NASA SP-3090

ASRDI OXYGEN TECHNOLOGY SURVEY

Volume IX:

Oxygen Systems Engineering Review

By Harold W. Schmidt and Donald E. Forney

Cryogenics Division, Institute for Basic Standards
National Bureau of Standards, Boulder, Colorado

Prepared for the
Aerospace Safety Research and Data Institute
NASA Lewis Research Center

Scientific and Technical Information Office 1975
NATIONAL AERONAUTICS AND SPACE ADMINISTRATION
Washington, D.C.

For sale by the National Technical Information Service
Springfield, Virginia 22161
Price – $7.50

PREFACE

This compendium is one of a series of publications on oxygen by the NASA Aerospace Safety Research and Data Institute. It is the result of an oxygen system engineering and technology review which was conducted to identify the special considerations for achieving safe and reliable oxygen systems. The document identifies the major problems affecting the reliability of oxygen systems, and it summarizes the basic oxygen technology applicable for the design, fabrication, and use of oxygen systems. Included is a compilation of data that helps to define the limiting conditions of use that oxygen "compatible" materials may be expected to withstand when used in oxygen systems.

The purpose of this volume is to show how oxygen systems may be designed and used safely and reliably by applying known engineering principles and past engineering experience.

Solomon Weiss, Acting Director
Aerospace Safety Research and Data Institute
National Aeronautics and Space Administration

Page intentionally left blank

FOREWORD

The design and operation of oxygen systems has been relatively routine, but the occasional accidents that have occurred during the handling and use of liquid and gaseous oxygen indicate a need for a better understanding of the reactivity of oxygen at temperatures and pressures beyond the familiar experience.

Technically, how to handle and use oxygen is primarily a matter of understanding the circumstances that cause oxygen to become reactive with its surroundings. Liquid and gaseous oxygen in contact with or mixed with most materials will not react or ignite without an ignition source. Therefore, problems are usually not experienced when designing for and operating oxygen systems at nominal pressures and temperatures. With higher oxygen system pressures and the resulting flow velocities, the severity of the oxygen environment is increased, the resulting sensitivity to ignition sources is increased, and the compatibility of materials with oxygen is decreased. The effect is a reduction in the number of candidate materials that can be used in such systems.

The environmental limits of time, temperature, pressure, flow rate, contamination, and other physical and chemical stresses that materials can be exposed to and withstand in oxidizer systems need to be defined and known for each application. This is necessary, too, for planning the research and development for extending the state-of-the-art in oxygen utilization. If compatibility data as functions of environmental conditions are provided, the state-of-the-art can be advanced with less risk of unknown factors, and engineering groups without high pressure oxygen experience will avoid the problems inherent in these systems.

Harold W. Schmidt

Page intentionally left blank

CONTENTS

Chapter		Page
	Preface	iii
	Foreword	v
1	Introduction	1
2	Characteristics of Oxygen	3
	2.1 PROPERTIES OF OXYGEN	6
	2.2 OXYGEN CONTAMINATION	6
	2.3 OXYGEN PURITY REQUIREMENTS	10
3	Materials Selection Criteria and Data	13
	3.1 OXIDE FILM FORMATION ON METALS	14
	3.2 CORROSION	18
	3.2.1 Chemical Corrosion	18
	3.2.2 Galvanic Corrosion	18
	3.2.3 Stress Corrosion	20
	3.3 CRACK PROPAGATION AND FATIGUE LIFE REDUCTION	20
	3.4 IGNITION OF MATERIALS	22
	3.4.1 Ignition Temperatures of Metals	24
	3.4.2 Ignition Temperature of Selected Nonmetal Materials	26
	3.4.3 Impact Energy Test Data for Metals and Nonmetals	29
	3.4.4 Ignition of Materials by Adiabatic Compression of Oxygen	31
	3.4.5 Ignition from Rupture of Materials	33
	3.4.6 Dynamic (Flow) Effects	35
	3.5 FLAMMABILITY AND COMBUSTION	37
	3.6 COMPATIBILITY TESTING	42
	3.6.1 NASA Specifications for Materials Compatibility Testing	42
	3.6.2 Tests Not Required by NASA	46

Chapter Page

3.7 PREFERRED POLYMERIC MATERIALS FOR OXYGEN SYSTEMS 51
3.7.1 Fluorocarbon Polymers 51
3.7.2 Silicone Polymers 54
3.7.3 Fiberglass 55
3.7.4 Polyimide Resins 55
3.7.5 Epoxy Resins 56

4 Oxygen Systems Engineering Considerations 57
4.1 FLUID SYSTEM LEAKAGE 57
4.1.1 Modes of Leakage 59
4.1.2 Leak Path Growth 60
4.1.3 Leak Clogging 60
4.1.4 Permeation 61
4.2 EROSION 63
4.3 SYSTEM DYNAMICS 67
4.4 GENERAL DESIGN CRITERIA 69
4.5 CLEANING REQUIREMENTS 72
4.6 COLD SHOCK CONDITIONING 73

5 Oxygen Tank Assemblies 75
5.1 GENERAL DESIGN AND SAFETY CONSIDERATIONS 77
5.1.1 Safety Standards and Specifications 77
5.1.2 Design Safety Factors and Proof Pressures 78
5.1.3 Corrosion 79
5.1.4 Stress Corrosion Cracking 80
5.1.5 Cyclic Stress and Cycle Life 80
5.1.6 Creep 81
5.1.7 Weld Joints 82
5.2 MATERIALS 84
5.3 INSULATION 84
5.4 TANK MAINTENANCE CONTROL 89
5.5 TANK OVERPRESSURE HAZARD 90

6 Oxygen Pumps 93
6.1 CENTRIFUGAL PUMPS 93
6.1.1 Pump Housing and Rotor Assembly 94
6.1.2 Turbopump Shaft Bearings 103
6.1.3 Turbopump Rotating Shaft Seals 107
6.2 POSITIVE DISPLACEMENT PUMPS 114

Chapter

7 Valve Assemblies 117
7.1 VALVE ELEMENT TYPES 118
7.2 GENERAL DESIGN CRITERIA 119
7.3 MATERIALS SELECTION 120
7.4 VALVE LIFE 122
7.5 INTERNAL LEAKAGE 122
7.5.1 Metallic Seats 123
7.5.2 Nonmetal Seats 124
7.6 VALVE ELEMENT ACTUATOR SEALS 124
7.7 EROSION 126
7.8 FILTRATION REQUIREMENTS 127

8 Lines, Connectors, Joints, and Fittings 129
8.1 ALLOWABLE WORKING PRESSURE 129
8.2 MATERIAL SELECTION 130
8.3 FLEXIBLE HOSE 131
8.4 BELLOWS 132
8.4.1 Flow Induced Vibration Failures 132
8.4.2 Bellows to Duct Attachment. 133
8.4.3 Bellows Materials. 133
8.5 COUPLINGS AND FITTINGS 134
8.5.1 AN, MS, and MC Couplings 134
8.5.2 Flanged Couplings 137
8.5.3 Threaded Pipe Couplings 139
8.6 WELDED AND BRAZED JOINTS 139
8.6.1 Welded Joints 139
8.6.2 Brazed Joints 141
8.7 LINE RUPTURE. 143

9 Seals 145
9.1 STATIC SEALS 145
9.2 DYNAMIC SEALS 149
9.2.1 Surface Finish Requirements 150
9.2.2 Friction of Dynamic O-Ring Seals 150
9.3 SEAL MATERIALS 150
9.3.1 Extrusion 152
9.3.2 Creep 155
9.3.3 Special Considerations for Very High Pressures 158
9.4 LEAK TESTS 160

Chapter | Page

10 Filters 163

Appendixes

A - Definition of Abbreviations and Acronyms and Trade Name Identification 167

B - Conversion Factors 173

C - Solubility of Hydrocarbons or Carbon Dioxide in Oxygen 179

D - Ignition Temperatures of Metals 181

E - Ignition Temperatures of Nonmetals 187

F - Combustion Rate Data 193

References 203

Index 212

CHAPTER 1. INTRODUCTION

The commercial availability and widespread use of oxygen by the general public, industry, NASA, and other federal agencies have made the handling of oxygen commonplace and routine. However, it has been stated that, in general, oxygen is so easy to handle that it can be dangerous. When an incident occurs with oxygen it can be catastrophic in nature, and the vigorous burning of a part of the system, or an explosion, can occur. Because they are rare, these occurrences are always unexpected. Oxygen system failures are most often associated with a change from a steady-state condition. They are also associated with contamination that is sensitive to ignition with oxygen.

Accident prevention in the use of oxygen requires understanding the characteristics of the fluid being handled, recognizing the limits of compatibility of materials with oxygen, and maintaining a clean system. The purpose of this volume is to provide the physical and chemical background information which will be helpful in meeting these requirements. It is the function of the designer to reduce or eliminate the possibility of oxygen system failure by anticipating potential operating problems and selecting appropriate materials, configurations, and controls. Accordingly, the emphasis of this review is on design. However, where they are pertinent, considerations for assembly, maintenance, and operations are an integral part of the review.

The following chapters discuss many of the special considerations that should be taken into account. They also attempt to provide an understanding of the characteristics of gaseous and liquid oxygen and how to deal with them under various circumstances. Understanding the behavior of oxygen with materials under use conditions reduces the possibility of system failures. Also reduced are the potential hazards and their resulting costs and time losses.

The subject is covered in four parts: (1) oxygen characteristics, purity, and specifications (ch. 2), (2) compatibility of materials with oxygen (ch. 3), (3) fluid flow phenomena and fluid system characteristics of special concern in oxygen systems (ch. 4), and (4) engineering review of oxygen systems and components (chs. 5 to 10). The first two parts provide an insight into the nature of oxygen - its characteristic behavior with other materials and how this behavior varies with operating conditions. The last two parts deal primarily with the application of oxygen technology to fluid systems and their components.

Special effort has been made to compile and correlate data on ignition energies and burning rates of materials in various oxygen environments. Although the data came from many sources using different techniques, good correlation was obtained on the effect of oxygen pressure (and partial pressure) on burning rates and ignition temperatures.

Operating pressure ranges as they are used in this document are defined as follows:

Low pressure	0 to 500 psia
Medium pressure	500 to 2000 psia
High pressure	2000 to 7500 psia
Very high pressure	7500 to 10 000 psia
Ultra-high pressure	10 000 to 15 000+ psia

While the general design considerations for oxygen systems for both flight and ground-based hardware are essentially the same, the problems encountered in flight hardware design are often more severe. This is true because of the weight limitations and lower structural margins of safety for flight hardware and the more critical nature of the flight environment. For this reason the two classes of hardware are usually treated separately in this review.

A microfiche supplement covering the pertinent pages of the references listed is attached to the back cover for the convenience of the reader. (Commonly available handbooks and copyrighted text books are not included.) An index to the microfiche supplement is included as a part of the list of references. Definitions of terms, acronyms, and trade names are included in appendix A. Also, since the units used throughout the volume are generally those of the references, conversion factors are included as appendix B.

CHAPTER 2. CHARACTERISTICS OF OXYGEN

Oxygen occurs naturally as one of the elements and is one of the five strongest elemental oxidizers along with fluorine, chlorine, bromine, and iodine (the halogens). Under most circumstances oxygen reacts very slowly or not at all. But under other circumstances it becomes highly reactive and will react with fuels at high energy release rates. It is this reactivity which is the primary reason for special concern when designing hardware to be used in oxygen service. Under certain conditions the elemental oxidizers oxygen and fluorine and the fluorine-oxygen mixtures (FLOX) have the same characteristics and behave in the same manner:

(1) They form oxidation films on metals that inhibit further reaction.

(2) They ignite spontaneously with fuels at their respective ignition temperatures.

(3) They burn metals and most nonmetals vigorously when ignited.

Oxygen reacts with nearly all materials that are not already fully oxidized. However, oxygen is more able to mix and form explosive mixtures with gases, liquids, and solids than with either FLOX or fluorine. Fluorine is too reactive (hypergolic) to mix with most materials and instead reacts on contact at whatever rate the reactants are combined. The passive mixing characteristics of oxygen are the basis for its greatest hazard: once the oxygen-fuel mixture is ignited, the reaction may proceed violently, even explosively. The most common hazard exists when gaseous oxygen is mixed with any vaporized fuel, thus forming an easily ignited and frequently explosive mixture. Of nearly equal concern is the absorption of oxygen by porous solids such as clothing which, when ignited, may burn vigorously. Similarly, a liquid oxygen spill may soak a solid fuel material, such as asphalt paving, and form an extremely reactive or explosive mixture. Oxygen in the liquid state is also potentially hazardous due to its extremely low temperature.

Recognition of these basic characteristics of oxygen is necessary to evaluate the safety of any oxygen system and is important in preventing system failure and the resulting hazards, cost, and time loss. The more subtle characteristics, that is, its potential reactivity in fluid systems due to pressure, temperature, and flow effects, are discussed in succeeding sections of this volume.

TABLE 2-I. - FIXED POINT PROPERTIES OF OXYGEN[a]

[Values in parenthesis are estimates.]

(a) Metric units (ref. 1, p. 314); gas constant, R = 62 365.4 cm^3-mm Hg/mole-K; molecular weight, 31.9988, mole = gram mole

Properties		Conditions							
		Triple point			Normal boiling point		Critical point	Standard conditions	
		Solid	Liquid	Vapor	Liquid	Vapor		STP (0° C)	NTP (20° C)
Temperature, K		54.351			90.180[b]		154.576	273.15	293.15
Pressure, mm Hg		1.138			760		37 823	760	760
Density, $(mole/cm^3)\times10^3$		42.46	40.83	0.000336	35.65	0.1399	13.63	0.04466	0.04160
Specific volume, $(cm^3/mole)\times10^{-3}$		0.02355	0.02449	2975	0.028047	7.1501	0.07337	22.392	24.038
Compressibility factor, Z = PV/RT		-------	0.0000082	0.9986	0.00379	0.9662	0.2879	0.9990	0.9992
Heats of fusion and vaporization, J/mole		444.8	7761.4		6812.3		0	-------	-------
Specific heat, J/mole-K	At saturation, C_s	46.07	53.313	-108.7	54.14	-53.2	(Very large)	-------	-------
	At constant pressure, C_r	--------	53.27	29.13	54.28	30.77	(Very large)	29.33	29.40
	At constant volume, C_v	--------	35.65	20.81	29.64	21.28	(38.7)	20.96	21.04
Specific heat ratio, $\gamma = C_p/C_v$		--------	1.494	1.400	1.832	1.446	(Large)	1.40	1.40
Enthalpy, J/mole		-6634.4	-6189.6	1571.8	-4270.3	2542.0	1032.2	7937.8	8525.1
Internal energy, J/mole		-6634.4	-6189.6	1120.0	-4273.1	1817.5	662.3	5668.9	6089.5
Entropy, J/mole-K		58.92	67.11	209.54	94.17	169.68	134.42	202.4	204.5
Velocity of sound, m/sec		--------	1159	141	903	178	164	315	326
Viscosity, μ	$(N\text{-}sec/m^3)\times10^3$	--------	0.6194	0.003914	0.1958	0.00685	(0.031)	0.01924	0.02036
	Centipoise[c]	--------	0.6194	0.003914	0.1958	0.00685	(0.031)	0.01924	0.02036
Thermal conductivity, k, mW/cm-K		--------	1.929	0.04826	1.515	0.08544	(d)	0.2428	0.2575
Prandtl number, $N_{pr} = uC_p/k$		--------	5.344	0.7392	2.193	0.7714	----------	0.7259	0.7265
Dielectric constant, ϵ		(1.614)	1.5687	1.000004	1.4870	1.00166	0.17082	1.00053	1.00049
Index of refraction,[e] $n = \sqrt{\epsilon}$		(1.271)	1.2525	1.000002	1.219	1.00083	1.0820	1.00027	1.00025
Surface tension, $(N/m)\times10^3$		--------	22.65	--------	13.20	-------	0	-------	-------
Equivalent volume/volume liquid at NBT		0.8397	0.8732	106 068	1	254.9	2.616	798.4	857.1

(b) English units (ref. 1, p. 414); gas constant, R = 0.335385 ft^3-psi/lb-^oR

Properties		Conditions							
		Triple point			Normal boiling point		Critical point	Standard conditions	
		Solid	Liquid	Vapor	Liquid	Vapor		STP (32^o F)	NTP (68^o F)
Temperature, ^oF		-361.84			-297.35[b]		-181.43	32.0	68.0
Pressure, psia		0.0220			14.696		731.4	14.696	14.696
Density, lb/ft^3		84.82	81.57	0.0006715	71.23	0.2794	27.23	0.0892	0.0831
Specific volume, ft^3/lb		0.01179	0.01226	1489.2	0.01404	3.5793	0.03673	11.21	12.03
Compressibility factor, Z = PV/RT		-------	0.0000082	0.9985	0.00379	0.9662	0.2879	0.9990	0.9992
Heats of fusion and vaporization, Btu/lb		5.967	104.348		91.588		0	-------	-------
Specific heat, Btu/lb-^oR	At saturation, C_s	0.345	0.398	-0.812	0.404	-0.397	(Very large)	-------	-------
	At constant pressure, C_p	-------	0.398	0.218	0.405	0.230	(Very large)	0.219	0.220
	At constant volume, C_v	-------	0.266	0.155	0.221	0.159	(0.289)	0.157	0.157
Specific heat ratio, $\gamma = C_p/C_v$		-------	1.496	1.406	1.833	1.447	(Large)	1.40	1.40
Enthalpy, Btu/lb		-89.192	-83.216	21.132	-57.412	34.176	13.88	106.72	114.62
Internal energy, Btu/lb		-89.192	-83.216	15.057	-57.450	24.435	8.90	76.22	81.875
Entropy, Btu/lb-^oR		0.4401	0.50122	1.5651	0.70339	1.2674	1.004	1.5123	1.5278
Velocity of sound, ft/sec		-------	3804	461	2963	583	537	1033	1070
Viscosity, μ	(lb/sec-ft)$\times 10^5$	-------	41.62	0.263	13.16	0.460	(2.1)	1.293	1.368
	Centipoise[c]	-------	0.6194	0.003914	0.1958	0.00685	(0.031)	0.01924	0.02036
Thermal conductivity, k, Btu/hr-ft-^oR		-------	0.11156	0.00279	0.08758	0.00494	(d)	0.01404	0.01489
Prandtl number, $N_{pr} = uC_p/k$		-------	5.3437	0.7392	2.1929	0.7714	----------	0.7259	0.7265
Dielectric constant, ϵ		(1.614)	1.5687	1.000004	1.4870	1.00166	1.17082	1.00053	1.00049
Index of refraction,[e] $n = \sqrt{\epsilon}$		(1.271)	1.2525	1.000002	1.219	1.00083	1.0820	1.00027	1.00025
Surface tension, (lb/ft)$\times 10^3$		-------	1.552	---------	0.9046	-------	0	-------	-------
Equivalent volume/volume liquid at NBT		0.8397	0.8732	106 068	1	254.9	2.616	798.4	857.1

[a] For basic data sources the reader is referred in ref. 1.

[b] Based on the NBS-1955 temperature scale using 90.180 K as a fixed point for the normal boiling temperature of oxygen. (The IPTS-1968 temperature scale used 90.188 K as the normal boiling temperature of oxygen but the reported data used in these tables has not yet been converted to the new temperature scale.) 273.15 K = 0^o C = 32^o F = 491.67^o R

[c] Units for poise, g/cm-sec.

[d] Anomalously large.

[e] Long wavelengths.

2.1 PROPERTIES OF OXYGEN

Fixed point properties of oxygen are included in table 2-I(a) (Metric Units) and 2-I(b) (U. S. Customary Units). More precise tabular data are presented in reference 1 (pp. 145-420).

2.2 OXYGEN CONTAMINATION

One cause of failure in oxygen systems is contamination. Contamination may be introduced during the manufacture of the oxygen or, subsequently, during the handling or final use. In liquid oxygen, dissolved contaminants are primarily hydrocarbons although other materials such as carbon dioxide (CO_2) are slightly soluble. Solid contaminants in both liquid and gaseous oxygen include particulates such as wear particles or dislodged oxides. In liquid oxygen, moisture and frozen undissolved contaminants, such as CO_2 or acetylene, may accumulate in the system.

Hydrocarbons are present in atmospheric air from which oxygen is generated. These are partially removed during oxygen production. The heavier (high molecular weight) hydrocarbons are removed to insignificant concentrations during initial distillation but light (low molecular weight) hydrocarbons such as methane, acetylene, ethane, ethylene, propane, and butane may remain with the oxygen. These are further decreased by further distillation and subsequently reduced to acceptable levels with silica gel absorbers.

Hydrocarbon contamination may be reintroduced through various means during subsequent handling and transfer. Since most of the common contaminants are less volatile than liquid oxygen they tend to increase in concentration during handling and storage. The normal (atmospheric) boiling points and freezing points of some air contaminants are given in table 2-II (ref. 2).

Whenever a hydrocarbon is present in LOX in quantities greater than its solubility limit it separates out as a liquid or a solid depending on the freezing point. It may also accumulate in the system. Solid hydrocarbons in liquid oxygen could be explosive if subjected to an ignition source such as friction, shock wave, or impact. Severe damage from explosion and fire could result. Subsequent warming of the system can vaporize the liquid oxygen and the contaminant which could result in an explosive mixture. In fact, the low molecular weight hydrocarbons (i.e., methane, ethane, and propane) have a solubility limit which exceeds their respective lower flammability limits when vaporized.

Tables 2-III and 2-IV (refs. 2 and 3) give solubility limits in liquid oxygen (at normal boiling point) and flammability limits in gaseous oxygen for some of the more common contaminants. Solubilities as a function of temperature are given in appendix C while table 2-V (ref. 4) lists the detonability limits of some fuels in gaseous oxygen.

TABLE 2-II. - PROPERTIES OF SOME AIR CONTAMINANTS[a]

Name	Density at -297.3° F, g/cm³	Normal boiling point		Freezing point	
		°F	°C	°F	°C
Helium	-----	-452.0	-268.89	[b]-455.8	-271.11
Hydrogen	-----	-423.0	-252.78	-434.5	-259.11
Neon	-----	-410.6	-245.99	-415.6	-248.57
Nitrogen	-----	-320.4	-195.75	-345.7	-209.75
Carbon monoxide	-----	-310.0	-190.00	-340.6	-206.95
Argon	-----	-302.3	-185.70	-308.7	-189.34
Oxygen	1.15	-297.3	-182.88	-361.1	-218.34
Methane	-----	-258.7	-161.53	-299.2	-183.99
Krypton	-----	-243.2	-152.98	-249.9	-156.57
Nitric oxide	-----	-241.2	-151.87	-262.5	-163.56
Ozone	-----	-169.4	-111.67	-313.8	-192.02
Xenon	-----	-160.8	-107.02	-169.6	-111.94
Ethylene	.727	-155.0	-103.89	-272.9	-169.34
Ethane	-----	-126.9	-88.23	-277.6	-171.97
Nitrous oxide	-----	-127.3	-88.53	-152.3	-102.42
Acetylene	.625	[c]-118.5	-83.51	-115.2	-81.87
Carbon dioxide	1.58	[c]-109.3	-78.53	-69.9 (5.2 atm)	-56.57
Hydrogen sulfide	-----	-79.2	-61.87	-117.2	-82.98
Carbonyl sulfide	1.65	-54.4	-47.98	-216.4	-137.98
Propylene	.775	-52.6	-46.97	-301.4	-185.25
Propane	-----	-43.9	-42.12	-309.8	-189.84
Ammonia	1.01	-28.0	-33.33	-107.9	-77.68
Formaldehyde	-----	-5.8	-20.91	-133.6	-91.97
iso-Butane	-----	10.4	-11.92	-229.0	-145.00
iso-Butylene	-----	21.2	-5.96	-220.5	-140.28
1-Butene	-----	23.0	-5.00	-202.0	-130.00
1,3-Butadiene	-----	26.7	-3.03	-164	-108.89
n-Butane	.770	31.1	-.49	-211.0	-135.00
2-Butene	-----	33.8 (cis)	1.01	-218	-138.89
Ethylene oxide	-----	51.3	10.76	-168.3	-111.31
Acetaldehyde	-----	69.8	21.01	-190.3	-123.53
Nitrogen dioxide	-----	70.3	21.31	15.3	-9.24
n-Pentane	-----	97.2	36.21	-204.7	-131.45
Acetone	-----	133.7	56.47	-139.0	-95.00
Methanol	.815	148.4	64.68	-144.0	-97.78
Hexane	.795	156.2	68.99	-137.7	-94.04
Benzene	-----	176.2	80.16	41.9	5.51
Water	-----	212.0	100.00	32.0	0.00
n-Decane	-----	345.2	173.99	-23.8	-30.91

[a]Ref. 2, p. 48.
[b]Lambda point.
[c]Sublimes.

TABLE 2-III. - SOLUBILITY LIMIT[a] OF HYDROCARBONS IN LIQUID OXYGEN[b]

Solubility at -297.3° F (-183° C).

Gas	Solubility	
	ppm - methane equivalent	ppm - moles
Methane	980 000.0	980 000.0
Ethane	430 000.0	215 000.0
Propane	150 000.0	50 000.0
Ethylene	55 000.0	27 500.0
Propylene	20 100.0	700.0
i-Butane	7 640.0	1 910.0
Butene-1	4 000.0	1 000.0
n-Butane	3 440.0	860.0
i-Butylene	530.0	135.0
n-Pentane	[c]100.0	[c]20.0
Acetylene	10.0	5.0 ([c]1.7)
n-Hexane	[c]12.0	[c]2.0
n-Decane	[c]6.0	[c].6
Acetone	[c]4.5	[c]1.5
Methanol	[c]12.0	[c]12.0
Ethanol	[c]30.0	[c]15.0
Carbon dioxide	[c]4.2	[c]4.2

[a]Solubility limits as function of oxygen temperature are presented graphically in appendix D.

[b]Ref. 2, p. 55.

[c]Ref. 3, p. 113-M.

TABLE 2-IV. - LOWER FLAMMABILITY LIMIT OF HYDROCARBONS SOLUBLE IN LIQUID OXYGEN[a]

Gas	Flammability units	
	ppm - methane equivalent	ppm - moles
Methane	50 000	50 000
Ethane	60 000	30 000
Propane	63 600	21 200
Ethylene	55 000	27 500
Propylene	60 000	20 000
i-Butane	72 000	18 000
Butene-1	64 000	16 000
n-Butane	74 400	18 600
i-Butylene	72 000	18 000
n-Pentane	70 000	14 000
Acetylene	50 000	25 000
n-Hexane	70 800	11 800
n-Decane	77 000	7 700

[a]Refs. 2 (p. 55) and 3 (p. 117-M).

TABLE 2-V. - DETONABILITY LIMITS OF GAS-OXYGEN MIXTURES, DETERMINED USING 400 J HIGH EXPLOSIVE DETONATOR FOR INITIATION[a]

Gas	Lower detonability limit[b] (volume percent gas)	Upper detonability limit[c] (volume percent gas)
Acetaldehyde	12 to 14	46 to 50
Acetylene	6.5 to 7	67 to 69
Carbon disulfide	12 to 13	[d]>46
Cyclopropane	6.5 to 7	38 to 40
Diethyl ether	4.5 to 5	28 to 30
Ethane	10 to 12	38 to 40
Ethylene	9 to 9.5	50 to 52
Ethylene oxide	8 to 9	64 to 66
Ethyl nitrite	4 to 4.5	58 to 62
Methylacetylene	5.5 to 6	48 to 50
Methyl vinyl ether	5 to 5.5	44 to 46
Propadiene	5 to 5.5	48 to 50
Propane	6.5 to 7.5	30 to 32
Propylene	6.5 to 7	36 to 38
Vinyl fluoride	11 to 12	54 to 56

[a]Ref. 4, p. 384.

[b]Detonation was observed at the higher gas concentration but was not observed at the lower gas concentration.

[c]Detonation was observed at the lower gas concentration but was not observed at the higher concentration.

[d]Experiments at higher gas concentration not possible due to vapor pressure limitations.

Note the very low solubility of acetylene in table 2-V. It is less dense than liquid oxygen and can readily accumulate in liquid oxygen systems. Also, acetylene is a highly unsaturated hydrocarbon (with a triple bond) which makes it unstable and highly reactive (shock and heat sensitive) in oxygen to a greater degree than the other hydrocarbons. Therefore, acetylene is highly undesirable as a contaminant and its presence in oxygen is generally limited to 0.05 ppm or less. Because of these characteristics it is generally measured separately from the rest of the hydrocarbons which are measured as a group and reported as an equivalent amount of methane based on carbon atom content.

Solid contaminants, in addition to the fire and explosion hazard, present the added hazards of mechanical malfunction and plugging or the restriction of flow. System fail-

ures due to these hazards can be minimized by controlling the purity of the oxygen and maintaining adequate system cleanliness. Most solid hydrocarbon impurities are lighter than LOX. (See contaminant densities in table 2-II.) They tend to float and accumulate at liquid level surfaces. This may be observed by examining the walls in a LOX storage tank. If impurities have been present, there may be a ring in the tank near the usual liquid level.

In general, the contamination of oxygen will increase as it is handled or stored. As liquid oxygen is lost by vaporization, contaminant concentration increases. Whenever a system is opened for repair or even for transfer line connect and disconnect operations contamination may enter the system. Long term wear and deterioration of mechanical components may contribute to particulates. Even residue from solvents used for cleaning may be a source of added contamination. These are the reasons why it is important to maintain rigid cleanliness practices and provide filters in stategic locations in some oxygen systems. (See chapter 10 on FILTERS.)

It is evident that control of the various sources of contamination mentioned previously is critical to the safe operation of oxygen systems. While specific control procedures are a function of system complexity and product end use, many techniques for such control have evolved. Contamination control procedures and specifications and oxygen quality control tests and test methods are listed in references 2 (appendix 3), 5 (sec. 4), 6, and 7 (secs. 2 and 3). Cleaning procedures and verification techniques are discussed in reference 8.

2.3 OXYGEN PURITY REQUIREMENTS

Oxygen purity-level requirements are dictated by the effect the contaminants have on the end use item. For example, fuel cells are sensitive to some impurities that would be acceptable for life support systems. The requirement for extremely high purity oxygen for fuel cells is necessitated to avoid contamination of the diffusion membranes. Toxic contaminants such as nitrous oxide and the chlorinated hydrocarbons are of concern for breathing oxygen.

The purity requirements for oxygen purchased by NASA for launch vehicle and spacecraft use are contained in MSFC (Marshall Space Flight Center) Specification 399A (ref. 6). Table 2-VI from this specification is a summary of those requirements including permissible specific contaminant levels. Procedures for purity verification are also included in reference 6. Oxygen systems cleanliness requirements and cleaning procedures are discussed in section 4.4.

TABLE 2-VI. - OXYGEN PURITY REQUIREMENTS[a]

[For grade A oxygen - all other impurities including inert gases and nitrogen, 30 ppm.]

Requirement	Grade A for fuel cells	Grade B for breathing	Grade C for propellant
Purity	99.995	99.60	99.60
Methane and ethane	Methane, 10 ppm Ethane, 2.0 ppm	Methane, 25.0 ppm Ethane, 2.0 ppm	No requirement
Propane and higher hydrocarbons	1.0 ppm as propane	1.0 ppm as propane	No requirement
Alkyne and acetylene hydrocarbons	0.05 ppm as acetylene	0.05 ppm as acetylene	0.25 ppm as acetylene
Total hydrocarbons	14.0 ppm as methane	29.0 ppm as methane	50.0 ppm as methane
Moisture	3.0 ppm	3.0 ppm	3.0 ppm
Nitrous oxide	1.0 ppm	1.0 ppm	No requirement
Halogenated hydrocarbons	1.0 ppm	1.0 ppm	No requirement
Odor	No odor	No odor	No requirement
CO and CO_2	1.0 ppm total	5.0 ppm carbon monoxide 5.0 ppm carbon dioxide	No requirement
Particulate	1.0 mg/liter max. (liquid only)	1.0 mg/liter max. (liquid only)	1.0 mg/liter max. (liquid only)

[a]Ref. 6, p. 2.

Page intentionally left blank

CHAPTER 3. MATERIALS SELECTION CRITERIA AND DATA

The reactivity of materials with oxygen depends on their conditions of exposure to oxygen and their physical and chemical properties. Except for most oxides and inert gases, most materials can react with oxygen. The reaction of oxygen with these materials may occur very slowly, such as the rusting of iron or oxidation of an aluminum surface, at a high rate, commonly observed as combustion or burning, or explosively, where the rate of reaction is nearly instantaneous. However, most materials will not burn when exposed to liquid or gaseous oxygen because their ignition temperatures are generally much higher than normal exposure temperatures. Oxygen system failures that occur during routine operations with oxygen are frequently characterized by an unexpected ignition of a part of the system from a localized energy source - the energy added being sufficient to reach the ignition temperature of the material involved.

If the energy input rate (power input) as converted to heat is greater than the rate of heat dissipation, and if it is continued for a sufficient time to reach the ignition temperature, ignition and combustion will occur. Sources of energy input per unit time (power) that may provide sufficient heat flux to cause ignition temperatures may include one or more of the following: mechanical impact, abrasion, rubbing friction, puncture, or rupture; surface shock from explosions, water hammer, pressure spikes, and shock waves; erosive fluid flow; electrical sparks or arcing; chemical reaction from sudden exposure of unoxidized surface or pockets of contamination; and heat transfer from an external source. Therefore, an understanding of the quantitative energy sources and energy release rates capable of causing combustion or explosion of a material is very important. If ignition temperature and burning rate data are considered, proper design and operational considerations can help eliminate potential ignition energy sources or accommodate them through the selection of proper materials. Existing data have been generated mainly by independent investigations to resolve the immediate problems of selecting the proper materials. Accordingly, because of varying techniques, procedures, specimen selection, and purpose, the data sometime appear to be scattered and incomplete. However, when all the data are used together, sufficient ignition temperature and burning rate data exist to evaluate the materials selected for given applications; these data are presented in the following sections. Although the burning rate of a material is an important factor when selecting materials for oxygen use (in the event an ignition would occur),

the ignition temperature is the most important parameter in preventing ignition and a possible fire hazard. To avoid ignition and fire with oxygen, it is desirable to use materials with ignition temperatures as high as possible. In addition, it is desirable to use materials and design criteria that would provide for maximum possible heat dissipation by thermal conduction. This would tend to require a greater power input to reach the ignition temperature. And finally, where possible, materials with the lowest heat of reaction with oxygen would contribute less energy to sustain combustion. The closer the initial temperature of the system is to the ignition temperature of the material the easier ignition becomes because less energy is required. The apparent ignition temperature may vary depending on exposure conditions such as the presence of an oxide film; the pressure, temperature, phase, and concentration of oxygen; and the rate of mechanical, electrical, or chemical energy input.

Therefore, it is desirable to provide engineering designs for fluid systems which preclude excessive energy releases, and it is necessary to provide a valid factor of safety by choosing materials to meet all possible environmental conditions. To do this, two things must be known: (1) the ignition temperature (or ignition energy requirements) of the material, and (2) the energy sources and energy release rates to which the material may be exposed under worst case combinations of power input. The selection of materials for use in oxygen systems has, up to the present time, been based largely on use experience and standardized impact and flammability tests. These tests are described in section 3.6. However, the final selection of a material for oxidizer applications is a trade-off between the chemical compatibility, the ignition and combustion characteristics, and the physical properties of the material. Material selection is based only on use experience, and precedence is acceptable if the use conditions are the same and ignition and burning rate data are not available. However, it is always better to review the possible ignition factors carefully to be sure the precedent is applicable.

The many trade-off factors to be considered when selecting materials are discussed in succeeding sections.

3.1 OXIDE FILM FORMATION ON METALS

Solid or quiescent liquid metals will form surface oxide films when exposed to oxygen environments. For a given metal the instantaneous rate of oxide film formation is primarily a function of temperature and pressure and of oxide film thickness. This is illustrated schematically in figure 3-1. The higher the initial surface temperature, the higher the rate of reaction and, thus, of initial oxide film growth. However, the oxide film tends to prevent the oxygen from contacting the base metal; for further reaction the oxygen must diffuse through the oxide film. Therefore, the reaction becomes diffusion rate limited, and the film growth reaction rate decreases and approaches zero with time.

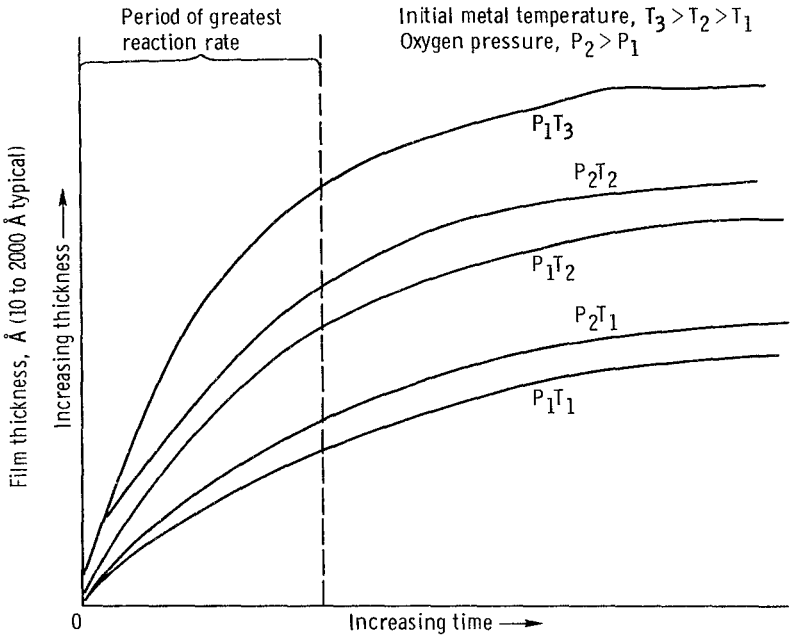

Figure 3-1. - Typical oxide film formation on metal surfaces.

The resulting film forms a protective barrier which inhibits further reaction. Increasing the oxygen partial pressure can increase the reaction rate by increasing the diffusion rate, but the protective film formed, although thicker than before, will continue to approach zero growth with time and provide protection from the higher pressure conditions.

Studies of oxide film growth on various materials indicate the rate of growth may be linear, parabolic, cubic, or logarithmic when the film thickness is plotted against time. For some materials and conditions the rate may follow a combination of all four profiles. Film formation on most metal surfaces approaches maximum thickness within a few minutes to several hours, depending on the materials and temperature.

Since the process of film formation is a chemical reaction, the heat of reaction may become significant in some cases. For example, powdered metals with a very high surface area to mass ratio may ignite when exposed to oxygen, or even air at room temperature, because the heat of reaction from film formation is sufficient to raise the metal particles to their ignition temperature. Similarly, if a bulk metal is exposed to a temperature near enough to its ignition temperature, sudden exposure of an unoxidized surface (such as from rupture or puncture) and subsequent heat of reaction may be sufficient to initiate combustion. The rate of film growth or oxidation, as illustrated in figures 3-2 and 3-3 (refs. 9 and 10), indicates an increase in reaction rate as the temperature is increased. Figure 3-3 illustrates a linear film growth rate which is typical of magnesium above the critical temperature (approximately 425° C). Note that the very high rate of oxide formation on magnesium is 550° to 575° C. The ignition temperature is only 625° C.

As illustrated by the data in figures 3-2 and 3-3, when the temperature of the materials exposed to oxygen approaches (but does not reach) the ignition temperature of the

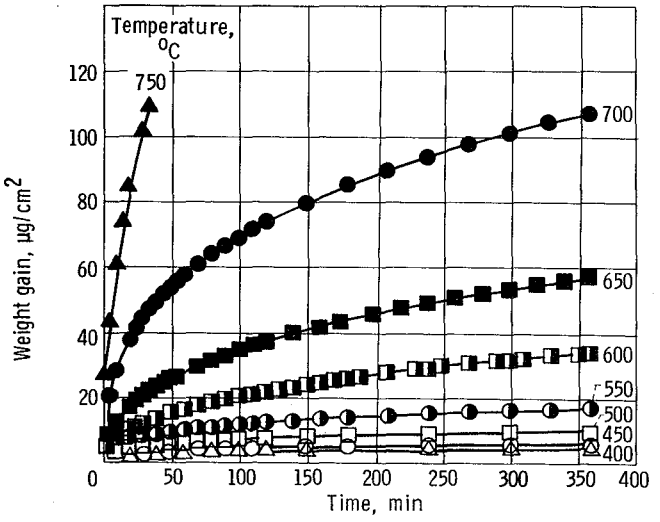

Figure 3-2. - Film growth on nickel as function of time and temperature (ref. 9, p. 492).

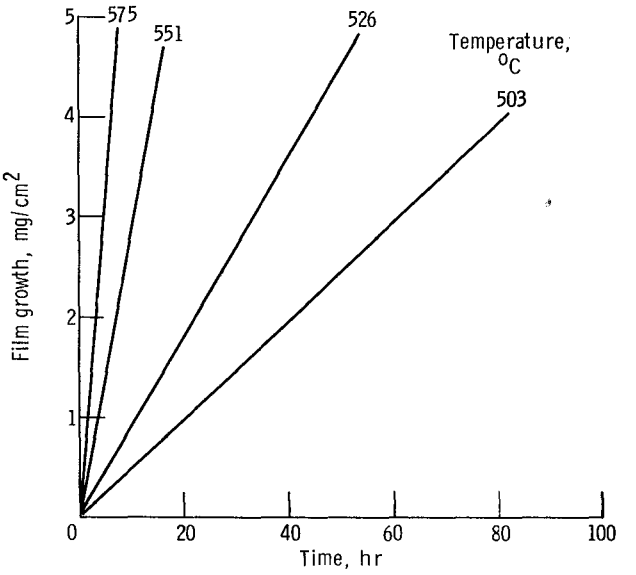

Figure 3-3. - Oxidation of pure magnesium in oxygen at various temperatures (ref. 10, p. 46). Ignition temperature, 625° C.

materials, the film formation rate may become catastrophic; that is, the film loses its protective capability and a continuous surface deterioration occurs. The rate of deterioration depends on the diffusion rate of the reactants through the oxide film.

A noncombustive, catastrophic reaction or film formation can occur when any of the following conditions exist:

(1) A metal or alloy is exposed to oxygen at a temperature approaching the ignition temperature of the alloy or one of its constituents[1].

(2) The material forms an oxide with a melting point below the exposure temperature[1].

(3) The exposure temperature exceeds the melting point of the base metal[1].

(4) A metal or alloy forms a relatively volatile oxide at the exposure temperature.

(5) The specific volume of the oxide formed is less than the specific volume of the base material, which would not permit complete coverage of the surface at any given time.

For example, the oxidation of iron alloy 15Mo-75Fe-10Cr exposed to oxygen at 910° and 1000° C is catastrophic (fig. 3-4 (ref. 11)). The oxides formed on the surface of this material are as follows:

[1]Ignition temperatures and melting points of selected metals and their oxides are given in the table on p. 17.

Oxide	Melting point, ^{o}C
Chromium oxide (Cr_2O_3)	2435
Iron oxide (Fe_2O_3)	1565
Molybdenum oxides:	
MoO_3	795
MoO_2	778
MoO_3 eutectic	778

In this case, the melting points of the oxide of one constituent (MoO_3) and its eutectic are below the test temperature. The MoO_3 formed can diffuse to the base metal and aid in oxidizing the surface. Not only does the MoO_3 formed aid in oxidizing the base metal, but, since it melts at the test temperature, it leaves the surface unprotected. At temperatures below the critical temperature (778° to 795° C) catastrophic oxidation does not occur. Above the critical temperature (910° to 1000° C), however, the rate of catastrophic oxidation increases very rapidly as shown in the example given in figure 3-4.

Another effect is the volatility of the oxide contributing to catastrophic oxidation as shown in figure 3-5 (ref. 12). Normal film formation occurs when tungsten is exposed to

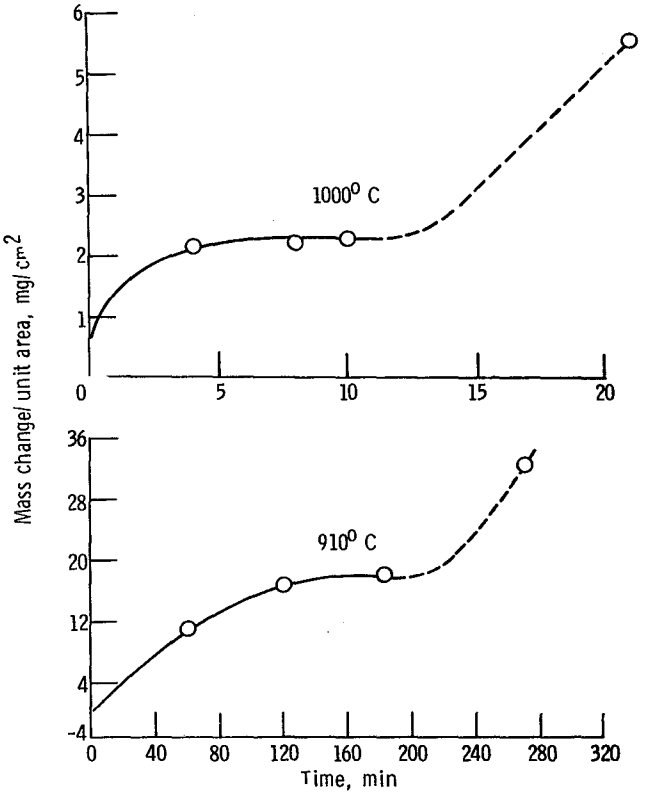

Figure 3-4. - Oxidation of 15Mo-75Fe-10Cr alloy (ref. 11, p. 18).

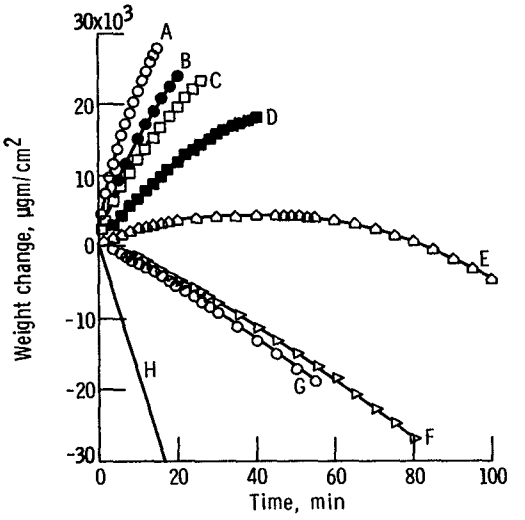

Figure 3-5. - Oxidation of tungsten at 1050° C. Effects of pressure: A, 0.1 atmosphere; B, 0.0512 atmosphere; C, 0.0263 atmosphere; D, 0.0112 atmosphere; E, 0.0066 atmosphere; F, 0.0033 atmosphere; G, 0.00131 atmosphere; H, volatility WO_3 (ref. 12, p. 623).

oxygen at 950° to 1050° C. The melting point of the oxide formed WO_3 is 1473° C; when the pressure is reduced as indicated, WO_3 is sufficiently volatile to sublime, and rapid weight loss is indicated.

For an additional discussion of surface oxidation phenomena and experimental test results see chapter 4 of reference 13.

3.2 CORROSION

The term corrosion is used to describe three surface reactions: stress corrosion, chemical corrosion, and galvanic corrosion. These could be classed as catastrophic. The phenomena should not be confused with film formation. As previously emphasized, film formation is a regressive, protective process; corrosion, on the other hand, is a progressive, destructive process that continues as long as both reactants are in contact.

3.2.1 Chemical Corrosion

The chemical corrosion is a straightforward chemical reaction of a fluid with the metal surface like the attack of salt solution on metal automobile bodies. The rate of attack or corrosion is determined by the temperature at the reaction zone and the type and concentration of the reactants. Although oxygen in a pure state is noncorrosive, the film formation phenomenon which is normally self-limiting can become propagating if the normal protective oxide film is compromised. For example, the presence of impurities such as moisture or other contaminants in the oxygen (or air) can result in serious chemical corrosion. Moisture is especially corrosive because the oxides are partially soluble in water which permits ionization: Consequently, an accelerated reaction results. For this reason oxygen systems must be kept clean and dry and their external surfaces protected from corrosion where necessary.

3.2.2 Galvanic Corrosion

Galvanic corrosion occurs where dissimilar metals are in contact in the presence of an electrolyte. Any fluid or substance that can conduct an electric current will do so by transferring ions from the cathode to the anode; in the process, the anode surface is destroyed. The presence of moisture or contaminants accelerates the corrosion of the dissimilar metal junction.

If metals are arranged in the order according to their electromotive potential, the more widely they are separated the greater the electromotive potential between them.

TABLE 3-I. - METAL COUPLES[a]

Group	Metallurgical category	Electro-motive force, V	Permissible couples[b]
1	Gold, solid and plated; gold-platinum alloys; wrought platinum	0.15	
2	Rhodium, graphite	0.05	
3	Silver, solid or plated; high silver alloys	0	
4	Nickel, solid or plated; Monel metal, high nickel-copper alloys, titanium	-0.15	
5	Copper, solid or plated; low brasses or bronzes; silver solder; German silver; high copper-nickel alloys; nickel-chromium alloys; austenitic stainless steels	-0.20	
6	Commercial yellow brasses and bronzes	-0.25	
7	High brasses and bronzes; Naval brass; Muntz metal	-0.30	
8	18 Percent chromium type corrosion-resistant steels	-0.35	
9	Chromium, plated; tin, plated; 12 percent chromium type corrosion-resistant steels	-0.45	
10	Tin-plate; terneplate; tin-lead solders	-0.50	
11	Lead, solid or plated; high lead alloys	-0.55	
12	Aluminum, wrought alloys of Duralumin type	-0.60	
13	Iron, wrought, gray, or malleable; plain carbon and low alloy steels, Armco iron	-0.70	
14	Aluminum, wrought alloys other than Duralumin type; aluminum, cast alloys of the silicon type	-0.75	
15	Aluminum, cast alloys other than silicon type; cadmium, plated and chromated	-0.80	
16	Hot-dip-zinc plate; galvanized steel	-1.05	
17	Zinc, wrought; zinc-base die-casting alloys; zinc, plated	-1.10	
18	Magnesium and magnesium-base alloys cast or wrought[c]	-1.60	

[a] Ref. 14, Std 63.

[b] Members of groups connected by lines are considered to form permissible couples. These permissible couples should not be construed to be totally devoid of galvanic action, but rather to represent an acceptably low galvanic effect. The ○ indicates the most cathodic member of the series, ● an anodic member, and the arrows the anodic direction.

[c] Aluminum alloys 5052, 5056, 5356, 6061, and 6063 are considered to form permissible couples with magnesium alloys.

Galvanic corrosion rates are a function of this potential. Therefore, metals with the lowest potential difference are preferred to minimize galvanic corrosion. A NASA table of preferred metal couples is given in table 3-I (ref. 14). Where dissimilar metals must be in contact, they should be insulated with gaskets, plating, or coatings. For additional detail, see reference 15.

3.2.3 Stress Corrosion

Stress corrosion, the phenomenon of crack formation and propagation that occurs in some metal alloys, is generally caused by intergranular corrosion at points of localized strain from high stress levels.

The occurrence of intergranular attack requires exposing the strained surface to an electrolytically active fluid such as moist oxygen, moist air, or water. The electrochemical potentials that exist across grain boundaries when the electrolyte is present cause the progressive attack. Since the reaction is chemical and the cause is stress, the rate of stress corrosion is determined by the amplitude and frequency of the strain, the temperature at the reaction zone, and the type and concentration of the reactant.

One problem is that the rate of attack or even the occurrence of stress corrosion varies in a specific alloy depending on the heat treatment. Therefore, care must be taken when selecting alloys and their heat treatments for any application where high localized stress can occur in the presence of an electrolytic fluid. Since the exterior of nearly all oxygen system components are exposed to moist air, an electrolyte is nearly always present on the outside of the system. Another related problem is the phenomenon of oxide film formation under stress. The strain resulting from the critical stress level permits the oxygen to undermine the surface film and thus allow bare metal oxidation rates. The critical stress is generally the stress required to exceed the elastic limit of the oxide film and, according to reference 16 (p. 17), corresponds to a strain of approximately 1 percent in 100 hours. The effect is very similar to catastrophic oxidation.

3.3 CRACK PROPAGATION AND FATIGUE LIFE REDUCTION

The presence of oxygen affects the rate of fatigue crack growth in metals as illustrated by the examples of stainless steel and nickel in figures 3-6 and 3-7 (refs. 17 and 18). In each case, as the oxygen pressure is increased, the fatigue life is reduced. Note that this phenomenon occurs at very low oxygen pressures. The significance of this is that an oxygen environment has a serious effect on fatigue life when compared to an inert gas environment. In the example given for stainless steel, the crack growth was almost negligible for 10^5 cycles at an oxygen pressure of 1×10^{-6} torr. When the oxygen

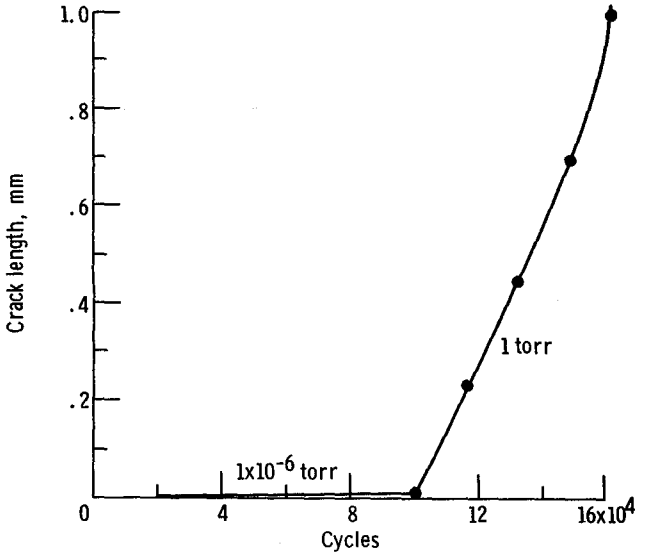

Figure 3-6. - Increase in rate of fatigue crack growth in 316 stainless steel upon introduction of 1 torr oxygen during fatigue at 800° C with 0.062 percent strain (ref. 17, p. 950).

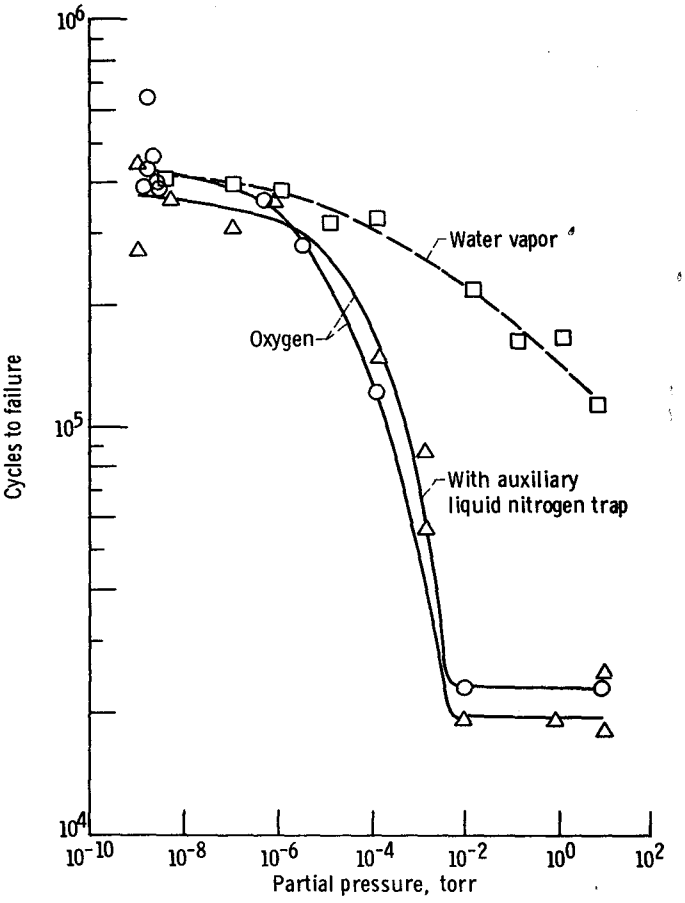

Figure 3-7. - Effect of oxygen and water-vapor pressure on fatigue life of nickel at 300° C at a plastic bending strain of 0.17 percent (ref. 18, p. 223).

pressure was increased to 1 torr, the crack growth increased abruptly. In the case of nickel, at oxygen pressures in the range of 10^{-6} torr or less, there was very little effect, but when oxygen was present at pressures of 10^{-3} torr or greater, the cycles to failure were reduced an order of magnitude.

The reaction of oxygen at crack boundaries, where fresh surface metal is exposed during stress cycles, weakens the metal and thus causes the cracks to grow faster. Metals which are more reactive with oxygen show this effect whereas the noble metals are not significantly affected (ref. 19, p. 170).

The presence of water vapor generally accelerates the effect of oxygen, and fatigue crack growth from the presence of both water and oxygen is greater than either alone. The failure of a D7AC alloy steel tank being tested under water was attributed to this phenomenon. (See section 5.1.4.)

Although the examples given in figures 3-6 and 3-7 were of results at elevated temperature, it is important to recognize that component metal parts subject to high stress cycles in moist oxygen or air environments may have a lower cycle life than would be ex-

pected. When cycle life is an important consideration, testing under exact environmental exposure may be indicated.

3.4 IGNITION OF MATERIALS

Ignition is defined by various researchers in slightly different ways, and there is even some controversy as to whether a particular material has a precise ignition temperature which is completely independent of all other parameters. In order to avoid this controversy, this document will employ the apparent or measured ignition temperature of materials.

The apparent ignition temperature of a given material is affected by its heat capacity, thermal conductivity, and heat of reaction and the rate of heat input, the method of temperature measurement, and measurement techniques. Other parameters affecting the ignition temperature include the thickness of the protective oxide film present before additional exposure and the surface to mass ratio of the exposed material (i.e., powdered material, surface finish, configuration, etc.). In addition, variables such as oxygen concentration, pressure, and temperature as well as exposure conditions (static or dynamic) affect measured ignition temperatures. Also, most materials often have localized imperfections such as contaminant inclusions (commonly found in both metals and nonmetals) as well as variations in polymeric chain endings and molecular irregularities (nonmetals). Such local imperfections may have much lower ignition temperatures than the bulk material and may serve as an igniter; this condition naturally causes variations in the measured ignition temperature.

The ignition temperature and ignition energy data presented in this chapter and in appendixes D and E are useful in selecting the most compatible material to meet the physical requirements for specific applications.

A summary of melting points, ignition temperatures, and thermal diffusivity and heat of combustion data for selected materials are presented in table 3-II (refs. 20 to 22).

The thermal diffusivity parameters, (i.e., thermal conductivity, density, and specific heat) may be used to calculate energy input rate or power input to reach the ignition temperature of the material. As the thermal conductivity, density, and heat capacity increase, the rate of energy (power) input to reach an ignition temperature increases. Also, if the heat of reaction is relatively high, the material, once ignited, burns with greater heat release which tends to propagate combustion more readily.

The melting points of the base metal and its oxide are important parameters since the protective effects of the oxide film are destroyed if the metal or its oxide melts.

These are some of the factors which must be considered in an engineering trade-off for selecting materials. The most advantageous of the previous factors for achieving an

TABLE 3-II. - IGNITION PARAMETERS FOR SELECTED METALS

Metal	Metal melting point (a)		Thermal conductivity at 20° C, $\frac{(cal)(cm)}{(sec)(cm^2)(^oC)}$ (b)	Density at 20° C, g/cm^3 (c)	Specific heat at 20° C cal/(g)(°C) (a)	Ignition temperature range at 1 atm oxygen, °C (d)	Heat of reaction (heat of oxide (formation), kcal/(g)(mole) (e)	Product (oxide)	Product melting point (f)	
	°C	°F							°C	°F
Aluminum	660	1220	0.53	2.699	0.215	>1000	-399.09	Al_2O_3	2015	3659
Antimony	631	1167	.045	6.62	.049	650	-166.5	Sb_2O_3	656	1213
Beryllium	1277	2332	.35	1.848	.45	1260 to 2500	-146	BeO	----	----
Chromium	1875	3407	.16	7.19	.11	1998	-269.7	Cr_2O_3	2435	4415
Copper	1083	1981	.941	8.96	.092	1083	-37.1	CuO	1326	2419
Iron	1537	2798	[g].18	7.87	.11	1310	-196.5	Fe_2O_3	1565	2849
Lead	327	621	[g].083	11.36	[g].0309	850 to 871	-52.07	PbO	888	1630
Magnesium	650	1202	.367	1.74	.245	625 to 640	-143.84	MgO	2800	5072
Manganese	1245	2273	----	7.43	[f].115	----------	-92	MnO	535	995
Molybdenum	2610	4730	.34	10.22	.066	745 to 780	-130	MoO_2	----	----
Nickel	1453	2647	[h].22	[h]8.902	.105	----------	-58.4	NiO	1990	3614
Platinum	1769	3217	[i].165	21.45	[g].0314	----------	--------	PtO	[j]550	1022
Silver	961	1762	[g]1.0	10.49	[g].0559	950	-7.306	Ag_2O	[j]300	572
Tantalum	2996	5425	.130	16.6	[h].034	1245 to 1270	-499.9	Ta_2O_5	1800	3272
Thorium	1750	3182	[k].090	[l]11.72	.034	500	-292	ThO_2	3050	5522
Tin	232	450	[g].15	[m]7.3	.054	865 to 970	-138.8	SnO_2	1127	2061
Titanium	1668	3035	[n].0372	4.507	.124	1310 to 1600	-218	TiO_2	1830 to 1850	3326 to 3362
Tungsten	3410	6170	[g].397	19.3	.033	1270 to 1300	-200.84	WO_3	1473	2683
Zinc	419	787	[h].27	[h]7.133	.0915	900 to 940	-83.17	ZnO	1975	3587

[a]Ref. 20, pp. 46 and 47.
[b]Ref. 20, pp. 48 and 49.
[c]Ref. 20, pp. 44 and 45.
[d]For additional data, see appendix D.
[e]Ref. 21, pp. 8 to 535.
[f]Ref. 22, pp. B-149 to B-242.
[g]At 0° C.
[h]At 25° C.
[i]At 17° C.
[j]Decomposes.
[k]At 100° C.
[l]Bomb-reduced
[m]Beta.
[n]At -240° C.

optimum chemical compatibility must be balanced against the required structural properties of materials.

3.4.1 Ignition Temperature of Metals

For most practical purposes, the measured ignition temperature of most metals varies only slightly over a wide range of pressures. For example, the ignition temperature of materials (both metal and nonmetal) tested at 2000 and 7500 psi in oxygen gas was essentially the same (ref. 23, p. 55). However, these data together with other available ignition temperature data plotted on a semi-logarithmic scale (to cover a wide pressure range) show slightly reduced ignition temperatures at high oxygen pressures for most metals (fig. 3-8). A few exceptions show an increase in ignition temperature with pressure. These exceptions and the variations in the slope of the curves are probably due primarily to the properties of the oxide film formed. (Nonmetal materials tend to be much more consistent.) These data are based on detailed information plotted in the figures in appendix D and are a composite compilation from the sources listed. In most cases the metal sample was placed in pressurized oxygen and heated slowly until the ignition temperature was reached and combustion occurred.

These data are useful in selecting the material most resistant to ignition. The highest possible localized temperature spike that could be anticipated in a given system should be less than the ignition temperature corrected for pressure per figure 3-8 and table 3-II plus an appropriate safety factor.

The apparent ignition temperature of most particulate metallic materials, which may be present in oxygen systems as contamination, is somewhat lower than that of the same material in bulk form. This is due primarily to the high specific surface or surface to mass ratio of the particulate. If the particles are small enough, the heat of oxide film formation alone may be sufficient to raise them to ignition temperature in gaseous oxygen. In any case, the power input required to raise particulates to their ignition temperature is lower than might be anticipated if only the bulk material ignition temperature is considered. For example, the ignition temperatures of chromium and copper are approximately 2000° and 1083° C, respectively, while the apparent ignition temperatures of 44 micron powders of the same materials in air are 580° and 700° C, respectively, as reported in reference 24 (p. 4).

Liquid oxygen, because of its cooling effect, makes particle ignition less likely. However, ignition may still occur in gaseous pockets or at sites of impact or friction, particularly when accumulated quantities of incompletely reacted wear particles or other contaminants are present.

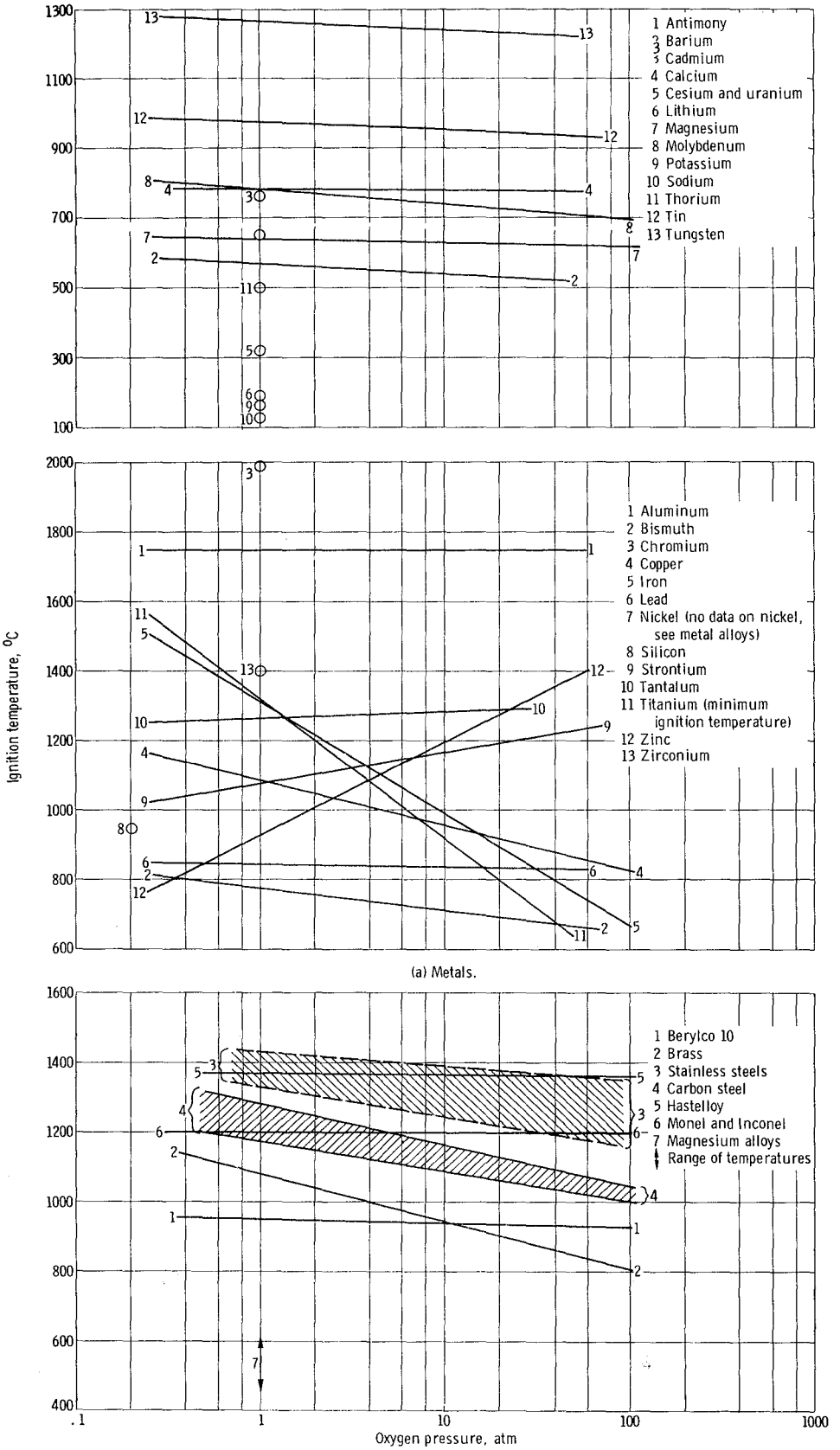

(a) Metals.

(b) Metal alloys.

Figure 3-8. - Average ignition temperature of metal and nonmetals.

3.4.2 Ignition Temperature of Selected Nonmetal Materials

The primary concern when using nonmetals in oxygen systems is their potential reactivity with oxygen. Their ignition temperatures are generally lower than those for metals and their low thermal conductivity and heat capacity make them much easier to ignite. For this reason, their use is more restricted.

The effect of oxygen pressure on the ignition temperature of polymeric materials is difficult to measure except over a wide range of pressures. As in the case of metals, when ignition temperatures of polymeric materials are plotted against pressure over a wide pressure range, a reduction in ignition temperature with increasing pressures be-

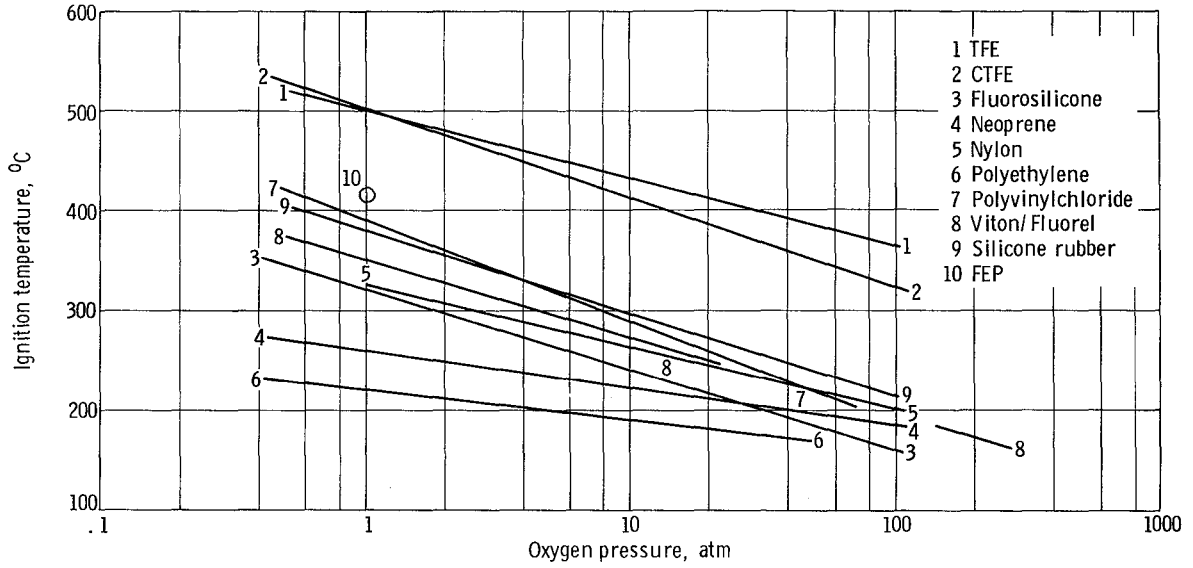

Figure 3-9. - Minimum ignition temperatures of nonmetal materials.

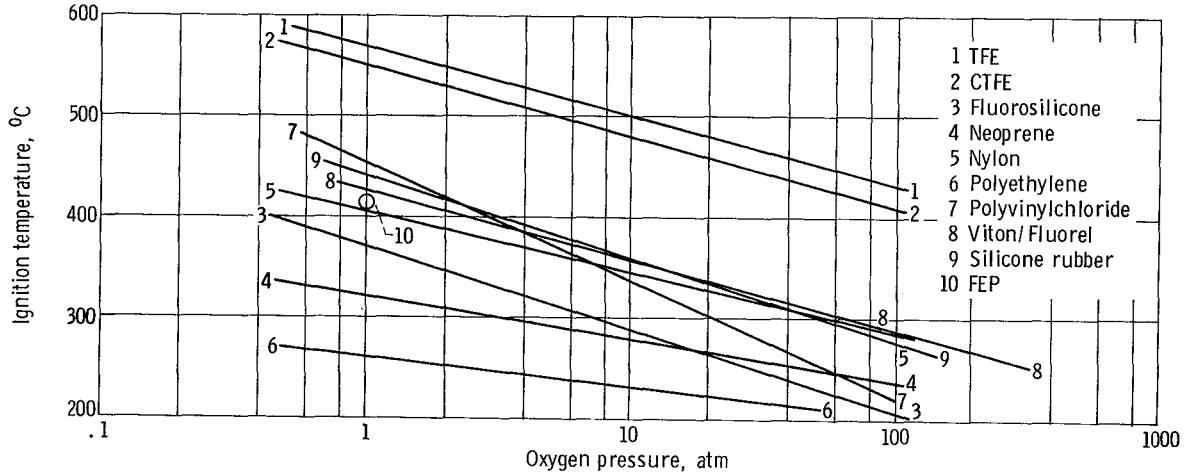

Figure 3-10. - Average ignition temperatures of nonmetal materials.

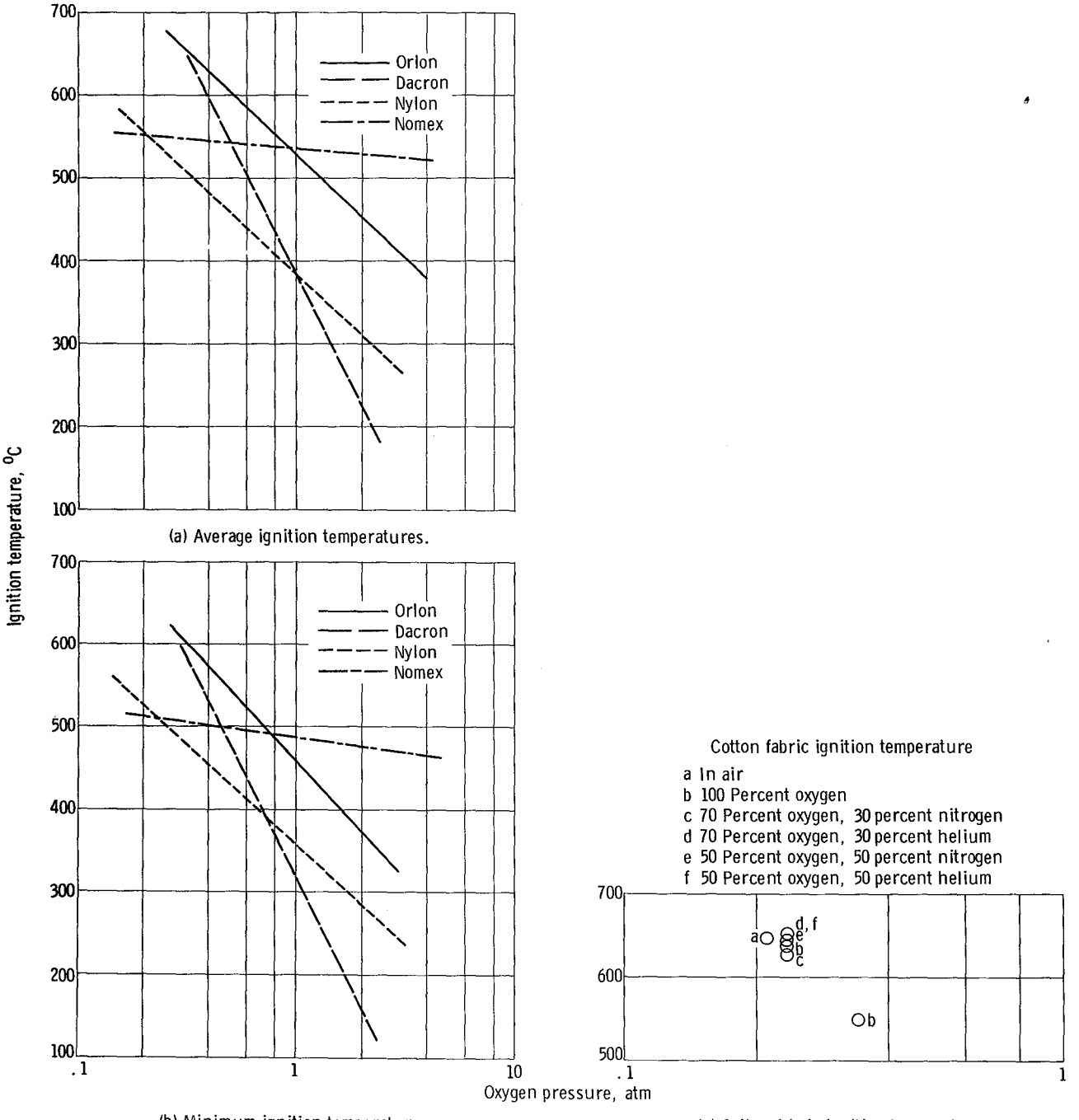

(a) Average ignition temperatures.

(b) Minimum ignition temperatures.

(c) Cotton fabric ignition temperatures.

Figure 3-11. - Ignition temperatures of fabric materials.

TABLE 3-III. - MINIMUM IGNITION TEMPERATURES OF MATERIALS IN OXYGEN AT 1-ATMOSPHERE PRESSURE[a]

Material	Minimum ignition temperature, °C
Selected plastics and elastomers	
Polyimide (Vespel)	500
Chlorotrifluoroethylene (TFE)	500
Tetrafluoroethylene (TFE)	500
Duroid 5600	468
Duroid 5813	463
Duroid 5870	452
Duroid 5650	444
Rulon A	463
Rulon B	460
Rulon C	458
Graphite asbestos	460
Vinylidene fluoride/hexafluoropropylene (Viton A/Fluorel)	[b]435 (see figs. E-1(p) and E-1(q))
Polymethylmethacrylate (Plexiglas)	430
TFE (carbon filled)	420
Fluorinated ethylene propylene copolymer (FEP)	412
Polyvinylalcohol	400
Silicone rubber	390
Kel-F 5500	340 to 352
Kel-F 3700	332 to 341
Carbon	330
Fluorosilicone	320
Polyvinylidene fluoride	(see fig. E-1(m))
Polyvinylchloride	390
Nylon[c]	345
Mylar[c]	320
Selected plastics and elastomers	
Butyl rubber[c]	275
Neoprene[c]	250 to 270
Polyethylene[c]	160 to 220
Natural rubber[c]	150
Selected lubricants	
TFE lubricant	505
CTFE grease	500
Halocarbon grease 25-10	431
Halocarbon oil 13-21	427
Mano pipe and joint	422 to 430
Oxyweld 64	410
Silicone grease	370
Selected adhesives	
Fused TFE	465
Eposy (3M EC 1469)	380
Oxyseal (2)	347 to 360
Epoxy (Armstrong A-6)	310
Selected fabrics	
Nomex	490
Orlon	430
Nylon	360
Dacron	310 to 390

[a]See introduction to appendix E for qualifications applicable to the data in this table.

[b]Ref. 25 data indicate this value could be as low as 335° C. Ref. 25 data also show ignition temperature to be 308° to 318° C at 3.4 atmospheres.

[c]Not recommended for oxygen - included for comparison only.

comes evident. On the other hand, the measured ignition temperature increases as the oxygen pressure or partial pressure is reduced below atmospheric pressure until a point is reached where no spontaneous ignition can occur since combustion can not be sustained.

Ignition temperatures as a function of oxygen pressure (or partial pressure) are presented in figures 3-9 to 3-11; these figures were compiled from the detailed data plotted in the figures of appendix E. Note that figure 3-9 shows the minimum ignition temperature, and figure 3-10 provides the average ignition temperature of the same materials. Average and minimum ignition temperatures for selected fabrics are included in figure 3-11.

It should be noted that materials which are not normally recommended for use with oxygen, such as nylon and cotton, have ignition temperatures nearly as high as some of the acceptable materials. Factors such as absorption characteristics, chemical deterioration, variations in the polymer structure, and contamination could explain the failure experience of some of the materials that are not recommended for oxygen. (For a discussion of recommended materials, see section 3.7.) In any case, the minimum ignition temperature (less an appropriate safety factor) should never be exceeded.

A summary of the minimum ignition temperatures for selected materials is presented in table 3-III (selected data from ref. 25).

3.4.3 Impact Energy Test Data for Metals and Nonmetals

As previously stated, the selection of materials for use in oxygen systems has been based on use experience and impact, ignition, and flammability testing with impact testing being a major source of compatability data. A description of impact test equipment and procedures may be found in the section 3.6.1.1.

When applying impact test data it should be recognized that the test was devised as a convenient and reproducible method for choosing materials from those that could withstand a selected impact energy level under standardized environmental conditions. This provided a form of "worst case" testing which has more recently been refined to permit measurement of impact limits or threshold data.

"Go-no-go" type impact ignition data in oxygen environments obtained by this test are compiled in reference 26 (pp. 42 to 220). Using fixed impact energies does not permit a determination of the limit of impact energy a material can withstand, nor does it permit a determination of how close to the limit a given test or operational condition may be. These data are helpful because they indicate the relative compatibility of a material when compared to the others tested. However, in order to make an engineering estimate of impact compatibility, the maximum level of impact that is possible in a given system must be determined, and the impact tolerance limit of the material must be known. With both factors known, a safety factor appropriate to the application can then be applied which would provide a more quantitative approach to compatibility determinations.

TABLE 3-IV. - IMPACT ENERGY FOR IGNITION OF SELECTED MATERIALS IN OXYGEN

Material	Impact energy, ft-lb/in.^{2}	Reference
Metals		
Zinc dust	380	27, p. 98
Aluminum 6061-T6	368+	26, p. 166
Rene 41	368+	26, p. 175
18 Percent nickel maraging steel	368+	26, p. 175
Stainless steel 347	368+	28, p. 7
Iron powder	357	27, p. 98
Columbium	357	27, p. 98
Aluminum chips	306	27, p. 98
Titanium	78	29, pp. 5 and 6
Titanium Ti-6Al-4V and Ti-25Zr	78	29, pp. 5 and 6
Nonmetals		
Polytetrafluoroethylene sheet	306 to 400	27, p. 97
Polytetrafluoroethylene (20 mil, sintered)	370	30, p. 102
Polytetrafluoroethylene tape	368+	26, p. 74
Polytetrafluoroethylene (glass filled)	368+	26, pp. 156 and 157
Polytetrafluoroethylene	368	31, p. 47
Polychlorotrifluoroethylene grease	368+	26, pp. 58 and 59
Polychlorotrifluoroethylene oil	368+	26, pp. 50 and 51
Fluorinated silicone (Drilube 822, 0.050 in. thick)	368+	26, p. 47
AFD-E-124D (experimental fluoroelastomer)	368	31, p. 49
Nonmetals		
CTFE (polychlorotrifluoroethylene)	357	27, p. 98
CTFE (20 mil)	210	30, p. 102
CTFE (10 mil)	160	30, p. 102
Vinylidene fluoride and hexafluoropropylene (cured)	357	27, p. 98
FEP (fluorinated ehtylene propylene, shredded)	306	27, p. 98
FEP (fluorocarbon resin, 10 mil)	145	30, p. 102
TFE (40 mil)	305	↓
TFE (30 mil)	300	
TFE (10 mil, unsintered)	220	
TFE (10 mil, sintered)		
Viton A	204 to 254	31, pp. 47 and 49
Fluorosilicone	204	31, p. 47
Phenylsilicone	204	31, p. 47
Mylar	122	32, p. 37
Trifluoropropylmethyl (Siloxane)	100	27, p. 98
Polyvinylidene fluoride (10 mil)	80	30, p. 102
Polyethylene (irradiated)	78	27, p. 97
Neoprene	55	30, p. 103
Nitrile rubber	39	30, p. 103
Fluorel[a]	368+	28, p. 6
Plexiglas[a]	368+	28, p. 6

[a]Ambient temperature GOX tests.

Some impact tolerance threshold data for metals and nonmetals are given in table 3-IV (refs. 26 to 32). The materials listed include those cases where an impact energy level has been reached without reaction in successive tests. For example, if the highest no reaction impact was 200 and the lowest impact at which reaction occurred was 215, the limit value used was 200. Therefore, since some of the values are not the absolute maximum of impact tolerance, the conservative value is considered to be close to the maximum.

Because of the variations in test results caused by sample thickness, material batches, apparatus types, and physical characteristics of striker and anvil materials, the test values are only approximate. Even different operators using the same equipment may get different results. An example of the effect of sample thickness for selected materials is illustrated in table 3-V (ref. 33). There are also chemical variations in compounded and processed materials - even materials with the same name. There are wide

TABLE 3-V. - EFFECT OF SPECIMEN THICKNESS OF VARIOUS MATERIALS AT 10-kg·m IMPACT ENERGY (IN GOX)[a]

Material	Thickness, cm	Oxygen pressure, N/m^2	Percent reaction	Increase in sensitivity
Silicone rubber	0.152	34×10^4	55	---
Silicone rubber	.050	34×10^4	100	1.8
Polytetrafluoroethylene	.157	6.8×10^6	10	---
Polytetrafluoroethylene	.086	6.8×10^6	20	2
Fluorinated rubber	.229	6.8×10^6	10	---
Fluorinated rubber	.152	6.8×10^6	33.3	3.3

[a]Ref. 33, p. 29.

variations in purity, chemical content, additives, and processing agents. This can also occur with different batches of the same material from the same source. For this reason, it is a common requirement that many materials be "batch" tested for acceptance for oxygen system applications.

Despite these variations, the data in table 3-IV are helpful in choosing a material and can help in achieving a good oxygen system component with less problems, redesign, and retesting.

3.4.4 Ignition of Materials by Adiabatic Compression of Oxygen

Adiabatic compression of gaseous phase oxygen from pressure spikes due to "water hammer," fast operation of valves in high pressure systems, oscillatory flow, or other

sudden pressurization can cause localized temperature increases sufficient to ignite many materials, especially organic contaminants or fine particles. Nonmetal materials especially should be protected from direct exposure to high pressure adiabatic compression of oxygen. Theoretical temperatures that can be reached by adiabatic compression of a gas are given in figure 3-12.

Not many data exist on adiabatic ignition of materials. Existing data for some materials generally compatible with oxygen are given in table 3-VI. Obviously, the samples which were exposed to a sudden compression of over 6000 psi ignited; figure 3-12 shows

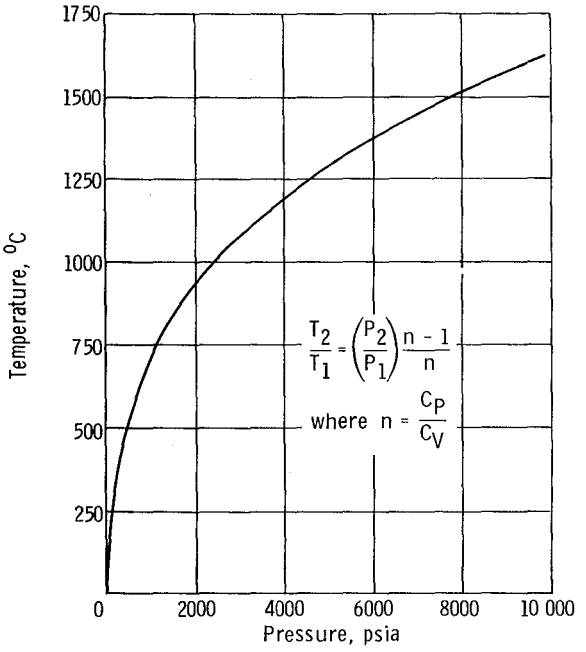

Figure 3-12. - Theoretical temperature attained by adiabatic compression (ref. 23, p. 60). Initial conditions: T_1 = 293 K (~20° C); P_1 = 14.7 psia.

TABLE 3-VI. - ADIABATIC COMPRESSION TESTS[a]

Pressure in storage vessel, psi		Sample	Weight of sample, g	Pressurization time of 51 in. length of 5/16 in. i.d. tubing and sample, sec	Remarks
Before test	Immediately after test				
7200	6900	Viton A (Virgin)	0.217	0.05	Sample ignited
7100	6700	Viton A (Virgin)	.223	↓	↓
7000	6500	Kel-F 81	.240		
6900	6300	Teflon (Virgin)	.161		

[a]Ref. 23, p. 80.

a temperature capability for that pressure approaching 1400^{o} to 1500^{o} C, and the ignition temperature for all these materials is less than 500^{o} C.

Extremely high pressures (as just shown) are generally required since the material to be ignited must absorb sufficient heat from the gas to reach the ignition temperature of the material (or a contaminant on the material). To do this, the final gas temperature must be considerably higher than the ignition temperature to allow sufficient time for the ignition temperature to be reached.

3.4.5 Ignition from Rupture of Materials

When material is overstressed to cause rupture, several things occur that can result in ignition in an oxygen environment. The temperature of the material increases in the area of rupture from strain, and the highest temperature develops at the rupture interface. The ruptured surface is generally very rough and has a very high local surface area to mass ratio. In addition, the newly exposed surface is subject to immediate additional heating from oxide film formation reaction. Finally, the faster the strain occurs leading to rupture, the higher the ruptured surface temperature will be. Although most materials (metal and nonmetal) can tolerate rupture in a moderate oxygen environment, some materials with poor ignition resistance characteristics may react if ruptured in a high pressure oxygen environment at a temperature near the ignition temperature.

Occurrences which are most likely to result in massive structural deformation, and thus possible ignition, are failed turbopump impeller assembly, water hammer, excessive overpressure, excessive g-forces, and the like.

Although titanium is a bad actor in an oxygen environment, it does serve to illustrate the rupture ignition phenomenon. Figures 3-13 (ref. 34) and 3-14 (ref. 34) show the limits of initial temperature and pressure combinations for rupture ignition of titanium and one of the titanium alloys. In this case, the data are based on tensile rupture. Tearing rupture would possibly result in a shift of position or slope of the curve. Other materials (whose ignition temperatures are lower than their melting points) would react in the same way at initial temperatures near their ignition temperature. "Molecular concentration" (or density) was used rather than pressure of oxygen only to illustrate that the effect of pressure on ignition is due to the higher concentration of oxygen molecules at the site of ignition.

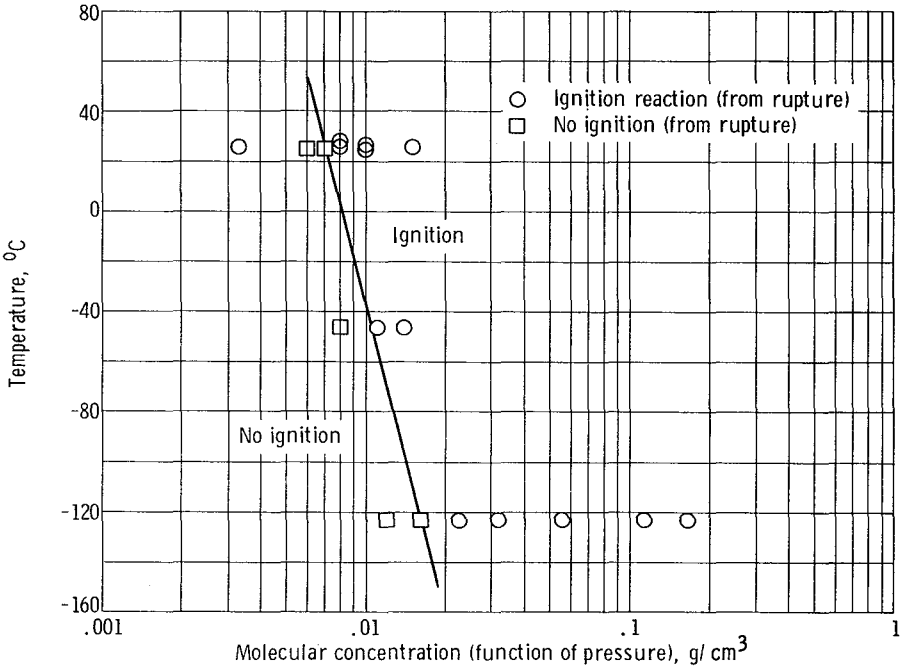

Figure 3-13. - Spontaneous ignition of titanium (Ti-75A) from rupture in oxygen (ref. 34, p. 10).

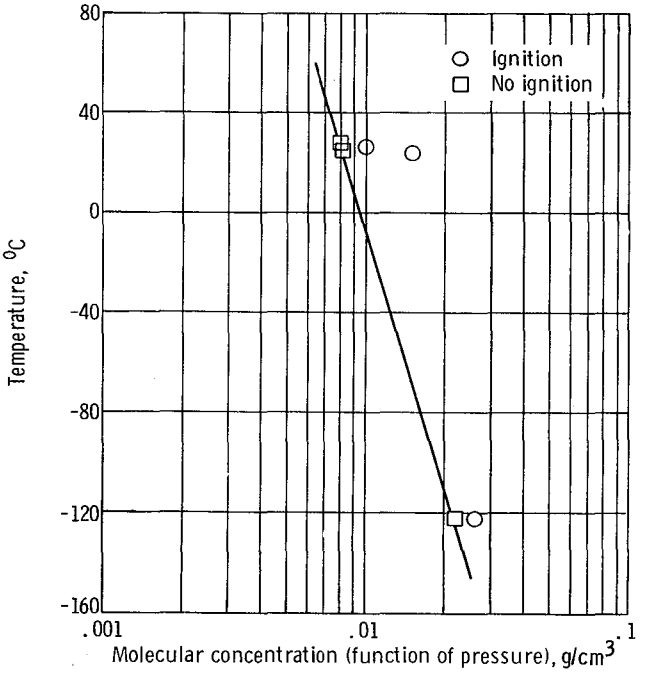

Figure 3-14. - Spontaneous ignition of titanium alloy (Ti-6Al-4V) from rupture in oxygen (ref. 34, p. 14).

3.4.6 Dynamic (Flow) Effects

Limited data and experience indicate that a high velocity flow of oxygen can effect ignition and increase the burning rates of materials. Also, solid particles entrained in a high velocity flow stream can cause surface erosion, and particle impact can cause, or be the source of, ignition.

Ignition of oxygen piping from impact and abrasion of entrained particulate matter has been a frequent occurrence in gaseous oxygen systems especially at room temperatures or higher. This is especially true where a high degree of cleanliness has not been maintained. Those organizations familiar with the problem maintain that the required cleanliness limits the flow velocity in the piping. In most cases, the oxygen flow velocity limits are set in consideration of past experience, the pipe material, and operating pressure and temperature. These vary with the organization. Typical values are listed in table 3-VII.

Actual tests (ref. 35) have confirmed what has been observed from experience: exceeding a velocity limit when entrained particulates are present results in ignition of the flow duct, and bends, valves, and other flow system obstructions or deviations are the most critical ignition sites. A summary of the actual test results is given in table 3-VIII (ref. 35).

TABLE 3-VII. - TYPICAL VELOCITY LIMITS FOR ENTRAINED PARTICULATES IN OXYGEN WITH CARBON STEEL PIPE

Pressure, atm	Temperature, °C	Maximum flow velocity	
		ft/sec	m/sec
10	175	150	46
10	150	175	53
10	120	200	61
20	175	75	23
20	150	85	26
20	120	100	30
20	65	130	40
40	120	50	15
40	100	60	18
40	65	65	20
60	100	30	9
60	65	35	10 to 11

TABLE 3-VIII. - IGNITION VELOCITIES OF ENTRAINED PARTICLES IN OXYGEN (STEEL PIPE)[a]

Pipe line configuration	Entrained material	No ignition velocity, m/sec	Ignition velocity, m/sec
Straight	Rust	[b]84	--
Straight	Sand	[b]84	--
Straight	Steel scale	28	52
Straight	Weld slag	[c]44	--
Curved	Weld slag	[d]53	--
Straight	Coke	30	--
Curved	Coke	17	53
Curved	Carbon	---	34
Straight	Carbon	---	13
Straight	80 Percent sand, 20 percent iron powder	13	31

[a]Ref. 35, pp. 13 to 16.
[b]Maximum test velocity attainable.
[c]Particles began to glow at this velocity.
[d]Some sparks at this velocity.

Although the added effect of the flow parameter on the total ignition energy may be small, especially for metals, it can become significant at higher temperatures and very high flow rates. While titanium is not normally suitable for use in oxygen, its sensitivity to oxygen makes it well suited to illustrate flow sensitivity to oxygen at relatively low pressures and flow rates. As illustrated in figure 3-15 (ref. 36), the reaction of titanium occurred at lower pressures and oxygen concentration under dynamic conditions than under static conditions. In this work (ref. 36, pp. 1 to 17) the static reaction data were obtained by tensile rupture of the specimen in a pressure vessel while dynamic reaction

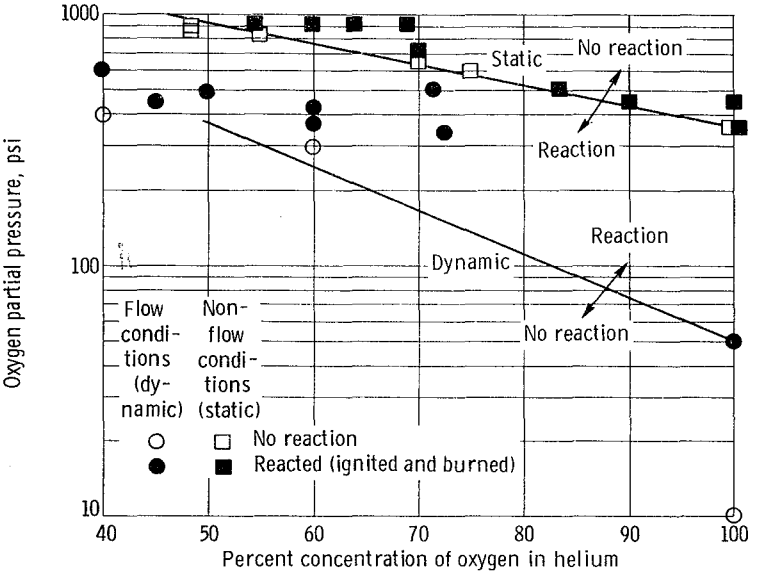

Figure 3-15. - Effect of flow and nonflow on the ignition of titanium foil as function of pressure and concentration (ref. 36, pp. 8 and 16). Tests at ambient temperature and with freshly exposed surface.

data were obtained by mechanical rupture of a diaphragm with subsequent gas flow through the rupture. This effect is also illustrated by tests with cryogenic oxidizers (oxygen-fluorine mixtures) on nonmetals (ref. 37, pp. 99 and 102). Sharp reductions in compatibility were measured, and ignition occurred as a function of flow velocities in both liquid and gaseous states. In both cases, flow conditions, in effect, added to the energy available to cause ignition or increased the sensitivity of the material to the exposure; this resulted in ignition under conditions where no ignition would occur statically.

Fluid shear forces, liquid cavitation, and sonic velocity effects in gases appear to be major causes of the sensitivity to high flow rates by various materials.

In summary, the primary source of concern under high velocity flow conditions is the entrainment of particulates and their subsequent impingement on a surface such as at bends in piping. However, the effects of extremes in flow velocity and pressure cannot

be ignored. Whether material erosion or ignition is due to entrained particulate impact and abrasion, to the erosive effects of the fluid flow, or to both, the fact remains that the effects exist and they increase with pressure and flow velocities. (See section 4.2 on erosion.)

Until a more quantitative limit can be established, the following practices are recommended:

(1) Where practicable, avoid sonic velocity in gases and cavitation in liquid oxygen; where this is impractical, use the preferred materials listed in section 3.7 and in chapters 5 to 9.

(2) If possible, avoid the use of nonmetals at locations within the system where sonic flow or cavitation can occur.

(3) Maintain fluid system cleanliness and limit entrained particulates as discussed in chapter 2, section 4.5.

3.5 FLAMMABILITY AND COMBUSTION

Despite the large volume of combustion and fire hazards research reported in the literature, very little information is directly applicable to or usable in oxygen system engineering, because most of it is the result of qualitative tests for specific applications rather than quantitative evaluation for general use.

Having standard flammability tests and procedures for testing solid materials is an important step in achieving more reliable and uniform data. This has been largely due to the needs of the Apollo program. These tests are specified in reference 38 and are summarized in section 3.6.

Gaseous phase flammability of fuels in air mixtures has been much more fully explored than solid phase reactions. Flammability limits for nearly all liquid and gaseous fuels are available in the literature. Data for selected fuels are given in table 2-V (p. 9). The data compiled in the following sections and in appendix F show fairly good quantitative correlations and indicate definite trends in the burning rate characteristics of solid materials in oxygen.

Burning rate data for selected polymeric materials are presented as a function of the oxygen pressure (or partial pressure for a mixtures with helium or nitrogen) in table 3-IX and figures F-1 to F-3 in appendix F.

The burning rate of a material varies depending on its initial temperature before ignition. If a material is uniformly heated close to its ignition temperature before ignition, its burning rate can be much higher than if it is ignited at room temperature. The entire surface may flash into flame if the material is ignited at a temperature near its ignition temperature. Therefore, it must be kept in mind that the burning rate data discussed

TABLE 3-IX. - COMBUSTION RATE OF SELECTED MATERIALS IN OXYGEN[a]

Material	Combustion rate, in./sec		
	Oxygen pressure		
	21 Percent oxygen, 1 atm	100 Percent oxygen, 0.2 atm	100 Percent oxygen, 1 atm
Cotton[b]	2.5	1.0	7.4
Dacron	.70	.90	2.30
Epoxy	----	----	.12
Neoprene	----	.10	.40
Nomex	.52	.31	.96
Nylon (fabric)	.32	.46	1.02
P.B.I.	----	.22	.40
Polyethylene	----	.06	.27
Polymethylmethacrylate (sheet)	.76	See figs F-1(k) and (l)	----
PVC	----	.30	1.0
Polyurethane	----	.56	.7
Silicone	----	.20	1.1
TFE (fabric)	----	See fig. F-1(q)	1.07
TFE (rod)	----	See fig. F-1(r)	No ignition
Viton-Fluorel	----	See fig. F-1(s)	----
Velcro	----	.24	.48

[a]See appendix F.

[b]Other than vertical burning, see fig. F-1(a).

here do not include the effect of initial temperature, since all the tests were begun at ambient temperature.

For any given oxygen partial pressure the burning rate is decreased by the presence of an inert diluent; at higher pressures the effect of the diluent increases, as indicated by the divergence of the burning rate curves in appendix F. However, the burning rate in all combustion supporting concentrations increases with pressure. For example, the partial pressure of oxygen in the normal atmosphere is about 0.2 atmosphere. From table 3-IX, in the case of Dacron, the combustion rate at 1.0 atmosphere total pressure for 20 percent oxygen (normal air) is about 0.7 inch per second and at 100 percent oxygen at the same partial pressure it is 0.9 inch per second. However, for 100 percent oxygen at 1 atmosphere it burns at 2.3 inches per second - about three times as fast. For nylon the rates are 0.32 inch per second for 20 percent oxygen at 1 atmosphere, 0.46 inch per second for 100 percent oxygen at the same partial pressure, and 1.02 inches per second for 100 percent oxygen at 1 atmosphere - over three times the normally expected burning

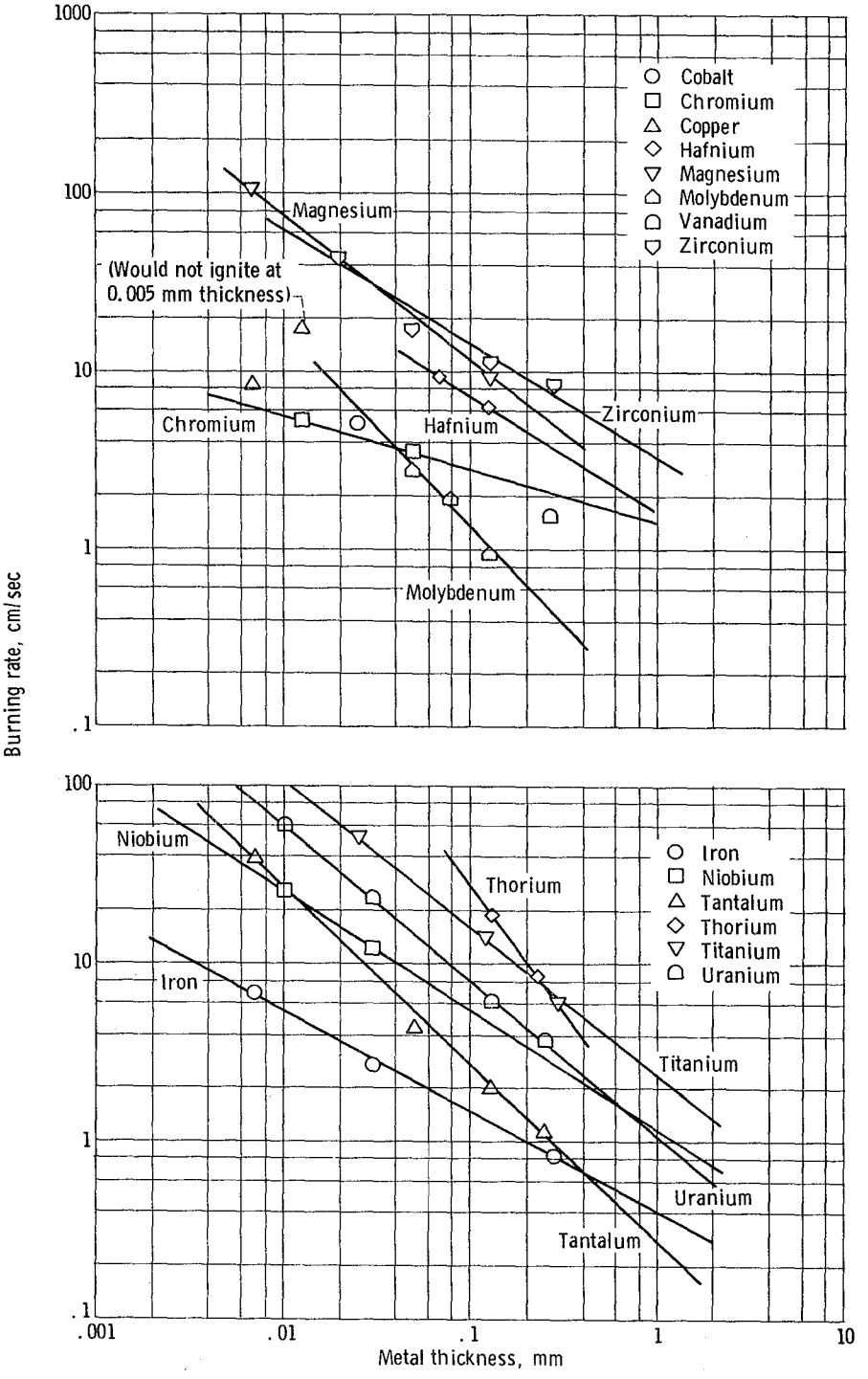

Figure 3-16. - Horizontal burning propagation rate for metals in 100 percent oxygen at pressure of 1 atmosphere (ref. 39, p. 151).

TABLE 3-X. - BURNING PROPAGATION RATE

FOR METAL RODS IN 1-ATMOSPHERE

OXYGEN PRESSURE

Material (1/16 to 3/16 in. diam)	Combustion rate, in./sec		
	Up	Down	Horizontal
Mild steel	0.3	0.5	0.435
Aluminum	10.0	-----	-----
309 Stainless steel	----	.171	.38
316 Stainless steel	.8	-----	.3
316L Stainless steel	.07	-----	-----
410 Stainless steel	.052	-----	.24
17-4PH Stainless steel	.12	-----	.3
4140 Stainless steel	.13	-----	.06
Nickel[b]	None	-----	None
Monel[b]	↓	-----	↓
Inconel[b]		-----	
Bronze[b]		-----	
Hastelloy	.06	-----	.08

[a]Ref. 40, vol. IV.

[b]These materials did not propagate combustion in oxygen at 1-atmosphere pressure.

rate. Teflon burns at 1.0 inch per second at 100 percent concentration and 1 atmosphere pressure. Nomex, a high temperature polyimide, and silicone rubber burn at about the same rate as Teflon.

An example of the effect of gravity on the burning rate is shown for cotton (fig. F-2) and Nomex (fig. F-8) in appendix F. There is a gradual increase in burning rate as the gravity level is increased; at zero gravity, the burning rate is the lowest.

In general, the burning rates of metals and nonmetals are the same order of magnitude; however, in most cases, the heat of reaction is greater for metals, resulting in a hotter fire. Burning rates for metals are shown in figure 3-16 (ref. 39) and table 3-X (ref. 40). The data in figure 3-16 show the effect of material thickness on the burning rate. Note that aluminum burned at 10 inches per second in a bottom ignition test (table 3-X) but that this burning was not propagated with the sample in the horizontal position (fig. 3-16).

A measure of the relative flammability of materials with oxygen is the oxygen index. The oxygen index value is the minimum percent concentration of oxygen in an oxygen-nitrogen mixture which will sustain combustion. Arithmetically, the oxygen index is expressed as

$$N = \frac{100 \times O_2}{O_2 + N_2} \text{ percent}$$

(The higher the number N, the greater the resistance to ignition.) The oxygen (O_2) and nitrogen (N_2) may be expressed in volume units or in moles. Table 3-XI (refs. 41 and 42) lists the oxygen index values for a number of materials. The oxygen index test is described in section 3.6.2.3.

TABLE 3-XI. - SELECTED OXYGEN INDEX FLAMABILITY TEST DATA[a]

Material	Oxygen index, N	Material	Oxygen index, N
Polyacetal, Celcon	14.9	Polypropylene (F.R.), Plaskon 1060	26.4
Polyethylene oxide, Polyox WSR-35	15.0	Nomex	26.7
Polyacetal plus 30 percent glass	15.6	Noryl SE-100	27.4
Cellulose acetate (dry = 0.1 percent water)	16.8	ABS (F.R.), Cycolac KL	27.4
Polymethyl methacrylate, Plexiglas	17.3	Noryl SE-1	28.0
Polypropylene, Profax 6505	17.4	Polypropylene (F.R.), Avisun 2356	29.2
Polyethylene[b]	17.5	Polycarbonate, Lexan 3412 plus 20 percent glass	29.8
Polystyrene, Shell 325	17.8	Polyphenylene oxide 534	30.0
Polypropylene, Profax P7401	17.8	Nylon 6-6 (saturated, about 8 percent water)	30.1
Cellulose acetate (wet = 4.9 percent water)	18.1	Polysulfone P1700	30.4
Polystyrene, Cosden 825 TV	18.2	Polyvinylchloride (PVC), Plaskon X2013	31.5
Polybutadiene[b]	18.3	ABS (F.R.), Cycovin KA	31.7
Polypropylene plus 30 percent glass	18.5	Epoxy-glass laminate, G.E. 11673FR-2	32.6
Acrylonitrile butadiene styrene (ABS), Cycolac T	18.8	Silicone rubber[b]	33.0
Cellulose butyrate (dry = 0.06 percent water)	18.8	Epoxy, Plenco 200D-B1242	38.3
Polystyrene, Dylene 8X	19.0	Polycarbonate, Lexan DL444	39.7
Cellulose butyrate (wet = 2.8 percent water)	19.9	PVC, Plaskon 2005	40.3
Arylon T-3198 natural	20.6	Alkyd resin, Plenco 1504-B6636	41.0
ABS plus 20 percent glass	21.6	Polyester, Atlac 711-050	41.5
Phenolic-paper laminate, Textolite 11571B	21.7	Polycarbonate, Lexan DL444 plus 20 percent glass	42.0
Polycarbonate, Lexan 191	22.5	Polyvinylidene fluoride	43.7
Arylon T-3198 white	22.8	PVC, Geon 101	45.0
Polypropylene (F.R.), Plaskon 1070X	23.7	Epoxy, Plenco 2000F-B6432	47.6
Polyphenylene oxide polymer, Noryl 731	24.3	Epoxy-glass laminate, G.E. 11635-FR-4	49.0
Nylon 6-6 (dry, as molded)	24.3	Phenolic (mica filled), Plenco 343-B817	52.8
Polycarbonate, Lexan 141	24.9	Porous carbon[b]	56.0
Epoxy-glass laminate, G.E. 11558G10	24.9	Polyvinylidene chloride, Saran	60.0
ABS (F.R.), Durez 2311	25.2	Polytetrafluoroethylene, Teflon	95.0
Polypropylene (F.R.), Plaskon 1050	25.6		
ABS (F.R.), Cycolac KT	25.8		

[a]Ref. 41, pp. 40 to 42.

[b]Ref. 42, p. 146.

3.6 COMPATIBILITY TESTING

There are several tests which are commonly used to obtain qualitative data pertaining to the compatibility of materials with oxygen. One of the most widely used compatibility tests is the mechanical impact test developed by the Army Ballistic Missile Agency for determining the compatibility of materials with liquid oxygen. There have been improvements in test equipment and techniques as described in reference 43. Ignition temperature determination is usually accomplished by means of some type of oxygen bomb test. Other types of tests, including flash and fire point, flow velocity, and pneumatic impact, are also employed in determining materials compatibility with gaseous oxygen. Furthermore, various flammability tests are used to determine burning characteristics of materials in oxygen environments such as spacecraft cabin atmospheres.

3.6.1 NASA Specifications for Materials Compatibility Testing

The Office of Manned Space Flight has issued a handbook (ref. 38) which establishes uniform material selection, evaluation, and control criteria for all materials that are under consideration for use in and around manned spacecraft during flight and test operations. Test specifications which were the basis for that handbook are references 44 to 46. These documents provide detailed descriptions of test equipment and procedures, some of which are summarized herein.

3.6.1.1 Mechanical impact testing. - This test is performed to determine the impact sensitivity of materials with liquid or gaseous oxygen (LOX or GOX). Tests are categorized as either ambient LOX mechanical impact or pressurized LOX or GOX mechanical impact. The basic test equipment for ambient LOX mechanical impact testing is described in reference 38 (pp. 4-60 to 4-66). For pressurized LOX or GOX testing appropriate modifications to incorporate a test chamber such as shown in reference 38 (pp. 4 to 82) must be made.

The test procedure involves dropping a 20-pound (9.04-kg) weight from known heights up to 43.3 inches (1.1 m) under near-frictionless conditions. The falling weight strikes a plunger (0.500-in. diameter) which delivers a blow to the material being tested as illustrated in figure 3-17. Complete test equipment description and procedures may be found in reference 38 (pp. 4-58 to 4-80).

Solid materials are tested in the form of 11/16-inch-diameter disks. Solid materials having up to 1/4 inch thicknesses are tested using disks in the thickness intended for actual use. Solid materials normally used in thicknesses greater than 1/4 inch are tested using disks having both 0.050 and 0.250 inch thicknesses. Greases, fluids, and other materials whose thicknesses are not dictated by conditions of use are tested as 0.050-inch layers. Paints and dry film lubricants are applied to 11/16-inch-diameter stainless

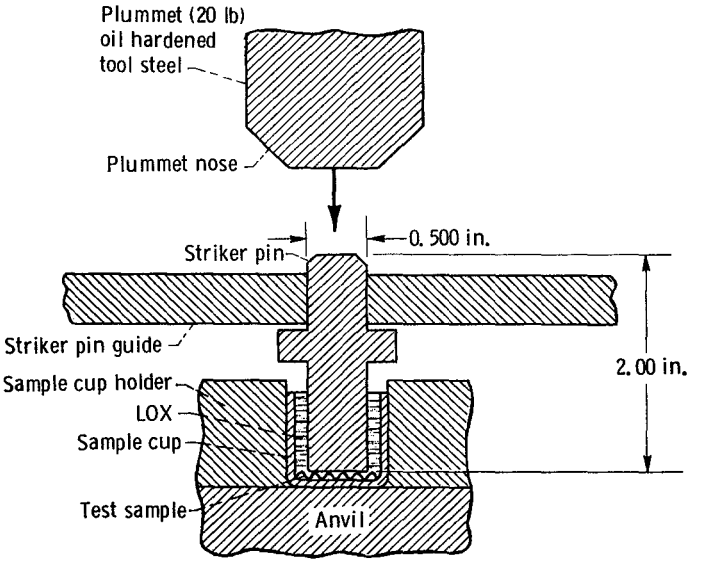

Figure 3-17. - Impact test striker assembly (ref. 45, p. 6).

steel disks in the same manner and thickness as intended for hardware application for testing. Leak check compounds, dyes, and dye penetrant systems are tested after application to 11/16-inch-diameter 6061-T6 aluminum disks which are unsealed and sulfuric acid anodized.

A material under test is subjected to twenty successive impacts at 72 foot-pounds (10 kg-m). More than one reaction in twenty impacts is cause for rejection. If one reaction occurs, the material is subjected to forty additional impacts. One reaction in the forty drops is cause for rejection. A reaction is defined as any of the following:

(1) Audible explosion

(2) Flash (electronically or visually detected)

(3) Evidence of burning (obvious charring)

(4) Major discoloration

A material proposed for use in liquid oxygen systems or subject to direct contact with liquid oxygen must be tested in a LOX environment and must meet the previous requirements. Materials proposed for use in high pressure (20 psia or above) LOX/GOX systems must meet the same requirements as a minimum. In addition, materials for use at 20 psia or above must meet mechanical impact acceptance requirements at the actual thickness (or thinner than actual) intended for use and at maximum use pressure and temperature. Material for use in high pressure environments (such as pressurized air) where the oxygen partial pressure is 20 psia or greater must meet pressurized LOX/GOX mechanical impact requirements.

A material which does not meet acceptance criteria for high pressure LOX/GOX systems is evaluated by determining its impact threshold level at maximum use pressure and temperature as outlined in reference 38 (p. 4-77). Based on this evaluation, the pro-

curing activity may approve the use of the material.

3.6.1.2 GOX pneumatic impact testing. - This test is used to determine the sensitivity and compatibility of materials with pure GOX when subjected to pneumatic impact. It is used in conjunction with mechanical impact threshold determination to verify acceptability for a specific application of a material which may be subjected to pneumatic impact loading (ref. 38, p. 2-5).

The material to be tested is placed in a sample chamber cavity where it is subjected to cyclic high pressure oxygen. This is accomplished by opening a quick acting supply valve, pressurizing the sample chamber cavity, equalizing the pressure at the test level, and then opening a chamber bleed valve. Standard impact frequency is 5 cycles within 60 seconds (automatically timed).

Materials are tested in an atmosphere of 95 (plus 5, minus 0 percent) GOX at pressures and temperatures equal to use pressures and temperatures. Standard tests are conducted at a temperature of $70^{o} \pm 10^{o}$ F. A detailed description of equipment and procedures may be found in reference 38 (pp. 4-83 to 4-87).

3.6.1.3 Upward propagation rate testing. - This test is intended to determine the flammability characteristics of materials when exposed along the bottom edge to an energized ignition source. The test is conducted at the highest pressure and oxygen concentration to which the material will be exposed.

The test is conducted in a chamber having sufficient volume to assure complete combustion of the test samples (minimum volume is 98 liters) and with pressure instrumentation and a viewing port. The test sample is supported within the chamber leaving an area 2 inches by 12 inches of the sample exposed. Ignition is accomplished by means of a standard silicone igniter (or equivalent) which is described in reference 38 (p. 4-3). Materials such as primers, paints, and coatings are applied on 3-mil-thick aluminum foil or the substrate material intended for use. Greases and fluids are applied to a substrate of 5-millimeter-thick fiberglass cloth for testing.

Materials are tested in a vertical position and exposed to an energized ignition source placed at the bottom of the sample for a period of 30 +20 or -10 seconds. Materials which fail to ignite or are self-extinguishing before 6 inches of the sample are consumed, with no sparking, sputtering, or dripping of flaming particles, are considered acceptable under this test. Flame propagation rates are measured and recorded on film. This test is described in detail in reference 38 (pp. 4-1 to 4-7).

3.6.1.4 Downward propagation rate testing. - This test is for determining the downward burning propagation rate of materials and their relative rankings. The test is similar to the upward propagation test except that the igniter is applied at the top edge of the test sample. The propagation rate is measured either by thermocouples or motion pictures (ref. 38, pp. 4-8 to 4-9).

3.6.1.5 Flash and fire point testing. - Flash and fire point testing is accomplished to evaluate the spark ignition characteristics of nonmetallic materials which have been

selected for application in and around manned spacecraft. Materials are normally considered acceptable if they exhibit a flash point above 400° F and a fire point above 450° F.

This test is conducted in a test chamber pressurized to at least 50 psia. A 0.5-gram sample is heated at a rate of 25 fahrenheit degrees per minute. A 2-millisecond, 50±20 millijoule spark is discharged between electrodes positioned 0.75 inch above the sample once for each 10 seconds.

Flash and fire occurrences are monitored visually through a glass viewport and electronically by a photoelectric cell detector. Flash point is defined as the lowest temperature at which the test specimen gives off sufficient flammable vapors that, when mixed with the test atmosphere and exposed to the spark ignition source, provides a non-self-sustaining flash or flame. The fire point is defined as that temperature atwhich the vapors continue to burn after ignition. As pressures are increased these temperatures tend to converge.

Data obtained from test rigs operating at pressures up to 50 psia when compared to those obtained at higher pressures are not identical. This anomaly is attributed to differences in spark generators because a higher spark voltage is required to obtain spark propagation at the higher pressures. While at low pressures the spark energy can be readily measured, at higher pressures even an approximate measurement is difficult (ref. 25, pp. 43 and 52). Accordingly, there is no assurance that test parameters are the same between high and low pressure setups. For a given pressure, however, the energy inputs appear repeatable which means that data for different materials under the same test pressure are consistent and permit ranking the materials. A description of test equipment and procedures may be found in reference 38 (pp. 4-10 to 4-16).

3.6.1.6 Electrical wire insulation testing. - This test is used to screen flammable wire insulation and electrical accessory materials such as wire bundle sleeving, heat shrinkable tubing, solder sleeves, bundle ties, cable clamps, and identification tags. The test is performed at use pressure and gas mixture conditions. Materials are considered acceptable if determined noncombustible in the test atmosphere during current overloads up to the melting point of the wire. The materials must also meet the requirements of the upward propagation test.

Testing is accomplished in a test chamber similar to the one used for the upward propagation test. Wires are assembled either in use configuration or in a bundle of seven insulated wires. Current is applied through one wire on the exterior of the bundle. Test current is increased in 5-ampere steps until either wire failure or ignition occurs. If the wire fails, voltage is maintained until it is positively established that current does not flow by bridging the gap to adjacent conductors. Equipment and procedures are described in reference 38 (pp. 4-17 to 4-20).

3.6.1.7 Connector potting flammability testing. - This test is intended to provide an evaluation of flammability characteristics of potting and coating compounds in a specific gas atmosphere environment. It simulates a short circuit or dielectric breakdown of

current carrying wires within a potting compound used to seal electrical connectors. Materials determined to be noncombustible under test conditions are considered acceptable.

The test is conducted at the highest pressure and oxygen concentration conditions for the intended use. The test chamber used is similar to the one used for the upward propagation test. Current is applied to one lead through a test connector potted with the test material. Current is increased until ignition of the potting compound occurs or the wire fails. If the wire fails, the voltage is maintained for 1 minute to establish that current does not flow by bridging the gap to adjacent conductors. For a description of procedures and equipment see reference 38 (pp. 4-21 to 4-29).

3.6.1.8 Other NASA compatibility testing. - Additional flammability tests are also required to determine combustion characteristics of materials in sealed and unsealed (vented) containers (ref. 38, pp. 4-42 to 4-48). Configuration testing to determine combustion characteristics, particularly propagation rates of materials as they are assembled in functional assemblies are also required (ref. 38, pp. 4-49 to 4-54). Such tests include simulated panel and assembly flammability tests and simulated crew bay configuration flammability verification tests.

In addition to the previously described tests, NASA also requires testing to verify compatibility with personnel, including odor and off-gassing products and carbon monoxide tests. These tests are to verify that, when heated, the materials do not give off products which will be toxic or objectional to crew members (ref. 38, pp. 4-30 to 4-36).

3.6.2 Tests Not Required by NASA

There are tests not necessarily required by NASA which are also of value in determining the compatibility of materials with oxygen. Generally these tests are designed to evaluate the ignition characteristics of materials in oxygen or combustion supporting environments.

3.6.2.1 Oxygen bomb test. - A typical autoignition test and test equipment, as described in reference 47 (pp. 2 to 6), include a reaction chamber about 12 inches in diameter by 18 inches high enclosed in a furnace. Temperature, pressure, and oxygen (gas) flow are the controlled parameters. Test samples are placed on a stainless steel tray located just above the gas inlet mixer. The tray may be independently temperature controlled or slaved to the main reaction chamber. Specimen temperature is measured by a thermocouple in contact with its exposed upper surface. Reaction chamber temperature is also monitored. The reaction chamber is pressurized with the test gas to the test pressure. A static or a dynamic test atmosphere may then be maintained. In the latter instance, the flow rate is controlled independent of operating pressure. After pressure and flow conditions are stabilized the furnace heater is activated to provide the

desired temperature profile and testing proceeds until ignition is obtained. Preignition and postignition reaction chamber atmospheres may also be sampled and analyzed for reaction products.

3.6.2.2 Thermogravimetric analysis testing. - The thermogravimetric analysis (TGA) technique may be employed for nonmetals in conjunction with flash and fire point testing techniques. In this test the weight or weight change of the sample being subjected to flash and fire point determination is determined by means of a precise spring balance. Sample weight loss and photoelectric cell output (for flash point determination) are plotted against test chamber temperature as illustrated in figure 3-18 (ref. 48). The

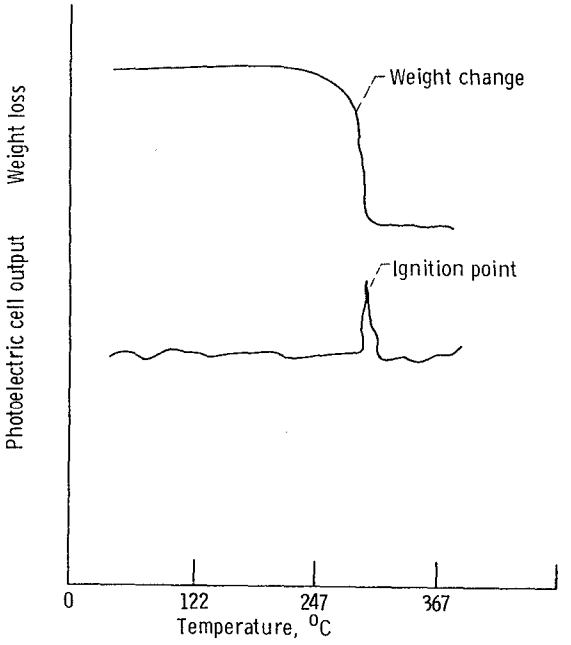

Figure 3-18. - Typical TGA ignition temperature determination (ref. 48, p. 107). Material, 85.5 milligrams polyvinyl chloride; test environment, 1.5 cubic centimeters per minute oxygen; heat rate, 24° C per minute.

temperature coincidence of an abrupt sample weight change and flash point indicator provides an ignition temperature determination. This test and associated equipment are described fully in reference 48 (pp. 101 to 104).

This test appears to provide a reproducible characterization of many nonmetal materials in oxygen atmospheres at a 1-atmosphere pressure or below.

3.6.2.3 Oxygen index testing. - The oxygen index test method is used to determine the relative flammability of materials. The test method is presently limited to physically self-supporting plastic test specimens. The oxygen index is the minimum concentration of oxygen, expressed as a volume percent, in a mixture of oxygen and nitrogen that will

just support combustion of the material under test.

Generally the test consists of igniting a specimen in a test column through which a slowly rising mixture of oxygen and nitrogen is flowing. The gas mixture is varied to determine the mixture which just supports combustion in the form of candle-like (top ignition) burning. This point is approached from both sides of the critical oxygen concentration in order to establish the oxygen index. The test and equipment are fully described in reference 49 (pp. 727 to 729). Data are tabulated in table 3-XI.

3.6.2.4 Velocity impact testing. - This test has been used by some investigators to rank materials according to their susceptibility to particle impact ignition. The test involves injecting a charge of metal particles (usually iron) into a flowing stream of oxygen. A sufficiently long flow path is provided to permit the particles to accelerate to the flowing gas velocity. At this point, the particles impinge a test specimen mounted in a cup-like holder in a combustion chamber vented to atmosphere. Ignition of a portion of the particles upon impact on the sample causes ignition of the particle cloud which then ignites the test specimen.

This test is rather limited in that there are many variables which affect the results, some of which are rather difficult to control. These include particle size and shape, distribution of particulate sizes and shapes within the flow pattern, and the thickness of the oxide film on both the particles and the sample. While test results generally confirm rankings obtained by other tests, the test is most useful as a verification test for specific applications, such as very high pressure, high velocity flow systems, where very high impact energies and possible ignition can occur. See also section 3.4.6.

3.6.2.5 Electrical arc ignition testing. - Tests to determine the susceptibility of materials to an electric arc have been conducted in a test chamber similar to the chamber used for high pressure flash and fire point testing described previously. An arc generator, electronic ignition sensing equipment, and temperature and pressure control equipment are also similar to that used for flash and fire point testing.

Test samples of varying thicknesses and a 0.500-inch diameter are prepared with a 3/32-inch hole in the center and supported between two electrodes. The electrodes are placed together through the hole. After pressure and temperature conditions are established, the electrodes are mechanically separated to initiate the arc. Ignition is monitored electronically. Tests are conducted at different arc current levels to determine current thresholds of no ignition and 100 percent ignition. The procedure for this test was developed by the White Sands Test Facility and is described in detail in reference 50.

Since actual power input to the test specimen cannot be accurately determined, this test also only provides a ranking of materials in terms of susceptibility to electric arc in proximity to the material. The power input can be accurately repeated, however, by controlling the arc current.

TABLE 3-XII. - PHYSICAL PROPERTIES OF PREFERRED POLYMERS

[Ref. 51, pp. 12.3.2-2 and 12.3.2-3.]

(a) Plastics

Common name	Fluorinated ethylene propylene	Polychlorotri-fluoroethylene	Polyvinylidene fluoride	Polytetrafluoro-ethylene	Polyimide
Trade name	Teflon FEP[a]	Kel-F[b]	Kynar[c]	Fluorosint[d,e] Teflon TFE[a] Halon TFE[f]	Kapton H[a] Kapton F[a] Vespel[a] Polymer SP-1[a]
Physical and mechanical properties:					
Specific gravity	2.14 to 2.17	2.1 to 2.2	1.76 to 1.77	2.13 to 2.22	1.42
Tensile strength, psi	2700 to 3100	4500 to 6000	7000	2000 to 4500	[g]25 000; 10 500
Elongation, percent	250 to 330	30 to 250	100 to 300	200 to 400	[g]70; 6 to 8
Tensile modulus, psi	0.5×10^5	1.5×10^5 to 3×10^5	1.2×10^5	0.58×10^5	4.3×10^5
Compressive strength, psi	2200	32 000 to 80 000	10 000	1700	24 400
Flexural strength, psi	----------	7400 to 9300	----------	----------	14 000
Impact strength, ft-lb/in. of notch	No break	0.8 to 5.0	3.5	3.0	0.9
Rockwell hardness	R25	R110 to R115	D80 (shore)	D50 to D65 (shore)	H85 to 95
Thermal conductivity, Btu/hr/ft^2/(^{o}F/in.)	1.75	0.9	0.9	1.75	2.2
Specific heat, Btu/lbm/^{o}F	0.28	0.22	0.33	0.25	0.27
Coefficient of linear expansion, in./in./^{o}F$\times10^{-5}$	4.7×10^{-5} to 5.8×10^{-5}	5×10^{-5} to 15×10^{-5}	6.7×10^{-5}	5.5×10^{-5}	28×10^{-5} to 35×10^{-5}
Volume resistivity, ohm-cm	$>2\times10^{18}$	1.2×10^{18}	2×10^{14}	$>10^{18}$	10^{18}
Clarity	Transparent to translucent	Transparent to translucent	Transparent to translucent	Opaque	Opaque
Processing properties:					
Molding qualities	Excellent	Excellent	Excellent	----------	----------
Injection molding temperature, ^{o}F	625 to 760	440 to 600	450 to 550	----------	----------
Mold shrinkage, in./in.	0.03 to 0.06	0.005 to 0.010	0.030	----------	----------
Machining qualities	Excellent	Excellent	Excellent	Excellent	----------
Resistance properties:					
Mechanical abrasion and wear Tabor CS 17 wheel mg, loss/1000 cycles	----------	0.01	17.6	----------	----------
Temperature:					
Flammability	None	None	Self-extinguishing	None	----------
Low temperature brittle point, ^{o}F	-420	-400	-80	-420	----------
Resistance to heat, ^{o}F (continuous)	400	350 to 390	300	550	500
Deflection temperature under load, ^{o}F	----------	258 (66 psi)	300 (66 psi), 195 (264 psi)	250 (66 psi)	----------
Chemical:					
Effect of sunlight	None	None	Slight bleaching on long exposure	None	Degrades after prolonged exposure
Effect of weak acids			None		None
Effect of strong acids			Attacked by fuming sulfuric		----------
Effect of weak alkalies			None		----------
Effect of strong alkalies			None		Attacked
Effect of organic solvents		Halogenated compounds cause slight swelling	Resists most solvents		Resistant to most organic solvents

[a] E. I. duPont de Nemours.
[b] Minnesota Mining and Manufacturing Co.
[c] Pennsalt Chemicals Corp.
[d] Polymer Corp. of Pennsylvania.
[e] Polypenco, Inc.
[f] Allied Chemical Corp.
[g] Film.

TABLE 3-XII. - Concluded. PHYSICAL PROPERTIES OF PREFERRED POLYMERS

[Ref. 51, pp. 12.3.2-2 and 12.3.2-3.]

(b) Elastomers

Elastomer types	Silicone rubber	Vinylidene fluoride hexa-fluoropropylene	Fluorosilicone	Polytrifluoro-chloroethylene
Trade name	Silastic[a] Silicone rubber[e,f]	Viton[b] Fluore[c]	Silastic LS-53[a]	Kel-F[c,d]
Physical and mechanical properties:				
Durometer range (shore A)	45 to 60	55 to 90	50 to 60	55 to 90
Specific gravity (base elastomer)	1.17 to 1.46	1.4 to 1.85	1.41 to 1.46	1.4 to 1.85
Density, lb/in.^{3} (base elastomer)	0.045	0.051 to 0.067	0.051	0.051 to 0.067
Tensile strength, psi:				
Pure gum	Under 400	>2000	1000	350 to 600
Reinforced	600 to 1500	----------	----------	----------
Elongation, percent:				
Pure gum	Under 200	>350	200	500 to 800
Reinforced	200 to 800	----------	----------	----------
Thermal conductivity, g, Btu/hr/sq ft/($^\circ$F/ft)	0.13	----------	0.13	----------
Coefficient of thermal expansion, cubical, in.^{3}/in.^{3}/$^\circ$F	45×10^{-5}	27×10^{-5}	45×10^{-5}	----------
Electrical insulation	Excellent	Excellent	Good	Excellent
Rebound:				
Cold	Very good	Good	Very good	----------
Hot	Very good	Excellent	Very good	----------
Compression set	Good to excellent	Good to excellent	Good	Good to excellent
Resistance properties:				
Temperature:				
Tensile strength at 250° F, psi	850	300 to 800	----------	300 to 800
Tensile strength at 400° F, psi	400	150 to 300	----------	150 to 300
Elongation at 250° F, percent	350	100 to 350	----------	100 to 350
Elongation at 400° F, percent	200	50 to 160	----------	50 to 160
Low temperature brittle point, $^\circ$F	-90 to -200	10 to -60	-90	10 to -60
Low temperature range of rapid stiffening, $^\circ$F	-60 to -120	20 to -30	----------	-20 to -30
Drift, room temperature	Poor to excellent	Good	----------	Good
Drift, elevated temperature (158° to 212° F)	Excellent	Good to excellent	Excellent	Good to excellent
Heat aging (212° F)	Excellent	Excellent	Excellent	Excellent
Maximum recommended continuous service temperature, $^\circ$F	480	450	500	400
Minimum recommended service temperature, $^\circ$F	-178	-50	-90	-60
Mechanical:				
Tear resistance	Poor	Poor to good	----------	Poor to good
Abrasion resistance	Poor	Good	Poor	Good
Impact resistance (fatigue)	Poor	Poor to good	Poor	Poor to good
Chemical:				
Sunlight aging	Excellent	Excellent	Excellent	Excellent
Weather resistance	Excellent	Excellent	Excellent	↓
Oxidation	Excellent	Excellent	Excellent	↓
Acids:				↓
Dilute	Very good	Excellent	Excellent	↓
Concentrated	Good	Good	Very good	↓
Alkali	Fair to excellent	Poor to fair	Fair to excellent	Poor to fair
Alcohol	Good	Excellent	Poor to good	Excellent
Petroleum products, resistance	Poor to fair	Good to excellent	Excellent	Good to excellent
Coal tar derivatives, resistance	Poor	Excellent	----------	Excellent
Chlorinated solvents, resistance	Good	Good	----------	Good
Hydraulic oils:				
Silicates	Poor	Good	----------	Good
Phosphates	Good	Poor	----------	Poor
Water swell resistance	Good	Good	Excellent	Good
Permeability to gases	Good	Excellent	Fair	Excellent

[a]Dow Corning Corp.
[b]E. I. duPont de Nemours.
[c]Minnesota Mining and Manufacturing Co.
[d]CTFE compounded with vinylidine fluoride.
[e]General Electric.
[f]Union Carbon and Carbide.

3.7 PREFERRED POLYMERIC MATERIALS FOR OXYGEN SYSTEMS

Of the three general classes of materials (metals, cermets, and polymers), the polymeric materials as a class are the most sensitive to possible ignition in oxygen. Metals have a significantly higher ignition temperature than polymeric materials and they have the advantage of the protective oxide film coating. Because these advantages are highly variable, depending on the circumstances, preferred metals are discussed in context with their application in chapters 5 to 10. The cermets (fused metal oxides) and fiberglass (a silicate) are already oxidized so they will not "burn" in oxygen.

All polymers will burn in oxygen and some of them will ignite very easily compared to most metals (see section 3.4). However, a few of the polymeric materials have relatively high ignition temperatures (up to 500° C) and are highly resistant to ignition and chemical deterioration in oxygen. Polymeric materials that are most resistant to reaction with oxygen are the fluorocarbon plastics and elastomers. Next in resistance to oxygen are the silicone elastomers and the polyimide and epoxy resins. Nearly all plastics and elastomers can be exposed to oxygen with no apparent reaction. They may even be highly resistant to deterioration or reaction for short exposure times. But, care must be taken that materials considered for use in oxygen systems have the necessary resistance to oxygen attack and degradation for long term exposure.

Selected physical properties of the preferred polymers are given in table 3-XII (ref. 51). For additional information see references 30, 52, and 53 (chs. 10, 11 and 12).

Although fiberglass is not a polymeric material, it is included in this discussion because of its special physical characteristics and its chemical inertness to oxygen.

3.7.1 Fluorocarbon Polymers

The fluorocarbon polymers are the most stable polymeric materials because the fluorine atom has the highest oxidation potential of any other oxidizer, and, therefore, the fluorocarbon structure cannot be broken by a weaker oxidizer under normal conditions. The higher the degree of substitution of fluorine for hydrogen in the polymer structure, the more resistant the polymer is to further oxidation.

A fully substituted fluorinated polymer, such as polytetrafluoroethylene,

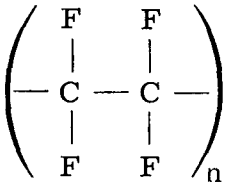

can only be reacted further by thermochemical degradation of the polymer which breaks the carbon-carbon bond. A partially substituted polymer, such as vinylidene fluoride,

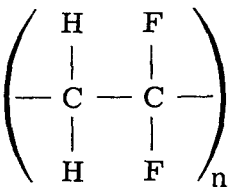

is less resistant to attack, and regular polyethylene

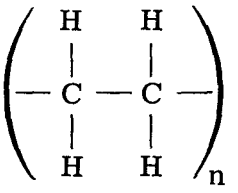

is more readily attacked by strong oxidizers. The substitution for the fluorine atom in the polymer, especially with hydrogen, results in a significant decrease in chemical inertness and causes thermal degradation at a lower temperature.

The physical properties of fluorocarbon polymers are highly variable depending on the specific material, the average molecular weight, and its degree of crystallinity. The higher the average molecular weight, the greater the viscosity, hardness, and toughness. Material of thin cross section can be quickly quenched to yield low crystallinity, some increase in chemical stability and density, and a decrease in the permeability to gases. The effects of crystallinity on physical properties of some fluorocarbon resins are shown in table 3-XIII and the effects of crystallinity on creep are discussed in section 9.3.2.

Polytetrafluoroethylene (TFE) has a crystalline structure below 327° C. If heated above 327° C it becomes amorphous, translucent, and plastic and begins to soften significantly. TFE begins to pyrolyze above 400° C; when heated above 650° C it decomposes into the monomer (C_2F_4), elemental fluorine (F_2), carbon tetrafluoride (CF_4), and other fragments. If oxygen is present, some COF_2 may be formed. Oxygen, fluorine, and hydrogen all react with polytetrafluoroethylene at the decomposition temperature (approximately 650° or 1202° F). The basic reactions are as follows:

$$(-CF_2-)_n \longrightarrow C_2F_4 + (F_2 + CF_4 + C)$$
$$(-CF_2-)_n + O_2 \longrightarrow COF_2$$
$$(-CF_2-)_n + H_2 \longrightarrow HF + C$$
$$(-CF_2-)_n + F_2 \longrightarrow CF_4$$

These reactions are typical of the fluorocarbon polymers. TFE is also prone to stress crazing when exposed to halogenated solvents and cleaning agents. When used as seals,

TABLE 3-XIII. - PHYSICAL PROPERTIES OF FLUOROCARBON RESINS OF VARYING CRYSTALLINITIES

[Values were obtained by reading data points from the original data curves. Values in parentheses ( ) were obtained by interpolation. No actual data were obtained with liquid-oxygen temperatures in the original study. Change in crystallinity indicated by asterisk.]

Mechanical property	Temperature, ^{o}F	Fluorocarbon resins											
		Kel-F				FEP Teflon			TFE Teflon				
		Crystallinity, percent											
		40	55	60	70	44	49	51	47	49	52.5	66.2	71
Notched Izod impact strength, ft-lb/in.	-423	---	---	1.4	1.2	---	1.95	1.7	---	---	1.25	---	1.55
	-320	---	---	1.3	1.1	---	1.9	1.5	---	---	1.17	---	1.35
	(-297)	---	---	(1.25)	(1.07)	---	(1.9)	(1.5)	---	---	(1.15)	---	(1.39)
Modulus of rigidity, psi×10^3	-423	262	222	---	230	935	---	695	267	---	275	377	---
	-320	232	197	---	203	305	---	305	224	---	190	200	---
	(-297)	(229)	(192)	---	(195)	(275)	---	(275)	(216)	---	(175)	(175)	---
Tensile yield strength, psi×10^3	-423	28.5	20.5	---	18.0	23.8	23.5	---	---	20.0	19.0	15.6	---
	-320	24.9	17.5	---	15.3	19.1	18.8	---	---	16.0	15.4	10.6	---
	(-297)	(24.4)	(17.0)	---	(15.0)	(17.9)	(17.6)	---	---	(14.2)	(14.1)	(9.0)	---
Ultimate tensile strength, psi×10^3	-423	29.0	22.5	---	17.95	24.0	23.6	---	---	20.05	19.0	15.7	---
	-320	24.9	17.6	---	15.8	18.1	17.9	---	---	17.9	15.4	11.8	---
	(-297)	(24.1)	(17.5)	---	(15.3)	(17.0)	(16.8)	---	---	16.0	14.2	11.0	---
Tensile modulus, psi×10^6	-423	1.26	0.975	---	0.830	0.825	0.620	---	---	0.600	0.645	0.625	---
	-320	1.11	0.802	---	0.760	0.700	0.450	---	---	0.500	0.520	0.435	---
	(-297)	(1.08)	(0.800)	---	(0.750)	(0.652)	(0.430)	---	---	(0.465)	(0.480)	(0.400)	---
Elongation, percent	-423	ca 2	ca 1	---	<1	ca 5	ca 5	---	---	ca 4	ca 3	ca 2	---
	-320	ca 4	2.5	---	ca 1	ca 7	ca 7	---	---	ca 9	ca 8	ca 4	---
	(-297)	(ca 4.5)	(3)	---	(ca 1)	(ca 8)	(ca 7)	---	---	(9)	(8)	(ca 5)	---
Flexural strength, psi×10^3	-423	74.0	55.5	---	50.5	35.9	39.6	---	---	33.8	25.7	22.8	---
	-320	58.0	42.7	---	37.0	25.7	27.7	---	---	30.0	24.0	21.5	---
	(-297)	(53.5)	(41.0)	---	(35.0)	(24.0)	(25.5)	---	---	(28.0)	(23.0)	(20.5)	---
Flexural modulus, psi×10^6	-423	2.09	1.94	---	1.84	0.78	0.75	---	---	0.778	0.72	0.695	---
	-320	1.83	1.70	---	1.64	0.68	0.68	---	---	0.720	0.70	0.64	---
	(-297)	(1.70)	(1.64)	---	(1.59)	(0.67)	(0.66)	---	---	(0.690)	(0.64)	(0.61)	---
		50*	55	60	70	44	49	51	47	50*	56*	68*	71
Compressive strength, psi×10^3	-423	42.5	---	44.5	28.8	36.3	35.2	---	---	30.4	32.5	33.2	---
	-320	35.0	---	37.5	38.8	30.0	30.0	---	---	20.0	21.2	22.0	---
	(-297)	(34.0)	---	(36.0)	(38.8)	(28.5)	(28.5)	---	---	(18.5)	(20.0)	(21.5)	---
Compressive modulus, psi×10^6	-423	1.67	---	1.76	1.48	1.01	1.04	---	---	0.81	0.90	0.97	---
	-320	1.48	---	1.52	1.65	0.91	0.91	---	---	0.75	0.79	0.84	---
	(-297)	(1.27)	---	(1.49)	(1.65)	(0.90)	(0.89)	---	---	(0.72)	(0.76)	(0.81)	---
Coefficient of thermal expansion (total contraction from 70^{o} F), in./in.	-423	0.011	---	---	---	0.017	---	---	---	0.0214	---	---	---
	-320	0.0093	---	---	---	0.0157	---	---	---	0.0205	---	---	---
	(-297)	(0.0090)	---	---	---	(0.0154)	---	---	---	0.0201	---	---	---

[a]Ref. 30, pp. 8 and 9.

gaskets, or other components in oxygen systems and under a stressed condition, halogenated solvents should not be used where exposure time is more than a few minutes. The threshold level of stress which can cause crazing is reported to be 4.1×10^6 to 5.5×10^6 newtons per square meter (600 to 800 psi) (ref. 54, p. 22).

Fluorinated ethylene propylene copolymer (FEP) is extrudable and is readily processed by common fabricating equipment. The notched Izod impact strength indicates that FEP is more resistant to impact fracture at cryogenic temperatures than either TFE or Kel-F.

Filled TFE and FEP have better resistance to deformation and cold flow, lower thermal coefficient of expansion, and better wear resistance than the unfilled Teflons (most common filler materials are metal powders and glass fiber). In the filled materials, elongation and impact strength are reduced. The glass-fabric-reinforced TFE and FEP are very strong and are used in applications involving tensile and flexural strength, as well as compression and shear. The room temperature mechanical properties of these materials are controlled by the strength of the glass fabric rather than the resin.

Chlorotrifluoroethylene (CTFE), an opaque colorless material, is exceptionally stable (comparable to TFE), highly temperature resistant, chemically inert, and a true thermoplastic. Chlorine in the molecule contributes to the translucency and the rigidity characteristics of the polymer. CTFE has superior resistance to cold flow over TFE; however, in most applications where creep or cold flow would be a problem, a fiberglass-filled fluorocarbon polymer may be preferred. The higher fluorocarbon has improved compressive yield and cold flow characteristics to some extent. However, the tensile yield and ultimate strength are decreased.

Vinylidene fluoride and hexafluoropropylene copolymer is a linear copolymer containing about 65 percent fluorine. It has excellent resistance to oxidation. O-rings molded from commercial compounds of this material make excellent static seals at temperatures from 260° to less than -184° C even though the material may be brittle at the lower temperatures.

3.7.2 Silicone Polymers

Silicone polymers are formed from a basic structure of alternating silicon and oxygen atoms cross linked with methyl, phenyl, or vinyl groups at each silicon atom. The silicone polymers are very stable at high temperatures (over 200° C). Reference 52 (p. 2-9) states that "at 500° F (260° C) after one-half hour exposure, silicone fiberglass laminates retain approximately 40 percent of initial strength." In a vacuum at 800° C, a 13 percent weight loss was measured, and at about 1200° C a 17 percent loss was obtained (ref. 52, pp. 2-9 and 2-10). The ignition temperature of silicone rubber is only 390° C. The permeability of silicone polymers to oxygen is very low even at

very high pressures. This is important to prevent rupture when suddenly depressurized after long periods of high pressure exposure. Experience with silicone O-rings in high pressure oxygen (over 6000 psia) has been very good in both static and dynamic seal applications. (See section 9.3.3.) However, the use of silicone rubber exposed to high velocity flow or possible high velocity particle impact is not recommended.

3.7.3 Fiberglass

Fiberglass materials are basically a mixture of oxidized silicon, metal silicates, phosphates, and borates, and because they are already oxidized, they will not burn or react with oxygen. However, processing agents and bonding materials for fiberglass laminates (such as epoxy resin) are flammable. Fiberglass is widely used as reinforcing filler in fluorocarbon materials to improve strength and reduce cold flow. Any application where fiberglass meets the physical requirements for temperature and stress may be considered for use in oxygen.

3.7.4 Polyimide Resins

Polyimides have the basic structure

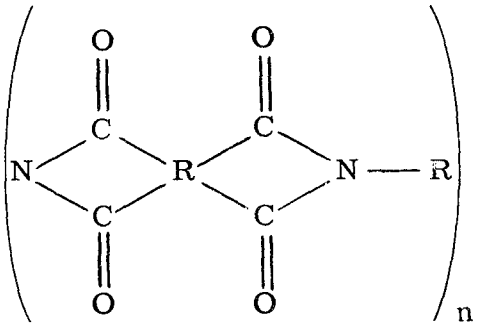

where R represents an aromatic groups which has a carboncyclic structure. Polyimides have a higher decomposition and ignition temperature than the epoxy resins and are used as wire insulation, film laminates, impregnants, and occasionally as bonding agents. They are stable at 315° C. Weight loss begins at about 370° C and reaches 40 percent at 815° C and over 90 percent when exposed to oxygen at 815° C (ref. 52, (p. 2-11).

3.7.5 Epoxy Resins

Epoxy polymers include a large family of materials having a basic epoxide structure of the form

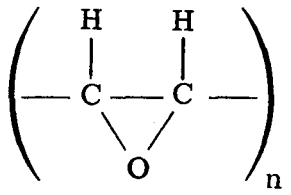

A wide variety of curing agents and additives provide variations in physical properties useful in many applications, mainly as bonding agents. However, decomposition begins at about 300° C. Total decomposition occurs by 900° C (ref. 52, p. 2-5).

Epoxy resins will ignite in oxygen at their initial decomposition temperatures (300° to 310° C, see table 3-III) unless a flame retardant is added to increase the ignition temperature. Antimony trioxide is generally added for this purpose with some decrease in mechanical properties (ref. 52, p. 2-6). Epoxy resins are not recommended where exposure to LOX or high pressure oxygen is possible because of its limited physical and chemical compatibility.

CHAPTER 4. OXYGEN SYSTEMS ENGINEERING CONSIDERATIONS

Oxygen system failures or malfunctions result from three possible causes: insufficiently compatible materials (chemical stress), structural failure (physical stress), and system contamination, which results in solid particle interference or clogging and ignition sensitivity (physical and chemical stress). Most fluid system hardware such as valves, lines, and fittings are made of materials and have design features that are suitable for a wide variety of fluids. Much of this hardware may be used with oxygen. On the other hand, there are many subtle requirements that must be met in specific oxygen systems that can disquality a material or design feature used in the available hardware. The designer can eliminate many potential problems by design and design modifications of existing hardware that accommodate the special characteristics of oxygen. Many of these subleties for an oxygen system have been reviewed in the previous chapter with respect to chemical compatibility and physical phenomena. The following sections discuss some of the special considerations for oxygen systems engineering with respect to system design, fabrication, and use. The concerns for oxygen systems discussed in this chapter include the problems of leakage and erosion, difficulties that arise from dynamic processes, and the sensitivity of oxygen systems to contamination and cleaning requirements. Subsequent chapters discuss individual fluid system components.

4.1 FLUID SYSTEM LEAKAGE

One of the continuing problems with fluid flow systems is leakage through valves and from joints, coupling, and component interfaces and from mechanical penetrations such as rotating shafts, valve stems, and actuators. Leak rate control is especially important in spacecraft where fluid loss can be critical to the mission. Oxygen system leaks present the additional problem of fire hazard from local oxygen enrichment and possible impingement of oxygen on a combustible material. The leakage rate and the resulting hazard increases because of the erosive effect which gradually enlarges the leak path. The rate of erosion also increases with increasing pressure. Extremes in temperature, temperature cycling, vibration, and mechanical stresses also contribute to the leakage problem since they can cause a leak and affect the rate of leakage increase. Finally, seal

wear in dynamic seals or deterioration from assembly-disassembly of static seals contributes to seal failure and leakage.

The possible leakage path between two surfaces pressed together to effect a seal depends on the relative dimensions of surface asperities (texture), waviness of the contacting surfaces, and the elasticity of the seal. Under light seal loads the leakage gap will be influenced by the amount of surface texture roughness, waviness, nodules, pits, and scratches that protrude above some average plane and thus prevent full contact of the surfaces. At higher loads the asperities yield and tend to allow closer conformity of the contacting surfaces. The predominant flow path will then be through the roughness, scratches, and interconnecting pits until sufficient yielding occurs to close all leakage paths.

The prevention of leaks and leak rate control can only be affected by the proper seal configuration and a choice of seal materials that meet the physical requirements and are not affected by the fluid being sealed.

This discussion presents a brief review of seal leakage, its causes and measurement, and the main issues in effecting a good seal. The application of these principles in both static and dynamic seal design is covered in chapter 9; those for high speed rotating shaft seals for turbopumps are covered in chapter 6.

The practical definition of zero leakage is less than the smallest amount of leakage measurable or detectable by the most accurate means available for the fluid involved.

The definition of zero liquid leakage is given in reference 55 (p. 3) as "that value of liquid leak or flow rate at which the surface tension of the liquid has just overcome the pressure acting on the liquid, and no flow occurs - assuming a given pressure and leak diameter." Although zero liquid leakage may exist under these conditions, gas could evolve due to vaporization.

Reference 56 (p. 11) suggests that "no leakage" or "zero leakage" is not a practical requirement and recommends that zero leakage be defined as "a measurable quantitative value that is insignificant in the operation of the system."

Zero gas leakage does not actually exist because the transition from gaseous flow to molecular flow or diffusion varies with the type of gas and the leak path of diffusion path through the material. However, an arbitrary zero gas leakage curve (fig. 4-1) was developed by the Jet Propulsion Laboratory for use as a specification standard (ref. 55, p. 10). Leak rates above the line are considered true leakage. Leakage rates below the line are actually molecular diffusion which for high molecular weight gases can approach zero. The lower portion of the curve is based on a leakage of 1 standard cubic centimeter per year at a 1 atmosphere differential pressure. The arbitrary displacement of the curve at 10^{-7} cubic centimeter per second was considered necessary for practical considerations. A zero gas leakage definition as given in reference 57 (p. 14) is "no more than 1.4×10^{-3} standard cubic centimeter per second at 300 psig at ambient temperature." An example of a leakage specification for oxygen tank assemblies (including

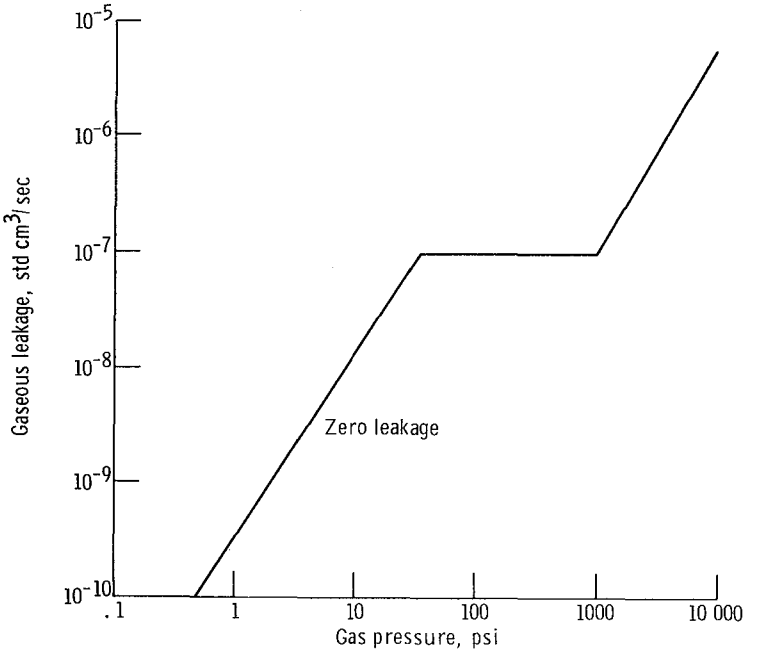

Figure 4-1. - Zero gas leakage (ref. 55, p. 10).

valve package) as used on the Skylab Orbital Workshop is 1×10^{-2} standard cubic centimeter per second helium at 3000 psig (ref. 58, p. 331).

4.1.1 Modes of Leakage

Fluid leakage can occur in four different flow modes: sonic or choked flow, turbulent flow, laminar flow, or molecular diffusion (permeation). Permeation is the diffusion of a fluid through a solid by molecular migration through the interstices of the material.

Equations for the various flow modes and flow characteristics as functions of pressure, temperature, and fluid properties are given in reference 56 (pp. 41 to 66).

Turbulent leakage flow occurs when the high velocity fluid cannot smoothly accommodate obstacles or disturbances in its natural flow path and pressure gradients are generated which tend to oppose flow. These pressure gradients cause the eddies and vortices characteristic of turbulent flow. Turbulent flow leakage generally results after erosion has enlarged the flow passage where viscosity and molecular forces are not effective and the flow passage length prevents choked flow. A Reynolds number greater than 2100 generally results in turbulent flow.

Choked flow or sonic flow in a gas occurs if the pressure drop across the leak passage or a constriction in the flow passage is greater than the ratio

$$\frac{\text{Pressure downstream}}{\text{Pressure upstream}} = \left(\frac{2}{K+1}\right)^{(K/K+1)}$$

where K is the ratio of specific heats of the fluid. The critical pressure ratio to achieve sonic flow for oxygen is in the range of 0.55 depending on the temperature of the gas.

The laminar flow equation is applicable for fluids when the Reynolds number is less than the laminar to turbulent flow transition value of approximately 1200.

The gradual transition of laminar flow to molecular flow is represented by combining the laminar flow equation and the molecular diffusion equation (ref. 59, pp. 55 to 63). However, the use of the combined equations should be limited to leaks where the flow path diameter is greater than 2×10^{-6} centimeter (ref. 59, p. 63).

Molecular flow occurs when the molecular mean free path at the average temperature is greater than the leak path diameter. When this condition exists, the average molecular motion as a result of the gas temperature and the molecular density gradient across the leak determines the flow rate.

4.1.2 Leak Path Growth

The most common characteristic of a leak is that it increases in rate with time because of erosion of the flow path and possible crack growth. The rate of leakage increase from erosion is affected by the differential pressure and type of fluid. As the pressure increases, the rate of leak path growth increases. The leak path growth is greater for turbulent liquid flow and two-phase liquid gas flow than for gaseous leakage. The erosion phenomenon is discussed in section 4.2 and crack growth from pressure stresses is discussed in section 5.1.5.

4.1.3 Leak Clogging

Very small leaks are sometimes blocked by very small particles or by liquids with a surface tension high enough to oppose the differential pressure. This blockage may be sufficient for a leak to go undiscovered.

"A phenomenon frequently observed is that if a container to be tested for leaks has at any time after manufacture been in contact with a liquid no leaks small in size (i.e., 10^{-7} atm cm^3/sec or smaller) will be found" (ref. 56, p. 74). If a liquid has entered a capillary tube, the pressure necessary to force it out of the tube is given by

$$P = \frac{4\theta}{d}$$

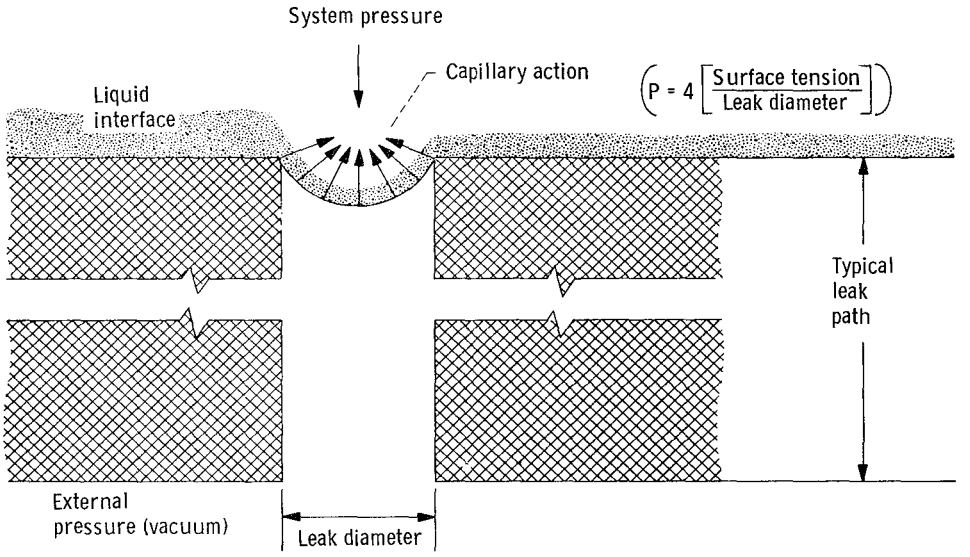

Figure 4-2. - Mechanism of clogging (ref. 55, p. 3).

(see also fig. 4-2) where θ is the surface tension of the liquid (usually expressed in dynes/cm), d the tube diameter (in cm), P the pressure (dynes/cm^2). (One atmosphere is equal to 1.01325×10^6 dynes/cm^2.) The phenomenon is of concern since water is generally used for hydrostatic testing. The differential pressure required to force water through a 1×10^{-6}-centimeter-diameter leak would be about 2.8 atmospheres (ref. 56, p. 75). However, since most leaks are not smooth round holes (they may be slits), it must be remembered that the leakage flow rate would be proportional to the cross-sectional areas. The pressure required to force the liquid through the leak is inversely proportional to the smallest cross-sectional dimension. Therefore, if the leak in the previous example were a slit with the smallest cross-sectional dimension one-tenth the diameter of the circle (of equal area), the pressure necessary to remove the water from such a slit would be approximately 28 atmospheres. For a liquid with a higher surface tension than water, the pressure could be much higher. On the other hand, the application of sufficient heat to vaporize the liquid would remove the clogged liquid and gaseous leak testing could then "discover" the leak.

4.1.4 Permeation

The permeation rate of contained gases through nonmetallic materials is an important consideration for low leakage sealing applications, since the permeability of the material may be considered a builtin leak. Permeation is measured as the volume of gas at standard temperature and pressure (STP) passing through a square centimeter of area per second per unit thickness of material per unit ΔP pressure where standard

temperature is 32° F and standard pressure is 1 atmosphere. The general formula for permeation given in reference 56 (p. 55) is

$$Q = \frac{K_p A \, \Delta P}{l}$$

where

Q flow rate, cm^3/sec

A area perpendicular to flow, cm^2

ΔP difference in partial pressure of gas across flow path, atm

l length of flow path, mm

K_p proportionality constant

(The units of K may be $(cm^3)(STP)(mm)/(sec)(cm^2)(atm)$.) Permeation rates for oxygen through selected materials are given in table 4-I (refs. 60 and 61).

TABLE 4-I. - PERMEABILITY OF POLYMERIC MATERIAL TO OXYGEN[a]

Material	Trade name or type	Permeation, P, $\frac{cm^3\ (STP)\text{-}mm}{cm^2\text{-}sec\text{-}atm}$	Temperature, °C
Vinylidene fluoride	X-500	0.0152×10^{-7}	25
chlorotrifluoro-ethylene	X-3700	.4150	25
Silicone rubber	RTV-502	420	23
	Silastic	448	25
	RTV-90	403	23
	RTV-501	409	23
Polyvinylidene fluoride hexafluoropropylene	Viton A	1.72	26
Polyvinyl fluoride	----------	.014	23
Polyvinyl chloride	Plasticized	.065	23
Fluorinated ethylene propylene	Teflon (FEP)	4.45	20 to 30
Polytetrafluoroethylene	Teflon (TFE)	7.6	25
Cellulose nitrate	----------	1.5	25
Polyvinylidene chloride	Saran 517	1.4	[b]25
Polychlorotrifluoro-ethylene	Kel-F	.023	[b]25

[a]Selected data from ref. 60.

[b]Ref. 61, p. XII-4.3.

4.2 EROSION

The phenomenon of surface damage and erosion from high velocity fluid flow is of particular concern in oxygen systems and occurs from several related flow processes. For example, erosion can be caused by

(1) Entrained liquid droplets in a high velocity gaseous flow impacting a solid

(2) Entrained bubbles or cavitation (two-phase flow) from localized reduced pressures or from excessive heat input to the fluid

(3) Entrained solid particles in a high velocity liquid or gaseous fluid

Reference 62 (pp. 239 and 240) states that "the cavitation damage process is very closely related to damage from droplet or particle impingement or conventional erosion."

Any dynamic condition that causes localized low pressure regions in the liquid that are lower than the local vapor pressure can cause cavitation. When very high relative velocities occur between the two- or three-phase fluid and the fluid handling hardware erosive impact forces are developed causing displacement of surface material.

Any example of erosion that is less common than the familiar high speed turbopump inducer cavitation was reported. It involved a high pressure fuel line in a J-57 turbojet engine. A small pin hole caused by cavitation erosion was attributed to a dent in the high pressure fuel line. In this failure the dent caused voids to form in the JP-4 (kerosene fuel) and then collapse downstream against the inner wall of the tube. The collapse of

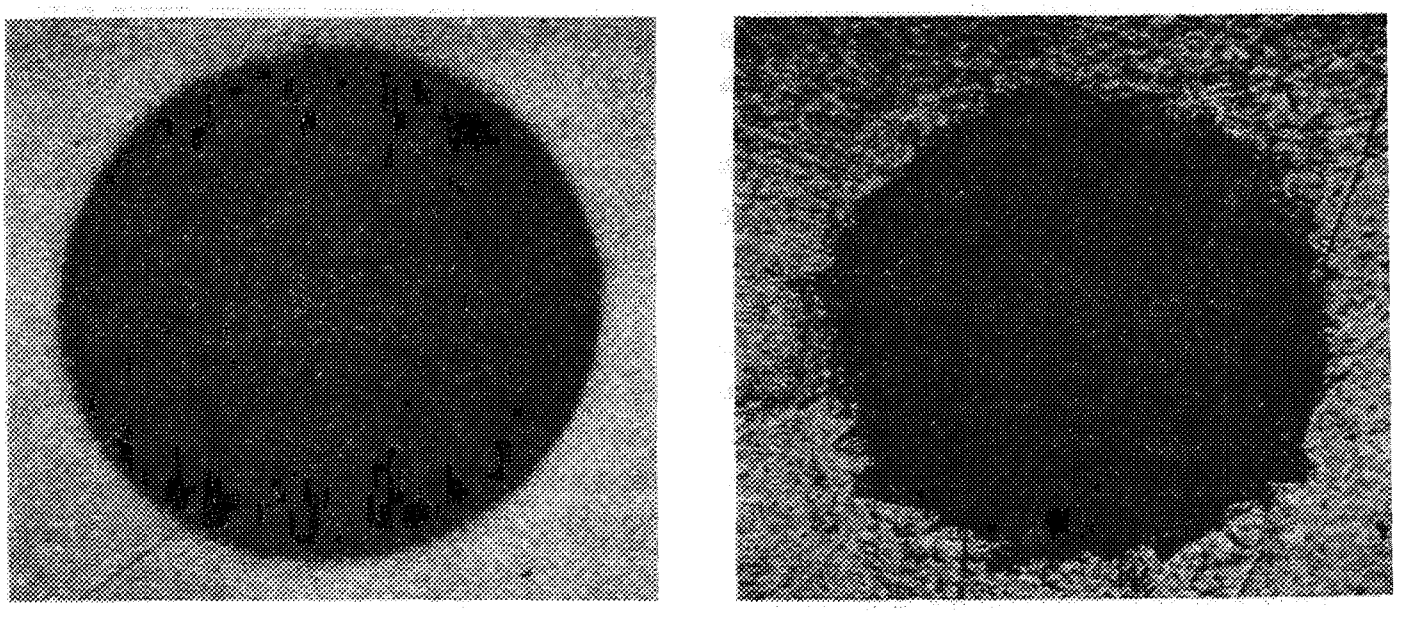

(a) Face view before exposure.

(b) Face view after 15 minutes of flow.

Figure 4-3. - Face views of 0.006-inch-diameter Kel-F orifice (ref. 64, p. 28).

cavitation voids can produce impact pressures by implosion exceeding the yield strength of most metals. When the voids collapse, the surface of the metal is subjected to repeated local plastic deformations that result in ultimate fracture and disintegration (ref. 63, p. 18).

To demonstrate the erosive effect of high velocity flow, Kel-F orifices (0.006-in. diam) were exposed to successive oxygen "blowdowns" or venting from a pressure of approximately 12 000 psi (ref. 64, pp. 19 to 29). Figure 4-3 illustrates the erosive nature of high velocity flow resulting from these pressures. The Kel-F was exposed to 15 minutes of flow from successive blowdowns from 10 000 to 1000 psi of approximately 1 minute in duration. The amount of surface erosion that was caused by entrained particulate material and the amount resulting from fluid friction and turbulence forces are not known. However, the effect should not be unexpected even in systems where the oxygen is carefully filtered.

Consideration for possible seal leak erosion and high velocity flow erosion should not be limited to nonmetal materials as shown by the damage to the brass orifice in figure 4-4. In this test, the brass orifice (0.005-in. diam) was exposed to ultra-high pressure oxygen blowdowns and resulting high velocity flow for only 35.5 minutes.

Absolute measurements of cavitation severity levels where surface deterioration begins for various materials in oxygen are not available. In general, erosion damage rates to materials in a dense liquid, such as mercury or liquid sodium, is considerably higher (3 to 20 times according to ref. 62, p. 239) than for a less dense liquid, such as water or liquid oxygen. Since liquid oxygen is less dense than water, its erosive impact on materials should be less. On the other hand, as a cryogenic fluid, liquid oxygen would tend to cavitate more readily in flowing systems since the temperature at which liquid oxygen is generally handled is near its boiling point.

Although every material has a critical velocity at which erosion will occur, this velocity is variable depending on the specific properties of the impact fluid, entrained material and its size and shape, and whether the fluid is liquid or gas. The following comparative data are helpful in confirming material selection for very high pressure applications.

Figure 4-5 shows the rate of erosion as a function of the amplitude of energy input. This was done by vibrating the test material at 20±1 kilohertz at varying amplitudes while in contact with the erosive fluid (water in this case).

Note that in all cases the materials most resistant to cavitation are stainless steels and nickel alloys that fortunately meet most of the other selection requirements for very high pressure, high velocity oxygen systems.

Four classes of materials in a general order of increasing resistance to erosion are glasses, plastics, cermets, and metals. A comparative listing of selected materials is given in table 4-II, which is a composite assembled from a wide range of test conditions and test fluids from reference 62.

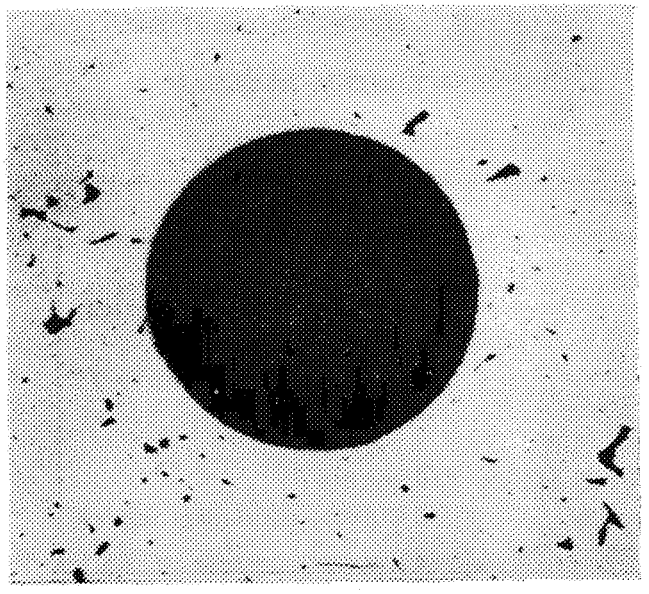

(a) Original 0.005-inch-diameter orifice.

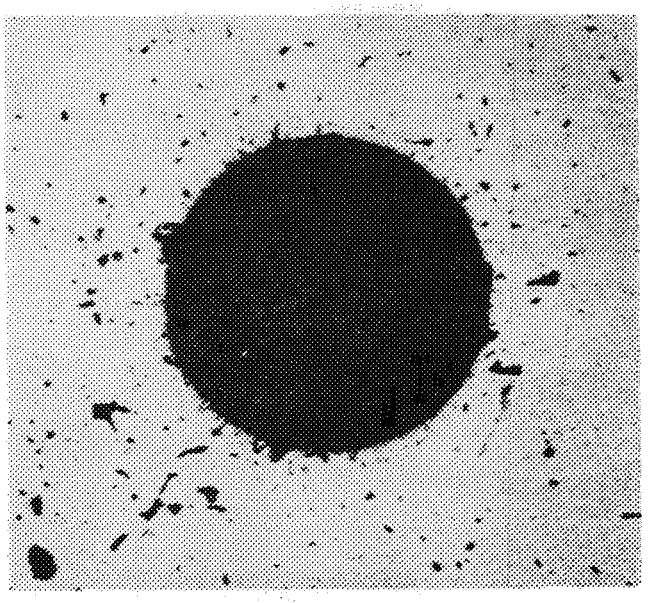

(b) After 3 minutes and 7 seconds.

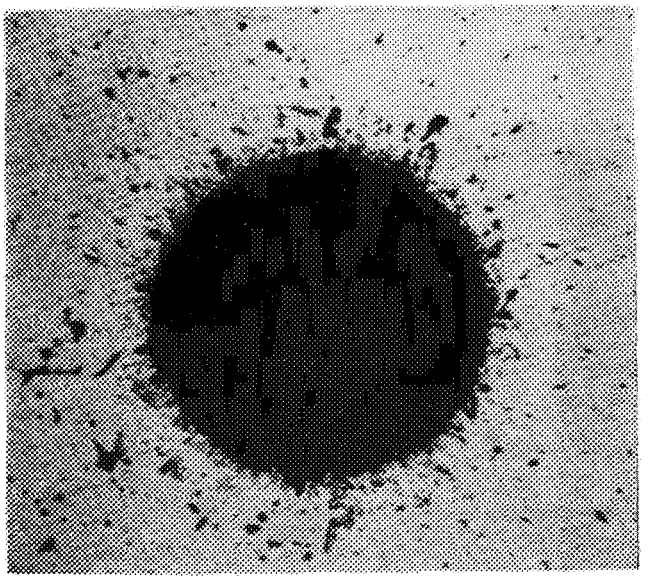

(c) After 13 minutes and 47 seconds.

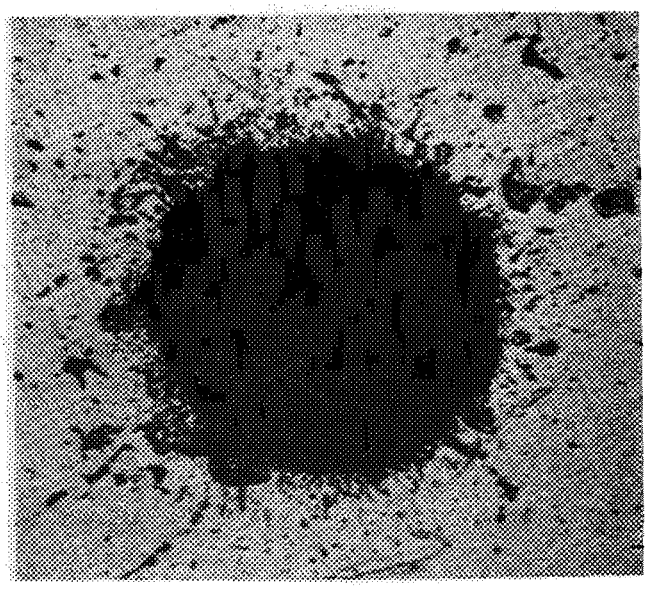

(d) After 35 minutes and 29 seconds.

Figure 4-4. - Progressive erosion of 0.005-inch-diameter brass orifice exposed to high-pressure high-velocity flow (ref. 64, p. 45).

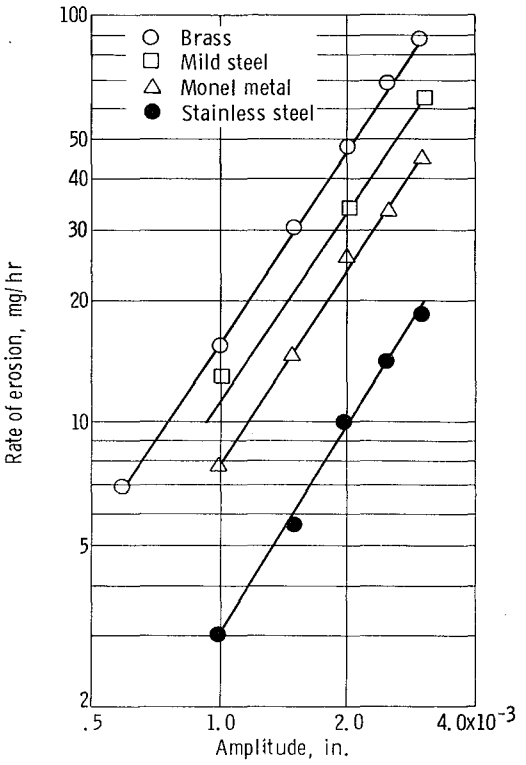

Figure 4-5. - Rate of erosion as function of amplitude (ref. 62, p. 167).

TABLE 4-II. - GENERAL ORDER OF INCREASING EROSION RESISTANCE OF SELECTED MATERIALS

Glass	Mild steel
Plexiglas	Stainless steel 400 series
Quartz	Monel
Polyethylene	Stainless steel 300 series
Aluminum 1100	Inconel 600
MgO	Steel A-286
Al_2O_3	Hastelloy X
Cast iron	Rene 41
Aluminum 2024-T4	Stellite
Bronze	Chrome plate (shot peened)
Brass	

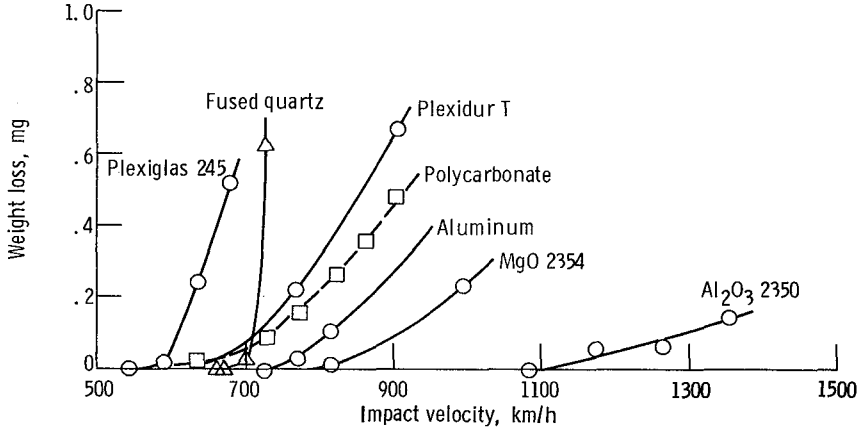

Figure 4-6. - Dependence of erosion depth on impact velocity (ref. 62, p. 46). Water droplet impact test time, 12 minutes.

The test results presented in figure 4-6 provide a relative "order of magnitude" velocity where erosion may occur from water. The nonmetals are affected between 500 and 700 kilometers per hour (455 and 638 ft/sec), and aluminum and the oxides are affected between 700 and 1100 kilometers per hour (638 and 1000 ft/sec).

The flow condition where cavitation and/or erosion begins for a given fluid temperature and ΔP is an important design consideration for oxygen systems and components.

Although cavitation as a destructive phenomenon is mainly associated with turbopumps, it may also occur any time the flow velocity is high and pressure falls below the vapor pressure of the liquid at the fluid temperature. When this occurs from throttling very high pressures (7500 to 10 000 psia) cavitation and impingement erosion may become damaging. In addition, in oxygen systems the erosion of the oxide surface and its continuous replacement would tend to accelerate the surface destructive phenomena.

Good design practice to prevent erosion damage would dictate good fluid dynamic contours, adequate filtration, materials selection most resistant to surface destructive phenomena, and assurance that the throttled pressure does not fall below the local vapor pressure when high differential pressures and flow velocities exist. This can be done by controlling the downstream minimum pressure or the downstream maximum temperature, or by decreasing the ΔP and the resulting velocity. Insulation to provide minimum heat transfer upstream of the throttling point and supercooling the liquid by jacketing are techniques to decrease the downstream vapor pressure. Filtration requirements are discussed in chapter 10.

4.3 SYSTEM DYNAMICS

Oxygen system deterioration or failure is frequently the result of dynamic forces generated within the system. These forces range from the well-known "water hammer" effect to thermal and physical stresses from cryogenic cycling and include many interacting combinations of forces. The potential damaging effect of these stresses are important enough that preventive measures should be considered at the earliest possible time in the design phase.

Failures of joints, couplings, seals, diaphragms, and bellows are most prevalent because they are the weakest part of the system. The most common causes of failure are due to over stresses from thermal expansion/contraction and water hammer. Water hammer forces in turn can cause adiabatic compression of gaseous pockets which can produce localized high temperatures. A combination of a fast acting valve closing against a column of liquid oxygen with high momentum can cause a water hammer pressure spike sufficient to force the fluid between the flange and seal. When this occurs in high pressure systems, experience has shown that autoignition sometimes occurs. Oftentimes, the metal seal between the flanges had taken a set from the strain of cryogenic to ambient temperature cycling thereby "loosening" the joint. Another form of fluid impact that can cause structural damage and possible reaction of oxygen with its container results from extremes of system size where very large masses of liquid can acquire extremely high momentum from very low pressure differentials. Very large flow systems such as the LOX fill drain system for the Saturn Booster or Shuttle at Kennedy Space Center require very long (1000+ ft) lines of large diameter. When a valve is opened allowing LOX to

flow into a line that long, the momentum of the column of liquid reaching the end can (and has) disintegrated the closure valve by a water hammer effect at the end of the line. Adiabatic compression of the gas in the line can also generate ignition temperatures. The potentially damaging momentum and resulting compression may also be generated by much smaller masses of liquid when accelerated by very high pressures. In both cases, flow rates and pressure buildups must be controlled by opening valves slowly enough or by providing a low flow rate bypass around major flow control valves.

A phenomenon which can be troublesome in the design of cryogenic systems is that of geysering. Geysering occurs when a long vertical tube with a reservoir at the top is filled with a cryogenic liquid such as oxygen. The heat transfer through the tube wall to the liquid causes gas bubbles to form. As the heating continues, the bubbles which form along the tube wall rise in the liquid and coalesce to form larger bubbles. If the tube is sufficiently long with respect to its diameter, the bubble formation and subsequent coalescence result in an expanding vapor slug which expels the liquid from the tube (almost explosively) into the reservoir above. Then, when the liquid in the reservoir drops back into the tube, a water hammer effect results which may cause structural damage to the system and the possible dumping of large quantities of liquid oxygen.

Tests were conducted (ref. 65, pp. 355 to 359) in which vertical tubes containing different fluids were heated at controlled rates to determine the predictability of geysering in order to avoid geysering by design. The geyser-nongeyser correlation shown in figure 4-7 resulted wherein the log of a parameter Z was plotted against the log of a parameter $(L/D)(D^{-0.68})$ where D is the pipe diameter, L is the heated pipe length; Z is defined as

$$Z = \frac{\frac{q}{A} L}{12\alpha(N_{pr})^{1/3}} \tag{1}$$

where A is the heat transfer area of the tube, N_{pr} the Prandtl number of the fluid, q the heat transfer rate, and α the thermal diffusivity.

While increased tank (ullage) pressure will decrease the frequency of geysering (ref. 65, p. 358), the tendency to geyser is not eliminated by the increased pressure. Therefore, it becomes feasible to design a propellant feedline in the normal manner to meet system requirements and then check the design against the correlation of figure 4-7 to determine if geysering will occur.

Having determined that for a particular design geysering will occur, there are several possibilities for eliminating the problem. First, the line diameter may be changed to take the design out of the geyser range. Second, the line may be insulated, as indicated by equation (1), to reduce the heat transfer rate in order to move the design out of

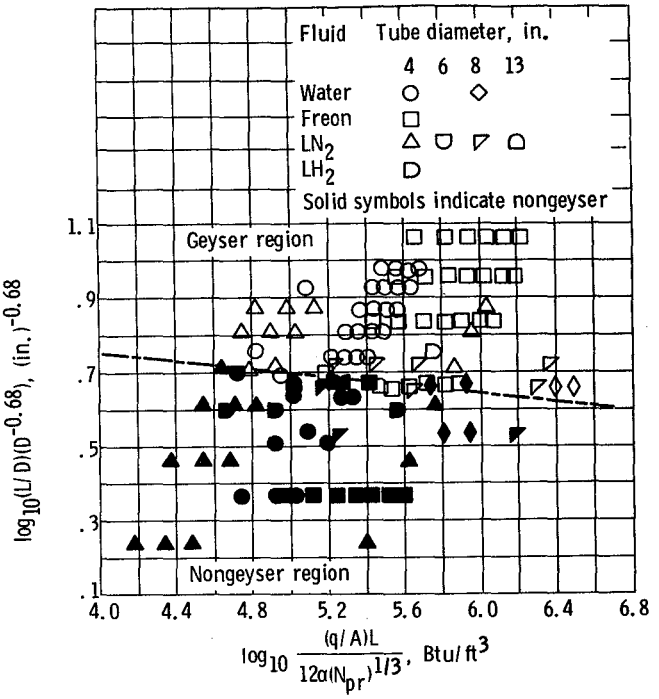

Figure 4-7. - Geyser-nongeyser correlation (ref. 65, p. 358).

the geyser range. A third method of preventing geysering is to recirculate the fluid from the reservoir through the tube at a rate high enough to prevent the fluid from reaching saturation temperature. Recirculation may be accomplished by thermal pumping, helium lift pumping, or mechanical pumping. Recirculation return lines may be added for the purpose, or if two or more feedlines from the same reservoir exist, one may serve as a return line.

4.4 GENERAL DESIGN CRITERIA

The design criteria summarized in this section are of a general nature and should be considered in the design of any oxygen system of component. They are applicable to the type of condition which is often inadvertently designed into a system but which could result in a hazardous situation or system malfunction, especially with high oxygen pressures (2000 to 7500 psi) or greater. Specific criteria applicable to various oxygen system components are reviewed in chapters 5 to 10.

The most important consideration in oxygen system design is the selection of materials which are compatible with oxygen. In addition to the compatibility and selection criteria developed in chapter 3, the design criteria and recommended practices for fluorine and fluorine-oxygen mixtures (FLOX) given in reference 37 (pp. 49 to 119) may also be used as aids in assuring a safe and reliable high pressure oxygen system. These

criteria are applicable because of the many commonalities between oxygen and the other elemental oxidizers.

When designing oxygen components or systems, every effort should be made to avoid cracks, crevices, pockets, and unnecessary cavities to prevent accumulating contamination and gas compressibility hazards. This is especially important for high pressure systems.

Contaminants caught between close clearances, accumulated in a cavity and impacted by high velocity particles, or even subjected to a gaseous compression or shock wave can ignite and burn and, in turn, ignite adjacent parts.

Filters should be installed at strategic locations to alleviate the hazard of particle impact ignition and clogging. The design and application of such filters are discussed in chapter 10.

Adiabatic compression of gaseous pockets, turbulent and erosive flow, entrained particles impinging and abrading the surfaces of the flow passage, and other local mechanical stress can all contribute to the failure and ignition of a local material. If the material is an ignition sensitive contaminant on a nonmetal component such as a gasket, ignition may occur more readily. Smooth, clean flow passages made of compatible materials preclude possible ignition. However, the maximum probable pipeline pressure spike should be such that the resulting adiabatic compression could not produce a final temperature in excess of the ignition temperature of any oxygen system component material.

Where possible, high pressure liquid oxygen systems that have gaseous oxygen pockets should be provided with liquid nitrogen jacketing. Adiabatic compression curves (see fig. 3-12 in section 3.4.4) show that the temperature of oxygen gas at atmospheric pressure and 0° C could be raised to the ignition temperature of Viton (400° C at 20 atm, fig. 3-10) at a pressure spike of 20 atmospheres or to the ignition temperature of a particulate contaminate at much lower pressure peaks. The selection of nonmetallic materials for use in gaseous pockets where pressure spikes could occur should be based on the highest possible adiabatic compression temperature and the ignition point of the material (see section 3.4.4).

When designing fittings, connections, and attachments, care must be taken with a connection interface of dissimilar metals. Metals which do not form acceptable couples (see table 3-I) should not be used in direct contact with each other when exposed to an electrolyte such as the moist atmosphere. When unacceptable couples are formed, a plating for one or both of the components may be selected from table 4-III to minimize galvanic action. Reference 66 contains specifications and criteria applicable to protective finishes (paints) and coatings and surface preparations appropriate to their application. However, the compatibility of coating materials with oxygen is not covered and must be determined by the user (see chapter 3 on materials compatibility). (Most paints and coatings should be restricted to external use in oxygen systems.)

TABLE 4-III. - SELECTED PLATING MATERIALS

Plating	Melting point, °C	Preferred base material	Application
Cadmium	321	Steels, iron, copper alloys	Widely used for bolts and fasteners to minimize corrosion and galvanic action
Chromium	1615	Steels, iron	Good for bearing surfaces and rubbing contact where resistance to wear, abrasion, and corrosion is needed; good for building up worn surfaces
Copper	1083	Ferrous alloys (improves adhesion where used as first coat for other plating)	Provides excellent undercoat base for chromium or nickel plate
Gold	1062	(a)	For maximum corrosion resistance
Nickel	1455	(a)	Optimum plating; highly corrosion resistant but low enough in cost for thick coatings, surface buildup, bearing refinishing, etc.
Platinum	1773	Copper alloys	
Silver	961	(a)	Bearing surfaces
TFE, FEP, and CTFE	(b)	(a)	Excellent chemical oxidation resistance; low friction; good for bearing surfaces and rubbing contact; sealing
Tin	232	Steels, iron	All purpose, low cost
Zinc	419		All purpose, low cost

[a]No restriction for use on oxygen compatible materials.
[b]For temperature limits see section 3.7.1.

The porosity of some materials, such as coatings, sintered materials, and some castings, may permit the absorption of gases, moisture, or other contaminants affecting their compatibility with oxygen. Whenever this possibility exists, care must be taken to assure no contamination. This can be accomplished by, first, heating the material in oxygen to the highest appropriate temperature and pressure which will oxidize the contaminant under controlled conditions, second, sealing the porosity by plating or coatings, or third, selecting an alternate material.

Many materials, especially nonmetal materials, have a variety of trade names for materials of the same or similar composition. Conversely, there are certain products

that have different chemical composition (and varying compatibility) but the same trade name. They are even similar in appearance. Worse yet, from an engineering control standpoint, materials of the same or similar composition are available in a variety of grades, purity, and quality. Some are excellent and some are poor, and their compatibility with oxygen can vary accordingly. Therefore, it is necessary that extreme care be used when selecting materials and verifying the quality of the fabrication material and the finished product. The designer and fabricator should verify the chemical composition of the materials selected by trade names, chemical names should be used for positive identification of the material, and the compatibility of the materials should be certified for use in the total environmental profile of pressure, temperature, flow rates, and exposure time to which they will be subjected.

Where the application is critical (such as with pressures over 2000 to 3000 psia or where the highest reliability is required in man-rated flight systems), the material to be used for fabrication of tanks and lines should be X-rayed to ensure quality material with freedom from unacceptable cracks and flaws.

4.5 CLEANING REQUIREMENTS AND PROCEDURES

One of the more critical aspects of engineering an oxygen system is the specification of and design for cleanliness. The appropriate level of cleaning must be specified by the designer. A detailed review of cleanliness requirements, cleaning procedures, and verification techniques is presented in volume II of this series (ref. 8). Criteria and data contained in chapter 3 of this volume may also be helpful when determining appropriate cleaning requirements. Provisions for maintenance and cleaning should be incorporated in system design.

When breaking into a system for maintenance or repair, the following must be done:

(1) Isolate, insofar as possible, the portion of the system to be entered.

(2) Verify that the system is drained and depressurized.

(3) Confirm that the entire system is at ambient temperature to avoid "breathing" contaminated air. That is particularly important if a part of the system is nitrogen jacketed. "Breathing" may also occur due to barometric pressure variations or temperature changes. A slight positive pressure or purge may be desirable to avoid "breathing."

(4) Cap or seal openings into the part of the system not being repaired as soon as possible.

(5) Purge and reclean repaired parts of the system prior to reinstallation.

It is desirable, also, to make provisions for periodic cleaning of possible contaminant traps in a system although every effort should be made to avoid such traps in the design.

4.6 COLD SHOCK CONDITIONING

All vessels and lines to be used for cryogenic service should be "cold-shocked" before final leak testing for operational use. The purpose of cold-shocking is to verify the integrity of the system for use at cryogenic temperatures. It is especially important that the expansion and contraction from ambient to cryogenic cycling does not impose excessive stresses on any component.

Components may be function tested while immersed in liquid nitrogen. Fluid systems should be conditioned with liquid nitrogen (preferably) or oxygen and function tested at operating conditions. After the system has been purged and vented and warmed to ambient temperature, all connections and threaded fittings should be retorqued.

The entire system should be inspected for evidence of cracking, distortion, or other anomaly. Special attention should be given to inspection of welds. After repairs, cold-shock tests may be repeated prior to final pressure test.

Page intentionally left blank

CHAPTER 5. OXYGEN TANK ASSEMBLIES

The tank assembly includes all the components necessary to contain and control the fluid. The complexity that an oxygen tank system can have is illustrated by the Saturn S-II stage flight weight liquid oxygen tank and the typical ground-based liquid oxygen tank shown in figure 5-1 (ref. 67). Failures of the tanks containing the oxygen have generally been caused by system contamination, structural failure, or incompatibility of tank components and component materials with oxygen for the conditions of use.

Accumulated system contamination can cause corrosion or can serve as a reaction initiator for ignition and combustion of the structural material with the oxygen. Structural failure of internal tank components, especially the rupture of metal components and the subsequent impact or collision of broken parts, can result in ignition and combustion of the material. Material compatibility considerations must include structural materials and component materials such as electrical conduits, insulation, and seals; these materials must be selected with consideration given to conditions that would exist for various component failure modes such as electrical shorts, overheating, rubbing, impact, and the like.

Tanks for liquid oxygen must be designed to withstand cryogenic temperatures and the slosh forces of the liquid. Tank component materials must be chemically compatible with oxygen, and appropriate cleanliness standards must be maintained. Thermal insulation requirements must be integrated with the design of any tank assembly that is to contain a cryogenic fluid. For example, the design of a tank assembly support system may be greatly influenced by the insulation requirements. Tanks for gaseous oxygen are pressure vessels so strength is a primary consideration as well as the factors of material compatibility and possible elevated operating temperatures. Weight is an important factor in flight weight tanks, whereas low cost and long life are more important than weight in ground based tanks. Therefore, design safety factors are lower for flight weight tanks than for ground-based tanks, and the probability of failure is increased unless rigid quality assurance measures are imposed.

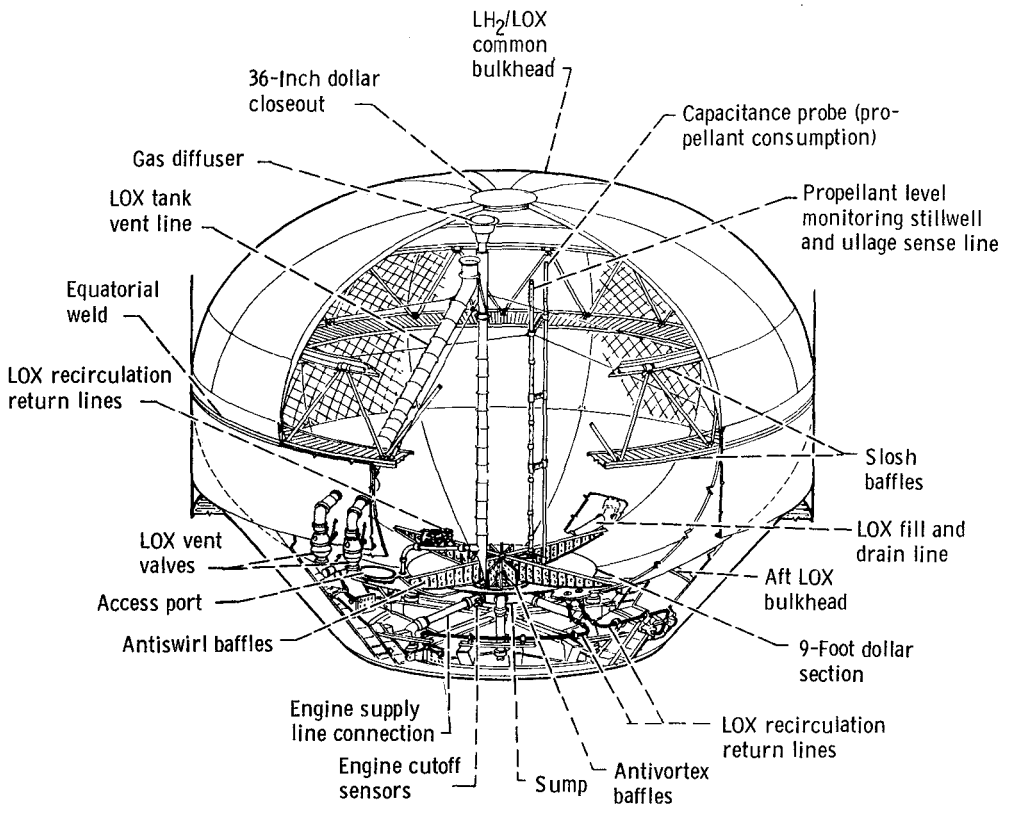

(a) Saturn S-II stage oxygen tank (ref. 67, p. 5-4).

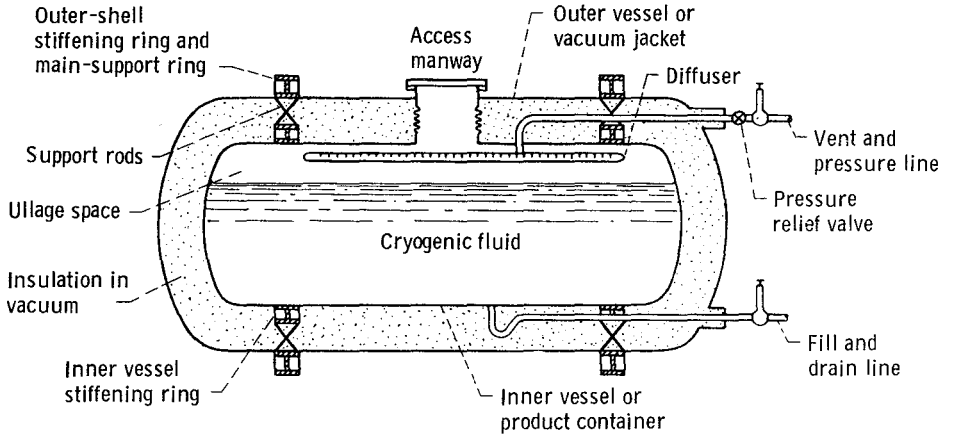

(b) Typical ground-based storage tank.

Figure 5-1. - Oxygen tank assemblies.

5.1 GENERAL DESIGN AND SAFETY CONSIDERATIONS

The most important factors in tank shell design and fabrication are the tank shape and method of support, material thickness control, alloy purity, weld strength, and assurance that the tank material is free of critical flaws. These factors are most critical in flight weight tanks where material thickness is minimized to keep the tank weight as low as practicable and where acceleration forces and structural stresses are generally greater.

References 52, 68, and 69 contain data on material properties applicable to tank systems. The structural design considerations and calculation methods for flight weight tanks are given in references 70 (pp. 329 to 352) and 71 (pp. 52 to 72).

Cycle life is an important consideration in the design of ground-based tanks which may be required to withstand many pressure cycles. Therefore, the design safety factors should include an allowance for the predicted cycle conditions.

Since design safety factors are generally higher for ground-based tanks, operating personnel are usually exposed to the pressurized system on a less restricted basis. Special considerations in ground-based mobile tank design include adequate load distribution in the tank suspension system to meet all road and load conditions and baffle mounting to withstand relatively high sloshing forces. A general minimum criteria used for mobile tank loadings is 2 g's vertically downward, 2 g's longitudinally, and 2 g's laterally. All tank components should be designed to meet the loads imposed plus the required safety factor. The structural design considerations for the tank shell and suspension system of ground-based storage and mobile tank systems are included in reference 72 (pp. 2-1 to 2-43).

5.1.1 Safety Standards and Specifications

Design standards and specifications have been established to assure adequate safety of ground-gased pressurized systems. These standards and specifications are generally applicable to cryogenic systems and should be considered in the design of stationary and mobile ground based liquid and gaseous oxygen tanks. They are listed here for convenience:

(1) ASME Boiler and Pressure Vessel Code, Section VIII, Division 1, 1971 (ref. 73)

(2) ASME Boiler and Pressure Vessel Code, Section VIII, Pressure Vessels, Division 2, Alternative Rules, 1971 (ref. 74)

(3) ASME Boiler and Pressure Vessel Code, Section IX, Welding Qualifications, 1971 (ref. 75)

(4) Air Force Technical Order T.O. 00-25-224, Welding High Pressure and Cryogenic Systems (ref. 76) (includes airborne and ground systems)

(5) American Petroleum Institute Standard No. 620, Design and Construction of Large, Welded, Low-Pressure Storage Tanks (ref. 77)

(6) Compressed Gas Association Tentative Specification for Insulated Tank Trucks, CGA-341 (ref. 78)

(7) Code of Federal Regulations, Title 49, Transportation Parts 100 to 199 (ref. 79)

The Code of Federal Regulations (Title 49) covers the rules and regulations governing transportation of explosives and dangerous materials by common carrier (ref. 79, section 170-179). Cargo tanks for liquid or gaseous oxygen must meet the specifications contained therein.

One of the more important considerations within the Code of Federal Regulations is the required retesting of cargo tanks every 5 years (ref. 79, section 173.33).

5.1.2 Design Safety Factors and Proof Pressures

Maximum allowable stress values for materials used for ground-based tanks are given in reference 73. The mechanical properties considered and the factors applied to establish the maximum allowable stresses are given here. At temperatures below the creep range, the maximum allowable stress value for ferrous materials and for nonferrous materials is the lowest of these:

(1) One-fourth of the specified minimum tensile strength at room temperature

(2) One-fourth of the tensile strength at operating temperature

(3) For ferrous materials, five-eighths of specified minimum yield strength at room temperature; for nonferrous materials, two-thirds of specified minimum yield strength at room temperature

(4) For ferrous materials, five-eighths of yield strength at operating temperature; for nonferrous materials, two-thirds of yield strength at operating temperature

For flight tanks, the design is optimized around the tank material strength to weight ratio parameter. Factors of safety normally used for booster tanks vary from 1.0 to 1.1 based on yield strength and 1.25 to 1.5 based on ultimate strength of the material. The higher values are applicable to manned vehicles. Table 5-I is a list of suggested safety factors for various circumstances.

In applying the safety factors listed in table 5-I, the maximum allowable working stress is computed for each safety factor pertaining to the particular circumstance or condition and the lower value is used. Proof test pressures are normally in the range of 105 to 150 percent of the maximum tank working pressure. To prevent general yielding of the tank shell during proof tests, stresses are normally limited to values equal to or less than the yield strength of the tank material or the welds. Procedures for determining an adequate proof test are outlined in reference 80 (pp. 12 to 17).

TABLE 5-I. - SUGGESTED SAFETY FACTORS FOR

FLIGHT WEIGHT OXYGEN TANKS[a]

Circumstance or condition	Yield safety factor	Ultimate safety factor
No hazard to personnel or vital equipment (unmanned)	1.0	1.25
Special safety devices provided for personnel (escape system or special shielding)	1.1	1.35
Hazard to personnel or vital equipment	1.33	1.65

[a]Ref. 70, p. 334.

Some typical design and test pressures and safety factors for flight oxygen tanks are presented in table 5-II.

TABLE 5-II. - TYPICAL OXYGEN TANK DESIGN DATA FOR FLIGHT WEIGHT TANKS

System	Vessel application	Vessel dimensions, in.	Vessel material	Design pressures, psig			Ultimate safety factor
				Limit	Proof	Burst	
Atlas	Propellant	120 diameter by 480 length then taper to 48 diameter over 120 length	301 stainless steel, extra full hard	26.0	33.0	49.0	1.88
Centaur		120 diameter by 87 length ellipsoid	301 stainless steel, extra full hard	48.0	------	60.0	1.25
Saturn I-C		396 diameter by 517 length	2219 aluminum	49.3	51.8	69.1	1.4
Saturn II		396 diameter by 264 length	2014 aluminum	84.4	------	118.0	1.4
Saturn IV		130 radius segments	2014 aluminum	70.4	------	98.5	1.4
Apollo ECS	Surge tank	14 by 13	Inconel 718	1020	1356	1530	1.5
Apollo ECS	Cabin pressurization	12.62 by 6.92	Inconel 718	1210	1600	1800	
Apollo SM	Fuel cell		Inconel 718	1020	1356	1530	
Apollo LM	Descent breathing	23.522 by 21.722	D6AC carbon steel	3000	3990	4500	
Apollo LM	Ascent breathing	14.500 by 11.968	Inconel 718	1000	1330	1500	

5.1.3 Corrosion

There is no possibility of significant chemical corrosion inside the tanks filled with uncontaminated liquid or gaseous oxygen. The problem of inside corrosion begins when the tank is empty and opened to the atmosphere. Exposure to atmospheric moisture and

contaminants is a serious corrosion hazard. The use of a purge or pressurant gas containing moisture or other contaminants will also contribute to the corrosion process. Purge and pressurant gases should have a dew point lower than -50° F and should be filtered to meet system requirements (see chapter 10).

Day-night temperature cycles and atmospheric pressure variations can cause extensive corrosion damage in a relatively short time due to the breathing of moist air. The breathing of tanks and oxygen systems in a standby or stored condition must be prevented to avoid contamination. This can only be prevented with certainty by maintaining a slight positive pressure inside the system at all times. Sections that have been isolated and opened for maintenance should be purged and appropriately cleaned following the maintenance operation. For additional discussion of corrosion refer to section 3.2.

5.1.4 Stress Corrosion Cracking

The possibility of stress corrosion cracking must be reviewed during oxygen tank design especially where high internal pressures or mounting load distributions can cause high stress concentrations. The resulting strain in the presence of an electrolytic agent such as moist air or water can result in structural failure. In addition, evidence indicates that the presence of oxygen and the process of oxide film formation aggravates stress corrosion cracking (see sections 3.1 and 3.3). An example of rapid stress corrosion failure is cited in reference 81 (p. 14). A type D6AC alloy steel heat treated to 220 to 240 ksi tensile strength was used to store very high pressure gaseous oxygen in the Apollo EVA system. During hydrostatic testing of one of the tanks, an external surface flaw was exposed to water. (The tank was tested under water for safety.) The tank subsequently failed, and failure was considered to be due to stress corrosion. The corrective action was to use oil for hydrostatic testing and discontinue the water immersion procedure.

5.1.5 Cyclic Stress and Cycle Life

Tanks that are pressurized and depressurized many times during testing and/or during their life are subject to fatigue failure due to crack propagation and flaw growth at stress concentration points. Stress concentrations usually occur in zones of discontinuity such as around inspection openings, flanges for manholes, and pipe entry bosses. Residual stresses from welding the tank assembly can also cause local areas of high stress.

Much work has been done in the field of fracture control for metallic pressure vessels. Although this work has helped to clarify the causes and characteristics of fracture processes and fracture mechanics, the full clarification is only evolving. However,

fracture mechanics theory has proven itself to be a valuable design tool for pressure vessels.

Cycle fatigue failures usually start at existing cracks, structural flaws, or material blemishes in areas of high stress concentration. The maximum stress occurs at the apex of the crack where the material is parting. The rate of failure is higher and the cycle life is lower for tank materials of low ductility. Since the crack growth is dependent on the level of stress at the apex, the tank should be designed with a factor of safety applied to the local maximum stress.

Critical flaw size and cyclic effects analysis techniques show that the size of flaws or surface cracks in the material of a finished tank may materially affect the expected tank life. The technique permits calculation of the critical flaw size and maximum crack tip stress required to cause failure at a given applied stress level. The mathematical equations and procedures for determining these limits are presented in reference 80 (pp. 5 to 10 and 23 to 25). Although these calculated stress intensity and crack growth predictions are only approximate, they provide valuable supporting information for design consideration.

Sheet stock for tanks should be screened to remove any material with visible flaws, cracks, or discontinuities greater than critical size. The remaining material is generally inspected by dye penetrants, X-ray, ultrasonic, or ferromagnetic methods as required for assurance that flaw sizes are less than the critical size.

An excellent source of practical fracture mechanics design data is reference 82. The data include state-of-the-art information on critical plane strain stress intensity factors, threshold stress intensity factors in corrosive media, sustained load crack growth rates, and fatigue crack growth rates.

5.1.6 Creep

Tanks for use at room temperatures or above may be subject to creep and should be evaluated for this possibility. Although creep in metals is usually associated with high temperatures, some materials such as aluminum exhibit a slight tendency to creep at room temperature. Therefore, if tank pressurization stresses are long in duration at stress levels near the yield stress, the possibility of significant creep exists. Creep data are usually obtained by subjecting a specimen of the material to a constant load at a specific temperature and measuring the change in length as a function of time. Typical creep and creep rupture curves are shown in figure 5-2 for selected aluminum alloys. Additional creep data are available in references 69 and 68.

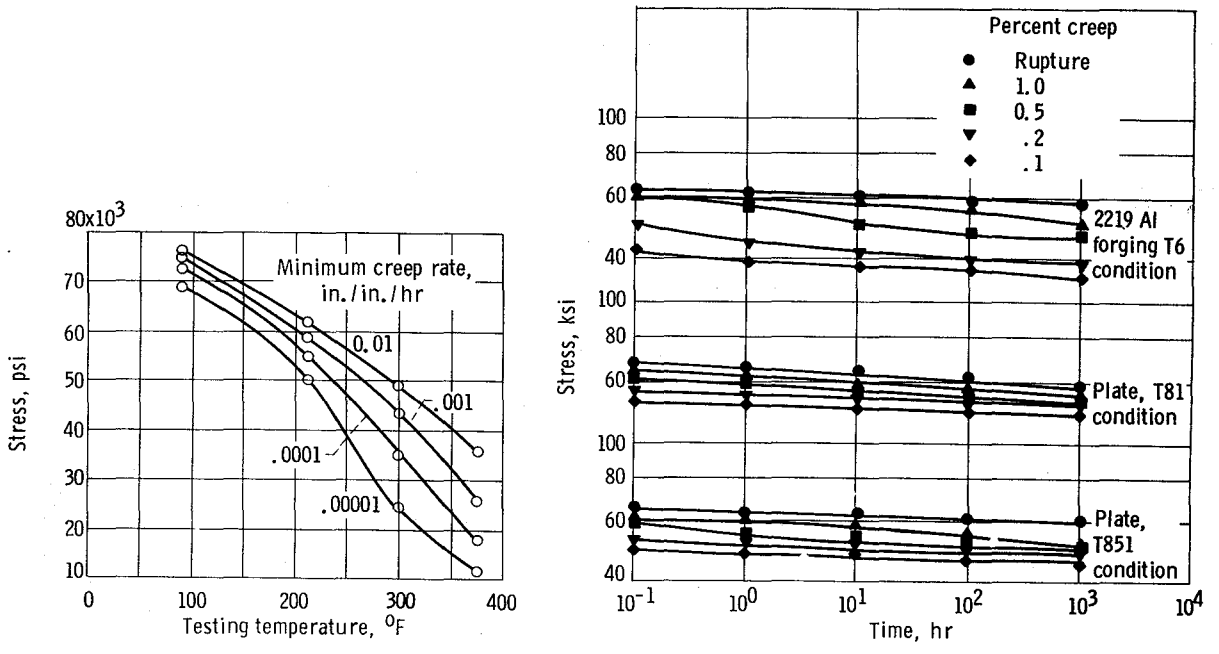

(a) Creep rates as function of temperature for 7075-T6 aluminum (ref. 20, p. 949). 0.040-Inch clad sheet.

(b) Creep and creep rupture curves for 2219 aluminum. Creep as function of time and stress at room temperature (ref. 69, code 3205, p. 17).

Figure 5-2. - Typical creep and creep rupture curves.

5.1.7 Weld Joints

Good weld joint design and welding techniques are necessary for a reliable tank structure. Since the strength of the heat affected zone at a weld joint is less than that of the parent material, increased thickness must be provided in this area to achieve a strength comparable to that of the parent material. Ideally, the weld zone thickness buildup should be symmetrical to minimize bending stresses (see fig. 5-3). Mismatch between butt welded components of pressure vessels can also result in substantial local increases in stress.

Bending stresses must also be considered at curvature discontinuities and abrupt changes in thickness that occur at tank wall penetrations, reinforcements, and bosses. Abrupt wall thickness changes are avoided by providing a tapered or stepped section between the tank membrane thickness and the weld land as shown in figure 5-3. For flight weight tanks, mounting pads and penetration reinforcements are usually butt welded to the tank with a tapered transition section on the reinforcement side of the weld and a stepped weld land on the membrane side of the weld as shown in figure 5-4. Ground-based tanks normally have a reinforcement pad fillet welded to the tank to provide additional strength around penetrations as shown in figure 5-5. This is less costly and more practical for ground-based tanks where the strength margin can be accommodated without concern for weight penalty.

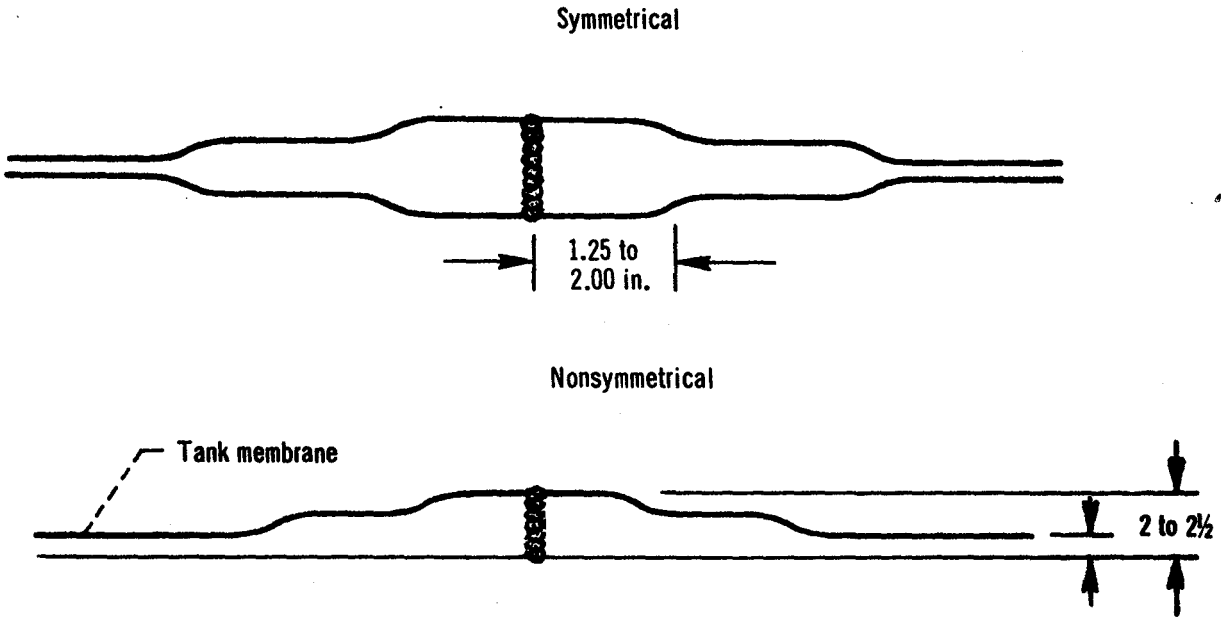

Figure 5-3. - Weld land configuration.

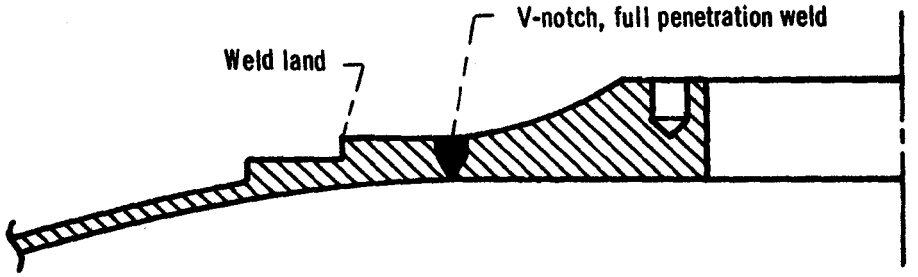

Figure 5-4. - Typical tank wall penetration for thin-walled tanks.

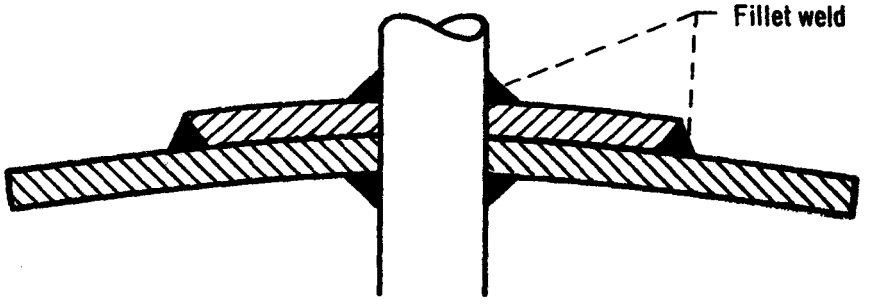

Figure 5-5. - Typical tank wall penetration for ground-based tanks.

Tank wall sheet stock and weld coupons of the material are generally tested statistically to provide a 99 percent strength reliability level for the tank material. A statistical confidence level of 95 percent is observed (ref. 71, pp. 25 to 28). Reference 83 (p. 71) provides additional statistical reliability for weld strength data by accounting for the differences in the individual weld coupon samples tested.

5.2 MATERIALS

Materials that have been used and may be considered for oxygen tanks include those listed in table 5-III. The lowest value for sheet stock gage recommended for propellant tanks is about 0.01 inch for steel alloys and 0.02 inch for aluminum alloys (ref. 70, p. 336).

TABLE 5-III. - TANK MATERIALS

Stainless steel: 301, 304, 316, 347
D6AC alloy steel[a]
Inconel 718
Monel
Mild steel (carbon steel)[b]
Magnesium: M-1, AZ31
Aluminum alloys: 6061-T-6, 6066-T-6, 2014-T-6, 2219-T-62, 2219-T-81, 2219-T-87, 5052

[a]Used for very high pressure oxygen gas storage in Apollo EVA system. See precautions against stress corrosion in section 3.2.3.

[b]Commercial gaseous oxygen cylinders (2200 psia max., -30° F min.).

5.3 INSULATION

Special concern is required when using oxygen system insulations that contain added combustible materials. These insulations can be hazardous in the event of an oxygen leak coupled with subsequent ignition. Most of the conventional insulations will not ignite readily but they will support combustion if they are ignited. All of the insulation materials listed in table 5-IV will burn in oxygen and each material will ignite in the presence of oxygen at its respective ignition temperature except those noted. The ignition temperatures and combustion rates of materials are given in chapter 3.

The use of metallic particles in combination with powdered oxide insulations for ox-

TABLE 5-IV. - TYPICAL THERMAL CONDUCTIVITY AND DENSITY DATA FOR VARIOUS INSULATIONS[a]

Insulation	Conductivity, K, $\frac{(Btu)(in.)}{(hr)(ft^2)(^oR)}$	Density, ρ, lb/ft^3	Kρ factor	Insulation pressure
Multilayer aluminum foil	0.00012 to	7.5	0.0009	10^{-4} mm Hg
(with glass or quartz fiber paper spacers)	0.00078	2.5	.002	10^{-4} mm Hg
Aluminized Mylar:				
24 layers/cm	0.049	2.8	.1375	
47 layers/cm	.104	5.85	.608	
Powders:				
Santocel-A[b]	.0011	6.0	.0066	10^{-4} mm Hg
Perlite[b]	.000864	8.0	.0069	10^{-4} mm Hg
Cab-O-Sil[b]	.0014	4.5	.0063	10^{-4} mm Hg
Fiberglass[b]	.01 to	4.0	.05	10^{-3} mm Hg
	0.21	4.0	.84	1 atm
Foams:				
Polystyrene	.18	2.88	.438	1 atm
	.056	2.88	.136	10^{-5} mm Hg
Epoxy	.229	5.0	1.14	1 atm
	.090	5.0	.45	4×10^{-3} mm Hg
Polyurethane	.229	5.0 to 8.74	1.14 to 2.0	1 atm
	.084	5.0 to 8.74	.42 to .734	10^{-3} mm Hg
Rubber	.25	5.0	1.25	1 atm

[a]Ref. 30, pp. 30 to 37.
[b]Nonflammable with oxygen.

ygen equipment is hazardous due to the flammability of the metals in such mixtures (see 3.4.1).

Tests have indicated that up to 20 percent aluminum powder may be used in Perlite in an oxygen atmosphere before combustion will be sustained (ref. 84, pp. 118 to 121). Since this may be affected by the particle size of the powdered metal, tests should be made of the material to determine the actual limit in each case.

Figure 5-6 illustrates the effect of gas pressure on the conductivity of a few of these insulations. Multilayer superinsulations have been developed with conductivities as low as 1×10^{-5} Btu-inch per hour-square foot-Rankine degrees (ref. 30, p. 32). However, this efficiency is extremely difficult to achieve in a practical ground-based tank application. In a 1-g environment the thermal conductivity of multilayer insulation decreases as each additional layer is added until the contact area between layers begins to increase from the added weight. Then the conductivity begins to increase. This is illustrated in figure 5-7 which shows the optimum number of layers to be between 50 and 90. Typical

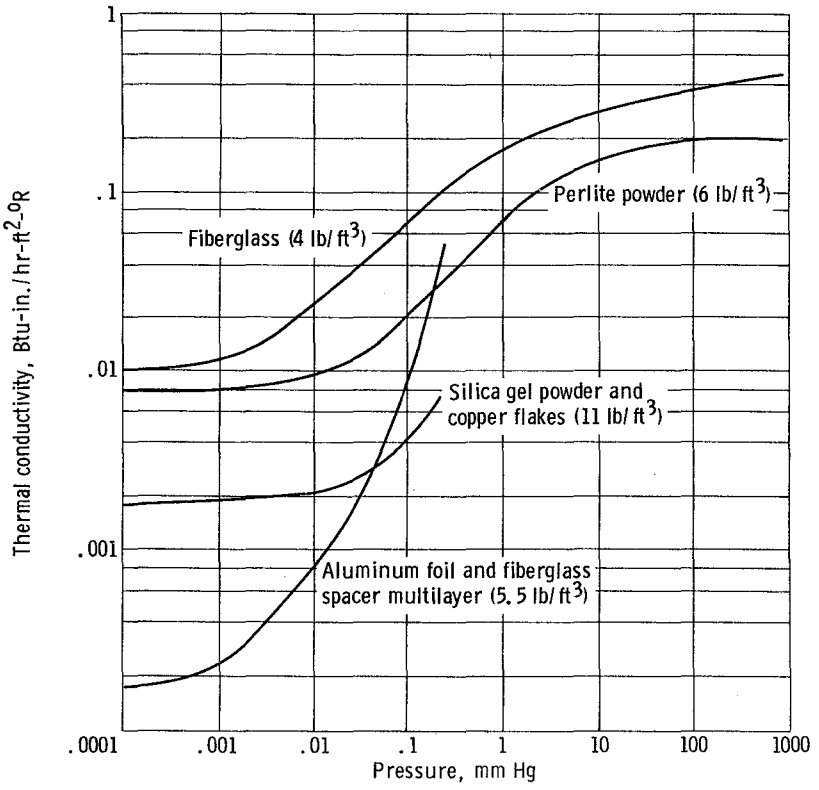

Figure 5-6. - Effect of gas pressure on thermal conductivities of various cryogenic insulations (ref. 72, pp. 2 to 9).

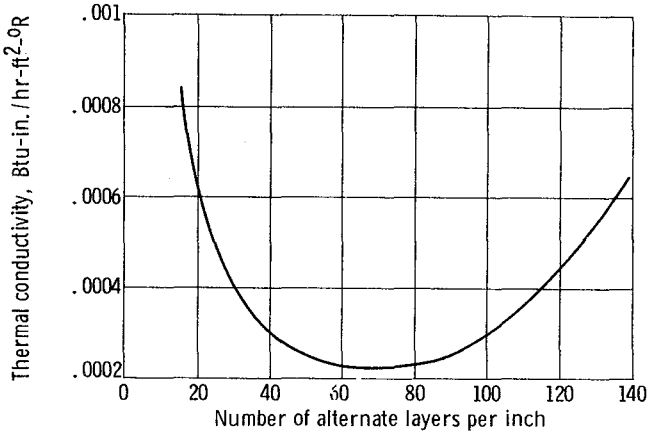

Figure 5-7. - Thermal conductivity against number of alternate layers of glass fiber paper and aluminum foil per inch thickness of insulation between 540^{0} and 140^{0} R (ref. 72, pp. 2 to 15).

TABLE 5-V. - MINIMUM VALUES OF EMITTANCES

FOR SELECTED METAL SURFACES[a]

Material[b]	Emittance[c]
Aluminum, 0.001-in. and 0.0015-in. household foil	0.02
Aluminum, vapor deposited on polyester film	.04
Brass, yellow 0.001-in. shim stock	.03
Cadmium, mossy plate	.03
Chromium, electroplate	.08
Copper, electrolytic, careful polish	.02
Copper, pure, carefully prepared	.01
Gold, 0.0015-in. foil	.01
Gold, vapor deposited on polyester film	.02
Lead, 0.004-in. foil	.04
Nickel, 0.004-in. foil	.02
Platinum	.02
Silver	.01
Stainless steel 302	.05
Tin, 0.001-in. foil	.01
Zinc, 0.0065-in. foil	.03
Solder, 50-50	.03

[a]Ref. 72, pp. 2 to 21.

[b]All materials solvent cleaned unless otherwise stated.

[c]For surface at 140° R from radiation source at 540° R.

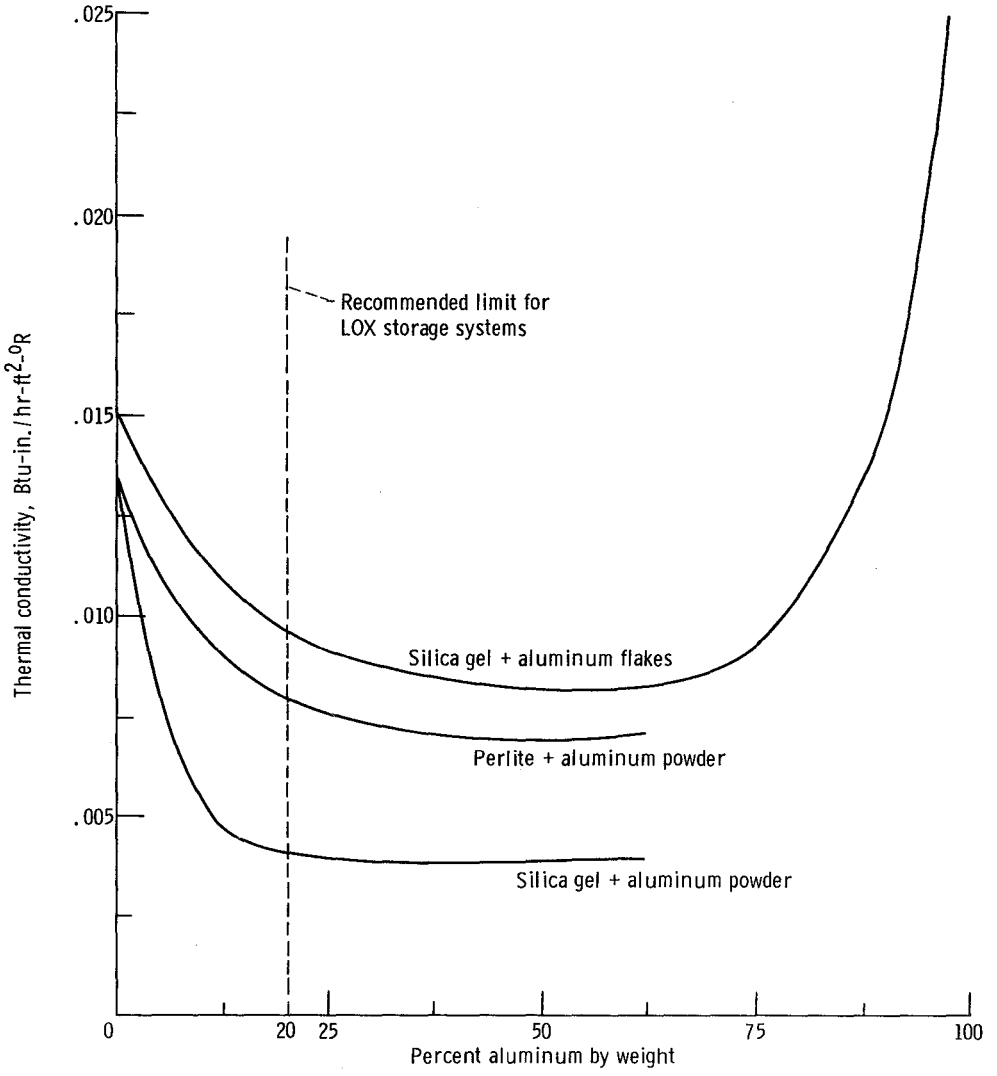

Figure 5-8. - Effect of metallic additives on apparent thermal conductivities of evacuated powder insulations between 540^0 and 140^0 R (ref. 72, pp. 2 to 11).

densities for various insulations are given in table 5-IV. The coating materials with the lowest emittance values for multilayer insulation are listed in table 5-V. The reduction of thermal conductivity of powdered insulations from the addition of metal powders is illustrated in figure 5-8. The optimum benefit results with aluminum powders in quantities of 20 to 70 percent by weight. As previously indicated, flammability is not generally sustained below 20 percent. Therefore, 20 percent appears to be an overall optimum for oxygen, but again, the actual limit would have to be determined by test in each particular case.

5.4 TANK MAINTENANCE CONTROL

In order to prevent exceeding the use limits of a tank, it is important to maintain a documentation of the tank's "life history" or "tank log." Every event in the life of the tank significant to engineering evaluation of the tank use limits should be recorded. The "log" should include the following:

(1) Original design specifications
(2) Raw materials record - source, quality test results, and processing record of the materials used to make the tank
(3) Fabrication record - record of the fabrication anomalies, weld rework, tank modifications, stress relief, and heat treat processes
(4) Test history - test data record
(5) Record of inspection anomalies
(6) Maintenance record, including cleaning and preparation
(7) Use and operation record
    (a) Cyclic use record - pressure cycles, temperature cycles, cumulative fill and drain data, cleaning, and inspection cycles
    (b) Record of use anomalies (especially accidental overpressure)

The need for these data is important in determining tank life inspection periods, cleaning, and reuse specifications. The raw materials record and fabrication record identify specific points for future inspection. Test history is important because pressurization testing can verify the tank reliability, but it can also contribute to cycle fatigue and reduced tank life. This is especially true for flight weight tanks where the margin between the working stress and yield stress is relatively small. Inspection anomalies and maintenance records aid in quality assurance. The use and operation record completes the total environmental effects profile useful in gaging the state of the tank system at any time.

5.5 TANK OVERPRESSURE HAZARD

It is difficult to predict the potential hazard that would result when a tank fails from accidental overpressure. Tanks fail by leaking local bursting or disintegrating into shrapnel. Some of the total energy is absorbed by the tank disintegration; some is absorbed to accelerate the tank parts (or shrapnel); and the rest of the energy is dissipated by a pressure wave. The amount of energy absorbed by the tank disintegration also varies with the tank wall thickness and the tank material, although this is relatively small compared to the total energy release.

The potential explosive energy equivalent of a pressurized tank is given by (ref. 85, p. 4)

$$E = 144 \left[\frac{V\left(\frac{P_1}{P_2}\right)\left(\frac{T_1}{T_2}\right)}{359} \right] RT_2 \ln \frac{P_1}{P_2}$$

where

E energy, ft-lb

P_1 tank pressure (absolute), lb/ft^2

P_2 atmospheric pressure (or ambient pressure) or zero pressure in space, lb/ft^2

R molar gas constant, 10.73 $lb\text{-}ft^3/(^oR)(in.^2)(lb)(mole)$

V tank volume, ft^3

T_1 ambient temperature, ^oR

T_2 temperature of contained gas, ^oR

This does not allow for the energy used in rupturing the tank and propelling its pieces.

The energy equivalent of TNT is 1.543×10^6 foot-pounds per pound TNT. Therefore, the TNT energy equivalent of a pressurized tank is

$$\text{lb TNT equivalent} = \frac{E}{1.543 \times 10^6}$$

An overpressure rupture of a tank in the atmosphere will cause a shock wave per distance relationship given by the Nomogram (fig. 5-9).

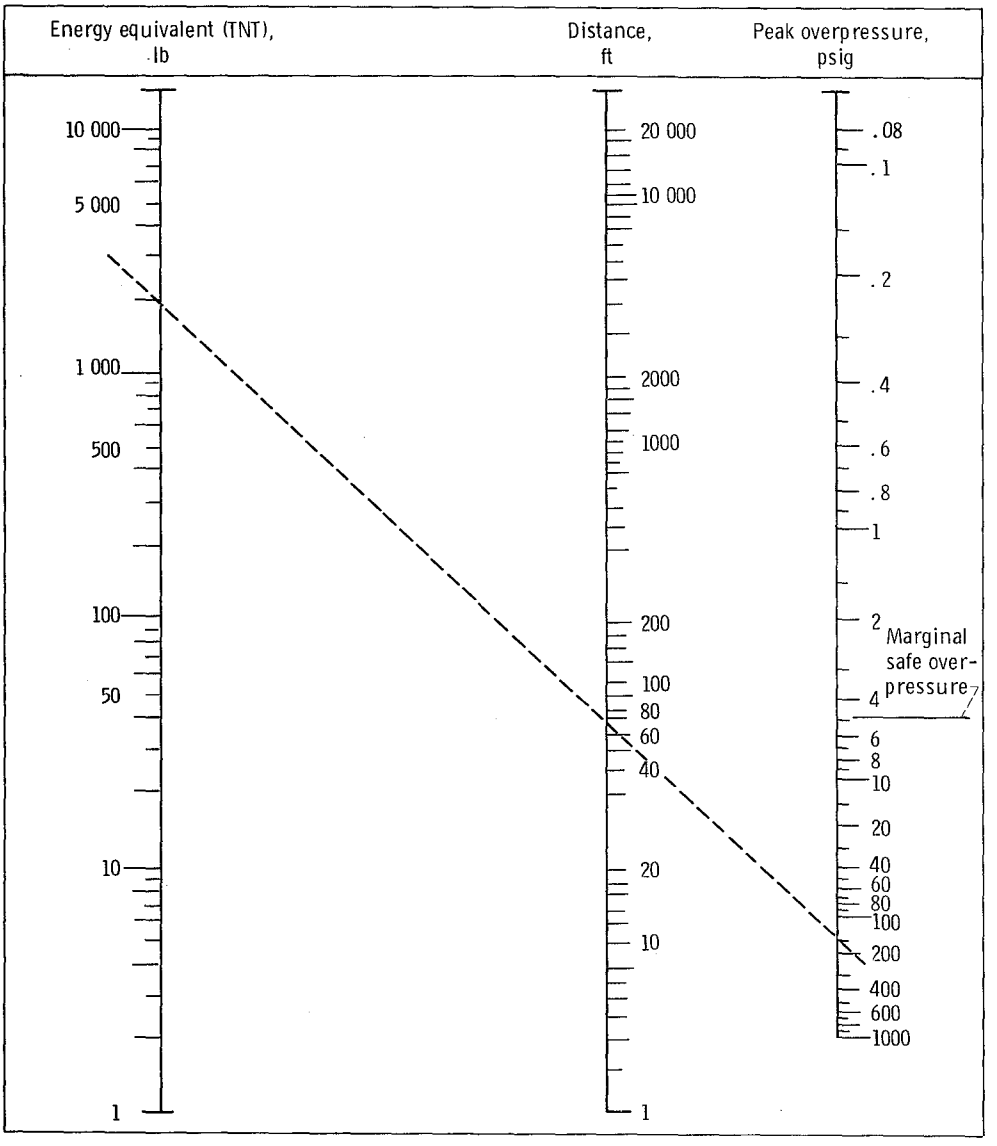

Figure 5-9. - Nomogram for magnitude of blast hazard from equivalent weights of TNT (ref. 85, p. 5). Missing factor (energy equivalent, distance, or peak overpressure) can be determined by locating two known factors on scales. Connect these points with straight line. Point of intersection of this line and third scale determines missing factor.

Page intentionally left blank

CHAPTER 6. OXYGEN PUMPS

The most commonly used pump for pumping liquid or gaseous oxygen is the centrifugal pump which is used almost exclusively in rocket engine systems. Centrifugal pumps are also widely used in ground applications for liquid oxygen pumping and as high flow rate gaseous oxygen compressors. Where very high pressures must be attained (usually at low flow rates), positive displacement piston-type pumps may be used; however, by means of staging, high pressures may be obtained from centrifugal pumps. Axial flow pumps tend to be impractical for pumping oxygen because of the relatively high density of the liquid and the complexity caused by bearing location and lubrication requirements for pumping gaseous oxygen. Diaphragm pumps can be designed to pump either liquid or gaseous oxygen, but practicality would generally dictate using a centrifugal or piston pump. This is because of problems such as diaphragm flexure fatigue, gaseous compression heating, and materials compatibility to meet the internal pump conditions. If for some purpose the axial or the diaphragm pump would be selected, the design criteria generated throughout this text would apply. To achieve high pressure liquid oxygen at very high flow rates, centrifugal pumps with one or more stages would be preferable. Most very high pressure oxygen requirements are for gaseous breathing oxygen storage purposes such as for life support systems. The easiest way to generate gaseous oxygen pressures up to 10 000 psi or higher is to pump liquid oxygen to that pressure through a vaporizer. Since this does not generally require high liquid flow rates, the positive displacement piston pump is the most appropriate.

Rotary pumps which may be exposed to an oxygen environment are generally used as vacuum pumps and as such are exposed to relatively low oxygen partial pressures.

6.1 CENTRIFUGAL PUMPS

Most experiences with centrifugal pump failures involve pump deterioration resulting from bearing or seal failure. Such failures often result in structural disintegration with resulting ignition and fire. The exposure of the pump materials to high-speed rubbing friction, pressure spikes, impact, and contamination is a risk in a centrifugal pump, and the sensitivity of the pump materials to these conditions in the presence of oxygen is always a potential for possible reaction.

The following sections review many of the special considerations to be given to the design, fabrication, and use of centrifugal pumps for liquid oxygen to avoid conditions that can lead to failure. Although the emphasis in this section is on turbine-driven centrifugal pumps for flight application, the principles discussed are generally applicable to ground-based pumps. Since ground-based centrifugal pumps are not weight limited, higher safety factors and long pump life can be achieved at lower cost. For example, geared electric motor drives may be used. By increasing the size and stiffness of the pump shaft, a longer impeller overhang can be tolerated thereby permitting use of conventionally lubricated rotor shaft bearings. The main drive shaft from the gear box may also support the pump impeller. This also permits the use of an integrated pump - gear box housing for greater strength.

6.1.1 Pump Housing and Rotor Assembly

The pump casing (fig. 6-1, ref. 86) which serves as the structural support of the turbopump assembly must withstand all of the torque and bending moments transmitted

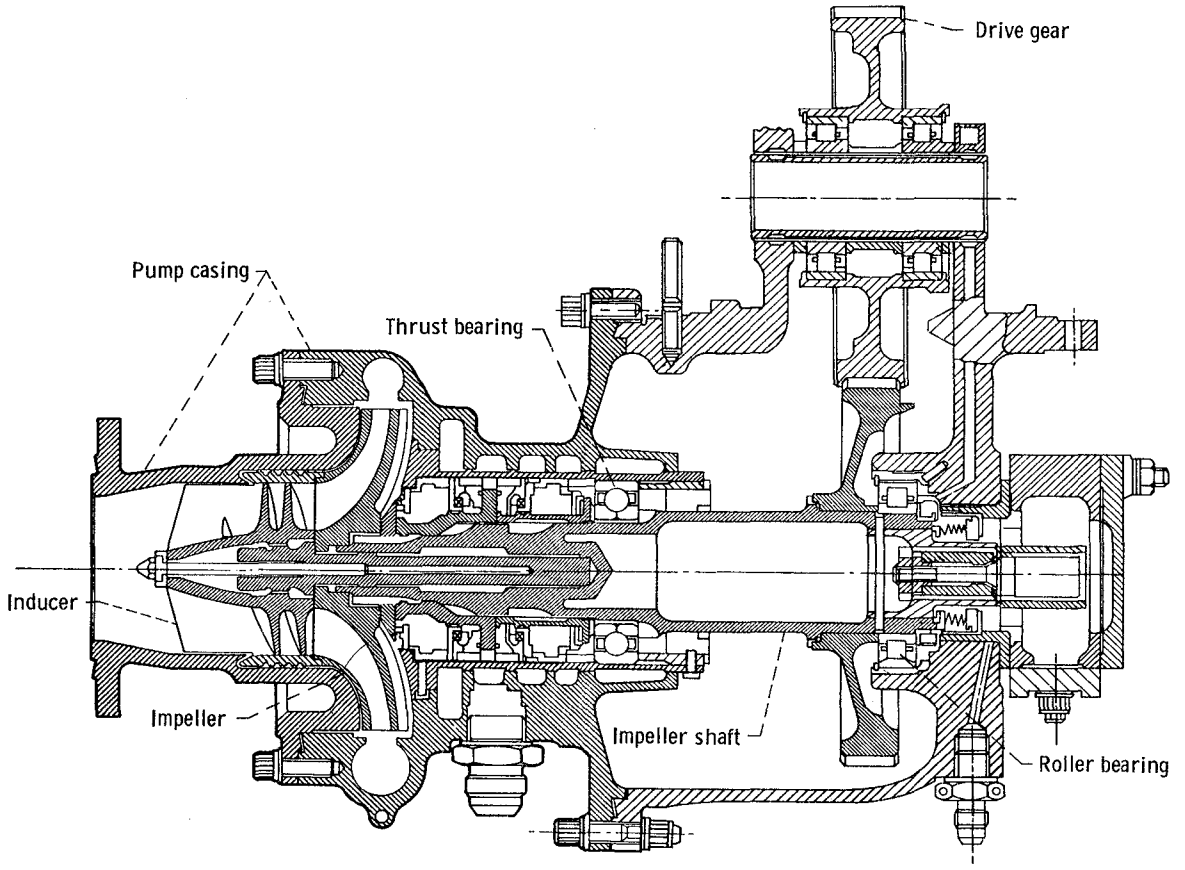

Figure 6-1. - Oxidizer pump assembly (based on ref. 86, fig. II-5).

through the structure in addition to the stresses from internal pressures. The casing must resist flexing from cyclic pressure variations, either circumferential or pulsing; otherwise, fatigue failure or excessive rotor rub could result. To avoid the large distortion associated with the resonance vibration of the pump case, the natural frequency of the pump case in any vibrational mode should be above any expected periodic driving force. Fluctuating pressure loads and perturbations in the inlet flow can be structurally damaging and should be avoided by design, operational procedures, and system monitoring.

The oxygen pump housing design is a matter of providing the strength necessary to prevent rotor contact while permitting the close clearances necessary for pump efficiency. In flight weight pumps this must be achieved without undo weight penalty. A discussion of centrifugal pump housing and rotor design is given in references 70 (pp. 219 to 225) and 87 (pp. 60 to 77 and 111 to 122). In addition, references 88 and 89 (ch. 7) are useful texts which may be consulted on design of pumps and turbomachinery.

6.1 1.1 Inducer - impeller-pump case clearance. - The practically attained minimum value for the blade tip clearance to blade length ratio for both inducers and impellers is 2.0 percent for oxygen pumps. When closer clearances are required which increase the possibility of rubbing, a "wear-in" seal or liner of polytetrafluoroethylene (TFE) or polychlorotrifluoroethylene (CTFE) liner (fig. 6-2) can be used to achieve the minimum clearance. These materials also reduce friction and abrasion should rubbing occur (ref. 90, pp. 70 and 71). The acceptance of this technique is primarily one of precedence. Therefore, the application of nonmetal rub rings and liners beyond the limit of experience should be with caution and verification testing. Initial wear-in of the seal or rub ring should be with liquid nitrogen. Although the average ignition temperature of TFE and CTFE in oxygen is between 410° and 540° C over the pressure range from 1 to 100 atmospheres (fig. 3-10) compared to 800° and 1000° C or higher for most metals and alloys, the heat sink provided by liquid oxygen and the lower coefficient of

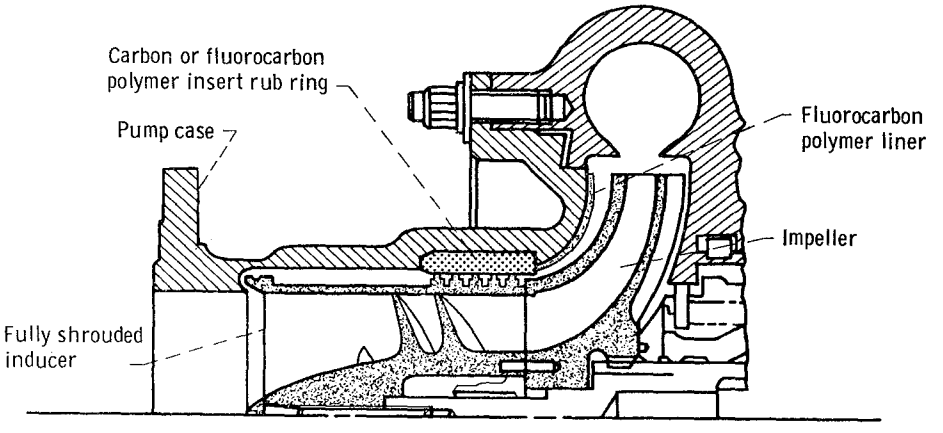

Figure 6-2. - Inducer impeller pump case lining (based on ref. 86, fig. I-1).

friction of TFE and CTFE permit their use in this application within present experience limits. A labyrinth seal is sometimes used to perform both sealing and rub liner functions. In such applications a labyrinth element is used in conjunction with a fluorocarbon polymer wear ring as illustrated in figure 6-2. The wear-in characteristics of this combination provide near optimum inducer to case clearances and reduce backflow to an acceptable level.

6.1.1.2 Turbopump shaft stability and critical speed. - Rotor stability is especially important in oxygen pumps in order to prevent rotor rub and bearing overstress while at the same time permitting the shaft diameter and weight to be minimum. With improved higher strength materials, the possibility of higher pump speeds in future pump developments increases the hazard of rubbing contact between the rotor and the pump case. The close clearances between the housing and the impeller and inducer blades must be maintained to assure pump efficiency. At current design speeds the inducer-impeller, shaft, and bearing system (rotor assembly) may pass through several critical speeds during spinup and shutdown. At critical speeds the rpm of the rotor assembly equals some multiple of the natural frequency of the rotor assembly or some forcing frequency. The shaft wobble accompanying critical speed operation may cause the impeller to rub the pump case. Accordingly, shaft radial balance and thrust balance are critical design requirements.

Although the primary driving force to shaft mount instability is rotor imbalance, other factors can induce forces which at resonant frequencies may cause the rotor to exceed its clearance envelope. Some of the factors that must be considered include variations in the bearing assembly stiffness, internal bearing friction, uneven pressure buildups in the pumped fluid around the rotor, resonant flexing of the casing, and variations in flow due to engine chugging or cyclic coupling of flow control loops. For oxygen, these factors must be anticipated as much as possible during the design stage to prevent pump failures. Initial runups of oxygen pumps should be programmed to verify a non-critical rub condition. In developmental pumps, testing should explore the complete operational profile with adequate instrumentation to determine the possibility of unacceptable impeller rub. For added safety, checkout runs may be made using liquid nitrogen.

There are two design philosophies currently applied in the design of rocket engine turbopump rotor assemblies. In one, the bearing and shaft system is designed with all of the turbopump operating speeds below rigid body, first whirling mode critical speed. To achieve this, high bearing mount spring rates are required. This requires stronger, stiffer shafts and increased shaft and bearing diameters. Roller bearings are used to provide high radial spring rates along with ball bearings for supporting axial thrust. Resonance problems are avoided, but there is a weight penalty. The second design philosophy calls for a design for pump operation above the first and second whirling mode critical speeds but below any mode where significant shaft bending occurs. This allows

smaller bearings and lighter shafts. The bearing mounting has a lower spring rate. The main advantage in this case is lower pump weight. In either design approach, a 20 percent margin is generally used between the shaft operating speed and the nearest whirling critical speed to assure rub free rotation (ref. 87, p. 11).

Because classical methods for computing rotor displacement when passing through critical speed are not accurate enough to predict rotor rub, digital computer programs for calculating the natural frequencies and amplitudes are generally used (ref. 91, pp. 31 to 48 and 82 to 88, and refs. 92 to 94). The use of such programs provides higher accuracy because more elaborate and accurate models may be used.

The rotor shaft is generally balanced initially as subcomponent and then as part of the assembled rotor on a balancing machine. The rotor assembly is then disassembled and reassembled in the turbopump. However, considerations such as pilot tolerances, runouts, and parallelism can alter the fine balance attained. In addition, fits may shift during operation due to thermal expansion differences between adjacent parts and mechanical deformations caused by centrifugal forces. Because these shifts may allow eccentric shifting of adjacent rotor parts, rotor imbalance results. For this reason, it is necessary to instrument for static and dynamic bearing loading and clearance measurements through the entire operating range as a part of the pump development testing. The assembled rotor should be balanced in the range of 50 to 100 microinches of mass eccentricity (μin.-lb out of balance/mass of rotor) (ref. 91, p. 88). When this procedure is used, actual rotor imbalance is rarely as great as the limits specified or permitted by the engineering drawings. Techniques for balancing turbomachinery are discussed in references 91 (pp. 48, 88, and 94 to 96) and 95.

Programs for computing critical speeds are given (with program description, user's manual, and FORTRAN listings) in reference 96. (Only the table of contents of this reference is included in the microfiche supplement. The text has been omitted because of its large size and small print.) Detailed discussions of shaft dynamics are presented in reference 91 (pp. 19 to 48 and 79 to 88).

6.1.1.2.1 *Torsional stability.* - Torsional vibration in turbopump shafts has not generally been a limiting or controlling design factor. But a comparison is usually made between the calculated values of torsional natural frequencies and possible forcing or coupling frequencies such as from gear teeth meshing, misalinements of couplings, or other torsional driving forces.

The calculated torsional natural frequencies are also compared with nontorsional system natural frequencies to avoid possible coupling (ref. 91, pp. 30 and 81). As in the case of whirling and bending instability, a 20 percent margin between the instability frequency and operating frequency should be provided.

6.1.1.2.2 *Axial thrust.* - Shaft axial thrust balance forces as high as 30 000 pounds per 1000 pound per second propellant flow can be required to keep the axial force on the rolling element thrust bearing to tolerable values. The impeller is generally balanced

by exposing its back face to a pressure distribution that matches that developed on the front face, as shown in figures 6-3 and 6-4. Up to 90 percent of the axial thrust load is sometimes required to be taken up by a thrust balance piston or back vanes on the pump impeller in support of a "ball" thrust bearing used to establish a fixed position for the rotor.

The pressure balancing arrangement shown in figure 6-3 incorporates a set of radial vanes on the back face of the impeller which constitutes a simple secondary centrifugal pump. The pressure field developed by this secondary pump is a rough match to the field developed on the front face of the impeller. The impeller back face vane system has been preferred from experience and is used in oxygen pumps on M-1, H-1, J-2, RL-10, and F-1 engines.

In the balance piston method (fig. 6-4) the balance chamber on the back face of the impeller is pressurized by flow communication with the pump exit. The exposed area on which this pressure acts, defined by the back wear rings and the shaft seal, is sized to provide the axial force opposing the force on the front face. For finer balancing, the piston chamber pressure is regulated by a vernier control. Techniques for determining the required balance chamber pressure level in the system shown in figure 6-4 are presented in reference 70 (pp. 223 and 224). Pressure balancing the pump impeller to support axial thrust loads using the balance piston method has caused frequent problems during turbopump development. Thrust loads could not be predicted within the desired accuracy, and small variations in impeller face pressures result in considerable variations in the magnitude of the net thrust. Because of the poor predictability of the thrust

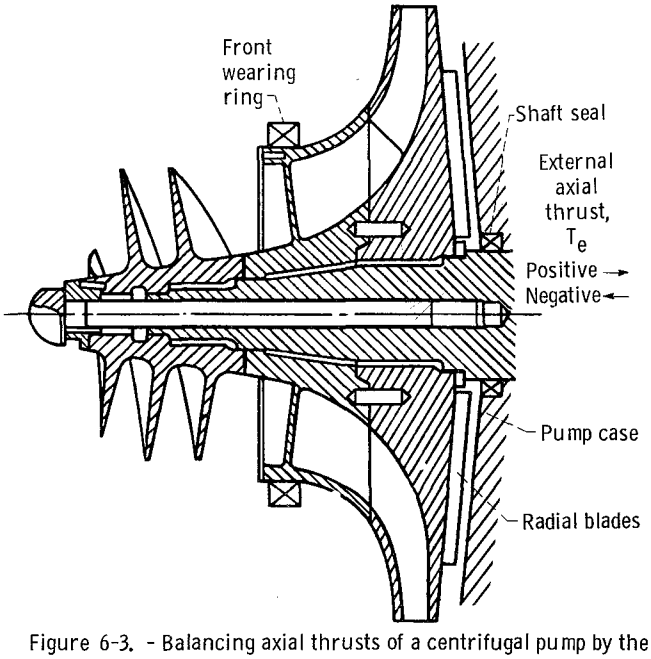

Figure 6-3. - Balancing axial thrusts of a centrifugal pump by the radial rib method (based on ref. 70, fig. 6-48).

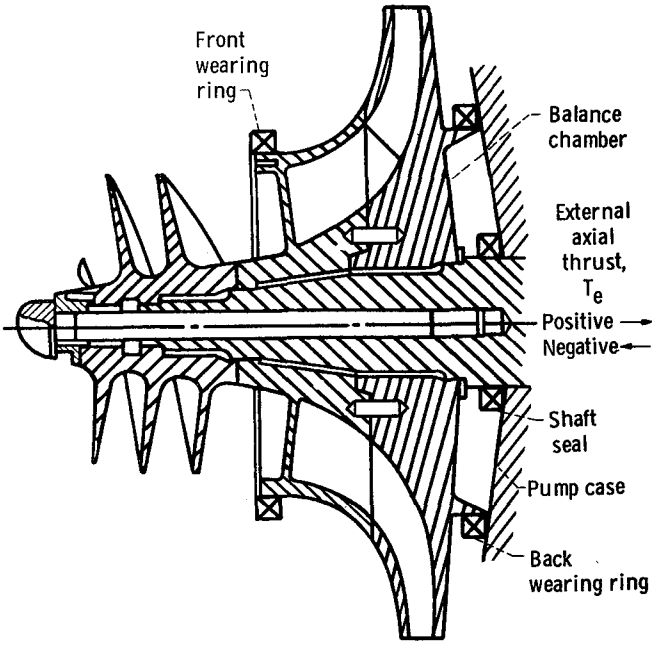

Figure 6-4. - Balancing axial thrusts of a centrifugal pump by the balance chamber method (based on ref. 70, fig. 6-47).

variations, especially during runup and stop transients, large tolerances to thrust force variations are generally provided in development models, and they are designed to be adjusted during tests. For this reason, pressure balancing with a controlled fluid back pressure has not been used in operational oxygen pumps.

Thrust balancing determinations for centrifugal pumps are discussed in references 70 (pp. 223 to 225) and 87 (pp. 82 to 89). Since experience has shown that actual and calculated thrust can vary considerably, initial runups should be done in steps with adequate instrumentation to verify thrust at operational speed.

For systems such as shown in figures 6-3 and 6-4, the balance of axial forces acting on the impeller may be approximated from equations given in reference 70 (pp. 223 to 225). A sample calculation of the axial thrust balance forces of the M-1 oxygen pump is presented in reference 97 (pp. 22 to 40).

6.1.1.3 Inlet flow dynamics. - Flow distortions and turbulence at the pump inlet introduced by valves, bellows, pipe bends, and poorly designed pipe entrance sections cause unsymmetrical hydrodynamic forces on the impeller. The unbalanced forces fluctuate with time and may cause an oscillation of the impeller-shaft system.

To avoid these unbalanced pumping forces, a straight run of pipe to the pump inlet of 5 pipe diameters is normally used (when space is available) to allow disturbances in the flow to subside before entering the pump. Valves, bellows, and elbows should be located upstream of this section. Straightening vanes are used in the inlet line if an adequate uninterrupted straight run immediately before the inlet cannot be installed. Bellows sections installed in the inlet line closer than 5 inlet line diameters should be fitted with a smooth liner to avoid the turbulence caused by the flow over the bellows convolutions. These considerations are discussed further in reference 90 (pp. 7 to 11 and 49 to 50). Problems associated with the use of convoluted sections in oxygen systems are discussed in section 8.4.

When turning vanes are used in elbows, the vane spacing to vane chord length ratio of 0.25 to 0.45 should be used for minimum pressure drop (ref. 70, p. 373). The exact value must be determined in flow tests.

6.1.1.3.1 *Inlet line cavitation.* - Cavitation in the inlet line fluid may result in a two-phase mixture of oxygen liquid and gas entering the pump. The nonuniform density of this mixture from blade to blade causes unbalanced forces on the inducer and impeller. Straightening vanes in the line do not correct this condition.

Cavitation in the line is avoided by providing a liquid oxygen tank pressure which is high enough to ensure that the static pressure at any point in the line never falls below the vapor pressure. Cavitation may also be prevented or reduced by subcooling the oxygen to reduce its vapor pressure or in some cases by reducing heat input with insulation of the pump and feedline. A boost pump may also be used to increase the inlet pressure.

In cases where the pump inlet pressure is very close to the local vapor pressure, and the feed system pressure drop is critical, filters and screens cannot be used. These would add to the pressure drop.

The relationship between the oxygen tank pressure and the maximum oxygen velocity in a loss-free inlet line is given by

$$V_{max} = \left[\frac{2g(P_t - P_v)}{\rho}\right]^{1/2} \quad (1)$$

where

P_t tank pressure, lb/ft^2

P_v oxygen vapor pressure, lb/ft^2

ρ oxygen density, lb/ft^3

g acceleration gravity, 32 ft/sec^2

To allow for pressure losses in the line and some static pressure margin for the acceleration of the flow over the pump blades without cavitation, the line cross-sectional area is taken large enough so that no more than one-third of the difference between tank pressure and vapor pressure is used to accelerate the flow in the line. The corrected line maximum velocity is computed from (ref. 90, p. 64)

$$V_m = \left[\frac{2g(P_t - P_v)}{3\rho}\right]^{1/2} \quad (2)$$

For more detail in inlet line design see references 70 (pp. 372 and 373) and 90 (pp. 7 to 11 and 64 and 65).

6.1.1.3.2 *Rotor blade cavitation.* - Two problems that can result from cavitation on inducer and impeller blades are vibration (ref. 90, pp. 39 and 40 and 76 and 77) and cavitation erosion. Although cavitation erosion is mainly a long term effect and is not normally a problem in short term turbopump operation, it could become more important in long time operation of high rpm - high discharge pressure pumps. The hazards associated with these effects in oxygen pumps are cracked or broken rotor blades from vibrations and erosion and ingested solid particles or blade parts which can fail the turbopump.

The suction surface of the impeller blade is normally the cavitation site. The pressure drop required to accelerate the flow over this surface can bring the static pressure

there to the liquid oxygen vapor pressure and cavitation occurs. A discussion of cavitation as it affects pump performance and damage is given in references 98 (pp. 81 to 101) and 99.

Blade surface roughness is also a factor in cavitation onset. Test results comparing surface finishes of 2 microinches to finishes of 160 microinches indicated a lowering of pump efficiency by 5.9 percent with chordwise striations and 7.2 percent with spanwise striations (ref. 100, p. 209). Cavitation onset and vibrations appeared to be advanced with increased roughness. Accordingly, it has been recommended (ref. 90, p. 58) that the blades be polished to a surface finish of 25 microinches rms.

Cavitation is avoided if the pressure of the oxygen entering the pump is high enough above the oxygen vapor pressure to accommodate the acceleration pressure drop. This higher pressure at the pump inlet can be obtained with higher tank pressures, use of a separate boost pump, or use of an inducer. The inducer usually mounted on the impeller shaft (fig. 6-1) and rotated at impeller speed provides only the relatively small pressure rise required to avoid cavitation on the impeller. Because of this modest pump work requirement from the inducer, its blading can be shaped to accommodate cavitation with useful pumping efficiency and high tolerance for cavitation erosion. A detailed discussion of inducer design is given in reference 90.

If tank pressure must be too low because of design trade-offs to prevent cavitation, the use of a separately driven boost pump or inducer at the liquid oxygen tank to raise the pump inlet pressure is necessary. The design of boost pumps is discussed in reference 101 (pp. 1 to 40); additional design studies are presented in references 102 to 104.

6.1.1.4 Safety factors

6.1.1.4.1 *Pump case.* - Safety factors recommended for preliminary design estimates of pump housings are summarized in this section. Usually these factors may be used for final design calculations and proof testing; however, design considerations such as fatigue effects and fracture toughness may justify using greater safety factors. As used here, the limit load is defined as the highest probable stress which the housing is expected to experience from external forces and pressure loading, including pressure spikes due to possible chugging, impeller overspeeding, and critical speed effects. The highest possible combination of forces must be included in estimating the highest probable stress. The recommended safety factors are as follows:

(1) The ratio of yield load to limit load should be equal to or greater than 1.1.

(2) The ratio of ultimate load to limit load should be equal to or greater than 1.5.

(3) The ratio of the ultimate fatigue strength to limit load should be equal to or greater than 1.33. (The ultimate fatigue strength is the maximum stress a component will withstand for the desired number of stress cycles without fatigue failure.) It may also be based on total strain.

(4) The proof pressure for testing the case should be obtained by multiplying the pressure used in determining the limit load by a factor of 1.2 (or as established by fracture mechanics analysis). Frequently, a value of two-thirds the calculated case burst pressure is used as an alternative proof pressure.

(5) For weldments, if joint efficiency test data are not available, use 85 percent of the material tensile and shear yield stress as well as ultimate stress in computing yield and ultimate safety factors.

Although not a design factor, a limit must be placed on operating pressure when special protection for personnel such as barriers is not provided. The following pressures are recommended:

(1) One-half ultimate

(2) Three-fourths the limit pressure

Additional criteria and recommended practices are provided in reference 87 (pp. 77 and 116 to 118).

6.1.1.4.2 *Pump rotor shaft.* - Table 6-I lists some examples of safety factors for existing rotor shaft designs of lightweight flight pumps with short service life requirements. Additional criteria and recommended practices are given in reference 91 (pp. 60 to 78).

6.1.1.5 Component materials. - Materials commonly used for pump components are listed in table 6-II.

TABLE 6-I. - ROTOR SHAFT SAFETY FACTORS

Pump application	Safety factor	
	Yield[b]	Ultimate[b]
Titan I and II	1.0	1.25
M-I	1.0	1.5
Titan III-M	1.0	1.4
Rocketdyne	1.1	1.5
ARES	1.2	1.6

[a]Ref. 91, p. 10.

[b]Based on highest potential stress possible under all testing and operating conditions.

TABLE 6-II. - COMMONLY USED CONSTRUCTION MATERIALS FOR LIQUID OXYGEN CENTRIFUGAL PUMPS

Component	Materials
Housing	Monel K and KR Inconel 718 Stainless steel 304, 347 Aluminum 356 (castings) and "Tens" 50-T-6
Impeller-inducer	Monel K Bronze and brass alloys Inconel 718, Inconel X Stainless steel 304, 347, 17-4PH Aluminum 7075-T73, 7079-T6, 2024-T4, 2014-T6, 356-T6
Shaft	Inconel 718, Inconel X Monel K Stainless steel 304, 347 4340 alloy steel
Case liner	TFE (Teflon), CTFE (Kel-F)
Wear ring	TFE (Teflon), CTFE (Kel-F), carbon

Oxygen compatible pump materials are normally alloys of nickel, aluminum, copper, or stainless steel. They allow a wide choice of material densities and strengths. However, allowances must be made for differences in the expansion-contraction coefficients and the dissimilar metals problem.

Monel K or Inconel 718 are preferred materials for pump rotors operating in the cavitation regime (ref. 90, p. 75). The blades can be thinner than those of aluminum and the resistance to bending and cavitation erosion is greater. Where cavitation is not severe and ease of fabrication and lower cost are desired, aluminum alloys are used. The preferred alloys are 7079-T6, 7075-T73, and 2024-T4. Alloy 7075-T73 is relatively free from stress corrosion cracking and would be preferred from that standpoint.

To improve surface hardness (and erosion resistance) the aluminum components should be anodized to a minimum depth of 70 microinches. For depths over 500 microinches, anodized surface films begin to lower the fatigue resistance of the aluminum. A practical maximum of 300 microinches is usually used.

6.1.2 Turbopump Shaft Bearings

The use of cryogenically cooled pump bearings in flight turbopumps results in an appreciable reduction in pump system complexity, weight, and cost. Use of conventional lubricants requires longer shaft overhang to isolate the bearing thermally from the cold region of the pump. Longer shaft and housing requirements can lead to excessive weight and pump critical speed problems (ref. 105, p. 309).

For ground operation where weight and efficiency are less important, ambient temperature conventional lubrication may be an advantage in achieving longer bearing life. When liquid oxygen is used to cool the bearing, a chemical reaction (i.e., surface oxidation, corrosion, ignition, and self-propagating combustion) is possible between the oxygen and the bearings, pump component material, and conventional lubricants and seals. In order to illustrate the precision and care that must be exercised in bearing design, the salient points of bearing design are reviewed briefly in the following sections. Additional detailed treatment of bearing design is given in reference 105 (chs. 6, 11, and 12); engineering design criteria and recommended practices are given in references 106 (pp. 31 to 68) and 107 (pp. 7 to 20).

6.1.2.1 Bearing materials. - Materials used successfully for bearings running in oxygen are given in table 6-III.

TFE coated or impregnated fiberglass requires greater web thickness than a metallic cage. Metallic cages are not recommended for submerged oxygen bearing. The coefficient of friction of the materials listed in table 6-III in cage applications is between 0.05 and 0.15 (ref. 106, p. 50). The web thickness to diameter ratio of 0.15 provides

TABLE 6-III. - COMMONLY USED MATERIALS FOR

BEARINGS IN LIQUID OXYGEN

Component	Material	Reference
Roller, ball, and races	440C steel 52100 steel	106, p. 19
Cages	Armalon (mandrel-wrapped glass fabric supported) (TFE)	
	Salox-M (40 percent bronze powder filled TFE)	106, p. 51
	15 to 25 Percent glass filled TFE	

the best performance. Minimum web thickness should be limited to 0.15 inch for strength reasons (ref. 106, pp. 29 and 67).

The 52100 steel is sensitive to moisture corrosion and accordingly AISI 440-C corrosion resistant steel is recommended for liquid oxygen cooled bearings (ref. 105, p. 321). While no known material ideally fulfills the requirements of hardness, ductility or toughness, machinability, and availability, 440-C best meets the requirements with the fewest limitations. Grade 440-C steel is not entirely corrosion resistant, and investigations are under way to develop a substitute. Nickel-based alloys are corrosion resistant but relatively soft. Although sintered carbides are corrosion resistant and hard, they are brittle. Stellite Star-J has been investigated as a cryogenic bearing material, but testing has not produced design recommendations (ref. 106, pp. 19 and 20). Further discussion of materials choice, heat treatment, and desired hardness and maximum working stress is contained in references 105 (ch. 12) and 107 (pp. 5 to 7).

6.1.2.2 Lubrication and cooling. - Bearings which run in liquid oxygen are generally lubricated by fluorocarbon solids which are wiped from the cage by the rolling elements then transferred to the races. These solid films serve as anti-weld agents which prevent cold welding of the balls to the races. Filled TFE (usually glass fiber filled) from which the remainer is made provides the solid TFE lubricants which serve this function.

The use of fluorocarbon polymers in the bearing cage construction permits the short term high-speed operation required by most present generation rocket engines. Their use is limited, however, for extended or repeated operation because of the limited supply of fluorocarbon lubricant due to cage wear. The requirements for bearing and cage design for solid lubrication are covered in references 106 (pp. 28 to 30 and 63 to 68) and 107 (pp. 7 to 20). Cooling is provided by liquid oxygen which is circulated through the bearing as illustrated by the M-1 oxygen pump design shown in figure 6-5.

The flow on the downstream side of oxygen cooled bearings should be throttled to prevent flash vaporization of the LOX by maintaining its pressure above vapor pressure. The M-1 oxygen pump bearings used a combination of flooding and jet impingement

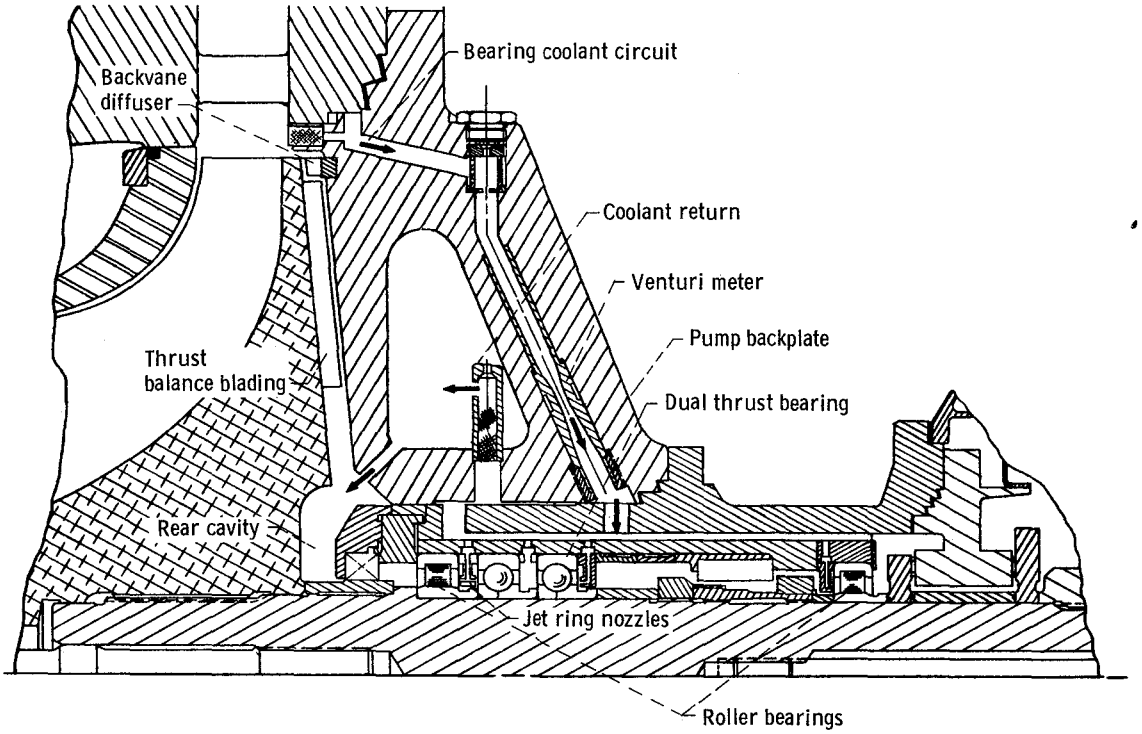

Figure 6-5. - Pump bearing cooling system (based on ref. 97, fig. 2).

(fig. 6-5). The jets were added to assure good circulation through the bearing (ref. 108, p. 1). Cooling is supplied through jet rings which direct the coolant on the rolling elements. The jet ring passage has an annular distribution channel with axial exit, cylindrical spray nozzles. For additional discussion of M-1 oxygen pump coolant system design see reference 108 (p. 12).

Typical cleanliness requirements for liquid rocket engines are given in reference 109, which gives the contamination per square foot of component as follows:

Particle size, μ	Number allowed per ft^2
175 to 700	5
700 to 2500	1
>2500	0
Nonvolatile residue	1 mg/ft^2 maximum

Since particles of the sizes permitted would have an adverse effect on bearings cooled by the LOX, filters ahead of the bearing cooling parts should screen out particles in excess of 40 microns; fluids used to clean the pump and bearings in preparation for oxygen service should be filtered through 10 micron filters (ref. 106, pp. 16 to 18 and 38 to 40).

6.1.2.3 Bearing life. - The life of an adequately lubricated bearing is limited by fatigue-induced pitting of the race and ball surfaces. Maximum stress appears at a depth of several thousandths of an inch below the surface. Fatigue failures begin as minute cracks at this depth which grow to the surface. Surface material is lost to this depth to produce a pitted surface. Once pitting occurs the rate of surface damage accelerates with each rotation cycle and the useful life of the bearing declines rapidly. However, oxygen cooled bearings are subject to an oxide film formation process where the oxide film is continually being replaced when virgin metal surface is exposed. This film promotes better boundary lubrication and helps to prevent galling and welding of the bearing surfaces.

The fatigue life of the bearing varies inversely with the ninth power of the maximum Hertz stress (ref. 105, pp. 383 to 384). For radial bearings the stress is due to preloading, impeller weight, shaft imbalance, and the centrifugal force of the balls against the outer race. Smaller balls will decrease the centrifugal force but increase the ball rotational speed. Hence, the number of fatigue inducing load cycles the ball surface will see will increase. A generally accepted life rating for ball and roller bearings is the "B-10 life," the operating life (hr) of a group of bearings at a given load and speed at which statistically 10 percent of them will have failed. Turbopump bearings are generally designed for a B-10 life of at least 10 times the required turbopump life (ref. 70, pp. 257 to 259). Figure 6-6 presents the centrifugal load DN (bearing bore in mm×rpm) limits in terms of 10 000 and 1000 hours of B-10 life for a typical ball bearing design.

Generally, rocket turbopump bearings have been successfully operated at DN values up to 1.5×10^6. Limited test information indicates possible satisfactory operation at 2.0×10^6 DN (ref. 70, p. 258). It is recommended in reference 106 (p. 31) that a DN of 3.0×10^6 should not be exceeded without prior testing. Ball sizes ranging from 3/16 to 7/8 inch in diameter and roller sizes from 1/4 to 1 inch in diameter are recommended

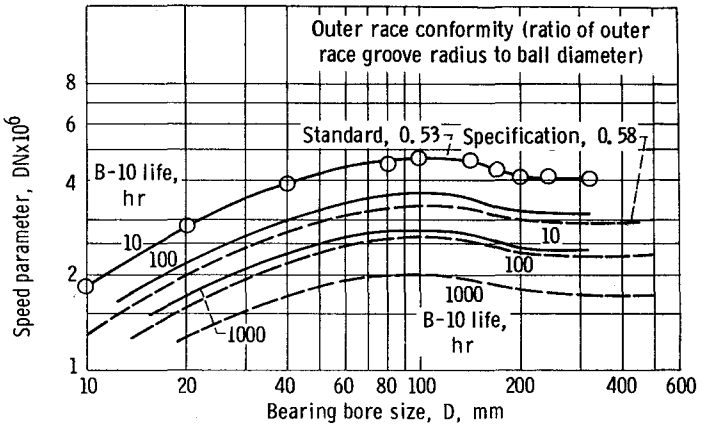

Figure 6-6. - Ball bearing centrifugal load DN limits (based on ref. 70, fig. 6-61).

(ref. 106, p. 23). Tests in liquid oxygen of the M-1 turbopump bearings reported a life expectancy of 5000+ seconds at a DN of 0.5×10^6 with ball diameters ranging from 23/32 to 3/4 inch and a bearing bore of 110 millimeters.

The maximum recommended Hertz compressive stress in balls, rollers, or races should be limited to 350 000 psi according to reference 107 (p. 7). Methods for computing the stress are discussed in reference 105 (pp. 150 to 158).

Higher bearing rotational speeds may be attainable in oxygen with unconventional designs presently under study. References 110 and 111 report recent experimental work on welded hollow and drilled hollow ball bearings. The hollow balls reduce the mass of the bearing and consequently allow higher rotational speeds before centrifugal loads become excessive.

6.1.3 Turbopump Rotating Shaft Seals

The primary concerns in oxygen pump rotating shaft seal design are the compatibility of materials with liquid oxygen in a rubbing environment and the possible seal face damage that can be caused by particulate contamination, thermal shock, and vibration.

The sliding surfaces of rotating shaft seals are subject to high thermal gradients, vibration from pump pulsations, shaft imbalance, and critical speed resonance. These rations can cause increased friction heating, surface breakdown, and seal failure. nerefore, the materials must be resistant to oxygen attack at high surface temperatures. The seal rubbing surfaces must have a low friction coefficient and the material should have high thermal conductivity, strength, and toughness and maintain good wear characteristics.

The contact pressure of a contact seal, as illustrated in figure 6-7, is controlled by balancing spring forces and hydraulic pressures. In this seal the spring closing force is supplied by the bellows secondary seal. Additional closing forces during pump operation are provided by pump delivery pressure being applied to the area on the high pressure side of the secondary seal and leakage pressure being applied to the low pressure side of the secondary seal. An interface pressure profile across the sealing surfaces (due to leakage flow pressure drop) tends to balance the closing forces with the resultant unbalance being the face contact load.

The seal design must not permit the maximum surface temperature to approach local ignition temperature. The oxygen pump seal integrity is of special concern because of the fire hazard from released high concentration oxygen and because of the possible ignition of the pump parts in the event of seal failure.

6.1.3.1 Seal types. - Primary seals are generally of the face contact type as illustrated in figure 6-7. While hydrostatic and hydrodynamic seals, which depend on fluid film support of the seal face, are potentially capable of extending the speed life limita-

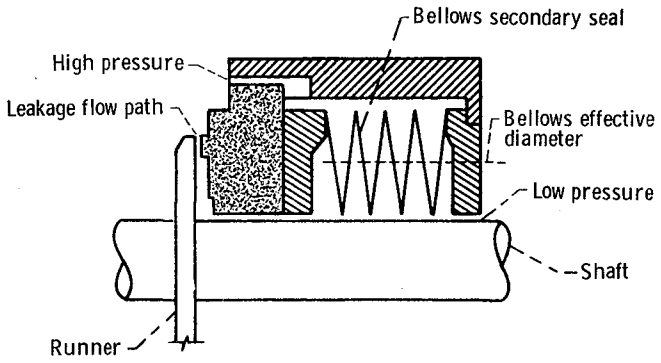

Figure 6-7. - Face contact seal.

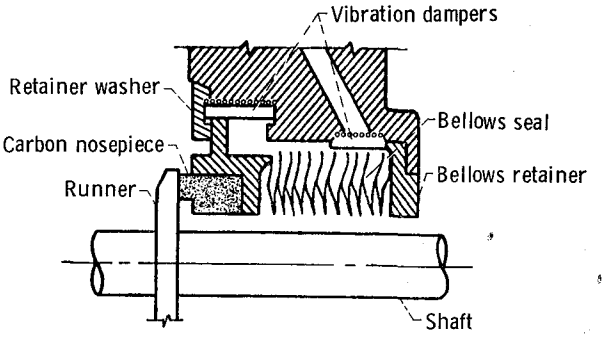

Figure 6-8. - Face contact/bellows.

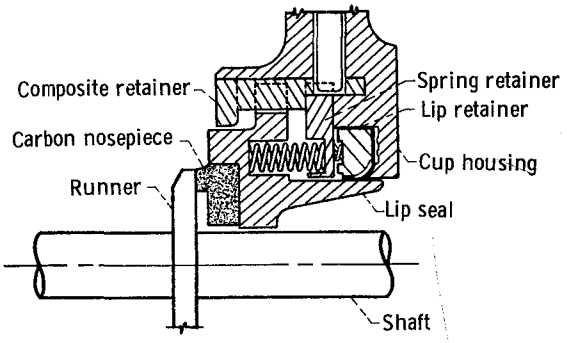

Figure 6-9. - Face contact/lip.

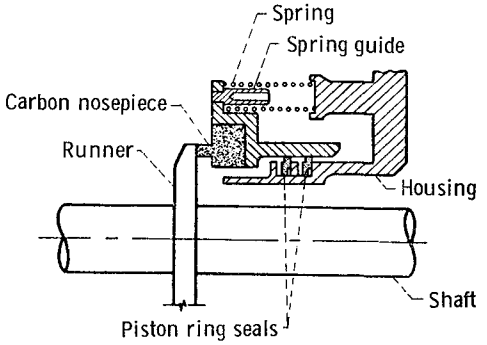

Figure 6-10. - Face contact/piston ring.

tions of seals, they have not yet been demonstrated to be suitable for oxygen service. However, the development of hydrostatic and hydrodynamic seals for oxygen service is continuing (ref. 112, pp. 15 to 18).

Secondary seal types include bellows, lip, and piston ring as illustrated in figures 6-8 to 6-10. The most common of these is the bellows seal which also provides spring and pressure loading to the primary seal. Bellows seals are subject to early fatigue failure unless damped to limit displacement under vibration. The lip seal provides good resistance to extreme vibration environments. It is, however, subject to damage and wear by accumulated contaminant particles. Piston ring seals are most resistant to oscillating pressure environments since they provide effective vibration damping. They, too, are sensitive to wear and leakage due to contaminant particles.

Labyrinth seals are not used as primary shaft seals in oxygen pumps because of the high leakage rates. This seal type is, however, often used to minimize backflow between inducer blading and pump housing. For long life seals and optimum compatibility, a back pressured purge at a controlled rate through the seal with helium or nitrogen warrants strong consideration in any oxidizer pump design.

6.1.3.2 Seal materials. - The most common nosepiece-runner materials for present generation oxygen turbopumps are graphitic (80 to 100 percent) carbon wear nose-

pieces riding on chromium-plated 4130 steel or annealed 440C stainless steel runners. Chrome plating has been shown to reduce the wear an order of magnitude. Also, 100 percent graphitic carbon has been shown to reduce wear significantly over amorphous carbon (ref. 113, p. 203). The influence of graphite content on seal wear and friction coefficient is shown in figure 6-11. The data for figure 6-11 were obtained by running carbon in sliding contact with chromium-plated 440C stainless steel in LOX at 2300 feet per minute (1000 g load with a 3/16-in. radius rider; ref. 113, p. 203). Experience with this seal combination in oxygen pumps is limited to pressures across the

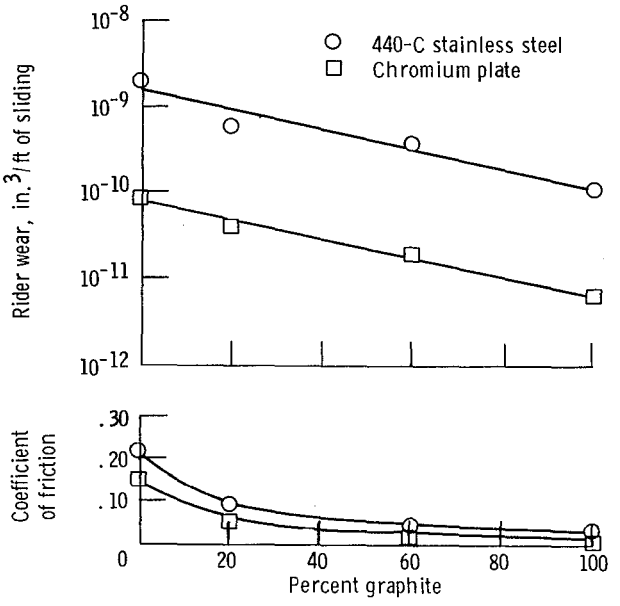

Figure 6-11. - Influence of graphite content on lubricating properties of carbon (based on ref. 113, fig. 2).

seal face of about 200 psi. If the trend toward higher pressures (and the higher pump rpm's) is considered, the continued use of carbon may be limited. Since higher pressure drops will require higher bearing forces between the graphite nosepiece and runner, the possibility exists that the ignition temperature of graphite in oxygen (about 450° C) may be reached if shaft speeds are increased over present practice.

Most failures to date have been due to cracking and breaking from thermal stress before reaching 450° C. Dense highly graphitic materials have the greatest resistance to ignition when compared to impregnated carbons. The use of impregnants must be verified by proof testing for chemical reactivity with oxygen under operating conditions (ref. 113, p. 207). The normally used materials for turbopump LOX seals are listed in table 6-IV.

Although the difference in wear rates between the various carbon face seals is

TABLE 6-IV. - LOX PUMP FACE SEAL MATERIALS

Component	Material
Nosepiece	Carbon P692, P5N, and 5AG
Runner surface coating	Chrome; tungsten chromium carbide
Runner base material	4130 steel; Inconel 750 and 1718; 440C stainless steel
Secondary seal:	
Lip seal	CTFE; Polyethylene terephthalate (Mylar)
Piston ring	CTFE; TFE
Bellows	Stainless steel 347; Inconel 750 and 718
Nosepiece base material and associated structural parts	Stainless steel 302, 303, 304, and 321; Inconel 750, 718, and 600; Invar 36; Carpenter 42
Insert adhesive (for attaching nosepiece)	Epon 901/B3; Teflon fusion

small, the best wear rates have been achieved with carbon P692. A generally preferred choice for the mating ring base material is 4130 steel (chrome plated) because of its higher thermal conductivity and lower cost. However, where pressure-velocity limits are approached (see sec. 6.1.3.3) and high temperatures and stresses are expected, Inconel 750 or Inconel 718 is preferred. These provide the higher strength and corrosion resistance for a more severe environment. The 440C stainless steel is also a suitable material. Tungsten chromium carbide (LW-5) was used in the development of the M-1 pump seal but the wear life was low (see table 6-V).

Invar 36 and Carpenter 42 have nearly the same expansion coefficient as carbon and are useful as nosepiece base materials in designs where expansion-contraction stresses would damage the carbon seal or its bond.

Of the two materials listed for bonding the carbon nosepiece to the metal base material, Epon 901/B3 is stronger but less compatible with oxygen than fused Teflon. Of the runner surface coating materials listed, chromium is the best material for wear characteristics and cost. To reduce the danger of carbon nosepiece ignition and to reduce wear rate for high pressure-velocity applications, seal combinations using aluminum oxide or calcium fluoride nosepieces operating on a nickel alloy runner have been used successfully in experimental pumps. The calcium fluoride - nickel combination also has worked well in high performance liquid fluorine pumps. Aluminum oxide, being brittle, must be properly supported on a metal substrate to avoid chipping. The use of carbon seals is discussed in reference 113. Aluminum oxide and calcium fluoride seals are covered in reference 114.

CTFE and Mylar are both used as secondary seal materials in operational pumps. Mylar is less resistant to ignition in oxygen then CTFE. Therefore, CTFE is preferable. TFE is also less likely to ignite than Mylar or other polymeric secondary seal

TABLE 6-V. - ROCKET ENGINE TURBOPUMP ROTATING SHAFT SEALS FOR LIQUID OXYGEN[a]

Program	Seal type	Materials				Seal diameter, in.	Fluid pressure, psig	Shaft speed, rpm	Rubbing speeds, ft/sec	Spring load, lb	Total load, lb	Unit load, psi	Pressure-velocity factor, (psi)(ft/sec)	Pressure balance ratio (b)	Wear life, hr	Dynamic leakage, standard ft^3/min
		Nose piece	Mating material	Secondary seal	Housing											
Thor	Fact contact welded bellows	Carbon P692	Chrome plated 4130	347 Stainless steel	304 Stainless steel	2.63	225	6 750	77	31	95	158	12.2×10^3	0.97	3	10
H-1	Face contact welded bellows	Carbon P692	Chrome plated 4130	Inconel 718	304 Stainless steel	2.63	200	6 800	78	82	106	176	13.7	.70	3	10
J-2	Face contact welded bellows	Carbon P5N	Chrome plated Inconel X	Inconel 718	321 Stainless steel	2.974	200	8 650	112	41	150	210	23.5	.85	2	15
J-25	Face contact welded bellows	Carbon P692	Chrome plated Inconel X	Inconel 718	321 Stainless steel	2.935	200	9 000	115	41	150	210	24	.85	2	15
M-1	Face contact welded bellows	Carbon P5N	LW5 (tungsten chromium carbide) on Inconel	Inconel 718	321 Stainless steel	6.902	450	4 000	120	20	471	196	23.5	.92	1.7	2.3
RL-10	Face contact welded bellows	Carbon 5AC	Chrome plated 5646 AMS	Inconel 750	5646 AMS	1.70	400	12 300	92	17	67	41	3.8	.05	---	----
F-1	Face contact lip seal (secondary)	Carbon P692	Chrome plated 4406	Mylar	303 Stainless steel	6.463	140	600	170	58	127	51	8.7	.7	3	25
Thor	Face contact lip seal (secondary)	Carbon P692	Chrome plated 4130	Kel-F	302 Stainless steel	2.65	225	6 800	78	32	82	120	10	.85	3	10
Atlas	Face contact lip seal (secondary)	Carbon P692	Chrome plated 4130	Kel-F	302 Stainless	2.63	250	10 000	115	32	86	137	15.8	.85	3	10

[a]Unpublished data obtained from Rocketdyne, Division of North American Rockwell, under NASA contract NAS3-13314.

[b]Pressure balance ratio = (closing area)/(face area).

materials, but its tendency toward cold flow and stress relaxation would require additional design innovations such as spring loading to maintain constant pressure.

The materials preferred for oxygen pump bellows seals are 347 stainless steel and Inconel. The 347 stainless steel is easy to weld and is preferable for lower pressures; where pressures (up to 500 psi) impose high stresses, Inconel 750 or 718 is used. Above 500 psi, piston ring seals are recommended.

6.1.3.3 Seal design factors. - Face contact seals have been used for oxygen pumps on the H-1, J-2, J-2S, M-1, and RL-10 engines. Seal pressures up to 500 psi were used and leakage ranged from 2.3 to 10 standard cubic feet per minute; wear life ranged from 1.7 to 3 hours with PV factors (pressure (lb/in.^{2}) $\times$ velocity (ft/sec)) up to 24 000. A state-of-the-art data summary is given in table 6-V. Seal life times of ground-based LOX pumps can be an order of magnitude greater than flight pumps since higher oxygen leakage rates are more acceptable and the designer has more flexibility for accommodation of oxygen leaks in ground-based systems.

6.1.3.3.1 *Leakage control and seal surface finish.* - Control of face contact seal leakage is achieved by carefully limiting surface waviness and roughness of nosepiece and runner. To compensate for waviness and roughness by increasing contact pressure to reduce leakage only increases the wear rate. Face seal mating surfaces are usually lapped flat to within 24 to 60 microinches in wave height; the resulting finish (surface roughness height) is approximately 10 to 20 microinches (ref. 115, p. 481). This surface finish appears to be optimum, and little or nothing is gained from a finer finish. According to references 51 (p. 6.4.3-2) and 115 (p. 481), an exceedingly smooth surface (in the range of 2 μin.) cannot support a lubricating film, and premature seal failure may occur. The lay on the mating surfaces for rotating shaft seals should be concentric circles across the seal face. As a general rule nonmetal seals (carbon or fluorocarbon polymer) will require a surface finish (roughness height) equal to 16 to 32 microinches.

6.1.3.3.2 *Seal rubbing speed, contact pressure, and wear.* - The allowable surface speed of contact seals is normally dictated by the amount of heat generation at the seal interface and the amount of cooling resulting from oxygen leakage and conduction through the structure. The temperature the seal may be allowed to attain is limited by thermal distortion, excessive wear rates, and the ignition temperature of the seal materials in oxygen. The heat generated at the seal mating surface is a direct function of the contact pressure, the coefficient of friction, and the velocity of the rubbing surfaces. Reference 116 presents a digital computer program which may be used to calculate temperature distribution in seal assemblies. These calculations are the first step in determining thermal deformation by means of the technique described in reference 117.

The face seal PV's (face pressure $\times$ velocity) for operational turbopumps are shown in table 6-V. The maximum recommended PV for a carbon seal in liquid oxygen for an expected life of 3 hours is 25 000 foot-pounds per second per square inch.

The current turbopump seal life is generally low (operating time, 2 to 3 hr) because of relatively high seal face unit loads required to meet leakage specifications. The average wear rate of the carbon nosepiece on the LOX side in the J-2 turbopump is approximately 0.010 inch per hour (unpublished data obtained from Rocketdyne, Division of North American Rockwell, under NASA contract NAS 3-13314). Allowance for high wear rate is provided by insuring that the nosepiece has sufficient height to wear away and continue to maintain seal capability during the operating life of the turbopump. Most wear and friction measurements with carbon material nosepieces indicate significantly higher wear rates and coefficients of friction during the initial seal "run-in period". During the "run-in period" a lubricating graphite film is transferred from the carbon nosepiece to the metal runner which reduces the friction and wear. The presence of stable, dense oxide film on a chromium-plated metal mating runner surface promotes adherence of the graphite transfer film.

6.1.3.3.3 *Shaft seal stability.* - Most LOX pump seals incorporate a bellows which allows the nosepiece to accommodate the face runout motions of the runner. The bellows-nosepiece combination, which constitutes a mass-spring system, is capable of vibrating in several modes, each with its characteristic natural frequency. To avoid seal leakage and rapid seal wear, resonant modes at shaft seal design speeds must be avoided. Bellows seal fatigue failures have been recorded less than 4.4 seconds after the onset of resonant vibrations (ref. 118, p. 7). If operation at or near resonance is unavoidable, vibration dampers are required. Vibration damping forces should be 5 to 10 percent of the seal spring (or bellows) load. Piston ring or lip seals used as secondary seals generally achieve enough damping forces. The subject of seal oscillations and methods for promoting seal stability are reviewed in references 112 (pp. 56 to 58 and 156) and 118.

6.1.3.3.4 *Contamination effect on seals.* - Foreign particle contamination can accumulate in the seal system cavities, and solid particle interference with sealing surfaces can cause abrasive wear of seal materials. The face contact bellows seals usually used in flight LOX turbopumps is the least sensitive to damage by particle contamination. The particles are generally too large to enter between the rubbing surfaces and usually there is very little if any damage due to seal face scoring. However, on a spring loaded face contact seal with a secondary lip seal (fig. 6-9) the tendency for particles to collect at the lip seal can cause erosive damage and excessive leakage of the lip seal. Hydrodynamic and self-energized hydrostatic type seals are also sensitive to abrasive wear from particle contamination. Particles tend to enter the face clearance gap and gouge or wear the seal face causing loss of life potential. System contamination limits specified for oxygen pump cryogenically cooled bearings (see sec. 6.1.2.2.1) also apply to face contact and lip seals for reliable operation. Contamination limits for seals are the same as those listed for oxygen cooled bearings.

6.2 POSITIVE DISPLACEMENT PUMPS

Single or multiple cylinder positive displacement pumps may be used to pump liquid oxygen to very high pressures (10 000 psi or greater). They have also been used to pump gaseous oxygen; but, because of compression heating they are generally limited to approximately a 1000 psi compression in this application. (See sec. 3.4.4 for adiabatic compression heating and secs. 3.4.1 and 3.4.2 for ignition temperatures of materials.)

The fundamental design considerations for piston pumps to be used for oxygen are the selection of materials that will function in the oxygen environment at operating conditions and the necessity of maintaining cleanliness to prevent component damage or ignition from contamination.

Positive displacement pumps are subject to most of the materials selection considerations as are centrifugal pumps. However, in centrifugal pump design, because of high speed operation, every effort is made to reduce or eliminate rubbing, while rubbing is inherent in piston-type pumps. The mitigating factor is that the rubbing in piston pumps is relatively low speed so that friction heating does not become a major problem. A schematic design drawing of a typical piston pump for liquid oxygen is shown in figure 6-12. A coolant jacketed version of the pump for gaseous oxygen compression is shown in figure 6-13 (ref. 119). In general, the pump will consist of a cylinder barrel and head, a piston with self-lubricating rings, inlet and outlet check valves, a screen filter, and a piston drive that may be any appropriate conventional power source.

The materials generally preferred for the piston pump components are given in table 6-VI.

The check valves for intake and exhaust are preferably all metal. For detailed valve design considerations see chapter 7.

Where vacuum pumps may be exposed to high concentrations of oxygen, the main concern is the possible reaction with pump lubricants.

This problem can be solved for most conventional vacuum pumps by proper cleaning and the substitution of the lubricant used to one that is resistant to oxygen. The preferred substitutes for the usual oils and greases used in vacuum pumps are one or more of the fluorocarbon lubricant oils or greases. Tricresylphosphate has also been used.

It is always good practice to review the materials used in the pump for general compatibility with oxygen and with moisture, as discussed in chapter 3.

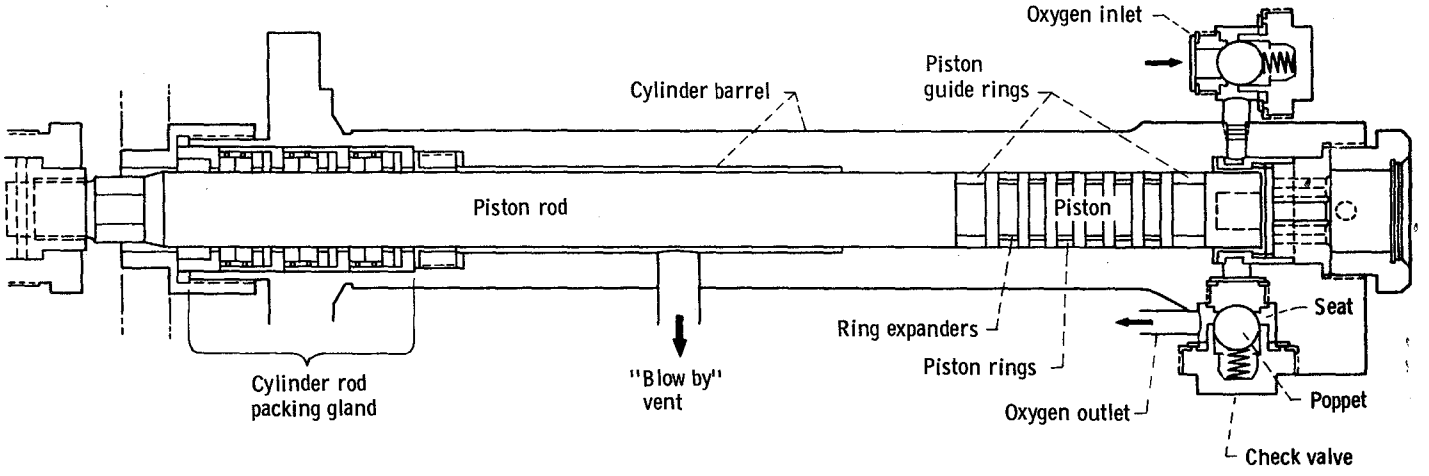

Figure 6-12. - Typical positive displacement piston pump for oxygen.

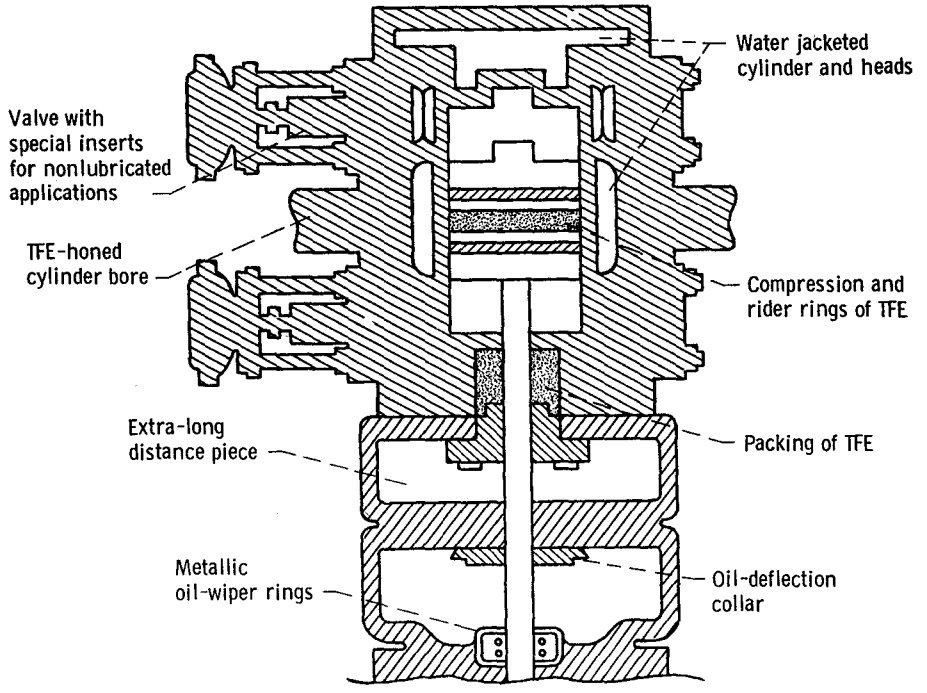

Figure 6-13. - Liquid cooled piston type oxygen compressor (ref. 119, p. 142).

TABLE 6-VI. - PREFERRED MATERIALS FOR PISTON

PUMP COMPONENTS FOR OXYGE USE

Component	Liquid oxygen	Gaseous
Cylinder and cylinder head	304 Stainless steel Monel	Cast iron 304 Stainless steel Monel
Gaskets and seals	Asbestos Copper Aluminum Glass-filled TFE CTFE Viton	Asbestos Copper Glass-filled TFE CTFE Viton
Piston	Brass	Brass
Piston rings	Glass-filled TFE Copper-filled TFE Lead-filled TFE	Glass-filled TFE Copper-filled TFE Lead-filled TFE
Piston rod packing	Asbestos TFE CTFE	Asbestos TFE CTFE

CHAPTER 7. VALVE ASSEMBLIES

The major problems with valves are their inherent tendency to leak, trap, and be affected by contaminants. Leakage through valve seats and through actuator seals is aggravated by wear, thermal cycling, erosive flow, water hammer, high pressures, and pressure spikes. The problem of sealing to prevent leakage through valve seats and valve element actuators (or valve stems) is one of the more challenging parts of fluid system design.

Valve assemblies incorporate nearly every type of seal - rotating shaft or sliding shaft seals, seals for many configurations of valve element - valve seat designs, and static seals. Since similar seals are required in many other fluid system components, the basic subject of sealing to prevent leakage is discussed separately in section 4.1 and considerations for seal design are discussed in chapter 9. However, a brief discussion of seals and sealing especially pertinent to valves is included in this chapter. In addition to leakage, many valve failures in liquid and gaseous oxygen systems are often due to the ignition of valve parts from collected contaminants or noncompatible material within the valve. This type of failure generally occurs at the instant that flow conditions begin when the valve is opened. Failures from overstress or abrasion and galling can also initiate a reaction with oxygen in addition to making the valve inoperative or causing leaks.

Most of the design requirements for valves for oxygen service are the same as those for other cryogenic liquid or ambient temperature gaseous systems. However, in oxygen service the consequences of a design weakness, a material incompatibility, or a contaminant can be more severe than for inert fluids or for most fuels.

Although valve design and material selection can increase contamination tolerance, contamination of any kind is still hazardous and recommended system cleanliness and oxygen purity must be maintained. Oxygen purity is discussed in chapter 2 and cleaning requirements are provided in section 4.5.

A review of valve design considerations is given in the following sections. High pressure requirements are emphasized because they serve best to illustrate the special considerations required for oxygen systems. The discussion is equally applicable to pressure and flow regulators, check valves, and relief valves since they all involve the regulation and control of fluids and they all use the same basic types of valving elements.

7.1 VALVE ELEMENT TYPES

Valve types are categorized by the manner in which they effect closure to flow or throttling. Figures 7-1 to 7-3 illustrate the three basic types of valves and valve elements: (1) rotating elements, (2) translational plug elements, and (3) gate elements.

The ball valve and the butterfly valve (fig. 7-1) are opened by rotating the valve element. The poppet or plug valve (fig. 7-2) simply closes an opening in the valve by a linear motion perpendicular to the seat. The gate or blade valve (fig. 7-3) closes much as a sliding door with the gate having a linear motion whereas the blade rotates into the closed position. The swing check valve (fig. 7-1) is a combination of the poppet and an offset butterfly element.

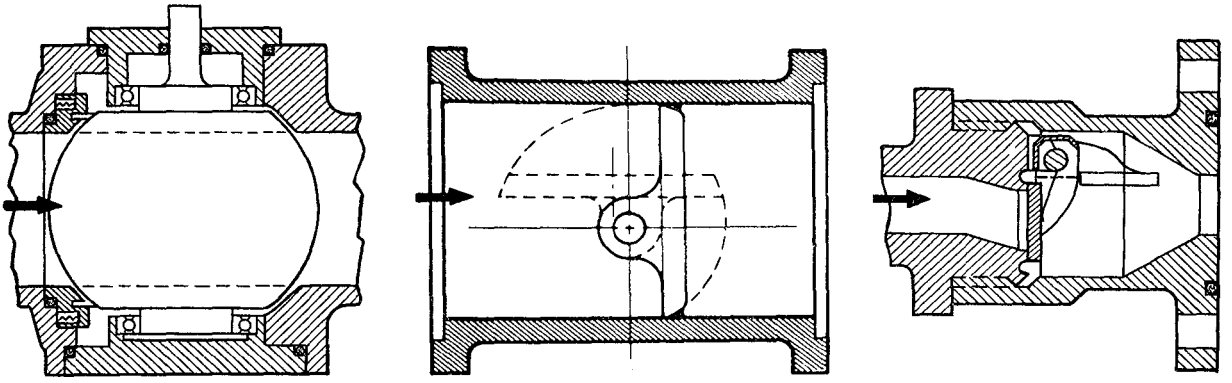

(a) Rotating ball. (b) Butterfly. (c) Swing check.

Figure 7-1. - Rotating element valves.

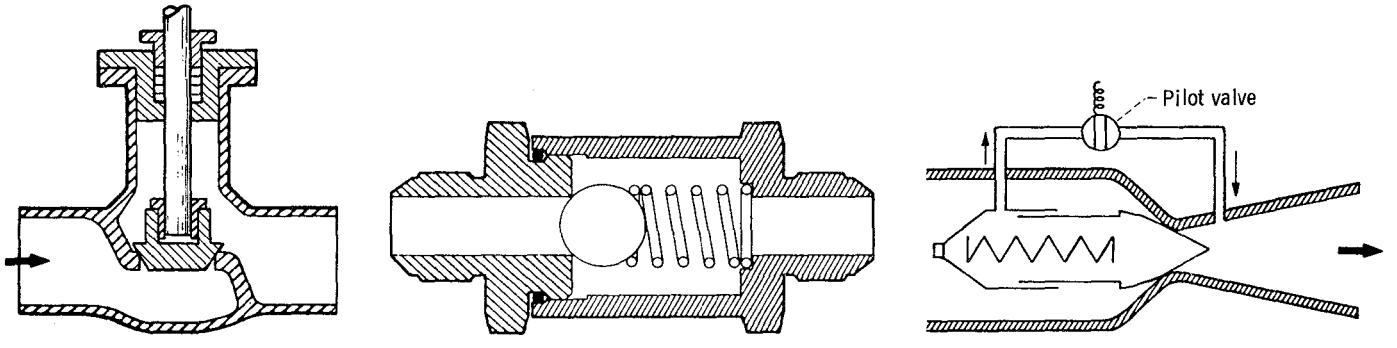

(a) Globe plug. (b) Ball check. (c) Venturi.

Figure 7-2. - Translational plug element valves.

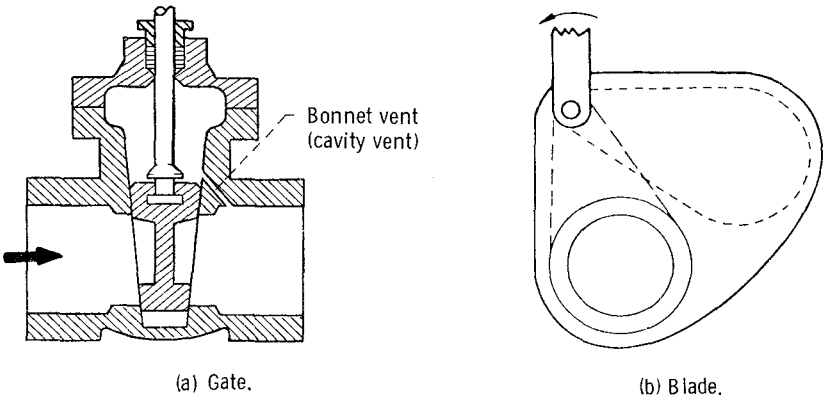

(a) Gate. (b) Blade.

Figure 7-3. - Gate element valves.

7.2 GENERAL DESIGN CRITERIA

Valves create a discontinuity in the flow line both fluid dynamically and structurally. The flow passage in many valve designs incorporate recesses, pockets, and crevices to accommodate the valve element actuating mechanism and the valve element supporting structure. Some valve designs require a cavity for the valve element to retract into when it is opened (fig. 7-3(a)). These valve mechanisms and the accommodations for them cause stagnation zones where particulate matter may accumulate and create a hazard in oxygen systems. Also, in liquid systems, the element may trap liquid in a closed cavity; unless the cavity is vented, an overpressure condition is created when the liquid vaporizes. Where they cannot be completely avoided, pockets and connecting passages should be designed to be self-cleaning by means of controlled fluid flow through the cavity. However, this criteria to avoid accumulation of contamination by means of a self-cleaning feature rather than by avoiding the cavity can increase pressure losses in the valve. By compromising a smooth fluid dynamic flow passage, turbulent flow can cause cavitation at high flow velocities. At extreme pressures and high flow velocities, such as very high pressure throttle valves, there is a possibility of erosive effects and possible ignition of nonmetal materials if contaminants or particulate matter are present. Therefore, the primary design criteria is to avoid valve design features that create stagnation zones or crevices where particulate matter can accumulate.

Engineering trade-offs to take advantage of available shelf hardware or low cost fabrication must be evaluated for each specific application. Most commercial valves were not designed for oxygen. However, they may be adapted for oxygen service by modifying some of the materials used in their components. An engineering valve design and selection trade study illustrating the factors which must be considered is discussed in reference 120 (pp. 5-46). Because of the thorough discussion contained in this study, no detailed discussion of valve selection is included here. However, considerations

such as material selection, valve life, and internal leakage are reviewed.

To achieve the minimum leakage possible in valves, the valve closure contacting surfaces must meet the basic design criteria for sealing discussed in section 4.1 and chapter 9. To maintain this capability, the design must incorporate features to minimize wear or distortion of the closure contacting surfaces.

7.3 MATERIALS SELECTION

Important considerations for valves for nonflight use are long life, high reliability, low component cost, and low maintenance cost. Since weight is no problem, a wide range of materials may be used because more massive parts can compensate for lower material strength. For flight valves, maximum reliability and low weight are the major design considerations. Weight and strength requirements restrict materials selection.

For higher pressures (3000 to 10 000+ psi) material selection is further reduced to those materials compatible with the severe dynamic conditions of abrasion, impact, and cavitation which cause surface damage, erosion, and the possible ignition of sensitive materials. Therefore, for very high pressures, the strength and compatibility of materials take precedence over low weight for flight hardware and low cost in ground hardware. High pressure service requires the same care in material selection and valve design for either ground or flight systems. The supporting data and detailed information for strength of materials are given in references 20, 69, and 121. Materials compatibility with oxygen is discussed in chapter 3 (see also refs. 23 and 37, pp. 140 to 148).

A list of materials that have been used for oxygen valves in major rocket engine propellant systems is given in table 7-I. It should be noted in table 7-I that Mylar has been used successfully as a secondary seal material in several operational valves even though it has been shown to react with oxygen in the NASA standard impact apparatus. Therefore, its use elsewhere in the valve or in valves of different design operating above 1500 psi should be reviewed carefully and validated by tests which cover all possible service conditions.

For very high and ultrahigh pressures (over 7500 psi), the preferred materials are metals and alloys which have high melting points, high ignition temperatures, a relatively high thermal conductivity, and a low heat of reaction with oxygen (see sec. 3.4). Copper, brass, Monel, 17-7 and 17-4 PH steels, 400 and 300 series stainless steel, and Hastelloy, in this approximate order, best meet these requirements. Aluminum and its alloys may be used, but caution should be exercised when using aluminum in gaseous oxygen in the very high pressure range (>7500 psia) because of its low melting point and very high heat of reaction. Therefore, Monel for strength requirements and

TABLE 7-I. - OXYGEN VALVE MATERIALS FOR ROCKET SYSTEMS

Vehicle and engine	Valve application	Fluid media	Valve element	Valve element material	Seal or seat material	Valve housing material	Dynamic seal type	Secondary seal material	Line size, in.	Operating pressure, psi	Flow rate, lb/sec	Actuator type	Response time, msec
Atlas MA-5	Booster main oxidizer value	LO_2	Butterfly	7075-T6 forging	CTFE	TENS-50 aluminum	Lip seal	Mylar[a]	4.0	782	424.5	Pneumatic piston	400
	Sustainer gas generator	LO_2	Blade	17-7 CRES	CTFE	356-T6 permanent mold casting	Face seal	Kel-F	.75	570	7.27	Pneumatic piston	100
	Vernier propellant valve	LOX	Poppet	2024-T4	CTFE	7075-T6	Lip seal	Kel-F	------	----	-------	---------	----
Saturn S-IB H-1	Main oxidizer value	LO_2	Butterfly	431 CRES	CTFE	356-T6 permanent mold casting	Lip seal	Mylar[a]	4.00	975	545	Hydraulic piston	333
	Gas generator (oxidizer)	LO_2	Poppet	A-286 CRES	FEP Teflon	347 CRES	Bellows	A286 CRES	.609	940	-------	Hydraulic piston	----
Saturn S-IC	Main oxidizer	LO_2	Poppet	6061-T6 aluminum forging	TFE Teflon	6151-T6 aluminum forging	Vented redundant lip seals	Mylar[a]	8.0	1600	2000	Hydraulic piston	600
F-1	Gas generator	LO_2	Ball	Two piece welded A-286	CTFE	7075-T73 die forging/TENS-50 permanent mold casting	Vented redundent lip seals	Kel-F	1.5	1600	121.5	Hydraulic piston	----
	Oxidizer prevalve	LO_2	Ball (visor)	----------	----------	----------	----------	----------	17.0	115	3970	Pneumatic piston	500
Saturn S-II	Main oxidizer valve	LO_2	Butterfly	431 CRES	CTFE	TENS-50 permanent mold casting	Lip seal	Mylar[a]	4.0	911	386	Pneumatic piston	50
	Gas generator (oxidizer)	LO_2	Poppet	A-286	FEP Teflon	6061-T6	Bellows	A-286	.531	1010	3.29	Pneumatic bellows	30
	Propellant utilization	LO_2	Rotating sleeve	440C	None	TENS-50 aluminum casting	Lip seal	Mylar[a]	2.0	1310	1 to 120	Electric motor	Throttling
	Prevalve	LO_2	Butterfly	A-286	CTFE	6061-T6	V-Seal	Teflon-coated Inconel X750	8.0	132	386	Pneumatic bellows	1000
	Propellant tank vent and relief	GO_2	Poppet	7075-T73	CTFE	356-T6	RACO and flat gaskets	Teflon with CRES and Kel-F and Mylar[a]	------	----	-------	---------	----

[a]Mylar generally not recommented for use in liquid oxygen valve seals because it has produced positive reactions in LOX impact sensitivity tests at high impact energy levels.

copper or brass for nonstructural requirements would provide the greatest resistance to ignition at high pressures and temperatures.

7.4 VALVE LIFE

Valve life is determined largely by the wear rate of the moving parts and the contacting surfaces. Valve element, valve seat, and actuator guide and seal wear can affect both external and internal leakage rates. Changes in the surface finish and shape of the valve element - valve seat interface from excessive closure forces can raise the leakage rate and increase the actuation force required to seal above acceptable limits. Useful valve life is achieved by careful specification of the valve element - valve seat materials, their surface finish, contact load, and by preventing relative motion as contact is made or broken. The easiest way to achieve a low leakage of "zero" leakage valve seal is to use a nonmetal seat or insert. This is also the lowest cost approach. All-metal valve elements including the seat can achieve the same leakage specifications but with less reliability and at greater cost. However, nonmetals become increasingly sensitive to erosion and particle impingement at higher oxygen pressures, especially with gaseous oxygen at room temperatures and above. Therefore, as pressures and/or temperatures are increased, material selection becomes more restricted and all-metal components are ultimately required. Limits of materials compatibility and materials selection criteria are given in chapter 3.

7.5 INTERNAL LEAKAGE

Sealing to prevent internal leakage is the most difficult part of valve design. A discussion of leakage through seals is presented in section 4.1. Sealing to prevent leakage and leakage flow tests are discussed in reference 122 (pp. 407 to 418). Considerations for sealing interface design are reviewed in chapter 9. "Zero" leakage as defined in section 4.1 is possible with both metallic and nonmetallic seats. However, the metallic valve element - valve seat is more easily damaged by solid particles trapped on the mating surfaces and from wear and plastic deformation during valve closure than the more compliant nonmetallic element seat. Increased leakage is a consequence of such surface damage. Specifications for permissible valve element - valve seat leak rates are a compromise between cost and performance requirements. Typical leak rates are listed in table 7-II (ref. 123).

TABLE 7-II. - ROCKET ENGINE LEAK RATES IN OPERATIONAL VALVES[a]

Engine system	Valve type and location	Service fluid	Seal type and material	Sealing diameter, in.	Leak test pressure, psig	Leakage, standard $in.^3/min$	Leakage, standard $in.^3/min$ per in. of seal
F-1	Poppet main oxidizer	LO_2	Captured Teflon poppet nose seal	8	80	$56GN_2$	2+
J-2	Butterfly main oxidizer valve		Kel-F lip seal	4	500	5He	.4
J-2S	Butterfly main oxidizer valve		Kel-F lip seal	4	500	3He	.25
S-11	Butterfly prevalve		Kel-F lip seal	8	50	450He	<20
MA-5	Blade gas generator		Machined Kel-F ring	1	500	$10GN_2$	3+

[a]Ref. 123, p. 18.

7.5.1 Metallic Seats

Metal seats are generally preferred for very high pressure applications because they are more resistant to damage from pressure stresses and erosive flow. Generally, the valve element in the plug or poppet-type valves is of a harder material than the seat material to prevent galling and contact surface deterioration from the stress of open-close cycling. But this is not critical when the contacting surfaces are not caused to rub or slide under pressure during closure and where closure pressure is within the elastic limit of the valve element - valve seat combination.

The design objective in metal-to-metal valve element - valve seat surfaces is complete contact between the surfaces since effective valve closure depends on close conformity of the mating seat and element surfaces. This is difficult to achieve, even with optically flat surfaces and assuming perfect alinement because of the surface asperities. Ideally, the height of these asperities is limited so that the local deformation required to seal is within the elastic limit of the seat-element materials, and work hardening of the contacting surfaces is minimized.

The real area of a surface may be many times greater than its apparent or projected area depending on the surface finish. The surfaces obtained by polishing and rolling are only slightly greater than their projected areas; a roughed surface from an abrasion process may have a total area three times its projected area (ref. 122, pp. 20 to 29). Even with relatively smooth polished surfaces the asperities prevent 100 percent surface contact. If sufficient pressure is applied to achieve 100 percent surface contact, the asperities are literally mashed beyond the elastic limit and work hardening and galling of the surface results.

The leakage paths are minimized by providing a valve element - valve seat contact surface finished with asperity heights small enough (less than 4 μin. rms) to prevent sig-

nificant localized work hardening. Average machine-finished surfaces have asperity heights of about 125 microinches rms. Metal-to-metal valve plug - valve seat combinations are usually finished to about 16 microinches by lapping the components together. But for high pressure, low leakage, multicycle operations a special care in lapping is taken to achieve surface finishes of 2 to 4 microinches. With additional effort, asperity heights between 1 and 2 microinches can be achieved using a diamond grinding and polishing compound of appropriate grade (ref. 122, p. 40). Even with the proper surface finish good seat life requires careful specifications of maximum seat closing forces to avoid surface damage. The valve element should contact the seat without friction to minimize wear and abrasion, and the quantity and size of particulate material in the oxygen must be controlled. Oxygen purity is discussed in section 2.3 and filtration is discussed in section 7.8 and chapter 10.

7.5.2 Nonmetal Seats

Polymeric valve seat materials are not specifically recommended for pressures above 2000 psi or flow velocities above 500 to 700 kilometers per hour (455 to 638 ft/sec) (see sec. 4.2). However, with proper protection, if the seat material is recessed in a high thermal conductivity metal, polymeric materials may be used after proof tests substantiate the design. This technique reduces the possibility of ignition and prevents "cold-flow" relaxation of the seat. This design technique was used successfully and confirmed in tests with liquid fluorine (ref. 37, p. 142). Nonmetal materials are particularly sensitive to the conditions associated with fluid flow at high pressures and flow velocities (i.e., particle impact, erosion, friction, and shock waves) because of their generally low ignition temperatures and low thermal conductivities.

While several nonmetallic materials have been used successfully in liquid and gaseous oxygen systems, tetrafluoroethylene (TFE), fluorinated ethylenepropylene copolymer (FEP), and chlorotrifluoroethylene (CTFE) filled with glass or metal fibers are preferred for most applications. For oxygen systems at pressures above 2000 psi, such nonmetallic seats should be qualified by proof tests which simulate the use cycle and environment (see ch. 3).

7.6 VALVE ELEMENT ACTUATOR SEALS

Schematic examples of dynamic seal designs generally used for oxygen valve stems and valve actuators are shown in figure 7-4 and in figure 9-1 in the chapter on seals.

In high pressure systems, oxidizer leakage through valve stem packing can be a problem; if leakage gets started, leak erosion enlarges the leak channel with a possibil-

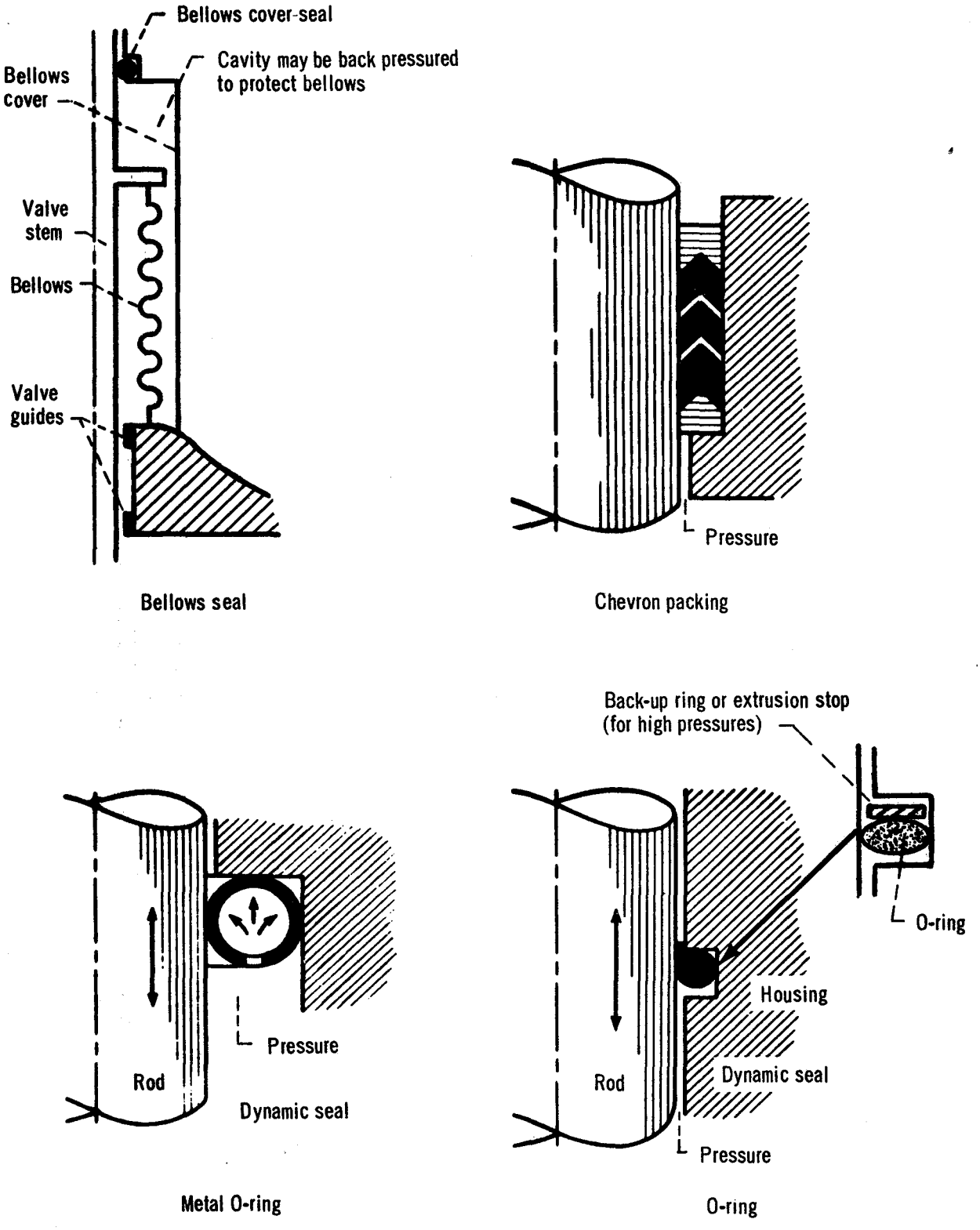

Figure 7-4. - Dynamic seals.

ity of igniting the seal material. To prevent valve packing leaks, frequent servicing and retightening are required. This is especially important for cryogenic valves because of thermal cycling effects. A spring loaded packing gland may be used to accommodate shrinkage and packing wear. A good valve stem packing is self-lubricating and wear resistant. The wear rate may be reduced by selecting packing with a low friction coefficient acting with a polished valve stem. The surface polish on the stem should be at least 8 to 10 microinches (ref. 70, p. 290). Stainless steel stems and Chevron or O-ring packing of tetrafluoroethylene (TFE) and chlorotrifluorethylene (CTFE) are preferred. For very high pressures dual or stepdown seals may be used. Silicone rubber does not pass the NASA standard impact test for ignition but has been used successfully in valves as a dynamic seal at pressures up to 7500 psia in the Apollo Personnel Life Support System. The Viton O-ring originally used failed because of oxygen absorption when exposed to 7500 psia oxygen pressure in the regulator valve. When the system was depressurized, the material fractured from the pressure of the absorbed gas (ref. 124). Section 9.3.3 discusses the qualification of silicone rubber for use in high pressure oxygen systems.

Bellows seals or diaphragms may be used for valve dynamic seals to achieve "zero" leakage. However, these present problems of fatigue cracking, accidental overpressure failure, differential pressure limits, and corrosion. Corrosion problems and prevention criteria are discussed in section 3.2. Internal corrosion can be prevented by maintaining dew point limits in the system and in any pressurant gas which contacts the bellows to -50° F or less.

Sliding surfaces in valves and regulators including dynamic O-ring seals and some valve stem packing may require a lubricant to reduce the breakout and running friction. The lubricant must be effective over the operating temperature range and be compatible with liquid or gaseous oxygen. The TFE lubricants or CTFE grease or oil (sparingly used) are preferred.

7.7 EROSION

In addition to entrained particulate erosion, erosion by cavitation may occur in valves handling liquid oxygen at very high pressures whose downstream static pressure is close to its vapor pressure. Very high pressure drops and the associated acceleration of the liquid over the valve element - valve seat surfaces or through packing leaks may cause erosion that can limit the seat-plug life or destroy an actuator seal (see sec. 4.2). The erosion rate increases with pressure at which cavitation occurs because of the increased driving force. Valve element - valve seat contours which avoid abrupt changes in flow direction are less subject to erosion damage. Erosive effects are most severe on lips and sharp edges exposed to the flow or on a static seal that begins to

leak. In addition to producing surface damage, high flow velocities have caused ignition of nonmetallic materials and all metal high pressure flange seals. The probability of ignition can be expected to increase with pressure because the apparent ignition temperature is reduced and because of the effect of flow on ignition of materials noted previously.

7.8 FILTRATION REQUIREMENTS

In very high pressure oxygen systems where near zero leakage is desired and where all-metal valve elements are used, filtration should remove particles within one or two orders of magnitude of the roughness of the valve seat interface surfaces to prevent seal deterioration. Additionally, valve stem guides, sleeve valve elements, butterfly lip seals, and ball valve seals are examples of valve components that are sensitive to solid particle contamination because of the close clearances. If solid particles become trapped, valve malfunction may result. Reference 123 (p. 94) records the case of a sticking poppet valve on a reaction control system engine. The poppet valve guide-stem clearance was 0.002 to 0.003 inch (2000 to 3000 μin.) and filtration was provided to remove particles down to 10 to 25 microns (400 to 1000 μin.). However, valve sticking continued until the poppet guide-stem clearance was increased to 0.008 inch (8000 μin.). Therefore, for this case, particles had to be removed that exceeded approximately one-eighth the clearance gap. If 10 percent is used as a nominal requirement, the original 0.003 inch clearance would have required filtration down to 300-microinch particles.

This example suggests that the established practices of filtering particles equal to or larger than the operating clearances in the valve are inadequate. While it is unsound to generalize from a single case, it is suggested that system cleaning and oxygen filtration of particle sizes no larger than 10 percent of the operating clearance may serve as an interim guide for systems where clearance clogging or possible binding from particulates could occur (see ch. 10). In most cases where motion exists between surfaces of close clearances, forces are such that particles would not bind the mechanism nor permit accumulation. However, the particulates would tend to increase the wear rate of the contacting surfaces.

Page intentionally left blank

CHAPTER 8. LINES, CONNECTORS, JOINTS, AND FITTINGS

Lines, tubing, pipes, ducting, and their associated hardware are subject to two conditions or circumstances that are of special concern in oxygen systems: unaccounted for overstress and high velocity flow of gaseous oxygen. Their length to diameter ratio allows very high leverage for excessive bending stresses in addition to stresses from internal pressure, thermal expansion-contraction, water-hammer, and cyclic stresses from vibration or chugging. Lines are often assembled without regard to slight misalinements (because it is so easy to do), and a prestress results which is additive to the working stress. These stresses are generally concentrated at a discontinuity such as a weld joint, connector, valve, elbow, or material flaw.

Sonic flow of gaseous oxygen in lines can impale entrained solid particles into an elbow or flow system component with sufficient energy to cause erosion or even ignition in sensitive materials.

This section is a review of the factors that should be taken into account to help assure a reliable oxygen transport system for liquid and gaseous oxygen for all possible pressures.

8.1 ALLOWABLE WORKING PRESSURE

The allowable working pressure for piping and tubing for ground-based systems is established in accordance with ANSI piping code for pressure piping (refs. 125, pp. 11 to 21, and 126, pp. 6 to 25).

For flight weight systems, the calculation of allowable stress is based on the material property and the required safety factor for each specific application. The structural integrity of the lines should be demonstrated by test as early in the prototype phase as possible. Recommended test practices are the following:

1. Subject the line to hydrostatic stress levels 1.25 to 1.5 times the maximum expected operating levels for proof testing and 2.5 times maximum operating levels for burst testing.

2. When thermal gradient tests or tests at operating temperatures are inconvenient, simulation of these stress levels or reduction in material strength should be accounted

for by additional pressure or loads at ambient temperature.

3. Vibration testing should be performed with the duct flowing the operating fluid at the maximum operating condition whenever possible to account for fluid mass and possible coupling of flow-induced and mechanical vibration.

Piping used to contain high pressure oxygen (over 2000 psia) should be X-rayed and visually inspected for imperfections. Unacceptable flaws should be cut out of the raw stock before fabrication processes. (Unacceptable flaws are discussed in sec. 5.1.5.)

8.2 MATERIAL SELECTION

Materials for pipe, tubing, or ducting for liquid oxygen systems are selected to meet the chemical compatibility requirements of the use environment as well as the required structural ductility and notch sensitivity characteristics at cryogenic temperatures.

Examples of preferred materials, based on the preceding criteria, and general experience for oxygen plumbing systems are presented in table 8-I for a range of pressures and temperatures.

TABLE 8-I. - MATERIALS FOR LINES FOR OXYGEN SYSTEMS

Material	Remarks
Aluminum 1114, 2024-0, 3003, 5052-0, 6061-0, 6061-T6, 6061-T4	Aluminum alloys used mainly as tubing with tube connectors; pressure limits determined by type of connector; not recommended for very high pressures (over 7500 psi)
Monel 400, K500	Tubing and pipe stock good for very high pressures and welded connections
Inconel 600, 718	Tubing and pipe stock good for very high pressures and welded connections
Stainless steel 304, 316, 317, 321, 347 Some 400 series stainless AM-350	Tubing and pipe stock good for very high pressures and welded connections
Rene 41	Tubing and pipe stock good for very high pressures and welded connections
Carbon steel	Welded joints or other; not usable below -30° F
Copper, copper alloys	Brazed joints or tube fitting connectors; not recommended for very high pressures

8.3 FLEXIBLE HOSE

For flexible hose requirements, wire reinforced stainless steel corrugated sections are generally used. Flexible metal ducting up to 18 inches in diameter is available for cryogenic liquid up to several atmospheres. The pressure drop through convoluted flexible tubing can be 10 to 15 times the pressure losses of straight wall tubing which suggests minimal use. Nonmetal materials are not generally used since they do not meet the flexibility requirements for use with low temperature gaseous or liquid oxygen. The brittle point of most oxygen compatible polymeric materials is above the temperature of liquid oxygen (-297° F). The TFE, CTFE, and FEP fluorocarbon polymers have brittle points lower than liquid oxygen temperature and could be used as a liner for flexible hose with liquid oxygen. However, this is not recommended because of the reduced cycle life at these temperatures. Brittleness temperatures are generally determined by impact tests (ASTM-D746-72, ref. 127, pp. 253-259). (The brittleness temperature limits are not the same as bending limits; some degree of bending can be tolerated at temperatures below the measured brittle point.) However, the brittle temperature may be used as a guide to determine the low temperature use limit of oxygen compatible polymer tubing or tubing liners for special test or laboratory applications. The brittle temperature of selected oxygen compatible polymers is presented in table 8-II.

For practical applications, the polymer lined flexible hose should be limited to ambient indoor and outdoor temperatures. Where cycle life is important, it should be predetermined by test.

TABLE 8-II. - BRITTLE POINT TEMPERATURES OF SELECTED POLYMERS[a]

Material	Brittle point temperature, °F
TFE	-420
FEP	-420
CTFE	-400
Silicone rubber	-90 to -200
Fluorosilicone rubber	-90
Polyvinylidene fluoride	-80
Vinylidene fluoride - hexafluoropropylene (Viton and Fluorel)	+10 to -60

[a]Ref. 51, pp. 12.3.2-2 and 3.

8.4 BELLOWS

Where flexible sections are necessary, bellows with conventional convoluted shape are recommended for liquid oxygen use. The convolution height, width, and shape may be varied to achieve the desired strength and flexibility. Welded bellows are more prone to overpressure damage and early fatigue failure than formed bellows, and they are generally more difficult to clean and keep clean. However, when greater flexibility is required in applications such as centrifugal pump secondary seals, welded spring bellows may be preferred (see table 6-V). An analysis of past fatigue failures indicates that mechanical and/or flow induced vibrations have caused cracking. Overdeflection due to mishandling has also contributed to some failures. Minor flaws have a tendency to propagate rapidly unless low magnitude stresses are maintained. Mechanical restraint linkage must be used to limit overflexure of the bellows beyond acceptable stress limits.

Dents, nicks, and scratches in the most highly stressed area of the bellows (the convolution crown) due to abusive handling during fabrication, shipment, or installation have also been a major contributor to bellows failures. The only solution to this problem is care in handling and suitable inspection to ensure quality control. Since excessive internal or external pressure causes buckling or buckling instability of the bellows, the design must permit the maximum surge pressure with the bellows in any operating position without exceeding the total stress limitations. Design criteria and sample calculations for bellows ducting and bulging stress limit calculations are provided in reference 70 (pp. 374 to 379).

8.4.1 Flow Induced Vibration Failures

Self-induced oscillation or vibration of bellows sections (or flexible lines) can occur at certain pressure - flow velocity combinations. Pressure variations of the fluid flowing over the convolutions at a given velocity can become resonant with the natural frequency of the bellows section and cause oscillations that result in cycle fatigue and cracking of the bellows.

An analytical method for determining the susceptibility of a bellows to flow induced vibration is given in references 128 to 130 (pp. 25 to 49). The observed frequency varies directly as a function of the fluid velocity and inversely with twice the bellows pitch distance. Preventing the impingement of the flow stream on the convolutions by using an internal sleeve has been used to prevent flow induced vibration. However, the installation of the sleeve presents complications in the design and fabrication and makes cleaning the duct for oxygen use more difficult. Damping devices such as external sleeves or travel limit braces can also prevent damaging oscillation.

8.4.2 Bellows to Duct Attachment

Wherever practical, the bellows to duct joint should be a full penetration V-notch butt-weld. If this is impractical, the design alternate should have all overlaps and crevices welded closed (see sec. 8.6.1).

A doubler contoured to fit snugly against the end convolution (fig. 8-1) is also an acceptable design; however, the convolution is partially inactivated, thus applying increased strain into the remaining convolutions.

If the end of the doubler is permitted to touch the convolution, a stress riser can be created when bellows are deflected or subjected to a vibration environment, which can promote early fatigue failure. A clearance of at least 0.05 inch is recommended as shown in figure 8-2.

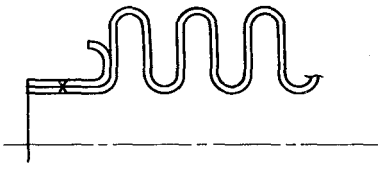

Figure 8-1. - Welding neck doublers.

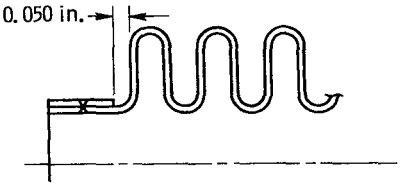

Figure 8-2. - Doubler clearance requirements.

8.4.3 Bellows Materials

Bellows materials suitable for oxygen use are given in table 8-III (refs. 70 and 131). The materials listed are primarily for formed bellows. Materials used most for

TABLE 8-III. - BELLOWS MATERIAL FOR OXYGEN USE[a]

Metal	Metal
304 Stainless steel	Aluminum 6061-T6
301 Stainless steel	Aluminum 7075
347 Stainless steel	Beryllium copper
A-286	Nonmetal[b]
Inconel 718	
Inconel X	TFE
Hastelloy-C	CTFE

[a]Refs. 70 (p. 376) and 131 (p. 46).
[b]Ambient temperature.

TABLE 8-IV. - ALLOWABLE STRESS FOR BELLOWS MATERIALS

Bellows materials	Operating temperature, °F	Estimated stress for failure in 106 cycles, psi	Suggested design values, psi
CRES 321	70	45 000	22 500
	-320	88 000	44 000
	-420	98 000	49 000
	400	40 000	20 000
Hastelloy-C	800	50 000	25 000
Inconel 718	70	55 500	27 750
	-320	65 400	32 800

electrodeposited bellows are nickel and copper.

Suggested design values of allowable stress are tabulated in table 8-IV for some of the common bellows materials. These suggested design values have been tabulated for a bellows life of 10^6 cycles. A life of 10^6 cycles was chosen because the S-N (stress-number of cycles) curves for most materials are relatively flat for greater than 10^6 cycles.

8.5 COUPLINGS AND FITTINGS

There are a multitude of coupling and threaded connector configurations available from many manufacturers incorporating various seal designs. In order to simplify the discussion of these components, this section is limited as much as possible to the coupling configuration, and the discussion of the seal design is covered in chapter 9.

8.5.1 AN, MS, and MC Couplings

The AN (Air Force/Navy Aeronautical), MS (Military Standard), and MC (NASA Marshall Center) connectors are the commonly used flared tube connectors which can be made to government or industry specifications. These connectors are basically the same except for their sealing interface specifications. The general configuration of these connectors is shown in figure 8-3.

The MS (Military Standard) version of the coupling has a 32-microinch finish on the 37° conical sealing surface.

The NASA Marshall Center (MC) connector (ref. 132, p. 5) has the following:

(1) Conical sealing surfaces are controlled to 8 microinch (rms) profile for steel and 16 microinch (rms) profile for aluminum.

(2) Sealing surfaces are round within 0.003 inch with maximum deviation of 0.0001 in any 60° arc.

(3) Concentricity of sealing surfaces are within 0.003 inch total indicator reading (TIR).

Standard AN's are excellent for low pressure requirements; for higher pressures, up to 3000 psia for larger sizes and 7500 psia for smaller sizes, the addition of conical seals are recommended (fig. 8-4). At the higher pressures, the possibility of coupling failure exists because of the tube slipping out of the fitting. This is more prevalent with aluminum or copper alloy fittings than with steel. A "rule of thumb" has evolved that recommends using these types of couplings be limited to 2 inches in diameter for steel tubing and 3/4 inch for aluminum or copper tubing at pressures in the range of 1500 psia. However, this is not a valid limitation because of the many variables in coupling designs.

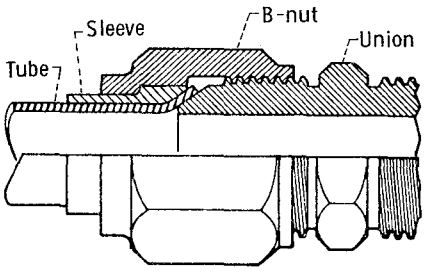

Figure 8-3. - AN, MS, and MC couplings. Materials available in 300 series stainless steel, 2024T-6 aluminum, and brass; seamless tubing preferred above 2000 psi.

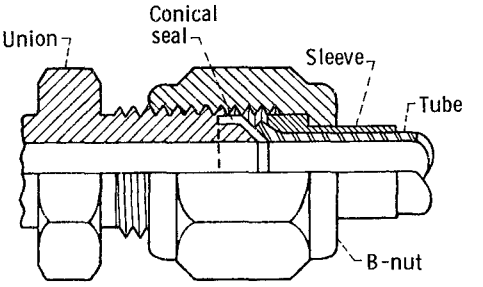

Figure 8-4. - Standard Air Force/Navy Aeronautical (AN) connector with metal conical seal. Materials available in 300 series stainless steel, 2024T-6 aluminum and brass; conical seal material - nickel, 6061-T4, 6061-T6, 6061-0, aluminum, or soft copper.

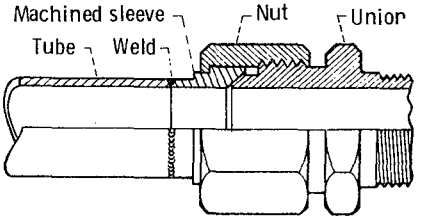

Figure 8-5. - Machined sleeve coupling.

But, greater care must be taken to effect a tight seal as the diameter is increased because of the longer seal interface and the increase in the possible leak paths. It is recommended that couplings for oxygen service meet a proof pressure test of 1.5 times the maximum expected working pressure. A better flared coupling is the machined flare where the flare and the ferrule, or sleeve, is one machined part (fig. 8-5); however, the tube must be welded to the fitting.

Threaded couplings for use in oxygen systems should be designed so that the threaded nuts, sleeves, and collars which provide the compression force may be lubricated without any portion of the seal interface being contaminated with lubricant; that is, the parts that effect the seal should not require lubricant for proper torque. Torque should always be specified for flight systems and for all high pressure systems. When torque values are specified, the specification should indicate whether or not a lubricant should be used. Preferred lubricants for oxygen systems are fluorocarbon polymers (solids, liquids, or grease) or molybdenum disulfide.

Thermal distortion of the connector will occur when the flow of liquid oxygen begins and ends. Repeated cycling of such distortion can cause sealing pressure relaxation and increase the leakage rate. An example of the magnitude of the relaxation that can occur during thermal cycling is shown in figure 8-6 (ref. 133). Examples of the increase in leakage rate with temperature cycles between 200° and -320° F are presented in reference 133 (pp. 243 to 246). To avoid such leaks, retorquing should be part of the stand-

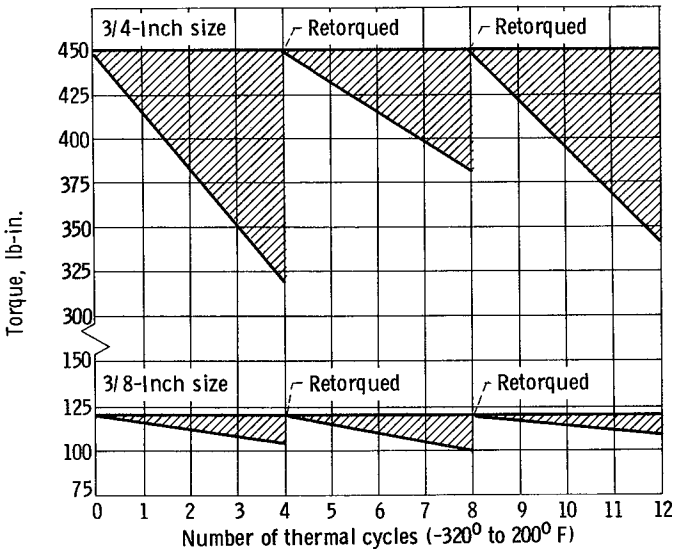

Figure 8-6. - Pressure relaxation from thermal cycling (ref. 133, p. 248). Tubing connectors (lubricated), 3/4 and 3/8 inch.

ard operating procedures for systems whose connectors are subjected to such temperature cycling.

Connector life and leakage rate are affected by the number of assembly-disassembly cycles, since each cycle may damage the surface finish. Also, as shown by the experimental data in reference 133 (pp. 252 to 259), the sensitivity of a fitting to repeated assembly and disassembly varies widely for the various designs tested. Redressing the mating surfaces before reassembly will extend the service life of a connector. It is also important to thoroughly clean the connection and lightly lubricate the male thread before each assembly. (Care must be taken not to contaminate the coupling passage.) The best practice is to use a connector which incorporates a replaceable seal and to always replace the seal (gasket) when reassembling the coupling.

B-nuts and sleeves of certain alloys develop stress corrosion cracks when exposed to seacoast atmosphere. B-nuts and/or sleeves manufactured of 2014, 2017, 2024, and 7075 aluminum alloys in the T4 or T6 tempers or type 303 stainless steel are not recommended for use for extended periods in a salt atmosphere.

Additional detail on the selection, design, and use of couplings and threaded connectors is provided in references 51 (secs. 5.11 and 5.12), 133 (pp. 182 to 202), and 134 (sec. I).

The design of an improved threaded connector using various ring seal materials and configurations is presented in figure 8-7. According to reference 135 the design combines the best features of many different connectors. The methods and techniques for calculating the design of each part of the connector are presented in reference 135 (pp. 3-1 to 3-18).

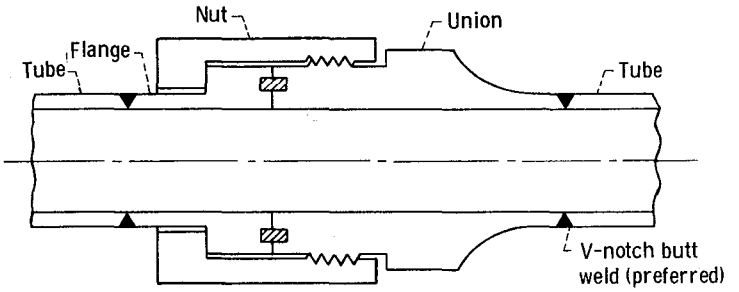

Figure 8-7. - Ring seal connector configuration (ref. 135, p. 3-3).

8.5.2 Flanged Couplings

Flanged couplings are the recommended fittings where connections must be frequently made and broken. Flange fittings are also applicable for semipermanent connections and are particularly suitable for high pressure systems and large diameter lines. Although these couplings are often sealed with flat soft aluminum or copper gaskets between serrated faces, they may also be designed to use single or dual ring seals, crush seals, or other compression type seals. Flanged connections for oxygen service should offer a minimum of pockets or cracks where residue or contaminants could accumulate. The design criteria and recommended design practice for the seal part of the coupling is covered in chapter 9 and in reference 37 (pp. 135 and 136) (see also fig. 9-2).

The degree of rigidity required for a coupling is directly related to the seal element which must compensate for deflections and distortions. Typical deflections and distortions which can cause leakage problems are shown in figure 8-8.

The ASME boiler code and the ANSI piping standards (refs. 73 (appendix 2), 104 (p. 20), 126 (pp. 26 and 27), and 136 (p. 27)) have been used as the standard for designing pressure vessels and piping systems that include flange joints. Where weight is not a special consideration, as with ground support equipment, the code provides safety factors of from 4 to 10. At the stress levels implied by these safety factors the deflection and distortion of the members are negligible.

For flight weight hardware and the temperature extremes of aerospace systems, deflections and distortions become important considerations. Since materials for aerospace application are subjected to 60 percent or more of their yield strength, distortions and deflections are greater than the corresponding flange designed according to the ASME code. Therefore, for flight weight flanged joints the determination of flange thickness, bolt size, and bolt spacing to prevent flange distortion and leakage becomes increasingly critical as flange diameter and fluid pressures increase. An example of flange and seal design calculations for medium pressure aerospace use is presented in reference 133 (pp. 69 to 83).

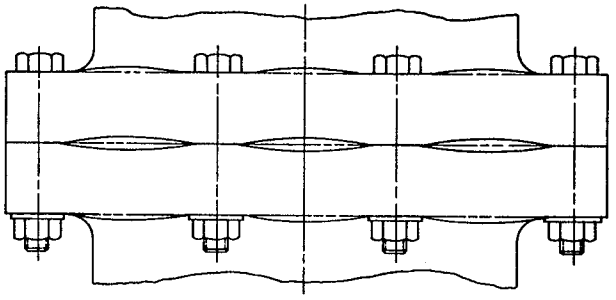

(a) Bowing (circular deflection or distortion).

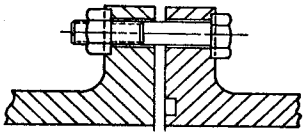

(b) Flange separation
(bolt strain and bolt hole distortion).

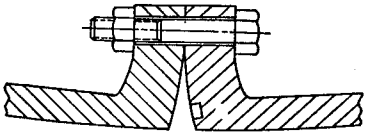

(c) Flange rotation
(angular and axial deflections or distortions).

Figure 8-8. - Types of deflections and distortions in flanged joints (ref. 133, p. 18).

Cryogenic cycling tends to loosen bolted connections; therefore, flange bolt tensions must be checked after 1 or 2 cycles and then again before each use interval. Many compression-type fittings and mechanical clamping techniques to hold the fitting together are commercially available. The design and choice of sealing materials in many of these fittings are suitable for use in oxygen systems.

The design loading of the seal faces by the flange assembly must include allowances for the mechanical stresses from thermal and mechanical forces. Proper assembly of the flanged coupling is equally important. Nonsymmetrical bolt loading can compress the gasket beyond yield locally so that subsequent torquing to even loading will still result in leakage past the yielded section. Suggested bolt torque values recommended for various bolt sizes and materials are tabulated in reference 137 (pp. 40 and 41). In general, the following practices and standards should be used:

(1) All bolts and nuts in the same bolt circle should be identical in material, size, length, and thread unless specifically designed otherwise.

(2) Avoid placing bolt fasteners in a shear stress; provide for shear or torque by splines, keyways, or coupling locks that permit the bolts to be loaded in tension.

(3) Where (2) cannot apply, use bolt hole sizes 0.5 percent larger than the bolt diameter maximum in order to provide a snug fit and prevent play. (This will require a bolt hole diameter tolerance of ±0.003 to 0.005 in.)

(4) One hundred percent of the nut threads should be loaded in contact with the bolt threads when tightened to specified torque values. (Specified values should include whether a lubricant should be used. Fluorocarbon or molybdenum disulfide lubricants are preferred.)

For additional discussion of design practice and analytical methods see references 51 (sec. 5.12.4) and 135 (pp. 2-1 to 2-50).

8.5.3 Threaded Pipe Couplings

Threaded pipe fittings should normally be avoided in high pressure oxygen service. But when it is necessary to use pipe fittings, they should be installed by welding or brazing in such a manner that the threads are completely isolated from the oxygen. The main concern in using pipe threaded fittings is the prevalent use of lubricants which, for oxygen, is undesirable and there is also the possibility of contaminants accumulating in the crevice formed. In addition, since the tapered threaded section of the fitting causes very high radial pressure on the female fitting, cracking from overstress is not uncommon. This problem is less for low pressure systems since less torque is required to effect a seal. With this taken into consideration, threaded pipe couplings for low pressure oxygen systems may be used. Where threaded couplings are used, Teflon tape may be safely employed as a thread lubricant.

8.6 WELDED AND BRAZED JOINTS

Properly welded or brazed joints have the highest potential for zero leakage and are the preferred method of joining pipe sections. But a common problem is the occurrence of cracks in welded and brazed joints. Cryogenic cycling and vibration commonly cause weld boundary cracking and stress corrosion. The latter can be more severe in oxygen especially when slight contamination is present. Therefore, inert gas shielded arc welding is generally preferred to avoid poor penetration and contamination (oxidation, flux, or slag inclusion).

8.6.1 Welded Joints

Pipe ends to be welded should be beveled suitable for full-penetration V-notch butt welding with minimum bead on the inside of the pipe. Sleeve joints (or socket joints) are unacceptable in oxygen systems and should be avoided unless the overlap joint can be brazed or isolated by welding. This is particularly important in high pressure systems and is good practice in any system. An inert gas backup should be used to prevent the pipe from being contaminated with slag that cannot be removed by normal cleaning procedures. The weld penetration or depth of fusion must be to the bottom of the V-groove:

the excess penetration of a bead 1/16 inch high on the inside of the pipe should be avoided or minimized.

Welded seams and connections used in oxygen installations over 150 psi require X-ray inspection of all welded joints. Welds with poor penetration, flux, or slag inclusion, pockets, bubbles, craters, or surface flaking cannot be permitted. Any visible imperfection should be ground out and rewelded. Inert gas shielding arc welding using tungsten electrodes (TIG welding) is the most widely used joining method. Both EB (electron beam) and GMA (gas metal arc) welding are being used where the unique characteristics of these welding methods are required. Resistance seam welding has been used on the Atlas and Thor engines, but manufacturing fit-up problems, corrosion susceptible crevices, and stress concentrations were experienced. Due to its flexibility, TIG welding has been used extensively on the J-2, F-1, Thor, and Atlas engines for fabricating joints. The F-1 engine was originally fabricated with the automatic, single pass, sleeve weld configuration for tube joints because of more repeatable weld quality and lower cost than welds produced by manual operation. However, sleeve joints are not the best practice from a system compatibility standpoint and were changed to the preferable butt weld joints in the J-2S. The in-service failures encountered with the F-1 tube sleeve weld configuration were in the form of fatigue cracks in the heat-affected zone of the weld. The cause was attributed to the high vibration environment of the engine and partial penetration welds. Addition of the fillet weld to the joint for increased fatigue strength and the use of vibration damping clamps on the tubing, located properly to reduce amplitudes, have resolved this problem.

The J-2S engine uses butt welded tube joints throughout with no weld stub-outs on components and no inplace welding. The J-2S, being a simplified version of the J-2, has fewer lines with less complicated routing and thus accommodated the installation of complete line assemblies without interference. Line assemblies are equipped with flanges at each end for makeup into static seal, bolted flange couplings.

Electron beam welding is generally used to join materials where a narrow weld bead and/or minimum heat input to the part is required. Electron beam welding is generally accomplished without the use of filler material and is limited to butt or sleeve-type tubular joints.

Control of weld repair requires some explanation since the effects on the joint are not obvious. The repair of a weld joint involves either completely restoring the component parts, then rejoining by the same method used for the original joint, or attempting a localized repair of the weld. Little or no difficulty can be expected with the part restoration - reweld procedure. However, a localized repair causes an enlarged heat-affected zone which may cause a local distortion resulting in residual stress sufficient to reduce the joint stress tolerance. Therefore, the complete restoration of the joint is preferable.

8.6.2 Brazed Joints

The preferred brazing methods for oxygen components are furnace brazing and induction brazing. To protect the metal from oxidation during the braze cycle, furnace brazing is done preferably in a vacuum or an argon hydrogen atmosphere. Similarily, induction brazing requires an argon shield on both the inside and the outside of the joint.

Figure 8-9 is a plot of shear strength as a function of temperature for selected braze alloys. These alloys are commonly used in design of tube joints for rocket propulsion fluid systems.

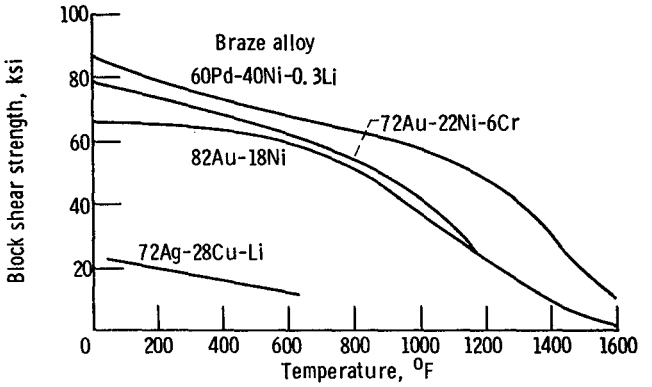

Figure 8-9. - Block shear strength as function of temperature properties of braze alloys (ref. 51, p. 5.12.5-3).

8.6.2.1 Stress corrosion of brazed joints. - The nickel alloys and chromium nickel steels are subject to stress corrosion cracking as a result of exposure to molten brazing filler metals. If there is residual or applied stress on the parts being brazed, or if stress is caused from thermal gradients during the brazing process, stress corrosion can occur. The braze material can penetrate the grain boundaries of the base alloy which reduces its strength.

Stress corrosion cracking can be prevented by the following:

(1) Use annealed materials for brazing.

(2) Prevent or remove externally applied stress during the brazing process.

(3) To reduce thermal stresses heat bulky parts to brazing temperature slowly enough to allow an even temperature to be reached.

Stainless steels containing chromium and carbon are subject to carbon precipitation when heated to temperatures between 800° and 1500° F. Carbon-chromium precipitation into the grain boundaries is particularily susceptible to stress corrosion from braze metals. Precipitated carbon may be redissolved before brazing by heat treating

at 1850° to 2000° F followed by rapid cooling.

If the brazing can be done rapidly (5 to 10 min), no appreciable amount of precipitation can occur. Preferred stainless alloys that are less affected by this phenomenon are types 347 and 321.

Preferred base metal - filler metal combinations are given in table 8-V (ref. 138).

TABLE 8-V. - BASE METAL FILLER METAL COMBINATIONS

[Ref. 138, (pp. 37 to 45) lists specific compositions of each filler material.]

	Al and Al alloys	Mg and Mg alloys	Cu and Cu alloys	Carbon and low alloy steels	Cast iron	Stainless steel	Ni and Ni alloys
Al and Al alloys	BAlSi						
Mg and Mg alloys	X	BMg					
Cu and Cu alloys	X	X	BAg, BAu, BCuP, RBCuZn				
Carbon and low alloy steels	BAlSi	X	BAg, BAu, RBCuZn	BAg, BAu, BCu, RBCuZn, BNi			
Stainless steel	BAlSi	X	BAg, BAu	BAg, BAu, BCu, BNi	BAg, BAu, BCu, BNi	BAg, BAu, BCu, BNi	
Ni and Ni alloys	X	X	BAg, BAu, RBCuZn	BAg, BAu, BCu, RBCuZn, BNi	BAg, BCu, RBCuZn	BAg, BAu, BCu, BNi	BAg, BAu, BCu, BNi

8.6.2.2 Braze joint cleanliness. - The usual cleaning procedure preparatory to brazing is to remove everything down to base metal (a thin oxide film will reform even at room temperature). It is important that the cleaned surface not be contaminated by handling prior to brazing. Since aluminum, magnesium, manganese, and beryllium oxides resist hydrogen reduction and some steels can become embrittled by hydrogen, brazing should be done in a helium or argon atmosphere, or better in a vacuum.

8.6.2.3 Clearances. - The clearance between surfaces to be brazed is generally held between 0.001 and 0.003 inch (ref. 139). A common practice in brazing pipe or tubing is to provide a brazed joint depth of 1 to $1\frac{1}{2}$ diameters.

8.7 LINE RUPTURE

A gas at ambient temperature escaping from the open end of a line or vessel yields a specific impulse of approximately 50 seconds, which is a considerable amount when it is realized that no chemical reaction is taking place. For example, a 1-inch line charged to 200 psi can develop approximately 175 pounds of thrust (see table 8-VI, ref. 140). Therefore, should a rupture occur in a line, flex hose, or bellows, the unrestrained sections may cause severe damage or injury. Restraints, fasteners, and braces should be used to prevent this type of occurrence especially in high pressure systems (over 2000 psia). From this example, the hazards of accidently uncoupling an "empty" line that in reality is under pressure become obvious.

TABLE 8-VI. - OPEN LINE THRUST FORCE[a]

To calculate the force acting on line opening, select applicable diameter and multiply right-hand column by the source pressure (psi).

Diameter opening, in.	Calculated force factor for each psi of source pressure	Diameter opening, in.	Calculated force factor for each psi of source pressure
1/8	0.18506	5/8	0.5777
1/4	.2832	3/4	.6759
3/8	.3814	7/8	.7741
1/2	.4796	1	.8723

[a]Ref. 140, Design Note 3G1.

Page intentionally left blank

CHAPTER 9. SEALS

Seals as applied to turbopump shafts, valve seats, and valve stems have been discussed in sections 6.1.3, 7.5, and 7.6, respectively. While the sealing principles and design considerations are generally the same, pump seals and valve seals have special requirements; these special requirements were discussed as a part of the component overall design.

The various types of seal configurations generally found in fluid systems are shown in figure 9.1. In order to achieve a seal, the contacting surfaces must be pressed together with sufficient force per unit area to close all leak paths. If a secondary material is used to achieve a seal between the surfaces, the material must maintain the pressure without being squeezed out or permitting pressure relaxation due to cold flow or creep. In the case of dynamic seals, the seal material must resist wear from rubbing friction to avoid seal surface damage by abrasion and pressure relaxation from wear.

9.1 STATIC SEALS

A good static seal is obtained when complete contact occurs between the mating surfaces at a uniform pressure, which is always greater than the contained pressure. This can be done either by forcing the two surfaces together such that plastic flow of the seal material results or by polishing the surface smooth enough so that elastic flow of the seal material will result in uniform surface contact. The plastic flow method is permissible for a single or a very limited number of sealing cycles, whereas the elastic yield method can be used when multicycle sealing is required, such as with a poppet valve.

Most of the leakage problems are caused by compromising the preceding principles. Typically, the seal surface pressure is reduced by cold flow or creep of seal material as a result of temperature cycling or over stressing. Other causes are inadequate confinement of seal material which permits extrusion, poor surface preparation, or improper material selection for the range of pressure and temperature conditions.

Flat gaskets are mainly used to seal flanged pipe connections, access covers for tanks, and assembled parts such as pump housings, clamshell valve housings, etc. A flat gasket must be thin enough to prevent extrusion or "blowout" from pressure and

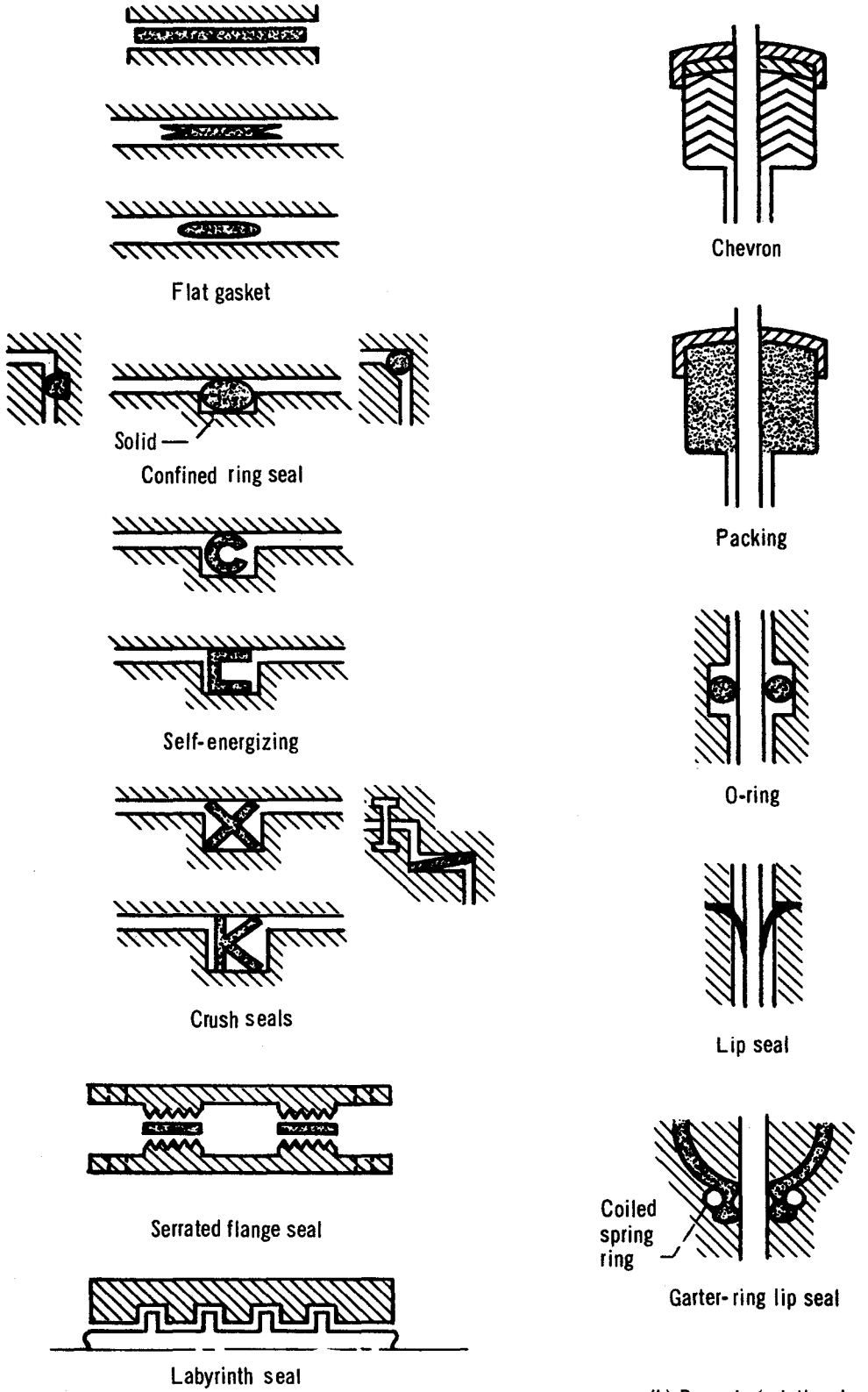

Figure 9-1. - Types of seals.

thick enough to seal surface irregularities and waviness.

The relatively large high surface area of flat gaskets makes uniform pressure distribution more difficult. Flange faces tend to bow out between the bolts, and surface waviness from any cause permits low sealing pressure zones that may allow leakage to begin (see sec. 8.5.2 and fig. 8-8). The use of serrations of the flange faces reduces cold flow, increases sealing pressure (force per unit contact area), and permits using metal materials in a flat gasket type application. The recommended design for the serrated seal is shown in figure 9-2.

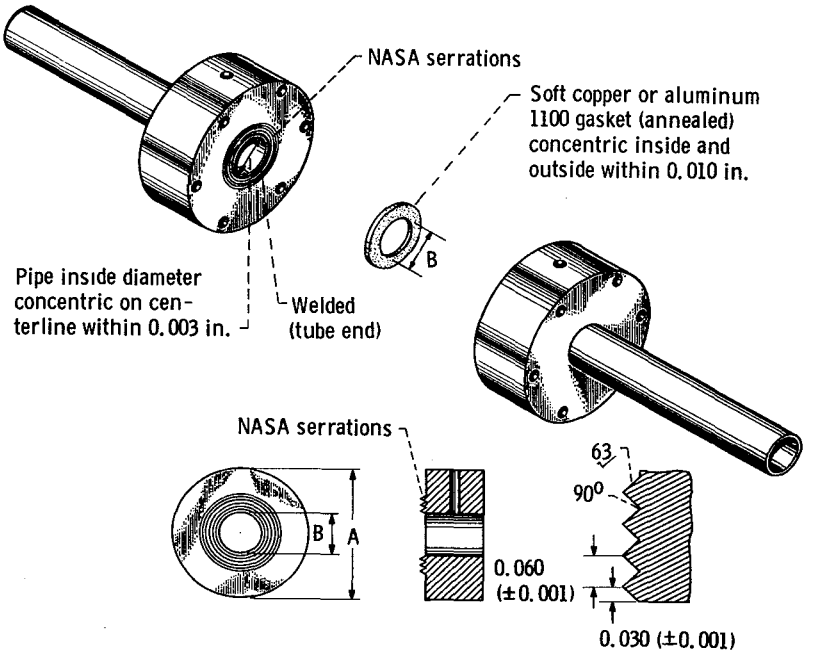

Figure 9-2. - Flange-type connectors for oxygen (ref. 37, p. 135). Flange connector bolts must be periodically retorqued since they tend to loosen under cryogenic-ambient temperature cycling.

Ring seals may have a wide variety of configurations. Some examples are shown in figure 9-1. Ring seals have a relatively low contact area; therefore, the force per unit area can be as high as desired and can be accurately controlled.

Providing a recess for the ring seals can prevent extrusion or blowout. In a V- or C-ring configuration, high pressure fluid can enter the open side and help provide a sealing pressure. The same applies to dynamic chevron seals or lip seals. For extra sealing pressure in lip seals, garter rings may be used.

Surface finishes for elastomer-metal contact surfaces are not too critical; that is, the average machine finish can be tolerated if the elastomer coating or thickness is greater than three times the maximum asperity height or surface finish roughness. However, depending on the application, 20 to 40 microinches is recommended for the

metal-nonmetal surfaces and 4 to 20 microinches for metal-metal surfaces. See section 7.5 for valve element - seat surface finishes.

Figure 9-3 shows the surface finish range that results from various processes.

Surface roughness measuring instruments and their measurement capability (ref. 122, pp. 11 to 22) are as follows:

(1) Electromechanical stylus (vertical readout, ×50 000). (Typical tip radius is 0.005 to 0.0001 in. or 500 to 100 μin. diam.)

(2) Optical interferometer (sensitive to 0.02 μin.)

(3) Electron microscope (0.2 μin.)

(4) Optical microscope (6.7 μin.)

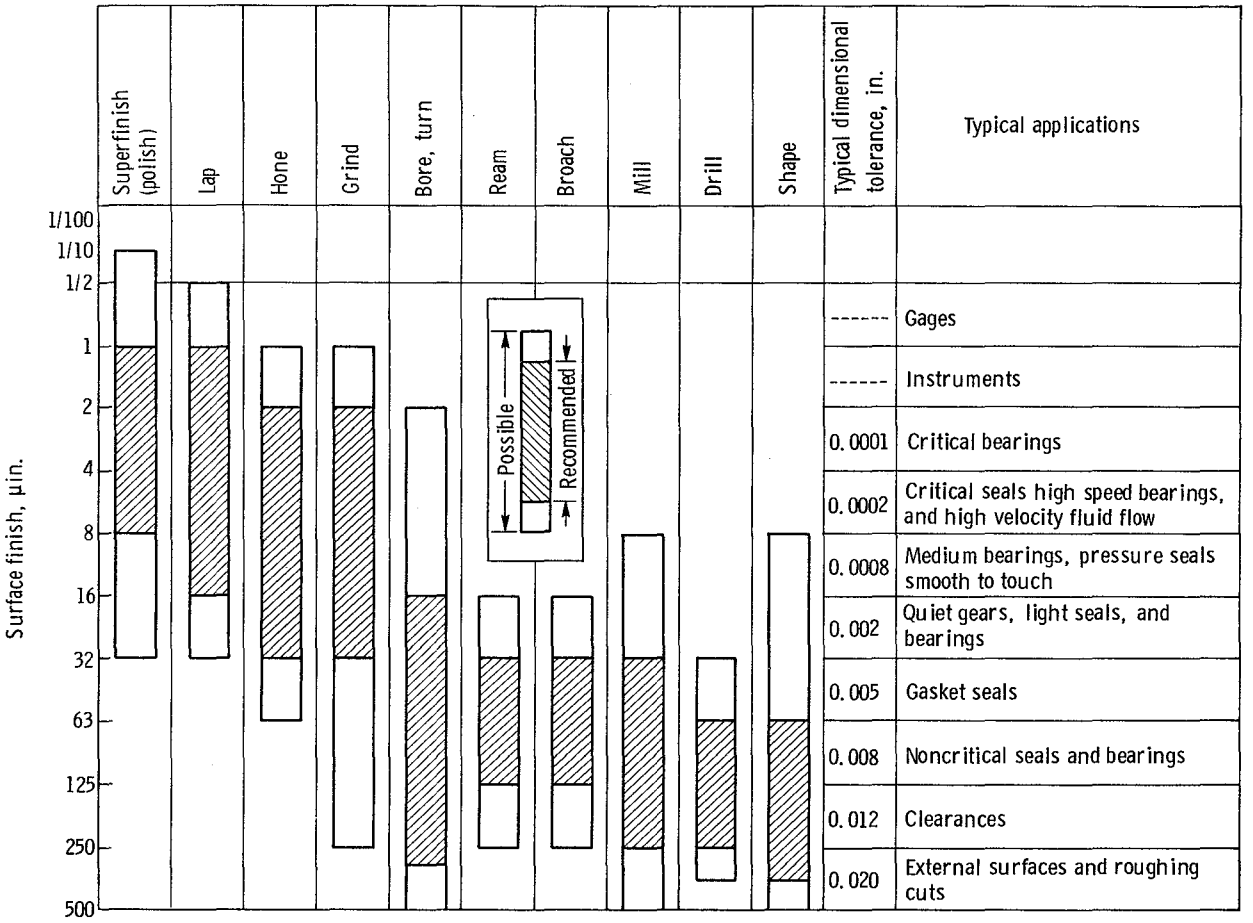

Figure 9-3. - Typical surface finishes produced by various manufacturing techniques (ref. 51, p. 6. 3. 2-7).

9.2 DYNAMIC SEALS

The basic requirement for a minimum leakage dynamic seal is the same as the static seal, except that the design condition must be maintained with relative motion between the seal and mating surface.

The dynamic joint design is the result of compromises between permissible leakage rates, joint life, and many other factors that affect these two variables. For example, the amount of rotation of a valve stem is extremely small compared to a turbopump shaft seal. In the case of the valve stem, near zero leakage can be obtained with relatively low seal wear. Zero leakage can be achieved with sliding shaft seal designs by using bellows or diaphragms.

Typical design specifications for dynamic O-ring seals are given in figure 9-4. Seal material selection for dynamic seals are discussed in sections 9.3 and in 6.3.2 and 7.3 for pumps and valves, respectively.

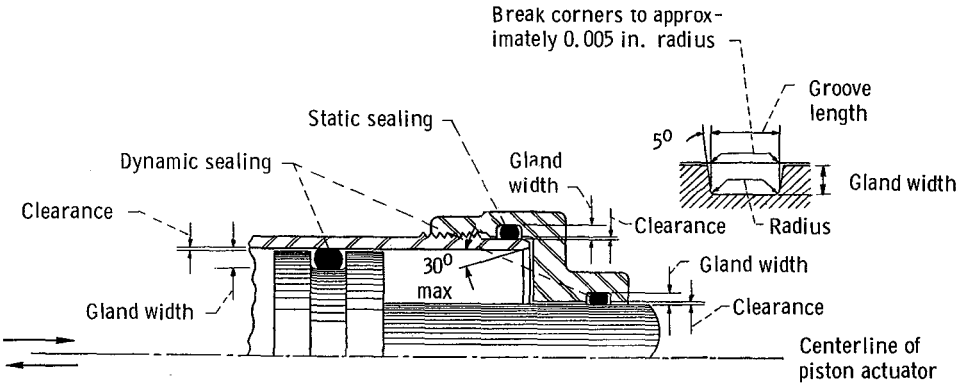

O-ring nominal section diameter, in.	O-ring section diameter, in.	Diametral squeeze, min.		Gland width, in.		Groove length, in.	Radius min	Two times diametral clearance (max), in.
		Dynamic	Static	Dynamic[a]	Static[b]			
1/16	0.070 ± 0.003	0.010	0.015	0.057	0.052	3/32	1/64	0.005
3/32	.103 ± .003	.010	.017	.090	.083	9/64	1/64	.005
1/8	.139 ± .004	.012	.022	.123	.113	3/16	1/32	.006
3/16	.210 ± .005	.017	.032	.188	.173	9/32	3/64	.007
1/4	.275 ± .006	.029	.049	.240	.220	3/8	1/16	.008

Fluid pressure	O-ring compound hardness
0-1000 psi	70 Shore "A" durometer
1000-2000 psi	80 Shore "A" durometer
2000 psi and higher	90 Shore "A" durometer

[a]Tolerance, +0.000, -0.001 in.
[b]Tolerance, +0.000, -0.005 in.

Figure 9-4. - Dynamic seal for translation or rotation (ref. 70, p. 290).

9.2.1 Surface Finish Requirements

The sliding surfaces in contact with dynamic O-ring seals should be ground, honed, or polished to a finish of 8 to 10 microinches rms. A finish within this range yields a longer life than either rougher or smoother finishes. Codirectional patterns, as produced by honing, have been proven to be the best surface finish for any type of dynamic sliding seal. For still better results, after an initial finishing, the surface could be hard chrome or nickel plated and again finished. The plating provides a hard, slippery surface that resists corrosion, wear, and scratching.

9.2.2 Friction of Dynamic O-Ring Seals

The breakaway friction of a dynamic O-ring seal is usually about three times the running friction. Breakaway and running frictions increase with fluid pressure, O-ring hardness, diametral squeeze, and temperature decrease. Accurate values of O-ring frictions can only be obtained experimentally for a given design.

9.3 SEAL MATERIALS

An example of the types of materials preferred for use in liquid or gaseous oxygen systems is given in table 9-I. Except for the silicone rubber, these materials meet MSFC Specification 106-B (ref. 45) for compatibility with oxygen. Their physical properties vary enough to meet almost any sealing requirement. Silicone rubber has been included based on service experience with the Apollo Personnel Life Support System. Viton was being used as a seal material in this system; however, the Viton O-rings exposed to a 7500 psia oxygen pressure in the regulator valve failed because of oxygen absorption. When depressurized, the material was fractured from the pressure of the absorbed gas. A modified Viton, identified as D-80, has been developed for use with oxygen at pressures up to 3000 psia (ref. 141, appendix II and p. 4).

The hardness and/or compressive strength of materials are the best physical properties when comparing the mechanical characteristics of materials for seal application. Where the sealing force or loading is high and the seal contact surface area is small, a harder material must be used to resist unwanted deformation and to resist creep. Where the sealing force or loading is low and the seal contact surface is large, a softer more compliant material must be used to permit maximum surface to surface contact. Figure 9-5 shows the hardness range of selected materials. The hardness and stiffness of each material increases with increasing shore or Rockwell value.

TABLE 9-I. - PREFERRED SEAL MATERIALS FOR OXYGEN

[Nonmetals may also be used as plating material.]

(a) Nonmetals

Trade name	Chemical name or description
Teflon TFE	Polytetrafluoroethylene
Halon TFE, G-80	Polytetrafluoroethylene
Rulon A	Polytetrafluoroethylene with MoS_2 filler
Nickel-filled Teflon	Polytetrafluoroethylene with nickel-powder filler
15-Percent glass-filled Teflon	Polytetrafluoroethylene with glass fibers
Teflon FEP	Fluorinated ethylene proplene
Kel-F 81	Polychlorotrifluoroethylene (CTFE)
Kel-F 82	Copolymer of CTFE and 3 mole percent vinylidene fluoride
Plaskon 2400	Polychlorotrifluoroethylene (CTFE)
Halon TVS (now called Plaskon 2200)	Polychlorotrifluoroethylene (CTFE)
Kynar	Vinylidene fluoride
Viton A	Copolymer of vinylidene fluoride and hexafluoropropylene
Fluorel	Copolymer of vinylidene fluoride and hexafluoropropylene
Silastic	Silicone rubber

(b) Metals

Aluminum	Copper alloys	Lead	Rhodium[a]
Aluminum alloys	Gold[a]	Monel	Silver[a]
Chromium[a]	Inconel	Nickel	Stainless steel
Copper	Indium[a]	Platinum[a]	Tin[a]

[a]Usually restricted to use as a surface plating material.

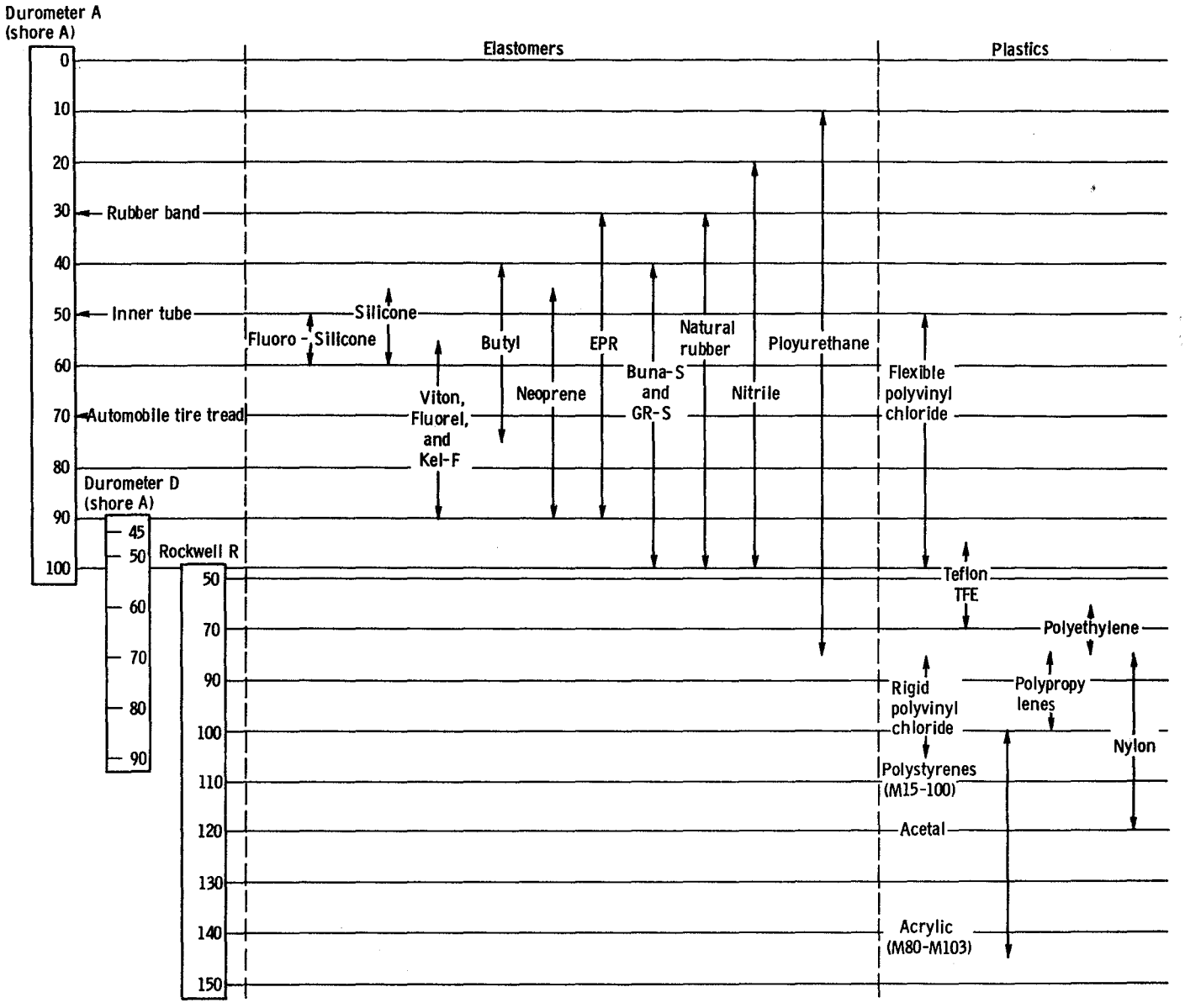

Figure 9-5. - Hardness spectrum for elastomers and plastics (ref. 51, p. 12. 3-1).

9.3.1 Extrusion

The problem of O-ring extrusion under various pressures and applications is shown pictorially in figure 9-6. The extrusion tendency of a material can be estimated from figure 9-7. This figure related the tendency to extrude or to resist extrusion as a function of the clearance gap and the pressure differential and shore hardness. A proper combination of clearance gap and O-ring hardness may prevent extrusion. Extrusion may also be avoided by providing a backup ring on the side of the O-ring opposite the high pressure source (fig. 9-6). For dynamic seals for pressures in excess of 800 psi,

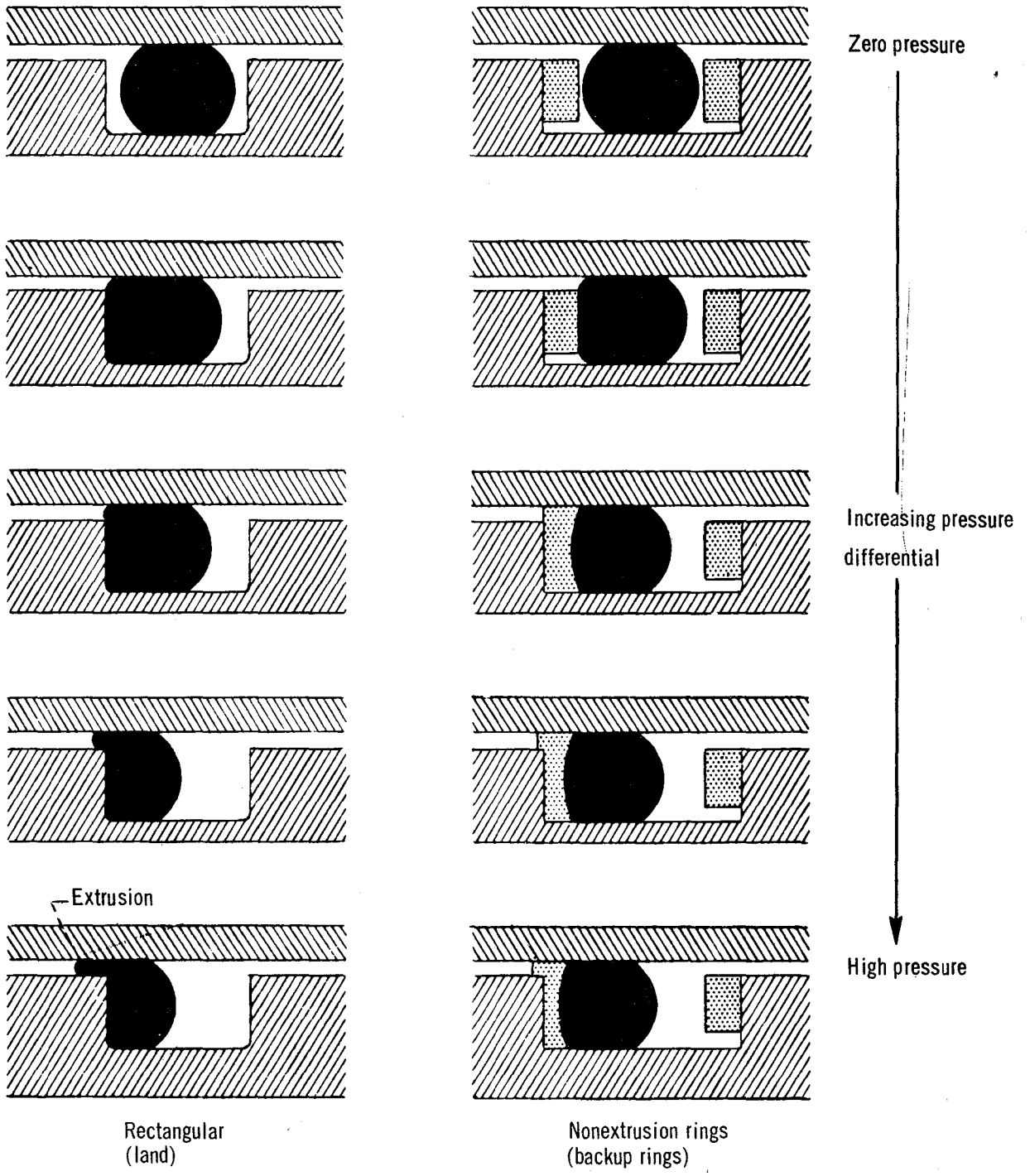

Figure 9-6. - O-ring extrusion (ref. 140, design note 3F2, p. 4).

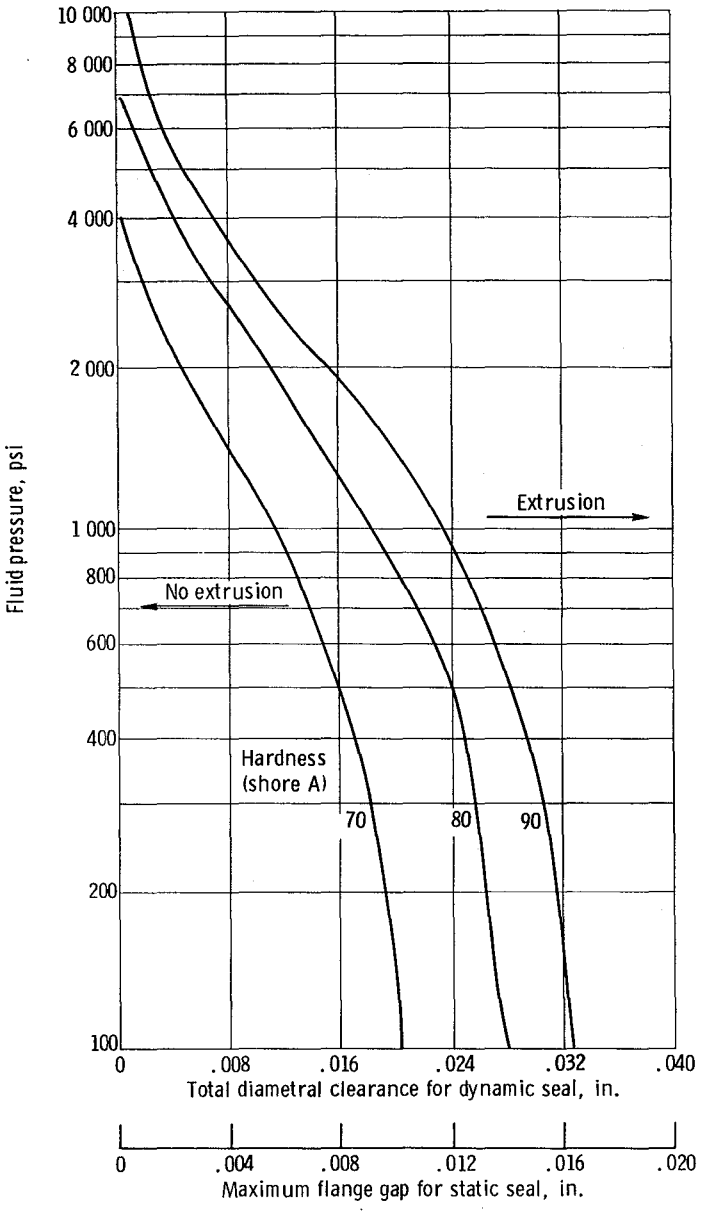

Figure 9-7. - Extrusion characteristics of O-rings (ref. 133, p. 60). Information originally from Seal Compound Manual, Parker Seal Co. Catalog C5702, July 1964.

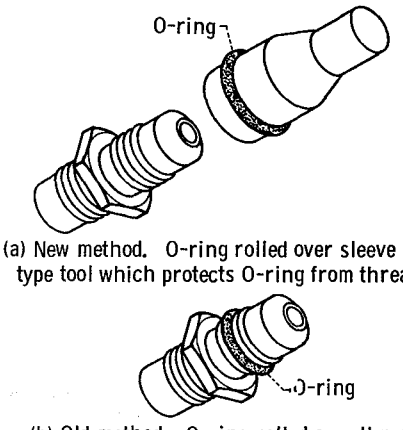

(a) New method. O-ring rolled over sleeve type tool which protects O-ring from threads.

(b) Old method. O-ring rolled over threads which can damage O-ring.

Figure 9-8. - Tool for preventing O-ring damage during installation (ref. 140, design note 3F2, p. 6).

Teflon or Kel-F backup rings are recommended. Where it is required that pressure be applied from either direction, a backup ring on both sides of the O-ring may be used. Sharp corners around, in, or near O-ring grooves should be avoided. Seals forced into sharp corners can damage the seal ring surface (see inset in fig. 9-4). Seal failures can also occur from cuts sustained by installation over sharp edges such as threads. An installation tool such as that shown in figure 9-8 can help to alleviate this problem.

9.3.2 Creep

Permanent dimensional changes (set) in a material due to an imposed load (below normal yield stress) are referred to as cold flow or creep. Such dimensional changes in seals can result in leakage. The effect of crystallinity, temperature, and pressure on the creep characteristics of materials commonly used in oxygen systems is shown in figures 9-9 to 9-15.

Creep data for selected materials at room temperature exposed to a 3000 psi stress are given in figure 9-9 (ref. 142). Figure 9-10 (ref. 143) illustrates the effect of crystallinity on the creep rate. For Teflon, a sharp reduction in creep rate exists over a narrow band of crystallinity between 70 and 80 percent. Thus, it can be helpful to specify the crystallinity of polymeric material where creep must be minimized. Additional

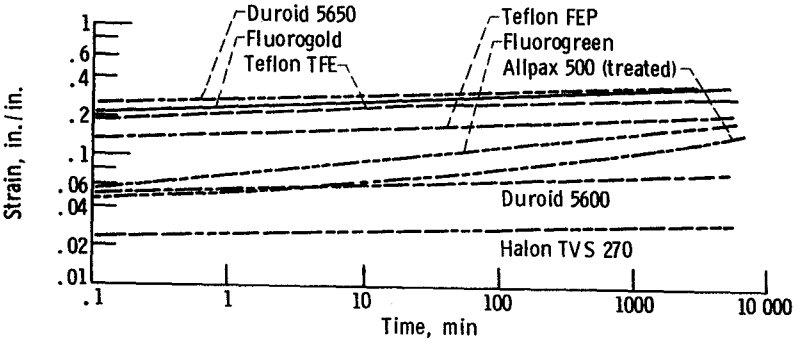

Figure 9-9. - Creep data for various gasket materials at ambient temperature and stress of 3000 psi (ref. 142, p. 20). Duroid 5600 and 5650, ceramic-filled Teflon; Fluorogold, fiberglass-filled Teflon; Fluorogreen, fiberglass-filled Teflon; Allpax 500, Fluorolub treated asbestos fiber with Styrene/Butadiene binder (not recommended for oxygen systems); Halon TVS, modified CTFE.

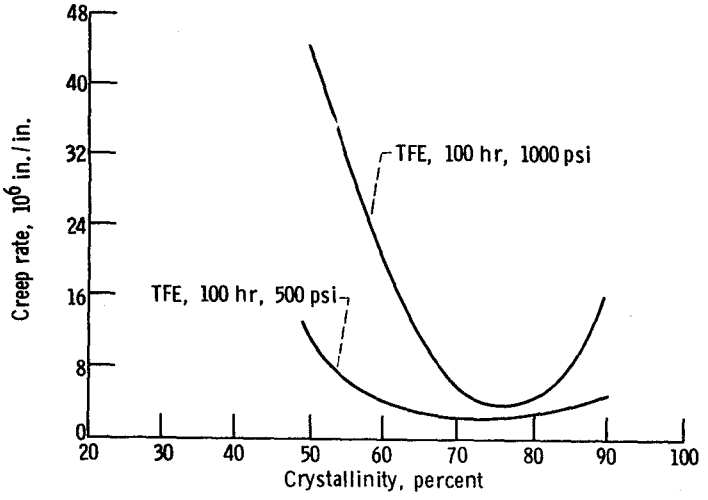

Figure 9-10. - Effect of crystallinity on creep rate (ref. 143, p. 98).

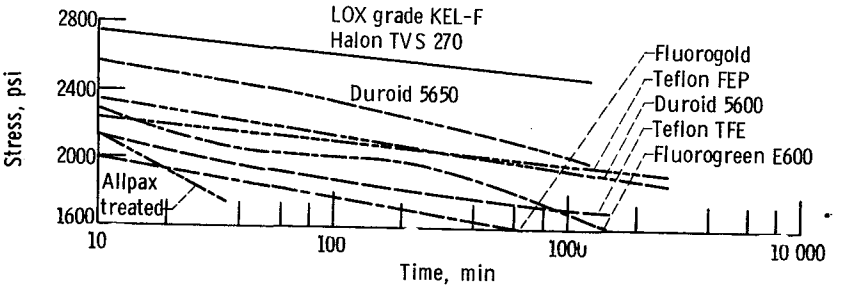

Figure 9-11. - Room temperature stress relaxation data (ref. 142, p. 21). Trade name designations in figure 9-9.

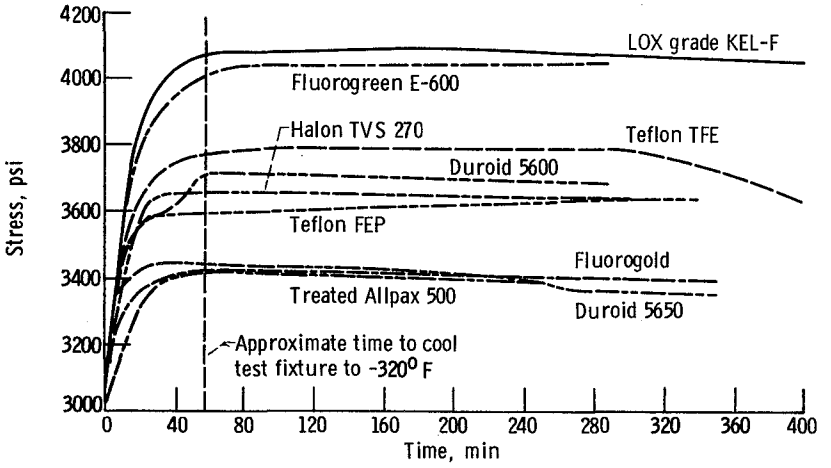

Figure 9-12. - Stress relaxation data for -320° F (-196° C) (ref. 133, p. 22). See figure 9-9 for trade name identifications.

data showing the effects of crystallinity on physical properties for selected materials are given in tables 3-XII and 3-XIII. Stress relaxation data for the same materials are given for room temperature and at -320° F in figures 9-11 and 9-12, respectively. Note that the creep at cryogenic temperature is nearly zero at the test loads. Creep data for selected metal candidates for seal application are given in figures 9-13 to 9-15.

The coefficient of thermal expansion-contraction of seal materials varies considerably and should also be taken into account in all seal design (see table 9-II).

A commonly used solution to the creep problem and the expansion-contraction problem is to use metal seals coated with the appropriate polymer (in most cases a fluorocarbon polymer). This provides a combination of the overall hardness, strength, and thermal expansion characteristics of a metal seal and the surface characteristics of a polymer seal. This technique is more successful in static seals than in dynamic seals, however, because the relatively thin polymeric coatings are more easily damaged in sliding seals.

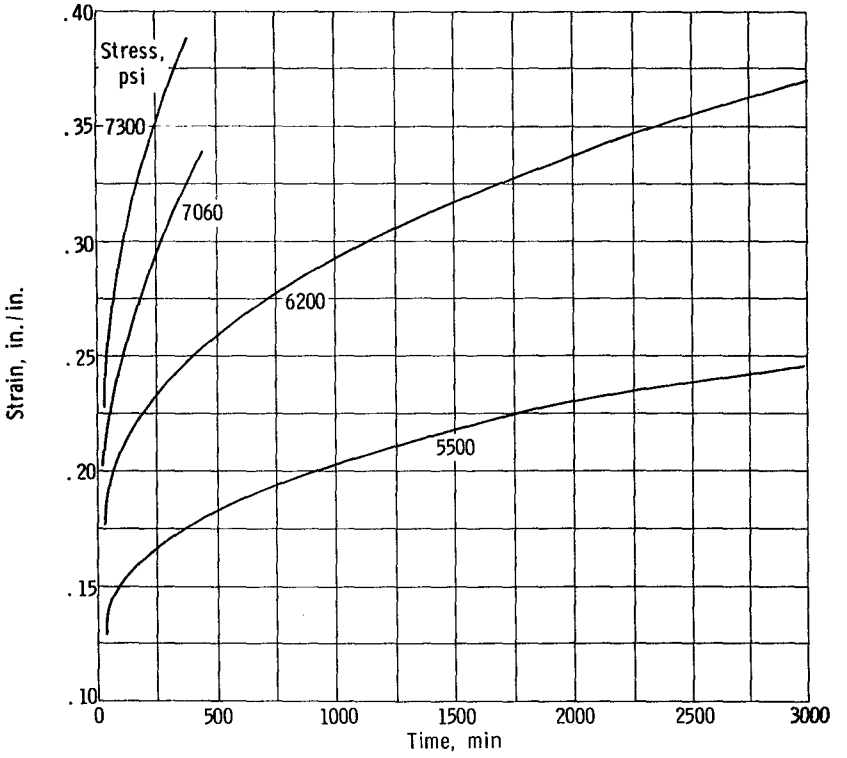

Figure 9-13. - Creep characteristics of 1100-0 aluminum at 196^{0} F (ref. 133, p. 21).

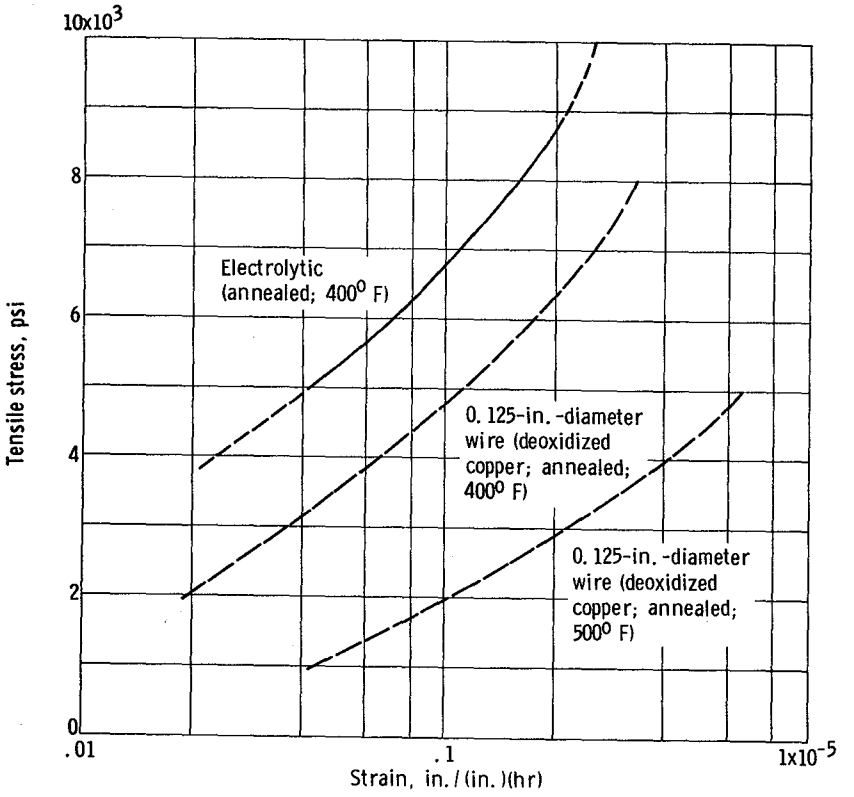

Figure 9-14. - Creep properties of copper (ref. 133, p. 19).

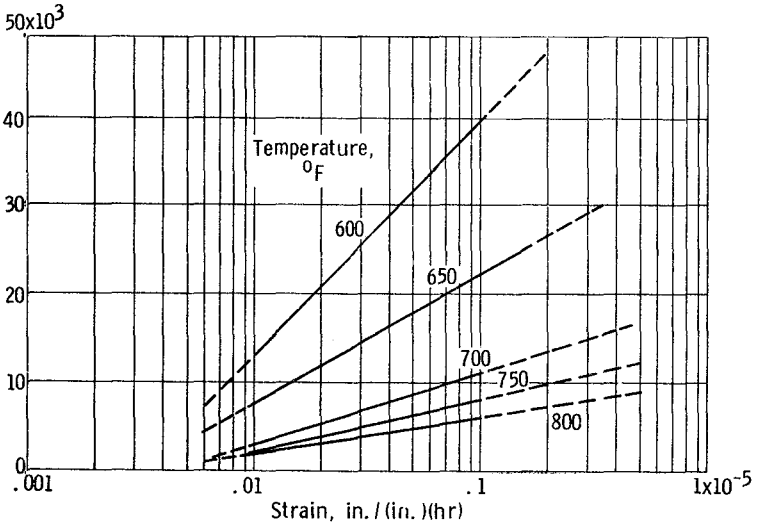

Figure 9-15. - Creep properties of "A" nickel (ref. 133, p. 20).

TABLE 9-II. - LINEAR THERMAL EXPANSION OF TYPICAL SEAL MATERIALS[a]

Material	Contraction (+75° to -65° F), in./ft	Expansion (-75° to +375° F), in./ft	Coefficient of expansion, in./(in.)(°F)
Teflon	0.093	0.148	5.5×10^{-5}
Nitrile, general purpose	.218	.468	13.0
Chloroprene	.190	.407	11.3
Viton-A	.130	.277	9.0
Kel-F	.064	.137	3.5
Silicone	.252	.540	15.0
High-temperature aluminum, 2017	.022	.047	13.0×10^{-6}
Stainless steel, type 302	.016	.035	9.6

[a]Ref. 51, sec. 6.3.2.7.

9.3.3 Special Considerations for Very High Pressures

During the early phases of the Apollo program silicone rubber O-ring seals were used for the high oxygen pressure applications in the personnel life support system (PLSS) and the emergency oxygen system. The material was selected because of the favorable experience gained during the Mercury and Gemini programs where silicone rubber was used for high pressure oxygen applications. Subsequent to the Apollo 7 fire, all of the silicone rubber seals in the high pressure (over 5000 psia) portable life support system and oxygen pressurization system applications were replaced by Viton be-

cause Viton passed the standard mechanical impact compatibility test and silicone rubber did not. However, the Viton seals were found to be functionally unsuitable at this pressure and silicone rubber O-ring seals were reinstituted.

The rationale exercised in reinstituting silicone rubber seals is completely explained in reference 124. Basically, the problem encountered with the Viton-A seal centered on its absorption of oxygen gas under high pressures and its subsequent inability to relieve the internal pressure from absorbed gases without rupture when the system was depressurized. Alternate materials were considered and rejected for various reasons: three such reasons are (1) similarity to Viton-A, (2) inadequate test data, and (3) poor compressive set characteristics. It was finally concluded that, based on extensive satisfactory experience (in excess of 19 500 hr of logged and estimated operating experience) in the Mercury, Gemini, and Apollo programs, at pressures exceeding 5000 psia, silicone rubber was the most satisfactory seal material available. Then, since the seals in this application were heat sinked and not exposed directly to oxygen flow, and in view of additional ignition tests successfully performed, silicone rubber seals were reinstituted. Representative high pressure (7500 psi and above) seal designs using silicone rubber are illustrated in figure 9-16 for both static and dynamic applications.

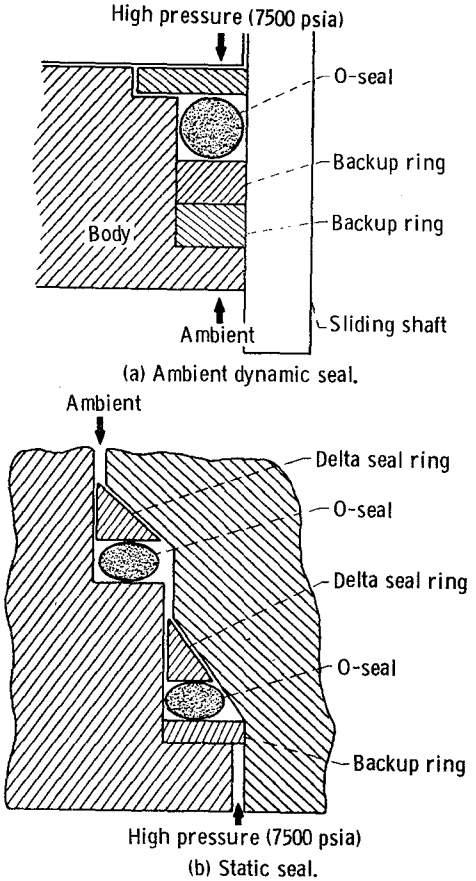

Figure 9-16. - Dynamic and static seals (ref. 124).

9.4 LEAK TESTS

Leak testing may be categorized as either leak measurement, the total leak measurement, or leak location. Generally, the procedure is to measure total leakage and then, if necessary, locate the individual leaks.

Laminar flow leaks can have very tortuous paths and, even for pressures above 3000 psi, a test time of 3 to 4 hours may be required for leak detection by measuring pressure loss in the system. Other commonly used test techniques vary widely in sensitivity and complexity: these techniques can vary from soap solution bubble testing (maximum sensitivity to 10^{-4} std cm^3/sec) to a bell jar - helium mass spectrometer (maximum sensitivity better than 10^{-9} std cm^3/sec, or 1 std cm^3/32 yr). Soap solution testing may be quite adequate for many oxygen propellant ground and flight systems using nitrogen as a pressurant gas. However, as leakage requirements become more stringent, as for a long duration interplanetary mission, it may become necessary to employ the more sensitive testing techniques such as the helium mass spectrometer. These techniques are discussed in references 55 (pp. 11 to 13) and 56.

Since helium is the most common tracer gas used for leak measurement, table 9-III is included showing some acceptable leak detection methods for various allowable helium

TABLE 9-III. - LEAKAGE MEASUREMENT USING GASEOUS HELIUM

Allowable leakage, standard cm^3/sec	Approximate equivalent	Leak detection method	Remarks
1.0×10^{-2}	0.6 cm^3/min (6 to 10 average size bubbles in 2 min)	Water submersion, wet test meter, or flowmeter	Detectable and measable with simple equipment
1.0×10^{-3}	1 cm in 17 min (no bubbles in 2 min)	Water submersion or wet test meter	Easy to get false indications; trapped gas between flanges, outside of seal, and desorbed gases from external surfaces may indicate leakage
1.0×10^{-6}	1.0 cm^3 in 12 days	Mass spectrometer	Leak check requires approximately 1/2 hr to set up and 1/4 hr to test
1.0×10^{-7}	1.0 cm^3 in 4 months	Mass spectrometer	Leak check requires approximately 1/2 hr to set up and 1/4 hr to test

leak rates. A discussion of leakage, including specification limits for system leakage in terms of helium gas, and a discussion of zero leakage, may be found in section 4.1.

A summary of commonly available test techniques and their approximate sensitivities are shown in figure 9-17.

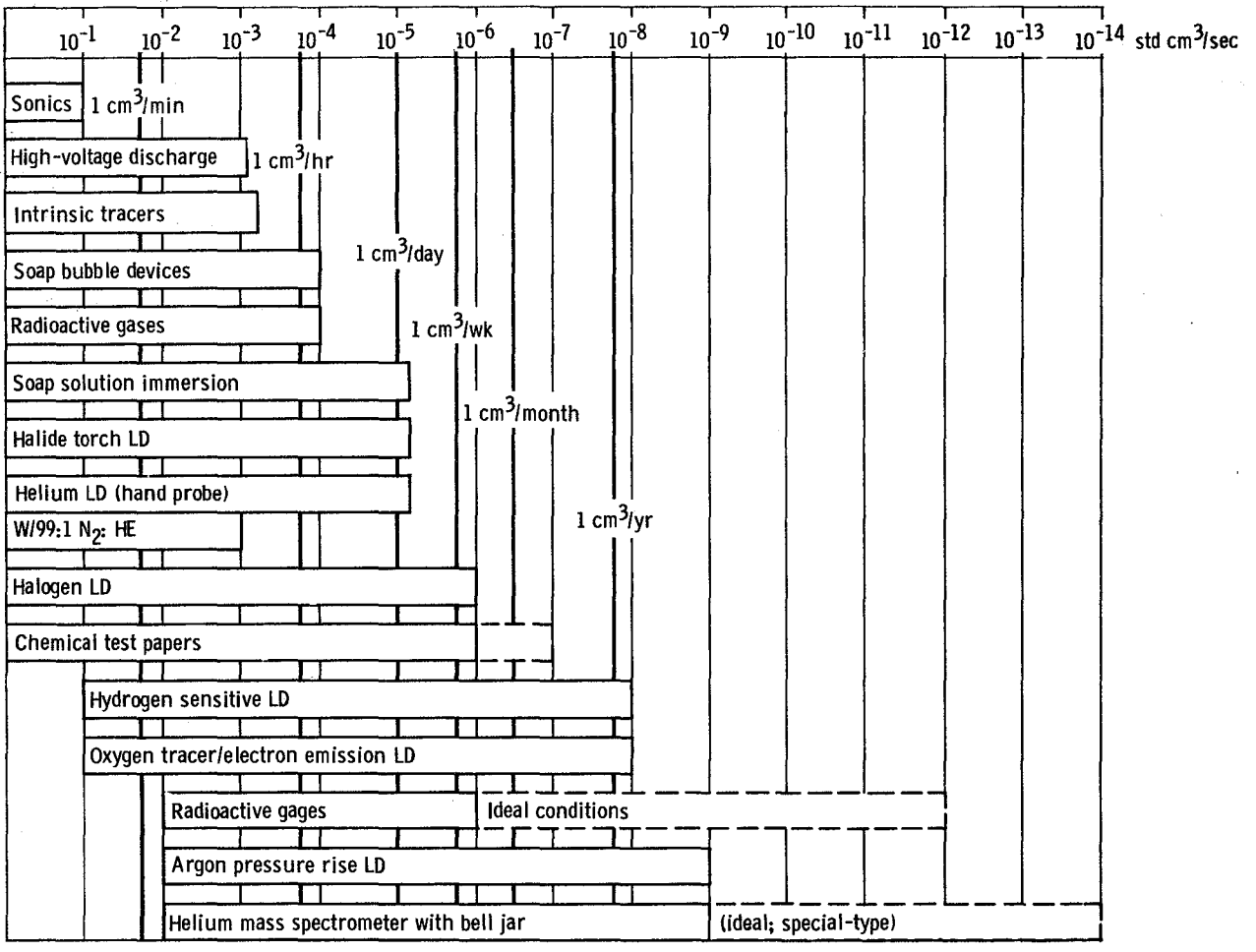

Figure 9-17. - Test methods and their test sensitivities (ref. 55, p. 12). Leak detector, LD.

Page intentionally left blank

CHAPTER 10. FILTERS

As noted earlier, solid particles in oxygen systems can cause abrasion and impact ignition of sensitive materials and clogging of close clearances. Generally, the oxygen as supplied by the vendor meeting MSFC Specification 399A (table 2-VII) has been filtered to remove particles greater than 10 microns nominal and 40 microns absolute. This is adequate for most oxygen system requirements provided that no additional contaminant is introduced by subsequent handling.

Particulate contamination is most critical in high pressure gaseous oxygen systems for two reasons: first, gaseous systems are generally at room temperature or higher, which reduces the energy requirement to cause ignition, and second, gaseous systems can easily accelerate particles to sonic or even supersonic velocities. This results in very high impact energies. Consequently, filters may be required, especially in high pressure gaseous oxygen systems. Where high reliability is required, careful control of particulate contamination and system cleanliness verification (sec. 4.5) must be maintained.

Where it is possible to provide contaminant-controlled oxygen to a contaminant-free system, system filters may not be required. Where filters are required to guarantee particle control, they should be installed in the section of the oxygen system which has a low flow velocity. This provides for a minimum ΔP, lower potential for high velocity particle impact, and minimal scrubbing action of the fluid through the filter. The degree of filtration is dictated by (1) size of orifices, pores, slots or passages, (2) clearances between sliding (or static) surfaces, and (3) the hazard of entrained material impacting or abraiding a surface.

Unless test data permit otherwise, the following criteria are suggested:

(1) Filter to a particle size that is 10 percent less than the smallest orifice, pore, or passage to remain unplugged.

(2) Remove by filtration particles that exceed 10 times the asperity height of the land surfaces where all metal valve surfaces are used in a shutoff valve application (see sec. 7.8).

(3) Solid particulates should be limited as follows:

4000 to 1000 microinches for low pressure gaseous oxygen systems (500 to 2000 psia)

1000 to 250 microinches for medium pressure (2000 to 7500 psia)
250 to 100 microinches for high pressure (7500 to 10 000 psia)
100 to 40 microinches for pressure above 10 000 psia

Oxygen filters require special design and maintenance considerations. Usually, filters are changed when the pressure loss across the element becomes too great. With oxygen filters it must be remembered that the unit is filtering and storing solid contaminants. If the contaminants include a high percentage of hydrocarbons, which may be increasing with each use, it should also be assumed that the filter could be sensitive to shock and ignition sources (ref. 144, p. 10).

Filter isolating valves should be installed in the line so that the pressure in the filter can be relieved and the filter element removed for cleaning. This may mean two filters in parallel where the flow of oxygen cannot be interrupted while the filter element is being cleaned. Bypass lines to permit removal of the filter element for cleaning are not recommended unless a high degree of control can be exercised over the use of the bypass line.

Since pressure losses across the filter increase with filter fineness and residue accumulation, system tolerance for such pressure loss must be provided. The standard procedure for monitoring the filter condition is by ΔP measurement.

Because of the pressure drop across a filter, filters may not be tolerable in liquid systems. However, components may be protected from damage due to large particulates by a screen which introduces only a slight pressure drop.

Some of the more common filter element types are listed in table 10-I. A chart of square mesh wire screen sizes is included as table 10-II and standard grades of twilled dutch double weave wire cloth in table 10-III.

Filter elements of bronze, nickel, monel, or stainless steel are preferred. Typical elements are sintered bronze or screens of materials as listed in table 10-III. In operation, the manufacturer's maximum recommended pressure drop must not be exceeded because the loss of filter element integrity in an oxygen line or component could easily result in a fire.

When conical wire mesh screens are used, the cone must point upstream so that the screen will be self-cleaning by washing debris to the wall of the pipe. This orientation will result in collecting particles in a location which will result in the least possible pressure drop across the screen.

TABLE 10-I. - FILTER ELEMENT TYPES[a]

Filter	Filtration	Filtration rating range available, μ[b]	
		Nominal[c]	Absolute
Square mesh wire cloth or twilled Dutch single weave wire cloth	Surface	--------	40 and up
Sintered square mesh wire cloth or sintered twilled Dutch single weave cloth	Surface	--------	40 and up
Wound wire cloth	Depth	2 and up	---------
Twilled Dutch double weave wire cloth	Surface		8 to 100
Sintered porous metal	Depth	2 to 60	5 to 135
Composite sintered porous metal and mesh	Depth	2 to 60	---------
Etched disk	Depth	0.5 to 75	1 to 150
Edge (ribbon or stacked washer)	Surface	40 to 125 25 to 500	---------

[a]Ref. 51. p. 5.10.4-2.

[b]1 μ = 39.4 μin.

[c]Nominal rate shown only for reference when absolute ratings are not commonly employed for medium.

TABLE 10-II. - SQUARE MESH WIRE SCREEN SIZES[a]

U. S. sieve number (mesh)	50	100	140	200	270	325	400
Wire per in.	52.36	101.01	142.86	200.0	270.26	323.00	400
Wire diameter, in.	0.0085	0.0043	0.0030	0.0021	0.0015	0.0012	0.0010
Sieve opening, in.	0.0117	0.0059	0.0041	0.0029	0.0021	0.0017	0.0015
Sieve opening, μ	297	149	105	74	63	44	37

[a]Ref. 51, p. 5.10.2-2.

TABLE 10-III. - STANDARD GRADES OF TWILLED DUTCH DOUBLE WEAVE WIRE CLOTH[a]

(a) Wire cloth specifications

Grade	Nominal mesh count	Absolute micron rating	Wire diameter, μ		Nominal thickness, in.	Nominal weight, lbf/ft^2
			Warp	Shute		
01	24 × 230	100.0	380	220	0.0350	-----
02	30 × 250	75.0	250	200	.0280	0.719
03	50 × 250	50.0	250	200	.0280	.633
04	80 × 745	35.0	100	76	.0110	.241
28	165 × 1350	20.0	70	40	.0057	.159
41	200 × 1350	15.0	70	40	.0057	.161
51	250 × 1350	12.5	55	40	.0051	.160
67	325 × 2100	10.0	38	25	.0033	.100
75	375 × 2150	7.5	34	24.5	.0031	.095

(b) Allowable tolerances

Warp wire mesh count		Shute wire mesh count		Wire diameter	
Warp wire mesh count	Number of tolerance wires per inch	Shute wire mesh count	Number of tolerance wires per inch	Wire diameter, μ	Diameter tolerance, μ
Up to 49	±0.3	Up to 250	±20	Up to 25	±1/2
50 to 74	±.5	251 to 1000	±25	26 to 99	±1
75 to 99	±1.1	1001 to 2000	±30	100 to 199	±2
100 to 400	±2.0	2001 to 3000	±50	200 to 400	±3

(c) Available materials

Finest available grade	Finest wire size, μ	Type of material
Grade 75: 375 × 2150	18	AISI 304, 304L stainless steel
Grade 41: 200 × 1350	25	AISI 316, Monel, nickel
Grade 04: 80 × 745	50	AISI 321, 347 stainless steel

[a]Ref. 51, p. 5.10.4-4.

APPENDIX A

DEFINITION OF ABBREVIATIONS AND ACRONYMS AND TRADE NAME IDENTIFICATION

This appendix contains a listing of acronyms and abbreviations used in the text along with their definitions. Also included is a listing of chemical terms used and their common trade names. This list of chemical terms is included only for assistance to the reader and is not meant to imply endorsement of the trade names listed nor disapproval of those which may have been omitted.

DEFINITION OF ABBREVIATIONS AND ACRONYMS

Term	Definition
ABS	acrylonitrile-butadiene-styrene copolymer
AN	Air Force/Navy Aeronautical
ANSI	American National Standards Institute
ASRDI	Aerospace Safety Research and Data Institute
ASTM	American Society for Testing and Materials
ASME	American Society of Mechanical Engineers
CGA	Compressed Gas Association
CM	command module
CNR	carboxy nitroso rubber
CTFE	(poly) chlorinatedtrifluoroethylene
DN	bearing bore × rpm
DOT	Department of Transportation
EB	electron beam
EPR	ethylene propylene rubber

Term	Definition
EVA	extravehicular activity
FEP	fluorinated ethylene-propylene (copolymer)
FLOX	fluorine-oxygen mixtures
FRC	Flight Research Center
g	acceleration of gravity (32.2 ft/sec^2)
GMA	gas metal arc
GN_2	gaseous nitrogen
GOX	gaseous oxygen
GSE	ground support equipment
GTA	gas tungsten arc
JP4	jet fuel grade kerosene
JPL	Jet Propulsion Laboratory
JSC	Johnson Space Center
KSC	Kennedy Space Center
LeRC	Lewis Research Center
LM	lunar module
LOX	liquid oxygen
MC	Marshall Center (Marshall Spaceflight Center)
MS	Military Standard
MSC	Manned Spacecraft Center, see JSC
MSFC	Marshall Space Flight Center
NASA	National Aeronautics and Space Administration
NBS	National Bureau of Standards
OPS	oxygen purge system
PBI	polybenzimidazole
PLSS	Personnel Life Support System
PV	pressure-velocity
PVC	polyvinylchloride

Term	Definition
RCS	reaction control system
RTV	room temperature vulcanizing
SCFM	standard cubic feet per minute
SCIM	standard cubic inches per minute
SM	service module
STP	standard temperature and pressure
TFE	(poly) tetrafluoroethylene
TGA	thermogravimetric analysis
TIG	tungsten inert gas
TNT	trinitrotoluene
T.O.	technical order
USAF	United States Air Force

TRADE NAME IDENTIFICATION

Trade or common name	Chemical name or definition
AFD-E-124D	terpolymer of perfluorovinyl ether and Teflon (TFE) (experimental fluoroelastomer)
Allpax 500	fluorolube treated asbestos fiber with styrene butadiene binder
Armalon	Teflon (TFE) coated glass fiber
Arylon T-3198	polyaryl ether
Atlac 711	polyester
Avisun 2356	polypropylene
Bakelite phenolic	phenolic resin
Buna-S	polybutadiene-styrene copolymer
Butyl rubber	isobutylene-isoprene copolymer
Cab-o-sil	sintered colloidal silica particles
Celcon	polyacetal

Trade or common name	Chemical name or definition
Cosden 825 TV	polystyrene
Cycolac KT and KL	acrylonitrile-butadiene-styrene copolymer (ABS)
Cycovin KA	acrylonitrile-butadiene-styrene copolymer (ABS)
Dacron	polyester fiber (polyethylene terephthalate)
DC-33	silicone grease
DC-41	silicone grease
Dowclene 10	emulsion of caustic soda, detergent, and sequestering agent
Drilube 822	fluorinated silicone
Durez 2311	acrylonitrile-butadiene-styrene copolymer (ABS)
Duroid (5000 series)	filled Teflon (TFE)
Dylene 8X	polystyrene
Epon	epoxy adhesive
Fluorel	vinylidene fluoride-hexafluoropropylene copolymer
Fluorogold	fiberglass filled Teflon (TFE)
Fluorogreen	fiberglass filled Teflon (TFE)
Fluorosilicone	fiberglass filled Teflon (TFE)
Formvar	polyvinyl formal
Geon 101	polyvinylchloride (PVC)
Glyptal	polyester plasticiser
Halocarbon	halogenated hydrocarbon
Halon	polytetrafluoroethylene (TFE)
Halon TVS	modified chlorotrifluoroethylene (CTFE)
Kel-F 81	chlorotrifluoroethylene (CTFE)
Kel-F 82	chlorotrifluoroethylene-vinylidene fluoride copolymer

Trade or common name	Chemical name or definition
Kynar	vinylidene fluoride
Lexan	polycarbonate
Lucite	polymethylmethacrylate
Mylar	polyester film (polyethylene terephthalate)
Natural rubber	polyisoprene
Neoprene	polychlorobutadiene
Nitrile rubber	polybutadiene acrylomitrile
Nomex	polyimide fiber (aromatic polyamide)
Noryl 731	polyphenylene oxide polymer
Nylon	polyamide
Orlon	polyacrylonitrile fiber
Oxyseal	graphite and chlorinated hydrocarbon
Perlite	volcanic glass
Plaskon 1070	polypropylene
Plaskon 2200 and 2400	chlorotrifluoroethylene
Plenco 200D	epoxy
Plexiglass	polymethylmethacrylate
Polyox WSR-35	polyethylene oxide
Profax 6505	polypropylene
RTV polymers	polysiloxane
Rulon	filled Teflon (TFE)
Salox-M	bronze-filled Teflon (TFE)
Santocel A	silica gel
Saran	polyvinylidene chloride
Shell 325	polystyrene
Silastic	polysiloxane
Silicone	polysiloxane
Teflon	polytetrafluoroethylene (TFE)

Trade or common name	Chemical name or definition
Textolite	phenolic-paper laminate
Turco	nonsilicated alkaline cleaner
Vespel	polyimide
Viton A	vinylidene fluoride-hexafluoropropylene copolymer

APPENDIX B

CONVERSION FACTORS

NASA policy dictates the use of the International System of Units (SI) as the standard in published documents. This volume, because of its wide use of references which present data in various systems of units, has deviated from that policy. Accordingly, the following tables of conversion factors for the most frequently used properties are included here. A more complete list of conversion factors for the SI system may be found in NASA SP-7012 - "International System of Units - Physical Constants and Conversion Factors."

ENERGY

abs J	int. J	cal	t.[a] cal	Btu	int. kW-hr	ft-lb (wt)	liter-atm	hp-hr
1	0.999835	0.239006	0.238849	0.947831×10^{-3}	2.77732×10^{-7}	0.737561	9.86896×10^{-3}	3.72505×10^{-7}
1.000165	1	0.239045	0.238889	0.947988×10^{-3}	2.777778×10^{-7}	0.737682	9.87058×10^{-3}	3.72567×10^{-7}
4.1840	4.1833	1	0.999346	3.96573×10^{-3}	1.162030×10^{-6}	3.08595	4.12917×10^{-2}	1.558562×10^{-6}
4.18674	4.18605	1.000654	1	3.96832×10^{-8}	1.162791×10^{-6}	3.08797	4.13187×10^{-2}	1.559582×10^{-6}
1055.040	1054.866	252.101	251.996	1	2.93018×10	778.156	10.41215	3.93008×10^{-4}
3 600 594	3 600 000	860 563	860 000	3412.76	1	2 655 656	35534.1	1.341241
2 684 525	2 684 082	641 617	641 197	2544.48	0.745578	1 980 000	26493.5	1
1.355821	1.355597	0.324049	0.323837	1.285089×10^{-3}	3.76555×10^{-7}	1	1.338054×10^{-2}	5.05051×10^{-7}
101.3278	101.3111	24.2179	24.2021	0.0960417	2.81420×10^{-5}	74.7354	1	3.77452×10^{-5}

[a]Thermochemical.

THERMAL CONDUCTIVITY

$\frac{(W)(cm)}{(cm^2)(K)}$	$\frac{(W)(in.)}{(in.^2)(^oF)}$	$\frac{(cal)(cm)}{(sec)(cm^2)(K)}$	$\frac{(Btu)(in.)}{(hr)(ft^2)(^oF)}$	$\frac{(Btu)(ft)}{(hr)(ft^2)(^oF)}$	$\frac{(Btu)(in.)}{(sec)(in.^2)(^oF)}$	$\frac{(Btu)(in.)}{(hr)(in.^2)(^oF)}$
1	1.411	0.2389	6.9340×10^{2}	57.79	1.338×10^{-3}	4.816
0.7087	1	0.1693	4.914×10^{2}	40.95	9.480×10^{-4}	3.413
4.1858	5.907	1	2.9027×10^{3}	2.419×10^{2}	5.602×10^{-3}	20.16
1.442×10^{-3}	2.035×10^{-3}	3.445×10^{-4}	1	8.33×10^{-2}	1.929×10^{-6}	6.944×10^{-3}
1.730×10^{-2}	2.442×10^{-2}	4.135×10^{-3}	12	1	2.315×10^{-5}	8.33×10^{-2}
7.4738×10^{2}	1.0548×10^{3}	1.785×10^{2}	5.184×10^{5}	4.3191×10^{4}	1	3.600×10^{3}
0.2076	0.2930	4.960×10^{-2}	1.44×10^{2}	12	2.778×10^{-4}	1

PERMEABILITY

$$\left[\text{Standard unit: } \frac{\text{cc(STP)cm}}{(\text{cm}^2)(\text{sec})(\text{bar})} = 1.\right]$$

Units system	Multiplication factor for converting to standard units	Units system	Multiplication factor for converting to standard units
$\frac{\text{scc cm}}{\text{cm}^2 \text{ sec cm Hg}}$	7.501×10^{1}	$\frac{\text{scc mil}}{\text{cm}^2 \text{ day atm}}$	2.901×10^{-8}
$\frac{\text{scc cm}}{\text{cm}^2 \text{ sec mm Hg}}$	7.501×10^{2}	$\frac{\text{scc mil}}{\text{in.}^2 \text{ hr lb/in.}^2}$	1.023×10^{-5}
$\frac{\text{scc mm}}{\text{cm}^2 \text{ sec sm Hg}}$	7.501	$\frac{\text{liter mm}}{\text{cm}^2 \text{ sec mm Hg}}$	7.501×10^{4}
$\frac{\text{scc mm}}{\text{m}^2 \text{ day atm}}$	1.142×10^{-10}	$\frac{\text{scc mm}}{\text{cm}^2 \text{ hr atm}}$	2.741×10^{-5}
$\frac{10^{-5} \text{ ft}^3 \text{ mil}}{\text{min ft}^2 \text{ atm}}$	1.273×10^{-8}	$\frac{\text{scc mil}}{100 \text{ in.}^2 \text{ day } 17.3 \text{ psi}}$	3.82×10^{-9}
$\frac{\text{scc mm}}{\text{cm}^2 \text{ sec atm}}$	9.8692×10^{-2}	$\frac{\text{scc mil}}{\text{in.}^2 \text{ day atm}}$	2.901×10^{-12}
$\frac{\text{scc mil}}{100 \text{ in.}^2 \text{ day atm}}$	4.497×10^{-11}	$\frac{\text{scc mil}}{100 \text{ m}^2 \text{ day } 17.7 \text{ psi}}$	2.408×10^{-14}
$\frac{\text{scc cm}}{\text{cm}^2 \text{ sec atm}}$	9.8692×10^{-1}		

LENGTH

cm	mm	μ	mμ	Å
1	10	10^{4}	10^{7}	10^{8}
10^{-1}	1	10^{3}	10^{6}	10^{7}
10^{-4}	10^{-3}	1	10^{3}	10^{4}
10^{-7}	10^{-6}	10^{-3}	1	10
10^{-8}	10^{-7}	10^{-4}	10^{-1}	1

cm	m	in.	ft
1	0.01	0.397	0.032808333
100	1	39.37	3.2808333
2.5400051	0.025400051	1	0.083333333
30.48061	0.30480061	12	1

SURFACE TENSION

dyne/cm	erg/cm^2	mg/mm	mg/in.	lb/ft
1	1	0.10197	2.5901	6.853×10^{-6}
9.80665	9.80665	1	25.400051	6.72×10^{-4}
0.38609	0.38609	0.03937	1	2.6459×10^{-5}
14592.15	14592.15	1488	37 794	1

VISCOSITY[a]

poise[b]	(lb force)(sec)/ft^2[c]	lb mass/ft-sec
1	2.0886×10^{-3}	0.0672
4.788×10^{2}	1	32.174
14.9	3.108×10^{-2}	1

[a]Absolute viscosity; kinetic viscosity = absolute viscosity/density.
[b]Poise = 1 (dyne)(sec)/cm^2 = 1 g/(cm)(sec).
[c]1 (lb force)(sec)/ft^2 = 1 slug/ft-sec.

FORCE[a]

	dynes	g	kg	J/cm	J/m	lb	poundals
dynes	1	980.7	9.807×10^{5}	10^{7}	10^{6}	4.448×10^{5}	1.383×10^{4}
g	1.020×10^{-3}	1	1000	1.020×10^{4}	102.0	453.6	14.10
kg	1.020×10^{-6}	0.001	1	10.20	0.1020	0.4536	1.410×10^{-2}
J/cm	10^{-7}	9.807×10^{-5}	9.807×10^{-2}	1	0.01	4.448×10^{-2}	1.383×10^{-3}
N/m or J/m	10^{-5}	9.807×10^{-3}	9.807	100	1	4.448	0.1383
lb	2.248×10^{-6}	2.205×10^{-3}	2.205	22.48	0.2248	1	3.108×10^{-2}
poundals	7.233×10^{-5}	7.093×10^{-2}	70.93	723.3	7.233	32.17	1

[a]Conversion factors between absolute and gravitational units apply only under standard acceleration due to gravity conditions.

AREA

cm^2	m^2	$in.^2$	ft^2
1	10^{-4}	0.15499969	1.0763367×10^{-3}
10^4	1	1549.9969	10.763867
6.4516258	6.4516258×10^{-4}	1	6.9444444×10^{-3}
929.03412	0.092903412	144	1

VOLUME

cm^3	$in.^3$	ft^3	mliter	liter	gal
1	0.061023378	3.5314455×10^{-5}	0.9999720	0.9999720×10^{-3}	2.6417047×10^{-4}
16.387162	1	5.7870370×10^{-4}	16.38670	1.638670×10^{-2}	4.3290043×10^{-3}
28317.017	1728	1	28316.22	28.31622	7.4805195
1.000028	0.06102509	3.531544×10^{-5}	1	0.001	2.641779×10^{-4}
1.000.028	61.02509	0.03531544	1000	1	0.2641779
3785.4345	231	0.13368656	3785.329	3.785329	1

MASS

g	kg	lb	metric ton	ton
1	10^{-3}	2.2046223×10^{-3}	10^{-6}	1.1023112×10^{-6}
10^3	1	2.2046223	10^{-3}	1.1023112×10^{-3}
453.59243	0.45359243	1	4.5359234×10^{-4}	5×10^{-4}
10^6	10^3	2204.6223	1	1.1023112
907184.86	907.18486	2000	0.90718486	1

SPECIFIC HEAT

cal/(g)(K)	J/(g)(K)	W-sec/(g)(K)	Btu/(lb)(^oR)
1	4.1840	4.1840	0.9995826
0.239006	1	1	0.238849
1.000654	4.18674	4.18674	1

ENTHALPY

cal/g	J/g	W-sec/g	Btu/lb
1	4.1840	4.1840	1.798823
0.239006	1	1	0.429929
0.555919	2.32597	2.32597	1

DENSITY

g/cm^3	$g/in.^3$	kg/gal	kg/ft^3	lb/gal	lb/ft^3
1	16.3872	3.78543	28.3170	8.34545	62.4283
0.0610232	1	0.23100	1.72800	0.509268	3.80959
0.264171	4.32900	1	7.48052	2.20462	16.4917
0.0353145	0.578704	0.133681	1	0.294715	2.20462
0.119826	1.96360	0.453592	3.39311	1	7.48052
0.0160184	0.262496	0.0606365	0.453592	0.133681	1

PRESSURE

	atm	bars or dynes/cm^2	cm Hg at 0^o C	in. Hg at 0^o C	in. H_2O at 4^o C	kg/m^2	lb/ft^2	lb/in.^{2}	tons (short)/ft^2	N/m^2	torr or mm Hg	micron	bar
atm	1	9.869×10^{-7}	1.316×10^{-2}	3.342×10^{-2}	2.458×10^{-3}	9.678×10^{-5}	4.725×10^{-4}	6.804×10^{-2}	0.9450	9.869×10^{-6}	1.316×10^{-3}	1.316×10^{-6}	0.9869233
bars or dynes/cm^2	1.013×10^{6}	1	1.333×10^{4}	3.386×10^{4}	2.491×10^{-3}	98.07	478.8	6.895×10^{4}	9.576×10^{5}	10	1333	1.333	10^{6}
cm Hg at 0^o C	76.00	7.501×10^{-5}	1	2.540	0.1868	7.356×10^{-3}	3.591×10^{-2}	5.171	71.83	7.501×10^{-4}	0.1	10^{-4}	75.006
in. Hg at 0^o C	29.92	2.953×10^{-5}	0.3937	1	7.355×10^{-2}	2.896×10^{-3}	1.414×10^{-2}	2.036	28.28	2.953×10^{-4}	3.937×10^{-2}	3.937×10^{-5}	29.52993
in. H_2O at 4^o C	406.8	4.015×10^{-4}	5.354	13.60	1	3.937×10^{-2}	0.1922	27.68	384.5	4.015×10^{-3}	0.5354	5.354×10^{-4}	402
kg/m^2	1.033×10^{4}	1.020×10^{-2}	136.0	345.3	25.40	1	4.882	703.1	9765	0.1020	13.60	1.360×10^{-2}	1.0197
lb/ft^2	2116	2.089×10^{-3}	27.85	70.73	5.202	0.2048	1	144	2000	2.089×10^{-2}	2.785	2.785×10^{-3}	2188
lb/in.^{2}	14.70	1.450×10^{-5}	0.1934	0.4912	3.613×10^{-2}	1.422×10^{-3}	6.944×10^{-3}	1	13.89	1.450×10^{-4}	1.934×10^{-2}	1.934×10^{-5}	14.5038
tons (short)/ft^2	1.058	1.044×10^{-6}	1.392×10^{-2}	3.536×10^{-2}	2.601×10^{-3}	1.024×10^{-4}	0.0005	0.0720	1	1.044×10^{-5}	1.392×10^{-3}	1.392×10^{-6}	1.044
N/m^2	1.013×10^{5}	10^{-1}	1.333×10^{3}	3.386×10^{3}	2.491×10^{-4}	9.807	47.88	6.895×10^{3}	9.576×10^{4}	1	133.3	0.1333	1×10^{5}
torr or mm Hg	760	7.501×10^{-4}	10	25.40	1.868	7.356×10^{-2}	0.3591	51.71	718.3	7.501×10^{-3}	1	10^{-3}	750.0617
micron	7.60×10^{5}	0.7501	10^{4}	2.540×10^{4}	1868	73.56	359.1	5.171×10^{4}	7.183×10^{5}	7.501	1000	1	7.5×10^{5}

Page intentionally left blank

APPENDIX C

SOLUBILITY OF HYDROCARBONS OR CARBON DIOXIDE IN OXYGEN

This appendix contains graphical presentations of the solubilities of some saturated and unsaturated hydrocarbons and carbon dioxide in liquid oxygen as a function of oxygen temperature.

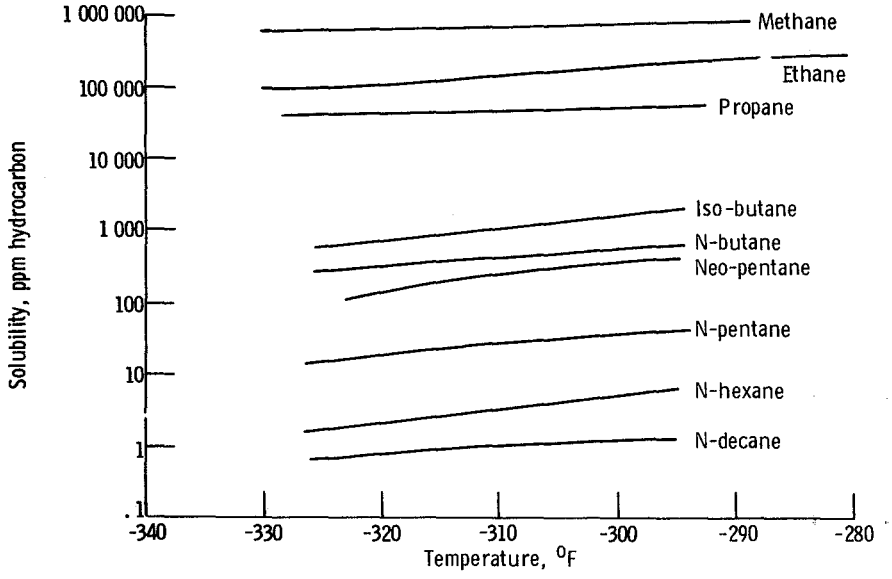

Figure C-1. - Solubility of saturated hydrocarbons in liquid oxygen (ref. 145, p. 19).

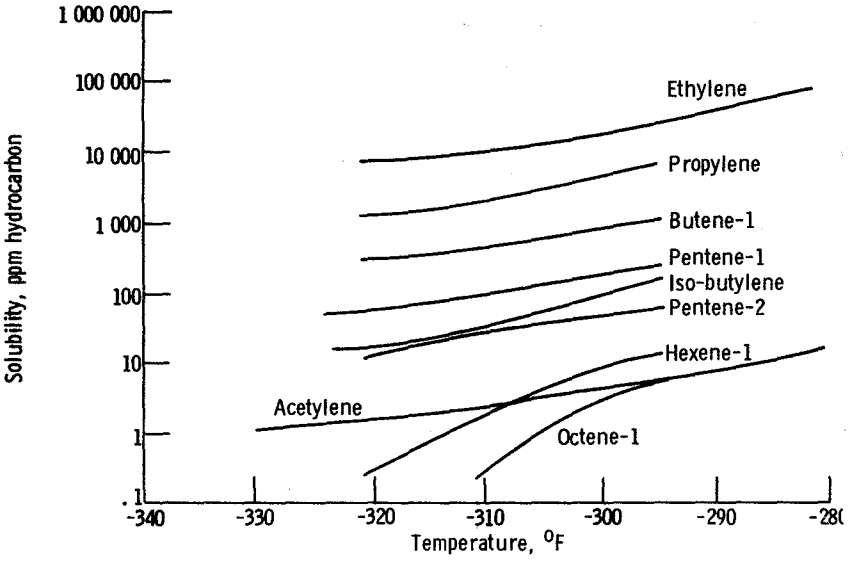

Figure C-2. - Solubility of unsaturated hydrocarbons in liquid oxygen (ref. 145, p. 20).

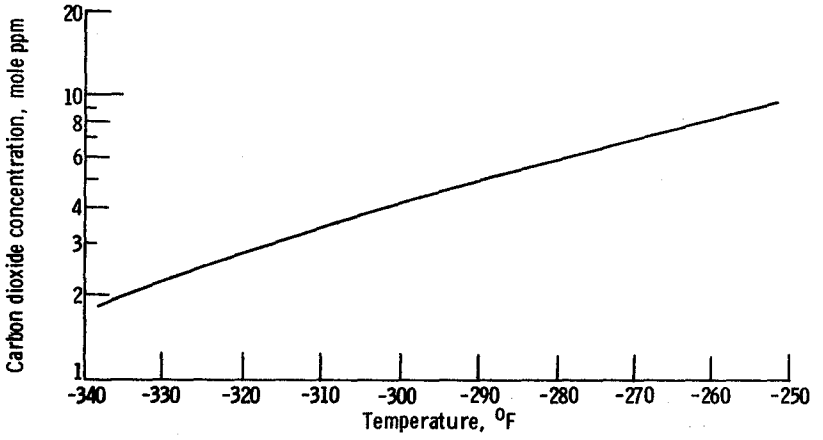

Figure C-3. - Solubility of carbon dioxide in liquid oxygen (ref. 2, p. 22).

APPENDIX D

IGNITION TEMPERATURES OF METALS

This appendix contains figures showing the measured ignition temperatures of metals and a table (from ref. 146) giving ignition temperature ranges for various magnesium alloys. The measured ignition temperatures of metals are plotted against the logarithm of oxygen pressure. In cases where the test environment was other than 100 percent oxygen, such as air, oxygen-nitrogen or oxygen-helium mixtures, the pressures plotted are oxygen partial pressures (i.e., if test gas is air at 1 atmosphere, the oxygen pressure plotted is 0.21 atmosphere).

The data plotted have been compiled from several references. These references are identified on the plots. Accordingly, such variables as test procedures and techniques, instrumentation, test specimen shape and purity, and quenching effects of the diluent gas are not accounted for.

The following table gives the pages on which the ignition temperature of the metals are shown:

Figure	Metal	Page	Figure	Metal	Page
D-1(a)	Aluminum	182	D-1(k)	Zinc	184
D-1(b)	Copper		D-1(l)	Bismuth and barium	
D-1(c)	Iron		D-1(m)	Strontium and calcium	
D-1(d)	Lead		D-1(n)	Beryclo-10	
D-1(e)	Magnesium		D-1(o)	Brass	
D-1(f)	Molybdenum	183	D-1(p)	Mild (carbon) steel	185
D-1(g)	Tantalum		D-1(q)	Nickel alloys	
D-1(h)	Tin		D-1(r)	Stainless steel	
D-1(i)	Titanium		D-1(s)	Miscellaneous	
D-1(j)	Tungsten				

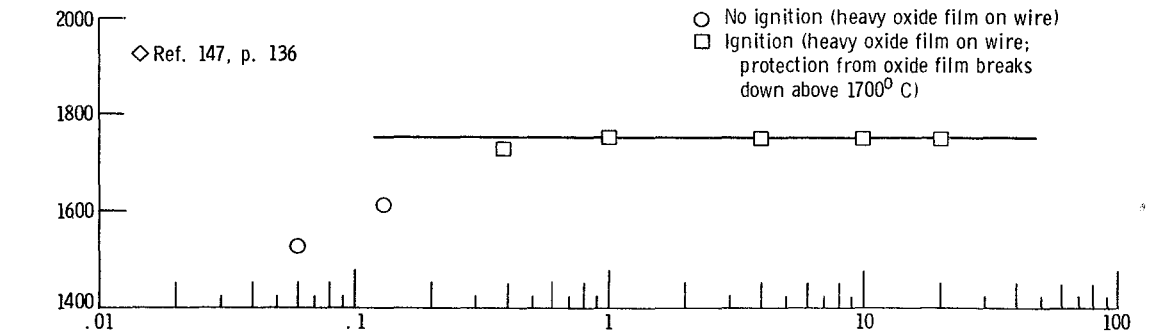

(a) Aluminum. Melting point of aluminum, ~680° C; boiling point of aluminum, 2467° C; melting point of Al_2O_3, 2045° C. Oxide film sufficiently strong to support molten aluminum wire until ignition conditions were reached.

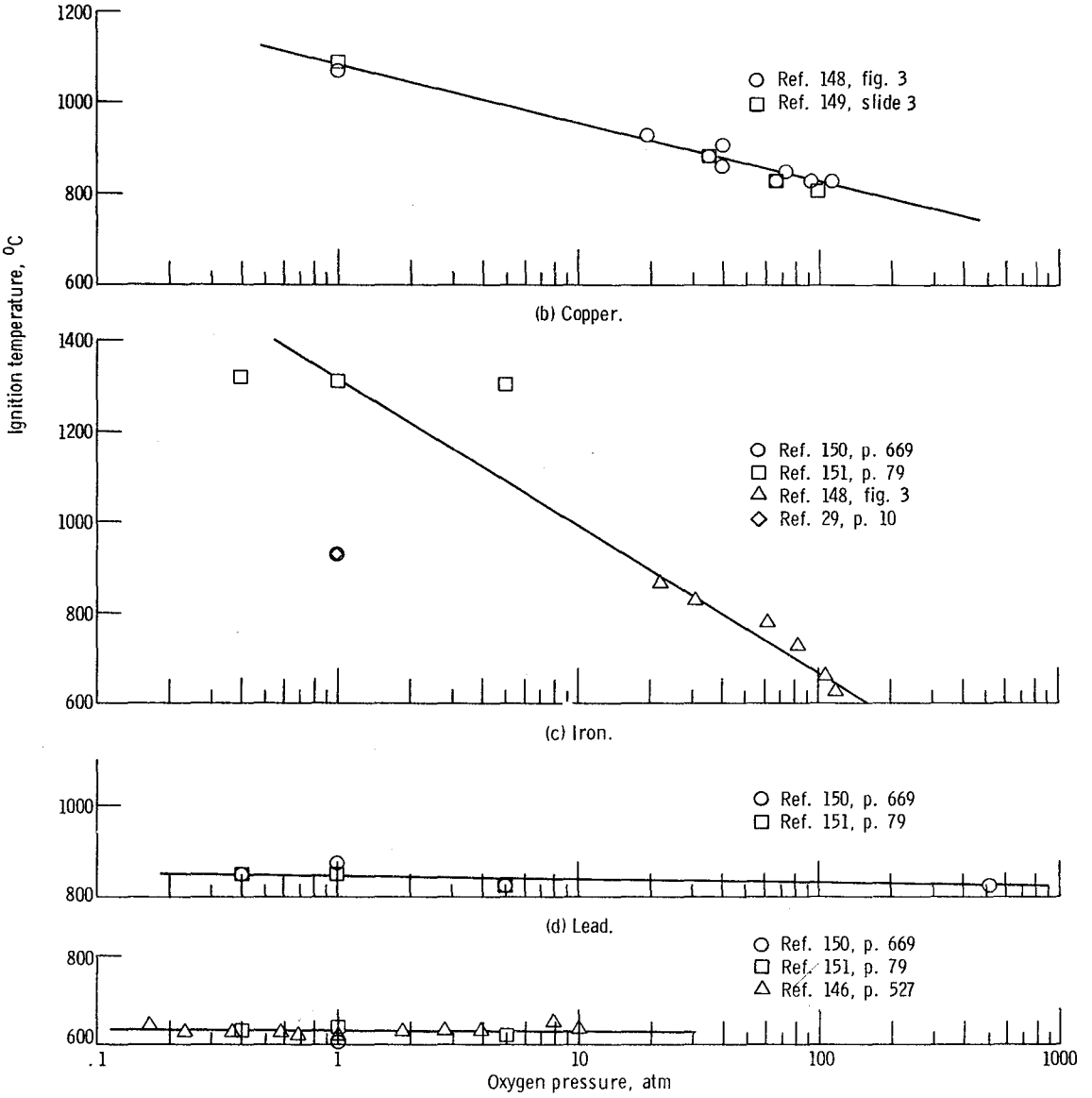

(b) Copper.

(c) Iron.

(d) Lead.

(e) Magnesium.

Figure D-1. - Ignition temperatures of metals.

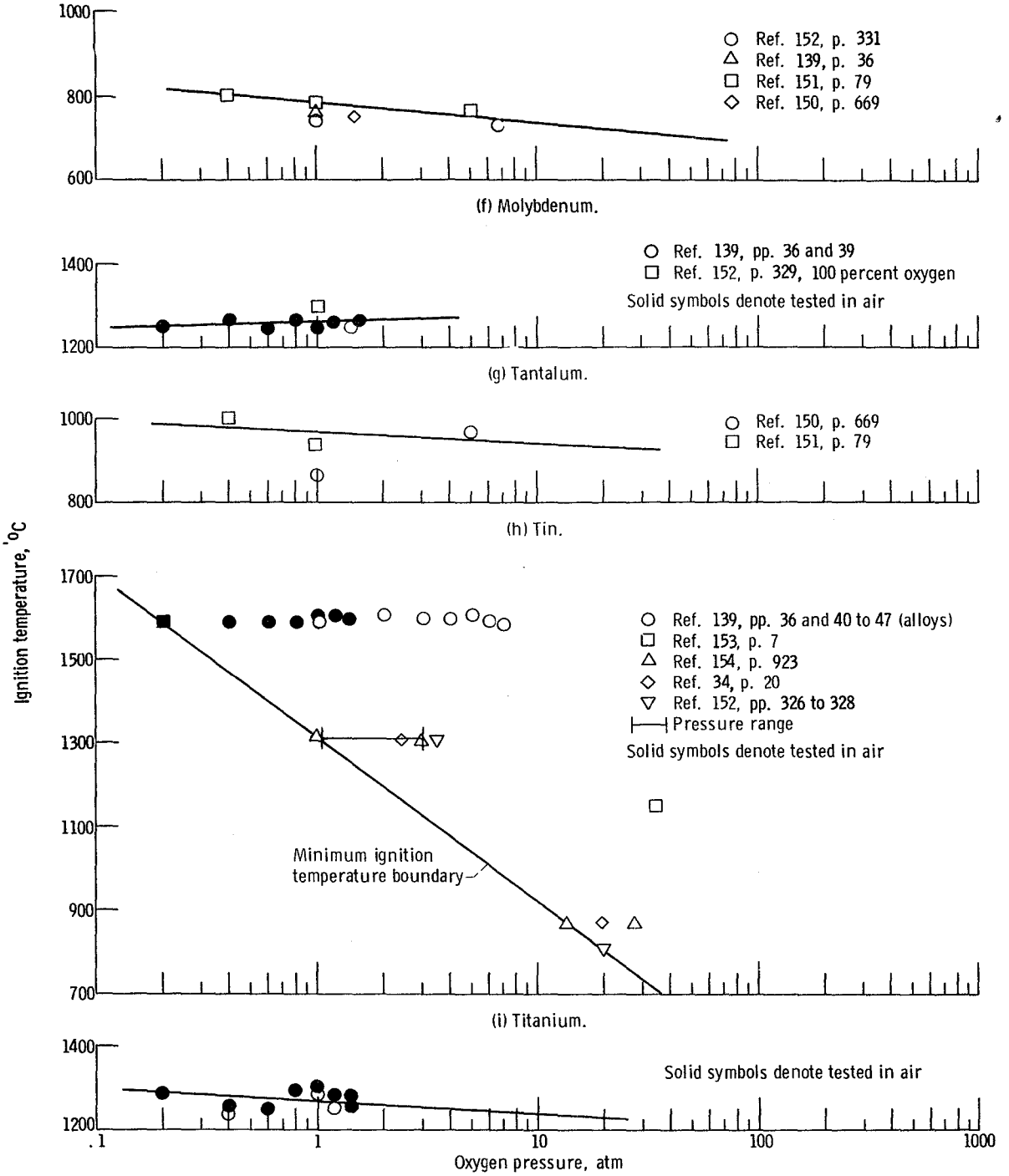

Figure D-1. - Continued.

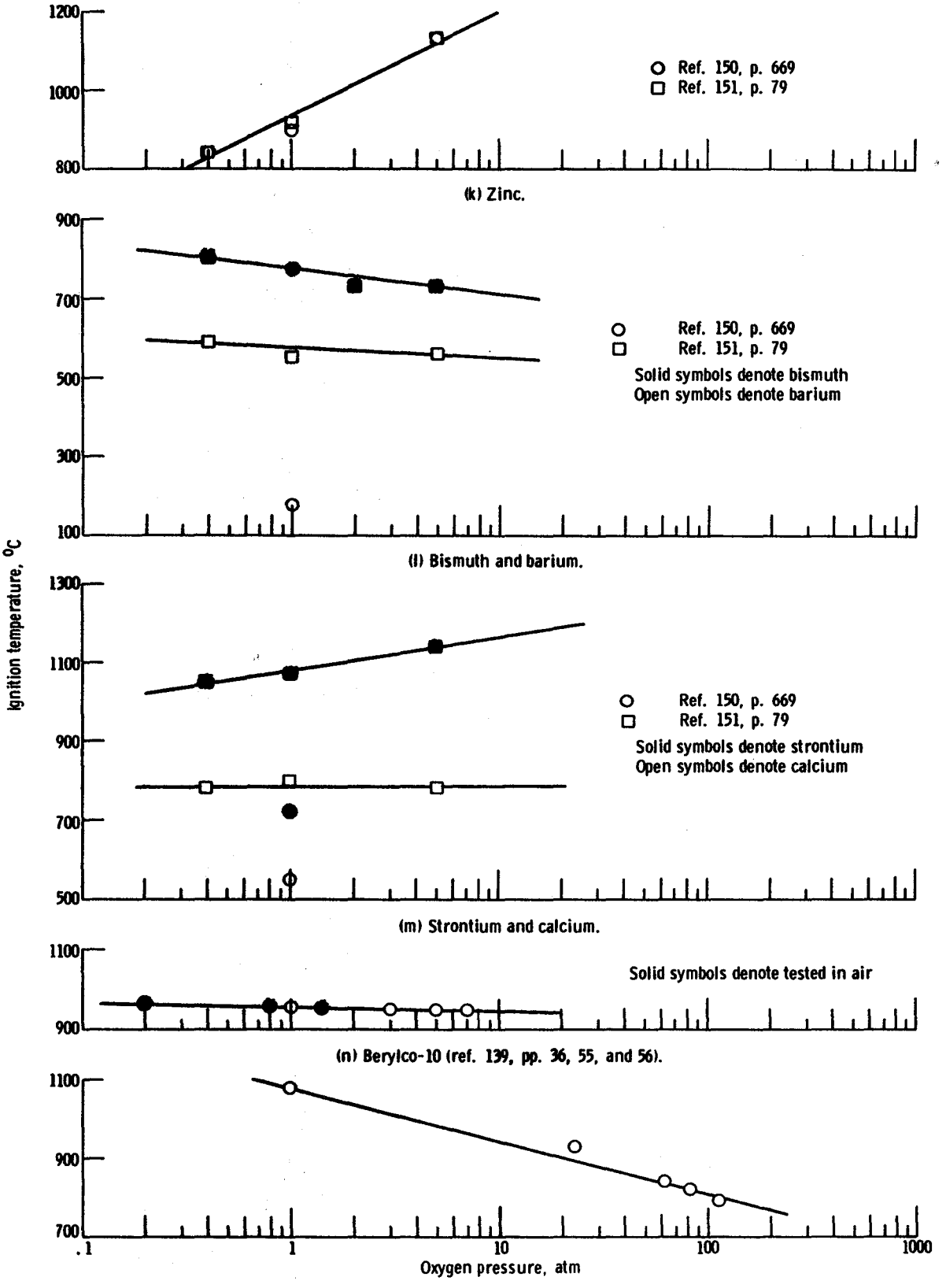

(k) Zinc.

(l) Bismuth and barium.

(m) Strontium and calcium.

(n) Berylco-10 (ref. 139, pp. 36, 55, and 56).

(o) Brass (ref. 148, fig 3).

Figure D-1. - Continued.

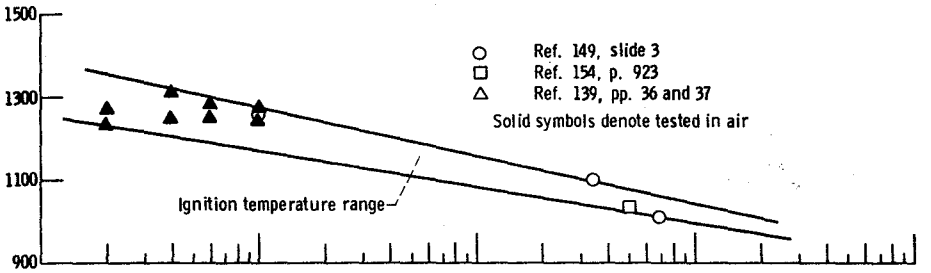

(p) Mild (carbon) steel.

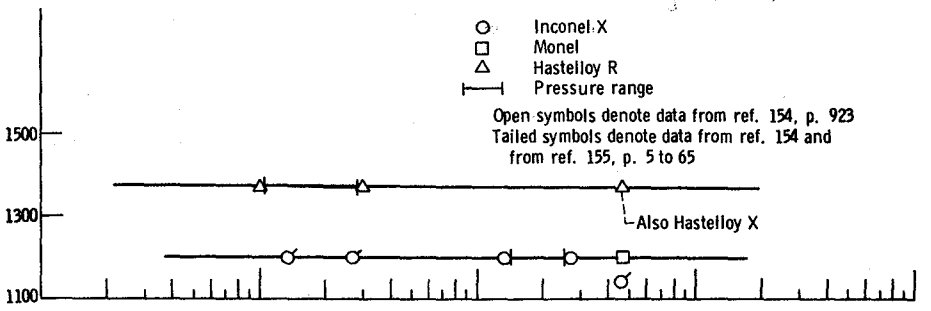

(q) Nickel alloys. (Ignition temperature of nickel above melting point, 1453° C.)

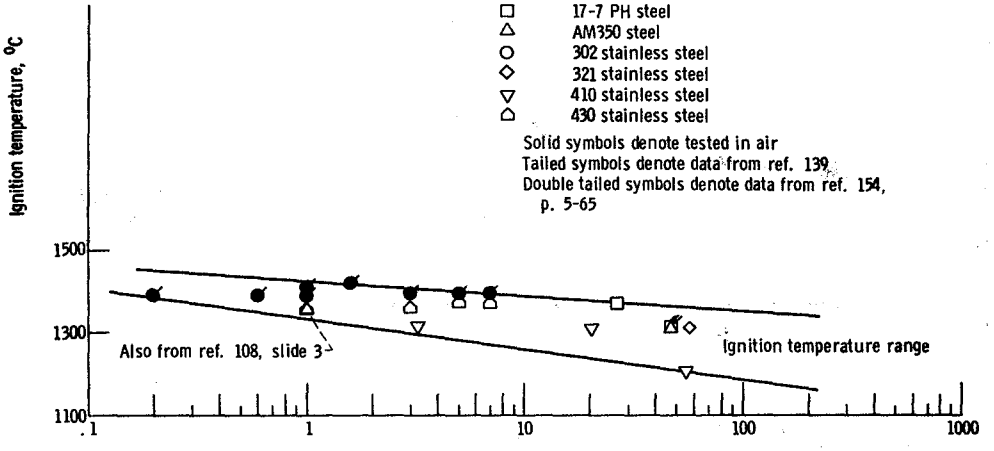

(r) Stainless steel.

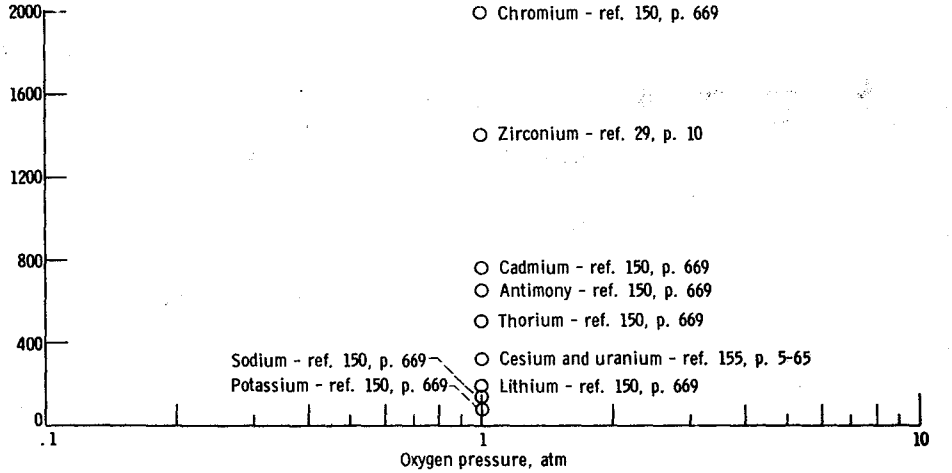

(s) Miscellaneous metals.

Figure D-1. - Concluded.

TABLE D-I. - IGNITION TEMPERATURE RANGES FOR VARIOUS MAGNESIUM ALLOYS AT 1-ATMOSPHERE OXYGEN PRESSURE[a]

Alloy	Ignition temperature range, °C
Mg - Ag (4.8 - 14.12 Ag)	537 to 550
Mg - Al (5.67 - 63.15 Al)	462 to 558
Mg - Al (80.33 - 93.73 Al)	>900
Mg - Cd (7.15 - 90.52 Cd)	517 to 612
Mg - Cu (10.3 - 30.76 Cu)	519 to 537
Mg - Ni (5.0 - 20.0 Ni)	508 to 517
Mg - Sn (9.88 - 25.62 Sn)	556 to 576
Mg - Pb (16.4 - 58.26 Pb)	504 to 575
Mg - Zn (3.04 - 89.33 Zn)	509 to 595

[a]Ref. 146, p. 524.

APPENDIX E

IGNITION TEMPERATURES OF NONMETALS

This appendix contains figures showing measured ignition temperatures of nonmetal (polymeric) materials. The measured ignition temperatures of nonmetal materials are plotted against the logarithm of oxygen pressure. In cases where the test environment was other than 100 percent oxygen, such as air, oxygen-nitrogen or oxygen-helium mixtures, the pressures plotted are oxygen partial pressures (i.e., if test gas is air at 1 atmosphere, the oxygen pressure plotted is 0.21 atmosphere).

The data plotted have been compiled from several references. These references are identified on the plots. Accordingly, such variables as test procedures and techniques, instrumentation, test specimen, shape and purity, and quenching effects of the diluent gas are not accounted for. Also, firepoint data from flash and firepoint testing have been included as ignition temperature data but are so identified on the plots.

The following table gives the pages on which the ignition temperatures of some nonmetals are shown:

Figure	Nonmetal	Page	Figure	Nonmetal	Page
E-1(a)	Butyl rubber	188	E-1(j)	Polytegrafluoroethylene (TFE)	190
E-1(b)	Fluorosilicone	↓	E-1(k)	Polyrinylalcohol	↓
E-1(c)	Neoprene		E-1(l)	Polyvinylchloride (PVC)	
E-1(d)	Nylon		E-1(m)	Polyvinylidene - fluoride	
E-1(e)	Polychlorotrifluoroethylene (CTFE)	189	E-1(n)	Silicone grease	191
			E-1(o)	Silicone rubber	↓
E-1(f)	Polyethylene		E-1(p)	Viton A	
E-1(g)	70 Percent polyethlene - 30 percent fiberglass		E-1(q)	Viton and Fluorel	
			E-1(r)	Dacron fabric	192
E-1(h)	Vespel		E-1(s)	Nomex fabric	↓
E-1(i)	Polymethylmethacrylate (Plexiglas or Lucite)	↓	E-1(t)	Nylon fabric	
			E-1(u)	Orlon fabric	

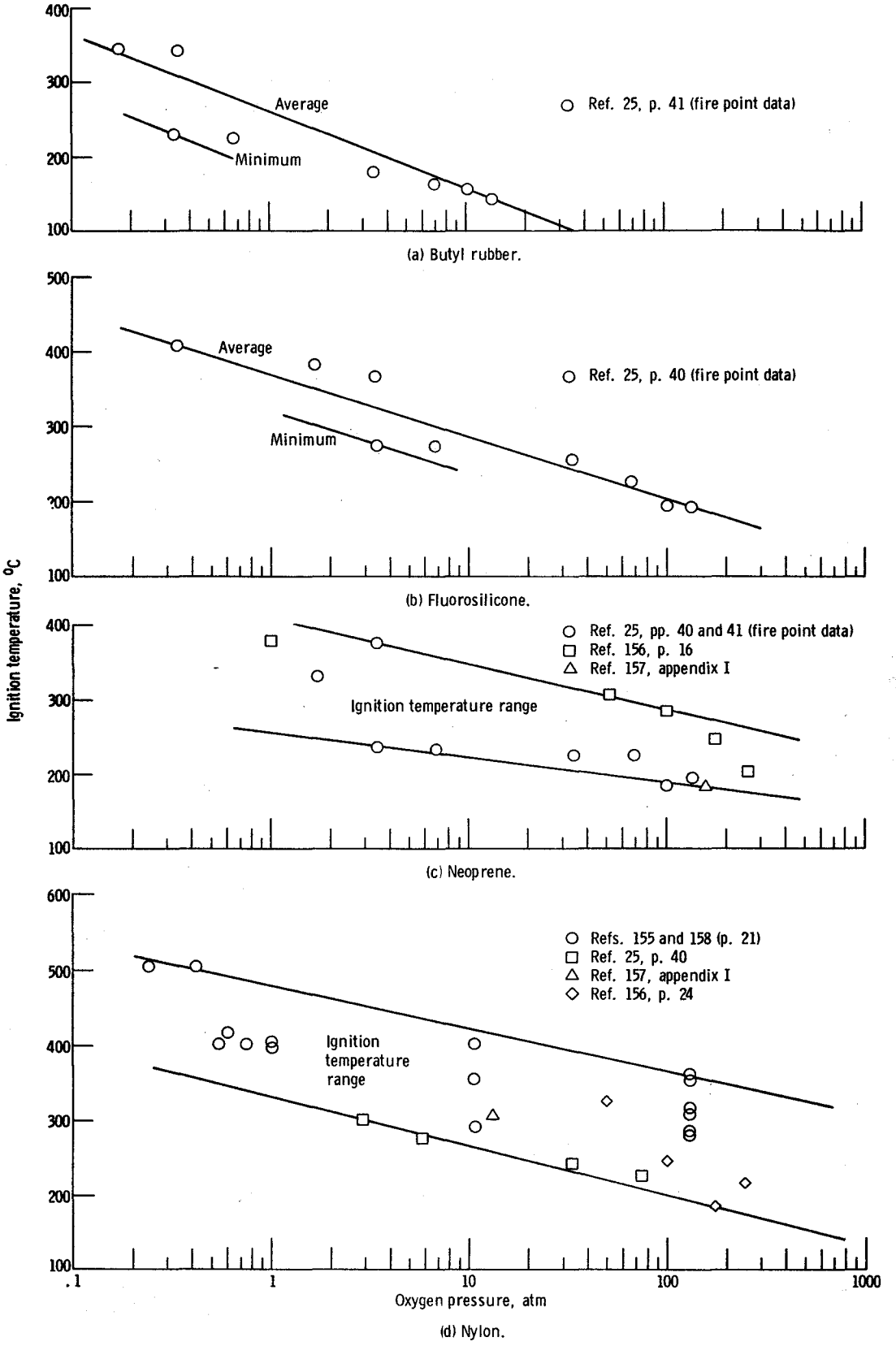

Figure E-1. - Ignition temperatures of nonmetals.

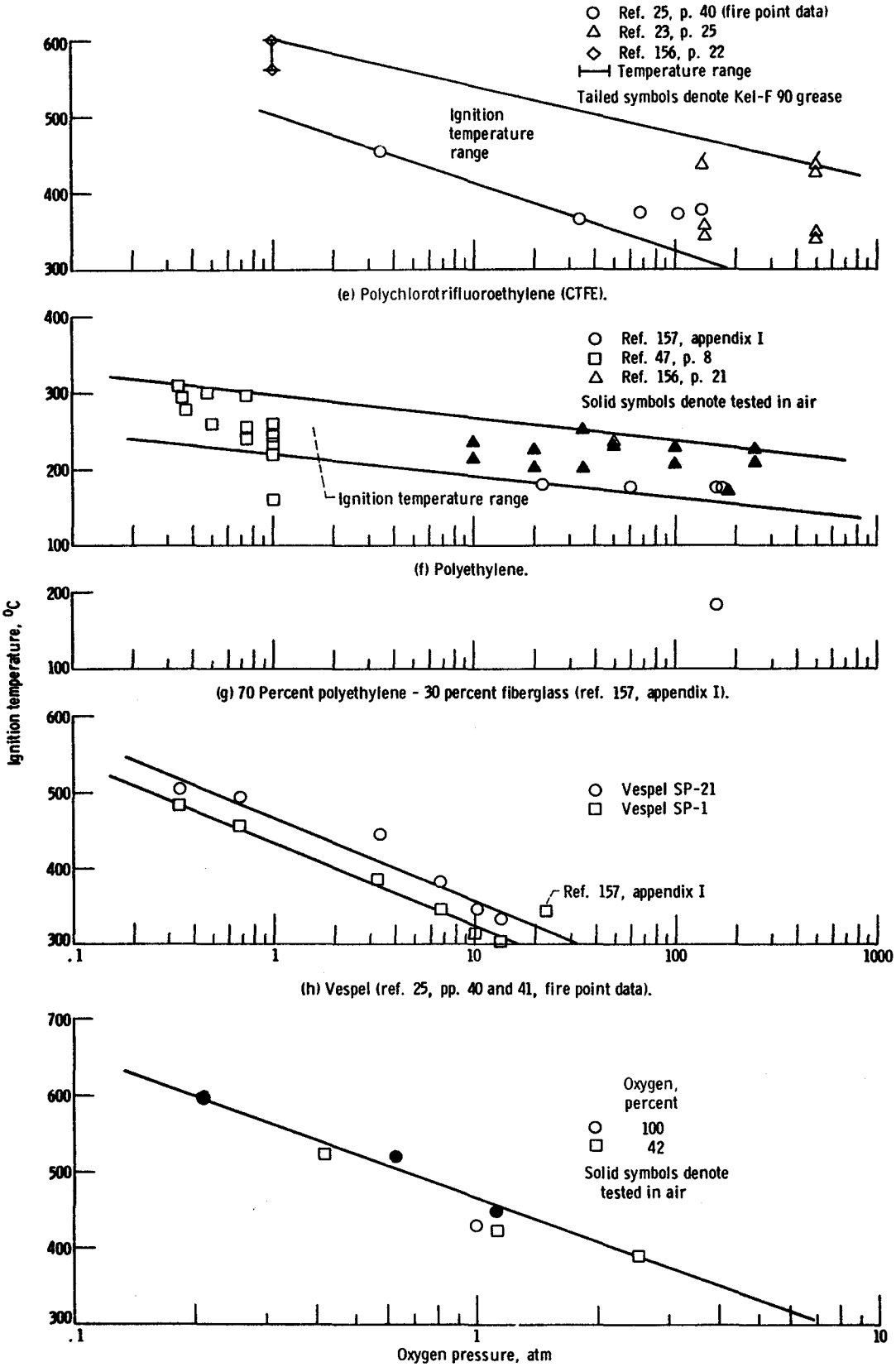

(e) Polychlorotrifluoroethylene (CTFE).

(f) Polyethylene.

(g) 70 Percent polyethylene - 30 percent fiberglass (ref. 157, appendix I).

(h) Vespel (ref. 25, pp. 40 and 41, fire point data).

(i) Polymethylmethacrylate (Plexiglas or Lucite) (ref. 159, p. 6).

Figure E-1. - Continued.

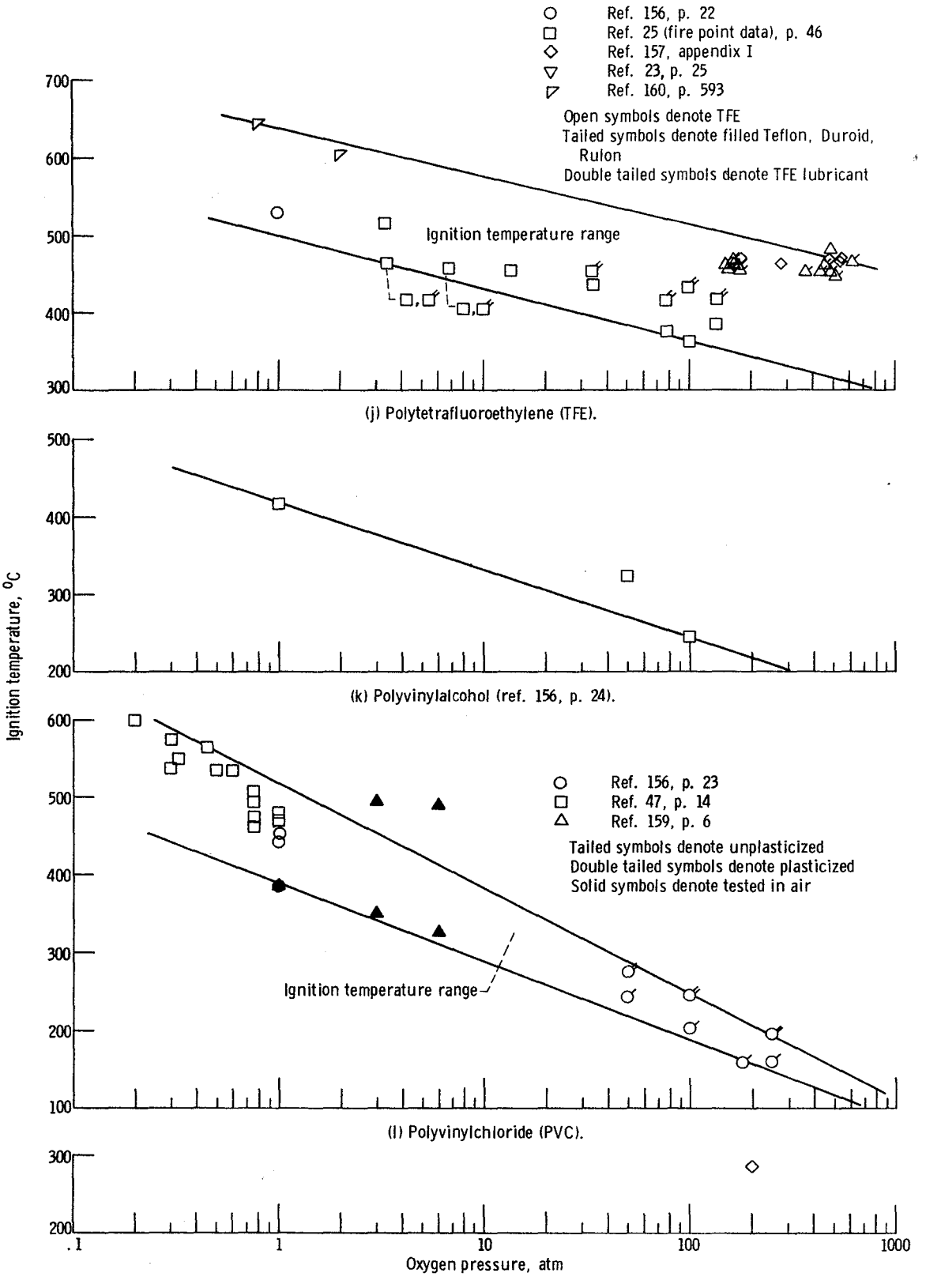

Figure E-1. - Continued.

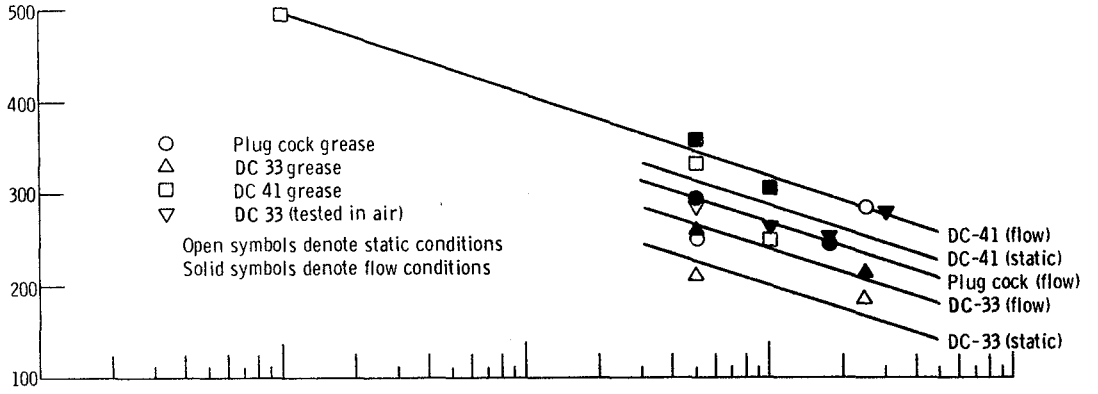

(n) Silicone grease (ref. 156, pp. 9 and 10).

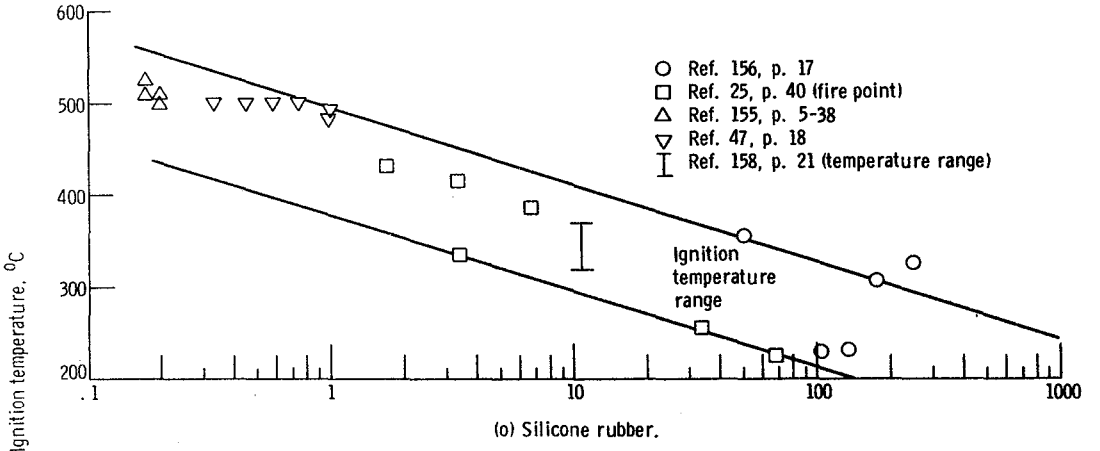

(o) Silicone rubber.

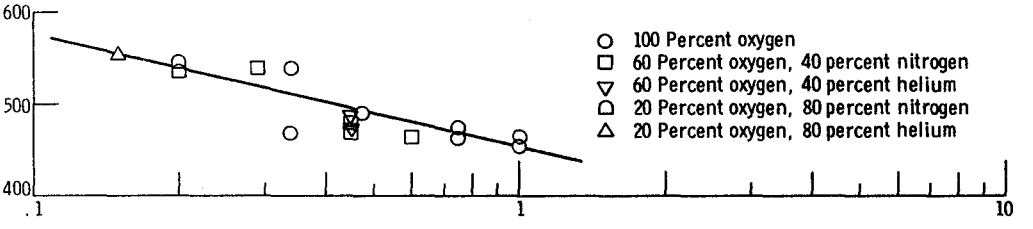

(p) Viton A (ref. 47, p. 31).

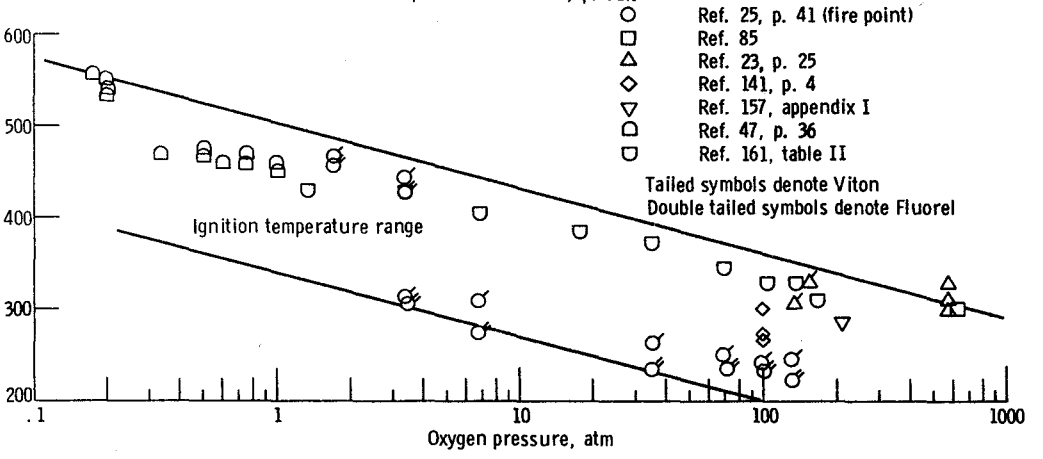

(q) Viton and Fluorel (copolymer of vinylidene fluoride and hexafluoropropylene).

Figure E-1. - Continued.

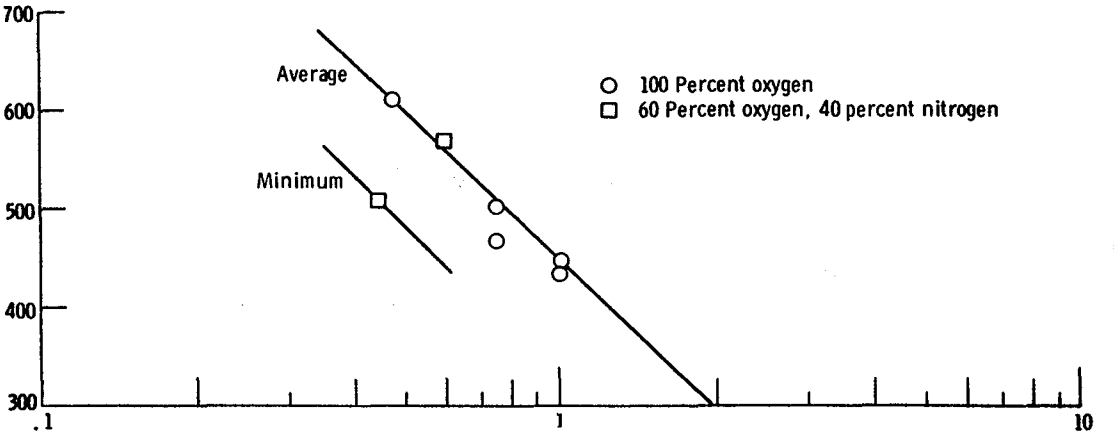

(r) Dacron fabric (ref. 47, p. 40).

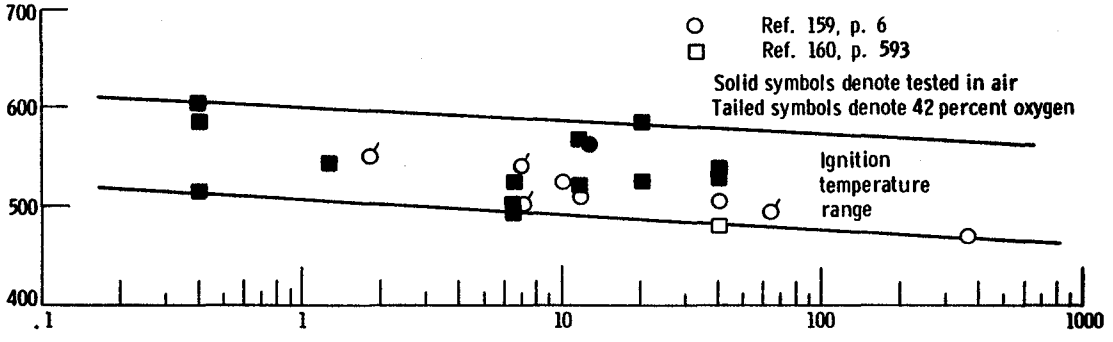

(s) Nomex fabric.

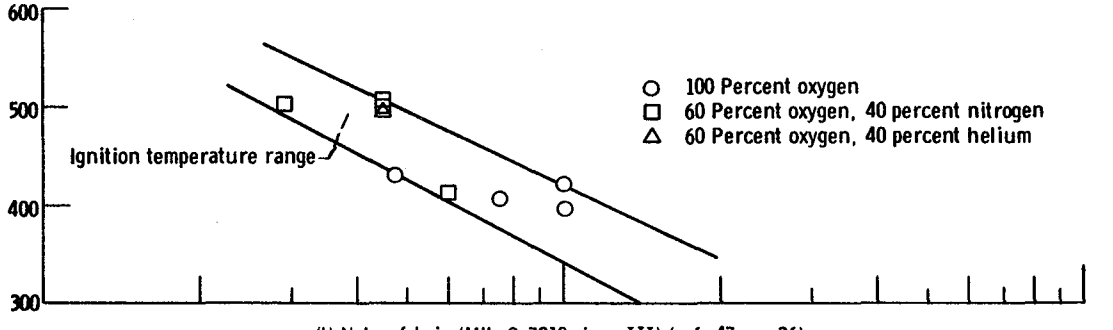

(t) Nylon fabric (MIL-C-7219, type III) (ref. 47, p. 36).

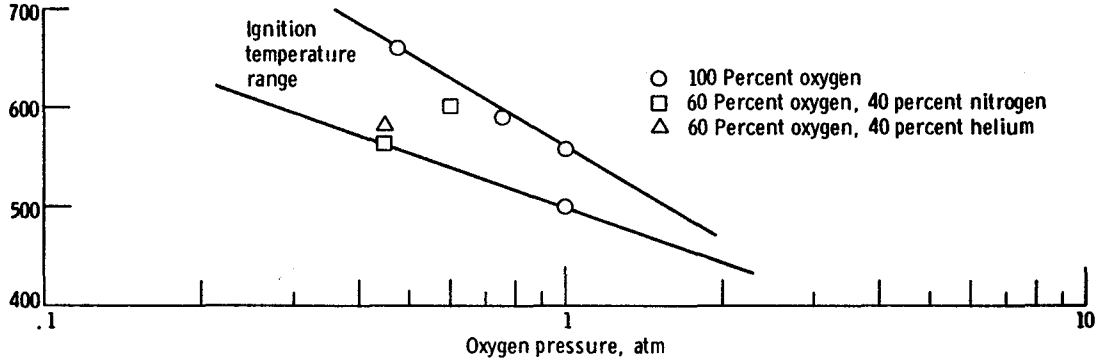

Ignition temperature, °C

(u) Orlon fabric.

Figure E-1. - Concluded.

APPENDIX F

COMBUSTION RATE DATA

This appendix contains figures showing the rate of burning of selected materials as a function of oxygen pressure (or partial pressure). In cases where the test environment was other than 100 percent oxygen, such as air or in mixtures with nitrogen or helium, the pressures plotted are partial pressures (i.e., if the test gas is air at 1 atmosphere pressure, the oxygen pressure plotted is 0.21 atmosphere).

The following table gives the pages on which the combustion rate data for selected materials are shown:

Figure	Material	Page	Figure	Material	Page
F-1(a)	Cotton fabric	194	F-1(k)	Polymethylmethacrylate (rod)	197
F-1(b)	Dacron fabric	194	F-1(l)	Polymethylmethacrylate (sheet)	197
F-1(c)	Epoxy	194	F-1(m)	Polysulfone	198
F-1(d)	Neoprene	195	F-1(n)	Polyurethane	198
F-1(e)	Nomex fabric	195	F-1(o)	Polyvinylchloride	198
F-1(f)	Nomex fabric	195	F-1(p)	Silicone	199
F-1(g)	Nylon	196	F-1(q)	Teflon fabric	199
F-1(h)	Nylon rod	196	F-1(r)	Teflon rod	200
F-1(i)	Poly-benzimidazole	196	F-1(s)	Viton-Fluorel	200
F-1(j)	Polyethylene	197	F-1(t)	Velcro	200

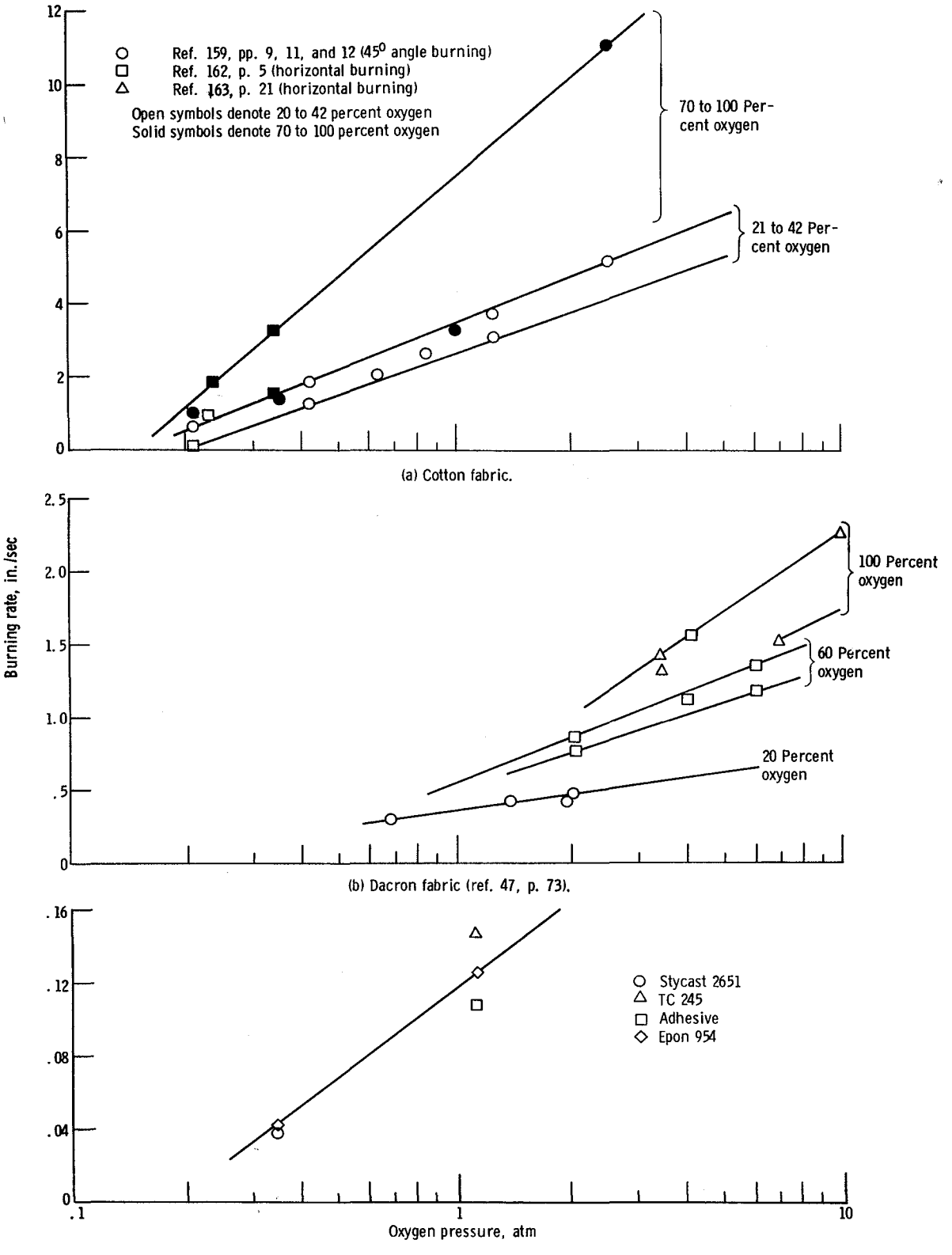

Figure F-1. - Combustion rate data. Lines represent the bestfit of the data based on the authors' interpretation.

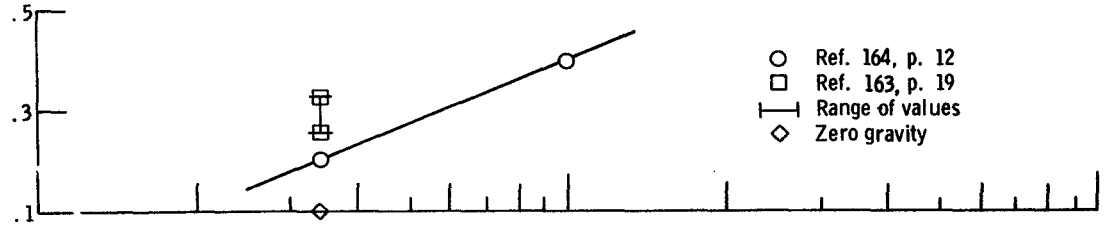

(d) Neoprene.

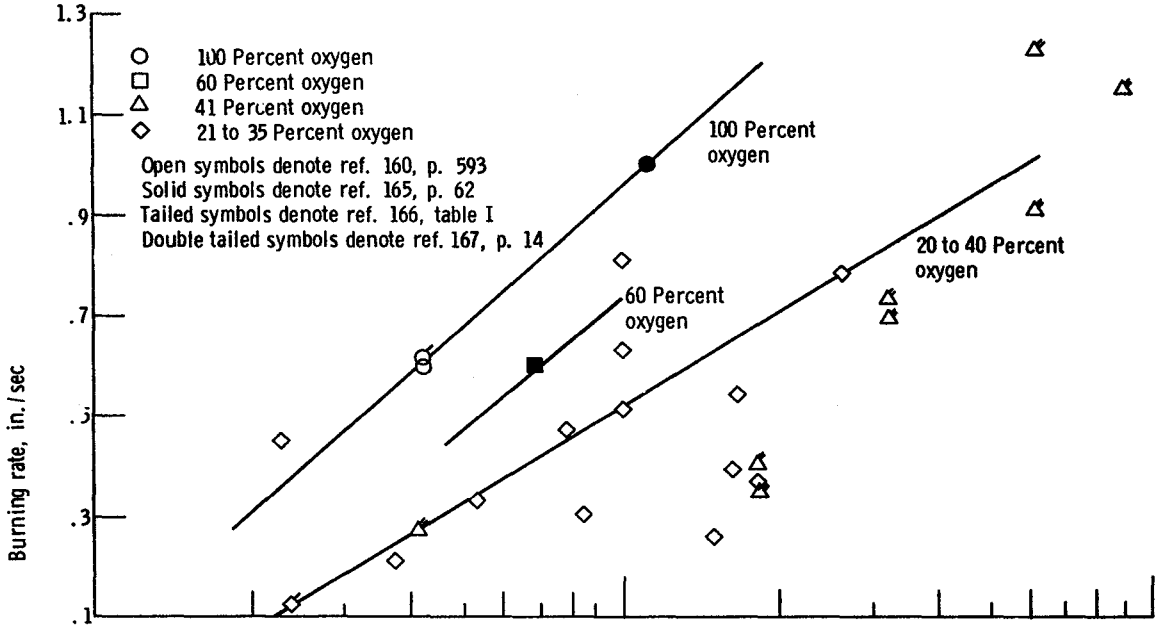

(e) Nomex fabric. Burning at various oxygen concentrations.

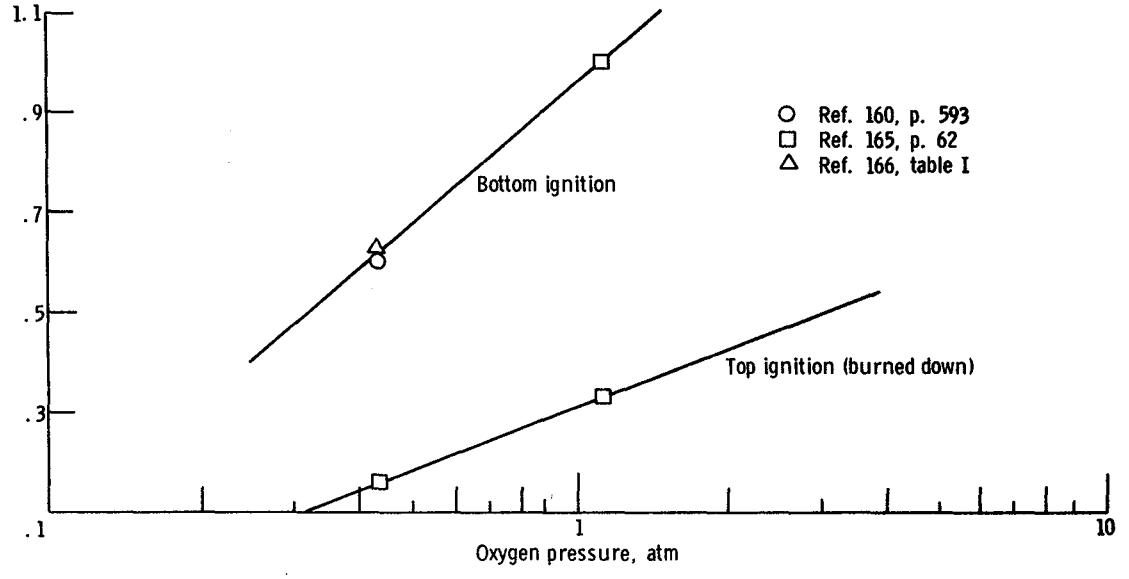

(f) Nomex fabric. Top and bottom ignitions in 100 percent oxygen.

Figure F-1. - Continued.

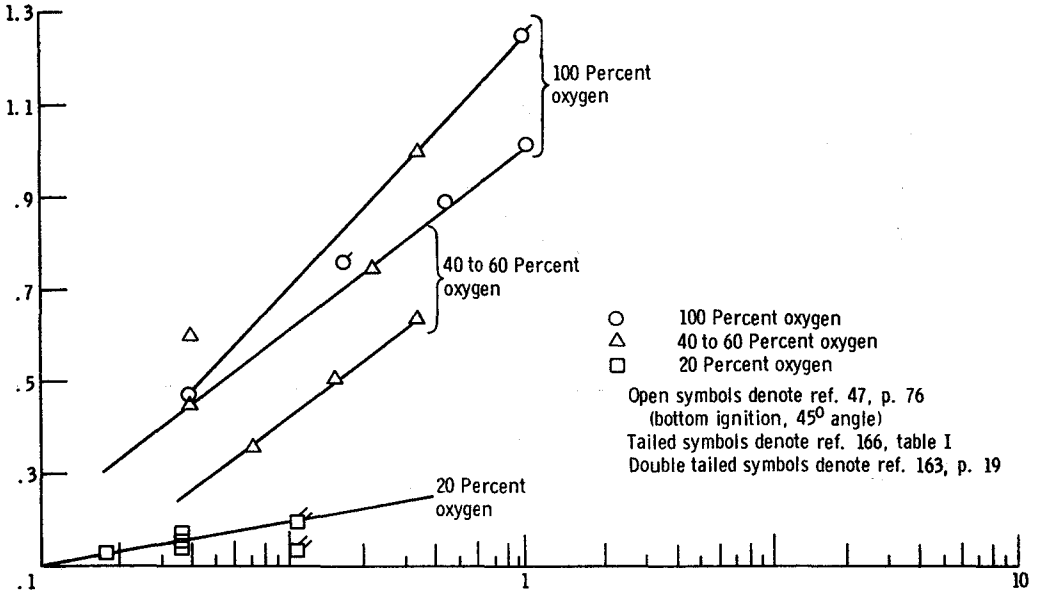

(g) Nylon.

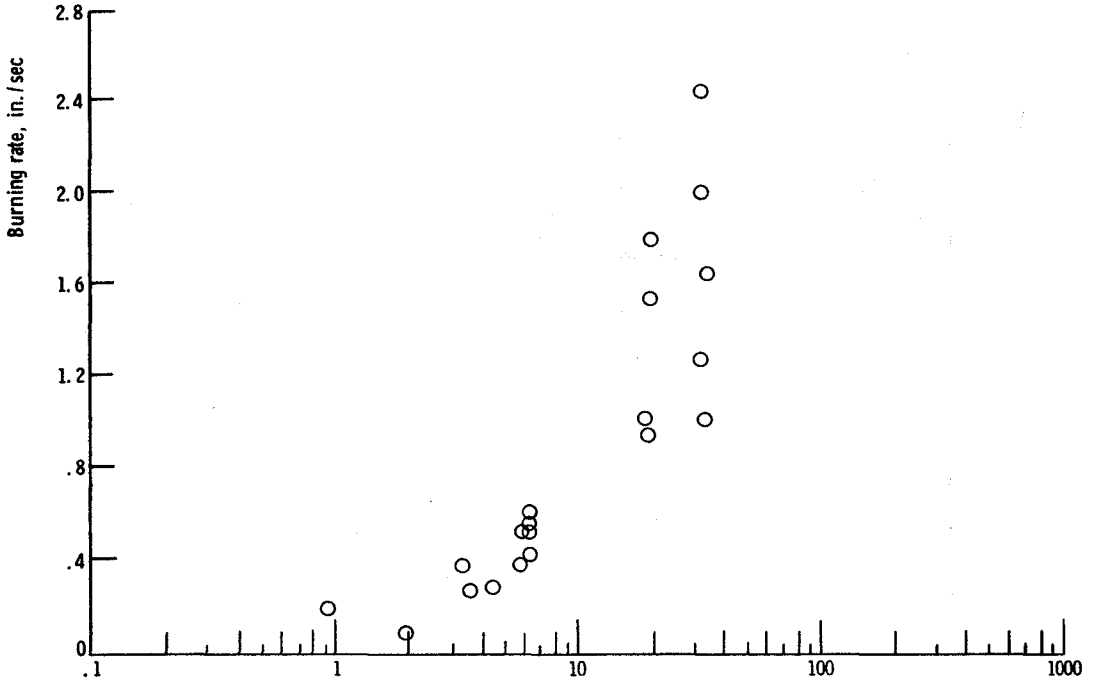

(h) Nylon rod (ref. 168, tables I to III, p. 10).

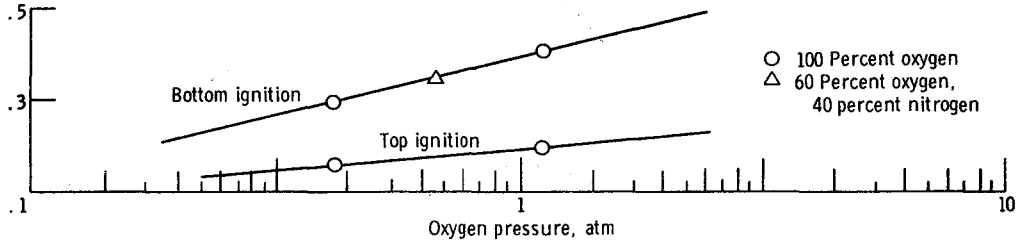

(i) Poly-benzimidazole (ref. 165, p. 62).

Figure F-1. - Continued.

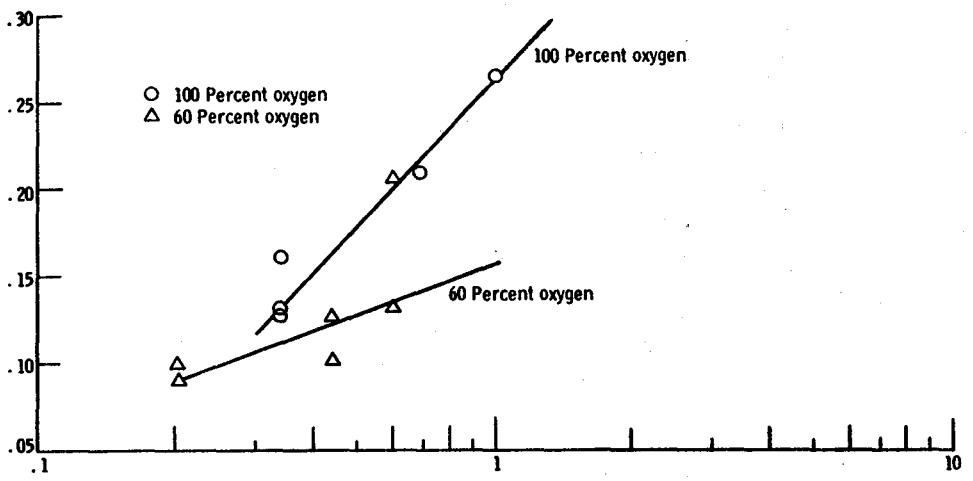

(j) Polyethylene (ref. 47, p. 70).

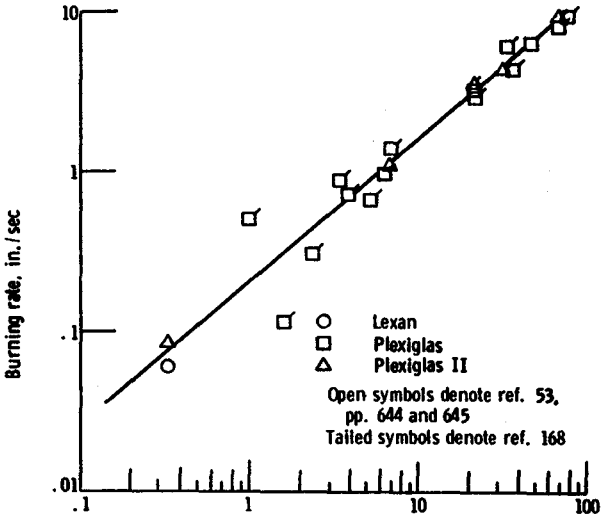

(k) Polymethylmethacrylate (rod).

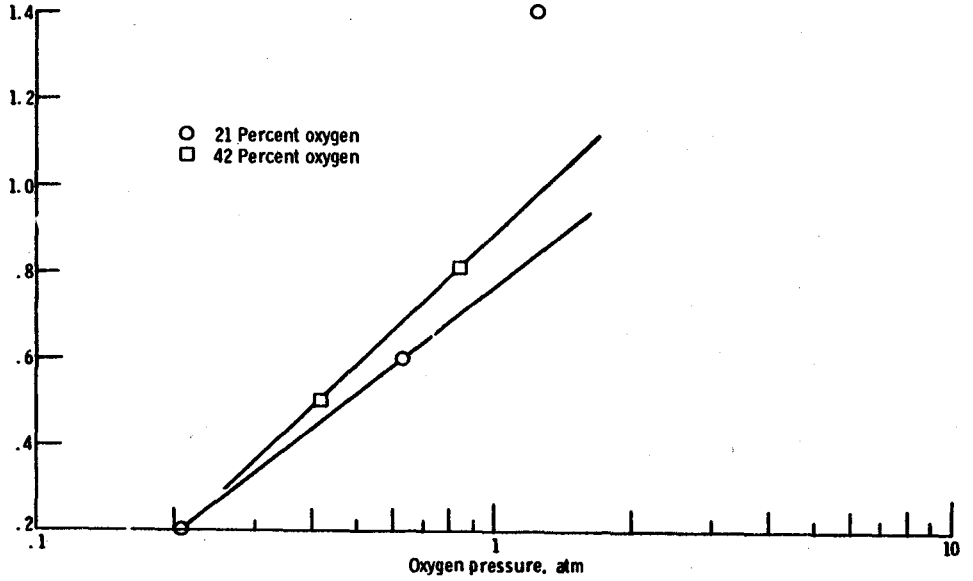

(l) Polymethylmethacrylate (sheet) (ref. 159, p. 11).

Figure F-1. - Continued.

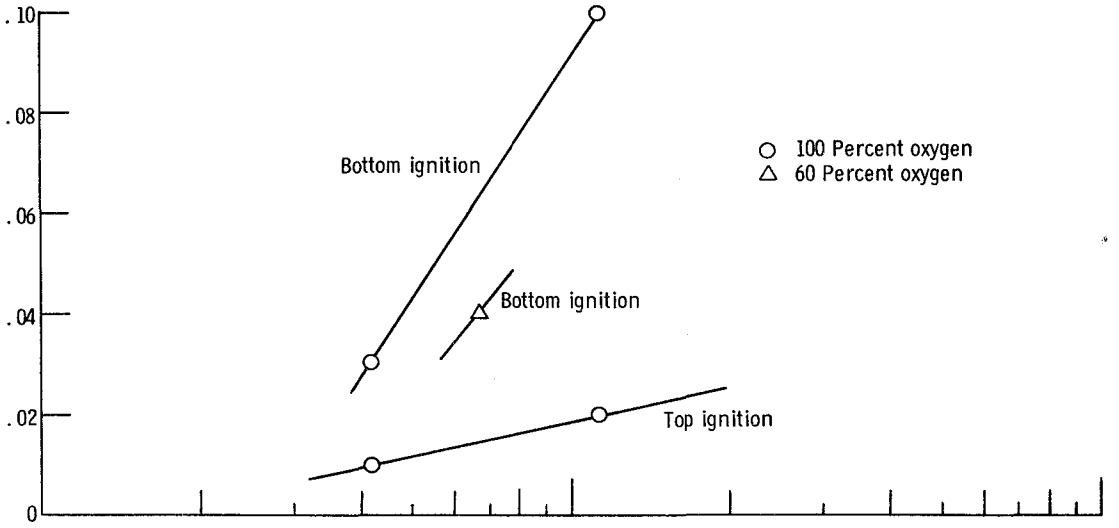

(m) Polysulfone (ref. 165, p. 63).

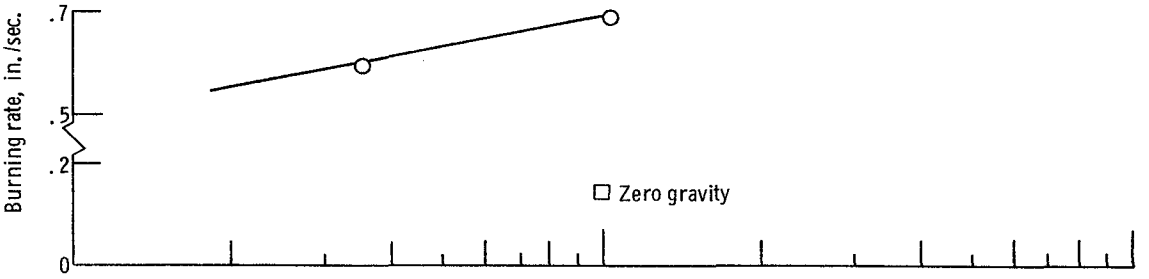

(n) Polyurethane (ref. 164, p. 12). 100 Percent oxygen.

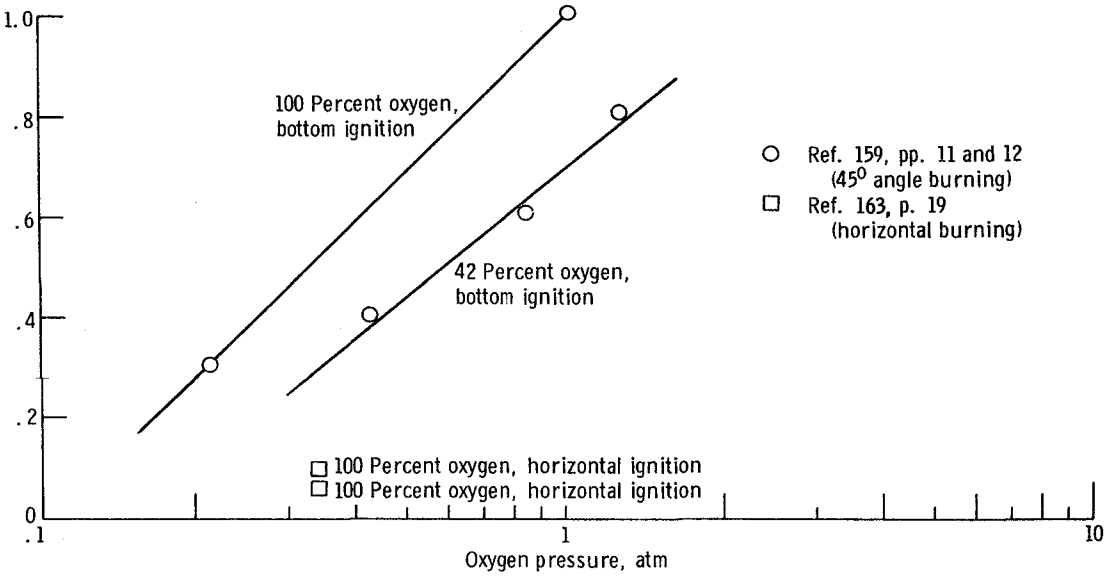

(o) Polyvinylchloride (PVC).

Figure F-1. - Continued.

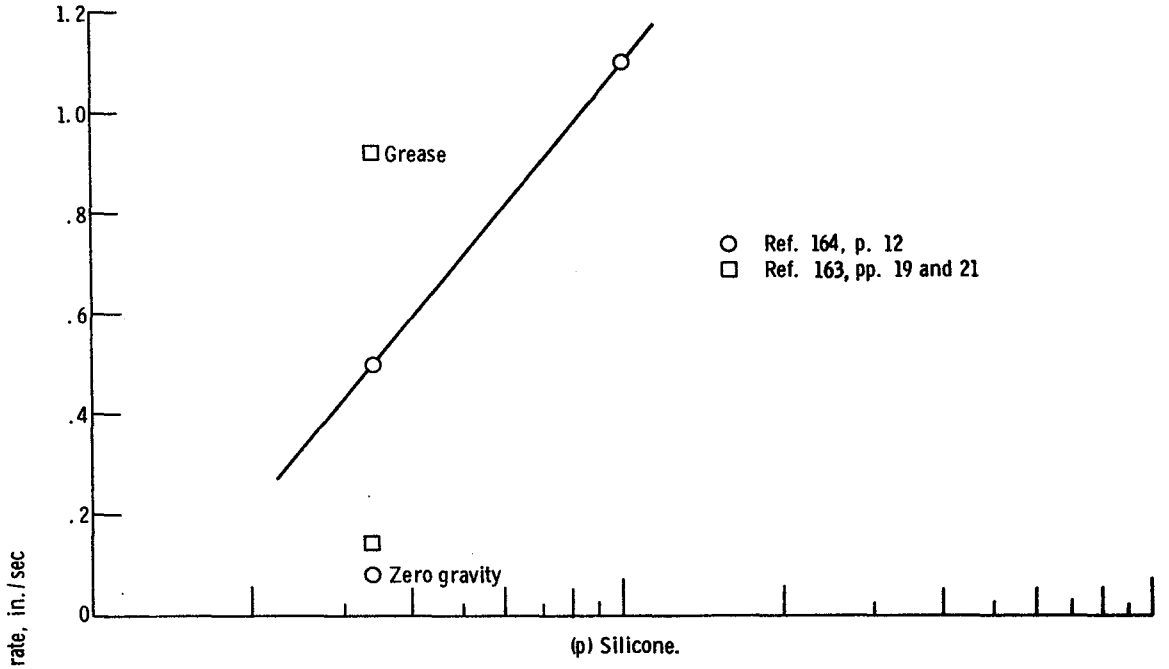

(p) Silicone.

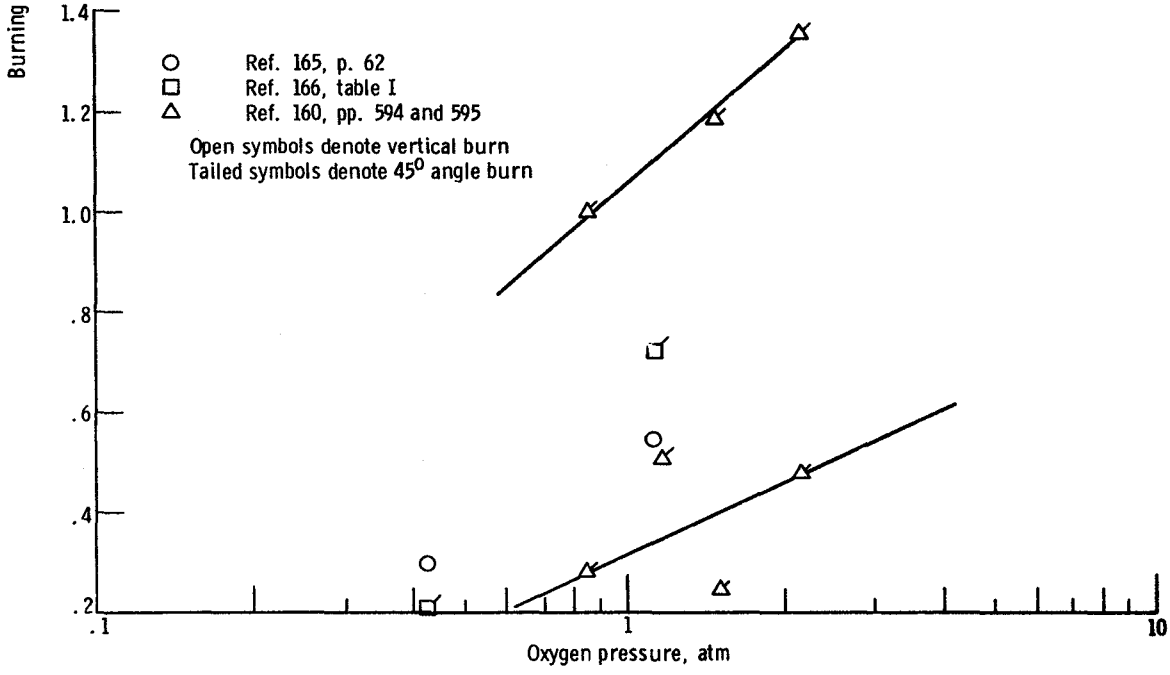

(q) Teflon fabric - bottom ignition (100 percent oxygen).

Figure F-1. - Continued.

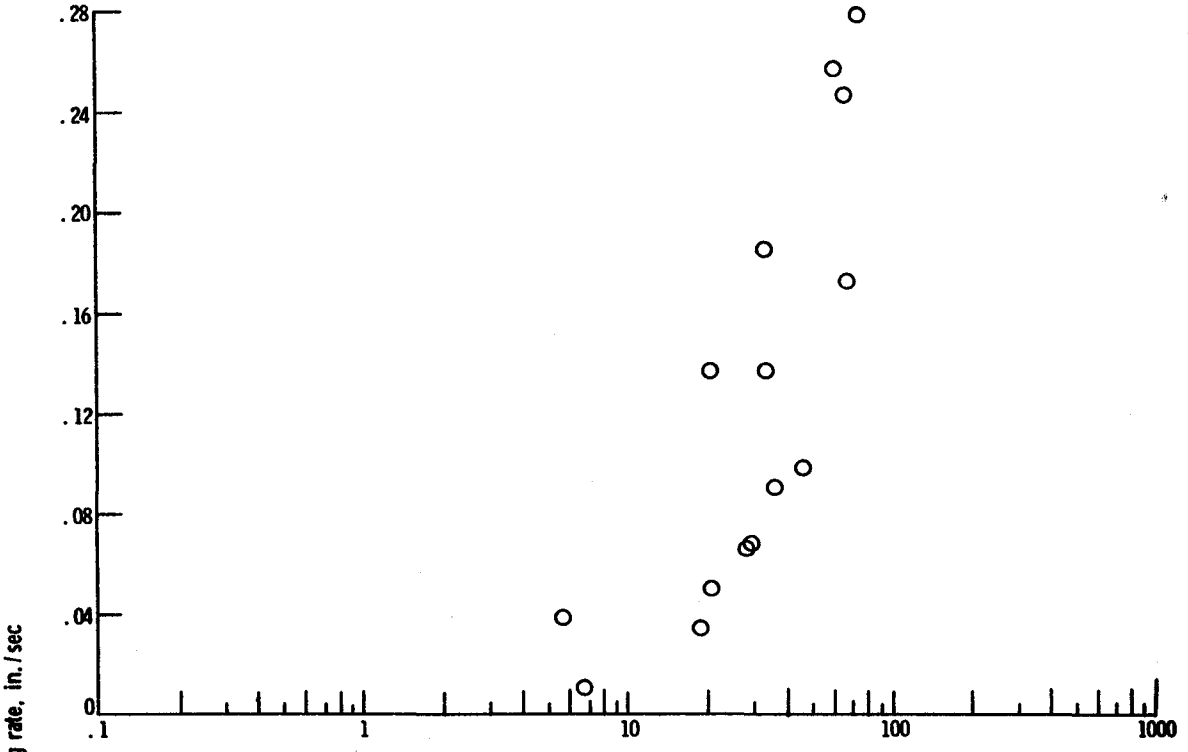

(r) Teflon rod - top ignition (ref. 168, p. 10).

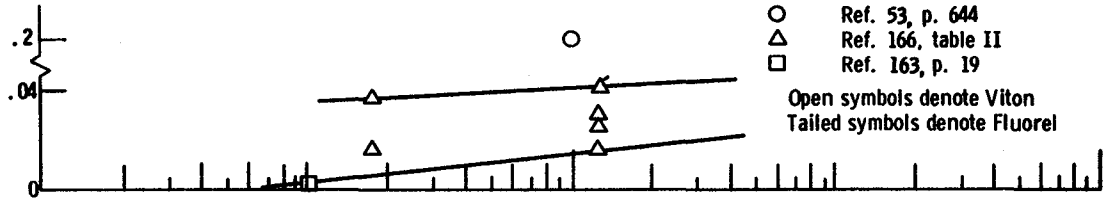

(s) Viton-Fluorel (copolymer of vinylidene fluoride-hexafluoropropylene).

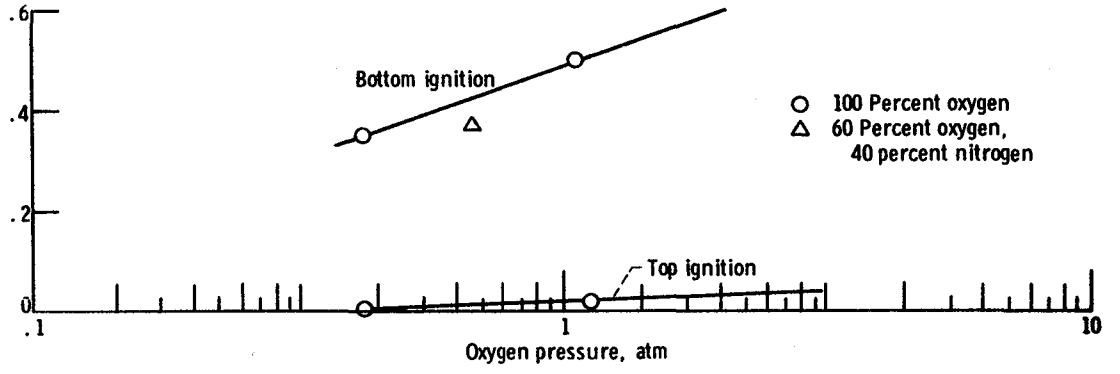

(t) Velcro (ref. 165, p. 62).

Figure F-1. - Concluded.

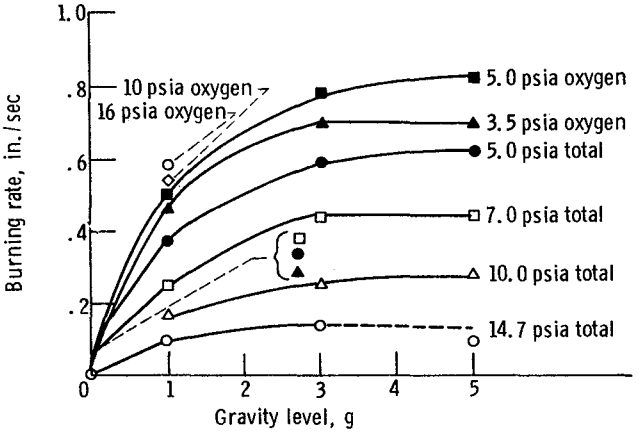

Figure F-2. - Effect of gravity level on burning rate in nitrogen-oxygen mixtures for cotton cloth (ref. 169, p. 26). Oxygen partial pressure in mixtures, 3.5 psia.

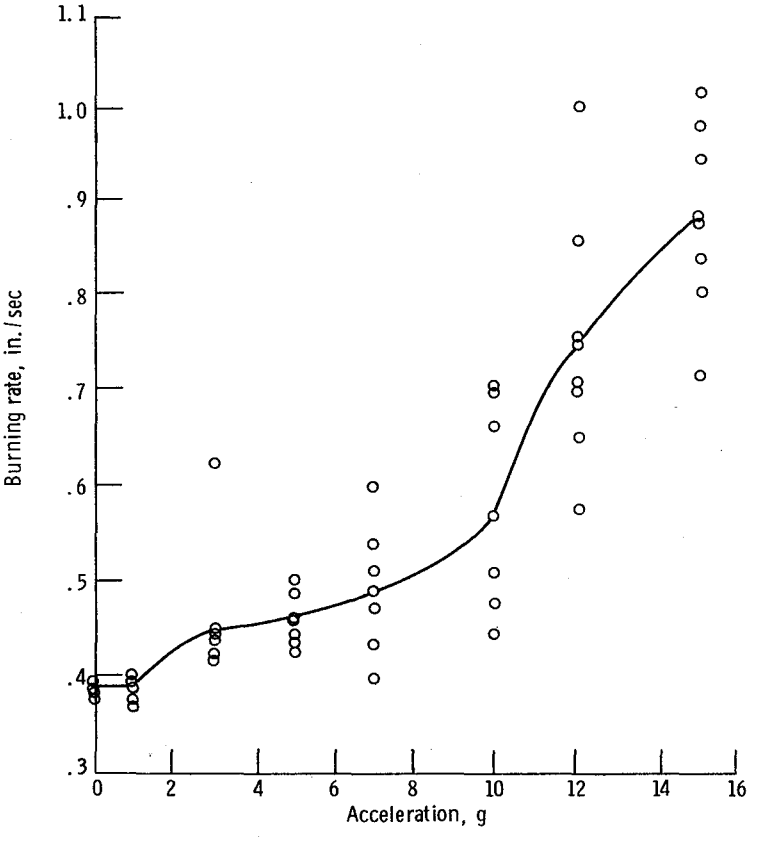

Figure F-3. - Burning rate as function of acceleration for Nomex standard cloth (ref. 170, fig. 1). Burning in direction of acceleration.

Page intentionally left blank

REFERENCES

In parentheses after most references are given the Microfiche card numbers denoting the location of the references in the Microfiche supplement and the pages of the references reproduced in the Microfiche supplement.

1. Roder, H. M.; and Weber, L. A., eds.: ASRDI Oxygen Technology Survey. Volume I: Thermophysical Properties. NASA SP-3071, 1972. (Card 1: pp. iii, v, 107-143.)

2. Bailey, B. M.; Sterner, C. J.; and Vignale, V. J.: Study of Liquid Oxygen Contamination, Summary Progress. Rep. 4, Air Products and Chem. Inc. (AD-253231), 1960. (Card 1: 46-59, 60-62.)

3. McKinley, C.; and Himmelberger, F.: The Role of Air Contaminants in Formulating Oxygen Plant Safety Principles. Chem. Eng. Prog., vol. 53, no. 3, Mar. 1957, pp. 112-M to 121-M.

4. Carlson, G. A.: Spherical Detonations in Gas-Oxygen Mixtures. Combustion and Flame, vol. 21, no. 3, Dec. 1973, pp. 383-385. (Card 1: All.)

5. Contamination Control Handbook. NASA SP-5076, 1969. (Card 2: pp. iii, IV-1 - IV-32.)

6. Oxygen. MSFC-SPEC-399B, NASA George C. Marshall Space Flight Center, Jan. 31, 1974. (Card 2: pp. 1-14.)

7. Quality Control of Oxygen Propellant, Liquid Oxygen, Aviator's Liquid Breathing Oxygen, and Aviator's Gaseous Breathing Oxygen. Rep. T. O. 42B6-1-1, Change 7, U.S. Air Force, May 1, 1969. (Card 2: pp. i, 1-1 - 3-6.)

8. Bankaitis, H.; and Schueller, C. F.: ASRDI Oxygen Survey. Volume II: Cleaning Requirements, Procedures, and Verification Techniques. NASA SP-3072, 1972. (Cards 2 and 3: pp. 1-15, 18-60.)

9. McGraw-Hill Encyclopedia of Science and Technology. Vol. 3, McGraw-Hill Book Co., 1966.

10. Tomashov, N. D.: Theory of Corrosion and Protection of Metals. MacMillan Co., 1966.

11. Brenner, S. S.: Catastrophic Oxidation of Some Molybdenum Containing Alloys. J. Electrochem., vol. 102, no. 1, Jan. 1955, pp. 16-21. (Card 3: All.)

12. Gulbransen, E. A.; and Andrew, K. F.: Kinetics of the Oxidation of Pure Tungsten from 500° to 1300° C. J. Electrochem. Soc., vol. 107, no. 7, July 1960, pp. 619-628.

13. Kubaschewski, O.; and Hopkins, B. E.: Oxidation of Metals and Alloys. Second ed., Butterworths, Inc., 1967.

14. Manned Spacecraft Criteria and Standards. MSCM 8080, NASA Manned Spacecraft Center, Apr. 1971 (changes, Oct. 1972).

15. Dissimilar Metals. MIL-STD-889A, Dept. Army, May 5, 1972. (Card 3: All.)

16. Richmond, J. C.; and Thornton, H. R.: Oxidation of Experimental Alloys. Rep. WADC TR-58-164, Part I, Wright Air Development Center, 1958. (Cards 3 and 4: pp. iii, 14-17, 33-45.)

17. Smith, H. H.; Shahinian, P.; and Achter, M. R.: Fatigue Crack Growth Rates in Type 316 Stainless Steel at Elevated Temperatures as a Function of Oxygen Pressure. Trans. Met. Soc. AIME, vol. 245, May 1969, pp. 947-953. (Card 4: All.)

18. Smith, H. H.; and Shahinian, P.: Effect of Oxygen and of Water Vapor on the Fatigue Life of Nickel at 300° C. Effects of Environmental and Complex Load History on Fatigue Life. STP-462, American Soc. Testing and Mater., 1970, pp. 217-233. (Card 4: pp. 217-225.)

19. Hartman, A.: On the Effect of Oxygen and Water Vapor on the Propagation of Fatigue Cracks in 2024-T3 Alclad Sheet. Int. J. Fract. Mech., vol. 1, Sept. 1965, pp. 167-188. (Card 4: pp. 167-170.)

20. Taylor, L., ed.: Metals Handbook. Vol. 1, Properties and Selection of Metals, eighth ed., American Soc. Metals, 1967.

21. Rossini, F. D.; Wagman, D. D.; Evans, W. H.; Levine, S.; and Jaffe, I.: Selected Values of Chemical Thermodynamic Properties, Part I. Tables. Circular 500-Part I, Nat. Bur. Stand., July 1961.

22. Weast, R. C.; and Selby, S. M., eds: Handbook of Chemistry and Physics. 48th ed., Chemical Rubber Co., 1967-1968.

23. Nihart, G. J.; and Smith, C. P.: Compatibility of Materials with 7500 PSI Oxygen. Union Carbide Corp. (AMRL TDR-64-76; AD608260), 1964. (Cards 4 and 5: pp. ii, iii, v, vi, vii, viii, 1-80.)

24. Jacobson, M.; Cooper, A. R.; and Nagy, J.: Explosibility of Metal Powders. BM-RI-6516, Bur. Mines, 1964. (Card 5: pp. 1, 4.)

25. Pippen, D. L.; and Stradling, J. S.: Techniques for Determination of Flash and Fire Points and Impact Sensitivity of Materials in a Gaseous Environment. Mat. Res. Stand., vol. 11, no. 6, June 1971, pp. 35-43, 52-53. (Card 5: All.)

26. Key, C. F.: Compatibility of Materials with Liquid Oxygen - Vol. I. NASA TM X-64711, Oct. 1972. (Cards 5, 6, and 7: pp. 11-13, 42-220.)

27. Hauser, R. L.; Sykes, G. E.; and Rumpel, W. F.: Mechanically Initiated Reactions of Organic Materials in Missile Oxidizers. ASD-TR-61-324, Aeronautical Systems Division, Wright-Patterson AFB, 1961. (Available from DDC as AD-268458.) (Card 7: pp. iii, 97-98.)

28. Key, C. F.: An Instrument for Determination of Impact Sensitivity of Materials in Contact with Gaseous Oxygen at Pressures up to 50 psia. NASA TM X-53846, 1969. (Card 7: pp. 5-7.)

29. Jackson, J. D.; Miller, P. D.; Boyd, W. K.; and Fink, F. W.: A Study of the Titanium-Liquid Oxygen Pyrophoric Reaction. WADD-TR-60-258, Wright Air Development Division, Air Research and Development Command, June 1960. (Card 7: pp. iii, 5-6, 10.)

30. Landrock, A. H.: Properties of Plastics and Related Materials at Cryogenic Temperatures. PLASTEC-20, Plastics Technical Evaluation Center, 1965. (Available from DDC as AD-469126.) (Card 7: pp. i, 8-9, 30-38, 101-103.)

31. Wright, H. W.; Howell, G. W.; and Lee, D. H.: Seal Material Development Program, Phase I. TRW Systems Group (NASA CR-114822), 1970. (Card 7: pp. vii, 47, 49, 59.)

32. Walker, W. R.: Design Handbook for O-Rings and Similar Elastic Materials. WADC-TR-59-428-PT-2, Wright Air Development Center, 1961. (Available from DDC as AD-265443.) (Card 8: pp. iii, 37.)

33. Key, C. F.: An Apparatus for Determination of Impact Sensitivity of Materials in Contact with Liquid and Gaseous Oxygen at High Pressures. Mat. Res. Stand., vol. 11, no. 6, June 1971, pp. 28-51. (Card 8: pp. 28-29, 51-52.)

34. A Study of the Mechanism of the Titanium-Liquid Oxygen Explosive Reaction. ASD-TR-61-479, Aeronautical Systems Div., Air Force Systems Command, 1961. (Card 8: pp. iii, 3-5, 7-8, 10, 14, 20.)

35. Wegener, W.: Investigations of the Admissible Oxygen Flow Velocity in Steel Pipes from a Safety Point of View. NASA TT F-14,831, 1973. (Card 8: pp. 1-22.)

36. Littman, F. E.; and Church, F. M.: Reactions of Titanium with Water and Aqueous Solutions. AECU-3825, Stanford Research Inst., 1958. (Card 8: pp. 1-17.)

37. Schmidt, H. W.; and Harper, J. T.: Handling and Use of Fluorine and Fluorine-Oxygen Mixtures in Rocket Systems. NASA SP-3037, 1967. (Cards 8 and 9: pp. vii, 49-119, 135-136, 140-148.)

38. Flammability, Odor, and Offgassing Requirements and Test Procedures for Materials in Environments that Support Combustion. NHB 8060.1A, NASA, Feb. 1974. (Cards 9 and 10: All.)

39. Chemical Engineering Division, Summary Report. Rep. ANL-6145, Argonne National Lab., Jan., Feb., Mar., 1960. (Card 10: p. 151.)

40. Lapin, A.: Liquid and Gaseous Oxygen Safety Review. Vol. IV. APCI-TM-184, Air Products and Chemicals, Inc. (NASA CR-120922), 1972. (Card 11: APCI Doc. No. 99000595, pp. 1-5.)

41. Isaacs, J. L.: The Oxygen Index Flammability Test. J. Fire and Flammability, vol. 1, Jan. 1970, pp. 36-47. (Card 11: pp. 36, 40-42.)

42. Fenimore, C. P.; and Martin, F. J.: Candle-Type Test for Flammability of Polymers. Mod. Plast., vol. 43, no. 11, Nov. 1966, pp. 141-192. (Card 11: pp. 141, 146.)

43. Blackstone, W. R.; and Ku, P. M.: Assessment of Impact Test Techniques for Determining the Fire or Explosion Hazards of Materials Exposed to Oxygen. Mat. Res. Stand., vol. 11, no. 6, June 1971, pp. 30-35, 52. (Card 11: All.)

44. Flammability, Odor, and Offgassing Requirements and Test Procedures for Materials in Environments which Support Combustion. MSFC-SPEC-101B, NASA George C. Marshall Space Flight Center, March 15, 1971.

45. Testing Compatibility of Materials for Liquid Oxygen Systems. MSFC-SPEC-106B, NASA Marshall Space Flight Center, Oct. 6, 1967. (Card 11: All.)

46. Apollo Spacecraft, Nonmetallic Materials Requirements. MSC-PA-D-67-13, NASA Manned Spacecraft Center, 1968; Addendas 1, 1A, 2, 2A, 1971.

47. Stevens, M. R.; Fisher, H. D.; and Breen, B. P.: Investigation of Materials Combustibility, Fire, and Explosion Suppression in a Variety of Atmospheres. AFAPL-TR-68-35, Air Force Aero Propulsion Lab., May 1968. (Card 11: pp. iii, 2-3, 5-8, 14, 18, 31, 36, 40, 45, 70, 73, 76.)

48. Kline, H. F.: A Study of Ignition Point Values of Nonmetallic Materials in Simulated Spacecraft Environment. Sci. Advanced Mater. Pro. Eng. Ser., vol. 11, 1967, pp. 101-109. (Card 11: pp. 101-104.)

49. Standard Method of Test for Flammability of Plastics Using the Oxygen Index Method. Part 27 of ASTM Annual Standards. ASTM Designation D 2863-70, 1973.

50. Stradling, Jack S.: Test Plan, Aerospace Safety Research and Data Institute (ASRDI), Ignition by Electrical Arc. TP-WSTF-192, rev. A., July 31, 1973. (Cards 11 and 12: All.)

51. Howell, Glen A.; and Weathers, Terry M., eds.: Aerospace Fluid Component Designers Handbook. TRW Systems Group, 1970.
Vol. I - Revision D. AFRPL-TDR-64-25-Vol-1D; AD-874542. (Card 12: pp. 5.11.1-1 - 5.11.4-5, 5.12.1-1 - 5.12.8-2, 6.4.3-2.)
Vol. II - Revision D. AFRPL-TDR-64-25-Vol-2D; AD-874543.

52. Plastics for Aerospace Vehicles. Part I. Reinforced Plastics. MIL-HDBK-17A, Dept. of Defense, Jan. 1971. (Card 12: pp. iii, 2-5 - 2-6, 2-9 - 2-11.)

53. Space Materials Handbook. Third ed., NASA SP-3051, 1969.

54. Testing Methods and Techniques: Strength of Materials and Components - A Compilation. NASA SP-5944(01). (Cards 12 and 13: All.)

55. Weiner, R. S.: Basic Criteria and Definitions for Zero Leakage. JPL-TR-32-926, Jet Propulsion Lab. (NASA CR-81189), 1966. (Card 13: pp. III, 1-7, 9-14.)

56. Marr, J. W.: Leakage Testing Handbook. NASA CR-952, 1968. (Card 13: pp. vii, viii, 11, 41-81.)

57. May, K. D.: Technology Survey Advanced Valve Technology. NASA SP-5019, 1965. (Card 13: pp. v, 14.)

58. Seventh Conference on Space Simulation. NASA SP-336, 1973. (Card 13: pp. 331-334.)

59. Burrows, G.: Flow Through and Blockage of Capillary Leaks. Trans. Inst. Chem. Engrs., vol. 39, 1961, pp. 55-63. (Card 13: All.)

60. Kelly, J. H.; et al.: Permeability Data for Aerospace Applications. IIT Research Institute (NASA CR-95393), 1968. (Cards 14 and 15: pp. I-1.1 - I-1.2, I-2.1 - I-2.2, IV-8.1 - IV-8.81, VII-1.1 - VII-1.16, VII-2.1 - VII-2.24.)

61. Design Data for Pressurized Gas Systems. Stanford Research Institute, Nov. 1963. (Card 15: pp. I-1 - I-2, XII-4.1 - XII-4.7.)

62. Erosion by Cavitation or Impingement. STP-408, American Soc. Testing and Mater., 1966.

63. Glenn, H. L.; and O'Neal, G.: Watch Those Dents. Aerosp. Safety, vol. 27, no. 8, Aug. 1971, p. 18. (Card 15: p. 18.)

64. Baum, J. V.; Goobich, B.; and Trainer, T. M.: An Evaluation of High-Pressure Oxygen Systems. AMRL-TDR-62-102, Aerospace Medical Research Lab., Sept. 1962. (Card 15: pp. iii, 19-29.)

65. Murphy, D. W.: An Experimental Investigation of Geysering in Vertical Tubes. Advances in Cryogenic Engineering, vol. 10. K. D. Timmerhaus, ed., Plenum Press, 1964, pp. 353-359. (Card 15: All.)

66. Protective Finishing Systems for Rockets, Guided Missiles, Support Equipment and Related Materials. MIL-STD-186C(MI), Dept. Army, Oct. 31, 1971. (Cards 15 and 16: pp. iii, iv, v, vi, 1-30.)

67. Saturn Flight Manual SA 506. MSFC-MAN-506, NASA Marshall Space Flight Center, Feb. 1969.

68. Metallic Materials and Elements for Aerospace Vehicle Structures. MIL-HDBK-5A, Dept. Defense, Feb. 8, 1966.

69. Aerospace Structural Metals Handbook. AFML-TR-68-115, Mechanical Properties Data Center, Belfour Stulen, Inc., 1971.

70. Huzel, D. K.; and Huang, D. H.: Design of Liquid Propellant Rocket Engines. NASA SP-125, 1971. (Card 16: pp. v, 219-225, 257-259, 289-292, 329-352, 372-379.)

71. Liquid Rocket Tanks and Components. NASA SP-8088, 1974. (Cards 16 and 17: pp. iii, v, vi, vii, 17-18, 52-72.)

72. Technical Manual of Oxygen/Nitrogen Cryogenic Systems. NAVAIR 06-30-501, Naval Air Systems Command, Mar. 1971. (Card 17: pp. i, ii, 2-1 - 2-43.)

73. ASME Boiler and Pressure Vessel Code, Section VIII, Pressure Vessels, Division 1. ASME, 1968.

74. ASME Boiler and Pressure Vessel Code, Section VIII, Pressure Vessels, Division 2 - Alternative Rules. ASME, 1971.

75. ASME Boiler and Pressure Vessel Code, Section IX, Welding Qualifications. ASME, 1971.

76. Welding High Pressure Systems and Cryogenic Systems. Tech. Order 00-25-224, Air Force, Aug. 30, 1965.

77. Recommended Rules for Design and Construction of Large, Welded, Low-Pressure Storage Tanks. API Standard 620, fourth ed., Feb. 1970; Supplement, Apr. 1971.

78. Tentative Standard - Insulated Tank Truck Specification. CGA-341, Compressed Gas Association, 1970.

79. Transporation. Code of Federal Regulations, Title 49, Pts. 100-199, Sup. Docs., Jan. 1, 1972.

80. Fracture Control of Metallic Pressure Vessels. NASA SP-8040, 1970. (Cards 17 and 18: pp. iii, iv, 1-37, 39-49, 51-55.)

81. Johnson, R. E.: Apollo Experience Report - The Problem of Stress-Corrosion Cracking. NASA TN D-7111, 1973. (Card 18: pp. 10-15.)

82. Campbell, J. E.; Berry, W. E.; and Feddersen, C. E.: Damage Tolerant Design Handbook. MCIC-HB-01, Metals and Ceramics Information Center, Battelle Memorial Inst., 1972.

83. Hood, D. W.; Eichenberger, T. W.; and Lovell, D. T.: An Investigation of the Generation and Utilization of Engineering Data on Weldments. AFML-TR-68-268, Air Force Materials Lab. (AD-851938), 1968. (Card 18: pp. iii, 55-73.)

84. Arnett, R. W.; Warren, K. A.; and Mullen, L. O.: Optimum Design of Liquid Oxygen Containers. WADC Rep. TR 59-62, Wright-Patterson A. F. Base (PB-181108), 1961. (Card 18: pp. 118-121.)

85. Olson, R. E.: Safety and Design Considerations for Gas Storage Vessels. M-64-137, Martin Co., Aug. 1964. (Cards 18: All.)

86. Letson, A. J.: RL10A-3-3 Rocket Engine Oxidizer Pump Development Program. Rep. PWA FR-1890, Pratt & Whitney Aircraft, 1966.

87. Liquid Rocket Engine Centrifugal Flow Turbopumps, NASA Space Vehicle Design Criteria (Chemical Propulsion). NASA SP-8109, 1973. (Card 19: pp. iii, 8-10, 39-53, 55-60, 74-80.)

88. Wislicenus, G. F.: Fluid Mechanics of Turbomachinery, vols. 1 and 2. Dover Publications, Inc., New York, 1965.

89. Stephanoff, A. J.: Centrifugal and Axial Flow Pumps, second ed., John Wiley & Sons, Inc., 1957.

90. Liquid Rocket Engine Turbopump Inducers. NASA SP-8052, 1971. (Cards 19 and 20: All.)

91. Rocket Engine Turbopump Shafts and Couplings. NASA Space Vehicle Design Criteria (Chemical Propulsion). NASA SP-8101, 1970. (Cards 20 and 21: pp. iii, v, vi, vii, viii, 12, 19-49, 66-71, 79-96.)

92. Prohl, M. A.: A General Method of Calculating Critical Speeds of Flexible Rotors. J. Appl. Mech., vol. 12, Sept. 1945, pp. A-142 - A-148. (Card 21: All.)

93. Mykelstad, N. O.: Numerical Analysis of Forced Vibrations of Beams. J. Appl. Mech., vol. 20, no. 11, Mar. 1953, pp. 53-56. (Card 21: All.)

94. Thomson, W. T.: Matrix Solution for the Vibration of Nonuniform Beams. J. Appl. Mech., vol. 17, no. 3, Sept. 1950, pp. 337-339. (Card 21: All.)

95. Satchwell, D. L.: More Accurate Balancing for High-Speed Rotors. Machine Design, vol. 37, Sept. 16, 1965, pp. 183-184. (Card 21: All.)

96. Eshleman, R. L.: Procedures for Calculating Natural Frequencies of Shafting Systems. IITRI-K6086, IIT Research Institute Technology Center, 1967. (Available from DDC as AD-811785.)

97. Brunner, J. J.: Analysis and Experimental Verification of Axial Thrust on the M-1 Liquid Oxygen Turbopump. Aerojet General Corp. (NASA CR-54817), 1966. (Card 21: pp. iii, 22-40.)

98. Pinkel, I. Irving; Hartmann, Melvin J.; Hauser, Cavour H.; Miller, Max J.; Ruggeri, Robert S.; and Soltis, Richard F.: Pump Technology. Selected Technology for the Petroleum Industry. NASA SP-5053, 1965, pp. 81-101. (Card 21: pp. v, 81-101.)

99. Ruggeri, R. S.; and Moore, R. D.: Method for Prediction of Pump Cavitation Performance for Various Liquids, Liquid Temperatures, and Rotative Speeds. NASA TN D-5292, 1969. (Card 22: pp. ii, 1-29.)

100. Numachi, F.: Effect of Surface Roughness on Cavitation Performance of Hydrofoils - Report 3. Trans. ASME, ser. B, J. Basic Eng., vol. 89, no. 1, Mar. 1967, pp. 201-209. (Card 22: All.)

101. King, J. A.; and Farrel, E. C.: The Transient Performance of a Hydraulic Turbine-Driven Inducer: Computer Predictions and Test Verification. Rep. R-7747, Rocketdyne (NASA CR-72518), 1969. (Card 22: pp. 1-40.)

102. Farquhar, J.; Lindley, B. K.; and Rostafiniski, W. A.: Transient Pumping Performance of a Two Speed, Hydraulic Turbine Driven/Inducer System. AIAA Paper 69-551, June 1969.

103. Farquhar, J.; Lindley, B. K.; McKinney, E. B.; Olson, G. K.; and Buckmann, P. S.: Inducer Dynamics: Full-Flow, Full-Admission Hydraulic Turbine Drive. Rep. AGC 7977-T1, Aerojet General Corp. (NASA CR-72378), 1969.

104. Bair, E. K.; and Campbell, W. E.: Evaluation of a Twin-Spool Hydrogen Turbopump at Zero NPSP. J. Spacecraft & Rockets, vol. 7, no. 1, Jan. 1970, pp. 49-53.

105. Bisson, E. E.; and Anderson, W. J.: Advanced Bearing Technology, NASA SP-38, 1964. (Cards 23 and 24: pp. v, vii, 139-173, 309-321, 371-450.)

106. Liquid Rocket Engine Turbopump Bearings, NASA SP-8048, 1971. (Cards 24 and 25: All.)

107. Scibbe, H. W.: Bearings and Seals for Cryogenics Fluids. NASA TM X-52415, 1968. (Card 25: pp. 5-20.)

108. Young, M. W.; and Kirby, L. F.: Development of Liquid Oxygen Cooled 110MM Roller and Tandem Ball Bearings at up to $.5 \times 10^6$ DN Values for the Oxidizer Turbopump of the M-1 Engine. Rep. AGC 8800-23, Aerojet General Corp. (NASA CR-54816), 1966. (Card 25: pp. iii, 1-12.)

109. Cleanliness of Components for Use in Oxygen, Fuel and Pneumatic Systems. MSFC-SPEC-164A, NASA George C. Marshall Space Flight Center, Oct. 1970. (Card 25: pp. 1-28.)

110. Coe, H. H.; Scibbe, H. W.; and Parker, R. J.: Performance of 75-Millimeter-Bore Bearings to 1.8 Million DN with Electron-Beam-Welded Hollow Balls. NASA TN D-5800, 1970. (Card 26: All.)

111. Coe, H. H.; Scibbe, H. W.; and Anderson, W. J.: Evaluation of Cylindrically Hollow (Drilled) Balls in Ball Bearings at DN Values to 2.1 Million. NASA TN D-7007, 1971. (Card 26: All.)

112. Ludwig, Lawrence P.: Self-Acting and Hydrodynamic Shaft Seals. NASA TM X-68214, 1973. (Card 26: pp. 1, 15-17.)

113. Hady, W. F.; Allen, G. P.; and Johnson, R. L.: Wear and Friction of Mechanical Carbons in Liquid Oxygen as Influenced by Transfer Films. ASLE Trans., vol. 6, no. 3, July 1963, pp. 201-208. (Card 26: All.)

114. Hady, W. F.; Allen, G. P.; Sliney, H. E.; and Johnson, R. L.: Friction, Wear, and Dynamic Seal Studies in Liquid Fluorine and Liquid Oxygen. NASA TN D-2453, 1964. (Card 26: All.)

115. Bernd, L. H.: Survey of the Theory of Mechanical Face Seals. Part 1 - Characteristics of Seals. Lubri. Eng., vol. 24, no. 10, Oct. 1968, pp. 479-484. (Card 26: All.)

116. Russel, T. E.; Allen, G. P.; Ludwig, L. P.; and Johnson, R. L.: Gas Turbine Face Seal Thermal Deformation and Computer Program for Calculation of Axisymmetric Temperature Field. NASA TN D-5605, 1969. (Cards 26, 27, and 28: All.)

117. Robinson, R. P.; and Burton, R.: Temperature Gradients in Seal Rings: A Method of Analysis. Proceedings of the Fourth International Conference on Fluid Sealing. A. L. King, B. S. Nau, and H. S. Stephens, eds., British Hydromechanics Res. Assoc. (England), 1969. (Card 28: All.)

118. Strom, T. N.; Ludwig, L. P.; and Hudelson, J. C.: Vibration of Shaft Face Seals and Stabilizing Effect of Viscous and Friction Damping. NASA TN D-5161, 1969. (Card 28: pp. ii, 1-18.)

119. Kauffmann, W. M.: Safe Operation of Oxygen Compressors. Chemical Engineering, vol. 76, no. 23, Oct. 20, 1969, pp. 140-148. (Card 28: pp. 140, 142, 144, 146, 148.)

120. Smith, G. M.: High Performance Space Shuttle Auxiliary Propellant Valve Program. Rep. R-9078, Rocketdyne Div., Rockwell International (NASA CR-120976), 1973. (Card 28: pp. 5-46.)

121. Schwatzberg, F. R.; Osgood, S. H.; Bryant, C.; and Knight, M.: Cryogenic Materials Data Handbook. Martin Marietta Corp., 1970.
Vol. 1 - Sections A, B, and C, Revised. AFML-TDR-64-280-Vol. 1-Rev.; AD-713619.
Vol. 2 - Sections D, E, F, G, H, and I, Revised. AFML-TDR-64-280-Vol. 2-Rev.; AD-713620.

122. Tellier, G. F.: Poppet and Seat Design Data for Aerospace Valves. AFRPL-TR-66-147, Air Force Rocket Propulsion Lab. (AD-488480), 1966. (Card 29: pp. iii, 11-41, 407-418.)

123. Liquid Rocket Valve Assemblies. NASA Space Vehicle Design Criteria (Chemical Propulsion). NASA SP-8097, 1973. (Card 29: pp. iii, 66-68.)

124. Engineering Memo - Hamilton Standard Div. of United Aircraft Corp. to NASA MSC. Subject: Silicone "O" Seals-PLSS and OPS High Pressure Oxygen Applications. Aug. 12, 1970. (Card 29: All.)

125. Power Piping. ASA B31.1, ANSI, 1973.

126. Petroleum Refinery Piping. B31.3, ANSI, 1973.

127. Standard Method of Test for Brittleness Temperature of Plastics and Elastomers by Impact. Part 27 of ASTM Annual Standards. ASTM Designation D 746-72, 1973.

128. Bass, R. L.; and Holster, J. L.: Bellows Vibration with Internal Cryogenic Flows. Trans. ASME, Ser. B; J. Eng. Ind., vol. 94, no. 1, Feb. 1972, pp. 70-75. (Card 30: All.)

129. Sack, L. E.: Analysis of Flow-Induced Vibration Associated with Bellows Convolutions. Rocketdyne, North Amer. Rockwell, IL8112-3175, Dec. 1968. (Card 30: All.)

130. F-1 Flexible Line Flow-Induced Vibration Verification Program. R-7897, Rocketdyne, North Amer. Rockwell, July 1969. (Card 30: pp. 1/2, 25-50.)

131. Hulbert, L. E.; Keith, R. E.; and Trainer, T. M.: State-of-the-Art Survey of Metallic Bellows and Diaphragms for Aerospace Applications. Battelle Memorial Inst. (AFRPL-TR-65-215), 1965. (Card 30: pp. iii, 45-46.)

132. Fittings, MC, Classification of Defects. MSFC-STD-437, NASA George C. Marshall Space Flight Center, February 11, 1965. (Card 30: pp. 1, 5.)

133. Henson, F. M.: An Evaluation of Gaskets, Seals, and Joints for Aerospace Hardware. Aerojet-General Corp. (NASA CR-93784), 1967.

134. Piping and Tubing Technology. NASA SP-5903(02). (Card 30: pp. i, 1-6.)

135. Rathbun, F. O., Jr., ed.: Separable Connector Design Handbook (Tentative): Design Criteria for Zero Leakage Connectors for Launch Vehicles. General Electric Co. (NASA CR-64944), 1964. (Cards 30 and 31: pp. i, ii, 2-1 - 2-50, 3-1 - 3-30.)

136. Refrigeration Piping. B31.5, ANSI, 1966.

137. Mechanical/Electrical Process Systems. Part B - Testing of Pressure Systems. Ch. 6 of NASA Lewis Operational Safety Manual. 1966. (Card 31: pp. 1, 40-41.)

138. Brazing Manual. American Welding Society Inc., 1963.

139. Reynolds, W. C.: Investigation of Ignition Temperatures of Solid Metals. NASA TN D-182, 1959. (Cards 31 and 32: pp. 1, 36, 39-50.)

140. System Safety. AFSC Design Handbook DH 1-6, third ed., July 1971.

141. Justl, O. J.: Development of Seal Material for Oxygen Systems. Tech. Rept. 28-22, Mare Island Naval Shipyard, 1972. (Available from DDC as AD-891963L.) (Card 32: pp. ii, 3-4, app. 2.)

142. Curry, J. E.: Status Report on Liquid Oxygen Seal Investigation. NASA TM X-53183, 1964.

143. Fluorocarbon Plastics. Materials and Process Manual No. 215. Materials in Design Engineering, Feb. 1964, pp. 93-104.

144. Joy, L. A.; and Baumer, R. E.: Safety Aspects of Using Oxygen in a Hazardous Environment. Engineering Rept. 037-70, Aerojet Liquid Rocket Co., 1970. (Card 32: pp. 1, 10.)

145. McKinley, C.; and Wang, E. S. J.: Hydrocarbon-Oxygen Systems Solubility. Advances in Cryogenic Engineering, vol. 4. K. D. Timmerhaus, ed., Plenum Press, Inc., 1960.

146. Fassell, W. M., Jr.; Gulbrasen, L. B.; Lewis, J. R.; and Hamilton, J. H.: Ignition Temperatures of Magnesium and Magnesium Alloys. J. Met., vol. 3, July 1951, pp. 522-528. (Card 32: pp. 522, 524, 527.)

147. Wolfhard, H. G.; Glassman, I.; and Green, L., eds.: Heterogeneous Combustion. Progress in Astronautics and Aeronautics. Vol. 15. Academic Press, 1964. (Card 32: pp. ix, x, xi, 136.)

148. Jakowsky, J. J.; and Butzler, E. W.: Oxygen-Oil Explosions. Preliminary Report II. Spontaneous Ignition of Metals in Oxygen under Pressure. BM-RI-2521, Bur. Mines, Sept. 1923. (Card 32: p. 1, fig. 3.)

149. Groves, W. E.: Safe Handling of Large Quantities of Gaseous Oxygen in Steel Pipelines. Iron and Steel Engr., vol. 42, no. 1, Jan. 1965, pp. 88-95. (Card 32: pp. 88-89.)

150. Grosse, A. V.; and Conway, J. B.: Combustion of Metals in Oxygen. Indus. Eng. Chem., vol. 50, no. 4, Apr. 1958, pp. 663-672. (Card 32: pp. 663, 669, 670.)

151. Laurendeau, N. M.; and Glassman, I.: Ignition Temperatures of Metals in Oxygen Atmospheres. Comb. Sci. Tech., vol. 3, 1971, pp. 77-82. (Card 32: pp. 77, 79-81.)

152. Mellor, A. M.: Heterogeneous Ignition of Metals: Model and Experiment. Ph.D. Thesis, Princeton University (NASA CR-93541), 1967. (Card 32: pp. 325-326, 328-329, 331-332.)

153. Hill, P. R.; Adamson, D.; Foland, D. H.; and Bressette, W. E.: High Temperature Oxidation and Ignition of Metals. NACA RM L55L23b, 1956. (Card 32: pp. 1, 7.)

154. Dean. L. E.; and Thompson, W. R.: Ignition Characteristics of Metals and Alloys. ARS J., vol. 31, no. 7, July 1961, pp. 917-923. (Card 32: pp. 917, 923.)

155. Nonmetallic Materials Design Guidelines and Test Data Handbook. NASA TM X-67639, 1970. (Available from DDC as AD-889181L.)

156. Guter. M.: Ignition in High Pressure Oxygen. S & T Memo 13/50, British Ministry of Aviation, 1967. (Card 32: pp. 9-10, 16-17, 21-24.)

157. Hust, J. G.; and Clark, A. F.: A Survey of Compatibility of Materials with High Pressure Oxygen Service. Rep. 275.03-72-11, NBS Institute for Basic Standards, Cryogenics Division, Oct. 1972. (Cards 32 and 33: pp. ii, 1-4, app. I.)

158. Attwood, H. C.; and Allen, G. R.: On the Spontaneous Ignition Temperature of Organic Materials in Oxygen. C. P. No. 1172, British Ministry of Defence (Aviation Supply), 1971. (Card 33: pp. 1-15, 21.)

159. Kuchta, J. M ; Litchfield, E. L.; and Furno, A. L.: Flammability of Materials in Hyperbaric Atmospheres, Final Report. Rep. No. 4016, Bur. Mines, 1967. (Card 33: pp. v, 6, 9, 11, 12.)

160. Cook, G. A.; Meierer, R. E.; and Shields, B. M.: Combustibility Tests on Several Flame-Resistant Fabrics in Compressed Air, Oxygen-Enriched Air, and Pure Oxygen. Text. Res. J., vol. 37, no. 7, July 1967, pp. 591-599. (Card 33: pp. 591-595.)

161. Pippen, D. L.; and Stradling, J. S.: Materials Testing in a Gaseous Oxygen Environment. Paper presented at 74th National Meeting, A. I. Ch. E. (New Orleans, LA), Mar. 1973. (Card 33: table 2.)

162. Huggett, C.; Von Elbe, G.; and Haggerty, W.: The Combustibility of Materials in Oxygen-Helium and Oxygen-Nitrogen Atmospheres. Rep. SAM-TR-66-85, Atlantic Res. Corp., 1966. (Card 33: pp. iii, 5.)

163. Huggett, C.; Von Elbe, G.; Haggerty, W.; and Grossman, J.: The Effects of 100 Percent Oxygen at Reduced Pressure on the Ignitibility and Combustibility of Materials. SAM-TR-65-78, Atlantic Research Corp. (AD-477338), 1965. (Card 33: pp. iii, 19, 21.)

164. Kimzey, J. H.: Flammability During Weightlessness. NASA TM X-58001, 1966. (Card 33: pp. 1, 12.)

165. Dawn, F. S.: Nonmetallic-Materials Development for Spacecraft Applications. Conference on Materials for Improved Fire Safety. NASA SP-5096, 1971, pp. 57-63. (Card 33: pp. III, VII, 62.)

166. Radnofsky, M. I.: New Materials for Manned Spacecraft, Aircraft, and Other Applications. Conference on Materials for Improved Fire Safety. NASA SP-5096, 1971, pp. 91-102. (Card 34: pp. VII, 91, 94, 95, 100, 101.)

167. Johnson, J. E.; and Woods, F. J.: Flammability in Unusual Atmospheres. Part II - Selected Materials in Oxygen-Nitrogen and Oxygen-Helium Mixtures at Pressures up to 315 psia. NRL-6606, Naval Research Laboratory, 1967. (Available from DDC as AD-823059L.) (Card 34: pp. iv, 14.)

168. Notardonato, J. J.; Burkhard, L. A.; and Cochran, T. H.: Effects of Pressure, Oxygen Concentration, and Forced Convection on the Flame Spread Rate of Plexiglas, Nylon, and Teflon. NASA TN D-7555, 1974. (Card 34: pp. 10-12.)

169. Neustein, R. A.; Mader, P. P.; Colombo, G. V.; and Richardson, D. E.: The Effect of Atmosphere Selection and Gravity on Burning Rate and Ignition Temperature. McDonnell Douglas Report DAC-62431, October 1968. (N70-10589).

170. Whitaker, D. H.: Effects of Acceleration Upon Combustion Rate Test, Nomex Standard Cloth. Rep. TF-WSTF-111A, White Sands Test Facility (Available as CR-129442), 1967.

Page intentionally left blank

INDEX

[Numbers refer to sections.]

Abrasion
  As ignition source, 3.4.6
  In pumps, 6.1.3.3.4
  Seal, 9.2
  In valves, 7.2.1.2
Adiabatic compression
  As ignition source, 3.4.4
  Ignition test (GOX pneumatic impact testing), 3.6.1.2
  Ignition test data, 3.4.4
  Temperature as function of pressure, 3.4.4
ANSI Piping Code, 8.1., 8.5.2
ASME Boiler and Pressure Vessel Code, 5.1.1, 8.5.2
Auto-ignition
  Ignition temperatures (see "Ignition temperatures")
  Tests (see "Tests")

Balance piston (see "Shaft stability, Axial thrust")
Bearings, 6.1.2
  Contamination limits of, 6.1.2.2.1
  DN limits, 6.1.2.3
  Life, 6.1.2.3
  Lubrication and cooling, 6.1.2.2
  Materials, 6.1.2.1
  Turbopump shaft, 6.1.2
Bellows
  As a rotating shaft seal, 6.1.3.1, 9.2
  As a valve stem seal, 7.6
  For lines, 8.4
    At pump inlet line, 6.1.1.3
    Bellow-to-duct attachment (see "Joints, Bellow-to-duct")
  Buckling instability, 8.4
  Design criteria, 8.4.2
  Flow-induced vibration failures, 8.4.1
  Vibration damping, 8.4.1
  Materials, 8.4.3
Brazed joints (see "Joints, Brazed")
Burning rates (see "Combustion rates")

Cavitation
  Definition and data, 4.2
  Design considerations for, 4.2
  Erosion, 4.2
  Flow, 7.7
  Inducer/impeller, 6.1.1.3.2
  Inlet line, 6.1.1.3.1
    Erosion of, 4.2
  Pump, 6.1.1.3
  Valve, 7.7
Centrifugal pumps (see "Pumps, centrifugal")
Chemical corrosion (see "Corrosion, Chemical")
Cleanliness
  For bearing coolant, 6.1.2.2.1
  For filters, 10.0
  For fuel cell oxygen, 2.3
  For oxygen systems, 2.3, 4.5, 5.1.3
  For pumps, 6.1.2.2.1
  For valves, 7.8
  Cleaning requirements, procedures, and verification techniques, 4.5
Cold-shock conditioning, 4.6
  Procedures, 4.6
Combustion, 3.5 (see "Flammability")
  Heat of, 3.4
  Of metals, 3.5
  Of nonmetals, 3.5
  Rates, 3.5
    Effect of oxygen concentration and pressure, 3.1.5
    Effect of material thickness, 3.1.5
Compatibility of materials with oxygen (see "Materials compatibility with oxygen")
Connectors (see also "Couplings and fittings" and "Joints")
  As site of stress, 8.0
Connector potting flammability testing, 3.6.1.7
Contaminants, oxygen (see also "Contamination")
  Boiling points, 2.2
  Corrosive, 3.2
  Dissolved, 2.2
  Flammability (see "Flammability, Limits of contaminants")
  Freezing points, 2.2
  In oxygen, 2.2
  Properties of, 2.2
  Solid, 2.2, 10.0
  Solubility of, 2.2, appendix C
Contamination (see also "Contaminants")
  In filters, 10.0
  In lines, joints, and fittings, 3.4.6, 8.0, 8.5.3, 8.6
  In pumps, 6.0, 6.1.2.2.1, 6.1.3.3.4
  In valves, 7.0, 7.2, 7.4
  Limits (levels), 2.2, 4.5, 6.1.2.2.1
  Of diffusion membranes, 2.2
  Particle, 2.2, 3.4.6, 4.2, 7.4, 7.8, 10.0
  Prevention of, 4.5, 5.1.3, 7.1, 8.5.1, 8.6.1
  Control, 2.1
Corrosion, 3.2
  Chemical, 3.2.1, 5.1.3, 6.1.2
  Galvanic, 3.2.2
  In oxygen systems, 3.2, 5.1.3, 5.1.4, 8.6.1
  Prevention, 5.1.3, 5.1.4
  Stress, 3.2.3, 3.3, 5.1.4, 8.6.2.1

Couplings and fittings, 8.5 (see also "Joints," Connectors," "Welds")
Cycle life, 8.5.1
Design, 8.5.1, 8.5.2
Failures of, 4.4, 8.5.2, 8.6
Leakage in, 4.1, 8.5.1, 8.5.2
Materials for, 8.5.1-8.5.3
Types:
AN, MS, and MC, 8.5.1
Flanged, 4.4, 8.5.2
Threaded, 8.5.1, 8.5.2
Coatings, thermal, 5.3, 6.1.1.1 (see "Insulation" and "Plating")
Crack propagation, 3.3
Critical flaw size, 3.3, 5.1, 5.1.5
Cyclic stress effects on, 5.1.5
Fatigue, 3.3, 5.1.5
Prevention, 5.1.5, 6.1.6
Creep
In tank materials, 5.1.6
In seal materials, 9.3.2
Critical speed (see "Pumps, centrifugal")
Critical flow (see "Cavitation")
Cycle life
Bellows, 8.4.3
Tank, 5.1.5
Valves, 7.4

Design criteria
Oxygen systems, general, 4.4
For bellows, 8.4
For lines, 8.1, 8.2
For tanks (see "Oxygen tank assemblies, Design and safety considerations")
For valves (see "Valve design criteria")
In relation to fluid dynamics, 4.2
In relation to stress intensity and crack propagation, 3.3
Detonability limits, fuels in oxygen, 2.2
Downward propagation rate testing, 3.6.1.4
Ducting (see "Lines")
Dynamic (flow) effects on ignition (see "Flow, Effect on ignition")
Dynamics, fluid system (see "Fluid system dynamics")

Electrical arc ignition testing, 3.6.2.5
Electrical wire insulation testing, 3.6.1.6
Epoxy resins (see "Polymers, Epoxy resins")
Erosion, 4.2
As ignition source, 3.0
Cavitation (see "Cavitation")
Definition and data, 4.2
In system leakage, 4.1
Particulate, 4.2
Seal, 4.2
Valve, 7.7

Face contact seal (see "Seals, dynamic")
Fatigue, effect of oxygen on
Crack growth (see "Crack propagation")
Cycle life, 3.3, 5.1.5, 6.1.2.3, 8.4
Fatigue failure, 5.1.2, 6.1, 6.1.4.1, 6.2.3, 6.3.1, 8.4, 8.4.3
Fatigue life, 3.1.3, 5.1.2, 6.2, 8.0, 8.4.2
Fatigue life reduction, 3.3
Fiberglass (see "Polymers, Fiberglass")
Filters
Design, 10.0
Materials, 10.0
Sizes, 10.0
Filtration requirements and criteria, 2.2, 2.3, 4.4, 4.5, 5.1.3, 6.1.2.2.1, 7.8, 10.0
Fittings (see "Couplings and fittings," "Joints," "Connectors")
Flame propagation rates, 3.5
Flammability, 3.5, 5.3 (see "Combustion")
Limits of contaminants, 2.2
Limits of fuels, 2.2
Rates and parameters, 3.5
Tests, 3.6.1
Data, 3.5
Flanged Couplings (see "Couplings and fittings")
Flash and fire point tests, 3.6.1.5
Flexible hose (see "Lines")
Flow (see also "Flow velocity," "Inlet flow dynamics," "System dynamics")
Cold flow (see "Creep")
Critical (see "Cavitation")
Effect on ignition, 3.4.6, 7.3
Erosion, 3.0, 4.2, 7.7
Leakage (see "Leakage")
Passages, design considerations, 4.4, 6.1.3, 7.2
Flow velocity
Effects on bellows, 8.4.2
Effects on compatibility, 3.4.6, 4.5, 7.7
Effects on flex hose, 8.3
Effects on geysering, 4.3.1
Effects on ignition, 3.4.6, 10.0
Erosive effects, 4.2, (see also "Erosion" and "Cavitation")
Limits in piping, 3.4.6
Tests, 3.6.2.4, 10.0
FLOX (Fluorine-oxygen mixtures), 4.4
Fluid system dynamics, 4.3
Flow oscillation, 4.4, 6.1.1.3, 7.3.2
Fluid system leakage, 4.1 (see also "Leakage" and "Seals")
Gaseous, 4.1
Leak clogging, 4.1.3
Leak erosion (see "Erosion")
Leak path, 4.1, 4.1.2, 5.1.5, 7.5, 7.6, 9.0
Liquid, 4.1
Modes of leakage (see "Leakage, Modes of")
Permeation, 4.1.4
Prevention, 4.1
Rate, 4.1, 9.4
Fluorine, 2.0, 9.4
Fluorocarbon polymers, 6.1.1.1, 6.1.2.2, 7.5.2, 8.3, 9.3.3
Chlorotrifluoroethylene (CTFE), 3.7.1.4

Filled TFE and FEP, 3.7.1.3
Fluorinated ethylene propylene copolymer (FEP), 3.7.1.2
Polytetrafluoroethylene (TFE), 3.7.1.1
Vinylidene fluoride and hexafluoropropylene copolymer - Viton, Fluorel, 3.7.1.5
Fracture mechanics, 5.1.5
Fracture toughness and cyclic effects, 5.1.5
Friction
As ignition source, 3.0
Erosive effects, 4.2
In pumps, 6.1.1.1, 6.1.1.2, 6.1.2.2., 6.1.3.3.2
In seals, 9.0, 9.2.2
In valves, 7.4, 7.6

Galvanic corrosion (see "Corrosion, Galvanic")
Geysering (see "Fluid system dynamics, Geysering")
GOX pneumatic impact testing, 3.6.1.2

Halogens, 2.0
Heat capacity (specific heat)
Data, 3.4
Effect on ignition of materials, 3.0
Heat transfer
As source of ignition, 3.0
As source of geysering, 4.3
As source of overstress, 4.4
Prevention of, 5.3
Hose (see "Lines")
Hydrocarbons (see "Contaminants, Dissolved," "Flammability, Limits of contaminants")
Properties of, 2.2

Ignition
By adiabatic compression, 3.4.4
By impact, 3.4.3
From flow effects, 3.4.6
From friction, 3.0
From rupture, 3.4.5
Of materials with oxygen, 1.0, 3.0, 3.4
Particle impact, 3.4.6
Tests, 3.6
Ignition temperature
Defined, 3.4
Determination (see "Ignition, Tests")
Of metals, 3.4
Of nonmetals, 3.4.2, 4.5, 6.3.2
Parameters, 3.4, 4.4, 7.3
Of particles as opposed to bulk material, 3.4.1
Impact
As ignition energy source, 3.0, 3.4.3, 3.4.6, 4.4, 5.0, 10.0
Fluid, 3.4.6, 4.2
In pumps, 6.1
In valves, 7.1
Particle, 1.0, 3.1.4.1.1, 3.1.4.4, 3.2.2.4, 3.3.2, 4.2, 7.5.2, 10.0
Pneumatic (see "Adiabatic compression" and "GOX pneumatic impact testing")
Testing, mechanical, 3.6.1.1

Impact energy
Limits of, 3.4.3
Effect of material thickness on, 3.4.3
Impeller/inducer, 6.1.1
Axial thrust, 6.1.2.2
Balancing of, 6.1.1.2
Cavitation, 6.1.1.3
Critical speed, 6.1.1.2
Materials, 6.1.1.5
Pump case clearance, 6.1.1.1, 6.1.1.2
Torsional stability, 6.1.1.2.1
Inlet flow dynamics, 6.1.1.3
Inducer/impeller cavitation, 6.1.1.3.2
Inlet line cavitation, 6.1.1.3.1
Insulation, 5.3
Emissivities of, 5.3 (see also "Thermal conductivities")
Fire Hazards of, 5.3

Joints (see also "Welds," "Couplings and fittings," "Connector")
Bellow-to-duct, 8.4.2
Brazed, 8.6, 8.6.1, 8.6.2
Materials, 8.6.2, 8.6.2.1
Cleanliness, 8.6.2.2
Fatigue strength, 6.1.4.1
Flanged joints, 8.5.2
Life, 4.4, 9.2
Pipe joints, 8.5.3
Sleeve or socket, 4.4, 8.6.1
Testing, 9.4
Welded, 4.4, 5.1.7, 6.1.1.4.1, 8.6, 8.6.1

Labyrinth seals, 6.1.1.1
Leak clogging, 4.1.3
Leak tests, 9.4
Leakage (see also "Fluid system leakage" and "Seals")
Coupling and fitting (see "Couplings and fittings, Leakage in")
Hose, 8.3
Modes of, 4.1.1
Laminar, 4.1.1
Molecular diffusion (see "Permeation")
Sonic or choked, 4.1.1
Transition, 4.1.1
Turbulent, 4.1.1
Seal (see "Seal leakage")
Valve element/seat leakage (see "Valve assembly, valve leakage")
Valve stem (see "Valve assembly")
"Zero leakage," 4.1
Lines, 6.1.4.1
Allowable working pressure for, 8.1
Assembly, 8.7
Bellows (see "Bellows")
Cavitation, 6.1.1.3.1, 4.2
Flexible hose, 8.3
Materials, 8.2, 8.3, 8.4.3, 8.5
Rupture, 8.7

Lip seal
Dynamic, 6.1.3.1, 9.1
Garter-ring lip seal, 9.1
In pump shafts, 6.1.3
Lubrication
Of bearings, 6.1.2.2
Of couplings, 8.5.1, 8.5.3
Of shaft seals, 7.6
Properties of carbon, 6.1.3.2

Materials
For bearings, 6.2
For bellows, 8.4.3
For connectors, lines, joints and fittings, 8.2, 8.3, 8.4.3, 8.5.1, 8.6.2.1
For filters, 10.0
For insulation, 5.3
For lines, 8.2
For pumps, 6.1.5
For pump shaft seals, 6.3.2
For tanks, 5.2
For valves, 7.3
For valves seals, 7.6
Materials compatibility with oxygen
Effect of flow on, 3.4.6
Limits of, 3.4
Metals, 3.4.1
Nonmetals, 3.4.2
Parameters affecting compatibility, 3.0
Preferred polymeric materials for oxygen system, 3.7
Materials, ignition of (see "Ignition" and "Ignition temperatures")
Materials selection criteria and data, 3.0 (see also "Materials compatibility")
Materials testing, 3.6
NASA Specifications for, 3.6.1
Connector potting flammability testing, 3.6.1.7
Downward propagation testing, 3.6.1.4
Electrical wire insulation testing, 3.6.1.6
Flash and fire point testing, 3.6.1.5
GOX pneumatic impact testing, 3.6.1.2
Mechanical impact testing, 3.6.1.1
Other NASA compatibility testing, 3.6.1.8
Upward propagation testing, 3.6.1.3
Tests not required by NASA, 3.6.2
Electrical arc ignition testing, 3.6.2.5
Oxygen bomb test, 3.6.2.1
Oxygen index testing, 3.6.2.3
Thermogravimetric analysis testing, 3.6.2.2
Velocity impact testing, 3.6.2.4
Mechanical impact test (see "Impact," "Testing")
Metals
Burning rate, 3.5
Dissimilar metals (see "Corrosion, Galvanic")
Ignition of, 3.4.1
Properties of, 3.4.1

NASA specifications for materials compatibility testing (see "Materials Compatibility with Oxygen")

Oxidation (see "Reactivity of oxygen" and "Oxide film formation")
Oxide films, characteristics of, 3.1, 3.4.1
Oxide film formation, 3.1
Catastrophic, 3.1.1.1
Heat of, 3.4
Rate of, 3.1
Thickness of, 3.1
Oxidizers, elemental
Characteristics, 1.0, 2.0
Oxygen (see "Oxygen")
Oxygen
Characteristics of, 1.0, 2.0
Contamination, 2.2 (see also "Contaminants")
Properties of, 2.1
Purity requirements and specifications, 2.3
Index:
Data, 3.5
Test, 3.6.2.3
Oxygen Bomb Test, 3.6.2.1
Oxygen systems
Cleaning requirements and procedures, 4.5
Cryogenic conditioning, 4.6
Design criteria (see "Design criteria")
Engineering considerations, 3.0, 4.0
Preferred nonmetal materials for, 3.7
Prevention of failures, 4.4
System dynamics (see "System dynamics")
Oxygen tank assemblies, 5.0
Design and safety considerations, 3.0, 4.4, 5.1, 5.1.1, 5.1.2
Corrosion, 3.2, 5.1.3-5.1.4
Creep, 5.1.6
Cyclic stress and cycle life, 5.1.5
Materials compatibility, 5.1.2, 5.2, 5.3
Safety factors and proof pressures, 5.1.2
Stress corrosion, 5.1.3
Tank wall penetrations, 5.1.7
Ullage allowances, 5.6
Weld joints, 5.1.6
Design standards and specifications, 5.1.1
Insulation, 5.3
Maintenance control, 5.4
Overpressure hazard, 5.5 (see also "TNT energy equivalent")

Permeability, of materials, 4.1.4
Data, 4.1.4
Permeation, 4.1.4
Piping (see "Lines")
Plating, 4.4, 5.3, 9.2.1 (see also "Coatings")
Polyimide resins (see "Polymers, polyimide resins")
Polymers, 3.7
Brittle point of, 8.3
Epoxy resins, 3.3.5

Fiberglass, 3.3.3, 6.2
Fluorocarbon (see "Fluorocarbon polymers")
Polyimide resins, 3.3.4
Silicone, 3.3.2, 9.3.3
Table of polymer trade names, appendix A
Polymer, permeability of, 4.1.4
Pneumatic impact (see "Impact, adiabatic compression")
Pressure balancing arrangement (see "Shaft stability, axial thrust")
Pressure ranges, definition of, 1.0
Propellant conditioning (see "Oxygen systems, propellant conditioning")
Pumps, oxygen, 6.0
Pumps, centrifugal, 6.1
Cleaning requirements, 6.1.2.2.1, 6.1.3.3.4
Critical speed, 6.1.1.2
Design requirements, 6.1.1, 6.1.2, 6.1.3, 6.2
Safety factors, 6.1.1.4
Materials, 6.1.1.5
Housing and rotor assembly, 6.1.1
Impeller/inducer (see "Impeller/inducer blade")
Inlet flow dynamics (see "Cavitation")
Turbopump shaft (see "Shaft")
Turbopump shaft bearings (see "Bearings")
Turbopump rotating shaft seals (see "Seals, dynamic")
Pumps, positive displacement, 6.2
Materials, 6.2
Purity requirements and specifications, 6.1.3.1

Reactivity of oxygen (see also "Material compatibility"), 3.0
Catastrophic oxidation, 3.1
Combustion (see "Combustion")
Corrosion (see "Corrosion")
Effect of oxygen on crack propagation (see "Crack propagation")
Flammability (see "Flammability")
Ignition (see "Ignition" and "Ignition temperature")
Oxide film formation (see "Oxide film formation")
Rate, 3.1
With common materials, 3.0, 3.1
With solid contaminants, 2.2
Ring seals, 9.1, 9.3.3 (see also "Seals")
Back-up ring, 3.3.1.5, 3.3.2, 9.3.1
Couplings, 8.5.1, 8.5.3
O-ring, 7.6, 9.2.1, 9.3, 9.3.1
Piston, 6.1.3.1, 6.2
Wear ring, 6.1.1.1
Nonextrusion seals (see "Ring seals, back-up")
Rotor (see also "Pumps, centrifugal, Housing and rotor assembly")
Assembly, 6.1.1, 6.1.1.1
Rub, 6.1.1.1, 6.1.1.2
Shaft designs, 6.1.1.4.2, 6.1.1.5
Stability, 6.1.1.2
Rupture, ignition, 3.0, 3.4.5, 5.0

Safety factors (see individual component)
Seal leakage, 6.3.3, 9.2 (see also "Fluid system leakage" and "Leakage")
Erosion, 4.2, 7.6
Permeation (see "Permeability")
Prevention, 4.4, 6.1.3
Testing techniques, 9.4
"Zero leakage" (see "Leakage, Zero leakage")
Seals, static (see also "Seal leakage," "Leakage"), 9.0, 4.1.2, 4.4
Creep, 9.3.2
Extrusion, 9.1, 9.3.1, 9.3.3
Hardness, 9.3.1
Materials, 3.7, 4.4, 8.5.2, 8.5.3, 9.0, 9.3
Surface finish, 6.3.3.1, 6.3.3.4, 8.5, 9.1.1, 9.2.1
Seals, dynamic, 9.2, 6.1.1.2, 6.3
Contamination effects on, 6.1.3.3.4
General design factors, 9.1, 9.2, 6.1.3.3
Leakage (see "Leakage")
Materials, 9.3, 6.1.3.2
Rubbing speed, contact pressure, wear, 9.2, 6.3.2, 8.5.1
Turbopump rotating shaft seals, 6.1.3
Stability of, 6.1.3.3.3
Surface finish (see "Seals, surface finish")
Types, 6.1.3.1 (see also "Bellows," "Lip seals," "Ring seals," "Labyrinth seals")
Shafts, rotating
Bearings (see "Bearings, turbopump shaft")
Design, 6.1.1, 6.1.1.2, 6.1.4.2
Lubricants, 7.2.2.1
Rotating shaft leakage, 4.1
Seal (see "Seals, dynamic")
Stability (see "Shaft stability")
Shaft stability, 6.1.1.1, 6.1.1.2
Axial thrust (load), 6.1.1.2.2 (see also "Impeller/inducer, Balancing of")
Critical speeds, 6.1.1.2
Impeller/shaft, 6.1.1
Torsional stability, 6.1.1.2.1
Shock wave, as ignition source, 1.0, 3.0, 4.3
Silicone polymers (see "Polymers, silicone")
Solubility limits
As a function of oxygen temperature, appendix C
Of hydrocarbons in oxygen, 2.2
Stress, 3.3.1.1, 4.7
Bending, 5.1.7, 6.1, 6.1.5, 8.0
Compressive, 4.4
Corrosion (see "Corrosion, stress")
Cyclic, 3.1.2.3, 3.1.3, 3.1.3.1, 3.1.3.3, 4.4, 5.1.5, 8.0
In bellows, 8.4.3
In joints, 8.4.4, 8.6.1
In piping and tubing, 8.1, 8.4, 8.4.4
In pumps, 6.1.1, 6.1.1.4, 6.1.2.3
In tanks, 5.1.2
In valves, 7.2
Levels for materials, 3.3, 5.1.2, 5.1.5
Mechanical, 1.0, 3.3, 4.4, 6.1, 8.5.3

Relaxation (see "Creep")
Thermal, 6.1.3.2, 7.2, 8.5.3
Surface damage, 4.2
Bearings, 6.1.2.3
Bellows, 8.4
Cavitation (see "Cavitation")
Erosion (see "Erosion")
From rupture, 3.4.5
Seals, 6.1.3.4, 9.0
Valve, 7.4, 7.5, 7.5.1
Surface finish
Coupling seal, 8.5.1
Pump impeller, 6.1.1.3.2
Seals (see "Seals, Surface finish")
Typical machined surface, 9.1.1
Valve components, 7.5.1, 7.6
System contamination, 2.2, 5.0
Control procedures, 2.3, 4.5, 5.1.3, 5.4, 6.3.3.4
System dynamics (see "Fluid system dynamics")

Tanks (see "Oxygen tank assemblies")
Testing (see specific subject/test name)
Thermal conductivity
Of insulation materials, 5.3
Of metals, 3.4, 6.3.2, 7.1, 7.2.1.4
Of nonmetals, 3.4, 7.1, 7.2.1.4
Of seals, 6.3
Thermal cycling, 4.1, 4.3, 7.0, 8.5.1, 9.1
Thermal diffusivity, 3.4
Thermogravimetric analysis testing (TGA), 3.6.2.2
TNT energy equivalent, 5.5
Tubing (see "Lines")
Turbopumps (see "Pumps, centrifugal")

Upward propagation testing, 3.6.1.3

Valve assembly, 7.0
Valve element types, 7.1
Valve seats (metallic), 7.5.1
Valve seats (nonmetallic), 7.5.2
Valve stem, 7.6
Valve seals, 7.5, 7.6
Erosion of, 7.7
Lubrication of, 7.6
Valve types, 7.1
Valve design criteria, 4.4, 7.0, 7.2, 7.4
Dynamic seals for valve actuators, 7.6
Filtration requirements, 7.8
Materials selection, 7.3
Valve leakage, 7.5, 7.6
Valve life, 7.6
Valve lubrication, 7.6
Valve wear, 7.4, 7.5
Valves (see "Valve assembly")
Velocity (see "Flow velocity")

"Water hammer"
As ignition source, 3.0, 4.3
From geysering, 4.3
In lines, connectors, joints, fittings, 8.0
In system failures, 1.0, 4.4, 7.0
Welding techniques, 5.1.7, 6.1.1.4.1, 8.6, 8.6.1
Butt welding, 8.6.1
Electron beam, 8.6.1
Gas metal arc, 8.6.1
Gas tungsten arc, 8.6.1
Resistance seam, 8.6.1
Welds, 4.4, 8.5.1 (see also "Joints")
In line assembly, 8.7
Weld joints (see "Joints, welded")
Lands, 5.1.7
Repair, 8.6.1
Weld neck doublers, 8.4.3
Wiring
Short circuits, sparks, arcing as source of ignition, 3.0, 5.0

Yield strength tank materials, 5.1.2

"Zero leakage" (see "Leakage, Zero leakage")

*U.S. GOVERNMENT PRINTING OFFICE: 1975 - 635-275/21

Card #1

REFERENCES

In parentheses after most references are given the Microfiche card numbers denoting the location of the references in the Microfiche supplement and the pages of the references reproduced in the Microfiche supplement.

1. Roder, H. M.; and Weber, L. A., eds.: ASRDI Oxygen Technology Survey. Volume I: Thermophysical Properties. NASA SP-3071, 1972. (Card 1: pp. iii, v, 107-143.)
2. Bailey, B. M.; Sterner, C. J.; and Vignale, V. J.: Study of Liquid Oxygen Contamination, Summary Progress. Rep. 4, Air Products and Chem. Inc. (AD-253231), 1960. (Card 1: 46-59, 60-62.)
3. McKinley, C.; and Himmelberger, F.: The Role of Air Contaminants in Formulating Oxygen Plant Safety Principles. Chem. Eng. Prog., vol. 53, no. 3, Mar. 1957, pp. 112-M to 121-M.
4. Carlson, G. A.: Spherical Detonations in Gas-Oxygen Mixtures. Combustion and Flame, vol. 21, no. 3, Dec. 1973, pp. 383-385. (Card 1: All.)
5. Contamination Control Handbook. NASA SP-5076, 1969. (Card 2: pp. iii, IV-1 - IV-32.)
6. Oxygen. MSFC-SPEC-399B, NASA George C. Marshall Space Flight Center, Jan. 31, 1974. (Card 2: pp. 1-14.)
7. Quality Control of Oxygen Propellant, Liquid Oxygen, Aviator's Liquid Breathing Oxygen, and Aviator's Gaseous Breathing Oxygen. Rep. T. O. 42B6-1-1, Change 7, U.S. Air Force, May 1, 1969. (Card 2: pp. i, 1-1 - 3-6.)
8. Bankaitis, H.; and Schueller, C. F.: ASRDI Oxygen Survey. Volume II: Cleaning Requirements, Procedures, and Verification Techniques. NASA SP-3072, 1972. (Cards 2 and 3: pp. 1-15, 18-60.)
9. McGraw-Hill Encyclopedia of Science and Technology. Vol. 3, McGraw-Hill Book Co., 1966.
10. Tomashov, N. D.: Theory of Corrosion and Protection of Metals. MacMillan Co., 1966.
11. Brenner, S. S.: Catastrophic Oxidation of Some Molybdenum Containing Alloys. J. Electrochem., vol. 102, no. 1, Jan. 1955, pp. 16-21. (Card 3: All.)
12. Gulbransen, E. A.; and Andrew, K. F.: Kinetics of the Oxidation of Pure Tungsten from 500° to 1300° C. J. Electrochem. Soc., vol. 107, no. 7, July 1960, pp. 619-628.
13. Kubaschewski, O.; and Hopkins, B. E.: Oxidation of Metals and Alloys. Second ed., Butterworths, Inc., 1967.
14. Manned Spacecraft Criteria and Standards. MSCM 8080, NASA Manned Spacecraft Center, Apr. 1971 (changes, Oct. 1972).
15. Dissimilar Metals. MIL-STD-889A, Dept. Army, May 5, 1972. (Card 3: All.)
16. Richmond, J. C.; and Thornton, H. R.: Oxidation of Experimental Alloys. Rep. WADC TR-58-164, Part I, Wright Air Development Center, 1958. (Cards 3 and 4: pp. iii, 14-17, 33-45.)
17. Smith, H. H.; Shahinian, P.; and Achter, M. R.: Fatigue Crack Growth Rates in Type 316 Stainless Steel at Elevated Temperatures as a Function of Oxygen Pressure. Trans. Met. Soc. AIME, vol. 245, May 1969, pp. 947-953. (Card 4: All.)

18. Smith, H. H.; and Shahinian, P.: Effect of Oxygen and of Water Vapor on the Fatigue Life of Nickel at 300° C. Effects of Environmental and Complex Load History on Fatigue Life. STP-462, American Soc. Testing and Mater., 1970, pp. 217-233. (Card 4: pp. 217-225.)

19. Hartman, A.: On the Effect of Oxygen and Water Vapor on the Propagation of Fatigue Cracks in 2024-T3 Alclad Sheet. Int. J. Fract. Mech., vol. 1, Sept. 1965, pp. 167-188. (Card 4: pp. 167-170.)

20. Taylor, L., ed.: Metals Handbook. Vol. 1, Properties and Selection of Metals, eighth ed., American Soc. Metals, 1967.

21. Rossini, F. D.; Wagman, D. D.; Evans, W. H.; Levine, S.; and Jaffe, I.: Selected Values of Chemical Thermodynamic Properties, Part I. Tables. Circular 500-Part I, Nat. Bur. Stand., July 1961.

22. Weast, R. C.; and Selby, S. M., eds: Handbook of Chemistry and Physics. 48th ed., Chemical Rubber Co., 1967-1968.

23. Nihart, G. J.; and Smith, C. P.: Compatibility of Materials with 7500 PSI Oxygen. Union Carbide Corp. (AMRL TDR-64-76; AD608260), 1964. (Cards 4 and 5: pp. ii, iii, v, vi, vii, viii, 1-80.)

24. Jacobson, M.; Cooper, A. R.; and Nagy, J.: Explosibility of Metal Powders. BM-RI-6516, Bur. Mines, 1964. (Card 5: pp. 1, 4.)

25. Pippen, D. L.; and Stradling, J. S.: Techniques for Determination of Flash and Fire Points and Impact Sensitivity of Materials in a Gaseous Environment. Mat. Res. Stand., vol. 11, no. 6, June 1971, pp. 35-43, 52-53. (Card 5: All.)

26. Key, C. F.: Compatibility of Materials with Liquid Oxygen - Vol. I. NASA TM X-64711, Oct. 1972. (Cards 5, 6, and 7: pp. 11-13, 42-220.)

27. Hauser, R. L.; Sykes, G. E.; and Rumpel, W. F.: Mechanically Initiated Reactions of Organic Materials in Missile Oxidizers. ASD-TR-61-324, Aeronautical Systems Division, Wright-Patterson AFB, 1961. (Available from DDC as AD-268458.) (Card 7: pp. iii, 97-98.)

28. Key, C. F.: An Instrument for Determination of Impact Sensitivity of Materials in Contact with Gaseous Oxygen at Pressures up to 50 psia. NASA TM X-53846, 1969. (Card 7: pp. 5-7.)

29. Jackson, J. D.; Miller, P. D.; Boyd, W. K.; and Fink, F. W.: A Study of the Titanium-Liquid Oxygen Pyrophoric Reaction. WADD-TR-60-258, Wright Air Development Division, Air Research and Development Command, June 1960. (Card 7: pp. iii, 5-6, 10.)

30. Landrock, A. H.: Properties of Plastics and Related Materials at Cryogenic Temperatures. PLASTEC-20, Plastics Technical Evaluation Center, 1965. (Available from DDC as AD-469126.) (Card 7: pp. i, 8-9, 30-38, 101-103.)

31. Wright, H. W.; Howell, G. W.; and Lee, D. H.: Seal Material Development Program, Phase I. TRW Systems Group (NASA CR-114822), 1970. (Card 7: pp. vi, 47, 49, 59.)

32. Walker, W. R.: Design Handbook for O-Rings and Similar Elastic Materials. WADC-TR-59-428-PT-2, Wright Air Development Center, 1961. (Available from DDC as AD-265443.) (Card 8: pp. iii, 37.)

33. Key, C. F.: An Apparatus for Determination of Impact Sensitivity of Materials in Contact with Liquid and Gaseous Oxygen at High Pressures. Mat. Res. Stand., vol. 11, no. 6, June 1971, pp. 28-51. (Card 8: pp. 28-29, 51-52.)

34. A Study of the Mechanism of the Titanium-Liquid Oxygen Explosive Reaction. ASD-TR-61-479, Aeronautical Systems Div., Air Force Systems Command, 1961. (Card 8: pp. iii, 3-5, 7-8, 10, 14, 20.)

35. Wegener, W.: Investigations of the Admissible Oxygen Flow Velocity in Steel Pipes from a Safety Point of View. NASA TT F-14,831, 1973. (Card 8: pp. 1-22.)

36. Littman, F. E.; and Church, F. M.: Reactions of Titanium with Water and Aqueous Solutions. AECU-3825, Stanford Research Inst., 1958. (Card 8: pp. 1-17.)

37. Schmidt, H. W.; and Harper, J. T.: Handling and Use of Fluorine and Fluorine-Oxygen Mixtures in Rocket Systems. NASA SP-3037, 1967. (Cards 8 and 9: pp. vii, 49-119, 135-136, 140-148.)

38. Flammability, Odor, and Offgassing Requirements and Test Procedures for Materials in Environments that Support Combustion. NHB 8060.1A, NASA, Feb. 1974. (Cards 9 and 10: All.)

39. Chemical Engineering Division, Summary Report. Rep. ANL-6145, Argonne National Lab., Jan., Feb., Mar., 1960. (Card 10: p. 151.)

40. Lapin, A.: Liquid and Gaseous Oxygen Safety Review. Vol. IV. APCI-TM-184, Air Products and Chemicals, Inc. (NASA CR-120922), 1972. (Card 11: APCI Doc. No. 99000595, pp. 1-5.)

41. Isaacs, J. L.: The Oxygen Index Flammability Test. J. Fire and Flammability, vol. 1, Jan. 1970, pp. 36-47. (Card 11: pp. 36, 40-42.)

42. Fenimore, C. P.; and Martin, F. J.: Candle-Type Test for Flammability of Polymers. Mod. Plast., vol. 43, no. 11, Nov. 1966, pp. 141-192. (Card 11: pp. 141, 146.)

43. Blackstone, W. R.; and Ku, P. M.: Assessment of Impact Test Techniques for Determining the Fire or Explosion Hazards of Materials Exposed to Oxygen. Mat. Res. Stand., vol. 11, no. 6, June 1971, pp. 30-35, 52. (Card 11: All.)

44. Flammability, Odor, and Offgassing Requirements and Test Procedures for Materials in Environments which Support Combustion. MSFC-SPEC-101B, NASA George C. Marshall Space Flight Center, March 15, 1971.

45. Testing Compatibility of Materials for Liquid Oxygen Systems. MSFC-SPEC-106B, NASA Marshall Space Flight Center, Oct. 6, 1967. (Card 11: All.)

46. Apollo Spacecraft, Nonmetallic Materials Requirements. MSC-PA-D-67-13, NASA Manned Spacecraft Center, 1968; Addendas 1, 1A, 2, 2A, 1971.

47. Stevens, M. R.; Fisher, H. D.; and Breen, B. P.: Investigation of Materials Combustibility, Fire, and Explosion Suppression in a Variety of Atmospheres. AFAPL-TR-68-35, Air Force Aero Propulsion Lab., May 1968. (Card 11: pp. iii, 2-3, 5-8, 14, 18, 31, 36, 40, 45, 70, 73, 76.)

48. Kline, H. F.: A Study of Ignition Point Values of Nonmetallic Materials in Simulated Spacecraft Environment. Sci. Advanced Mater. Pro. Eng. Ser., vol. 11, 1967, pp. 101-109. (Card 11: pp. 101-104.)

49. Standard Method of Test for Flammability of Plastics Using the Oxygen Index Method. Part 27 of ASTM Annual Standards. ASTM Designation D 2863-70, 1973.

50. Stradling, Jack S.: Test Plan, Aerospace Safety Research and Data Institute (ASRDI), Ignition by Electrical Arc. TP-WSTF-192, rev. A., July 31, 1973. (Cards 11 and 12: All.)

51. Howell, Glen A.; and Weathers, Terry M., eds.: Aerospace Fluid Component Designers Handbook. TRW Systems Group, 1970.
Vol. I - Revision D. AFRPL-TDR-64-25-Vol-1D; AD-874542. (Card 12: pp. 5.11.1-1 - 5.11.4-5, 5.12.1-1 - 5.12.8-2, 6.4.3-2.)
Vol. II - Revision D. AFRPL-TDR-64-25-Vol-2D; AD-874543.

52. Plastics for Aerospace Vehicles. Part I. Reinforced Plastics. MIL-HDBK-17A, Dept. of Defense, Jan. 1971. (Card 12: pp. iii, 2-5 - 2-6, 2-9 - 2-11.)

53. Space Materials Handbook. Third ed., NASA SP-3051, 1969.

54. Testing Methods and Techniques: Strength of Materials and Components - A Compilation. NASA SP-5944(01). (Cards 12 and 13: All.)

55. Weiner, R. S.: Basic Criteria and Definitions for Zero Leakage. JPL-TR-32-926, Jet Propulsion Lab. (NASA CR-81189), 1966. (Card 13: pp. III, 1-7, 9-14.)

56. Marr, J. W.: Leakage Testing Handbook. NASA CR-952, 1968. (Card 13: pp. vii, viii, 11, 41-81.)

57. May, K. D.: Technology Survey Advanced Valve Technology. NASA SP-5019, 1965. (Card 13: pp. v, 14.)

58. Seventh Conference on Space Simulation. NASA SP-336, 1973. (Card 13: pp. 331-334.)

59. Burrows, G.: Flow Through and Blockage of Capillary Leaks. Trans. Inst. Chem. Engrs., vol. 39, 1961, pp. 55-63. (Card 13: All.)

60. Kelly, J. H.; et al.: Permeability Data for Aerospace Applications. IIT Research Institute (NASA CR-95393), 1968. (Cards 14 and 15: pp. I-1.1 - I-1.2, I-2.1 - I-2.2, IV-8.1 - IV-8.81, VII-1.1 - VII-1.16, VII-2.1 - VII-2.24.)

61. Design Data for Pressurized Gas Systems. Stanford Research Institute, Nov. 1963. (Card 15: pp. I-1 - I-2, XII-4.1 - XII-4.7.)

62. Erosion by Cavitation or Impingement. STP-408, American Soc. Testing and Mater., 1966.

63. Glenn, H. L.; and O'Neal, G.: Watch Those Dents. Aerosp. Safety, vol. 27, no. 8, Aug. 1971, p. 18. (Card 15: p. 18.)

64. Baum, J. V.; Goobich, B.; and Trainer, T. M.: An Evaluation of High-Pressure Oxygen Systems. AMRL-TDR-62-102, Aerospace Medical Research Lab., Sept. 1962. (Card 15: pp. iii, 19-29.)

65. Murphy, D. W.: An Experimental Investigation of Geysering in Vertical Tubes. Advances in Cryogenic Engineering, vol. 10. K. D. Timmerhaus, ed., Plenum Press, 1964, pp. 353-359. (Card 15: All.)

66. Protective Finishing Systems for Rockets, Guided Missiles, Support Equipment and Related Materials. MIL-STD-186C(MI), Dept. Army, Oct. 31, 1971. (Cards 15 and 16: pp. iii, iv, v, vi, 1-30.)

67. Saturn Flight Manual SA 506. MSFC-MAN-506, NASA Marshall Space Flight Center, Feb. 1969.

68. Metallic Materials and Elements for Aerospace Vehicle Structures. MIL-HDBK-5A, Dept. Defense, Feb. 8, 1966.

69. Aerospace Structural Metals Handbook. AFML-TR-68-115, Mechanical Properties Data Center, Belfour Stulen, Inc., 1971.

70. Huzel, D. K.; and Huang, D. H.: Design of Liquid Propellant Rocket Engines. NASA SP-125, 1971. (Card 16: pp. v, 219-225, 257-259, 269-292, 329-352, 372-379.)

71. Liquid Rocket Tanks and Components. NASA SP-8088, 1974. (Cards 16 and 17: pp. iii, v, vi, vii, 17-18, 52-72.)

72. Technical Manual of Oxygen/Nitrogen Cryogenic Systems. NAVAIR 06-30-501, Naval Air Systems Command, Mar. 1971. (Card 17: pp. i, ii, 2-1 - 2-43.)

73. ASME Boiler and Pressure Vessel Code, Section VIII, Pressure Vessels, Division 1. ASME, 1968.

74. ASME Boiler and Pressure Vessel Code, Section VIII, Pressure Vessels, Division 2 - Alternative Rules. ASME, 1971.

75. ASME Boiler and Pressure Vessel Code, Section IX, Welding Qualifications. ASME, 1971.

76. Welding High Pressure Systems and Cryogenic Systems. Tech. Order 00-25-224, Air Force, Aug. 30, 1965.

77. Recommended Rules for Design and Construction of Large, Welded, Low-Pressure Storage Tanks. API Standard 620, fourth ed., Feb. 1970; Supplement, Apr. 1971.

78. Tentative Standard - Insulated Tank Truck Specification. CGA-341, Compressed Gas Association, 1970.

79. Transporation. Code of Federal Regulations, Title 49, Pts. 100-199, Sup. Docs., Jan. 1, 1972.

80. Fracture Control of Metallic Pressure Vessels. NASA SP-8040, 1970. (Cards 17 and 18: pp. iii, iv, 1-37, 39-49, 51-55.)

81. Johnson, R. E.: Apollo Experience Report - The Problem of Stress-Corrosion Cracking. NASA TN D-7111, 1973. (Card 18: pp. 10-15.)

82. Campbell, J. E.; Berry, W. E.; and Feddersen, C. E.: Damage Tolerant Design Handbook. MCIC-HB-01, Metals and Ceramics Information Center, Battelle Memorial Inst., 1972.

83. Hood, D. W.; Eichenberger, T. W.; and Lovell, D. T.: An Investigation of the Generation and Utilization of Engineering Data on Weldments. AFML-TR-68-268, Air Force Materials Lab. (AD-851938), 1968. (Card 18: pp. iii, 55-73.)

84. Arnett, R. W.; Warren, K. A.; and Mullen, L. O.: Optimum Design of Liquid Oxygen Containers. WADC Rep. TR 59-62, Wright-Patterson A. F. Base (PB-181108), 1961. (Card 18: pp. 118-121.)

85. Olson, R. E.: Safety and Design Considerations for Gas Storage Vessels. M-64-137, Martin Co., Aug. 1964. (Cards 18: All.)

86. Letson, A. J.: RL10A-3-3 Rocket Engine Oxidizer Pump Development Program. Rep. PWA FR-1890, Pratt & Whitney Aircraft, 1966.

87. Liquid Rocket Engine Centrifugal Flow Turbopumps, NASA Space Vehicle Design Criteria (Chemical Propulsion). NASA SP-8109, 1973. (Card 19: pp. iii, 8-10, 39-53, 55-60, 74-80.)

88. Wislicenus, G. F.: Fluid Mechanics of Turbomachinery, vols. 1 and 2. Dover Publications, Inc., New York, 1965.

89. Stephanoff, A. J.: Centrifugal and Axial Flow Pumps, second ed., John Wiley & Sons, Inc., 1957.

90. Liquid Rocket Engine Turbopump Inducers. NASA SP-8052, 1971. (Cards 19 and 20: All.)

91. Rocket Engine Turbopump Shafts and Couplings. NASA Space Vehicle Design Criteria (Chemical Propulsion). NASA SP-8101, 1970. (Cards 20 and 21: pp. iii, v, vi, vii, viii, 12, 19-49, 66-71, 79-96.)

92. Prohl, M. A.: A General Method of Calculating Critical Speeds of Flexible Rotors. J. Appl. Mech., vol. 12, Sept. 1945, pp. A-142 - A-148. (Card 21: All.)

93. Mykelstad, N. O.: Numerical Analysis of Forced Vibrations of Beams. J. Appl. Mech., vol. 20, no. 11, Mar. 1953, pp. 53-56. (Card 21: All.)

94. Thomson, W. T.: Matrix Solution for the Vibration of Nonuniform Beams. J. Appl. Mech., vol. 17, no. 3, Sept. 1950, pp. 337-339. (Card 21: All.)

95. Satchwell, D. L.: More Accurate Balancing for High-Speed Rotors. Machine Design, vol. 37, Sept. 16, 1965, pp. 183-184. (Card 21: All.)

96. Eshleman, R. L.: Procedures for Calculating Natural Frequencies of Shafting Systems. IITRI-K6086, IIT Research Institute Technology Center, 1967. (Available from DDC as AD-811785.)

97. Brunner, J. J.: Analysis and Experimental Verification of Axial Thrust on the M-1 Liquid Oxygen Turbopump. Aerojet General Corp. (NASA CR-54817), 1966. (Card 21: pp. iii, 22-40.)

98. Pinkel, I. Irving; Hartmann, Melvin J.; Hauser, Cavour H.; Miller, Max J.; Ruggeri, Robert S.; and Soltis, Richard F.: Pump Technology. Selected Technology for the Petroleum Industry. NASA SP-5053, 1965, pp. 81-101. (Card 21: pp. v, 81-101.)

99. Ruggeri, R. S.; and Moore, R. D.: Method for Prediction of Pump Cavitation Performance for Various Liquids, Liquid Temperatures, and Rotative Speeds. NASA TN D-5292, 1969. (Card 22: pp. ii, 1-29.)

100. Numachi, F.: Effect of Surface Roughness on Cavitation Performance of Hydrofoils - Report 3. Trans. ASME, ser. B, J. Basic Eng., vol. 89, no. 1, Mar. 1967, pp. 201-209. (Card 22: All.)

101. King, J. A.; and Farrel, E. C.: The Transient Performance of a Hydraulic Turbine-Driven Inducer: Computer Predictions and Test Verification. Rep. R-7747, Rocketdyne (NASA CR-72518), 1969. (Card 22: pp. 1-40.)

102. Farquhar, J.; Lindley, B. K.; and Rostafiniski, W. A.: Transient Pumping Performance of a Two Speed, Hydraulic Turbine Driven/Inducer System. AIAA Paper 69-551, June 1969.

103. Farquhar, J.; Lindley, B. K.; McKinney, E. B.; Olson, G. K.; and Buckmann, P. S.: Inducer Dynamics: Full-Flow, Full-Admission Hydraulic Turbine Drive. Rep. AGC 7977-T1, Aerojet General Corp. (NASA CR-72378), 1969.

104. Bair, E. K.; and Campbell, W. E.: Evaluation of a Twin-Spool Hydrogen Turbopump at Zero NPSP. J. Spacecraft & Rockets, vol. 7, no. 1, Jan. 1970, pp. 49-53.

105. Bisson, E. E.; and Anderson, W. J.: Advanced Bearing Technology, NASA SP-38, 1964. (Cards 23 and 24: pp. v, vii, 139-173, 309-321, 371-450.)

106. Liquid Rocket Engine Turbopump Bearings, NASA SP-8048, 1971. (Cards 24 and 25: All.)

107. Scibbe, H. W.: Bearings and Seals for Cryogenics Fluids. NASA TM X-52415, 1968. (Card 25: pp. 5-20.)

108. Young, M. W.; and Kirby, L. F.: Development of Liquid Oxygen Cooled 110MM Roller and Tandem Ball Bearings at up to $.5\times10^6$ DN Values for the Oxidizer Turbopump of the M-1 Engine. Rep. AGC 8800-23, Aerojet General Corp. (NASA CR-54816), 1966. (Card 25: pp. iii, 1-12.)

109. Cleanliness of Components for Use in Oxygen, Fuel and Pneumatic Systems. MSFC-SPEC-164A, NASA George C. Marshall Space Flight Center, Oct. 1970. (Card 25: pp. 1-28.)

110. Coe, H. H.; Scibbe, H. W.; and Parker, R. J.: Performance of 75-Millimeter-Bore Bearings to 1.8 Million DN with Electron-Beam-Welded Hollow Balls. NASA TN D-5800, 1970. (Card 26: All.)

111. Coe, H. H.; Scibbe, H. W.; and Anderson, W. J.: Evaluation of Cylindrically Hollow (Drilled) Balls in Ball Bearings at DN Values to 2.1 Million. NASA TN D-7007, 1971. (Card 26: All.)

112. Ludwig, Lawrence P.: Self-Acting and Hydrodynamic Shaft Seals. NASA TM X-68214, 1973. (Card 26: pp. 1, 15-17.)

113. Hady, W. F.; Allen, G. P.; and Johnson, R. L.: Wear and Friction of Mechanical Carbons in Liquid Oxygen as Influenced by Transfer Films. ASLE Trans., vol. 6, no. 3, July 1963, pp. 201-208. (Card 26: All.)

114. Hady, W. F.; Allen, G. P.; Sliney, H. E.; and Johnson, R. L.: Friction, Wear, and Dynamic Seal Studies in Liquid Fluorine and Liquid Oxygen. NASA TN D-2453, 1964. (Card 26: All.)

115. Bernd, L. H.: Survey of the Theory of Mechanical Face Seals. Part 1 - Characteristics of Seals. Lubri. Eng., vol. 24, no. 10, Oct. 1968, pp. 479-484. (Card 26: All.)

116. Russel, T. E.; Allen, G. P.; Ludwig, L. P.; and Johnson, R. L.: Gas Turbine Face Seal Thermal Deformation and Computer Program for Calculation of Axisymmetric Temperature Field. NASA TN D-5605, 1969. (Cards 26, 27, and 28: All.)

117. Robinson, R. P.; and Burton, R.: Temperature Gradients in Seal Rings: A Method of Analysis. Proceedings of the Fourth International Conference on Fluid Sealing. A. L. King, B. S. Nau, and H. S. Stephens, eds., British Hydromechanics Res. Assoc. (England), 1969. (Card 28: All.)

118. Strom, T. N.; Ludwig, L. P.; and Hudelson, J. C.: Vibration of Shaft Face Seals and Stabilizing Effect of Viscous and Friction Damping. NASA TN D-5161, 1969. (Card 28: pp. ii, 1-18.)

119. Kauffmann, W. M.: Safe Operation of Oxygen Compressors. Chemical Engineering, vol. 76, no. 23, Oct. 20, 1969, pp. 140-143. (Card 28: pp. 140, 142, 144, 146, 148.)

120. Smith, G. M.: High Performance Space Shuttle Auxiliary Propellant Valve Program. Rep. R-9078, Rocketdyne Div., Rockwell International (NASA CR-120976), 1973. (Card 28: pp. 5-46.)

121. Schwatzberg, F. R.; Osgood, S. H.; Bryant, C.; and Knight, M.: Cryogenic Materials Data Handbook. Martin Marietta Corp., 1970.
Vol. 1 - Sections A, B, and C, Revised. AFML-TDR-64-280-Vol. 1-Rev.; AD-713619.
Vol. 2 - Sections D, E, F, G, H, and I, Revised. AFML-TDR-64-280-Vol. 2-Rev.; AD-713620.

122. Tellier, G. F.: Poppet and Seat Design Data for Aerospace Valves. AFRPL-TR-66-147, Air Force Rocket Propulsion Lab. (AD-488480), 1966. (Card 29: pp. iii, 11-41, 407-418.)

123. Liquid Rocket Valve Assemblies. NASA Space Vehicle Design Criteria (Chemical Propulsion). NASA SP-8097, 1973. (Card 29: pp. iii, 66-68.)

124. Engineering Memo - Hamilton Standard Div. of United Aircraft Corp. to NASA MSC. Subject: Silicone "O" Seals-PLSS and OPS High Pressure Oxygen Applications. Aug. 12, 1970. (Card 29: All.)

125. Power Piping. ASA B31.1, ANSI, 1973.

126. Petroleum Refinery Piping. B31.3, ANSI, 1973.

127. Standard Method of Test for Brittleness Temperature of Plastics and Elastomers by Impact. Part 27 of ASTM Annual Standards. ASTM Designation D 746-72, 1973.

128. Bass, R. L.; and Holster, J. L.: Bellows Vibration with Internal Cryogenic Flows. Trans. ASME, Ser. B; J. Eng. Ind., vol. 94, no. 1, Feb. 1972, pp. 70-75. (Card 30: All.)

129. Sack, L. E.: Analysis of Flow-Induced Vibration Associated with Bellows Convolutions. Rocketdyne, North Amer. Rockwell, IL8112-3175, Dec. 1968. (Card 30: All.)

130. F-1 Flexible Line Flow-Induced Vibration Verification Program. R-7897, Rocketdyne, North Amer. Rockwell, July 1969. (Card 30: pp. 1/2, 25-50.)

131. Hulbert, L. E.; Keith, R. E.; and Trainer, T. M.: State-of-the-Art Survey of Metallic Bellows and Diaphragms for Aerospace Applications. Battelle Memorial Inst. (AFRPL-TR-65-215), 1965. (Card 30: pp. iii, 45-46.)

132. Fittings, MC, Classification of Defects. MSFC-STD-437, NASA George C. Marshall Space Flight Center, February 11, 1965. (Card 30: pp. 1, 5.)

133. Henson, F. M.: An Evaluation of Gaskets, Seals, and Joints for Aerospace Hardware. Aerojet-General Corp. (NASA CR-93784), 1967.

134. Piping and Tubing Technology. NASA SP-5903(02). (Card 30: pp. i, 1-6.)

135. Rathbun, F. O., Jr., ed.: Separable Connector Design Handbook (Tentative): Design Criteria for Zero Leakage Connectors for Launch Vehicles. General Electric Co. (NASA CR-64944), 1964. (Cards 30 and 31: pp. i, ii, 2-1 - 2-50, 3-1 - 3-30.)

136. Refrigeration Piping. B31.5, ANSI, 1966.

137. Mechanical/Electrical Process Systems. Part B - Testing of Pressure Systems. Ch. 6 of NASA Lewis Operational Safety Manual. 1966. (Card 31: pp. 1, 40-41.)

138. Brazing Manual. American Welding Society Inc., 1963.

139. Reynolds, W. C.: Investigation of Ignition Temperatures of Solid Metals. NASA TN D-182, 1959. (Cards 31 and 32: pp. 1, 36, 39-50.)

140. System Safety. AFSC Design Handbook DH 1-6, third ed., July 1971.

141. Justl, O. J.: Development of Seal Material for Oxygen Systems. Tech. Rept. 28-22, Mare Island Naval Shipyard, 1972. (Available from DDC as AD-891963L.) (Card 32: pp. ii, 3-4, app. 2.)

142. Curry, J. E.: Status Report on Liquid Oxygen Seal Investigation. NASA TM X-53183, 1964.

143. Fluorocarbon Plastics. Materials and Process Manual No. 215. Materials in Design Engineering, Feb. 1964, pp. 93-104.

144. Joy, L. A.; and Baumer, R. E.: Safety Aspects of Using Oxygen in a Hazardous Environment. Engineering Rept. 037-70, Aerojet Liquid Rocket Co., 1970. (Card 32: pp. 1, 10.)

145. McKinley, C.; and Wang, E. S. J.: Hydrocarbon-Oxygen Systems Solubility. Advances in Cryogenic Engineering, vol. 4. K. D. Timmerhaus, ed., Plenum Press, Inc., 1960.

146. Fassell, W. M., Jr.; Gulbrasen, L. B.; Lewis, J. R.; and Hamilton, J. H.: Ignition Temperatures of Magnesium and Magnesium Alloys. J. Met., vol. 3, July 1951, pp. 522-528. (Card 32: pp. 522, 524, 527.)

147. Wolfhard, H. G.; Glassman, I.; and Green, L., eds.: Heterogeneous Combustion. Progress in Astronautics and Aeronautics. Vol. 15. Academic Press, 1964. (Card 32: pp. ix, x, xi, 136.)

148. Jakowsky, J. J.; and Butzler, E. W.: Oxygen-Oil Explosions. Preliminary Report II. Spontaneous Ignition of Metals in Oxygen under Pressure. BM-RI-2521, Bur. Mines, Sept. 1923. (Card 32: p. 1, fig. 3.)

149. Groves, W. E.: Safe Handling of Large Quantities of Gaseous Oxygen in Steel Pipelines. Iron and Steel Engr., vol. 42, no. 1, Jan. 1965, pp. 88-95. (Card 32: pp. 88-89.)

150. Grosse, A. V.; and Conway, J. B.: Combustion of Metals in Oxygen. Indus. Eng. Chem., vol. 50, no. 4, Apr. 1958, pp. 663-672. (Card 32: pp. 663, 669, 670.)

151. Laurendeau, N. M.; and Glassman, I.: Ignition Temperatures of Metals in Oxygen Atmospheres. Comb. Sci. Tech., vol. 3, 1971, pp. 77-82. (Card 32: pp. 77, 79-81.)

152. Mellor, A. M.: Heterogeneous Ignition of Metals: Model and Experiment. Ph.D. Thesis, Princeton University (NASA CR-93541), 1967. (Card 32: pp. 325-326, 328-329, 331-332.)

153. Hill, P. R.; Adamson, D.; Foland, D. H.; and Bressette, W. E.: High Temperature Oxidation and Ignition of Metals. NACA RM L55L23b, 1956. (Card 32: pp. 1, 7.)

154. Dean. L. E.; and Thompson, W. R.: Ignition Characteristics of Metals and Alloys. ARS J., vol. 31, no. 7, July 1961, pp. 917-923. (Card 32: pp. 917, 923.)

155. Nonmetallic Materials Design Guidelines and Test Data Handbook. NASA TM X-67639, 1970. (Available from DDC as AD-889181L.)

156. Guter, M.: Ignition in High Pressure Oxygen. S & T Memo 13/50, British Ministry of Aviation, 1967. (Card 32: pp. 9-10, 16-17, 21-24.)

157. Hust, J. G.; and Clark, A. F.: A Survey of Compatibility of Materials with High Pressure Oxygen Service. Rep. 275.03-72-11, NBS Institute for Basic Standards, Cryogenics Division, Oct. 1972. (Cards 32 and 33: pp. ii, 1-4, app. I.)

158. Attwood, H. C.; and Allen, G. R.: On the Spontaneous Ignition Temperature of Organic Materials in Oxygen. C. P. No. 1172, British Ministry of Defence (Aviation Supply), 1971. (Card 33: pp. 1-15, 21.)

159. Kuchta, J. M ; Litchfield, E. L.; and Furno, A. L.: Flammability of Materials in Hyperbaric Atmospheres, Final Report. Rep. No. 4016, Bur. Mines, 1967. (Card 33: pp. v, 6, 9, 11, 12.)

160. Cook, G. A.; Meierer, R. E.; and Shields, B. M.: Combustibility Tests on Several Flame-Resistant Fabrics in Compressed Air, Oxygen-Enriched Air, and Pure Oxygen. Text. Res. J., vol. 37, no. 7, July 1967, pp. 591-599. (Card 33: pp. 591-595.)

161. Pippen, D. L.; and Stradling, J. S.: Materials Testing in a Gaseous Oxygen Environment. Paper presented at 74th National Meeting, A. I. Ch. E. (New Orleans, LA), Mar. 1973. (Card 33: table 2.)

162. Huggett, C.; Von Elbe, G.; and Haggerty, W.: The Combustibility of Materials in Oxygen-Helium and Oxygen-Nitrogen Atmospheres. Rep. SAM-TR-66-35, Atlantic Res. Corp., 1966. (Card 33: pp. iii, 5.)

163. Huggett, C.; Von Elbe, G.; Haggerty, W.; and Grossman, J.: The Effects of 100 Percent Oxygen at Reduced Pressure on the Ignitibility and Combustibility of Materials. SAM-TR-65-78, Atlantic Research Corp. (AD-477338), 1965. (Card 33: pp. iii, 19, 21.)

164. Kimzey, J. H.: Flammability During Weightlessness. NASA TM X-58001, 1966. (Card 33: pp. 1, 12.)

165. Dawn, F. S.: Nonmetallic-Materials Development for Spacecraft Applications. Conference on Materials for Improved Fire Safety. NASA SP-5096, 1971, pp. 57-63. (Card 33: pp. III, VII, 62.)

166. Radnofsky, M. I.: New Materials for Manned Spacecraft, Aircraft, and Other Applications. Conference on Materials for Improved Fire Safety. NASA SP-5096, 1971, pp. 91-102. (Card 34: pp. VII, 91, 94, 95, 100, 101.)

167. Johnson, J. E.; and Woods, F. J.: Flammability in Unusual Atmospheres. Part II - Selected Materials in Oxygen-Nitrogen and Oxygen-Helium Mixtures at Pressures up to 315 psia. NRL-6606, Naval Research Laboratory, 1967. (Available from DDC as AD-823059L.) (Card 34: pp. iv, 14.)

168. Notardonato, J. J.; Burkhard, L. A.; and Cochran, T. H.: Effects of Pressure, Oxygen Concentration, and Forced Convection on the Flame Spread Rate of Plexiglas, Nylon, and Teflon. NASA TN D-7555, 1974. (Card 34: pp. 10-12.)

169. Neustein, R. A.; Mader, P. P.; Colombo, G. V.; and Richardson, D. E.: The Effect of Atmosphere Selection and Gravity on Burning Rate and Ignition Temperature. McDonnell Douglas Report DAC-62431, October 1968. (N70-10589).

170. Whitaker, D. H.: Effects of Acceleration Upon Combustion Rate Test, Nomex Standard Cloth. Rep. TF-WSTF-111A, White Sands Test Facility (Available as CR-129442), 1967.

REFERENCE

1

RODER, H. M.; AND WEBER, L. A., EDS.: ASRDI OXYGEN TECHNOLOGY SURVEY. VOLUME I: THERMOPHYSICAL PROPERTIES. NASA SP-3071, 1972.

ASRDI OXYGEN TECHNOLOGY SURVEY

Volume I:

Thermophysical Properties

NATIONAL AERONAUTICS AND SPACE ADMINISTRATION

NASA SP-3071

ASRDI OXYGEN TECHNOLOGY SURVEY

Volume I: Thermophysical Properties

Edited by

Hans M. Roder and Lloyd A. Weber

Cryogenics Division, Institute for Basic Standards
National Bureau of Standards, Boulder, Colorado

Prepared for the
Aerospace Safety Research and Data Institute
NASA Lewis Research Center

Scientific and Technical Information Office 1972
NATIONAL AERONAUTICS AND SPACE ADMINISTRATION
Washington, D.C.

Page intentionally left blank

Preface

This publication is part of a major oxygen safety review in progress by the NASA Aerospace Safety Research and Data Institute (ASRDI). The objectives of the review include:

1. Recommendations to improve NASA's oxygen handling practices by comparing NASA and contractor oxygen systems including the design, inspection, operation, maintenance and emergency procedures.

2. Assessment of the vulnerability to failure of oxygen equipment from a variety of sources so that hazards may be defined and remedial measures formulated.

3. Contributions to safe oxygen handling techniques through research.

4. Formulation of criteria and standards on all aspects of oxygen handling storage and disposal.

This Special Publication is composed of the thermodynamic functions, transport properties, and physical properties of both liquid and gaseous oxygen. The low temperature regime is emphasized. Because the data are detailed beyond that previously available, this handbook should fill an existing need for both the scientific and technical communities.

I. I. Pinkel, Director
Aerospace Safety Research and Data Institute
National Aeronautics and Space Administration

Page intentionally left blank

Contents

Preface iii

Contents v

Key Words vi

1. Introduction 1

2. Description of the Volume on Thermophysical Properties 1

   2.1 Pagination 2

   2.2 The Descriptive Sheets, Section A. 2

   2.3 The Figures, Section B. 2

   2.4 The Tables, Section C. 3

   2.5 The Appendices 3

   2.6 The Index 3

3. Computer Programs and Extrapolation 3

4. Evaluation of Existing Literature 6

   4.1 Preliminary Work 7

   4.2 The Evaluation Process 7

   4.3 Comments on the Critical Selection of "Best" Values 7

   4.4 Properties Calculated for This Volume 8

5. Acknowledgement 9

6. Appendices 11

   6.1 Appendix 1, Unit Conversions 11

   6.2 Appendix 2, Bibliography of References 13

   6.3 Appendix 3, CDC - ASRDI Numbers 35

7. Section A, Descriptive Sheets 41

8. Section B, Figures 107

9. Section C, Tables 145

10. Index 421

8. Section B, Figures

LIST OF FIGURES

Compressibility Factor B-3
Dielectric Constant B-5
Dielectric Constant (Saturated Liquid and Vapor) B-5a
Corona Onset Voltage B-8
Electrical Conductivity B-8a
Specific Heat at Constant Pressure (Heat Capacity) B-15
Specific Heat of Solid, Below 4 K (Heat Capacity) B-15a
Specific Heat of Solid, 14-54 K (Heat Capacity) B-15b
Specific Heat at Constant Volume, Isotherms B-16
Specific Heat at Constant Volume, Isobars B-16a
Joule-Thomson Inversion Curve B-22
Heat of Vaporization B-25
Melting Curve for Oxygen B-27
Prandtl Number B-29
Specific Volume (P-V-T) B-30
Density (P-V-T) B-30a
P vs T Phase Diagram (Skeleton) (P-V-T) B-30b
Emissivity vs. Temperature (Radiative Properties) B-31
Total Band Absorptance (Radiative Properties) B-31a
Velocity of Sound B-33
Surface Tension B-35
Thermal Conductivity B-36
Temperature-Entropy Chart (Thermodynamic Diagrams). B-37
Mollier Diagram (Thermodynamic Diagrams) B-37a
Mollier Diagram (Supercritical) (Thermodynamic Diagrams) B-37b
Enthalpy-Entropy Chart (Thermodynamic Diagrams) B-37c
Pressure-Temperature Phase Diagram (Thermodynamic Diagrams) . . B-37d
Temperature-Entropy Chart (Metric) (Thermodynamic Diagrams) . . . B-37e
Vapor Pressure (psia/°R) B-38
Vapor Pressure (Atm, Torr/K) B-38a
Viscosity (Dynamic) B-39
Rotational Band (Infrared Absorption) B-42
Fundamental (Vibration-Rotation) Band (Infrared Absorption) B-42a

REFERENCE 1

PAGE 108 BLANK

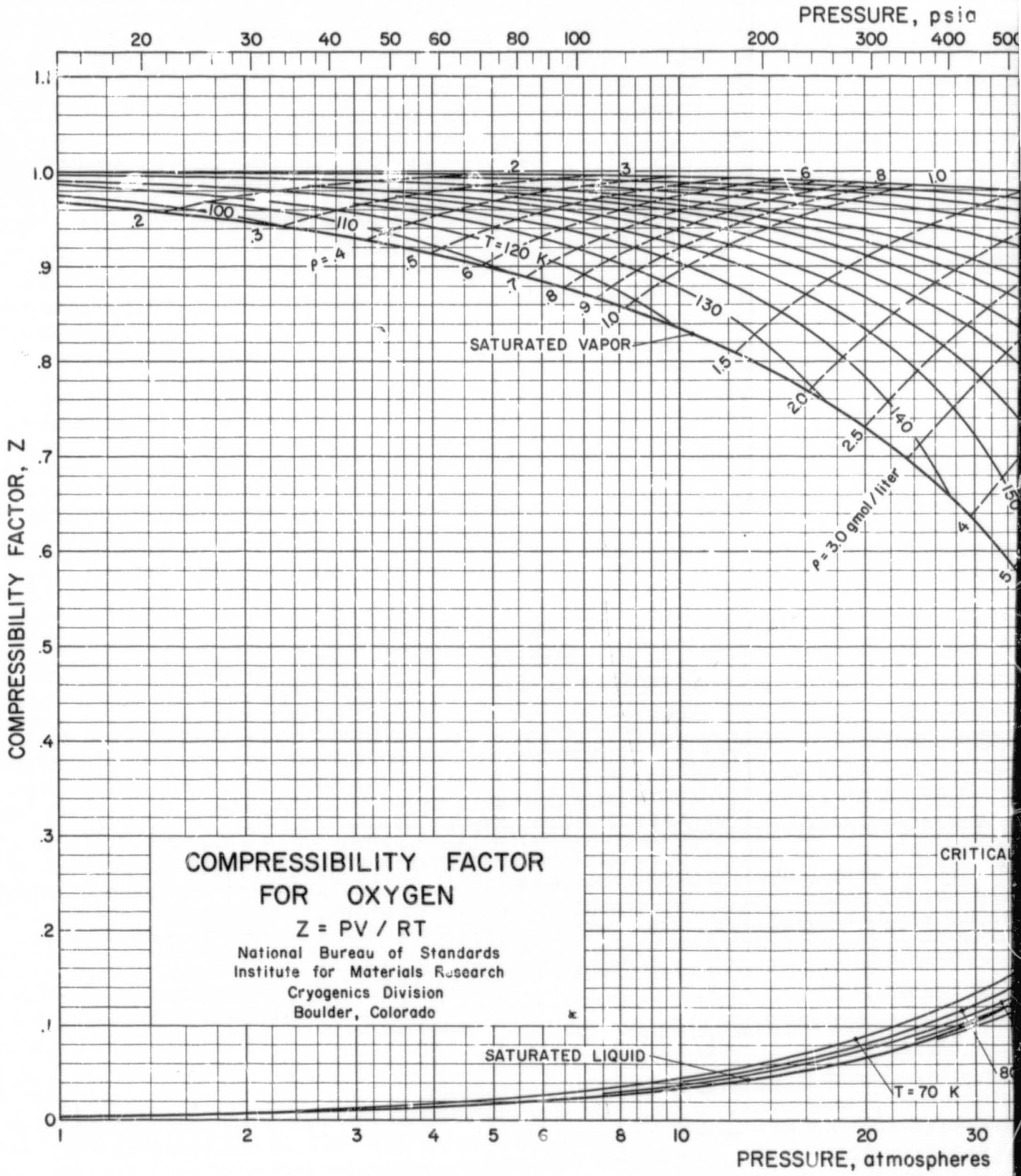
PRESSURE, psia
20
30
40
50
60
80
100
200
300
400
COMPRESSIBILITY FACTOR, Z
1.0
.9
.8
.7
.6
.5
.4
.3
.2
.1
0
SATURATED VAPOR
SATURATED LIQUID
T = 120 K
T = 70 K
ρ = .4
ρ = 3.0 gmol / liter
CRITICAL
COMPRESSIBILITY FACTOR
FOR OXYGEN
Z = PV / RT
National Bureau of Standards
Institute for Materials Research
Cryogenics Division
Boulder, Colorado
1
2
3
4
5
6
8
10
20
30
PRESSURE, atmospheres

B-3

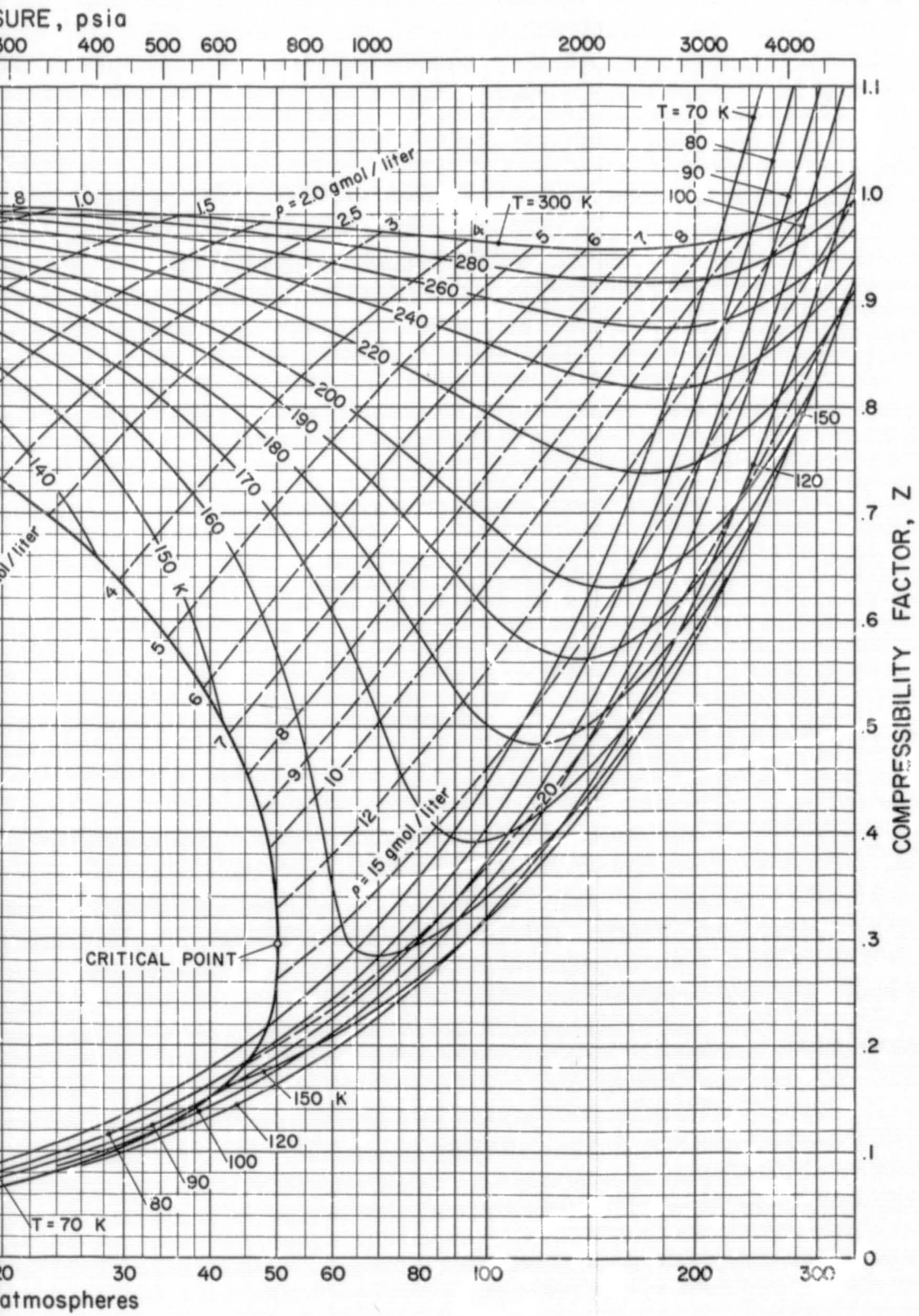
SURE, psia
300 400 500 600 800 1000 2000 3000 4000
T = 70 K
80
90
100
T = 300 K
ρ = 2.0 gmol / liter
1.0
1.5
2.5
3
4
5
6
7
8
280
260
240
220
200
190
180
170
160
150 K
140
120
150
ol / liter
4
5
6
7
8
9
10
12
20
ρ = 15 gmol / liter
CRITICAL POINT
150 K
120
100
90
80
T = 70 K
1.1
1.0
.9
.8
.7
.6
.5
.4
.3
.2
.1
0
COMPRESSIBILITY FACTOR, Z
20 30 40 50 60 80 100 200 300
atmospheres

REFERENCE 1

PAGE 110 BLANK

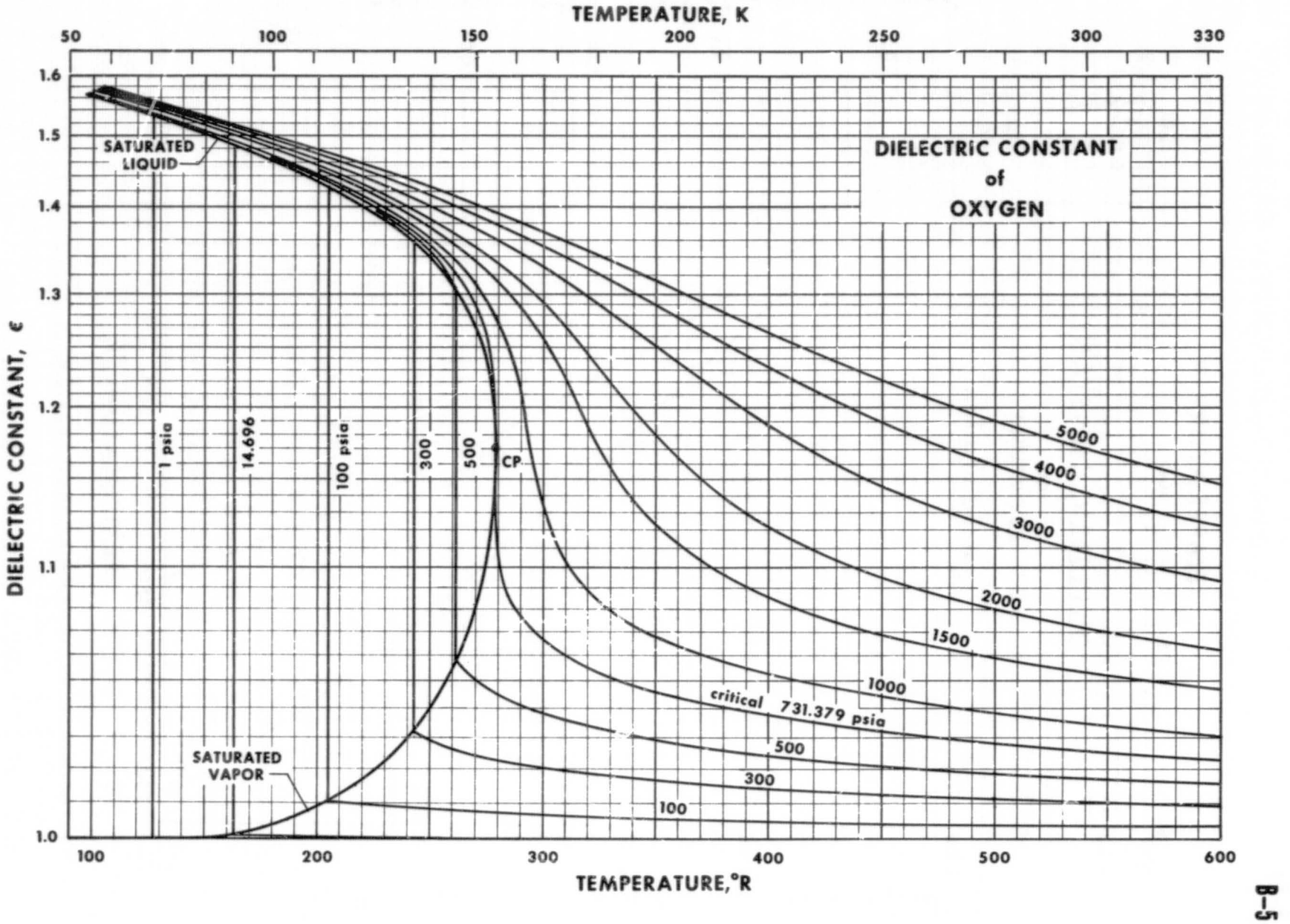
TEMPERATURE, K
50
100
150
200
250
300
330
DIELECTRIC CONSTANT
of
OXYGEN
DIELECTRIC CONSTANT, ε
1.6
1.5
1.4
1.3
1.2
1.1
1.0
SATURATED LIQUID
SATURATED VAPOR
1 psia
14.696
100 psia
300
500
CP
5000
4000
3000
2000
1500
1000
critical 731.379 psia
500
300
100
100
200
300
400
500
600
TEMPERATURE, °R

B-5a

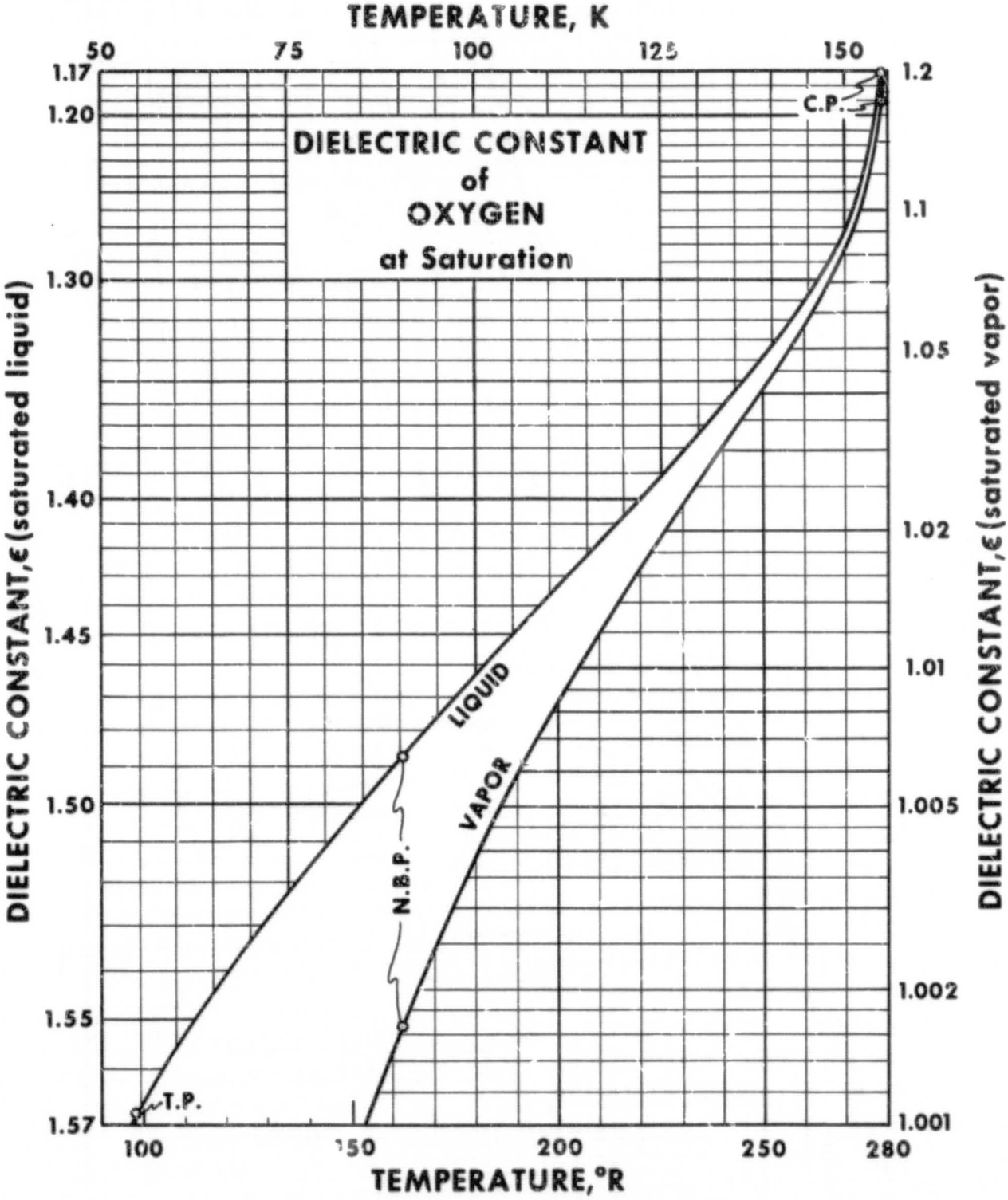
TEMPERATURE, K
50
75
100
125
150
DIELECTRIC CONSTANT
of
OXYGEN
at Saturation
C.P.
LIQUID
VAPOR
N.B.P.
T.P.
DIELECTRIC CONSTANT, ε (saturated liquid)
1.17
1.20
1.30
1.40
1.45
1.50
1.55
1.57
DIELECTRIC CONSTANT, ε (saturated vapor)
1.2
1.1
1.05
1.02
1.01
1.005
1.002
1.001
100
150
200
250
280
TEMPERATURE, °R

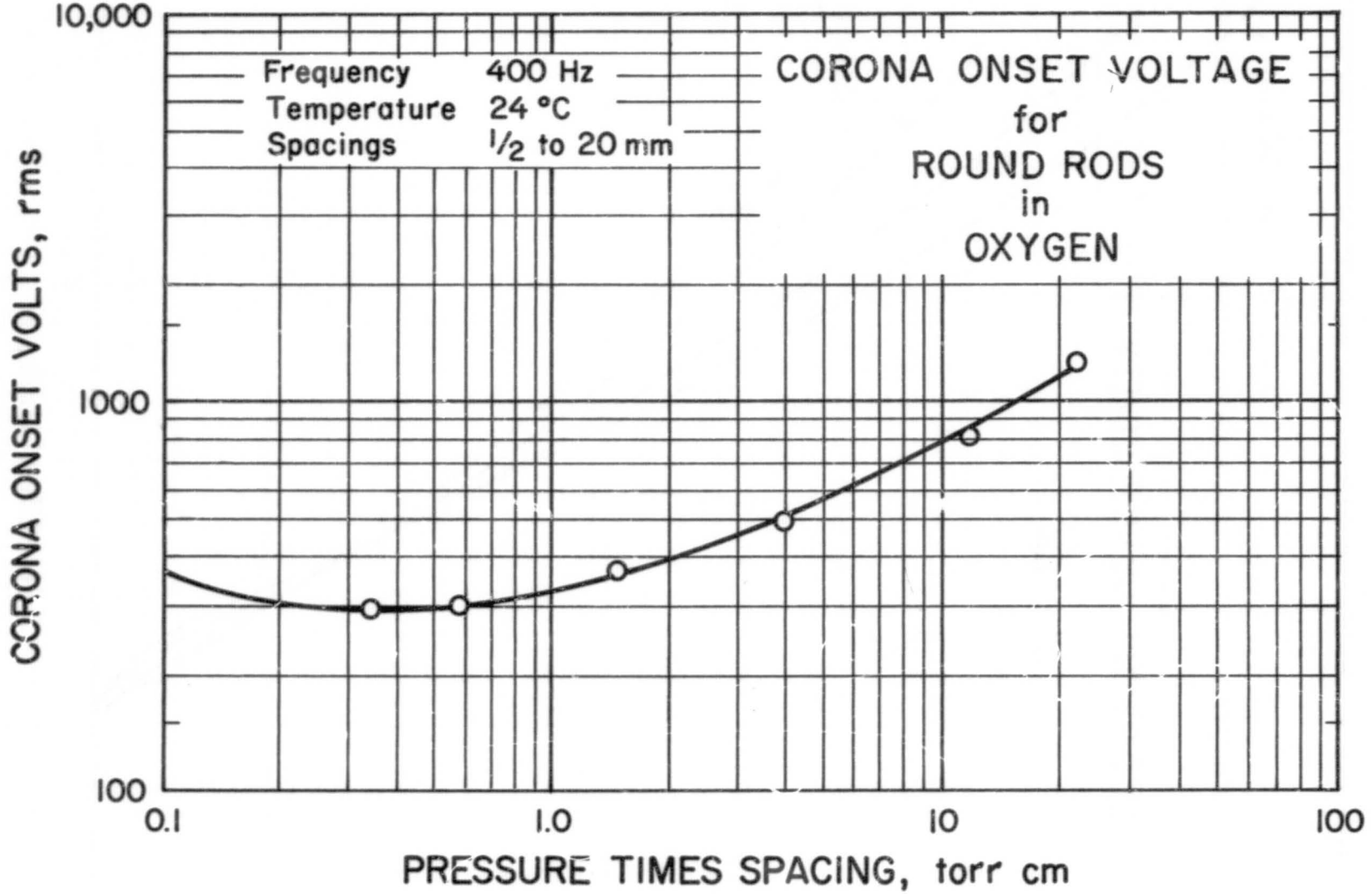
CORONA ONSET VOLTAGE
for
ROUND RODS
in
OXYGEN
Frequency 400 Hz
Temperature 24 °C
Spacings 1/2 to 20 mm
CORONA ONSET VOLTS, rms
10,000
1000
100
0.1
1.0
10
100
PRESSURE TIMES SPACING, torr cm

B-8a

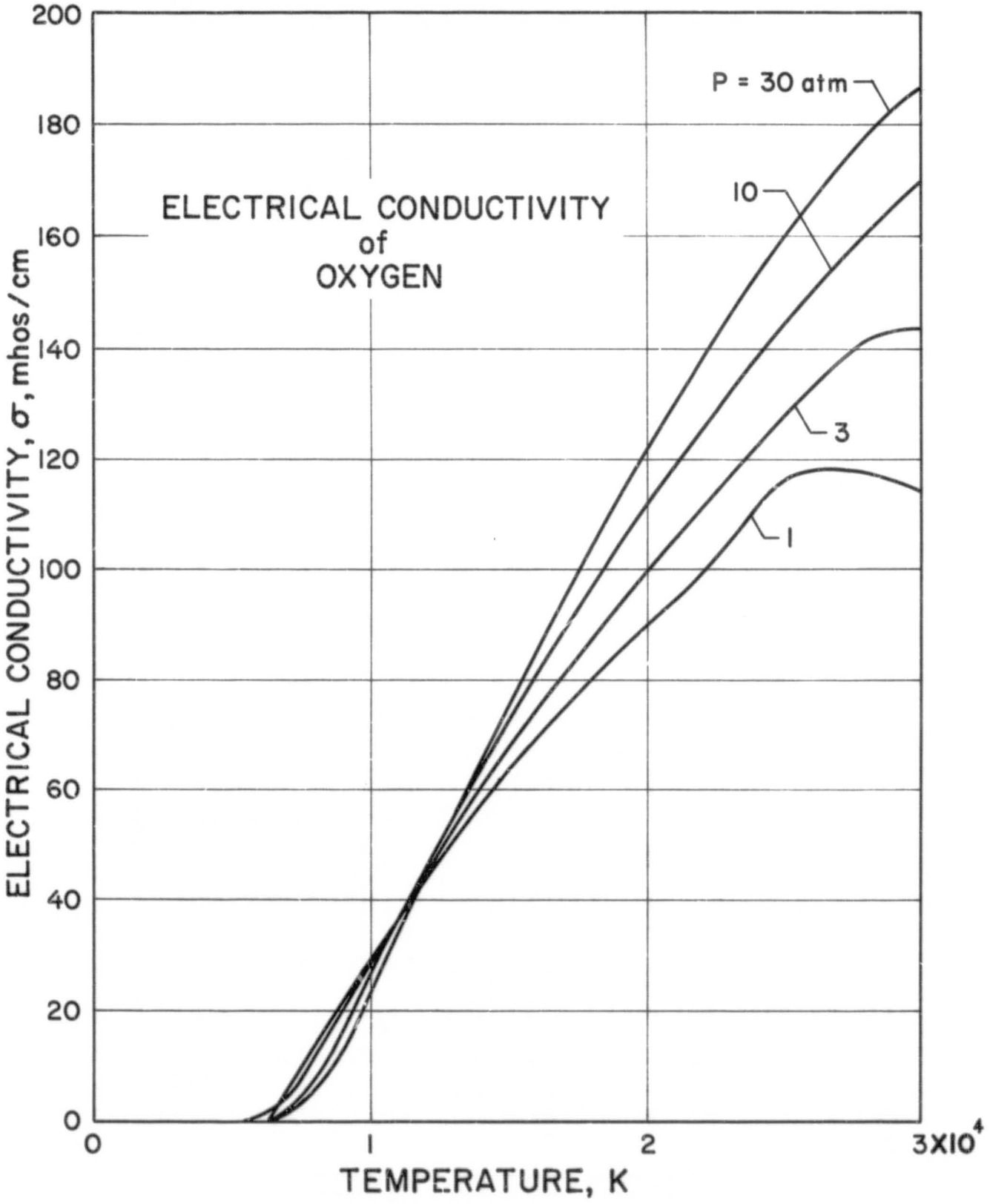
ELECTRICAL CONDUCTIVITY
of
OXYGEN
P = 30 atm
10
3
1
ELECTRICAL CONDUCTIVITY, σ, mhos/cm
TEMPERATURE, K
0
20
40
60
80
100
120
140
160
180
200
0
1
2
3X10⁴

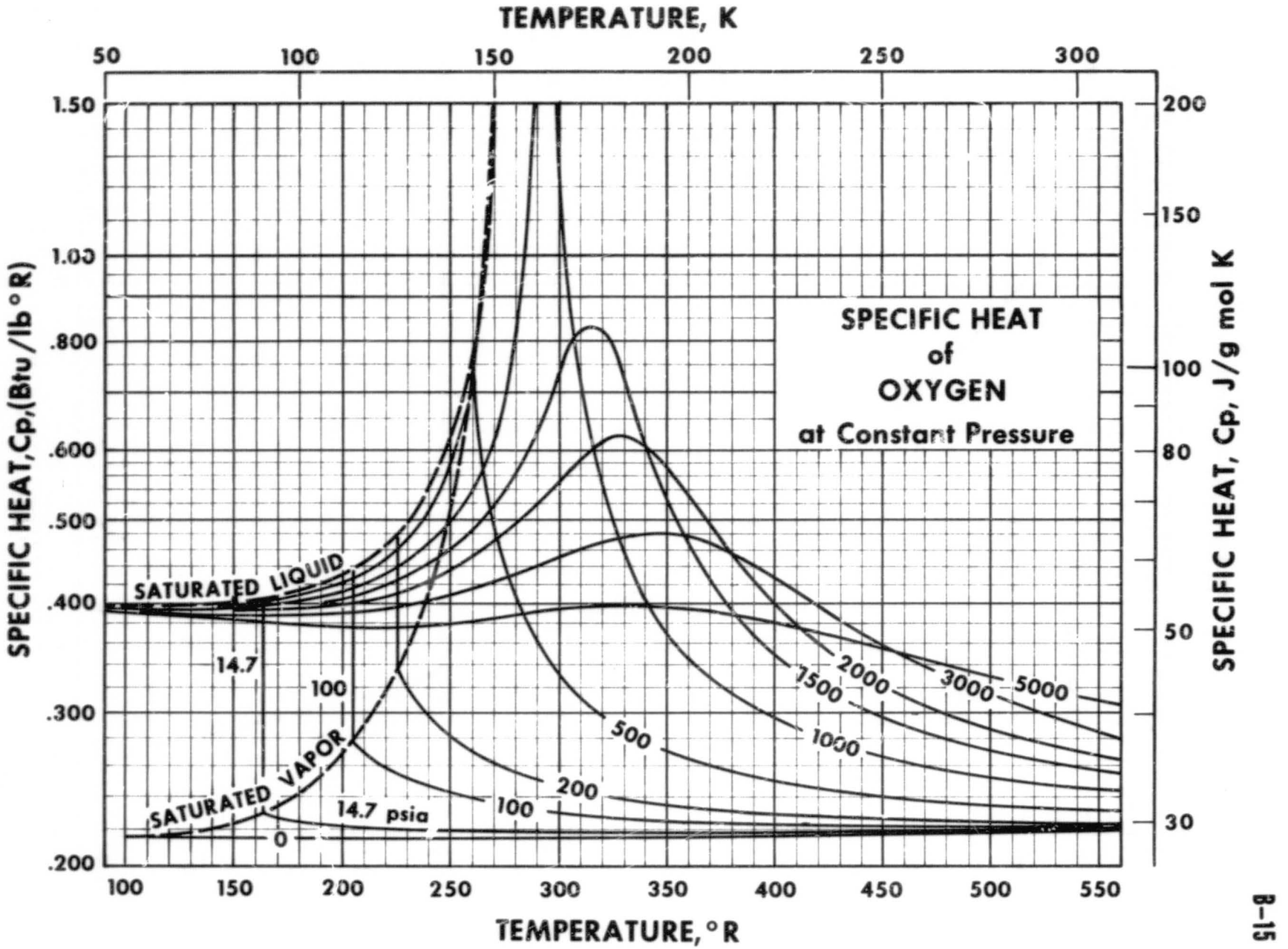
TEMPERATURE, K
50
100
150
200
250
300
1.50
1.00
.800
.600
.500
.400
.300
.200
SPECIFIC HEAT,Cp,(Btu/lb°R)
200
150
100
80
50
30
SPECIFIC HEAT, Cp, J/g mol K
SPECIFIC HEAT
of
OXYGEN
at Constant Pressure
SATURATED LIQUID
SATURATED VAPOR
14.7
100
14.7 psia
0
100
200
500
1000
1500
2000
3000
5000
100
150
200
250
300
350
400
450
500
550
TEMPERATURE, °R

B--15a

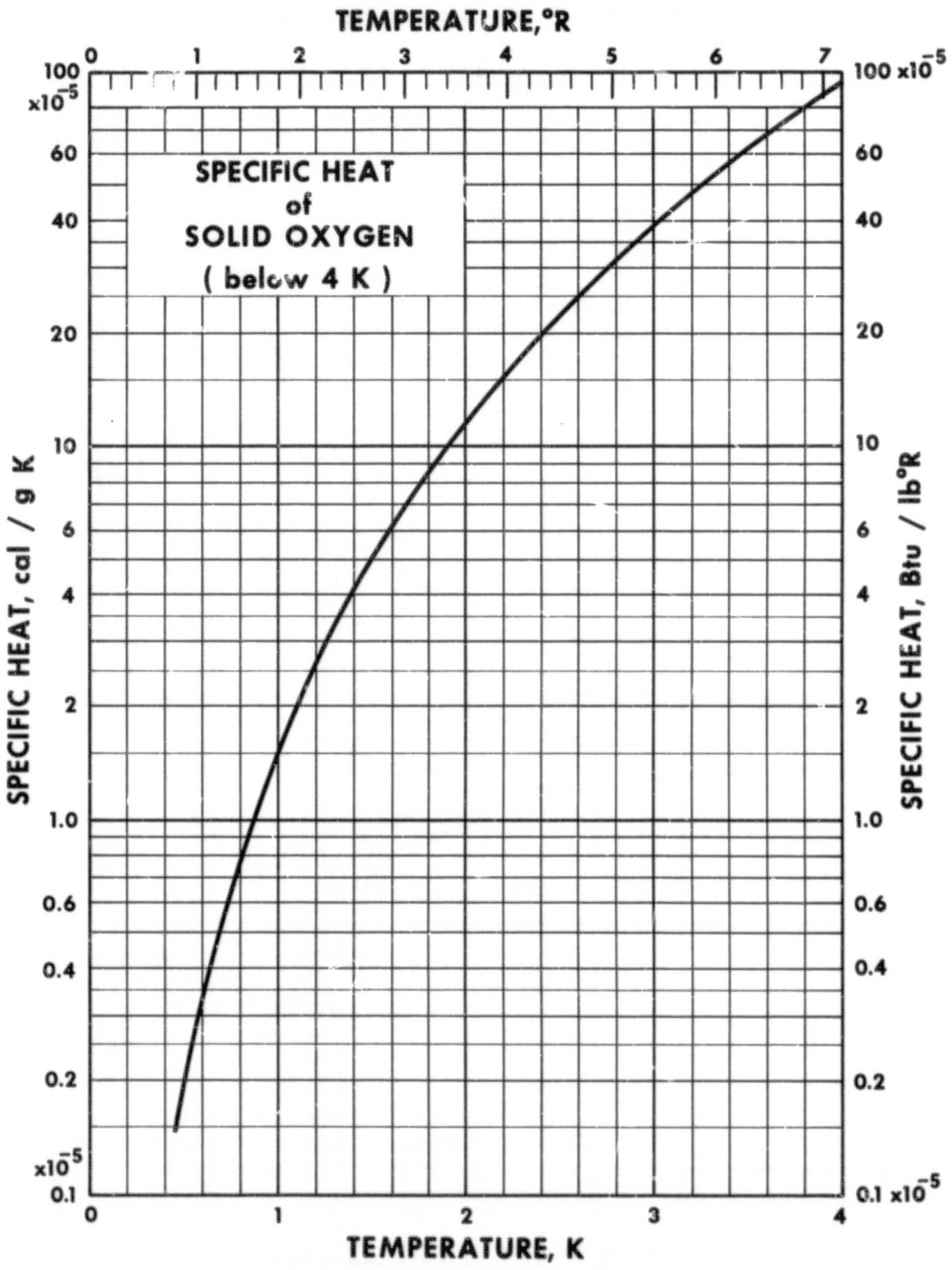
TEMPERATURE,°R
0
1
2
3
4
5
6
7
SPECIFIC HEAT
of
SOLID OXYGEN
(below 4 K)
SPECIFIC HEAT, cal / g K
100 x10⁻⁵
60
40
20
10
6
4
2
1.0
0.6
0.4
0.2
x10⁻⁵
0.1
SPECIFIC HEAT, Btu / lb°R
100 x10⁻⁵
60
40
20
10
6
4
2
1.0
0.6
0.4
0.2
0.1 x10⁻⁵
0
1
2
3
4
TEMPERATURE, K

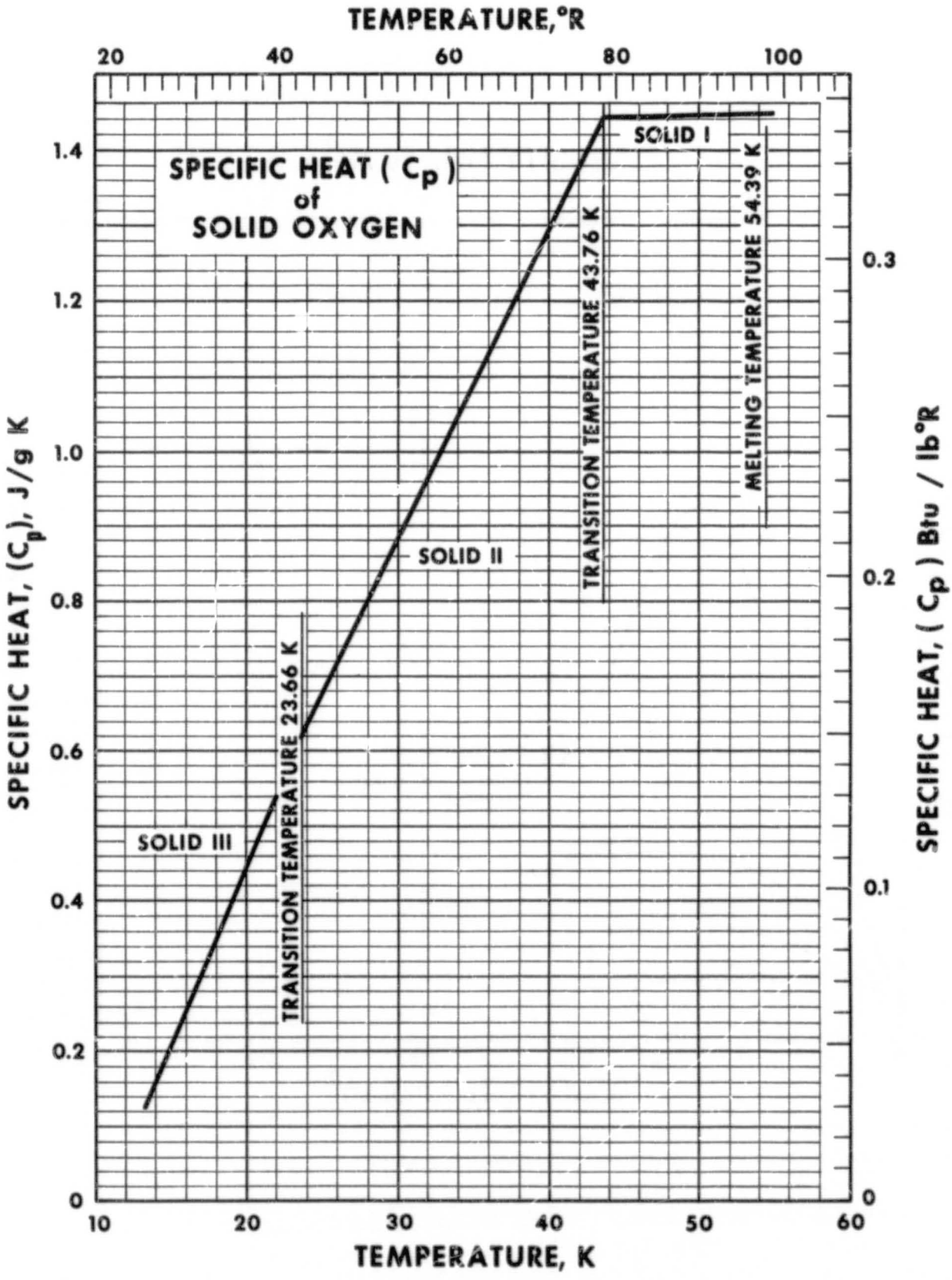
TEMPERATURE,°R
20
40
60
80
100
SPECIFIC HEAT (C_p)
of
SOLID OXYGEN
SOLID I
MELTING TEMPERATURE 54.39 K
TRANSITION TEMPERATURE 43.76 K
SOLID II
TRANSITION TEMPERATURE 23.66 K
SOLID III
SPECIFIC HEAT, (C_p), J/g K
SPECIFIC HEAT, (C_p) Btu / lb°R
1.4
1.2
1.0
0.8
0.6
0.4
0.2
0
0.3
0.2
0.1
0
10
20
30
40
50
60
TEMPERATURE, K

B-16

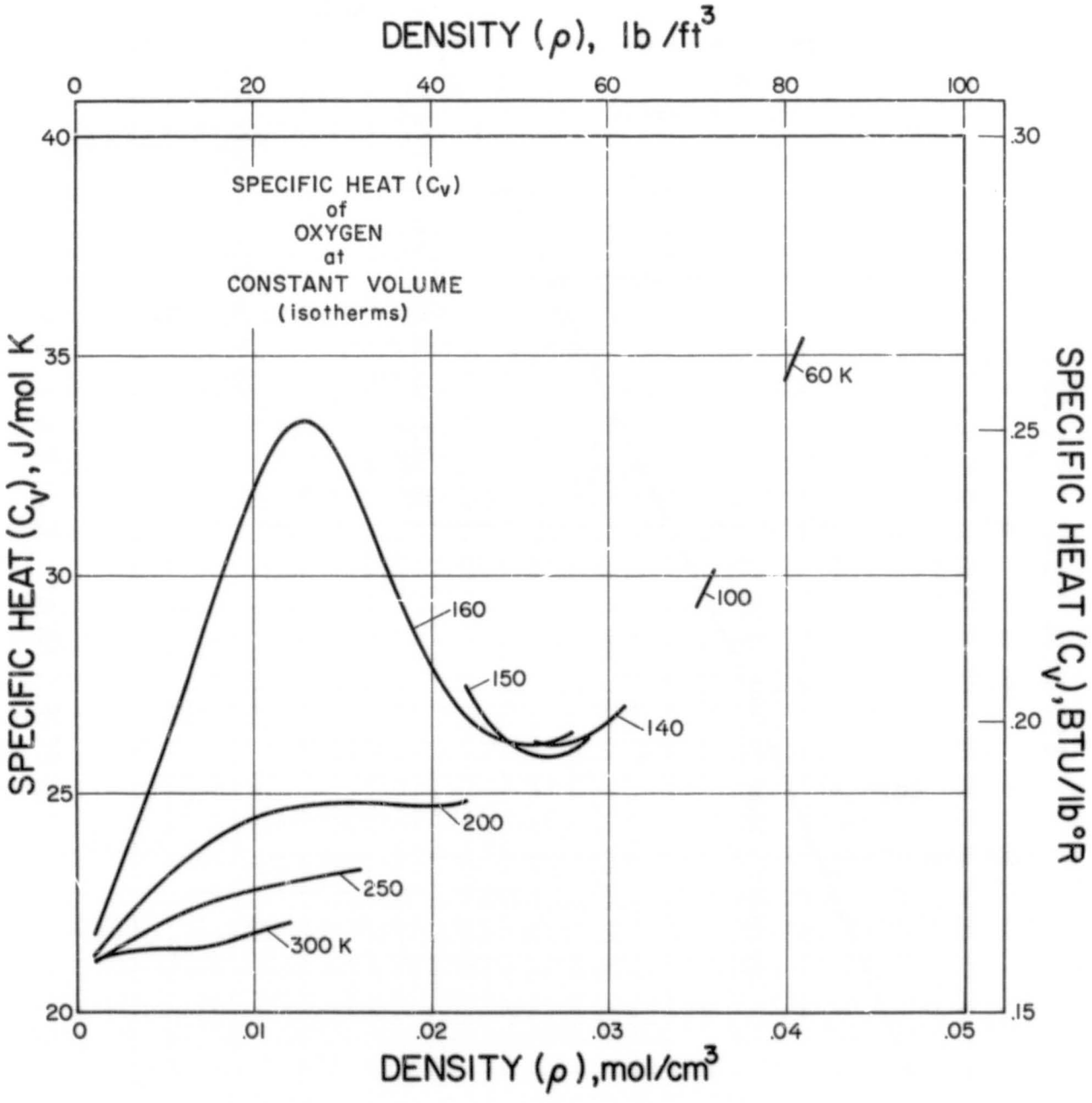
DENSITY (ρ), lb /ft³
0
20
40
60
80
100
SPECIFIC HEAT (Cv)
of
OXYGEN
at
CONSTANT VOLUME
(isotherms)
60 K
100
160
150
140
200
250
300 K
SPECIFIC HEAT (Cv), J/mol K
40
35
30
25
20
SPECIFIC HEAT (Cv), BTU/lb °R
.30
.25
.20
.15
0
.01
.02
.03
.04
.05
DENSITY (ρ), mol/cm³

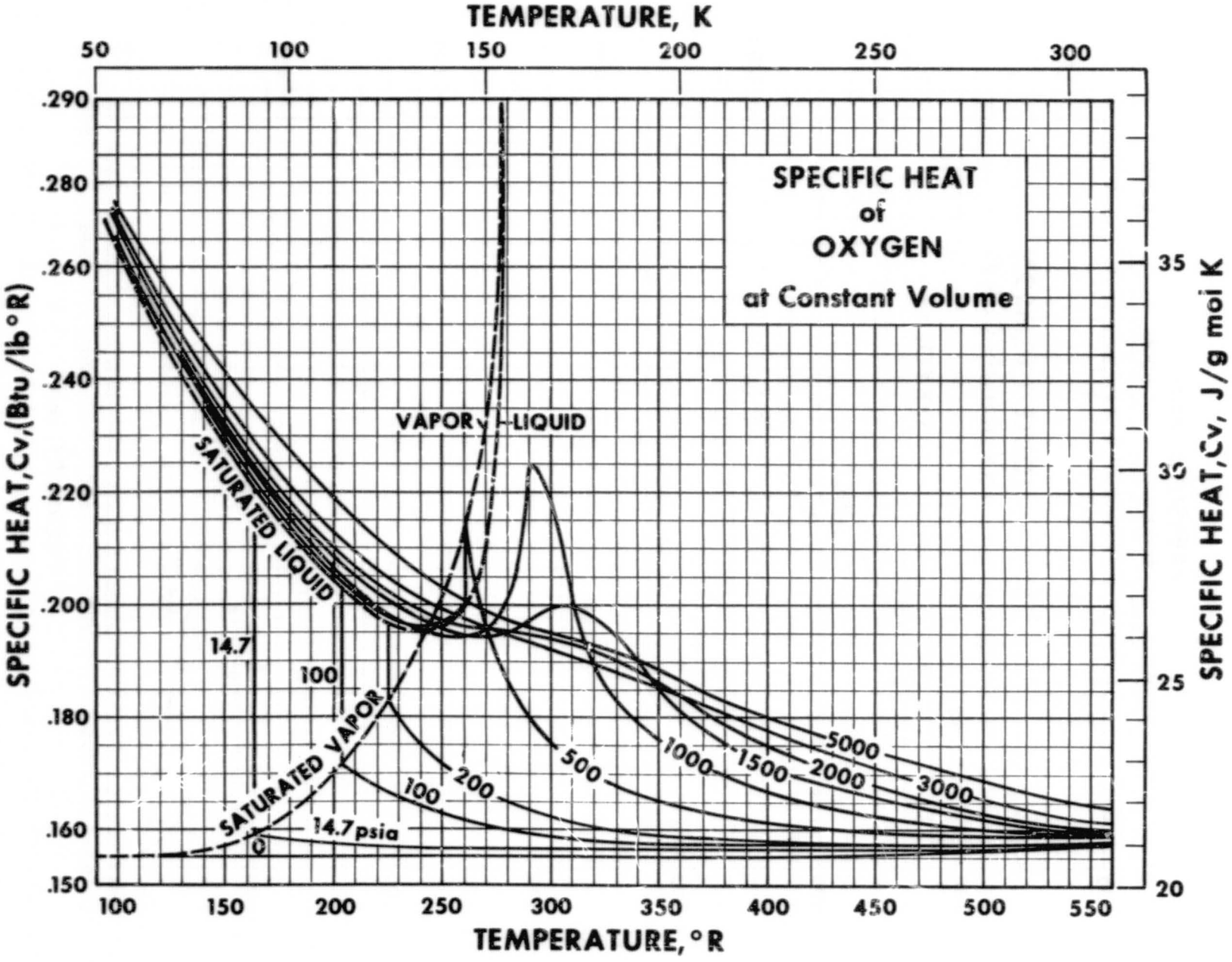
TEMPERATURE, K
50
100
150
200
250
300
SPECIFIC HEAT
of
OXYGEN
at Constant Volume
SPECIFIC HEAT,Cv,(Btu/lb°R)
.290
.280
.260
.240
.220
.200
.180
.160
.150
SPECIFIC HEAT,Cv, J/g moi K
35
30
25
20
VAPOR
LIQUID
SATURATED LIQUID
SATURATED VAPOR
14.7
100
14.7 psia
100
200
500
1000
1500
2000
3000
5000
100
150
200
250
300
350
400
450
500
550
TEMPERATURE, °R

B-22

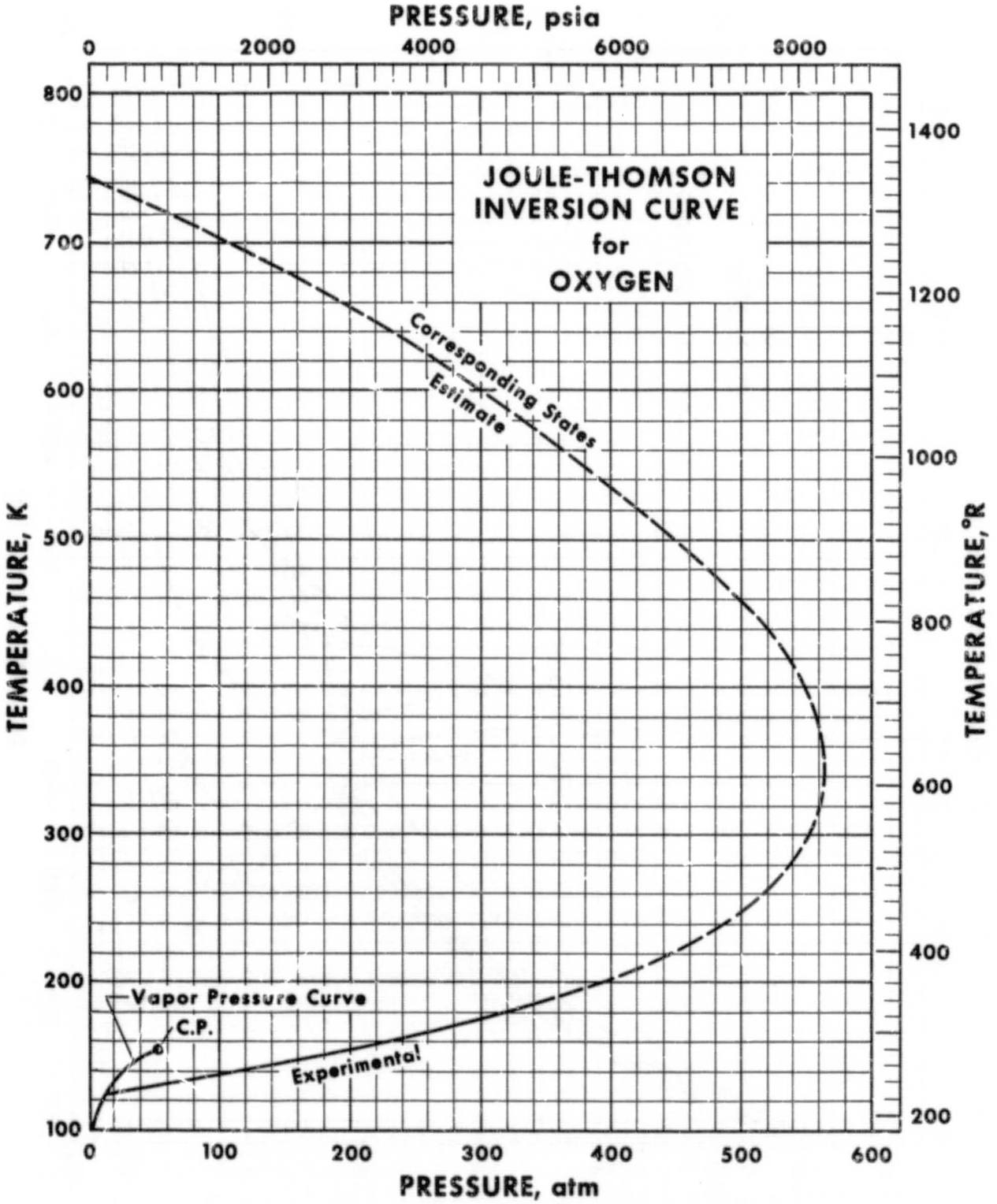
PRESSURE, psia
0
2000
4000
6000
8000
JOULE-THOMSON
INVERSION CURVE
for
OXYGEN
Corresponding States
Estimate
Vapor Pressure Curve
C.P.
Experimental
TEMPERATURE, K
800
700
600
500
400
300
200
100
TEMPERATURE, °R
1400
1200
1000
800
600
400
200
0
100
200
300
400
500
600
PRESSURE, atm

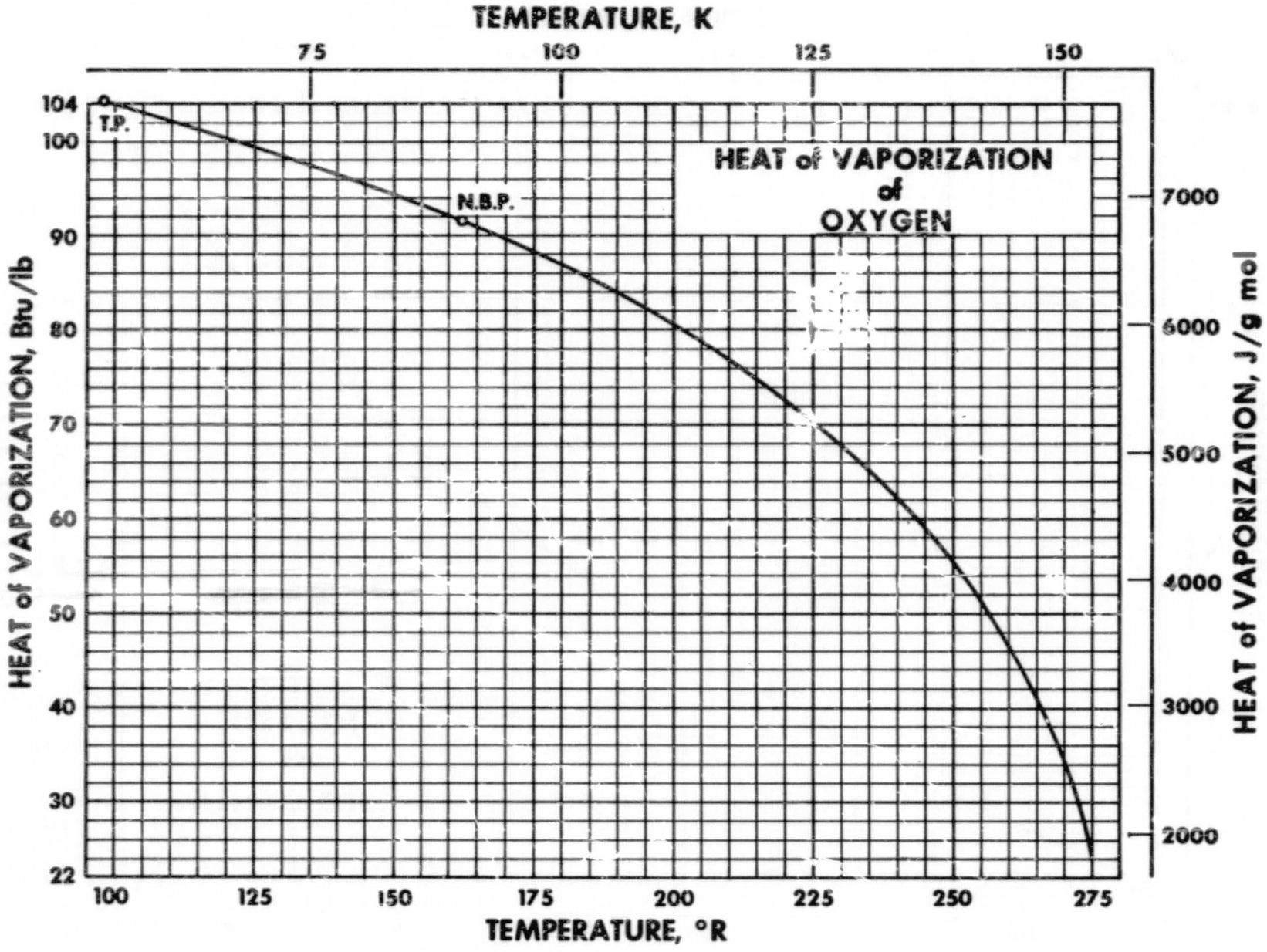
TEMPERATURE, K
75
100
125
150
HEAT of VAPORIZATION
of
OXYGEN
T.P.
N.B.P.
HEAT of VAPORIZATION, Btu/lb
104
100
90
80
70
60
50
40
30
22
HEAT of VAPORIZATION, J/g mol
7000
6000
5000
4000
3000
2000
100
125
150
175
200
225
250
275
TEMPERATURE, °R

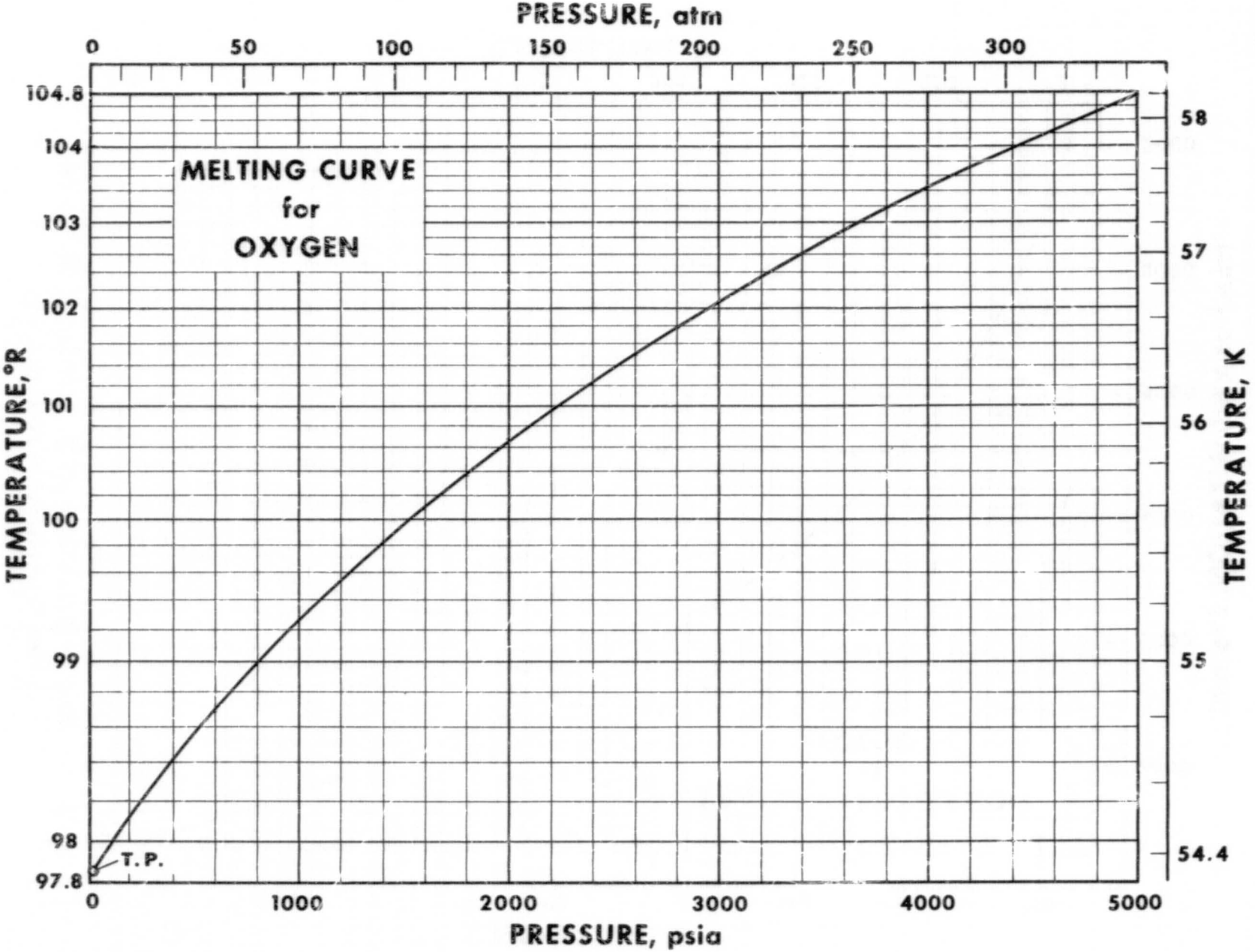
PRESSURE, atm
0
50
100
150
200
250
300
MELTING CURVE
for
OXYGEN
TEMPERATURE, °R
104.8
104
103
102
101
100
99
98
97.8
T.P.
TEMPERATURE, K
58
57
56
55
54.4
0
1000
2000
3000
4000
5000
PRESSURE, psia

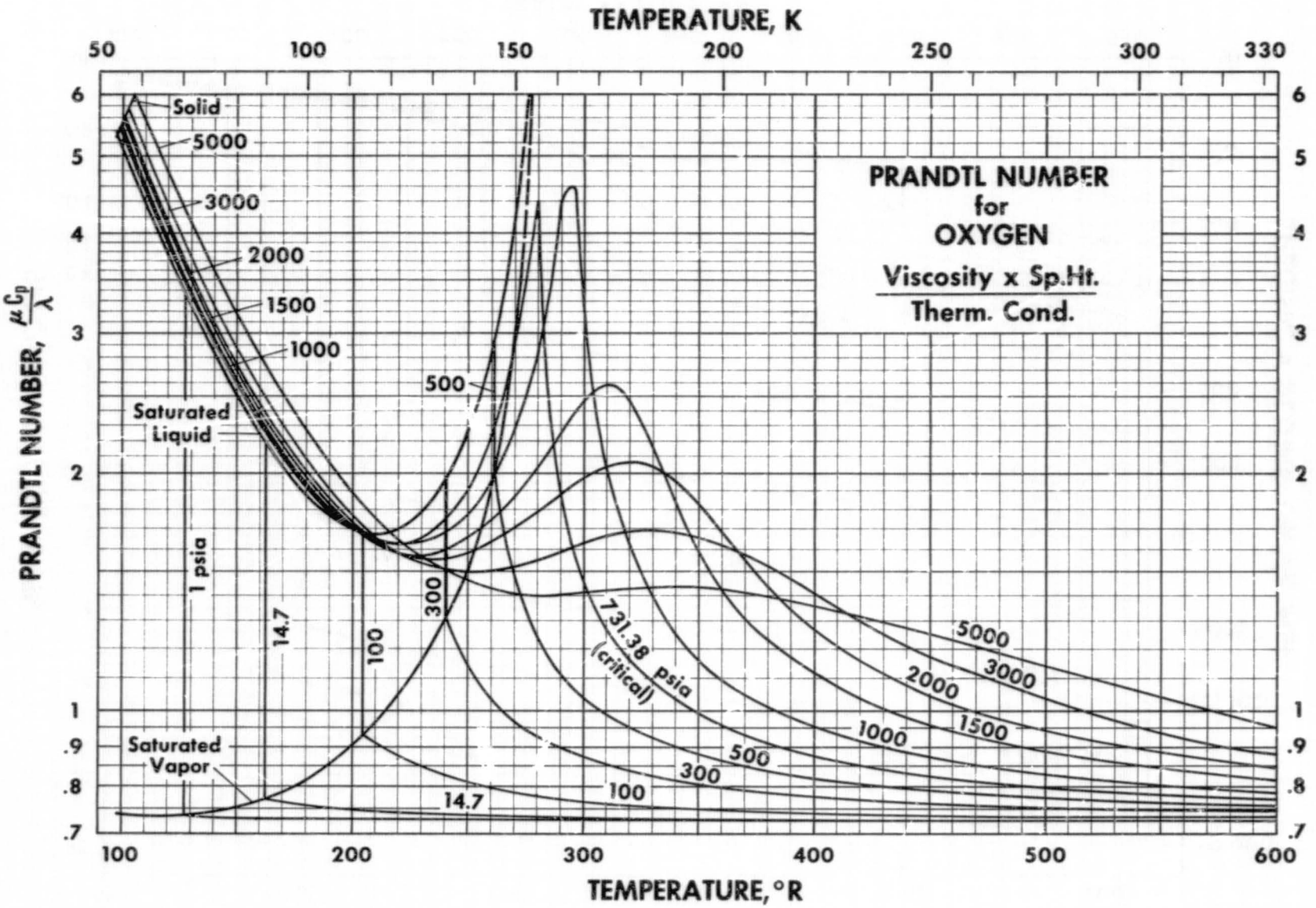
TEMPERATURE, K
50
100
150
200
250
300
330
PRANDTL NUMBER
for
OXYGEN
Viscosity x Sp.Ht.
Therm. Cond.
PRANDTL NUMBER, $\frac{\mu C_p}{\lambda}$
Solid
5000
3000
2000
1500
1000
500
Saturated
Liquid
1 psia
14.7
100
300
731.38 psia
(critical)
5000
3000
2000
1500
1000
500
300
100
14.7
Saturated
Vapor
6
5
4
3
2
1
.9
.8
.7
100
200
300
400
500
600
TEMPERATURE, °R

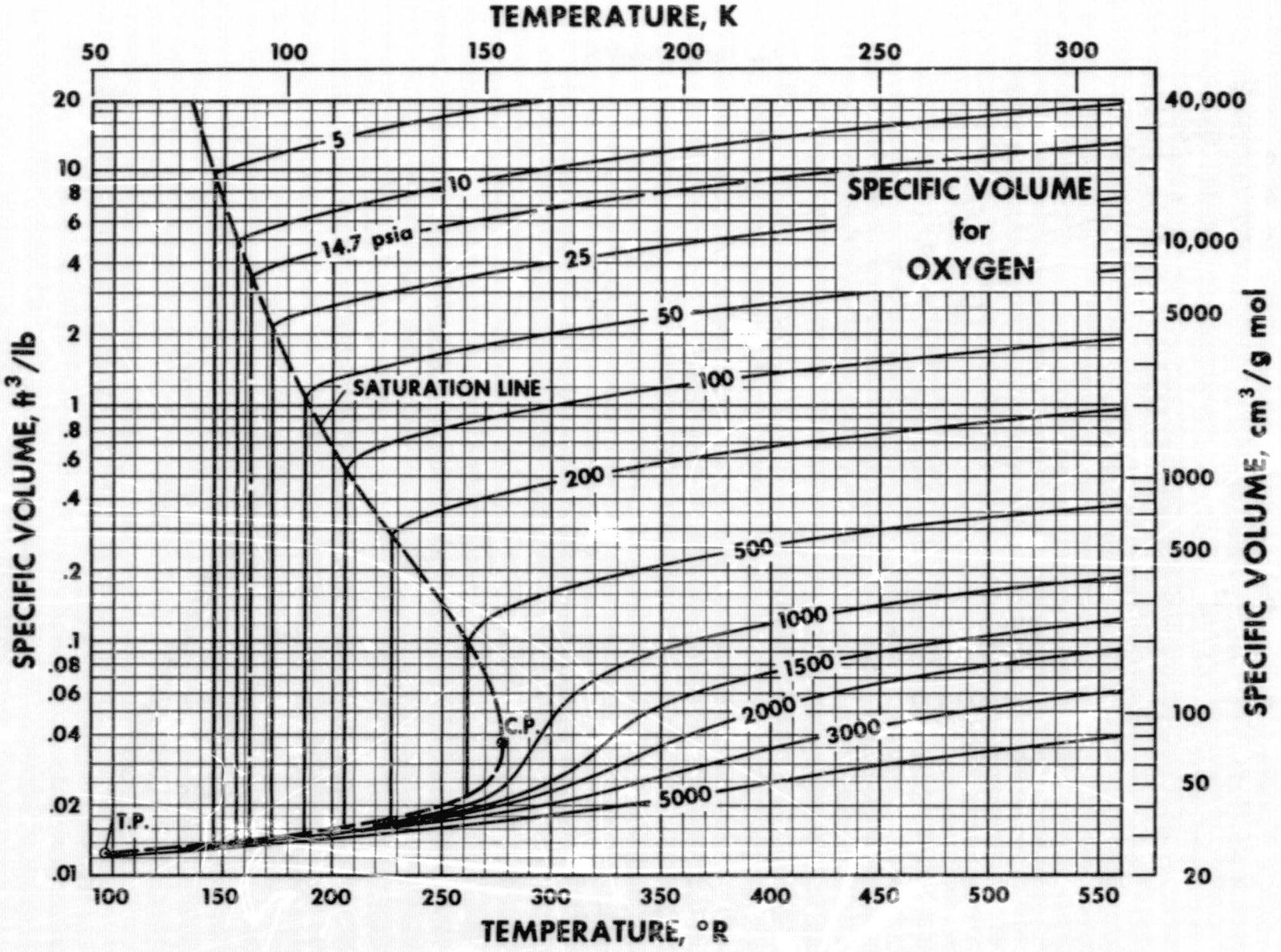
TEMPERATURE, K
50
100
150
200
250
300
SPECIFIC VOLUME
for
OXYGEN
5
10
14.7 psia
25
50
100
200
500
1000
1500
2000
3000
5000
SATURATION LINE
C.P.
T.P.
SPECIFIC VOLUME, ft³/lb
20
10
8
6
4
2
1
.8
.6
.4
.2
.1
.08
.06
.04
.02
.01
SPECIFIC VOLUME, cm³/g mol
40,000
10,000
5000
1000
500
100
50
20
100
150
200
250
300
350
400
450
500
550
TEMPERATURE, °R

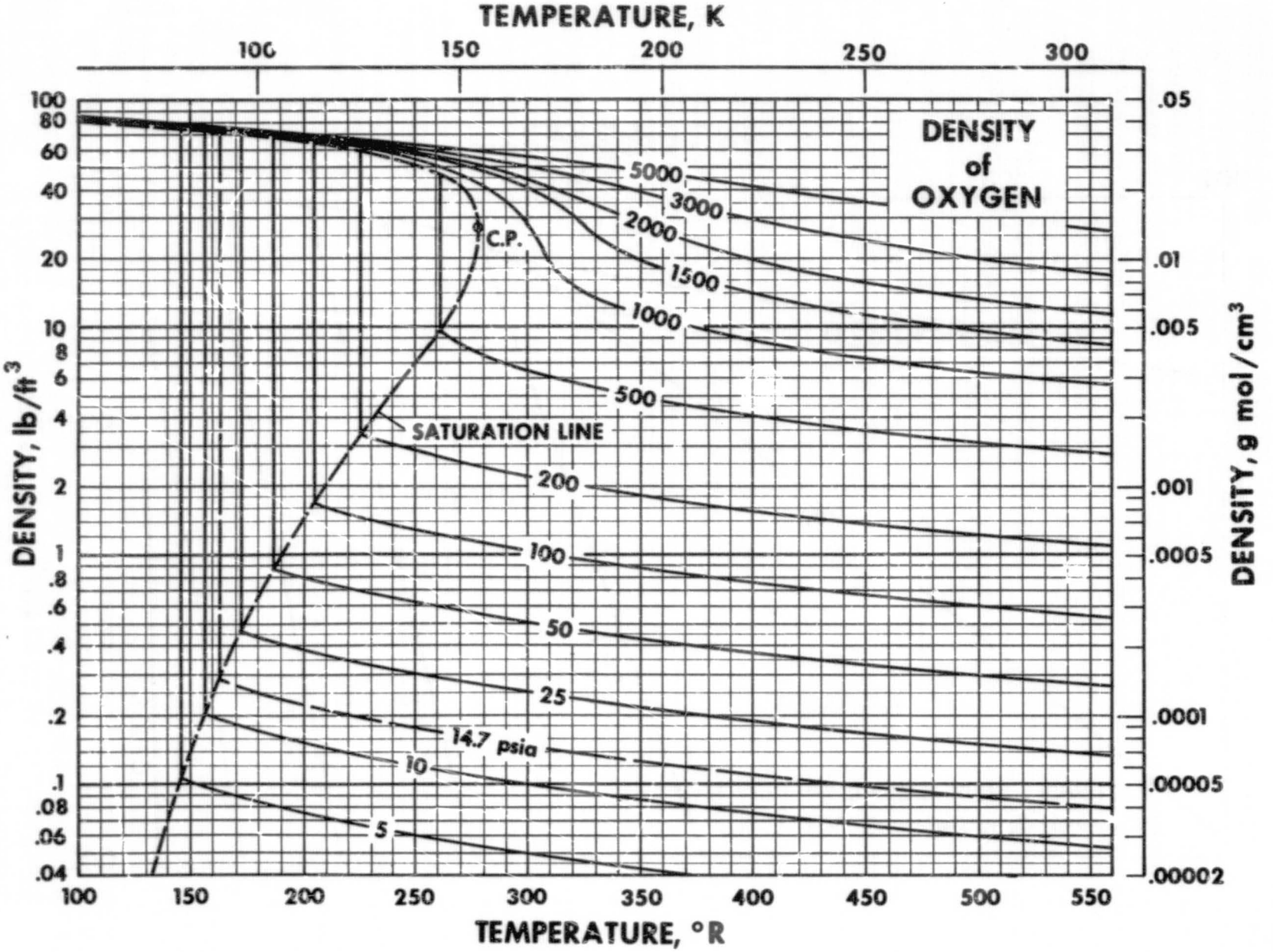
TEMPERATURE, K
100
150
200
250
300
DENSITY of OXYGEN
5000
3000
2000
1500
1000
500
200
100
50
25
14.7 psia
10
5
C.P.
SATURATION LINE
DENSITY, lb/ft³
100
80
60
40
20
10
8
6
4
2
1
.8
.6
.4
.2
.1
.08
.06
.04
DENSITY, g mol/cm³
.05
.01
.005
.001
.0005
.0001
.00005
.00002
100
150
200
250
300
350
400
450
500
550
TEMPERATURE, °R

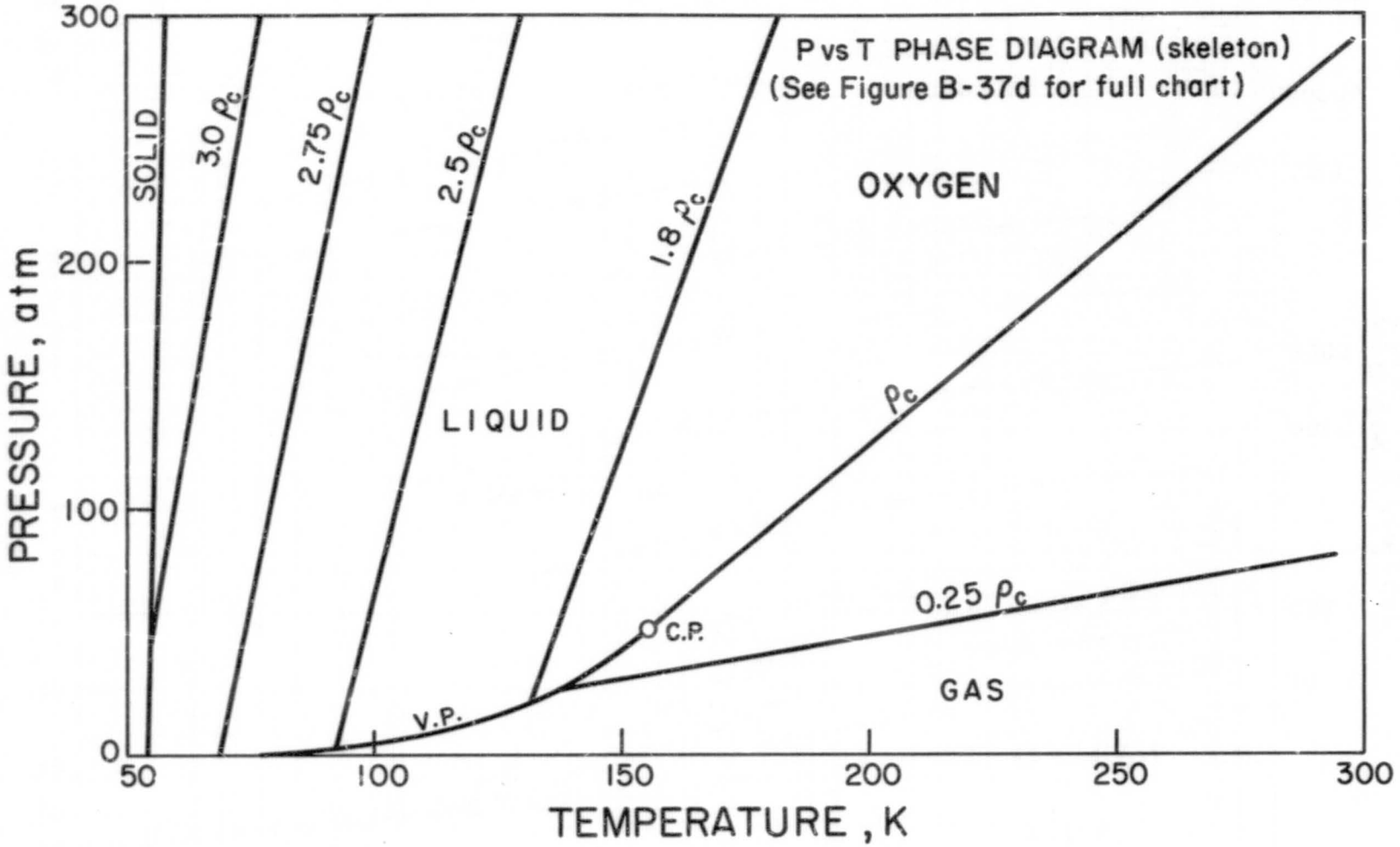
P vs T PHASE DIAGRAM (skeleton)
(See Figure B-37d for full chart)
OXYGEN
SOLID
LIQUID
GAS
3.0 ρc
2.75 ρc
2.5 ρc
1.8 ρc
ρc
0.25 ρc
C.P.
V.P.
PRESSURE, atm
TEMPERATURE , K
300
200
100
0
50
100
150
200
250
300

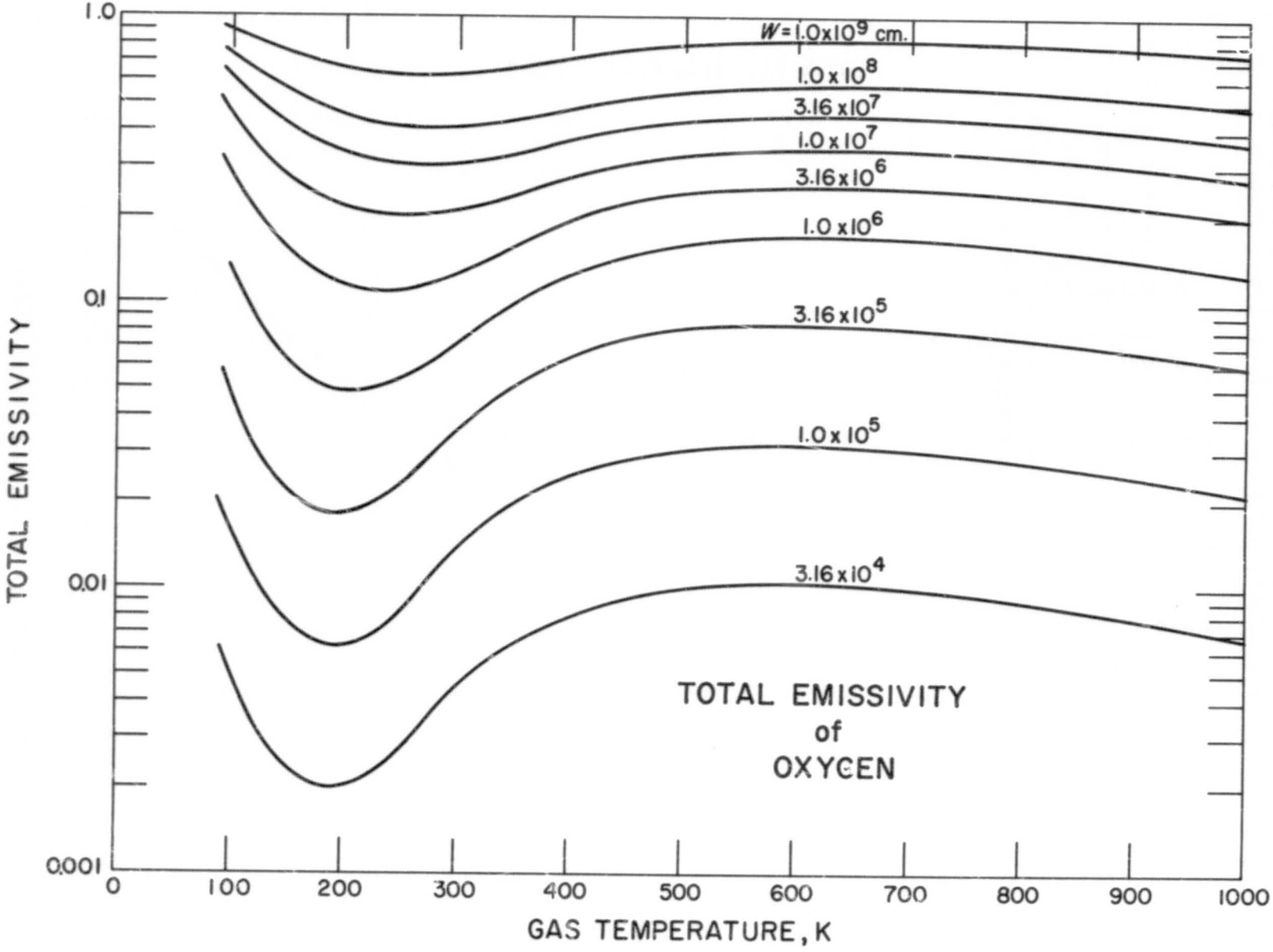
1.0
0.1
0.01
0.001
TOTAL EMISSIVITY
W = 1.0x10^9 cm.
1.0 x 10^8
3.16 x 10^7
1.0 x 10^7
3.16 x 10^6
1.0 x 10^6
3.16 x 10^5
1.0 x 10^5
3.16 x 10^4
TOTAL EMISSIVITY
of
OXYGEN
0
100
200
300
400
500
600
700
800
900
1000
GAS TEMPERATURE, K

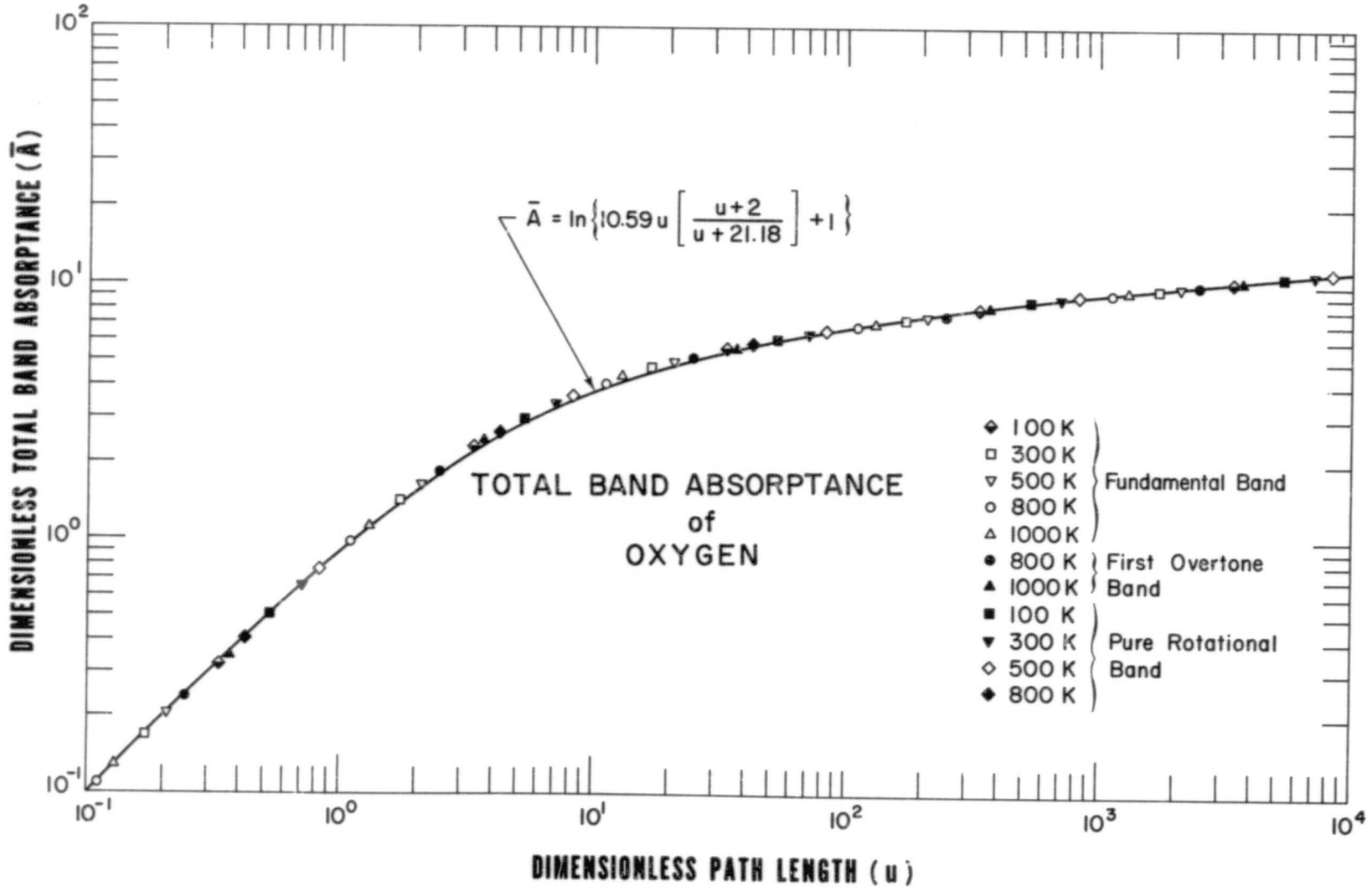
$\bar{A} = \ln\left\{10.59\,u\left[\frac{u+2}{u+21.18}\right]+1\right\}$
TOTAL BAND ABSORPTANCE
of
OXYGEN
100 K
300 K
500 K
800 K
1000 K
Fundamental Band
800 K
1000 K
First Overtone Band
100 K
300 K
500 K
800 K
Pure Rotational Band
DIMENSIONLESS TOTAL BAND ABSORPTANCE ($\bar{A}$)
DIMENSIONLESS PATH LENGTH (u)
10^{-1}
10^{0}
10^{1}
10^{2}
10^{3}
10^{4}

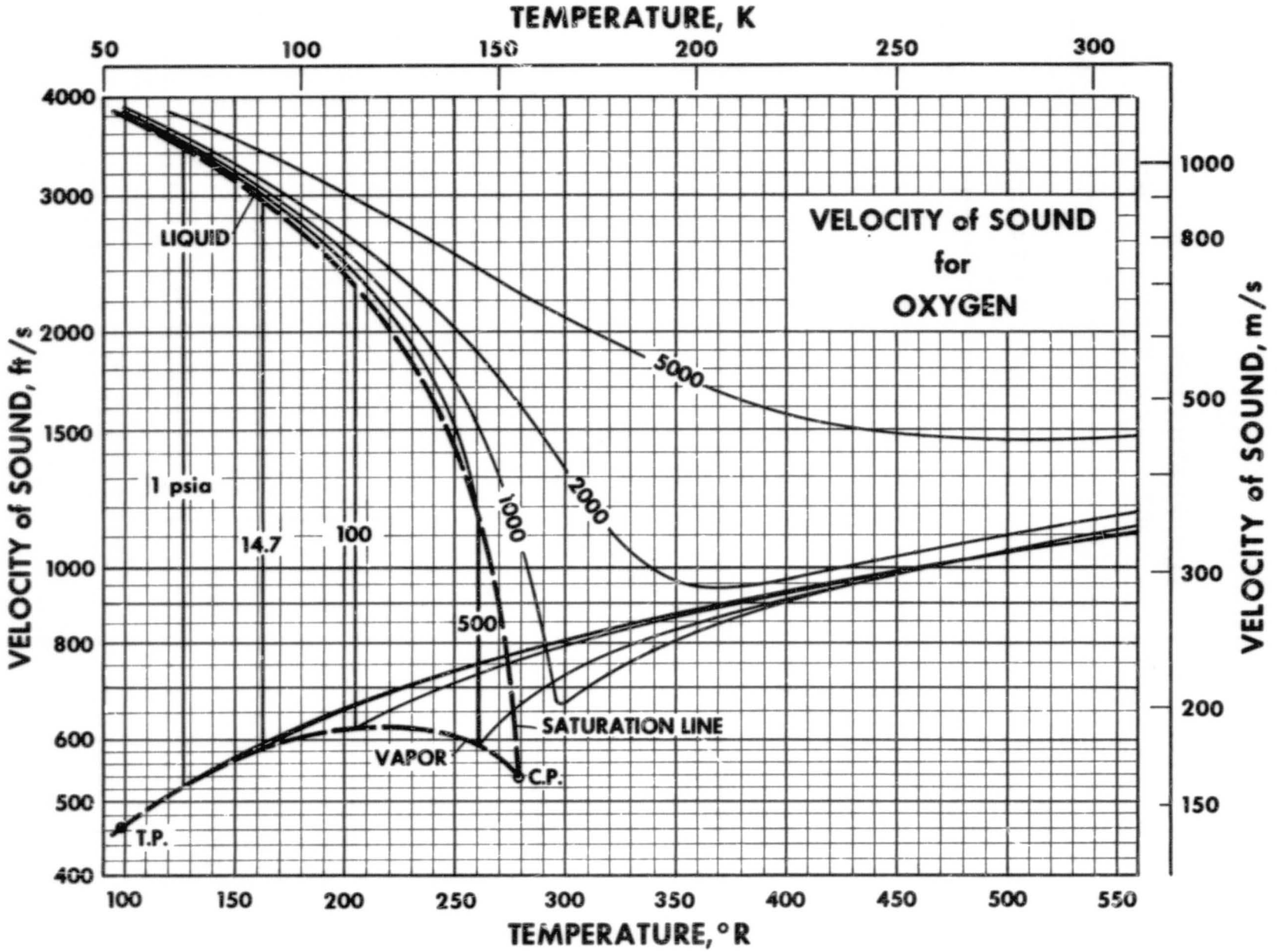
TEMPERATURE, K
50
100
150
200
250
300
VELOCITY of SOUND, ft/s
4000
3000
2000
1500
1000
800
600
500
400
VELOCITY of SOUND, m/s
1000
800
500
300
200
150
VELOCITY of SOUND
for
OXYGEN
LIQUID
1 psia
14.7
100
500
1000
2000
5000
SATURATION LINE
VAPOR
C.P.
T.P.
100
150
200
250
300
350
400
450
500
550
TEMPERATURE, °R

B-35

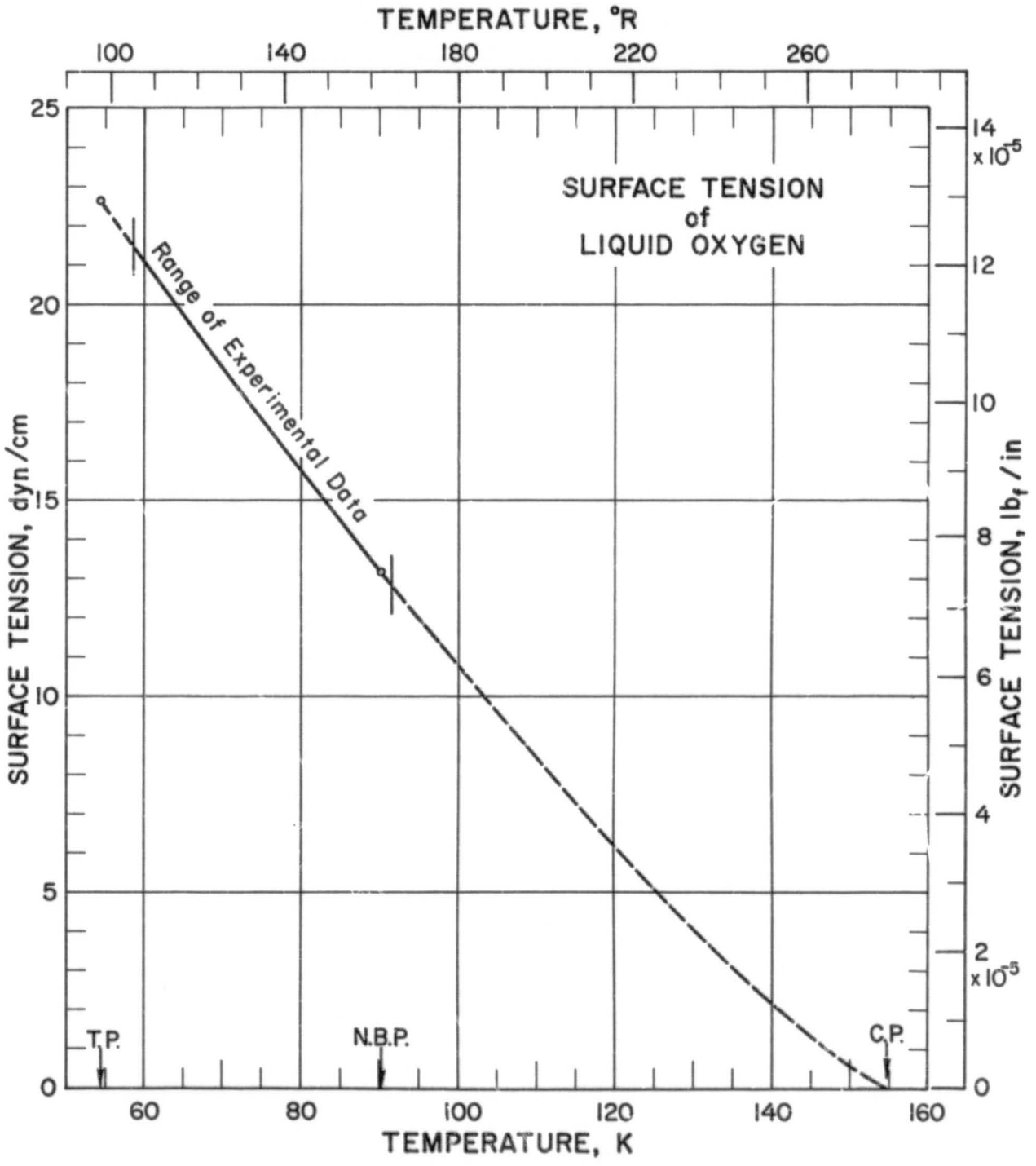
TEMPERATURE, °R
100
140
180
220
260
SURFACE TENSION
of
LIQUID OXYGEN
Range of Experimental Data
SURFACE TENSION, dyn/cm
SURFACE TENSION, lbf / in
14 x 10⁻⁵
12
10
8
6
4
2 x 10⁻⁵
0
25
20
15
10
5
0
T.P.
N.B.P.
C.P.
60
80
100
120
140
160
TEMPERATURE, K

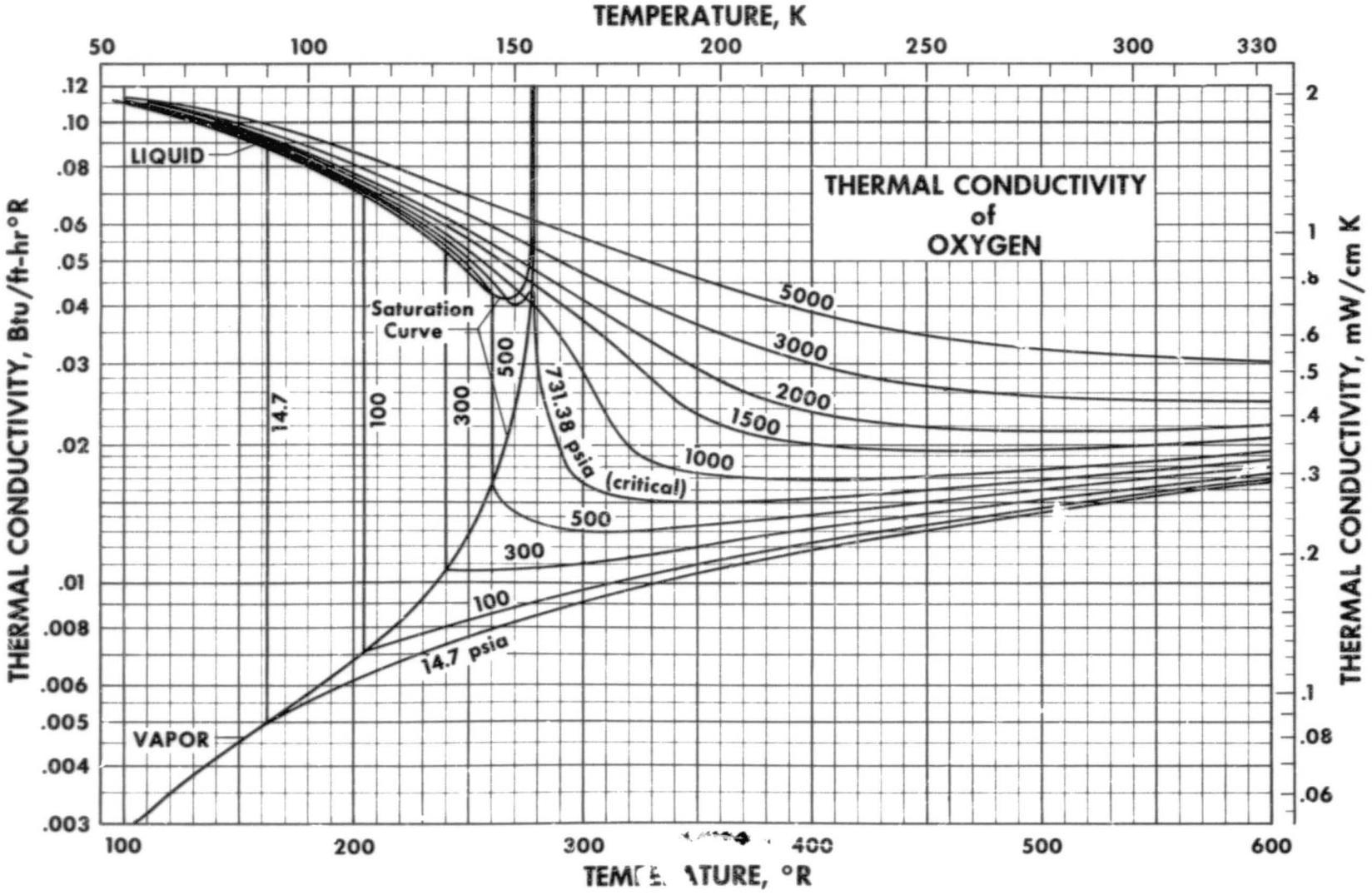
TEMPERATURE, K
50
100
150
200
250
300
330
THERMAL CONDUCTIVITY, Btu/ft-hr°R
.12
.10
.08
.06
.05
.04
.03
.02
.01
.008
.006
.005
.004
.003
THERMAL CONDUCTIVITY, mW/cm K
2
1
.8
.6
.5
.4
.3
.2
.1
.08
.06
THERMAL CONDUCTIVITY of OXYGEN
LIQUID
VAPOR
Saturation Curve
14.7
100
300
500
731.38 psia (critical)
5000
3000
2000
1500
1000
500
300
100
14.7 psia
100
200
300
400
500
600
TEMPERATURE, °R

REFERENCE 1

PAGE 132 BLANK

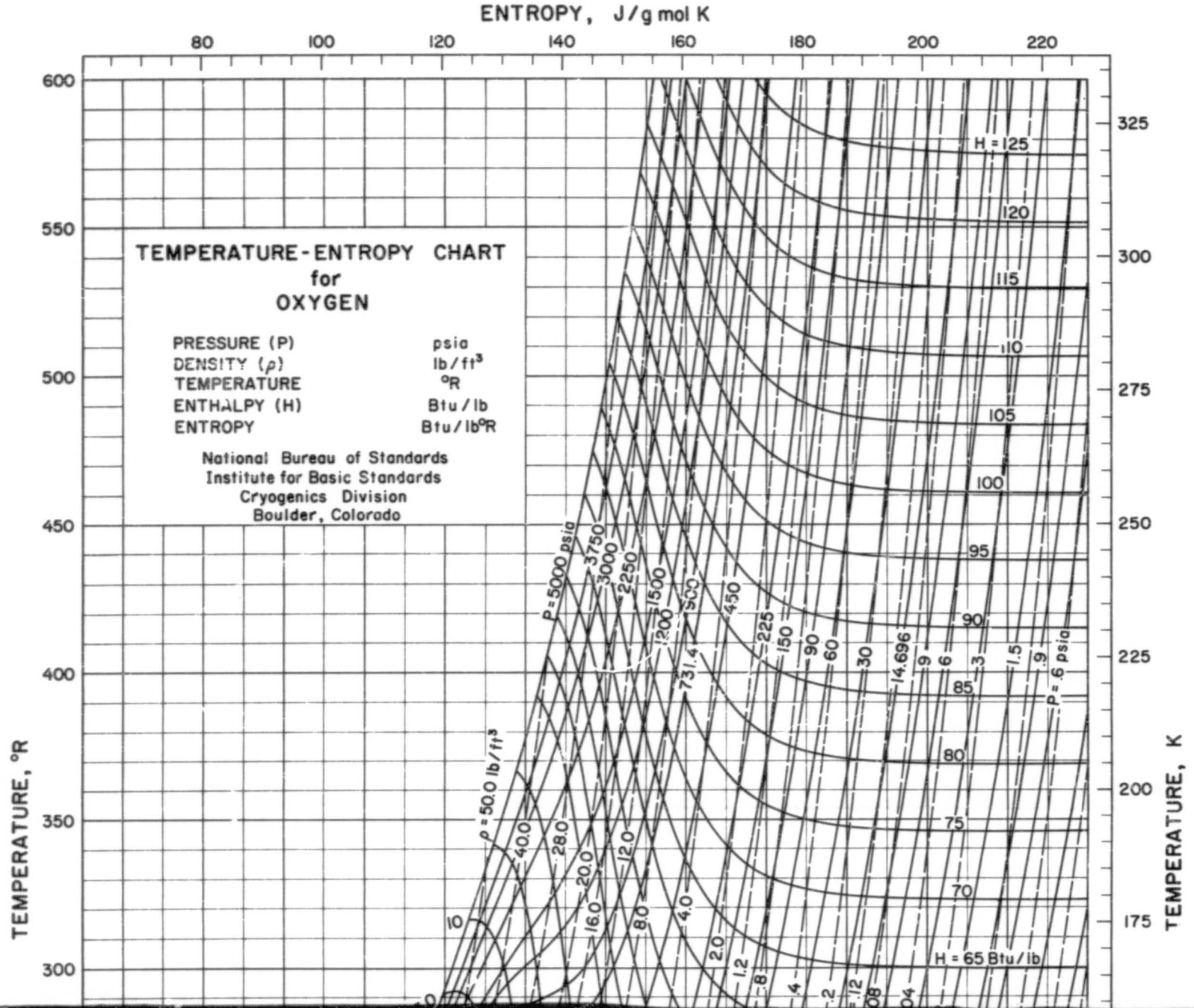
ENTROPY, J/g mol K
80
100
120
140
160
180
200
220
TEMPERATURE, °R
600
550
500
450
400
350
300
TEMPERATURE, K
325
300
275
250
225
200
175
TEMPERATURE-ENTROPY CHART
for
OXYGEN
PRESSURE (P) psia
DENSITY (ρ) lb/ft³
TEMPERATURE °R
ENTHALPY (H) Btu/lb
ENTROPY Btu/lb°R
National Bureau of Standards
Institute for Basic Standards
Cryogenics Division
Boulder, Colorado
H = 125
120
115
110
105
100
95
90
85
80
75
70
H = 65 Btu/lb
P = 5000 psia
3750
3000
2250
1500
1200
731.4
450
225
150
90
60
30
14.696
9
6
3
1.5
.9
P = .6 psia
ρ = 50.0 lb/ft³
40.0
28.0
20.0
16.0
12.0
8.0
4.0
2.0
1.2
.8
.4
.2
.12
.08
.04
10

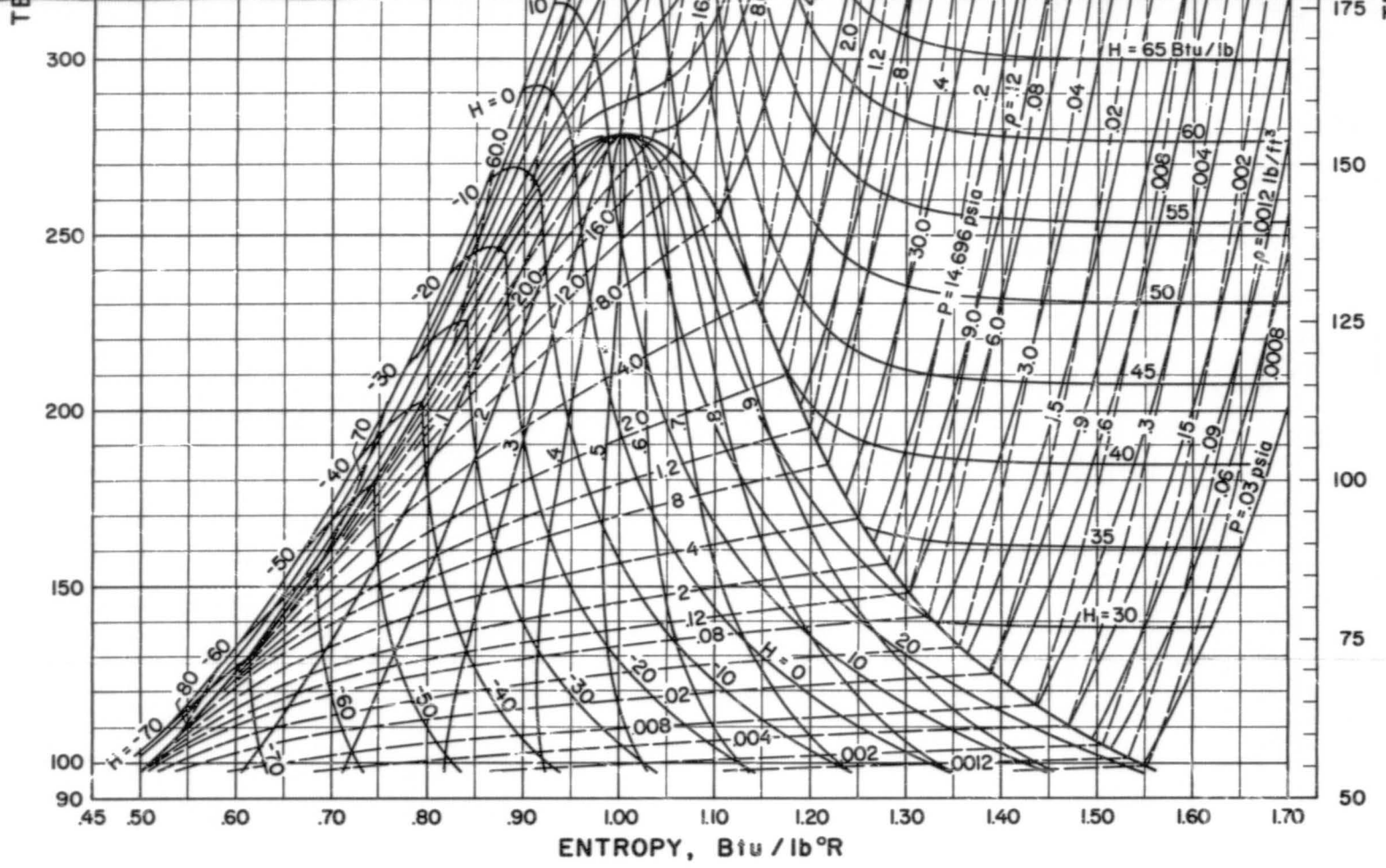
TEMPERATURE, °R
ENTROPY, Btu / lb °R
H = 65 Btu / lb
H = 30
H = 0
H = -70
P = 14.696 psia
P = .03 psia
ρ = .0012 lb/ft³
90
100
150
200
250
300
50
75
100
125
150
175
.45
.50
.60
.70
.80
.90
1.00
1.10
1.20
1.30
1.40
1.50
1.60
1.70

B-37a

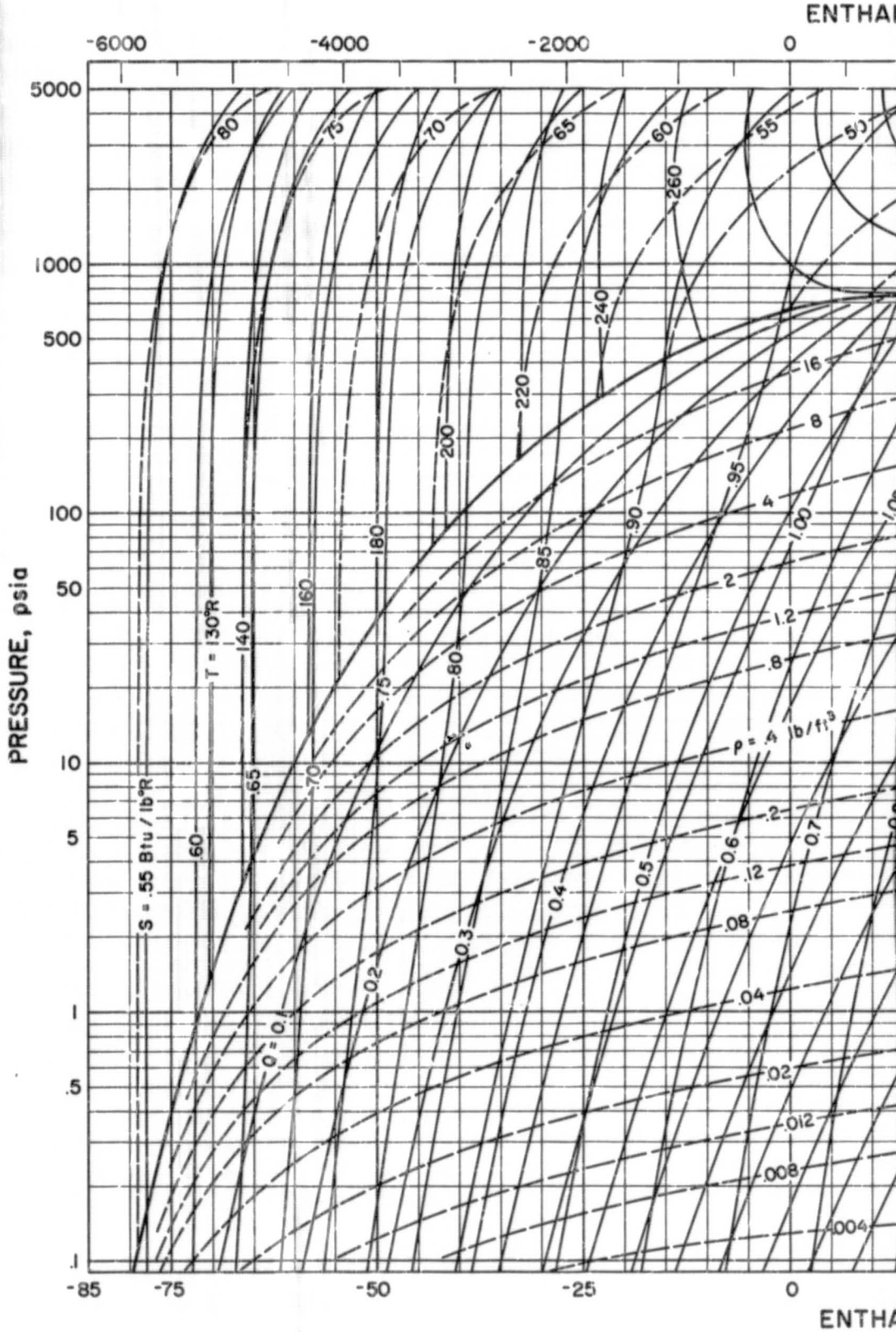
ENTHA
-6000
-4000
-2000
0
5000
1000
500
100
50
10
5
1
.5
.1
PRESSURE, psia
-85
-75
-50
-25
0
ENTHA
T = 130°R
S = .55 Btu / lb°R
ρ = .4 lb/ft³

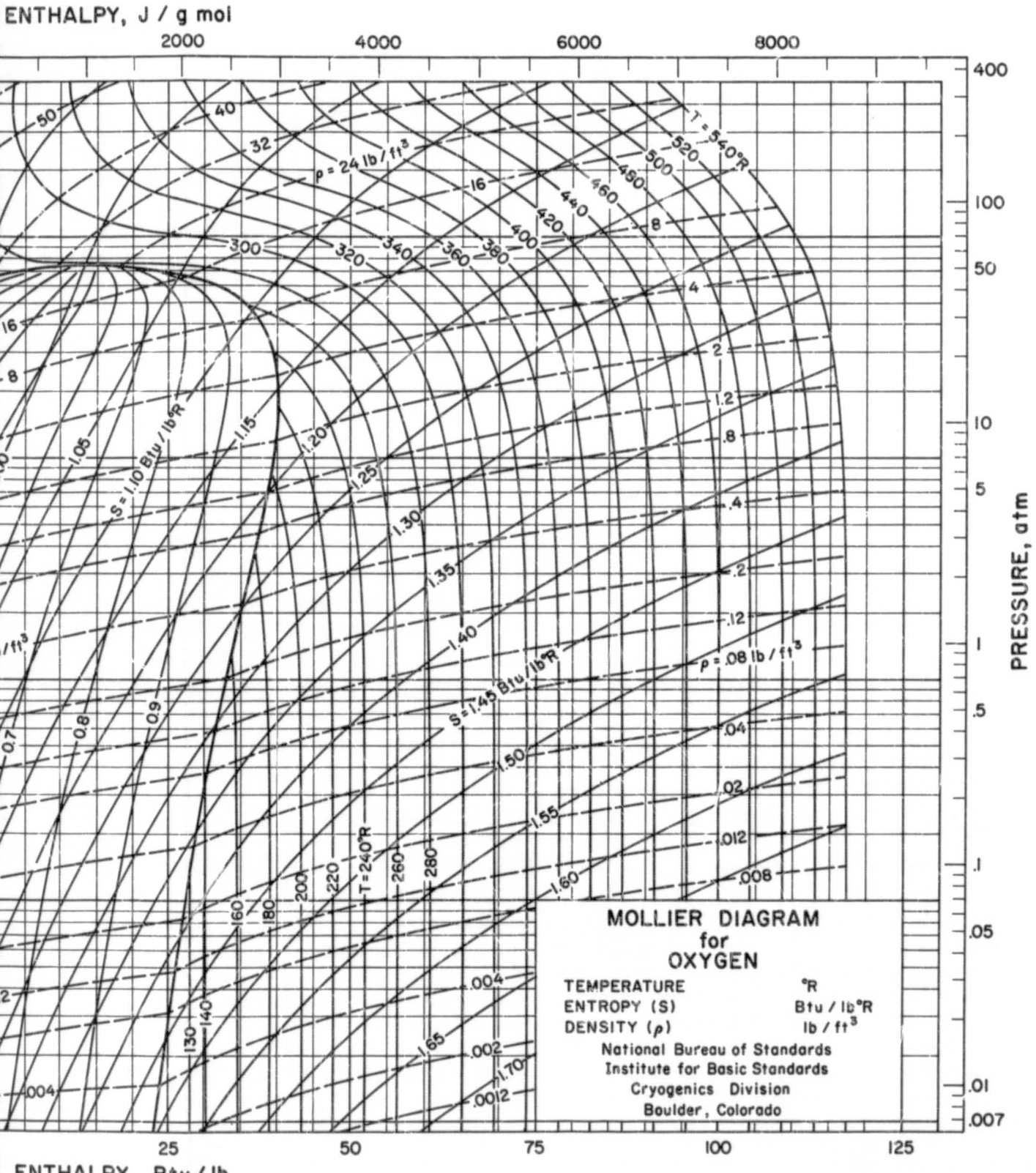
ENTHALPY, J / g mol
2000
4000
6000
8000
400
100
50
10
5
1
.5
.1
.05
.01
.007
PRESSURE, atm
ρ = 24 lb / ft³
ρ = .08 lb / ft³
T = 540°R
T = 240°R
S = 1.10 Btu / lb°R
S = 1.45 Btu / lb°R
MOLLIER DIAGRAM
for
OXYGEN
TEMPERATURE °R
ENTROPY (S) Btu / lb°R
DENSITY (ρ) lb / ft³
National Bureau of Standards
Institute for Basic Standards
Cryogenics Division
Boulder, Colorado
25
50
75
100
125
ENTHALPY, Btu / lb

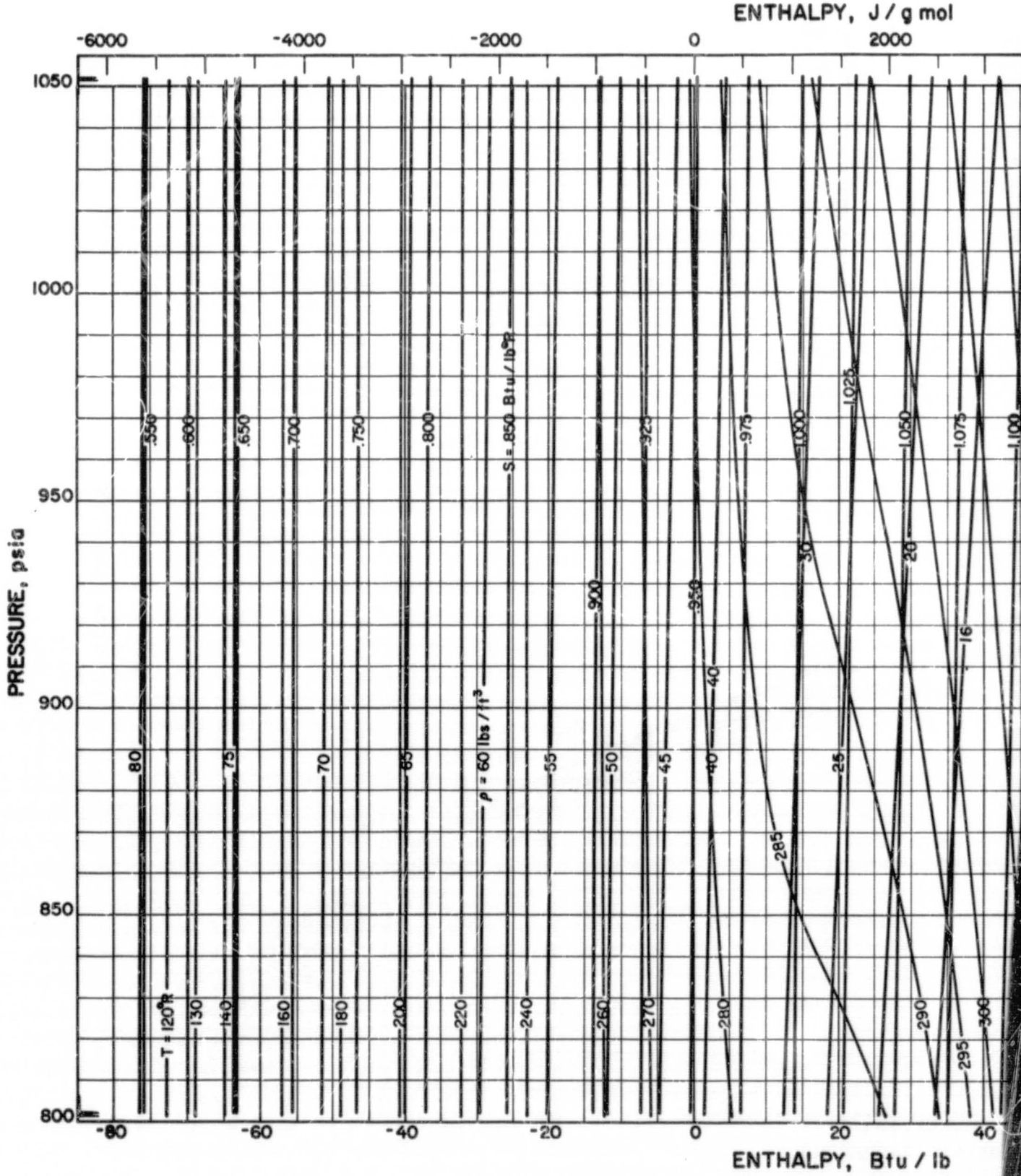
ENTHALPY, J / g mol
-6000
-4000
-2000
0
2000
1050
1000
950
900
850
800
PRESSURE, psia
S = .850 Btu / lb°R
ρ = 60 lbs / ft³
T = 120°R
-80
-60
-40
-20
0
20
40
ENTHALPY, Btu / lb

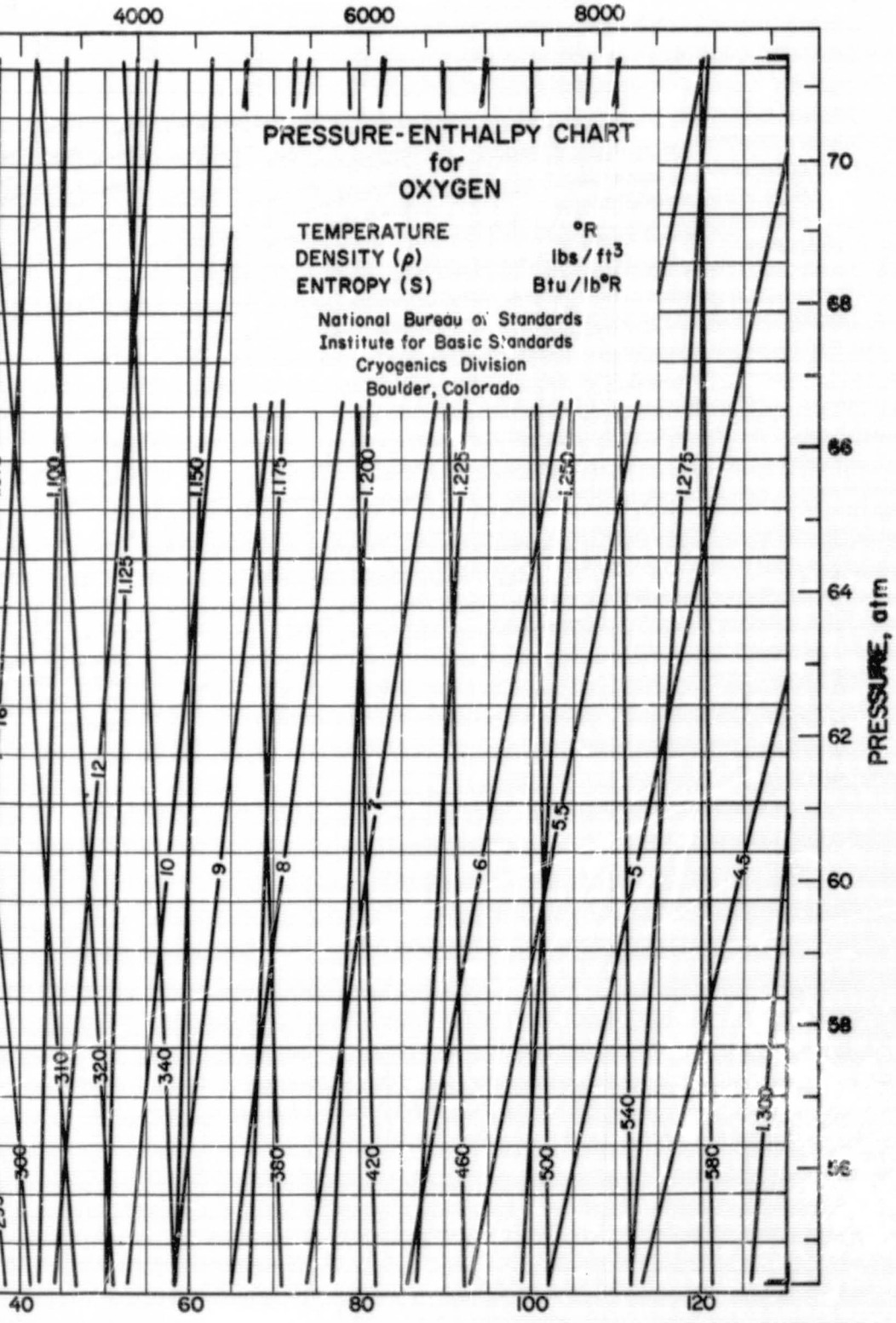
PRESSURE-ENTHALPY CHART
for
OXYGEN
TEMPERATURE °R
DENSITY (ρ) lbs / ft³
ENTROPY (S) Btu / lb°R
National Bureau of Standards
Institute for Basic Standards
Cryogenics Division
Boulder, Colorado
PRESSURE, atm
4000
6000
8000
40
60
80
100
120
70
68
66
64
62
60
58
56
1.100
1.125
1.150
1.175
1.200
1.225
1.250
1.275
1.300
12
10
9
8
7
6
5.5
5
4.5
300
310
320
340
380
420
460
500
540
580

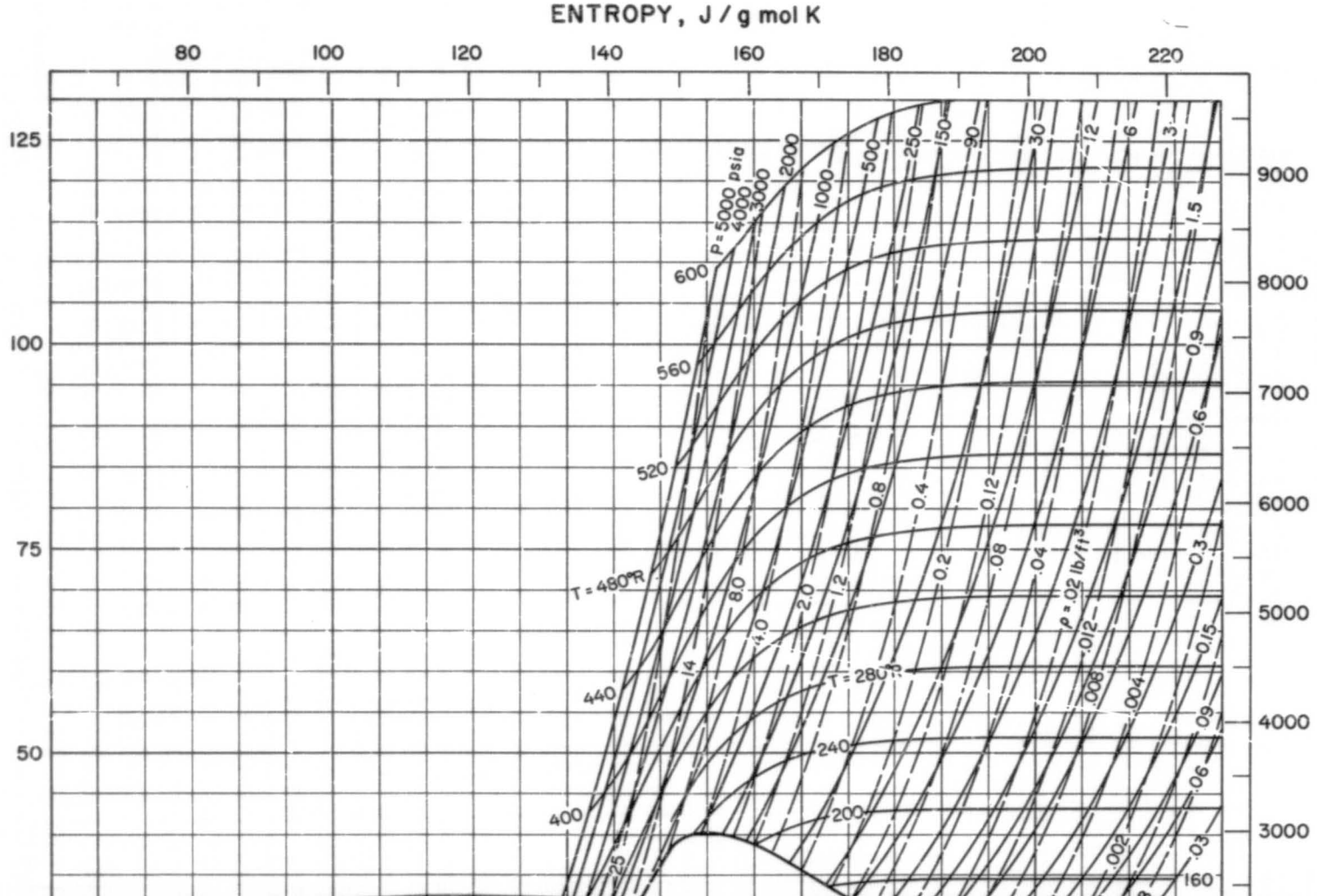
ENTROPY, J / g mol K
80
100
120
140
160
180
200
220
125
100
75
50
Btu / lb
9000
8000
7000
6000
5000
4000
3000
P = 5000 psia
4000
3000
2000
1000
500
250
150
90
30
12
6
3
1.5
0.9
0.6
0.3
0.15
0.09
0.06
0.03
600
560
520
440
400
T = 480°R
T = 280°R
240
200
160
0.8
0.4
0.2
0.12
0.08
0.04
0.012
0.008
0.004
0.002
ρ = .02 lb/ft³
8.0
4.0
2.0
1.2
.14
.25

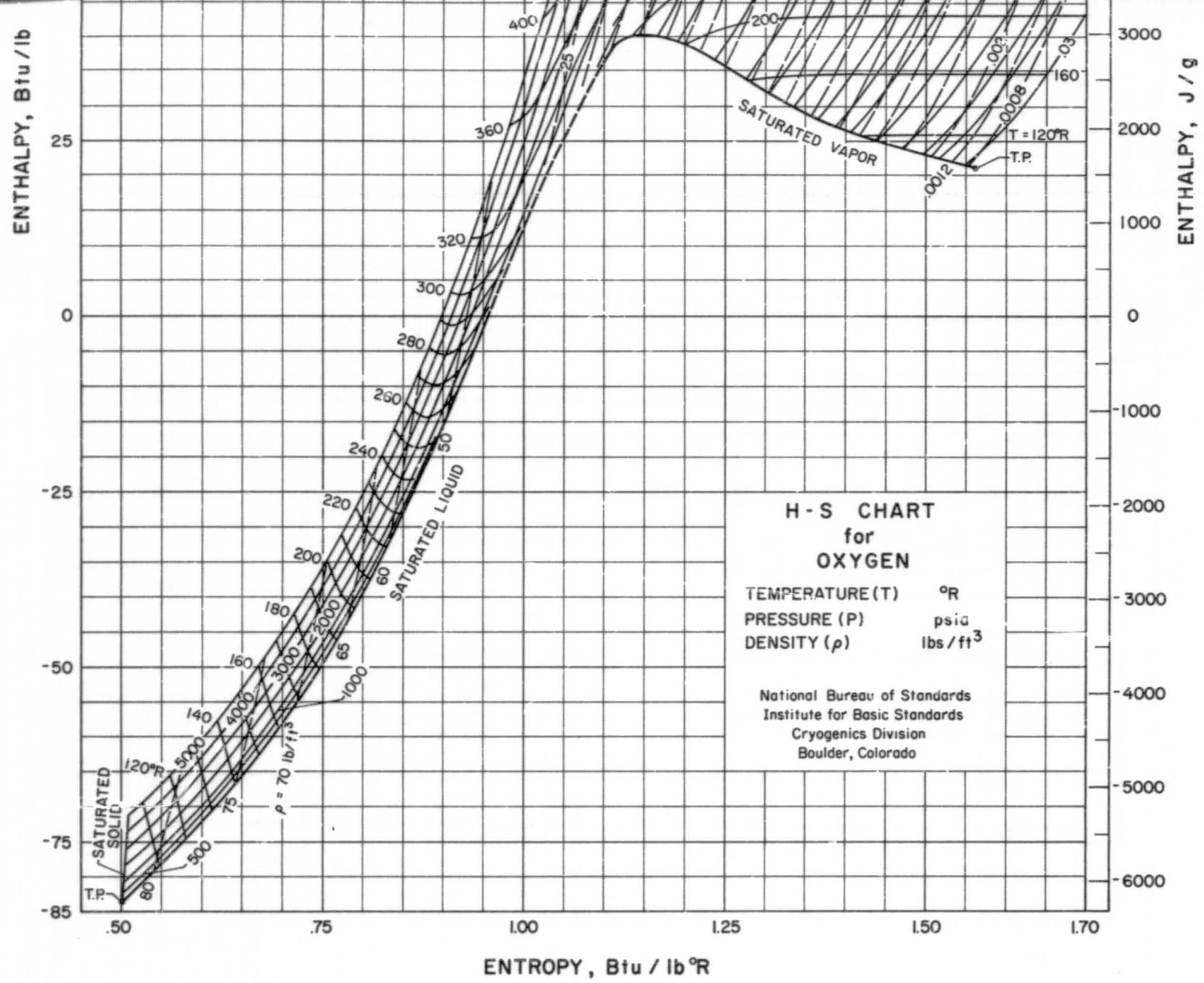
H-S CHART
for
OXYGEN
TEMPERATURE (T) °R
PRESSURE (P) psia
DENSITY (ρ) lbs/ft³
National Bureau of Standards
Institute for Basic Standards
Cryogenics Division
Boulder, Colorado
ENTHALPY, Btu/lb
ENTHALPY, J/g
ENTROPY, Btu/lb°R
SATURATED VAPOR
SATURATED LIQUID
SATURATED SOLID
T.P.
T = 120°R
ρ = 70 lb/ft³
.50
.75
1.00
1.25
1.50
1.70
25
0
-25
-50
-75
-85
3000
2000
1000
-1000
-2000
-3000
-4000
-5000
-6000

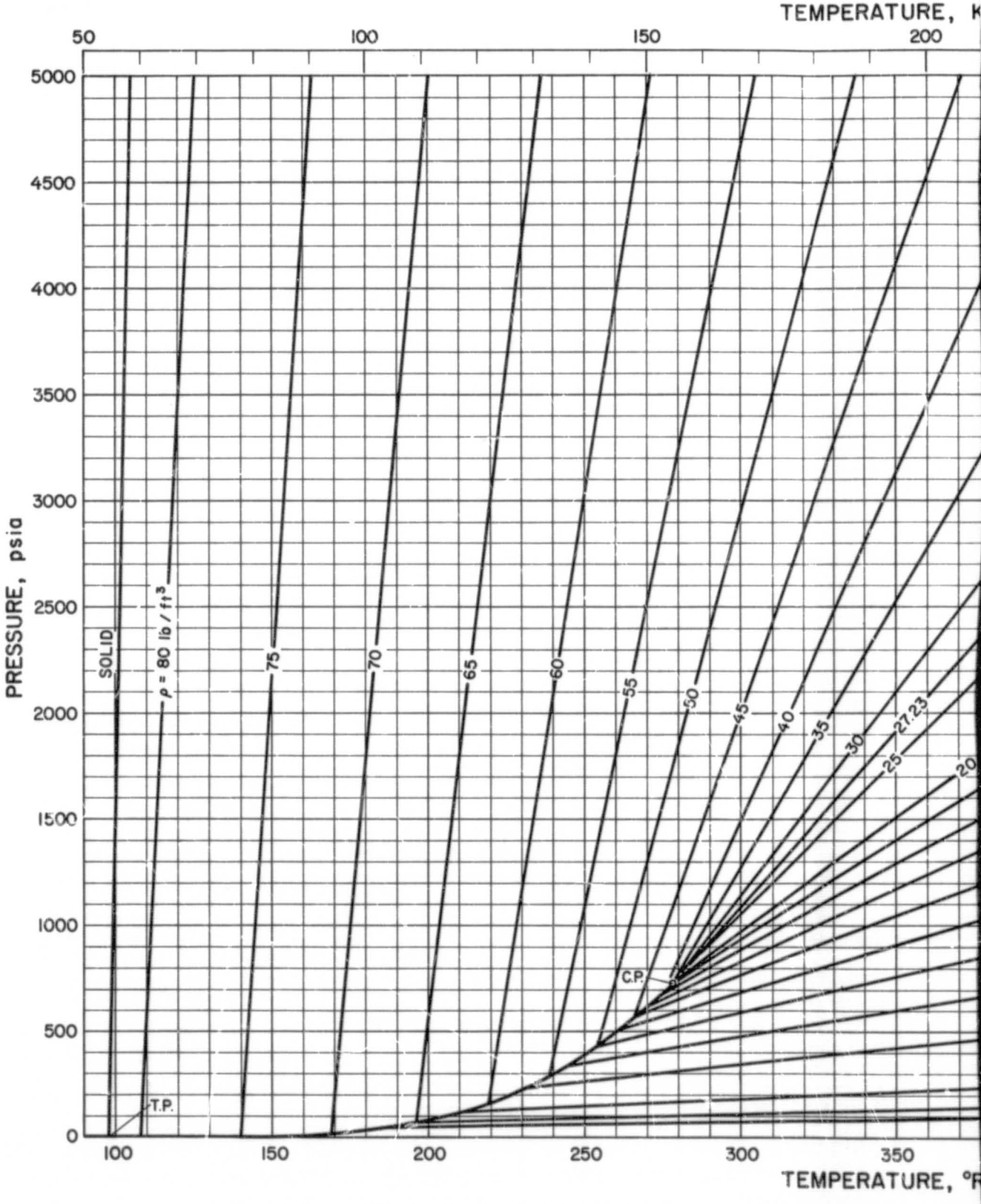
TEMPERATURE, K
50
100
150
200
5000
4500
4000
3500
3000
2500
2000
1500
1000
500
0
PRESSURE, psia
SOLID
ρ = 80 lb / ft³
75
70
65
60
55
50
45
40
35
30
27.23
25
20
C.P.
T.P.
100
150
200
250
300
350
TEMPERATURE, °R

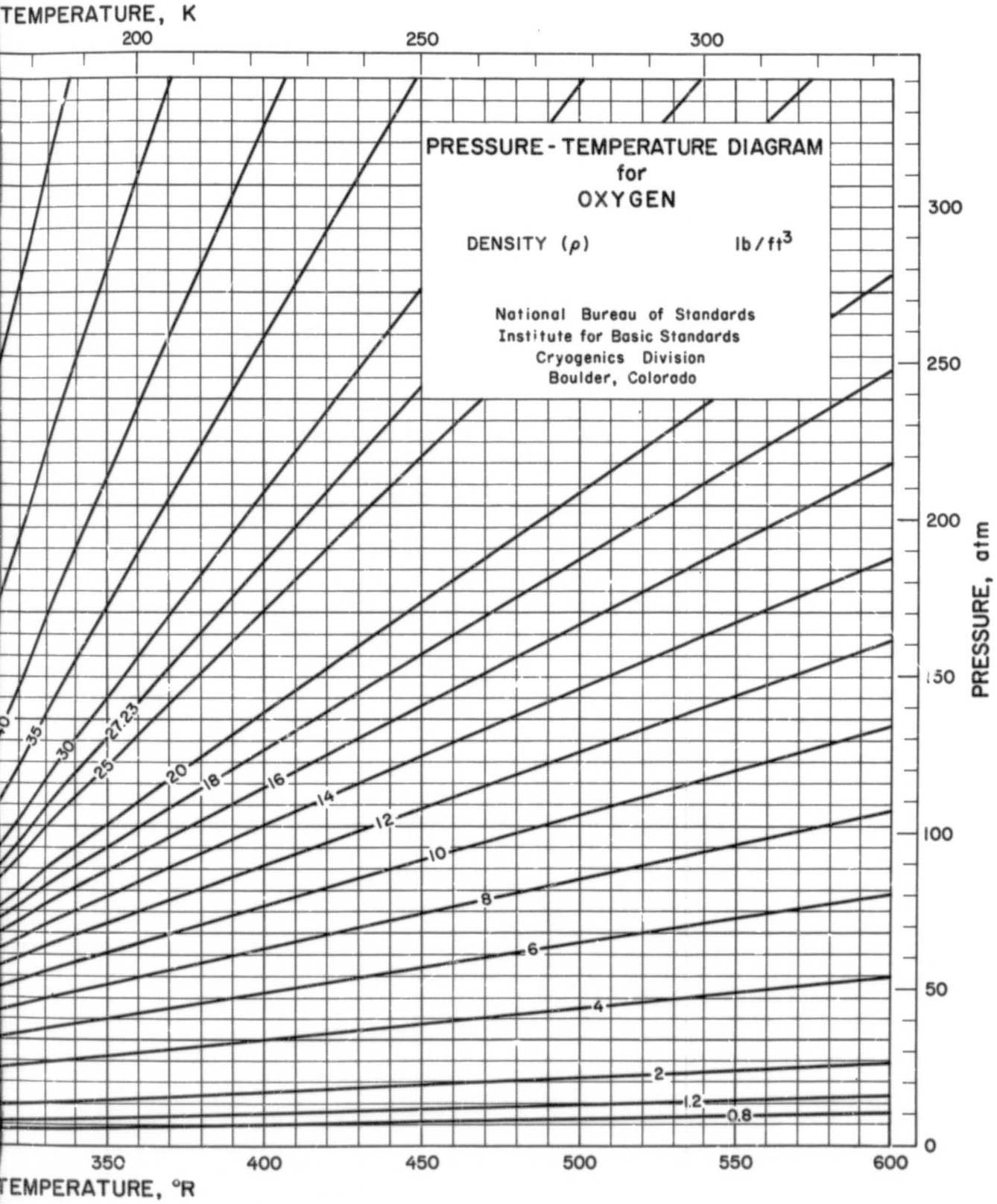
TEMPERATURE, K
200
250
300
PRESSURE - TEMPERATURE DIAGRAM
for
OXYGEN
DENSITY (ρ) lb / ft³
National Bureau of Standards
Institute for Basic Standards
Cryogenics Division
Boulder, Colorado
40
35
30
27.23
25
20
18
16
14
12
10
8
6
4
2
1.2
0.8
300
250
200
150
100
50
0
PRESSURE, atm
350
400
450
500
550
600
TEMPERATURE, °R

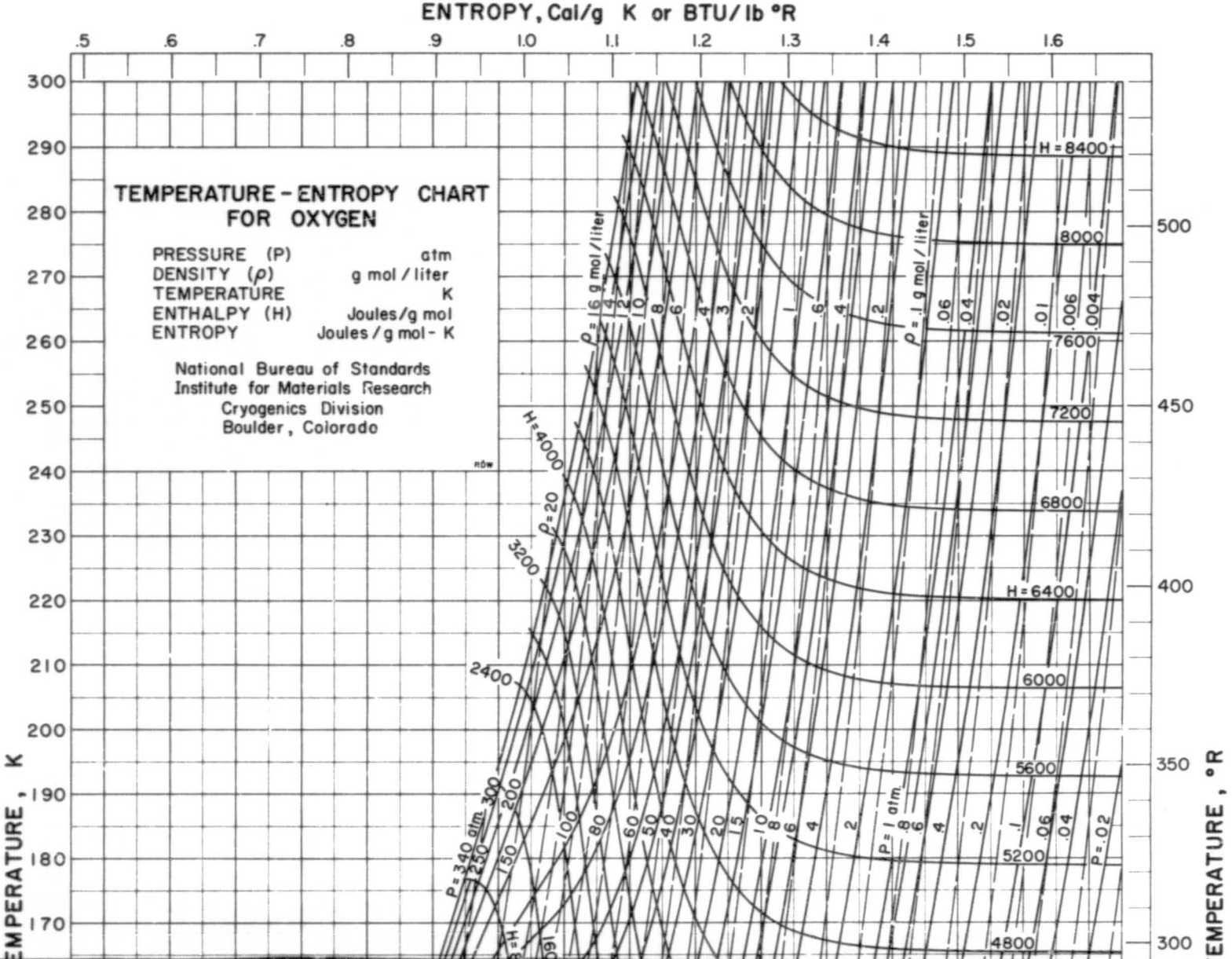
ENTROPY, Cal/g K or BTU/lb °R
.5
.6
.7
.8
.9
1.0
1.1
1.2
1.3
1.4
1.5
1.6
TEMPERATURE - ENTROPY CHART FOR OXYGEN
PRESSURE (P) atm
DENSITY (ρ) g mol / liter
TEMPERATURE K
ENTHALPY (H) Joules/g mol
ENTROPY Joules / g mol - K
National Bureau of Standards
Institute for Materials Research
Cryogenics Division
Boulder, Colorado
TEMPERATURE, K
TEMPERATURE, °R
300
290
280
270
260
250
240
230
220
210
200
190
180
170
500
450
400
350
300
H = 8400
8000
7600
7200
6800
H = 6400
6000
5600
5200
4800
H = 4000
3200
2400
ρ = 16 g mol / liter
ρ = .1 g mol / liter
P = 340 atm
P = 1 atm
P = .02

B-37e

TEMPERATURE, °R
TEMPERATURE, K
ENTROPY, Joules/g mol - K
H=4400 Joules/g mol
H = 2400
H=800
H=0
H=-800
H=-1600
H=-2400
H=-3200
H=-4000
H=-4800
P = 340 atm
P = 0.1 g mol / liter
P = 1 g mol / liter
P = 2.4 g mol / liter
P = 1 atm
P = 0.1 atm

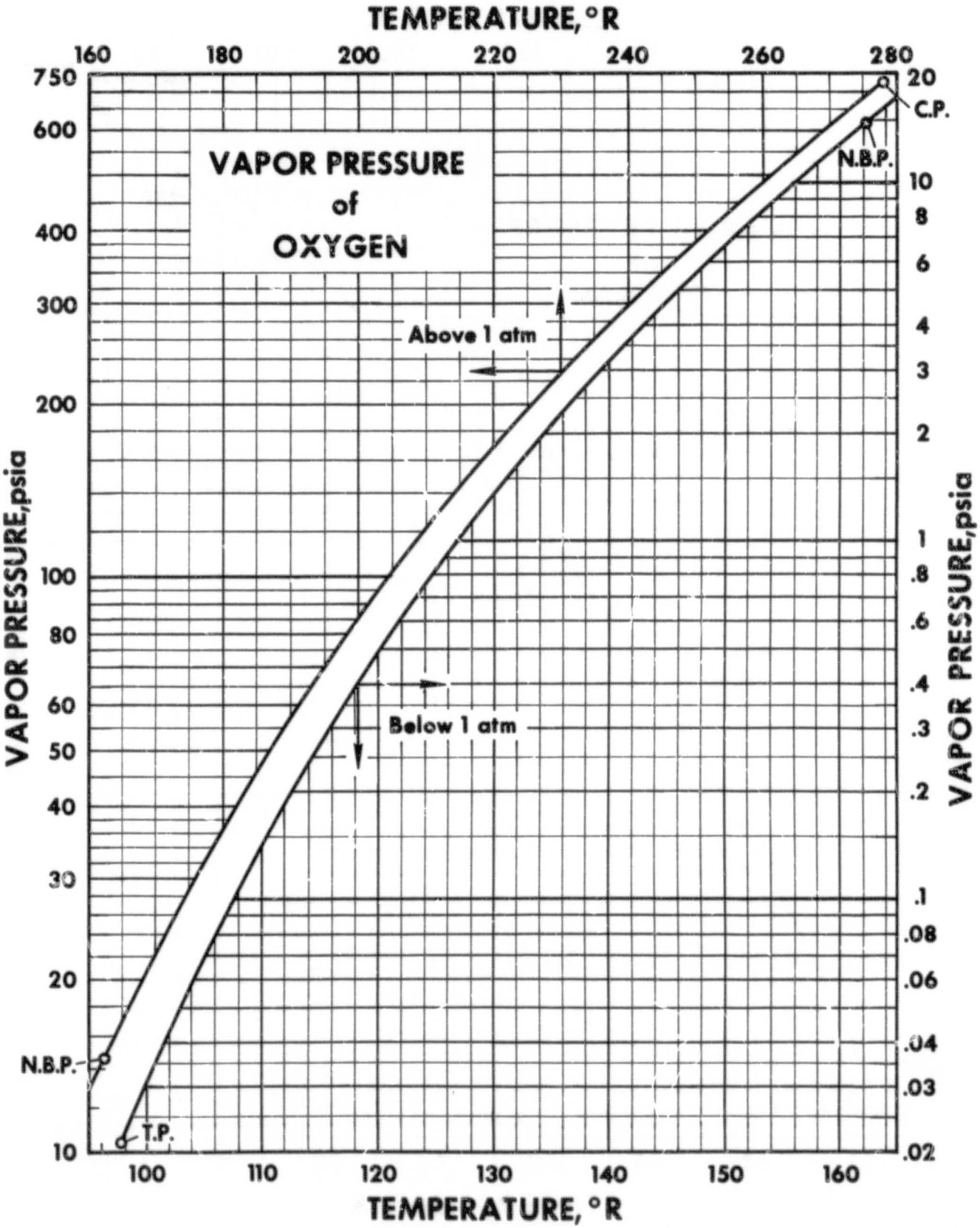
TEMPERATURE, °R
160
180
200
220
240
260
280
VAPOR PRESSURE of OXYGEN
Above 1 atm
Below 1 atm
C.P.
N.B.P.
N.B.P.
T.P.
VAPOR PRESSURE, psia
750
600
400
300
200
100
80
60
50
40
30
20
10
20
10
8
6
4
3
2
1
.8
.6
.4
.3
.2
.1
.08
.06
.04
.03
.02
VAPOR PRESSURE, psia
100
110
120
130
140
150
160
TEMPERATURE, °R

B-38a

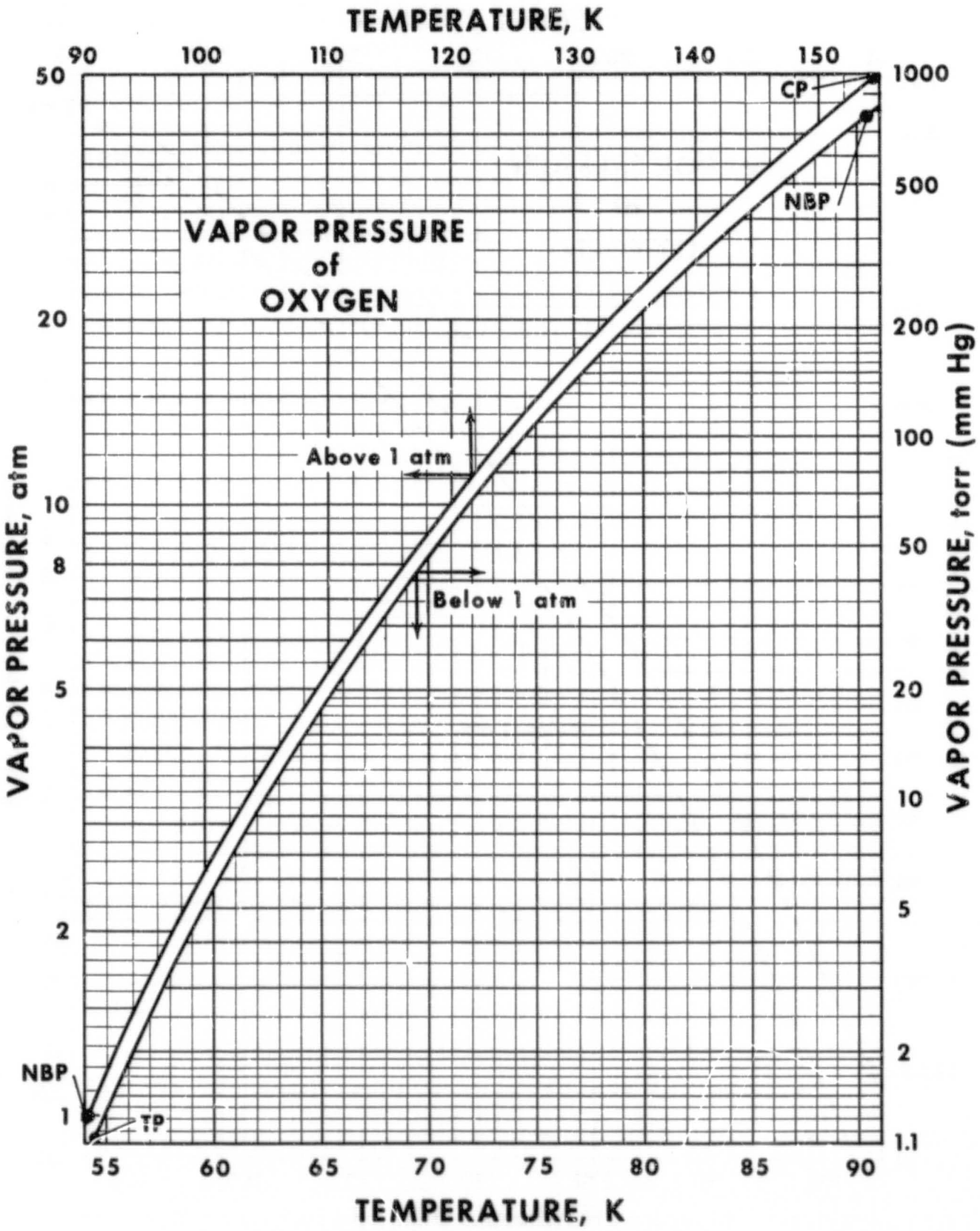
TEMPERATURE, K
90
100
110
120
130
140
150
50
20
10
8
5
2
1
1000
500
200
100
50
20
10
5
2
1.1
CP
NBP
VAPOR PRESSURE
of
OXYGEN
Above 1 atm
Below 1 atm
VAPOR PRESSURE, atm
VAPOR PRESSURE, torr (mm Hg)
NBP
TP
55
60
65
70
75
80
85
90
TEMPERATURE, K

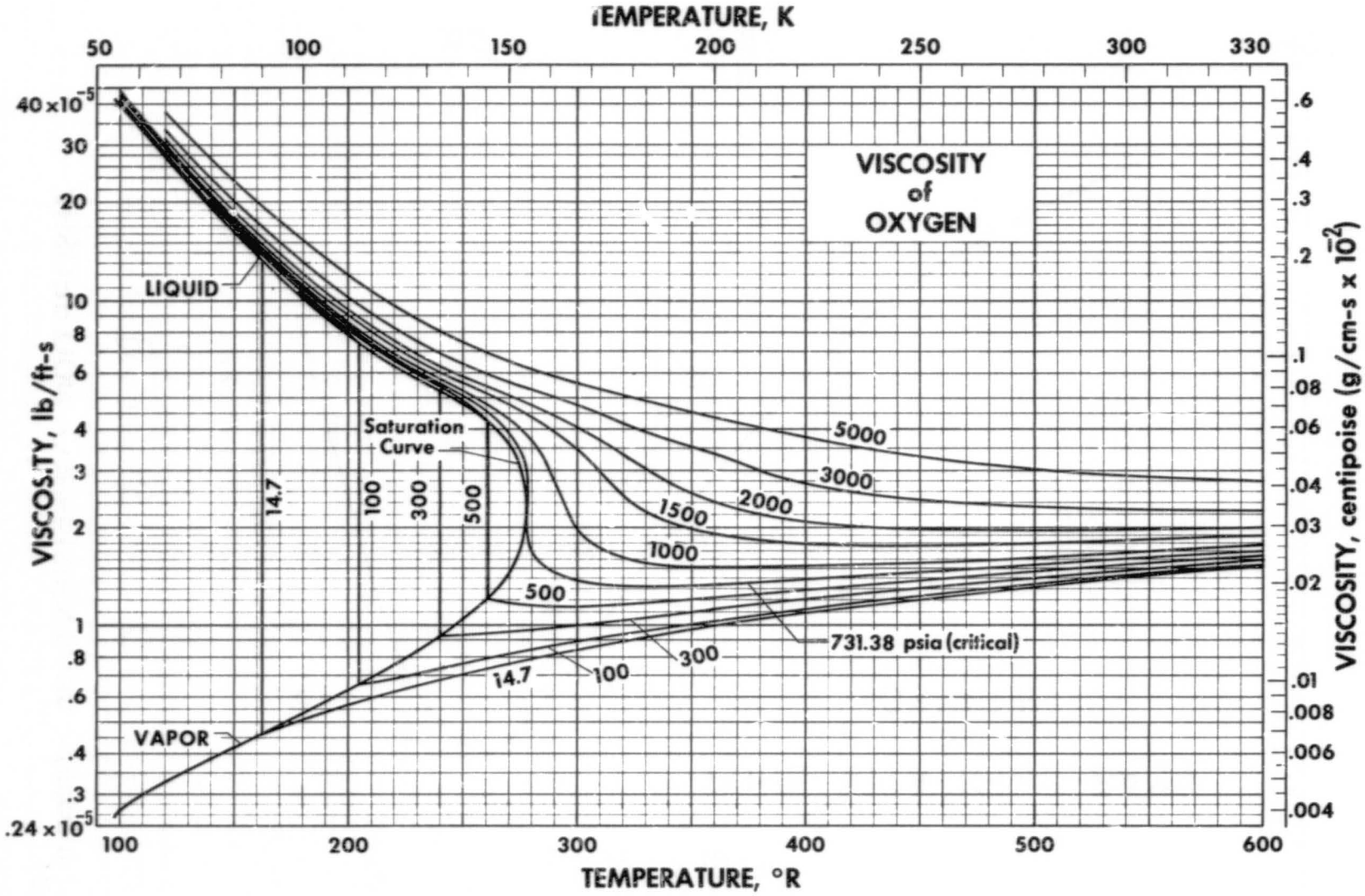
TEMPERATURE, K
50
100
150
200
250
300
330
VISCOSITY
of
OXYGEN
VISCOSITY, lb/ft-s
40 x 10⁻⁵
30
20
10
8
6
4
3
2
1
.8
.6
.4
.3
.24 x 10⁻⁵
VISCOSITY, centipoise (g/cm-s x 10⁻²)
.6
.4
.3
.2
.1
.08
.06
.04
.03
.02
.01
.008
.006
.004
LIQUID
VAPOR
Saturation Curve
14.7
100
300
500
5000
3000
2000
1500
1000
500
731.38 psia (critical)
300
100
14.7
100
200
300
400
500
600
TEMPERATURE, °R

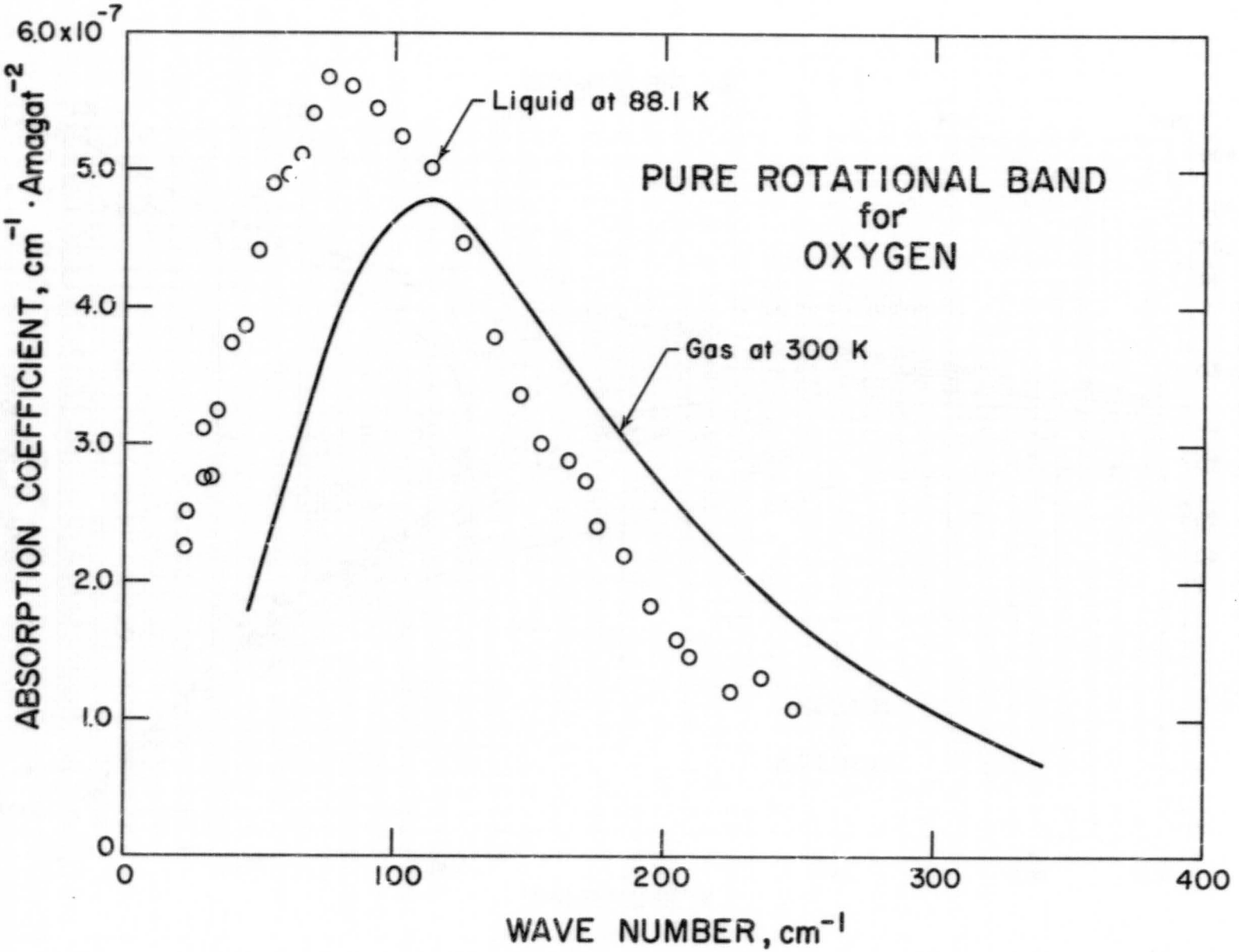
6.0x10^-7
5.0
4.0
3.0
2.0
1.0
0
ABSORPTION COEFFICIENT, cm^-1 · Amagat^-2
Liquid at 88.1 K
PURE ROTATIONAL BAND
for
OXYGEN
Gas at 300 K
0
100
200
300
400
WAVE NUMBER, cm^-1

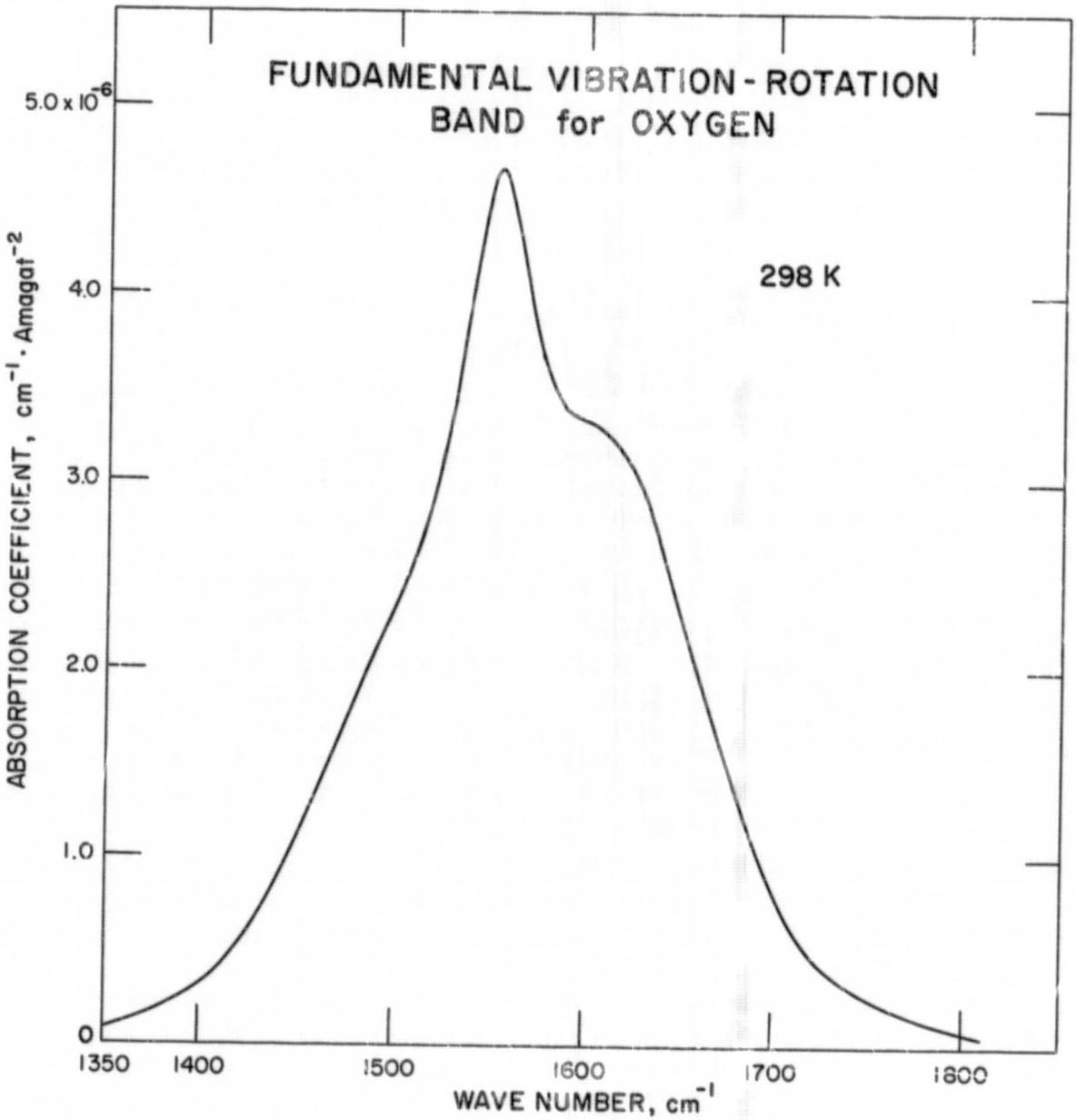
FUNDAMENTAL VIBRATION - ROTATION
BAND for OXYGEN
298 K
ABSORPTION COEFFICIENT, cm⁻¹ · Amagat⁻²
5.0 x 10⁻⁶
4.0
3.0
2.0
1.0
0
1350
1400
1500
1600
1700
1800
WAVE NUMBER, cm⁻¹

END OF REFERENCE

1

REFERENCE

2

BAILEY, B. M.; STERNER, C. J.; AND VIGNALE, V. J.: STUDY OF LIQUID OXYGEN CONTAMINATION, SUMMARY PROGRESS. REP. 4, AIR PRODUCTS AND CHEM., INC. (AD-253231), 1960.

THIS MATERIAL HAS BEEN APPROVED FOR PUBLICATION PER LETTER FROM KENNETH F. STERLING, AIR FORCE ROCKET PROPULSION LABORATORY TO JOANNE FOLK DATED AUG. 27, 1974.

STUDY OF LIQUID OXYGEN CONTAMINATION

Summary Progress Report No. 4

B. M. Bailey, C. J. Sterner, and V. J. Vignale

AIR PRODUCTS, INCORPORATED

Allentown, Pennsylvania

A. P. I. Research Project No. 03-9-2880

Contract No. AF 33(616)-6730

Project No. 3148

Task No. 30196

JULY 1960

Directorate of Rocket Propulsion

AIR FORCE FLIGHT TEST CENTER

AIR RESEARCH AND DEVELOPMENT COMMAND

UNITED STATES AIR FORCE

Edwards Air Force Base, California

ABSTRACT

This Summary Progress Report No. 4 presents a review of the work performed in accordance with Contract AF 33(616)-6730. The purpose of this study is to develop a better understanding of the physical-chemical and mechanical relationships involved and to develop realistic parameters for specification purposes for the applications of oxygen to missiles.

The significance, sources, and degree of contamination, and the current specifications for liquid oxygen and equipment are discussed. Recommendations for liquid oxygen specifications and for equipment operation are presented. An extensive bibliography is included, as well as appendices which amplify the general discussion.

APPENDIX I

GENERATION OF LIQUID OXYGEN

Composition of Feed

Air, the raw material for the production of liquid oxygen, consists of a mixture of 78.03 percent nitrogen, 20.99 percent oxygen, and 0.94 percent argon by volume. The remainder, approximately 0.04 percent, consists of various gases, vapors, and dust or particulate matter. Table VII presents a partial list of gases and vapors which may make up the remaining 0.04 percent or 400 ppm of the air feed to a liquid oxygen generator. This table indicates the magnitude of concentration of these gases and is based on composite values obtained from the literature (14 through 18). Table VIII presents the normal boiling and freezing points of compounds frequently present in the atmosphere and of compounds which may sometimes appear in the system.

Not every air separation plant feed contains all the materials listed nor in the concentrations shown in Tables VII and VIII. Naturally, some regions will contain certain contaminants while others will contain different contaminants. The air feed to a plant in a rural area would be expected to contain carbon dioxide, moisture and the rare gases, but only traces of hydrocarbons, organic compounds, ammonia and acidic gases. In locating an air plant, or at least the source of the air feed, particular consideration must be given to the possibility of combustible contaminants. In an industrial area, such as near a refinery, it is not unusual to find high concentrations of hydrocarbons. At a metallurgical site, acidic gases will be present. Other industrial sites would be expected to have their atmospheres contaminated from venting or spillage of volatile compounds which are used as raw materials, intermediates, and solvents.

Experience (38) has shown that, normally, one should expect air feed streams to obey the following general rules: the concentration of individual hydrocarbons will decrease as the number of carbon atoms in the molecule increases; methane concentration is frequently greater than the total concentration of all of the other hydrocarbons combined; concentrations of combustibles above 30 ppm are unusual.

Figure 9 is a flow diagram of one type of liquid oxygen-nitrogen plant process. Air from the atmosphere first passes through filters for the removal of

TABLE VII

SOME GASES AND VAPORS WHICH MAY BE PRESENT IN THE AIR FEED TO LIQUID OXYGEN GENERATORS*

(Concentrations in parts per million by volume)

Gas or Vapor	Composition of Literature Reported
Carbon Dioxide	200 to 500
Rare Gases:	
Helium	4 to 5
Neon	12 to 18
Krypton	1.1
Xenon	0.08
Hydrocarbons:	
Methane	5 to 38
Acetylene	0.001 to 30
Others	<1 to 100
Organic Compounds	1
Acidic Gases:	
Carbon Monoxide	1
Hydrogen Sulfide	1
Hydrogen Cyanide	1
Nitrogen Oxides	1
Ammonia	1

*References 14 through 18

TABLE VIII

PROPERTIES OF POSSIBLE INGREDIENTS OF AIR

Name	Normal Boiling Point °F	Freezing Point °F
Helium	-452.0	-455.8**
Hydrogen	-423.0	-434.5
Neon	-410.6	-415.6
Nitrogen	-320.4	-345.7
Carbon Monoxide	-310.0	-340.6
Argon	-302.3	-308.7
Oxygen	-297.3	-361.1
Methane	-258.7	-299.2
Krypton	-243.2	-249.9
Nitric Oxide	-241.2	-262.5
Ozone	-169.4	-313.8
Xenon	-160.8	-169.6
Ethylene	-155.0	-272.9
Ethane	-126.9	-277.6
Nitrous Oxide	-127.3	-152.3
Acetylene	-118.5*	-115.2
Carbon Dioxide	-109.3*	- 69.9 (5.2 atm)
Hydrogen Sulfide	- 79.2	-117.2
Carbonyl Sulfide	- 54.4	-216.4
Propylene	- 52.6	-301.4
Propane	- 43.9	-309.8
Ammonia	- 28.0	-107.9
Formaldehyde	- 5.8	-133.6
iso-Butane	10.4	-229.0
iso-Butylene	21.2	-220.5
1-Butene	23.0	-202.0
1, 3-Butadiene	26.7	-164
n-Butane	31.1	-211.0
2-Butene	33.8 (cis)	-218
Ethylene Oxide	51.3	-168.3
Acetaldehyde	69.8	-190.3
Nitrogen Dioxide	70.3 (d)	+ 15.3
n-Pentane	97.2	-204.7
Acetone	133.7	-139.0
Methanol	148.4	-144.0
Hexane	156.2	-137.7
Benzene	176.2	41.9
Water	212.0	32.0
n-Decane	345.2	- 23.8

*Sublimes
**Lambda point

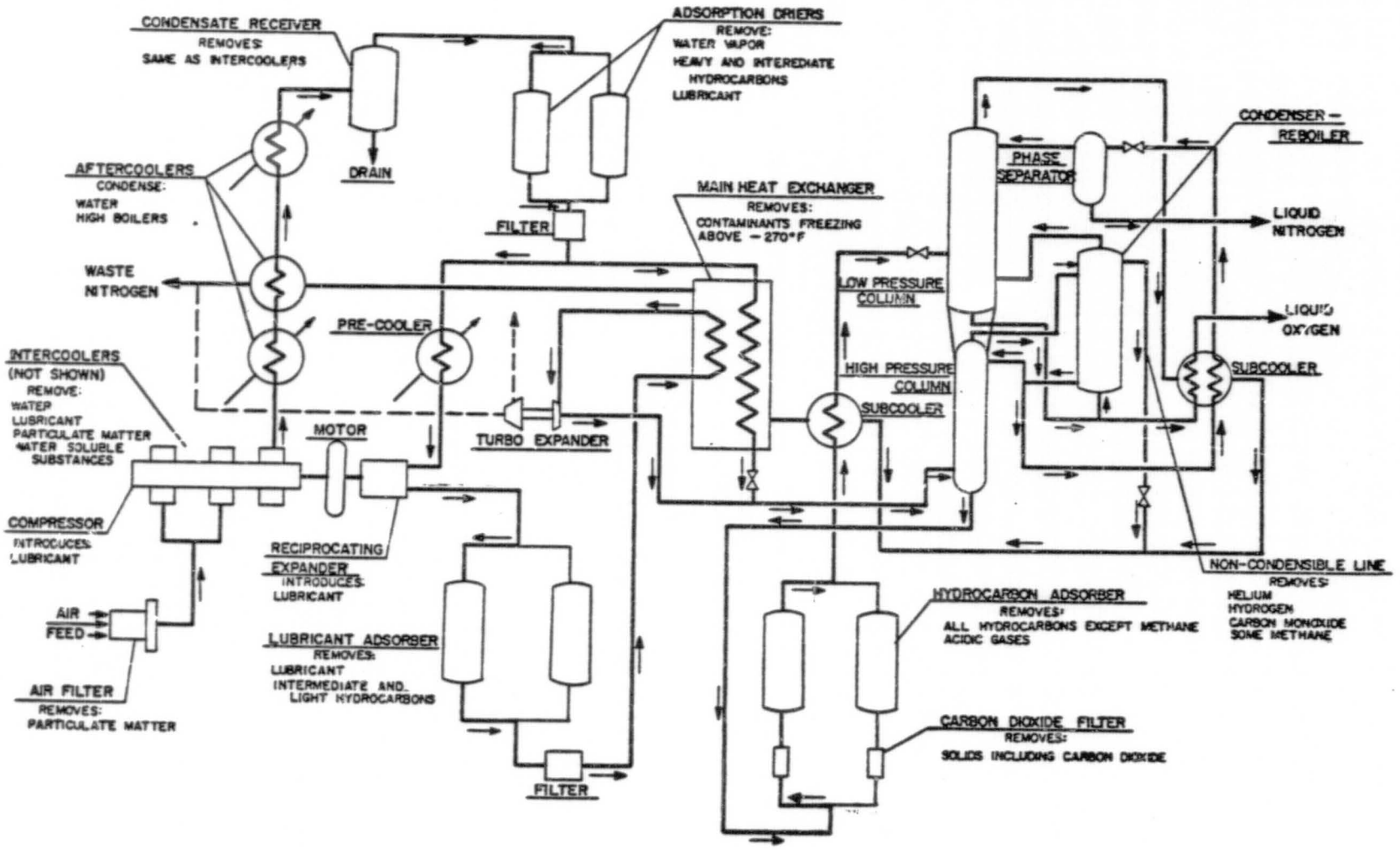

FIGURE 9 - FLOW DIAGRAM OF A LIQUID OXYGEN GENERATOR

particulate matter before undergoing compression. Lubricants used in the compressor will contaminate the air by entrainment of oil droplets. These lubricants may break down into lighter fractions which vaporize into the air stream. This source of contamination and the hazards associated with it are reduced by proper choice of lubricant and by designing the compressor to avoid high temperatures. Condensation of moisture in the compressor intercoolers and aftercoolers strips the air of substantial fractions of soluble substances, such as acetone and ammonia, as well as entrained lubricant and particulate matter which passed through the intake filter. The condensed moisture and oil accumulate in traps after each cooler and are drained from the system.

The compressed air passes through adsorption driers where heavy hydrocarbons and other organic compounds, including residual compressor lubricants, are removed along with the water vapor. These driers are effective also in reducing to a large degree the intermediate hydrocarbons, such as pentane and hexane.

The dried air is cooled to about -270°F by two different paths. The larger quantity of air passes through the main heat exchanger where most compounds having a freezing point above -270°F will freeze out onto the walls of the exchanger. During defrost, these solids will be vaporized and swept out of the exchanger into the atmosphere by waste nitrogen. Residual quantities of the frozen compounds, depending upon their solid vapor pressures at about -270°F, will remain in the air stream, such as carbon dioxide and acetylene.

A smaller quantity of dried air is cooled by expansion in a lubricated reciprocating expander followed by further expansion in a lubricated turbo-expander which uses an air-seal to prevent entry of lubricant into the main air stream. Between the two stages of expansion, the air passes through a lubricant separator and adsorber which removes the lubricant picked up in the reciprocating expander. Residual intermediate hydrocarbons and large portions of lighter hydrocarbons will be removed at the same time.

The air from the turbo-expander joins the air from the main heat exchanger before entering the high-pressure column. The air leaving the main heat exchanger is partially liquefied by undergoing Joule-Thomson expansion. Entering the high-pressure column with the air will be: the very low boiling gases such as helium and hydrogen; the compounds which have high vapor pressures at -270°F such as methane, nitric oxide and ozone; the compounds which are liquid at this temperature such as propane and propylene; and the entrained solids in the air stream. Of these, the more volatile compounds and some carbon monoxide and argon will leave the high-pressure column with the nitrogen. The remainder will leave with the oxygen-enriched air.

The enriched air is passed through carbon dioxide filters and hydrocarbon adsorbers for final cleanup. Theoretically, besides nitrogen and argon, only a portion of the carbon monoxide and methane should be left in the feed to the low-pressure column. The carbon monoxide and a portion of the argon should leave the low-pressure column with the nitrogen overhead and the remainder with the pure liquid oxygen at the bottom.

It is possible, especially in industrial areas, for contaminants in the air feed to increase unexpectedly. At such times, the hydrocarbon adsorbers in the liquid feed to the low-pressure column may become overloaded and breakthrough may occur, particularly if this stream is not monitored. In the event of breakthrough, the lower hydrocarbons, methane, ethane, and ethylene, will be displaced on the adsorbers by the higher hydrocarbons such as propane, propylene and butane.

A typical analysis of the liquid oxygen from such a plant operating in a relatively clean atmosphere is approximately as following:

Carbon Dioxide	1 to 2 ppm
Acetylene	0.05 ppm
Total Hydrocarbons	5 to 10 ppm, occasionally 30 ppm

APPENDIX II

LIMITS FOR FLAMMABLE CONTAMINANTS

1. Flammability Limits

For a mixture to be flammable, that is, to support its own combustion without external aid, several conditions must exist (20, 21). Proper quantities of fuel and oxidant must be present as well as a source of ignition. If any one of these is absent, inflammation cannot take place. An exception to this rule is the decomposition under certain conditions of some chemicals which have negative heats of formation - acetylene, silver acetylide, ozone, and others - without the need of any agent. These materials are hazardous by themselves and play a part in ignition. Hazardous conditions, in general, are avoided by preventing the simultaneous appearance of all three factors -- fuel, oxidant, ignitor. This philosophy of control is one generally practiced by industry.

In the case of liquid oxygen, obviously, the oxygen serves as the potential oxidizer and cannot be eliminated. Not all sources of ignition are known, so positive control of the mechanism of ignition is difficult. Control of the fuel remains as the safest means of avoiding a hazardous condition. However, the avoidance of fuels does not necessarily mean that ignition sources or initiators are to be ignored.

Much is known about flammable limits of gases in air (20), and the underlying theory of combustion has been studied extensively (21). Data on combustible limits in gaseous oxygen, although not as complete as in air, are also available. However, data on combustible limits in liquid oxygen are very meager, although this is not as great a handicap as it might seem. Further discussion will show that safe generalizations may be used as guides for combustible limits with liquid oxygen.

Table IX presents the lower flammability limits for various gases in both air and oxygen at ambient temperature and atmospheric pressure. It can be seen that the limits for all of the gases listed are practically the same for both cases, indicating that the limits are set by the concentration of fuel, providing sufficient oxygen is present. On this evidence, it may be presumed that flammability data obtained with air may be used as if it were obtained with gaseous oxygen. It is also interesting to note that,

TABLE IX

LOWER FLAMMABILITY LIMITS OF COMBUSTIBLES

Gas	Air*	Oxygen (Gas) *	Oxygen (Liquid)**
Hydrogen	4.0	4.0	----
Methane	5.0	5.1	11.0
Ethane	3.0	3.0	4.0
Propane	2.2	2.3	----
Butane	1.9	1.8	----
iso-Butane	1.8	1.8	----
Ethylene	2.7	3.0	----
Propylene	2.0	2.1	----
Butene-1	1.6	1.8	----
Butene-2	1.8	1.7	----
i-Butylene	1.8	---	----
Carbon Monoxide	12.5	15.5	----

All values are given in mole percent (not methane equivalent).

* Reference (20), ambient temperature, atmospheric pressure.
** Reference (22), -297°F, atmospheric pressure.

on a methane equivalent basis, flammability limits for the hydrocarbons are all approximately the same.

Experimental results (22, 23) for the lower flammability limits of methane and ethane in liquid oxygen are also presented in Table IX. Comparing flammability limits in liquid oxygen versus flammability limits in gaseous oxygen, it may be predicted that, in general, more fuel will be needed with liquid oxygen than with warm gaseous oxygen. This prediction is supported by a consideration of the requirements of combustion. For combustion to be self-supporting, sufficient energy must be produced by the burning portion to raise the adjacent mass to kindling temperature. If liquid oxygen is used in place of gaseous oxygen, additional heat is required both to vaporize the oxygen and fuel and to warm the vapors to ambient temperature. This additional heat can only come from additional fuel. This, it may be assumed that, where experimental flammability data is lacking for liquid oxygen, an additional margin of safety is supplied by using data obtained with air or gaseous oxygen.

2. Solubility

In the above discussion of flammability limits, it was assumed that the mixtures of fuel and oxygen were homogeneous. However, in actual circumstances it is unlikely that concentrations of hydrocarbons would be permitted to approach the flammability limit. Table X presents the solubilities of the various hydrocarbons in liquid oxygen compared with their lower flammability limits. Solubility as a function of temperature is presented for the saturated hydrocarbons in Figure 10 and for the unsaturated hydrocarbons in Figure 11. It can be seen that, except for methane, ethane, and propane, the solubility limit is reached well below the flammability limit. As was mentioned in the Discussion (Section A, Subsection 2, Combustible Contaminants), concentrations above the solubility limit are as hazardous as concentrations above the flammability limit. This means that hazard tolerance should be based on solubility limits instead of flammability limits.

Although solubility is generally thought of as equilibrium between solid and liquid phases, it can also be considered to be equilibrium between immiscible liquid phases. Ethane, propane, ethylene, and propylene are all reported (22, 24, 25) to form conjugate phases with liquid oxygen. In the cases of ethylene and propylene, the formation of a second, fuel-rich, liquid must be considered in the same category as the formation of

TABLE X

SOLUBILITY OF HYDROCARBONS IN LIQUID OXYGEN
Parts Per Million by Mole

Gas	Solubility* at -297.3°F (Methane Equivalent)	Lower Flammability Limit (Methane Equivalent)
Methane	980,000	50,000
Ethane	430,000	60,000
Propane	150,000	63,600
Ethylene	55,000	55,000
Propylene	20,100	60,000
i-Butane	7,640	72,000
Butene-1	4,000	64,000
n-Butane	3,440	74,400
i-Butylene	530	72,000
Acetylene	10	50,000

* Reference 24

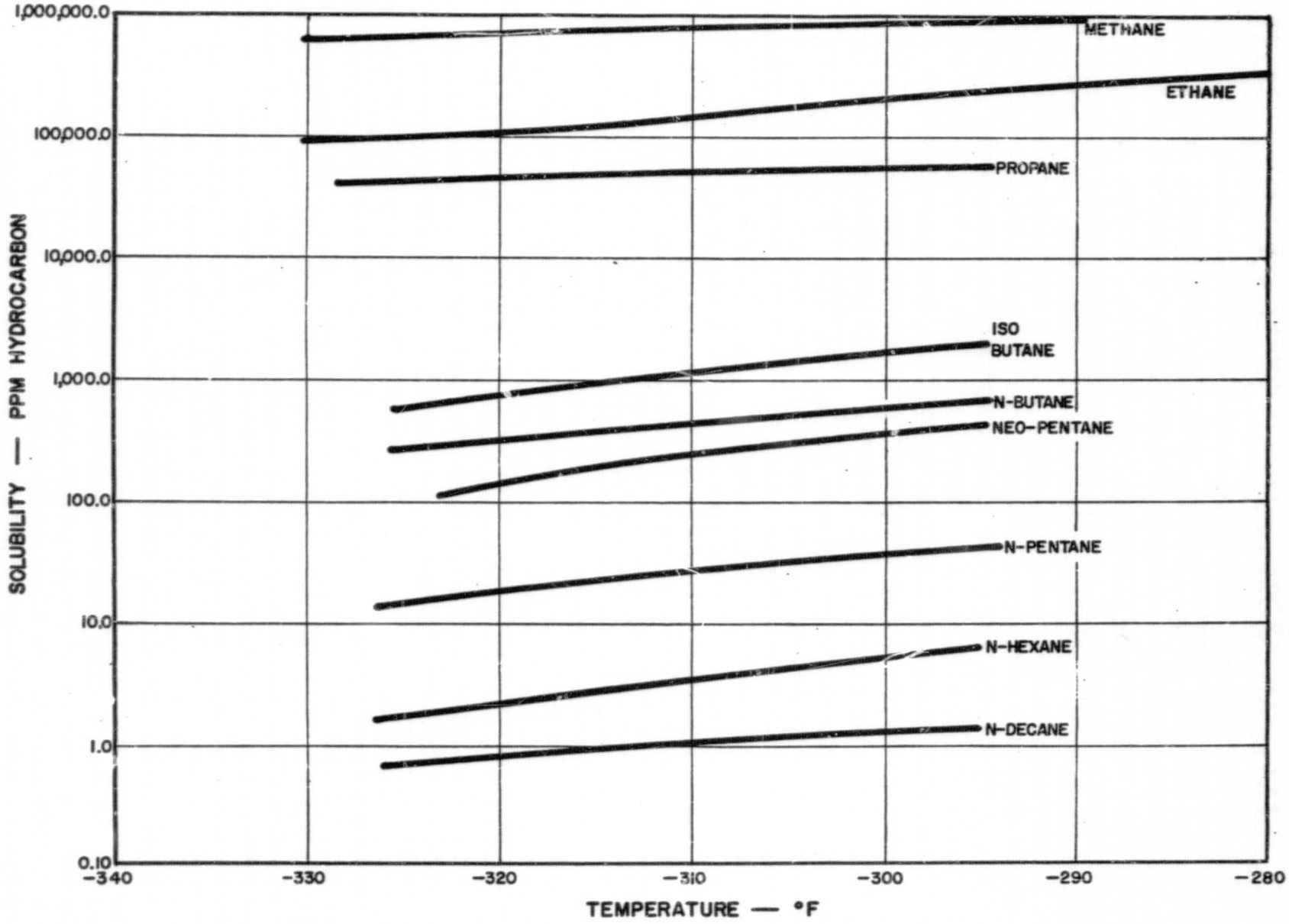

FIGURE 10 - SOLUBILITY OF SATURATED HYDROCARBONS IN LIQUID OXYGEN (24)

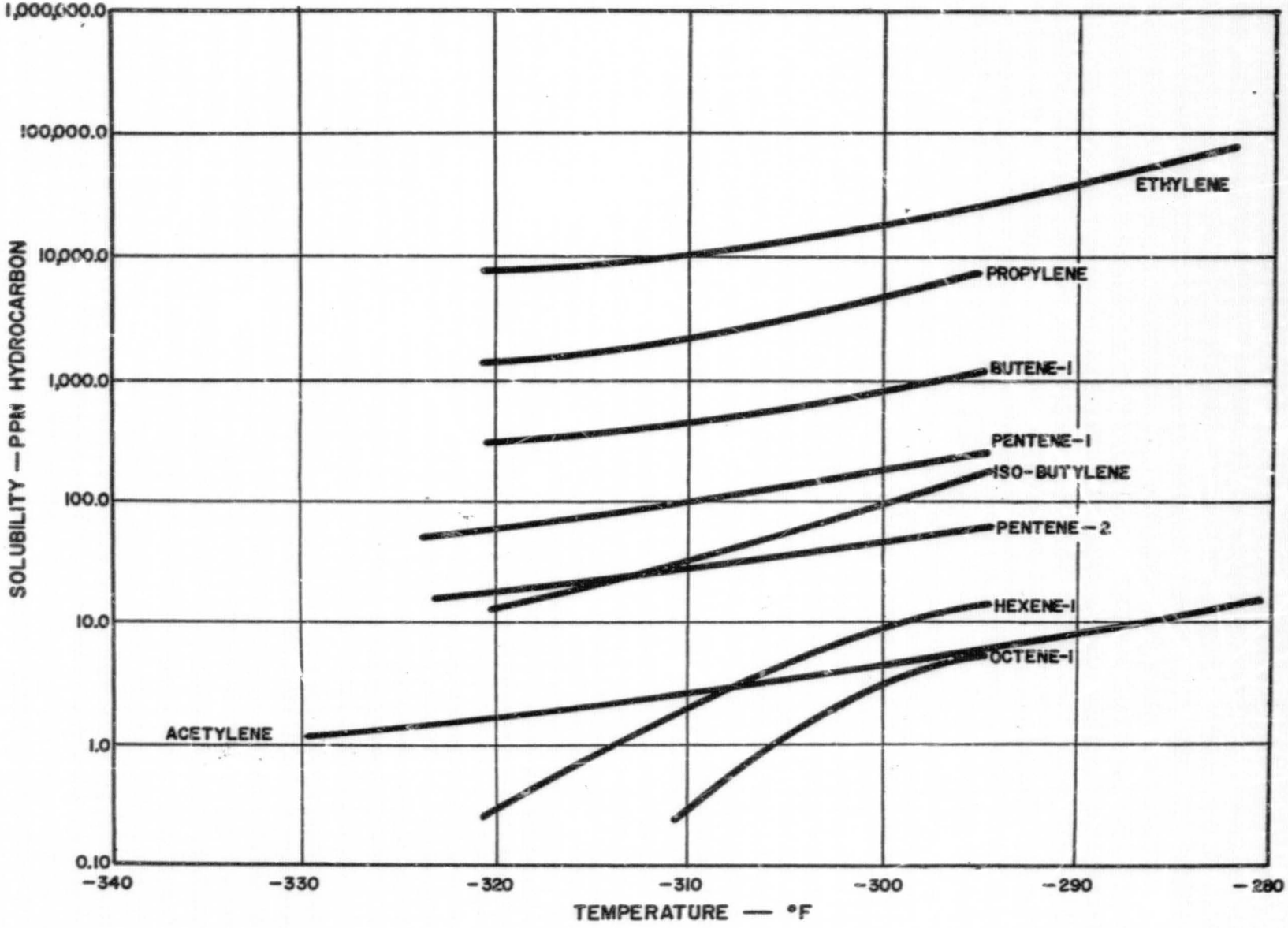

FIGURE 11 - SOLUBILITY OF UNSATURATED HYDROCARBONS IN LIQUID OXYGEN (24)

a solid phase, and with the same degree of hazard. The concentration of hydrocarbon in the oxygen rich phase would be termed the solubility. Considerable data on solubilities of combustibles in liquid oxygen are available in the literature (7, 8, 21, 22, 24, 25, 26, 27, 28, 29, 30, 31, 32).

3. Initiators

An initiator is defined as an energy source of such a magnitude and intensity that a fuel-oxidant reaction can occur providing the fuel-oxidant mixture concentration is within the flammability region. Initiators can be chemical, thermal, electrical, and mechanical in nature. The intensity of the energy source refers to the energy (or temperature) level, and magnitude refers to the total quantity of energy released as kindling. The potential chemical initiators, ozone, and the nitrogen oxides are discussed at length below. A discussion of thermal initiators such as electric matches, blasting caps, external heat, and thermite bombs is beyond the scope of this project. Electrical initiators such as static electricity discharge, which is generated within the liquid oxygen handling system, are a part of this project and will be studied under Supplement No. 1 of this project. Mechanical initiators such as adiabatic bubble compression, fluid friction of high velocity solid particles, mechanical friction of valves, and pump bearings and shock waves induced by 'water hammer' are a part of this project and will be studied under Supplement No. 1 of this project.

Ozone has been shown experimentally to react with unsaturated hydrocarbons at liquid oxygen temperatures and to increase the ignition sensitivity of liquid oxygen-fuel mixtures in the flammable region, that is, the energy level for ignition is reduced (27). Flammable mixtures of liquid oxygen-fuel have been ignited by ozone (22, 27, 29, 34, 35). Explosive reactions between ozone and nitrogen trioxide or tetroxide at temperatures well above -297°F (36) and explosive decomposition of ozone itself at -150°F (37) have been reported. In all experimental work, relatively large quantities of ozone were used. However, despite the evidence of its ability to initiate combustion, there is no reported evidence in the literature of the presence of ozone in liquid oxygen. One team of investigators report the possibility of trace quantities (30).

Experiments with nitric oxide and nitrogen dioxide show that neither react with unsaturated hydrocarbons at -297°F and that they do not increase the ignition sensitivity (in some cases, even lowering the sensitivity) of flammable liquid oxygen-hydrocarbon mixtures (27). If ozone (at least more than 200 ppm ozone for mixtures studied) is introduced into flammable liquid oxygen-unsaturated hydrocarbon mixtures containing nitrogen dioxide,

the ignition sensitivity is increased to a greater extent than that due to ozone alone (27). Nitrogen dioxide added to a liquid oxygen-ethane mixture just below the lower-flammable-limit concentration had no effect on the limit (22). Nitric oxide reacts with oxygen at temperatures slightly above -297°F and very violently at -265°F (36).

Experiments with gaseous nitrous or nitric oxides have shown them to be flammable but no ignition occurred when each solid oxide was slurried in liquid oxygen (22). Cocrystals of nitrous oxide and acetylene containing more than 25 mol percent of the latter were observed experimentally to have the same ignition sensitivity in liquid oxygen as acetylene (39).

Data on the presence of initiators and sensitizers in liquid oxygen and knowledge of their effects are meager. The safest course appears to be the avoidance of flammable liquid oxygen-fuel mixtures and the prevention of the occurrance of chemical, thermal, and mechanical initiators. The former results in the ineffectiveness of the initiator by removing the fuel and the latter reduces the possibility of occurance of initiation which experimental data have shown to be hazardous.

APPENDIX III

ADSORPTION REPURIFICATION OF LIQUID OXYGEN

Since low-temperature adsorption-purifiers are already used in air-separation plants to remove hydrocarbon contaminants and carbon dioxide, adsorptive purifiers can be designed for stored liquid oxygen based on this experience. The difference between the purification of stored liquid oxygen and purification in an air-separation plant lies in the different temperatures used for the process. The hydrocarbon adsorbers in a generating plant normally operate at about -280°F and 75 psia whereas adsorbers purifying stored liquid oxygen would operate at about -297°F and slightly above atmospheric pressure. The effect of temperature on adsorber capacity has not been completely established, but it may be particularly important for the components with low solubilities which are of interest.

Available data show that the adsorptive capacity for contaminants decreases moderately with a decrease in inlet concentration. Since the concentrations to be handled in launch-site storage are lower than the concentrations dealt with in air plants, the concentration difference must also be considered in adsorber design. Although conservative criteria may be used for the safe design of adsorptive repurification systems, it is desirable to obtain more quantitative data on adsorbent characteristics before establishing final designs.

Since the build-up of contamination in stored liquid oxygen is generally a gradual process, it would not be economically desirable to build individual repurification units which would be idle much of the time. Instead, a central unit might be used to service, in rotation, a number of storage tanks through long-distance lines, or, alternatively, a mobile unit could be designed to service tanks periodically, as required.

Repurification Rate

The purification rate of a recirculation-adsorber depend primarily upon the size of the circulation pump and the extent of mixing in the storage tanks. During repurification through an external adsorber the liquid oxygen would be subject to additional heat influx due to the adsorption operation. Liquid-nitrogen refrigeration could be used to recondense any boil-off resulting from such heating.

In the simplified analysis of repurification rates which follows, liquid-nitrogen recondensation of the boil-off oxygen is assumed. (The amount of liquid nitrogen

required would be small.) In addition, it is assumed that the circulating oxygen leaves the adsorber completely free of contamination, although it is recognized that this is true only for a perfect absorbent.

The following simplified models are considered in evaluating the probable repurification rate:

1. Complete By-Passing

If the positions of the inlet and outlet lines leading to and from the repurification system are close to each other in the storage tank, it is possible that complete by-passing will occur. Liquid oxygen flowing to the adsorber will have been already purified and essentially no purification will take place after an initial active volume has been circulated through the purifier. The positions of the inlet and outlet lines in the storage tank, therefore, must be arranged to promote thorough mixing of the contents. (Refer to Figure 3, Page 13, and Section II, Part C, Paragraph 1, Change in Contaminant Concentration, Page 11.)

2. Complete Mixing

For the case of complete mixing, the concentration of contaminant will decrease according to the equation:

$$-\frac{dC}{dt} = kC \qquad \text{(III-1)}$$

where

C = concentration of contaminant in liquid oxygen.

t = time after start of purification, hours.

k = purification coefficient (capacity of pump per hour divided by storage tank capacity).

The integrated form of this equation yields the new concentration, C, of the impurity in question:

$$\ln \frac{C_o}{C} = kt \qquad \text{(III-2)}$$

where

C_o = initial concentration of contaminant.

The "half-life" of the purification system, i.e., the time required to reduce the contaminant concentration by a factor of two is:

$$t_{1/2} = \frac{0.694}{k} \qquad \text{(III-3)}$$

Thus a tank containing 24,000 gallons and connected to an external repurifier circulating liquid oxygen at a rate of 100 gpm will have a "half-life" of:

$$t_{1/2} = 2.78 \text{ hours}$$

3. Plug Flow

In the case of plug flow, the time to remove all the contaminant is proportional to the volume of liquid in the vessel divided by the pump rate. For a 24,000 gallon tank and 100 gpm pump, the liquid will be completely purified in 240 minutes, or 4 hours. This, of course, is for ideal conditions and will not happen except when pumping the entire contents from one tank to another. Interestingly, the "half-life" for plug flow is not much less than that for complete mixing, i.e., concentration decreases linearly with time:

$$t_{1/2} = \frac{0.5}{k} \qquad \text{(III-4)}$$

For the example cited, the "half-life" would be 2.00 hours as compared to 2.78 hours for complete mixing.

4. Actual Flow

Actual recirculation-flow will be a mixture of the three possible flow conditions with the decrease in contaminant concentration being somewhere between the rates for the two extreme cases of flow, i.e., plug flow and complete by-passing. In launch-site storage-tanks equipped with inlet and outlet piping arrangements such as illustrated previously in Figure 3(b), the flow pattern should be more favorable to rapid repurification; the rate of decrease in contaminant concentration could be expected to be closer to that for plug flow and complete mixing than for complete by-passing.

END OF REFERENCE

2

REFERENCE

3

McKINLEY, C.; AND HIMMELBERGER, F.: THE ROLE OF AIR CONTAMINANTS IN FORMULATING OXYGEN PLANT SAFETY PRINCIPLES. CHEM. ENG. PROG., VOL. 53, NO. 3, MAR. 1957.

THIS REFERENCE IS MATERIAL THAT IS READILY AVAILABLE AND THEREFORE THE CONTENTS HAVE NOT BEEN REPRODUCED.

END OF REFERENCE

3

REFERENCE

4

CARLSON, G. A.: SPHERICAL DETONATIONS IN GAS-OXYGEN MIXTURES. COMBUSTION AND FLAME, VOL. 21, NO. 3, DEC. 1973.

COURTESY OF COMBUSTION AND FLAME JOURNAL

COMBUSTION AND FLAME 21, 383–385 (1973)

Spherical Detonations in Gas-Oxygen Mixtures*

G. A. CARLSON

Applied Material Science Division 5323, Sandia Laborntories, Albuquerque, NM 87115

Studies of the spherical detonation of a variety of gases with oxygen are reported. Detonability limits for 15 gas-oxygen mixtures in a 20-cm-i.d. sphere have been determined, using small high explosive detonators to initiate detonation. The minimum energy for initiation of detonation in 14 stoichiometric gas-oxygen mixtures has been determined, using exploding wires to initiate detonation.

Flammability limits have been determined for a wide variety of gases in air and oxygen. Detonability limits, on the other hand, have been established for relatively few gases [1–8]. We report here detonability limits and minimum energies for initiation of detonation for a number of gases in oxygen.

The gas mixtures were detonated within a 20-cm-i.d. spherical vessel consisting of two 1.9-cm-wall stainless steel 304L flanged hemispheres bolted together and sealed with an O-ring (see Fig. 1). Gases were introduced into the sphere tangent to the wall, resulting in a swirling, mixing action. A high explosive detonator or an exploding wire, positioned in the center of the sphere, was used to initiate detonation of the gas mixture. A calibrated piezoelectric transducer (Susquehanna ST-4, 0-700 bars), was used to monitor the resulting pressure waves at the vessel wall.

Detonators containing about 400 J of stored chemical energy were used in the measurement of detonability limits. Exploding wires were used to determine minimum initiation energies for detonation of near-stoichiometric mixtures. Capacitively stored energies from 0.11 to 12.5 J (0.025 to 1 μF at 3 to 5 kV) were discharged through 0.71-cm-long uncoated copper wires, ranging in diameter from 1.27×10^{-3} to 1.15×10^{-2} cm. Absorption of electrical energy by the exploding wires was determined from the current and voltage across the wires to be completed within 0.2 μsec. Energy transfer into the exploding wires was calculated to be about 50%, judging from the resulting shock wave intensity [9].

Upper and lower detonability limits were determined for 15 gases in oxygen. In all experiments, detonation was differentiated from combustion by the appearance of the pressure waves recorded at the vessel wall. Detonation resulted in a well-defined shock front traveling at supersonic velocity, while combustion always proceeded at subsonic velocities and was not accompanied by a well-defined shock wave. Figure 2 shows pressure records for ethylene-oxygen mixtures run slightly below and slightly above the lower detonability limit. In Fig. 2a, below the detonability limit, only the shock wave attributable to the high explosive detonator is observed. A pressure increase due to combustion was only observed in records taken at slower sweep speeds. The duration of the combustion reaction was about 900 μsec. In contrast, at a slightly higher ethylene concentration, detonation occurs. In Fig. 2b, a sharp spike at 48 μsec marks the arrival of a well-defined gas detona-

*This work was supported by the United States Atomic Energy Commission.

Copyright © 1973 by The Combustion Institute
Published by American Elsevier Publishing Company, Inc.

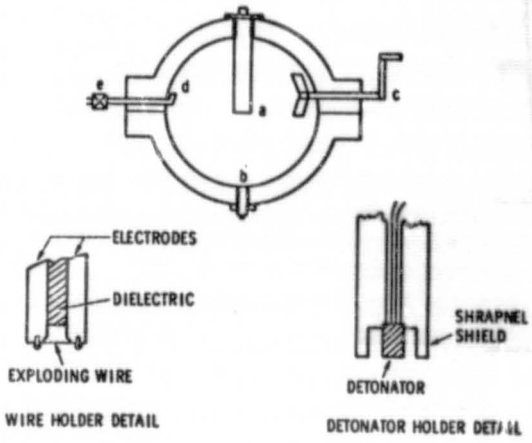

Fig. 1. Spherical reaction vessel used for gas detonation studies. (a) detonator or wire holder (see detail drawings); (b) pressure transducer; (c) gas mixer; (d) tangential gas inlet; (e) valve connection to vacuum manifold.

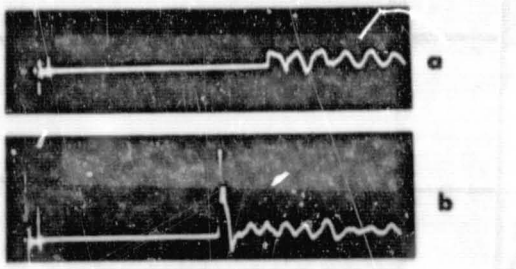

Fig. 2. Pressure records of detonability limits experiments. Trace a, 9.0% ethylene in oxygen at 760 Torr; Trace b, 9.5% ethylene in oxygen at 760 Torr. Both traces, 156 bars/div. 10 μsec/div.

tion wave. The shock wave velocity of 2100 m/sec, determined from the arrival time, compares favorably with gas detonation wave velocities reported for ethylene-methane-oxygen mixtures [1]. The results of the detonability limits study are given in Table 1.

TABLE 1
Detonability Limits of Gas-Oxygen Mixtures, Determined Using a 400 J High Explosive Detonator for Initiation

Gas	Lower Detonability Limit[a] (Volume % gas)	Upper Detonability Limit[b] (Volume % gas)
Acetaldehyde	12 –14	46–50
Acetylene	6.5– 7	67–69
Carbon disulfide	12 –13	> 46[c]
Cyclopropane	6.5– 7	38–40
Diethyl ether	4.5– 5	28–30
Ethane	10 –12	38–40
Ethylene	9 – 9.5	50–52
Ethylene oxide	8 – 9	64–66
Ethyl nitrite	4 – 4.5	58–62
Methylacetylene	5.5– 6	48–50
Methyl vinyl ether	5 – 5.5	44–46
Propadiene	5 – 5.5	48–50
Propane	6.5– 7.5	30–32
Propylene	6.5– 7	36–38
Vinyl fluoride	11 –12	54–56

[a] Detonation was observed at the higher gas concentration, but was not observed at the lower gas concentration.
[b] Detonation was observed at the lower gas concentration, but was not observed at the higher concentration.
[c] Experiments at higher gas concentration not possible due to vapor pressure limitations.

TABLE 2
Minimum Initiation Energy for Detonation of Gas-Oxygen Mixtures Using Exploding Wire Initiation

Gas	Gas Concentration (Volume %)	Minimum[a] Initiation Energy (Joules)
Acetylene	40	< 0.11
Ethyl nitrite	31	0.31
Propadiene	28.6	0.31
Methylacetylene	28.6	0.31
Ethylene oxide	40	0.31
Methyl vinyl ether	28.6	0.62
Cyclopropane	25	0.62
Ethylene	33	0.62
Vinyl fluoride	40	0.88
Propylene	25	1.25
Diethyl ether	20	2.5
Propane	22.2	2.5
Ethane	28.6	8.75
Acetaldehyde	40	12.5

[a]Capacitively stored energy, determined as $CV^2/2$. The actual energy expended in the shock wave from the exploding wire is about 50% of the stored energy [9].

The minimum energy required for initiation of detonation was determined for intermediate compositions of each gas mixture investigated. The mixtures chosen for study contained somewhat less oxygen than stoichiometric mixtures, since earlier detonation studies by Litchfield [6–8] indicated that such mixtures were more sensitive to detonation initiation. This is probably due to the importance of CO as a reaction product in detonation reactions, as is indicated by thermodynamic calculations.

The results of the study of minimum energies for initiation of detonation are shown in Table 2. In general, these energies are somewhat lower than previous investigators have found [1, 4, 6, 7, 8]. However, it has been demonstrated [10] that different methods of initiating detonation (i.e., spark, exploding wire, laser pulse), as well as different experimental geometries, can have a substantial effect on the minimum energy for initiation of detonation. Thus, the present results should be interpreted as establishing the order of difficulty of initiating detonation in the gases studied, rather than the absolute magnitude of the initiation energy.

References

1. Manson, N., and Ferrie, F., *Fourth Symposium (International) on Combustion*, Williams and Wilkins, Baltimore (1953) p. 486.
2. Kogarko, S. M., Adushkin, V. V., and Lyamin, A. G., *Comb., Expl. and Shock Waves* 1, 15 (1965).
3. Zel'dovich, I. B., Kogarko, S. M., and Simonov, N. N., *Sov. Phys.–Tech. Phys.* 1 1689 (1956).
4. Freiwald, H., and Koch, H. W., *Ninth Symposium (International) on Combustion*, Academic Press, New York (1963) p. 275.
5. Maček, A., *AIAA J.* 1, 1915 (1963).
6. Litchfield, E. L., Hay, M. H., and Forshey, D. R., *Ninth Symposium (International) on Combustion*, Academic Press, New York (1963), p. 282.
7. Litchfield, E. L., and Hay, M. H., Detonation initiation in alkane-oxygen mixtures, BuMines Rpt. No. 6840 (1966).
8. Litchfield, E. L., Hay, M. H., and Cohen, D. J., Initiation of Spherical Detonation in Acetylene-Oxygen Mixtures, BuMines Report No. 7061 (1967).
9. Carlson, G. A., *J. App. Phys.* 42, 2155 (1971).
10. Bach, G. G., Knystautas, R., and Lee, J. H., *Thirteenth Symposium (International) on Combustion*, The Combustion Institute, Pittsburgh, Pennsylvania, (1971) p. 1097.

(Received December 11, 1972; revised June 22, 1973)

END OF REFERENCE

4

Card #2

REFERENCE

5

CONTAMINATION CONTROL HANDBOOK. NASA SP-5076, 1969.

NASA SP-5076

TECHNOLOGY UTILIZATION

COPY 2

CONTAMINATION CONTROL HANDBOOK

LEWIS RESEARCH CENTER
Aerospace Safety Research
and Data Institute

NATIONAL AERONAUTICS AND SPACE ADMINISTRATION

NASA SP-5076

CONTAMINATION CONTROL HANDBOOK

Prepared by Sandia Laboratories
under NASA Order Number H-13245A
for Marshall Space Flight Center

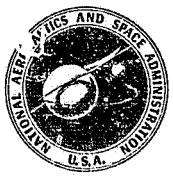

Technology Utilization Division
OFFICE OF TECHNOLOGY UTILIZATION 1969
NATIONAL AERONAUTICS AND SPACE ADMINISTRATION
Washington, D.C.

FOREWORD

Rigid control of contamination has contributed to the reliability and precision of vehicles and instruments sent out to explore space. Experience gained in the aerospace community also can be helpful in the pharmaceutical, electronic, and many other industries in which extreme cleanliness is important. This is one of three Special Publications issued by the NASA Office of Technology Utilization to help extend and diffuse current concepts and techniques of rigorous contamination control.

The first of these documents, Contamination Control Principles, SP-5045, was issued in 1967 when a NASA Contamination Control Panel called attention to the widespread need for guideline information. The George C. Marshall Space Flight Center, the Manned Spacecraft Center, and the John F. Kennedy Space Center were represented on that panel by, respectively, Frederick J. Beyerle, Quintin T. Ussery, and Dr. John Gayle. Since then a number of special courses for technicians and supervisors employed in clean rooms have been given, and the lectures prepared by James W. Useller for one of those courses at the Lewis Research Center have been published in Clean Room Technology, SP-5074.

This handbook deals in more detail with many of the same matters discussed in SP-5045 and SP-5074. It was prepared for the George C. Marshall Space Flight Center under the direction of H. D. Sivinski, Manager of the Planetary Quarantine Department at the Sandia Laboratories and one of the authors of Contamination Control Principles. He was assisted in this work by a team that included D. M. Garst, K. F. Lindell, W. J. Whitfield, and J. A. Paulhamus and their associates at the Sandia Laboratories; Dr. John Beakley and L. Hughes of the University of New Mexico, and Mrs. Dorothee Drury, technical editor.

The authors' purpose was to assemble in one volume the information and data most likely to be of practical help to persons engaged in contamination control in industrial and related operations. Although commercial names have been used, mention of them does not constitute endorsement by the authors or any Government agency. The group responsible for this work drew on many sources of information and has included matters about which there may still be controversy, but the information presented has been verified to the extent believed practical.

Ronald J. Philips, Director
Technology Utilization Division
Office of Technology Utilization

SECTION 4

CONTAMINATION CONTROL IN GASES AND LIQUIDS

Controlling contamination in gases and liquids requires methods applicable to the type and quantity of contaminants and the cleanliness level required for a particular application. Gases and liquids may be grouped according to their two major uses:

a. As part of a system, such as hydraulic fluids and actuating or control gases, fuels, coolants, lubricants, and refrigerants.

b. In processing and in support of system operations such as cleaning solvents, flush gases and liquids, cutting oils, and lubricants.

When used as part of a system, the gas or liquid may be recycled or reused often. In such cases, methods for controlling contamination with capabilities for monitoring or verifying the cleanliness level may be designed as part of the system.

Specifications for procurement of gases and liquids should include the required purity level and tolerable concentrations of specific impurities.

Contamination controls should include methods of verifying the purity levels prior to use and monitoring the cleanliness levels periodically during use, to assure that acceptable levels are being maintained.

The storage, transportation, handling, and transfer of gases and liquids should not contribute to their contamination. These operations require well-defined control techniques and practices to maintain the required purity levels.

4.1 Contaminants in Gases

Gases discussed herein are those defined by the U.S. Interstate Commerce Commission as "Compressed or Liquefied" in the interest of safe handling and transportation in interstate commerce. These gases are segregated into the following major groups, as they differ in physical state when contained.

Nonliquefied gases are those which do not liquefy in containers at normal temperatures and under pressures up to 2000 to 2500 psig, normally attained in commercially used containers. However, these gases will liquefy at cryogenic temperatures (approximate range from -200° to -459°F).

Liquefied gases are those which do become liquids, to a very large extent, in containers at or near normal temperatures and under pressures ranging from 25 to 2500 psig, normally attained in commercially used containers.

4.1.1 Description of Gases

Pertinent information on each of the compressed gases is essential to the effective application of a specific gas as part of a system or in processing and in support of system activities. General information is available from the gas producer or distributor. More detailed information is contained in much of the open literature (see Paragraph 4.3, Bibliography). Essential information is provided below:

a. Physical properties include boiling points, critical temperatures and pressures, specific heat, density, and other data for each gas. Table 4-1 lists some of the common gases and their properties. The data given generally represent the properties of a pure gas. Therefore, the values of certain of these properties will vary somewhat with various purity levels. It should also be noted that the factors used in expressing values of properties will vary depending on the source of the data.

b. Formulation includes elements of gas mixtures and impurities, with concentrations of each gaseous element, water, oil, and particulates in each available grade.

c. Materials of construction which are suitable or not suitable for containment of the gas as related to pressure, temperature, and corrosive limitations.

d. Physiological effects are odor, toxicity, threshold limit values, contact irritation to skin, eyes, etc.

e. Precautions in handling and storage include containers, safety devices, temperatures, flammability, etc.

f. Marking and identification of containers include methods of marking, type of data marked on containers, and color marking. These methods may vary with the different producers.

4.1.2 Purity Levels and Grades

Minimum purity levels of gases are normally defined by percent by volume. Maximum impurities are defined by parts per million by volume. Factors for interconversion of the various concentration units are shown in Table 4-2.

Analysis of individual impurities may be automatically supplied with the higher purity grades or may be available on request from the producer.

Terms or nomenclature used by the compressed gas industry to define grades of gases relative to the purity levels vary widely among producers, and often between gases from one producer. A grade term defining a purity level for one gas may define a different purity level for another. Therefore, a single grade term defines a purity

TABLE 4-1

Low Temperature Physical Properties of Gases

Name	Formula	Molecular Weight	Normal Boiling Point			Critical Point		Triple Point or (Melting Point)		Specific Heat Cp @ 70°F, 14.7 PSIA	Gas Density @70°F 14.7 PSIA
			Temp. °F.	Liquid Density lb./cu. ft.	Latent Heat BTU/ lb.-mole	Temp. °F.	Pressure PSIA	Temp. °F.	Pressure PSIA	BTU/ (lb. mole) (°F)	lb./cu. ft.
Acetylene	C_2H_2	26.04	—119.2 (3)	38.7 (3)	9180 (3)	96.0	906	—114.6	17.4	10.6	0.0680
Air (1)	(2)	28.96	—317.9	54.56	2556					7.0	0.07493
Ammonia	NH_3	17.03	— 28.1	42.6	10037	270.3	1639	—108.0	$8.8x10^{-1}$	8.6	0.0445
Argon (1)	A	39.95	—302.6	86.98	2804	—187.6	705	—308.9	9.99	4.98	0.1034
Carbon Dioxide	CO_2	44.01	—109.3 (3)	97.5 (3)	10854 (3)	87.9	1071	— 69.9	75.1	8.95	0.1144
Carbon Monoxide	CO	28.01	—311.9	49.3	2597	—220.4	508	—337.1	2.23	6.97	0.0725
Carbonyl Sulfide	COS	60.07	— 58.3	73.0	7961	221.0	896	(—217.8)		9.92	0.1521
Chlorine	Cl_2	70.91	— 29.3	97.4	8780	291.2	1118	—149.8	$2.02x10^{-1}$	8.2	0.1853
Deuterium	D_2	4.03	—417.3	10.7	540	—390.8	239	—426.0	2.48	6.97	0.0104
Ethane	C_2H_6	30.07	—127.6	33.8	6315	90.1	708	—297.9	$1.20x10^{-4}$	12.6	0.0783
Ethylene	C_2H_4	28.05	—154.8	35.2	5826	49.1	735	—272.5	$1.70x10^{-2}$	10.4	0.0729
Fluorine	F_2	38.00	—306.6	93.8	2815	—200.2	808	(—363.3)		7.49	0.0983
Freon—12	CCl_2F_2	120.92	— 21.6	92.9	8592	233.6	597	(—252.4)		17.66	0.318
Freon—13	$CClF_3$	104.46	—114.6	95.0	6670	83.9	561	(—294.0)		16.09	0.273
Freon—14	CF_4	88.01	—198.4	122.4	5160	— 49.9	542	—299.2	$1.70x10^{-3}$	14.6	0.228
Freon—22	$CHClF_2$	86.47	— 41.4	88.2	8704	204.8	716	(—256.0)		13.35	0.229
Helium (1)	He	4.00	—452.13	7.798	36	—450.2	33	—455.8 (4)	$7.35x10^{-1}$(4)	4.98	0.01034
Hydrochloric Acid	HCl	36.46	—120.9	74.3	6948	124.5	1199	(—173.)		6.9	0.0950
Hydrogen (1)	H_2	2.02	—422.99	4.418	389	—399.8	188	—434.5	1.044	6.89	0.005209
Hydrogen Sulfide	H_2S	34.08	— 75.4	60.0	8033	212.7	1307	—122.0	3.36	8.2	0.0892
Krypton (1)	Kr	83.80	—244.0	150.6	3884	— 82.8	796	—250.9	10.62	4.98	0.2172
Methane	CH_4	16.04	—258.6	26.5	3519	—116.6	670	—296.5	1.69	8.6	0.0416
Methyl Chloride	CH_3Cl	50.49	— 11.5	62.2	9293	289.6	967	—144.0	1.27	9.97	0.133
Neon (1)	Ne	20.18	—410.7	75.35	748	—379.7	395	—415.4	6.27	4.98	0.05215
Nitric Oxide	NO	30.01	—241.0	79.3	5953	—137.2	945	—263.6	3.16	7.1	0.0777
Nitrogen (1)	N_2	28.01	—320.5	50.46	2405	—232.6	491	—345.9	1.82	6.98	0.07245
Nitrogen Trifluoride	NF_3	71.01	—199.2	96.0	4984	— 38.7	657	(—343.3)	$1.77x10^{-5}$		0.1864
Nitrous Oxide	N_2O	44.01	—127.2	76.8	7110	97.7	1054	—131.6	12.74	9.2	0.1146
Oxygen (1)	O_2	32.00	—297.3	71.27	2932	—181.1	737	—361.8	$2.10x10^{-2}$	7.02	0.08281
Ozone	O_3	48.00	—169.4	101.8	6174	10.2	791	(—314.5)			0.124
Propane	C_3H_8	44.10	— 43.7	36.2	8076	206.2	617	—305.8	$8.39x10^{-11}$	17.4	0.1154
Propylene	C_3H_6	42.08	— 53.8	37.5	7925	197.4	667	—301.0	$2.44x10^{-8}$	15.3	0.1070
Sulfur Dioxide	SO_2	64.06	13.9	89.3	10728	315.0	1142	—103.8	$2.43x10^{-1}$	9.6	0.1687
Xenon (1)	Xe	131.30	—163.0	190.8	5436	61.9	847	—169.2	11.82	4.98	0.3416

(1) Based on data from the Compressed Gas Association Meeting June 19, 1962

(2) Proximate composition of dry air (Mole Percent): 78.09 N_2, 20.95 O_2, 0.93 Ar, 0.03 CO_2

(3) Denotes sublimation and solid density

(4) λ (lambda) point

Copyright by Air Products and Chemicals Inc. Reprinted with permission.

TABLE 4-2

Factors for Interconversion of Concentration Units of Gases and Vapors

Desired Units ↓ / Present Units →	Percent by Volume	Parts per Million by Volume	Moles per Liter	Milligrams per Cubic Centimeter	Milligrams per Liter	Milligrams per Cubic Meter	Milligrams per Cubic Foot
Percent by volume	-	10^{-4}	2450	24,500/M	2.45/M	2.45×10^{-3}/M	0.0863/M
Parts per million by volume	10^{4}	-	24.5×10^{6}	24.5×10^{6}/M	24,500/M	24.5/M	863/M
Moles per liter	4.1×10^{-4}	4.1×10^{-8}	-	1/M	10^{-3}/M	10^{-6}/M	35.3×10^{-6}/M
Milligrams per cubic centimeter	$4.1\ M \times 10^{-4}$	$4.1\ M \times 10^{-8}$	M	-	10^{-3}	10^{-6}	35.3×10^{-6}
Milligrams per liter	0.41 M	$4.1\ M \times 10^{-5}$	$M \times 10^{3}$	10^{3}	-	10^{-3}	0.0353
Milligrams per cubic meter	410 M	0.041 M	$M \times 10^{6}$	10^{6}	10^{3}	-	35.3
Milligrams per cubic foot	11.6 M	$1.16\ M \times 10^{-3}$	28,300 M	28,300	28.3	0.0283	-

How to use table:

1. Locate column along top of table which gives present unit.
2. Locate row along left of table which gives desired unit.
3. Read down and across to locate multiplying factor.
4. Multiply present quantity by factor.

Example: Given 700 ppm to convert to moles per liter:
$700 \times 4.1 \times 10^{-8} = 2.87 \times 10^{-5}$ moles/liter.

Note: In table, M is molecular weight of the gas or vapor.

From Process Instruments and Controls Handbook,
by Douglas M. Considine, Copyright 1957 by the
McGraw Hill Book Co., Inc.
used by permission of the McGraw Hill Book Co.

level of a single gas from a single producer. The same grade term may define a different purity level when used by other producers. Some of the most commonly used terms for gas grades are listed below in alphabetic order and do not imply any relative order of purity.

Grades	
Analytical	Research
Commercial	Technical
High purity	Ultrapure
Instrument	Zero
Prepurified	

Impurities found in various gases may be generally classified as gaseous and aerosol (liquid and solid particulates). Gaseous impurities are principally small concentrations of the constituents of gaseous or liquid media from which the basic gas is extracted or from other substances used in production processes.

In some gases forms of hydrocarbons may be an intolerable element. Sources of hydrocarbons when not a normal element are residues of cleaning solvents from containers and system equipment, and from lubricants used in processing equipment and containment systems.

Water in either liquid or vapor form is usually a major significant containment in all gases. The water content of a gas is usually reduced to an extremely low level by the normal gas production processes. However, additional amounts of water are easily introduced into the gas from the air both by inboard leakage into the system and during transfer to a container or from a container to the user's system. Another source of water is inadequately dried containers, transfer equipment, and materials and equipment used in gas systems.

Oils in liquid or vapor form may be introduced into the gas from lubricants and packing materials or sealants and inadequately cleaned equipment used in the production processes and the containment system.

Solid particulates are not normally found in any significant volume in newly produced and purified gases. Principle sources of particulates are corrosion, rust, scaling, and flaking of containers used to transport the gas or to contain the gas in the user's system. For this reason, gas producers are reluctant to certify any maximum concentration of particulate matter in gases.

Table 4-3 is a list of some commonly used gases with typical minimum purity levels that exist in the higher purity grades available from most producers. The impurities, which are those normally found, are given with the maximum values for each, and are typical of the concentrations that may be expected for the designated purity level. Actual analysis will vary with each batch or container of a specific gas and may reveal some impurities not shown.

Producers in the compressed gas industry with highly developed, well-controlled processes for separation and purification are capable of providing gases of extremely high purity levels which meet most use requirements. Research and development in this field are constantly refining these processes to a point where some impurities can be

TABLE 4-3

Typical Purity Levels and Impurity Concentrations of Gases

NAME	(a) PURITY LEVEL % VOLUME	(b) IMPURITIES IN PPM													
		Acetylene (C_2H_2)	Argon (Ar)	Carbon Dioxide (CO_2)	Carbon Monoxide (CO)	Helium (He)	Hydrogen (H_2)	Krypton (Kr)	Methane (CH_4)	Neon (Ne)	Nitrogen (N_2)	Nitrous Oxide (N_2O)	Oxygen (O_2)	Xenon (Xe)	Water (H_2O)
Argon	99.999	0.05	-	0.5	1.0	5.0	1.0	-	0.5	-	3.0	0.1	1.0	-	1.0
Helium	99.9995	0.05	-	0.5	1.0	-	1.0	-	0.5	2.0	5.0	0.1	1.0	-	1.0
Hydrogen	99.999	0.05	5.0	0.5	1.0	5.0	-	-	0.5	-	5.0	0.1	1.0	-	1.0
Krypton	99.99	0.5	-	0.5	10.0	5.0	1.0	-	5.0	50.0	25.0	0.1	2.0	25.0	1.0
Neon	99.998	0.5	-	0.5	1.0	25.0	1.0	-	0.5	-	5.0	0.1	1.0	-	1.0
Nitrogen	99.999	0.05	5.0	0.5	1.0	5.0	1.0	-	0.5	-	-	0.1	1.0	-	1.0
Oxygen	99.995	0.05	5.0	0.5	1.0	5.0	5.0	5.0	0.5	5.0	15.0	0.1	-	-	1.0
Xenon	99.99	0.5	-	5.0	10.0	5.0	1.0	25.0	5.0	5.0	5.0	0.1	5.0	-	1.0

(a) Purity levels may be equal to or greater than (≥) the values shown.

(b) Impurity concentrations may be equal to or less than (≤) the values shown.

reduced to a virtually undetectable level. The major problem, then, is maintaining the gas purity level in containers and containment systems to the ultimate use point. Initial potential sources of impurities in gases are producer storage containers, transfer equipment, shipping containers, and handling practices.

It may be reasonable to assume that a container of gas is of that purity level labeled or certified by the producer. However, when the use requirements are critical, a complete and accurate analysis by a qualified laboratory may be needed.

4.1.3 Gas Systems

The gas user is responsible for maintaining or purifying a gas within the cleanliness level compatible with end use requirements. Gases which do not meet needed purity levels may require extensive purification facilities, which are not economically feasible except for the high volume user. Hence, the most economical gas for the lower volume user is one obtained within the required purity level. Techniques for contamination control in this paragraph are limited to the user gas system.

A gas system used for the containment, control, and distribution of a compressed gas includes the following components:

Tanks	Tubing
Fittings	Nozzles
Regulators	O-rings and packing
Valves	Filters and other purification equipment

The assemblage of the above parts and components in a system constitutes the principal source of contaminants to the gas. Types of contaminants, examples of each, and some of the principal sources are shown in Table 4-4.

Effective contamination controls must be considered in the design stage of a gas system and implemented throughout the assembly operations. (See Section 2 for product design considerations.) In addition to general design considerations, some characteristics unique to a gas system that should be considered are given below:

a. All materials exposed to the gas should not be adversely effected by the particular gas.

b. Parts and equipment such as regulators, valves, flow meters, safety devices, tubing, etc., should have a minimum of entrapment areas and should be suitable for the pressures involved.

c. For oxygen systems, eliminate sharp bends in parts and system configuration to prevent erosion, hot spots, and ignition; and provide special conditioning procedures to assure removal and exclusion of all combustible substances.

d. Seals or packing and lubricants in operating parts should be minimum contributors of contaminants to the gas system.

e. Cleaning agents should be minimum contributors of contamination and easily removed from the system.

f. Provide procedures and equipment to prevent contaminants from entering the system when it is opened for any reason.

g. After system cleaning a final rinse, flush or purge should be used to assure removal of cleaning agents and residue (e.g., removal of hydrocarbons by steam flushing and water by heating, dry gas purging, and evacuating).

TABLE 4-4

Contaminants in Gas Systems

Types	Examples and Sources
Gases and vapors (Adsorbed on surfaces or otherwise trapped or generated within the system)	Vapors from cleaning solvents Vapors from assembly process materials Atmospheric air Products from chemical reactions of materials in the system with cleaning agents, process materials, atmospheric air, etc.
Particulates (Solid and liquid droplets)	Residue from cleaning agents and processes Residue from assembly processes and materials Condensates from air, gases, and vapors by temperature and pressure changes Airborne particles Wear particles from valves, regulators, and other equipment operated in the system Corrosion products generated in the system

The following factors should be considered in determining requirements for gas purification equipment:

a. Specified purity level for end use

b. Purity levels available from the producers

c. Specific contaminants or impurities in gases as received that must be removed or reduced in concentration

d. Economics involved--e.g., cost of producer delivering gas of the required purity level versus cost of design, installation, and maintenance of purification equipment

e. Capabilities of purification equipment to remove specific impurities to the levels required

f. Types and concentrations of contaminants introduced by the gas system.

The principal contaminants present in gases as procured and those introduced by a gas system are:

a. Particulates such as corrosion products, rust, scale, wear products, shedding, and flaking of materials from shipping containers and from the gas system

b. The water content of most gases can normally be reduced to an acceptable maximum concentration by the producer. Inboard leakage of the ambient atmosphere into gas systems is a primary source of moisture. Inadequately dried containers and systems and particulate filter equipment are other sources.

Equipment for use in-line with a gas system to remove the principal contaminants, as well as special design equipment, is available from gas equipment companies.

a. Selection and design of particulate filters should consider compatibility with the gas, flow rate, pressure, and temperatures involved. Special consideration should be given to the filter media with regard to:

(1) removal rating

(2) working pressure

(3) material

(4) migration or unloading

(5) water-vapor and oil-vapor content

(6) other characteristics that may contribute contaminants to the system.

In-line filters are usually located at the point of egress from shipping container or point of ingress to the gas system, or both if the transfer equipment and line are extensive, to exclude particulates from the system, or at or near the point of gas usage to remove particulates to an acceptable level for final use.

b. Some adsorptive materials used in drying equipment (for water vapor removal) may have a water content in excess of that in the gas, resulting in an increase of water content rather than the intended decrease.

Molecular sieves that have been adequately dehydrated are very effective media for drying gas to low levels of water content.

Drying equipment should be located as near as possible to the point of gas usage to preclude additional moisture being introduced between the dryer and point of use.

c. Other purification equipment employing various methods of absorption, adsorption, phase separation, and chemical catalysis may be used in removing or reducing gaseous impurities. Most of these processes require highly specialized techniques and complex equipment, which are not normally economically feasible for a low volume user.

4.1.4 Specifications and Analysis of Gases

The needed cleanliness level or purity of a gas used as part of a system or process is determined by the cleanliness level requirements of the specific application. To facilitate this determination and to formulate a gas specification that will adequately describe the requirements, the following factors should be considered:

a. Chemical and physical properties of the gas as they may affect usage requirements

b. Normal impurities in the gas as they may affect usage requirements

c. Purity levels with concentrations of impurities of the gas normally supplied by producers

d. Cautions and hazards in handling, containment, and use of the gas

e. Facilities and methods required for monitoring or verifying purity levels or concentrations of specific contaminants

f. Facilities required for the removal of specific contaminants

g. Contamination potential of the gas containment or distribution system.

A procurement specification for a gas should adequately describe the acceptable purity level and impurity concentrations in terms such as the following (see Table 4-3):

a. Gas purity level--specify minimum percent by volume

b. Normal gas impurities--specify allowable maximum concentration by parts per million or percent by volume

c. Water content--specify allowable maximum concentration by dew point (°F or °C) or parts per million

d. Other gaseous impurities that must be limited--specify allowable maximum concentration by parts per million or percent by volume

e. Particulate matter (fiber and nonfiber)--specify allowable maximum particle sizes with maximum allowable number per unit volume

f. Particulate matter (viable)--specify allowable maximum limits. (See Section 6 on microbial contamination and control.)

Gas analysis is the identification and/or quantitative measurement of gas constituents. These analytical measurements are significant to the producer and user. When applied, the measurements:

a. Provide a check on production processes and controls

b. Determine quality of end product

c. Provide a comparison with specifications

d. Detect trace impurities and contaminants

e. Provide continuous analysis or monitoring for compatibility with use requirements.

All analytical methods and techniques are fundamentally based on the interactions between matter and energy. Energy states, characteristic of the composition of any particular substance, are readily inferred by observing the consequences of interaction between the substance and an external source of energy. External energy sources may be grouped according to their basic modes of interaction with matter. A variety of analytical techniques and instrumentation is available depending on the type of energy, the means of using the energy, and the elements to be measured. Some of the techniques for gas analysis for each mode of energy used are shown in Table 4-5.

Methods for completely analyzing a specific gas may employ a variety of physical and chemical techniques and instrumentation, in different combinations, to provide identification and measurement of all constituents. The basic steps of analysis for a practical application consist of:

a. Obtaining a true representative sample of the gas stream

b. Separating the sample into its components or constituents or identifying those constituents of analytical interest

c. Determining the quantity of each constituent with relation to the whole sample or to one another

d. Recording the analysis results.

TABLE 4-5

Analysis Techniques for Gases

Techniques	Type Interaction	Definition	Energy Used
Ultraviolet spectrophotometry	Transmission and reflection	Measurement of the quantity and quality of electromagnetic radiation emitted, reflected, transmitted, or diffracted by the sample	Electromagnetic radiation
Light scattering			
Infrared spectrophotometry			
Microwave spectroscopy			
Orsat analyzer	Consumption of sample or reactant	Measurement of results in terms of amount of sample or reactant consumed, product formed, thermal energy liberated, or equilibrium attained	Reaction with other chemicals
Automatic titrators			
Impregnated tape	Measurement of reaction products		
Photometry			
Colorimetry			
Gas chromatography			
Combustion	Thermal energy liberation		
Other thermic reaction			
Mass spectroscopy Nier type Omegatron Time of flight	Ion separation	Measurement of the current, voltage, or flux changes produced in energized electrical and magnetic circuits containing the sample	Electrical and magnetic fields
Gaseous conduction	Electrical properties		
Paramagnetism	Magnetic properties		
Nuclear magnetic resonance			
Conductivity	Thermal	Measurement of results of applying thermal or mechanical energy to a system in terms of energy transmission, work done, or physical state	Thermal or mechanical energy
Dew point			
Sound velocity	Mechanical		

The selection of methods and instrumental techniques for gas analysis involves consideration of a number of factors. The factors include:

a. How the techniques will be employed:

   (1) laboratory analysis

   (2) continuous analysis (automated).

b. Knowledge of the probable composition of the sample:

   (1) a knowledge of the constituents of analytical interest permits selection of instrumentation for a quantitive measurement of each known element

   (2) identification of unknown elements requires instrumentation for both identification and quantitive measurement.

c. The physical state of the gas, which is normally gaseous. However, some constituents or impurities may be in other states such as:

   (1) particulates--solid

   (2) moisture or water--liquid.

d. Instrument performance which includes the following:

   (1) sensitivity -- the smallest change that can be reliably detected and distinguished from background noise or drift

   (2) range -- the span of concentrations of which the instrument is capable of measuring

   (3) accuracy -- the accuracy of instrument readings with respect to the actual value being measured

   (4) temperature effects -- ambient temperature effects on instrument and requirements to compensate for temperature of sample.

The selection of methods and instrumentation for a complete analysis instrument must be tailored to the sample composition and the information requirements. Some techniques are rather universal, permitting identification and measurement of most constituents. These are known as specific type techniques and are usually more complex and costly, and sometimes less sensitive. The less specific types are usually simpler but are less able to distinguish between related substances having similar interactions with energy. The nonspecific instruments usually have greater sensitivity to extremely small concentrations of the element being measured and are usually more adaptable to continuous analysis operations and automation. Instruments and techniques used to measure concentrations of water vapor or moisture and to size and count particulates

suspended in the gas are usually limited to these applications. However, in selecting this type specifically for moisture or particulate analysis, consideration must be given to other elements in the gas that will interfere with the instrument sensitivity.

Moisture monitoring instruments and techniques must be capable of measurements within the range of concentrations expected and the limits required. Other elements of the gas should not interfere or affect the sensitivity of the instrument. The adaptability to continuous and automated analysis should be considered if this is a requirement. Some of the instruments or techniques for humidity or water-vapor analysis are: (a) dew point -- other corrosive gases and vapors having dew points relatively close will cause errors; (b) electrical conductivity -- sample flow must be low, may be affected by other vapors, and corrosive or water soluble gases; (c) hygrometers -- affected by contaminants absorbed on wet-bulb wick (mechanical hygrometers are also available); and (d) volumetric absorption (pneumatic bridge).

Instruments and techniques for determining sizes and quantity of particulates suspended in the gas must have measurement capabilities within the ranges required. Two of the instruments and techniques are the light-scattering photometer which determines particle size or concentration level, and the microscopic measurement which consists of collecting the sample on a filter media for measurement; usually a grab sample technique.

4.1.5 Safe Handling of Compressed Gases

Compressed gas users should comply with all applicable regulatory standards in the use, handling, and storage of compressed gases. Regulatory standards include:

a. ICC regulations on the transportation of explosives and other dangerous articles

b. FAA regulations on the transportation of compressed gases by air

c. U.S. Coast Guard regulations on the transportation of compressed gases by water

d. ASME code on pressure vessels

e. ASME code on pressure piping

f. Compressed Gas Association standards

g. Local, state, and municipal codes and standards applicable to the use and storage of compressed gases.

These standards are considered minimum requirements. Supplemental procedures for the safety of operational personnel and the protection of equipment and facilities must be compatible with these minimum requirements, and should include such other procedures that are required for a particular operation or gas usage.

Compressed gases, like high explosives, are a form of stored energy and are potentially hazardous. Strict compliance with safe-handling practices, procedures, and standards by all personnel involved will ensure control of all potential hazards and incidents.

Five basic practices interdependent in achieving a high degree of safety in a compressed gas system are:

a. Engineering design compatible with pressure, volume, and particular gas used

b. Assembly practices and processes with good quality control

c. Proper assembly in accordance with design specifications

d. Proper operation in accordance with safe practices

e. Adequate maintenance and inspection to assure continued safety.

Compressed gas containers most commonly encountered by the user are cylinders. Rules and regulations pertaining to cylinders apply equally to spheres and drums where their alternate use is authorized by ICC regulations. Cylinder safety begins with the supplier by his adherence to ICC regulations covering:

a. Inspection and testing

b. Proper filling

c. Valves

d. Safety relief devices

e. Marking and labeling

f. Transportation.

4.2 Contaminants in Liquids

In rough cleaning operations, contamination in the cleaning solution may be a normal condition. In precision cleaning, however, the contaminant level is of definite concern and should be monitored periodically to assure that the required purity level is maintained. Contaminants in liquids consist of five primary types:

a. Nonvolatile residue

b. Other liquids in suspension or solution

c. Absorbed gases

d. Particulate matter

e. Microbial matter (viable particulates).

These contaminants normally originate from the following sources:

a. May be contained in the liquid as received from the producer

b. May be generated by use in cleaning processes or system operation

c. May be contributed by storage tanks, pipes, valves, and other system components

d. May be contributed by exposure to ambient air (particularly high-purity water).

The effects of contaminants in liquids are similar to the effects of the same contaminants in any other environment. However, the method of migration is different, and the contaminant may in some cases assume different forms. A representative list of the effects of contaminants in liquids is shown in Table 4-6.

TABLE 4-6

Effects of Contaminants in Liquids

Contaminant	Effects
Nonvolatile residue	Contact resistance Increased wear Corrosion Noncompatible with LOX systems
Particulate	Increased friction, wear, and erosion Mechanical restriction Electrical malfunction Photographic process degradation Corrosion
Microbial	Deterioration of material Cross infection Creation of nonsterile conditions Water and food pollution Purity dilution of pharmaceutical products
Other liquids	Dilution; reduced effectiveness Corrosion Chemical reactions; acidity, safety hazards

4.2.1 Hydraulic Systems

The performance of hydraulic systems is directly related to the level of contamination within the system. Contaminants may induce wear on critical components, affect the forces necessary to drive valves or servomechanisms, and directly obstruct hydraulic lines.

An effective method of contaminant removal can be designed only when the types and effects of contaminants have been identified. Some sources and effects of significant types of contaminants are shown in Table 4-7.

a. Design Considerations for a Hydraulic Filtration System -- The life of systems whose accuracy or reliability does not warrant recirculating fluid filtration may be extended by careful cleaning and periodic fluid changes. The cleaning techniques used for components in the system (ultrasonics, vapor degreasing, chemical, etc.) are covered in Section 3 of this handbook. In assembled systems, a cleaning procedure may consist of flushing the lines with a cleaning solution, rinsing with deionized water, and drying with nitrogen. This procedure, however, is only typical; various steps may need to be added or repeated.

   When a hydraulic system requires a recirculating liquid filter assembly, the following factors should be considered in the system design:

   (1) level of contamination permitted

   (2) type and amount of contaminants present

   (3) available space

   (4) volume and type of liquid to be filtered

   (5) type of service and conditions of operation

   (6) adaptability of the unit for adding auxiliary equipment.

b. Design Considerations for a Cleanable Hydraulic System -- In the design and assembly of hydraulic systems, several basic, but sometimes overlooked, factors should be considered in constructing a system that can be cleaned to the tolerances specified. These factors are as follows:

   (1) the materials of construction must be such to permit cleaning to the level required with the cleaning materials and processes needed

   (2) the materials should be identified as to composition

   (3) the materials should be compatible with the liquid used in the system

TABLE 4-7

Sources and Effects of Contaminants in Hydraulic Systems

Types	Sources	Effects
Dirt and dust	Area of operation of the system Environment of components before assembly or during assembly During manufacture of the components, such as core sand in castings	Wear by abrasion Wear by erosion Obstructs passages Activating force of valves and servomechanisms may be increased or erratic Acts as a chemical catalyst to promote oxidation of the hydraulic fluid
Water	Condensate resulting from low operating temperatures Introduced with fluid used in the system Improper drying of system after cleaning Enters through seals immersed in water or high-humidity environments	Oxidizes some metals used in hydraulic systems Accelerates oil oxidation with a metal catalyst present
Metal particles	Generated during manufacturing of components Generated during assembly of the system Generated during operation of the system	Similar to dirt and dust
Rust	Improper use of carbon steel in the system Flash rust formed during cleaning of carbon steel parts	Similar to dirt and dust
Hydrocarbons		
Oil oxidation	Presence of air with the hydraulic fluid Accelerated by high temperatures Accelerated by presence of fine particles Accelerated by presence of water	Similar to dirt and dust
Polymerization	Generated by high temperatures Accelerated by presence of fine particles Accelerated by presence of water	Similar to dirt and dust Increases viscosity to change forces required for the system
Sheaves (crystal-like growths)	Formed in presence of Buna-N rubber, oil, and metal High temperatures accelerate the reaction Still fluid accelerates the reaction	Similar to dirt and dust Generation of sheaves may etch away metal even between close tolerance parts such as pistons and cylinder walls
Miscellaneous contaminants	Parts packing material Paint on inside of pipe Surface coatings from improper preparation and cleaning before assembly	Similar to dirt and dust

(4) welds should be placed so as to be cleanable if at all possible

(5) welds should be checked for impurities (scale, spatter)

(6) drain and bleed-out ports should be provided for ease in cleaning

(7) the system should not contain dead end plumbing

(8) the components should be cleaned before assembly

(9) the system should be assembled in a clean area, if possible.

c. Liquid Filtration -- Several types of particle separators are used with hydraulic systems such as gravity settling and centrifugation. However, the main method of separating particles from liquid is filtration. Two major types of filters are surface and depth, and a combination of the two may be used in recirculating hydraulic systems.

Surface filters remove solid particulate matter from liquids by a straining action which does not absolutely filter soluble contaminants and fine particles. The different types and uses of surface filters are described below:

(1) Extended area membrane-type filters are made from paper folded into an accordion pleat and enclosed within a housing. Consequently, this type of filter has a large surface area. By changing the density of the paper and the density of packing, particles of various size ranges can be removed.

(2) Bag filters are made from reinforced cloth in a configuration suitable for insertion in a housing. The filter characteristics are similar to (1).

(3) Wire screens, perforated metal, and discs of pressed sintered powdered metal are generally used to filter gross particulate contaminants and as support for other types of filter material.

(4) Magnetic fields may be used to separate magnetic materials from liquids.

Depth filters allow the liquid to pass through a filter medium. Absorbent and adsorbent filtering action are used in different types of depth filters.

(1) Absorbent filters use materials such as cotton, felt, paper, and hair. Filtration is accomplished as particles are trapped in the filter media. These types of

filters are inactive chemically and remove only solid particles.

(2) Adsorbent filters use materials such as charcoal, bone-black, and clay. This filter adsorbs some dissolved contaminants as well as removes particles by trapping. Adsorbent filters are, however, water-sensitive and must be used only where the system can be kept water-free.

(3) Combination filters can employ most of the above filter types to achieve a combination of filter effects.

d. Contaminant Measurement Methods -- Water-vapor content of an empty system can be measured directly by using standard dew-point measurement techniques on the air in the system.

The general method for measuring particulate contamination is to collect a sample of fluid from the hydraulic system, filter it through a membrane filter, and count and size the particles.* Individual components can be installed in special test systems to test for contaminants in the part or generated by the part. The components may be submersed in ultrasonic tanks to simulate the worst case of particle contamination due to vibration of the component. The Dual Volume sampling method is useful for reducing background count in these types of tests.** In taking samples, many precautions must be taken to avoid particle generation and inaccurate test results.†

4.2.2 Analysis of Contaminants in Liquids

Some of the contaminants found in liquids and particularly those contributed by the system are discussed in Paragraph 4.2.1, Hydraulic Systems. See Paragraph 6.3.2, Monitoring Methods for Microbial Contamination - Liquids, for the microbial detection methods.

---

*Procedure for the Determination of Particulate Contamination of Hydraulic Fluids by the Particle Count Method, Society of Automotive Engineers, Inc., ARP 598, March 1, 1960.

**A Method for Determining the Degree of Cleanliness of the Interior of Hydraulic Components and of the Downstream Side of Hydraulic Filter Elements, Field Service Report No. 4, APM-FSR-4A, Aircraft Porous Media, Inc., Glen Cove, N.Y., January 24, 1958.

†A Systematic Approach to Obtaining Meaningful Contamination Data from System Fluid Samples, Field Service Report No. 24, APM-FSR-24A, Aircraft Porous Media, Inc., Glen Cove, N.Y., September 30, 1964.

Liquid dilution by unwanted constituents will not be discussed in detail in this handbook, since this is a matter that can be regulated to a large degree by using definitive specifications in either purchasing or formulating a liquid solution. Periodic chemical analysis is required to assure that prescribed quality levels are maintained. Such analysis may be necessary during and after formulation by the manufacturer, as an acceptance procedure by the user, and periodically during use.

Particulates and other nonvolatile residue present the other greatest concern in contamination control. Gross particulate matter can be seen visually, and smaller particles can be detected by the use of membrane filters and microscopes. One method for detecting particles 5 microns and larger is described in Aerospace Recommended Practice (ARP) 598. A more quantitative method is generally required, however, for most contamination control work. This is described in the following discussion of nonvolatile residue.

Nonvolatile residue (NVR) is defined as the soluble (or suspended) material and insoluble particulate matter remaining after temperature-controlled evaporation of a filtered volatile liquid. The amount of NVR content in solvents must be controlled in cleaning processes in order to obtain desired cleanliness of the product since the NVR will remain on the product after the solvent evaporates.. The final rinse stage of any precision cleaning process must utilize only solvent with an extremely low NVR content. Earlier stages in a multistage cleaning operation may be less critical in the control of NVR.

Some typical contaminants encountered in NVR control are:

Skin oils
Solder fluxes
Cutting fluids
Plasticizers
Cleaning solvents
Lubricants.

The primary methods of NVR detection are:

Gravimetric
Nephelometer
Solvent purity meter
Chromatography
Spectrophotometry.

Figures 4-1 through 4-5 depict the apparatus and steps involved in each NVR detection method. These methods are described and compared in Table 4-8.

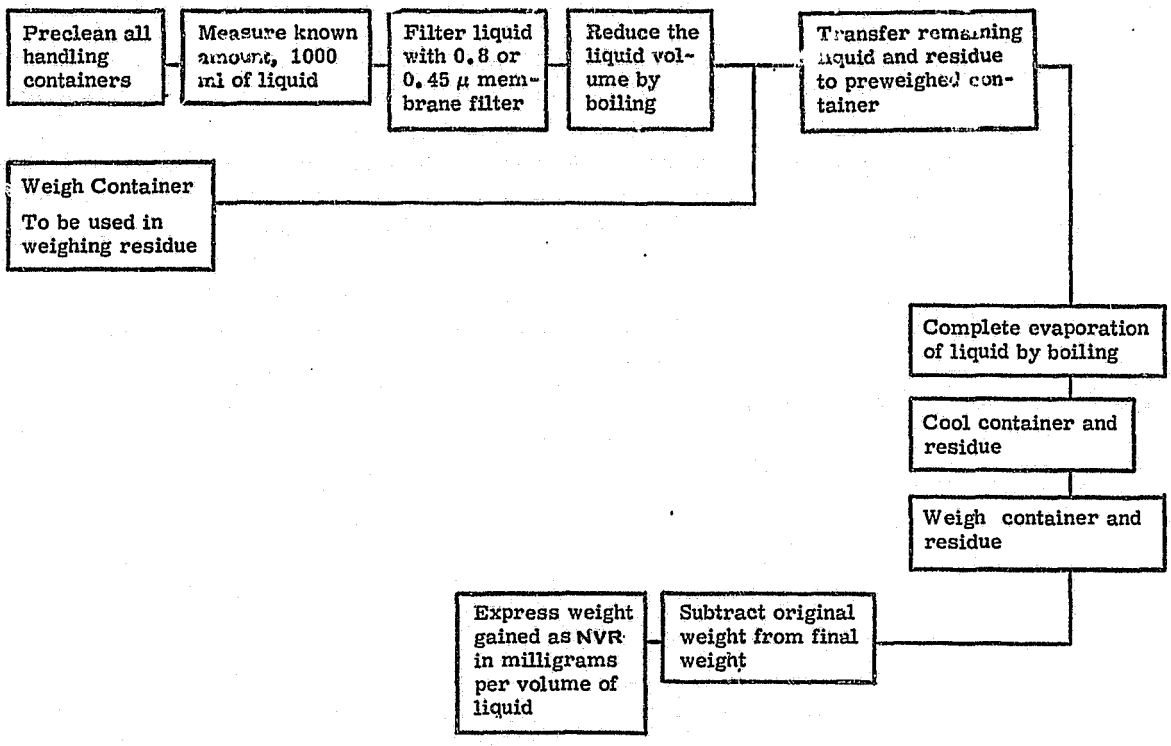

Figure 4-1. Typical gravimetric flow diagram

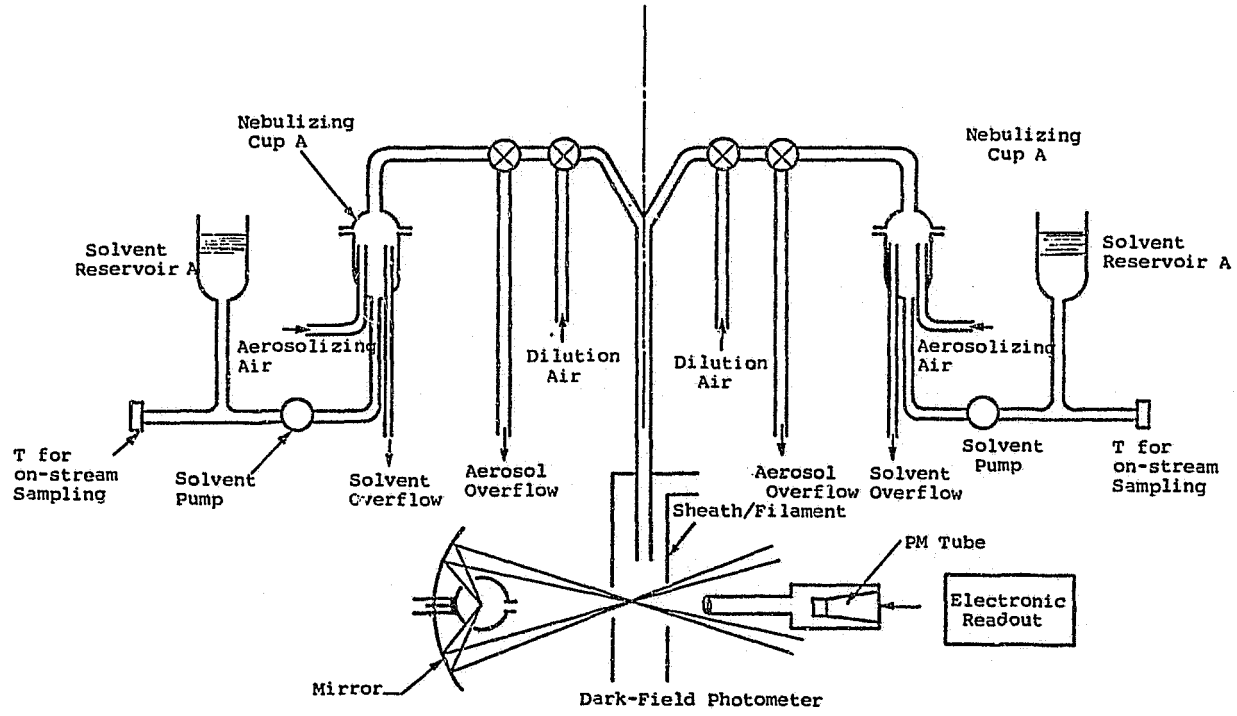

Figure 4-2. Schematic layout of NVR nephelom

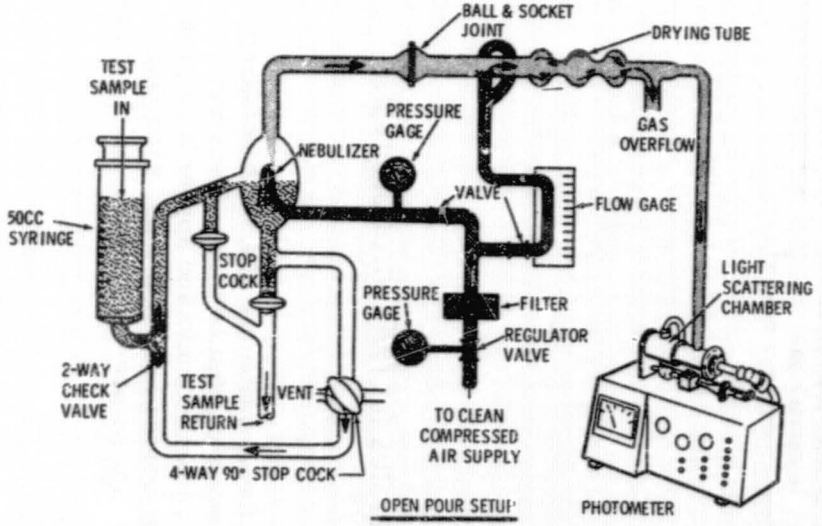

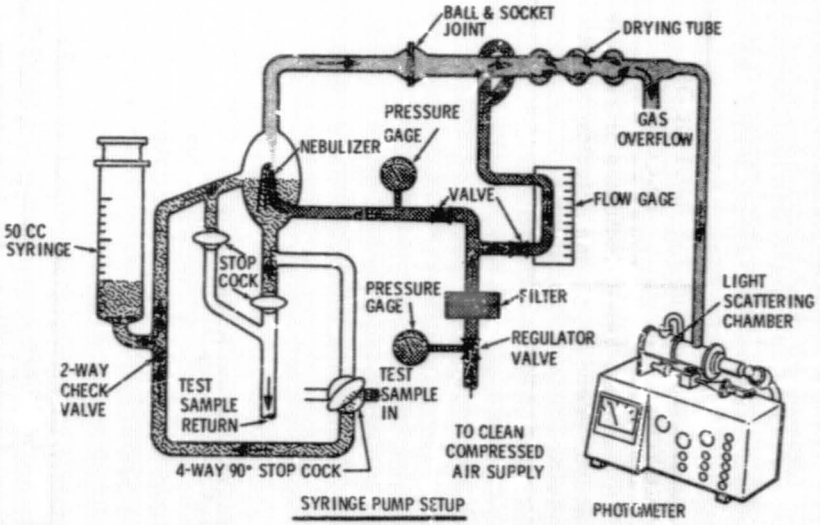

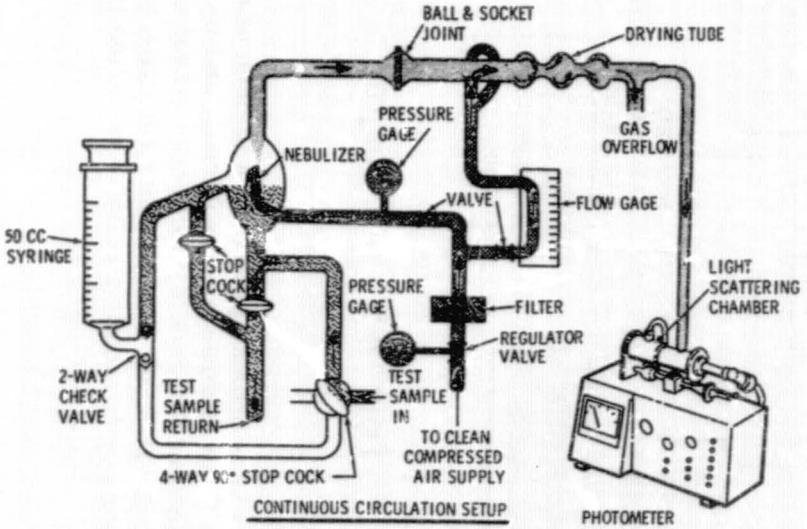

Figure 4.3. Solvent purity meter diagram

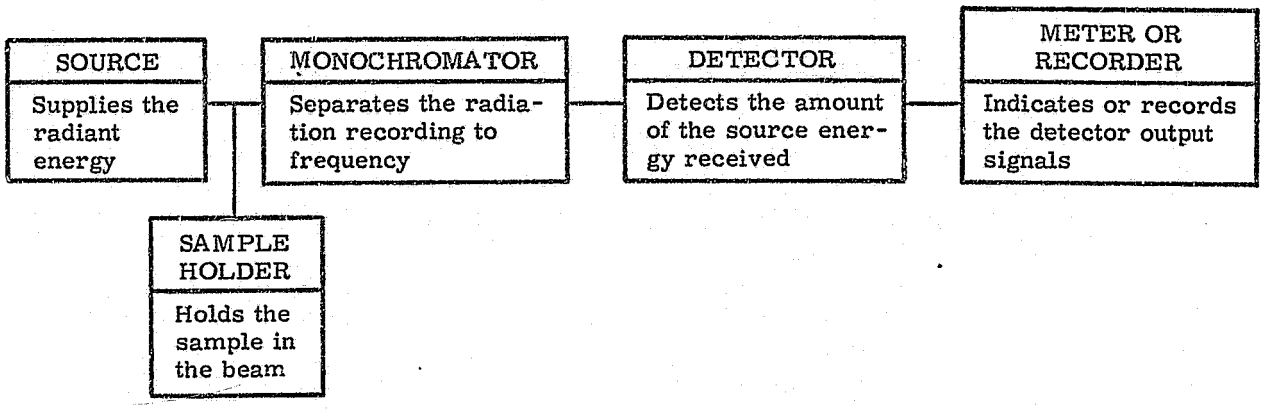

Figure 4-4. Block diagram of typical spectrophotometer

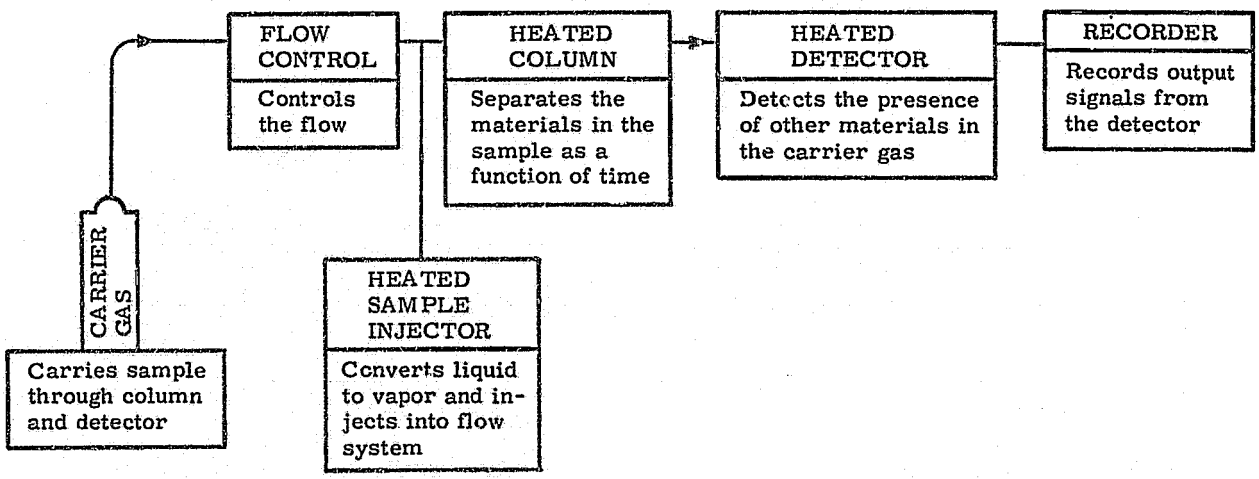

Figure 4-5. Block diagram of typical apparatus for NVR chromatography

Chromatography is a method of separating the constituents of a mixture based on their differences in solubility and mobility through a packed column. The time required for each component to travel through the packed column and appear as a peak on the recording trace is its retention time. Under controlled conditions, each component will exhibit a definite retention time, and this time provides significant information to its identity.

TABLE 4-8

NVR Detection Techniques

Comparison Characteristic	Gravimetric	Nephelometer	Solvent Purity Meter	Spectrophotometry	Chromatography
Principles of operation	Performed by weighing a container and evaporating (by boiling) a known amount of solvent and reweighing the container. The weight gain is NVR.	Solvent is aerosolized by clean air and sampled by forward light-scattering photometer. As NVR content is increased, the rate of evaporation is decreased resulting in larger droplets at the point of scattering, which produces larger signal output of the photometer	Same as nephelometer	Absorption of electromagnetic radiation	Multitheoretical plate Distillation Selective adsorption
Sensitivity	~0.01 ppm by weight	1 ppm	1 ppm	Varies from solvent to solvent; ~1 ppm optimized	1 ppm
Time for determination	May vary from 0.75 to 8.0 hours	~5 minutes	1 minute	5 minutes to 1 hour	5 minutes to 1 hour
Units of measurement	Milligrams per volume, and may be converted to ppm by weight	ppm either by weight or by volume after converting photometer reading by use of calibration curves	ppm either by weight or by volume after converting photometer reading by use of calibration curves	Percent transmittance converted to ppm or actual weight	Retention volume and direct readout are difficult
Operator aspect	Well versed in laboratory techniques, contamination control practices, and precise measurements	On development models was found simple to operate but somewhat difficult to maintain	Extremely simple to operate. Production personnel operate with no difficulty	Comprehensive knowledge of chemistry required for setup and interpretation	Comprehensive knowledge of chemistry required for setup and interpretation
General information	Widely used, recognized by ASTM Standards, may be costly in time and labor. Batch sampling only	Developed by IITRI for NASA. Shows great promise. Batch or continuous sampling	Developed by Sandia and is being marketed by commercial firms. Batch or continuous sampling	Can be quite expensive. Quite specific in application.	May be somewhat limited in identifying the variety of contaminants in a residue

Specifications and tests for NVR follow:

ASTM-NVR-66, Tentative Method of Test for Nonvolatile Residue of Halogenated Solvent Extract from Aerospace Components (Using Rotary Flash Evaporator)

MSFC-QUAL-AMC-5, Analysis of Liquid Samples for Nonvolatile Residue

MSFC-SPEC-164, Cleanliness of Components for Use in Oxygen, Fuel, and Pneumatic Systems, Specifications for

MSFC-PROC-195, Cleanliness Level Requirements and Inspection Methods for Determining Cleanliness Level of Gas Bearing, Gas Supply, and Slosh Measuring Systems, Procedure for

MSFC-DWG-10M01671, Cleanliness Levels, Cleaning, Protection, and Inspection Procedures for Parts, Field Parts, Assemblies, Subsystems and Systems for Pneumatic Use in Support Equipment, Specification for

MSFC-PROC-245, Carbon Tetrachloride Scrubber Method for Analysis of Condensable Hydrocarbon Contamination in Compressed Gases, Procedure for

MSFC-DWG-A10419906, Cleanliness of Components for Use in Gyro Air Supply System, Specification for

ASTM D 1025-52, Nonvolatile Residue of Polymerization Grade Butadiene

ASTM D 1353-65, Nonvolatile Matter in Lacquer Solvents and Diluents

ASTM D 2109-64, Nonvolatile Matter in Halogenated Organic Solvents and Their Admixtures

FST-2, Quality Specifications and Methods of Analysis for Freon Precision Cleaning Agent.

4.2.3 Removal of Contaminants from Liquids

Contaminants may be removed from liquids by physical, thermal, or chemical processes. The complexity of the process may be fairly simple (for some particulates) or highly involved (for liquids having similar vapor pressures).

Contaminants may be removed from liquids in many ways, any one of which may be the most feasible for a given situation. Some of the factors which will influence the selection of a particular method are:

a. The volume of liquid to be processed

b. The type of contaminants to be removed

c. The boiling point and vapor pressure of the liquid (and of the contaminant also, if it is a liquid)

d. The specific gravity of the contaminant

e. The degree of purity required

f. The time required for purification or output rate of the process

g. Economic considerations of space, initial purchase, operation, personnel, and maintenance.

The primary methods of removing contaminants from liquids are summarized in Table 4-9.

TABLE 4-9

Methods for Removing Contaminants from Liquids

Removal Method	Principle	Type of Contaminant Removed
Distillation	Evaporation and condensation	Liquids Nonvolatile residue Particulates Microbial organisms
Sedimentation and drain off	Gravity settling	Particulates
Filtration	Straining Adsorption Absorption Magnetic attraction	Particulates Microbial organisms
Centrifugation	Gravity	Particulates Microbial organisms
Deionization	Ion exchange	Dissolved minerals in water

Some of the characteristics, limitations, and applications of these methods are described as follows.

a. Distillation -- Apparatus for this method can vary from a simple laboratory setup to large, sophisticated distillation systems. Along with filtration, this is probably the most universally used method for purifying liquids because it will remove most of the contaminants normally found in liquids in a relatively economical manner. Distillation plays an important role in the reclamation of manufacturing grade solvents and in the repurification of technical or precision grade solvents. A typical distillation process and system are shown in Figures 4-6 and 4-7.

b. Sedimentation -- This is a time-consuming but effective method for removing particulate matter from liquids. It is generally applied to removing gross particulates and is not recommended when extremely high purity is required. The purity attainable is a function of:

(1) the time allowed for settling

(2) the specific gravity of the contaminant as compared to that of the liquid

(3) the degree to which agitation of the liquid can be controlled and minimized.

The purified liquid is usually drawn off at a point in the upper portion of the container and the sediment is discarded. An exception to this procedure is the removal of heavy sludge from industrial washers by sludge conveyors.

c. Filtration -- All filters perform the basic function of collecting and retaining contaminants. The type of filter selected for a particular application should be determined by the type and size of contaminant encountered, flow rates, and purity level desired, and the anticipated filter cleaning or replacement frequency. Some filters such as wire screens, perforated metal, and the larger pore size porous metal can be cleaned; most other types must be discarded and replaced. Filters may be used in-line to filter the entire volume of liquid in either batch or recirculating systems, or they may continuously filter only a portion of the liquid, as in the case of some ultrasonic cleaners. Membrane filters in flat or extended area configurations are used almost exclusively for filtering ultrapure liquids. Additional information on the types of filters available is contained in Paragraph 4.2.1.

d. Centrifugation -- This principle is similar to that of sedimentation. The primary difference is the time required for particulate removal. High-speed centrifuges greatly accelerate removal time for even those substances with very little difference in specific gravity. Centrifugation is used widely in removing microbial organisms from a liquid.

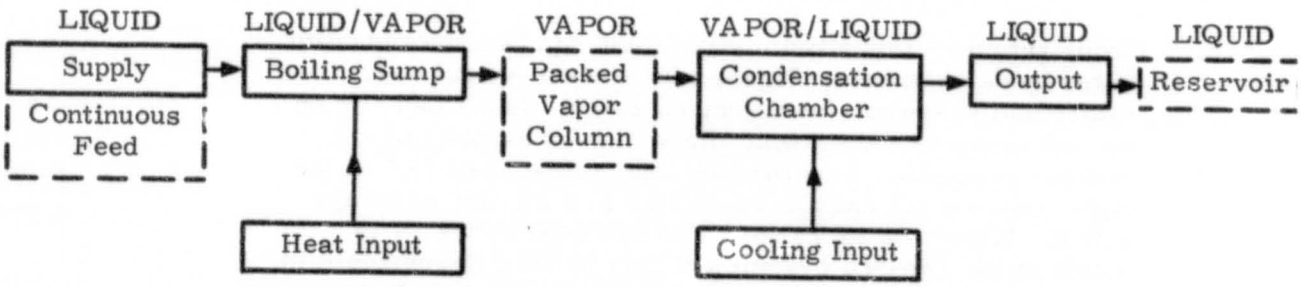

Solid lines indicate basic components and dashed lines optional components. Notations above the blocks indicate the physical state of the contents at that point in the process.

Figure 4-6. Diagram of a typical distillation process

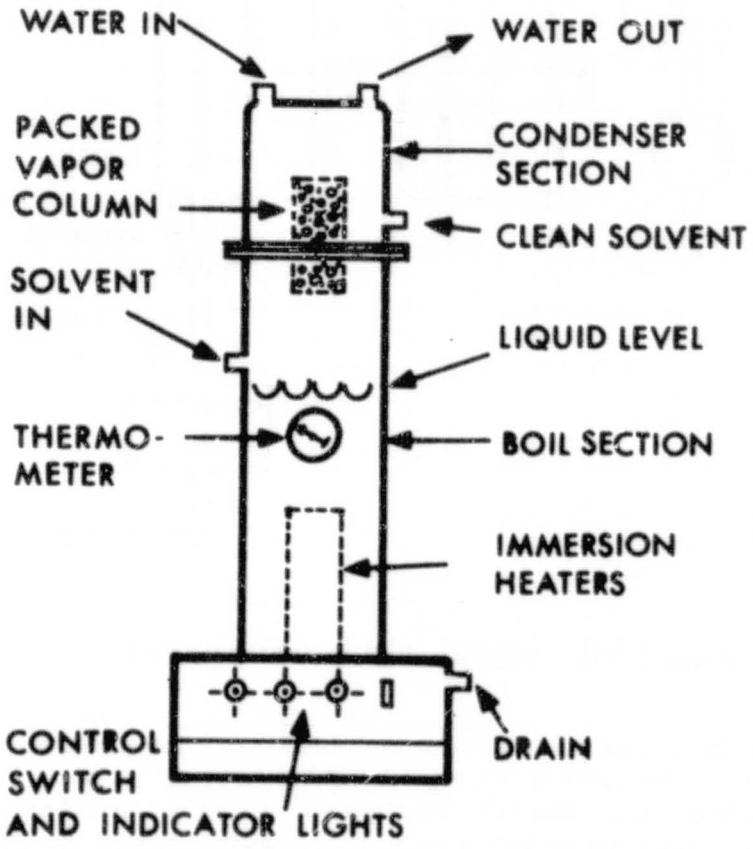

Courtesy of Baron-Blakeslee, Inc.

Figure 4-7. Typical distillation system

e. Deionization -- Dissolved mineral ions can be removed from water by deionization. Figure 4-8 shows a typical continuous recirculation system for deionized water. Resin bed "C" on the left removes the cationic impurities by exchanging the cationic impurities for hydrogen ions. Resin bed "A" on the right removes the anionic impurities in a similar exchange action. Mixed bed exchangers can accomplish the same result as the two-bed system and may be used downstream in addition to the two-bed system. Virtually, all dissolved contaminants can be removed from water in this manner. Further information on deionized water is found in Paragraph 3.4.1.

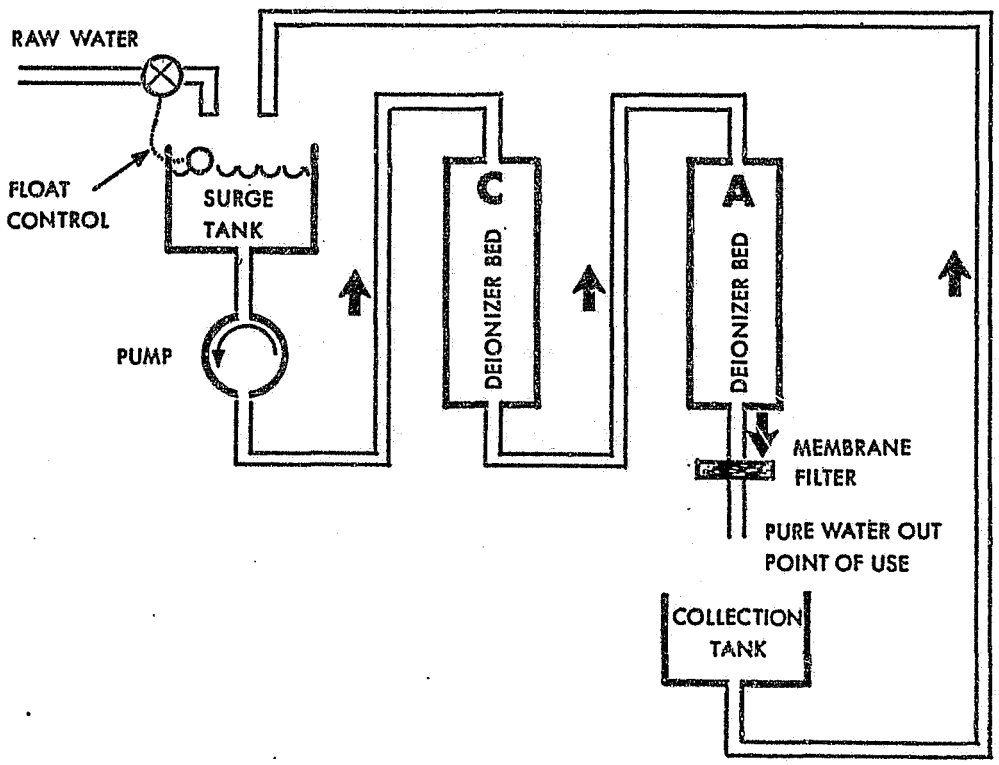

Figure 4-8. Typical deionized water system

Dilution and replacement contribute to the control of contaminants, although they are not methods for separating and removing contaminants from liquids. Dilution in this case is partial replacement of a contaminated liquid with a clean liquid of the same type. This may be done on a continuous or batch basis to maintain a minimum cleanliness level. Total replacement is commonly used when other methods of purification are not practical.

4.3 Bibliography

Analysis of the Cleanliness of Teflon Lined High Pressure Hose Using a Bend Test: J. A. Farris; Field Service Report No. 8, APM-FSR-8, Aircraft Porous Media, Inc., Glen Cove, New York; April 24, 1960.

Applied Instrumentation, Handbook of: Douglas M. Considine and S. D. Ross (Ed); McGraw-Hill Book Co., Inc., N. Y. C., N. Y.; 1964.

Chemical Engineers Handbook: J. H. Perry (Ed); McGraw-Hill Book Co., Inc., N. Y.; 1963.

Cleanliness Meter and Its Application to Solvent Cleaning: R. C. Marsh and F. C. Oswalt; SC-R-66-865, Sandia Corporation; March 1966.

Combination Final Rinsing Station Using Freon TF Solvent, A: R. C. Marsh; SC-TM-64-604, Sandia Corporation; May 1964.

Compressed Gases, Handbook of: Compressed Gas Association, Inc.; Reinhold Publishing Corp., N. Y. C., N. Y.; 1966.

Contamination Analysis and Control: James L. Dwyer; Reinhold Publishing Corp., N. Y. C., N. Y.; 1966.

Contamination Detection by Analytical Instrumentation: N. L. Crump and T. T. Bartels; Proceedings of the 6th Annual AACC Technical Meeting, Washington, D. C.; May 1967.

"Contamination Removal from Circulating Oil Systems: I:" Lubrication, Vol. 52, No. 8; August 1966.

Determination of Particulate Contamination of Hydraulic Fluids by the Particle Count Method, Procedure for the: Aerospace Recommended Practice, ARP-598, Society of Automotive Engineers, Inc.; March 1, 1960.

Determining the Degree of Cleanliness of the Interior of Hydraulic Components and of the Down-stream Side of Hydraulic Filter Elements, A Method for: J. A. Farris and E. A. Kirnbauer; Field Service Report No. 4, APM-FSR-4A, Aircraft Porous Media, Inc., Glen Cove, N. Y.; January 24, 1958.

Determining the Degree of Contamination of Sampling Valves, A Method of: E. A. Kirnbauer; APM-FSR-9B, Aircraft Porous Media, Inc., Glen Cove, N. Y.

Fluid Filters, Media and Contamination: H. L. Wheeler, Jr.; BFD 168, Bendix Filter Division, Bendix Aviation Corporation, Madison Heights, Mich.; 1960.

Fluid Sampling, Specification for: MSC-SPEC-C-13; November 1966 (or latest issue).

Fluid System Components, The Effect of Contamination on: Bulletin A 50, Aircraft Porous Media, Inc., Glen Cove, N. Y.; April 20, 1967.

Gas Data Book, Matheson: The Matheson Co., Inc., E. Rutherford, N.J.; 1966.

Gas Purification Processes: G. Nonhebel (Ed); George Newness Ltd., London, England; 1964.

High Purity De-Ionized Water Cleaning Stations: R. C. Marsh; SC-TM-66-49, Sandia Corporation; February 1966.

Hydraulic System Contamination: J. W. Parker; Aeronautical Systems Division, Wright-Patterson Air Force Base.

Mechanical Engineers Handbook, Marks: T. Baumeister (Ed); McGraw-Hill Book Co., Inc., N.Y.; 1958.

Obtaining Meaningful Contamination Data from System Fluid Samples, A Systematic Approach to: E. A. Kirnbauer; Field Service Report No. 24, APM-FSR-24A, Aircraft Porous Media, Inc., Glen Cove, N.Y.; September 30, 1964.

Process Instruments and Controls Handbook: Douglas M. Considine (Ed); McGraw-Hill Book Co., Inc., N.Y.C., N.Y.; 1957.

"Sheaves, A Growth Contaminant in Hydrocarbon Systems:" J. L. Bicknell; Missile Systems Division, The Bendix Corporation, Mishawaka, Inc.; Proc. Soc. Automotive Engineers, Aerospace Systems Conf., Los Angeles, Calif.; June 1967.

Spacecraft Fluid Analysis, Specification for: MSC-SPEC-C-14; November 1966.

Surface Chemistry, Theory and Applications: J. J. Bikerman; Academic Press, Inc., N.Y.C., N.Y.; 1958.

END OF REFERENCE
5

REFERENCE

6

OXYGEN. MSFC-SPEC-399B, NASA GEORGE C. MARSHALL SPACE FLIGHT CENTER, JAN. 31, 1974.

A00390-3

MSFC-SPEC-399B
January 31, 1974
SUPERSEDING
MSFC-SPEC-399A
July 31, 1967 and
Amendment 1
April 9, 1971

GEORGE C. MARSHALL SPACE FLIGHT CENTER
NATIONAL AERONAUTICS AND SPACE ADMINISTRATION

SPECIFICATION

OXYGEN

This specification has been approved by the George C. Marshall Space Flight Center (MSFC) and is available for use by MSFC and associated contractors.

1. SCOPE

1.1 Scope. - This specification covers the procurement requirements for oxygen used in space vehicles and associated ground support equipment.

1.2 Classification. - Oxygen shall be of the following types and grades, as specified (see Table I and 6.2):

Type I - Gaseous

Grade A - Fuel cell
Grade B - Breathing
Grade C - Propellant

Type II - Liquid

Grade A - Fuel cell
Grade B - Breathing
Grade C - Propellant

2. APPLICABLE DOCUMENTS

2.1 The following documents form a part of this specification to the extent specified herein. Unless otherwise indicated, the issue in effect on date of invitation for bids or request for proposals shall apply.

TABLE I. OXYGEN REQUIREMENTS

Requirement	Grade A for fuel cells	Grade B for breathing	Grade C for propellant
Purity	99.99	99.60	99.60
Methane and ethane	Methane 16.0 ppm* Ethane 2.0 ppm	Methane 25.0 ppm Ethane 2.0 ppm	No requirement
Propane and higher hydrocarbons	1.0 ppm as propane	1.0 ppm as propane	No requirement
Alkyne and acetylene hydrocarbons	0.05 ppm as acetylene	0.05 ppm as acetylene	0.25 ppm as acetylene
Total hydrocarbons	20.0 ppm as methane	29.0 ppm as methane	50.0 ppm as methane
Moisture	3.0 ppm	3.0 ppm	3.0 ppm
Nitrous oxide	1.0 ppm	1.0 ppm	No requirement
Halogenated hydrocarbons	1.0 ppm	1.0 ppm	No requirement
Odor	No odor	No odor	No requirement
CO and CO_2	1.0 ppm total	5.0 ppm carbon monoxide 5.0 ppm carbon dioxide	No requirement
Other Impurities (Nitrogen, Argon & Helium)	75.0 ppm total	No requirement	No requirement
Particulate	1.0 milligrams per liter (mg/l) max. (type II only)	1.0 milligrams per liter (mg/l) max. (type II only)	1.0 milligrams per liter (mg/l) max. (type II only)

* Ppm in table I represents parts per million by volume.

STANDARDS

Federal

FED-STD-209	Clean Room and Work Station Requirements, Controlled Environment

Military

MIL-STD-129	Marking for Shipment and Storage

(Copies of specifications, standards, drawings, and publications required by contractors in connection with specific procurement functions should be obtained from the procuring activity or as directed by the contracting officer.)

2.2 Other Publications. - The following documents form a part of this specification to the extent specified herein. Unless otherwise indicated, the issue in effect on date of invitation for bids or request for proposals shall apply.

Interstate Commerce Commission

49 CFR 71-90	Interstate Commerce Commission Rules and Regulations for the Transportation of Explosives and Other Dangerous Articles.

National Bureau of Standards

Miscellaneous Publication M-191 (1948)	Charts of Compressibility Factors and Charts Showing the Quantities Delivered by Commercial Cylinders for Hydrogen, Nitrogen, and Oxygen.

(Application for copies should be addressed to the Superintendent of Documents, Government Printing Office, Washington, D. C. 20402.)

3. REQUIREMENTS

3.1 Samples.

3.1.1 Quality Assurance Sample. - The quality assurance sample shall meet those requirements and quality assurance tests of this specification specified in the contract or order (see 6.2) for the type and grade purchased.

3.1.2 Acceptance Sample. - The acceptance sample shall meet all the requirements of this specification for the type and grade purchased.

3.2 Performance and Product Characteristics.

3.2.1 Types I and II.

3.2.1.1 Purity. - The minimum per cent purity for each grade of oxygen shall be as follows:

(a) Grade A - 99.99 by volume

(b) Grade B - 99.60 by volume

(c) Grade C - 99.60 by volume

3.2.1.2 Specific Impurities.

3.2.1.2.1 Methane and Ethane. - Methane and ethane for Grade A oxygen shall not be greater than 16 ppm by volume methane and 2 ppm by volume ethane. Methane and ethane for Grade B shall not be greater than 25.0 ppm by volume methane and 2 ppm ethane.

3.2.1.2.2 Propane and Higher Molecular Weight Hydrocarbons. - Propane and higher molecular weight hydrocarbons shall not be greater than 1.0 ppm by volume expressed as propane for Grades A and B.

3.2.1.2.3 Alkyne Hydrocarbons. - Alkyne hydrocarbons shall not be greater, expressed as acetylene, than the following:

(a) Grade A - 0.05 ppm by volume

(b) Grade B - 0.05 ppm by volume

(c) Grade C - 0.25 ppm by volume

3.2.1.2.4 Total Hydrocarbons. - The total hydrocarbons as methane shall not be greater than the following:

(a) Grade A - 20 ppm by volume

(b) Grade B - 29.0 ppm by volume

(c) Grade C - 50.0 ppm by volume

3.2.1.2.5 Moisture. - The moisture content shall not be greater than the following:

(a) Grade A - 3.0 ppm by volume

(b) Grade B - 3.0 ppm by volume

(c) Grade C - 3.0 ppm by volume

3.2.1.2.6 Carbon Monoxide and Carbon Dioxide. - The total carbon monoxide and carbon dioxide shall not be greater than 1.0 ppm by volume in Grade A oxygen. Carbon monoxide and carbon dioxide shall not be greater than 5.0 ppm by volume for Grade B.

3.2.1.2.7 Nitrous Oxide. - The nitrous oxide (N_2O) in Grades A and B oxygen shall not be greater than 1.0 ppm by volume.

3.2.1.2.8 Halogenated Hydrocarbons. - The total halogenated hydrocarbons for Grades A and B shall not be greater than 1.0 ppm by volume.

3.2.1.2.9 Other Impurities (Nitrogen, Argon & Helium). - The amount of nitrogen, argon and/or helium contained in Grade A oxygen shall not be greater than 75 ppm by volume.

3.2.1.2.10 Odor Test. - Grades A and B oxygen shall give no indication of odor.

3.2.1.2.11 Particulate. - The particulate (see 6.4.1) content of Type II, Grades A, B, and C, shall not exceed 1.0 mg/l.

3.3 Filling Containers.

3.3.1 Filters. - Approved stainless steel filters, 10 micron nominal and 40 micron absolute, shall be used between the manufacturer's plant and the shipping container.

3.3.2 Filling Containers. - Cylinders shall be filled with Type I oxygen to a pressure of 1,800, 2,015, or 2,200 psig as specified in the contract or order (see 6.2). When filling cylinders having a stabilized temperature other than 21°C (70°F), the fill pressure shall be as specified in Table II for the applicable temperature and nominal fill pressure. When cylinders are tested as specified in 4.4.3.1, the cylinder pressure shall not vary more than ± 25 psig from the pressure specified in Table II that corresponds to the stabilized temperature of the cylinder being filled.

3.4 Product Identification. - A tag shall be firmly attached to each container in a conspicuous location. The tag shall contain the following information:

Product Oxygen Type _____ Grade _____.
Specification MSFC-SPEC-399B.

TABLE II. TABLE OF TEMPERATURES AND GAGE PRESSURES (POUNDS PER SQUARE INCH GAGE (PSIG))

(Modified NBS Publication M-191 (1948))

*Temp °C	Temp °F	*Filling pressures at 21 °C (70 °F) 1800	2015	2200	*Temp °C	Temp °F	*Filling pressures at 21 °C (70 °F) 1800	2015	2200
-46	-50	1240	1370	1479	10	50	1707	1909	2082
-44	-48	1249	1381	1491	11	52	1717	1920	2093
-43	-46	1258	1392	1503	12	54	1726	1930	2105
-42	-44	1268	1403	1516	13	56	1735	1941	2117
-41	-42	1277	1414	1528	14	58	1745	1951	2129
-40	-40	1287	1425	1540	16	60	1754	1962	2141
-39	-38	1296	1436	1552	17	62	1763	1972	2153
-38	-36	1306	1440	1565	18	64	1773	1983	2164
-37	-34	1315	1457	1577	19	66	1782	1994	2176
-36	-32	1325	1468	1589	20	68	1790	2004	2188
-34	-30	1334	1479	1601	21	70	1800	2015	2200
-33	-28	1344	1490	1613	22	72	1809	2026	2212
-32	-26	1353	1500	1625	23	74	1818	2036	2224
-31	-24	1362	1511	1637	24	76	1828	2047	2236
-30	-22	1372	1522	1649	26	78	1837	2057	2248
-29	-20	1381	1533	1662	27	80	1846	2068	2260
-28	-18	1391	1544	1674	28	82	1855	2078	2272
-27	-16	1400	1555	1686	29	84	1864	2089	2283
-26	-14	1409	1565	1698	30	86	1874	2100	2295
-24	-12	1419	1576	1710	31	88	1883	2110	2307
-23	-10	1428	1587	1723	32	90	1892	2121	2318
-22	- 8	1437	1598	1735	33	92	1901	2132	2330
-21	- 6	1447	1608	1747	34	94	1910	2142	2342
-20	- 4	1456	1619	1759	36	96	1920	2153	2354
-19	- 2	1466	1630	1771	37	98	1929	2163	2366
-18	0	1475	1641	1783	38	100	1938	2174	2378
-17	2	1484	1654	1795	39	102	1947	2184	2389
-16	4	1494	1663	1807	40	104	1956	2195	2401
-15	6	1503	1673	1819	41	106	1965	2205	2413
-13	8	1512	1684	1831	42	108	1975	2216	2425
-12	10	1522	1695	1843	43	110	1984	2226	2436
-11	12	1531	1706	1855	44	112	1993	2237	2448
-10	14	1540	1716	1867	46	114	2002	2247	2460
- 9	16	1550	1727	1878	47	116	2011	2258	2471
- 8	18	1559	1738	1890	48	118	2020	2268	2483
- 7	20	1568	1749	1902	49	120	2030	2279	2495
- 6	22	1578	1759	1914	50	122	2039	2289	2507
- 4	24	1587	1770	1926	51	124	2048	2300	2518
- 3	26	1596	1781	1938	52	126	2057	2310	2530
- 2	28	1606	1791	1950	53	128	2066	2321	2542
- 1	30	1615	1802	1962	54	130	2075	2331	2554
0	32	1624	1813	1974	56	132	2084	2342	2566
1	34	1634	1823	1986	57	134	2093	2352	2577
2	36	1643	1834	1998	58	136	2102	2363	2589
3	38	1652	1845	2010	59	138	2112	2373	2600
4	40	1661	1856	2022	60	140	2121	2384	2612
6	42	1671	1866	2034	61	142	2130	2394	2623
7	44	1680	1877	2046	62	144	2139	2405	2635
8	46	1689	1888	2058	63	146	2148	2416	2647
9	48	1698	1898	2070	64	148	2157	2426	2659
					66	150	2166	2437	2671

*These values are rounded off to the nearest whole number.

Contract or order number _____.
Manufacturer _____ Supplier _____.
Lot identification _____ Filling date _____.

Certification of filled containers of Type I oxygen:

(1) Quantity (cubic feet at NTP)[1] _____.
(2) Container pressure after filling _____.
(3) Container temperature after filling _____.

Certification of filled containers of Type II oxygen:

(1) Quantity _____ tons.
Quality certifying manufacturer _____.
Quality certifying agent _____.

4. QUALITY ASSURANCE PROVISIONS

4.1 The supplier is responsible for the performance of all inspection requirements as specified herein. Except as otherwise specified, the supplier may utilize his own or any other inspection facilities and services acceptable to the procuring activity that are covered by an inspection or quality control plan as required by the contract. Unless otherwise specified, the inspection plan shall be submitted for review with the supplier's bid or proposal. Inspection and test records shall be kept complete and, upon request, made available to the procuring activity or its designated representative, in accordance with provisions of the contract or the procurement document. The procuring activity or its designated representative reserves the right to perform any or all of the inspections set forth in the specification for individual contaminants or requirements.

4.2 Lot. -

4.2.1 Type I in cylinders filled from gas source. - When Type I oxygen cylinders are filled, each set of cylinders charged on the same manifold at the same time shall constitute a lot. The number of samples per lot shall conform to Table III. Each cylinder selected for testing shall have approximately 1 standard cubic foot of gas withdrawn before sampling for all tests.

[1]Normal temperature and pressure is defined as 21.11°C (70°F), and 760 millimeters of mercury (mm Hg) pressure (14.7 pounds per square inch absolute (psia).

TABLE III. TEST SAMPLES

Lot Sizes	Number of Samples
1 to 10	1
11 to 40	2
41 to 70	3
71 and up	4

4.2.2 Type I in Cylinders Filled from Liquid Source. - When gaseous oxygen is compressed into cylinders from the vaporization of liquid oxygen, the following sampling procedure shall apply:

4.2.2.1 Procedure. - Each day, after initial filling or any additional filling of the liquid storage system, samples from the first set of cylinders charged on the manifold shall be selected in accordance with Table III. Between the initial or any additional filling, one sample cylinder shall be taken at random for test from each lot of 20 filled cylinders. Each cylinder selected for testing shall have approximately 1 standard cubic foot of gas withdrawn before sampling for all tests.

4.2.3 Type II Filled Containers. - When Type II oxygen containers are filled, each container shall constitute a lot. Two samples shall be drawn from each lot. The samples are required for acceptance tests and shall be taken at the lowest outlet of the container.

4.2.4 Continuous Service, Type II, Grade C only. - Continuous service is continuous deliveries under Government contract of a single product complying with the propellant specification.

4.2.4.1 Sampling Option. - Unless otherwise specified, the following sampling option for Type II, Grade C propellant oxygen shall be used for storage and transport containers engaged in continuous propellant service. The contractor shall sample the contents of each transport container engaged in continuous service at least once every 7 days at uniform intervals of time. Samples shall be taken from the filled transport containers. The contractor shall sample the contents of each transport container when entering continuous oxygen service and when the transport container has remained empty for a period greater than 24 hours. When empty, all ports and vents shall remain closed to the atmosphere. In continuous propellant service, compliance with quality conformance tests specified herein shall be determined by sampling the filling point storage container after each addition or, in case of continuous production, at established intervals not less than once every 24 hours (see 6.2). A storage container that is in the process of being filled during a change of duty shift, shall be sampled after filling at the option of the Government inspector.

4.3 Samples. -

4.3.1 Quality Assurance Sample. - The quality assurance sample (when required by the contract (see 6.2)), shall be selected at random from the production lots submitted for acceptance.

4.3.1.1 Quality Assurance Sample Rejection. - If any specimen of the quality assurance sample fails to meet the requirements specified herein, a detailed report shall be required by the procuring activity describing the action taken by the supplier to insure conformance to this specification. The corrective action taken shall be the basis for resuming normal procurement activity.

4.3.2 Acceptance Sample. - Unless otherwise specified by the procuring activity, the sample shall be taken at the point of filling, prior to shipment. Samples shall be drawn from each lot of oxygen.

4.3.2.1 Acceptance Sample Certification. - The contractor shall furnish with each Form DD250, or applicable shipping document, a certified copy of the actual laboratory analysis of each sample taken.

4.3.2.2 Acceptance Sample Rejection. - Any sample that fails any acceptance test specified herein shall be cause for rejection of the lot submitted.

4.4 Testing. -

4.4.1 Quality Assurance Testing. - When quality assurance testing is required by the contract or order (see 6.2), testing shall be performed by the supplier under MSFC surveillance, or as directed by the procuring activity. Specific tests and the installation where the tests are to be conducted shall be as specified in the contract or order (see 3.1.1 and 6.2).

4.4.2 Acceptance Test Plan. - The contractor or supplier shall utilize acceptance test procedures that have been approved by the procuring activity to perform the tests specified herein. Unless otherwise specified in the contract or order (see 6.2), a detailed test plan, including schematic diagrams of test setups and a list of equipment to be utilized for test, shall be submitted by the contractor to the procuring activity and approved before tests are performed. When the contractor is unable to provide approved test procedures for determining the particulate content of Type II oxygen, the recommended MSFC procedure described in 6.3 shall be used. Identifiable test plans that have received approval under contracts the previous year need not be resubmitted.

4.4.3 Acceptance Tests. -

4.4.3.1 Filling pressure test. - Samples shall be tested for proper filling pressure by attaching a gage of the type described below to the valve outlet and by attaching either a thermocouple or thermometer of the type described below to the cylinder wall. If a thermometer is used, the bulb shall be protected from alien temperatures by a fireproof insulating material secured by either spring clips or tape. The insulation shall not be applied between the bulb and the cylinder wall. The cylinder shall stand until it stabilizes at approximately room temperature. The cylinder valve shall be opened and the internal pressure observed on the gage. If the internal pressure differs from the applicable pressure value shown in Table II corresponding to the stabilized cylinder temperature by more than 25 psig, the sample cylinder, and all other cylinders filled from the same manifold at the same time shall be rejected. Pressures shall be measured by means of accurately calibrated Bourbon tube gages or other laboratory-type pressure measuring device capable of being accurately read to within $\pm$ 5 psig. For the purpose of this specification, a gage or other pressure measuring device having scale increments of 10 psig is considered satisfactory for reading within the $\pm$ 5 psig requirement. Temperatures shall be measured using thermocouples or thermometers. Thermocouples shall be of laboratory accuracy and shall have a sufficient number of scale divisions to be read within $1/2^{o}$.

4.4.3.2 Purity. - The purity of Grade A oxygen shall be determined by indirect measurement to determine conformance to 3.2.1.1. The conformance certification shall be based on instrumental analysis utilizing analytical equipment having sensitivity capability of separating and/or determining the specified maximum allowable concentration of each component. This equipment may include gas chromatographic, mass spectrometric, infrared, or other analytical equipment having adequate sensitivity characteristics for specific component analysis. The purity of Grades B and C oxygen shall be by direct measurement for conformance to 3.2.1.1. The difference between the sum of the oxygen and contaminant concentration will be assumed to be inert gases and nitrogen.

4.4.3.2.1 Methane and Ethane. - Tests shall be performed to determine conformance to 3.2.1.2.1.

4.4.3.2.2 Propane and Higher Molecular Weight Hydrocarbons. - Tests shall be performed to determine conformance to 3.2.1.2.2.

4.4.3.2.3 Alkyne Hydrocarbons. - Tests shall be performed to determine conformance to 3.2.1.2.3.

4.4.3.2.4 Total Hydrocarbons. - Tests shall be performed to determine conformance to 3.2.1.2.4.

4.4.3.2.5 Moisture. - Tests shall be performed to determine conformance to 3.2.1.2.5.

4.4.3.2.6 Carbon monoxide and Carbon Dioxide. - Tests shall be performed to determine conformance to 3.2.1.2.6.

4.4.3.2.7 Nitrous Oxide. - Tests shall be performed to determine conformance to 3.2.1.2.7.

4.4.3.2.8 Halogenated Hydrocarbons. - Tests shall be performed to determine conformance to 3.2.1.2.8.

4.4.3.2.9 All Other Impurities (Nitrogen, Argon and Helium). - All other impurities for Grade A oxygen including inert gases and nitrogen shall be by appropriate instrumental analysis to determine conformance to 3.2.1.2.9.

4.4.3.2.10 Odor Tests. - Odor tests shall be checked to determine conformance to 3.2.1.2.10.

4.4.3.2.11 Particulate Content. - The particulate content for Type II, Grades A, B, and C, oxygen shall be tested to determine conformance to 3.2.1.2.11. (see 6.3).

4.4.4 Examination. - All oxygen submitted shall be examined to determine conformance to 3.4, and the marking requirements of Section 5.

5. PREPARATION FOR DELIVERY

5.1 Filling and Transporting. - An approved filter (see 3.3) shall be connected to the inlet side of all transfer containers during filling.

5.2 Marking. - All containers shall be marked in accordance with ICC Regulation 49 CFR 71-90, Standard MIL-STD-129, and properly tagged and identified (see 3.4).

5.3 Transfer Equipment. - Oxygen containers shall be approved by the procuring activity with respect to design, insluation, and compatibility for the type and grade of oxygen. Any equipment found to be defective shall be repaired or rejected for future deliveries as required by the procuring activity. All liquid oxygen containers shall be insulated to effect a maximum loss not greater than 0.5 per cent for 24 hours.

6. NOTES

6.1 Intended Use. - The oxygen furnished in accordance with this specification is intended for three uses: fuel cell, breathing, and propellant.

6.2 Ordering Data. - Procurement documents should specify the following:

(a) Title, number, and date of this specification.

(b) Type and grade oxygen required (see 1.2).

(c) Sampling option for continuous propellant transport container service (see 4.2.4.1).

(d) Whether quality assurance testing is required and if so, what tests are to be conducted (see 3.1.1).

(e) Where quality assurance testing will be accomplished (see 4.4.1).

(f) Whether acceptance test plan is required or identify the approved test plan (see 4.4.2).

(g) Whether special packaging, packing, a nd marking is required (see Section 5.)

(h) Container pressure for Type I at 21° C.

6.3 MSFC Test Procedure. - The MSFC recommended equipment, material, and test procedures for determining particulate content of Type II, Grades A, B, and C oxygen shall be as specified below.

6.3.1 Particulate. - Type II, Grades A, B, and C oxygen shall be sampled and tested for contamination in accordance with the following method.

NOTE

Particulate content determination should be made in a controlled environment meeting the particulate level of Standard FED-STD-209. "Class 30,000."

6.3.1.1 Test Equipment. - The test equipment or its equivalent shall consist of the following:

(a) Flask: dewar, five-liter capacity, round configuration, 2-inch opening, and slotted chloro fluorocarbon stopper which serves to relieve internal pressure.

(b) Holder: filter, stainless steel; complete with stainless steel base, chloro fluorocarbon stopper, integral locking ring, and 650 ml stainless steel funnel.

(c) Filter disc: Teflon or glass fiber, 1.50 micron or less with grid.

(d) Foil: aluminum.

(e) Aspirator: water.

(f) Dish: petri, plastic.

(g) Forceps: unserrated tips.

(h) Balance: analytical, 0.1 mg sensitivity.

(i) Flask: filter, Pyrex, heavy-wall, two-liter, with side arm.

(j) Oven: vacuum.

6.3.1.2 Dewar Cleaning. - Clean a five-liter dewar flask by rinsing three times with 200 ml of filtered freon TF, or equal; dry the flask with filtered gaseous nitrogen; close the flask with a slotted chloro fluorocarbon stopper covered with degreased aluminum foil.

6.3.1.3 Sample. - Remove the stopper from the cleaned dewar flask and collect a five-liter sample of Type II oxygen. Immediately close the flask with the stopper.

6.3.1.4 Procedure. -

6.3.1.4.1 Filter Disc Tare. - Using forceps, one 1.50-micron or less Teflon or glass fiber filter disc and back-up pad shall be placed in an open petri dish. Place the dish in a vacuum oven at 70°C (158°F) for 30 minutes. Remove the dish and place in a desiccator containing dustless calcium sulfate for 30 minutes. Using forceps, remove the filter disc (without the back-up pad) from the desiccator and place on a balance. Allow a 2-minute interval, permitting the filter disc to come to constant weight. Record the weight to the nearest 0.1 mg. Using forceps, remove the filter disc from the balance and replace in the covered petri dish.

6.3.1.4.2 Filtration. - Connect a heavy-wall two-liter Pyrex filter flask to a water aspirator with Teflon or chloro fluorocarbon tubing and place in a hot water bath 10 cms in depth. Place the stainless steel base on the filter assembly on the top of the Pyrex flask. Using forceps, remove the filter disc and back-up pad from the petri dish and place them on the stainless steel base. Immediately lower the filter funnel onto the base; secure with the locking ring and place a degreased aluminum-foil cover on top of the filter funnel. Turn on the water aspirator. Remove the aluminum-foil cover and pour three or four drops of the Type II sample from the dewar flask into the filter funnel to prevent shattering of the filter disc. Pour the remaining contents of the dewar flask into the filter funnel but not directly on the filter disc. Between pourings, cover the filter funnel with the aluminum-foil cover. During filtration, frost will form on the filter flask and aspiration shall be continued until frost disappears. Rinse the filter funnel with filtered freon TF. Disconnect the funnel and discontinue water aspiration. Using forceps, transfer the filter disc to the open petri dish and place in a vacuum oven at 70°C (158°F) for 30 minutes.

NOTE

A sudden change in vacuum oven pressure should be avoided as it may remove particles from the filter and cause erroneous results.

Remove the dish and place in a desiccator for 30 minutes. Using forceps, remove the filter disc from the desiccator and place on a balance. Allow a 2-minute interval permitting the filter disc to come to constant weight. Record the weight to the nearest 0.1 mg. A particulate content of the sample shall not exceed 1.0 mg/l.

6.4 Definition. -

6.4.1 Particulate. - The [illegible]dissolved solids retained on a 10.0 microns filter disc.

6.5 Changes, Deviations, or Waivers. - No technical changes, deviations, or waivers will be [illegible]de to the requirements of this document without the approval of the cogni[illegible]ant design engineering activity of MSFC. All changes, deviations, or wai[illegible]rs will be submitted to the Requirements Integration Division, S&E-S/P-S[illegible] Marshall Space Flight Center, Alabama 35812, for coordination with the [illegible]ognizant design activity.

Notice. - When Governmen[illegible]drawings, specifications, or other data are used for any purpose other [illegible]an in connection with a definitely related Government procurement opera[illegible]on, the United States Government thereby incurs no responsibility nor [illegible]ligation whatsoever; and the fact that the Government may have form[illegible]ated, furnished, or in any way supplied the said drawings, specificatio[illegible] or other data is not to be regarded by implication or otherwise as in a[illegible] manner licensing the holder or any other person or corporation, or [illegible]onveying any rights or permission to manufacture, use, or sell any p[illegible]ented invention that may in any way be related thereto.

Custodian:

NASA - George C. Marshall Sp[illegible]e Flight Center

Preparing Activity:

George C. Marshall Space Flight Center

NAS[illegible]—MSFC—C

END OF REFERENCE

6

REFERENCE

7

QUALITY CONTROL OF OXYGEN PROPELLANT, LIQUID OXYGEN, AVIATOR'S LIQUID BREATHING OXYGEN, AND AVIATOR'S GASEOUS BREATHING OXYGEN. REP. T.O. 42B6-1-1, CHANGE 7, U.S. AIR FORCE, MAY 1, 1969.

THIS MATERIAL HAS BEEN APPROVED FOR PUBLICATION PER LETTER DATED AUG. 30, 1974 FROM GRIFFIN L. JONES, KELLY AIR FORCE BASE.

T.O. 42B6-1-1

7.4-8-0

TECHNICAL MANUAL

QUALITY CONTROL OF OXYGEN PROPELLANT LIQUID OXYGEN, AVIATOR'S LIQUID BREATHING OXYGEN, AND AVIATOR'S GASEOUS BREATHING OXYGEN

PLEASE NOTE: SUPPLEMENTS ATTACHED TO THIS PAMPHLET.

F41608-67-D-7509

CHANGE NOTICE

LATEST CHANGED PAGES SUPERSEDE THE SAME PAGES OF PREVIOUS DATE

Insert changed pages into basic Publication. Destroy superseded pages.

PUBLISHED UNDER AUTHORITY OF THE SECRETARY OF THE AIR FORCE

BASIC AND ALL CHANGES HAVE BEEN MERGED TO MAKE THIS A COMPLETE PUBLICATION.

AFPS SA OCT 70, 1200 REPRINT

15 MAY 1963

CHANGE 7 1 MAY 1969

Reproduction for nonmilitary use of the information or illustrations contained in this publication is not permitted without specific approval of the issuing service. The policy for use of Classified Publications is established for the Air Force in AFR 205-1.

Technical orders are normally distributed promptly after printing. Date(s) shown on the title page (lower right) are for identification only. This is not a distribution date. Processing time sometimes causes distribution to only appear to have been delayed.

LIST OF EFFECTIVE PAGES

INSERT LATEST CHANGED PAGES. DESTROY SUPERSEDED PAGES.

NOTE: The portion of the text affected by the changes is indicated by a vertical line in the outer margins of the page. Changes to illustrations are indicated by miniature pointing hands. Changes to wiring diagrams are indicated by shaded areas.

Dates of issue for original and changed pages are:

Original	0	15 May 63	
Change	1	15 Oct 65	
Change	2	7 Nov 66	
Change	3	20 Dec 66	
Change	4	29 Sep 67	
Change	5	1 May 68	
Change	6	1 Sep 68	
Change	7	1 May 69	

TOTAL NUMBER OF PAGES IN THIS PUBLICATION IS 46 CONSISTING OF THE FOLLOWING:

Page No.	Change No.	Page No.	Change No.	Page No.	Change No.
*Title	7				
*A	7				
i	0				
ii	4				
1-1 – 1-2	6				
1-3 – 1-5	0				
1-6 Blank	0				
2-1	0				
2-2	4				
2-2A Added	4				
2-2B Blank	4				
2-3	1				
2-4	0				
2-5 – 2-6	6				
*2-7	7				
2-8	5				
2-9	0				
2-10	5				
2-10A Added	5				
2-10B Blank	5				
2-11 – 2-13	0				
2-14 Blank	0				
3-1	0				
3-2 – 3-3	6				
3-4	5				
*3-5	7				
3-6	6				
4-1 – 4-2	6				
5-1	6				
5-2 – 5-3	0				
*5-4	7				
5-5 – 5-7	4				
5-8 Blank	0				
6-1 – 6-2	0				

Upon receipt of the second and subsequent changes to this technical order, personnel responsible for maintaining this publication in current status will ascertain that all previous changes have been received and incorporated. Action should be taken promptly if the publication is incomplete.

* The asterisk indicates pages changed, added, or deleted by the current change.

ADDITIONAL COPIES OF THIS PUBLICATION MAY BE OBTAINED BY USAF ACTIVITIES IN ACCORDANCE WITH T.O. 00-5-2.

USAF

SECTION I

GENERAL

1-1. PURPOSE AND SCOPE. The purpose of this technical manual is to provide information, guidance, instructions, and procedures for on-base quality control of liquid oxygen used as a missile propellant, and liquid and gaseous oxygen used for aviator's breathing purposes.

1-2. GENERAL. The quality control requirements of oxygen supplied as a propellant are different from those of oxygen supplied for breathing purposes. This difference is defined and dictated by the kinds and amounts of contaminants permitted in oxygen, according to use. Therefore, a knowledge and understanding of this difference is essential to the quality control of oxygen in accordance with intended use.

1-3. DESCRIPTION AND PROPERTIES OF OXYGEN. Oxygen can exist as a solid, liquid, or gas, depending upon the temperature and pressure to which it is subjected. At atmospheric pressure, oxygen exists as a solid at temperatures below its melting point, -361°F (-218°C). Solid oxygen turns into a liquid at its melting point and remains in this state until the temperature rises to its boiling point, -297°F (-183°C). At this latter temperature, liquid oxygen vaporizes into the gaseous state. Conversely, gaseous oxygen will turn into liquid, at atmospheric pressure, by cooling to a temperature below -297°F. By increasing the pressure, gaseous oxygen can be liquefied at higher temperatures, up to its critical temperature, -182°F (-119°C). Oxygen will not condense to a liquid at temperatures above its critical temperature regardless of the pressure applied. The pressure required to liquefy oxygen at its critical temperature is known as its critical pressure, 736.5 psia. The application of high pressure and ultra-low temperatures to convert gases into their liquid state is known as the science and technology of cryogenics. Liquid oxygen is a cryogenic fluid.

1-4. SOURCE OF OXYGEN. Air, which contains about 21 percent oxygen by volume, is the principal source of liquid and gaseous oxygen. Air is compressed and cooled to liquefaction, whereupon the liquid oxygen is separated by distillation and taken off as liquid product, or gasified for gaseous product.

1-5. PHYSICAL PROPERTIES OF OXYGEN. Gaseous oxygen is colorless, odorless, tasteless and about 1.1 times as heavy as air. Liquid oxygen is an extremely cold (approximately 395 degrees below body temperature) pale blue fluid, which flows like water. One gallon of liquid oxygen weighs 9.519 pounds which is approximately 1.14 times the weight of one gallon of water. (See figure 1.1.) Liquid oxygen is stored and handled at atmospheric pressure in well-insulated containers which maintain the liquid at its boiling point. Therefore, liquid oxygen is always boiling as it slowly turns into gaseous oxygen. As the expanding gas from the boiling liquid increases in amount, it builds up pressure within the container. Therefore, the expanding gas must be vented to the atmosphere, because confinement is both dangerous and impractical. When the cold and colorless gas is vented to the atmosphere, it produces a fog as it immediately condenses moisture and carbon dioxide in the air.

1-6. CHEMICAL PROPERTIES OF OXYGEN. Oxygen is a very reactive material, combining with most of the chemical elements. The union of oxygen with another substance is known as oxidation. Extremely rapid or spontaneous oxidation is known as combustion. While oxygen is non-combustible in itself, it strongly supports and rapidly accelerates the combustion of all flammable materials; some to an explosive degree. Oxygen, as supplied, contains a minimum of 99.5 percent by volume of pure oxygen. The remaining 0.5 percent consists principally of argon, plus various organic and inorganic compounds in amounts measured in the parts per million range.

1-7. PRODUCTION (GENERATION) OF OXYGEN. Air, the raw material for the production of oxygen is principally a mixture of 78.09 percent nitrogen, 20.95 percent oxygen and 0.93 percent

OXYGEN						
MASS		LIQUID VOLUME AT BOILING POINT			GAS VOLUME AT ONE ATMOSPHERE AND 70°F	
Grams	Pounds	Liters	Gallons	Cubic Feet	Liters	Cubic Feet
1.000	0.002205	0.0008766	0.0002316	0.00003096	0.7540	0.02663
453.6	1.000	0.3976	0.1050	0.01404	342.0	12.08
1141.0	2.515	1.000	0.2642	0.03532	860.11	30.38
4318.0	9.519	3.785	1.000	0.1337	3256.0	115.0
32300.0	71.21	28.32	7.481	1.000	24355.0	860.1
1.326	0.002924	0.001163	0.0003072	0.00004106	1.000	0.03532
37.55	0.08280	0.03292	0.008697	0.001163	28.32	1.000

Figure 1-1. Oxygen Weight-Volume Equivalents

argon, by volume. The remaining 0.03 percent consists of various gases, vapors, and particulate matter in varying concentrations, depending upon locality and climatic conditions. Air is compressed and cooled to liquefaction. The liquid oxygen in the liquefied air is separated by fractional distillation, whereupon it is withdrawn as liquid oxygen product or passed to a vaporizer for conversion to gaseous oxygen product. The equipment and facilities used in producing oxygen are known as liquid oxygen generating plants.

1-8. LIQUID OXYGEN GENERATING PLANTS. Atmospheric air is passed through a liquid oxygen generating plant in five basic steps: compression, purification, refrigeration, expansion and distillation. A brief description of the basic steps is as follows:

a. Air from the atmosphere is first passed through filters before undergoing compression in the air compressor and then is cooled by a heat exchanger.

b. The cooled compressed air is purified and dried by removal of carbon dioxide, hydrocarbons, solid particles, and moisture as it is passed through carbon dioxide scrubbers, filters, drying tubes and hydrocarbon absorbers.

c. The cold and purified compressed air is further cooled by passage through a heat exchanger.

d. The air is then passed through an expansion valve where it liquefies as it becomes as cold as its temperature of liquefaction.

e. The liquid air is fed to the fractional distillation column where it flows through numerous trays, boiling off nitrogen and releasing liquid oxygen. The liquid oxygen collects at the bottom of the column, where it is drawn off as product or diverted to a vaporizer for conversion to gaseous oxygen product.

1-9. SUPPLY SOURCES OF OXYGEN. Liquid and gaseous oxygen supplied to the Air Force are obtained from the following generating plants.

1-10. COMMERCIAL PLANTS. Liquid and gaseous oxygen generated at commercial plants are procured according to the military specification that is specific to the intended use:

a. Liquid oxygen for propellant use is procured in accordance with the current issue of Specification MIL-P-25508.

b. Liquid and gaseous oxygen for aviator's breathing purposes are procured in accordance with the current issue of Specification MIL-O-27210.

1-11. GOVERNMENT OWNED - CONTRACTOR OPERATED PLANTS. Liquid oxygen generated at government owned-contractor operated plants is procured according to the current issue of Specification, MIL-P-25508.

1-12. GOVERNMENT OWNED - GOVERNMENT OPERATED PLANTS. Liquid and gaseous oxygen plants which are government owned-government operated and are located on Air Force bases are hereinafter referred to as AF Operated Generating Plants or Base Generating Plants. These plants are designed and built to generate liquid or gaseous oxygen according to the following production capacities and product quality:

a. Twenty, Twenty-five, and Fifty Tons Per Day. Produces both liquid oxygen and liquid nitrogen for support of missile sites. Generated liquid oxygen must meet the requirements of the current issue of Specification MIL-P-25508.

b. One Ton Per Day. Produces liquid and gaseous oxygen for breathing purposes in support of aircraft. Generated liquid and gaseous oxygen must meet the requirements of the current issue of Specification MIL-O-27210.

1-13. CONTAMINANTS AND CONTAMINATION. The following discussion on contaminants and contamination applies to propellant liquid oxygen and aviator's liquid breathing oxygen. Contaminants in, and contamination of aviator's gaseous breathing oxygen is discussed in Section V. Liquid oxygen as produced by generating plants contains contaminants which are not completely removed by the generating process. Atmospheric air, from which liquid oxygen is generated, is the primary source of contamination. An additional source of contamination is the compressors and other equipment of the generating plants. Airborne contaminants and those added by the generating plants are partially removed by a system of filters, absorbers, driers, and heat exchangers before the air is finally liquefied. When the liquid oxygen separates from the liquefied air, it carries with it those contaminants which are not completely removed. The variety and quantity of contaminants which separate with the liquid oxygen depend on how effective their removal has been during the generating process. Generating plants are designed to remove contamination to the lowest limits possible both for safety of operation and for quality of product. The contamination limits of liquid oxygen produced by any generating plant for Air Force Supply as a propellant or as breathing oxygen are specified as procurement limits. Procurement limits and the ultimate use limits of contamination are based on the types and significance of contaminants, and the sources of increasing contamination in liquid oxygen during storage, handling, and transfer.

1-14. TYPES AND SIGNIFICANCE OF CONTAMINANTS. The types and significance of contaminants in liquid oxygen are described in paragraphs 1-15 through 1-17.

1-15. HYDROCARBONS. These contaminants are present in atmospheric air, and are also added by the compressors and other equipment of the generating plant. They are only partially removed by the low-temperature hydrocarbon absorption-purifiers of the generating plants. Those which separate with the liquid oxygen are called light hydrocarbons because they contain four carbon atoms or less, such as methane, acetylene, ethane, ethylene, propane, and butane. Heavier hydrocarbons are removed to insignificant concentrations in properly operating plants. However, through mistakes, carelessness, or breakdown of equipment during storage, handling and transfer of liquid oxygen, heavy hydrocarbons can cause contamination in the form of solvents, oils, greases or fumes. The presence of hydrocarbons in liquid oxygen constitutes a potential fire and explosion hazard. The hazard increases during storage and handling because all of the common hydrocarbon contaminants, except carbon monoxide, are less volatile than liquid oxygen and, therefore, increase in concentration. If either the solubility limit or the low flammability limit of a hydrocarbon is exceeded, the condition is especially hazardous. A source of ignition can initiate a fire or explosion if the hydrocarbon is present in sufficient concentration to sustain combustion. Ignition sources can be static electricity, mechanical and fluid friction, and shock waves introduced by impact. Whenever a hydrocarbon is present in quantities greater than its solubility in liquid oxygen, it separates out of the liquid as a solid. Even the smallest grain of hydrocarbon solid in liquid oxygen has the potential of continued burning upon suitable ignition. Although one tiny particle may not be dangerous in itself, a collection of such particles could be serious, since ignition may propagate from particle to particle. Acetylene is especially hazardous in this respect.

a. Acetylene. Acetylene is the most hazardous hydrocarbon contaminant because: it is very insoluble; it can readily be triggered into ignition; and, since it is chemically unstable, it can decompose under certain conditions and become its own source of ignition. Therefore, a special test has been developed to determine acetylene concentration in propellant liquid oxygen.

b. Significance in Aviator's Liquid Breathing Oxygen. Hydrocarbon contaminants in liquid oxygen create, in addition to their potential fire and explosion hazards, potential psychological and physiological hazards to aircrews when liquid oxygen is used for breathing purposes. Depending upon the type and concentrations of hydrocarbons, psychologically, the effects may be uneasiness, apprehension or possible panic, resulting from detecting their presence by odor; physiologically, the effects may be nausea, illness, intoxication or possible asphyxia.

1-16. INERT SOLIDS. These contaminants are classified as inert solids because they do not react with oxygen to create a fire and explosion hazard, and to distinguish them from hydrocarbons, which become solids when their solubility limits are exceeded. Inert solids consist of three distinct forms:

a. Particulate Matter. These solids consist of rust, metal fragments, dust and fibers derived from the equipment or the environment of the liquid oxygen supply system. These contaminants are solids at normal temperatures as well as at liquid oxygen temperature.

b. Moisture. In its liquid or vaporous form, moisture condenses to ice on contact with liquid oxygen or with the cold surfaces of equipment. Atmospheric moisture is an ever-present source of contamination.

c. Carbon Dioxide. This contaminant is slightly soluble in liquid oxygen but separates out of liquid oxygen as a solid when its solubility limit is exceeded. Inert solid contaminants in liquid oxygen are hazardous for a number of reasons. First, they may cause mechanical malfunctions or failures. Second, they may cause plugging of filters, lines, injectors, valves, etc. Third, they may accumulate charges of static electricity.

1-17. TOXIC AND ODOROUS CONTAMINANTS. The odorous and toxic characteristics of hydrocarbons have already been discussed in paragraph 1-15, above. In addition to the hydrocarbons, there are other contaminants which, if present in aviator's liquid breathing oxygen, may also affect the mental and physical well-being of aircrews. In particular, these contaminants are nitrous oxide and chlorinated hydrocarbons.

1-18. SOURCES OF INCREASING CONTAMINATION. The initial contamination of liquid oxygen in the generating plant increases continuously after generation, as non-volatile contaminants are concentrated by the evaporation of liquid oxygen. This gradual process of increasing contamination is accelerated if contaminants are introduced during storage, handling and transfer operations, all of which are potential sources of increasing contamination. The added contaminants are concentrated as liquid oxygen vaporizes and the increasing contamination of liquid oxygen is therefore compounded each time contaminants are introduced. This means that the problem of controlling contaminants becomes more severe as the liquid oxygen passes through both the propellant liquid oxygen supply system and the aviator's breathing oxygen supply system. With respect to the former, the problem is increased by large scale transfers of liquid oxygen and by long periods of storage. In regard to the latter, the problem is increased by the potential toxicity and lower maximum limits of contaminants in liquid oxygen. Thus, an acceptable concentration of contaminants in liquid oxygen as generated or procured can increase to a point which may threaten the safety or reliability of the mission. Therefore, procurement limits establish higher quality for both propellant liquid oxygen and aviator's breathing oxygen to allow for increase of contamination to established use limits. This margin of safety does not provide a margin for error or for unexpected contamination, and personnel should not relax their vigilance in quality control against the ever present sources of increasing contamination of liquid oxygen.

1-19. INCREASING CONCENTRATION DUE TO EVAPORATION OF LIQUID OXYGEN. Liquid oxygen in the supply system is always boiling and evaporating. Non-volatile contaminants in

liquid oxygen are always increasing in concentration as the amount of liquid decreases. This ever-present process of increasing contamination is intensified by cool-down vaporization looses associated with liquid transfer operations. Concentration of contaminants will increase in approximate proportions to the amount of liquid oxygen loss by vaporization. In the case of large scale transfers of propellant liquid oxygen, the increases of concentration of contaminants can be of considerable magnitude. For example, if a 10 percent vaporization loss occurs, the concentration of contaminants will automatically increase by a factor of 1.11. Obviously, repeated losses will increase contamination to dangerous levels.

1-20. HANDLING AND TRANSFER OPERATIONS. These operations are a continuing source of increasing contamination by contaminant addition. The types of contaminants range from dust and dirt to moisture and carbon dioxide and other atmospheric constituents. Whenever transfer operations require the connection or disconnection of a transfer line, the opportunity for introducing additional contamination arises. At the time of connection, atmospheric contaminants or dust and dirt may be trapped in a section of the transfer line, to be carried into the supply system by the flowing liquid. At the time of disconnection, atmospheric contamination may become deposited inside the cold transfer equipment, ready to enter the rest of the system during the next transfer operation. Field and laboratory experiments have shown that strong convective currents are formed by the density difference between cold oxygen vapors and warm ambient air. As the cold, denser oxygen vapors flow out of the low points of cold transfer equipment, the warm, less dense air flows in at the high points, depositing moisture and other condensables in the form of frost. Both mechanisms of contamination can be controlled by strict adherence to proper procedures. The trapped portion of the atmosphere may be removed by adequate purging before transferring, and condensables may be prevented from entering cold transfer connections by allowing the connections to warm up before disconnecting. The making and breaking of transfer connections should be accomplished as quickly as careful handling will permit.

1-21. EQUIPMENT. The sources of increasing contamination of liquid oxygen from equipment are variable both as to time and origin. Long-term deterioration of mechanical equipment must be expected. The moving parts of valves and pumps will wear and contribute to particulate contamination. Other sources of potential contamination are the solvents and solids which may remain from repair or cleaning operations.

SECTION II

QUALITY CONTROL OF PROPELLANT LIQUID OXYGEN

2-1. INTRODUCTION. The quality control of propellant liquid oxygen requires frequent and continuous surveillance over its constantly increasing contamination. Quality control of propellant liquid oxygen begins with base-generation or procurement to assure that its contamination is within procurement limits. Surveillance continues throughout the supply system to assure that, at any time during storage, handling, and transfer, the contamination of propellant liquid oxygen is within use limits. Adequate and reliable quality control of liquid oxygen demands that each operation in the missile liquid oxygen-supply-system must be carried out in strict compliance with procedures established to assure safety of operations and reliability of the propellant.

2-2. SCOPE. This section established procedures and requirements for the quality control of oxygen that is procured or base generated, transferred, and stored for use as a propellant. This section is applicable to base personnel who are responsible for supervising or performing the operations associated with receipt, generation, storage, transportation, or transfer of propellant liquid oxygen.

2-3. PERSONNEL. Personnel selected to perform operations in the supply system should be trained in a thorough knowledge of the characteristics of liquid oxygen and its contaminants, and of the system to be quality controlled. Only those personnel who demonstrate understanding of the operations involved, and capable and reliable performance, should be assigned duties and responsibilities in the supply system.

2-4. CONTROL OF CONTAMINATION. A knowledge and understanding of how contaminants are concentrated in liquid oxygen by the sources of increasing contamination is essential to the effective control of contamination.

2-5. VAPORIZATION. The concentration of contaminants due to liquid oxygen vaporization cannot, of course, be prevented. However, the rate of increasing contamination from this source shall be controlled by minimizing heat additions in handling and transfer through proficient and careful performance of operations.

2-6. EQUIPMENT. Addition of contaminants from equipment shall be reduced or prevented by operating and maintaining generators, storage tanks, trailers and propellant loading systems in accordance with the applicable operation and service technical orders. This source of added contamination shall be further controlled by assuring that all equipment is inspected and cleaned in accordance with T.O. 42C-1-11.

2-7. DISPOSITION OF DETERIORATED PROPELLANT LIQUID OXYGEN. When the contaminants in liquid oxygen reach or exceed the Use Limits, the liquid oxygen shall be condemned and proper disposition of the material shall be made. Occasion may arise when safety and reliability may be insured through condemnation and disposal of liquid oxygen that is not contaminated beyond Use Limits but which does not have sufficient quality to undergo required transfers and storage. As an example, it would not be in the best interests of safety and reliability to fill a launch site storage tank with "perishable" propellant which, today, is within Use Limits but, which at a later time when about to service a missile will have deteriorated beyond the Use Limits. Estimating when propellant liquid oxygen will deteriorate beyond Use Limits can be based only on past affecting conditions and facts; these pertinencies vary from Base to Base, and within each Base. The "when", "how", and "point" of proper disposal of liquid oxygen, whether or not its deterioration is too close to Use Limits to allow for a margin of safety, is a Base managerial problem. The specific action to be taken is determined after examination of all pertinent conditions and facts.

2-8. QUALITY CONTROL REQUIREMENTS OF PROPELLANT LIQUID OXYGEN.

2-9. PROCUREMENT LIMITS. The procurement limits for purity and contamination of

propellant liquid oxygen must meet the requirements of the current issue of Specification MIL-P-25508 (USAF). Liquid oxygen, space vehicle grade (99.60% purity) in accordance with AFPID 9135-8 meets the requirements of MIL-P-25508 and may be substituted for military specification oxygen.

2-10. USE LIMITS.

Total Hydrocarbons ppm by weight measured as carbon	Acetylene ppm by weight	Purity % by volume when gasified	Moisture at 70°F and 760 mm	Particulate
75 (max) (200 ppm by volume as methane equivalent)	1.5 (max)	99.2 (min)	26.3 ppm of water vapor (max) (-63.5°F Frostpoint)	2.5 mgm/Liter (max), total particles and fibers

2-11. SUPPLY SOURCES OF PROPELLANT LIQUID OXYGEN.

2-12. PROCURED FROM CONTRACTORS.

a. Commercial Generating Plants. Propellant liquid oxygen procured from commercial generating plants must meet the requirements of the current issue of Specification MIL-P-25508 as determined by tests conducted on the contents of each filled shipping container prior to leaving contractors' plants.

b. Government Owned-Contractor Operated Generating Plants. Propellant liquid oxygen procured from Government owned-contractor operated generating plants must meet the requirements of the current issue of Specification MIL-P-25508 as determined by testing each Government-owned storage container after each addition of a new batch of material; or, in the case of continuous production, at established intervals, but not less than once every 24 hours.

2-13. AIR FORCE OPERATED GENERATING PLANTS. Propellant liquid oxygen produced by on-base generating plants must meet the requirements of the current issue of Specification MIL-P-25508 as determined by the Continuous-Recording, Oxygen Purity and Total Hydrocarbons Analyzers, and by tests for acetylene, moisture, and particulate performed at least once a day.

2-14. SAMPLING AND TESTING. Sampling and testing at intervals and points in the supply system provide the continuous monitoring of contamination that is so essential to the quality control of propellant liquid oxygen. Tests, both singly and collectively, serve many needs and purposes; in fact, they are the basis for the performance of all operations in supply. No operation in the supply system shall be performed until a basis for action is established by tests. The basis for action at any point in supply is the degree of contamination of propellant liquid oxygen as shown by tests. Tests, or records of tests will show: contaminant concentration upon receipt, and during on-base-generation of propellant; the contamination, and rate of increase, from vaporization and from contaminant additions during storage, handling and transfer; the point of added contamination and whether occurrence was due to mishandling or equipment malfunction; the presence or imminence of a hazardous condition; the necessity for investigation and corrective action; and ultimately, the reliability of the propellant at the moment of use.

2-15. TESTS, METHODS, AND EQUIPMENT. The analysis for contamination of propellant liquid oxygen, which consists of tests for content of purity, total hydrocarbons, acetylene, moisture and particulate matter, is performed principally by instruments, designated as major equipment. The required tests, methods, and major equipment are listed in paragraph 2-23. The complete list of required equipment which includes accessory laboratory equipment is listed in paragraph 2-24.

2-16. SAMPLING EQUIPMENT AND METHODS.

a. Sampler, Liquid Oxygen, TTU-131/E (Cosmodyne). (Federal Stock No. 6695-895-1348). Operate, maintain and clean the sampler in accordance with T.O. 33D2-10-34-1.

b. Collective Dewar - Liquefied Gas Container. (Federal Stock No. 7330-205-1415, 2-liter capacity; all metal.) This method simply consists of permitting a flow of the liquid into the Dewar. A

tube, which ends in a vertical direction, shall be fixed at the opening of the sampling point. Purge the sampling point and attached tube with flowing liquid oxygen. Fill the Dewar half full with liquid oxygen and precool the Dewar by swirling the liquid. Discard the precooling liquid. Immediately collect the sample, and quickly close the container with vented closure. Perform tests on the sample as soon as possible to prevent excessive concentration of contaminants. The Dewar is used to collect samples for the acetylene and particulate tests.

NOTE

Before sampling, clean the Dewar by rinsing three times with 200 milliliters of filtered methylene chloride or trichlorotrifluoroethane ("Freon TF Solvent") solvent; dry with filtered gaseous nitrogen; close with clean closure.

CAUTION

A catch pan shall be placed under sampling valve to contain LOX drippings or spillage during filling of Cosmodyne and Dewar samplers.

CAUTION

A suitable protective cover shall be placed over sampling valves after sample is taken and shall be removed only for taking samples or for repairing valves.

2-17. LABORATORY CLEANLINESS AND SAFETY. Environmental cleanliness is essential and required to prevent airborne contamination of test samples and of testing and sampling equipment. The potential hazards associated with handling liquid oxygen, and cylinders of compressed gases require strict compliance with established safety measures and precautions. Therefore work shall be performed in the laboratory, and the laboratory shall be operated and maintained, in accordance with the following requirements:

a. The laboratory shall contain a fume hood.

b. The filtering of liquid oxygen shall be performed at the fume hood.

c. Two exits from the laboratory shall be provided.

d. The floor shall be damp-mopped at least once every 24 hours, or more frequently if required by outside environment. When considered necessary, the floor shall be cleaned with a detergent and water.

e. All fixtures, testing instruments, table tops, cabinets, and desks shall be damp-wiped every 24 hours. Do not use a dry cloth or feather duster which increases the content of airborne dust and redistributes it about the area.

f. Good housekeeping is essential to the efficient and safe operation of the laboratory. Testing and sampling equipment which requires cleaning shall be cleaned as soon as possible after use and placed in its assigned storage space. Metal waste cans with self-closing covers shall be conveniently located for the disposal of waste. Accumulation of odds and ends on work surfaces and in-out-away places shall be avoided.

g. Smoking shall be positively prohibited in the laboratory.

h. Personnel shall be prohibited from carrying sources of flames and sparks, such as matches and lighters into the laboratory.

i. Personnel shall wear protective clothing and equipment when handling liquid oxygen.

j. A carbon dioxide extinguisher and a bucket of sand shall be present in the laboratory to fight fires.

k. In the event of a fire, if the fire cannot be quickly controlled, personnel shall evacuate the area immediately.

l. In the event of an accidental spillage involving large quantities of liquid oxygen, the area shall be evacuated.

m. Safety equipment and protective clothing shall be inspected periodically and frequently for suitable operation and use.

n. Safety precautions shall be observed at all times when operating the Perkin-Elmer 213 in the laboratory. Fittings shall be leak-tested frequently and regularly. Personnel shall become thoroughly familiar with safety precautions in handling high-pressure gas cylinders and connections. Safety instructions are contained in T.O. 42B5-1-2, Gas Cylinders, Use, Handling and Maintenance.

2-18. RECEIPT OF PROPELLANT LIQUID OXYGEN FROM A CONTRACTOR. Propellant liquid oxygen procured from contractor owned-contractor operated plants is sampled from the

transport container and tested prior to shipment. The delivery of the product is accompanied by a procurement limits test report, signed by an authorized representative of the contractor. Propellant liquid oxygen procured from government owned - contractor operated plants is sampled from the storage tanks, after the addition of each new batch or, in the case of continuous production, at established intervals, but not less than once every 24 hours, and tested for procurement limits. The delivery of the product is accomplished by the latest test reports of the storage tanks from which the shipment was filled. In addition, the contractor samples the contents of each transport trailer on a once-a-week schedule, and tests for procurement limits. A record of tests on each trailer is maintained by the contractor. Upon receipt of commercial product, on-base sampling and testing is not required before unloading, unless there is evidence of possible contamination of the product enroute. When evidence of possible contamination enroute exists, before unloading is permitted, sample and test the contents of the shipping container as follows:

a. Sampling Location: Outlet port of the shipping container.

b. Samplers: Collect one set of samples with the TTU-131/E and Dewar sampler.

c. Tests: Nos. 3, 4, 5, 6 and 7 of paragraph 2-23.

d. Quality Control Requirements. Propellant liquid oxygen procured from a contractor shall not exceed the Procurement Limits of the current issue of Specification MIL-P-25508.

NOTE

Test results differing objectionably from Procurement Limits shall be reported to the Air Force Quality Control Representative concerned and to MAAMA (MAOQT) requesting immediate investigation and appropriate action. If the "excessively" contaminated shipment cannot be returned, permit unloading for disposal purposes only. Tank cars or tank trucks which are unloaded into a storage tank and which are received by a contractor containing product in amounts greater than approximately 200 gallons, shall be reported by the Air Force Quality Control Representative concerned to the responsible Supply Officer by letter as follows: Name of propellant producing or distributing plant. Identification of transportation equipment. Date received. Approximate amount of produc. in container when received. Action taken.

2-19. AIR FORCE OPERATED GENERATING PLANTS. Sample and test propellant liquid oxygen during generation as follows:

a. Sampling and Testing Frequency: Continuous-Recording Oxygen Purity and Total Hydrocarbons Analyzers; and tests for acetylene, moisture and particulate at least once a day.

b. Sampling Location: In accordance with the applicable Oxygen-Nitrogen Generating Plant, Operation and Service Manual.

c. Samplers: Collect sample for moisture test with the TTU-131/E Sampler and sample for acetylene and particulate matter tests with the Dewar.

d. Tests: Nos. 1, 2, 5, 6 and 7 of paragraph 2-23.

e. Quality Control Requirements: Propellant liquid oxygen during generation shall not exceed the Procurement Limits of the current issue of Specification MIL-P-25508.

2-20. AIR FORCE OPERATED GENERATOR STORAGE TANK. Sample and test the contents of the generator storage tank as follows:

a. Sampling and Testing Frequency: At least once per week.

b. Sampling Location: At the 10 percent sampling try cock. Tanks which are not so equipped shall be sampled at the lowest accessible point.

c. Samplers: Collect one set of samples with the TTU-131/E and Dewar Samplers.

d. Tests: Nos. 3, 4, 5, 6, and 7 of paragraph 2-23.

e. Quality Control Requirements: The contents of the generator storage tank shall not exceed the Use Limits specified in paragraph 2-10.

NOTE

If the contents of the generator storage tank exceed the Use Limits, make proper disposition of the contents and ascertain the cleanliness of the storage tank in accordance with T.O. 42C-1-11. If the storage tank does not meet the cleanliness criteria of T. O. 42C-1-11, appropriate cleaning action shall be taken.

2-21. ON-BASE AIR FORCE MAINTAINED TRAILERS. Sample and test on-base trailers as follows:

a. Sampling and Testing Frequency: At least once per week.

b. Sampling Location: Outlet port of the filled trailer.

c. Samplers: Collect one set of samples with the TTU-131/E and Dewar Samplers.

d. Tests: Nos. 3, 4, 5, 6, and 7 of paragraph 2-23.

e. Quality Control Requirements: The contents of the trailer shall not exceed the Use Limits specified in paragraph 2-10.

NOTE

If the contents of the trailer exceed the Use Limits, make proper disposition of the contents and, before re-use, clean the trailer tank in accordance with T.O. 42C-1-11.

2-21A. BASE STORAGE TANKS. Sample and test the contents of the base storage tanks as follows:

a. Sampling and Testing Frequency: At least once every 30 days.

b. Sampling Location: At the ten percent sampling trycock. Tanks which are not so equipped shall be sampled at the lowest accessible point.

c. Samplers: Collect one set of samples with the TTU-131/E and Dewar Samplers.

d. Tests: Nos. 3, 4, 5, 6, and 7 of paragraph 2-23.

e. Quality Control Requirements: The contents of the base storage tanks shall not exceed the Use Limits specified in paragraph 2-10.

2-22. LAUNCH SITE STORAGE TANK. When launch site storage tank is not protected by a suitable in-line filter, liquid oxygen shall be unloaded through the following filters, as applicable, located between the trailer and the fill connection of the launch storage tank:

Atlas Sites: Filter, Portable, Liquid Oxygen; 10 Micron, Nominal; 25 Micron, Absolute; FSN 1450-818-5251AC, Manufacturer's Code 81331; part No. 8003506.

Titan I Sites: Filter, Portable, Liquid Oxygen; 10 Micron, Nominal; 25 Micron, Absolute; FSN 4930-857-1110; Manufacturer's Code 81321; part No. 002105.

Operation and maintenance instructions are contained in applicable missile technical orders. Sample and test the launch site storage tank as follows:

a. Sampling and Testing Frequency: The following sampling and testing frequencies shall be performed when a single Propellant Loading Exercise (PLX) is carried out, or when a series of PLX's is to be run on a single missile within a 72-hour period as indicated below:

(1) Single PLX. No longer than 72 hours prior to PLX.

(2) Single PLX. Immediately after completing PLX and prior to topping launch storage tank.

(3) Single PLX. Immediately after topping launch storage tank following completion of PLX.

(4) Single PLX. Immediately after resupply when contents of storage tank are discarded.

(5) Series of PLX's. Sample and test only the first PLX of series, no longer than 72 hours prior to start of series.

(6) Series of PLX's. After each third topping of storage tank during PLX series.

(7) Series of PLX's. After completing last PLX of series and prior to topping storage tank.

(8) Series of PLX's. Immediately after topping storage tank following last PLX of series.

(9) Series of PLX's. Immediately after resupply when contents of storage tank are discarded.

(10) Immediately after each third topping of storage tank between single PLX's or series of PLX's, but in no instance shall the storage tank be sampled less than once in 90 days.

NOTE

Test results of sampling required by (1) and (5) above shall be reported to the maintenance activity prior to starting the PLX or series of PLX's. When PLX's are performed with liquid nitrogen in lieu of Lox, the same procedures above will apply.

b. Sampling Location: At the empty trycock located at the lower level of the tank.

c. Samplers: Collect one set of samples with the TTU-131/E and Dewar Samplers.

d. Tests: Nos. 3, 4, 5, 6, and 7 of paragraph 2-23.

e. Quality Control Requirements: The contents of the launch storage tank shall not exceed the use limits specified in paragraph 2-10.

WARNING

Liquid propellant oxygen must not be loaded into the missile if the contents of the launch storage tank exceed the use limits. Make proper disposition of the contents. If the use limits for any of the following: total hydrocarbons, acetylene, moisture, or particulate have been exceeded, ascertain the cleanliness of the propellant loading system (PLS) in accordance with T.O. 42C-1-11. If the PLS does not meet the cleanliness criteria of T.O. 42C-1-11, appropriate cleaning action shall be taken.

2-23. TESTS, METHODS, AND MAJOR TEST EQUIPMENT FOR QUALITY CONTROL OF PROPELLANT LIQUID OXYGEN.

No.	Test	Equipment	Test Methods
1	Purity	Continuous Oxygen Purity Analyzer	In accordance with the applicable Oxygen Generating Plant Operation and Service Manual.
2	Total Hydrocarbons	Continuous Oxygen Total Hydrocarbons Analyzer	In accordance with applicable Manufacturer's Instruction Manual.
3	Purity	Portable Oxygen Purity Analyzer Kit (Orsat Type).	In accordance with applicable Oxygen Generating Plant Operation and Service Manual.
4	Total Hydrocarbons	Portable Hydrocarbon Analyzer; Perkin-Elmer Model 213	In accordance with applicable Manufacturer's Instruction Manual.
5	Acetylene	Acetylene Test Kit (Ilosvay Type-Short Method).	In accordance with applicable Manufacturer's Instruction Manual
6	Moisture	Dewpoint Indicator (Electrolytic hygrometer type, Consolidated Electrodynamics part No. 26-350-6000)	In accordance with Consolidated Electrodynamics Instruction Manual
7	Particulate Matter	Filtration and Millipore Equipment	In accordance with Specification MIL-P-25508 (A 2-liter sample is acceptable)

2-24. LABORATORY EQUIPMENT.

Item No.	Stock No. and Part No.	Nomenclature
1	6630-714-2457, Perkin-Elmer part No. 213-0001	Hydrocarbon Content Analyzer
2	6685NC824089PYB, Consolidated Electrodynamics Corp, part No. 26-304	Moisture Tester
3	6640-829-5812, Millipore, part No. XX50-047-00	Filter Holder, Aerosol Standard
4	3655-893-3096, Millipore, part No. XX20-047-20SS	Filter Holder, Hydrosol
5	3655-893-3092, Precision Scientific Co., Cat. No. 68351	Oven, Vacuum Dessicator
6	3655-893-3097, Millipore Type RAWGO 04700 Package	Filter Paper
7	3655-893-3088, Cahn Elec., part No. 1404	Balance
8	3655-893-3098, Corning LG-2, 3160, Arthur H. Thomas, part No. 4333-A	Dishes, Petri, Pyrex
9	3655-893-3089, Braun, part No. 28630	Aspirator
10	3655-856-8941	Collection Dewar - Metal Liquefied Gas Container
11	6640-855-8866, A. H. Thomas, part No. 2110	Sample Evaporation Beaker
12	6640-855-8865, Braun part No. 29416	Filter, Flask
13	6640-855-8864, A.H. Thomas, part No. 2214	Bottle, 8 oz.
14	3655-893-3093, Tygon S22-1, Arthur H. Thomas, part No. 9766	Tubing, 1/4 in. ID, 1/16 in. Wall
15	3655-893-3094, Tygon S22-1, Arthur H. Thomas, part No. 9766	Tubing, 1/4 in. ID, 1/2 in. Wall
16	6640-855-8765, Braun, part No. 25040-5, Coors, part No. 580, Size 5	Desiccator Plate, Porcelain, 230 mm
17	6640-420-9170, Braun, part No. 25045-4, Coors, part No. 570, Size 4	Desiccator Plate, Porcelain, 190 mm

Item No.	Stock No. and Part No.	Nomenclature
18	6640-418-0680, Fisher Scientific, part No. 5-875-A or Humbolt Mfg. Co., No. H-8700	Clamp, Hoffman, Open Side
19	6640-855-8764, Fisher Scientific, part No. 5-743	Clamp, Versatile, Asbestos Sleeves
20	6640-855-8763, Fisher Scientific, part No. 5-756	Clamp, Holder, Regular Model
21	6640-855-8863, Braun part No. 60110-6x9 or A. S. Aloe No. V77000C	Support, Iron, Rectangular Base
22	6640-805-8354, Harshaw Chemical, part No. 5 or Chicago Apparatus Co., No. 49500B (#5)	Stopper, Bottle, Rubber
23	6640-855-8862, Braun part No. 23455 or Aloe part No. V34750	Cork Borer, Hand Set
24	5110-897-8355, Braun part No. 23475 or Aloe part No. V34800	Sharpener, Cork Borer
25	3655-525-5920 Air Products part No. 3-979-13-0001.	Wire, Copper, B&S 22 5 lb box
26	7310-245-0927, Braun part No. 33938 or Fisher, part No. 11-499-50 or Lindberg No. HR-8A	Hot Plate, 8 in. diameter
27	6640-426-0315, Millipore part No. XX62000 06	Forceps, Microscope Slide
28	6640-855-8861, Millipore part No. YY-22-142-00	Holder, Test Filter, 142 mm
29	6640-855-8860, Millipore part No. WH 14200	Filter, Microweb, 142 mm pkg.
30	6640-855-8859, Millipore part No. WS 14200	Filter, Microweb, 142 mm pkg.
31	6640-855-8762, Emil Greiner part No. G2754D, Nalge part No. 2402	Bottle, Wash or Dispensing
32	6640-855-8754, Emil Greiner part No. G2230H, Nalge part No. 2176	Spouts, Pouring

Item No.	Stock No. and Part No.	Nomenclature
33	6640-855-8755, Emil Greiner part No. T3867P, N alge part No. 2340	Jugs, Dispensing, 2 gal
34	6640-855-8756, Emil Greiner part No. T3867P, Nalge part No. 2340-5	Jugs, Dispensing, 5 gal
35	6640-855-8823, Emil Greiner part No. G21598, Nalge Part No. 6190	Stopper, Polyethylene, Size 10, doz.
36	6640-855-8760, Emil Greiner part No. G21598, Nalge part No. 6190-8	Stopper, Polyethylene, Size 8, doz.
37	6640-855-8758, Emil Greiner part No. G21598, Nalge part No. 6190-4	Stopper, Polyethylene, Size 4, doz.
38	4710-863-9096, A. H. Thomas part No. 9767	Tubing, Polyethylene, 1/4 in, OD. 100 ft. roll
39	6640-855-8770, Corning Glass Works part No. LG-2-5340	Flask, Filtering, 4,000 ml
40	6640-855-8769, Corning part No. LG-22080	Bulb, Levelling
41	6640-515-6064, Corning part No. LG-2-3075	Cylinder, Graduated, 100 ml
42	6640-420-3000, Corning part No. LG-2-3022	Cylinder, Graduated, 1000 ml
43	6640-527-7342, Corning part No. LG-2-3120	Desiccator, Glass
44	6640-855-8768, A. H. Thomas, part No. 5474C, Corning part No. 5650	Flask, Volumetric, 100 ml
45	6640-855-8767, A.H. Thomas, part No. 5474-C, Corning part No. 5650-1000	Flask, Volumetric, 1000 ml
46	6640-403-6000, Corning part No. LG-2-1000	Beaker, Laboratory, 2000 ml
47	6640-855-8766, Braun part No. 13912-600, Corning part No. 1000	Beaker, Griffin Low Form 600 ml
48	6650-530-0022, American Optical Model 2MG-H2	Microscope, Optical Vertical
49	6650-490-2702, Fisher Scientific part No. 12-455	Stage, Micrometer, Microscope

Item No.	Stock No. and Part No.	Nomenclature
50	6650-540-9018, American Optical Model 353	Light, Microscope
51	6650-897-7083, Bausch & Lomb Catalog No. 31-16-50-01 (Catalog D184)	Eyepiece, Filar, Micrometer
52	5120-897-8358, Master Appliance part No. 12300	Heatgun
53	6640-855-8876, Bell & Gossett Model SYC 10-1	Compressor, Oilless
54	6640-855-8875, A. H. Thomas part No. 1040-A or Fisher part No. 1-100-A or Welch Mfg. Co., No. 1402B	Air Pump, Two Stage
55	7920-897-8356, Emil Greiner part No. G-1412	Brush, Staticmaster, 1 in.
56	6670-855-8753, Braun part No. 12445A or Ahaus No. 750-S	Balance, Triple Beam, 1610 gr
57	8415-897-7086, A. H. Thomas part No. 6103F	Gloves, Polyethylene
58	6640-855-8761, A. S. Lapine part No. 190-96, Corning part No. 3950	Glass Wool
59	6850-281-1837, Emil Greiner part No. G7688D	Drierite, Indicating $CaSO_4$, 5 lb bottle
60	8415-897-7087, Standard Safety Co., part No. Sta-Safe 822W	Gloves, Cryogenic Type, pr.
61	6506-106-5000, Fisher Scientific No. A-660	Ammonium Chloride, 25 lb drum
62	6810-753-4784, McKesson & Robbins No. 73-631, Fisher part No. A-669	Ammonium Hydroxide, pint bottle
63	6810-897-8473, Baker Chemical Co., No. 1656, Fisher part No. C-457	Cuprous Chloride, 1 lb bottle
64	6810-033-8851	Trichlorotrifluoroethane ("Freon TF-Solvent") Solvent
65	6640-855-8874, Millipore part No. AAWGO 4700	Paper, Filter (100 per pkg)
66	6630-507-0584, Air Products part No. 5-869-12-0006	Test Set Assembly, Oxygen Orstat Type

Item No.	Stock No. and Part No.	Nomenclature
66A	6630-404-2500 Air Products part No. 4-104-27-0001	Bulb, Leveling
66B	6630-399-2958 Air Products part No. 4-894-27-0001	Tube, Reacting
66C	6630-399-2959 Air Products part No. 4-717-27-0001	Reservoir
66D	6630-490-1731 Air Products part No. 4-105-27-0001	Burette, 100 ml.

Item No.	Stock No. and Part No.	Nomenclature
67	6640-855-8873, Fisher Scientific part No. 3-403	Wash Bottle (12 per case)
68	6505-823-7877, Fisher Scientific part No. 4-320 or Braun part No. 60142 Cat. No. 21850	Detergent (12 3-1/4 lb cartons per case)
69	6810-241-1203, Fisher Scientific part No. C-493	Copper Sulfate (5-lb bottle)
70	6630-855-8872, Air Products part No. 4-999-51-001; 6185 DC-16	Acetylene Test Check Color Standard, set; ppm: 0.1, 0.25, 0.5, 1.0, 1.5
71	6640-855-8871, Nalge part No. 2302	Bottle, Aspirator
72	6850-680-2234, Fisher Scientific part No. S-156	Silica Gel (5-lb bottle)
73	6810-275-8126, Fisher Scientific part No. S-516	Soluble Starch (1-lb bottle)
74	6810-262-8577, Fisher Scientific part No. H-330	Hydroxylamine, Hydrochloride (1 pkg. btl.)
75	6810-223-2727, Fisher Scientific part No. D-37	Methylene Chloride (55 gal drum)
76	6640-855-8870, Fisher Scientific part No. 10-595	Clamps, Cyl Support
77	6640-855-8869, Fisher Scientific part No. 9-050	Distilled Water Storage Tank
78	6640-855-8868, Fisher Scientific part No. 9-039-5A or Braun part No. 26172	Still, Water
79	6640-855-8867, Nalge Co. part No. 2202	Bottle, Nalgene (6 per case)
80	6830-855-9427, AFPID No. 6806	Oxygen, Methane, 90 $\pm$10 PPM
81	6830-855-9430, AFPID No. 6809	Oxygen,Methane, 5 to 10 PPM
82	4730-775-9716, part No. 202-1 Crawford Fitting	Fitting, Nut, 1/8 in. OD
83	4730-863-9100, part No. 203-1, Crawford Fitting	Fitting, Front Ferrule, 1/8 in. OD
84	4730-772-1662, part No. 204-1, Crawford Fitting	Fitting, Back Ferrule, 1/8 in. OD

Item No.	Stock No. and Part No.	Nomenclature
85	4730-783-8846, part No. 400-6-2, Crawford Fitting	Fitting, Reducing Union, 1/4 in. OD to 1/8 in. OD
86	4730-793-2746, part No. 600-6-4, Crawford Fitting	Fitting, Reducing Union, 3/8 in. OD to 1/4 in. OD
87	4730-863-9095, part No. 600-A-6ANF, Crawford Fitting	Fitting to AN Adapter, 3/8 in. to 3/8 in. OD AN Tube
88	4730-722-1371, part No. 400-7-4, Crawford Fitting	Fitting, Female Connector, 1/4 in. OD to 1/4 in. OD Female
89	4730-588-2687, part No. 400-1-4, Crawford Fitting	Fitting, Male to Connector, 1/4 in. OD to 1/4 in. OD
90	4730-701-2886, part No. 200-1-2, Crawford Fitting	Fitting, Male to Connector. 1/8 in. OD to 1/8 in.
91	4730-863-9090, part No. 810-A-8ANF, Crawford Fitting	Fitting to AN Adapter, 1/2 in. OD to 1/2 in.
92	4730-793-2748, part No. 810-6-4, Crawford Fitting	Fitting, Reducing Union, 1/2 in. OD to 1/4 in. OD
93	4730-691-5444, part No. 810-1-4, Crawford Fitting	Fitting, Male Connector, 1/2 in. OD to 1/4 in.
94	4730-775-9718, part No. 402-1, Crawford Fitting	Fitting, Nut, 1/4 in. OD
95	4730-863-9091, part No. 403-1, Crawford Fitting	Fitting Front Ferrule, 1/4 in. OD
96	4730-772-1664, part No. 404-1, Crawford Fitting	Fitting, Back Ferrule, 1/4 in. OD
97	4710-277-7581	Tube, Copper
98	4820-863-9097, Matheson part No. 58	Needle Valve
99	4820-863-9104, Matheson part No. 52B	Needle Valve
100	6680-804-9042, API part No. 26590-805A	Regulator, Pressure for 0_2
101	6680-855-9479, Matheson part No. 3	Regulator, High Pressure - Inlet Connection No. 350
102	6640-863-6766, Fisher part No. 13-258-18A	Oven, Drying

Item No.	Stock No. and Part No.	Nomenclature
103	4730-870-1175, Victor Equipment part No. 974-0102	Fitting Spare Inlet CGA/590
104	8120-823-7986, Specification ICC 3E1800	"Lecture Bottle", Cylinder, Compressed Gas, Valve Outlet, 5/16 in. - 32 thds/inch
105	6695-895-1348, Cosmodyne part No. CS 4.4	Sampler, Liquid Oxygen, TTU-131/E
106	8115-224-7935	Container Assy
107	7920-634-1745 Kimberly Clark part No. 900L	Kimwipes, Disposable Wipers, Case
108	4940-771-3213, Air Products part No. 63965A	Acetylene Test Kit (Ilosvay, short method)
109	6830-264-6748	Hydrogen, Technical, FED Specification BB-H-886

NOTE: Allowances for laboratory equipment are included in ECL 460.

SECTION III

QUALITY CONTROL OF AVIATOR'S LIQUID BREATHING OXYGEN

3-1. INTRODUCTION. During flight, the lives of aircrews, and even persons on the ground in the path of flight, depend on the quality control of aviator's liquid breathing oxygen. The quality control of aviator's liquid breathing oxygen requires frequent and continuous surveillance over its constantly increasing contamination. Surveillance begins with base generation or procurement and continues throughout storage, handling, transfer and servicing of the aircraft. Adequate and reliable quality control of aviator's liquid breathing oxygen demands that each operation in the aircraft liquid oxygen supply system must be carried out in strict compliance with procedures established to assure flight safety and mission completion.

3-2. SCOPE. This section established procedures and requirements for the quality control of liquid oxygen that is procured or base generated, stored, transferred, and used for breathing purposes by aircrews. This section is applicable to base personnel who are responsible for supervising or performing the operations associated with receipt, generation, storage, and transferring of, and servicing aircraft with, aviator's liquid breathing oxygen.

3-3. PERSONNEL. Personnel selected to perform operations in the supply system should be trained in a thorough knowledge of the characteristics of liquid oxygen, the significance of contamination when used for breathing purposes, and of the supply system to be quality controlled. Only those personnel who demonstrate understanding of the operations involved, and capable and reliable performance, should be assigned duties and responsibilities in the supply system.

3-4. CONTROL OF CONTAMINATION. A knowledge and understanding of how contaminants are concentrated in liquid oxygen by the sources of increasing contamination are essential to the effective control of contamination.

3-5. VAPORIZATION. The concentration of contaminants due to liquid oxygen vaporization cannot, of course, be prevented. However, the rate of increasing contamination from this source shall be controlled by minimizing heat additions in handling and transfer through proficient and careful performance of operations.

3-6. EQUIPMENT. Addition of contaminants from equipment shall be reduced or prevented by operating and maintaining generators, storage tanks, servicing carts, and aircraft liquid oxygen systems in accordance with applicable technical manuals.

3-7. HANDLING AND TRANSFER. The addition of contaminants from the environment shall be prevented by careful and proficient handling and transfer operations. Liquid oxygen strongly attracts and absorbs atmospheric gases, some of which are odorous and which may be present in the atmosphere, due to an environmental source.

3-8. QUALITY CONTROL REQUIREMENTS OF AVIATOR'S LIQUID BREATHING OXYGEN

3-9. PROCUREMENT LIMITS. The procurement limits for purity and contamination, which include the absence of odor, of aviator's liquid breathing oxygen must meet the requirements of the current issue of Specification MIL-O-27210(USAF).

3-10. USE LIMITS. The use limits of liquid aviator's breathing oxygen are as follows:

Odor	None	
Purity (percent by volume)	99.5	(Min.)
Carbon Dioxide (ppm by volume)	10	(Max.)
Methane (ppm by volume)	50	(Max.)
Acetylene (ppm by volume)	0.1	(Max.)
Ethylene (ppm by volume)	0.4	(Max.)
Ethane and other hydrocarbons (ppm by volume)	6	(Max.)
Nitrous Oxide (ppm by volume)	2	(Max.)
Halogenated Compounds:		
Refrigerants (freons, etc.) (ppm by volume)	2	(Max.)
Solvents (trichloroethylene, carbon tetrachloride, etc.) (ppm by volume)	0.2	(Max.)
Other (ppm by volume)	0.2	(Max.)

3-11. SUPPLY SOURCES OF AVIATOR'S LIQUID BREATHING OXYGEN.

3-12. COMMERCIAL GENERATING PLANTS. Aviator's liquid breathing oxygen procured from commercial generating plants must meet the requirements of the current issue of Specification MIL-O-27210(USAF).

3-13. AIR FORCE OPERATED GENERATING PLANTS. Aviator's liquid breathing oxygen produced by Generating Plants must meet the requirements of the current issue of Specification MIL-O-27210(USAF).

3-14. SAMPLING AND TESTING. Sampling and testing at intervals and points in the supply system provides the continuous monitoring of contamination that is essential to the quality control of aviator's liquid breathing oxygen. Tests, both singly and collectively, serve many needs and purposes; in fact, they are the basis for the performance of all operations in supply. No operation in supply shall be performed until a basis for action is established by tests.

3-15. ON-BASE TESTING. Air Force Bases which produce liquid oxygen from on-base generating plants shall sample and test the contents of the on-base generator tanks in accordance with paragraph 3-19. Receipt of aviator's liquid breathing oxygen from a contractor shall be tested in accordance with paragraph 3-18, and by the following tests for odor and particulate. Continuous surveillance of storage tanks, servicing trailers and aircraft converter systems for the presence of odor shall be made by the test for odor.

a. Odor Test. A liquid sample shall be tested for odor by pouring approximately 200 ml of the sample into a clean 400-ml beaker or similar container after covering the bottom of the beaker with a clean, dry filter paper or other absorbent paper. A watchglass cover or some other means of partially covering the top of the beaker shall be provided as the 200 ml of liquid evaporates to dryness. This will prevent atmospheric constituents from being absorbed by the exposed liquid. The liquid shall be permitted to evaporate to dryness and warm up to approximately room temperature in an area free from air currents or extraneous odors. When the liquid has completely evaporated, the watchglass shall be removed and the beaker contents smelled at frequent intervals until the accumulated frost on the outside of the beaker has completely melted. Odors will be most prevalent when the beaker has warmed to nearly room temperature.

b. Particulate Test. Concurrent with the odor test, 200 mls of the sample shall be poured into a clean 400 ml beaker or similar container, without a filter paper in the bottom. A watchglass cover or some other means of partially covering the top of the beaker shall be used as the 200 mls of liquid evaporate to dryness. When the frost on the outside of the beaker has melted, the outside of the beaker shall be wiped with a clean dry cloth and the beaker placed on a clean white paper. The interior of the beaker shall be visually examined, without the aid of magnification, for the presence of particles.

3-16. PERIODIC OR REQUESTED TESTS FOR PURITY AND KINDS AND AMOUNTS OF CONTAMINANTS. The tests are performed in the continental United States by the Air Force Aerospace Fuels Laboratories and the Materials Laboratory, SMAMA. Laboratories are listed in paragraph 3-25. Tests are performed in overseas Commands by laboratories designated by Command Headquarters.

3-17. TESTS AFTER INCIDENTS AFFECTING FLYING PERSONNEL. Samples taken after incidents in which flying personnel are affected, and any additional samples deemed necessary by the Director of Base Medical Services, will be submitted through the Base Medical Service to the appropriate Regional Environmental Health Laboratory in accordance with AFR 161-17. Laboratories are listed in paragraph 3-25.

3-18. RECEIPT OF AVIATOR'S LIQUID BREATHING OXYGEN FROM A CONTRACTOR. Before unloading is permitted, sample and test the contents of each shipping container as follows:

a. Sampling Location: Outlet port of the shipping container.

b. Test: Test for odor in accordance with paragraph 3-15, step a., and for particles in accordance with paragraph 3-15, step b.

c. Quality Control Requirements: The contents of the shipping container shall contain no odor or particles.

NOTE

When the test reveals the presence of either odor or particles in the contents of the shipping container, as tested above, do not unload the contents into base storage. Contact the Government representative responsible for quality contol surveillance over the contractor. Permit unloading for disposal purposes only if the shipment cannot be returned.

3-19. AIR FORCE OPERATED GENERATOR TANKS. Air Force Bases which produce liquid oxygen from on-base generating plants shall sample and test the contents of the on-base generator tanks as follows:

a. Sampling Location: At the drain valve.

b. Tests and Frequencies:

(1) When a tank which is connected continuously to the generator is functioning as a receiver for the product stream, the contents of the tank shall be tested for odor and purity after each addition or, if on continuous production, once each 24 hours. If the production record for purity of the quantity added has been stable and above the minimum requirement, the purity test is not necessary. Once every 90 days and whenever contamination is suspected, a sample from the tank then functioning as a receiver shall be sent to a designated laboratory (paragraphs 3-16 and 3-25) and tested for compliance with the procurement limits for minor constituents, Specification MIL-O-27210. Identify sample by completing, as applicable, AFTO Form 176 and attaching it to the sampler.

(2) During the period a tank is functioning as storage, the contents of the tank shall be tested for odor once each week in accordance with paragraph 3-15.a. Once every 90 days and whenever contamination is suspected, a sample of the contents of the tank functioning, at the time, as storage shall be sent to a designated laboratory (paragraphs 3-16 and 3-25) and tested for use limits specified in paragraph 3-10. Identify sample by completing, as applicable, AFTO Form 176 and attaching it to the sampler.

c. Quality Control Requirements:

(1) Odor - none.

(2) When functioning as receivers for the product stream of the generator, the contents of the on-base generator tanks shall not exceed the procurement limits.

(3) When functioning as storage containers, the contents of the on-base generator tanks shall not exceed the use limits.

NOTE

When tests show the contents of the on-base generator tanks have an odor, or exceed the Procurement or Use Limits, whenever applicable as above, the contents shall be drained and the tanks purged in accordance with the applicable storage tank operation and service technical manual.

3-20. BASE STORAGE TANKS. Sample and test the base storage tanks as follows:

NOTE

When Liquid Oxygen Sampler, TTU-131/E, FSN 6695-895-1348, cannot be obtained because of a supply difficulty, periodic purging of the base storage tanks must be accomplished by procedures described in the applicable technical manuals for the operation and maintenance of the equipment and on the following frequencies:

Capacity of Storage Tank	Minimum Frequency of Purging
2000 gallons and under	Once each 6 months
Over 2000 gallons	Once each 12 months

a. Sampling Location: At the drain valve.

b. Tests and Frequencies: Test for odor, once each week, in accordance with paragraph 3-15.a. Once every 90 days and whenever contamination is suspected, a sample of the contents of base storage tanks shall be sent to a designated laboratory (paragraphs 3-16 and 3-25) and tested for use limits specified in paragraph 3-10. Identify sample by completing AFTO Form 176 and attaching it to the sampler (omit procurement data).

c. Quality Control Requirements:

(1) Odor - none.

(2) The contents of the base storage tanks shall not exceed the use limits specified in paragraph 3-10.

NOTE

When tests show the contents of the base storage tanks have an odor, or exceed the use limits, the contents shall be drained and the tanks purged in accordance with the applicable storage tank operation and service technical manual.

3-21. SERVICING TRAILERS. Sample and test the aircraft liquid oxygen servicing trailers as follows:

a. Sampling Location: At the drain valve.

b. Tests and Frequencies: Test for odor in accordance with paragraph 3-15.a., as follows:

(1) Immediately after first transfer each day of Liquid Oxygen into a servicing trailer.

(2) When six days have elapsed since the servicing trailer was used to service aircraft, or was filled with liquid oxygen.

NOTE

AFTO Form 134 will be maintained on all liquid oxygen servicing trailers. These forms may be destroyed two weeks after the date of the last recorded aircraft servicing.

c. Quality Control Requirements: Odor – None.

NOTE

When tests show the presence of odor in the contents of servicing trailer, the contents shall be drained and the trailer purged in accordance with the applicable operation and service technical manual.

3-22. AIRCRAFT CONVERTER SYSTEM. Sample and test the aircraft liquid oxygen converter system as follows:

a. Sampling Location: At the drain valve.

b. Tests and Frequencies: Test for odor in accordance with paragraph 3-15.a. as follows:

(1) As soon as possible after report of in-flight odors by aircrews.

(2) In accordance with applicable aircraft manuals.

3-23. PURGING FREQUENCIES AND METHODS

a. Frequencies:

(1) Storage Tanks and Servicing Trailers. Any time tests show the contents of a storage tank or servicing trailer are odorous, or exceed the Procurement or Use Limits whenever applicable. (See paragraphs 3-19.c.(2) and (3).) Periodic purging shall be performed in accordance with the applicable technical manuals for the operation and maintenance of the equipment.

(2) Aircraft Converter System. In accordance with the applicable technical manuals.

b. Methods. In accordance with the instructions of the applicable technical manuals.

3-24. TESTING AND SAMPLING EQUIPMENT.

Item No.	Stock No. and Part No.	Nomenclature
1	6640-403-3500	Beaker, 400 ml
2	6640-290-6811	Watch Glass, 100 mm
3	6640-NL Fisher Scientific Co. Pgh., Pa. Part No. 9-805 or A.H. Thomas Co., Phila., Pa., Part No. 5200	Filter Paper, Whatman No. 1, Unwashed Medium Diam., 5.5 CM., Package - 100 sheets
4	6630-507-0584 Air Products and Chemicals, Inc., Allentown, Pa., Part No. 5-869-12-0006	Analyzer Kit, Oxygen Purity, Orsat Type
4A	6630-404-2500 Air Products, Part No. 4-104-27-0001	Bulb, Leveling
4B	6630-399-2958 Air Products, Part No. 4-894-27-0001	Tube, Reacting
4C	6630-399-2959 Air Products, Part No. 4-717-27-0001	Reservoir
4D	6630-490-1731 Air Products, Part No. 4-105-27-0001	Burette, 100 ml
8	Deleted.	
9	6695-895-1348 Cosmodyne CS.4.4	Sampler, Liquid Oxygen, TTU-131/E

3-25. AIR FORCE TESTING LABORATORIES FOR AVIATOR'S LIQUID BREATHING OXYGEN.

a. Directorate of Air Force Aerospace Fuels Laboratories:

(1) Wright-Patterson Air Force Base Shipping Address:

Transportation Officer
Wright-Patterson AF Base
Ohio
Attn: MAOQLA, Bldg 70, Area "B"
Telephone: Dayton, Ohio - CLEAR-WATER 3-7111, Ext. 21106 or 26287

Mail Address - Correspondence pertaining to samples.

Commander
Wright-Patterson AF Base
Ohio
Attn: MAOQLA

(2) Searsport, Maine, Laboratory - shipping and correspondence.

Chief
Searsport Air Petroleum and Chemical Laboratory
Searsport, Maine
Telephone: Searsport, Maine, KIngswood 8-2451

(3) Tampa, Florida, Laboratory:

Chief
AF Petroleum and Chemical Laboratory
Building 1121 - Shipping Address, Express
P.O. Box 6051 - Mailing Adress - letters, parcel post.

Call No. 82030 - Wire Address.

Mac Dill Air Force Base
Tampa, Florida
Telephone: Tampa, Florida
Area Code 813,
830-3645 or 830-2138

(4) Mukilteo, Washington, Laboratory:

Shipping Address - Express

Chief, Mukilteo AF Petroleum and Chemical Laboratory
Everett, Washington

Wire Address -

Commander
326th Air Defense Group
Attn: Chief, Mukilteo AF Petroleum and Chemical Laboratory
Paine Air Force Base, Washington

Mailing Address - Letters, Parcel Post:

Chief, AF Petroleum and Chemical Laboratory
Attn: MAOQLD
P.O. Box 357
Mukilteo, Washington
Telephone, Everett, Washington, Fairview 6-4122

(5) Materials Laboratory, SMAMA

Shipping and Mailing Address:

Sacramento Air Materiel Area
Attn: Materials Laboratory, SMMQSL
McClellan Air Force Base, California

b. Regional Environmental Health Laboratories:

(1) LSGHM

McClellan Air Force Base, California

(2) SGHK

Kelly Air Force Base, Texas

NOTE

Send samples for testing to Regional Environmental Health Laboratories only in those incidents in which flying personnel are affected.

END OF REFERENCE

7

REFERENCE

8

BANKAITIS, H.; AND SCHUELLER, C. F.: ASRDI OXYGEN SURVEY. VOLUME II: CLEANING REQUIREMENTS, PROCEDURES AND VERIFICATION TECHNIQUES. NASA SP-3072, 1972.

NASA SP-3072

ASRDI OXYGEN TECHNOLOGY SURVEY

Volume II: Cleaning Requirements, Procedures, and Verification Techniques

BANKAITIS and SCHUELLER

NATIONAL AERONAUTICS AND SPACE ADMINISTRATION

NASA SP–3072

ASRDI OXYGEN TECHNOLOGY SURVEY

Volume II: Cleaning Requirements, Procedures, and Verification Techniques

By H. Bankaitis and Carl F. Schueller

Aerospace Safety Research and Data Institute
Lewis Research Center, Cleveland, Ohio

Scientific and Technical Information Office 1972
NATIONAL AERONAUTICS AND SPACE ADMINISTRATION
Washington, D.C.

INTRODUCTION

Cleanliness requirements for mechanical systems have been undergoing a continuous evolution. With the advent of the airplane hydraulic and pneumatic systems and their associated close tolerances, special requirements had to be instituted to prevent malfunction or excessive wear due to particulate matter or contaminants. When man prepared to venture into the hostile environment of space more stringent requirements were necessary. With the more recent widespread use of oxygen, both in industry and space, additional scope had to be added to the cleanliness requirements. Recognition of oxygen's inherent reactivity characteristic as well as the fact that relatively small quantities of contaminants could serve as ignition sources and thus cause the burning of otherwise satisfactory containment materials led to these necessary additional requirements.

During this evolution a proliferation of cleanliness requirements has been generated. In part, this has occurred because the applications vary in scope from industrial use, with the least stringent requirements, to manned space vehicles, with the most demanding requirements. It has also been caused by the fact that the actual degree of cleanliness required has a small scientific base. Thus, many groups in both industry and government have generated cleaning specifications by trial and have verified them by operating experience accumulated with particular applications.

This report displays the oxygen system cleaning specifications drawn from 23 industrial and government sources, cleaning processes employed for meeting these specifications, and recommended postcleaning inspection procedures for establishing the cleanliness achieved.

It is the purpose of this document to collate and examine areas of agreement and difference in the specifications, procedures, and inspection. Also, the lack of clarity or specificity will be discussed. This absence of clarity represents potential safety hazards due to misinterpretation. Also, it can result in exorbitant expenditures of time and money in satisfying unnecessary requirements.

CLEANLINESS REQUIREMENTS

The degree of required cleanliness depends on the intended application of the component or system and is usually expressed in terms of allowable limits of contaminants. A contaminant is defined as any material which by being present in a system or component may cause mechanical malfunction, fire, or explosion. The types of most common contaminants and their relative sizes are illustrated in figure 1 (ref. 1). Techniques

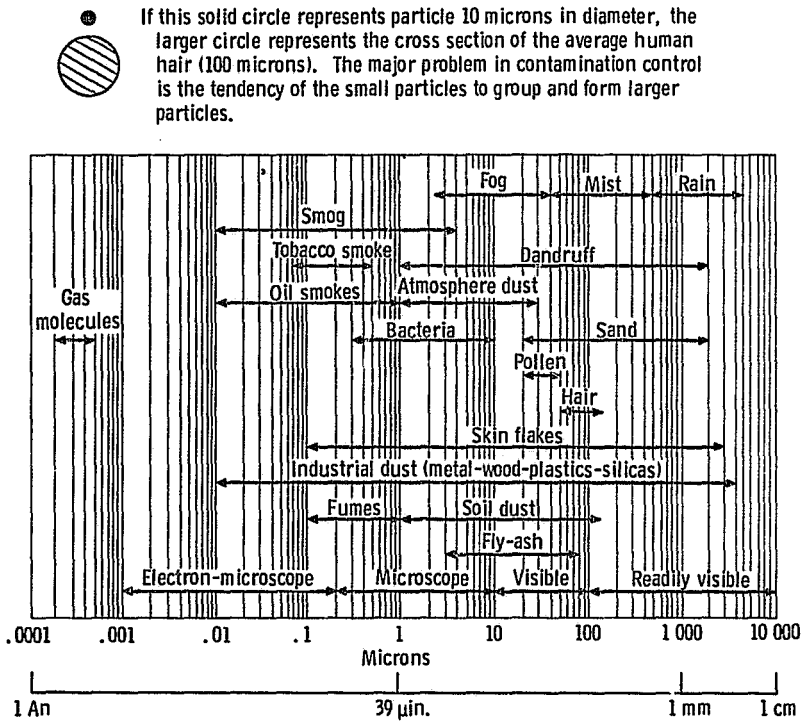

Figure 1. - Approximate sizes of common particles (ref. 1).

required to detect these contaminants as a function of their size are also indicated. Sources of contaminants which are probably the most difficult to predict are the fabrication and assembly operations such as grinding, cutting, welding, etc. Effective cleaning will

(1) Prevent functional interference with components by particles deposited on moving parts, valve seats, and system sensors and controls

(2) Reduce the likelihood of fire by rubbing friction which might occur if the clearance between moving system parts fills with contaminants

(3) Avoid accumulations of finely divided contaminants which are more easily ignited in oxygen than the bulk system materials

The cleanliness requirements can be placed in the following two general categories:

(1) Aerospace clean - applies to flight systems, components, ground service equipment for flight systems, environmental chambers, space cabins, and breathing apparatuses.

(2) Commercial clean - applies to industrial and process systems in which the threat, or consequences, of failure are low.

Wherever possible, the specifications, cleaning processes, and verification procedures are grouped in this report according to these cleanliness grades. Unfortunately, the originators of the cleaning requirements seldom classified them according to this scheme, but this pattern is discernible in the accumulated cleaning information.

Description of Contaminants

The following five contaminants are mentioned in the 33 cleanliness requirements (refs. 2 to 22) reviewed:

(1) Particulate matter - general term applied to finely divided solid matter of dimensions measured in microns (10^{-6} m or 3.9×10^{-5} in.). Its population in a system (or component) is determined by counting the particles in a unit volume of wash fluid (liquid or gas) that passed through the system at the end of the cleaning process. The cleanliness of the system (or components) is reported in terms of the number of particles of a given size range per unit area of the surface rinsed or washed. If the internal surfaces are accessible after cleaning, then the particle count can be made from a wipe of the surface and reported on the basis of the particle distribution per unit area of the internal system surface.

(2) Fiber - particle having a length of 100 microns or greater with a length to width ratio of 10:1 or greater. Fibers are classed according to length in microns and reported as a population number per square foot of internal surface area. (The internal surface which is exposed to the service media is often referred to in the literature as the "critical surface area.")

(3) Condensable hydrocarbons - usually refers to hydrocarbons capable of going from a gaseous to a liquid or solid state at system temperature and pressure. They are measured and reported as parts per million by weight of system fluid. In chemical use it usually refers to 1 microgram per gram.

(4) Solvent soluble organic residue - usually refers to hydrocarbons remaining on a surface after cleaning. It is measured in milligrams per milliliter of rinse solvent and reported in milligrams per square foot of critical surface area.

(5) Total solids - constitute the sum total of solid material obtained by filtering and evaporating a unit volume of the cleaning solvent. Total solids are reported in units of weight per unit area of the system or component.

Cleanliness Requirements for Particulate Matter Contaminants

In the reviewed cleanliness requirements particulate matter is given the greatest emphasis. The cleanliness requirements listed in table I (pp. 63 to 66) show considerable variation in the specification for particulate cleanliness. In some cases acceptable particle sizes and population are small and carefully defined; in other cases only the population of the largest acceptable sizes are specified. The differences are suspected to relate to the clearance dimensions of the moving parts of the system of concern when the specifications were first prepared. Permissible particle sizes are kept well below

these clearance dimensions. Also, it is desirable to point out that generally the smallest particles have the tendency to group and form larger particles. However, if they do not agglomerate and become suspended in the wash fluid, they are most easily washed from the system since the smallest particles are more readily maintained suspended in the wash fluid. Removal of the smallest particles from the surface becomes increasingly less effective as particle size decreases because of their ability to tenaciously adhere to the surface. This adherence is further enhanced by the wetting action of the wash fluid through the formation of residual film and corresponding surface tension. Any attempt to remove the particle must overcome this surface tension. By placing an upper limit on the permissible size and population of the larger particles, one is reasonably assured that the population of smaller particles will not be troublesome. The designer must judge the range of permissible particle sizes remaining in his system after cleaning on the basis of the sensitivity of the system components to interference by particles (ref. 23). It might be noted that past experience (described in the proposed Lewis Research Center design criteria monograph on liquid rocket valve assemblies) indicates that the particle size should be restricted to one-eighth of the clearances available. Furthermore, a John F. Kennedy Space Center (KSC) study of cleanliness specification (ref. 24, p. 26) states that for a given cleanliness level a standard particle distribution can be calculated per MIL-STD-1246A to obtain the total particle volume. This calculated volume used in conjunction with the available clearance can then be related to the allowable particulate contamination level and thus the degree of cleanliness required for the system. The pore size of the filters that can be used to protect these components and the ignition hazard posed by cavities in the system where particles may drop out of suspension in the process fluid and form dangerous accumulations must also be taken into consideration. The particulate specifications given in table I have served successfully for the systems indicated. The designer may use the one which comes closest to matching his system.

Overall cleanliness requirements for manned and unmanned space flight hardware systems (tanks, pipes, propulsion units, etc.) are presented in figure 2. The particle cleanliness requirements for manned space flight hardware are inconclusive for particles smaller than 175 microns. For unmanned ballistic flight systems these requirements are inconclusive for particles smaller than 300 microns. However, the limits of the largest allowable size of contaminants are very specific: 1000 microns for unmanned ballistic flight systems, and 2500 microns for systems used in manned space flight applications. According to KSC personnel, the largest allowable size of contaminant acceptable for manned space flight applications derived from actual "field tests" at the KSC complexes represents the maximum cleanliness results obtainable in the field during the 1960 to 1964 time period.

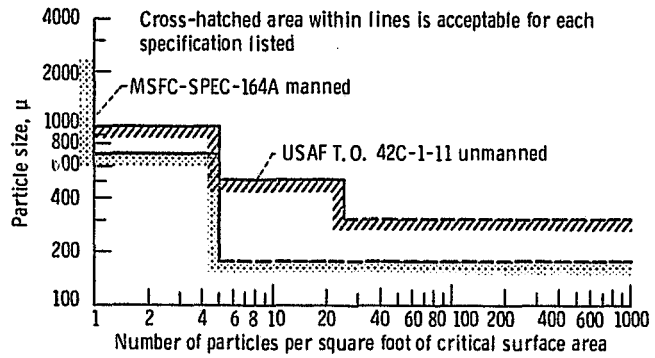

Figure 2. - Particulate matter - cleanliness requirements for space hardware.

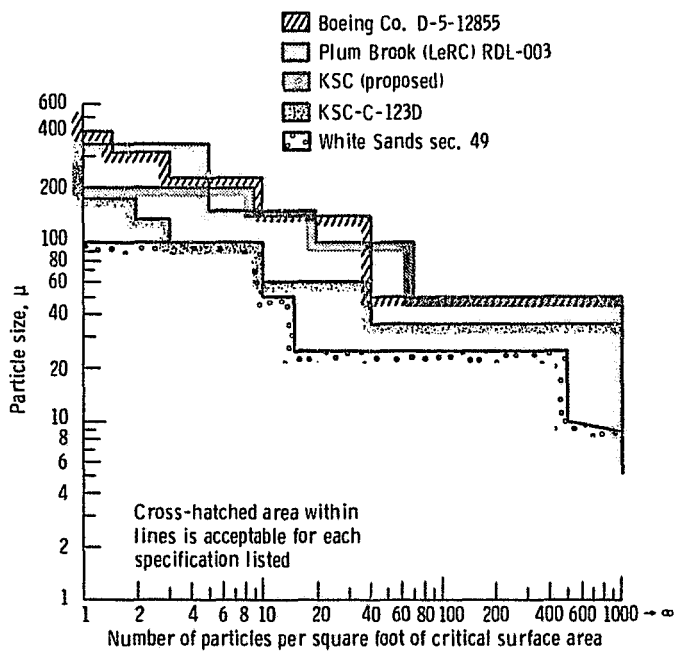

Figure 3. - Particulate matter - cleanliness requirements for ground based components and systems that may interface with flight systems.

Figure 3 shows the particulate cleanliness requirements for systems in the fabrication phase or test apparatus operations. Some of the systems in fabrication may be interfaced with space flight hardware or may be ground support equipment for space flight hardware. In the latter case the contaminant control is a very significant part of operations because of the extensive reuse of the equipment and the associated hazard of contaminant accumulation. In comparison to space flight systems cleanliness requirements, the requirements for ground service equipment illustrated in figure 3 allow fewer larger size particulate matter contaminants. Reasons for this are not readily obvious from the

available literature. A comparison of the KSC-C-123D (ref. 10) cleanliness requirements with the KSC proposed cleanliness requirements (ref. 11) indicates that the cleanliness requirements may be relaxed somewhat.

Figure 4 shows the particulate cleanliness requirements for environmental chambers, space cabins, and breathing oxygen components. The wide spread in allowable population of particulate matter is emphasized. However, this may be understandable because more contaminants must be accommodated by the design because man is a source of contamination in these cases. Rationale for abrupt changes in permitted size of population of particulate matter could not be established from the available literature.

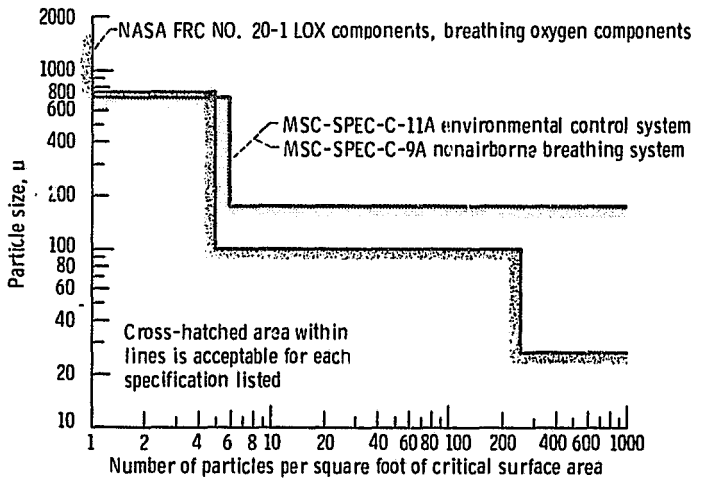

Figure 4. - Particulate matter - cleanliness requirements for space cabins, environmental chambers, breathing oxygen components.

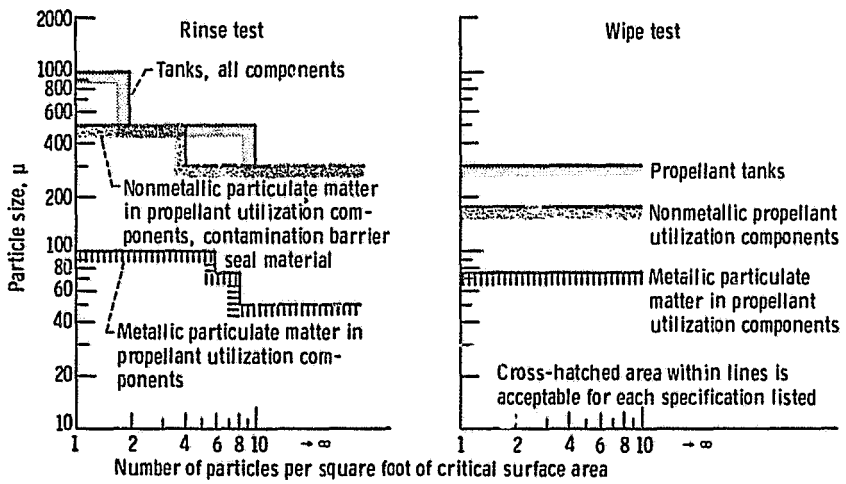

Figure 5. - Particulate matter - cleanliness requirements as function of material and inspection technique (spec. 075192B GDA-Convair, Dec. 13, 1967).

Figure 5 presents particulate cleanliness requirements specified by General Dynamics - Convair Division (ref. 19). The outstanding feature of these requirements is the classification of cleanliness requirements according to cleanliness verification techniques and the nature of the contaminant. The cleanliness requirements are more stringent for metallic particles than for nonmetallic regardless of verification techniques used.

Figure 6 is an example of the particulate cleanliness requirements established by commercial industry engaged in oxygen production. Three distinct classes of cleaning requirements are defined:

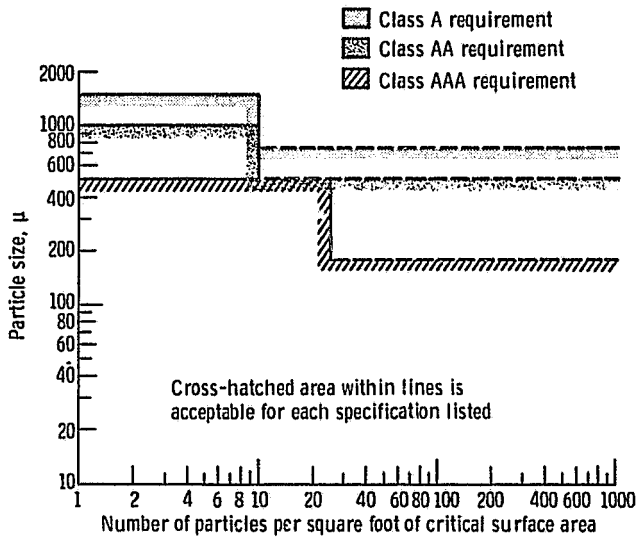

Figure 6. - Particulate matter - air products and chemicals cleanliness requirements.

(1) Class AAA is the most demanding class of cleanliness requirements; it is applicable to equipment or apparatus with moving surfaces which contact liquid or gaseous oxygen. In relation to the government and aerospace industry cleanliness requirements, this class is within the general space flight hardware limits.

(2) Class AA is the more general cleanliness requirements; it is applicable to shop fabricated or purchased equipment where fixed surfaces contact liquid or gaseous pure oxygen.

(3) Class A is the least strigent class of cleanliness requirements; it is applicable to surfaces which through use will contact fluids other than pure oxygen, for example, liquid air or crude oxygen.

Cleanliness Requirements for Fiber Contaminants

The cleanliness requirements for fiber contaminants are not as extensive as for the particulate matter. The information listed in table I clearly indicates that stated requirements vary from disallowing presence of any fiber contaminants at all (White Sands Test Facility, sec. 49) (ref. 6) to the very explicit requirements exemplified by Plum Brook (Lewis Research Center, LeRC) RDL-003 (ref. 3). In this realm of variations the following are noteworthy:

(1) Nine sets of cleanliness requirements do not state allowable fiber contaminant limits.

(2) Eight sets of cleanliness requirements state one point limits above which fiber contaminants cannot be tolerated, namely, no fibers greater than 2000, 4000, or 6000 microns in length.

(3) The KSC (proposed, ref. 11) cleanliness requirements permit the fiber contaminants to be classed and counted as particulate matter contaminant.

(4) The GDA 0-75192B (ref. 19) cleanliness requirements, consistent with particulate matter contaminant treatment, explicitly differentiate between metallic and nonmetallic fiber allowable limits. These limits are also adjusted on the basis of verification techniques used. Metallic fiber contaminants are totally disallowed, while nonmetallic fiber contaminant limits vary from none greater than 2000 microns in length

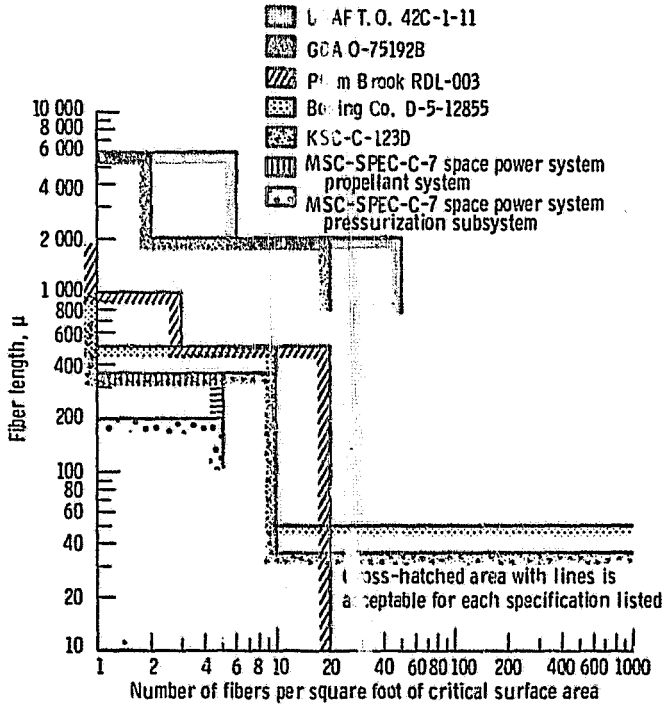

Figure 7. - Fiber-cleanliness requirements.

to none greater than 6000 microns in length depending on the systems involved.

The more explicit fiber contaminant requirements are illustrated in figure 7. The allowable fiber length limits are plotted as functions of the allowable population per square foot of critical surface area. Maximum allowable limits are indicated by the solid lines. Plum Brook (LeRC) cleanliness requirement limits for fiber type contaminants are the most explicit (ref. 3). These requirements limit fiber contaminant to 20 fibers of 0 to 500 microns in length, three fibers of 501 to 1000 microns in length, and one fiber to 1001 to 1875 microns in length. Thus, these specifications leave no doubt about the cleanliness level to be attained. Other requirements illustrated in the figure are less explicit.

Cleanliness Requirements for Condensable Hydrocarbons

Most of the cleanliness requirements do not indicate the condensable hydrocarbon type contaminant limits. In the few instances where the allowable contaminant limits are specified they vary from very explicit to extremely vague requirements. For example, from the data presented in table I the statements are as follows:

(1) Very explicit.

(a) 2.0 ppm by weight of test gas[1] (KSC-C-123D, ref. 10).

(b) 1.0 ppm by weight of test gas[1] (KSC proposed, ref. 11).

(c) 0 ppm by weight of test gas[1] (Plum Brook RDL-003, ref. 3).

(2) Explicit - no fluorescence on the cleaned surface using ultraviolet light (USAF T.O. 42C-1-11, (ref. 12); GDA 0-75192B (ref. 19); QCL 107F Air Products (ref. 4)).

(3) Vague.

(a) Low intensity fluorescence on the cleaned surface is acceptable (QCL 105F Air Products, ref. 4).

(b) No fluorescence (QCL 106F Air Products, ref. 4). (However, the specification allows isolated particles of lint on the cleaned surfaces.)

Cleanliness Requirements for the Remaining Types of Contaminants

Cleanliness requirements for solvent soluble organic residue, total solids, and other contaminants are either totally not stated or specified in the 1 to 5 milligram per square foot range of critical surface area. An exception is the Linde cleanliness requirement (ref. 8). It specifically limits nonvolatile residue to 500 milligrams per

---

[1]A sample of purge gas used to dry the system as part of the cleaning procedure.

square foot of critical surface area and solvent soluble organic residue to 10 milligrams per square foot of critical surface area. (The techniques used for measuring are discussed in the VERIFICATION OF CLEANLINESS section.)

For all the previously described contaminant limits the relation between the realistic cleanliness level and the specified cleanliness level is not defined in any of the requirements reviewed. There is no record in the documents reviewed of the basis for the selection of the cleanliness requirements generated by the separate groups within government and industry.

CLEANING PROCEDURES

Twenty-three cleaning procedures have been reviewed (refs. 2 to 22 and 25) to compare their approach to cleaning problems and highlight similarities or differences. A complete set of summaries of the procedures is given in the appendix and a complete set of detailed procedures is included in the attached microfiche supplement. Several general comments can be made regarding these cleaning procedures:

(1) All cleaning procedures except USAF T.O. 42C-1-11 (ref. 12) are written as guidelines and not as explicit specifications.

(2) Cleaning procedures vary according to the cleanliness requirements, the system components being cleaning, and the system materials.

(3) Cleaning procedures may be classified as aerospace clean or commercial clean.

(4) Cleaning procedures are most involved and costly for aerospace clean and least involved and costly for commercial clean.

A precautionary remark regarding cleaning agents and equipment used in these procedures is appropriate at this point. The toxicity of the cleaning solvents and the bodily harm associated with ultrasonically activated equipment or solutions present personnel health hazards which require protective measures.

There are five distinct steps that may be repeated several times in a given cleaning procedure. These steps are listed in table II (p. 66) with the associated information regarding cleaning agents, mechanical methods used with each step, and the purpose of each step. The particular sequence or number of these steps in a given procedure is a direct function of the cleanliness requirements and intended application or prior cleaning history of the item being cleaned.

The chemicals, cleaning agents, and mechanical aides used from table II vary as functions of materials of the components or systems being cleaned. In some instances cleaning procedures are specified according to the material used in the construction of the component, whereas in other instances the procedures are specified according to the components. The latter approach is most often used where two or more dissimilar ma-

terials (such as a metal and a nonmetal) or two different metals are used in fabricating the component. Not all cleaning agents can be used with such combinations of materials. For example, a highly acidic or alkaline cleaning agent may be suitable for one metal but not for the other, whereas some organic solvents may cause nonmetallic materials to swell and possibly degrade the physical or chemical properties due to solvent absorption or leaching action. Table III (ref. 26, pp. 68 to 71) illustrates some of the effects the common cleaning agents have on system materials. When all parts of a system cannot tolerate the same cleaning agent, they are cleaned separately before assembly. Subsequent assembly under clean conditions (clean room, etc.) avoids the need for further cleaning with strong agents.

An example of the cleaning procedures specified according to material as given in the appendix is presented in tables IV and V. Table IV (pp. 72 and 73) presents procedures for components made from various steel alloys, while table V (pp. 74 and 75) presents procedures for aluminum and its alloys. The procedures range from highly complex (i. e., numerous repetitions of basic steps) to very simple. The difference in metals to be cleaned affects the choice of cleaning agents, their concentrations, and metal exposure times and temperature ranges at which exposure to cleaning chemicals is made. This is evident, for example, by an examination of step 10 in table IV and step 8 in table V. For the steel alloys (step 10, table IV), cleaning agent formulation contains a quantity of phosphoric acid (exposure times range from 15 to 20 min) at temperatures between 80° and 175° F. For the aluminum and its alloys (step 8, table V), the cleaning formulation is mildly alkaline and exposure times are 30 to 120 minutes at 80° to 95° F or as short as 1 to 3 minutes at 140° to 180° F. Comparing the aforementioned individual cleaning steps for the given material, one becomes aware of the variations in cleaning agent concentrations, temperatures, and exposure times from one procedure to another. On the basis of the documents available at this time, technical justification for these differences cannot be established.

The information presented in tables IV and V must mirror the cleanliness requirements previously established. Thus, the cleaning procedures fall into the same general classes as the cleanliness requirements. The following are some examples:

(1) Aerospace clean. This category of cleaning procedures must meet the most demanding cleanliness requirements to ensure system reliability and safety. Cleaning procedures in this category can be further grouped into four distinct groups:

(a) Manned space flight. Preparation for such flights involves the greatest number of cleaning steps and related inspections to meet the most stringent cleanliness requirements for both space flight hardware and ground support equipment.

(b) Short duration space flight. For these flights the cleaning procedures are simplified somewhat by using fewer repetitive steps and inspections.

Card #3

(c) Environmental chambers. These chambers could be environmental simulators on the ground or spacecraft cabins. A new factor, the human body, becomes an additional source of contamination. It is a living source of contamination which cannot be eliminated by cleaning. Therefore, the problems it presents must be accommodated by a very careful choice of materials, detailed design considerations, and corresponding operating procedures. The floors and walls, where feasible, are thoroughly scrubbed to remove visible soils (ref. 26). People are required to wear lintless protective clothing, booties, and head gear in the environmental chambers and the spacecraft prior to launch. This protective equipment is cleaned to oxygen service requirements.

(d) Research test apparatus. Relatively simple procedures are used if the apparatus is small and the consequences of fire or system failure are limited to tolerable levels.

(2) Commercial clean. This cleaning category generally involves the simplest cleaning procedures since the consequences of failure are designed to be small in ground-base commercial equipment built to large safety factors. Commercial oxygen processors do achieve aerospace clean conditions when required.

Cleaning is expensive. Cleaning requirements which are more exacting than the risk involved in system failure would justify are not cost effective.

VERFICATION OF CLEANLINESS

The verification methods for determining the cleanliness achieved are reviewed in references 2 to 22 and 25. A list of the more common verification tests are presented in table VI (pp. 76 to 78) along with a general description of the procedures used in each test, the results that should be expected, and the limitations of the test method. Verification of cleanliness usually involves a sequence of tests; these tests are presented separately in table VI. The types and sequence of verification methods to be used are usually specified along with the cleanliness requirements by the originating agency.

The tests described in the table are of two categories:

(1) Direct determination. The verification techniques are based on direct determination of the cleanliness condition of the critical surface:

(a) pH paper - to determine the acidity or alkalinity of the surface

(b) Wipe - to detect particulate matter

(c) Visual

(i) Ultraviolet light or black light - to detect hydrocarbons by means of fluorescence

(ii) Water break - to determine the presence of contaminant film by the water's inability to wet the surface

(iii) Flood light - to detect particulates

These are all qualitative in nature and are effective only in situations where the critical surface areas are easily accessible to sight or touch.

(2) Indirect determination. The verification techniques are based on the analysis of a sample of the final rinse fluid (gas or liquid) to indirectly determine the cleanliness condition of the critical surface. The test methods in this category are the following:

(a) Gas blowdown - to determine by filtering and counting the particulate contaminants collected on the filter paper

(b) Solvent flush - to determine by filtering and counting the particulate contaminants collected on the filter paper

(c) Solvent soluble organic residue - to detect and determine organic contaminants such as oils, hydrocarbons, protective film coatings, etc.

(d) Condensable hydrocarbons - to determine presence and quantity of hydrocarbons

(e) Nonvolatile residue - to determine the quantity of solid matter contaminants

Sampling and analysis of the final rinse fluid using the aforementioned tests constitute the entire basis for determining the cleanliness condition of the critical surface area. The fluid used in the final rinse operations has to be of exceptional purity to facilitate a reasonably accurate determination of the quantity of contaminants entrained by the fluid. Also, the sampling technique must be properly executed to obtain a highly representative sample of the rinse fluid. A properly executed sampling technique means the following:

(1) The quantity and number of samples taken must be commensurate with the sensitivity and precision of the cleanliness verification method used.

(2) The samples taken must be representative of the entire fluid used in flushing the critical surface area. Also, the sampling should be done at normal operating conditions of the system or component, and the sampling points must be properly located.

(3) The samples must be clear of extraneous contamination such as unclean sampling equipment.

Otherwise, the results achieved may be erroneous and an acceptably clean part may be rejected or unacceptably clean part may be accepted.

The gas blowdown and solvent flush tests are qualitative in nature, because the particle count is an estimate of an average count. The remaining three tests in this category are quantitative in nature because the infrared spectrophotometric or gravimetric determinations are used in establishing the quantity of the contaminants in the representative sample. The condensable hydrocarbon test, however, is probably the least accurate of the three. This is because of the intricate manipulations required to isolate

the condensable hydrocarbons and because an arbitrary factor called "compensating evaporation factor" must be used in the computation to determine the concentration of the contaminants. These combine to severely degrade the test results.

In general, the reproducibility and accuracy of all the test results described in table VI vary widely and are functions of sampling procedures, the test methodology itself, and the ability and attitude of the technician performing the test.

A limited amount of verification methodology evaluation was performed by Hayes International under contract from Marshall Space Flight Center (ref. 27). This evaluation showed that evaporation of the solvent for nonvolatile residue content was erratic because of the effects of partial vapor pressures of the organic constituents, whereas infrared differential absorption spectroscopy yielded reproducible and accurate data. The evaluation also showed that the basic theoretical parameters required to provide for accurate and reproducible verifications have not been adequately defined.

The summary of a paper by J. P. McDonald of Martin Marietta Corporation (ref. 28) very aptly describes the current state-of-the-art:

> ...It is not a well understood fact (outside of contamination control circles) that the sole quantitative content of all vehicle fluid system cleanliness criteria specifications for components lies in the content of the final rinse, the parameters for which have never been quantitatively defined. All effort expended on this activity in the vehicle aerospace field has relied on criteria that have not been dimensionally defined by determinative parameters, at least with regard to force of impingement, velocity (or "volume" of flow), orientation of surface being sampled, accessory sampling energy (e.g., insonation), or other characteristics that vitally affect the validity of results. The effort has depended almost totally on operator interpretation.

CONCLUDING REMARKS

The review of the cleanliness requirements, cleaning procedures, and verification techniques indicates the following:

1. Existing cleaning requirements generally allow the quantity of particulate contaminants to increase with a corresponding decrease in size of the particle whether metallic or nonmetallic.

2. Cleanliness requirements for manned space flight are the most stringent as regards allowable maximum particle size and quantity of particles, while general industrial requirements are the least demanding.

3. The quantitative justification for most of the requirements was not presented in the documents reviewed. Whether such justification exists or testing is required to es-

tablish the requirements cannot be stated from this review.

4. Large areas of uncertainty or areas subject to interpretation exist in some of the cleanliness requirements reviewed. For example, at a given particle size the permissible quantity is not specified in some cases.

5. The various cleaning procedures are all based on five steps: degrease, clean, rinse, inspect, and dry. The sequence and repetition of these steps in a given cleaning procedure depends on the stringency of the cleaning requirements.

6. The tests used to verify a required level of cleanliness are, in general, unsupported by adequate quantitative test data and are subject to the introduction of errors by the test technician.

7. Although very difficult to achieve, the proper balance between cleaning requirements, procedures, and verification techniques is quite necessary. Without it one may expend an unwarranted amount of time and effort unnecessarily recleaning an item or may damage the system by introducing an inadequately cleaned item.

8. Consideration should be given to establishing joint National Aeronautics and Space Administration - Department of Defense - American Medical Association - Environmental Protection Agency - industry effort to develop a series of uniform procedures. These should be based on actual test and experimental data and would establish the level of cleanliness required, methods of accomplishment, and verification as a function of the final application.

CLEANING METHODS AND PROCESSES, NASA FRC PROCESS SPECIFICATION 20-1, NOVEMBER 1, 1970 (REF. 22)

Specific Cleaning Processes for Breathing Oxygen Components - Metallic

Step	Process	Agent	Time, min	Temperature, ^{o}F	Remarks	Reference paragraph
1	Preclean				By hand wiping, brushing, and scraping.	6.3.1.1 (5.1.1)
2	Clean	Trichloroethylene	5		Ultrasonic or vapor degrease or flush with 5μ filtered solvent at circulation rate of 20 component volumes per minute. When flush procedure is used, heated solvent of 120^{o} - 140^{o} F is desired, but in no case shall temperature be less than 60^{o} F.	6.3.1.1 (5.1.2)
3	Rinse	Trichloroethylene			Solvent shall be fresh filtered (5μ nominal). Step omitted if flush procedure used in step 2.	6.3.1.1 (5.1.3)
4	Dry	Dry nitrogen and/or heating to		180 (max)	Nitrogen filtered to 5μ nominal.	6.3.1.1 (5.1.4)
5	Flush	Ethyl alcohol			Filtered 5μ nominal.	6.3.1.2
6	Rinse	Demineralized or distilled water				6.3.1.3
7	Dry	Dry nitrogen or by heating to		180 (max)		6.3.1.4
8	Check	Halogen detector			Sniff check or equivalent to ensure that all traces of trichloroethylene or other halogen vapors are removed.	6.3.1.5

CLEANING METHODS AND PROCESSES, NASA FRC PROCESS SPECIFICATION 20-1, NOVEMBER 1, 1970 (REF. 22)

Basic Cleaning Process for Metallic Articles

Step	Process	Agent	Time, min	Temperature, ^{o}F	Remarks	Reference paragraph
1	Preclean				By wiping, brushing, and scraping.	5. 1. 1
2	Clean	Trichloroethylene	5		Ultrasonic or vapor degrease or flush with 5μ filtered trichloroethylene at circulation rate of 20 component volumes per minute. When flush procedure is used heated trichloroethylene of 120^{o} - 140^{o} F is desired, but in no case shall temperature be less than 60^{o} F.	5. 1. 2
3	Rinse	Trichloroethylene			Solvent shall be fresh, filtered (5μ nominal). Step omitted if flush procedure used in step 2.	5. 1. 3
4	Dry	Dry nitrogen and/or heat to		180 (max)	Nitrogen filtered to 5μ nominal.	

CLEANING METHODS AND PROCESSES, NASA FRC PROCESS SPECIFICATION 20-1, NOVEMBER 1, 1970 (REF. 22)

Specific Cleaning Processes for Breathing Oxygen Components - Nonmetallic

Step	Process	Agent	Time, min	Temperature, ^{o}F	Remarks	Reference paragraph
1	Preclean	Paper			Hand wipe clean of any visible grease, oil, or contaminants.	6.3.2 (5.2.1)
2	Clean	1% nonionic detergent and water solution		140 (max)	Either scrub with nonmetallic brush, flush with detergent solution at flow rate of 20 component volumes per minute for 3 minutes, or ultrasonic clean in detergent solution.	6.3.2 (5.2.2)
3	Dry	Dry, oil-free nitrogen gas or air				6.3.2 (5.2.3)
4	Rinse	Demineralized or distilled water		140 (max)		6.3.2 (5.2.4)
5	Dry	(a) Dry, oil-free nitrogen gas			Filtered through 5μ filter.	6.3.2 (5.2.5)
		(b) Heat in oven		120 - 140	Nonmetallic gaskets or parts, such as O-rings, shall not be subjected to temperature above 140^{o} F.	
		(c) Vacuum				
6	Check	Halogen detector			Sniff check of equivalent to ensure that all traces of trichloroethylene or other halogen vapors are removed.	6.3.2

CLEANING METHODS AND PROCESSES, NASA FRC PROCESS SPECIFICATION 20-1, NOVEMBER 1, 1970 (REF. 22)

Basic Cleaning Process for Nonmetallic Articles

Step	Process	Agent	Time, min	Temperature, ^{o}F	Remarks	Reference paragraph
1	Preclean	Paper			Hand wipe clean of any visible grease, oil, or contaminants.	5.2.1
2	Clean	1% nonionic detergent and water solution		140 (max)	Either scrub with nonmetallic brush, flush with detergent solution at flow rate of 20 component volumes per minute for 3 minutes, or ultrasonic clean in detergent solution.	5.2.2
3	Dry	Dry, oil-free nitrogen gas or air				5.2.3
4	Rinse	Demineralized or distilled water		140 (max)		5.2.4
5	Dry	(a) Dry, oil-free nitrogen gas			Filtered through 5μ filter.	5.2.5
		(b) Heat in oven		120 - 140	Nonmetallic gaskets or parts, such as O-rings, shall not be subjected to temperatures above 140^{o} F.	

KSC (PROPOSED)
NONMETALLIC MATERIALS (REF. 11)

[Ref. par. 3.10.2.1.2 and others as noted. Removable nonmetallic parts may be cleaned as separate items. When nonmetallic parts cannot be removed it shall be cause to clean the item as a nonmetallic.]

Step	Process	Agent	Time, min	Temperature, °F	Remarks	Reference paragraph
1	Clean	0.5% solution of detergent per MIL; D-16791 and deionized water	5 - 15	110 - 130	Clean by flushing, soaking, spraying, or sonic energy.	3.9.3.3
2	Rinse	Water	5	90 - 110		
3	Rinse	Deionized water	5		If ultrasonic cleaning used, rinse for additional 10 minutes in ultrasonic cleaner.	
4	Inspect	Narrow range pH paper			pH must be between 6 and 8, otherwise repeat steps 1 - 3.	4.3
5	Dry	Gaseous nitrogen or vacuum drying oven		100 - 120	Type I, class 1, grade B of spec. BB-N-411.	3.10.2.4
6	Clean	Trichlorotrifluoroethane or isopropyl alcohol	1		Use only compatible solvent-material combinations.	
7	Inspect				Particle count of fluid from step 6, in accordance with 4.3.	
8	Dry	Gaseous nitrogen or vacuum oven		100 - 120	Remove all traces of solvent (see spec. BB-N-411).	

SYSTEMS AND EQUIPMENT CLEANING, CPIA PUBLICATION 194
ROCKET PROPELLANTS(B) OXYGEN (REF. 21)

Plastic Parts

Step	Process	Agent	Time, min	Temperature, ^{o}F	Remarks	Reference paragraph
1	Disassemble				To separate aluminum steel and plastic parts.	10. a. 1
2	Clean	4% detergent solution	30	120		10. b. 1
3	Rinse	Distilled water			Several times.	10. b. 2
4	Dry	Nitrogen gas				10. b. 3

CLEANING AND INSPECTION PROCEDURES FOR BALLISTIC MISSILE SYSTEMS T. O. 42C-1-11 CHANGE 2, NOVEMBER 15, 1967 (REF. 12)

Electroplated Parts and Components Containing Dissimilar Metals

Step	Process	Agent	Time, min	Temperature, °F	Remarks	Reference paragraph
1	Degrease	Trichloroethylene or trichlorotrifluoroethane	As required	Ambient		3-15 3-75
2	Vapor degrease	Trichloroethylene or trichlorotrifluoroethane		Boiling	Immerse parts in vapor until condensation ceases. Flush with freshly condensed degreaser solvent.	3-15 3-64
3	Alkaline clean	Alkaline cleaner: 5 - 10 oz/gal tap water	15 - 25	150 - 175	Parts shall be completely free of step 2 solution because of explosion hazard.	3-77
4	Rinse	Tap water	5 - 10	150		3-84
5	Rinse	Demineralized water	5 - 10	150		3-84
6	Dry	Oven, nitrogen gas, or vacuum		180 - 200 140		3-87
7	Rinse	Detergent solution: 1/2 - 1 oz/gal tap water, demineralized water, or trichloroethylene	15 - 25 As required	120 - 140	MIL-D-16791 type I.	3-86 3-85
8	Flush	Demineralized water	As required	150	Do not flush of solvent used in step 7.	
9	Inspect					
10	Dry	Oven, nitrogen gas, or vacuum		180 - 200 140		3-87

CLEANING AND INSPECTION PROCEDURES FOR BALLISTIC MISSILE SYSTEMS T. O. 42C-1-11 CHANGE 2, NOVEMBER 15, 1967 (REF. 12)

Nonmetallic Parts and Components Containing Nonmetallic Parts

Step	Process	Agent	Time, min	Temperature, °F	Remarks	Reference paragraph
1	Detergent clean	Detergent solution: 1/2 - 1 oz/gal of tap or demineralized water	5 - 10	120 - 140	MIL-D-16791 type I.	3-86
2	Rinse	Tap water	5 - 10	150		3-84
3	Rinse	Demineralized water	5 - 10	150		3-84
4	Dry	Oven, nitrogen gas, or vacuum		180 - 200 140		3-87
5	Detergent rinse	Detergent solution: 1/2 - 1 oz/gal of tap or demineralized water	15 - 20	120 - 140		3-86
6	Inspect					3-89
7	Dry	Oven, nitrogen gas, or vacuum		180 - 200 140		3-86

CLEANING AND INSPECTION PROCEDURES FOR BALLISTIC MISSILE SYSTEMS T. O. 42C-1-11 CHANGE 2, NOVEMBER 15, 1967 (REF. 12)

Metal Filter Elements

Step	Process	Agent	Time, min	Temperature, °F	Remarks	Reference paragraph
1	Vapor degrease	Trichloroethylene or trichlorotrifluoroethane	As required	Boiling	MIL-T-27602 (FSN 6850-681-5688).	3-64
2	Dry	Oven, nitrogen gas, or vacuum		180 - 200 140		3-87
3	Ultrasonic clean	Trichloroethylene or trichlorotrifluoroethane	3 - 5	10° below boiling point		3-15 3-79
4	Rinse	Trichloroethylene	5 - 7	Ambient	Solvent filtered through 10μ filter.	3-85
5	Inspect					
6	Dry	Oven, nitrogen gas, or vacuum		180 - 200 140		3-87

CLEANING, TESTING, AND HANDLING OF OXYGEN, FUEL, AND PNEUMATIC COMPONENTS
D5-12855, BOEING CO., MAY 15, 1968 (REF. 9)

Dead-End Components (Pressure Gages, Transducers, etc.)

[Ref. par. 3.0 and others as noted. Components not to be immersed in cleaning media, and, also, components not to be exposed to acid (ref. par. 3.1).]

Step	Process	Agent	Time, min	Temperature, °F	Remarks	Reference paragraph
1	Inspection	Prior to precleaning			Inspect exterior and visible interior.	5.2
2	Precleaning	Trichloroethylene precision cleaning agent, Dowclene WR			Alternating vacuum solvent flush (28 in. of Hg min. vacuum). Fill and drain component a minimum of 20 times. Fresh solvent for each fill. Two other methods are also stated.	6.2.2
3	Final cleaning	Trichloroethylene precision cleaning agent, Dowclene WR, use minimum quantity of solvent per 7.3.1			Rinse significant surfaces using one of the methods in 3.2. Must be in controlled environment per 6.3.2.	3.3
4	Drying	Nitrogen gas per BB-N-411; air or other gas to be specifically approved by engineering		130 - 250	Temperature dependent on parts (see 6.2.6). Vacuum oven drying is preferred.	3.3 6.2.7

CLEANING AND INSPECTION PROCEDURES FOR BALLISTIC MISSILE SYSTEMS T.O. 42C-1-11 CHANGE 2, NOVEMBER 15, 1967 (REF. 12)

Transducers, Pressure Gages, and Other Dead-End Cavity Parts

Step	Process	Agent	Time, min	Temperature, °F	Remarks	Reference paragraph
1	Fill	Trichloroethylene			3/4 full and rotate component gently to circulate fluid. Repeat fill and rotate procedure two times.	3-15
2	Rinse	Petroleum ether				
3	Inspect					3-89
4	Dry	Oven, nitrogen gas, or vacuum		180 - 200 140		3-87

CLEANING OF OXYGEN PRESSURE GAGE COMPONENTS, NAVAL BOILER, AND TURBINE LABORATORY, MARCH 26, 1965 (REF. 18)

Step	Process	Agent	Time, min	Temperature, °F	Remarks	Reference paragraph
1	Disassemble				Disconnect from piping system, remove back of gage, elongate coil of capillary tubing, and open capillary tubing filing off tip.	1-6
2	Clean	Freon PCA			Forced by air pressure (5 psig) flow 150 ml of Freon PCA at approximately 50 ml/min. Repeat with two additional 124 ml portions and reverse flush with 100 ml of solvent.	7-10
3	Rinse	Freon PCA			Introduce 50 ml of solvent through connection end of gage, collect effluent in white porcelain dish, and evaporate to dryness.	11
4	Inspect	Ultraviolet light (3600 - 3900 Å)			White dish from step 3 checked for fluorescence. If fluorescence observed, continue flushing.	11-12
5	Assemble					13-15

CLEANING AND TESTING OF OXYGEN AND NITROGEN GAS PIPING SYSTEMS
MIL-STD-1330 (SHIPS), MAY 10, 1968 (REF. 20)

Bourdon C Tube Pressure Gages

Step	Process	Agent	Time, min	Temperature, ^{o}F	Remarks	Reference paragraph
1	Disassemble					4.5.1.1
2	Clean	Trichlorotrifluoroethane			MIL-C-81302 type I ultra-clean at flow rate of 50 mil/min.	4.5.1.8
3	Check	Ultraviolet light (3600 - 3900 Å)			Continue flushing if fluorescence is evident.	4.5.1.10
4	Dry	Dry, oil-free nitrogen				4.5.1.11

CLEANING METHODS AND PROCESSES, NASA FRC PROCESS
SPECIFICATION 20-1, NOVEMBER 1, 1970 (REF. 22)

Specific Cleaning Process for Pressure Transducers and Bourdon Tubes

Step	Process	Agent	Time, min	Temperature, ^{o}F	Remarks	Reference paragraph
1	Preclean	Trichloroethylene			Hot solvent.	6.5.1.1
2	Clean	Trichloroethylene	1	180±5	Soak in hot solvent.	6.5.1.2
			1	Ambient	Place in ambient solvent. Repeat cycle 10 times. Ambient solvent not to exceed 85° F.	6.5.1.3
3	Dry	Oven	150	250±10	For Bourdon tubes.	6.5.1.4
			150	180±10	For pressure transducers.	

B. Material

1. Aluminum
2. Brass, bronze, copper
3. Carbon steel and carbon steel alloys

CLEANING AND INSPECTION PROCEDURES FOR BALLISTIC MISSILE SYSTEMS T.O. 42C-1-11 CHANGE 2, NOVEMBER 15, 1967 (REF. 12)

Aluminum

Step	Process	Agent	Time, min	Temperature, °F	Remarks	Reference paragraph
1	Mechanical descaling		As required			3-39
2	Degrease	Trichloroethylene	As required	Ambient	MIL-T-27602.	3-15 3-75
3	Vapor degrease	Trichloroethylene or trichlorotrifluoroethane			MIL-T-27602 (FSN 6850-681-5688).	
4	Alkaline clean	Sodium carbonate (3 oz/gal), trisodium phosphate (3 oz/gal), remainder tap water	1 - 3	140 - 180		
5	Rinse	Tap water		150		
6	Pickle	HNO_3 (12% by volume), HF (1% by volume), remainder tap water		Ambient		
7	Rinse	Demineralized water		150		
8	Dry	Oven heated nitrogen or vacuum		180 - 200 140	MIL-P-27401; filtered through 10μ filter.	
9	Rinse	Detergent solution: 1/2 - 1 oz of sol/gal tap or demineralized water or trichloroethylene	15 - 25	120 - 140	MIL-D-16791 type I. MIL-T-27602.	
10	Flush	Demineralized water	As required	150	Do not flush if solvent used in step 9.	
11	Inspect					
12	Dry	See step 8				

CLEANING PROCEDURES - METALS CLEANING SPI-49.111
LINDE COMPANY, DIV. OF UNION CARBIDE, DECEMBER 28, 1965 (REF. 8)

Aluminum

Step	Process	Agent	Time, min	Temperature, °F	Remarks	Reference paragraph
1	Preclean	Diversey 1319 (1) 3 oz/gal		Ambient	(1) Code 3008-2825: step 1, preclean with solution gun only if aluminum is contaminated with oil or other heavy soil.	02.1
2	Rinse	Cold water (2) or hot water (2)			(2) Water shall be potable. (3) Code 3008-3000.	.02.2
3	Clean/etch	Aluminux: Diversey aluminum (6 oz/gal) Diversey 202(4) (2 oz/gal of water)	(5) 1 - 2	160	(4) Code 3008-2775. (5) For light gage material; heavy gage material not to be soaked longer than necessary.	.02.3
4	Rinse	Hot water				.02.4
5	Deoxidize or desmut	Diversey 596(6) (7 oz/gal water), H_2SO_4 (7% by volume), remainder water			(6) Code 3002-1300.	.02.5
6	Rinse	Hot water				.02.6
7	Dry	Air (7)			(7) Clean, dry, oil free.	

SYSTEMS AND EQUIPMENT CLEANING, CPIA PUBLICATION 194
ROCKET PROPELLANTS(B) OXYGEN (REF. 21)

Aluminum, Aluminum Alloys

Step	Process	Agent	Time, min	Temperature, °F	Remarks	Reference paragraph
1	Disassembly				To separate aluminum plastic and steel parts.	10. a. 1
2	Degrease	Perchloroethylene	30			10. a. 2
3	Rinse	Alcohol				10. a. 2
4	Rinse	Water				10. a. 2
5	Clean	4% solution of aluminum cleaner	30			10. a. 3
6	Rinse	Water				10. a. 3
7	Final clean	Steam				10. a. 5a
8	Dry	Nitrogen				10. a. 5b

ALUMINUM CLEANED BY SOLUTION SPRAYING
KSC (PROPOSED) (REF. 11)

[Ref. Par. 3.10.3.5 and others as noted.]

Step	Process	Agent	Time, min	Temperature, °F	Remarks	Reference paragraph
1	Precleaning	Trichloroethylene type II, trichlorotrifluoroethane, or 0.5% solution of a detergent in deionized water	5 - *15	110 - *130	Conform to MSFC-SPEC-217. Conform to MSFC-SPEC-237. *For detergent solution only.	3.10.3.5.1a (3.9.3 & 3.10.3.1)
2	Clean	Formula IV: % by wt Material: 9±0.4 2-butoxyethanol solvent; 1.5±0.1 Na_2HPO_4; 0.5±0.05 Surfactant (alkyl aryl polyethylene glycol ether); Remainder deionized water	60 - 120	80 - 95	Spray minimum flow of 6 gal/min/ft at item; maximum i.d. at a spray head delivery; P = 150 - 200 psig.	3.10.3.5.1b (3.10.3.3.3)
3	Rinse	Deionized water	30	Ambient	Delivery rate same as step 2. Continue rinse until evidence of surfactant disappears.	
4	Brighten	Formula V: % by vol Material: 23±0.5 61% HNO_3; Remainder deionized water	20 - 40	Ambient	Spray delivery rate same as step 2.	3.10.3.5.1c (3.10.3.3)
5	Rinse	Steps 1 and 3			Steps 4 and 5 to be accomplished if smut has developed on the part during steps 1 - 3.	3.10.5.1d

Continued. ALUMINUM CLEANED BY SOLUTION SPRAYING
KSC (PROPOSED) (REF. 11)

Step	Process	Agent	Time, min	Temperature, ^{o}F	Remarks	Reference paragraph
6	Final rinse	Deionized water			(1) For rotating head spray machine - (a) Lower spray head to lowest point of item cleaned. (b) Spray at rate 2.2 gal/min/ft. (c) Delivery P = 150 - 200 psig. (d) Rinse spray head vertically at rate of 1 ft/min. (e) Take test samples from lowest point. (f) 2500 ml sample to be obtained in 58 - 62 sec. (g) Steps (a) - (e) must be correlated so that 2500 ml test sample will represent 1 ft^2 of critical surface area. (h) Collect first 2500 mil sample at start of spray; second when spray head traversed 50% of vertical distance; collect third sample as spray head approaches highest point. (2) For rotating spray wand - same as step 6 except 2500 ml samples will be taken at first, third, and fifth minutes of spray.	3.10.3.3.1d

Concluded. ALUMINUM CLEANED BY SOLUTION SPRAYING
KSC (PROPOSED) (REF. 11)

Step	Process	Agent	Time, min	Temperature, ^{o}F	Remarks	Reference paragraph
7	pH test	Narrow range pH paper			All samples analyzed to to 4.3. pH sensitive to 0.1 pH unit. pH range, 6.0 - 8.0. If non-conformance flush 15 minutes and test, on second failure re-clean steps 1 - 6.	3.10.3.5.1e (3.10.3.3i)
8	Dry	Gaseous nitrogen			To a dew point of -65° F at all critical parts per 4.3. Final 5 minutes gaseous nitrogen at system operating pressure; if unattainable, purge velocity at farthest downstream exit port, shall be 35 SCFM.	(3.10.3.3j) (3.10.3.3k)
9	Repeat rinse	Trichloroethylene; trichlorotrifluoroethane	15		Flow rate of 6 gal/min/ft. Spray head pressure 80 - 100 psig.	
10	Drain					
11	Repeat rinse	Step 6 (1) or 6 (2)			Delivery pressure, 20 - 100 psig. Test solvent - if unacceptable, repeat steps 1 - 11.	
12	Test					
13	Dry	Same as step 8				

KSC (PROPOSED) (REF. 11)

Aluminum

[Ref. par. 3.10.2.3 and others as noted.]

Step	Process	Agent	Time, min	Temperature, °F	Remarks	Reference paragraph
1	Mechanical descale	Brushing, shot peening, etc.			As required.	3.9.2
2	Degrease	Trichloroethylene or trichlorotrifluoroethane			Solvent or vapor MSFC-SPEC-217 or MSFC-SPEC-237.	3.9.3.1
3	Dry	Gaseous nitrogen			Type I, class 1, grade B of spec. BB-N-411.	3.10.2.4
4	Remove corrosion	23±5% by volume of 61% nitric acid, remainder is deionized water	10 - 60	Ambient	Formula V.	3.10
5	Rinse	Water	5	90 - 110		
6	Rinse	Deionized water	3			
7	Dry	Gaseous nitrogen		120 - 140		
[a]8	Clean	By weight: 9% 2-Butoxyethanol solvent 1.5% Sodium phosphate, dibasic, anhydrous 0.5% Surfactant Remainder is deionized water	30 - 120	80 - 95	Flush, soak, brush, or sonic clean.	3.10
9	Rinse	Water	5	90 - 110		
10	Rinse	Deionized water	3		If ultrasonic cleaning used, rinse additional 10 minutes in ultrasonic cleaner.	
11	Brighten and passivate	Same as step 4	10 - 30	Ambient	Step 8, cleaning is usually adequate.	
12	Rinse	Water	5	90 - 110	Only if step 11 used.	

[a]All fluids used in steps 8 to 18 shall be prefiltered prior to use to meet the cleanliness level specified for the item when tested according to 4.5.2.

Concluded. KSC (PROPOSED) (REF. 11)

Step	Process	Agent	Time, min	Temperature, °F	Remarks	Reference paragraph
13	Rinse	Deionized water	5		Only if step 11 used.	
14	pH test	Narrow range pH paper			Repeat steps 2 - 13 if pH not between 6.0 and 8.0.	
15	Dry	Gaseous nitrogen		120 - 140	Vacuum drying oven also acceptable.	
16	Flush	Trichlorotrifluoroethane	1		MSFC-SPEC-237.	
17	Inspect				By analysis of fluid from 16.	
18	Dry	Gaseous nitrogen		120 - 140	Vacuum drying oven also acceptable.	

CLEANING, TESTING, AND HANDLING OF OXYGEN, FUEL, AND PNEUMATIC COMPONENTS
DS-12855, BOEING CO., MAY 15, 1968 (REF. 9)

Coated Aluminum

[Not to be subjected to temperatures exceeding 130° F.]

Step	Process	Agent	Time, min	Temperature, °F	Remarks	Reference paragraph
1	Rough cleaning				Clean per BAC5765.	7.5.2a
2	Solvent flush	Trichloroethylene, precision cleaning agent, or Dowclene WR				6.2.2
3	Ultrasonic detergent	Detergent-water solution (1)	5	130 (max) (2)	(1) Water distilled or deionized having minimum specific resistance of 50 000 Ω. Detergents conform to MIL-D-16791 type I. Detergent concentration, 0.1 - 0.6 oz/gal of water. (2) Solution may be heated to 130° F (max), provided it is followed by a heated (max, 130° F) water rinse.	6.2.4
4	Ultrasonic water rinse	Distilled or deionized water (3)	5		(3) Must have minimum specific resistance of 50 000 Ω and pH 6.0 - 8.0.	6.2.5
5	Dry	Nitrogen gas, air, or other gas specifically approved by engineering			(4) Gas shall meet requirements of 6.2.1.1: shall not contain considerable hydrocarbons in excess of 3 ppm by weight, shall not exceed 60% relative humidity at ambient temperature. (5) Drying gas may be heated providing parts do not exceed 130° F for MIL-C-5541 coated parts.	6.2.6 or 6.2.7

Concluded. CLEANING, TESTING, AND HANDLING OF OXYGEN, FUEL, PNEUMATIC COMPONENTS DS-12855, BOEING CO., MAY 15, 1968 (REF. 9)

Step	Process	Agent	Time, min	Temperature, ^{o}F	Remarks	Reference paragraph
6	Visual acceptance inspection					4.9
7	Final flush	Step 2	3			6.2.2
8	Dry	Step 5				6.2.6 or 6.2.7

CLEANING AND INSPECTION PROCEDURES FOR BALLISTIC MISSILE SYSTEMS T. O. 42C-1-11 CHANGE 2, NOVEMBER 15, 1967 (REF. 12)

Brass, Copper, and Bronze

Step	Process	Agent	Time, min	Temperature, °F	Remarks	Reference paragraph
1	Mechanical descaling		As required			3-39
2	Degrease	Trichloroethylene	As required	Ambient	MIL-T-27602.	3-15 3-75
3	Vapor degrease	Trichloroethylene or trichlorotrifluoroethane			MIL-T-27602 (FSN 6850-681-5688).	3-15 3-16 3-64
4	Alkaline clean	Alkaline cleaner: 5 - 10 oz/gal tap water		150 - 175	Fed. spec. P-C-436.	3-59
5	Rinse	Tap water	5 - 10	150		
6	Pickle	H_2SO_4, 8.6% by volume; HNO_3, 1.4% by volume; demineralized water, 90% by volume; or HF, 10 - 15% by volume; demineralized water for remainder		120 - 140	Solution temperature and immersion time to be determined from test coupons.	3.61
7	Rinse	Demineralized water	5 - 10	150		
8	Dry	Oven, nitrogen gas, or vacuum		180 - 200 140		3-87
9	Rinse	Detergent solution: 1/2 - 1 oz/gal of tap water, demineralized water, or trichloroethylene	15 - 25	120 - 140	MIL-D-16791 type I.	3-86 3-85
10	Flush	Demineralized water	As required	150	Do not flush if solvent used in step 9.	
11	Inspect					3-89
12	Dry	Same as step 8				3-87

KSC (PROPOSED) (REF. 11)

Copper and Copper Alloys (3. 10. 2. 4)

Step	Process	Agent	Time, min	Temperature, °F	Remarks	Reference paragraph
1	Mechanical descale	Brushing, shot peening, etc.			As required.	3. 9. 2
2	Degrease	Trichloroethylene or trichlorotrifluoroethane			MSFC-SPEC-217. MSFC-SPEC-237.	3. 9. 3. 1
3	Dry	Gaseous nitrogen			Type I, class 1, grade B of spec. BB-N-411.	3. 10. 2. 4
4	Corrosion removal	6. 5 - 93% Sulfuric acid 17 - 61% Nitric acid Remainder is deionized water	10 - 30	Ambient	For heavy corrosion.	3. 10. 1. 7
5	Rinse	Water	5	90 - 110		
6	Rinse	Deionized water	3		One if step 4 is used.	
7	Dry	Gaseous nitrogen		120 - 140		
8	Clean	30 - 85% Orthophosphoric acid 20 - 2% 2-Butoxyethanol solvent 1% Surfactant Remainder is deionized water	60 - 90	80 - 105	Will remove light corrosion and oxidation so that step 4 may not be required.	3. 10. 2. 4
9	Rinse	Water	5	90 - 110		
10	Rinse	Deionized water	3		If ultrasonic cleaner used, rinse additional 10 minutes in ultrasonic cleaner.	3. 10. 2. 4
11	Brighten	Same as 4	10 - 30	Ambient	For cupro-nickel alloys and silicon bronzes	3. 10. 2. 4
12	Rinse	Water	5	90 - 110	Only if step 11 is used.	3. 10. 2. 4
13	Rinse	Deionized water	5			
14	pH test	pH paper (narrow range)			Repeat steps 2 - 13 if pH not between 6. 0 and 8. 0.	3. 10. 2. 4

Concluded. KSC (PROPOSED) (REF. 11)

Step	Process	Agent	Time, min	Temperature, °F	Remarks	Reference paragraph
15	Dry	Gaseous nitrogen or vacuum drying oven		120 - 140		3.5.7.2
16	Flush	Trichlorofluoroethane	1		MSFC-SPEC-237.	3.10.2.4
17	Inspect				By analysis of fluid from 16 in accordance with 4.3.	
18	Dry	Gaseous nitrogen (same as step 15)				

CLEANING AND INSPECTION PROCEDURES FOR BALLISTIC MISSILE SYSTEMS T. O. 42C-1-11 CHANGE 2, NOVEMBER 15, 1967 (REF. 12)

Carbon Steel and Carbon Steel Alloys

Step	Process	Agent	Time, min	Temperature, °F	Remarks	Reference paragraph
1	Mechanical degrease		As required			3-39
2	Degrease	Trichloroethylene			MIL-T-27602.	3-15 3-75
3	Vapor degrease	Trichloroethylene or trichlorotrifluoroethane	As required	Degreaser operating temperature	MIL-T-27602 (FSN 6850-681-5688).	3-15
4	Alkaline clean	Alkaline cleaner 5 - 10 oz/gal of tap or demineralized water	15 - 20	150	Fed. spec. P-C-436. Parts shall be completely free of step 3 solvents because of possible explosion hazard.	3-77
5	Rinse	Tap water	5 - 10	150		3-84
6	Pickle	HF, 15 - 20% by volume; Rodine 50 or equivalent inhibitor, 0.25 - 0.50% by volume; tap water, balance.	15 - 30	Ambient		3-51
7	Rinse	Tap water	5 - 7	150	Omit if step 6 omitted.	3-84
8	Rinse	Demineralized water	3 - 5	150		3-84
9	Bake		180	375±25	Required only for steels harder than Rockwell C32 to prevent hydrogen embrittlement.	
10	Protective coat	Corrosion preventative	As required	Ambient		3-55
11	Dry	Oven, nitrogen gas, or vacuum	As required	180 - 200 140 -		3-87
12	Rinse	Detergent solution, 1/2 - 1 oz/gal tap water, demineralized water, or trichloroethylene	15 - 25	120 - 140	MIL-D-16791 type I.	3-86

Concluded. CLEANING AND INSPECTION PROCEDURES FOR BALLISTIC MISSILE SYSTEMS T. O. 42C-1-11 CHANGE 2, NOVEMBER 15, 1967 (REF. 12)

Step	Process	Agent	Time, min	Temperature, °F	Remarks	Reference paragraph
13	Flush	Demineralized water	As required	150	Do not flush if solvent used in step 12.	
14	Inspect					
15	Dry	Same as step 10.				3-87

PLUM BROOK RDL-003 (REF. 3)

Carbon/Steel

Step	Process	Agent	Time, min	Temperature, °F	Remarks	Reference paragraph
1	Degrease	Trichloroethylene (Fed. spec. O-T-634b)			As required.	3. 1. 1
		or detergent-water solution		140 - 160	As required.	
2	Rinse	Distilled or deionized water			Until detergent is no longer evident.	3. 1. 2
3	Clean	20% by volume of inhibited hydrochloric acid (Fed. spec. O-A-86)			Until area is clean and free of rust and scale.	3. 1. 3
4	Rinse	0. 02% by weight of citric acid solution			Continue rinse until effluent pH = influent pH.	3. 1. 4
5	Flush	By weight a solution of 0. 5% sodium hydroxide, 0. 5% sodium nitrate, 0. 25% monosodium phosphate with distilled or deionized water.	30			3. 1. 5
6	Inspect					4. 0
7	Dry	Dry, hydrocarbon-free, gaseous nitrogen	2		As required.	3. 1. 6
8	Package					

C. Tanks

1. Aluminum and aluminum alloy tanks
2. Cryogenic tanks

SYSTEMS AND EQUIPMENT CLEANING, CPIA PUBLICATION 194
ROCKET PROPELLANTS(B) OXYGEN (REF. 21)

Aluminum and Aluminum Alloy Tanks

Step	Process	Agent	Time, min	Temperature, °F	Remarks	Reference paragraph
1	Preclean				Remove burns, grease, dirt, scale.	10.d.1
2	Degrease	Solvent	30			10.d.2
3	Rinse	Alcohol				10.d.3
4	Wash	Water				10.d.4
5	Clean	4% aluminum cleaning solution	20	Room		10.d.5
6	Wash	Water or steam clean				10.d.7
7	Dry	Dry nitrogen				10.d.7

CLEANING PROCEDURES - METALS CLEANING SPI-49.111
LINDE COMPANY, DIV. OF UNION CARBIDE, DECEMBER 28, 1965 (REF. 8)

Aluminum Shells

Step	Process	Agent	Time, min	Temperature, °F	Remarks	Reference paragraph
1	Etch	Diversey aluminux, (1) 6 oz/1 gal water; Diversey 202 (2) 2 oz/gal water		160	Swab with solution: (1) Code 3008-3000 (2) Code 3008-2775	.08.1
2	Rinse	Cold water (3)			(3) Water shall be potable.	.08.2
3	Deoxidize/ desmut	Diversey 596, 7 oz/gal water; H_2SO_4 7% by volume; remainder water		Ambient	Swab with solution inside and outside of the shell.	.08.3
4	Rinse	Cold water				.08.4

CLEANING OF CRYOGENIC TANKS FOR LO_2, LN_2, AND LH_2 SERVICE, AIR FORCE ROCKET PROPULSION LABORATORY TECHNICAL INSTRUCTION, AFRPL TI 5-4-3, NOVEMBER 1967 (REF. 25)

Step	Process	Agent	Time, min	Temperature, ^{o}F	Remarks	Reference paragraph
1	Clean	Solvent			Hot vapors of unspecified solvent until inlet and outlet temperatures are within 5^{o} F.	6. c. 1
2	Dry	Nitrogen gas			Purge with warm gas filtered through 10 μ filter until escaping gas smells sweet (no evidence of characteristic solvent fumes) and registers a dew point of -63^{o} F or less.	6. c. 2

CLEANING OF CRYOGENIC TANKS FOR LO_2, LN_2, and LH_2 SERVICE, AIR FORCE ROCKET PROPULSION LABORATORY TECHNICAL INSTRUCTION, AFRPL TI 5-4-3, NOVEMBER 1967 (REF. 25)

Detergent or Alkaline Solution Cleaning

Step	Process	Agent	Time, min	Temperature, ^{o}F	Remarks	Reference paragraph
1	Preclean	Vacuum			NO SWEEPING, dust cannot be removed from the vessel.	6.a.1
2	Clean[a]	Hot solution	30	175 - 180	Unspecified.	6.b.1
3	Rinse	Demineralized water		Ambient	Filtered through 10μ filter. (a) For alkaline solutions, use pH meter or transmitted light examination to determine when the alkalinity of outlet equals inlet. (b) For neutral solutions, flow a volume at least 6 times the capacity of the vessel.	6.b.5
4	Dry	Warm dry nitrogen gas			Purge until escaping gas registers a dew point of -63^{o} F or less.	6.b.6

[a]Do not clean aluminum alloy vessels with caustic or alkaline solutions unless specifically approved.

CLEANING OF CRYOGENIC TANKS FOR LO_2, LN_2, AND LH_2 SERVICE, AIR FORCE ROCKET PROPULSION LABORATORY TECHNICAL INSTRUCTION, AFRPL TI 5-4-3, NOVEMBER 1967 (REF. 25)

Manual Cleaning

Step	Process	Agent	Time, min	Temperature, ^{o}F	Remarks	Reference paragraph
1	Preclean	Vacuum			NO SWEEPING, dust cannot be removed from the vessel.	6. a. 1
2	Clean	Unspecified solvent			Solvent if not certified must pass through 10μ filter; in all cases surfaces shall be thoroughly wiped or scrubbed with rags or brushes.	6. a. 3
3	Rinse	Potable or demineralized water				6. a. 3
4	Pressure check	Dry nitrogen			Pressurize to operating pressure; hold 24 hours within 3 psig corrected for temperature. Closure shall not leak.	6. a. 7
5	Purge	Gaseous nitrogen			Repeatedly pressurize and dump until effluent gas smells sweet (no evidence of characteristic odors of cleaning solution used and dew point = -63^{o} F or less).	6. a. 8. a

D. Tubing

1. Aluminum alloy tubing
2. Nonferrous pipe assemblies, tubing
3. Steel pipe, pipe assemblies, tubing

MSFC SPEC-164A (REF. 5)

Aluminum Alloy Tubing

Step	Process	Agent	Time, min	Temperature, °F	Remarks	Reference paragraph
1	Cleaning		10	160±10	Circulation rate at least 20 tubing or hose volumes per min.	3.5.2.6 3.5.1.6
2	Flushing	Tap water	10	Room		
3	Cleaning	3.0 - 5.0% nitric acid	5 (min) 7 (max)	85 - 95	Spec. O-N-350: Phosphoric acid solution 0.5% by wt to remove heavy soils.	3.5.2.6
4	Flushing	Demineralized water	10	Room	No particle over 175 microns, etc.	3.2.10 3.5.1.6 3.5.2.6 4.4.3.1
5	Dry					

CLEANING PROCEDURES - METALS CLEANING SPI-49.111
LINDE COMPANY, DIV. OF UNION CARBIDE, DECEMBER 28, 1965 (REF. 8)

Nonferrous Pipe Assemblies and Parts

Step	Process	Agent	Time, min	Temperature, °F	Remarks	Reference paragraph
1	Preclean	Diversey 1319 (1) 3 oz/gal water		Ambient	(1) Code 3008-2825; step 1 optional.	.03
2	Rinse	Hot water (2)			Remove flux; (2) water shall be potable	.03.1
3	Pickle	$Na_2Cr_2O_7$, 9 oz/gal water; H_2SO_4, 16% by volume water		Ambient	Soak until uniformly pickled.	.03.2
4	Rinse	Cold or hot water				.03.3
5	Clean	Step 1				.03.4
6	Rinse	Step 4				.03.5
7	Dry					

CLEANING PROCEDURES - METALS CLEANING SPI-49.111
LINDE COMPANY, DIV. OF UNION CARBIDE, DECEMBER 28, 1965 (REF. 8)

Nonferrous Pipe and Tubing - Straight Lengths

Step	Process	Agent	Time, min	Temperature, °F	Remarks	Reference paragraph
1	Preclean	Diversey 1319: (1) 3 oz/gal water		Ambient	(1) Code 3008-2825.	.04.1
2	Rinse	Cold water (2)			(2) Water shall be potable.	.04.2
3	Pickle	$Na_2Cr_2O_2$, 9 oz/gal water; H_2SO_4, 16% by volume in water		Ambient	Soak until uniformly pickled.	.04.3
4	Rinse	Step 2				.04.4
5	Clean	Step 1				.04.5
6	Dry					.04.6

CLEANING AND TESTING OF OXYGEN AND NITROGEN GAS PIPING SYSTEMS
MIL-STD-1330 (SHIPS) MAY 10, 1968 (REF. 20)

Oxygen System Flush

Step	Process	Agent	Time, min	Temperature, °F	Remarks	Reference paragraph
1	Disassemble					5.2.3
2	Flush	Trichlorotrifluoroethane	30		MIL-C-81302 type I, ultraclean. Repeat flushing if more than 5 ppm total contamination is found.	5.2.4.1
3	Drain					5.3.1.4
4	Dry	Dry, oil-free nitrogen, air, or vacuum				5.3.1.4

MSFC-SPEC-164A (REF. 5)

Corrosion-Resistant Steel Tubing

Step	Process	Agent	Time, min	Temperature, °F	Remarks	Reference paragraph
1	Cleaning	Nonetch alkaline: e.g., Turco 4215 - concentration, 10±2 oz/gal	10	160±10	Circulation rate at least 20 tubing or hose volumes of liquid per min.	3.5.1.6
2	Flushing	Tap water	10	Room		3.5.1.6
3	Cleaning	Nitric acid solution, 10±2% by wt	5 (min) 10 (max)	170 - 190	See spec. D-N-250.	3.5.1.6
4	Flushing	Demineralized water	10	Room	No particle over 175 microns; no more than 5 particles from 100 - 175 micron size; specific resistance, 50 000 Ω; pH rating between 6 and 8.	3.2.10
5	Dry					

CLEANING OF PIPING AND EQUIPMENT - SECTION 49
WHITE SANDS (REF. 6)

Piping Steel

Step	Process	Agent	Time, min	Temperature, °F	Remarks	Reference paragraph
1	Mechanical	Grinding, brushing, sandblasting (Al_2O_3 sand), vacuum clean, flushing with clean water.				49-07a
2	Degreasing[a]	Trichloroethylene or mild commercial alkaline cleaner		140 - 160	MIL-T-27602: 5 - 7 oz/gal water solvent reused until contaminant concentration reaches 0.1% by wt.	49-07b
3	Rinsing	Clean water until cleaning solvent not evident			For alkaline cleaner only.	49-07c
4	First inspection	Visual			Presence of rust, scale etc. Proceed to step 5.	49-07d
5	Chemical descaling	Solution of fluorides and HNO_3			Steel surfaces - conditions to be determined by tests on representative specimens.	49-07e
		Method A: 20% NaOH in water		140 - 160	Remove varnish from surfaces. Flush until effluent pH stabilizes between 3.0 to 4.0.	49-074

[a]Valves and accessories are to be disassembled and cleaned in accordance with this specification (49-07i). Parts, such as gaskets and seals, that might be harmed by cleaning chemicals shall be cleaned by dipping in isopropyl alcohol.

Concluded. CLEANING OF PIPING EQUIPMENT - SECTION 49
WHITE SANDS (REF. 6)

Step	Process	Agent	Time, min	Temperature, ^{o}F	Remarks	Reference paragraph
6	Passivation	(1) 0.0.1% citric acid (2) 0.25 - 0.50% NaOH solution (3) Rinse with demineralized water			Rinse with alkaline.	
		(4) 0.25% monosodium phosphate, 0.25% disodium phosphate; 0.50% sodium nitrite; 99.0% demineralized water	60		Surface treat.	
		Method B: (1) 0.10% Na_2CrO_4 solution (2) Rinse with demineralized water (3) Dry	15 - 20		Surface treat.	49-07f
7	Final rinse	Demineralized water			Until pH effluent = pH influent.	49-07g
8	Dry	(1) Air or (2) Vacuum evacuation		140 - 250		49-07h
9	Final dry	Purge gas		140	Until a dew point of -60^{o} F is reached.	49-07h

CLEANING, TESTING, AND HANDLING OF OXYGEN, FUEL, AND PNEUMATIC COMPONENTS
D5-12855, THE BOEING CO., MAY 15, 1968 (REF. 9)

Small Tubing (1 in. i.d. max) Length to Inside Diameter Ratio Greater Than 10

[Tubing over 1 in. i.d. and with length i.d. ratio less than 10 will be processed as parts.]

Step	Process	Agent	Time, min	Temperature, ^{o}F	Remarks	Reference paragraph
1	Rough clean					5.2
2	Solvent flush	Trichloroethylene precision cleaning agent or Dowclene WR	5		Processing times given are minimum; flushing solution flow rates shall be 10 ft/sec minimum.	6.2.2
3	Alkaline flush	Turco 4215, 4215S, 4142, or 4142S or comparable nonsilicated alkaline cleaner, 1.0 - 2.0 oz/gal in water	10	150 - 170	Water distilled or deionized; minimum spec. resistance, 50 000 Ω.	6.2.3
4	Dry	Nitrogen, air, or other gas specifically approved by engineering			Shall meet 6.2.1.1; shall not contain condensable hydrocarbons in excess of 3 ppm by weight; shall not exceed 60% RH at ambient temperature.	6.2.6 or 6.2.7
5	Visual acceptance inspection					4.9
6	Final flush	Step 2	3			6.2.2
7	Dry	Step 4				6.2.6 or 6.2.7

CLEANING PROCEDURE - METALS CLEANING SPI-49.111
LINDE CO., DIV. OF UNION CARBIDE, DECEMBER 28, 1965 (REF. 8)

Steel Pipe and Steel Pipe Assemblies and Steel Parts

Step	Process	Agent	Time, min	Temperature, ^{o}F	Remarks	Reference paragraph
1	Strip paint	Diversey aluminum: (1) 12 oz/gal of water Diversey G-60: (2) 4 oz/gal of water		165	(1) Code 3008-3000. (2) Code 3008-2770. Soak until all paint is removed or loosened.	.06.1
2	Preclean	Diversey 1319: (3) 3 oz/gal water		Ambient	(3) Code 3008-2825.	.06.2
3	Rinse	Cold or hot water (4)			(4) Water shall be potable.	.06.3
4	Pickle	Diversey Everite: 20% by volume in water	120	Ambient	(5) If solution is at 140^{o} F soak for 60 minutes. Sheet steel parts should not be soaked any longer than is necessary to remove rust and scale.	.06.4
5	Rinse	Step 3				.06.5
6	Rust proof	Oakite 87, 6 oz/gal of water	5	170		.06.6
7	Rinse	Step 3				.06.7
8	Rust proof	H_2CrO_4, 0.1 oz/gal water	2		DO NOT RINSE	.06.8
9	Dry					.06.9

REFERENCES

In parentheses after each reference are given the Microfiche card numbers denoting the location of the reference in the Microfiche supplement and the pages of the reference reproduced in the Microfiche supplement. A reference to a proposed KSC specification indicates that only preliminary work has been accomplished and the specification is subject to change until finalized.

1. May, Kenneth D.: Advanced Valve Technology. NASA SP-5019, 1965. (Card 1: pp. 80 and 81.)
2. Anon.: Cleaning and Inspection of Oxygen and Nitrogen Piping Systems. BUSHIPS Instruction 9230.12A, Feb. 8, 1961. (Card 1: All.)
3. Anon.: Cleanliness of Cryogenic Systems, Cleaning for Cryogenic Fluids. NASA Plum Brook Station RDL-003, May 10, 1968. (Card 1: All.)
4. Anon.: Cleaning Procedures 05.04 and QCL's. Air Products, July 1, 1971. (Card 1: All.)
5. Anon.: Cleaning for Oxygen, Fuel and Pneumatic Systems. MSFC-SPEC-164A, NASA, Oct. 1, 1970. (Card 1: All.)
6. Anon.: Specification for LEM Test Facility. Vol. IV, Sec 49. White Sands Test Facility. (Card 2: All.)
7. Anon.: Precision Cleaning. MSC-SPEC-C-11A, NASA, June 9, 1967. (Card 2: All.)
8. Anon.: Cleaning Procedures. Union Carbide Corp., Linde Div. (Card 2: pp. 2-62 - 2-112.)
9. Anon.: Cleaning, Testing and Handling of Oxygen, Fuel and Pneumatic Components. Rep. D5-12855, Rev. G, Boeing Co., May 15, 1968. (Cards 2 and 3: Sec. I, pp. 5 - 22; Sec. I, pp. A-1 - A-7; Sec. II, pp. 1 - 12.)
10. Anon.: Cleanliness Levels, Cleaning, Protection and Inspection Procedures for Parts, Field Parts, Assemblies, Subsystems, and Systems for Fluid Use in Support Equipment. KSC-C-123(D), NASA, Mar. 14, 1968. (Card 3: All.)
11. Anon.: Proposed Specification for Surface Cleanliness of Fluid Systems. NASA Kennedy Space Center. (Cards 3, 4, and 5: All.)
12. Anon.: Cleaning and Inspection Procedures for Ballistic Missile Systems, Change 2. USAF T.O. 42C-1-11, Nov. 15, 1967. (Card 5, pp. 3-1 - 3-24.)
13. Anon.: Spacecraft Chemical and Fluid Cleanliness Requirements. MSC-SPEC-C-6B, NASA, Jan. 14, 1969. (Card 5: All.)

14. Anon.: General Specification for Cleanliness of Environmental Test Chambers (Oxygen Rich, Physiological or Vacuum). MSC-SN-C-0024, NASA, Mar. 3, 1969. (Card 5: All.)

15. Anon.: Cleanliness of Non-Airborne Breathing Systems. MSC-SPEC-9A, NASA, June 9, 1967. (Card 6: All.)

16. Anon.: Spacecraft On-Board Equipment Cleanliness. MSC-SPEC-C-8, NASA, Jan. 5, 1967. (Card 6: All.)

17. Anon.: Apollo Spacecraft Fluid Systems Surface Cleanliness. MSC-SPEC-C-7, NASA, Nov. 17, 1966. (Card 6: All.)

18. Anmuth, M.: Cleaning of Oxygen Pressure Gage Components. Naval Boiler and Turbine Lab., Mar. 26, 1965. (Card 6: All.)

19. Anon.: Cleanliness Criteria, Critical Components. Spec. No. 075192B, General Dynamics/Convair, Dec. 13, 1967. (Card 6: All.)

20. Anon.: Cleaning and Testing of Oxygen and Nitrogen Gas Piping Systems. MIL-STD-1330 (SHIPS), May 10, 1968. (Card 6: All.)

21. Anon.: Liquid Propellant Handling, Storage and Transportation. Vol. 3 of Chemical Rocket/Propellant Hazards. Rep. CPIA Publ. 194, vol. 3, Applied Physics Lab., Johns Hopkins Univ. (AD-870259L), 1970. (Cards 6 and 7: pp. 18-6 - 18-7.)

22. Anon.: Cleaning Methods. Process Specification 20-1, NASA Flight Research Center. (Card 7: All.)

23. Anon.: Cleanliness Level Requirements for Pneumatic and Hydraulic Components: Service Arm Systems, Complex 39. Rep. MCR-69-484, Martin Marietta Corp. (NASA CR-107216), Sept. 1969. (Card 7: p. I-1.)

24. Anon.: Standard Cleanliness Specification, Phase II, Final Report. Dowell Div., Dow Chemical Co. (NASA-JFK-TR-1137), Sept. 1970. (Card 7: pp. 26-42.)

25. Anon.: Technical Instruction 5-4-3, Air Force Rocket Propulsion Lab. (Card 7: All.)

26. Anon.: Contamination Control Handbook. NASA SP-5076, 1969. (Card 7: Sec. 2, p. II-1; Sec. 3, pp. III-94 - III-97.)

27. Ellenburg, Janus Y.: Monitoring Cleaning Processes and Procedures. Contamination Control: Current and Advanced Concepts in Instrumentation and Automation. Rep. SC-M-68-94, Sandia Corp. (NASA CR-95657), Sept. 1967, pp. 123-136. (Card 7: pp. 123-136.)

28. Anthony, H. V.; McDonald, J. P.; and Piccone, M.: Automated Final Cleaning, Rinsing, and Drying Station. Contamination Control: Current and Advanced Concepts in Instrumentation and Automation. Rep. SC-M-68-94, Sandia Corp. (NASA CR-95657), Sept. 1967, pp. 137-148. (Card 7: pp. 137-148.)

END OF REFERENCE

8

REFERENCE

9

McGRAW-HILL ENCYCLOPEDIA OF SCIENCE AND TECHNOLOGY.
VOL. 3, McGRAW-HILL BOOK CO., 1966.

THIS REFERENCE IS COPYRIGHTED MATERIAL AND THEREFORE
THE CONTENTS HAVE NOT BEEN REPRODUCED FROM THE TEXT.

END OF REFERENCE

9

REFERENCE

10

TOMASHOV, N. D.: THEORY OF CORROSION AND PROTECTION OF METALS. MACMILLAN CO., 1966.

THIS REFERENCE IS COPYRIGHTED MATERIAL AND THEREFORE THE CONTENTS HAVE NOT BEEN REPRODUCED FROM THE TEXT.

END OF REFERENCE

10

REFERENCE

11

BRENNER, S. S.: CATASTROPHIC OXIDATION OF SOME MOLYBDENUM CONTAINING ALLOYS. J. ELECTROCHEM., VOL. 102, NO. 1, JAN. 1955.

PHOTOSTAT FILE

Catastrophic Oxidation of Some Molybdenum-Containing Alloys[1]

S. S. Brenner

Research Laboratory, General Electric Company, Schenectady, New York

ABSTRACT

When nickel or chromium is added to binary iron-molybdenum alloys, catastrophic oxidation occurs in certain concentration regions. Chromium is more effective than nickel in inducing this rapid type of oxidation.

Catastrophic oxidation occurs because of the formation of liquid MoO_3 along the metal-oxide interface. This is preceded by the cracking of the chromium or nickel-containing oxide.

Catastrophic oxidation does not occur with alloys containing large amounts of nickel.

Introduction

Catastrophic oxidation of certain alloys containing appreciable amounts of molybdenum has been reported. It is postulated that this rapid type of attack is due to the formation of MoO_3. The presence of other volatile and low melting oxides such as V_2O_5 (670°C), Bi_2O_3 (820°C), PbO (888°C), WO_3 (1473°C), and mixtures of these oxides can also induce this type of attack in the absence of molybdenum (1–4).

While several workers (2–4) are of the opinion that catastrophic oxidation stems from the presence of a liquid oxide layer, none of these postulates how the liquid film is formed and what the oxidation process is, in the case where the liquid oxide is formed by the alloying element.

This paper presents results on the oxidation of some molybdenum-containing materials and proposes a mechanism of catastrophic oxidation. A previous paper (5) showed that binary nickel-molybdenum alloys up to 30% (weight) molybdenum and binary iron-molybdenum alloys up to 20% molybdenum do not oxidize catastrophically at 1000°C. In both cases, MoO_2 and molybdate, in addition to nickel oxide or iron oxide, are formed during oxidation. To induce catastrophic oxidation, additions of nickel or chromium or both were made to binary iron-molybdenum alloys.

Experimental

Specimen preparation.—All alloys were prepared by arc melting in a multiple hearth arc furnace. Their nominal compositions are given in Table I. In most cases, nominal compositions deviate less than 5% from analyzed compositions. Nominal weight percentages are used throughout this paper.

The 100 g alloy buttons were ground on two faces, hot rolled, sand blasted, cold rolled if possible, and finally annealed. Specimens 0.020 in.–0.040 in. were cut from the rolled strips.

Procedure.—Oxidation of the alloys was determined by measuring the weight loss of the metal. Weighed specimens were placed in covered alundum filtering crucibles which were seated in a 4-in. diameter crucible furnace. The purpose of the alundum crucible was to minimize contamination from the neighboring samples and from the fire brick plug. Oxygen was passed through the crucible furnace at a rate of about 2 l/min to insure against oxygen depletion. The temperature was constant to better than ±5°C.

The amount of metal oxidized was determined as follows. After the bulk oxide was removed, the weight of the metal core with the residual oxide remaining on it was determined. The residual oxide was then reduced in hydrogen and its original weight was calculated by assuming that the oxide contained 25% oxygen.

Results

When nickel was substituted for iron in the 20Mo80Fe alloy, the striking and unexpected results shown in Fig. 1 occurred. Up to 10% nickel there is only a small change in the oxidation rate; beyond 15% there is a sudden increase with a maximum at about 25Ni. At this composition the oxidation is about 15 times as fast as with the 20Mo70Fe10Ni alloy. Beyond 25Ni, the oxidation rate again decreases rapidly, approaching that of the 20Mo70Fe-10Ni alloy at 40Ni. An increase to 60Ni gives only a small change in the oxidation rate.

Additions of chromium to the iron-molybdenum alloys initiated rapid oxidation even more readily. Only small amounts of chromium in the order of 5% are sufficient to accelerate attack. Some alloy samples oxidized completely in the 2-hr testing

[1] Manuscript received March 22, 1954.

TABLE I. *Loss of metal by oxidation during 2 hr at 1000°C*

Alloy	$\Delta m/A$ (mg/cm²)
20Mo80Fe	16.1
20Mo75Fe5Ni	9.4
20Mo70Fe10Ni	9.9
20Mo65Fe15Ni	27.9
20Mo60Fe20Ni	93.8
20Mo55Fe25Ni	152.5
20Mo50Fe30Ni	46.2
20Mo40Fe40Ni	11.2
20Mo20Fe60Ni	3.7
25Ni75Fe	18.2
25Ni70Fe5Mo	14.1
25Ni65Fe10Mo	23.9 (uneven attack)
25Ni45Fe30Mo	122.5
50Ni20Fe30Mo	4.8
10Mo5Cr85Fe	128.5 (uneven attack)
5Mo15Cr80Fe	112.0 (uneven attack)
15Mo10Cr75Fe	>365.0 (completely oxidized)
25Cr75Fe	1.0
20Mo5Cr75Fe	31.3
15Mo15Cr70Fe	>361.0 (completely oxidized)
20Mo10Cr70Fe	>198.0 (completely oxidized)
5Mo25Cr70Fe	1.0
10Mo25Cr65Fe	58.4 (uneven attack)
30Mo5Cr65Fe	34.3
40Ni20Mo35Fe5Cr	10.3
40Ni20Mo30Fe10Cr	10.5
40Ni20Mo20Fe20Cr	5.7

period. The effect of chromium additions in excess of 25% could not be evaluated because of the difficulty of fabrication of the alloys.

The three quaternary alloys containing 40% nickel did not exhibit catastrophic oxidation even though the chromium and molybdenum content were as high as 20% each.

Table I lists for every alloy the amount of metal oxidized during 2 hr of oxidation at 1000°C. These values are plotted as a function of composition in Fig. 2, the shaded areas indicating the regions of catastrophic oxidation.

The amounts of metal oxidized as given in Table I are single values, not averages. Several duplicate determinations were made on most of the alloy samples, generally giving a reproducibility of within 30% of the reported values. Where oxidation was not uniform, the reproducibility was less satisfactory; however, the relative degree of attack was not altered. Several of the duplicate determinations were made in the absence of other specimens and in different furnaces. In all cases the amount of oxidation was within the normal reproducibility, indicating that contamination of one sample by another was kept to a minimum.

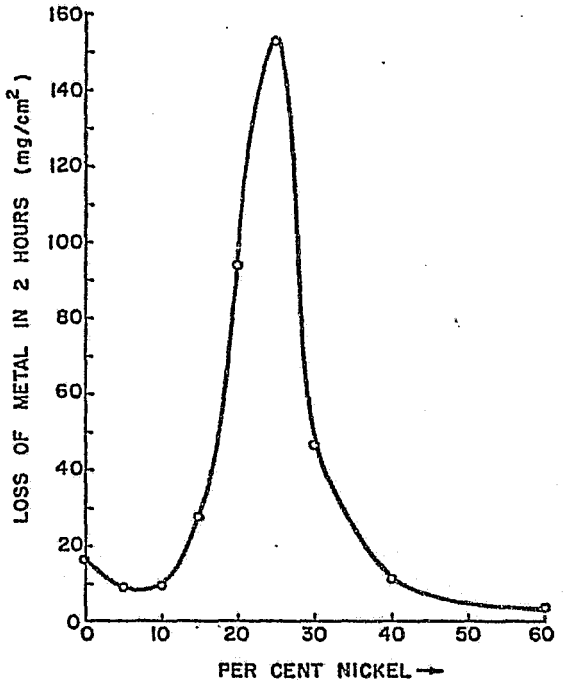

FIG. 1. Oxidation of 20MoFeNi alloys, 1000°C. (Nickel is substituted for iron in the original 20Mo80Fe alloy.)

MECHANISM OF CATASTROPHIC OXIDATION

The results on oxidation of iron-molybdenum alloys and on nickel-molybdenum alloys, as reported previously (5), show that, due to the enrichment of molybdenum, MoO_2 is formed immediately adjacent to the alloy surface. As long as the MoO_2 is prevented from oxidizing to MoO_3, normal oxidation

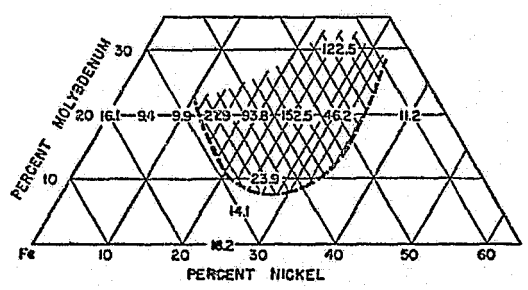

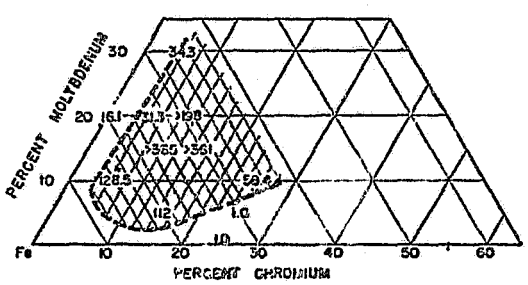

FIG. 2. Oxidation of FeMoNiCr alloys. Numbers indicate weight loss per unit area after 2 hr at 1000°C. Shaded areas indicate regions of rapid oxidation.

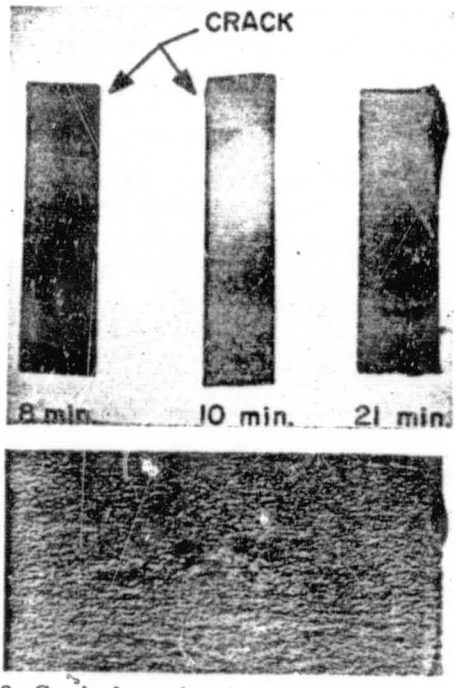

FIG. 3. Crack formation in oxide on 15Mo75Fe10Cr Alloy at 1000°C. Top, crack growth as a function of time. (2× before reduction for publication); bottom, oxidation after 8 min. (10× before reduction for publication.)

occurs. However, as soon as the MoO_2 has access to a large supply of oxygen, the low melting and highly volatile MoO_3 is formed.

The simplest method of supplying the MoO_2 layer with oxygen is by means of a crack or pore in the main oxide. Pore formation does occur with the MoFeCr alloys as shown in Fig. 3. After the initially very rapid formation of the chromium-rich oxide, a crack appears exposing the molybdenum-enriched surface. Molten MoO_3 is formed which penetrates along the metal-oxide interface. Being less noble, the chromium and iron in contact with the MoO_3 constantly reduces the MoO_3 according to

$$MoO_3 + 2Fe \rightarrow Mo + Fe_2O_3$$

$$MoO_3 + 2Cr \rightarrow Mo + Cr_2O_3$$

Being an excellent flux, liquid MoO_3 probably dissolves the chromium and iron oxide at the $MoO_{3(l)}$-metal interface. Fluxing is further facilitated by the

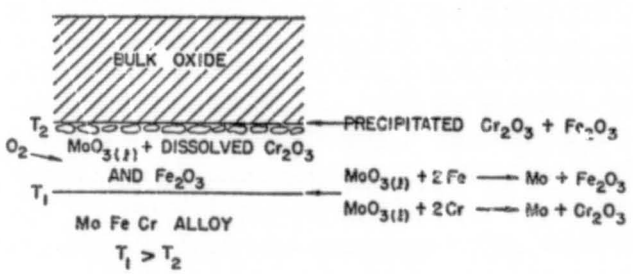

FIG. 4. Mechanism of catastrophic oxidation

FIG. 5. Oxidation of 15Mo75Fe10Cr alloy, 2 hr at 1000°C. Top, top view of oxidized specimen; center, side view of oxidized specimen; bottom, original alloy specimen. (1½× before reduction for publication.)

released heat of formation of chromium and iron oxide which tends to increase the temperature at the metal-$MoO_{3(l)}$ interface. The dissolved iron and chromium oxide nucleate and precipitate again in

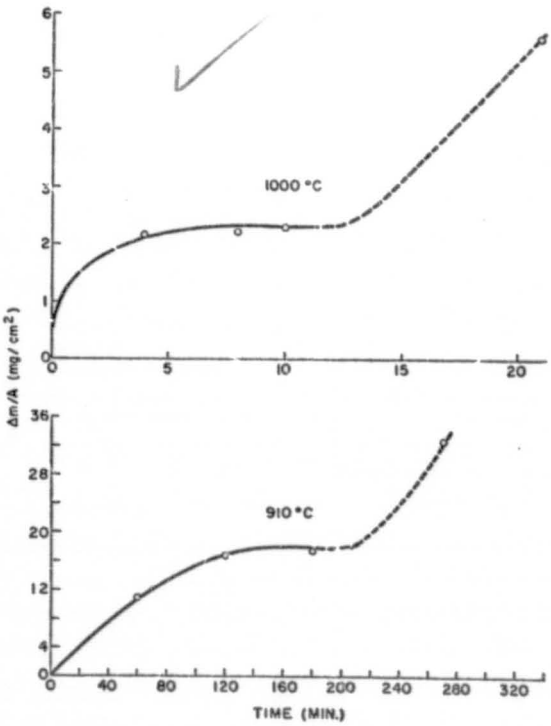

FIG. 6. Oxidation of 15Mo75Fe10Cr alloy

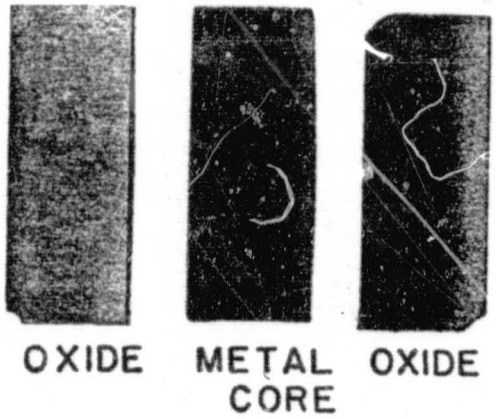

FIG. 7. Oxidation of 20Mo55Fe25Ni alloy, 2 hr at 1000°C. (1½× before reduction for publication.)

the cooler region near the $MoO_{6(l)}$-bulk oxide interface. This process is shown schematically in Fig. 4.

Thus, the original crack or pore is never healed and both MoO_2 and Mo have continual access to the oxygen. As the metal is oxidized along the edges, the oxide curls up until, after complete oxidation, it appears as shown in Fig. 5.

The cracking of the Cr-rich oxide is in agreement with the findings of McCullough, Fontana, and Beck (6). In their investigation on the oxidation of some stainless steels, they found that at 980°C there was an abrupt increase in the oxygen pickup after an initial period ranging from 10 to 45 min. At 925°C the time to rupture increased to about 4 hr.

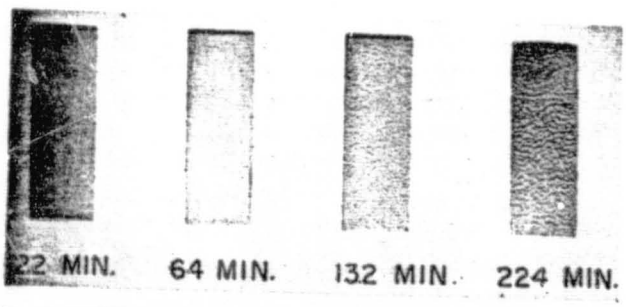

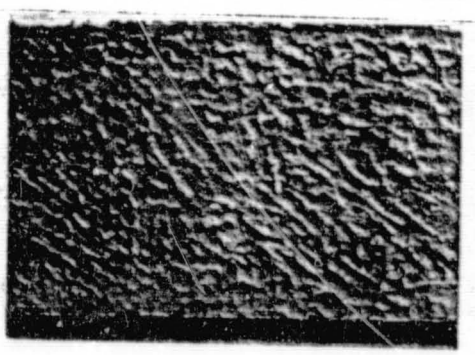

FIG. 8. Surface roughening of the 20Mo55Fe25Ni alloy during oxidation at 910°C. Top, surface roughening as a function of time (1× before reduction for publication); bottom, surface after 224 min. (5× before reduction for publication.)

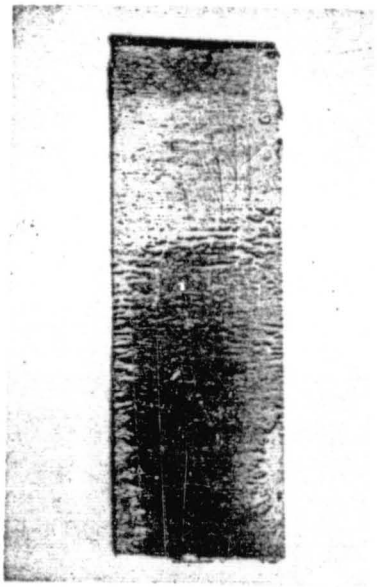

FIG. 9. Nonuniform oxidation of 20Mo55Fe25Ni alloy, 1 hr at 1000°C.

Fig. 6 shows the weight loss of 15Mo10Cr75Fe alloy as a function of time at 1000° and 910°C. The two curves show clearly the abrupt increase of oxidation after about 15 min at 1000°C and 3½ hr at 910°C.

That the crack should appear at the edges is quite reasonable. Presumably the crack formation comes by the stress relieving of the compressed oxide. Since a sharp edge offers little constraint, the oxide tends to pull away from it.

X-ray analysis of the oxide formed on the MoFeCr alloys showed it to consist of a mixture of Fe_2O_3 and Cr_2O_3. No $Cr_2O_3 \cdot FeO$ could be detected even before the cracking of the oxide occurred.

At first it appeared that the mechanism of the rapid oxidation of the MoFeNi alloys was different from that of the MoFeCr alloys. Oxidation is less violent and more uniform. This behavior is shown

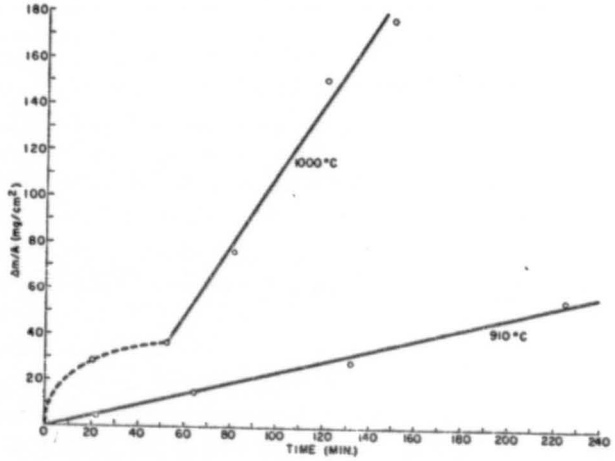

FIG. 10. Oxidation of 20Mo55Fe25Ni alloy

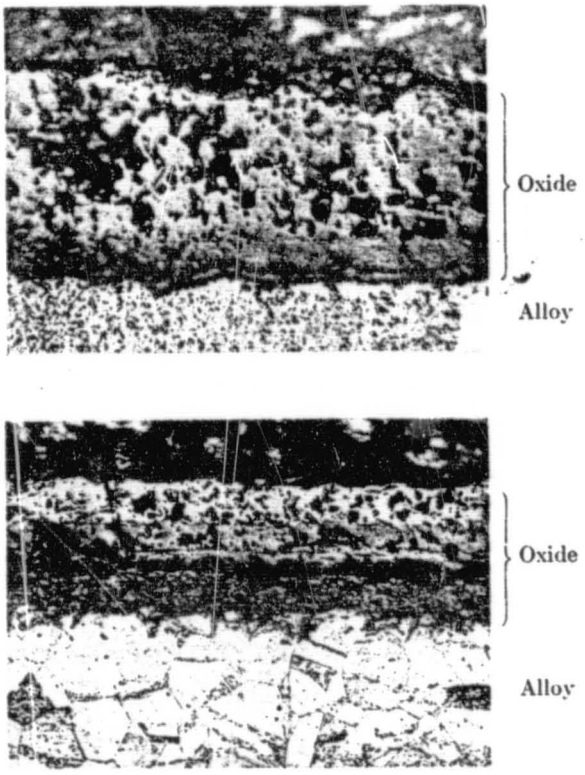

FIG. 11. Top, rapid oxidation, oxide on 30Mo45Fe25Ni alloy, 2 hr at 1000°C; bottom, retarded oxidation, oxide on 5Mo70Fe25Ni alloy, 5 hr at 1000°C. (250× before reduction for publication.)

in Fig. 7 which shows the metal core and the two oxide plates removed from the 20Mo55Fe25Ni alloy sample after 2-hr oxidation at 1000°C. However, it was noticed that in many cases the oxide had pulled away slightly from the edges. An investigation of the surface of the 20Mo55Fe25Ni alloy after oxidation for varying periods at 910°C revealed the development of a rough and ridged surface (Fig. 8) suggesting the presence of a liquid phase. It was also observed that at the higher temperature (1000°C) some areas of the specimen were sometimes attacked more severely than others, as shown in Fig. 9.

In view of these facts, it is believed that the oxidation mechanism is similar to that of the MoFeCr alloys. After the metal surface is enriched by molybdenum, oxygen obtains access to the surface and forms liquid MoO_3. The MoO_3 penetrates along the metal-oxide interface, constantly being reduced by the less noble iron and oxidized by the ambient oxygen. Iron oxide is dissolved in the molten MoO_3 and re-precipitated along the bottom surface of the bulk oxide (see Fig. 4). Since nickel is considerably more noble than molybdenum, nickel-rich ridges form on the surface. This process can, therefore, be described as a selective oxidation by a liquid phase. Since the oxygen affinity of chromium is much larger than that of iron, it can readily be seen that the oxidation of the chromium alloys should be much more violent.

An effort was made to indicate more clearly the cracking or pore formation of the oxide on the 20Mo55Fe25Ni alloy. Oxidation measurements as a function of time were made at both 910° and 1000°C (Fig. 10). Neither of the two measurements definitely shows that cracking occurs, although there is good indication of it at 1000°C. At both temperatures oxidation is linear with time.

Returning to Fig. 1, it can now be said in view of the foregoing discussion, that in the range of 15–35% nickel, a liquid film of MoO_3 is formed, while with the other compositions molybdenum is prevented from oxidizing to the higher oxide. The difference between the oxide structure of the 45Fe30Mo25Ni alloy exhibiting rapid oxidation and the 5Mo70Fe25Ni alloy exhibiting normal oxidation is pointed out in Fig. 11. The normally oxidized sample exhibits the MoO_2 rich oxide layer adjacent to the alloy surface, while the rapidly oxidized sample shows only one homogeneous layer.

The question remains why there is a critical nickel composition range in which rapid oxidation occurs. It was hoped that x-ray diffraction analysis of the oxides formed on the alloys would give some clue. However, the main oxide on all the MoFeNi alloys beyond 10% nickel consisted primarily of a Fe_3O_4 spinell-type phase. The oxide is undoubtedly $(Fe, Ni)O \cdot Fe_2O_3$ with nickel ions replacing the ferrous ions as the nickel content is increased.

An analysis of the oxide formed on the 20Mo55Fe25Ni alloy (maximum rate of oxidation) gave the following composition:

	Wt %
Fe	50.0
Ni	22.0
Mo	0.7
O	balance

This indicates that the ratio of nickel to iron is practically the same in the oxide as in the alloy. Furthermore, with this amount of nickel in the oxide, ferrous ions are almost completely replaced by nickelous ions and $NiO \cdot Fe_2O_3$ is formed exclusively. It is, therefore, hypothesized that $(FeNi)O \cdot Fe_2O_3$ is more prone to cracking than is the pure $FeO \cdot Fe_2O_3$. The oxide on the alloys with more than 35% nickel may still crack, but now the alloy surface below the oxide is sufficiently diluted with nickel to prevent the formation of MoO_3. This reasoning is in agreement with results reported previously (5) that nickel-molybdenum alloys containing 30% molybdenum do not exhibit catastrophic oxidation.

Similar analysis is extended to the three MoFeNiCr alloys. If the oxide does crack, there is enough nickel

on the alloy surface to prevent the formation of liquid MoO_3, and healing of the crack can occur.

Summary and Conclusions

When chromium or nickel is added to binary iron-molybdenum alloys which oxidize normally, catastrophic oxidation can occur within certain composition regions. Chromium induces catastrophic oxidation more readily than nickel.

It is postulated that immediately after the initial oxidation, the metal surface becomes enriched in molybdenum. The oxide on the alloy cracks, allowing the formation of liquid MoO_3 along the alloy oxide interface. $MoO_{3(l)}$ constantly oxidizes the iron and chromium in the alloy to Fe_2O_3 and Cr_2O_3. Fe_2O_3 and Cr_2O_3 dissolve in the MoO_3 and re-precipitate along the MoO_3-bulk oxide interface. Healing of the crack cannot, therefore, occur.

When the alloy contains a sufficient amount of nickel, formation of MoO_3 is prevented in a similar manner as in the nickel-rich nickel-molybdenum alloys. Thus, MoFeNiCr alloys with 40% nickel and 20% molybdenum do not oxidize catastrophically. These alloys may be of industrial use.

Acknowledgment

The author is grateful to Dr. David Turnbull for his valuable suggestions and criticisms.

Any discussion of this paper will appear in a Discussion Section to be published in the December 1955 Journal.

References

1. W. C. Leslie and M. G. Fontana, *Trans. Am. Soc. Metals*, **41**, 1213 (1949).
2. A. de S. Brasunas and N. J. Grant, *Iron Age*, 85, Aug. 17, 1950.
3. G. W. Rathenau and J. L. Meijering, *Metallurgia*, **42**, 167 (1950).
4. P. Amgwerd, Eidgenössische Materials prüfungs- und Versuchsanstalt fur Industrie, Bauwesen und Gewerbe, Zurich/St. Gallen, Report No. 171, September 1949.
5. S. S. Brenner, *This Journal*, 102, 7 (1955).
6. H. M. McCullough, M. G. Fontana, and F. H. Beck, *Trans. Am. Soc. Metals*, **43**, 404 (1951).

END OF REFERENCE

11

REFERENCE

12

GULBRANSEN, E. A.; AND ANDREW, K. F.: KINETICS OF THE OXIDATION OF PURE TUNGSTEN FROM 500° TO 1300°C. J. ELECTROCHEM. SOC., VOL. 107, NO. 7, JULY 1960.

THIS REFERENCE IS MATERIAL THAT IS READILY AVAILABLE AND THEREFORE THE CONTENTS HAVE NOT BEEN REPRODUCED.

END OF REFERENCE

12

REFERENCE

13

KUBASCHEWSKI, O.; AND HOPKINS, B. E.: OXIDATION OF METALS AND ALLOYS. SECOND ED., BUTTERWORTHS, INC., 1967.

THIS REFERENCE IS COPYRIGHTED MATERIAL AND THEREFORE THE CONTENTS HAVE NOT BEEN REPRODUCED FROM THE TEXT.

END OF REFERENCE

13

REFERENCE

14

MANNED SPACECRAFT CRITERIA AND STANDARDS. MSCM 8080, NASA MANNED SPACECRAFT CENTER, APR. 1971 (CHANGES, OCT. 1972).

THIS REFERENCE HAS A LIMITED DISTRIBUTION AND MAY NOT BE REPRODUCED.

END OF REFERENCE

14

REFERENCE

15

DISSIMILAR METALS. MIL-STD-889A, DEPT. ARMY, MAY 5, 1972.

MIL-STD-889A
5 MAY 1972
SUPERSEDING
MIL-STD-889
25 September 1969

MILITARY STANDARD

DISSIMILAR METALS

FSC MISC

DEPARTMENT OF DEFENSE
Washington, D. C. 20301

Dissimilar Metals

MIL-STD-889

1. This Military Standard has been approved by the Department of Defense and is mandatory for use by all Departments and Agencies of the Department of Defense.

2. Recommended corrections, additions, or deletions should be addressed to Air Force Materials Laboratory, Attn: LAA, Wright-Patterson Air Force Base, Ohio 45433.

CONTENTS

Paragraph	1.	SCOPE	Page 1
	1.1	Purpose	1
	1.1.1	Supersession	1
	1.1.2	Applicability	1
	1.2	Classification	1
	1.2.1	Type I	1
	1.2.1.1	Grouping of type I metals and their alloys	1
	1.2.2	Type II	1
	2.	REFERENCED DOCUMENTS	4
	3.	DEFINITIONS	4
	3.1	Dissimilar metals	4
	3.2	Galvanic (two or more metals) (electrolytic corrosion)	5
	3.3	Galvanic series	5
	3.4	Anode	5
	3.5	Cathode	5
	4.	GENERAL STATEMENTS	5
	5.	DETAILED REQUIREMENTS	5
	5.1	Type I requirements, dissimilar metals	5
	5.2	Type II requirements	
	5.2.1	Class 1	5
	5.2.2	Class 2	6
	5.2.3	Class 3	6
	5.2.4	Class 4	6
	5.2.5	Class 5	6
	5.3	Protection against electrolytic corrosion	6
	6.	NOTES	8

TABLES

Table	I	Grouping of Metals, Type I	2
	II	Dissimilar Metals Compatibility in Seawater at Ambient Temperature, Type II	3

MILITARY STANDARD

DISSIMILAR METALS

1. SCOPE

1.1 Purpose. This standard establishes requirements for the definition of dissimilar metals and selection of anti-corrosion, protective systems for dissimilar metals couples.

1.1.1 Supersession. This standard shall supersede MS33586 and shall be construed to replace it wherever called out in specifications and other documents.

1.1.2 Applicability. This military standard does not apply to standard attaching parts such as rivets, bolts, nuts, and washers which are component parts of assemblies which will be painted prior to being placed in service.

1.2 Classification

1.2.1 Type I. Applicable to components and systems conforming to MIL-F-7179 requirements.

1.2.1.1 Grouping of type I metals and their alloys.

1.2.1.1.1 Metals listed in the same group in table I are similar and shall be considered compatible when in contact and when protected in accordance with MIL-F-7179. Metals not in the same group are dissimilar and incompatible.

1.2.2 Type II. Applicable to all other equipment, parts and systems.

1.2.2.1 Table II shall be used to determine the compatibility of two metals in intimate contact.

1.2.2.2 The environmental conditions to which surfaces are exposed are classified as follows in order of generally decreasing severity.

Class 1 - Surfaces of equipment in direct contact with seawater, such as the exterior surfaces of dipped sonar equipment, and equipment including aircraft weapon systems used on ships.

Class 2 - Surfaces of equipment exposed or subject to the direct action of climatic conditions. Such climatic conditions include but

are not limited to rain, snow, salt-laden air, direct solar radiation, industrial atmospheres, dust, and wind-blown sand. For example, both the exterior and interior surfaces of the frame of an open-frame motor directly exposed to climatic conditions would be classified as class 2.

Class 3 - Sheltered surfaces of equipment not exposed or subject to the direct action of climatic conditions as described for class 2.

Class 4 - Surfaces of equipment exposed only to an unusually mild environment such as might exist in a temperature and humidity controlled room.

Class 5 - Surfaces of equipment subject to unusual chemical or temperature environments.

Table I. Grouping of Metals, Type I.

Group I	Group II	Group III	Group IV
Magnesium alloys	Aluminum	Zinc	Copper and its alloys
	Aluminum alloys (all)	Cadmium	Nickel and its alloys
Aluminum alloys 5052, 5056, 5356, 6061, and 6063	Zinc	Steel	Chromium
	Cadmium	Lead	Stainless steel (passive)
Tin	Tin	Tin	Gold
	Stainless steel (active)	Stainless steel (active)	Silver
	Tin lead (solder)	Nickel and its alloys	
		Tin lead (solder)	
	Titanium	Titanium	Titanium

NOTE: 1. Caution is required on use of zinc in contact with aluminum alloys in class 1 and 2 environments. Alkaline corrosion products of zinc are particularly deterimental to aluminum alloys. An alkali resistant coating for the aluminum faying surface is required.

2. Caution is required on use of cadmium or cadmium plate in contact with titanium in class 1 and 2 environments. Alkaline corrosion products of cadmium are particularly detrimental to titanium. An alkali resistant coating for titanium faying surface is required.

TABLE II. Dissimilar Metals Compatibility in Seawater at Ambient Temperature, Type II

	*	1	2	3	4	5	6	7	8	9	10	11	12	13	14	15	16	17	18	19	20
Gold, Platinum, Gold Platinum Alloys	1	C	C	C	C	No	No	No	No	No	No	No	C	No	No	No	Pr	Pr	No	No	Pr
Rodium, Graphite, Palladium	2	C	C	C	C	C	C	C	C	No	No	No	C	No	No	No	Pr	Pr	No	No	Pr
Silver, Silver Base Alloys	3	C	C	C	C	C	C	C	C	C	No	No	C	No	No	No	Pr	Pr	No	No	Pr
Titanium	4	C	C	C	C	C	C	C	C	C	C	C	C	C	C	No	Pr	Pr	C	C	Pr
Nickel, Nickel Base Alloys, Cobalt Alloys	5	No	C	C	C	C	C	C	C	C	C	C	C	S/No	S/No	No	Pr	Pr	S/No	No	Pr
Nickel Copper (QQ-N-281 & QQ-N-286), Monel	6	No	C	C	C	C	C	C	C	C	C	C	C	No	No	No	Pr	Pr	No	No	Pr
Steel AISI 300 Series, A-286, Nickel Chrome Steels Ti(6Al-4V)	7	No	C	C	C	C	C	C	C	C	C	C	C	C	S/No	No	Pr	Pr	S/No	S/No	Pr
Copper, Bronze, Brass Copper Alloys, Silver Solder	8	No	C	C	C	C	C	C	C	C	C	C	C	C	No	No	Pr	Pr	No	No	Pr
Commercial Yellow Brass & Bronze	9	No	No	C	C	C	C	C	C	C	C	C	C	C	C	No	Pr	Pr	No	No	Pr
High Alloy, Leaded, Naval Brass, Leaded Bronze	10	No	No	No	C	C	C	C	C	C	C	C	C	C	C	No	Pr	Pr	No	No	Pr
Cres Steel (431, 440), AISI 400 Series, P-H Steels	11	No	No	No	C	C	C	C	C	C	C	C	C	C	C	C	Pr	Pr	S/No	No	Pr
Chromium Plate, w. Mo.	12	C	C	C	C	C	C	C	C	C	C	C	C	C	C	C	Pr	Pr	C	S/No	Pr
Cres Steel, AISI 410, 416 420	13	No	No	No	C	S/No	No	C	C	C	C	C	C	C	C	C	Pr	Pr	No	No	Pr
Tin, Tin Plate, Indium, Tin-Lead Alloys	14	No	No	No	C	S/No	No	S/No	No	C	C	C	C	C	C	C	Pr	Pr	C	S/No	Pr
Lead, Lead Base Alloys	15	No	No	No	No	No	No	No	No	No	No	C	C	C	C	C	Pr	Pr	C	C	Pr
Aluminum 2024, 2014, 7075	16	Pr	Pr	Pr	Pr	Pr	Pr	Pr	Pr	Pr	Pr	Pr	Pr	Pr	Pr	Pr	Pr	Pr	Pr	Pr	Pr
All Steels Except Cres	17	Pr	Pr	Pr	Pr	Pr	Pr	Pr	Pr	Pr	Pr	Pr	Pr	Pr	Pr	Pr	Pr	Pr	Pr	Pr	Pr
Aluminum 1100, 3003, 5052, 6063, 6061, 356	18	No	No	No	C	S/No	No	S/No	No	No	No	S/No	C	No	C	C	Pr	Pr	C	C	Pr
Cadmium, Zinc Plate Galvanize, Clad Al, Be	19	No	No	No	C	No	No	S/No	No	No	No	No	S/No	No	S/No	C	Pr	Pr	C	C	Pr
Magnesium	20	Pr	Pr	Pr	Pr	Pr	Pr	Pr	Pr	Pr	Pr	Pr	Pr	Pr	Pr	Pr	Pr	Pr	Pr	Pr	Pr

LEGEND: C = Compatible (no barrier needed)
No = Incompatible
S = Compatible 2 miles away from seawater
Pr = Must have primer coat and special treatment due to inherent chemical corrosion susceptibility of the metals.

* Identification of horizontal groups are identical with numbered vertical group.

2. REFERENCED DOCUMENTS

2.1 The issues of the following documents in effect on the date of invitation for bids form a part of this standard to the extent specified herein.

SPECIFICATION

Federal

QQ-N-281	Nickel-Copper-Alloy Bar, Plate, Rod, Sheet, Strip, Wire, Forgings and Structural and Special Shaped Sections
QQ-N-286	Nickel-Copper-Aluminum Alloy, Wrought

Military

MIL-S-5002	Surface Treatments and Metallic Coatings for Metal Surfaces of Weapons Systems
MIL-F-7179	Finishes and Coatings: General Specification for Protection of Aerospace Weapon Systems, Structures and Parts
MIL-S-8802	Sealing Compound, Temperature-Resistant, Integral Fuel Tanks and Fuel Cell Cavities, High-Adhesion
MIL-S-23586	Sealing Compound, Electrical, Silicon Rubber, Accelerator Required
MIL-S-81733	Sealing Compound, Corrosion Preventive

Other

SD-24	General Specification for Design and Construction of Aircraft Weapon Systems

(Copies of specifications, standards, drawings, and publications required by suppliers in connection with specific procurement functions should be obtained from the procuring activity or as directed by the contracting officer.)

3. DEFINITIONS

3.1 Dissimilar metals. Materials classified in different groups are considered dissimilar or incompatible with one another. The tendency toward galvanic corrosion is greater between widely separated groups than between adjacent groups. Metals from different groups may be placed in contact where suitable protection against galvanic action is provided. The method of protection required will be largely dependent on design and usage environments. The surface composition of a part should be considered when determining dissimilarity; a cadmium-plated copper part is considered similar to aluminum.

3.2 Galvanic (two or more metals) (electrolytic corrosion). Accelerated corrosion of a metal because of an electrical contact with a more noble metal or a nonmetallic conductor in an electrolyte.

3.3 Galvanic series. A list of metals and alloys arranged according to their relative corrosion potentials in a given environment.

3.4 Anode. The electrode of an electrolytic cell at which oxidation is the principal reaction. It is usually the electrode where corrosion occurs and metal ions enter solution.

3.5 Cathode. The electrode of an electrolytic cell at which reduction is the principal reaction. It is usually the electrode where metal ions do not enter solution.

4. GENERAL STATEMENTS

4.1 The classification of types I and II metals not listed herein shall be as released by the Naval Air Systems Command (Code AIR-52031C) or the Air Force Systems Command (Code 11), as applicable.

4.2 All nonmetals in contact with metals shall be considered dissimilar unless there is technical data supporting compatibility. This includes both plastic and metal matrix composites.

5. DETAILED REQUIREMENTS

5.1 Type I requirements, dissimilar metals.

5.1.1 Metals in the same group are considered compatible. Metals in different groups are considered incompatible.

5.2 Type II requirements

5.2.1 Class 1. Metals exposed to a seawater environment shall be corrosion and stress-corrosion resistant or shall be processed to resist corrosion and stress-corrosion cracking.

5.2.1.1 Where incompatible metals as defined in table II are used, an interposing material compatible with each shall be used. In addition, irrespective of the metals involved, all exposed edges shall be sealed with a suitable (e.g., temperature compatible) sealant material, such as material conforming to MIL-S-8802, MIL-S-23586 or MIL-S-81733, provided design integrity of the assembly is not, thereby, compromised.

5.2.1.2 Characteristics to satisfy performance requirements for the Naval Air Systems Command shall be in accordance with SD-24.

5.2.2 Class 2. Metals exposed to the environment described for class 2 shall be corrosion and stress-corrosion resistant or shall be processed to resist corrosion and stress-corrosion cracking.

5.2.2.1 Where incompatible metals are defined in table II are used, an interposing material compatible with each shall be used. In addition, where magnesium is one of the metals involved in a dissimilar metal combination, all exposed edges shall be sealed with a suitable sealant such as material conforming to MIL-S-8802 or MIL-S-81733.

5.2.3 Class 3. Metals exposed to the environment described for class 3 shall be corrosion and stress-corrosion resistant or shall be processed to resist corrosion and stress-corrosion cracking.

5.2.3.1 Where incompatible metals as defined in table II are used, an interposing material compatible with each shall be used.

5.2.4 Class 4. For class 4, some relaxation of the requirements of class 3 may be applicable. Plans for the use of metals and metal combinations in class 4 applications shall be submitted to the procuring activity for approval, if relaxation of the requirements of class 3 is requested. The request for approval shall include all necessary technical information concerning the application with data supporting adequate resistance to deterioration.

5.2.5 Class 5. Metals and metal combinations proposed for use in unusual temperature or chemical environments shall be submitted to the procuring activity for approval. The request for approval shall include all necessary technical information concerning the application with data supporting adequate resistance to deterioration.

5.3 Protection against electrolytic corrosion.

5.3.1 Dissimilar metals shall not be used in intimate contact unless suitably protected against electrolytic corrosion. Because of the seriousness of galvanic corrosion, every effort shall be made to avoid the use of dissimilar metals, to exclude moisture or other electrolyte from the system, and to protect metal surfaces in the contact area.

5.3.1.1 Table II lists metals in seawater at ambient temperature; relative positions may vary in other environments; where it is necessary that metals not shown as compatible in table II be assembled, the following measures, as applicable, shall be used to prevent corrosion.

5.3.1.1.1 Interposition of a material compatible with each to decrease electrolytic potential differences, such as cadmium plate on steel in contact with aluminum.

5.3.1.1.2 Interposition of an inert material between the dissimilar metals to act as a mechanical and insulating barrier, including potting or lubricating material.

5.3.1.1.3 Application of organic coatings to the contact faces of each of the dissimilar metals, such as paint coats on steel and aluminum surfaces in contact.

5.3.1.1.4 Application of corrosion inhibitors to the faces of the dissimilar metals, such as zinc-chromate paste on nickel-plated brass screws in contact with aluminum.

5.3.1.1.5 Design of dissimilar metal contacts so that the area of the cathodic metal is relatively smaller than the area of the anodic metal, such as screws of stainless steel or nickel-plated brass in contact with aluminum but not the reverse. NOTE: Only applicable for immersed conditions.

5.3.1.1.6 Limitation of amount of aeration and of electrolyte reaching the dissimilar metal faces, such as steel bolts in aluminum with all surfaces of contact sealed with zinc-chromate primer, vinyl films, sealing in dry gas or air, or equivalent.

5.3.1.1.7 For welded and brazed assemblies, overcoating to at least 1/3 inch beyond the heat-affected zone with a metal compatible with both the parent metal and the weld or braze, as applicable.

5.3.1.1.8 Application of inorganic coatings such as phosphate and zinc-rich coatings on steel.

5.3.2 Any other systems of protection which are designed to alleviate electrolytic corrosion shall be subject to the approval of the procuring activity. If other environments are concerned, it shall be the responsibility of the contractor to establish the actual compatibility (reference to MIL-S-5002 is suggested).

5.3.3 Insulate dissimilar metals from each other in accordance with MIL-F-7179.

6. NOTES

6.1 For further background information, reference is made to the following publications:

Behavior of Coupled Dissimilar Metals

Corrosion Handbook, Edited by H. H. Uhlig (Wiley 1948)
Corrosion and Corrosion Control, Edited by H. H. Uhling (Wiley 1963)
Corrosion by L. L. Shrier (Wiley 1963)
Corrosion and Oxidation of Metals by U. R. Evans
(St. Martins Press 1960)

Corrosion Control and Surface Treatment

Air Force T.O. 1-1-2	Corrosion Control and Treatment for Aerospace Equipment
NAVAIR 01-1A-509	Corrosion Control for Aircraft

CUSTODIANS:
Army - EL
Navy - AS
Air Force - 11

REVIEW ACTIVITIES:
Army - MU
Navy - EC, OS
Air Force - 13, 17, 84

USER ACTIVITIES:
Army - MR
Navy - None
Air Force - None

PREPARING ACTIVITY:
Air Force - 11

PROJECT NUMBER: MISC-0697

☆ U.S. GOVERNMENT PRINTING OFFICE: 1972-714-167/7788

END OF REFERENCE

15

REFERENCE

16

RICHMOND, J. C.; AND THORNTON, H. R.: OXIDATION OF EXPERIMENTAL ALLOYS. REP. WADC TR-58-164, PART I, WRIGHT AIR DEVELOPMENT CENTER, 1958.

JAN 6 '59

1.6-0-0

#1 SUPER ALLOYS
OXIDATION RESISTANCE

#2 Oxidation Misc

WADC TECHNICAL REPORT 58-164
PART I
ASTIA DOCUMENT No. 155688

LEWIS RESEARCH CENTER
Aerospace Safety Research
and Data Institute
DEC 18 1973
CLEVELAND, OHIO

COPY 1

OXIDATION OF EXPERIMENTAL ALLOYS

COMPOSITE MAT'LS BRANCH

N 66908
Pt I

JOSEPH C. RICHMOND
H. RICHARD THORNTON
NATIONAL BUREAU OF STANDARDS

JUNE 1958

N 1

LIBRARY COPY

LEWIS LIBRARY, NASA
CLEVELAND, OHIO

WRIGHT AIR DEVELOPMENT CENTER

(1)

NOTICES

When Government drawings, specifications, or other data are used for any purpose other than in connection with a definitely related Government procurement operation, the United States Government thereby incurs no responsibility nor any obligation whatsoever; and the fact that the Government may have formulated, furnished, or in any way supplied the said drawings, specifications, or other data, is not to be regarded by implication or otherwise as in any manner licensing the holder or any other person or corporation, or conveying any rights or permission to manufacture, use, or sell any patented invention that may in any way be related thereto.

- - - - -

Qualified requesters may obtain copies of this report from the Armed Services Technical Information Agency, (ASTIA), Arlington Hall Station, Arlington 12, Virginia.

- - - - -

This report has been released to the Office of Technical Services, U. S. Department of Commerce, Washington 25, D. C., for sale to the general public.

- - - - -

Copies of WADC Technical Reports and Technical Notes should not be returned to the Wright Air Development Center unless return is required by security considerations, contractual obligations, or notice on a specific document.

WADC TECHNICAL REPORT 58-164
PART I
ASTIA DOCUMENT No. 155688

OXIDATION OF EXPERIMENTAL ALLOYS

JOSEPH C. RICHMOND
H. RICHARD THORNTON
NATIONAL BUREAU OF STANDARDS

JUNE 1958

MATERIALS LABORATORY
CONTRACT No. AF 33(616) 56-19
PROJECT No. 9964

Copy No.
HQ
LAL
LFL
AAL
HSFS

WRIGHT AIR DEVELOPMENT CENTER
AIR RESEARCH AND DEVELOPMENT COMMAND
UNITED STATES AIR FORCE
WRIGHT-PATTERSON AIR FORCE BASE, OHIO

McGregor & Werner Midwest Corp., Dayton, O.
3-44-400-10-16-58

ABSTRACT

A study was made of the oxidation resistance of ten high-temperature alloys; 1) aluminum-modified Nichrome V, 2) Nichrome V, 3) niobium-modified Nichrome V, 4) an iron-chromium-aluminum alloy, 5) Inconel 702, 6) Hastelloy R235, 7) Hastelloy W, 8) type 316 stainless steel, 9) Inconel X and 10) Inconel. Tests included the measurement of the average depth of external oxidation and maximum depth of oxide penetration on specimens that had been subjected to stress in air at high temperature for 100 hours, and on specimens that had been subjected to stress in air under fluctuating-temperature conditions for an equivalent length of time, plus continuous recording of the weight change of specimens oxidized in air at high temperatures.

The depth of oxidation was found to increase with temperature and with stress. There was little effect of stress at stresses below that required to produce 1% extension in 100 hours. All of the alloys conformed reasonably well to the parabolic rate law in the weight-gain oxidation tests.

PUBLICATION REVIEW

This report has been reviewed and is approved.

FOR THE COMMANDER:

Richard R. Kennedy

RICHARD R. KENNEDY
Chief, Metals Branch
Materials Laboratory

E. Microscopic Evaluation. The depth of oxide penetration on specimens that had been subjected to the load-extension test or to the fluctuating-temperature load test was determined by microscopic evaluation of metallographic sections prepared from treated and untreated portions of each specimen.

A sample about 3/8 x 1/4 inch in size was sheared from near the center of the reduced section of each tested specimen, one edge of the sample corresponding to an edge of the tested specimen. A similar sample was cut from the untested portion of the same specimen that was removed in shearing it to the contour shown in figure 1, for those alloys for which such samples were available. The edge of the untreated sample that was next to the specimen in the original sheet was marked for identification. These two samples, with those of other specimens of the same alloy, were mounted side by side in plastic, with the marked edge of the untreated sample and the edge of the treated sample that was an edge of the treated specimen, nearest the surface of the mount. The mounted specimens were ground and polished to produce the metallographic sections for examination. About 1/16 inch of material was removed in the grinding process. The metallographic sections were made parallel to the direction of loading, and the two sections of any one specimen were parallel to each other and were about 1/8 inch apart in the original sheet.

The overall thickness of the untreated metal was measured at three locations, and the average of these three measurements was taken as the original thickness, D, (see figure 5) of the specimen before treatment. There was some variation in the thickness of the original specimens, hence a small error in the determination was introduced because of the difference in thickness of the specimen at the locations of the two sections. It was not possible to make microscopic measurements of the thickness of the untreated specimen before test, because preparation of metallographic sections involves cutting the specimen.

There was no untreated sample for each specimen of Hastelloy R235 having the same thickness as the treated portion of the specimen. For this alloy the overall thickness of the untreated sample, D, was taken as the average of four measurements of the thickness of the untreated specimen made with a micrometer caliper before test. For this alloy the error in the measurement D is on the order of ±0.1 mil.

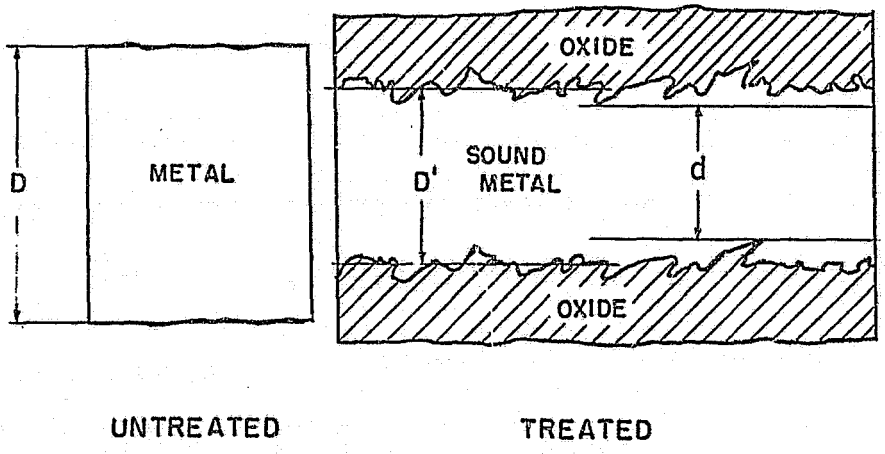

Figure 5. Sketches illustrating the measurement of D, D' and d on metallographic sections of tested and untested portions of specimens.

There was no sheared-out portion of the niobium-modified 80 nickel-20 chromium alloy, since these specimens were milled to the contour indicated in figure 1. For these specimens the untreated sample was cut from a portion of the specimen that was outside of the furnace during test, hence for this alloy the metallographic sections of treated and untreated metal were located about eight inches apart in the original sheet.

Two measurements were made on the treated sample, D' and d. These measurements are illustrated in figure 5.

The average thickness of metal remaining after treatment, D', was measured as the distance between two lines on the respective sides of the section, each parallel to the original surface of the metal and each located at the metal-oxide interface. Each line was positioned so that there was an area of metal on the side toward the oxide as large as the area of oxide on the side toward the metal. Measurements were made at five different locations picked at random along each section, and the average was computed. The average depth of oxide penetration was computed as $(D-D')/2$.

The thickness of the oxide-free sound metal remaining after treatment, d, was measured as the distance between two lines on the respective sides of the section, each parallel to the original surface of the metal and each located on the metal side of the oxide-metal interface on the respective sides of the specimen. Each line was positioned so that it just touched the deepest point of oxide penetration on that side of the specimen in that field of view. Measurements were made at five different locations picked at random along the section, and the average was computed. The maximum depth of oxide penetration was computed as $(D-d)/2$.

Oxide inclusions in the metal were not considered as oxide penetration from the surface unless there appeared to be a direct connection to the surface layer of oxide.

The magnification of the microscope was such that the length of each section in one field of view was approximately twice the width of the section. The filar eyepiece used for these measurements had a calibration factor of 0.027 mils per division.

In addition to the measurements of D, D' and d, counts were made of the number of stringers per inch over one mil in depth. In this case, the depth was measured from the oxide-metal interface on the treated specimen, and not from the original surface of the specimen. In addition, the presence of fissures and voids was noted.

Voids, fissures and stringers were completely different in apperance. Voids were spherical, or at least rounded in shape. Fissures appeared to have been formed mechanically, by pulling apart the grains of the metal, and were usually relatively wide, with straight angular sides that match. Stringers were narrow, and appeared to have been formed without disturbing the crystal structure of the metal. Stringers were usually connected to the surface, while fissures frequently were not, and voids never were. Voids and fissures were usually hollow, with a very thin layer of oxide on the interior surface. Stringers were not hollow, but consisted of a separate crystalline phase, usually an oxide, and occurred at grain boundaries. Stringers appeared to be intergranular oxidation.

A statistical study was made of the various measurements in order to determine the error of measurement and to select a reliable parameter to indicate the statistical scatter of the measured quantities.

Three sets of measurements of D, D' and d were made, each set consisting of 10 measurements made on the same field of the same specimen. The reproducibility of the measurements, expressed as the standard deviation of the 10 values, varied from 0.6 to 1.6 divisions, the average for the 9 sets being 1.03 divisions, or 0.028 mils. There was no significant difference in the error of measurement of D, D' and d.

The standard deviations of 30 sets of 3 values each of D were computed, the 3 values in each set being from different locations on the same section. These standard deviations varied from 0 to 4.18 divisions, the average for the 30 sets being 1.36 divisions, or 0.037 mils.

The standard deviations of 10 sets of five values each of D' were computed, the five values in each case being from different locations on the same section. These standard deviations varied from 0.98 to 3.61 divisions, the average of the ten sets being 1.76 divisions, or 0.047 mils.

The standard deviations of 40 sets of five values each of d were computed, the five values in each set being from different locations on the same section. These standard deviations varied from 1.68 to 22.1 divisions, the average for the 40 sets being 5.73 divisions, or 0.115 mils.

The total variance (the square of the standard deviation) of a quantity such as (D - D'), in which both D and D' are averages, will be the sum of the variances of D and D' taken separately. Each of these two variances, in turn, will be made up of two components, one due to the error of measurement and the other due to the true variation in the quantity being measured.

The expected value for the true average standard deviation of D - D' corrected for the error of measurement, would be 1.71 divisions, compared to the observed value of 1.76 divisions for the standard deviation of D'. In a like manner, the expected value of the true average standard deviation of D - d would be 5.71 divisions, compared to the observed value of 5.73 divisions for the standard deviation of d.

The net effect is that the contribution to the variance of (D - D') or (D - d) made by the variance of D is almost exactly equal to the correction that must be made for the known error of measurement, and the two corrections nearly cancel each other.

On the basis of this analysis, it was decided to use the observed values of the standard deviation of D' as the standard deviation of (D - D'), and that of d as the standard deviation of (D - d) in computing 95% confidence errors.

The values for depth of oxide penetration, either (D - D')/2 or (D - d)/2, are in error by an amount equal to the difference in the original thicknesses of the treated and untreated portions of the specimen at the locations where metallographic sections were made. This error is due to the natural variation in the thickness of the original sheet of metal, and is inherent in the method of evaluation. There is no direct method for evaluating the size of this error, but a statistical analysis

based on comparison of pairs of specimens receiving identical treatment indicates that the average value of this error is on the order of ±0.1 mil. This error is in addition to the error e based on the statistical scatter in the individual values of D' or d for each specimen. Because this error will be nearly constant for all of the measurements made on a single specimen, it probably does not have any appreciable effect on the size of e.

V PRESENTATION AND DISCUSSION OF DATA

A. Load-Extension Tests. Results of the load extension tests are given in Table II. The data show increasing depth of oxide penetration with increasing temperature, and with increasing stress at any one temperature. However, the reported values include the reduction in thickness that occurred on specimens that underwent high extension, and this reduction in thickness undoubtedly accounts for at least a portion of the observed increase in apparent depth of oxide penetration with an increase in initial stress.

When depth of oxide penetration, either average depth of external oxidation or maximum depth of oxide penetration, is plotted as a function of the initial stress on the specimen as in figures 6 and 7 for Hastelloy R235, the effects of stress and temperature are brought out more clearly. While the scatter in individual points is rather large there was a definite trend in each case for an increase in stress above a certain minimum value to cause an increase in the depth of oxide penetration. The critical stress value for each alloy at each temperature is given in Table III. It can be seen in the table that in general there is excellent agreement between the critical stress for average depth of external oxidation and that for maximum depth of oxide penetration. The critical stress, above which depth of oxide penetration increases with an increase in stress, corresponds generally to the stress required to produce approximately 1% extension in 100 hours. There was a definite trend for the observed depth of oxide penetration, either average depth of external oxidation or maximum depth of oxide penetration, to be greater under no-load conditions than under moderate stress. A protective oxide film usually forms under compression. It may be that a moderate tensile stress in the metal relieved part of the compressive stress in the oxide, and permitted a thicker layer of protective oxide to form before it ruptured due to build up of compressive stress as the oxide increased in thickness.

Siebert, Sinnott, De Smyter and Keith (Reference 2) also found that for the alloys Chromel ASM, ARM and D and type 310 stainless steel there was a minimum stress level for each material, above which a noticeable increase in intergranular oxidation was observed. Their measurements were made under conditions such that the effect of the reduction in area of the specimen due to extension was not a part of the measurement.

The metallographic sections were examined for stringers, and those over 1 mil in depth were counted. Only on the specimens of the niobium-modified Nichrome V, Hastelloy R235, type 316 stainless steel, Inconel and Inconel X were any stringers noted, and even on these alloys the number of stringers per inch of oxide-metal interface was low. After completion of the microscopic evaluation, the metallographic sections were etched and again examined to determine whether the stringers were intercrystalline or transcrystalline. There was no evidence of any transcrystalline stringers.

TABLE II

RESULTS OF LOAD-EXTENSION TESTS

Alloy	Spec. No.	Test Temp. °F	Stress psi	Extension in 100 hrs. %	Depth of Oxide Penetration Avg. mils	e [1] mils	Max. mils	e [1] mils	Stringers per inch [2]
Al. Modified Nichrome V	21	1800	0	0.15	0.00	0.03	0.12	0.12	0
	22	1800	0	0.05	0.09	0.04	0.36	0.09	0
	23	1800	500	0.90	0.02	0.03	0.35	0.11	0
	24	1800	500	1.00	0.19	0.02	0.56	0.18	0
	25	1800	575	1.05	0.27	0.03	0.56	0.09	0
	26	1800	575	1.20	0.07	0.07	0.38	0.16	0
	27	1800	675	1.55	0.06	0.04	0.30	0.16	0
	28	1800	675	1.10	0.40	0.02	0.69	0.08	0
	29	1800	850	1.95	0.24	0.02	0.58	0.14	0
	30	1800	850	2.45	0.64	0.04	0.89	0.18	0
	67	1800	900	4.40	0.87	0.06	1.12	0.07	0
	68	1800	900	3.90	0.70	0.03	1.00	0.19	0
	69	1800	1000	5.75	0.39	0.09	0.67	0.14	0
	70	1800	1000	5.60	0.00	0.09	0.09	0.11	0
	31	2000	350	1.45	0.30	0.05	0.51	0.10	0
	32	2000	350	1.60	0.21	0.07	0.41	0.09	0
	33	2000	450	2.15	0.42	0.06	0.67	0.05	0
	34	2000	450	1.85	0.32	0.31	0.59	0.08	0
	35	2000	500	2.00	0.59	0.05	0.73	0.10	0
	36	2000	500	2.20	0.32	0.05	0.99	0.05	0
	37	2000	550	2.50	0.61	0.04	0.72	0.41	0
	38	2000	550	2.50	0.67	0.05	0.90	0.09	0
	39	2000	0	0.35	0.41	0.08	0.56	0.07	0
	40	2000	0	0.35	0.82	0.30	1.00	0.12	0
	61	2000	600	3.85	0.19	0.01	0.40	0.05	0
	62	2000	600	4.10	0.70	0.06	0.89	0.09	0
	63	2000	650	4.75	0.00	0.09	0.30	0.11	0
	64	2000	650	4.30	0.00	0.00	0.12	0.07	0
	65	2000	700	5.35	0.76	0.04	1.02	0.04	0
	66	2000	700	5.57	0.57	0.09	0.74	0.08	0
	41	2100	525	12.15	0.90	0.09	1.22	0.15	0
	42	2100	525	5.45	0.90	0.04	1.08	0.06	0
	43	2100	460	5.60	0.61	0.07	0.96	0.07	0
	44	2100	460	5.25	0.30	0.02	0.58	0.06	0
	45	2100	300	2.25	0.27	0.03	0.46	0.14	0
	46	2100	300	2.35	0.47	0.07	0.67	0.09	0
	47	2100	100	0.70	0.54	0.02	0.74	0.06	0
	48	2100	100	0.65	0.65	0.03	0.75	0.03	0
	49	2100	0	0.15	0.01	0.02	0.18	0.06	0
	50	2100	0	0.00	0.58	0.03	0.75	0.06	0

[1] and [2] See end of Table II

TABLE II (continued)

Alloy	Spec. No.	Test Temp. °F	Stress psi	Extension in 100 hrs. %	Depth of Oxide Penetration Avg. mils	e 1/ mils	Max. mils	e 1/	Stringers per inch 2/
Al.Modified Nichrome V	51	2200	375	3.75	0.54	0.07	0.78	0.06	0
	52	2200	375	3.85	0.62	0.13	0.86	0.11	0
	53	2200	325	3.85	0.23	0.11	0.40	0.16	0
	54	2200	325	3.35	0.61	0.02	0.79	0.06	0
	55	2200	225	2.00	0.27	0.08	0.52	0.06	0
	56	2200	225	1.85	0.31	0.08	0.45	0.13	0
	57	2200	100	0.90	0.49	0.09	0.79	0.13	0
	58	2200	100	0.75	0.31	0.07	0.56	0.13	0
	59	2200	0	0.15	0.14	0.08	0.29	0.10	0
	60	2200	0	0.30	0.27	0.06	0.43	0.07	0
Nichrome V	21	1800	0	0.00	0.02	0.02	0.35	0.13	0
	22	1800	0	0.10	0.00	0.03	0.27	0.12	0
	23	1800	900	0.80	0.12	0.01	0.42	0.09	0
	24	1800	900	0.30	0.06	0.08	0.45	0.09	0
	25	1800	1025	0.40	0.02	0.05	0.41	0.21	0
	26	1800	1025	1.50	0.09	0.02	0.67	0.36	0
	27	1800	1200	2.60	0.26	0.06	1.80	0.83	0
	28	1800	1200	2.80	0.14	0.03	3.42	1.01	0
	29	1800	1240	3.50	0.28	0.03	Fissures		0
	30	1800	1240	5.50	0.18	0.02	Fissures		0
	31	2000	425	1.40	0.17	0.03	0.77	0.52	0
	32	2000	425	1.40	0.17	0.03	0.55	0.21	0
	33	2000	575	3.40	0.21	0.09	Fissures		0
	34	2000	575	2.80	0.10	0.05	Fissures		0
	35	2000	610	3.00	0.19	0.07	Fissures		0
	36	2000	610	4.50	0.15	0.04	Fissures		0
	37	2000	640	3.90	0.25	0.06	Fissures		0
	38	2000	640	6.30	0.56	0.03	Fissures		0
	39	2000	0	0.00	0.09	0.03	0.40	0.11	0
	40	2000	0	0.00	0.00	0.05	0.24	0.09	0
	41	2100	225	0.80	0.23	0.02	0.52	0.10	0
	42	2100	225	0.80	0.17	0.07	0.48	0.10	0
	43	2100	310	1.30	0.26	0.06	0.61	0.19	0
	44	2100	310	1.30	0.28	0.06	0.67	0.05	0
	45	2100	415	3.00	0.46	0.09	0.76	0.12	0
	46	2100	415	3.00	0.37	0.11	0.78	0.17	0
	47	2100	455	3.60	0.47	0.06	1.13	0.24	0
	48	2100	455	3.30	0.35	0.05	0.88	0.26	0
	49	2100	0	0.00	0.25	0.06	0.51	0.10	0
	50	2100	0	0.10	0.26	0.06	0.74	0.35	0

1/and 2/ See end of Table II

TABLE II (continued)

Alloy	Spec. No.	Test Temp. °F	Stress psi	Extension in 100 hrs. %	Depth of Oxide Penetration Avg. mils	e 1/ mils	Max. mils	e 1/ mils	Stringers 2/ per inch
Nichrome V	51	2200	120	0.80	0.38	0.07	0.70	0.11	0
	52	2200	120	0.90	0.37	0.05	0.80	0.16	0
	53	2200	205	1.50	0.59	0.06	0.92	0.09	0
	54	2200	205	1.80	0.34	0.06	0.74	0.11	0
	55	2200	285	3.10	0.55	0.02	1.68	0.84	0
	56	2200	285	3.70	0.55	0.12	1.59	0.91	0
	57	2200	315	4.60	0.52	0.12	1.80	1.03	0
	58	2200	315	4.30	0.54	0.12	1.63	0.93	0
	59	2200	0	0.30	0.38	0.07	0.76	0.23	0
	60	2200	0	0.20	0.22	0.12	0.68	0.11	0
Nb.Modified Nichrome V	21	1800	0	0.00	0.00	0.04	0.01	0.08	0
	22	1800	0	0.00	0.00	0.03	0.15	0.06	3
	23	1800	650	0.10	0.00	0.06	0.09	0.07	0
	24	1800	650	0.20	0.00	0.04	0.13	0.06	3
	25	1800	725	0.70	0.00	0.03	0.06	0.03	5
	26	1800	725	0.30	0.01	0.03	0.16	0.02	1
	27	1800	840	0.80	0.08	0.04	0.27	0.04	2
	28	1800	840	0.70	0.08	0.05	0.23	0.06	4
	29	1800	925	0.80	0.13	0.02	0.28	0.05	1
	30	1800	925	4.70	0.22	0.07	0.46	0.07	5
	31	2000	550	2.70	0.20	0.04	1.02	0.24	13
	32	2000	550	2.50	0.20	0.04	0.99	0.10	3
	33	2000	500	1.80	0.26	0.04	0.91	0.26	10
	34	2000	500	2.00	0.19	0.06	1.08	0.25	11
	35	2000	450	1.70	0.23	0.02	1.34	0.29	7
	36	2000	450	1.60	0.30	0.09	0.89	0.12	3
	37	2000	350	1.00	0.04	0.05	0.87	0.10	8
	38	2000	350	0.90	0.08	0.07	0.65	0.34	8
	39	2000	0	0.10	0.03	0.03	0.83	0.12	2
	40	2000	0	0.10	0.17	0.04	0.98	0.17	3
	41	2100	525	5.90	0.45	0.03	1.28	0.14	5
	42	2100	525	6.10	0.45	0.05	1.32	0.17	2
	43	2100	475	4.10	0.40	0.03	1.26	0.33	6
	44	2100	475	3.70	0.36	0.01	1.40	0.41	2
	45	2100	375	1.80	0.19	0.07	1.15	0.20	3
	46	2100	375	1.60	0.37	0.03	1.23	0.35	4
	47	2100	300	1.10	0.21	0.02	1.01	0.03	0
	48	2100	300	1.10	0.17	0.07	0.98	0.22	2
	49	2100	0	0.00	0.18	0.04	0.86	0.27	3
	50	2100	0	0.00	0.19	0.03	0.86	0.09	2

1/and 2/ See end of Table II

TABLE II (continued)

Alloy	Spec. No.	Test Temp. °F	Stress psi	Extension in 100 hrs. %	Depth of Oxide Penetration Avg. mils	e 1/ mils	Max. mils	e 1/ mils	Stringers per inch 2/
Nb.Modified Nichrome V	51	2200	335	4.00	0.56	0.03	1.37	0.26	4
	52	2200	335	4.20	0.47	0.06	0.77	0.25	7
	53	2200	310	3.50	0.65	0.02	1.29	0.22	5
	54	2200	310	2.90	0.60	0.07	1.17	0.16	8
	55	2200	235	1.80	0.22	0.05	1.05	0.24	1
	56	2200	235	1.90	0.56	0.04	1.13	0.23	2
	57	2200	150	1.30	0.30	0.01	0.86	0.07	1
	58	2200	150	1.10	0.42	0.08	0.99	0.19	3
	59	2200	0	0.40	0.45	0.03	1.03	0.08	2
	60	2200	0	0.10	0.09	0.06	1.08	0.24	1
	62	1800	900	0.50	0.00	0.01	0.28	0.26	1
	63	1800	900	1.30	0.00	0.02	0.38	0.14	6
	66	1800	1000	4.60	0.52	0.04	0.85	0.04	1
	71	1800	1000	3.80	0.01	0.06	0.46	0.26	4
	72	1800	1050	2.20	0.00	0.05	0.41	0.20	6
	73	1800	1050	7.30	0.08	0.04	0.93	0.76	2
	67	2000	600	2.80	0.58	0.02	1.36	0.21	18
	68	2000	600	2.00	0.45	0.04	1.18	0.23	14
Iron-Chromium-Aluminum Alloy	21	1800	150	0.90	0.21	0.05	0.37	0.03	0
	22	1800	150	1.00	0.31	0.07	0.41	0.08	0
	23	1800	225	1.90	0.26	0.03	0.44	0.07	0
	24	1800	225	2.00	0.22	0.06	0.37	0.13	0
	25	1800	385	6.00	0.69	0.06	0.95	0.09	0
	26	1800	385	5.00	0.60	0.09	0.84	0.09	0
	27	1800	410	5.10	0.60	0.17	0.76	0.17	0
	28	1800	410	7.80	0.64	0.12	0.89	0.14	0
	29	1800	0	0.00	0.05	0.02	0.28	0.09	0
	30	1800	0	0.10	0.03	0.03	0.15	0.05	0
	31	2000	50	0.60	0.17	0.06	0.34	0.11	0
	32	2000	50	0.60	0.06	0.09	0.29	0.11	0
	33	2000	75	1.20	0.26	0.11	0.52	0.07	0
	34	2000	75	1.40	0.36	0.06	0.57	0.09	0
	35	2000	105	2.40	0.19	0.11	0.44	0.14	0
	36	2000	105	2.40	0.28	0.07	0.61	0.10	0
	37	2000	120	2.90	0.20	0.12	0.61	0.13	
	38	2000	120	3.20	0.21	0.05	0.60	0.13	0
	39	2000	0	0.00	0.06	0.05	0.23	0.08	0
	40	2000	0	0.00	0.02	0.03	0.46	0.21	0

1/ and 2/ See end of Table II

TABLE II (continued)

Alloy	Spec. No.	Test Temp.	Stress	Extension in 100 hrs.	Depth of Oxide Penetration				Stringers per inch[2]
					Avg.	e[1]	Max	e[1]	
		°F	psi	%	mils	mils	mils	mils	
Iron-Chromium-Aluminum Alloy	41	2200	30	0.60	0.02	0.15	0.36	0.24	0
	42	2200	30	0.50	0.21	0.17	0.62	0.23	0
	43	2200	55	2.90	0.32	0.25	0.65	0.18	0
	44	2200	55	2.10	0.26	0.14	0.94	0.15	0
	45	2200	65	3.20	0.37	0.06	0.85	0.24	0
	46	2200	65	3.00	0.17	0.09	0.75	0.30	0
	47	2200	70	5.00	0.46	0.10	1.94	2.03	0
	48	2200	70	4.80	0.53	0.20	1.76	1.01	0
	49	2200	0	0.00	0.30	0.08	0.53	0.13	0
	50	2200	0	0.00	0.21	0.08	0.95	0.30	0
	51	2100	42.5	0.90	0.26	0.04	0.48	0.10	0
	52	2100	42.5	1.00	0.22	0.03	0.43	0.13	0
	53	2100	67.5	1.70	0.29	0.08	0.55	0.13	0
	54	2100	67.5	2.00	0.46	0.09	0.78	0.14	0
	55	2100	82.5	2.30	0.41	0.03	0.70	0.13	0
	56	2100	82.5	2.60	0.16	0.08	0.45	0.13	0
	57	2100	90	3.40	0.47	0.16	0.75	0.24	0
	58	2100	90	3.90	0.50	0.13	0.74	0.15	0
	59	2100	0	0.00	0.28	0.07	0.52	0.07	0
	60	2100	0	0.00	0.27	0.04	0.52	0.08	0
Inconel 702	127	1500	0	0.00	0.01	0.04	0.17	0.04	0
	128	1500	0	0.00	0.01	0.03	0.24	0.06	0
	105	1500	10,000	0.15	0.11	0.03	0.37	0.13	0
	116	1500	10,000	0.10	0.04	0.04	0.33	0.17	0
	117	1500	10,500	0.10	0.09	0.04	0.28	0.14	0
	118	1500	11,000	0.20	0.12	0.07	0.26	0.08	0
	129	1500	11,000	0.15	0.03	0.02	0.30	0.21	0
	119	1500	11,500	0.35	0.11	0.04	0.26	0.09	0
	120	1500	12,000	0.35	0.23	0.03	0.54	0.11	0
	130	1500	12,000	0.35	0.00	0.03	0.23	0.12	0
	121	1500	12,500	0.15	0.00	0.11	0.22	0.11	0
	122	1500	13,000	1.15	0.20	0.11	1.23	1.75	0
	126	1500	13,000	1.15	0.21	0.04	0.47	0.07	0
	86	1600	0	0.00	0.11	0.03	0.43	0.14	0
	87	1600	0	0.00	0.08	0.03	0.51	0.08	0
	35	1600	4,500	0.20	0.05	0.05	0.28	0.13	0
	34	1600	5,000	0.25	0.12	0.07	0.54	0.18	0
	33	1600	5,500	0.65	0.19	0.07	0.43	0.04	0
	32	1600	6,000	0.45	0.05	0.03	0.18	0.10	0

1/ and 2/ See end of Table II

TABLE II (continued)

Alloy	Spec. No.	Test Temp. °F	Stress psi	Extension in 100 hrs. %	Depth of Oxide Penetration Avg. mils	e 1/ mils	Max. mils	e 1/ mils	Stringers 2/ per inch
Inconel 702	51	1600	6,500	0.95	0.12	0.09	0.53	0.31	0
	31	1600	6,500	0.70	0.12	0.04	0.55	0.25	0
	36	1600	6,750	1.00	0.11	0.04	0.37	0.04	0
	52	1600	6,750	0.55	0.04	0.02	0.19	0.11	0
	53	1600	7,000	0.90	0.10	0.03	0.30	0.13	0
	71	1600	7,000	0.85	0.04	0.03	0.21	0.03	0
	39	1600	7,500	1.80	0.27	0.02	0.55	0.09	0
	55	1600	7,500	1.60	0.21	0.03	0.59	0.18	0
	73	1600	7,500	1.60	0.18	0.06	0.39	0.14	0
	106	1700	0	0.00	0.12	0.13	0.52	0.31	0
	107	1700	0	0.00	0.02	0.03	0.37	0.11	0
	108	1700	1,500	0.80	0.07	0.06	0.42	0.25	0
	109	1700	1,500	0.60	0.22	0.07	0.47	0.10	0
	100	1700	1,600	1.20	0.21	0.10	1.00	0.26	0
	99	1700	1,800	1.85	0.26	0.09	0.62	0.31	0
	110	1700	1,850	1.35	0.16	0.08	0.47	0.16	0
	111	1700	1,850	1.35	0.23	0.06	0.50	0.12	0
	98	1700	2,000	2.55	0.06	0.05	0.71	0.18	0
	112	1700	2,100	2.45	0.23	0.04	0.62	0.29	0
	113	1700	2,100	2.80	0.31	0.02	1.03	0.39	0
	97	1700	2,200	4.50	0.44	0.06	0.98	0.32	0
	114	1700	2,200	3.20	0.06	0.05	0.73	0.20	0
	115	1700	2,200	2.35	0.16	0.06	0.79	0.04	0
	96	1700	2,500	6.90	0.63	0.04	1.90	0.61	0
	76	1800	0	0.00	0.38	0.04	0.90	0.17	0
	77	1800	0	0.00	0.05	0.08	0.35	0.23	0
	78	1800	1,100	1.00	0.17	0.11	0.61	0.38	0
	79	1800	1,100	0.95	0.08	0.10	0.56	0.54	0
	80	1800	1,350	1.75	0.24	0.04	0.71	0.44	0
	81	1800	1,350	1.35	0.38	0.16	1.12	0.36	0
	82	1800	1,600	3.25	0.53	0.07	1.21	0.24	0
	83	1800	1,600	3.45	0.45	0.06	1.26	0.21	0
	84	1800	1,750	4.50	0.65	0.15	1.56	0.65	0
	85	1800	1,750	3.95	0.64	0.12	1.72	0.78	0
Hastelloy R235	24	1500	0	0.00	1.11	0.25	1.44	0.36	0
	25	1500	0	0.00	0.65	0.12	0.93	0.18	0
	26	1500	23,000	1.00	0.69	0.13	1.01	0.06	0
	14	1500	23,000	1.15	0.81	0.06	1.27	0.29	0

1/ and 2/ See end of Table II

TABLE II (continued)

Alloy	Spec. No.	Test Temp. °F	Stress psi	Extension in 100 hrs. %	Depth of Oxide Penetration Avg. mils	e[1] mils	Max. mils	e[1] mils	Stringers[2] per inch
Hastelloy R235	15	1500	24,500	2.00	0.28	0.14	0.66	0.27	0
	27	1500	24,500	1.85	0.50	0.14	0.74	0.20	0
	28	1500	26,000	3.75	1.19	0.15	1.43	0.22	0
	17	1500	26,000	3.55	1.17	0.14	1.54	0.17	0
	29	1500	27,000	4.45	0.55	0.00	0.93	0.22	0
	30	1500	27,000	4.90	1.31	0.16	1.72	0.33	0
	57	1600	0	0.00	0.75	0.14	1.09	0.32	0
	58	1600	0	0.00	0.89	0.07	1.23	0.23	2
	59	1600	15,000	0.70	0.66	0.13	0.87	0.12	1
	46	1600	15,000	0.70	0.68	0.08	1.08	0.13	7
	47	1600	16,000	2.05	0.77	0.09	1.52	0.42	15
	60	1600	16,000	1.35	1.66	0.03	2.00	0.15	5
	63	1600	17,000	2.90	1.00	0.06	2.17	0.58	2
	64	1600	17,000	3.35	0.65	0.07	1.93	0.71	0
	74	1600	18,000	10.90	2.05	0.34	5.15	0.53	0
	75	1600	18,000	4.00	0.97	0.19	1.83	0.41	0
	39	1700	0	0.00	0.99	0.17	1.40	0.27	0
	40	1700	0	0.00	0.55	0.04	0.99	0.23	0
	70	1700	12,000	0.90	0.70	0.07	1.24	0.21	0
	71	1700	12,000	0.80	0.66	0.07	1.13	0.26	1
	72	1700	13,000	2.35	1.25	0.13	2.22	0.59	0
	80	1700	13,000	1.60	0.61	0.18	1.23	0.18	1
	87	1700	13,500	6.85	0.95	0.58	1.77	1.08	0
	88	1700	13,500	2.80	0.51	0.07	1.39	0.34	0
	94	1700	13,750	2.10	0.70	0.18	1.38	0.65	0
	95	1700	13,750	4.95	1.01	0.14	2.29	0.44	0
	102	1800	0	0.00	0.66	0.08	1.46	0.15	0
	103	1800	0	0.00	0.31	0.10	1.26	0.22	0
	89	1800	5,000	0.70	0.78	0.06	1.76	0.33	0
	101	1800	5,000	0.50	0.70	0.09	1.54	0.17	0
	97	1800	5,750	1.90	0.46	0.06	1.35	0.34	0
	107	1800	5,750	1.70	0.77	0.11	1.96	0.15	0
	98	1800	5,750	1.30	0.51	0.11	1.42	0.19	0
	90	1800	6,000	5.00	0.97	0.17	2.31	0.47	0
	96	1800	6,000	2.55	0.61	0.08	2.04	0.31	0
	104	1800	6,000	3.75	1.21	0.14	2.37	0.30	0
	105	1800	6,250	7.25	1.51	0.23	3.22	0.47	0
	106	1800	6,250	7.55	1.32	0.28	2.84	0.63	0

1/ and 2/ See end of Table II

TABLE II (continued)

Alloy	Spec. No.	Test Temp. °F	Stress psi	Extension in 100 hrs. %	Depth of Oxide Penetration Avg. mils	e 1/ mils	Max. mils	e 1/ mils	Stringers per inch 2/
Hastelloy W	119	1300	0	0.00	0.05	0.04	0.14	0.07	0
	120	1300	0	0.00	0.04	0.02	0.18	0.11	0
	35	1300	15,000	0.60	0.21	0.05	0.33	0.08	0
	121	1300	15,000	0.70	0.00	0.03	0.09	0.05	0
	34	1300	20,000	1.55	0.12	0.04	0.29	0.08	0
	122	1300	20,000	1.80	0.19	0.02	0.27	0.02	0
	33	1300	25,000	3.70	0.30	0.04	0.41	0.04	0
	123	1300	25,000	4.10	0.39	0.04	0.52	0.06	0
	124	1300	26,000	4.20	0.35	0.06	0.48	0.07	0
	125	1300	26,000	6.15	0.56	0.04	0.66	0.06	0
	66	1500	0	0.00	0.09	0.03	0.28	0.06	0
	67	1500	0	0.10	0.18	0.03	0.31	0.03	0
	71	1500	6,500	1.05	0.26	0.01	0.37	0.07	0
	76	1500	6,500	0.95	0.24	0.02	0.38	0.07	0
	63	1500	8,300	1.65	0.32	0.03	0.45	0.10	0
	64	1500	8,300	2.05	0.23	0.08	0.33	0.03	0
	77	1500	8,300	1.80	0.28	0.03	0.37	0.03	0
	80	1500	9.500	3.10	0.34	0.02	0.48	0.06	0
	81	1500	9,500	2.25	0.23	0.07	0.37	0.05	0
	90	1500	10,500	5.10	0.41	0.05	0.53	0.03	0
	91	1500	10,500	5.10	0.33	0.06	0.44	0.04	0
	127	1650	0	0.00	0.27	0.03	0.55	0.07	0
	128	1650	0	0.00	0.16	0.04	0.25	0.07	0
	96	1650	2,000	0.90	0.06	0.13	0.40	0.14	0
	103	1650	2,000	1.20	0.16	0.06	0.31	0.03	0
	110	1650	3,000	1.60	0.37	0.07	0.53	0.09	0
	129	1650	3,000	1.20	0.27	0.03	0.40	0.03	0
	130	1650	4,000	1.85	0.32	0.07	0.47	0.06	0
	131	1650	4,000	2.60	0.33	0.06	0.49	0.06	0
	132	1650	4,750	5.95	0.64	0.04	0.86	0.06	0
	133	1650	4,750	2.50	0.70	0.04	0.89	0.02	0
	59	1800	0	0.00	0.12	0.08	0.58	0.07	0
	60	1800	0	0.00	0.00	0.10	0.42	0.20	0
	101	1800	710	0.55	0.27	0.02	1.01	0.11	0
	102	1800	710	0.75	0.28	0.05	0.66	0.17	0
	103	1800	1,000	1.50	0.75	0.10	1.10	0.10	0
	104	1800	1,000	1.20	0.41	0.04	0.76	0.09	0
	105	1800	1,150	1.80	0.73	0.04	1.02	0.04	0
	106	1800	1,150	1.45	0.57	0.04	0.95	0.13	0
	115	1800	1,650	3.50	0.71	0.03	1.20	0.24	0
	116	1800	1,650	4.00	1.31	0.07	1.74	0.16	0

1/ and 2/ See end of Table II

TABLE II (continued)

Alloy	Spec. No.	Test Temp.	Stress	Extension in 100 hrs.	Depth of Oxide Penetration				Stringers 2/ per inch
					Avg.	e 1/	Max.	e 1/	
		°F	psi	%	mils	mils	mils	mils	
Type 316	61	1450	0	0.15	0.22	0.09	0.53	0.10	0
Stainless	62	1450	0	0.05	0.12	0.03	0.26	0.11	0
Steel	63	1450	4750	0.60	0.66	0.08	1.04	0.35	2
	64	1450	4750	1.95	0.63	0.05	1.02	0.21	2
	65	1450	5800	0.90	0.15	0.02	0.34	0.04	0
	66	1450	5800	0.50	0.14	0.03	0.42	0.07	0
	79	1450	6000	4.40	0.45	0.06	0.72	0.17	0
	80	1450	6000	3.45	0.27	0.06	0.57	0.06	0
	77	1450	6500	5.50	0.55	0.06	0.90	0.12	0
	78	1450	6500	5.40	0.48	0.07	0.83	0.11	0
	1	1450	6500	2.65	0.26	0.07	0.51	0.09	0
	2	1450	7000	3.10	0.34	0.07	0.62	0.05	0
	68	1450	7250	1.35	0.21	0.02	0.43	0.05	0
	3	1450	7500	5.60	0.49	0.09	0.83	0.12	0
	70	1450	7750	1.40	0.20	0.03	0.53	0.04	0
	41	1500	0	0.00	0.07	0.02	0.28	0.04	0
	42	1500	0	0.00	0.07	0.03	0.27	0.03	0
	49	1500	3750	1.40	0.14	0.04	0.39	0.10	0
	50	1500	3750	1.10	0.14	0.03	0.37	0.06	0
	21	1500	4500	2.00	0.30	0.04	0.63	0.12	0
	47	1500	4500	2.60	0.25	0.01	0.55	0.12	0
	48	1500	4500	2.35	0.33	0.08	0.60	0.20	0
	81	1500	4750	2.20	0.22	0.03	0.42	0.04	0
	83	1500	4750	2.00	0.19	0.02	0.41	0.06	0
	22	1500	5000	2.65	0.41	0.03	0.71	0.09	0
	82	1500	5000	3.35	0.28	0.03	0.48	0.07	0
	84	1500	5000	2.50	0.21	0.04	0.48	0.07	0
	45	1500	5250	5.30	0.46	0.09	0.85	0.20	2
	46	1500	5250	5.05	0.46	0.04	0.80	0.16	0
	23	1500	5500	4.30	0.53	0.07	0.88	0.17	0
	31	1550	0	0.00	0.15	0.05	0.54	0.08	0
	32	1550	0	0.00	0.14	0.04	0.44	0.10	0
	33	1550	3000	1.35	0.20	0.03	0.53	0.08	0
	34	1550	3000	1.20	0.17	0.05	0.50	0.10	0
	11	1550	3500	1.60	0.30	0.04	0.71	0.22	0
	35	1550	3700	3.15	0.46	0.09	0.93	0.20	1
	36	1550	3700	2.85	0.35	0.02	0.68	0.10	0
	12	1550	4000	2.30	0.36	0.07	0.82	0.29	0
	86	1550	4000	3.80	0.38	0.05	0.59	0.05	0
	85	1550	4000	3.70	0.41	0.05	0.72	0.17	0

1/ and 2/ See end of Table II

Card #4

TABLE II (continued)

Alloy	Spec. No.	Test Temp.	Stress	Extension in 100 hrs.	Depth of Oxide Penetration Avg.	e 1/	Max.	e 1/	Stringers per inch 2/
		°F	psi	%	mils	mils	mils	mils	
Type 316 Stainless Steel	87	1550	4200	4.10	0.41	0.05	0.71	0.21	0
	88	1550	4200	5.60	0.44	0.06	0.91	0.31	3
	89	1550	4400	6.10	0.49	0.05	0.90	0.24	2
	90	1550	4400	5.15	0.50	0.05	0.92	0.22	1
	13	1550	4500	3.35	0.55	0.09	0.78	0.13	0
	37	1550	4525	5.75	0.58	0.07	0.95	0.20	1
	38	1550	4525	5.75	0.57	0.08	1.03	0.34	5
	14	1550	5000	5.70	0.62	0.07	1.13	0.15	0
	60	1600	0	0.00	0.22	0.12	0.63	0.21	0
	59	1600	0	0.00	0.22	0.07	0.59	0.08	0
	58	1600	2325	1.00	0.31	0.06	0.77	0.13	0
	57	1600	2325	1.05	0.29	0.07	0.73	0.15	0
	56	1600	2630	1.45	0.25	0.05	0.63	0.08	0
	55	1600	2630	1.65	0.24	0.05	0.60	0.08	0
	54	1600	3125	2.50	0.34	0.11	0.67	0.19	0
	53	1600	3125	2.75	0.45	0.05	1.13	0.71	6
	52	1600	3450	4.25	0.57	0.09	1.06	0.32	2
	51	1600	3450	4.95	0.65	0.12	1.02	0.18	8
Inconel X	79	1450	0	0.00	0.01	0.04	0.26	0.05	1
	80	1450	0	0.00	0.01	0.02	0.21	0.13	0
	57	1450	20,000	0.10	0.04	0.04	0.33	0.08	1
	71	1450	20,000	0.05	0.02	0.05	0.17	0.07	0
	25	1450	22,500	0.05	0.03	0.03	0.22	0.05	0
	45	1450	22,500	0.20	0.07	0.06	0.25	0.03	0
	56	1450	22,500	0.10	0.00	0.04	0.23	0.06	0
	24	1450	25,000	0.00	0.01	1.02	0.31	0.20	0
	62	1450	25,000	0.05	0.00	0.03	0.13	0.05	5
	23	1450	27,500	0.00	0.05	0.05	0.26	0.04	0
	63	1450	27,500	0.40	0.03	0.03	0.19	0.05	6
	81	1500	0	0.00	0.03	0.11	0.38	0.22	0
	82	1500	0	0.00	0.00	0.07	0.12	0.13	0
	50	1500	16,000	0.00	0.02	0.10	0.26	0.08	0
	88	1500	16,000	0.10	0.00	0.06	0.60	0.11	0
	6	1500	17,500	0.10	0.09	0.08	0.41	0.23	0
	49	1500	17,500	0.15	0.05	0.06	0.39	0.12	0
	8	1500	19,000	0.15	0.11	0.08	0.24	0.07	0
	48	1500	19,000	0.25	0.11	0.02	0.29	0.04	0
	7	1500	20,500	0.30	0.04	0.05	0.38	0.06	0
	47	1500	20,500	0.10	0.09	0.07	0.25	0.06	0

1/ and 2/ See end of Table II

TABLE II (continued)

Alloy	Spec. No.	Test Temp.	Stress	Extension in 100 hrs.	Depth of Oxide Penetration				Stringers 2/ per inch
					Avg.	e 1/	Max.	e 1/	
		°F	psi	%	mils	mils	mils	mils	
Inconel X	46	1500	21,500	0.05	0.03	0.03	0.27	0.05	0
	87	1500	21,500	0.40	0.02	0.03	0.21	0.03	0
	77	1550	0	0.05	0.03	0.05	0.46	0.05	0
	78	1550	0	0.00	0.00	0.02	0.20	0.05	0
	98	1550	14,000	0.10	0.00	0.02	0.30	0.09	0
	99	1550	14,000	0.15	0.04	0.09	0.27	0.10	0
	76	1550	15,000	0.40	0.04	0.04	0.23	0.10	0
	93	1550	15,000	0.15	0.06	0.11	0.63	0.40	10
	91	1550	16,000	0.25	0.05	0.03	0.49	0.41	0
	96	1550	16,000	0.05	0.00	0.03	0.23	0.10	0
	13	1550	17,000	0.15	0.14	0.10	0.56	0.06	0
	97	1550	17,000	0.20	0.03	0.03	0.37	0.10	0
	83	1600	0	0.05	0.04	0.06	0.78	0.45	1
	84	1600	0	0.00	0.04	0.05	0.62	0.13	0
	20	1600	7,000	0.15	0.12	0.07	0.54	0.35	12
	55	1600	7,000	0.05	0.21	0.09	0.90	0.11	5
	19	1600	8,000	0.00	0.08	0.04	1.04	0.14	28
	54	1600	8,000	0.15	0.15	0.10	1.00	0.23	22
	18	1600	9,000	0.50	0.28	0.04	0.88	0.21	0
	95	1600	9,000	0.15	0.25	0.05	0.73	0.18	3
	52	1600	10,000	0.15	0.02	0.03	0.50	0.13	7
	94	1600	10,000	0.20	0.00	0.04	0.33	0.10	0
Inconel	66	1450	0	0.00	0.00	0.04	0.40	0.63	0
	67	1450	0	0.05	0.00	0.03	0.21	0.09	0
	64	1450	2500	1.65	0.10	0.06	0.30	0.05	0
	63	1450	2750	1.95	0.14	0.04	0.29	0.03	0
	62	1450	3000	3.60	0.26	0.05	0.64	0.19	0
	61	1450	3500	5.30	0.36	0.02	0.93	0.38	1
	76	1450	3500	0.75	0.02	0.03	0.19	0.05	0
	77	1450	3500	0.80	0.03	0.05	0.25	0.06	0
	78	1450	3750	1.70	0.18	0.02	0.40	0.06	0
	79	1450	3750	0.85	0.00	0.01	0.23	0.07	0
	84	1450	4000	1.05	0.10	0.01	0.23	0.02	0
	85	1450	4000	1.05	0.13	0.01	0.26	0.10	0
	57	1450	4325	1.90	0.05	0.04	0.28	0.04	0
	58	1450	4325	2.30	0.21	0.06	0.39	0.10	0
	106	1450	4900	2.65	0.18	0.03	0.34	0.04	0
	107	1450	4900	2.90	0.24	0.02	0.43	0.09	0
	108	1450	5300	4.35	0.36	0.09	0.65	0.04	1
	109	1450	5300	4.70	0.35	0.08	0.56	0.10	0

1/ and 2/ See end of Table II

TABLE II (continued)

Alloy	Spec. No.	Test Temp.	Stress	Extension in 100 hrs.	Depth of Oxide Penetration				Stringers per inch 2/
					Avg.	e 1/	Max.	e 1/	
		°F	psi	%	mils	mils	mils	mils	
Inconel	31	1500	0	0.00	0.03	0.02	0.31	0.13	0
	32	1500	0	0.00	0.09	0.00	0.28	0.15	0
	51	1500	3000	0.75	0.10	0.03	0.21	0.05	0
	52	1500	3000	0.90	0.12	0.03	0.23	0.04	0
	101	1500	3050	2.00	0.18	0.03	0.35	0.08	0
	102	1500	3050	2.15	0.22	0.03	0.41	0.09	0
	91	1500	3100	3.50	0.31	0.04	0.54	0.10	1
	92	1500	3100	3.50	0.30	0.04	0.47	0.09	0
	93	1500	3200	3.05	0.26	0.02	0.49	0.06	0
	94	1500	3200	4.80	0.29	0.02	0.69	0.21	0
	41	1550	0	0.00	0.06	0.03	0.33	0.08	0
	42	1550	0	0.00	0.00	0.04	0.17	0.05	0
	15	1550	2400	0.65	0.14	0.03	0.29	0.07	0
	103	1550	2400	0.95	0.04	0.06	0.17	0.09	0
	96	1550	2600	2.05	0.22	0.03	0.39	0.07	0
	97	1550	2600	2.15	0.19	0.03	0.41	0.10	0
	49	1550	2900	3.30	0.31	0.06	0.77	0.16	1
	50	1550	2900	2.50	0.10	0.06	0.30	0.07	0
	47	1550	3300	4.30	0.33	0.04	0.71	0.33	1
	48	1550	3300	3.70	0.31	0.04	0.64	0.17	0
	45	1550	3550	5.20	0.36	0.05	0.85	0.27	0
	46	1550	3550	4.85	0.36	0.06	0.71	0.06	0
	19	1600	0	0.00	0.03	0.03	0.22	0.04	0
	25	1600	0	0.00	0.00	0.05	0.33	0.15	0
	17	1600	1400	0.35	0.09	0.02	0.36	0.03	0
	21	1600	1400	0.40	0.03	0.02	0.21	0.05	0
	18	1600	2000	1.45	0.12	0.03	0.37	0.07	0
	22	1600	2000	1.40	0.13	0.03	0.31	0.09	0
	20	1600	2600	4.65	0.31	0.05	0.59	0.09	0
	24	1600	2600	3.90	0.30	0.06	0.68	0.05	0
	16	1600	2800	4.75	0.39	0.04	0.62	0.05	0
	23	1600	2800	4.60	0.30	0.02	0.55	0.12	0

1/ 95% confidence error

2/ over 1 mil in depth

TABLE III

STRESS IN PSI, AT WHICH DEPTH OF OXIDE PENETRATION BEGAN TO INCREASE WITH STRESS

Alloy	Average Depth of External Oxide Penetration				Maximum Depth of Oxide Penetration			
Temperature, °F	1800	2000	2100	2200	1800	2000	2100	2200
Al Mod. - Nichrome V	700	500	400	225	700	500	400	100
Nichrome V	1000	575	300	100	1000	575	400	200
Nb Mod. - Nichrome V	700	400	300	150	700	400	300	150
Fe-Cr-Al	150	75	50	40	200	75	50	50
Temperature, °F	1500	1600	1700	1800	1500	1600	1700	1800
Inconel 702	10,000	5500	1800	1350	10,000	5500	2000	1100
Hastelloy R 235	23,000	15,000	12,000	5000	23,000	15,000	12,000	5000
Temperature, °F	1450	1500	1550	1600	1450	1500	1550	1600
Type 316 S.S.	4750	3750	3000	2300	4750	3750	3000	2300
Inconel X	20,000	17,500	15,000	7000	20,000	16,000	15,000	7000
Inconel	3500	3000	2400	1400	3500	3000	2400	1400
Temperature, °F	1300	1500	1650	1800	1300	1500	1650	1800
Hastelloy W	15,000	6500	2000	700	15,000	6500	2000	700

END OF REFERENCE

16

REFERENCE

17

SMITH, H. H.; SHAHINIAN, P.; AND ACHTER, M. R.: FATIGUE CRACK GROWTH RATES IN TYPE 316 STAINLESS STEEL AT ELEVATED TEMPERATURES AS A FUNCTION OF OXYGEN PRESSURE. TRANS. MET. SOC. AIME, VOL. 245, MAY 1969.

Fatigue Crack Growth Rates in Type 316 Stainless Steel at Elevated Temperature as a Function of Oxygen Pressure

H. H. Smith, P. Shahinian, and M. R. Achter

Crack growth rates are measured at elevated temperature in a resonant fatigue machine from vibration frequency decreases calibrated in terms of crack depth. Crack growth rates in Type 316 stainless steel at 500° and 800°C show a sharp increase with oxygen pressure in an intermediate pressure range and little or no change at high and low pressures. At 500°C, 1 torr of oxygen reduces the fatigue life by almost a factor of 100 in comparison to that in vacuum and raises the growth rate of shallow cracks by the same amount. At 800°C the effects are smaller. Changes in slope in the crack growth rate curves are discussed in terms of a model in which rates of surface production and of surface coverage by gas are compared. The use of a calculation method in which the surface exposure time is equal to χ/v, where χ is the interatomic spacing and v is the growth rate, makes it possible to obtain order of magnitude agreement at 500°C between the observed pressure and the predicted pressure at these slope changes. At 800°C oxidation becomes a factor and the data cannot be treated by simple adsorption theory.

THE decrease in the fatigue life of metals as a function of gas pressure usually follows a stepped curve with virtually all of the decrease concentrated in a sharp drop in a transition zone at intermediate pressures and little or no change at low and high ranges. A number of models, differing in the details of the mechanism, have been offered to explain the shape of the curve. Measurements of crack growth in aluminum as a function of gas pressure by Bradshaw and Wheeler[1] and Hordon[2] demonstrated opportunities for quantitative comparison to evaluate the proposed models.

Since comparable data were lacking at high temperatures, in the present work rates of crack propagation were measured in Type 316 stainless steel at 500° and 800°C as a function of oxygen pressure. Choice of this material was dictated by two considerations; it is stiff enough at these elevated temperatures to resonate with the regenerative drive on our fatigue machine and it is known to display a large effect of environment. A new method of calculation is described to predict the gas pressure at the critical point.

EXPERIMENTAL PROCEDURE

Because of the difficulty of measuring crack depths directly at high temperatures, an indirect method was developed based on the decrease in the resonant frequency with the growth of a crack. A reversed bending, constant amplitude fatigue machine, described previously,[3] vibrates a specimen at its resonant frequency, automatically records any changes in it and shuts itself off after it has reached a preset value of frequency decrease. The record of frequency change is used to determine the rate of crack growth.

Sheet type specimens of Type 316 stainless steel, Fig. 1, incorporated a sharp, shallow notch to localize the formation of a single crack. After machining, they were annealed in a vacuum of 10^{-6} torr either at 1066° (lot A) or 871°C (lot B) and then electropolished in an acetic-chromic acid solution. Bending strains were measured at 500° and 800°C by an optical technique[4] and reported as total strain without correction for the notch. At 500°C, the 0.141 pct strain was 0.085 pct elastic and the remainder plastic. At 800°C the 0.062 pct strain was all elastic. To convert frequency decrease to crack length, calibration curves were obtained by interrupting the vibration at stated intervals of frequency decrease. The crack depth was measured microscopically at a magnification of X400 and reported as the average of the measurement on each edge. Some specimens were sectioned for crack measurement while others were returned to the machine and fatigued further. There was good agreement between the two methods.

Before beginning the vibration, the vacuum chamber was first evacuated cold to 1×10^{-6} torr, then heated to the operating temperature and held there until the pressure was again reduced to 1×10^{-6} torr at which time oxygen was introduced to the desired pressure. In this investigation the vibration frequency was nominally 10 cps and a decrease of 0.6 cps was taken as the failure point. The choice of the frequency decrease to represent failure has no appreciable effect on the fatigue life because the crack is growing very fast at this point.

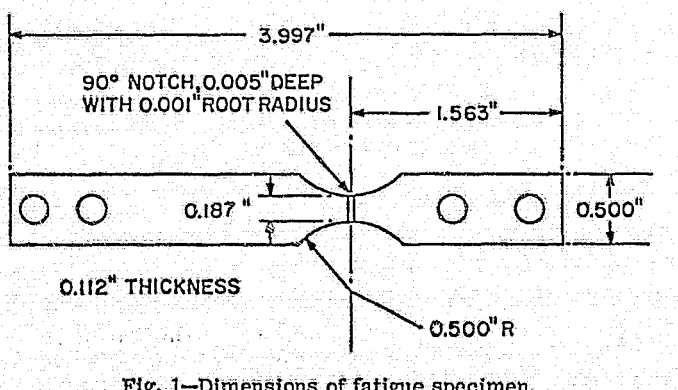

Fig. 1—Dimensions of fatigue specimen.

H. H. SMITH, P. SHAHINIAN, Member AIME, and M. R. ACHTER, Member AIME, are Research Physical Metallurgist, Supervisory Research Physicist, and Head, respectively, Thermostructural Materials Branch, Metallurgy Division, Naval Research Laboratory, Washington, D. C.

Manuscript submitted August 22, 1968. IMD

At low gas pressures, in the so-called molecular flow region, below 10^{-3} torr in our system, the pressure at the gage is slightly lower than the actual pressure in the hot zone. Since the pressure difference is too small to affect significantly the shape of the curve, being proportional to the square root of the ratio of the temperatures,[5] a correction was not made.

RESULTS

Correlation of Frequency Change and Crack Length. Fig. 2 illustrates the change in frequency with the duration of the vibration. Lot B material displays a slight increase in frequency at the start, reflecting strain hardening, followed by a slow decrease, indicating the beginning of crack growth. As indicated by the faster change which follows, crack growth then accelerates. Lot A material displays a somewhat different behavior. Since it has been annealed at a higher temperature, and is therefore softer, there is more strain hardening, as shown by the steep increase in frequency at the start. For purposes of measurement of crack growth rate and of fatigue life, the reference frequency is taken as the maximum reached before the decrease starts. At the maximum frequency, optical examination disclosed no measurable crack, even though discontinuous crack segments were observed in the root of the notch.

Correlations between frequency change and crack length measured on interrupted test specimens are shown in the calibration curves in Figs. 3(*a*) and 3(*b*). A straight line relationship is indicated on the log-log plots at both temperatures. Although the curves differ from each other slightly in slope and position, it is not clear whether the differences are significant. Crack lengths are approximately proportional to the square root of the change in frequency. Since the data represent measurements in vacuum, oxygen pressures from 10^{-5} to 810 torr, and in air at total strains from 0.055 to 0.141 pct, it is clear that one calibration plot at each temperature, despite some scatter, is sufficient for the determination of crack lengths from frequency changes. Refinement of the method would be required, however, to detect crack initiation at a very early stage.

Fatigue Data. Crack lengths, determined from frequency changes, show the effect of oxygen pressure at 800°C, Fig. 4, and demonstrate the high growth rates in the terminal stages. The slight inflection in the curve at 10^{-1} torr is reflected in the growth rate vs crack length curve in Fig. 5. Here there are two groups of curves, one group at low gas pressures and the other at high pressures. The 10^{-1} torr curve

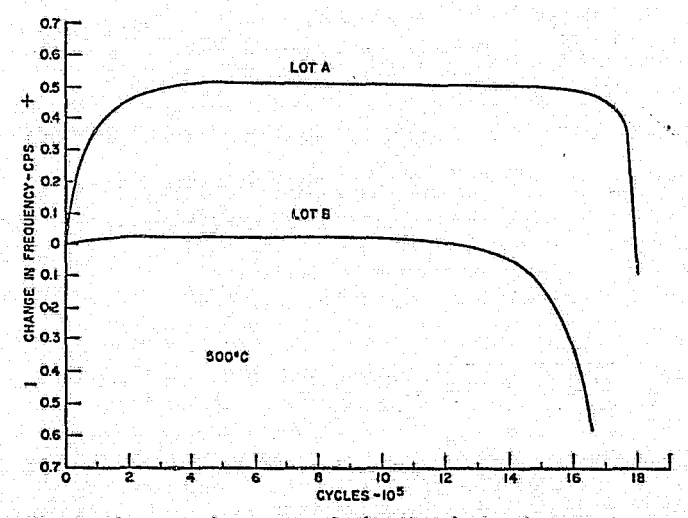

Fig. 2—Change in frequency of vibration during fatigue at 500°C of Type 316 stainless steel annealed at 1066°C (Lot A) and annealed at 871°C (Lot B).

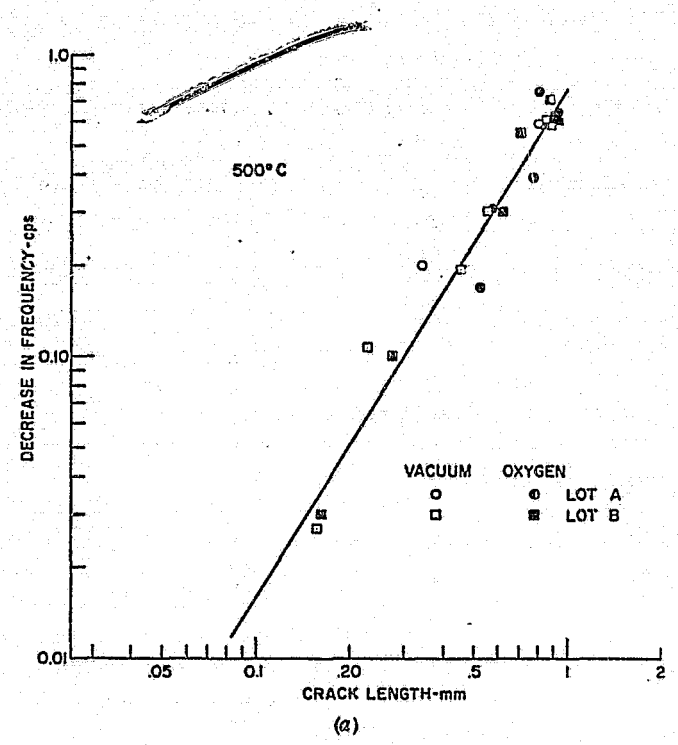

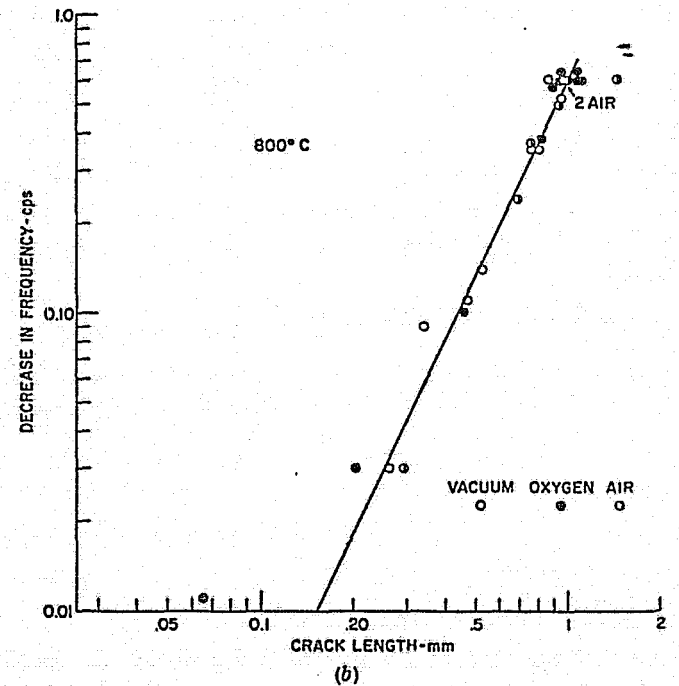

Fig. 3—Correlation of crack length and frequency decrease for Type 316 stainless steel fatigued at various strains in vacuum of 10^{-6} torr, in air, and in oxygen at pressures from 10^{-5} to 810 torr (*a*) at 500°C and (*b*) at 800°C.

has growth rates representative of the high pressure curve for short cracks but that of low pressure curves for long cracks. There are also two groups at 500°C in Fig. 6.

There was some concern that the strain hardening of the stainless steel at 500°C, annealed at 1066°C (lot A), might have some effect on crack propagation characteristics and affect the response of growth rate to gas pressure. Therefore, growth rates at two oxygen pressures were measured for lot B material, which was annealed at 871°C and did not strain harden appreciably. As shown in Fig. 7, the increase in growth rate by the increase in gas pressure from 10^{-6} to 1 torr is very close to that for lot A material in Fig. 6 except for very small cracks.

If now the crack growth rates are plotted as a function of oxygen pressure one obtains a family of curves for constant crack lengths, as in Figs. 8 and 9, which display the familiar stepped form, similar to the curves of fatigue life vs oxygen pressure in Fig. 10.

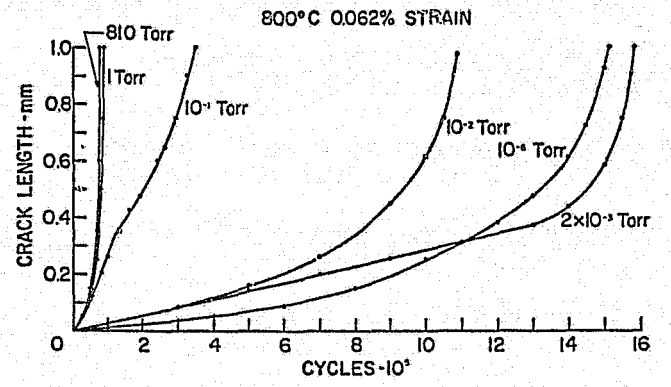

Fig. 4—Crack growth during fatigue at 800°C in oxygen pressures ranging from 10^{-6} to 810 torr.

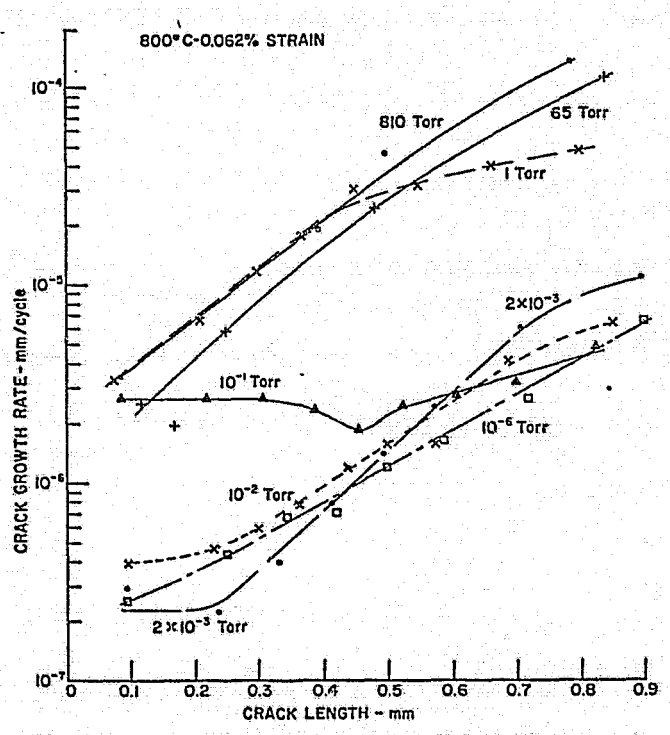

Fig. 5—Fatigue crack growth rate at 800°C as a function of crack length in oxygen.

The point where the curve bends upward from the low pressure plateau is called the lower transition and the point of leveling off at the high pressure plateau is the upper transition or critical point.

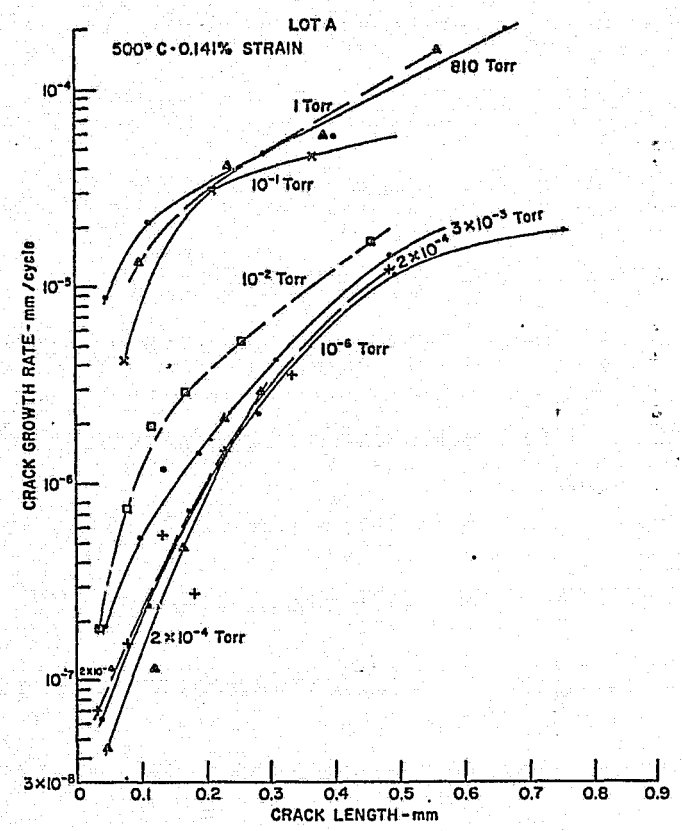

Fig. 6—Fatigue crack growth rate in Lot A material at 500°C as a function of crack length in oxygen.

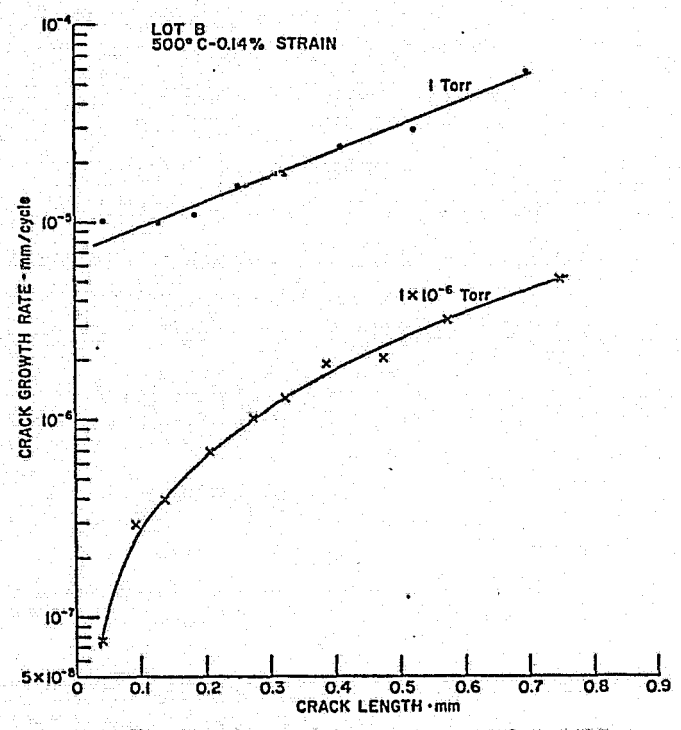

Fig. 7—Fatigue crack growth in Lot B material at 500°C as a function of crack length in oxygen.

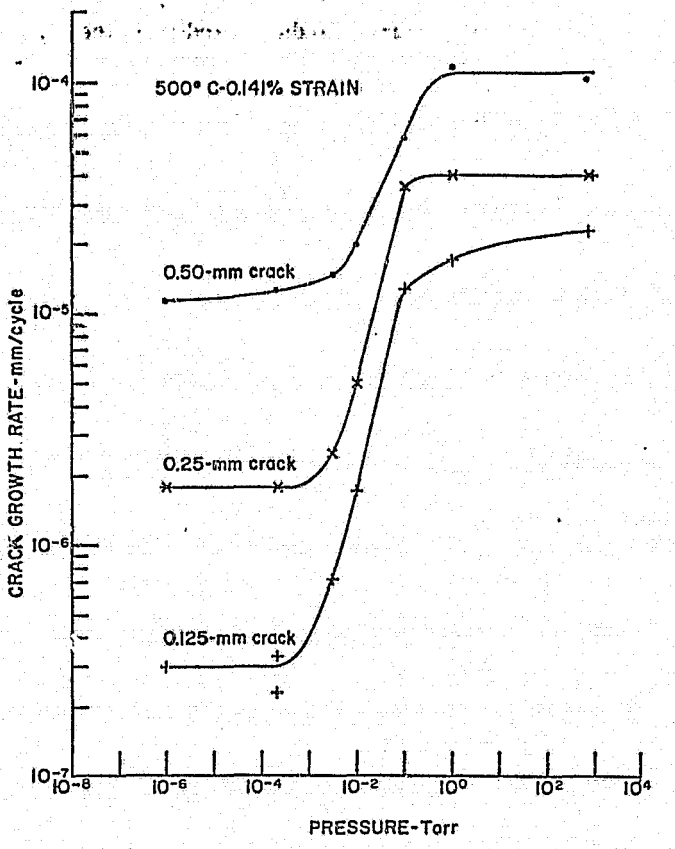

Fig. 8—Effect of oxygen pressure on rate of fatigue crack growth in Lot A material at 500°C.

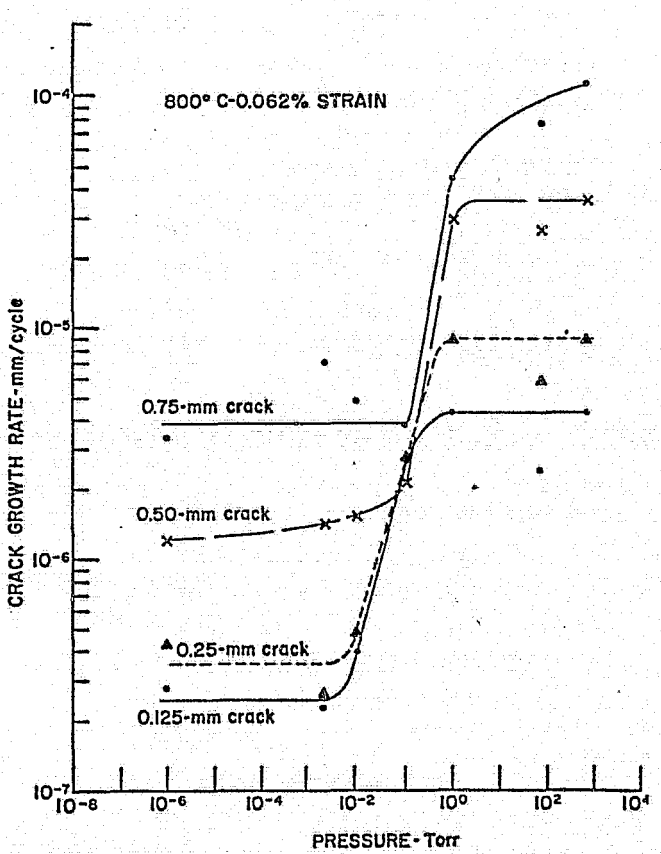

Fig. 9—Effect of oxygen pressure on rate of fatigue crack growth at 800°C.

At 500°C the endurance in the ultimate vacuum of 10^{-6} torr is almost 100 times longer than in 1 torr O. From the fact that the ratio of crack growth rate in oxygen to that in vacuum for the smallest crack is almost of the same magnitude, one can conclude that

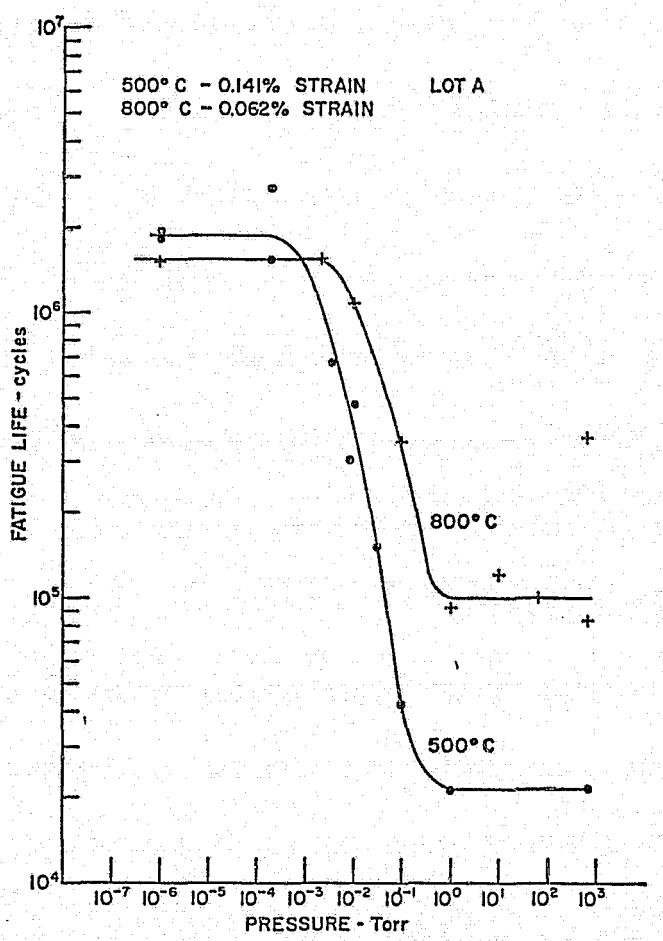

Fig. 10—Effect of oxygen pressure on fatigue life at 500°C (Lot A) and 800°C.

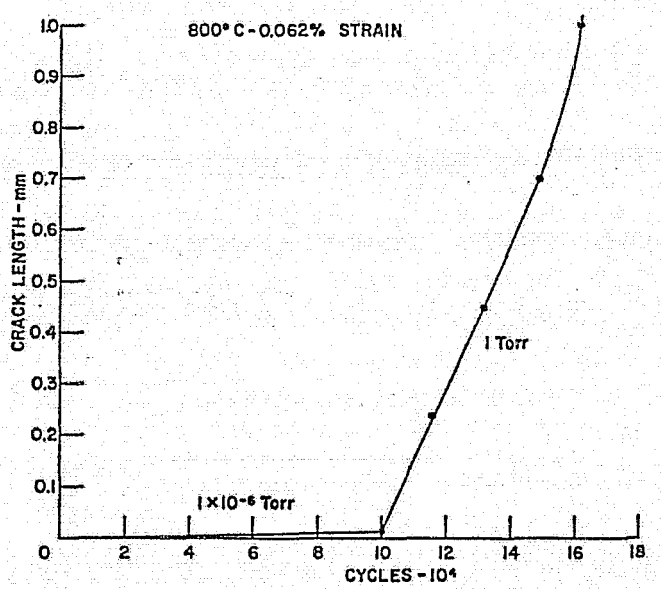

Fig. 11—Increase in rate of fatigue crack growth upon introduction of 1 torr oxygen during fatigue at 800°C.

most of the lifetime is spent in the growth of a small crack. The curves in Fig. 8 resemble those of Bradshaw and Wheeler[1] for aluminum in H_2O vapor in two respects. As the cracks become longer, and grow faster, the effect of gas pressure on growth rate becomes smaller. Secondly, the transition pressures are higher for the longer cracks.

In some ways the fatigue lives and crack propagation rate curves at 800° differed from those at 500°C. At the higher temperature the effect of environment on fatigue lives was considerably smaller. At temperatures this high, a competing reaction, oxidation strengthening, has been found to reduce the crack accelerating effect of oxygen. In fact, a reversal is sometimes observed, with fatigue lives longer in an oxidizing environment than in vacuum.[4] However, the lack of an increase in fatigue life with oxygen pressure at high pressures is not in accord with oxidation strengthening. Also, the transition pressures are higher at 800° than at 500°C. Neither is there the same reduction in environmental effect with increase in crack length as at 500°C.

Changes in Atmosphere. To determine whether the history of previous environments had any effect, crack growth rates were measured before and after the atmosphere was changed. In each case, the rate of propagation in the new environment was the same as that for a specimen which had been fatigued in that environment its entire life. In Fig. 11, the curve, after the introduction of 1 torr O, is the same as that for the same pressure in Fig. 4. For the experiment represented by Fig. 12, the vibration was stopped during the evacuation of the oxygen and not restarted until the ultimate vacuum was reached. Except for a short transition period, perhaps ascribable to completion of degassing of the crack, the growth rate corresponded to the curve for 10^{-6} torr in Fig. 4. In Fig. 12 and in Fig. 4, close to 1.8×10^5 cycles were required for the crack to grow from 0.53 to 1.0 mm at 10^{-6} torr. It was surprising that the oxidation suffered by the stainless steel had no effect upon its subsequent behavior in vacuum.

Metallographic Observations. All cracks at both temperatures were transgranular. There was no obvious effect of gas pressure on crack geometry observed to explain faster growth rates in oxygen, although increasing pressure resulted in relatively straighter cracks. In the examination of interrupted test specimens for the calibration plots of Fig. 3(*a*) and 3(*b*), small cracks were found after a few hours in vacuum even when the lifetime was long. Therefore, it is the rate of propagation and not initiation which determines the effect of environment on life.

DISCUSSION

According to the general adsorption model, crack propagation is accelerated with increasing gas pressure until the rates of surface generation and of coverage by gas are equal. At this so-called critical point increases of pressure should have no further effect. A number of detailed mechanisms have been proposed to explain how this general model operates. One deals with dislocations piled up against the oxide layer,[6] another with the prevention of rewelding of the crack surfaces,[7] and still another with the generation of hydrogen by the reaction of water vapor with clean aluminum on the crack surfaces.[1,8,9] Another proposed mechanism holds that reaction of the gas with the interatomic bonds at the crack tip would reduce the work required to break these bonds.[10]

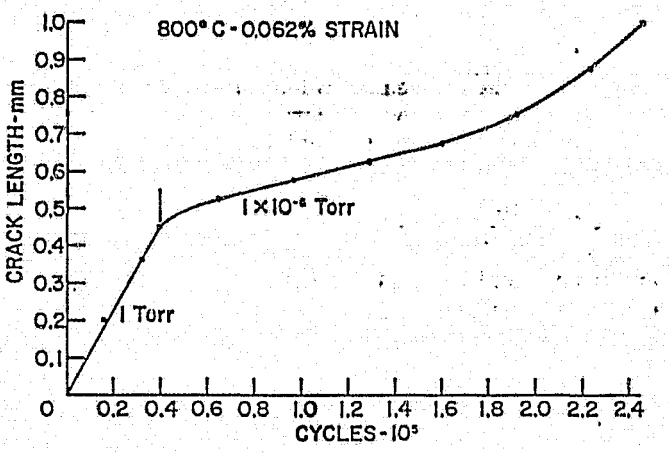

Fig. 12—Decrease of rate of fatigue crack growth at 800°C as pressure is reduced from 1 torr to 1×10^{-6} torr.

Let alone distinguishing between these detailed mechanisms, it has not as yet been possible to relate crack growth rate with gas pressure to substantiate the general adsorption model. In this paper we present a calculation method, modified from one proposed earlier for creep,[11] which considerably narrows the spread between the predicted and observed critical pressure. Crack propagation is visualized as the uncovering of successive rows of atomic sites by breaking of interatomic bonds at the crack tip. At the critical point, the rate of impingement of gas molecules at the crack tip must equal the rate of bond breaking. The rate of breaking of bonds, per length of crack edge equal to the interatomic spacing, is given by v/χ where v is the crack tip velocity and χ the interatomic spacing. In effect each site in the row of atomic sites uncovered by the breaking of bonds at the crack tip must adsorb a gas atom before the next row is uncovered. At the critical point the time in which adsorption must be completed is χ/v. To predict the critical pressure one would then compute from kinetic theory of gases the pressure required to saturate the surface in time χ/v, or to bombard each lattice site of a surface at the rate v/χ.

To compute the predicted pressure it is first necessary to convert the measured growth rate to the effective rate since the crack grows only during a part of the cycle. It seems reasonable to estimate that it grows during $\frac{1}{2}$ the tensile part of the cycle or $\frac{1}{4}$ the complete period. Then the time in which coverage must be completed is given by

$$t = \frac{\chi}{v} = \frac{\chi}{4f\, da/dN} \text{ sec} \qquad [1]$$

where f is 10 cps and da/dN is the measured crack tip velocity in cm per cycle, corrected to the effective velocity by the factor 4.

Taking 2.5Å as the interatomic spacing for γ iron, the density of sites becomes 1.9×10^{15} cm^{-2} and the impingement rate per site is

$$\nu = \frac{3.5 \times 10^{22} P}{1.9 \times 10^{15} (MT)^{1/2}} \text{ sec}^{-1} \quad [2]$$

where M is the molecular weight of gas, P the pressure in torr, and T the temperature.

Remembering that only 1 molecule of oxygen is required to cover 2 atoms of iron, the saturation time is

$$t = \frac{1.9 \times 10^{15} (MT)^{1/2}}{2 \times 3.5 \times 10^{22} P} \text{ sec} \quad [3]$$

and from Eqs. [3] and [1] we get for the predicted oxygen pressure

$$P_p = 2.5 \times 10^2 \, (da/dN) \, T^{1/2} \quad [4]$$

To illustrate, for the 0.25 mm crack at 500°C in Fig. 8, at the upper transition or critical pressure where P_p should equal the observed pressure P_o, we take $da/dN = 4 \times 10^{-6}$ cm per cycle and get $P_p = 2.8 \times 10^{-2}$ torr. Here $P_o = 1.1 \times 10^{-1}$ torr and $R = P_o/P_p = 4$. Similarly, the R values were calculated at three places on each curve in Figs. 8 and 9, at the upper and lower transition points and a point midway between them.

In Table I, the R values for the upper transition, or critical point, at 500°C are >1. That is, the observed pressure is greater than the predicted. The agreement between P_o and P_p is roughly an order of magnitude. Bradshaw and Wheeler[1] and Hordon,[2] in attempting to explain values of R of about 10^3 for aluminum, considered the attenuation of gas flow by a capillary crack, as suggested by Snowden.[12] Bradshaw,[13] in addition, discussed the possibility that more than 1 layer of oxygen is required before the crack growth rate becomes constant. However, when our calculation procedure is applied to the data of Bradshaw and Wheeler, agreement of their P_o and P_p is also within an order of magnitude;[14] P_o/P_p is 10, 9, and 5 for their 3 curves. With this agreement between P_o and P_p it does not appear necessary to resort to a large correction for the attenuation in a capillary crack. If it were necessary, R would increase with crack length, and it does not.

Much of the discussion of the events at the tip of the crack depends upon the value of R and its response to the conditions of the measurement. In our calculation the greatest uncertainty is the factor used to convert measured crack growth rate to effective rate. In reversed bending the factor must be >2. We used a value of 4. If we had used a number <4, R would be larger than reported but the R values in Table I could not be much greater than 10 at 500°C. At our present state of knowledge, it is not possible to know what part of the value of R is ascribable to attenuation by a capillary crack and what part to the sticking coefficient, which may be appreciably less than one. However, the variation in R with the conditions of measurement may be interpreted with confidence in a discussion of the model.

Table I. Comparison of Predicted Saturation Pressures P_p Based on Crack Growth Rate and Observed Transition Pressures P_o

		R (P_o/P_p)			
		Crack Length – mm			
		0.125	0.25	0.50	0.75
500°C	Upper transition (critical point)	12	4	5	
	Mid transition	9	3	2	
	Lower transition	5	2	0.5	
800°	Upper transition (critical point)	58	79	42	37
	Mid transition	40	40	49	33
	Lower transition	28	22	53	36

Certain features of the data at 500°C in Fig. 8 fit the model. The transition pressures increase with crack length. It would be expected that a faster growing crack would require a higher gas impingement rate. Also, R increases with increasing gas pressure. According to the model, at the upper transition the rates of surface generation and coverage should be equal and $R = 1$. Now R, at the lower transition at 500°C, is anywhere from 10 to 50 pct of the value at the upper transition for the three crack lengths. Therefore, we conclude that the rate of crack growth is a function of impingement rate only when the gas pressure is large enough for coverage of at least 10 pct of the sites in time χ/v.

At 800°C, R is considerably greater than at the lower temperature. Recent results on nickel[15] also show a similar change in environmental response with temperature; the high pressure transition shifts to higher pressures as temperature is raised. This pressure shift was attributed to oxidation along the crack surfaces at the higher temperature, causing a reduced rate of arrival of oxygen molecules at the tip of the advancing crack. To provide sufficient oxygen to produce the maximum crack growth rate, a higher pressure is required at higher temperatures, resulting in higher values of R.

At 500°C, where no visible oxidation is present, the order of magnitude agreement between P_o and P_p, as well as the similar results in treating the data for aluminum, attests to the validity of the calculation method and supports the general adsorption model. With the continuing development of new metallographic techniques there is hope that it will be possible before too long to distinguish between the detailed mechanisms.

SUMMARY AND CONCLUSIONS

Crack growth rates in Type 316 stainless steel show a sharp increase with oxygen pressure in an intermediate range and little or no change at high and low pressures. According to a general model for environmental effects, the high pressure transition or critical pressure, where the curve levels off again, represents the point where the surface is being covered by oxygen at the same rate it is being produced. A method of calculating the predicted pressure is described which results in order of magnitude agreement between it and the observed pressure at 500°C. With this agreement it is concluded that large corrections for the attenuation of gas flow by a capillary crack are not needed.

At 800°C the agreement is not as good as at 500°C, although considerably better than two orders of magnitude. This apparent change in the environmental effect with increase in temperature may be attributed to greater oxidation at crack surfaces at the higher temperature. Therefore, the data cannot be treated by simple adsorption theory.

REFERENCES

[1]F. J. Bradshaw and C. Wheeler: *Appl. Mat. Res.*, 1966, vol. 5, pp. 112-20.

[2]M. J. Hordon: *Acta Met.*, 1966, vol. 14, pp. 1173-78.

[3]M. R. Achter, H. H. Smith, R. J. Riley, and R. L. Stegman: *Rev. Sci. Instr.*, 1966, vol. 37, pp. 311-15.

[4]G. J. Danek, Jr., H. H. Smith, and M. R. Achter: *Proc. ASTM*, 1961, vol. 61, pp. 775-88.

[5]S. Dushman: *Scientific Foundations of Vacuum Technique*, p. 14, John Wiley & Sons, New York, 1962.

[6]H. Shen, S. E. Podlaseck, and I. R. Kramer: *Acta Met.*, 1966, vol. 14, pp. 341-46.

[7]N. Thompson, N. Wadsworth, and N. Louat: *Phil. Mag.*, 1956, vol. 1, Ser. 8, pp. 113-26.

[8]T. Broom and A. Nicholson: *J. Inst. Met.*, 1960-61, vol. 89, pp. 183-90.

[9]A. Hartman: *Inter. J. Fracture Mech.*, 1965, vol. 1, pp. 167-87.

[10]M. R. Achter: *Proc., Institute of Environmental Sciences*, 1963, pp. 385-94.

[11]M. R. Achter and H. W. Fox: *Trans. TMS-AIME*, 1959, vol. 215, p. 295.

[12]K. U. Snowden: *Acta Met.*, 1964, vol. 12, pp. 295-303.

[13]F. J. Bradshaw: *Scripta Met.*, 1967, vol. 1, p. 41.

[14]M. R. Achter: *Scripta Met.*, 1968, vol. 2, pp. 525-28.

[15]R. L. Stegman and P. Shahinian: Naval Research Laboratory, Washington, D. C., unpublished research, 24 Dec. 1968.

END OF REFERENCE

17

REFERENCE

18

SMITH, H. H.; AND SHAHINIAN, P.: EFFECT OF OXYGEN AND OF WATER VAPOR ON THE FATIGUE LIFE OF NICKEL AT 300°C. EFFECTS OF ENVIRONMENTAL AND COMPLEX LOAD HISTORY ON FATIGUE LIFE. STP-462, AMERICAN SOC. TESTING AND MATER., 1970.

THIS MATERIAL HAS BEEN APPROVED FOR PUBLICATION PER LETTER DATED AUG. 19, 1974, ASTM TO JOANNE FOLK.

EFFECTS OF ENVIRONMENT AND COMPLEX LOAD HISTORY ON FATIGUE LIFE

A symposium
presented at the
Fall Meeting
AMERICAN SOCIETY FOR
TESTING AND MATERIALS
Atlanta, Ga., 29 September–4 October, 1968

ASTM SPECIAL TECHNICAL PUBLICATION 462

LIBRARY COPY
RETURN TO
LEWIS LIBRARY
CLEVELAND, OHIO

List Price $22.00

AMERICAN SOCIETY FOR TESTING AND MATERIALS
1916 Race Street, Philadelphia, Pa. 19103

Introduction

In keeping with a well established precedent, Committee E-9 on Fatigue again sponsored a triennial symposium on aircraft structural fatigue problems at the Fall Meeting held in Atlanta, Ga., 29 Sept.–4 Oct. 1968.

Previous symposia have concentrated on the basic mechanism of fatigue, the effects of stress concentrations, and the behavior of full-scale structural assemblies and components under simulated service loadings.

This symposium was divided into three broad categories: (1) cumulative damage; (2) random load effects; and (3) the effects of corrosive environments.

In general, the papers in the first two categories approach the basic problem of life estimation in a more rational manner than heretofore. The papers on the effects of corrosive environments reflect the current concern with the superposition of environmental simulation on the fatigue problem.

M. S. Rosenfeld

Research Aerospace Engineer,
Aero Structures Department,
Naval Air Development
Center; symposium chairman.

H. H. Smith[1] *and P. Shahinian*[1]

Effect of Oxygen and of Water Vapor on the Fatigue Life of Nickel at 300 C

REFERENCE: Smith, H. H. and Shahinian, P., "Effect of Oxygen and of Water Vapor on the Fatigue Life of Nickel at 300 C," *Effects of Environment and Complex Load History on Fatigue Life, ASTM STP 462*, American Society for Testing and Materials, 1970, pp. 217–233.

ABSTRACT: The fatigue behavior of high-purity nickel, vibrated in reversed bending, was studied at 300 C in oxygen and in water vapor at pressures from 10^{-9} to 10 torr. Fatigue life was reduced in both oxygen and water vapor, but the variation in life with pressure differed somewhat for the two. The curve of fatigue life *versus* oxygen pressure is step-shaped with little or no dependence of life on pressure at very low and high pressures, the major reduction taking place at intermediate pressures. In contrast, the fatigue life in water vapor drops off gradually throughout the entire high-pressure range, but the maximum reduction is much less than in oxygen. Evidence obtained by residual gas analysis shows that a hot ionization gage filament may change the composition of the environment which, in turn, may affect fatigue life. Metallographic examination of failed specimens disclosed a relation between deformation and cracking characteristics and oxygen pressure. A calculation of the pressure required to saturate the crack surfaces at an estimated rate of crack growth showed that the predicted pressure agreed with the highest transition pressure, at which the reduction in fatigue life approaches a maximum.

KEY WORDS: fatigue, nickel, high temperature, gaseous environment, vacuum, oxygen, water vapor

Introduction

The question of whether it is oxygen or water vapor which is detrimental to fatigue life in air has been studied by a number of investigators [*1–5*].[2] Most of the metals investigated have been found to be affected more by oxygen than water vapor except aluminum and its alloys which are reported to be especially susceptible to water vapor. However, in these studies the exact composition of the environment was not known with certainty because it was

[1] Research Physical Metallurgist and Supervisory Research Physicist, respectively, Thermostructural Materials Branch, Metallurgy Division, U.S. Naval Research Laboratory, Washington, D.C. 20390.

[2] The italic numbers in brackets refer to the list of references appended to this paper.

not analyzed. In all but one of the studies the effect of water vapor was examined in the presence of oxygen. In addition, other impurity gases were of course present but their possible effect was not considered. Because of these factors there is some uncertainty in the interpretation of results.

The purpose of this investigation was to distinguish between the effects of oxygen and water vapor on the fatigue life of high-purity nickel at 300 C. Composition of the environment was carefully controlled and analyzed to isolate the effects of oxygen and water vapor from those of the impurity gases, CO, CO_2, H_2, and N_2. The observed variation of fatigue life with pressure of gas is discussed in terms of the surface-gas-adsorption model.

Experimental Procedure

The 99.99 percent nickel strip used in this study had the following percentages of impurities: 0.006 C, 0.001 S, <0.001 Mn, <0.001 Cu, 0.0005 Co, 0.0004 Fe, 0.0003 Si, and 0.0002 Cr. From the cold-rolled material, sheet specimens, 0.060 in. thick with a 0.187-in. wide reduced section, were machined, vacuum-annealed at 870 C for 2 h, and electropolished in a solution 57 percent by volume sulfuric acid.

Fatigue experiments were conducted at 300 C in oxygen and in water vapor at a series of partial pressures from 10^{-9} to 10 torr. The fatigue machine used, described in detail previously [6], was of the reversed-bending, constant-deflection type incorporating an electromagnetic drive to facilitate testing in a controlled environment. In the control circuit of the machine there is a feedback loop to maintain a constant vibration amplitude. All of the experiments were run at a nominal vibration frequency of 5 cps and a plastic bending strain of 0.17 percent. The bending strain was determined by means of an elevated-temperature optical technique [7]. Current to the electromagnets was interrupted when the power required to maintain a constant amplitude increased to the predetermined level taken as the fatigue life.

An oil-diffusion pump system containing two liquid-nitrogen traps, one at the pump and an auxiliary one adjacent to the hot zone, provided ultimate vacuums in the 10^{-9} torr range after an overnight bake. Two oxygen series were run, one with both liquid-nitrogen traps in the system and one without the auxiliary trap. In the water-vapor series, liquid-nitrogen traps were not used. Pressure was measured in the fatigue chamber as close as feasible to the hot zone using a Bayard Alpert type ionization gage at pressures below 1×10^{-4} torr and a NRC Type 530 Alphatron gage at pressures above this value. The ion gage was turned on only momentarily to measure pressure because it affected the composition of the environment. This will be discussed further in the "Results" section.

The pressure in the fatigue chamber was varied by admitting gas through a variable-conductance high-vacuum valve, after the chamber was first

evacuated to the ultimate vacuum. Analyses of the atmosphere were made before and after the specimen was fatigued at pressures below 1×10^{-4} torr using a magnetic sector-type residual-gas analyzer to determine the impurity content. The sensitivity of the instrument to O_2, H_2O, CO, CO_2, H_2 and N_2 was determined along with the spectrum patterns for each gas. A spectrum pattern shows the relation of the peaks of a mass spectrum to the principal or base peak, expressed as percentages of the base peak. Spectrum patterns are necessary to determine the partial pressures of gas species, such as carbon monoxide and nitrogen, which have a base peak at the same mass number.

To ascertain whether the main impurities, CO, CO_2, N_2, and H_2, produced an effect on fatigue, specimens were cycled in these individual gases at 1×10^{-4} torr. Additional pressure levels of 5×10^{-7} and 1×10^{-2} torr were used for the carbon monoxide. The purities of the gases in percentages were 99.5 oxygen, 99.995 nitrogen, 99.5 carbon monoxide, 99.5 carbon dioxide, and 99.9 hydrogen. Distilled and degassed water was used in the water-vapor-pressure series. Since at reduced pressure the impurity content of the gases is low, no further purification was attempted. To minimize contamination of the gas, however, gas-cylinder to leak-valve distances were kept short. Initially, a liquid-nitrogen trap was placed in the oxygen line, but it did not reduce the level of water vapor measured in the chamber and was discarded.

A metallographic study was made on failed specimens in an attempt to relate mode and other features of cracking to the environment.

Results

Environment

In assessing the effects of oxygen and water vapor on fatigue life it was necessary to follow the compositional changes of the environment as experimental conditions were varied. As the gas was admitted, as liquid-nitrogen traps were introduced, or as ion gages were turned on, the concentrations of the impurity gases were altered. The findings dictated to some extent the experimental procedures required and the interpretation of the fatigue data.

At the ultimate vacuum the environment was composed mainly of H_2, CO, N_2, and H_2O, as shown in Fig. 1 by the typical residual-gas analyses of the system with and without the auxiliary trap at pressures of 6×10^{-9} and 1×10^{-8} torr, respectively. Because of inaccuracies introduced by extrapolating the gas sensitivities to these low pressures, the sum of the partial pressures is slightly higher than the ion-gage pressure. The use of a liquid-nitrogen trap at the diffusion pump and an auxiliary trap near the hot zone removed mainly the condensibles, water vapor and carbon dioxide. Other gases were also reduced by "pumping" at the cold walls. Each trap provided a measure of improvement to the vacuum. During the analyses the ion gages remained off for reasons which will become evident later.

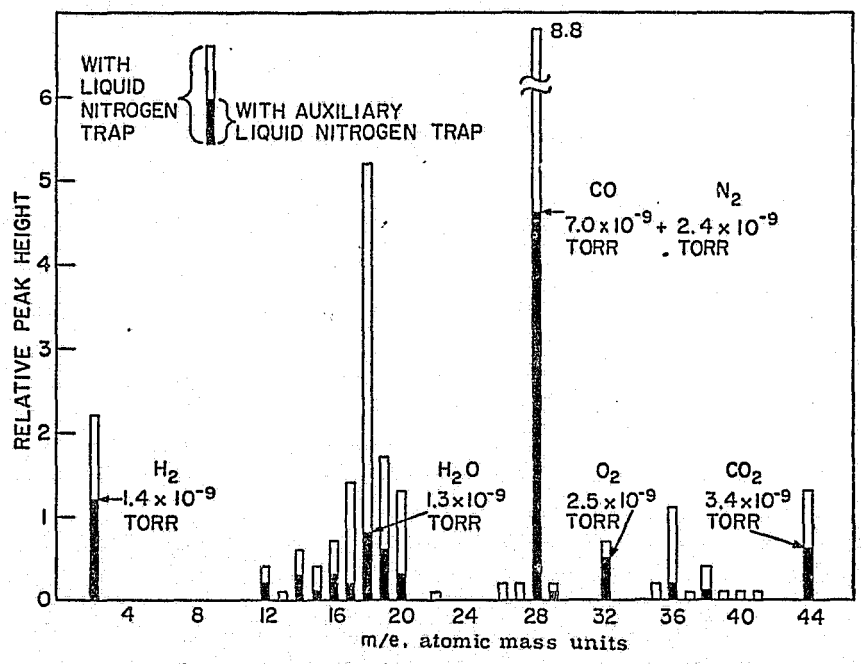

FIG. 1—*Typical gas analyses at the ultimate vacuum at 300 C with the liquid nitrogen trap* (1×10^{-8} *torr*) *and including the auxiliary trap* (6×10^{-9} *torr*).

When oxygen is admitted to the system, even in small amounts, the partial pressures of many of the residual gases increase, particularly CO, CO_2, and H_2O (Table 1). Carbon monoxide increased substantially more than the other gases, but its ratio to oxygen became smaller at higher oxygen pressures. The increase in water vapor as oxygen pressure is raised is held by the liquid-nitrogen traps to levels of about three orders of magnitude lower than that of oxygen. The increase in these gases cannot be accounted for by their concentrations in the tank oxygen. In the case of water vapor neither does it appear that it is being dislodged from the walls of the system by impinging oxygen molecules because the ratio of water vapor to oxygen remains constant over long periods of time. Adsorbed water vapor should eventually decrease. Thus these gases appear to form in the system. The compositional changes may be attributed to hot filaments which can cause thermal decomposition and chemical reactions to take place.

In the water-vapor experiments which were run without liquid-nitrogen traps, the partial pressures of the impurity gases rose as water vapor was admitted to a pressure of 1×10^{-5} torr (Table 2). The increases in the amounts of H_2, CO, O_2, and CO_2 were much greater when the ion gage was on than

TABLE 1—*Fatigue life of nickel in various environments.*

Environment Pressure, torr	Fatigue Life, cycles	Impurity Gases, Partial Pressure, torr					
		O_2	H_2O	CO_2	CO	N_2	H_2
Vacuum							
6×10^{-9}	4.4×10^5	1.6×10^{-9}	3.5×10^{-9}	6.0×10^{-9}	4.0×10^{-9}	2.6×10^{-9}	1.3×10^{-9}
H_2O							
1×10^{-4}	3.1×10^5	3.0×10^{-9}	1×10^{-4}	1.4×10^{-7}	1.6×10^{-7}	2.0×10^{-8}	4.0×10^{-9}
CO_2							
1×10^{-4}	3.7×10^5	3.0×10^{-8}	8.8×10^{-8}	$1. \times 10^{-4}$	6.6×10^{-7}	...	5.0×10^{-9}
H_2							
1×10^{-4}	3.3×10^5	1.4×10^{-7}	3.0×10^{-7}	1.2×10^{-8}	...	8.1×10^{-7}	1×10^{-4}
N_2							
1×10^{-4}	2.8×10^5	1.8×10^{-6}	5.6×10^{-9}	1.0×10^{-8}	...	1×10^{-4}	3.4×10^{-9}
O_2							
1×10^{-4}	1.2×10^5	1×10^{-4}	1.3×10^{-7}	4.5×10^{-7}	1.8×10^{-7}	...	4.7×10^{-8}
O_2							
1×10^{-2}	0.2×10^5	1×10^{-2}					
CO							
5×10^{-7}	3.7×10^5	3.5×10^{-9}	1.6×10^{-9}	4.0×10^{-9}	4.6×10^{-7}	...	1.2×10^{-8}
CO							
1×10^{-4}	3.1×10^5	1.0×10^{-7}	5.4×10^{-9}	1.0×10^{-10}	1.0×10^{-4}	1.0×10^{-7}	7.2×10^{-10}
CO							
1×10^{-2}	2.8×10^5						
$H_2O + CO$							
1×10^{-5}	4.9×10^5	2.7×10^{-8}	5.3×10^{-6}	4.7×10^{-8}	6.0×10^{-6}	...	1.0×10^{-8}
$O_2 + H_2O$							
2.4×10^{-6}	3.4×10^5	1.0×10^{-6}	1.0×10^{-6}	7.8×10^{-8}	1.0×10^{-7}	1.4×10^{-7}	1.0×10^{-9}

TABLE 2—*Effect of hot ion-gage filament on peak heights of the major masses when water vapor is present.*

	Peak Heights—Divisions			
	Ion Gage Off		Ion Gage On	
			Water Vapor Leak, 1×10^{-5} torr	
m/e	Ultimate at 6×10^{-8} torr	Water Vapor Leak, 1×10^{-5} torr	10 ma Emission[a]	0.1 ma Emission
2.....	5.5	86	470	250
18.....	35	>1 000	>1 000	>1 000
28.....	11	110	200	120
32.....	0.9	1.0	220	100
44.....	4.1	13	47	20

[a] Normal operation.

when off. In fact, with the ion gage off, the partial pressure of oxygen was the same in the 10^{-5} torr water-vapor atmosphere as in the ultimate vacuum. The effect of the hot filament on gases was further demonstrated when the filament temperature was reduced (Table 2). Lowering the temperature by about 100 C by reducing the emission current to 0.1 ma decreased H_2, CO, O_2, and CO_2, but generally not as low as when the gage was off. The filament had a very small effect at the ultimate vacuum. At the hot filament, water vapor can dissociate and carbon monoxide and carbon dioxide can be formed by reaction of oxygen with available carbon in the filament.

In addition to the reactions at the thoria-coated iridium filament of the ion gage it is known [*8*] that similar reactions may occur at the hot tungsten filament of the residual gas analyzer. A difference between the reactions at the two filaments is that oxygen will combine readily with tungsten but not with thoria. Because of these possible filament effects, the specimens were fatigued normally with the ion gages and gas analyzer off. Implicit in these findings is that the amounts of many of the impurity gases may actually be lower than measured with the gas analyzer. Nevertheless, when considering the effects of the gases on fatigue life, the impurity levels as observed with the gas analyzer were used.

Fatigue Life

Oxygen and water vapor both reduce the fatigue life of nickel at 300 C (Fig. 2), but the variation of life with pressure differs for the two gases. In oxygen most of the reduction in life occurs over an intermediate pressure range. Increasing the pressure at the high range does not affect life while at

the low range fatigue life continues to improve slightly as pressure is reduced. This is in contrast to many metals which exhibit distinct plateaus at both high and low pressures in their fatigue life *versus* pressure curves. An auxiliary liquid-nitrogen trap in the system which reduced the condensibles did not significantly affect the variation of life with oxygen pressure. This is an indication that the water vapor at the levels present in the oxygen environment was not detrimental. In water vapor, fatigue life gradually decreases with increase in pressure without an abrupt transition range. A clear reduction in life initially occurs at about 10^{-5} torr of water vapor. The life in vacuum

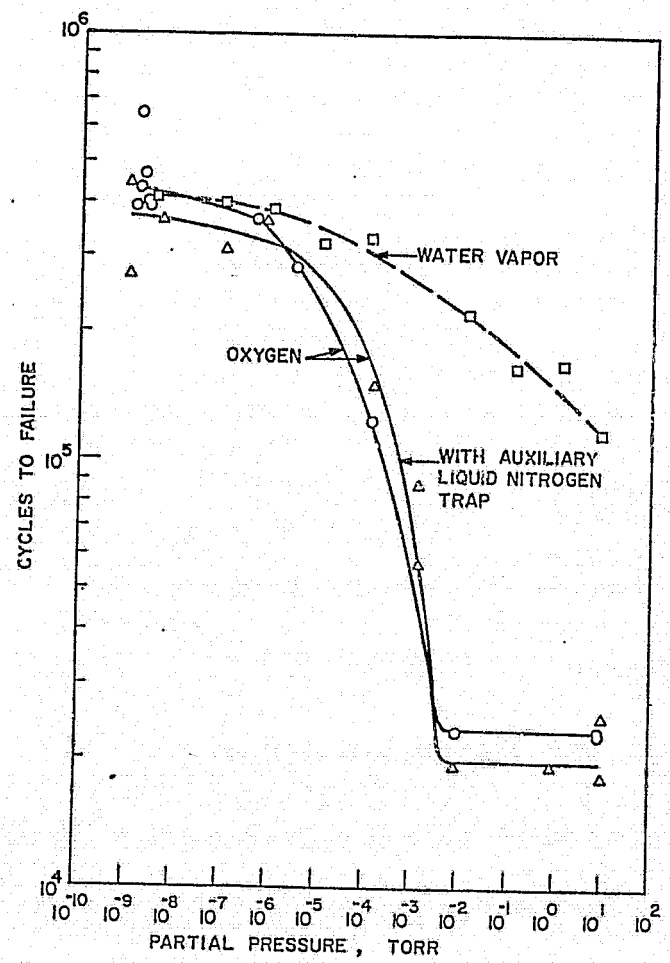

FIG. 2—*Effect of oxygen and water-vapor pressure on fatigue life at 300 C at a plastic bending strain of 0.17 percent.*

is approximately twenty times longer than in oxygen and four times longer than in water vapor at a pressure of 10 torr.

Fatigue life of nickel in reduced pressures of CO, CO_2, H_2, and N_2 is slightly lower than in vacuum, but the reductions are considerably less than in oxygen at the same pressure (Table 1). If the reduction in life found in an oxygen environment of 10^{-4} torr is, in fact, caused by that gas, most of the weakening observed in the impurity gases can be accounted for by the presence of small amounts of oxygen. If the adjustment for the weakening by oxygen is made, then the fatigue lives in the impurity gases are only at the most about 10 percent lower than in vacuum. Since this apparent difference is within the range of experimental scatter it might not be real. Thus, it may be concluded that the gases CO, CO_2, H_2, and N_2 in the concentrations studied have little or no effect on fatigue life. It is possible of course that these gases at higher pressures may produce an effect on nickel.

Since apparently there is no significant effect by the impurity gases, the reduction of life observed in an oxygen atmosphere may be attributed to the oxygen. At an oxygen pressure of 10^{-4} torr where an appreciable decrease in life occurs, to one third of that in vacuum, the partial pressures of the impurity gases including water vapor are at least two orders of magnitude lower (Table 1). At these pressures of $< 10^{-6}$ torr it is clear from our data that the impurity gases are not effective. Further support may be obtained at 10^{-2} torr oxygen where the reduction in life is a maximum, if it is assumed that the partial pressures of the impurities remain at least two orders of magnitude lower than the oxygen. Then the reduction in life possible in the impurity gases at 1×10^{-4} torr would be only a small fraction of that observed in oxygen at 1×10^{-2} torr. It is thus clear that the oxygen reduces fatigue life as represented by the curve in Fig. 2 and is more effective than the other gases at least at lower pressures.

In the water-vapor series of experiments the partial pressures of the main impurities, carbon monoxide and carbon dioxide, were almost three orders of magnitude lower than the water vapor at 1×10^{-4} torr (Table 1). Again, assuming a similar concentration ratio of the gases exists at 1×10^{-1} torr water vapor, it is evident that the impurities at 10^{-4} torr would not contribute significantly to the observed reduction in fatigue life at 1×10^{-1} torr. Fortunately, in the water-vapor series the partial pressure of oxygen did not change but remained essentially the same as in vacuum.

It is of interest to note that with the ion gage on during a water-vapor experiment at 1×10^{-5} torr the oxygen pressure is high enough to reduce fatigue life. This effect at pressures of 1×10^{-5} and 1×10^{-4} torr of water vapor is demonstrated in Table 3. The life in water vapor was approximately 25 percent lower with the ion gage on than with the gage off, entirely accountable by the oxygen present.

TABLE 3—*Reduction in fatigue life of nickel in water vapor at 300 C as a result of ion-gage operation.*

Pressure, torr	Fatigue Life (cycles)	
	Ion Gages Off	Ion Gages On
1×10^{-5}.....	3.5×10^5	2.7×10^5
1×10^{-4}.....	3.1×10^5	2.3×10^5

The possibility of a combination effect of gases was examined. For example, Wadworth and Hutchings [*1*] reported that water vapor increases the effect of oxygen in the weakening of copper although it alone shows no effect. And Snowden [*2*] showed that the presence of water vapor reduces the effect of oxygen on the fatigue life of lead. Since in the oxygen experiments water vapor was present and in water-vapor experiments carbon monoxide was a major impurity, fatigue life was determined in equal mixtures of these combinations of gases. No additional weakening was evident due to the nature of the combination (Table 1), indicating that each reactive gas weakens independently of the other.

Metallographic Observations

In the metallographic study of failed specimens certain features of the cracking and structure appeared to be related to oxygen pressure. The nature of cracking and deformation that occurred in the low pressure region, transition region, and high pressure plateau are shown in Figs. 3 through 6. Severe rumpling was observed on the surface in vacuum but not in oxygen at high pressure. It is not known whether the variation in the degree of rumpling was due to the environment itself, or entirely to differences in the number of cycles to failure. At 10^{-9} torr it was not possible to distinguish whether the cracks were transgranular or intergranular because of the heavily deformed structure. The distribution of cracks in the specimen surface is indicated in Fig. 3*a* where the dark void-like areas are valleys remaining after the removal of 0.0035 in. of the heavily deformed surface layer. Many of these valleys contain small cracks, and at the minimum section some of these cracks have joined together. Although a few cracks are broad and deep at failure, most of them are shallow as shown in Fig. 3*b*. In addition to the rumpled surface, extensive polygonization in the interior occurred at this low pressure.

At the transition pressure of 1×10^{-4} torr cracks are deeper and more numerous than at the lower pressure (Fig. 4). Cracks can be seen in Fig. 4*b* originating from the valleys which appear to be preferential sites, but it was not possible to ascertain the mode of cracking. At this pressure the surface as

END OF REFERENCE

18

REFERENCE

19

HARTMAN, A.: ON THE EFFECT OF OXYGEN AND WATER VAPOR ON THE PROPAGATION OF FATIGUE CRACKS IN 2024-T3 ALCLAD SHEET. INT. J. FRACT. MECH., VOL. 1, SEPT. 1965.

THIS MATERIAL HAS BEEN APPROVED FOR PUBLICATION PER LETTER FROM STEPHANIE VENEMA, NOORDHOFF INTERNATIONAL PUBLISHING (NETHERLANDS) TO JOANNE FOLK DATED SEPT. 30, 1974.

ON THE EFFECT OF OXYGEN AND WATER VAPOR ON THE PROPAGATION OF FATIGUE CRACKS IN 2024-T3 ALCLAD SHEET

A. Hartman*

ABSTRACT

The propagation of fatigue cracks in 2024-T3 alclad sheet under fluctuating tension in different atmospheres has been studied. Of the principal contituents of air, water vapor had a much more severe effect than oxygen; in wet pure argon the endurance was much shorter than in dry pure oxygen. In air, other circumstances remaining unaltered, the endurance increased continuously at a reduction of the water vapour content; the endurance at a water content of the air of 20 ppm being about 6 times as long as in air saturated with water. Between the limits of 30% and 100% relative humidity, as occurring in normal air, the endurance was only slightly affected. The thermodynamics and the mechanisms of the reactions of oxygen and water vapor with the metal are discussed.

INTRODUCTION

In recent years the interest in the propagation of fatigue cracks has increased considerably as a consequence of the development of the so called fail-safe design philosophy for aircraft. This philosophy admits the possibility of the initiation of fatigue cracks during the estimated service life of the aircraft, but it requires a structure which excludes the danger of fatal damage as a consequence of such cracks. Hence, the rate of crack propagation and the residual static strength of the cracked structure need to be known.

The factors which may affect the propagation of fatigue cracks are numerous, one of them being the environment. The usual environment in fatigue tests is air. Normal air consists for the greater part of the rather inert gas nitrogen; it contains about 20% of the rather active gas oxygen and, depending on the temperature and the relative humidity, small varying amounts of water vapor. Corrosive effects during fatigue tests in air, although usually ignored, cannot be ruled out, particularly on metals like aluminium, situated near to the base of the electromotive force series. These effects have been demonstrated as early as 1932 by Gough and Sopwith [1] who showed that the fatigue strengths of several metals were higher in vacuum than they were in the normal indoor atmosphere.

This paper will be mainly concerned with an investigation carried out at the National Aero- and Astronautical Research Institute (NLR) on the effects of oxygen and water vapor on the propagation of fatigue cracks in sheet material of the aluminium alloy 2024-T3 Alclad. The description of the experimental procedure and the presentation and discussion of the principal results of the investigation will be preceded by a summary of the available information on the effects of the atmospheric constituents on the fatigue strength of aluminium and its alloys. Some thermodynamics of the reactions of oxygen and water vapor with metals and a discussion of the reaction of aluminium with the environment are given at the end of the paper.

SURVEY OF PREVIOUS INVESTIGATIONS

Several investigators have studied the effect of a gas environment like air on the fatigue life of specimens from aluminium and its alloys. Generally the effect of the gas environment was determined by comparison of the fatigue life in gases at normal atmospheric pressure and in vacuum

* National Aero- and Astronautical Research Institute, Amsterdam.

with pressures as low as 10^{-9} torr (1 torr = 1 mm Hg). A disadvantage of this vacuum technique is that only the total pressure of the gases is measured and not the partial pressures of the different components of the gas mixture. The investigations aimed at a study of crack initiation and total life of the specimen rather than a study of crack propagation.

The tests of Wadsworth and Hutchings[2,3] were conducten on electropolished specimens of high purity metals and alloys under reversed bending deformation. Metals used were annealed copper, iron, aluminium, gold, and a heat-treated Al-Zn-Mg-Cu alloy. The specimens were fatigued at a frequency of loading of 3000 cycles per min in various pressures of air and other gases. In a vacuum of 10^{-5} torr the endurance of the aluminium alloy specimens increased by factors lying between 5 and 15, depending on the strain amplitude.

Wadsworth and Hutchings concluded from their results that only gases combining easily with the metal had an effect on the endurance of the specimens. Oxygen affected copper, aluminium, aluminium alloy and iron, but had no effect on gold. Water vapor was as effective as oxygen on aluminium but without effect on copper. Wadsworth and Hutchings have attributed the effect of gases on the endurance of metals to a chemical action of the gas making slip irreversible. During repeated loading, microcracks are formed at the surface of the specimen. They assume that at high pressures oxidation of the freshly exposed surface of the crack is rapid and occurs within a fraction of a cycle. The oxidized surface of the crack cannot heal during the subsequent reversal of the load and the crack grows progressively until failure results. They suppose that in the complete absence of an atmosphere a microcrack forming during the tension part of the cycle will probably heal during the succeeding compression part of the cycle, tending to reduce the crack rate considerably. This oxidation theory, however, is not adequate to explain the specific effect of water vapor.

Broom and Nicholson[4] studied the effect of a gas atmosphere on the endurance of smooth aluminium alloy (Al-Cu, Al-Cu-Mg, Al-Zn-Mg-Cu) specimens under axial loading with zero mean stress and a frequency of loading of approximately 10,000 cycles per minute. The gases used were hydrogen, air, oxygen and nitrogen; the pressures ranged from 760 to 10^{-6} torr. They used a cold trap in conjunction with their vacuum chamber which permitted them to reduce the water content of the gas environment to a very low value.

In the virtual absence of water vapor, a variation in oxygen pressure in the approximate range from 10^{-6} to 10^{2} torr did not appear to have an effect on the endurance of the aluminium-alloy specimens. Significant effects within the range of the experiments were caused only by water vapor and hydrogen. A given pressure of hydrogen as a test atmosphere caused an appreciably smaller reduction in endurance than the same pressure of water vapor. Contrary to the findings of Wadsworth and Hutchings it was observed that absence of a deleterious environment slowed down crack initiation more conspicuously than crack growth; the latter, however, was also retarded. Both crack initiation and crack growth were affected by the presence of water vapor.

The deleterious effect of the water vapor in the air on the endurance of the aluminium alloy specimens could be prevented by coating the specimens with a layer of butyl rubber, which is rather impervious to water.

Broom and Nicholson think it probable that hydrogen ions are responsible for the specific effect of hydrogen and water and that these ions are released by dissociation of hydrogen molecules or by the reaction of water vapor with aluminium. They tentatively propose that the introduction of hydrogen ions from the surface into the metal may be responsible in some way for the reduction in endurance. As the most probable mechanism by which hydrogen may assist crack initiation and propagation it is suggested that a building up of pressure occurs in any voids found or formed near

the active slip planes. This involves formation of H_2 ions on an external surface, their diffusion to an internal surface, and their recombination with a low probability of dissociation. When a reaction between water molecules and a clean aluminium surface produced by slip provides the hydrogen ions, such a process can lead to a considerable internal pressure which has to be superimposed on the stresses caused by the external load.

In the United States, Bennett and his associates[5,6,7] have studied the effect of the indoor atmosphere on fatigue failure of metals, including aluminium alloys, in rotating bending and in reversed plane bending. By using specimens partially covered with pressure-sensitive tape they could show that gas evolution occurred, which was associated with fatigue damage. The gas bubbles did not start forming until a considerable portion of the fatigue life had elapsed but fatigue cracks still could not be detected. No bubbles were observed if the stress amplitude was lower than necessary to form a fatigue crack. Gas evolution started earlier in the fatigue life in the high stress, low cycle range than in the lower stress ranges. The gas trapped under the tape was analyzed by mass spectrometry means and found to be hydrogen. The evolution of hydrogen appeared to be dependent on the presence of water. Their observation that hydrogen is evolved on the surface of aluminium or steel fatigue specimens suggests that a reaction between the environment and the metal is operative, involving the displacement of hydrogen from water by the metal.

For aluminium alloys they found, in agreement with the results of Broom and Nicholson, that the fatigue strength was affected almost exclusively by the water vapor content of the environment. They also found that the deleterious effect of water vapor was operative during both crack initiation and crack propagation stages of the fatigue tests. It could be eliminated by the application of certain polar organic liquids, like dodecylalcohol, which form protective films on the metal.

Ham and Reichenbach[8] studied the fatigue life and surface appearance of strips of cold rolled commercial aluminium at pressures down to 7×10^{-9} torr and compared them with that in dry air, wet air and room air at 760 torr. The specimens were subjected to reversed bending at about 8000 cycles/minute. The endurance was about seven times longer in high vacuum than in wet air and about four times longer in high vacuum than in dry air (unknown water content). Before failure occurred the cyclic strain caused more surface roughening and more fatigue cracks in vacuum than in air.

In dry air, life was independent of pressure in the range from 760 to 10^{-2} torr, increased rapidly in the range from 10^{-2} to 10^{-4} torr and was again independent of pressure in the range from 10^{-4} to 7×10^{-9} torr. If we neglect any influence of traces of water vapor in the dry air the results of Ham and Reichenbach indicate that the oxygen in the air has an accelerating effect on fatigue crack initiation and propagation in aluminium and that an air pressure exceeding 10^{-2} torr already yields the maximum effect. At lower pressures the effect of oxygen decreases and the positive effect on crack growth has almost disappeared at air pressures less than 10^{-4} torr.

Ham and Reichenbach propose an explanation of their results based on the hypothesis of a larger strain capacity of metals in vacuum than in the presence of contaminating molecules. If tested in vacuum the material near the local strain concentration, which ordinarily would lead to a fatigue crack in air, will have a greater strain capacity and work hardening capacity than it would have in air. Either a crack may never start if the extra capacity is enough to accommodate the strain elastically after work hardening, or possibly a crack may start and propagate into a region of less strain where it is arrested. If the number of cycles applied without contamination is large enough, the material in that region can work-harden sufficiently to accommodate the required strain elastically and in a sense heal up the

bad spot. After the material is work-hardened, the contaminating gas will no longer do any damage. The environment will affect the fatigue life if during the work-hardening period a monolayer of adsorbed molecules can be built up in the crack which reduces stress and strain required for continued crack propagation. In this theory the specific effect of the constituents of the gas atmosphere is determined by the concentration of the constituent and the decrease in surface tension caused by an adsorbed monolayer of the constituent on the metal.

Jenkins and Roberts[9] made push-pull fatigue tests on smooth uncoated and coated specimens from extruded DTD 5044 aluminium alloy (Al-Zn-Mg type) with zero mean stress and a stress amplitude of 25 kg/mm^2 in air. They found that, by excluding the effects of the environment by means of a butyl rubber coating, the fatigue lives were increased four to five times. The exclusion of the environmental effects favored crystallographic crack propagation (transcrystalline). Atmospheric corrosion facilitated non-crystallographic fatigue crack propagation (intercrystalline).

Kramer and Podlaseck[10] present experimental data for aluminium single crystals showing an improvement in fatigue life at decreasing pressure for the pressure range 760 to 10^{-8} torr. Due to the absence of grain boundaries, the use of single crystals has the advantage that the effect of the environment on the surface of the metal can be studied without interaction with a grain boundary effect. The tests were of the constant strain amplitude, reverse bending type using cantilever specimens and a frequency of loading of 2500-4000 cycles per minute.

Contrary to the conclusion of Ham and Reichenbach[8], Kramer and Podlaseck conclude from their results that within the range of pressures used in the experiments there was a continuous increase in fatigue life at decreasing pressure.

In addition to fatigue tests Kramer and Podlaseck also performed static tensile tests and creep tests. They draw the tentative conclusion that both the stress-strain curves and the creep curves show a decrease in the rate of strain hardening with decreasing pressure. This conclusion does not agree well with the hypothesis put forward by Ham and Reichenbach[8], *i.e.*, in vacuum, more work hardening at the tip of a crack occurs than in air.

Summarizing the data in the literature it is fairly certain that for aluminium and its alloys both the fatigue crack initiation and fatigue crack propagation are affected by a normal air environment. The dominant factor in air is the water vapor content. For less reactive metals, like copper, the dominant factor is the oxygen content of the environment. For the noble metals, like gold, air does not affect the fatigue life. The deleterious effect of the environment can be prevented by coating the metal surface with a film like butyl rubber, which is almost impervious to water. Several mechanisms have been proposed to explain the effect of the environment on the fatigue process but none can explain the effects satisfactorily.

The constituents which might affect the fatigue life of aluminium alloy specimens in normal air by corrosive action are most likely oxygen and water vapor. In the NLR investigation the effects of these two gases on the propagation of fatigue cracks in 2024-T3 alclad sheet have been determined experimentally by measuring the growth of fatigue cracks in gas environments of about 760 torr pressure with known contents of oxygen and water vapor. Table 1 gives a summary of the six series of tests.

END OF REFERENCE
19

REFERENCE

20

TAYLOR, L., ED.: METALS HANDBOOK. VOL. I. PROPERTIES AND SELECTION OF METALS, EIGHTH ED., AMERICAN SOCIETY FOR METALS, 1967.

THIS REFERENCE IS COPYRIGHTED MATERIAL AND THEREFORE THE CONTENTS HAVE NOT BEEN REPRODUCED FROM THE TEXT.

END OF REFERENCE

20

REFERENCE

21

ROSSINI, F. D.; WAGMAN, D. D.; EVANS, W. H.; LEVINE S.; AND JAFFE, I.: SELECTED VALUES OF CHEMICAL THERMODYNAMIC PROPERTIES, PART I. TABLES. CIRCULAR 500-PART I, NATIONAL BUREAU OF STANDARDS, JUL. 1961.

THIS REFERENCE IS MATERIAL THAT IS READILY AVAILABLE AND THEREFORE THE CONTENTS HAVE NOT BEEN REPRODUCED.

END OF REFERENCE

21

REFERENCE

22

WEAST, R. C.; AND SELBY, S. M., EDS.: HANDBOOK OF CHEMISTRY AND PHYSICS. FORTY-EIGHTH ED., CHEMICAL RUBBER CO., 1967-1968.

THIS REFERENCE IS COPYRIGHTED MATERIAL AND THEREFORE THE CONTENTS HAVE NOT BEEN REPRODUCED FROM THE TEXT.

END OF REFERENCE

22

REFERENCE

23

NIHART, G. J.; AND SMITH, C. P.: COMPATIBILITY OF MATERIALS WITH 7500 PSI OXYGEN. UNION CARBIDE CORP. (AMRL TDR-64-76; AD-608260), 1964.

N65-11897

AMRL-TDR-64-76

COPY 1

COMPATIBILITY OF MATERIALS WITH 7500 PSI OXYGEN

G. J. NIHART
C. P. SMITH

UNION CARBIDE CORPORATION, LINDE DIVISION

OCTOBER 1964

BIOMEDICAL LABORATORY
AEROSPACE MEDICAL RESEARCH LABORATORIES
AEROSPACE MEDICAL DIVISION
AIR FORCE SYSTEMS COMMAND
WRIGHT-PATTERSON AIR FORCE BASE, OHIO

COMPATIBILITY OF MATERIALS WITH 7500 PSI OXYGEN

G. J. NIHART
C. F. SMITH

FOREWORD

This investigation was initiated by the Biomedical Laboratory of the Aerospace Medical Research Laboratories, Aerospace Medical Division, Wright-Patterson Air Force Base, Ohio. The research was conducted by Union Carbide Corporation, Linde Division, Cryogenic Development Laboratory, Tonawanda, New York under Contract No. AF33(657)-11686. Mr. C. P. Smith, Section Engineer, and Mr. G. J. Nihart, Staff Chemist, were the principal investigators for Union Carbide Corporation. Contract monitor for the Aerospace Medical Research Laboratories was Mr. Irving H. Lantz. The work was performed in support of Project No. 6373, "Equipment for Life Support in Aerospace," and Task No. 637302, "Respiratory Support Equipment." The work sponsored by this contract was started in June 1963 and was completed in June 1964.

The authors acknowledge the invaluable assistance of Mr. R. M. Thayer, Mr. C. M. Heath, Mr. C. F. Gottzmann, Mr. E. S. Kordyban, and Mr. J. Notaro of Union Carbide Corporation, Linde Division.

This technical report has been reviewed and is approved.

WAYNE H. McCANDLESS
Technical Director
Biomedical Laboratory

ABSTRACT

A research program was conducted to develop ignition data on thread lubricants, thread sealants, fluorocarbon plastics, and metals. Spontaneous ignition temperatures were determined in both 2000 psi and 7500 psi oxygen for all the above materials except metals. The spontaneous ignition temperatures for these materials were found to be essentially the same in 7500 psi oxygen and in 2000 psi oxygen. Only three of the tested lubricants are recommended for possible use in 7500 psi systems. None of the thread sealants are recommended. Glass-filled polytetrafluoroethylene is usable only if tightly confined. The relative ease of ignition of metals and alloys was determined by promoted ignition methods in oxygen at 7500 psi. Inconel alloy 600, brass, Monel alloy 400, and nickel were found to have the highest resistance to ignition and combustion among the common alloys and metals. Of the materials tested, stainless steel and aluminum are the least satisfactory for use at oxygen pressures of 7500 psi. A test system was constructed to evaluate the hazards in rapidly charging a 65 cubic inch nickel-lined vessel with high pressure oxygen. A series of rapid charging tests up to as high as 8000 psi proceeded without incident. Electrostatic charges measured during the charging were negligible.

TABLE OF CONTENTS

	Page
INTRODUCTION	1
PROGRAM DEVELOPMENT	1
Selection of Test Methods	1
Oxygen Bomb Test	2
Impact Sensitivity Test	2
Velocity Impact Test	2
Hot Wire Test	2
Promoted Ignition Test	3
Adiabatic Compression Test	3
Selection of Materials for Test	3
Thread Lubricants and Thread Sealants	3
Fluorocarbon Plastics and Elastomers	5
Metals and Alloys	6
Design of Equipment	8
High Pressure Oxygen Warm Converter	11
High Pressure Oxygen Bomb	11
Valves, Fittings, and Tubing	11
Simulated System	11
EXPERIMENTAL PROGRAM	14
High Pressure Laboratory	14
Construction of Laboratory	14
Physical Arrangement of Test Equipment	14
Cleaning and Assembly of Equipment	14
High Pressure Oxygen Bomb Tests	14
Purpose	14
Procedure	17
Preliminary Tests of Prototype Bomb and Final Bomb	17
7500 psi Tests	20
Adiabatic Compression Tests	26
Purpose and Discussion	26
Preliminary Tests	26
7500 psi Tests	28
Promoted Ignition Tests	28
Purpose	28
Procedure	28
Preliminary Tests	30
7500 psi Tests	32
Simulated System Tests	45
Purpose	45
Philosophy	45
Materials of Construction and Arrangement of Equipment	45
Procedure	49
7500 psi Tests	50
Evaluation of Hardware Used in the Experimental Program	52
Gemini Regulator	52
High Pressure Valves	52
Tubing Connection and Fittings	53
Miscellaneous	55

TABLE OF CONTENTS
(Continued)

	Page
CONCLUSIONS	55
RECOMMENDATIONS	56
REFERENCES	57
APPENDICES	59
I. CALCULATION OF THEORETICAL TEMPERATURE ATTAINED BY ADIABATIC COMPRESSION.	59
II. CALCULATION OF COMPRESSIBILITY FACTORS FOR OXYGEN.	61
III. ADIABATIC COMPRESSION - A CONTROLLED IGNITION MECHANISM	63
IV. TABLES OF EXPERIMENTAL DATA	67

LIST OF FIGURES

Figure 1.	Warm Converter for High Pressure Oxygen	12
Figure 2.	High Pressure Oxygen Bomb: A. Assembled B. Disassembled	12
Figure 3.	High Pressure Valve	13
Figure 4.	Tubing Connection	13
Figure 5.	High Pressure Laboratory	15
Figure 6.	Control Area of High Pressure Test Equipment	15
Figure 7.	Physical Arrangement of Test Equipment in High Pressure Bays.	16
Figure 8.	Sand-bagged Warm Converter	16
Figure 9.	Prototype High Pressure Oxygen Bomb	17
Figure 10.	Schematic of Prototype Oxygen Bomb in Horizontal Position	18
Figure 11.	Schematic of Linde Standard Oxygen Bomb	18
Figure 12.	Schematic of Prototype Oxygen Bomb in Vertical Position	18
Figure 13.	Prototype Bomb as Used for Preliminary Tests	19
Figure 14.	10,000 psi Oxygen Bomb With Test Tube Enclosed	21
Figure 15.	Schematic for 7500 psi Oxygen Bomb Test	22

LIST OF FIGURES
(Continued)

		Page
Figure 16.	High Pressure Oxygen Bomb Test Set-up: A. Complete Set-up B. Close-up of Bomb in Furnace . . .	23
Figure 17.	Preliminary Adiabatic Compression Test Set-up	27
Figure 18.	7500 psi Adiabatic Compression Test Set-up	27
Figure 19.	Schematic for Adiabatic Compression Test	29
Figure 20.	Pressure Profile of Adiabatic Compression Test	30
Figure 21.	Physical Configurations Used with Promoter Material and Metal Specimens in Pyrex Test Tube During Promoted Ignition Tests	31
Figure 22.	Pressure Profile of Promoted Ignition Test	33
Figure 23.	Promoted Ignition Test, Stainless Steel	35
Figure 24.	Promoted Ignition Test, Inconel X-750	36
Figure 25.	Promoted Ignition Test, Aluminum	37
Figure 26.	Promoted Ignition Test, Copper and Lead	38
Figure 27.	Promoted Ignition Test, Brass	39
Figure 28.	Promoted Ignition Test, Inconel 600	40
Figure 29.	Promoted Ignition Test, Monel 400	41
Figure 30.	Promoted Ignition Test, Nickel	42
Figure 31.	Promoted Ignition Test, Gold and Silver	43
Figure 32.	Promoted Ignition Test: . . . . . A. Stainless Steel Sealed in KEL-F B. Stainless Steel Sealed in TEFLON FEP C. Aluminum Coated with KEL-F	44
Figure 33.	Schematic for Simulated System Tests	46
Figure 34.	Picture of Simulated System Test	47
Figure 35.	View of Gemini Regulator Location in Simulated System. . .	47
Figure 36.	Pressure Profile of Simulated System Test	51
Figure 37.	Typical Photographic Record of Electrostatic Charge Developed in Simulated Test	51
Figure 38.	High Pressure Valve Stems	54

LIST OF FIGURES
(Continued)

		Page
Figure 39.	Ruptured 10,000 psi Bursting Discs	54
Figure 40.	Theoretical Temperature Attained by Adiabatic Compression	60
Figure 41.	Compressibility Factor for Oxygen at 293° K	62
Figure 42.	Sketch	63
Figure 43.	Sketch	63

LIST OF TABLES

Table 1.	Relative Resistance of Metals and Alloys to Ignition and Combustion in Oxygen in Decreasing Order	9
Table 2.	Metals and Alloys Selected for Test in 7500 psi Oxygen	10
Table 3.	Lowest Spontaneous Ignition Temperature Found in 7500 psi Oxygen and in 2000 psi Oxygen	25
Table 4.	Metals and Alloys Arranged in Order of Decreasing Resistance to Ignition and Combustion in 7500 psi Oxygen	33
Table 5.	Theoretical Temperature Attained by Adiabatic Compression	59
Table 6.	Compressibility Factor for Oxygen at Various Pressures	61
Table 7.	Summary of Preliminary High Pressure Oxygen Bomb Tests and Correlation with 2000 psi Prototype Bomb Tests and Linde Standard 2000 psi Oxygen Bomb Tests	68
Table 8.	Summary of High Pressure Oxygen Bomb Tests	69
Table 9.	Preliminary Data - Promoted Ignition Test	74
Table 10.	Promoted Ignition Test	75
Table 11.	Pressurization of Simulated System with Oxygen	78
Table 12.	Adiabatic Compression Tests	80

COMPATIBILITY OF MATERIALS WITH 7500 PSI OXYGEN

INTRODUCTION

The ease with which materials of construction ignite and combust in a gaseous oxygen environment has been a problem of long standing to those concerned with the safe design of oxygen handling equipment. Use of oxygen containing equipment has generally been limited to pressures below 3000 psi due to lack of knowledge of behavior of materials at higher pressures.

The use of gaseous oxygen at higher pressures in aerospace breathing systems (4), (17)* has increased the hazards inherent in an oxygen system (13) and additionally introduced several unknown entities. Some of these unknowns were investigated and evaluated by Baum, Goobich, and Trainer (1).

The present investigation was initiated to obtain further data on the behavior of materials in high pressure oxygen. Specifically, the purpose of the study was threefold:

1. Develop ignition data on thread lubricants, thread sealants, fluorocarbon plastics, and metals in 7500 psi oxygen.

2. Determine the hazards in charging a simulated system to 7500 psi with oxygen.

3. Measure the electrostatic charge developed during the charging of the simulated system.

PROGRAM DEVELOPMENT

The program was divided into three major areas of investigation and information was developed in each of these areas:

1. Selection of Test Methods.
2. Selection of Materials for Test.
3. Design of Equipment

Selection of Test Methods

Evaluation of various test methods was made to determine the amount of useful information which might be derived from a particular type of test in order to select the tests which would yield the most information in the time interval of the contract. It was recognized that each test would require development of parameters at 7500 psi which would give reliable and consistent data for comparison of materials.

---

* Numbers in parentheses refer to references on page 57.

The tests considered for use in testing relative compatibility of materials in this program were:

1. Oxygen Bomb Test
2. Impact Sensitivity Test
3. Velocity Impact Test
4. Hot Wire Test
5. Promoted Ignition Test
6. Adiabatic Compression Test

Oxygen Bomb Test

The oxygen bomb test is a standard test used to determine the spontaneous ignition temperature of organic materials in 2000 psi oxygen. A specimen of the material to be tested is placed in an oxygen bomb and subjected to 2000 psi oxygen pressure; the bomb is then heated until spontaneous ignition of the sample material occurs or until the temperature reaches 500° C, whichever occurs first.

This test is considered to be an excellent test for thread lubricants, thread sealants, and fluorocarbon plastics. By comparing tests at 2000 psi and at 7500 psi, the effect of oxygen pressure on the spontaneous ignition temperature of the material could be determined.

Impact Sensitivity Test

This test is made by impregnating a specimen of the material with liquid oxygen and dropping a known weight through a given distance so that a hammer with a specified area impacts the sample. This test yields values denoting the amount of kinetic energy required to produce a reaction. This subject has been well covered by Reynales [11], [12], and it was not felt that enough additional information would be derived from the test to justify its use.

Velocity Impact Test

The velocity impact test can be used to test either non-metallic material or metallic material. The test is made in the following manner: A standard powdered material is injected into a high velocity oxygen stream and, after being accelerated to the velocity of the stream, is impacted against a specimen of the material to be tested. The heat generated during the impact ignites the powdered material and subjects the specimen to a known quantity of energy at an oxygen pressure variable from 50 to 700 psig.

This test has been used at Linde as a sorting tool to provide information on metals and alloys and the results concur with Linde experience. However, the specimen itself is in comparatively low-pressure oxygen and further tests by this method were not expected to yield as much additional information as other tests.

Hot Wire Test

This test was first used in 1923 by the Bureau of Mines [7], [8] to determine the ignition temperature of metals in oxygen at various pressures. It is based on the measurement of the electrical resistance of a wire specimen of the metal or alloy at its ignition point. Prior calibration of

the resistance of wire specimens versus temperature must be made.

The test suffers from a number of deficiencies and has yielded anomalous results in Linde tests which were made in 2000 psi oxygen. It might be possible to overcome the deficiencies of this test if enough time were available but even then there would be no guarantee that the results would be satisfactory.

Promoted Ignition Test

The promoted ignition test is designed to determine the resistance to ignition and the amount of burning after ignition of the more resistant metals. It has been used previously at Linde to develop information on the combustion of metals and the ability of a given system to resist conflagration. Its use in this program would be an extension of the test to higher pressures to supplement the information which has been developed to date.

The test is made by subjecting the metal specimen to the energy released when a promoter material is heated to its spontaneous ignition temperature in oxygen. This test has considerable built-in flexibility by varying the weight of the promoter material, the weight of the metal, or the configuration of the metal specimen.

Adiabatic Compression Test

This test could be used to test either metal specimens or non-metallic specimens. The sample contained in a test vessel at 15 psia of oxygen is subjected to the temperature developed when the vessel is rapidly pressurized to oxygen pressures ranging from 2000 psi to 8000 psi. Theoretically, extremely high temperatures may be reached by adiabatic compression (Appendix I) and it was expected that this test would yield some good data.

This type of test was also expected to be applicable in defining the hazards in charging a simulated system.

The test methods selected for use in this program were:

1. Oxygen Bomb Test
2. Promoted Ignition Test
3. Adiabatic Compression Test

Selection of Materials for Test

The number of materials available for testing in a program of this type is almost unlimited. Therefore, it was necessary to select those materials which it was thought would yield the most information. Selection was made by correlation of information found in the literature and that derived from unpublished Linde test programs.

Thread Lubricants and Thread Sealants

The subject of available thread lubricants and thread sealants has been covered quite well by Reynales (12). Using this information and that available from Linde files, a number of materials were chosen to be tested.

It was known beforehand that most of the materials selected for test would not be suitable for use in 7500 psi oxygen. In fact, a few are not suitable for 2000 psi oxygen. However, the most useful information expected from the oxygen bomb test was whether the spontaneous ignition temperature of a material in 7500 psi oxygen would differ from its spontaneous ignition temperature in 2000 psi oxygen. By testing some materials which would ignite at low temperatures as well as some which would ignite at high temperatures, the effect of pressure on the spontaneous ignition temperature of typical materials could be determined.

The materials selected for test are as follows:

1. Thread Lubricants

a. Aroclor 1254 - A chlorinated phenyl compound produced by Monsanto Chemical Company

b. Dixon's Flake Graphite No. 1 - Dixon Corporation, Bristol, Rhode Island

c. Oxweld Anti-Friction Compound No. 54 - A proprietary compound of Union Carbide Corporation, Linde Division. It is not recommended for service above 150° F or 300 psi of oxygen.

d. Kel-F 90 Grease - A formulation of poly chlorotrifluoroethylene oils and waxes with an inert gelling agent manufactured by Minnesota Mining and Manufacturing Company.

e. Halocarbon Grease Series 25-10 - A polychlorotrifluoroethylene formulation manufactured by Halocarbon Products Corporation, Hackensack, New Jersey.

f. Halocarbon Oil Series 13-21 - A polychlorotrifluoroethylene oil marketed by Halocarbon Products Corporation.

g. Molykote Z - Molybdenum disulfide in dry powder form produced by The Alpha Corporation, Greenwich, Connecticut.

h. Burnil Brand Microplates - Thin platelets of synthetic mica available as a powder, as a suspension of the powder in water, or as a thin paper from Minnesota Mining and Manufacturing Company.

i. Oxweld Anti-Friction Compound No. 64 - A proprietary product of Union Carbide Corporation, Linde Division. It is not recommended for service above 250° F or 500 psi of oxygen.

j. Almasol Powder (325 mesh) - This powder is composed of aluminum-magnesium-silicate of laminar lattice structure. It is used as an ingredient in solid film lubricants marketed by The Almasol Corporation, Fort Worth, Texas.

k. High Purity Goop - A proprietary lubricant made by Crawford Fitting Company, Cleveland, Ohio.

l. Everlube Solid Film Lubricant No. 811 - A molybdenum disulfide dispersion available from Everlube Corporation of America, North Hollywood, California.

m. Oxylube No. 703 - A dry film lubricant based on molybdenum disulfide which is marketed by Drilube Company, Glendale, California.

2. Thread Sealants

a. Oxyseal - Parker-Hannifin Corporation, Cleveland, Ohio.

b. Rectorseal No. 15 - Rector Well Equipment Company, Fort Worth. Texas

c. Key Abso-lute - W. K. M. Division of ACF Industries, Houston, Texas

d. Mano Pipe and Joint Compound - Mano Industries, Woodside, Long Island, New York

e. Linde Green Pipe Joint Compound - Union Carbide Corporation, Linde Division.

f. 50/50 Soft Solder

Fluorocarbon Plastics and Elastomers

1. There were three types of fluorocarbon plastics which were of interest:

a. Polytetrafluoroethylene(TFE) - Marketed under the trade name of "Teflon" by E. I. du Pont de Nemours and Company, Inc. and as "Halon" TFE by Allied Chemical Corporation.

b. Polychlorotrifluoroethylene(CTFE) - Marketed as "Kel-F" by Minnesota Mining and Manufacturing Company,as "Polyfluoron" by Acme Resin Corporation, and as "Halon" VK and TVS by Allied Chemical Corporation.

c. Polyfluoroethylenepropene (FEP) - A copolymer of tetrafluoroethylene and hexafluoropropylene marketed under the trade name "Teflon" 100X by E. I. du Pont de Nemours and Company, Inc.

2. There were two types of fluoroelastomers of interest:

a. Copolymers of vinylidene fluoride and hexafluoropropylene - Available as "Fluorel" from Minnesota Mining and Manufacturing Company, and as "Viton" A, "Viton" A-HV, and "Viton" B from E. I. du Pont de Nemours and Company, Inc.

b. Copolymers of vinylidene fluoride and chlorotrifluoroethylene - Marketed by Minnesota Mining and Manufacturing Company, in two types, "KEL-F" Elastomer 3700 and "KEL-F" Elastomer 5500.

3. Additionally there are numerous companies which supply filled, formulated, or reinforced TFE.

4. The following materials were selected for test: *

a. Teflon (Virgin TFE) - E. I. du Pont de Nemours and Company, Inc.
b. Teflon 100X (FEP) - E. I. du Pont de Nemours and Company, Inc.
c. Viton A (Virgin) - E. I. du Pont de Nemours and Company, Inc.
d. Viton B (Virgin) - E. I. du Pont de Nemours and Company, Inc.
e. Rulon A (Reinforced TFE) - Dixon Corporation
f. Rulon B (Reinforced TFE) - Dixon Corporation
g. Rulon C (Reinforced TFE) - Dixon Corporation
h. Duroid 5600 (60% Teflon, 40% aluminum silicate ceramic fibers) - Rogers Corporation
i. Duroid 5650 (75% Teflon, 25% aluminum silicate ceramic fibers) - Rogers Corporation
j. Duroid 5870 (85% Teflon, 15% glass fibers) - Rogers Corporation
k. Duroid 5813 (60% Teflon, 40% glass fibers with MoS_2 filler) - Rogers. Corporation
m. Kel-F 81 (CTFE) - Minnesota Mining and Manufacturing Company
n. Kel-F Elastomer 3700 - Minnesota Mining and Manufacturing Company
o. Kel-F Elastomer 5500 - Minnesota Mining and Manufacturing Company

Metals and Alloys

The oxidation, ignition, and combustion of metals in air and oxygen have received considerable attention in the past decade, but the ignition and burning of metals is still poorly understood. Knowledge of reaction kinetics and mechanics is sadly lacking. There are many investigators who have made significant contributions to this field. Their work is reviewed by Smeltzer and Perrow [16] and by Markstein [10]. Because it is not the purpose of this investigation to become involved in the complicated mechanisms of ignition and combustion, only those articles which were considered to be of direct value to the present work have been referenced [1, 3, 6, 9, 14, 15].

The investigation of Dean and Thompson [3] yielded data which was directly applicable in helping to select the metals to be tested in the present investigation. Metal tubes were electrically heated to destruction in 50, 300, and 800 psia of oxygen, in a 50-50 mixture of oxygen and carbon dioxide, and in 100% carbon dioxide. Color motion picture photography recorded the manner in which the tubes heated and failed. The results of their tests showed that:

1. Stainless steels ignited within their melting range.

2. Steel alloys with no nickel content ignited at temperatures below their melting points.

3. Most of the nickel-based alloys tested did not ignite until the melting point was reached. At 800 psia both Inconel X and Monel failed at temperatures 250° to 500° F below their respective melting points.

---

* Appreciation is expressed to the following companies for samples furnished for these tests: E. I. du Pont de Nemours and Company, Inc., Rogers Corporation, Dixon Corporation, The Fluorocarbon Company, Minnesota Mining and Manufacturing Company.

4. Nickel A did not ignite, only melted.

5. Copper ignited slightly below its melting point At a pressure of 300 psia approximately 70% of the test specimen was destroyed.

6. No ignition or burning of the aluminum alloy occurred, only melting.

7. For all the ferrous alloys tested, the rate of burning increased with the oxygen pressure.

8. Cobalt-based alloys ignited within their melting point range.

9. Titanium was the only metal which ignited in an atmosphere of carbon dioxide.

Reynolds [14] found that 18-8 stainless steel, copper, nickel, Inconel, and Inconel X melted before igniting in oxygen at pressures up to eight atmospheres.

Hill, Adamson, Foland, and Brissette [9] report that Inconel, copper, Monel, and aluminum did not have a spontaneous ignition temperature in the solid phase, and that iron, carbon steel, and common iron alloy had spontaneous ignition temperatures in the solid phase (below their melting points) and melted very rapidly while burning.

Baum, Goobich, and Trainer [1] found Monel and Type 316 stainless steel acceptable alloys of construction for 7500 psi oxygen systems but copper and brass possessed some undesirable characteristics.

Riehl, Key, and Gayle [15] report aluminum in gaseous oxygen to be sensitive to explosive shock while stainless steel is not.

Investigations previously made at Linde using the "Velocity Impact Test" (e.g. A known weight of powdered material was accelerated in a high velocity oxygen stream and impacted against the metal specimen) yielded the following results:

1. Carbon steel, cast iron, stainless steel, and aluminum could be ignited and completely consumed with the evolution of large quantities of energy.

2. Stainless steel and aluminum burned with explosive violence.

3. Copper, copper alloys, and Monels had a decided quenching effect on combustion.

The "Promoted Ignition Test" has been used in earlier work at Linde to investigate the resistance to ignition and the amount of burning after ignition of various metals in 2000 psi oxygen. In this test the metal specimen was subjected to the energy released when a promoter material was spontaneously ignited. Although this test does not provide absolute values it does effectively sort the metals in regard to their relative resistance to combustion. The results of this work are:

1. In general, metal alloys with a high percentage of nickel such as the Monels and Inconels have the highest resistance to combustion.

2. The resistance to combustion appeared to be related to the percentage of iron in an alloy.

3. The size of the metal sample will affect its resistance to combustion (e.g. the more subdivided a metal specimen, the easier it will ignite).

The results of Dean and Thompson [3] referred to earlier were evaluated in regard to the relative resistance to ignition and combustion of each metal tested and the metals are listed in Table 1 in the order of their decreasing resistance, with the most resistant metal at the top of the list.

The relative resistance of metals as determined by the "Velocity Impact Test" and the "Promoted Ignition Test" at Linde are also listed in Table 1 for comparison. It should be pointed out that there might be some shifting in the position of the metals in the "Promoted Ignition Test" column because in those cases where two or more metals showed similar resistance to ignition, the violence of the combustion determined the position. Also if a large enough number of tests were to be performed on each metal, statistically the position of a metal might be changed.

Of particular interest is the position occupied by aluminum. Dean and Thompson's work would place it at the top of the list while it is at the bottom of the list in the Linde tests. This is no doubt due to the fact that Dean and Thompson only heated the tube to its melting point. Grosse and Conway [6] have shown the ignition temperature of aluminum to be > 1000° C which is considerably above its melting point of 660° C. Aluminum is at the bottom of the ladder on the Linde tests because of its violent reaction once it becomes ignited.

It will be noted that nickel and copper alloys are at the top of the list in all three columns.

For the present investigation, metals and alloys were selected which would be representative of materials already tested in oxygen pressures up to 2000 psi. Results at 7500 psi could thus be compared to those obtained at the lower pressures. Additionally some other metals were chosen because of their possible usefulness in high pressure systems.

The metals and alloys selected for test, the melting point of each, and the reported ignition temperature in oxygen are presented in Table 2.

Design of Equipment

The materials of construction and the design of the equipment to be used in the test program was an area that received considerable attention. Because of the inherent hazards with gaseous oxygen and the magnification of these hazards with 7500 psi oxygen, it was necessary to select those materials which would be considered relatively safe by present available knowledge. Consequently nickel alloys were used in all critical pieces of apparatus. This resulted in considerable delay in initial construction of equipment.

TABLE 1.

RELATIVE RESISTANCE OF METALS AND ALLOYS TO IGNITION AND COMBUSTION IN OXYGEN IN DECREASING ORDER

Dean and Thompson (3)	Velocity Impact	Promoted Ignition
50-800 psi	50-100 psi	2000 psi
Aluminum	**Monel	**Monel
Nickel A	**K-Monel	**Inconel 600
*Hastelloy C	***Tobin bronze	**Monel S
**Monel	Copper	***Tobin bronze
*Hastelloy X	Steel	**Duranickel
**Inconel X	18-8 stainless steel	*****Ampco alloy No. 15
*Hastelloy R	Aluminum	**Permanickel
Copper		**K-monel
*Haynes 25		*Hastelloy R-235
*Multimet		Maraging Steel
18-8 Stainless Steel		Beryllium Copper
Other Stainless Steel		******Elgiloy
Carbon Steel		****Rene' 41
Titanium		**Inconel X-750
		*Multimet
		*Hastelloy X
		*Haynes 25
		***Everdur
		18-8 Stainless Steel
		Aluminum

TRADEMARKS

*Union Carbide Corporation, Stellite Division
**The International Nickel Company, Inc.
***Anaconda American Brass Company
****General Electric Company
*****Ampco Metal, Inc.
******Elgin National Watch Company

TABLE 2.

METALS AND ALLOYS SELECTED FOR TEST IN 7500 PSI OXYGEN

METAL OR ALLOY	MELTING POINT °C	IGNITION TEMPERATURE IN OXYGEN, °C
1. Stainless Steel		
Type 316	1375-1400	----
Type 304	1400-1475	M.P. (a)
Type 301	1400-1425	----
2. Age-Hardening Stainless Steel		
*Type 17-7 PH	1415-1450	150-275 below M.P. (a)
3. Nickel-Chromium Alloys		
Inconel alloy 600 (formerly Inconel)	1400-1425	M.P. (b)
Inconel alloy X-750 (formerly Inconel X)	1400-1425	150-275 below M.P. (a)
4. Nickel - Copper Alloy		
Monel alloy 400 (formerly Monel)	1300-1350	150-275 below M.P. (a)
5. Other Metals and Alloys		
Aluminum	660	>1000 (c)
Nickel	1455	M.P. (a)
Copper	1082	<M.P. (a) (d)
Brass	932	<850 (d)
Silver	960	----
Gold	1063	----
Lead	327	870 (c)

(a) Reference 3
(b) Reference 14
(c) Reference 6
(d) Reference 7

* Trademark of Armco Steel Corporation

High Pressure Oxygen Warm Converter

High pressure oxygen was generated in a warm converter. Required quantities of liquid oxygen were introduced into the warm converter and vaporized into the gaseous state to provide the necessary pressure. The warm converter was contained in a water bath with an inlet and outlet through which tap water flowed.

The converter was patterned after a previous Linde design which was modified to provide a larger capacity and a higher working pressure. The internal geometric volume of the converter is 425 cubic inches. Pressures up to 15,000 psi oxygen have been generated. Materials of construction were Inconel alloy X-750 and Monel alloy 400 which provided the strength for the pressures to be developed and also furnished a definite measure of safety because of their relative resistance to ignition. Figure 1 shows the top of the converter extending out of the water bath. All high pressure oxygen for the entire test program was generated in this warm converter.

Compressibility factors were calculated for oxygen at various pressures (Appendix II) for use during the test program.

High Pressure Oxygen Bomb

The original consideration given to a high pressure oxygen bomb was a design patterned after the one presently used at Linde for tests at 2000 psi. This bomb has a high mass with built-in cooling passages and integral heating unit. However, the use of a smaller bomb had several advantages relative to the present program and a small high pressure bomb was designed after substantial testing of a prototype bomb.

Figure 2 shows the high pressure bomb assembled and disassembled. Inconel X-750 was the material of construction because of the strength needed at the high temperatures to which the bomb would be heated.

Valves, Fittings, and Tubing

Initially all valves were constructed of Monel alloy 400 with stems of Monel alloy K-500. Packing was glass filled TFE. All fittings and tubing were made of Monel 400. Fabrication was by a commercial vendor of high pressure equipment. At a later date, some stainless steel parts were substituted to expedite test work and to evaluate the use of stainless steel.

All valves were rated at 30,000 psi with the exception of an air-operated valve which was rated at 10,000 psi. All valves were of standard construction as shown in Figure 3.

All fittings and tubing were rated at 30,000 psi with the exception of some 9/16" O.D. x 5/16" I.D. tubing which was only rated for 10,000 psi. The standard threaded and coned tubing connection was used as shown in Figure 4.

Simulated System

Construction of the simulated system will be discussed later under the experimental program.

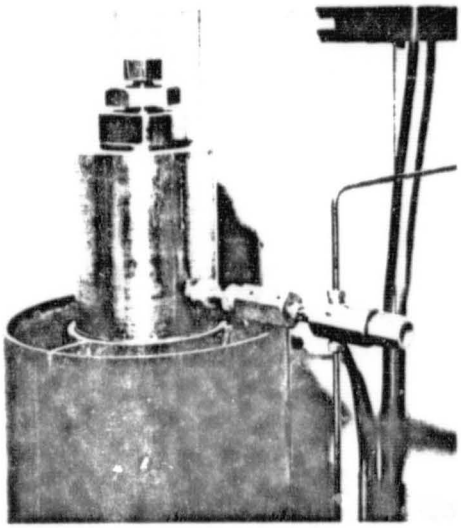

FIGURE 1. WARM CONVERTER FOR HIGH PRESSURE OXYGEN

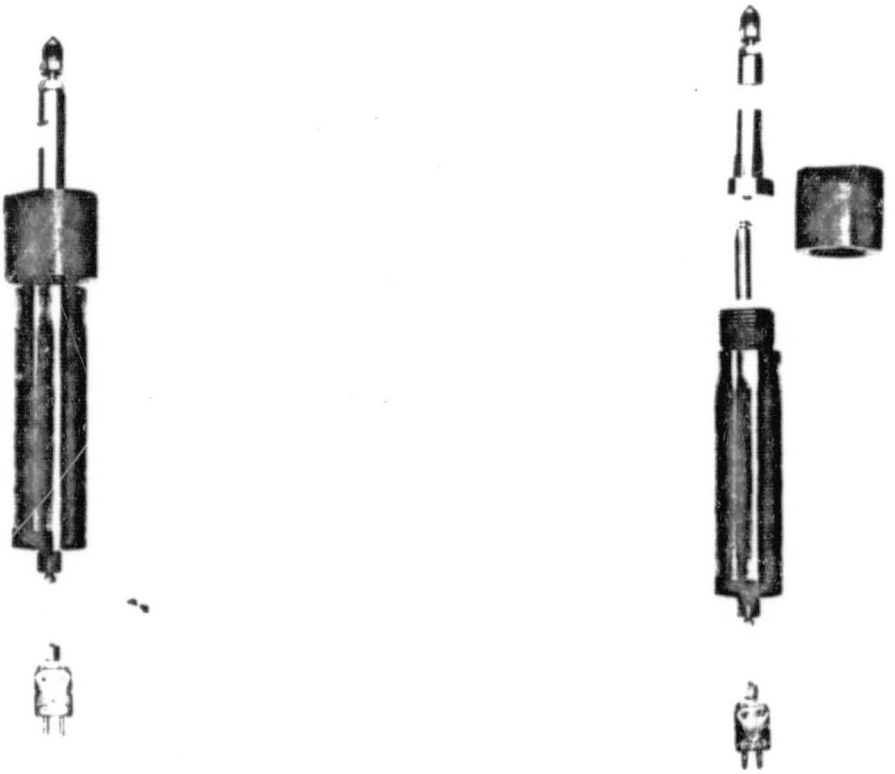

A. ASSEMBLED

B. DISASSEMBLED

FIGURE 2. HIGH PRESSURE OXYGEN BOMB

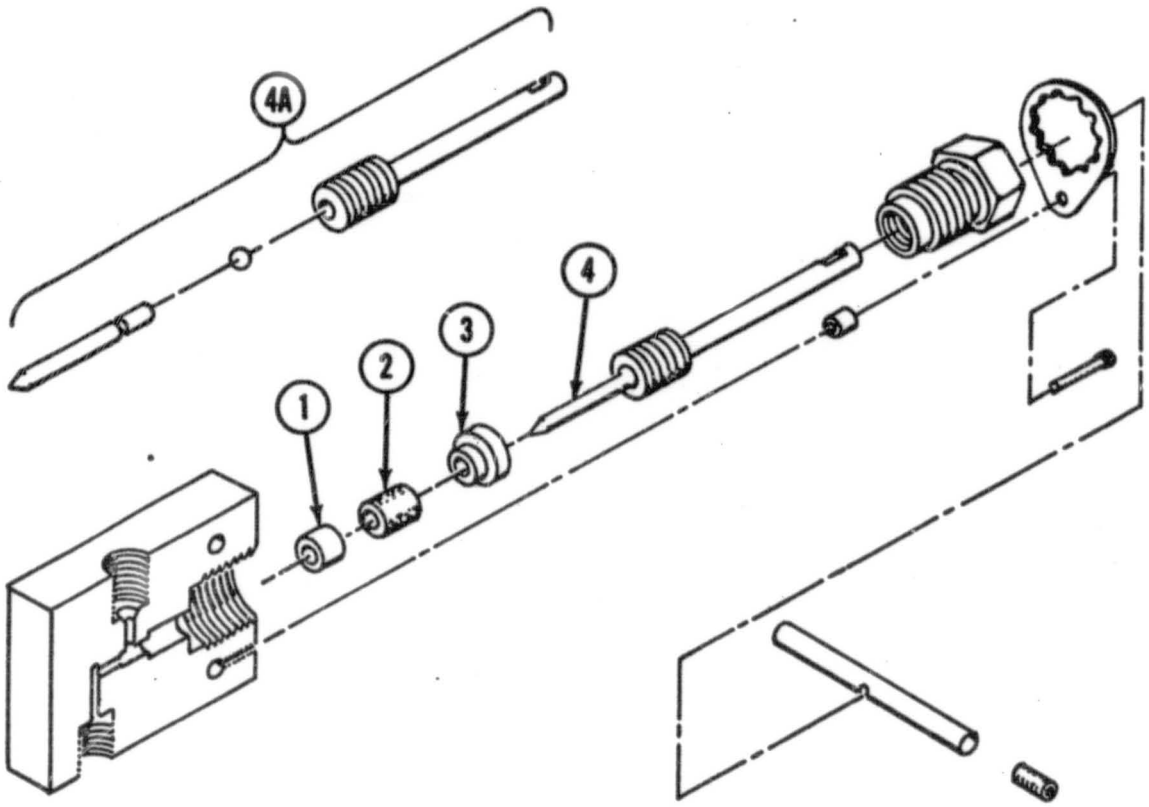

KEY

1. Bottom Packing Washer
2. Glass Filled Teflon Packing
3. Top Packing Washer
4. Rotating Stem
4A. Non-Rotating Stem

FIGURE 3. HIGH PRESSURE VALVE

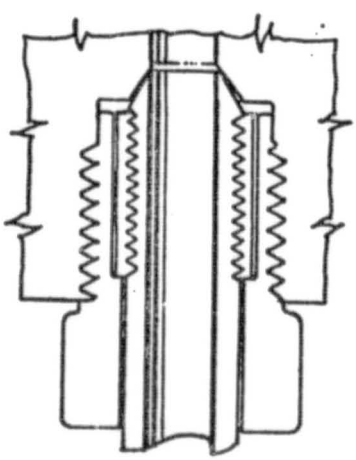

FIGURE 4. TUBING CONNECTION

EXPERIMENTAL PROGRAM

High Pressure Laboratory

Construction of Laboratory

All experimental tests were performed in two high pressure bays of a high pressure laboratory shown in Figure 5.

The bays of the laboratory are constructed of reinforced concrete walls with one blow-out wall. The blow-out wall faces a dirt hill at the rear of the laboratory. Heavy blast mats extend upward from the top of the hill to stop flying projectiles. The same type of blast mat is used to cover the ceiling and other critical points in each bay.

All valves and controls are operated from outside the test area by extensions through the heavy concrete wall (Figure 6). All visual observations are made from the operating area with the use of mirrors.

Physical Arrangement of Test Equipment

A common entrance door from the operating area serves both high pressure bays with the entry way separated from each bay by heavy steel plate. The warm converter was placed in one bay and the test equipment was placed in the other bay so as to isolate the high pressure oxygen generating equipment from the test equipment in the event of a failure in either section. Tubing connection was carried via a small tunnel between the two bays. Additionally the warm converter was sandbagged. This physical arrangement can be seen in Figure 7 which shows test equipment set up for the high pressure oxygen bomb test. Figure 8 shows the sandbagged warm converter.

Cleaning and Assembly of Test Equipment

All valves, fittings, tubing, and apparatus were disassembled and cleaned for oxygen service by standard vapor degreasing and washing methods. Threads of valve stems, tubing, and gland nuts were given a very thin film of fluorocarbon lubricant immediately prior to assembly. These threads are normally not exposed to high pressure oxygen because of weep holes in the fittings.

All liquid oxygen entering the warm converter was passed through a filter which is rated to remove 99.5% of all particles greater than one micron.

High Pressure Oxygen Bomb Tests

Purpose

The oxygen bomb test determines the spontaneous ignition or explosion temperature of a material in contact with oxygen at some given pressure. The test provides a means for determining the allowable temperature to which a material may be exposed in oxygen at the given pressure without the possibility

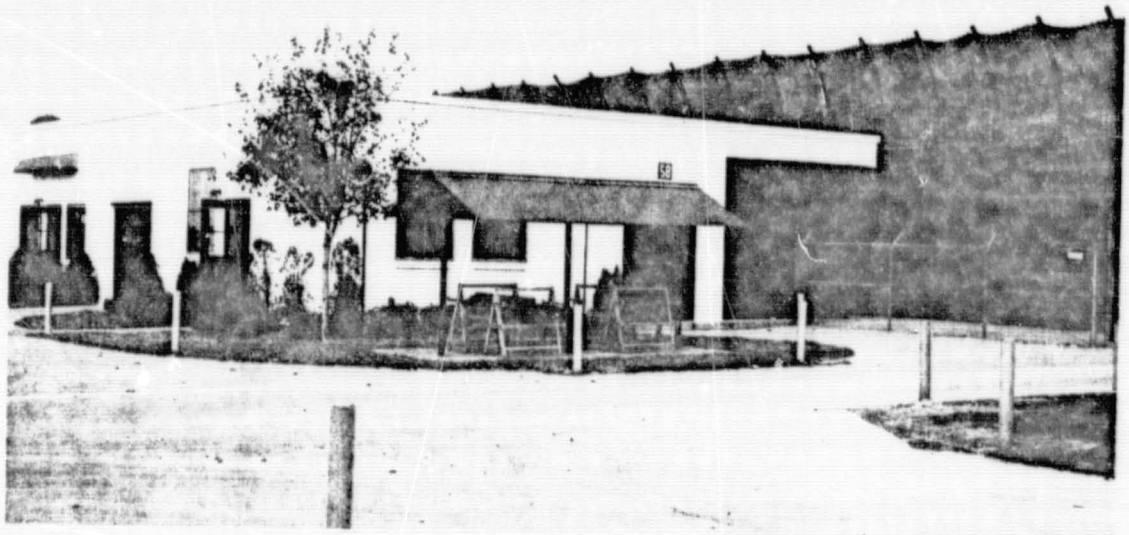

FIGURE 5. HIGH PRESSURE LABORATORY

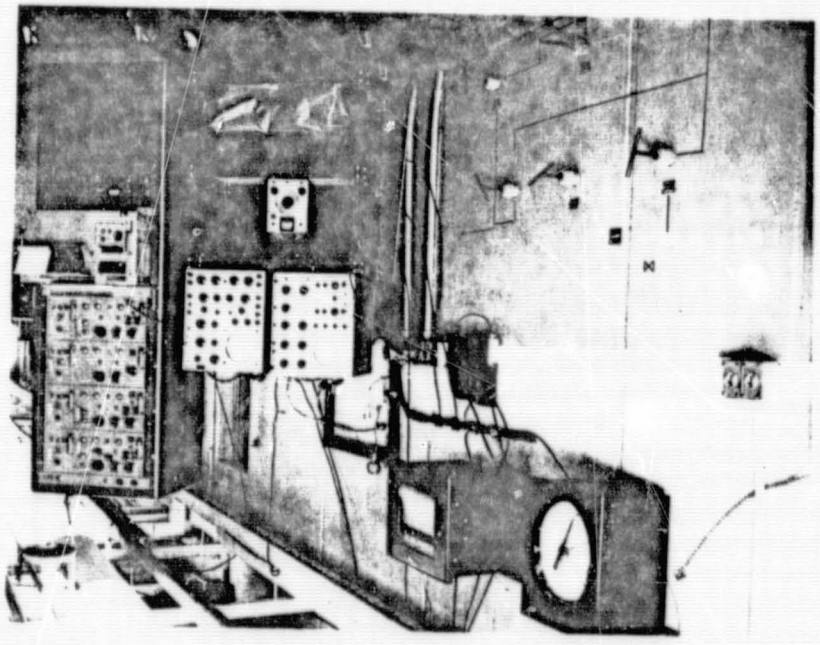

FIGURE 6. CONTROL AREA OF HIGH PRESSURE TEST EQUIPMENT

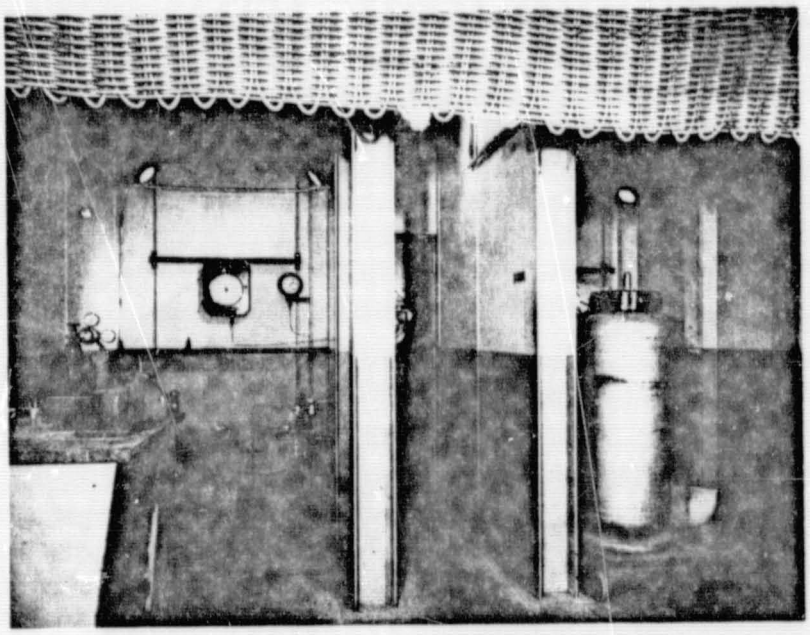

FIGURE 7. PHYSICAL ARRANGEMENT OF TEST EQUIPMENT IN HIGH PRESSURE BAYS

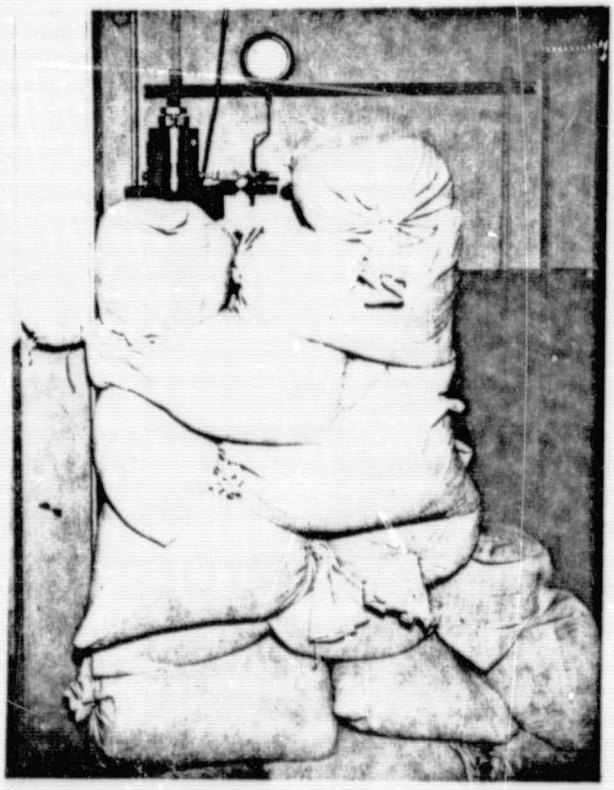

FIGURE 8. SANDBAGGED WARM CONVERTER

of spontaneous ignition. A material should not be used in oxygen service where its spontaneous ignition temperature might be approached; a substantial safety factor is normally provided.

Procedure

The test is made by placing a sample of the material in the oxygen bomb, pressurizing with oxygen, and heating the bomb until the spontaneous ignition occurs. The temperature and pressure are recorded at which the ignition takes place.

Preliminary Tests of Prototype Bomb and Final Bomb

1. Prototype Bomb

As mentioned earlier the use of an oxygen bomb with a small mass would have some advantages in the 7500 psi program over the design used for the standard Linde 2000 psi bomb which has a large mass. Therefore, a prototype bomb (Figure 9) was purchased for making preliminary tests at 2000 psi. It was rated for 10,000 psi at a temperature of 1000°F.

This bomb was essentially a piece of high pressure stainless steel tubing having a one-half inch inside diameter. Each end of the tubing was coned and threaded into a hexagonal cap with a coned seating surface. The opposite end of each cap had a 1/4" high pressure connection. A pencil iron-constantan thermocouple with an Inconel shield was introduced through one end and oxygen gas through the other end.

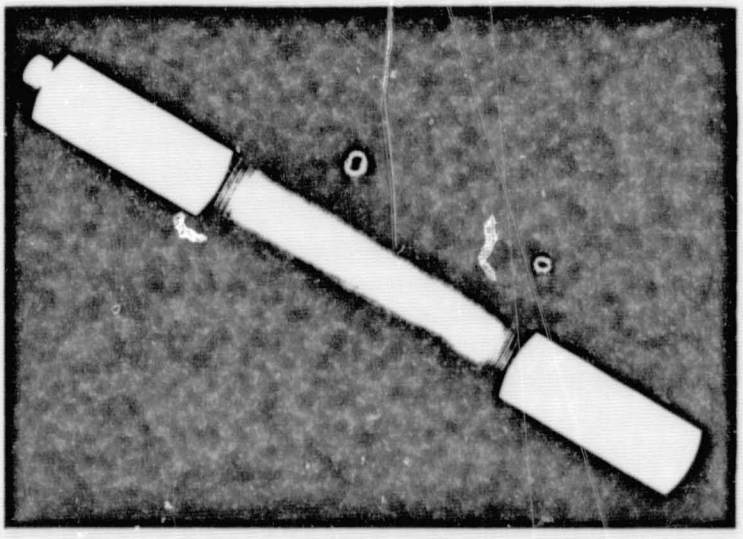

FIGURE 9. PROTOTYPE HIGH PRESSURE OXYGEN BOMB

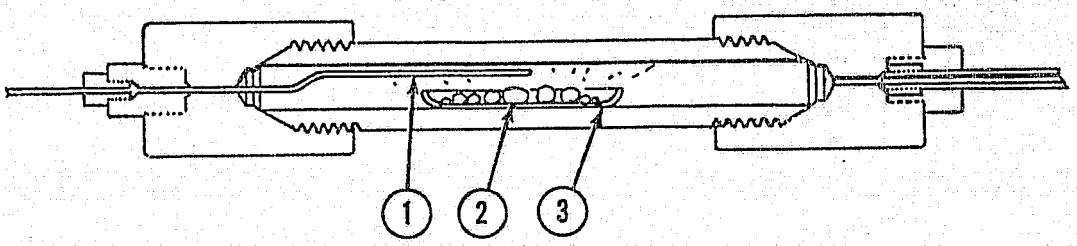

FIGURE 10. SCHEMATIC OF PROTOTYPE OXYGEN BOMB IN HORIZONTAL POSITION

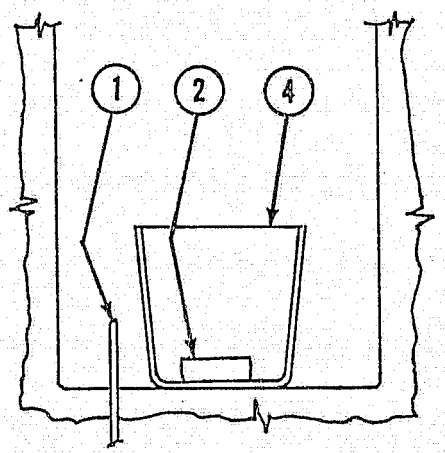

FIGURE 11. SCHEMATIC OF LINDE STANDARD OXYGEN BOMB

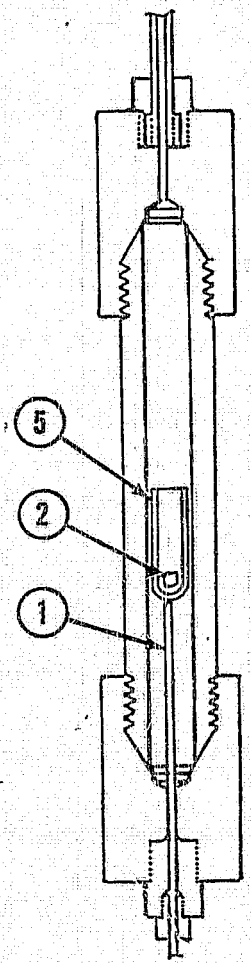

KEY

1. Thermocouple
2. Specimen
3. Specimen Boat
4. Specimen Crucible
5. Specimen Test Tube

FIGURE 12. SCHEMATIC OF PROTOTYPE OXYGEN BOMB IN VERTICAL POSITION

By testing materials which had previously been tested in the Linde standard bomb, it was possible to determine if comparable ignition temperatures were obtained. Initially the prototype bomb was tried in a horizontal position as shown in the schematic of Figure 10. The sample was placed in a quartz boat and slid in one end of the tube which was then placed in a tube furnace and heated. Results were unpredictable and one low-ignition material decomposed without the occurrence of spontaneous ignition.

Because spontaneous ignition is thought to occur in the gas phase by the decomposition products of the test material reaching an explosive concentration in the oxygen, it was postulated that the decomposition products were diffusing through the bomb as it lay in the horizontal position and not reaching an explosive concentration. In the Linde standard bomb (shown schematically in Figure 11), the sample is contained in a crucible and the gases collecting above the sample are confined to the crucible where they reach an explosive concentration.

By placing the prototype bomb in a vertical position (schematically shown in Figure 12) and using a 10 mm x 35 mm Pyrex glass test tube (without lip) as a sample holder, it was found that the spontaneous ignition temperature obtained on typical materials was the same as that found in the standard Linde bomb.

The prototype bomb, as pictured in Figure 13, was used to investigate many parameters of the bomb test to determine the effect on the spontaneous

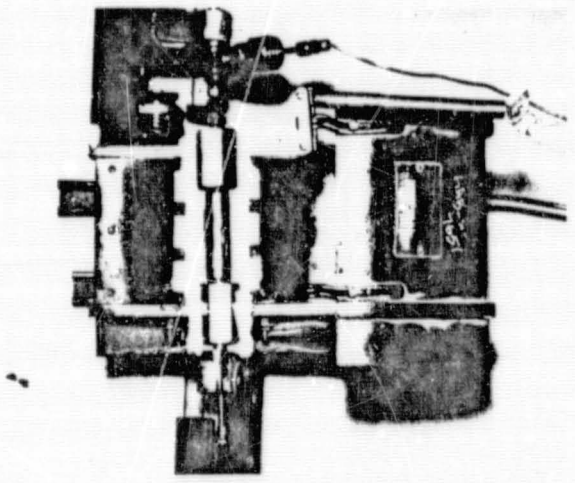

FIGURE 13. PROTOTYPE BOMB AS USED FOR PRELIMINARY TESTS

ignition temperature caused by variations in sample weight, heating rates, etc. The results of these tests are presented in Table 7 of Appendix IV. Heating rate and sample size of the materials tested were found to have little effect on the spontaneous ignition temperature.

During these tests the prototype bomb began to leak because scoring occurred at the seating interfaces of the tube and cap. The leakage could be stopped by resurfacing the seating surfaces or by the use of thin copper gaskets, but the leakage was severe enough at 2000 psi to make a new bomb design desirable for the 7500 psi tests.

2. Final Bomb

The geometric configuration of the prototype bomb had been proven out in preliminary tests, so the final bomb was designed using a 1/2" I.D. opening. Inconel X-750 was used as the material of construction because of its strength at high temperatures. A lens ring was used to provide a leak-tight seal as shown in a schematic of the bomb in Figure 14B.

A few tests with standard materials in the new bomb yielded high spontaneous ignition temperatures. This was demonstrated to be due to convection currents set up in the bomb by part of the bomb cavity at the top being outside the heating zone of the furnace. (The entire cavity of the prototype bomb was physically in the furnace.) A convection from the cold zone at the top to the warm zone at the bottom caused the decomposition products to diffuse. Thus an explosive concentration did not materialize until a higher temperature was reached.

This situation was corrected by making a lens ring plug as shown schematically in Figure 14A. This is the design finally used for all the high pressure tests. In preliminary tests made with this design at 2000 psi, it was found that the spontaneous ignition temperature of standard materials compared favorably with those determined in the standard Linde bomb and in the prototype bomb. Preliminary tests made on these same standard materials at oxygen pressures of 5500 to 9000 psi indicated that their spontaneous ignition temperatures at these higher pressures were going to be the same as that at 2000 psi.

This preliminary data is also presented in Table 7 of Appendix IV.

7500 psi Tests

1. Test Set-up and Procedure

A schematic of the test set-up for the high pressure oxygen bomb is shown in Figure 15 and a pictorial view of the set-up is shown in Figure 16.

With the sample in the bomb, the bomb is successively pressurized with cylinder oxygen and blown down to atmospheric pressure four times. This is done slowly. Finally the bomb is pressurized with high pressure oxygen from the converter. The fill lines from the converter and the 2000 psi cylinder oxygen are blown down to isolate the bomb from oxygen sources. The bomb is then heated in the furnace until spontaneous ignition occurs.

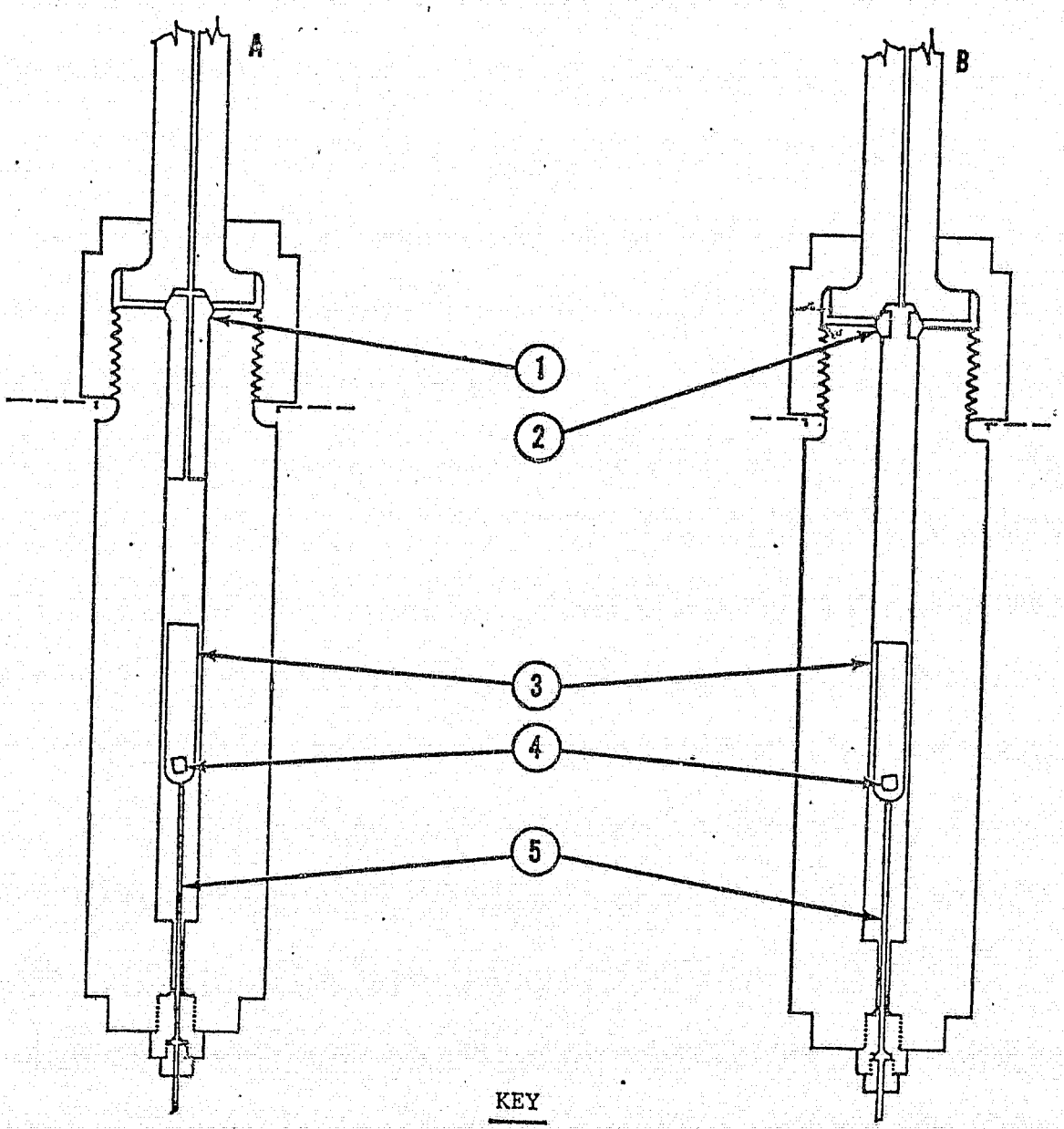

KEY

1. Lens Ring Plug ("A" Only)
2. Lens Ring ("B" Only)
3. Pyrex Test Tube, 10 mm X 35 mm
4. Specimen
5. Thermocouple

FIGURE 14. 10,000 PSI OXYGEN BOMB WITH TEST TUBE ENCLOSED

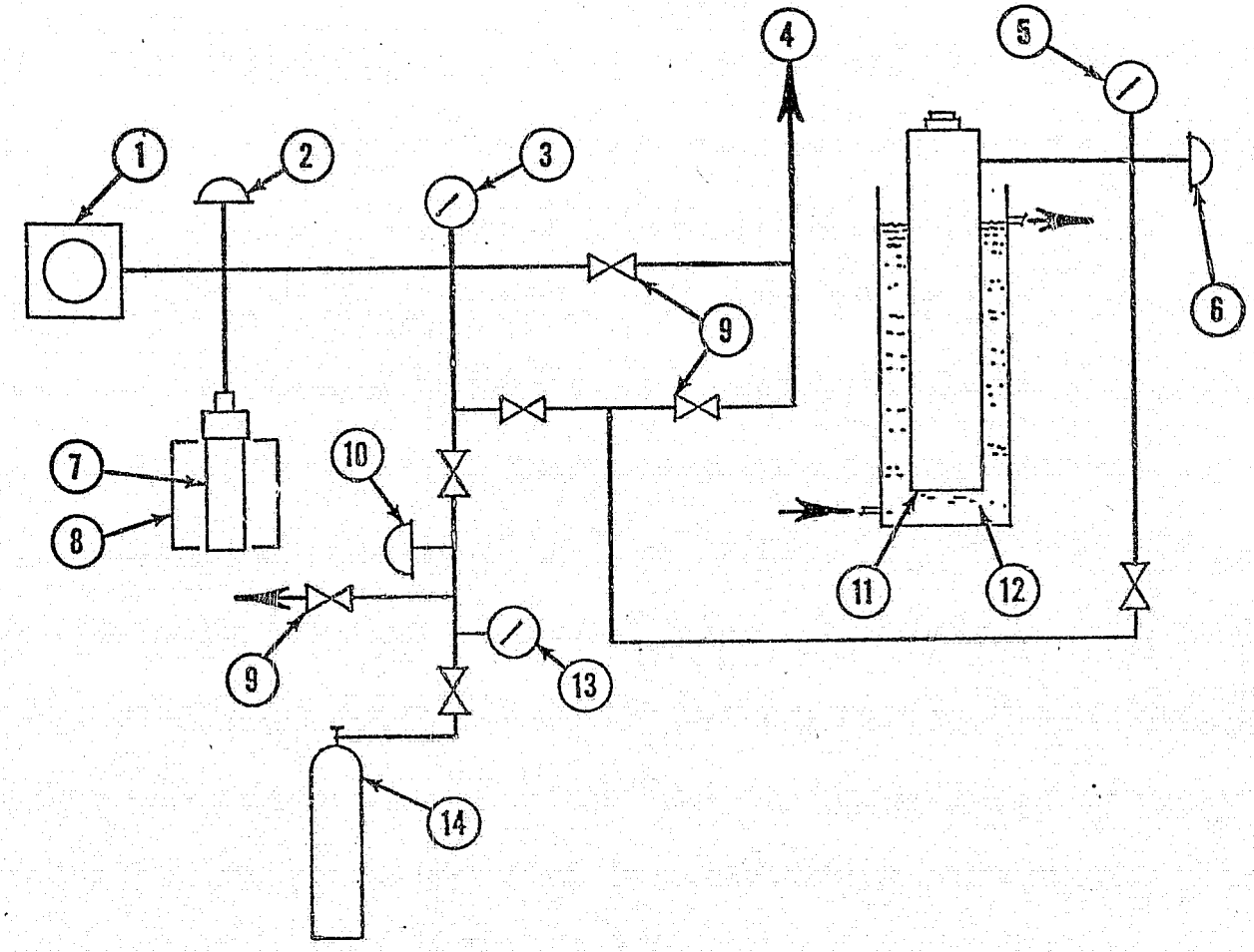

KEY

1. 10,000 psi Pressure Recorder
2. 10,000 psi Bursting Disc
3. 15,000 psi Pressure Gage
4. Blowdown to Outside
5. 50,000 psi Pressure Gage
6. 16,500 psi Bursting Disc
7. Oxygen Bomb
8. Furnace
9. Blow Down Valve
10. 3,000 psi Safety Disc
11. Warm Converter
12. Water Bath
13. 3,000 psi Oxygen Gage
14. Cylinder Oxygen- 2,000 psi

FIGURE 15. SCHEMATIC FOR 7500 PSI OXYGEN BOMB TEST

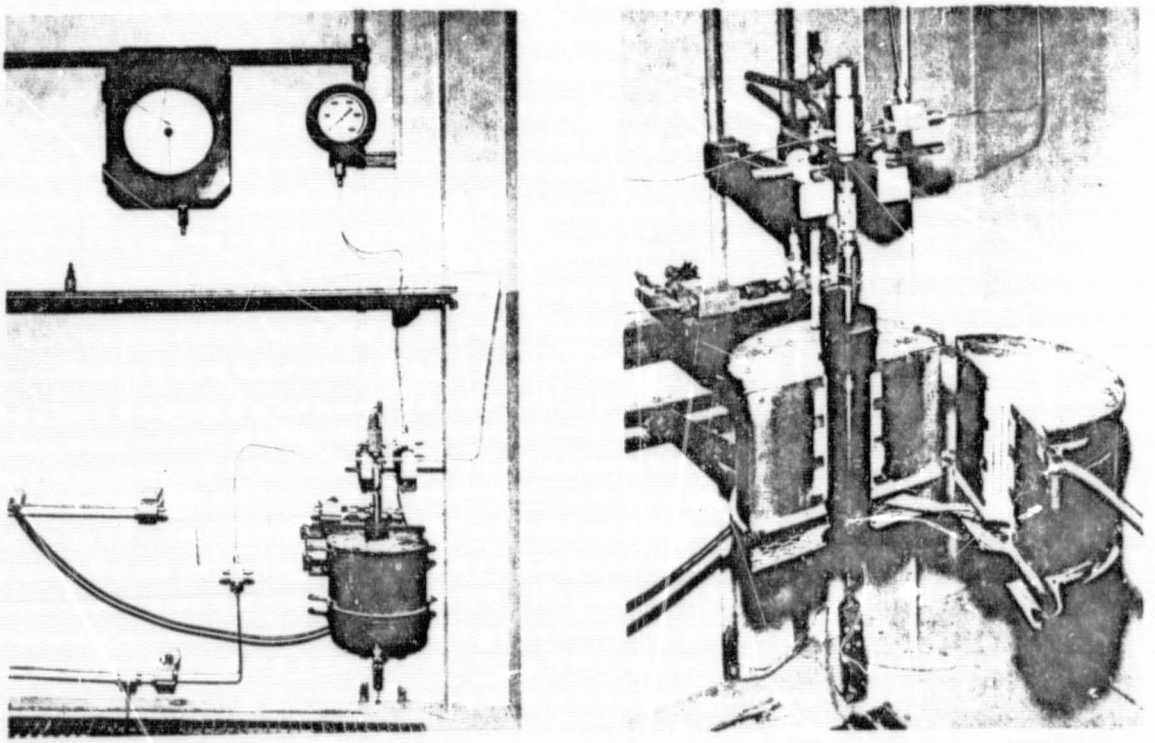

A. COMPLETE SET-UP

B. CLOSE-UP OF BOMB IN FURNACE

FIGURE 16. HIGH PRESSURE OXYGEN BOMB TEST SET-UP

Because the pressure in the bomb increases with temperature, it is necessary to select a starting pressure which will yield a final pressure of 7500 psi at the spontaneous ignition temperature of the material under test.

A variac was used to control the rate of heating of the furnace. For expected low ignition temperatures, the variac was set at a lower value than for expected high ignition temperatures. This produced comparable heating rates over the last twenty minutes prior to ignition.

2. Spontaneous Ignition Temperatures

Ignition temperatures were determined for each material in 7500 psi oxygen and in 2000 psi oxygen using the high pressure bomb and the same test parameters. The lowest ignition temperature found for each material in 7500 psi oxygen and in 2000 psi oxygen are presented in Table 3. Complete information on all materials tested may be found in Table 8 of Appendix IV. In general, the ignition temperatures at 7500 psi were found to be the same as those at 2000 psi.

Results with Oxylube No. 703 demonstrate the fact that with some materials the weight of the sample is significant in determining its spontaneous ignition temperature in the bomb. Results with Oxweld Anti-Friction Compound

No. 64 also demonstrate the effect of weight with some materials and results with Everlube No. 811 demonstrate the effect that the physical geometry of the sample can have on the ignition point.

After a conversation with personnel of the Swagelok Company, the results with High Purity Goop were attributed to the possible non-homogeneity of the product. High Purity Goop is a mixture of fluorocarbon materials and one test sample may have contained more of one component than that contained in another sample.

3. Evaluation of Results

a. Thread Lubricants

A study of ignition temperatures presented in Table 3 shows the fluorocarbon lubricants to have high spontaneous ignition temperatures.

Dixon's Flake Graphite, Burnil Brand Microplates, and Almasol Powder did not ignite at 500°C and therefore may be applicable to lubrication problems in high pressure oxygen. However, experience with these materials is lacking and other problems that might be associated with their use would need to be ascertained.

Molykote Z and products formulated with molybdenum disulfide, Everlube No. 811 and Oxylube No. 703, have low ignition temperatures and are not recommended for use in either 7500 psi or 2000 psi oxygen service.

b. Thread Sealants

Ignition temperatures of those thread sealants tested are all approximately the same except for Mano Pipe and Joint Compound and 50-50 soft solder. If the temperature rise and pressure rise when ignition occurs (Table 8 of Appendix IV) are evaluated in reference to the sample weight, it appears that ignition of Key Abso-Lute or Linde Green Pipe Joint Compound results in the liberation of less energy than the ignition of Rectorseal No. 15 or Parker Oxyseal.

Mano Pipe and Joint Compound has a relatively high ignition temperature and a comparatively small amount of energy release but Linde experience with the sealing characteristics of the product show that it does not meet the specifications required for high pressure oxygen service. However, further development of this product might make its sealing characteristics acceptable.

Soft solder did not ignite at 500°C, but its melting point is 225°C. It would not present any ignition hazard but evaluation of its use as a sealant by tinning of threads would need to be made.

c. Fluorocarbon Plastics and Elastomers

Teflon (TFE) and filled TFE products have the highest spontaneous ignition temperatures with Kel-F 81 being next highest. The ignition temperatures of the fluorocarbon elastomers are substantially lower than those of the fluorocarbon plastics.

TABLE 3

LOWEST SPONTANEOUS IGNITION TEMPERATURE FOUND
IN 7500 PSI OXYGEN AND IN 2000 PSI OXYGEN, °C

	7500 psi	2000 psi
Thread Lubricants		
Aroclor 1254	355	376
Dixon's Flake Graphite No. 1	No ignition 500°C	No ignition 500°C
Kel-F 90 Grease	435	435
Oxweld Anti-Friction Compound No. 54	230	237
Burnil Brand Microplates	No ignition 500°C	No ignition 500°C
Molykote Z	267	277
Halocarbon Oil Series 13-21	435	427
Halocarbon Grease Series 25-10	438	431
Oxweld Anti-Friction Compound No. 64	410	410
Everlube No. 811	216	250
Oxylube No. 703	190	238
High Purity Goop	411	398
Almasol Powder	No ignition 500°C	No ignition 500°C
Thread Sealants		
Oxyseal	347	360
Mano Pipe and Joint Compound	422	430
Key Abso-lute	342	355
Rectorseal No. 15	355	374
Linde Green Pipe Joint Compound	362	356
50-50 Soft Solder	No ignition 500°C	No ignition 500°C
Fluorocarbon Plastics and Elastomers		
Viton A (Virgin)	300	310
Viton B (Virgin)	316	325
Teflon (Virgin)	465	469
Teflon 100 X	410	413
Rulon A	465	463
Rulon B	460	466
Rulon C	465	458
Duroid 5600	470	468
Duroid 5650	444	461
Duroid 5870	463	452
Duroid 5813	463	463
Kel-F 81	425	431
Kel-F Elastomer 3700	332	341
Kel-F Elastomer 5500	340	352
Rubber Compound		
Neoprene	190	200

TFE products and Kel-F 81 both liberate only a small amount of energy on ignition, indicated by the low temperature and pressure rise on ignition when compared to that of other materials.

4. Conclusions

a. Because the spontaneous ignition temperatures of the majority of the materials tested can be attained by adiabatic compression, only those that did not ignite at 500°C can be recommended as not presenting a hazard. Further investigation would be required to determine other problems that might be associated with their use.

b. It is recognized that some type of material is needed for dynamic and static seals. The use of TFE or glass-filled TFE in these instances would be recommended because of the low energy release of TFE. However, these would be recommended only if tightly confined. Because TFE, per se, cold flows, the glass-filled TFE would receive a higher recommendation.

Adiabatic Compression Tests

Purpose and Discussion

Originally it was thought that this test could be used to test specimens of various metallic and non-metallic materials to show that the material could or could not be ignited by adiabatic compression. Calculation of theoretical temperatures attainable by adiabatic compression (Appendix I) indicated that the melting points of most metals to be tested would be exceeded. Because these temperatures would not be reached in actual practice, it was thought that experimental tests would be in order to determine the peak temperatures attainable.

Reynales [13] reports that temperature rises of 560°F were measured by sudden opening of a shut-off valve and pressurizing with 2200 psi nitrogen. In shock tube experiments with oxygen, peak temperatures of over 2000°F were recorded and all materials tested including Teflon, Kel-F, Buna-n, and butyl rubber were burned. Greenspan[5] reported ignition of Teflon and Kel-F by adiabatic compression.

A shock tube could have been used in the present program for this type of experiment but this would require the use of a bursting disc and the likely probability that a piece of the bursting disc might impact the specimen and invalidate results. It was also thought that a shock tube would not duplicate any condition that might exist during charging of a receiver at 7500 psi. Therefore, a quick-opening air-operated valve was purchased for use in adiabatic tests.

Preliminary Tests

Before the air-operated valve was received, a few crude tests were made at 2000 psi to determine possible test parameters. The tests were made using the apparatus shown in Figure 17. Both nitrogen and oxygen at 2000 psi were used for these tests and a small test volume varying from 10 cc to 50 cc was suddenly charged to 2000 psi by opening a ball-cock valve by hand as quickly

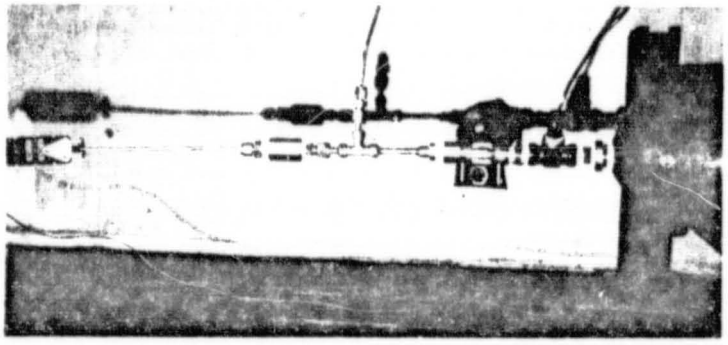

FIGURE 17. PRELIMINARY ADIABATIC COMPRESSION TEST SET-UP

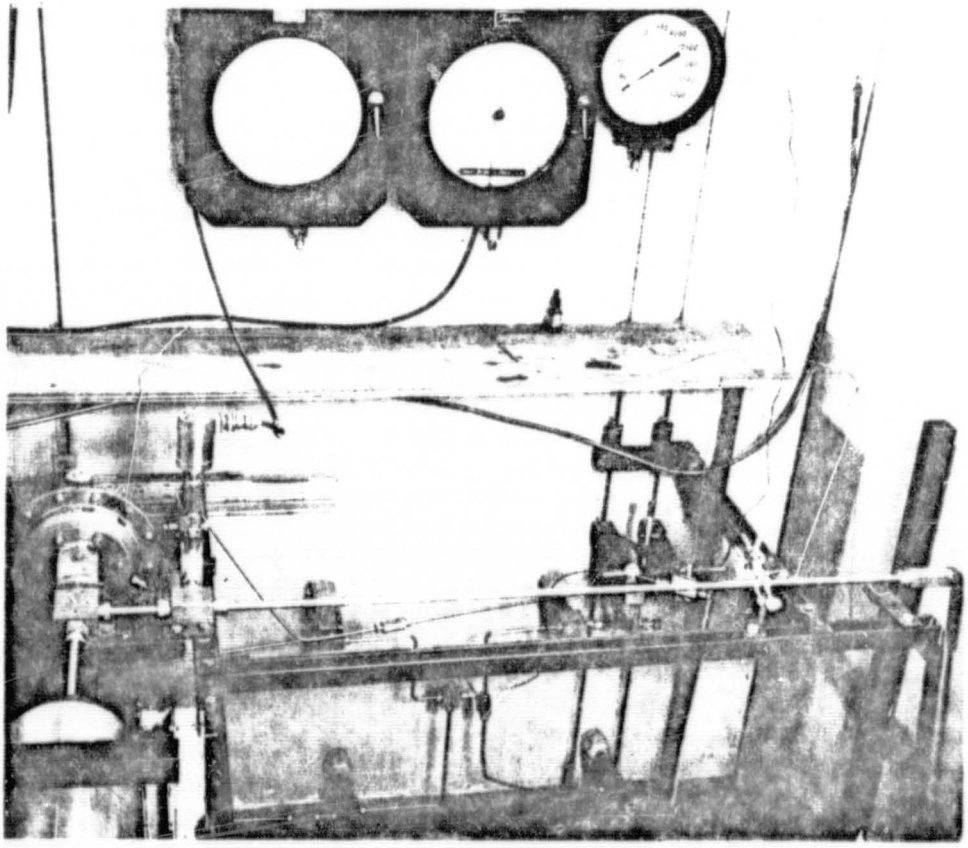

FIGURE 18. 7500 PSI ADIABATIC COMPRESSION TEST SET-UP

as possible. Results of these tests are not tabulated because of information which was developed later. It will suffice here to say that the maximum rise in temperature measured was only 93°C but that two-milligram slivers of lead were melted in this apparatus which indicated that temperatures in the order of 327°C were momentarily reached.

7500 psi Tests

When the quick-opening air-operated valve was received, experimental tests at 2000 psi showed that the opening time of the valve was in the order of 0.5 second and the pressurization time of a 20-inch section of 5/16" I.D. tubing required 0.05 second. Calculations based on these measurements indicated that the temperatures developed would not begin to approach theoretical. (See Appendix III). Consequently the use of this test became unattractive in the testing of metals, and because it was already known that organic materials could be raised to their spontaneous ignition temperatures by 2000 psi oxygen,[5] there was no advantage in further use of the test.

The air-operated valve (with 5/16" I.D. ports) was purchased for a dual purpose. It was to be used in the charging of a simulated system. While setting up for the simulated system the opportunity to make some quick temperature measurements presented itself. The tip of a 1/16" inconel shielded pencil thermocouple was removed to expose the bare iron-constantan junction. This was placed at the end of various lengths of 5/16" I.D. tubing. The tubing was then suddenly pressurized from an intermediate storage vessel by opening the air-operated valve. During these quick tests a maximum temperature of 378°C was recorded when a 51-inch section of tubing was pressurized to 6650 psi. Temperature measurements beyond this pressure were not made. The arrangement for the test is shown in Figure 18 and a schematic of the set-up in Figure 19.

At a later date, samples of Kel-F 81, virgin Viton A, and virgin Teflon were quickly tested in the same set-up by placing the specimens at the dead end of the tube and suddenly pressurizing them to pressures ranging from 6300 to 6900 psi with oxygen. All specimens spontaneously ignited. Results are reported in Table 12 of Appendix IV. During these tests a pressure transducer and recorder in the system indicated that pressurization occurred in 0.05 sec. (Figure 20). Results of these tests only proved that the ignition temperatures of these materials could be reached in this set-up which was expected.

Promoted Ignition Tests

Purpose

The promoted ignition test is a means of evaluating the relative resistance to ignition and combustion of various metals by subjecting the metal specimen to the energy released when a promoter material is heated to its spontaneous ignition temperature in oxygen at a given pressure. The test from a practical standpoint shows what can happen when an elastomeric material, such as a gasket or O-ring, ignites in an oxygen system.

Procedure

The procedure for this test is the same as the procedure for the oxygen bomb test but a metal specimen as well as the promoter material is placed in the Pyrex test tube. Refer to Figure 15 for a schematic of the test set-up.

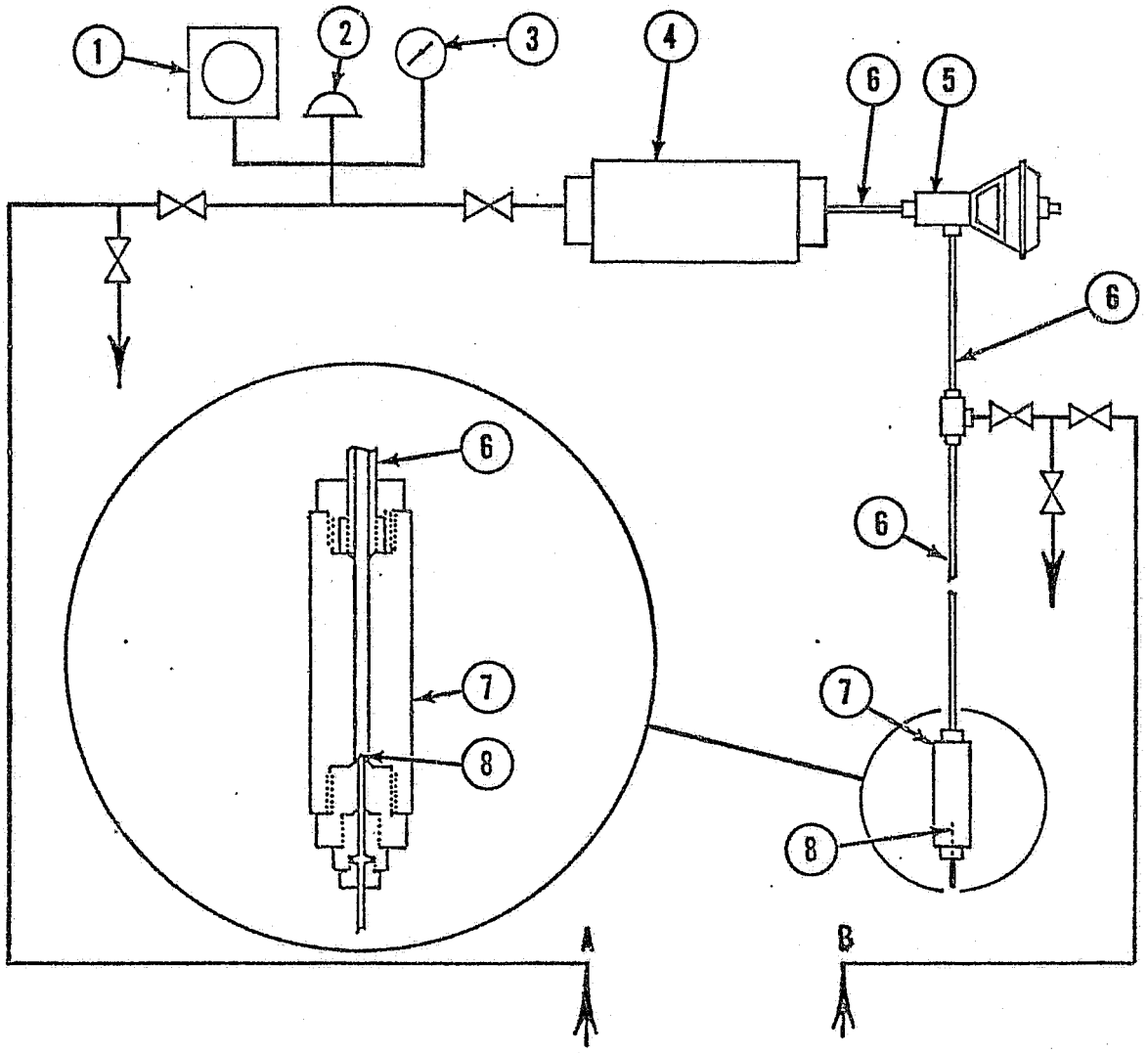

KEY

1. 0-10,000 psi Recorder
2. 10,000 psi Bursting Disc .
3. 10,000 psi Gage
4. Storage Vessel
5. Air-Operated Valve
6. 5/16" I.D. Tubing
7. 5/16" I.D. Coupling
8. 1/16" Thermocouple or Specimen of Material

A. High Pressure Oxygen from Converter
B. 2000 psi Cylinder Oxygen

FIGURE 19. SCHEMATIC FOR ADIABATIC COMPRESSION TEST

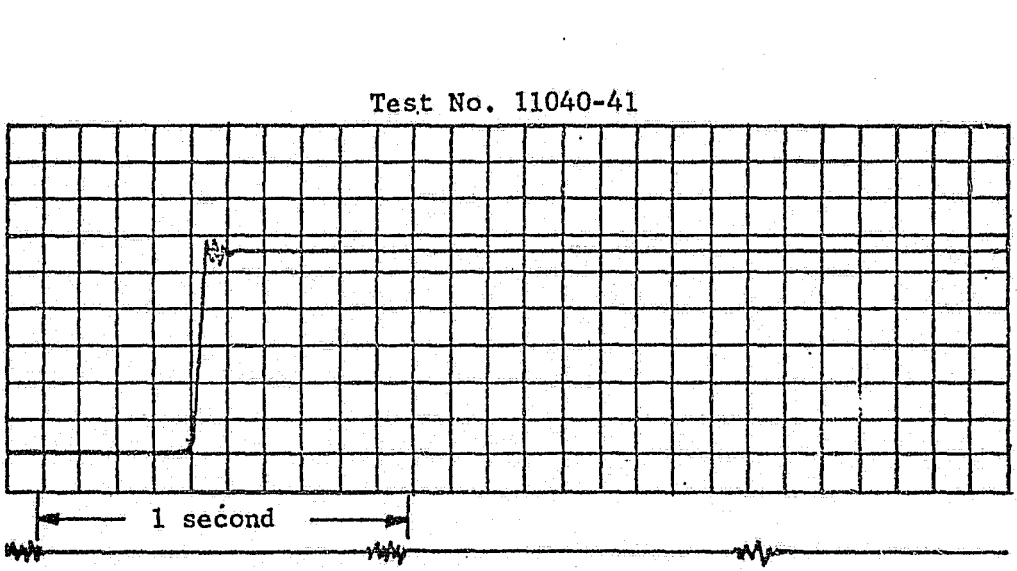

FIGURE 20. PRESSURE PROFILE OF ADIABATIC COMPRESSION TEST

Preliminary Tests

It was necessary to determine the parameters which would give reproducible and comparable results on the various metals to be tested. Preliminary tests were carried out at 2000 psi. A review of promoter materials had narrowed the choice to neoprene or Viton A. Two or three tests were made with Viton A but neoprene was selected because of its lower ignition temperature and the possibility that decomposition products from the Viton A might effect the outcome of the test.

Neoprene O-rings were ordered for these tests and purchased with the understanding that all O-rings would be from the same batch of neoprene in order to obtain uniform spontaneous ignition temperatures. However, difficulty was experienced in that the ignition temperature of the neoprene varied substantially which is typical with this type of compound. This did not seem to materially affect the test results but it did cause the pressure at the spontaneous ignition temperature to vary because of the pressure dependency on the temperature of the bomb.

Various weight and size combinations as well as physical relationships were tried until one was found which would yield comparable results. These various configurations are schematically shown in Figure 21.

Metal specimens of 0.005-inch thick foil were used. Certified analyses of the metal foils were obtained. Original plans were either to use a constant weight of promoter and vary the physical dimensions of the metal specimen or to use fixed physical dimensions for the metal specimen and vary the weight of the promoter. The latter condition appeared to be more attractive after completion of all the 2000 psi tests and some of the 7500 psi tests. The final physical configuration chosen for the 7500 psi tests is that shown in Figure 21F.

Twenty-nine preliminary tests were performed at 2000 psi (Table 9 of Appendix IV). However, when tests were started at 7500 psi it was discovered

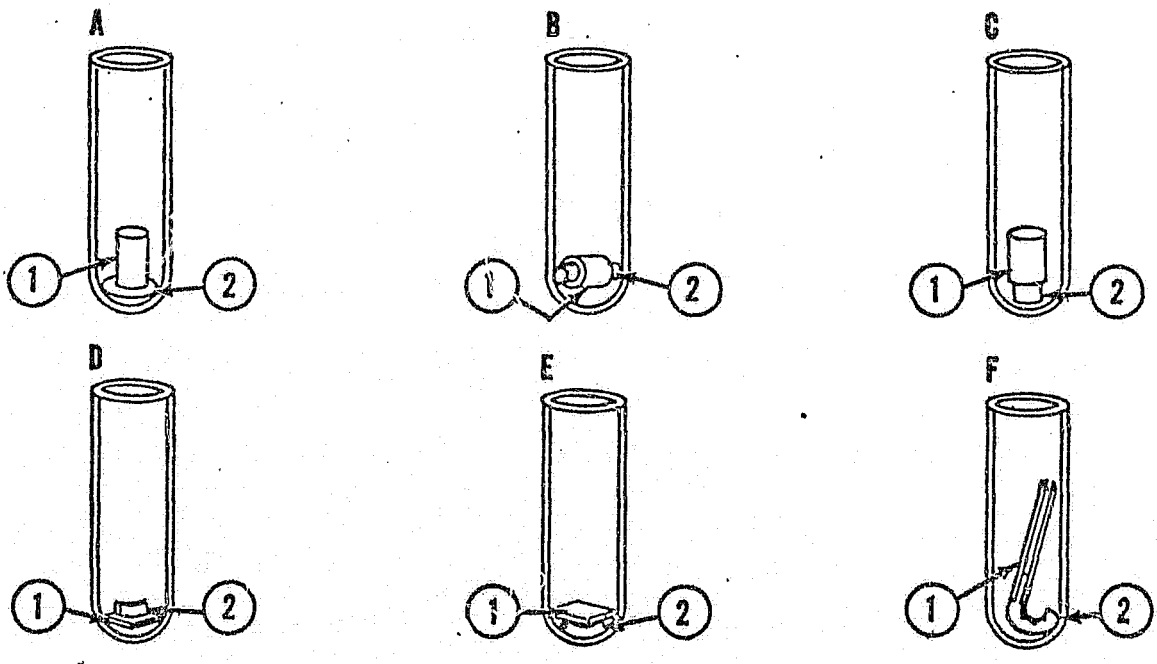

KEY

A. Formed a cylinder of the metal specimen to fit inside the neoprene O-ring. Specimen in a vertical position.

B. Rolled the neoprene O-ring within a cylinder of the metal specimen. Ends were open and specimen in a horizontal position.

C. Formed a cylinder of the metal specimen and lightly crimped the promoter into the bottom of the specimen which was in a vertical position.

D. Metal specimen in a flat horizontal position and the neoprene on top of the specimen.

E. Metal specimen in a flat horizontal position and the neoprene underneath the specimen.

F. Formed a half-cylinder from a long metal specimen with the neoprene crimped into the bottom of the specimen which was always in a semi-vertical position.

1. METAL 2. NEOPRENE

FIGURE 21. PHYSICAL CONFIGURATIONS USED WITH PROMOTER MATERIAL AND METAL SPECIMENS IN PYREX TEST TUBE DURING PROMOTED IGNITION TESTS

that results were significantly different from those obtained in the 2000 psi tests in that the weight of neoprene required to bring about combustion of the metal was less. This was attributed to the geometric configuration of the bomb, the physical position of the metal specimen in the test tube during preliminary tests, and the difference in oxygen pressures. All of these factors would favor the blanketing of the metal specimen by the ignition products of CO_2 and H_2O formed during combustion of the neoprene. At the lower pressure of 2000 psi the combustion products would occupy a much greater volume than at 7500 psi.

Although the tests at 2000 psi were informative it was necessary to develop new parameters at 7500 psi. Original intentions had been to perform identical tests at 2000 psi and at 7500 psi for comparison purposes, but tests at 2000 psi now had to be eliminated and only the 7500 psi tests were made.

7500 psi Tests

1. Discussion of Test

After completion of a number of tests at 7500 psi, a geometrical configuration of 5 millimeters by 30 millimeters was selected as the standard size for the 5-mil metal foil samples. By determining the weight of neoprene necessary to combust, partially combust, melt, or partially melt a specimen, the relative resistance to ignition and combustion was obtained for the metals and alloys.

The metals and alloys have been arranged in Table 4 in order of their decreasing resistance to ignition as determined by these tests in 7500 psi oxygen. Complete data on the tests is presented in Table 10 of Appendix IV.

It had been hopefully expected that we might be able to extract some temperature data from the pressure profiles in the bomb during the ignitions and a pressure transducer was connected into the bomb system. The pressure was recorded on a Sanborn 150 recorder which permitted suppression of several thousand pounds of pressure and, by means of an attenuator, the recorder could be spanned over a narrow pressure range if it were so desired. After a large number of tests and a study of the pressure profiles, the conclusion was reached that prediction of ignition temperatures could not be determined from the profiles. A typical pressure profile is shown in Figure 22.

2. Discussion of Results

a. From Table 4 it can be seen that nickel is by far the most resistant to ignition (gold and silver excepted) but if enough energy is present nickel will burn.

b. A standard specimen of Monel alloy 400 was never completely combusted so the amount of neoprene shown in Table 4 to completely combust the standard size specimen was estimated. The required weight of neoprene might actually be higher than the estimate which would improve the relative position of Monel 400.

TABLE 4

METALS AND ALLOYS ARRANGED IN ORDER OF DECREASING RESISTANCE TO IGNITION AND COMBUSTION IN 7500 PSI OXYGEN

Metal or Alloy	Weight of Neoprene to Completely Combust Standard Specimen 5 mm x 30 mm x 0.005"
Gold	Only melts
Silver	Only melts
Nickel	48 to 56 mg*
Monel alloy 400	18 to 19 mg*
Yellow Brass (partial combustion only)	11.8 to 15.2 mg
Inconel alloy 600	13.2 mg
Aluminum	11.0 to 16.4 mg
Copper	10.5 mg*
Inconel alloy X-750	9.0 mg
Stainless steels	7.1 to 8.5 mg

*Estimated from results of a number of tests which were either standard with only part of the specimen consumed or were not standard and either complete or partial combustion occurred.

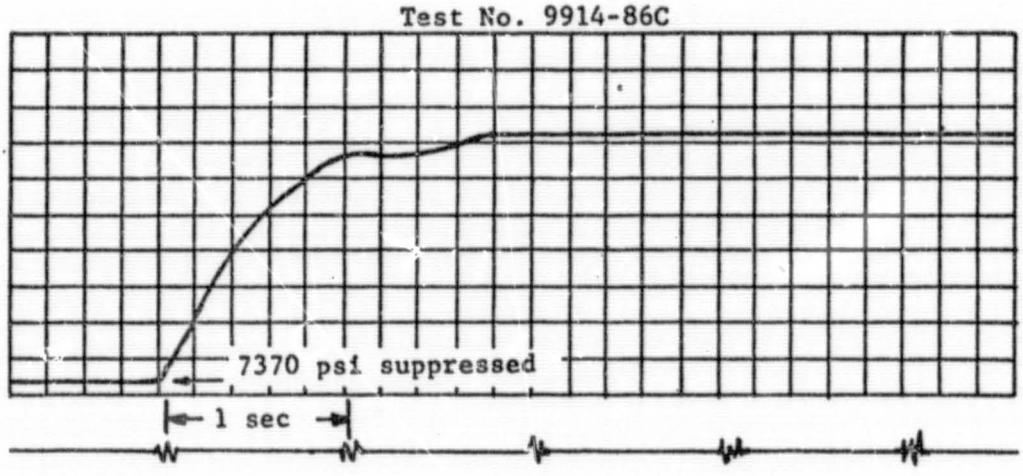

FIGURE 22. PRESSURE PROFILE OF PROMOTED IGNITION TEST

c. It has been possible to demonstrate with some of the metals (e.g. copper, brass, Monel 400, and nickel) that ignition can be started and part of the specimen combusted without consuming all of the specimen. By varying the weight of neoprene only slightly, it has been possible to combust a small part of the specimen, a large part of the specimen, or all of the specimen. This is characteristic of these metals and demonstrates their quenching effect once ignition has started. This is no doubt due to the low heats of combustion of these materials. Evidence of this is shown in Figures 26, 27, 29, and 30. Figures 23, 24, 25, 28, 31 and 32 show other ignition results.

d. Lead was not listed in Table 4 because 12.6 mg of neoprene melted the specimen into a ball with very little oxidation and no further tests were run. Therefore it was difficult to position it in the table.

e. Aluminum was tested with two different anodized surface thicknesses and also with what was thought to be normal surface condition if just exposed to the atmosphere. The amount of neoprene necessary to ignite the aluminum was not as clear cut as with other metals. However a range was established between 11.0 and 16.4 mg. Once ignited, the aluminum burned violently.

f. Gold and silver required more neoprene to melt the specimens than was required to ignite most of the other metals.

g. Brass had high resistance to ignition but it was always heavily oxidized.

h. Stainless steels were least resistant to ignition.

i. Samples of stainless steel enclosed in 5-mil Kel-F and 5-mil Teflon FEP were tested. This was intended to simulate a coating of these materials on the metal. Complete ignition occurred in all cases.

j. Two samples of aluminum coated on one side with Kel-F were tested. The Kel-F disappeared in one case without ignition and ignited in the other case. The aluminum was not affected in either case.

3. Evaluation of Test Results

a. With the exception of aluminum, results of these tests generally agree with those previously made at Linde in 2000 psi oxygen and with those of Dean and Thompson (3). (See Table 1.)

b. Nickel has the highest resistance to ignition and combustion. Therefore it would be the first choice for construction of a high pressure oxygen receiver from the standpoint of compatibility with oxygen.

c. Monel alloy 400, Inconel alloy 600, and brass, would be rated as the next best materials.

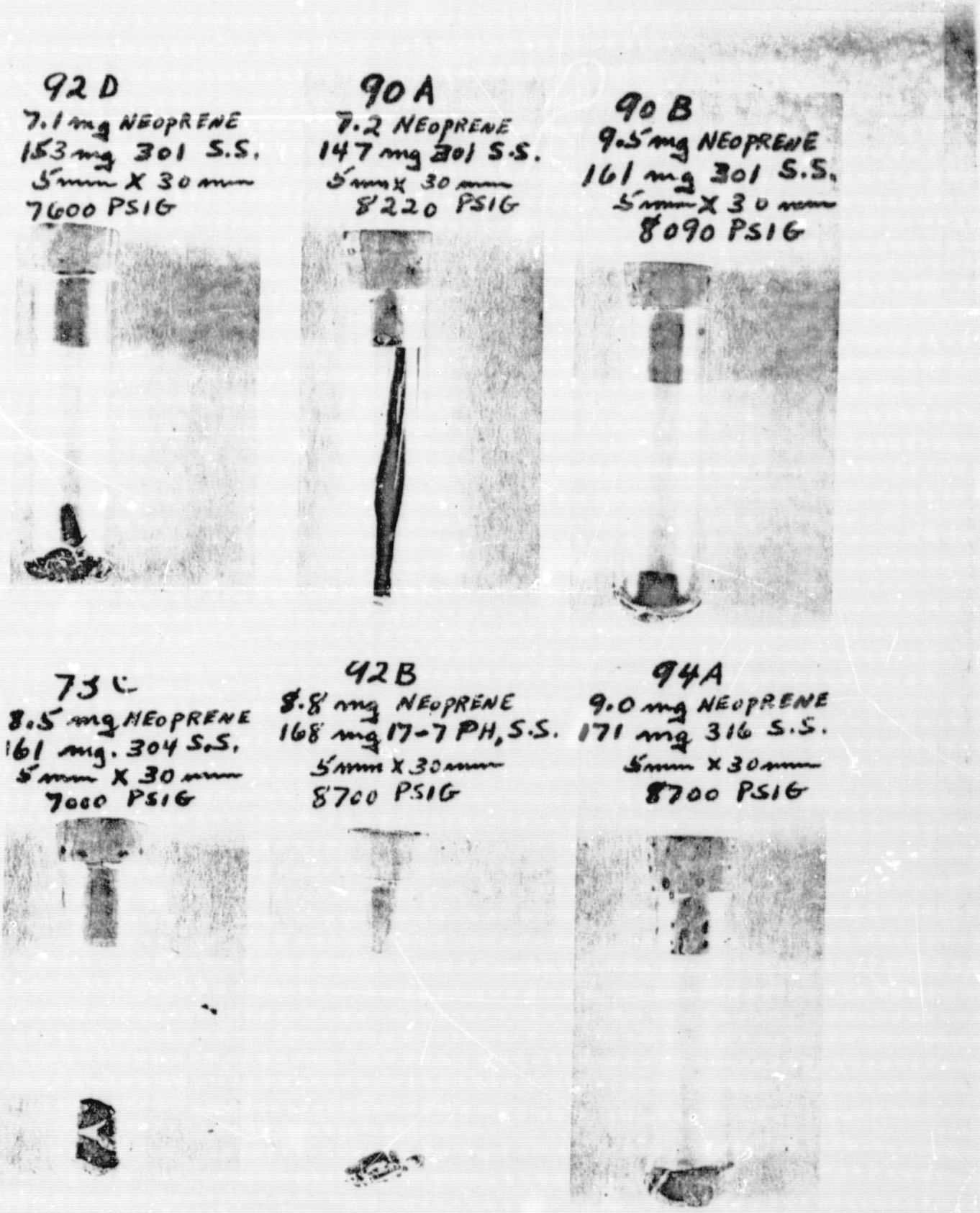

FIGURE 23. PROMOTED IGNITION TEST, STAINLESS STEEL (ENLARGED 2X)

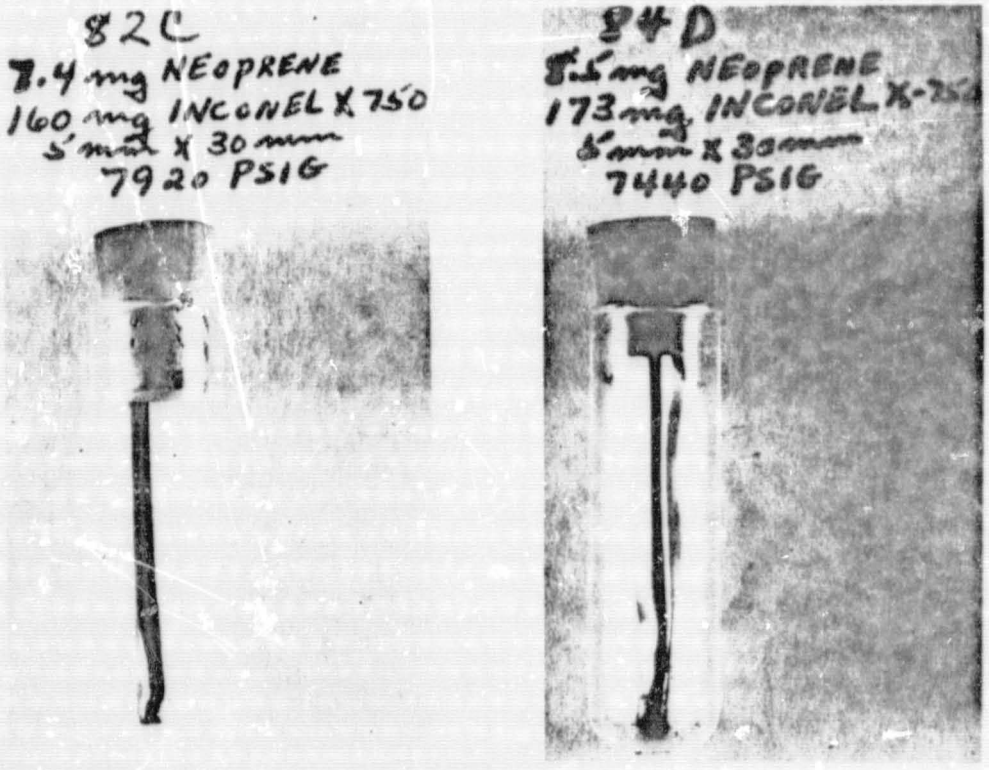

FIGURE 24.

PROMOTED IGNITION TEST

INCONEL X-750 (ENLARGED 2X)

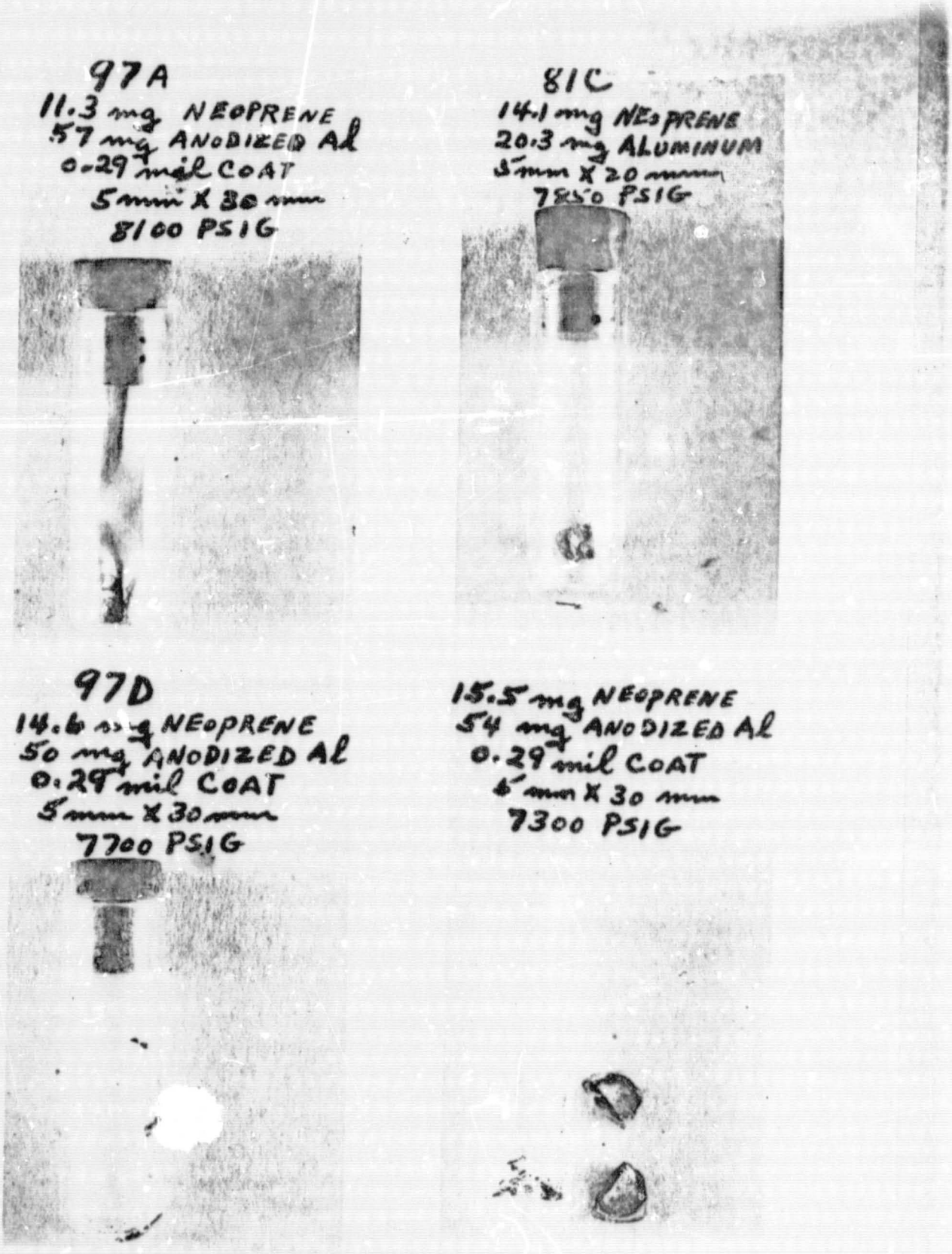

FIGURE 25. PROMOTED IGNITION TEST, ALUMINUM (ENLARGED 2X)

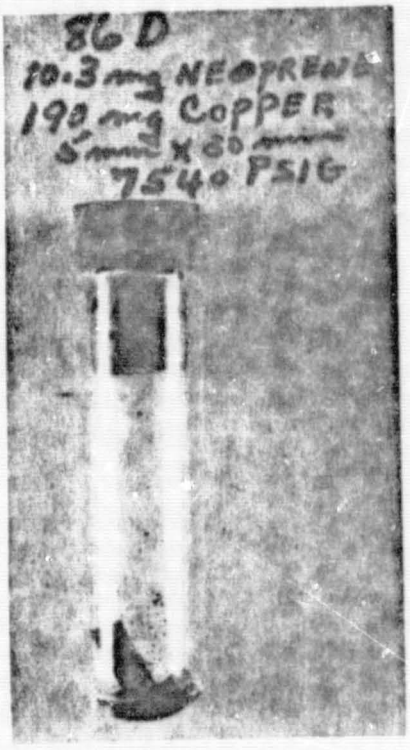

FIGURE 26.

PROMOTED IGNITION TEST

COPPER AND LEAD (ENLARGED 2X)

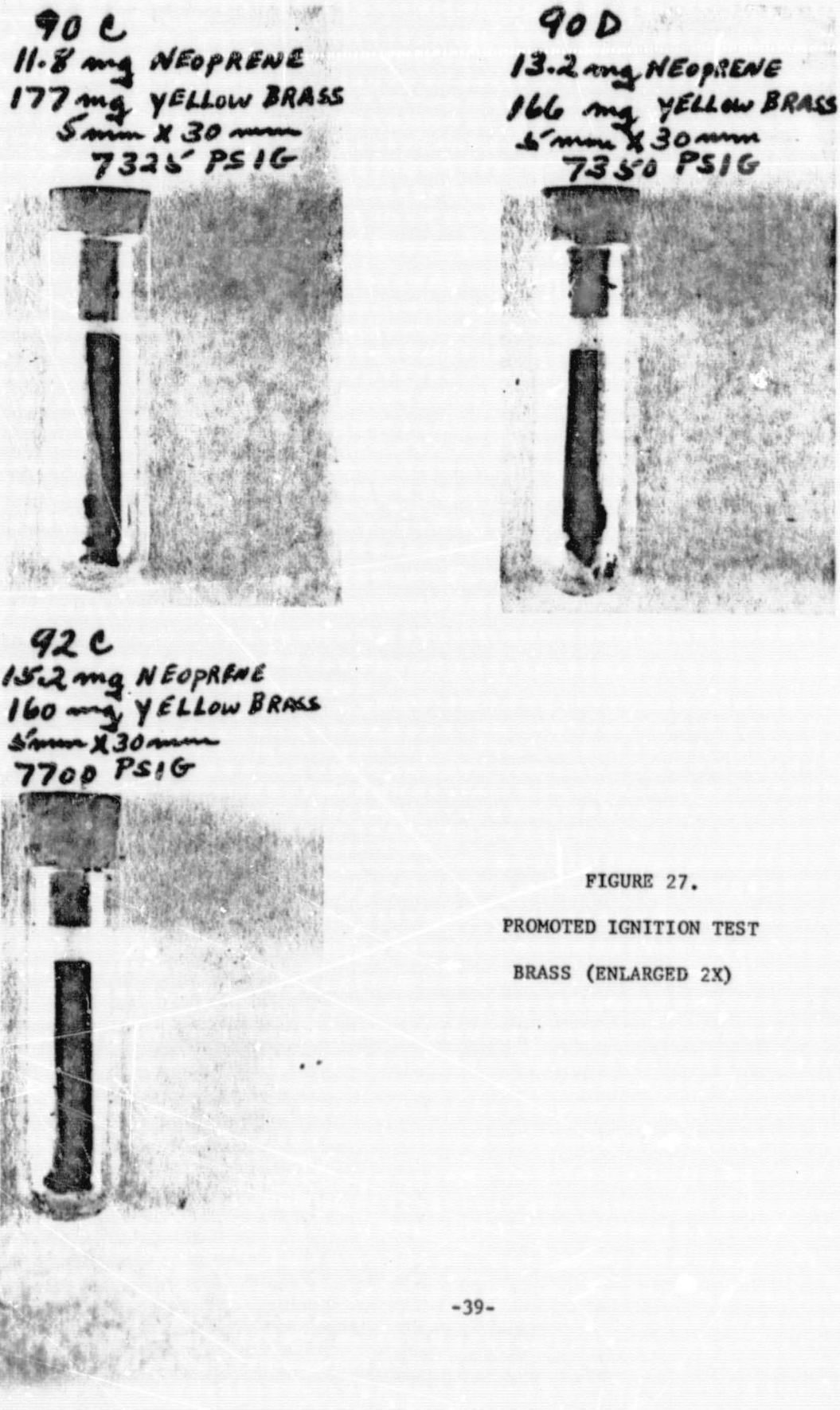

FIGURE 27.

PROMOTED IGNITION TEST

BRASS (ENLARGED 2X)

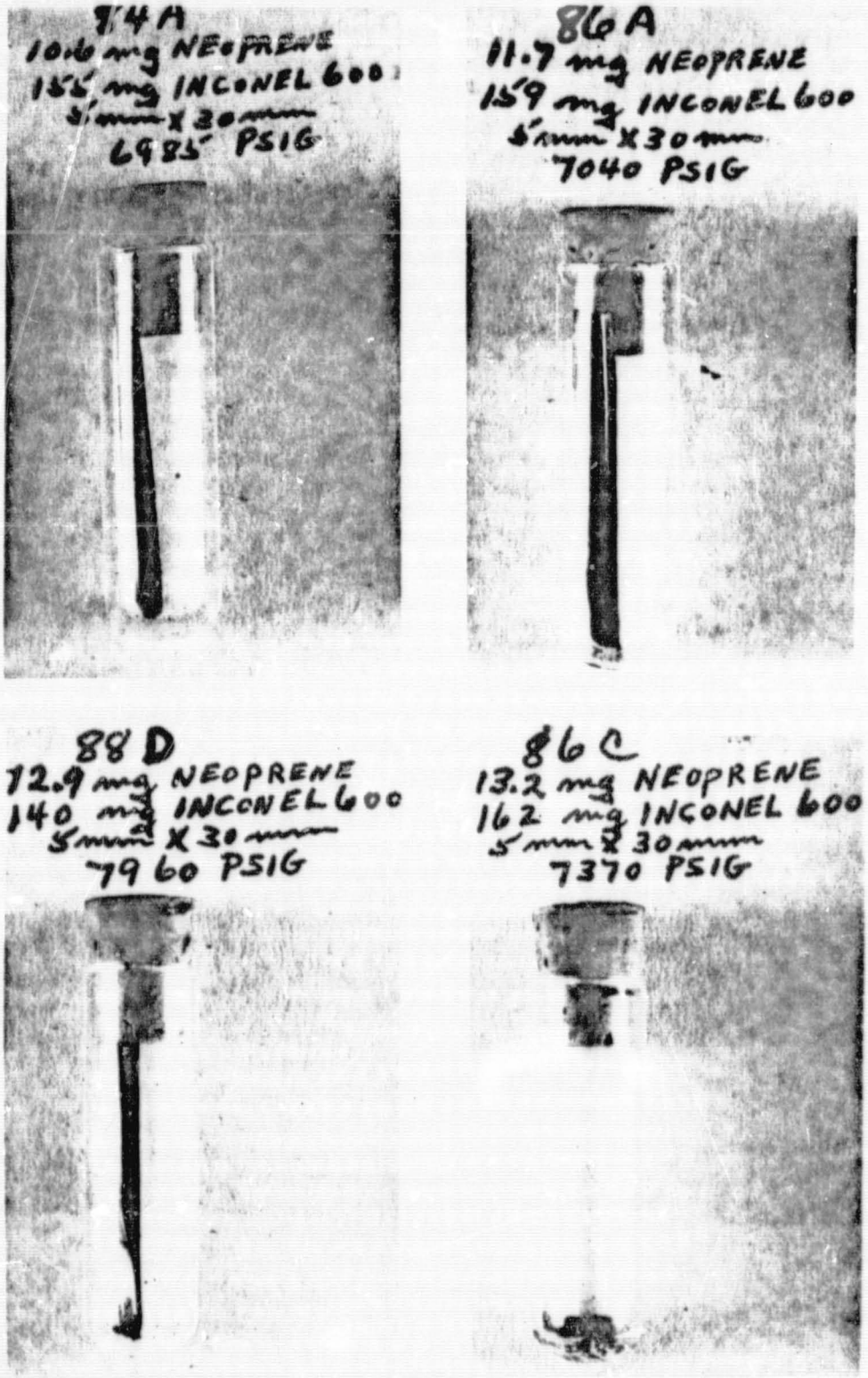

FIGURE 28. PROMOTED IGNITION TEST, INCONEL 600 (ENLARGED 2X)

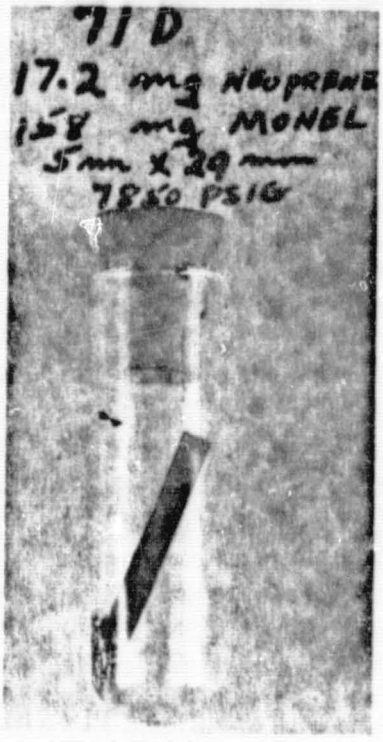

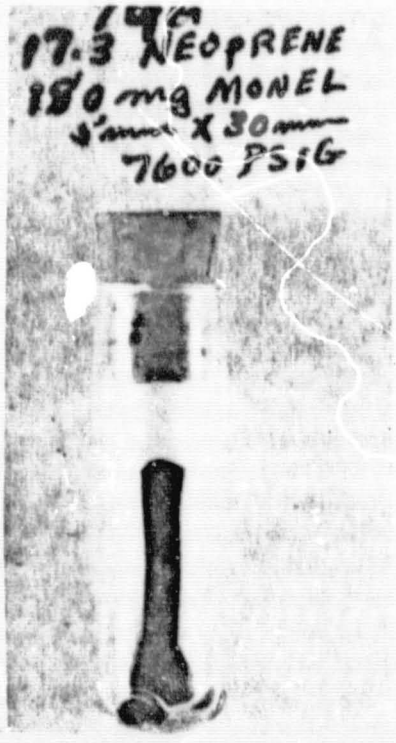

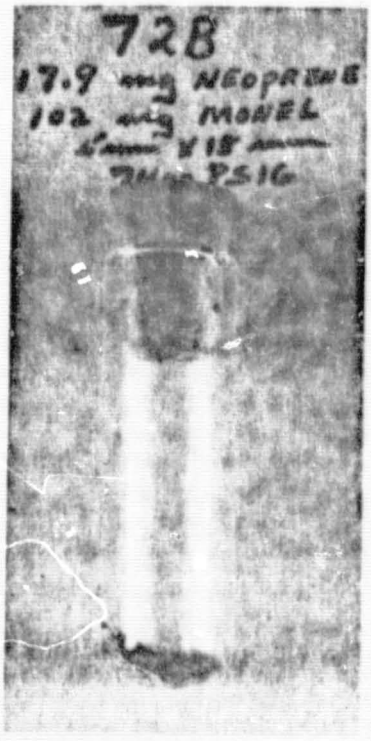

FIGURE 29. PROMOTED IGNITION TEST, MONEL 400 (ENLARGED 2X)

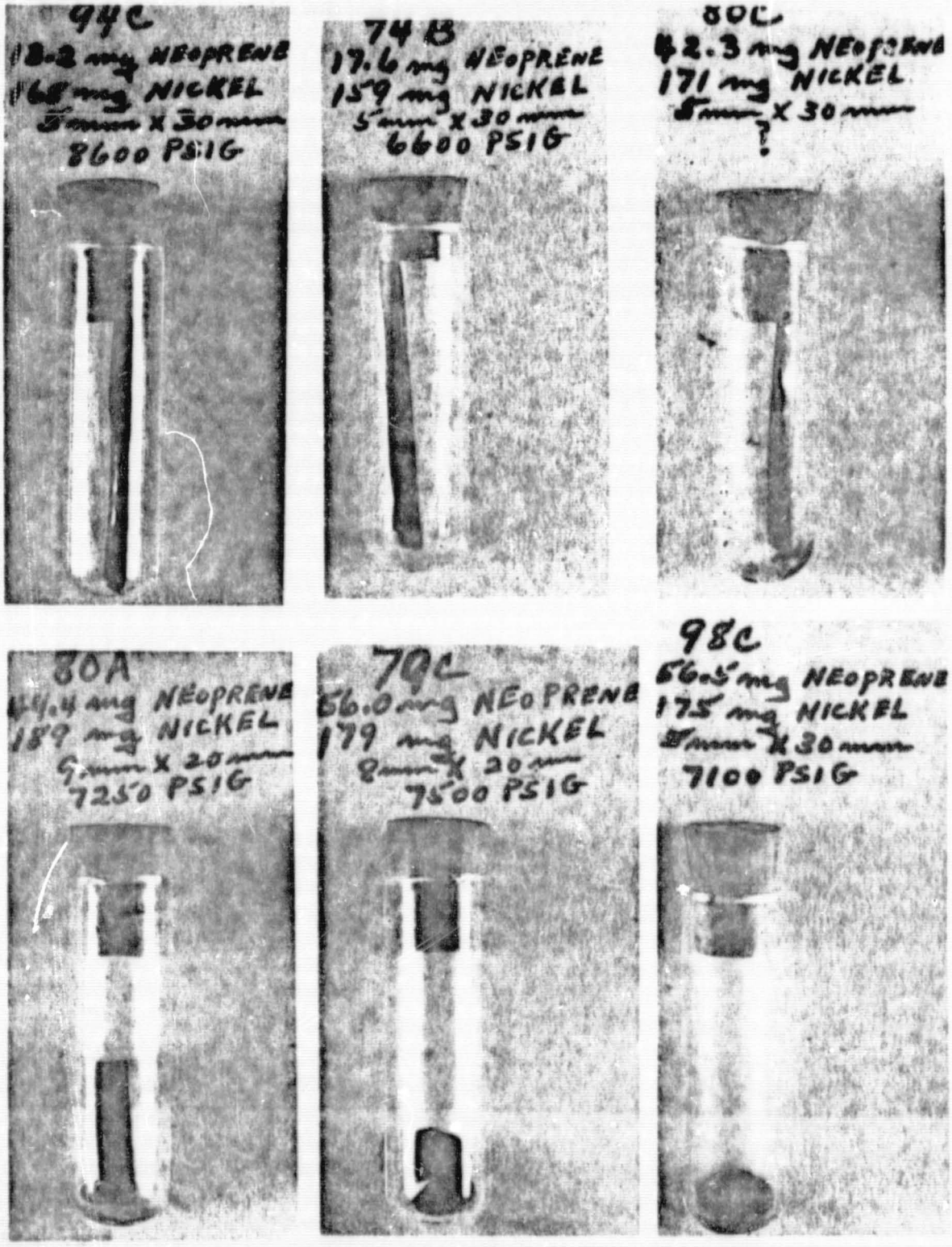

FIGURE 30. PROMOTED IGNITION TEST, NICKEL (ENLARGED 2X)

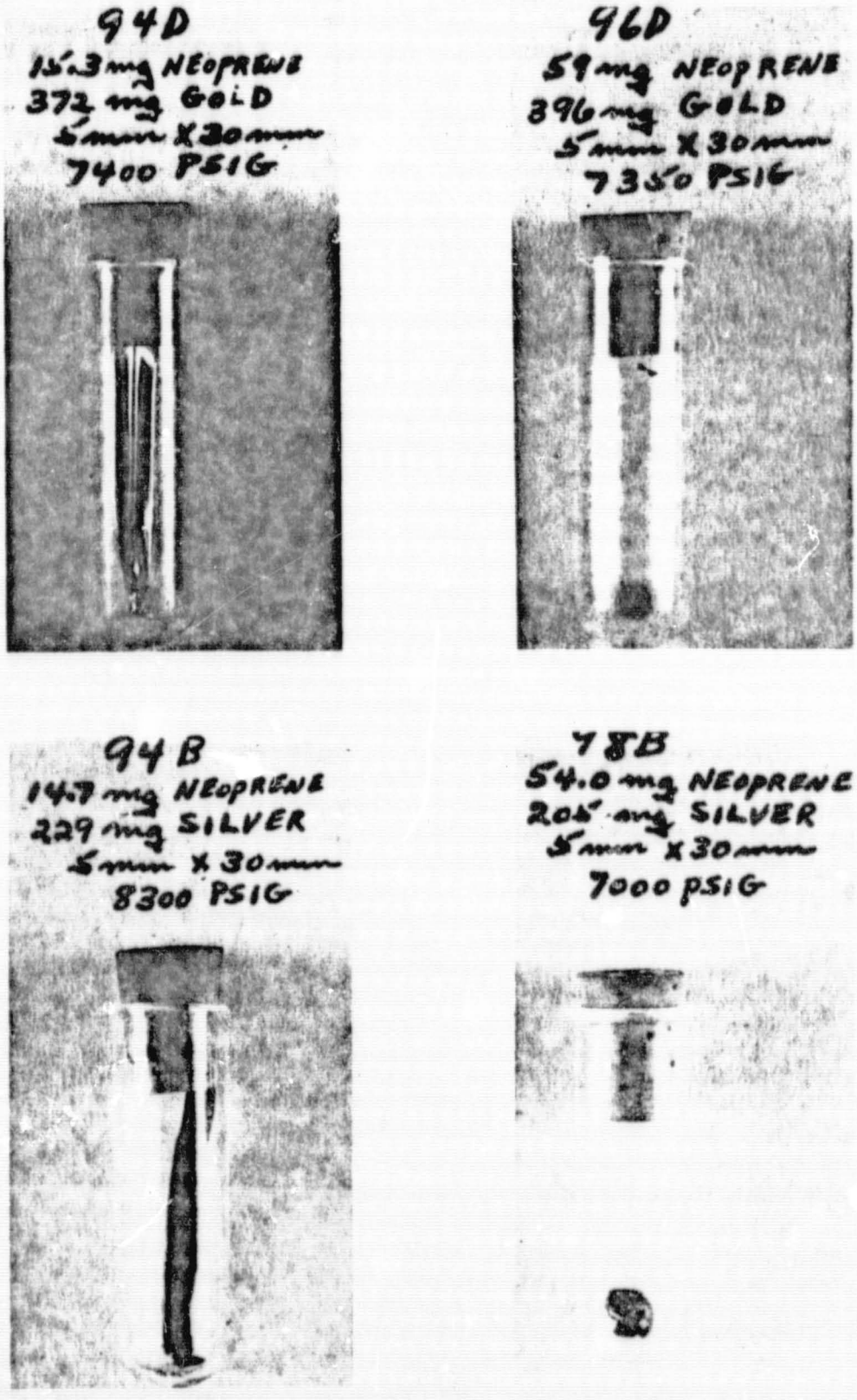

FIGURE 31. PROMOTED IGNITION TEST, GOLD AND SILVER (ENLARGED 2X)

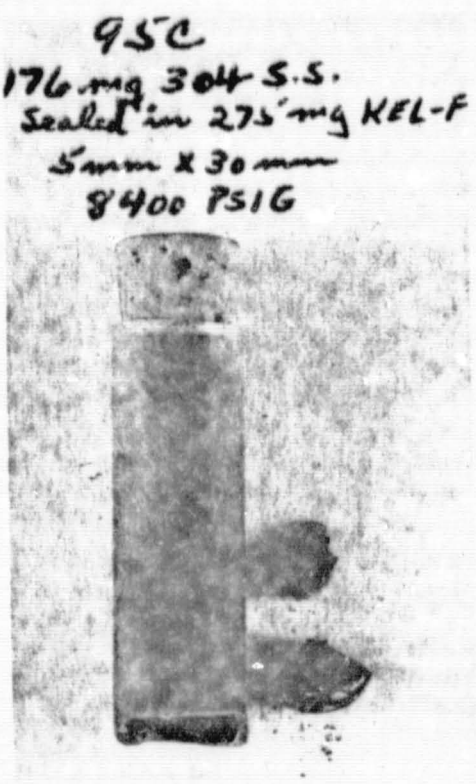

A.

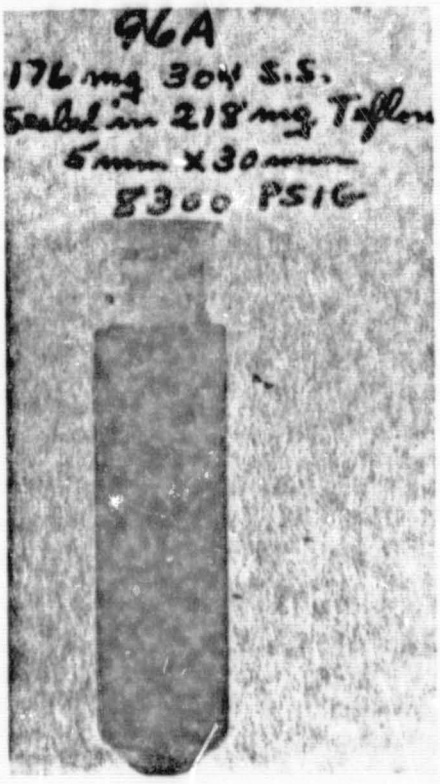

B.

C.

FIGURE 32.

PROMOTED IGNITION TEST

A. STAINLESS STEEL SEALED IN KEL-F

B. STAINLESS STEEL SEALED IN TEFLON FEP

C. ALUMINUM COATED WITH KEL-F

(ENLARGED 2X)

d. Gold and silver might have applications in plating other metals. Their use would not present an ignition hazard.

e. Copper is not recommended because of other shortcomings.[1]

f. Of the materials tested, stainless steel and aluminum are the least satisfactory for use at oxygen pressures of 7500 psi.

Simulated System Tests

Purpose

The simulated system tests had three objectives:

1. To experimentally determine the hazards involved in charging a simulated system with 7500 psi oxygen.

2. To determine any electrostatic charge developed during charging of the simulated system.

3. To determine the flow rate at which a hazardous condition is approached.

Philosophy

The philosophy used in constructing and testing the system was as follows:

1. Use the best possible materials as determined by previous test data.

2. Use equipment and arrange it in a manner which would best simulate an actual system.

3. Pressurize the system rapidly with oxygen to various pressure levels and measure the pressure rise by means of a pressure transducer and recorder. This information will permit calculation of flow rates.

4. By means of a probe and oscilloscope, measure the electrostatic charge of the high pressure oxygen gas in the receiver as it is charged.

Materials of Construction and Arrangement of Equipment

The schematic of the test set up is shown in Figure 33. Figures 34 and 35 are pictorial presentations. The equipment, its material of construction and the reason for its position are:

1. Storage Vessel

The storage vessel was used as a source of high pressure oxygen after it had been charged by the converter. It was used for two reasons:

a. As an intermediate vessel between the converter and the simulated system to isolate the converter in case of a mishap.

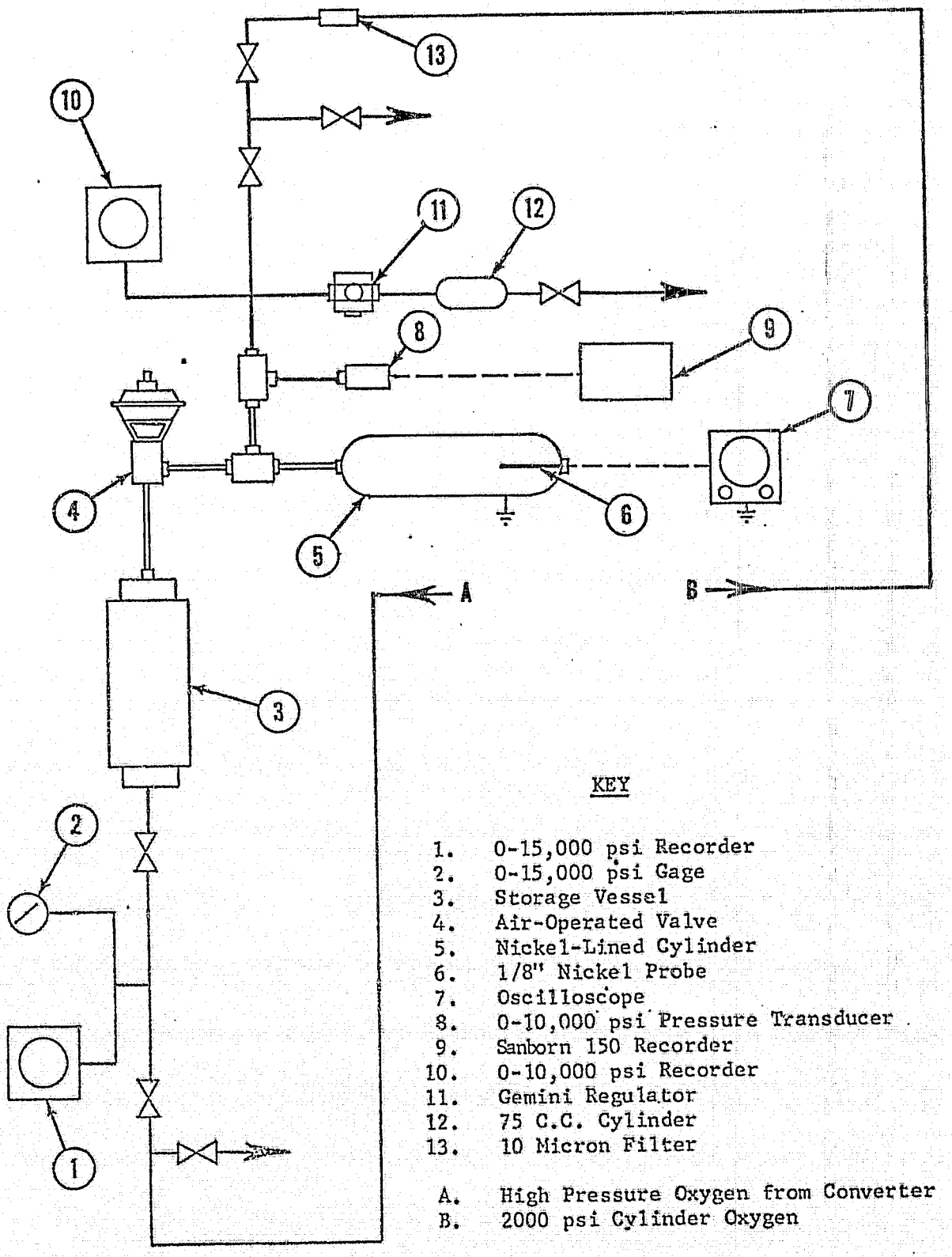

KEY

1. 0-15,000 psi Recorder
2. 0-15,000 psi Gage
3. Storage Vessel
4. Air-Operated Valve
5. Nickel-Lined Cylinder
6. 1/8" Nickel Probe
7. Oscilloscope
8. 0-10,000 psi Pressure Transducer
9. Sanborn 150 Recorder
10. 0-10,000 psi Recorder
11. Gemini Regulator
12. 75 C.C. Cylinder
13. 10 Micron Filter

A. High Pressure Oxygen from Converter
B. 2000 psi Cylinder Oxygen

FIGURE 33. SCHEMATIC FOR SIMULATED SYSTEM TESTS

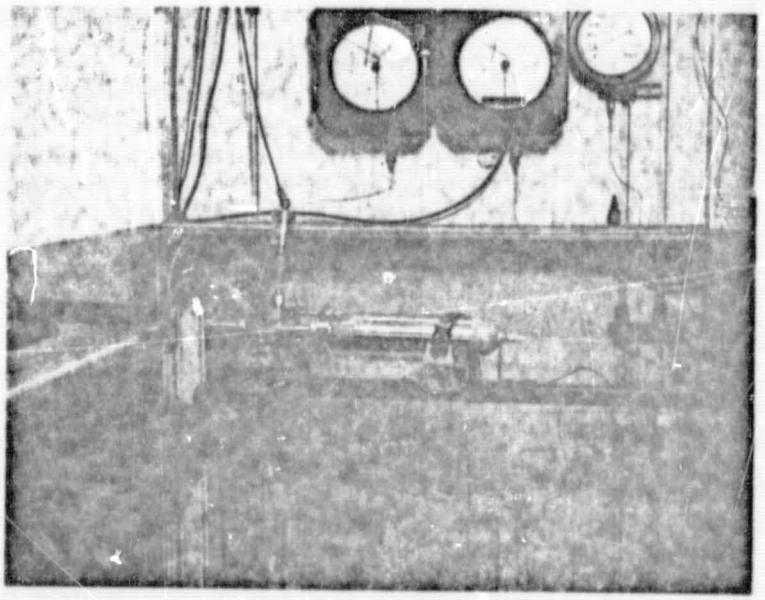

FIGURE 34. PICTURE OF SIMULATED SYSTEM TEST

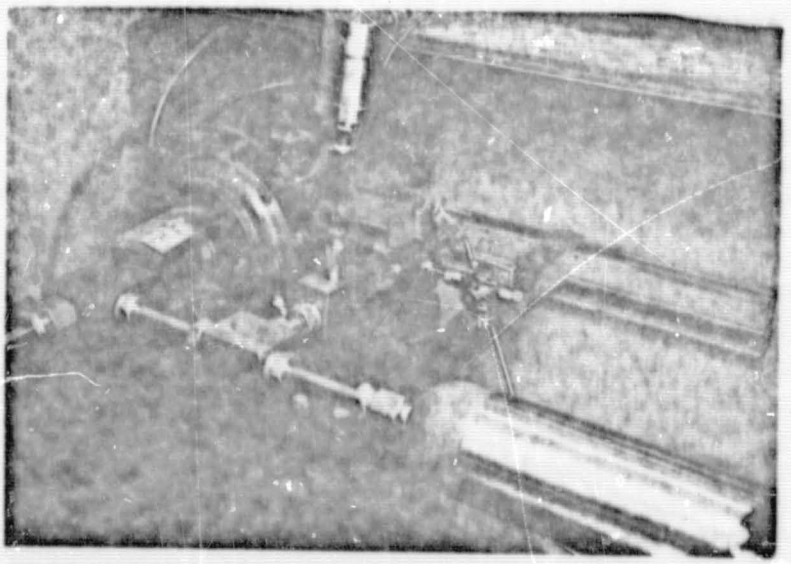

FIGURE 35. VIEW OF GEMINI REGULATOR LOCATION IN SIMULATED SYSTEM

b. To warm up the oxygen by pressurization and provide gas at essentially ambient temperature.

The storage vessel had an internal geometric volume of 341 cubic inches, was constructed of 316 stainless steel and was rated at 15,000 psi. It was considered expendable in the event of a mishap. A 5/16-inch diameter hole through the head of the vessel was given a funnel-shaped, curved radius on the inside face of the head to facilitate gaseous flow.

2. Air-operated valve

The valve body, removeable seat, stem, and packing washers were made from Monel 400 and Monel K-500. The packing was glass-filled TFE. The valve contained 5/16-inch I.D. ports and was rated at 10,000 psi. It was actually necessary to use the valve at higher pressures for these tests but because the tests were conducted in a high pressure area and the valve had a built in safety factor we were able to do so. Valves rated for higher pressures contained smaller port openings which would not have been as satisfactory for the tests.

The upstream port of the valve was placed in a direct line with the storage vessel and the downstream port was placed in a direct line with the receiver to provide the minimum resistance to gas flow.

3. Receiver

Because nickel was found to be the best material of construction, a nickel-lined stainless steel cylinder was purchased. The cylinder wall consisted of 0.20 inch of nickel and 0.30 inch of stainless steel. The cylinder was rated for 7500 psi. Internal geometric volume was 65 cubic inches. The receiver was placed in direct line with the air-operated valve to minimize pressurization time.

4. Probe

A 1/8-inch nickel rod was selected for the electrostatic probe because of its resistance to ignition. It entered the receiver through an insulated fitting and was sealed with TFE packing. A nickel washer fastened to the rod on the inside prevented its being blown out by the combination of high pressure and the lubricity of the TFE.

5. 10,000 psi Pressure Transducer

The transducer was used to measure the pressurization time of the simulated system. Because it was made of stainless steel it was placed in a physical position to minimize its being impacted by any particles that might be in the system.

6. Regulator

Because we were trying to simulate a system, it was felt that a pressure regulator which is currently used in high pressure oxygen should be included.

The regulator used was identical to that which will be used in the Gemini capsule. The regulator is only used at 5000 psi in the Gemini capsule but is similar in construction to the regulator used in the Mercury capsule at 7500 psi. Aluminum was used for the body of the Mercury regulator while stainless steel is used for the body of the Gemini regulator.

The regulator contains a relief device on the downstream side to handle all the flow in the event of catastrophic failure in the regulator itself. The relief device limits pressure downstream to a maximum of 200 psi.

Elastomeric materials are used in the regulator for static and dynamic seals.

The regulator was placed in a position which was thought to be comparable to one that would be used in a system: not too far from the receiver but not in a direct line with the charging line.

7. Valves, Fittings, and Tubing

All valve bodies were Monel 400 but some of the valve stems were Monel K-500 and some were 17-4 PH stainless steel. Likewise packing washers were either Monel 400 or stainless steel. Packing for the valve stems was glass-filled TFE.

All fittings were Monel 400 except for two stainless steel tees to connect the 9/16" O.D. x 5/16" I.D. tubing. All tubing was also Monel 400.

8. Lubricants and Thread Sealants

TFE tape was used both as a lubricant and a sealant for pipe threads on both ends of the receiver and at the transducer because other materials were either considered to be unsuitable or sealing characteristics were unknown.

A thin film of fluorocarbon oil was used to lubricate the threads of the tubing, gland nuts and valve stems. However, these points are not exposed to high pressure oxygen either because of weep holes or isolation by the valve stem packing.

9. 10,000 psi Pressure Recorder

This recorder contained a stainless steel bourdon tube but shock effects on it were minimized by using 1/8-inch O.D. tubing to connect it to the system.

Procedure

The following steps were followed in making a simulated test:

1. High pressure oxygen from the warm converter was used to pressurize the storage vessel to the desired pressure.

Card #5

2. Initially the receiver was successively pressurized and blown down several times with 2000 psi oxygen to be certain an oxygen atmosphere existed. This was also done with the Gemini regulator after the first series of tests. (For immediate succeeding tests, step 2 was eliminated.)

3. The blowdown valves were closed and the air-operated valve was opened.

4. The rate of pressure build-up was recorded on a Sanborn 150 recorder and any electrostatic charge developed was recorded photographically with an oscilloscope. A typical pressure profile is shown in Figure 36, and a typical photographic record of the electrostatic charge is shown in Figure 37.

5. The air-operated valve was closed and the simulated system and the downstream side of the Gemini regulator were blown down.

6. The electrostatic probe was grounded for several minutes between tests to be certain there was no charge on it at the beginning of the next test.

7. Steps, 1, 3, 4, 5, and 6 were repeated for the next test.

8. Temperature of the gas in the storage vessel just prior to making a test was always between 10°C and 20°C.

7500 psi Tests

1. Results

a. The simulated system was pressurized with oxygen to instantaneous pressures ranging from 665 psi to 7100 psi without any mishaps. Pressurization time varied from 0.5 second to 0.21 second.

b. Ten pressurizations were made to instantaneous pressures of 7000 psi. Final pressures of 8000 psi were developed when the air-operated valve was left open and the receiver and storage vessel were permitted to equalize pressures over a period of a few minutes. The gas in the storage vessel (initially at 12,000 psi) was cooled tremendously during pressurization of the simulated system. The temperature of the gas in the storage vessel was not measured but Byrnes, Reid and Ruccia [2] have shown that the temperature of a gas in a cylinder during depressurization may be lowered substantially.

c. Electrostatic charges measured varied from 0.0 volt to -0.32 volt.

d. Substituting thirty inches of 1/4-inch O.D. x 0.083-inch I.D. tubing for the 9/16-inch O.D. by 5/16-inch I.D. charging line between the air-operated valve and the receiver did not increase the electrostatic charge developed. The pressurization time recorded for the receiver when 1/4-inch tubing wasused for the charging line is in error because of the position occupied by the transducer during these tests.

e. Temperature measurement of gas in the receiver during pressurization showed a maximum temperature rise of 80°C.

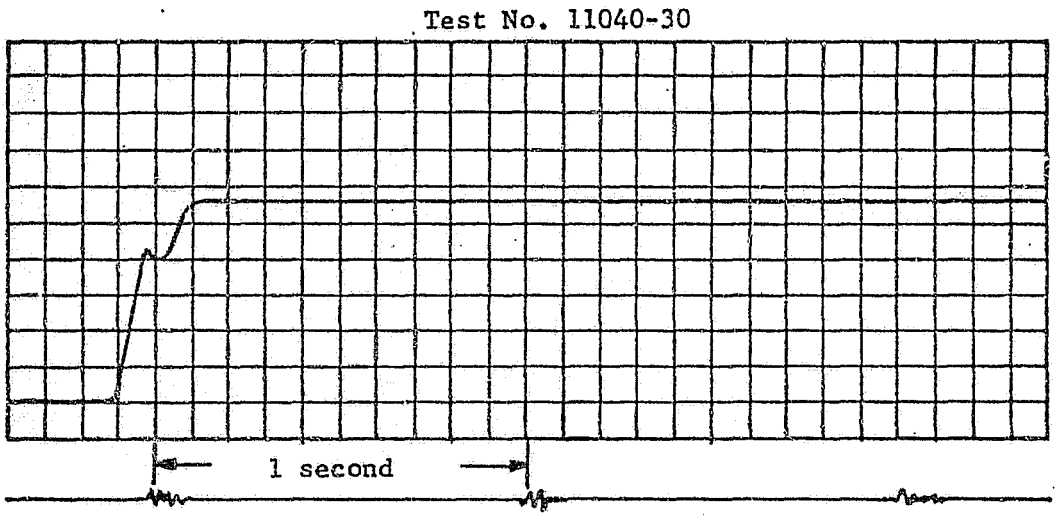

FIGURE 36. PRESSURE PROFILE OF SIMULATED SYSTEM TEST

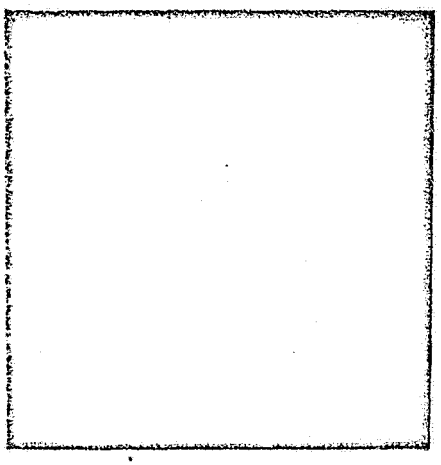

FIGURE 37.

TYPICAL PHOTOGRAPHIC RECORD OF ELECTROSTATIC CHARGE DEVELOPED IN SIMULATED TEST

f. Complete data may be found in Table 11 of Appendix IV.

2. Evaluation of Results

a. The fact that the simulated system was tested thoroughly without any malfunctions does not alter the fact that charging of a system of this type always carries with it the inherent hazards associated with high pressure gaseous oxygen nor does it imply that oxygen can be handled in the system with absolute safety.

b. Because there were no malfunctions, the flow approaching a hazardous condition cannot be defined.

c. There were no significant electrostatic charges developed during these tests. Therefore, it must be concluded that this does not represent a hazard in the system as it was tested. If the gas were to travel through lengthy lines before reaching the receiver, more of a charge might be developed.

d. A dip always occurred in the pressure profile (Figure 36) and correlated with a hissing sound from the test area. This was found to be due to the relief valve opening on the downstream side of the Gemini regulator. Apparently because of the rapid pressurization, the downstream pressure exceeded 200 psi before the regulator could shut off the flow. This momentarily caused a dip in the pressure curve until the regulator started to control, then the relief valve would close and the pressure in the system would rise. Of course this all happened in a small fraction of a second.

e. The Gemini regulator performed perfectly during all the tests. However, in view of the results of oxygen bomb tests and promoted ignition tests, some of its materials of construction are not recommended for 7500 psi oxygen service.

f. After one of the tests, the receiver started to leak around the threads where the fitting for the probe threaded into the receiver. It was thought that the TFE tape might have partially ignited but when the fitting was removed it was not possible to determine that any ignition had taken place.

Evaluation of Hardware Used in the Experimental Program

Gemini Regulator

As previously mentioned this regulator performed perfectly but some of the materials of construction are not recommended for 7500 psi oxygen service.

High Pressure Valves

1. Serious galling occurred between the packing rings and the stem of the original Monel valves (Figure 38 A, B, C, D, and F). These valves were standard construction but custom-made. The difficulty was attributed to improper machining and surface finish of the parts, as well as tolerances which were too close. Reworking of the pieces provided better operation, but

the problem was never completely eliminated. No doubt use of similar metals together contributed to the over-all galling problem.

2. The seating surfaces of the Monel K-500 stem and the Monel 400 body tended to gall so that it was necessary to tighten the valve more and more to obtain a leak-tight seal. Finally it would be necessary to reface the seating surfaces of both the stem and the body. Figures 38 A, C, and D show galling as it occurred on the seating surface of the stem.

3. During the latter part of the program, 17-4PH stainless steel valve stems were substituted for the Monel K-500 valve stems in the Monel 400 bodies and stainless steel packing rings were substituted for Monel packing rings. This was done both to expedite test work and to permit some experience to be gained. The 17-4 PH valve stems performed better mechanically than the Monel K-500 stems because the seating surface did not gall as severely. Both rotating stems and non-rotating stems were used. (See Figure 3). The non-rotating stem gives good leak-tight seals with no scoring of the seating surface but it gives very poor control over gas flow because of backlash.

4. Complete stainless steel valves (body and stem) were used at times to keep the test work going and to gain some experience with their use in high pressure oxygen.

5. On occasion, when a valve was taken apart, there would be a slick dark film on the valve stem below the bottom packing washer (Figure 38 E). This appeared to be TFE which had coated the stem as it was opened and closed. This represents a possible source of ignition and, because it is not confined, would be more likely to be exposed to ignition conditions.

6. In spite of the fact that no mishaps occurred, stainless steel valves are the least satisfactory for use in 7500 psi oxygen service because of the low resistance of stainless steel to ignition.

7. Considerable effort needs to be expended to design a high pressure valve from materials that are more compatible with high pressure oxygen but still will not gall.

Tubing Connection and Fittings

The mechanical connection shown in Figure 4 was used throughout the tests except in those places that required pipe connections. This is a standard high pressure connection and, although there are some problems associated with its use, in general it performed satisfactorily and provided leak-tight seals.

It is recommended that some consideration be given to a means of locking the gland nut in position after the fitting has been tightened. This would prevent loosening due to vibration.

For maximum safety, all welded connections are recommended.

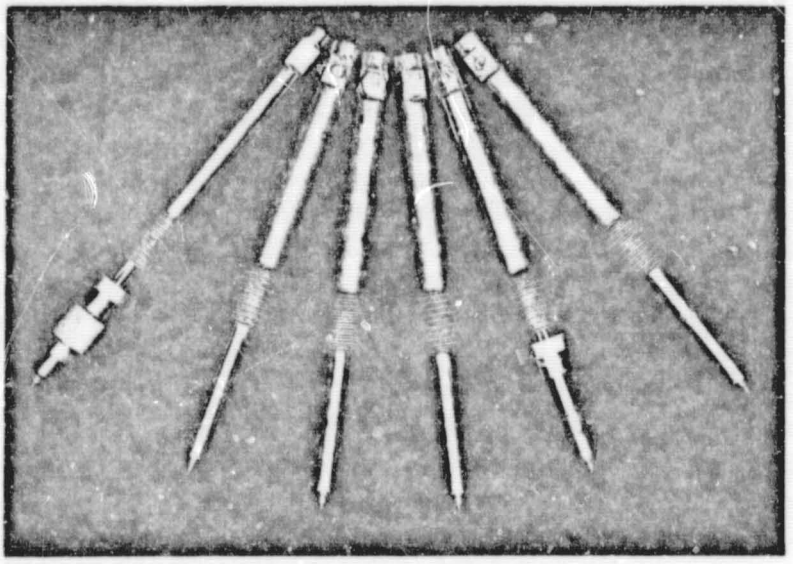

FIGURE 38. HIGH PRESSURE VALVE STEMS

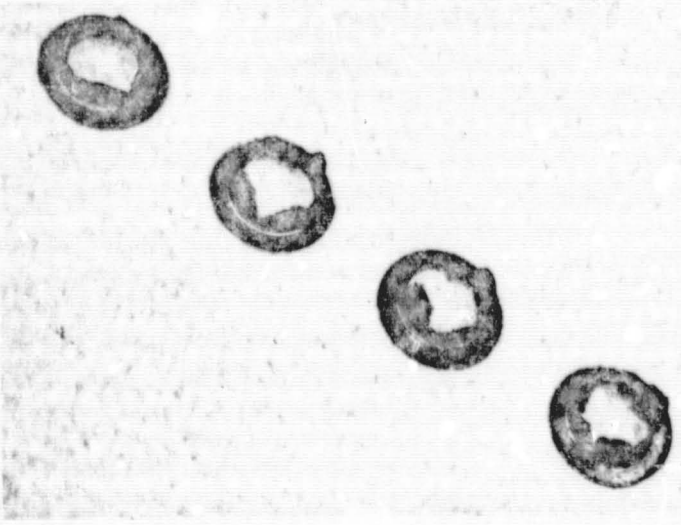

FIGURE 39. RUPTURED 10,000 PSI BURSTING DISCS

Miscellaneous

Four 10,000 psi safety discs were ruptured during the experimental test program. These are shown in Figure 39. These discs were fabricated from Monel alloy 400. The torn edges of these discs showed no evidence of ignition or combustion being caused by the rupture.

CONCLUSIONS

The following conclusions are based upon the results of the present experimental test program and other data referenced in this report.

1. The spontaneous ignition temperatures of the materials tested are essentially the same in 7500 psi oxygen as in 2000 psi oxygen.

2. The relative resistance of metals and alloys to ignition and combustion in 7500 psi oxygen agrees in general with results obtained in earlier Linde test work at 2000 psi and with the results of Dean and Thompson [3] except for aluminum.

3. Only three thread lubricants might have possible safe application in 7500 psi oxygen. These lubricants are Dixon's Flake Graphite No. 1, Burnil Brand Microplates, and Almasol Powder. Further information on their lubricating properties and thermal stability would need to be known before a complete recommendation could be made. One drawback to this type of lubricant is that there is always a possibility of particulate matter inadvertently getting into the high pressure system.

4. The only thread sealant tested in this program which might be recommended for 7500 psi oxygen service would be 50-50 soft solder (which could be used in tinning threads). TFE tape is not recommended because of the possibility of pieces getting into the gas stream.

5. Recognizing that some type of packing is needed for static and dynamic seals, glass-filled TFE would be the only material presently recommended for use. Even its use presents a hazard and it should only be used when tightly confined.

6. Inconel alloy 600, brass, Monel alloy 400, and nickel are recommended for use in 7500 psi oxygen. Other metals might be acceptable if plated with nickel, silver, or gold. Monel alloy K-500 might also be acceptable but it was not given the promoted ignition test in 7500 psi oxygen.

7. Of the materials tested, stainless steel and aluminum are the least satisfactory for use at oxygen pressures of 7500 psi.

8. Copper is not recommended because of the results of Baum, Goobich, and Trainer [1]. Other copper alloys might be acceptable material but would need to be tested.

9. Electrostatic charges developed during the charging of a small high pressure receiver were found to be negligible.

10. The simulated system was pressurized with oxygen to instantaneous pressures ranging from 665 psi to 7100 psi without incident. Pressurization time varied from 0.5 to 0.21 seconds.

The hazards considered to be most responsible for ignitions in oxygen systems are:

a. Adiabatic Compression - High temperatures may be produced when low pressure oxygen is suddenly brought to a high pressure, such as when a valve is suddenly opened between a high pressure and a low pressure portion of the system. These temperatures can be high enough to ignite organic materials or small particles of metal.

b. Particulate Matter - Particles may be accelerated in a high velocity stream and impacted against organic materials or metallic burrs, projections, etc. Their energy is converted to high local temperatures by this impact with subsequent ignition of associated materials. Even the particles themselves might be ignited if they were either organic or metallic in nature.

These hazards may be substantially reduced by proper cleaning of the equipment initially, use of filters (especially ahead of regulators) minimum use of organic material, and judicious operation of valves and regulators to prevent rapid increases in pressure.

There are other mechanisms by which ignition may occur but these have been well covered by Reynales [13].

RECOMMENDATIONS

1. Further study should be made on the copper alloys to define more clearly their compatibility and applicablility in 7500 psi systems.

2. More tests should be conducted on metals and alloys to determine the effect of geometric configuration on the relative ignition temperatures.

3. There is need for further investigation into thread lubricants and thread sealants. This study would need to cover their physical properties such as lubrication and sealing qualities as well as their compatibility with oxygen. Development of special lubricants and sealants might be required.

4. A program is needed to develop and build better hardware constructed of materials more compatible with high pressure oxygen. The program should cover any and all equipment which would be used in a 7500 psi oxygen system.

REFERENCES

(1) Baum, J. V., Goobich, B., and Trainer, T. M., An Evaluation of High-Pressure Oxygen Systems, AMRL Technical Documentary Report 62-102, Aerospace Medical Research Laboratories, Wright-Patterson Air Force Base, Ohio, September 1962.

(2) Byrnes, W. R., Reid, R. C., and Ruccia, F. E., The Rapid Depressurization of a Gas Storage Cylinder, Preprint No. 214, Massachusetts Institute of Technology, Cambridge, Mass., 1963.

(3) Dean, L. E., and Thompson, W. R., "Ignition Characteristics of Metals and Alloys," Journal of the American Rocket Society, 31 (7), 917-23, July 1961.

(4) Gillerman, J. B., "Telescoped Testing of Environmental System Speeded Mercury Design," Space/Aeronautics, 35, 76-79, May 1961.

(5) Greenspan, Lewis, "Ignition of Kel-F and Teflon," Review of Scientific Instruments, 29, 172-3, February 1958.

(6) Grosse. A. V., and Conway, J. B., "Combustion of Metals in Oxygen," Industrial and Engineering Chemistry, 50 (4), 663-672, April 1958.

(7) Hersey, M. D., "Study of the Oxygen-Oil Explosion Hazard," Am. Soc. Naval Engineers, 36, 231-243, 1924.

(8) Hersey, M. D., Oxygen - Oil Explosions, Department of Interior, Bureau of Mines, Preliminary Reports 1, 2, and 3, U. S. Bureau of Mines, Washington, D.C., July 1923.

(9) Hill, P., Adamson, D., Foland, D., and Brissette, W., High Temperature Oxidation and Ignition of Metals, NACA, R. M. L55L23b, National Advisory Committee for Aeronautics, Langley Research Center, Langley Field, Va., March, 1956.

(10) Markstein, G. H., "Combustion of Metals, AIAA Journal, 1 (3), 550-562, March 1963.

(11) Reynales, C. H., Compatibility of Materials with Oxygen, Report No. D81-444, Douglas Aircraft Company, Inc., Long Beach, Calif., Oct. 1, 1958.

(12) Reynales, C. H., "Selection of Lubricants and Thread Compounds for Oxygen Missile Systems," Advances in Cryogenic Engineering, Pages 117-129, Vol.6, K. D. Timmerhaus, Ed., Plenum Press. 1961, New York.

REFERENCES
(Continued)

(13) Reynales, C. H., Safety Aspects in the Design and Operation of Oxygen Systems, Engineering Paper No. 741, Douglas Aircraft Co., Inc., Santa Monica, Calif., 1959.

(14) Reynolds, W. C., Investigation of Ignition Temperatures of Solid Metals, NASA Technical Note D-182, National Aeronautics and Space Administration, Washington, D.C., October, 1959.

(15) Riehl, W. A., Key, C. F., and Gayle, J. B., Reactivity of Titanium with Oxygen, NASA Technical Report R-180, National Aeronautics and Space Administration, Washington, D. C., 1963.

(16) Smeltzer, W. W., and Perrow, J. M., "Oxidation of Metals," Industrial and Engineering Chemistry, 53 (4), 319-324, April 1961.

(17) Watkins, H. D., "Basic Gemini ECS Keyed to 14-day Flight," Aviation Week and Space Technology, 79, 52-69, August 19, 1963.

APPENDIX I

CALCULATION OF THEORETICAL TEMPERATURE ATTAINED BY ADIABATIC COMPRESSION

The theoretical temperature attained by adiabatic compression was calculated using the expression:

$$\frac{T_2}{T_1} = \left(\frac{P_2}{P_1}\right)^{\frac{n-1}{n}} \qquad \text{where} \quad n = \frac{C_P}{C_V}$$

substituting for n, we obtain:

$$\frac{T_2}{T_1} = \left(\frac{P_2}{P_1}\right)^{\frac{1.4-1}{1.4}} = \left(\frac{P_2}{P_1}\right)^{0.286}$$

Using an initial pressure of 14.7 psia and an initial temperature of 293°K:

$$T_2 = 293\left(\frac{P_2}{14.7}\right)^{0.286}$$

This equation was solved for various pressures to obtain the theoretical temperature rise. These are presented in Table 5 and Figure 40.

TABLE 5

THEORETICAL TEMPERATURE ATTAINED BY ADIABATIC COMPRESSION

CALCULATED FROM THE EXPRESSION $\frac{T_2}{T_1} = \left(\frac{P_2}{P_1}\right)^{\frac{n-1}{n}}$

P_2, psia	Temperature	
	T_2, °K	T_2, °C
100	506	233
200	622	349
400	761	488
800	922	649
1,200	1036	763
1,600	1122	849
2,000	1199	926
2,400	1266	993
2,800	1313	1040
3,200	1363	1090
4,000	1455	1182
5,000	1561	1288
6,000	1639	1366
7,000	1711	1438
7,500	1750	1477
10,000	1900	1627
15,000	2123	1850

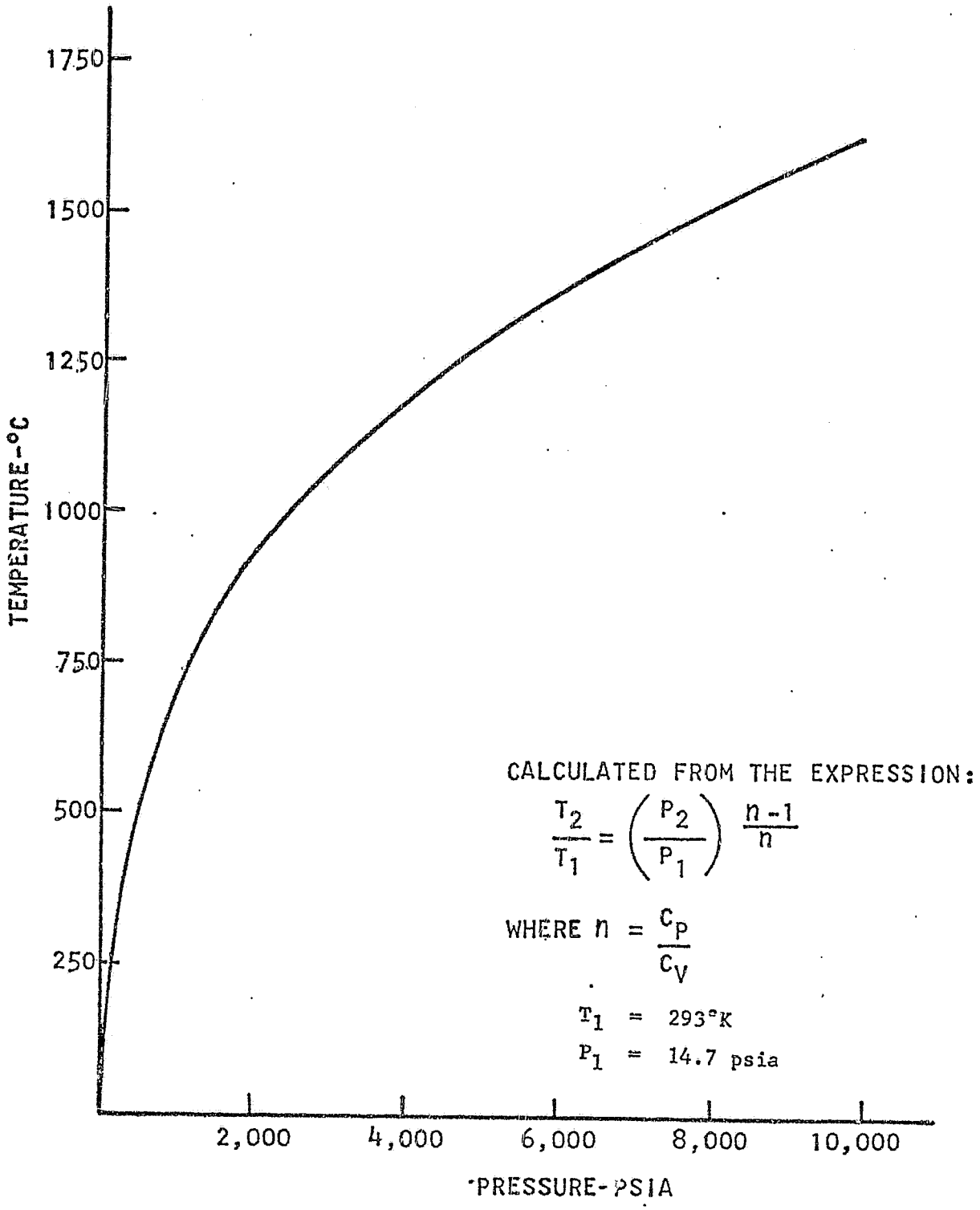

FIGURE 40. THEORETICAL TEMPERATURE ATTAINED BY ADIABATIC COMPRESSION

APPENDIX II

CALCULATION OF COMPRESSIBILITY FACTORS FOR OXYGEN

The compressibility factor (Z) for oxygen was calculated for various pressures using charts[1] which comprised a series of lines representing compressibility factor, $Z = \left[\frac{PV}{P_oV_o}\right]_{T = \text{const.}}$, plotted against reduced pressure, $P_r = \frac{P}{P_c}$, for different values of reduced temperature, $T_r = \frac{T}{T_c}$

The pressures and compressibility factor for each are presented in Table 6 and Figure 41 for $T_r = 1.9$.

TABLE 6

COMPRESSIBILITY FACTOR FOR OXYGEN AT VARIOUS PRESSURES

P, psia	P_R	Z
200	0.271	0.995
400	0.543	0.99
600	0.815	0.985
800	1.08	0.97
1,000	1.36	0.965
1,200	1.63	0.955
1,400	1.90	0.95
1,600	2.17	0.942
2,000	2.71	0.938
2,400	3.26	0.935
2,800	3.80	0.938
3,200	4.35	0.945
4,000	5.42	0.97
5,000	6.78	1.02
6,000	8.15	1.07
7,000	9.50	1.125
8,000	10.85	1.193
9,000	12.20	1.272
10,000	13.58	1.35
11,000	14.92	1.42
12,000	16.30	1.49
13,000	17.65	1.56
14,000	19.0	1.63
15,000	20.4	1.71
16,000	21.7	1.78
17,000	23.1	1.85
18,000	24.4	1.92
19,000	25.8	1.99
20,000	27.2	2.06

(1) "Compressibility Charts and Their Application to Problems Involving Pressure-Volume-Energy Relation for Real Gases" - Research Bulletin P-763J, Worthington Corporation, Harrison, New Jersey (1952)

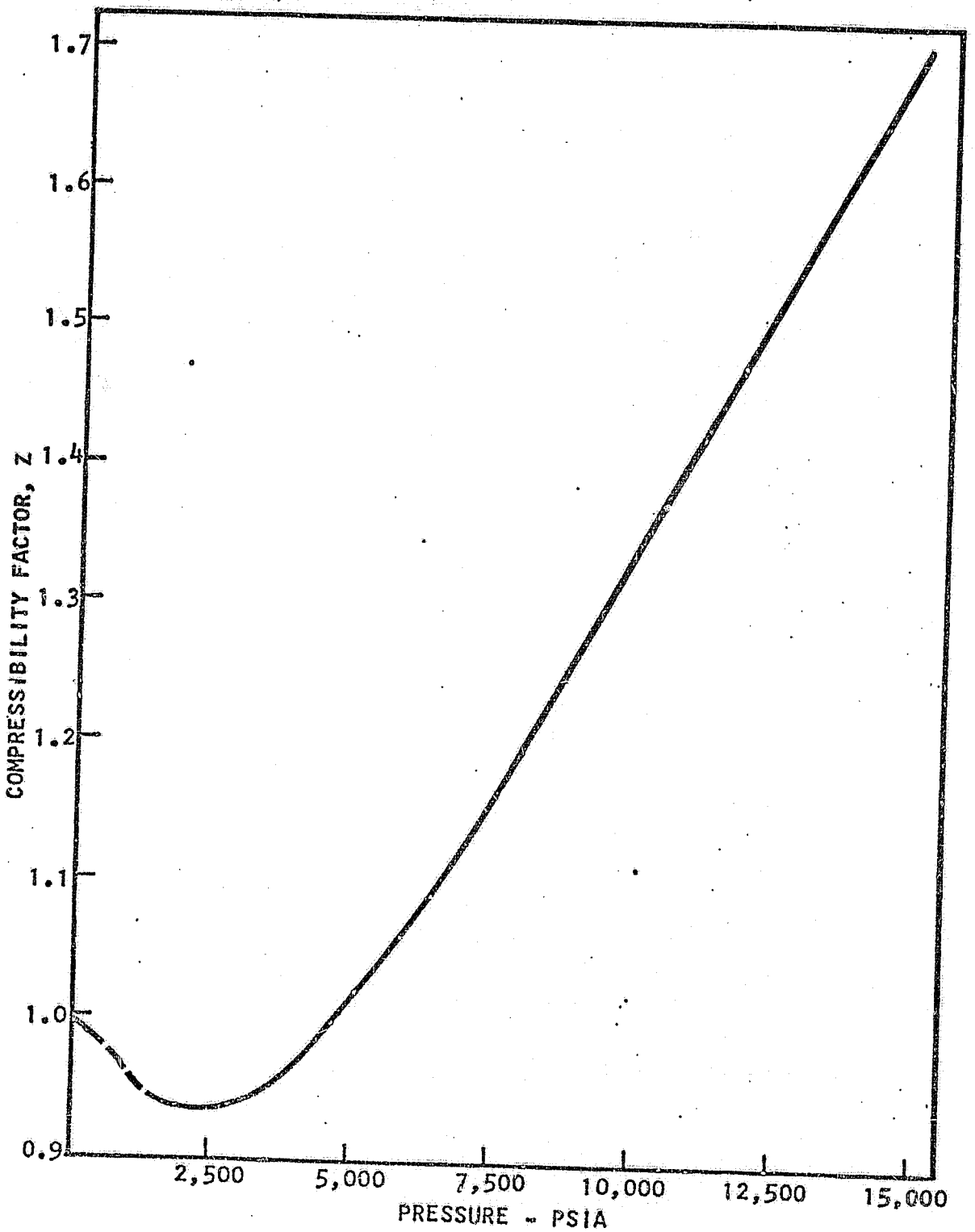

FIGURE 41. COMPRESSIBILITY FACTOR FOR OXYGEN AT 293°K

APPENDIX III

ADIABATIC COMPRESSION - A CONTROLLED IGNITION MECHANISM

Compression Apparatus

The envisioned apparatus as shown in Fig. 42 was considered equivalent to the model of Fig. 43 where the advancing high pressure gas front is equivalent to a piston moving at the velocity of sound (C_o). In this case a shock wave advances into the gas at rest at a velocity (V_W) greater than the velocity of the piston (V_p). The values for these velocities and resulting pressure and temperature rise behind the shock wave can be calculated.

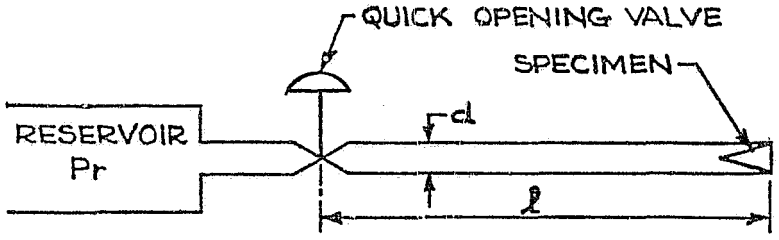

FIGURE 42

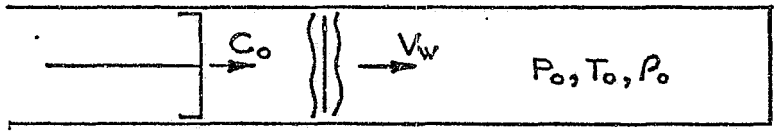

FIGURE 43

When the shock wave preceeding the piston reaches the wall at the end of the tube it is reflected giving rise to further compression.

1st Shock

$$V_W = \frac{1}{2}\frac{V_p}{1-\mu^2} + C_o^2 + \frac{1}{4}\left(\frac{V_p}{1-\mu^2}\right)^2 \qquad (1)\ \text{(Ref. 1)}$$

where:

$$\mu^2 = \frac{k-1}{k+1}$$

for $V_p = C_o$ and representative values of $K = 1.4$ and $C_o = 1130$ ft./sec.

$$V_W = 1990 \text{ ft./sec.}$$

$$M_o = \frac{V_W}{C_o} = 1.76 \qquad (2)$$

Ref. 1: R. Courant, K. O. Friedricks - Supersonic Flow and Shock Waves Interscience Publishers Inc., 1948.

$$\frac{P_1}{P_o} = (1 + \mu^2) M_o^2 - \mu^2 = 3.494 \qquad (3)$$

$$\frac{\rho_1}{\rho_o} = \frac{P_1 + \mu^2 P_o}{P_o + \mu^2 P_1} = 2.3 \qquad (4)$$

$$\frac{T_1}{T_o} \cdot = \frac{P_1}{P_o} \frac{\rho_o}{\rho_1} = 1.52 \qquad (5)$$

from (5) $T_1 = 1.52\ (530°R) = 805°R$

2nd Shock

$$\frac{P_2}{P_1} = \frac{(2\mu^2 + 1) \frac{P_1}{P_o} - \mu^2}{\mu^2 \frac{P_1}{P_o} + 1} = 5.06 \qquad (6)$$

and from expressions similar to (4) and (5)

$T_2 = 1430\ °R$

The conclusion is that in the assumed model a series of shock reflections will rapidly tend to build up pressures and corresponding high temperatures in the tube. Actually friction effects would tend to dampen the shock waves fairly soon.

To determine how clearly the above model can be simulated tests were run on the quick-opening valve. The observed results are indicated below.

Preliminary Tests with "Quick Opening" Valve

Measurements made of the rate of pressure build-up in the actual tube indicates flow velocities substantially below sonic so that the actual mechanism of compression cannot utilize the idealized piston described above.

Valve opening time - 0.5 sec.

Pressure build-up to 2000 psi in 20 in. long 5/16 in. diameter tube takes - 0.05 sec.

The rate of pressure build-up is nearly linear and approximately proportional to the length of test section.

In this instance, the mechanism of pressure build-up involves mixing of the gas at rest in the tube and the inrushing gas.

In view of the fact that a high degree of mixing takes place the anticipated temperature rise becomes uncertain and of questionable reproducibility.

Comparison of Gas Heat Capacity to Heat Loss to Surroundings

In this case a control volume of 1.07×10^{-3} ft.^{3} was taken representing a tube 5/16 in. I. D. and 24 in. long.

then $Q = V \rho C_p$ (7)

$$= 1.07 \times 10^{-3} (.089) .3 = .29 \times 10^{-4} \text{ Btu/°F}$$

The heat transfer from the tube can be expressed as:

$$dQ = h A \Delta T \, dt \quad (8)$$

where both the heat transfer area (A) and the temperature gradient are time dependent.

then: $$Q = \int_0^t h \, A(t) \, \Delta T(t) \, dt \quad (9)$$

From thermodynamic considerations an expression for ΔT was derived as follows:

$$\frac{T_2}{T_1} = \left(\frac{V_1}{V_2}\right)^{k-1} \quad (10)$$

$$\Delta T = T_2 - T_1 = T_1 \left[\left(\frac{V_1}{V_2}\right)^{k-1} - 1 \right] \quad (11)$$

since:

$$V_2 = V_1 - AX \quad (12)$$

where $X = \frac{dX}{dt} t$ and letting $\frac{dX}{dt} = K$

$$V_2 = V_1 - AKt \qquad (13)$$

Substituting (13) in (11) and simplifying:

$$\Delta T = T_1 \left[\left(\frac{\rho}{\rho - kt} \right)^{k-1} - 1 \right] \qquad (14)$$

The heat transfer area made up of the tube ends and the varying surface area is expressed as:

$$A = 2 \frac{\pi}{4} d^2 + \pi d (\rho - x)$$

$$= 2 \frac{\pi}{4} d^2 + \pi d (\rho - kt) \qquad (15)$$

Substituting (14) and (15) in (9) and simplifying the heat transfer to the surroundings is expressed as:

$$Q = h T_1 \frac{\pi d^2 l (k-1)}{2k (2-k)} \left[l^{2-k} - (1-kt)^{2-k} \right] + \frac{\pi d l}{(3-k) k} \left[l^{3-k} - (1-kt)^{3-k} \right]$$

$$- \frac{\pi}{2} d^2 t - \pi d \left(l t - \frac{k}{2} t^2 \right) \qquad (16)$$

for the representative values of:

$d = \frac{.31}{12} = .026$ ft.

$l = 2$

$t = .04$ sec.

$k = 25$ ft./sec.

$T_1 = 530$ °R

$Q = .06$ Btu

This heat loss to the surroundings is too large compared to the heat capacity of the gas to maintain adiabatic conditions during compression.

APPENDIX IV.

TABLES OF EXPERIMENTAL DATA

TABLE 7

SUMMARY OF PRELIMINARY HIGH PRESSURE OXYGEN BOMB TESTS

AND CORRELATION WITH 2000 PSI PROTOTYPE BOMB TESTS AND LINDE STANDARD 2000 PSI OXYGEN BOMB TESTS

HIGH PRESSURE BOMB								PREVIOUS DATA						
								PROTOTYPE BOMB					LINDE STANDARD BOMB	
Test date 1963	Sample material and test No.	Notes	Sample weight in grams	Ignition temp. °C	Ignition pressure psi	Temp. rise on ignition °C	Pressure rise on ignition psi	Average ht'g rate °C/min during last 20 min.	Test date 1963	Sample weight in grams	Ignition temp. °C	Ignition pressure psi	Average ht'g rate °C/min.	Ignition temp. °C	Ignition pressure psi
	Durabla Gasket														
10-7	9914-14D		0.1	156	2300	20	50	8.0	8-6	0.1	147	2275	3	165	1900
10-18	9914-16A		0.1	153	2500	20	200	4.8	8-7	0.1	152	2200	4		
10-18	9914-16B		0.1	149	8100	12	500	4.4	8-14	0.1	160	2230	10		
									8-14	0.1	146	2230	5		
									8-14	0.3	155	2200	6		
									8-14	0.3	165	2230	12		
									8-15	0.1	146	2250	6		
	Filled Teflon														
10-2	9914-14A		0.3	461	2200	30	50	5.0	8-13	0.3	446	2280	4	No explosion at 410°C and 2000 psi	
10-7	9914-14B		0.3	460	2300	30	50	5.5	8-13	0.3	451	2140	9		
10-7	9914-14C		0.3	460	2170	30	70	1.8	8-13	0.3	455	2160	10		
10-18	9914-16C		0.3	456	5550	17	1000	4.3	8-13	0.15	451	2200	10		
10-21	9914-17A	(1)	0.3	455	7200	--	---	4.0	8-14	0.3	446	2300	10		
10-22	9914-18A	(2) (3)	0.15	N.E.340	---	--	---	--	8-14	0.5	459	2280	10		
10-22	9914-18B	(4)	0.15	469	9000	--	---	5.2	8-15	0.3	446	2300	10		
10-22	9914-18C		0.15	456	6450	23	600	4.1							
10-23	9914-19A	(5)	0.15	218	5500	40	400	7.8							
10-23	9914-19B		0.15	460	8000	15	1000	4.7							
10-24	9914-21A	(6)	0.15	471	8050	16	900	5.8							
	Viton A Compound														
10-8	9914-14E		0.1	330	2220	60	40	7.2	8-12	0.1	310	2300	5	330	2250
10-23	9914-19C		0.1	330	8600	50	600	8.8	8-14	0.1	325	2250	6		
									8-15	0.3	310	2100	10		
	Tricresyl Phosphate														
10-18	9914-16D		0.1	254	6900	32	1200	8.4	8-7	0.1	240	2400	4	260	2150
	Leather		---	---	-----	---	---	---	8-12	0.1	163	2300		170	2100
									8-12	0.1	160	2280			

(1) High pressure oxygen leaked through valve into bomb and pressure in bomb was reduced by blowing to atmosphere three times during test.
(2) N.E. - means no explosion at the indicated temperature
(3) Test stopped at 340°C because of leakage. Sample had started to decompose.
(4) High pressure oxygen leaked through valve into bomb.
(5) It is thought that this sample may have been contaminated.
(6) This sample was composed entirely of shavings.

TABLE 8

SUMMARY OF HIGH PRESSURE OXYGEN BOMB TESTS

Test date 1963	Sample material and test No.	Notes	Sample weight in grams	Ignition temp °C	Ignition pressure psi	Temp. rise on ignition °C	Pressure rise on ignition psi	Initial oxygen press. in bomb before ht'g	Voltage setting on furnace variac	Average ht'g rate °C/min. during last 20 min.
	Oxweld Anti-Friction Compound No. 54									
10/23	9914-20A		0.1	235	7400	40	900	5550	95	8.5
10/25	9914-23B		0.12	230	7600	31	950	6000	80	6.0
10/25	9914-23C		0.11	237	2300	50	200	1900	80	5.9
	Aroclor 1254									
10/23	9914-20B		0.15	355	7550	35	1400	5150	95	8.3
10/23	9914-20C		0.11	355	8100	17	1000	5750	95	7.8
10/24	9914-21B		0.14	376	2300	31	300	1750	95	6.7
10/24	9914-21C		0.13	385	2400	90	400	1800	95	8.3
	Virgin Teflon									
10/25	9914-22A		0.1	474	7870	16	600	4850	95	5.6
10/25	9914-22B	(leak)	0.1	471	7150	12	600	4830	95	5.6
10/25	9914-22C		0.2	465	7750	16	1200	5150	95	5.3
10/25	9914-23A		0.1	469	2650	20	100	1950	95	6.3
	Teflon 100X									
10/30	9914-24A		0.1	414	7800	9	800	4600	95	5.2
10/30	9914-24B	(leak)	0.1	412	6600	10	600	4600	95	5.1
10/30	9914-24C		0.1	410	8150	10	800	5250	95	4.8
10/30	9914-25A		0.1	413	1800	32	50	1400	95	6.8
	Kel-F 5500									
10/31	9914-25B		0.1	345	7650	11	600	5050	90	6.5
10/31	9914-25C	(leak)	0.1	340	7200	16	600	5400	85	5.7
10/31	9914-25D		0.1	352	2200	38	100	1900	85	5.9
	Kel-F 3700									
10/31	9914-26A		0.1	332	7600	15	800	5300	85	5.9
10/31	9914-26B		0.1	331	6900	15	700	5050	85	5.8
10/31	9914-26C		0.1	341	2350	30	100	1900	85	5.8
	Kel-F 81									
11/1	9914-26D	(1)	0.1	433	8300	10	500	5150	85	3.8
11/1	9914-27A	(1)	0.1	433	7300	8	400	4750	95	6.2
11/1	9914-27B	(1)	0.1	431	2500	15	200	1850	87	4.2
11/4	9914-27C	(1)	0.1	432	7800	10	500	4900	95	5.9
11/11	9914-32B	(2)	0.1	425	8100	10	400	5050	95	5.9
		(1) 1/8" rod from Adam Spence Corp.								
		(2) 1/16" sheet from Fluorocarbon Company.								
	Kel-F 90 Grease									
11/4	9914-27D		0.14	435	7200	10	500	4800	95	6.6
11/4	9914-30A	(leak)	0.12	448	7200	5	300	5000	95	6.7
11/5	9914-30B		0.13	445	8500	7	500	5150	95	5.8
11/5	9914-30C		0.11	435	2500	16	300	1900	95	8.0

TABLE 8 (Cont'd)

SUMMARY OF HIGH PRESSURE OXYGEN BOMB TESTS

Test date 1963	Sample material and test No.	Notes	Sample weight in grams	Ignition temp °C	Ignition pressure psi	Temp. rise on ignition °C	Pressure rise on ignition psi	Initial oxygen press. in bomb before ht'g	Voltage setting on furnace variac	Average Ht'g rate °C/min during last 20 min.
	High Purity Goop									
11/5	9914-28A	(1) (2)	0.1	N.E.500	8300	---	---	5100	95	5.5
11/5	9914-28B		0.22	411	6100	21	800	4400	95	7.0
11/5	9914-28C		0.1	419	2550	7	300	1950	95	6.8
11/6	9914-28D	(1) (2) (leak)	0.15	N.E.500	6000	--	---	5000	95	5.0
11/7	9914-30D	(1) (2)	0.18	N.E.500	8200	--	---	5050	90	3.8
11/8	9914-31A	(1) (2)	0.1	N.E.450	2900	--	---	1900	95	5.8
11/8	9914-31B	(2) (3)	0.3	N.E.440	7500	--	---	4850	86	2.8
	(1) When bomb disassembled, sample had disappeared and evidence of ignition, but no indication of ignition on charts- slight fumes were also noticed when bomb disassembled.									
	(2) N. E. - means no explosion at indicated temperature									
	(3) A residue of .03 gram of sample remained									
	Halocarbon Grease 25-10									
11/6	9914-29A	(leak)	0.12	438	7000	12	500	4800	90	5.0
11/6	9914-29B		0.13	444	7650	7	600	5000	90	5.0
11/6	9914-29C		0.12	431	2750	14	200	1850	95	6.6
11/6	9914-29D		0.11	439	7700	5	500	4900	95	6.2
	Holykote Z									
11/8	9914-31C		0.13	270	7000	140	350	5000	95	9.6
11/8	9914-31D		0.12	267	7300	120	400	5300	85	4.1
11/8	9914-32A		0.11	277	2700	103	50	1900	85	6.9
	Duroid 5600									
11/11	9914-32C		0.1	480	7300	10	300	4900	95	5.5
11/11	9914-32D		0.2	470	8100	12	600	5200	95	5.5
11/12	9914-33A	(1)	0.2	468	2450	12	400	1900	95	6.2
	(1) Residue same shape as initial sample, but it collapsed to dust when touched									
	Duroid 5650									
11/12	9914-33B		0.2	458	8000	17	1000	4900	95	5.7
11/12	9914-33C	(leak)	0.2	444	7450	17	900	4850	95	5.7
11/12	9914-33D	(1)	0.2	461	2450	20	150	1750	95	6.7
	(1) White residue same shape as initial sample									
	Duroid 5813									
11/13	9914-34A		0.2	464	8050	16	1000	4850	95	6.5
11/13	9914-34B	(leak)	0.2	463	7000	17	800	4900	95	6.3
11/13	9914-34C		0.2	463	2300	16	200	1650	95	6.0
	Duroid 5870									
11/13	9914-34D	(leak)	0.2	463	7550	18	1200	5000	95	6.3
11/14	9914-35A		0.2	469	7900	16	1200	4850	95	6.0
11/14	9914-35B		0.2	452	2650	39	250	1800	95	5.9

N.E. - means no explosion at the indicated temperature.

TABLE 8 (Cont'd)

SUMMARY OF HIGH PRESSURE OXYGEN BOMB TESTS

Test date 1963	Sample material and Test No.	Notes	Sample weight in grams	Ignition temp. °C	Ignition pressure psi	Temp. rise on ignition °C	Pressure rise on ignition, psi	Initial oxygen press. in bomb before ht'g.	Voltage setting on furnace variac	Average ht'g rate °C/min during last 20 min.
	Rulon A									
11/15	9914-35C	(leak)	0.2	465	7200	22	800	4900	95	6.1
11/15	9914-35D		0.2	466	7700	20	900	4800	95	6.8
11/18	9914-36A		0.2	463	2600	22	150	1900	90	4.9
	Rulon B									
11/18	9914-36B		0.2	460	7900	25	600	4850	95	6.0
11/18	9914-36C		0.2	465	7400	25	500	4700	95	7.0
11/18	9914-36D		0.2	466	2600	20	200	1900	85	3.8
	Rulon C									
11/19	9914-37A		0.2	465	7300	15	700	4600	95	5.9
11/19	9914-37B		0.2	471	7750	16	750	4750	95	6.3
11/19	9914-37C		0.2	458	2600	25	300	1900	95	7.0
	Everlube Solid Film Lubricant No. 811 (Dried)									
11/19	9914-37D	(Powder)	0.21	216	6200	220	600	4800	92	7.3
11/19	9914-38A	(1/16" chunks)	0.20	250	2350	240	100	1850	88	7.5
11/20	9914-38B	(1/16" chunks)	0.20	254	8700	175	900	6000	88	7.0
	Halocarbon Oil Series 13-21									
11/20	9914-38C		0.17	442	7700	10	600	4800	95	7.6
11/20	9914-38D	(1)	0.11	N.E.500	7800	---	---	4800	92	5.0
11/20	9914-39A		0.18	435	7800	15	800	4800	92	6.3
11/21	9914-39B		0.18	427	2400	23	400	1700	88	5.0
	(1) Sample ignited without any indication being evident on the recorder charts									
	Burnil Brand Microplates									
11/21	9914-39C (1)	(2) (Powder)	0.08	N.E.500	9200	---	---	5600	90	4.0
11/21	9914-39D (1)	(2) (Powder)	0.09	N.E.500	2400	---	---	1700	95	5.6
11/21	9914-40A	(2) (Paper)	0.2	N.E.500	8000	---	---	4700	95	5.4
	(1) Unable to get any more weight of powder into test tube									
	(2) All samples were still intact when the bomb was disassembled									
	Viton A (Virgin)									
11/22	9914-40B		0.11	310	7200	16	500	4900	90	7.6
11/22	9914-40C		0.12	310	2400	80	100	1900	85	6.4
11/22	9914-40D		0.13	300	7000	60	600	5000	85	6.8
	Viton B (Virgin)									
11/22	9914-41A		0.11	318	7000	47	600	4800	85	6.2
11/22	9914-41B		0.11	316	7700	19	800	5300	85	7.0
11/23	9914-41C		0.11	325	2350	30	100	1700	85	5.0

N.E. - means no explosion at the indicated temperature.

TABLE 8 (Cont'd)

SUMMARY OF HIGH PRESSURE OXYGEN BOMB TESTS

Test date 1963	Sample Material and Test No.	Notes	Sample weight in grams	Ignition temp. °C	Ignition pressure psi	Temp. rise on ignition °C	Pressure rise on ignition psi	Initial oxygen press. in bomb before ht'g	Voltage setting on furnace variac	Average ht'g rate °C/min during last 20 min
	Mano Pipe and Joint Compound									
11/26	9914-41D	(1)	0.17	N.E.500	8150	---	---	4950	95	6.0
11/26	9914-42A	(2)	0.21	422	7700	12	100	4900	95	6.5
11/26	9914-42B	(2)	0.19	427	7900	10	100	5050	95	6.7
11/27	9914-42C	(2)	0.20	430	2600	16	25	1850	95	5.4
		(1) Sample may be partly decomposed. Color changed from dark to light gray.								
		(2) Sample sintered								
	Dixon's Flake Graphite No.1									
11/27	9914-43A		0.23	N.E.500	7500	---	---	4650	95	3.5
11/27	9914-43B		0.24	N.E.500	7500	---	---	4650	95	5.0
11/27	9914-43C		0.23	N.E.500	2700	---	---	2000	95	6.0
	Oxylube No. 703 (Dried)									
12/2	9914-43D	(1)	0.11	N.E.500	8600	---	---	4900	95	5.0
12/2	9914-44A	(1)	0.23	N.E.500	2400	---	---	1700	90	4.0
12/2	9914-44B	(1)	0.20	N.E.500	7550	---	---	4650	92	3.0
12/4	9914-45B	(6)(2) estimated wt.	0.5+	190	6200	45	300	4700	95	7.7
12/4	9914-45C	(3)(4)	0.22	N.E.500	8800	---	---	5150	95	4.0
12/4	9914-45D	(5)(2)	0.21	N.E.310	7300	---	---	4900	95	7.2
12/4	9914-46A	(6)(2)	0.53	200	6500	40	500	4900	95	8.0
12/13	9914-51D	(6)(2)	0.40	238	2200	42	25	1800	95	8.0
		(1) Sample tested as chunk; some oxidation on outside of chunk evidenced by yellow color.								
		(2) Sample powdered in mortar and tested in powdered state.								
		(3) Sample composed of small pieces and powder as present in original dried sample.								
		(4) Sample intact when bomb disassembled; slight oxidation on bottom of sample evidenced by yellow color.								
		(5) Sample intact, no discoloration. Powder slightly sintered.								
		(6) Sample completely disappeared. Bomb thoroughly gunked with combustion products and corrosion.								
	Oxyseal (dried)									
12/3	9914-44C	(1)	0.15	347	7900	153	500	4950	95	7.4
12/3	9914-44D	(1) (leak)	0.20	348	6800	160	500	4900	90	6.4
12/3	9914-45A	(1)	0.20	360	2700	160	500	2000	90	4.2
		(1) Enough heat was liberated to melt the bottom of the pyrex test tube.								
	Oxweld Anti-Friction Compound No. 64									
12/6	9914-47A	(1)	0.22	N.E.500	8500	---	---	5000	95	5.0
12/8	9914-47B	(2)	0.21	N.E.400	8000	---	---	5000	95	5.0
12/8	9914-47C		0.80	414	6700	46	1900	4400	95	5.0
12/8	9914-47D		0.74	410	7600	Bursting Disc Ruptured		4800	95	5.0
12/8	9914-47E		0.52	410	2500	65	1000	1900	95	4.1
		(1) Sample completely disappeared when bomb disassembled.								
		(2) Sample partly decomposed, but mostly intact.								

N.E. - means no explosion at the indicated temperature.

TABLE 8 (Cont'd)

SUMMARY OF HIGH PRESSURE OXYGEN BOMB TESTS

Test date 1963	Sample material and test No.	Notes	Sample weight in grams	Ignition temp. °C	Ignition pressure psi	Temp. rise on ignition °C	Pressure rise on ignition psi	Initial oxygen press. in bomb before ht'g	Voltage setting on furnace variac	Average ht'g rate °C/min during last 20min.
	Rectorseal No. 15 (Dried). MIL-T-5542B (ASG)									
12/10	9914-48A		0.28	374	7700	104	2500	4900	98	6.3
12/10	9914-48B		0.18	355	6800	80	1000	4600	96	6.9
12/10	9914-48C		0.16	374	2500	70	400	2000	96	6.9
	50/50 Soft Solder									
12/10	9914-48D	(1)	0.6	N.E.500	7500	---	---	4700	96	3.4
12/10	9914-49A	(1)	0.5	N.E.500	7600	---	---	4800	100	5.0
12/10	9914-49B	(1)	0.5	N.E.500	2600	---	---	1900	100	6.3
	(1) Solder melted and a considerable amount of oxide formed.									
	Almasol Powder (325 Mesh)									
12/11	9914-49C	(1)	0.10	N.E.500	8000	---	---	4600	100	7.8
12/11	9914-49D	(1) (leak)	0.14	N.E.500	7000	---	---	4600	100	6.0
12/11	9914-49E	(1)	0.15	N.E.500	2900	---	---	2000	100	5.5
	(1) Sample intact. No evidence of oxidation.									
	Key Absolute (Dried) MIL-T-5542-B (ASG)									
12/11	9914-49F	(1)	0.12	N.E.500	7300	---	---	4550	95	3.0
12/12	9914-50A		0.56	342	6600	40	1200	4300	95	6.1
12/12	9914-50B	(2)	0.75	355	2500	40	500	1900	92	5.8
	(1) Sample decomposed, white ash left. (2) Bursting disc ruptured.									
	High Purity Goop									
12/12	9914-50C	(1)	0.51	N.E.420	8500	---	---	5100	95	4.0
12/13	9914-51A		0.50	398	2800	55	900	1900	95	5.0
	(1) Decomposition occurred, clear oily liquid condensed on bomb head, part of sample remaining. Fumes issued from bomb when it was disassembled.									
	Neoprene O-Ring (MIL-R-1149, Type II, Class I)									
12/13	9914-51B		0.11	200	2500	175	200	2000	95	7.4
12/13	9914-51C		0.05	190	7100	90	900	5500	89	6.0
	Linde Green Pipe Compound									
12/5	9914-46B		0.26	373	7450	14	250	4650	95	7.4
12/5	9914-46C		0.52	362	6900	30	600	4500	92	6.9
12/5	9914-46D		0.31	356	2350	54	200	1750	90	5.1

N.E. - means no explosion at the indicated temperature.

TABLE 9

PRELIMINARY DATA - PROMOTED IGNITION TEST

1964 date	Test No.	Promoter	Promoter wt. mg.	Specimen	Specimen wt. mg.	Physical configuration	Ignition temp. °C	Ignition pressure psig.	Approximate specimen size width x length mm.	Remarks
1-3	9914-59A	Neoprene	61	Stainless Steel Type 304	54	A	N.E.340	2400	6 x 8	O-ring charred and hard but original shape
1-3	9914-59B	"	55	Stainless Steel Type 304	52	A	200	2100	6 x 8	Complete combustion
1-3	9914-59C	"	59	Stainless Steel Type 304	53	A	325	2300	6 x 8	Complete combustion
1-3	9914-59D	"	57	Monel	50	A	N.E.220	2200	6 x 8	O-ring hard but original shape
1-6	9914-60A	"	57	Monel	51	A	N.E.350	2250	6 x 8	Ignition occurred as oxygen pressure reduced from bomb.
1-6	9914-60B	"	59	Monel	52	A	198	2000	6 x 8	Monel melted and oxidized.
1-6	9914-60C	"	57	Monel	49	A	350	2300	6 x 8	Monel melted into ball and oxidized on outer surface.
1-6	9914-60D	"	55	Monel	50	A	358	2250	6 x 8	Monel melted into ball and oxidized on outer surface.
1-7	9914-61A	"	59	----	--	--	360	2250	------	----------
1-7	9914-61B	"	55	----	--	--	360	2300	------	----------
1-7	9914-61C	"	55	Monel	150	A	360	2300	8 x 20	Monel melted and surface oxidation
1-7	9914-61D	"	55	Monel	150	A	200	2050	8 x 20	Monel melted and surface oxidation
1-8	9914-62A	"	55	Silver	140	A	349	2200	6 x 15	Silver melted, slight oxidation
1-8	9914-62B	"	56	Gold	170	A	200	2000	7 x 9	Gold melted into ball, no oxidation.
1-8	9914-62C	"	29	----	--	--	365	2000	------	----------
1-8	9914-62D	"	15	----	--	--	374	1950	------	----------
1-9	9914-63A	"	6	----	--	--	378	2150	------	----------
1-9	9914-63B	"	6	Stainless Steel Type 304	60	D	365	2300	7 x 8	Slight oxidation no ignition of stainless steel
1-9	9914-63C	"	7	Stainless Steel Type 304	44	D	375	1950	5 x 8	Slight oxidation no ignition of stainless steel
1-9	9914-63D	"	15	Stainless Steel Type 304	60	D	366	2000	7 x 8	Slight oxidation no ignition of stainless steel
1-10	9914-64A	"	29	Stainless Steel Type 304	49	D	343	2100	7 x 7	Oxidation of metal in contact with Neoprene.
1-10	9914-64B	"	29	Stainless Steel Type 304	55	E	365	2200	7 x 8	Complete combustion.
1-10	9914-64C	"	13	Stainless Steel Type 304	51	E	318	2200	7 x 7	Slight oxidation of stainless steel.
1-10	9914-64D	"	28	Stainless Steel Type 304	60	E	378	2000	7 x 8	Complete combustion.
1-13	9914-65A	"	19	Stainless Steel Type 304	59	E	358	1650	7 x 8	Stainless steel oxidized but did not burn.
1-13	9914-65B	"	21	Stainless Steel Type 304	56	E	327	1900	7 x 8	Stainless steel oxidized but did not burn.
1-13	9914-65C	"	24	Stainless Steel Type 304	57	E	316	2100	7 x 8	Stainless steel oxidized but did not burn.
1-13	9914-65D	"	26	Stainless Steel Type 304	55	E	378	1800	7 x 8	Stainless steel oxidized but did not burn.
1-15	9914-66A	"	26	Stainless Steel Type 304	55	E	345	2500	6 x 8	Complete combustion
1-15	9914-66B	Viton A	51	Stainless Steel Type 304	51	C	316	2200	6 x 8	Complete combustion
1-15	9914-66C	Viton A	50	Monel	50	C	310	2200	6 x 8	Monel melted, slight oxidation.
1-15	9914-66D	Viton A	73	Monel	52	C	307	2000	6 x 8	Monel melted, partly oxidized.
1-15	9914-67A	Viton A	50	Monel	50	C	312	7500	5 x 10	Monel melted some and surface oxidized.
1-15	9914-67B	Viton A	34	Stainless Steel Type 304	50	C	332	2200	5 x 10	Complete combustion.

TABLE 10

PROMOTED IGNITION TEST

1964 date	Test No.	Neoprene wt. mg.	Specimen	Specimen wt. mg.	Physical configuration	Ignition temp. °C	Ignition pressure psig.	Specimen size width x length mm.	Remarks
1-15	9914-67C	35	Monel	49	C	345	1900	5 x 10	Monel melted into ball.
1-16	9914-67D	31	Stainless Steel Type 304	51	C	194	6000	5 x 10	Complete combustion
1-16	9914-68A	21	Stainless Steel Type 304	51	C	310	8000	5 x 10	Complete combustion
1-16	9914-68B	30	Monel	50	C	315	7500	5 x 10	Monel melted and oxidized.
1-16	9914-68C	18	Stainless Steel Type 304	52	C	189	6750	5 x 10	Complete combustion
1-16	9914-68D	15	Monel	50	C	190	6700	5 x 10	Monel melted and oxidized.
1-16	9914-69A	13	Stainless Steel Type 304	50	C	189	7400	5 x 10	Complete combustion
1-16	9914-69B	12	Monel	51	C	190	7450	5 x 10	Monel partly oxidized, not melted.
1-17	9914-69C	7.6	Stainless Steel Type 304	49	C	190	7400	5 x 10	Complete combustion
1-17	9914-69D	7.0	Gold	128	C	189	7400	5 x 10	Gold melted at bottom where promoter contacted it.
1-17	9914-70A	4.4	Stainless Steel Type 304	50	C	192	7200	5 x 10	Complete combustion
1-17	9914-70B	1.8	Stainless Steel Type 304	50	C	N.E.280	7700	5 x 10	O-ring oxidized but still intact. No oxidation of stainless steel.
1-17	9914-70C	14.5	Monel	98	C	190	7000	5 x 18	Monel melted at bottom and oxidized 1/2 way up.
1-17	9914-70D	14.4	Monel	60	C	191	7200	5 x 10	Monel melted at bottom and side. Heavy oxidation.
1-17	9914-71A	2.5	Stainless Steel Type 304	49	C	316	7450	5 x 10	Stainless oxidized but did not burn.
1-17	9914-71B	14.0	Monel	41	C	191	5650	5 x 7	Oxidized, started to melt one corner.
1-17	9914-71C	4.3	Stainless Steel Type 304	49	C	306	7100	5 x 10	Stainless oxidized, but did not burn.
1-20	9914-71D	17.2	Monel	158	F	184	7850	5 x 29	13 mm burned 16 mm remained.
1-20	9914-72A	17.6	Monel	50	C	186	7450	5 x 10	Complete combustion.
1-20	9914-72B	17.9	Monel	102	C	185	7400	5 x 18	Complete combustion.
1-20	9914-72C	7.8	Stainless Steel Type 304	47	C	194	7250	5 x 10	Oxidized 5 mm from bottom but did not burn.
1-20	9914-72D	11.0	Stainless Steel Type 304	150	F	186	7500	5 x 30	Complete combustion.
1-20	9914-73A	8.5	Stainless Steel Type 304	50	C	190	7400	5 x 10	Complete combustion.
1-20	9914-73B	6.5	Gold	86	C	195	6700	5 x 7	Gold partly melted.
1-20	9914-73C	8.5	Stainless Steel Type 304	161	F	190	7000	5 x 30	Complete combustion.
1-21	9914-73D	10.0	Nickel	159	F	298	7350	5 x 30	Oxidation inside and out where neoprene touched. Hole burned through nickel.
1-21	9914-74A	13.4	Nickel	159	F	190	6800	5 x 30	Bottom 3 or 4 mm melted with surface oxidation.
1-21	9914-74B	17.6	Nickel	159	F	189	6600	5 x 30	Bottom 2 or 3 mm melted with light surface oxidation.
1-21	9914-74C	24.0	Nickel	158	F	185	6600	5 x 30	Light oxidation of bottom
1-21	9914-74D	31.7	Nickel	160	F	188	6500	5 x 30	Light yellow oxidation lower 1/3 of specimen.
1-22	9914-75A	6.5	-------	---	--	190	7150	-------	----------
1-22	9914-75B	7.0	-------	---	--	192	6100	-------	----------
1-23	9914-75C	17.3	Nickel	55	C	185	7400	5 x 10	Slight oxidation. Bottom corner melted.
1-23	9914-75D	17.0	Monel	58	C	185	7300	5 x 10	Complete combustion.
1-23	9914-79A	17.3	Monel	180	F	178	7600	5 x 30	Partial combustion 15 mm length left.
1-23	9914-79B	8.3	Stainless Steel Type 304	109	F	185	7400	5 x 20	Heavy oxidation at bottom of specimen but did not ignite.

N.E. - means no explosion at the indicated temperature.

TABLE 10 (Cont'd)

PROMOTED IGNITION TEST

1964 date	Test No.	Neoprene wt. mg.	Specimen	Specimen wt. mg.	Physical configuration	Ignition temp. °C	Ignition pressure psig.	Specimen size width x length mm	Remarks
1-23	9914-79C	56.0	Nickel	179	A	178	7500	8 x 20	Complete combustion.
1-23	9914-79D	17.0	Monel	189	F	280	7550	5 x 30	Partial combustion, 18 mm length left.
1-24	9914-80A	44.4	Nickel	189	A	180	7250	9 x 20	Partial combustion, 14 mm length left.
1-24	9914-80B	41.6	Nickel	113	C	178	8450	5 x 20	Nickel did not ignite. (Neoprene completely wrapped in metal)
1-24	9914-80C	42.3	Nickel	171	F	Recorder not operating.		5 x 30	Nickel partly ignited. 24 mm left. (Only part of neoprene wrapped in metal.)
1-27	9914-80D	40.9	Nickel	42	C	367	8375	5 x 10	Nickel 1/2 melted, some oxidation. 750 psi blow down when pressure too high.
1-27	9914-81A	47.7	Nickel	45	C	174	6810	5 x 10	Nickel 1/2 melted, some oxidation.
1-27	9914-81B	19.2	Aluminum	12.1	C	177	7200	5 x 10	Complete combustion. oxide fused.
1-27	9914-81C	14.1	Aluminum	20.3	C	174	7850	5 x 20	Aluminum just started to melt. Little oxidation.
1-27	9914-81D	16.4	Aluminum	13.0	C	179	7600	5 x 10	Complete combustion.
1-28	9914-82A	10.9	Stainless Steel Type 304	110	C	T st stopped at 226	Pressure to high	5 x 20	Neoprene and specimen intact. Neoprene charred.
1-28	9914-82B	10.8	Inconel X-750	171	F	259	8315	5 x 30	Complete combustion, magnetic oxide.
1-28	9914-82C	7.4	Inconel X-750	160	F	276	7920	5 x 30	Heavy oxidation and small corner missing at bottom but did not ignite.
1-28	9914-82D	13.0	Stainless Steel Type 304	111	F	177	7460	5 x 20	Complete combustion.
1-28	9914-83A	10.6	Inconel 600	155	F	179	6985	5 x 30	Melting and some oxidation at bottom. 25 mm left.
1-29	9914-84B	9.4	Inconel X-750	171	F	185	7810	5 x 30	Complete combustion.
1-29	9914-84C	13.7	Inconel 600	153	F	185	6310	5 x 30	Complete combustion magnetic oxide.
1-29	9914-84D	8.5	Inconel X-750	173	F	185	7440	5 x 30	Started to melt and heavy oxidation at bottom.
1-29	9914-86A	11.7	Inconel 600	159	F	170	7040	5 x 30	Started to melt and oxidize at bottom.
1-29	9914-86B	9.0	Inconel X-750	183	F	285	8360	5 x 30	Complete combustion.
1-30	9914-86C	13.2	Inconel 600	162	F	190	7370	5 x 30	Complete combustion.
1-30	9914-86D	10.3	Copper	190	F	227	7560	5 x 30	Almost complete combustion. 5 mm left. Surface oxidation.
1-31	9914-88A	8.7	Inconel X-750	186	F	183	7000	5 x 30	Complete combustion.
1-31	9914-88B	8.2	Copper	183	F	170	8440	5 x 30	Partial combustion. 22 mm left - surface oxidation. Black and red crystals in slag.
1-31	9914-88C	12.5	Inconel 600	164	F	83	6380	5 x 30	Bottom 2 or 3 mm melted out of one side with surface oxidation only at bottom.
2-3	9914-88D	12.9	Inconel 600	140	F	183	7960	5 x 30	Bottom two or three mm melted with heavy surface oxidation on melted portion.

TABLE 10 (Cont'd)

PROMOTED IGNITION TEST

1964 date	Test No.	Neoprene wt. mg.	Specimen	Specimen wt. mg.	Physical configuration	Ignition temp. °C	Ignition pressure psig.	Specimen size width x length mm.	Remarks
2-3	9914-90A	7.2	Stainless Steel Type 301	147	F	303	8220	5 x 30	No ignition. Only slight discoloration of upper part. Heavy oxidation inside at bottom.
2-4	9914-90B	9.5	Stainless Steel Type 301	161	F	188	8090	5 x 30	complete combustion.
2-3	9914-90C	11.8	Yellow brass	177	F	186	7325	5 x 30	Bottom 7 or 8 mm melted with heavy oxidation. Heavy black oxidation over entire length of specimen.
2-4	9914-90D	13.2	Yellow brass	166	F	180	7350	5 x 30	Melted bottom 10 mm into ball with heavy oxidation. Black oxidation over entire length of specimen.
2-4	9914-92A	8.0	Stainless Steel Type 301	157	F	190	7860	5 x 30	Complete combustion.
2-18	9914-92B	8.8	Stainless Steel Type 17-7PH	168	F	320	8700	5 x 30	Complete combustion. Bottom of test tube melted.
2-18	9914-92C	15.2	Yellow brass	160	F	185	7700	5 x 30	Bottom 8mm completely combusted-Heavy oxidation over entire length of specimen.
2-18	9914-92D	7.1	Stainless Steel Type 301	153	F	188	7600	5 x 30	Complete combustion. Bottom of test tube melted.
2-18	9914-93A	16.4	Anodized aluminum (<0.1 mil coat)	50	F	181	7700	5 x 30	Complete combustion. Side of test tube melted.
2-18	9914-93B	11.0	Anodized aluminum (<0.1 mil coat)	47	F	185	7450	5 x 30	Complete combustion. Side of test tube melted..
2-18	9914-93C	8.2	Anodized aluminum (<0.1 mil coat)	50	F	185	7500	5 x 30	No melting or significant oxidation .
2-18	9914-93D	9.8	Anodized aluminum (<0.1 mil coat)	52	F	185	7300	5 x 30	No melting or significant oxidation.
2-18	9914-94A	9.0	Stainless Steel Type 316	171	F	324	8700	5 x 30	Complete combustion.
2-18	9914-94B	14.7	Silver	229	F	376	8300	5 x 30	Bottom 6 mm melted.
2-18	9914-94C	13.2	Nickel	168	F	361	8600	5 x 30	2 mm melted out of each of lower corners.
2-19	9914-94D	15.3	Gold	372	F	183	7400	5 x 30	Bottom 3 or 4 mm melted.
2-19	9914-95A	12.6	Lead	209	F	186	7700	5 x 30	Melted into ball. Very little oxidation.
2-19	9914-95B	15.2	Anodized 25 mil aluminum (0.2mil coat)	163	F	185	7200	5 x 20	No ignition.
2-19	9914-95C	176 mg stainless steel Type 304 sealed in 275 mg of Kel-F			--	380	8400	5 x 30	Complete combustion.
2-19	9914-95D	176 mg stainless steel Type 304 sealed in 300 mg of Kel-F			--	415	7500	5 x 30	Complete combustion.
2-19	9914-96A	176 mg stainless steel Type 304 sealed in 218 mg of Teflon FEP			--	419	8300	5 x 30	Complete combustion.
2-19	9914-96C	1 x 4 x 4 mm Kel-F coated on 4 x 4 x 4 mm aluminum		---	--	N.E.500	9000	-------	Aluminum intact. No Significant oxidation. Kel-F gone.
2-25	9914-96D	59	Gold	396	A	180	7350	5 x 30	Melted into ball.
2-25	9914-97A	11.3	Anodized aluminum (0.3 mil coat)	57	F	184	8100	5 x 30	Lower 2 or 3 mm melted. No significant oxidation.
2-25	9914-97B	13.8	Anodized aluminum (0.3 mil coat)	53	F	189	8000	5 x 30	Bottom few mm started to melt.
2-27	9914-97C	15.5	Anodized aluminum (0.3 mil coat)	54	F	184	7800	5 x 30	Complete combustion.
2-27	9914-97D	14.6	Anodized aluminum (0.3 mil coat)	50	F	180	7700	5 x 30	Complete combustion.
2-28	9914-98A	1 x 4 x 4 mm Kel-F coated on 1 x 4 x 4 mm aluminum		--	--	385	8000	-------	Kel-F ignited.aluminum intact
2-28	9914-98B	54.0	Silver	205	A	182	7040	5 x 30	Entire specimen melted
2-28	9914-98C	56.5	Nickel	175	A	186	7100	5 x 30	Complete combustion.

N.E. - means no explosion at the indicated temperature.

TABLE 11

PRESSURIZATION OF SIMULATED SYSTEM WITH OXYGEN

Date 1964	Test No.	Pressure in Storage Vessel: Before Test psi	Pressure in Storage Vessel: Immediately after test psi	Pressure in Storage Vessel: On Warming after test psi	Pressure in Simulated System: Immediately after test psi	Pressure in Simulated System: On Cooling after test psi	Pressure in Simulated System: When Completely equalized with storage vessel psi	Initial Pressurization time of simulated system, sec.	Electrostatic charge measured volts
	9/16" O.D. x 5/16" I.D. tubing. Gemini Regulator blanked on low pressure side.								
3-4	11040-3-1	approx. 1100	----	----	900	----	----	0.52	*N.D.
3-4	11040-3-2	approx. 900	----	----	775	----	----	0.51	*N.D.
3-4	11040-3-3	approx. 775	----	----	665	----	----	0.55	*N.D.
3-4	11040-3-4	approx. 1100	----	----	875	----	----	0.52	*N.D.
3-5	11040-3-5	approx. 1200	----	----	975	----	----	0.5	*N.D.
3-5	11040-3-6	approx. 975	----	----	850	----	----	0.5	*N.D.
3-5	11040-3-7	approx. 850	----	----	750	----	----	0.5	*N.D.
3-5	11040-6	2200	----	----	1700	----	----	0.3	< -0.05
3-5	11040-7	1800	----	----	1500	----	----	0.4	< -0.05
3-5	11040-8	3000	----	----	2400	----	----	0.30	< -0.05
3-5	11040-9	2500	2100	2200	2100	1800	----	0.30	< -0.05
3-5	11040-10	3800	2950	3200	2950	----	----	0.30	< -0.05
3-5	11040-11	5100	3850	4200	3850	3250	----	0.26	< -0.05
3-5	11040-12	4700	3600	3800	3600	3100	----	0.28	-0.05
3-5	11040-13	5900	4200	4700	4200	3900	----	0.26	-0.25
3-5	11040-14	7400	5050	5800	5050	4200	----	0.24	----
3-5	11040-15	8500	5600	6500	5600	4800	----	0.24	-0.20
3-5	11040-16	6500	4600	5200	4600	3850	----	0.26	-0.15
3-5	11040-17	5200	3850	4300	3850	3300	----	0.28	-0.14
3-5	11040-18	4300	3300	----	3300	2850	----	0.30	-0.10
	Geometric volume of 80 cc added to low pressure side of Gemini Regulator and valve installed to blow down low pressure side.								
3-6	11040-19	3200	2600	2800	2700	2300	----	0.28	-0.10
3-6	11040-20	6300	4400	5100	4400	3500	----	0.26	-0.10
3-6	11040-21	9000	5750	6600	5750	----	----	0.24	-0.14
3-6	11040-22	10700	6600	7500	6600	----	----	0.22	-0.15
3-6	11040-23	11000	6500	7350	6500	----	7350	0.21	-0.13
	30 inches of 1/4" O.D. x 0.083" I.D. tubing substituted for 9/16" O.D. x 5/16" I.D. tubing.								
3-6	11040-24	9200	6200	6800	5700	----	6800	0.14	< -0.05
3-6	11040-25	6800	----	5000	4600	----	5000	0.16	< -0.05
3-6	11040-26	3800	----	3100	2800	----	3100	0.20	< -0.05
	Reinstalled 9/16" O.D. x 5/16" I.D. tubing.								
3-9	11040-27	12000	7000	8000	7000	----	8000	0.22	-0.08
3-9	11040-28	12000	7000	8000	7000	----	8000	0.22	-0.08
3-9	11040-29	12000	7000	8000	7000	----	8000	0.22	-0.09
3-9	11040-30	12000	7000	8000	7000	----	8000	0.23	-0.11
3-9	11040-31	12100	7100	8100	7100	----	8100	0.22	-0.09
3-9	11040-32	10500	6300	7250	6300	----	7250	Not recorded	-0.09

*N.D. - None detected

TABLE 11 (Cont'd)

PRESSURIZATION OF SIMULATED SYSTEM WITH OXYGEN

Date 1964	Test No.	Pressure in Storage Vessel			Pressure in Simulated System			Initial Pressurization time of simulated system,. sec.	Electrostatic charge measured volts
		Before Test psi	Immediately after test psi	On Warming after test psi	Immediately after test psi	On Cooling after test psi	When Completely equalized with storage vessel psi		
3-10	11040-33	12000	7000	8000	7000	----	8000	0.22	-0.14
3-10	11040-34	12000	7000	8000	7000	----	8000	0.22	-0.16
3-10	11040-35	12200	7100	----	7100	----	----	0.22	-0.12
3-10	11040-36	12000	7000	----	7000	----	----	0.22	-0.12
3-10	11040-37	12000	7000	----	7000	----	----	0.22	-0.32
	1/16" Dia. inconel shielded iron-constantan thermocouple substituted for nickel probe. Thermocouple extended approximately two inches into gas space of receiver.								Increase in Temperature, °C
3-10	11040-38	10200	6200	----	6200	----	----	0.23	Not recorded
3-10	11040-39	9000	5600	----	5600	----	----	0.23	68°C
	1/16" Dia. unshielded iron-constantan thermocouple substituted for inconel shielded thermocouple.								
3-10	11040-40	8100	5200	----	5200	----	----	0.24	80°C

TABLE 12

ADIABATIC COMPRESSION TESTS

Date 1964	Pressure in Storage Vessel		Sample	Weight of sample in grams	Pressurization time of 51" length of 5/16" I.D. tubing and sample, sec	Remarks
	Before test psi	Immediately after test psi				
3-10	7200	6900	Viton A (Virgin)	0.217	0.05	Sample ignited
3-10	7100	6700	Viton A (Virgin)	0.223	0.05	Sample ignited
3-10	7000	6500	Kel-F 81	0.240	0.05	Sample ignited
3-10	6900	6300	Teflon (Virgin)	0.161	0.05	Sample ignited

END OF REFERENCE

23

REFERENCE

24

JACOBSON, M.; COOPER, A. R.; AND NAGY, J.: EXPLOSIBILITY OF METAL POWDERS. BM-RI-6516, BUREAU OF MINES, 1964.

1965 2913

RI bureau of mines
report of investigations 6516

EXPLOSIBILITY OF METAL POWDERS

By Murray Jacobson, Austin R. Cooper, and John Nagy

UNITED STATES DEPARTMENT OF THE INTERIOR
BUREAU OF MINES
1964

EXPLOSIBILITY OF METAL POWDERS

By Murray Jacobson, Austin R. Cooper, and John Nagy

* * * * * * * * * * * * report of investigations 6516

UNITED STATES DEPARTMENT OF THE INTERIOR
Stewart L. Udall, Secretary

BUREAU OF MINES
Marling J. Ankeny, Director

EXPLOSIBILITY OF METAL POWDERS

by

Murray Jacobson,[1] Austin R. Cooper,[2] and John Nagy[3]

ABSTRACT

Data obtained in the Bureau's study of dust explosions of 313 elemental metals, alloys, catalysts, and ores comprising 54 types of material are summarized. Information is given on ignition temperature, spark energy for ignition, minimum explosion concentration, explosion pressure, rate of pressure rise, and in some instances, the admixed inert dust and oxygen concentration in an atmosphere required to prevent ignition of dust dispersions. The effects of particle diameter on explosibility and pyrophoricity are also discussed.

INTRODUCTION

Explosion hazards of numerous dusts have been evaluated during the past 25 years by the Bureau of Mines. These data are being grouped according to type of material and are being made available to industry. Publications on agricultural[4] and plastics[5] dusts have been released. The present report lists laboratory data on 313 metal, alloy, catalyst, and ore samples comprising 54 separate types of material; it supersedes earlier reports in which limited

[1]Supervisory research physicist, Health and Safety Research and Testing Center, Bureau of Mines, Pittsburgh, Pa.

[2]Physical science technician, Dust Explosions Research Section, Branch of Dust Explosions, Health and Safety Research and Testing Center, Bureau of Mines, Pittsburgh, Pa.

[3]Chief, Branch of Dust Explosions, Health and Safety Research and Testing Center, Bureau of Mines, Pittsburgh, Pa.

[4]Jacobson, Murray, John Nagy, Austin R. Cooper, and Frank J. Ball. Explosibility of Agricultural Dusts. BuMines Rept. of Inv. 5753, 1960, 23 pp.

[5]Jacobson, Murray, John Nagy, and Austin R. Cooper. Explosibility of Dusts Used in the Plastics Industry. BuMines Rept. of Inv. 5971, 1962, 30 pp.

Work on manuscript completed March 1964.

TABLE 1. - Ignition and explosibility of metal powders

Material	Line No.	Ignition temperature,[1] °C		Minimum explosive concentration, oz/cu ft	Minimum[1] igniting energy for dust cloud, millijoules	Maximum pressure, psig	Maximum rate of pressure rise, psi/sec	Index of explosibility
		Cloud	Layer					
Severe								
Aluminum, atomized	1	650	760	0.045	50	73	20,000+	>10
Aluminum-magnesium alloy	249	430	480	.020	80	86	10,000	>10
Magnesium	159	620	490	.040	40	90	9,000	>10
Thorium hydride	191	260	20	.080	3	60	6,500	>10
Zirconium	228	20	190	.045	[2]15	55	6,500	>10
Uranium hydride	212	20	20	.060	[2]5	43	6,500	>10
Titanium	194	330	510	.045	25	70	5,500	>10
Uranium	211	20	[2]100	.060	[2]45	53	3,400	>10
Thorium	190	270	280	.075	5	48	3,300	>10
Strong								
Titanium hydride	205	480	540	0.070	60	96	12,000	6.0
Zirconium hydride	232	350	270	.085	60	69	9,000	3.7
Aluminum-silicon alloy	258	670	-	.040	60	74	7,500	3.6
Calcium silicide	267	540	540	.060	150	73	13,000	2.0
Iron, carbonyl	126	320	310	.105	20	41	2,400	1.6
Ferrotitanium	281	370	400	.140	80	53	9,500	1.3
Coal, Pittsburgh seam	-	610	180	.055	60	83	2,300	1.0
Moderate								
Silicon	184	-	790	0.110	100	82	12,000	0.9
Boron	98	470	400	<.100	60	90	2,400	.8
Aluminum-nickel alloy	253	950	540	.190	80	79	10,000	.6
Aluminum-lithium alloy	244	470	400	<.100	40	96	3,700	.6
Aluminum-cobalt alloy	236	950	570	.180	100	78	8,500	.4
Ferromanganese	272	450	290	.130	80	47	4,200	.4
Aluminum-copper alloy	237	-	830	.100	100	68	2,600	.3
Chromium	107	580	400	.230	140	55	4,000	.1
Manganese	170	460	240	.125	305	48	2,800	.1
Tantalum	186	630	300	<.200	120	50	2,600	.1
Tin	193	630	430	.190	80	37	1,300	.1
Zirconium alloy	289	420	340	-	30	43	300	-
Weak								
Aluminum-iron alloy	241	870	750	-	720	62	1,800	-
Zinc	217	680	460	0.500	960	48	1,800	<0.1
Gold bronze	284	370	190	1.000	-	44	1,300	-
Ferrosilicon	278	860	-	.425	400	50	700	<.1
Vanadium	213	500	490	.220	60	48	600	<.1
Antimony	90	420	330	.420	1,920	8	100	<.1
Cadmium	101	570	250	-	4,000	7	100	-
Iron ore, pyrite	305	420	-	-	-	-	-	-
Ferrovanadium	282	440	400	1.300	400	-	-	<.1
Ferrochromium	269	790	670	2.000	-	-	-	-
Lead	138	710	270	-	-	-	-	<<0.1
Manganese ore (sulfide)	312	320	300	-	-	-	-	<< .1
Tellurium	189	550	340	-	-	-	-	<< .1
Nickel ore (sulfide)	313	-	340	-	-	-	-	<< .1
Molybdenum	171	720	360	-	-	-	-	<< .1
Cobalt	109	760	370	-	-	-	-	<< .1
Copper ore (sulfide)	299	-	390	-	-	-	-	<< .1
Tungsten	208	730	470	-	-	-	-	<< .1
Lead ore (sulfide)	308	-	<500	-	-	[3]9	200	<< .1
Beryllium	95	910	540	-	-	-	-	<< .1
Copper	110	700	-	-	-	-	-	<< .1
None								
Aluminum-bronze alloy	234	-	990	-	-	-	-	-
Beryllium-copper alloy	259	-	-	-	-	-	-	-
Manganese-bronze alloy	285	-	910	-	-	-	-	-
Nickel	172	-	-	-	-	-	-	-
Selenium	174	-	-	-	-	-	-	-
Stainless steel	286	-	-	-	-	-	-	-

[1]These data apply to relatively coarse dust (through a No. 200 sieve) but not to submicron powder.
[2]In this test less than 1 gram of powder was used. Larger quantities ignited spontaneously.
[3]Ignition by guncotton flame; electrical spark source used for ignition of other metals.

END OF REFERENCE

24

REFERENCE

25

PIPPEN, D. L.; AND STRADLING, J. S.: TECHNIQUES FOR DETERMINATION OF FLASH AND FIRE POINTS AND IMPACT SENSITIVITY OF MATERIALS IN A GASEOUS ENVIRONMENT. MAT. RES. STAND., VOL. 11, NO. 6, JUNE 1971.

ture on this test, the words "compatibility," "reactivity," and "sensitivity" seem to be used as though they were interchangeable. As a matter of fact, they are not equivalent terms, and, further, the type of impact test utilized to measure one of these qualities is not necessarily appropriate to the others.

As a starting point, we can define a compatible material reasonably as one that will not produce unacceptable damage or malfunction in the lox system in which it will be used. Further, we shall disregard for the moment differences between the test and service systems. Then the sequence of events in the test can be diagrammed as shown on page 34.

Here we see that the first step involves the conversion of mechanical energy into heat and that the question of whether ignition occurs is decided primarily by whether we impart enough energy to effect ignition at some localized site in the test material. It is important to note that we cannot apply directly a known amount of energy; rather, we must apply a deliberately excessive amount in order to have a small portion show up as a hot spot in the material. Further, the only way we can determine whether a hot spot has occurred is by observing a fire during the test or by noting small char marks on the specimen afterward. If either response is observed, we have answered one question, Will this amount of energy input result in ignition? Such a test is of course a quantal response test, and we have therefore defined the sensitivity of the material.

The second step in the sequence involves the question of whether an ignition will propagate or die out. In a test involving dynamic energy inputs, the heat source will be applied and then removed quickly. Therefore, the propagation will depend to a large extent on the exothermicity of the reaction started plus the heat transfer characteristics of the test system (From this, it can be surmised that the degree of propagation after ignition does *not* depend a great deal on the original energy

(*continued on page 52*)

REFERENCE: Pippen, D. L. and Stradling, J. S., **"Techniques for Determination of Flash and Fire Points and Impact Sensitivity of Materials in a Gaseous Oxygen Environment,"** *Materials Research and Standards*, MTRSA, Vol. 11, No. 6, p. 35.

ABSTRACT: The test techniques developed at the NASA White Sands Test Facility, New Mexico, for determining the flash and fire points of materials, as well as the sensitivity of materials to gaseous oxygen pneumatic and mechanical impact, are discussed. Test pressures up to 2000 psia have been used in the flash and fire testing and test pressures up to 5000 psia in the impact sensitivity tests. Data obtained from the flash and fire system and the impact sensitivity test apparatus are included. Each test system provides a rapid means for evaluating materials for possible use in oxygen environments and a method for material screening. The systems described can be used with various gas mixtures as well as with 100 percent oxygen. The data from the test techniques described presently are being used for determining the compatibility of materials with the high pressure oxygen systems in the Apollo spacecraft.

KEY WORDS: impact strength, flash point, fire point, mechanical shock, oxygen, spark ignition, pneumatic equipment, electrical sparks, oscilloscopes, photoelectric cells, compatibility, spacecraft

Techniques for Determination of Flash and Fire Points and Impact Sensitivity of Materials in a Gaseous Oxygen Environment

D. L. Pippen and J. S. Stradling

Manned space flight has brought about new techniques for testing materials for use in inhabited areas of a spacecraft as well as for determining compatibility of materials with various pressurized oxygen environments. Liquid oxygen (lox) impact testing, which has been performed successfully for several years, has overshadowed most impact tests involving gaseous oxygen (gox). However, because lox test data do not correlate necessarily with gox test data and because most oxygen systems use oxygen in both its liquid and gaseous phases, gox testing should be given equal consideration.

Recent attention also has been given to tests that permit the evaluation of a material in proximity to an electrical discharge in the form of a spark. Such tests effectively determine the combustibility of the offgassed products of a material as a function of temperature. Thus, flash and fire point testing at the application pressure of a material can provide meaningful data in all areas in which electrical conductors are routed as well as in areas in which static electrical discharges may occur. This paper presents the test techniques presently being used at the NASA Manned Spacecraft Center White Sands Test Facility (WSTF) to evaluate the reactivity of materials to gox impact and also describes a technique for determining the flash and fire points of materials under various oxygen pressures.

Gaseous Oxygen Impact Testing

Materials used in high pressure systems may be subjected to a mechanical impact or a pneumatic impact. The mechanical impact is imparted when a material specimen is struck with a steel striker pin, the pneumatic impact when a material is subjected to a rapid pressure increase (step function).

Mechanical Impact Test Equipment/ The WSTF gox mechanical impact testing apparatus uses a drop weight impact tester devised by the Army Ballistic Missile Agency (ABMA), currently the NASA George C. Marshall Space Flight Center. The basic ABMA tester was modified by replacing the 20-lb plummet with a 7½-lb plummet and by replacing the anvil with a high pressure test chamber designed by the WSTF. This tester, hereafter referred to as the WSTF mechanical impact tester, is shown in Fig. 1. Figure 2 is a photograph of the completed system installation.

A complete description of the basic ABMA impact tester may be found in several references[1,2]; thus, no further description is given here. The modification required to convert the ABMA impact tester to the WSTF mechanical impact tester is given in the following paragraphs.

The anvil region assembly (Fig. 1) consists of the gox mechanical impact test chamber shown in Fig. 3. As are all of the parts except the seals and diaphragm, the chamber frame (*1*) is constructed of 300 series stainless steel. The equalizer pin (*2*) is used to assure that equal force is im-

[1] Lucas, W. R. and Riehl, W. A., *AS7M Bulletin*, ASTBA, No. 244, Feb. 1960, pp. 29–34.

[2] "Liquid Oxygen Compatibility Impact Sensitivity Test Method," USAF Specification Bulletin 527, U.S. Air Force, 1 May 1961.

D. L. Pippen, acting chief, Laboratories Branch, National Aeronautics and Space Administration White Sands Test Facility, Las Cruces, N. Mex.

J. S. Stradling, test operations director, Laboratories Branch, National Aeronautics and Space Administration White Sands Test Facility, Las Cruces, N. Mex.

Table 1—Gaseous Oxygen High Energy Impact Test Results*

Material	Energy, ft-lb/in.²	Mechanical			Pneumatic		
		Test Pressure, psia	Reactions/Tests	Remarks	Test Pressure, psia	Reactions/Tests	Remarks
EA-40 adhesive epoxy	200	250	4/4	Total burn	3500	0/1	No reaction
	200	500	1/1	Total burn	4000	0/4	No reaction
					4500	4/4	Total burn
Polyisoprene sheet	200	Ambient	2/2	Slight odor, discoloration	500	0/2	No reaction
	200	100	1/1	Odor, slight residue, decomposition	1000	1/2	Partial burn and odor
	200	1500	1/1	Violent explosion, total specimen decomposition	1500	4/4	Partial burn and odor
Polyurethane plastic	200	2000	0/4	No reaction	200	0/4	No reaction
					500	1/2	Total burn and odor
					3000	4/4	Total burn and odor
2T adhesive epoxy	200	100	2/2	Partial burn, barely detectable odor	5000	0/4	No reaction
	200	250	4/4	Partial burn, barely detectable odor			
Red fiber sheet	200	1000	0/4	No reaction	1500	0/4	No reaction
	200	1500	4/4	Total burn, black residue	2000	1/2	Total burn
					2500	1/2	Black residue
					3000	4/4	Black residue
Fluorosilicone elastomer	200	3000	0/2	No reaction	2500	0/4	No reaction
		4000	0/2	No reaction	3000	1/4	
		5000	0/8	No reaction	3500	1/2	
					4000	1/2	
					4500	4/4	
Glass-filled teflon	200	500	1/2	Severe discoloration, odor, charred residue	2500	0/4	No reaction
					3000	1/1	Total burn, no residue, no odor
	200	1000	1/1	Severe discoloration, odor, charred residue	3500	1/1	Total burn, no residue, no odor
	200	3000	1/2	Total burn, odor, very little residue			

*Table 1 continued on Page 37.

parted to the diaphragm pin (*3*) by the plummet. A rubber diaphragm (*4*) is connected to the diaphragm pin to form a pneumatic amplifier chamber (*5*). The shaft extension (*6*) provides mechanical coupling through a high pressure seal (*7*) to the striker pin (*8*), which is located in the high pressure test chamber (*9*). The striker pin is tapered from approximately 0.5 to 0.25 in. and fits into the specimen cup (*10*), which is held in place by the anvil nut (*11*). The anvil nut seal (*12*) prevents loss of chamber pressure. Chamber ports (*13* and *14*) are used for pressurizing and exhausting the chamber and provide a means for pressure instrumentation. Striker pin position is monitored by a position indicator (*15*). The lower side (*16*) of the pneumatic amplifier chamber is vented to the atmosphere. The holding pin (*17*) retains the striker pin in the chamber during the loading operation.

The unique "pneumatic amplifier" concept (patent applied for by WSTF) enables offsetting the upward chamber pressure force on the striker pin by an equal and opposite force with the pneumatic amplifier diaphragm. This principle has been used with success by WSTF and other government agencies to whom this concept has been supplied.

The major advantages of this type of system over those designs with the plummet inside the test chamber are that (1) the smaller chamber is manipulated more easily; (2) the small chamber volume permits safer, more economical, and faster operation; and (3) chamber accessibility with specimen cup and striker pin removability permit easier cleaning. The position indicator allows precision adjustment of the striker pin with respect to the specimen.

Mechanical Impact Sensitivity Test Procedure/ A prepared and cleaned test material specimen is placed in the specimen cup, which is positioned within the test chamber by the anvil nut (see Fig. 3). The impact energy to which the specimen is to be subjected is determined. The plummet drop height then is adjusted by positioning the magnetic plate (Fig. 1) so that the specified impact energy will be

(continued on page 37)

Table 1—(Continued)

Material	Energy, ft·lb/in.²	Mechanical			Pneumatic		
		Test Pressure, psia	Reactions/Tests	Remarks	Test Pressure, psia	Reactions/Tests	Remarks
Glass-filled teflon	200	3500	4/4	Total burn, odor, very little residue			
Silicone elastomer[a]	200	1000	0/4	No reaction	3000	0/4	No reaction
	200	1500	1/2	Offensive odor, total burn	3500	4/4	Total burn, small amount of white residue
	200	2000	4/4	Offensive odor, total burn			
GEMON 3010 polyimide laminate	200	4500	0/4	No reaction	4000	0/1	No reaction
	200	5000	1/3	White residue formed on upper surface of specimen, strong odor	4500	0/4	No reaction
					5000	1/3	Gray-white residue, no odor
Delrin plastic	200	250	1/2	Surface burning, slight odor	250	1/2	Considerable surface burn and odor
	200	500	3/4	Soot, strong odor, entire surface burned	500	3/4	Considerable surface burn and odor
	200	1000	4/4	Soot, strong odor, entire surface burned	1000	4/5	Specimen melted, producing odor and black soot
					1500	1/2	Specimen melted, producing odor and black soot
					2000	4/4	Specimen melted, producing odor and black soot
EPR ethylene propylene rubber	200	500	4/4	Total burn, no residue, bad odor	1500	0/4	No reaction
					2000	4/4	Total burn, no residue, bad odor
Epibond 70-1768 adhesive paste	200	500	4/4	Total burn, no odor, no residue	1000	0/4	No reaction
					1500	1/2	Total burn, no odor, no residue
					2000	1/3	Total burn, no odor, no residue
					2500	4/4	Total burn, no odor, no residue
L9/3T grease	200	5000	0/4	No reaction	5000	0/4	No reaction
Glass fabric	200	5000	0/4	No reaction	5000	0/4	No reaction

[a] All specimens lubricated with Krytox 240AC grease per test requirements.

delivered to the test specimen. The test chamber then is purged with oxygen and pressurized to the test pressure by the system shown in Fig. 4. Pressure in the test chamber forces the striker pin into an upward position as shown in Fig. 3. The pneumatic amplifier chamber is then pressurized with gaseous nitrogen (GN_2) (Fig. 4) until the shaft position indicator shows that the upward force exerted on the striker pin has been equalized by the downward force from the pneumatic amplifier.

Energizing the electromagnet automatically releases the plummet safety catch shown in Fig. 1. The electromagnet then is deenergized and the plummet drops onto the equalizer pin (see Fig. 3). The impact energy is transmitted directly to the specimen. After the test chamber and the pneumatic amplifier chamber are depressurized, the anvil nut and the specimen cup are removed. The specimen then is inspected for evidence of reaction.

Determination of Mechanical Impact Reaction/ Tests to date have indicated reactions varying from slight discoloration to complete consumption of the specimen. The odor of the specimen residue varies from nothing detectable to a strong one of burning. Based on these specimen residue observations, WSTF considers a specimen to have reacted when, upon completion of an impact test, the specimen residue exhibits discoloration, charring, burning, or an odor indicative of burning.

Mechanical Impact Test Results and Discussion/ The results of the mechanical impact testing of 14 materials are given in Table 1. They were obtained by dropping a plummet weighing 7½ lb from a height of 16 in.; thus, a 200-ft·lb/in.² impact was imparted to the 0.25-in.-diameter test specimen. The pneumatic impact data also are given in Table 1 to enable comparison of results from the two systems.

Apollo Program testing is now being performed with 50-ft·lb/in.² impact on a 0.25-in.-diameter specimen. Few reactions have occurred at this low impact energy, thus a limited number of data are included in Table 2. Many of the materials that exhibited no reaction at 50-ft·lb/in.² in-

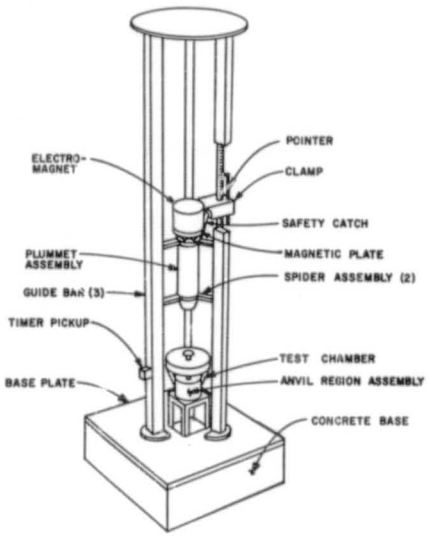

Fig. 1—*WSTF mechanical impact test chamber installed on basic ABMA tester.*

dicated reactions at 200-ft • lb/in.^{2}. The best example is visible in Fig. 5, which shows the reaction residue of polyisoprene after testing at 1500-psia oxygen and 200-ft • lb/in.^{2} energy. Figure 6 shows the condition of the 12,000-psia working pressure, oxygen supply flex line after the test. Needless to say, the chamber also was damaged extensively during this test. This same material indicated no reaction when tested at 1500-psia oxygen and 50-ft • lb/in.^{2} energy. No study of material reactivity as a function of cleanliness has been conducted on the mechanical impact sensitivity test. All specimens are cleaned by using techniques that are identical to those used for pneumatic impact specimen preparation. In brief, cleaning is accomplished by soaking and agitating (not ultrasonically) solid, nonporous specimens in a mild detergent and warmed, deionized water solution for 5 min. They then are rinsed thoroughly with deionized water and dried with filtered nitrogen and packaged in precleaned Teflon bags. Unwashable specimens (liquids, porous nonmetallics) are tested in the as-received condition.

Pneumatic Impact Testing/ A diagram of the WSTF pneumatic impact test system is shown in Fig. 7. The specimen cup assembly and the thermocouple (Fig. 8) consist of stainless steel high pressure fittings. A specimen 0.188 in. in diameter by 0.075 in. thick is common. A high speed valve that opens in approximately 2 ms provides the test chamber with high velocity oxygen flow. The high pressure reactor maintains the volume of gas at test pressure during test chamber pressurization. The low pressure oxygen purge conditions the specimen and chamber to assure an essentially 100 percent concentration of oxygen during the test.

Gaseous Oxygen Pneumatic Impact Sensitivity/ The test pressure at which the specimen is to be tested is established. Oxygen compression equipment pressurizes the reactor to the test pressure. A test material specimen then is placed in the specimen cup, and the specimen cup assembly is installed loosely on the specimen holder fitting. Low pressure oxygen then purges the system and flows around the specimen cup assembly for 60 s.

The specimen cup then is tightened and reactor test pressure and instrumentation

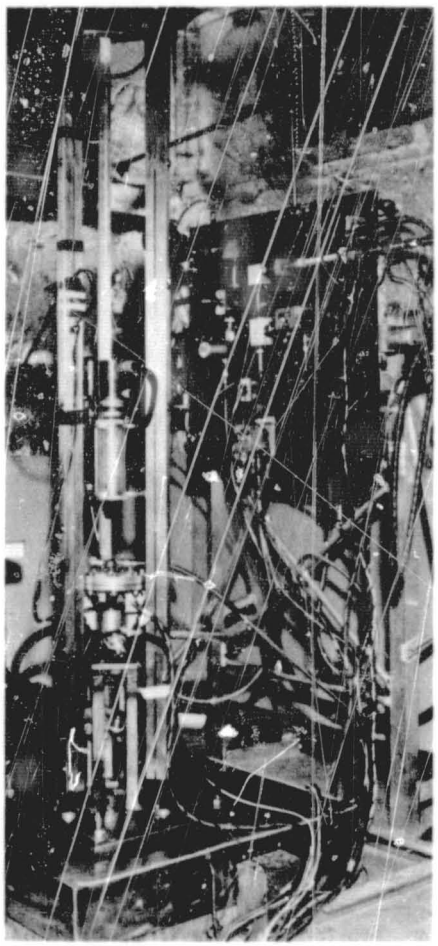

Fig. 2—*Photograph of mechanical impact test system.*

readiness are verified. A galvanometer-type recorder then is energized to record chamber pressure, chamber temperature, and valve cycle times, and an automatic valve sequencer designed to provide identical pressure cycles is actuated. The sequencer first commands the high speed valve to open for 50 ms. The high speed valve is closed and test pressure is retained in the test chamber for 5 s. The sequencer then opens the test chamber vent valve for 5 s to permit the test chamber to return to ambient atmospheric pressure (approximately 12.4 psia at WSTF). This pressure-vent sequence is repeated four more times for a total of five cycles per material specimen. The specimen then is removed and inspected for evidence of reaction.

Determination of Pneumatic Impact Reaction/ Tests to date have displayed reactions producing effects ranging from odor and slight discoloration to total combustion. Again, based on specimen residue observations and specimen cup temperature records, WSTF considers a specimen to have reacted when, upon completion of an impact test, the specimen residue exhibits discoloration, charring, burning, or an odor indicative of a reaction.

Pneumatic Impact Test Results and Discussion/ The results of the pneumatic impact testing, using the system configuration shown in Fig. 7 at test pressures up to 5000 psia, of 20 different materials are presented in Tables 1 and 2. Comparison of mechanical impact data on the same materials indicates no apparent correlation between the two test methods.

Test specimen cleanliness is extremely important in these tests. As an example, one Teflon specimen tested at 2000 psia in its as-received condition was consumed completely. Another specimen of material that had been cleaned with Freon showed no reaction up to 5000 psia.

Flash and Fire Point Testing

Materials used in physical systems generally are subject to exposure to an electrical discharge of energy in the form of a spark or arc. This discharge could be the result

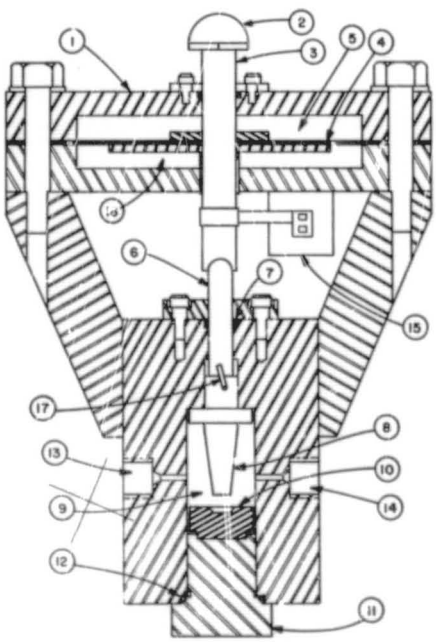

Fig. 3—*WSTF mechanical impact test chamber.*

Table 2—Gaseous Oxygen Low Energy Impact Test Results

Material	Energy, ft-lb/in.²	Mechanical			Pneumatic		
		Test Pressure, psia	Reactions/Tests	Remarks	Test Pressure, psia	Reactions/Tests	Remarks
Viton rubber	50	4000	0/1	No reaction	3500	0/4	No reaction
	50	5000	0/4	No reaction	4000	1/3	Total burn, odor, white ash
Red fiber sheet	50	5000	0/4	No reaction	1500	0/4	No reaction
					2000	1/2	Total burn, black residue
					2500	1/2	Total burn, black residue
					3000	4/4	Total burn, black residue
2T adhesive epoxy	50	4500	0/4	No reaction	5000	0/4	No reaction
	50	5000	1/3	Total burn, black residue			
Virgin teflon sheet	50	5000	0/4	No reaction	4000	0/4	No reaction
					4500	4/4	Total burn, no odor, no residue
Neoprene rubber	50	5000	0/4	No reaction	1000	0/4	No reaction
					1500	2/3	Total burn, odor, black residue
					4500	4/4	Total burn, odor, black residue
Buna-N rubber	50	5000	0/4	No reaction	1500	0/4	No reaction
					2000	2/4	Slight odor, no residue, total burn
					2500	4/4	Slight odor, no residue, total burn
Silicone elastomer	50	4500	0/4	No reaction	1000	0/4	No reaction
	50	5000	1/2	Strong odor, partial burn	1500	1/1	Total burn, no residue, no odor
Krytox 240AC grease	50	5000	0/4	No reaction	5000	0/4	No reaction
Polyisoprene sheet	50	1500	0/4	No reaction	500	0/2	No reaction
					1000	1/2	Partial burn and odor
					1500	4/4	Partial burn and odor

of static electricity buildup, electrical wiring short circuit, high voltage arcing, or other such phenomena. The flash and fire point test was developed to determine the relative reactivity of materials when subjected to a given impulse of energy in the form of an electrical discharge. While the test pressure and the atmospheric mixture are maintained constant and the temperature is increased at a linear rate, an electrical spark is discharged periodically across a spark gap located above the test specimen.

Test Equipment/ Flash and fire point testing is done in the test fixture shown in Fig. 9. This chamber has a volume of approximately 0.5 liter. A specimen is placed in the aluminum specimen cup (*1*). A glass chimney (*2*) is used between the cup and the spark electrodes (*3*) to prevent spark arc over to the cup. The chimney also is used to direct the offgassed products of the specimen past the spark electrodes. An asbestos washer (*4*) prevents heat sinking of the specimen by the stainless steel test chamber (*5*). A 1500-W heater (*6*) is coiled around the cup. This heater is insulated from the test chamber with an asbestos liner. A thermocouple (*7*) monitors the cup temperature and provides the control temperature signal to the temperature rate controller (*8*). The spark generator (*9*) applies the spark high voltage across the high voltage chamber feedthroughs (*10*). The temperature rate controller (*8*) applies sufficient heater power to the heater coil (*6*) through the heater-power chamber feedthroughs (*11*) to maintain a 25 F/min temperature rise rate over the test temperature range. A pressure port (*12*) supplies the test atmospheric environment and evacuates the chamber. A safety pressure relief valve also is connected to a port opposite the one shown as *12*.

Flash and fire occurrence can be monitored visually through the glass viewport (*13*) and electronically by the photoelectric cell detector (*14*)-storage oscilloscope (*15*) arrangement. The flash and fire occurrences are coupled to the photocell detector through a quartz rod (*16*). This rod penetrates the viewport through a Teflon feedthrough bushing (*17*). Chamber pressure is maintained constant by the 120-liter ballast tank (*18*). Figure 10 is a photograph of the flash and fire chamber.

Flash and Fire Point Determination Test Procedure/ A 0.5 ± 0.005-g specimen is loaded in the specimen cup and

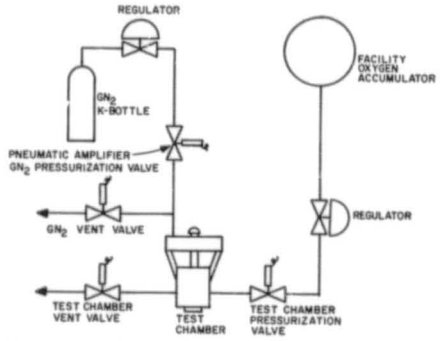

Fig. 4—*WSTF mechanical impact test system.*

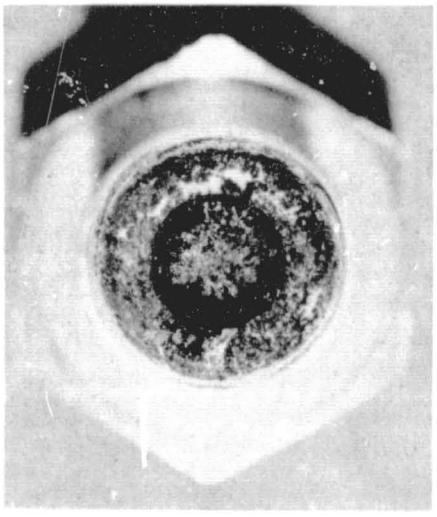

Fig. 5—*Reaction residue of polyisoprene.*

the glass chimney is installed. The spark electrodes are adjusted to 0.75 ± 0.025 in. above the top surface of the specimen and the spark gap is adjusted to 0.125 ± 0.025 in. The chamber is evacuated to at least 0.1 psia and backfilled to the required test pressure (Test materials with low vapor pressures are not subjected to the evacuation process. For these materials, the chamber is first purged for 1 min with the test atmosphere at ambient pressure and then pressurized to the test pressure.). The temperature rate controller and spark generator are energized.

The specimen temperature is programed automatically to increase from room temperature to the upper test temperature at a 25 ± 5 F/min rate. A 2 ± 1-ms, 50 ± 20-mJ spark (average energy) is discharged for each 4 ± 1 F increase in temperature. Three specimens of each material are tested. The chamber is cooled and the specimen cup and fixture are cleaned before each test is performed.

The chamber is monitored visually for

Table 3—Flash and Fire Point Test Results[a]

Material	Test Pressure, psia	Flash Point, deg F	Fire Point, deg F	Test Fixture	Remarks
Fluorosilicone L-449-6	5	738	770	L[b]	
	25	717	717	L	
	50	692	692	L	
	50	528	528	H[c]	
	100	521	521	H	
	500	494	494	H	
	1000	438	438	H	
	1500	379	379	H	
	2000	376	376	H	
TFE Teflon	5	None	None	L	
	25	876	None	L	
	50	900	None	L	
	50	865	865	H	
	100	861	861	H	
	200	852	852	H	
	500	815	815	H	
	1000	703	703	H	
	1500	688	688	H	
	2000	730	730	H	
Nylon sheet	5	740	None	L	
	25	760	773	L	
	50	737	737	L	
	50	568	568	H	
	100	529	529	H	
	500	464	464	H	
	1087	432	432	H	Chamber damaged
PLV-2000 viton cement	25	None	None	L	
	50	804	804	L	
	50	653	653	H	
	100	679	679	H	
	500	576	576	H	
	1000	547	547	H	
	1500	455	455	H	
Vespel SP-1	2000	470	470	H	
	5	None	None	L	
	25	842	None	L	
	50	841	None	L	
	50	901	901	H	
	100	845	845	H	
	500	727	727	H	
	1000	657	657	H	
	1500	601	601	H	
Drilube 822	2000	589	589	H	
	5	840	None	L	
	25	709	760	L	
	50	636	636	L	
	50	551	551	H	
	100	578	578	H	
	500	486	486	H	
	1000	461	461	H	
	1500	394	394	H	
Kel-F-81	2000	411	411	H	
	5	883	None	L	
	25	798	None	L	
	50	790	846	L	
	500	692	692	H	
	1000	707	707	H	
	1500	700	700	H	
Silicone O ring	2000	706	706	H	
	5	None	None	L	
	25	774	806	L	
	50	780	780	L	
	50	639	639	H	
	100	723	723	H	
	500	490	490	H	
	1000	434	434	H	
	1500	447	447	H	
Neoprene	2000	444	444	H	
	5	643	None	L	
	25	622	626	L	
	50	710	710	L	

Table 3—(Continued)

Material	Test Pressure, psia	Flash Point, deg F	Fire Point, deg F	Test Fixture	Remarks
	50	454	454	H	
	100	452	452	H	
	500	435	435	H	
	1000	436	436	H	
	1500	369	369	H	
Viton A	2000	379	379	H	
	5	660	None	L	
	25	640	874	L	
	50	731	828	L	
	50	604	604	H	
	100	591	591	H	
	500	513	513	H	
	1000	483	483	H	
	1500	472	472	H	
Nicrobraze 50	2000	469	469	H	
	1500	713	713	H	Chamber rupture occurred from ignition of test chamber internal components
Butyl rubber					
	5	713	None	L	
	25	656	656	L	
	50	652	650	L	
	50	448	448	H	
	100	431	431	H	
	500	356	356	H	
	1000	332	332	H	
	1500	317	317	H	
Glass-filled	2000	292	292	H	
Teflon	5	None	None	L	
	25	874	None	L	
Vespel Sp-21	50	790	955	L	
	5	566	None	L	
	25	953	None	L	
	50	529	None	L	
	50	935	935	H	
	100	921	921	H	
	500	835	835	H	
	1000	730	730	H	
	1500	658	658	H	
L9/3T grease	2000	631	631	H	
	5	696	None	L	
	25	750	763	L	
	50	775	775	L	
	50	600	600	H	
	100	534	534	H	
	500	474	474	H	
	1000	464	464	H	
	1500	453	453	H	
Krytox 240AC	2000	468	468	H	
grease	5	660	None	L	
	25	313	None	L	
	50	None	None	L	
	50	873	873	H	
	100	858	858	H	
	500	847	847	H	
	1000	782	782	H	
	1500	808	808	H	
Fluorel	2000	783	783	H	
	5	744	None	L	
	25	766	852	L	
	50	704	801	L	
	50	587	587	H	
	100	528	528	H	
	500	453	453	H	
	1000	453	453	H	
	1500	451	451	H	
	2000	430	430	H	

[a] All tests terminated at 1000 F.
[b] Low pressure.
[c] High pressure.

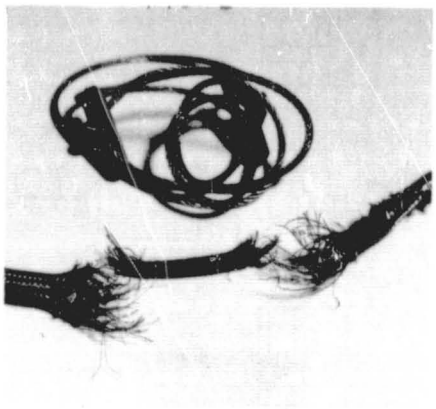

Fig. 6—*Flex line damage due to polyisoprene reaction.*

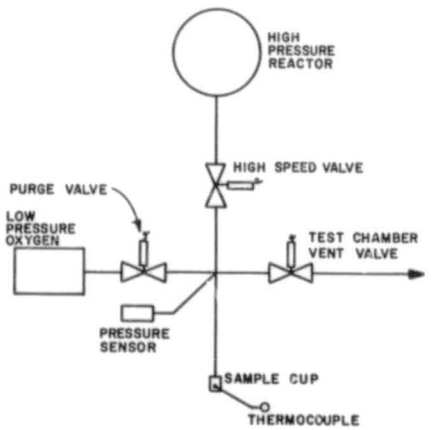

Fig. 7—*WSTF pneumatic impact test system.*

flash points and for fire points. Additionally, the storage oscilloscope displays a basic "spark background" for each spark occurrence. A change in this basic pattern occurs whenever a flash or fire occurs.

Determination of Reaction/ The flash point of a material is defined as the lowest temperature at which a material will give off flammable vapors that, when mixed with the test atmosphere and exposed to the spark ignition source, will provide a nonself-sustaining flash or flame. The fire point of a material is defined as the lowest temperature at which a material will give off flammable vapors that, when mixed with the test atmosphere and exposed to the spark ignition source, will continue to burn after ignition.

The oscilloscope displays for a flash point vary considerably; however, it has been possible to categorize reactions as shown in Fig. 11. The photographs are of actual occurrences, whereas the drawings that are located under each photograph represent the pattern seen on the oscillo-

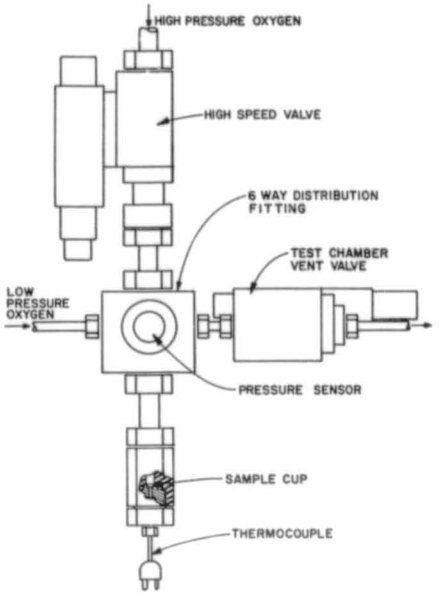

Fig. 8—*WSTF pneumatic impact test system.*

scope screen. Figure 11*a* shows a phenomenon designated as the "halo" effect. This terminology is taken from ASTM Test for Flash and Fire Points by Cleveland Open Cup (D 92–57); however, whether the physical phenomena that have occurred in the WSTF test are identical to the phenomena described in the ASTM procedure is not known. It appears that the spark supplies sufficient energy to the offgassed vapors so that ionization occurs, yet no flame propagation is evident. The result, as displayed on the oscilloscope, is an increase in signal amplitude without an increase in signal duration (with respect to the basic spark pattern). Visually, the halo effect usually is evident as a bluish glow around the spark electrodes coincident with the spark.

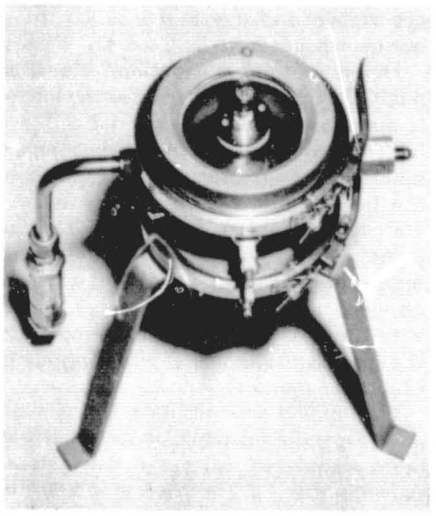

Fig. 10—*Photograph of flash and fire chamber.*

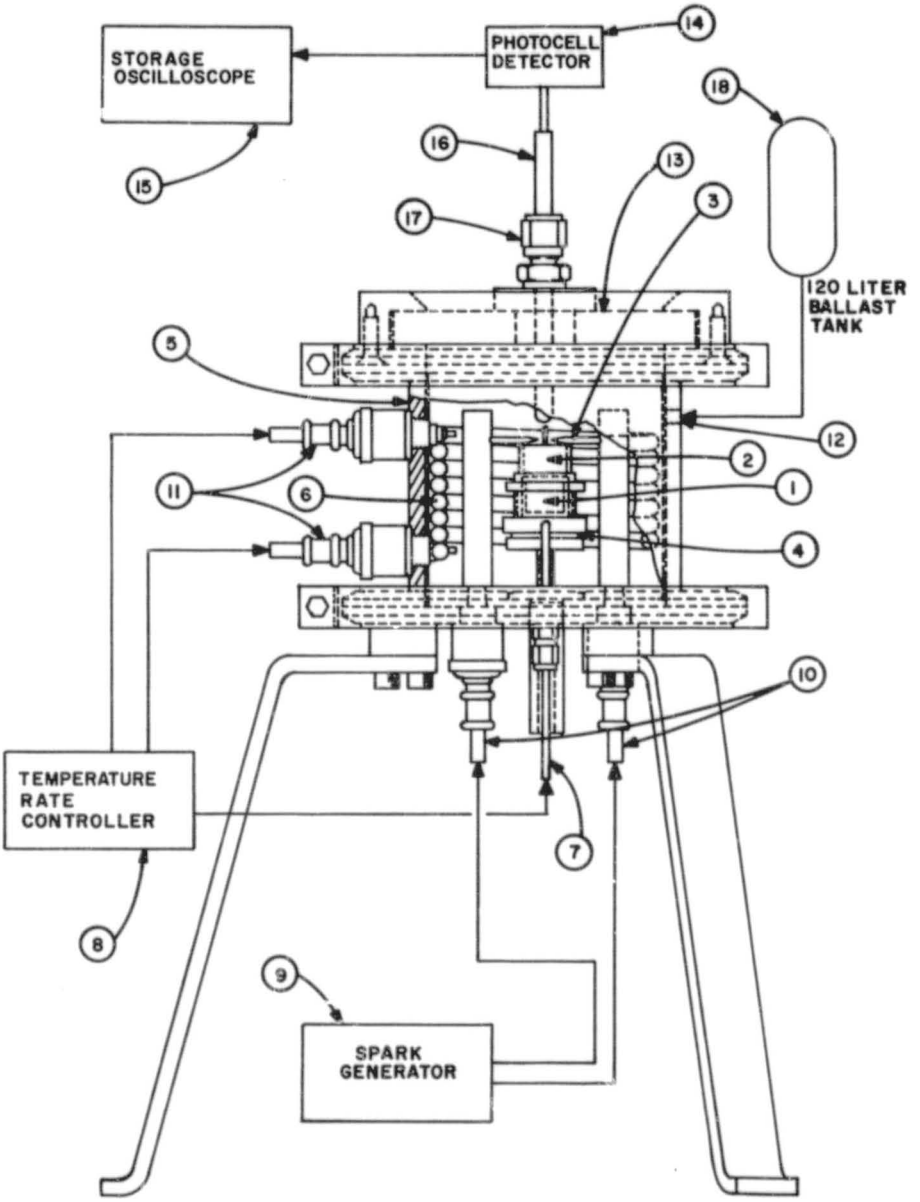

Fig. 9—*WSTF flash and fire point test apparatus and control system.*

Figure 11*b* displays a flash point. The amplitude of the signal (as monitored by the oscilloscope) is maintained for a longer period of time than is that of the basic spark. The signal amplitude can be greater or less than the amplitude of the basic spark, depending upon photocell response to the light wavelength of the flash and to the light output of the flash. Because the oscilloscope vertical amplifier is d-c coupled, a fire is indicated by a d-c level increase that lasts for the duration of the fire, as shown in Figs. 11*c* and 11*d*.

Flash and Fire Test Results and Discussion/ A comprehensive study of the repeatability of flash and fire points has been accomplished by using materials chosen as chemically stable standards. Figure 12 gives the test results for four of these materials. Spark energy, chamber pressure, spark electrode height above the specimen, and spark gap distance were maintained constant throughout the tests. The test results indicate excellent reproducibility.

Preliminary tests indicate that the flash point is dependent upon spark intensity, test pressure, and temperature but relatively independent of the height of electrodes above the specimen. The flash point dependence upon spark intensity creates some problems, because the amount of available spark voltage must be increased and spark gap distance decreased as test pressure requirements increase so that the spark will jump the gap. This results in a change of energy. Likewise, as the tem-

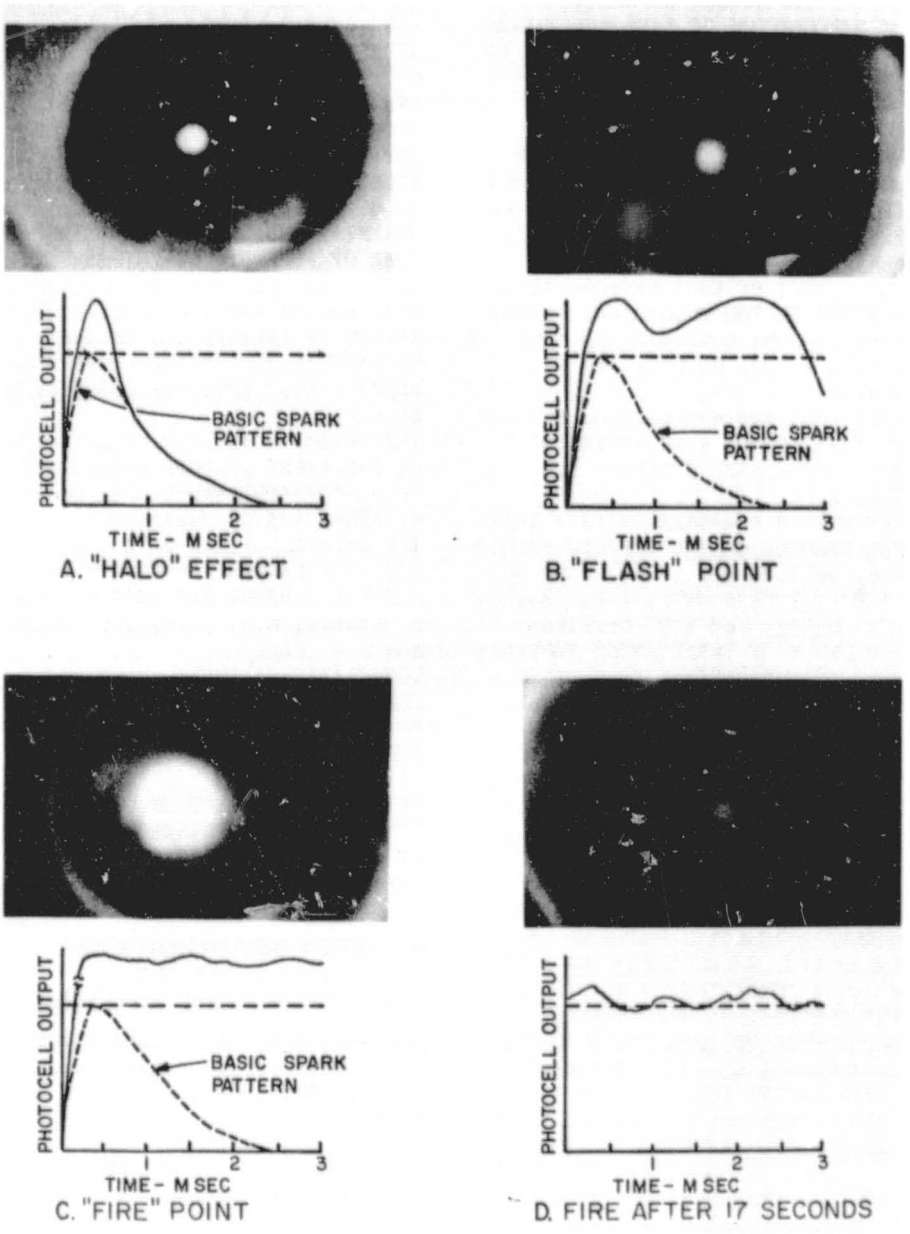

Fig. 11—*Typical oscilloscope displays and actual photographs of flash and fire point test.*

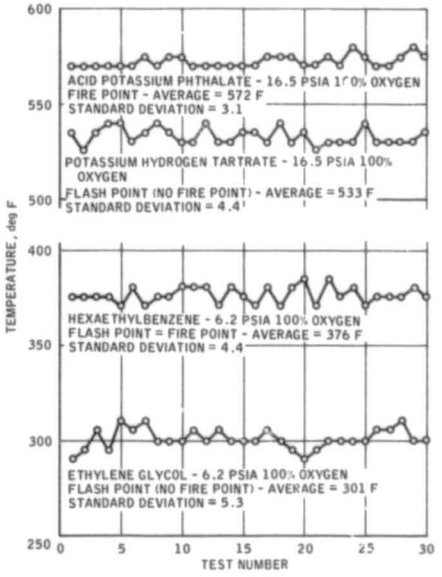

Fig. 12—*Flash and fire point repeatability test.*

perature is increasing, the voltage required to initiate a spark is less; thus, spark energy also varies with temperature.

WSTF now is performing two series of flash and fire tests. The first series is designated as the low pressure test and uses the system described herein. Testing to 50 psia and 1000 F is possible with this system. The second series uses a test chamber of the same volume but with much thicker walls and a 5500-W heater power capability. Testing to 3000 psia and 1000 F is possible with this high pressure test system. Reactions and flash and fire points from the two systems are different. This difference is attributed to the increased spark voltage and current and to the decreased spark gap distance required at high pressures to enable the spark to cross the gap. Another possibility is that materials may autoignite before the flash point is reached.

An illustration of this difference is shown in Fig. 13, which shows the high pressure flash and fire chamber after the severe reaction incurred while testing powdered Nicrobraze 50 alloy at 1500 psia in a 100 percent oxygen atmosphere. The flash and fire points occurred simultaneously at 715 F. The intense flame temperature from the burning specimen ignited the spark electrodes and the heater. Burning, in conjunction with the corresponding pressure increase, forced the oxygen inlet fitting to blow out. Molten metal was spewed about the test area, causing the damage seen in the photograph. When tested in 50-psia, 100 percent oxygen with the low pressure system, the same material had no flash or fire point. The basic difference in the two systems is a factor of three to four increase in spark generator output for the high pressure system as well as, in this instance, a considerable difference in test pressure.

The WSTF has performed flash and fire pressure-profile tests as well as materials screening tests on many materials. Table 3 gives results for several materials tested at various pressures. The apparent anomaly at 50 psia between data from the two fixtures is attributed to the required change of spark generators when switching from the low to high pressure systems. As was noted previously, the high pressure tests require much more spark voltage to obtain

(*continued on page 52*)

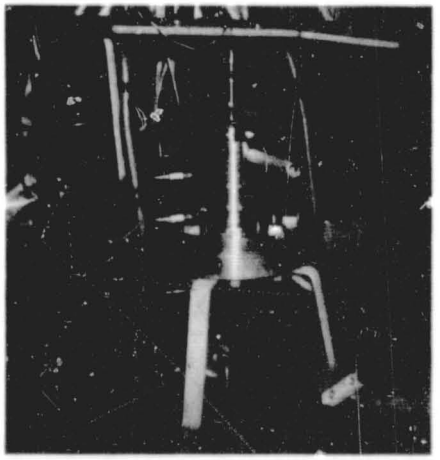

Fig. 13—*Photograph of high pressure flash and fire chamber after Nicrobraze 50 reaction.*

(*continued from page 51*)

Table 3—Effect of Pressure on Impact Sensitivity in Gaseous Oxygen

Material	Thickness, cm	% Reaction at Pressure, N/cm^2			
		6.8×10^6	3.4×10^6	68×10^4	34×10^4
Fluorinated hydrocarbon	0.188	66.6	50	20	0
Fluorinated silicone	0.328	100	100	50	50
Silicone	0.152	. . .	100	100	50

Table 4—Impact Sensitivity of Selected Materials in Liquid and Gaseous Oxygen at 10 kg·m

Material	Thickness, cm	Pressure, N/m^2	% Reaction in	
			lox	gox
Nylon	0.008	3.4×10^6	20	50
Silicone	0.152	68×10^4	100	100
Polytetrafluoroethylene	0.165	3.4×10^6	0	10
Chlorotrifluorocarbon plastic	0.317	6.8×10^6	0	0

2. The impact sensitivity of materials in gaseous oxygen varies directly with pressure.

3. The relative rating of the materials tested in lox at pressures up to 6.8×10^6 N/m^2 is the same as lox at 9.5×10^4 N/m^2.

4. This tester provides flexibility of test conditions for evaluation of a wide variety of materials in fuels and oxidizers.

5. The above data are tentative and, as such, constitute preliminary test results for the conditions noted. A much more comprehensive test program, structured to yield statistically meaningful cardinal data over a wide variety of materials of interest currently is in progress at the Marshall Space Flight Center. ■ ■ ■

Assessment of Impact Test Techniques

(*continued from page 35*)

input.). By our previous definition of compatibility, it follows that there are two categories of compatible materials: those that are insensitive and those that are sensitive but do not propagate. Incompatible materials, of course, are those that exhibit both sensitivity and a tendency to propagate.

Clearly, if we are to define the compatibility of a material by test, we must measure both sensitivity and the tendency to propagate, that is, the potential reaction intensity.

Conclusions

We have attempted herein to review the development of the two lox impact test methods appearing in Part 18 of the ASTM Standards and to present some of the aspects involved in using such tests to choose materials for lox systems. Hopefully, we have presented a conclusive case to the effect that both sensitivity and reaction intensity measurements are necessary for credible choices between materials.

Noting that one of the above methods purports to measure sensitivity and the other yields reaction intensity, it would seem that the use of both would solve the problem. We have attempted to show, however, that the sensitivity test violates so many fundamental aspects that its inability to yield acceptable precision is not surprising. The reaction intensity test appears to yield meaningful results, but the method is so new that it has not been used outside the laboratory where it was developed, and we know nothing about its reproducibility. Moreover, even if the reaction intensity test does prove to be reproducible through interlaboratory testing, it will not constitute a complete measure of compatibility; precise sensitivity information also is needed. Therefore, we must conclude that a new test for sensitivity with better precision than now available is needed urgently.

REFERENCES

[1] Africano, A. in *Advances in Cryogenic Engineering*, Vol. 5, Plenum Press, New York, 1960.

[2] "Liquid Oxygen Compatibility Impact Sensitivity Test Method," USAF Specification Bulletin 527, U.S. Air Force, 1 May 1961.

[3] "Testing Compatibility of Materials for Liquid Oxygen Systems," NASA Specification MSFC-SPEC-106B, National Aeronautics and Space Administration, 16 Sept. 1966.

[4] Crow, E. L., Davis, F. A., and Maxfield, M. W., *Statistics Manual*, Dover Publications, New York, 1960.

[5] Brown, J. A. et al, "Sensitivity and Rheology Studies on Lead Azide-RDX-Silica Mixtures," Final Technical Report No. GR-1SRS-69 for U.S. Army Picatinny Arsenal, Esso Research and Engineering Co., Jan. 1969.

[6] Blackstone, W. R., Baber, B. B., and Ku, P. M., *Transactions*, American Society of Lubrication Engineers, ASLTA, Vol. 11, No. 3, July 1968.

[7] Rothman, D., Alexander, M. J., and Zimmerman, J. M., "The Design and Analysis of Sensitivity Experiments," NASA CR-62026, Vols. I and II, National Aeronautics and Space Administration, May 1965. ■ ■ ■

Determination of Flash and Fire Points and Impact Sensitivity

(*continued from page 43*)

spark propagation; thus, arcing at the points occurs during the spark discharge. Because this arcing causes a higher temperature spark, it is expected that the flash and fire points occur at lower temperatures.

Another interesting observation is that, whereas numerous flashes but few fires occur with the low pressure system, flash and fire points generally occur simultaneously when the high pressure system is used. This variance is attributed to the difference in spark generators or perhaps the greater possibility of autoignition under high pressure conditions. WSTF is performing studies to determine the relationship of flash and fire points to spark characteristics as well as autoignition properties under high pressure oxygen environments.

It should be pointed out that a difficulty arose when we attempted to specify spark energy as a control parameter. Energy measurement in the low pressure system is straightforward and can be accomplished by measuring the spark current and voltage compared to time, plotting a power envelope, and then obtaining the area under the curve. This measurement can be performed readily because, at the low pressures involved, the spark is in the form of a "normal glow discharge" as described by Cobine[3]; thus, the voltage wave form is fairly smooth and easy to define. At higher pressures, however, the required increase in spark voltage causes an erratic, frequent transition from normal glow to arcing during the spark period. Because different energies exist for the two conditions, even an approximate measurement of energy is difficult. Nonetheless, a quantity that is measured easily is spark gap current as a function of time, which can be displayed on a storage oscilloscope by using a current probe or a current sampling resistor. Although this current measurement does not describe directly the spark energy delivered (as is desired), it does give a means for calibrating individual spark generators to ensure that the same energy profile is used for different test setups.

General conclusions

Gaseous Oxygen Impact Testing/ Testing to date using the WSTF mechanical and pneumatic impact systems has provided reproducible, repeatable data for test pressures up to 5000 psia in a 100

[3]Cobine, J. D., *Gaseous Conductors, Theory and Engineering Applications*, Dover Publications, New York, 1958, p. 250.

percent gaseous oxygen environment. The systems now are being used to provide data for screening and evaluation of materials considered for use in manned spacecraft, high pressure oxygen systems. The data indicate no correlation between gaseous oxygen mechanical and pneumatic impact test results; thus, each provides valuable data for materials evaluation. However, there are materials that do not react to either test.

Further evaluation of both test methods is required before standardization can be accomplished. Variables to be investigated include, for mechanical impact, the effects of specimen size, specimen configuration, impact energy, plummet drop height, and specimen temperature upon material reactivity and, for pneumatic impact, the effects of specimen size, specimen configuration, specimen chemical composition, system response time, and shock/adiabatic compression upon material reactivity.

Flash and Fire Point Testing/ The low and high pressure flash and fire point determining systems also have provided repeatable, reproducible test results. Variables requiring close control are distance between spark electrodes, spark output, and chamber pressure. Two of the outstanding characteristics of the apparatus are that visual flash and fire data are augmented with electronically obtained data and that any test environment compatible with the test chamber material can be used.

Further investigations of the effects of spark output upon flash and fire points are required to establish a realistic standard value. Once this has been accomplished, a standard test procedure should be established. ■ ■ ■

A Shock Sensitivity Tester

(*continued from page 21*)

[2] English, W. D. and Spicer, D. R., *Materials Research and Standards*, MTRSA, Vol. 9, No. 1, Jan. 1969, p. 30.

[3] *Military Explosives*, Technical Manual TM 9-1910/TO 11A-1-34, Department of the Army and the Air Force, April 1955.

[4] Green, J., Levine, N. B., and Sheehan, W. R., "Polymers for Use in Fluorine-Containing Oxidizers," *Bulletin of the 6th Liquid Propulsion Symposium*, Chemical Propulsion Information Agency, Sept. 1964.

[5] Robertson, A. B., *Transactions of the Faraday Society*, TFSOA, Vol. 44, 1948, p. 977.

[6] Macek, A., *Chemical Reviews*, CHREA, Vol. 62, 1962, p. 41.

[7] Zippermayer, M., *Chemica*, Vol. 13, 1959, p. 190.

[8] Cook, M. A., Pack, D. M., and McEwans, W. S., *Transactions of the Faraday Society*, TFSOA, Vol. 56, 1960, p. 1028.

[9] *Liquid Propellant Test Methods*, Joint Army, Navy, NASA, Air Force Working Group, Chemical Propulsion Information Agency, 1960, with supplements at irregular intervals.

[10] *Liquid Propellant Test Methods*, Joint Army, Navy, NASA, Air Force Working Group, Test 1, "Card Gap Test for Shock Sensitivity of Liquid Monopropellants," 1960.

■ ■ ■

Seminars

Jun. 10–12—Pennsylvania State University, Built-Up Roof Design, Roofing Problems and Their Solution, University Park, Pa., Fee—$80. Contact: C. Charriere, Architectural Engineering, Continuing Education Coordinator, 101 Engineering A Building, University Park, Pa. 16802 or Tele: (814) 865-6394.

Jun. 28–July 2—American Iron and Steel Institute, Cold Formed Steel Design, Cornell University, Ithaca, N.Y., Fee—$125. Contact: Prof. J. C. Smith, Director of Continuing Engineering Education, 251 Carpenter Hall, Cornell University, Ithaca, N.Y. 14850.

Jun. 28–July 2—Tustin Institute of Technology, Inc., Vibration and Shock Test Fixture Design, Los Angeles, Calif., Fee—$290. Contact: Tustin Institute of Technology, Inc., 22 E. Los Oliros St., Santa Barbara, Calif. 93105 or Tele: (805) 963-1124.

July 12–16—Massachusetts Institute of Technology, Strain Gage Techniques, Cambridge, Mass. Contact: Director of the Summer Session, Rm. E19-356, MIT, Cambridge, Mass. 02139.

July 12–16—University of Southern California, Computer and Communication Statistical Reliability, Los Angeles, Calif., Fee—$300. Contact: University of Southern California University College, Noncredit Programs, University Park, Los Angeles, Calif. 90007.

July 19–23—Engineering Foundation of the United Engineering Trustees, Inc., Clinical Engineering, Deerfield Academy, Deerfield, Mass., Fee—$160. Contact: Engineering Foundation, 345 E. 47th St., New York, N.Y. 10017.

July 19–23—American Society for Metals, Metallographic Interpretation, Red Carpet Inn, Milwaukee, Wis. Contact: Dr. William M. Mueller, Director of Education, ASM, Metals Park, Ohio 44073.

July 19–23—Ohio State University, Applications of Human Factor Principles in Systems Design, Columbus, Ohio, Fee—$225. Contact: R. D. Frasher, Coordinator of Continuing Engineering Studies, Ohio State University, 2070 Neil Ave., Columbus, Ohio 43210 or Tele: (614) 422-7469.

July 19–23—Georgia Institute of Technology, Computer Engineering, Course I—Digital Process Control, Atlanta, Ga., Fee—$200. Contact: Director, Dept. of Continuing Education, Georgia Institute of Technology, Atlanta, Ga. 30332 or Tele: (404) 873-4211, Ext. 343.

July 26–30—Pennsylvania State University, Fundamental and Applied Aspects of Metal Fatigue, University Park, Pa. Contact: Pennsylvania State University, University Park, Pa. 16802 or Tele: (814) 865-6585.

July 26–30—Georgia Institute of Technology, Computer Engineering, Course II—Signal Processing, Passive, Active, and Digital, Fee—$200. Contact: Director, Dept. of Continuing Educa-

(*continued on page 54*)

cleaner
quieter
gradation
analysis

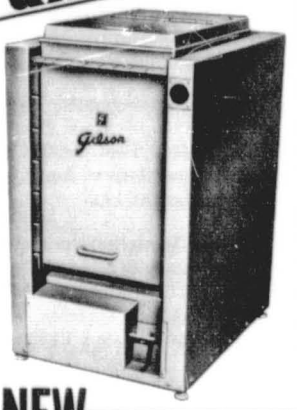

The NEW
GILSON TEST-MASTER

For gradation testing of stone, slag, coal, ores, sand, gravel and similar materials, or for mass separations for research purposes.

- Operates free-standing; no permanent mounting necessary
- Vibration-free outer case, for smooth, quiet operation
- Dustproof, fully enclosed
- Low maintenance; near-zero downtime with ordinary care

Other features include:
• Built-in timer • Hydraulic foot pedal tray clamping • Optional built-in speed control accessory • Optional sand attachment for 3" sieves • Size range 4" to No. 200 • Sample capacity up to 1 cu. ft.

Made by the makers of the GILSON Testing Screen, test-sizing standard of the industry for over 30 years.

WRITE OR PHONE FOR LITERATURE
PHONE (419) 256-7711

4
Name
Title
Company
Address
City
State Zip

GILSON SCREEN COMPANY
P.O. BOX 99 · MALINTA, OHIO 43535

CIRCLE 1959 ON READER SERVICE CARD

END OF REFERENCE

25

REFERENCE

26

KEY, C. F.: COMPATIBILITY OF MATERIALS WITH LIQUID OXYGEN - VOL. I. NASA TM X-64711, OCTOBER 1972.

NASA TECHNICAL MEMORANDUM

NASA TM X-64711

COMPATIBILITY OF MATERIALS WITH LIQUID OXYGEN – VOLUME I

By. C. F. Key
Astronautics Laboratory

(NASA-TM-X-64711) COMPATIBILITY OF MATERIALS WITH LIQUID OXYGEN, VOLUME 1 (NASA) 227 p GP-0 CSCL 11D

X73-10133

Unclas 53441

October 1, 1972

DISTRIBUTION UNLIMITED PER J3/18 NASA TECHNICAL DIRECTIVE 75-40, 9-26-74

SPECIAL RELEASE

Not to be indexed, referenced, or given further distribution without approval of NASA

NASA

George C. Marshall Space Flight Center
Marshall Space Flight Center, Alabama

TECHNICAL REPORT STANDARD TITLE PAGE

1. REPORT NO.	2. GOVERNMENT ACCESSION NO.	3. RECIPIENT'S CATALOG NO.
NASA TM X-64711		

4. TITLE AND SUBTITLE	5. REPORT DATE
COMPATIBILITY OF MATERIALS WITH LIQUID OXYGEN — VOLUME I	October 1, 1972
	6. PERFORMING ORGANIZATION CODE
7. AUTHOR(S) C. F. Key	8. PERFORMING ORGANIZATION REPORT #
9. PERFORMING ORGANIZATION NAME AND ADDRESS George C. Marshall Space Flight Center Marshall Space Flight Center, Alabama 35812	10. WORK UNIT, NO.
	11. CONTRACT OR GRANT NO.
	13. TYPE OF REPORT & PERIOD COVERED Technical Memorandum
12. SPONSORING AGENCY NAME AND ADDRESS National Aeronautics and Space Administration Washington, D.C. 20546	14. SPONSORING AGENCY CODE

15. SUPPLEMENTARY NOTES

Prepared by Astronautics Laboratory,
Science and Engineering

16. ABSTRACT

The test instrument and procedure developed by Lucas and Riehl (Ref. 1) was used to determine the compatibility of a wide variety of materials with liquid oxygen (LOX). This method is based upon the tendency of materials to react with LOX on impact and is commonly known as the "ABMA Tester." Within the past 15 years' use, over 240,000 individual test drops have been made on approximately 2,000 different materials.

Pertinent data from these tests have been compiled, and the findings are presented in this report. Recommendations are made for the guidance of designers and others in the selection of safe materials for use in oxygen systems. Materials are discussed according to the following classifications: (1) Lubricants, (2) Sealants and Threading Compounds, (3) Thermal and Electrical Insulation, (4) Elastomers, Plastics and Adhesives, (5) Gaskets and Packing, (6) Metals, Alloys, and Solders, (7) Solvents, Cleaning Solutions, and Miscellaneous, and (8) Dye Penetrants.

DISTRIBUTION UNLIMITED PER NASA TECHNICAL DIRECTIVE 75-40, 9-26-74

17. KEY WORDS	18. DISTRIBUTION STATEMENT
LOX Compatibility Materials Oxidizer	SEE DOCUMENT RELEASE FORM

19. SECURITY CLASSIF. (of this report)	20. SECURITY CLASSIF. (of this page)	21. NO. OF PAGES	22. PRICE
Unclassified	Unclassified	227	NTIS

MSFC - Form 3292 (May 1969)

a substantial body of data including more than 240,000 tests.

RESULTS

The results obtained by application of the foregoing test procedure to a wide variety of different products are tabulated according to categories in Tables I through VIII.

There are two ratings given for each material: one for the individual sample or lot evaluated; the other for the material in general. For example, it should be noted that Viton "A" has an overall batch test rating even though individual samples or batches may be satisfactory or unsatisfactory. The materials are rated as follows when evaluated in accordance with the provisions of MSFC-SPEC-106B:

Satisfactory (S) - Approved for LOX service if cleaned and/or processed by applicable MSFC standards.

Jar Test (JT) - Satisfactory as stated above with the provision that each jar or sample within a manufacturer's batch must be individually tested and found acceptable.

Batch Test (BT) - Satisfactory with the provision that each manufacturer's batch of the product must be individually tested and found acceptable.

Incomplete (I) - Insufficient test experience to rate sample adequately.

Unsatisfactory (U) - Capable of vigorous burning or exploding in contact with LOX.

The batch test, jar test, and incomplete categories deserve special mention. Materials which are basically compatible with LOX can be rendered incompatible by trace amounts of impurities. The policy of MSFC is to rate as satisfactory specific lots of new materials found to be insensitive, if the chemical composition of these materials is available. However, such materials generally are placed in the batch test category until tests have been completed on samples from a sufficient number of different lots to indicate adequate quality control. The large number of materials included in the batch test category reflects the practice of testing new products as they appear on the market even when no immediate application is indicated. Materials for which the chemical composition is not available, and for which samples from only one of two lots have been tested, are placed in the incomplete category.

Such materials are not approved for LOX service until additional information becomes available. In addition, it has been found that variations can occur within a given lot or batch. Therefore, it is necessary to test each sample within a certain batch or lot.

Three notes of caution are in order. (1) Whenever possible, a complete identification is made of the materials tested. Although some general conclusions can be drawn relative to certain classes or chemical families of materials, it is definitely unsafe to predict the behavior of any totally new product on this basis. Even materials normally inert to LOX can be rendered unsafe by minute amounts of processing additives, pigments, etc., that may be favored by one manufacturer or processor. It is equally unsafe to define a material for a specific application in liquid oxygen solely on the basis of a military or other specification for a general purpose product, since most of such specifications do not limit sufficiently the chemical constitution of the product. (2) Assuming there is freedom from deleterious additives or contaminants, the chemical nature of the product primarily governs its behavior toward LOX. For these reasons, the tabulated test data are applicable only to the specific proprietary products mentioned and may not apply to other similar materials or to other products meeting the same specification. (3) It has been determined that most material specifications on the fluorinated plastics are not sufficient to determine that they are of virgin, unfilled, or undyed variety. This has necessitated a change in some of the ratings listed in the tables to reflect this concern. Fluorinated plastics are generally given a rating of batch test unless it has a manufacturer identification number. Under no circumstances should a rating of satisfactory be inferred for all polytetrafluoroethylene, fluorinated ethylene propylene, or chlorotrifluorocarbon polymers unless the specific manufacturer's or vendor's product has been evaluated in its use thickness.

An additional factor that must be kept in mind in evaluating the data is that only the chemical compatibility of the material with oxygen systems is reported herein. This criterion will apply to all materials which may contact oxygen. However, many other factors usually must be considered before a final material selection can be made. For example, if a lubricant were to be used on an O-ring in a valve in an oxygen system at low temperature, at least four additional factors must be investigated as follows:

1. Corrosivity of the lubricant and metal components which it may contact during storage and use,

2. Compatibility of the lubricant and elastomer O-ring or other seals,

3. Low temperature behavior of the lubricant,

4. Lubricity of the material under operating conditions.

Naturally, the factors to be considered in final selection of any material are dependent upon the service intended. Selection and evaluation of these factors will vary widely. Thus, it is not feasible to attempt to provide in this report all of the information necessary to assess fully the adequacy of a material for specific applications. However, unless extenuating circumstances exist, this Center will not approve the use of any material listed as "Unsatisfactory" in the attached tables in oxygen systems.

The selection of the specific material to use among those rated as satisfactory will depend upon the particular application intended. This Center should be consulted directly for such assistance.

DISCUSSION

Lubricants

Lubricants tested for impact sensitivity in LOX are shown in Table 1. It is realized that none of the fluids or greases that withstood the impact test would actually function as lubricants at LOX temperature (-297°F). However, all materials withstanding this test are considered safe for use in gaseous oxygen, which also is a hazardous environment. The only type of lubricant capable of functioning at LOX temperature would be a solid or dry film lubricant. Although a number of these appear insensitive to impact, their adhesion and functional characteristics at LOX temperature have not yet been proven through use at this Center.

All petroleum-derived lubricants tested to date have proven to be impact sensitive, as expected. The conventional silicone greases and fluids constitute a similar hazard.

All completely flourinated and/or chlorinated fluids and greases tested to date have proven satisfactory for LOX service from the standpoint of impact sensitivity. This includes materials now being marketed under the trade names of "Fluorolube", "Kel-F," and "Halocarbon." * However, any specific fluorocarbon lubricant for which no data are tabulated should be tested prior to use to insure that its inherent compatibility will not be affected adversely by additives that may be present.

*The names of the manufacturers of all proprietary prodects mentioned in the test of this report are provided in Tables 1 through 8.

TABLE I. LUBRICANTS

Material	Manufacturer or Source	Test No.	Composition	Remarks	Thickness (inch)	No. Reactions/ No. Tests	Energy Level Kg-M	Batch Or Jar Rating	Material Rating
Aerolon G Dry Film Lubricant	Acheson Colloids Company	4072	Colloidal graphite, isopropanol and Freon 11 and 12	Spray coat on stainless steel inserts		0/40	10	S	BT
Aerolon M Dry Film Lubricant	Acheson Colloids Company	4074	Colloidal molydisulfide, Freon 11 and 12, isopropanol and methylene chloride	Spray coat on stainless steel inserts		0/40	10	S	BT
Anderol Lubricant L-118	Lehigh Chemical Company	1445	Molybdenum disulphide and vehicle	Violent explosion	0.050	1/8 1/2 0/10	10 5 2	U U U	U U U
Anderol Grease L-182	Lehigh Chemical Company	1336			0.050	2/5 1/15	10 5	U U	U U
Anderol Solvent Resistant Grease L-237	Lehigh Chemical Company	1452			0.050	0/20	5	U	U
Anderol Synthetic Multi-Purpose Grease L-278	Lehigh Chemical Company	1446		Test halted because of reaction violence	0.050	1/4	10	U	U
Anderol Grease L-419	Lehigh Chemical Company	1338		Violent explosion	0.050	1/2 1/1	10 5	U U	U U
Anderol Low Temperature Oil L-451	Lehigh Chemical Company	1335			0.050	1/2 1/4	10 5	U U	U U
Anderol Thixotropic Grease L-730	Lehigh Chemical Company	1443			0.050	2/8 1/2 1/10	10 5 2	U U U	U U U
Anderol Synthetic Long Fiber Grease L-752	Lehigh Chemical Company	1447			0.050	1/7 0/13	5 2	U U	U U
Anderol Synthetic Long Fiber Grease L-754	Lehigh Chemical Company	1444		Violent explosion	0.050	2/20	10	U	U
Anderol Grease (MIL-G-15793) L-793	Lehigh Chemical Company	875			0.050	0/20	10	I	I
Anderol Grease L-795	Lehigh Chemical Company	1339			0.050	2/9	5	U	U
Anderol Fluid X-1368	Lehigh Chemical Company	811	Halogenated hydrocarbon	Experimental product	0.050	0/20	10	I	BT
Apiezon L Grease	A.H. Thompson Company	739	Long chain aliphatic hydrocarbon		0.050	2/12 2/2 2/4	10 8 5	U U U	U U U

TABLE I. LUBRICANTS (Continued)

Material	Manufacturer or Source	Test No.	Composition	Remarks	Thickness (inch)	No. Reactions/ No. Tests	Energy Level Kg/m	Batch or Jar Rating	Material Rating
Apiezon M Grease	A.H. Thompson Company	740	Long chain aliphatic		0.050	2/12	10	U	U
Apiezon Q Wax	A.H. Thompson Company	8726	Long chain aliphate		0.050	10/20	10	U	U
Aroclor 1242	Monsanto Chemical Company	8215	Chlorinated biphenyl	Violent Reactions	0.050	11/34	10	U	U
Belco No-Flame Grease	Bel Ray Corporation	5845			0.050	1/20	10	I	I
Belco 1245 Grease	Bel Ray Corporation	5840	Polymers of trifluo· vinyl chloride		0.050	0/20	10	S	BT
Belco 1260 Grease	Bel Ray Corporation	5846	Polymers of trifluoro-vinyl chloride		0.050	0/20	10	S	BT
Bestoil	Oster Manufacturing Company	5649		Violent Reaction	0.050	10/20 9/20 14/20 11/20 6/20 2/20	10 8 6 4 2 1	U U U U U U	U U U U U U
Bestoil	Oster Manufacturing Company	8442		Violent Reactions	0.050	51/100 43/100 51/100 41/100 22/100 21/100	10 8 6 4 2 1	U U U U U U	U U U U U U
CBS Dry Film Lubricant 5940	Columbia Broadcasting Company Laboratory	2723	Copper, silver, and molydisulfide	Coating on stainless steel inserts		0/19	10	BT	S
CBS Dry Film Lubricant CLD 5940	Columbia Broadcasting Company Laboratory	3797	Copper, silver, and molydisulfide	Applied to stainless steel inserts		0/20	10	S	S
Cellulube Oil 220	Celanese Corporation	1057		Violent reactions	0.050	2/5	10	U	U
Celvacene Light Vacuum Grease	Consolidated Electrodynamics Corporation	1788		Violent reactions	0.050	4/20	10	U	U
Chrysler-Chapman Processed Oil Chrysler-Chapman Processed Oil	Chrysler Corporation Chrysler Corporation	9832 10281			0.050 0.050	0/20 0/20	10 10	S S	BT BT
Cimcool AL	Cincinnati Milling Products Company	4408	Hydrocarbon oil base		0.050	2/4 1/1 1/2 0/20	10 7 6 5	U U U U	U U U U
Compound Rust and Corrosion Inhibiting (MIL-C-12178)		1616			0.050	3/20	10	U	U

TABLE I. LUBRICANTS (Continued)

Material	Manufacturer or Source	Test No.	Composition	Remarks	Thickness (inch)	No. Reactions/ No. Tests	Energy Level Kg/m	Batch or Jar Rating	Material Rating
Conducto Lube Grease	Conducto Lube Company	600		Electrically conductive grease		2/5 1/4 1/6	10 5 1	U U U	U U U
Cosmoline Grease 1044	E.F. Houghton Company	1337		Violent explosion	0.050	1/1	10	U	U
Cosmolube No. 1 Grease	E.F. Houghton Company	793		Violent explosion	0.050	2/6	10	U	U
Cosmolube Grease 101	E.F. Houghton Company	794		Violent explosions	0.050	2/11	10	U	U
Cosmolube (MIL-L-4343A) 615	E.F. Houghton Company	798		Violent explosions	0.050	2/9 1/11	10 5	U U	U U
CTFE Polymer Oil	Hauser Research and Engineering Company	6765		Reprocessed Oil	0.5 ml	0/20	10	S	BT
CX-1 Lubricant	Kennedy Space Center	9156			0.050	14/20	10	U	U
Dag Dispersion Dip Coating 154	Acheson Colloids Company	3451	Colloidal graphite in alcohol	Applied to stainless steel inserts		0/20	10	I	I
Dag Dispersion 155	Acheson Colloids Company	3448	Colloidal graphite and Triclene D	Applied to stainless steel inserts		0/20	10	S	BT
Dag Dispersion 210	Acheson Colloids Company	3453	Colloidal molydisulfide in isopropyl alcohol	Applied to stainless steel inserts		4/20 2/5 0/20	10 5 3	U U U	U U U
Dag Dispersion 211	Acheson Colloids Company	3449	Colloidal molydisulfide in trichloroethylene	Applied to stainless steel inserts		0/20	10	S	BT
Dag Dispersion 217	Acheson Colloids Company	844	Graphite and organic vehicle	Violent explosion		1/10	10	U	U
Desco Formulation TF-48	Delta-Desco Company	9220	Fluorocarbon base	Stem packing lubricant	0.050	0/20	10	S	BT
Dow Corning Grease 3	Dow Corning Corporation	831	Silicone		0.050	2/6 4/10 1/14	10 8 5	U U U	U U U
Dow Corning Grease 4	Dow Corning Corporation	809	Silicone		0.050	3/13 1/17	10 5	U U	U U
Dow Corning Grease 5	Dow Corning Corporation	832	Silicone		0.050	2/2 2/6	10 5	U U	U U
Dow Corning Grease 6	Dow Corning Corporation	835	Silicone		0.050	2/3 1/17	10 5	U U	U U

TABLE I. LUBRICANTS (Continued)

Material	Manufacturer or Source	Test No.	Composition	Remarks	Thickness (inch)	No. Reactions/ No. Tests	Energy Level Kg/m	Batch or Jar Rating	Material Rating
Dow Corning Grease 7	Dow Corning Corporation	930	Silicone		0.050	2/2 2/3 0/15	10 5 2	U U U	U U U
Dow Corning Grease 11	Dow Corning Corporation	445	Silicone		0.050	2/3 0/15	10 5	U U	U U
Dow Corning Grease 33 (Light Consistency)	Dow Corning Corporation	159	Silicone		0.050	2/11 1/6 0/20	10 5 3	U U U	U U U
DC-33 Grease (Light Consistency) Lot M-347	Dow Corning Corporation	8412	Silicone	Cell III	0.050	26/100 26/100 16/100 8/100 3/100 0/100	10 8 6 4 2 1	U U U U U U	U U U U U U
DC-33 Grease	Dow Corning Corporation	10333	Silicone		0.050	7/20	10	U	U
DC-33 Grease Lot M-347 (Light Consistency)	Dow Corning Corporation	7299 7300 7301 7303 7302	Silicone	Standard grease cups Standard grease cups Standard grease cups Standard grease cups Standard grease cups	0.050	4/20 3/20 1/20 1/20 0/20	10 7.62 5.54 4.16 3.46	U U U U U	U U U U U
DC-33 Grease Lot M-347 (Light Consistency)		7304 7305 7306 7308 7307		Two piece cups Two piece cups Two piece cups Two piece cups Two piece cups	0.050	6/20 5/20 2/20 1/20 0/20	10 7.62 5.54 4.16 3.46	U U U U U	U U U U U
Dow Corning 33 Grease	Dow Corning Corporation	5641	Silicone	Light consistency	0.050	5/20 5/20 3/20 3/20 0/20 0/20	10 8 6 4 2 1	U U U U U U	U U U U U U
Dow Corning Grease 41	Dow Corning Corporation	829	Silicone		0.050	2/20	10	U	U
Dow Corning Grease 44	Dow Corning Corporation	158	Silicone		0.050	2/20	10	U	U
Dow Corning Grease 55	Dow Corning Corporation	420	Silicone		0.050	1/2 1/6 0/8	10 5 2	U U U	U U U
Dow Corning Fluid 200 (200 cs)	Dow Corning Corporation	177	Silicone		0.050	7/20	10	U	U
Dow Corning Fluid 550	Dow Corning Corporation	838	Silicone		0.050	2/8	10	U	U

TABLE I. LUBRICANTS (Continued)

Material	Manufacturer or Source	Test No.	Composition	Remarks	Thickness (inch)	No. Reactions No. Tests	Energy Level Kg.m	Batch or Jar Rating	Material Rating
Dow Corning Fluid 560	Dow Corning Corporation	4636	Silicone		0.050	6/20 7/20 2/20 2/20 0/20	10 5 4 3 1	U U U U U	U U U U U
Dow Corning Fluid 702	Dow Corning Corporation	383	Silicone		0.050	2/9 1/5	10 5	U U	U U
Dow Corning Fluid 703	Dow Corning Corporation	384	Silicone		0.050	2/4	10	U	U
Dow Corning Fluid 710	Dow Corning Corporation	781	Silicone		0.050	2/6 2/4 2/20 0/20	10 5 3 2	U U U U	U U U U
Dow Corning Fluid 710	Dow Corning Corporation	4730	Silicone		0.050	2/6 2/4 2/20 0/20	10 5 3 2	U U U U	U U U U
Dow Corning Valve Seal A	Dow Corning Corporation	444	Silicone		0.050	2/20	10	U	U
Dow Corning High Vacuum Grease	Dow Corning Corporation	213	Silicone		0.050	10/20	10	U	U
Dow Corning Electric Motor Grease	Dow Corning Corporation	593	Silicone		0.050	1/6 1/20	10 5	U U	U U
Dow Corning E-4-3112 (Lot B-1723-4)	Dow Corning Corporation	7451 7450	Fluorosilicone Fluorosilicone	Experimental Compound	0.025 ml 0.050 ml	0/20 0/20	10 10	S S	I I
Dow Corning E-322-62-I-2	Dow Corning Corporation	7859	Fluorosilicone		0.050	4/20 2/20 0/20 0/20 0/20	10 5.6 4.9 4.2 3.5	U U U U U	U U U U U
Dow Corning E-322-62-I-3	Dow Corning Corporation	7965	Fluorosilicone		0.050	7/20 3/20 1/20 0/20 0/20	10 5.6 4.9 4.2 3.5	U U U U U	U U U U U
Drilube 701 (Oxylube)	Voi-Shan Manufacturing Company	8266	Coated on cadmium plated A 286 steel		0.050	0/20	10	S	S
Drilube 701 (Oxylube)	Drilube Company	2116 1469	Molydisulfide in ethyl alcohol and ethyl acetate	Spray coating on stainless steel inserts		0/35	10	S	S

TABLE I. LUBRICANTS (Continued)

Material	Manufacturer or Source	Test No.	Composition	Remarks	Thickness (inch)	No. Reactions/ No. Tests	Energy Level Kg/m	Batch or Jar Rating	Material Rating
Drilube 702 (Oxylube)	Drilube Company	1650	Molydisulfide in chromous and phosphoric acid		0.050	0/20	10	S	S
Drilube 703 (Oxylube)	Drilube Company	825	Molydisulfide in chromous and phosphoric acid		0.050	0/20	10	S	S
Drilube Dip Coating 90	Drilube Company	1368		Dip coating on stainless steel inserts		2/3 1/17	10 5	U U	U U
Drilube 822	Drilube Company	4490	Fluorinated silicone	Dispensed in poly-ethylene tube	0.010	5/20	10	U	U
Drilube 822	Drilube Company	4080	Fluorinated silicone	Dispensed in poly-ethylene tube	0.050	0/20	10	U	U
Drilube Type 822, MMS N306A (Lot 3034)	Drilube Company	7589	Fluorinated silicone	Twenty-four tubes tested; sensitivity varies from tube to tube	0.050	0-2/20	10	U	U
Dry Lube	V.B. Products, Incorporated	6641		On aluminum discs		0/20	10	I	I
Du Metal	Garlock Packing Company	814	Teflon and sintered metal	For bearing surfaces	0.063	0/20	10	S	BT
Dumore "O" Cool Bearing Oil	Dumore Company	1334			0.050	1/1 1/3	10 5	U U	U U
Duo Vacuum Pump Oil	Welch Scientific Company	376			0.050	1/9 0/11	10 7	U U	U U
Ecoalube Dry Film Lubricant	Everlube Corporation	7824	Organic bonded dry film lubricant	Air dried 45 min, 1 hour at 400°F	0.008	19/20	10	U	U
Electrofilm Lubribond A	Electrofilm, Incorporated	9430	Organic bonded molydi-sulfide and graphite		0.005	8/20	10	U	U
Electrofilm Lubribond A	Electrofilm, Incorporated	4433	Resin bonded dry film lubricant	Air dry. Spray coat on stainless steel inserts		3/20 2/20 0/20	10 5 3	U U U	U U U
Electrofilm Lubribond B (Batch 171042 3-9-64)	Electrofilm, Incorporated	5874	Dry film lubricant with resin binder	Stainless steel inserts dipped and air dried		10/20 4/20 7/20 7/20 0/20 0/20	10 10 6 4 2 1	U U U U U U	U U U U U U
Electrofilm Lubribond M	Electrofilm, Incorporated	6651	Dry film lubricant in a volatile carrier	Sample sprayed on stainless steel inserts		0/20	10	S	BT

TABLE I. LUBRICANTS (Continued)

Material	Manufacturer or Source	Test No.	Composition	Remarks	Thickness (inch)	No. Reactions/ No. Tests	Energy Level Kg/m	Batch or Jar Rating	Material Rating
Electrofilm Lube-Lok M-1266	Electrofilm, Incorporated	5872		Stainless steel inserts dipped and air dried		0/20 0/20	10 10	S S	BT BT
Electrofilm Lubribond M	Electrofilm, Incorporated	4432	Spray bomb dry film lubricant	Air dry. Spray coat on stainless steel inserts		0/20	10	S	BT
Electro-Moly Powder Grade 1	Electrofilm, Incorporated	4625	Molybdenum disulphide solid lubricant	Stainless steel inserts used		0/20	10	S	S
Electro-Moly Powder Grade 2 Electro-Moly Powder Grade 2	Electrofilm, Incorporated Electrofilm, Incorporated	4624 6647	Molydisulfide powder Molydisulfide powder	Stainless steel inserts used		0/20 0/20	10 10	S S	S S
Electrofilm 66-C	Electrofilm, Incorporated	1310	Molydisulfide and organic vehicle	Spray coating		1/80	10	S	BT
Electrofilm 17-S	Electrofilm, Incorporated	981	Solid film lubricant with thermosetting resin			2/20	10	U	U
Electrofilm 99A	Electrofilm, Incorporated	4426	Resin bonded solid film lubricant	Dip coat on stainless steel inserts		2/60	10	U	U
Spray Bomb Lubricant G 7.8 in A.C. Propellant Freon 12	Electrofilm, Incorporated	4425		Dip coat on stainless steel inserts		0/20	10	S	BT
Electrofilm 1000	Electrofilm, Incorporated	535	Ceramic bonded molydisulfide	Spray coating		0/20	10	U	U
Electrofilm 1005 (Lot No. 149532)	Electrofilm, Incorporated	4431	Ceramic-bonded molydisulfide solid film lubricant	Dip coat on stainless steel inserts		0/20	10	S	BT
Electrofilm 2006	Electrofilm, Incorporated	534	Molydisulfide, synthetic graphite with silicone and formaldehyde resins	Violent explosions		2/2 2/2 1/3	10 5 3	U U U	U U U
Electrofilm Lube-Lok 2306	Electrofilm, Incorporated	6647	Inorganic bonded molydisulfide	Stainless steel inserts	Smear	0/20	10	S	BT
Electrofilm Lube-Lok 2306 (Batch 1678)	Electrofilm, Incorporated	5867	Inorganic bonded molydisulfide	Stainless steel inserts dipped and air dried		0/20 0/20	11.3 10	S S	BT BT
Electrofilm Lube-Lok No. 2306 (Lot No. 146031)	Electrofilm, Incorporated	4429	Inorganic-bonded molydisulfide	Dip coat on stainless steel inserts		0/20	10	S	BT
Electrofilm Lube-Lok 2396	Electrofilm, Incorporated	4256	Molydisulfide and graphite with sodium silicate	Coating applied to stainless steel inserts	0.001	0/40	10	S	BT
Electrofilm Lube-Lok 2396 (Batch 1459)	Electrofilm, Incorporated	5863	Molydisulfide graphite with sodium silicate	Stainless steel inserts dipped and air dried		0/20 0/20	11.3 10	S S	BT BT

TABLE I. LUBRICANTS (Continued)

Material	Manufacturer or Source	Test No.	Composition	Remarks	Thickness (inch)	No. Reactions/ No. Tests	Energy Level Kg/m	Batch or Jar Rating	Material Rating
Electrofilm Lube-Lok 2396 (Batch 145931)	Electrofilm, Incorporated	6648	Molydisulfide graphite with sodium silicate	Stainless steel inserts	Smear	0/20	10	S	BT
Electrofilm Lube-Lok 2406 (Batch 1711)	Electrofilm, Incorporated	5865	Inorganic bonded dry film lubricant	Stainless steel inserts dipped and air dried		0/20 0/20	11.3 10	S	BT
Electrofilm Lube-Lok 2406 (Batch 171142)	Electrofilm, Incorporated	6659		Stainless steel inserts	Smear	0/20	10	S	BT
Electrofilm 4396	Electrofilm, Incorporated	2724	Molydisulfide and graphite with vinyl binder		0.001	7/20 4/20 3/20 0/20	10 5 3 2	U U U U	U U U U
Electrofilm 5396, Diluted (Batch 203353)	Electrofilm, Incorporated	7380	Dry film lubricant with resin binder	Brushed on stainless steel inserts		2/20 1/20 0/20 0/20 0/20	10 9 8.31 7.62 6.93	U U U U U	U U U U U
Electrofilm 5396	Electrofilm, Incorporated	4430	Resin bonded solid film lubricant	Dip coat on stainless steel inserts		3/20	10	U	U
Everlube Dry Film Lube 811	Everlube Corporation	6971	Molydisulfide and sodium silicate binder	Stainless steel inserts . brush coated, 24 hours air dry		0/20	10	S	S
Everlube Dry Film Lube 811 (Batch 020905)	Everlube Corporation	7361	Molydisulfide and sodium silicate binder	Stainless steel inserts dipped and air dried (1-inch and 2-inch anvil used)		0/20	10	S	S
Everlube 811	Everlube Corporation	1829	Molydisulfide and sodium silicate	Dip coating, cured at 400°F		0/20	10	S	S
Everlube 811 (Sample No. 1)	Everlube Corporation	5417	Dry film lubricant consisting of moly-disulfide and inorganic binder	Dip coating on stainless steel inserts		0/20	10	S	S
Everlube 811 (Sample No. 2)	Everlube Corporation	5418	Dry film lubricant consisting of moly-disulfide and inorganic binder	Dip coating on stainless steel inserts		0/20	10	S	S
Everlube 811-B2	Everlube Corporation	4424	Dry film lubricant consisting of moly-disulfide and inorganic binder	Dip coating on stainless steel inserts		0/20	10	S	S

TABLE I. LUBRICANTS (Continued)

Material	Manufacturer or Source	Test No.	Composition	Remarks	Thickness (inch)	No. Reactions/ No. Tests	Energy Level Kg/m	Batch or Jar Rating	Material Rating
Everlube 811B	Everlube Corporation	4306	Molydisulfide and sodium silicate	Coating applied to stainless steel inserts		0/20	10	S	S
Esso Grease M-100 Super MIL ASU	Esso Oil Company	1317			0.050	3/10 1/10	10 5	U U	U U
Fel Pro C-100	Felt Products Company	3761	Molydisulfide and organic vehicle		0.010	2/3 1/4 1/3 1/5 0/7	10 4 3 2 1	U U U U U	U U U U U
Flexonic Bearing P/N 6080-295-60	Garlock Packing Company	7208	Lead impregnated Teflon with copper backing		0.121	0/20	10	S	BT
Fluid Dome P/N A-15431-76	Gilmore Industries	7944		Violent	0.050	7/20	10	U	U
Fluorocarbon Lubricant 95-1 (Lot 12)	Dixon Corporation	5572	Fluorocarbon; Teflon filled		0.050	0/20	10	S	BT
Fluorocarbon Lubricant 95-1 (Lot 12)	Dixon Corporation	5571			0.010	0/20	10	S	BT
Fluorocarbon Lubricant No. 95-1 (Tube 3)	Dixon Corporation	7447	Fluorocarbon	Three tubes tested	0.050	0/20	10	S	BT
Fluoro-Chem A0369 (Oil)	Hal· :bon Products Corporation	6969	Chlorofluorocarbon		0.5 ml	0/20	10	S	BT
Fluorochemical FC-75	Minnesota Mining and Manufacturing Company	448	Fluorinated cyclic ether		0.050	0/20	10	S	S
Fluorochemical FC-101	Minnesota Mining and Manufacturing Company	939			0.050	0/20	10	S	S
Fluorochemical FC-43	Minnesota Mining and Manufacturing Company	447	Heptacosafluoro-tributylamine		0.050	0/20	10	S	S
Fluorinated Grease	Minnesota Mining and Manufacturing Company	2149			0.005	0/20	10	S	S
Fluorochemical FX-45	Minnesota Mining and Manufacturing Company	3233			0.050	0/20	10	S	S
Fluorolube FS-5	Hooker Chemical Company	8257	Chlorofluorocarbon		0.050	0/20	10	S	S
Fluorolube FS-5	Hooker Chemical Company		Chlorofluorocarbon		0.5 ml	0/20	10	S	S
Fluorolube T-45	Hooker Chemical Company	1173	Chlorofluorocarbon		0.050	0/20	10	S	S

TABLE I. LUBRICANTS (Continued)

Material	Manufacturer or Source	Test No.	Composition	Remarks	Thickness (inch)	No. Reactions/ No. Tests	Energy Level Kg/m	Batch or Jar Rating	Material Rating
Fluorolube T-80	Hooker Chemical Company	9895	Chlorofluorocarbon		0.050	0/20	10	S	S
Fluorolube T-80	Hooker Chemical Company	1852	Chlorofluorocarbon	Three batches tested	0.050	0/60	10	S	S
Fluorolube T-80	Hooker Chemical Company	3335	From Allpax treating bath	Four batches tested	0.050	0/20	10	S	S
Fluorolube T-80	Hooker Chemical Company	6756	Chlorofluorocarbon	Taken from Allpax bath	0.5 ml	0/20	10	S	S
Fluorolube T-80	Hooker Chemical Company	6972	Chlorofluorocarbon	Taken from Allpax bath	0.5 ml	0/20	10	S	S
Fluorolube T-80 C5-27-63	Hooker Chemical Company	4663	Chlorofluorocarbon		0.050	0/20	10	S	S
Fluorolube T-80	Hooker Chemical Company	5892	Chlorofluorocarbon	Taken from Allpax bath	0.5 ml	0/20	10	S	S
Fluorolube HO-125	Hooker Chemical Company	5878	Chlorofluorocarbon		0.5 ml	0/20	10	S	S
Fluorolube HO-125	Hooker Chemical Company	4827	Chlorofluorocarbon		0.5 ml	0/20	10	S	S
Fluorolube MO-10	Hooker Chemical Company	5891	Chlorofluorocarbon		0.050	0/20	10	S	S
Fluorolube GR-544	Hooker Chemical Company	2208	Chlorofluorocarbon		0.050	0/20	10	S	S
Fluorolube LG	Hooker Chemical Company	3876	Chlorofluorocarbon	Two batches tested	0.050	0/20	10	S	S
Fluorolube GR-362	Hooker Chemical Company	437	Chlorofluorocarbon		0.050	0/20	10	S	S
Fluorolube GR-362	Hooker Chemical Company	2528	Chlorofluorocarbon		0.050	0/20	10	S	S
Fluorolube S-30 (Lot No. 2-7-63)	Hooker Chemical Company	4422	Chlorofluorocarbon		0.050	0/20	10	S	S
Fluorolube S-30 (Lot No. 2-7-63)	Hooker Chemical Company	4355	Chlorofluorocarbon		0.050	0/20	10	S	S
Fluorolube 350	Hooker Chemical Company	3760	Chlorofluorocarbon		0.050	0/20	10	S	S
Fluorolube 350 (Lot No. 6-7-62)	Hooker Chemical Company	4423	Chlorofluorocarbon		0.050	0/20	10	S	S
Fluorosilicone Fluid No. 1	Dow Corning Corporation	6997 6998 6999 7181	Fluorosilicone		0.5 ml	5/20 3/20 2/20 3/20	10 8 6 4	U	U
Fluorosilicone Fluid No. 2	Dow Corning Corporation	6996 7182 7183	Fluorosilicone		0.5 ml	2/20 3/20 1/20	10 8 6	U	U
Fluorosilicone Fluid No. 3	Dow Corning Corporation	6953 7184 7185 7186	Fluorosilicone		0.5 ml	3/40 2/20 3/20 2/20	10 10 8 6	U	U

TABLE I. LUBRICANTS (Continued)

Material	Manufacturer or Source	Test No.	Composition	Remarks	Thickness (inch)	No. Reactions/ No. Tests	Energy Level Kg/m	Batch or Jar Rating	Material Rating
Fluorosilicone Fluid No. 4	Dow Corning Corporation	6995	Fluorosilicone		0.5 ml	0/20	10	S	I
Fluorosilicone Fluid No. 5	Dow Corning Corporation	6994 7188	Fluorosilicone		0.5 ml	2/24 0/20	10 8	U	U
Fluorosilicone Fluid No. 6	Dow Corning Corporation	6993 7189	Fluorosilicone		0.5 ml	2/20 0/20	10 8	U	U
Fluorosilicone Fluid No. 7	Dow Corning Corporation	6992	Fluorosilicone		0.5 ml	0/20	10	S	I
Fluorosilicone Fluid No. 8	Dow Corning Corporation	6991 7190 7191	Fluorosilicone		0.5 ml	1/20 2/20 1/20	10 8 6	U	U
FS-1265, Lot 49, 10,000cs	Dow Corning Corporation	5830	Fluorosilicone		0.5 ml	1/80	10	S	U
FS-1265, Lot 58, 10,000cs	Dow Corning Corporation	6261	Fluorosilicone		0.5 ml	4/20	10	U	U
FS-1265, Lot 73, 10,000cs	Dow Corning Corporation	6454	Fluorosilicone		0.5 ml	6/20	10	U	U
FS-1265, Lot E-322-58	Dow Corning Corporation	7581 7580 7579 7578 7577 7576	Fluorosilicone Fluorosilicone Fluorosilicone Fluorosilicone Fluorosilicone Fluorosilicone	Sample No. G Sample No. D Sample No. C Sample No. B Sample No. A Sample No. A	0.5 ml 0.5 ml 0.5 ml 0.5 ml 0.5 ml 0.5 ml	3/20 3/20 2/20 0/20 3/20 1/20	10 10 10 10 10 10	U U U S U I	U U U U U U
FS1265 (Lot No. 23) Jar No. 1	Dow Corning Corporation	4637	Fluorosilicone oil	Viscosity 200 cs at 25°C	0.050	2/26 1/20 3/20 1/20	10 5 4 3	U U U U	U U U U
FS-1265, Lot E 32262M	Dow Corning Corporation	7657	Fluorosilicone		0.050	2/20	10	U	U
FS-1265, Lot E 32262N	Dow Corning Corporation	7658	Fluorosilicone		0.050	0/20	10	S	U
XF-1-0184 Fluid (Lot 28) Jar No. 1	Dow Corning Corporation	4865	Fluorinated silicone		0.050	5/20 7/20 1/20 0/20	10 5 4 3	U U U U	U U U U
XF-1-0266 (Lot 35)	Dow Corning Corporation	5037	Fluorinated silicone	Viscosity 300 cs at 25°C	0.050	2/20 3/20 1/20 0/20	10 8 5 4	U U U U	U U U U
XF-1-0267 (Lot 34)	Dow Corning Corporation	5031	Fluorinated silicone	Viscosity 1000 cs at 25°C	0.050	4/60 1/20 0/20	10 9 8	U U U	U U U

TABLE I. LUBRICANTS (Continued)

Material	Manufacturer or Source	Test No.	Composition	Remarks	Thickness (inch)	No. Reactions/ No. Tests	Energy Level Kg/m	Batch or Jar Rating	Material Rating
XF-6-7012 Fluid (Lot L-9) Jar No. 1	Dow Corning Corporation	4629	Fluorinated silicone		0.050	9/20 6/20 2/20 0/20	10 5 4 3	U U U U	U U U U
XG-5-0032 (Lot 1)	Dow Corning Corporation	5295	FS1265 and silica		0.050	2/60	10	U	U
XG-5-0033 (Lot 1)	Dow Corning Corporation	5291	FS1265 and ASU thickener		0.050	2/40	10	U	U
XG-5-0034 (Lot 1)	Dow Corning Corporation	5293	FS1265 and Teflon		0.050	2/60	10	U	U
FS1265 (Lot 26) Jar No. 1	Dow Corning Corporation	4634	Fluorosilicone	Viscosity 300 cs at 25°C	0.050	2/20 5/20 3/20 0/20	10 5 4 3	U U U U	U U U U
FS1265 (Lot 34) Jar No. 1	Dow Corning Corporation	4646	Fluorosilicone	Viscosity 1000 cs at 25°C	0.050	3/60 0/20 0/20 3/20 0/20	10 9 8 5 3	U U U U U	U U U U U
FS1265 (Lot 34) Jar No. 2	Dow Corning Corporation	4642	Fluorosilicone	Viscosity 1000 cs at 25°C	0.050	2/60 0/20 0/20 0/20	10 8 6 5	U U U U	U U U U
FS1265 (Lot Y535) Jar No. 1	Dow Corning Corporation	4654	Fluorosilicone	Viscosity 140 cs at 25°C	0.050	4/20 6/20 1/20	10 5 4	U U U	U U U
FS1265 (Lot Y535) Jar No. 2	Dow Corning Corporation	4650	Fluorosilicone	Viscosity 140 cs at 25°C	0.050	2/9 1/33 2/20 0/20	10 5 4 3	U U U U	U U U U
FS1265 (Lot Y540)	Dow Corning Corporation	4843	Fluorosilicone	Viscosity 10,000 cs at 25°C	0.025	1/60	10	S	U
FS1265 (Lot Y540)	Dow Corning Corporation	4628	Fluorosilicone	Viscosity 10,000 cs at 25°C	0.050	0/40	10	S	U
FS1280 (Lot 1D)	Dow Corning Corporation	4620	Fluorosilicone	Glass jar	0.050	2/28	10	U	U
FS1280 (Lot 2E)	Dow Corning Corporation	4785	Fluorosilicone	Glass jar	0.050	0/20	10	S	U
FS1280 (Lot 3F)	Dow Corning Corporation	4784	Fluorosilicone	Glass jar	0.050	2/44	10	U	U

TABLE I. LUBRICANTS (Continued)

Material	Manufacturer or Source	Test No.	Composition	Remarks	Thickness (inch)	No. Reactions/ No. Tests	Energy Level Kg/m	Batch or Jar Rating	Material Rating
FS1280 (Lot 5H)	Dow Corning Corporation	4782	Fluorosilicone	Glass jar	0.050	2/25	10	U	U
FS1280 (Lot 12)	Dow Corning Corporation	4871	Fluorosilicone	Glass jar	0.050	2/38	10	U	U
FS-1280, Lot 26	Dow Corning Corporation	6008	Fluorosilicone		0.050	0/20	10	S	U
FS-1280, Lot 36, Tube 1	Dow Corning Corporation	5651	Fluorosilicone		0.050	0/20	10	S	U
FS-1280, Lot 36, Tube 2	Dow Corning Corporation	5650	Fluorosilicone		0.050	0/20	10	S	U
FS-1281	Dow Corning Corporation	6207	Fluorosilicone		0.050	0/20	10	S	U
FS-1281, Lot 27, Jar No. 1 Jar No. 2	Dow Corning Corporation	6009	Fluorosilicone		0.050	3/20 0/20	10 10	U S	JT JT
FS-1281, Lot 31	Dow Corning Corporation	5947	Fluorosilicone		0.050	6/20	10	U	JT
FS-1281, Lot 32	Dow Corning Corporation	6036	Fluorosilicone		0.050	0/20	10	S	JT
FS-1281, Lot 33	Dow Corning Corporation	7000	Fluorosilicone		0.050	0/20	10	S	JT
FS-1281, Lot 28	Dow Corning Corporation	3621	Fluorosilicone	Sensitivity varies from jar to jar	0.050	0-5/20	10		JT
FS-1281, Lot 28	Dow Corning Corporation	4308	Fluorosilicone		0.005	4/9 4/9 3/24 1/11	10 5 3 1	U U U U	JT JT JT JT
FS-1281, Lot 35, Jar B	Dow Corning Corporation	7906	Fluorosilicone		0.050	11/200	10	U	JT
FS-1281, Lot 36, Jars ME-5 to ME-15	Dow Corning Corporation	8089	Fluorosilicone	Three jars accepted	0.050	0-3/20	10	–	JT
FS-1281, Lot 35, Jars KSC-108 to KSC-111	Dow Corning Corporation	10022	Fluorosilicone	Two jars accepted	0.050	0-5/20	10	–	JT
FS-1281, Lot 36, Jars CB-53 to CB-73	Dow Corning Corporation	8178	Fluorosilicone	Eight jars accepted	0.050	0-3/20	10	–	JT
FS-1281, Lot 37, Jars KSC-1 to KSC-48	Dow Corning Corporation	7677	Fluorosilicone	Twenty-five jars accepted	0.050	0-5/20	10	–	JT
FS-1281, Lot 37, Jar KSC-42	Dow Corning Corporation	7834	Fluorosilicone		0.050	9/100	10	–	JT
FS-1281, Lot 37, Jars CB-50 to CB-52	Dow Corning Corporation	8152	Fluorosilicone	One jar accepted	0.050	0-2/20	10	–	JT
FS-1281, Lot 37, Jars AR-2 to AR-14	Dow Corning Corporation	7847	Fluorosilicone	Five jars accepted	0.050	0-3/20	10	–	JT

TABLE I. LUBRICANTS (Continued)

Material	Manufacturer or Source	Test No.	Composition	Remarks	Thickness (inch)	No. Reactions/ No. Tests	Energy Level Kg/m	Batch or Jar Rating	Material Rating
FS-1281, Lot 38, Jars CB-74 to CB-193	Dow Corning Corporation	8373	Fluorosilicone	Twenty-two jars accepted	0.050	0-5/20	10	–	JT
FS-1281, Lot 38, Jars ME-17 to ME-28	Dow Corning Corporation	8239	Fluorosilicone	Three jars accepted	0.050	0-3/20	10	–	JT
FS-1281, Lot 38, Jars AR-1 to AR-10	Dow Corning Corporation	8698	Fluorosilicone	Six jars accepted	0.050	0-3/20	10	–	JT
FS-1281, Lot 39, Jar DC-1	Dow Corning Corporation	7882	Fluorosilicone		0.050	3/20 3/20 2/20 0/20 0/20	10 5.6 4.9 4.2 3.5	U	JT
FS-1281, Lot 39, Jar DC-2	Dow Corning Corporation	7887	Fluorosilicone		0.050	5/20 2/20 1/20 0/20 0/20	10 5.6 3.5 2.8 2.1	U	JT
FS-1281, Lot 39, Jars KSC-116 to KSC-119	Dow Corning Corporation	10030	Fluorosilicone	None accepted	0.050	1-4/20	10	U	JT
FS-1281, Lot 39, Jars KSC-49 to KSC-107	Dow Corning Corporation	7163 9275	Fluorosilicone	Thirty-two jars accepted	0.050	0-4/20	10	–	JT
FS-1281, Lot 40, Jars ME-56 to ME-58	Dow Corning Corporation	9136	Fluorosilicone	One jar accepted	0.050	0-3/20	10	–	JT
FS-1281, Lot 40, Jars KSC-25 to KSC-40	Dow Corning Corporation	8648	Fluorosilicone	Six jars accepted	0.050	0-4/20	10	–	JT
FS-1281, Lot 41, Jars ME-29 to ME-52	Dow Corning Corporation	8732	Fluorosilicone	Fifteen jars accepted	0.050	0-3/20	10	–	JT
FS-1281, Lot 41, Jars TEST-1 to TEST-12	Dow Corning Corporation	8786	Fluorosilicone	Nine jars accepted	0.050	0-3/20	10	–	JT
FS-1281, Lot 44, Jars CB-194 to CB-211	Dow Corning Corporation	10046	Fluorosilicone	Thirteen jars accepted	0.050	0-3/20	10	–	JT
FS-1281, Lot E-322-62-Q	Dow Corning Corporation	7656	Fluorosilicone		0.050	3/20	10	U	JT
FS-1281, Lot E-322-62K-2	Dow Corning Corporation	7871	Fluorosilicone		0.050	2/40 2/20 2/20 0/20 0/20	10 7.7 7.0 6.3 5.6	U	JT

TABLE I. LUBRICANTS (Continued)

Material	Manufacturer or Source	Test No.	Composition	Remarks	Thickness (inch)	No. Reactions/ No. Tests	Energy Level Kg/m	Batch or Jar Rating	Material Rating
FS-1281, Lot E-322-62K-3	Dow Corning Corporation	7876	Fluorosilicone		0.050	2/20 1/20 1/20 0/20 0/20	10 7.7 7.0 6.3 5.6	U	JT
FS-1281, Lot E-322-62-0	Dow Corning Corporation	7655	Fluorosilicone		0.050	2/20	10	U	JT
FS-1281, Lot E-322-62L	Dow Corning Corporation	7654	Fluorosilicone		0.050	3/20	10	U	JT
FS-1281, Lot E-322-62K	Dow Corning Corporation	7653	Fluorosilicone		0.050	0/20	10	S	JT
FS-1281, Lot E-322-62H	Dow Corning Corporation	7651	Fluorosilicone		0.050	2/20	10	U	JT
FS-1281, Lot 33, Jar K-1	Dow Corning Corporation	6223	Fluorosilicone		0.050	0/20	10	S	JT
Jar K-2			Fluorosilicone		0.050	2/32	10	U	JT
Jar K-3			Fluorosilicone		0.050	2/20	10	U	JT
Jar K-4			Fluorosilicone		0.050	0/20	10	S	JT
Jar K-5			Fluorosilicone		0.050	0/20	10	S	JT
Jar K-6			Fluorosilicone		0.050	2/37	10	U	JT
Jar K-7			Fluorosilicone		0.050	2/20	10	U	JT
Jar K-8			Fluorosilicone		0.050	0/20	10	S	JT
Jar K-9			Fluorosilicone		0.050	0/20	10	S	JT
Jar K-10			Fluorosilicone		0.050	0/20	10	S	JT
Jar K-11			Fluorosilicone		0.050	0/20	10	S	JT
Jar K-12			Fluorosilicone		0.050	0/20	10	S	JT
FS-1281, Lot 35	Dow Corning Corporation	7001	Fluorosilicone		0.050	0/20	10	S	JT
FS-1281, Lot 35, Jar A		6763	Fluorosilicone		0.050	2/34	10	U	JT
Jar B		6760	Fluorosilicone		0.050	2/52	10	U	JT
Jar C		6758	Fluorosilicone		0.050	2/37	10	U	JT
FS-1281, Lot 36, Jar I	Dow Corning Corporation	7468	Fluorosilicone		0.050	3/20	10	U	JT
Jar II		7469	Fluorosilicone		0.050	5/60	10	U	JT
FS-1281, Lot 37	Dow Corning Corporation	7505	Fluorosilicone		0.050	2/30	10	U	JT
FS-1281, Lot E-322-59									
Jar F	Dow Corning Corporation	7575	Fluorosilicone		0.050	0/20	10	S	JT
Jar E		7573	Fluorosilicone		0.050	3/60	10	U	JT
FS-1292 Grease, Lot 45	Dow Corning Corporation	8719	Fluorosilicone		0.050	2/100	10	U	U
FS-1292 Grease, Lot 52	Dow Corning Corporation	9774	Fluorosilicone		0.050	2/20	10	U	U
FX 46 Grease (Lot 1)	Minnesota Mining and Manufacturing Company	3873			0.010	0/20	10	S	BT
FX-46 Grease (Lot 1)	Minnesota Mining and Manufacturing Company	3874			0.002	0/20	10	S	BT

TABLE I. LUBRICANTS (Continued)

Material	Manufacturer or Source	Test No.	Composition	Remarks	Thickness (inch)	No. Reactions/ No. Tests	Energy Level Kg/m	Batch or Jar Rating	Material Rating
Fluorolube S-30	Hooker Chemical Company	4355	Chlorofluorocarbon		0.050	0/20	10	S	S
Fluoro-Glide	Chemplast Incorporated	1876	Teflon-Freon	Two batches tested		0/20	10	S	S
Garlock Bearing Material	Garlock Packing Company	5680			0.130	9/20	10	U	BT
Garlock Bearing Material (with Teflon and Lead removed)	Garlock Packing Company	5679			0.100	0/20	10	S	BT
Garlock Du Metal (with Brass backing)	Garlock Packing Company	5850	Teflon and sintered metal		0.0125	0/20	10	S	BT
Goop-High Purity Swag Lock Thread Lubricant Antiseize Compound	Crawford Fitting Company	4819	Chlorofluorocarbon with Teflon filler		0.010	1/60	10	S	BT
Grease (GAA-MIL-C-10924)	Sta-Vis Oil Company	908			0.050	2/5 2/10 0/5	10 5 2	U – –	U U U
Grease (GL · MIL-G-3278A)	Socony Mobil Oil Company	599	Petroleum base grease		0.050	2/10	10	U	U
Grease, Lubricating, O.D. No. 00	Warren Refining and Chemical Company	611		Violent reaction	0.050	1/20	10	U	U
Halocarbon Oil, Series 4-11	Halocarbon Products Corporation	5996	Chlorofluorocarbon		0.5 ml	0/20	10	S	S
Halocarbon Oil, Series 4-11E	Halocarbon Products Corporation	5995	Chlorofluorocarbon		0.5 ml	0/20	10	S	S
Halocarbon Oil, Series 2.3/100	Halocarbon Products Corporation	4511	Chlorofluorocarbon		0.050	0/20	10	S	S
Halocarbon Oil, Series 10-25	Halocarbon Products Corporation	5994	Chlorofluorocarbon		0.5 ml	0/20	10	S	S
Halocarbon Oil, Series 10-25E	Halocarbon Products Corporation	6041	Chlorofluorocarbon		0.5 ml	0/20	10	S	S
Halocarbon Oil, Series 11-14	Halocarbon Products Corporation	6037	Chlorofluorocarbon		0.5 ml	0/20	10	S	S
Halocarbon Oil, Series 11-14E	Halocarbon Products Corporation	5993	Chlorofluorocarbon		0.5 ml	0/20	10	S	S
Halocarbon Oil, Series 11-21	Halocarbon Products Corporation	1287	Chlorofluorocarbon		0.5 ml	0/20	10	S	S
Halocarbon Oil, Series 11-21E	Halocarbon Products Corporation	6040	Chlorofluorocarbon		0.5 ml	0/20	10	S	S
Halocarbon Oil, Series 11-21E	Halocarbon Products Corporation	7402	Chlorofluorocarbon		0.5 ml	0/20	10	S	S
Halocarbon Oil, Series 13-21E	Halocarbon Products Corporation	6453	Chlorofluorocarbon		0.5 ml	0/20	10	S	S
Halocarbon Oil, Series 13-21E	Halocarbon Products Corporation	6038	Chlorofluorocarbon		0.5 ml	0/20	10	S	S
Halocarbon Oil, Series 14-25	Halocarbon Products Corporation	5970	Chlorofluorocarbon		0.5 ml	0/20	10	S	S

TABLE I. LUBRICANTS (Continued)

Material	Manufacturer or Source	Test No.	Composition	Remarks	Thickness (inch)	No. Reactions/ No. Tests	Energy Level Kg/m	Batch or Jar Rating	Material Rating
Halocarbon Oil, Series 14-25	Halocarbon Products Corporation	6042	Chlorofluorocarbon		0.5 ml	0/20	10	S	S
Halocarbon Oil, Series 14-25E	Halocarbon Products Corporation	6039	Chlorofluorocarbon		0.5 ml	0/20	10	S	S
Halocarbon Oil, Series 208	Halocarbon Products Corporation	5832	Chlorofluorocarbon		0.5 ml	0/20	10	S	S
Halocarbon Oil, Series 208	Halocarbon Products Corporation	7395	Chlorofluorocarbon		0.5 ml	0/20	10	S	S
Halocarbon Oil, Series 208	Halocarbon Products Corporation	7394	Chlorofluorocarbon		0.5 ml	0/20	10	S	S
75% Halocarbon 208 Oil – 25% Bestoil	Chemistry Branch	8505			0.050	6/20 3/20 4/20 3/20 2/20 0/20	10 7.7 5.6 3.5 1.4 0.7	U	U
80% Halocarbon 208 Oil – 20% Bestoil	Chemistry Branch	8591			0.050	4/20 3/20 2/20 2/20 0/20 0/20	10 7.7 5.6 4.9 4.2 3.5	U	U
83% Halocarbon 208 Oil – 17% Bestoil	Chemistry Branch	8650			0.050	15/140 13/140 1/140 0/140	10 9.1 8.4 7.7	U	U
80% Halocarbon 208 Oil – 20% DC 200 Oil	Chemistry Branch	8654			0.050	5/40	10	U	U
90% Halocarbon 208 Oil – 10% DC 200 Oil	Chemistry Branch	8983			0.050	11/160 9/160 0/160 0/160	10 9.1 8.4 7.7	U	U
Halocarbon Grease, Series 11B3	Halocarbon Products Corporation	7059	Chlorofluorocarbon		0.050	0/20	10	S	S
Halocarbon Grease, Series 25-10M	Halocarbon Products Corporation	6045	Chlorofluorocarbon		0.050	0/20	10	S	S
Halocarbon Grease, Series 25-20M	Halocarbon Products Corporation	6046	Chlorofluorocarbon		0.050	0/20	10	S	S
Halocarbon Grease X90-10	Halocarbon Products Corporation	6043	Chlorofluorocarbon		0.050	0/20	10	S	S
Halocarbon Grease X90-15M	Halocarbon Products Corporation	6044	Chlorofluorocarbon		0.050	0/20	10	S	S
Halocarbon Grease X90-15M-5A	Halocarbon Products Corporation	6519	Chlorofluorocarbon		0.050	0/20	10	S	S
Halocarbon Grease 25-5S	Halocarbon Products Corporation	10264	Chlorofluorocarbon	Three batches tested	0.050	0/60	10	S	S

TABLE I. LUBRICANTS (Continued)

Material	Manufacturer or Source	Test No.	Composition	Remarks	Thickness (inch)	No. Reactions/ No. Tests	Energy Level Kg/m	Batch or Jar Rating	Material Rating
Halocarbon Oil 13-21	Halocarbon Corporation	989	Chlorofluorocarbon		0.050	0/20	10	S	S
Halocarbon Oil 11-21	Halocarbon Corporation	1287	Chlorofluorocarbon		0.050	0/20	10	S	S
Halocarbon Grease 25-20MB	Halocarbon Corporation	1262	Chlorofluorocarbon	Contains rust inhibitor	0.050	0/20	10	S	S
Halocarbon Grease 25-20MA	Halocarbon Corporation	1261	Chlorofluorocarbon	Contains rust inhibitor	0.050	0/20	10	S	S
Halocarbon Grease 25-20MZ	Halocarbon Corporation	1244	Chlorofluorocarbon	Contains rust inhibitor	0.050	0/20	10	S	S
Halocarbon Grease 25-10MZ	Halocarbon Corporation	1243	Chlorofluorocarbon	Contains rust inhibitor	0.050	0/20	10	S	S
Halocarbon Grease 25-20M-5A	Halocarbon Corporation	1831	Chlorofluorocarbon with a barium sulfonate inhibitor		0.050	0/20	10	S	S
Houghton Hi-Temp Grease 2409	E.H. Houghton Company	4421	Polyglycol		0.050	3/20	10	U	U
Invelco-33	Drilube Company	1357			0.050	2/20	10	U	U
Johnson's No. 250 J-Cool		6653			0.5 ml	5/20	10	U	U
Kay Lube Dry Film Lube	Kaynar Manufacturing Company	7067	Molydisulfide with organic binder	Coated inserts		6/20	10	U	U
Kay Lube Dry Film Lube	Kaynar Manufacturing Company	7203 7207		Coated inserts Coated inserts	0.0024 0.0024	4/20 0/20	7.62 3.46	U U	U U
Kel-F Polymer Oil, Lot 509	Minnesota Mining and Manufacturing Company	6755	Chlorofluorocarbon		0.5 ml	0/20	10	S	S
Kel-F-90 Grease	Minnesota Mining and Manufacturing Company	5908	Chlorofluorocarbon		0.050	0/20	10	S	S
Kel-F-90 Grease, Lot 532	Minnesota Mining and Manufacturing Company	7002	Chlorofluorocarbon		0.050	0/20	10	S	S
Kel-F-90 Grease, Lot 534	Minnesota Mining and Manufacturing Company	7401	Chlorofluorocarbon		0.050	1/60	10	S	S
Kel-F 90 Grease, Lot 540	Minnesota Mining and Manufacturing Company	9130	Chlorofluorocarbon	Three jars evaluated	0.050	0/60	10	S	S
Kel-F-90 Grease, Lot 1224	Minnesota Mining and Manufacturing Company	5988	Chlorofluorocarbon		0.050	0/20	10	S	S

TABLE I. LUBRICANTS (Continued)

Material	Manufacturer or Source	Test No.	Composition	Remarks	Thickness (inch)	No. Reactions/ No. Tests	Energy Level Kg/m	Batch or Jar Rating	Material Rating
Kel-F-90 Grease, Lot 529 (with rust inhibitor)	Minnesota Mining and Manufacturing Company	6652	Chlorofluorocarbon		0.050	0/20	10	S	S
Kel-F-90 Grease	Minnesota Mining and Manufacturing Company	3243	Chlorofluorocarbon	Two batches tested	0.050	0/20	10	S	S
Kel-F-90 Grease, Lot 507	Minnesota Mining and Manufacturing Company	4419	Chlorofluorocarbon		0.050	0/20	10	S	S
Kel-F-90 Grease, Lot 1222	Minnesota Mining and Manufacturing Company	5030	Chlorofluorocarbon		0.050	0/20	10	S	S
Kel-F-Grease L1477 NB14781-9	Minnesota Mining and Manufacturing Company	5482	Chlorofluorocarbon		0.050	0/20	10	S	S
Kel-F-Polymer Oil Grade KF-10	Minnesota Mining and Manufacturing Company	4420	Chlorofluorocarbon		0.050	0/20	10	S	S
Kel-F-Polymer Oil Grade KF-10 (Lot 1273)	Minnesota Mining and Manufacturing Company	5480	Chlorofluorocarbon		0.050	0/20	10	S	S
Kel-F-Polymer Oil, Lot 502	Minnesota Mining and Manufacturing Company	5573	Chlorofluorocarbon		0.050	0/20	10	S	S
Kel-F Oil No. 1	Minnesota Mining and Manufacturing Company	451	Chlorofluorocarbon		0.050	0/20	10	S	S
Kel-F-10-200 Wax	Minnesota Mining and Manufacturing Company	356	Chlorofluorocarbon		0.050	0/20	10	S	S
Kel-F Polymer Oil No. 10	Minnesota Mining and Manufacturing Company	2744	Chlorofluorocarbon	Two batches tested	0.050	0/20	10	S	S
Kel-F-10, Oil Lot 516	Minnesota Mining and Manufacturing Company	7586	Chlorofluorocarbon		0.5 ml	0/20	10	S	S
Kel-F Polymer Oil KF-3	Minnesota Mining and Manufacturing Company	2721	Chlorofluorocarbon	Contains rust inhibitor	0.050	1/60	10	S	S
Kel-F Polymer Oil KF-1	Minnesota Mining and Manufacturing Company	2722	Chlorofluorocarbon	Contains rust inhibitor	0.050	0/20	10	S	S
Kel-F 10 Polymer Oil Lot 1006-1	Minnesota Mining and Manufacturing Company	2897	Chlorofluorocarbon		0.050	0/20	10	S	S
KX-262 NB-1247-36	Minnesota Mining and Manufacturing Company	3604	Chlorofluorocarbon		0.050	0/40	10	S	S
KX-245 Lot 2	Minnesota Mining and Manufacturing Company	3606	Chlorofluorocarbon		0.050	0/40	10	S	BT
Kel-F Polymer Oil KF-10, Lot 523	Minnesota Mining and Manufacturing Company	8385	Chlorofluorocarbon		0.050	0/20	10	S	S

TABLE I. LUBRICANTS (Continued)

Material	Manufacturer or Source	Test No.	Composition	Remarks	Thickness (inch)	No. Reactions/ No. Tests	Energy Level Kg/m	Batch or Jar Rating	Material Rating
KX-245 Polymer Oil	Minnesota Mining and Manufacturing Company	8599			0.050	0/20	10	S	BT
Krytox 143AA Oil, Lot 8	E.I. du Pont de Nemours and Company	9894	Fluorocarbon		0.050	0/20	10	S	S
Krytox 143AB Oil, Lot 16	E.I. du Pont de Nemours and Company	9900	Fluorocarbon		0.050	0/20	10	S	S
Krytox 143AC Oil, Lot 12	E.I. du Pont de Nemours and Company	9898	Fluorocarbon		0.050	0/20	10	S	S
Krytox 143AD Oil, Lot 6	E.I. du Pont de Nemours and Company	9902	Fluorocarbon		0.050	0/20	10	S	S
Krytox 143AZ Oil, Lot 3	E.I. du Pont de Nemours and Company	9901	Fluorocarbon		0.050	0/20	10	S	S
Krytox 240AB Grease, Lot 4	E.I. du Pont de Nemours and Company	9896	Fluorocarbon		0.050	0/20	10	S	S
Krytox 240 AC Grease, Lot 17	E.I. du Pont de Nemours and Company	9897	Fluorocarbon		0.050	0/20	10	S	S
PR-143AB Oil, Lot 6	E.I. du Pont de Nemours and Company	8715	Fluorocarbon	Krytox 143AB	0.050	0/20	10	S	S
PR-143AC Oil, Lot 6	E.I. du Pont de Nemours and Company	8714	Fluorocarbon	Krytox 143AC	0.050	0/20	10	S	S
PR-240AB Grease, Lot 4	E.I. du Pont de Nemours and Company	8716	Fluorocarbon	Krytox 240AB	0.050	0/20	10	S	S
PR-240AC Grease, Lot 4	E.I. du Pont de Nemours and Company	8717	Fluorocarbon	Krytox 240AC	0.050	0/20	10	S	S
PR-240AC Grease, Lot 7	E.I. du Pont de Nemours and Company	8841	Fluorocarbon	Krytox 240AC	0.050	0/20	10	S	S
PR-240AC Grease, Lot 9	E.I. du Pont de Nemours and Company	9148	Fluorocarbon	Krytox 240AC	0.050	0/20	10	S	S
PR-143 Oil	E.I. du Pont de Nemours and Company	7631	Fluorocarbon		0.5 ml	0/20	10	S	S
PR-143 Oil	E.I. du Pont de Nemours and Company	7632	Fluorocarbon	Stainless steel inserts	Smear	0/20	10	S	S
PR-240 Grease	E.I. du Pont de Nemours and Company	7633	Fluorocarbon		0.050	0/20	10	S	S

TABLE I. LUBRICANTS (Continued)

Material	Manufacturer or Source	Test No.	Composition	Remarks	Thickness (inch)	No. Reactions/ No. Tests	Energy Level Kg/m	Batch or Jar Rating	Material Rating
Lapping Compound 38-1200	United States Products Company	1960			0.050	2/4 2/16	10 5	U	U
Liquid O-Ring 1231, Lot 54S	Oil Research Center	8619	Teflon-chlorofluorocarbon		0.050	0/20	10	S	BT
Liquid O-Ring, Lot 52S	Oil Research Center	7956	Teflon-chlorofluorocarbon	Three tubes evaluated	0.050	0/60	10	S	BT
Lubeco 905 Dry Film Lubricant	Hi Shear Corporation	6980			0.063	0/20	10	S	BT
Lubeco 905 Dry Film Lubricant	Hi Shear Corporation	6981			0.063	0/20	10	S	BT
Lubeco 905 Dry Film Lubricant	Parker Aircraft	8236			0.050	0/20	10	S	BT
Lube Rex	General Cement Company	597	Hydrocarbon grease		0.050	2/6	10	U	U
Lubriko MD-T-419	Masden-Lubricant Company	588	Hydrocarbon grease		0.050	3/12	10	U	U
Lubriplate	Fiske Brothers Incorporated	643	Hydrocarbon grease		0.050	2/10	10	U	U
Lubriseal	A.H. Thomas Company	637	Hydrocarbon grease		0.050	2/6 0/20	10 5	U –	U –
McLube 99	McGee Chemical Company	3895			0.050	0/40	10	S	S
McLube 2010	McGee Chemical Company	3896	Molydisulfide with graphite and Fluorolube		0.050	0/20	10	S	BT
McLube 2023	McGee Chemical Company	3897	Molydisulfide with graphite and Fluorolube		0.050	0/20	10	S	BT
Metco Valvelube	Metallizing Engineering Co.	562	Hydrocarbon grease	Very violent reaction	0.050	1/20	5	U	U
Midwest Research Institute Dry Film Lubricant	Midwest Research Institute	3614	Molydisulfides, graphite, and bismuth in sodium silicate 10:1:5/7			0/20	10	S	S
Midwest Research Institute Dry Film Lubricant	Midwest Research Institute	3613	Molydisulfide, graphite, and bismuth in sodium silicate 10:1:2:5/7			0/20	10	S	S
Midwest Research Institute Dry Film Lubricant	Midwest Research Institute	3612	Molydisulfide, graphite, and bismuth in sodium silicate 10:1:5/7			0/20	10	S	S
Midwest Research Institute Dry Film Lubricant	Midwest Research Institute	3611	Molydisulfide and graphite in sodium phosphate 10:1/7			0/20	10	S	S
ML-554 Grease	Kennedy Space Center	8235			0.050	0/20	10	S	I

TABLE I. LUBRICANTS (Continued)

Material	Manufacturer or Source	Test No.	Composition	Remarks	Thickness (inch)	No. Reactions/ No. Tests	Energy Level Kg/m	Batch or Jar Rating	Material Rating
~~Micro-Seal Process 100-1~~	~~Microseal Products Co.~~	6638		On stainless steel inserts		0/20	10	S	S
Microseal Dry Film Lubricant 100-1	Microseal Products Sales	4660		Stainless steel inserts used		0/40	10	S	S
MLF-9 Dry Film Lubricant	Midwest Research Institute	6928	Molydisulfide, graphite, bismuth, aluminum phosphate	On stainless steel inserts		0/20	10	S	S
MLF Dry Film Lubricant	Midwest Research Institute	8694	Polyimide bonded		0.002	10/20	10	U	U
MLF Dry Film Lubricant	Midwest Research Institute	8695	Polyimide bonded		0.002	5/20	10	U	U
MLF-2 Dry Film Lubricant	Midwest Research Institute	8859	Polyimide bonded dry film lubricant containing antimony oxide and molydisulfide		0.002	0/20	10	S	I
Mogul Taper Valvelube	Metallizing Engineering Co.	561			0.050	2/20	10	U	U
Mold Release Lubricant S-122	Miller-Stephenson Company	2736				0/20	10	S	S
Molylube Spray Dry Powder Lubricant Can No. 1	Bel-Ray Company Incorporated	5431	Molydisulfide in spray bomb	Sprayed on inserts		0/20	10	S	S
Molylube Spray Dry Powder Lubricant Can No. 2	Bel-Ray Company Incorporated	5430	Molydisulfide in spray bomb	Sprayed on inserts		0/20	10	S	S
Molylube Spray Dry Powder Lubricant	Bel-Ray Company Incorporated	4418	Molydisulfide in spray bomb	Sprayed on inserts		0/20	10	S	S
Molylube Spray Dry Powder Lubricant	Bel-Ray Company Incorporated	4781	Molydisulfide in spray bomb	Sprayed on stainless steel inserts		0/20	10	S	S
Molylube Spray (Sample No. 1)	Bel-Ray Company Incorporated	4777	Molydisulfide in spray bomb	Sprayed on stainless steel inserts		0/20	10	S	S
Molylube Spray (Sample No. 2)	Bel-Ray Company Incorporated	4776	Molydisulfide in spray bomb	Sprayed on stainless steel inserts		0/20	10	S	S
Molylube Spray (Sample No. 3)	Bel-Ray Company Incorporated	4775	Molydisulfide in spray bomb	Sprayed on stainless steel inserts		0/20	10	S	S
Molylube Spray (Sample No. 4)	Bel-Ray Company Incorporated	4774	Molydisulfide in spray bomb	Sprayed on stainless steel inserts		0/20	10	S	S
Molylube Spray (Sample No. 5)	Bel-Ray Company Incorporated	4773	Molydisulfide in spray bomb	Sprayed on stainless steel inserts		0/20	10	S	S

TABLE I. LUBRICANTS (Continued)

Material	Manufacturer or Source	Test No.	Composition	Remarks	Thickness (inch)	No. Reactions/ No. Tests	Energy Level Kg/m	Batch or Jar Rating	Material Rating
Molylube N	Bel-Ray Company, Incorporated	9293	Graphite-molydisulfide in an inorganic binder	Cured at 175°C for 30 minutes	0.004	0/20	10	S	BT
Molylube Spray Versatile Dry Powder Lubricant	Bel-Ray Company, Incorporated	6196		Sprayed on stainless steel inserts		0/220	10	S	S
Molylube 1612	Bel-Ray Company, Incorporated	5844			0.5 ml	3/60	10	U	U
Molylube	Bel-Ray Company, Incorporated	2735	Molydisulfide Freon propellant			0/20	10	S	BT
Molylube AR	Bel-Ray Company, Incorporated	2734	Molydisulfide and binder			8/80	10	U	U
Molub Alloy 379, Dry Film Lubricant	Imperial Oil and Grease Company	8807			0.050	9/20	10	U	U
Molub Alloy 369, Dry Film Lubricant	Imperial Oil and Grease Company	8808			0.050	17/20	10	U	U
Molykote G Grease	Alpha Molykote Corporation	716	Molydisulfide and petroleum base oil	Violent reactions	0.050	3/4	10	U	U
Molykote Grease M-55	Alpha Molykote Corporation	518	Molydisulfide and organic vehicle		0.050	2/20	10	U	U
Molykote Spray Lube	Alpha Molykote Corporation	772	Molydisulfide with Freon propellant			0/20	10	S	BT
Molykote M-8800	Alpha Molykote Corporation	3363				5/20 2/20 0/20	10 5 3	U U U	U U U
Molykote X-15	Alpha Molykote Corporation	3362	Sodium silicate, molydisulfide, and graphite			0/60	10	S	BT
Molykote Z	Alpha Molykote Corporation	1655	Molydisulfide powder	Two batches tested		0/20	10	S	S
Molykote Z	Alpha Molykote Corporation	1654		Without stainless steel inserts		2/20	10	—	—
Molykote Z, MIL-M-7866A	Alpha Molykote Corporation	6449	Molydisulfide	On stainless steel inserts		0/20	10	S	S
Moly Spray Kote Lubricant No. 1	Alpha Molykote Corporation	4780	Molydisulfide in spray bomb	Sprayed on stainless steel inserts		2/60	10	U	U
Moly Spray Kote Lubricant No. 2	Alpha Molykote Corporation	4772	Molydisulfide in spray bomb	Sprayed on stainless steel inserts		0/20	10	S	BT

TABLE I. LUBRICANTS (Continued)

Material	Manufacturer or Source	Test No.	Composition	Remarks	Thickness (inch)	No. Reactions/ No. Tests	Energy Level Kg/m	Batch or Jar Rating	Material Rating
Moly Spray Kote Lubricant No. 3	Alpha Molykote Corporation	4771	Molydisulfide in spray bomb	Sprayed on stainless steel inserts		0/20	10	S	BT
Moly Spray Kote Lubricant No. 4	Alpha Molykote Corporation	4770	Molydisulfide in spray bomb	Sprayed on stainless steel inserts		0/20	10	S	BT
Moly Spray Kote Lubricant No. 5	Alpha Molykote Corporation	4769	Molydisulfide in spray bomb	Sprayed on stainless steel inserts		0/20	10	S	BT
Moly Spray Kote Lubricant No. 6	Alpha Molykote Corporation	4882	Molydisulfide in spray bomb	Sprayed on stainless steel inserts		4/20	10	U	U
Moly Spray Kote Lubricant No. 7	Alpha Molykote Corporation	4883	Molydisulfide in spray bomb	Sprayed on stainless steel inserts		3/20	10	U	U
Moly Spray Kote Lubricant No. 8	Alpha Molykote Corporation	4884	Molydisulfide in spray bomb	Sprayed on stainless steel inserts		2/20	10	U	U
Moly Spray Kote Lubricant No. 9	Alpha Molykote Corporation	4885	Molydisulfide in spray bomb	Sprayed on stainless steel inserts		0/20	10	S	BT
Molynamel E	Lockrey Company	3239	Molydisulfide, teflon, and toluene			7/60 2/20	10 5	U U	U U
Oil-ES-Oil	American Durafilm Company	4626	Teflon spray bomb	Sprayed on stainless steel inserts		0/20	10	S	BT
Orlox 200 P	Bel-Ray Company, Incorporated	5304			0.050	0/20	10	S	BT
Orlox 200 P	Bel-Ray Company, Incorporated	5839	Aroclor, graphite, and molydisulfide		0.050	0/20	10	S	BT
Orlox 500 C	Bel-Ray Company Incorporated	5300			0.050	0/20	10	S	BT
Orlox 500 C	Bel-Ray Company, Incorporated	5843	Fluorolube, graphite, and molydisulfide		0.5 ml	0/20	10	S	BT
Orlox 1800 P	Bel-Ray Company, Incorporated	5837	Aroclor, graphite, and molydisulfide		0.050	3/60	10	U	BT
Orlox 1800 P	Bel-Ray Company, Incorporated	5302			0.050	0/20	10	S	BT
Oxylube	Drilube Company		(See Drilube)						
Parker "O" Lube	Parker Appliance Company	788			0.050	2/5	10	U	U
Parker Water Oil Lube Grease 50	Parker Appliance Company	274			0.050	1/2 1/2 1/4	10 5 3	U – –	U – –
P.D. 785	Frankford Arsenal	2079	Mixture of perfluoro-trialkylamines		0.050	0/20	10	S	BT

TABLE I. LUBRICANTS (Continued)

Material	Manufacturer or Source	Test No.	Composition	Remarks	Thickness (inch)	No. Reactions/ No. Tests	Energy Level Kg/m	Batch or Jar Rating	Material Rating
P.D. 786	Frankford Arsenal	2080	Grease consisting of polytetrafluorcethylene gelling agent (P.D. 787) and perfluorotri-alkylamine oil (P.D. 785)		0.050	0/20	10	S	BT
P.D. 787	Frankford Arsenal	2105	Polytetrafluoroethylene gelling agent			0/20	10	S	BT
P.D. 788	Frankford Arsenal	2081	Grease consisting of P.D. 787 and P.D. 789		0.050	0/20	10	S	BT
P.D. 789	Frankford Arsenal	2077	Mixture of perfluorotri-alkylamines		0.050	0/20	10	S	BT
P.D. 797	Frankford Arsenal	3553	Perfluorotrialkylamine base oil and silica gelling agent		0.050	0/20	10	S	BT
P.D. 791	Frankford Arsenal	2106	Purified sample of perfluorotrialkylamine		0.050	0/10	10	I	I
P.D. 792	Frankford Arsenal	2078	Grease consisting of graphite gelling agent and perfluorotrialkyl-amine base oil (P.D. 789)		0.050	0/20	10	S	BT
P.D. 800	Frankford Arsenal	3561	Perfluorotrialkylamine base oil and silica gelling agent		0.050	0/20	10	S	BT
P.D. 801	Frankford Arsenal	3552	Perfluorotrialkylamine base oil and silica gelling agent		0.050	0/20	10	S	BT
P.D. 808	Frankford Arsenal	3560	Silica gelling agent			0/20	10	S	BT
P.D. 809	Frankford Arsenal	3563	Silica gelling agent			0/20	10	S	BT
P.D. 810	Frankford Arsenal	3564	Silica gelling agent			0/20	10	S	BT
P.D. 811	Frankford Arsenal	3570	Special grade graphite			0/20	10	S	BT
P.D. 812	Frankford Arsenal	3569	Perfluorotrialkylamine blend			0/20	10	S	BT
P.D. 816	Frankford Arsenal	3991	Fluorinated amine oil and fluorinated polymer gelling agent		0.050	0/20	10	S	BT

TABLE I. LUBRICANTS (Continued)

Material	Manufacturer or Source	Test No.	Composition	Remarks	Thickness (inch)	No. Reactions/ No. Tests	Energy Level Kg/m	Batch or Jar Rating	Material Rating
P.D. 817	Frankford Arsenal	3992	Fluorinated oils and polymer gelling agent		0.050	0/20	10	S	BT
P.D. 819	Frankford Arsenal	3993	Fluorinated oil and polymer gelling agent		0.050	0/20	10	S	BT
P.D. 820	Frankford Arsenal	3994	Fluorinated polymer		0.050	0/20	10	S	BT
P.D. 821	Frankford Arsenal	3995 7628	Fluorinated Polymer		0.050 0.5 ml	0/20 0/20	10 10	S S	BT BT
P.D. 822	Frankford Arsenal	3996	Fluorinated polymer		0.050	4/20	10	U	BT
PD-838	Frankford Arsenal	5893			0.050	0/20	10	S	BT
PD-838A	Frankford Arsenal	7629			0.050	0/20	10	S	BT
PD-838A	Frankford Arsenal	7630		Stainless steel inserts	Smear	0/20	10	S	BT
PD-839 Oil	Frankford Arsenal	5971			0.5 ml	0/20	10	S	BT
PD-855 Oil	Frankford Arsenal	7641			0.5 ml	2/40	10	U	U
PD-856 Grease	Frankford Arsenal	7637			0.050	0/20	10	S	BT
PD-857 Grease	Frankford Arsenal	7639			0.050	0/20	10	S	BT
P.D. 826A	Frankford Arsenal	7638			0.050	0/20	10	S	BT
Pydraul AC (Lot E4)	Monsanto Chemical Company	4417			0.050	3/5 2/15	10 5	U –	U –
Polyglycol 11-200 Lot 8-6	Dow Chemical Company	1940	Polyglycol		0.050	0/20	10	I	I
QC-2-0093	Dow Corning Corporation		Fluorosilicone	Sensitivity varies from jar to jar	0.050	0-5/20	10	JT	JT
QC-2-0026	Dow Corning Corporation		Fluorosilicone	Sensitivity varies from jar to jar	0.050	0-3/20	10	JT	JT
QC-2-0026, Lot 37	Dow Corning Corporation	7454	Fluorosilicone	Twenty-four jars tested 18 rejected	0.050	0-4/20	10	JT	JT
QC-2-0093, 1280, Jar No. 1 Jar No. 2	Dow Corning Corporation	7392 7393	Fluorosilicone		0.050	0/20 0/20	10 10	S S	JT JT
QF-1-0065 Fluid (2500 cs)	Dow Corning Corporation	1288	Fluorosilicone		0.050	3/12 0/8	10 5	U –	U –

TABLE I. LUBRICANTS (Continued)

Material	Manufacturer or Source	Test No.	Composition	Remarks	Thickness (inch)	No. Reactions/ No. Tests	Energy Level Kg/m	Batch or Jar Rating	Material Rating
QF-1-0065 (7500 cs)	Dow Corning Corporation	4438	Fluorosilicone		0.050	0/20	10	S	U
Rulon Spray	Dixon Corporation	9152			0.001	1/60	10	S	BT
R & R Teflon Lubricant No. 30 Colloidal Dispenser Stock No. 499	Ideal Design Company	5051			0.050	0/20	10	S	BT
Sealube Grease	Parker Appliance Company	550			0.050	2/2	10	U	U
						1/4	5	U	U
						3/10	3	U	U
Semco No. 551		1442			0.050	0/20	10	S	U
Shell SAE-30 Oil	Shell Oil Company	9764	Hydrocarbon	Violent	0.050	10/20	10	U	U
						8/20	7.7		
						5/20	5.6		
						3/20	3.5		
						1/20	1.4		
						0/20	0.7		
Silgon 6 (1000 cs)	Anderson Chemical Company	4415			0.050	7/20	10	U	U
Silgon Fluid 6 (300 cs)	Anderson Chemical Company	965			0.050	2/5	10	U	U
						2/3	5	–	–
Silgon 6 (500 cs)	Anderson Chemical Company	4413			0.050	2/20	10	U	U
Silgon Grease 10	Anderson Chemical Company	4410			0.050	2/20	10	U	U
Silicone Lubricant 398-38-1114	General Electric Company	955			0.050	2/3	10	U	U
						1/1	5	–	–
						1/5	1	–	–
Silicone Lubricant 20057	Electromechanics Corporation	478			0.050	2/10	10	U	U
Silicone Lubricant 81717	General Electric Company	569			0.050	2/3	10	U	U
						1/1	5	–	–
Silicone Fluid SF 96 (275 cs)	General Electric Company	564			0.050	2/10	10	U	U
						0/10	5	–	–
Silicone Fluid SF 96 (100 cs)	General Electric Company	565			0.050	2/5	10	U	U
						4/6	5	–	–
Silicone Fluid SF 96 (40 cs)	General Electric Company	566			0.050	2/6	10	U	U
						2/6	5	–	–
Silicone Fluid SF 81 (40 cs)	General Electric Company	493			0.050	2/4	10	U	U
						2/3	5	–	–

TABLE I. LUBRICANTS (Continued)

Material	Manufacturer or Source	Test No.	Composition	Remarks	Thickness (inch)	No. Reactions/ No. Tests	Energy Level Kg/m	Batch or Jar Rating	Material Rating
Slick Spray Lubricant	Oil Center Research	9149			0.001	0/60	10	S	BT
S-122 Fluorocarbon Lubricant	Miller Stephenson Company	9757				0/20	10	S	BT
Syntex 48	Bel-Ray Company Incorporated	5476			0.050	4/20 1/3	10 9	U –	U –
Syntex 54	Bel-Ray Company Incorporated	5478			0.050	0/20	10	S	BT
Syntex 54	Bel Ray Company Incorporated	5838	Aroclor 1254		0.5 ml	0/20	10	S	BT
Templube Grease 124	National Engineering Products Company	542			0.050	2/7	10	U	U
Ucon Lubricant 50 HB-280X	Union Carbide Corporation	3214	Polyalkylene glycol		0.050	4/20 0/20	10 5	U –	U –
Ucon Lubricant 50-HB-280X	Union Carbide Corporation	785	Polyalkylene glycol		0.050	2/2 1/18	10 5	U –	U –
Ucon Lubricant 50 HB-280X	Union Carbide Corporation	3207	Polyalkylene glycol		0.030	2/20	10	U	U
Ucon Fluid LB-300X	Union Carbide Corporation	4416	Polyalkylene glycol		0.050	5/20	10	U	U
Ucon Fluid 50-LB-65	Union Carbide Corporation	433	Polyalkylene glycol		0.050	1/3 1/3 1/3	10 5 3	U – –	U – –
Ucon Fluid LB-135	Union Carbide Corporation	434	Polyalkylene glycol		0.050	1/2	10	U	U
Ucon Lubricant LB300X	Union Carbide Chemical Company	4411	Polyglycol base lubricant		0.050	5/20	10	U	U
Valve Seal A	Dow Corning Corporation	10335	Silicone		0.050	7/20	10	U	U
Versilube Fluid F-50	General Electric Company	238	Silicone		0.050	2/2 2/2	10 5	U –	U –
Versilube Fluid G-300	General Electric Company	270	Silicone		0.050	2/10	10	U	U
Viscasil Fluid 5000	General Electric Company	552	Silicone	Violent explosion	0.050	1/20	10	U	U
Vydax 525	E.I. du Pont de Nemours & Company, Incorporated	7391	Fluorocarbon Telomer Dispersion	Stainless steel inserts Dipped and dried 24 hours		0/20	10	S	BT
Vydax 550	E.I. du Pont de Nemours & Company, Incorporated	7390	Fluorocarbon Telomer Dispersion	Stainless steel inserts Dipped and dried 24 hours		0/20	10	S	BT
Vydax 550	E.I. du Pont de Nemours & Company, Incorporated	7211	Fluorocarbon Telomer Dispersion		0.5 ml	0/20	10	S	BT

TABLE I. LUBRICANTS (Concluded)

Material	Manufacturer or Source	Test No.	Composition	Remarks	Thickness (inch)	No. Reactions/ No. Tests	Energy Level Kg/m	Batch or Jar Rating	Material Rating
Vydax AR	E.I. du Pont de Nemours & Company, Incorporated	7388	Fluorocarbon Telomer Dispersion	Stainless steel inserts Dipped and dried 24 hours		0/20	10	S	BT
Vydax AR	E.I. du Pont de Nemours & Company, Incorporated	7389	Fluorocarbon Telomer Dispersion	Stainless steel inserts Spray-Coated, dried 24 hours		0/20	10	S	BT
WD-40 Stoprust	Rocket Chemical Company	2667		Violent explosions	Spray Film	3/24 2/15	10 5	U –	U –
Whytekote 505	Alpha Molykote Corporation	3469			0.002	1/1 1/1 1/1 1/2	10 5 3 1	U – – –	U – – –
Wire-lube Pulling Lubricant	Ideal Industries Incorporated	4080			0.050	0/20	10	S	I
XLE-42 Fluid	Union Carbide Corporation	926	Silicone		0.050	0/20	10	S	I
X520	Union Carbide Corporation	876	Silicone		0.050	2/20	10	U	U
Sample IIF	Union Carbide Corporation	1449	70% Ucon 65LB		0.050	5/20 4/20	10 5	U –	U –
X-15 Inorganic Bonded Dry Film Lubricant	Alpha Molykote Corporation	7362		Stainless steel inserts dip coated		0/20	10	S	S
X-15 Inorganic Bonded Dry Film Lubricant	Alpha Molykote Corporation	6970		Stainless steel inserts brush coated, 24 hours air dry		0/20	10	S	S
XG-5-0034	Dow Corning Corporation	5833			0.050	2/100	10	S	BT
25% Bestoil – 75% Halocarbon 208		6966			0.5 ml	4/20	10	U	U

TABLE II. SEALANTS AND THREADING COMPOUNDS

Material	Manufacturer or Source	Test No.	Composition	Remarks	Thickness (inch)	No. Reactions/ No. Tests	Energy Level Kg/m	Batch or Jar Rating	Material Rating
All-Purpose Tape-Unyte	J.C. Whitlam Manufacturing Co.	6649		Stainless steel inserts	0.003	0/20	10	S	S
Anderol 1333	Lehigh Chemical Company	704	Antimony compound in fluoro-silicone fluid	Corrosive to aluminum alloys	0.050	0/34	10	S	U
Anti-scoring Extreme Pressure Lube No. 3	Chicago Manufacturing and Distributing Company	3772			0.050	2/20	10	U	U
Anti-scoring Extreme Pressure Lube No. 3	Chicago Manufacturing and Distributing Company	3773			Thin film	10/20	10	U	U
Anti-seize Compound 32-Z	Materials Division, MSFC	2192			0.050	0/20	10	S	BT
AR-1F (Lot 67)	Materials Division, MSFC	1462	Arochlor 1254 and graphite		0.050	0/20	10	S	BT
AR-1F	Hayes Aircraft Corporation	3129	Arochlor 1254 and graphite		0.050	0/20	10	S	BT
AR-1F	Hayes Aircraft Corporation	4507			0.050	0/20	10	S	BT
Blue Goop Thread Lubricant	Crawford Fitting Company	8216	Chlorofluorocarbon oil base		0.050	0/20	10	S	BT
Conley Teflon Paste	Conley Corporation	9139	Tetrafluoroethylene base		0.050	0/20	10	S	BT
Dag Dispersion No. 217	Acheson Colloids Company	84			0.050	1/10	10	I	I
Dag Dispersion 1730	Acheson Colloids Company		Arochlor 1254 and graphite	Thirty-three batches tested	0.050	0/20	10	S	BT
Dag Dispersion 1730, Lot 500	Acheson Colloids Company	9122	Arochlor 1254, graphite	Eight tubes evaluated	0.050	0/160	10	S	BT
Dag Dispersion 1730, Lot 500	Acheson Colloids Company	8709	Arochlor 1254, graphite	Seven tubes evaluated	0.050	0/140	10	S	BT
Dag Dispersion 1730, Lot 500	Acheson Colloids Company	9157	Arochlor 1254, graphite	Six tubes evaluated	0.050	0/120	10	S	BT
Dag Dispersion 1730, Lot 500	Acheson Colloids Company	9276	Arochlor 1254, graphite	Four tubes evaluated	0.050	0/80	10	S	BT
Dag Dispersion 1730, Lot 500	Acheson Colloids Company	10285	Arochlor 1254, graphite	One tube evaluated	0.050	0/20	10	S	BT

TABLE II. SEALANTS AND THREADING COMPOUNDS (Continued)

Material	Manufacturer or Source	Test No.	Composition	Remarks	Thickness (inch)	No. Reactions/ No. Tests	Energy Level Kg/m	Batch or Jar Rating	Material Rating
Dag Dispersion 1730, Lot 501	Acheson Colloids Company	10286	Arochlor 1254, graphite	Three tubes evaluated	0.050	0/60	10	S	BT
Dag Dispersion 1730	Acheson Colloids Company								
Lot 60-139		5907	Aroclor 1254 & graphite		0.050	0/20	10	S	BT
Lot 500		7072	Aroclor 1254 & graphite		0.050	0/20	10	S	BT
Lot 501		7005	Aroclor 1254 & graphite		0.050	0/20	10	S	BT
Dag Dispersion 1730, Lot 500	Acheson Colloids Company	4662			0.050	0/20	10	S	BT
Easy Wrap Pipe Joint Tape	J.A. Sexauer Manufacturing Co.	4368	Teflon	No adhesive	0.003	0/20	10	S	BT
Fluoroseal	Industrial Plastic Fabricators Incorporated	485	Water dispersion of Teflon and ammonia		0.050	0/20	10	S	BT
Liquid O-ring No. 1235	Oil Center Research				0.050	0/20	10	S	BT
Leak Lock	Highside Chemical Company Incorporated	545		Two batches tested	0.050	1/11	10	U	U
Loctite A	American Sealants Company	827			0.050	2/7	10	U	U
						2/2	5	–	–
LOX-Lube (Spec NA-2-20502)	North American Aviation	249	Graphite and chlorinated hydrocarbon	Sensitivity varies from batch to batch	0.050	10/20	10	U	BT
LOX-Sealant (Spec NA-2-20502)	North American Aviation		15% Dixon 200-10 graphite, 85% Arochlor 1254	Sensitivity varies from batch to batch	0.050	2/20	10	U	BT
LOX-Safe	Redel Incorporated	7959	Graphite and chlorinated hydrocarbon	Sensitivity varies from batch to batch	0.050	2/20	10	U	BT
LOX Sealant	Rolls Royce Limited	935	Graphite, chlorinated hydrocarbon		0.050	0/20	10	U	BT
Oxyseal	Parker Appliance Company	217	Graphite and chlorinated hydrocarbon		0.050	6/10	10	U	U
						0/12	3	–	–
Permatex 1516	Permatex Company Incorporated	861	Graphite and chlorinated hydrocarbon		0.050	4/60	10	U	U
Plastic Lead Seal No. 1	Crane Packing Company	234	Lead compounds in rubber binder		0.050	3/10	10	U	U
						1/20	8	–	–
						1/10	7	–	–

TABLE II. SEALANTS AND THREADING COMPOUNDS (Continued)

Material	Manufacturer or Source	Test No.	Composition	Remarks	Thickness (inch)	No. Reactions/ No. Tests	Energy Level Kg/m	Batch or Jar Rating	Material Rating
Plastic Lead Seal No. 2	Crane Packing Company	744	Lead compounds in runner binder		0.050	2/6	10	U	U
Plastic Lead Seal No. 4	Crane Packing Company	236	Lead compounds in rubber binder		0.050	2/3 2/10 0/10	10 5 3	U – –	U – –
Potting Compound No. 420	Carl Biggs Company	520			0.050	3/14 1/20	10 5	U –	U –
Rectorseal 25X-1	Rector Well Equipment Company Incorporated	169	Graphite and chlorinated hydrocarbon		0.050	2/10	10	U	U
Rectorseal No. 15	Rector Well Equipment Company Incorporated		Graphite and chlorinated hydrocarbon		0.050	1-5/20	10	U	[illegible]
Reddy-Lube No. 2	Redel Incorporated	245	Graphite and chlorinated hydrocarbon	Sensitivity varies from batch to batch	0.050	0-2/20	10	—	BT
Reddy-Lube No. 2	Redel Incorporated		Graphite and chlorinated hydrocarbon	Thin samples		3-5/20 1/12	10 7	U –	BT –
Sauereisen No. 1	Sauereisen Cements Company	744			0.050	2/2 1/18	10 5	U –	U –
Sauereisen No. 51	Sauereisen Cements Company	351			0.050	0/20	10	S	BT
Sauereisen No. 52	Sauereisen Cements Company	289			0.050	1/1 1/1 1/1 1/2	10 7 5 3	U – – –	U – – –
Seal-Rite No. 5	Macksons Company	241	Graphite, aluminum silicate binder, and carbohydrate vehicle	Sensitivity varies from batch to batch	0.050	0-2/20	10	–	BT
Sexauer "Easy Wrap" Pipe Joint Tape	J.A. Sexauer Manufacturing Company	5894	Teflon	Stainless steel inserts	0.0035	0/20	10	S	S
Sexauer "Easy Wrap" Pipe Joint Tape	J.A. Sexauer Manufacturing Company	6389	Teflon	Stainless steel inserts	0.0035	0/20	10	S	S

TABLE II. SEALANTS AND THREADING COMPOUNDS (Concluded)

Material	Manufacturer or Source	Test No.	Composition	Remarks	Thickness (inch)	No. Reactions/ No. Tests	Energy Level Kg/m	Batch or Jar Rating	Material Rating
Sodium Silicate and Graphite	Materials Division, MSFC	580	Sodium silicate and graphite		0.050	0/20	10	S	BT
Sodium Silicate and Talc	Materials Division, MSFC	723	Sodium silicate and talc		0.050	0/20	10	S	BT
Thread Compound No. 265	Valley Products Company	9295			0.050	2/20	10	U	U
Thread Compound No. 265	Valley Products Company	507			0.050	2/37	10	U	U
Thread Lube	Parker Appliance Company	273			0.050	1/2 1/2 1/2 1/2	10 7 5 3	U – – –	U – – –
Tape Tite	Blue Seal Chemical Company	7919	Sintered Teflon		0.004	0/20	10	S	BT
Teflon Thread Seal Tape 121	Dodge Fibers Corporation	8381	Sintered Teflon	Eight rolls evaluated	0.003	0/160	10	S	S
Thread Seal Tape No. 121	Dodge Fibers Corporation	6952				0/20	10	S	S
Thread Seal Tape No. 121	Dodge Fiber Company	4371	Teflon	No adhesive	0.010	0/20	10	S	S
Teflon Thread Sealant S-22, Lot 66AME1-B	Saunders Engineering Company	8620	Sintered Teflon	Nine rolls evaluated	0.003	0/180	10	S	S
T-Film Thread Compound	Eco Engineering Company	820	Teflon-water dispersion		0.050	0/20	10	S	BT
Torq Compound	Torq Manufacturing Company	5481		Stainless steel inserts used	0.050	16/20	10	U	U
TFE Fluorocarbon Thread Sealing Tape	Raybestos-Manhattan Company	7058	TFE Teflon		0.003	0/20	10	S	BT
Universal Thread Seal Teflon Ribbon	W.S. Shamban and Company	2554	Teflon			0/20	10	S	BT
X-Pando	X-Pando Corporation	641	Silicate cement		0.050	0/20	10	S	BT

TABLE III. THERMAL AND ELECTRICAL INSULATIONS

Material	Manufacturer or Source	Test No.	Composition	Remarks	Thickness (inch)	No. Reactions/ No. Tests	Energy Level Kg/m	Batch or Jar Rating	Material Rating
AI-220	Anaconda Wire and Cable Company	7661	Amide-imide copolymer	Applied to 0.008-inch thick aluminum	0.001	8/20	10	U	U
AI-220	Anaconda Wire and Cable Company	7662	Amide-imide copolymer	Applied to 0.02-inch thick copper	0.007	6/20	10	U	U
Aluminum and Mylar Covering from Fibrous Glass Insulation	Fibrous Glass Incorporated	3799	Aluminum and Mylar			2/2 2/4 2/4 2/4 2/7	10 5 3 1 1/2	U – – – –	U – – – –
Alsimag Ceramic Insulation 196	American Lava Corporation	1006	Clinonstatite crystals			2/20	10	U	U
Anaconda AI-200 Magnet Wire	Anaconda Wire and Cable Company	6925	Copper with amide-imide copolymer insulation	Stainless steel inserts	0.005	6/20	10	U	U
Armstrong Cork Style 7326	Armstrong Cork Company	9792			0.065	6/20 3/20 1/20 2/20 1/20 0/20	10 7.7 5.6 3.5 2.8 1.4	U	U
Armstrong Cork Style 9250	Armstrong Cork Company	8711			0.131	20/20	10	U	U
Ban-Roc Mineral Wool	Johns Manville Corporation	10247			0.090	0/20	10	S	BT
B-115 Coating	Westinghouse Corporation	7665		Applied to 0.008-inch copper	0.0005	5/20	10	U	U
AWG No. 22 Copper Wire Coated with Aluminum Phosphate Impregnated Felt Asbestos	General Electric Company	3197	Aluminum phosphate, asbestos, and copper			0/20	10	S	BT
Cable, Type 4TX-22-1934	Hi-Temp Wires Incorporated	1705				0/20	10	S	BT
Cable, Type 4TX-22-1934 Outside Covering	Hi-Temp Wires Incorporated	1778				3/20	10	U	BT
Cable Transonics, Type 1932	Suprenant Manufacturing Co.	1706				0/20	10	S	BT

TABLE III. THERMAL AND ELECTRICAL INSULATIONS (Continued)

Material	Manufacturer or Source	Test No.	Composition	Remarks	Thickness (inch)	No. Reactions/ No. Tests	Energy Level Kg/m	Batch or Jar Rating	Material Rating
Chromel-Alumel, Teflon Singles, Nylon Wrap	Revere Corporation of America	1691	Chromel-Alumel, Teflon, and Nylon			3/20	10	U	U
Chromel-Alumel, Teflon Singles, Asbestos Jacket	Revere Corporation of America	1686	Chromel-Alumel, Teflon, and asbestos			2/2 2/2 2/10 1/6	10 5 3 2	U – – –	U – – –
Copper-Constantan Sinterex Teflon Tape Cover	Revere Corporation of America	1687	Copper Constantan, and Teflon			1/60	10	S	BT
Copper-Constantan Conductor with Polyvinyl Insulation	Revere Corporation of America	1682	Copper Constantan, and polyvinyl plastic			2/2 2/2 1/1 1/7	10 5 3 2	U – – –	U – – –
20-2 Conductor Standard No. 1741 Shielded	Alpha Wire Corporation	1681				3/4 2/15	10 5	U –	U –
Cellular Glass Insulation with Aluminum Vapor Barrier	Pittsburg-Corning Corporation	6247		Stainless steel inserts	0.4	17/20	10	U	U
Centaur Insulation		5972		Stainless steel inserts	0.407	11/20 11/20 14/20 20/20 18/20 9/20	10 8 6 4 2 1	U	U
Convair Liquid Hydrogen Insulation	Convair Division General Dynamics	3189	Phenolic resin, fiberglass honeycomb, epoxy fiberglass sealer, epoxy adhesive		0.313	2/2 11/11 20/20 7/20 0/20	10 5 2 1 1/2	U – – – –	U – – – –
Coast Pro-Seal 777 Potting Compound	Coast Pro-Seal Manufacturing Company	5211		Two coats sprayed on aluminum inserts	0.025	18/20	10	U	U
Coast Pro-Seal 777 Potting Compound	Coast Pro-Seal Manufacturing Company	5212		One coat sprayed on aluminum discs	0.015	15/20	10	U	U

TABLE III. THERMAL AND ELECTRICAL INSULATIONS (Continued)

Material	Manufacturer or Source	Test No.	Composition	Remarks	Thickness (inch)	No. Reactions/ No. Tests	Energy Level Kg/m	Batch or Jar Rating	Material Rating
Coast Pro-Seal 777P Primer and One Coat Coast Pro-Seal 777 Potting Compound	Coast Pro-Seal Manufacturing Company	5213		Sprayed on aluminum discs	0.015	17/20	10	U	U
Coast Pro-Seal 776 Primer and One Coat Proseal 777 Potting Compound	Coast Pro-Seal Manufacturing Company	5214		Sprayed on aluminum discs	0.015	19/20	10	U	U
Corning 7052 Glass	Corning Glass Compony	7858			0.060	0/20	10	S	S
CPR-20 Insulation	Chemical Plastics Research International Corporation	4362		Density 4 lbs/ft^3	0.250	17/20 15/20 8/20 4/20 0/20	10 7 5 3 1	U – – – –	U – – – –
CPR-314 Foam	Upjohn Company	9810	Isocyanate		0.100	3/20	10	U	U
CPR-314 Foam	Upjohn Company	9846	Isocyanate		0.500	10/20	10	U	U
CPR-358-2 Foam	Upjoh Company	9883	Isocyanate		0.250	4/20	10	U	U
CPR-368 Foam	Upjohn Company	9830	Isocyanate		0.250	2/20	10	U	U
CPR-9005-2 Foam	Minnesota Mining and Manufacturing Company	9841	Isocyanate		0.500	7/20	10	U	U
CPR-1021-2 S-II Insulation	Chemical Plastics Research International Corporation	4573	Polyurethane		0.250	3/40 2/40 2/20 0/20 0/20	10 9 8 7 5	U – – – –	U – – – –
Dimplar Aluminized Mylar	Quality Electric Company	8377			0.001	15/80	10	U	U
Dynatherm D-65 Tape with Fiberglass Braid	Kennedy Space Center	7955	Filled polyurethane		0.075	0/20	10	S	BT
Dynatherm D-65	Dynatherm Chemical Corporation	5667		On aluminum discs	0.008 to 0.010	15/20 2/20	10 5	U –	BT
Dynatherm D-65 plus a Modified Fluorinated Coating	Dynatherm Chemical Corporation	7178		Stainless steel inserts	0.045	20/20	10	U	U

TABLE III. THERMAL AND ELECTRICAL INSULATIONS (Continued)

Material	Manufacturer or Source	Test No.	Composition	Remarks	Thickness (inch)	No. Reactions/ No Tests	Energy Level Kg/m	Batch or Jar Rating	Material Rating
Dynatherm D-65 and Fiberglass Tape with Dynatherm No. 905	Dynatherm Chemical Corp.	7179		Stainless steel inserts	0.045	20/20	10	U	U
Dynatherm D-65 Tape	Dynatherm Chamical Corp.	6258		Stainless steel inserts	0.038	0/20 0/20	12 10	S	BT
Dyna-Therm D65	Dyna-Therm Chemical Corporation	3668	Filled polyurethane	8 to 10 mils on aluminum discs		15/20 2/20	10 5	U –	BT –
Dyna-Therm D-65	Dyna-Therm Chemical Corporation	2321	Polyurethane, sodium phosphate, sodium borate, and carbon		0.063	0/40	10	S	BT
Dyna-Therm D-65	Dyna-Therm Chemical Corporation	3250	Polyurethane, sodium phosphate, sodium borate, and carbon		0.125	0/20	10	S	BT
Dyna-Therm D-65	Dyna-Therm Chemical Corporation	3255	Polyurethane, sodium phosphate, sodium borate, and carbon	Aged 8 months	0.063	0/20	10	S	BT
Dyna-Therm D-65 with 904 Coating	Dyna-Therm Chemical Corporation	3251	Polyurethane, sodium phosphate, sodium borate, and carbon		0.063	0/20	10	S	BT
Dyna-Therm D-904	Dyna-Therm Chemical Corporation	2323	Polyurethane		0.050	6/20 2/15 0/20	10 5 4	U – –	U – –
Dyna-Therm D-100	Dyna-Therm Chemical Corporation	1801	Polyurethane		0.063	2/20 1/40	10 2	U –	U –
Dynatherm 4327	Dynatherm Chemical Corp.	5669		Applied on aluminum discs		1/60	10	S	BT
Dynatherm Custom Compound, LOX Compatible Coating D-4327, (New Formulation) Batch 54-89-1	Dynatherm Chemical Corp.	6955		Stainless steel inserts dipped, air dried 48 hours		2/20	10	U	U
Dynatherm C-4327 (New Formulation) Batch 54-89-3		6954		Stainless steel inserts dipped, air dried 48 hours		5/20	10	U	U

TABLE III. THERMAL AND ELECTRICAL INSULATIONS (Continued)

Material	Manufacturer or Source	Test No.	Composition	Remarks	Thickness (inch)	No. Reactions/ No. Tests	Energy Level Kg/m	Batch or Jar Rating	Material Rating
Electroplast	Duetsch Laboratories	4523		On stainless steel strips		13/17	10	U	U
Electroplast 202	Du tsch Laboratories	4800		Stainless steel cups used		2/2 2/3 2/3 2/12	10 5 3 1	U – – –	U – – –
EPI Resin 560	Jones Debney Corporation	7660	Epoxy	Applied to 0.012-inch thick copper	0.005	9/20	10	U	U
EPI Resin 560	Jones Debney Corporation	7659	Epoxy	Applied to 0.008-inch thick aluminum foil	0.001	9/20	10	U	U
Fiber Frax	Carborundum Company	2355	Mineral fiber	With aluminum foil backing		4/40	10	U	U
Fiber Frax (XSW)	Carborundum Company	2381	Mineral fiber			2/20	10	U	U
Fiber Frax	Carborundum Company	2410	Mineral fiber	Heat treated 3 hours at 1000°F		0/20	10	S	BT
Fibrous Glass Insulation	Fibrous Glass Incorporated	3798	Glass		0.125	2/2 2/2 2/2 2/2	10 5 3 1	U – – –	U – – –
Fiberglass Insulation No. 1000	Gustin-Bacon Ultralite	5057			0.050	2/3 3/5 6/20 4/20	10 5 3 1	U – – –	U – – –
Flamemastic No. 700	Dynatherm Chemical Corp.	4384			0.050	3/40	10	U	U
Foamglass Insulation	Pittsburgh-Corning Corporation	799	Cellular glass			0/20	10	S	S
Foamseal Joint Sealer 30-45	Benjamin Foster Company	923				2/2 2/3 2/2	10 5 2	U – –	U – –
Foamsil Insulation	Pittsburgh-Corning Corporation	878	Cellular glass			0/20	10	S	S

TABLE III. THERMAL AND ELECTRICAL INSULATIONS (Continued)

Material	Manufacturer or Source	Test No.	Composition	Remarks	Thickness (inch)	No. Reactions/ No. Tests	Energy Level Kg/m	Batch or Jar Rating	Material Rating
Formvar	Astrionics Laboratory	7664		Applied to 0.016-inch thick copper	0.0004	12/20	10	U	U
Foster Fire Resistive Coating 60-30N	Benjamin Foster Company	1017				2/2 2/5 2/2	10 5 2	U – –	U – –
Foster Flexfas Bonding Agent 82-10	Benjamin Foster Company	970				0/20	10	S	U
Foster Fire Resistive Coating 60-65	Benjamin Foster Company	1016				2/2 2/2 2/7	10 5 2	U – –	U – –
Foster Sealfas Insulation Coating 31-96	Benjamin Foster Company	968				2/4 2/4 2/5	10 5 2	U – –	U – –
Frit No. 1	Lear Siegler Corporation	4491	80-85% lead oxide, 15% silicon dioxide, less than 5% unknown oxide	Tested on nickel strips		0/20	10	S	S
Frit No. 1 Modified with Cerium Oxide	Lear Siegler Corporation	4470		Tested on nickel strips	0.025	0/20	10	S	S
Glass Fiber "B" No. 621	Owens-Corning Corporation	2357	Glass		0.063	0/40	10	S	S
Glass No. 621	Owens-Corning Corporation	2378	Glass		0.063	0/20	10	S	S
Hexcell 91LD	Hexcell Products Company	4234	Honeycomb phenolic and epoxy		0.063	20/20 20/20 20/20 15/20	10 5 3 1	U – – –	U – – –
Hexcell Polyurethane Insulation 1414-2	Hexcell Products Company	3680	Polyurethane		0.250	20/20 19/20 8/20 0/20	10 5 3 2	U – – –	U – – –
HRP Honeycomb Filled with CPR-1021-2		4570		Bonded to 2014T-6 aluminum with Aerobond 430-7	0.250	20/20 20/20 2/20	10 3 1	U – –	U – –

TABLE III. THERMAL AND ELECTRICAL INSULATIONS (Continued)

Material	Manufacturer or Source	Test No.	Composition	Remarks	Thickness (inch)	No. Reactions/ No. Tests	Energy Level Kg/m	Batch or Jar Rating	Material Rating
H-Film Conductor Cable		4471 5203	H-Film insulation, copper conductor, FEP adhesive		0.030 0.030	4/20 4/20	10 10	U U	U U
H-Foam 490	E.I. du Pont de Nemours & Company, Incorporated	5655 5654		Stainless steel inserts Stainless steel inserts	0.065 0.11	0/20 0/40	10 10	S S	I I
H-Foam 536	E.I. du Pont de Nemours & Company, Incorporated	5652 5657		Stainless steel inserts Stainless steel inserts	0.055 0.13	0/20 0/20	10 10	S S	I I
Inserts, Fired Durock Type D117-063	Physical Science Corporation	3220	Lead oxide, cobalt oxide, nickel oxide, and bismuth oxide			0/20	10	S	S
Insulation		5405	Vitel PE-20% adhesive and resin (polyester) foam Freon blown polyurethane in the skin of 1/2 mil Mylar and 1/2 mil aluminum		0.400	42/120 22/100 25/100 71/100 78/100 55/100	10 8 6 4 2 1	U – – – – –	U – – – – –
Isowood	North American Aviation	3209	Quartz spheres and epoxy		0.125	15/20 7/20 2/20 0/20	10 7 5 3	U – – –	U – – –
Johns-Manville Rock Cork Insulation	Johns-Manville Company	800	Mineral fiber			2/5 2/7 1/8	10 5 2	U – –	U – –
Johns-Manville Thermobestos Insulation	Johns-Manville Company	795	Calcium silicate			0/20	10	S	S
Johns-Manville Thermomat Style 281	Johns-Manville Company	3228	Asbestos felt saturated with phenolic resin and inorganic filler		0.063	11/20 6/20 5/20 3/20 0/20	10 5 3 2 1	U – – – –	U – – – –

Card #6

TABLE III. THERMAL AND ELECTRICAL INSULATIONS (Continued)

Material	Manufacturer or Source	Test No.	Composition	Remarks	Thickness (inch)	No. Reactions/ No. Tests	Energy Level Kg/m	Batch or Jar Rating	Material Rating
Kaowool	Babcock and Wilcox Company	2346	Ceramic	Two batches tested		2/20 0/20	10 5	U –	U –
Kaowool	Babcock and Wilcox Company	2488	Ceramic fiber	Heat treated 2 hours at 1000°F	0.063	0/40	10	S	BT
Kaowool	Babcock and Wilcox Company	6945	Ceramic fiber	Heat treated 2 hours at 1000°F	0.415	0/20	10	S	BT
Larodyne Foam	North American Rockwell Corporation	9352	Polyurethane	NAA-3310-23-4	0.050	34/40	10	U	U
Magnolia Foam 7015-1	Magnolia Plastics Incorporated	4558			0.250	20/20 20/20 17/20 4/20 0/20	10 5 4 3 2	U – – – –	U – – – –
Marinite 23A	Johns-Manville Company	5665			Approx. 0.0625	0/20	10	S	BT
Micro-Fibrous Felt No. 108	Johns-Manville Company	4027	Glass		0.125	0/20	10	S	BT
Microlite Fiber Glass Insulation	Johns-Manville Company	3126	Fiberglass		0.094	0/20	10	S	BT
Micro-Quartz	Johns-Manville Company	2347	Quartz fibers			5/40	10	U	U
Micro-Quartz	Johns-Manville Company	2382	Quartz fibers	Heat treated inserts used		1/20	10	I	I
ML Enamel	E.I. du Pont de Nemours and Company	7666		Applied to 0.002-inch thick aluminum	0.001	3/60	10	U	BT
Potassium Titanate		2221	Potassium titanate		0.063	8/40	10	U	U
Potassium Titanate		2728	Potassium titanate	Heated 4 hours at 1000°F	0.063	0/20	10	S	BT
RL-2405 Foam 5#/ft³ density	Raybestos Manhattan Corporation	6098			0.402	13/20 11/20 19/20 20/20 18/20 2/20	10 8 6 4 2 1	U – – – – –	U – – – – –

TABLE III. THERMAL AND ELECTRICAL INSULATIONS (Continued)

Material	Manufacturer or Source	Test No.	Composition	Remarks	Thickness (inch)	No. Reactions/ No. Tests	Energy Level Kg/m	Batch or Jar Rating	Material Rating
RL 2405 Foam	Raybestos-Manhattan Corporation	5982	3 mil aluminum foil, Adiprene L-100	Stainless steel inserts	0.500	20/20 14/20 20/20 20/20 14/20 0/20	10 8 6 4 2 1	U	U
Styrofoam 1/6#/ft³ density	Dow Chemical Company	6237		Stainless steel inserts	0.401	4/20 3/20 4/20 8/20 10/20 7/20	10 8 6 4 2 1	U	U
Styrofoam 1.6#/ft³ density	Dow Chemical Company	6322		Stainless steel cups	0.401	2/20 2/20 5/20 10/20 16/20 7/20	10 8 6 4 2 1	U	U
Silvered Gage Twenty Four Conductor Wire	Revere Corporation of America	1688	Silvered gage twenty-four conductor wire, Inner wire insulation-revcothene. Outer covering Geon Shield-Tinned Copper		0.594	2/2	10	U	U
Silicone RTV Foam QR 7131	Dow-Corning Corporation	3769	Silicone		0.250	4/20 3/20 0/20	10 5 3	U – –	U – –
Scotch Foam I Insulation	Minnesota Mining and Manufacturing Company	798	Foamed plastic		0.060	2/2 2/12 0/5	10 5 3	U – –	U – –
Smooth On Cement	Smooth On Manufacturing Company	1646			0.050	0/20	10	S	S
Snap-On Insulation	Gustin-Bacon Company	796	Glass fiber-organic filled			2/20	10	U	U
Stafoam Insulation AA202	Dayton Rubber Company	781				3/20	10	U	U

TABLE III. THERMAL AND ELECTRICAL INSULATIONS (Continued)

Material	Manufacturer or Source	Test No.	Composition	Remarks	Thickness (inch)	No. Reactions/ No. Tests	Energy Level Kg/m	Batch or Jar Rating	Material Rating
Stafoam Insulation C-02	Dayton Rubber Company	782				2/8	10	U	U
						2/4	5	–	–
						0/8	3	–	–
Styrofoam Insulation No. 33	Styrofoam Plastics Corporation	707	Styrofoam			2/3	10	U	U
						3/4	5	–	–
Silvered Gage Twenty Four Conductor Wire	Revere Corporation of America	1688	Silvered gage twenty-four conductor wire, Inner wire insulation-revcothene. Outer covering Geon Shield-Tinned Copper		0.594	2/2	10	U	U
Teflon Type 2857, No. 18 Strained Copper, Silver Coated		1690	Teflon, copper, and silver			0/20	10	S	BT
Tensolite Alpha Type 2812-2	Alpha Wire Corporation	1684				2/11	10	U	BT
						2/3	5	–	–
						1/6	3	–	–
Tensolite Alpha Type 2812-4	Alpha Wire Corporation	1683				0/20	10	S	BT
Type 2TX-22-1934ZX Wire	Hi-Temp Wires Incorporated	1679	Stranded silver-plated copper conductor with extruded Teflon insulation, shielded in tinned copper. Outside polyvinyl chloride			2/2	10	U	U
						1/1	5	–	–
						2/12	3	–	–
						0/5	2	–	–
		1680				2/11	5	–	–
						1/9	3	–	–
Thermo-Resist 69	Thermo Resist Company	3674	Phenylated nylon			11/20	10	U	U
						8/10	5	–	–
						4/10	3	–	–
Thermofil TFE (Size No. 10; Control No. C415-63-2)	Rayclad Tubes Incorporated	4810		Stainless steel inserts used		0/20	10	S	S
Thermolag T-230	Emerson Electric Manufacturing Company	5381		Stainless steel inserts coated with Thermolag	0.116	20/20	10	U	U
Thermolag T-500	Emerson Electric Manufacturing Company	5382		Stainless steel inserts coated with Thermolag	0.015	8/20	10	U	U

TABLE III. THERMAL AND ELECTRICAL INSULATIONS (Continued)

Material	Manufacturer or Source	Test No.	Composition	Remarks	Thickness (inch)	No. Reactions/ No. Tests	Energy Level Kg/m	Batch or Jar Rating	Material Rating
Unicrest Insulation, Outer Covering	United Cork Company	788				2/2 2/2 2/3	10 5 3	U – –	U – –
Unicrest Insulation	United Cork Company	747				2/2 2/4 0/14	10 5 3	U – –	U – –
Unicrest Type S E Insulation	United Cork Company	709				2/20 2/20	10 5	U –	U –
Vimasco Insulation Coating WC-1	Vimasco Corporation	921				2/3 2/2 2/4	10 5 3	U – –	U – –
Vimasco Carlon Insulation Coating 500	Vimasco Corporation	919				3/20	10	U	U
White Mercury Resistant Electrical Insulation Coating 168-W-20	W.P. Fuller and Company	4012	Modified silicone	Baked on stainless steel inserts	Brush coat	2/20	10	U	U
Wire, Ceramic Coated Nickel-Clad Copper	General Cable Corporation	3218	Ceramic coated, nickel-clad copper			23/40	10	U	U
Wire, Ceramic Coated Nickel-Clad Copper	General Cable Corporation	3322	Ceramic coated, nickel-clad copper			20/40 9/20	10 5	U –	U –
Wire Coated with ML Enamel	General Cable Corporation	4009				0/20	10	S	BT
Wire Coated with ML Enamel and Covered with Felt Asbestos	General Cable Corporation	4008				0/20	10	S	BT
ML Wire Enamel RC-5019	E.I. du Pont de Nemours & Company, Incorporated	6769		Thin coat applied on stainless steel inserts, air dry 30 minutes, bake 60 min at 105°C, bake 10 min at 400°C		0/20	10	S	BT
Wire: MIL-W-16878C, Type E [3 conductor No. 20, twisted and shielded (complete wire)] [3 small conductor wires] [outside cover]		6631 6629 6630		Stainless steel inserts, cleaned with trichloro-ethylene Same as above	0.163 0.063 0.010	0/20 0/20 0/20	10 10 10	S S S	BT BT BT

TABLE III. THERMAL AND ELECTRICAL INSULATIONS (Concluded)

Material	Manufacturer or Source	Test No.	Composition	Remarks	Thickness (inch)	No. Reactions/ No. Tests	Energy Level Kg/m	Batch or Jar Rating	Material Rating
Wire: MIL-C-27500-20T-3-N-6	ITT Suprenant, Incorporated	6636		Same as above	0.230	0/20	10	S	BT
[Teflon covered, 3 conductor No. 20 twisted and shielded]		6633		Same as above					
[3 small conductor wires]		6632		Same as above	0.082	7/20	10	U	BT
[] small conductor wire]		6634		Same as above	0.0015	0/20	10	S	BT
[Label]		6635		Same as above	0.025	0/20	10	S	BT
[Outside cover]									
Zeolite 5A	Kennedy Space Center	9351			0.050	0/20	10	S	BT

TABLE IV. PLASTICS, ELASTOMERS, AND ADHESIVES

Material	Manufacturer or Source	Test No.	Composition	Remarks	Thickness (inch)	No. Reactions/ No. Tests	Energy Level Kg/m	Batch or Jar Rating	Material Rating
Aclar 22	Allied Chemical Company	5308	Chlorofluorocarbon	Stainless steel inserts used	0.020	0/20	10	S	S
Aclar 22	Allied Chemical Company	5309	Chlorofluorocarbon	Stainless steel inserts used	0.010	0/20	10	S	S
Aclar 22	Allied Chemical Company	5310	Chlorofluorocarbon	Stainless steel inserts used	0.003	0/20 0/20	11.3 10	S –	S –
Aclar 22A	Allied Chemical Company	4520	Chlorofluorocarbon	Stainless steel inserts used	0.030	0/20	10	S	S
Aclar 22A	Allied Chemical Company	4521	Chlorofluorocarbon	Stainless steel inserts used	0.015	0/20	10	S	S
Aclar 22A	Allied Chemical Company	4522	Chlorofluorocarbon	Stainless steel inserts used	0.010	0/20	10	S	S
Aclar 22A	Allied Chemical Company	3997	Fluorohalocarbon	Stainless steel inserts used	0.005	0/20	10	S	S
Aclar 22A	Allied Chemical Company	3998	Fluorohalocarbon	Stainless steeel inserts used	0.002	0/40	10	S	S
Aclar 22C Film	Allied Chemical Company	7062	Fluorohalocarbon	Stainless steel inserts	0.0015	0/20	10	S	S
Aclar 33C	Allied Chemical Company	6643	Fluorohalocarbon	Stainless steel inserts	0.001	0/20	10	S	S
Aclar 33C	Allied Chemical Company	6645	Fluorohalocarbon	Stainless steel inserts	0.002	0/20	10	S	S
Aclar 33C	Allied Chemical Company	6644	Fluorohalocarbon	Stainless steel inserts	0.005	0/20	10	S	S
Aclar Type 191 (MIL-F-22191)	Allied Chemical Company	4185	Fluorohalocarbon	Stainless steel inserts	0.002	0/20	10	S	S
Aero Quip Black	Aeroquip Corporation	1012	Erradiated polyvinyl chloride	Liner for flex hose		2/4 2/12 0/4	10 5 2	U – –	U – –
Aero Quip Orange		1011	Teflon	Liner for metal flex hose		0/20	10	S	BT
Aerospace Sealant 92-012	Dow Corning Corporation	7282			0.005	6/20 6/20 4/20 2/20 1/20	10 7.62 5.54 3.46 1.39	U	U

TABLE IV. PLASTICS, ELASTOMERS, AND ADHESIVES (Continued)

Material	Manufacturer or Source	Test No.	Composition	Remarks	Thickness (inch)	No. Reactions/ No. Tests.	Energy Level Kg/m	Batch or Jar Rating	Material Rating
Aluminum discs cemented with polyurethane and edge coated with Dynatherm D-65		5734 5736				0/20 0/20	10 5	S S	BT BT
Aluminum discs cemented with polyurethane and potted with Dynatherm D-65		5737			0.5	2/12 2/2 1/20	10 8 6	U	BT
Aluminized Nylon		6253 6255		Stainless steel inserts	0.003	8/20 9/20	10 10	U	U
Aluminized Mylar	Kennedy Space Center	9915		Ten sheets stacked	0.003	7/20	10	U	U
Amco Adhesive F-88	American Consolidated Manufacturing Company	3404	Fluorohalocarbon		0.050	2/3 2/11 0/20	10 5 1	U – –	U – –
Armstrong Cement	Armstrong Products Company	657			0.050	2/2 1/1	10 5	U –	U –
Araldite 6010 and Catalyst 125	CIBA Chemical Company	743	Epoxy		0.050	3/3 2/4 2/2	10 5 2	U – –	U – –
Armalon PDX7700B	Du Pont	4802	Teflon felt	Bleach	0.063	0/20	10	S	S
Anaphrene (urethane rubber)	E.I. du Pont de Nemours & Company, Incorporated	6067		Stainless steel inserts	0.172	20/20	10	U	U
Ben-Har Lacing Tape	Bently Harris Manufacturing Company	7063		Stainless steel inserts as received	0.015	0/20	10	S	S
B.F.C. Transparent Blue Liquid Envelope	Better Finishing Company Incorporated	3840		Film on stainless steel inserts		2/10 2/13 0/20	10 5 2	U – –	U – –
Blastguard Tape Grade AAA	H.K. Porter Company Incorporated	2327		Treated pressure sensitive tape	0.125	12/20 2/11 0/5	10 5 3	U – –	U – –
Blastape MX4647	Johns-Manville Company	2328			0.125	0/20	10	S	BT
Buna-N Rubber		656				2/3	10	U	U

TABLE IV. PLASTICS, ELASTOMERS, AND ADHESIVES (Continued)

Material	Manufacturer or Source	Test No.	Composition	Remarks	Thickness (inch)	No. Reactions/ No. Tests	Energy Level Kg/m	Batch or Jar Rating	Material Rating
Butyl Fairprene	E.I. du Pont de Nemours & Company, Incorporated	618	Fabric impregnated with butyl rubber			4/6 2/20	10 5	U –	U –
Caram Cement	Caram Manufacturing Company	5728	1 part E918A butyl adhesive, Component A, 1 part E918B butyl adhesive, Component B, and 1 part toluene	Cured 48 hours at room temperature	0.035	18/20 18/20 16/20 11/20 1/20 0/20	10 8 6 4 3 2	U	U
Celcon	Celanese Corporation	5914			0.003	12/20 9/20 5/20 3/20 4/20 1/20	10 8 6 4 2 1	U	U
Chemlok 203, Set No. 1	Hughson Chemical Company	6623		Stainless steel inserts, cured for 1/2 hour at 50°C, 1 hour at 100°C, 16 hours at 150°C	0.062	4/20 3/20 2/20 2/20 0/20 0/20	10 8 6 4 2 1	U	U
Chemlok 203, Set No. 2	Hughson Chemical Company	6616		Stainless steel inserts cured for 1/2 hour at 50°C, 1 hour at 100°C, 1 hour at 150°C, 16 hours at 200°C		3/40 2/60 0/20 0/20	10 8 6 4	U	U
Chemlok 220-123	Hughson Chemical Company	6943		Stainless steel inserts	0.062	5/20 2/20 2/20 3/20 0/20 0/20	10 8 6 4 2 1	U	U
Chemlok 220-205	Hughson Chemical Company	6937		Stainless steel inserts	0.064	4/20 5/20 4/20 2/20 0/20 0/20	10 8 6 4 2 1	U	U

TABLE IV. PLASTICS, ELASTOMERS, AND ADHESIVES (Continued)

Material	Manufacturer or Source	Test No.	Composition	Remarks	Thickness (inch)	No. Reactions/ No. Tests	Energy Level Kg/m	Batch or Jar Rating	Material Rating
Cotton Fabric Treated with THPC	Hooker Chemical Company	6979			0.018	19/20 13/20 2/20 0/20	10 5 2 1	U	U
CS 2727 Epoxy and Accelerated 9817	Chem-Seal Corporation of America	6932	100 gms epoxy 21 gms catalyst	Air Dried 72 hours	0.050	9/20 8/20 6/20 6/20	10 8 6 4	U	U
Coast Pro Seal 793	Coast Pro Seal Manufacturing Company	2759	Polyurethane		0.063	2/7	10	U	U
Compound Rubber X-58	Bacon Industries Incorporated	280	Teflon impregnated silicone rubber			2/3	10	U	U
C328 RTV	Connecticut Hard Rubber Company	4822	Viton base adhesive		0.015 to 0.025	2/4 2/6 2/6 2/11 0/20	10 5 3 2 1	U – – – –	U – – – –
Compound TH-1057 Rubber	Stillman Rubber Company	5729	Fluorinated silicone		0.100	15/20 10/20 11/20 3/20 0/20	10 8 6 4 2	U – – – –	U – – – –
Compound TH-1057 Rubber	Stillman Rubber Company	2385	Fluoro-silicone		0.063	0/20	10	U	U
Crystal MG Inorganic Paper	Minnesota Mining and Manufacturing Company	3195			0.003	2/20	10	U	U
Crystal MP Inorganic Paper	Minnesota Mining and Manufacturing Company	3196			0.003	0/20	10	S	BT
Crystal M Inorganic Paper	Minnesota Mining and Manufacturing Company	3194			0.003	0/20	10	S	BT
Cryo-Mastic IC-531	Insul-Coustic Company	9215		Vapor barrier	0.025	15/20 11/20 14/20 14/20 12/20	10 7.7 5.6 3.5 1.4	U	U

TABLE IV. PLASTICS, ELASTOMERS, AND ADHESIVES (Continued)

Material	Manufacturer or Source	Test No.	Composition	Remarks	Thickness (inch)	No. Reactions/ No. Tests	Energy Level Kg/m	Batch or Jar Rating	Material Rating
Cycolac LT-1000	Marbon Chemical Corporation	8513	Styrene		0.010	20/20 20/20 20/20 18/20 14/20	10 7.7 5.6 3.5 1.4	U	U
Cycolac LT-1000	Marbon Chemical Corporation	8518	Styrene		0.020	20/20 20/20 20/20 16/20 9/20	10 7.7 5.6 3.5 1.4	U	U
Cycolac LT-1000	Marbon Chemical Corporation	8523	Styrene		0.030	20/20 19/20 17/20 13/20 10/20	10 7.7 5.6 3.5 1.4	U	U
Cycolac LT-1000	Marbon Chemical Corporation	8528	Styrene		0.040	19/20 20/20 14/20 8/20 3/20	10 7.7 5.6 3.5 1.4	U	U
Cycolac LT-1000	Marbon Chemical Corporation	8533	Styrene		0.050	19/20 19/20 10/20 8/20 1/20	10 7.7 5.6 3.5 1.4	U	U
Cycolac LT-1000	Marbon Chemical Corporation	8538	Styrene		0.060	20/20 15/20 19/20 10/20 1/20	10 7.7 5.6 3.5 1.4	U	U
Cycolac LT-1000	Marbon Chamical Corporation	8543	Styrene		0.080	15/20 4/20 2/20 3/20 2/20 2/20 0/20	10 7.7 5.6 4.2 3.5 2.3 1.4	U	U

TABLE IV. PLASTICS, ELASTOMERS, AND ADHESIVES (Continued)

Material	Manufacturer or Source	Test No.	Composition	Remarks	Thickness (inch)	No. Reactions/ No. Tests	Energy Level Kg/m	Batch or Jar Rating	Material Rating
Dalbon Fluorocarbon Resin	Diamond Alkali Company	8795	Polyvinyl Fluoride	Applied on stainless steel discs	0.005	9/20	10	U	U
D.C. 274 Adhesive	Dow Corning Corporation	640	Silicone			2/8 0/12	10 5	U –	U –
D.C. 325	Dow Corning Corporation	4480	Silicone		0.050	3/3 2/11 1/13 1/2 0/21	10 5 4 3 2	U – – – –	U – – – –
DC 94-017	Dow Corning Corporation	7981	Fluorosilicone		0.050	2/20	10	U	U
DC 94-017	Dow Corning Corporation	7985	Fluorosilicone		0.075	0/20	10	I	U
DC 94-017	Dow Corning Corporation	7984	Fluorosilicone		0.106	4/20	10	U	U
DC 94-018	Dow Corning Corporation	7982	Fluorosilicone		0.050	5/20	10	U	U
DC 94-018	Dow Corning Corporation	7982	Fluorosilicone		0.084	4/20	10	U	U
DC 94-018	Dow Corning Corporation	7986	Fluorosilicone		0.100	4/20	10	U	U
DC 94-019	Dow Corning Corporation	7983	Fluorosilicone		0.060	3/20	10	U	U
DC 94-019	Dow Corning Corporation	7988	Fluorosilicone		0.090	0/20	10	S	BT
DC 94-019	Dow Corning Corporation	7991	Fluorosilicone		0.224	1/60	10	S	BT
DC 93-019	Dow Corning Corporation	8208	Silicone ablative material		0.115	4/20 1/20 0/20	10 7.7 5.6	U	U
DC 93-019 and DC 94-003	Dow Corning Corporation	8213	Silicone ablative material		0.070	6/20 4/20 8/20	10 7.7 5.6	U U	U U
Dow Corning No. 780 Sealant	Dow Corning Corporation	6931	Silicone	Air dried 72 hours	0.050	16/20 10/20 9/20 8/20 4/20	10 8 6 4 2	U – – – –	U – – – –

TABLE IV. PLASTICS, ELASTOMERS, AND ADHESIVES (Continued)

Material	Manufacturer or Source	Test No.	Composition	Remarks	Thickness (inch)	No. Reactions/ No. Tests	Energy Level Kg/m	Batch or Jar. Rating	Material Rating
Dodge Fibers Lacing Tape (E775-476)		7057	Teflon	Washed in F-33	0.010	0/20	10	S	BT
Dip Pak No. 661	Fidelity Chemical Corporation	3762	Cellulose acetate butyrate		0.063	2/10	10	U	U
Dip Pak No. 661	Fidelity Chemical Corporation	3764	Cellulose acetate butyrate	Stainless steel inserts dipped in molten Dip Pak	0.001	9/20 3/20 7/20 0/20	10 2 5 1	U – – –	U – – –
Du Pont H Film	E. I. du Pont de Nemours and Company, Incorporated	3647			0.002	0/20	10	S	BT
Du Pont H Film No. 67011 (361A)	E. I. du Pont de Nemours and Company, Incorporated	4192			0.002	14/20 2/20 2/20 0/20	10 5 3 1	U – – –	U – – –
Du Pont HT-1 No. 67014(171A)	E. I. du Pont de Nemours and Company, Incorporated	4198			0.010	4/4 4/4 2/8	10 5 1	U – –	U – –
Du Pont HT-1 Felt No. 1280-74-0	E. I. du Pont de Nemours and Company, Incorporated	4195			0.125	2/2 2/2 2/14 1/20	10 5 2 1	U – – –	U – – –
Du Pont HT-1 No. 380 369-370	E. I. du Pont de Nemours and Company, Incorporated	4197			0.030	2/2 2/2 2/2 3/3	10 5 2 1	U – – –	U – – –
Du Pont No. 97-001A	E. I. du Pont de Nemours and Company, Incorporated	3596	0.005 FEP laminated to TFE fabric and metalized with aluminum		0.010	0/20	10	S	S
Du Pont No. 506A112	E. I. du Pont de Nemours and Company, Incorporated	3595	Armalon and FEP dispersion coated glass		0.006	0/20	10	S	S
Du Pont ML Film	E. I. du Pont de Nemours and Company, Incorporated	3558			0.008	2/20 0/20	10 5	U –	BT –

TABLE IV. PLASTICS, ELASTOMERS, AND ADHESIVES (Continued)

Material	Manufacturer or Source	Test No.	Composition	Remarks	Thickness (inch)	No. Reactions/ No. Tests	Energy Level Kg/m	Batch or Jar Rating	Material Rating
Du Pont ML Film	E. I. du Pont de Nemours and Company, Incorporated	3536			0.004	0/40	10	S	BT
Du Pont ML Film	E.I. du Pont de Nemours and Company, Incorporated	3555			0.002	0/40	10	S	BT
Dynatherm D-65A Primer	Dynatherm Chemical Corporation	9427			0.005	7/20 6/20 4/20	10 7.7 5.6	U – –	U – –
Dynatherm D-4327, Lot 30017	Dynatherm Chemical Corporation	9806		39 percent solids	0.010	2/20 3/20	10 7.7	U –	BT –
Dynatherm D-4327, Lot 30017	Dynatherm Chemical Corporation	9808		10 percent solids	0.010	0/20	10	S	BT
Dynatherm D-4327, Lot 10356	Dynatherm Chemical Corporation	8839		Ten coats brushed on stainless steel discs with 30 min. drying between coats 72 hrs. drying after final coat.	0.009	3/20	10	U	BT
Dynatherm D-4327, Lot 10346	Dynatherm Chemical Corporation	8830		Stainless steel discs dip coated, dried for 45 hours	0.011	6/20 4/20 3/20 2/20 0/20	10 7.7 7.0 6.3 5.6	U – – – –	BT – – – –
Dynatherm D-4327, Lot 10346	Dynatherm Chemical Corporation	8836		Stainless steel discs, dip coated and oven dried at 95°F for 12 hours	0.007	12/40	10	U	BT
Dynatherm D-4327, Lot 10346	Dynatherm Chemical Corporation	8773		Stainless steel discs, dip coated and air dried for 72 hours	0.004	5/20	10	U	BT
Dynatherm D-4327, Lot 10346	Dynatherm Chemical Corporation	8663		Stainless steel discs, dip coated and air dried for 24 hours	0.002	3/20	10	U	BT
Dynatherm D-4327, Lot 10346	Dynatherm Chemical Corporation	8804		Stainless steel discs, dip coated and air dried for 18 hours	0.002	3/20	10	U	BT
Dynatherm D-4327, Lot 10346	Dynatherm Chemical Corporation	8664		Stainless steel discs, dip coated and air dried for 30 minutes	0.002	4/20	10	U	BT

TABLE IV. PLASTICS, ELASTOMERS, AND ADHESIVES (Continued)

Material	Manufacturer or Source	Test No.	Composition	Remarks	Thickness (inch)	No. Reactions/ No. Tests	Energy Level Kg/m	Batch or Jar Rating	Material Rating
Dynatherm D-4327, Lot 10346	Dynatherm Chemical Corporation	8801		Stainless steel discs, dip coated in 10 percent solid D-4327 and air dried for 18 hours	0.002	0/40	10	S	BT
Dynatherm D-4327	Dynatherm Chemical Corporation	4381		Brushed on stainless steel inserts and air dried		0/60	10	S	BT
E-Bond Rubber Sealant	International Epoxy Corporation	4199	Epoxy and polysulfide	LP/32 activator	0.050	10/20 14/20 10/20	10 5 1	U — —	U — —
EC1944 B	Minnesota Mining and Manufacturing Company	2745			0.063	3/20 0/20	10 5	U —	U —
Ecco Bond No. 45 and Catalyst No. 15	Emerson and Cuming Incorporated	742	Epoxy Cement	Violent reactions	0.050	2/2 2/2 2/2	10 5 2	U — —	U — —
EC-1252 Adhesive	Minnesota Mining and Manufacturing Company	8252			0.050	20/20	10	U	U
Eimac 221	Eitel McCollough, Incorporated	7729	Polyphenyl		0.280	6/20	10	U	U
Epoxy Topping without Seal Coat	Toch Brothers Company	8374			0.35	11/20	10	U	U
Epoxy Topping with Seal Coat	Toch Brothers Company	8375			0.40	11/20	10	U	U
Epibond 123 and Hardner 952A	Furane Plastics Incorporated	741	Epoxy Cement	Violent reactions	0.050	5/20	10	U	U
Epon Glass Terminal Board		659				2/3 1/1	10 5	U —	U —
Epoxy Potting Compound	Bendix Corporation	1945	Epoxy		0.063	1/1 1/1 1/1	10 5 2	U — —	U — —
Epoxy Filled Glass Fabric (MIL-P-18177)	General Electric Company	3790	Epoxy-Glass	Type G.E.E. Grade G-10	0.063	19/20 4/20 3/20 0/20	10 5 2 1	U — — —	U — — —

TABLE IV. PLASTICS, ELASTOMERS, AND ADHESIVES (Continued)

Material	Manufacturer or Source	Test No.	Composition	Remarks	Thickness (inch)	No. Reactions/ No. Tests	Energy Level Kg/m	Batch or Jar Rating	Material Rating
Epoxy Filled Glass Fabric (MIL-P-18177)	General Electric Company	4289	Epoxy-Glass	Type G.E.E. Grade G-10	0.063	20/20	10	U	U
Epon 901	Shell Chemical Company	5432	11 parts curing agent B-3 to 100 parts resin. Cured 1/2 hour at 240°F, then 1-1/2 hours at 350°F		0.050	27/40 10/40 4/20 5/20 2/20 0/20	10 8 6 4 2 1	U – – – – –	U – – – – –
Eimac 221	Eitel-McCullough, Incorporated	7587	Parapoly phenyl	Total 6/20	Approx. 0.2	6/20	10	U	U
Estane 5470X-1 Molded at 290°F	Goodyear Corporation	7552		Stainless steel inserts washed with F-33	0.005	13/20 7/20 8/20 2/20 2/20	10 7.62 5.54 3.46 1.39	U – – – –	U – – – –
Estane 5470X-1 Molded at 290°F	Goodyear Corporation	7552		Stainless steel inserts washed with F-33	0.010	12/20 9/20 7/20 2/20 1/20	10 7.62 5.54 3.46 1.39	U – – – –	U – – – –
Estane 5470X-1 Molded at 290°F	Goodyear Corporation	7552		Stainless steel inserts washed with F-33	0.020	6/20 1/20 6/20 3/20 1/20	10 7.62 5.54 3.46 1.39	U – – – –	U – – – –
Estane 5470X-1 Molded at 290°F	Goodyear Corporation	7552		Stainless steel inserts washed with F-33	0.030	8/20 7/20 6/20 4/20 2/20 0/20 0/20	10 7.62 5.54 4.85 4.16 3.46 2.77	U – – – – – –	U – – – – – –
Estane 5470X-1 Molded at 290°	Goodyear Corporation	7552		Stainless steel inserts washed with F-33	0.040	4/20 2/20 1/20 1/20 0/20 0/20	10 7.62 5.54 4.85 4.16 3.46	U – – – – –	U – – – – –

TABLE IV. PLASTICS, ELASTOMERS, AND ADHESIVES (Continued)

Material	Manufacturer or Source	Test No.	Composition	Remarks	Thickness (inch)	No. Reactions/ No. Tests	Energy Level Kg/m	Batch or Jar Rating	Material Rating
Extane 5470X-1 Molded at 290°F	Goodyear Corporation	7552		Stainless steel inserts washed with F-33	0.050	4/20	10	U	U
						4/20	7.62	–	–
						1/20	5.54	–	–
						0/20	4.85	–	–
						0/20	4.16	–	–
						0/20	3.46	–	–
Estane 5470X-1 Molded at 290°F	Goodyear Corporation	7552		Stainless steel inserts washed with F-33	0.060	6/20	10	U	U
						2/20	7.62	–	–
						1/20	6.93	–	–
						0/20	6.24	–	–
						0/20	5.54	–	–
						0/20	5.54	–	–
Estane 5470X-1 Molded at 290°F	Goodyear Corporation	7552		Stainless steel inserts washed with F-33	0.080	3/20	10	U	U
						1/20	7.62	–	–
						1/20	5.54	–	–
						0/20	4.85	–	–
						0/20	4.16	–	–
						0/20	3.46	–	–
Ethyl Cellulose		6354	Ethyl cellulose	Stainless steel inserts	0.005	17/20	10	U	U
						9/20	8	–	–
						8/20	6	–	–
						3/20	4	–	–
						0/20	2	–	–
Ethyl Cellulose		6354	Ethyl cellulose	Stainless steel inserts	0.010	19/20	10	U	U
						16/20	8	–	–
						10/20	6	–	–
						6/20	4	–	–
						0/20	2	–	–
Ethyl Cellulose		6354	Ethyl cellulose	Stainless steel inserts	0.020	18/20	10	U	U
						11/20	8	–	–
						12/20	6	–	–
						7/20	4	–	–
						0/20	2	–	–
Ethyl Cellulose		6354	Ethyl cellulose	Stainless steel inserts	0.030	16/20	10	U	U
						14/20	8	–	–
						11/20	6	–	–
						7/20	4	–	–
						3/20	2	–	–
						0/20	1	–	–

TABLE IV. PLASTICS, ELASTOMERS, AND ADHESIVES (Continued)

Material	Manufacturer or Source	Test No.	Composition	Remarks	Thickness (inch)	No. Reactions/ No. Tests	Energy Level Kg/m	Batch or Jar Rating	Material Rating
Ethyl Cellulose		6354	Ethyl cellulose	Stainless steel inserts	0.050	16/20	10	U	U
						12/20	8	–	–
						7/20	6	–	–
						4/20	4	–	–
						2/20	2	–	–
						0/20	1	–	–
Ethyl Cellulose		6354	Ethyl celluloses	Stainless steel inserts	0.060	14/20	10	U	U
						10/20	8	–	-
						9/20	6	–	–
						3/20	4	–	–
						0/20	2	–	–
Ethyl Cellulose		6354	Ethyl cellulose	Stainless steel inserts	0.080	17/20	10	U	U
						13/20	8	–	–
						9/20	6	–	–
						2/20	4	–	–
						0/20	2	–	–
Ethylene Propylene Compound E-617-9	Parker Seal Company	9894			0.078	7/20	10	U	U
Exon-461	Firestone Plastics Company	7785	Polyvinyl chloride resin		0.080	5/20	10	U	U
						2/20	7/7	–	–
						0/20	7.0	–	–
						0/20	5.6	–	–
Exon-461	Firestone Plastics Company	7813	Polyvinyl chloride resin		0.060	6/20	10	U	U
						5/20	7.7	–	–
						4/20	5.6	–	–
						1/20	4.9	–	–
						0/20	4.2	–	–
						0/20	3.5	–	–
Exon-461	Firestone Plastice Company	7806	Polyvinyl chloride resin		0.050	2/20	10	U	U
						1/20	7.7	–	–
						5/20	5.6	–	–
						3/20	4.9	–	–
						1/20	2.8	–	–
						0/20	2.1	–	–
						0/20	1.4	–	–

TABLE IV. PLASTICS, ELASTOMERS, AND ADHESIVES (Continued)

Material	Manufacturer or Source	Test No.	Composition	Remarks	Thickness (inch)	No. Reactions/ No. Tests	Energy Level Kg/m	Batch or Jar Rating	Material Rating
Exon-461	Firestone Plastics Company	7799	Polyvinyl chloride resin		0.040	6/20	10	U	U
						5/20	7.7	–	–
						3/20	5.6	–	–
						0/20	2.8	–	–
						0/20	2.1	–	–
						0/20	1.4	–	–
Exon-461	Firestone Plastics Company	7792	Polyvinyl chloride resin		0.030	9/20	10	U	U
						5/20	7.7	–	–
						6/20	5.6	–	–
						2/20	3.5	–	–
						0/20	2.8	–	–
						0/20	2.1	–	–
Exon-461	Firestone Plastics Company	7785	Polyvinyl chloride resin		0.020	10/20	10	U	U
						10/20	7.7	–	–
						7/20	5.6	–	–
						3/20	3.5	–	–
						1/20	2.8	–	–
						0/20	2.1	–	–
Exon-461	Firestone Plastics Company	7784	Polyvinyl chloride resin		0.010	11/20	10	U	U
						8/20	7.7	–	–
						8/20	5.6	–	–
						3/20	3.5	–	–
						2/20	1.4	–	–
						1/20	0.7	–	–
Exon-461	Firestone Plastics Company	4614	PVC		0.032	4/20	10	U	U
Exon-461	Firestone Plastics Company	4615	PVC		0.020	2/20	10	U	U
Exon-461	Firestone Plastics Company	4616	PVC		0.022	2/20	10	U	U
Exon-461	Firestone Plastics Company	4377	PVC		0.088	2/80	10	U	U
Fairprene 85-001	Du Pont	4609	Viton A on 116 glass	Stainless steel inserts used	0.011	5/20	10	U	U
FEP 120	Du Pont	4585	Teflon suspension fluorinated ethylene propylene	Material coated on brass disc; stainless steel inserts used		0/20	10	S	BT

TABLE IV. PLASTICS, ELASTOMERS, AND ADHESIVES (Continued)

Material	Manufacturer or Source	Test No.	Composition	Remarks	Thickness (inch)	No. Reactions/ No. Tests	Energy Level Kg/m	Batch or Jar Rating	Material Rating
Fibrous Glass Tubing	Taylor Fibre Company	3812	Epoxy-Glass		0.063	2/2 2/2 2/3	10 5 2	U – –	U – –
Fibrous Glass Tubing	Taylor Fibre Company	3810	Epoxy-Glass		0.063	2/2 2/2 2/3	10 5 2	U – –	U – –
Fiberglass Epoxy Pipe	Test Laboratory	8770			0.22	20/20	10	U	U
Fiberglass Plus A Fluoro-silicone Coating		7177	Glass, coated with fluorinated vinyl resin	Stainless steel inserts	0.012	20/20	10	U	U
Fiberglass Thread	Corning Glass	7180	Glass with parafin wax lubricant	Stainless steel inserts	0.033	20/20	10	U	U
Fluoroflex-T Extruded Hose	Resistoflex Corporation	6957	Teflon with 0.05% carbon black		0.050	0/20	10	S	BT
Fluoroglass E-775-303	John L. Dore Company	4376	Teflon and ground glass			0/20	10	S	S
Flaymbar 477	Ocean Chemical, Incorporated	9842			0.010	14/20	10	U	U
Fluoro-Ray Ceramic Filled TFE, Batchess 101, 102, and 103	Raybestos-Manhattan Company	9775	Ceramic Filled TFE		0.025	2-4/20	10	U	BT
Fluoro-Brown	John L. Dore Company	1393	Reprocessed Teflon		0.063	0/20	10	S	BT
Fluorel Elastomer O-Ring, Size 006	Seal Eastern Company	10239				0/20	10	S	BT
Fluorel Elastomer O-Ring, Size 016	Seal Eastern Company	10240				4/20	10	U	BT
Fluorel Elastomer O-Ring Size 160	Seal Eastern Company	10241				4/20	10	U	BT
Fluorosilicone LS-53-24-300	Dow Corning Corporation	9957	Fluorosilicone		0.070	7/20	10	U	U

TABLE IV. PLASTICS, ELASTOMERS, AND ADHESIVES (Continued)

Material	Manufacturer or Source	Test No.	Composition	Remarks	Thickness (inch)	No. Reactions/ No. Tests	Energy Level Kg/m	Batch or Jar Rating	Material Rating
Fluorel KX2141	Minnesota Mining and Manufacturing Company	2262			0.094	0/20	10	S	U
Fluorel-Elastomer (orange, brown, black, white)	Minnesota Mining and Manufacturing Company	1318 1067	Chlorofluoro-carbon	Five batches tested	0.063	0/20	10	S	U
Fluorolin Tape 101	Joclin Manufacturing	773	3 mil Teflon and 3 mil adhesive			2/3 2/17	10 5	U –	U –
Fluorolin Tape 303	Joclin Manufacturing Company	770	6 mil Teflon impregnated glass fibers and 4 mil adhesive			2/2 2/6 0/12	10 5 2	U – –	U – –
Fluorolin Tape	Joclin Manufacturing company	771	3 mil aluminum foil 4 mil Teflon, 2 mil adhesive			2/3 0/2 2/4	10 5 2	U – –	U – –
FM 1000 Adhesive	Bloomingdale Rubber Company	4057	Nylon Epoxy	Violent reactions	0.010	17/20 11/20 9/20	10 5 2	U – –	U – –
Garlock 8573, Lot 65, AME-8N	Aerospace Mechanical Equipment, Incorporated	8600	Filled Teflon		0.105	0/20	10	S	BT
Garlock 8573	Garlock Packing Company	7943	Filled Teflon		0.097	0/20	10	S	BT
Garlock 8573	Garlock Packing Company	9155	Filled Teflon		0.117	0/20	10	S	BT
G.E. Formulation II	General Electric Company	3863	Potting compound of Adiprene L - 100 parts Castor oil - 10 parts Teflon 7X - 100 parts Quadrol - 5.7 parts	Sample B	0.028	2/2 2/8 2/9 2/10 0/20	10 5 3 2 1	U – – – –	U – – – –
G.E. Formulation II	General Electric Company	2952		Sample C	0.034	2/5 0/20	10 5	U –	U –
G.E. Formulation II	General Electric Company	3866		Sample D	0.043	6/20 2/8 0/20	10 5 1	U – –	U – –

TABLE IV. PLASTICS, ELASTOMERS, AND ADHESIVES (Continued)

Material	Manufacturer or Source	Test No.	Composition	Remarks	Thickness (inch)	No. Reactions/ No. Tests	Energy Level Kg/m	Batch or Jar Rating	Material Rating
G.E. Formulation II	General Electric Company	2951		Sample E	0.063	0/20	10	I	U
G.E. Formulation II	General Electric Company	2955		Sample F	0.070	0/20	10	I	U
G.E. Formulation II	General Electric Company	3869		Sample F aged 1 year	0.070	2/4 2/4 0/20	10 7 5	U – –	U – –
G. E. Formulation II	General Electric Company	3871	Potting compound of Adeprene L - 100 parts Castor oil - 10 parts Teflon 7X - 100 parts Quadrol - 5.7 parts	Sample G	0.105	2/20 0/20	10 8	U –	U –
G. E. Formulation II	General Electric Company	2743		Sample H	0.125	0/20	10	I	U
G.E. Formulation I	General Electric Company	2945	Potting compound of Adeprene L - 100 parts Castor oil - 10 parts Quadrol - 5.7 parts		0.063 0.125	2/11 1/3 0/11 3/0 0/20	10 5 3 10 5	U – – – –	U – – – –
G.E. Formulation III	General Electric Company	2954	Potting compound of Adeprene L - 100 parts Castor oil - 10 parts Quadrol - 4.5 parts Fluorolube - 30 parts		0.152	0/20	10	S	U
G.E. Formulation IIIA	General Electric Company	3040	Same as above except Fluorolube increased to 45 parts		0.063	6/20 2/7 0/20	10 5 3	U – –	U – –
G.E. Formulation IIIA	General Electric Company	3041	Same as above except Fluorolube increased to 45 parts		0.032	10/20 2/4 0/20	10 5 3	U – –	U – –
Gen-Flex Plastic Tubing No. 603	General Cements Company	1678				2/4 2/2 1/14	10 5 2	U – –	U – –
Glid Air	Glidden Company	1900			0.063	5/8 1/1 1/1 1/1	10 5 2 1	U – – –	U – – –

TABLE IV. PLASTICS, ELASTOMERS, AND ADHESIVES (Continued)

Material	Manufacturer or Source	Test No.	Composition	Remarks	Thickness (inch)	No. Reactions/ No. Tests	Energy Level Kg/m	Batch or Jar Rating	Material Rating
Glass Lacing Tape No. 075127B476	Dodge Fiber Corporation	6068	Glass with Teflon coat	Stainless steel inserts	0.010	1/60	10	S	BT
Glass and Ceramic Adhesive	Dow Corning Corporation	9831	Silicone base	Cured for 24 hours at room temperature	0.050	9/20	10	U	U
Glass Resin 100	Illinois Glass Company	10040			0.050	20/20	10	U	U
Gylon S-50-S	Garlock Packing Company	10265	Filled Teflon		0.100	0/20	10	S	BT
Gylon	Garlock Packing Company	8718	Filled Teflon		0.095	0/20	10	S	BT
GR266, 2H/2 FEP	Du Pont	5566		Code 10-63-13	0.002	0/20	10	S	BT
Gudebrade Style 256 (Lacing Tape)	Gudebrade Silk Company	7075 6391	Teflon TFE	As received	0.010	1/60	10	S	BT
Halon TFE, Batch 3-41-3	Allied Chemical Corporation	7466 7467			0.066 0.070	0/20 0/20	10 10	S S	BT BT
Heat Shrink LS-53	Dow Corning Corporation	5925 5924 5923			0.050 0.063 9.125	20/20 17/20 9/20	10 10 10	U U U	U U U
H Cement	W. T. Bean	5440		H cement applied to stainless steel inserts over dried at 140°F for 15 minutes; then at 600°F for 30 minutes	0.010	0/20	10	S	BT
H-Film 295-1A-3	Du Pont	5191			0.001	11/20 11/20 4/20 0/20	10 8 7 6	U – – –	BT – – –
H-Film 147-2A-2	Du Pont	5193			0.003	4/20 5/20 2/20 0/20	10 8 6 4	U – – –	BT – – –
H-Film 380-2-2	Du Pont	5568		Aged 24 hours at 300°C	0.002	0/20	10	S	BT

TABLE IV. PLASTICS, ELASTOMERS, AND ADHESIVES (Continued)

Material	Manufacturer or Source	Test No.	Composition	Remarks	Thickness (inch)	No. Reactions/ No. Tests	Energy Level Kg/m	Batch or Jar Rating	Material Rating
H-Film 380-2-2	Du Pont	5567		No extra drying	0.002	4/20	10	U	BT
H-Film 227-1A-1	Du Pont	5195			0.005	4/20	10	U	BT
						8/20	8	–	–
						0/20	7	–	–
						0/20	6	–	–
H-Film	Custom Component Switches, Incorporated	6642			0.001	0/20	10	S	BT
Hercocel A	Hercules Powder Company	7729			0.080	2/20	10	U	U
						3/20	7.7	–	–
						3/20	7.0	–	–
						0/20	6.3	–	–
						0/20	5.6	–	–
Hercocel A	Hercules Powder Company	7734			0.060	3/20	10	U	U
						2/20	7.7	–	–
						2/20	5.6	–	–
						0/20	4.9	–	–
						0/20	4.2	–	–
Hercocel A	Hercules Power Company	7739			0.050	4/20	10	U	U
						3/20	7.7	–	–
						2/20	5.6	–	–
						2/20	4.9	–	–
						0/20	4.2	–	–
						0/20	3.5	–	–
Hercocel A	Hercules Powder Company	7746			0.040	4/20	10	U	U
						4/20	7.7	–	–
						1/20	5.6	–	–
						1/20	4.2	–	–
						0/20	3.5	–	–
						0/20	2.8	–	–
Hercocel A	Hercules Powder Company	7752			0.030	5/20	10	U	U
						6/20	7.7	–	–
						2/20	5.6	–	–
						2/20	4.9	–	–
						0/20	4.2	–	–
						0/20	3.5	–	–

TABLE IV. PLASTICS, ELASTOMERS, AND ADHESIVES (Continued)

Material	Manufacturer or Source	Test No.	Composition	Remarks	Thickness (inch)	No. Reactions/ No. Tests	Energy Level Kg/m	Batch or Jar Rating	Material Rating
Hercocel A	Hercules Powder Company	7758			0.020	10/20	10	U	U
						9/20	7.7	–	–
						8/20	5.6	–	–
						3/20	3.5	–	–
						0/20	2.8	–	–
						0/20	2.1	–	–
Hercocel A	Hercules Powder Company	7765			0.010	10/20	10	U	U
						6/20	7.7	–	–
						6/20	5.6	–	–
						2/20	4.9	–	–
						0/20	4.2	–	–
						0/20	3.5	–	–
Hercocel A	Hercules Powder Company	7772			0.005	8/20	10	U	U
						7/20	7.7	–	–
						6/20	5.6	–	–
						2/20	3.5	–	–
						2/20	2.8	–	–
						0/20	1.4	–	–
Hinac G1-FS Coating		6006		Applied by Boeing, Wichita		3/40	10	U	U
Hinac G-1S	Pennsalt Company	6061				15/20	10	U	U
HT-3 High Temperature Sealant	Organocerams Inc.	7202			0.012	5/20	10	U	U
						2/20	7.62	–	–
						2/20	5.54	–	–
						2/20	4.85	–	–
				Threshold	0.012	0/20	4.16	–	–
						0/20	3.46	–	–
HT-5 High Temperature Sealant	Organocerams Inc.	7196			0.050	2/20	10	U	U
						1/20	7.62	–	–
						0/20	6.93	–	–
						0/20	6.24	–	–
						0/20	5.54	–	–
HT-424 Adhesive	E. I. du Pont de Nemours and Company, Incorporated	4220	Epoxy phenolic	Violent reactions	0.013	20/20	10	U	U
						20/20	5	–	–
						20/20	3	–	–
						6/20	1	–	–

TABLE IV. PLASTICS, ELASTOMERS, AND ADHESIVES (Continued)

Material	Manufacturer or Source	Test No.	Composition	Remarks	Thickness (inch)	No. Reactions/ No. Tests	Energy Level Kg/m	Batch or Jar Rating	Material Rating
Hypalon Rubber	E. I. du Pont de Nemours and Company, Incorporated	1958			0.094	2/3 2/5 2/6 1/8	10 5 3 2	U – – –	U – – –
Hypalon-Asbestos	E. I. du Pont de Nemours and Company, Incorporated	1959			0.063	2/10 1/10	10 5	U –	U –
Hypalon Rubber	E. I. du Pont de Nemours and Company, Incorporated	1946			0. 094	2/2 2/4 2/7 0/7	10 5 3 2	U – – –	U – – –
Hysol Cement 6020	Houghton Labs Incorporated	1003	Epoxy Cement	Violent reactions	0.050	2/3 2/2 2/4	10 5 2	U U –	U U –
Kel-F (Plasticized)	Minnesota Mining and Manufacturing Company	3320	Polytrifluorochloro-ethylene		0.032	0/20	10	S	BT
Kel-F (Unplasticized)	Minnesota Mining and Manufacturing Company	822	Polytrifluorochloro-ethylene			0/20	10	S	BT
Kel-F Plastics, Unplasticized	Minnesota Mining and Manufacturing Company	7648			0.075	0/20	10	S	BT
Kel-F (Sheet) Cadillac Plastic Lot No. A30994	Cadillac Plastic Company	6071			0.63	0/20	10	S	BT
Kel-F AMS3650 Part No. 20M30252		6072		Stainless steel inserts	0.042	0/20	10	S	BT
Kel-F FX-703	Minnesota Mining and Manufacturing Company	7978	Fluorochemical lacquer	Baked on stainless steel inserts at 250°C for 2 hours	0.002	0/20	10	S	BT
Kel-F L-1380	Minnesota Mining and Manufacturing Company	3999	Polytrifluorochloro-ethylene		0.005	0/20	10	S	BT
Kel-F L-1381	Minnesota Mining and Manufacturing Company	4006	Polytrifluorochloro-ethylene		0.005	0/20	10	S	BT

TABLE IV. PLASTICS, ELASTOMERS, AND ADHESIVES (Continued)

Material	Manufacturer or Source	Test No.	Composition	Remarks	Thickness (inch)	No. Reactions/ No. Tests	Energy Level Kg/m	Batch or Jar Rating	Material Rating
Kel-F Film Type 8105	Minnesota Mining and Manufacturing Company	4003	Polytrifluorochloro-ethylene		0.005	0/20	10	S	BT
Kel-F Film Type KX202	Minnesota Mining and Manufacturing Company	4000	Polytrifluorochloro-ethylene		0.002	0/20	10	S	BT
Kel-F Film Type KX8110	Minnesota Mining and Manufacturing Company	4004	Polytrifluorochloro-ethylene		0.010	0/20	10	S	BT
Kel-F Film Type 8210	Minnesota Mining and Manufacturing Company	4002	Polytrifluorochloro-ethylene		0.010	0/20	10	S	BT
Kel-F Film Type 8205	Minnesota Mining and Manufacturing Company	4001	Polytrifluorochloro-ethylene		0.005	0/20	10	S	BT
Kel-F81 Plastic	Minnesota Mining and Manufacturing Company	3045	Polymer based on chlorotrifluoro carbon		0.063	0/20	10	S	BT
Kel-F800 (Pressurized can)	Sprayon Products, Incorporated	2601		Sprayed on stainless steel inserts. Dried 72 hours		2/60	10	U	BT
Kel-F 800 Spray	Sprayon Products, Incorporated	7979	Chlorofluorocarbon	Baked on stainless steel inserts at 250°C for 2 hours	0.002	0/20	10	S	BT
Kel-F 800 Spray	Sprayon Products, Incorporated	5713		Stainless steel inserts Spray-coated, aged 17 days		0/20	10	S	BT
Kel-F800 Resin	Minnesota Mining and Manufacturing Company	1421	Polytrifluorochloro-ethylene		0.063	0/20	10	S	BT
Kel-F800 Plastic	Minnesota Mining and Manufacturing Company	3060	Polytrifluorochloro-ethylene		0.062	0/20	10	S	BT
Kel-F800 Plastic	Minnesota Mining and Manufacturing Company	3319	Polytrifluorochloro-ethylene	Soaked in petroleum ether and dried	0.125	6/20	10	U	BT
Kel-F-800 Hot Melt Primer and Kel-F-800 Impregnated Glass Cloth	Hughes Aircraft Company	4414			0.063	3/4 0/16	10 5	U —	U —

TABLE IV. PLASTICS, ELASTOMERS, AND ADHESIVES (Continued)

Material	Manufacturer or Source	Test No.	Composition	Remarks	Thickness (inch)	No. Reactions/ No. Tests	Energy Level Kg/m	Batch or Jar Rating	Material Rating
Kel-F Hot Melt Primer and Polyurethane Impregnated Glass Cloth	Hughes Aircraft Company	4475			0.063	2/2 2/2 2/2 0/14	10 5 3 1	U — — —	U — — —
Kel-F-800 Hot Melt Primer	Hughes Aircraft Company	4374		Stainless steel inserts used	0.063	2/7 1/2 1/3 0/8	10 5 3 1	U — — —	U — — —
Kel-F Primer 640 Top Coat L-1431 (KX636)	Minnesota Mining and Manufacturing Company	4809		Sprayed on stainless steel inserts		0/20	10	S	S
KX640 Primer KX635 Top Coat	Minnesota Mining and Manufacturing Company	4808		Sprayed on stainless steel inserts		0/20	10	S	S
Kel-F-PN25 Primer	Minnesota Mining and Manufacturing Company	1676		One coat sprayed on stainless steel inserts		0/20	10	S	S
Kel-F PN25 Primer and NW-25TN Coating	Minnesota Mining and Manufacturing Company	1675		Two coats sprayed on stainless steel inserts		0/20	10	S	S
Kel-F Dispersion 625	Minnesota Mining and Manufacturing Company	3518	Polytrifluorochloro-ethylene	Film	0.005	0/20	10	S	S
Kel-F Dispersion KX633	Minnesota Mining and Manufacturing Company	4005	Polytrifluorochloro-ethylene	Film	0.003	0/20	10	S	S
Kel-F Elastomer	Minnesota Mining and Manufacturing Company	3852	Polytrifluorochloro-ethylene		0.125	0/20	10	S	S
Kel-F Elastomer	Minnesota Mining and Manufacturing Company	3853	Polytrifluorochloro-ethylene		0.063	0/20	10	S	S
Koroseal	B.F. Goodrich Company	4286	Vinyl rubber		0.125	2/20	10	U	U
Krylon Crystal Clear Spray Coating	Krylon Incorporated	3226	Acrylic resin and aromatic hydrocarbons		0.002	2/3 2/6 0/20	10 5 1	U — —	U — —
Kynar (RC-2525)	Pennsalt Chemical Company	2874	Vinylidene Fluoride		0.063	0/10	10	I	U
Kynar	The Fluorocarbon Company	5364	Vinyledine fluoride		0.016	5/20 2/20	10 8	U —	U —

TABLE IV. PLASTICS, ELASTOMERS, AND ADHESIVES (Continued)

Material	Manufacturer or Source	Test No.	Composition	Remarks	Thickness (inch)	No. Reactions/ No. Tests	Energy Level Kg/m	Batch or Jar Rating	Material Rating
Kynar (Lot 6210-9E; Annealed)	The Fluorocarbon Company	5364	Vinyledine fluoride		0.016	5/20 2/20 2/20	10 8 6	U – –	U – –
Kynar (Lot 6210-9E; Annealed)	The Fluorocarbon Company	5367	Vinyledine fluoride		0.032	4/20 11/40	11.3 10	U –	U –
Kynar (Lot 6210-9E; Annealed)	The Fluorocarbon Company	5370	Vinyledine fluoride		0.063	2/20	10	U	U
Kynar (Lot 6210-9E; Annealed)	The Fluorocarbon Company	5361	Vinyledine fluoride		0.025	2/20 1/20 1/20	10 8 6	U – –	U – –
Kynar (Lot 6210-9E)	The Fluorocarbon Company	4839	Vinyledine fluoride		0.063	1/60	10	S	U
Kynar	Connecticut Hard Rubber Company	4824	Vinyledine fluoride		0.025	21/40	10	U	U
Kynar	Connecticut Hard Rubber Company	4834	Vinyledine fluoride		0.025.	18/20	10	U	U
Kynar	Connecticut Hard Rubber Company	4836	Vinyledine fluoride		0.002	20/20	10	U	U
Kynar	Connecticut Hard Rubber Company	4835	Vinyledine fluoride		0.002	20/20	10	U	U
Lamicold	Minnesota Mining and Manufacturing Company	3169	Teflon glass cloth		0.125	0/20	10	S	S
Lefkoweld 109 Adhesive	Leffingwell Chemical Company	10012	Adhesive-activator ratio 1 to 1	Cured 2-1/2 hours at 150°F	0.050	18/20	10	U	U
Leno Weave (Sample No. 1)	Connecticut Hard Rubber Company	5356	Polytetrafluoroethylene fabric impregnated with Kynar		0.015	4/20 3/20 3/20 3/20 0/20	10 8 6 4 2	U – – – –	BT – – – –
Leno Weave (Sample No. 2)	Connecticut Hard Rubber Company	4831	Polytetrafluoroethylene fabric impregnated with Kynar		0.015	0/20	10	I	BT

TABLE IV. PLASTICS, ELASTOMERS, AND ADHESIVES (Continued)

Material	Manufacturer or Source	Test No.	Composition	Remarks	Thickness (inch)	No. Reactions/ No. Tests	Energy Level Kg/m	Batch or Jar Rating	Material Rating
Leno Weave (Sample No. 3)	Connecticut Hard Rubber Company	4832	Polytetrafluoroethylene fabric impregnated with Kynar		0.015	1/20	10	I	BT
Leno Weave (Sample No. 4)	Connecticut Hard Rubber Company	4826	Polytetrafluoroethylene fabric impregnated with Kynar		0.015	0/20	10	S	BT
Lexan Polycarbonate Resin	General Electric Company	2730	Polycarbonate resin		0.063	20/20 16/20 0/20 3/17	10 5 2 4	U – – –	U – – –
Liquid Envelope, Aluminum Cold Spray	Better Finishing and Coating Company	3854			0.050	2/2 2/2 2/8 0/20	10 5 2 1	U – – –	U – – –
Liquid Envelope, Aluminum Cold Spray 675-291-A	Better Finishing and Coating Company	3858			0.050	2/2 2/2 2/4 2/10	10 5 2 1	U – – –	U – – –
Liquid Envelope, Coverlac S.C. 224	Better Finishing and Coating Company	3856		Dip coating on stainless steel inserts		3/20 2/14 0/20	10 5 3	U – –	U – –
LS-53	Dow Corning Corporation	5330	Fluorosilicone elastomer		0.070	4/20 6/20 3/20 8/20	10 8 6 4	U – – –	U – – –
LS-53	Dow Corning Corporation	5334	Fluorosilicone elastomer		0.035	11/20 10/20 6/20 4/20 5/20 0/20	10 8 6 4 2 1	U – – – – –	U – – – – –

TABLE IV. PLASTICS, ELASTOMERS, AND ADHESIVES (Continued)

Material	Manufacturer or Source	Test No.	Composition	Remarks	Thickness (inch)	No. Reactions/ No. Tests	Energy Level Kg/m	Batch or Jar Rating	Material Rating
LS-53	Dow Corning Corporation	5340	Fluorosilicone elastomer		0.016	16/20	10	U	U
						13/20	8	–	–
						9/20	6	–	–
						10/20	4	–	–
						6/20	2	–	–
						2/20	1	–	–
O-Rings, Sample No. 6071	Nichols Engineering Company	5732	Dow Corning LS-53 Modified with Teflon		0.131	17/20	10	U	U
LS-63	Dow Corning Corporation	6047		Washed with F-33 Alkaline cleaned, heat treated at 180°C for 5 hours and at 115°C for 48 hours (stainless steel inserts)	0.055	6/20	10	U	U
						2/20	8	–	–
LS-63, Lot 129	Dow Corning Corporation	5935			0.050	4/20	10	U	U
LS-63, Lot 129	Dow Corning Corporation	5934			0.063	12/20	10	U	U
LS-63, Lot 129	Dow Corning Corporation	5933			0.125	3/20	10	U	U
LS-70	Dow Corning Corporation	5315	Fluorosilicone rubber		0.070	2/20	10	U	U
						8/20	8	–	–
						4/20	6	–	–
						0/20	4	–	–
LS-70	Dow Corning Corporation	5319	Fluorosilicone rubber		0.035	4/20	10	U	U
						6/20	8	–	–
						3/20	6	–	–
						8/20	4	–	–
						7/20	2	–	–
						7/20	1	–	–
LS-70	Dow Corning Corporation	5325	Fluorosilicone rubber		0.016	16/20	10	U	U
						15/20	8	–	–
						8/20	6	–	–
						11/20	4	–	–
						4/20	2	–	–
LS-2249, Lot 130	Dow Corning Corporation	5937			0.050	19/20	10	U	U

TABLE IV. PLASTICS, ELASTOMERS, AND ADHESIVES (Continued)

Material	Manufacturer or Source	Test No.	Composition	Remarks	Thickness (inch)	No. Reactions/ No. Tests	Energy Level Kg/m	Batch or Jar Rating	Material Rating
LS-2249, Lot 130	Dow Corning Corporation	5936			0.063	14/20	10	U	U
LS-2249, Lot 130	Dow Corning Corporation	5938			0.125	6/20	10	U	U
M.L. Enamel	E. I. du Pont de Nemours and Company, Incorporated	5428	A polyimide from a pyrolytic anhydride		0.005	3/20	10	U	BT
Micarta	Westinghouse Electric Corporation	5490	Tested in cell II		0.063	15/20 16/20 7/20 4/20	10 8 6 4	U – – –	U – – –
Micarta	Westinghouse Electric Corporation	2530	Phenolic laminate, fabric base		0.063	16/20 16/20 6/20 0/20	10 5 2 1	U – – –	U – – –
Mox-Tuff Cryogenic Material	Moxness Products, Incorporated	6262		Stainless steel inserts	0.097	10/20	10	U	U
Mylar (from Polyester Powder)		6380	Polyester			17/20	10	U	U
Mylar (Doped with 10% FEP and 90% PET)		6381	Polyester		0.08	7/20	10	U	U
Mylar A	E.I. du Pont de Nemours & Company, Incorporated	6166	Polyester	Stainless steel inserts Vacuum exposed at 250°F		2/20 5/20 3/20 1/20 0/20	10 8 6 4 2	U – – – –	U – – – –
Mylar A	E.I. du Pont de Nemours & Company, Incorporated	6669	Polyester	Stainless steel inserts Cleaned with Trike	0.003	4/20 1/20 1/20 1/20 0/20	10 7.62 5.54 4.16 3.46	U – – – –	U – – – –
Mylar A	E.I. du Pont de Nemours & Company, Incorporated	6691	Polyester	No stainless steel inserts used, cleaned with Trike	0.003	4/20 1/20 1/40 1/40 0/20	10 7.62 6.93 6.24 5.54	U	U

TABLE IV. PLASTICS, ELASTOMERS, AND ADHESIVES (Continued)

Material	Manufacturer or Source	Test No.	Composition	Remarks	Thickness (inch)	No. Reactions/ No. Tests	Energy Level Kg/m	Batch or Jar Rating	Material Rating
Mylar A	E.I. du Pont de Nemours & Company, Incorporated	6680	Polyester	Stainless steel inserts cleaned with Trike	0.005	11/20 7/20 5/20 2/20 1/20	10 7.62 5.54 3.46 2.08	U	U
Mylar A	E.I. du Pont de Nemours & Company, Incorporated	6704	Polyester	Stainless steel cups	0.005	50/100 44/100 34/100 10/100 3/80 0/2	10 8 6 4 2 2	U	U
Mylar A	E.I. du Pont de Nemours & Company, Incorporated	6562 6700	Polyester	No stainless steel inserts, cleaned with Trike	0.005	5/20 5/20 2/20 1/20 2/20 0/20 1/20	10 7.62 5.54 4.16 3.46 3.46 2.08	U	U
Mylar A	E.I. du Pont de Nemours & Company, Incorporated	6522 6742	Polyester	Stainless steel inserts	0.005	50/100 41/100 22/100 12/100 3/100	10 8 6 4 2	U	U
Mylar A	E.I. du Pont de Nemours & Company, Incorporated	6716	Polyester	No stainless steel inserts	0.005	2/120	10		
Mylar A	E.I. du Pont de Nemours & Company, Incorporated	6148	Polyester	Stainless steel inserts	0.006	15/20 6/20 7/20 4/20 4/20 0/20	16 14 12 10 8 6	U	U
Mylar A	E.I. du Pont de Nemours & Company, Incorporated	6675	Polyester	Stainless steel inserts cleaned with Trike	0.0075	14/20 10/20 14/20 6/20 4/20	10 7.62 5.54 3.46 2.08	U	U

TABLE IV. PLASTICS, ELA. .OMERS, AND ADHESIVES (Continued)

Material	Manufacturer or Source	Test No.	Composition	Remarks	Thickness (inch)	No. Reactions/ No. Tests	Energy Level Kg/m	Batch or Jar Rating	Material Rating
Mylar A	E.I. du Pont de Nemours & Company, Incorporated	6565	Polyester	No stainless steel inserts, cleaned with Trike	0.0075	2/20 5/20 1/20 1/40 1/40 1/20 1/40	10 7.62 6.93 6.24 5.54 3.46 2.77	U	U
Mylar A	E.I. du Pont de Nemours & Company, Incorporated	6686	Polyester	Stainless steel inserts cleaned with Trike	0.010	18/20 14/20 14/20 11/20 4/20	10 7.62 5.54 3.46 2.08	U	U
Mylar A	E.I. du Pont de Nemours & Company, Incorporated	6575	Polyester	No stainless steel inserts, cleaned with Trike	0.010	7/20 7/20 2/20 2/20 2/40 1/20 1/60 0/40	10 7.62 6.93 6.24 5.54 4.85 4.16 3.46	U	U
Mylar D	E.I. du Pont de Nemours & Company, Incorporated	6405			0.003	2/20 1/20	10 8	U	U
Mylar D	E.I. du Pont de Nemours & Company, Incorporated	6588		No stainless steel inserts, cleaned with Trike	0.003	5/20 4/20 1/20 1/20 0/60	10 7.62 6.93 6.24 5.54	U	U
Mylar D	E.I. du Pont de Nemours & Company, Incorporated	6407		Stainless steel inserts	0.005	2/20 2/20 2/20 1/20 0/20	10 8 6 4 2	U – – – –	U – – – –

TABLE IV. PLASTICS, ELASTOMERS, AND ADHESIVES (Continued)

Material	Manufacturer or Source	Test No.	Composition	Remarks	Thickness (inch)	No. Reactions/ No. Tests	Energy Level Kg/m	Batch or Jar Rating	Material Rating
Mylar D	E. I. du Pont de Nemours and Company, Incorporated	6595		No stainless steel inserts, cleaned with Trike	0.005	3/20	10	U	U
						2/20	7.85	–	–
						1/20	6.93	–	–
						2/20	6.24	–	–
						2/60	5.54	–	–
						1/20	3.46	–	–
						1/60	2.77	–	–
						0/20	2.08	–	–
Mylar D	E. I. du Pont de Nemours and Company, Incorporated	6412		Stainless steel inserts	0.0075	9/20	10	U	U
						11/20	8	–	–
						7/20	6	–	–
						6/20	4	–	–
						2/20	2	–	–
						0/20	1	–	–
Mylar D	E. I. du Pont de Nemours and Company, Incorporated	6392		No stainless steel inserts, cleaned with Trike	0.0075	3/20	10	U	U
		6607				1/20	7.62	–	–
						2/20	5.54	–	–
						1/20	5.54	–	–
						1/20	4.85	–	–
						1/20	4.16	–	–
						0/60	3.46	–	–
Mylar D	E. I. du Pont de Nemours and Company, Incorporated	6418			0.010	14/20	10	U	U
						11/20	8	–	–
						11/20	6	–	–
						9/20	4	–	–
						2/20	2	–	–
						0/20	1	–	–
Mylar D	E. I. du Pont de Nemours and Company, Incorporated	6398		No stainless steel inserts, cleaned with Trike	0.010	10/20	10	U	U
						8/20	7.62	–	–
						6/20	5.54	–	–
						1/20	3.46	–	–
						2/20	2.08	–	–
						0/20	1.39	–	–
Mylar R22 Plastic Film	E. I. de Pont de Nemours and Company, Incorporated	722	Polyester film			2/20	10	U	U
Mylar Film	E. I. du Pont de Nemours and Company, Incorporated	4545	Polyester film		0.001	4/20	10	U	U

TABLE IV. PLASTICS, ELASTOMERS, AND ADHESIVES (Continued)

Material	Manufacturer or Source	Test No.	Composition	Remarks	Thickness (inch)	No. Reactions/ No. Tests	Energy Level Kg/m	Batch or Jar Rating	Material Rating
Mylar Film	E. I. du Pont de Nemours and Company, Incorporated	3414	Vapor coated with aluminum on both sides 400 Å thick		0.002	4/20 3/20 0/20	10 5 3	U – –	U – –
Mylar Film	E. I. du Pont de Nemours and Company, Incorporated	3444	Vapor coated on one side with 200Å aluminum 400 Å aluminum on other side		0.006	5/20 5/20 0/20	10 5 3	U – –	U – –
Mylar Film	E. I. du Pont de Nemours and Company, Incorporated	3409	Vapor coated with 400 Å aluminum on one side		0.002	2/25 0/20 2/20	10 5 6	U – –	U – –
Mylar Film	E. I. du Pont de Nemours and Company, Incorporated	3442	Vapor coated with 400 Å aluminun on one side		0.006	2/23 0/20	10 5	U –	U –
Mylar, Aluminized	B. F. Goodrich Company	3397	Aluminized Mylar reinforced with No. 477 vedine adhesive between filaments			1/1 1/1 1/5	10 5 3	U – –	U – –
Mylar, Aluminized	B. F. Goodrich Company	3398	Aluminized Mylar reinforced with No. 476 Vedine adhesive between filaments			1/1 1/1 1/1 0/6	10 5 2 1	U – – –	U – – –
Mylar, Aluminized	B. F. Goodrich Company	3399	Aluminized Mylar reinforced with No. 52042			1/1 1/6 1/1	10 3 2	U – –	U – –
Mylar, Aluminized	B. F. Goodrich Company	3396	Aluminized Mylar reinforced with No. 15345			1/1 1/1 1/2 0/1	10 5 2 1	U – – –	U – – –
Mylar, Aluminized	B. F. Goodrich Company	3395	Aluminized Mylar reinforced with No. 15094			2/2 1/1 1/2 0/3	10 5 2 1	U – – –	U – – –
Mylar, Aluminized	B. F. Goodrich Company	3394	Aluminized Mylar reinforced with No. 482			2/2 2/3 1/4	10 5 3	U – –	U – –

TABLE IV. PLASTICS, ELASTOMERS, AND ADHESIVES (Continued)

Material	Manufacturer or Source	Test No.	Composition	Remarks	Thickness (inch)	No. Reactions/ No. Tests	Energy Level Kg/m	Batch or Jar Rating	Material Rating
Mylar		3493	1-1/2 mil Mylar between two pieces of 0.0035 aluminum polyester adhesive	Three batches tested		2/8 2/9 1/3 0/20	10 5 3 2	U – – –	U – – –
Mystik Foil No. 7402 Tape	Mystik Adhesive Products Company	835 426	Aluminum, silicone adhesive			2/3 2/3 1/14	10 5 2	U – –	U – –
Mystik Foil No. 7402 Tape	Mystik Adhesive Products		Aluminum, silicone adhesive	Baked 100°F overnight and stripped		0/20	10	S	U
Mystik Foil No. 7402 Tape	Mystik Adhesive Products		Aluminum, silicone adhesive	Aged 1 week and stripped		1/20	10	I	U
Narmco Experimental Adhesive No. 1	Narmco Research and Development Company	4082	Chlorinated polyester cured with 2% MEK, peroxide and cobalt naphtenate		0.050	7/10 4/10 2/20 0/20	10 5 3 2	U – – –	U – – –
Narmco Experimental Adhesive No. 2	Narmco Research and Development Company	4085	Chlorinated polyester with 33.3% antimony trichloride, cured with 2.0% MEK, peroxide and cobalt naphtenate		0.050	9/10 2/5 1/10 2/10 0/20	10 5 3 2 1	U – – – –	U – – – –
Narmco Experimental Adhesive No. 3	Narmco Research and Development Company	4088	ERL 0625 epoxy cured with 10.6 Phr meta-phenylene diamine		0.050	7/10 2/10 0/20	10 5 3	U – –	U – –
Narmco Experimental Adhesive No. 4	Narmco Research and Development Company	4090	ERL 0625 epoxy, cured with 14.5 phr chlorendic anhydride and 0.5% benzyldimethylamine		0.050	6/10 6/20 2/10 1/10 0/20	10 5 3 2 1	U – – – –	U – – – –
Narmco Resin 3135	Narmco Research and Development Company	3624	Aluminum alloy 7075-T6 cross laminated with layers of adhesive, two pieces of 1 mil FEP Type 544 between aluminum		0.050	2/20 3/20 2/20	10 5 1	U – –	U – –

TABLE IV. PLASTICS, ELASTOMERS, AND ADHESIVES (Continued)

Material	Manufacturer or Source	Test No.	Composition	Remarks	Thickness (inch)	No. Reactions/ No. Tests	Energy Level Kg/m	Batch or Jar Rating	Material Rating
Narmco Resin 3135	Narmco Research and Development Company	3512	Adhesive consisting of 50% epoxy and 50% polyamide		0.050	3/3	10	U	U
						2/2	5	–	–
						2/7	2	–	–
						0/12	1	–	–
Narmco Metlbond 3170	Narmco Research and Development Company	3508	Adhesive consisting of 50% filled epoxy, 50% filled polyamine		0.050	16/24	10	U	U
						2/8	5	–	–
						2/14	3	–	–
						0/20	1	–	–
Narmco 2-Part Adhesive	Narmco Research and Development Company	3514	Adiprene L-100 polyurethane prepolymer, Moca curing agent		0.050	5/5	10	U	U
						3/5	5	–	–
						4/5	3	–	–
						2/5	1	–	–
Narmco C	Narmco Research and Development Company	5707		0.050" thick in bottom of aluminum cup	0.050	20/20	10	U	U
						20/20	8	–	–
						20/20	6	–	–
						20/20	4	–	–
						19/20	2	–	–
						14/20	1	–	–
Narmco 7343	Narmco Research and Development Company	9228		10 pound plummet	0.050	8/20	0.5	U	U
						5/20	0.25	–	–
						0/20	0.13	–	–
Narmco 7343	Narmco Research and Development Company	9377		2.2 pound plummet	0.050	10/20	1	U	U
						2/29	0.25	–	–
						0/20	0.13	–	–
Potting Compound Narmco 7343	Whittaker Corporation, Division of Telecomputing Corporation	5666			0.030	2/20	10	U	U
		6002			0.030	8/20	10	U	U
Neoprene Rubber	Non-Metallics Materials Branch	9353			0.040	16/20	10	U	U
						10/20	7.7	–	–
						8/20	5.6	–	–
						2/20	4.9	–	–
						2/20	4.2	–	–
						0/20	3.5	–	–
						0/20	2.8	–	–
Neoprene Rubber A-522	Non-Metallics Materials Branch	6081			0.065	3/20	10	U	U
						3/20	8	–	–
						0/20	6	–	–
Nitroso Copolymer	Thiokol, Reaction Motors Division	7563			0.19	0/12	10	I	I

TABLE IV. PLASTICS, ELASTOMERS, AND ADHESIVES (Continued)

Material	Manufacturer or Source	Test No.	Composition	Remarks	Thickness (inch)	No. Reactions/ No. Tests	Energy Level Kg/m	Batch or Jar Rating	Material Rating
Nitroso Vulcanizate	Thiokol, Reaction Motors Division	7562			0.080	1/6	10	I	I
Nitroso Terepolymer Vulcanizate	Thiokol Chemical Company	8980			0.036	2/20	10	I	I
Non-metallic Inserts (MSFC Stock No. 127-912-4200)		4285			0.063	2/2 2/6 2/2	10 5 3	U – –	U – –
Nylon Hooks		9227			0.035	4/4	10	U	U
Nylon Basket Weave No. 1803		2250	Polyamide		0.032	2/2 2/2 2/2 2/12	10 5 2 1	U – – –	U – – –
Nylon Type 127-1		3545	Polyamide		0.250	8/20 1/1 1/2 0/20	10 5 3 1	U – – –	U – – –
Nylon "C" Lot 8762	Specialty Converting, Incorporated	4184	Polyamide		0.001	13/20	10	U	U
Nylon, Zytel	E. I. du Pont de Nemours and Company, Incorporated	4180	Polyamide		0.001	10/20	10	U	U
Nylon, Zytel	E. I. du Pont de Nemours and Company, Incorporated	4183	Polyamide		0.002	3/20	10	U	U
Nylon, Zytel	E. I. du Pont de Nemours and Company, Incorporated	4182	Polyamide		0.004	8/20	10	U	U
Nylon Extruded Rod		855			0.063	2/2 2/2 2/3	10 5 2	U – –	U – –
Nylon		6250			0.004	2/40	10	U	U
Nylon and Polyethylene Composite		6254		Stainless steel inserts	0.017	11/20	10	U	U
Nylon and Polyethylene Composite		6252		Stainless steel inserts	0.019	8/20	10	U	U

TABLE IV. PLASTICS, ELASTOMERS, AND ADHESIVES (Continued)

Material	Manufacturer or Source	Test No.	Composition	Remarks	Thickness (inch)	No. Reactions/ No. Tests	Energy Level Kg/m	Batch or Jar Rating	Material Rating
Nylon and Polyethylene Composite		6257		Stainless steel inserts	0.120	2/20	10	U	U
O-Ring (neoprene)		7015			0.068	20/20	10	U	U
O-Ring	Disogrin Ind. Div of Pellon Corporation	5731		Stainless steel inserts	0.145	15/20	10	U	U
Parco "O" Rings 947-70	Plastics and Rubber Product Company	1430	Viton A		0.063	0/20	10	S	BT
Permacel P421 Tape	Permacel Tape Corporation	1261				1/6	10	U	U
						0/2	5	–	–
Permafil		3529				7/20	10	U	U
						7/20	5	–	–
						0/20	3	–	–
P.C. No. 925, Teflon MB	Raybestos-Manhattan	7474			0.063	0/20	10	S	BT
Penton Chlorinated Polyethylene	Hercules Powder Company	7442	Chlorinated Polyethylene	Stainless steel inserts	0.005	18/20	10	U	U
						16/20	7.62	–	–
						13/20	5.54	–	–
						8/20	3.46	–	–
						3/20	1.39	–	–
Penton Chlorinated Polyethylene	Hercules Powder Company	7437	Chlorinated Polyethylene	Stainless steel inserts	0.010	18/20	10	U	U
						15/20	7.62	–	–
						15/20	5.54	–	–
						9/20	3.46	–	–
						3/20	1.39	–	–
Penton Chlorinated Polyethylene	Hercules Powder Company	7430	Chlorinated Polyethylene	Stainless steel inserts	0.020	18/20	10	U	U
						13/20	7.62	–	–
						7/20	5.54	–	–
						6/20	3.46	–	–
						3/20	1.39	–	–
Penton Chlorinated Polyethylene	Hercules Powder Company	7427	Chlorinated Polyethylene	Stainless steel inserts	0.030	17/20	10	U	U
						15/20	7.62	–	–
						4/20	5.54	–	–
						3/20	3.46	–	–
						1/20	1.39	–	–

TABLE IV. PLASTICS, ELASTOMERS, AND ADHESIVES (Continued)

Material	Manufacturer or Source	Test No.	Composition	Remarks	Thickness (inch)	No. Reactions/ No. Tests	Energy Level Kg/m	Batch or Jar Rating	Material Rating
Penton Chlorinated Polyethylene	Hercules Powder Company	7422	Chlorinated Polyethylene	Stainless steel inserts	0.040	13/20	10	U	U
						10/20	7.62	–	–
						4/20	3.46	–	–
						2/20	3.46	–	–
						2/20	1.39	–	–
Penton Chlorinated Polyethylene	Hercules Powder Company	7415	Chlorinated Polyethylene	Stainless steel inserts	0.050	14/20	10	U	U
						9/20	7.62	–	–
						5/20	5.54	–	–
						2/20	3.46	–	–
						0/20	2.77	–	–
						0/20	2.08	–	–
						0/20	1.39	–	–
Penton Chlorinated Polyethylene	Hercules Powder Company	7409	Chlorinated Polyethylene	Stainless steel inserts	0.060	11/20	10	U	U
						5/20	7.62	–	–
						2/20	5.54	–	–
						1/20	4.85	–	–
						0/20	4.16	–	–
						0/20	3.46	–	–
Penton Chlorinated Polyethylene	Hercules Powder Company	7403	Chlorinated Polyethylene	Stainless steel inserts	0.075	12/20	10	U	U
						13/20	7.62	–	–
						6/20	5.54	–	–
						2/20	4.16	–	–
						0/20	3.46	–	–
						0/20	2.77	–	–
Plaskon 2200 CTFE Caps	Aero-Dynamics, Incorporated	8264	Polytrifluorochloro-ethylene resin		0.080	2/20	10	U	BT
Plaskon 2400 CTFE	Allied Chemical Corporation	5588	Formerly known as Halon TVS (300) High ZST	Stainless steel inserts Used	0.128	0/20	10	S	BT
Plaskon 2400 CTFE	Allied Chemical Corporation	5590	Formerly known as Halon TVS (300) High ZST	Stainless steel inserts Used	0.058	0/20	10	S	BT
Plaskon Alkyd 440 Sheet Plastic	Barrett Division Allied Chemical Company	1004	Glass and polyester			2/5	10	U	U
						2/13	5	–	–
						0/2	1	–	–
Plastic KF52 (MIL-B-131B Class 2)	Plastic Film Corporation	300		Lot No. 46		1/2	10	U	U
						1/4	5	–	

TABLE IV. PLASTICS, ELASTOMERS, AND ADHESIVES (Continued)

Material	Manufacturer or Source	Test No.	Composition	Remarks	Thickness (inch)	No. Reactions/ No. Tests	Energy Level Kg/m	Batch or Jar Rating	Material Rating
Plastic P35A (MIL-B-131B Class 1)	Plastic Film Corporation	301		Lot No. 150		1/2	10	U	U
						2/2	5	–	–
Plastic Rod (MIL-P-79B)		857		Electrical insulation		2/2	10	U	U
						2/2	5	–	–
						1/16	2	–	–
Plastic Plugs		3501	Dyed polyethylene		0.063	4/11	10	U	U
						2/10	5	–	–
						2/14	3	–	–
						0/20	1	–	–
Plastic Steel Putty Type A	Devcon Corporation	3390	80% Steel with epoxy binder	Violent reactions	0.050	5/5	10	U	U
						5/5	5	–	–
						9/12	2	–	–
						4/20	1	–	–
Plexiglass		558		Three batches tested		2/2	19	U	U
						1/3	5	–	–
						1/4	3	–	–
Polyken No. 110 Tape	Kendall Company					2/2	10	U	U
						2/2	5	–	–
Polyethylene		1698			0.032	4/7	10	U	U
						2/19	5	–	–
						1/3	2	–	–
						0/17	1	–	–
Polyethylene Tubing		2627				2/11	10	U	U
						2/10	5	–	–
						2/20	2	–	–
Polyethylene		5719		Stainless steel inserts	0.006	16/20	10	U	U
						16/20	8	–	–
						16/20	6	–	–
						8/20	4	–	–
						6/20	2	–	–
						0/20	1	–	–
Polyethylene	Du Pont	5175		Shore hardness 25	0.005	7/20	10	U	U
						10/20	8	–	–
						9/20	6	–	–
						11/40	4	–	–

TABLE IV. PLASTICS, ELASTOMERS, AND ADHESIVES (Continued)

Material	Manufacturer or Source	Test No.	Composition	Remarks	Thickness (inch)	No. Reactions/ No. Tests	Energy Level Kg/m	Batch or Jar Rating	Material Rating
Polyethylene	Du Pont	5141		Shore hardness 52	0.137	3/20	11.3	U	U
						1/20	10	–	–
						1/20	8	–	–
						0/20	6	–	–
Polyethylene	Du Pont	5163		Shore hardness 35	0.020	15/20	10	U	U
						16/20	8	–	–
						13/20	6	–	–
						11/20	4	–	–
						7/20	2	–	–
						3/20	1	–	–
Polyethylene	Du Pont	5157		Shore hardness 40	0.075	4/20	11.3	U	U
						7/20	10	–	–
						3/20	8	–	–
						6/20	6	–	–
						0/20	4	–	–
Polyethylene 1220	Allied Chemical Company	5205		High density	0.063-075	7/20	10	U	U
						2/20	8	–	–
						1/20	6	–	–
						2/20	4	–	–
						1/20	2	–	–
						0/20	1	–	–
Polyethylene	Du Pont	5606		Stainless steel insert used	0.006	19/20	10	U	U
						18/20	8	–	–
						17/20	6	–	–
						11/20	4	–	–
						11/20	2	–	–
						0/20	1	–	–
Polyethylene Construction Film		8472			0.006	88/100	10	U	U
						50/100	8	–	–
						42/100	6	–	–
						30/100	4	–	–
						9/100	2	–	–
						0/100	1	–	–
Polypropylene Caps	Aero-Dynamics, Incorporated	8265			0.063	20/20	10	U	U
Polyphenyle Oxide	General Electric Company	8618			0.065	20/20	10	U	U

TABLE IV. PLASTICS, ELASTOMERS, AND ADHESIVES (Continued)

Material	Manufacturer or Source	Test No.	Composition	Remarks	Thickness (inch)	No. Reactions/ No. Tests	Energy Level Kg/m	Batch or Jar Rating	Material Rating
Polypropylene	Non-Metallics Materials Branch	8585			0.080	15/20	10	U	U
						12/20	7.7	–	–
						4/20	5.6	–	–
						2/20	4.9	–	–
						0/20	4.2	–	–
						0/20	3.5	–	–
Polypropylene	Non-Metallics Materials Branch	8578			0.060	17/20	10	U	U
						12/20	7.7	–	–
						6/20	5.6	–	–
						3/20	3.5	–	–
						1/20	2.8	–	–
						0/20	1.4	–	–
Polypropylene	Non-Metallic Materials Branch	8573			0.050	17/20	10	U	U
						12/20	7.7	–	–
						8/20	5.6	–	–
						7/20	3.5	–	–
						2/20	1.4	–	–
Polypropylene	Non-Metallic Materials Branch	8568			0.040	18/20	10	U	U
						15/20	7.7	–	–
						9/20	5.6	–	–
						7/20	3.5	–	–
						3/20	1.4	–	–
Polypropylene	Non-Metallic Materials Branch	8563			0.030	18/20	10	U	U
						17/20	7.7	–	–
						14/20	5.6	–	–
						14/20	3.5	–	–
						8/20	1.4	–	–
Polypropylene	Non-Metallic Materials Branch				0.020	19/20	10	U	U
						18/20	7.7	–	–
						15/20	5.6	–	–
						14/20	3.5	–	–
						8/20	1.4	–	–
Polypropylene	Non-Metallic Materials Branch	8552			0.010	18/20	10	U	U
						18/20	7.7	–	–
						16/20	5.6	–	–
						12/20	3.5	–	–
						8/20	1.4	–	–
						3/20	0.7	–	–

TABLE IV. PLASTICS, ELASTOMERS, AND ADHESIVES (Continued)

Material	Manufacturer or Source	Test No.	Composition	Remarks	Thickness (inch)	No. Reactions/ No. Tests	Energy Level Kg/m	Batch or Jar Rating	Material Rating
Polysulfide Compound 380M	Products Research Corporation	8649			0.017	20/20	10	U	U
P-101-S Composite	Snyder Manufacturing Company	8812			0.020	0/20	10	S	I
Polyurethane Wiping Material		2502			0.016	2/3	10	U	U
						2/9	3	–	–
						0/20	1	–	–
Polyvinyl Chloride	Teledyne Corporation	3785			0.125	2/2	10	U	U
						2/9	5	–	–
						2/14	2	–	–
						0/20	1	–	–
Polyvinyl Chloride		4280		Tested in air 11/20 charge noted	0.050				
Polyvinyl Chloride		4279		Tested in air 8/20 charge noted	0.025				
Polyvinyl Chloride		3782		Cotton cloth coated with PVC 0.015 inches per side	0.050	2/2	10	U	U
						2/2	5	–	–
						2/5	3	–	–
						1/20	1	–	–
Polyvinyl Chloride Electrical Insulation	Revere Corporation of America	1692	Polyvinyl chloride		0.063	2/3	10	U	U
						2/3	5	–	–
						2/11	2	–	–
						1/3	3	–	–
Potting Compound	Bendix Corporation	1945	Epoxy		0.063	1/1	10	U	U
						1/1	5	–	–
						1/1	2	–	–
						1/2	1	–	–
Polyvinyl and Butyl-Coated Nylon		6256		Stainless steel inserts	0.005	9/20	10	U	U
Pro-Seal 994, Lot T0306	Coast Pro-Seal Manufacturing Company	9820			0.050	5/20	10	U	U

TABLE IV. PLASTICS, ELASTOMERS, AND ADHESIVES (Continued)

Material	Manufacturer or Source	Test No.	Composition	Remarks	Thickness (inch)	No. Reactions/ No. Tests	Energy Level Kg/m	Batch or Jar Rating	Material Rating
Pro-Seal 994, Lot L8666	Coast Pro-Seal Manufacturing Company	9825			0.050	6/20	10	U	U
Pro-Seal 994, Sand Mix	Kennedy Space Center	10037			0.100	12/20	10	U	U
Pro-Seal 994, Sand Mix	Kennedy Space Center	9839	Three Parts of 994, one part of graded sand		0.500	11/20	10	U	U
Pro-Seal 994, Expansion Joint Sealant	Coast Pro-Seal Manufacturing Company	3221	Polyurethane		0.050	8/20	10	U	U
Pro-Seal 994	Coast Pro-Seal Manufacturing Company	3221			0.063	7/20 6/20 2/20 0/20	10 5 2 1	U – – –	U – – –
PR341 Casting Resin	Product Research Corporation	713				3/3 2/3 2/7	10 5 3	U – –	U – –
PR-1732	Product Research Corporation	9243			0.001	6/20	10	U	U
PR-1540 1 Part A, 2 Parts D	Product Research Corporation	6990			0.050	18/20	10	U	U
PR-1525	Product Research Corporation	2939	Polyurethane		0.063	3/20 0/20	10 5	U –	U –
PR-1525	Product Research Corporation	2932	Polyurethane		0.125	2/20	10	U	U
PR-1527	Product Research Corporation	2937	Polyurethane		0.063	7/20 3/20	10 5	U –	U –
PR-1527	Product Research Corporation	2936	Polyurethane		0.032	11/20	10	U	U
PR-1538	Product Research Corporation	2935	Polyurethane		0.063	10/20	10	U	U
PR-1538-T	Product Research Corporation	2934	Polyurethane		0.063	5/20 1/20	10 5	U –	U –
PR-1732 with Dynatherm-4327 Top Coat	Non-Metallic Materials Branch	9244			0.002	2/20	10	U	U

TABLE IV. PLASTICS, ELASTOMERS, AND ADHESIVES (Continued)

Material	Manufacturer or Source	Test No.	Composition	Remarks	Thickness (inch)	No. Reactions/ No. Tests	Energy Level Kg/m	Batch or Jar Rating	Material Rating
PR-1910	Product Research Corporation	990	Silicone		0.050	2/2	10	U	U
						2/2	5	–	–
						0/16	2	–	–
PR-1902 Primer	Product Research Corporation	2332				2/11	10	U	U
						0/9	5	–	–
PR-1955	Product Research Corporation	3931			0.063	2/4	10	U	U
						2/16	5	–	–
						2/12	3	–	–
						0/20	1	–	–
PR-1955 BT	Product Research Corporation	9379			0.050	18/20	10	U	U
						17/20	7.7		
						14/20	5.6		
						9/20	3.5		
						4/20	1.4		
						0/20	0.7		
PR-1955 BT	Product Research Corporation	9120			0.066	15/20	10	U	U
						12/20	7.7		
						4/20	5.6		
						6/20	3.5		
						1/20	1.4		
PR-1955 BT	Product Research Corporation	8863			0.250	12/20	10	U	U
						7/20	7.7		
						8/20	5.6		
PR-1955 BT	Product Research Corporation	9385			0.350	14/20	10	U	U
						11/20	7.7		
						5/20	5.6		
						1/20	3.5		
PR-1955 with Top Coat P-81-2018	Product Research Corporation	4601			0.050	2/3	10	U	U
						2/5	8	–	–
						2/15	5	–	–
PR-1955 with Top Coat P-81-2018	Product Research Corporation	4594			0.030	2/2	10	U	U
						2/2	8	–	–
						2/3	6	–	–
						2/2	4	–	–
						2/2	2	–	–
						2/9	1	–	–

TABLE IV. PLASTICS, ELASTOMERS, AND ADHESIVES (Continued)

Material	Manufacturer or Source	Test No.	Composition	Remarks	Thickness (inch)	No. Reactions/ No. Tests	Energy Level Kg/m	Batch or Jar Rating	Material Rating
PR-1955 with Top Coat P-81-2018	Product Research Corporation	492			0.025	2/2	10	U	U
						2/2	8	–	–
						2/2	6	–	–
						2/2	4	–	–
						2/2	2	–	–
						2/2	1	–	–
PR-1955 with Top Coat P-81-2018	Product Research Corporation	4591			0.015	2/2	10	U	U
						2/4	8	–	–
						2/4	6	–	–
						2/6	4	–	–
						2/8	2	–	–
PR-1955 with Top Coat P-81-208	Product Research Corporation	4582			0.050	2/2	10	U	U
						2/8	8	–	–
						2/5	6	–	–
						2/10	4	–	–
						2/8	3	–	–
						2/20	2	–	–
PR-1955 with Top Coat P-81-2020	Product Research Corporation	4584			0.025	2/2	10	U	U
						2/2	8	–	–
						2/2	6	–	–
						2/5	4	–	–
						2/4	2	–	–
						2/6	1	–	–
PR-1955 with Top Coat P-81-2035	Product Research Corporation	4587			0.015	2/2	10	U	U
						2/2	8	–	–
						2/2	6	–	–
						2/4	4	–	–
						2/2	2	–	–
						0/20	1	–	–
PT-201 and Solvent PT-1001	Product Techniques Incorporated	1893	Phenolic epoxy			1/1	10	U	U
						1/1	5	–	–
						1/2	2	–	–
PT-201 Coated Coil Spring	Product Techniques Incorporated	3615				3/10	10	U	U
						2/9	5	–	–
						0/4	3	–	–

TABLE IV. PLASTICS, ELASTOMERS, AND ADHESIVES (Continued)

Material	Manufacturer or Source	Test No.	Composition	Remarks	Thickness (inch)	No. Reactions/ No. Tests	Energy Level Kg/m	Batch or Jar Rating	Material Rating
Pyro Prey AC-81 Type 1 Plastic	Cordo Molding Products Incorporated	916	Phenolic impregnated fiberglass		0.060	2/2 2/2 2/3	10 5 3	U – –	U – –
Quanted 1682	Quantum, Incorporated	8502	Polyimide		0.005	0/40	10	S	BT
Q90-002A/B	Dow Corning Corporation	4486	Fluorosilicone	Rubber sealant	0.050	2/7 2/20 0/20	10 5 4	U – –	U – –
Q90-031	Dow Corning Corporation	4484	Fluorosilicone		0.050	2/5 2/6 0/18 0/20	10 5 4 3	U – – –	U – – –
Q2-0103	Dow Corning Corporation	4482			0.050	2/2 2/4 2/17 0/5 1/20	10 5 3 2 1	U – – – –	U – – – –
Q9-002A and B Adhesive	Dow Corning Corporation	3532	Fluorosilicone rubber	RTV cured	0.050	0-2/20	10	U	U
Q-2-0046 Adhesive	Dow Corning Corporation	3339	Fluorosilicone rubber	RTV cured	0.050	1/140	10	S	U
Q-2-0046 Adhesive	Dow Corning Corporation	3788	Fluorosilicone rubber	RTV cured	0.025	38/40	10	U	U
Q94-002	Dow Corning Corporation	5314	Fluorosilicone rubber	Rubber sealant	0.050	2/20	10	U	U
Q94-002	Dow Corning Corporation	5503	Fluorosilicone rubber	Rubber sealant	0.013	1/20 0/20	11.3 10	— S	U –
Q94-002	Dow Corning Corporation	5505	Fluorosilicone rubber	Rubber sealant	0.058	3/20 3/20	10 8	U –	U –
Q94-002	Dow Corning Corporation	5507	Fluorosilicone rubber	Rubber sealant	0.032	12/20 12/20	10 8	U –	U –
Q94-002	Dow Corning Corporation	5509	Fluorosilicone rubber	Rubber sealant	0.020	13/20 15/20	10 8	U –	U –
Q2-0046, Lot 010101	Dow Corning Corporation	6924		Samples aged for 2 weeks	0.050	4/20	10	U	U

TABLE IV. PLASTICS, ELASTOMERS, AND ADHESIVES (Continued)

Material	Manufacturer or Source	Test No.	Composition	Remarks	Thickness (inch)	No. Reactions/ No. Tests	Energy Level Kg/m	Batch or Jar Rating	Material Rating
Q94-002	Dow Corning Corporation	5921	Fluorosilicone	Not cured	0.050	3/20	10	U	U
Q94-002 (old sample)	Dow Corning Corporation	5910	Fluorosilicone		0.050	3/20	10	U	U
Q94-002, Lot NB06-5	Dow Corning Corporation	6975	Fluorosilicone		0.050	2/20	10	U	U
Q94-002, Lot 1531	Dow Corning Corporation	5920	Fluorosilicone		0.050	4/20	10	U	U
Q94-002, Lot 1531	Dow Corning Corporation	5927	Fluorosilicone		0.050	11/20	10	U	U
Q94-002, Lot 1531	Dow Corning Corporation	5926	Fluorosilicone		0.085	10/20	10	U	U
Q94-002, Lot 1531	Dow Corning Corporation	5928	Fluorosilicone		0.105	5/20	10	U	U
Raycom 2148 RPR	Raytheon Company	3853			0.125	2/20	10	U	U
Red Wing Silicone Rubber		1907			0.063	20/20 20/20 14/20 1/20	10 5 3 1	U – – –	U – – –
Red Wing Silicone Rubber		1921		Two 0.063 inches stacked to make 0.125	0.125	17/20 4/20 0/20	10 3 1	U – –	U – –
Relco A (50%) + Relco B (50%)	Reliance Steel Products Co.	2962	Epoxy		0.063	2/20	10	U	U
Relco A + Relco B + Grit	Reliance Steel Products Co.	2963	Epoxy		0.063	3/5 2/5 2/3 1/8	10 5 3 2	U – – –	U – – –
Ricote (MIP) 10[illegible]-C-1	Modern Industrial Plastics Division of the Durison Co., Incorporated	4010		Brush coating on stainless steel inserts		7/20	10	U	U
RTV 511, 20/480°F	General Electric	5903 5954 5980		Stainless steel inserts	0.031	14/20 4/20 2/20 2/20 2/20	10 8 6 2 1	U	U

TABLE IV. PLASTICS, ELASTOMERS, AND ADHESIVES (Continued)

Material	Manufacturer or Source	Test No.	Composition	Remarks	Thickness (inch)	No. Reactions/ No. Tests	Energy Level Kg/m	Batch or Jar Rating	Material Rating
RTV 511, 20/480°F	General Electric	5901 5956		Stainless steel inserts	0.062	2/40 7/20 0/20	10 8 4	U	U
RTV-560, 20/480°F	General Electric	5895 5958		Stainless steel inserts	0.031	14/20 18/20 15/20 20/20 6/20 4/20	10 8 6 4 2 1	U	U
RTV-560, 20/480°F	General Electric	5896 5961		Stainless steel inserts	0.062	3/20 4/20 5/20 4/20 2/20 0/20	10 8 6 4 2 1	U	U
No. 601 Rubber	Raybestos-Manhattan	5809		Stainless steel inserts	0.035	1/20	10	I	I
RT/Duroid 5813	Rogers Corporation	7397		Stainless steel inserts	0.036	0/20	10	S	BT
RT/Duroid 5870	Rogers Corporation	7398		Stainless steel inserts	0.053	0/20	10	S	BT
RTV-S-53V-70 Density = 10 lb/ft^3	Dow Corning Corporation	6239		Flexible foam	0.400	20/20 20/20 20/20 20/20 11/20 0/20	10 8 6 4 2 1	U	U
Rulon A, Lot PA-2 (Dixon No. E-3846)	Dixon Corporation	5922			0.050	0/20	10	S	S
Rulon Sheet	Dixon Corporation	5589	Teflon composite	Stainless steel inserts used	0.060	0/20	10	S	BT
Rulon A	Dixon Corporation	9131	Filled tetrafluoro-ethylene		0.063	0/20	10	S	S
Sauereisen Low Expansion Cement No. 29	Sauereisen Cement Company	2495	Zirconium base		0.050	0/20	10	S	S

TABLE IV. PLASTICS, ELASTOMERS, AND ADHESIVES (Continued)

Material	Manufacturer or Source	Test No.	Composition	Remarks	Thickness (inch)	No. Reactions/ No. Tests	Energy Level Kg/m	Batch or Jar Rating	Material Rating
Scotchcast Resin No. 11	Minnesota Mining and Manufacturing Company	9913			0.050	6/20	10	U	U
Scotch Ply Type 1002	Minnesota Mining and Manufacturing Company	9240	Epoxy resin with non-woven glass filament		0.113	20/20 20/20	10	U	U
Scotch Tape No. Y-9089	Minnesota Mining and Manufacturing Company	2853	Pluton fabric, neoprene base adhesive		0.063	20/20 2/2 0/20	10 5 1	U – –	U – –
Scotch Pressure Sensitive Tape No. Y-9050	Minnesota Mining and Manufacturing Company	2852				17/20 9/10 0/20	10 5 1	U – –	U – –
Scotch Plastic Film, Type 546	Minnesota Mining and Manufacturing Company	6249	Adhesive free Teflon	Stainless steel inserts	0.010	0/20	10	S	S
Scotch Electrical Tape No. 27	Minnesota Mining and Manufacturing Company	631	White glass cloth with thermosetting adhesive		0.007	4/5 5/6 3/3	10 5 1	U – –	U – –
Scotch Electrical Tape No. 33	Minnesota Mining and Manufacturing Company	516	Black vinyl plastic with pressure sensitive adhesive		0.010	2/4 2/3 0/2	10 5 2	U – –	U – –
Scotch Electrical Tape No. 60	Minnesota Mining and Manufacturing Company	496	Teflon and silicone adhesive		0.006	2/3 2/7	10 5	U –	U –
Scotch Electrical Tape No. 61	Minnesota Mining and Manufacturing Company	1271	Teflon and silicone adhesive		0.006	2/2 2/4	10 5	U –	U –
Scotch Resin No. CRP-235	Minnesota Mining and Manufacturing Company	712	Epoxy	One part "A" and two parts "B" cured at 30°C for 1/2 hour		3/6 1/14	10 5	U –	U –
Scotch Electrical Tape No. 27	Minnesota Mining and Manufacturing Company	517				3/4 2/2	10 3	U –	U –
Scotch Tape No. 506	Minnesota Mining and Manufacturing Company	630				3/4 2/5	10 5	U –	U –
Scotch Teflon Tape No. 536	Minnesota Mining and Manufacturing Company	149				3/10 1/10 1/7	10 5 8	U – –	U – –

TABLE IV. PLASTICS, ELASTOMERS, AND ADHESIVES (Continued)

Material	Manufacturer or Source	Test No.	Composition	Remarks	Thickness (inch)	No. Reactions/ No. Tests	Energy Level Kg/m	Batch or Jar Rating	Material Rating
Scotch Teflon Tape No. 547	Minnesota Mining and Manufacturing Company	37				0/10	10	I	I
Scotch Teflon Tape No. 549	Minnesota Mining and Manufacturing Company	786				2/2 2/5 1/13	10 5 2	U – –	U – –
Series R, Spun Bonded Olefin Paper	E.I. du Pont de Nemours and Company	8217			0.005	19/20	10	U	U
Silastic RTV 94-002, Lot 162116 (lab. run)	Dow Corning Corporation	6611		Cured 30 days at 110°C	0.111	7/20	10	U	U
Silicone Tape S-5638	Dow Corning Corporation	6637		Stainless steel inserts	0.022	19/20	10	U	U
Silastic No. 50 Rubber	Dow Corning Corporation	736	Silicone rubber			2/2 2/6 2/4	10 5 2	U – –	U – –
Silastic No. 675	Dow Corning Corporation	163				2/3 2/2 1/1	10 5 2	U – –	U – –
Silastic No. 50-24-480	Dow Corning Corporation	514				8/10	10	U	U
Silastic No. 80-24-480	Dow Corning Corporation	164				7/10	10	U	U
Silastic No. 290-24-480	Dow Corning Corporation	321				2/10 1/10	10 5	U –	U –
Silastic No. 916-4-480	Dow Corning Corporation	980				2/2 3/15	10 5	U –	U –
Silastic LS-53	Dow Corning Corporation	549				2/7 2/8 0/5	10 5 2	U – –	U – –
Silastic LS-53-24-300	Dow Corning Corporation	1007			(illegible)	2/3 2/5	10 5	U –	U –
Silastic LS-13-8-400	Dow Corning Corporation	547				2/8 3/10 0/2	10 5 2	U – –	U – –

TABLE IV. PLASTICS, ELASTOMERS, AND ADHESIVES (Continued)

Material	Manufacturer or Source	Test No.	Composition	Remarks	Thickness (inch)	No. Reactions/ No. Tests	Energy Level Kg/m	Batch or Jar Rating	Material Rating
Silastic S-2098-24-480	Dow Corning Corporation	546				2/3	10	U	U
						0/17	5	–	–
Silastic S-9711-2-480	Dow Corning Corporation	545				2/2	10	U	U
						2/2	5	–	–
						0/2	3	–	–
Silastic LS-63	Dow Corning Corporation	1232				3/20	10	U	U
Silicone Impregnated Fiberglass Panel 83-5	Dow Corning Corporation		Silicone and glass			2/2	10	U	U
						3/3	5	–	–
						2/2	2	–	–
Silicone Rubber Flexible Tubing	Dow Corning Corporation	2740	Silicone			5/5	10	U	U
						5/5	5	–	–
						5/5	3	–	–
						3/5	1	–	–
Silverprene Coated Asbestos	Jamac Incorporated	2877			0.015	2/2	10	U	U
						2/2	5	–	–
						2/5	3	–	–
						2/6	2	–	–
						1/20	1	–	–
SP Polymer with 20% Copper Fibers Plus 10% MoS_2 (by Weight) (NASA Batch)		6967				0/20	10	S	BT
SP-1 Unfilled Polymer SP		6963	Polyimide		0.050	0/20	10	S	U
SP-21 Polymer with 15% Graphite (by weight)	E.I. du Pont de Nemours & Company, Incorporated	6964	Polyimide		0.050	0/20	10	S	BT
SP-41 Polymer SP with 40% Bronze (by weight)	E.I. du Pont de Nemours & Company, Incorporated	6968	Polyimide		0.050	0/20	10	S	BT
Stillman Rubber TH 1057	Stillman Rubber Company	5730			0.100	16/20	10	U	U
						10/20	8		
						11/20	6		
						3/20	4		
						0/20	2		
S-2273 Fluorosilicone Rubber	Dow Corning Corporation	6950			0.200	10/20	10	U	U

TABLE IV. PLASTICS, ELASTOMERS, AND ADHESIVES (Continued)

Material	Manufacturer or Source	Test No.	Composition	Remarks	Thickness (inch)	No. Reactions/ No. Tests	Energy Level Kg/m	Batch or Jar Rating	Material Rating
Stycast 2651		2757	Epoxy		0.063	2/2 2/2 2/3 0/20	10 5 3 1	U – – –	U – – –
Teflon (virgin)	E.I. du Pont de Nemours & Company, Incorporated	3402	Polytetrafluoroethylene		0.002	0/20	10	S	S
Teflon (virgin)	E.I. du Pont de Nemours & Company, Incorporated	3403	Polytetrafluoroethylene		0.006	0/20	10	S	S
Tedlar 50 SG20TR	E.I. du Pont de Nemours & Company, Incorporated	4874	Polyvinyl fluoride film	Stainless steel inserts used	0.005	18/20 17/20 18/20	10 8 7	U – –	U – –
Tedlar 100S30	E.I. du Pont de Nemours & Company, Incorporated	4613	Polyvinyl fluoride film	Stainless steel inserts used	0.001	8/20	10	U	U
Tedlar 150A1 30 WH	E.I. du Pont de Nemours & Company, Incorporated	4873	Polyvinyl fluoride film	Stainless steel inserts used. Tested in air	0.002	0/20	10	S	U
Tedlar 150A1 30 WH	E.I. du Pont de Nemours & Company, Incorporated	4797	Polyvinyl fluoride film	Stainless steel inserts used	0.002	3/20	10	U	U
Tedlar 200 AM 30 WH	E.I. du Pont de Nemours & Company, Incorporated	4890	Polyvinyl fluoride film		0.002	4/29 1/20 0/20 0/13	10 9 8 5	U – – –	U – – –
Tedlar 200BG 30 WH	E.I. du Pont de Nemours & Company, Incorporated	4886	Polyvinyl fluoride film		0.002	4/25 1/20 0/20 1/35	10 8 7 5	U – – –	U – – –
Tedlar 200 BP	E.I. du Pont de Nemours & Company, Incorporated	4610	Polyvinyl fluoride film		0.002	3/60	10	U	U
Tedlar 200S 30 WH	E.I. du Pont de Nemours & Company, Incorporated	4611	Polyvinyl fluoride film		0.002	3/20	10	U	U
Tedlar 200S 40	E.I. du Pont de Nemours & Company, Incorporated	4612	Polyvinyl fluoride film		0.002	5/20	10	U	U

TABLE IV. PLASTICS. ELASTOMERS. AND ADHESIVES (Continued)

Material	Manufacturer or Source	Test No.	Composition	Remarks	Thickness (inch)	No. Reactions/ No. Tests	Energy Level Kg/m	Batch or Jar Rating	Material Rating
Tenite II	MSFC	6469	Cellulose acetate butyrate	Stainless steel inserts	0.005	15/20 12/20 6/20 4/20 0/20	10 8 6 4 2	U	U
Tenite II	MSFC	6464	Cellulose acetate butyrate	Stainless steel inserts	0.010	13/20 6/20 8/20 3/20 0/20	10 8 6 4 2	U	U
Tenite II	MSFC	6459	Cellulose acetate butyrate	Stainless steel inserts	0.020	14/20 9/20 7/20 0/20 0/20	10 8 6 4 2	U	U
Tenite II	MSFC	6456	Cellulose acetate butyrate	Stainless steel inserts	0.030	12/20 8/20 11/20 4/20 0/20	10 8 6 4 2	U	U
Tenite II	MSFC	6537	Cellulose acetate butyrate	No stainless steel inserts	0.040	2/20 5/20 4/20 3/20 0/20	10 8 6 4 2	U	U
Tenite II	MSFC	6556	Cellulose acetate butyrate	Stainless steel inserts	0.040	12/20 6/20 4/20 0/20	10 8 6 4	U	U
Tenite II	MSFC	6551	Cellulose acetate butyrate	Stainless steel inserts	0.050	7/20 7/20 3/20 0/20 0/20	10 8 6 4 2	U	U
Tenite II	MSFC	6542	Cellulose acetate butyrate	Stainless steel inserts	0.080	6/20 3/20 3/20 0/20	10 8 6 4	U	U

TABLE IV. PLASTICS, ELASTOMERS, AND ADHESIVES (Continued)

Material	Manufacturer or Source	Test No.	Compositi	Remarks	Thickness (inch)	No. Reactions/ No. Tests	Energy Level Kg/m	Batch or Jar Rating	Material Rating
Titan II Space Suit Material, DuPont HT-7 and Butyl Rubber	Arrowhead Products Company	5659			0.015	20/20 20/20 20/20 20/20 20/20 4/20	10 8 6 4 2 1	U	U
Teflon 403-108	E.I. du Pont de Nemours & Company, Incorporated	5576	Polytetrafluoroethylene coated glass fabric		0.003	0/20 0/20	11.3 10	S –	BT –
Teflon 405-113	E.I. du Pont de Nemours & Company, Incorporated	5582	Polytetrafluoroethylene coated glass fabric		0.005	0/20 0/20	11.3 10	S	BT –
Teflon 406-116	E.I. du Pont de Nemours & Company, Incorporated	5580	Polytetrafluoroethylene coated glass fabric		0.006	0/20 0/20	11.3 10	S –	BT –
Teflon 408-128	E.I. du Pont de Nemours & Company, Incorporated	5584	Polytetrafluoroethylene coated glass fabric		0.008	0/20 0/20	11.3 10	S –	BT –
Teflon 410-112	E.I. du Pont de Nemours & Company, Incorporated	5577	Polytetrafluoroethylene coated glass fabric		0.010	0/20	11.3	S	BT
Teflon 414-141	E.I. du Pont de Nemours & Company, Incorporated	5578	Polytetrafluoroethylene coated glass fabric		0.014	0/20	11.3	S	BT
Teflon TFE, Fiber 400-60-0 (Merge 10419)	E.I. du Pont de Nemours & Company, Incorporated	6829	Fluorocarbon			4/20 2/20	10 10	U	U
Teflon TFE, Fiber 1350-180-0 (Merge 10458)	E.I. du Pont de Nemours & Company, Incorporated	6831	Fluorocarbon			0/20	10	S	BT
Teflon TFE Hose No. 1		7613			0.070	0/20	10	S	BT
Teflon TFE Hose No. 1 14B		7295		Washed with F-33 Stainless steel inserts	0.082	0/20	10	S	BT
Teflon TFE Hose No. 2		7614			0.070	0/20	10	S	BT
Teflon TFE Hose No. 2 14B		7296		Washed in F-33 Stainless steel inserts	0.072	0/20	10	S	BT
Teflon TFE Hose No. 3		7297		Washed in F-33 Stainless steel inserts	0.060	0/20	10	S	BT

TABLE IV. PLASTICS, ELASTOMERS, AND ADHESIVES (Continued)

Material	Manufacturer or Source	Test No.	Composition	Remarks	Thickness (inch)	No. Reactions/ No. Tests	Energy Level Kg/m	Batch or Jar Rating	Material Rating
Teflon TFE Hose No. 4		7298		Washed in F-33 Stainless steel inserts	0.060	0/20	10	S	BT
GRGA-0213	Non-Metallic Materials Branch	10256			0.015	20/20	10	U	U
Teflon TFE Sheet	Chemplast, Incorporated	8799		Virgin, unfilled, undyed	0.002	0/20	10	S	BT
Teflon TFE Sewing Thread DXHE MT400	The Mason Silk Company	5992				14/20	10	U	U
Teflon-TFE Coated 6061-T6 Aluminum Coating: DuPont 850-311 Catalyst: VM-7799	Trans-Sonics	6455	Teflon	Stainless steel inserts	0.007	0/20	10	S	S
5% Teflon TFE Dispersion	Dow Corning Corporation	5848				0/20	10	S	BT
Teflon TFE Coated Glass Cloth No. 410-128	E.I. du Pont de Nemours & Company, Incorporated	5484			0.010	2/20	10	U	BT
Teflon TFE Coated Glass Cloth No. 405-112	E.I. du Pont de Nemours & Company, Incorporated	5354			0.005	1/20 0/20	11.3 10	– S	BT BT
Teflon TFE Coated Glass Fabric No. 410-112	E.I. du Pont de Nemours & Company, Incorporated	5485			0.010	0/20	10	S	BT
Teflon TFE Coated Glass Fabric No. 414-141	E.I. du Pont de Nemours & Company, Incorporated	5486			0.014	0/20	10	S	BT
Teflon Lacing Tape Temp-Lace Style 256	Gudebrad Brothers Silk Company	4794				0/20	10	S	BT
Teflon Sleeve from Adel Clamp		3389		Virgin, unfilled, undyed	0.032	0/20	10	S	BT
Teflon XA102A522	Goodyear Corporation	3492	Polytetrafluoroethylene	Spray film	0.006	2/20 1/2 0/20	10 9 8	U – –	BT – –
Teflon XA102A522	Goodyear Corporation	3491	Polytetrafluoroethylene	Spray film	0.015	0/20	10	S	BT
Teflon FEP (virgin)	E.I. du Pont de Nemours & Company, Incorporated	1247	Fluorinated ethylene-propylene polymer			0/20	10	S	S

TABLE IV. PLASTICS, ELASTOMERS, AND ADHESIVES (Continued)

Material	Manufacturer or Source	Test No.	Composition	Remarks	Thickness (inch)	No. Reactions/ No. Tests	Energy Level Kg/m	Batch or Jar Rating	Material Rating
Teflon, TFE Virgin	E.I. du Pont de Nemours & Company, Incorporated	3489	Polytetrafluoroethylene		0.032	0/20	10	S	S
Teflon, TFE White Sheet Stock	E.I. du Pont de Nemours & Company, Incorporated	5128	Polytetrafluoroethylene		0.063	0/40	10	S	S
Teflon, TFE White Hose Lining	E.I. du Pont de Nemours & Company, Incorporated	95	Polytetrafluoroethylene			0/20	10	S	BT
Teflon, Red Hose Lining	E.I. du Pont de Nemours & Company, Incorporated	96	Polytetrafluoroethylene	Pigmentation affects test results		0-2/20	10	–	BT
Teflon Tube (Thermofit TFE)	Rayclad Tubes Incorporated	1830	Polytetrafluoroethylene		0.016	0/20	10	S	BT
Teflon FEP Film with Teflon TFE Felt	E.I. du Pont de Nemours & Company, Incorporated	4190	Polytetrafluoroethylene	0.005 in. film between two pieces 0.125 in. felt	0.255	0/40	10	S	BT
Teflon FEP Type 544	E.I. du Pont de Nemours & Company, Incorporated	3527	Polytetrafluoroethylene	not filled, not dyed	0.001	0/20	10	S	S
Teflon FEP Virgin	E.I. du Pont de Nemours & Company, Incorporated	3366	Polytetrafluoroethylene	not filled, not dyed	0.01	0/20	10	S	S
Teflon FEP Virgin	E.I. du Pont de Nemours & Company, Incorporated	3367	Polytetrafluoroethylene	not filled, not dyed	0.021	0/20	10	S	S
Teflon FEP Virgin	E.I. du Pont de Nemours & Company, Incorporated	3365	Polytetrafluoroethylene	not filled, not dyed	0.005	0/20	10	S	S
Teflon FEP and Aluminum	E.I. du Pont de Nemours & Company, Incorporated	4188	Aluminum and Polytetrafluoroethylene	FEP-2 mils, aluminum 2 mils, FEP-2 mils	0.006	0/40	10	S	BT
Teflon 30 TFE	E.I. du Pont de Nemours & Company, Incorporated	3516	Polytetrafluoroethylene	Two batches tested		0/20	10	S	BT
Teflon 856-200	E.I. du Pont de Nemours & Company, Incorporated	3641	Polytetrafluoroethylene		0.006	0/20	10	S	S
Teflon TFE Dupont Enamel 852-202	E.I. du Pont de Nemours & Company, Incorporated	3504	Polytetrafluoroethylene		0.001	0/20	10	S	S
Teflon, Dupont Clear Lacquer No. 852-202 over Dupont Primer No. 850-204	E.I. du Pont de Nemours & Company, Incorporated	1597	Polytetrafluoroethylene	321 stainless inserts used		0/20	10	S	S

TABLE IV. PLASTICS, ELASTOMERS, AND ADHESIVES (Continued)

Material	Manufacturer or Source	Test No.	Composition	Remarks	Thickness (inch)	No. Reactions/ No. Tests	Energy Level Kg/m	Batch or Jar Rating	Material Rating
Teflon, Dupont Primer No. 850-204	E.I. du Pont de Nemours & Company, Incorporated	1596	Polytetrafluoroethylene	321 stainless inserts used		0/20	10	S	S
Teflon, Dupont Green Primer No. 850-204 and Clear Lacquer No. 850-202	U.S. Aircraft Products Co.	1777	Polytetrafluoroethylene	On 321 stainless steel inserts		0/20	10	S	S
Teflon Covering from Cable		3802	Polytetrafluoroethylene		0.020	0/20	10	S	BT
Teflon Coated Flat Conductor Shielded Type A NASA-POH-41286	Methode Cable Company	4287	Teflon and copper	Organic adhesive	0.028	5/40	10	U	U
Teflon Coating No. 852-201 over Primer No. 850-201	E.I. du Pont de Nemours & Company, Incorporated	1308	Polytetrafluoroethylene	Applied to stainless steel discs		0/20	10	S	S
Teflon Coating No. 251-214	E.I. du Pont de Nemours & Company, Incorporated	1282	Polytetrafluoroethylene	Applied to stainless steel discs		0/20	10	S	S
Teflon O-Ring	Various	1927	Polytetrafluoroethylene			0/20	10	S	BT
Teflon Helix	Connecticut Hard Rubber Co.	4508	Teflon with bonding agent		0.025	18/20 2/10 1/2 0/20	10 3 2 1	U — — —	U — — —
Teflon-Resin Spray 852-204	E.I. du Pont de Nemours & Company, Incorporated	4473		Sprayed on stainless steel inserts	0.003	0/20	10	S	U
Telcon	Alyin Products Incorporated	3850	Fluorocarbon	Spray film		0/20	10	S	BT
Thermo-Dip		5063		Stainless steel inserts dipped in melted thermoplastic		12/20	10	U	U
Thermoplaz Formula 1500	Sargent Engineering Corp.	3775			0.050	5/5 5/5 5/5 5/5 5/5	10 5 3 2 1	U — — — —	U — — — —
Thermoplaz Formula 1501	Sargent Engineering Corp.	3778			0.050	0/40	10	S	BT
Thermo-Resist 69		3875			0.063	11/20	10	U	U
Temporell No. 741	Orell Incorporated	1656				2/2 2/2 2/2 4/14	10 5 2 1	U — — —	U — — —
Temporell No. 740	Orell Incorporated	1657				1/1 1/1 7/7	10 2 1	U — —	U — —

TABLE IV. PLASTICS, ELASTOMERS, AND ADHESIVES (Continued)

Material	Manufacturer or Source	Test No.	Composition	Remarks	Thickness (inch)	No. Reactions/ No. Tests	Energy Level Kg/m	Batch or Jar Rating	Material Rating
Temp-R-Tape I	Connecticut Hard Rubber Co.	3643	Polytetrafluoroethylene with silicone polymer adhesive			3/20 2/20 3/20 0/20	10 5 4 1	U – – –	U – – –
Union Carbide 40-S Dimethylsilicone	Union Carbide Chemical Corporation	4804			0.063	2/20	10	U	U
Vinylloyd No. 5909	Vinylloyd Company	143	Chlorofluorocarbon		0.032	0/20	10	S	BT
Viton A on Teflon 86007	E.I. du Pont de Nemours & Company, Incorporated	914			0.020	2/7 0/15	10 5	U –	BT –
Velcro Hi Grade	Velcro Corporation	9287	Stainless steel backs, Eligilog hooks, and Inconel pile		0.063	0/20	10	S	BT
Velcro Hi Meg	Velcro Corporation	9288	Hook, pile, and backing Nylon		0.063	20/20	10	U	U
Vespel Discs (Polymer SP-1)	E.I. du Pont de Nemours & Company, Incorporated	8712	Polyimide	Batch SP-1-45	0.050	6/20	10	U	U
Vespel Discs (Polymer SP-1)	E.I. du Pont de Nemours & Company, Incorporated	9784	Polyimide	Batch 10246-29-2	0.050	1/60	10	S	U
Vespel Discs (Polymer SP-1)	E.I. du Pont de Nemours & Company, Incorporated	9221	Polyimide	Batch 10246-11-2	0.050	4/20	10	U	U
Vespel Discs (Polymer SP-1)	E.I. du Pont de Nemours & Company, Incorporated	9904	Polyimide	Batch 1089-0-79-2	0.050	0/20	10	S	U
Vespel Discs (Polymer SP-1)	E.I. du Pont de Nemours & Company, Incorporated	9966	Polyimide	Batch 10890-197-1	0.050	3/20	10	U	U
Vespel Discs (Polymer SP-3)	E.I. du Pont de Nemours & Company, Incorporated	9223	Polyimide	Batch 10077-138-3	0.050	0/20	10	S	BT
Vespel Discs (Polymer SP-21)	E.I. du Pont de Nemours & Company, Incorporated	9905	Polyimide filled with 15 percent graphite	Batch 10890-115-2	0.050	0/20	10	S	BT
Vespel Discs (Polymer SP-21)	E.I. du Pont de Nemours & Company, Incorporated	8713	Polyimide filled with 15 percent graphite	Batch P-530	0.050	0/20	10	S	BT
Vespel Discs (Polymer SP-21)	E.I. du Pont de Nemours & Company, Incorporated	10067	Polyimide filled with 15 percent graphite	Batch SRB-184	0.050	0/20	10	S	BT

TABLE IV. PLASTICS, ELASTOMERS, AND ADHESIVES (Continued)

Material	Manufacturer or Source	Test No.	Composition	Remarks	Thickness (inch)	No. Reactions/ No. Tests	Energy Level Kg/m	Batch or Jar Rating	Material Rating
Vespel Discs (Polymer SP-21)	E.I. du Pont de Nemours & Company, Incorporated	10402	Polyimide filled with 15 percent graphite	Batch 11052-37-2-M-64	0.050	0/20	10	S	BT
Vespel Discs (Polymer SP-21)	E.I. du Pont de Nemours & Company, Incorporated	10404	Polyimide filled with 10 percent graphite	Batch 1122-78	0.050	0/20	10	S	BT
Velostat, Conductive Polyolefin	Custom Materials, Incorporated	6011			0.005	8/20 7/20 3/20 0/20	10 8 6 4	U	U
Vin-LOX Sealant	Vin-LOX Corporation	7289	Vinyl polymer emulsion	Cured 10 days at room temperature	0.050	20/20 20/20 20/20 17/20 6/20 2/20	10 7.62 5.54 3.46 1.39 0.70	U	U
Vithane No. 1		6615			0.025	18/20	10	U	U
Vithane No. 2 (Viton Coated)		6614			0.25	19/20	10	U	U
Vinyl Covered Nylon		616				2/8 1/10	10 5	U –	U –
Vinyl Tubing		674				2/8 3/5	10 5	U –	U –
Vynakote	Spectra-Strip Wire and Cable Corporation	976				2/6 4/14	10 5	U –	U –
XR 5033	Minnesota Mining and Manufacturing Company	2748	Epoxy		0.063	2/25 0/35	10 5	U –	U –

TABLE IV. PLASTICS, ELASTOMERS, AND ADHESIVES (Continued)

Material	Manufacturer or Source	Test No.	Composition	Remarks	Thickness (inch)	No. Reactions/ No. Tests	Energy Level Kg/m	Batch or Jar Rating	Material Rating
Vimasco WC-1		5404			0.050	19/20	10	U	U
Viton A-80-001	E.I. du Pont de Nemours & Company, Incorporated	4603		Stainless steel inserts used	0.047	0/40	10	S	BT
Viton A Plus Teflon No. 86007	E.I. du Pont de Nemours & Company, Incorporated	4606		Stainless steel inserts used	0.025	0/40	10	S	BT
Viton A Hose	E.I. du Pont de Nemours & Company, Incorporated	4798			0.063	3/20	10	U	BT
Viton Sponge	Connecticut Hard Rubber Co.	4806			0.250	9/20	10	U	U
Viton A		5946			0.125	0/20	10	S	BT
Viton A, A-34470	R-P&VE-M	6080			0.065	0/20	10	S	BT
Viton A O-Ring Z-100, 19535-1		6075		Stainless steel inserts	0.104	0/20	10	S	BT
21625-1		6074		Stainless steel inserts	0.104	0/20	10	S	BT
Viton A, MIL-R-25897	Aeroquip Corporation	6520		Stainless steel inserts	0.100	0/20	10	S	BT
		6521		Stainless steel inserts	0.100	0/20	10	S	BT
Viton Compound V702-0, Batch 12304	I. B. Moore Company	6956			0.047	2/20	10	U	BT
Viton A Compound 17107A	Precision Rubber Company	7309			0.144	0/20	10	S	BT
Viton A O-Ring HS-8-513-16		7396		Fibro Seal Batch SR 277-70		0/20	10	S	BT
Viton A O-Ring	B.H. Hadley, Inc.	6333		Stainless steel inserts Washed with F-33		0/20	10	S	BT

TABLE IV. PLASTICS, ELASTOMERS, AND ADHESIVES (Continued)

Material	Manufacturer or Source	Test No.	Composition	Remarks	Thickness (inch)	No. Reactions/ No. Tests	Energy Level Kg/m	Batch or Jar Rating	Material Rating
Viton A O-Ring									
Batch 01284	B.H. Hadley, Inc.	7023		Same as above		0/20	10	S	BT
Batch 01382		7283		Same as above		2/20	10	U	BT
Batch 01382		7021		Stainless steel inserts As received		6/20	10	U	BT
Batch 02656		7020		Same as above		9/20	10	U	BT
Batch 03919		7019		Same as above		3/20	10	U	BT
Batch 04204		7025		Stainless steel inserts Washed in F-33		0/20	10	S	BT
Batch 05549		7022		Same as above		0/20	10	S	BT
Batch 05764		7024		Same as above		0/20	10	S	BT
Batch 05828		7018		Same as above		7/20	10	U	BT
Batch P HS-8513-224		7360		As Received		2/20	10	U	BT
Viton A O-Ring, Batch No. 01911, MIL-R-25897, NAS 1593-11	Parker-Hannifin Corp.	6768		Stainless steel inserts		3/20	10	U	BT
Viton A O-Ring, Batch No. 01911, MIL-R-25897, NAS 1593-13	Parker-Hannifin Corp.	6767		Stainless steel inserts		1/20	10	I	BT
Viton A O-Ring, Batch No. 01911, MIL-R-25897, NAS 1593-16	Parker-Hannifin Corp.	6766		Stainless steel inserts		2/20	10	U	BT
Viton A O-Ring, Batch No. 02404, Part No. SP133-7	Parker Aricraft	6076			0.063	2/27 2/20	10 8	U	BT
Viton A O-Ring, Batch No. 02460, Part No. SP-133-3	Parker Aircraft	6078	DuPont 77-545			2/20 3/20	10 8	U	BT
Viton A O-Ring, Batch No. 03447, NAS 1593 2-16	Parker-Hannifin Corp.	6933		Stainless steel inserts	0.066	5/20	10	U	BT
Viton A O-Ring, Batch No. 05018, NAS 1593 2-12	Parker-Hannifin Corp.	6935		Stainless steel inserts	0.066	5/20	10	U	BT
Viton A O-Ring, Batch No. 05427, NAS 1593 2-13	Parker-Hannifin Corp.	6934		Stainless steel inserts	0.068	2/20	10	U	BT
Viton A O-Ring, Batch No. 05483, NAS 1593 2-11	Parker-Hannifin Corp.	6936		Stainless steel inserts	0.064	9/20	10	U	BT

TABLE IV. PLASTICS, ELASTOMERS, AND ADHESIVES (Continued)

Material	Manufacturer or Source	Test No.	Composition	Remarks	Thickness (inch)	No. Reactions/ No. Tests	Energy Level Kg/m	Batch or Jar Rating	Material Rating
Viton A O-Ring, Compound 920-70 OC, Batch 23632	Plastic & Rubber Products Company	6388				2/20	10	U	BT
Viton A O-Ring, Compound 920-90 OC, Batch 24884	Plastic & Rubber Products Company	6386				2/22	10	U	BT
Viton O-Rings, Size 2-34	Parker Seal Company	9953	Compound 77-545	Batch 02107Z		0-1/20	10	–	BT
Viton O-Rings, Size 2-38	Parker Seal Company	9979	Compound 77-545	Batch 02095Z		18/300	10	U	BT
Viton O-Rings, Size 2-115	Parker Seal Company	10282	Compound 77-545	Batch 02181		17/40	10	U	BT
Viton O-Rings, Size 2-155	Parker Seal Company	8260	Compound 77-545	Batch 06780		2/20	10	U	BT
Viton O-Rings, Size 2-466	Parker Seal Company	8261	Compound 77-545	Batch 06739		0/20	10	S	BT
Viton O-Rings, Size 2-160	Parker Seal Company	9942	Compound 77-545	Batch 021072		2/20	10	U	BT
Viton O-Rings, Size 2-161	Parker Seal Company	9956	Compound 77-545	Batch 2142H		0/20	10	S	BT
Viton O-Rings	Plastics and Rubber Products Company	10232		Fives sizes evaluated		2-4/20	10	U	BT
Viton O-Rings, Size 2-34	Parker Seal Company	9953	Compound 77-545	Batch 02107Z		0-1/20	10	–	BT
Viton O-Rings, Size 2-38	Parker Seal Company	9979	Compound 77-545	Batch 02095Z		18/300	10	U	BT
Viton O-Rings, Size 2-115	Parker Seal Company	10282	Compound 77-545	Batch 02181		17/40	10	U	BT
Viton O-Rings, Size 2-155	Parker Seal Company	8260	Compound 77-545	Batch 06780		2/20	10	U	BT
Viton O-Rings, Size 2-466	Parker Seal Company	8261	Compound 77-545	Batch 06739		0/20	10	S	BT
Viton O-Rings, Size 2-160	Parker Seal Company	9942	Compound 77-545	Batch 021072		2/20	10	U	BT
Viton O-Rings, Size 2-161	Parker Seal Company	9956	Compound 77-545	Batch 2142H		0/20	10	S	BT
Viton O-Rings	Plastics and Rubber Products Company	10232		Five sizes evaluated		2-4/20	10	U	BT
Viton O-Rings, Size 013	Precision Rubber Products Company	8814	Compound 17107			0/20	10	S	BT

TABLE IV. PLASTICS, ELASTOMERS, AND ADHESIVES (Continued)

Material	Manufacturer or Source	Test No.	Composition	Remarks	Thickness (inch)	No. Reactions/ No. Tests	Energy Level Kg/m	Batch or Jar Rating	Material Rating
Viton O-Rings, Size 121	Precision Rubber Products Company	8815	Compound 17107			0/20	10	S	BT
Viton O-Rings, Size 222	Precision Rubber Products Company	8816	Compound 17107			3/20	10	U	BT
Viton O-Rings, Size 228	Precision Rubber Products Company	8823	Compound 17107			4/40	10	U	BT
Viton O-Rings, Size 010	Precision Rubber Products Company	9971	Compound 19009	Cured 3rd Qtr 1967		0/40	10	S	BT
Viton O-Rings, Size 014	Precision Rubber Products Company	9790	Compound 19009	Cured 3rd Qtr 1967		0/40	10	S	BT
Viton O-Rings, Size 006	Precision Rubber Products Company	9914	Compound 1900-X44	Batch 6L and 9L		7/80	10	U	BT
Viton O-Rings, Size 009	Precision Rubber Products Company	9931	Compound 1900-X44	Lot C-3019		0/20	10	S	BT
Viton O-Rings, Size 010	Precision Rubber Products Company	9999	Compound 1900-X44	Batch 9L		4/20	10	U	BT
Viton O-Rings, Size 010	Precision Rubber Products Company	9932	Compound 1900-X44	Lot C-3033		0/20	10	S	BT
Viton O-Rings, Size 013	Precision Rubber Products Company	9945	Compound 1900-X44	Batch 9L		2/20	10	U	BT
Viton O-Rings, Size 016	Precision Rubber Products Company	9929	Compound 1900-X44	Batch 8L		0/20	10	S	BT
Viton O-Rings, Size G17	Precision Rubber Products Company	9927	Compound 1900-X44	Cured 2nd Qtr 1967		0/20	10	S	BT
Viton O-Rings, Size 018	Precision Rubber Products Company	9925	Compound 1900-X44	Cured 2nd Qtr 1967		2/20	10	U	BT
Viton O-Rings, Size 024	Precision Rubber Products Company	9922	Compound 1900-X44	Batch 6L		0/40	10	S	BT
Viton O-Rings, Size 027	Precision Rubber Products Company	9937	Compound 1900-X44	Batch 9L		0/40	10	S	BT

TABLE IV. PLASTICS, ELASTOMERS, AND ADHESIVES (Continued)

Material	Manufacturer or Source	Test No.	Composition	Remarks	Thickness (inch)	No. Reactions/ No. Tests	Energy Level Kg/m	Batch or Jar Rating	Material Rating
Viton O-Rings, Size 031	Precision Rubber Products Company	9938	Compound 1900-X44	Lot C-3024		2/20	10	U	BT
Viton O-Rings, Size 032	Precision Rubber Products Company	10002	Compound 1900-X44	Batch 9L		0/20	10	S	BT
Viton O-Rings, Size 032	Precision Rubber Products Company	9915	Compound 1900-X44	Batch 6L, 1 strip		2/20	10	U	BT
Viton O-Rings, Size 032	Precision Rubber Products Company	9915	Compound 1900-X44	Batch 6L, 7 strips		3/20	10	U	BT
Viton O-Rings, Size 034	Precision Rubber Products Company	9920	Compound 1900-X44	Batch 6L, 7 strips		0/20	10	S	BT
Viton O-Rings, Size 034	Precision Rubber Products Company	9921	Compound 1900-X44	Batch 6L, 1 strip		0/20	10	S	BT
Viton O-Rings, Size [illegible]	Precision Rubber Products Company	10005	Compound 1900-X44	Batch 9L		2/20	10	U	BT
Viton O-Rings, Size 038	Precision Rubber Products Company	9441	Compound 1900-X44	Lot C-3027		0/20	10	S	BT
Viton O-Rings, Size 161	Precision Rubber Products Company	9954	Compound 1900-X44	Batch 6L		3/20	10	U	BT
Viton Strips	Precision Rubber Products Company	10014	Compound 17107	Batch 121464	0.070	0/20	10	S	BT
Viton Discs	Precision Rubber Products Company	10015	Compound 17107	Batch 121464	0.070	0/20	10	S	BT
Viton Sheet Material Discs	Precision Rubber Products Company	10231	Compound 1900-X44	Batch 11L	0.070	0/20	10	S	BT
Viton Sheet Material Strip	Precision Rubber Products Company	10230	Compound 1900-X44	Batch 11L	0.070	0/20	10	S	BT
Viton A Discs (New)	Precision Rubber Products Company	7945	Compound 1900-X44		0.070	2/20	10	U	BT

TABLE IV. PLASTICS, ELASTOMERS, AND ADHESIVES (Continued)

Material	Manufacturer or Source	Test No.	Composition	Remarks	Thickness (inch)	No. Reactions/ No. Tests	Energy Level Kg/m	Batch or Jar Rating	Material Rating
Viton A Discs (Old)	Precision Rubber Products Company	7949	Compound 1900-X44		0.070	5/20	10	U	BT
Viton A Discs	Precision Rubber Products Company	7954	Compound 1900-X44		0.070	5/20	10	U	BT
Viton A O-Rings, A-18	Stillman Rubber Company	7916	Compound SR-277-7	Batch 61400		7/20	10	U	BT
Viton A O-Ring	Precision Rubber Company	7284				0/20	10	S	BT
		7285				0/20	10	S	BT
		7286				0/20	10	S	BT
		7287				0/20	10	S	BT
Viton A O-Ring Compound 17107A	Precision Rubber Company								
Batch 011165		7016			0.103	0/20	10	S	BT
Batch 020865		7163			0.070	0/20	10	S	BT
Batch 020865		7162			0.070	0/20	10	S	BT
Batch 040565.3		7245		Washed in F-33	0.047	0/20	10	S	BT
Batch 121464		6960			0.103	0/20	10	S	BT
Batch 121464		6959			0.139	0/20	10	S	BT
Batch 121464		6958			0.139	0/20	10	S	BT
Batch 121464		7017			0.139	0/20	10	S	BT
Viton O-Rings, Size 013	Precision Rubber Products Company	8814	Compound 17107			0/20	10	S	BT
Viton O-Rings, Size 121	Precision Rubber Products Company	8815	Compound 17107			0/20	10	S	BT
Viton O-Rings, Size 222	Precision Rubber Products Company	8816	Compound 17107			3/20	10	U	BT
Viton O-Rings, Size 228	Precision Rubber Products Company	8823	Compound 17107			4/40	10	U	BT
Viton O-Rings, Size 010	Precision Rubber Products Company	9971	Compound 19009	Cured 3rd Qtr 1967		0/40	10	S	BT
Viton O-Rings, Size 014	Precision Rubber Products Company	9790	Compound 19009	Cured 3rd Qtr 1967		0/40	10	S	BT

TABLE IV. PLASTICS, ELASTOMERS, AND ADHESIVES (Continued)

Material	Manufacturer or Source	Test No.	Composition	Remarks	Thickness (inch)	No. Reactions/ No. Tests	Energy Level Kg/m	Batch or Jar Rating	Material Rating
Viton O-Rings, Size 006	Precision Rubber Products Company	9914	Compound 1900-X44	Batch 6L and 9L		7/80	10	U	BT
Viton O-Rings, Size 009	Precision Rubber Products Company	9931	Compound 1900-X44	Lot C-3019		0/20	10	S	BT
Viton O-Rings, Size 010	Precision Rubber Products Company	9999	Compound 1900-X44	Batch 9L		4/20	10	U	BT
Viton O-Rings, Size 010	Precision Rubber Products Company	9932	Compound 1900-X44	Lot C-3033		0/20	10	S	BT
Viton A on Glass Fibers 85001	E.I. du Pont de Nemours & Company, Incorporated	912			0.011	2/2 2/5 2/3	10 5 2	U – –	BT – –
Viton A on Dacron Fabric	E.I. du Pont de Nemours & Company, Incorporated	915				2/2 2/4 2/11	10 5 1	U – –	U – –
Viton A Elastomer	E.I. du Pont de Nemours & Company, Incorporated		Copolymer of vinylidene fluoride and hexa-fluoropropylene	Sensitivity varies from batch to batch		0-4/20	10	–	BT
X-70	Hadbar Incorporated	5424	Fluorosilicone rubber		0.125	2/20	10	U	U
X-70	Hadbar Incorporated	5425	Fluorosilicone rubber		0.100	0/20	10	I	U
X-70	Hadbar Incorporated	5426	Fluorosilicone rubber		0.033	19/20	10	U	U
X-70	Hadbar Incorporated	5352	Fluorosilicone rubber	Teflon coated	0.085	2/20 1/20	10 8	U –	U –
X-72	Hadbar Incorporated	5423	Fluorosilicone rubber		0.035	19/20	10	U	U
X-72	Hadbar Incorporated	5348	Fluorosilicone rubber		0.070	2/20 2/20	10 8	U –	U –
X-72	Hadbar Incorporated	5421	Fluorosilicone rubber		0.125	2/40	10	U	U
X-73	Hadbar Incorporated	5346	Fluorosilicone rubber		0.064	1/20 1/20	10 8	U –	U –

TABLE IV. PLASTICS, ELASTOMERS, AND ADHESIVES (Concluded)

Material	Manufacturer or Source	Test No.	Composition	Remarks	Thickness (inch)	No. Reactions/ No. Tests	Energy Level Kg/m	Batch or Jar Rating	Material Rating
X-73	Hadbar Incorporated	5420	Fluorosilicone rubber		0.030	20/20	10	U	U
X-73	Hadbar Incorporated	5419	Fluorosilicone rubber		0.125–0.130	2/20	10	U	U
Compound 1200-140	Hadbar Incorporated	5350	Fluorosilicone rubber	Teflon coated	0.078	4/40 2/20	10 8	U –	U –
Zero Perm		5487		Stainless steel inserts used	0.003	5/20 2/20 0/20	10 8 6	U – –	U – –
XR5038	ZMCO	2748	Epoxy		0.003	2/25	10	U	U

TABLE V. GASKETS AND PACKINGS

Material	Manufacturer or Source	Test No.	Composition	Remarks	Thickness (inch)	No. Reactions/ No. Tests	Energy Level Kg/m	Batch or Jar Rating	Material Rating
Accopac No. 812	Armstrong Cork Company	1419	Teflon and asbestos		0.063	0/20	10	S	BT
Accopac No. 816	Armstrong Cork Company	1421	Teflon and asbestos	Two batches tested	0.063	0/20	10	S	BT
Allpax 500 Superheat Sheet (as received)	Allpax Company		Styrene-butadiene copolymer with asbestos fiber	Highly variable. Average range of test results shown for each thickness	0.250 0.125 0.094 0.063 0.016	0-2/20 0-3/20 0-5/20 3-10/20 5-15/20	10 10 10 10 10	– – – – –	U U U U U
Allpax 500 Superheat Sheet (impregnated with Fluorolube T-80)	Allpax Company		Styrene-butadiene copolymer with asbestos fiber		0.250 0.125 0.063 0.031	0/20 0/20 0/20 0-2/20	10 10 10 10	S S S –	U U U U
Allpax 500	Allpax Company	1567	Styrene-butadiene copolymer with asbestos fiber	Not Fluorolubed	0.250	30/120	10	U	U
Allpax 500	Allpax Company		Styrene-butadiene copolymer with asbestos fiber	Fluorolubed per MS 750. Highly variable. Test results show range of results for each thickness	0.250 0.125 0.094 0.063 0.031 0.016	0-18/20 0-2/20 0-1/20 0-8/20 0-11/20 0-4/20	10 10 10 10 10 10	– – – – – –	BT BT BT BT BT BT
Allpax 500	Allpax Company	1572	Stryene-butadiene copolymer with asbestos fiber	AR-1F treated	0.250	3/40	10	U	U
Allpax 500	Allpax Company	1899		Aging test. Fluorolubed 3/9/60. Tested 3/23/61	0.063	0/20	10	S	BT
Allpax 500	Allpax Company	2004		Aging test. Fluorolubed 3/9/60. Tested 4/19/61	0.063	0/20	10	S	BT
Allpax 500	Allpax Company	3560		Aging test. Fluorolubed 3/5/60. Tested 6/13/62	0.063	0/20	10	S	BT
Allpax 500 Gasket	Chemistry Branch	3561	Fluorolube treated per MS-750 (3/26/60)		0.063	0/20	10	S	BT

TABLE V. GASKETS AND PACKINGS (Continued)

Material	Manufacturer or Source	Test No.	Composition	Remarks	Thickness (inch)	No. Reactions/ No. Tests	Energy Level Kg/m	Batch or Jar Rating	Material Rating
Ankorite 425	Anchor Packing Company	1345	Asbestos-rubber composite		0.063	0/20	10	S	BT
Annin Valve Company Valve Packing	Annin Valve Company	4489	25% fiberglass and 75% Teflon		0.050	0/20	10	S	BT
Armalon 97-001	E.I. du Pont de Nemours & Company, Incorporated	3642	0.005 in. TFE fiber, 0.005 in. FEP film		0.010	0/20	10	S	BT
Armalon PDX 7550		3517	Teflon TFE felt and FEP film		0.125	0/20	10	S	BT
Armalon No. 410-128	E.I. du Pont de Nemours & Company, Incorporated	1689	Teflon and glass		0.016	0/20	10	S	BT
Armalon Teflon Glass	E.I. du Pont de Nemours & Company, Incorporated	1674	Teflon and glass		0.016	2/2 2/5 1/13	10 5 3	U – –	U – –
Armalon	E.I. du Pont de Nemours & Company, Incorporated	762	Fluorocarbon felt	Bleached sheet	0.063	0/20	10	S	BT
Armalon	E.I. du Pont de Nemours & Company, Incorporated	1070	Fluorocarbon felt	Unbleached sheet	0.063	2/4	10	U	U
Asbestos Textile Style 3603 Sheet	Asbestos Textile Company	1343			0.063	0/20	10	S	BT
Asbestos Textile Style 3604 Sheet	Asbestos Textile Company	1344			0.063	2/20	10	U	U
Asbestos Textile Style 3605 Sheet	Asbestos Textile Company	1342			0.063	2/6 0/14	10 5	U –	U –
Asbestos from Flexitallic Gasket		2220	Asbestos	Stainless steel inserts used		0/20	10	S	BT
Asbestos Sheeting with GRS Binder	Allpax Company	2151	Asbestos and synthetic rubber	Samples from Test Division	0.063	2/120	10	–	U
Asbestos Sheeting with GRS Binder	Allpax Company	2157	Asbestos and synthetic rubber	Samples from Test Division	0.063	0/60	10	S	U
Avronite 5B7 Sheet	Kalendex Corporation	1008	Fiber coated with Buna-N		0.032	2/4 2/3 0/13	10 5 3	U – –	U – –

TABLE V. GASKETS AND PACKINGS (Continued)

Material	Manufacturer or Source	Test No.	Composition	Remarks	Thickness (inch)	No. Reactions/ No. Tests	Energy Level Kg/m	Batch or Jar Rating	Material Rating
Avronite Sheet 5B10	Kalendex Corporation	993	Fiber core coated with Buna-N		0.093	2/3 2/2 2/4	10 5 3	U – –	U – –
Avronite Sheet 5B20	Kalendex Corporation	922	Fiber core coated with Buna-N		0.063	2/2 2/3 0/15	10 5 3	U – –	U – –
Avronite Sheet 10B20	Kalendex Corporation	991	Fiber core coated with Buna-N		0.063	2/2 2/2 2/3	10 5 3	U – –	U – –
Carbon Seal		6648		Stainless steel cups	0.134	0/20	10	S	BT
Carbon Seal from Bingham LOX Pump Seal, MOD-CADS		5931		No stainless steel inserts	0.062	0/20	10	S	BT
Carbon Seal from Bingham LOX Seal, MOD-CADS		5932		Stainless steel inserts	0.062	0/20	10	S	BT
Carbon Seal from Bingham LOX Seal, MOD-CADS		5930		Fragments from previous impact tests		10/20	10	U	BT
Carbon Seal from Bingham LOX Seal, MOD-CADS		5929		Ground to powder in a Wiley Mill		5/20	10	U	BT
Chesterton Packing No. 324	A.W. Chesterton Company	2911		Very violent reaction	0.250	1/1 1/1	10 5	U –	U –
Convair Gasket, Green	Convair Division General Dynamics Incorporated	1285	Metal gasket with green coating		0.063	2/2 0/18	10 5	U –	U –
Convair Gasket, Brown	Convair Division General Dynamics Incorporated	1280	Metal gasket with brown coating		0.062	0/20	10	S	BT
Extruded Cryal "S"	Johns-Manville Company	4517	Filled Teflon		0.063	0/20	10	S	BT
Extruded Cryal "M"	Johns-Manville Company	4518	Filled Teflon		0.063	0/20	10	S	BT
Durabla Gasket Material	Durabla Manufacturing Company	2491	Compressed asbestos and fluorosilicone rubber	Sensitivity varies from batch to batch	0.063	3/40 0/20	10 2	U –	BT BT

TABLE V. GASKETS AND PACKINGS (Continued)

Material	Manufacturer or Source	Test No.	Composition	Remarks	Thickness (inch)	No. Reactions/ No. Tests	Energy Level Kg/m	Batch or Jar Rating	Material Rating
Durabla Gasket Material	Durabla Manufacturing Company	3506	Compressed asbestos and fluorosilicone rubber	Sensitivity varies from batch to batch	0.032	2/8 2/19 0/20	10 5 3	– – –	BT – –
Duroid Sheet 900	Rogers Corporation	1346	Cellulose fibers and Buna-N		0.032	2/2 2/2 2/16	10 5 3	U – –	U – –
Duroid Sheet 910	Rogers Corporation		Similar to Duroid 900		0.032	2/2 2/2 2/16	10 5 3	U – –	U – –
Duroid Sheet 3102	Rogers Corporation	1347	Neoprene latex and asbestos fibers	Conforms to (MIL-G-7021 Class 2)	0.032	2/3 2/2 0/14	10 5 3	U – –	U – –
Duroid Sheet 3110	Rogers Corporation	1349	Similar to Duroid 3102		0.032	2/2 2/2 1/16	10 5 3	U – –	U – –
Duroid Sheet 3200	Rogers Corporation	1351	Buna-N latex and asbestos fibers		0.032	2/2 2/2 2/3	10 5 3	U – –	U – –
Duroid Sheet 3210	Rogers Corporation	1352	Similar to Duroid 3200		0.032	2/2 2/2 2/16	10 5 3	U – –	U – –
Duroid Sheet 3300	Rogers Corporation	1353	Buna-S and asbestos fibers		0.032	2/2 2/2 0/16	10 5 3	U – –	U – –
Duroid Sheet 3310	Rogers Corporation	1354	Similar to Duroid 3300		0.032	2/3 2/3 0/14	10 5 3	U – –	U – –
Duroid Sheet 3350	Rogers Corporation	1355	Similar to Duroid 3300		0.063	2/2 2/6 0/11	10 5 3	U – –	U – –
Duroid Sheet 3400	Rogers Corporation	1473	Viton A and asbestos fibers		0.063	0/20	10	S	BT

TABLE V. GASKETS AND PACKINGS (Continued)

Material	Manufacturer or Source	Test No.	Composition	Remarks	Thickness (inch)	No. Reactions/ No. Tests	Energy Level Kg/m	Batch or Jar Rating	Material Rating
Duroid Sheet 5600	Rogers Corporation	480	Teflon and ceramic fibers		0.063	0/20	10	S	BT
Duroid Sheet 5613	Rogers Corporation	492	Similar to Duroid 5600; contains molybdenum disulfide		0.063	2/6 0/14	10 2	U –	BT –
Duroid Sheet 5650	Rogers Corporation	481	Similar to Duroid 5600; has higher Teflon content		0.063	0/20	10	S	BT
"E" Felt	Unit Cork Company	709			0.063	2/20	10	U	U
FEP on Surface of Glass Fabric	Non-Metallic Materials Branch	7567 7568		Stainless steel inserts	0.060 0.050	0/20 0/20	10 10	S S	BT BT
Flexrock Type 420 Packing,									
SPT-13-64	Flexrock Company	5968			0.25	0/20	10	S	BT
SPT-14-64		5967			0.25	0/20	10	S	BT
SPT-15-64		5966			0.25	0/20	10	S	BT
SPT-16-64		5953			0.25	0/20	10	S	BT
SPT-17-64		5952			0.25	0/20	10	S	BT
SPT-18-64		5951			0.25	0/20	10	S	BT
Flexitallic Gasket	Flexitallic Gasket Company	348	Stainless steel and Teflon		0.063	0/20	10	S	BT
Flexitallic Gasket	Flexitallic Gasket Company	349	Stainless steel and blue asbestos		0.063	0/20	10	S	BT
Flexrock 420 Packing	Flexrock Company	2887	Braided Teflon		0.250	0/20	10	S	BT
Flexrock 420 Packing	Flexrock Company	2886	Braided Teflon		0.500	0/40	10	S	BT
Flexrock 420 Packing	Flexrock Company	2376	Braided Teflon	Stainless steel inserts used	0.188	0/20	10	S	BT
Flexrock 420 Packing	Flexrock Company	2377	Braided Teflon	Stainless steel inserts used	0.313	0/20	10	S	BT
Flexrock 420 Packing	Flexrock Company	2880	Braided Teflon		0.125	0/40	10	S	BT
Flexrock 420 Packing	Flexrock Company	2884	Braided Teflon		0.375	0/40	10	S	BT

TABLE V. GASKETS AND PACKINGS (Continued)

Material	Manufacturer or Source	Test No.	Composition	Remarks	Thickness (inch)	No. Reactions/ No. Tests	Energy Level Kg/m	Batch or Jar Rating	Material Rating
Fluorobestos LS-7598	Raybestos-Manhattan Inc.	2068	Teflon and asbestos		0.030	0/20	10	S	BT
Fluorobestos, Unsintered	Raybestos-Manhattan Inc.	1918	Teflon and asbestos		0.063	0/20	10	S	BT
Fluoroblue Sheet	John L. Dore Company	1391	Compounded Teflon		0.063	0/20	10	S	BT
Fluoroblack Sheet	John L. Dore Company	1312	Compounded Teflon		0.063	0/20	10	S	BT
Fluorobrown	John L. Dore Company	1393	Reprocessed filled Teflon		0.063	0/20	10	S	BT
Fluorogold Gasket Material	Fluorocarbon Products Company	3336	Chlorofluorocarbon		0.125	0/20	10	S	BT
Fluorogreen E-600	John L. Dore Company	3372	Teflon and inorganic filler	Seven different batches tested	0.063	0/40	10	S	S
Fluorogreen E-600	John L. Dore Company	2066	Teflon and inorganic filler	Seven different batches tested	0.063	0/20	10	S	S
Fluorogreen E-600, (12 sheets)	John L. Dore Company	5818		Stainless steel inserts 6 sheets at 0.062 inch		0/20	10	S	S
SPT-1 through SPT-12				Stainless steel inserts 6 sheets at 0.125 inch		0/20	10	S	S
Fluorogreen E-600, SPT 3-65 through SPT 26-65 (24 sheets)	John L. Dore Company	6495		7 sheets at 0.062 inch		0/20	10	S	S
				1 sheet at 0.065 inch		0/20	10	S	S
				1 sheet at 0.066 inch		0/20	10	S	S
				1 sheet at 0.072 inch		0/20	10	S	S
				1 sheet at 0.080 inch		0/20	10	S	S
Fluorogreen E-600 SPT 3-65 through SPT 26-65	John L. Dore Company	6495		2 sheets at 0.120 inch		0/20	10	S	S
				6 sheets at 0.125 inch		0/20	10	S	S
				1 sheet at 0.130 inch		0/20	10	S	S
				1 sheet at 0.132 inch		0/20	10	S	S
				1 sheet at 0.135 inch		0/20	10	S	S
				1 sheet at 0.150 inch		0/20	10	S	S
Fluorogreen E-600 (30 sheets) SPT 27-65 through SPT 56-65	John L. Dore Company	7104		Wash with F-33					
				2 sheets at 0.060 inch		0/20	10	S	S
				2 sheets at 0.062 inch		0/20	10	S	S
				5 sheets at 0.063 inch		0/20	10	S	S
				4 sheets at 0.064 inch		0/20	10	S	S
				1 sheet at 0.065 inch		0/20	10	S	S

TABLE V. GASKETS AND PACKINGS (Continued)

Material	Manufacturer or Source	Test No.	Composition	Remarks	Thickness (inch)	No. Reactions/ No. Tests	Energy Level Kg/m	Batch or Jar Rating	Material Rating
Fluorogreen E-600 (continued)	John L. Dore Company	7104		3 sheets at 0.066 inch		0/20	10	S	S
				3 sheets at 0.066 inch		0/20	10	S	S
				1 sheet at 0.070 inch		0/20	10	S	S
				1 sheet at 0.115 inch		0/20	10	S	S
				3 sheets at 0.125 inch		0/20	10	S	S
				1 sheet at 0.126 inch		0/20	10	S	S
				1 sheet at 0.127 inch		0/20	10	S	S
				1 sheet at 0.128 inch		0/20	10	S	S
				1 sheet at 0.129 inch		0/20	10	S	S
				2 sheets at 0.135 inch		0/20	10	S	S
				1 sheet at 0.136 inch		0/20	10	S	S
				1 sheet at 0.138 inch		0/20	10	S	S
Fluorogreen E-600	John L. Dore Company	10013			0.030	0/20	10	S	S
Fluorogreen Gasket No. 10426445	John L Dore Company	4375		Fluorogreen E-600	0.063	0/20	10	S	S
Fluorocarbon Standard "O" Rings	The Fluorocarbon Company	4803				0/20	10	S	BT
Fluoro-Ray	Raybestos-Manhattan Company	9775	Ceramic filled Teflon	Three batches tested	0.025	2-4/20	10	U	BT
Fluoro-Ray Blue Ceramic-Filled Teflon	Raybestos-Manhattan	4588		Stainless steel inserts	0.063	0/20	10	S	BT
Garlock 605 Sheet	Garlock Packing Company	1230	Wire Reinforced asbestos		0.063	2/2	10	U	U
						2/5	5	–	–
						0/13	2	–	–
Garlock 900 Sheet	Garlock Packing Company	315	Asbestos-rubber composite		0.063	2/2	10	U	U
						2/3	5	–	–
						2/4	2	–	–
Garlock 5875	Garlock, Incorporated	5989	Astestos and Teflon						
SPT 21-64					0.375	0/20	10	S	BT
SPT-19-64					0.50	0/20	10	S	BT
SPT-20-65					0.50	0/20	10	S	BT
Garlock 7021 Sheet	Garlock Packing Company	1231	Asbestos-rubber composite	Violent reactions	0.063	2/2	10	U	U
						2/3	5	–	–
						2/2	2	–	–
						0/2	1	–	–
Garlock 7228 Sheet	Garlock Packing Company	1395	Asbestos-Neoprene rubber		0.063	2/2	10	U	U
						0/14	5	–	–

TABLE V. GASKETS AND PACKINGS (Continued)

Material	Manufacturer or Source	Test No.	Composition	Remarks	Thickness (inch)	No. Reactions/ No. Tests	Energy Level Kg/m	Batch or Jar Rating	Material Rating
Garlock 7705 Sheet	Garlock Packing Company	1229	Blue asbestos-rubber composite	Violent reactions	0.063	2/2 2/2 2/2 1/2	10 5 2 1	U – – –	U – – –
Garlock 8573	Garlock Packing Company	8600	Filled Teflon	Three batches tested	0.092	0/20	10	S	BT
Garlock 8573 Sheet	Garlock Packing Company	3321	Glass-filled Teflon		0.063	0/20	10	S	BT
Gatke Buna-PAK I-26 Sheet	Gatke Corporation	1340	Compressed asbestos with binder		0.063	2/20 0/10	10 5	U –	U –
Gylon S-50-S	Garlock Packing Company	10265	Filled Teflon		0.100	0/20	10	S	BT
John Crane Style C-30 Packing	Crane Packing Company	442	Braided Teflon		0.250	0/20	10	S	BT
John Crane Style C-30 Packing	Crane Packing Company	2910	Braided Teflon		0.250	0/20	10	S	BT
John Crane Style C-94 Packing	Crane Packing Company	2909	Braided asbestos lubricated with Teflon suspensoid		0.025	0/20	10	S	BT
John Crane Style 177J7 Packing	Crane Packing Company	839	Braided asbestos over graphited asbestos core	Sensitivity varies from batch to batch	0.250	0/20	10	S	BT
John Crane Style 333 Sheet	Crane Packing Company	1199	Compressed asbestos with binder		0.063	4/20	10	U	U
John Crane Style 444 Sheet	Crane Packing Company	1211	Chemically treated compressed vegetable plant fiber		0.063	2/4 0/16	10 5	U –	U –
John Crane Style 888 Sheet	Crane Packing Company	1213	Compressed asbestos with oil resistant binder		0.063	2/20	10	U	U
John Crane Style 2150 Sheet	Crane Packing Company	1214	Asbestos with heat resisting binder		0.063	2/3 2/17	10 5	U –	U –
John Crane Style 2151 Sheet	Crane Packing Company	1212	Similar to Style 2150		0.063	2/2 2/4 0/4	10 5 3	U – –	U – –

TABLE V. GASKETS AND PACKINGS (Continued)

Material	Manufacturer or Source	Test No.	Composition	Remarks	Thickness (inch)	No. Reactions/ No. Tests	Energy Level Kg/m	Batch or Jar Rating	Material Rating
Johns-Manville No. 60 Sheet	Johns-Manville Company		Compressed asbestos with binder	Variable	0.063	0-2/20	10	–	BT
Johns-Manville No. 61 Sheet	Johns-Manville Company	1652			0.063	3/9 3/11	10 5	U –	U –
Johns-Manville No. 76 Sheet	Johns-Manville Company	1360	Compressed asbestos with binder	Variable	0.063	0-5/20	10	–	BT
Johns-Manville No. 76 Sheet	Johns-Manville Company	1474 1922	Compressed asbestos with binder	Sensitivity varies from batch to batch	0.063	0/20 0/20	10 10	S S	BT BT
Johns-Manville No. 76 Sheet	Johns-Manville Company	1926 1925	Compressed asbestos with binder		0.032	2/5 2/5	10 10	U U	U U
Johns-Manville No. 84 Sheet	Johns-Manville Company	1653			0.063	2/2 2/2 2/2	10 5 3	U – –	U – –
Johns-Manville Style 91 Sheet	Johns-Manville Company	1059	Chrysolite asbestos cloth with Teflon suspensoid		0.063	2/3 0/17	10 5	U –	U –
Johns-Manville Style 92 Sheet	Johns-Manville Company	1203	Crocidolite asbestos cloth with Teflon suspensoid		0.063	2/2 2/2 0/16	10 5 2	U – –	U – –
Johns-Manville No. 219 Sheet	Johns-Manville Company	1649			0.063	2/3 0/11	10 5	U –	U –
Johns-Manville Lo Flo Sheet	Johns-Manville Company	1673	Teflon reinforced with glass fiber		0.032	0/20	10	S	BT
Johns-Manville Lo Flo Sheet	Johns-Manville Company	1673	Teflon-ground glass		0.063	0/20	10	S	BT
Johns-Manville Style 2024 Packing	Johns-Manville Company	1585		Formerly known as Johns-Manville MX 3681 Packing	0.250	2/4 1/16	10 5	– –	U –
Johns-Manville MX-3681	Johns-Manville Company	1589	Compressed asbestos with binder	Variable	0.500	0/20	10	S	BT

TABLE V. GASKETS AND PACKINGS (Continued)

Material	Manufacturer or Source	Test No.	Composition	Remarks	Thickness (inch)	No. Reactions/ No. Tests	Energy Level Kg/m	Batch or Jar Rating	Material Rating
Johns-Manville MX-3681	Johns-Manville Company		Compressed asbestos with binder	Variable	0.375	0-13/20	10	–	U
Johns-Manville MX-3681	Johns-Manville Company		Compressed asbestos with binder	Variable	0.313	5-13/20	10	U	U
Johns-Manville MX-3681	Johns-Manville Company		Compressed asbestos with binder	Variable	0.250	20-5/20	10	–	U
Johns-Manville MX-3681	Johns-Manville Company		Compressed asbestos with binder		0.188	26/40 5/60	10 5	– –	U –
Johns-Manville MX-3681	Johns-Manville Company	1944	Compressed asbestos with binder	Variable	0.125	3-7/20	10	U	U
Kel-F Elastomer Gasket 3-5986-1	Arrowhead Products	6450		Stainless steel inserts		0/20	10	S	BT
Kel-F Elastomer Gasket 3-5986-3	Arrowhead Products	6451		Stainless steel inserts	0.039	0/20	10	S	BT
Kel-F Lip Seal, QR 717A, Lot A31584	W.S. Shamblee Company	6073		Stainless steel inserts	0.128	0/20	10	S	BT
Heat Cleaned Glass Fabric		7566		Stainless steel inserts	0.010	0/20	10	S	BT
K&M 238 Sheet	Keasby and Mattison Company	1332			0.063	2/4 0/11	10 5	U –	U –
K&M 239 Sheet	Keasby and Mattison Company	1333	Asbestos with GR-5 elastomer	Meets MIL-A-17472	0.063	4/20	10	U	U
Leather Chrome-Tanned	Obtained from Bell Aircraft Company	1201	Leather	Violent explosions	0.125	2/5 2/7	10 5	U –	U –
Leather, Chrome-Tanned, Fluorolube Impregnated	Bell Aircraft Company ("Turkhide")	1202			0.125	0/20	10	–	U
Naflex Seal with Teflon Tape and Adhesive	Rocketdyne	3696	Teflon, silicone adhesive	Seven batches tested (typical data)	0.060	2/4 2/2 2/12 0/20	10 5 3 1	U – – –	U – – –
Narmco Seal, Serial No. 003 Serial No. 005	Narmco Research and Development Company	10041 7570 7571	TFE-FEP TFE-FEP fiberglass Teflon-fiberglass	 Stainless steel inserts Stainless steel inserts	0.125 0.100 0.100	0/20 0/20 0/20	10 10 10	S S S	S S S

TABLE V. GASKETS AND PACKINGS (Continued)

Material	Manufacturer or Source	Test No.	Composition	Remarks	Thickness (inch)	No. Reactions/ No. Tests	Energy Level Kg/m	Batch or Jar Rating	Material Rating
Serial No. 016		7582	Teflon-fiberglass	Stainless steel inserts	0.100	0/20	10	S	S
Serial No. 017		7583	Teflon-fiberglass	Stainless steel inserts	0.100	0/20	10	S	S
Serial No. 018		7584	Teflon-fiberglass	Stainless steel inserts	0.100	0/20	10	S	S
Serial No. 061		7585	Teflon-fiberglass	Stainless steel inserts	0.100	0/20	10	S	S
Serial No. 064		7642	Teflon-fiberglass	Stainless steel inserts	0.11	0/20	10	S	S
Serial No. 065		7643	Teflon-fiberglass	Stainless steel inserts	0.10	0/20	10	S	S
Serial No. 066		7644	Teflon-fiberglass	Stainless steel inserts	0.11	0/20	10	S	S
Serial No. 070		7645	Teflon-fiberglass	Stainless steel inserts	0.10	0/20	10	S	S
Novabestos 7511T	Raybestos-Manhattan Company	6277	Dispersed asbestos TFE fiber paper	Cleaned per MSFC-SPEC-106B	0.50	0/20	10	S	BT
Novabestos 7511T	Raybestos-Manhattan Company	4837	Dispersed asbestos TFE fiber paper	Cleaned per MSFC-SPEC-106B	0.020	0/20	10	S	BT
Novabestos 7511T	Raybestos-Manhattan Company	2729	Dispersed asbestos fiber paper		0.020	0/20	10	S	BT
Novabestos 7711T	Raybestos-Manhattan Company	5979	Dispersed asbestos fiber paper	Stainless steel inserts	0.020	0/20	10	S	BT
		5978			0.030	0/20	10	S	BT
Mylar Seat Assembly Gasket	Hadley Valve Company	5586			0.008	16/20	10	U	U
"O" Ring 2 pc 29513-231-1000-80 on Mark Couplings		5189	Fluorosilicone		0.131	20/20	10	U	U
						11/14	8	–	–
Quinorgobord	Johns-Manville Company	4516	Asbestos-Rubber Composite		0.125	0/20	10	S	BT
Parco O-ring Sheet No. 945-70	Plastic and Rubber Products Company		Fluorinated elastomer		0.063	0/20	10	S	BT
Raybestos-Manhattan Fluorobestos Sheet	Raybestos-Manhattan Company	1918	Teflon impregnated asbestos	Available as special LOX grade	0.063	0/20	10	S	BT
Raybestos-Manhattan K-68 Sheet	Raybestos-Manhattan Company	1924	Asbestos with sulfur-free neoprene binder		0.063	0/20	10	S	BT
Raybestos-Manhattan K-68 Sheet	Raybestos-Manhattan Company	1923	Asbestos with sulfur-free neoprene binder		0.094	4/20	10	U	U
Raybestos-Manhattan 655 Sheet	Raybestos-Manhattan Company	1209			0.063	2/8	10	U	U
						1/12	8	–	–

TABLE V. GASKETS AND PACKINGS (Continued)

Material	Manufacturer or Source	Test No.	Composition	Remarks	Thickness (inch)	No. Reactions/ No. Tests	Energy Level Kg/m	Batch or Jar Rating	Material Rating
Raybestos-Manhattan 670 Sheet	Raybestos-Manhattan Company	1140		Violent reactions.	0.063	2/4 2/3 2/5	10 8 2	U – –	U – –
Raybestos-Manhattan 673 Sheet	Raybestos-Manhattan Company	1207			0.063	2/4 1/16	10 8	U –	U –
Raybestos-Manhattan 10,000 Sheet	Raybestos-Manhattan Company	1069	Crude asbestos fibers with binder		0.063	2/2 2/2	10 8	U –	U –
Raybestos-Manhattan RL-395	Raybestos-Manhattan Company	2067	Teflon asbestos cloth		0.063	0/20	10	S	BT
Raybestos-Manhattan RL-80	Raybestos-Manhattan Company	2474	Teflon impregnated asbestos cloth	RM-607	0.125	0/40	10	S	BT
Raybestos-Manhattan RL-80	Raybestos-Manhattan Company	2476	Teflon impregnated asbestos cloth	RM-607	0.063	0/40	10	S	BT
Raybestos-Manhattan RL-1356	Raybestos-Manhattan Company	2069	Asbestos sheet with 0.009 in. Teflon film		0.063	0/20	10	S	BT
L-2094-1 Gasket	Raybestos-Manhattan Company	5804		Stainless steel inserts	0.080	15/20 7/20 6/20	10 8 6	U U U	U U U
Packing P/N 00526-78	Annin Packing Company	5969			0.275	5/20	10	U	U
RL-1355	Raybestos-Manhattan Company	5803		Stainless steel inserts	0.080	10/20 3/20 0/20	10 8 6	U U U	U U U
RL-1735	Raybestos-Manhattan Company	5810		Stainless steel inserts	0.060	9/20 2/20 0/20	11 10 8	U U U	U U U
RM 10-M-351	Raybestos-Manhattan Company	5949			0.074	0/20	10	S	BT
RM 10-M-351, Aluminized	Raybestos-Manhattan Company	5950		Stainless steel inserts	0.082	0/20	10	S	BT
RM 12T-370	Raybestos-Manhattan Company	5948			0.077	0/20	10	S	BT
RM 827-M-B	Raybestos-Manhattan Company	5909		Stainless steel inserts	0.060	0/20	10	S	BT
Rulon A	Dixon Corporation	9131	Filled Teflon		0.063	0/20	10	S	S

TABLE V. GASKETS AND PACKINGS (Continued)

Material	Manufacturer or Source	Test No.	Composition	Remarks	Thickness (inch)	No. Reactions/ No. Tests	Energy Level Kg/m	Batch or Jar Rating	Material Rating
Sacoma 715 Packing	American Asbestos Company	556		Variable	0.250	0-2/20	10	—	U
Sepco 200 Gasket	Southern Products Corporation	4801			0.063	2/4 2/20	10 5	U –	U –
Teflon Gasket		7553	Virgin Teflon		0.107	0/20	10	S	S
Tetrabest Gasket Seal Carter P/N 3913	Anchor Packing Company	6828			0.020	0/20	10	S	BT
Teflon-Coated Viton "O" Rings	Hadbar Incorporated	5215	No. 954-70 Viton and Teflon coat			0/20	10	S	BT
Teflon-Coated Naflex Seal AMS4340		4812	Virgin Teflon			0/40	10	S	BT
EOR 76574-3 Teflon-coated Naflex gasket	Orbit Machine Corporation	2383			0.063	2/20	10	U	BT
EOR 76574-5 Teflon-coated Naflex gasket	Orbit Machine Corporation	2384			0.063	5/20	10	U	BT
Teflon TFE Filled with 25% Glass	Arrowhead Products	5050	Teflon TFE–75% Glass–25%		0.050	0/20	10	S	BT
Teflon Lip Seal	Hadley Valve Company	5587	Virgin Teflon	Stainless steel inserts used	0.180	0/20	10	S	BT
Tetrabest	Anchor Packing Company	5491	Asbestos and Teflon		0.021	0/20	10	S	BT
Viton A "O" Ring		4370			0.063	0/20	10	S	BT
Viton A "O" Ring PN7170-19009 Compound 19009		5313			0.110	0/20	10	S	BT
Viton A "O" Ring		5312			0.133	0/20	10	S	BT
Viton A "O" Ring HS8-513-111	B.H. Hadley Incorporated	5384			0.093	0/20	10	S	BT
Viton A "O" Ring HS8-513-232	B.H. Hadley Incorporated	5383			0.031	0/20	10	S	BT
Viton A "O" Ring	B.H. Hadley Incorporated	5385			0.060	0/20	10	S	BT
Viton A "O" Ring VLF34 for replenishing Tank Safety Head	Hadbar Incorporated	5513			0.268	0/20	10	S	BT

TABLE V. GASKETS AND PACKINGS (Concluded)

Material	Manufacturer or Source	Test No.	Composition	Remarks	Thickness (inch)	No. Reactions/ No. Tests	Energy Level Kg/m	Batch or Jar Rating	Material Rating
Viton A "O" Ring VLF34 for LOX System	Hadbar Incorporated	5514			0.266	0/20	10	S	BT
Viton A 3Q63-MS29513-255	Du Pont	5062			0.125	0/20	10	S	BT

TABLE VI. METALS, ALLOYS, AND SURFACE TREATMENTS

Material	Manufacturer or Source	Test No.	Composition	Remarks	Thickness (inch)	No. Reactions/ No. Tests	Energy Level Kg/m	Batch or Jar Rating	Material Rating
Aluminum Alloy 1100-"0"		11447			0.032	0/20	10	S	S
Aluminum Alloy 1100-"0"		11448			0.063	0/20	10	S	S
Aluminum Alloy 2014-T6		3110			0.010 0.010	0/10 0/100	10 5	S –	S –
Aluminum Alloy 2014-T6		3084			0.025 0.025	0/120 0/100	10 5	S –	S –
Aluminum Alloy 2014-T6		2969 2854			0.063 0.063 0.063	1/100 0/100 0/100	10 10 5	S S –	S S –
Aluminum Alloy 2024-T6-Alodine 1200	American Chemical Paint Co.	957			0.063	0/20	10	S	S
Aluminum Alloy 2024-T3 Anodized, Sandoz Blue B	Sandoz Chemical Co.	491	MIL-A-8625A Type II Nickel Acetate Sealed		0.081	0/20	10	S	S
Aluminum Alloy 2024-T3		11444			0.032	0/20	10	S	S
Aluminum Alloy 2024-T3		11445			0.063	0/20	10	S	S
Aluminum Alloy 2024-T3		11446			0.090	0/20	10	S	S
Aluminum Alloy 2024-T3 Anodized, Sandoz Green AX	Sandoz Chemical Co.	490	Nickel Acetate Sealed MIL-A-8625A, Type II		0.063	0/20	10	S	BT
Aluminum Alloy 2219-T87		3616			0.094	0/20	10	S	S
Aluminum Alloy 2219-T37 Iridite 14-4 Coated		6003			0.063	0/20	10	S	S
Aluminum Alloy 5052-H32-LOX Test Cups		1511		LOX test cups	0.063	0/20	10	S	S
Aluminum Alloy 5052-H32-LOX Test Cups		6973		Vapor, degreased, alkaline cleaned and acid etched	0.063	0/20	10	S	S
Aluminum Alloy 5052-H32-LOX Test Cups		9116		Vapor, degreased, alkaline cleaned and acid etched	0.063	0/20	10	S	S

TABLE VI. METALS, ALLOYS, AND SURFACE TREATMENTS (Continued)

Material	Manufacturer or Source	Test No.	Composition	Remarks	Thickness (inch)	No. Reactions/ No. Tests	Energy Level Kg/m	Batch or Jar Rating	Material Rating
Aluminum Alloy 5052-H32-Iridite-14-2 Coated		2826			0.063	0/20	10	S	S
Aluminum Alloy 5052-Iridite 14-2 Coated		572			0.063	0/20	10	S	S
Aluminum Alloy 5086-H34		2869		Hand deburred	0.063	1/147 0/80	10 5	S —	S
Aluminum Alloy 5086		506			0.063	0/20	10	S	S
Aluminum Alloy 5086-H34-Alodine 1200 Coated		958	Nickel-Acetate sealed		0.063	0/20	10	S	S
Aluminum Alloy 5086 - Iridited-Gold		500			0.063	2/24 1/20	10 8	U —	BT
Aluminum Alloy 5456-M343		2771			0.063 0.063	1/120 0/80	10 5	S —	S
Aluminum Alloy 6061-T6		5511		Samples, striker & anvil not precooled	0.063	0/20	10	S	S
Aluminum Alloy 6061-T6		5512		Samples precooled	0.063	0/20	10	S	S
Aluminum Alloy 6061-T6 Sulfuric Acid Anodized		8601		Not sealed	0.063	0/100	10	S	BT
Aluminum Alloy 6061-T6 Anodized, Sandoz Gold	Sandoz Chemical Co.	9209	MIL-A8625A Type II Nickel acetate sealed		0.063	0/60	10	S	BT
Aluminum Alloy 6061-T6-Anodized Sandoz Yellow	Sandoz Chemical Co.	9205	MIL-A-8625A Type II Nickel acetate sealed		0.063	0/60	10	S	BT
Aluminum Alloy 6061-T6-Anodized, Sandoz Black BK	Sandoz Chemical Co.	999	MIL-A-8625A Type II Nickel acetate sealed		0.063	0/20	10	S	BT
Aluminum Alloy 6061-T6-Anodized, Sandoz Blue B	Sandoz Chemical Co.	1737	MIL-A-8625A Type II Nickel acetate sealed		0.063	3/40	10	U	BT
Aluminum Alloy 6061-T6 Anodized, Sandoz Green AX	Sandoz Chemical Co.	1000	MIL-A-8625A Type II Nickel acetate sealed		0.063	0/20	10	S	BT

TABLE VI. METALS, ALLOYS, AND SURFACE TREATMENTS (Continued)

Material	Manufacturer or Source	Test No.	Composition	Remarks	Thickness (inch)	No. Reactions/ No. Tests	Energy Level Kg/m	Batch or Jar Rating	Material Rating
Aluminum Alloy 6061-T6 Iridite 14-2 Coating	Associated Products Lab.	7918			0.063	0/20	10	S	S
Aluminum Alloy 6061-T6 Iridite 14-2 Coating	Allied Research Product	1002	Nickel acetate sealed		0.063	0/20	10	S	S
Aluminum Alloy 6061-T6-Alodine MTL Modified 401-45	Metallic Materials Branch	9903	Applied to 0.063 discs		0.005	0/20	10	S	BT
Aluminum Alloy 6061-T6 Alodine 1200S		11402			0.063	0/20	10	S	S
Aluminum Alloy Tens-50		11450			0.125	0/20	10	S	S
Aluminum Alloy Tens-50		11453			0.032	0/20	10	S	S
Aluminum Foil	Kaiser-Aluminum Co.	7726			0.001	0/20	10	S	S
Aluminum Black Magic No. 1	Metallic Materials Branch	9799	Applied to 2 mil aluminum		0.001	4/20	10	U	BT
Aluminum Black Swab No. A-14	Metallic Materials Branch	9805	Conversion coating on 2 mil aluminum foil		0.001	0/20	10	S	BT
Alpha 238 Solder	Alpha Metals Inc.					2/3 9/17	10 5	U	U
Alpha 10/88/2 AG Solder	Alpha Metals Inc.	7651	10% tin, 88% lead 2% silver		0.025	2/20	10	U	U
Ampco 2013 (filings)	Metallic Materials Branch	4401		In stainless steel cups	–	0/20	10	S	S
Ampco 2013 (filings)	Metallic Materials Branch	4402		In aluminum cups	–	0/20	10	S	S
Ampco 2013		4399			0.032	0/20	10	S	S
Ampco-24 Alloy		3481	5% iron, 15% aluminum 80% copper		0.063	0/20	10	S	S
Barium metal plus copper oxide	Space DIV, NAR Corp.	MC-1483	1.16 gms barium 0.3875 gm copper oxide			0/20	10	S	–

TABLE VI. METALS, ALLOYS, AND SURFACE TREATMENTS (Continued)

Material	Manufacturer or Source	Test No.	Composition	Remarks	Thickness (inch)	No. Reactions/ No. Tests	Energy Level Kg/m	Batch or Jar Rating	Material Rating
Aluminum Alloy 6061-T6, Anodized Sandoz Yellow 2D	Sandoz Chemical Co.	1735	MIL-A-8625A Type II Nickel acetate sealed		0.063	0/20	10	S	BT
Aluminum Alloy 6061-T6, Anodized Sandoz Black V-Orange 3A	Sandoz Chemical Co.	1733	MIL-A-8625A Type II Nickel acetate sealed		0.063	4/20	10	U	BT
Aluminum Alloy 6061-T6, Anodized Sandoz Gold (Black V, Orange 3A)	Sandoz Chemical Co.	1841	MIL-A-8625A Type II Nickel acetate sealed		0.063	0/20	10	S	BT
Aluminum Alloy 6061-T6 – Treated	Sandoz Chemical Co.	584		Soaked 24 hours in 0.1% sulfuric acid followed by 24 hours in 0.2% sodium dichromate	0.063	0/20	10	S	BT
Aluminum Alloy 6061-T6-Anodized Sandoz 00319	Sandoz Chemical Co.	1726	MIL-A-8625A Type II Nickel acetate sealed		0.063	5/40	10	U	BT
Aluminum Alloy 6061-T6, Anodized Sandoz Bordeaux Red	Sandoz Chemical Co.	1847	MIL-A-8625A Type II Nickel acetate sealed		0.063	0/20	10	S	BT
Aluminum Alloy 6061-T6, Anodized Sandoz Orange 2B	Sandoz Chemical Co.	1846	MIL-A-8625A Type II Nickel acetate sealed		0.063	0/20	10	S	BT
Aluminum Alloy 6061-T6-Anodized Cyanamide Black WA	American Cyanamid	1842	MIL-A-8625A Type II Nickel acetate sealed		0.063	0/20	10	S	BT
Aluminum Alloy 6061-T6 Anodized Eaton Scarlet	Eaton Chemical Co.	998	MIL-A-8625A Type II Nickel acetate sealed		0.063	0/20	10	S	BT
Aluminum Alloy 6061-T6 Anodized Black	Eaton Chemical Co.	3165	MIL-A-8625A Type II Nickel acetate sealed		0.063	2/20 1/20	10 5	U —	BT
Aluminum Alloy 6061-T6 Anodized Krieger 15285	Krieger Color & Chemical Co.	1732 1895	MIL-A-8625A Type II Nickel acetate sealed		0.063 0.063	3/20 0/20	10 10	U S	BT BT
Aluminum Alloy 6061-T6 Anodized Krieger Blue B	Krieger Color & Chemical Co.	1734 1844	MIL-A-8625A Type II Nickel acetate sealed		0.063 0.063	1/40 1/40	10 10	I I	BT BT
Aluminum Alloy 6061-T6 Iridite 14-2 Coating		3851			0.063	0/20	10	S	BT

TABLE VI. METALS, ALLOYS, AND SURFACE TREATMENTS (Continued)

Material	Manufacturer or Source	Test No.	Composition	Remarks	Thickness (inch)	No. Reactions/ No. Tests	Energy Level Kg/m	Batch or Jar Rating	Material Rating
Beryico 25 (4485, 1/2 hard, NAS8-8672)		6639			0.052	0/20	10	S	S
Beryllium		3125			0.063	0/20	10	S	S
Beryllium Copper Alloy 25	Brush Beryllium Company	9411			0.063	0/20	10	S	S
Bronze Filter, Sintered		2517			0.060	0/20	10	S	S
Brass Inserts		3016	65% copper, 34% zinc, 2%		0.063	0/20	10	S	S
Cadmium		1902		Electroplated	0.001	0/20	10	S	S
Carboloy No. 608 Coated with Everlube 811	Haward Corporation	4398	Chrome carbide coated on one side with Everlube 811 Dry Lubricant		0.063	0/20	10	S	S
Carboloy No. 883 Coated with Everlube 811	Haward Corporation	4397	Tungsten carbide coated with Everlube 811 on one side		0.063	0/20	10	S	S
Cerrobend Low Melting Alloy		852	Contains bismuth, lead, tin	Low melting alloy	0.063	2/3 1/17	10 5	U –	U –
Cherry Lock Rivet, NAS-1398 D5-4, D5-Z	Cherry Rivet Company	5677	Coated with dry film lube C-23			7/20	10	U	U
Cherry Lock Rivet NAS-1398, D5-3	Cherry Rivet Company	5678	Coated with dry film lube C-23			3/20	10	U	U
Copper Wire		9140			0.005	0/20	10	S	S
CN-346 Copper Nickel Alloy	International Nickel Co.	3849	70% copper, 30% nickel		0.050	0/20	10	S	S
Chromium		1896		Electroplated	0.5 mil	0/20	10	S	S
Columbium	Space Division, NAR	ME659				0/20	10	S	BT
Durlite Black Oxide	Durlite Company	9369			0.001	0/20	10	S	BT
Dutch Boy Resin Solder	National Lead Company	5686	40% tin/60% lead		0.010	12/20 9/20 7/20 4/20 2/20 0/20	10 8 6 4 2 1	U – – – – –	U – – – – –

TABLE VI. METALS, ALLOYS, AND SURFACE TREATMENTS (Continued)

Material	Manufacturer or Source	Test No.	Composition	Remarks	Thickness (inch)	No. Reactions/ No. Tests	Energy Level Kg/m	Batch or Jar Rating	Material Rating
Dutch Boy Fluxrite Solder	National Lead Company	5687	60% tin/40% lead with NUAX Flux		0.014	20/20	10	U	U
						17/20	8	–	–
						17/20	6	–	–
						12/20	4	–	–
						5/20	2	–	–
						0/20	1	–	–
Easy Flo-Solder		5693	High silver content		0.005	0/20	11.3	S	BT
						0/20	10	S	BT
EZ Fo Alloy AMS 4771	Rocketdyne	463-25C			0.005	0/20	10	S	BT
Ersins 5 Core Solder, Non-Corrosive Flux	Ersin Multicore Solder Limited	5695	60% tin/40% lead		0.005	14/20	10	U	U
						12/20	8	–	–
						7/20	6	–	–
						7/20	4	–	–
						5/20	2	–	–
						0/20	1	–	–
Eutectic No. 151B Solder	Eutectic Welding Alloy Corporation	3534	90% tin, zinc, nickel		0.032	10/20	10	U	U
						3/20	4	–	–
						0/20	2	–	–
Eutectic No. 153 Solder	Eutectic Welding Alloy Corporation	3538	90% lead, 10% silver		0.032	3/20	10	U	U
						2/22	7	–	–
						0/20	5	–	–
Eutectic No. 155 Solder	Eutectic Welding Alloy Corporation	3541			0.032	2/35	10	U	U
						2/20	8	–	–
Eutectic 157 Solder	Eutectic Welding Alloy Corporation	705		Low melting alloy	0.050	3/4	10	U	U
						2/3	5		
						2/3	3		
						0/6	6		
Eutectic 1800 Solder	Eutectic Welding Alloy Corporation	757			0.050	0/20	10	S	BT
Eutectic 115B Solder with Eutectic 151B Flux	Eutectic Welding Alloy Corporation	2903			0.050	13/60	10	U	U
GSB-156		7482	0.03 mil tin plate over brass		0.067	4/20	10	U	U

TABLE VI. METALS, ALLOYS, AND SURFACE TREATMENTS (Continued)

Material	Manufacturer or Source	Test No.	Composition	Remarks	Thickness (inch)	No. Reactions/ No. Tests	Energy Level Kg/m	Batch or Jar Rating	Material Rating
GSC-232		7483	0.03 mil tin plate over brass		0.038	0/20	10	S	BT
Handy Solder flux for high temp Soldery	Handy & Horsmen	6270			0.050	0/20	10	S	BT
Haynes Alloy Tubing Sleve Soldered to Mu Metal		4505			0.063	0/20	10	S	BT
Haynes Alloy Tubing		4506			0.063	0/20	10	S	S
Indium Foil	National Bureau of Standards	5482	Indium		0.003	11/40	10	U	U
Indalloy Flux No. 2	Indium Corporation of America	6329		Baked @ 100°C for one hour	Smear on stainless steel inserts	15/20	10	U	U
Inconel 69 Weld Wire	Space Division NAR	MC-2050			–	0/20	10	S	S
K-6 Alloy	Karl-Harrison Co.	11368	Nickel, Lead & Tin on stainless steel		0.066	4/4	10	U	BT
K-6 Alloy	Karl-Harrison Co.	2141	Nickel, Lead & Tin on stainless steel		0.066	0/40	10	S	BT
K-Seal (PE)	Karl-Harrison Co.	11392	Tin plated on stainless		0.063	6/20	10	U	U
Kelite Process 235	Kelite Company	8233			0.050	2/20	10	U	U
Kester Solder No. 955 Flux 44 Core 16 QQ-S-571	Kester Solder Company	5559	95% tin/5% silver		0.005	15/20 12/20 8/20 5/20 2/20 1/20	10 8 6 4 2 1	U – – – – –	U – – – – –
Kester Solder Tin 20 Core 66 Flux 44 (QQ-S-571-C Spec)	Kester Solder Company	5553	20% tin/1.2% antimony. Remainder lead	Stainless steel inserts used	0.009	6/20 7/20 7/20 2/20 2/20 0/20	10 8 6 4 2 1	U – – – – –	U – – – – –

TABLE VI. METALS, ALLOYS, AND SURFACE TREATMENTS (Continued)

Material	Manufacturer or Source	Test No.	Composition	Remarks	Thickness (inch)	No. Reactions/ No. Tests	Energy Level Kg/m	Batch or Jar Rating	Material Rating
Kirkson No. 20 Alloy with Indalloy No. 2 Flux on Stainless Steel	Southwestern Industries	6447		Cleaned per ES-195 procedure		0/20	10	S	BT
Kirkson Solid Wire Solder TEC	Morris P. Kirk and Sons, Incorporated	6055	95% cadmium/5% silver	Heated and rolled	0.012	0/20 0/20	11.3 10	S	BT
Kirkson Solid Wire Solder No. 20	Morris P. Kirk and Sons, Incorporated	6057	97.5% lead/1% tin	Heated and rolled	0.012	0/20 0/20	11.3 10	S	BT
Kirkson Solid Wire Solder No. 390	Morris P. Kirk and Sons, Incorporated	6049		Heated and rolled	0.005	3/20 1/20	10 8	U	U
Kirkson Solid Wire Solder No. 625	Morris P. Kirk and Sons, Incorporated	6051	Cadmium-zinc composite	Heated and rolled	0.015	0/20	11.3	S	BT
Kirkson Solid Wire Solder No. B-95AG	Morris P. Kirk and Sons, incorporated	6059	94% lead/5.5% silver	Heated and rolled	0.010	0/20 0/20	11.3 10	S	BT
Kirkson Solid Wire Solder No. B-975G	Morris P. Kirk and Sons, Incorporated	6053	97.5% lead/2.5% silver	Heated and rolled	0.015	0/20	10	S	BT
Kovar-A Alloy		962	Nickel, Cobalt, Iron		0.063	0/20	10	S	S
LA-91 Rod Stock	Micro-Systems, Incorporated	5852		Stainless steel inserts	0.25	13/20	10	U	U
Laminated Shim Stock		6004			0.125	0/20	10	S	BT
LAZ 933 Alloy	Battelle Memorial Institute	5997	Magnesium-aluminum-zinc alloy	Stainless steel inserts	0.068	20/20 18/20 15/20 9/20 0/20	10 8 6 4 2	U	U
LA-91		4392	Lithium-aluminum magnesium alloy		0.050	17/20 4/20 0/20 0/20	10 5 4 3	U – – –	U – – –
LA-91		4391	Lithium-aluminun magnesium alloy		0.100	12/20 0/20 0/20 0/20	10 7 6 5	U – – –	U – – –

TABLE VI. METALS, ALLOYS, AND SURFACE TREATMENTS (Continued)

Material	Manufacturer or Source	Test No.	Composition	Remarks	Thickness (inch)	No. Reactions/ No. Tests	Energy Level Kg/m	Batch or Jar Rating	Material Rating
LA-141		4493	Lithium-aluminum magnesium alloy		0.050	18/20 3/20 2/20 0/20	10 5 4 3	U – – –	U – – –
LA-141		4498	Lithium-aluminum magnesium alloy		0.100	15/20 1/20 1/20 0/20	10 7 6 5	U – – –	U – – –
Lead Sheet		4799			0.125	0/20	10	S	BT
Lead Slugs		4811A			0.063	0/20	10	S	BT
Lead		4811		Previously tested as slugs 0.063 inch thick (See 4811A)	0.012 to 0.014	0/20	10	S	BT
Lead Oxide Slurry	Kennedy Space Center	8857		Dried at 100°C	0.050	0/40	10	S	BT
Lemcote LCB	Metallic Materials Branch	9892		Air dried 90 hours	0.010	0/20	10	S	BT
Magnesium-Lithium Alloy LA-91		1222			0.063	2/3 1/2 1/3 1/12 0/20	10 8 7 6 3	U – – – –	U – – – –
Magnesium-Lithium Alloy LA-141		1221			0.063	1/2 0/20	10 3	U –	U –
Magnesium Cups, Untreated		540				2/7	10	U	U
Magnesium Alloy HK 31	Dow Metal Products Company	1703	Magnesium, thorium, zirconium alloy		0.063	0/20	10	I	I
Magnesium Alloy M-1	Dow Metal Products Company	1702	Magnesium, aluminum, manganese alloy		0.063	2/20	10	U	U
Magnesium Alloy AZ-31	Dow Metal Products Company	1701	Magnesium, zinc, manganese alloy		0.063	2/3 1/4 0/11	10 5 3	U – –	U – –

TABLE VI. METALS, ALLOYS, AND SURFACE TREATMENTS (Continued)

Material	Manufacturer or Source	Test No.	Composition	Remarks	Thickness (inch)	No. Reactions/ No. Tests	Energy Level Kg/m	Batch or Jar Rating	Material Rating
Magnesium Alloy M-1		1702	1/5% manganese			2/20	10	U	U
Magnesium HK-31XA-H24 Alloy	Metallic Materials Branch	9281	Magnesium-Thorium alloy		0.062	9/60	10	U	U
Magnesium HM-21XA Alloy	Metallic Materials Branch	9284			0.063	4/20 2/20 1/20	10 7.7 5.6	U	U
Mu Metal		4519			0.033	0/20	10	S	S
Metro LOX Rust Inhibitor	Metallic Materials Branch	9132	Calcium carbonate		0.050	0/20	10	S	BT
Mercury		11429			0.003	0/20	10	S	S
Neatpak Wire Solder 95/5	Federated Metal Division of American Smelting and Refining Company	5565	95% tin/5% silver	Stainless steel inserts used	0.007	10/20 11/20 3/20 2/20 3/20 0/20	10 8 6 4 2 1	U – – – – –	U – – – – –
P/M 452 ' Shim Spacer LOX Induce		3848			0.020	0/20	10	S	BT
Phos-IT	Wyandotte Chemical Company	10328			0.050	0/20	10	S	BT
34137 Connectors		7484		Stainless steel inserts Stainless steel inserts	0.072 0.090	0/17 1/20	10 10	I I	I I
Phoson 15 Hard Solder		5701	High silver content	Stainless steel inserts	0.020	0/20 0/20	11.3 10	S	BT
Q-21 Flux	Zophor Mills, Incorporated	6271			0.5 ml	12/20 9/20 9/20 4/20 2/20 0/20	10 8 6 4 2 1	U	U
Red-16 ACS Solution	General Dynamics Company	7980			0.050	0/20	10	S	BT
Sermetal (Type W) Inorganic Coating		7475		Stainless steel inserts dipped and air dried		0/20	10	I	BT

TABLE VI. METALS, ALLOYS, AND SURFACE TREATMENTS (Continued)

Material	Manufacturer or Source	Test No.	Composition	Remarks	Thickness (inch)	No. Reactions/ No. Tests	Energy Level Kg/m	Batch or Jar Rating	Material Rating
Silbond No. 45 Solder	United Wire and Supply Co.	758				0/20	10	S	BT
Silicon Carbide Abrasive in Bottom of Aluminum Cup		3173		150 mesh	0.032	0/20 0/20	10 5		
SN-10 Rosin Core Solder	Ray Manufacturing Alpha Metals	7625		Stainless steel insqrts Stainless steel inserts	0.031 0.001	4/20 0/20	10 10	U U	U U
Solder 60/40 Lead Tin Solder		5204	60% lead/40% tin		0.050	17/20	10	U	U
Solder No. 151B	Eutectic Welding Alloy Corporation	3534	90% tin, zinc, nickel		0.032	10/20 3/20 0/20	10 4 2	U – –	U – –
Solder No. 153	Eutectic Welding Alloy Corporation	3538	90% lead, 10% silver		0.032	3/20 2/22 0/20	10 7 5	U – –	U – –
Solder No. 155	Eutectic Welding Alloy Corporation	3541			0.032	2/35 2/20	10 8	U –	U –
Solder		34	50% tin, 50% lead	No flux		3/5 0/5	10 5	U	U
Solder		76	60% tin, 40% lead			2/6 1/6	10 3	U	U
Solder			60% tin, 40% lead	With flux		3/5 0/5	10 5	U	U
Solder, High Silver				Paste heated to 1000°F 5 minutes. Droplets degreased with trichloroethylene		0/20	10	S	BT
Speed Nuts Type C41055-632-27	Tennerman Products, Inc.	9294		Degreased with trichloroethylene	0.017	0/20	10	S	S
Steel, Rene 41 Stainless steel		4488			0.063	0/20	10	S	S
Steel, 18% Nickel Maraging Steel	Bethlehem Steel Company	4617		Heat Treatment 120D163		0/20	10	S	S

TABLE VI. METALS, ALLOYS, AND SURFACE TREATMENTS (Continued)

Material	Manufacturer or Source	Test No.	Composition	Remarks	Thickness (inch)	No. Reactions/ No. Tests	Energy Level Kg/m	Batch or Jar Rating	Material Rating
Steel, 19-9 DL Stainless Steel		4487			0.125	0/20	10	S	S
Steel Alloy No. CN-346	International Nickel Co.	3849	70% copper, 30% nickel		0.050	0/20	10	S	S
Steel – 17-4PH Alloy						0/20	10	S	S
Steel – 17-7PH Alloy		11431			0.020	0/20	10	S	S
Steel – 17-7PH Alloy		11430			0.030	0/20	10	S	S
Steel 440A	Space Division NAR	MC-1970				0/20	10	S	S
Stainless Steel Wool No. 4-33		379			0.50	1/2	10	U	U
						0/12	7	–	–
Steel Wool		380				3/4	10	U	U
						0/16	7	–	–
Stainless Steel 301 Alloy		2829			0.012	0/100	10	S	S
						0/100	5	–	–
Stainless Steel 301 Alloy		2818		Hand deburred	0.063	0/200	10	S	S
						0/100	5	–	–
Stainless Steel 302 Alloy		3603			0.094	0/20	10	S	S
Stainless Steel 304		11434			0.062	0/20	10	S	S
Stainless Steel 304		11435			0.030	0/20	10	S	S
Stainless Steel 304		11440			0.093	0/20	10	S	S
Stainless Steel 321		11441			0.030	0/20	10	S	S
Stainless Steel 321		11442			0.062	0/20	10	S	S
Stainless Steel 321		11443			0.093	0/20	10	S	S
Stainless Steel 347 Alloy		3631			0.062	0/20	10	S	S
Silver Plated Stainless Steel		2449			0.063	0/20	10	S	S
Steel Inserts MXB 1113		3018			0.063	0/20	10	S	S

TABLE VI. METALS, ALLOYS, AND SURFACE TREATMENTS (Continued)

Material	Manufacturer or Source	Test No.	Composition	Remarks	Thickness (inch)	No. Reactions/ No. Tests	Energy Level Kg/m	Batch or Jar Rating	Material Rating
Tin Plate (0.004 in.) on 421 Stainless Steel Inserts		1612			0.063	2/20	10	U	U
Tin Plate (0.001 in.) on Stainless Steel Inserts		2244			0.125	2/20 0/20	10 4	U –	U –
Tin Plate (0.002 in.) on Stainless Steel Inserts		2246			0.125	3/20 1/20 0/20	10 8 5	U – –	U – –
Tin Plate (0.0005 in.) in Stainless Steel Inserts		2235			0.125	2/5 1/20 0/20	10 5 4	U – –	U – –
Tin Plate (0.00025 in.) on Stainless Steel Inserts		2230			0.125	2/5 3/18 0/20	10 7 5	U – –	U – –
Titanium Alloy, 6Al-4V				Deburred	0.063	7/40 1/2 2/3 2/60 0/20	10 8 7 5 1	U – – – –	U – – – –
Titanium Alloy, 6Al-4V				Deburred	0.250	18/20 8/20 1/20	10 2 1	U – –	U – –
Titanium Alloy, 4Al-3 Mo-1V				Deburred	0.063	2/2 1/1 2/5 1/3 0/4	10 5 3 2 1	U – – – –	U – – – –
Titanium Alloy, RC55				Deburred	0.063	15/20 1/20 2/20 0/20	10 3 2 1	U – – –	U – – –
Titanium Alloy, 13V-11 Cr-3Al				Deburred	0.063	15/20 5/20 2/20 0/20 0/20	10 7 5 3 2	U – – – –	U – – – –

TABLE VI. METALS, ALLOYS, AND SURFACE TREATMENTS (Continued)

Material	Manufacturer or Source	Test No.	Composition	Remarks	Thickness (inch)	No. Reactions/ No. Tests	Energy Level Kg/m	Batch or Jar Rating	Material Rating
Titanium Alloy, 5Al-2.5 Sn				Deburred	0.125	15/20	10	U	U
						17/20	5	–	–
						8/20	3	–	–
						1/1	2	–	–
						2/20	1	–	–
Titanium Alloy, 5Al-2.5 Sn				Deburred	0.063	11/20	10	U	U
						3/20	5	–	–
						1/20	3	–	–
						1/20	2	–	–
						0/20	1	–	–
Titanium Alloy, 5 Al-2.5 Sn				Deburred	0.063	4/20	10	U	U
						1/20	5	–	–
Titanium Alloy, 5Al-2.5 Sn				Deburred	0.025	7/20	10	U	U
						2/20	5	–	–
						0/20	1	–	–
Titanium Alloy, 5Al-2.5 Sn				Deburred	0.010	2/40	10	U	U
						2/20	5	–	–
						0/20	3	–	–
Titanium Alloy, 75A	Allegheny Ludlum Steel Corporation			Steel inserts		2/2	10	U	U
						2/2	5	–	–
						2/4	3	–	–
Titanium Alloy, 140A	Allegheny Ludlum Steel Corporation			Steel inserts		4/4	10	U	U
						2/3	5	–	–
						2/3	3	–	–
Titanium Alloy	Ram Cru		Ram Cru-245	Steel inserts		2/2	10	U	U
						2/3	5	–	–
						1/15	3	–	–
Washer AN960PD416		2143	Anodized Type II Aluminum			1/60	10	S	BT
Young's Alloy Metal Washers	Ardel Corporation	3825			0.063	0/20	10	S	BT

Card #7

TABLE VI. METALS, ALLOYS, AND SURFACE TREATMENTS (Concluded)

Material	Manufacturer or Source	Test No.	Composition	Remarks	Thickness (inch)	No. Reactions/ No. Tests	Energy Level Kg/m	Batch or Jar Rating	Material Rating
Zirconium		3648			0.083	14/20	10	U	U
						8/20	5	–	–
						2/20	3	–	–
						2/20	2	–	–
						0/20	1	–	–
Wire Ceramic EZE-MO33AW9	Phelps Dodge Co.	4367				0/20	10	S	–
Wire AWG 38 Ceramic Coated Nickel clad silver	Physical Services Corp.	4369			0.01	0/20	10	S	S

TABLE VII. CHEMICALS, SOLVENTS, PAINTS, LEAK CHECK COMPOUNDS, DETERGENTS, AND MISCELLANEOUS MATERIALS

Material	Manufacturer or Source	Test No.	Composition	Remarks	Thickness (inch)	No. Reactions/ No. Tests	Energy Level Kg/m	Batch or Jar Rating	Material Rating
Acetic Acid		6035	Acetic acid		0.050	0/20	10	S	I
Acetone (Spectro Grade) Lot 30A		6910	Acetone		0.5 ml	12/20 12/20 5/20 4/20 8/20 4/20 3/20 1/20 3/20 0/20	10 9.0 7.62 6.24 4.85 3.46 2.08 2.08 1.39 1.39	U	U
Activated Charcoal	Kennedy Space Center	9862		Contract 8-030158	0.050	30/40 11/20 2/20 4/20 1/20	10 5.6 3.5 1.4 0.7	U	U
Activated Charcoal, AC-7096	Kennedy Space Center	9371			0.050	12/20	10	U	U
Activated Charcoal, AC-7096	Barnaby-Chaney Corp.	7843			0.050	12/20 10/20 10/20 13/20 9/20 3/20	10 7.7 5.6 3.5 1.4 0.7	U	U
Activated Charcoal 592	Barnaby-Chaney Corp.	9849			0.050	4/20 2/20 1/20 0/20	10 7.7 6.7 5.6	U	U
Aluminum Octoate	Witco Chemical Co., Inc.					6/20 0/20	10 5	U	U
Amyl Acetate, Normal		357				2/10	10	U	U
American Crown Soap, Type 6061	Hewitt Soap Company	10273			0.050	2/20	10	U	U

TABLE VII. CHEMICALS, SOLVENTS, PAINTS, LEAK CHECK COMPOUNDS, DETERGENTS, AND MISCELLANEOUS MATERIALS (Continued)

·ial	Manufacturer or Source	Test No.	Composition	Remarks	Thickness (inch)	No. Reactions/ No. Tests	Energy Level Kg/m	Batch or Jar Rating	Material Rating
Amvoy Solvent Detergent	Amvoy Soap Company	9772			0.050	0/20	10	S	BT
Aroclor 1254	Monsanto Chemical Corp.	657	Chlorinated hydrocarbon		0.050	0/20	10	U	BT
Aroclor 1254	Monsanto Chemical Corp.	656	Chlorinated hydrocarbon		0.001	9/20	10	U	BT
Asbestos Cement Composite	Test Laboratory	9910			0.125	0/20	10	S	BT
Benzene	Eastman Organic Chemical Company	9602		Violent Reactions	0.050	19/20 14/20 12/20 7/20 3/20 0/20	10 7.7 5.6 3.5 1.4 0.7	U	U
Benzene	Eastman Organic Chemical Company	9607		Violent reactions	0.025	20/20 10/20 10/20 8/20 4/20 0/20	10 7.7 5.6 3.5 1.4 0.7	U	U
Benzaldoxine	Eastman Organic Chemical Company	10203		Violent reactions	0.050	14/20 5/20 13/20 5/20 1/20	10 7.7 5.6 3.5 1.4	U	U
Benzyl Acetate	Eastman Organic Chemical Company	9296		Violent reactions	0.050	13/20 14/20 12/20 7/20 3/20 0/20	10 7.7 5.6 3.5 1.4 0.7	U	U
Benzyl Acetate	Eastman Organic Chemical Company	9307		Violent reactions	0.025	12/20 14/20 14/20 11/20 7/20 1/20	10 7.7 5.6 3.5 1.4 0.7	U	U

TABLE VII. CHEMICALS, SOLVENTS, PAINTS, LEAK CHECK COMPOUNDS, DETERGENTS, AND MISCELLANEOUS MATERIALS (Continued)

Material	Manufacturer or Source	Test No.	Composition	Remarks	Thickness (inch)	No. Reactions/ No. Tests	Energy Level Kg/m	Batch or Jar Rating	Material Rating
Benzyl Alcohol	Eastman Organic Chemical Company	9319		Violent reactions	0.050	20/20 14/20	10 7.7	U	U
	Company					14/20 20/20 20/20 20/20 20/20	7.7 5.6 3.5 1.4 0.7		
Benzyl Alcohol	Eastman Organic Chemical Company	9308		Violent reactions	0.025	20/20 20/20 20/20 20/20 20/20 20/20	10 7.7 5.6 3.5 1.4 0.7	U	U
Benzyl Methyl Ether	Eastman Organic Chemical Company	9512		Violent reactions	0.051	16/20 18/20 19/20 10/20 3/20 0/20	10 7.7 5.6 3.5 1.4 0.7	U	U
Benzyl Methyl Ether	Eastman Organic Chemical Company	9518		Violent reactions	0.025	13/20 15/20 17/20 13/20 3/20 0/20	10 7.7 5.6 3.5 1.4 0.7	U	U
Blast 3 Ultrasonic Cleaner	Narda Ultrasonic Corporation			Steel samples heated to 100°C in cleaner, rinsed, and dried		0/20	10	S	BT
Blast 3 Ultrasonic Cleaner	Narda Ultrasonic Corporation			50% solution evaporated dry		2/2 1/18	10 5	U –	U –
Blue Layout Dye	Octagon Process, Incorporated	9238		Lot B-2693		21/40	10	U	U
Black Marking Ink 73X	Independent Ink Company	7818		On anodized discs		25/40	10	U	U
Black Paint, Type Q36K802	Rinshed Mason Corporation	9395			0.005	15/20	10	U	U
Black Paint, Type Q36K802	Rinshed Mason Corporation	9396		Heat treated at 800°C for 370 sec.	0.005	2/30	10	U	U

TABLE VII. CHEMICALS, SOLVENTS, PAINTS, LEAK CHECK COMPOUNDS, DETERGENTS, AND MISCELLANEOUS MATERIALS (Continued)

Material	Manufacturer or Source	Test No.	Composition	Remarks	Thickness (inch)	No. Reactions/ No. Tests	Energy Level Kg/m	Batch or Jar Rating	Material Rating
Bromobenzene	Eastman Organic Chemical Company	9545		Violent reactions	0.054	11/20 16/20 15/20 9/20 2/20 0/20	10 7.7 5.6 3.5 1.4 0.7	U	U
Bromobenzene	Eastman Organic Chemical Company	9551		Violent reactions	0.026	15/20 17/20 11/20 5/20 8/20 4/20 0/20	10 7.7 5.6 3.5 2.8 2.1 1.4	U	U
Ortho-Dichlorobenzene	Eastman Organic Chemical Company	9328		Violent reactions	0.025	16/20 13/20 11/20 9/20 7/20 3/20 0/20	10 7.7 5.6 3.5 2.8 2.1 0.7	U	U
Para-Dichlorobenzene	Eastman Organic Chemical Company	9587		Violent reactions	0.050	8/20 9/20 5/20 5/20 4/20 2/20 0/20	10 7.7 5.6 3.5 2.8 2.1 0.7	U	U
1-Bromobutane	Eastman Organic Chemical Company	10105		Violent reactions	0.050	10/20 9/20 11/20 7/20 4/20 0/20	10 7.7 5.6 3.5 2.8 1.4	U	U
1-Bromobutane	Eastman Organic Chemical Company	10112		Violent reactions	0.025	15/20 10/20 13/20 10/20 5/20 0/20	10 7.7 5.6 3.5 2.8 1.4	U	U

TABLE VII. CHEMICALS, SOLVENTS, PAINTS, LEAK CHECK COMPOUNDS, DETERGENTS, AND MISCELLANEOUS MATERIALS (Continued)

Material	Manufacturer or Source	Test No.	Composition	Remarks	Thickness (inch)	No. Reactions/ No. Tests	Energy Level Kg/m	Batch or Jar Rating	Material Rating
Chlorobenzene	Eastman Organic Chemical Company	9623		Violent reactions	0.050	14/20 20/20 18/20 12/20 2/20 0/20	10 7.7 5.6 3.5 1.4 0.7	U	U
Chlorobenzene	Eastman Organic Chemical Company	9623		Violent reactions	0.025	14/20 20/20 18/20 12/20 2/20 0/20	10 7.7 5.6 3.5 1.4 0.7	U	U
Ortho-Dichlorobenzene	Eastman Organic Chemical Company	9320		Violent reactions	0.051	10/20 8/20 7/20 13/20 2/20 2/20 0/20 0/20	10 7.7 5.6 3.5 2.8 2.1 0.7 1.4	U	U
Cab-O-Sil HS-5		6610		Slurry of LOX and Cab-O-Sil		0/20	10	S	S
HT-56 Carbon Seal	Kennedy Space Center	7670	See Graphitor		0.063	0/20	10	S	BT
Carbon Seal	Borg Warner Corporation	10329	See HT-56		0.32	0/20	10	S	BT
Cleaner No. I	Davis Young Company	10277			0.010	7/40	10	S	BT
Ceramic No. 19 Inserts	Stathoms Instruments	5851		Stainless steel inserts	0.126	0/20	10	S	BT
Crud from LOX Tank West Area, F-1 Test Stand		6930				3/20	10	U	U
Carbon Tetrachloride, Technical Grade	Fisher Scientific Company	384				0/10	10	—	—
Carbon Tetrachloride, C.P.	Fisher Scientific Company	385		Residue from 5 ml.		0/20	10	S	S

TABLE VII. CHEMICALS, SOLVENTS, PAINTS, LEAK CHECK COMPOUNDS, DETERGENTS, AND MISCELLANEOUS MATERIALS (Continued)

Material	Manufacturer or Source	Test No.	Composition	Remarks	Thickness (inch)	No. Reactions/ No. Tests	Energy Level Kg/m	Batch or Jar Rating	Material Rating
Carbon Tetrachloride	Fisher Scientific Company	383		Evaporated to 5% original weight		0/20	10	S	S
Chloroethene Solvent, 1,1,1 Trichloroethane	Dow Chemical Company	353				0/20	10	S	S
Chlorinated Polyether		821				2/2 2/2	10 5	U —	BT —
Chloroform		354				0/20	10	S	BT
Chlorotrifluoro Hydrocarbon	Halocarbon Corporation					0/20	10	S	BT
Chromic Acid Anodizing Solution		233				0/10	10	U	U
Chlorinated Paraffin	Hercules Powder Company	568				1/7	10	U	U
Corning Glass Type 9010	Corning Glass Co.	2950				0/20	10	S	S
Corning Glass 0088	Corning Glass Co.	4472			0.125	0/20	10	S	S
1-Bromodecane	Eastman Organic Chemical Company	9729		Violent reactions	0.050	15/20 17/20 16/20 5/20 3/20 0/20	10 7.7 5.6 3.5 2.8 1.4	U	U
1-Bromodecane	Eastman Organic Chemical Company	9736		Violent reactions	0.025	10/20 9/20 11/20 5/20 2/20 0/20	10 7.7 5.6 3.5 2.8 1.4	U	U
1-Chlorodecane	Eastman Organic Chemical Company	9679		Violent reactions	0.050	16/20 16/20 15/20 8/20 4/20 0/20	10 7.7 5.6 3.5 2.8 1.4	U	U

TABLE VII. CHEMICALS, SOLVENTS, PAINTS, LEAK CHECK COMPOUNDS, DETERGENTS, AND MISCELLANEOUS MATERIALS (Continued)

Material	Manufacturer or Source	Test No.	Composition	Remarks	Thickness (inch)	No. Reactions/ No. Tests	Energy Level Kg/m	Batch or Jar Rating	Material Rating
1-Chlorooctadecane	Eastman Organic Chemical Company	9691		Violent reactions	0.050	19/20 20/20 20/20 7/20 5/20 0/20	10 7.7 5.6 3.5 2.8 1.4	U	U
Deak No. I		1959			0.050	2/20	10	U	U
Dioctyl Phthalate		340		Violent reaction	0.050	2/10	10	U	U
Dowell F-33	Dow Chemical Company	7118		Concentrate	0.050	6/20	10	U	U
Dowell F-33	Dow Chemical Company	9119		0.1% solution		0/20	10	S	BT
Dyna-Therm 7275	Dyna-Therm Chemical Corporation	5058			0.010	1/20 2/6 2/4 2/7 2/14 0/20	10 5 4 3 2 1	U	U
Ethylene Glycol Ethylene Glycol 25% in water		625		Violent reaction	0.050 0.050	1/20 0/20	10 10	U BT	U BT
Ferrite Core Material 3C		3617				0/6	10	I	I
Ferrox Safety Floor Covering	American Abrasive Metal Company	1917				1/1 2/2 2/2 2/6	10 5 2 1	U – – –	U – – –
Flo-Master Ink	Cushman & Denison Manufacturing Company	5427		Violent reaction	0.050	8/20	10	U	U
Floor Sealer	Texize Corporation	8766		On anodized discs		11/20	10	U	U
Flaxsoap Detergent	Kennedy Space Center	9907	Vegetable oil detergent			6/20	10	U	U
Fluorescein		511	Disodium salt	2 1/2 ml of 5% solution evaporated to dryness		2/2 2/5	10 5	U	U

TABLE VII. CHEMICALS, SOLVENTS, PAINTS, LEAK CHECK COMPOUNDS, DETERGENTS, AND MISCELLANEOUS MATERIALS (Continued)

Material	Manufacturer or Source	Test No.	Composition	Remarks	Thickness (inch)	No. Reactions/ No. Tests	Energy Level Kg/m	Batch or Jar Rating	Material Rating
Fluoroalkyl Camphorate	E.I. du Pont de Nemours & Company, Incorporated					2/14 0/6	10 5	U –	U –
Fluorosilicone Polymer, Distilled						2/2 2/9 0/9	10 5 2	U – –	U – –
F-33 Detergent	Dow Chemical Company	993		0.1% solution		0/20	11	BT	BT
F-33 Detergent	Dow Chemical Company	6965		Concentrate	0.5 ml	2/20	10	U	U
FN Leak Detector	Fluid Scientific, Inc.	9391		On anodized discs		0/20	10	S	BT
Freon 113 (PCA)	E.I. du Pont de Nemours & Company, Incorporated	8256			0.050	0/20	10	S	S
Freon 113 (PCA)	E.I. du Pont de Nemours & Company, Incorporated	10266		Lot 81-7M	0.050	0/20	10	S	S
Genesolv D	Allied Chemical Company	10267		Electronic grade	0.050	1/60	10	S	S
Graphitor LOX Pump Seal	Kennedy Space Center	9908	See HT56	As received	0.050	9/20	10	U	BT
Graphitor LOX Pump Seal	Kennedy Space Center	9909	See Carbon Seal	Washed in F-33	0.050	1/20	10	S	BT
Getter Material	Union Carbide, Linde Division	6260	Palladium oxide	Stainless steel cups, Powder		0/20	10	S	S
Heck Check, Type I	The Heckerman Corporation	7558		Atuminum discs drained at 90° angle		2/20	10	U	U
Heck Check, Type II	The Heckerman Corporation	7560		Aluminum discs drained at 90° angle		2/20	10	U	U
Hexafluoropentamethylene Adipate Polyester	Hooker Electrochemical Company					2/11 0/9	10 5	U –	U –
1-Bromoheptane	Eastman Organic Chemical Company	10119			0.030	9/20 10/20 12/20 9/20 4/20	10 7.7 5.6 4.2 3.2	U	U

TABLE VII. CHEMICALS, SOLVENTS, PAINTS, LEAK CHECK COMPOUNDS, DETERGENTS, AND MISCELLANEOUS MATERIALS (Continued)

Material	Manufacturer or Source	Test No.	Composition	Remarks	Thickness (inch)	No. Reactions/ No. Tests	Energy Level Kg/m	Batch or Jar Rating	Material Rating
1-Bromoheptane	Eastman Organic Chemical Company	10128		Violent reactions	0.025	9/20 11/20 8/20 3/20 0/20	10 7.7 4.2 3.5 1.4	U	U
1-Chloroheptane	Eastman Organic Chemical Company	9667		Violent reactions	0.050	15/20 12/20 12/20 3/20	10 7.7 5.6 4.2	U	U
Bromocyclohexane	Eastman Organic Chemical Company	10219		Violent reactions	0.050	7/20 2/20 1/20	10 7.7 7	U	U
1-Bromohexane	Eastman Organic Chemical Company	9705		Violent reactions	0.050	16/20 17/20 15/20 11/20 3/20 2/20 0/20	10 7.7 5.6 3.5 2.8 2.1 1.4	U	U
Hexanoic Acide	Eastman Organic Chemical Company	9432		Violent reactions	0.050	13/20 8/20 11/20 10/20 2/20 0/20	10 7.7 5.6 3.5 1.4 0.7	U	U
Hexanol 2	Eastman Organic Chemical Company	9534		Violent reactions	0.050	17/20 14/20 10/20 8/20 2/20 0/20	10 7.7 5.6 3.5 1.4 0.7	U	U

TABLE VII. CHEMICALS, SOLVENTS, PAINTS, LEAK CHECK COMPOUNDS, DETERGENTS, AND MISCELLANEOUS MATERIALS (Continued)

Material	Manufacturer or Source	Test No.	Composition	Remarks	Thickness (inch)	No. Reactions/ No. Tests	Energy Level Kg/m	Batch or Jar Rating	Material Rating
N-Hexyl Ether	Eastman Organic Chemical Company	9495		Violent reactions	0.025	18/20 16/20 15/20 13/20 3/20 0/20	10 7.7 5.6 3.5 1.4 0.7	U	U
N-Hexyl Formate	Eastman Organic Chemical Company	10196		Violent reactions	0.050	11/20 15/20 14/20 3/20 1/20 0/20	10 7.7 5.6 3.5 2.8 1.4	U	U
Ink, Tech Pen, Black	Mark-Tex Corporation	437				3/17	10	U	U
Joy Detergent, 5% Solution Evaporated to Dryness		472				2/2 2/5	10 5	U –	U –
K-1008 Red Ink	Minnesota Mining and Manufacturing Company	6382		Novabestos		0/20	10	S	BT
Lauric Acid Solution		6064	Lauric acid (Dodecanoic acid)	Smeared on stainless steel inserts, air dried	Approx. 0.002	4/20 5/20 2/20	10 5 2	U	U
Lauric Acid Solution		6063	Lauric acid (Dodecanoic acid)		0.050	2/2 2/4 2/6 2/8	10 8 6 4	U	U
Liberty Stamp Pad Ink	Liberty Ink Company	6263		Evaporated to paste	0.25 ml	3/20	10	U	U
MX-15 Rust Inhibitor	Cee Bee Chemical Company	6016 6452		Powder Powder	Approx. 0.050	2/20 0/20	10 10	U S	I I
Methyl and Fluoro Silicone Copolymer		808				2/2 2/4 2/7	10 5 2	U – –	U – –
Mothand Caulking Compound	Moore-Handley Hardware Company	3328				19/20 10/20 9/20 0/20	10 5 2 1	U – – –	U – – –

TABLE VII. CHEMICALS, SOLVENTS, PAINTS, LEAK CHECK COMPOUNDS, DETERGENTS, AND MISCELLANEOUS MATERIALS (Continued)

Material	Manufacturer or Source	Test No.	Composition	Remarks	Thickness (inch)	No. Reactions/ No. Tests	Energy Level Kg/m	Batch or Jar Rating	Material Rating
N-Hexyl Ether	Eastman Organic Chemical Company	9495		Violent reactions	0.025	18/20 16/20 15/20 13/20 3/20 0/20	10 7.7 5.6 3.5 1.4 0.7	U	U
N-Hexyl Formate	Eastman Organic Chemical Company	10196		Violent reactions	0.050	11/20 15/20 14/20 3/20 1/20 0/20	10 7.7 5.6 3.5 2.8 1.4	U	U
Ink, Tech Pen, Black	Mark-Tex Corporation	437				3/17	10	U	U
Joy Detergent, 5% Solution Evaporated to Dryness		472				2/2 2/5	10 5	U —	U —
K-1008 Red Ink	Minnesota Mining and Manufacturing Company	6382		Novabestos		0/20	10	S	BT
Lauric Acid Solution		6064	Lauric acid (Dodecanoic acid)	Smeared on stainless steel inserts, air dried	Approx. 0.002	4/20 5/20 2/20	10 5 2	U	U
Lauric Acid Solution		6063	Lauric acid (Dodecanoic acid)		0.050	2/2 2/4 2/6 2/8	10 8 6 4	U	U
Liberty Stamp Pad Ink	Liberty Ink Company	6263		Evaporated to paste	0.25 ml	3/20	10	U	U
MX-15 Rust Inhibitor	Cee Bee Chemical Company	6016 6452		Powder Powder	Approx. 0.050	2/20 0/20	10 10	U S	I I
Methyl and Fluoro Silicone Copolymer		808				2/2 2/4 2/7	10 5 2	U — —	U — —
Morhand Caulking Compound	Moore-Handley Hardware Company	3328				19/20 10/20 9/20 0/20	10 5 2 1	U — — —	U — — —

TABLE VII. CHEMICALS, SOLVENTS, PAINTS, LEAK CHECK COMPOUNDS, DETERGENTS, AND MISCELLANEOUS MATERIALS (Continued)

Material	Manufacturer or Source	Test No.	Composition	Remarks	Thickness (inch)	No. Reactions/ No. Tests	Energy Level Kg/m	Batch or Jar Rating	Material Rating
Magnesium Oxide		1951				0/20	10	S	S
Oxylene Evaporated to 5% Original Volume	John B. Moore Corporation	664	Freon 11 and Methylene chloride			0/20	10	S	BT
Methyl Fluorosiloxane	General Precision Company	10068		Violent reactions	0.040	18/40	10	U	U
Nero-Fill (S-2) Carbon	Great Lakes Carbon Products Company	10038			0.050	0/20	10	S	BT
Nessin Metal Marker	J.P. Nessin, Jr. Company	8725			0.004	6/20	10	U	U
Oakite 33 Cleaner	6962	6962			0.5 ml	0/20	10	S	BT
Oakite 34		6961		Granules		0/20	10	S	BT
Oxy-Tec, Type 1, (Oxygen Leak Detector)	American Gas and Chemical Company								
Bottle No. 1		7311			0.5 ml	0/20	10	S	BT
Bottle No. 1		7312		Aluminum discs drained at 90° angle		0/20	10	S	BT
Bottle No. 2		7310			0.5 ml	0/20	10	S	BT
Bottle No. 2		7313		Aluminum discs drained at 90° angle		0/20	10	S	BT
Paper Pockets	Straza Industries	10039			0.009	7/20	10	U	U
Paint, White		5740	One coat Indurall (MIL-P-8585A) and one coat Glidden white (MIL-E-5556)			3/20	10	U	U
Paint, Black		5739	One coat Indurall (MIL-P-8585A) and one coat Warren black			2/20 8/20	10 6	U —	U —
Paint, Green		5742	Indurall (MIL-P-8585A) Color No. 34151-S-3035 (one coat)			5/20 6/20	10 6	U —	U —

TABLE VII. CHEMICALS, SOLVENTS, PAINTS, LEAK CHECK COMPOUNDS, DETERGENTS, AND MISCELLANEOUS MATERIALS (Continued)

Material	Manufacturer or Source	Test No.	Composition	Remarks	Thickness (inch)	No. Reactions/ No. Tests	Energy Level Kg/m	Batch or Jar Rating	Material Rating
Paint, White		5744	Glidden white (MIL-E-5556)			5/20	10	U	U
Passivating Solution (Steel)		5429	Solution consisting of 0.25% disodium phosphate, 0.25% monosodium phosphate, 0.50% sodium nitrate and water			0/20	10	S	S
Chloronapthalene	Eastman Organic Chemical Company	10214		Violent reactions	0.050	13/20 5/20 1/20 0/20	10 7.7 7.0 5.6	U	U
Bromocyclopentane	Eastman Organic Chemical Company	10189		Violent reactions	0.050	7/20 8/20	10 7.7	U	U
1-Bromopentane	Eastman Organic Chemical Company	10069		Violent reactions	0.050	19/20 19/20 14/20 4/20 2/20 0/20	10 7.7 5.6 3.5 2.8 1.4	U	U
1-Bromopentane	Eastman Organic Chemical Company	10076		Violent reactions	0.025	14/20 11/20 12/20 3/20 0/20	10 7.7 3.5 2.8 1.4	U	U
1-5-Dibromopentane	Eastman Organic Chemical Company	10208		Violent reactions	0.050	8/20 4/20 5/20 3/20 1/20 0/20	10 7.7 5.6 3.5 2.1 1.4	U	U
1-Bromopropane	Eastman Organic Chemical Company	10191		Violent reactions	0.050	9/20 4/20 8/20 7/20 1/20	10 7.7 5.6 3.5 1.4	U	U

TABLE VII. CHEMICALS, SOLVENTS, PAINTS, LEAK CHECK COMPOUNDS, DETERGENTS, AND MISCELLANEOUS MATERIALS (Continued)

Material	Manufacturer or Source	Test No.	Composition	Remarks	Thickness (inch)	No. Reactions/ No. Tests	Energy Level Kg/m	Batch or Jar Rating	Material Rating
2-Chloropropane	Eastman Organic Chemical Company	9645		Violent reactions	0.050	17/20 18/20 18/20 13/20 5/20 0/20	10 7.7 5.6 3.5 1.4 0.7	U	U
2-Chloropropane	Eastman Organic Chemical Company	9651		Violent reactions	0.025	15/20 16/20 15/20 11/20 3/20 0/20	10 7.7 5.6 3.5 1.4 0.7	U	U
1-2-Dibromopropane	Eastman Organic Chemical Company	10136		Violent reactions	0.050	8/20 6/20 7/20 1/20 0/20	10 7.7 5.6 3.5 1.4	U	U
1-2-Dibromopropane	Eastman Organic Chemical Company	10143		Violent reactions	0.025	11/20 12/20 13/20 4/20 1/20 0/20	10 7.7 5.6 3.5 2.8 1.4	U	U
1-3-Dibromopropane	Eastman Organic Chemical Company	10182		Violent reactions	0.050	8/20 7/20 3/20 1/20 0/20	10 7.7 5.6 3.5 1.4	U	U
Bromoctane	Eastman Organic Chemical Company	10175		Violent reactions	0.050	11/20 14/20 16/20 9/20 2/20 0/20	10 7.7 5.6 4.9 4.2 2.8	U	U
Perchloroethylene Liquid	Hooker Electrochemical Company	358				0/20	10	S	S

TABLE VII. CHEMICALS, SOLVENTS, PAINTS, LEAK CHECK COMPOUNDS, DETERGENTS, AND MISCELLANEOUS MATERIALS (Continued)

Material	Manufacturer or Source	Test No.	Composition	Remarks	Thickness (inch)	No. Reactions/ No. Tests	Energy Level Kg/m	Batch or Jar Rating	Material Rating
Perchloropentacyclo Decane	Hooker Electrochemical Company	817				0/20	10	S	BT
No. 67 Purified	Pittman-Dunn Laboratory					0/20	10	S	BT
Perfluorotributylamine, (Purified)	Pittman-Dunn Laboratory	812				0/20	10	S	BT
Perfluorotributylamine and Chlorotrifluorohydrocarbon (1:1)	Frankford Arsenal	3569				0/20	10	S	BT
Pluronic L-62-F Detergent	Wyandotte	7616		0.1 percent solution, on aluminum discs drained at 90° angle		0/20	10	S	BT
Pluronic L-62-F Detergent	Wyandotte	7615		Concentrated solution, on aluminum discs, drained at 90° angle		16/20	10	U	U
Pluronic L-62-LF Nonionic Detergent	Wyandotte	7650		0.5 percent solution	0.5 ml	0/20	10	S	BT
Pluronic L-62-LF Nonionic Detergent	Wyandotte	7649		Aluminum discs drained at 90° angle, 0.5% solution		0/20	10	S	BT
Polyglycol 11-200, Lot 261	Dow Chemical Company	931		Violent	0.050	1/20	10	U	U
Polyglycol 15-200	Dow Chemical Company	932	Polyoxyalkylene ethers with methyl side chains and terminal hydroxyl groups		0.050	2/12	10	U	U
Polyglycol 166-900	Dow Chemical Company	1940			0.050	0/20	10	I	I
Polyglycol 174-500	Dow Chemical Company	929	Polypropylene glycol	Violent	0.050	1/20	10	I	U
Polyglycol P-400	Dow Chemical Company	934	Polypropylene glycol		0.050	2/20	10	U	U
Polyglycol P-2000	Dow Chemical Company	933	Polypropylene glycol		0.050	2/2	10	U	U
Quartz (Clear Fused) Sample I-1551-A-20X		1776			0.050	0/20	10	S	S

TABLE VII. CHEMICALS, SOLVENTS, PAINTS, LEAK CHECK COMPOUNDS, DETERGENTS, AND MISCELLANEOUS MATERIALS (Continued)

Material	Manufacturer or Source	Test No.	Composition	Remarks	Thickness (inch)	No. Reactions/ No. Tests	Energy Level Kg/m	Batch or Jar Rating	Material Rating
Rely-On Caulking Compound	DAP Incorporated	3331				12/20 13/20 13/20 3/20	10 5 2 1	U – – –	U – – –
Rust Oleum A-4208-50 Launch Grey Paint	Rust Oleum Corporation	5180		Dip coat	0.005	0/40	10	S	BT
Safety Walk Type B	Minnesota Mining and Manufacturing Company	1916				1/1 2/2 4/20	10 5 0.75	U – –	U – –
Semco Bubble Check DPS 4.905	Semco Sales and Service	3450				0/40	10	S	BT
Sherlock Leak Detector, Type I	Winton Products Company	8258		Batch 12135		0/20	10	S	BT
Sherlock Lead Detector, Type II	Winton Products Company	8259		Batch 3564		5/20	10	U	BT
Sherlock, 5 Second Leak Detector, Type II	Winton Products Company	5672		2.5 ml evaporated at 100°C	2.5 ml	1/60	10	S	BT
Sherlock C G-1 Bubble Tester		3419				0/40	10	S	BT
Silica Gel, Indicating 6-16 Mesh	E.H. Sargent and Company	2492				0/20	10	S	S
Spotcheck Cleaner Type SKC-2-1	Magnaflux Corporation		Chlorinated hydrocarbon			0/60	10	S	S
Snoop Leak Detector	Nuclear Products Company	430				0/20	10	S	BT
Skript Writing Fluid Permanent No. 54, Royal Blue	Shaeffer Pen Company	6264		Evaporated to dryness	0.25 ml	0/20	10	S	BT
Skript Writing Fluid, Permanent No. 54, Royal Blue	Shaeffer Pen Company	6266			0.25 ml	0/20	10	S	BT
Skydrol 500	Monsanto Chemical Company	455				1/4 0/20	10 7	U –	U –

TABLE VII. CHEMICALS, SOLVENTS, PAINTS, LEAK CHECK COMPOUNDS, DETERGENTS, AND MISCELLANEOUS MATERIALS (Continued)

Material	Manufacturer or Source	Test No.	Composition	Remarks	Thickness (inch)	No. Reactions/ No. Tests	Energy Level Kg/m	Batch or Jar Rating	Material Rating
Swift Soap 40/45	Swift and Company	10280			0.050	3/20	10	U	U
Soap 6606	Hewitt Soap Company	10279			0.050	12/20	10	U	U
Soap 6602	Hewitt Soap Company	10274			0.050	3/20	10	U	U
Soap 6603 Easy Flow	Hewitt Soap Company	10275			0.050	2/20	10	U	U
Sodium-Dichromate		584				0/20	10	S	S
Sodium Silicate	Fisher Scientific Company	3393				0/20 0/40	10 5	S —	S —
Solution of 30 percent NaOH and 9 g/L of Gum Tragacanth		6929	30 percent solution NaOH and gum tragacanth	Stainless steel cups	0.5 ml	0/20	10	S	I
Stoddard Solvent		553		Extremely violent explosion		1/9	10	U	U
Tech-Pen Ink Type K	Mark-Tex Corporation	7060			0.10	15/20	10	U	U
Work Glove MSA 87633	Mine Safety Appliances	6248		Stainless steel inserts	0.075	20/20	10	U	U
Tetrone AC	E.I. du Pont de Nemours & Company, Incorporated	1952				3/20	10	U	U
Tenamene – 3	Dow Chemical Company	3544				1/1 1/3 1/4	10 2 1	U — —	U — —
Torque Paint	Eronel Industries	8251		Room temperature cured for 20 hrs.	0.012	8/20	10	U	U
Triton X-100	Kennedy Space Center	8845			0.050	6/20	10	U	U
Triclene WR	Metallic Materials Branch	10257	1-1-1 Trichloroethylene		0.050	0/20	10	S	BT
1-1-1-Trichloroethane	Metallic Materials Branch	8380			0.050	0/20	10	S	S
Thermocolor Number 34 Temperature Sensitive Point	Bodishe Awilin-Soda Fabrik	430				3/20	10	U	U

TABLE VII. CHEMICALS, SOLVENTS, PAINTS, LEAK CHECK COMPOUNDS, DETERGENTS, AND MISCELLANEOUS MATERIALS (Continued)

Material	Manufacturer or Source	Test No.	Composition	Remarks	Thickness (inch)	No. Reactions/ No. Tests	Energy Level Kg/m	Batch or Jar Rating	Material Rating
Thermocolor Number 15 Temperature Sensitive Point	Bodishe Awilin-Soda Fabrik	431				0/20	10	I	I
Tide Detergent	Proctor and Gamble Company	417		2 ml 1% solution evaporated to dryness		4/20	10	U	U
Trichloroethylene Evaporation Residue	Du Pont Trichloroethylene			Four batches tested		3/17 2/2	10 10	U –	BT –
Trichloroethylene, Extraction Grade, Evaporation Residue		544				0/2	10	C	I
Trichloroethylene, Missile Grade, Liquid		396				0/20	10	S	S
Trichloroethylene, Liquid	Dow Chemical Company	486		Liquid		0/20	10	S	S
Trichloroethylene (Perma-A-Chlor-NA) Residue	E.I. du Pont de Nemours & Company, Incorporation	397		10 mg		2/5 2/15	10 5	U –	BT –
Trichloroethylene (Perma-A-Chlor-NA) Residue	E.I. du Pont de Nemours & Company, Incorporated			5 mg		2/4 1/16	10 5	U –	BT –
Trichloroethylene (Perma-A-Chlor-NA) Residue	E.I. du Pont de Nemours & Company, Incorporated			25 mg		1/20	10	C	BT
Trichloroethylene (Triclene D)	E.I. du Pont de Nemours & Company, Incorporated	361		Sensitivity varies from batch to batch		0-2/20	10	C	BT
Trichloroethylene Evaporation Residue	Detrex Trichloroethylene			Liquid		0/20	10	S	S
Trichloroethylene Evaporation Residue Lot No. 218	Detrex Trichloroethylene			Liquid		0/20	10	S	S
Trichloroethylene Evaporation Residue Lot No. WB83	Detrex Trichloroethylene	544		Liquid		0/20	10	S	S
Tricresyl Phosphate		954				5/20	10	U	U
Trilauryl Silicon Fluoride	Frankford Arsenal					2/5 1/4	10 5	U –	U –

TABLE VII. CHEMICALS, SOLVENTS, PAINTS, LEAK CHECK COMPOUNDS, DETERGENTS, AND MISCELLANEOUS MATERIALS (Concluded)

Material	Manufacturer or Source	Test No.	Composition	Remarks	Thickness (inch)	No. Reactions/ No. Tests	Energy Level Kg/m	Batch or Jar Rating	Material Rating
Vycor Glass, Corning Type 7913	Corning Glass Works	1693				0/20	10	S	S
Vermiculite (hydrated) Magnesium, Aluminum, Iron Silicate						0/20	10	S	S
Vel Pink Liquid Detergent	Colgate-Palmolive Peet Co.	4898	Novabestos 7511T soaked in Vel for one hour. Dried for one hour at 60°C			17/20	10	U	U
Vel Pink Liquid Detergent	Colgate-Palmolive Peet Co.	4497			0.050	0/20	10	U	U
Warren Spray Enamel Primer (Brown)	Warren Paint and Color Company	3245				4/20 2/20	10 5	U –	U –
Warren Spray Enamel Yellow Zinc Chromate	Warren Paint and Color Company	3247				2/20	10	U	U
Zinc Chromate Paste	389	389				3/20 1/20 2/20	10 5 2	U – –	U – –
Zinc Chromate (SPEC-MIL-P-8585	Chromatone Corporation	3526				2/20 2/20 0/20	10 5 1	U – C	U – C
1,3,5-Trimethyl, 2,4,6-Trifluoro Benzene	Illinois State Geological Survey					1/20	10	C	C

TABLE VIII. PENETRANTS AND PENETRANT COMPONENTS

Material	Manufacturer or Source	Test No.	Sample Preparation	Remarks	Thickness (inch)	No. Reactions/ No. Tests	Energy Level Kg/m	Batch or Jar Rating	Material Rating
Fluoro Finder FL-50 Penetrant	Testing Systems, Incorporated	8597		On anodized discs		20/20	10		U
D-492A (24-44-4) Developer	Shannon Luminous Materials Company	4895	0.50 cc volume in in test cup	High sensitivity mixed 1/2 pound per gallon		0/20	10	–	BT
D-492A (24-44-4) Developer	Shannon Luminous Materials Company	4894	0.25 cc volume in test cup			0/20	10	–	BT
D-492A (24-44-4) Developer	Shannon Luminous Materials Company	4893	0.50 cc volume oven dried 30 minutes at 100°C			0/20	10	–	BT
D-492A (24-44-4) Developer	Shannon Luminous Materials Company	4892	0.50 cc volume vacuum dried for 45 minutes			0/20	10	–	BT
D-498 Developer	Shannon Luminous Materials Company	4913	0.05 inch in test cup	High sensitivity mixed 1/2 pound per gallon		0/20	10	–	BT
E-159 (25-7-3) E[illegible]sifier	Shannon Luminous Materials Company	4914	0.50 cc volume in test cup	Emulsifier for P-505 Penetrant		0/20	10	–	U
E-159 (25-7-3) Emulsifier	Shannon Luminous Materials Company	4909	0.25 cc volume in test cup			3/20	10	–	U
E-159 (25-7-3) Emulsifier	Shannon Luminous Materials Company	4907	0.50 cc volume, oven [illegible] at 100°C for 3 hours, 30 minutes			5/20	10	–	U
E-159 (25-7-3) Emulsifier	Shannon Luminous Materials Company	4900	0.50 cc volume, vacuum dried			2/20	10	–	U
E-159 (25-7-3) Emulsifier	Shannon Luminous Materials Company	4910	Novabestos 7511T soaked in E-159 for 1 hour, oven dired at 60°C for 30 minutes	Emulsifier for P-505 Penetrant		20/20	10	–	U
Tracer Tech Cleaner K-4-10A	Shannon Luminous Materials Company	10384		On anodized discs		0/20	10		BT
E-153 Emulsifier	Consolidated American Services, Inc.	4239	0.50 cc volume in test cup	Emulsifier for P-148 Penetrant		14/20 1/7 1/8	10 5 3		U

TABLE VIII. PENETRANTS AND PENETRANT COMPONENTS (Continued)

Material	Manufacturer or Source	Test No.	Sample Preparation	Remarks	Thickness (inch)	No. Reactions/ No. Tests	Energy Level Kg/m	Batch or Jar Rating	Material Rating
P-138 Penetrant	Consolidated American Services, Inc.	4242	0.50 cc volume in test cup	Water-washable		2/4 2/12	10 5	– –	U –
P-148 Penetrant	Consolidated American Services, Inc.	4241	0.50 cc volume in test cup	Post emulsifiable		3/8 2/5 1/1	10 5 3		U
P-236 (22-83-2) Shannon Glow Penetrant	Consolidated American Services, Inc.	4249	0.50 cc volume in test cup	Corrodes aluminum alloys		0/40	10	–	BT
P-236 (22-83-2) Shannon Glow Penetrant	Consolidated American Services, Inc.	4248	0.25 cc volume in test cup	Corrodes aluminum alloys		0/20	10	–	BT
P-236 (22-83-2) Shannon Glow Penetrant	Consolidated American Services, Inc.	4302	0.25 cc volume in test cup	Batch No. 1		0/40	10	–	BT
P-236 (22-83-2) Shannon Glow Penetrant	Consolidated American Services, Inc.	4300	0.25 cc volume in test cup	Batch No. 2		0/40	10	–	BT
P-236 (22-83-2) Shannon Glow Penetrant	Consolidated American Services, Inc.	4298	0.25 cc volume in test cup	Batch No. 3		0/40	10	–	BT
P-236 (22-83-2) Shannon Glow Penetrant	Consolidated American Services, Inc.	4244	2 cc volume evaporated to dryness	Batch No. 3		0/20	10	–	BT
P-236 (22-83-2) Shannon Glow Penetrant	Consolidated American Services, Inc.	4297	2.50 cc volume evaporated to dryness	Batch No. 3		0/20	10	–	BT
Tracer Tech P-133 Penetrant	Shannon Luminous Materials Company	9394		On anodized discs		20/20	10	U	U
P-505 (25-7-5) Penetrant	Shannon Luminous Materials Company	4919	0.50 cc volume in test cup			0/20	10	–	BT
P-505 (25-7-5) Penetrant	Shannon Luminous Materials Company	4908	0.25 cc volume in test cup			0/20	10	–	BT
P-505 (25-7-5) Penetrant	Shannon Luminous Materials Company	4918	0.50 cc volume oven dried for 1 hour			0/20	10	–	BT
P-505 (25-7-5) Penetrant	Shannon Luminous Materials Company	4735	0.50 cc volume oven at 100°C for 11 hours			1/6	10	–	BT

TABLE VIII. PENETRANTS AND PENETRANT COMPONENTS (Continued)

Material	Manufacturer or Source	Test No.	Sample Preparation	Remarks	Thickness (inch)	No. Reactions/ No. Tests	Energy Level Kg/m	Batch or Jar Rating	Material Rating
P-505 (25-7-5) Penetrant	Shannon Luminous Materials Company	4911	Novabestos 7511T (0.020) soaked in penetrant for 1 hour, oven dried at 60°C for 30 minutes, left in oven overnight with heat off			0/20	10	–	BT
Tracer Tech P-545 (30-7-2) Penetrant	Shannon Luminous Materials Company	10383		On anodized discs		0/20	10	–	BT
P-600 (25-40-5) W/W Diamorphic Tracer-Tech Penetrant	Shannon Luminous Materials Company	5278	0.50 cc volume in test cup			0/20	10	–	BT
P-600 (25-40-5) W/W Diamorphic Tracer-Tech Penetrant	Shannon Luminous Materials Company	5279	0.25 cc volume in test cup			2/20	10	–	BT
P-600 (25-40-5) W/W Diamorphic Tracer-Tech Penetrant	Shannon Luminous Materials Company	5277	0.50 cc volume oven dried for 3 hours at 100°C			7/20	10	–	BT
P-605 (25-40-4) W/W Diamorphic Tracer-Tech Penetrant	Shannon Luminous Materials Company	5286	0.50 cc volume in test cup			0/20	10	–	U
P-605 (25-40-4) W/W Diamorphic Tracer-Tech Penetrant	Shannon Luminous Materials Company	5285	0.25 cc volume in test cup			0/20	10	–	U
P-605 (25-40-4) W/W Diamorphic Tracer-Tech Penetrant	Shannon Luminous Materials Company	5281	0.50 cc volume oven dried at 100°C for 3 hours			6/20	10	–	U
P-605 (25-40-4) W/W Diamorphic Tracer-Tech Penetrant	Shannon Luminous Materials Company	5284	0.50 cc volume vacuum dried for 3 hours			6/20	10	–	U
P-605-W (25-40-4) Diamorphic Tracer-Tech Penetrant	Shannon Luminous Materials Company	5879	0.50 cc volume in test cup			0/20	10	–	U
P-605-W (25-40-4) Diamorphic Tracer-Tech Penetrant	Shannon Luminous Materials Company	5884 5883	0.25 cc volume in test cup			5/20	10	–	U
P-605-W (25-40-4) Diamorphic Tracer-Tech Penetrant	Shannon Luminous Materials Company	5876	0.50 cc volume oven dried at 100°C to approximately 0.25 cc			15/40	10	–	U

TABLE VIII. PENETRANTS AND PENETRANT COMPONENTS (Continued)

Material	Manufacturer or Source	Test No.	Sample Preparation	Remarks	Thickness (inch)	No. Reactions/ No. Tests	Energy Level Kg/m	Batch or Jar Rating	Material Rating
P-605-W (25-40-4) Diamorphic Tracer-Tech Penetrant	Shannon Luminous Materials Company	5882 5881 5880	Novabestos 7511T soaked in penetrant for 1 hour, drained for 30 minutes, dried at 60°C for 30 minutes			20/20 20/20 20/20	10 2 1	– – –	U – –
P-605-W (25-40-4) Diamorphic Tracer-Tech Penetrant	Shannon Luminous Materials Company	5941 5940 5939	Anodized aluminum discs dipped in penetrant, drained on edge 15 min.	Per Shannon Luminous Materials Co. Specification		20/20 13/20 4/20	10 2 1	– – –	U – –
P-605-W (25-40-4) Tracer-Tech Penetrant (10:1 Dilution)	Shannon Luminous Materials Company	6020	0.25 cc volume in test cup	Diluted 10 to 1		0/20	10	–	BT
P-605-W (25-40-4) Tracer-Tech Penetrant (10:1 Dilution)	Shannon Luminous Materials Company	6019	Novabestos 7511T soaked in penetrant for 1 hour, drained for 30 minutes, dried at 60°C for 30 minutes	Diluted 10 to 1		0/20	10	–	BT
P-610 (25-40-3) W/W Diamorphic Tracer-Tech Penetrant	Shannon Luminous Materials Company	5273	0.50 cc volume in test cup			4/20	10	–	U
P-610 (25-40-3) W/W Diamorphic Tracer-Tech Penetrant	Shannon Luminous Materials Company	5272	0.25 cc volume in test cup			5/20	10	–	U
P-610 (25-40-3) W/W Diamorphic Tracer-Tech Penetrant	Shannon Luminous Materials Company	5270	0.50 cc volume oven dried at 100°C for 3 hours			8/20	10	–	U
P-610 (25-40-3) W/W Diamorphic Tracer-Tech Penetrant	Shannon Luminous Materials Company	5271	0.50 cc volume vacuum dried			10/20	10	–	U
P-615 (25-40-1) W/W Diamorphic Tracer-Tech Penetrant	Shannon Luminous Materials Company	5270	0.50 cc volume in test cup			0/20	10	–	U
P-615 (25-40-1) W/W Diamorphic Tracer-Tech Penetrant	Shannon Luminous Materials Company	5276	0.25 cc volume in test cup			2/20	10	–	U
P-615 (25-40-1) W/W Diamorphic Tracer-Tech Penetrant	Shannon Luminous Materials Company	5274	0.50 cc volume oven dried at 100°C for 3 hours			3/20	10	–	U

TABLE VIII. PENETRANTS AND PENETRANT COMPONENTS (Continued)

Material	Manufacturer or Source	Test No.	Sample Preparation	Remarks	Thickness (inch)	No. Reactions/ No. Tests	Energy Level Kg/m	Batch or Jar Rating	Material Rating
P-615 (25-40-1) W/W Diamorphic Tracer-Tech Penetrant	Shannon Luminous Materials Company	5275	0.50 cc volume vacuum dried			2/20	10	–	U
PGP + STS Penetrant	Space Information and Development Division of North American Aviation Co.	4903	0.50 cc volume in test cup			0/20	10	–	BT
PGP + STS Penetrant	Space Information and Development Division of North American Aviation Co.	4960	0.50 cc volume oven dried at 100°C for 2 hours			0/20	10	–	BT
PGP + STS Penetrant	Space Information and Development Division of North American Aviation Co.	4961	0.50 cc volume vacuum dried for 1 hour, 30 minutes			0/20	10	–	BT
PGP + STS Penetrant	Space Information and Development Division of North American Aviation Co.	4901	Novabestos 7511T soaked in penetrant for 1 hour, drained for 30 minutes, oven dried at 60°C for 1 hour			0/20	10	–	BT
PGP-10-T Penetrant	Space Information and Development Division of North American Aviation Co.	4904	0.50 cc volume in test cup			0/20	10	–	BT
PGP-10-T Penetrant	Space Information and Development Division of North American Aviation Co.	4958	0.50 cc volume oven dried at 100°C for 2 hours			0/20	10	–	BT
PGP-10-T Penetrant	Space Information and Development Division of North American Aviation Co.	4959	0.50 cc volume vacuum dried for 1 hour, 27 min.			0/20	10	–	BT
PGP-10-T Penetrant	Space Information and Development Division of North American Aviation Co.	4902	Novabestos 7511T (0.020) soaked in penetrant for 1 hour, dried at 60°C for 1 hour			0/20	10	–	BT
PGP-26 AF Penetrant	Space Information and Development Division of North American Aviation Co.	4954	5 drops oven dried at 100°C for 1 hour, 45 minutes			0/20	10	–	BT

TABLE VIII. PENETRANTS AND PENETRANT COMPONENTS (Continued)

Material	Manufacturer or Source	Test No.	Sample Preparation	Remarks	Thickness (inch)	No. Reactions/ No. Tests	Energy Level Kg/m	Batch or Jar Rating	Material Rating
PGP-26 BF Penetrant	Space Information and Development Division of North American Aviation Co.	4953	5 drops oven dried at 100°C for 1 hour, 36 minutes			0/20	10	–	BT
PGP-26-BF Penetrant	Space Information and Development Division of North American Aviation Co.	4949	Novabestos 7511T soaked in penetrant for 30 minutes, oven dried at 60°C for 1 hour			0/20	10	–	BT
PGP-30-T80	Space Information and Development Division of North American Aviation Co.	4951	Novabestos 7511T soaked in penetrant for 30 minutes, oven dried at 60°C for 1 hour			0/20	10	–	BT
PGP-26 BF-6	Space Information and Development Division of North American Aviation Co.	10332	On anodized discs			1/280	10	–	BT
SKL-4 Penetrant	Magnaflux Corporation	4936	0.50 cc volume in test cup	Concentrate		0/20	10	–	BT
SKL-4 Penetrant	Magnaflux Corporation	4934	0.25 cc volume in test cup	Concentrate		2/20	10	–	BT
SKL-4 Penetrant	Magnaflux Corporation	4731	0.125 cc volume in test cup	Concentrate		0/20	10	–	BT
SKL-4 Penetrant	Magnaflux Corporation	4935	0.50 cc volume oven dried at 100°C for 4 hours	Concentrate		6/20	10	–	BT
SKL-4 Penetrant	Magnaflux Corporation	4745	0.50 cc volume oven dried at 100°C for 2 hours	Concentrate		0/20	10	–	BT
SKL-4 Penetrant	Magnaflux Corporation	4716	0.50 cc volume oven dried just to dryness	Concentrate		0/20	10	–	BT
SKL-4 Penetrant	Magnaflux Corporation	4715	1.00 cc volume oven dried just to dryness	Concentrate		3/20	10	–	BT

TABLE VIII. PENETRANTS AND PENETRANT COMPONENTS (Continued)

Material	Manufacturer or Source	Test No.	Sample Preparation	Remarks	Thickness (inch)	No. Reactions/ No. Tests	Energy Level Kg/m	Batch or Jar Rating	Material Rating
SKL-4 Penetrant	Magnaflux Corporation	4933	0.50 cc volume vacuum dried .	Concentrate		1/40	10	–	BT
SKL-4 Penetrant	Magnaflux Corporation	4732	2 cc volume vacuum dried	Concentrate		0/20	10	–	BT
SKL-4 Penetrant	Magnaflux Corporation		0.50 cc volume in test cup	Diluted with 3 parts water to 1 part SKL-4					
SKL-4 Penetrant (3 to 1 Dilution)	Magnaflux Corporation	4599	0.125 cc volume in test cup	Diluted with 3 parts water to 1 part SKL-4		0/20	10	–	BT
SKL-4 Penetrant (3 to 1 Dilution)	Magnaflux Corporation	4915	Novabestos 7511T soaked in penetrant for 1 hour, drained for 3 hours, oven dried at 60°C overnight	Diluted with 3 parts water to 1 part SKL-4		0/20	10	–	BT
SKL-4 Penetrant	Magnaflux Corporation	4733	2.00 cc volume evaporated to dryness, 3 hours at 100°C	Concentrate		1/20	10	–	U
SKL-4 Penetrant	Magnaflux Corporation	4595	2.50 cc volume evaporated at 100°C to 0.25 cc volume	Concentrate		3/16 2/17 2/15	10 5 3	–	U
SKL-4 Penetrant	Magnaflux Corporation	4905	Novabestos 7511T soaked in penetrant for 1 hour, drained for 1 hour, oven dried at 50°C for 1 hour	Concentrate		20/20	10	–	U
SKL-4 Penetrant	Magnaflux Corporation	4926	Novabestos 7511T soaked in penetrant for 1 hour, drained for 3 hours, oven dried at 60°C overnight	Concentrate		6/20	10	–	U
SKL-4 Penetrant (3 to 1 Dilution)	Magnaflux Corporation	4924	Novabestos 7511T soaked in penetrant for 1 hour, dried at 60°C for 30 minutes	Diluted with 3 parts water to 1 part SKL-4		0/20	10	–	BT
SKD-NF Spotcheck Developer	Magnaflux Corporation	4942	0.50 cc volume in test cup	Concentrate		0/20	10	–	BT

TABLE VIII. PENETRANTS AND PENETRANT COMPONENTS (Continued)

Material	Manufacturer or Source	Test No.	Sample Preparation	Remarks	Thickness (inch)	No. Reactions/ No. Tests	Energy Level Kg/m	Batch or Jar Rating	Material Rating
SKD-W Developer	Magnaflux Corporation	4930	0.50 cc volume in test cup	Concentrate		0/20	10	–	BT
SKD-W Developer	Magnaflux Corporation	4931	0.50 cc volume oven dried at 100°C	Concentrate		0/20	10	–	BT
SKD-W Developer	Magnaflux Corporation	4930	0.50 cc volume vacuum dried	Concentrate		0/20	10	–	BT
SPX-21 Spotcheck Developer	Magnaflux Corporation	4945	0.25 cc volume in test cup	Concentrate		0/20	10	–	BT
Turco Dy-Chek Remover 4441 Green Label	Turco Products, Inc.	5264	0.25 cc volume in test cup	Concentrate		0/20	10	–	BT
Turco Dy-Chek Remover 4441 Green Label	Turco Products, Inc.	5262	0.50 cc volume oven dried at 100°C	Concentrate		0/20	10	–	BT
Turco Dy-Chek Remover 4441 Green Label	Turco Products, Inc.	5263	0.50 cc volume vacuum dried	Concentrate		0/20	10	–	BT
Turco Dy-Chek Developer Green Label	Turco Products, Inc.	5261	0.50 cc volume in test cup	Concentrate		2/20	10	–	BT
Turco Dy-Chek Developer Green Label	Turco Products, Inc.	5260	0.25 cc volume in test cup	Concentrate		2/40	10	–	BT
Turco Dy-Chek Developer Green Label	Turco Products, Inc.	5258	0.50 cc volume oven dried at 100°C	Concentrate		0/20	10	–	BT
Turco Dy-Chek Developer Green Label	Turco Products, Inc.	5259	0.50 cc volume vacuum dried	Concentrate		0/20	10	–	BT
Turco Dy-Chek Penetrant 4449 Green Label	Turco Products, Inc.	5265 5269	0.50 cc volume in test cup	Concentrate		0/40 0/40	10 10	– –	BT BT
Turco Dy-Chek Penetrant 4449 Green Label	Turco Products, Inc.	5269	0.25 cc volume in test cup	Concentrate		0/20	10	–	BT
Turco Dy-Chek Penetrant 4449 Green Label	Turco Products, Inc.	5266	0.50 cc volume oven dried at 100°C for 30 minutes	Concentrate		0/20	10	–	BT

TABLE VIII. PENETRANTS AND PENETRANT COMPONENTS (Continued)

Material	Manufacturer or Source	Test No.	Sample Preparation	Remarks	Thickness (inch)	No. Reactions/ No. Tests	Energy Level Kg/m	Batch or Jar Rating	Material Rating
Turco Dy-Chek Penetrant 4449 Green Label	Turco Products, Inc.	5267	0.40 cc volume vacuum dried	Concentrate		0/20	10	–	BT
Turco Dy-Chek Penetrant 4449 Green Label	Turco Products, Inc.	5608	Novabestos 7511T soaked in penetrant for 1 hour, drained for 30 minutes, oven dried at 60°C for 30 minutes	Concentrate		0/80	10	–	BT
Turco Fluoro-Chek Penetrant	Turco Products, Inc.	4251	0.50 cc volume in test cup	Regular		2/6 2/3 0/20	10 5 3	–	U
Turco Fluoro-Chek Penetrant	Turco Products, Inc.	4252	0.50 cc volume in test cup	High Sensitivity		5/20 3/20 0/20	10 5 3	–	U
Turco Fluoro-Chek Emulsifier	Turco Products, Inc.	4295	0.50 cc volume in test cup	Extremely violent reactions		2/13	10	–	U
Turco Fluoro-Chek Penetrant (WW)	Turco Products, Inc.	4296	0.50 cc volume in test cup	Extremely violent reactions		2/4	10	–	U
Visi-Safe Penetrant	Turco Products, Inc.	9778		On anodized discs		0/20	10	–	BT
Visi-Safe Developer	Turco Products, Inc.	8603	Non-aqueous	On anodized discs		0/20	10	–	BT
Visi-Safe Developer	Turco Products, Inc.	8604	Dry			3/20	10	–	BT
Special Penetrant 137-115	Magnaflux Corporation	3804	0.50 cc volume in test cup			0/20	10	–	U
Special Penetrant 137-115	Magnaflux Corporation	3819	0.25 cc volume in test cup			2/10 12/15	10 3	–	U
Special Penetrant 137-115	Magnaflux Corporation	3910	Two drops 1% solution evaporated to dryness			2/7 0/13	10 5	–	U
Special Penetrant 137-115	Magnaflux Corporation	3819 3283	Porous aluminum castings soaked in penetrant and dried			2/9 2/11	10 5	–	U

TABLE VIII. PENETRANTS AND PENETRANT COMPONENTS (Continued)

Material	Manufacturer or Source	Test No.	Sample Preparation	Remarks	Thickness (inch)	No. Reactions/ No. Tests	Energy Level Kg/m	Batch or Jar Rating	Material Rating
Special Penetrant 137-115	Magnaflux Corporation	3822	Porous stainless steel inserts soaked in penetrant and dried			2/3 2/9 2/8	10 5 2	–	U
Special Penetrant 137-89	Magnaflux Corporation	3683	0.50 cc volume in test cup	Violent explosions		6/20	10	–	U
Special Emulsifier 137-90	Magnaflux Corporation	3682	0.50 cc volume in test cup			0/20	10	–	U
Special Emulsifier 137-95	Magnaflux Corporation	3821	0.50 cc volume in test cup			0/20	10	–	U
Special Emulsifier 137-95	Magnaflux Corporation	3922	One drop on 2014-T6 aluminum alloy			3/20	10	–	U
ZE-43 Emulsifier	Magnaflux Corporation	4766	0.50 cc volume in test cup	For use with ZL-42 Penetrant		0/40	10	–	U
ZE-43 Emulsifier	Magnaflux Corporation	4724	0.25 cc volume in test cup	For use with ZL-42 Penetrant		3/20	10	–	U
ZE-43 Emulsifier	Magnaflux Corporation	4938	0.50 cc volume oven dried at 100°C for 3 hours	For use with ZL-42 Penetrant		6/20	10	–	U
ZE-43 Emulsifier	Magnaflux Corporation	4730	0.50 cc volume vacuum dried for 1 hour, 30 minutes	For use with ZL-42 Penetrant		2/20	10	–	U
ZE-43 Emulsifier	Magnaflux Corporation	4922	Novabestos 751 T soaked 1 hour in emulsifier, dried 3 hours in air	For use with ZL-42 Penetrant		3/20	10	–	U
ZE-43 Emulsifier	Magnaflux Corporation	4912	Novabestos 751T soaked in emulsifier for 1 hour, oven dried at 60°C for 30 minutes	For use with ZL-42 Penetrant		20/20	10	–	U
ZE-43 Emulsifier	Magnaflux Corporation	4765	0.50 cc volume concentrated to 0.25 cc	For use with ZL-42 Penetrant		2/13 2/7	10 5	–	U

TABLE VIII. PENETRANTS AND PENETRANT COMPONENTS (Continued)

Material	Manufacturer or Source	Test No.	Sample Preparation	Remarks	Thickness (inch)	No. Reactions/ No. Tests	Energy Level Kg/m	Batch or Jar Rating	Material Rating
ZL-42 Penetrant	Magnaflux Corporation	4768 4728	0.50 cc in test cup			0/20 0/20	10 10	– –	BT BT
ZL-42 Penetrant	Magnaflux Corporation	4760	0.25 cc volume in test cup			0/100	10	–	BT
ZL-42 Penetrant	Magnaflux Corporation	4739 4722	0.50 cc volume oven dried for 11 hours at 100°C			0/20 0/20	10 10	– –	BT BT
ZL-42 Penetrant	Magnaflux Corporation	4764	2.50 cc evaporated to 1.5 cc			0/20	10	–	BT
ZL-44 Penetrant (10 to 1 Dilution)	Magnaflux Corporation	5289	0.50 cc volume in test cup	Diluted 10 parts water to 1 part ZL-44		0/20	10	–	BT
ZL-44 Penetrant (10 to 1 Dilution)	Magnaflux Corporation	5287	0.25 cc volume in test cup			0/20	10	–	BT
ZL-44 Penetrant (10 to 1 Dilution)	Magnaflux Corporation	5288	0.50 cc volume oven at 100°C			0/20	10	–	BT
ZL-44 Penetrant (10 to 1 Dilution)	Magnaflux Corporation	5282	0.50 cc volume vacuum dried	Diluted 10 parts water to 1 part ZL-44		0/40	10	–	BT
ZL-44 Penetrant	Magnaflux Corporation	4746	0.50 cc volume in test cup	Concentrate		0/20	10	–	U
ZL-44 Penetrant	Magnaflux Corporation	4725	0.25 cc volume in test cup	Concentrate		0/20	10	–	U
ZL-44 Penetrant	Magnaflux Corporation	4740	0.50 cc volume oven dried at 100°C for 11 hours	Concentrate		2/20	10	–	U
ZL-44 Penetrant	Magnaflux Corporation	4738	0.50 cc volume dried for 1 hour, 30 minutes	Concentrate		3/20	10	–	U
ZL-44 Penetrant	Magnaflux Corporation	4929	Novabestos 7511T soaked in penetrant 1 hour, drained for 3 hours	Concentrate		20/20	10	–	U

TABLE VIII. PENETRANTS AND PENETRANT COMPONENTS (Continued)

Material	Manufacturer or Source	Test No.	Sample Preparation	Remarks	Thickness (inch)	No. Reactions/ No. Tests	Energy Level Kg/m	Batch or Jar Rating	Material Rating
ZL-44 Penetrant	Magnaflux Corporation	4906	Novabestos 7511T soaked in penetrant for 1 hour, oven dried at 60°C for 30 minutes	Concentrate		20/20	10	–	U
ZL-44B	Magnaflux Corporation	4758	0.50 cc volume in test cup			0/40	10	–	U
ZL-44B	Magnaflux Corporation	4755 4726	0.25 cc volume in test cup			0/40 0/20	10 10	– –	U U
ZL-44B	Magnaflux Corporation	4721	0.50 cc volume evaporated in oven at 100°C for 7 hours			0/40	10	–	U
ZL-44B	Magnaflux Corporation	4744	0.50 cc volume vacuum dried			5/20	10	–	U
ZL-44B	Magnaflux Corporation	4925	Novabestos 7511T soaked in penetrant for 1 hour, oven dried at 60°C for 30 minutes			31/40	10	–	U
ZL-44B	Magnaflux Corporation	4928	Novabestos 7511T soaked in penetrant for 1 hour, dried for 3 hours			0/20	10	–	U
ZL-44B, Batch IW9	Magnaflux Corporation	7935		Diluted 1 to 1 with water		0/20	10	–	BT
ZL-44B, Batch IW10	Magnaflux Corporation	7936		Diluted 1 to 1 with water		2/20	10	–	BT
ZL-44B	Magnaflux Corporation	4754	Five drops in test cup			0/20	10	–	U
ZL-44B	Magnaflux Corporation	5393	0.25 volume concentrate			3/20	10	–	U
ZL-44B (1 to 1 Dilution)	Magnaflux Corporation	6015	Novabestos 7511T soaked in penetrant for 1 hour, drained for 30 minutes, dried at 60°C for 30 minutes	Diluted 1 part ZL-44B to 1 part water		0/20	10	–	BT

TABLE VIII. PENETRANTS AND PENETRANT COMPONENTS (Continued)

Material	Manufacturer or Source	Test No.	Sample Preparation	Remarks	Thickness (inch)	No. Reactions/ No. Tests	Energy Level Kg/cm	Batch or Jar Rating	Material Rating
Zyglo ZL-2 Penetrant	Magnaflux Corporation	4022	0.50 cc volume in test cup	Violent reactions		2/6 1/6 1/9 0/20	10 5 3 1	–	U
Zyglo ZL-2 Penetrant	Magnaflux Corporation	4024	0.25 cc volume in test cup	Violent reactions		1/5 1/13 2/6 1/9 0/20	10 5 3 1 5	–	U
Zyglo ZL-22 Penetrant	Magnaflux Corporation	4020	0.50 cc volume in test cup	Violent reactions		2/3 3/13 2/3 1/5	10 5 3 2	–	U
Zyglo ZL-22 Penetrant	Magnaflux Corporation	4016	0.25 cc volume in test cup	Violent reactions		2/4 2/18	10 5	–	U
Zyglo ZL-22 Penetrant	Magnaflux Corporation	4018	One drop of 1% solution, 99% trichloroethylene in test cup	Violent reactions		2/4 2/7 0/12	10 5 3	–	U
Zyglo ZL-22 Penetrant	Magnaflux Corporation	4019	One spray coat on aluminum inserts	Violent reactions		4/4 1/6 1/10	10 5 3	–	U
Zyglo ZL-4A Penetrant	Magnaflux Corporation	2059	0.50 cc volume evaporated to dryness			2/6 0/14	10 5	–	U
Zyglo ZL-1A Penetrant	Magnaflux Corporation	4021	One drop in test cup			2/3 3/5 1/12	10 3 3	–	U
Zyglo ZL-4B Penetrant	Magnaflux Corporation		On anodized discs	Diluted 9:1 with water		0/20	10	–	BT
Zyglo ZL-4B Penetrant	Magnaflux Corporation	4737	0.50 cc volume in test cup			0/20	10	–	BT
Zyglo ZL-4B Penetrant	Magnaflux Corporation	4723	0.25 cc volume in test cup			0/20	10	–	U

TABLE VIII. PENETRANTS AND PENETRANT COMPONENTS (Continued)

Material	Manufacturer or Source	Test No.	Sample Preparation	Remarks	Thickness (inch)	No. Reactions/ No. Tests	Energy Level Kg/m	Batch or Jar Rating	Material Rating
Zyglo ZL-4B Penetrant	Magnaflux Corporation	4736	0.50 cc volume vacuum dried			3/20	10	–	U
Zyglo ZL-4B Penetrant	Magnaflux Corporation	4743	0.50 cc volume evaporated to dryness at 100°C			2/20	10	–	U
Zyglo ZL-4B Penetrant	Magnaflux Corporation	4920	Novabestos 7511T soaked in penetrant for 1 hour, oven dried for 30 minutes at 60°C			14/20	10	–	U
Zyglo ZP-4 Developer	Magnaflux Corporation	5474	0.50 cc dispersion, oven dried			0/20	10	–	BT
Zyglo ZP-4A Developer	Magnaflux Corporation	5475	0.50 cc dispersion, oven dried			0/20	10	–	BT
Zyglo ZP-45 Developer	Magnaflux Corporation	4719	0.50 cc volume in test cup	1 ounce to pint of water		0/20	10	–	BT
Zyglo ZP-45 Developer	Magnaflux Corporation	4720	0.50 cc volume oven dried at 100°C	28.4 gms in 473.2 cc of water		0/20	10	–	BT
Zyglo ZP-45 Developer	Magnaflux Corporation	4718	0.50 cc volume vacuum dried	28.4 gms in 473.2 cc of water		0/20	10	–	BT
Zyglo ZP-45 Developer	Magnaflux Corporation	4747	Stainless steel inserts dipped in solution and dried	28.4 gms in 473.2 cc of water		0/20	10	–	BT
Zyglo ZP-5 Penetrex Developer	Magnaflux Corporation	3826	Residue of approximately 0.030 in test cup			0/40	10	–	BT
Zyglo ZLX 38 Penetrant	Magnaflux Corporation	5913	Novabestos 7511T soaked in solution for 1 hour, drained for 30 minutes, and dried at 60°C for 30 minutes			0/20	10	–	BT
Zyglo ZPX 404 Developer	Magnaflux Corporation	5912	Novabestos 7511T soaked in solution for 1 hour, drained for 30 minutes, and dried at 60°C for 30 minutes			0/20	10	–	BT

TABLE VIII. PENETRANTS AND PENETRANT COMPONENTS (Continued)

Material	Manufacturer or Source	Test No.	Sample Preparation	Remarks	Thickness (inch)	No. Reactions/ No. Tests	Energy Level Kg/m	Batch or Jar Rating	Material Rating
Zyglo KXS Cleaner	Magnaflux Corporation	5911	Novabestos 7511T soaked in solution for 1 hour, drained for 30 minutes, and dried at 60°C for 30 minutes			0/20	10	–	BT
Zyglo ZL-10 Colorless Dye	Magnaflux Corporation	510	0.50 cc volume in test cup	Full strength		2/11 2/11 1/13	10 7 5	–	U
Zyglo ZL-10 Colorless Dye	Magnaflux Corporation	537	2.5 ml of 5% water solution evaporated to dryness			1/17 1/13	6 4	–	U
Oil Red "O" Dye	Magnaflux Corporation	3757	Paste made of trichloroethylene and Oil Red "O" 0.050 inch in test cup, dried 48 hours	Violent reactions		3/9 1/2 1/9	10 3 2	–	U
Oil Red "O" Dye	Magnaflux Corporation	3759	Residue from 2.5 saturated solution of Oil Red "O" and methyl isobutyl ketone	Violent reactions		5/12 2/7	10 5	–	U
137-115 Special Penetrant	Magnaflux Corporation	3923	2219-T87 aluminum dipped in Special Penetrant 137-115 emulsified with 137-95, rinsed, and dried			5/20 0/20 2/20	10 10 10	–	U
137-115 Special Penetrant	Magnaflux Corporation	3900	Aluminum cups scratched with emery wheel, soaked in Special Penetrant 137-115, emulsified with 137-95, rinsed with trichloroethylene, water, and dried			3/20	10	–	U
137-115 Special Penetrant	Magnaflux Corporation	3916	2014-T6 aluminum discs scratched with emery wheel, soaked in Special Penetrant 137-115 for 30 minutes, and emulsified with 137-95 for 5 minutes, rinsed in water, placed in developer for 10 minutes, rinsed with water, and dried			0/20	10	–	U

TABLE VIII. PENETRANTS AND PENETRANT COMPONENTS (Continued)

Material	Manufacturer or Source	Test No.	Sample Preparation	Remarks	Thickness (inch)	No. Reactions/ No. Tests	Energy Level Kg/m	Batch or Jar Rating	Material Rating
137-115 Special Penetrant	Magnaflux Corporation	3898	Aluminum cups scratched with X-acto No. 24 knife, soaked in Special Penetrant 137-115 for 30 minutes, emulsified with 137-95 for 10 minutes, rinsed with water, and dried			2/2 2/2 2/10	10 5 2	–	U
137-115 Special Penetrant	Magnaflux Corporation	3899	Aluminum cups 0.032 inch thick scratched with X-acto No. 24 knife, soaked in Special Penetrant 137-115 for 1 hour, emulsified for 10 minutes, rinsed with water, and dried at 100°C			2/3 3/4 2/3 0/10	10 5 2 1	–	U
137-115 Special Penetrant	Magnaflux Corporation	3919	Aluminum discs (cracked) soaked in Special Penetrant 137-115 for 30 minutes, soaked in emulsifier for 2 minutes, rinsed, dipped in developer, rinsed with water, and dried			0/20	10	–	U
137-115 Special Penetrant	Magnaflux Corporation	3904	2014-T6 aluminum 0.063-inch thick, scratched with emery wheel, soaked 30 minutes in Special Penetrant 137-115, emulsified with 137-95 for 10 minutes, rinsed with water, and dried			2/6 2/14	10 5	–	U
137-115 Special Penetrant	Magnaflux Corporation	3908	1 cc of 1% solution of Penetrant trichloroethylene evaporated to dryness			0/20	10	–	U
137-115 Special Penetrant	Magnaflux Corporation	3902	Aluminum casting 0.250-inch thick, soaked in Zyglo 137-115, washed in Emulsifier 137-95, rinsed with water, and dried			0/20	10	–	U

TABLE VIII. PENETRANTS AND PENETRANT COMPONENTS (Continued)

Material	Manufacturer or Source	Test No.	Sample Preparation	Remarks	Thickness (inch)	No. Reactions/ No. Tests	Energy Level Kg/m	Batch or Jar Rating	Material Rating
137-115 Special Penetrant	Magnaflux Corporation	3912	1 cc of 1% penetrant in trichloroethylene in scratched aluminum cups, evaporated to dryness			2/20	10	–	U
137-115 Special Penetrant	Magnaflux Corporation	3918	Special Penetrant 137-115 placed in 0.032-inch hole, emulsified with 137-95, rinsed with water, placed in developer, rinsed with water, and dried			1/20	10	–	U
137-115 Special Penetrant	Magnaflux Corporation	3917	2014-T6 aluminum discs scratched with emery wheel, soaked in Special Penetrant 137-115 overnight, soaked in emulsifier 137-95 for 10 minutes, rinsed with water, placed in developer, rinsed with water, and dried			0/20	10	–	U
137-115 Special Penetrant	Magnaflux Corporation	3928	2014-T6 aluminum (cracked) soaked in Special Penetrant 137-115, emulsified with 137-95, rinsed, and dried			0/40	10	–	U
137-115 Special Penetrant	Magnaflux Corporation	3920	2014-T6 aluminum discs (cracked) soaked in Special Penetrant 137-15 for 24 hours, emulsified with 137-95 for 10 minutes, rinsed with water, dipped in developer, rinsed with water, and dried			1/40	10	–	U
137-115 Special Penetrant	Magnaflux Corporation	3926	356 aluminum soaked in Special Penetrant 137-115, emulsified with 137-95, rinsed, dipped in developer, rinsed, and dried			2/40	10	–	U

TABLE VIII. PENETRANTS AND PENETRANT COMPONENTS (Continued)

Material	Manufacturer or Source	Test No.	Sample Preparation	Remarks	Thickness (inch)	No. Reactions/ No. Tests	Energy Level Kg/m	Batch or Jar Rating	Material Rating
137-115 Special Penetrant	Magnaflux Corporation	3905	2014-T6 aluminum 0.063-inch thick, scratched with emery wheel, emulsified with 137-95 for 30 minutes, washed, soaked in trichloroethylene for 1 hour, washed with 137-95, rinsed, dried, washed with trichloroethylene, and dried at 150°C			0/20	10	–	U
137-115 Special Penetrant	Magnaflux Corporation	3903	Aluminum casting 0.063-inch thick, soaked in Emulsifier for 10 minutes, and dried at 200°F for 10 minutes			2/2 1/2 2/3	10 5 2	–	U

TABLE VIII. PENETRANTS AND PENETRANT COMPONENTS (Continued)

Material	Other Comments	Manufacturer	Results			Component Rating	System Rating
			No. Reactions/No. Tests at 10 kg-m				
				Anodized Aluminum Disc			
			Novabestos	Drained at 45°C	Drained at 93°C		
Dye Penetrants							
P-133		Shannon Luminous Materials Company			20/20	U	U
P-505 (27-7-5)	Emulsifier E-159, Developers D-492, 498	Shannon Luminous Materials Company	0/20	0/20	0/20	BT	U
P-545 (30-7-2)	Cleaner K-4-10A	Shannon Luminous Materials Company			0/20	BT	BT
P-600 (25-40-5) W/W Diamorphic (9:1 dilution)	Water Washable, Developers D-492, 498	Shannon Luminous Materials Company	0/20	4/20, 4/20	0/20, 1/20	BT	BT
P-605 (25-40-4) Concentrate	Water Washable, Developers D-492, 498	Shannon Luminous Materials Company	20/20	20/20	20/20	U	U
P-605 (25-40-4) (10:1 dilution)	Water Washable, Developers D-492, 498	Shannon Luminous Materials Company	0/20, 0/20	7/20, 6/20, 5/20	2/20	BT	BT
P-610W (25-40-3) Concentrate	Water Washable, Developers D-492, 498	Shannon Luminous Materials Company	20/20	13/20	11/20	U	U
P-610W (24-40-3) (9:1 dilution)	Water Washable, Developers D-492, 498	Shannon Luminous Materials Company	2/20	6/20	6/20	U	U
P-615W (25-40-1)	Water Washable, Developers D-492, 498	Shannon Luminous Materials Company	20/20, 20/20	20/20, 20/20	20/20, 19/20	U	U
P-615W (25-40-1) (9:1 dilution)	Water Washable, Developers D-492, 498	Shannon Luminous Materials Company	0/20, 0/20	6/20, 3/20, 4/20, 5/20	7/20, 4/20, 4/20, 3/20	U	U
POP 26-BF-3	–	Space Information Division, NAA			0-11/20	BT	BT

TABLE VIII. PENETRANTS AND PENETRANT COMPONENTS (Continued)

Material	Other Comments	Manufacturer	Results: No. Rejections/No. Tests at 10 kg-m			Component Rating	System Rating
				Anodized Aluminum Disc			
			Novabestos	Drained at 45°C	Drained at 90°C		
S&ID Penetrant NAA-M-103-565H	Emulsifier 563-C	Space Information Division, NAA	0/20	0/20	5/20	U	BT
PCP-26BF-6		Space Information Division, NAA			1/280	BT	BT
Spot Check SKL-4 Concentrate	Water Washable, Developers Recommended by Manufacturer	Magnaflux Corporation	20/20, 20/20	14/20	10/20, 13/20	U	U
Spot Check SKL-4 (3:1 dilution)	Water Washable, Developers Recommended by Manufacturer	Magnaflux Corporation	0/20, 0/20	0/20, 0/20	0/20, 0/20	BT	BT
Turco 4499 Green Label	Turco Dy-Chek Remover 4441 and Dy-Chek Developer	Turco Products, Incorporated	0/20	0/20	0/20	BT	BT
Visi-Safe	Visi-Safe Developer	Turco Products, Incorporated			0/20	BT	BT
Zyglo ZL-44B	Water Washable, Developers Recommended by Manufacturer	Magnaflux Corporation	18/20, 13/20	4/20	7/20	U	U
Zyglo ZL-44B (1:1 dilution)	Water Washable, Developers Recommended by Manufacturer	Magnaflux Corporation	0/20	0/20, 1/20	3/20, 1/20, 0/20	BT	BT
Zyglo ZL-4BL (9:1 dilution)	Water Washable, Developers Recommended by Manufacturer	Magnaflux Corporation			0/20	BT	BT
Zyglo ZL-46	Cleaner ZC-46 and Developer ZP-46	Magnaflux Corporation	0/20, 0/20, 0/20	0/20	0/20	BT	BT
Zyglo ZL-42*	Emulsifier ZE-43, Developer Recommended by Manufacturer	Magnaflux Corporation	2/20, 0/20	3/20, 0/20	4/20, 7/20	U	U

*This material may have been contaminated with ZE-43

TABLE VIII. PENETRANTS AND PENETRANT COMPONENTS (Continued)

Material	Other Comments	Manufacturer	Results: No. Reactions/No. Tests at 10 kg-m			Component Rating	System Rating
				Anodized Aluminum Disc			
			Novabestos	Drained at 45°C	Drained at 90°C		
Fluoro-Finder FL-50		Testing Systems, Inc.			20/20	U	U
Emulsifiers or Cleaners							
Emulsifier 563 C	Penetrant NAA-M-103-565H	Space Information Division NAA	0/20	3/20	2/20	BT	BT
Emulsifier E-159 (25-7-3)	Penetrant P-505	Shannon Luminous Materials Company	20/20	19/20	20/20	U	U
Zyglo Cleaner ZC-46	Penetrant ZL-46	Magnaflux Corporation	0/20	0/20	0/20	BT	BT
Zyglo Emulsifier ZE-43	Penetrant ZL-42	Magnaflux Corporation	20/20	10/20	15/20	U	U
Cleaner K-4-10A	Penetrant P545	Shannon Luminous Materials Company			0/20	BT	BT
Developers							
D-492 (24-44-4)		Shannon Luminous Materials	0/20			BT	
D-498		Shannon Luminous Materials Company	0/20			BT	
SKDW		Magnaflux Corporation	0/20			BT	
SKDNF		Magnaflux Corporation	0/20			BT	
SPX-21		Magnaflux Corporation	0/20			BT	
Zyglo ZP-4		Magnaflux Corporation	0/20			BT	

TABLE VIII. PENETRANTS AND PENETRANT COMPONENTS (Concluded)

Material	Other Comments	Manufacturer	Results: No. Reactions/No. Tests at 10 kg-m			Component Rating	System Rating
				Anodized Aluminum Disc			
			Novabestos	Drained at 45°C	Drained at 90°C		
Zyglo ZP-4A		Magnaflux Corporation.	0/20			BT	
Zyglo ZP-5		Magnaflux Corporation	0/20			BT	
Zyglo ZP-46		Magnaflux Corporation	0/20			BT	
Zyglo ZP-45		Magnaflux Corporation	0/20			BT	
Zyglo ZPX-404		Magnaflux Corporation	0/20			BT	
Visi-Safe Developer		Turco Products, Inc.			0/20	BT	
Dyes							
Florescing Agent GPC	1 cc saturated solution evaporated to dryness	G.W. Gates Company	4/20	10			
Oil Red "O" Dye	Residue from 0.5 cc of saturated solution in methyl isobutyl ketone		5/12	10			
Oil Red "O" Dye	Residue from 0.5 cc dissolved in trichlcro-ethylene. Dried 48 hours		2/9	10			
ZL-10 Colorless Dye	Full strength	Magnaflux Corporation	2/11	10			
ZL-10 Colorless Dye	2-1/2 cc of 5% water solution evaporated to dryness	Magnaflux Corporation	1/7	10			

END OF REFERENCE

26

REFERENCE

27

HAUSER, R. L.; SYKES, G. E.; AND RUMPEL, W. F.: MECHANICALLY INITIATED REACTIONS OF ORGANIC MATERIALS IN MISSILE OXIDIZERS. ASD-TR-61-324, AERONAUTICAL SYSTEMS DIVISION, WRIGHT-PATTERSON AFB, 1961. (AVAILABLE FROM DDC AS AD-268458.)

THIS MATERIAL HAS BEEN APPROVED FOR PUBLICATION PER LETTER FROM R. H. MALTBY TO JOANNE FOLK DATED AUG. 27, 1974.

ASD TECHNICAL REPORT 61-324
ASD-CR-61-19

MECHANICALLY INITIATED REACTION OF ORGANIC MATERIALS IN MISSILE OXIDIZERS

R. L. Hauser
G. E. Sykes
W. F. Rumpel

Martin Company

Directorate of Materials and Processes
Contract No. AF 33(616)-7271
Project No. 7340

AERONAUTICAL SYSTEMS DIVISION
AIR FORCE SYSTEMS COMMAND
UNITED STATES AIR FORCE
WRIGHT-PATTERSON AIR FORCE BASE, OHIO

ABSTRACT

This report presents the results of impact testing of 24 organic materials with liquid oxygen. In addition, nine of these same materials were tested with gaseous oxygen, and seven were tested with liquid ~~oxygen~~ Nitrogen tetroxide. Pure polymers, plasticizers, and antioxidants were studied and their threshold sensitivity levels and detonation energies were determined. Procedures and equations for calibrating impact testing machines were developed and used to calculate the rates of energy transfer into test materials. A full record of test procedures is included.

In addition, 18 of the given materials in contact with liquid oxygen were subjected to shear forces with a modified Shell Four-Ball Wear Tester to determine whether reactions could be initiated by friction.

PUBLICATION REVIEW

This report has been reviewed and is approved.

FOR THE COMMANDER:

J. M. Kelble, Chief
Elastomers and Coatings Branch
Nonmetallic Materials Laboratory
Directorate of Materials and Processes

Table 22. Industry Survey of Pure Materials Tested for Impact Sensitivity with Liquid Oxygen

Material	w (lb)	h (in.)	b (in.)	A $in.^2$	E (ft-lb)	E/A	q	$h\left(\frac{w}{bA}\right)^{\frac{1}{2}}$	$h\left(\frac{w}{A}\right)^{\frac{1}{2}}$	Source
A. Chemicals										
Acetone (reagent grade)	20	42		0.196	70	357	6/20		424	M-D
Butyl Alcohol	10	12		0.196	10	51	0/20		121	AGC
Carbon (activated charcoal)	20	42		0.196	70	357	2/2		424	M-D
	20	42		0.196	40	204	2/2		424	
	20	42		0.196	20	102	2/2		424	
	20	42		0.196	10	51	2/2		424	
Carbon tetrachloride	4.5	32		0.030	12	400	0/10		391	T-RMD
	10	72		0.196	60	306	0/10		514	AGC
Chlorinated biphenyl	20	45.8	0.050	0.442	76.4	172	0/10	4360	302	Red
Chloroform	35	63.4	0.015	0.500	185	370	0/10	4330	532	D-SM
Dibutyl Sebacate	20	42	0.010	0.196	70	357	2/8	4240	424	M-D
	20	42	0.002	0.196	70	357	4/10	9500	424	M-D
Diethyl Phthalate	20	42		0.196	70	357	2/4		424	M-D
Dioctyl Phthalate	20	42	0.010	0.196	70	357	2/10	4240	424	M-D
	20	42	0.002	0.196	70	357	8/20	9500	424	M-D
Dioxane	10	12		0.196	10	51	0/10		86	AGC
Iron Oxide (Fe_2O_3)	35	65	0.015	0.500	190	380	0/10	4430	545	D-SM
Iron Oxide (Fe_2O_3, FeO, Fe_3O_4)	20	42		0.196	70	357	0/5		424	M-D
Methylene Chloride	10	72		0.196	60	306	0/10		514	AGC
	35	63.4	0.015	0.500	185	370	0/10	4330	532	D-SM
Methyl Ethyl Ketone (reagent grade)	20	42		0.196	70	357	9/20		424	M-D
Molybdenium Disulfide	20	42		0.196	70	357	0/136		424	M-D
	35	55	0.015	0.500	165	330	0/10	3760	461	D-SM
Perfluoroalkyl Camphorate	20	42		0.196	70	357	0/40		424	M-D
Perfluoroalkyl Pyromellitate	20	42		0.196	70	357	0/60		424	M-D
Perfluoro Tributylamine	35	63.4	0.015	0.500	185	370	0/10	4330	532	D-SM
Propylene Glycol $C_3H_6(OH)_2$	20	42		0.196	70	357	2/13		424	M-D
95% P.G, 5% Water	20	42		0.196	70	357	2/12		424	M-D
90% P.G, 10% Water	20	42		0.196	70	357	1/20		424	M-D
85% P.G. 15% Water	20	42		0.196	70	357	0/20		424	M-D
Silica Aerogel	25.7	72		1.74	170	98	0/10		277	ADL
Sodium Acetate	20	42		0.196	70	357	0/20		424	M-D
Sodium Stearate	35	12.7	0.015	0.500	37	74	2/2	867	107	D-SM
Sugar	35	25.3	0.015	0.500	74	148	2/2	1728	212	D-SM
1,1,1, Trichloroethane	20	42		0.196	70	357	2/7		424	M-D
Trichloroethylene	4.5	32		0.030	12	400	0/10		391	T-RMD
	26	11.3		1.74	28	1.60	1/10		138	ADL
	26	17.5		1.74	38	21.8	0/10		218	
	26	22.1		1.74	48	27.5	4/10		269	
	26	28.5		1.74	62	35.6	5/10		276	
	26	40.5		1.74	88	50.5	7/10		494	
Tricresyl Phosphate	12	4.94		0.441	59.3	132	0/2		26	GE
	20	43.8	0.050	0.442	73	165	2/2	4170	295	Red
	20	12	0.050	0.442	20	45.2	2/2	1140	81	
	25.7	33		1.74	85	48.8	0/10*		127	ADL
B. Polymers										
Methyl Methacrylate	20	42		0.196	70	357	6/17		424	M-D
Polycarbonate	20	42	0.0045	0.196	70	357	4/4	6325	424	M-D
Polyethylene	25.7	12		1.74	25	14.5	0/10*	46		ADL
Polyethylene, irradiated	20	42		0.196	70	357	1/6		424	M-D
	20	42	0.015	0.196	70	357	5/5	3464	424	M-D
Polyethylene, irradiated shredded	4.5	6.13		0.030	2.34	78	0/10*		75	T-RMD
Polyethylene Terephthalate	4.5	10.9		0.030	3.99	133	0/10*		133	T-RMD
	20	42	0.010	0.196	70	357	2/30	4240	424	M-D
	10	72		0.196	60	306	0/10		514	AGC
Polystyrene	25.7	24		1.74	[illegible]	29	0/10*		92	ADL
Polyvinylidene Chloride	10	24		0.196	20	102	0/10		171	AGC
Tetrafluoroethylene (sheet)	4.5	32	0.010	0.030	12	400	0/10	1238	391	T-RMD
	20	42	0.005	0.196	70	357	0/67		424	M-D
	10	72		0.196	60	306	0/10		514	AGC

Table 22. (concl)

Material	w (lb)	h (in.)	b (in.)	A $in.^2$	E (ft-lb)	E/A	q	$h\left(\frac{w}{bA}\right)^{\frac{1}{2}}$	$h\left(\frac{w}{A}\right)^{\frac{1}{2}}$	Source
Tetrafluoroethylene (shredded)	4.5	14.2		0.030	5.34	178	0/10*		173	T-RMD
Tetrafluoroethylene-hexafluoropropylene (shredded)	4.5	15.1		0.030	5.67	189	0/10*		185	T-RMD
	10	72		0.196	60	306	0/10		514	AGC
Trifluorochloroethylene (sheet)	70	12	0.050	0.196	70	357	0/20			M-B
	20	42	0.025	0.196	70	357	0/20	8484	424	M-D
	10	72		0.196	60	306	0/10*		514	AGC
(shredded)	4.5	12.4		0.030	4.65	155	0/10*		151	T-RMD
Oil, AO-369	20	42		0.196	70	357	0/120		424	M-D
HG1200-L6-160	20	42		0.196	70	357	0/20		424	M-D
MO536	20	42		0.196	70	357	2/67		424	M-D
S-30	20	42		0.196	70	357	0/40		424	M-D
Kel-F-#1	20	42		0.196	70	357	1/80		424	M-D
Kel-F-10	20	42		0.196	70	357	0/380		424	M-D
4-11v	4.5	32		0.030	12	400	0/10		308	T-RMD
	20	45.8	0.050	0.442	76.4	173		4465	975	Red
	20	42		0.196	70	357	0/50		424	M-D
6-25-Z Wax	4.5	32		0.030	12	400	0/10		391	T-RMD
10-25	20	42		0.196	70	357	0/60		424	M-D
11-14	4.5	32		0.030	12	400	0/10		391	T-RMD
	20	42		0.196	70	357	0/10		424	M-D
Trifluoropropylmethyl Siloxane, 0.75% Benzoyl peroxide	4.5	8		0.030	3	100	0/10*		97.8	T-RMD
	20	42	0.060	0.196	70	357	2/51	1732	424	M-D
Vinylidene Fluoride-Hexafluoropropylene, cured	20	42	0.070	0.196	70	357	0/20	1603	424	M-D
	20	42		0.196	70	357	0/20		424	M-D
	20	42	0.10	0.050	70	357	0/20	1340	424	M-D
C. Metals										
Aluminum (chips)	10	72		0.196	60	306	0/10		514	AGC
Columbium	20	42	0.005	0.196	70	357	0/18	2040	424	M-D
10% Titanium	20	42	0.007	0.196	70	357	0/18	1603	424	M-D
0.75% Zirconium	20	42	0.005	0.196	70	357	1/18	2040	424	M-D
Iron (reagent grade) Powder	20	42		0.196	70	357	0/20		424	M-D
Steel (chips) 17-7 PH	10	72		0.196	60	306	0/10		514	AGC
Steel (chips) 304 - Stainless	10	72		0.196	60	306	-		514	AGC
Titanium (pure)	4.5					78	0/10			T-RMD
6Al-4 V Alloy	20	42	0.060	0.196	70	357	20/22	1732	424	M-D
	20	36	0.060	0.196	60	306	2/2	1484	363	
	20	30	0.060	0.196	50	255	2/2	1237	303	
	20	24	0.060	0.196	40	204	2/2	989	242	
	20	18	0.060	0.196	30	153	2/2	742	181	
	20	12	0.060	0.196	20	102	2/2	494	121	
	20	6	0.060	0.196	10	51	1/4	247	60	
	4.5	6.2		0.030	2.3	78	0/10		76	T-RMD
Titanium-Alloy Bl20VCA										
Solution treated	4.5			0.030		122	0/10			T-RMD
Aged	4.5			0.030		67	0/10*			T-RMD
2.5%-Zirconium alloy	4.5			0.030		78	0/10*			T-RMD
Zinc (dust) Tech grade	35	65	0.015	0.050	190	380	1/10	4430	532	D-SM

*Refers to threshold level of impact sensitivity

Sources: ADL, Arthur D. Little, Inc
AGC, Aerojet-General Corp
D-SM, Douglas Aircraft Corp, Santa Monica
GE, General Electric Co
M-B, Martin Company, Baltimore
M-D, Martin Company, Denver
Red, Redel Corporation
T-RMD, Thiokol Chemical Corp, Reaction Motors Div

END OF REFERENCE

27

REFERENCE

28

KEY, C. F.: AN INSTRUMENT FOR DETERMINATION OF IMPACT SENSITIVITY OF MATERIALS IN CONTACT WITH GASEOUS OXYGEN AT PRESSURES UP TO 50 PSIA. NASA TM X-53846, 1969.

G.1-1-8-1

NASA TECHNICAL
MEMORANDUM

Report No. 53846

AN INSTRUMENT FOR THE DETERMINATION OF IMPACT SENSITIVITY OF MATERIALS IN CONTACT WITH GASEOUS OXYGEN AT PRESSURES UP TO 50 PSIA

By C. F. Key
Astronautics Laboratory

DISTRIBUTION UNLIMITED PER
NASA TECHNICAL DIRECTIVE
75-40, 9-26-74

May 21, 1969

SPECIAL RELEASE

Not to be indexed, referenced,
or given further distribution
without approval of NASA

NASA

George C. Marshall Space Flight Center
Marshall Space Flight Center, Alabama

TECHNICAL REPORT STANDARD TITLE PAGE

1. Report No. NASA TM X-53846	2. Government Accession No.	3. Recipient's Catalog No.
4. Title and Subtitle An Instrument for the Determination of Impact Sensitivity of Materials in Contact with Gaseous Oxygen at Pressures up to 50 PSIA		5. Report Date May 21, 1969 6. Performing Organization Code
7. Author(s) C. F. Key		8. Performing Organization Report No.
9. Performing Organization Name and Address George C. Marshall Space Flight Center Marshall Space Flight Center, Alabama 35812		10. Work Unit No. 11. Contract or Grant No.
12. Sponsoring Agency Name and Address		13. Type of Report and Period Covered NASA Technical Memorandum 14. Sponsoring Agency Code
15. Supplementary Notes		

16. Abstract

An apparatus developed by Marshall Space Flight Center for use in determining the compatibility of materials in gaseous oxygen pressurization systems is described. The MSFC impact tester provides flexibility of testing conditions and reproducible results. Test results illustrating variables which must be controlled in gaseous oxygen impact testing are also presented.

DISTRIBUTION UNLIMITED PER NASA TECHNICAL DIRECTIVE 75-40, 9-26-74

17. Key Words	18. Distribution Statement
	CSTAR, Requests must be approved by the author

19. Security Classif. (of this report)	20. Security Classif. (of this page)	21. No. of Pages	22. Price
U	U	13	

TABLE I. IMPACT SENSITIVITY OF MATERIALS IN GASEOUS OXYGEN

Material	Manufacturer or Source	Thickness, (Inch)	Potential Energy kg-m	No. Reactions/ No. Tests	Comments
Aluminum Grease Cups		0.035	10	0/20	
Andox C Grease		0.003	10	16/20	6 SBs*
Cycolac LT-1000	Marbon Chemical Corporation	0.080	10	16/20	6 SBs
Cycolac LT-1000	Marbon Chemical Corporation	0.060	10	18/20	7 SBs
Cycolac LT-1000	Marbon Chemical Corporation	0.050	10	20/20	12 SBs
Cycolac LT-1000	Marbon Chemical Corporation	0.040	10	19/20	14 SBs
Cycolac LT-1000	Marbon Chemical Corporation	0.030	10	17/20	11 SBs
Cycolac LT-1000	Marbon Chemical Corporation	0.020	10	4/20	4 SBs
Cycolac LT-1000	Marbon Chemical Corporation	0.010	10	2/20	3 SBs
CPR-385-2	Upjohn Company	0.250	10	0/20	
DC-33 Grease, Lot M356	Dow Corning Corporation	0.050	10	2/20	
Ethylene Propylene Rubber		0.070	10	2/20	
FS-1265 Fluid, 300 cs	Dow Corning Corporation	0.025	10	1/20	Flash
FS-1281	Dow Corning Corporation	0.050	10	0/20	
Fluorel Sponge 1062	Mosite Rubber Company	0.200	10	0/20	
Grex Polyolefin	Grace Chemical Company	0.080	10	40/40	10 SBs
Grex Polyolefin	Grace Chemical Company	0.060	10	16/20	7 SBs
Grex Polyolefin	Grace Chemical Company	0.050	10	12/20	9 SBs
Grex Polyolefin	Grace Chemical Company	0.040	10	9/20	7 SBs
Grex Polyolefin	Grace Chemical Company	0.030	10	7/20	4 SBs
Grex Polyolefin	Grace Chemical Company	0.020	10	4/20	3 SBs
Grex Polyolefin	Grace Chemical Company	0.010	10	4/20	3 SBs

* SB - Sustained Burning

TABLE I. IMPACT SENSITIVITY OF MATERIALS IN GASEOUS OXYGEN (Continued)

Material	Manufacturer or Source	Thickness, (Inch)	Potential Energy kg-m	No. Reactions/ No. Tests	Comments
H-4001		0.080	10	8/20	Flashes
H-4001		0.060	10	10/20	6 SBs
H-4001		0.050	10	11/20	6 SBs
H-4001		0.040	10	11/20	8 SBs
H-4001		0.030	10	8/20	6 SBs
H-4001		0.020	10	5/20	3 SBs
H-4001		0.010	10	6/20	5 SBs
Houghton Safe 1120		0.003	10	8/20	4 SBs
LS-53 Fluorosilicone	Dow Corning Corporation	0.062	10	4/25	
L-3251 Fluorel	Raybestos-Manhattan, Incorporated	0.080	10	0/20	
Mylar Tape 49133	Minnesota Mining & Manufacturing Company	0.003	10	2/20	1 SB
Mystic Tape		0.003	10	4/20	4 SBs
Narmco 7343		0.050	10	20/20	1 SB
Neoprene		0.040	10	4/20	1 SB
Neoprene Coated Nylon	Manned Spacecraft Center	0.010	10	2/20	1 SB
Neoprene Gasket		0.100	10	2/10	2 SBs
Plexiglass		0.063	10	0/20	
Reschal Net		0.035	10	2/3	16.7 psia
Silicone Fabric 10470	Manned Spacecraft Center	0.110	10	1/20	
Silicone Hose (Wire)	Manned Spacecraft Center	0.110	10	0/20	

TABLE I. IMPACT SENSITIVITY OF MATERIALS IN GASEOUS OXYGEN (Concluded)

Material	Manufacturer or Source	Thickness, (Inch)	Potential Energy kg-m	No. Reactions/ No. Tests	Comments
Silicone Sl-503, White	Manned Spacecraft Center	0.110	10	1/20	1 SB
Silicone Rubber RTV-60	Manned Spacecraft Center	0.075	10	0/20	
Solder, 60% Tin-40% Lead		0.025	10	0/20	
Stainless Steel 347		0.063	10	0/20	
Tape #65	Minnesota Mining & Manufacturing Company	0.003	10	0/20	Burnt Odors
Teflon	Cadillac Plastic Company	0.010	10	0/20	
Teflon Sheet	E. I. du Pont de Nemours & Company	0.010	10	1/21	
T-Film Thread Compound		0.002	10	2/20	
Thermal Barrier, SRGA-0213		0.010	10	7/20	
Tenite II		0.080	10	18/20	2 SBs
Tenite II		0.060	10	14/20	5 SBs
Tenite II		0.050	10	18/20	17 SBs
Tenite II		0.040	10	20/20	20 SBs
Tenite II		0.030	10	20/20	20 SBs
Tenite II		0.020	10	5/20	3 SBs
Tenite II		0.010	10	0/20	
Tenite II		0.005	10	0/20	
Velcro Nylon Pile and Hook on Aluminum Disc		0.200	10	1/4	1 SB, 16.7 psia
Vespel Discs, Batch SRB-184	E. I. du Pont de Nemours & Company	0.050	10	0/20	
Viton A		0.070	10	1/20	1 SB
Zirconium		0.063	10	15/20	12 SBs

END OF REFERENCE

28

REFERENCE

29

JACKSON, J. D.; MILLER, P. D.; BOYD, W. K.; AND FINK, F. W.: A STUDY OF THE TITANIUM-LIQUID OXYGEN PYROPHORIC REACTION. WADD-TR-60-258, WRIGHT AIR DEVELOPMENT DIVISION, AIR RESEARCH AND DEV. COMMAND, JUNE 1960.

THIS MATERIAL HAS BEEN APPROVED FOR PUBLICATION PER LETTER FROM WALTER K. BOYD, BATTELLE COLUMBUS LABORATORIES TO JOANNE FOLK DATED OCT. 28, 1974.

F. W. FINK

WADD TR 60-258

A STUDY OF THE TITANIUM-LIQUID OXYGEN PYROPHORIC REACTION

J. D. Jackson
P. D. Miller
W. K. Boyd
F. W. Fink
BATTELLE MEMORIAL INSTITUTE
Columbus, Ohio

June 1960

WRIGHT AIR DEVELOPMENT DIVISION

NOTICE

When Government drawings, specifications, or other data are used for any purpose other than in connection with a definitely related Government procurement operation, the United States Government thereby incurs no responsibility nor any obligation whatsoever; and the fact that the Government may have formulated, furnished, or in any way supplied the said drawings, specifications or other data, is not to be regarded by implication or otherwise as in any manner licensing the holder or any other person or corporation, or conveying any rights or permission to manufacture, use, or sell any patented invention that may in any way be related thereto.

WADD TR 60-258

A STUDY OF THE TITANIUM-LIQUID OXYGEN PYROPHORIC REACTION

J. D. Jackson
P. D. Miller
W. K. Boyd
F. W. Fink
BATTELLE MEMORIAL INSTITUTE
Columbus, Ohio

June 1960

Materials Central
Contract No. AF 33(616)-6345
Project No. 7351

Wright Air Development Division
Air Research and Development Command
United States Air Force
Wright-Patterson Air Force Base, Ohio

ABSTRACT

A review of the literature indicates that titanium is impact sensitive under liquid oxygen below the acceptable limit for other metals.

An experimental program was begun to determine the mechanism of the titanium-LOX reaction. Several factors were investigated singly in a controlled manner using unalloyed titanium (75A) and an alloy (6Al-4V) that were carefully cleaned. The factors were:

(1) Exposure of a fresh surface by fracture and tearing

(2) Deformation by impact using steel balls

(3) Impact of smooth specially cleaned flat surfaces

(4) LOX pressure and velocity

(5) Galling.

The results from this program indicate that ~~no one of the above, per se,~~ is a primary cause of this reaction. A proposed mechanism is that heat generated by impact produces gaseous oxygen, which is compressed at local sites. A fresh surface exposed by the impact reacts with the high-pressure gaseous oxygen. Propagation is dependent on the amount of heat generated and the rate of heat loss from the affected area.

PUBLICATION REVIEW

This report has been reviewed and is approved.

FOR THE COMMANDER:

W. J. TRAPP
Chief, Strength and Dynamic Research
Metals and Ceramics Laboratory
Materials Central

the 70-foot-pound level, B-120VCA was more reactive than Ti-6Al-4V, and Ti-75A was least reactive.

Battelle Memorial Institute (BMI)[7] reported that Ti-75A and 6Al-4V exhibit sensitivity at the 70-foot-pound level with a loud report and a bright flash. The sensitivity seemed to be about the same whether the specimen was struck with stainless steel or with a piece of titanium similar to the specimen. When the Ti-75A specimen and striker were abraded, sensitivity was noted at levels of 10 and 30 foot-pounds. No change in sensitivity was found with abraded Ti-6Al-4V. One specimen of Ti-110AT exhibited no sensitivity with an impact of 70 foot-pounds.

Convair Astronautics[8] reported finding sensitivity with annealed A-110AT in the 30 to 70-foot-pound range. When Convair used a pointed striker instead of a flat face, little sensitivity was found for this alloy.[9]

Reaction Motors, Inc.[10], has reported what it calls threshold values for titanium in LOX. The threshold value is the lowest impact level at which no reactions occur out of 20 tries. Data are as follows:

Material	LOX Threshold, ft-lb/in.^{2}
Unalloyed titanium	78
Ti-6Al-4V	78
Ti-25Zr	78
B-120VCA (solution treated)	122
B-120VCA (aged 72 hr at 900 F)	67

These data indicate that the harder (aged) B-120VCA is more sensitive than its softer counterpart, and more reactive than 6Al-4V and Ti-75A.

Anodized Titanium. Both Battelle[7] and Martin[11] have investigated the impact sensitivity of anodized titanium disks of Ti-75A, B-120VCA, and Ti-6Al-4V supplied by WADD. These samples, which had been punched from treated sheets, were slightly dished and had sharp burrs at the exposed edges. Battelle filed the edges to remove the larger burrs, which slightly damaged some of the anodized coatings at the edge. Martin applied a proprietary plastic material to the edges. Both report that burning or detonation occurred at the 70-foot-pound level. However, anodizing significantly reduced the sensitivity.

Impact of Other Materials Under LOX

In general, other materials of construction, such as steel, stainless steel, and aluminum, do not exhibit the same reactivity at low energy levels as does titanium. Convair[8] noted no sensitivity for Type 301 stainless steel at an impact of 70 foot-pounds. Reaction Motors[12] found no reaction with aluminum up to an impact level of 400 foot-pounds per square inch.

Convair[8] has reported impact results using a pointed striker that pierces the specimen. No reactions have been obtained at the 25-foot-pound level for 301-XF stainless steel, K-Monel, or Alclad 2024-O. Two nonmetallics, Epoxylite and Conolon 506 (fiber glass-phenolic laminate), which are normally impact sensitive for a conventional flat striker, exhibited no reaction at the 75-foot-pound level.

ABMA[5] reported that, under proper conditions, some materials can be made to react at low impact levels. For example, when particles of grit were present on aluminum, burning was initiated at an impact level of 72 foot-pounds. The sensitivity increased as the hardness of the grit increased. Particle size seemed to be important also. For sand, a size of 50 to 60 mesh gave the greatest number of reactions. In decreasing order of reactivity were found: Carborundum, sand, Alundum, bentonite, and asbestos. No reactivity was found with talc or NaCl.

ABMA also found that aluminum wool, steel wool, stainless steel wool, and magnesium wool exhibit reactivity at the 72-foot-pound level. They report that soft solders have an extremely high sensitivity to LOX. Magnesium, even when treated with Dow 17 fluoride-chromate coating, was reactive at 72 foot-pounds.

Impact Using Other Propellants

Reaction Motors[10] also reported threshold values of titanium and its alloys in 90 per cent hydrogen peroxide, as follows:

Material	Threshold, ft-lb/in.^{2}
Unalloyed titanium	122
Ti-6Al-4V	144
Ti-25Zr	122
B-120VCA (solution treated)	211
B-120VCA (aged 72 hr at 900 F)	167

"(5) Gaseous oxygen reacts more readily with metals than any other element except fluorine. However, in the liquid state oxygen is a very inactive material; a cold iron wire immersed in liquid oxygen remains unaffected; a hot wire is quenched, and only a burning wire will continue to burn and explode."

The physical properties of titanium suggest that it might be more reactive in LOX than other structural materials. First, titanium has a very low heat capacity, both on a mole basis and on a volume basis. Second, titanium has a low thermal conductivity when compared with other materials. Third, titanium has a low ignition point in oxygen, as reported by Grosse and Conway[19]. These data are shown below:

Material	Heat Capacity[a] Cal/Degree C/Mole	Heat Capacity[a] Cal/Degree C/Cu Cm	k, Thermal Conductivity[a], Btu/hr/sq ft/(degree F/ft)	Approximate Ignition Point in Oxygen, C
Al	5.8	0.58	117	Over 1000
Cu	10.8	1.51	220	
Cr	5.7	0.78		2000
Fe	6.1	0.84	26	930
Mg	5.9	0.42	92	540-625
Ni	6.2	0.93	35	
Stain. steel	6.6	0.96	9	
Ti	4.4	0.42	14	610
Zr				1400

(a) Room temperature.

At least one theory has been advanced for the explosive behavior of titanium in LOX. This theory, as discussed by Alfred Africano, of the Space Technology Laboratory, depends on energy considerations of a point contact of titanium. An impact results in a temperature rise of a single cry .al that has broken apart. With materials having a high coefficient of heat transfer, the heat is rapidly dissipated, whereas with those, such as titanium, that have a low coefficient of heat transfer, the heat is transferred less rapidly. Thus, the reaction with LOX is more likely to begin. A mathematical relationship has been proposed.[20]

Reaction of Titanium in Gaseous Oxygen

Titanium has been shown to be reactive under certain conditions to gaseous oxygen. One example is the burning of titanium in a system designed to handle uranyl sulfate solution pressurized with oxygen at ORNL.[21,22] Galling was believed to lead to the formation of pyrophoric material, which was ignited by impact. These reactions were noted in valves and valve seats. The ignition was shown to have occurred in the gas phase at high oxygen pressures.

END OF REFERENCE

29

REFERENCE

30

LANDROCK, A. H.: PROPERTIES OF PLASTICS AND RELATED MATERIALS AT CRYOGENIC TEMPERATURES. PLASTEC-20, PLASTICS TECHNICAL EVALUATION CENTER, 1965. (AVAILABLE FROM DDC AS AD-469126.)

THIS MATERIAL HAS BEEN APPROVED FOR PUBLICATION PER LETTER FROM ARTHUR H. LANDROCK TO HAROLD W. SCHMIDT DATED SEPT. 10, 1974.

DEC 7 '65

COPY 1*

PLASTEC REPORT 20

X65-19322
AD 469126

PROPERTIES OF PLASTICS AND RELATED MATERIALS AT CRYOGENIC TEMPERATURES

LIBRARY COPY
SEP 3 1965
LEWIS LIBRARY, NASA
CLEVELAND, OHIO

JULY 1965

PLASTEC
PLASTICS TECHNICAL EVALUATION CENTER
PICATINNY ARSENAL
DOVER, NEW JERSEY

PLASTEC REPORT 20

PROPERTIES OF PLASTICS AND RELATED MATERIALS AT CRYOGENIC TEMPERATURES

by
ARTHUR H. LANDROCK

JULY 1965

PLASTICS TECHNICAL EVALUATION CENTER
PICATINNY ARSENAL, DOVER, NEW JERSEY

DISCLAIMERS:

The findings in this report are not to be construed as an official Department of the Army position, unless so designated by other authorized documents.

Mention of a particular commercial product neither constitutes an endorsement by the Plastics Technical Evaluation Center, nor a voucher for the accuracy of a manufacturer's claim, unless specifically noted.

NOTICE:

Trade designations appearing in the references cited have been included in this report if such inclusion was felt to be essential to an understanding of the original reference.

ABSTRACT

This report reviews the effects of cryogenic temperatures on plastics and such related materials as elastomers and adhesives. It presents an annotated bibliography of 319 references from the open literature, government project and contract reports, and conference papers. A detailed subject index and a number of supplemental indexes are included. Topics covered are: Molded Polymeric Materials (Plastics); Cryogenic Insulation; Structural Plastic Laminates; Elastomers, Seals and Sealants; Adhesives; Plastic Films, Film Laminations and Vapor Barriers; Fibers; Electrical Applications; Wear and Friction; Liquid Oxygen (LOX) Compatibility; Radiation and Combined Effects; and Miscellaneous Applications. Test Methods are not treated in a separate section in the discussion, but the subject index refers to many references with information on test procedures and apparatus.

TABLE 2. MECHANICAL AND THERMAL PROPERTIES OF FLUOROCARBON RESINS OF VARYING CRYSTALLINITIES
(From Mowers, Rocketdyne, Ref 237) X-65-19322

Mechanical Property	Temp., °F	Kel-F Crystallinity, %				FEP Teflon Crystallinity, %			TFE Teflon Crystallinity, %				
		40	55	60	70	44	49	51	47	49	52.5	66.2	71
Notched Izod Impact Strength, ft-lb/in.	-423	--	--	1.4	1.2	--	1.95	1.7	--	--	1.25	--	1.55
	-320	--	--	1.3	1.1	--	1.9	1.5	--	--	1.17	--	1.35
	(-297)	--	--	(1.25)	(1.07)	--	(1.9)	(1.5)	--	--	(1.15)	--	(1.39)
Modulus of Rigidity, psi x 10^3	-423	262	222	--	230	935	--	695	267	--	275	377	--
	-320	232	197	--	203	305	--	305	224	--	190	200	--
	(-297)	(229)	(192)	--	(195)	(275)	--	(275)	(216)	--	(175)	(175)	--
Tensile Yield Strength, psi x 10^3	-423	28.5	20.5	--	18.0	23.8	23.5	--	--	20.0	19.0	15.6	--
	-320	24.9	17.5	--	15.3	19.1	18.8	--	--	16.0	15.4	10.6	--
	(-297)	(24.4)	(17.0)	--	(15.0)	(17.9)	(17.6)	--	--	(14.2)	(14.1)	(9.0)	--
Ultimate Tensile Strength, psi x 10^3	-423	29.0	22.5	--	17.95	24.0	23.6	--	--	20.05	19.0	15.7	--
	-320	24.9	17.6	--	15.8	18.1	17.9	--	--	17.9	15.4	11.8	--
	(-297)	(24.1)	(17.5)	--	(15.3)	(17.0)	(16.8)	--	--	16.0	14.2	11.0	--
Tensile Modulus, psi x 10^6	-423	1.26	0.975	--	0.830	0.825	0.620	--	--	0.600	0.645	0.625	--
	-320	1.11	0.802	--	0.760	0.700	0.450	--	--	0.500	0.520	0.435	--
	(-297)	(1.08)	(0.800)	--	(0.750)	(0.652)	(0.430)	--	--	(0.465)	(0.480)	(0.400)	--
Elongation, %	-423	ca 2	ca 1	--	< 1	ca 5	ca 5	--	--	ca 4	ca 3	ca 2	--
	-320	ca 4	2.5	--	ca 1	ca 7	ca 7	--	--	ca 9	ca 8	ca 4	--
	(-297)	(ca 4.5)	(3)	--	(ca 1)	(ca 8)	(ca 7)	--	--	(9)	(8)	(ca 5)	--
Flexural Strength, psi x 10^3	-423	74.0	55.5	--	50.5	35.9	39.6	--	--	33.8	25.7	22.8	--
	-320	58.0	42.7	--	37.0	25.7	27.7	--	--	30.0	24.0	21.5	--
	(-297)	(53.5)	(41.0)	--	(35.0)	(24.0)	(25.5)	--	--	(28.0)	(23.0)	(20.5)	--

TABLE 2. MECHANICAL AND THERMAL PROPERTIES OF FLUOROCARBON RESINS OF VARYING CRYSTALLINITIES (From Mowers, Rocketdyne, Ref 237) (CONT) X65-19322

Mechanical Property	Temp., °F	Kel-F Crystallinity, %				FEP Teflon Crystallinity, %			TFE Teflon Crystallinity, %				
		40	55	60	70	44	49	51	47	49	52.5	66.2	71
Flexural Modulus, psi x 10^6	-423	2.09	1.94	--	1.84	0.78	0.75	--	--	0.778	0.72	0.695	--
	-320	1.83	1.70	--	1.64	0.68	0.68	--	--	0.720	0.70	0.64	--
	(-297)	(1.70)	(1.64)	--	(1.59)	(0.67)	(0.66)	--	--	(0.690)	(0.64)	(0.61)	--
		50*	55	60	70	44	49	51	47	50*	56*	68*	71
Compressive Strength, psi x 10^3	-423	42.5	--	44.5	28.8	36.3	35.2	--	--	30.4	32.5	33.2	--
	-320	35.0	--	37.5	38.8	30.0	30.0	--	--	20.0	21.2	22.0	--
	(-297)	(34.0)	--	(36.0)	(38.8)	(28.5)	(28.5)	--	--	(18.5)	(20.0)	(21.5)	--
Compressive Modulus, psi x 10^6	-423	1.67	--	1.76	1.48	1.01	1.04	--	--	0.81	0.90	0.97	--
	-320	1.48	--	1.52	1.65	0.91	0.91	--	--	0.75	0.79	0.84	--
	(-297)	(1.27)	--	(1.49)	(1.65)	(0.90)	(0.89)	--	--	(0.72)	(0.76)	(0.81)	--
Coefficient of Thermal Expansion (Total contraction from 70°F), in./in.	-423	0.011	--	--	--	0.017	--	--	--	0.0214	--	--	--
	-320	0.0093	--	--	--	0.0157	--	--	--	0.0205	--	--	--
	(-297)	(0.0090)	--	--	--	(0.0154)	--	--	--	0.0201	--	--	--

The above values were obtained by PLASTEC by reading off data points from the original data curves. The values in parentheses ( ) were obtained by interpolation. No actual data was obtained with liquid-oxygen temperatures in the original study.

Note change in crystallinity, indicated by asterisk (*)

TABLE 6. APPARENT MEAN THERMAL CONDUCTIVITY OF SOME SELECTED FOAMS (FromKropschot, National Bureau of Standards, Ref 124.) X-65-19322

Foam	Density (g/cm^3)	Boundary Temps. (°K)	Test Space Pressure	Thermal Conductivity ($\mu w/cm/°K$)
Polystyrene	0.039	300-77	1 atm	330
	0.046	300-77	1 atm	260
	0.046	77-20	10^{-5} mm Hg	81
Epoxy	0.080	300-77	1 atm	330
	0.080	300-77	10^{-2} mm Hg	168
	0.080	300-77	4×10^{-3} mm Hg	130
Polyurethane	0.08-0.14	300-77	1 atm	330
		300-77	10^{-3} mm Hg	120
Rubber	0.08	300-77	1 atm	360
Silica	0.16	300-77	1 atm	550
Glass	0.14	300-77	1 atm	350

their conductivity by as much as 30%. If H_2 or He is allowed to permeate the cells, the conductivity can be increased by a factor of 3 or 4. Even under evacuation, foam insulations have much higher conductivities than other types of insulation.

Cryo-pumping effects are responsible for the partial evacuation of foam insulations upon exposure to liquid hydrogen (142). For this reason precautions must be taken to assure that gas-tight barriers are provided to stop the penetration of moisture and air into the insulation. Such penetration would result in a marked increase in thermal conductivity and the possible disruption of the cells if the surface temperature were to suddenly increase. An explosion hazard might also be created if hydrogen were to leak from the tank and come in contact with any condensed air. To reduce such a hazard a helium purge can be introduced to carry away any diffusing atmospheric gases. Such a purge will, however, lead to a substantial decrease in the insulating effectiveness of the foam. Polyurethane foams rank poorly when compared to other insulating materials such as multiple-layers, opacified powders, glass fibers and Perlite over the range 60° to -320°F.

Studies have been carried out on the use of evacuation to reduce the thermal conductivity of load-bearing plastic foams for use in cryogenic applications (267). Urethane foams showed the greatest decrease in conductivity, while the reduction in the case of styrene foams was only moderate. Most closed-cell rigid foams could be evacuated to give conductivity values as low as 1/3 to 1/2 those of the unevacuated foams.

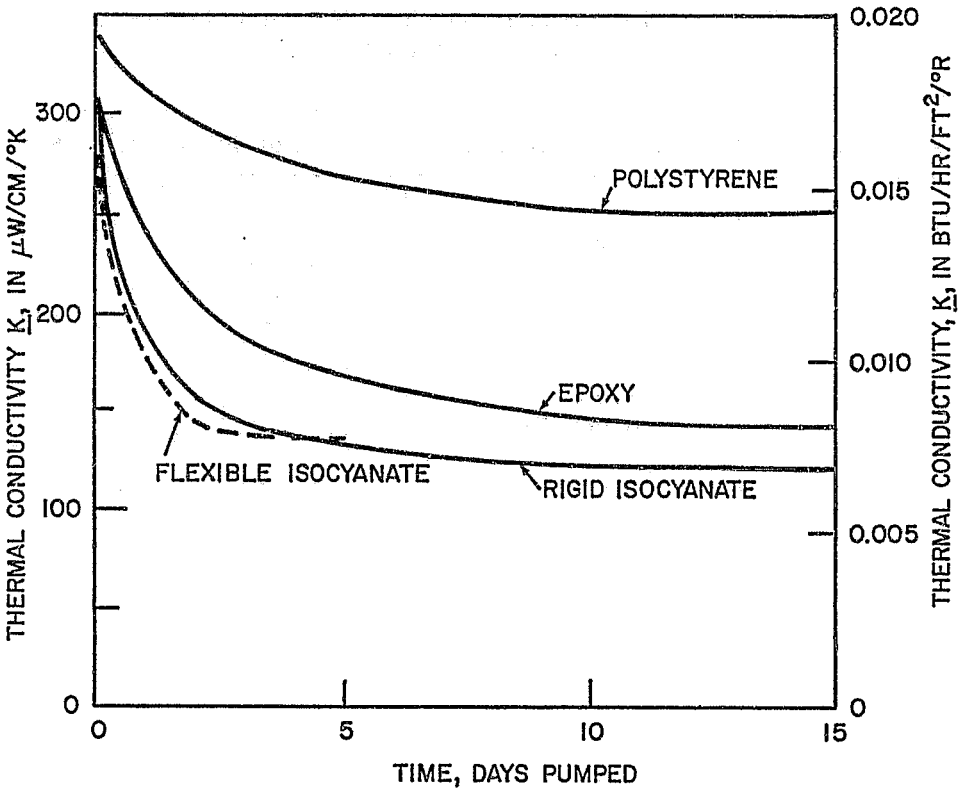

Figure 21. Apparent Mean Thermal Conductivity between 300° and 76°K of Selected Foams as a Function of Time under Evacuation. (From Kropschot, National Bureau of Standards, Ref 124.)

The range of values for thermal conductivities of typical foams used for cryogenic insulation is shown in Table 7, which includes values for vacuum powder and multiple-layer insulation (124). The relatively high conductivities of the foams is readily apparent.

MULTIPLE-LAYER INSULATIONS

Multiple-layer insulations are composed of highly reflective radiation shields of thin-gage foil separated by low-conductivity spacer materials such as glass or quartz. In some cases multilayers of aluminized polyester film (Mylar) are used without spacers. When evacuated, multiple-layer insulations have very high thermal efficiency for both cryogenic and high-temperature service because of their radiation attenuation characteristics (7). Some foams of multiple-layer insulations have yielded the lowest thermal conductivity of any bulk insulations developed to date (124). The lowest thermal conductivity values have been obtained by using layers of aluminum foil separated by glass fiber paper. Many other materials can be used, such as glass fiber mat (bonded and unbonded), glass fabric, nylon net, and finely divided powder.

TABLE 7. RANGE OF THERMAL CONDUCTIVITIES FOR VARIOUS INSULATIONS (From Kropschot, National Bureau of Standards, Ref 124.) X-65-193-2

μ w/cm/°K	Btu-ft/hr/ft^2/°F	Btu-in./hr/ft^2/°F	
300	0.0173	0.208	Foam
200	0.0116	0.139	
100	0.00578	0.0693	
50	0.00288	0.0347	
20	0.00116	0.0139	Vacuum powder
15	0.000867	0.0104	
10	0.000578	0.00693	
5	0.000288	0.00347	
3	0.000173	0.00208	
2	0.000116	0.00139	
1	0.0000578	0.000693	Multiple layer
0.3	0.0000173	0.000208	

Note: 1 w/cm/°K = 57.79 Btu-ft/hr/ft^2/°F = 693.5 Btu-in./hr/ft^2/°F

There are problems in the use of multiple-layer composites. Evacuation to relatively high vacuum levels is required, necessitating the use of encapsulation. As with powder insulations, these composites are sensitive to acoustic vibrations, compressive loading, and thermal cycling (7). When evacuated, these so-called "super-insulations" have by far the lowest thermal conductivity of any systems developed to date (10^{-4} to 10^{-5} BTU in./hr-ft^2-°F (118). Although extremely efficient from a thermal viewpoint, multiple-layer high-vacuum insulations suffer from serious physical and design limitations which may preclude their application in many liquid propulsion systems. The structural integrity of two surfaces with an evacuated space between them is limited by the strength of the massive feed-through supports. These supports provide the major heat leak in the system. In such a system an outer shell of large area and light weight must be supported against the load resulting from the pressure differential between the evacuated shell and the external environment. This results in severe design limitations. A large weight penalty may be imposed to maintain structural stability with large, low-pressure propellant tanks. Large evacuated structures are considered to be inherently unreliable. Film bladders have been used to compress the multilaminar insulations into stacks in order to circumvent some of these difficulties. Unfortunately the thermal conductivity of such a system is increased by about two orders of magnitude (118).

Table 8 lists thermal conductivity and density values of a number of insulating materials, including multilayer insulations (174). The kρ or density-thermal conductivity factor included in this table is useful in initial screening of candidate insulation materials. This factor is really a statement of the relative weight per unit area for equal performance and is a measure of overall insulation

TABLE 8. TYPICAL THERMAL CONDUCTIVITY (k), DENSITY (ρ) AND kρ FACTORS OF VARIOUS THERMAL INSULATIONS (From McGrew, Martin-Marietta Corp, Ref 174.) X-65-19322

Insulation	k*	ρ**	kρ	Insulation Pressure
Materials				
Silica Aerogel	0.12	8.5	1.02	Air environment (1 atm)
Polyurethane foam	0.20	2.0	0.40	Air environment (1 atm)
Kapok	0.24	0.88	0.21	Air environment (1 atm)
Corkboard	0.30	20.0	6.0	Air environment (1 atm)
Balsa wood	0.36	8.0	3.88	Air environment (1 atm)
Rubber	0.98	75.0	73.0	Air environment (1 atm)
Multilayer (S-I) Insulation				
S-I 10	0.00078	2.5	0.0020	10^{-4} mm Hg
S-I 12	0.00108	2.0	0.0020	10^{-4} mm Hg
S-I 44 (formerly 4)	0.00024	4.7	0.0011	10^{-4} mm Hg
S-I 62	0.00022	5.5	0.0012	10^{-4} mm Hg
S-I 62	0.0072	---	---	15 psi external load
S-I 91	0.00012	7.5	0.009	10^{-4} mm Hg
Opacified Powders				
Santocel "A"	0.0011	6.0	0.0066	10^{-4} mm Hg
Perlite	0.000864	8.0	0.0069	10^{-4} mm Hg
Cab-o-sil	0.0014	4.5	0.0063	10^{-4} mm Hg
Fiberglass				
AAAA 2.2×10^{-5} in. diameter fiber-heat felt	0.01	4.0	0.05	10^{-3} mm Hg
AAAA 2.2×10^{-5} in. diameter fiber-heat felt	0.03	1.04	0.03	10^{-3} mm Hg
AAAA 2.2×10^{-5} in. diameter heat felt	0.21	4.0	0.84	1 atm

* Btu/hr-ft^2-°F/in.
** lb/ft^3

efficiency for a particular material or composite. Final material selection, however, should be made on the basis of heat transfer rates and the weight of the total insulation.

The use of vacuum-coated aluminum on 25-gage Mylar provides low bulk density and the advantages of a single-component system (136). At atmospheric pressure this system performs as a good bulk, sponge or fiber insulation. When the interstitial pressure is reduced to 10^{-5} Torr or below, performance is about three orders of magnitude better. Such a system offers extremely low $k\rho$ products. The tolerance in weight per square foot of the metallized Mylar is a variable of critical interest in space applications (136). The gage of the Mylar base material can be controlled to within $\pm 32\%$ by the film manufacturer. The aluminum coating adds only about 0.8% to this variation, and from a weight standpoint, is not a controlling factor. The Mylar substrate is not normally subject to requirements for close weight control. Its extremely thin gage makes high percentages of variation difficult to avoid in manufacture. For space applications there is a definite need for tightening control of specific weight of this material.

In multilayer insulations radiative heat transfer becomes important once gas conduction and solid conduction have been reduced (142). Ideally, radiation shields of the highest reflectivity are separated by nearly nonconducting spacers in a high vacuum. Representative multilayer insulations are described in some detail in Table 9. Multilayer insulations have been used successfully in cryogenic storage and transportation problems of large tanks on earth. In all likelihood they can be used successfully for thermal protection of liquid hydrogen during long periods of space travel. Multiple-layer insulations of quite reasonable thickness will probably be adequate to reduce the boil-off losses to acceptable proportions.

Large-scale tests in liquid-hydrogen service have been carried out using model space tankage and a compressible superinsulation (137). Such insulation, which requires very low residual gas pressure in its interstices for proper thermal performance, is obviously applicable in the vacuum environment of space. As a design compromise to satisfy the atmospheric storage problem the insulation volume is encapsulated within a hermetically sealed, flexible plastic laminate jacket, which is evacuated to the required degree of vacuum. In this system an external bearing pressure of one atmosphere will compress the insulation, reducing its thickness and increasing its thermal conductivity.

Aluminized Mylar in multiple-layer insulations may not be as effective as aluminum foil, since the coated plastic is somewhat transparent to infrared energy (268). Tests carried out at the National Bureau of Standards indicated that several layers of aluminized Mylar separated by a spacer were required to indicate an emissivity equivalent to thin aluminum foil. The utilization of multiple-shield insulations presents advantages in weight savings, increased pay load, and shorter cool-down time. Present evacuated powder-insulated 28,000-gallon liquid-oxygen tanks have a loss rate of about 35% per year. It may be possible to reduce this to 1/10 of this value with multiple-layer insulations. This advantage is offset by the considerably lower cost of the powder insulation.

TABLE 9. TYPICAL MULTILAYER INSULATIONS (From A. D. Little, Inc., Ref 142)

Radiation Shield	Spacer
0.002-inch thick H-19 tempered aluminum, bright on two sides (Alcoa)	0.020-inch thick vinyl-coated glass-fiber screen, grid dimensions 1/8 x 1/8 inch (Owens-Corning)
0.00025-inch thick crinkled polyester film, aluminized on one side (Nat. Res. Corp.)	0.020-inch thick vinyl-coated glass-fiber screen, grid dimensions 1/8 x 1/8 inch (Owens-Corning)
0.002-inch thick H-19 tempered aluminum, bright on two sides (Alcoa)	0.008-inch thick glass-fiber mat (Dexter Paper) with 50% perforations
0.00025-inch thick crinkled polyester film, aluminized on one side (Nat. Res. Corp.)	0.001-inch thick glass-fiber cloth (J.P. Stevens)
0.00025-inch thick crinkled polyester film, aluminized on one side (Nat. Res. Corp.)	----- none -----
0.00025-inch thick crinkled polyester film, aluminized on one side (Nat. Res. Corp.)	0.008-inch thick glass-fiber mat with 50% perforations (Dexter Paper)
0.0005-inch thick soft aluminum, bright on one side (Alcoa)	0.003-inch thick polyester fiber spacers (Dexter Paper)

Recent work with vacuum fiberglass and superinsulation using a flexible type of vacuum jacket is encouraging (62). Even though the materials are compressed due to the atmospheric load on the flexible vacuum jacket, they have excellent thermal resistance and recover almost completely when the load is removed as the insulated cryogenic tankage leaves the earth's atmosphere. Crinkling of aluminized Mylar is sometimes carried out to minimize interlayer contact (258). A patented superinsulation method involving "quilted superinsulation" has been used to insulate a 105,000-gallon liquid-hydrogen tank (119). Blankets of the quilted material can be readily installed in position in an essentially field-erected tank. Total expected heat leak of this system is 1480 Btu/hr, which is equivalent to 0.3% of total capacity per day.

A jacketed multilayer insulation system has been applied to a 150-gallon cylindrical cryogenic tank and tested under compression due to atmospheric pressure with vacuum within the insulation (SI-62) (222). This condition simulated the effect of the ground-hold condition on the insulation. Additional studies were

carried out at reduced pressures, simulating the condition in space. The flexible vacuum jacket material is a laminate of 1-mil aluminum sandwiched between two layers of a 1/2-mil Mylar. Heat flux with 1-atmosphere compressive load on the tank was 20 Btu/hr-ft^2 (vacuum within the insulation about 5 μ Hg). Under a reduced pressure of 10^{-4} atm it was 0.83 Btu/hr-ft^2 (vacuum within the insulation about 0.5 μ Hg). These results show that heat flux is increased by a factor of about 25 when the insulation is compressed under ground-hold conditions. The preliminary tests indicate the applicability of this type of insulation system.

An interesting development involves the use of a honeycomb-reinforced foam insulation next to a liquid-hydrogen tank wall, followed by a layer of multi-foil reflective insulation. This system is enclosed in a Mylar sheath, which serves as a vacuum jacket prior to launch, protects the fragile multi-foil insulation during ascent, and serves as a meteroroid bumper in space. The Mylar sheath is held in place with a piece of nylon netting until the vehicle is in the parking orbit (144).

Table 10 gives the apparent mean thermal conductivities of a number of multiple-layer insulations (122, 124).

Super insulation appears to be most attractive for intermediate duration (greater than 1 day but less than 1 year) space flights (90A). Super insulation systems such as NRC-2 and Linde SI-62 have apparent thermal conductivity values when measured under high vacuum between room temperature and -320°F of 1 to 3 x 10^{-5} Btu-ft/hr-ft^2-°F. In comparison to these values, evacuated fiberglass and evacuated powder insulations have k-factors approximately 30 to 50 times higher, and plastic foams 500 to 1000 times higher. The differences between the systems are reduced if comparison is made on a $k\rho$ or $(k\rho)^{\frac{1}{2}}$ basis, but the super insulations are still significantly better than the other passive systems. One of the most critical problems arising in insulating large tanks with multilayer insulation is the manner of attaching the insulation to the tank. Heat leaks through attachments as well as through interconnecting structural members and plumbing can negate all the advantages of a "super insulation" system. No more than 30% of the total heat leak into a tank insulated with multilayer insulation should be caused by discontinuities such as joints, supports and piping attachments.

POWDER INSULATIONS

Powder insulations consist of finely divided particulate materials such as perlite, expanded silicone dioxide, calcium silicate, and diatomaceous earth. Phenolic spheres are also used. At one atmosphere pressure, powder reduces the total heat transport across the insulation by reducing both convection and radiation, and, if the particle size is small enough, by reducing the mean free path of the gas molecules (124). When the powder is at low pressures (10 μ of Hg or less), gas conduction is negligible and heat transport is chiefly by radiation and solid conduction. Phenolic spheres of 25-100 μ particle size, 0.2 g/cm^3 density and $< 10^{-3}$ mm Hg gas pressure give conductivity values of 13 $\pm$1 μw/cm/°K. At pressures above 10^{-2} mm the conductivity of phenolic spheres rises rapidly (41c, 124).

The vacuum required with powder insulations is much less extreme than in the high-vacuum or multiple-layer insulations. However, most powders can

TABLE 10. THE APPARENT MEAN THERMAL CONDUCTIVITY OF ALUMINIZED MYLAR AND SELECTED MULTIPLE-LAYER INSULATIONS OF ALUMINUM FOIL SPACED WITH VARIOUS MATERIALS
(From Kropschot, National Bureau of Standards, Ref 122, 124)

Sample Thickness (cm)	Number of Layers or Shields (per cm)	Density (g/cm^3)	Cold-Wall Temp.* (°K)	Thermal Conductivity ($\mu w/cm/°K$)	Spacer Material
Aluminized Mylar					
3.5	24	0.045	76	0.85	None; Al one side
1.3	47	0.09	76	1.8	None; Al one side
Multiple-Layer Insulations of Aluminum Foil Spaced with Various Materials					
3.7	26	0.12	76	0.7	Glass fiber
3.7	26	0.12	20	0.5	Glass fiber
2.5	24	0.09	76	2.3	Nylon net
1.5	76	0.76	76	5.2	Glass fiber
4.5	6	0.03	76	3.9	Glass fiber (unbonded)
2.2	6	0.03	76	3.0	Glass fiber (unbonded)

* Warm-wall temperature 300°K

X-615-69-322

absorb considerable moisture and, therefore, must be thoroughly dried before the required vacuum can be attained.

Powder insulations tend to pack and therefore change in volume when subjected to vibration for extended periods (118). They also require an external supporting shell. When the temperature does not fall below that of liquid nitrogen, gas-filled powder insulations may be used.

Tables 7 and 11 give some data on the insulating properties of powders. "Multiple-layer Insulations" should be consulted for additional information.

TABLE 11. TYPICAL THERMAL CONDUCTIVITY, DENSITY AND k x ρ FACTORS OF VARIOUS THERMAL INSULATIONS AT A MEAN TEMPERATURE OF -250° F (From Minges, Aeronautical Systems Div., WPAFB, Ref 7)

Insulation	Thermal Conductivity, k*	Density, ρ**	k x ρ Factor
Organic Foam	1×10^{-1}	2.0	2.0×10^{-1}
Fibrous Insulation (Evacuated)	1×10^{-1}	7.0	7×10^{-1}
Air	7×10^{-2}	0.2	1.4×10^{-2}
Evacuated Powder	8×10^{-3}	6.0	4.8×10^{-2}
Multilayer Composite (Evacuated)	3×10^{-4}	4.7	1.4×10^{-3}

* Btu-in./hr/ft^2/°F
** lbs/ft^3

REINFORCED PLASTICS

Several studies have been carried out on the applicability of reinforced plastics for use in structural insulations (90A, 266). Such insulations include the following:

Ref 90A:

Narmco 570/143 (E glass)	"E" glass-cloth-reinforced epoxy
Insurok T-601	Medium weave cotton fabric (canvas) base phenolic

SECTION 11. LIQUID OXYGEN (LOX) COMPATIBILITY

In addition to performing satisfactorily, polymeric materials in a cryogenic system must withstand the effects of the cryogenic fluids themselves. Materials subject to contact with LOX may be evaluated by the ABMA Impact Sensitivity Test, primarily designed for application to materials used in missiles, but which yields results which may also be used as a criterion for most other cryogenic applications (29, 190). The test is performed by subjecting a sample of the material, immersed in LOX, to impact at various levels up to 70 foot-pounds. Any signs of oxidation, such as odor, change of color, evolution of light, or audible sound, are called detonations, and, as such, are considered to be failures of the sample. For a material to be considered compatible with LOX, it must withstand 70 foot-pound impacting of 20 samples with no more than one detonation. The degree of compatibility for those samples producing more than one detonation in 20 tries is dependent on the number and violence of the reactions.

All hydrocarbons are considered to be sensitive to LOX to some degree (67). The degree of sensitivity is an inverse function of the amount of substitution of various strongly bonded atoms, especially halogens, for the hydrogen atom. Hydrocarbons immersed in LOX are susceptible to explosions under impact loading because the C-H bond is easily broken, with oxygen reacting with both C and H. The susceptibility to explosion is decreased by replacing the H with an element that forms a stronger bond with the C. This is the situation in Kel-F, where the H atoms are replaced by fluorine and chlorine atoms in the ratio of 3:1, and Teflon (TFE), where H is completely replaced by fluorine. These C-F bonds are very strong, and therefore such materials show no impact sensitivity (67).

The LOX impact sensitivity of fluorocarbon plastic films is shown in Fig. 46 (33). The data was obtained on an RMD impact tester. The rather low value for polyvinylidene fluoride points up the effect of hydrogen on the molecule. The figure also shows that sample thickness has a strong effect on impact sensitivity. Reactions of organic materials with LOX, using relatively pure elastomeric and thermoplastic polymers, have been extensively studied and reported (105, 159). Plasticizers and antioxidants were also studied in this recent work. The flash of light resulting from impact was measured with a photocell, and the sound intensity or pressure pulse was monitored with a microphone. Many of the pure polymers were found to be resistant, although, in the compounded form, they may have been fairly reactant on contact with LOX. Table 29 shows the results of these tests.

Fluorinated polymers, primarily Teflon, have been in wide use for cryogenic seals. The development of a new cryogenic gasket for LOX service has recently been described (99, 187, 293). The gasket is a glass-fiber-laminated structure in which the glass fiber bundle is not completely saturated with fluorocarbon (Teflon) polymer binder (See also Ref 234). Most elastomers are not satisfactory for service in LOX because of their reactivity. Several fluorinated elastomers (Viton, Kel-F and Fluorel) have shown high sensitivity to LOX, however, and have been considered for cryogenic seals. The results of LOX compatibility tests on various polymers used as gaskets are shown in Table 30 (29). Note the non-reactivity of Mylar A in this table. In an earlier program of study 2/30 detonations were obtained for an impact level of 70 foot-pounds (219).

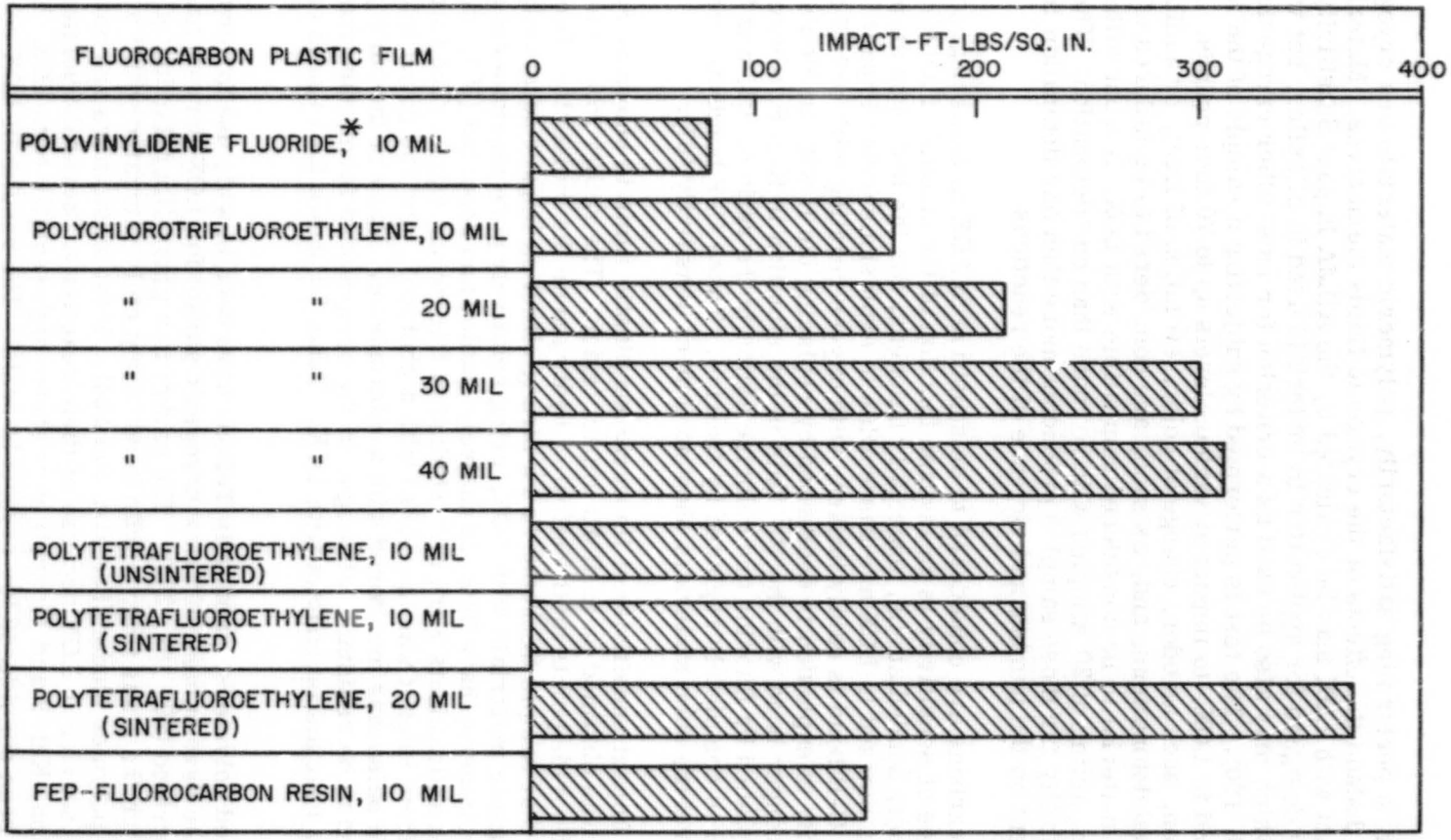

* HAS UNSATURATED VINYLIDENE GROUP, $-(CF_2 = CH_2)-$

X-65-19322

Figure 46. LOX Impact Sensitivity of Fluorocarbon Plastics - RMD Impact Tester (After Bringer, 3M Co, Ref 33, based on data by Reaction Motors Div, Thiokol Chemical Corp)

R-59

TABLE 29. DETONATION FREQUENCIES OF MATERIALS IN LIQUID OXYGEN* (USING ALUMINUM CUPS, A-286 STRIKERS). (From Hauser and Rumpel, Hauser Res & Eng Co and Martin-Marietta Corp Resp, Ref 105, 159)

Material	Impact Energy, ft-lb							
	70	60	50	40	30	20	10	5
Polymers								
Acrylonitrile-butadiene 1000 x 132	1/20	1/13	4/20	3/10	--	2/2	0/20	--
Chlorinated polyether (Penton)	0/20	--	--	--	--	--	--	--
Polyacetal (Delrin)	0/20	--	--	--	--	--	--	--
Polybutadiene	0/20	--	0/5	--	--	--	--	--
Polychloroprene	0/20	--	--	--	--	--	--	--
Poly (cyanoethyl) siloxane	1/29	1/10	0/20	--	--	--	--	--
Polydimethylsiloxane	1/30	0/20	0/5	--	--	--	--	--
Polyethylene, branched	0/20	--	0/5	--	--	--	--	--
Polyethylene, linear (Marlex)	0/20	--	--	--	--	--	--	--
Polyisoprene	0/20	--	0/5	--	--	--	--	--
Polypropylene	0/20	--	0/5	--	--	--	--	--
Polystyrene	2/11	3/4	4/5	4/5	--	4/10	0/20	--
Poly (trifluoropropyl) methylsiloxane	0/20	--	--	--	--	--	--	--
Polyvinyl chloride	0/20	--	0/5	--	--	--	--	--
Polyvinylidene chloride	0/20	--	--	--	--	--	--	--
Polyvinylidene fluoride (Kynar)	0/20	--	--	--	--	--	--	--
Vinylidene fluoride-hexafluoropropylene (Viton A)	0/20	--	--	--	--	--	--	--
Plasticizers								
Dibutyl phthalate	1/10	1/15	3/10	--	--	--	1/15	0/5
Dibutyl sebacate	0/20	--	0/5	--	--	--	--	--
Tri-o-cresyl phosphate	1/10	1/10	3/3	--	--	--	1/10	0/5

* Frequencies measured by number of detonations/number of trials

TABLE 30. IMPACT SENSITIVITY OF MATERIALS IN LIQUID OXYGEN (From Walker, Boeing Airplane Co, Ref 29)

Specimen Material	Specimen Form, in.	Weight Dropped, lbs	Distance Dropped, ft	Impact, ft-lbs	No. of Trials	No. of Reactions
Nitrile Rubber	.75 dia x .035	5.0	3.5	17.5	3	3
Neoprene Rubber 2-0006	.75 dia x .035	7	3.5	24.5	3	3
Mylar Type A	.75 dia x .007 thick	12	2	24	10	0
Teflon felt and Teflon 100X Laminate	Teflon 100X sandwiched in Teflon felt - .75 dia x .12	20	3.5	70	3	0
Silicone Rubber DC 916 60268	.75 dia x .03	20	.7	14	3	3
Butyl Rubber	.75 dia x .045	20	.6	12	10	2 (Violent detonation)
Kel-F	1 dia x .5	20	3.5	70	40	0
Viton A	1 dia x .5	20	3.5	70	20	0
Polydimethylsiloxane	1 dia x .5	20	3.5	70	3	3
Fluorinated Siloxane LS-53	1 dia x .5	20	3.5	70	51	2

END OF REFERENCE

30

REFERENCE

31

WRIGHT, H. W.; HOWELL, G. W.; AND LEE, D. H.: SEAL MATERIAL DEVELOPMENT PROGRAM, PHASE I. TRW SYSTEMS GROUP (NASA CR-114822), 1970.

N71-16577

JUN 21 '71

COPY 1

N71-16577

REPORT NO. 14771-6001-R0-00 31 DECEMBER 1970

70-7
21 JAN '71

SEAL MATERIAL DEVELOPMENT PROGRAM

FINAL REPORT

PHASE I

LEWIS RESEARCH CENTER
Aerospace Safety Research
and Data Institute
JUL 22 1971
CLEVELAND, OHIO

LIBRARY COPY
JUN 21 1971
LE ..ND, OHIO

PREPARED FOR
NATIONAL AERONAUTICS AND SPACE ADMINISTRATION
MANNED SPACECRAFT CENTER
HOUSTON, TEXAS 77058

CONTRACT NO. NAS 9-10481

TRW
SYSTEMS GROUP

Report No. 14771-6001-R0-00
31 December, 1970

FINAL REPORT

SEAL MATERIAL DEVELOPMENT PROGRAM
PHASE I

Prepared for

NASA Manned Spacecraft Center
Houston, Texas

H. W. Wright, Program Manager

Approved by: G. W. Howell
Laboratory Staff Engineer

Approved by: D. H. Lee, Manager
Combustion Systems Laboratory

ABSTRACT

The Seal Material Development Program is planned as a three-phase program. This report covers Phase I which was conducted to identify and characterize materials which would advance the state of the art for oxygen-hydrogen propulsion system seals. The temperature range to be covered was from -423°F (37°R) to +200°F (660°R). A total of nineteen materials were evaluated, with fourteen being tested at least once during the program. Included in the materials tested were Teflon (as the control material), ethylene propylene terpolymer compounds, two silicone compounds, HYSTL (a TRW polyurethane resin), an experimental fluorinated elastomer (AF-E-124D), and Viton-A. Although the goal of the program was to identify a single material for use in both oxygen and hydrogen over the entire temperature range, a number of materials were characterized for use in either oxygen or hydrogen.

The experimental fluoroelastomer AF-E-124D generally indicated superior performance to other materials for use in both oxygen and hydrogen systems. The Teflon TFE performed satisfactorily in both propellants. Viton A and HYSTL exhibited excellent seal characteristics for use in liquid hydrogen systems. Tests conducted included liquid hydrogen seal tests, ABMA LO_2 impact sensitivity tests, and cleaning and flushing fluid and elevated temperature exposure tests.

Further characterization of AF-E-124D as well as other promising materials is recommended to establish design parameters for these materials. In addition, fabrication and test of materials in various seal configurations are the next steps in developing promising materials as advanced oxygen-hydrogen propulsion system seals.

Table 5-6. ABMA LO_2 Impact Sensitivity Test Results, First Series

Material	Impact Load (ft-lb)					
	72	60	50	40	30	20
Teflon TFE (control)	0/10	-	-	-	-	-
255-2 Viton-A	3/3*	2/10*	0/4	0/2	-	-
AF-E-71-2 EPT Compound	3/3*	-	-	2/5	2/2*	1/1
263-2 EPT-Hydrin	3/3*	-	-	3/5	2/2	2/2
310-1 Phenyl Silicone	6/10	-	3/3	0/3	-	-
316-1 Fluorosilicone	3/3	-	2/4	0/3	-	-
1904-85 HYSTL	4/5	-	-	2/2	2/5	2/8

*Indicates an audible detonation.

Code: Fractions depict number of reactions/total impact tests.

Table 5-7. ABMA LO_2 Impact Sensitivity Test Results Summary

Material	Impact Load (ft-lb)						
	72	60	50	40	30	20	10
Teflon TFE (control)	0/40						
AF-E-124D	0/20						
255-2 Viton-A	3/3*	2/10*	8/46	0/2			
310-1 Phenyl Silicone	6/10	-	3/3	12/24	2/2*	2/20	
1904-85 HYSTL	4/5	-	-	2/2	2/5	2/8	1/20
316-1 Fluorosilicone	3/3	-	2/4	7/11*	3/3	4/10	1/10
AF-E-71-2 EPT-HYSTL	3/3*	-	-	2/5	2/2*	1/1	1/10
263-2 EPT-Hydrin	3/3*	-	-	3/5	2/2	2/2	2/10

*Indicates an audible detonation.

Code: Fractions depict number of reactions/total impact tests.

Although it was difficult to obtain realistic seat impression photographs, Figures 5-19 through 5-25 give a relative comparison of the seat conditions after being subjected to equal test conditions.

The data provided in Table 5-8 reflects average data derived from various test samples. The apparent significant superiority of the HYSTL over the other materials in the group was unexpected and may not be a result of relative materials capability. Since HYSTL is a plastic, the surface finish is normally very smooth. At the other extreme, the AF-E-124D samples available for test (since material is in limited supply) had relatively uneven surfaces, as may be seen in Figure 5-19. This may account for the variation in seat stress required to effect a seal as shown in Table 5-8 both at ambient temperature and -423°F. Other material surfaces were of approximately equal quality with the HYSTL surface.

5.4 SOLVENT AND CLEANING FLUID EXPOSURE TEST DESCRIPTION

Each candidate seal material was subjected to a series of solvent exposure tests to establish fluids compatibility. The fluids used in this test are common cleaning and test fluids normally used in propellant systems. They are:

- Distilled water
- Freon TF
- Isopropyl Alcohol (IPA)
- Trichlorethylene

The test procedures used were as follows: First, samples were obtained in standard test sample sizes. Measurements of length, thickness and weight were taken. The samples were placed in individual containers with each fluid. The samples were exposed to the fluids for the following lengths of time:

- One hour
- Four hours
- One day
- Three days
- Seven days
- Fourteen days

END OF REFERENCE

31

Card #8

REFERENCE

32

WALKER, W. R.: DESIGN HANDBOOK FOR O-RINGS AND SIMILAR ELASTIC MATERIALS. WADC-TR-59-428-PT-2, WRIGHT AIR DEVELOPMENT CENTER, 1961. (AVAILABLE FROM DDC AS AD-265443.)

THIS MATERIAL HAS BEEN APPROVED FOR PUBLICATION PER LETTER FROM R. H. MALTBY TO JOANNE FOLK DATED AUG. 27, 1974.

NOV 21 61

D. F.

N-8029
N-8029

WADC TECHNICAL REPORT 59-428
PART II

COPY 2

DESIGN HANDBOOK FOR O-RINGS AND SIMILAR ELASTIC SEALS

WILLIAM R. WALKER

BOEING AIRPLANE COMPANY

LEWIS RESEARCH CENTER
Aerospace Safety Research
and Data Institute
MAR 27 1973
CLEVELAND, OHIO

(5) N-8029

APRIL 1961

This report is not to be announced
or distributed automatically
to foreign governments
(AFR 205-43A, paragraph 6d).

AERONAUTICAL SYSTEMS DIVISION

NOTICES

When Government drawings, specifications, or other data are used for any purpose other than in connection with a definitely related Government procurement operation, the United States Government thereby incurs no responsibility nor any obligation whatsoever; and the fact that the Government may have formulated, furnished, or in any way supplied the said drawings, specifications, or other data, is not to be regarded by implication or otherwise as in any manner licensing the holder or any other person or corporation, or conveying any rights or permission to manufacture, use, or sell any patented invention that may in any way be related thereto.

ASTIA release to OTS not authorized.

Qualified requesters may obtain copies of this report from the Armed Services Technical Information Agency, (ASTIA), Arlington Hall Station, Arlington 12, Virginia.

Copies of ASD Technical Reports and Technical Notes should not be returned to the Aeronautical Systems Division unless return is required by security considerations, contractual obligations, or notice on a specific document.

WADC TECHNICAL REPORT 59-428
PART II

DESIGN HANDBOOK FOR O-RINGS AND SIMILAR ELASTIC SEALS

WILLIAM R. WALKER

BOEING AIRPLANE COMPANY

APRIL 1961

MATERIALS CENTRAL
CONTRACT No. AF 33(616)-5722
PROJECT No. 7381

AERONAUTICAL SYSTEMS DIVISION
AIR FORCE SYSTEMS COMMAND
UNITED STATES AIR FORCE
WRIGHT-PATTERSON AIR FORCE BASE, OHIO

McGregor & Werner, Inc., Dayton, O.
300 - October 1961 - 4-95 & 96

ABSTRACT

This is a continuation of the summation of work accomplished under Air Force Contract AF 33(616)-5722, Task No. 73810. It is presented as Part II of a handbook covering the mechanism of O-ring sealing. Data presented herein is concerned with hydraulic and pneumatic systems utilizing static and dynamic type seals at temperatures exceeding 275°F and for static applications at cryogenic temperatures. The effect of vibration, pressure cycling, seal materials and fluids on the operational efficiency of seals and back-up rings are discussed. Sections are devoted to cryogenic, fuel, and, vacuum system seals, and aging and age control. It also includes physical properties of elastomers at high temperatures and a bibliography.

PUBLICATION REVIEW

This report has been reviewed and is approved.

FOR THE COMMANDER:

J. M. Kelble, Chief
Elastomers and Coatings Branch
Non-Metallic Materials Laboratory
Materials Central

TABLE XV

IMPACT SENSITIVITY OF MATERIALS IN LIQUID OXYGEN

Specimen Material	Specimen Form (in.)	Weight Dropped	Distance Dropped	Impact (Ft. Lbs.)	No. of Trials	No. of Reactions
Nitrile Rubber	.75 Dia. x .035	5.0 lbs.	3.5 ft.	17.5	3	3
Neoprene Rubber 2-0006	.75 Dia. x .035	7	3.5	24.5	3	3
Mylar Dupont Type A	.75 Dia. x .007 Thick	12	2	24	10	0
Teflon Felt and Teflon 100X Laminate	Teflon 100X sandwiched in Teflon Felt .75 Dia. x .12	20	3.5	70	3	0
Silicone Rubber DC 916 60263	.75 Dia. x .03	20	.7	14	3	3
Butyl Rubber	.75 Dia. x .045	20	.6	12	10	2 (Violent Detonation)
Kel-F	1 Dia. x .5	20	3.5	70	40	0
Viton A	1 Dia. x .5	20	3.5	70	20	0
Polydimethylsiloxane	1 Dia. x .5	20	3.5	70	3	3
Fluorinated Siloxane LS-53	1 Dia. x .5	20	3.5	70	51	2

END OF REFERENCE

32

REFERENCE

33

KEY, C. F.: AN APPARATUS FOR DETERMINATION OF IMPACT SENSITIVITY OF MATERIALS IN CONTACT WITH LIQUID AND GASEOUS OXYGEN AT HIGH PRESSURES. MAT. RES. STAND., VOL. 11, NO. 6, JUNE 1971.

An Apparatus for Determination of Impact Sensitivity of Materials in Contact with Liquid and Gaseous Oxygen at High Pressures

C. F. Key

REFERENCE: Key, C. F., "An Apparatus for Determination of Impact Sensitivity of Materials in Contact with Liquid and Gaseous Oxygen at High Pressures," *Materials Research and Standards*, MTRSA, Vol. 11, No. 6, p. 28.

ABSTRACT: An apparatus developed by the Marshall Space Flight Center for use in determining the impact sensitivity of engineering materials in liquid and gaseous oxygen at pressures greater than 1 atm is described. This apparatus uses the basic impact tester described in ASTM D 2512, with the addition of a pressurized specimen holder in place of the D 2512 anvil region. A certain flexibility in test conditions is allowed for in that drop height can be varied as specified and reproducible results can be obtained. In addition, two view ports allow both operational viewing of results and film documentation.

The use of a uniquely balanced striker pin arrangement with less than 0.31 kg • m energy loss allows the direct comparison of results of all tests with pressure as a variable. It is anticipated that this tester can be used for evaluation of materials in other reactive propellants such as nitrogen tetroxide, Toflox, and fluorine.

KEY WORDS: oxygen, liquid oxygen, liquid propellants, cryogenic rocket propellants, impact tests, low temperature tests, ignition, hypergolic ignition

Liquid and gaseous oxygen (lox and gox) are used extensively in both the space program and industry in general. Pure liquid and gaseous oxygen are stable and not subject to detonation; however, mixing with most organic and some inorganic materials can cause ignition or explosion under stimuli such as impact or puncture. Many fires and explosions involving gaseous or liquid oxygen have been reported.

Organic materials of the type conventionally used as adhesives, lubricants, gaskets, elastomers, etc., are particularly hazardous. However, this hazard is not confined to them alone, it applies to many totally inorganic substances in contact with lox or gox. The environmental and structural demands inherent in space vehicle systems make it a matter of prime urgency to characterize all materials precisely with regard to lox/gox sensitivity.

Accordingly, a lox impact test device was developed at the George C. Marshall Space Flight Center (MSFC) to provide information on the relative hazards presented by these materials. The development of this test method and device was described by W. R. Lucas and W. A. Riehl in the *ASTM Bulletin*, February 1960. This device has been used successfully at MSFC over the past decade for the selection of materials in liquid or gaseous oxygen systems. The test procedure and criteria of acceptability have been issued as MSFC-SPEC-106B. The basic parameters also have been accepted as ASTM Test for Compatibility of Materials with Liquid Oxygen (Impact Sensitivity Threshold Technique (D 2512-68)).

While impact, or mechanical energy, is the basis for this test method, other forms of energy also are capable of triggering the mixtures. These energy forms can arise from virtually unforseen, unpredictable, and seemingly unknown sources. The mere fact that an unsatisfactory or "sensitive" component or material in a liquid or gaseous oxygen system is not expected to encounter impact energy at the location where it is to function cannot be considered sufficient justification for its use.

An earlier report, NASA TM X-53846, described the development of the first-generation gox impact tester for use at low pressures up to 34×10^4 N/m^2. A device for transmitting impact energy was favored for this test program because basically it is the simplest method of transmitting a measurable amount of energy to a test fixture. This paper describes the second-generation tester, which is designed for use at higher pressures.

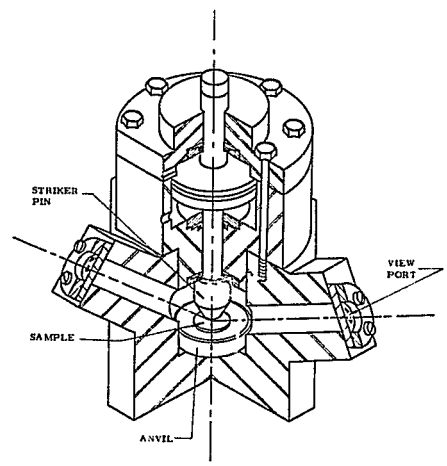

Fig. 1—*High pressure oxygen tester.*

Theoretical

It generally is accepted that the high temperatures resulting from nearly adiabatic compression are the cause of ignition in an impact tester. It should be noted that these conditions also can be produced by the rapid pressurization of a line. The theoretical temperature due to adiabatic compression can be calculated from the following equation:

$$\frac{T_f}{T_i} = \left[\frac{P_f}{P_i}\right]^{[n-1/n]}$$

C. F. Key, projects officer, Materials Div., Astronautics Lab., NASA, Marshall Flight Space Center, Ala.

where

P_i = initial pressure,
T_i = initial temperature,
P_f = final pressure,
T_f = final temperature, and
$n = c_p/c_v$ (specific heat ratio).

For oxygen $n = 1.4$, thus

$$\frac{T_f}{T_i} = \left[\frac{P_f}{P_i}\right]^{1.4-1/1.4} = \left[\frac{P_f}{P_i}\right]^{0.286}$$

Assume an initial pressure of 9.5×10^4 N/m^2 and an initial temperature of 20 C (293 K), then

$$T_f = 293\left[\frac{P_f}{9.5 \times 10^4}\right]^{0.286}$$

The final temperature for various pressures is shown below.

Temperature, T_f		Pressure, N/m^2
deg C	(deg K)	
233	(506)	68×10^4
488	(761)	2.72×10^6
649	(922)	5.44×10^6
763	(1036)	10.88×10^6
926	(1199)	13.6×10^6
1182	(1455)	27.2×10^6

It is obvious from the above that rapid pressurization of lines with gox may generate high temperatures which are sufficient to ignite a large number of materials.

Because adiabatic compression constitutes yet another potential source of energy for ignition or detonation, the development of a high pressure gox tester was undertaken at MSFC. This report describes in some detail the design and operation of this tester. Comparison of test results with those obtained with the Army Ballistic Missile Agency (ABMA) lox tester also are presented.

Description of Tester

The gox tester utilizes the basic ABMA tester assembly with a pressurized specimen holder. The tester is designed to allow a 9.04-kg plummet to fall through a distance of 1.1 m onto a striker pin protruding from the specimen holder. The maximum allowed deviation from free fall is 3 percent. Figure 1 shows details and orientation of striker pin and specimen. The basic instrument as shown consists of a plummet guided in its vertical fall by two sets of bearings, one set at each end of the plummet. The bearings arranged at the vertices of equilateral triangles roll freely in tracks milled in steel bars. These tracks are bolted rigidly to steel tubing supports and are aligned accurately with shims so that uniform contact with the ball bearings is maintained at all points along the length of the track. The supports are anchored securely to the top and base plate. The 2.54-cm-thick base plate is anchored in a 0.028-m^3 cube of concrete.

The control panel is separated from the instrument by a reinforced concrete wall containing an observation window aligned with the viewing port of the specimen holder so the operator has a view of the specimen. Another viewing port is provided on the holder for photographic coverage of test evaluation. The room is darkened to a predetermined level during the tests to enhance observation of reactions.

The plummet is held at the desired height by an electromagnet and a safety catch spring loaded in the holding position. When power is delivered to the solenoid the safety catch is released. The drop height may be varied from 0 to 1.1 m. A height indicator is located on the electromagnet support strut and must be reset to zero with the plummet resting on the striker pin and specimen whenever the drop height or specimen thickness are changed.

The plummet is released by activating two switches on the control panel, one releases the safety catch and the other reverses the electromagnetic field, whose collapse releases the plummet. The plummet delivers the impact to a stainless steel striker pin resting on the specimen. The specimen holder is pressurized to the desired pressure by a remotely controlled solenoid valve.

The striker pin is 20.65 cm long and has a 1.27-cm-diameter impacting surface area. The position striker assembly has a 12.4 to 1 pressure ratio to balance system. This provides a method for decreasing the stable friction losses of the system to less than 0.31 kg • m.

Procedure for Test Evaluation

The physical nature of the specimen determines the manner in which it is prepared for test evaluation. Solids and sheet materials are cut into 1.90 to 2.54-cm-diameter disks. Oils, greases, and other semisolids are evaluated as thin films in the bottom of the specimen holder. It is imperative that the specimens and holders be precleaned prior to test. After each test, the specimen holder is dismantled and cleaned with a pure chlorinated hydrocarbon solvent and dried. A clean striker pin, whose face must be free of pits and scratches, is used for each test. The striker pin is cleaned by vapor degreasing and alkaline soak, followed by rinsing in water and drying.

Table 1—Drop Height Schedule for Approximate Threshold Value Determination

Measurement	Drop Height, cm
First height	109.98
Second height	83.82
Third height	60.96
Fourth height	38.10
Fifth height	15.24

A precleaned specimen is placed in the holder. The cap is placed on the specimen holder and bolted in place. The system is purged and pressurized to the desired pressure with the test fluid. Twenty specimens are tested at each decreasing impact level from 10 kg • m until there is no evidence of reaction at the pressure of interest. One of the following will serve as evidence of reaction:

An audible explosion
A visible flash in a darkened room
Discoloration
Evidence of burning (charring)

The approximate threshold value is obtained by testing 20 specimens at each of the drop heights listed in Table 1. The first height at which no reactions are obtained in 20 consecutive drops is called the "approximate threshold value." The "definitive threshold value" is determined by 20 tests at drop height increments of 7.62 cm starting at a height of 14.24 cm above the approximate threshold value; it is the higher of the two adjacent heights at which no reaction was obtained.

Test Results

Effect of Specimen Thickness/ A series of test evaluations were made to determine the effect of specimen thickness on impact sensitivity at pressures up to 1000 psi in room temperature gaseous oxygen. The results are tabulated in Table 2. It is obvi-

(continued on page 51)

Table 2—Effect of Specimen Thickness of Various Materials at 10-kg • m Impact Energy

Material	Thickness, cm	Pressure, N/m^2	% Reaction	Increase in Sensitivity
Silicone rubber	0.152	34×10^4	55	...
Silicone rubber	0.050	34×10^4	100	1.8
Polytetrafluoroethylene	0.157	6.8×10^6	10	...
Polytetrafluoroethylene	0.086	6.8×10^6	20	2
Fluorinated rubber	0.229	6.8×10^6	10	...
Fluorinated rubber	0.152	6.8×10^6	33.3	3.3

Infrared Sensor Materials

(*continued from page 15*)

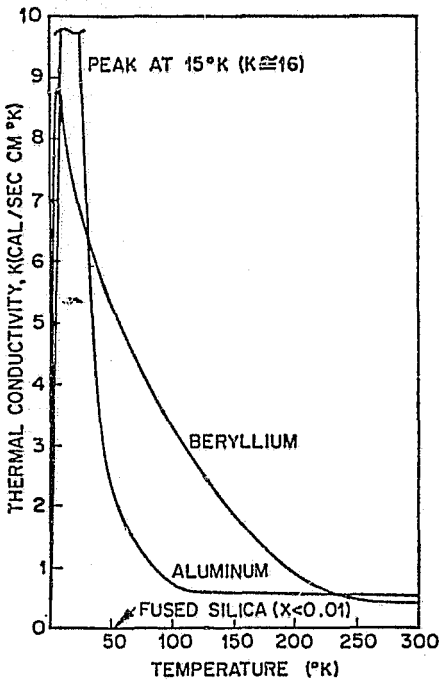

Fig. 12—*Thermal conductivity of mirror substrate materials.*

quirements of High Performance Infrared Sensors," presented at the Space Technology and Heat Transfer Conference of the American Society of Mechanical Engineers, Los Angeles, June 1970.

[8] Ballard, S. S. and Browder, J. S., *Applied Optics*, APOPA, Vol. 5, 1966, p. 1873.

[9] Herzberger, M. and Salzberg C. D., *Journal of the Optical Society of America*, JOSAA, Vol. 52, 1962, p. 420.

[10] Bulletin No. DLA-1333, Texas Instruments, Inc., Oct. 1967.

[11] Cardona, M., Paul, W., and Brooks, H., *Journal of the Physics and Chemistry of Solids*, JPCSA, Vol. 8, 1959, p. 204.

[12] Salzberg, C. D. and Villa, J. J., *Journal of the Optical Society of America*, JOSAA, Vol. 48, 1958, p. 579.

[13] Rank, D. H., Bennett, H. E., and Cronemeyer, D. C., *Journal of the Optical Society of America*, JOSAA, Vol. 44, 1954, p. 13.

[14] Briggs, H. B., *Physical Review*, PHRVA, Vol. 77, 1950, p. 287.

[15] Salzberg, C. D. and Villa, J. J., *Journal of the Optical Society of America*, JOSAA, Vol. 47, 1957, p. 244.

[16] Rodney, W. S. and Malitson, I. H., *Journal of the Optical Society of America*, JOSAA, Vol. 46, 1956, p. 956.

[17] Pamphlet No. U-71, Eastman Kodak Co., 1967.

[18] Hilton, A. R. and Jones, C. E., *Applied Optics*, APOPA, Vol. 6, 1967, p. 1513.

[19] Private communication with P. E. Natale, Eastman Kodak Co., 1968.

[20] Stierwalt, D. L. and Potter, R., *Journal of the Physics and Chemistry Solids*, JPCSA, Vol. 23, 1962, p. 99.

[21] Stierwalt, D. L., Bernstein, J. B., and Kirk, D. D., *Applied Optics*, APOPA, Vol. 2, 1963, p. 1169.

[22] Stierwalt, D. L. in AIAA *Progress in Astronautics and Aeronautics Series*, Vol. 18, Academic Press, N.Y., 1966, p. 21.

[23] Stierwalt, D. L., *Applied Optics*, APOPA, Vol. 5, 1966, p. 1911.

[24] Personal communication with D. L. Stierwalt, Naval Electronic's Laboratory Center, San Diego, Calif., 1968.

[25] Ladd, L. S., *Infrared Physics*, INFPA, Vol. 6, 1966, p. 145.

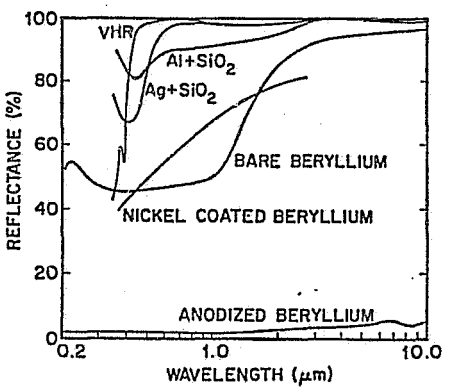

Fig. 13—*Spectral reflectance of mirror coatings.*

[26] Stierwalt, D. L. and Potter, R. in *Proceedings of the International Conference on the Physics of Semiconductors*, the Institute of Physics and the Physical Society, London, 1962, p. 513.

[27] Hass, G. in *Applied Optics and Optical Engineering*, R. Kingslake, Ed., Vol. III, Academic Press, 1965, p. 309.

[28] Goggin, W. R. and Schroeder, J. B., "Beryllium in the Optics Industry," presented at Beryllium Symposium, National Materials Advisory Board meeting, Washington, D.C., March 1970.

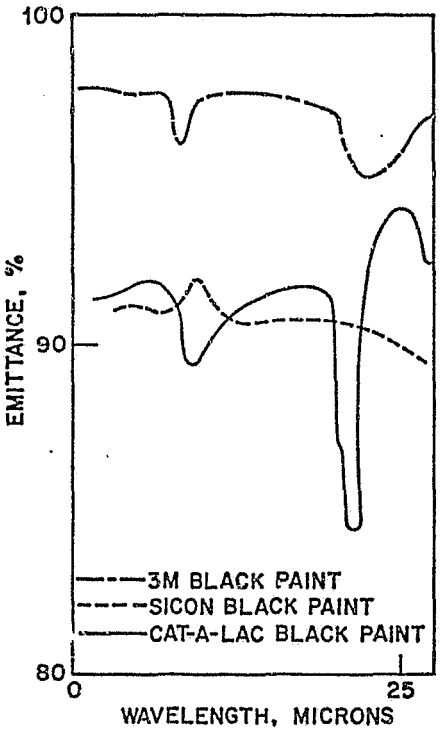

Fig. 14—*Spectral absorptance of baffle coatings.*

[29] Goggin, W. R. and Schroeder, J. B., "Be Mirror Technology," Proceedings, Electro-Optical Systems Design Conference, New York. Sept. 1969.

[30] Aronson, J. R. McLinden, H. G., "Far-Infrared Spectra of Solids," Symposium on Thermal Radiation of Solids, NASA Report SP-55, 1965.

[31] Blackburn, H. and Campbell, D. S. in *Transactions of the 8th Vacuum Symposium 1961*, Vol. 2, Pergamon Press, [illegible]

[32] Hilton, A. R. and [illegible], *Applied Optics*, APOPA, Vol. 6, 1967, p. 1513.

[33] Volf, M. B., *Technical Glasses*, Pitman, 1961.

[34] Bernstein, J. B. and Stierwalt, D. L., "Infrared Spectral Emittance of Five Black Coatings," Naval Weapons Center, China Lake, 1970.

[35] Janssen, J. E. et al, "Normal Spectral Reflectance of Anodized Coatings on Aluminum, Titanium and Beryllium," ASD Technical Report TR 61-147, Honeywell Research Center, Sept. 1961.

[36] Hering, R. G. and Smith, T. F. in *Progress in Astronautics and Aeronautics*, Vol. 23, Thermophysics, Academic Press, 1970, p. 337.

■ ■ ■

An Apparatus for the Determination of Impact Sensitivity

(*continued from page 29*)

ous from the data that the impact sensitivity of materials varies inversely with thickness; consequently, it is mandatory that materials be evaluated for impact sensitivity in the thickness of interest. This is a fact which cannot be overstressed.

Effect of Pressure/ The effect of pressure on test results was observed by dropping a 10-kg • m plummet through a distance of 1.1 m. The results given in Table 3 indicate that the impact sensitivity of the materials evaluated increases rapidly as pressure is increased.

Effect of lox/gox Impact Tests/ There always have been questions about the relative severity of impact testing in gaseous and liquid oxygen. Some workers believe that lox impact testing is more severe than gox impact testing at a given pressure. A series of test evaluations were conducted to determine the relative differences between lox and gox tests with a 10-kg • m impact energy. The results (Table 4) indicate that materials generally are more impact sensitive in gaseous than in liquid oxygen at a given pressure.

Conclusions

An impact sensitivity tester has been developed for determination of impact sensitivity of selected materials in liquid and gaseous oxygen and other propellants at various pressures. The preliminary data indicate the following:

1. The impact sensitivity of the materials tested tends to be more pressure dependent in gaseous oxygen than in liquid oxygen.

(*continued on page 52*)

(continued from page 51)

Table 3—Effect of Pressure on Impact Sensitivity in Gaseous Oxygen

Material	Thickness, cm	% Reaction at Pressure, N/cm²			
		6.8 × 10⁶	3.4 × 10⁶	68 × 10³	34 × 10³
Fluorinated hydrocarbon	0.188	66.6	50	20	0
Fluorinated silicone	0.328	100	100	50	50
Silicone	0.152	...	100	100	50

Table 4—Impact Sensitivity of Selected Materials in Liquid and Gaseous Oxygen at 10 kg·m

Material	Thickness, cm	Pressure, N/m²	% Reaction in	
			lox	gox
Nylon	0.008	3.4 × 10⁶	20	50
Silicone	0.152	68 × 10³	100	100
Polytetrafluoroethylene	0.165	3.4 × 10⁶	0	10
Chlorotrifluorocarbon plastic	0.317	6.8 × 10⁶	0	0

2. The impact sensitivity of materials in gaseous oxygen varies directly with pressure.

3. The relative rating of the materials tested in lox at pressures up to 6.8 × 10^6 N/m² is the same as lox at 9.5 × 10^4 N/m².

4. This tester provides flexibility of test conditions for evaluation of a wide variety of materials in fuels and oxidizers.

5. The above data are tentative and, as such, constitute preliminary test results for the conditions noted. A much more comprehensive test program, structured to yield statistically meaningful cardinal data over a wide variety of materials of interest currently is in progress at the Marshall Space Flight Center. ■ ■ ■

Assessment of Impact Test Techniques

(continued from page 35)

input.). By our previous definition of compatibility, it follows that there are two categories of compatible materials: those that are insensitive and those that are sensitive but do not propagate. Incompatible materials, of course, are those that exhibit both sensitivity and a tendency to propagate.

Clearly, if we are to define the compatibility of a material by test, we must measure both sensitivity and the tendency to propagate, that is, the potential reaction intensity.

Conclusions

We have attempted herein to review the development of the two lox impact test methods appearing in Part 18 of the ASTM Standards and to present some of the aspects involved in using such tests to choose materials for lox systems. Hopefully, we have presented a conclusive case to the effect that both sensitivity and reaction intensity measurements are necessary for credible choices between materials.

Noting that one of the above methods purports to measure sensitivity and the other yields reaction intensity, it would seem that the use of both would solve the problem. We have attempted to show, however, that the sensitivity test violates so many fundamental aspects that its inability to yield acceptable precision is not surprising. The reaction intensity test appears to yield meaningful results, but the method is so new that it has not been used outside the laboratory where it was developed, and we know nothing about its reproducibility. Moreover, even if the reaction intensity test does prove to be reproducible through interlaboratory testing, it will not constitute a complete measure of compatibility; precise sensitivity information also is needed. Therefore, we must conclude that a new test for sensitivity with better precision than now available is needed urgently.

REFERENCES

[1] Africano, A. in *Advances in Cryogenic Engineering*, Vol. 5, Plenum Press, New York, 1960.

[2] "Liquid Oxygen Compatibility Impact Sensitivity Test Method," USAF Specification Bulletin 527, U.S. Air Force, 1 May 1961.

[3] "Testing Compatibility of Materials for Liquid Oxygen Systems," NASA Specification MSFC-SPEC-106B, National Aeronautics and Space Administration, 16 Sept. 1966.

[4] Crow, E. L., Davis, F. A., and Maxfield, M. W., *Statistics Manual*, Dover Publications, New York, 1960.

[5] Brown, J. A. et al, "Sensitivity and Rheology Studies on Lead Azide-RDX-Silica Mixtures," Final Technical Report No. GR-1SRS-69 for U.S. Army Picatinny Arsenal, Esso Research and Engineering Co., Jan. 1969.

[6] Blackstone, W. R., Baber, B. B., and Ku, P. M., *Transactions*, American Society of Lubrication Engineers, ASLTA, Vol. 11, No. 3, July 1968.

[7] Rothman, D., Alexander, M. J., and Zimmerman, J. M., "The Design and Analysis of Sensitivity Experiments," NASA CR-62026, Vols I and II, National Aeronautics and Space Administration, May 1965. ■ ■ ■

Determination of Flash and Fire Points and Impact Sensitivity

(continued from page 43)

spark propagation; thus, arcing at the points occurs during the spark discharge. Because this arcing causes a higher temperature spark, it is expected that the flash and fire points occur at lower temperatures.

Another interesting observation is that, whereas numerous flashes but few fires occur with the low pressure system, flash and fire points generally occur simultaneously when the high pressure system is used. This variance is attributed to the difference in spark generators or perhaps the greater possibility of autoignition under high pressure conditions. WSTF is performing studies to determine the relationship of flash and fire points to spark characteristics as well as autoignition properties under high pressure oxygen environments.

It should be pointed out that a difficulty arose when we attempted to specify spark energy as a control parameter. Energy measurement in the low pressure system is straightforward and can be accomplished by measuring the spark current and voltage compared to time, plotting a power envelope, and then obtaining the area under the curve. This measurement can be performed readily because, at the low pressures involved, the spark is in the form of a "normal glow discharge" as described by Cobine[3]; thus, the voltage wave form is fairly smooth and easy to define. At higher pressures, however, the required increase in spark voltage causes an erratic, frequent transition from normal glow to arcing during the spark period. Because different energies exist for the two conditions, even an approximate measurement of energy is difficult. Nonetheless, a quantity that is measured easily is spark gap current as a function of time, which can be displayed on a storage oscilloscope by using a current probe or a current sampling resistor. Although this current measurement does not describe directly the spark energy delivered (as is desired), it does give a means for calibrating individual spark generators to ensure that the same energy profile is used for different test setups.

General conclusions

Gaseous Oxygen Impact Testing/ Testing to date using the WSTF mechanical and pneumatic impact systems has provided reproducible, repeatable data for test pressures up to 5000 psia in a 100

[3]Cobine, J. D., *Gaseous Conductors, Theory and Engineering Applications*, Dover Publications, New York, 1958, p. 250.

END OF REFERENCE

33

REFERENCE

34

A STUDY OF THE MECHANISM OF THE TITANIUM-LIQUID OXYGEN EXPLOSIVE REACTION. ASD-TR-61-479, AERONAUTICAL SYSTEMS DIV., AIR FORCE SYSTEMS COMMAND, 1961.

CATALOGED BY ASAPRL
AD 65,357

ASD-TR-61-479

FILE COPY

DO NOT DESTROY
RETURN TO
TECHNICAL INFORMATION LIBRARY
ASAPRL

A STUDY OF THE MECHANISM OF THE TITANIUM-LIQUID OXYGEN EXPLOSIVE REACTION

WRIGHT AIR DEV. DIV.
TECHNICAL LIBRARY
WRIGHT-PATTERSON AIR FORCE BASE, OHIO

TECHNICAL REPORT ASD-TR-61-479

DIRECTORATE OF MATERIALS AND PROCESSES
AERONAUTICAL SYSTEMS DIVISION
AIR FORCE SYSTEMS COMMAND
WRIGHT-PATTERSON AIR FORCE BASE, OHIO

PROJECT No. 7351, TASK No. 73521

(Prepared under Contract No. AF 33(616)-7595 by
Battelle Memorial Institute, Columbus, Ohio;
J. D. Jackson, P. D. Miller, W. K. Boyd, F. W. Funk, Authors)

NOTICES

When Government drawings, specifications, or other data are used for any purpose other than in connection with a definitely related Government procurement operation, the United States Government thereby incurs no responsibility nor any obligation whatsoever; and the fact that the Government may have formulated, furnished, or in any way supplied the said drawings, specifications, or other data, is not to be regarded by implication or otherwise as in any manner licensing the holder or any other person or corporation, or conveying any rights or permission to manufacture, use, or sell any patented invention that may in any way be related thereto.

Qualified requesters may obtain copies of this report from the Armed Services Technical Information Agency, (ASTIA), Arlington Hall Station, Arlington 12, Virginia.

This report has been released to the Office of Technical Services, U. S. Department of Commerce, Washington 25, D. C., for sale to the general public.

Copies of ASD Technical Reports and Technical Notes should not be returned to the Aeronautical Systems Division unless return is required by security considerations, contractual obligations, or notice on a specific document.

ABSTRACT

A mechanism for the LOX-titanium reaction was proposed during a previous investigation (WADD TR 60-258). It was postulated that the impact of a titanium surface immersed in LOX generates sufficient heat to gasify a pocket of oxygen. In addition, the impact tends to compress the oxygen at the local impact sites. A rapid reaction occurs at the fresh surface formed by the impact.

The present investigation has established that a fresh titanium surface, formed by rupture of a tensile specimen, would react in gaseous oxygen under approximately 100 psig pressure at temperatures as low as about -250 F. These results tend to substantiate the proposed mechanism.

Means of eliminating or minimizing the reaction of titanium when ruptured in gaseous oxygen were investigated. The addition of HF as a gas to the oxygen resulted in some inhibition. Argon reduced the reactivity of oxygen gas by dilution. Coating the tensile specimens with fluoride-phosphate or with vapor-deposited aluminum did not affect the reactivity. These same coatings furnished some protection to titanium from reactivity during impact under LOX.

PUBLICATION REVIEW

This report has been revised and is approved.

FOR THE COMMANDER:

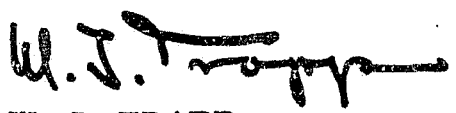

W. J. TRAPP
Chief, Strength & Dynamics Branch
Metals & Ceramics Laboratory
Directorate of Materials & Processes

A literature survey showed that the impurity content of LOX is very low. Only solid impurities in LOX are believed to affect the impact sensitivity of titanium.

The experimental program included an investigation of means of eliminating or minimizing the reaction of titanium when ruptured in gaseous oxygen. Two means were tried, namely (1) gaseous additions to the oxygen atmosphere and (2) the coating of titanium surfaces. These experiments were conducted under conditions of oxygen pressure at which reactions had occurred previously. It was found that the addition of 2 per cent HF gas to oxygen at room temperature raised the threshold pressure for the reaction from 75 to about 200 psig. An inert gas also reduced the titanium sensitivity by acting as a diluent. However, the addition of about 5 per cent or more of argon was required to raise the threshold to about 200 psig. Fluorine additions apparently increased the reactivity of the fresh titanium surface.

Coated titanium tensile specimens were ruptured in gaseous oxygen at room temperature. No reduction in reactivity was noted when using coatings of a fluoride-phosphate or a vapor-deposited aluminum. In fact, the experiments indicated that somewhat greater damage occurred with an aluminum coating than with uncoated specimens.

Impact studies showed some effectiveness for the fluoride-phosphate and vapor-deposited aluminum coatings for inhibiting reactions in LOX, particularly for 75A material.

EXPERIMENTAL PROGRAM

Tensile Rupture of Titanium in High-Pressure Oxygen

The following paragraphs describe an experimental program which was designed to investigate the reactivity of a fresh titanium surface in gaseous oxygen over a wide range of temperatures. The fresh surface was obtained by breaking a titanium tensile specimen, and the atmosphere was maintained in a specially outfitted autoclave system.

Equipment and Operation

A standard 1-liter AISI Type 316 stainless steel autoclave was used as the container. It was fitted with a holder so that a tensile specimen could be fractured while being exposed to high-pressure gaseous oxygen at low temperature. Figure 1 is a schematic diagram of the autoclave system used.

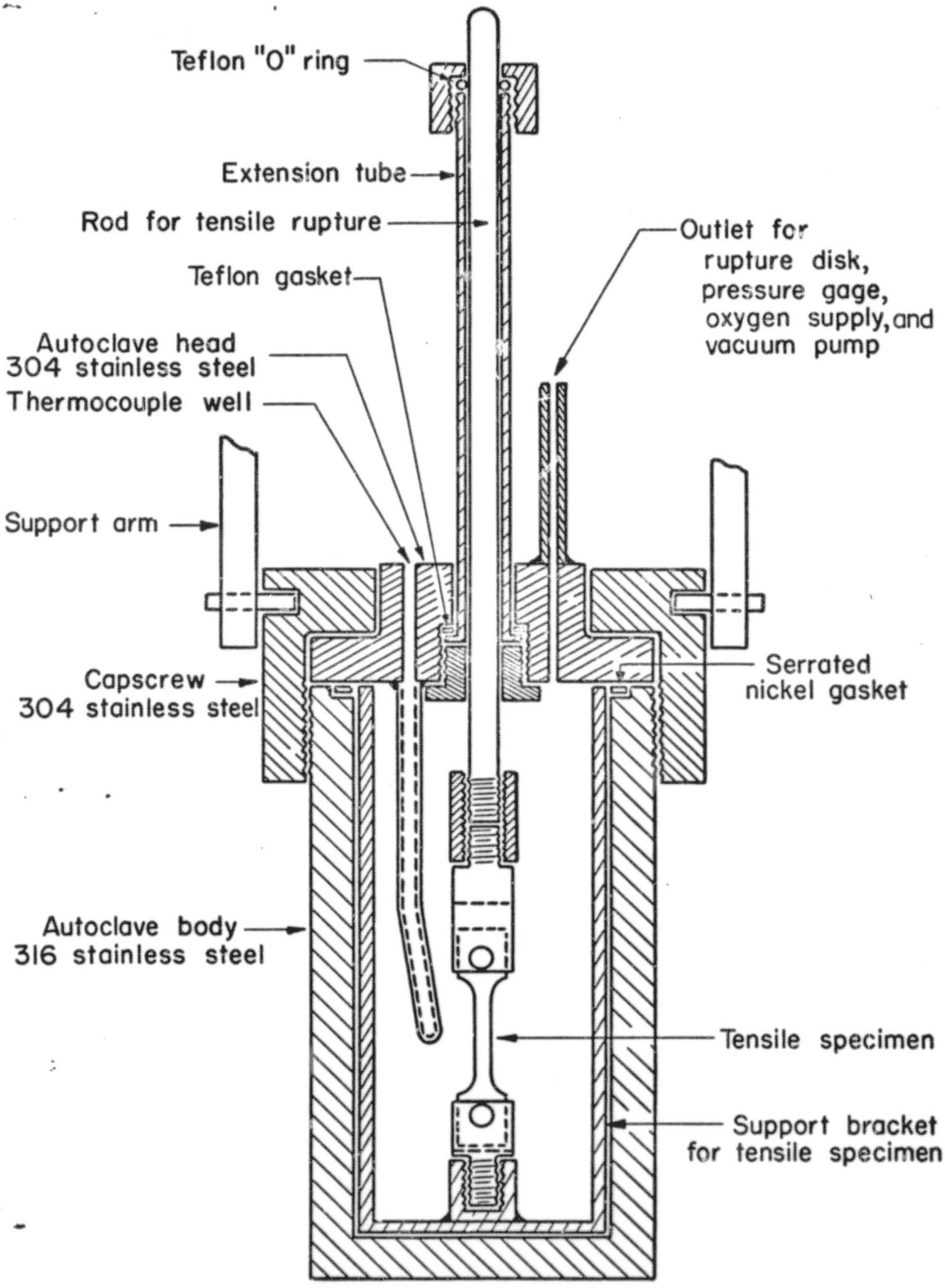

FIGURE 1. SCHEMATIC DIAGRAM OF STRESS-RUPTURE ASSEMBLY

The load was applied to the system from a hydraulic ram connected to the specimen through the pull rod. The relative size and shape of the components are shown in Figure 2.

The top of the specimen was attached to the pull rod and the bottom of the specimen to the stainless steel support bracket by use of stainless steel pins about 0.25 inch in diameter. To protect the autoclave in the event of a violent increase in temperature, a Pyrex cylinder was placed around the specimen within the support bracket, as shown in Figure 2. In later experiments, it became expedient to use a ceramic liner between the walls of the autoclave and the support bracket.

Figure 3 shows the support used for mounting the autoclave and pull jack. The pull rod was sealed at the top of the extension tube with a Teflon O-ring. The autoclave was cooled in a large stainless steel Dewar, shown in the photograph. The temperature was measured with a copper-Constantan thermocouple located about 1 inch from the center of the specimen. Additional thermocouples were attached to the outer autoclave surface at several other areas.

Procedure

Both Ti-75A and Ti-6Al-4V tensile specimens were prepared from sheet stock. The physical properties and the chemical analysis for each alloy is listed in Table 1. The specimens were machined 2-11/16 inch long by 9/16 inch wide with a reduced section 1 inch long by 0.19 inch wide and 0.050 inch thick. The original surface was left in the as-received condition, and the edges were surface ground.

TABLE 1 ANALYSES OF TITANIUM MATERIALS (a)

Specimens were 0.050 inch thick

Physical Analysis										
Yield Strength, psi	Tensile Strength, psi	Elongation, per cent	Bend Test (b)	Surface Roughness, microinches	Chemical Analysis, % C	Fe	N_2	H_2	Al	V
				Ti-75A, Heat M7826						
L-80,500	100,150	22	2.0T	15-20	.025	0.08	.009	.005	--	--
T-91,600	105,800	21	2.0T	35-40						
				Ti-6Al-4V, Heat M8545						
L-138,300	147,400	14	2.8T	18-20	.020	0.17	.020	.007	6.0	4.1
T-143,700	150,500	15	3.6T	25-30						

(a) Produced by TMCA

(b) Press brake at 105 degrees.

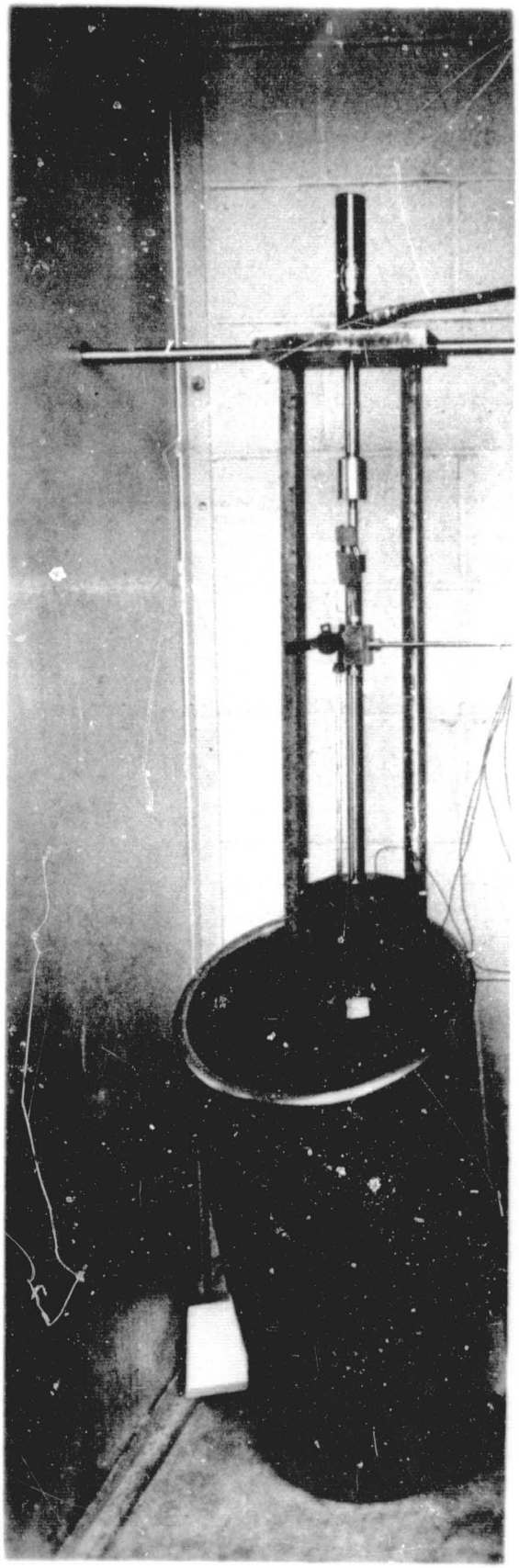

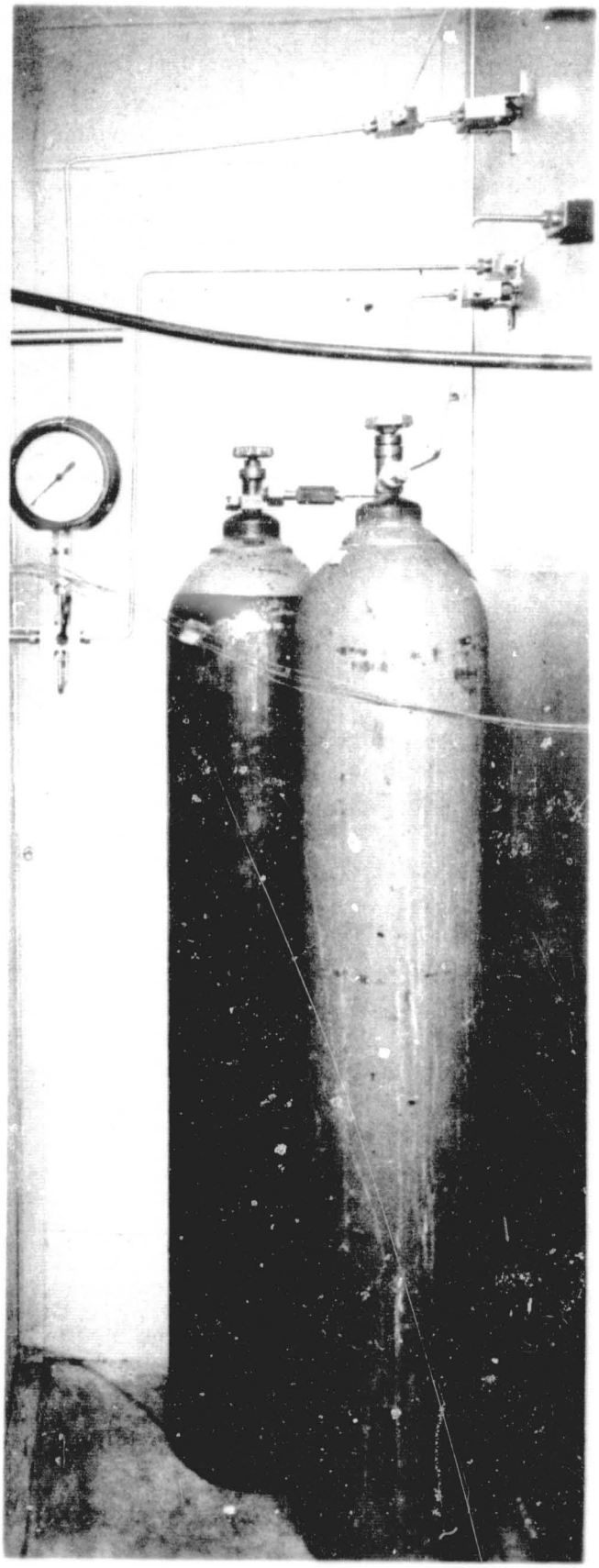

All materials used in contact with high-pressure oxygen were cleaned thoroughly by first scrubbing with soap and water, followed by degreasing for 1/2 to 1 hour in a boiling alkaline cleaner*. After rinsing in water and drying, the materials were given a final degreasing for 1/2 to 1 hour in distilled carbon tetrachloride. After cleaning, these materials were handled only by clean metal tools.

In the conduct of an experiment, a standard sheet tensile specimen was first fastened in place using stainless steel pins. Next, the specimen assembly was inserted into the autoclave and sealed. The hydraulic jack assembly was then fastened in place (see Figure 3).

In the early experiments, the system was leak tested by adding high-pressure helium. If no significant pressure drop occurred, the pressure was released. The system was evacuated by a vacuum pump and flushed with helium two to three times. After the final evacuation, the system was pressurized with gaseous oxygen.

In later experiments, the atmosphere was obtained by repeated flushing with oxygen under pressure. This modification avoided the possibility of nitrogen from the air leaking into the system during the evacuation cycle. The final pressure adjustment was made when the autoclave had been cooled to the desired temperature.

The autoclave was cooled in a stainless steel Dewar by using liquid nitrogen. The liquid level was adjusted to 2 to 3 inches above the bottom of the autoclave. The upper portion of the autoclave remained in the cold nitrogen-vapor phase. The top of the Dewar was closed with a thick Styrofoam insulating cover. The temperature in the vapor phase of the Dewar was controlled with tank nitrogen gas and a circulating fan. When the temperature, measured inside the autoclave near the specimen, was close to the desired value, the Dewar was lowered so that the autoclave was completely in the vapor phase.

Then, the oxygen pressure was adjusted to the desired level and the system was allowed to reach an equilibrium temperature. The specimen was ruptured by pumping the hydraulic system. The force required to break the specimen was indicated by the recording needle on the hydraulic system gage.

The temperature, indicated by the thermocouple in the well near the specimen, was registered on a fast-response recorder. The system pressure was observed on the pressure gage by use of a mirror. A reaction was indicated by an immediate temperature rise and possibly a change in pressure. Experience showed that it was desirable to release the oxygen pressure, usually within 10 to 30 seconds after rupture. This stopped the burning-titanium reaction, and thus prevented serious damage to the stainless steel autoclave fittings.

*The alkaline cleaner consisted of 30 g/l sodium metasilicate, 7.5 g/l sodium hydroxide, and 0.5 g/l Duponol.

TABLE 2. RESULTS OF TENSILE-RUPTURE EXPERIMENTS IN GASEOUS OXYGEN WITH UNALLOYED TITANIUM (Ti-75A)

Experiment	Temperature, F	Initial Pressure, psig	Oxygen Concentration, g/cc	Final[a] Pressure, psig	Reaction ?	Remarks
1	-250	100	0.031	80	No	Pressure drop due to ram movement
2	-190	550	0.162	>2000[b]	Yes	Rupture disk blew; autoclave damaged
3[c]	-190	450	0.116	655	Yes	Specimen grips ignited; severe autoclave damage
4[c]	-190	250	0.055	325	Yes	Moderate damage to specimen grips
5	-190	150	0.032	150	Yes	Moderate damage to specimen grips
6[c]	-190	100	0.022	100	Yes	Portions of titanium specimen remain[d]
20	-190	75	0.016	75	No	Bright metallic surface at fracture
7[c]	-190	50	0.012	50	No	Bright metallic surface at fracture
24	-50	100	0.014	100	Yes	Severe damage to specimen grips
25	-50	75	0.011	75	Yes	Small piece of titanium specimen remains
26	-50	50	0.008	50	No	Bright metallic surface at fracture
8[c]	77	350	0.033	275	Yes	Severe damage to specimen grips
9[c]	78	150	0.015	150	Yes	Moderate damage to specimen grips; some of titanium specimen remains[d]
12	79	100	0.010	75	Yes	Small piece of titanium specimen remains; grips damaged
18	76	100	0.010	100	Yes	Large piece of titanium specimen remains
13	83	75	0.008	65	Yes	Upper half of specimen showed no reaction
14	80	75	0.008	70	Yes	Large pieces of titanium specimen remain
16	78	60	0.007	60	No	Very small burned spot on fractured face
15	77	50	0.006	50	No	Bright metallic surface at fracture

(a) Oxygen pressure released 10 to 30 seconds after rupture in all experiments except 1, 2, and 3.
(b) LOX may have been condensed during cooling. Rapid evaporation may have produced the pressure rise.
(c) Stainless steel pins brazed in titanium specimens.
(d) See Figure 6.

Reactivity at -50 F and at Room Temperature. Reactions were obtained at both -50 F and at room temperature for oxygen pressures of 75 psig and above. In Experiment 13 conducted at room temperature, however, only one-half of the specimen burned.

In Experiment 16 conducted at room temperature at 60 psig, no propagating reaction was obtained. However, one very small burned spot was found on the fractured face upon examination (see Figure 7). This shows that the reaction initiated but did not propagate, and apparently represents a borderline case for propagation.

With a pressure of 50 psig, at both -50 F and room temperature, no indication of any reaction was observed. Thus the threshold pressure is between 50 and 75 psig at both these temperatures.

Rupture of Alloyed Titanium

Tensile specimens of Ti-6Al-4V were ruptured in gaseous oxygen at -190 F and at room temperature using the same techniques as for the unalloyed titanium experiments. The results are given in Table 3.

TABLE 3. RESULTS OF TENSILE RUPTURE EXPERIMENTS IN GASEOUS OXYGEN WITH ALLOYED TITANIUM (Ti-6Al-4V)

Experiment	Temperature, F	Initial Pressure, psig	Oxygen Concentration, g/cc	Final[a] Pressure, psig	Reaction?	Remarks
30	-190	125	0.026	115	yes	Specimen largely consumed; grips damaged
29	-190	100	0.022	--	No	Bright metallic surface at fracture
10[b]	75	150	0.015	150	yes	Some of titanium specimen remains; grips damaged[c]
28	79	100	0.010	100	yes	Specimen largely consumed; grips damaged
27	77	75	0.008	75	no	Bright metallic surface at fracture
11[b]	80	75	0.008	75	no	Bright metallic surface at fracture

(a) Oxygen pressure released 10 to 30 seconds after rupture.
(b) Stainless steel pins brazed in titanium specimens.
(c) See Figure 6.

Generation of Heat. One factor, which should be considered in the discussion of the mechanism, is whether the generation of heat is sufficient to initiate the propagating reaction without the exposure of a fresh surface. The temperature of the surface may be raised, as during impact, to some point where rapid oxidation and subsequent burning will occur without necessarily rupturing the surface, as proposed in the hypothesis.

Dean and Thompson[2] reported that titanium was the most reactive material, in high-pressure atmospheres, of the common metals and alloys. It was shown that titanium tubing (about 0.5-inch OD x 0.03-inch wall) would react at 35-psig oxygen pressure when the specimen was heated electrically (within 1 to 2 minutes) to 2400 F. At 285-psig oxygen pressure, reaction occurred at 1600 F. In addition, titanium reacted in a 50 per cent O_2-50 per cent CO_2 mixture, at a temperature of 1400 F, under 285-psig pressure. In 100 per cent CO_2, reaction occurred at 2600 F at 285 psig.

On the basis of the results of these tests, it would appear that titanium heated in LOX at atmospheric pressure would not react until temperatures in excess of 2400 F were obtained over some large area. At these temperatures, rapid diffusion of the oxide coating into the metal would occur, and a fresh surface could actually be formed to initiate the reaction. However, no evidence, such as oxidized or discolored surfaces, has been found to indicate that temperatures in this range can be achieved by impact alone. In addition, the low temperature of the system and vaporization of LOX would tend to remove the heat rapidly.

The experimental results show that a titanium specimen, even when at low temperature, will ignite under pressure if a fresh surface is presented by fracture. According to the hypothesis prepared, the temperature of gaseous oxygen needs only to be high enough so that it will not be condensed when the pressure reaches about 100 psig. This temperature is about -250 F, as shown by the threshold-pressure graph of Figure 8.

It should also be mentioned that the driving force for the reaction is actually greater at low temperature than at room temperature, as shown by thermodynamic considerations. The difference in the free-energy values is only about 5 per cent however; so the effect probably could not be detected. Therefore, the reaction is, essentially, as probable thermodynamically at room temperature or above as at low temperatures, as demonstrated by the experimental results.

Effect of Strain Rate. Previous tensile-rupture experiments, using titanium specimens submerged in LOX, showed that no reactivity at the break was obtained at strain rates from 100 to 10,000 inches per inch per minute. In the present investigation, reactions were obtained under high-pressure gaseous oxygen at a strain rate of about 2 inches per inch per minute. The

END OF REFERENCE

34

REFERENCE

35

WEGENER, W.: INVESTIGATIONS OF THE ADMISSIBLE OXYGEN FLOW VELOCITY IN STEEL PIPES FROM A SAFETY POINT OF VIEW. NASA TT F-14,831, 1973.

APR 9 '73

NASA TT F-14,831

NASA TECHNICAL TRANSLATION NASA TT F-14,831

8.4-0-0

INVESTIGATIONS OF THE ADMISSIBLE OXYGEN FLOW VELOCITY IN STEEL PIPES FROM A SAFETY POINT OF VIEW

W. Wegener

LEWIS RESEARCH CENTER
Aerospace Safety Research
and Data Institute
APR 9 1973
CLEVELAND, OHIO

Translation of: "Untersuchungen über die sicherheitstechnisch zulässige Strömungsgeschwindigkeit von Sauerstoff in Stahlrohrleitungen," Stahl und Eisen, Vol. 84, No. 8, April 9, 1964, pp. 469-475.

LIBRARY COPY
APR 9 1973
LEWIS LIBRARY, NASA
CLEVELAND, OHIO

NATIONAL AERONAUTICS AND SPACE ADMINISTRATION
WASHINGTON, D. C. 20546 MARCH 1973

INVESTIGATIONS OF THE ADMISSIBLE OXYGEN FLOW VELOCITY IN STEEL PIPES FROM A SAFETY POINT OF VIEW*

W. Wegener

Operational Dangers and Safety Requirements /469**

The use of steel pipe in pipe systems for compressed oxygen has been subjected to certain safety requirements in Germany since the year 1942.*** It has only been modified slightly since that time. One of the important restrictions is the limitation of the flow velocity of oxygen to 8 meters/second. The reason for this restriction is that at higher velocities there is a danger of pipe fires. This occurs when scale and corrosion products separate when moist oxygen is being transported. These products are then carried along by the flow and can start to glow because of friction at the pipe walls. The existence of this danger has /470 been verified in a certain sense. When new pipelines which are somewhat contaminated are cleaned by a high-pressure flow, one can observe fire phenomena at the two ends. The oxygen flow velocities which occur are then considerably higher than those usually used in the operation of the system. On the other hand,

*Communication No. 6 of the Machine Installation and Report No. 360 of the Machine Board of the German Association of Iron Miners. Reprint requests should mention the Group No. D No. 758. Communication of the Federal Institute for Material Testing.

**Numbers in the margin indicate pagination of the original foreign text.

***Joint Bulletin of the Reichs Business Ministry and Reichs Labor Ministry of November 28, 1942, as well as directives for the use of steel pipes in pipe systems (distribution networks for compressed oxygen). Reichsarbeitsbl. (1943) Nr. 1, P. III, 1, u. Bundesarbeitsbl. (1955) Nr. 12, P. 481/84.

the oxygen pressure is relatively low.

The operational dangers which did occur at the time were tested by experiments. However, the experimental results were not published. Therefore today we can no longer determine what the exact conditions were for which flashes occurred in pipes. Other investigations showed that the oxygen lines installed up to the year 1942 were made of unalloyed steel almost without exception. Also we found that the systems were operated at flow velocities below 8 meters/second. Apparently the oxygen fluxes corresponded to the operational requirements. This could have been the reason why the highest permissible velocity was specified at 8 meters/second. According to present technical requirements, this limiting value is too low.

The directives for Germany were in part taken over by other countries. For example, in the United States and Great Britain, other recommendations have been published. In these cases, they were usually in the form of plant specifications or they were specified by insurance companies. They are different from the German specifications because they allow higher flow velocities which are specified independent of the pressure.

Good results have been obtained with flow velocities over 8 meters/second. For this reason and because oxygen is being used in metallurgical installations to an ever increasing degree, the Association of German Iron Miners and the Mining and Rolling Mill Associations decided many years ago to again test the safety aspects for oxygen steel pipe systems. The purpose was to reduce the restrictions. A research contract was awarded to the German Institute for Material Testing (BAM) after a joint conference with the Ministries for Labor and Social Order, the BAM and other occupational associations and operators of air-separation plants.

Experiment Planning

The experiment planning was structured into three phases.

1. A suitable test set-up had to be developed for experiments under laboratory conditions. This installation was operated at differing flow velocities. Solids were introduced into the oxygen stream and their influences in straight and curved pipes was observed. The experimental set-up had to be designed so that it could be transferred to larger scales with as little change as possible.

2. Subsequent to this, a large test section should be operated, in which experiments made with the installation mentioned in Paragraph 1 could be made.

3. Finally a continuous test section is to be installed, in which oxygen, having the conventional purity, i.e., without any solid additives, was to be operated over a time period of several weeks at a high velocity.

The experiments carried out under laboratory conditions were performed in the open air ground installation of the German Ministry for Material Testing in Berlin-Dahlem. They were concluded approximately two years ago. The experimental set-up and the essential results were reported in [1]. This is why we will now report on the second and third phases of the experiments.

The test sections were built at the Duisburg-Ruhrort factory of the Phoenix-Rheinrohr AG.

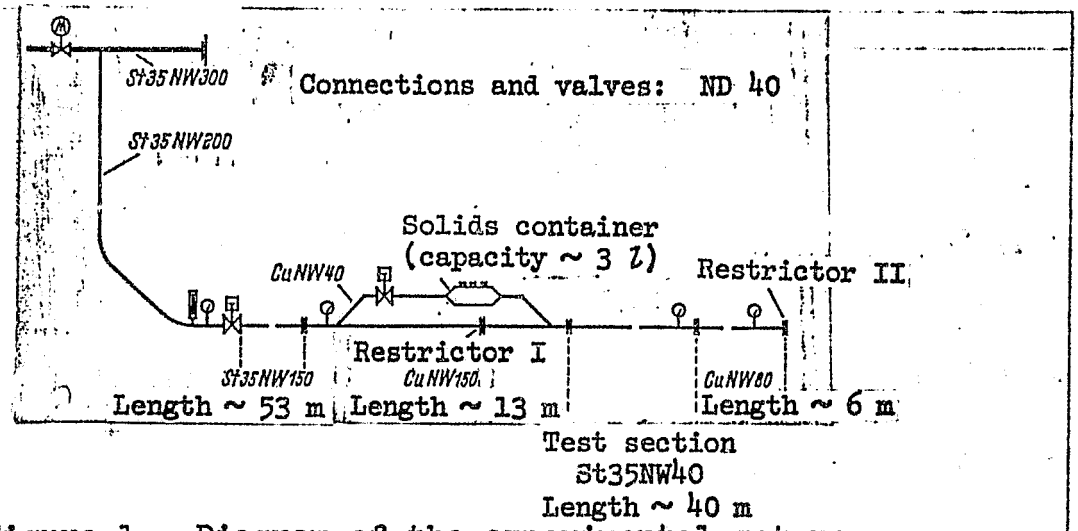

Figure 1. Diagram of the experimental set-up.

Experimental Set-Up

From an approximately 15-meter high NW 300 (nominal width 300 mm) oxygen pipe there is a NW 200 bend which drops down perpendicular to it. It runs into a vertical NW 150 pipe through a sleeve valve. After 53 m, the steel pipe is extended by means of a 13 m long copper tube pipe having the same dimensions. From this main line there is a bypass line, which can be closed off by means of a sleeve valve. It contains a container for introduced solids (Figure 2). Just before the connection flanges for the test section, there is a connection between the bypass line and the main line. The adjacent test section ends with a 6-m long safety section, which has exchangeable restrictors in it. The restrictor diameter determines the amount of oxygen flowing per unit of time and therefore also determines the flow velocity in the

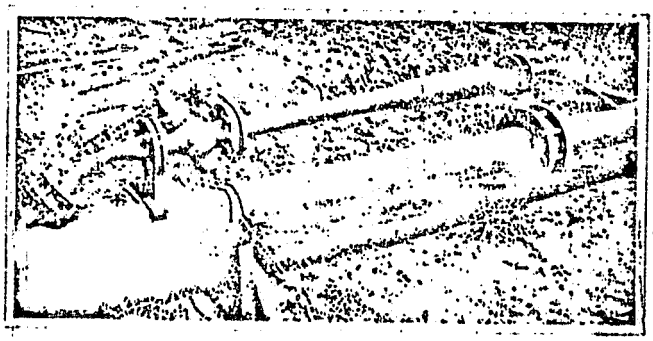

Figure 2. Bypass pipes with container for collection of solids.

test section. The safety line and the restrictors are made of copper. If steel were used, the solids carried along by the oxygen flow could trigger an undesirable fire in the pipe when they impact the restrictor vertically. /471

The oxygen flows into the free atmosphere. Because of the considerable noise levels, it later on became necessary to install a sound absorber at the pipe end. It also seemed appropriate to install the restrictors in an eccentric manner along the lower parts of the tube end, so that the introduced foreign particles could not accumulate there.

There is an additional restrictor in the main line between the tap and reentry point of the bypass line. Because of the restricted tube cross section at this point, part of the oxygen flows through the bypass line and carries along the materials introduced into the container. Manometers are installed ahead of the test section as well as at its end. These measure the pressure decrease in the line. All the lines and the valves are designed for ND 40 (nominal pressure 40 atmospheres gauge pressure). The valves are operated from a secured panel with a pneumatic system.

Forty-meter long straight steel pipes having nominal dimensions of 40, 50, 65 and 80 were available for the test section. However, as we will show later on, only the NW 40 line could be used. During the experiments in the middle of the test section, i.e., that is about 20 meters from the beginning, either two 5s bends (arc radius = 5 x tube radius) or an expansion arc with four 3s or 5 D bends (arc radius = 5 x pipe radius) were welded in.

Determination of the Flow Velocity

A uniform flow velocity, which was not known at first, was adjusted by means of the restrictors (Figure 1), which were installed at the ends of the safety line. This meant that repeatable experimental conditions were produced. The oxygen flux could not be determined with measurement restrictors, because there was a danger that the writing instruments would be damaged because of the pressure shocks in the line which occur when the slide is open and closed before and after each experiment. Since the aperture ratio of the measurement restrictor should correspond to the expected flux, it would have been necessary to exchange it with a considerable expenditure in time when other velocities were tested.

Another possibility for calculating the oxygen flux was then considered. This is based on the fact that compressed gases flow into the atmosphere at the speed of sound, as long as the pressure ratio is above the critical pressure ratio. The amount of outlet flow is primarily determined by the pressure and temperature of the gas ahead of the restrictor as well as the restrictor cross section. The discharge ratio α must be introduced as a correction factor. It considers the jet constriction due to sharp edges and similar effects. Therefore it essentially depends on the geometric shape of the restrictor. Because of the unknown discharge ratios in the restrictors, the calculated discharge amounts were uncertain.

Finally another method was used. It led to exact values. The NW 300 oxygen line mentioned and used in the experimental arrangement could be closed off over a distance of about 360 m by means of a slide. This closed off part of the tube including the main line ahead of the test section forms a "container"

having a volume V_B of about 27 m^3. After the slide in the main line is opened, the oxygen flows through the test section and through the final restrictor to the outside air. The line pressure decreases from about 28 atmospheres operational pressure to about 10 atmospheres depending on the cross section of the final restrictor and during a time interval of about 5 to 20 minutes. If the recorded pressure p values are plotted as a function of time t in the form $\lg p = f(t)$, we obtain a straight line. The inclination of this line is proportional to the flow velocity at the beginning of the test section. The somewhat simplified derivation is as follows (notations see Table 1):

TABLE 1

NOTATIONS USED

F	= cross section of the test section in m^2
V_B	= volume of the pipe segment which can be blocked ahead of the test section in m^3
P_0	= normal pressure (= 1.033 at)
T_0	= normal temperature (= 273° K = 0° C)
V_0	= gas flow in Nm^3/sec reduced to normal conditions (p_0, T_0)
p	= gas pressure in at
T	= absolute gas temperature in °K
w	= gas velocity in meters/second
t	= time in seconds
1, 2, 3	= subscripts characterizing the experimental conditions at the following points: 1 — at the beginning of the test section; 2 — at the end of the test section; 3 — in front of the final restrictor
p', t', T'	= for unsteady flow [$(dp/dt) \neq 0$], p and p' are the gas pressures at the times t and t', respectively, in the range of constant temperature T'.

The gas volume flowing through the NW 300 line per unit of time and recalculated per normal conditions is specified by the equation

$$V_0 = -V_B \cdot \frac{1}{p_0} \cdot \frac{T_0}{T_1} \cdot \frac{dp_1}{dt} \tag{1}$$

The same pressure and the same temperature exist at the beginning of the test section. The equation which specifies the gas volume, also recalculated for normal conditions, flowing through the cross section F per unit of time at the velocity w_1 — if the pressure change dp is ignored — is

$$V_0 = F \cdot w_1 \cdot \frac{p_1}{p_0} \cdot \frac{T_0}{T_1} \cdot \tag{2}$$

Since the gas fluxes specified by Equations (1) and (2) must be the same, the differential quotient has the value

$$\frac{dp_1}{dt} = -\frac{F}{V_B} \cdot w_1 \cdot p_1 \cdot \tag{3}$$

After transforming the above, we obtain the following equation which must be integrated

$$\int_{p_1'}^{p_1} \frac{dp_1}{p_1} = -\frac{F}{V_B} \cdot w_1 \cdot \int_{t'}^{t} dt \tag{4}$$

and after carrying out the integration we find

$$\ln p_1 - \ln p_1' = \frac{F}{V_B} \cdot w_1 \cdot (t' - t). \tag{5}$$

Using base ten logarithms, we finally obtain the following equation for the flow velocity at the beginning of the test section

$$w_1 = 2{,}3026 \cdot \frac{V_B}{F} \cdot \frac{\lg p_1 - \lg p_1'}{t' - t} \cdot \tag{6}$$

/472

In the determination of w_1 it is necessary to consider the fact that the oxygen cools off ($T_1 \rightarrow T'_1$) during expansion in the NW 300 line. It was found that for a pressure drop from 28 atmospheres to about 20 atmospheres the temperature dropped from between 8 to 10 degrees C below the outside temperature. However, because of the increase in heat transfer, from the atmosphere, it remained constant along the line. The function $\lg p = f(t)$ is therefore only linear in the range of the final temperature T'_1. Figure 3 shows such a curve.

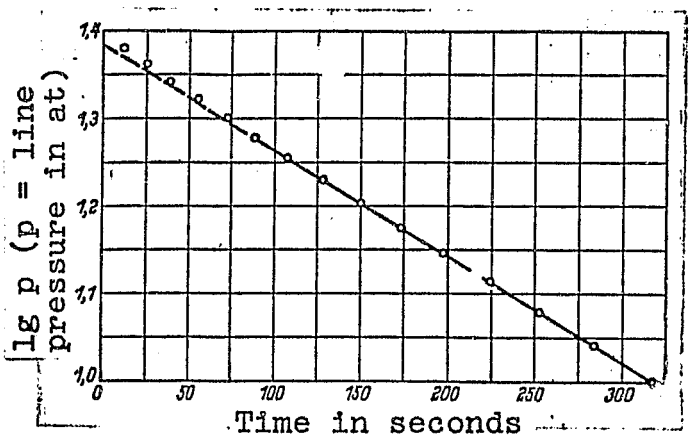

Figure 3. Pressure decrease in the pipe NW 300.

The velocity w_1 calculated according to Equation (6), which is only valid for T'_1, can be corrected for any other temperature T_1 by multiplying it with $\sqrt{T_1/T'_1}$. This correction factor is found from the temperature dependence of the velocity of sound which exists at the final constrictor. It is not important whether the gas temperatures T_3 or T'_3 (ahead of the final restrictor) agree with the gas temperature T_1 or T'_1 (at the beginning of the test section), respectively, This is because the value of the quotient T_n/T'_n remains almost unchanged. This then results in the final relationship for the flow velocity at the beginning of the test section

$$w_1 = 2{,}3026 \cdot \frac{V_B}{F} \cdot \frac{\lg p_1 - \lg p'_1}{t' - t} \cdot \sqrt{\frac{T_1}{T'_1}} \qquad (7)$$

The pressure p_2 at the end of the test section can be calculated according to the flow velocity which exists there

$$w_2 = w_1 \cdot \frac{p_1}{p_2} \qquad (8)$$

w_1 to be substituted is taken from Equation (7). No temperature correction is necessary because there were no measurable differences between T_1 and T_2.

The values of w_1 and w_2 determined in this way for various restrictor cross sections have a maximum possible error of ±3%. It is important to realize that for steady flow, the velocity found is independent of the absolute pressure in the main line. This means that fluctuations in the average 28 atmospheres operational pressure could be ignored.

Experimental Procedure

Before each test series we determined the flow velocity w_1 and measured the pressures p_1 and p_2 at the beginning and end of the test section. It was especially important to make sure that there were no differences when the bypass line was opened or closed. Otherwise the cross section of the restrictor in the main line had to be enlarged. The measurements after each test series gave values within the experimental error bounds.

During the test series, the slide in the NW 300 line remained open. Thus the same pressure prevailed at all times (27 to 29 atmospheres, corresponding to the operational pressure).

The container in the bypass line was filled with 1 to 2 kg of solids while the main line was not under pressure. It was then again hermetically closed. After the slide was opened in the main line, we first had to wait until there were stationary flow conditions. Then the slide in the bypass line, which had

been closed up to that time, was operated and the solids were introduced from the container into the test section. Depending on the material, the container was emptied after 0.5 to 1 minutes. As soon as there was only pure oxygen in the test section, the experiment could be terminated.

We used roll scale, welding cinders and rust as solids. These are materials which can be introduced into the lines by modification, operation or displacement of the systems. In addition, we also used sand. For example, sand is used for sand blasting storage containers. We used flue dust as a comparison material because of its high iron oxide content. We also used coke, stone coal, and sand and iron powder mixtures, which are more or less combustible materials. The solids were sometimes in powder form or in granular form. The grain sizes were as high as 5 mm. The dry oxygen used had a purity of about 99.6%.

The first experiments were carried out in a straight pipe segment at a flow velocity of 30 meters/second at the beginning and 33 meters/second at the end of the test section. According to results of earlier laboratory experiments [1], these conditions were still not dangerous for the lines. Later on we increased the initial velocity up to 53 meters/second when various lines, both curved and straight, were installed. The final velocity calculated from a pressure loss of 38% amounts to 85 meters/second. It was not possible to obtain steady velocities because of the capacity of the air-separation installation. This is why we were not able to use lines larger than NW 40 as initially planned. In order to give a fair representation of the operational conditions, we primarily carried out experiments with curved lines. In contrast to this, it was only necessary to carry out a small number of experiments with straight lines. This was because in lines having curved segments, there was a 20-meter long straight pipe segment after them.

Experimental Results

Table 2 shows the results obtained with various materials for various oxygen flow velocities for the straight test section. Table 3 shows the same thing for the lines with curved segments. It is not necessary to further classify them according to radii of the pipe bends, because we were not able to detect differences in the experimental results.

The final restrictors used to limit the discharged amounts of oxygen had diameters of 12, 13, 15, 20, 26, and 32 mm. Accordingly, there were stepped flow velocities in the test section. As the number of experiments was increased, the restrictor cross section gradually increased because of erosion, so that the flow velocity also increased. The oxygen temperature /473 which depends on the outside temperature also had a small influence on the flow velocity. In addition, the oxygen pressure fluctuated according to operational conditions. Nevertheless, all experimental conditions remained within small limits.

Rust, Flue Dust, Sand

The solids rust, flue dust and sand were found to be safe. We were not able to find glowing particles at the end of pipes or flashes in the pipes themselves in either straight lines or lines having several bends. Flow velocity values up to 53 meters/second and oxygen pressures up to 28 atmospheres prevailed at the beginning, and the maximum values at the end of the test section were 85 meters/second and 17 atmospheres. We could only observe dense dust clouds.

TABLE 2

EXPERIMENTAL CONDITIONS AND RESULTS FOR A STRAIGHT TEST SECTION

Added solid	Flow velocity w and pressure p of oxygen at the beginning (subscript 1) and at the end of the test section (subscript 2)				Number of experiments and results*
	w_1 in m/s	p_1 in ata	w_2 in m/s	p_2 in ata	
Sand	18 33 51	28 26 27	19 37 84	27 23 16	1 – 2 – 3 –
Rust	33 44 51	25 28 27	37 57 84	22 22 16	2 – 2 – 2 –
Flue dust (deposited)	29 — 33 44 51	25 28 27	33 — 37 57 84	22 22 16	3 – 2 – 2 –
Roll scale	33 44 51	25 28 27	37 57 84	22 22 16	1 – 2 – 2 –
Welding cinders	33 44 51	25 29 27	37 57 84	22 23 16	1 – 2 – 2 +
Coke	29 — 33 44 51	25 29 27	33 — 37 57 84	22 23 16	2 –, 1 + 2 + 3 +
Stone coal	11 13 18	29 22 — 29 20 — 29	11 13 19	29 22 — 29 19 — 28	1 – 3 –, 1 + 4 +

*+ = sparks observed; – = sparks not observed

Roll Scale

The same is true for roll scale in the case of straight lines only. In curved lines, glowing particles emerged from the pipe ends at an initial velocity of 28 meters/second. In the case of an increased initial velocity of 52 meters/second in one

TABLE 3

EXPERIMENTAL CONDITIONS AND RESULTS

FOR A CURVED TEST SECTION

Added solid	Flow velocity w and pressure p of oxygen at the beginning (subscript 1) and at the end of the test section (subscript 2)				Number of experiments and results*
	w_1 in m/s	p_1 in ata	w_2 in m/s	p_2 in ata	
Sand	30—32 43—44 52	28—29 26—28 28—29	33—36 55—57 82	25—26 21—22 18	4— 3— 12—
Rust	30—32 43—44 52—53	28—29 26—28 27—29	33—36 55—57 82—85	25—26 21—22 17—18	4— 3— 18—
Flue dust (deposited)	30—32 43—44 52—53	28—29 26—28 28—29	33—36 55—57 82—85	25—26 21—22 17—18	4— 3— 16—
Roll scale	28—32 42—44 52 52	28—29 27—29 29 29	30—36 55—57 82 82	25—26 21—22 18 18	11—, 2+ 5—, 9+ 3—, 4+
Welding cinders	13 17 28 42—44 50—53	29 29 29 27—29 28—29	13 18 31 55—57 82—85	29 28 26 21—22 17—18	Fire after the first bend 2— 2+ 6—, 4+ 1—, 5+ 2—, 13+
Submerged arc welding cinders	42—44 50—52	27—29 27—29	55—57 82—83	21—22 17—18	3—, 3+ 9—, 1+
Coke	17 30—32 42—44 52—53 53	29 28—29 27—29 27—28 29	18 33—36 55—57 82—85 85	28 25—26 21—22 17—18 18	2—, 1+ 5+ 18+ 13+
Stone coal	13 13 32	29 29 29	13 13 36	29 29 26	Fire after the fifth bend 2— Fire at many points Fire after second bend
Mixture of 20% iron dust and 80% sand	13 28 28 42	29 29 29 29	13 31 31 56	29 26 26 22	2+ 4 1—, 2+ 3 Fire after the third bend 2 Fire after third bend 1

*+ = sparks observed; — = sparks not observed.

case the pipe line sparked. The fire occurred just behind the first bend of the expansion arc (Figure 4a) consisting of four 3s bends. This divided the test section into two parts. The oxygen emerged at a very high velocity from the segment ahead of the fire point. It blew away the resulting liquid iron oxide slag. As other investigations have shown, the presence of this slag is required in order for the burning of the steel to progress [2]. Consequently the fire in this section subsided immediately after the line was broken. The test section segment downstream of the fire location was continuously bathed by the expelled oxygen. At the same time, the glowing slag was blown into the line. This is why the fire continued until the oxygen stream was cut off by closing the slide in the main line.

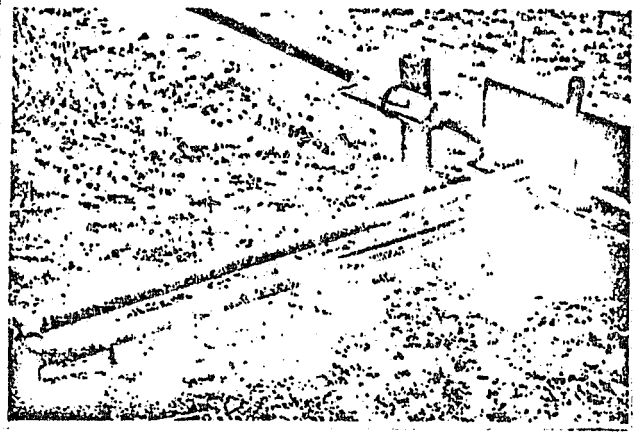

(a) Fire caused by roll scale after the first bend.

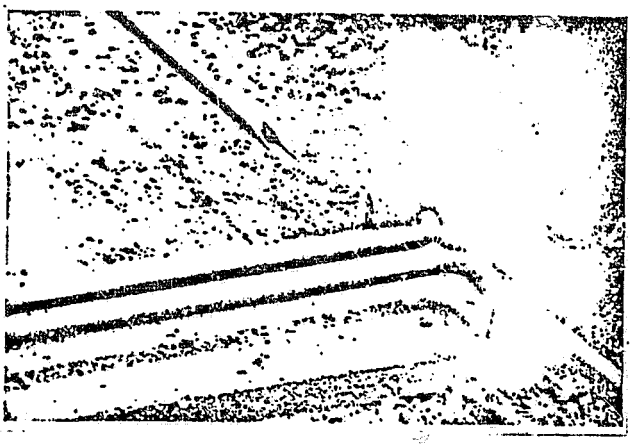

(b) Fire caused by coke behind the fourth bend.

Figure 4. Fire in the test section.

Welding Cinders

Some welding cinder particles began to glow in the straight line at initial velocities of 44 meters/second. In curved lines, some sparks occurred at 17 meters/second. However, we were not able to trigger a fire in the pipe for initial velocities up to 53 meters/second. In curved tubes and with sillicate slag from

submerged arc welding, which contained almost no free iron, we were able to observe individual weak sparks for initial velocities of 44 meters/second.

Coke, Stone Coal, Iron Powder

As expected, much more dangerous conditions prevailed when coke, stone coal and iron powder were used than before. In the straight tube, we were able to observe glowing of the coke particles at initial velocities of 30 meters/second. In curved pipes this occurred beginning with 17 meters/second. At an initial velocity of 53 meters/second, the pipe burned out behind the fourth 3s bend of the expansion arc (see Figure 4b). With stone /474 coal , during the first experiment with the line having two 5s bends, a fire occurred behind the second bend. The flow velocity was approximately 34 meters/second. Further experiments showed that stone coal ignites in straight as well as in curved pipes at velocities above about 13 meters/second. In one case, ignition occurred very close to the entrance of the bypass line into the test section. Apparently a dust explosion originated at this point, because the test section as well as the bypass line with the solids container was broken into many parts. In addition, various burned points were found in the destroyed pipe ahead of the expansion arc. When an 80% sand and 20% iron powder (flame powder) was used, some sparks were observed at flow velocities of 13 meters/second. At 28 meters/second initial velocity, the line behind the third 3s end of the expansion arc burned off. In the experiments carried out under laboratory conditions [1] with iron powder, ignitions were obtained only above 43 meters/second.

The course of the line fire in the experiment with roll scale was similar to what was observed with coke, stone coal or iron powder. We also found here that the fire does not advance in the direction opposite to the oxygen flow direction. In one experiment, we were only able to observe a fire phenomenon which lasted a short time. In this case the recoil produced by rupture of the line which was transferred perpendicular to the main flow direction because of the installed bend tore the line out of the foundation and bent it greatly. The emerging oxygen was no longer able to reach the part of the line downstream of the fire. After the oxygen remaining in this line segment had been reduced to normal pressure by expansion into the atmosphere, the fire could no longer be maintained because of insufficient oxygen supply.

Continuous Run Test Section

In order to install a continuous run test section, which was to have been operated at flow velocities of more than 8 meters/second, an oxygen line installed in the factory was bridged by means of a low cross section bypass line. The bypass line consisted of two 20-meter long ND 40 and NW 50 steel pipes. At first, the reversal point was connected by a large copper arc. The oxygen flux was increased over two days until a velocity of w_1 = 29 meters/second was reached at the beginning of the line at a pressure of p_1 = 36 atmospheres. The corresponding conditions at the end of the line were p_2 = 33 atmospheres and w_2 = 32 meters/second. After a time period of 36 days, the copper arc was replaced by a connection piece made of steel pipe containing two 3s bends. This bypass line, which was made entirely of steel, remained in continuous operation for another 28 days under the stated conditions. No complaints were recorded over the time span which extended over more than two months. No changes could be observed inside the line compared with the earlier state.

Consequences for the Test Results

In the experiments described above, we did not determine after what path length the velocity of the introduced solids reached a certain constant fraction of the flow velocity of the oxygen. According to other investigation results,* we may assume that there is a uniform velocity ratio after only a few meters. The question of the eigen velocity of the solids remains unanswered as well as their dependence on certain parameters such as density, drain size and shape of the particles, as well as pressure and velocity of the oxygen. These questions were not investigated further because we believed that even if the kinetic energy of the particles were known, for example, the production of sparks in the lines could not be adequately explained. In addition, the kinetic energy of identical particles would only have resulted in a statistical average value. This is because in all test conditions used, there were turbulent flow conditions in which the materials moved not only parallel but also perpendicular to the tube axis. In addition, we must consider the fact that it would be difficult to experimentally verify theoretical models because processes which occur inside the pipes could not be directly observed. For this reason it is not possible even for experiments with the straight line to state where and at what velocity and pressure the particles start to glow because of friction or where they start to burn. We can even assume that some sparks are produced by impact of the particles along the restrictors at the tube ends. The fact that there are significantly more sparks in curved lines even at low velocities leads us to believe that they are produced in the bends. In addition the observed line fires always begin just behind the bends. We were clearly able to show /475 that glowing particles will only occur in the lines, or line fires.

*Private communication of the British Oxygen Company, London.

will only occur when the velocity carries along combustible solids at a sufficiently high velocity. Among these materials we have roll scale and welding slag, because they contain some amounts of free metal. Non-combustible materials such as rust and sand only lead to mechanical damage to the pipes at the velocities used here.

We could imagine that adding stone coal, coke and iron powder would considerably intensify the experimental conditions. If we consider the fact that often easily combustible materials can be contained in newly laid lines, then the experimental results are important for two reasons. First of all, they show how necessary it is to carefully remove all foreign material by pressure cleaning before the lines are used. They also show that it is dangerous to use oxygen for this purpose. This is why it is best to blow out the pipes using inert gases with no oil or with air containing no oil. On the other hand, there is no reason for alarm if combustible materials are sucked into the line after setting it into operation. There is the possibility that seal particles will enter the gas stream, but only experience can show whether this danger really exists. In any case, we did not obtain any information on such a danger during the experiments with the continuous test section.

It is not absolutely certain that all scale in pipes can be removed by staining before they are laid. It is also not certain whether welding slag can be removed by blowing the pipes out after they are laid. These materials can separate from the pipe wall even after the line has been set into operation. However, there is immediate danger to the lines only at high velocities, which will probably not be used during operation because of the considerable pressure losses.

We do not have any reservations in using flow velocities greater than 8 meters/second in steel pipelines for pressure stages up to ND 40. If an upper value were specified, it would be easy to consider the safety aspects because of the economical limitations.

Danger to the Valves

Valves are required components of pipeline networks. In general they contain combustible seals which of necessity will be in contact with the oxygen stream. Such seals can start to burn much more easily than the metallic components. Therefore there is the danger that the sparks which can be produced under the given conditions will cause them to ignite. Not only the energy determines this, but also the duration over which they are effective. The questions related to this must be investigated in separate experiments.

In addition to danger to the seals by glowing particles, there is another danger for the valves. At pressure ratios of about 1.9 and up, flow velocities can occur which come close to the speed of sound. Under these conditions, thermodynamic effects can occur which will lead to a division of the gas stream into hot and cold partial streams if the valve has an unfavorable fluid-dynamic shape. These processes were already described a few years ago [3]. They must be given special attention because of numerous cases of damage caused by oxygen slides.

As long as no information and experience is available on the question of how an increased oxygen flow velocity in the lines will affect the operational safety of the valves, we must introduce appropriate measures in order to avoid accidents caused by valve fires.

In oxygen networks which are operated at flow velocities above 8 meters/second, new installations should only have valves in which the housings are made of special brass or other copper alloys. Pipe bends ahead of these valves should be avoided.

In existing lines, the installed valves with steel housings should be replaced by housings made of copper alloy if this is not too difficult. They can also be converted to remote control or at least have a fireproof covering so the operating personnel will be protected.

* *
*

We would like to thank the Federal Ministry for Labor and Social Order, the Association of German Miners and the firms Phoenix-Rheinrohr AG (Werk Ruhrort, oxygen plant), Gesellschaft für Linde's Eismaschinen AG (Sauerstoffwek Berlin-Borsigwalde) and Knapsack-Griesheim AG (Weksgruppe Sauerstoff) for providing the research material, test material and personnel. I would like to thank Mr. R. Dreissig and Mr. W. Grünwald for their help.

Summary

By means of experimental investigations we wanted to clarify whether the oxygen flow velocity limit of 8 meters/second in steel pipes according to safety regulations could be increased without the danger of pipe fires. We were able to determine the conditions required to produce pipe fires by an appropriately designed test section in which the usual operational conditions were simulated and sometimes exceeded by introducing impurities such as rust, sand, welding slag, roll scale, etc., into the line. According to the experimental results, there is a danger

to the lines by the usual expected impurities only at high velocities which are usually not used in operational installations for reasons of economy (large pressure decrease). On the other hand, valves are exposed to more danger. Therefore special requirements must be placed on the design, selection of material and method of operation.

References

1. Wegener, W. Arbeitsschutz, No. 7, 1962, pp. 164-168; and Moderne unfallverhütung, No. 6, 1962, pp. 57-61.

2. Kirschfeld, L. Arch. eisenhuttenwes, Vol. 32, 1961, pp. 57-62.

3. Sprenger, H. Z. schweisstechn, Vol. 46, 1956, p. 227.

Translated for National Aeronautics and Space Administration under contract No. NASw 2483, by SCITRAN, P. O. Box 5456, Santa Barbara, California, 93108.

END OF REFERENCE

35

REFERENCE

36

LITTMAN, F. E.; AND CHURCH, F. M.: REACTIONS OF TITANIUM WITH WATER AND AQUEOUS SOLUTIONS. AECU-3825, STANFORD RESEARCH INST., 1958.

AECU - 3825

June 15, 1958

Final Report | *March 15, 1957 - June 15, 1958*

REACTIONS OF TITANIUM WITH WATER AND AQUEOUS SOLUTIONS

By: Fred E. Littman Frank M. Church

SRI Project No. SD-2116

Prepared for:

UNION CARBIDE NUCLEAR COMPANY OAK RIDGE, TENNESSEE

Union Carbide Nuclear Co. Subcontract No. 1088
(Prime Contract No. W-7045-ENG-26)

Approved:

R. B. VAILE, JR., CHAIRMAN DEPARTMENT OF PHYSICS

DONALD L. BENEDICT, DIRECTOR PHYSICAL SCIENCES RESEARCH

Copy No. 71

PERMANENT COPY #2
FILE No. 3665

Final Report

REACTIONS OF TITANIUM WITH WATER AND AQUEOUS SOLUTIONS

I. Introduction

For the past fifteen months the Institute has been investigating the conditions under which relatively massive shapes of titanium undergo spontaneous ignition and continue to react with systems containing oxygen and water. This investigation grew out of concern arising from several incidents in which titanium parts suddenly failed in the course of a prolonged test[1,2]. These failures were quite unexpected in view of titanium's corrosion and erosion resistance, which seemed to make it a choice material of construction for homogeneous reactors and fuel recovery systems. Examination of the physical evidence at the damaged site indicated that a violent brief reaction had occurred, resulting in melting of a portion of the titanium part.

On the theory that these reactions were initiated by exposure of a fresh titanium surface (formed mechanically by abrasion or galling) to the oxygenated solutions, a series of tests was conducted to delineate the conditions of pressure, oxygen concentration, and temperature which are conducive to initiation and propagation of such reactions.

II. Summary

The work described in this report delineates the engineering conditions under which it is safe to use titanium as a material of construction in the presence of oxygen. These conditions apply not only to the atomic energy industry but to chemical processing as well.

The working hypothesis stated in the introduction, was in part confirmed by the experimental results. A freshly formed titanium surface reacted rapidly with oxygen and the energy released by this reaction resulted in an ignition of the titanium sample, which then continued to burn until either the metal was consumed or the supply of oxygen exhausted. Water, however, played only a very minor role in this reaction. Some of the more significant results of this investigation are:

[1]Hammond, J.P., T.J. Vegley, Jr., and G.M. Adamson. Failures of Titanium Alloy Trim in HRP Dump Valve Loop. ORNL 56-8-214.
[2]Griess, J.C., et al. Report on Corrosion of Titanium Impeller Number One. ORNL 55-9-65.

A fresh titanium surface produced, for example, by the rupture of a sample in tension at room temperature, will react with oxygen and ignite. If the oxygen is diluted with steam or an inert diluent, higher oxygen pressures are required than for pure oxygen. For example, with 100% oxygen a minimum pressure of 350 psi is necessary for the ignition of a titanium sample. With 90% oxygen a total pressure of 500 psi is required; with 65% oxygen a pressure of 1000 psi; and with 50% oxygen, 1700 psi. Helium and steam behave as diluents. If a fresh surface is produced on a sample submerged in oxygenated water containing up to 3000 ppm of oxygen, no observable reaction resulted.

In some experiments a rupture disk made of 12-mil titanium foil was used as a closure of the pressure vessel. When this disk was broken by puncturing it with a spring-loaded knife, the freshly formed surfaces were exposed to a stream of the compressed gases contained in the bomb as the bomb discharged. The limits of ignition under these dynamic conditions are lower than those of samples in a static atmosphere. Ignition occurred at pressures above 50 psi with pure oxygen, at 500 psi with 60% oxygen, at 1000 psi with 45% oxygen, and at 1700 psi with 38% oxygen. The shape of the curves separating the ignition region from the "safe" region is such that no autoignition is likely to occur at room temperature unless the oxygen concentration exceeds 35% irrespective of pressure.

The ignition limits described above were not markedly affected by changes in the surface-to-volume ratio of the sample, the alloy used, or its temperature in the range up to 300°C.

When a sample of titanium ignited in the vapor space was allowed to burn down into a pool of water, the primary result seemed to be a quenching of the reaction. The presence of hydrogen in the residual atmosphere indicated some thermal decomposition of water.

The limits of propagation of the reaction between metal and oxygen (as distinct from the ignition limits) were also investigated. They were found to be much lower than ignition limits, particularly in the presence of steam. Although pure steam did not react even with molten titanium the presence of a small amount of oxygen (>1%) produced a self-sustaining reaction.

The autoignition of metals on fresh surfaces seems to be restricted to only a few metals. Of those tested, only titanium and zirconium exhibited autoignition. It is believed that this property is related to the mutual solubility of the molten metal and its oxide, which forestalls the formation of a protective oxide.

III. Experimental Results

A. Autoignition Studies

1. Static Tests

a. Equipment and Procedures

A stainless steel reactor was built for the ignition work. It was designed to contain aqueous solutions at pressures up to 2000 psi and temperatures up to 300°C. As shown in Figures 1 and 2 it consisted of a cylindrical body with two removable heads. A pullrod sealed with four O-rings held one end of the test specimen, and a hydraulic pullram in a heavy frame provided the means for breaking the titanium. The assembled arrangement is shown in Figure 3.

The reactor was heated with clamp-on heaters supplied with a variable current. The temperature of the solutions was measured by a thermocouple connected to a direct-reading gauge. The pressure was measured with a transducer (Taber Teledyne). The output of the transducer, as well as that of the thermocouple, was recorded at will on a Varian strip chart recorder.

The samples were about 5 in. long and made of 1/4 in., round stock, which was reduced to a 1/8 in. diameter in the middle, to provide a definite breaking point as well as to stay within the capacity of the ram. When foil was used, strips about 5 in. long and 1/2 in. wide were cut and notched to provide a definite place for the break.

The inside of the reactor was lined on the bottom with a short section of ceramic pipe and a concrete-asbestos disk. This lining successfully prevented erosion of the reactor. A new lining was used for each run.

The gas mixtures were prepared in the reactor. Commercial grades of helium and oxygen were used. When steam was used as a diluent, it was generated in the bomb by heating water to a temperature corresponding to the proper partial pressure. When helium-oxygen mixtures were used, adequate mixing was obtained only if the oxygen was introduced last; otherwise a badly stratified charge resulted. Mass spectrometer samples were taken occasionally to verify the composition of the mixture.

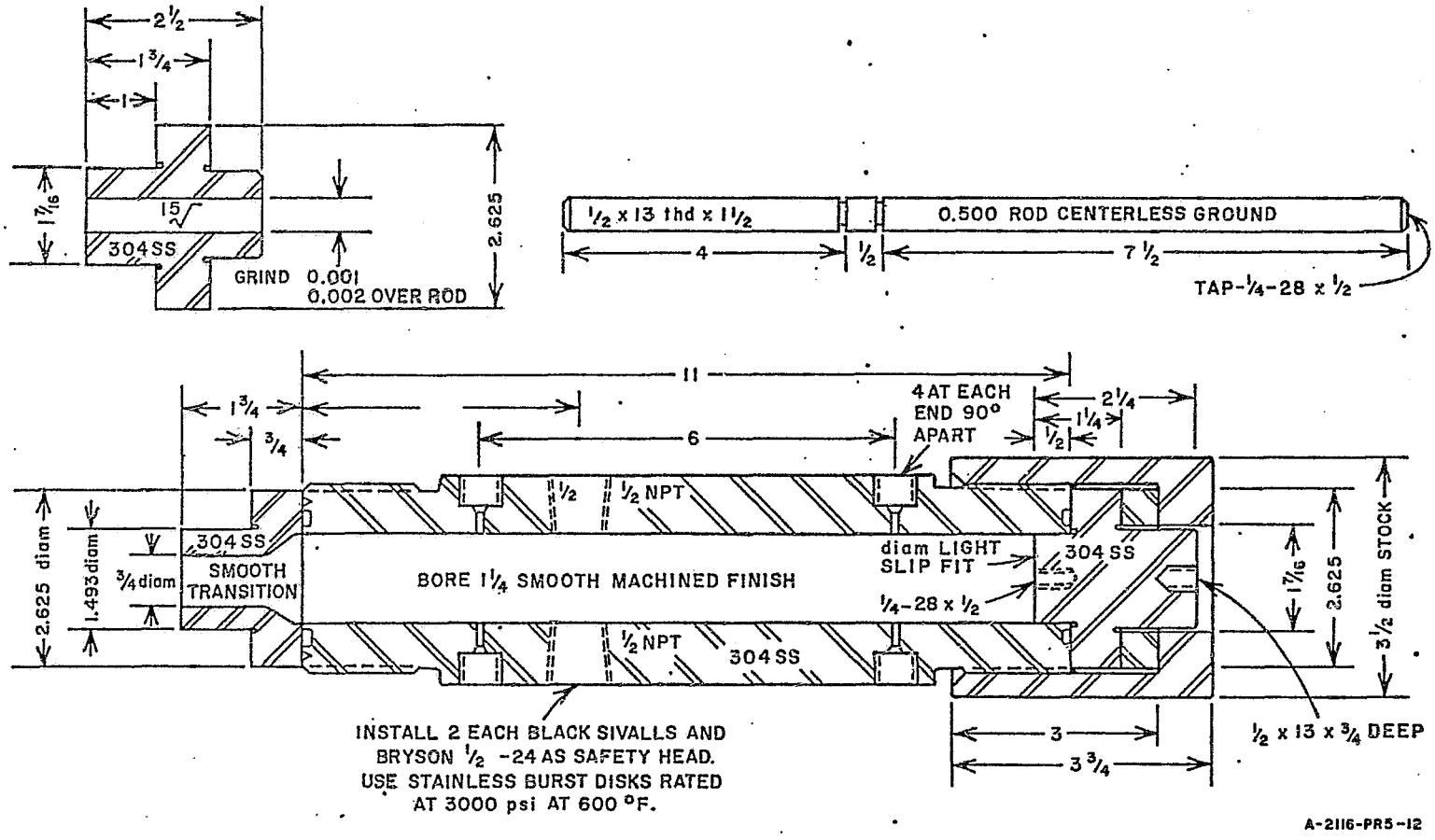

FIG. 1

REACTION VESSEL

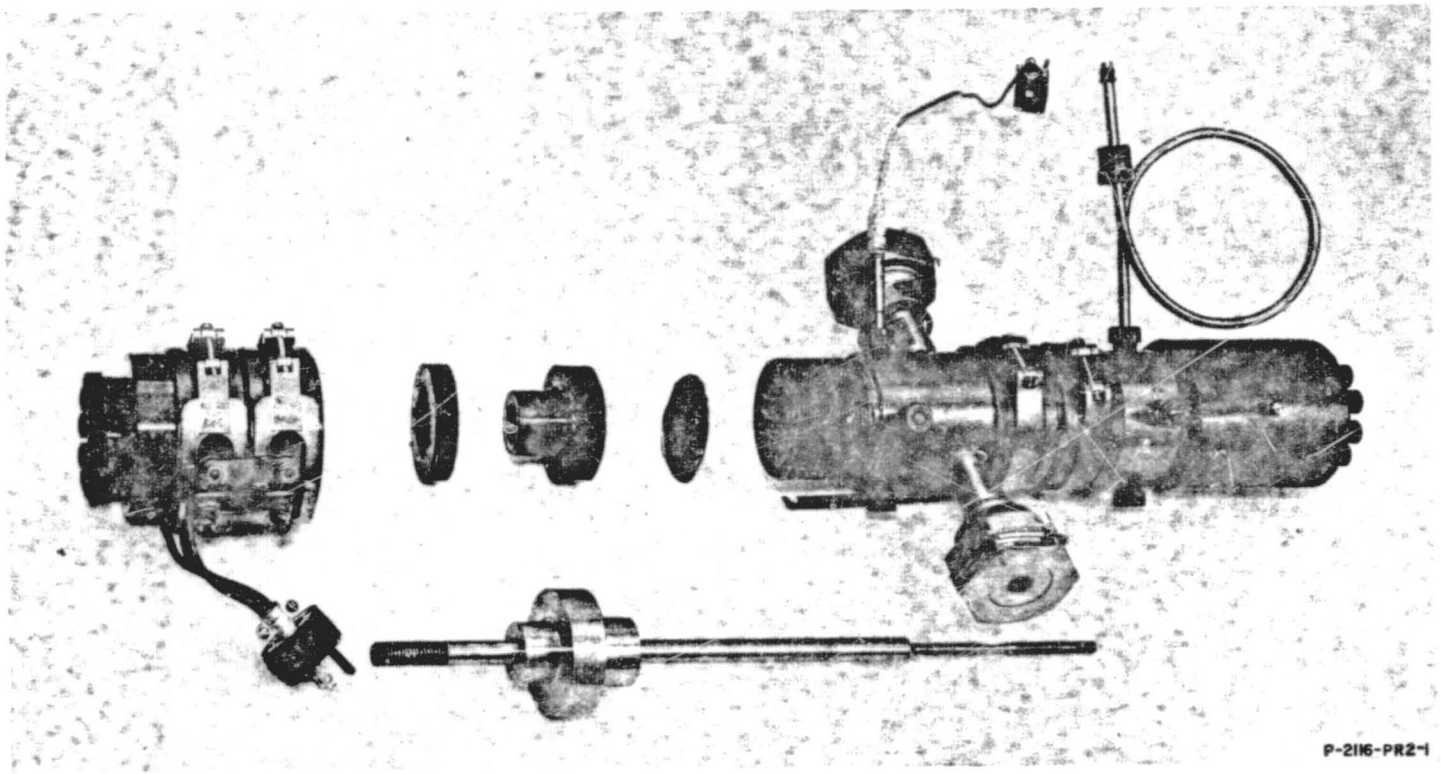

FIG. 2
EXPLODED VIEW OF THE REACTOR

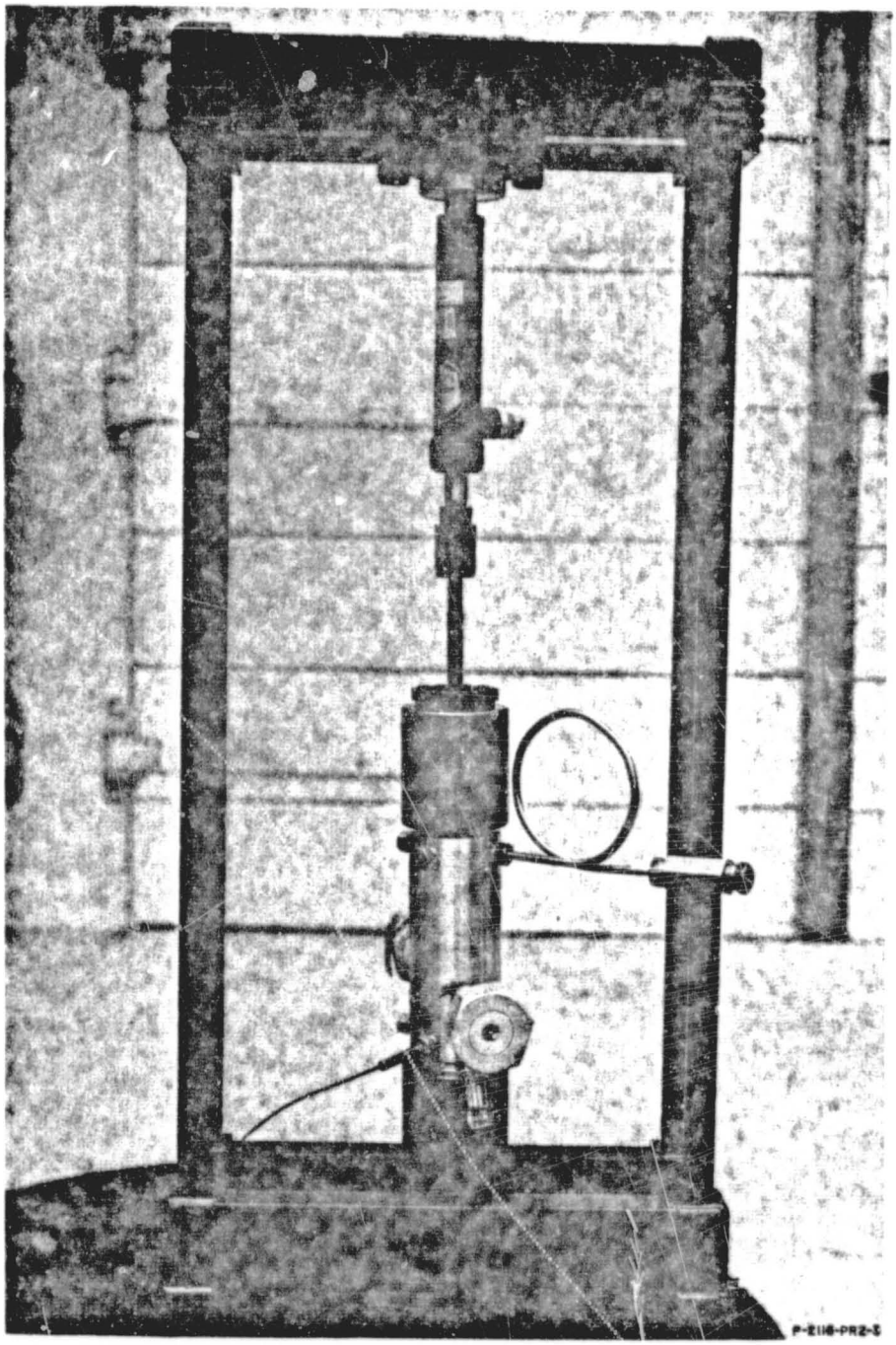

FIG. 3

REACTOR ASSEMBLY WITH HYDRAULIC PULL-RAM IN POSITION

The procedure consisted of placing a sample in the reactor, securing the reactor in the steel frame located in an explosion test pit, and pressurizing to the desired pressures. The reactor was then heated, if runs at elevated temperatures were to be made. When proper conditions of pressure and temperature were attained, the sample was broken in tension using the hydraulic pull-ram. The occurrence of a reaction was indicated mainly by a sudden decrease of the gas pressure. The reactor was then vented and opened up. Visual inspection verified the occurrence or nonoccurrence of a reaction.

b. Ignition Limits of Titanium in Dilute Oxygen

The lower ignition limits were established by breaking successive titanium samples. The pressure for a given composition of oxygen plus diluent was increased from run to run, until ignition occurred. Sometimes "initial" ignition was noted: that is, the test sample would show burned spots, usually on the edges of the fresh surface, but the entire sample did not burn. The "initial" ignition results were observed under conditions close to the borderline shown in Figure 4. The results of tests with helium-oxygen mixtures are shown in Table I. Table II shows results obtained under otherwise similar conditions using 1/2 in. strips of 12 mil titanium foil in place of the 1/4 in. rod. A third set of results is shown in Table III, where steam was used as a diluent in place of helium.

Table I

REACTIONS OF 1/4 IN. TITANIUM ROD
WITH HELIUM-OXYGEN MIXTURES

(Static Conditions)

Run No.	Type	P_{O_2} (psi)	P_{He} (psi)	P_{total} (psi)	O_2 (%)	Reaction
58	A-55	300	200	500	60	--
59	A-55	400	100	500	80	--
60	A-55	300	100	400	75	--
61	A-55	400	--	400	100	√*
62	A-55	500	100	600	83	initial
63	A-55	500	50	550	91	initial
73	A-110 AT	900	100	1000	90	√
74	A-110 AT	800	200	1000	80	√
75	A-110 AT	700	300	1000	70	initial
76	A-110 AT	750	250	1000	75	(1/2 only)
77	A-110 AT	950	950	1900	50	√
78	A-110 AT	900	1000	1900	47.5	--

*√ denotes ignition

Table II

REACTIONS OF 0.012 IN. TITANIUM FOIL
WITH HELIUM-OXYGEN MIXTURES

Run No.	Type	P_{O_2} (psi)	P_{He} (psi)	P_{total} (psi)	O_2 (%)	Reaction
97	A-55	500	---	500	100	✓*
98	A-55	450	---	450	100	✓
99	A-55	350	---	350	100	--
100	A-55	350	---	350	100	✓
101	A-55	900	950	1850	48.5	--
102	A-55	900	750	1650	54.5	✓
103	A-55	900	600	1500	60.0	✓
104	A-55	900	400	1300	69.0	✓
105	A-55	900	500	1400	64.0	✓
106	A-55	700	300	1000	70	✓
107	A-55	450	50	500	90	✓
108	A-55	850	900	1750	48.5	--
109	A-55	850	700	1550	55.0	--
110	A-55	650	280	930	70	--
111	A-55	600	200	800	75	--
112	A-55	500	100	600	83.5	✓

Table III

IGNITION IN PRESENCE OF STEAM

Run No.	Type	P_{O_2} (psi)	P_{steam} (psi)	P_{total} (psi)	O_2 (%)	Temp	Reaction
67	A-55	500	15	515	97	100°C	initial
68	A-55	500	100	600	83	165	initial
79	A-110 AT	650	225	875	74	200	initial
80	A-110 AT	950	600	1550	61	250	✓*
83	A-110 AT	1000	1000	2000	50	285	✓
169	6 Al-4V	525	175	700	75	188	--
170	6 Al-4V	750	500	1250	60	241	--
171	6 Al-4V	850	750	1600	53	275	✓

*✓ denotes ingnition

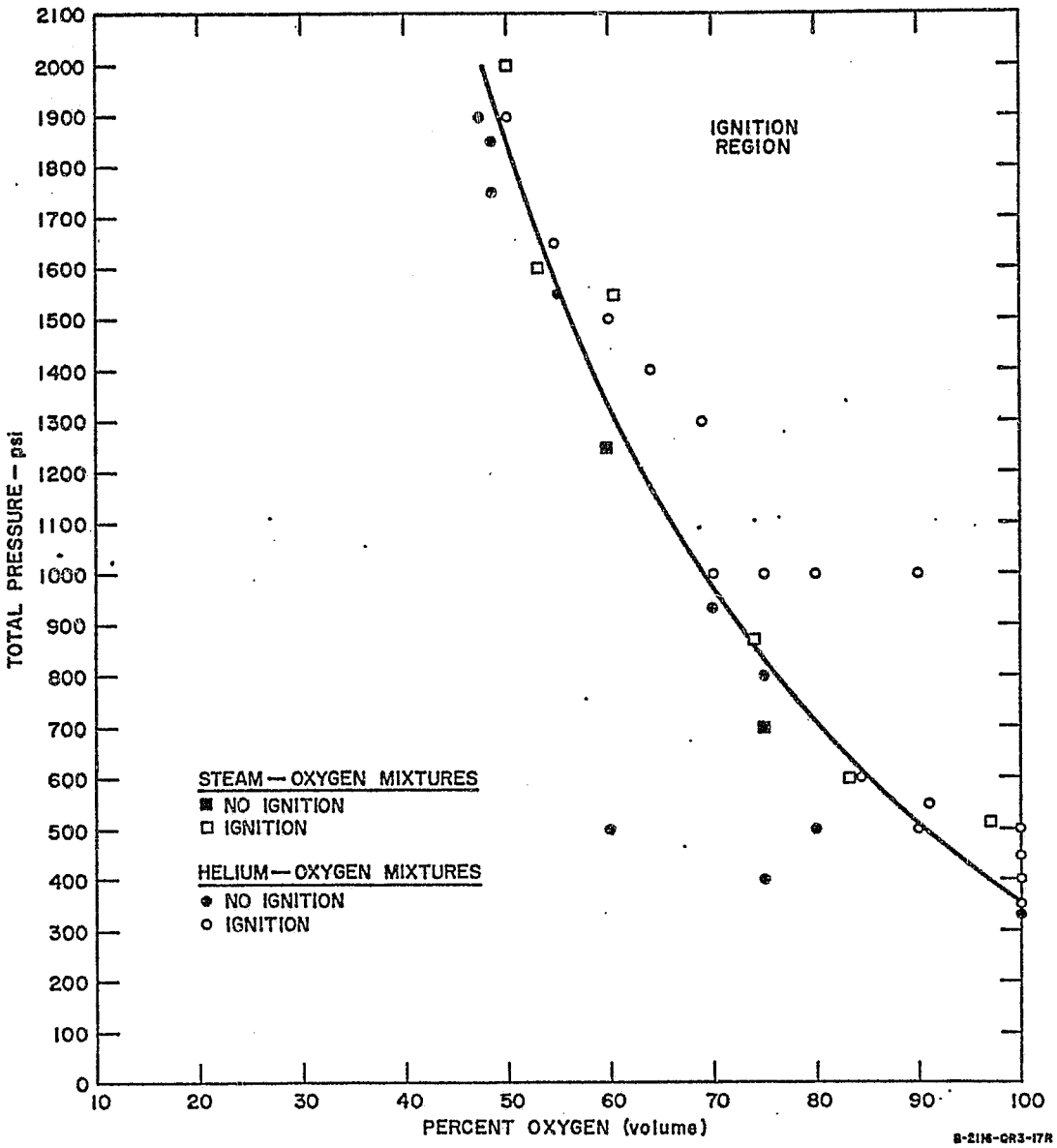

FIG. 4

REACTIONS OF TITANIUM WITH HELIUM-OXYGEN AND STEAM-OXYGEN MIXTURES
Static Tests

All of these data are shown graphically in Figure 4. The line drawn through these points indicates the boundary between the go and no-go regions. There seems to be no difference between the behavior of titanium foil and rod, nor between helium and steam as a diluent. The boundary line appears to become asymptotic to an ordinate drawn through a concentration of 35% oxygen; this would indicate that, at room temperature, no autoignition would occur at any pressure as long as the oxygen concentration is below 35%. A more exact definition of the asymptote would require higher pressure and special equipment which was not available at the time.

c. Effect of Surface-to-Volume Ratios and Alloying

Most of the samples of titanium used in the static experiments consisted of 5 in. lengths of 1/4 in. diameter rod, reduced to a 1/8 in. diameter cross section near the middle, with a 1/2 in. taper. Several runs were made with differently shaped specimens. Some rods were reduced to 1/8 and 1/16 in. respectively by a square-cut groove near the center, resulting in a very abrupt change in diameter. Another sample was machined from 1 in., round stock to resemble the poppet in the valves mentioned in ORNL report No. 56-8-214. Its cylindrical section was about 1 in. long, with a 60° taper coming to a 1/8 in. point attached to a 1/4 in. rod. (See Figure 5: the burned sample had a longer cylindrical section.) This sample weighed 72 g. Still other runs were made using 1/2 in. strips of 12 mil titanium foil. All of these samples ignited readily upon breaking and were completely consumed or melted, even though in the case of the large poppet only 25% of the required amount of oxygen was present. These tests indicate that in the presence of oxygen at the necessary pressures the exposure of a very small fresh area can result in a self-sustaining reaction.

As indicated in Tables I-III several different titanium alloys were used, such as A-55, A-110 AT, and 6 Al-4V. The results obtained with these samples show no differences within the limits of experimental error. These limits are of the order of $\pm$ 25 psi.

d. Reactions with Water

Since the incidents which first directed attention to titanium were apparently metal-water reactions, the behavior of titanium toward water at elevated temperatures and pressures was examined quite carefully.

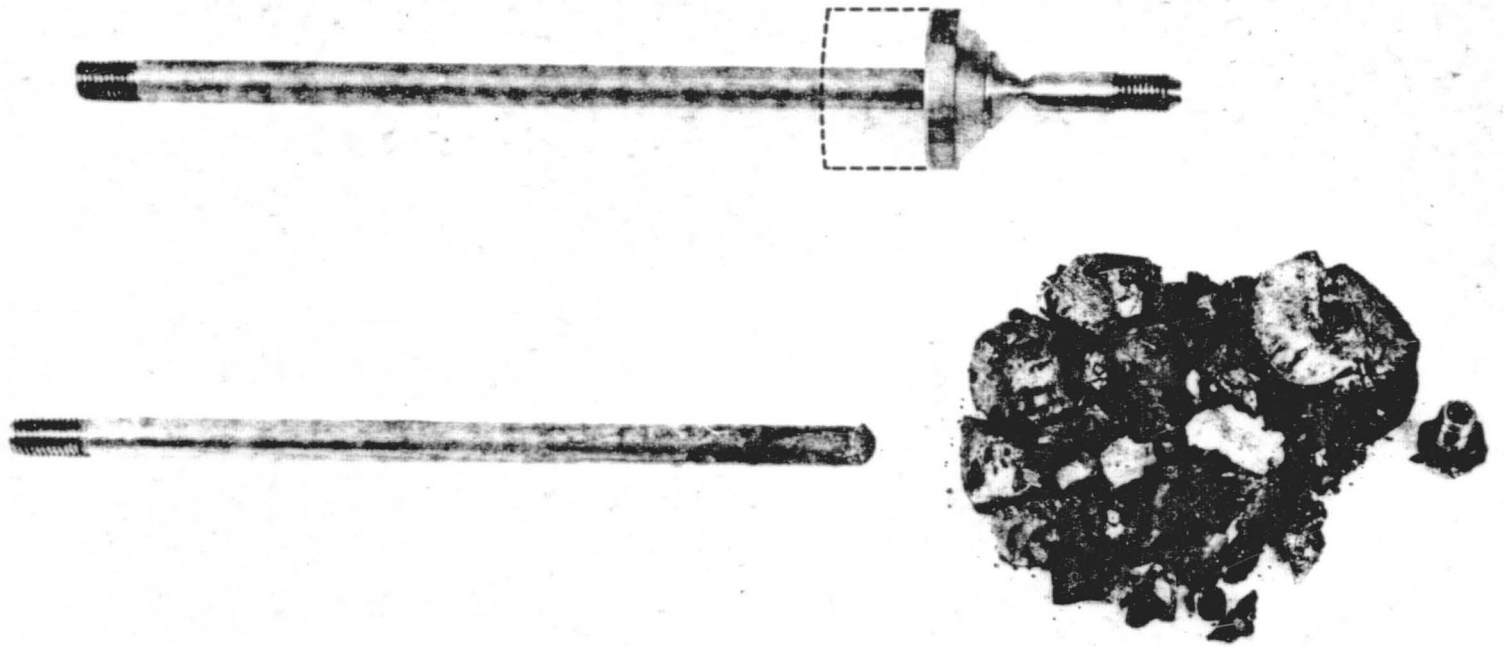

P-2116-QR3-19

FIG. 5
IGNITION OF TITANIUM POPPET

For the first static tests in the presence of water, small test specimens were used to reduce the danger of excessive steam pressures during the burning of titanium. Strips 1/2 in. wide and 3 in. long were cut from 0.012 in. titanium (A-55) foil with notches at the desired breaking point. Thus, by adjusting the water level with respect to the notched area, the strips could be broken either in the gas or in the liquid phase. The results are summarized in Table IV. Ignition occurred only when the strips were broken in the vapor space. The top half of the strip was completely consumed (Run No. 38); the lower half, partly submerged in water, appeared to have been quenched (Figure 6). In order to study this phenomenon under the most favorable conditions, titanium rods were ignited in the gas phase and the burning titanium was permitted to come into contact with liquid water. For this purpose, 10 ml of water was placed in the pressure vessel, oxygen added to the desired pressure and, after equilibration for 1/2 hour, the reaction was initiated by breaking the test sample. Fastax movies of some of these experiments were taken. The composition of the resulting atmosphere was determined mass spectroscopically for some experiments.

Examination of the residues (Figure 7) and of the movies did not show anything striking. The molten metal did not appear to react violently with water; the analytical results indicated, however, the presence of some hydrogen, amounting to about 3% of the reacted titanium. This may be due to a direct metal-water reaction, but could be the result of thermal decomposition of water by the very hot metal (>2000°C). When a sufficiently long rod and enough water were used, the reaction was quenched. It appears, therefore, that even under the optimum conditions of these tests the reaction of titanium with water was not self-sustaining.

2. Dynamic Tests

a. Equipment and Procedures

The reactor described in Section III-1-a was equipped with a special head to hold down a titanium rupture disk, which was broken by a spring-loaded plunger. Either water or steam could be selected as the material initially in contact with the disk, depending upon the orientation of the reactor. A very high degree of turbulence exists as the contents of the reactor are discharged through the break in the rupture disk. The thickness of the disks varied from 4 to 12 mils. Figure 8 shows the arrangement with the rupture disk facing downward.

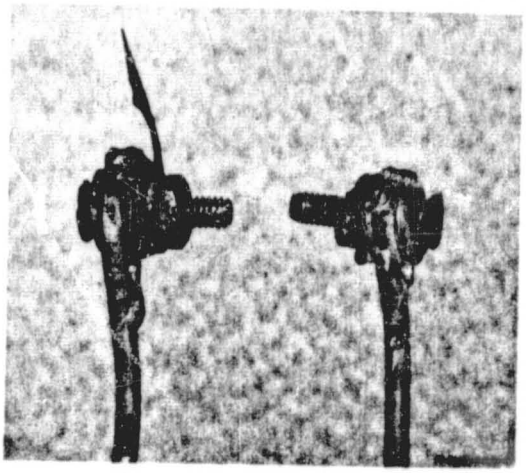

FIG. 6

QUENCHING OF TITANIUM STRIPS
Run No. 38

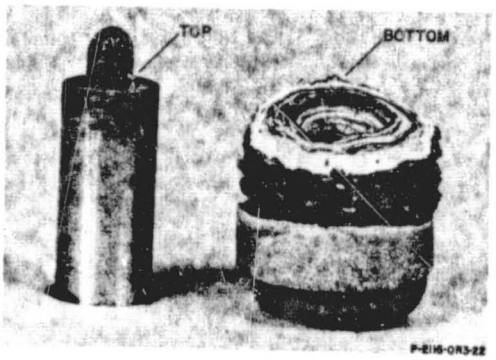

FIG. 7

TITANIUM SLAG FROM IGNITION
IN PRESENCE OF WATER

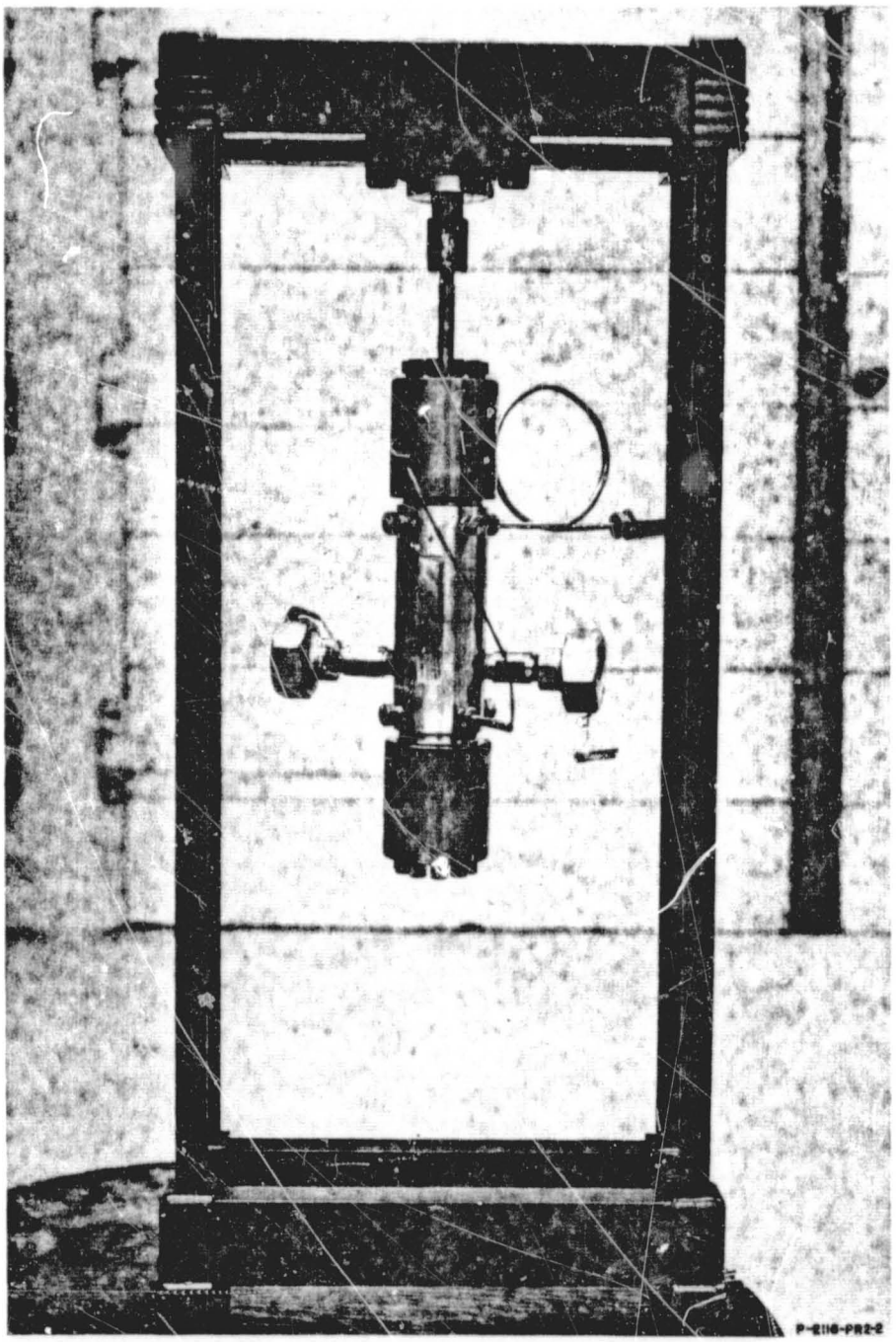

FIG. 8

REACTOR ASSEMBLY
With Rupture Disk Facing Downward

Table IV

REACTIONS OF TITANIUM IN THE PRESENCE OF WATER

Run No.	Oxygen Pressure (psi)	Temperature (°C)	Remarks
36	500	RT	Blank test without water; reaction occurred
37	500	RT	Submerged below break-point; reaction occurred
38	750	RT	Submerged below break-point; reaction occurred
38b	1000	RT	Sample completely submerged; no reaction
39	500	180°	Sample completely submerged; no reaction
40	500	200°	Sample completely submerged; no reaction
41	1000	200°	Sample completely submerged; no reaction

For experiments at elevated temperatures two thermocouples were used, one in the solution and one in contact with the titanium disk. The latter was removed just prior to puncturing the disk. Heating was again accomplished with circular strip heaters.

b. Ignition Limits of Titanium Foils in Dilute Oxygen

The relationship between oxygen pressure and concentration necessary to produce autoignition of a titanium specimen under dynamic conditions of gas flow was determined in a series of runs in which the oxygen concentration at a given total pressure of oxygen and diluent was increased until ignition occurred. The results given in

Figure 9 and Table V show that ignition occurs much more readily under dynamic than under static conditions: pure oxygen at 50 psi pressure streaming past a fresh surface produced autoignition. The ignition limits are much lower throughout the whole range of oxygen concentrations. Figure 10 shows the appearance of a reacted disk.

Table V

REACTIONS OF TITANIUM WITH HELIUM-OXYGEN MIXTURES
(Dynamic Conditions)

Run No.	Foil (in.)	P_{O_2} (psi)	P_{He} (psi)	P_{total} (psi)	O_2 (%)	Reaction
131	.003	350	--	350	100	√*
132	.003	300	--	300	100	√
133	.003	250	--	250	100	√
134	.003	200	--	200	100	√
135	.003	150	--	150	100	√
136	.003	100	--	100	100	√
137	.003	50	--	50	100	√
138	.003	10	--	10	100	--
141	.012	50	--	50	100	√
156	.008	500	500	1000	50	√
157	.008	400	600	1000	40	--
158	.008	450	550	1000	45	√
159	.008	420	280	700	60	√
160	.008	370	250	620	60	√
161	.008	340	130	470	72.5	√
162	.008	300	200	500	60	--
163	.012	450	1050	1500	30	--
164	.012	450	1050	1500	30	--
165	.012	540	960	1500	36	--
166	.012	600	900	1500	40	√
167	.012	630	1170	1800	35	--
168	.012	500	200	700	71.5	√

*/ denotes ignition

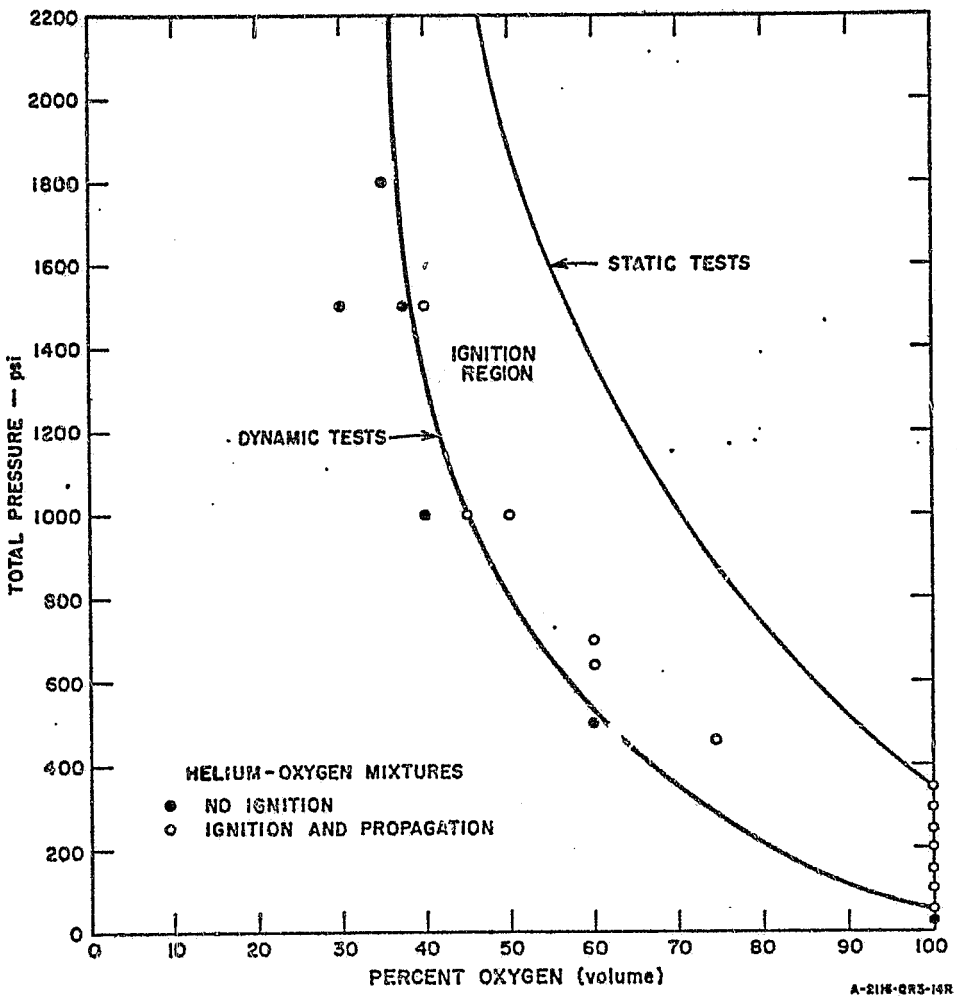

FIG. 9

REACTIONS OF TITANIUM WITH HELIUM-OXYGEN MIXTURES
Dynamic Tests

END OF REFERENCE

36

REFERENCE

37

SCHMIDT, H. W.; AND HARPER, J. T.: HANDLING AND USE OF FLUORINE AND FLUORINE-OXYGEN MIXTURES IN ROCKET SYSTEMS. NASA SP-3037, 1967.

NASA SP-3037

HANDLING AND USE OF

FLUORINE AND FLUORINE-OXYGEN MIXTURES IN ROCKET SYSTEMS

SCHMIDT

NATIONAL AERONAUTICS AND SPACE ADMINISTRATION

NASA SP-3037

HANDLING AND USE OF

FLUORINE AND FLUORINE-OXYGEN MIXTURES IN ROCKET SYSTEMS

by Harold W. Schmidt
with assistance of Jack T. Harper

Lewis Research Center
Cleveland, Ohio

Scientific and Technical Information Division
OFFICE OF TECHNOLOGY UTILIZATION 1967
NATIONAL AERONAUTICS AND SPACE ADMINISTRATION
Washington, D.C.

CONTENTS

CHAPTER		PAGE
1	*INTRODUCTION*	1
	1.1 HISTORICAL BACKGROUND	2
	1.2 FLUORINE STUDIES AT LEWIS RESEARCH CENTER	2
	REFERENCES	6
2	*PROPERTIES OF FLUORINE AND FLUORINE-OXYGEN (FLOX) MIXTURES*	7
	2.1 THERMODYNAMIC, CHEMICAL, AND PHYSICAL PROPERTIES OF ELEMENTAL FLUORINE	7
	2.2 PROPERTIES OF FLUORINE-OXYGEN (FLOX) MIXTURES	8
	2.3 INDEX TO PROPERTIES	9
	REFERENCES	46
3	*COMPATIBILITY OF MATERIALS*	49
	3.1 CHARACTERISTICS OF FLUORINE AND FLOX	49
	3.2 COMPATIBILITY OF METALS WITH FLUORINE AND FLOX	54
	3.3 COMPATIBILITY OF NONMETALS WITH FLUORINE AND FLOX MIXTURES	81
	3.4 FLOX SPILL TESTS ON COMMON MATERIALS	110
	REFERENCES	119
4	*COMPONENTS AND SUBSYSTEMS DESIGN, FABRICATION, AND INSTALLATION CONSIDERATIONS*	121
	4.1 LIQUID-FLUORINE AND FLOX STORAGE TANK AND TRANSFER LINES	121
	4.2 INSULATION	133
	4.3 LINES, JOINTS, AND FITTINGS	134
	4.4 VALVES	140
	4.5 FLUORINE PUMPS	148
	4.6 INSTRUMENTATION	157
	4.7 REFRIGERATION SYSTEMS	163
	4.8 FLUORINE DISPOSAL METHODS AND DESIGN	165
	4.9 SYSTEM FABRICATION AND COMPONENT INSTALLATION	173
	REFERENCES	175
5	*FACILITY DESIGN CRITERIA*	177
	5.1 GENERAL CONSIDERATIONS IN FACILITY DESIGN	177
	5.2 FACILITY DESIGN	183
	REFERENCES	208

Chapter 3. Compatibility of Materials

In the early stages of fluorine technology development, a number of failures occurred that were characterized by a chemical ignition between the fluorine and its containment system. Since the zone where ignition occurred was usually consumed in the reaction, the exact cause of failure was often obscured. Evidence indicated that either the incompatibility of materials or contamination was the cause.

To define compatibilities of materials (metals and nonmetals), a series of investigations was conducted at Lewis with both fluorine and FLOX. Test results indicated that, with proper design and selection of materials, reliable systems can be built. Successful operation can then be assured by scrupulously maintaining the system free of contamination.

Most common metals of construction are compatible for use in a fluorine environment. Metals can burn with fluorine (or oxygen) only if the reaction is initiated by inducing combustion at the reaction zone by reaction of a secondary material (contaminant) or by localized addition of energy, such as friction, impact, or heating to ignition temperature. The choice of metals for use in fluorine systems is primarily based on property requirements for a given application, such as strength and shock resistance at cryogenic temperatures, welding and brazing or soldering characteristics, and thermal conductivity. Considerations peculiar to the fluorine environment would include exposure to friction (film characteristics), the ignition temperature of the metal in fluorine, and resistance to hot and cold hydrogen fluoride.

Many inorganic nonmetals can be used in limited applications with fluorine, including fused metal oxides and fluorides (cermets), Pyrex, and all fully fluorinated compounds. Partially fluorinated materials must be considered as a special case. Most notable of these are polytetrafluoroethylene (TFE) and polychlorotrifluoroethylene (PCFE) because of their resistance to reaction with fluorine and FLOX. These polymers have been used successfully for gaskets and seals in limited applications.

3.1 CHARACTERISTICS OF FLUORINE AND FLOX

3.1.1 Chemical

Fluorine is one of the most powerful oxidizing agents known and can react with practically all organic and inorganic substances. The few

exceptions include the inert gases (under normal conditions of contact), fluorinated compounds in their highest state of oxidation, and a few fluorinated polymers. Even these polymers may burn in fluorine atmospheres if reaction is initiated. The reaction characteristics of FLOX are similar to those of fluorine, except that, at lower concentrations, FLOX mixtures tend to become less hypergolic as the percent fluorine in the mixture is decreased.

The activation energy required to initiate combustion with fluorine is generally much lower than that required for any other oxidant. Fluorine molecules in a fluorine system are always at a state of energy (with respect to a possible reactant) that is closer to their activation energy than other oxidizers in comparable systems. In fact, many materials react spontaneously on exposure to fluorine even at very low temperatures. In concentrations as low as 5 to 10 percent, FLOX ignites spontaneously with many materials and reacts with charcoal at concentrations of less than 1 percent fluorine (ref. 1).

Whether or not a substance will burn spontaneously on exposure to fluorine or FLOX depends on the conditions of exposure. The most important parameters affecting these conditions are

(1) Initial temperature and pressure of the system

(2) Thermal conductivity of the substance, if the reacting material is a solid

(3) Particle size (or surface area exposed, with respect to the mass of substance)

(4) Degree of dynamic or static exposure

(5) Concentration of fluorine in a mixture such as FLOX

3.1.1.1 *Temperature effects.*—Partially oxidized material may be fully oxidized by exposure to an oxidizing atmosphere at a suitable temperature; this is particularly true with fluorine (ref. 2). Fluorine has the highest oxidation potential of all the elements, and ordinary oxides may be considered to be in a state less than maximum oxidation since fluorine can replace the oxygen atoms with sufficient heat release to maintain combustion. Even firebrick (Al_2O_3-SiO_2) will burn in fluorine as was demonstrated at Lewis. A fluorine-hydrogen torch was used to heat the firebrick to a high temperature. The hydrogen was then shut off, and the brick began to burn vigorously with the fluorine.

The reaction of fluorocarbon polymers with fluorine is another example of reaction to a higher state of oxidation. Polytetrafluoroethylene $(CF_2\text{-}CF_2)_x$, for example, is a fluorocarbon chain polymer, but fluorine is capable of breaking the carbon-carbon bond and reacting the carbon to a higher degree of saturation, forming carbon tetrafluoride (CF_4). Reaction may be initiated by reaching the ignition temperature or by

providing activation energy mechanically by impact, friction, high flow velocities, or by reaction with a contaminant.

3.1.1.2 *Pressure effects.*—A pressure increase can also promote reaction initiation with fluorine (ref. 3). A group of nonmetallic materials was tested under static conditions for compatibility with both liquid and gaseous fluorine at atmospheric pressure and 1500 pounds per square inch gage (ref. 4). In most of the tests in which no reaction occurred at atmospheric pressure, reaction was initiated by a pressure increase. These tests are discussed in section 3.3.1.

3.1.1.3 *Thermal conductivity.*—Materials with a high thermal conductivity resist ignition with fluorine more readily than materials with low conductivity. Combustion with fluorine will not occur if the heat of reaction can be dissipated from the point of ignition fast enough to maintain the temperature below the ignition point of the material involved (ref. 5). In an actual case, a brass flowmeter was installed in a stainless-steel, liquid-fluorine flow line (fig. 3–1). Ignition occurred at the flange connection between the two metals and resulted in destructive combustion of the flange materials as well as a considerable length of the stainless-steel line. At the surface of contact between the two metals, the steel material was reacted completely away, leaving the end of the brass fitting unaffected.

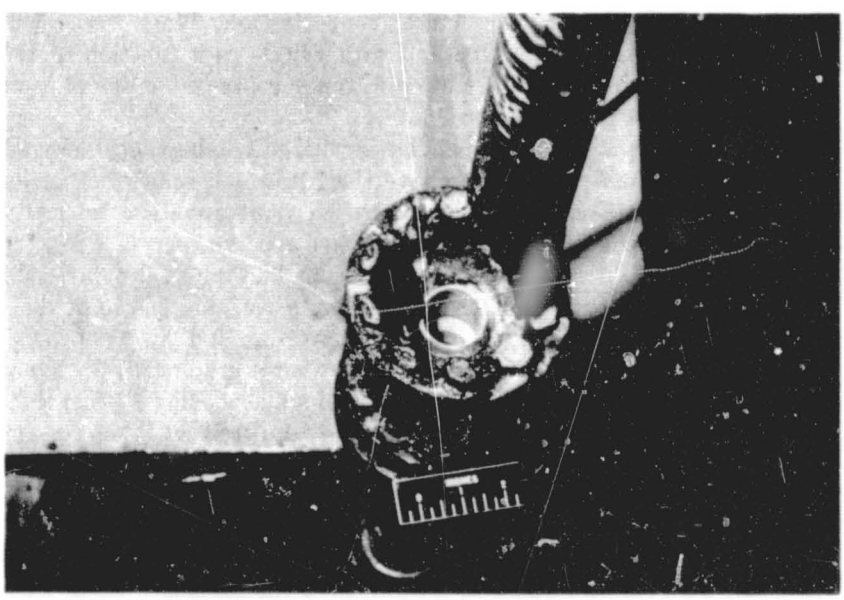

FIGURE 3–1.—Results of fluorine burnout between stainless-steel flange and brass fitting (ref. 2).

3.1.1.4 *Surface-area effects.*—Fluorine will react with the surface of nearly all solid materials. If the material is not spontaneously combustible (like most metals), surface reaction simply forms a fluoride film on or in the surface. If, however, the surface area exposed to fluorine is very large in proportion to its mass (e.g., fine-mesh screen or finely divided material such as powdered metal or spun glass) the heat of surface reaction may initiate combustion and the material becomes spontaneously reactive because the rate of heat dissipation is reduced.

3.1.1.5 *Dynamic and static effects.*—Tests at Lewis have shown that most materials are less resistant to reaction when exposed to a fluorine or FLOX environment under kinetic (flow) conditions than under static conditions. These tests show that

(1) Flow conditions contribute to the activation energy required to initiate reaction (i.e., reactivity increases with increase in rate of flow).

(2) Activation energy and/or flow conditions required to initiate reaction with FLOX is/are greater than that required for fluorine.

3.1.2 Reactions

3.1.2.1 *Reaction with water.*—Tests at Lewis (unpublished data) have shown that two types of reaction can occur with water: a slow noncombustive reaction and a fast combustion reaction. The occurrence of combustive reaction in these tests was determined to be a function of the water droplet size and the fluorine concentration. Water *vapor* will react combustively with fluorine and with FLOX as a function of the FLOX concentration. (FLOX concentration is expressed as the percent fluorine by weight in the mixture.)

Fluorine can be bubbled through water without combustion; however, at room temperature, the vapor above the liquid will sometimes ignite and burn with the fluorine. As ice, water shows no apparent reactivity with gaseous fluorine; however, an explosive reaction occurs when ice is exposed to liquid fluorine (or when liquid fluorine is dropped into water). This reaction is usually preceded by a variable and unpredictable induction period, which is affected by pressure and flow conditions.

The results of a fluorine-ice reaction are shown graphically in figure 3–2. The section of tubing shown was part of a fluorine flow system that, was evacuated while partly immersed in liquid nitrogen. When an unknown leak permitted air to get into the system, atmospheric moisture apparently condensed and froze in the tubing at the liquid-nitrogen level. The resulting explosion occurred when liquid fluorine contacted the ice during tank pressurization. *Water, in the form of moisture in the atmosphere or contained in pressurant or purge gases which were inadvertently introduced into a cryogenic fluorine or FLOX system, has been a major cause of fluorine system failures* (*see sec. 5.2.6.1*).

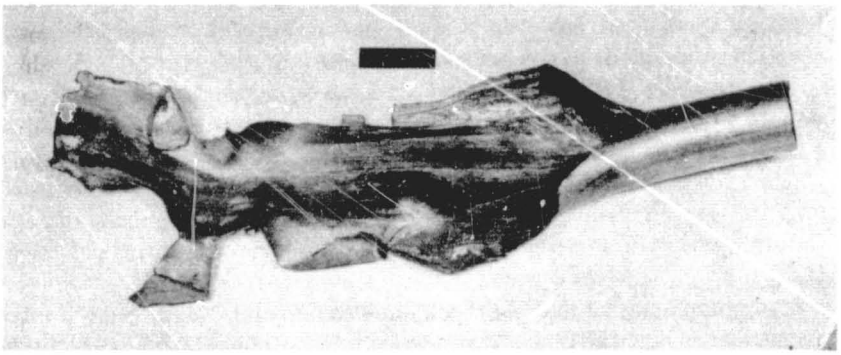

FIGURE 3-2.—Result of contamination in Monel propellant line carrying liquid fluorine (ref. 2).

Spill tests have demonstrated that 30-percent FLOX will not usually react combustively with water (refer to section 3.4). However, that some reaction does occur is shown by the decrease in pH (increase in acidity) in the water during these spill tests. Lewis tests involved dumping FLOX into a pan of water and into a showerhead spray. Unpublished data from Rocketdyne Inc. indicated that similar results occurred when FLOX was dumped into a water fog; a combustive reaction did not occur in either case. It is concluded that some FLOX concentration higher than 30 percent would be required to obtain reliable ignition with a water spray. In general, the reactivity of fluorine at any given concentration is a function of particle size, being more pronounced with fine water sprays or fogs than with coarse sprays. When the water present is in vapor form (e.g., humid air), the reactivity is a function of fluorine-moisture concentration, temperature, and rate of mixing or diffusion.

3.1.2.2 *Reaction with carbon.*—The reaction of fluorine with carbon has been the subject of considerable investigation. Experience at Lewis has shown that the characteristics of reaction-ignition obtained with carbon are determined largely by its state of crystallinity (ref. 6). In addition, the reactivity of carbon is dependent on its state of subdivision (particle size) and the temperature. Graphitic or crystallized carbon tends to react explosively with fluorine after an indeterminate induction period in a manner similar to that of ice; amorphous carbon and charcoal are highly hypergolic with fluorine and react smoothly at all conditions, even at very low fluorine concentrations (refer to section 3.3.3.6 and ref. 6).

The higher activation energy of crystalline carbon, as opposed to amorphous carbon, is probably a result of the carbon-carbon bond,

which forms an orderly hexagonal pattern with a lamellar structure. If reaction is initiated, however, it is self-sustaining and produces the same reaction products as amorphous carbon does.

The reaction between fluorine and amorphous carbon is a most important and useful chemical reaction in the handling of fluorine or FLOX, since it provides a feasible method for reacting fluorine to a chemically inert and relatively nontoxic gas that can be vented to the atmosphere. Fluorine and carbon react to produce primarily carbon tetrafluoride (CF_4) with trace amounts of other fluorocarbons (e.g., C_2F_6).

The nontoxicity of fluorocarbons has been established in some limited experiments, and reference 7 states that "The fluorocarbons are probably the most non-toxic organic compounds possible. . . ." Reference 8 gives carbon tetrafluoride a toxicity rating of moderate (temporary effects, not severe enough to threaten life or cause permanent physical impairment). The source data for this rating are not given, and it may be that the indicated toxicity might take into account heating of the fluorocarbon above its decomposition temperature. Polytetrafluoroethylene $(C_2F_4)_n$ begins to dissociate at about 842° F (ref. 9) and these fluorocarbons have been in wide use as cooking utensil coatings without reported ill effects to users.

A recent experiment at the von Kármán Center of Aerojet-General Corporation (unpublished data) involved piping the effluent from a fluorine-charcoal reactor into a cage of laboratory rats. No ill effects to the animals were observed. In earlier studies (ref. 10), 2,2-difluoropropane (which is a less stable fluorocarbon than carbon tetrafluoride) was used as a substitute for nitrogen in the breathing atmosphere for guinea pigs. In these tests, no ill effects were observed either. Thus it seems reasonable to assume that, under the normal conditions of exposure that might be expected at a rocket facility, the carbon tetrafluoride effluent from a charcoal disposal system would be relatively nontoxic.

3.2 COMPATIBILITY OF METALS WITH FLUORINE AND FLOX

Many studies have been performed to determine the compatibility of various metals with fluorine and FLOX. There is considerable variation in the reaction of fluorine with the surface of metals reported in these studies, which was probably a result of the difference in experimental conditions employed, and particularly in the purity of fluorine used and the amount of hydrogen fluoride or other contamination present. Fluorine will form hydrogen fluoride when brought into contact with any hydrogen-bearing compound, including atmospheric moisture. In fact, the *primary* contaminant that must be carefully guarded against in fluorine systems is moisture. Thus, in maintaining fluorine and FLOX purity, it

is vitally important to exclude all atmospheric contamination from fluorine or FLOX systems.

The following paragraphs summarize the results of various studies on the effect of fluorine or FLOX on the surface of metal materials.

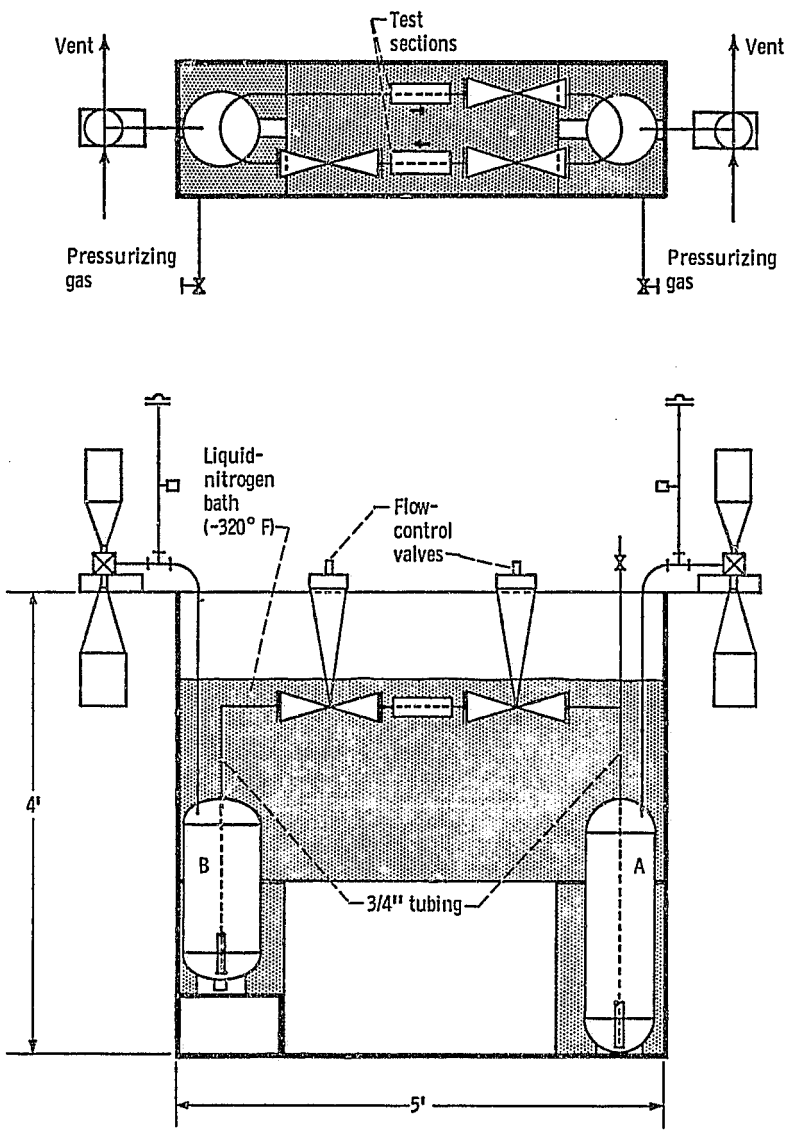

FIGURE 3-3.—High-pressure fluorine-flow apparatus.

ing high velocities and simulating leaks, flat-faced plugs for impact tests, and triangular wedges for turbulence effects and exposure of sharp edges and corners to fluorine flow.

These specimens were exposed to a range of flow velocities and pressures. The following results were obtained:

(1) Flow velocities of up to 400 feet per second at a temperature of −320° F and pressures up to 1500 pounds per square inch gage caused no measurable physical erosion, and no chemical attack occurred with nickel, stainless-steel, aluminum, or brass specimens.

(2) All configurations tested were found acceptable for fluorine systems under the conditions imposed.

(3) Sudden release of high-pressure liquid fluorine in metal tubes containing gaseous fluorine without liquid-nitrogen jacketing (ambient temperature) had no effect on the system.

In addition, turbulence, fluid friction, and impact effects resulting from high-pressure high-velocity liquid-fluorine flow through clean tubing or past irregularly shaped or sharp-edged objects will not initiate fluorine system failures. The successful operations achieved in this series of compatibility tests were attributed to the care taken in the assembly, cleaning, and operating techniques used before exposing the system to severe dynamic fluorine service (ref. 3).

3.2.2 Chemical Effects on Metals Exposed to Fluorine

3.2.2.1 *Corrosion studies.*—When metals are exposed to fluorine, one of two chemical effects can be expected to occur, film formation or corrosion. In the presence of pure fluorine, metals form a fluoride film in the surface, with film formation occurring almost entirely in the first few hours of exposure. Fluoride films, like the oxide films that form on aluminum in air, are so closely bonded to the metal surface that they are considered "in" rather than "on" the surface of the metal.

Corrosion of metals occurs when moisture is present in any quantity. The moisture reacts with fluorine and fluorides to form hydrogen fluoride and fluoride complexes; this in turn destroys the metal fluoride film, and corrosion will occur from exposure to hydrogen fluoride. Since the film immediately re-forms, a cycle is set up whereby the base metal is reacted away. The process continues until the hydrofluoric acid is exhausted or the base metal is destroyed.

The fact that corrosion can occur in fluorine systems is the reason for extreme stress herein on cleanliness and on selection of procedures to keep fluorine or FLOX systems free of moisture contamination.

LONG-TERM EXPOSURE: Several test programs have been run to determine "corrosion" of metals exposed to fluorine environments. Some early tests showed excessive rates of apparent corrosion in metals

exposed to fluorine, though this high rate was later attributed to the presence of contaminants in the fluorine. The most important result from more recent studies (ref. 11) is that most metals show little or no sign of corrosion following prolonged exposure to contaminant-free liquid fluorine. (However, most metals are attacked severely by hydrogen fluoride, particularly in the presence of free moisture, ref. 12.) Corrosion problems involved in handling fluorine of FLOX will be relatively insignificant if hydrogen fluoride is excluded from the system and the fluorine or FLOX is kept in a high state of purity. Table 3-I lists results of U. S. Air Force tests in which test specimens of various metals were immersed in liquid fluorine for 1 year.

TABLE 3-I.—CORROSION [a] OF METAL SPECIMENS IMMERSED IN LIQUID FLUORINE FOR 1 YEAR (REF. 11)

[Area of specimen, 4.20 sq in.]

Metal	Sample	Sample weight		Weight difference after cleaning, g
		Before exposure, g	After exposure, g	
Stainless steel 304	1	18.6849	18.6873	0.0009
	2	18.5512	18.5540	—.0026
	3	18.7305	18.7298	—.0002
	4	18.6154	18.6210	.0009
	5	18.5245	18.5325	.0022
Stainless steel 410	6	17.8507	17.8298	—0.0483
	7	18.1199	18.0981	—.0427
	8	17.8918	17.8766	—.0342
	9	17.9080	17.8005	—.0223
	10	18.0191	18.0123	—.0207
Monel 15–7	11	17.9713	17.9760	0.0008
	12	17.9272	17.9371	—.0006
	13	18.1022	18.1104	.0022
	14	17.9481	17.9553	.0029
	15	17.9088	17.9144	.0001
Copper	16	19.5659	19.5715	—0.0027
	17	19.7531	19.7639	.0005
	18	19.6306	19.6379	—.0008
	19	19.7691	19.7752	.0006
	20	19.6955	19.7001	—.0017
Aluminum 1100	21	6.3930	6.3616	—0.0488
	22	6.4349	6.4106	—.0422
	23	6.3277	6.3046	—.0399
	24	6.3876	6.3688	—.0315
	25	6.3828	6.3675	—.0314

[a] Based on weight difference after cleaning.

TABLE 3-I.—CORROSION [a] OF METAL SPECIMENS IMMERSED IN LIQUID FLUORINE FOR 1 YEAR (REF. 11)—Concluded

[Area of specimen, 4.20 sq in.]

Metal	Sample	Sample weight		Weight difference after cleaning, g
		Before exposure, g	After exposure, g	
Aluminum 6061	26	6.0088	5.9928	—0.0315
	27	5.9816	5.9697	—.0295
	28	6.0216	6.0163	.0432
	29	5.9744	5.9578	—.0333
	30	5.9193	5.8984	—.0333
Nickel	31	20.4919	20.4952	—0.0035
	32	20.4087	20.4149	—.0006
	33	20.6207	20.6281	.0014
	34	20.5791	20.5999	.0032
	35	20.6101	20.6206	.0038
Monel	36	20.5294	20.5366	—0.0010
	37	20.4504	20.4604	—.0004
	38	20.4651	20.4715	—.0035
	39	20.6064	20.6157	—.0021
	40	20.6896	20.6916	—.0036
Titanium A-110 AT	41	10.4057	10.3207	—0.0900
	42	10.3669	10.2730	—.1008
	43	10.4500	10.3724	—.0847
	44	10.3437	10.2718	—.0795
	45	10.2572	10.1847	—.0795
Titanium C-120 AV	46	10.3558	10.2710	—0.0897
	47	10.3333	10.2516	—.0877
	48	10.3732	10.3085	—.0730
	49	10.4072	10.3659	—.0654
	50	10.3463	10.3091	—.0516
Magnesium AZ-31	51	3.9513	3.9416	—0.0460
	52	3.9398	3.9696	—.0175
	53	3.9748	3.9706	—.0485
	54	3.9345	3.9097	—.0501
	55	3.9334	3.9261	—.0431
Magnesium HM-31	56	3.9925	3.9491	—0.0307
	57	4.0097	3.9558	—.0892
	58	4.0078	3.9671	—.0843
	59	4.0017	3.9215	—.1022
	60	3.9625	3.9942	—.0973

[a] Based on weight difference after cleaning.

Studies at Lewis (ref. 13) involved exposure of test specimens (tubes) of 3S-O and 52S-O aluminum, 347 and 321 stainless steels, A-nickel, and low-leaded brass alternately to liquid and gaseous fluorine for periods up

to 3½ months. Results of these tests were confirmed by the recent tests described in reference 11. For conditions that involved very clean systems and high purity in the fluorine used, the amount of specimen weight change was relatively slight and for most purposes could be con-

TABLE 3-II.—CORROSION DATA (REF. 13)

Metal	Weight, g		Weight change, g	Internal area, sq in.	Time, hr
	Before exposure	After exposure			
Aluminum 3S-O	18.9033	18.9033	0	7.20	[a]1055
	18.6296	18.6322	.0026	7.12	1055
	16.4636	16.4744	.0108	5.83	[b]2730
	16.3856	16.3962	.0106	5.83	2730
	18.8299	18.8313	.0014	7.20	2730
	18.6457	18.6563	.0106	7.20	2730
Aluminum 52S-O	28.6731	28.6750	0.0019	8.36	1055
	27.8926	27.9019	.0093	8.21	1055
	27.7912	27.8075	.0163	8.06	2730
	27.9204	27.9041	—.0163	8.06	2730
	28.1495	28.1594	.0099	8.36	2730
	26.5484	26.5579	.0095	7.77	2730
Stainless steel AISI 347	42.2858	42.2870	0.0012	7.29	1055
	41.8131	41.8132	.0001	7.12	1055
	35.4984	35.5015	.0031	5.83	2730
	35.6087	35.6121	.0034	5.91	2730
	42.1893	42.1932	.0039	7.12	2730
	42.6253	42.6275	.0022	7.20	2730
Stainless steel AISI 321	27.3230	27.3249	0.0019	7.20	1055
	26.9847	26.9865	.0018	7.03	1055
	23.4952	23.4980	.0028	5.91	2730
	23.5475	23.5523	.0048	5.83	2730
	27.2577	27.2587	.0010	7.12	2730
	27.7913	27.7934	.0021	7.20	2730
A-nickel	43.5582	43.5587	0.0005	7.20	1055
	43.6383	43.6387	.0004	7.20	1055
	36.3945	36.4005	.0060	5.74	2730
	41.4378	43.4404	.0026	7.12	2730
	38.8173	38.8203	.0030	6.34	2730
Low-leaded brass	57.7751	57.7800	0.0049	6.58	1055
	59.2956	59.2993	.0037	6.82	1055
	48.5486	48.5662	.0176	5.39	2730
	48.4982	48.5133	.0151	5.39	2730
	58.6092	58.6168	.0076	6.66	2730
	59.0067	59.0116	.0049	6.66	2730

[a] Exposed 783 hr to gas, 272 hr to liquid.
[b] Exposed 1714 hr to gas, 1016 hr to liquid.

sidered insignificant. Data from these tests (table 3-II) show a small weight gain for each specimen that includes the gain expected from normal fluoride film as well as any reaction products from hydrogen fluoride corrosion.

Metallurgical examination of the test specimens did not reveal any intergranular corrosion except for nickel. Very slight intergranular corrosion was observed; however, this was considered negligible for the time period involved. The physical appearance of the test specimens was

TABLE 3-III.—TEMPERATURE EFFECTS ON CORROSION OF METALS AND ALLOYS IN FLUORINE FOR 5-DAY EXPOSURE (REF. 14)

Material	Type	Average temperature, °F	Area, sq in.	Weight change, g
Aluminum	1100 H-14	79	2.082	0.0004
		79	2.088	.0002
		394	2.079	.0001
		394	2.069	.0001
		673	1.990	.1871
		673	1.998	.1976
		1009	2.021	.7470
		1009	1.989	.7308
	2024 T-3	79	2.020	0.0001
		79	2.019	0
		394	2.014	.0001
		394	2.016	.0003
		673	1.740	.0113
		673	1.733	.0171
		1020	1.725	.0028
		1020	1.740	.0033
	5154 H-34	79	1.608	0
		79	1.612	—.0003
		356	1.601	—.0004
		356	1.612	—.0003
	5154-O	640	1.989	0.0012
		640	2.007	.0012
		1017	1.991	.0031
		1017	1.999	.0030
Magnesium	M1A	79	2.002	0.0003
		79	2.002	.0001
		358	1.981	.0002
		358	2.002	.0001
		653	1.926	.0010
		653	1.968	.0011
		1006	1.972	.0128
		1006	1.954	.0121

reported (ref. 13) as follows:

(1) Both exposed and unexposed surfaces of nickel appeared identical.

(2) Both aluminum samples appeared considerably lighter in color but appeared unchanged otherwise.

TABLE 3-III.—TEMPERATURE EFFECTS ON CORROSION OF METALS AND ALLOYS IN FLUORINE FOR 5-DAY EXPOSURE (REF. 14)—Concluded

Material	Type	Average temperature, °F	Area, sq in.	Weight change, g
Magnesium	AZ81A-T6	79	2.735	0.0003
		79	2.806	0
		363	2.762	—.0002
		363	2.772	—.0002
		691	2.762	.0003
		691	2.737	.0005
		1000	2.780	.0060
		1000	2.783	.0039
	1C-T6	79	2.558	—0 0002
		79	2.552	.0002
		406	2.640	0
		406	2.664	—.0002
		691	2.656	.0020
		691	2.629	.0015
		1002	2.642	.0012
		1002	2.644	.0026
Monel		79	2.002	0.0005
		79	2.003	.0003
		396	1.996	.0004
		396	2.003	.0001
		684	2.009	.0027
		684	1.951	.0031
		1020	1.991	.0179
		1020	1.984	.0180
Nickel	A	79	1.988	0
		79	1.997	0
		396	2.002	.0002
		396	2.004	0
		684	1.997	.0010
		684	2.007	.0008
		1026	1.982	.0350
		1026	1.984	.0349
Stainless steel	304L	79	2.086	0
		79	2.093	.0001
		406	2.088	.0942
		406	2.094	.0891

(3) Iridescence that occurred in some areas of the stainless steels indicated the presence of fluoride films. This was most prevalent in 347-series steels; however, occurrence was not general in test specimens.

(4) A low-leaded brass was lightly covered with a reddish film that was not continuous, but generally covered the entire surface.

There was no visual difference reported between those portions of the test specimens exposed only to the gaseous phase and those exposed to both liquid and gas, nor was the gas-liquid demarcation line detectable on the specimens.

TEMPERATURE EFFECTS: Some data on the effects of temperature on surface reactivity obtained under U. S. Air Force contract (ref. 14) is presented in table 3-III. The weight change column in the table shows the general effect that can be expected from temperature increase. The data appear to fall within the scatter band that could be expected in the experimental process.

The effect of hydrogen fluoride (anhydrous hydrofluoric acid) in causing corrosion of various metals has been discussed in reference 15 and is presented in table 3-IV (from ref. 15). This reference states that, for Monel and nickel, the rates of corrosion for mixtures of water and hydrofluoric acid are of the same order.

3.2.2.2 *Fluoride film studies.*—According to reference 11, fluoride film formation on the surface of metals in fluorine occurs mostly in the first few minutes of exposure, after which time the reaction rate drops off sharply. Thus, this film acts to inhibit further attack of the base metal.

TABLE 3-IV.—CORROSION RATES OF HYDROGEN FLUORIDE WITH VARIOUS METALS (REF. 15)

Metal	Temperature, °C		
	500	550	600
	Penetration, in./month		
Stainless steel:			
430	0.005	0.030	0.038
304	----	----	.044
347	0.6	1.5	.58
309 Cb	.019	.14	.55
310	.04	.33	1.0
Nickel	.003	----	.003
Monel	.004	----	.006
Copper	.005	----	.004
Inconel	.005	----	----
Aluminum 2S (2 percent manganese)	.016	----	0.005
Magnesium	.042	----	.048

Figures 3–5 to 3–12 illustrate the typical film formation that can be expected when various metals are exposed to fluorine. The film thickness was measured in angstroms as a function of time. It should be remembered that the measurements taken during these studies included the normal fluoride film formation as well as any possible "corrosion" or formation of chemical complexes by hydrogen fluoride or trace amounts of other system contaminants.

Figures 3–5 to 3–9 generally show a film formation in the range of 2 to 14 angstroms during a period of 230 minutes (or about 4 hr) at temperatures from −113° to 183° F. Figure 3–10 shows an extension of the exposure time under similar conditions (86° F) up to 90 hours. As shown, slight increases in film thickness were measured (now in the range of 10 to 30 Å) but again a constant thickness is approached. Figures 3–11 and 3–12 repeat the exposure of selected metals at the maximum temperature (183° F) but show little significant effect.

Generally, the variations in film thickness with respect to the exposure variables were slight, though exposure time has the greatest effect. In

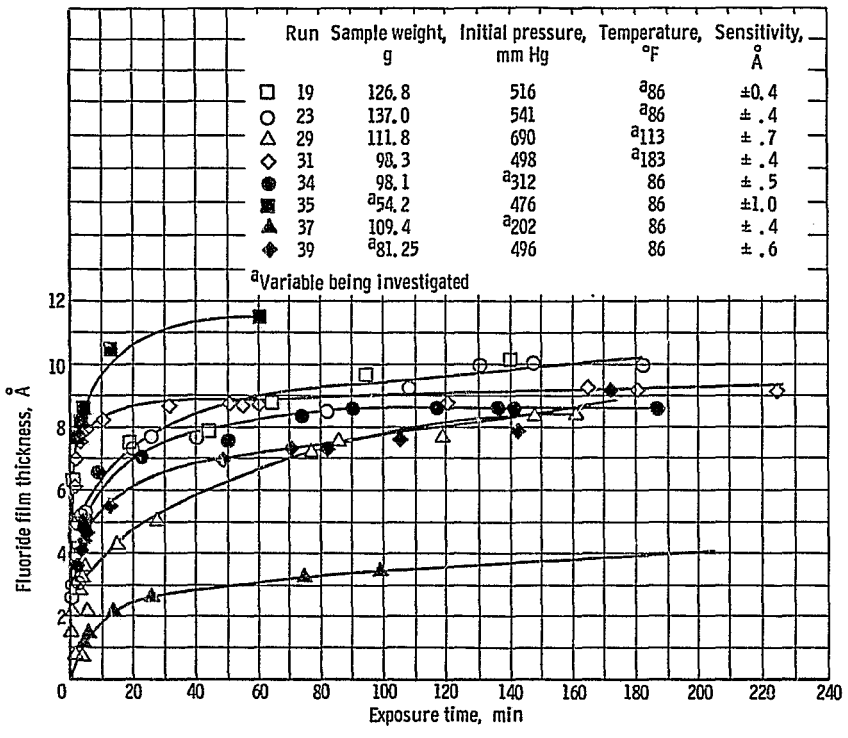

FIGURE 3–5.—Variation of fluoride film thickness on Monel powders to time of exposure to fluorine (ref. 11).

all cases, film thickness tended to become constant at less than 50 angstroms.

The characteristics of metallic surface films and surface reaction are as follows:

(1) Aluminum and aluminum alloys form a tenacious and protective oxide film when the bare metal is exposed to air or oxygen. A similar

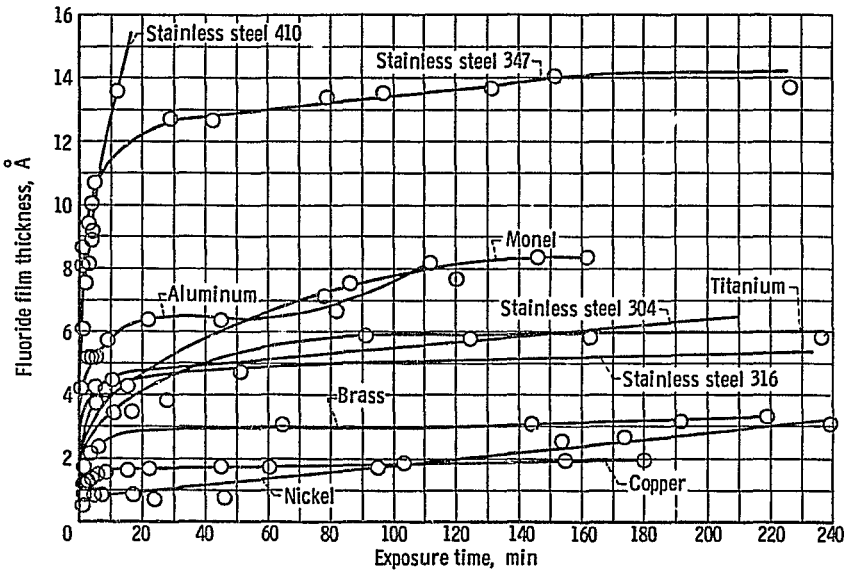

FIGURE 3-6.—Variation of film thickness on metal powders at —113° F with time of exposure to fluorine (ref. 11).

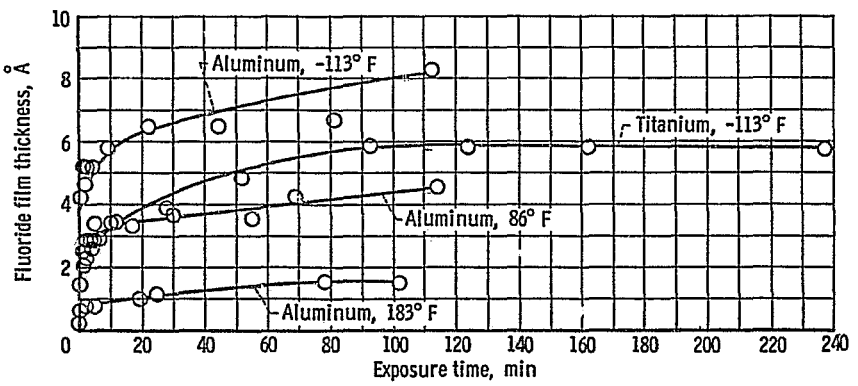

FIGURE 3-7.—Variation of film thickness on aluminum and titanium with time of exposure to fluorine (ref. 11).

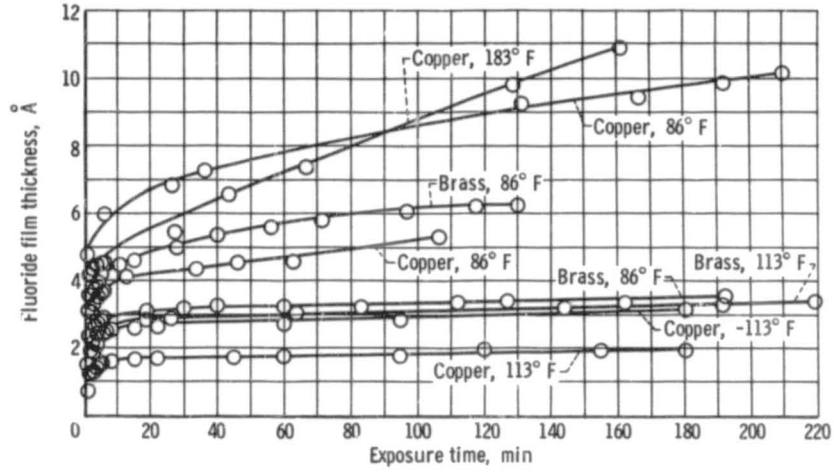

FIGURE 3-8.—Variation of fluoride film thickness on copper and brass powders at two different temperatures (ref. 11).

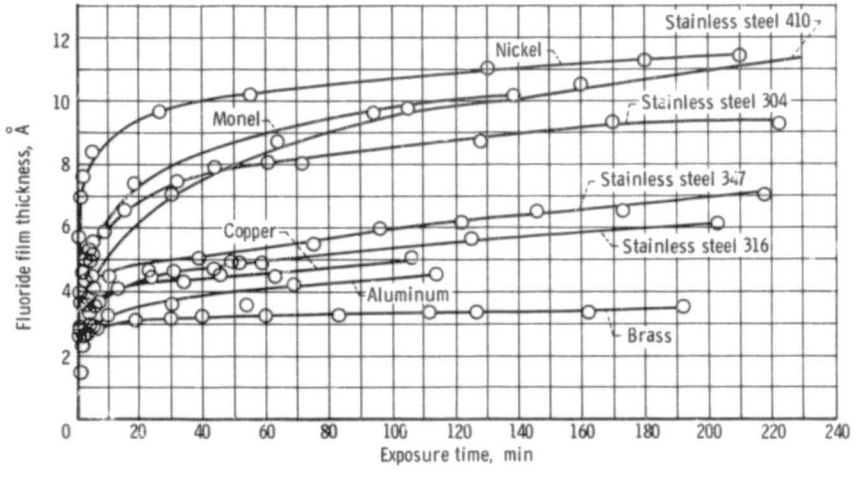

FIGURE 3-9.—Variation of film thickness on metal powders at 86° F with time of exposure to gaseous fluorine in initial period (ref. 11).

film (AlF_3) is formed on exposure to fluorine; if the oxide film is present, fluorine will replace this film. Although the replacement mechanism is not known, the most probable method is by diffusion through the oxide film to react with the bare metal, by replacement of the oxygen, or by both of these. The melting point of aluminum is below its ignition point with fluorine gas (ref. 16); fluoride formation on molten aluminum

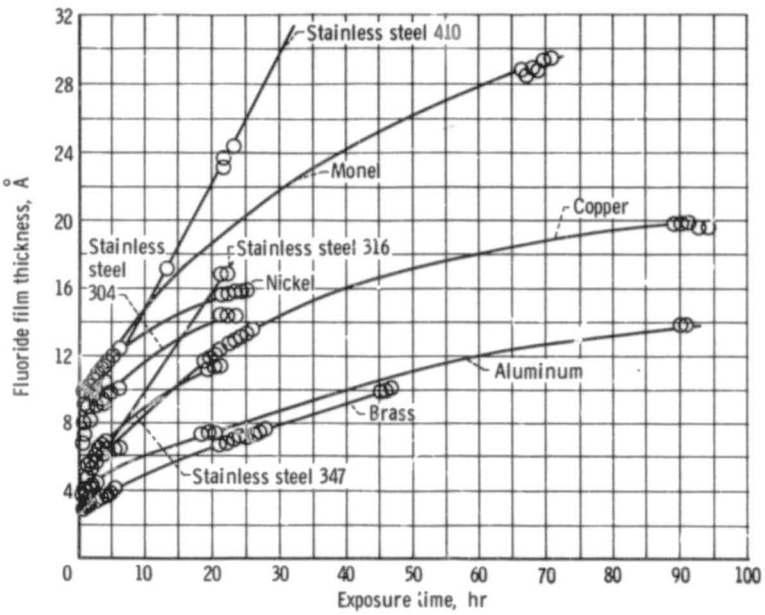

FIGURE 3-10.—Variation of film thickness on metal powders at 86° F with time of exposure to gaseous fluorine for total run (ref. 11).

would probably be similar to the oxide formation on mercury.

(2) Fluorine reacts with the surface of iron, iron alloys, and mild steels to form ferrous and ferric fluoride films at a higher rate and depth than with the more resistant metals. The films are less stable than those of more resistant metals, particularly when exposed to moisture (ref. 17). Susceptibility to corrosion from hydrogen fluoride is also greater.

(3) Stainless steels are more resistant to attack by hydrogen fluoride than mild steels and form stable fluoride films similar to those formed on Monel, though less stable at elevated temperatures. Stainless-steel welds have the same characteristics as the parent material.

(4) Nickel (A, D, and L) and Monel form films similar to those formed on aluminum, but are particularly stable for use at high temperatures (1200° F; refer to section 3.2.4). Welding does not reduce the corrosion resistance of nickel or Monel if fluxes either are not used or are completely removed. Inconel, Illium, Illium "R", and Duranickel are less resistant than either nickel or Monel at higher temperatures but are generally similar to stainless steels.

(5) Copper has a high resistance to fluorine attack. The copper alloys, red brass, and yellow brass are also highly resistant. Cupric

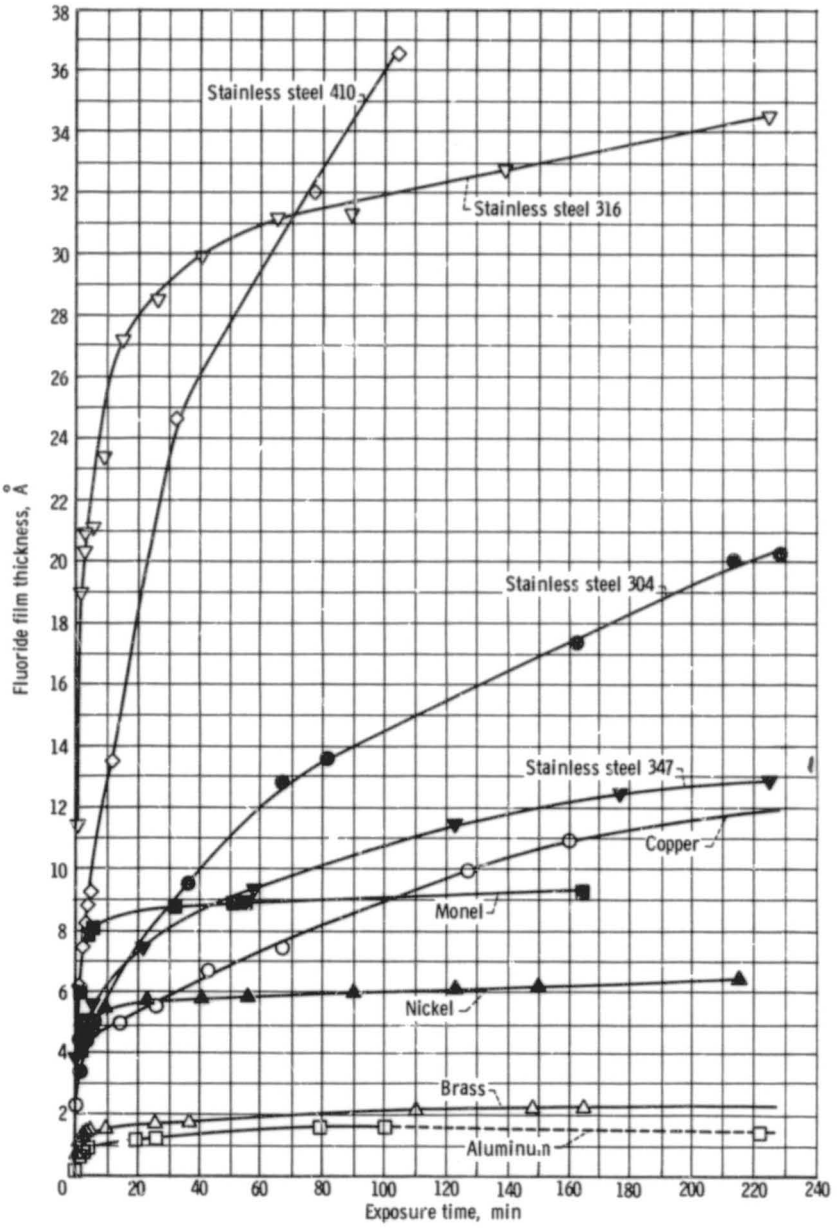

FIGURE 3–11.—Variation of film thickness on metal powders at 183° F with time of exposure to gaseous fluorine (ref. 11).

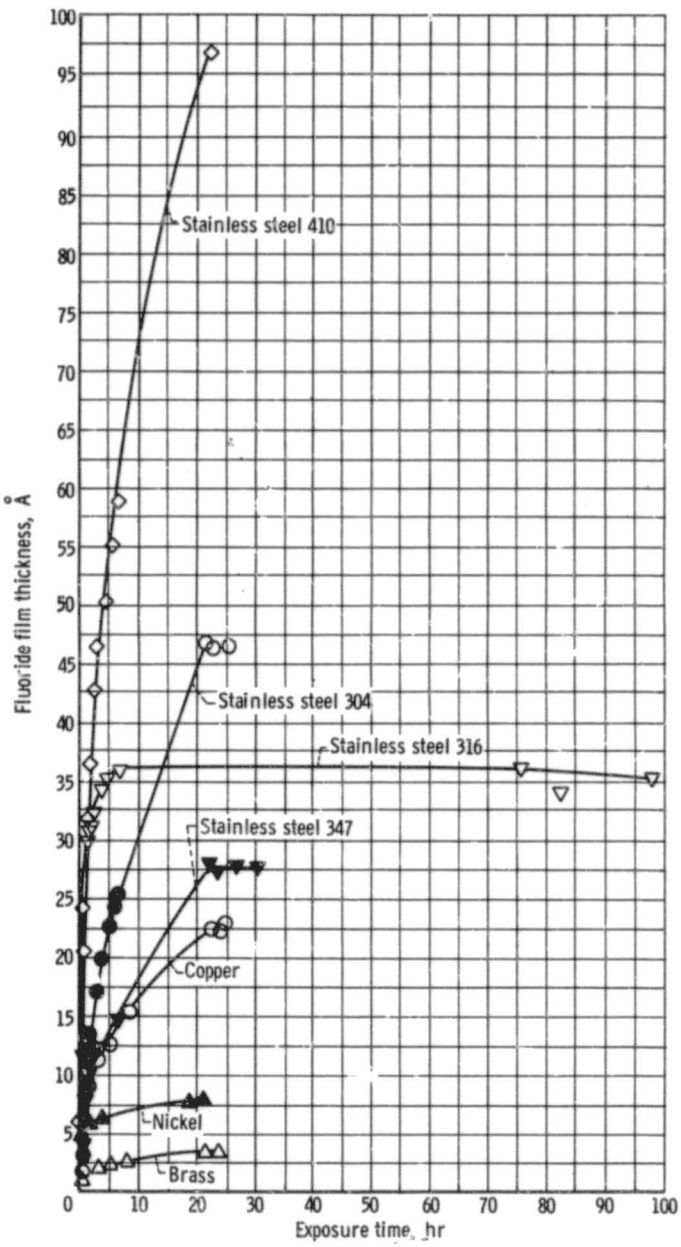

FIGURE 3–12.—Variation of film thickness on metal powders at 183° F with time of exposure to gaseous fluorine for total run (ref. 11).

fluoride film is very stable in the presence of dry fluorine or dry hydrogen fluoride, but hydrolyzes readily in moisture to form hydrofluoric acid, which attacks all copper alloys.

(6) Magnesium, like aluminum, is always coated with a tenacious oxide film. Fluoride film formation is similar to that on aluminum.

(7) Limited experience with titanium indicates poor resistance to hydrogen fluoride and film characteristics similar to stainless steels. In fracture tests with titanium in liquid fluorine (ref. 18), specimens did not ignite, and in other tests (ref. 19) the ignition of titanium was more severe in liquid oxygen than in liquid fluorine. However, gaseous fluorine will rapidly attack titanium at temperatures above 300° F (149° C), according to reference 11, and there have been cases reported where titanium was ignited at −113° F (−81° C), although these authors noted that *catalysis* was necessary and that the reaction was smothered by the fluoride film (refs. 11 and 17).

(8) Silver solder and Nicrobraze are recommended for most of the joining where welding is impractical or impossible. (Flux should *not* be used; refer to section 4.9.3.) Exact film characteristics of these materials have not been determined; however, these metals have been widely used and have provided highly reliable connections.

(9) Chromium forms four fluorides (ref. 20): (1) divalent, (2) trivalent, (3) tetravalent, and (4) pentavalent ((3) and (4) are volatile). When chromium is reacted with fluorine below 300° F (149° C) it forms a protective divalent fluoride similar to the film on nickel plate. Above 300° F, the fluoride is converted from a divalent to a volatile tetravalent fluoride form (ref. 20) and loses its protective ability. Chromium may be used below 300° F with no problems other than those associated with nickel plate.

(10) Beryllium behaves much the same as nickel in fluoride film formation (ref. 20). Tantalum should not be used at temperatures above 150° F (66° C). Because of its low ignition point, little research data are available on tantalum.

(11) Lead forms a nontenacious fluoride film. In passive exposure, however, it has been used successfully as seal or gasket material.

(12) Tin reacts in a manner similar to lead and has had some use for soft gaskets in cryogenic service (ref. 20).

(13) Rhodium, palladium, and platinum can be used in contact with fluorine at room temperature essentially without attack (ref. 20). These metals are used in some equipment because they are inert to hydrogen fluoride.

Some additional information on the effects of exposure temperatures on metal surfaces exposed to fluorine is given in table 3-V. The reason for the contradictory information on Monel is not known; however, this as well as other inconsistencies may be partly a result of the different

Card #9

TABLE 3-V.—COMPATIBILITY OF MATERIALS IN FLUORINE

Material	Resistant at temperature (material unaffected), °F, of—	Attack at temperature, °F, of—			Combustion temperature, °F
		Slight	Moderate	Severe	
Iron	-----	----------	----------	----------	[a]1242
Carbon steel	[b]700	----------	----------	[b]930	---------
Stainless steel 302	-----	----------	----------	[b]400 to 500	[d]1258
Chromium plate	[c]302	----------	----------	----------	---------
Molybdenum	-----	----------	----------	----------	[a]401
Monel	-----	[d]1382	----------	[b]930 to 1100	[a]797
Tungsten	-----	----------	----------	----------	[a]580
Inconel	[b]750	[d]1022	----------	[d]1382	---------
Dow metal (G)	[b]930	----------	----------	[a]900	---------
Copper	-----	[b]930 to 1100	----------	[c]1290	[a]1277
Copper wool	-----	----------	----------	----------	[a]200–250
Aluminum (2S)	[b]850 / [b]930	----------	[c]1110	----------	Above melting point
Nickel	[b]1100	----------	[c]1290 / [d]1382	----------	[a]2097
Soda glass	[e]302	----------	----------	----------	---------
Borosilicate	[e]392	----------	----------	----------	---------
Silica	[e]482	----------	----------	----------	---------
Metallic oxides	-----	----------	----------	----------	[c]482

[a] Ref. 20 (for further information refer to section 3.2.4).
[b] Ref. 12.
[c] Ref. 27.
[d] Ref. 28.
[e] Ref. 29.

methods used by the various investigators in obtaining the data. The reaction of copper foil and gaseous fluorine was studied in an all-glass apparatus at pressures to about 200 millimeters of mercury and temperatures from 800° to 1200° F (refs. 21 and 22). The rate of reaction in film formation increased at elevated temperatures in this study; however, the apparent final film thickness (as measured by fluorine consumption) was less than at lower temperatures.

3.2.3 Effects of Fluorine Exposure on Mechanical Properties of Metals

3.2.3.1 *Tensile properties.*—Studies that involved comparison of the effects on test specimens from immersion in liquid nitrogen and liquid fluorine (ref. 11) indicated that the tensile properties of metals were not affected by exposure to the fluorine environment. The corrosion (ref. 11, p. 45) for most of the test specimens was less than 1 mil per year. Thus, the conclusions drawn earlier (section 3.2.2.1) regarding the corrosive effects of fluorine exposure were confirmed. (The 1 mil/yr "rate" assumes that this corrosion would continue, which is unlikely. Again, too, the fluoride film penetration may be what is indicated by ref. 11 as corrosion; this penetration, as indicated by the data, is negligible.)

Samples were tested after removal from liquid-fluorine and liquid-nitrogen baths following the 1-year soaking period. According to reference 11, the mechanical properties of 120 specimens were determined in a standard tensile testing machine. As shown by values given in table 3-VI, there were no significant differences in mechanical properties between samples immersed in liquid nitrogen or liquid fluorine. Long-term exposure to cryogenic (−320° F) temperatures appeared to improve tensile properties over the handbook values. Table 3-VI, from these studies, displays scatter within the limits that could be expected for the particular data. Recent studies at General Dynamics/Convair (unpublished data) have shown these earlier conclusions regarding tensile properties to be true.

3.2.3.2 *Stressed samples.*—In tests by the U. S. Air Force (ref. 19), specimens of the same metals listed in table 3-VII were stressed to just below their yield points and suspended in liquid fluorine for 2 weeks. None of the test specimens showed signs of stress-corrosion cracking under the test conditions and exposure time (ref. 19).

Tests were run at Lewis on stressed tensile specimens to study the effects of liquid-fluorine environment on the mechanical properties of several sheet alloys (ref. 18). The smooth and notch tensile strengths and the elongation properties of steel, nickel, aluminum, and titanium alloys were determined in a liquid-fluorine environment at −320° F. Mechanical properties data obtained in fluorine were compared with data on specimens of the same sheet and heat treatment tested in an

TABLE 3-VI.—AVERAGE TENSILE PROPERTIES OF 1-YEAR TEST SPECIMENS (REF. 11)

Metal	Treatment (liquid at −320° F)	Average yield stress, psi	Average ultimate stress, psi
Stainless steel 304	Nitrogen	60 620	93 960
	Fluorine	63 440	94 100
Stainless steel 410	Nitrogen	74 680	88 920
	Fluorine	73 700	89 380
Armco steel 15–7 Ph-Mo	Nitrogen	71 660	143 420
	Fluorine	70 700	141 900
Copper	Nitrogen	53 580	57 640
	Fluorine	54 080	58 660
Aluminum 1100	Nitrogen	21 480	23 120
	Fluorine	21 700	22 940
Aluminum 6061	Nitrogen	41 840	45 820
	Fluorine	41 480	46 360
Nickel	Nitrogen	89 960	96 900
	Fluorine	89 680	96 420
Monel	Nitrogen	58 020	93 740
	Fluorine	58 120	93 040
Titanium A110 AT	Nitrogen	125 400	151 600
	Fluorine	126 200	152 000
Titanium C120 AV	Nitrogen	124 000	153 200
	Fluorine	121 400	152 200
Magnesium AZ31	Nitrogen	35 500	41 600
	Fluorine	34 160	41 720
Magnesium HK-31	Nitrogen	49 000	49 960
	Fluorine	46 000	48 240

environment of liquid nitrogen (−320° F).

Short-term (2 hr) exposure of stressed tensile specimens to liquid fluorine (ref. 18) indicated possible slight deterioration of some mechanical properties when compared with similar tests in a nonreactive environment (liquid nitrogen) at the same temperature, as shown in table 3-VII. This indicated deterioration was believed to be a result of contaminants in the gaseous-fluorine supply. The data described in detail in table 3-VII show scatter within the limits that can be expected for the particular test. The results of the Lewis tests (ref. 18) are summarized as follows:

TABLE 3-VII.—TEST RESULTS OF MECHANICAL PROPERTIES AFTER 2-HOUR EXPOSURE IN LIQUID NITROGEN AND LIQUID FLUORINE AT —320° F (REF. 18)

Alloy	Liquid nitrogen			Liquid fluorine		
	Smooth tensile strength, psi	Elongation, percent	Notch tensile strength, psi	Smooth tensile strength, psi	Elongation, percent	Notch tensile strength, psi
Stainless steel AM 350	298×10^3	21.0	79×10^3	262×10^3	6.7	76×10^3
	293	22.5	104	252	7.0	101
	272	6.0	90	256	7.0	--------
	270	9.0	--------	242	8.5	--------
	293	21.0	--------	--------	----	--------
Av. ----	285×10^3	15.9	91×10^3	253×10^3	7.3	88.5×10^3
Stainless steel ASM 6434	276×10^3	6.8	52.2×10^3	271×10^3	2.0	--------
	293	----	65.2	270	2.1	--------
	290	4.0	--------	277	2.5	--------
	276	4.0	--------	274	3.0	--------
Av. ----	285×10^3	4.9	58.7×10^3	273×10^3	2.4	--------
Inconel X ----	192×10^3	10.7	--------	179×10^3	19.0	--------
	199	18.0	--------	195	21.0	--------
	189	13.5	--------	192	18.0	--------
Av. ----	193×10^3	14.1	--------	189×10^3	19.3	--------
Stainless steel AISI 301 70 percent Cr	340×10^3	1.5	219×10^3	349×10^3	1.0	216×10^3
	344	1.3	226	--------	----	--------
Av. ----	342×10^3	1.4	223×10^3	--------	----	--------
Stainless steel AISI 304L	257×10^3	----	256×10^3	240×10^3	2.0	250×10^3
	253	1.5	254	251	2.0	--------
	264	1.5	--------	--------	----	--------
Av. ----	258×10^3	1.5	255×10^3	246×10^3	2.0	--------

(1) Exposure of several alloys to liquefied commercial fluorine gas produced a detrimental effect on the tensile strength of some alloys. A limited number of tests indicated that 2 hours of exposure lowered tensile strength from insignificant amounts to as much as 11 percent. The elongations showed similar trends.

(2) The sharp-notch strengths were not significantly affected.

(3) The presence of contaminants (probably mainly hydrogen fluoride) could have been the cause of the degradation, and different amounts of contaminants could account for the variations in mechanical properties observed.

(4) The surface appearance of specimens exposed to liquid fluorine

TABLE 3-VII.—TEST RESULTS OF MECHANICAL PROPERTIES AFTER 2-HOUR EXPOSURE IN LIQUID NITROGEN AND LIQUID FLUORINE AT —320° F (REF. 18)—Concluded

Alloy	Liquid nitrogen			Liquid fluorine		
	Smooth tensile strength, psi	Elongation, percent	Notch tensile strength, psi	Smooth tensile strength, psi	Elongation, percent	Notch tensile strength, psi
Aluminum 2014-T6 clad	84.0×10^3	13.0	56.4×10^3	82.0×10^3	12.0	58.5×10^3
	86.0	14.0	60.7	83.3	12.0	59.7
	83.0	13.5	--------	79.5	11.0	--------
Av. ----	84.3×10^3	13.5	58.6×10^3	81.6×10^3	11.7	59.1×10^3
Aluminum 6061-T6 bare	60.6×10^3	24.0	55.5×10^3	60.2×10^3	20.5	58.2×10^3
	61.3	22.5	58.7	56.0	16.5	55.5
	--------	----	54.7	62.0	17.5	--------
	--------	----	56.0	--------	----	--------
Av. ----	61.0×10^3	23.3	56.2×10^3	59.4×10^3	18.2	56.9×10^3
Aluminum 7075-T6 clad	94.5×10^3	14.5	38.7×10^3	89.8×10^3	10.5	--------
	94.0	14.0	34.2	93.0	11.0	--------
	94.0	----	39.6	--------	----	--------
Av. ----	94.2×10^3	14.3	37.5×10^3	91.4×10^3	10.8	--------
Titanium alloy Ti-6Al-4V annealed	207×10^3	6.0	183×10^3	183×10^3	6.5	181×10^3
	203	11.0	199	180	6.0	187
	205	11.7	196	--------	----	--------
Av. ----	205×10^3	9.6	193×10^3	182×10^3	6.3	184×10^3
Titanium alloy Ti-6Al-4V solution-treated	226×10^3	17.0	--------	199×10^3	14.0	--------
	225	17.0	--------	185	7.0	--------
	218	14.0	--------	208	5.0	--------
	--------	----	--------	220	8.0	--------
	--------	----	--------	219	4.5	--------
Av. ----	223×10^3	16.0	--------	206×10^3	7.7	--------

ranged from clean to discolored. Etched surfaces had occasional deposits of corrosion products.

Figure 3–13 shows a schematic drawing of the tensile loading apparatus, the test chamber, the liquid-nitrogen cryostat, and the supply piping for purging, filling, and emptying the test chamber. The tensile load was generated by a hydraulic ram mounted at the top of the loading frame. Hydraulic fluid under pressure was metered to the ram by a needle valve from a previously charged accumulator. The tensile load on the specimen was measured by a load cell that utilized strain gages for load indication. This load cell was mounted so that it was in compression when load was applied to the test section (fig. 3–13).

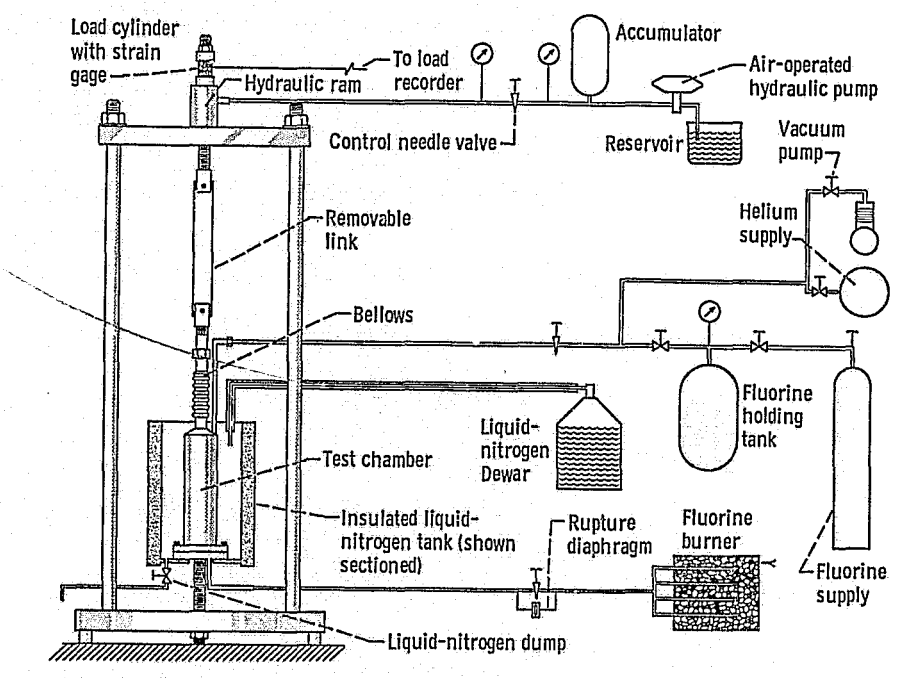

FIGURE 3–13.—Schematic diagram of test setup for Lewis tensile stress tests (ref. 18).

When the test chamber was filled with liquid fluorine, the smooth specimens were loaded to a stress value equal to 90 percent of the yield strength of the material at a temperature of −320° F (liquid-nitrogen boiling temperature). The notch specimens were loaded to 90 percent of the failure stress of duplicate notch specimens in liquid nitrogen. This load was maintained for 2 hours so that the specimens were under stress during the time of exposure to fluorine. After this time, the load was increased until fracture resulted. All specimens were loaded to fracture at strain rates of about 0.005 inch per inch per minute.

For smooth tensile specimens, the hold stress applied was 90 percent of the 0.2 percent yield strength of the material tested in liquid nitrogen. For notch specimens, the hold stress was 90 percent of the failure stress in liquid nitrogen. The time of exposure was 2 hours in this case also.

An interesting aspect of these tests (ref. 18) was that titanium specimens were tested to failure in liquid fluorine without ignition (despite the exposure of a nonpassivated surface by the fracture). Titanium has shown a tendency to ignite when subjected to impact in a liquid-oxygen environment (table 3-VIII), and thus its use in liquid fluorine has been discouraged. The Lewis tests indicated that the use of titanium is feasi-

TABLE 3-VIII.—SUMMARIZED IMPACT IGNITION (REF. 19)

Number of tests	Striker configuration	Number of samples at impact	Energy level, ft-lb	Degree of ignition		
				Moderate	Slight	None
Monel striker, titanium sample						
5	Flat, smooth	5	2.6	--	--	5
2	Flat, rough	2		1	--	1
2	Hemispherical	2		[a]1	--	1
2	Chisel point	2		--	[a]2	--
3	Pointed, conical	3		--	[a]3	--
Titanium striker, titanium sample						
8	Flat, smooth	2	40.0	1	1	--
		2	55.0	1	1	--
		4	58.0	--	1	3
4	Flat, grooved	2	55.0	1	--	1
		2	58.0	2	--	--
16	Pointed, conical	3	2.6	--	1	2
		3	6.0	2	1	--
		2	9.0	1	1	--
		1	35.0	1	--	--
		2	50.0	1	1	--
		2	55.0	1	1	--
		2	58.0	--	1	1
		1	61.0	--	--	1
9	Hollow, pointed	4	6.0	--	1	3
		4	10.0	1	1	2
		1	38.0	1	--	--
Stainless-steel or aluminum striker, aluminum sample						
8	Flat, grooved	8	58.0	1	--	7
4	Pointed, conical	2	30.0	--	--	2
		[b]2	58.0	--	--	2
Titanium striker, titanium sample, liquid oxygen						
10	Flat, smooth	1	60.0	--	1	--
		1	55.0	--	1	--
		8	65.0	--	--	8
9	Conical, pointed	9	65.0	[c]5	4	--
3	Flat, rough	3	65.0	--	1	2
4	Flat, grooved	4	65.0	2	--	2

[a] Ignition indicated by disappearance of striker tip. No evidence of sample igniting.
[b] Aluminum striker.
[c] One sample caught fire and burned almost completely.

ble in liquid-fluorine systems, but it should be thoroughly tested for the particular application before use with fluorine.

3.2.3.3 *Flexure tests.*—In several tests lasting up to 6 hours, flexing thin metal strips in liquid fluorine once per second produced no measurable effects (ref. 19). The flexure tests were performed on copper, brass, aluminum, and Monel immersed in liquid fluorine and were intended to provide some information on the flexibility of the fluoride film. If increased corrosion had resulted, it would have provided evidence that a fluoride film was being lost and re-formed, and that the film was not flexible. The negative results indicate that the fluoride film is not affected by the flexing of metals exposed to fluorine.

3.2.3.4 *Impact tests.*—As reported in reference 19, results were obtained that "were not very reproducible and in no case with liquid fluorine did ignition become general." These tests involved the impact of various shapes of strikers on impact plates beneath the surface of liquid fluorine or liquid oxygen (table 3-VIII).

Ignition was observed by all types of strikers at different impact levels on two titanium alloys tested in liquid fluorine. It should be noted that ignition of titanium with liquid oxygen was more severe than with fluorine (ref. 19). In one case (of 26 tests with oxygen) ignition became general, and the sample burned completely; in each case with fluorine, though reaction was initiated, it failed to propagate itself. Reference 19 states, "Ignition, when it was observed, was indicated by the formation of small craters and gullies together with droplets of melted metal [either] on the sample or on the striker face."

The data (table 3-VIII) provided little information for the compatibility of metals with fluorine; however, when compared with equivalent data for liquid oxygen or when impact ignition energies are compared for different materials, relative reactivities may be obtained for comparable energy values. These values may also be used in comparison with calculated localized energies that may be present in a given system.

As another part of the same series of tests (ref. 19), tubes of various metals were filled with liquid fluorine and struck on the outside at known impact levels. The degree of reaction on the inside of these tubes was not affected by intensive impact by pointed strikers on the outside of the tubes. Vibration of several samples after impacts, at 30 cycles per second, also produced no effects (ref. 19).

3.2.4 Ignition Temperatures of Metals in Fluorine Atmospheres

An experiment was performed (in cooperation with NASA Lewis) to determine ignition temperatures of metals in fluorine atmospheres (ref. 16). In these tests, metal wires were heated electrically in a chamber

TABLE 3-IX.—IGNITION TEMPERATURES OF METALS IN FLUORINE (REF. 16)

(a) Technique A.

Metal	Wire diameter, in.	Ignition temperatures, °C	Average ignition temperature, °C	Maximum variation from average, percent
Aluminum	0.010 .016	----	(a)	----
Copper	0.0123	725 645 670 670 747	692	8.0
Iron	0.014	677 667 667 676	672	0.8
Molybdenum	0.0149	214 207 188 220 188	205	8.3
Monel	0.010	437 423 348 377	396	12.0
Nickel	0.008 .0155 .0154 .0155 .0155 .0152	1168 1096 1219 1195 1209 1084	1162	6.0
Stainless steel 302	0.020	749 796 611 570	681	13.0
Tungsten	0.0153	260 332 263 275	283	18.0

TABLE 3-IX.—IGNITION TEMPERATURES OF METALS IN FLUORINE (REF. 16)—Concluded

(b) Technique B.

Metal	Wire diameter, in.	Maximum wire temperature, °C	Ignition delay, sec	Ignition temperature range, °C	Activation energy, kcal/mole
Copper	0.012	905 852 810 767 701 689	0.8 1.0 .6 .8 1.2 No ignition	689 to 701	39.5
Iron	0.014	730 676 648 644 618	1.0 1.6 2.0 2.2 No ignition	618 to 644	16.3
Nickel	0.015	1357 1306 1266 1253	0.6 1.2 .6 No ignition	1253 to 1266	----

[a] An average of four tests gave an ignition temperature greater than the melting point.

(bomb) containing fluorine, and temperatures were calculated from current and voltage readings by using resistivity-temperature data. Two procedures were used, and a comparison of results is given in table 3-IX.

Technique A.—An evacuated bomb was filled with gaseous fluorine at atmospheric pressure, and the temperature of the specimen was gradually increased by the variable resistor. The voltage and current at which the wire burned out were used, in conjunction with resistivity data, to calculate the temperature at ignition (table 3-IX).

Technique B.—The test specimen was brought to a predetermined temperature in the evacuated bomb before the introduction of fluorine. Fluorine was then admitted and the time (ignition delay) required for the reaction to go to completion was measured with a stop watch (table 3-IX). As shown in the table, ignition occurred at different temperatures for the different metals, but only the range is given. This procedure was used to obtain ignition-delay—temperature curves.

In general, molybdenum, Monel, and tungsten exhibited the lowest ignition points of the metals tested, with values ranging from 200° to

400° C. Aluminum, copper, iron, and 302 stainless steel ignited between 600° and 700° C. Nickel ignited at 1153° C.

3.3 COMPATIBILITY OF NONMETALS WITH FLUORINE AND FLOX MIXTURES

Fluorine-compatible nonmetallic materials would be extremely desirable for use in fluorine or FLOX systems, particularly when the design problem involves modification of an existing launch vehicle to make it fluorine or FLOX compatible. In this case, the problem would be to find materials for given seal, gasket, and other applications to replace currently used materials. For this reason, investigations were required to define the compatibility of materials suitable for use in fluorine or FLOX environments. These studies were conducted at Lewis in three separate programs:

(1) Studies of the effects of exposure of various nonmetals to gaseous and liquid-fluorine atmospheres at atmospheric pressure and 1500 pounds per square inch gage under static conditions

(2) Studies of the effects of exposure of various nonmetals to gaseous and liquid fluorine and FLOX under static conditions and atmospheric pressure

(3) Studies of the effects of gaseous and liquid fluorine and FLOX under flow conditions with pressures up to 1250 pounds per square inch gage and flow velocities of 280 feet per second (liquid) and pressures to 400 pounds per square inch gage and flow velocities to 900 feet per second (gaseous)

Results of the static exposure tests are discussed in the following sections. The dynamic tests are discussed in detail in section 3.3.3. Samples were deliberately tested to destruction to determine compatibility limits as affected by the various parameters.

3.3.1 Static Studies

In the early phases of fluorine work at Lewis, investigations were conducted (refs. 4 and 23) to determine the compatibility of nonmetals with fluorine (1) to classify relative compatibility of nonmetals and (2) to determine any nonmetals suitable for use as bearings and seal materials, sealants, and lubricants for possible fluorine service. These studies involved static exposure to both gaseous and liquid fluorine and were conducted first at atmospheric pressure and later at 1500 pounds per square inch gage. Liquid-fluorine tests were conducted at −320° F, and gaseous fluorine tests were conducted at room temperature. The materials investigated and the results are given in table 3-X.

TABLE 3-X.—NONMETALS EXPOSED TO GASEOUS AND LIQUID FLUORINE
(REFS. 4 AND 23)

Sample [a]	Sample exposed to–				Sample injected into liquid fluorine at 1500 psig pressure
	Liquid fluorine at atmospheric pressure	Gaseous fluorine at atmospheric pressure [b]	Liquid fluorine at 1500 psig pressure	Gaseous fluorine at 1500 psig pressure [b]	
	Liquid				
Kel-F LO No. 10 (M. W. Kellogg Co.)	No reaction	No reaction	No reaction	Reaction [c]	Reaction [d]
Fluorolube HO (Hooker Electrochemical Co.)	↓	↓	↓	Reaction [c]	Reaction
N-43, $(C_4F_9)_3N$ (Minnesota Mining & Mfg. Co.)	↓	↓	↓	Reaction [c]	No reaction
Tap water	↓	↓	↓	Reaction	↓
Cenco Hyvac Oil (Central Scientific Co.)	Not tested	Burned	Not tested	Not tested	Not tested
Glyptal (General Electric Co.)	Not tested	Burned	Not tested	Not tested	Not tested
Dow Corning 200 fluid (20 centistokes)	Exploded	Burned	Not tested	Not tested	Not tested
Water glass	Not tested	Burned	Not tested	Not tested	Not tested
Safety Solvent 178 (Fine Organics, Inc.)	↓	↓	↓	↓	↓
Leak-Tec (American Gas & Chemicals, Inc.)	↓	↓	↓	↓	↓
Leak-Tec with glycerine	↓	↓	↓	↓	↓
Dry JP-4 fuel	↓	↓	↓	↓	↓
Carbon tetrachloride	↓	Exploded	↓	↓	↓

Grease					
Kel-F Med. Wax (M. W. Kellogg Co.) Kel-F No. 1 Grease (M. W. Kellogg Co.) Fluorolube LG (Hooker Electrochemical Co.) Fluorolube MG (Hooker Electrochemical Co.)	No reaction [d] [d] [d]	No reaction	Reaction [f] [d] [d] [d]	Reaction [d] [d] [d]	Not tested
Permatex No. 3 (Permatex Co.) Q-Seal (Quigley Co.) Blue Goop (Crawford Fitting Co.) Molylube (Bel-Ray Co., Inc.) Plast-O-Seal (The Colonial Plastics Mfg. Co.)	No reaction No reaction Exploded Exploded Burned	No reaction	Reaction No reaction Not tested Not tested Not tested	Reaction	Not tested
Permatex No. 1 (Permatex Co.) Permatex No. 2 (Permatex Co.) X-Pando seal coating (X-Pando Corp.) Tyte Unyte (J. C. Whitlam Mfg. Co.) White lead	Not tested	Burned	Not tested	Not tested	Not tested
Solid					
Ruby (Al_2O_3) Teflon (E. I. du Pont de Nemours & Co.) Fel-F Solid (M. W. Kellogg Co.) Kel-F Elastomer 5500 (M. W. Kellogg Co.) Graphitar (United States Graphite Co.)	No reaction	No reaction	No reaction No reaction Reaction [f] No reaction No reaction	No reaction No reaction Reaction Reaction Reaction	Not tested

[a] Samples are listed by trade name in most cases; the compositions were not available.
[b] Ref. 4.
[c] Reacted when exposed surface area was increased.
[d] Not tested; Kel-F and Fluorolube materials are all polymers of chlorotrifluoroethylene.
[e] Reacted in two of four tests.
[f] Reacted in one of two tests.

TABLE 3-X.—NONMETALS EXPOSED TO GASEOUS AND LIQUID FLUORINE (REFS. 4 AND 23)—Concluded

Sample [a]	Sample exposed to–				Sample injected into liquid fluorine at 1500 psig pressure
	Liquid fluorine at atmospheric pressure	Gaseous fluorine at atmospheric pressure [b]	Liquid fluorine at 1500 psig pressure	Gaseous fluorine at 1500 psig pressure [b]	
Powdered Graphitar (United States Graphite Co.)	Not tested	Burned	Not tested	Not tested	Not tested
Neoprene-covered Fiberglas	Exploded	No reaction	↓	Reaction	↓
N-43 plus neoprene-covered Fiberglas	Not tested	No reaction		Reaction	
Plexiglas (Rohm & Haas Co.)	No reaction	No reaction	Reaction	Reaction	Not tested
Tygon tubing (U. S. Stoneware Co.)	↓	↓	Reaction	↓	↓
Vinylite (Carbide and Carbon Chemicals Co.)			No reaction		
Pennsalt PCC (Pennsylvania Salt Mfg. Co.)			No reaction		
Pennsalt PCI (Pennsylvania Salt Mfg. Co.)			Reaction [c]		
Flux on silver-soldered copper-to-brass joint			Not tested		
Slag on stainless-steel weld joint	No reaction	No reaction	No reaction	Reaction	Not tested
Flux on silver-soldered stainless-steel joint	No reaction	No reaction	Reaction	Reaction	↓
Dow Corning Elastomer	Not tested	Burned	Not tested	Not tested	
Molykote Type Z Powder (Bel-Ray Co., Inc.)	↓	↓	↓	↓	
Litharge and glycerine					
Palmetto (Greene, Tweed & Co.)					

[a] Samples are listed by trade name in most cases; the compositions were not available.
[b] Ref. 4.
[c] Reacted in one of two tests.

Most of the materials were not sufficiently compatible for use in fluorine systems; however, the tests did demonstrate the typical characteristics of fluorine in showing remarkable inhibition to reaction with many nonmetals under nonflow or static conditions. Recognition of this fact is important in dealing with fluorine. Later investigations under dynamic conditions with some of the more resistant materials (section 3.3.3) substantiate this conclusion.

Consistent results were obtained in both liquid and gaseous tests in indicating that an increase in pressure (0 to 1500 psig) increased reactivity. Under gaseous conditions, all but two of the materials reacted when the pressure was increased to 1500 pounds per square inch gage.

3.3.2 Static Compatibility Tests

Reactivity of elemental fluorine had been defined by earlier work (section 3.3.1), but little information existed on the effects of reactivity to be expected from addition of oxygen to fluorine. To define these effects, a program involving static exposure of nonmetals to both fluorine and FLOX was conducted (ref. 24). The resulting information was the basis for later dynamic studies (section 3.3.3).

In the static liquid FLOX compatibility test program (ref. 24), the sample was placed on the movable sample holder rod (fig. 3–14),

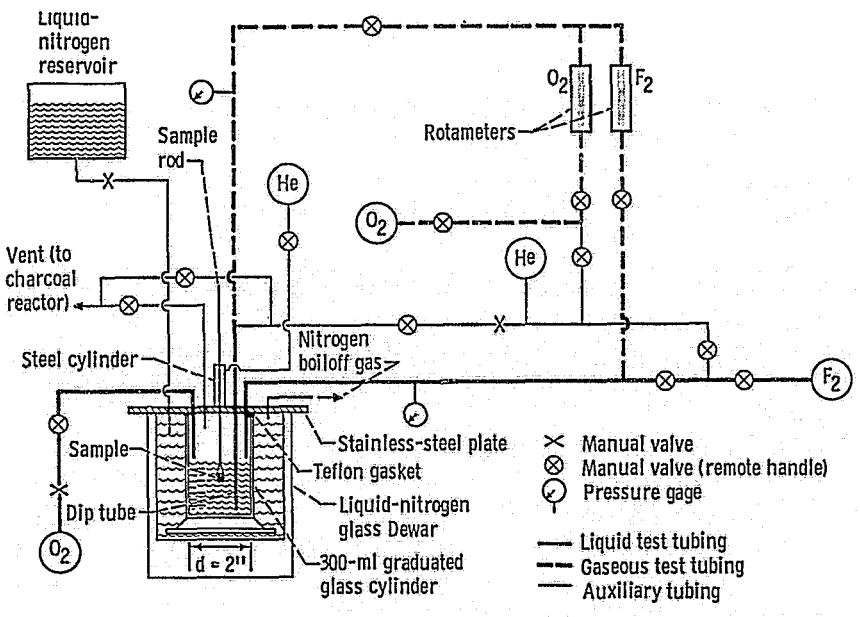

FIGURE 3–14.—Schematic drawing of FLOX system for static tests.

inserted by remote control into the FLOX mixture, and exposed to FLOX for 15 seconds. The sample was then agitated for another 45 seconds. If no reaction occurred, the sample was withdrawn into the helium-inerted tube. More fluorine was added to increase the FLOX concentration and the sample reimmersed. If the sample survived the maximum FLOX concentration used (80 to 85 percent), it was then immersed and agitated in pure liquid fluorine for 5 minutes. If the sample survived, it was removed, inspected, and reweighed.

In the gaseous tests, the sample was held stationary on the sample holder (fig. 3–14). Gaseous FLOX, at controlled concentration and pressure (2 psig or less), was slowly passed through the test chamber for 3 minutes at each concentration. The concentration was increased by increasing the rate of fluorine flow relative to the oxygen flow.

Results for all the materials tested statically in gaseous and liquid FLOX are given in the form of a bar graph in figure 3–15 (ref. 24). Identification and structures of materials tested are given in table 3-XI. In the figure, the gap between nonreaction and the reaction symbols is explained by the fact that concentration was increased incrementally, and this gap represents an unknown region of reactivity. Examination of the results indicates that reactivity with FLOX is a function of fluorine concentration. It must be emphasized, however, that these results were obtained under carefully controlled conditions. The reaction point in the figure represents the *maximum* concentration these materials may withstand under ideal static conditions. In practice, a wide margin of safety should be used to allow for variation of quality control in production of the material.

In the liquid testing, when a reaction occurred it was either an explosive reaction or a relatively slow-burning surface reaction. The nature of the reaction seems related to the degree of porosity of the material and its ability to absorb fluorine. When a reaction occurred between a porous material and fluorine or FLOX, it was usually quite violent. Therefore, in the physical makeup of the nonmetallic materials porosity appears to have an important effect on the type of reaction. The reactions that occurred after longer time delays seem dependent on a surface initiation with a highly variable and unpredictable induction period. The explosive reactions observed were similar to those observed between fluorine and water or crystalline carbon (refer to section 3.1.2).

The gaseous static FLOX tests were run at atmospheric temperature and pressure conditions. Since a temperature difference of about 350 F° existed between liquid and gaseous FLOX, it was initially expected that, with gaseous FLOX at the higher temperature, the fluorine concentration required for reaction would be less than that required for the liquid exposure. Normally, an increase in temperature increases the possibility of ignition as well as the reaction rate; however, as figure 3–15 shows,

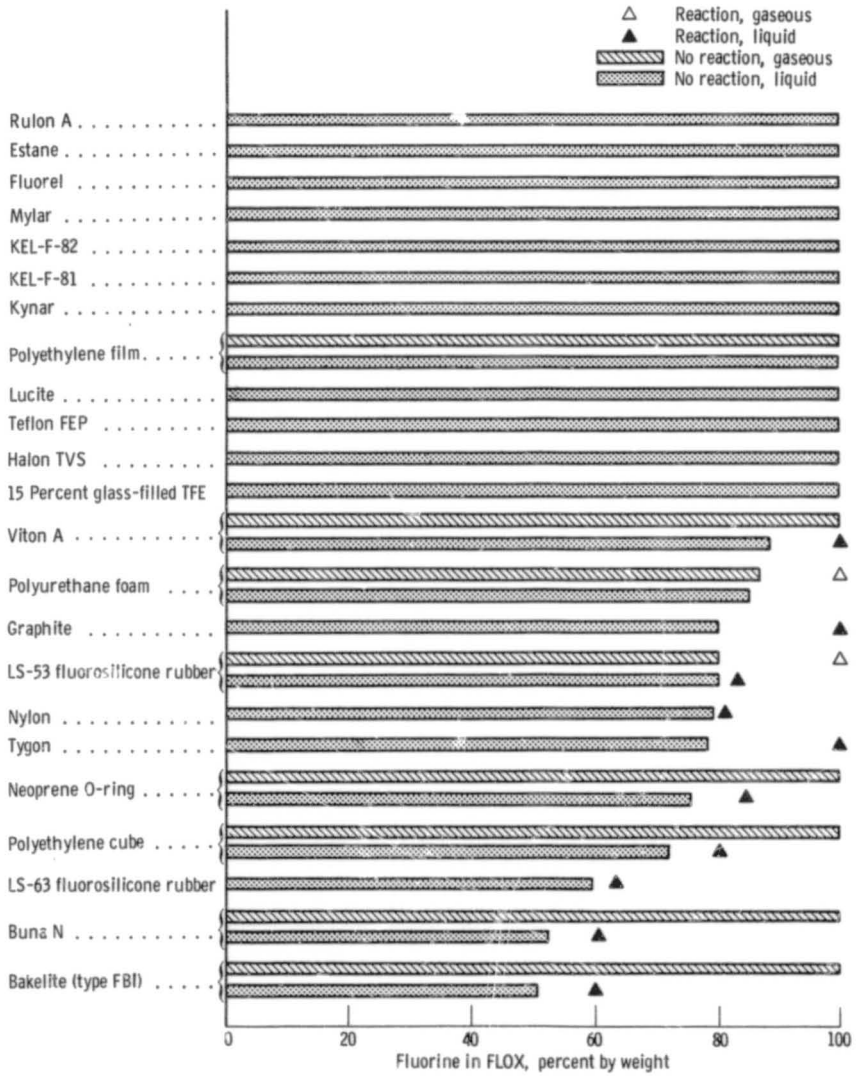

FIGURE 3–15.—Static compatibility test results for solid nonmetals in FLOX. Liquid FLOX temperature, —320° F; gaseous FLOX temperature, 20° to 40° F; pressure, atmospheric (ref. 24). (These results should not be used as a guide in selecting materials to withstand dynamic conditions or pressures greater than atmospheric.)

reactions occurred more readily in liquid than in gas for particular concentrations. Since the only parameter changed here was temperature, the greater reactivity appears to be caused by the higher molecular density (fluorine molecules per unit volume) of the liquid; that is, the

TABLE 3-XI.—TEST MATERIALS IDENTIFICATION (REF. 24)

Trade name	Chemical name or description	Molecular structure
Teflon TFE	Polytetrafluoroethylene	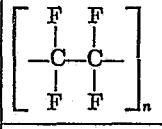
Halon TFE, G-80	Polytetrafluoroethylene	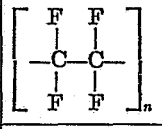
Rulon A	Polytetrafluoroethylene with MoS_2 filler	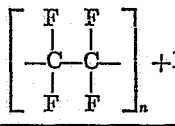 $+MoS_2$
Nickel-filled Teflon	Polytetrafluoroethylene with nickel-powder filler	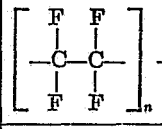 +Ni
15-Percent glass-filled Teflon	Polytetrafluoroethylene with glass fibers	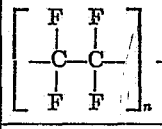 +Glass
Kel-F 81	Polychlorotrifluoroethylene (CTFE)	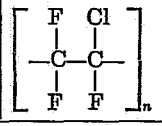

Plaskon 2400	Polychlorotrifluoroethylene (CTFE)	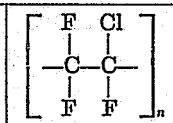
Halon TVS (now called Plaskon 2200)	Polychlorotrifluoroethylene (CTFE)	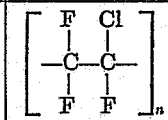
Teflon FEP	Fluorinated ethylene propylene	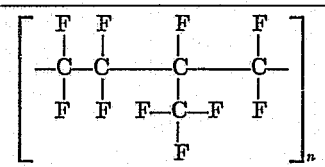
Kynar	Vinylidene fluoride	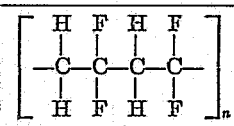
Kel-F 82	Copolymer of CTFE and 3 mole percent vinylidene fluoride	----------
Mylar	Polyethylene terephthalate	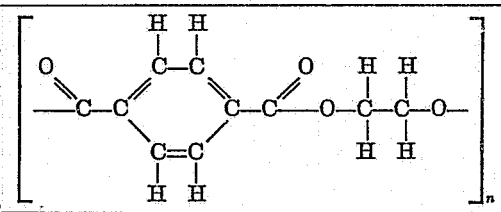

TABLE 3-XI.—TEST MATERIALS INDENTIFICATION (REF. 24)—Continued

Trade name	Chemical name or description	Molecular structure
Lucite	Polymethyl methacrylate	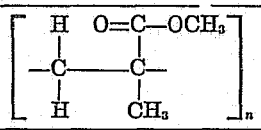
Tygon	Polyvinyl chloride-acetate	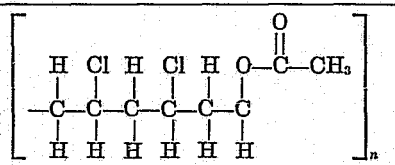
Nylon	Polyamide	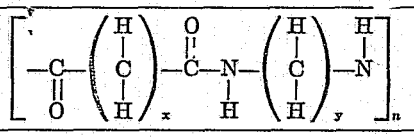
Bakelite	Phenol formaldehyde	Not available
Polyethylene	Polyethylene	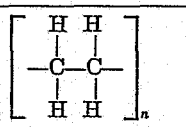
Neoprene	Polychloroprene	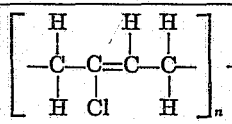 +Carbon black (a)

Buna N	Copolymer of acrylonitrile and butadiene	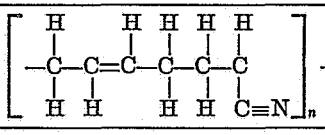 +Carbon black	(a)
LS-63 Rubber	Trifluoropropyl methyl polysiloxane	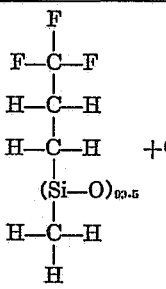 +Curing agents	(a)
LS-53 Rubber	Trifluoropropyl methyl polysiloxane		
Viton A	Copolymer of vinylidene fluoride and hexafluoropropylene	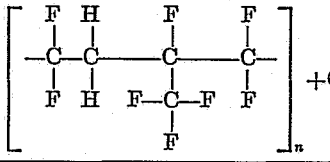 +Carbon black	(a)
Fluorel	Copolymer of vinylidene fluoride and hexafluoropropylene	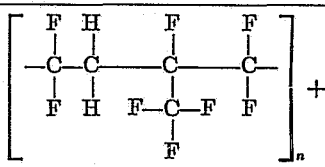 +Carbon black	(a)

* Simplified structure in uncured state.

TABLE 3-XI.—TEST MATERIALS IDENTIFICATION (REF. 24)—Concluded

Trade name	Chemical name or description	Molecular structure
Polyurethane foam	Polyurethane	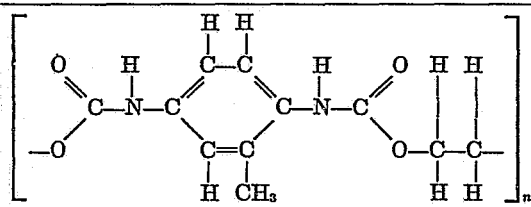 +Curing agents (a)
Estane	Polyurethane rubber	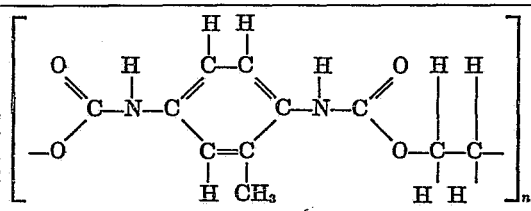 +Carbon black (a)

Graphite	Crystalline carbon	
CPE 401 (BR 93) with EPON 828	Amorphous chlorinated polyethylene	Unknown
CPE 402 (TDX 176) with tribase E	Amorphous chlorinated polyethylene	Unknown
CPE 403 with EPON 828	Semicrystalline chlorinated polyethylene	Unknown

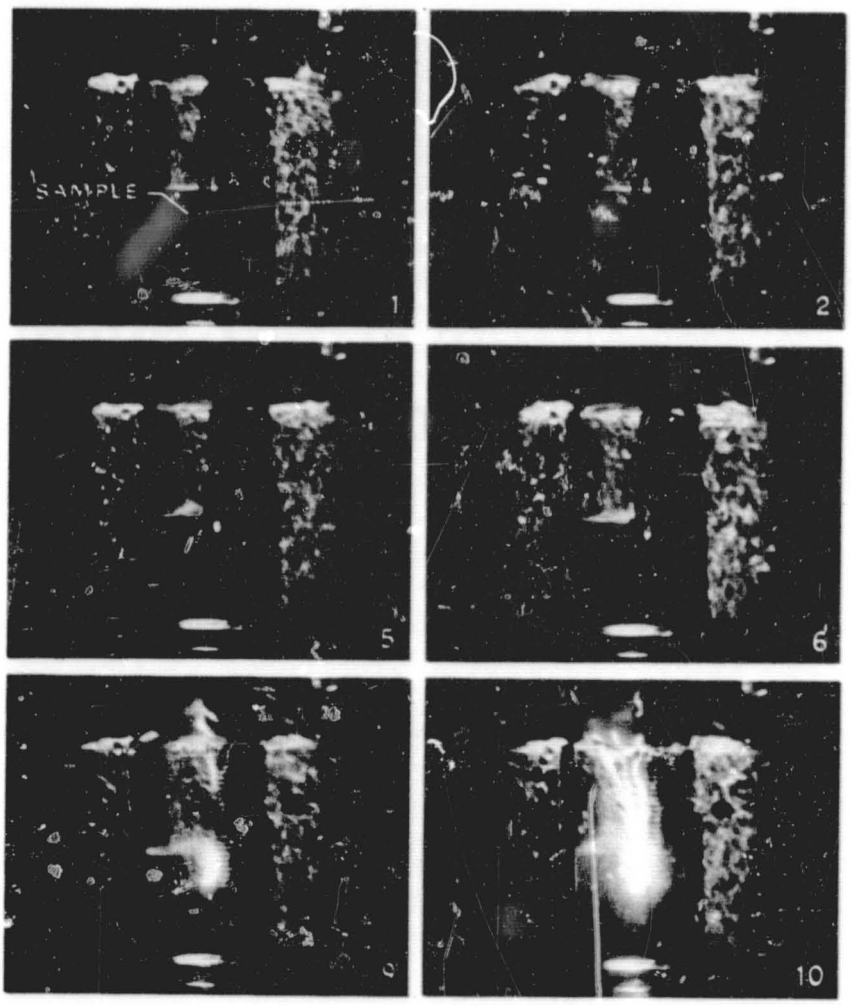

FIGURE 3–16.—Typical slow-burning surface reaction of neoprene

effect of the greater availability of fluorine atoms to participate in the reaction in the liquid case seems to exceed the effect on reactivity normally obtained from an increase in temperature. This explanation was also supported by the results of the high-pressure tests (section 3.3.1). In that series of tests, the increase in the molecular density of the gas at 1500 pounds per square inch gage, as well as the temperature effect, caused a higher reactivity than in the liquid case. Therefore, the higher enthalpy of the room-temperature gaseous system at atmospheric pres-

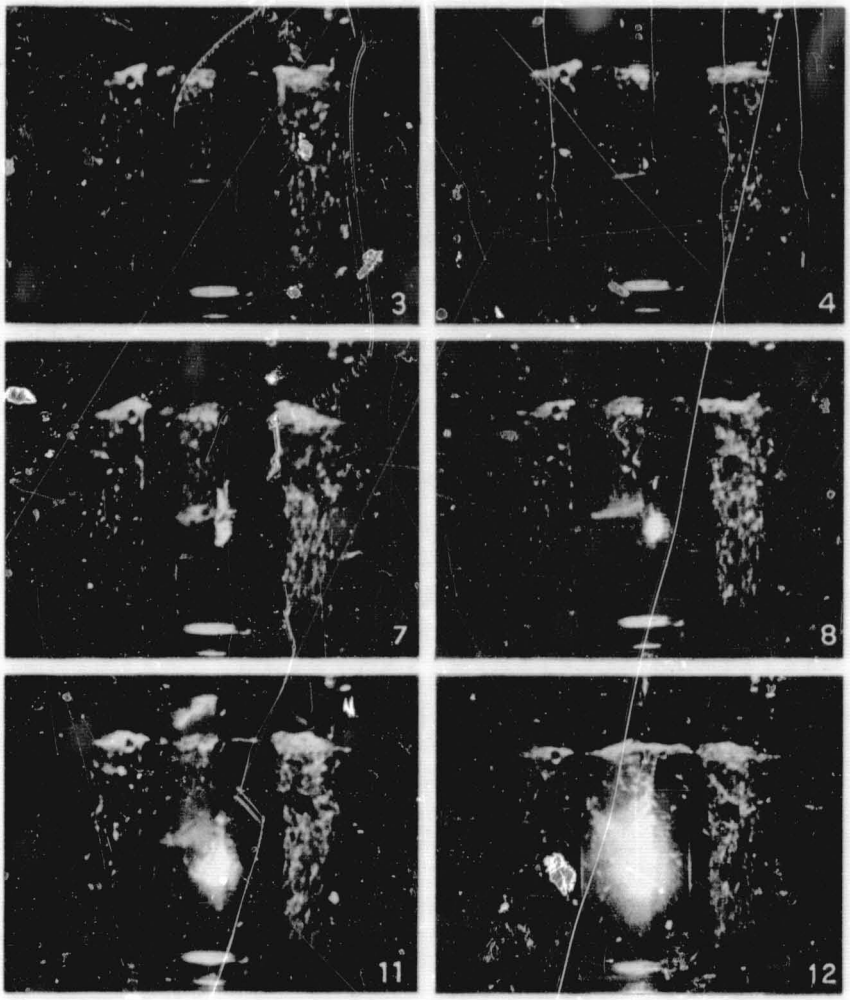

O-ring in 83.5 percent FLOX. Film speed, 24 frames per second.

sure was not in itself sufficient to cause higher reactivity of the gas, but by increasing the pressure to 1500 pounds per square inch gage with resulting increase in molecular density, the reactivity exceeded that of the liquid. This reactivity factor is further discussed in section 3.3.3.5.

A typical slow-burning surface-reaction sequence (fig. 3–16) shows a neoprene O-ring being tested in 83.5-percent liquid FLOX (83.5 percent fluorine by weight in a fluorine-oxygen mixture). The reaction, once initiated, seemed to propagate itself over an increasingly large area;

burning was smooth and quiet. The sequence shown occurred in 1/2 second.

Samples that exhibited reaction delay in the gaseous tests were observed to smolder before igniting. In other words, the material reacted slowly until its combustion temperature was reached, at which time it ignited.

3.3.3 Dynamic Tests

A dynamic test program (ref. 24) was carried out to define velocity effects on reactivity of selected nonmetals with various FLOX concentrations, since experience with fluorine system failures showed that most

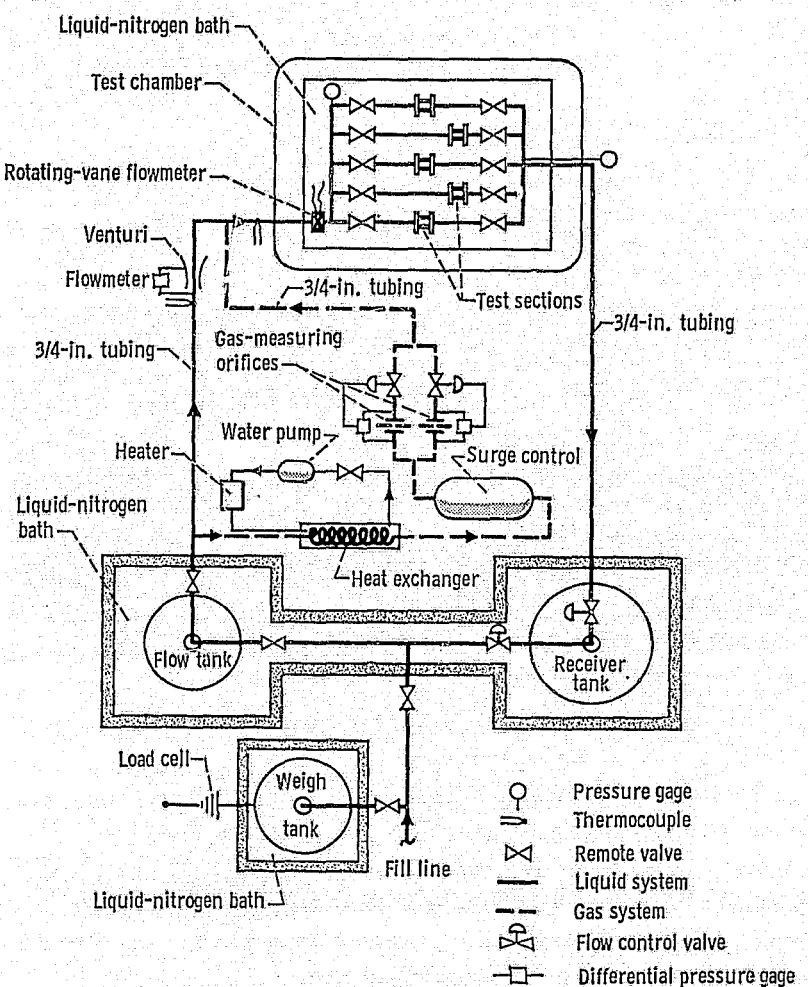

FIGURE 3-17.—Schematic drawing of FLOX system for dynamic tests (ref. 24).

ignitions occurred with combinations of high pressures and high velocity. Test data from this program revealed that reactivity varies as a function of increasing flow velocity and increasing FLOX concentration in a predictable manner. Generally, the fluorocarbon polymers, particularly the fully fluorinated straight-chain polymers, were most compatible with fluorine and FLOX (ref. 24). The test program was essentially divided into three phases: (1) an initial study to determine the effects of pressure at flow velocity, (2) a series of liquid-phase FLOX tests to define the effects of flow velocity and concentration on the reactivity of FLOX with selected nonmetals, and (3) a series of gaseous-phase tests to define the effects of flow velocity, FLOX concentration, and ambient temperature on the reactivity of FLOX with selected nonmetals.

The test apparatus used for the dynamic tests is shown schematically in figure 3–17. The specimen materials were fabricated into tubular orifices (see fig. 3–18) and installed in the test legs of the apparatus.

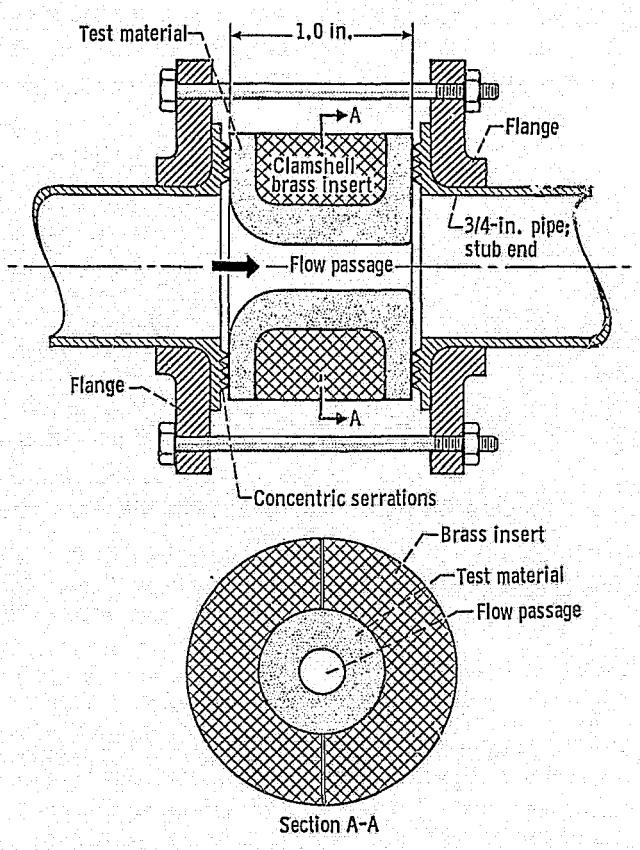

FIGURE 3–18.—Dynamic FLOX test-specimen holder (ref. 24). (Not drawn to scale.)

Flow through the specimen was achieved by pressurizing the flow tank with helium gas to the required pressure to obtain maximum flow, while maintaining only slightly more than atmospheric pressure in the receiver tank. The flow rate was then controlled by operation of a flow-control valve located downstream from the specimen. Flow quantities were measured by the turbine flowmeter and venturi meter.

The testing procedure for this program involved increasing velocity in increments (for each FLOX concentration); smaller increments were chosen as the suspected reaction point was approached. Successive runs were made through each specimen (at increasingly higher pressures in the flow tank to provide higher maximum velocities) until reaction occurred.

The first phase of testing involved varying pressures up to 400 pounds per square inch gage at a flow velocity of 12.2 feet per second. Since no reactions occurred for the materials tested, it was concluded that the effects of pressure on reactivity (from the pressurization required to achieve flow) would be negligible when compared with the effect from velocity. Since a pressure effect is present in any confined flow situation, the velocity effects on reactivity should be valid for an equivalent condition in an operational system.

The main conclusions drawn from the dynamic tests (ref. 24) are as follows:

(1) Some nonmetallic materials may be considered for use in rocket systems with fluorine or FLOX under controlled conditions of exposure; however, because of possible variations in quality and because nonmetals are more sensitive to contamination than metals in a fluorine environment, a margin of safety should be provided based on the acceptable level or risk for the particular application. Where flight reliability is required, qualification testing must be performed.

(2) Generally, the highly fluorinated and highly chlorinated materials are more suitable for use in fluorine or FLOX systems than materials containing atoms such as hydrogen in their molecular structures or materials impregnated with some noncompatible additive. Of all materials tested, the polytetrafluoroethylenes, Halon TFE and Teflon TFE, are the most promising for practical application in fluorine or fluorine-oxygen environments.

(3) The strong significance of flow velocity on reactivity of nonmetallic materials with fluorine or FLOX indicates that some of these materials are suitable for use as static seals if it is assumed that no contamination is present. Exposure to direct flow (particularly in the liquid phase) should be avoided except under conditions where the risk is acceptable.

(4) The orderly molecular arrangement of the more crystalline

materials makes them less susceptible to fluorine attack than the amorphous materials with their irregular molecular alinement. A material selected for use should therefore be of the highest crystalline form available for the particular material.

(5) The reactivity of nonmetallic materials with fluorine and FLOX increases as a function of molecular density (number of molecules per unit volume) present at the point of reaction initiation.

3.3.3.1 *Reactivity profiles from liquid tests.*—From data obtained in the dynamic tests, reactivity profiles (flow velocity at burnout as a function of FLOX concentration at burnout) were generated for selected materials (ref. 24). Since a material must be tested to burnout at several concentrations in order to generate a reactivity profile, only the materials of greatest interest were chosen. A composite of these reactivity profiles is shown in figure 3–19. (Fig. 3–20 shows those materials for which only a single test was made.)

It should be emphasized that the data were obtained under carefully controlled conditions. The reaction line in the figure represents the *maximum* concentration and/or velocity these materials may withstand under ideal conditions. In practice, a wide margin of safety should be used. Differences in reactivity with fluorine are possible with supposedly identical materials because of variations in fabrication processes, which may produce voids, impurities, or other differences in the material. Therefore, materials selected for use in a fluorine or FLOX environment

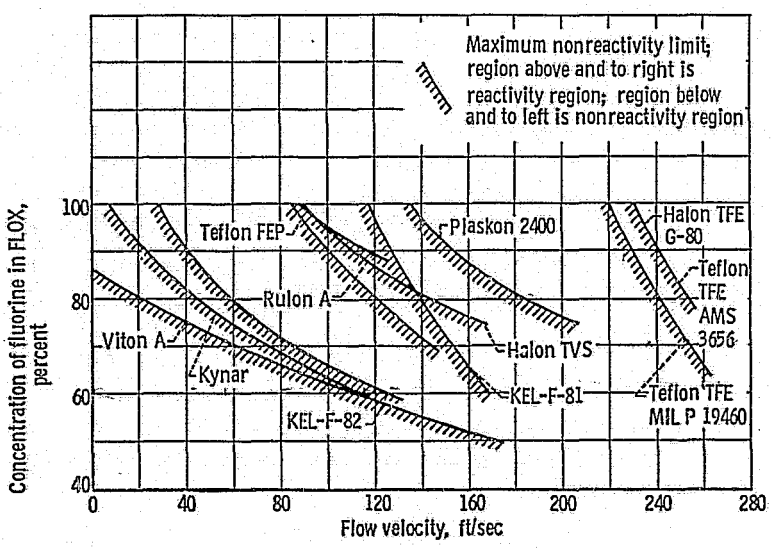

FIGURE 3–19.—Composite liquid FLOX reactivity profiles.

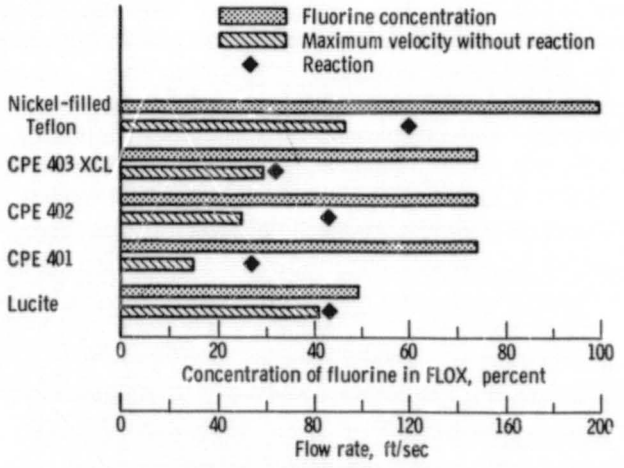

FIGURE 3–20.—Dynamic liquid FLOX compatibility tests (single data points, ref. 24). Pressure range, 100 to 400 pounds per square inch gage; temperature, —320°F; specimen configuration, 0.25-inch orifices.

should be of the highest possible quality. It should be remembered that the activation energy required to initiate reaction with these nonmetallic materials is not appreciably greater than the energy level that exists under some normal exposure conditions. This is particularly true when these materials are exposed to the flow of liquid fluorine or FLOX. Therefore, when exposure includes a high flow rate of liquid fluorine (or FLOX of high concentration) only a relatively small increase in flow rate, or the presence of a minor amount of contamination, could result in reaction initiation. Because of the lack of statistical test information, no fixed factor of safety can be given; the margin to be used should depend on the acceptable level of risk for the particular application. In all applications of nonmetallic materials, the severity of environmental conditions should be minimized by avoiding direct exposure to flow if possible. The most FLOX-compatible materials that fulfill physical requirements should be chosen when nonmetals must be used.

3.3.3.2 *Typical reaction.*—A specimen of Lucite was tested to failure under dynamic conditions (ref. 24) because it is transparent and the reaction initiation and propagation can be photographed easily. Reaction of this material occurred at a flow velocity of 84 feet per second and is shown in figure 3–21. (Distortion was caused by photographing through liquid nitrogen.) In this close-up view, the first frame shows FLOX passing through the specimen. The second frame shows reaction initiation (about 1/24 sec later). A projection review of the original film showed that this reaction was initiated at the inlet near the end of

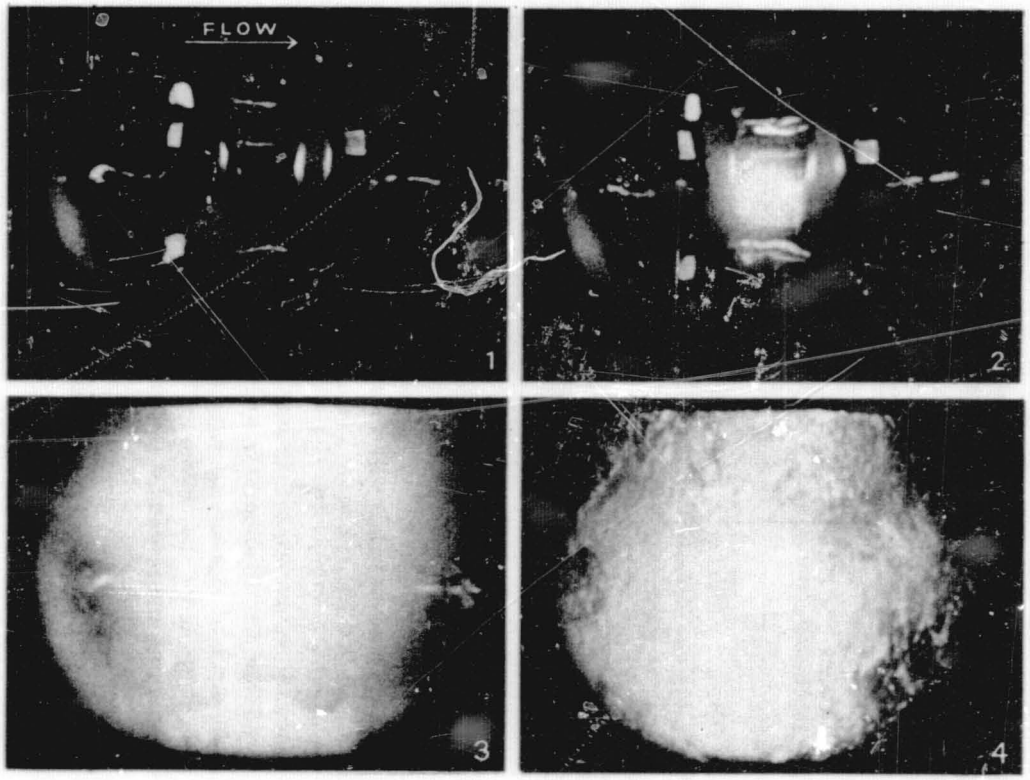

FIGURE 3-21.—Dynamic FLOX compatibility test of Lucite specimen. Film speed, 24 frames per second; time interval between frames, 1 and 2, and 3 and 4, 9 seconds (ref. 24).

the throat curvature (see fig. 3–21) of the test specimen (not visible in the figure since contrast was lost in making the print). Reaction was then propagated over the entire surface of the channel in the specimen. The remaining frames in figure 3–21 show the reaction at increasing stages in its progression.

3.3.3.3 *Gaseous dynamic testing.*—High-velocity flow tests were performed with pure gaseous fluorine to explore the effect of velocity on reactivity (ref. 24). Table 3-XII shows nine materials that were fabri-

TABLE 3-XII.—GASEOUS FLUORINE COMPATIBILITY TESTS (REF. 24)

Material (1/4-in. tubular orifices)	Duration of sonic velocity of 900 ft/sec, sec	Average velocity for 30-sec period, ft/sec
Halon TFE	10	825
Teflon TFE	[a]Unknown	[a]Unknown
Rulon A	11	750
Kel-F-81	4	825
Teflon FEP	5	750
Halon TVS	8	700
Kel-F-81 amorphous	9	850
Kel-F-82	16	880
Kynar	2	825

[a] Instrument malfunction.

cated into 1/4-inch orifices and exposed to 30-second test runs at increasing velocities. These materials withstood maximum conditions of gaseous fluorine flow of 900 feet per second (sonic flow) for several seconds and average velocities of 700 to 880 feet per second for the test run. Table 3-XIII shows three materials that were fabricated into 1/8-inch orifices and exposed from 5 to 30 minutes to sonic flow rates. While all the materials tested survived exposure to sonic flow rates, only the TFE (table 3-XIII) held up under the maximum 30-minute time obtainable with the test apparatus and procedure (see section 3.3.3.5).

TABLE 3-XIII.—GASEOUS FLUORINE TIME-EXPOSURE TESTS (REF. 24)

Material (1/8-in. tubular orifice)	Velocity without reaction, ft/sec	Time, min	Velocity that caused reaction, ft/sec	Time, min
TFE	900 (sonic)	30	No reaction	30
Kel-F-81 amorphous	372	30	900 (sonic)	5
Kel-F-82	279	30	900 (sonic)	15

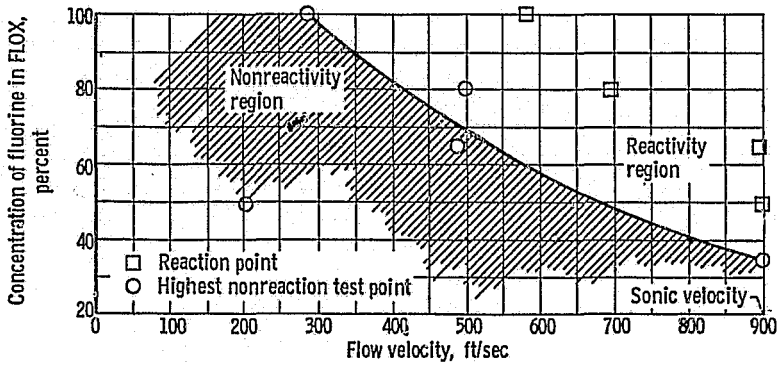

FIGURE 3-22.—Gaseous FLOX reactivity profile for Viton A (ref. 24). Temperature, 60° F; sample configuration, 0.20-inch orifice.

A reactivity profile for Viton A is shown in figure 3-22 (the only material for which the required test runs were made). The explanations of the curve and precautions given for application of the liquid reactivity profiles also apply for this figure. From these limited data, it appears possible that a step occurs in the reactivity profile for Viton A at sonic velocity, although the curve does not indicate this. Reactions for this material usually occurred at sonic velocity, before the backpressure buildup reduced the velocity. Only at the 34-percent-FLOX concentration was sonic flow maintained (for 9 sec) without reaction; after this time, the velocity decreased to an average of 700 feet per second for 60 seconds.

3.3.3.4 *Crystallinity effects on reactivity.*—Tests of chlorotrifluoroethylenes in crystalline and amorphous forms revealed that the crystalline form was more resistant to reaction than the amorphous form (ref. 24). This led to an attempt to control crystallinity in materials.

X-ray diffraction photographs were taken in the Lewis diffraction laboratory in an attempt to measure the crystallinity of Kel-F and other materials. These studies provided a means for making comparisons of crystallinity among different materials. Figure 3-23 shows X-ray diffraction photographs of five different materials. The relative degree of crystallinity is estimated from the relative sharpness of the diffraction rings. Teflon TFE appears to be more crystalline than Teflon FEP. The difference in crystallinity is similarly apparent between crystalline and amorphous Kel-F-81. The figure also shows that heat-treated Kel-F-81 amorphous has a degree of crystallinity similar to crystalline Kel-F-81. These photographs demonstrate that the heat-treating process transforms the amorphous material to a more crystalline state. Also, this crystalline form is more resistant to reaction than the amorphous form from which it was created.

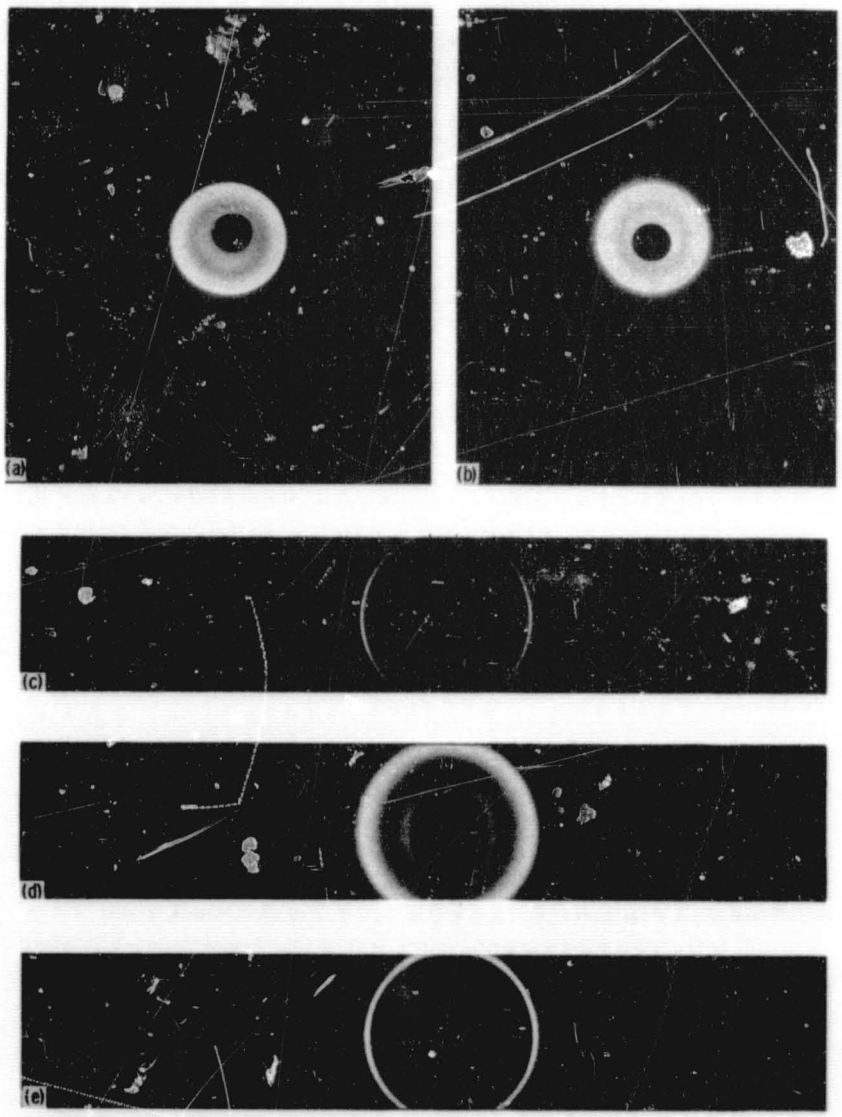

(a) Teflon TFE. (b) Teflon FEP.

(c) Crystalline Kel-F-81.

(d) Kel-F-81 amorphous.

(e) Kel-F-81 amorphous (heat treated).

FIGURE 3-23.—X-ray diffraction patterns (ref. 24).

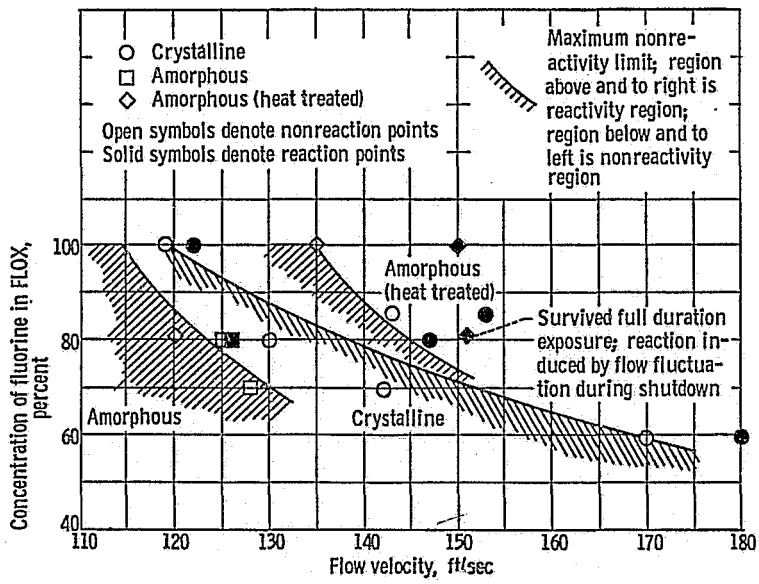

FIGURE 3-24.—Liquid FLOX compatibility profiles for crystallinity effects for Kel-F-81 (ref. 24).

Different degrees of crystallinity are obtained by varying the cooling rate during the molding process, where faster cooling rates produce more amorphous materials. Since test data show that Kel-F-81 amorphous reacted under less severe conditions than crystalline Kel-F-81, an attempt was made to transform Kel-F-81 from the amorphous to the crystalline form by heating two amorphous specimens to a temperature just below the melting point and allowing them to cool slowly (33 F°/hr). Theoretically, this treatment should transform the material from amorphous to crystalline. These specimens were tested in the same manner as the other Kel-F-81 specimens and gave a reactivity profile that falls in the same general position as that of the crystalline Kel-F-81 (fig. 3-24). On the basis of the limited number of data points taken, the heat-treating process increased the resistance of the material to FLOX (which indicates that the orderly arrangement of the molecules in the crystalline form makes the material less susceptible to fluorine attack than in the amorphous form with its irregular molecular alinement). When one of the fluorocarbons is being selected for use in fluorine systems, the most crystalline form available should be used.

3.3.3.5 *Other factors affecting reactivity.*—Some factors other than velocity and FLOX concentrations were also observed as affecting reactivity (ref. 24):

(1) Exposure time: In order to attain sustained high velocities to gain information on the effect of exposure time, it was necessary to reduce the specimen orifice diameter from 1/4 to 1/8 inch to provide longer run times. Three specimens were tested (table 3-XIII), and sustained velocities up to a maximum of sonic were attained in each case. TFE successfully withstood pure gaseous fluorine flow at sonic velocity of 900 feet per second for 30 minutes; Kel-F-81 amorphous ignited after 5 minutes at 900 feet per second. All three specimens had just previously been exposed to lower flow velocities (see table 3-XII) for 30 minutes without reacting.

A Viton A specimen was exposed to gaseous 50-percent-FLOX flow at 200 feet per second for 30 minutes. There was no reaction at this velocity during the extended time run. In order to obtain an additional data point for this material, the specimen was then subjected to sonic velocity of 900 feet per second. The specimen reacted almost immediately.

The effect of exposure time on reactivity of liquid FLOX was not specifically examined; however, many short-duration test runs were consistently made on the same test specimen with no effect until the reaction conditions for the material (concentration and velocity) were reached. The reaction points seemed to be independent of the total exposure time leading up to the reaction conditions. Additionally, past Lewis experience has shown that TFE can be used successfully in valves for packing and seals for prolonged time periods (several months of intermittent use without effect is not uncommon). Therefore, exposure time in itself is probably not a significant factor in reactivity of either gaseous or liquid fluorine or FLOX. It may have some effect at marginal FLOX concentrations and flow velocities; however, some very long run times, hours rather than minutes, would be needed to verify this possibility.

(2) Phase effects: Normally, at a higher temperature, a material is closer to its enthalpy of activation. However, reviews of both static and dynamic test results revealed that both FLOX and fluorine were much more reactive as cryogenic liquids than as ambient gases. According to reference 24, the higher molecular density in the liquid phase had more of an effect on reaction initiation than did the higher temperature of the gaseous phase. The decreased reactivity due to the diluent effect of oxygen in a FLOX mixture also seems to substantiate the premise that reactivity is partly a function of the molecular density of fluorine at a potential reaction zone.

The effect observed during static tests is discussed in section 3.3.3. The greater reactivity of the cryogenic liquid was also noticed in the dynamic tests. A comparison between the liquid and the gaseous reactivity profiles for Viton A (figs. 3–19 and 3–22) shows that much higher velocities were required to obtain reactions with gaseous FLOX than

with liquid FLOX at similar concentrations. This fact, together with the fact that many other materials which did not react with gaseous fluorine at sonic velocity did react with liquid FLOX at much lower velocities, is evidence that the cryogenic liquid is more reactive than ambient temperature gas at pressures up to 400 pounds per square inch gage. The effect of higher molecular density for the liquid seems to exceed the effect on reactivity that is normally characteristic of increases in temperature and enthalpy.

(3) Contamination: The importance of cleanliness in a fluorine system is generally well recognized. All fluorine or FLOX systems should be free from moisture, dirt, oil, grease, and other such contaminants. Reactions of fluorine or FLOX with significant accumulations of foreign materials can trigger a reaction with the system, and particularly with any nonmetallic components. (Cleaning procedures for fluorine systems are included in chapter 6. The cleaning procedure used for the nonmetallic samples tested in this program is included in section 6.2.1.)

3.3.3.6 *Reaction rates.*—With explosive reactions, it was observed that a large portion of the test specimen usually remained after reaction (with either the liquid or the gas). Graphite, which is a very porous material, reacted explosively with 100-percent liquid fluorine after a 1½-minute delay. After the test, 85 percent of the sample remained intact. Reaction characteristics of crystalline and amorphous carbon are not alike. Amorphous carbon is hypergolic with fluorine even at very low concentrations and will burn smoothly even with liquid fluorine or FLOX, while crystalline carbon shows a strong initial inhibition to reaction with fluorine, but reacts explosively when reaction occurs. If reaction is initiated, however, it is self-sustaining and produces the same reaction products as amorphous carbon (mainly carbon tetrafluoride gas, refer to section 3.1.2.2).

Rulon A, which is polytetrafluoroethylene (TFE) impregnated with a molybdenum disulfide filler (for better wear characteristics), reacted explosively, whereas the nonimpregnated polytetrafluoroethylene burned smoothly. Fluorine should have the tendency to react with molybdenum disulfide (see Molylube in table 3-X), and therefore the presence of the filler affected not only the material reaction point but also its rate of reaction. Kynar, which is an unimpregnated resin, also reacted explosively. As shown in table 3-XII, however, this material contains many hydrogen atoms in the side links of its molecular structure. There was a general tendency for materials with high hydrogen content to react explosively. As in the case of graphite, the materials may absorb FLOX interstitially to a certain depth, and the ensuing reaction may involve only the portion of the material that has absorbed FLOX. The explosive reaction then separates the reacted material from the unreacted material

and prevents further reaction. In slower burning reactions, ignition began at the surface of the material, progressed over an increasingly large area, and burned inward until the source of reactant was depleted.

3.3.3.7 *FEP-TFE discrimination.*—During compatibility tests for polymeric materials (ref. 24), polytetrafluoroethylene (TFE) proved to be preferable to FEP (fluorinated ethylene propylene) for use in fluorine or FLOX systems (fig. 3–19). However, a reliable method was required to discriminate between the two basic types, since a particular stock item (with the same physical appearance) could be formed from either material. To define some simple tests to differentiate between these two materials, studies were conducted at Lewis with the following results:

(1) TFE characteristics: At ambient temperatures, polytetrafluoroethylene (TFE) resin tends to be crystalline and very opaque. If no pigments have been added, it is normally a milky-white color that can vary to light gray or light brown. Unless some type of cold-forming process is used, the material will not adhere to itself below 620° F; above this temperature it becomes amorphous and sublimes. The molecular structure for this material is

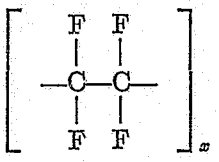

(2) FEP characteristics: Fluorinated ethylene propylene (FEP) tends to be more translucent (than TFE) at ambient conditions. It does not sublime like TFE, but becomes a very viscous fluid above a 500° to 530° F range. In addition, the material adheres to itself above this melting point range. The structure of the material is

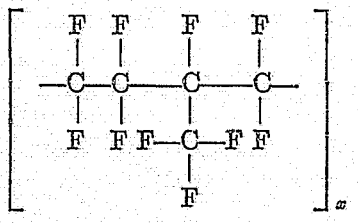

(3) Sample differentiation tests: To determine whether the material to be used is TFE or FEP, the following general tests were used and can be applied in the field:

(a) Melting point test: The sample is heated to between 530° and 600° F. The Lewis tests indicated that the sample will melt if it is FEP, while if it is TFE, corners will remain sharp and no signs of slumping will be apparent.

(b) Adherence test: When samples are stacked on top of each other and heated to 600° F, the FEP samples will fuse together, while TFE samples will show no signs of cohesion.

(c) Deformation test: A weight (15 g) is suspended from the sample by a wire looped over the sample. The sample is then furnace heated to 550° F to check deformation from an applied load. After 10 minutes at 554° F, the TFE should show no signs of elongation, while the FEP sample should be completely cut through by the weight.

3.3.4 Investigation of Soft-Seal Material Applications

In the course of developing a zero-leak shutoff valve design concept (section 4.4.1), tests were run on six soft-seal materials in 100-percent-fluorine environments (ref. 5). The tests employed a minimum-exposure technique, in which the specimen was surrounded to a maximum degree with metal to increase local thermal conductivity (see section 3.1.1.3). It was expected that reaction of the fluorine with seal materials would thus be minimized. That this occurs is borne out by the test results with nitroso rubber, which could normally be expected to burn when exposed to the flow of liquid fluorine.

The materials tested included

(1) Nitroso rubber
(2) High-percentage glass-filled tetrafluoroethylene (Fluorogreen E-600 and Fluorobrown)
(3) High-percentage metal-filled tetrafluoroethylene
    (a) Nickel filled
    (b) Copper filled
    (c) Bronze filled

In the design of the test-valve seal retainer, the soft-seal material was protected by minimizing its exposed surface area (refer to section 4.4.1). This, together with the heat-dissipating characteristic of the surrounding metal, tended to inhibit a combustion reaction (refer to section 3.1.1.3).

Test results showed surface decomposition in the nitroso rubber sample over its shielded area as well as over its exposed annulus. A layer of porous, gumlike parent material covered the entire specimen after an exposure of 61 seconds. After 178 seconds of exposure, the annulus of the glass-filled polytetrafluoroethylene (Fluorobrown) was pitted because of noncombustive reaction with the fluorine. Approximately one-sixth of the specimen was lost in this manner. The Fluorogreen E-600 showed no evidence of deterioration after 63 seconds of exposure.

Under visual examination after exposure, neither chemical change nor

fiber migration due to erosion was observed in the metal-filled polytetrafluoroethylene sample. A comparison of the weights of the samples before and after testing quantitatively confirmed the observation. Thus, no conclusion could be made regarding any inhibiting effect on chemical reaction from addition of metal fillers to polytetrafluoroethylene.

The major value of these tests was in demonstrating

(1) That fluorine compatibility of a material can be enhanced by protecting it from the flow stream and by minimizing surface exposure
(2) That high thermal conductivity reduces the tendency to combustive reactions

3.4 FLOX SPILL TESTS ON COMMON MATERIALS

The use of fluorine or FLOX as an oxidizer at rocket installations requires data on reaction characteristics to be expected if fluorine or FLOX is spilled on some common materials (sand, slag, etc.). To gain information on hypergolicity, cloud formation, and other reaction characteristics with some of these materials, tests were conducted at Plum Brook in 1964 (ref. 25), by spilling 5- to 10-pound quantities of fluorine, FLOX, and liquid oxygen onto test specimens of representative materials that might be used in rocket installations.

The test apparatus, shown in figure 3–25, consisted of a $3\frac{1}{2}$-gallon liquid-nitrogen-jacketed stainless-steel tank with appropriate fill and vent lines, a remotely controlled spill valve, and a spill pipe. The valve was insulated with asbestos padding, and the spill pipe was cooled by a liquid-nitrogen coil and purged with helium. Spills were made on samples contained in 12-inch-deep 3-foot-square stainless-steel pans.

The results of the tests (ref. 25) are included in tables 3-XIV and 3-XV. Spills listed are those made with 100-percent fluorine and 30-percent FLOX (30-percent fluorine by weight in liquid oxygen). Spills were also made with liquid oxygen to gain comparative data and these are included in table 3–XVI.

In the spills involving use of 30-percent FLOX, 10-pound quantities were spilled on various materials. It was observed that when no reaction occurred, the toxic vapors merely drifted downwind close to the ground. In other cases, with spills on asphalt, for example, there was a small reaction with little heat release. In such cases, the reaction cloud rose at very low angles. In some reactions, for example, 30-percent FLOX with JP-4 fuel, several rapid microexplosions occurred over a period of 1 to 2 seconds. A yellow fireball formed and expanded to a diameter of 25 to 30 feet (fig. 3–26), and a turbulent black cloud emerged

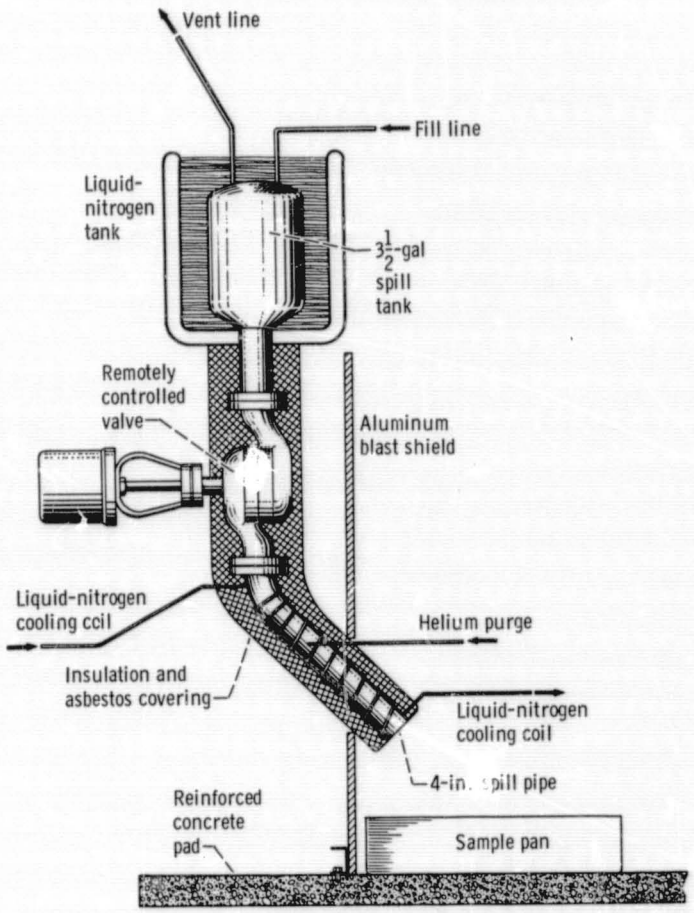

FIGURE 3-25.—Apparatus used for FLOX spill tests (ref. 25).

from the fireball. A marked "stack" effect was produced as the cloud rose rapidly and almost vertically. An atmospheric fire on the JP-4 fuel surface continued for more than 1 minute before it was manually extinguished. The loud sputtering effect or multiple explosions were also noticed when FLOX was spilled on JP-4-fuel-soaked sand and oil-soaked sand. Slow-motion close-up motion pictures of the reaction with oil-soaked sand distinctly showed three large reactions and about five smaller ones, all of which occurred within less than 1 second. In an attempt to smooth out the multiple explosion effect of the FLOX–JP-4 fuel reaction, 30-percent FLOX was spilled into a JP-4 fuel stream. As shown in table 3-XIV, the multiple explosions still occurred. A similar test was made with a coarse spray of JP-4 fuel. Multiple

TABLE 3-XIV.—RESULTS OF 30-PERCENT-FLOX SPILL TESTS (REF. 25)
[FLOX spill quantity, 10 lb.]

Test material		Weather conditions		Reaction	Cloud or vapor	Moisture content, percent		Acid content, pH	
Substance	Weight, lb	Wind speed, mph	Temperature gradient from 2.5 to 30 ft			Before	After	Before	After
Concrete slab	480.0	8	—0.8 F°	None	Vapors drifted close to ground	----	----	----	----
Sand	475.0	3	—2.0 F°	None	Vapors drifted close to ground	1.00	1.34	----	----
Rich soil	311.0	8	0	Bright flame	White cloud rose high at about 45° angle	8.81	12.17	----	----
Asphalt (from building)	177.0	8	0	Sputtered, small flames	Gray cloud drifted close to ground	----	----	----	----
Oil-soaked sand	478.0	8	0	Several loud, rapid explosions	Gray cloud rose high at about 45° angle	1.03	1.31	----	----
Charcoal	180.0	8	0	Large, smooth, brilliant fireball	White cloud rose high at about 60° angle and disappeared	5.94	17.95	----	----

Limestone slab -----	332.0	5	—1.0 F°	None ----------	Vapors drifted close to ground	----	----	----	----
Lake water (5 gal)--	41.7	1	—1.0 F°	None ----------	Vapors drifted close to ground	----	----	8.30	2.30
JP-4 fuel-soaked sand	478.4	2	0.5 F°	Loud sputtering, large flames	Dark cloud rose high at about 60° angle	14.23	1.83	----	----
JP-4 fuel (3 gal)---	20.1	2	0	Several loud, rapid explosions; large fireball	Black cloud rose high, almost vertically	----	----	----	----
Asphalt (from road)	258.0	2	1.0 F°	Loud sputtering, small flashes	Gray cloud rose at about 15° angle	0.08	0.37	----	----
Water-soaked sand--	552.0	1	1.0 F°	None ----------	Vapors drifted close to ground	19.28	14.97	8.40	7.60
Lake-water spray --	Not measured	5	—1.9 F°	None ----------	Vapors drifted close to ground	----	----	6.70	1.30
JP-4 fuel stream (bad timing)	6.7	5	—1.9 F°	Several loud, rapid explosions; large fireball	Black cloud rose high at about 60° angle	----	----	----	----

TABLE 3-XIV.—RESULTS OF 30-PERCENT-FLOX SPILL TESTS (REF. 25)
[FLOX spill quantity, 10 lb.]—Concluded

Test material		Weather conditions		Reaction	Cloud or vapor	Moisture content, percent		Acid content, pH	
Substance	Weight, lb	Wind speed, mph	Temperature gradient from 2.5 to 30 ft			Before	After	Before	After
JP-4 fuel (coarse spray)	6.7	5	—2.0 F°	Very rapid, smooth explosions; large fireball	Black cloud rose high at about 70° angle; smoke ring formed	----	----	----	----
JP-4 fuel stream (good timing)	6.7	5	—2.2 F°	Several loud, rapid explosions; large fireball	Black cloud rose high at about 50° angle	----	----	----	----
Coke (low grade)---	265.0	3	—2.0 F°	Small reaction, small flame	Gray cloud had very little rise	2.56	5.77	----	----
Crushed limestone--	462.0	3	—2.0 F°	None ----------	Vapors drifted close to ground	----	----	----	----

TABLE 3-XV.—RESULTS OF 100-PERCENT-FLOX (PURE FLUORINE) SPILL TESTS (REF. 25)

Test material		Weather conditions		Liquid-fluorine spill quantity, lb	Reaction	Cloud or vapor	Moisture content, percent		Acid content, pH	
Substance	Weight, lb	Wind speed, mph	Temperature gradient from 2.5 to 30 ft				Before	After	Before	After
Crushed limestone	411.0	15	0	10	Sputtered, small yellow flames	Gray cloud rose at low angle	----	----	----	----
Sand	320.0	5	—0.7 F°	10	Bright flame	White cloud rose at about 45° angle	2.70	4.20	----	----
Water-soaked sand	321.0	5	0	10	Strong explosion	Light gray cloud rose at about 40° angle	16.30	12.68	8.70	3.55
Asphalt (from road)	275.0	5	0	5	Sputtered, small flashes	Gray cloud rose at low angle	0.03	0.05	----	----
Lake water (5 gal)	41.7	12	—1.1 F°	5	Loud, sharp detonation	White cloud rose at about 30° angle	----	----	8.15	1.35
JP-4 fuel (2 gal)	13.4	5 to 10	0	5	Smooth, fast-burning, large fireball	Black cloud rose almost vertically	----	----	----	----

TABLE 3-XVI.—LIQUID-OXYGEN COMPARISON SPILL TESTS (REF. 25)

Test material		Weather conditions		Liquid-oxygen spill quantity, lb	Reaction	Cloud or vapor
Substance	Weight, lb	Wind speed, mph	Temperature gradient from 2.5 to 30 ft			
JP-4 fuel (1 gal)	6.7	8	—2.0 F°	5	None	Vapors drifted close to ground
JP-4 fuel (2 gal) with spark-plug igniter	13.4	8	—2.0 F°	10	Loud, sharp detonation	Black cloud rose fast and high, almost vertically

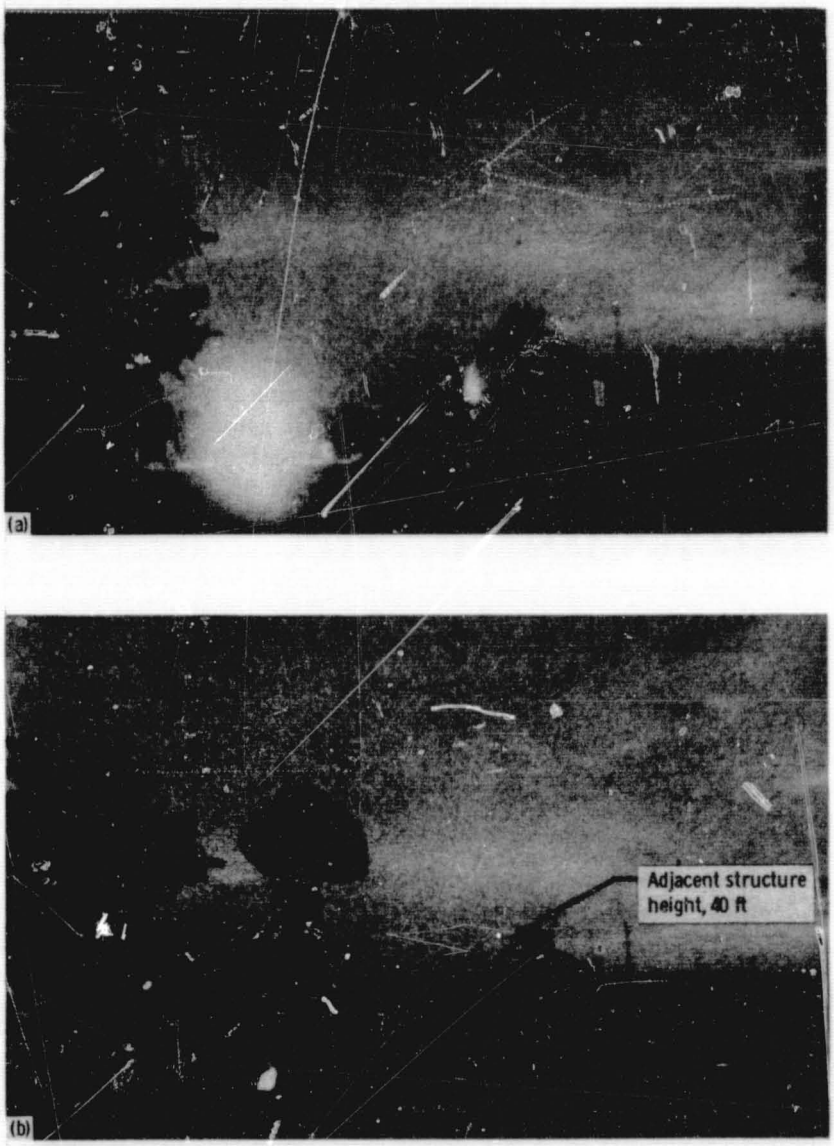

(a) Fireball.

(b) Reaction cloud (2.5 sec later).

FIGURE 3–26.—Spill tests of 30-percent FLOX onto JP-4 fuel at Plum Brook.

explosions were again noticed but the reactions were very rapid, less severe, and considerably smoother. In this test, a large, distinct, horizontal smoke ring formed and moved slowly upward.

When 30-percent FLOX was spilled into lake water, there was no reaction; however, a later chemical analysis revealed that the acid content (presumably hydrogen fluoride) of the water had increased considerably after the spill. In order to obtain greater contact surface area, 30-percent FLOX was also spilled into a shower-head spray of lake water. Again there was no reaction, and again the acid content of the water was increased considerably.

When 30-percent FLOX was spilled onto charcoal, a smooth, quiet, brilliant flame occurred over a period of 2 to 3 seconds. Many minute sparks swept upwards within the flame. A faint white cloud rose rapidly at about a 50° angle and disappeared. The flame was so brilliant that observers approximately 140 yards away viewing through 7x50 binoculars experienced a delay of about 10 minutes in return to normal vision. For results of this and other FLOX spills, see tables 3-XIV and 3-XV.

In all cases, 100-percent fluorine reacted with the materials on which it was spilled, even crushed limestone (table 3-XV). These results are also given in table 3-XIV. A strong detonation occurred when fluorine was spilled on lake water. An almost instantaneous small flash of white light was observed, and a strong shock wave was felt by observers 140 yards away. The white cloud formed after the explosion rose at an angle of only about 30°, indicating a relatively small heat release from reaction of only a limited amount of the fluorine spilled with the water; the rapid energy release from the blast apparently blew the remaining fluorine from the reaction site before it could react. The heat content of the cloud then represented the heat release from a small instantaneous reaction.

It was observed that when 100-percent fluorine was spilled on JP-4 fuel, smooth burning occurred, as opposed to the multiple explosions previously mentioned with the 30-percent-FLOX spills. A yellow fireball about 25 feet in diameter was observed and the resultant black cloud rose rapidly, almost vertically, then drifted downwind and slowly dissipated.

Several significant trends were noticed in these spill tests. When there was no reaction, the FLOX, liquid oxygen, fluorine, or hydrogen fluoride vapors drifted slowly downwind close to the ground. When a reaction did occur, the rate of rise and angle of rise of the resultant toxic cloud were dependent on the amount of heat produced by the reaction.

The smoothness of the 100-percent fluorine–JP-4 fuel reaction compared with the multiple explosion effect of the 30-percent-FLOX–JP-4 fuel spill and the violent detonation of the liquid-oxygen–JP-4 fuel spill

indicated that the reaction was smoother with more fluorine present in the FLOX mixture.

In spills on lake water, it was noted that no reaction occurred with 30-percent FLOX, even into a water spray; yet a violent explosion occurred when 100-percent fluorine was spilled on lake water. The indication is that there is some concentration between 30 and 100 percent at which FLOX will react with water, and the reaction will probably be very rapid.

Additional work has been conducted in studies (ref. 26) involving large-scale FLOX spills; results of these tests are discussed in sections 5.2.1.4 and 5.2.3.

REFERENCES

1. SCHMIDT, HAROLD W.: Design and Operating Criteria for Fluorine Disposal by Reaction with Charcoal. NASA MEMO 1-27-59E, 1959.
2. SCHMIDT, HAROLD W.; AND ROTHENBERG, EDWARD A.: Some Problems in Using Fluorine in Rocket Systems. Spec. Rept. No. 12, Proc. Propellant Thermodynamics and Handling Conf., Ohio State Univ., June 1960, pp. 183–202.
3. SCHMIDT, HAROLD W.: Compatibility of Metals with Liquid Fluorine at High Pressures and Flow Velocities. NACA RM E58D11, 1958.
4. PRICE, HAROLD G., JR.; AND DOUGLASS, HOWARD W.: Nonmetallic Material Compatibility with Liquid Fluorine. NACA RM E57G18, 1957.
5. DEWITT, RICHARD L.; AND SCHMIDT, HAROLD W.: Experimental Evaluation of Liquid-Fluorine System Components. NASA TN D-1727, 1963.
6. SCHMIDT, HAROLD W.: Reaction of Fluorine with Carbon as a Means of Fluorine Disposal. NACA RM E57E02, 1957.
7. SIMONS, J. H.: Scientific and Utilitarian Value of Fluorine Chemistry. Ind. Eng. Chem., vol. 39, no. 3, Mar. 1947, pp. 238–241.
8. SAX, N. IRVING: Dangerous Properties of Industrial Materials. Reinhold Pub. Corp., 1957.
9. HAZELDINE, R. N.; AND SHARPE, A. G.: Fluorine and Its Compounds. John Wiley & Sons, Inc., 1951, p. 143.
10. MCBEE, E. T.: Fluorine Chemistry. Ind. Eng. Chem., vol. 39, no. 3, Mar. 1947, pp. 236–237.
11. KLEINBERG, SIDNEY; AND TOMPKINS, JAMES F.: The Compatibility of Various Metals with Liquid Fluorine. Rept. No. ASD-TDR-62-250, Air Products and Chemicals, Inc., Mar. 1962.
12. BROWN, M. H.: Resistance of Materials to Fluorine and Hydrogen Fluoride. Rept. No. MDDC-144, AEC.
13. GUNDZIK, RICHARD M.; AND FEILER, CHARLES E.: Corrosion of Metals of Construction by Alternate Exposure to Liquid and Gaseous Fluorine. NACA TN 3333, 1954.
14. JACKSON, R. B.: Corrosion of Metals and Alloys by Fluorine. Rept. No. NP-8845, Allied Chem. Corp., Mar. 1960.
15. MELLOR, J. W.: Comprehensive Treatise on Inorganic and Theoretical Chemistry, Suppl. II, Pt. I, Longmans, Green and Co., 1956, p. 138.
16. GODWIN, THOMAS W.; AND LORENZO, CARL F.: Ignition of Several Metals in Fluorine. Paper No. 740-58, ARS, 1958.

fittings (i.e., ¾-in. AN-type fittings have been satisfactory to 1500 psig. Sizes larger than ¾ in. should be limited to appropriately reduced pressures). Causes of failures at Lewis were traced to high-pressure inadequacy of the fitting design, to mechanical failure from overtightening to achieve zero-leak seals, and to other causes of overstress failure (e.g., tubing pulls out of compression fitting). In all fluorine or FLOX installations where these fittings are used, torque values should be specified as a function of fitting size, type, and material. Of course, lubricants *may* be used on the threaded portion of the fitting because the threads are external to the fluorine system and therefore are not exposed; however, a subsequent leak in the fitting *may* result in ignition and line failure.

4.3.2 Flange Fittings

Flange fittings have been used quite extensively in gaseous- and liquid-fluorine installations and portable equipment. They are recommended fittings where connections must be frequently made and broken. Flange fittings are also applicable for semipermanent connections and are particularly suitable for high-pressure systems. The preferred facing

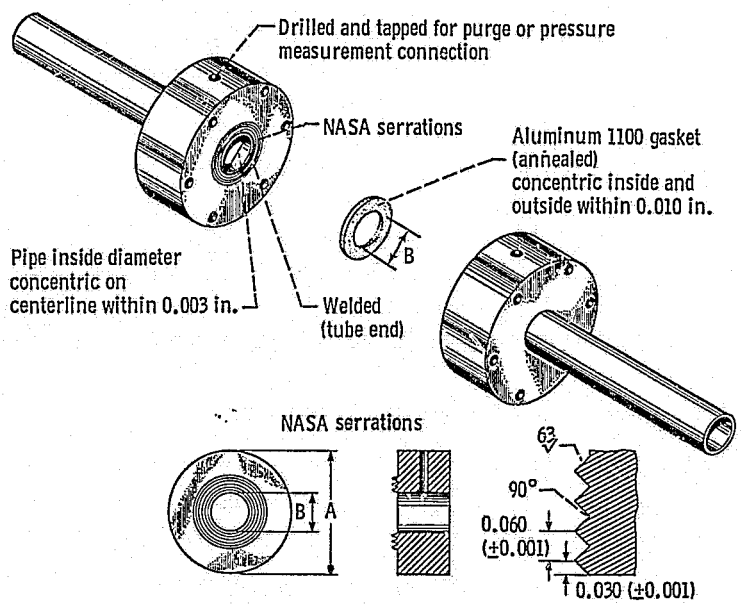

FIGURE 4-5.—Flange-type connectors for fluorine service. (Flange connector bolts must be periodically retorqued since they tend to loosen under cryogenic-ambient temperature cycling.)

on flanged fittings is concentrically serrated with a raised face; the seal is provided by soft annealed aluminum (or soft copper) gaskets (fig. 4–5). In this fitting, all surfaces, where not otherwise specified, should have a number 125 finish.

In addition to meeting the general design criteria, which apply to the selection of flange types for any service (size, working pressure, and temperature), flanged connections for fluorine service should offer a minimum of pockets, cracks, or restrictions where residue or contaminants could accumulate. Cryogenic cycling tends to loosen bolted connections; therefore, *flange bolt tensions must be checked frequently to correct tension,* especially after several extreme temperature cycles. Metallic confined ring gaskets (O-rings, U-rings, crush gaskets, etc.) have been used successfully in bolted flange fittings to provide zero-leak seals.

Nonmetals, such as polytetrafluoroethylene (TFE), have been successfully applied in fluorine systems but are normally used in applications where metals are not feasible (e.g., valve-stem packing). Nonmetals have been tested under severe exposure conditions (see section 3.3) that define the extreme limits within which they can be applied; their use would probably be normally restricted to zero-leak-seal applications in gaseous service. In any application, care should be taken to protect nonmetals from direct contact with liquid fluorine, and direct contact with the fluorine or FLOX flow stream should be avoided. Studies described in section 3.3.4 indicate the feasibility of the use of soft-seal materials in exposed-seal liquid-fluorine or FLOX applications, although the reliability of seals directly exposed to the liquid or to flow conditions is reduced.

Many compression-type fittings and mechanical clamping techniques to hold the fitting together are commercially available. The design and choice of sealing materials in many of these fittings are suitable for use in fluorine systems. The choice of using these fittings must be made on the basis of criteria in this text on the specific application.

4.3.3 Threaded Fittings

Threaded pipe fittings should normally be avoided in fluorine or FLOX service. When it is necessary to use pipe fittings because of size considerations, they should be installed (by welding, silver soldering, or brazing, as described in section 4.9.3) so that the threads are removed or completely isolated from the fluorine or FLOX.

Threaded fittings and thread compounds and/or lubricants should be used only where risk of possible reaction and line or component failure is acceptable.

static labyrinth seal cavity. No pressure rise was measured over an entire series of liquid-fluorine transfers, which indicated that the inner seal was completely effective; in addition, no external leakage was observed at the plane of separation of the coupling during the steady-state flow periods (ref. 5).

4.4 VALVES

Most of the standard globe, plug, or needle valves can be adapted for gaseous fluorine (or FLOX) service by using polytetrafluoroethylene valve-stem packing. In most cases, liquid fluorine or FLOX applications would require diaphragm or bellows-seal valves to ensure that the liquid does not contact the stem-seal material. Packed-stem valves are subject to leakage because of thermal shrinkage when they are exposed to cryogenic fluids, but they have been applied in liquid-fluorine service by using extended stem bonnets. Vertically mounted valve-bonnet extensions reduce the possibility that liquid fluorine or FLOX will contact the stem packing, since heat transfer into the valve maintains a gas pocket in the area of the packing, provides relatively higher packing temperatures, and thus prevents leaks that might cause spontaneous ignition. Preferred valve materials are shown in table 4-III.

Packless valves use a flexible metallic seal to isolate the valve-operating mechanism. Bellows seals permit greater motion of the valve stem and plug. Diaphragm seals have been used successfully in the smaller valve sizes.

Packless valves are inherently more reliable in both liquid and gaseous fluorine service; consequently, they are often used in fluorine installations and handling equipment. It is highly recommended that valves used in high-pressure liquid-fluorine service be restricted to packless bellows or diaphragm sealed. Valves should be completely disassembled for thorough cleaning prior to use, and while the valve is apart, it is a good practice to lap the valve plug into its mating seat to ensure perfect mating.

All bolted connections on valves, flanges, etc., should be retightened periodically to ensure proper torque for sealing. Temperature cycling from ambient to cryogenic temperature tends to loosen bolted connections. In most cases, valve failures at Lewis were traced to high-pressure leaks from loosened bolt connections or from extreme pressure surges (such as might result from a reaction and failure elsewhere in the system). It should be pointed out that leaks can occur without ignition or catastrophic failure; however, loosened connections or points of leakage are particularly susceptible to contamination and subsequent high-pressure ignition and failure.

TABLE 4-III.—PREFERRED MATERIALS FOR VALVE COMPONENTS

Valve component	Service	
	Gaseous	Liquid
Bodies	Nickel (300 series) Stainless steel Monel Aluminum Inconel Brass	Copper (low pressure) Monel Nickel Aluminum Stainless steel (300 series) Inconel
Plugs	Stainless steel (300 series) Monel Aluminum	Stainless steel (300 series) Monel
Bellows	Monel Stainless steel 347	Monel Stainless steel 347
Diaphragms	Stainless steel 347	Stainless steel 347
Gaskets	Soft aluminum Soft copper Polytetrafluoroethylene (TFE) Lead	Soft aluminum Soft copper
Seats[a]	Nickel Copper Aluminum Brass	Nickel Copper Aluminum Brass
Chevron packing	Polytetrafluoroethylene (TFE) Copper braid and TFE	Not recommended
O-rings, V-rings, etc., (refer to section 4.3.2)	Aluminum Polytetrafluoroethylene (TFE) Stainless steel	Copper Aluminum Stainless steel

[a] All-stainless-steel valves have been used, but they have a tendency to gall and bind under high closure forces; therefore, stainless-steel valve seats are usually avoided for fluorine or FLOX service.

4.4.1 Soft-Seal Valve Design

The use of soft seals to permit adaption of standard valves to a zero-leak application is often desirable. However, exposure of the seals to the fluorine environment, to the rubbing friction of closure conditions, and to the flow of fluorine (all of which present ignition hazards) has made

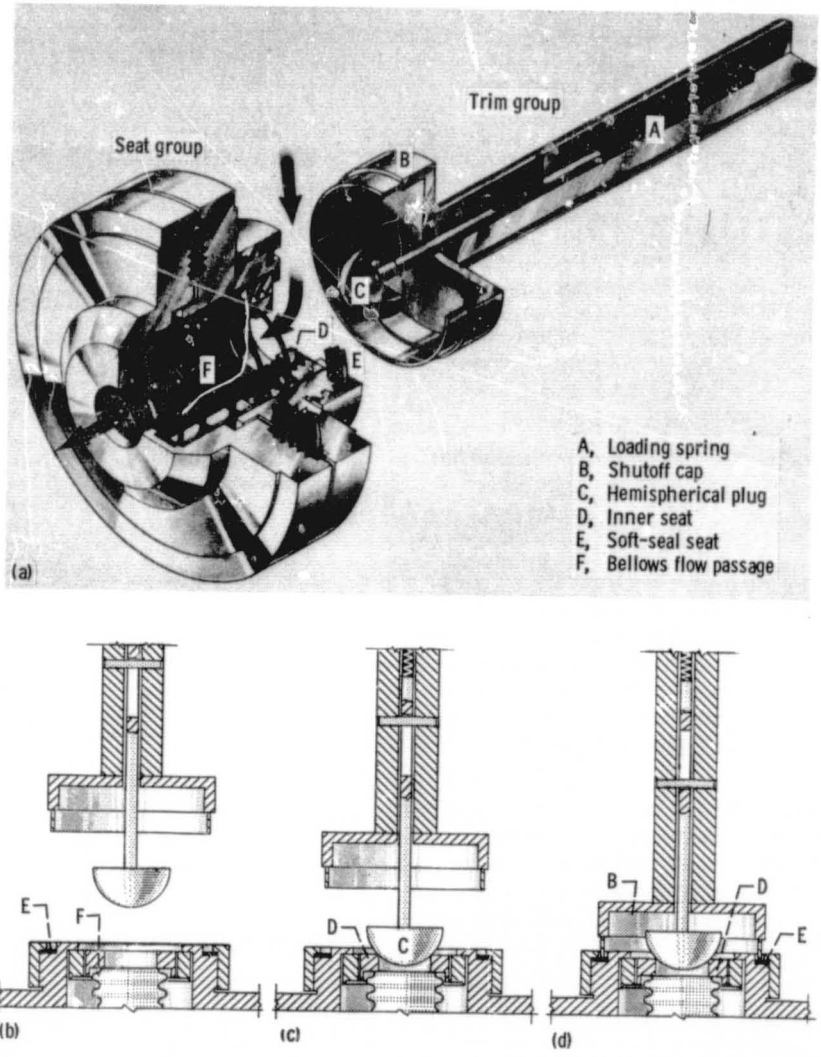

(a) Cutaway of soft-seal valve in opening position.

(b) Valve open. (c) Bulk flow stopped. (d) Valve closed.

FIGURE 4–8.—Soft-seal valve developed at Lewis.

the use of soft seals generally unreliable.

As part of a testing program to develop and evaluate liquid-fluorine components (ref. 5), a zero-leak valve employing a soft-seal material at the flow shutoff interface was developed (fig. 4–8). It was successfully tested with liquid fluorine at flow rates up to 2 pounds per second and inlet pressure up to 97 pounds per square inch absolute. This valve was tested under dynamic liquid-fluorine conditions with soft-seal materials, including glass-filled and metal-filled tetrafluoroethylene, and nitroso rubber. (The metal- and glass-filled polymers were chosen arbitrarily, but in support of compatibility studies; the nitroso rubber was purposely selected as a normally noncompatible material.) By designing the valve for minimum exposure to fluorine and by surrounding the seal with metal to provide good thermal conductivity for heat transfer, it was expected that material compatibility could be enhanced. The test results confirmed this assumption.

A sectional view and schematic drawing of the soft-seal valve in its open position are shown in figure 4–8. A standard commercial valve actuator and housing was used for the testing. In operation, liquid-fluorine flow was directed past valve plug C, through the bellows flow passage F to the housing exhaust port. As the trim group was lowered, the spring-loaded hemispherical plug C contacted the floating spring-loaded inner metal seat D, which shut off the bulk of fluorine flow (fig. 4–8(c)). Continued downward movement of the trim group allowed the shutoff cap B to contact the soft seal E and completely seal the valve to fluorine flow (fig. 4–8(d)). Any of the cryogenic liquid trapped between the shutoff cap and the hemispherical plug vented itself to the downstream side of the valve assembly through the spring-loaded seal formed between the hemispherical plug and the inner seat D.

The design was tested at flow rates up to 2.06 pounds per second and a valve inlet pressure of 97.7 pounds per square inch absolute. At the conclusion of the testing, the valve soft-seal material was inspected for signs of erosion or chemical action. Results of the tests with various seal materials with respect to compatibility are discussed in section 3.3.4.

Principles demonstrated by this valve design indicated that limited application could be made by using soft-seal materials to achieve a zero-leak valve. Extensive testing would be required to assure adequate reliability, however.

4.4.2 All-Metal Conical Valve Design

Some limited work has been done to explore the possibility of an all-metal zero-leak valve design (ref. 6). This investigation was based on meeting the following specifications:

(1) The valve configuration must be all metal in order to have maximum compatibility with fluorine.

(2) The valve design must feature zero-leak capability under extreme conditions of environment and must not be affected by repeated open-close cycling.

(3) The valve design must permit the use of a wide range of valve actuator forces to permit easy adaption to flight-weight hardware.

A valve was designed based on the concept that the elasticity of metal could be used in the same fashion as the elasticity of soft seals to achieve zero-leak capability in a valve.

The general, physical characteristics of the design which evolved (fig. 4–9) are that (1) the cone is tapered so that (for circular cross sections) a constant total rim area is present from the lip back to the cone apex (the valve plug has a constant-thickness center section where the actuator stem is attached and the stem force is applied) and (2) the valve seat has a spherical seating surface.

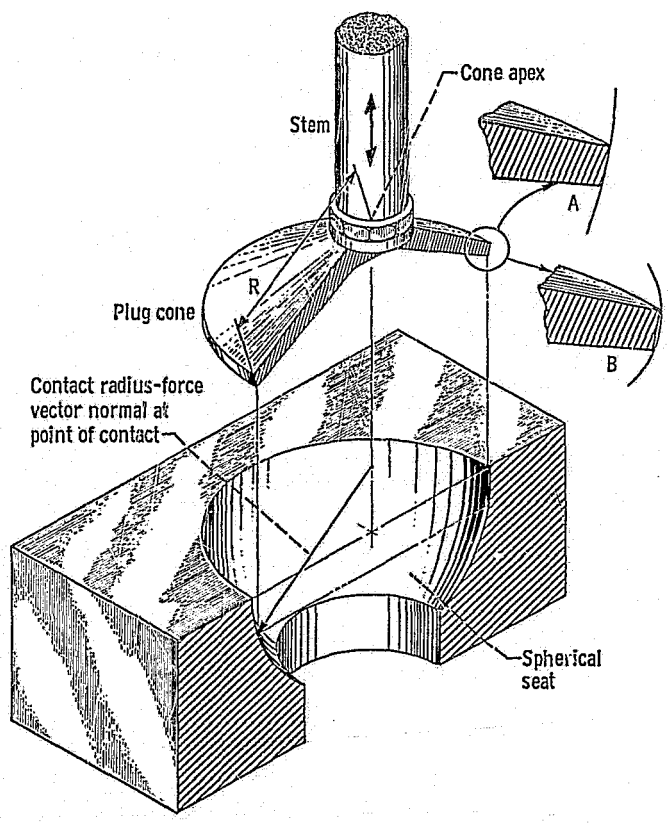

FIGURE 4–9.—Schematic drawing of conical valve design and operation.

For this type of valve, any desired mechanical advantage can be obtained for plugstem force applied by selecting an angle α from 0° (a cylinder) to an angle approaching 90° (fig. 4–9). (The sealing force is equal to the plugstem force divided by cosine α.) Since the distance R (fig. 4–9) is the same for the plug cone and the valve seat, this sealing force is applied normal to the valve seat and eliminates the sliding contact found in most valve plug-seat combinations. The mechanical advantage permits use of light plugstem pressures to achieve zero-leak seals.

Major design parameters for this valve can be widely varied. As one approach, after selecting the materials to be used, the cross-sectional area of the cone lip, and the force to be applied, the designer can choose the optimum cone angle so that the elastic limits of the cone material are not exceeded. In general, a minimum lip width is desirable to avoid stress concentration on sharp corners (see inset B in fig. 4–9) with resultant strain-hardening of the material. If thicker cross sections are used, the cone lip should be ground and lapped to provide a spherical surface to mate with the spherical valve seat (inset A, fig. 4–9).

Contact faces between the valve plug and seat must be smooth and round with 100 percent contact. For this reason, machining must be held to close tolerances to maintain roundness of plug rim and seat and proper plug taper, since underloading an out-of-round protrusion on either the rim or seat could cause local strain beyond the elastic limit of the material. A #4 finish (American Standard B46) was used for the contacting surface of the plug and seat to reduce the possibility of localized work hardening of hills and valleys on the contacting surfaces. The design shows a number of attractive features:

(1) It can be used in fluorine (or other reagent) environments.

(2) The elastic properties of the conical plug afford zero-leak seals under repeated cycling.

(3) A slight angular misalinement or rotation of the valve plug in the seat will not affect the sealing properties of the valve.

(4) Normal passivation film does not affect the sealing properties of the valve.

(5) The conical plug characteristic is adaptable to a wide range of sealing forces (from valve operators) because of the inherent mechanical advantage supplied by the plug shape.

Leak tests were performed with aluminum, magnesium, and stainless-steel plugs in stainless-steel seats (seat material should be as hard as, or harder than, the plug material). The test fluids were helium and fluorine gas at ambient temperatures (fig. 4–10). Zero leakage was obtained with both fluids at pressures up to 200 pounds per square inch gage during and after 100 operating cycles (open-close). This capability is a result of another important feature of this valve; open-close cycling does

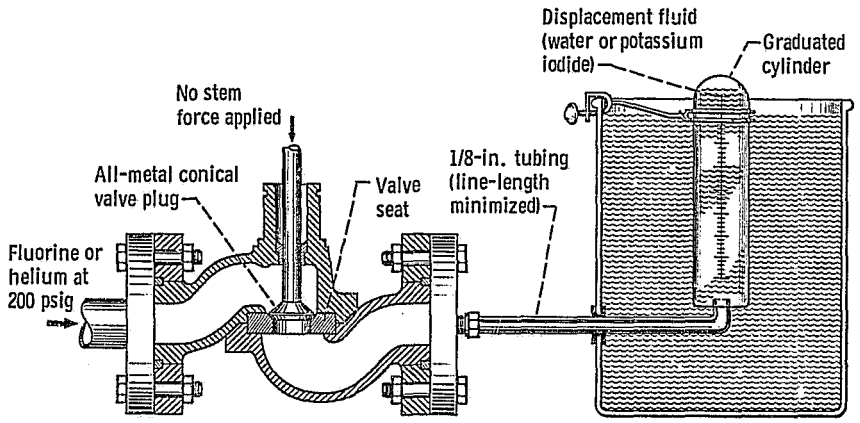

FIGURE 4–10.—Schematic drawing of apparatus used to verify zero-leak capability (24 hr) with no plugstem pressure applied.

not cause plug-seal material deformation or wear of contacting surfaces. All materials used were capable of achieving zero leakage as long as the elastic load limits were not exceeded.

Zero leakage was measured for periods up to 24 hours by using a water displacement method for helium and a potassium iodide solution for fluorine detection. This development effort was limited to demonstrating the design concept. No effort was made to optimize the design for minimum pressure drop across the valve or to develop a specific hardware item.

4.4.3 Pressure Regulating Valves

Pressure regulating valves as such have not been used for fluorine because of the nonmetallic parts normally included in these valves. Where automatic flow control is required, fluorine-compatible valves with flow- or pressure-sensing actuator-controllers have been used. If gaseous fluorine is used, pressure is reduced and throttled with throttling valves. (The gas cylinder shutoff valves should *never* be used for throttling fluorine gas flow, because this results in undue wear and stress of the primary shutoff valve.)

4.4.4 Pressure Relief

The fluorine containment system in mobile storage operations does not use pressure-relief devices (refer to section 4.1.3). In fixed tank facility storage applications, both burst diaphragms and pressure-relief valves have been used for pressure relief in fluorine containment systems. Burst

diaphragms are preferred for pressure-relief devices, since they are generally more reliable and less prone to leakage than relief valves. This is important both in subcooled fluorine containment systems (vapor pressure is below atmospheric) and during any evaluation procedures, since an inward leak of moist air can occur. Monel diaphragms, sized to relieve at the desired overpressure in the particular system, are commonly used at Lewis. If repressurization following burst disk failure would be a requirement (e.g., to transfer fluorine from a containment vessel), two burst disks can be hooked up to the outlets of a three-way valve or a normally open automatically actuated valve can be installed upstream of the burst disk. Outlets from the burst diaphragms should be connected to the disposal system to prevent any release of fluorine contaminant to the atmosphere.

Automatic valves, modified to open on sensing an upstream overpressure, have been used as pressure-relief valves at Lewis. Since the possibility of inward air leakage through the seat exists in this device, however, its use is usually avoided. Whichever relief device is selected, the practice of regular inspection should be followed to ensure reliability.

4.4.5 Check Valves

Most commercial all-metal check valves are suitable for either gaseous or liquid fluorine. Selection should be based on the general criteria discussed in chapter 3 and in this section. Check valves that tend to "chatter" should not be used.

4.4.6 Valve Operators

4.4.6.1 *Manually operated valves.*—For safety considerations in handling gaseous fluorine under pressure, manual valves should be used with a protective barrier separating the operator from the valve. Valve handle extensions are generally used, and, where necessary, a bevel gear arrangement is included to change the direction of valve closure force.

4.4.6.2 *Pneumatic, hydraulic, and motor-operated valves.*—There is a great variety of actuators applicable to valve operation in fluorine systems. The only special requirements would be design considerations for possible exposure to fluorine or hydrogen fluoride vapors.

4.4.6.3 *Solenoid operators.*—In general, solenoid operators are restricted to smaller valves and to pilot-valve applications. Most solenoid valves cannot be used with fluorine or FLOX because the materials used for sealing solenoid windings are not compatible with fluorine. If solenoid valves are used in a fluorine line, the solenoid must be hermetically sealed with a compatible (preferably metal) sealing system to prevent

contact with the fluorine. Also, precautions should be taken to ensure that the connecting wiring is protected from the effects of fluorine or hydrogen fluoride vapors (refer to section 5.2.5.3).

4.5 FLUORINE PUMPS

Although design data for liquid-fluorine pumps are limited, the extensive development of liquid-oxygen pumps (and recent work with seals for fluorine and FLOX pumps) has indirectly provided information for most areas of a liquid-fluorine-pump design.

The most difficult barrier in using existing conventional cryogenic pump designs for FLOX or fluorine lies in the lack of a compatible and reliable shaft seal that will operate for extended periods in the reactive fluorine or FLOX environment. Development testing of a fluorine pump at Bell Aircraft Corporation demonstrated that such seals were feasible. One seal accumulated over 27 minutes running time in liquid fluorine, and another seal operated well through three 300-second runs in a single 2-hour period (ref. 7). Work performed at Lewis and by Rocketdyne Division of North American Aviation and by the Florida Research and Development Center of Pratt & Whitney Aircraft has contributed to resolution of the seal problem (refer to section 4.5.2). Other major problem areas in pump design are the seal configuration and the impeller-inducer design.

4.5.1 Dynamic Seals

The most critical problem in designing a seal for a liquid-fluorine pump is controlling the leakage of fluorine to prevent contact of fluorine or FLOX with noncompatible elements of the pump (particularly the bearing lubricant, since no known lubricants are compatible with liquid fluorine). Leakage control can be maintained (1) by providing a more compatible environment for the seal by a backpressure inerting technique, bleeding an inert pressurant through the seal cavity and past the seal into the impeller cavity, or (2) by venting and purging the seal cavity overboard with or without use of a purge gas sweep. Both these methods, discussed subsequently, have been successfully demonstrated in pump tests (ref. 7).

Mechanical seals, bellows or spring-loaded, appear to be the better choice to incorporate in a positive shaft-seal design. This type of seal has been used successfully in liquid-oxygen pumps (ref. 8). In the following discussion it is assumed that the bellows seal is used, but if spring-loaded seals were considered, the discussion would still generally apply.

END OF REFERENCE

37

REFERENCE

38

FLAMMABILITY, ODOR, AND OFFGASSING REQUIREMENTS AND TEST PROCEDURES FOR MATERIALS IN ENVIRONMENTS THAT SUPPORT COMBUSTION. NHB 8060.1A, NATIONAL AERONAUTICS AND SPACE ADMINISTRATION, FEB. 1974.

OFFICE OF
MANNED SPACE FLIGHT

NHB 8060. 1A
February 1974
Edition

FLAMMABILITY, ODOR, AND OFFGASSING REQUIREMENTS AND TEST PROCEDURES FOR MATERIALS IN ENVIRONMENTS THAT SUPPORT COMBUSTION

NATIONAL AERONAUTICS AND SPACE ADMINISTRATION
WASHINGTON, D.C. 20546

PREFACE

This publication establishes uniform material selection, evaluation and control criteria for all materials that are under consideration for use in and around Manned Space Vehicles, ground support equipment and facilities, during assembly, test and flight operations. It supercedes the November 1971 issue of NHB 8060.1. Included herein are revised criteria for material applications in high pressure LOX/GOX systems and in combustion supporting environments other than oxygen. Other changes to improve the content of the document include elimination of duplicate procedures and incorporation of requirements previously referenced. This publication, based on the materials technology developed during the Apollo and Skylab programs, provides:

a. Standard requirements for control of flammability, odor and offgassing of materials to be used in the design and development of Manned Space Vehicles.

b. Guidelines and directions for material selection.

c. Testing procedures for the candidate materials.

The provisions of this handbook are applicable to the NASA installations responsible for hardware design and development of Manned Space Vehicles and related hardware.

Provisons of this handbook will be included as applicable in all future contracts and programs involving Manned Space Vehicles. However, the supply of this document within NASA is limited. Therefore, for those procurement actions involving only a certain portion (or portions) of this handbook, the cognizant NASA installations shall abstract or reproduce only such portions as apply to a given RFP or contract action in lieu of furnishing copies of this handbook.

Any questions or comments concerning the provisons of this document should be directed to Reliability, Quality Assurance, and System Safety (Code MQ), NASA Headquarters.

Dale D. Myers
Associate Administrator for
Manned Space Flight

For sale by the Superintendent of Documents, U.S. Government Printing Office, Washington, D.C. 20402

CONTENTS

Par.		Page
	CHAPTER 1 INTRODUCTION	
100	Scope	1-1
101	Approach	1-1
102	Relation to NASA Centers Material Programs	1-2
103	Abbreviations and Acronyms	1-2
104	Related Documents	1-2
	CHAPTER 2 REQUIREMENTS	
200	Materials Selection	2-1
201	Batch/Lot Approval	2-2
202	Material Categories and Requirements	2-2
203	Stowed/Life Support Equipment Interface	2-8
204	Test Requirements	2-8
205	System Flammability Requirements	2-11
206	Spacecraft Offgassing Requirements	2-13
207	Related Considerations	2-13
	CHAPTER 3 MATERIALS PROGRAM MANAGEMENT	
300	General	3-1
301	Material Control Program Plan	3-2
302	Quality Assurance (QA) Provisons	3-4
	CHAPTER 4 REQUIRED TESTS	
400	General	4-1
401	Test No. 1 - Upward Propagation Test	4-1
402	Test No. 2 - Downward Propagation Rate Test	4-8
403	Test No. 3 - Flash and Fire Point Test	4-10
404	Test No. 4 - Electrical Wire Insulation and Accessory Flammability Test	4-17
405	Test No. 5 - Electrical Connector Potting and Conformal Coatings Flammability Test	4-23
406	Test No. 6 - Odor Test	4-30
407	Test No. 7 - Determination of Offgassing Products and Carbon Monoxide Test	4-37
408	Test No. 8 - Flammability Test for Materials in Vented Containers	4-42
409	Test No. 9 - Electrical Overload Test for Sealed Containers	4-47
410	Test No. 10 - Guidelines for Simulated Panel and Assembly Flammability Test	4-49
411	Test No. 11 - Guidelines for Simulated Crew Bay Configuration Flammability Verification Test	4-53
412	Test No. 12 - Guidelines for Total Spacecraft Offgassing Test	4-55

Par.		Page
413	Test No. 13 - Ambient Liquid Oxygen and Pressurized Liquid and Gaseous Oxygen Mechanical Impact Test	4-58
414	Test No. 14 - Gaseous Oxygen Pneumatic Impact Test	4-83
415	Test No. 15 - Constant Temperature Immersion of Materials in Type J Fluids	4-88

FIGURES

2-1	Test Record Sample Form	2-15
4-1	WSTF Flash & Fire Point Test Apparatus & Control System	4-11
4-2	Typical Oscilloscope Displays	4-15
4-3	Potting Flammability Test Equipment Schematic	4-21
4-4	Sample Configuration	4-22
4-5	Conformal Coating Sample Configuration	4-27
4-6	ABMA Impact Tester	4-61
4-7	Details of Striker, Sample Cup, and Sample	4-62
4-8	Samples In Test Cups	4-64
4-9	Grease Insert Cup Holder	4-65
4-10	Sample Freezing Box	4-67
4-11	Free Fall Timing Circuit	4-68
4-12	Dye Penetrant Rack	4-74
4-13	Typical Mechanical Impact Test Chamber	4-82
4-14	Pneumatic Impact Test System	4-84
4-15	Pneumatic Impact Test System	4-85

TABLES

2-1	Materials Usage Types and Materials Group Classification	2-4

APPENDICES

APPENDIX A	Abbreviations and Acronyms	A-1
APPENDIX B	Related Documents	B-1
APPENDIX C	Precision Cleaning Guidelines for Oxygen Impact Test Specimens and Test Apparatus	C-1

CHAPTER 1 INTRODUCTION

100 SCOPE

This publication establishes the criteria for selection of materials for use in future manned space vehicles and in equipment involving personnel in ground test facilities with environments that support combustion. It establishes the flammability, odor, and offgassing limitations for testing candidate materials. Chapter 2 provides material selection criteria and evaluation requirements for the various material usage categories. It also relates the various test techniques to the applicable material usage categories. Detailed procedures to be utilized for screening candidate materials are provided in Chapter 4. The major elements of a Materials Control Program are presented in Chapter 3. It is intended that the NASA Center Program Office and material specialists shall select the appropriate elements of this publication and establish a materials control program tailored to the needs of the specific programs.

Note: The designer and materials engineer must exercise care in evaluating the data from the tests specified herein since final acceptance of materials depends on their application in the spacecraft. Generally, the materials are tested in their final configuration or a thorough analysis is performed of the test data in relation to the applications of the materials in the spacecraft to assure that no hazards exist.

101 APPROACH

The selection of materials which are used in and around manned spacecraft during flight and test operations must include consideration of the flammability properties and offgassing limitations of the candidate materials. The materials evaluation should be conducted at the most hazardous gas mixture and pressure conditions anticipated for the application environment. This should be established by the responsible Program Office in accord with Program requirements.

The material selection is to be based on the following general fire control criteria:

1. The probability of ignition shall be reduced through design measures that include elimination of low flash and fire point materials.

2. Any potential fire shall be restricted to minimum and well defined isolated areas without propagation paths.

3. The rate and magnitude of pressure and temperature increase in any potential fire shall not cause structural damage to the vehicle.

102 RELATION TO NASA CENTERS MATERIAL PROGRAMS

The NASA Manned Space Flight Centers (George C. Marshall Space Flight Center, Johnson Space Center, and John F. Kennedy Space Center) shall use this document and develop implementation plans for Center-peculiar operations to ensure the disciplines specified herein are standardized.

Implementation of the requirements of this document are considered the responsibility of the appropriate center materials representative and the applicable Program Office. Revisions to the requirements of this publication shall be approved by the Center Materials Representative convened by OMSF (MQ).

103 ABBREVIATIONS AND ACRONYMS

Abbreviations and acronyms used in this publication are included in Appendix A.

104 RELATED DOCUMENTS

Appendix B lists the documents that form a part of this publication to the extent specified herein. Unless otherwise indicated, the issue in effect on date of invitation for bids or request for proposals shall apply.

(Copies of specifications, standards, drawings, and publications required by contractors in connection with specific procurement functions should be obtained from the procuring activity or as directed by the contracting officer.)

CHAPTER 2 REQUIREMENTS

200 MATERIALS SELECTION

1. GENERAL

All materials considered for use in a manned spacecraft including the materials of the spacecraft, stowed equipment, or experiments shall be evaluated for flammability, odor, and offgassing characteristics and shall meet the applicable requirements specified in this publication. Materials shall be evaluated in accordance with the applicable test methods specified herein. A minimum of three specimens (excluding black boxes) of the materials in the thickness intended for use shall be subjected to each applicable test in the most hazardous usage environment as specified by the responsible program office. Material applications previously tested, reviewed, and approved shall be considered to minimize additional testing.

Materials in Type D and J applications which can also be exposed to the pertinent fluid as the result of a single barrier failure must be reported. An engineering evaluation and analysis of test data shall be provided to justify the use of the materials or a configuration test must be performed. A single barrier failure is defined as a failure which will be restricted to potential leaks within a component; e.g., leaks from the pressurized fluid enclosure to an adjacent electrical enclosure within the component.

Failures of structural parts such as pressure lines and tanks are not considered single barrier failures. These structural parts shall be reviewed on an individual design basis.

2. MATERIALS GROUPING AND RESTRICTIONS

Materials considered for use shall be grouped as follows based upon the results of screening tests and shall be approved for specific applications by the NASA Center responsible for the spacecraft/hardware development.

GROUP I - Materials that are noncombustible or self-extinguishing when tested for flammability properties in accordance with the applicable required tests shown in Table 2-1. Group I materials will be verified in end item configuration and/or full scale tests in accordance with Paragraph 205 unless it can be shown by the rationale resulting from an engineering evaluation and analysis of

test data that configuration/full scale tests are not required. In addition, these materials shall also meet the requirements of Tests 6 and 7.

Note: There are no restrictions on Group I materials in design.

GROUP II - Materials that do not meet the Group I flammability requirement. Group II materials shall not be used unless functional requirements preclude the use of Group I types and the materials are specifically approved by the cognizant NASA Center on an individual basis. Should it be imperative to use Group II materials in habitable environments, the functionally acceptable material with the lowest flame propagation rate and the lowest production rate for offgassed products shall be used. The Group II materials shall be subjected to the applicable required tests shown in Table 2-1 including Tests 6 and 7. All pertinent test and design data including drawings, photographs, specifications, environmental and functional requirements, and one-square foot samples of materials in the proper thickness shall be submitted to the cognizant NASA Center for review and approval. Systems using Group II materials in the design shall be subjected to configuration testing in accordance with Paragraph 205. The use of Group II materials in the system design shall be approved by the cognizant NASA Center before use in the spacecraft.

201 BATCH/LOT APPROVAL

Unless specified otherwise by the procuring activity, all materials considered for use in environments which support combustion shall be batch/lot tested in their minimum use thickness until such time as reactivity characteristics traceable to batch/lot variations are determined. Batch/lot test specifications or procedures and disposition of batch/lot test data shall be specified by the NASA procuring activity.

202 MATERIAL CATEGORIES AND REQUIREMENTS

Table 2-1 Material Usage Types and Material Group Classifications presents the relationship of material usage types and material group classifications with respect to each required test. Material usage is categorized as follows:

1. TYPE A EXPOSED MATERIALS IN THE CREW BAY ENVIRONMENT

   a. This category shall include the material applications that are unlimited with respect to quantity, proximity

to ignition sources, or exposure to the crew bay atmosphere and are used over wide areas of the spacecraft. To prevent flame propagation, these materials or their applications must be self-extinguishing as defined herein.

b. Materials shall meet Group I requirements and shall be nonpropagating in their usage configuration by test or analysis.

2. TYPE B SPECIAL MATERIALS APPLICATIONS AND MINOR EXPOSED MATERIALS

a. This category includes those materials applications in the spacecraft arranged in discrete locations and exposed to the crew bay atmosphere. The amount and arrangement of materials shall be limited to prevent the spread of fire in the pressurized vehicle. The requirements presented in Table 2-1 are applicable.

b. Materials, whether Group I or Group II, shall be shown to be nonhazardous in their usage configuration by test or analysis.

3. TYPE C LOW PRESSURE OXYGEN SUPPLY MATERIALS

This category includes those materials used in the systems exposed to less than 20 psia oxygen. It includes those materials in the suit loop, emergency oxygen mask and the oxygen delivery system exposed to the crew bay environment.

All materials used in this category shall meet Group I requirements except in those special cases where authorization is given by the program office to use Group II materials which shall then be shown to be nonhazardous in their usage configuration by test or analysis.

4. TYPE D MATERIALS IN HIGH PRESSURE LOX/GOX SYSTEMS

As a goal, the design should not have an ignition source normally interfacing with the media. If the design does not meet this goal in the particular system it is mandatory that configuration tests be run or that a comprehensive configuration analysis showing that no hazard exists be submitted to NASA for approval.

a. This category shall include those materials used in greater than 20 psia oxygen systems and materials used in oxygen storage and GSE systems supplying oxygen. They shall meet the requirements of Test 13, Part 1, ambient LOX, as a minimum. Data for materials previously

Table 2-1 Materials Usage Types and Materials Group Classifications

MATERIALS USAGE CATEGORIZATION	GROUP I MATERIALS REQUIRED TESTS (SEE NOTE 1)	GROUP II MATERIALS (NASA CENTER APPROVAL FOR USE REQUIRED) REQUIRED TESTS (SEE NOTE 1)
Type A - Exposed Materials in the Crew Bay Environment	Test 1 or 4 or 5 (see note 4) Tests 6 and 7	None (see note 5)
Type B - Special Applications and Minor Exposed Materials	Test 1 or 4 or 5 (see note 4) Tests 6 and 7	Tests 2 and 3 and 6 and 7
Type C - Low Pressure Oxygen Supply Materials	Test 1 or 4 or 5 Tests 6 and 7 (See Note 2)	Tests 2 and 3 and 6 and 7 (See Note 2)
Type D - Materials in High Pressure LOX/GOX/Systems	Tests 4 and 5 and 6 and 7 (See Note 2) (See Note 2) and 13 and 14	None (see note 5)
Type E - Sealed Containers	Tests 1 and 9	Tests 2 and 3 and 9 (See Note 3)
Type F - Vented Containers	Tests 1 and 8 and 6 and 7	Tests 2 and 3 and 6 and 7 and 8 (See Note 3)
Type G - Materials Applications in Nonflight Equipment	Test 1 or 4 or 5 Tests 6 and 7	Tests 2 and 3 and 6 and 7
Type H - Material in Unpressurized Portions of the Spacecraft	Test 1 or 4 or 5	Tests 2 and 3
Type J - Materials in Combustion Supporting Environments Other than Oxygen	Test 15	None (see note 5)

NOTE:
1. End item configuration-type test 10 or 11 and 12 or an analysis required for final materials acceptance for use in manned spacecraft except type H for which Test 12 is not required.
2. Tests 6 and 7 applicable to LOX systems which could affect crew atmosphere.
3. Tests 2 and 3 applicable to material selection and not End Item Sealed or Vented Container.
4. Both tests 1 and 5 are applicable to potting compounds and conformal coatings.
5. Normally, only Group I materials may be used in these applications. When Group II materials must be used, specific program office approval is required. The materials are then subjected to all the tests required for the Type application.

tested to the requirements of Test 13, Part 1, are listed in NASA publication TMX 64711. All materials considered for use shall be batch tested until the capability of the material to meet the requirements of this category is established.

Candidate materials which meet the requirements of Test 13, Part 1, and are proposed for use in high pressure LOX/GOX systems shall also meet the mechanical impact acceptance requirements of Test 13, Part 2, at the actual thickness, (or thinner than actual), intended for use at maximum use pressure and temperature. Materials which do not meet the acceptance criteria of Paragraph 413.B and remain candidates shall undergo threshold determinations at the actual thickness intended for use and at the maximum use pressure and temperature in accordance with Paragraph 413.C.17.

All Type D materials shall be approved by the procuring activity prior to use in design.

b. The acceptance requirements for mechanical LOX/GOX impact tests at actual thickness intended for use and at the maximum use pressure and temperature are given in Paragraph 413.B.

c. In addition, materials intended to be used in proximity to sources of electrical energy shall be evaluated in configuration using "worst case" electrical and environmental conditions applying the techniques of Test No. 4. To be acceptable, materials must be self-extinguishing. If additional information (especially where pneumatic impact loading is possible) is required, Test No. 14 may be used. Materials that do not meet the requirements of the above tests and which are essential to the application shall be analyzed and the approximate energy levels, to which they can be exposed, calculated to form the basis for additional testing.

d. Materials which will be used in high pressure environments (such as pressurized air) containing oxygen and some inert gas at a partial pressure of or greater than 20 psia shall be evaluated according to Test No. 13, Part 2 only, in the use environment at the actual thickness intended for use and at maximum use pressure and temperature.

5. TYPE E MATERIALS IN SEALED CONTAINERS

a. This category shall include those material applications inside sealed containers, sealed with inert gas, and/or potting compounds inside, with no method of receiving or replenishing a supply of combustion supporting atmosphere.

b. Where the evaluation analyses of existing data are inadequate, all materials used in sealed containers shall meet the requirements of Test No. 9. The container shall not rupture.

c. Tests No. 6 and 7 are generally not required for materials applications inside sealed containers.

6. TYPE F MATERIALS IN VENTED CONTAINERS

a. This category shall include those materials applications used inside unsealed containers with or without an internal ignition source. Removal of materials shall be for operational use only.

b. Where the evaluation analyses of existing data are inadequate, materials applications used in closed (but not sealed) containers shall meet the requirement of Test No. 8. The container shall not rupture or permit the escape of flames or burning debris. The container shall not emit gasses and heat to an extent that would cause a pressure rise in the module or vehicle which might cause structural damage.

7. TYPE G MATERIAL APPLICATIONS IN NONFLIGHT EQUIPMENT

a. This category shall include those materials used in nonflight equipment such as that introduced into the flight spacecraft for closed hatch, power on tests. The cognizant design organization shall identify all nonflight equipment and provide the rationale that supports the use of the material in question in an environment that will support combustion.

b. Type G materials shall meet the requirements of Group I (refer to Paragraph 200.B) in their use configuration.

8. TYPE H MATERIAL IN UNPRESSURIZED PORTIONS OF THE SPACECRAFT

a. The material applications included in this category shall be those in uninhabited portions of the spacecraft.

b. Materials outside the crew bay area shall meet the requirements specified herein, as applicable. The use of materials that fail to meet the applicable flammability requirements shall require design measures to minimize fire hazards. The materials shall be self-extinguishing in air when evaluated in accordance with the applicable flammability tests. The details of the design measures (drawings, specifications, photographs, etc.), the rationale for use of the material, and the experimental proof of acceptability under the worst practical conditions shall be approved by the procuring activity prior to inclusion of the materials in the design. The data based on ASTM, Underwriters Laboratory (references listed in Appendix B) and FAA flammability procedures may be used as a basis for determining the flammability characteristics of materials in unpressurized areas of the spacecraft provided the test atmosphere is at least as severe as that proposed for use.

9. TYPE J MATERIALS FOR COMBUSTION SUPPORTING ENVIRONMENTS OTHER THAN OXYGEN

a. As a goal, the design should not have an ignition source normally interfacing with the media. If materials screening tests indicate a potential hazard when used within 1 inch of an ignition source, it is mandatory that configuration tests be run or that a comprehensive configuration analysis showing that no hazard exists be submitted to NASA for approval/disapproval.

b. This category shall include all materials exposed to fluids other than oxygen such as N_2O_4, N_2H_4 and other oxidizers and fuels that are theoretically capable of undergoing exothermic reactions with the environment in which used.

c. Materials shall be shown to be compatible with the environment in question at 160°F. A material is considered compatible if exposure of the material to that environment at 160°F (under maximum use pressure) for a period of 48 hours does not result in chemical or physical changes such as tackiness, flaking, complete dissolution, etc. (Data obtained according to general guidelines similar to that of Test No. 15 are included in the Titan II Storage Propellant Handbook and are considered directly applicable.) Materials shown to be

incompatible at temperatures less than 160°F shall be considered incompatible. All materials for which no compatibility data exists shall be evaluated using the procedure of Test Number 15.

d. If the materials are exposed to a source of energy such as mechanical impact, pneumatic impact, heat source, etc. then a configuration test or a special test applicable to the unique conditions shall be devised and performed to ensure the material's compatibility. A configuration analysis may be performed to ensure adequate compatibility.

Note: Not all the detailed test procedures can be provided for this category due to the wide variation in the chemical behavior of the environments involved. In the design of specific test equipment for each environment, care must be taken to ensure compatibility of all exposed instrumentation.

203 STOWED/LIFE SUPPORT EQUIPMENT INTERFACE

All equipment programmed for spacecraft mission usage that is stowed in containers (such as life support and experiment equipment) must conform to the applicable requirements specified in this publication.

204 TEST REQUIREMENTS

The following test requirements summarize and scope the Required Tests presented in Chapter 4.

1. TEST NO. 1 - UPWARD PROPAGATION TEST

Materials shall be nonflammable or shall be self-extinguishing within 6 inches of the ignition source when ignited at the bottom of a vertically oriented specimen and shall not spark, sputter, or drip flaming particles.

2. TEST NO. 2 - DOWNWARD PROPAGATION RATE TEST

Materials failing to comply with the requirements of Test No. 1 shall be ignited at the top of a vertically oriented specimen and the flame propagation rate shall be determined and the occurrence of a spark, sputter, drip, or transfer of solid mass during burning shall be recorded.

3. TEST NO. 3 - FLASH AND FIRE POINT TEST

Group II materials shall be evaluated according to Test No. 3 and shall be acceptable for design if they exhibit a flash point above 400°F and a fire point above 450°F.

4. TEST NO. 4 - ELECTRICAL WIRE INSULATION AND ACCESSORY FLAMMABILITY TEST

Materials shall be nonflammable in the test atmosphere during the application of current overloads up to the melting point of the conductor. In addition, the configuration shall meet the requirements of Test No. 1.

5. TEST NO. 5 - ELECTRICAL CONNECTOR POTTING FLAMMABILITY TEST

Materials used as potting compounds shall be nonflammable in the test atmosphere during the application of current overloads up to the melting point of the conductor. In addition, the configuration shall meet the requirements of Test No. 1.

6. TEST NO. 6 - ODOR TEST

The nature and quantity of odor products as measured in the test chamber for a given sample size shall not exceed the rating of 2.5 as expressed in the acceptability criteria of Test No. 6. This test shall determine the odor characteristics of materials. The results of Test No. 7 shall be reviewed before conducting this test so that members of the odor team are not inadvertently exposed to toxic offgassing products.

7. TEST NO. 7 - DETERMINATION OF OFFGASSING PRODUCTS AND CARBON MONOXIDE TEST

Nonmetallic materials shall be screened to determine their suitability for use in the space vehicle crew compartment environments. Materials shall be tested for the production of potentially toxic, or objectionable, and condensible volatiles. Carbon monoxide, total organics, certain inorganics, and condensates shall be determined.

8. TEST NO. 8 - FLAMMABILITY TEST FOR MATERIALS IN VENTED CONTAINERS

The combustion characteristics of a fire in a closed (unsealed) container must be determined before the container is used in a spacecraft. The containers shall be tested

by internal or external igniters unless it can be demonstrated by evaluation, analyses, and rationale of all known test data that the materials applications will not introduce any flammability hazards that will jeopardize the mission. Potentially hazardous materials or instruments that contain such materials, which are removed from the container for operational purposes, must meet the requirements of Group I materials. This requirement is applicable if the materials remain out of the container beyond a time limit to be set by agreement among the program offices and Flight Crew Operations.

9. TEST NO. 9 - ELECTRICAL OVERLOAD TEST FOR SEALED CONTAINERS

The ability of sealed containers to withstand the effects of a fire initiated within the container resulting from an electrical overload requires testing of the materials in the container to ensure the container will not rupture. However, testing may be waived if it can be demonstrated by evaluation, analysis, and rationale of all test data that the materials applications will not introduce any flammability hazards that will jeopardize the mission.

10. TEST NO. 10 - GUIDELINES FOR SIMULATED PANEL AND ASSEMBLY FLAMMABILITY TEST

Spacecraft-exposed assemblies shall undergo fire tests that represent the most hazardous situation unless it can be demonstrated by evaluation, analyses, and rationale of all known test data that the materials applications will not introduce any flammability hazards that will jeopardize the mission. The combustion characteristics, particularly the propagation rate, of a number of different sizes and areas of nonmetallic materials of similar or different types that comprise a functional assembly, subsystem, or system in the spacecraft shall be determined.

11. TEST NO. 11 - GUIDELINES FOR SIMULATED CREW BAY CONFIGURATION FLAMMABILITY VERIFICATION TEST

Panels and assemblies of "worst case" materials must be tested for the purpose of determining the propagation, combustion phenomena, and behavior of the materials in the event a fire started in the spacecraft unless it can be demonstrated by evaluation, analyses, and rationale of all test data that the materials applications will not introduce any flammability or toxicological hazards that will jeopardize the mission. A mockup vehicle, configured in the same manner as the flight vehicle, shall be used for this test.

12. TEST NO. 12 - GUIDELINES FOR TOTAL SPACECRAFT OFFGASSING TEST

This test is designed to measure the total quantity and individual components of the products offgassed by a spacecraft during manned and unmanned chamber tests for determining the toxicological safety of the spacecraft during manned flight.

13. TEST NO. 13 - LIQUID AND GASEOUS OXYGEN MECHANICAL IMPACT TEST

All materials selected for use in contact with high pressure LOX and/or GOX whether directly or as a result of a single barrier failure must be acceptable for oxygen impact sensitivity according to the requirements and guidelines of this test procedure. Both ambient LOX and pressurized LOX and GOX test methods are included.

14. TEST NO. 14 - GASEOUS OXYGEN PNEUMATIC IMPACT TEST

This test is performed to determine the sensitivity of materials in contact with gaseous oxygen, whether directly or as the result of a single barrier failure, when subjected to pneumatic impact. The materials are tested over the pressure range of 50 psia to approximately 10,000 psia as directed by program requirements.

15. TEST NO. 15 - CONSTANT TEMPERATURE IMMERSION OF MATERIALS IN TYPE J FLUIDS

Materials used or considered for use in hazardous fluid systems other than oxygen, whether in direct contact with the fluid or as a result of a single barrier failure, shall be tested according to the guidelines of this procedure. The test determines the gross compatibility of materials in Type J fluids and it does not preclude the use of other tests to determine critical compatibilities. The data from other tests will be used for information purposes.

205 SYSTEM FLAMMABILITY REQUIREMENTS

Materials will be verified in end item configuration such as stowage in vented containers and simulated crew bay configuration flammability verifications, unless it can be demonstrated by evaluation, analyses, and rationale of all test data that the materials applications will not introduce any flammability and offgassing hazards that will jeopardize the mission. Prior to initiating tests, the cognizant design organization shall submit to the cognizant NASA Center for review and approval,

specific and detailed proposals that include drawings, photographs, specifications, test plans, and procedures for all items that require system tests. Systems tests shall duplicate contiguous materials and "worst case" operating conditions. The test plan shall identify the worst probable failure modes and the proposed test shall reflect the use of these modes. Test analyses and documentary records that include instrumentation data, photographic coverage, etc. shall be provided to the cognizant NASA Center at the conclusion of each systems test for review and approval. Test No. 10, "Guidelines for Simulated Panel and Assembly Flammability Test" and Test No. 11, "Guidelines for Simulated Crew Bay Configuration Flammability Verification Test" shall be used in planning the system flammability tests. For required systems or configuration tests, the use of a piece of functional equipment is not mandatory. Noncritical electronic and nonflammable parts can be simulated with respect to mass and geometry. The simulation must be approved by the cognizant NASA Center. Any assembly may be selected for test based on "worst case" configurations of potentially flammable materials. "Worst Case" shall include consideration of geometry, spatial relationships and material quantities. "Worst Case", is defined as an assembly or materials that present a maximum potential ignition/propagation hazard as indicated by analyses. This selection must consider:

1. Proximity of potential ignition hazards.
2. Propagation paths formed by proximal materials.
3. The quantity of flammable material in any given area.
4. The most hazardous oxidizing atmosphere and pressure to which it will be exposed.
5. Consequences of ignition.
6. Heat sink effects.
7. Single-barrier failure considerations shall be limited to potential leaks within a component that permit the fluid to directly contact the materials behind the barrier, for example, leaks from a fluid enclosure to an adjacent enclosure such as through the following:

   a. Welded or brazed joints
   b. Mechanical joints (e.g., B-nuts)
   c. O-rings, gaskets and bladders
   d. Metal and nonmetal diaphragms

   Redundant seals in series which have been acceptance pressure tested individually prior to flight shall not be considered.

206 SPACECRAFT OFFGASSING REQUIREMENTS

The spacecraft or its individual modules shall be offgassed during manned and unmanned chamber tests. The individual offgassed components shall be identified and measured, and the total quantity of the products shall be reported to the responsible NASA Medical Office. The test shall be conducted at the lowest habitable operating pressure. Where it is not feasible, as determined by the procuring agency, to test a complete spacecraft or a specified module, an analysis of the data obtained from offgassing tests on systems, modules, and spacecraft that contain the same or similar materials may be performed by the cognizant design activity and medical office to establish the safety of the spacecraft atmosphere.

207 RELATED CONSIDERATIONS

1. METALLIC MATERIALS

Metallic materials used in the design of equipment that will be exposed to the habitable environments shall be nonflammable or self-extinguishing in the designated spacecraft atmosphere and actual use thickness when determined by Test No. 1 and, if used in an oxygen system, they shall be oxygen compatible when tested in accordance with Test No. 13.

2. ISOLATION OF GROUP II MATERIALS

All efforts shall be made to isolate Group II materials from the crew bay environment and potential ignition sources by suitable design means. The resulting design shall be nonflammable when tested in accordance with the required applicable tests.

3. ELECTRICAL/ELECTROMECHANICAL EQUIPMENT

Electrical or electromechanical devices such as motors, heaters, control panels, lights, etc., shall meet the requirements of the applicable flammability, odor, and offgassing configuration tests.

208 TEST DISCIPLINE, RECORDS, AND REPORTING

1. TEST DISCIPLINE

a. Test plans and procedures will be written before each test and submitted to the cognizant NASA Center and testing agency.

b. Each test rationale, plan and procedure will be approved by the cognizant NASA Center before tests start.

c. Each test shall be directed by the cognizant Test Engineer/Conductor or his appointed alternate.

d. The Test Engineer/Conductor shall ensure that testing is accomplished in accordance with approved test plans and procedures and that recording of data and test results is complete and accurate. Each material to be tested shall be identified through one of the following:

(1) Manufacturer's Certification or Identification

(2) NASA Certification or Identification

(3) Contractor Certification or Identification

e. The test setup shall simulate the actual conditions that the materials under test will be subjected to during flight or ground tests.

Note: If response is not received in (time as specified in the contract) days following receipt of the test plans/procedures by the cognizant NASA Center, test programs may be initiated and test approval assumed.

2. TEST RECORDS

Complete test records shall be prepared by the contractor or NASA design/test activity for each material or system tested. The test conductor assigned for the conduct of each test is responsible for the acquisition, recording, and control of all test data. Records of applicable data are presented on the Test Record form similar to Figure 2-1. The test record format is flexible; however, all pertinent test data are to be recorded and maintained for test history purposes on all materials tested.

3. TEST REPORTING

Complete test records and additional supporting data, which could influence the acceptability of the material, shall be submitted to the cognizant Program Office before use or stowage in space vehicles. Test records should be available not later than hardware delivery to a contractor/NASA Center. The hardware cognizant NASA Center shall ensure that test data is distributed to all interested centers. Specific test data required for each test are presented in Chapter 4.

Test Title _____ Test Agency _____

Test Conductor _____ Test Number _____

Test Team Member _____ Date _____

Quality Assurance _____

Safety _____

Material (Chemical) Genesis _____

Chemical Composition _____

Manufacturer _____

Sample Size (Including Thickness in inches) _____

Power _____

Igniter _____

Chamber Volume in liters _____ Media _____ Vacuum _____

_____ Top Ignition _____ Bottom Ignition _____

Sample Number _____

GOX (%) _____

Chamber Pressure, (psia) _____

Sample Weight (grams) _____

Time to Ignition (seconds) _____

Total Burning Time (seconds) _____

Time to Propagate, 5 inches (seconds) _____

Self-Extinguishing _____

Weight Consumed (grams) _____

Burning Length (inches) _____

Time to Propagate 12 inches (seconds) _____

Flame Propagation Rate (inch/seconds) _____

Camera Coverage PPS/CPS _____

Combustion Pressure _____

Increase (psia) _____

Description of Test (Narrative) _____

Figure 2-1 Test Record Sample Form

CHAPTER 3 MATERIALS PROGRAM MANAGEMENT

300 GENERAL

The total materials control program involves the identification, evaluation, and resolution of potential flammability and off-gassing hazards resulting from the use of materials in manned or test spacecraft and associated test equipment. The major elements of a total program are:

1. MATERIALS IDENTIFICATION

   Identification and documentation of all materials used, both in original design and in any change, including weights, surface areas and applications both inside and outside the spacecraft.

2. USAGE EVALUATION

   Documentation of material applications and the comparison of test data to establish selection and test requirements to identify potential hazards.

3. TESTING

   Logic, procedures, and data documentation for the test program to support evaluation and full scale verification of modules, vehicles, or experiments, if warranted.

4. HAZARD REMOVAL

   Procedures involved in the removal of identified hazards.

5. DEVIATION PROCEDURES

   Procedures involved in documenting and approving materials that do not meet the established requirements but are proposed for use in the spacecraft due to lack of replacement materials or other considerations.

6. AS-BUILT CONTROL

   Procedures involved in assuring that no material hazards are introduced between initial design and mission completion.

7. FORMAL REVIEW PROCEDURES

   Procedures used to summarize the status of materials to permit certification of acceptability of a given design or a given configuration.

8. NEW TECHNOLOGY

Identify areas of new test technology or technique improvement for consideration.

301 MATERIAL CONTROL PROGRAM PLAN

Preparation and implementation of material control program plans are the joint responsibility of the cognizant NASA Centers and their respective contractors of contractor-furnished equipment and suppliers of Government-furnished equipment and experiments. The final control plan shall be approved by NASA Center assigned program responsibility. The contractor/supplier shall define in the control plan a systematic and continuing program to report and control material use, status, test, evaluation, substitution, and verification. The plan shall also contain detailed procedures for submitting deviation requests including drawing numbers, weights, surface areas as applicable, location, environment, etc. Before any evaluation testing is conducted, the applicable NASA Center Program Office must review and approve the need for the test. Such control plans shall contain as a minimum:

1. TEST FACILITIES

Before initiation of a test program, each facility must demonstrate to the cognizant NASA Center that equipment to be used is properly calibrated and will produce the same or equivalent results as related equipment used by other testing agencies. Equivalence in testing will also be demonstrated by each facility performing tests on standard material samples furnished by the cognizant NASA Center.

2. TEST ENVIRONMENT

All tests shall be conducted at the most hazardous test pressure and gas mixture conditions designated for the applicable program environment. A definition of these conditions shall be included as part of the program plan.

3. SYSTEM VERIFICATION AND TESTING

Materials requiring system verification shall be tested and accepted in accordance with Paragraph 205. Test plans shall be prepared for all contemplated configuration tests, simulated crew bay configuration tests, and total spacecraft tests. These test plans shall be submitted to the appropriate NASA Center Program Office for approval before initiation of test. If verification testing is required, the representative usage configuration and assemblies shall be tested.

4. NONFLIGHT EQUIPMENT

The contractor shall identify nonflight equipment, used during closed hatch tests, and the rationale supporting its use.

5. MATERIALS EVALUATION

Materials used in the design and fabrication of manned spacecraft and in facilities must be evaluated against the requirements of the proper groups (refer to Paragraph 200.B). Materials that do not meet the criteria of the pertinent material screening test shall be processed by one of the following selections:

a. The materials shall be rejected and substitute materials selected and tested.

b. The materials shall be subjected to configuration testing or analysis.

c. A deviation shall be required when:

(1) The nonmetallic materials at the configuration level will not pass the required application test or analysis based on similarity to other test configurations which indicate a possible hazard exists.

(2) The nonmetallic materials will not be subjected to a configuration test and the analyses are inconclusive.

6. PROCEDURES AND REQUIREMENTS CHANGE CONTROL

Procedures shall be established to resolve materials questions, problems, and deviation requests.

7. AS BUILT CONTROL

The contractor/supplier shall identify the activities that involve review of post design release documentation, control of material access to the spacecraft crew bay, and physical examination of the spacecraft by material specialists. Post release documentation review should include material review dispositions, test preparation sheets, which introduce materials without an engineering order, discrepancy reports, standard repair practices, and all applicable process specifications. Periodic examinations of the spacecraft/equipment at various stages

of manufacture shall be conducted as a part of a Fire Safety Inspection Procedure to identify violations of hazardous material usages.

8. FORMAL REVIEW PROCEDURE

A formal review procedure shall be established by the contractor as part of the materials control program to verify materials acceptability. The data presentation shall include applicable drawing identification, verification of drawing review, material status, deviation status, applicable test data, and hazard removal status.

302 QUALITY ASSURANCE (QA) PROVISIONS

Unless otherwise specified in the contract or order, the cognizant NASA Center is responsible for the performance of all test requirements as specified herein (performance of tests may be delegated to a test activity approved by NASA). The NASA or its designated representative reserves the right to perform any or all of the tests set forth in this specification where such tests are deemed necessary to assure that materials and systems conform to the prescribed requirements. If other than NASA test facilities are used, the contractor shall be responsible to the cognizant NASA Center for assuring that the testing agency conducts the tests in accordance with the following requirements:

1. All instrumentation used in these tests shall be in current calibration and shall bear appropriate documentation to this effect from an approved calibration laboratory.

2. All materials tested shall be accompanied by manufacturer's identification and the test specimens shall represent the materials proposed for use in construction of the spacecraft.

3. If assemblies or subassemblies are to be tested, the supplier shall certify that the test articles contain identical materials and potential ignition sources with equivalent geometrical configurations to those produced for use in the spacecraft or that they are identical to the installed equipment.

4. The testing capability of the laboratories and personnel involved shall be certified in accordance with applicable Center certification requirements that relate to the requirements of this document.

5. The complete results of each test shall be recorded in accordance with instructions contained in Paragraph 208 on a form similar to Figure 2-1.

6. The designated NASA materials control representative of the cognizant NASA Center will evaluate the test data and approve the materials/systems based on the criteria established herein.

CHAPTER 4 REQUIRED TESTS

400 GENERAL

Table 2-1 identifies the required tests for material usage types and materials group classifications. The test procedures and related test disciplines for tests Number 1 through 15 are presented in Paragraphs 401 through 415.

401 TEST NO. 1 - UPWARD PROPAGATION TEST

1. PURPOSE

The purpose of the upward propagation test is to determine the flammability characteristics of candidate materials when exposed along the bottom edge to an energized ignition source. Determination shall be made during the tests as to the sample's combustibility, self-extinguishing properties, and total burn time if not self-extinguishing.

2. CRITERIA OF ACCEPTABILITY

Materials shall be classified as Group I if determined noncombustible, or self-extinguishing before 6 inches of the sample are consumed, the time of burning not to exceed 10 minutes. There shall be no sparking, sputtering, or dripping of flaming particles from the test sample. The sample shall be hung vertically in the test chamber and the igniter placed at the bottom of the sample for a period of 30^{+20}_{-10} seconds. Materials that fail the above criteria shall be subjected to Test No. 2.

3. TEST CONDITIONS - PRESSURES AND ATMOSPHERE

The test pressure and gas mixture conditions for the pertinent materials category shall be designated by the program office. These conditions shall represent the most hazardous atmosphere anticipated in the spacecraft.

4. TEST EQUIPMENT

Materials applied in nonoxygen enriched atmospheres (such as air, 79% N_2 + 21% O_2) at 14.7 psia may be tested in a hood or in a chamber similar to that described in (a) below. The chamber described below is used for testing materials in oxygen or oxygen enriched atmospheres at other than the above pressure.

a. Chamber. The test chamber shall have a volume sufficient to assure complete combustion of the sample under test. It shall have a minimum volume of 98 liters and shall be suitably constructed and protected to ensure safe operation. A window or viewing port for visual observation shall be included. The test chamber shall contain inlets for vacuum, ignition wire, instrumentation, air, oxygen, test gas mixtures, and suitable elements for heating the chamber when required. The chamber shall be fully protected against the possibility of operator injury in the event of explosive rupture. Organic materials used in the construction of the chamber, such as gaskets and seals, shall be of a type that contribute little or no outgassing to the chamber or that can be pre-outgassed by vacuum cycling to a minimal identifiable amount (less than 10 parts per million (ppm) based on chamber volume). A vertical sample holder as specified in Paragraph 401.4.e below shall be positioned within the test chamber.

b. Pressure Gage. A pressure gage capable of measuring operating pressures with an accuracy of 0.2 psia or a pressure transducer and recorder with comparable capability shall be used.

c. Oxygen Supply. Oxygen used in conducting the test shall be commercially available and shall conform to Specification MIL-O-27210, Type 1, or MIL-P-25508, Type 1. Equipment used to transfer the oxygen to the test chamber shall be efficient and safe and conform to Type D requirements.

d. Gas Supply. Test gases, other than oxygen, shall conform to the appropriate specifications as required. Efficient and safe equipment shall be used for measuring the gas flow and for transferring the gas to the test chamber.

e. Sample Holder. The sample holder shall consist of a vertically mounted steel clamp that overlaps 1/4-inch on each side of a specimen along the full 12-inch minimum length of the sample, leaving a 2-inch wide by 12-inch long exposed center section. The sample material shall be located in the sample holder such that the bottom of the sample materials is located at least 3-inches from the chamber base to preclude the aid in propagation derived from a build-up of burning residue.

f. Ignition Source. Ignition of the sample shall be accomplished by employing a regulated energy source.

The ignition source for tests performed in an oxygen enriched atmosphere (other than air) shall consist of a length of No. 20 gage bare nichrome wire, which has a nominal resistivity of 0.7 ohms per foot, sufficient to wind six to eight turns around a standard silicone ignitor* or equivalent. (To be considered equivalent to a silicone ignitor an alternate ignitor shall provide a flame temperature in excess of 1500°F, a flame duration of 30^{+20}_{-10} seconds, a flame envelope 1 x 1/2 x 1 inch and shall not drip, sputter, or otherwise expel flaming particles.) At least one inch of wire shall be left at each end to permit fastening to the power source lugs. The ignition of the ignitor shall be accomplished by employing a regulated direct current power source. The upper edge or surface of the ignitor shall be placed approximately 0.25 inch from the bottom edge of the sample.

* The silicone rubber rod shall be prepared according to the following procedure:

82.5 parts by weight RTV-560 or equivalent shall be blended with 17.5 of RTV-577 or equivalent. To the mix, 0.5 parts by weight of Thermolite T-12 shall be added and thoroughly mixed. The blend shall be immediately deaerated in a vacuum of not less than 28 inches mercury for a period of not more than ten minutes. The compound shall then be cast in a mold that will provide rods, when cured and finished, of 0.22 inch diameter and 1.25 inch length.

The compound shall be cured either for 24 hours at room temperature or for four hours at room temperature followed by 10 hours at 130 $\pm$ 10°F. The cured material shall show a Shore A durometer reading of not less than forty (40).

For tests conducted in atmospheres which are not oxygen enriched, such as air, the silicone igniter cannot be used. An igniter, for example a Brunsen burner, which provides a temperature of 1500°F and a burn time of 30^{+20}_{-10} seconds in the selected atmosphere shall be employed.

g. Propagation Indicators. When requested by the Program Office, motion picture records shall be evaluated and retained on propagation tests. The camera shall be 16mm or equivalent, operating at a rate suitable to provide an accurate indication of the test. The equipment shall be calibrated to the manufacturer's specifications and shall be positioned such that an accurate determination of the total burn characteristics can be made from the films. As an alternative, a pulse camera may be used in conjunction with the stop watch used in (h) below.

h. Propagation Timers. All burning tests shall be visually observed for ignition and combustion characteristics. A stop watch shall be started at the first visual indication of combustion and stopped when the flame front reaches the top of the sample or the sample self-extinguishes, whichever occurs first.

5. SAMPLE PREPARATION

Samples shall be prepared for test as follows:

a. Inspection, Cleaning, Marking. Material samples shall be evaluated in the thickness intended for use whenever possible and shall be free of cuts, abrasions, or other flaws are determined by close visual inspection. Before testing, the samples shall be cleaned by brushing or by flowing an inert gas over them to remove loose surface contamination. Gage marks (wire or fiberglass threads) shall be placed across the samples at one inch intervals starting at the bottom of the sample.

b. Sizing. Sizing shall be accomplished in accordance with the following:

(1) Films, fabrics, sheets, and composites shall be tested in the "as received" condition. Samples shall be cut in the form of rectangles 2-1/2 inches wide by 12 inches long minimum. Foams and high bulk materials shall be tested in the "as applied" thickness and have the same minimum dimensions as specified above.

(2) Primers, coating materials, paints, and pressure sensitive tapes shall be applied on the substrate material intended for use, if known. The coatings shall be applied in a thickness equivalent to normal use and post cured in accordance with prescribed manufacturing practices. If the spacecraft substrate material is not available, the coatings shall be applied to 2.5 x 12.0 x 0.003 inch aluminum panels.

(3) Fluids and greases shall be applied to a suitable noncombustible substrate such as 0.005 inch thick fiberglass cloth. The substrate shall be allowed to soak in the fluid for a period of 30 minutes. Greases shall be applied to the substrate in a thickness of 0.010 inch.

Note: Materials and components that will be used in an irregular size or shape shall be tested in the "as purchased" configuration. Such samples shall be attached to the sample holder by fiberglass or metal threads when the sample cannot be held by the sample holder. This includes coaxial cable, thermocouple wire, other low energy signal wiring, and electrical wiring.

6. PRETEST PROCEDURE

The following pretest checks shall be performed before test start:

a. Verify that all test equipment is clean and is in current calibration, and that analytical equipment is calibrated and operative.

b. Observe placement of motion picture camera(s).

c. Verify that all other instrumentation is operative.

d. Verify that oxygen comforms to the classification specified in Paragraph 401.4.c and other gases are certified as required.

e. Verify that sample is correctly identified.

f. Prepare (3) samples as specified in Paragraph 401.5.

g. If samples are irregularly shaped, describe the shapes.

h. Weigh the samples and record the weight.

i. Record volume of the test chamber in liters verifying that it has a volume of at least 98 liters and is sufficient to assure complete combustion of the sample under test.

j. Mount the sample in the sample holder and verify that the exposed center section is 2.0 ± 0.1 inches wide.

k. Position the sample holder within the chamber.

1. Place the ignitor horizontally 0.25 ± 0.03 inches from the bottom of the sample at the midpoint of the (2 inch) exposed width.

7. TEST PROCEDURE

Testing of the candidate samples shall be accomplished in accordance with the following basic procedure for materials which will be applied in atmospheres at pressures less than 14.7 psia. Materials applied in atmosphere at 14.7 psia (such as air) may be tested in the chamber but the leak check steps can be deleted. These materials may also be tested in a hood but precautions must be taken to baffle the test sample from drafts. The applicable steps of the procedure shall then be followed.

a. Evacuate the chamber to less than absolute 0.2 psia.

b. Isolate the chamber and monitor the pressure for one minute. Testing shall not begin until all leaks are corrected (a leak is indicated if an increase in pressure of more than 0.2 psia occurs in two minutes).

c. Pressurize the chamber with test gas mixtures at the maximum use pressure.

d. Verify composition of the test gas mixture using analytical methods that are accurate and appropriate for the test conditions.

e. Allow the chamber to stabilize at the test pressure, then soak the samples in test gas mixture for a period of at least three minutes.

f. Verify that the chamber pressure is the desired test pressure, then isolate the chamber.

g. Start the motion picture camera and other applicable instruments.

h. Apply current to the ignition wire until the silicone rod ignites.

i. Record whether sample is noncombustible, self-extinguishing, and/or extent of burning.

j. Note combustion characteristics (nature and color of flame, soot, residue and other pertinent observations).

k. Record the final pressure in the chamber and the final temperature rise.

l. Return the chamber to the normal state.

8. REPORTING

The data shall be reported in accordance with instructions contained in Paragraph 208 on a form similar to Figure 2-1. The following special data are required:

a. Combustion Characteristics. Distance that flame progressed before extinguishing, flame phenomena and temperature, etc.

402 TEST NO. 2 - DOWNWARD PROPAGATION RATE TEST

1. PURPOSE

The purpose of this test is to determine the downward propagation rate of materials.

2. CRITERIA OF ACCEPTABILITY

Materials shall be evaluated for individual flame propagation properties to provide relative rankings for materials review and selection.

3. TEST CONDITIONS - PRESSURES AND ATMOSPHERE

The test pressure and gas mixture conditions for the pertinent materials category shall be designated by the program office. These conditions shall be representative of the most hazardous atmosphere anticipated in the spacecraft.

4. TEST EQUIPMENT

The test equipment shall be the same as that in 401.4.

5. PROPAGATION RATE INDICATORS

a. A vertical bank of a minimum of four thermocouple indicators positioned on the back of the sample combined with a recorder may be used in lieu of data from other devices. A precision of at least 5 percent shall be obtained with the measuring device. Loss of more than one thermocouple or loss of either end point thermocouple will invalidate the test.

b. Motion picture measurements may be used in lieu of thermocouples to measure the propagation rate.

c. Visual observations using manually activated timing devices may supplement the use of thermocouples or motion picture measurements.

6. SAMPLE PREPARATION

Samples shall be prepared in the same manner as described in Section 401.5.

7. PRETEST PROCEDURE

The pretest procedure shall be the same as that described Section 401.6.

8. TEST PROCEDURE

The test procedure shall be the same as that described in Section 401.7, except that the bottom edge or surface of the igniter shall be placed in contact with the top edge of the sample.

9. REPORTING

Test data shall be reported in accordance with instructions contained in Paragraph 208 on a form similar to Figure 2-1. The special information shall be the same as required under Section 401.8.

Card #10

403 TEST NO. 3 - FLASH AND FIRE POINT TEST

1. PURPOSE

The flash and fire test is designed to evaluate the spark ignition characteristics of materials selected for application in and around manned spacecraft.

2. CRITERIA OF ACCEPTABILITY

Flash and fire points shall be measured and recorded. Candidate materials shall be acceptable for design if they exhibit a flash point above 400°F and a fire point above 450°F.

3. TEST CONDITIONS - PRESSURE AND ATMOSPHERE

The test pressure and gas mixture conditions for the pertinent materials category shall be designated by the program office. These conditions shall represent the most hazardous atmosphere anticipated in the spacecraft.

4. DEFINITIONS

a. Flash Point. The flash point is the lowest temperature at which a material will give off, at or near its surface, flammable vapor which, when mixed with the test atmosphere and exposed to an ignition source, will provide a nonself-sustaining flash or flame.

b. Fire Point. The fire point is the lowest temperature at which the mixture of vapors from the surface of the material and the test atmosphere continue to burn after ignition. A self-sustaining self-propagating glow shall be considered equivalent to flaming combustion.

5. TEST EQUIPMENT

a. Test Chamber. The test chamber shall be the same or equivalent to that described in Section 401.4.

b. Spark Ignition Equipment. Spark needles shall be made of tungsten shaped to 0.004 inch radius point. Spark energy shall be supplied to the electrodes using the high voltage spark generator circuit. The total spark energy per pulse shall be 50 $\pm$ 20 millijoules with a spark duration of 2 $\pm$ 1 milliseconds.

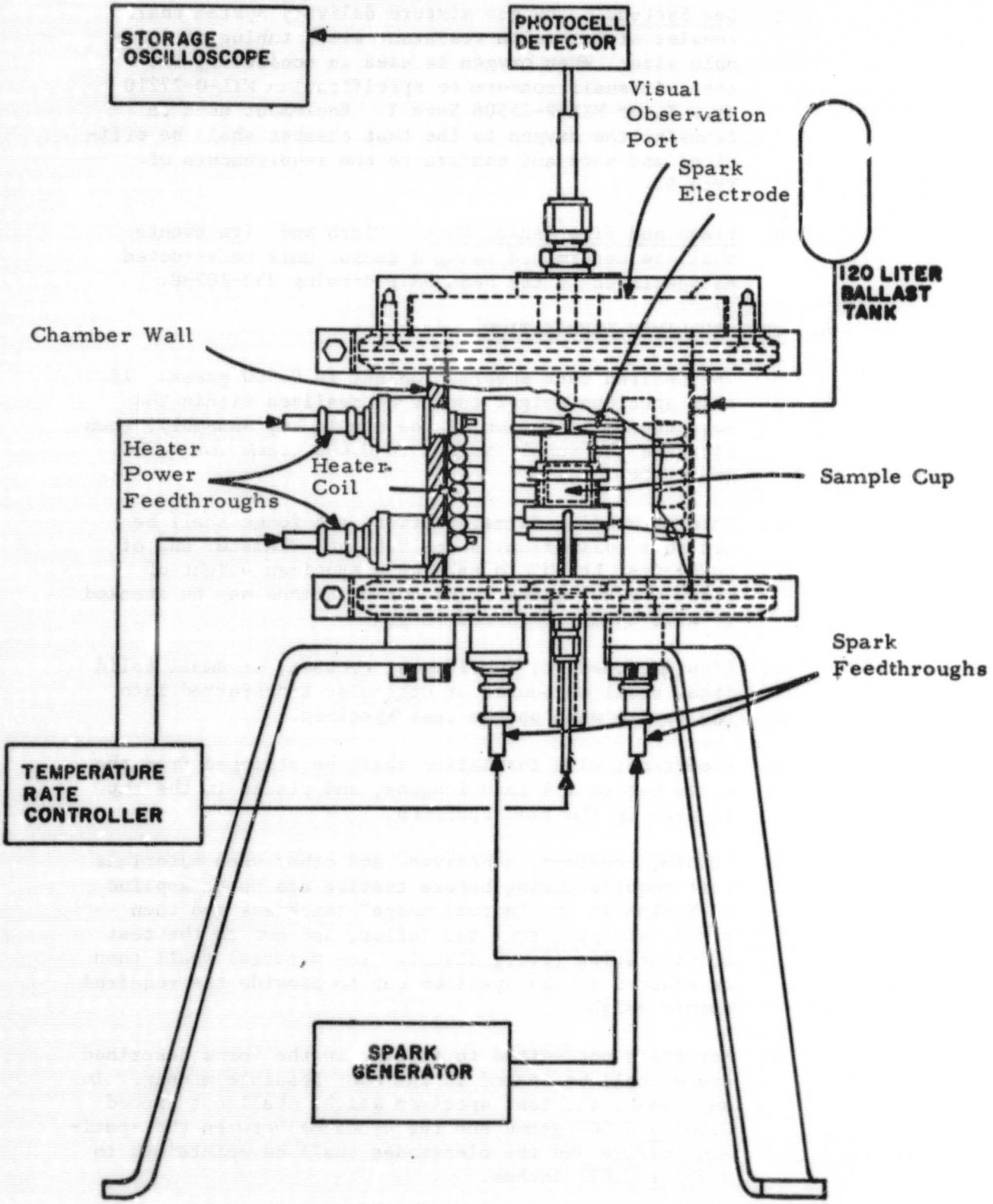

FIGURE 4-1 WSTF FLASH & FIRE POINT TEST APPARATUS & CONTROL SYSTEM

c. Gas Systems. The gas mixture delivery system shall consist of corrosion resistant steel tubing of suitable size. When oxygen is used in conducting the test, it shall conform to specification MIL-O-27210 Type I, or MIL-P-25508 Type I. Equipment used to transfer the oxygen to the test chamber shall be efficient and safe and conform to the requirements of Type D.

d. Flash and Fire Sensor Unit. Flash and fire events shall be determined using a sensor unit constructed as specified in the NASA WSTF drawing 252-10298.

6. TEST SPECIMEN PREPARATION

a. The desired test specimen weight is 0.500 grams. If this specimen weight cannot be realized within the adjustment limitation of the sample cup assembly, then decrease the sample weight to 0.400 grams (or 0.300 grams.etc.).

b. Bulk materials, films, fabrics, and foams shall be cut to a cylindrical shape 0.6 inch diameter and of sufficient height to make up a specimen weight of 0.500 ± 0.005 grams. The cut specimens may be stacked to make up the required weight.

c. Liquids, powders, lubricants, greases, or small solid items shall be poured or otherwise transferred into the cup to make up the test specimen.

d. Electrical wire insulation shall be stripped from the wire, cut to 1/4 inch lengths, and placed in the cup to make up the test specimen.

e. Paints, coatings, adhesives, and other such materials that require curing before testing are to be applied to Teflon in the "normal usage" thickness and then cured, stripped from the Teflon, and cut to the test configuration (i.e., discs). The material shall then be stacked in the specimen cup to provide the required sample weight.

f. Materials not suited to testing in the forms described above shall be tested in the most feasible manner. In any event, the test specimen weight shall not exceed 0.500 ± 0.005 grams and the distance between the specimen surface and the electrodes shall be maintained to 0.750 ± 0.025 inches.

g. The specimens shall be cleaned by blowing with dry nitrogen or air.

7. TEST PROCEDURE

a. The test chamber shall be thoroughly cleaned before each test. Black light may be used to detect the presence of residue.

b. Place 0.500 $\pm$ 0.005 grams of the test specimen into the cup.

c. Place the cup in the cup assembly.

d. Insert the spark electrodes and adjust the spark gap to 0.125 $\pm$ 0.025 inches.

e. Adjust the specimen cup assembly so that the distance between the specimen surface and the spark gap is 0.750 $\pm$ 0.025 inches.

f. Seal the test chamber and evacuate to at least 0.2 psia.

Note: A pressure rise greater than 0.2 psia in two minutes indicates a leak that must be corrected before proceeding with the test.

g. Pressurize the chamber to the desired test atmosphere and pressure.

h. Allow the spark to discharge across the electrodes for a total of 20 times before thermal programming. This step will establish spark uniformity.

i. Heat the specimen at the rate of 25 $\pm$ 5°F per minute. A single spark shall be discharged once for each 10^{+3}_{-0} seconds.

j. Record flash and fire points as detected.

k. Testing for flash and fire points shall be stopped when the maximum test temperature of 1000°F has been reached.

l. Depressurize and cool the chamber to ambient temperature.

m. Thoroughly clean the sample cups and interior of the chamber.

n. Repeat steps 403.7.a through m until the required number of samples has been tested.

8. ELECTRONIC DETECTION OF FLASH AND FIRE

A major advantage of the test system shown in Figure 4-1 is that sensitive instrumentation and visual observation are both used to monitor flash occurrences within the chamber. Some materials exhibit an apparent flash which has been defined as a "halo". The system described in Paragraph 403.5 records this halo effect and differentiates between the halo effect and a true flash point. This is accomplished by means of an oscilloscope, operated in the storage mode so that the spark output can be analyzed and retained on the scope's display console after its occurrence. Typical spark energy outputs observed on the oscilloscope are presented in Figure 4-2. The basic spark output is characterized as shown in "A" of Figure 4-2. When a material that exhibits the halo is being tested, the amplitude of the basic spark output generally increases by some small increment with each spark after a certain temperature is reached as shown in "B" and "D" of Figure 4-2. During a period when the halo is being observed, the displacement (horizontal) axis is vertically constant; only the energy amplitude increases. The halo does not propagate as does an actual flash. The halo appears like an ionized gas that adds energy to the spark only for the duration of the spark. An actual flash self-propagates for a time period longer than the spark time; hence, an increase in the time displacement will be observed. This is illustrated in "C" and "D" of Figure 4-2. Characteristics exhibited by materials as illustrated in "C" and "D" of Figure 4-2 are difficult to differentiate visually from the halo; however, the instrumentation display clearly indicates the occurrence of a flash. Examples "E" and "F" of Figure 4-2 illustrates the shape of flashes that can easily be distinguished. A sustained flash shall be considered as the fire point.

9. REPORTING

The test data shall be reported in accordance with instructions contained in Paragraph 208 on a form similar to Figure 2-1. The following special information shall be reported:

a. Maximum test temperature.

b. Flash point temperature °F.

c. Fire point temperature °F.

d. Observations (temperature of observed halo, sample discoloration, etc.)

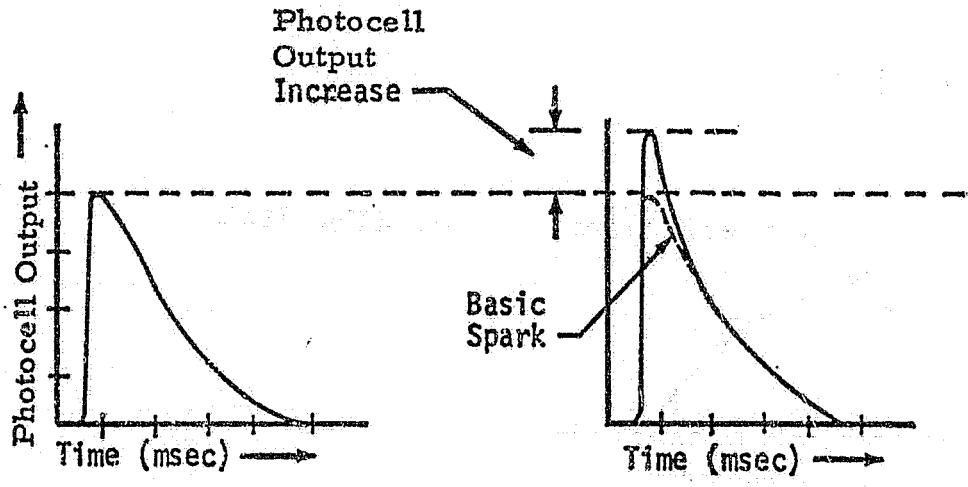

A. BASIC SPARK

B. "HALO" EFFECT

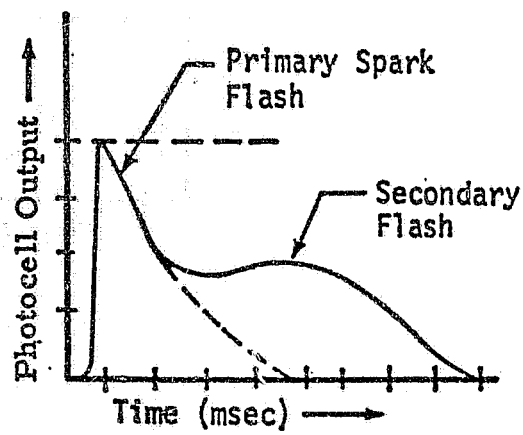

C. ACTUAL FLASH

Figure 4-2 Typical Oscilloscope Displays (Sheet 1 of 2 Sheets)

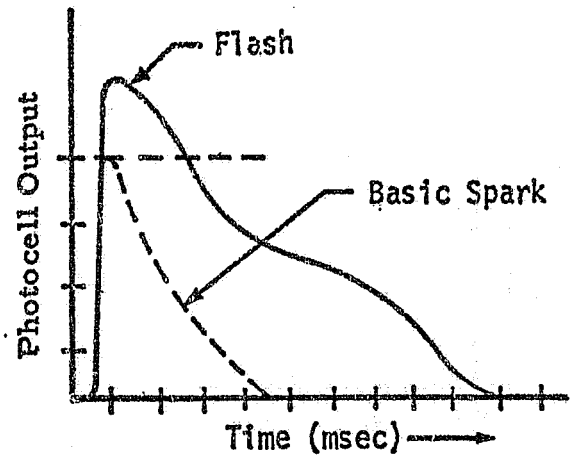

D. ACTUAL FLASH

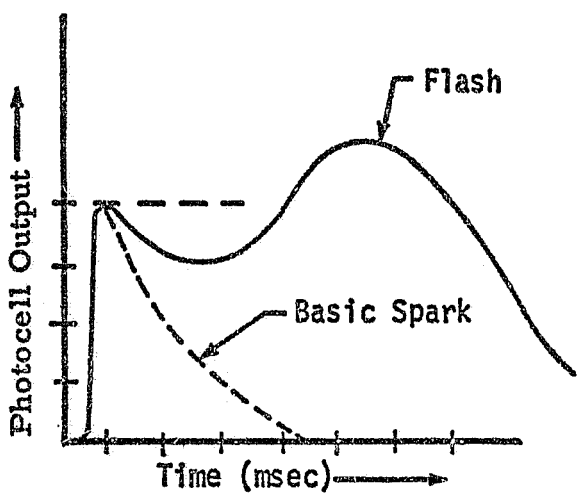

E. ACTUAL FLASH

F. ACTUAL FLASH

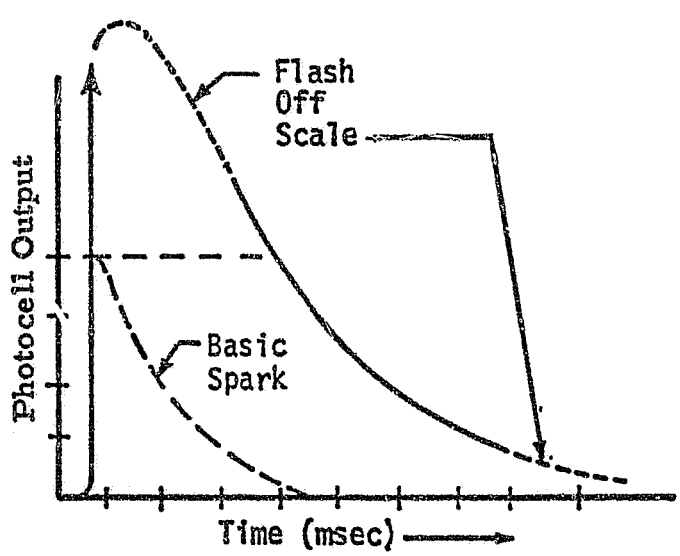

Figure 4-2 Typical Oscilloscope Displays (Sheet 2 of 2 Sheets)

404 TEST NO. 4 - ELECTRICAL WIRE INSULATION AND ACCESSORY FLAMMABILITY TEST

1. PURPOSE

This test is designed to screen wire insulation and electrical accessory material for flammability characteristics. Electrical accessory material consists of wire bundle sleeving, heat shrinkable tubing, solder sleeves, bundle ties, cable clamps, and identification tags.

2. CRITERIA OF ACCEPTABILITY

Electrical wire insulation and accessories shall be noncombustible in the test atmosphere during the application of current overloads up to the melting point of the electrical conductor and in addition, meet the requirements of Test No. 1.

3. TEST CONDITIONS - PRESSURES AND ATMOSPHERES

The test pressure and gas mixture conditions for the pertinent materials category shall be designated by the program office. These conditions shall represent the most hazardous atmosphere anticipated in the spacecraft.

4. TEST EQUIPMENT

The test equipment shall be the same as that described in 401.4, items a through d.

a. Sample Holder. The sample holder shall consist of two horizontally mounted electrical connections, i.e., knurled bolts, spaced 12 inches apart. Three nonflammable center supports shall be provided to support the center and end of the sample wire bundle. The electrical terminals shall be connected to the ignition power source.

b. Ignition Source. An external electrical power supply shall be provided which is capable of providing a large steady current through one wire of the sample bundle so that a high temperature will be achieved quickly. The power source must be capable of supplying a current 10% above the nominal fusion current for the gage wire being tested in accordance with the following schedule.

Wire Gage No.	Initital Test Current (amps)	Nominal Fusion Current (amps)
28	10	15
26	15	20
24	20	30
22	25	40
20	40	60
18	60	80
16	100	120
14	140	160
12	205	225
10	230	300

5. SAMPLE PREPARATION

a. Wire Insulation Samples

(1) Insulated wire samples shall be free of cuts, abrasions, or other flaws as determined by close visual inspection.

(2) Prior to testing, the samples shall be cleaned of foreign matter and residue using a method compatible with the insulation being tested.

(3) A test bundle of seven insulated wires, six of which are 12 inches in length and the seventh wire 13 inches in length, shall be tightly bound together, using Bently-Harris STFE-30 or equivalent lacing tape, in four places approximately 3 inches apart. The 13 inches length of wire shall be positioned on the exterior of the bundle in intimate contact with adjacent wires and shall be stripped of 1/2 inch of insulation on each end. A crimp spade lug terminal shall be used at each end to terminate the overload wire and provide a heat sink. The wires shall be laid up parallel to each other and one end of the bundle shall be twisted 180° relative to the other. Electrical harnesses and accessories as used in actual applications, including connectors, may be used in lieu of the above configuration. The mating connector with electrical wiring to power electrode must be either ceramic insulated wire or bare copper wire of lower gage number than that used in the test bundle.

b. Electrical Wire Accessories

(1) Accessory specimens shall be free of cuts, abrasions or other flaws as determined by close visual inspection.

(2) Accessory specimens shall be installed over or adjacent to wire bundles, prepared per Paragraph 404.5, in the manner in which they are intended to be installed in the spacecraft.

6. PRETEST PROCEDURE

a. Verify that all test equipment is clean and in current calibration.

b. Verify gas certification.

c. Visually inspect each sample (there shall be no cuts, abrasions, or other flaws).

d. Prepare three samples per Paragraph 404.5.a.

e. Install wire accessories per Paragraph 404.5.b. Document installation configuration details.

f. The sample bundle shall be mounted in the sample holder and positioned within the test chamber by fastening one end of the stripped wire to each of the electrical connection posts. The sample bundle shall be supported in the middle by a center support, constructed with a nonflammable material.

g. Record wire gage number.

h. Record power supply current capability in amps. Power supply must meet the requirement of Paragraph 404.4.b for the gage wire being tested.

i. Record thickness of wire insulation in mm.

j. Record volume of chamber in liters.

7. TEST PROCEDURE

Testing of the candidate samples shall be accomplished in accordance with the following basic procedure for materials which will be used in atmospheres at pressures less than 14.7 psia. Materials used in an atmosphere at 14.7 psia (such as air) may be tested in the chamber but

the leak check steps can be deleted. These materials may also be tested in a hood but precautions must be taken to baffle the test samples from drafts. The applicable steps of the procedure shall then be followed.

a. Evacuate the chamber to 0.2 psia or less.

b. Allow the chamber to stand for two minutes. A leak is indicated if an increase in the test chamber of greater than 0.2 psia is observed at the end of that time. If a leak occurs, the chamber will be brought to atmospheric pressure, leak corrected, and steps 404.7.a and 404.7.b repeated. Repressurize the chamber to test pressure with the test gas.

c. After the chamber has stabilized at test pressure, soak the specimen for at least three minutes. Record soak time.

d. Verify chamber pressure is test pressure and isolate the chamber.

e. Apply a current per initial test current of Paragraph 404.4.b to the wire. If ignition is not obtained in one minute, the current shall be increased in 5 amp steps at one minute intervals until the wire fails or ignition occurs. If the wire fails, the voltage shall remain applied to the overloaded wire until it is positively established that current does not flow by bridging the gap to adjacent conductors.

f. Record current level at which ignition occurred or the wire failed. Record if combustion was sustained or halted upon removal of ignition source.

g. Return the chamber to the normal state.

8. REPORTING

Test data shall be reported in accordance with instructions contained in Paragraph 208 on a form similar to Figure 2-1. The following special data shall be reported:

a. Configuration of the test item.

b. Combustion characteristics and phenomena; self-extinguishing or burned.

c. Current level at end of test.

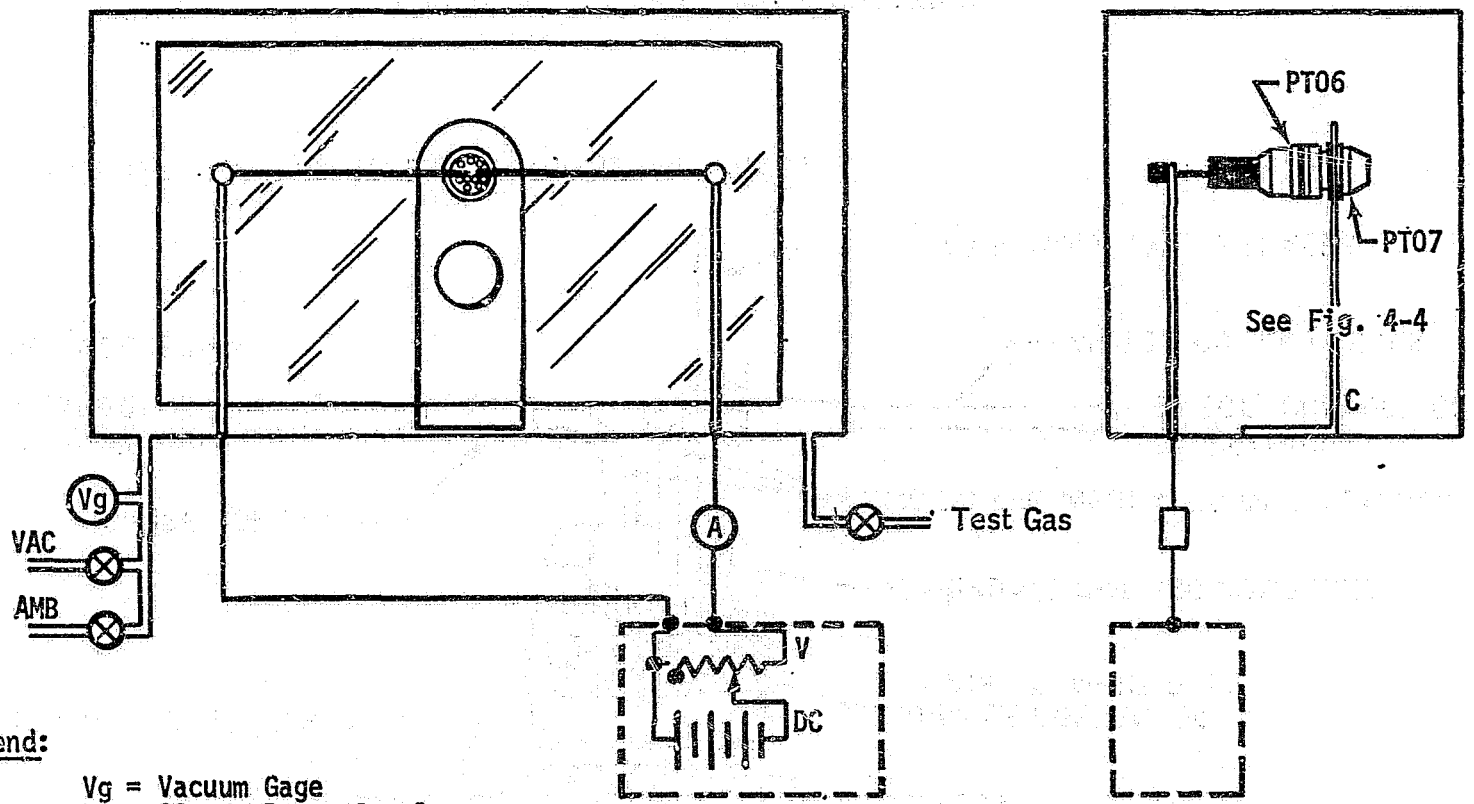

Legend:

Vg = Vacuum Gage
DC = 28 vdc Power Supply
V = Variable Resistor
A = 0 to 100 Amp Ammeter
C = Central Connector Mount
PT06 = Bendix PT 06-CP-18-11P Straight Plug
PT07 = Bendix PT 07-CP-18-11S Jam Nut Receptacle

Figure 4-3 Potting Flammability Test Equipment Schematic

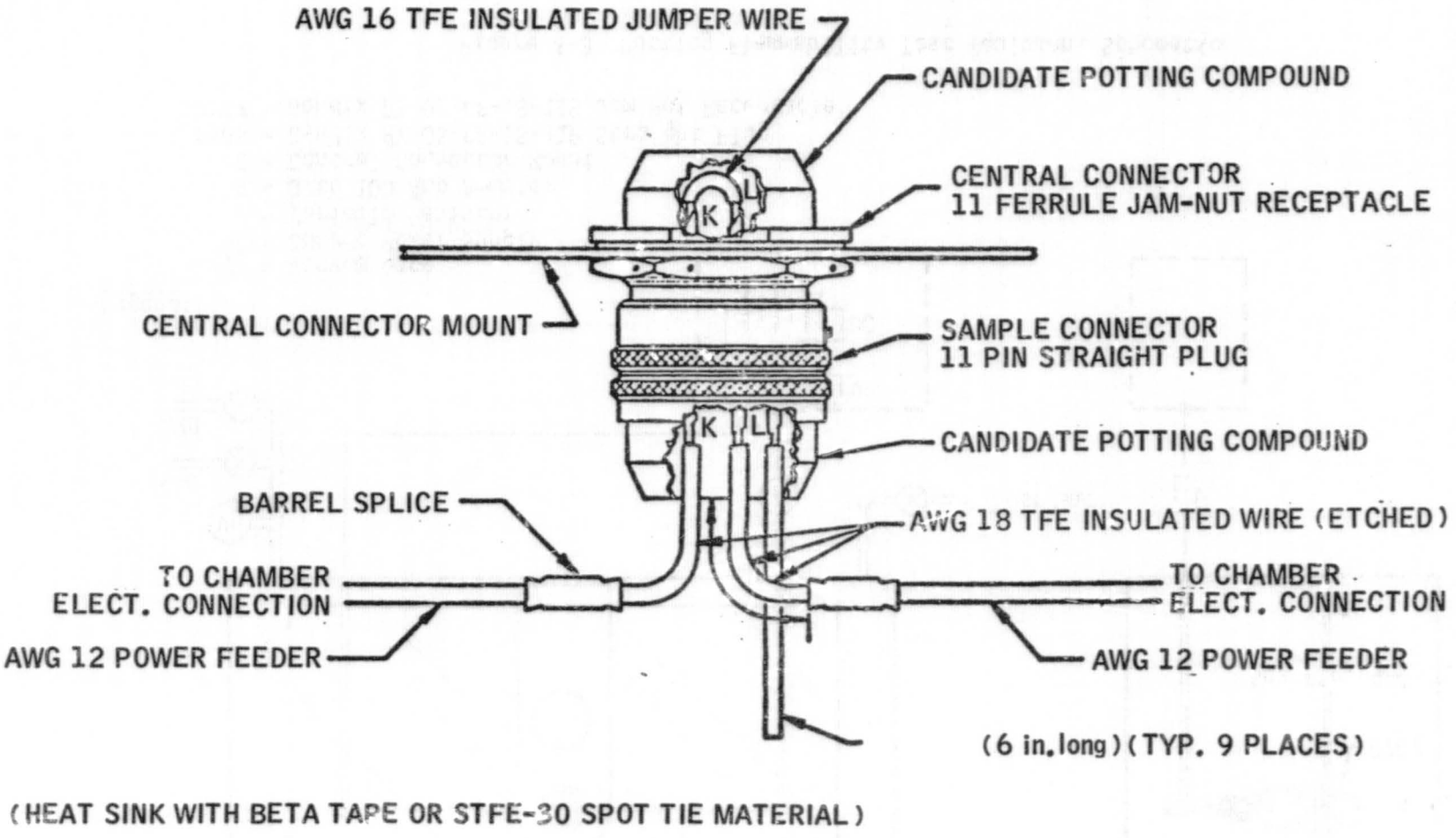

FIGURE 4-4. SAMPLE CONFIGURATION

405 TEST NO. 5 - ELECTRICAL CONNECTOR POTTING AND CONFORMAL COATINGS FLAMMABILITY TEST

1. PURPOSE

This test evaluates the flammability characteristics of spacecraft potting and coating compounds in a specific gas atmosphere environment. It is designed to simulate a short circuit or dielectric breakdown of current carrying wires, or connector contacts within the potting or coating used to environmentally seal electrical connectors and circuit boards.

2. CRITERIA OF ACCEPTABILITY

Connector potting, and coating compounds shall be noncombustible in the test atmosphere during the application of current overloads up to the melting point of the electrical conductor and in addition, meet the requirements of Test No. 1.

3. TEST CONDITIONS - PRESSURES AND ATMOSPHERES

The test pressure and gas mixture conditions for the pertinent materials category shall be designated by the program office. The conditions shall represent the most hazardous atmosphere anticipated in the spacecraft.

4. TEST EQUIPMENT

The test equipment shall be the same as that described in 401.4, items a through d.

a. Sample Holder and Connector Mount. The sample holder shall consist of two horizontally mounted electrical connections (bolt with knurled nuts) spaced 12 inches apart. The electrical terminals shall be connected to the ignition power source. A central connector consisting of a vertical panel drilled to receive a horizontal Bendix PT07 Jam Nut Receptacle or equivalent shall be provided. See Figures 4-3 and 4-4.

b. Ignition Source. An external power supply shall be provided which is capable of providing a large steady current so a high temperature will be achieved quickly. The power source must be capable of supply 100 amperes of current through the No. 18 AWG overload conductor.

5. SAMPLE PREPARATION FOR POTTING COMPOUNDS

a. Prepare three samples for each candidate potting compound per Paragraphs 405.5.b through 405.5.j below.

Note: Electrical harness and accessories as used in actual applications including connectors may be used in lieu of the hardware called out below. A direct short must be built into this system.

b. Prepare a 6 inch length of AWG 18 white Teflon insulated wire (MIL-W-16878, Type E, or MIL-W-22759, Type MS21985) as follows:

(1) Form a U-bend in the middle of the wire and etch the center 4 inches per JSC Specification Q-3.

(2) Strip 1/4 inch insulation from each end.

(3) Cut the wire in half such that 2 inches of etched insulation remain on the unstripped end of each 3 inch length.

c. Prepare two 6 inch lengths of AWG 12 white TFE Teflon insulated wire. Strip 1/2 inch of insulation from one end of each wire 1/4 inch from the other end.

d. Crimp the 1/4 inch exposed AWG 12, 6 inch wire to the 1/4 inch exposed AWG 18, 3 inch wire using a standard copper barrel crimp sleeve. Repeat for the second wire.

e. Slide a 1 inch length of FEP Teflon heat shrinkable sleeving over each barrel crimp; shrink using a hot air gun.

f. Obtain a Bendix Pygmy PT06CP-18-11P Straight Plug or equivalent. Take the wires prepared and stripped per Paragraph 405.5.b above and crimp one wire to contact K and the second wire to adjacent contact L (see Figure 4-4).

g. Crimp nine etched white AWG 18 Teflon insulated wires, each 6 inches long, in the remaining contacts.

h. Place the potting boot on the connector and fill with the candidate potting compound, per the manufacturer's instructions. Ensure that the potting compound is within the recommended shelf life. Ensure that all

steps are followed exactly as they would be in flight hardware, including cleaning and priming of connector rear insert for bondable capability, degassing potting compound, proper humidity control, etc.

i. Cure per applicable user's procedure or manufacturer's recommended time/temperature for optimum properties.

j. Remove potting boot.

6. CENTRAL CONNECTOR PREPARATION

a. Prepare three central connectors per Paragraph 405.6.b through e.

b. Obtain a Bendix Pygmy PT07CP-18-11S Jam Nut Receptacle or equivalent. Crimp a short AWG 16 Teflon insulated jumper between contact K and contact L (see Figure 4-4).

c. Place the potting boot on the connector and fill with the compound to be tested.

d. Cure per manufacturer's instruction.

e. Remove potting boot.

7. SAMPLE PREPARATION FOR COATING COMPOUNDS

a. Prepare three samples for each candidate conformal coating compound as follows:

(1) Obtain an eight lug NAS1066-3-8 terminal block. Mount to a 4 x 15 x 0.020 inch aluminum base plate. See Figure 4-5.

(2) Prepare a 14 inch length of AWG 18 white Teflon insulated wire (MIL-W-22759, Type MS21985) as follows:

(a) Form a U-bend in the middle of the wire and etch the center 4 inches per JSC-SPEC-Q-3.

(b) Cut the wire in half and strip 1/2 inch of insulation from all four ends.

(3) Etch 2 inches of one end of each of six additional AWG 18 Teflon insulated wires, each 6 inches long, per JSC-SPEC-Q-3. Strip 1/2 inch of insulation from the etched ends.

(4) Form a U-bend in the middle of a 10 inch length of AWG 20 white Teflon insulated wire and etch the center 4 inches per JSC-SPEC-Q-3. Cut the etched portion of the wire to obtain a jumper 3 inches long, all of which is etched. Strip 1/2 inch from each end.

(5) Obtain ten MS20659 terminal lugs and crimp per manufacturer's instructions to conductors at etched ends of wires prepared per 7.a.(3) and (4) above.

(6) Fasten the nine wires to the terminal block as shown in Figure 4-5, using standard terminal board hardware.

(7) Overcoat the base plate, terminal block, wire lugs, and wire insulation to within 1/8 inch of the end of the etched portion with the candidate primer (if applicable) and conformal coating compound, applied to recommended thickness and in accordance with recommended application techniques.

(8) Cure per recommended time/temperature process.

8. TEST PROCEDURE FOR POTTED CONNECTORS

Testing of the candidate connector samples shall be accomplished in accordance with the following basic procedure for materials which will be applied in atmospheres at pressures less than 14.7 psi absolute. Materials applied in an atmosphere at 14.7 psia may be tested in the chamber but the leak check (step 2) can be deleted. These materials may also be tested in a hood but precautions must be taken to baffle the test samples from drafts. The applicable steps of the procedure shall then be followed.

a. After verifying the test gas certification, the sample prepared per Paragraph 405.5 and 405.6 shall be mounted in the sample holder by locking the PT06CP plug to the PT07CP receptacle which has been placed in the vertical panel provided for it, and fastened with a threaded locknut. The stripped ends of the lengths of wire crimped into the plug shall be fastened to the current supply terminals of the sample holder.

b. The test chamber shall be evacuated to a pressure of 0.2 psia or less and repressurized to the test pressure with the test atmosphere. Allow the chamber to stand for one minute. A leak is indicated if an increase in test chamber pressure of 0.2 psia is observed during

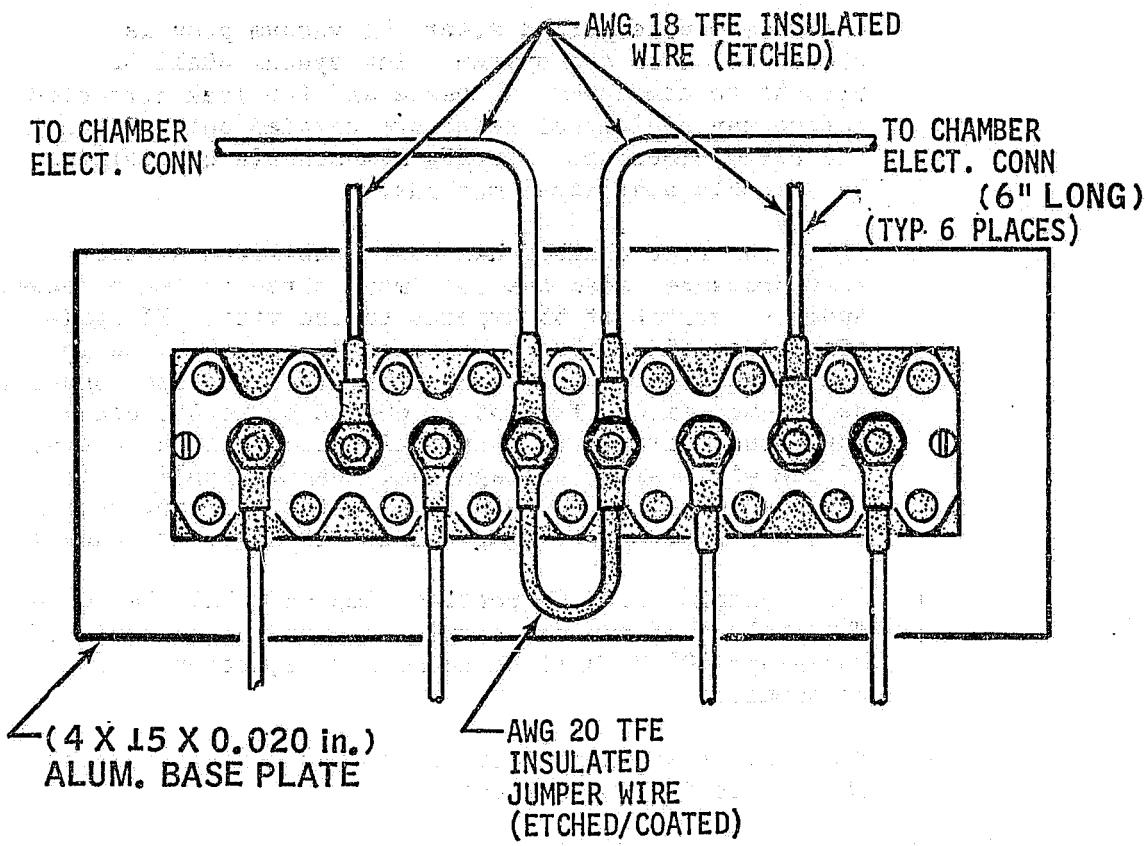

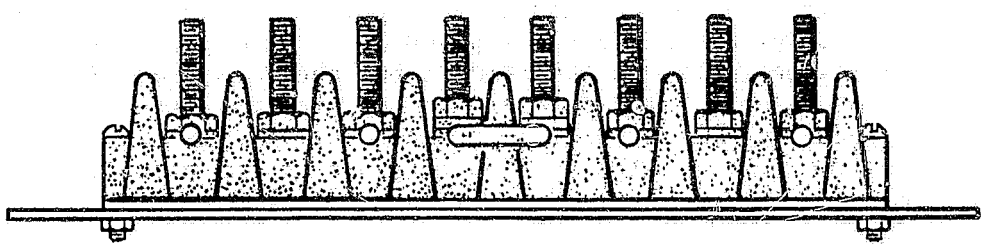

NAS1066-3-8 TERMINAL BLOCK ASSEMBLY*

*Procurable from Olympic Plastic Co.,
3471 So. La Cienega Blvd., Los Angeles, Calif.,
or Seastrom Mfg Co., 701 Sonora, Glendale, Calif.

Note: Shaded areas to be coated with candidate conformal coating.

FIGURE 4-5 . CONFORMAL COATING SAMPLE CONFIGURATION

the five minute period after the vacuum pump is closed off from the system. The system shall be brought to atmosphere pressure and the leak corrected before any additional tests are carried out. Repeat the above procedure. Verify atmospheric composition by suitable analytical methods.

c. After the test chamber has been stabilized at the test pressure, soak the specimens three to ten minutes. Apply a current of 55 amperes to the wire. If ignition or considerable degradation is not obtained in one minute, the current shall be increased five amperes per minute (i.e., from 55 to 60 and 60 to 65, etc.) until such time as the wire fails or ignition occurs. If the wire fails, voltage shall remain applied to the open wire for one minute to establish that current does not flow by bridging the gap to adjacent conductors.

d. Three samples of each potting compound shall be tested. The failure of any one sample to meet the criteria of Paragraph 405.2 shall be cause for rejection of that compound.

e. The chamber shall be returned to the normal state at the conclusion of the test.

9. TEST PROCEDURE FOR COATING COMPOUNDS

Testing of the candidate coating samples shall be accomplished in accordance with the following basic procedure for materials which will be applied in atmospheres at pressures less than 14.7 psia. Materials applied in an atmosphere at 14.7 psia may be tested in the chamber but the leak check (step 2) can be deleted. These materials may also be tested in a hood but precautions must be taken to baffle the test samples from drafts. The applicable steps of the procedure shall then be followed.

a. The sample, prepared per Paragraph 405.7, shall be placed in the chamber and the stripped end of each 7 inch wire shall be fastened to a chamber electrical connection.

b. After verifying the test gas certification, the test chamber shall be evacuated to a pressure of 0.2 psia and repressurized to the test pressure with test atmosphere. Allow the chamber to stand for two minutes. A leak is indicated if an increase in test chamber pressure of 0.2 psia is observed during the two minute period after the vacuum pump is closed off from the system. The system shall be brought to atmospheric pressure and the leak corrected before any additional tests are carried out. Repeat the above procedure.

c. After the test chamber has been stabilized at the test pressure, soak the specimens 3 to 10 minutes. Apply a current of 40 amperes to the wire. If ignition or considerable degradation is not observed in one minute, the current shall be increased 5 amperes per minute (i.e., from 40 to 45 to 50, etc.) until such time as the wire fails or ignition occurs. If the wire fails, voltage shall remain applied to the open wire until it is positively established that current does not flow by bridging the gap to adjacent conductors.

d. Three samples of each candidate conformal coating shall be tested. The failure of any one sample to meet the criteria of Paragraph 405.2 shall be caused by rejection of that coating.

10. REPORTING

Test data shall be reported in accordance with instructions contained in Paragraph 208 on a form similar to Figure 2-1. The following special information shall be reported.

a. Current level at the end of the test.

b. Results of each test including combustion phenomena if ignition occurs.

406 TEST NO. 6 - ODOR TEST

1. PURPOSE

The purpose of this test is to determine the odor characteristics of materials. A material that fails these requirements shall not be used.

Note: The results of Test No. 7 shall be reviewed before conducting this test so that members of the odor team are not inadvertently exposed to toxic offgassing products.

2. ODOR TEST REQUIREMENTS AND CRITERIA

a. Prerequisites to Selection of Odor Evaluation Test Panel.

(1) Review NMI7100.8 "Human Research Policy and Procedures" to determine applicable procedure.

(2) Prepare protocol and authorization of human research where required by Paragraph 8, NMI7100.8.

(3) Prepare voluntary consent forms for signature of test panel members where required by Paragraph 6, NMI7100.8.

b. Selection of Test Panel for Odor Evaluation

(1) The test conductor shall establish a pool of qualified personnel composed entirely of either NASA or contractor personnel.

(2) Where contractor personnel are used, NASA contracts shall include human research activity within the statements of work in order that applicable state workmen's compensation statutes will apply in the event of injury.

(3) Each member of the pool shall be capable of detecting seven basic odors from the following solutions:

Primary Odor	Standard Compound	Amount Dilution In Water
Ethereal	1,2-Dichloroethane	0.4 ml in 500 ml
Camphoraceous	1,8-Cineole	5 µl in 500 ml
Musky	15-Hydroxpentadecanoic acid lactone	1 mg in 1,000 ml
Floral	1-methyl-1-ethyl-2 phenyl propanol-1	0.075 ml in 500 ml
Minty	methone (dl)	2 µl in 333 ml

Primary Odor	Standard Compound	Amount Dilution In Water
Pungent	Formic acid	25 ml of 90 percent solution in 500 ml
Putrid	Methyl disulfide (Methyl dithiomethane)	1 ul in 10,000 ml

(4) Members of the pool shall be given three odorless solutions along with the seven primary standards for detection of odor.

(5) The solutions shall be freshly prepared once a month or as needed and stored in closed amber bottles away from heat sources and direct sunlight.

(6) The established pool for odor evaluation shall be requalified every three months.

(7) A panel of at least five members shall be selected from the pool for odor evaluations.

(8) Odor panel members shall receive a nose and throat examination by a medical staff member before and after each odor test session.

(9) Members of the pool shall not participate on the panel if their sense of smell is affected in any manner such as by recent smoking, ingestion of highly flavored foods, and exposure to pungent vapors.

(10) At least one of the seven odors shall be presented to the panel as a standard for sensing odor before evaluation of odors from any sample material.

(11) Panel members shall not be permitted to see the material, nor to know the gas sample being evaluated for odor, nor to see the ratings of the other panelists.

(12) Odor evaluation on sample materials shall be performed in a room actively ventilated and free from extraneous odors.

(13) Odor evaluations shall be performed on every new bottle of oxygen or gas used for the tests.

(14) Provisions shall be made for flushing the face mask of residual odors.

c. Odor Evaluations and Acceptance Criteria

Members Rating	Test Conductor's Rating
Undetectable	0
Barely Detectable	1
Easily Detectable	2
Objectionable	3
Irritating	4

An average rating of 2.5 or lower of any sample material by the panel members, signifies the material passes the odor test.

3. TEST CONDITIONS - PRESSURES AND ATMOSPHERE

a. The test pressure and gas atmosphere conditions for the pertinent materials category shall be designated by the program office.

b. Leak Check. The test system shall not increase in pressure more than 0.2 psia while remaining at a reduced pressure of 0.2 psia for a time period of one hour after isolation from the pump.

c. The sample materials shall be heated at test temperature corresponding to their maximum use temperature $^{+10^\circ}_{-0^\circ}$F for a test duration of at least 72 hours.

d. Odor evaluations shall be performed within 72 hours of the conclusion of the thermal treatment.

e. All measuring equipment shall have the proper calibration stickers.

f. All equipment shall be cleaned in accordance with commonly accepted laboratory practices and shall be given a distilled water rinse and oven dried at a minimum temperature of 200°F. The equipment shall be free of extraneous odors and contaminants before each use.

4. TEST EQUIPMENT

a. Test Chamber. The test chamber shall be made of Pyrex glass and its internal volume shall be two liters minimum. The test chamber shall have the following:

(1) A gas tight removable cover.

(2) A sampling valve.

(3) A sampling port capable of being sealed with a septum. A laboratory vacuum dessicator may be used as a test chamber.

b. Oven. The oven shall be capable of providing a constant interior temperature from 70 ± 2°F up to 200 ± 5°F.

c. Test Gas Supply. The test gas shall be commercially available and conform to the appropriate specifications. Suitable equipment for transferring gas to the test chamber shall be used.

d. Sample Transfer Equipment. Glass syringes, of 3 cm^3 minimum capacity, shall be used for measuring and transferring sample atmospheres from the test chambers to the panel members' face mask.

e. Pressure Gage. The pressure gage shall be capable of measuring absolute pressures to within 0.2 psia accuracy.

f. Olfactometer. The olfactometer shall consist of a mask made of odorless flexible material which can be applied to a panel member's face.

g. Odor Testing Equipment. All odor testing equipment shall be nonproducers of odor and carbon monoxide, as set forth under the test conditions in Paragraph 406.3.

5. TEST SPECIMENS PREPARATION

a. Categories. All the materials to be tested shall be classified into four categories; surface, volume, weight, or specialized items.

b. Samples Based on Surface. This classification is defined as all those materials that are essentially two dimensional. This would include films, fabrics, coating, finishes, inks, primers, adhesives, thin film lubricants, tapes, and electrical insulating materials.

(1) The sample tested shall have a surface area of 46.5 ± 2.5 square inches per liter of test chamber. Coatings, finishings, etc., shall be coated on clean aluminum substrate of 0.020 ± 0.001 inch thickness. Material thickness, curing process,

and method of application shall be accordance with the manufacturer's recommendations. Material may be coated on both sides of the aluminum panel. Tapes and other similar materials with an adhesive surface shall be fastened to a similar aluminum panel. In all cases, only the outer surfaces of a material on the aluminum panel is counted in the surface area determinations. Films, fabrics, and, similar materials shall be cut to give 46.5 ± 2.5 square inches surface. Because these materials are two surfaced in use, both the top and bottom surface shall be counted in determining total surface area. Heat shrinkable tubing shall be applied and shrunk to simulate actual use configuration.

c. Samples Based on Volume

(1) This classification is defined as all those materials having a definite volume but having a large real surface area due to surface convolutions or matting. These shall include foams and other blown or foamed materials and insulation padding.

(2) Samples of these materials shall be cut to a thickness of 0.50 ± 0.05 inch unless the existing thickness is less than 0.50 inch. In this case, the existing thickness shall be used. The material shall be cut to such a size as to give 7.75 ± 0.75 square inches of total surface per liter of test container volume. All surfaces, tops, bottoms, and sides shall be used to compute total surface area. In cases where the natural thickness is such that the material cut would be too large to be placed into the container, two or more pieces may be cut as long as the total surface area requirement is met.

d. Samples Based on Weight

(1) This classification is defined as all those materials having a definite bulk and not falling into the volume classification. This shall include potting compounds, molding compounds, cast or formed objects, solid wires, and thick plastics. Liquids that are not used or applied as coatings or thin films shall be included.

(2) The samples shall be used as much as possible in the supplied configuration and cut to give 5.0 ± 0.25 grams per liter of chamber volume. Potted or molded materials shall be prepared and cured

per manufacturer's directions and cut to weight. Liquids shall be placed in suitable nonreactive dishes 2.25 ± 0.25 inches in diameter. Sample weight shall be 5.0 ± 0.25 grams per liter of test chamber volume.

e. Specialized Items. It must be recognized that some materials will not meet the above classifications and must be specially handled. This will most often occur with nonhomogeneous materials. These cases will be tested in the manner designated by the Test Engineer in charge. The manner of testing and sample preparation shall be fully reported.

6. PRETEST PROCEDURE

Before odor testing, candidate materials must have been tested for total organics and carbon monoxide and must meet those criteria of acceptability.

7. TEST PROCEDURE

The procedure shall be conducted in the following order:

a. Sample materials shall be prepared according to the conditions outlined under sample preparation in Paragraph 406.5.

b. After placing the sample material in the test chamber, the chamber shall be evacuated to 0.2 psia or less. The test chamber shall then be pressurized to test pressure and test atmosphere.

c. The test chamber shall be exposed to a temperature not to exceed the actual use temperature $^{+10}_{-0}$°F in an oven for a time period at least 72 hours, allowing time for initial warm-up.

d. Following the isothermal exposure, the test chamber shall be removed from the oven and allowed to return to room temperature.

e. The pressure in the test chamber shall be measured and recorded after return to room temperature.

f. Observation of distillable residues on interior chamber walls shall be made and recorded.

g. The test chamber shall be pressurized to ambient atmospheric pressure with test gas and a sampling septum installed.

h. Odor Test. Known volumes of sample atmosphere shall be extracted from the test chamber by means of a syringe and diluted with fresh gas in the following proportions.

(1) One part of sample atmosphere to 29 parts of test gas.

(2) One part of sample atmosphere to 9 parts of test gas.

(3) No dilution, or as drawn from the flask.

(4) Odor dilutions shall be administered to panel members at random.

8. REPORTING

Test data shall be reported in accordance with instructions contained in Paragraph 208 on a form similar to Figure 2-1. The following special information shall be reported:

a. Average rating numbers determined by the panel members.

b. Definition of the odor as interpreted by each panel member.

c. Material category per Paragraph 406.5.

407 TEST NO. 7 - DETERMINATION OF OFFGASSING PRODUCTS AND CARBON MONOXIDE TEST

1. PURPOSE

This test establishes the criteria for a screening test, which will determine the suitability of nonmetallic materials for use in the space vehicle crew compartment environments. The criteria are established with respect to production of offgassing of potentially toxic, or objectionable, and condensable volatiles. The products are separated into three categories: carbon monoxide, organics and inorganics, and condensates.

2. DEFINITIONS

The following definitions apply to the terms as used in this test procedure.

a. Offgassing. The evolution of gaseous products from a liquid or solid material.

b. Condensables. The portions of offgassed products which condense on a cooled surface.

c. Total Organic Offgassing. The total of the organic gaseous and condensed products which offgassed from a material. This does not include carbon monoxide, water or carbon dioxide.

d. Total Inorganic Offgassing. The total of the inorganic gaseous and condensed products which offgassed from a material.

3. CRITERIA FOR ACCEPTABILITY

a. The maximum allowable level of total organics, excluding water, in the tested configuration shall not exceed 100 micrograms per gram of sample.

b. The maximum allowable level of carbon monoxide in the tested configuration shall not exceed 25 micrograms of carbon monoxide per gram of sample.

c. Inorganic gases such as HCN, ammonia, HCI, shall be recorded and evaluated by a toxicologist for potential toxicity levels.

4. TEST CONDITIONS - PRESSURES AND ATMOSPHERES

The test pressure and gas mixture conditions for the pertinent materials category shall be designated by the program office. These conditions shall represent the most hazardous atmosphere anticipated in the spacecraft.

5. TEST EQUIPMENT

a. Test Chamber. The test chamber shall have a minimum volume of two liters. It shall have a configuration and be fabricated of materials which allow ready cleaning. A thermometer or thermocouple and pressure gage for temperature and pressure determination, respectively, shall be included in the test chamber. The pressure gage shall be capable of measuring operating pressures with an accuracy of $\pm$ 0.2 psi absolute, a pressure transducer and recorder with comparable capability may be used. The chamber shall be connected so as to permit direct gas sample introduction from the chamber to a gas chromatograph and/or mass spectrometer.

b. Heating Source. The heating unit or oven shall maintain the temperature in the test chamber uniformly constant at the designated test temperatures. The temperature during sample exposures shall be recorded.

c. Vacuum Pump. The vacuum pump shall be capable of producing a vacuum in the test system of less than 0.2 psia.

d. Analytical Equipment. The analytical equipment shall consist of the following types of equipment and any other instruments that the tester desires to use efficiently to increase the accuracy, reliability, and confidence in the offgassing products evaluation.

(1) Gas Chromatograph System. The gas chromatograph system shall use a minimum of two detectors, viz., thermal conductivity and hydrogen flame ionization units with appropriate recorders. As a supplementary detector, the electron capture attachment/recorder is recommended. The separatory columns shall have the capability of separating light organic and inorganic gases, organic sulfides and mercaptans, halogenated hydrocarbons, representative aliphatic and aromatic hydrocarbons including aldehydes, ketones, alcohols, and esters. The hydrogen flame ionization detector has greater sensitivity to

organic materials. Conversely, because of the flame ionization detector's lack of sensitivity to the inorganic compounds listed above, the thermal conductivity detector is used for their identification.

(2) Recording Infrared Spectrophotometer capable of analyzing 3 microliters (3 µl) or less of liquid with accessories that include an infrared gas cell with 10m path length.

(3) Mass spectrometer.

(4) Cold trapping system suitable for trapping and transfer of microliter quantities of liquid to suitable analytical equipment.

(5) Gas Sampling System suitable for the transfer of measured volumes of gas samples from the test chamber to the gas chromatograph.

(6) Calibration Gas Samples as required to qualify detector sensitivity and readout. The calibrated gas samples may be obtained from a manufacturer or made up in the laboratory. The basic calibration gas to be used shall be methane.

6. SAMPLE PREPARATION

a. Prerequisites. Before loading the sample into the chamber, the chamber shall be filled to test pressure with the test atmosphere, heated at 150 ± 5°F for 24 hours, and the gas analyzed for a total organic off-gassing and carbon monoxide. The chamber shall be certified as clean for use if the total organics and carbon monoxide values are no higher by volume as methane equivalents, than that of the test atmosphere. After use, the chamber shall be reused without cleaning if the sample values are equal to or less than the above. If not, the chamber shall be heated and purged with air or nitrogen by some convenient method, such as a heat gun equipped with a blower. The chamber then shall be loaded to test pressure with test atmosphere, and tested to the above specifications.

b. Leak Check. The test systems shall not increase in pressure more than 0.2 psia while remaining at a reduced pressure of 0.2 psia for a time period of one hour.

c. Test Specimens. The materials to be tested shall be classified into four categories and prepared as detailed in 406.5.a through e.

7. TEST PROCEDURE

a. Purge the test chamber until the minimum purity of the test atmosphere is 95 percent of the use environment and then begin heating. Bring the chamber to 120.0 ± 3.5°F or to the designated test temperature, and adjust the chamber pressure to test pressure.

b. After 24 hours, check the test gas for contaminants with the gas chromatograph. Proceed to Paragraph 407.7.c if the total contamination is no more by volume then the test atmosphere. If the contamination exceeds the above value, the test chamber shall be flushed and rechecked after an additional 24 hours. This procedure shall be continued until the contamination is below the specific level. If the gassing contamination continues indefinitely, modification of the test chamber is indicated.

c. Place a clean, weighed specimen prepared per Paragraph 407.6.c in the test chamber.

d. The chamber shall be evacuated through a liquid nitrogen trap to below 0.2 psia. The chamber shall then be closed off and the test gas shall be filtered through a 13X Molecular Sieve and bled into the chamber to test pressure. The conditions of exposure are maximum use temperature, when designated, or 120 ± 5.0°F for a total period of 72 hours. Allow the chamber to cool until ready for test. After the final gas samples are taken, the test specimen is removed from the chamber and weighed. The gases are then analyzed for the following:

(1) Total organic offgassing expressed as pentane equivalents.

(2) All offgassing components exceeding 10 ug/g, excluding water vapor and carbon dioxide, shall be identified and quantified. These shall include but not be limited to the following:

Organic - benzene, xylene, methyl ethyl ketone, n-butanol, chloroform, dichloromethane, 1-4 dioxane, formaldehyde, and trichloroethylene.

Inorganic - hydrogen cyanide, hydrogen chloride, ammonia.

(3) Condensables - the identity and quantity of condensables shall be determined.

(4) Quantity of carbon monoxide evolved.

e. Condensables (organic and inorganic) shall be determined at room temperature. The condensed products shall be flushed from the test cell by solvent rinse or an equivalent method.

f. Offgassing components, including those listed in Paragraph 407.7.d.2 that exceed 10 ug/g shall be identified and the quantities recorded in the reporting format.

g. The carbon monoxide content or the evolved gases shall be determined above by using an appropriate separation and analytical technique having the sensitivity to detect within 0.5 ug/g CO.

h. All charts, equipment calibration information, and test data are to be retained in the event that further identification or evaluation is necessary.

8. REPORTING

Test data shall be reported in accordance with instructions contained in Paragraph 208 on a form similar to Figure 2-1. The following special data and pertinent information shall be reported:

a. Carbon monoxide in micrograms per gram.

b. Total gas phase organic offgassing in micrograms per gram as pentane equivalents.

c. Identity of all gas phase organic products greater than 10 ug/g.

d. Total inorganic gas phase species in micrograms/gram.

e. Identity and quantity of condensables.

408 TEST NO. 8 - FLAMMABILITY TEST FOR MATERIALS IN VENTED CONTAINERS

1. PURPOSE

This test describes the method for determining the ability of a closed (unsealed) container to withstand the effects of a fire internal or external to the containers. This test is applicable to containers with both internal ignition sources and external ignition sources.

Potentially hazardous materials, or instruments containing such materials, that are removed from the container for a period longer than established between the program offices and Flight Crew Operations must meet the requirements for Group I materials.

2. CRITERIA FOR ACCEPTABILITY

In the event of an internal fire, the container:

a. Shall not rupture and thus permit the escape of flames, burning debris or the scattering of flaming contents outside the chamer.

b. Shall not permit flames or burning materials to be emitted through vents.

c. The container shall not emit gases and heat to the extent that a rise in pressure measured in the test chamber when related to a corresponding rise in the module or vehicle might be sufficient to cause rupture of the walls of the habitable areas of the spacecraft.

3. TEST CONDITIONS - PRESSURES AND ATMOSPHERES

The test shall be performed on materials configured in a container in the same manner as the flight item. The most hazardous ("worst case") configuration of materials shall be determined and used in the test. The test pressure and gas mixture conditions shall be designated by the program office. These conditions shall represent the most hazardous atmosphere anticipated in the spacecraft.

4. TEST EQUIPMENT

a. Test Chamber. The test chamber shall be the same or similar to that described in 401.4.a.

b. Thermal Characteristics Indicators

(1) Temperature Monitoring. Thermocouple readings may be monitored by multiple point recorders or any equally accurate method. The desired accuracy is ± 10°F. The thermocouples may be placed inside the container spaced one inch apart along and in contact with the conductor selected for overloading. Where the external igniter is used, the thermocouples shall be placed on and around the material selected for ignition in accordance with the test engineer's direction. Additional thermocouples shall be placed approximately at the center of the top, bottom, and four sides of the interior. Thermocouples shall be placed on the exterior of the container against the top, bottom, and four sides, approximately in the middle of each panel.

c. Pressure Gage. A pressure gage capable of measuring operating pressures with an accuracy of ± 0.2 psia, or a pressure transducer and recorder with comparable capability, shall be used.

d. Motion or still pictures of the test are required.

5. IGNITION SOURCE

a. Internal Ignition. Ignition of the materials in the container with electrical wiring shall be accomplished by using a power supply that is capable of providing a large current through one wire of the conductor bundle so a high temperature will be achieved quickly. The power source must be capable of supplying a current for that gage wire being tested. Refer to Test No. 4, Paragraph 404.4.b, for the initial test current for wire gage number 28 through 12. Materials in a non-electrical container shall be treated as described in Paragraph 408.5.b.

b. External Ignition. Ignition of materials in a container without an internal ignition source shall be accomplished in the following manner. A silicone igniter or equivalent which is representative of the worst possible spacecraft fire shall be placed outside the container at a point closest to the most combustible material in the test configuration. Sufficient energy shall be supplied to ignite the igniter. The igniter shall be left in contact with the container until it burns out. The contractor shall furnish analyses to support the selection of ignition sources.

Note: In the event that the worst service condition specified above cannot be determined, the igniter shall be appropriately placed inside the container to serve as the ignition source.

6. SAMPLE PREPARATION

a. The container shall be the same size, geometry, and material as the flight container.

b. The equipment to be tested shall be the same as the flight equipment, with regard to nonmetallics. Electronic parts and similar expensive metallic or ceramic entities may be simulated.

c. The equipment shall be packaged and positioned in the container in the same manner as in the flight article. Thermocouples shall be exited through bushings or any adequately sealable means.

7. PRETEST PROCEDURE

a. Verify that all test equipment is in current calibration.

b. Verify that the container is the required item.

c. Verify proper attachment of thermocouples in the designated area.

d. Verify proper packaging and positioning of the materials and equipment.

e. Verify the gas certification.

f. Position the container in the chamber.

g. Verify the placing of the ignition wire in the designated spot in the container or that the conductor to be overloaded is hooked up to the proper, high current power supply.

h. Observe that the ignition wire, thermocouples and other instrument leads are hooked up to the pertinent outlets.

8. TEST PROCEDURE

Testing of the containers shall be accomplished in accordance with the following basic procedures for containers which will be exposed to atmospheres at pressures less than 14.7 psia. Materials applied in an atmosphere at 14.7 psia may be

tested in the chamber but the leak check steps (1 and 2) below can be omitted. These containers may also be tested in a hood but precautions must be taken to baffle the test area from drafts. The applicable steps of the procedure shall then be followed.

a. The chamber shall be evacuated to a minimum of 0.2 psia.

b. Isolate the chamber and monitor the pressure for five minutes to check for leaks. A rise of 0.2 psia during that time indicates a leak that must be rectified before going to the next step.

c. Pressurize the chamber to test pressure $\pm$ 0.2 psia with the test atmosphere.

d. After the chamber has stabilized at the proper pressure, permit the container to equilibrate for 15 minutes.

e. Start all applicable instruments.

f. For containers with an internal ignition source such as an electrical conductor, current shall be applied to the conductor at the amperage shown for that size conductor in the table in 404.4.b. If no effect is shown, the current shall be increased in five ampere steps at one minute intervals until the wire fails or ignition occurs.

g. For containers requiring external ignition, apply current to the igniter until ignition occurs or will not occur.

h. Observe all phenomena occurring in and around the container.

Note: The test shall be terminated if the container ruptures or if obviously excessive quantities of fire and smoke are emitted from the vents.

i. Record any pressure rise and the final pressure in the chamber.

j. Remove the container from the test chamber and examine it and its contents and record all observations.

9. REPORTING

Test data shall be reported in accordance with instructions contained in Paragraph 208 on a form similar to Figure 2-1. The following special test data and information shall be reported.

a. Identification by generic name of all the materials tested in the container.

b. Vendor and vendor designation for the materials.

c. Construction and source of container.

d. Presence or absence of flame or ignition failure.

e. Color of flame.

f. Evolution of smoke from the container.

g. Evolution of flame from the vents.

h. Length of time flame persisted from the container.

i. Length of time smoke evolved.

j. Rate of temperature and pressure rise and final temperature and pressure in the test chamber.

k. Condition of container after the test.

l. Condition of contents of the container after the test.

409 TEST NO. 9 - ELECTRICAL OVERLOAD TEST FOR SEALED CONTAINERS

1. PURPOSE

This procedure describes the method for testing materials packaged in sealed containers and the ability of the container to withstand, without rupturing, the effects of a fire initiated within the container as a result of an electrical overload. For containers with no internal electrical energy sources, the ignition system described in Paragraph 408.5.b. shall be used.

2. CRITERIA FOR ACCEPTABILITY

The sealed container shall not rupture and emit flame, burning particles, smoke or gas as a result of the test.

3. TEST CONDITIONS - PRESSURES AND ATMOSPHERES

The test conditions shall be the same as those described in 408.3.

4. TEST EQUIPMENT

1. Test Chamber. The test chamber shall be the same or similar to that described in 401.4.a.

2. Thermal Characteristics Indicators. The temperature monitoring shall be the same as described in Section 408.4.b.(1).

3. 16 millimeter motion picture camera(s) shall film the phenomena in case the container distorts or ruptures.

5. IGNITION SOURCE

The ignition of the materials shall be accomplished in the same manner as described in 408.5.

6. SAMPLE PREPARATION

The samples preparation shall be the same as that described in 408.6.

7. PRETEST PROCEDURE

The pretest procedure shall be the same as described in 408.7.

8. TEST PROCEDURE

The test procedure shall be the same as that in 408.8 except that the "Note" under 408.8.h. shall be changed to read, "The test shall be terminated if the container ruptures."

9. REPORTING

Test data shall be reported in acordance with instructions contained in Paragraph 208 on a form similar to Figure 2-1. The following special test data and information shall be reported:

a. Identification by generic and trade names of all the materials tested in the container.

b. Construction, configuration, and source of the container.

c. Presence or absence of ignition or fusion of the conductor.

d. Temperature changes inside the container and those measured on the outer walls of the container.

e. Phenomena associated with rupture of container, if rupture occured:

(1) Presence or absence of flame and smoke.

(2) Extent of scatter of burning or smoking materials.

(3) Part of container where rupture occurred.

(4) Pressure and temperature rise in chamber.

(5) Presence of gases and method of detection.

f. Condition of container after the test.

g. Condition of the contents after the test.

410 TEST NO. 10 - GUIDELINES FOR SIMULATED PANEL AND ASSEMBLY FLAMMABILITY TEST

1. PURPOSE

This procedure describes the method for determining the combustion characteristics particularly the propagation rate, of a number of different sizes and areas of non-metallic materials of similar or different types that make up a functional assembly, subsystem, or system in the spacecraft. (Each item usually requires a specifically developed procedure. Guidelines for establishing the parameters of the test follow). The purpose of flammability tests on assemblies is to determine the behavior of the assembly under the particular test conditions which shall be representative of the most hazardous situation to which the assembly will be exposed in the spacecraft.

2. CRITERIA FOR ACCEPTABILITY

The results of the burning of the assembly must be considered in light of their effects on the spacecraft external to the assembly, as well as the effects of the fire internal to the assembly. Acceptability shall be determined by the procuring activity on the basis of the results obtained during the testing of individual assemblies, subsystems, and systems.

3. TEST CONDITIONS - PARAMETERS AND INSTRUMENTATIONS

a. Configuration and materials of the test assembly will duplicate exactly the flight article.

b. Test assembly (combustion element) will be oriented in the chamber as it will be in the operational spacecraft at launch.

c. The test chamber volume will be sufficient to provide for complete combustion per the fire hazard analysis, and to accommodate the largest assembly to be tested with adequate space around the assembly to allow observation of the extent of projection of burning pieces due to sputtering and expansion of gases internal to the burning mass.

d. The test assembly will be operational before and during the test and will be tested for operation after the test.

(1) The "worst case" mode of operation, determined by the fire hazard analysis, will be selected.

(2) The test assembly will be in operation before the test until steady state conditions are reached.

e. For assemblies containing substitute materials or new designs, the test configuration need not be operational unless economically feasible. The materials shall be configured as in the flight article. Expensive components may be simulated, but the basic material, geometry, and simulated mass of the components must be the same as in the flight assembly.

f. All thermal interfaces will be simulated.

(1) Cold plates.

(2) Structure.

(3) Convection due to the cabin fan.

(4) Cabin radiation characteristics.

g. Environment. Pressure and temperature.

(1) Test chamber ambient temperature will be as anticipated in actual use conditions.

(2) Gas environments and pressures shall be defined by program requirements.

h. Instrumentation. Instrumentation requirements for each test assembly will be determined on an individual basis as part of overall combustion hazard analysis.

(1) Temperature Measurement. Temperatures will be continuously recorded during testing.

(a) Temperature measuring recording equipment will have response times equal to or greater than the rate of change of temperature at the location being measured as predicted by thermal calculations.

(b) Locations of temperature measurement devices will depend on the configuration of the assembly being tested. These should provide a temperature profile of the assembly and location of ignition sites.

(c) Measure ambient gas temperature.

(d) Measure chamber wall temperature.

(2) Pressure Measurement. Continuously measure and record the chamber gas pressure.

(3) Determine quantity and composition of combustion gas generated. Use gas chromatography, mass spectrometry, and other applicable methods as outlined in Test No. 7, Paragraph 407.5.d. above.

4. IGNITION SOURCE

In general, two modes of ignition must be considered.

a. Ignition from an internal source; i.e., wire overload or short circuit.

b. Ignition from an external source; i.e., flame or fire propagated from another nearby burning entity.

5. PRETEST PROCEDURE

a. Define or select the test assembly. This should be a portion of the spacecraft which is a meaningful and convenient package for fire hazard testing and analysis. The portion selected shall be that definable area vulnerable to a potential fire.

b. Perform a fire hazard analysis on the test assembly.

(1) Material inventory.

(2) Configuration analysis.

(3) Thermal analysis.

c. Design the flammability test to obtain the required information. The experimental design will be based on the fire hazard analysis.

d. Write detailed test procedure.

6. TEST PROCEDURE

a. Ignition. The ignition source shall be that detailed in Test No. 8, Paragraph 408.5. Ignition will be accomplished at appropriate sites (determined by combustion hazard analysis) and will simulate the following fire conditions.

(1) Momentary heat source produced by any suitable method other than the constant burning silicone igniter.

(2) Ignition source with continous heat input (internal).

(3) External heat input. A rationale justifying selection of ignition points will accompany each test report.

b. Post Test Inspection. The following comparable test data will be obtained before and after the test.

(1) Color still photographs.

(2) Weight of individual materials.

(3) Operational characteristics.

(4) Visual inspection.

(5) Motion pictures as required by the test engineer.

7. REPORTING

Test data shall be reported in accordance with instructions contained in Paragraph 208 on a form similar to Figure 2-1. The following special test data and information shall be reported:

a. Identification by generic name of all materials.

b. Vendor and vendor designation for the materials.

c. Weight and surface area of the nonmetallic materials.

d. Combustion characteristics (burning rate, sparks, dripping, flame color and size, etc.).

e. Initial point of ignition.

f. Flame propagation paths within the assembly.

g. Heat transport paths away from the assembly.

h. Total heat generated.

i. Quantity and composition of combustion product gases.

j. Evaluation of the effects of the fire on the performance of the assembly according to spacecraft hazard categories.

411 TEST NO. 11 - GUIDELINES FOR SIMULATED CREW BAY CONFIGURATION FLAMMABILITY VERIFICATION TEST

1. PURPOSE

This procedure will use panels and assemblies of "worst case" materials configured in a mockup vehicle in the same manner as the flight vehicle for the purpose of determining the propagation, combustion phenomena and behavior of the materials in the event of fire in the spacecraft.

2. CRITERIA FOR ACCEPTABILITY

The results of the test should demonstrate that there can be no propagation of the fire to adjacent equipment by radiation, conduction, or mass transfer. There shall be no sputter, drip, or release of hot or burning particles.

3. TEST CONDITIONS - PRESSURES AND ATMOSPHERES

The test shall be conducted at the most hazardous pressure and gas mixture conditions designated for the materials applications.

4. TEST EQUIPMENT

The test shall be performed using a full scale spacecraft mockup vehicle.

5. TEST CONFIGURATION

a. The equipment tested shall be similar in configuration to the flight article. As described in Test No. 10, Paragraph 410.3.e., the electronic parts can be mock-ups of the same material mass and geometry as the flight part or instrument.

b. All potential propagation paths shall be simulated.

c. Geometric and spatial proximity to spacecraft panels and enclosures shall be simulated.

6. IGNITION SOURCE

a. A standard silicone ignition source or equivalent, as noted in Test No. 8, Paragraph 408.5 shall be used to produce as hot a flame as might occur in the spacecraft.

b. The source shall be placed as close as possible to or in contact with the most combustible material in the assembly.

c. Sufficient energy shall be supplied to the wire to ignite the igniter and the test configuration.

7. PRETEST PROCEDURES

The pretest procedures will describe, step-by-step, the preparation of the chamber and the assembly and configuration of the materials within the vehicle. Ignition locations and test termination criteria shall be established. The pretest documents shall be prepared by the contractor and submitted to the testing agency and the program office for concurrence before the test is run.

8. TEST PROCEDURES

The test procedures will describe, step-by-step the final instrumentation of the test items and the chamber, the performance of the test and the post test disassembly of the test panels for observation. The procedures shall be written by the contractor and submitted to the program office and testing agency for concurrence before the test is run.

9. REPORTING

Test data shall be reported in accordance with instructions contained in Paragraph 208 on a form similar to Figure 2-1. The following test data and information shall be reported:

a. Identification and dimensions of the assemblies tested.

b. Identification by generic name of all materials tested in the complete mockup test.

c. Vendor and vendor designation for the materials.

d. Weight and surface area of the nonmetallic materials.

e. Combustion characteristics.

f. Flame propagation paths within the assemblies and the chamber.

g. Total heat generated.

h. Quantity and composition of combustion product gases.

i. Evaluation of the effects on the performance of the assembly in relation to spacecraft hazard categories.

412 TEST NO. 12 - GUIDELINES FOR TOTAL SPACECRAFT OFFGASSING TEST

1. PURPOSE

This test is designated to measure the total quantity and individual components of the products offgassed by a spacecraft during manned and unmanned chamber tests to determine the toxicological safety of the spacecraft during manned flights.

2. CRITERIA FOR ACCEPTABILITY

The results of this test shall be evaluated and analyzed by the responsible medical office and the safety of the spacecraft atmosphere shall be established with respect to the measured contaminants. A report confirming the status shall be sent to the cognizant NASA program office.

3. TEST CONDITIONS - PRESSURES AND ATMOSPHERES

The test pressure and gas mixture conditions to be used during the test shall be designated in accordance with the requirements of each program and shall not be less, quantitatively, than those used in the manned flight vehicle.

4. PRETEST PROCEDURES

a. The instrumentation for monitoring the heater control network of the gas sampling lines and measuring the temperature shall be applied.

b. The gas sampling lines from the spacecraft to the gas sampling station shall be leak checked. (A leak rate no greater than 1×10^{-6} Torr-liters/second will be allowed).

c. The gas sampling lines of the gas sampling station shall be leak checked. (A leak rate of no greater than 1×10^{-6} Torr-liters/second will be allowed).

d. A functional checkout shall be performed to determine the following:

(1) That the temperature of the gas sampling lines can be maintained at ambient plus 18 $\pm$ 9.0°F.

(2) That an adequate flow rate can be maintained for the cabin gas sampling line.

e. The gas sampling lines shall be verified as clean by assuring that no gaseous contaminants are present at concentration levels greater than one ppm. The gas sampling lines shall be heated at 160 $\pm$ 20°F during this verification. (This will require introducing high purity nitrogen into the cabin sampling port).

f. The capability for continuous and intermittent gas sampling shall be provided. Each set of cryogenic traps shall include a dry ice solvent cooled trap and a liquid argon cooled trap.

g. For manned tests, the capability for continuous on-line, real-time monitoring of concentrations of CO_2, N_2, O_2 and other spacecraft atmospheric contaminants shall be provided. This will necessitate the use of:

(1) CO_2 analyzer.

(2) O_2 analyzer.

(3) N_2 analyzer.

(4) Mass Spectrometer.

(5) Any necessary instruments selected from Paragraph 407.5.d of Test No. 7.

5. TEST PROCEDURE

a. Before Manning

(1) The heater control network shall be monitored and line temperatures recorded hourly during the cryogenic trapping period and immediately before obtaining gas samples. The Test Director shall be notified if the line temperature is out of tolerance.

(2) Gas samples shall be obtained before each manning of the vehicle. It is recommended that the samples be taken before any cabin depressurization below 3 psia.

b. Manned Phase

(1) The Medical Office shall provide a toxicological evaluation of the analytical data to the program office.

(2) The heater control network shall be monitored and line temperatures recorded hourly. The Test Director shall be notified if the line temperatures are out of tolerance. (The allowable temperature for the gas sampling lines shall be spacecraft ambient temperature plus 18.0 $\pm$ 9°F.

(3) After each ingress, an initial gas sample shall be obtained as soon as operational pressure is reached.

Subsequent samples shall be collected from the cabin. Exception: If a collection time occurs when the crew is isolated in the suit loop, a sample shall be collected therefrom.

(4) Continuous monitoring of the on-line real-time analytical instrumentation for the duration of the manned phases shall be maintained to obtain data on the concentrations of CO_2, N_2, O_2, and other atmospheric contaminants in the cabin. Any unusual mass spectrometric or other analytical data shall be supplied to the medical office as soon as available.

6. POST TEST REQUIREMENTS

a. The analytical data from the gas samples shall be reported to the medical office within 26 days of completion of the testing.

7. REPORTING

The tests shall be directed by the cognizant test engineer or his appointed alternate. Approval of the test and verification of data transcribed to the data sheets shall be indicated at the end of the test procedure by the responsible test engineer's signature.

A final report containing the complete evaluation and analysis of the test results and data and the recommendations of the Medical Office shall be submitted to the appropriate program office.

413 TEST NO. 13 - AMBIENT LIQUID OXYGEN AND PRESSURIZED LIQUID AND GASEOUS OXYGEN MECHANICAL IMPACT TESTS

1. PURPOSE

The purpose of this test is to determine the impact sensitivity of materials with liquid or gaseous oxygen (LOX or GOX). The test is applicable to materials selected for use in high pressure LOX or GOX systems. (Type D).

The test methods are separated as follows:

a. Ambient LOX Mechanical Impact. (Part 1)

b. Pressurized LOX or GOX Mechanical Impact. (Part 2)

2. CRITERIA FOR ACCEPTABILITY FOR AMBIENT LOX MECHANICAL AND PRESSURIZED LOX AND GOX MECHANICAL IMPACTS

a. The material shall be subjected to twenty (20) successive impact tests at 72 ft lbs using the equipment described in Paragraph 3. More than one reaction in 20 impacts rejects the material. If there is no more than one reaction in 20 impacts, the material shall be subjected to 40 additional impacts. No further reactions shall place the material in the acceptable category. The material shall show none of the following reactions:

(1) Audible explosion.

(2) Flash (electronically or visually detected).

(3) Evidence of burning (obvious charring).

(4) Major discoloration.

Note: A burnt odor alone is not considered a reaction. If any reaction occurs due to rebound of plummet, it shall be reported as evidence of sensitivity.

b. All Type D materials that fail Paragraph 2.a criteria must be subjected to LOX or GOX mechanical impact threshold determinations in the thickness of actual use.

3. PART 1 - AMBIENT LOX MECHANICAL IMPACT SCREENING TEST

a. Sample Preparation

(1) Sampling. Sufficient material shall be available to permit preparation and testing of at least 240 separate 11/16-inch diameter disc samples. Sheet materials up to 1/4 inch in thickness shall be

tested as 11/16 inch diameter discs in the thickness intended for actual use. Materials normally used in thicknesses greater than 1/4 inch shall be sized and tested as 11/16 inch diameter discs of two thickness 0.050 ± 0.005 inch and 0.250 ± 0.025 inch. Failure of samples of either thickness to meet requirements of this specification shall be cause for rejection of the material. Greases, fluids, and other materials, whose thicknesses are not dictated by conditions of use, shall be tested as 0.050 ± 0.005 inch layers in test cups. Materials not readily available in sheet form shall be tested in the available configuration.

"Stainless steel inserts shall be used as a false bottom in the aluminum specimen cups when testing all materials with the exception of greases, oils, other liquids, dye penetrants, coatings, and solders. The latter materials shall be tested as specified in other sections of this specification."

(2) O-Rings. Each size from each batch of O-rings and/or o-ring materials shall be sampled and tested as follows unless it can be demonstrated that test results on different sizes and batches are comparable when tested as specified in Section 413.3.o.

(a) Extruded O-Rings. At least 240 discs 16 inch diameter by thickness of o-rings shall be cut from a strip after the chopping operation. The discs shall be processed and deflashed with the same equipment used for the o-rings. The discs shall be cleaned as specified for the material and its use and tested after precooling as specified in 413.3.i.

(b) Molded O-Rings. At least 240 discs 11/16 inch diameter by the thickness of the o-rings, and which have been processed and deflashed, shall be furnished.

(c) O-Rings from standard stock or where above procedures are impractical. O-rings 1/2 inch outside diameter or less shall be sampled and tested as a complete o-ring. O-rings larger than 1/2 inch outside diameter shall be tested as one segment (approximately 3/4 inch long on a stainless steel insert. The

samples shall be cleaned and precooled as specified above. If a sample is not impacted during testing, it shall be placed in a new cup with a stainless steel insert and precooled prior to re-testing. As an alternative, sufficient samples may be prepared to account for the normal impact misses.

b. Test Equipment

(1) ABMA Impact Tester (see Figure 4-6). The impact tester shall have a rugged structural frame with three vertical guides capable of maintaining accurate vertical alignment under repeated shock conditions, a solenoid-operated mechanism for dropping a plummet which weighs 20 ± 0.05 pounds through a distance of 43.3 ± 0.02 inches (this will transmit to the test sample an approximate impact energy of 72 foot-pounds, a striker pin (see Figure 4-7) 1/2 inch in diameter and 2 inches long, and test cup (see Figure 4-8) approximately 7/8 inch inside diameter by approximately 7/8 inch inside depth made of 1/16 inch thick aluminum alloy. The initial alignment and subsequent operation of the impact tester shall be such that the plummet falls uniformly under essentially friction-free conditions. This shall be verified by determining the drop interval across a measured distance. The observed plummet acceleration shall not deviate more than 3 percent from the prevailing gravitational acceleration.

Note: The weight X drop-height product specified is not duplicated for the purposes of this test by combinations other than 20 ± 0.05 pounds and 43.3 ± 0.2 inches. For example, doubling the weight and halving the drop height would not duplicate the specified requirement.

c. Drop Tester Components

(1) Electromagnet. The electromagnet shall be designed with a sufficient safety factor to hold over 20 pounds of weight with a minimum energizing wattage.

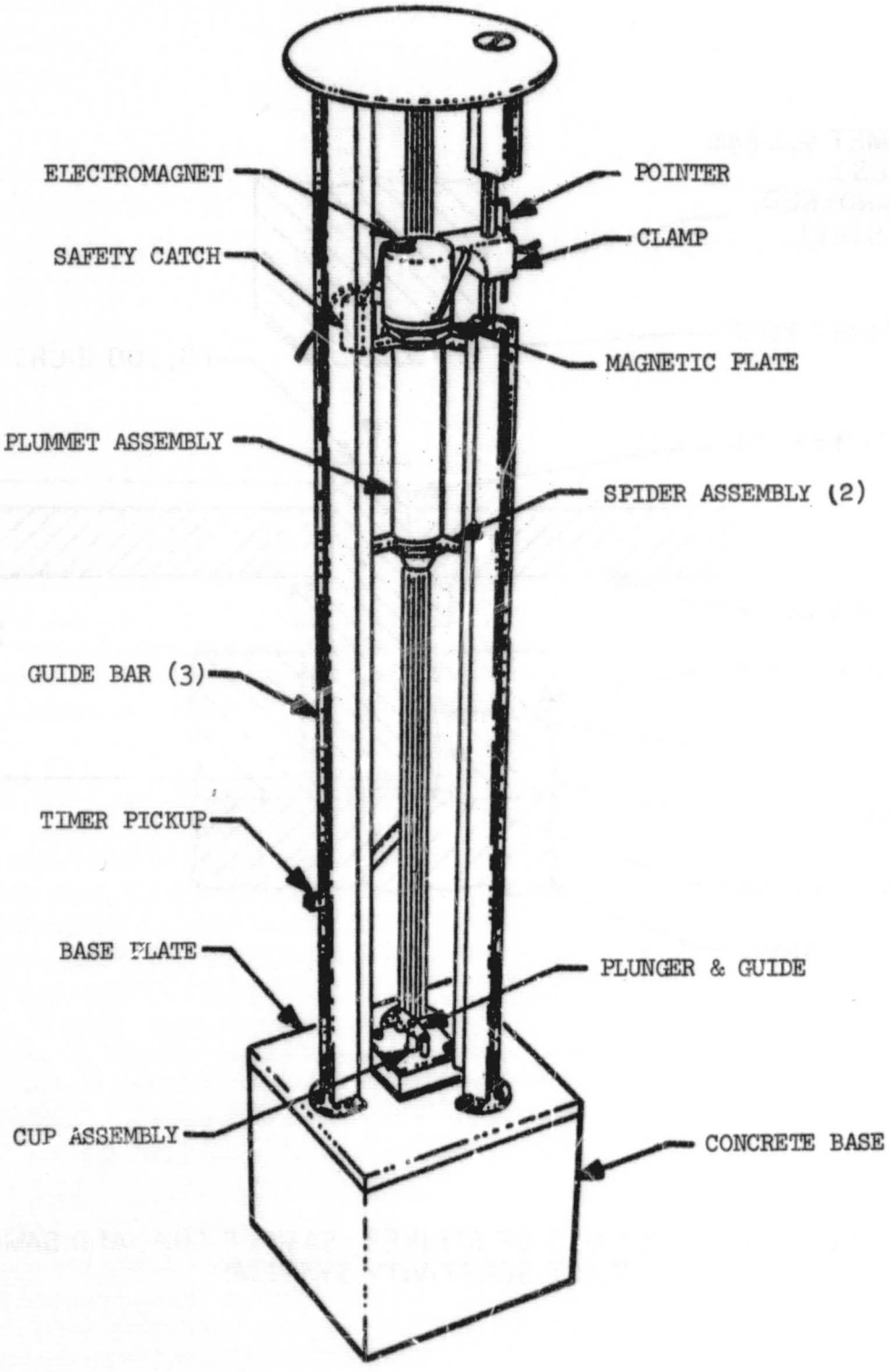

FIGURE 4-6. ABMA IMPACT TESTER

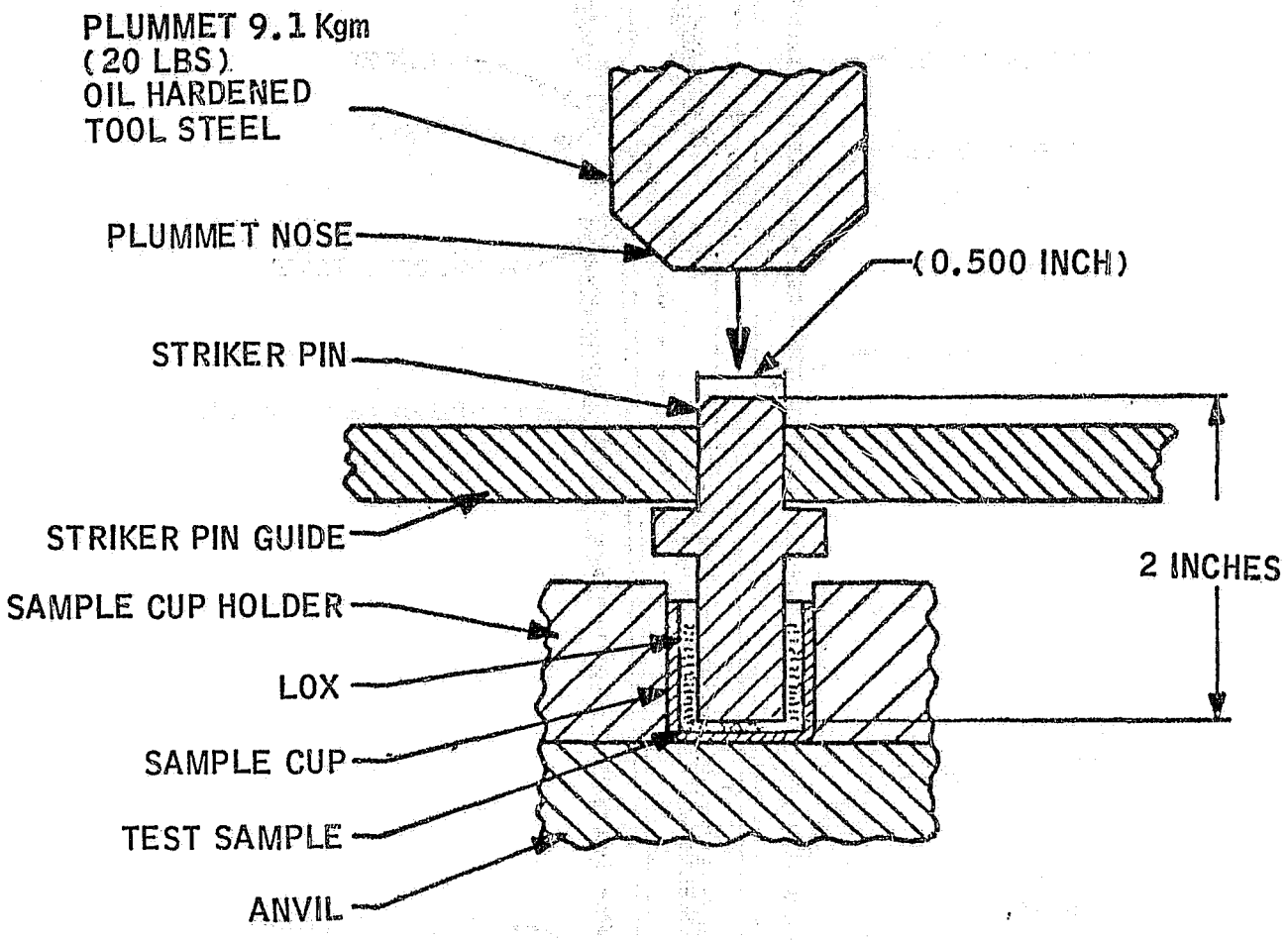

FIGURE 4-7. DETAILS OF STRIKER, SAMPLE CUP, AND SAMPLE (IMPACT SENSTIVITY SYSTEM)

(2) Safety Catch. The solenoid-operated safety catch shall be designed to hold the plummet near the base of the magnet in the event of a power failure.

(3) Base Plate. The base plate shall be constructed from 1-inch thick stainless steel plate and shall rest solidly and level on a 2-foot cube base of reinforced concrete. Four stainless steel foundation bolts shall be used to anchor the plate to the concrete.

(4) Anvil Plate and Specimen Cup Holder. A stainless steel, type 440B heat treated anvil plate 5 by 5 by 2 inches thick, shall be bolted to the base plate in the center of the machine. This plate shall center the specimen cup holder and provide the base plate with protection from denting upon impact. A 5 by 5 inch stainless steel specimen cup holder, 1-inch thick, shall be bolted on top of the anvil plate. The specimen cup holder shall have a slightly tapered hole into which the test cup can be placed.

(5) Specimen Cups (See Figure 4-8). One-piece specimen cups shall be made of 5052-H32 aluminum alloy. A special insert cup (see Figure 4-9) with an inside depth of 0.050 + 0.005 inch shall also be used when testing semi-solid materials. These special insert cups shall be placed inside the one-piece specimen cups.

(6) Striker Pins. The striker pins shall be made from 17-4 PH stainless steel with hardness in accordance with the applicable detail drawings. A sufficient number of pins shall be provided for testing and discard.

(7) Auxiliary Equipment. The auxiliary equipment shall consist of stainless steel forceps for handling the specimen cups and striker pins, stainless steel spatulas, and LOX handling equipment (e.g., stainless steel Dewar flasks, fireproof lintless laboratory coats, safety goggles, gloves, and LOX storage containers). Additional handling equipment shall include a

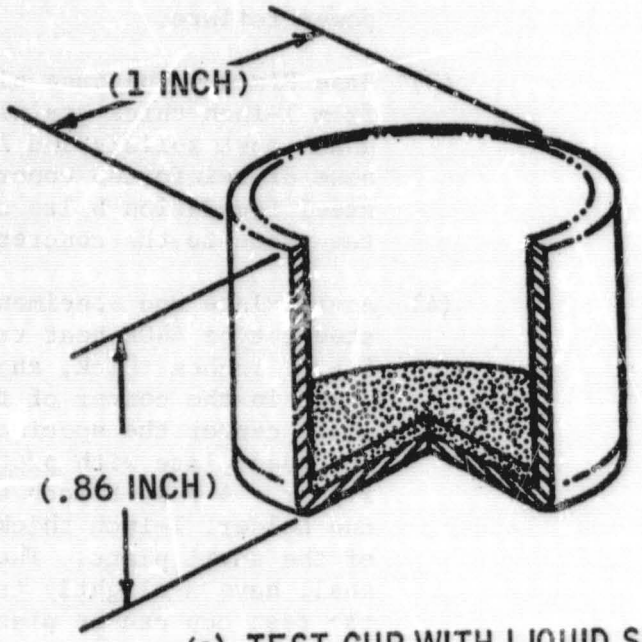

(a) TEST CUP WITH LIQUID SAMPLE

(0.050 ± 0.005 INCH THICK

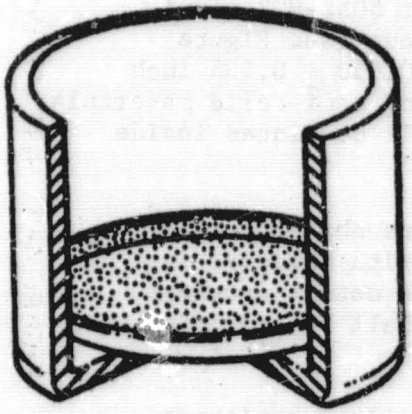

(b) TEST CUP WITH GREASE SAMPLE SHOWING INSERT CUP

FIGURE 4-8 SAMPLES IN TEST CUPS

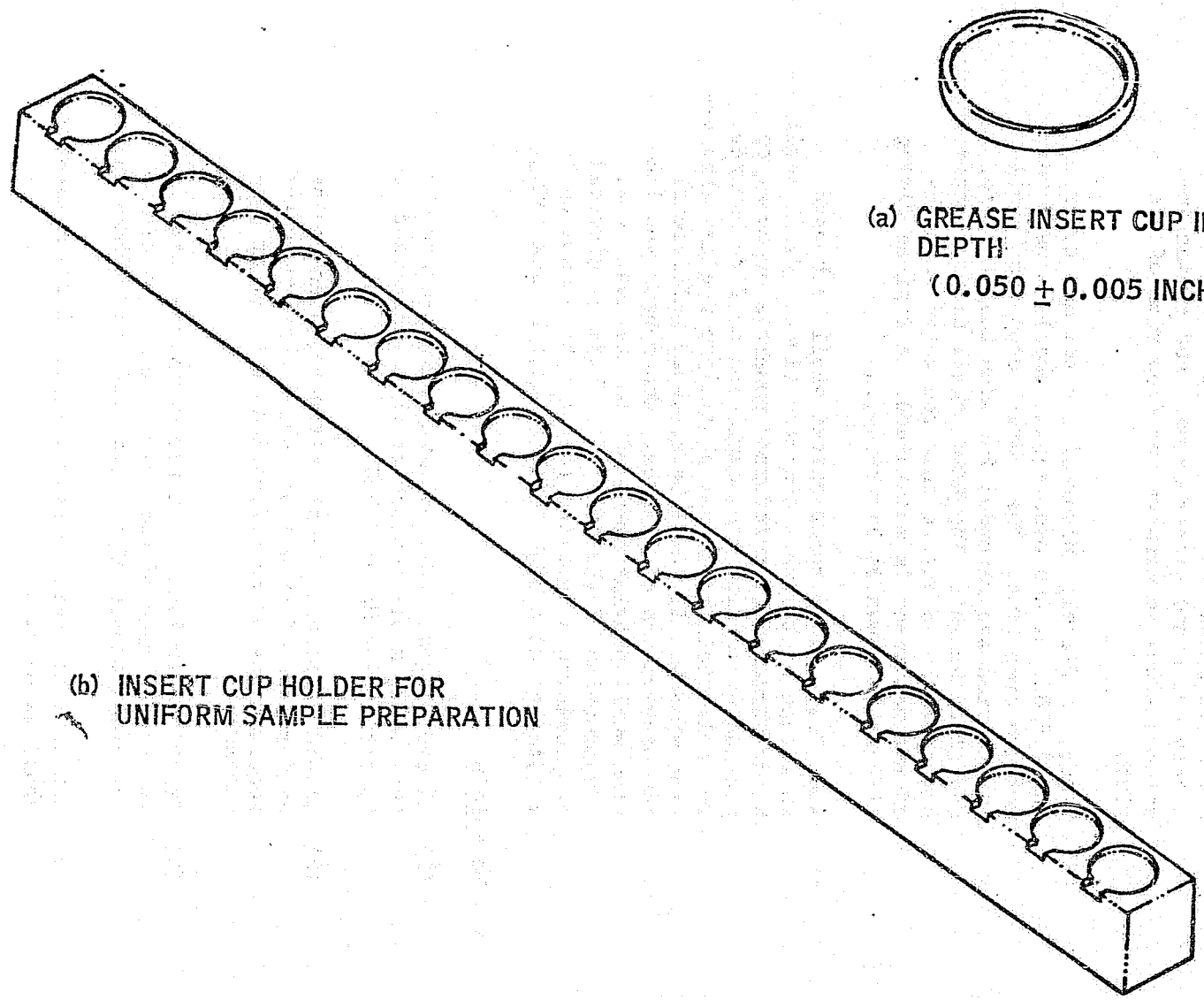

(a) GREASE INSERT CUP INSIDE DEPTH
(0.050 ± 0.005 INCH)

(b) INSERT CUP HOLDER FOR UNIFORM SAMPLE PREPARATION

FIGURE 4-9. GREASE INSERT CUP HOLDER

grease insert cup holder (see Figure 4-9), sample freezing box (see Figure 4-10), striker pin baskets, specimen cup trays, microburettes, syringes, a test cell for the impact tester with a protective window for observation of test drops, a control panel for the operator to activate the safety catch and electromagnet, and timing instrumentation to measure the drop time of the plummet.

(8) Timer. A Berkely Universal counter and timer, Model 5500, or approved equal, shall be used to measure drop time. The overall drop time shall be measured and recorded for each test drop for any given height. The timer shall be calibrated periodically to ensure that the rated accuracy of the equipment is maintained. A typical timing circuit is shown on Figure 4-11.

(9) Test Cell. The impact tester shall be housed in a test cell with a concrete floor. Walls shall be constructed of reinforced concrete or metal to provide protection from explosion or fire hazards. The cell shall contain a shatterproof-glass observation window. It shall be darkened sufficiently for observation of flashes. Continuous ventilation shall provide fresh air to the test cell. Construction of the test cell shall be directed at providing a facility that can be economically maintained at a high level of good housekeeping.

d. Materials

(1) Liquid Oxygen. LOX, used in the performance of this test, shall conform to the requirements of Specification MIL-P-25508.

(2) Liquid Nitrogen. Liquid nitrogen, used in the performance of this test, shall conform to the requirements of Specification BB-N-411 or MIL-P-27401.

(3) Trichloroethylene. Trichloroethylene, used in the performance of this test, shall conform to the requirements of Specification MSFC-SPEC- 217.

(4) Alkaline Cleaner. A nonetch-type alkaline cleaner shall be used.

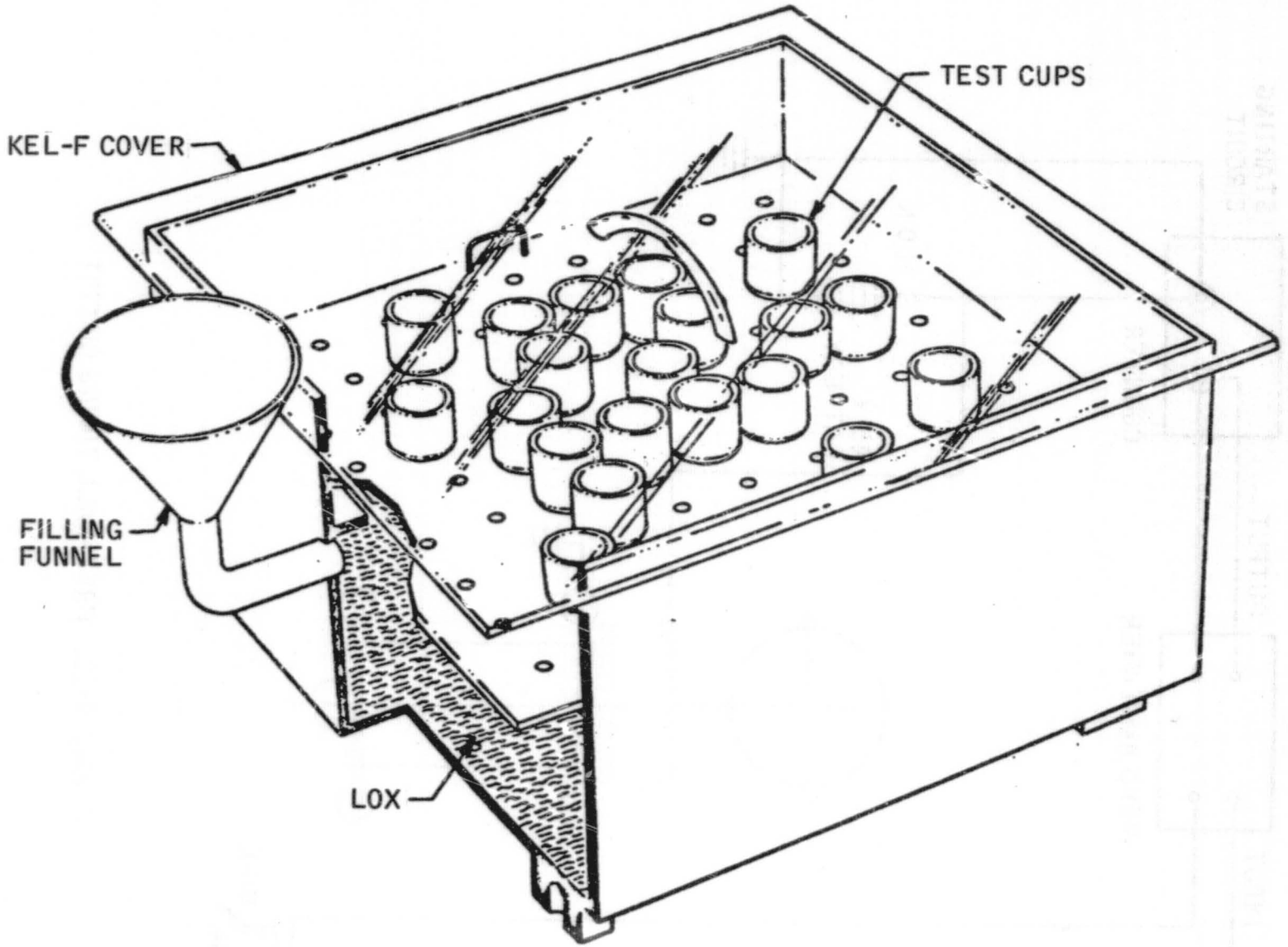

FIGURE 4-10. SAMPLE FREEZING BOX

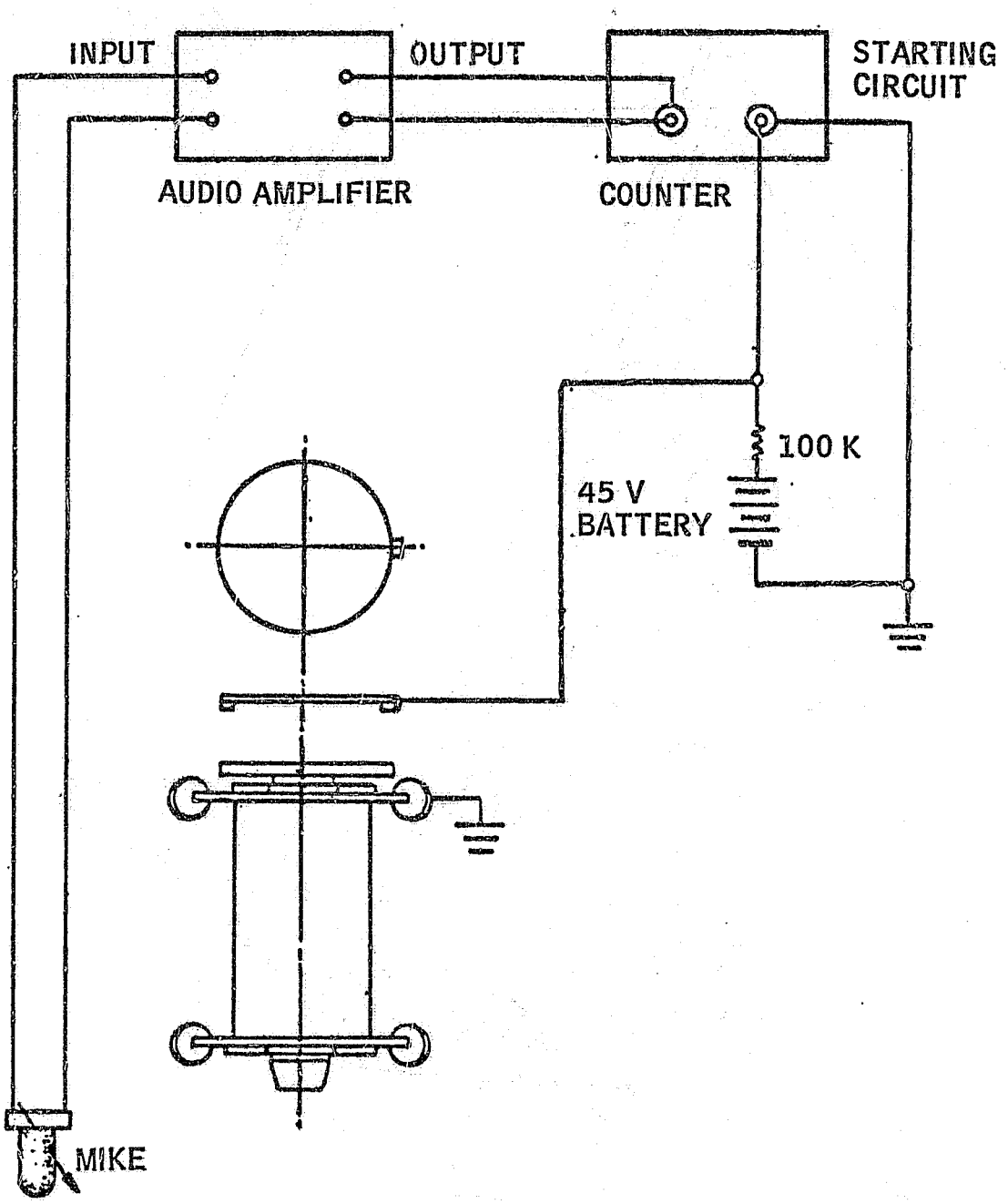

FIGURE 4-11. FREE-FALL TIMING CIRCUIT

e. Preparation of Equipment for Testing

(1) Impact Tester. The guide tracks, plummet, anvil plate, striker pin guide, sample cup holder, and base plate of the impact tester shall be cleaned thoroughly at the start of each test and between tests of different materials, and shall be rinsed with clean extraction grade trichloroethylene at least after impact test of every tenth sample. After completion of testing for the day, the impact tester shall be thoroughly cleaned. Cleanliness shall be maintained throughout any series of impact tests to minimize erroneous results.

(2) Striker Pins. Striker pins shall be used only once and then cleaned. Before each test the striker pins shall be checked for dimensional conformance to the applicable drawing and then examined to ensure freedom from scratches, nicks, metallic slivers, and other imperfections. When required, the pins shall be remachined to ensure freedom from scratches and pits. Prior to use, all striker pins shall be vapor degreased in perchlorethylene or extraction grade trichlorothylene for at least 30 minutes. After use, they shall be thoroughly cleaned by soaking in trichloroethylene and scrubbed with a detergent solution. Following this treatment, the striker pins shall be soaked in an alkaline cleaner, rinsed with water, dried, and stored in a suitable container to ensure cleanliness.

(3) Remachined Striker Pins. The length of remachined striker pins shall be 2.000 (plus 0.010 or minus 0.100) inches. Striker pins shall be remachined if the striking area exhibits scratches or pits or both. It may be necessary to remachine pins that are bent or flattened during impact tests. Badly bent and remachined pins, in which the diameter near the striking area is greater than 0.505 inch or is less than 0.495 inch, shall be discarded.

(4) Type 347 Stainless Steel Inserts. Type 347 stainless steel inserts shall be cleaned in accordance with the method specified for striker pins.

(5) Specimen Cups. A test cup shall be used only once and discarded. Prior to use, specimen cups should be cleaned as follows:

(a) Vapor degrease in perchloroethylene or extraction grade trichloroethylene for 15 minutes (cups should be in an inverted position).

(b) Rinse with deionized water.

(c) Soak in nonetch-type alkaline cleaner 180-200°F for 20 minutes.

(d) Rinse thoroughly with deionized water.

(e) Immerse in water solution containing 0.5 percent of hydrofluoric acid (48 percent) by volume and 5.0 percent of nitric acid (70 percent) by volume for 2 to 5 minutes at room temperature.

(f) Rinse with deionized water.

(g) Desmut by immersing at room temperature in a 50-percent (by volume) solution of nitric acid (70 percent) for 5 minutes or until smut is removed.

(h) Rinse thoroughly with deionized water.

(i) Dry in a moderately hot oven 250-300°F to avoid staining.

(j) Store in a clean container until ready for use.

The cups shall not be used for at least 72 hours after cleaning.

f. Blank Test. The effectiveness of the cleaning procedure shall be checked by testing a series of twenty blank cups (filled with LOX) and striker pins from each batch of clean cups and striker pins at the 72-foot-pound level. In addition to these blank tests, four blank tests shall be made at random during the testing of any materials. Additional blank tests may be made at the discretion of the operator. The striker pins and sample cups shall be handled by forceps or tongs and kept out of contact with the operator's hands or other sources of contamination.

g. Cleaning Procedure for Auxiliary Equipment

(1) Test Cell. The ceiling, walls, and any fixture in the test cell shall be rinsed with water at the end of the working day. The concrete floor shall be scrubbed daily with a detergent.

(2) Stainless Steel Ware. Stainless steel ware, such as striker pin baskets, forceps, tongs, spatulas, and inserts, shall be cleaned in the same manner as the striker pins. Once integrated into the handling procedure, a thorough rinse of the stainless steel ware with clean, extraction grade trichloroethylene should be the only cleaning necessary.

(3) Classware Check. Any glassware, such as microburettes, beakers, and syringes, shall be cleaned by soaking in a alkaline cleaner, rinsed with water, and dried. Immediately prior to use, they shall be vapor degreased with trichloroethylene for at least 30 minutes.

h. Preparation of Test Samples

(1) Number of Samples. At least 20 samples shall be used for each series of test drops. It may be desirable to prepare more than 20 samples because of rejection due to samples floating or breaking up during precooling.

(2) Liquid Samples. Liquid samples shall be applied to form a layer in the bottom of the specimen cups 0.050 $\pm$ 0.010 inch thick.

(3) Greases and Semisolids. Grease samples shall be prepared as follows:

(a) Special specimen cups with inside depths of 0.050 $\pm$ 0.005 inch shall be provided (see Figure 4-9).

(b) The special specimen cups shall be cleaned as specified in 413.5.e.

(c) Place special cups into the cup holder (see Figure 4-9). Press sufficient sample material into the special cups with a clean, stainless steel spatula to form a sample that is free of air bubbles and void spots.

(d) Scrape off the excess sample with the spatula until a smooth surface, level with the edge of the cup, is achieved.

(e) Remove the special cup from the holder and place it inside the regular specimen cups.

(4) Solid Samples. Solid samples shall be cleaned, rinsed, dried as specified below, and placed in the bottom of the specimen cups.

(5) Metallic and Solvent-Resistant Samples. Metallic and solvent-resistant samples shall be scrubbed in detergent water, rinsed, dried, and vapor degreased with tricholoroethylene before placing in the specimen cups.

(6) Nonmetallic Samples. Nonmetallic samples shall be cleaned with a detergent solution followed by water rinsing and oven drying at 212 ± 18°F for 1 hour or until dry. The particular detergent used shall be impact sensitive in accordance with the requirements of this specification in the concentration used when tested as outlined in 413.3.h.(8).

(7) Coatings

(a) Paints and Dry Film Lubricants. Coating samples, such as paints and dry film lubricants, shall be prepared as follows:

(1) Apply the coating to 11/16 inch diameter stainless steel inserts in the same manner and to the same thickness that is intended for hardware application.

(2) After the samples have dried, place them in the regular specimen cups and test.

(b) Elastomerics. Elastomeric coating samples shall be prepared as follows:

(1) Thin with reagent grade methyl isobutyl ketone or other compatible solvent to 10 percent of total weight of solids, or to manufacturer's recommendations.

(2) Apply the coating to 11/16 inch diameter stainless steel inserts as follows:

(a) METHOD 1 (Single Dip Coat). Dip coat inserts to approximately 0.0005 inch and place on clean aluminum foil to air dry. The coated inserts shall be removed from the foil and turned over after 30 minutes to allow both sides to dry completely. The specimens shall be air dried for a minimum of 24 hours prior to testing. The coating thickness shall be checked on at least four samples and recorded.

(b) METHOD 2 (Brush Coat). Apply 22 coats (10 percent solids) using a single brush stroke with a soft nonshedding brush. Allow a minimum of 30-minute drying time between coats. If the thickness of the coating is greater than 0.015 inch, the specimen shall be rejected; if less than 0.015 inch, additional coats shall be applied as required to achieve the specified thickness. Each specimen shall be visually examined for contamination following application of each coat (especially bristles from the brush). The coated specimens shall be air dried for a minimum of 24 hours following application of the final coat before testing.

(8) Leak Check Compounds, Dyes, and Dye Penetrant Systems. Clean, unsealed, sulfuric-acid-anodized, 6061-T6 discs 11/16 inch in diameter by 0.063 inch thick shall be used as a carrier. Prior to use, the discs shall be vapor degreased in extraction grade trichloroethylene. To check the effectiveness of the cleaning procedure, a minimum of 20 blank discs shall be tested as specified in 413.3.f. The discs shall then be soaked in the leak check compound, dye, dye penetrant, emulsifier, or developer for 15 minutes; drained for 15 minutes at an angle of 90 degrees in the fixture shown on Figure 4-12, and tested by placing the specimen discs on stainless steel inserts in the bottom of the test cups.

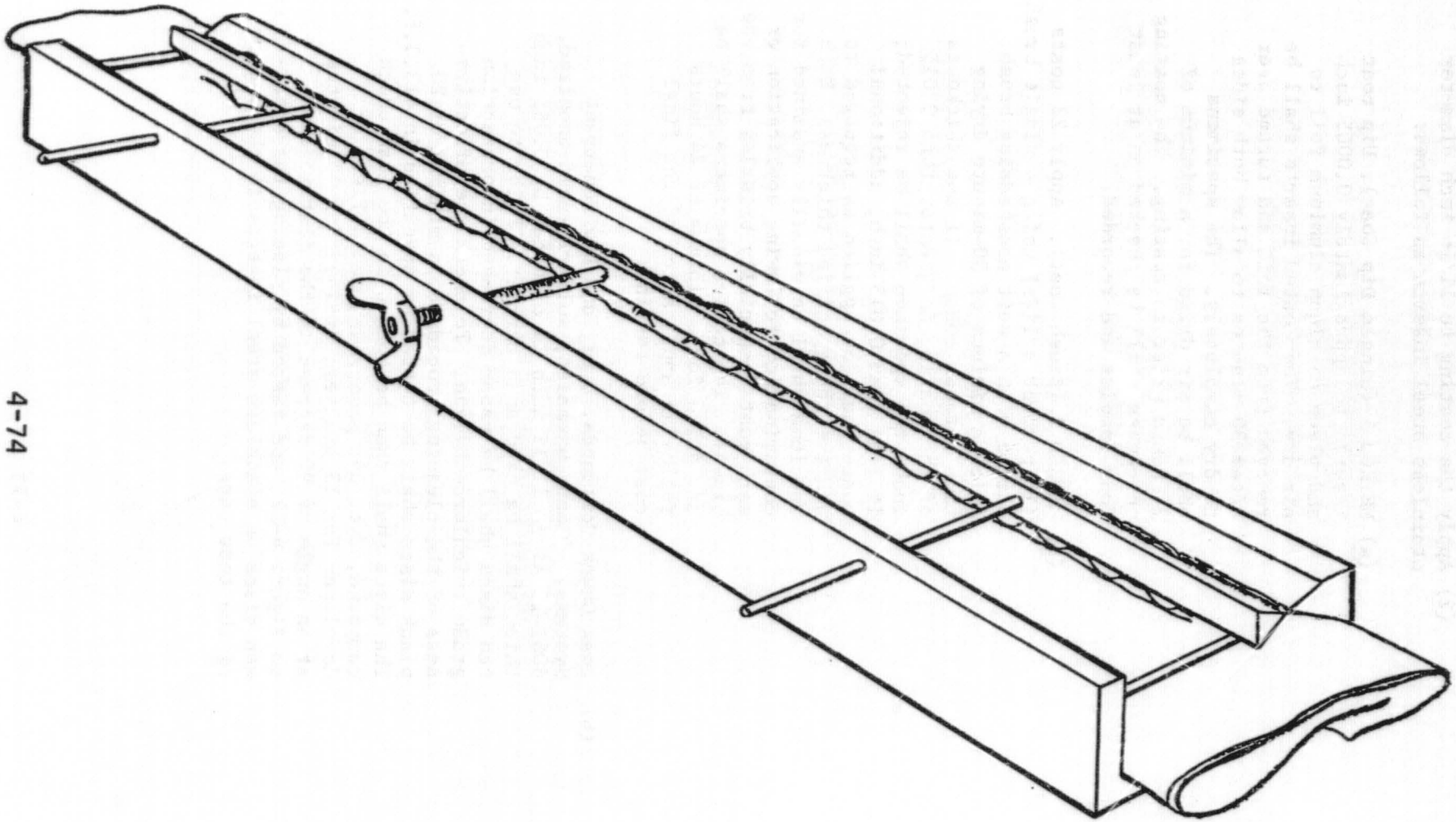

FIGURE 4-12. DYE PENETRANT RACK

(9) Solders. Solders shall be tested as flat sheets. The sheets shall be prepared by melting and casting the solders to form ingots and by rolling the ingots into sheets of 0.020 ± 0.005 inch in thickness. Discs 11/16 inch in diameter shall be punched from the sheets, cleaned as outlined in Paragraph h.(4) above and test by placing the dics on stainless steel inserts in the bottom of the test cups. If rosin core solder is used, care should be taken to ensure that the rosin is burned off or completely removed prior to test.

i. Precooling. Precooling shall be accomplished by lowering the temperature of the material to the boiling point of LOX at one atmospheric pressure (minus 298°F)

j. Dewar Flasks. Stainless Steel Dewar flasks shall be precooled by slowly pouring LOX into the flask until the LOX ceases to boil. When cooled, the flask shall be filled with LOX and covered with clean aluminum foil or a stainless steel cover. Since glass Dewar flasks are easily broken, they should not be used.

k. Specimen Cups

(1) Blank Specimen Cups. The clean, blank specimen cups shall be precooled by slowly pouring LOX into a sample trap until the LOX covers and fills the cups.

(2) Specimen Cups Containing Sample Material. To minimize cracking of the samples during freezing, the cups containing the samples shall be precooled slowly by using the freezing box shown on Figure 4-10. The box should be leveled prior to use. The procedure shall be as follows:

(a) Place approximately 40 specimen cups over the holes in the retainer plate.

(b) Using an automatic delivery tube with a 25-liter Dewar flask, pressurize the Dewar flask to approximately 2.5 pounds per square inch gage (psig) with oil-free oxygen.

(c) While maintaining the pressure at approximately 2.5 psig, open the discharge valve approximately halfway and start to fill the freezing box.

The time required to fill the cups and the freezing box 1/8 inch from the top shall be 35 to 40 minutes. After this step, a careful inspection shall be made. Any sample that separates from the bottom of the cup

and floats or shatters due to thermal shock shall be discarded. The thickness of at least five frozen samples shall be measured and recorded. The samples shall be transferred to a suitable (precooled) container for storage until tested. Additions of LOX shall be made, as necessary, while tests are in progress to ensure that each sample cup is completely filled at time of testing.

l. Striker Pins. Cleaned striker pins shall be precooled by placing pins in a Dewar flask and adding liquid nitrogen to the flask until the pins are covered with liquid nitrogen.

m. Specimen Cup Holder and Base Plate. The specimen cup holder and anvil plate shall be precooled by adding liquid nitrogen to the stainless steel moat surrounding the specimen cup holder and base plate. The moat should be filled with liquid nitrogen to approximately 1/2 inch below the top of the specimen cup holder.

n. Pretest Procedure

(1) Critical test parameters shall be as follows:

(a) Plummet Weight. Plummet weight shall be 20 ± 0.05 pounds.

(b) Drop Height. Drop height shall not deviate more than ± 0.2 inch from the specified height.

(c) Striker Pin Diameter. Striker pin diameter near the striking area shall be 0.500 ± 0.005 inch.

(d) Energy Loss. The energy loss due to friction shall be controlled by measuring and recording the drop time of each drop of any given height. The observed plummet acceleration shall not deviate more than 3 percent from the prevailing gravitational acceleration.

(l) Blank Drop. The effectiveness of the cleaning procedure shall be checked by testing blank cups as outlined in 413.3.f.

o. Test Procedure for Ambient LOX Mechanical Impact Determination

(1) The magnet shall be adjusted to proper drop height 43.3 inches for 72 foot-pounds.

(2) Clean tongs shall be used to set the precooled specimen cups into the specimen cup holder.

(3) A visual check shall be made to assure that the frozen sample has not separated from the bottom of the cup. Samples that have separated shall be discarded.

(4) Place the striker pin in the cup and hold it in place by the striker pin guide.

(5) Add LOX to the specimen cup to ensure that the specimen cup is full.

(6) Cover the exposed container of LOX.

(7) Close the test cell door, turn off the cell lights, and set the timer.

(8) Release the safety catch and plummet by means of the control panel located outside the test cell near the observation window.

(9) Observe and record the results of the impact reaction as defined in 413.2.

(10) Record the drop time of the plummet for each drop.

p. Interpretation of Results. A material proposed for use in LOX systems or subject to direct contact with LOX shall conform to the requirements of Section 413.2.

q. Threshold Levels. For materials sensitive at 72 foot-pounds, it may be desirable to determine threshold values. The approximate threshold value shall be obtained by testing 20 samples at each of the drop heights listed in Table 4-1. The first height at which no reactions are obtained in 20 drops shall be the approximate threshold value. The definitive threshold value shall be determined by 20 tests at drop-height increments of 3 inches starting at a height of 6 inches above the approximate threshold value. The definitive threshold value shall be the higher of the two adjacent heights at which no reaction was obtained.

r. Rejection and Retest. Failure of any sample to meet the requirements of this specification shall be cause for rejection of the lot represented. Rejected materials shall not be submitted for approval without full details being furnished concerning the previous rejection and measures taken to correct the defects. If not more than one test unit of the original test sample fails to meet the test requirements specified herein, the manufacturer may request a retest. If all test units of the retest meet the requirements specified herein, the material shall be considered compatible for use in LOX systems.

TABLE 4-1. DROP HEIGHT SCHEDULE FOR THRESHOLD VALUE DETERMINATION

Energy (Ft Lbs)	Drop Height (Inches)
72	43.3
65	39.0
60	36.0
55	33.0
50	30.0
45	27.0
40	24.0
35	21.0
30	18.0
25	15.0
20	12.0
15	9.0
10	6.0

4. PART 2 - TEST METHOD FOR PRESSURIZED LOX OR GOX MECHANICAL IMPACT

a. Purpose. This procedure determines the compatibility of materials used in pressurized LOX or GOX systems.

b. Criteria of Acceptability. The material when subjected to mechanical impacts at the maximum use pressure and temperature shall meet the criteria described in 413.2. Materials which fails to meet those criteria shall be subjected to threshold determinations in LOX or GOX at maximum use pressure and temperature at the drop heights shown in Table 4-1.

c. Test Atmosphere. Candidate materials shall be tested in 95^{+5}_{-0} percent LOX or GOX (MIL-O-27210C).

d. Test Equipment. All tests shall be performed utilizing the basic ABMA impact tester described in Paragraph 413.3.b with appropriate modifications.

e. Sample Identification. The following information shall accompany each material submitted for test.

(1) Generic name.

(2) Manufacturer and manufacturer's designation.

(3) Composition.

(4) Batch/lot number.

(5) Previous cleaning and conditioning processes.

(6) Test pressure.

(7) Test temperature.

f. Sample Preparation. The materials samples shall be prepared according to the procedures described in Paragraph 413.3.a.

g. Sample Cleanliness. Materials submitted shall be cleaned in accordance with the cleaning guidelines established for the material and its application.

h. Pre-Test Procedure. Verify that all test equipment is in current calibration.

(1) The ABMA test equipment, fixtures, striker pins, etc. shall be thoroughly cleaned before each test according to the procedure utilized by the testing agency. If such a procedure has not been established, the cleaning guidelines outlined in Appendix C shall be followed.

i. Test Procedures

(1) Place the sample in position within the sample retainer cavity. Verify that the sample is contained in a specimen holder and cup assembly which will allow for the transfer of impact energy to the subject specimen in a repetitious manner.

(2) Pass gaseous oxygen from the high pressure oxygen source into the chamber and pressurize the test chamber to the applicable test pressure.

(3) Adjust the plummet drop height. The plummet's weight shall be standardized at 20 pounds and dropped from heights shown in Table 4-1.

(4) Adjust the chamber pressures to the specified levels.

(5) Maintain the pressures in the test chamber at $^{+5}_{-0}$ percent of the specified pressure.

(6) Counterload the equalizer chamber to permit the striker pin to "float" in the test chamber.

(7) Maintain the temperature at $\pm$ 10 percent of the specified temperature.

(8) Activate the plummet release mechanism.

(9) Record the pressure and temperature in the chamber before, during, and after the test.

(10) Record audible explosions.

(11) Record any flashes electronically or visually detected.

(12) At the conclusion of the test, release the residual GOX pressure in the assembly.

(13) Diassemble the test apparatus.

(14) Examine the sample specimen and cup specimen holder for visible signs of reaction.

(15) Record all observations; photographs of a visual change in the sample specimen shall be at the discretion of the test engineer.

(16) Repeat the above procedure, each time employing a new sample and assuring cleanliness requirements are maintained until the total number of samples are tested.

j. Threshold Level Determination. Materials sensitive at 72 ft lbs shall be subjected to threshold level determinations according to the procedure detailed in Section 413.3.q. The determinations shall be made starting at the maximum use pressure and temperature.

k. Reporting. Test data shall be reported in accordance with instructions contained in Paragraph 208 on a form similar to Figure 2-1. The following special test data and information shall be reported:

(1) Lot/batch numbers of each material.

(2) Impact energy for each test.

(3) Temperature change in the test chamber.

(4) Condition of sample after test.

(5) Number of mechanical impacts.

(6) Number of failures versus number of samples tested.

(7) Definitive threshold value.

(8) Pertinent comments and observations of test.

TYPICAL MECHANICAL IMPACT TEST CHAMBER

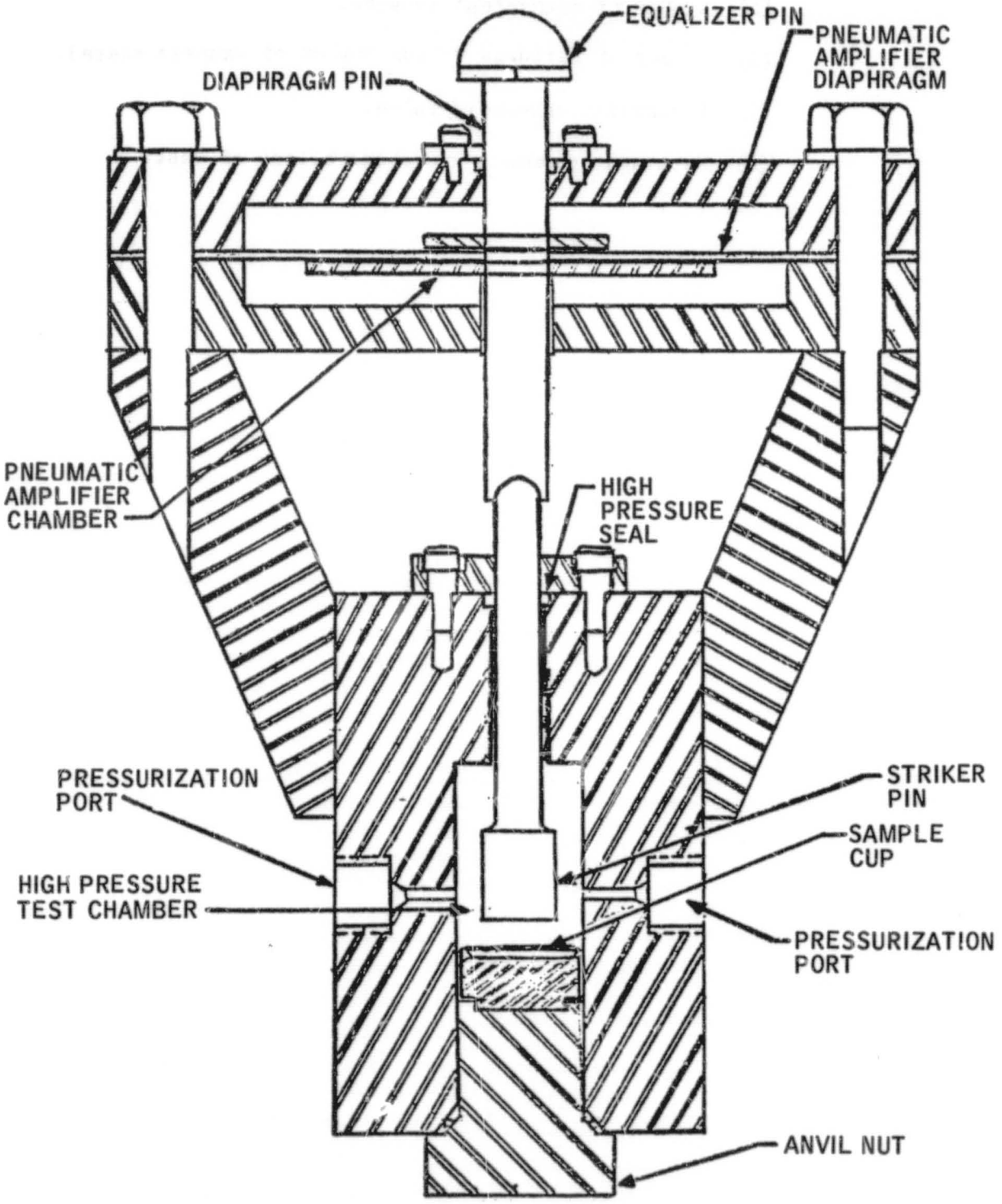

FIGURE 4-13

414 TEST NO. 14 - GASEOUS OXYGEN PNEUMATIC IMPACT TEST

1. PURPOSE

The purpose of this test is to determine the sensitivity of materials to pure gaseous oxygen (GOX) when subjected to pneumatic impact. The test is applicable to materials selected for use in high pressure oxygen systems (Type D).

2. CRITERIA FOR ACCEPTABILITY

a. A candidate material shall exhibit no reactions at the specified use pressure times 1.5, and maximum temperature to which it can be exposed in the thickness intended for use.

b. If a material does react at the test pressure and temperature, a review will be required to ascertain the level of pneumatic impact conditions that exist within the system in which the material is applied.

3. TEST CONDITIONS - PRESSURES AND ATMOSPHERES

a. Candidate materials shall be tested in 95^{+5}_{-0} percent GOX (MIL-O-27210C) at the specified use pressure and temperature. Test pressures ranging from 50 psia to 10,000 psia will be utilized. Intermediate pressure increments of 500 psia will normally be used.

b. Standard test conditions employed in performance of the pneumatic impact test are as follows: (Other conditions require special notation)

(1) Test chamber temperature 70 $\pm$ 10°F.

(2) Five pneumatic impact cycles within 60 seconds, automatically timed.

(3) The pressure in the test chamber shall be raised to 95 percent of test pressure within 20 $\pm$ 7 milliseconds.

c. The pneumatic test equipment is presented schematically in Figures 4-14 and 4-15.

4. SAMPLE IDENTIFICATION

The following information shall accompany each material submitted for test.

a. Generic name

b. Manufacturer and manufacturer's designation.

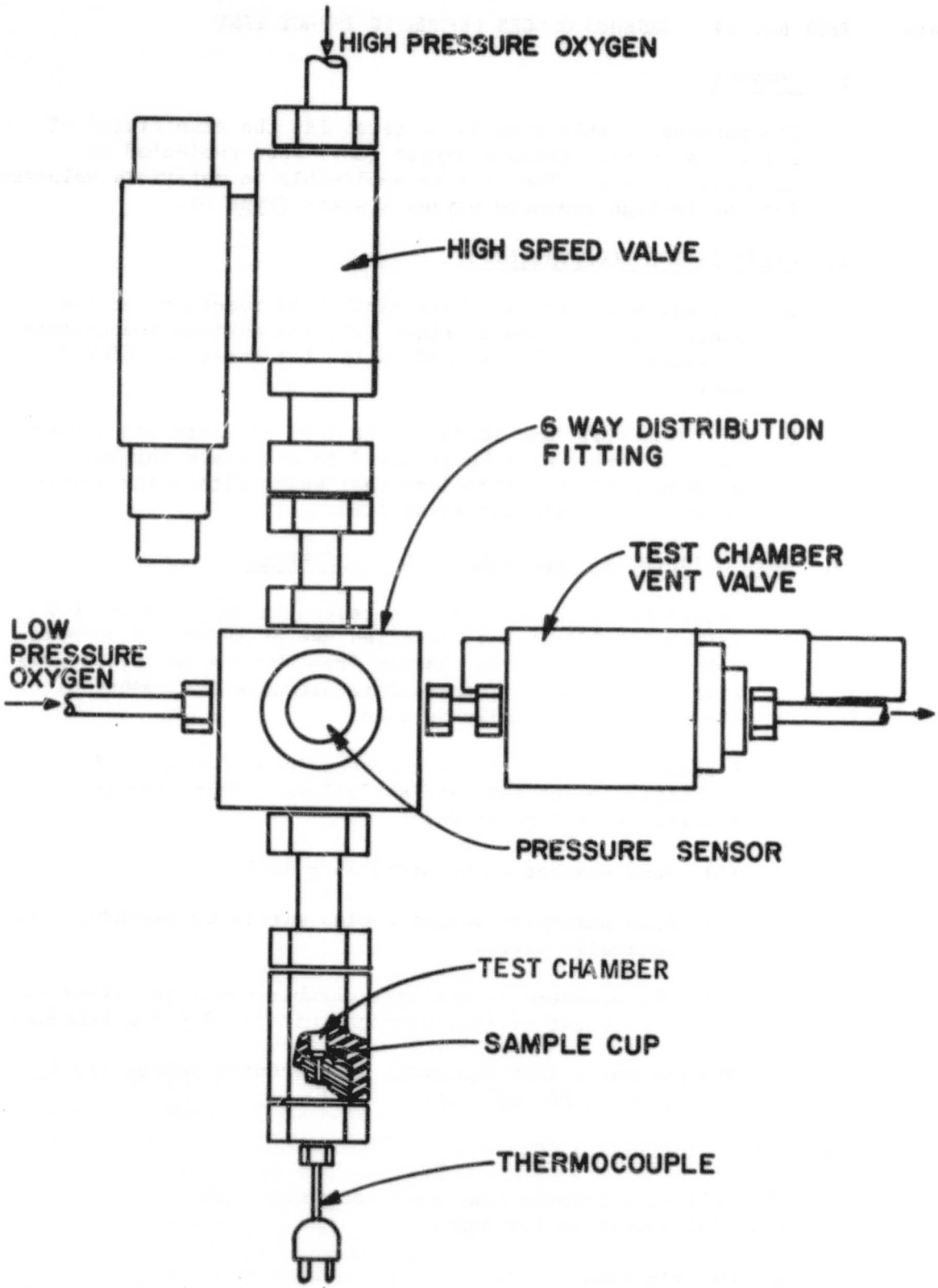

FIGURE 4-14 PNEUMATIC IMPACT TEST SYSTEM

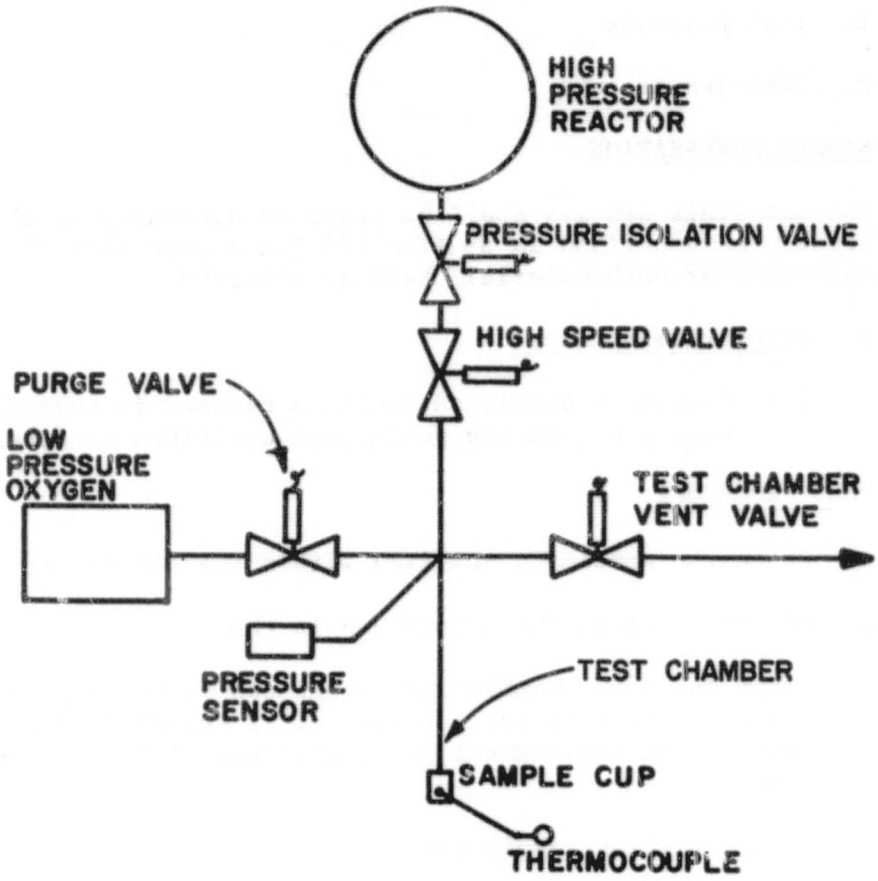

FIGURE 4-15 PNEUMATIC IMPACT TEST SYSTEM

c. Composition

d. Batch/lot number

e. Previous cleaning and conditioning processes

f. Test pressure

g. Test Temperature

5. SAMPLE PREPARATION

The materials samples shall be prepared according to the procedures described in Section 413.3.a except that 80 specimens of each material shall be prepared.

a. Sample Cleanliness

(1) Materials submitted shall be cleaned in accordance with the cleaning guidelines described in Appendix C.

6. TEST PROCEDURE

a. Place the sample in position within the sample cup.

b. Loosely install the sample cup in the test chamber.

c. Purge the test chamber and sample cup with low pressure oxygen by opening purge valve V-1 to ensure that a 95^{+5}_{-0} percent oxygen environment is established within the test chamber.

d. Wrench-tighten sample cup.

e. Pressurize the high pressure accumulator to the desired test pressure with oxygen.

f. Stabilize the test chamber temperature at the desired test conditions.

g. Subject the material specimen to cyclic high pressure oxygen as follows:

(1) Ensure purge valve V-1 is closed.

(2) Open vent valve V-4 until chamber pressure sensor indicates atmospheric pressure, then close V-4.

(3) Open pressure isolation valve V-2.

(4) Cycle high speed valve V-3 open until test chamber pressure sensor indicates the same pressure as the accumulator, then close.

(5) Maintain pressure in test chamber for five seconds.

(6) Open vent valve V-4 for five seconds to allow the test chamber pressure to decay to atmosphere pressure.

(7) Repeat Steps (4),(5), and (6) until five complete cycles have been accomplished.

(8) Close pressure isolation valve V-2.

(9) Open vent valve V-4 and high speed valve V-3.

(10) When test chamber pressure sensor indicates atmospheric pressure, close V-3 and V-4.

h. Remove sample cup from test chamber.

i. Remove the material specimen and examine for evidence of reaction.

j. Record all observations on the data sheet. Photographs of a visual change in the sample shall be at the discretion of the test engineer.

k. Repeat the above sequence to obtain data on a total of 20 specimens at each specified test pressure.

7. REPORTING

Test data shall be reported in accordance with instructions contained in Paragraph 208 on a form similar to Figure 2-1. The following special test data and information shall be reported:

a. Lot/batch number

b. Pressure change before and after test

c. Temperature change in the test chamber

d. Condition of sample after test

e. Number of test cycles

f. Number of failures versus number of samples tested

g. Pertinent comments and observations of the test agency

415 TEST NO. 15 - CONSTANT TEMPERATURE IMMERSION OF MATERIALS IN TYPE J FLUIDS

1. PURPOSE

The purpose of this test is to determine the gross compatibility of materials with Type J fluids.

2. SCOPE

This test is applicable for materials being considered for use in all Type J fluids. The test technique is hazardous in nature and requires remote propellant handling and control.

3. CRITERIA FOR ACCEPTABILITY

The criteria for acceptability is based on exposure to a test environment consisting of a 48-hour conditioning period in the test fluid at a temperature of 160°F. All materials are to be tested at their maximum use pressure. A material is considered to be compatible with the test fluid if exposure of a minimum of three test specimens to these conditions results in no obvious changes in the material, i.e., dissolution, separation, etc.

Materials shown to be incompatible at test fluid temperatures of less than 160°F are also considered incompatible and testing at 160°F is not required.

4. TEST CONDITIONS

Test pressure will be adjusted to simulate maximum applied system use pressure at a temperature of 160°F + 5.5°F - 0°F. The samples will be immersed for 48 $\pm$ 1 hours then removed for post test observations.

5. TEST EQUIPMENT

The test fixture shall be constructed of 300 series stainless steel or equivalent. It shall contain a rupture disc suitable for protecting personnel and test equipment in the event a sample ignition occurs. The fixture shall have penetrations for filling, pressurization, pressure and temperature measuring devices. The test fixture volume shall be a minimum of 1.5 liters with a minimum of two-thirds of this volume as ullage.

6. SAMPLE PREPARATION

A minimum of three samples shall be prepared in lengths of two inches. The normal sample size shall be 2" X 1/4" X 1/4".

Cleaning shall conform to the applicable vehicle specification. The sample shall be mounted in the test fixture with a stainless steel wire in a position where it will be fully submerged in the test fluid medium.

7. TEST PROCEDURE

a. Verify that all test equipment is in current calibration.

b. Position sample in the text fixture.

c. Complete test fixture assembly (with rupture disc) and perform leak test.

d. Fill test fixture completely with the test fluid to ensure all interior surfaces are wet.

e. Draw ullage and pressurize test fixture with gaseous helium to desired test pressure.

f. Isolate test fixture and monitor pressure for 10 minutes. A decay in pressure of more than one percent is unacceptable.

g. Start recording instrumentation (pressure and temperature).

h. Initiate power to the heaters. Ensure a temperature rise rate of 9 to 18°F per minute. Ensure temperature stabilizes at 160°F + 5.5°F, - 0°F.

i. Continue immersion test for 48 $\pm$ 1 hours after temperature stabilizes.

j. After 48 hours, vent the test fixture, de-energize heaters, secure recording instrumentation.

k. Purge test fixture with GN_2 until no liquid or vapor is visible at the vent line.

l. Disassemble test fixtures and examine test sample.

m. Record all observations on the data sheet. Photographs of the sample shall be at the discretion of the test engineer. Recorded observations shall include comments pertaining to any sample color changes, physical deformation, dissolution characteristics, separation, apparent size changes, etc.

n. Chamber shall be decontaminated and cleaned per the applicable test agency requirements.

8. REPORTING

Test data shall be reported in accordance with instructions contained in Paragraph 208 on a form similar to Figure 2-1. The following special test data and information shall be reported:

a. Lot/batch number

b. Temperature change in test fixture

c. Condition of samples after test

d. Pertinent comments and observations of the test agency

APPENDIX A -- ABBREVIATIONS AND ACRONYMS

ABMA	Army Ballistic Missile Agency
amps	amperes
ASTM	American Society for Testing Materials
AWG	American Wire Gage
FAA	Federal Aviation Administration
FAR	Federal Aviation Regulation
FEP	Fluorinated Ethylene Propylene
GFE	Government Furnished Equipment
GSE	Ground Support Equipment
GOX	Gaseous Oxygen
JSC	Johnson Space Center
KSC	John F. Kennedy Space Center
LOX	Liquid Oxygen
MQ	Reliability, Quality Assurance and System Safety (OMSF)
MSFC	George C. Marshall Space Flight Center
N_2O_4	Nitrogen tetroxide
N_2H_4	Hydrazine
OMSF	Office of Manned Space Flight
ppm	parts per million
psia	pounds per square inch absolute
QA	Quality Assurance
RFP	Request for Proposal
SBF	Single Barrier Failure
SPEC	Specification
TFE	polytetrafluoroethylene resin
Vg	Vacuum Gage
WSTF	White Sands Test Facility

APPENDIX B - RELATED DOCUMENTS

The following publications contain applicable information relating to the selected requirements and criteria prescribed herein:

SPECIFICATIONS

Military

MIL-W-16878	Wire, Electrical, Insulated, High Temperature
MIL-W-22759	Wire, Electrical, Fluorocarbon-Insulated, Copper and Copper Alloy
MIL-P-25508	Propellant Oxygen, Type I
MIL-O-27210	Oxygen, Aviators Breathing, Liquid and Gas, Type I

Lyndon B. Johnson Space Center (JSC)

JSC-SPEC-Q3	Pretreatment (Etching) of Teflon Surfaces prior to Potting Processes, Specification for
JSC-02681	Nonmetallic Materials Design Guidelines and Test Data Handbook
JSC-C-20A	Water, High Purity and Distilled
JSC-C-23	Surface Cleanliness Levels for Sampling Equipment.

American Society for Testing Materials (ASTM)

ASTM-D56	Standard Method of Test for Flash Point by Tag Closed Tester
ASTM-D568	Standard Method of Test for Flammability of Flexible Plastics
ASTM-D635	Standard Method of Test for Flammability of Self-Supporting Plastics

PUBLICATIONS

George C. Marshall Space Flight Center (MSFC)

TMX 64711	Compatibility of Materials with Liquid Oxygen - Volume I
MSFC-SPEC-234A	Nitrogen, Space Vehicle Grade

Federal Aviation Administration (FAA)

FAR25	Airworthiness Standards (Part 25)

DRAWINGS

National Aeronautics and Space Administration/White Sands Test Facility (NASA/WSTF)

222-10167C	Modified High Voltage Spark Generator
251-10234-2A	Flash and Fire Test Apparatus
252-10235D	Flash and Fire Temperature Controller System Assembly
252-10298	Flash and Fire Point Sensor Unit
3552	WSTF Instruction Manual

APPENDIX C

PRECISION CLEANING GUIDELINES FOR OXYGEN IMPACT TEST SPECIMENS AND TEST APPARATUS

1.0 PURPOSE. These requirements are written to assure that cleaniness conditions are maintained and testing of materials is undertaken under uniformly clean conditions. These cleaning guidelines shall assure that nonmetallic materials specimens are subjected to uniform cleaning methods which are repeatable. The method is intended to remove hydrocarbons which contaminate the surface during manufacturing, handling, processing, and shipping.

2.0 SCOPE. These guidelines describe methods of cleaning material test specimens. The constraints implied by cleaning and the techniques of cleaning are only generally covered. Particulate contamination shall be controlled by assuring freshly prepared cleaning solutions. These guidelines are not an operating procedure or job instruction which details every specific step required to perform a cleaning operation. These operating procedures/job instructions are the responsibility of the operating element and are not within the scope of this document.

3.0 VISUAL EXAMINATION

3.1 All material specimens and test apparatus shall be visually inspected to detect signs of contamination. Methods employed within the sample preparation area shall be those which can be utilized during inspection and verification to determine the amount of precleaning required. Any contamination shall be cause for recleaning (see Section 4.0). Observations must be made with the unaided eye and light of sufficient intensity to illuminate the area being inspected during the initial material cleanliness inspection.

3.2 All material specimens shall be free of cuts, abrasions, and other flaws as determined by close visual inspection without magnification.

4.0 CLEANING

4.1 Before any GOX impact test, the material specimens shall be precleaned by brushing with a nylon brush and by flowing an inert gas over them to remove loose surface contamination, followed by reinspection as specified in Section 3.2

4.2 Only lubricant and grease test specimens shall be tested in their "as used" condition; that is, no special cleaning processes other than those used to prepare the material for application or assembly test are required.

4.3 All other test specimens shall be subjected to the following general cleaning provisons consisting of the removal of such gross surface contaminants as scale, grease marks, manufacturing residues, excess plasticizers, corrosion and oxidation products, etc., prior to final precision cleaning per this specification. Solvent cleaning shall be limited to water and mild detergent since further solvent action can change the physical and chemical properties of materials by leaching or solvent absorption, thus altering the sensitivity to GOX impact. The cleaning method proposed here is uniformly applied to all materials (see 4.7) prior to performing GOX impact tests and correlates with existing contractor cleanliness specifications.

4.4 Rubber gloves, or equivalents, shall be worn during all cleaning operations. Cleaned surfaces shall not be handled with bare hands. Clean (low-lint) white nylon gloves, or equivalent, shall be worn when handling cleaned items. During and subsequent to cleaning, care shall be taken not to recontaminate parts. Cleaned parts shall be placed and sealed in a Teflon, or equivalent, package which has been cleaned in accordance with JSC-C-23, Level 1.

4.5 Cleaning and inspection processes per this specification are designed not to be detrimental to nonmetallic materials or test apparatus parts. When a procedure herein is not directly applicable to nonmetallic material specimens, those specimens shall not be processed per this specification.

4.6 Cleaning Materials

4.6.1 Rinse Water. Rinse water shall be of the distilled or deionized variety conforming to JSC-SPEC-C-20A, except that a minimum resistance of 50,000 ohm-cm is acceptable. Water shall be filtered through a 25 micron (absolute) filter or better, prior to use for spraying or flushing.

4.6.2 Detergent. Detergent shall be added to deionized water in accordance with concentration requirements of Section 4.9.3 and then passed through a 25 micron (absolute) filter, or better, prior to use, for flushing/decontamination purposes. The following detergent types are acceptable; Liqui-Det. #2, Turco 4215S, Ivory Liquid Detergent.

4.6.3 Cleaning Solvents. Cleaning Solvents shall be Freon TF for cleaning test fixture and apparatus and shall be filtered through a 4.5 micron (absolute) filter, or better, prior to use. The NVR content of the Freon solvent shall not exceed 1.0 mg per 100 ml. Nonmetallic materials shall be suitably cleaned with water and mild detergent solution.

4.7 Cleaning Methods. Where applicable, WSTF Instruction Manual, No. 3552, Process No. 3, shall be followed. When cleaning elastomeric parts (rubber, elastomers, O-rings, and other plastic or synthetic nonmetallic parts).

4.8 Precleaning. Where applicable, (Section 4.1), samples and test apparatus shall be precleaned prior to conducting any GOX mechanical or pneumatic tests.

4.9 Cleaning Procedure

4.9.1 Samples and test apparatus shall be first inspected for any signs of abrasion, etc., and brushed clean, using a nylon brush.

4.9.2 The material specimens shall then be decontaminated, using cold tap water. Flush with water until pH of effluent is within 0.5 pH unit of influent, but do not flush less than two minutes.

4.9.3 Perform detergent cleaning using 1/2 to 1 oz. of detergent/gallon of deionized water. Assist cleaning with nylon brush. Immersion time shall be 5 + 1 minute at bath temperature of 120-150° F. Agitation, not ultrasonic, shall be effected for a period not less than 30 seconds prior to removal from detergent bath.

4.9.4 Soak and agitate for not less than two minutes with deionized water (see Section 4.6.1) 140°F maximum until no evidence of detergent solution is apparent when checked by a suitable ASTM or equivalent method.

4.9.5 Rinse-spray using deionized water for at least ten thorough applications.

4.9.6 Place samples in clean Petri dish.

4.9.7 Dry for 5 minutes with nitrogen (GN_2) conforming to MSFC-SPEC-234A, filtered through a membrane filter not exceeding a 4.5 micron pore size, and package in a Teflon package.

4.9.8 Samples have now been uniformly cleaned and are ready for GOX mechanical/pneumatic testing.

5.0 TEST APPARATUS

5.1 Prior to performing any GOX impact test, the test chamber and components, where necessary as determined by Section 3.0, shall be degreased in a solution of detergent and demineralized water or Freon, depending upon the contaminants. Rinsing or flushing shall be thorough, followed by adequate drying, such as passage of dry nitrogen, air, or inert gas over the components.

5.2 Application of any cleaning solution must be restricted to usages where problems subsequent to cleaning will not occur as a result of the application; e.g., corrosion from entrapped cleaning fluids that might alter a material's GOX impact characteristics, etc.

5.3 All steps in any procedure must progress in an uninterrupted series of operations through the final rinse and drying operation. Precautions must be taken to assure that cleanliness is maintained until testing commences.

☆ U. S. GOVERNMENT PRINTING OFFICE : 1974 732-186/192

END OF REFERENCE

38

REFERENCE

39

CHEMICAL ENGINEERING DIVISION, SUMMARY REPORT. REP. ANL-6145, ARGONNE NATIONAL LAB., JAN., FEB., MAR., 1960.

ANL-6145
Chemistry - Separation Processes
for Plutonium and Uranium
(TID-4500, 15th Ed.)
AEC Research and
Development Report

ARGONNE NATIONAL LABORATORY
9700 South Cass Avenue
Argonne, Illinois

CHEMICAL ENGINEERING DIVISION SUMMARY REPORT

January, February, March, 1960

Stephen Lawroski, Division Director
W. A. Rodger, Associate Division Director
R. C. Vogel, Associate Division Director
V. H. Munnecke, Assistant Division Director

Preceding Quarterly Reports:
ANL-6101 October, November, December, 1959
ANL-6068 July, August, September, 1959
ANL-6029 April, May, June, 1959

Operated by The University of Chicago
under
Contract W-31-109-eng-38

Table 37

COMPARISON OF BURNING-PROPAGATION RATES IN OXYGEN FOR VARIOUS METALS
Samples in form of either foil or wire. See ANL-5959, page 71, for method

Metal	Thickness (mm)	Width (mm)	Diameter (mm)	Burning-propagation Rate (cm/sec)
Aluminum	0.015	~3.0		-[a]
Cadmium	0.005	~3.0		-[a]
Cobalt	0.30	~3.0		-[a]
Cobalt	0.025	2.9		5.09
Chromium	0.05	2.9		3.56
Chromium	0.013	2.8		5.37
Copper	0.05	~3.0		-[a]
Copper	0.007	3.1		8.32
Hafnium	0.13	~3.0		6.40
Hafnium	0.07	3.0		9.27
Indium	0.05	~3.0		-[a]
Iron	0.28	3.0		0.87
Iron	0.030	3.0		2.74
Iron	0.007	3.2		6.96
Iron			0.23	5.09
Lead	0.17	~3.0		-[a]
Magnesium	0.13	2.8		9.32
Magnesium	0.007	3.2		109
Molybdenum	0.13	3.2		0.96
Molybdenum	0.08	3.1		1.96
Molybdenum	0.05	3.0		2.75
Molybdenum			0.25	2.13
Nickel	0.01	~3.0		-[a]
Niobium	0.030	3.0		12.6
Niobium	0.010	3.1		26.5
Niobium			0.05	49.5
Rhenium			0.52	-[a]
Tantalum	0.25	3.2		1.15
Tantalum	0.13	3.1		2.01
Tantalum	0.05	3.0		4.32
Tantalum	0.007	3.0		39.9
Thorium	0.23	3.0		8.75
Thorium	0.13	3.1		19.4
Tin	0.01	~3.0		-[a]
Titanium	0.29	3.2		6.11
Titanium	0.12	3.1		14.3
Titanium	0.025	3.3		53.3
Titanium	0.007	3.1		138
Tungsten	0.13	~3.0		-[a]
Uranium	0.25	3.0		3.75
Uranium	0.13	3.0		6.04
Uranium	0.03	3.0		24.5
Uranium	0.01	3.0		60.6
Uranium			0.48	5.96
Vanadium	0.28	3.0		1.51
Zinc	0.02	~3.0		-[a]
Zirconium	0.27	3.0		8.24
Zirconium	0.13	3.0		11.1
Zirconium	0.05	3.0		17.3
Zirconium	0.02	3.0		42.8
Zirconium	0.007	4.2		177
Zirconium			0.39	19.9

[a]Combustion not sustained, therefore no burning propagation rate measurable.

END OF REFERENCE

39

Card #11

REFERENCE

40

LAPIN, A.: LIQUID AND GASEOUS OXYGEN SAFETY REVIEW. VOL. IV. APCI-TM-184, AIR PRODUCTS AND CHEMICALS, INC. (NASA CR-120922), 1972.

NASA CR-120922
APCI TM 184

LIQUID AND GASEOUS OXYGEN SAFETY REVIEW

FINAL REPORT

Vol. IV

JUNE 1972

A. LAPIN
AIR PRODUCTS AND CHEMICALS, INC.
ALLENTOWN, PENNSYLVANIA 18105

Prepared for
AEROSPACE SAFETY RESEARCH AND DATA INSTITUTE
LEWIS RESEARCH CENTER
NATIONAL AERONAUTICS AND SPACE ADMINISTRATION
CLEVELAND, OHIO 44135

Under
NASA Contract NAS3–15083
Paul M. Ordin, Program Manager

1. Report No.	2. Government Accession No.	3. Recipient's Catalog No.
NASA CR-120922 Vol. IV		

4. Title and Subtitle	5. Report Date
Liquid and Gaseous Oxygen Safety Review Final Report, Vol. I to IV (1320 pages - Total)	June 1972
	6. Performing Organization Code
7. Author(s)	8. Performing Organization Report No.
Abraham Lapin	APCI TM 184
	10. Work Unit No.
9. Performing Organization Name and Address	11. Contract or Grant No.
Air Products and Chemicals, Inc. P. O. Box 538 Allentown, Pennsylvania	NASA NO. NAS3-15083
	13. Type of Report and Period Covered
12. Sponsoring Agency Name and Address	Contractor Report April 1971 - June 1972
National Aeronautics and Space Administration Washington, D.C. 20546	14. Sponsoring Agency Code

15. Supplementary Notes

Project Manager, Paul M. Ordin
Aerospace Safety Research and Data Institute
Lewis Research Center
Cleveland, Ohio

16. Abstract

A thorough and detailed study of Air Products and Chemicals, Inc. and Air Products Ltd. practices in the design and use of equipment in oxygen service, was performed. The report includes Liquid and Gaseous Oxygen Safety Review information covering: Material Compatibility, Operational Hazards, Maintenance Programs, Systems Emergencies, and Accident/Incident Investigations and Reports, and a set of references. Areas requiring further research and development for systems involving exposure to oxygen environment have been identified. An index to the Liquid and Gaseous Safety Review Data Forms and a General Index have been included to allow for easy retrieval of the reported information.

17. Key Words (Suggested by Author(s))	18. Distribution Statement
Liquid and Gaseous Oxygen Safety Review, Material Compatibility, Compatibility Checks, Operational Hazards, Maintenance Programs, Systems Emergencies, Accident and Incident Investigations and Reports, Transportation Systems, Storage Systems.	Unclassified Unlimited

19. Security Classif. (of this report)	20. Security Classif. (of this page)	21. No. of Pages	22. Price*
Unclassified	Unclassified	Vol. IV - 340	$6.00 Vol. IV only

* For sale by the National Technical Information Service, Springfield, Virginia 22151
$21.00 for all four volumes.

NASA CR-120922
APCI TM 184

LIQUID AND GASEOUS OXYGEN SAFETY REVIEW

Final Report

Volume IV of Four Volumes

June 1972

A. Lapin

Air Products and Chemicals, Inc.
Allentown, Pennsylvania 18105

Prepared for

Aerospace Safety Research and Data Institute
Lewis Research Center
National Aeronautics and Space Administration
Cleveland, Ohio 44135

Under

NASA Contract NAS3-15083

Paul M. Ordin, Program Manager

Air Products and Chemicals INC.

COMPANY CONFIDENTIAL

THE BURNING OF METALS IN OXYGEN ATMOSPHERES

(80 TO 100%)

Technical Memorandum No. 186

EA-2156

March 1972

John Daly

DISTRIBUTION:

W. L. Ball
L. S. Gaumer
J. M. Geist
M. H. Halsted/G. W. Robinson/H. E. Wynn
A. Lapin
C. McKinley
A. W. Mellen
W. J. Scharle
D. Spencer (APL)
E. P. Thomas
K. Wilson (APL)
APCI Library (2)
APL Library
R&D Central Files

APPROVALS:

A. Lapin — 3/24/72 (Date)

C. McKinley — 4/2/72 (Date)

APCI DOCUMENT NO. 922455

SUMMARY

An exploratory experimental program has been carried out in the Allentown laboratories between February and May 1970 in order to observe and measure the burning rates of several metals. The test runs did not involve any equipment for measuring temperature, heat input, or heat evolved. The observations made for the most part were qualitative but there were some combustion rates measured in two of the experimental apparatuses.

There were five basic set-ups used in this experimental program (Figures 1 to 5), four involving gaseous oxygen at atmospheric pressures and one using LOX at atmospheric pressure. Experimental results for two of the set-ups, Figures 2 and 5, are recorded on 16mm movies. Typical runs for mild steel, stainless steel, and aluminum were filmed.

There were two ignition methods used. Initially an oxyacetylene torch was used to heat the sample to ignition or melting whichever the case might be. Later an ignition "pill" made of compressed steel wool, stainless steel wool, or aluminum wool was used. This pill was ignited by means of a 6 volt battery and two electrodes. The second method was the better of the two since the oxygen atmosphere around the sample was not disturbed as much as in the case of the torch, which emits a high velocity flame.

Table I lists the metals with their compositions, which were tested. All metals were tested in every set-up except Apparatus No. 3. Mild steel and stainless steel were run in this set-up.

In addition to the experimentation, a literature survey was conducted on the combustion of metals. The Appendix contains a list of pertinent reports along with abstracts. Some of the more important articles are the eight papers by Dr. L. Kirschfeld, who has done extensive work in the field of combustion of metals.

CONCLUSIONS

For the most part, metals will react with oxygen if exposed to the right conditions. The degree with which a specific metal reacts depends on a number of variables. Pressure, temperature, phase of oxygen and oxygen concentration are among the most important ones. It appeared that the metals tested reacted faster and to a greater degree in liquid than in gaseous oxygen. The reason for this is not clear but two possible answers are: higher oxygen concentrations or better contacting of oxygen in the reaction zone. Combustion rates increase as the flow rate of oxygen increases, at least in the case of mild steel as shown in figure 6.

The data taken during these series of tests agree in a qualitative way with those of other researchers in the field of combustion of metals (4,5,6,7). In general most agree that mild steel is the easiest to ignite and burns readily in oxygen. Nickel and its alloys appear at the other end of the scale, being the most resistive to burning in oxygen regardless of conditions. Aluminum lies somewhere in the middle, being a very reactive metal in oxygen after ignition, but its low melting point and high ignition temperature make it one of the hardest metal to ignite and keep burning. The list of metals which were tested, is arranged, in Table II, in order of decreasing resistance to ignition and burning in oxygen atmospheres.

Air Products and Chemicals INC.

TABLE I

Compositions of Metals Tested

Stainless Steel	C (Max) %	Mg (Max) %	Composition Si (Max) %	Cr %	Ni %	Others %
309	0.2	2.00	1.00	22-24	12-15	--
316	0.1	2.00	1.00	16-18	10-14	Mo 2-3
316 L	0.03	2.00	1.00	16-18	10-14	Mo 1.75-2.5
410	0.15	1.00	1.00	11.5-13.5	---	--
17-4 Ph	0.04	--	--	16.5	3.5-4.0	Cu 3.4-4.0

Commercial Leaded Bronze: 89% Cu, 1.75% Pb, 9.25% Zn

Monel 400: 66.5% Ni, 0.12% C, 1.0% Mn, 1.35% Fe, 0.15% Si, 31.5% Cu

Inconel 600: 76.0% Ni, 0.04% C, 0.2% Mn, 7.2% Fe, 0.20% Si, 0.10% Cu, 15.8% Cr

Nickel 200: 99.5% Ni, 0.06% C, 0.25% Mn, 0.15% Fe, 0.05% Si, 0.05% Cu

Hastelloy B: 65% Ni, 0.1% C, 0.5% Mn, 6% Fe, 0.5% Si, 28% Mo

Aluminum 5357: 1.0% Mg, 0.25% Mn, 98.75% Al

Carbon Steel 1010: 0.08-0.13% C, 0.30-0.60% Mn, 0.040% P, 0.050% S, Balance Fe

Molybdenum Steel 4140: 0.33-0.43% C, 0.75-1.0% Mn, 0.040% P, 0.040% S, 0.2-0.33% Si, 0.8-1.10% Cr, 0.15-0.25% Mo, Balance Fe

TABLE II

Metals Tested Arranged in Order of Decreasing Resistance to Ignition and Burning

Nickel 200	- only melted
Commercial bronze	- only melted
Inconel 600	- very little reaction
Monel 400	- very little reaction
Hastelloy B	- very slow reaction rate
Aluminum	- hard to ignite but very reactive after ignition
Stainless steel	- self-sustaining reaction in some runs
Mild steel	- very easy to ignite--complete combustion of sample

RESULTS

Variations in burning characteristics of metals were determined in each of the tests in the five experimental set-ups. These characteristics are classified into five catagories.

1. Metals for which self-sustaining burning was sufficient to allow a combustion rate to be measured. In addition these metals burned until oxygen was removed (√).

2. Metals which burned in a long enough self-sustaining manner, that a rate of combustion was measured, but differed from number 1 in that they were eventually self-extinguishing in nature (√+).

3. Metals which burned or reacted in a manner which did not allow the determination of a rate of combustion. For example, stainless would melt off the sample rod and react with the oxygen in the molten form at the base of the experimental equipment (√*).

4. Metals which reacted only when outside heat was supplied (S.R.).

5. Metals which did not react; the test sample only melted (N.R.).

Table III has a listing of all the metals tested and the testing apparatuses. In addition, the metals are classified into the above mentioned categories, and some typical burning rates are mentioned.

With regard to the resistance of metals in reacting with oxygen, nickel and its alloys are probably the most resistive, while steel, stainless steel, and aluminum are the least resistive of the metals tested. Aluminum, although reacting most violently with oxygen, was very hard to ignite. This is a factor in its favor for its use in some oxygen atmosphere applications.

EXPERIMENTATION AND DISCUSSION OF RESULTS

Apparatus No. 1 (Figure 1)

In this equipment although very simple, three types of reactions could be distinguished (see Table III). Mild steel is the easiest of the metals to ignite. Once heated to glowing red and lowered into the beaker containing oxygen it would continue to burn as long as there was oxygen available. The reason being, mild steel ignites and burns in oxygen at, or just below its melting point, causing the reaction to remain on the rod. Stainless steel on the other hand, reacts with oxygen at, or just above its melting point, therefore, it was very difficult to sustain a reaction on the rod for a long period of time. Stainless steel because it reacts with oxygen at a higher temperature and in a different phase than mild steel, was very sensitive to positioning. Combustion rates for stainless steel were obtained when the stainless steel rod was burning horizontally and vertically from bottom to top. Aluminum, like stainless steel ignites above its melting point (5). It is estimated in the literature that its ignition temperature in oxygen is around 3700°F (5,6). Since aluminum's melting point is about 1220°F there was very little chance of getting the test piece hot enough to cause ignition in this type of equipment. Nickel and its alloys are other metals which ignite above their melting point, so ignition of these metals was again not achieved. Low oxygen concentration,

Air Products and Chemicals INC.

TABLE III

Metals Tested Classified into Degrees with which they Reacted with Oxygen in Each Apparatus

Metal		Apparatus 1	2	3	4	5
Mild Steel 1/16", 1/8" & 1/4" rod	Data on 1/16" rod	√*	√ .3 in/sec (up) .5 in/sec (down)	√* No Data	√*	√ .435 in/sec
Aluminum 1/16" rod		N.R.	√+ 10 in/sec (up) approximate	-----	√*	√*
309 Stainless Steel 1/16" rod		√*	√ .171 in/sec (down)	-----	√*	√ .38 in/sec
316 Stainless Steel 1/16" rod		√*	√+ .08 in/sec (up)	-----	√*	√ .3 in/sec
316 L Stainless Steel 3/32" rod		√*	√+ .07 in/sec (up)	-----	√*	S.R.
410 Stainless Steel 1/16" rod		√*	√+ .052 in/sec (up)	-----	√*	√+ .24 in/sec
17-4 Ph Stainless Steel 1/16" rod		√*	√+ .12 in/sec (up)	-----	√*	√ .3 in/sec
4140 Steel 3/16" rod		√*	√ .013 in/sec (up)	-----	√*	√ .06 in/sec
Nickel 200 1/16" & 1/8" Rod		N.R.	N.R.	N.R.	N.R.	N.R.
Monel 400 1/16" rod		S.R.	S.R.-9 sec of glowing	-----	N.R.	S.R. - 4 sec of glowing
Inconel 600 1/16" & 1/8" Rod		S.R.	N.R.	-----	N.R.	S.R.-4 sec of glowing
Commercial Bronze 1/16" rod		N.R.	N.R.	-----	N.R.	N.R.
Hastelloy B 5/64" rod		S.R.	√ .06 in/sec (up)	-----	S.R.	√ .08 in/sec

Note: See Results on page 4 for explanation of symbols

END OF REFERENCE

40

REFERENCE

41

ISAACS, J. L.: THE OXYGEN INDEX FLAMMABILITY TEST.
J. FIRE AND FLAMMABILITY, VOL. 1, JAN. 1970.

COURTESY OF THE JOURNAL OF FIRE AND FLAMMABILITY,
TECHNOMIC PUBLISHING CO., INC., 265 W. STATE ST.,
WESTPORT, CT, 06880.

6.2-c

The Oxygen Index Flammability Test

Jack L. Isaacs

General Electric Co.
Louisville, Ky. 40225

(Received October 1, 1969)

ABSTRACT

The Oxygen Index Flammability Test was developed by Fenimore and Martin because they found that none of the generally accepted tests gave the precise measurement of the relative flammability of polymeric materials necessary for flammability research. This paper will describe their test, give some typical results for the various types of materials which can be studied by this method, and compare results from this test with those obtained on other tests. Some examples to show how the method can be applied to almost every phase of flammability testing from quality control to pure research will also be presented.

INTRODUCTION

In 1966, Drs. C. P. Fenimore and F. J. Martin of the General Electric Research and Development Center published an article [1] introducing the Oxygen Index Test, which they had developed for studying the flammability of polymeric materials. Since that time, the test has become widely recognized as a significant addition to the field of polymer flammability testing. At the present time over 100 different industrial firms are using the test to study not only polymers, but fabrics, woods and many other materials. In this paper we will show how the test can be applied to almost every phase of flammability testing from pure research to everyday quality control.

THE OXYGEN INDEX TEST METHOD

Before discussing the test, it is necessary to first define Oxygen Index and explain its meaning. The Oxygen Index, n, of a material is the percentage concentration of oxygen in a mixture of oxygen and nitrogen which will maintain equilibrium burning conditions, i.e., the heat produced during combustion just balances the heat lost to the surroundings. Physically, this is the lowest concentration of oxygen which will support sustained combustion of the material, and is calculated from the following equation:

$$n\,(\%) = \frac{100 \times O_2}{O_2 + N_2}$$

where O_2 is the oxygen concentration at equilibrium and N_2 is the associated nitrogen concentration.

Table 2. Typical Oxygen Index Results for Rigid Plastics.

Material	Oxygen Index	Source
Polyacetal, Celcon	14.9	19
Polyethylene Oxide, Polyox WSR-35	15.0	19
Polyacetal plus 30% glass	15.6	14
Cellulose Acetate (dry = 0.1% water)	16.8	24
Polymethyl Methacrylate, Plexiglas	17.3	1
Polypropylene, Profax 6505	17.4	19
Polystyrene, Shell 325	17.8	21
Polypropylene, Profax P7401	17.8	22
Cellulose Acetate (wet = 4.9% water)	18.1	24
Polystyrene, Cosden 825 TV	18.2	21
Polypropylene plus 30% glass	18.5	14
ABS, Cycolac T	18.8	21
Cellulose Butyrate (dry = 0.06% water)	18.8	24
Polystyrene, Dylene 8X	19.0	22
SAN	19.1	14
Cellulose Butyrate (wet = 2.8% water)	19.9	24
Arylon T-3198 Natural	20.6	14
ABS plus 20% glass	21.6	14
Phenolic—Paper Laminate, Textolite 11571B	21.7	21
Polycarbonate, Lexan 191	22.5	14
Arylon T-3198 White	22.8	14
Polypropylene (F.R.), Plaskon 1070X	23.7	21
Noryl 731	24.3	14
Nylon 6-6 (dry, as molded)	24.3	23
Polycarbonate, Lexan 141	24.9	21
Epoxy-Glass Laminate, G.E. 11558G10	24.9	22
ABS (F.R.), Durez 2311	25.2	14

has been hampered by the failure of the test to measure flame spread rate and ease of ignition. In the future, attempts will be made to modify the procedure to overcome these drawbacks. Typical examples are given in Table 3.

6. *Rubber*—The method for rigid and flexible plastics has been applied to rubbers. Some results are shown in Table 4.

7. *Wood*—Table 4 also contains examples of the results for woods. The experimenter must be careful, as with many plastics, to avoid misleading results due to the formation of char. Reference 3 suggests the use of a statistical testing method for erratically burning materials such as these.

8. *Coated Products*—Wire coatings are being tested with the conductor removed [8] or replaced with a non-conductor, such as glass, so that conduction does not change the heat balance at equilibrium burning conditions i.e., Oxygen Index changes. Other coated products with the substrate present are being tested but results are not yet available for discussion.

9. *Other Areas*—Oxygen Index values for various materials at other pressures and temperatures are being determined for use in several areas including aerospace. Gases other than nitrogen and combinations of gases have also been used to study various materials [1].

Table 2. Typical Oxygen Index Results for Rigid Plastics.

Material	Oxygen Index	Source
Polypropylene (F.R.), Plaskon 1050	25.6	21
ABS (F.R.), Cycolac KT	25.8	21
Polypropylene (F.R.), Plaskon 1060	26.4	21
Noryl SE-100	27.4	22
ABS (F.R.), Cycolac KL	27.4	21
Noryl SE-1	28.0	15
Polypropylene (F.R.), Avisun 2356	29.2	21
Polycarbonate, Lexan 3412 plus 20% glass	29.8	15
Polyphenylene Oxide 534	30.0	15
Nylon 6-6 (saturated, about 8% water)	30.1	23
Polysulfone P1700	30.4	15
PVC, Plaskon X2013	31.5	21
ABS (F.R.), Cycovin KA	31.7	21
Epoxy—Glass Laminate, G.E. 11673FR-2	32.6	22
Epoxy, Plenco 200D-B1242	38.3	21
Polycarbonate, Lexan DL444	39.7	15
PVC, Plaskon 2005	40.3	22
Alkyd, Plenco 1504-B6636	41.0	21
Polyester, Atlac 711-050	41.5	16
Polycarbonate, Lexan DL444 plus 20% glass	42.0	15
Polyvinylidene Fluoride	43.7	15
PVC, Geon 101	45.0	1
Epoxy, Plenco 2000F-B6432	47.6	21
Epoxy—Glass Laminate, G.E. 11635 FR-4	49.0	22
Phenolic (Mica Filled), Plenco 343-B817	52.8	21
Polyvinylidene Chloride, Saran	60.0	1
Polytetrafluoroethylene, Teflon	95.0	1

RELATION TO OTHER TESTS

When a new test is developed, results are usually checked against those obtained on some generally accepted test. There are few tests which will numerically measure the relative flammability of a material. Several accepted tests presumably bracket materials into several broad classifications (burning, self-extinguishing and non-burning) according to their ability to support combustion. Two of the best known are the ASTM D-635 Test and the U.L. Subject 94 Test [10]. In Table 5, we compare the results obtained on these two tests with the Oxygen Index for the material.

It is apparent from these data that neither test correlates with the Oxygen Index Test or with each other. This leads to confusing results such as those for Dylene 85 which has an Oxygen Index equal or greater than all of the polypropylenes tested yet it rates only self-extinguishing (SE) while the polypropylenes are non-burning (NB). It is evident that the results are affected by factors other than the materials inherent flammability. A similar situation exists with the Subject 94 test where certain types of materials need an Oxygen Index near 27 to guarantee an SE rating [9]. In both cases, we have

Table 3. Typical Oxygen Index Results for Non-Rigid Plastics, Cellular Materials and Fabrics.

Material Designation	Oxygen Index	Sample Size	Remarks	Source
Non-rigid plastics				
Delrin	16.1	0.125" × 1" × 4"	—	5
Plexiglas G	16.7	0.030" × 1" × 6"	—	5
Plexiglas G	16.8	0.050" × 1" × 6"	—	5
Plexiglas G	17.4	0.125" × 1" × 6"	—	5
Polystyrene, Koppers 8	18.0	0.062" × 0.875" × 4"	—	5
Cellulose Acetate Butyrate	19.6	0.125" × 1" × 4"	—	5
Lexan 8000-111	21.3	0.005" × 2" × 6"	—	5
Lexan 8070-112	22.2	0.010" × 2" × 6"	—	5
Lexan, commercial sheet	26.1	0.062" × 1" × 4"	—	5
Kapton Polyimide 100H	36.5	0.001" × 1" × 4"	—	5
Effect of plasticizer on flammability		(100 parts PVC, 70 parts plasticizer, 12 parts $CaCO_3$ or flame retardant)		
D.O.P. Plasticizer	21.6	—	$CaCO_3$ filler	11
63 Parts D.O.P./7 Parts TCP	22.4	—	$CaCO_3$ filler	11
49 Parts D.O.P./21 Parts Santicizer 140	23.9	—	$CaCO_3$ filler	11
56 Parts D.O.P./14 Parts Santicizer 148	25.0	—	8 parts $CaCO_3$ filler 4 parts antimony oxide	11
Cellular Materials				
Unmodified Polyurethane Foam	16.5			7
SBR Foam	16.9			7
Polybutadyene Foam	17.1			7
Natural Rubber Foam	17.2			7
PVC Foam (adhesive backing)	22.3			21
Fabrics				
Cotton	18.6	—	—	5
Rayon Felt	18.7	—	—	17
Rayon	18.9	—	—	17
Acrylic	19.6	1" × 6"	Glass Filament	5
Polyester	20.6	1" × 6"	Glass Filament	5
Wool	23.8	1" × 6"	Glass Filament	5
Nomex	26.7	1½" × 4"	Metal Frame	5
Flame Treated Cotton, U.S. Army	27.3	2" × 5"	Metal Frame	5
Dynel	29.8	1" × 6"	Metal Frame	5
Polybenzimidazole	40.6	1½" × 4"	Metal Frame	5

END OF REFERENCE

41

REFERENCE

42

FENIMORE, C. P.; AND MARTIN, F. J.: CANDLE-TYPE TEST FOR FLAMMABILITY OF POLYMERS. MOD. PLAST., VOL. 43, NO. 11, NOV. 1966.

COURTESY OF MODERN PLASTICS JOURNAL

PHOTOSTAT FILE

Candle-type test for flammability of polymers

By C. P. Fenimore* and F. J. Martin*

Limiting oxygen index, defined as the minimal volume fraction of oxygen in a slowly rising gaseous atmosphere that will sustain the candle-like burning of a stick of polymer, is a convenient, reproducible, numerical measure of polymer flammability. A simple apparatus and technique for its determination are described. Measured indices for commercial plastics, used in conjunction with a postulated flame model, permit some conclusions about the mode of action of commonly used flame retardants. Some retardants act by affecting pyrolysis reactions in the condensed phase and, in so doing, slow the rate of generation of fuel gases necessary to sustain the flame; chlorine incorporated into polyethylene acts in this way. Other flame retardants poison the gaseous flame reactions, e.g., antimony in halogenated polyethylene, and in certain other plastics materials.

THE GROWING USE of plastics for structural applications emphasizes the need for greater knowledge of the chemistry and physics involved in their burning. Such knowledge hopefully will lead to the development of new flame retardant materials and to greater insight into their selection, formulation, and use in the manufacture of plastic products. A new technique for evaluating the flammability of polymers is described in this article and examples are given of the application of this technique to the study of a series of practical flame retardant systems.

A variety of techniques to evaluate flammability and flame spread has been described in the literature (1-3).[1] In many of these, a sample of specified geometry is ignited in air in a specific manner and after the ignition source has been removed, the time or distance burned before extinction is used as a measure of flammability. These tests generally have been used in practice to rate materials roughly into groups such as "slow burning" or "self-extinguishing," Class I or II. Neither these nor other tests described in the literature seemed to meet our requirements for a simple, reproducible, informative measure of the relative flammability of polymers. Consequently, other techniques were tried including an adaptation of a test used by H. G. Wolfhard and coworkers to compare flammabilities of some gaseous and volatile liquid fuels.

Wolfhard et al. (4, 5) determined the limiting mixture of air and nitrogen in which a given fuel could just burn. They described the mixtures by their oxygen indices:

$$\text{Oxygen index} = n = \frac{[O_2]}{[O_2] + [N_2]}$$

where the brackets indicate the volume concentrations of the oxygen and nitrogen. For air, n = 0.21. The smaller the limiting n, the more flammable the fuel since the more its flames survived cooling by nitrogen. Some of Wolfhard's limiting indices for diffusion flames at atmospheric pressure were:

n = 0.054 for hydrogen gas,
= 0.056 for an equimolar mixture of hydrogen and carbon monoxide,
n = 0.071 for monomeric formaldehyde,
= 0.133 to 0.134 for benzene and normal paraffins containing 6 to 10 carbon atoms.

We have found that the limiting oxygen indices, determined for sticks of polymers burning in a candle-like manner, constitute a convenient rating of flammability for solid polymers. For materials that do not continue to burn after ignition in air, the value of n is greater than 0.21; the air must be enriched with oxygen to investigate them. The indices for all polymers we burned fall within the range of 0.150 for polyoxymethylene to 0.95 for polytetrafluoroethylene.

Test procedures and variables

Known atmospheres were prepared by metering air and either nitrogen or oxygen through critical flow ori-

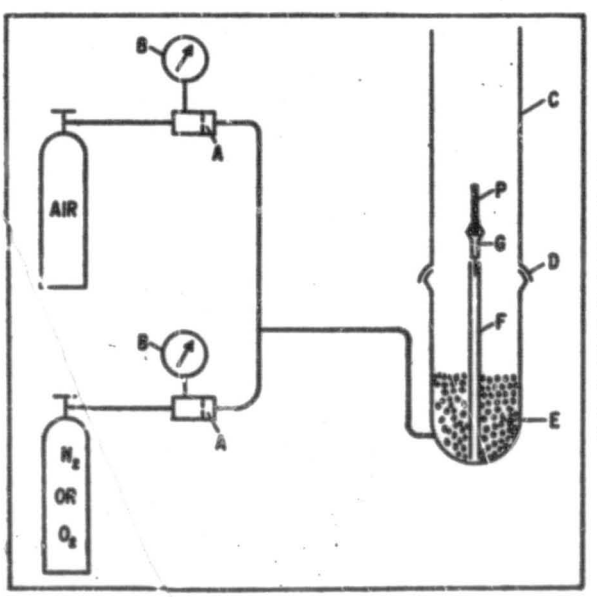

FIG. 1: Schematic diagram of apparatus. A—metering orifice; B—Bourdon test gate, O-100 p.s.i.g.; C—Pyrex tube, 3.5 in. ID; D—tapered ground glass joint; E—bed of glass beads; F—Pyrex tube, 7 mm. ID; G—spring clamp; P—polymer sample, about 0.6 × 0.3 × 8 centimeters.

*Research and Development Center, General Electric Co.
1—Numbers in parentheses designate references at end of article.

index was characteristic of polypropylene was shown by burning a strip of higher molecular weight polymer (Profax 6505) which did not undergo excessive melting and gave $n = 0.174 \pm 0.002$. We tried to avoid excessive melting by using high-molecular-weight polymers, but in some cases they were not available to us and hence have not been evaluated, e.g., high-molecular-weight poly-α-methylstyrene.

A less troublesome experimental problem arose in tests in which relatively small quantities of residue occurred at the burning surface, either because of inert fillers or because of char formation. On these samples a cap formed which led to extinction unless the index was high enough to permit periodic shedding of the residue. Even though the flame could not be considered steady in such cases, it was usually possible to establish a useful extinction limit. On the other hand, with samples heavily loaded with inert filler, small flames stabilized by a zone of glowing ash progressed steadily down the specimen and resulted in very reproducible limits; however, longer times (around 5 min.) were required to establish the steady state.

Before presenting the experimental data, a comment on the significance of the candle-like flames observed in the absence of combustion residues seems appropriate. These appear to be gaseous diffusion flames standing above the polymer surface. Heat from the flame is transported down to the polymer surface (mostly by molecular conduction) and results in pyrolysis of the polymer to yield gaseous fuels which sustain the flame. Flame and surface temperatures and also pyrolysis gas compositions have been reported for PE, PMMA, and polyoxymethylene (6) burned at 5 cm. of Hg in argon/oxygen mixtures. Flame temperatures were in the range 1200 to 1500° C. and the temperature at the burning polymer surface was around 500 to 600° C. These data support this proposed flame model. In terms of this model, flame retardants might act by 1) slowing down pyrolysis reactions in the condensed phase which generate fuel gases, 2) slowing the gas-phase flame reactions, and 3) interfering with the heat transfer from the flame to the condensed phase.

The use of the candle-like flame to evaluate flammability differs in one important respect from some other measures of flammability, namely, the candle-like flame propagates down over a polymer surface not previously heated by convection of hot products over it. The hot products rise above the polymer so that convection heating is negligible. To illustrate the importance of convection, we held some polymer sticks vertically at the top end and ignited them at the bottom, i.e., the inverse of the usual procedure. Under these conditions, and even with minimum ignition of polymers such as polyoxymethylene, PE, and PMMA, the flame spread rapidly and enveloped the whole stick, although the oxygen content of the atmosphere was below that required for candle-like burning at the top. In many cases, the heat from the bottom part of the flame melted the polymer above it and the whole lower end of the stick dropped off carrying the flame with it, or else dripping polymer disturbed the stability causing the flame to suddenly blow off. In only a few instances was it possible to obtain meaningful oxygen indices under these conditions.

More success was obtained, however, with Plexiglas G. The polymer softened but did not lose its shape rapidly. The flame enveloped the

Table I: Limiting oxygen indices (n) of various materials (at atmospheric pressure unless otherwise stated)

Material	*n*
Polyoxymethylene	
Delrin, Du Pont	0.150 ± 0.003
Celcon, Celanese	
0.1 cm. thick	0.148 ± 0.001
0.3 cm. thick	0.149
At 14 cm. of Hg pressure	0.190
Polyethylene oxide,	
Polyox WSR-35, Union Carbide	0.150
Kitchen candle (wick in paraffin)	0.16
Polymethyl methacrylate,	
Plexiglas, Rohm and Haas	0.173 ± 0.001
Polypropylene,	
Profax 6505, Hercules	0.174 ± 0.002
Asbestos-filled, "slow-burning"	
JMDC-4400, Union Carbide	0.205 ± 0.005
"Self-extinguishing" JMDA-9490,	
Union Carbide (probably contains chlorine and antimony oxide)	0.282 ± 0.003
Polyethylene	
1220, Allied Chemical	0.174 ± 0.001
Marlex - 5002, Phillips	0.175 ± 0.001
Marlex at 14 cm. of Hg pressure	0.210
Polystyrene	
0.1 cm. thick from stock	0.181
0.6 cm. thick, Westlake high-temperature sheet	0.183
Polybutadiene, cross-linked with 2 parts of dicumyl peroxide	0.183
Polyvinyl alcohol, Elvanol 70-05, Du Pont	0.225 ± 0.004
Chlorinated polyether, Penton, Hercules $[-CH_2-C(CH_2Cl)_2-CH_2-O-]$	0.232
Polycarbonates, various clear Lexan resins, General Electric $[-C_6H_4-C(CH_3)_2-C_6H_4-OC(O)O-]$	0.26 to 0.28
Polyphenylene oxide, General Electric $[-C_6H_2(CH_3)_2-O-]$	0.28 to 0.29
Carbon	
Porous carbon, PC-25, National Carbon	0.559 ± 0.003
Carbon electrode, L 8109, National Carbon	0.635
Carbon electrode at 50 cm. of Hg pressure	0.80
Carbon electrode at 24 cm. of Hg pressure	1.00
Silicone rubber, General Electric	0.30 to 0.33
Polyvinyl chloride, Geon-101 without plasticizer, Goodrich	0.45
Polyvinylidene chloride, Saran 281S905, Dow	0.60
Teflon, Du Pont	0.95

END OF REFERENCE

42

REFERENCE

43

BLACKSTONE, W. R.; AND KU, P. M.: ASSESSMENT OF IMPACT TEST TECHNIQUES FOR DETERMINING THE FIRE OR EXPLOSION HAZARDS OF MATERIALS EXPOSED TO OXYGEN. MAT. RES. STAND., VOL. 11, NO. 6, JUNE 1971.

J-0143

An Assessment of Impact Test Techniques for Determining the Fire or Explosion Hazards of Materials Exposed to Liquid Oxygen*

W. R. Blackstone and P. M. Ku

REFERENCE: Blackstone, W. R. and Ku, P. M., "An Assessment of Impact Test Techniques for Determining the Fire or Explosion Hazards of Materials Exposed to Liquid Oxygen," *Materials Research and Standards*, MTRSA, Vol. 11, No. 6, p. 30.

ABSTRACT: Historically, the qualification of materials for liquid oxygen service has included a drop weight impact test to measure ignition susceptibility. However, recent incidents have focused attention upon the possibility that the currently used impact test methods occasionally fail to identify potentially hazardous materials, and such an error can have extremely grave consequences. In this context, the development of the current ASTM impact sensitivity test is traced, and it is shown that the extremely poor precision exhibited by this method is due largely to the use of inappropriate statistical procedures. Next, the development of a new impact reaction intensity test method presently being considered by ASTM is outlined. Finally, fundamental aspects of liquid oxygen impact testing are discussed, including the generally accepted ignition mechanism, the system-specific nature of the test, the sequence of events during impact ignition, and the meaning of these aspects in measuring hazard.

KEY WORDS: liquid oxygen, impact, impact tests, impact sensitivity, ignition, combustion, statistics, chemical reactions

It is common knowledge that many materials can burn or explode if subjected to external stimuli in the presence of oxygen. The aerospace industry in particular, with its widespread use of both liquid and gaseous oxygen, is concerned with this problem, and much effort has been expended in attempting to define the degree of hazard associated with various materials under various types of external stimuli. Impact in an oxygen environment is one mode of stimulus receiving considerable attention.

One of the first problem areas to be recognized was that of the severe mechanical or hydraulic impact conditions or both in liquid oxygen (lox) systems. Consequently, much research has gone into the development of lox impact test methods to aid in the selection of materials for these systems, and from this a more or less standardized lox impact test technique has evolved. Three similar versions of this technique—NASA MSFC-SPEC-106B, AF Specification Bulletin 527, and ASTM Test for Compatibility of Materials with Liquid Oxygen (Impact Sensitivity Threshold Technique) (D 2512-69)—are the most widely used. They all rate a material in terms of its "lox impact sensitivity," the level of impact energy required to initiate a reaction between the test material and the liquid oxygen.

Until recently, the idea of measuring reaction propagation rates in lox largely was ignored and materials were rated solely on the basis of the standard lox impact test. In 1969, however, ASTM published for information a new method for rating materials on the basis of reaction intensity (*Annual Book of ASTM Standards*, Part 18, October 1970), which still is under ballot for adoption as an ASTM standard. The test uses impact as the ignition stimulus but does not attempt to measure minimum ignition levels; rather, the material is impacted from a height known to be sufficient to produce ignition, and a measurement is made of the explosive shock pressure produced.

Thus, it appears that designers will soon have a choice between two different ASTM impact test methods for use in selecting "safe" materials for lox systems. Considering the potentially grave consequences of using an "unsafe" material, it is probable that both tests will be applied. For most materials, the use of both tests will present no particular problems, for the two tests will produce similar overall safety ratings. For example, both tests will demonstrate the reactivity of most petroleum based greases or the relative inertness of compounds such as chlorofluorocarbon oils and greases. Even here, however, it is clear that something is amiss. In the impact sensitivity method a petroleum based grease usually will react on *less than half* of the test drops at an energy input of about 357 ft • lb/in.^{2}. In the reaction intensity test, the same material usually will react on *all* of the test drops at an energy input of about 122 ft • lb/in.^{2}.

There are a significant number of situations in which the use of some material other than the chlorofluorocarbons is attractive from an economic or performance standpoint. It is in the testing of such materials that the designer will be faced with just what one might expect from the above: contradictory material ratings from two tests. Consider his dilemma at this point: one test rates the material as highly explosive while the other yields a safe rating. Which test does he believe? He can accept the material only if there is some assurance that the conditions leading to the explosions in one of the tests will not occur in the intended application (Whoever has such assurance?). If he rejects the material, the lack of other material that

*Portions of this paper were excerpted from "Development of an Improved Gaseous Oxygen Impact Test System" by W. R. Blackstone, N70-32875, NASA-CR-108529, Southwest Research Institute, San Antonio, Tex., July 1970.

W. R. Blackstone, senior research engineer, Department of Structural Research, Southwest Research Institute, San Antonio, Tex.

P. M. Ku, director, Department of Fluids and Lubrication Technology, Southwest Research Institute, San Antonio, Tex.

would be functional in the intended application may force a costly and time consuming redesign of the system to eliminate the need for such a material.

In the following sections, the development of the impact sensitivity and reaction intensity test methods will be reviewed briefly, followed by discussions of such fundamental aspects as statistical procedures appropriate to quantal response testing, the system-specific nature of such testing, and the meaning of these aspects in measuring hazard.

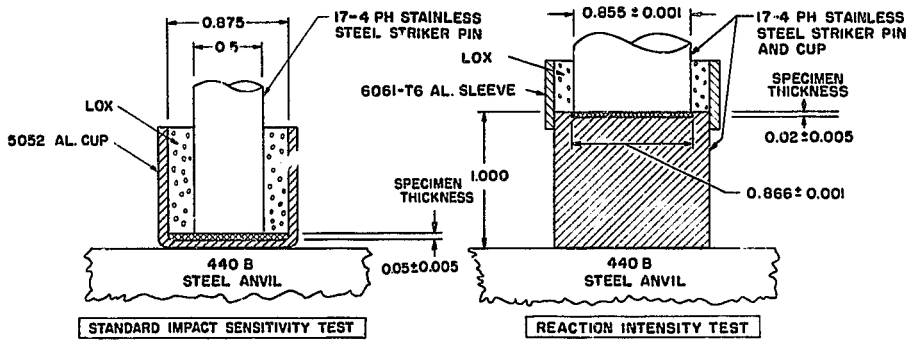

Fig. 1—*Comparison of design parameters.*

Current Technology

The Impact Sensitivity Test/ According to Africano [*1*],[1] representatives of the Army Ballistic Missile Agency (ABMA),[2] the Air Force, and various contractors met several times during 1957 for the purpose of standardizing the various lox impact tests in use at that time. The version agreed upon was based generally on the machine in use at ABMA, with the following principal test parameters:

Total dropped weight, 20 lb
Drop distance, 42 in.
Specimen thickness, 0.05 in.
Striker pin-specimen contact area, 0.196 in.^{2}
Specimen cup material, 1100 aluminum alloy

The agreed criterion for an acceptably insensitive material was that it survive a minimum of 20 consecutive tests with "no detonation, or other positive reaction, as indicated by an audible report, a visible flash in a darkened room, discoloration, or other evidence of burning..." Africano also mentions that the above parameters and criterion were recognized as a tentative solution which might be changed if warranted by subsequently accumulated data.

Two comments are in order at this point concerning this last qualification. First, the criterion for acceptability was of necessity a tentative and arbitrary requirement based upon the fact that a certain lubricant, considered at the time to be the only safe available lubricant, would "pass" these test conditions. Interestingly, that same lubricant "failed" in subsequent testing by essentially the same test method and is no longer considered acceptable; the criterion, however, remains the same. Second, upon evaluation of the accumulated data, a number of investigators have suggested that the principal test parameters were in need of reevaluation. However, the very fact that such accumulated data exist was and is used to deter such reevaluation, for it is argued that changes in the parameters would obviate the accumulated data! As a result, the original criterion and basic parameters survive today essentially unchanged as standard impact sensitivity test methods in the forms of USAF Specification Bulletin 527 [2] and NASA Specification M -SPEC-106B [3]. More recently, the sin r characteristics of these two methods have been combined in ASTM Test Method D 2512-69.

All of these test methods utilize the same basic drop weight type of tester with only minor variations in test procedures and handling the test materials. The test material is placed in an aluminum specimen cup in the presence of liquid oxygen, and a ½-in.-diameter stainless steel striker pin is placed upon the test material. A 20-lb plummet released from a known height falls on the striker pin, rebounds, and strikes again several times. After each test drop the specimen remains are discarded, and a new specimen is positioned for the next drop. In all three methods, the basic concept is that of attempting to measure the "threshold value" of a material by finding the greatest height at which the material will withstand 20 consecutive test drops without reaction. This value becomes the relative sensitivity rating for the material.

As mentioned previously, in the Air Force and NASA methods a variation of the threshold value technique is used widely to qualify materials for service; here, 20 or more drops are made from a fixed height of 42 in. (or 43.3 in.), and the materials are accepted or rejected on a go-no go basis. Clearly, for a material that yields no reactions in this test, its threshold value is, by definition, 42 in. (or 43.3 in.) or more.

At this point, even the lay reader already will sense intuitively that there is something wrong in allowing the plummet to rebound and strike again, for one must then decide how to differentiate between reactions occurring on the initial impact (where the drop height and specimen condition, and hence the energy input, are known) and those occurring on subsequent impacts (where neither drop height nor specimen condition is known). As a matter of fact, no differentiation is made, and all reactions are given the same value. Thus, from this alone (and there are other contributing factors), it is not surprising that these methods have been plagued from their inception with poor repeatability and reproducibility, as is brought out in the precision statement published in ASTM Method D 2512:

Threshold Value Drop Height, in.	Repeatability, one Operator/ Apparatus, in.	Reproducibility, different Operator/ Apparatus, in.
24	17.0	40.8
15	10.6	25.2
6	4.3	10.1

To illustrate the meaning of the above values, let us assume that we have a material on which we have conducted many hundreds of threshold value determinations and that the average of all these is 24 in. Assume that we then send out specimens of this material to two other laboratories and ask each to conduct one threshold value determination. According to the stated test reproducibility (and this was derived from the best available Air Force and NASA test data), the two determinations must differ by *more than 40 in.* before we can consider them suspect. As a matter of fact, the highest available drop height on the tester is 48 in., and test drops are not made at less than 6 in. because of timing problems. True, the table says that the precision gets better for the lower threshold values, but "qualification" testing is done at the other end of the scale, where the progression of values suggests that the precision may be even worse.

Clearly, such figures by themselves show that this test method does not yield results sufficiently precise for reliable compati-

[1] Italic numbers in brackets refer to the list of references at the end of this paper.

[2] Now Marshall Space Flight Center, National Aeronautics and Space Administration.

bility evaluations. In spite of its record, however, this test method is still the primary method by which materials are chosen for lox systems.

The Reaction Intensity Test/ The test facility at Southwest Research Institute was installed originally in the late 1950's, and for some years was operated in accordance with the standard procedure described above. Generally, the research program followed during this period was similar to those of other organizations in the field: a systematic investigation of the effects of various equipment adjustments in an attempt to determine the cause or causes of the poor precision of the threshold value method. In the mid 1960's, however, it became clear that the prime source of trouble lay not in the equipment but in the procedure itself. This conclusion came as a result of reviewing impact sensitivity research in the field of condensed phase explosives and liquid monopropellants. It was learned that workers in this field had at first followed the threshold value approach but had long since abandoned this as unworkable from the standpoint of the statistical theory involved. The much more efficient replacement involved measurement of the 50-50 go-no go point, with fundamental principles of probability mathematics being applied in determining the S curve from which to establish this point. Apparently, lox impact sensitivity testing had run afoul of the same problem and possibly could benefit from the same solution. In order to use the new technique, however, it was necessary to make three significant equipment changes:

1. The specimen cup material was changed from aluminum to 17-4 PH stainless steel.
2. A "rebound catcher" was installed.
3. The striker pin-specimen contact area was increased from 0.196 in.^{2} to 0.575 in.^{2}.

The specimen cup material was changed because aluminum specimen cups undergo considerable plastic deformation under impact. The amount of deformation is highly variable from test to test and this introduces an undesirable variation in the energy absorbed by the specimen. The deformation of the cup also affects the energy transfer on initial impact to the extent that few reactions occur on initial impact in liquids and greases in the standard impact sensitivity test even when the material is known to be sensitive. Such a change was necessary if the reaction normally occurring on the second or third rebound (under unknown energy input conditions) were to occur instead on the initial impact. With this accomplished, the rebound catcher was installed to eliminate the secondary impacts. These two steps did not, however, reduce test variation to an acceptable level. In fact, this goal was not accomplished until it was discovered quite by accident that it also was necessary to increase the striker pin-specimen contact area to the value indicated above.

Figure 1 shows the new test design parameters resulting from the above steps compared with those of the standard impact sensitivity test. It also will be noted that the bottom thickness of the specimen cup was increased greatly; this was done to retard the onset of violent boiling of the lox and the attendant specimen disturbance during the test. Another change involved a decrease of specimen thickness from 0.05 in. to 0.02 in. This change was made to compensate for the impact energy dilution caused by the large increase in striker pin-specimen contact area.

To illustrate the effects of the several changes in the area of the specimen, we can compare the reaction frequencies obtained with the energy inputs. For this purpose it is both convenient and informactive to use Africano's [*1*] maximum rate theory of impact sensitivity. This theory holds that the maximum energy transfer rate per unit area is the condition accompanying the highest locally induced temperature and, therefore, is the most likely measure of the probability of ignition. For drop weight impact, the maximum energy rate function X is

$$X = h\left(\frac{gE_BW}{Ab}\right)^{1/2}$$

where

h = drop height, ft,
g = acceleration of gravity, in./s^2,
E_B = bulk modulus of elasticity, lb/in.^{2},
W = drop weight, lb,
A = striker pin-specimen contact area, in.^{2}, and
b = specimen thickness, in.

For a silicone oil initially at −297 F, we can assume a bulk modulus of 10^6 lb/in.^{2}. It does not matter if this assumption is in error, since the following results were all obtained with large numbers of test drops on this same specimen material.

For the standard impact sensitivity test configuration, and considering only initial impacts, we obtained

$$X = (3.5)\left[\frac{(386)(10^6)(20)}{(0.196)(0.05)}\right]^{1/2}$$

$$= 3.11 \times 10^6 \text{ ft} \cdot \text{lb/in.}^2\text{-s}$$

and an expected reaction frequency of 3.4 percent.

For the standard impact sensitivity test configuration, and considering only rebound impacts,

X = unknown
Reaction frequency = 34.0 percent

Changing the specimen cup from aluminum to stainless steel and reducing the specimen thickness,

$$X = (1.667)\left[\frac{(386)(10^6)(20)}{(0.196)(0.02)}\right]^{1/2}$$

$$= 2.34 \times 10^6 \text{ ft} \cdot \text{lb/in.}^2\text{-s}$$

Reaction frequency = 49.0 percent

Taking the additional step of increasing the striker pin diameter,

$$X = (1.583)\left[\frac{(386)(10^6)(20)}{(0.575)(0.02)}\right]^{1/2}$$

$$= 1.296 \times 10^6 \text{ ft} \cdot \text{lb/in.}^2\text{-s}$$

Reaction frequency ≃ 80 percent (projected from up-and-down test results)

Going one step further and reducing the plummet weight, we obtain

$$X = (1.583)\left[\frac{(386)(10^6)(7.75)}{(0.575)(0.02)}\right]^{1/2}$$

$$= 0.807 \times 10^6 \text{ ft} \cdot \text{lb/in.}^2\text{-s}$$

Reaction frequency ≃ 80 percent (projected from up-and-down test results)

While it is not evident in the manner in which the above data are presented, all of the steps except the last were necessary to the previously stated goal of reducing test variation to an

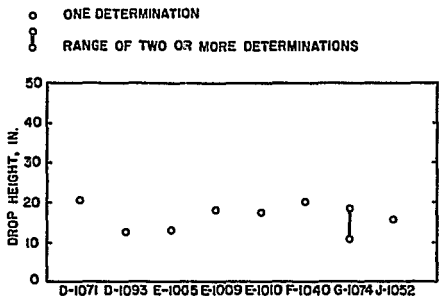

Fig. 2—*Fifty percent point of liquids.*

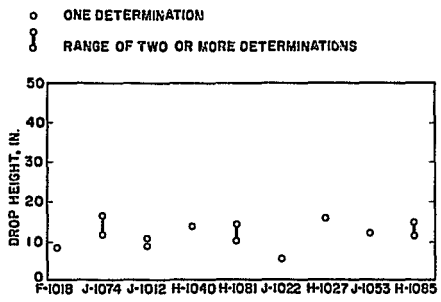

Fig. 3—*Fifty percent point of greases.*

doing this, however, we noted the significant trend which the last step emphasizes; namely, the fact that we were reducing total energy input rates but obtaining higher reaction frequencies. The meaning of this will be discussed in a later section. Once operational, the new test technique, which is known as the "up-and-down" or Bruceton [4], method, proved to be efficient and repeatable. Figures 2 and 3 present some typical results for various liquids and greases, ranging from common hydrocarbons to fluorochemicals,[3] which demonstrated that the precision with which sensitivity could be rated by the up-and-down test was much improved over that of the current test methods. However, with improved precision, it also can be seen that the sensitivities of most of these materials are so close together as to make significant distinction between them difficult. Moreover, just as one would suspect intuitively (from the types of materials tested), some of these were violent reactors while others yielded at worst only small char marks—no flash, no sound. Clearly, in a lox system the violent reactors would be more hazardous than the mild reactors; yet, this intuitively obvious difference was not being defined quantitatively by sensitivity measurements alone. This in turn made it clear that the degree, or intensity, of reaction not only is a fundamental part of the full definition of hazard per se but further in some cases is the only property which can distinguish unambiguously between "good" and "bad" materials. Significantly, Brown et al [5] independently and simultaneously arrived at the same conclusion with regard to the impact sensitivity testing of condensed phase explosives.

After considering the above, the next logical step seemed to be the development of some means for making quantitative measurements of reaction intensity during impact tests. The equipment subsequently developed for this purpose proved satisfactory, and the results of an extensive test program utilizing this apparatus were published in July 1968 [6]. The method also appears for information only in the *Annual Book of ASTM Standards*, Part 18, October 1970 and currently is under ballot as an ASTM standard method by Committee F-7 on Aerospace Industry Methods.

Briefly, the reaction intensity measuring system consists of a probe device which makes a relative measurement of the peak air shock pressure generated by a reaction. For test drops, two such devices are located near the specimen cup at points 180 deg apart. The standard test procedure calls for 20 test drops from 43.3 in., which yields a total of 40 peak pressure readings.

[3]Specimen materials are identified in Table 1.

Table 1—Test Materials

Specimen Code	Specimen Type	Description
D-1071	Liquid	Heptacosafluorotributylamine
D-1093		Silicone
E-1005		Fluorosilicone
E-1009		Chlorinated biphenyl
E-1010		Fluorinated polymers of chlorotrifluoroethylene
F-1040		A fluorochemical, composition unknown
G-1074		Silicone
J-1050		Mineral oil, MIL-L-6032, grade 1100
J-1052		A fluorochemical, composition unknown
J-1080		Polyglycol
K-1081		Different lot of J-1080
K-1082		Different lot of E-1010
F-1018	Grease	MoS_2 and petroleum-base oil
G-1051		Unknown
G-1052		Unknown
G-1071		Unknown
G-1077		Graphite in fluorocarbon oil
H-1012		MoS_2 in fluorocarbon oil
H-1013		Tetrafluoroethylene in fluorocarbon oil
H-1027		Unknown
H-1032		Chlorinated polymer of chlorotrifluoroethylene
H-1040		Graphite in chlorinated biphenyl
H-1081		Fluorosilicone
H-1085		Different lot of H-1032
J-1012		Graphite and chlorinated biphenyl
J-1022		Silicone
J-1053		Hydrocarbon
J-1074		Different lot of H-1032
J-1120		Unknown
K-1001		Fluorosilicone
K-1002		Different lot of H-1032
K-1015		Polymeric fluorinated oil with PTFE thickener
K-1022		Perfluorotrialkylamine with PTFE thickener

The highest individual peak pressure reading of the 40 thus obtained is defined as the maximum peak pressure and is taken as the reaction intensity rating of the material under test.

Figure 4 presents typical reaction intensity test results on 23 liquids and greases. For each material, the two circles connected by a line show the range of maximum peak pressures (the maximum peak pressure is the highest individual peak pressure reading of the 40 such readings taken in a 20-drop test) obtained in all tests on that material. For example, one 20-drop test on H-1081 yielded a maximum peak pressure of 50 psi, another test gave 32 psi, while the remaining eight tests yielded maximum peak pressures somewhere between these two values.

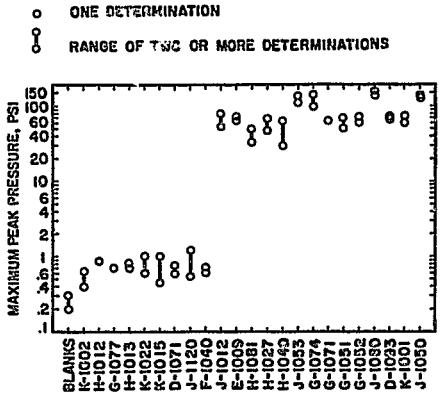

Fig. 4—*Maximum peak pressures of liquids and greases.*

At this point some physical frames of reference for the various levels of peak pressure would be helpful. First, the maximum peak pressure readings obtained in two 20-drop tests on "blanks" (specimen cup with liquid oxygen but without any specimen material) are included in Fig. 4. These readings (0.2 to 0.3 psi) amount to background noise—the sound pressure generated by the steel-on-steel impact. Second, the readings from about 0.4 to about 2 psi are those of sounds only slightly above the background noise. Toward the lower part of this range, these sounds are practically indistinguishable from the background noise. Toward the upper part, the sounds are distinct but still low and usually are not accompanied by any visible flash. Third, readings in the neighborhood of 5 to 9 psi are the same as those produced by Chinese firecrackers (approximately $\frac{3}{16}$ in. in diameter by 1.5 in. long) exploded individually in the specimen cup. Finally, readings of 50 to 70 psi are the same as those produced by cherry bombs (spherical firecrackers of about

1.0-in. diameter) exploded in the specimen cup.

With this background, the significance of the maximum peak pressure readings produced by the various materials can be evaluated. Most noteworthy is the separation of the 23 materials into two distinct groups: one with high maximum peak pressures and the other with low maximum peak pressures. Judging from the physical references discussed, it is not unreasonable to assume that the 30 to 160-psi reactions are dangerous explosions, and it appears that this group of materials can be classified as extremely hazardous. On the other hand, the reactions of the other group of materials in Fig. 4 in no instance yielded peak pressures exceeding 1.2 psi; reactions of this order are so mild that this group can be classified as relatively inert.

Also notable is the fact that no less than five of the materials shown to be capable of powerful explosions in Fig. 4 have previously passed the standard impact sensitivity test. These are J-1012, H-1081, H-1027, H-1040, and K-1001. Considering the fact that for the past several years this test method has handled nearly all the acceptance testing in this area, it is a logical assumption that some potentially hazardous materials may be in service at present.

In contrast to liquids and greases, the sensitivity of various solid materials (plastics, elastomers, etc.) was found to vary over a significant range with different energy inputs. Thus, sensitivity as well as reaction intensity appears to be a significant parameter in the evaluation of such materials.

Discussion

It might seem at first glance that lox impact testing should be a simple and straightforward procedure. As seen in the foregoing sections, however, the impact-ignition-explosion event is complex and there are a number of well hidden pitfalls in the path of one seeking a safe material for some application. To avoid these one must take into account certain fundamental aspects of impact sensitivity testing in general and of the lox impact test in particular. Foremost among these are the system-specific nature of the test, the statistical problems peculiar to quantal response testing, and the inherent inability of a quantal response test to characterize safety quantitatively. These aspects will be reviewed briefly in the following paragraphs.

System Dependence/ It generally is accepted that impact produces ignition through concentration of energy into hot spots; not through general compression of the bulk material. Since much of the total impact energy delivered does, however, go into deformation of the specimen, specimen cup, etc., it follows that only a portion shows up at a hot spot site as an ignition stimulus. From this, it can be seen that the amount of actual ignition stimulus delivered depends not only upon the gross impact stimulus applied but also on how efficiently that stimulus is localized into hot spots. This, in turn, is a function of test method, specimen cup, striker pin, compression, state of the substance tested, and so on. Clearly, then, it can be dangerous to conclude from an impact test that a certain material is safe at a given level of energy input; in the service system, a much smaller energy input might cause ignition through better localization. Impact sensitivity, in other words, is a highly system-dependent phenomenon.

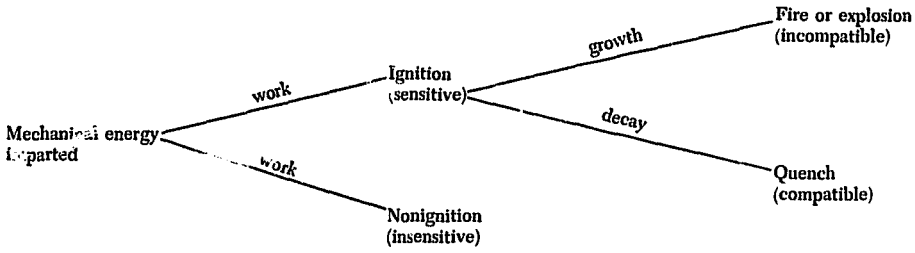

It was seen previously that an increase in striker pin-specimen contact area brought about a significant increase in reaction frequency in spite of the attendant reduction in total energy input. A possible explanation of this is that a liquid or grease specimen tends to have a low density of potential hot spot sites per unit area. Thus in a given test drop, the larger contact area raises the probability that a potential hot spot site will be under the striker pin.

Quantal Response Testing/ A particularly glaring weakness of the standard impact sensitivity tests is evident from the probability distributions one is obliged to work with in any type of sensitivity experiment. One cannot measure the precise energy input level (threshold value) that barely would initiate a reaction but can observe only whether an applied drop height does, or does not, initiate a reaction in a given specimen. The specimen used is consumed or changed as a result of the trial; therefore, a new specimen must be prepared for the next trial. It is highly improbable that the original specimen can be duplicated exactly; thus, the new specimen will have most probably a threshold value different from that of the original. Consequently, in a whole population of specimens, there is a probability distribution of threshold values with the result that, in a test of a number of specimens impacted from a given height, some will react and others will not. A plot of the frequency of reactions over a range of drop height yields a cumulative probability distribution. Any of several reliable methods [7] may be used to estimate the mean of such a distribution with a small number of tests such as ordinarily required in a practical test method. To measure a point in either tail of the probability curve, however, one must make large numbers of tests to achieve reasonable accuracy. It so happens that the standard lox impact sensitivity test attempts measurements in this area of the curve with relatively small numbers of tests. The result, of course, is poor precision.

As an illustration of the consequences of failing to recognize these statistical parameters, consider the fact that some materials presently are categorized in the current standard impact tests as having "batch-to-batch variation" in sensitivity. For one grease it has been reported that, on the average, about 40 percent of the specimens of this material are rated as "acceptable" for lox service. The remainder are rejected as "unacceptable." However, the overall reaction frequency of this material, counting satisfactory and unacceptable results together, is about 5 percent. With a table of the cumulative binomial probabilities, we find that, for a probability of reaction in a single trial of 0.05, the probability of obtaining zero reactions in 20 trials (the familiar pass criterion) is 0.3585, or about 36 percent. Thus, there is apparently no justification for concluding that some of the batches are acceptable while others are not, for the results are close to what one would expect to obtain in *repeated tests* on a *single batch* of material with a reaction frequency of 5 percent!

From the above, it should be clear that the current standard method for measuring sensitivity is in need of drastic overhaul. One alternative would be to increase greatly the number of trials the candidate material must endure without reaction; this, however, seems impractical. A better solution would be to adopt one of the previously referenced methods for measuring the mean; one of these, the up-and-down method, has given good results on condensed phase explosives and liquid monopropellants for many years now.

The Sequence of Events/ In the litera-

ture on this test, the words "compatibility," "reactivity," and "sensitivity" seem to be used as though they were interchangeable. As a matter of fact, they are not equivalent terms, and, further, the type of impact test utilized to measure one of these qualities is not necessarily appropriate to the others.

As a starting point, we can define a compatible material reasonably as one that will not produce unacceptable damage or malfunction in the lox system in which it will be used. Further, we shall disregard for the moment differences between the test and service systems. Then the sequence of events in the test can be diagrammed as shown on page 34.

Here we see that the first step involves the conversion of mechanical energy into heat and that the question of whether ignition occurs is decided primarily by whether we impart enough energy to effect ignition at some localized site in the test material. It is important to note that we cannot apply directly a known amount of energy; rather, we must apply a deliberately excessive amount in order to have a small portion show up as a hot spot in the material. Further, the only way we can determine whether a hot spot has occurred is by observing a fire during the test or by noting small char marks on the specimen afterward. If either response is observed, we have answered one question, Will this amount of energy input result in ignition? Such a test is of course a quantal response test, and we have therefore defined the sensitivity of the material.

The second step in the sequence involves the question of whether an ignition will propagate or die out. In a test involving dynamic energy inputs, the heat source will be applied and then removed quickly. Therefore, the propagation will depend to a large extent on the exothermicity of the reaction started plus the heat transfer characteristics of the test system (From this, it can be surmised that the degree of propagation after ignition does *not* depend a great deal on the original energy

(continued on page 52)

J-0144

Techniques for Determination of Flash and Fire Points and Impact Sensitivity of Materials in a Gaseous Oxygen Environment

D. L. Pippen and J. S. Stradling

REFERENCE: Pippen, D. L. and Stradling, J. S., "Techniques for Determination of Flash and Fire Points and Impact Sensitivity of Materials in a Gaseous Oxygen Environment," *Materials Research and Standards*, MTRSA, Vol. 11, No. 6, p. 35.

ABSTRACT: The test techniques developed at the NASA White Sands Test Facility, New Mexico, for determining the flash and fire points of materials, as well as the sensitivity of materials to gaseous oxygen pneumatic and mechanical impact, are discussed. Test pressures up to 2000 psia have been used in the flash and fire testing and test pressures up to 5000 psia in the impact sensitivity tests. Data obtained from the flash and fire system and the impact sensitivity test apparatus are included. Each test system provides a rapid means for evaluating materials for possible use in oxygen environments and a method for material screening. The systems described can be used with various gas mixtures as well as with 100 percent oxygen. The data from the test techniques described presently are being used for determining the compatibility of materials with the high pressure oxygen systems in the Apollo spacecraft.

KEY WORDS: impact strength, flash point, fire point, mechanical shock, oxygen, spark ignition, pneumatic equipment, electrical sparks, oscilloscopes, photoelectric cells, compatibility, spacecraft

Manned space flight has brought about new techniques for testing materials for use in inhabited areas of a spacecraft as well as for determining compatibility of materials with various pressurized oxygen environments. Liquid oxygen (lox) impact testing, which has been performed successfully for several years, has overshadowed most impact tests involving gaseous oxygen (gox). However, because lox test data do not correlate necessarily with gox test data and because most oxygen systems use oxygen in both its liquid and gaseous phases, gox testing should be given equal consideration.

Recent attention also has been given to tests that permit the evaluation of a material in proximity to an electrical discharge in the form of a spark. Such tests effectively determine the combustibility of the offgassed products of a material as a function of temperature. Thus, flash and fire point testing at the application pressure of a material can provide meaningful data in all areas in which electrical conductors are routed as well as in areas in which static electrical discharges may occur. This paper presents the test techniques presently being used at the NASA Manned Spacecraft Center White Sands Test Facility (WSTF) to evaluate the reactivity of materials to gox impact and also describes a technique for determining the flash and fire points of materials under various oxygen pressures.

Gaseous Oxygen Impact Testing

Materials used in high pressure systems may be subjected to a mechanical impact or a pneumatic impact. The mechanical impact is imparted when a material specimen is struck with a steel striker pin, the pneumatic impact when a material is subjected to a rapid pressure increase (step function).

Mechanical Impact Test Equipment/ The WSTF gox mechanical impact testing apparatus uses a drop weight impact tester devised by the Army Ballistic Missile Agency (ABMA), currently the NASA George C. Marshall Space Flight Center. The basic ABMA tester was modified by replacing the 20-lb plummet with a 7½-lb plummet and by replacing the anvil with a high pressure test chamber designed by the WSTF. This tester, hereafter referred to as the WSTF mechanical impact tester, is shown in Fig. 1. Figure 2 is a photograph of the completed system installation.

A complete description of the basic ABMA impact tester may be found in several references[1,2]; thus, no further description is given here. The modification required to convert the ABMA impact tester to the WSTF mechanical impact tester is given in the following paragraphs.

The anvil region assembly (Fig. 1) consists of the gox mechanical impact test chamber shown in Fig. 3. As are all of the parts except the seals and diaphragm, the chamber frame (*1*) is constructed of 300 series stainless steel. The equalizer pin (2) is used to assure that equal force is im-

[1] Lucas, W. R. and Riehl, W. A., *ASTM Bulletin*, ASTBA, No. 244, Feb. 1960, pp. 29–34.

[2] "Liquid Oxygen Compatibility Impact Sensitivity Test Method," USAF Specification Bulletin 527, U.S. Air Force, 1 May 1961.

D. L. Pippen, acting chief, Laboratories Branch, National Aeronautics and Space Administration White Sands Test Facility, Las Cruces, N. Mex.

J. S. Stradling, test operations director, Laboratories Branch, National Aeronautics and Space Administration White Sands Test Facility, Las Cruces, N. Mex.

(*continued from page 51*)

Table 3—Effect of Pressure on Impact Sensitivity in Gaseous Oxygen

Material	Thickness, cm	% Reaction at Pressure, N/cm²			
		6.8×10^6	3.4×10^6	68×10^4	34×10^4
Fluorinated hydrocarbon	0.188	66.6	50	20	0
Fluorinated silicone	0.328	100	100	50	50
Silicone	0.152	. . .	100	100	50

Table 4—Impact Sensitivity of Selected Materials in Liquid and Gaseous Oxygen at 10 kg·m

Material	Thickness, cm	Pressure, N/m²	% Reaction in	
			lox	gox
Nylon	0.008	3.4×10^6	20	50
Silicone	0.152	68×10^4	100	100
Polytetrafluoroethylene	0.165	3.4×10^6	0	10
Chlorotrifluorocarbon plastic	0.317	6.8×10^6	0	0

2. The impact sensitivity of materials in gaseous oxygen varies directly with pressure.

3. The relative rating of the materials tested in lox at pressures up to 6.8×10^6 N/m² is the same as lox at 9.5×10^4 N/m².

4. This tester provides flexibility of test conditions for evaluation of a wide variety of materials in fuels and oxidizers.

5. The above data are tentative and, as such, constitute preliminary test results for the conditions noted. A much more comprehensive test program, structured to yield statistically meaningful cardinal data over a wide variety of materials of interest currently is in progress at the Marshall Space Flight Center. ■ ■ ■

Assessment of Impact Test Techniques

(*continued from page 35*)

input.). By our previous definition of compatibility, it follows that there are two categories of compatible materials: those that are insensitive and those that are sensitive but do not propagate. Incompatible materials, of course, are those that exhibit both sensitivity and a tendency to propagate.

Clearly, if we are to define the compatibility of a material by test, we must measure both sensitivity and the tendency to propagate, that is, the potential reaction intensity.

Conclusions

We have attempted herein to review the development of the two lox impact test methods appearing in Part 18 of the ASTM Standards and to present some of the aspects involved in using such tests to choose materials for lox systems. Hopefully, we have presented a conclusive case to the effect that both sensitivity and reaction intensity measurements are necessary for credible choices between materials.

Noting that one of the above methods purports to measure sensitivity and the other yields reaction intensity, it would seem that the use of both would solve the problem. We have attempted to show, however, that the sensitivity test violates so many fundamental aspects that its inability to yield acceptable precision is not surprising. The reaction intensity test appears to yield meaningful results, but the method is so new that it has not been used outside the laboratory where it was developed, and we know nothing about its reproducibility. Moreover, even if the reaction intensity test does prove to be reproducible through interlaboratory testing, it will not constitute a complete measure of compatibility; precise sensitivity information also is needed. Therefore, we must conclude that a new test for sensitivity with better precision than now available is needed urgently.

REFERENCES

[1] Africano, A. in *Advances in Cryogenic Engineering*, Vol. 5, Plenum Press, New York, 1960.

[2] "Liquid Oxygen Compatibility Impact Sensitivity Test Method," USAF Specification Bulletin 527, U.S. Air Force, 1 May 1961.

[3] "Testing Compatibility of Materials for Liquid Oxygen Systems," NASA Specification MSFC-SPEC-106B, National Aeronautics and Space Administration, 16 Sept. 1966.

[4] Crow, E. L., Davis, F. A., and Maxfield, M. W., *Statistics Manual*, Dover Publications, New York, 1960.

[5] Brown, J. A. et al, "Sensitivity and Rheology Studies on Lead Azide-RDX-Silica Mixtures," Final Technical Report No. GR-1SRS-69 for U.S. Army Picatinny Arsenal, Esso Research and Engineering Co., Jan. 1969.

[6] Blackstone, W. R., Baber, B. B., and Ku, P. M., *Transactions*, American Society of Lubrication Engineers, ASLTA, Vol. 11, No. 3, July 1968.

[7] Rothman, D., Alexander, M. J., and Zimmerman, J. M., "The Design and Analysis of Sensitivity Experiments," NASA CR-62026, Vols. I and II, National Aeronautics and Space Administration, May 1965. ■ ■ ■

Determination of Flash and Fire Points and Impact Sensitivity

(*continued from page 43*)

spark propagation; thus, arcing at the points occurs during the spark discharge. Because this arcing causes a higher temperature spark, it is expected that the flash and fire points occur at lower temperatures.

Another interesting observation is that, whereas numerous flashes but few fires occur with the low pressure system, flash and fire points generally occur simultaneously when the high pressure system is used. This variance is attributed to the difference in spark generators or perhaps the greater possibility of autoignition under high pressure conditions. WSTF is performing studies to determine the relationship of flash and fire points to spark characteristics as well as autoignition properties under high pressure oxygen environments.

It should be pointed out that a difficulty arose when we attempted to specify spark energy as a control parameter. Energy measurement in the low pressure system is straightforward and can be accomplished by measuring the spark current and voltage compared to time, plotting a power envelope, and then obtaining the area under the curve. This measurement can be performed readily because, at the low pressures involved, the spark is in the form of a "normal glow discharge" as described by Cobine[3]; thus, the voltage wave form is fairly smooth and easy to define. At higher pressures, however, the required increase in spark voltage causes an erratic, frequent transition from normal glow to arcing during the spark period. Because different energies exist for the two conditions, even an approximate measurement of energy is difficult. Nonetheless, a quantity that is measured easily is spark gap current as a function of time, which can be displayed on a storage oscilloscope by using a current probe or a current sampling resistor. Although this current measurement does not describe directly the spark energy delivered (as is desired), it does give a means for calibrating individual spark generators to ensure that the same energy profile is used for different test setups.

General conclusions

Gaseous Oxygen Impact Testing/ Testing to date using the WSTF mechanical and pneumatic impact systems has provided reproducible, repeatable data for test pressures up to 5000 psia in a 100

[3]Cobine, J. D., *Gaseous Conductors, Theory and Engineering Applications*, Dover Publications, New York, 1958, p. 250.

END OF REFERENCE

43

REFERENCE

44

FLAMMABILITY, ODOR, AND OFFGASSING REQUIREMENTS AND TEST PROCEDURES FOR MATERIALS IN ENVIRONMENTS WHICH SUPPORT COMBUSTION. MSFC-SPEC-101B, NASA GEORGE C. MARSHALL SPACE FLIGHT CENTER, MARCH 15, 1971.

THIS REFERENCE IS MATERIAL THAT IS READILY AVAILABLE AND THEREFORE THE CONTENTS HAVE NOT BEEN REPRODUCED.

END OF REFERENCE

44

REFERENCE

45

TESTING COMPATIBILITY OF MATERIALS FOR LIQUID OXYGEN SYSTEMS. MSFC-SPEC-106B, NASA MARSHALL SPACE FLIGHT CENTER, OCT. 6, 1967.

MSFC-SPEC-106B
September 16, 1966
SUPERSEDING
MSFC-SPEC-106A
May 5, 1964
AMENDMENT 1
June 18, 1964

GEORGE C. MARSHALL SPACE FLIGHT CENTER

NATIONAL AERONAUTICS AND SPACE ADMINISTRATION

SPECIFICATION

TESTING COMPATIBILITY OF MATERIALS FOR LIQUID OXYGEN SYSTEMS

This specification, dated September 16, 1966, has been approved by the George C. Marshall Space Flight Center (MSFC) and is available for use by MSFC and associated contractors.

1. SCOPE

1.1 This specification establishes acceptance criteria of materials for use in liquid oxygen and gaseous oxygen systems and provides a method to be used in determining the impact sensitivity of such materials.

2. APPLICABLE DOCUMENTS

2.1 The following documents form a part of this specification to the extent specified herein. Unless otherwise indicated, the issue in effect on date of invitation for bids or request for proposals shall apply.

SPECIFICATIONS

Federal

BB-N-411	Nitrogen, Technical.

Military

MIL-P-25508	Propellant, Oxygen.
MIL-P-27401	Propellant Pressurizing Agent, Nitrogen.

George C. Marshall Space Flight Center

MSFC-SPEC-217	Trichloroethylene, Technical, Specification for.

(Copies of specification, standards, drawings, and publications required by contractors in connection with specific procurement functions should be obtained from the procuring activity or as directed by the contracting officer.)

2.2 Other publications. - The following documents form a part of this specification to the extent specified herein. Unless otherwise indicated, the issue in effect on date of invitation for bids or request for proposals shall apply.

George C. Marshall Space Flight Center

NASA Technical Memorandums	Compatiblity of Materials with Liquid Oxygen.

(Applications for copies should be addressed to Propulsion and Vehicle Engineering Laboratory, Materials Division, George C. Marshall Space Flight Center, Huntsville, Alabama 35812.)

3. REQUIREMENTS

3.1 Qualification. - The material shall pass all tests described herein and in the applicable detailed documents prior to use in liquid oxygen (LOX) and gaseous oxygen (GOX) systems. This specification also shall apply to the materials of systems supplying other gases (air, helium, nitrogen, etc.) intended for use in purging or pressurizing LOX systems. Unless otherwise specified, new materials considered for use shall be batch-tested until the capability of the new material to meet the requirements of this specification is established.

3.1.1 Approved materials list. - National Aeronautics and Space Administration (NASA) Technical Memorandums entitled, "Compatiblity of Material with Liquid Oxygen," contain a listing of approved materials and should be consulted before a new material is tested. These memorandums are available to all contractors who specify a "need to know" in writing.

3.2 Serviceability. - When subjected to simulated service conditions, the material shall not crack, spall, nor undergo any other adverse physical change that will preclude its use at the temperature of LOX.

3.3 Impact sensitivity. - The material shall be subjected to 20 successive tests at 72 foot-pounds (10 kilogram-meters) using the test equipment described in 4.3.1, and test procedure described in 4.6. The material shall show none of the following reactions:

(a) An audible explosion.
(b) A visible flash in a darkened room.
(c) Discolorations.
(d) Evidence of burning (charring).

If no reactions occur during the 20 tests, the material shall be accepted. If more than one reaction occurs in 20 tests, the material shall be rejected. If one reaction occurs during the 20 tests, the material shall be subjected to an additional 40 tests. If any reaction occurs during the 40 tests, the material shall be rejected.

NOTE

A burnt odor alone is not considered a reaction. If any reaction occurs due to rebound of plummet, it shall be reported as evidence of sensitivity.

4. QUALITY ASSURANCE PROVISIONS

4.1 Responsibility for inspection. - Unless otherwise specified in the contract or the purchase order, the supplier is responsible for the performance of all inspection requirements as specified herein. The supplier may utilize his own facility or any commercial laboratory if acceptable to MSFC. The procuring activity, or its designated representative, reserves the right to perform any or all of the inspections set forth in the specification where such inspections are deemed necessary to ensure that supplies and services conform to prescribed requirements.

4.2 Sampling. - Sufficient material shall be available to permit preparation and testing of at least 60 separate 11/16-inch diameter disc samples. Sheet materials up to 1/4 inch in thickness shall be tested as 11/16-inch diameter discs in the thickness intended for actual use. Materials normally used in thicknesses greater than 1/4 inch shall be sized and tested as 11/16-inch diameter discs of two thicknesses, 0.050

±0.005 inch and 0.250 ±0.025 inch. Failure of samples of either thickness to meet requirements of this specification shall be cause for rejection of the material. Greases, fluids, and other materials, whose thicknesses are not dictated by conditions of use, shall be tested as 0.050 ±0.005-inch layers in test cups. Materials not readily available in sheet form shall be tested in the available configuration. The O-rings shall be tested in the configuration intended for use unless it can be demonstrated that test results on both sheet material and the O-rings are comparable when tested as specified in 3.3.

NOTE

When testing hard samples that are sometimes capable of initiating false reactions with the aluminum cup material, expendable type 347 stainless steel discs, 11/16 inch in diameter by 1/16 inch in thickness, shall be placed in the bottom of the cup. Stainless steel discs shall be used for all tests whenever different thicknesses of the same material are tested.

4.3 Test equipment. - The tester described in this specification is the ABMA impact tester. Drawings contained herein are for general information only. Materials and configuration of the tester shall conform to the applicable detail drawings that may be obtained from Propulsion and Vehicle Engineering Laboratory, Materials Division, (R-P&VE-MCA) George C. Marshall Space Flight Center, Huntsville, Alabama 35812.

4.3.1 ABMA impact tester (see figure 1). - The impact tester shall have a rugged structural frame with three vertical guides capable of maintaining accurate vertical alignment under repeated shock conditions, a solenoid-operated mechanism for dropping a plummet which weighs 20 ±0.05 pounds through a distance of 43.3 ±0.2 inches (this will transmit to the test sample on approximate impact energy of 72 foot-pounds (10 kilogram-meters)), a striker pin (see figure 2) 1/2 inch in diameter and 2 inches long, and test cup (see figure 3) approximately 7/8-inch inside diameter by approximately 7/8-inch inside depth made of 1/16-inch thick aluminum alloy. The initial alignment and subsequent operation of the impact tester shall be such that the plummet falls uniformly under essentially friction-free conditions. This shall be verified by determining the drop interval across a measured distance. The observed plummet acceleration shall not deviate more than 3 percent from the prevailing gravitational acceleration.

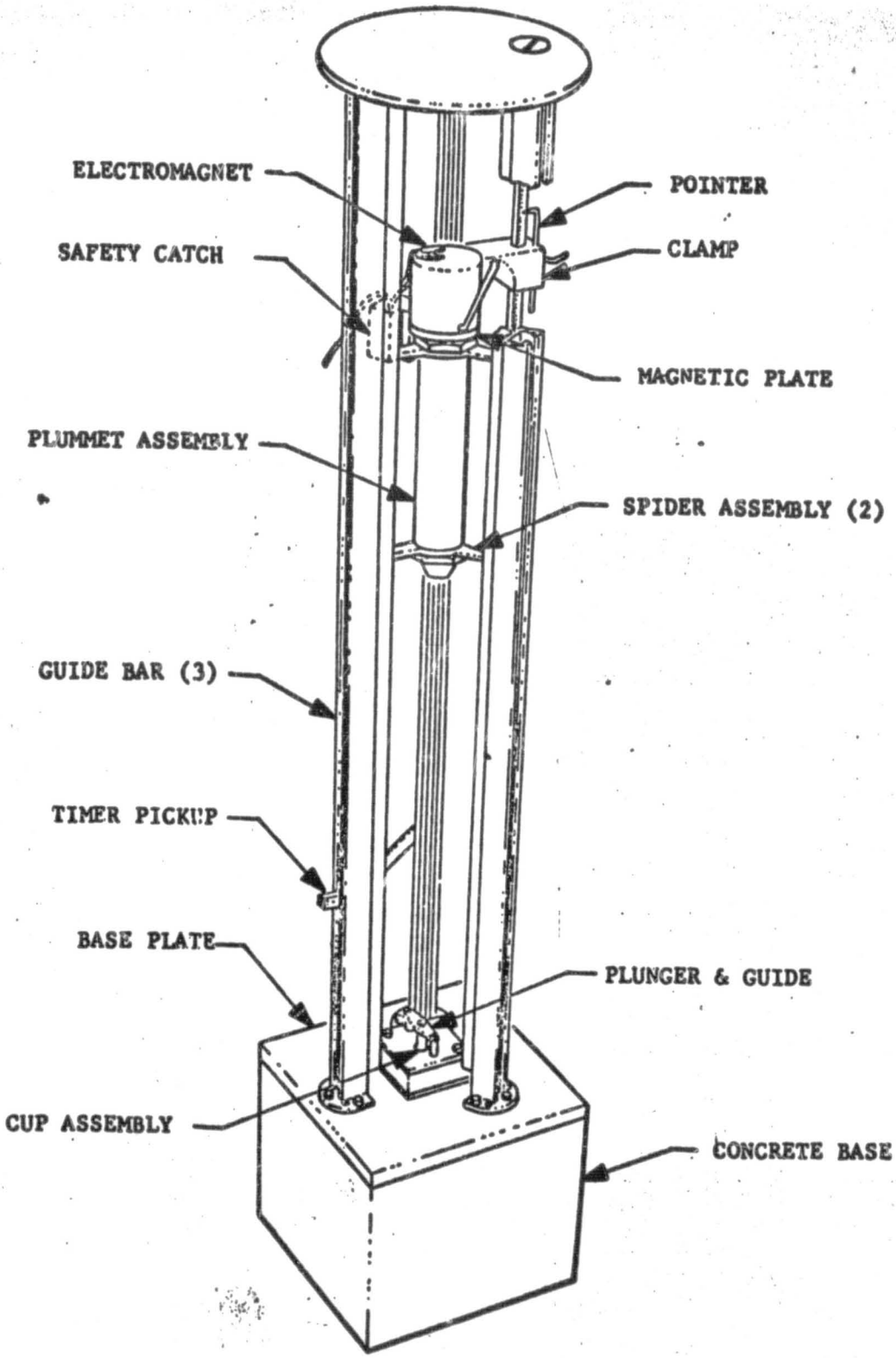

Figure 1. ABMA impact tester.

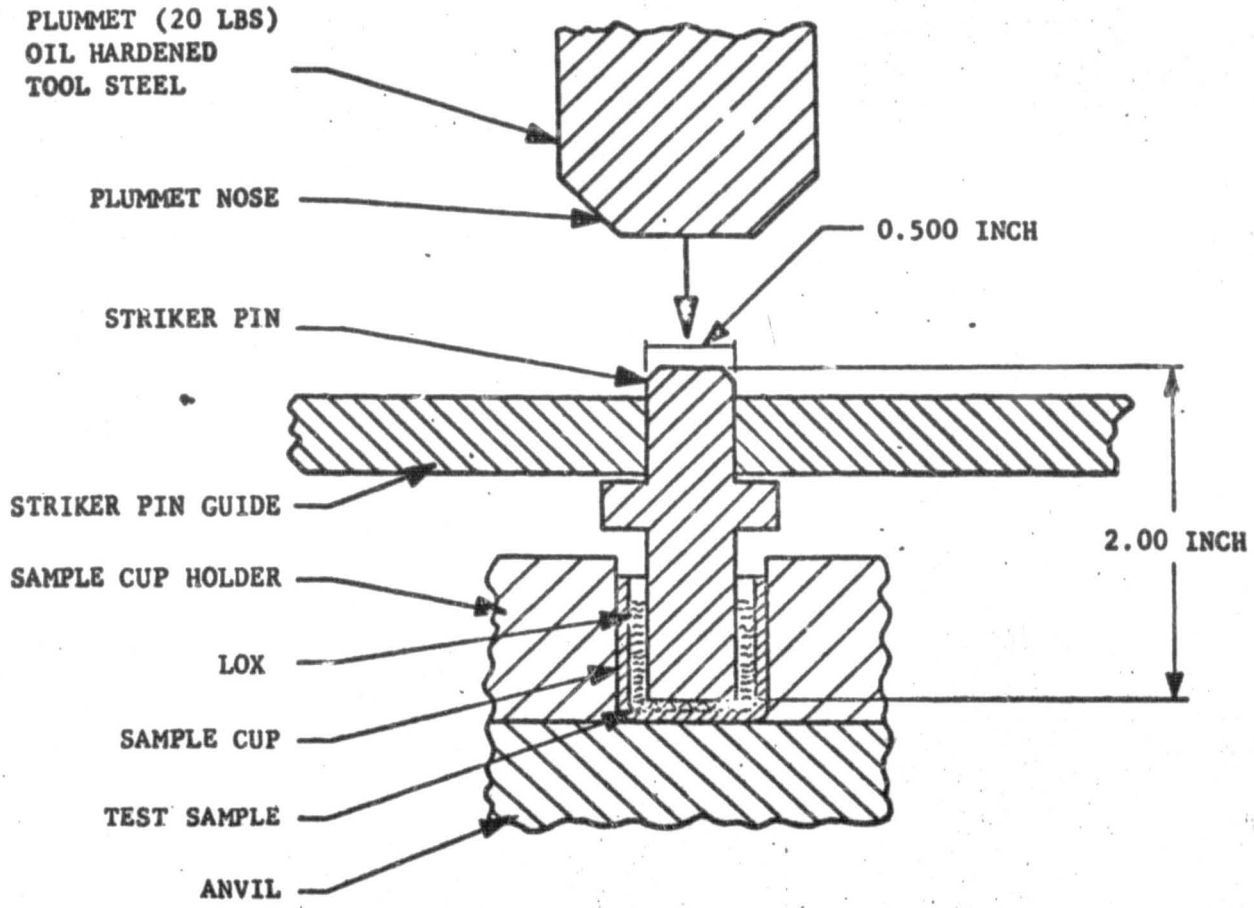

Figure 2. Details of striker, sample cup, and sample (impact sensitivity system).

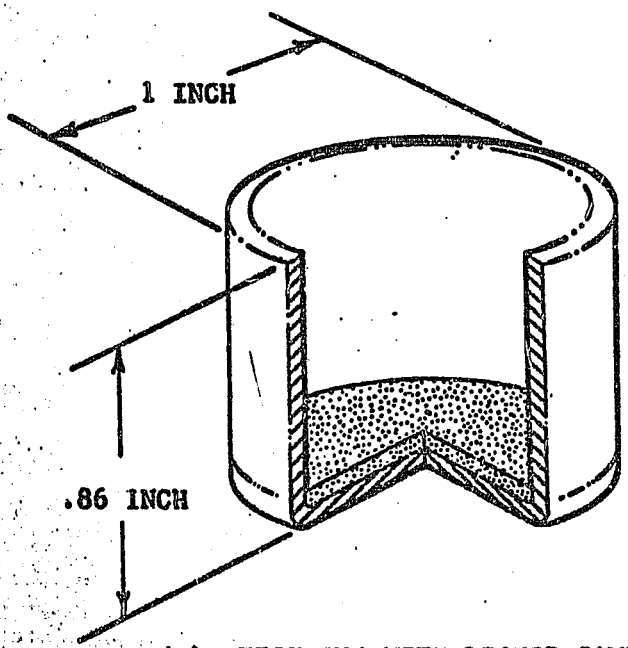

(a) TEST CUP WITH LIQUID SAMPLE (0.050 ± 0.005 INCH THICK)

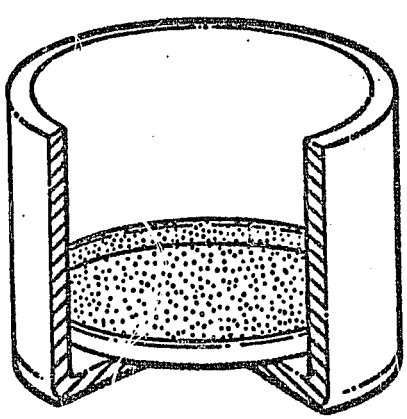

(b) TEST CUP WITH GREASE SAMPLE SHOWING INSERT CUP

Figure 3. Samples in test cups.

NOTE

The weight x drop-height product specified is not duplicated for the purposes of this test by combinations other than 20 ±0.05 pounds and 43.3 ±0.2 inches. For example, doubling the weight and halving the drop height would not duplicate the specified requirement.

4.3.1.1 Details of drop tester components.

4.3.1.1.1 Electromagnet. - The electromagnet shall be designed with a sufficient safety factor to hold over 20 pounds of weight with a minimum energizing wattage.

4.3.1.1.2 Safety catch. - The solenoid-operated safety catch shall be designed to hold the plummet near the base of the magnet in the event of a power failure.

4.3.1.1.3 Base plate. - The base plate shall be constructed from 1-inch thick stainless steel plate and shall rest solidly and level on a 2-foot cube base of reinforced concrete. Four stainless steel foundation bolts shall be used to anchor the plate to the concrete.

4.3.1.1.4 Anvil plate and specimen cup holder. - A stainless steel, type 440B heat treated anvil plate, 5 by 5 by 2 inches thick, shall be bolted to the base plate in the center of the machine. This plate shall center the specimen cup holder and provide the base plate with protection from denting upon impact. A 5-by-5-inch stainless steel specimen cup holder, 1 inch-thick, shall be bolted on top of the anvil plate. The specimen cup holder shall have a slightly tapered hole into which the test cup can be placed.

4.3.1.1.5 Specimen cups (see figure 3). - One-piece specimen cups shall be made of 5052-H32 aluminum alloy. A special insert cup (see figure 4) with an inside depth of 0.050 ±0.005 inch shall also be used when testing semisolid materials. These special insert cups shall be placed inside the one-piece specimen cups.

4.3.1.1.6 Striker pins. - The striker pins shall be made from 17-4 PH stainless steel with hardness in accordance with the applicable detail drawings. A sufficient number of pins shall be provided for testing and discard.

4.3.2 Auxiliary equipment. - The auxiliary equipment shall consist of stainless steel forceps for handling the specimen cups and striker pins, stainless steel spatulas, and LOX handling equipment (e.g., stainless steel Dewar flasks, fireproof lintless laboratory coats, safety goggles, gloves, and LOX storage containers). Additional handling equipment shall include a grease insert cup holder (see figure 4), sample freezing box (see figure 5), striker pin baskets, specimen cup trays, microburettes, syringes, a test cell for the impact tester with a protective window for observation of test drops, a control panel for the operator to activate the safety catch and electromagnet, and timing instrumentation to measure the drop time of the plummet.

4.3.2.1 Timer. - A Berkely Universal counter and timer, Model 5500, or approved equal, shall be used to measure drop time. The overall drop time shall be measured and recorded for each test drop for any given height. The timer shall be calibrated periodically to ensure that the rated accuracy of the equipment is maintained. A typical timing circuit is shown on figure 6.

4.3.3 Test cell. - The impact tester shall be housed in a test cell with a concrete floor. Walls shall be constructed of reinforced concrete or metal to provide protection from explosion or fire hazards. The cell shall contain a shatterproof-glass observation window. It shall be darkened sufficiently for observation of flashes. Continuous ventilation shall provide fresh air to the test cell. Construction of the test cell shall be directed at providing a facility that can be economically maintained at a high level of good housekeeping.

4.4 Materials.

4.4.1 Liquid oxygen. - LOX, used in the performance of this test, shall conform to the requirements of Specification MIL-P-25508.

4.4.2 Liquid nitrogen. - Liquid nitrogen, used in the performance of this test, shall conform to the requirements of Specification BB-N-411 or MIL-P-27401.

(a) GREASE INSERT CUP INSIDE DEPTH - 0.050 ± 0.005 INCH

(b) INSERT CUP HOLDER FOR UNIFORM SAMPLE PREPARATION

Figure 4. Grease insert cup holder.

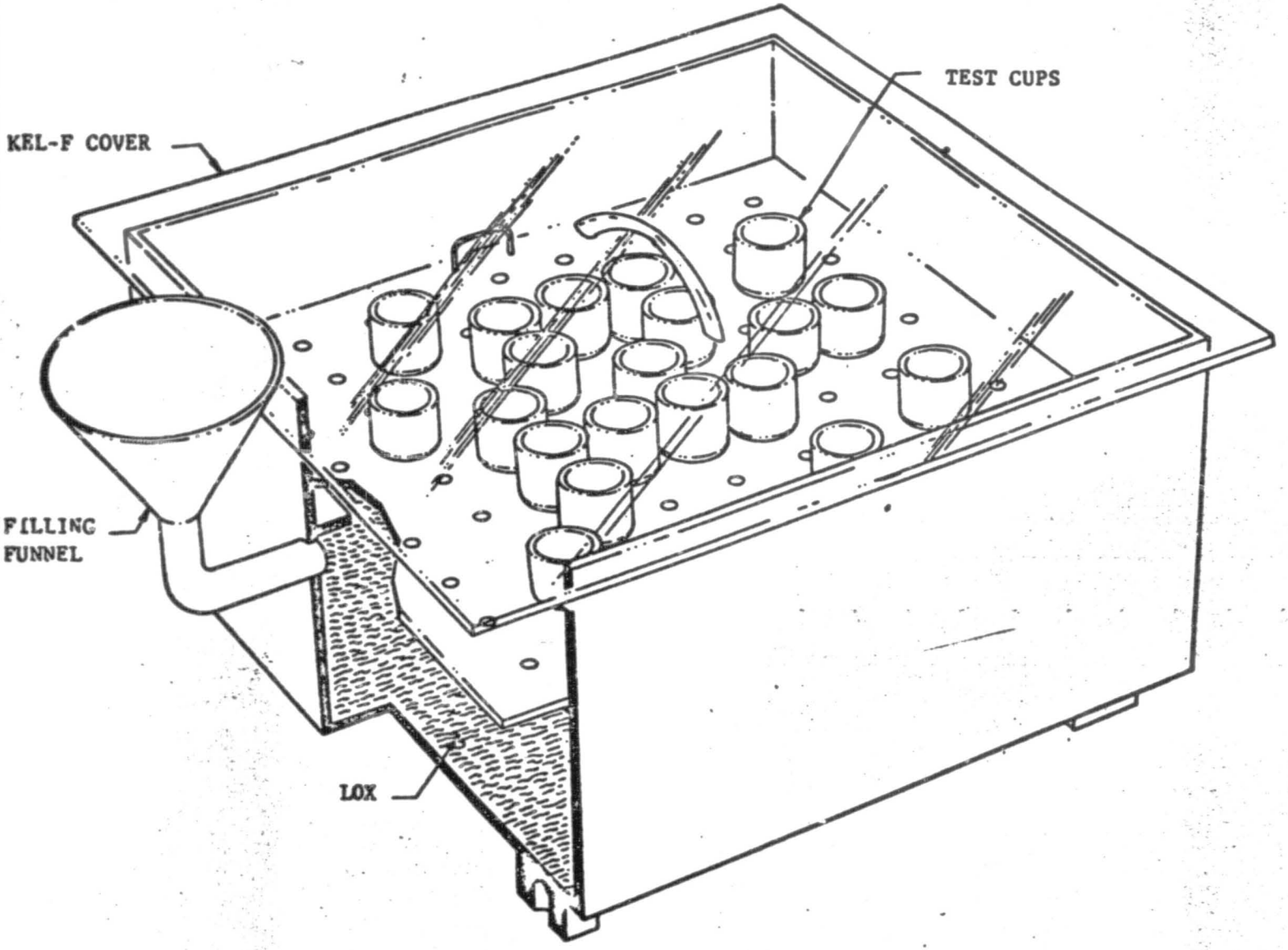

Figure 5. Sample freezing box.

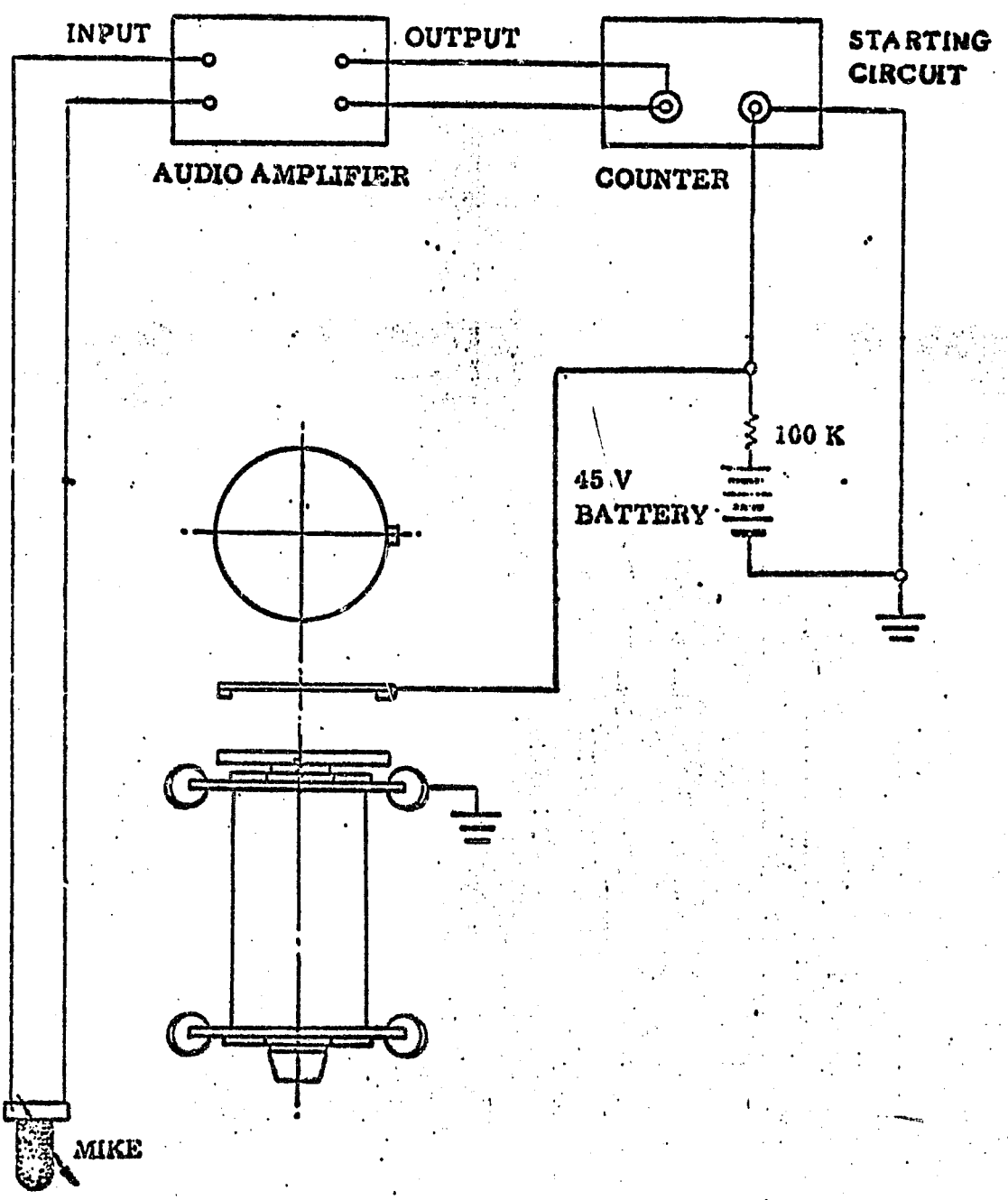

Figure 6. Free-fall timing circuit.

4.4.3 Trichloroethylene. - Trichloroethylene, used in the performance of this test, shall conform to the requirements of Specification MSFC-SPEC-217.

4.4.4. Alkaline cleaner. - A nonetch-type alkaline cleaner shall be used.

4.5 Preparation of equipment for testing.

4.5.1 Impact tester. - The guide tracks, plummet, anvil plate, striker pin guide, sample cup holder, and base plate of the impact tester shall be cleaned thoroughly at the start of each test and between tests of different materials, and shall be rinsed with clean extraction grade trichloroethylene at least after impact test of every tenth sample. After completion of testing for the day, the impact tester shall be thoroughly cleaned. Cleanliness shall be maintained throughout any series of impact tests to minimize erroneous results.

4.5.1.1 Striker pins. - Striker pins shall be used only once and then cleaned. Before each test the striker pins shall be checked for dimensional conformance to the applicable drawing and then examined to endure freedom from scratches, nicks, metallic slivers, and other imperfections. When required, the pins shall be remachined (see 4.5.1.1.1) to ensure freedom from scratches and pits. Prior to use, all striker pins shall be vapor degreased for at least 30 minutes. After use, they shall be thoroughly cleaned by soaking in trichloroethylene and scrubbed with a detergent solution. Following this treatment, the striker pins shall be soaked in an alkaline cleaner, rinsed with water, dried, and stored in a suitable container to ensure cleanliness.

4.5.1.1.1 Remachined striker pins. - The length of remachined striker pins shall be 2.000 (plus 0.010 or minus 0.100) inches. Striker pins shall be remachined if the striking area exhibits scratches or pits or both. It may be necessary to remachine pins that are bent or flattened during impact tests. Badly bent and remachined pins, in which the diameter near the striking area is greater than 0.505 inch or is less than 0.495 inch, shall be discarded.

4.5.1.2 Type 347 stainless steel inserts. - Type 347 stainless steel inserts shall be cleaned in accordance with the method specified for striker pins in 4.5.1.1.

4.5.1.3 Specimen cups. - A test cup shall be used only once and discarded. Prior to use, specimen cups should be cleaned as follows:

(a) Vapor degrease in perchloroethylene or extraction grade trichloroethylene for 15 minutes (cups should be in an inverted position).

(b) Rinse with deionized water.

(c) Soak in nonetch-type alkaline cleaner (82 to 93 degrees Celsius (^{o}C)) for 20 minutes.

(d) Rinse thoroughly with deionized water.

(e) Immerse in water solution containing 0.5 percent of hydrofluoric acid (48 percent) by volume and 5.0 percent of nitric acid (70 percent) by volume for 2 to 5 minutes at room temperature.

(f) Rinse with deionized water.

(g) Desmut by immersing at room temperature in a 50-percent (by volume) solution of nitric acid (70 percent) for 5 minutes or until smut is removed.

(h) Rinse thoroughly with deionized water.

(i) Dry in a moderately hot oven (121 to 149 ^{o}C) to avoid staining.

(j) Store in a clean container until ready for use.

The cups shall not be used for at least 72 hours after cleaning.

4.5.1.4 Blank test. - The effectiveness of the cleaning procedure shall be checked by testing a series of twenty blank cups (filled with LOX) and striker pins from each batch of clean cups and striker pins at the 72-foot-pound (10-kilogram-meter) level. In addition to these blank tests, four blank tests shall be made at random during the testing of any materials. Additional blank tests may be made at the discretion of the operator. The striker pins and sample cups shall be handled by forceps or tongs and kept out of contact with the operator's hands or other sources of contamination.

4.5.2 Auxiliary equipment.

4.5.2.1 Test cell. - The ceiling, walls, and any fixture in the test cell shall be rinsed with water at the end of the working day. The concrete floor shall be scrubbed daily with a detergent.

4.5.2.2 Stainless steel ware. - Stainless steel ware, such as striker pin baskets, forceps, tongs, spatulas, and inserts, shall be cleaned in the same manner as the striker pins (see 4.5.1.1). Once integrated into the handling procedure, a thorough rinse of the stainless steel ware with clean, extraction grade trichloroethylene should be the only cleaning necessary.

4.5.2.3 Glassware check. - Any glassware, such as microburettes, beakers, and syringes, shall be cleaned by soaking in an alkaline cleaner, rinsed with water, and dried. Immediately prior to use, they shall be vapor degreased with trichloroethylene for at least 30 minutes.

4.5.2.4 Cleanliness check. - The effectiveness of the cleaning procedure shall be checked as outlined in 4.5.1.4.

4.6 Test procedure.

4.6.1 Preparation of test samples.

4.6.1.1 Number of samples. - At least 20 samples shall be used for each series of test drops. It may be desirable to prepare more than 20 samples because of rejection due to samples floating or breaking up during precooling.

4.6.1.2 Liquid samples. - Liquid samples shall be applied to form a layer in the bottom of the specimen cups 0.050 $\pm$0.010 inch thick.

4.6.1.3 Greases and semisolids. - Grease samples shall be prepared as follows:

(a) Special specimen cups with inside depths of 0.050 $\pm$0.005 inch shall be provided (see figure 4a).

(b) The special specimen cups shall be cleaned as specified in 4.5.1.3.

(c) Place special cups into the cup holder (see figure 4). Press sufficient sample material into the special cups with a clean, stainless steel spatula to form a sample that is free of air bubbles and void spots.

(d) Scrape off the excess sample with the spatula until a smooth surface, level with the edge of the cup, is achieved.

(e) Remove the special cup from the holder and place it inside the regular specimen cups.

4.6.1.4 Solid samples. - Solid samples, prepared as specified in 4.2, shall be cleaned, rinsed, dried as specified below, and placed in the bottom of the specimen cups.

4.6.1.4.1 Metallic and solvent-resistant samples. - Metallic and solvent-resistant samples shall be scrubbed in detergent water, rinsed, dried, and vapor degreased with tricholoroethylene before placing in the specimen cups.

4.6.1.4.2 Nonmetallic samples. - Nonmetallic samples shall be cleaned with a detergent solution followed by water rinsing and oven drying at 100 ± 10°C for 1 hour or until dry. The particular detergent used shall be impact insensitive in accordance with the requirements of this specification in the concentration used when tested as outlined in 4.6.1.6.

4.6.1.5 Coatings. - Coating samples, such as paints and dry film lubricants, shall be prepared as follows:

(a) Apply the coating to 11/16-inch diameter stainless-steel inserts in the same manner and to the same thickness that is intended for hardware application.

(b) After the samples have dried, place them in the regular specimen cups and test.

4.6.1.6 Leak check compounds, dyes, and dye penetrate systems. - Clean, unsealed, sulfuric-acid-anodized, 6061-T6 discs 11/16-inch in diameter by 0.063 inch thick shall be used as a carrier. Prior to use, the discs shall be vapor degreased in extraction grade trichloroethylene. To check the effectiveness of the cleaning procedure, a minimum of 20 blank discs shall be tested as specified in 3.3. The discs shall then be soaked in the leak check compound, dye, dye penetrate, emulsifier, or developer for 15 minutes; drained for 15 minutes at an angle of 90 degrees in the fixture shown on figure 7; and tested by placing the specimen discs on stainless steel inserts in the bottom of the test cups.

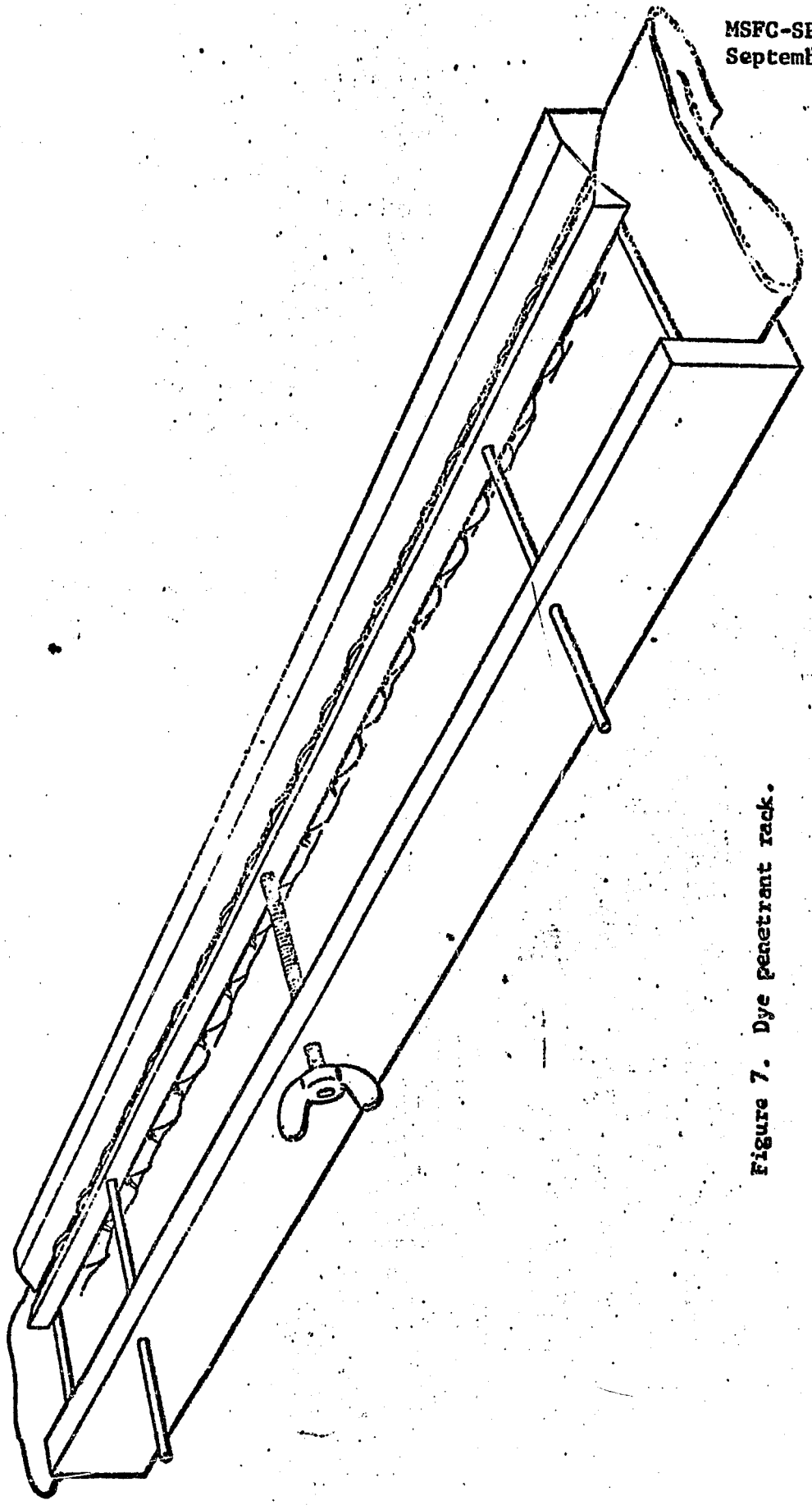

Figure 7. Dye penetrant rack.

4.6.1.7 Solders. - Solders shall be tested as flat sheets. The sheets shall be prepared by melting and casting the solders to form ingots and by rolling the ingots into sheets of 0.020 ±0.005 inch in thickness. Discs 11/16 inch in diameter shall be punched from the sheets, cleaned as outlined in 4.6.1.4.1, and tested by placing the discs on stainless steel inserts in the bottom of the test cups. If rosin core solder is used, care should be taken to ensure that the rosin is burned off or completely removed prior to test.

4.6.2 Precooling. - Precooling shall be accomplished by lowering the temperature of the material to the boiling point of LOX at one atmospheric pressure (minus 183°C).

4.6.2.1 Dewar flasks. - Stainless steel Dewar flasks shall be precooled by slowly pouring LOX into the flask until the LOX ceases to boil. When cooled, the flask shall be filled with LOX and covered with clean aluminum foil or a stainless steel cover. Since glass Dewar flasks are easily broken, they should not be used.

4.6.2.2 Specimen cups.

4.6.2.2.1 Blank specimen cups. - The cleaned, blank specimen cups shall be precooled by slowly pouring LOX into a sample tray until the LOX covers and fills the cups.

4.6.2.2.2 Specimen cups containing sample material. - To minimize cracking of the samples during freezing, the cups containing the samples shall be precooled slowly by using the freezing box shown on figure 5. The box should be leveled prior to use. The procedure shall be as follows:

(a) Place approximately 40 specimen cups over the holes in the retainer plate.

(b) Using an automatic delivery tube with a 25-liter Dewar flask, pressurize the Dewar flask to approximately 2.5 pounds per square inch gage (psig) with oil-free oxygen.

(c) While maintaining the pressure at approximately 2.5 psig, open the discharge valve approximately halfway and start to fill the freezing box.

The time required to fill the cups and the freezing box 1/8 inch from the top shall be 35 to 40 minutes. After this step, a careful inspection shall be made. Any sample that separates from the bottom of the cup and floats or shatters due to thermal shock shall be discarded. The thickness of at least five frozen samples shall be measured and recorded. The samples shall be transferred to a suitable (precooled) container for storage until tested. Additions of LOX shall be made, as necessary, while tests are in progress to ensure that each sample cup is completely filled at time of testing.

4.6.2.3 Striker pins. - Cleaned striker pins shall be precooled by placing pins in a Dewar flask and adding liquid nitrogen to the flask until the pins are covered with liquid nitrogen.

4.6.2.4 Specimen cup holder and base plate. - The specimen cup holder and anvil plate shall be precooled by adding liquid nitrogen to the stainless steel moat surrounding the specimen cup holder and base plate. The moat should be filled with liquid nitrogen to approximately 1/2 inch below the top of the specimen cup holder.

4.6.3 Impact test. - Critical test parameters shall be as follows:

(a) Plummet weight. - Plummet weight shall be 20 $\pm$0.05 pounds.

(b) Drop height. - Drop height shall not deviate more than $\pm$0.2 inch from the specified height.

(c) Striker pin diameter. - Striker pin diameter near the striking area shall be 0.500 $\pm$0.005 inch.

(d) Energy loss. - The energy loss due to friction shall be controlled by measuring and recording the drop time of each drop of any given height. The observed plummet acceleration shall not deviate more than 3 percent from the prevailing gravitational acceleration.

4.6.3.1 Blank drop. - The effectiveness of the cleaning procedure shall be checked by testing blank cups as outlined in 4.5.1.4.

4.6.3.2 Test drop. - The following steps shall be accomplished with sufficient care and speed so that the specimen cup will be full of LOX at all times prior to and during impact:

(a) The magnet shall be adjusted to proper drop height (43.3 inches for 72 foot-pounds).

(b) Clean tongs shall be used to set the precooled specimen cups into the specimen cup holder.

(c) A visual check shall be made to assure that the frozen sample has not separated from the bottom of the cup. Samples that have separated shall be discarded.

(d) Place the striker pin in the cup and hold it in place by the striker pin guide.

(e) Add LOX at the specimen cup to ensure that the specimen cup is full.

(f) Cover the exposed container of LOX.

(g) Close the test cell door, turn off the cell lights, and set the timer.

(h) Release the safety catch and plummet by means of the control panel located outside the test cell near the observation window.

(i) Observe and record the results of the impact reaction as defined in 3.3.

(j) Record the drop time of the plummet for each drop.

4.6.3.3 Interpretation of results. - A material proposed for use in LOX systems or subject to direct contact with LOX shall conform to the requirements of 3.3.

4.6.3.4 Threshold levels. - For materials sensitive at 72 foot-pounds (10 kilogram-meters), it may be desirable to determine threshold values. The approximate threshold value shall be obtained by testing 20 samples at each of the drop heights listed in table I. The first height at which no reactions are obtained in 20 drops shall be the approximate threshold value. The definitive threshold value shall be determined by 20 tests at drop-height increments of 3 inches starting at a height of 6 inches above the approximate threshold value. The definitive threshold value shall be the higher of the two adjacent heights at which no reaction was obtained.

Table I. Drop height schedule for approximate threshold value determination.

Measurement	Inches
First Height	43.3 (10 kilogram-meter)
Second Height	33
Third Height	24
Fourth Height	15
Fifth Height	6

4.7 Rejection and retest. - Failure of any sample to meet the requirements of this specification shall be cause for rejection of the lot represented. Rejected materials shall not be resubmitted for approval without full details being furnished concerning the previous rejection and measures taken to correct the defects. If not more than one test unit of the original test sample fails to meet the test requirements specified herein, the manufacturer may request a retest. If all test units of the retest meet the requirements specified herein, the material shall be considered compatible for use in LOX systems.

5. PREPARATION FOR DELIVERY

5.1 When it is necessary to ship samples of materials for testing, the preservation, packaging, and packing shall be such that contamination of samples and materials will be prevented. Initial wraps shall be of the same cleanliness as the sample materials.

6. NOTES

6.1 Intended use. - This specification is intended for use with the ABMA impact tester in determining the compatibility of materials with LOX.

6.2 Ordering data. - Procurement documents should specify the following:

(a) Title, number, and date of this specification.

(b) Where tests are to be conducted.

(c) Whether certified test data is required.

6.3 Changes, deviations, or waivers. - No technical changes, deviations, or waivers will be made to the requirements of this document without the approval of the cognizant design engineering activity of MSFC. All changes, deviations, or waivers will be submitted to the Engineering Specifications and Standards Section of the Propulsion and Vehicle Engineering Laboratory (R-P&VE-VNR) for coordination with the cognizant design activity.

Notice. - When Government drawings, specifications, or other data are used for any purpose other than in connection with a definitely related Government procurement operation, the United States Government thereby incurs no responsibility nor any obligation whatsoever; and the fact that the Government may have formulated, furnished, or in any way supplied the said drawings, specifications, or other data is not to be regarded by implication or otherwise as in any manner licensing the holder or any other person or corporation, or conveying any rights or permission to manufacture, use, or sell any patented invention that may in any way be related thereto.

Custodian:	Preparing activity:
NASA - George C. Marshall Space Flight Center	George C. Marshall Space Flight Center

NASA-MSFC-C

MSFC-SPEC-106B
Amendment 1
October 6, 1967

GEORGE C. MARSHALL SPACE FLIGHT CENTER

NATIONAL AERONAUTICS AND SPACE ADMINISTRATION

SPECIFICATION

TESTING COMPATIBILITY OF MATERIALS FOR LIQUID OXYGEN SYSTEMS

This amendment forms a part of George C. Marshall Space Flight Center (MSFC) Specification MSFC-SPEC-106B, September 16, 1966, and has been approved by MSFC and is available for use by MSFC and associated contractors.

(1) Page 4, paragraph 4.2: Delete the last sentence of paragraph 4.2 and substitute the following:

"Stainless steel inserts shall be used as a false bottom in the aluminum specimen cups when testing all materials with the exception of greases, oils, other liquids, dye penetrants, coatings, and solders. The latter materials shall be tested as specified in other sections of this specification."

(2) Page 4, paragraph 4.2: Add the following paragraphs:

"4.2.1 O-rings. - Each size from each batch of O-rings and/or O-ring materials shall be sampled and tested as follows unless it can be demonstrated that test results on different sizes and batches are comparable when tested as specified in 3.3.

"4.2.1.1 Extruded O-rings. - At least 60 discs (11/16-inch diameter by thickness of O-rings) shall be cut from a strip after the chopping operation. The discs shall be processed and deflashed with the same equipment used for the O-rings. The discs shall be cleaned as specified in 4.6.1.4.2 and tested after precooling as specified in 4.6.2.2.2.

"4.2.1.2 Molded O-rings. - At least 60 discs (11/16-inch diameter by thickness of O-rings) shall be furnished that have been processed and deflashed in the same equipment used for the O-rings. The discs shall be cleaned as specified in 4.6.1.4.2 and tested after precooling as specified in 4.6.2.2.2.

"4.2.1.3 O-rings from standard stock or where above procedures are impractical. - O-rings 1/2-inch outside diameter or less shall be sampled and tested as a complete O-ring. O-rings larger than 1/2-inch outside diameter shall be tested as one segment (approximately 3/4-inch long) on a stainless steel insert. The samples shall be cleaned and precooled as specified above. If a sample is not impacted during testing, it shall be placed in a new cup with a stainless steel insert and precooled prior to testing. As an alternative, sufficient samples may be prepared to account for the normal misses. If additional cleaning procedures are used, they must be specified on the test data sheets."

(3) Page 16, paragraph 4.6.1.5: Delete and substitute the following:

"4.6.1.5 Coatings.

"4.6.1.5.1 Paints and dry film lubricants. - Coating samples, such as paints and dry film lubricants, shall be prepared as follows:

"(a) Apply the coating to 11/16-inch diameter stainless steel inserts in the same manner and to the same thickness that is intended for hardware application.

"(b) After the samples have dried, place them in the regular specimen cups and test.

"4.6.1.5.2 Elastomerics. - Elastomeric coating samples shall be prepared as follows:

"(a) Thin with reagent grade methyl isobutyl ketone or other compatible solvent to 10 percent of total weight of solids, or to manufacturer's recommendations.

"(b) Apply the coating to 11/16-inch diameter stainless steel inserts as follows:

"(1) METHOD 1 (SINGLE DIP COAT). - Dip coat (approximately 0.0005 inch) and place on clean aluminum foil to air dry. The coated inserts shall be removed from the foil and turned over after 30 minutes to allow both sides to dry completely. The specimens shall be air dried for a minimum of 24 hours prior to testing. The coating thickness shall be checked on at least four samples and recorded.

"(2) METHOD 2 (BRUSH COAT). - Apply 22 coats (10 percent solids) using a single brush stroke with a soft nonshedding brush. Allow a minimum of 30-minutes drying time between coats. If the thickness of the coating is greater than 0.015 inch, the specimen shall be rejected; if less than 0.015 inch, additional coats shall be applied as required to achieve the specified thickness. Each specimen shall be visually examined for contamination following application of each coat (especially bristles from the brush). The coated specimens shall be air dried for a minimum of 24 hours following application of the final coat before testing."

Custodian:

NASA - George C. Marshall Space Flight Center

Preparing activity:

George C. Marshall Space Flight Center

END OF REFERENCE

REFERENCE

46

APOLLO SPACECRAFT, NONMETALLIC MATERIALS REQUIREMENTS. MSC-PA-D-67-13, NASA MANNED SPACECRAFT CENTER, 1968; ADDENDAS 1, 1A, 2, 2A, 1971.

THIS REFERENCE HAS A LIMITED DISTRIBUTION AND MAY NOT BE REPRODUCED.

END OF REFERENCE

46

REFERENCE

47

STEVENS, M. R.; FISHER, H. D.; AND BREEN, B. P.: INVESTIGATION OF MATERIALS COMBUSTIBILITY, FIRE, AND EXPLOSION SUPPRESSION IN A VARIETY OF ATMOSPHERES. AFAPL-TR-68-35, AIR FORCE AERO PROPULSION LAB., MAY 1968.

N68-30134

COPY 1

N68-30134

INVESTIGATION OF MATERIALS COMBUSTIBILITY, FIRE, AND EXPLOSION SUPPRESSION IN A VARIETY OF ATMOSPHERES

M. R. STEVENS, H. D. FISHER, AND B. P. BREEN

DYNAMIC SCIENCE
A DIVISION OF MARSHALL INDUSTRIES
MONROVIA, CALIFORNIA

LEWIS RESEARCH CENTER
Aerospace Safety Research
and Data Institute

TECHNICAL REPORT AFAPL-TR-68-35

MAY 1968

LIBRARY
OCT 26 1969
LEWIS LIBRARY, NASA
CLEVELAND, OHIO

This document has been approved for public release and sale. Its distribution is unlimited.

AIR FORCE AERO PROPULSION LABORATORY
AIR FORCE SYSTEMS COMMAND
WRIGHT—PATTERSON AIR FORCE BASE, OHIO

NOTICE

When Government drawings, specifications, or other data are used for any purpose other than in connection with a definitely related Government procurement operation, the United States Government thereby incurs no responsibility nor any obligation whatsoever; and the fact that the Government may have formulated, furnished, or in any way supplied the said drawings, specifications, or other data, is not to be regarded by implication or otherwise as in any manner licensing the holder or any other person or corporation, or conveying any rights or permission to manufacture, use, or sell any patented invention that may in any way be related thereto.

Copies of this report should not be returned unless return is required by security considerations, contractual obligations, or notice on a specific document.

AFAPL-TR-68-35

INVESTIGATION OF MATERIALS COMBUSTIBILITY, FIRE, AND EXPLOSION SUPPRESSION IN A VARIETY OF ATMOSPHERES

M. R. Stevens, H. D. Fisher, and B. P. Breen

DYNAMIC SCIENCE
A Division of Marshall Industries
Monrovia, California

TECHNICAL REPORT AFAPL-TR-68-35

May 1968

AIR FORCE AERO PROPULSION LABORATORY
AIR FORCE SYSTEMS COMMAND
WRIGHT-PATTERSON AIR FORCE BASE, OHIO

ABSTRACT

Combustibility studies of materials of construction employed in space flight vehicle cabins have been carried out as a function of various simulated cabin atmospheric environments. The program was conducted under three distinct phases. Phase I efforts were directed at defining the spontaneous ignition temperature, of the individual materials, under dynamic atmospheric conditions for the various atmospheres employed. Phase II centered about the burning characteristics of the respective materials as a function of atmospheric and gravitational environments. These studies also involve the effects of various extinguishants upon the burning characteristics under the influence of several atmospheric environments and gravitational variations. Phase III focused upon the flame spread behavior of the material, under the influence of various atmospheric environments and in the presence of Halon 1301 flame extinguishant. Detailed analyses of the work clearly show the dependency of the combustion behavior of the materials upon the atmospheric environment utilized.

II. EXPERIMENTAL PROGRAM

A. PHASE I. DETERMINATION OF THE SPONTANEOUS IGNITION TEMPERATURE OF SELECTED MATERIALS

1. Introduction

The rapid evolution of spacecraft has rendered it increasingly difficult to design flight vehicle cabins with regard to fire and explosion prevention. Utilization of oxygen enriched, low pressure atmospheres within a sealed cabin makes it imperative to determine the flammable characteristics of the materials employed therein. Of prime importance, in this regard, are the ignition characteristics of materials. Therefore, the first phase of this study is devoted to the determination of the ignition behavior of relevant materials as a function of oxygen concentration and total environmental pressures.

The overall atmospheric environment within the sealed flight cabin is generally subject to a recirculating or recycling process. It was, therefore, felt that the most pertinent ignition data is that obtained under similar conditions, i.e., a dynamic environment. However, under the influence of a dynamic atmospheric environment, the observed minimum ignition temperatures will differ from those generally associated with the ASTM Autogeneous Ignition Temperature designation. Therefore, the minimum ignition temperatures reported here are designated as Spontaneous Ignition Temperatures and are defined as being the lowest temperature of the test specimen at which the material will ignite, under the particular test condition and apparatus employed, without the application of an igniting source, i.e., flame or spark.

In general, the Spontaneous Ignition Temperatures, (S.I.T.) reported here will be higher than those attained by application of the static A.S.T.M. method. This follows from the fact that the sequence of oxidative chemical reactions, which liberate heat and lead to combustion, is disturbed by the removal of heat and chemical intermediates from the vicinity of the test specimen by the circulating flow imposed on the system. Thus, additional heat must be supplied to the test specimen, (raising its temperature) in order

to make up and exceed this loss and thus so permit ignition to take place.

2. Apparatus

Determination of the Spontaneous Ignition Temperature of each test specimen was carried out employing a Combustion Monitor, designed and constructed by Dynamic Science for the Air Force under an earlier contract (AF 33(657)-11075). This unit was specifically designed to investigate the ignition and burning characteristics of combustible materials. Temperature, pressure, and fluid flow are controlled from a console, located immediately in front of two furnace reaction chambers, identified as Furnace No. 1 and Furnace No. 2. Figure 1 illustrates the overall facility. A complete description of this system, together with operating procedures, may be found in Reference 1.

For the present study, Furnace No. 2 was utilized. The furnace reaction chamber is 12 inches in diameter and approximately 18 inches high. Access to the chamber is through a flanged cover sealed with an asbestos gasket which is double-jacketed with 304 stainless steel and tightened with 1/2 inch bolts. A 3-inch diameter viewing port permits observation of the experiment's performance within the chamber. Figure 2 illustrates the No. 2 Furnace Reaction Chamber. Fluid inlets, exhaust ports, electrical leads, and thermocouples enter the chamber from 3 tubes in the bottom of the chamber, as shown. The enclosing furnace is 28 inches square (viewed from the top) and 32 inches high. The solid samples, employed for this work, were placed upon a tray located just above the inlet side of the incoming fluid mixer unit. This stainless steel tray is equipped with a self contained heating unit, allowing the tray temperature to be controlled independently or slaved to that of the main reaction chamber.

In practice, the reaction chamber may be operated under conditions of static atmosphere environments or dynamic atmosphere environments. Both modes of operation may be carried out at constant pressure or variable pressures. The spontaneous ignition temperature determinations reported below were carried out under dynamic atmospheric environments at constant pressure. To accomplish this, the main reaction chamber is equipped with a differential pressure regulator, (a Sterer Valve), manufactured by the Sterer Engineering

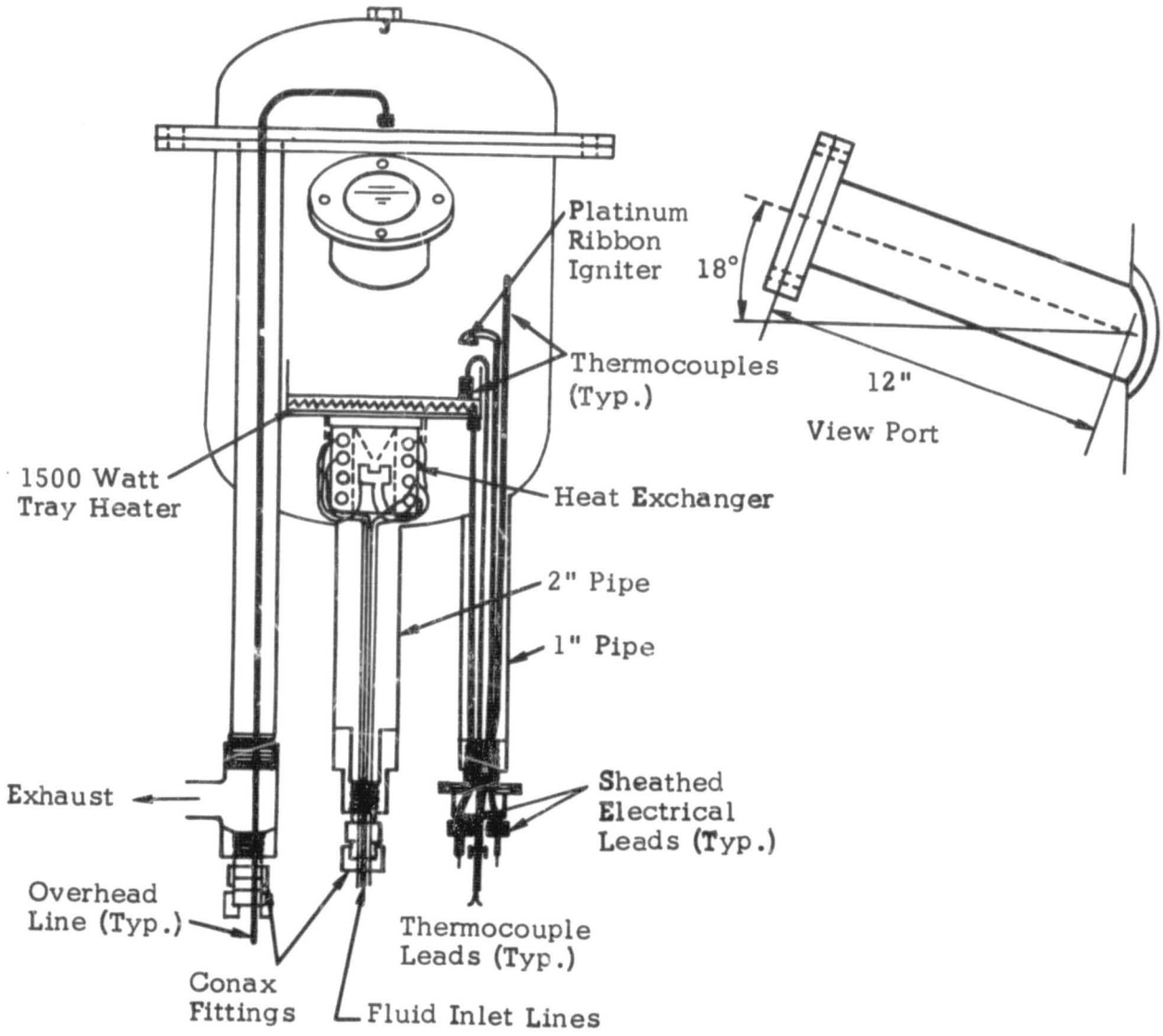

FIGURE 2. No. 2 Furnace Chamber.

Company of Los Angeles.

Additional equipment employed for these tests were a Vacuum Manifold System, a Gas Chromatograph, and a Beckman Oxygen Analyzer. The vacuum manifold system was connected to the No. 2 Furnace Reaction Chamber. This system was employed to obtain samples of preignition and post-ignition atmospheres from the reaction chamber. Gaseous samples, so taken, are analyzed by the Gas Chromatograph. The chromatograph utilized was a Micro Tech 2500R, and was directly connected to the vacuum manifold system. It was fitted with molecular sieve and silica gel columns, both 10 feet long by 1/4 inch in diameter. The columns were operated at 150°C with helium carrier gas at a flow rate of 60 cc/min. The Beckman Oxygen Analyzer was employed to monitor the oxygen content of the incoming environmental gases.

Suitable thermocouples were used to control and/or indicate temperature at critical areas within the reaction chamber. One such unit monitored the overall environmental temperature. A second unit monitored the tray temperature, while a third unit monitored the test specimen temperature. Total pressure within the chamber was continuously monitored by means of a Statham Pressure Transducer of 0-30 psia range.

3. Procedure

The test sample is placed upon the surface of the tray heater, located in the No. 2 Furnace Reaction Chamber. The specimen thermocouple is placed in contact with the upper (exposed) surface of the sample. At this point, the reaction chamber is sealed, evacuated, and leak checked. With the chamber isolated from the vacuum, the desired atmosphere is introduced and the chamber pressure is then set by adjusting the reference pressure on the Sterer Valve to the desired operating level.

When the operating pressure level is reached, the gas flow rate is adjusted such that the chamber atmosphere is changed at a constant rate, independent of the operating pressure. The S.T.P. flow rates used at various chamber pressures are shown in Table I.

The furnace heater is now activated and the power level adjusted as required. The tray heater is then activated and its power level adjusted. Recorders monitoring chamber pressure and temperatures are activated. The test run has started.

TABLE I

GAS FLOW RATES THROUGH REACTION CHAMBER
AT STP AT VARIOUS CHAMBER PRESSURES

Operating Pressure, mm Hg.		Flow Rate, Liters/Minute
760	14.7 psia	4
569	11 "	3.2
362	7 "	1.87
259	5 "	1.33

4. Experimental Results

Eleven materials were selected for study under this phase of the program. They were selected on the basis that each represented a basic material present within the flight vehicle cabin. The Spontaneous Ignition Temperature (SIT) of each material was determined primarily as a function of oxygen concentration and total environmental pressures. Eight were subjected to intensive study, three were spot checked only. Data for only three of the materials have been previously reported (2).

(a) Polyethylene

The polyethylene S.I.T. study was the first to be carried out. Table II presents all the data obtained in the course of the polyethylene experimental test program. In these initial experiments an effort was made to ascertain the relative importance of such variables as sample size, heating rate, flow rate, pressure, and oxygen concentration upon observed S.I.T. values. This data had been reported in Summary Report No. SN-6401(2). As presented in Table II, the data have been rearranged for purposes of clarity and evaluation. Several variables previously considered (2) have been omitted here since

TABLE II. SPONTANEOUS IGNITION TEMPERATURE OF POLYETHYLENE

Run No.	Atm. Composition (%) O_2	N_2	He	Pressure (mm Hg)	Flow Rate l/Min.	Size (Inches)	Heating Rate °C/min	S.I.T. °C	Remarks
118	100	-	-	760	0	1x1x3/8	6	248	Increase of flow rate
119	100	-	-	760	0	4x4x3/8	5.5	250	increases S.I.T.
104	100	-	-	760	2.3	1x1x3/8	3	250	Compare runs 104 and
115	100	-	-	760	4.2	1x1x3/8	7.5	223	120, 131.
120	100	-	-	760	6.5	1x1x3/8	10.0	264	Sample surface area
131	100	-	-	760	0	1x1x3/8	3.5	230	does not affect S.I.T.
106	50	50	-	760	4.8	1x1x3/8	3.5	262	Compare runs 118 and
112	75	-	25	760	4.1	1x1x3/8	-	242	119.
114	25	-	75	760	4.0	1x1x3/8	7.5	No ignition	
125	100	-	-	569	0	3x3x3/8	9.8	300	S.I.T. function of
103	100	-	-	569	1.9	1x1x3/8	2.0	250	oxygen concentration.
113	75	25	-	569	4.4	1x1x3/8	12.0	244	Compare runs 113, 108
108	50	50	-	569	5.3	1x1x3/8	-	282	and 110.
110	20	80	-	569	5.2	1x1x3/8	-	No ignition	
111	20	80	-	569	5.6	1x1x3/8	-		
102	100	-	-	362	1.4	1x1x3/8	5.4	300	Run 102 appears
116	75	25	-	362	4.2	1x1x3/8	14.0	291	out of line. Compare
107	50	50	-	362	3.0	1x1x3/8	-	No ignition	102 with 125.
121	100	-	-	259	0	1x1x3/8	10	319	Within narrow limits
128A	100	-	-	259	1.4	1x1x3/8	4	310	sample thickness will
129	100	-	-	259	1.4	1x1x3/8	4	No ignition	affect S.I.T.
130	100	-	-	259	1.4	1x1x1/8	6	311	Runs 128A, 101 and
101	100	-	-	259	1.1	1x1x3/8	4.4	305	121 definitely discount
105	100	-	-	259	2.9	1x1x3/8	4	302	affect of flow on S.I.T. as a parameter in these experiments.

TABLE III. SPONTANEOUS IGNITION TEMPERATURE OF POLYVINYLCHLORIDE
DIMENSIONS: 4 PIECES, EACH 1 x 1 x 1/16

Run No.	Atm. Composition (%)			Pressure (mm Hg)	Flow Rate (l/min)	Heating Rate °C/min	S.I.T. °C	Remarks
	O_2	N_2	He					
201	100	--	--	760	4	5	480	
204	100	--	--	760	4	3.5	452	
205	100	--	--	760	4	3.5	462	Sample in O_2 Atm. 30 days
206	100	--	--	569	3.2	4	462	
206A	100	--	--	569	3.2	5	452	
209	100	--	--	569	5.2	7.5	502	Inc. of Flowrate, Inc. S.I.T.
220	100	--	--	569	3.2	6.5	510	
212	100	--	--	362	1.9	8	539	
215	100	--	--	259	1.3	5	552	
202	60	40	--	760	4	5	537	
207	60	40	--	569	3.2	5	562	
213	60	40	--	362	1.9	5	535	Value low.
218	60	40	--	362	1.9	5	572	
216	60	40	--	259	1.3	5	600	
203	20	80	--	760	4	5	No ignition	Runs below 760 mmHg of this series were not needed.
203A	20	80	--	760	4	5	"	
208	20	80	--	569	3.2	5	"	
208A	20	80	--	569	5.2	5	"	
211	20	80	--	569	5.2	5	"	
217	20	80	--	259	1.3	5	"	
219	20	80	--	259	1.3	5	"	
214	20	80	--	362	1.9	5	"	
210	60	--	40	569	5.2	5	568	Helium, as diluent, does not have great effect upon S.I.T.

TABLE IV. SPONTANEOUS IGNITION TEMPERATURE OF SILICONE RUBBER
DIMENSIONS: 2 PIECES, EACH 1 x 1 x 1/8 INCHES

Run No.	Atm. Composition (%)			Pressure (mm Hg)	Flow Rate (l/min)	Heating Rate °C/min	S.I.T. °C	Remarks
	O_2	N_2	He					
301A	100	--	--	760	4	3.5	496	
301B	100	--	--	760	4	3.3	498	
310	100	--	--	760	4	4	488	Sample aged in O_2 for 30 days
311	100	--	--	760	4	4	492	
318	100	--	--	760	4	--	485	
302	100	--	--	569	3.2	5	498	
302A	100	--	--	569	3.2	3.3	495	
313	100	--	--	569	3.2	4	505	
303	100	--	--	362	1.9	3.3	No ignition	Faulty run
303A	100	--	--	362	1.9	3.3	510	
303B	100	--	--	362	1.9	3.5	500	
304	100	--	--	259	1.3	3	500	
305	60	40	--	760	4	3.3	495	
306	60	40	--	569	3.2	4	498	
307	60	40	--	362	1.9	2.5	498	
308	60	40	--	259	1.3	3.3	498	
308A	60	40	--	259	1.3	3.4	505	
309	20	80	--	760	4	3.3	510	
319	20	80	--	760	4	--	515	
312	20	80	--	569	3.2	3.5	512	
315	20	80	--	569	3.2	--	528	
316	20	80	--	362	1.9		No ignition	
317	20	80	--	259	1.3	--	No ignition	
320	20	80	--	569	1.9	--	502	
314	60	--	40	569	3.2	4.3	508	

TABLE VIII. SPONTANEOUS IGNITION TEMPERATURE OF VITON A--ELASTOMER
DIMENSIONS--2 PIECES OF 1 x 1 x 1/16 INCH MATERIAL

Run No.	Atm. Composition (%)			Pressure (mm Hg)	Flow Rate (l/min)	Heating Rate °C/min	S.I.T. °C	Remarks
	O_2	N_2	He					
401	100	--	--	760	4	4.1	460	
416	100	--	--	760	4	--	458	Sample crusty at end; No change in shape
421	100	--	--	760	4	--	455	Sample "soaked" in 100% oxygen gas
422	100	--	--	760	4	--	462	for 30 days.
404	100	--	--	569	3.2	4	463	
407	100	--	--	569	3.2	4	472	
410	100	--	--	362	1.9	4	480	Glow, no flame
413	100	--	--	259	1.3	4	540	
423	100	--	--	259	1.3	--	470	
402	60	40	--	760	4.0	4.1	462	
405	60	40	--	569	3.2	4	480	
418	60	40	--	569	3.2	4	470	
411	60	40	--	362	1.9	5	540	Glow, no flame
403	20	80	--	760	4	5	545	Glow, no flame
417	20	80	--	760	4	--	535	Glow, no flame
406	20	80	--	569	3.2	4	No ignition	
412	20	80	--	362	1.9	--	No ignition	Slight exothermic reaction
420	20	80	--	362	1.9	--	No ignition	
414	60	40	--	259	1.3	--	No ignition	
415	20	80	--	259	1.3	--	No ignition	
408	60	--	40	569	3.2	5	475	
419	60	--	40	569	3.2	--	485	
409	20	--	80	569	3.2	3.5	552	Glow, no flame

TABLE X. SPONTANEOUS IGNITION TEMPERATURE OF MIL-C-7219 TYPE III NYLON FABRIC
DIMENSIONS: 14 PIECES OF 1" SQUARES

Run No.	Atm. Composition (%)			Pressure (mm Hg)	Flow Rate (l/min)	Heating Rate	S.I.T. °C	Remarks
	O_2	N_2	He					
501	100	--	--	760	4	7.5	392	
519	100	--	--	760	4	7.0	414	Aged 30 days in 100% O_2
520	100	--	--	760	4	7.5	420	Aged 30 days in 100% O_2
504	100	--	--	569	3.2	5.0		Second ignition at 430 °C
507	100	--	--	569	3.2	10.0	402	
510	100	--	--	362	1.9	--	No ignition	
502	60	40	--	760	4	8	412	Had second flame at 448 °C
505	60	40	--	569	3.2	5	502	
517	60	40	--	569	3.2	4	508	Had double glow, second at 500 °C
511	60	40	--	362	1.9	3.5	502	Had no flame, only "glow"
510A	100	--	--	362	1.9	11	430	
515	100	--	--	259	1.3	--	No ignition	
514	60	40	--	259	1.3	--	No ignition	
503	20	80	--	760	4	--	No ignition	Sample reduced to carbon
516	20	80	--	760	4	--	No ignition	
518	20	80	--	569	3.2	--	No ignition	Black film on tray
506	20	80	--	569	3.2	--	No ignition	All samples consumed, carbon trace
512	20	80	--	362	1.9	--	No ignition	Black residue in system
508	60	--	40	569	3.2	5	495	Glow, no flame
509	20	--	80	569	3.2	--	No ignition	Sample consumed, carbon trace remains

TABLE XII. SPONTANEOUS IGNITION TEMPERATURE OF 7400 DACRON FABRIC
DIMENSIONS: 19 PIECES, EACH 1" x 1" SQUARES

Run No.	Atm. Composition (%)			Pressure (mm Hg)	Flow Rate (l/min)	Heating Rate °C/min	S.I.T. °C	Remarks
	O_2	N_2	He					
601	100	--	--	760	4	8	448	
604	100	--	--	569	3.2	5.5	488	
604A	100	--	--	569	3.2	7.5	468	Second ignition at 492°C
607	100	--	--	569	3.2	5	500	
610	100	--	--	362	1.9	6	610	
613	100	--	--	259	1.3	--	No ignition	
617	100	--	--	760	4	--	432	O_2 soaked 30 days
616	100	--	--	760	4	--	438	O_2 soaked 30 days
602	60	40	--	760	4	6.5	468	
605	60	40	--	569	3.2	6.5	508	Also 512 and 515. This is due to "stacking" of sample
603	20	80	--	760	4	--	No ignition	
606	20	80	--	569	3.2	--	No ignition	
608	60	--	40	569	3.2	--	No ignition	

TABLE XIV. SPONTANEOUS IGNITION TEMPERATURE OF ORLON FABRIC
DIMENSIONS: 9 PIECES OF 1" SQUARES

Run No.	Atm. Composition (%)			Pressure (mm Hg)	Flow Rate (l/min)	Heating Rate $^{o}C/min$	S.I.T. ^{o}C	Remarks
	O_2	N_2	He					
701	100	--	--	760	4	5	518	Quite a spread in values.
701A	100	--	--	760	4	6.5	560	Most likely due to degree of compaction.
704	100	--	--	569	3.2	5	590	
710	100	--	--	362	1.9	3	660	Glow only, no flame
713	100	--	--	259	1.33	--	No ignition	
716	100	--	--	760	4	3.5	515	Soaked in O_2 - 30 days,
717	100	--	--	760	4	5	500	No apparent effect on S.I.T.
702	60	40	--	760	4	5	600	
705	60	40	--	569	3.2	5	568	Glow
703	20	80	--	760	4	--	No ignition	
715	20	80	--	259	1.4	--	No ignition	
708	60	--	40	569	3.2	2	580	Red glow only

TABLE XX. BURNING RATE OF POLYETHYLENE IN VARIOUS AMBIENT ATMOSPHERES AND AT VARIOUS PRESSURES IN ABSENCE OF EXTINGUISHANTS

Run No.	Atm. Composition (%)			Pressure (mm Hg)	Time to Ignition	Variac Setting	Watt-Sec.	% of Standard	Time to 1" Line From Ignitor on - Sec.	Time to 6" Line (From 1" Line) - Sec.	Burning Rate- In/Sec	Remarks
	N_2	O_2	He									
SN-64-1	80	20	--	745	35	80	1120	100	--	--	--	Standard run
SN-64-2	80	20	--	745	30	80	960	100	--	--	--	Standard run
				Standard is 32.5 sec. @ 1040 watt-sec.								
SN-64-3	--	100	--	259	11.5	80	368	35.38	12.4	37.9	0.132	
SN-64-4	--	100	--	259	--	80	--	--	--	--	--	*
SN-64-5	--	100	--	259	8.5	80	272	26.15	19.2	31.0	0.161	Flame dripped
SN-64-6	--	100	--	259	--		Faulty Ignitor		--	--	--	
SN-64-7	--	100	--	259	11.9	80	380.8	36.62	23.5	39.6	0.126	Flame dripped
				Average ignition time:			10.6 sec.		Average burning rate:		0.139	
				Average % standard:			32.71%					
SN-64-8	--	100	--	517	13.2	80	42.2	40.58	21.5	23.7	0.211	
SN-64-9	--	100	--	760	12.3	80	393.6	37.85	17.1	18.6	0.269	Sparks
SN-64-10	40	60	--	259	29.7	80	950.4	91.38	44.9	54.8	0.091	Flame dripped
SN-64-11	40	60	--	517	16.9	80	540.8	52.00	29.2	48.1	0.104	
SN-64-12	40	60	--	760	11.9	80	380.8	36.62	21.5	38.1	0.131	
SN-64-13	--	60	40	259	37.8	80	1209.6	116.3	46.8	50.5	0.099	
SN-64-14	--	60	40	517	20.8	80	665.6	64.0	25.1	39.1	0.128	
SN-64-15	--	60	40	760	14.1	80	451.2	43.38	21.5	23.9	0.209	

* No ignition, faulty ignitor.

TABLE XXI. BURNING RATE OF 7400 DACRON FABRIC IN VARIOUS AMBIENT ATMOSPHERES AND AT VARIOUS PRESSURES IN ABSENCE OF EXTINGUISHANT

Run No.	Atm. Composition (%)			Pressure (mm Hg)	Time to Ignition Sec.	Watts	Watt-Sec.	% of Standard	Time to 1" Line From Igniter on - Sec.	Time to 6" Line (From 1" Line) - Sec.	Burning Rate-In/Sec.	Remarks
	O_2	N_2	He									
SN-64-16	20	80	--	740	10.2	44	448.8	--	6.9	11.6	0.423	Standard run
SN-64-17	20	80	--	740	10.8	44	475.2	--	6.3	11.9	0.420	Standard run
Average watt sec = 462, taken as standard for this series.												
SN-64-18	100	--	--	259	8.5	44	374	80.91	1.2	3.8	1.31	Dripped flame
SN-64-19	100	--	--	259	9.0	44	396	85.71	1.2	3.5	1.42	
SN-64-20	100	--	--	517	8.5	44	374	80.91	0.72	3.3	1.51	
SN-64-21	100	--	--	760	7.5	44	330	71.43	2.3	2.2	2.27	
SN-64-26	60	--	40	259	4.6	72	331.2	71.68	1.5	5.8	0.862	
SN-64-24	60	--	40	517	4.0	72	288	62.33	1.5	3.2	1.56	
SN-64-25	60	--	40	760	4.7	72	338	73.15	0.66	4.2	1.19	
SN-64-27	60	40	--	259	9.6	44	422.4	91.42	1.3	6.3	0.79	
SN-64-28	60	40	--	517	10.2	44	448.8	97.14	1.2	4.4	1.14	
SN-64-29	60	40	--	760	9.3	44	409.2	88.57	1.1	3.7	1.35	Dripped flame
SN-64-30	20	80	--	740	10.6	44	466.4	--	5.1	10.5	0.476	Treat as standard
SN-64-31	20	80	--	517	14.2	44	624.8	135.2	6.7	12.0	0.416	
SN-64-32	20	80	--	259	18.3	44	805.2	174.3	9.7	16.4	0.305	Very smokey

TABLE XXII. BURNING RATE OF MIL-C-7219, TYPE III NYLON FABRIC IN VARIOUS ATMOSPHERES AND AT VARIOUS PRESSURES IN ABSENCE OF EXTINGUISHANT

Run No.	Atm. Composition (%)			Pressure (mm Hg)	Time to Ignition Sec.	Watts	Watt-Sec.	% of Standard	Time to 1" Line From Ignitor on - Sec.	Time to 6" Line (From 1" Line) - Sec.	Burning Rate-In/Sec.	Remarks
	O_2	N_2	He									
SN-64-33	20	80	--	740	7.4	72	532.8	--	7.4	6.5	0.173	*
SN-64-34	20	80	--	740	6.1	72	444.2	--	11.1	32.4	0.154	Flame drippe
SN-64-46	20	80	--	740	7.0	72	504	--	5.0	30.0	0.166	
				Average watt sec. = 493.6, take as standard value.								
SN-64-35	100	--	--	760	5.4	72	388.2	78.65	1.6	4.9	1.02	
SN-64-36	100	--	--	517	5.7	72	410.4	83.64	1.7	5.6	0.89	
SN-64-37	100	--	--	155	8.0	72	576	116.5	3.4	10.7	0.47	
SN-64-38	100	--	--	259	7.4	72	532.8	100.0	2.1	6.7	0.75	Drip flame
SN-64-39	60	40	--	760	7.0	72	504	102.1	2.3	7.8	0.64	Drip flame
SN-64-40	40	60	--	517	8.0	72	576	116.5	2.9	13.9	0.36	Drip flame
SN-64-41	60	40	--	517	6.1	72	444.2	90.0	2.8	9.7	0.51	
SN-64-42	60	40	--	259	7.6	72	547.2	110.9	2.5	11.2	0.45	Drip flame
SN-64-43	60	--	40	760	7.0	72	504	102.1	--	6.0	1.00	
SN-64-44	60	--	40	517	8.0	72	576	116.5	--	8.0	0.75	
SN-64-45	60	--	40	259	8.0	72	576	116.5	--	10.0	0.60	
SN-64-47	20	80	--	517	8.0	72	576	116.5	7.0	40.0	0.125	
SN-64-49	20	80	--	259	--	--	--	--	--	--	---	No ignition

* Flame out 1-1/8" over base.

END OF REFERENCE

47

REFERENCE

48

KLINE, H. F.: A STUDY OF IGNITION POINT VALUES OF NON-METALLIC MATERIALS IN SIMULATED SPACECRAFT ENVIRONMENT. SCI. ADVANCED MATER. PROC. ENG. SER., VOL. 11, 1967.

Society of Aerospace Material and Process Engineers

Science of Advanced Materials and Process Engineering Proceedings

VOLUME 11

THE EFFECTS OF THE SPACE ENVIRONMENT ON MATERIALS

11TH NATIONAL SYMPOSIUM
AND EXHIBIT

Chase-Park Plaza Hotel – St. Louis
April 19–20–21, 1967

A STUDY OF IGNITION POINT VALUES OF NONMETALLIC MATERIALS IN SIMULATED SPACECRAFT ENVIRONMENT

by

H. F. Kline

Structures and Mechanics Division
National Aeronautics and Space Administration
Manned Spacecraft Center
Houston, Texas

ABSTRACT

A thermogravimetric analyzer combined with a photoelectric cell has been employed to study the thermal stability of elastomeric materials and to determine their ignition points in a pure oxygen environment at 5 psia pressure. Results show that elastomer ignition points can be determined reproducibly within 4° C. In addition, the loss of volatile materials by elastomers during heating can be monitored up to the ignition point. The method appears to be suitable for the characterization of elastomeric materials in oxygen atmospheres; this is illustrated by tests with a fluoro elastomer, a polyvinyl chloride, and a polyisoprene. It is proposed that this method be adopted as a standard for the elimination of conflicting results from laboratory to laboratory.

1. INTRODUCTION

The evaluation of the thermal stability of nonmetallic materials is of major concern in the construction of spacecraft. This concern deepens as the lengths of flight times increase. Relatively little data are available on ignition points of nonmetallic materials, and there is poor correlation of available data.

The poor sensitivity and the lack of reproducibility in previously employed methods for determining ignition points have been largely responsible for the lack of information on nonmetallic materials used in simulated spacecraft environments. To date, the life environment condition has been based on aviators breathing oxygen at 5 psia.

It might be concluded that an absolute value does not exist in regard to the ignition point of a material. Most so-called ignition-point values give only the relative numerical rankings of materials considered under a specific laboratory conditions; comparison of values on a material is exceedingly difficult in passing from one laboratory to another. The inescapable conclusion is that certain procedures have inherent errors which make reproducibility almost impossible in ignition-point testing.

2. EVALUATION OF COMMON IGNITION-POINT DETERMINATION METHODS

In considering some of the usual methods used in determining these ignition values, first, figure 1 shows one of the common types of test fixtures. This type of equipment is usually placed in a bell jar,

or other type of chamber, containing the required environment. Electric power is applied to the nichrome heater wire to supply heat to the specimen surface. The ignition value is determined by using thermocouples embedded in the specimen surface.

The errors observed in the operation of this type of equipment are varied. As an example, the coils must be evenly spaced and the material must be located at the same position relative to the coil on each test; otherwise, the values obtained do not correlate from test to test.

Further, the temperature rise of the thermocouple, caused by the heat from the heater coil, is greater than the temperature increase of the material surface because of different thermal properties. Therefore, unless the coil temperature is raised very slowly to allow for thermocouple-sample temperature equilibration, the temperature shown by the thermocouple is greater than the actual surface value. If the thermocouples are embedded in the interior of the material, they are insulated from the source of heat, and the values obtained are not representative of the actual temperature of the material surface. Another necessary precaution to insure very accurate results is that the size and shape of the samples must be the same for the duplication of test results.

A more sophisticated approach requires equipment of the type shown in figure 2.[1] The heat source of this item is a dc arc between two carbon electrodes. This heat energy is focused on the specimen by reflections from mirrors A and B. A weight is attached to the specimen; the burning through of its suspension material releases the weight allowing it to strike on a microswitch, accurately marking the burn-through time. A multiple-filter system controls the heat incident upon the specimen.

This system lends itself to testing in air. In pure oxygen environments it has obvious disadvantages. The system must be placed in a well-insulated chamber to maintain the thermal environment. When this is done the controls become cumbersome. Further, the operation of a carbon arc within a pure oxygen atmosphere is a hazardous operation.

An even more complicated device is shown in figure 3.[2] The oxygen gas used in this testing device is preheated. Heavy metal is usually required for the construction of this apparatus. Again, the main objection to this type of apparatus is the use of thermocouples in contact with the specimen. Results with this type of apparatus have shown that tested samples act as heat sinks for thermocouples, giving misleading results. Assuming that it is possible to counteract the heat-sink effect by the use of extremely fine thermocouples, the use of a surface-contact thermocouple is objectionable because it senses only a limited area of a material that frequently is relatively nonhomogeneous. Further, the observation of results is visual and leads to the possibility of human error.

Anyone who has worked in this field may recall other schemes or systems which have been used to determine ignition points. Only a few of the more common ones are presented for the purpose of illustration.

3. THERMOGRAVIMETRIC ANALYSIS METHOD

Considerable time has been spent in developing a method for determining meaningful ignition values. This technique is basically a thermogravimetric analysis (TGA) method. For discussion purposes, thermogravimetry is defined as a continuous measurement of the weight or change in weight of a specimen as it is subjected to a temperature program. This change in weight is continuously recorded. The determination of thermal profiles by TGA of nonmetallic materials, particularly polymers, is becoming increasingly more common. However, certain meritorious modifications have been made in the TGA equipment.

Figure 4 outlines the equipment in schematic form. The apparatus is a modified Thermo-Grav.[a] It consists of a precise spring balance enclosed in a glass sample chamber. It may be operated at programed temperatures in almost any noncorrosive gaseous environment either at 1 atmosphere or at

[a]Thermo-Grav is a Trade Mark of the American Instrument Co., Inc., 8030 Georgia Avenue, Silver Spring, Maryland.

reduced pressures. Spring deflections proportional to changes in sample weight are converted into electrical signals by movement in the transducer coil. These signals are presented as weight changes on the Y-axis of an XY recorder. The X-axis of the recorder senses an input which is related to the sample chamber temperature.

A photoelectric cell focused on the sample tube has been added to the above standard equipment. This photoelectric cell senses any flash or flame within the sample chamber, and this signal is sensed by a second recorder. Spark needles of nichrome wire are mounted as closely as possible to the sample without interfering with the weight-loss mechanism. The specimen is either mounted on a glass holder or in a crucible as shown. The sample chamber is purged, then filled with the gas or gas mixture required by the test. Furnace heating power, sufficient to cause the internal gas temperature to rise, is applied.

Two recorders are used as indicated in the illustration. The first recorder plots the temperature of the sample chamber on the X-axis and the corresponding weight loss of the material on the Y-axis. The second recorder plots the temperature of the sample chamber on its X-axis exactly as the temperature scan on the first X-axis. The Y-axis of the second recorder plots any ignition light sensed by the photoelectric cell.

The flash point of a material will be detected by a discernible rise from an established baseline on the Y-axis of the second recorder. The fire point value will be indicated in the same manner by a sustained, discernible rise. These points can be expressed as temperature values.

4. EXPERIMENTAL RESULTS

To illustrate the operation, data obtained from specimens subjected to this method are shown in figures 5 to 16. Figure 5 illustrates a test of a fluorocarbon rubber compound which has been compounded for flame resistance. This figure relates the instant of ignition of this material to the temperature to which it has been subjected. Figure 6 shows the weight loss of the material with the abscissa of this graph synchronized with the abscissa of figure 5. Figure 7 shows the two graphs combined and indicates the relationship of the moment of ignition to the weight loss. The accepted theory relative to flammability of nonmetallic materials, particularly elastomers, is that flash points and ignition points are dependent upon loss of volatile materials and that the ignition of these volatiles is the basis of combustion of the given material. As illustrated, this system pinpoints the temperature at which combustion occurs for a given set of parameters. A more exact ignition value would be difficult to obtain.

In the same manner as in figure 5, figure 8 shows the relationship between the moment of ignition and the temperature. Figure 9 again shows the weight loss of the material. Figure 10 is a combined presentation of the graphs from the two recorders. Note the increased height of the ignition-point rises in figures 8 and 10 as compared with the rise in figure 5. As previously indicated, the compound for figure 5 was flame retarded; the polyvinyl chloride elastomers shown in figures 8, 9, and 10 were not flame retarded. Indications are that the intensity of the energy released can be rated by this method based on the relative height of the ignition peaks.

Figure 11 represents a highly flammable type of elastomer. Note the height of the ignition-point ordinate rise. Figure 12 is the corresponding weight loss, and figure 13 is the combined presentation. It would be possible to run this type of thermal analysis using a two-pen recorder. The work presented here was limited to the equipment available. Figures 15 and 16 are runs of the same material under the same parameters and are introduced to illustrate the reproducibility of the method. Note that the difference in ignition temperatures between the two runs is only 3° C.

5. PROBLEM AREAS

There are certain conditions that must be specified in the use of a photoelectric cell as a detector to record the ignition temperature of material specimens. The photoelectric cell used was calibrated in the middle of the visual light spectrum considering range and sensitivity. An example is given in figure 14. It shows that the signal intensity of the photoelectric cell is somewhat dependent upon the type of light emitted from the specimen when ignition occurs. The specimens emitting light in the

green, yellow, or red spectrum offer the easiest detection. The lower blue spectrum is difficult to detect with the standard photoelectric cell used in this work. Visual observation has shown that the use of two photoelectric cells would improve the accuracy of the suggested ignition-determination method. One could be used for the specific spectra not covered by the standard cell. This will be evaluated in an extension of this work.

Radiation at higher temperatures imposes a problem with photoelectric cells because of the sensitivity of photoelectric cells to heat radiation. This is manifested as noise on recorders, or as a drifting baseline. Thus, the photoelectric cell must be isolated from the furnace heat to maintain a level baseline and prevent signal distortion. The photoelectric cell used in this work was water-jacketed for cooling.

6. CONCLUSIONS

Ignition points obtained by this method can be closely related to the loss of volatiles by a given material while this material is being subjected to a programed heat input. In effect, a third point is established on a thermo-analytical graph or a thermal profile of any given nonmetallic material. The resulting thermal profile establishes a very meaningful view of the thermal stability of a given nonmetallic material.

Further, the thermogravimetric analyzer equipment used is standard and commercially available. Parameters can be closely controlled and varied. These last facts should lead to closer agreement in reported ignition values from laboratory to laboratory if this method is put into general use.

REFERENCES

(1) Thompson, D. C.; Hagman, J. F.; and Mueller, N. N.: Article prepared for Division of Rubber Chemistry, A.C.S. (New York, N.Y.), September 11, 1957.

(2) Development of Specifications for Testing Nonmetallic Materials for Use in Manned Spacecraft: R&D Department, General Dynamics/Electric Boat, Groton, Connecticut, Contract NAS 9-1629, for NASA/MSC.

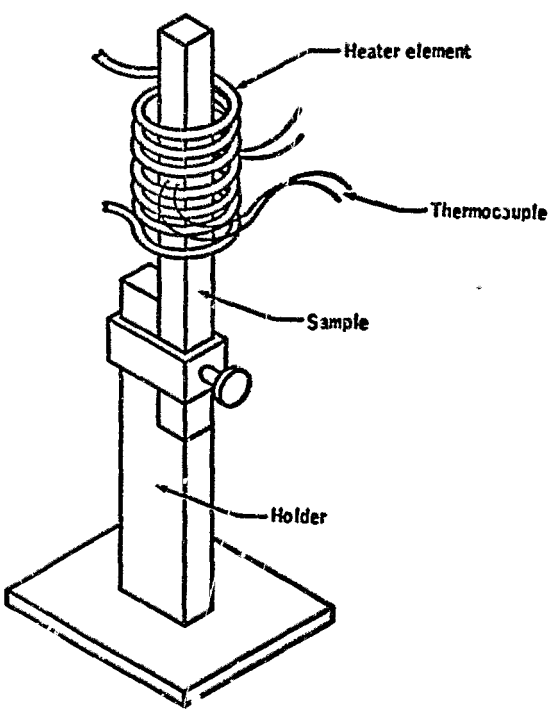

Figure 1. - Heater coil detail.

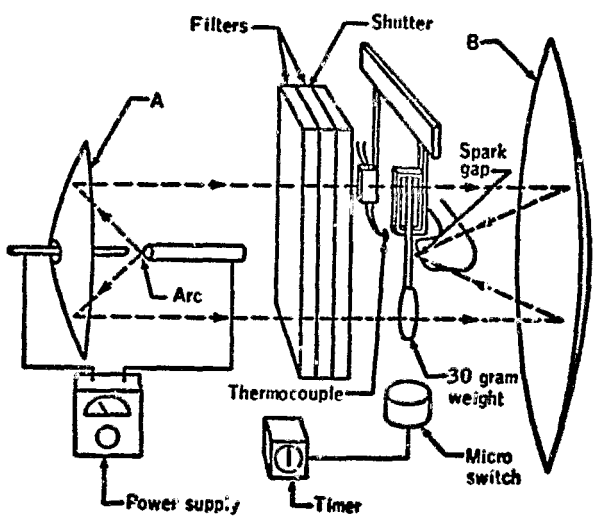

Figure 2. - A more sophisticated testing apparatus.

END OF REFERENCE

48

REFERENCE

49

STANDARD METHOD OF TEST FOR FLAMMABILITY OF PLASTICS USING THE OXYGEN INDEX METHOD. PART 27 OF ASTM ANNUAL STANDARDS: ASTM DESIGNATION D 2863-70, 1973.

THIS REFERENCE IS COPYRIGHTED MATERIAL AND THEREFORE THE CONTENTS HAVE NOT BEEN REPRODUCED FROM THE TEXT.

END OF REFERENCE

REFERENCE

50

STRADLING, J. S.: TEST PLAN, AEROSPACE SAFETY RESEARCH AND DATA INSTITUTE (ASRDI), IGNITION BY ELECTRICAL ARC. TP-WSTF-192, REV. A., JULY 31, 1973.

TP-WSTF-192
Revision A
July 31, 1973

Test Plan

Aerospace Safety Research and Data Institute

(ASRDI)

Ignition by Electrical Arc

Issued by

Laboratories Office

NASA Johnson Space Center

White Sands Test Facility

Prepared by: _____
Jack S. Stradling
Laboratory Manager

Approved by: _____
David L. Pippen
Chief, Laboratories Office

Approved by: _____
Frank E. Belles
Director, Aerospace Safety
Research & Data Institute

Ignition by Electrical Arc

Background

Since December 1971, WSTF has actively supported the ignition by electrical arc test effort as defined in Test Plan WSTF-192. A detailed review of the test data obtained to date was conducted on June 26, 1973. As a result of this review, several modifications to the test matrix and initial materials selection were required. The changes are hereby included in this test plan revision.

Introduction

This test provides a method of determining various metallic and nonmetallic materials' susceptibility to ignition in a 100 percent oxygen atmosphere when subjected to an electrical arc. This condition in actual systems can be realized when static electrical discharges, lightning, or electrical wiring shorts occur. The tests described herein are designed to simulate various material thicknesses, environmental temperatures and pressures, and arc energies under controlled laboratory conditions so that a measure of the safety hazards involved can be obtained.

Test Philosophy

The following variables will be considered in this study.

a. Temperature - Tests will be conducted at -250°F, 70°F and 500°F (nonmetallics) or 1000°F (metallics).

b. Pressure - Tests will be performed initially at 100, 1000 and 2000 psia. A limited number of tests will be conducted at 500 and 5000 psia.

c. Atmosphere - A 100 percent oxygen atmosphere will be established for all tests. Mil-O-27210C oxygen will be provided.

d. Arc current will be varied from 50 milliamperes to a maximum of 500 milliamperes in 50 milliampere steps.

e. Specimen configuration shall be as follows:

(1) Nonmetallics: 0.5-inch diameter circular discs, concentrically drilled with 3/32-inch diameter drill. Test thicknesses of 0.010 and 0.100 inch will be employed.

(2) Metallics: 0.25-inch diameter circular discs shall be mechanically attached to an electrode. Initial test thicknesses of 0.010 and 0.100 inch will be used. An optional thickness of 0.070 inch may be utilized.

Test Materials

Material types to be employed include nonmetallics and metallics. The materials and their order of test are as follows:

a. Teflon TFE

b. Viton

c. Vespel SP-21

d. Series 304 Stainless Steel

e. Series 6061-T6 Aluminum

Test Apparatus Description

A specially designed chamber is employed in this test. The chamber has provisions for installation of heating or cooling coils, a pressure-activated electrode separating mechanism, and feedthroughs for thermocouples, photoelectric devices, arc current and thermal conditioning.

Other equipment employed in the test includes a constant-current arc generator, a storage oscilloscope for display of the photoelectric cell responses, temperature and pressure instrumentation, and thermal control equipment.

Sample Preparation

Nonmetallic samples will be prepared in one-half inch diameter circular discs of the required thickness. Each sample will be concentrically drilled with a 3/32-inch diameter drill to permit a short circuit condition to be established between the electrodes (see Figure 1).

Metallic samples will be fabricated in one-quarter inch diameter circular discs, then mechanically attached to a fixed electrode (see Figure 1).

Each sample will be precision-cleaned after preparation. The present procedure used to prepare samples for gaseous oxygen impact tests will be used. After preparation, the materials will be placed in hermetically sealed polyethylene bags and handled with noncontaminating manipulators.

Test Sequence

a. The test chamber and associated hardware will be cleaned prior to each sample test.

b. The test material will be loaded into the test chamber, then the chamber will be assembled, purged, leak checked and pressurized with gaseous oxygen.

c. The required temperature and pressure will be obtained by utilizing the appropriate environmental conditioning equipment.

d. The electrical arc will be initiated by providing a "short circuit" current between the electrodes then mechanically separating the electrodes. The constant-current arc generator will provide a controlled two-second duration arc.

e. When sample ignition is observed, all data and observations will be recorded. The test chamber will be vented and any remaining test sample shall be removed and examined.

f. A minimum of four tests will be conducted at both the ignition and the nonignition thresholds. The two thresholds may span a range of several hundred milliamperes for repeatable ignition and nonignition values.

Reporting

Data and pertinent operational comments will be supplied upon completion of each material matrix. A final report will be prepared which summarizes the entire ignition by electrical arc test program within two months after test completion as defined by the included test matrix (see Table 1).

Distribution

	No. of Copies
RA/Manager	1
RC/Chief, Engineering Office	1
RD/Chief, Test Programs Office	2
RF/Chief, Laboratories Office	5
NH/Chief, Quality Assurance Office	1
ES5/R. L. Johnston	1
ES5/M. W. Steinthal	1
KT/T. P. Larkin	1
LA/Chief, Shuttle Program Office	1

	No. of Copies
Dyna/H. Fearing	1
Dyna/D. Whitaker	5
Documentation	13
NASA Aerospace Safety Research and Data Institute Attn: Messrs. F. Belles/P. Ordin 21000 Brookpark Road Cleveland, Ohio 44135	10

Card #12

Ignition by Electrical Arc Test Matrix

		Thickness (inches)			Pressure (psia)					Temperature (°F)			
Nonmetallics	0.003	0.010	0.070	0.100	100	500	1000	2000	5000	-250	70	500	1000
Teflon TFE	x	x		x	x	x	x	x	*	x	x	x	
Viton		x	x	x	x		x	x		x	x	x	
Vespel SP-21		x	x	x	x		x	x		x	x	x	
Metallics													
304 Stainless Steel		x	*	x	x		x	x	*	x	x		x
6061 Aluminum		x	*	x	x		x	x	*	x	x		x

* These tests are to be performed only if required after review of data obtained at other parameter values.

NOTE: Ignition threshold shall be determined in 50 milliamp increments or decrements to a maximum arc current of 500 milliamps. A minimum of four tests shall be conducted at both the ignition and the nonignition threshold.

Table 1

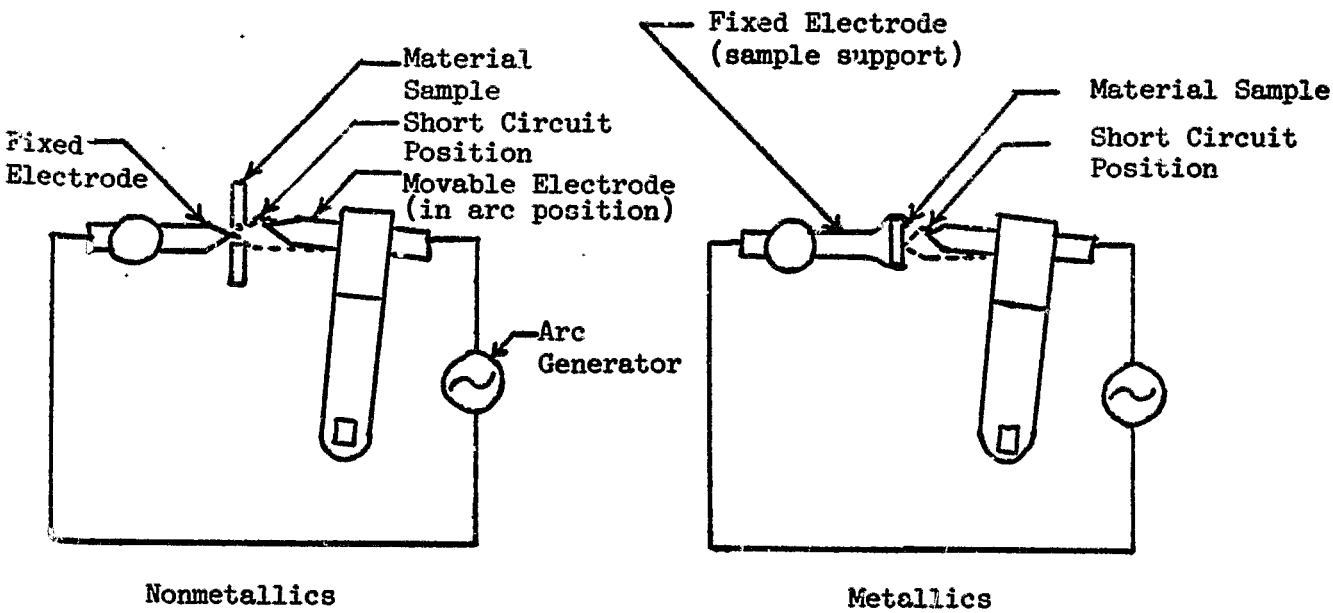
Material
Sample
Short Circuit
Position
Fixed
Electrode
Movable Electrode
(in arc position)
Arc
Generator
Nonmetallics
Fixed Electrode
(sample support)
Material Sample
Short Circuit
Position
Metallics

Figure 1

END OF REFERENCE

50

REFERENCE

51

HOWELL, G. A.; AND WEATHERS, T. M., EDS.: AEROSPACE FLUID COMPONENT DESIGNERS HANDBOOK. TRW SYSTEMS GROUP, 1970. VOL. I - REVISION D. AFRPL-TDR-64-25-VOL-1D; AD-874542.

RPL-TDR-64-25

AEROSPACE FLUID COMPONENT DESIGNERS' HANDBOOK

VOLUME I

Revision D

APPROVED FOR PUBLIC RELEASE; DISTRIBUTION UNLIMITED PER AFRPL LTR, 17 FEB 72, TAB, 72-10, PP.A17.

TECHNICAL DOCUMENTARY REPORT NO. RPL-TDR-64-25

FEBRUARY 1970

AIR FORCE ROCKET PROPULSION LABORATORY

RESEARCH AND TECHNOLOGY DIVISION

AIR FORCE SYSTEMS COMMAND

Edwards, California

PROJECT NO. 3058

Prepared Under

Contracts AF04(611)-8385,
AF04(611)-11316,
F04611-67-C-0062, and
F04611-68-C-0065
by

TRW
SYSTEMS GROUP

RPL-TDR-64-25

COPY NO. 086

AEROSPACE FLUID COMPONENT DESIGNERS' HANDBOOK

VOLUME I

Revision D

TRW SYSTEMS GROUP
One Space Park
Redondo Beach, California

Glen W. Howell
Terry M. Weathers
Editors

Notice: This document is subject to special export controls and each transmittal to foreign governments or foreign nationals may be made only with prior approval of AFRPL (RPPR-STINFO), Edwards, California 93523.

FEBRUARY 1970

Prepared for
AIR FORCE ROCKET PROPULSION LABORATORY
RESEARCH AND TECHNOLOGY DIVISION
AIR FORCE SYSTEMS COMMAND
Edwards, California

Contract Number AF 04(611)-8385
AF 04(611)-11316
F04611-67-C-0062
F04611-68-C-0065

APPROVED FOR PUBLIC RELEASE; DISTRIBUTION UNLIMITED PER AFRPL LTR, 17 FEB 72, TAB, 72-10, PP.A17.

AEROSPACE FLUID COMPONENT DESIGNERS' HANDBOOK

© Copyright 1970 by
TRW Systems Group, TRW Inc.
All rights reserved

First Issue: MAY 1964
Revised: OCTOBER 1965
Revised: MARCH 1967
Revised: NOVEMBER 1968
Revised: FEBRUARY 1970

Qualified requesters may obtain copies of this report from the
Defense Documentation Center (DDC), Cameron Station
Alexandria, Virginia

TABLE OF CONTENTS

FOREWORD

ACKNOWLEDGEMENTS

ABSTRACT

Section

1.0 INTRODUCTION

2.0 HEAT TRANSFER

3.0 FLUID MECHANICS

4.0 FLUID SYSTEMS

5.0 FLUID COMPONENTS

6.0 MODULES

7.0 DYNAMIC ANALYSIS OF FLUID COMPONENTS

8.0 COMPUTERS

9.0 SPECIFICATIONS

10.0 CONTAMINATION AND CLEANING

11.0 RELIABILITY

12.0 MATERIALS

13.0 ENVIRONMENTS

14.0 STRESS ANALYSIS

15.0 COMPONENT TESTING

16.0 FLUIDICS

APPENDIX A – ENGINEERING DATA and CONVERSION FACTORS

APPENDIX B – REVISION RECORD

BIBLIOGRAPHY

INDEX

FOREWORD

This handbook is the result of a program which was originated to document state of the art information on aerospace fluid component technology. The program consists of compiling, organizing, and editing basic information concerning the design and selection of aerospace fluid components. The program was initiated in June 1962, and has been conducted under contract by TRW Systems Group (formerly TRW Space Technology Laboratories), Science and Technology Division, for the Air Force Rocket Propulsion Laboratory, Air Force Systems Command. Mr. Jack G. Hartley succeeded Captain John L. Feldman who succeeded Messrs. Roy A. Silver and James R. Lawrence as the Air Force Program Manager. Mr. Terry M. Weathers succeeded Mr. Glen W. Howell as the Project Manager directing the program at TRW Systems Group, Although Mr. Howell retained overall responsibility for the handbook program as Manager of the Fluid and Electrical Systems Department. Subsequent editions of the handbook will be published and updated in a new format as part of the Air Force Design Handbook (DH) series. The handbook, to be identified as AFSC DH 3-6, Fluid Components, will be published and distributed by the Design Handbooks Branch (ASNPS-40), Aeronautical Systems Division, Wright-Patterson AFB, Ohio 45433.

A first edition of this new handbook will be available about mid-1970 (see subsection 1.7).

SPECIAL NOTICE

Subsequent Editions of This Handbook will Appear in a New Format as Explained in the Foreword Above.

ISSUED FEBRUARY 1970
SUPERSEDES NOVEMBER 1968

5.11 QUICK-DISCONNECT COUPLINGS

5.11.1 INTRODUCTION

5.11.2 WHEN TO USE QUICK-DISCONNECT COUPLINGS

5.11.3 QUICK-DISCONNECT SELECTION FACTORS

5.11.3.1 General

5.11.3.2 Valve Configurations

5.11.3.3 Body Materials and Seals

5.11.3.4 Locking Devices

5.11.4 COMMON TYPES OF QUICK-DISCONNECT COUPLINGS

5.11.4.1 Plain Quick-Disconnect Couplings

5.11.4.2 Single Valve Quick-Disconnect Couplings

Single Poppet Quick-Disconnect Couplings

Single Sleeve Quick-Disconnect Coupling

5.11.4.3 Double Valve Quick-Disconnect Coupling

Double Rotating Ball Quick-Disconnect Coupling

Double Poppet (Drilled) Quick-Disconnect Coupling

Double Poppet (Solid) Quick-Disconnect Coupling

Tube-Sleeve and Poppet Quick-Disconnect Coupling

5.11.1 Introduction

A quick-disconnect coupling consists of a male plug and a female socket with a locking device for rapid connecting and disconnecting of fluid lines. The coupling or de-coupling operation normally requires less than one second time and is executed by a simple slide and/or rotary motion of the coupling ring.

In this Sub-Section the basic types of quick-disconnect couplings are described and compared, and cross-sectional drawings are presented to illustrate their construction and operation. In addition, factors to consider in choosing materials, seals, and locking devices are discussed.

5.11.2 When to Use Quick-Disconnect Couplings

Quick-disconnect couplings are used in hydraulic, pneumatic, storable propellant, and cryogenic systems, when one or more of the following conditions prevail:

Ease of installation is required
Rapid connecting and disconnecting is required
Filling or draining of lines is to be eliminated
The entry of contamination is to be prevented
Fluid components are frequently removed for repair or replacement
Breakaway connections are required
Remote disconnecting of fluid lines is required

5.11.3 Quick-Disconnect Selection Factors

5.11.3.1 GENERAL. The selection of a quick-disconnect coupling involves determining the valve configuration best suited, the body materials and seals compatible with the system characteristics, and the locking device capable of withstanding the required number of operations, adaptable to remote disconnection, and operable in the required space envelope.

5.11.3.2 VALVE CONFIGURATIONS. The "Quick-Disconnect Coupling Selection Diagram" in Figure 5.11.3.2a is a flow diagram intended to serve as a guide in selecting valve configurations for fluid quick-disconnect coupling applications. Three parameters are considered in construction of the diagram in the order of their importance: self-sealing features, air inclusion and fluid loss, and pressure drop. Each parameter is discussed below:

Self-Sealing Requirements. Based on system requirements, self-sealing of both ends of the disconnected line may be mandatory, required for one end only, or may be unnecessary for either disconnected end. When the requirement is established, the field of coupling configurations is narrowed to a few types, differing principally in the valve arrangement (Figure 5.11.3.2a).

Air Inclusion and Fluid Loss During Connecting and Disconnecting. The air inclusion and fluid loss characteristics apply only to self-sealing, double valved couplings where a discrete volume of air is trapped within the coupling during connecting, and an equivalent volume of fluid is lost during disconnecting. This results in air being forced into the system during coupling and fluid being lost during coupling. Typical values for these characteristics for one-half inch tube size quick-disconnect couplings are presented in the "Fluid Quick-Disconnect Characteristic Chart" in Table 5.11.3.2. Additional fluid is lost in disconnecting due to leakage past the valves during closing. This quantity will depend upon such factors as fluid properties, fluid temperature, fluid pressure, valve closure rate, wear, and valve seal design. This additional leakage can be determined accurately by test, and must be added to the trapped volume to determine the total fluid loss.

Quick-Disconnect Coupling Pressure Drop. The pressure drop across a quick-disconnect coupling is determined by the shape of the flow path through the coupling, the fluid flow rate, and the fluid properties. The flow-path differs markedly between the various types of valve designs (Fig-

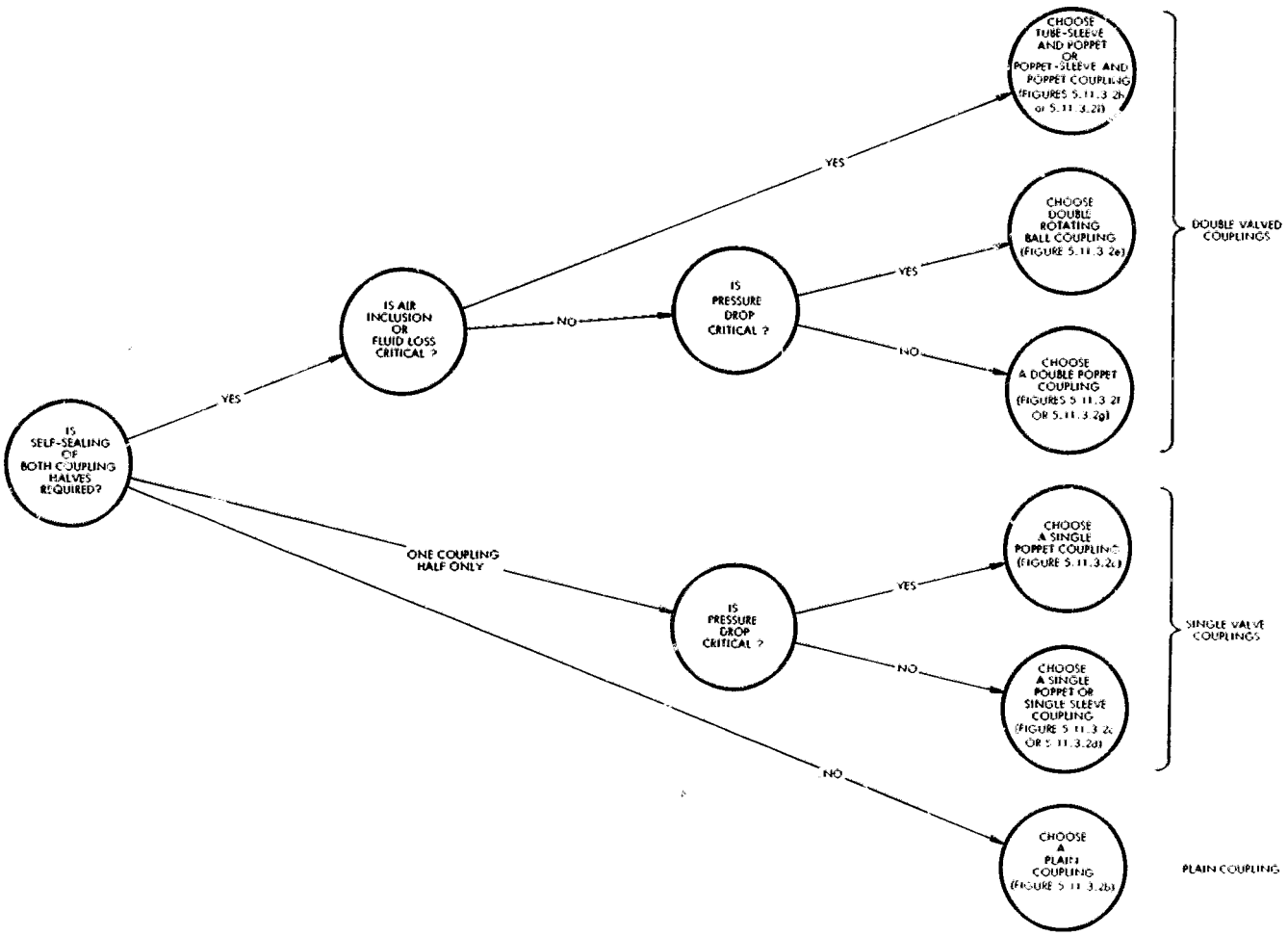

Figure 5.11.3.2a. Quick-Disconnect Couplings Selection Diagram

Table 5.11.3.2. Fluid Quick-Disconnect Comparison Chart

QUICK-DISCONNECT CONFIGURATION	FIGURE	SELF-SEALING		TYPICAL SIZE RANGES AVAILABLE TUBING O.D. (in.)	
		BOTH COUPLING HALVES	ONE COUPLING HALF ONLY	MINIMUM	MAXIMUM
Plain	5.11.3.2b			1/4	6
Single poppet	5.11.3.2c		X	1/4	6
Single sleeve	5.11.3.2d		X	1/4	3/4
Double rotating ball	5.11.3.2e	X		1/4	2
Double poppets (drilled)	5.11.3.2f	X		1/4	2
Double poppets (solid)	5.11.3.2g	X		1/4	6
Tube-sleeve and poppet	5.11.3.2h	X		1/4	1-1/4
Stem-sleeve and poppet	5.11.3.2i	X		3/16	2-1/2

QUICK-DISCONNECT CONFIGURATION	LOCKING ACTION			TYPICAL CHARACTERISTICS FOR ONE-HALF INCH TUBE SIZE		
	ROTARY	ROTARY AND PUSH-PULL	PUSH-PULL	PRESSURE DROP, psi AT 6 GPM MIL-H-5606 AT 60F	VOLUME TRAPPED DURING CONNECTING OR DISCONNECTING (cc)	WEIGHT (STEEL, 2000 PSI RATING) (lb)
Plain		X	X	0.6	NA*	0.5
Single poppet		X	X	3.4	NA*	0.6
Single sleeve			X	3.6	NA*	0.6
Double rotating ball	X			3.0	3.5	1.1
Double poppets (drilled)			X	3.3	5.8	1.7
Double poppets (solid)	X	X	X	4.8	3.3	0.8
Tube-sleeve and poppet			X	5.5	0.8	1.3
Stem-sleeve and poppet			X	6.0	0.03	1.2

*N.A: Not applicable

ures 5.11.3.2b through 5.11.3.2i), and also varies to some degree between different designs of the same valve type. The latter may be due to streamlining of poppets for reduced pressure drop, or reduction in flow area (for strengthening internal parts) causing increased pressure drop. For comparative purposes, typical pressure characteristics for one-half inch tube size couplings are presented in Table 5.11.3.2.

5.11.3.3 BODY MATERIALS AND SEALS. The selection of body materials and seals is dependent upon the following factors:

System Fluid and Temperatures. Materials commonly used for coupling bodies are steel, stainless steel, aluminum, and brass. Other body materials used for special application include plastics, bronze alloys, titanium, Monel, and copper. Seal materials commonly used in quick-disconnect couplings are the natural and synthetic rubbers, Teflon and Teflon products, and metals. Which of the above or other materials is chosen is based on fluid-material compatibility, a subject to be included in Section 12.0, "Materials."

System Pressure. The system pressure dictates the coupling's strength requirement, which is a function of the yield strength and thickness of the stressed materials. The material thicknesses in turn affect the coupling weight, pressure drop, and size. The material chosen is of such strength that the thicknesses of the stressed parts do not

result in excessive weight, restricted flow causing excessive pressure drop, or excessive space. This is significant in that an unrealistic restriction on weight, size, or pressure drop will result in unwarranted compromising of the other factors and/or the body material.

5.11.3.4 LOCKING DEVICES. Locking devices have two functions to perform: to lock the plug and socket together, and to hold the coupling valves open. The strength of the locking device is determined by the type of locking materials and the size and number of locking balls, threads, fingers, pins, or other devices incorporated within the socket which mate with a locking groove or slot in the plug. In selecting a locking device, other factors which are to be considered are number of required operating cycles while pressurized and depressurized; the mode of locking and unlocking; forces required to connect and disconnect; and space allowed for actuation of the locking device. Consideration should also be given to remote disconnection using pneumatics, squibs, or lanyards.

5.11.4 Common Types of Quick-Disconnect Couplings

5.11.4.1 PLAIN QUICK-DISCONNECT COUPLINGS. The plain, quick-disconnect coupling is an open, straight-through flow coupling without shutoff valves in the plug or socket. A typical plain coupling is shown in Figure 5.11.3.2b, which utilizes a cam ring, ball and groove device for locking, and an O-ring for sealing. The coupling is connected by mating the plug and socket and rotating the cam ring, forcing the balls radially into the plug groove. This action draws the coupling halves together, compressing the O-ring to achieve an external seal. The coupling is unlocked and disconnected by rotating the cam ring in the opposite direction (allowing the balls to move from the plug groove into the ball cage) and pulling the coupling halves apart.

5.11.4.2 SINGLE VALVE QUICK-DISCONNECT COUPLINGS. Two types are described:

Single Poppet Quick-Disconnect Coupling. The single poppet, quick-disconnect coupling consists of an open plug and a valved socket (Figure 5.11.3.2c). The mating parts are pushed together, first forming an external seal between the plug and socket. Further travel of the plug forces the poppet valve open, and retraction of the actuating ring confines the balls in the groove, locking the coupling halves. Disconnecting is accomplished by retracting the actuating ring and pulling the coupling halves apart.

Single Sleeve Quick-Disconnect Coupling. The single sleeve, quick-disconnect coupling consists of a valved socket and plain plug, (Figure 5.11.3.2d). Connecting is accomplished by mating the plug and socket, retracting the coupling ring, and pushing the coupling halves together. The outer diameter of the plug forms a seal with an O-ring on the inner diameter of the socket as the plug slides into the socket and opens the sleeve valve. When the valve is fully opened, the plug ball groove is aligned with the locking balls which drop into the groove. The coupling ring is then released, locking the coupling. The coupling is disconnected by retracting the coupling ring and pulling the plug and socket apart.

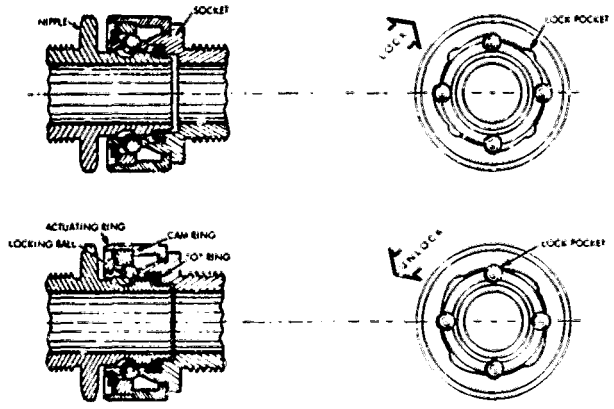

Figure 5.11.3.2b. Plain Quick-Disconnect Coupling
(Courtesy of Roylyn, Inc., Glendale, California)

5.11.4.3 DOUBLE VALVE QUICK-DISCONNECT COUPLINGS. Five types are discussed:

Double Rotating Ball Quick-Disconnect Coupling. The double rotating ball, quick-disconnect coupling consists of two coupling halves, each containing a ball valve, (Figure 5.11.3.2e). It is connected by mating the coupling halves and twisting the coupling ring. The coupling ring actuates a pinion gear, which rotates the ball valves to the open position. Disconnecting is accomplished by rotating the coupling ring, shutting the ball valves and unlocking the coupling.

Double Poppet (Drilled) Quick-Disconnect Coupling. The double poppet (drilled) quick-disconnect coupling consists of a plug and socket, each containing a drilled poppet valve, (Figure 5.11.3.2f). The mating parts are pushed together forming an external seal between the plug and socket. Further movement of the plug causes the poppet valves to butt against each other, opening the valves. When the poppet valves are in the full open position, the locking fingers snap into position forming a lock between the plug and socket. The coupling is disconnected by retracting the actuating ring and pulling the coupling halves apart.

Double Poppet (Solid) Quick-Disconnect Coupling. The double poppet (solid) quick-disconnect coupling (Figure 5.11.3.2g) consists of a plug and socket, each containing a solid poppet valve. The coupling halves are pushed together, first forming an external seal and next opening both poppet valves. Retraction of the coupling ring allows the balls to drop in the plug locking race. Release of the coupling ring confines the balls, locking the coupling halves together. Disconnecting is accomplished by retracting the coupling ring and pulling the coupling apart.

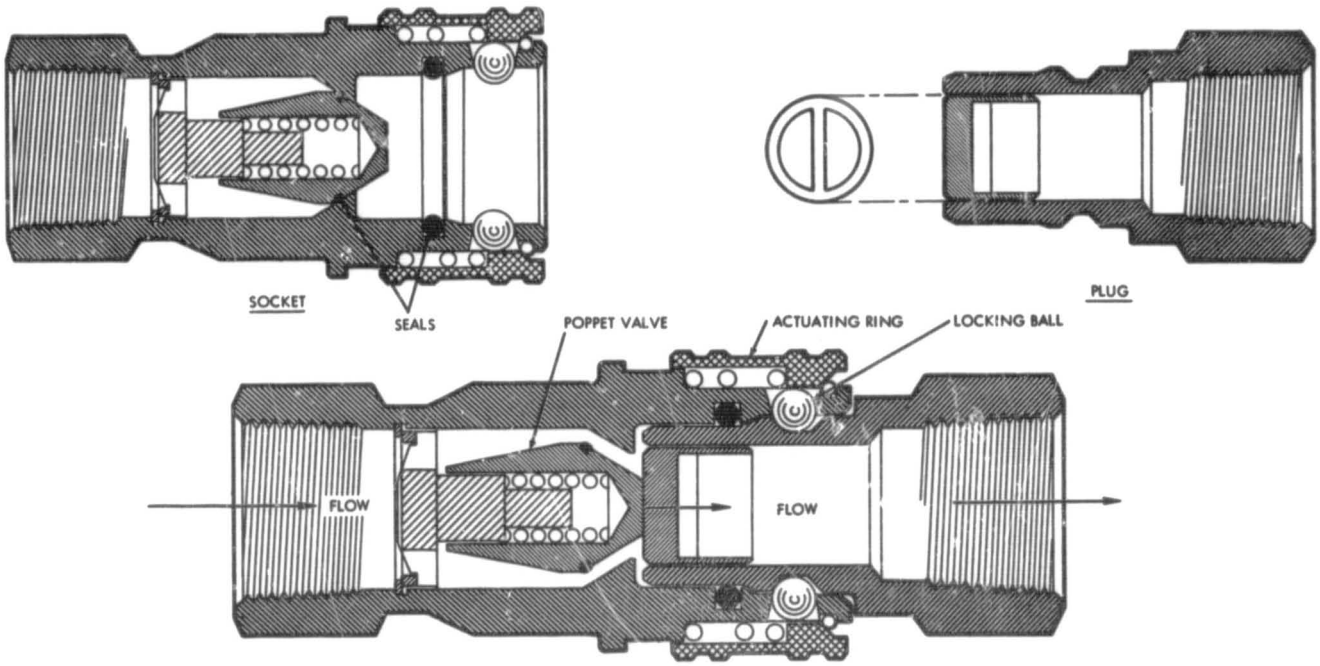

Figure 5.11.3.2c. Single Poppet Quick-Disconnect Coupling
(Courtesy of the Hansen Manufacturing Company, Cleveland, Ohio)

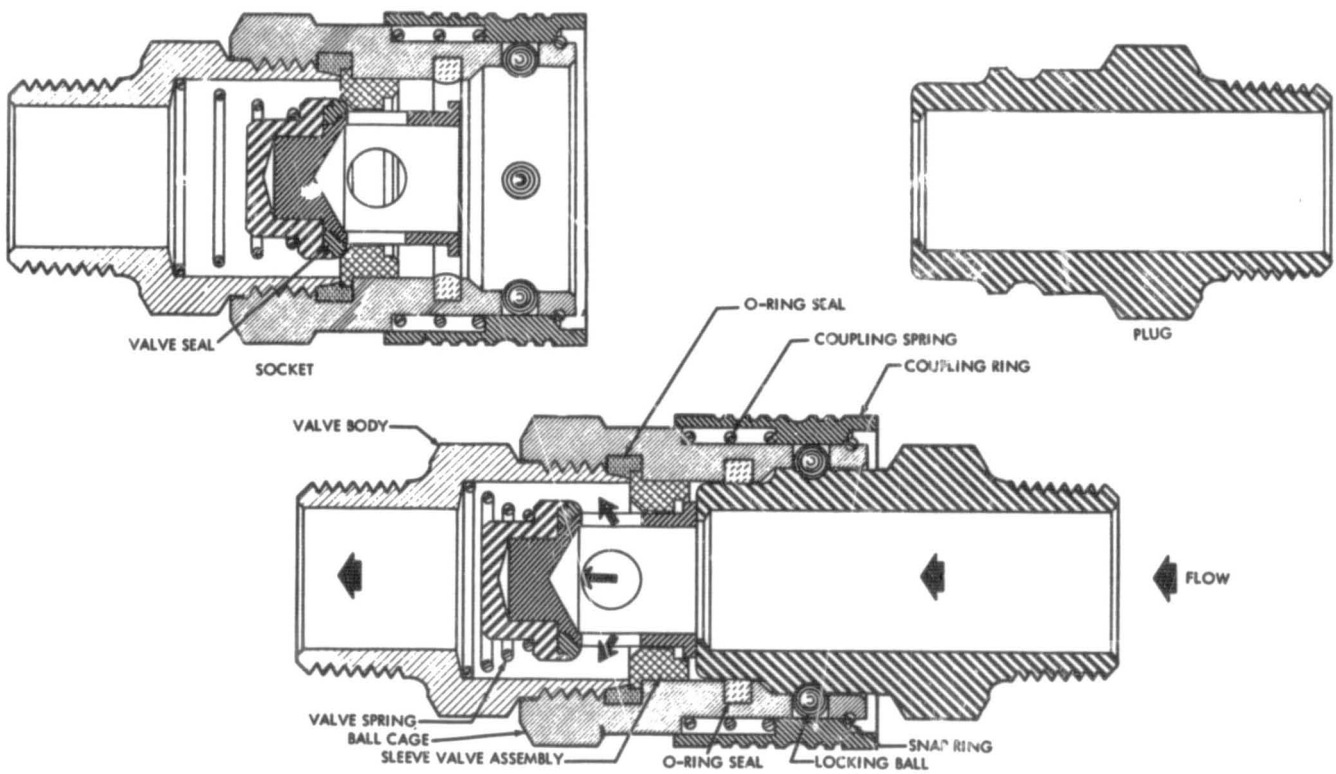

Figure 5.11.3.2d. Single Sleeve Quick-Disconnect Coupling
(Courtesy of Tru-Flate, Inc., Oakland, California)

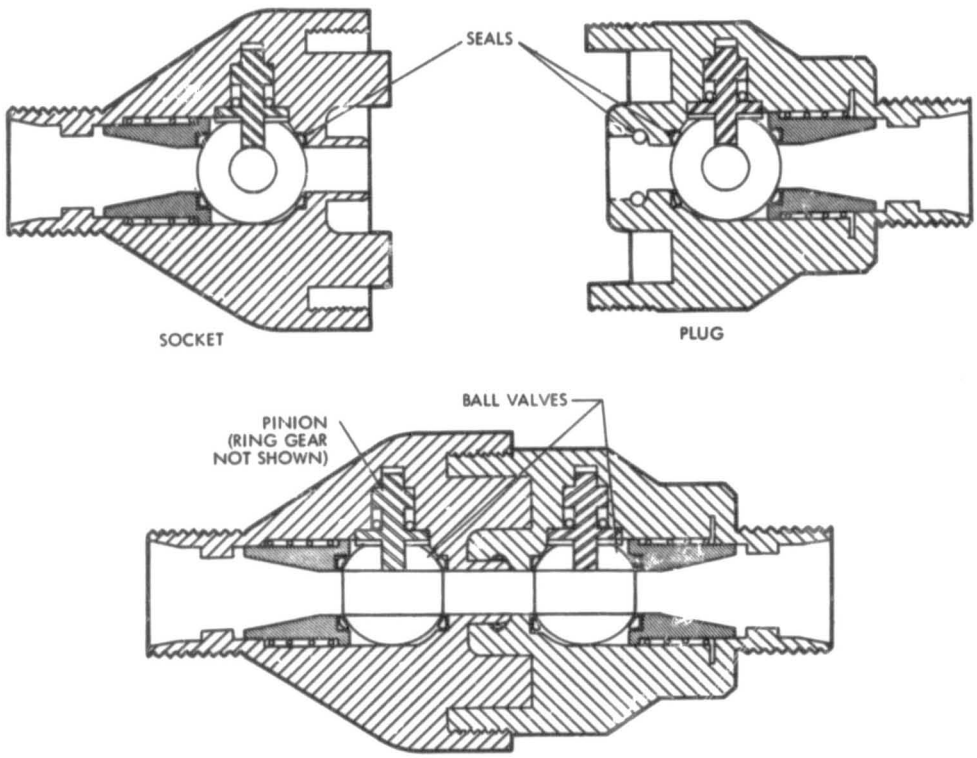

Figure 5.11.3.2e. Double Rotating Ball Quick-Disconnect Coupling

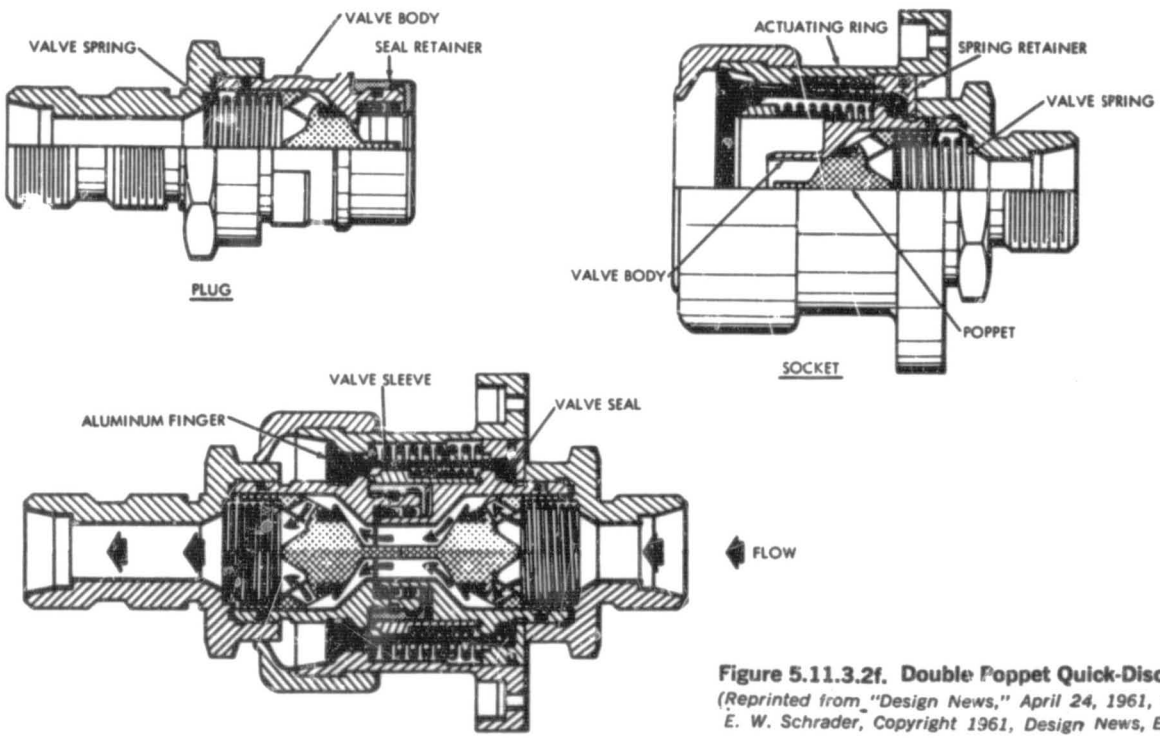

Figure 5.11.3.2f. Double Poppet Quick-Disconnect Coupling
(Reprinted from "Design News," April 24, 1961, vol. 16, no. 9, E. W. Schrader, Copyright 1961, Design News, Englewood, Colorado)

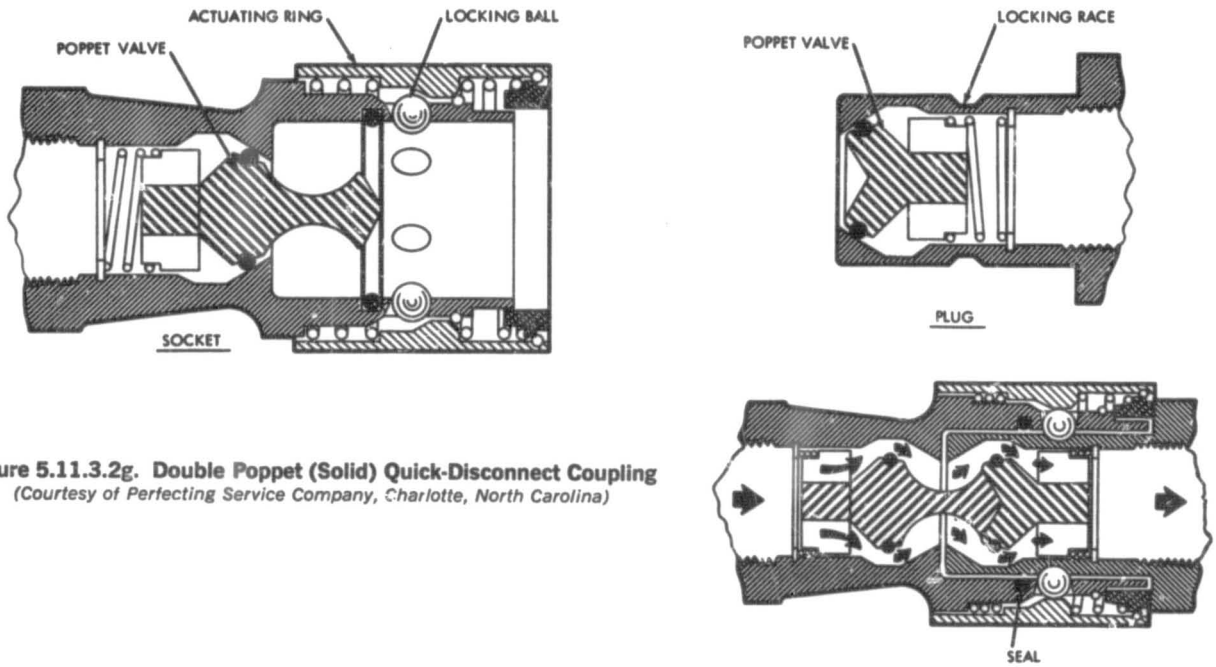

Figure 5.11.3.2g. Double Poppet (Solid) Quick-Disconnect Coupling
(Courtesy of Perfecting Service Company, Charlotte, North Carolina)

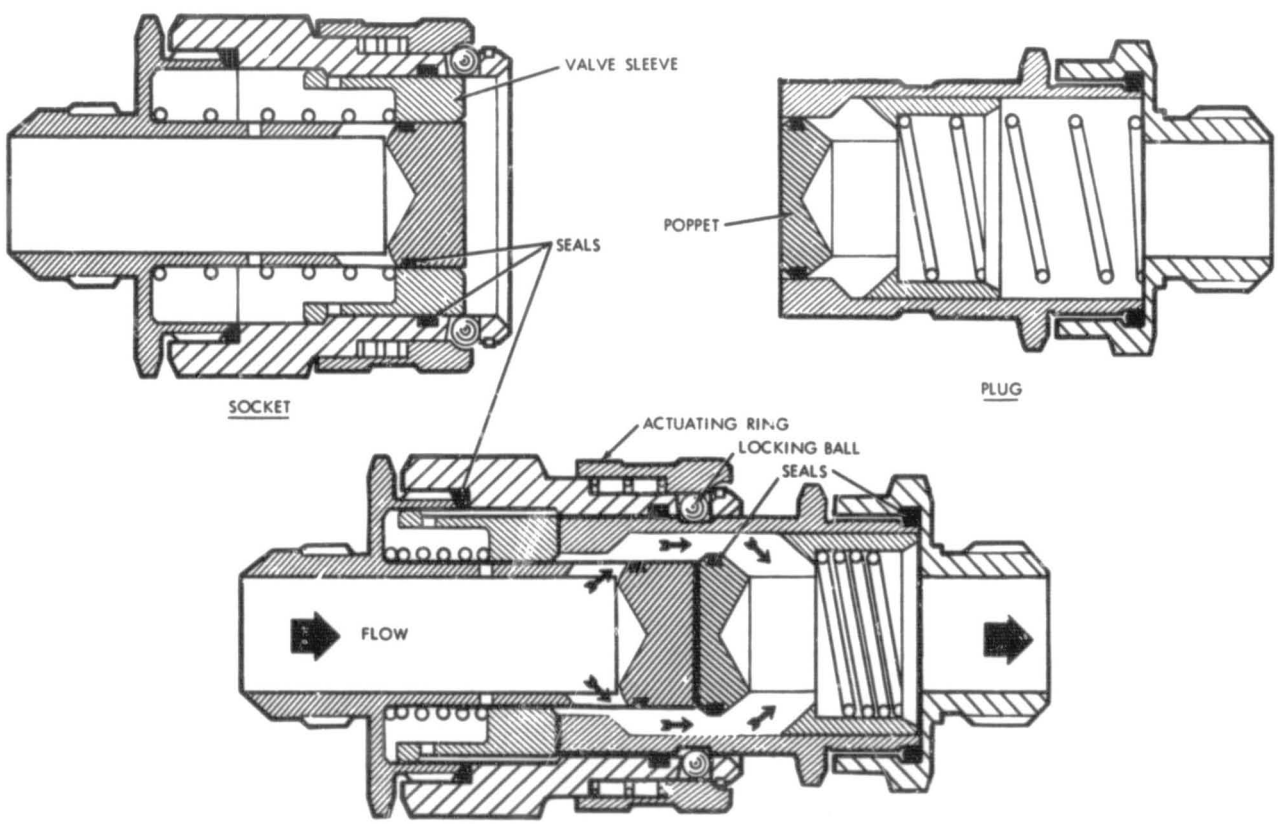

Figure 5.11.3.2h. Tube Sleeve and Poppet Quick-Disconnect Coupling
(Courtesy of Snap-Tite, Inc., Union City, Pennsylvania)

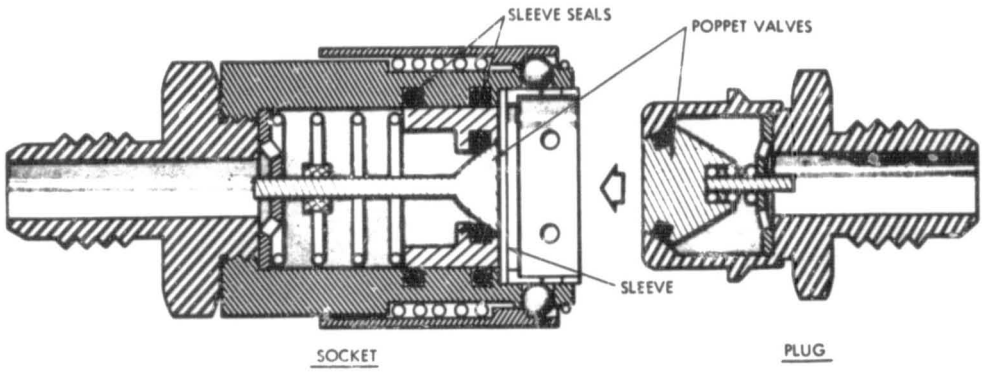

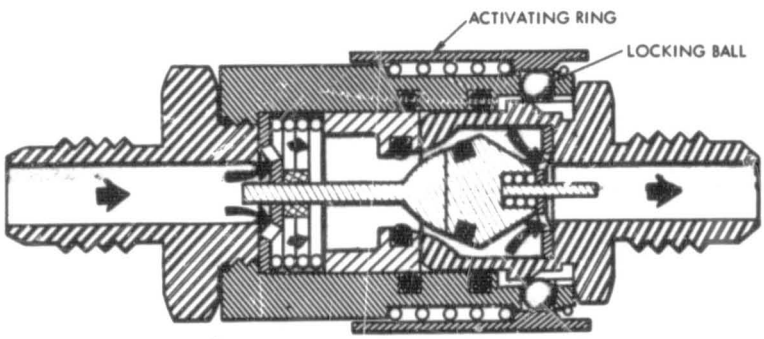

Figure 5.11.3.2i. Poppet Sleeve and Poppet Quick-Disconnect Coupling
(Courtesy of Seaton-Wilson Manufacturing Company, Inc., Burbank, California)

Sleeve and Poppet Quick-Disconnect Coupling. The sleeve and poppet quick-disconnect coupling (Figure 5.11.3.2h) consists of a plug containing a poppet valve and a socket containing a tubular stem and sleeve valve. The plug and socket are pushed together, first forming an external seal between the plug outside diameter and the O-ring seal on the inside diameter of the ball cage. The valve sleeve is pushed into the socket by the plug, which open the tubular stem and sleeve valve. Simultaneously, the tubular stem butts against and opens the poppet valve in the plug. When the valves are fully opened, the balls drop into the locking groove of the plug and the actuating ring slides over the balls, locking the coupling halves together. The coupling is disconnected by retracting the actuating ring and pulling the coupling halves apart.

Poppet-Sleeve and Poppet Quick-Disconnect Coupling. The poppet-sleeve and poppet quick-disconnect coupling (Figure 5.11.3.2i) consists of a socket containing a combination poppet and sleeve shutoff valve, and a plug containing a poppet shutoff valve. The coupling halves are pushed together forming an external seal between the outer diameter of the plug and the inner diameter of the socket. On initial contact, the poppet and sleeve in the socket retract until the poppet has reached its full open position as determined by the stop located on the poppet stem. Further travel of the plug causes the socket poppet to open the poppet in the plug. The plug, in turn, forces the socket sleeve to the full open position. Retraction of the actuating ring allows the locking balls to pass over the locking ridge on the plug. Release of the actuating ring confines the balls in the locking race, forming a positive lock between the coupling haves. Disconnecting is accomplished by retracting the actuating ring pulling the coupling halves apart.

REFERENCES

Plain
6-59, 19-89, V-103, V-106, V-250

Single Poppet
6-59, 19-52, 19-89, V-72, V-103, V-214, V-235

Single Sleeve
6-59, V-252

Double Rotating Ball
1-31, 6-59, V-97

Double Poppets (Drilled)
6-59, V-69, V-212

Double Poppets (Solid)
1-31, 6-59, 19-52, V-72, V-98, V-103, V-116, V-153, V-106, V-180

Tube-Sleeve and Poppet
1-31, 6-59, 19-52, 19-89, V-103, V-116, V-160, V-180

Stem-Sleeve and Poppet
1-31, 73-95, V-30, V-130

TABLE OF CONTENTS

5.12 CONNECTORS

5.12.1 INTRODUCTION

5.12.2 CONNECTOR SELECTION CONSIDERATIONS
- 5.12.2.1 Permanent or Separable Connectors
- 5.12.2.2 Permanent Connector Selection
- 5.12.2.3 Separable Connector Selection

5.12.3 THREADED CONNECTORS
- 5.12.3.1 Design and Selection Criteria
- 5.12.3.2 Connector Preload
- 5.12.3.3 Seal Seating Load
- 5.12.3.4 Pressure End Load
- 5.12.3.5 Bending Moment Load
- 5.12.3.6 External Axial and Torsional Loads
- 5.12.3.7 Vibration
- 5.12.3.8 Connector Assembly
- 5.12.3.9 Contamination
- 5.12.3.10 Temperature and Thermal Shock
- 5.12.3.11 Additional Factors
- 5.12.3.12 Threaded Connector Types
- 5.12.3.13 Flared Tube Seal Connectors
- 5.12.3.14 Sleeve Seal Connectors
- 5.12.3.15 Separate Seal Connectors

5.12.4 BOLTED FLANGE CONNECTORS
- 5.12.4.1 General Description
- 5.12.4.2 Environmental and Service Considerations
- 5.12.4.3 Bolt Torquing
- 5.12.4.4 Flange Deflections and Distortions
- 5.12.4.5 Allowable Bolted Flange Connector Stresses
- 5.12.4.6 Facing Considerations
- 5.12.4.7 Bolting Dimensional Details
- 5.12.4.8 Bolted Flange Connector Handling and Assembly
- 5.12.4.9 Gasket Considerations
- 5.12.4.10 Flange Design Procedures
- 5.12.4.11 Ring Clamp Flanges

5.12.5 BRAZED JOINTS AND CONNECTORS
- 5.12.5.1 General
- 5.12.5.2 The Brazing Process
- 5.12.5.3 Brazed Connector Design Factors
- 5.12.5.4 Brazing Parameters
- 5.12.5.5 Joint Rebrazing
- 5.12.5.6 Brazed Joint Inspection
- 5.12.5.7 Brazed Joint and Connector Configurations

5.12.6 WELDED JOINTS AND CONNECTORS
- 5.12.6.1 General
- 5.12.6.2 The Welding Process
- 5.12.6.3 Welded Connector Design Factors
- 5.12.6.4 Welding Techniques
- 5.12.6.5 Welded Connector and Joint Types

5.12.7 SWAGED CONNECTORS
- 5.12.7.1 General
- 5.12.7.2 Swaged Connector Types

5.12.8 ADHESIVE BONDED JOINTS AND CONNECTORS
- 5.12.8.1 General
- 5.12.8.2 Application
- 5.12.8.3 Design Factors

5.12.1 Introduction

Connectors, commonly referred to as fittings, are devices used in fluid systems for the purpose of joining lines or components and sealing the joint thus made. Connectors may be used for line-to-line, line-to-component, or component-to-component applications. All connectors, regardless of type, employ three functional elements: (1) a seal, (2) the connector-to-line joint, and (3) the load carrying structure. The distinction between connectors involves the manner by which these three functions are accomplished. In some separable connectors there is a direct relation between the functional elements and the mechanical parts of the connector, while in permanent connectors all three functions may be combined, as in a single welded joint.

Connectors can be broadly categorized as separable, permanent, and semi-permanent. *Separable connectors* have at least one mechanical joint which can be easily separated and reconnected a number of times. In addition to the mechanically separable joint, separable connectors may employ a permanent (swaged, welded, or brazed) connection for joining the connector mating halves to the tube and/or component. The separable connector category includes threaded connectors (Sub-Topic 5.12.3) and bolted-flange connectors (Sub-Topic 5.12.4). Quick disconnects, which are a special type of separable connector, are covered in Sub-Section 5.11. *Permanent connectors* employ welded, brazed, soldered, swaged, or adhesive-bonded connections rather than mechanical joints, and are used where reduced weight and reliability are more important than ease of separation. Two most common types of permanent connectors are brazed and welded connectors, covered respectively in Sub-Topics 5.12.5 and 5.12.6. Swaged and adhesive-bonded connectors are treated in Sub-Topics 5.12.7 and 5.12.8.

Semi-permanent connectors are a special class of permanent connectors consisting of permanent joints (welded, brazed, or swaged) which can be used for a limited number of separation and reconnection cycles without requiring removal or replacement of lines, or special adapters or fittings in making reconnections. Discussion of semi-permanent connectors is included under the welded, brazed, and swaged connector types.

The purpose of this sub-section is to present design and selection factors for separable, permanent, and semi-permanent connectors, and to present data on specific connector designs within each category.

5.12.2 Connector Selection Considerations

Numerous factors, often conflicting, enter into the selection of a connector for a given fluid system application. The following paragraphs discuss factors to be considered in selection of connectors.

As a general rule, the number of connectors in any system, regardless of type, should be kept to a minimum. Any connector is a potential source of problems. In addition it adds to system weight and costs.

5.12.2.1 PERMANENT OR SEPARABLE CONNECTORS. The first decision which must be made in selecting a connector is whether the joint or joints under consideration should be made separable or permanent. The fundamental distinction between permanent and separable connectors involves the manner in which the connector seal is effected. The seal of a permanent connector is effected by intermolecular cohesion at the sealing interface, whereas the separable connector seal involves mechanical mating, usually involving local deformation of one of the sealing surfaces. The intermolecular bond effected in the permanent connector has a far higher probability of sealing than the mechanical mating of surfaces with the separable connector; however, the permanent connector seal cannot be easily separated, whereas the separable connector can be readily disconnected with a minimum of tooling and, in many instances, reused.

In addition to higher probability of sealing due to lack of mechanical parts, permanent connectors also offer a weight advantage over most separable connectors, often second in importance only to reliability for flight systems. Other attributes of permanent connectors are small envelope and resistance to shock and vibration.

On the other hand, the distinct advantage of separable over permanent connectors is the ease of making and breaking joints, often a very important consideration during system development, as well as for component replacement, repair, and system maintenance.

The heat required for making most permanent joints must be carefully considered regarding any possible detrimental effects on the system. Heat damage to polymeric seals in valves and thermal distortion are common problems in welded installations. Loss of strength in heat-affected areas must also be considered. Accessibility of the connectors to the necessary welding or brazing tools can be another limitation to the application of permanent connectors, depending upon the system configuration. Permanent connectors which join dissimilar materials such as titanium-stainless steel, or aluminum-stainless steel, present problems which can more readily be overcome with mechanical-type joints. Susceptibility of brazed or welded joints to corrosion is another potential problem which must be considered in selecting permanent connectors.

5.12.2.2 PERMANENT CONNECTOR SELECTION. The choice of permanent connectors offers several possible joining techniques including welding, brazing, bonding, soldering, and swaging with welding and brazing the most common. Factors which influence the selection between types of permanent joints include permanence of the joint, temperature range, fluid compatibility, and suitability of the connector and/or tube materials and geometry for either welding or brazing. Although providing a permanent connection, brazing lends itself more readily than welding to making a joint which can be separated and rejoined if necessary, since a brazed connection can sometimes be reheated, separated, and later rebrazed. At the expense of added weight, however, it is possible to provide welded joints with limited reusability. Such joints are commonly referred to as semi-permanent welded joints. Elevated temperature and joint strength are two of the major limitations with brazed joints, resulting from the relatively low melting points of brazing alloys. A practical upper temperature limit for most brazed joints is approximately 1000 F, the actual limit for specific applications being dependent upon the materials used.

5.12.2.3 SEPARABLE CONNECTOR SELECTION. Most separable connectors fall into one of two categories: (1) threaded connectors and (2) bolted flange connectors (in which category clamped flange connectors are considered for the purpose of this discussion).

A basic difference between threaded connectors and bolted flange connectors is the number of tension (or tensile) members in the separable joint. Threaded connectors utilize a single nut, while flanged connectors use several bolts. The choice between threaded and flanged connectors is determined by line size and the amount of preloading required to establish a satisfactory seal over the entire range of connector loads. In smaller line sizes, threaded connectors have a weight advantage. As the line size approaches 1 inch, applied torque limitations reduce the preloading ability of the threaded connector structural members, and only by increased size (and, therefore, increased weight) of these structural members can satisfactory preloading be maintained.

In general, a 2000 inch-pound torque limitation is used for a threaded connector because of wrench size and nut strength limitations. Thus, a practical limitation exists for the amount of torque applied to a single threaded connector and, consequently, the use of threaded connectors is limited

by system fluid pressure and line size (Sub-Topic 5.12.3 further discusses preload limitations). Size and weight of the connector are other factors which place a line size limitation on the use of threaded connectors. For smaller line sizes (less than 1 inch) threaded connectors have a weight advantage over flanged connectors. A practical limitation on the use of flanged connectors in small line sizes is the fact that in small flange sizes the bolt becomes too small for reliable torquing. Threaded connectors are favored for use with smaller line sizes because of their relative ease of installation and the simplicity with which the tube may be joined to the connector, especially with flared connectors. One disadvantage of threaded connectors is the danger of damage to the tube or line if the threaded flange is not restrained while the nut is torqued down.

In addition to nuts and bolts, clamps offer a method for joining flanges. Ring clamps, such as the V-band clamp, and snap-on clamps provide advantages with respect to simplicity of installation and ease of removal. Snap clamps, however, have no capability for providing variable preload, while ring clamps are limited to relatively low preloads, thus they are used primarily for low pressure ducting or in small line sizes.

5.12.3 Threaded Connectors

A threaded connector is a line fitting which provides a separable mechanical joint secured by a single threaded nut, whereas a bolted flange connector uses several bolts, a clamp, or combinations of these to secure the joint.

Figures 5.12.3a and b illustrate the functional similarities of typical connectors with separate seals. Both connectors contain three functional elements: (1) the seal, (2) the tube-to-connector joint(s). The functional elements are not necessarily restricted to specific mechanical components of the connectors (Reference 44-14). In the bolted-flange connection shown in Figure 5.12.3a, the seal as a functional element consists of the two flanges and the seal; in the threaded connector shown in Figure 5.12.3b, the stub end flange, seal, and threaded flange constitute the seal. The functional similarity between the bolts in Figure 5.12.3a and the nut in Figure 5.12.3b, the tension member of the load-carrying structure, is apparent. The tube-to-connector joints are effected in both instances by weld joints.

Detailed Topics 5.12.3.1 through 5.12.3.11 discuss considerations which are equally applicable to threaded and bolted flange connectors. Detailed Topics 5.12.3.12 through 5.12.3.15 treat threaded connectors only.

5.12.3.1 DESIGN AND SELECTION CRITERIA. Table 5.12.3.1 summarizes important factors relevant to the design and selection of threaded and bolted flange connectors. Some of the factors noted are discussed in greater detail in the following detailed topics. It should be noted that the design and selection criteria listed under each of the five major headings do not necessarily appear in their order of importance.

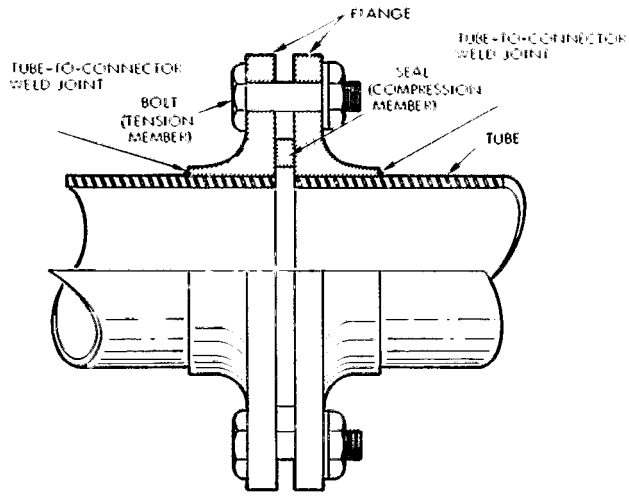

Figure 5.12.3a. Typical Bolted Flange Connector Components

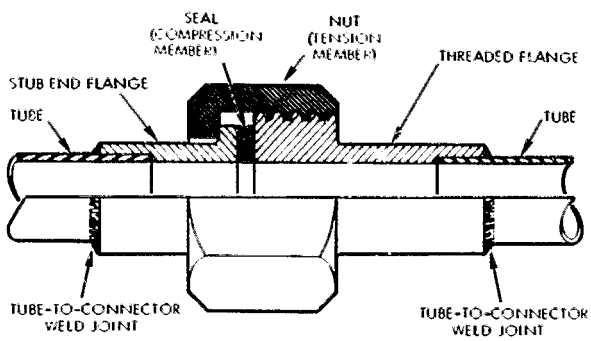

Figure 5.12.3b. Typical Threaded Connector Components

5.12.3.2 CONNECTOR PRELOAD. Connector preload is the axial structural load which is required to maintain sealing in any connector; it is provided by tightening the tension member. Preload requirements commonly control the basic design of the connector. The preload has three functions: (1) to seat the seal, (2) to provide force to resist applied structural loads tending to separate the connector joint, and (3) to provide stored elastic energy to maintain sealing load, in spite of dimensional changes resulting from axial and bending loads, stress relaxation, and thermal gradients.

In order to maintain adequate seal load it is necessry to preload the connector to an amount greater than the combined expected axial pressure end load and other externally applied loads. In addition, sufficient load must be provided for dimensional changes caused by thermal gradients. A

ISSUED: MARCH 1967
SUPERSEDES: OCTOBER 1965

Table 5.12.3.1. Threaded and Bolted Flange Connector Design and Selection Criteria

Performance and Environmental Criteria
- Leakage
- Temperature Range
- Temperature Cycling
- Pressure Range
- Reverse Bending, or Flexure
- Impulse-Vibration Cycling
- Torque Relaxation
- Vacuum-Radiation Tolerance
- Material Degradation

Configuration Criteria
- Weight
- Envelope
- Cost
- Tube Entry Clearance
- Suitable Materials
- Preload Relationship
- Angularity Tolerance

Manufacturing Criteria
- Tolerances Required
- Machines Required
- Tooling Required
- Inspection Required
- Tubing Requirements

Reliability and Quality Assurance Criteria
- Torque Latitude for Sealing
- Torque Latitude for Preload
- Effect of Axial Load on Seal
- Failure Mode, Effect on System
- Inspectability

Assembly Criteria
- Torque Required
- Cleanliness Required
- Care Required
- Special Tools Required
- Inspectability
- Reconnectability

balance must be achieved, however, between a preload which is sufficient to prevent connector separation or seal leakage, and a preload so large that it may cause eventual failure of the tensile members of the connector.

Connector preload can be classified as either series or parallel, as illustrated by the arrangements shown in Figure 5.12.3.2a. In the series arrangement, all of the compressive force of the preload is transmitted through the sealing element, and any change in applied load is felt by the seal. In the series arrangement, therefore, the tension member must have sufficient spring follow-up to account for seal flow or relaxation without the load being reduced below the minimum sealing load. In the parallel arrangement, the seal carries all of the load only until the seal is compressed to the point where the two connector flange halves are drawn together; further application of axial force preloads the connector directly through the flanges and very little additional load is carried by the seal.

Factors the designer should consider in determining the connector preloads are discussed below and illustrated with simplified preload diagrams in Figures 5.12.3.2b, c, d, and e.

Minimum Compressive Seal Load Needed to Prevent Leakage. After the seal has been subjected to an initial seal load, a minimum residual compressive seal load must be maintained during service conditions to prevent leakage. The residual load should give an apparent seal stress greater than the counteracting tensile stresses caused by system operating conditions, including pressure end load and bending, which tend to separate the sealing surfaces. In theory, ideal sealing surfaces would remain in contact until the apparent seal stress decreased to zero. In practice, however, a certain prescribed minimum residual compressive load must be maintained at all times in order to maintain a satis-

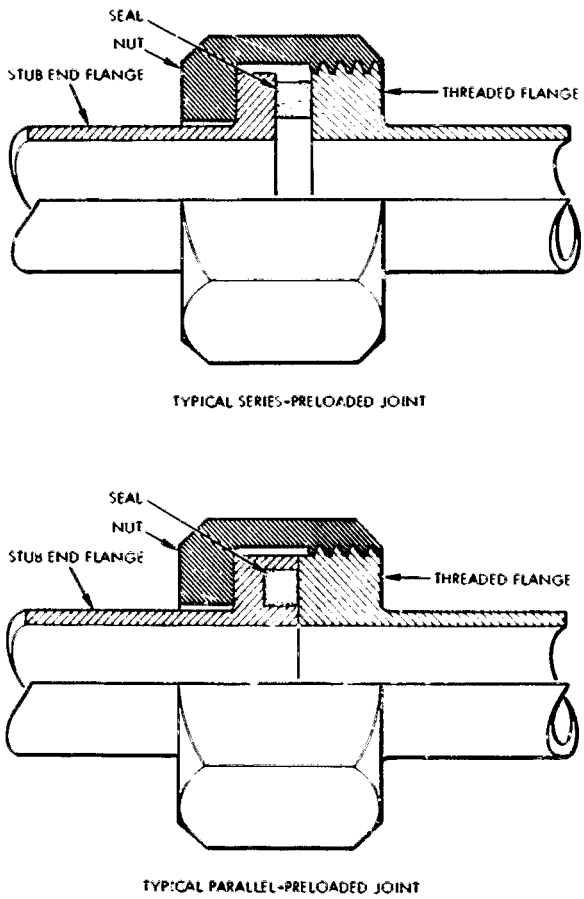

Figure 5.12.3.2a. Series and Parallel Preloaded Joints

ISSUED: MARCH 1967
SUPERSEDES: OCTOBER 1965

factory seal. The required seal load is the major factor affecting connector design for small line sizes and low system pressures. For large sizes and high pressures, pressure end loads have a more important influence on connector design than seal seating load.

Maximum Allowable Stress in the Tensile Members. The maximum allowable stress in a connector is based on the connector tensile member material yield stress at maximum operating temperature, derated by some safety factor. In an optimized connector design, the maximum operational load considered as an upper limit for connector operation would coincide with the maximum allowable tensile member load.

Deflection Rates of Compression and Tension Members. The deflection rate, which is the reciprocal of the spring rate, is a measure of change in deflection for a given change in load. The deflection rate for the compression members of a connector is invariably much less than the deflection rate of the tensile member in any connector.

Effects of Thermal Gradients. A thermal gradient, caused by the passage of a hot fluid through a connector, generally causes the connector compression members to become hotter than the tension members. This results in an increase in preload, since the compression members expand, transferring load to the tension members. If the tension members are overstressed, material yielding may occur. Such a condition could result in immediate connector structural failure or eventual structural failure as a result of thermal cycling. Material yielding, or creep, might also result in leakage when thermal equilibrium is restored, because the seal load is decreased. In the case where a cold fluid passes through the connector, a contraction of the compression members occurs, resulting in a relaxation of load on the tension members. The load relaxation must not be so great that the sealing load is reduced below the minimum necessary to prevent leakage. Since the connector structure is rather complex from a thermal analysis standpoint, an experimental determination of the thermal gradients expected in a particular connector service application may be necessary.

Magnitude of Structural Loads. Connector structural loads are a function of axial, torsional, and bending loads, each of which is discussed in greater detail in subsequent sub-topics. For an optimum connector design, the maximum tensile load anticipated on the tension members would coincide with the maximum allowable connector load determined from material properties. In addition, the compressive load on the seal interface must never be reduced below the minimum required seal load. The maximum allowable load in the tension member occurs when the maximum hot thermal gradient and maximum tensile end load are applied simultaneously. The minimum compressive load on the seal interface exists when the maximum cold thermal gradient and the maximum tensile end load occur simultaneously.

Variations in Initial Preload. The initial preload on a connector is dependent on many factors, e.g., thread form, thread alignment, thread fit, amount of lubrication, surface finishes of parts, type of lubrication, environment, etc. It is important for the designer to prescribe a preload that will meet the requirements of a satisfactory connector, one which is not so large or small as to cause connector failure (structural or leakage) at temperature extremes under full load. An acceptable preload range can be built into a connector by proper selection of the tension member(s) deflection rate, i.e., selection of tension member(s) with a greater than optimum deflection rate. (The optimum deflection rate is defined as that which produces coincidence of (a) the maximum allowable tensile load, with the tensile load created by the maximum hot thermal gradient, combined with the maximum connector end load, and/or (b) the minimum compressive seal load, with the load created by the maximum cold thermal gradient, combined with the maximum connector end load.

A preload diagram provides a convenient design tool for correlating the factors described above. It is basically a plot of load versus deflection for the tension and compression members of a connector. In the preload diagram shown in Figure 5.12.3.2b the line O-T is a stress-strain type curve for the tension member showing the expected deflection for applied load. Note that the load-deflection curve for tension member(s), O-T, goes through the origin, i.e., zero deflection at zero load. The load deflection curve for connector compression member(s), c-c', has a negative slope, indicating that increasing load deflection of the compression member(s) is opposite in direction to the deflection of the tension member(s). Note that the intersection of the load deflection curve of the compressive member(s) with the deflection axes at zero load is quite arbitrary. That is, when a connector nut is tightened or torqued so as to produce a tension member load corresponding to O-a, the compression member(s) of the connector deflect an amount δ_o. When the

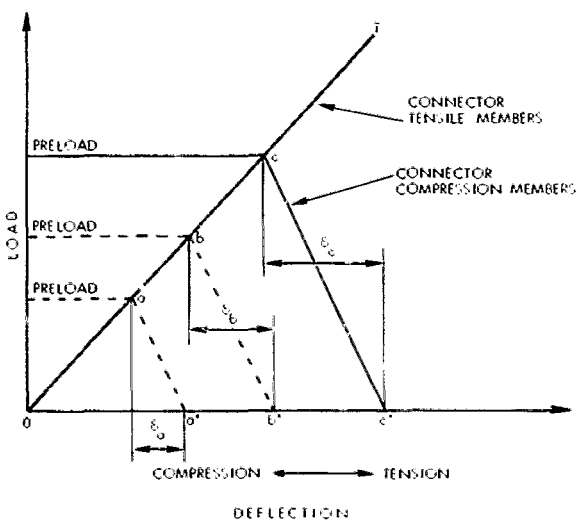

Figure 5.12.3.2b. Load-Deflection Curve

connector nut is further tightened to O-B, the compression members deflect an amount δ_b, and so on until the nut is tightened to the desired preloaded value, producing δ_c deflection. In all instances the slope or deflection rate of the compression members is constant, but as increasing preload is applied the deflection increases as indicated.

To elaborate further on the load deflection diagram, consider Figure 5.12.3.2c. Three values of preload, designated 1, 2, and 3, are indicated. These preloads establish the deflection of tension and compression members of the connector. When additional load is imposed on the connector in the form of fluid pressure, bending, axial loads, etc., the connector tends to separate. The tension member deflection increases, and the compression member deflection decreases. At preload 1 in Figure 5.12.3.2c, a load L_1 is required to reduce the compression member deflection to zero (by stretching the tension member sufficiently to relieve the preload). If preload 2 or 3 is initially applied, it is necessary to apply a load L_2 or L_3, respectively, to cause connector separation, i.e., zero deflection of compression members.

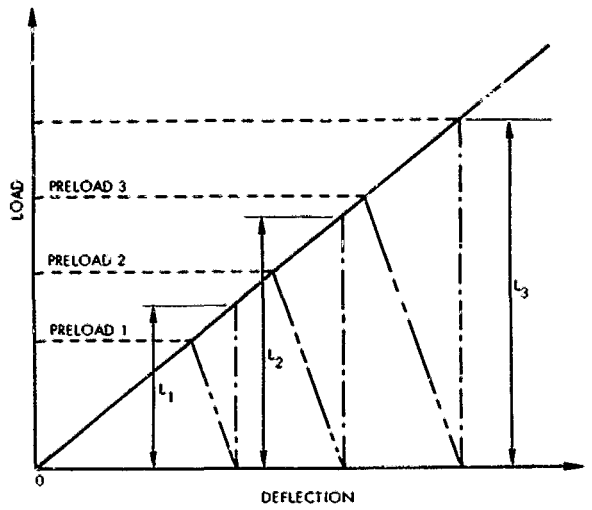

Figure 5.12.3.2c. Preload and External Loading

The foregoing example considers only constant temperature cases. If an initially preloaded connector is subjected to thermal shock, a temperature gradient will exist between the tension and compression members. Most often the thermal shock is imposed from within the line; as a result, the case where tension members are suddenly cooled or heated is generally of less consequence than when the compression members of the connector are cooled or heated. When the compression members are suddenly heated they will expand and transfer load to the tension members. When the compression members are suddenly cooled they will contract, and load will be removed from the tension members. These cases are illustrated in Figure 5.12.3.2d. In addition, this figure shows how an externally applied load, L, affects the connector when thermal shock is imposed.

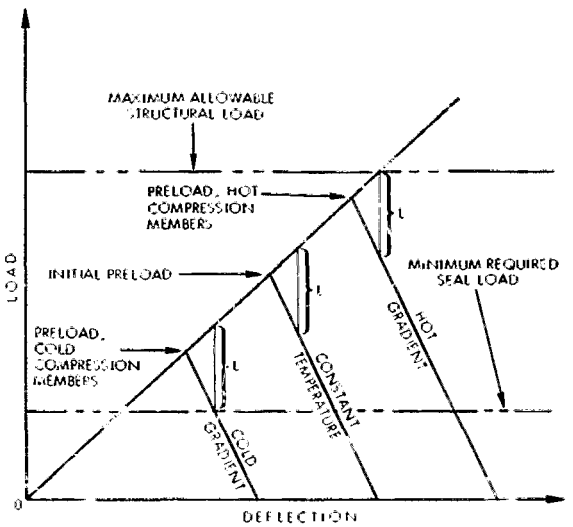

Figure 5.12.3.2d. Effect of Thermal Gradients

The system-imposed tensile end load, L, in conjunction with the maximum hot thermal gradient (gradient from inside to outside of connector) establishes the maximum load on the connector, controlled by structural limitations. The load, L, in conjunction with the maximum cold thermal gradient, establishes the minimum load on the connector, controlled by sealing requirements.

Another point worth noting in considering the preload in a separable connector is the proper selection of the tensile member deflection rate. As previously noted, the tensile member deflection rate is the measure of change in length (deflection) with change in load. Several different deflection rates for separable connector tensile members are illustrated in Figure 5.12.3.2e.

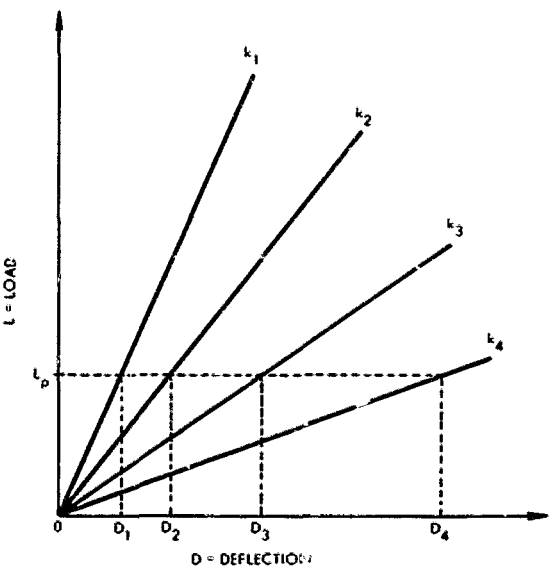

Figure 5.12.3.2e. Tensile Member Deflection Rates

As seen from Figure 5.12.3.2e, a given initial load, L_1, creates differing levels of deflection D_1, D_2, D_3, and D_4 in the tensile members dependent upon the deflection rates k_1, k_2, k_3, and k_4 of each tensile member. When selecting a tensile member deflection rate for a particular application, it is always conservative to use an actual deflection rate greater than the desired deflection rate, except for the case when the anticipated deflection causes yield of the tensile member.

5.12.3.3 SEAL SEATING LOAD. The seal seating load is the initial axial compression load on the seal required to produce intimate contact between sealing surfaces. The seal seating load should not be confused with the minimum residual compressive load necessary to maintain a leak-tight seal under operating conditions. The minimum residual compressive load need only provide an apparent seal stress slightly greater than the total seal unloading due to connector operating loads. The seal seating load can be estimated as

$$F_S = \pi D_{eff} G \qquad \text{(Eq 5.12.3.3a)}$$

where

D_{eff} = effective seal diameter, in.

G = initial required seal seating load, pounds-per-inch of seal length

The value of G in pounds-per-inch for the gasket seating load is a function of the seal material and geometry. Tables 6.3.3.2b,c, and d in Sub-Section 6.3, "Static Seals," list recommended seal stress for several types of seals. Figure 5.12.3.3 is a plot of the required seal seating load as a function of line diameter for representative values of G, assuming D_{eff} equals 1.1 times the line outside diameter.

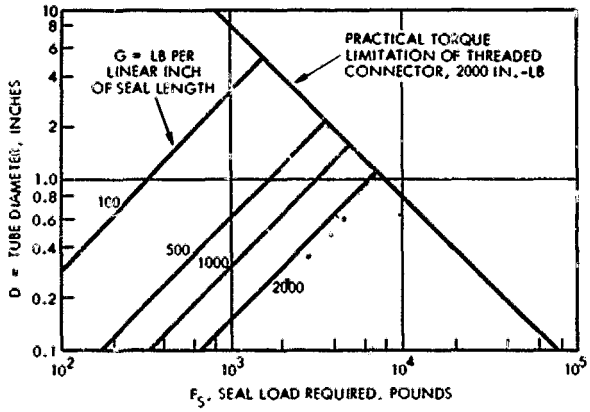

Figure 5.12.3.3. Required Seal Load as a Function of Seal Diameter

To obtain the seal seating load in threaded connectors, it is necessary to apply torque to the connector nut. The amount of torque necessary to obtain some required preload, assuming standard connector threads, may be approximated by the following equation (Reference 44-14):

$$\tau = 0.2d\,F \qquad \text{(Eq 5.12.3.3b)}$$

where

τ = required preload torque, in-lb

d = nominal thread diameter, in.

F = required preload, lbs

Unless better information is available, d may be approximated as 1.30 times the tube outside diameter. Using the upper limit of torque applied to a threaded connector as 2000 in-lb (see Detailed Topic 5.12.2.3) an upper limit of connector loading due to preload may be established as

$$F_{max} = \frac{7690}{D} \qquad \text{(Eq 5.12.3.3c)}$$

Figure 5.12.3.3 shows this upper limit as a function of tube diameter. When F_{max} is used in conjunction with the required seal seating loads shown on the same curve, the designer is able to determine whether a given seal, with a specified value of G, can be used in a particular size tubing system since gasket seating load is torque limited.

5.12.3.4 PRESSURE END LOAD. The pressure end load is a result of system pressure, and is equal to

$$F_e = \frac{\pi}{4} D_{eff}^2 P \qquad \text{(Eq 5.12.3.4)}$$

where

F_e = pressure end load, lbs

D_{eff} = effective seal diameter, in.

P = internal pressure, psi

Assuming that D_{eff} = 1.1 times the tubing outside diameter, because the effective diameter of most connector seals is about this much larger than the tube OD, Figure 5.12.3.4 gives values of the pressure end load, F_e, for various combinations of tubing diameter and internal fluid pressure.

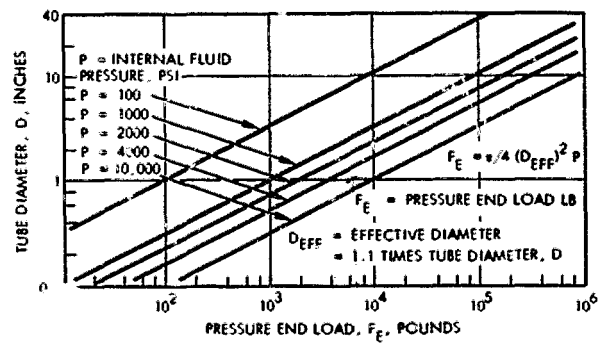

Figure 5.12.3.4. Connector Pressure End Load as a Function of Tube Diameter and Design Pressure

The system operating pressure is a major determining factor in the design or selection of a threaded connector. In a ground-based system, the pressure end load is frequently the design load for the connector. Although anchors, fluid components, and other restraints absorb a part of the pressure end load, design practice necessitates the connector be made to withstand the entire pressure end loading. Pressure impulses must be considered from this same standpoint, i.e., the connector must be designed to withstand the impulse load. The system pressure in conjunction with the tubing diameter will also be a major selection factor in choosing between a threaded connector or a flanged separable connector. Structural limitations of the threaded connector and practical means of applying large torques commonly restrict applications of threaded connectors to tube sizes of one inch or less.

5.12.3.5 BENDING MOMENT LOAD. A bending moment, M, producing bending loads, F_B, may be present because of tubing misalignment, thermal expansion or contraction of the tubing system, vibration, displacement of anchors, or acceleration forces. Bending moments imposed on a fitting in a tubing system cannot usually be determined in advance, since these moments depend upon the specific tubing system, its operating conditions, and the location of the threaded connector in the system. However, some limits, even if arbitrary, must be established so that the designer can gain a feeling for the bending loads imposed on a connector. In general, the bending load can be expressed, in terms of the maximum stress that can be transmitted by the tubes, as

$$F_B = \pi D t \sigma_m \qquad \text{(Eq 5.12.3.5a)}$$

where

D = tubing outside diameter, in.

t = tube wall thickness, in.

σ_m = limiting longitudinal stress of tube material, psi

In the previous equation, the value of t (tube wall thickness) is obtained, if not already known, from the tubing design considerations. For thin-walled tubing, t may be evaluated (Reference 44-14) from

$$t = \frac{PD}{2\sigma_c} \qquad \text{(Eq 5.12.3.5b)}$$

where

P = internal pressure rating of system, psi

D = tube outside diameter, in.

σ_c = limiting circumferential (hoop) stress of tube material, psi

The bending load limit then becomes

$$F_B = \frac{\pi}{2} PD^2 \frac{\sigma_m}{\sigma_c} \qquad \text{(Eq 5.12.3.5c)}$$

The problem of determining the maximum allowable bending load now becomes one of determining the appropriate limiting values for σ_m and σ_c in Equation (5.12.3.5c).

For aerospace applications it is desirable to maintain minimum weight throughout. In this respect, σ_c may be taken as either two-thirds of the material yield strength or one-half of the material ultimate strength, whichever is less. This is based on a proof pressure rating of 1.5 times system operating pressure and a burst pressure rating of 2 times system operating pressure.

The value of σ_m in a moderate application could be taken as the tube material yield strength. However, the severity of an aerospace environment usually imposes more stringent limitations on values of σ_m. For example, cyclic loading resulting from vibration would require σ_m to be selected on the basis of tube material fatigue strength. Additional factors such as impact loads, temperature extremes, etc., would further modify the value chosen for σ_m. A typical value for σ_m might therefore be based on one-half the tube material endurance strength.

5.12.3.6 EXTERNAL AXIAL AND TORSIONAL LOADS. As with bending loads, external axial and torsional loads imposed upon the connector assembly by the line are largely a function of the line diameter. Usually the axial loads which may be transmitted by small diameter tubing to a threaded connector are minor in comparison with preload and pressure forces, and may be discounted. Torsional loads may present a problem if sufficiently large to cause rotation of one part of the joint with respect to the other.

The larger lines normally associated with bolted-flange applications may transmit forces to the connector appreciably in excess of those associated with internal pressure and seal preload requirements. As with bending loads, this is particularly true of short, large diameter lines whose terminal points are subjected to significant displacements, as shown in Section VIII-B-3 of Reference 34-10.

5.12.3.7 VIBRATION. The vibration spectrum for a threaded connector is wholly dependent on the intended system application. Some representative vibration environments are presented in Sub-Topic 13.3.5 and Sub-Section 7.3. In any threaded connector application involving thin walled tubing, experience has shown that a simple vibration loading may be expected to induce structural failure in the tubing or piping before connector structural failure occurs. However, leakage, the most common type of threaded connector failure, may develop prior to structural failure of the tube Reference 147-1 describes a number of vibration tests of threaded connectors and shows tube rupture to be more prevalent with flared-tube connectors, whereas sleeve seal connectors tended to leak under vibration. A low system pressure in the presence of vibration, inadequate seal seating stresses may lead to separation of sealing surfaces and subsequent leakage. At elevated system pressures, the vibration-induced bending load, in addition to the pressure end load, may cause fatigue failure of a connector or may cause material yield and eventual leakage due to insufficient preload.

The precise location of tubing failure due to vibration is largely a function of the connector type. In the connectors that incorporate tube flaring, the root of the flare becomes the most likely point of failure. This is due to the cold working of the tube material in the flaring process. For connectors that utilize a swaging process to hold the tube in place, the point where the tube is held is most likely to fail because of stress concentration induced in swaging. For connectors utilizing a weld joint to the tubing, the weld area is susceptible to failure under vibration as the result of exposure to extreme heat in the welding process. For connectors using brazed joints, the brazing process must insure adequate wetting of surfaces or tube pull-out may result from insufficient shear strength. Although other failure modes exist and must be investigated, those mentioned above represent the most commonly encountered failure modes under vibration.

5.12.3.8 CONNECTOR ASSEMBLY. The need for special assembly tools may be a determining factor in the design or selection of a connector. The tube-to-connector joint may necessitate special welding, brazing, swaging, holding, or other tools. The connector-to-connector joint may also require some form or combination of the above-mentioned tools. Therefore, before the type of connector is selected, consideration must be given to the method of assembly. See SAE ARP 683, "Installation Procedures and Torques for Fluid Connections."

In addition to the special tools requisite in a connector assembly, the methods in which these tools are used bear consideration. The critical steps in connector-to-tube assembly, connector-to-connector assembly, and proper handling and installation of seals must be evaluated. Details of torquing and the effect of over- or under-torquing a connector must also be investigated. Tube material properties and the ability of the tube to be cold-worked for flaring or swaging as well as weldability, brazability, and bondability may also be a consideration in a connector selection or design.

5.12.3.9 CONTAMINATION. At any point in a tubing or piping system where a connector is installed, there exists a point of potential system contamination. When a connector is disconnected, adequate protection of the tubing or piping immediately surrounding the fitting must be provided in order to prevent foreign particulate matter from entering the system. In addition to environmentally introduced contamination, potential contamination emanating from the connector must be considered. Some connectors generate and collect more contamination than others, due to notches, grooves, recesses, or other cavities where contamination is likely to collect. The threads of a threaded connector are prime candidates for contamination generation, as are certain weld and braze joints. In this regard, the method of assembly may become a critical factor. The performance of the threading operation in joining the threaded connector, as well as the use of thread lubricants and sealants, may necessitate limitations, controls, special methods, etc. Aside from any special precautions, it is good practice to wash the connector and the immediately surrounding tubing or piping with an acceptable solvent prior to making a disconnect (opening the system).

5.12.3.10 TEMPERATURE AND THERMAL SHOCK. The temperature environment is a determining factor in the selection of materials of construction for a separable connector. At elevated temperatures, the connector must be designed to withstand the effects of material creep and stress relaxation. At low temperatures, material ductility must be sufficient to prevent brittle failure. As discussed in Detailed Topic 5.12.3.2, "Connector Preload," thermal shock and the associated thermal gradients must be taken into account when determining an appropriate preload range for a separable connector.

5.12.3.11 ADDITIONAL FACTORS. Some additional factors in a threaded or bolted flange connector design worth consideration are:

a) The total number of parts involved in a particular connector and the associated storage, handling, availability, and logistics problems

b) The critical dimensions and/or critical surfaces, with related machining, handling, and protection

c) The necessity of special containers and/or individual handling of separate seals, special connector devices, etc.

d) The overall size and weight of the connector

e) The quality control necessary in the production, procurement, and installation of a given connector

f) The ease with which a given connector can be inspected when installed, and the associated equipment necessary to accomplish inspection.

g) The necessity for insuring that assembly and inspection personnel are thoroughly familiar with both the design and functional characteristics of the connector. This factor is essential if reliable, leak-tight systems are to be consistently achieved.

5.12.3.12 THREADED CONNECTOR TYPES. Major distinguishing features between various types of threaded connector designs are the seals, both tube-to-connector seals and connector-to-connector separable joint seals. Probably the most common classification of threaded connectors is the flared tube seal connector, a design which combines features of the tube-to-connector seal and separable joint seal by using the flared tube as a gasket clamped between the connector halves.

A second threaded connector type is the sleeve seal connector, employing a sleeve which is attached to the tube; instead of the tube forming the separable joint seal, the sleeve and connector together form the seal. Sleeve seal connectors include those commonly referred to as flareless connectors.

A third and distinctive type of connector is the separate seal connector, employing a separate removable sealing element between the connector halves (flanges) to make the separable joint seal. In this connector design, a permanent

type joint (i.e., welded or brazed) is commonly employed to provide the tube-to-connector seal. Swaging is also employed in some separate seal connector designs to accomplish the tube-to-connector seal.

In the following sub-topics, samples of specific connector design types which can be classified under each of the above-mentioned threaded connector seals are described. In these descriptions, reference to a "tube-to-tube joint" has been adopted for simplicity, and use of the term "union" is adhered to in this case, although other types of joints such as tube-to-component, etc., exist.

5.12.3.13 FLARED TUBE SEAL CONNECTORS. The flared tube seal type connector is probably the most common threaded connector. This connector utilizes the tubing flare to accomplish both the connector-to-connector seal and the tube-to-connector seal. This design has numerous variations, most of which employ the same basic geometry but differ in the manufacturing and quality control requirements. The AN (Air Force Navy Aeronautical), MS (Military Standard), and MC (Marshall Center) connectors are common flared tube connectors which can be procured to government or industry specifications. These connectors and others are discussed in the following paragraphs.

AN Flared Connectors. The AN flared connector, illustrated in Figure 5.12.3.13a, consists of a sleeve, a connecting nut, and a union. This connector is manufactured in accordance with military specification MIL-F-5509B, titled "Fitting, Flared Tube, Fluid Connection." In making a tube connection with this type of connector, the following sequence of operations is generally followed: (1) The nut and the sleeve are placed on the tubing, (2) the tubing is flared by a hand tool or by a machine, and (3) the connection is secured by placing the flared tubing in contact with the nose of the union, sliding the sleeve and nut against the flared tubing end, and threading the nut into place on the union. The sleeve is forced against the back of the tube flare by the nut as it is threaded onto the union. As the nut is tightened, the sleeve compresses the back of the tube flare against the nose of the union, thus forming the seal. Actual sealing is accomplished by deformation of the flared tube against the mating surface of the union.

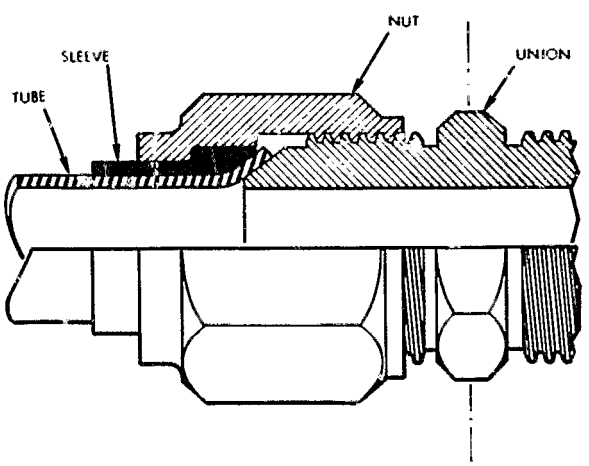

Figure 5.12.3.13a. AN Flared Connector

A major advantage of the AN flared connector is its simplicity; however, several disadvantages have given rise to modifications and even completely new connector design concepts. Some of the outstanding disadvantages include:

a) The torque relaxation with time characteristics. This is a tendency of the flared fitting to lose the initial assembly torque after a period of time, resulting in a loose connection.

b) The inability to obtain sufficient sealing stresses in ½ inch and larger connector sizes. To obtain satisfactory metal-to-metal sealing against helium leakage, recent work indicates that a contact stress of 1 to 3 times the yield strength of the softer material is required. Using the minimum torque requirements given in AND 10064 for steel tubing and the relation $T = 0.2\ dF$ (see Detailed Topic 5.12.3.3), values of available seating stress can be obtained and compared with those values of seating stress required for specific applications.

c) Inadequate quality control requirements. The inspection sampling frequency is generally considered insufficient, and surface finish requirements on sealing surfaces are inadequate for satisfactory sealing in the presence of helium, low leakage requirement, high pressure, or cryogenic temperature.

d) The tendency of hard steel tubing to crack when subjected to flaring operations. Aerospace applications frequently demand the use of high strength tubing. This type of material is frequently not capable of being cold worked without having extremely high residual stress levels result, therefore requiring stringent material and manufacturing specifications.

To solve the problem of the AN connector a modification in the form of a separate seal has been devised. This seal, shown in Figure 5.12.3.13b, is a truncated cone, and fits over the end of the 37-degree union nose. The seal is made of a soft material, generally copper or aluminum, offering lower required seating stresses. While presenting a solution to the required seating stress problem, the separate seal has the disadvantage of adding another piece to the connector (which could be omitted if proper care is not taken during assembly), and it does not eliminate the disadvantages previously identified in (a), (c), or (d).

MS Flared Connector. The MS flared connector, often referred to as a precision flared fitting, utilizes the same nut and sleeve as the AN connector, and is procured to the same military specification. The primary difference between the MS and AN connector exists in the union: the MS union (and other parts to which the connector nut attaches) is procured to MS (Military Standards), whereas the AN union is procured by Air Force/Navy Aeronautical Standards. Some important characteristics of the MS unions are:

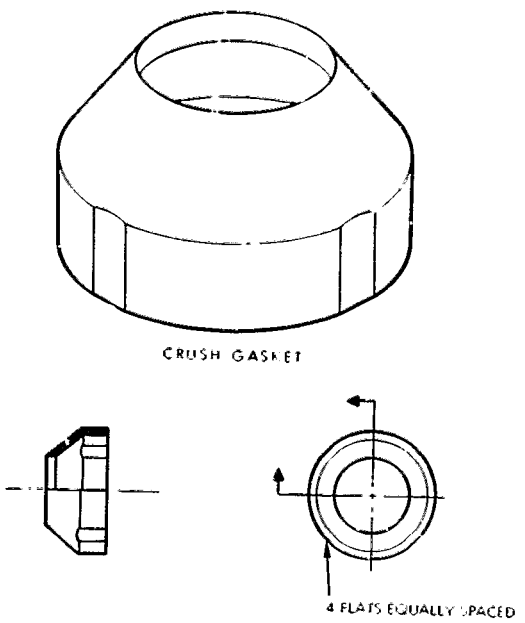

Figure 5.12.3.13b. Conical Seal for AN Connector
(Courtesy of Voi Shan Industries, Culver City, California)

a) Finer finish on the 37-degree cone of the sealing surface
b) 100 percent inspection of unions for thread concentricity to each other, thread relief lengths and diameters, surface smoothness of thread reliefs and hex faces, and surface finish of cone ends
c) Tighter dimensional tolerances restricting the overall length of the connector (union or other) hex nut-to-tip dimension.

These changes were incorporated as an attempt to obtain better sealing quality by imposing tighter quality control, but they do not resolve the sealing stress requirement problem mentioned above under the discussion of the AN flared connector.

MC Fittings. MC fittings, which were developed by NASA, are basically similar in appearance and operation to the AN and MS flared fittings shown in Figure 5.12.3.13a. The MC connector is procured to NASA Specification MC 146. Some of the refinements incorporated into the MC fittings in order to increase reliability are:

a) The finish of the conical sealing surface is limited to 10 to 14 microinches rms profile for steel, and 22 to 28 microinches rms for aluminum.
b) The sealing surfaces are round, within 0.0002 inch, and limited to a maximum deviation of 0.0001 inch in any 60-degree arc.
c) Concentricity of the sealing surface with the thread pitch diameter is within 0.003 inch TIR (total indicator reading).

Globe Aerospace Connector. This connector, shown in Figure 5.12.3.13c, uses the standard AN, MS, or MC sleeve and union, but employs a different concept in the locking nut. The nut is composed of two parts: a hex nut similar to an AN818 with a groove in the shoulder length, and a locking nut with the same size hex and six barbed fingers. The fingers of the lock nut fit over the shoulder of the nut proper in such a way that all six fingers of the lock nut engage the groove in the nut proper. Both nuts are threaded onto the union when forming a connection. The nut proper is torqued first and accomplishes the seal between tube flare and union. The lock nut is then torqued to an equal or greater value, and the barbed fingers grip the lip of the groove on the nut proper and lock it in position. The lock nut innovation precludes the necessity for safety wiring in the presence of a vibration environment.

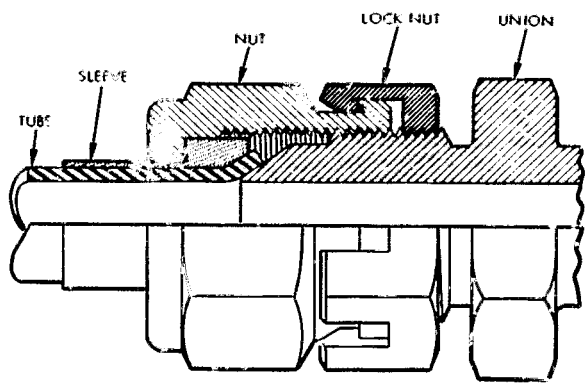

Figure 5.12.3.13c. Globe Aerospace Connector
(Courtesy of Globe Aerospace, North Hollywood, California)

DL Connector. The DL connector, as shown in Figure 5.12.3.13d, is in essence an AN connector, but with two modifications:

a) The sleeve of the DL connector is the same thickness throughout its entire length.
b) The nut of the DL connector has a groove in the outer periphery at about the midway point of its length, and has greater material volume at the point where it contacts the sleeve.

These modifications remove material from the sleeve, place it in the nut, and the nut is thus able to carry heavier loading.

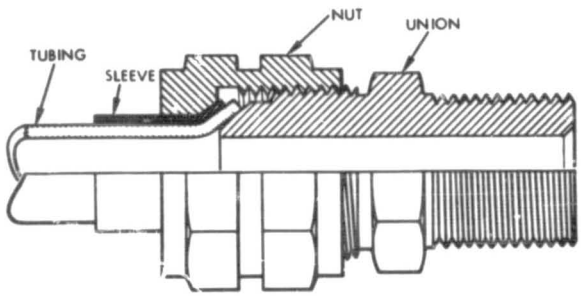

Figure 5.12.3.13d. DL Connector
(Courtesy of E. B. Wiggins, Inc., Los Angeles, California)

5.12.3.14 SLEEVE SEAL CONNECTORS. The sleeve seal connector is characterized by effecting a seal between the union and a sleeve. In some cases two parallel seals are required, the first as previously mentioned and the second between the tube and the sleeve. The sleeve is usually attached permanently to the tubing by swaging, brazing, or welding. The following paragraphs describe various sleeve seal connectors.

MS Flareless. The MS flareless connector shown in Figure 5.12.3.14a is made up of a union, a sleeve (often referred to as a ferrule), and a nut. As the tubing is inserted into the union, it is seated on an internal shoulder; the ferrule is then slid along the tube and seated against the internal taper of the union. Following this, the nut is tightened and the sharp edge of the ferrule is driven into the tubing, forming a seal and forcing the tube forward against the shoulder. At this same time, the seal of ferrule-to-internal taper of the union is formed, as the ferrule bows up to make contact with the internal taper. After the initial connection, the ferrule is locked on the tubing. Upon disassembly, a certain amount of springback takes place in the ferrule, and as long as the connector is not overtorqued, reuse is acceptable. Overtorquing can cause yielding of the ferrule, loss of the ferrule, and/or springback, and may result in poor sealing.

It has been found that machine presetting the ferrule on the tubing results in a better quality connector. However, even this operation requires a certain degree of skill, although machines such as the Weatherhead fixed stop or Parker hydraulic pressure-balanced preset machines are well suited for repeatability and rapid, uniform presets. Another limitation of this connector is the fact that the exterior surfaces of the tubing and ferrule must be protected from damage if a leak-free connector is to be insured.

Flodar Fitting. The Flodar connector, manufactured by the Flodar Corporation and shown in Figure 5.12.3.14b, is similar to the MS flareless connector in external appearance. The Flodar, like the MS connector, uses a union,

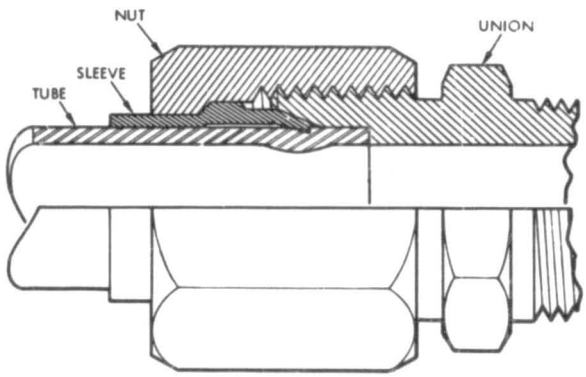

Figure 5.12.3.14a. MS Flareless Connector

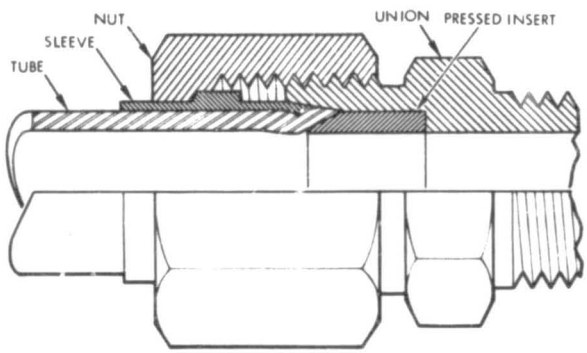

Figure 5.12.3.14b. Flodar Connector
(Courtesy of Flodar Corporation, Cleveland, Ohio)

sleeve, and nut. In the Flodar fitting, as the nut is tightened onto the union the tube is flared slightly at the end, a result of the internal part of the union having a V-shaped seating surface. The sleeve bears against the back of the tube flare to retain the tubing, preventing tube "pull out" and forming a secondary seal. The rear portion of the sleeve is slotted every 90 degrees to give a "collet grip," which aids in dampening vibration.

Swagelok. The Swagelok connector, manufactured by the Crawford Fittings Corporation and shown in Figure 5.12.3.14c, is also similar to the MS flareless connector. As in the MS connector, the tube is seated against an internal shoulder within the union. However, instead of a single piece sleeve, the Swagelok employs two pieces, the front ferrule and the rear ferrule, both of which are contained within the nut.

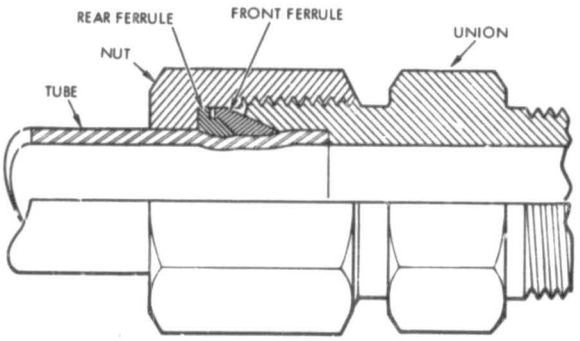

Figure 5.12.3.14c. Swagelok Connector
(Courtesy of Crawford Fitting Corporation, Cleveland, Ohio)

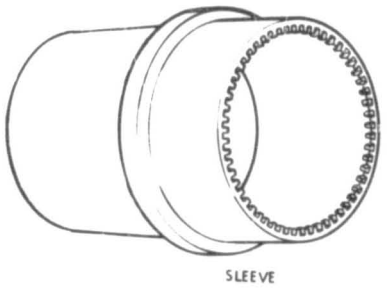

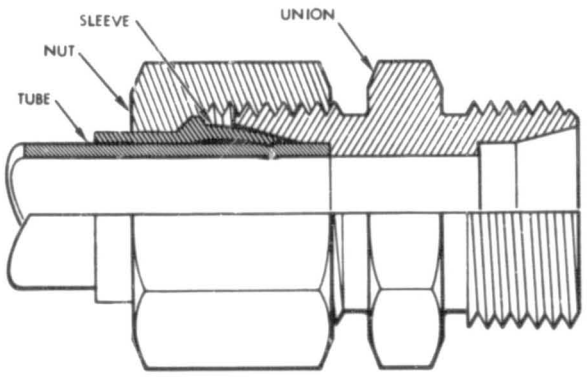

Figure 5.12.3.14d. Sermeto Serrated-Sleeve Connector
(Courtesy of The Weatherhead Company, Cleveland, Ohio)

In seating the tube against the union, the nut forces the rear ferrule against the front ferrule and both ferrules bite into the tube, forcing the tube against the inner shoulder of the union. A secondary seal of front ferrule-to-union is also formed upon tightening the connector nut. The double ferrule offers greater tube holding than the MS flareless connector.

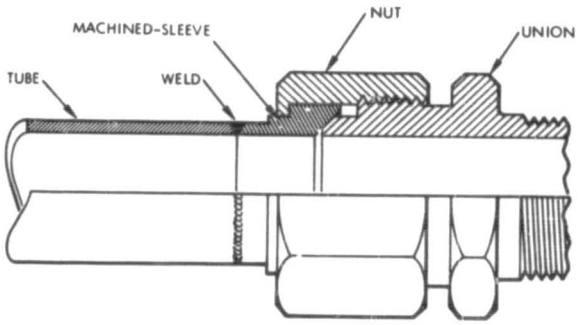

Figure 5.12.3.14e. Machined-Sleeve Connector
(Reference 36-11)

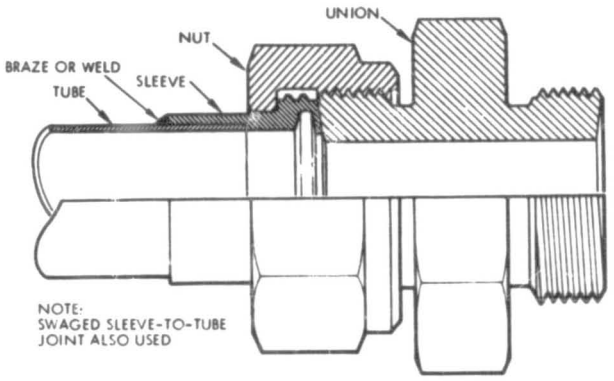

Figure 5.12.3.14f. Dynatube Connector
(Courtesy of Resistoflex Corporation, Roseland, New Jersey)

Sermeto Serrated Sleeve. The Sermeto Serrated Sleeve, manufactured by the Weatherhead Company and shown in Figure 5.12.3.14d, seats the tubing against the inner shoulder of the union in exactly the same fashion as the MS connector. The sleeve of this connector is a single piece, but is similar to the combination of front and rear ferrule in the Swagelok connector in that it is contained completely within the nut. In addition, the leading edge on the sleeve inner diameter is serrated, giving a greater cutting edge area than a smooth sleeve, and providing additional retention of the tube.

Machined Sleeve. This type of connector, as shown in Figure 5.12.3.14e, utilizes standard AN nuts and mating parts. The sleeve, however, is a specially machined piece that is permanently attached to the tubing. In this connector, the sleeve mates with the tapered nose of the union to form the seal. The machined sleeve connector is generally considered to be a stronger connector than standard AN or MS flared connectors, and is less sensitive to vibration environments.

Dynatube. The Dynatube connector, manufactured by the Resistoflex Corporation and shown in Figure 5.12.3.14f,

utilizes as the sealing member a specially designed sleeve which is directly and permanently connected to the tubing. The face of the sleeve seals against the union (mating part) as the nut is drawn tight. Internal pressure assists in making the seal during operation. A feature of this connector is the small threaded portion on the exterior of the sleeve which engages the threads of the nut when the fitting is disconnected, preventing the sealing surface from being exposed, as well as preventing the nut from slipping back on the tubing.

Hi-Seal. The Hi-Seal connector, manufactured by Imperial Eastman Corporation and shown in Figure 5.12.3.14g, is composed of a sleeve, a nut, and a union. The sleeve has a precision 12-degree cone which slides into the union and provides the seal as the nut is drawn onto the union. The nut also drives the serrated edges on the inside of the sleeve into the tubing, thus swaging the sleeve permanently to the tubing.

Lo-Torque. The Lo-Torque connector, manufactured by Parker Aircraft Company and shown in Figure 5.12.3.14h, is similar to the machined sleeve connector previously described. Generally, the sleeve and threaded flange are brazed to the tubing instead of being welded.

5.12.3.15 SEPARATE SEAL CONNECTORS. The separate seal connector employs an individual piece, functionally identical to a flange gasket, to accomplish connector sealing. This type of connector generally has all components except the seal attached to the tubing system, thus the seal is the only "loose" piece. The major disadvantage of separate seal connectors is the possibility of omitting the seal at assembly. Several types of separate seal connectors are described in the following paragraphs.

AFRPL Connector. The AFRPL connector, shown in Figure 5.12.3.15a, was developed for the Air Force by Battelle Memorial Institute (Reference 44-14) to temperature and environment specifications beyond the capability of most commercially available connectors. In this connector, a separate seal, referred to as the "bobbin seal," is used as the sealing member, so named because of its resemblance to the bobbin of a sewing machine.

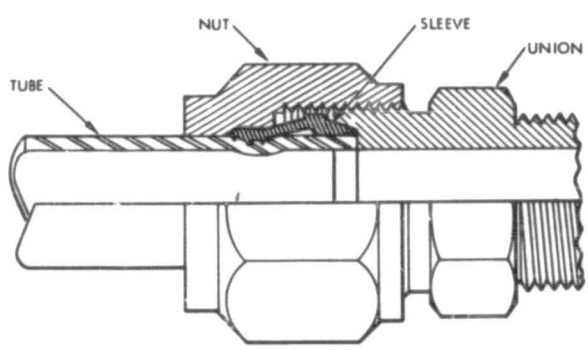

Figure 5.12.3.14g. Hi-Seal Connector
(Courtesy of Imperial Eastman Corporation, Chicago, Illinois)

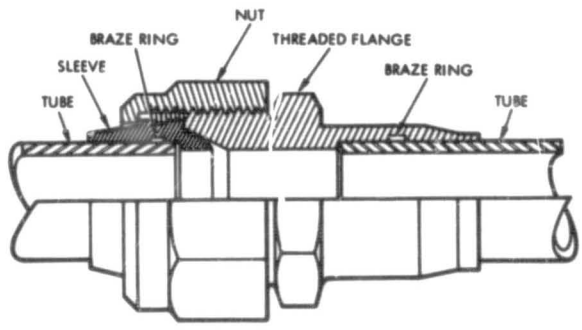

Figure 5.12.3.14h. Parker Lo-Torque Connector
(Courtesy of Parker Aircraft Co., Los Angeles, California)

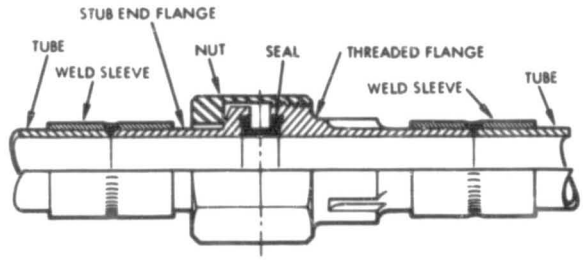

Figure 5.12.3.15a. AFRPL Connector, Showing Tube-to-Tube Connection

The conical discs of the bobbin seal mate with the plain stub end on one side, and with the threaded stub end on the other. As the connector is tightened, plastic deformation of the seal legs occurs on the radial surfaces and the necessary connector seal is created. Reuse of the seal is not recommended, since the sealing surfaces have been deformed and an intimate mating of surfaces cannot be guaranteed. Depending upon the materials involved and the intended usage, the bobbin seal may or may not be plated. The AFRPL connector is normally welded to the tube, as illustrated.

Advantages of this connector are: (1) positive sealing can be achieved by the development of sufficient sealing stresses without excessive torque, and (2) this design affords a wide range of preloading values and can be made to give parallel loading. The major disadvantage of this connector is that the seal must be replaced after a single usage. The connector can be inspected for possible seal omission: if the seal is left out, the nut will be threaded well beyond the thread form on the threaded flange, thus providing obvious detection.

Gamah Connector. This connector, manufactured by the the Gamah Corporation and shown in Figure 5.12.3.15b, employs a seal member which is essentially a belleville spring. Sealing is accomplished by plastic deformation of the seal member. In this connector, the seal can be reversed and used a second time, but further use is not recommended. To achieve a minimum envelope size, the connector uses a circular nut, which requires a spanner wrench for tightening. The connector parts that are joined to the tubing are usually swaged on to the tube, but may be welded or brazed.

Astro-Weight Connector. This connector, manufactured by Harrison Manufacturing Company and shown in Figure 5.12.3.15c, utilizes a K-seal which attains sealing by metallic elasticity as well as pressure energization. Upon assembly, the seal makes intimate contact with the sleeve and the connector. When system pressure is applied the seal is forced against the sleeve and the connector to assist sealing still further. The sleeve and male nut of the connector can be swaged, welded, or brazed to the tubing.

Roylyn Connector. This connector, manufactured by Roylyn Incorporated and shown in Figure 5.12.3.15d, is a four-piece unit that generally has the male fitting and the sleeve welded to the tubing, with the nut loose on the tubing but prevented from falling off by the position of the sleeve. The separate seal is of the belleville spring type.

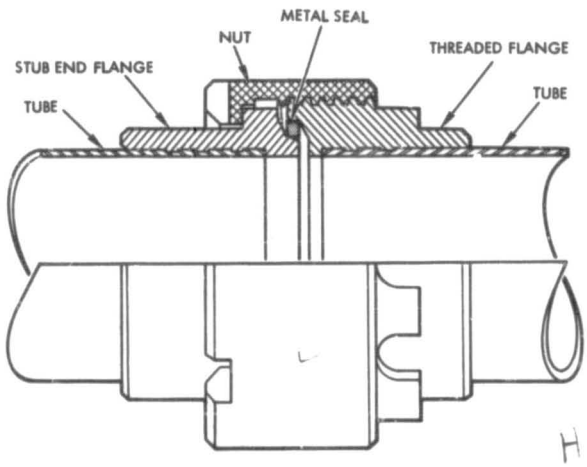

Figure 5.12.3.15b. Gamah Connector, Showing Tube-to-Tube Connection

(Courtesy of Gamah Corporation, Denver, Colorado)

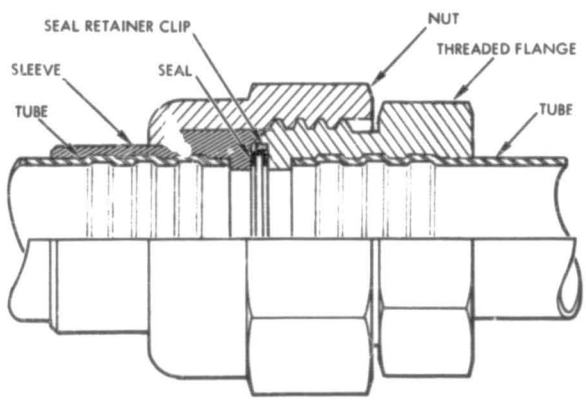

Figure 5.12.3.15c. Astro-Weight Connector Showing Tube-to-Tube Connection

(Courtesy of Harrison Manufacturing Co., Burbank, California)

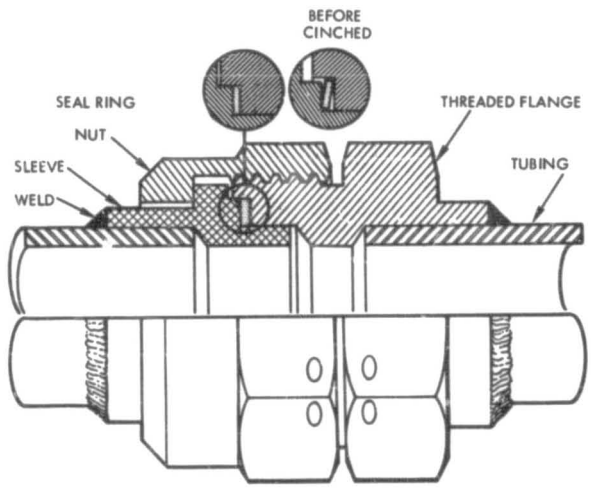

Figure 5.12.3.15d. Roylyn Connector, Showing Tube-to-Tube Connection

(Courtesy of Roylyn Incorporated, Glendale, California)

Rubbernek Connector. This connector, manufactured by the Chicago Fittings Corporation and shown in Figure 5.12.3.15e, is another of the flareless tube type that employs a special five-piece sealing and tube-retaining element in addition to the standard union and connecting nut. The seal is molded from synthetic rubber compounds. In connecting the nut to the union, the retainer and guide force the anchor to clamp the tubing while the seal is forced against the union. The anchor is essentially a belleville spring with a sharp edge that provides the means for tube retention.

Aeroquip Marman Conoseal Connector. This connector, manufactured by Aeroquip Corporation/Marman Division and shown in Figure 5.12.3.15f, is a four-piece unit that has the male flange and the sleeve flange welded to the tubing. The connector nut is loose on the tubing, but is prevented from falling off by the position of the sleeve. The separate seal is of the belleville spring type.

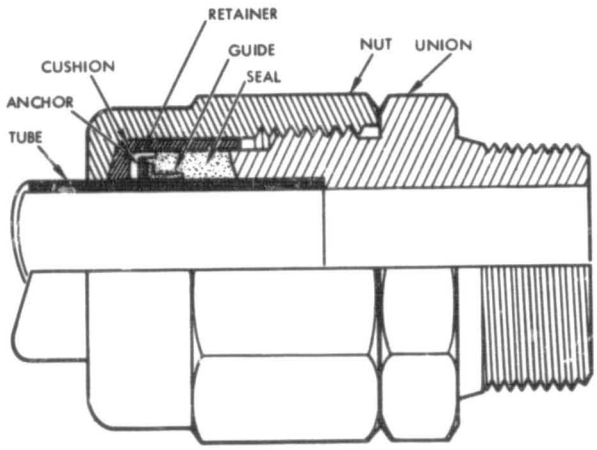

Figure 5.12.3.15e. Rubbernek Connector
(Courtesy of Chicago Fittings Corporation, Broadview, Illinois)

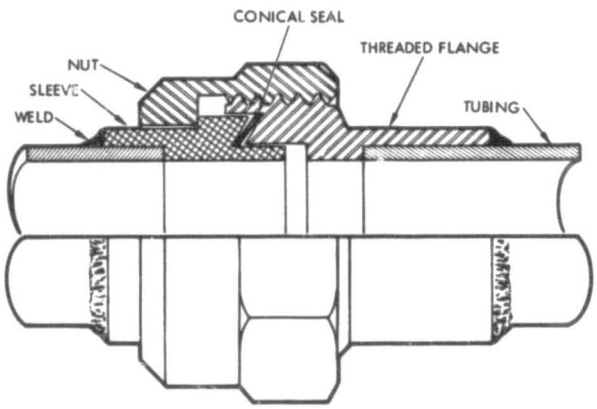

Figure 5.12.3.15f. Aeroquip Marman Conoseal Connector, Showing Tube-to-Tube Connection
(Courtesy of Marman Division, Aeroquip Corporation, Jackson, Michigan)

5.12.4 Bolted Flange Connectors

5.12.4.1 GENERAL DESCRIPTION. Bolted flange connectors incorporate the same three basic elements found in threaded connectors: the seal, the connector-to-line joint, and the load-carrying structure (see Sub-Topic 5.12.3). The outstanding difference between bolted flange connectors and threaded connectors is the number of tensile members in the load-carrying structure. Whereas threaded connectors have a single threaded element, in flanged connectors the tensile load is normally divided between four or more threaded elements. Static seals are usually used between the flanges, while the flange is usually welded or brazed to the line.

Bolted flange connectors can be generally classed as having either integral or separate flanges (see Figure 5.12.4.1). For the same flange material, the integral type will usually be lighter than a corresponding separate flange connector; however, alignment of bolt holes is easier with the separate type flange. Separate flanges are also referred to as loose or floating flanges. In some cases it may be possible to select a higher strength material for the separate flange, since it need not be compatible with the fluid in the system, nor weldable or brazable to the line material. With both integral and separate flange connectors there are numerous possible specific designs utilizing various seal and facing configurations, some of which are illustrated in Figure 6.3.2.4b.

In the following detailed topics, some of the more important factors related to the design and selection of a bolted flange connector for aerospace applications are considered.

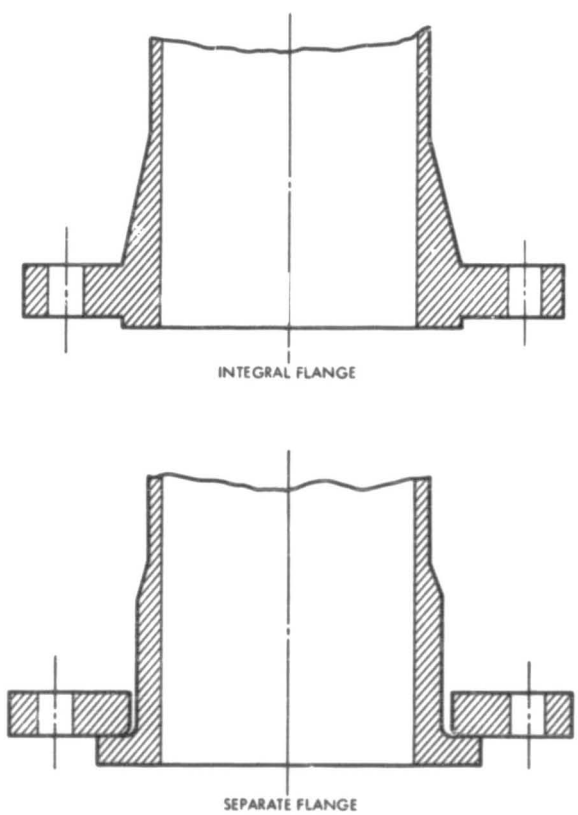

Figure 5.12.4.1. Integral Flange and Separate (Loose) Flange

Those basic separable connector considerations equally applicable to threaded and bolted flange connectors are treated under "Threaded Connectors" as follows:

Factor	Detailed Topic
Threaded Connector Design and Selection Criteria	5.12.3.1
Connector Preload	5.12.3.2
Seal Seating Load	5.12.3.3
Pressure End Load	5.12.3.4
Bending Moment Load	5.12.3.5
External Axial and Torsional Load	5.12.3.6
Vibration	5.12.3.7
Connector Assembly	5.12.3.8
Contamination	5.12.3.9
Temperature and Thermal Shock	5.12.3.10
Additional Factors	5.12.3.11

5.12.4.2 ENVIRONMENTAL AND SERVICE CONSIDERATIONS. Prior to designing or selecting any bolted flanged connector, the anticipated environment and service must be known. Important parameters include:

a) Maximum and minimum operating pressure

b) Maximum and minimum operating temperature

c) Chemical compatibility of flange materials with contained fluid

d) Vibration environment

e) Compatibility of flange and tubing from the standpoint of welding or brazing

f) Required service life, anticipated material creep

g) Maximum thermal gradients anticipated

h) Types and magnitudes of external loads

i) Maximum permissible leakage rate(s)

j) Size and weight limitations.

5.12.4.3 BOLT TORQUING. Bolt torque is determined by flange preload requirements. The preload must be high enough to properly seat the seal and provide greater compressive strain than the expected strain relaxation caused by tensile loads, yet must not be too high so that overstressing of the gasket and/or flange tensile members results. Parallel gasket loading, described in Detailed Topic 5.12.3.2, protects the gasket from over-torquing, but also places extreme importance on seal gland design. Establishing the proper preload value is essential in obtaining seal seating and maintaining a seal during operation. The factors that must be considered in determining the required preload are:

a) Spring constants of the compression and tension members

b) Minimum compressive load on the flange members needed to prevent leakage

c) Maximum allowable stress in the tensile member

d) Magnitude of the structural loads effects on thermal gradients.

A detailed discussion of preload is given in Detailed Topic 5.12.3.2.

Table 5.12.4.3 shows the relationship between bolt stress and torque. It should be noted that this table makes no allowance for friction, therefore the values given represent upper limits, actual values being lower depending on friction. Because of the loss of torque caused by friction, and the variable it introduces, every attempt should be made to minimize friction by lubricating bolts and nuts, and to avoid the use of high-friction self-locking nuts.

The sequence of bolt tightening is discussed in Detailed Topic 5.12.4.8.

5.12.4.4 FLANGE DEFLECTIONS AND DISTORTIONS. Three problems common to bolted flange joints which can be avoided by proper flange design and selection procedures are (1) flange rolling, (2) flange scrubbing, and (3) flange bowing (see Figure 5.12.4.4). Flange rolling describes the tendency of a bolted flanged connector to separate at the sealing surface while simultaneously making more intimate contact outside the bolt circle. Flange rolling may

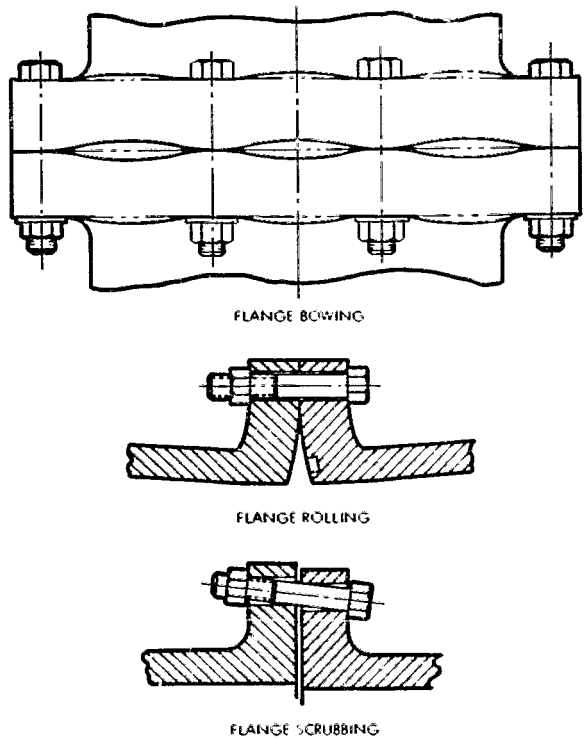

Figure 5.12.4.4. Deflections and Distortions in Flanges

Table 5.12.4.3. Relationship of Bolt Stress to Torque for Various Bolt Sizes

(This table makes no allowance for friction, therefore the values of torque and stress given here represent upper limits)

Bolt Size (in.)	No. Threads per inch			Root Area (in^2)	Tensile Stress for Torque of 1 in-lb (psi)	Axial Load with Torque of 1 in-lb on Nut (lbs)
	Coarse	Fine	Extra Fine			
1/4	20	28	32	0.0269 0.0326 0.0352	1,115 879 807	20.6 21.5 21.7
5/16	18	24	32	0.0454 0.0524 0.0590	512 432 377	16.6 17.1 17.6
3/8	16	24	32	0.0678 0.0809 0.0890	292 261 213	14.3 14.9 15.3
7/16	14	20	28	0.0933 0.1090 0.1217	179 150 132	12.2 12.6 13.0
1/2	13	20	28	0.1257 0.1486 0.1634	118 97 86	10.9 11.4 11.7
9/16	12	18	24	0.1620 0.1888 0.2054	82.3 68.8 63.3	9.9 10.3 10.5
5/8	11	18	24	0.2018 0.2400 0.2586	59.3 48.2 44.3	8.72 9.24 9.33
3/4	10	16	20	0.3020 0.3513 0.3725	32.1 27.0 25.3	7.34 7.64 7.68
7/8	9	14	20	0.4183 0.4805 0.5200	20.4 17.6 16.1	6.52 6.78 6.92
1	8	14	20	0.5510 0.6464 0.6921	13.6 11.6 10.6	5.73 5.99 6.09
1-1/8	7	12	18	0.6931 0.8118 0.8772	9.61 8.06 7.43	5.08 5.32 5.43
1-1/4	7	12	18	0.8698 1.0238 1.0969	6.71 5.73 5.35	4.62 4.80 4.90
1-3/8	6	12		1.0541 1.2602	5.17 4.24	4.18 4.40
1-1/2	6	12	18	1.2938 1.5212 1.6101	3.84 3.31 3.17	3.86 4.16 4.32

result where tube walls are thin and afford little resistance to rolling moments; where flanges lack sufficient rigidity and consequently deflect under high end loads; or where there is no flange contact outside of the bolt circle, in which case the outermost point of flange contact serves as a fulcrum. Flange rolling can be minimized by making flanges rigid, by making the bolt circle as close to the pipe or tube as possible, and through the use of full face gaskets. The adverse effects of flange rolling can be minimized through the use of raised face flanges.

Flange scrubbing is a condition where there is radial displacement of one flange with respect to the other, i.e., motion of flanges in a direction perpendicular to the tubing axis. This condition can result from differential contraction or expansion of dissimilar flange materials, or from flange misalignment. Scrubbing causes motion at the sealing interface, which can materially degrade the seal.

Bowing is a problem that results from spacing bolts too far apart and/or insufficiently rigid flanges.

5.12.4.5 ALLOWABLE BOLTED FLANGE CONNECTOR STRESSES. In flange design where creep is not a factor, allowable stresses may be related to the short-time yield strength of the material. Yield strength selected as a basis for design should be that at the maximum anticipated service temperature.

An allowable stress for flange material, equal to two-thirds of the material yield strength, conforms to general pressure vessel design practice. (The ASME Code, Reference 68-70, uses 62.5 percent for ferrous materials, two-thirds for non-ferrous materials.) Since in flanged joints the criterion of failure involves excessive deformation rather than rupture, ultimate tensile strength of the material is not directly considered. An allowable stress of two-thirds of the yield strength implies that at a proof test pressure of 1.5 times the operating pressure, the stress may reach the yield strength of the material.

Allowable bolt stresses no higher than 50 percent of the material yield strength are suggested. The allowable stress for bolting is set lower than for the flanges for the following reasons:

a) Bolts are loaded in tension with no ability to transfer load to some other part of the structure in case of overload

b) The only bolt stress calculated is that due to the axial forces whereas, in service, the bolts will have some bending and shear stresses due to rotation of the flanges

c) The threads on the bolts form a notch with accompanying stress intensification

d) In service, the bolts are loaded in initial bolt make-up by tightening with a wrench, which introduces shear stresses and a reduction in axial yield strength.

For a proof test pressure of 1.5 times the operating pressure, it will be necessary to tighten the bolts beyond the recommended 50 percent up to 75 to 90 percent of their yield strength. Typical allowable stress values for several materials based on the above criteria are given in Table 5.12.4.5. It should be noted that materials which obtain their strength by heat treatment may be altered in welding or brazing flanges to the tube. However, if the joining process is such as to limit the heat-affected zone to a small volume of material, design of the bolted flange connection may be based on the heat treatment properties of the material.

5.12.4.6 FACING CONSIDERATIONS. The subject of flange facing types is discussed in Detailed Topic 6.3.2.4, "Gland Design," where seal glands are classified as unconfined, semi-confined, and fully-confined and are illustrated in Figure 6.3.2.4b. Some additional considerations influencing the selection flange facing are discussed in the following paragraphs.

Fully confined (tongue-and-groove) or semi-confined facings aid in locating and holding the gasket during assembly and reduce the possibility of gasket blowout. Also, at least one of the faces is partially protected against damage during handling and assembly of the joints. With metal gaskets, and where low-leakage rates with gases are desired, protecting the flange seating surface during shipment, storage, fabrication, assembly, and possible reassemblies, becomes very important. The ring joint or double groove facing provide particularly good protection of the flange sealing surfaces.

Where the joints will be subjected to high temperatures in service, there is a possibility of partial welding of metal gaskets to the flange faces. Use of dissimilar metals will help to prevent this problem, and in cases where fluid compatibility permits, a graphite lubricant film on the seating surfaces may aid in disassembly. Nonmetallic gaskets will generally harden after long periods of high-temperature service. The raised face configuration has some advantage in this respect, since a much-used gasket of this design can be removed more easily than one with the tongue-and-groove or semiconfined facings.

5.12.4.7 BOLTING DIMENSIONAL DETAILS. Tables 5.12.4.7a and b give pertinent details on bolting suitable for bolted-flanged connections designed for minimum weight. It is desirable to locate the bolts as close to the tube wall as possible. The bolting listed requires a minimum of radial clearance between bolts and flange hub or stub-end wall. In some instances it may be desirable to spot-face the hub or stub end wall to minimize bolt-to-tube wall distance. Socket-head cap screws are suggested in small sizes (No. 5 through No. 12 Am. Std. socket-head cap screws), and NAS 624/636 external wrenching bolts in larger sizes ($\frac{1}{4}$-inch through one inch). NAS-type bolts are suggested for larger sizes since standard socket-head cap screws may have inadequate bearing areas. The radial and between-bolts minimum clearances shown in the table are based on allowances for fillets, use of standard socket wrenches, and for minimum space between bolts. The "rule-of-thumb" is that the distance between bolt holes should be at least equal to the bolt hole diameter.

Table 5.12.4.5. Typical Allowable Stress Values Using the Following Criteria:
Allowable Stress for Flanges = Two-Thirds Yield Strength
Allowable Stress for Bolts = One-Half Yield Strength

Material (Yield strengths are specified minimums)	Allowable Stress for Indicated Temperature, psi			
	Up to 100 °F	150 °F	200 °F	250 °F
Aluminum alloy, 6061-T6				
35,000-psi yield strength				
38,000-psi ultimate tensile strength				
Flanges	23,300	23,000	22,700	21,900
Bolts	17,500	17,200	17,000	16,400
Aluminum alloy, 2014-T6				
55,000-psi yield strength				
65,000-psi ultimate tensile strength				
Flanges	36,700	35,800	34,500	31,200
Bolts	27,500	26,800	25,700	23,400
	Up to 100 °F	300 °F	500 °F	700 °F
Type 347, annealed stainless steel				
35,000-psi yield strength				
75,000-psi ultimate tensile strength				
Flanges	23,300	20,000	18,900	18,900
Bolts	17,500	15,100	14,200	14,200
Type 301, cold-rolled stainless steel				
90,000-psi yield strength				
115,000-psi ultimate tensile strength				
Bolts	45,000	40,000	38,000	36,000
	Up to 100 °F	300 °F	500 °F	600 °F
AM 355, precipitation hardened				
150,000-psi yield strength				
290,000-psi ultimate tensile strength				
Flanges	100,000	85,000	79,000	73,000
Bolts	75,000	63,000	59,000	54,000
	Up to 100 °F	400 °F	600 °F	800 °F
Rene' 41, nickel-base alloy				
130,000-psi yield strength				
170,000-psi ultimate tensile strength				
Flanges	86,000	84,000	82,000	80,000
Bolts	65,000	63,000	61,000	60,000

Table 5.12.4.7a. Flange Bolting Dimensions for Socket Head Capscrews

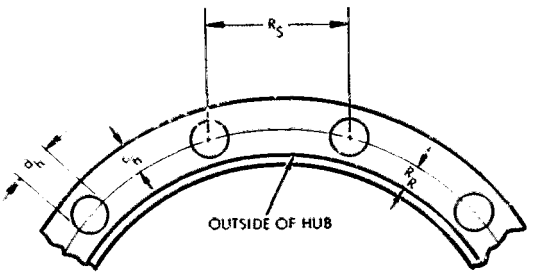

INTEGRAL FLANGE

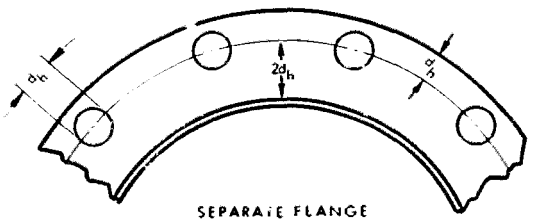

SEPARATE FLANGE

Nominal Size* (in.)	Threads per inch	Root Area, A_{BJ} (sq. in.)	Radial Clearance, R_R	Minimum Space, R_S	Hole Size, d_h	Maximum Head Diameter (in.)
#5	44	0.00716	0.132	0.396	0.141	0.200
#6	40	0.00874	0.143	0.429	0.152	0.221
#8	36	0.01285	0.165	0.495	0.180	0.265
#10	32	0.0175	0.186	0.558	0.209	0.306
#12	28	0.0226	0.202	0.606	0.240	0.337
1/4	28	0.0326	0.259	0.657	0.281	0.438
5/16	24	0.0524	0.306	0.796	0.344	0.531
3/8	24	0.0809	0.365	0.974	0.406	0.649
7/16	20	0.109	0.415	1.125	0.469	0.750
1/2	20	0.149	0.464	1.242	0.532	0.828
9/16	18	0.189	0.519	1.407	0.594	0.938
5/8	18	0.240	0.575	1.575	0.687	1.050
3/4	16	0.351	0.665	1.845	0.812	1.230
7/8	14	0.480	0.779	2.157	0.937	1.438
1	12	0.625	0.870	2.437	1.062	1.620

* Sizes #5 through #12, American Standard Socket Head Cap Screws, ASA B18.3-1954

R_R = (Max Head Dia./2) + 0.030 inches

$R_S = 3 R_R$

Sizes 1/4" through 1" Dimensionally to National Aircraft Standards, NAS 624 through 636

R_R = 1/2 (Maximum Head Diameter) + 0.040 inches for 1/4" through 7/16" nominal size

1/2 (Maximum Head Diameter) + 0.050 inches for 1/2" through 3/4" nominal size

1/2 (Maximum Head Diameter) + 0.060 inches for 7/8" and 1" nominal size

R_S = 1.5 + Maximum Head Diameter

Table 5.12.4.7b. Estimation of Bolt Size and Spacing for External-Wrenching Bolts
(Reference 46-29)

(1) Total Bolt Area (Bolt Circle Radius)			(2)	(3) Root Area			(4)	(5)
Fine (in.)	Coarse (in.)	8-Thread (in.)	Bolt Size (in.)	Fine (in^2)	Coarse (in^2)	8-Thread (in^2)	Bolt Spacing* (in.)	Edge Distance (in.)
0.273	0.225	-	1/4	0.0326	0.0269	-	3/4	3/8
0.406	0.352	-	5/16	0.0524	0.0454	-	13/16	7/16
0.508	0.426	-	3/8	0.0809	0.0678	-	1	1/2
0.609	0.521	-	7/16	0.1090	0.0953	-	1-1/8	9/16
0.748	0.633	-	1/2	0.1486	0.126	-	1.25	0.62
1.007	0.845	-	5/8	0.2400	0.202	-	1.50	0.75
1.262	1.083	-	3/4	0.3513	0.302	-	1.75	0.81
1.464	1.278	-	7/8	0.4805	0.419	-	2.06	0.94
1.743	1.537	1.537	1	0.6245	0.551	0.551	2.25	1.06
2.040	1.740	1.828	1-1/8	0.8118	0.693	0.728	2.50	1.12
2.29	1.988	2.08	1-1/4	1.024	0.890	0.929	2.81	1.25
2.69	2.16	2.37	1-3/8	1.260	1.054	1.155	3.06	1.37
2.94	2.50	2.71	1-1/2	1.521	1.294	1.405	3.25	1.50

*This spacing can be reduced with internal-wrenching bolts, or by use of special thin-wall wrenches, causing an appreciable reduction in flange weight, since the bolt size can be reduced one or two sizes.

A maximum spacing between bolts equal to $2(d_h + t)$ is suggested, where d_h is the bolt hole diameter and t is the flange thickness. If bolts are too far apart, flange bowing may result in gasket leakage.

Bolting shown in Table 5.12.4.7a may be used with nuts, or the bolts may be studded into tapped holes in a mating flange. The studded design is advantageous from the standpoint of assembly, and provides a slight weight reduction. Use of bolts and nuts also permits easier replacement in case of damaged or seized threads. This is a particularly important consideration if disassembly and re-assembly are required after service at high temperature or under a hard vacuum, since thread seizing under these conditions is a strong possibility.

5.12.4.8 BOLTED FLANGE CONNECTOR HANDLING AND ASSEMBLY. Bolt load should be controlled by using a torque wrench when tightening bolts. Since torque-bolt load relationships vary with such factors as material, thread class, surface finishes, and lubricant, the relationship for the particular combination of bolting, surfaces, and lubricant should be checked. The magnitude of bolt torque to be used is covered in Detailed Topic 5.12.4.3.

To facilitate proper assembly, whether using a nut and bolt or a stud-end nut arrangement, it is necessary to clean the threads and to be sure that the nuts do not bind when assembled. Flange seating surfaces and gasket should be checked for cleanliness. The gasket should be carefully placed in position and all bolts inserted and tightened finger tight. Bolts should then be tightened in sequence, as indicated in Figure 5.12.4.8. The number of tightening rounds (the number of times each bolt is tightened in sequence) will vary depending upon the specific application. With some aerospace applications involving o-rings, it is standard practice to torque all bolts to 100 percent of final torque on the first round. In other instances, such as some critical joints using laminated asbestos gaskets, bolts are torqued down in increments of 10 percent of final torque

per round. The majority of aerospace applications call for bolt tightening in increments of one-third or one-fourth of final torque per round. It is desirable to recheck the bolt torque after a period of 24 to 48 hours and, if possible, after a short period of operation under service conditions.

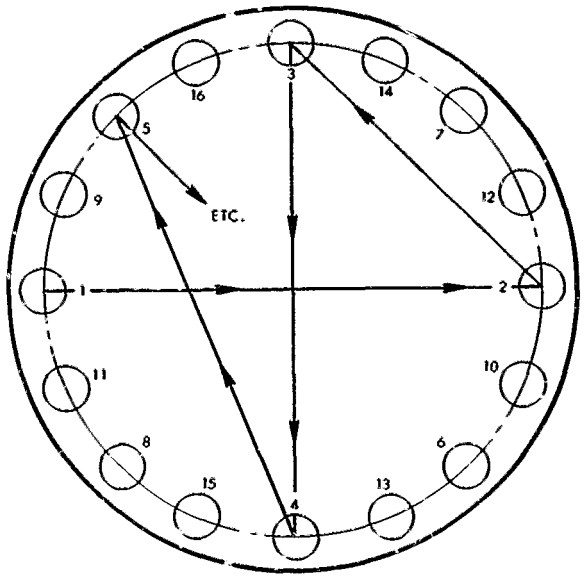

TIGHTENING SEQUENCE FOR 16-BOLT FLANGE

Figure 5.12.4.8. Example of Bolt-Tightening Sequence

5.12.4.9 GASKET CONSIDERATIONS. The types of gaskets employed with flanges consist generally of (1) annular ring gaskets, (2) pressure energized gaskets, and (3) full face gaskets. The most widely used gasket for bolted-flange connections is the annular ring type. The pressure energized gasket (gaskets with sealing action aided by internal pressures) are shown in Table 6.3.3.5b, (Sub-Section 6.3). Full face gaskets generally require higher bolt loads than comparable connections using "inside gaskets" (i.e., annular ring gaskets). Disadvantages of full faced gaskets include less tolerance against thermal gradients and a tendency for the load on the gasket to be concentrated at the bolt holes and on the portion of the gasket outside the bolt circle. Full faced gaskets are widely used for mild service conditions, but seldom for severe service conditions involving either high (above 450°F) or low (cryogenic) temperatures, or pressures above 300 psig.

Gasket thickness must be sufficient enough to provide adequate "conformity," since thicker gaskets generally are able to conform to surface scratches and to compensate for sealing waviness. However, gaskets must be thin enough to provide stability and prevent "blowout" when residual stresses are low and internal pressures high.

Two important design criteria related to gaskets and their proper selection are (1) seating stress, and (2) residual stress. Suggested design values for seating stresses are given in Detailed Topic 6.3.3.2.

5.12.4.10 FLANGE DESIGN PROCEDURES. Step-by-step design procedures for bolted flanges, specifically oriented toward aerospace applications, are contained in the following documents:

"Tentative Separable Connector Design Handbook," Contract NAS 8-4012 Advanced Technology Laboratories, General Electric Company (46-29)

"Development of Mechanical Fittings, Phases I and II," Technical Documentary Report RTD-TDR-63-1115, Battelle Memorial Institute (44-14)

Other references dealing with bolted flanged connector design for general applications are:

Taylor Forge Bulletin 502, 5th Edition (V-357)

ASME Boiler and Pressure Vessel Code, Section VIII (68-70)

5.12.4.11 RING CLAMP FLANGES. Ring clamps (see Figure 5.12.4.11) were devised in an attempt to duplicate a flanged connection without using a great number of bolts. Generally, the ring clamp is made of two mating flanges with tapered outer surfaces, over which is fitted a split hoop whose inside surfaces are tapered at the same angle as the flange. Small projections with bolt holes are provided where the two halves of the hoop are mated; usually two bolts are used, but if one side of the ring is pivoted, a single bolt may be used. When the bolt(s) are tightened, a clamping force normal to the tapered faces is imposed. The axial component of the clamping force is the only force available for sealing and preloading. The ring clamp is used extensively for many commercial applications and has been used in missile systems, usually for large-diameter, low-pressure, lightweight joints. Its major limitations are:

a) It is difficult to attain high preloads and control initial preload within narrow limits. This is largely due to the friction in the V-band clamp, which results in uneven loading around the circumference.

b) The weight of a fitting of this type would far exceed that of standard-type flanges for high-pressure applications.

Advantages of ring clamp flanges include speed of assembly or disassembly, and the lack of requirements for wrench accessability around the entire perimeter of the connector.

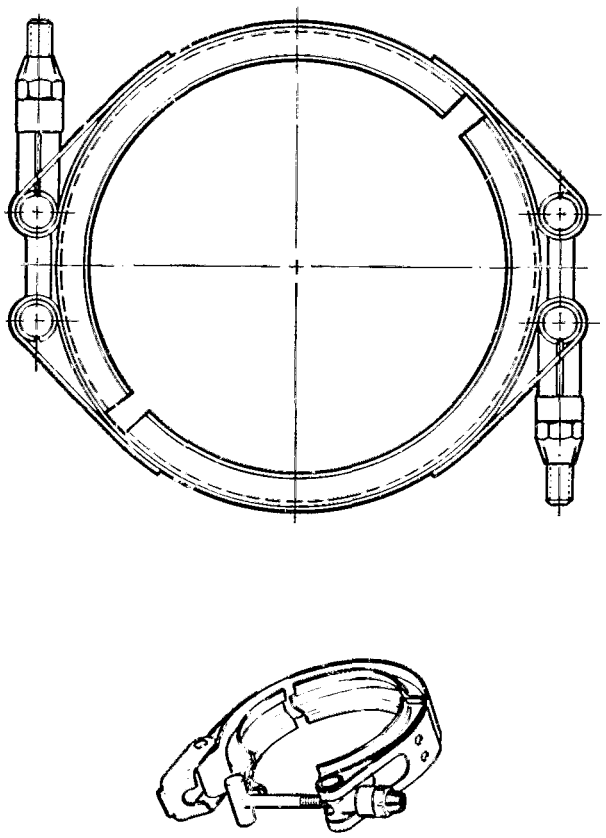

Figure 5.12.4.11. Typical Ring Clamp
(Courtesy of Marman Division, Aeroquip Corporation, Los Angeles, California)

Ring clamp flanges may be expected to perform well in those non-critical low-pressure applications requiring frequent disassembly, especially in large diameters which would require either large numbers of bolts or heavy flanges (for stiffness) if conventional bolted-flange designs were used.

5.12.5 Brazed Joints and Connectors

5.12.5.1 GENERAL. Brazed joints are being used increasingly in aerospace fluid system applications because of their advantages of low leakage under extremes of temperature, pressure, and vibration while providing a capability for disconnecting and rejoining. Brazing is used in making tube-to-connector joints in both threaded and flanged-type connectors, as well as to perform both the joining and sealing functions in brazed connectors. Brazed connectors include a variety of brazed sleeves used for joining tubing. This sub-topic describes various brazed connector configurations, and considers brazed-joint desig and installation parameters.

5.12.5.2 THE BRAZING PROCESS. Brazing is a metal-joining operation performed at temperatures ranging between those of welding and soft soldering, with soft soldering temperatures considered to be below 800 F. Brazing differs from welding in that (1) bonding results from wetting rather than melting the base alloy, (2) the brazing filler metal (brazing alloy) is made to flow into the joint capillary, and (3) the brazing filler metal is an alloy having a composition different from that of the metals being joined. Almost all similar metals and alloys, or metals and alloys with similar coefficients of expansion above 1100 F, may be joined by brazing.

The American Welding Society and the American Society for Testing Materials list brazing filler metals under the following seven classifications:

1) Aluminum-silicon (used only on grades of aluminum with relatively high melting temperatures)

2) Copper-phosphorous (used primarily for joining copper and copper alloys)

3) Silver (used on virtually all ferrous and non-ferrous metals except aluminum, magnesium, and several other low melting-point metals)

4) Copper-gold (used primarily in electron tube assembly)

5) Copper and copper-zinc (used for joining both ferrous and non-ferrous metals)

6) Magnesium (used for magnesium alloy base material)

7) Heat-resistant brazing filler metals (used primarily where extreme heat or corrosion resistance is required).

There are other special purpose filler metals in addition to these seven classes, some of which are listed in the Welding Handbook, 4th Edition, Section 3, Chapter 46, (Reference 504-2).

Some of the commonly used filler metals are listed in Table 5.12.5.2, along with their composition and working temperature range.

5.12.5.3 BRAZED CONNECTOR DESIGN FACTORS. Proper design (or selection) of a brazed connector demands consideration of several factors, some of the more important of which are discussed in the following paragraphs.

Braze Alloy Compatibility with Tube, Connector, and Fluids. Compatibility of a braze alloy with tubing and connector materials should be considered in terms of wettability, flow, and corrosion. The wettability and flow characteristics of candidate brazing alloys may be determined by heating small specimens of the tube and fitting materials on which have been placed samples of the brazing alloy. The specimens are heated to progressively higher

Table 5.12.5.2. Composition Melting Temperatures and Brazing Temperatures of Common Brazing Alloys

(Reference 320-7)

Brazing Alloy	Chemical Composition (Percent)										Melting Temperature Range (°F)	Minumum Recommended Brazing Temperature (°F)
	Au	Ag	Ni	Pd	Cr	Cu	Si	Li	B	Fe		
72Ag-28Cu-Li	-	71.8	-	-	-	28	-	0.2	-	-	1410	1450
72Au-22Ni-6Cr	72	-	22	-	6	-	-	-	-	-	1785 to 1835	1950
35Au-3Ni-62Cu	35	-	3	-	-	62	-	-	-	-	1787 to 1886	1890
82Au-18Ni	82	-	18	-	-	-	-	-	-	-	1742	1850
Ni-Cr-B	-	-	81.5	-	15	-	-	-	3.5	-	1930	2150
Ni-Cr-B-Si-Fe	-	-	83.5	-	6	-	5	-	3	2.5	1830	1900
60Pd-40Ni-0.3Li	-	-	40	59.7	-	-	-	0.3	-	-	2100	2150
82Au-18Ni-Li	81.7	-	18	-	-	-	-	0.3	-	-	1710	1825
70Au-22Ni-8Pd	70	-	22	8	-	-	-	-	-	-	1825 to 1910	1950

Table 5.12.5.3. Wettability and Flow of Braze Alloys

(Reference 320-7)

Base (Tube) Material	Brazing Alloy	Wettability	Flow
AISI Type 321 or 347 Stainless Steel	72Ag-28Cu-Li	Good	Good
	72Au-22Ni-6Cr	Good	Fair
	82Au-18Ni	Good	Fair
AM 350 Stainless Steel	72 Ag-28Cu-Li	Good	Good
	82Au-18Ni-Li	Excellent	Excellent
Rene' 41	72Au-22Ni-6Cr	Good	Fair
	35Au-3Ni-62Cu	Good	Fair
	82Au-18Ni	Good	Fair
	60Pd-40Ni-0.3Li	Good	Good
	Ni-Cr-B	Fair	Poor
	Ni-Cr-B-Si-Fe	Fair	Poor
	82Au-18Ni-Li	Excellent	Excellent
	70Au-22Ni-8Pd	Excellent	Excellent

temperatures in a controlled atmosphere furnace and, after the desired temperature is reached, are withdrawn from the furnace in order to evaluate the melted braze alloys. Unaided visual examination will reveal how well the braze alloy flows, and to what degree the specimen tube metal surface has been wetted. Micrographic examination will show how well the braze metal and the base metal have joined. The wettability and flow characteristics of several brazing alloys and companion tubing materials are presented in Table 5.12.5.3. Although the results of this type of test are qualitative in nature, they establish both the wetting compatibility and an approximate brazing temperature of the braze alloy and tube materials.

The effect of braze alloy on the base metal is of particular concern when brazing 300-series stainless steels, for the use of certain braze alloys with stainless steel can lead to intergrannular attack of the steel by the alloy. Another problem in selecting a brazing alloy is the possibility of carbide precipitation, caused by the alloy, which results in reduced corrosion resistance. Unless special protection is to be provided, the braze alloy selected must be compatible with the fluids with which it is to be used, just as the tube and connector materials must be compatible.

Strength of Brazed Joint. For a particular application, the selection of a specific alloy should be based upon experience of previous users, or upon results of a preliminary block-shear test, conducted to determine the joint strength and using the specific metals involved. Details on how these tests may be conducted are included in Reference 320-7. Figure 5.12.5.3a is a plot of shear strength versus temperature for palladium-nickel-lithium, gold-nickel, and silver-copper based braze alloys. These alloys are used in design of tube joints for rocket propulsion fluid systems. The figure shows that the palladium-nickel based alloy exhibits greater strength than the silver and gold based alloys.

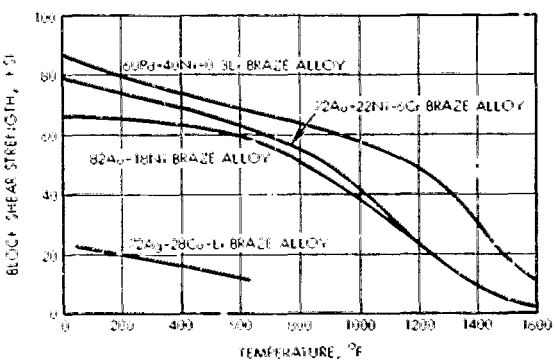

Figure 5.12.5.3a. Block Shear Strength Versus Temperature Properties of Braze Alloys
(Reference 320-7)

Connector Wall Thickness. The wall thickness of brazed joint sleeves will vary depending upon the design configuration. Sleeves which have no braze alloy retention grooves, or grooves which are outboard of the prepared surfaces, need not have wall thicknesses any greater than the wall thickness of the tubing being joined. Sleeves which have braze alloy retention grooves cut in the middle of, or inboard from, the prepared surfaces should generally have a wall thickness equal to or greater than the tubing, to compensate for the stress concentrations caused by the braze alloy grooves.

Connector Length. The lengths of the brazed connector sleeve and the prepared surfaces are critical to the strength of the brazed joint. Primary concern is that the joint be able to withstand bending loads, together with axial loading, which tends to pull the tube ends out of the sleeve. This combined loading condition is the result of stresses produced by a vibration and/or impulse environment while the tubing is under full internal pressure. Development of the maximum percentage of tube strength under flexure and impulse loading at elevated temperatures is probably the most difficult test which brazed fittings must pass. Under such conditions the tubing tends to fail just at the point where it enters the fittings. To overcome this tendency, (1) the ends of the fittings are tapered or stepped to relieve stress concentrations, and (2) the flow of brazed alloy is usually stopped short of the end of the connector by concentrating the brazing heat towards the center of the sleeve, or by using sleeve locating lands for capillary control. Concentrating the heat toward the center helps to prevent thermal degradation of the strength properties of the tubing at the location where it enters the connector sleeve.

The shear strength of the brazing alloy and accessability give a first approximation for sizing the connector sleeve length.

Tube Sizing. Machine sizing of tubing and connectors is generally required to control the variation in diametrial spacing between the braze connector and the tube OD. Sizing is also necessary because the tolerances on diameter and roundness of commercial tubing are not within those required to form a satisfactory capillary gap between the brazed connector and tubing wall.

Tube sizing can be accomplished satisfactorily in a number of ways, such as by the use of hydraulic presses and sizing dies, swaging operations, machining, and hand fitting. The first three methods require the use of fairly heavy forming equipment, used primarily for in-shop work. In field maintenance and repair operations, however, hand sizing methods using portable sizing tools are generally employed. One configuration of hand sizing tool using an explosive cartridge is shown in Figure 5.12.5.3b. The energy required to size the tubing is obtained by the expansion of gases from a .22, .32, or .38 caliber cartridge. High energy tube sizing tools such as this can be used in the field, providing normal safety precautions are observed. The tools may be fitted with a variety of split dies

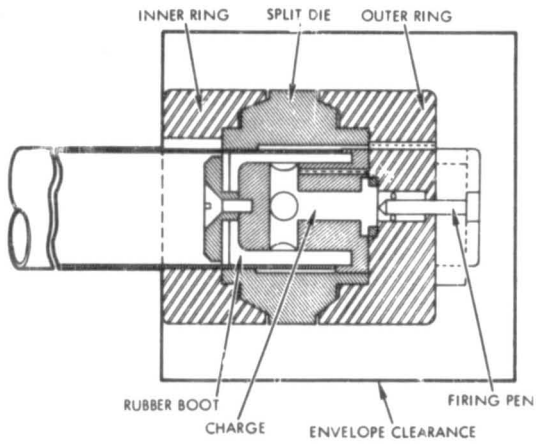

Figure 5.12.5.3b. Portable High-Energy Tube-Sizing Tool
(Reference 320-7)

to hold the tubing to correct diameter and wall thickness. These tools are designed to size tubing to 0.010 (+0.003, −0.000) inches above the nominal tubing diameter. Sizing tools have been made for tubing up to approximately 2 inches in diameter with wall thicknesses up to approximately 0.065 inches. For heavier wall thicknesses sizing is usually accomplished by machining.

Clearance Between Members of the Joint. The clearance between members of the joint determines the thickness of the alloy film that will be formed between the parts during brazing, and thus has an important influence on the joint strength. The clearance must be large enough to allow entrance of the molten braze alloy, and escape of the molten flux and gases developed during heating. On the other hand, if the joint clearance is too large, the braze alloy will not flow in the joint by capillary attraction. Clearance should normally be in the range of 0.001 to 0.005 inches, and should be maintained at the brazing temperature to get proper flow.

When determining what clearances to use for brazing dissimilar metals, the thermal expansion of the parts must be considered, allowing sufficient clearance for entrance of the braze alloy at the brazing temperature.

Line Size. The line size limitation for brazed connectors depends on design parameters which include:

a) Total expected end loading
b) Braze alloy material available
c) Shear strength of braze alloy
d) Power requirements to accomplish a satisfactory braze joint.

While brazed tube connections have been made in line sizes ranging up to six inches in diameter, non-aerospace applications have utilized brazing of much larger diameter joints, such as in the copper ducting of steam condenser cooling water systems. In considering the application of brazed connectors to any particular line size, the expected design end loads will determine the lower limits of strength required by the brazed joint, making it possible to provide a suitable braze alloy for these strength limitations. Once this information has been obtained, it is then necessary to determine whether or not sufficient heat and/or power can be provided to accomplish the brazing operation. Heat rate and power requirements are discussed further in Detailed Topic 5.12.5.4.

Theoretically, there is no upper limit of line diameter for brazed joints, nor for the length of the braze sleeve. Normal practice, as recommended in Reference 320-7, is for braze sleeve length not to exceed 1.5 times the line outside diameter. For any given braze sleeve length-to-diameter ratio, it is apparent that the maximum system pressure is not a function of line diameter, since the total shear area of the connector will increase as the line diameter increases, at the same rate as will the cross-sectional area of the line. At the larger diameters, however, it may be found that the problems associated with applying the necessary heat to accomplish the brazing operation will limit line diameters more often than will the length of braze sleeve and the larger number of braze rings required with longer sleeves.

5.12.5.4 BRAZING PARAMETERS. Important brazing parameters which affect considerably the degree of success in making a brazed tube joint are:

a) Parameters Independent of Material Properties
   Surface cleanliness
   Atmosphere control
   Heating rate and power requirements

b) Parameters Dependent on Material Properties
   Connector sleeve design
   Induction heating coil design (or other heat source)
   Tube sizing

Those parameters independent of material properties are discussed in the following paragraphs.

Surface Cleanliness. An effective tube braze cannot be made unless conditions of absolute cleanliness are maintained. Impurities or foreign deposits on surfaces to be brazed will decompose upon heating and give off contaminating and bubble forming gases, thus leaving residues which prevent adhesion of the brazing alloy. Procedures for pre-braze cleaning of high strength stainless steel alloys are outlined in Reference 320-7.

Atmosphere Control. An inert gas envelope or fluxing is necessary for tube brazing, in order to minimize oxidation of the metal surfaces and provide maximum possible adhesion of the brazing alloy. Any one of several different methods may be used for inert gas shielding, all of which are generally based upon providing a plenum chamber of some form around the brazed area, which is then purged and kept under a positive pressure with inert gas such

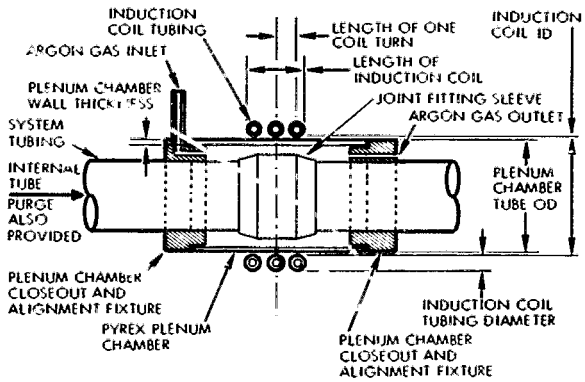

Figure 5.12.5.4. Schematic of Braze Tube Joining Induction Coil and Plenum Chamber
(Reference 320-7)

as nitrogen, helium, or argon (see Figure 5.12.5.4). In addition, it is usually necessary to purge the inside of the tubing with the same inert atmosphere. Inert gas pressure inside and outside of the brazed joint should be the same, so that no gas can pass through the molten brazing alloy, causing voids or the expelling of molten brazing alloy from the joint capillary.

The inert gas used for purging during brazing operations must be free of moisture. If even small amounts of water are present in the purge gas, the continuous flow introduces enough moisture in the braze area to create a serious contamination problem. To prevent this, a drying train should be used in the inert gas feed systems to insure that not more than 10 parts per million of moisture remain.

During the braze operation, a continuous low flow of inert gas should be maintained to sweep off any adsorbed gases which may be released from the metal surfaces upon heating, and to prevent possible leakage of air into the brazed area. The gas flow rate should be continued even after the brazing operation has taken place, and during cooling of the joint, to prevent air from entering the area upon contraction of the cooling inert gas.

Another method for controlling brazing atmosphere is by use of a brazing flux. Upon the application of heat, the flux decomposes, forming a gaseous envelope around the braze area. A disadvantage of using flux for aerospace fluid system brazing is the difficulty of removing the flux residue from the brazed joint, particularly from the inside of the tubing. If the flux is not removed, it serves as a nucleus for corrosion and can generate particulate contamination in the fluid system. An important advantage of using flux is that it greatly simplifies the brazing operation by eliminating the cumbersome inert gas system and stringent prebraze joint cleaning requirements. Self-fluxing braze alloys, such as those containing lithium, are available which eliminate the necessity of using a separate brazing flux.

Heat Rate and Power Requirements. Induction heating is currently the most widely used method of generating heat for in-place fluid systems brazing. Methods such as resistance heating, gas torches, furnaces, and exothermic reactions, are also used, but to a lesser extent. Induction heating is a process by which heat is produced in a metal which is in proximity to a rapidly varying magnetic field produced by an alternating current. The heat is generated by the resistance of the metal to the flow of eddy currents induced by the varying magnetic field, and also because of hysteresis effects in the metal. The required magnetic field is produced by conducting high frequency current through a work coil, or inductor, which acts as the primary winding of a simple transformer, while the workpiece acts as a secondary. By shaping the coil properly, the heat can be localized, or spread throughout the work, as required. The work coil may consist of a single turn, or of many turns, depending on the desired heat pattern, the work material, the current frequency, and the distance from the coil to the work. Heat distribution patterns can be obtained which are not possible with conventional methods of heating.

When performing initial production brazing runs on a specific material and tubing system, power settings of the induction heating machine should be kept sufficiently low, to insure uniform heating of the tube and connector assemblies. Slow heating rates will allow time to observe visually the wetting and flow action of the brazing alloy. Once the characteristics of the materials have been established, heating rates can be increased and times reduced to the point where effective brazes can be made in seconds. Table 5.12.5.4 gives some typical brazing times for several aerospace tubing and connector materials.

The choice of frequency in induction heating depends upon the particular application. The degree to which the induced currents and, in turn, the heating effect, penetrate the work is generally an inverse function of the frequency of the applied alternating current. Frequencies from 60 cps into the megacycle range have been used for induction heating. The higher frequencies from radio frequency (RF) generators, in the approximate range from 200,000 to 450,000 cps, usually produce a very intense, fast, and localized heat pattern, desirable for brazing thin-walled tubing. A more diffuse and slower heating effect with a deeper heating penetration is produced by the lower motor-generator frequencies in the range from 1000 to 10,000 cps. The choice of a particular frequency to be used for a given application may be determined by the characteristics of the equipment available, rather than by more strictly technical consideration (see Reference 320-7). In many cases it is not critical, and almost any frequency may be used.

5.12.5.5 JOINT REBRAZING. Experience with brazed joints to date indicates that debrazing and rebrazing of joints can be accomplished easily and result in a satisfactory joint, providing the necessary steps are taken to insure that oxidation of the joining surfaces does not occur. The number of times which a joint may be rebrazed depends considerably upon the brazing alloys involved and their

Table 5.12.5.4. Brazing Parameters for Induction Braze Joining of Tubing
(Reference 320-7)

Tubing Material	AISI 347 Stainless Steel	AISI 347 Stainless Steel	AM 350 CRT Stainless Steel	AM 350 SCT Stainless Steel	Rene' 41 Alloy
Tube Size:					
Outside diameter	1.000	3.000	0.250	1.000	0.125
Wall thickness	0.083	0.250	0.042	0.134	0.010
Fitting Sleeve Material	AISI 347 Stainless Steel	AISI 347 Stainless Steel	AM 355 SCT Stainless Steel	AM 355 SCT Stainless Steel	Rene' 41 Alloy
Composition of Brazing Alloy	71.8 Ag 28.0 Cu 0.2 Li	71.8 Ag 28.0 Cu 0.2 Li	81.7 Au 18.0 Ni 0.3 Li	81.7 Au 18.0 Ni 0.3 Li	81.7 Au 18.0 Ni 0.3 Li
Brazing Control Temperature*	1450 F	1500 F	1500 F	1450 F	1900 F
Brazing Heating Time	47 seconds	360 seconds	15 seconds	45 seconds	45 seconds
Induction Heating Machine Information:					
Frequency	250 Kc	250 Kc	450 Kc	250 Kc	450 Kc
Rated capacity	30 Kw	30 Kw	2.5 Kw	30 Kw	2.5 Kw
Power setting	20 percent	45 percent	75 percent	35 percent	65 percent
Plate voltage	3.5 Kv	6 Kv	2.7 Kv	4 Kv	2.3 Kv
Plate amperage	1.8 amperes	2.3 amperes	0.7 amperes	2.0 amperes	0.7 amperes

*Control temperature measured by thermocouple tack welded to tube OD 1/32 inch from edge of fitting sleeve

susceptibility to oxidation. With gold-nickel alloys, rebrazing can be accomplished as many as 5 to 8 times with a satisfactory joint resulting each time. With lead-nickel-lithium brazing alloys, however, rebrazing using the original alloy is difficult because the lithium in the brazing alloy dissipates with heat. In this case, the lithium (which serves as a volatile flux and improves wettability and flow characteristics of the alloy) is dissipated by evaporation. Rebrazing results in poor wetting and flow characteristics and, thus, an unsound joint. For any brazing alloy containing small amounts of an essential ingredient which can be dissipated or otherwise degraded by reheating, it is not recommended that rebrazing be attempted.

Repairs of brazed joints can be accomplished successfully in ways other than rebrazing. For example, a repair can be made by completely removing the defective joint by cutting the tubing at both sides of the joint, then replacing the cut-out section by brazing a new section in place using new connectors, as required. Although successful, this method does add weight to the fluid system. Where weight considerations are overriding it may be desirable to rebraze the original joint.

Rebrazing should be undertaken only when absolutely necessary. New braze alloy should be used when possible, even when the original connector sleeves are reused because of mechanical loss and degradation of the original brazing alloy in the reheat cycle and during the cleaning operation. Reasons why rebrazing is not desirable are:

a) Repeated heating exposes the joint components to more opportunities for contamination, oxidation, and adverse heat treating.

b) Fluxing agents in the original braze alloy become depleted either by evaporation or by a reaction with the surface oxides on the joint components, and effect on the brazing operation is lost.

c) At elevated temperatures there is a gradual diffusion of the braze alloy into the base metal, which changes the composition and properties of both the remaining alloy and the joint component materials. These material changes can be detrimental both from a strength and corrosion standpoint.

d) Extended times at brazing temperatures can produce damaging metallurgical changes such as carbide precipitation in certain stainless steels, or overaging and loss of strength in precipitation hardening materials such as AM 350 and René 41.

Further information on rebrazing may be obtained from Reference 320-7.

5.12.5.6 BRAZED JOINT INSPECTION. Probably the single most important objection to the use of brazed connectors is the difficult problem of inspecting joints for integrity, following the brazing process. The use of visual inspection holes in a connector only assures proper flow of the braze alloy in the joint (see Figures 5.12.5.7c and d, and Table 5.12.5.7). The most reliable methods developed to date for inspecting the integrity of joints involve the use of X-ray and sonic inspection equipment. Complete inspection using X-rays requires two photographs taken at positions 90 degrees apart. Because both the near and far sides of the tubing joint will appear on the X-ray plate, considerable skill is required of the inspector to determine in which quadrant a defect may be located. In general, the main item which shows up in the X-ray photograph is the extent of alloy distribution and existence of voids on the prepared surfaces of the joint. The X-ray photograph, in effect, indicates the extent of braze alloy wetting, but it does not indicate whether a satisfactory bond exists. This can be determined by use of an ultrasonic inspection technique which involves the transmission of high frequency sound to the brazed joint and monitoring of the time interval and frequency of the sound echo. If a solid joint has been

Table 5.12.5.7. Dimensions of Brazed Connector Sleeves
(Reference 320-7)

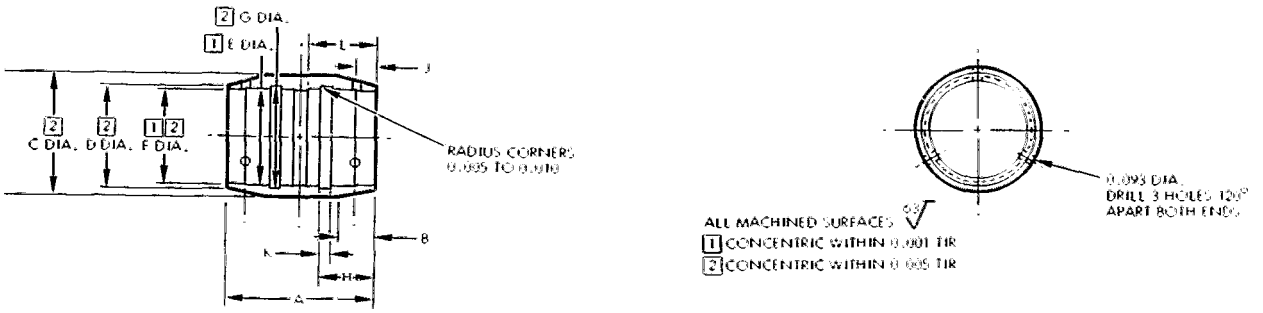

Sleeve Material	Tube OD	Sleeve Dimensions										
		A	B	C	D	E	F	G	H	J	K	L
AISI Type 347 Stainless Steel	1	1.500 ±0.005	0.375 ±0.010	1.255 ±0.005	1.082 +0.005 -0.000	1.002 +0.001 -0.000	1.0005 +0.001 -0.000	1.055 +0.005 -0.000	0.550 ±0.005	0.195 ±0.005	0.100 +0.005 -0.000	0.6875 +0.005 -0.000
	3	3.335 ±0.005	0.875 ±0.010	3.720 +0.010 -0.000	3.130 ±0.010	3.003 +0.001 -0.000	3.001 +0.001 -0.000	3.200 +0.005 -0.000	1.200 ±0.005	0.245 ±0.005	0.205 +0.005 -0.000	1.550 ±0.005
AM 355 SCT Stainless Steel	1 4	0.559 ±0.005	0.156 ±0.010	0.400 +0.005 -0.000	0.321 +0.005 -0.000	0.254 +0.001 -0.000	0.251 +0.001 -0.000	0.276 +0.005 -0.000	0.223 ±0.005	0.100 ±0.005	0.040 +0.005 -0.000	0.245 +0.005 -0.000
	1	1.500 ±0.005	0.375 ±0.010	1.304 +0.005 -0.000	1.082 +0.005 -0.000	1.007 +0.001 -0.000	1.004 +0.001 -0.000	1.055 +0.005 -0.000	0.550 ±0.005	0.195 ±0.005	0.100 +0.005 -0.000	0.6875 +0.005 -0.000
Rene' 41	1 8	0.500 ±0.010	0.125 ±0.010	0.187 ±0.005	0.158 +0.005 -0.000	0.128 +0.001 -0.000	0.128 +0.001 -0.000	-	-	-	-	-

made, the echo will originate from the inside wall of the tubing, but if a poor joint or lack of bonding exists, the echo will emanate from the unbonded surface between the connector and the outside wall of the tubing. By knowing the precise distance from the sound emitter to the brazed joint, and accurately determining the time interval between signal transmission and receipt of the echo, it can be determined quite reliably if a satisfactory bond exists at the joint.

Although usable information regarding the structure of the brazed joint is obtained from X-ray and ultrasonics, only a final leak test and proof pressure test can determine the brazed joint integrity.

5.12.5.7 BRAZED JOINT AND CONNECTOR CONFIGURATIONS. A brazed connector is basically a sleeve which fits over the ends of the tubes to be joined. The sleeve may contain internal grooves for the braze alloy rings. Figure 5.12.5.7a illustrates the use of braze alloy rings in various locations in several typical brazed tube joints.

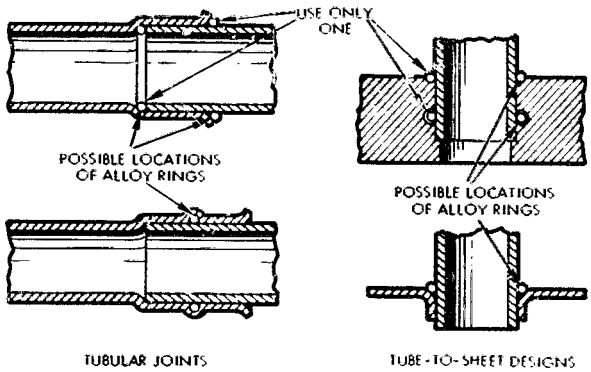

Figure 5.12.5.7a. Typical Designs for Brazed Joints
(Reference 46-16)

Brazed connectors generally assume one of two shapes. The first, illustrated in Figure 5.12.5.7b, is a simple through bore connector with the braze alloy ring butted between the ends of the tube to be brazed. The second, shown in Figure 5.12.5.7c, contains two braze alloy rings in the sleeve and employs three capillary clearance lands.

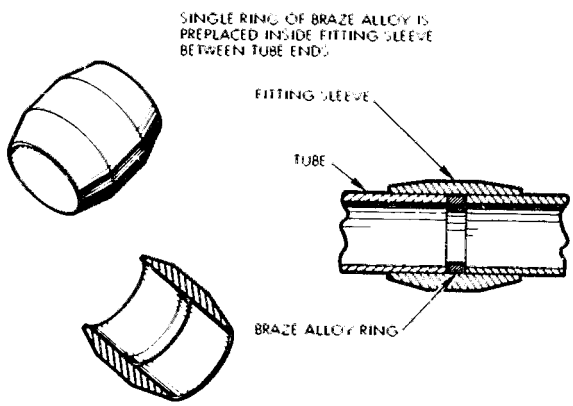

Figure 5.12.5.7b. Straight-Through Bore Connector Sleeve
(Reference 320-7)

The diameter and length of the braze alloy retention grooves must be selected so that the notch effect is minimized and fracture of the connector sleeve under load is avoided. The dimensions of the grooves must also be chosen to provide for the containment of sufficient braze alloy to assure complete filling of the joint capillary under any brazing condition. A braze alloy groove volume of approximately three to seven times the maximum joint capillary volume is recommended.

Because of difficulties which would be encountered in machining the connectors and assembling the joint, it is recommended that one-quarter-inch diameter tube be the smallest size using internal braze alloy retention grooves. The braze alloy retention groove should always be located slightly closer to the interior end of the joint capillary than to the outer end. Thus, if the braze alloy is observed to have flowed the longer distance to the edge of the sleeve, some assurance is provided for a full braze alloy flow to the sleeve center. Inspection holes are usually placed in the connector sleeve to permit a more complete evaluation of the extent of alloy flow.

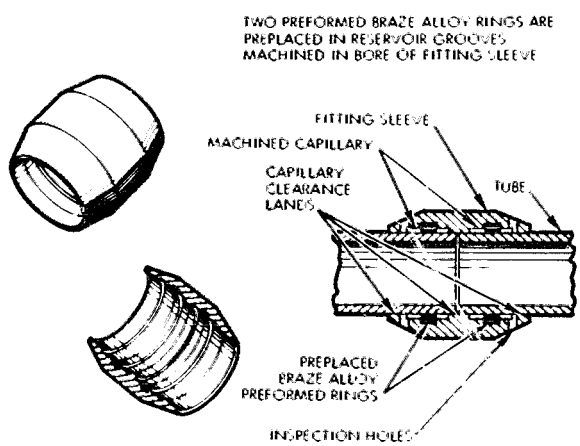

Figure 5.12.5.7c. Groove Bore Connector Sleeve
(Reference 320-7)

The capillary clearance lands at the center and ends of the connector shown in Figure 5.12.5.7c serve to align the tube ends as well as provide a positive capillary dimension in the assembled joint. The locating lands should have sufficient area to withstand the socket loads applied by misalignment of the installed tubing. When a sleeve is designed with locating lands, the overall length of the sleeve will be the length of the braze capillary plus the total length of the locating lands. Dimensions of grooved bore connector sleeves are shown in Table 5.12.5.7.

Two other variations of connector sleeves are shown in Figures 5.12.5.7d and 5.12.5.7e, both employing the use of preplaced brazing alloy and alloy retention grooves. The configuration in Figure 5.12.5.7d is generally restricted to lightweight tubing which can be upset beaded to form the brazing alloy groove. The configuration in Figure 5.12.5.7e is a machined connector which employs an exothermic reaction pack (shown) to provide brazing heat. The primary advantage of this connector is that in-place joints can be made in remote or limited space locations with no equipment other than the reaction pack and a 6-volt battery. Also, because of the fast reaction time and rapid temperature rise in exotherm brazing, the deleterious effects of time-at-temperature on heat treatment and grain structure of the tubing are reduced. This connector is presently commercially available for use with one-half-inch OD tubing.

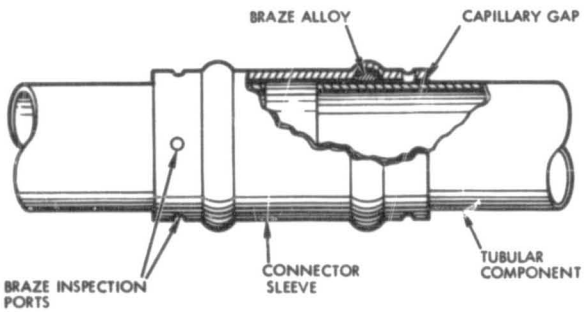

Figure 5.12.5.7d. Brazed Connector Featuring Upset Bead Braze Alloy Retention Grooves
(Courtesy of Marman Division, Aeroquip Corporation, Jackson, Michigan)

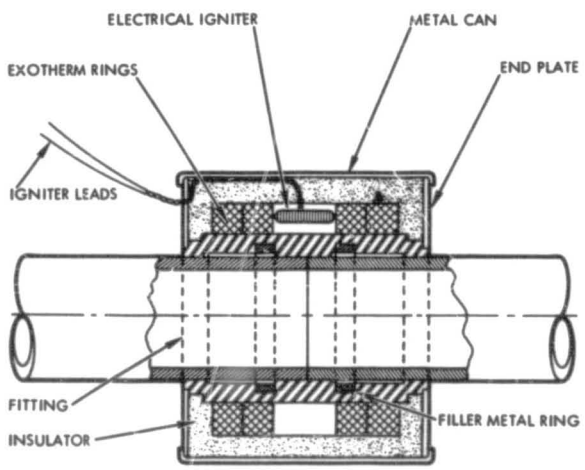

Figure 5.12.5.7e. Exotherm Brazed Connector
(Courtesy of The Deutsch Co., Los Angeles, California)

5.12.6 Welded Joints and Connectors

5.12.6.1 GENERAL. Welded connectors provide minimum weight, leak-tight joints with maximum joint strength, and avoid the dissimilar metals compatibility problems associated with brazed joints. The primary drawback of a welded connector or joint is that due to its permanent nature, physical cutting or machining is required for separation. Basic information related to the design of welded connectors and joints, as well as applicable tube weld methods, is discussed in this sub-section.

5.12.6.2 THE WELDING PROCESS. Welding is the process of joining two pieces of metal by establishing a metallurgical bond between each piece. Welding is accomplished by the application of heat and/or pressure, leading to the classification of (1) pressure welding, and (2) fusion welding. Pressure welding may be accomplished with or without a heat source; however, the time required to accomplish the weld is lessened with a heat source. The temperature requirements for pressure welding normally fall in the plastic forging range, as opposed to the melting temperature range for fusion welding.

5.12.6.3 WELDED CONNECTOR DESIGN FACTORS. The designer must be aware of a number of factors when considering the use of welded connectors and/or joints in a tubing or piping system. The factors which follow are considered to be of major significance.

Connector Material. The type of materials to be welded is the most important factor in any weldment, dictating the type of welding process(es) available. For example, when welding lines and connectors made of ferrous materials, consideration must be given to:

a) The tendency of the weld metal and/or base metal to crack during the welding operation or while cooling after welding

b) Changes in mechanical properties of weld or base metals due to welding process

c) Changes in metallurgical structure of base metal due to welding

d) Changes in chemical composition of base metal due to volatilization of alloying components, air oxidizing, or reactions with shielding gases.

One of the most commonly used materials for aerospace tubing applications is austenitic stainless steel. For this class of metals, Table 5.12.6.3 gives recommendations for electrode or welding rod types to be used with various grades of stainless steel.

Tube Thickness. Tube thickness influences the selection of weld method. Thick sections that require multiple passes to form a weld seam are usually best welded with an inert-gas shielding-arc using a consumable electrode. Sections of lesser thickness, in the one-sixteenth to three-sixteenth-inch range may be welded by a number of processes, depending on the overall size and maneuverability of the workpiece. Detailed Topic 5.12.6.4 further discusses this aspect of welding.

Table 5.12.6.3. Welding Rod or Electrode Recommendations for Wrought Austentitic Stainless Steel Pipe Grades

(From "Welding Handbook," 4th Ed., Section II, American Welding Society, New York, 1962)

AISI Designation	Popular Designation	Recommended Electrode or Welding Rod*
304	19-9	E, ER 308
304L	19-9 (extra low carbon)	E, ER 308L
309	25-12	E, ER 309
309 Cb	25-12 Cb	E 309 Cb
310	25-20	E, ER 310
310 Cb	25-20 Cb	E, ER 310 Cb
310 Mo	25-20 Mo	E, ER 310 Mo
316	18-12 Mo	E, ER 316
316L	18-12 Mo (extra low carbon)	E, ER 316L, or ER 318
317	19-13 Mo	E, ER 317
318	18-12 Mo Cb	ER 318
321	18-8 Ti	E, ER 347, ER 321
347	18-8 Cb	E, ER 347
348	18-8 Cb	E, ER 347, ER 348

*AWS and ASTM Specifications: E means grade recognized by AWS-ASTM as covered electrode; ER as bare electrode and welding rod

Joint Strength. From a strength standpoint, a welded joint can be analyzed by the use of standard strength of materials formulas. The allowable working stresses to use for the weld joint in the case of many standard materials can be obtained from several sources, including the American Welding Society "Welding Handbook."

The designer should use caution, however, in the design of welded joints utilizing the super-strength alloys such as austenitic and semiaustenitic stainless steels, nickel base alloys, and high-strength aluminum, because of the detrimental effects of weld heat on the strength of these metals. When welded joints and connectors are to be used extensively in a fluid system, it is recommended that test specimens utilizing the actual materials and joining techniques be prepared and tested to verify design calculations.

Fluid Compatibility. The fluid to be contained and its corrosive nature must be considered in selecting a weld method. Although the microstructure of the parent metal may be compatible with the operating fluid, changes in microstructure resulting from the welding process may make this area of the tubing more susceptible to corrosion. Stress corrosion may take place in weld areas if stress concentrations are allowed to occur. Therefore, the designer should take into consideration the changes in material composition resulting from the welding process, and ascertain the compatibility of any such material changes in the presence of the system fluid.

Welding Equipment Portability. The location and position of welds affects the choice of welding method, primarily from the standpoint of size and portability of the welding equipment. Gas welding equipment is highly portable, whereas resistance welding equipment for flash butt welding is usually permanently installed. Also, metal arc welding equipment is quite portable, requiring only a standard motor-driven DC generator. The inert gas shielded methods require more elaborate equipment, including a gas supply; however, this type of welding can be carried out in all positions, including overhead which is advantageous when in-place welding must be conducted. Other fusion welding methods which depend on floating oxides out of the molten weld puddle are usually limited to downhand welding in the horizontal position.

Production Requirements. The number of like welds to be made considerably influences the selection of the welding method. Large production quantities justify making an investment in elaborate tooling, and automatic welding machines, whereas low production usually requires the use of standard equipment for hand-welding methods. The tubing size also influences the choice of weld method, since practicality will limit the use of automatic equipment in large diameter tubing. The welding methods that lend themselves to automation are the inert gas, atomic hydrogen, and all resistance welding processes. For random in-place tube welding or one-of-a-kind welds, gas welding is often employed because of the simplicity of the equipment involved. This is also true for hand-operated inert shielded-arc welding, with this method offering the advantage of not contaminating the work with corrosive flux that has to be removed. Inert gas metal-arc welding, which uses an automatically fed consumable electrode, is a method often used for production welding because it sets a pace for the welding operator.

5.12.6.4 WELDING TECHNIQUES. Any one of several tried and proven welding techniques can be used for the joining of fluid system lines and components. Equipment for welding tubing includes hand-held tools, semi-automatic welding equipment, and fully automatic equipment.

The success of any welded joint in a fluid system depends to a large extent upon selection of the proper welding method and execution of the weld in a satisfactory manner. Following are discussions of those methods that are the most likely to be used for fluid system welding.

Gas Tungsten-Arc Welding. This process, often referred to as TIG welding, is an inert gas shielded, metal-arc process using a nonconsumable tungsten electrode. The inert gas shield is usually provided by helium or argon. The weld is accomplished by fusing workpieces with a tungsten arc without adding filler material. The primary advantage of this method is that it does not require a flux to form a satisfactory weld, obviating post cleaning of the weld area. This is important for closed fluid systems where flux removal would be difficult. If flux is used it must be removed, otherwise it will accelerate corrosion of the weld metal and contaminate the system.

Because there is no flux to absorb impurities in the TIG welding process, cleanliness is an important consideration. Combustible materials in the path of the arc will burn and generate gases that contaminate the inert shroud, causing scum to form over the molten metal and making it difficult for the welding operator to obtain smooth flow. Also, it is a potential cause of cracks and porosity in the weld. Tubing which is to be joined by the TIG process should be cleaned mechanically, when necessary, and with solvent.

Another advantage of TIG welding is that it can be accomplished in all positions, because there is no slag to be worked out of the weld puddle by gravity. Consequently, overhead welding is entirely feasible, solving practical work problems when it is difficult or impossible to position the work. In addition, visual control of the weld area is excellent, as the gas envelope around the arc is transparent and the weld puddle clean. An operator making a weld by hand can do an excellent job because he does not have to contend with smoke and fumes and can see more clearly what he is doing. In addition, this process provides minimum distortion of the metal near the weld because the heat is concentrated at the weld area. The intensity of the average tungsten arc is approximately 10,000 to 15,000 amps per square inch of electrode.

Table 5.12.6.4a lists a number of weld parameters for joining, by the TIG process, tubing materials which are most commonly found in aircraft and rocket propulsion fluid systems. Materials included in this table are AISI Type 347, AM 350 CRT, and AM 350 SCT stainless steels, René 41 Alloy, and 6061-T6 aluminum. Further details for joining these materials by TIG welding can be obtained from Reference 320-7.

Table Weld Parameters for Joining Tubing by TIG Process for Aerospace Fluid Systems

(Reference)

Tubing System Material	Tube Size (in.) OD	Tube Size (in.) Wall	Sleeve Thickness (in.)	Weld Type and No. of Passes	Diameter of Electrode (in.)	Weld Current (amperes)	Arc Voltage (volts)	Travel Speed (sec per revolution)	Welding Start Position	Shielding Gas and Flow Rate: Torch	Shielding Gas and Flow Rate: Backup	Purge Time (min)
AISI Type 347 Stainless Steel	1	0.083	0.030	External 1 pass	3/32	84	10.0	26.5	6 (b)	75% Argon 25% Helium 20 cfh	Helium 40 cfh	5
	3	0.250	None	Internal 1 pass plus External 1 pass	3/32	100	9.5	180	6	75% Argon 25% Helium 50 cfh	Helium 50 cfh	3
					3/32	110	9.5	210	12	75% Argon 25% Helium 60 cfh	Helium 40 cfh	3
AM 350 CRT Stainless Steel	1/4	0.042	0.015	External 1 pass	1/16	15 (c)	12.0	17	Traveling	75% Argon 25% Helium 20 cfh	Helium 50 cfh	10
AM 350 SCT Stainless Steel	1	0.134	None	External 1st pass 2nd pass	3/32	95 55	14.0 14.0	45 45	7:30	75% Argon 25% Helium 40 cfh	Helium 50 cfh	15
René' 41 Alloy	1/8	0.010	0.010	External 1 pass	1/16	5 (c)	18.0	8.5	Traveling	75% Argon 25% Helium 15 cfh	Helium 30 cfh	10
	1	0.065	0.031 (d)	External 1 pass	1/16	52	15.0	27	9	75% Argon 25% Helium 35 cfh	Helium 10 cfh	15
6061-T6 Aluminum	1	0.058	0.045 Diam. 4043 Alum. Alloy Wire	External Wire Feed (e)	1/16	26 (f)	13.0	48	11 (e)(f)	Helium 50 cfh	Argon 30 cfh (g)	1

Notes: (a) All welds made with two percent thoriated electrodes.
(b) Number denotes electrode position in terms of hour positions of clock, electrode travel is clockwise direction unless otherwise noted.
(c) Electrode travel started before weld current initiated.
(d) Wire feed was at rate of 12 inches per minute for electrode traveling speed of 4 inches per minute, counterclockwise travel.
(e) Current of 20 amperes was used to preheat start area for 20 seconds, current was then increased to 26 amperes after which electrode travel and wire feed were started within five seconds. Approximately two-thirds around, circumference weld current was reduced to compensate for effect of preheating ahead of electrode. After overlapping weld start, wire feed was sloped off, then weld current was sloped off to zero by the time approximately one-half a revolution was made.
(f) Solar 202 flux was also used for inside surfaces of tube and joint at joint area.

Gas Metal-Arc Welding. This welding process is an offspring of the TIG welding process. Gas metal-arc welding (more appropriately termed gas-shielded consumable metal-electrode welding) utilizes a consumable metal electrode and a gas shield, usually CO_2, helium, or argon. In this process, a special welding tool feeds the electrode, usually of the same composition as the material being welded, as it is consumed. The use of electrode in the form of coiled wire increases the speed of this welding process, and a further time savings is effected since no weld slag forms which must later be removed.

When using helium or argon for a gas shield, this process can be used for welding a great variety of materials. However, cost usually limits the use of these gases to the welding of aluminum, magnesium, or stainless steels where a completely inert atmosphere is required.

For welding heavy-walled steel tubing, a granular flux is often combined with a CO_2 gas shield. Hollow electrodes with a self-contained flux in the center are also used. Another method uses a magnetic flux added to the inert gas, which adheres to the electrode wire as a result of magnetic force caused by current flow in the wire.

Gas Welding. This is another welding process which can be adapted sufficiently well for in-place fabrication of fluid systems. It is a versatile process in that existing portable torches and equipment can be used. Generally speaking, oxyacetylene and oxyhydrogen flames are used, however, natural gas and propane may also be utilized. When gas welding is employed, it is often necessary to supply a filler material to build up the weld area to the necessary volume and strength. In addition, the use of a flux is required to prevent oxidation of the molten weld metal, as discussed above. However, this imposes the disadvantages of post-weld cleaning. Since the development of shielded arc welding, the gas welding process has been largely limited to applications where portability of welding equipment is a must.

Flash Welding. Flash welding is a resistance welding process. In joining two pieces by this process, the welding voltage is first applied between the pieces, a flashing or arcing follows for a prescribed time, and finally the pieces are forced together upsetting the metal and forming a weld joint. Although this is a rapid method of welding, when tubing is welded in this manner it is often impossible to remove the flash that is formed on the inside of the tubing. Flash welding schedules for welding tubing of thicknesses from 0.010 to 1.0 inch are given in Table 5.12.6.4b.

Electron Beam Welding. A recently developed welding technique which has proven invaluable for the welding of high strength and high refractory metals and alloys is the electron beam welding method (EB welding). An electron beam welding machine consists of a vacuum chamber in which electrons are produced and directed toward the work piece. The heart of the electron beam welder is an electron gun in the form of a triode. Its components are an electron-emitting cathode, an accelerating electrode, and a focusing electrode or lens. Figure 5.12.6.4 illustrates schematically the Pierce electron gun and shows how the beam of electrons can be focused on a small area.

Three primary advantages of the electron beam process are:

1) In addition to forming welds under ideal conditions of purity, a large amount of heat can be concentrated in a very small area. This means that the fuse zone which forms the weld bead can be deep and narrow with a depth-to-width ratio of from 4 to as high as 25, compared to about 1 for other welding processes such as TIG and gas.

2) Because the weld zone is so narrow, there is less molten metal to give off heat during cooling, and consequently, there is less distortion in the weld zone, and the microstructure of the parent metal adjacent to the weld zone

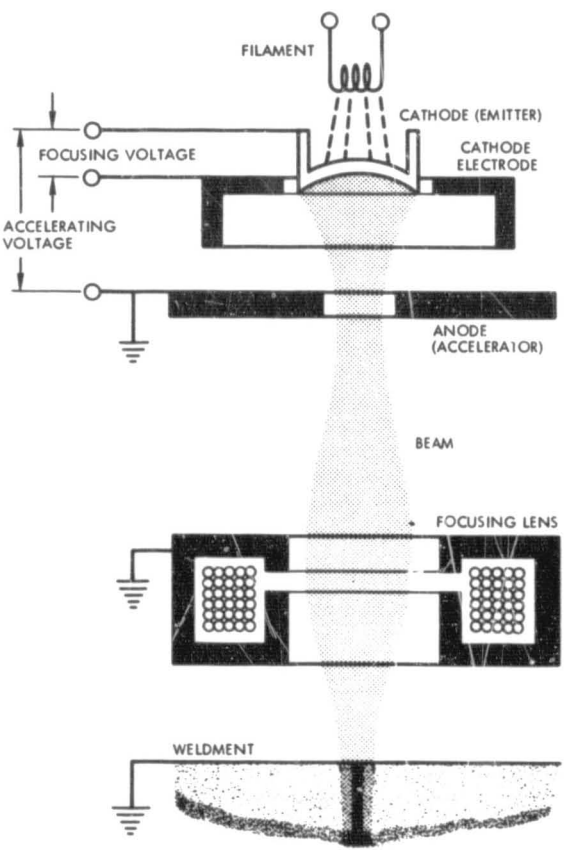

Figure 5.12.6.4. Sketch of Pierce Electron Gun
(Reprinted with permission from "International Science and Technology," No. 4, April 1962, R. F. Bunshah, Conover-Mast Publications, New York, New York)

is less affected. This is important because the heat-affected zone adjacent to the fusion zone is very often the location where welds fail because of the inability to control the micro-structure of this area.

3) The amount of heating can be varied smoothly and precisely by varying the control voltages. This means that preheating and post-heating can be accomplished easily and weld spatter is seldom a problem.

The major drawback or disadvantage of using the electron beam process for in-place welding is that all welding must be accomplished in a vacuum of approximately 10^{-4} torr. This requires remote manipulation of the work piece, or electron gun, and greatly limits the work which can be welded by this process. To date, this welding method has been confined primarily to special welding tasks requiring design of special equipment and set-up, or to general welding of small components. Additional information on this process can be obtained from References 411-2 and 65-42.

Atomic Hydrogen Welding. This welding process is a type of arc welding. Although the inert-gas welding processes have displaced atomic-hydrogen welding to a large extent, the process is worthy of note in that it is particularly suited to welding high alloy steels and relatively thin materials, while maintaining the same composition in the weld as in the base metal. Atomic-hydrogen welding is usually accomplished with a special hand-held tool that contains two tungsten electrodes and a hydrogen gas feed through one or both of the electrode holders. No filler metal is used in this process. As the workpieces are positioned, the two electrodes are energized and an AC arc is maintained with a hydrogen gas envelope. The hydrogen dissociates in the arc and then combines with the cooler base metal. In combining with the base metal, substantial heat is released. The heat of combination plus the heat of the arc produces a higher temperature than is available from ordinary arc welding processes. The hydrogen gas also provides a reducing envelope that shields the weld area from oxygen and nitrogen in the free atmosphere.

5.12.6.5 WELDED CONNECTOR AND JOINT TYPES. Basically, there are two types of welded joints used in aerospace fluid systems. One is the plain joint in which the tube ends or components are fitted together, either butted or lapped, and then welded by the application of heat with or without the use of a flux and filler material. The other type of joint is termed a sleeve joint, employing the use of a separate connector, or sleeve, which is slipped over the ends of the two parts to be joined and welded to the parts, usually at the joint interface. Some specific joint types are discussed below.

Butt Joints. When using the arc welding method to form the straight butt joint illustrated in Figure 5.12.6.5a, no surface preparation of tube ends is necessary if relatively thin-walled tubing is used and joining is accomplished by a single pass of the electrode. Preparation of the tube ends is required, however, when wall thickness makes more than one weld pass necessary (see Figure 5.12.6.5b).

A straight butt joint may also be made by any of several other welding methods, as discussed in Detailed Topic 5.12.6.4.

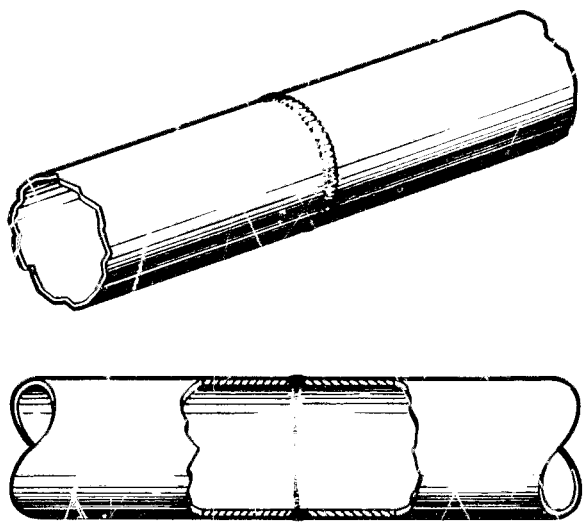

Figure 5.12.6.5a. Straight Butt Tube Weld Joint

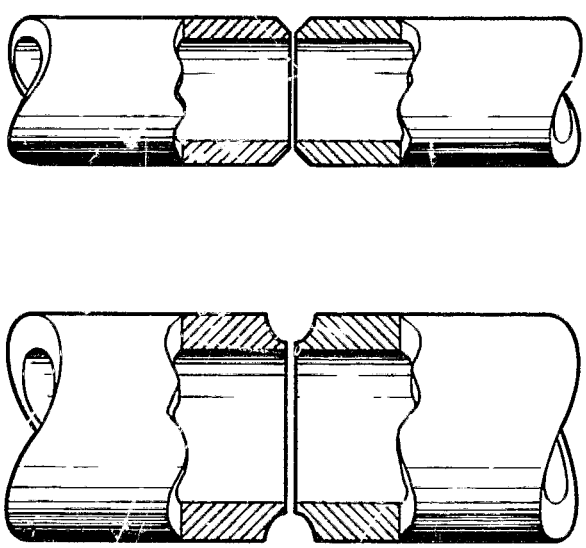

Figure 5.12.6.5b. Edge Preparation Required for Welding Thick-Walled Tubing

Table 5.12.6.4b. Flash Welding of Tubing and Flat Sheets

(From "Welding Handbook," 4th Ed., Section II, American Welding Society, New York, 1962)

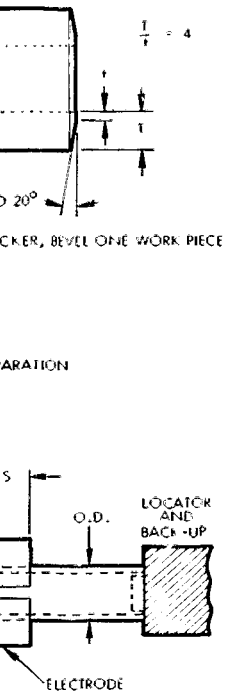

T, In.	A, In.	B, In.	C, In.	D, In.	H, In.	J = K, In.	L = M, In.	Flashing Time, Sec.	O.D., In.	S With Locator	S Without Locator
0.010	0.110	0.060	0.050	0.040	0.020	0.030	0.055	0.40	0.250	0.375	1.00
0.020	0.215	0.115	0.100	0.080	0.035	0.058	0.108	0.80	0.312	0.375	1.00
0.030	0.325	0.175	0.150	0.125	0.050	0.088	0.163	1.25	0.375	0.375	1.50
0.040	0.430	0.230	0.200	0.165	0.065	0.115	0.215	1.75	0.500	0.375	1.75
0.050	0.530	0.280	0.250	0.205	0.075	0.140	0.265	2.25	0.750	0.500	2.00
0.060	0.630	0.330	0.290	0.240	0.090	0.165	0.310	2.75	1.000	0.750	2.50
0.070	0.715	0.385	0.330	0.280	0.105	0.193	0.358	3.50	1.50	1.000	3.00
0.080	0.805	0.435	0.370	0.315	0.120	0.218	0.403	4.00	2.00	1.250	
0.090	0.885	0.475	0.410	0.345	0.130	0.238	0.443	4.50	2.50	1.750	
0.100	0.970	0.520	0.450	0.375	0.145	0.260	0.485	5.00	3.00	2.000	
0.110	1.060	0.570	0.490	0.410	0.160	0.285	0.530	5.75	3.50	2.25	
0.120	1.140	0.610	0.530	0.440	0.170	0.305	0.570	6.25	4.00	2.50	
0.130	1.225	0.650	0.575	0.470	0.180	0.325	0.613	7.00	4.50	2.75	
0.140	1.320	0.700	0.620	0.510	0.190	0.350	0.660	7.75	5.00	2.75	
0.150	1.390	0.730	0.660	0.530	0.200	0.365	0.695	8.50	5.50	3.00	
0.160	1.470	0.770	0.700	0.560	0.210	0.385	0.735	9.00	6.00	3.25	
0.170	1.540	0.800	0.740	0.580	0.220	0.400	0.770	9.75	6.50	3.50	
0.180	1.620	0.840	0.780	0.610	0.230	0.420	0.810	10.50	7.00	3.75	
0.190	1.690	0.870	0.820	0.630	0.240	0.435	0.845	11.25	7.50	4.00	
0.200	1.760	0.900	0.860	0.650	0.250	0.450	0.880	12.00	8.00	4.25	
0.250	2.010	1.010	1.000	0.730	0.280	0.505	1.005	16.00	8.50	4.50	
0.300	2.245	1.120	1.125	0.810	0.310	0.560	1.123	21.00	9.00	4.75	
0.350	2.460	1.210	1.250	0.880	0.330	0.605	1.230	27.00	9.50	5.00	
0.400	2.640	1.290	1.350	0.930	0.360	0.645	1.320	33.00	10.00		
0.450	2.780	1.350	1.430	0.970	0.380	0.675	1.390	38.00			
0.500	2.910	1.410	1.500	1.020	0.390	0.705	1.455	45.00			
0.550	3.040	1.465	1.575	1.055	0.410	0.733	1.520	50.00			
0.600	3.135	1.505	1.630	1.085	0.420	0.753	1.568	56.00			
0.650	3.245	1.555	1.690	1.125	0.430	0.778	1.623	63.00			
0.700	3.360	1.615	1.750	1.160	0.450	0.805	1.680	70.00			
0.800	3.525	1.675	1.850	1.210	0.465	0.838	1.763	83.00			
0.900	3.660	1.730	1.930	1.250	0.480	0.865	1.830	97.00			
1.000	3.800	1.800	2.000	1.300	0.500	0.900	1.900	110.00			

Not Recommended Without Use of Locator

* Data based on welding, without preheat, two pieces of the same welding characteristics. See Fig. 31.12 for assembly of parts.

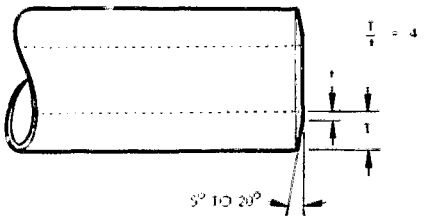

NOTE: WHEN "T" IS 3/16 IN. OR THICKER, BEVEL ONE WORK PIECE

RECOMMENDED END PREPARATION
TUBING

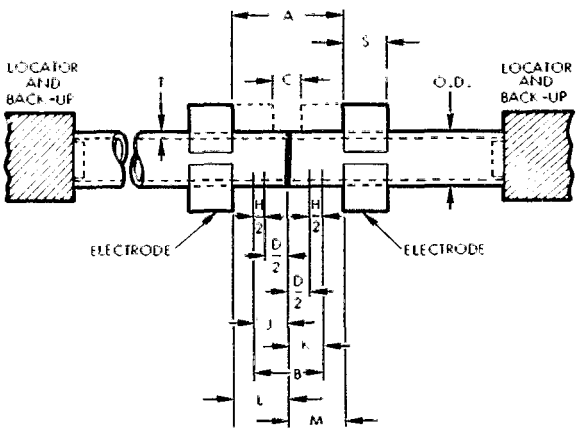

T = TUBE WALL OR SHEET THICKNESS
A = INITIAL DIE OPENING
B = MATERIAL LOST
C = FINAL DIE OPENING
D = TOTAL FLASH-OFF
H = TOTAL UPSET
J = K = MATERIAL LOST PER PIECE
L = M = INITIAL EXTENSION PER PIECE
O.D. = OUTSIDE DIA. OF TUBING
S = MINIMUM NECESSARY LENGTH OF ELECTRODE CONTACT

Table 5.12.6.4b. Flash Welding of Tubing and Flat Sheets
(From "Welding Handbook," 4th Ed., Section II, American Welding Society, New

T, In.	A, In.	B, In.	C, In.	D, In.	H, In.	J = K, In.	L = M, In.	Flashing Time, Sec.	O. I
0.010	0.110	0.060	0.050	0.040	0.020	0.030	0.055	0.40	0.
0.020	0.215	0.115	0.100	0.080	0.035	0.058	0.108	0.80	0.
0.030	0.325	0.175	0.150	0.125	0.050	0.088	0.163	1.25	0.
0.040	0.430	0.230	0.200	0.165	0.065	0.115	0.215	1.75	0.
0.050	0.530	0.280	0.250	0.205	0.075	0.140	0.265	2.25	0.
0.060	0.620	0.330	0.290	0.240	0.090	0.165	0.310	2.75	1.
0.070	0.715	0.385	0.330	0.280	0.105	0.193	0.358	3.50	1.
0.080	0.805	0.435	0.370	0.315	0.120	0.218	0.403	4.00	2.
0.090	0.885	0.475	0.410	0.345	0.130	0.238	0.443	4.50	2.
0.100	0.970	0.520	0.450	0.375	0.145	0.260	0.485	5.00	3.
0.110	1.060	0.570	0.490	0.410	0.160	0.285	0.530	5.75	3.
0.120	1.140	0.610	0.530	0.440	0.170	0.305	0.570	6.25	4.
0.130	1.225	0.650	0.575	0.470	0.180	0.325	0.613	7.00	4.
0.140	1.320	0.700	0.620	0.510	0.190	0.350	0.660	7.75	5.
0.150	1.390	0.730	0.660	0.530	0.200	0.365	0.695	8.50	5.
0.160	1.470	0.770	0.700	0.560	0.210	0.385	0.735	9.00	6.
0.170	1.540	0.800	0.740	0.580	0.220	0.400	0.770	9.75	6.
0.180	1.620	0.840	0.780	0.610	0.230	0.420	0.810	10.50	7.
0.190	1.690	0.870	0.820	0.630	0.240	0.435	0.845	11.25	7.
0.200	1.760	0.900	0.860	0.650	0.250	0.450	0.880	12.00	8.
0.250	2.010	1.010	1.000	0.730	0.280	0.505	1.005	15.00	8.
0.300	2.245	1.120	1.125	0.810	0.310	0.560	1.123	21.00	9.
0.350	2.460	1.210	1.250	0.880	0.330	0.605	1.230	27.00	9.
0.400	2.640	1.290	1.350	0.930	0.360	0.645	1.320	33.00	10.
0.450	2.780	1.350	1.430	0.970	0.380	0.675	1.390	38.00	
0.500	2.910	1.410	1.500	1.020	0.390	0.705	1.455	45.00	
0.550	3.040	1.465	1.575	1.055	0.410	0.733	1.520	50.00	
0.600	3.135	1.505	1.630	1.085	0.420	0.753	1.568	56.00	
0.650	3.245	1.555	1.690	1.125	0.430	0.773	1.623	63.00	
0.700	3.360	1.610	1.750	1.160	0.450	0.805	1.680	70.00	
0.800	3.525	1.675	1.850	1.210	0.465	0.838	1.763	83.00	
0.900	3.660	1.730	1.930	1.250	0.480	0.865	1.830	97.00	
1.000	3.800	1.800	2.000	1.300	0.500	0.900	1.900	110.00	

*** Data based on welding, without preheat, two pieces of the same welding**
Fig. 31.12 for assembly of parts.

Lap Joints. The plain lap weld joint, as shown in Figure 5.12.6.5c, is not normally used in high-pressure/high-temperature aerospace fluid systems because of the increased weight and increased pressure drop as a result of turbulence across the male tube end. Another disadvantage is that system fluid can become trapped between the mating tube surfaces because both ends of the joint are generally not welded. Trapped fluids can cause corrosion and cleaning problems. As shown in Figure 5.12.6.5c, the joint can be made by either expanding the female member or reducing the male member. Expansion and reduction of tubing can be accomplished by such methods as swaging, or explosive forming. One advantage of the lap joint is that it is generally stronger in bending than the butt joint because the moment of inertia is increased by the double wall. The change in diameter of the tube wall must be gradual, however, to avoid stress concentrations. This type of joint is normally restricted to easily worked tubing which can withstand the forming operations without cracking or excessive thinning.

When the longitudinal forces in a fluid system are the determining strength consideration, the female member of the lap joint may be serrated, notched, or slotted (see Figure 5.12.6.5c) to afford greater weld bead length and hence a greater allowable shear force. If a lap joint has been made properly, it will seldom fail radially under burst pressure; the main mode of failure will be in tension as the weld is placed in shear.

Burn-Down Flange Joints. A third type of plain weld joint used in the aerospace industry is the burn-down flange joint, depicted in Figure 5.12.6.5d. This joint is used for relatively thin wall tubing which is difficult to butt weld because of burn-through tendencies. Fabrication of this joint requires forming a flange on each of the two parts to be joined. Welding is accomplished by butting the flanges together and applying concentrated heat at the peripheral intersection, thereby melting or burning down the two flanges to form a weld bead. The advantage of this joint is that burn-through and loss of weld puddle control are eliminated because material is specifically provided to form the weld

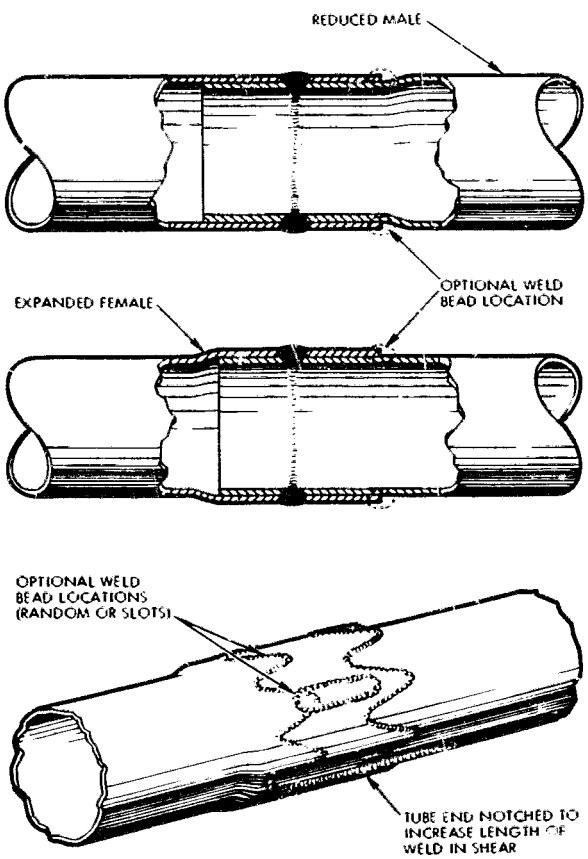

Figure 5.12.6.5c. Plain Lap Weld Joints for Tubing

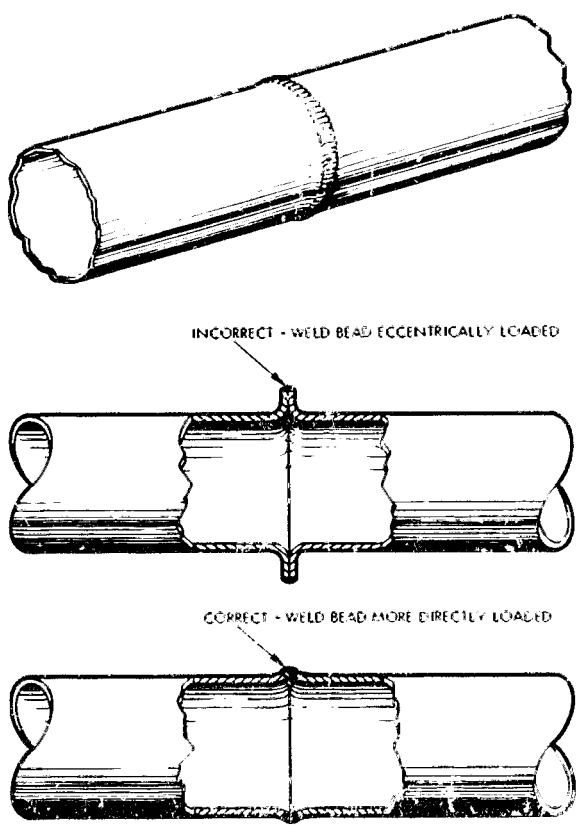

Figure 5.12.6.5d. Burn-Down Flange Weld Joint

bead at a greater diameter than the tube wall. The strength of such a joint will not be as great as that of a straight butt joint, unless the weld bead extends down to the tubing wall OD to prevent eccentric loading (see Figure 5.12.6.5d). The burned-down flange joint is more expensive than a butt joint because joint preparation requires an extra forming operation.

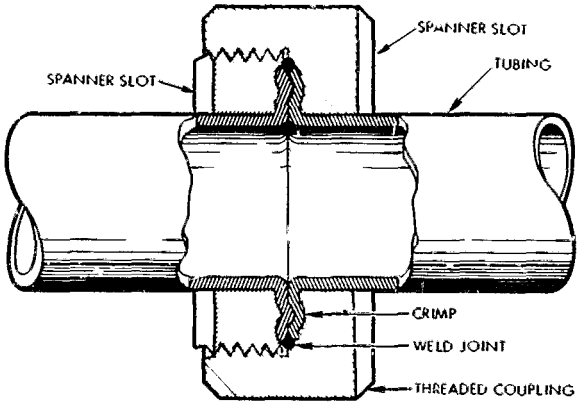

Figure 5.12.6.5e. Modified Burn-Down Flange Joint

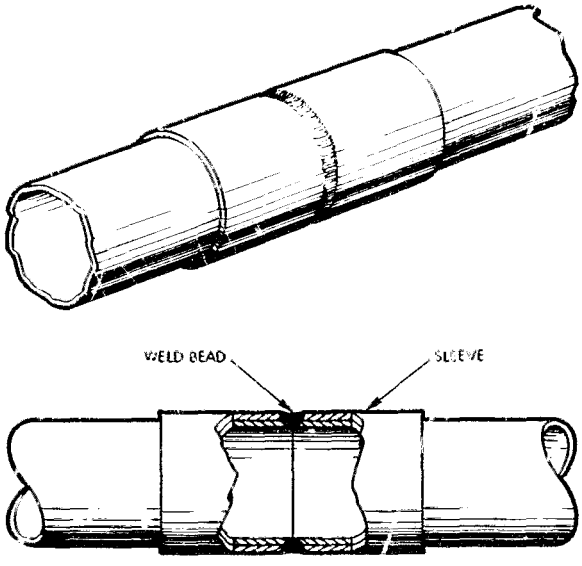

Figure 5.12.6.5f. Welded Sleeve Joint

Modified Burn-Down Flange Joints. A modification of the burn-down flange joint is shown in Figure 5.12.6.5e. Since in this connection the weld is used only to accomplish sealing and is not relied on for strength of the connection, a very small weld is all that is required. In making this type of tube connection the tube ends are first flared to make a butt joint; next a set of aluminum split ring chill blocks are installed onto the tube joint for the purpose of clamping the tube ends together and providing a heat sink during the welding of the flared tube ends. Note that a slight crimp in the flared tube ends is created by the chill blocks, preventing welding contamination from entering the inside of the tubing. After the weld has been made, a threaded coupling is slipped over the weld joint for the purpose of carrying pressure loading. This threaded coupling can be very light, since it is not required to maintain any gasket sealing load, but merely adds the requisite material to resist pressure loading. This type of connection may be classified as semi-permanent, since the seal weld can be broken and rewelded if necessary.

Sleeve Joints. When high strength alloys are used, it is often difficult to form or machine tubing and connectors in preparation for welding. In addition, the butt welding of thin wall high strength tubing is difficult without burn-through or sagging of the weld bead into the tube. To circumvent these problems, a weld connector or sleeve may be provided over the joint area, as shown in Figure 5.12.6.5f. The weld is made by heating the sleeve just over the joint between the two tubes, fusing the sleeve and tubes together in one operation. The connector sleeve is generally made from a piece of tubing the next size larger than the tubing being welded, or is an expanded piece of the same tubing. The wall thickness of the weld sleeve may be the same as or thinner than the tubes being joined. The length of the sleeve is not critical but should be long enough to give support to the heat-affected zone adjacent to the weld bead. Reference 320-7 contains additional details on weld sleeve design.

To assure that the weld is made in the proper location when using a sleeve, it is necessary to position and hold it so that when the weld bead is laid it will fall just above the gap between the two parts being joined. The difference between the outside diameter of the tubing and the inside diameter of the sleeve is not critical, providing that the gap between the two does not exceed 0.005 to 0.010 inch. Because of variations in tolerances on seamless steel tubing diameter, mismatch between two joined tubes can be as great as 0.003 inch on one- and two-inch diameter tubing without causing difficulty in welding, providing that weld penetration is approximately equivalent on both sides of the joint. When extremely heavy sections of tubing are welded, it often is necessary to provide a backup torch to make a weld pass on the inside diameter. This, of course, can only be accomplished when there is access to the inside of the tubing. When using a weld sleeve, the tubes should be butted together rather than allowing a gap, although satisfactory welds can be made with gaps as high as 0.030 inch. Gaps larger than this may cause weld bead concavity, which can result in stress concentration in the weld area.

5.12.7 Swaged Connectors

5.12.7.1 GENERAL. Swaging, as applied to connectors, is the process of joining two pieces by the cold forming of metal to both make a seal and form a connection to carry the structural load. This type of connection is generally considered to be permanent in nature, although recent developments have exploited the technique for obtaining a semi-permanent connector which does not require the addition of heat (Reference 36-14). The swaging process as such is utilized in some existing connectors as a means of locating a ferrule or sleeve on a piece of tubing, and is receiving increasing attention in new connector concepts. As an example of present usage, the MS flareless connector ferrule is swaged to the tubing during the initial connector assembly process.

The swaging process offers some distinctive advantages over other permanent connectors, such as:

a) Heat is not required to make the connection, and therefore tubing is not weakened as a result of heat concentration or annealing.

b) Inspection to assure proper mechanical locations of swaged connector parts can be readily accomplished by visual operation.

5.12.7.2 SWAGED CONNECTOR TYPES. One type of swaged connector is the Parker "H" fitting shown in Figure 5.12.7.2a. In this connector, the tubing is inserted into the ends of the connector body. The sleeves, or slides in this case, are then pulled up onto the tapered lands of the connector body resulting in the tubing being locked in place by the sharp edges of the connector body inner diameter. Either a special hand-operated or hydraulically operated tool is required to set the sleeves onto the connector body. A more recent development, also from Parker Aircraft, is the "X" connector illustrated in Figure 5.12.7.2b. The development of this connector for NASA's Marshall Space Flight Center (as a potential improvement over MC connectors) is described in Reference 36-14. This concept is unique in that it is under development for not only the one-half-inch tubing size illustrated, but for a 4-inch duct size. The concept is being considered for all sizes of lines from one-quarter-inch tubing to the largest diameter ducts currently visualized in launch vehicle design (about 20-inch diameter, according to Reference 34-10). The sleeves of high strength stainless steel are stretched beyond their yield stress when the tubing ends are swaged into place. During assembly, the gold-plated primary seals of the stainless steel collar are seated against the sleeve seating surfaces by the axial force resulting from radial deformation of the collar by an assembly tool. This toggle action results in negligible relaxation of the axial sealing force when the collar lips spring radially outward slightly after the assembly tool is removed. Upon disassembly the collar is either "unswaged" or cut off and discarded, a new collar (and hence new gold-plated seals) is used for each subsequent reassembly.

5.12.8 Adhesive Bonding Joints and Connectors

5.12.8.1 GENERAL. Adhesive bonding is a process suitable for joining metal-to-metal, metal-to-nonmetal, or nonmetal-to-nonmetal. The types of adhesives used include thermosetting resins, thermoplastic resins, and various artificial elastomers. Joints that can be brazed can generally be adhesive bonded also, with the exception that high-temperature applications and high-tensile strength requirements are limiting factors for adhesive bonds.

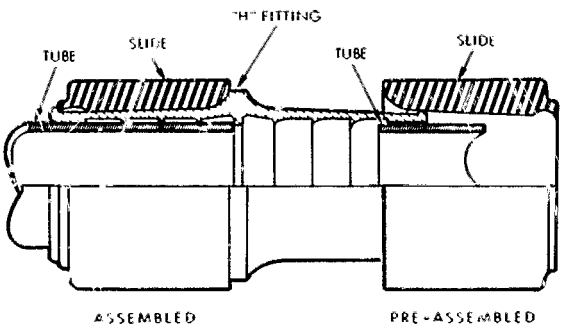

Figure 5.12.7.2a. Parker "H" Connector
(Courtesy of Parker Aircraft Co., Los Angeles, California)

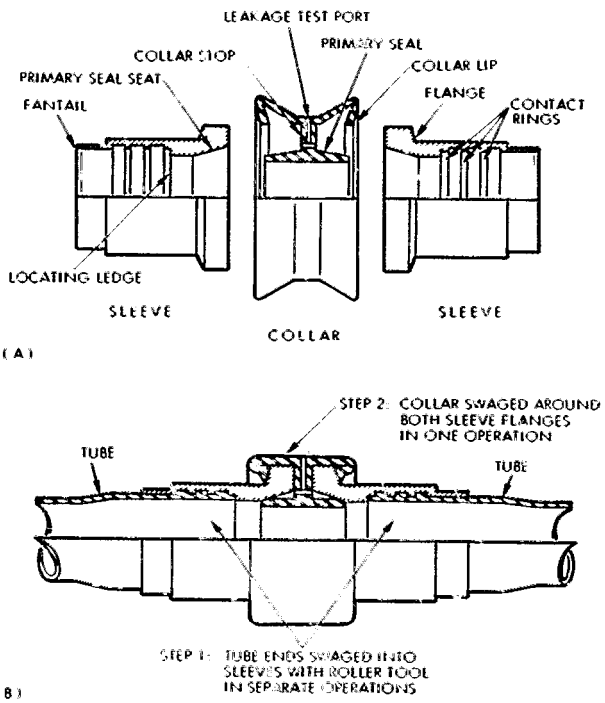

Figure 5.12.7.2b. Parker "X" Connector
(Reference 36-14)

5.12.8.2 APPLICATION. Adhesive bonding has seen limited usage in aerospace fluid connector applications to date, although it has been used in related components, such as liners for filament-wound reinforced-plastic helium pressure vessels. Adhesive bonding of relatively low-pressure plastic pipe using sleeve or socket-type connectors has been widely used in numerous military, industrial, and commercial applications for reasons of chemical compatibility, weight, or cost.

Increased interest in the use of filament-wound reinforced plastic for liquid-propellant tankage and even high-pressure rocket engine fluid-transfer lines (Reference 34-10) may be expected to focus more attention on the use of adhesive bonding in future aerospace applications.

5.12.8.3 DESIGN FACTORS. The design of an adhesive bonded joint is similar to that of a brazed joint, in that full advantage must be taken of the shear strength of the adhesive. Butt joints are therefore avoided in preference to lap type joints.

As with brazing, a satisfactory bonded design must also give consideration to surface preparation. Generally acceptable methods in preparing surfaces to be adhesively bonded include:

a) Cleaning all contaminants and grease from surfaces
b) Etching surfaces to make them chemically receptive to adhesives and to provide good wetting characteristics
c) Rinsing
d) Drying
e) Applying a primer.

Thin materials may be successfully joined by adhesive bonding. In addition, adhesive bonding allows a smooth contour at the joint, can provide thermal and electrical insulation, can protect against galvanic action between dissimilar metals, and may be used as a dampener against vibration or sound.

Three factors that severely limit the use of adhesively bonded connectors and joints are:

a) Instability of many adhesives at temperatures above about 400°F
b) Poor tensile strength
c) Limited compatibility of the adhesive with fluid media.

REFERENCES

*References added March 1967

Threaded Connectors

1-216
6-30
6-100
6-111
6-130
6-154
6-161
6-187
6-209
18-1
19-76
23-38
23-55
36-11
36-12
36-14
44-14
44-15
46-6
46-7
46-29
46-31
147-1
151-2
151-3
151-4
233-1
447-4
V-97
44-24*

Connecter Preload Theory

36-11
36-12
36-14
44-14
44-15
46-29
46-31
44-24*

Flanged Connector Design

19-76
23-38
26-213
26-214
36-11
36-12
36-14
44-14
46-6
46-7
46-29
46-31
68-62
132-1
196-1
400-1

Swaged Connectors

36-14
36-20*
46-31

Welded and Brazed Connectors

65-42
68-62
77-5
77-6
36-20*
320-9*
132-1
320-7
504-1
504-2
513-2*

Adhesive Bonded Connectors

26-209
34-10
93-8
132-1
400-1

6.4 DYNAMIC SEALS

6.4.1 Introduction

6.4.2 Dynamic Seal Classifications

6.4.3 Design and Selection Factors

- 6.4.3.1 Sealing Interface
- 6.4.3.2 Materials
- 6.4.3.3 Contamination
- 6.4.3.4 Fluid Compatibility
- 6.4.3.5 Temperature
- 6.4.3.6 Pressure
- 6.4.3.7 Resiliency and Rate of Return

6.4.4 Design Data

- 6.4.4.1 Lip Seals
- 6.4.4.2 Molded Shape Packings
- 6.4.4.3 O-Rings
- 6.4.4.4 Compression Packings
- 6.4.4.5 Split Ring Seals
- 6.4.4.6 Special Sealing Concepts

6.4.1 Introduction

A dynamic seal is a mechanical device used to minimize, or reduce to an acceptable level, leakage of a fluid from one region to another when there is relative motion between the sealing interfaces. In normal dynamic seal operation, relative motion will exist between a static or stationary interface and a moving interface. The basic types of motion which may occur singly or in combination are:

a) Sliding motion, in which the direction of motion is perpendicular to or across the seal interface. The contact interface is continuously changing location on the gland. If the motion occurs in both directions it is called reciprocating.

b) Rotary motion, in which the direction of motion is along the seal interface. The contact interface is limited to one location on the gland. Where reversal of motion occurs, it is termed oscillating.

The motion may be continuous, but in most instances it will be intermittent with varying periods of time, during which the seal will function in a static condition. A special case of intermittent action, in which the interfaces are separated and remated, occurs in some valve closure seals. Typical applications of valve closure seals are shown in Sub-Section 6.2, "Valving Units."

In addition to meeting the sealing requirements, a dynamic seal must also be designed for acceptable friction and wear at the interface. No escape of the sealed fluid is desirable from a sealing standpoint. However, in order to get reasonable friction and wear characteristics at the seal interface with the current state-of-the-art of dynamic seal design, a small amount of leakage must be tolerated for lubrication. Results of one of the latest studies on dynamic sealing are described in Reference 152-4. In some dynamic seal applications it is possible only to minimize leakage, not prevent it. Friction coefficients for various material combinations are given in Sub-Section 12.7.

If leakage cannot be tolerated, the use of bellows or diaphragms can be used in certain applications to replace conventional dynamic seals. The use of bellows or diaphragms will be controlled by the physical limitations of the design, such as length of stroke required, power available to move the seal, i.e., bellows compression force, and by the envelope available. Application of bellows is described in Sub-Section 6.6 and diaphragms in Sub-Section 6.7.

Dynamic seals considered in this sub-section are limited primarily to seals used in valve applications, including such typical applications as valve actuator seals involving relatively low rotary and linear speeds. These paragraphs do not include a discussion of dynamic seals which are primarily intended for high speed rotary applications, such as pumps and turbines.

A discussion of the application of face or mechanical seals is covered in References 112-12 and 46-27; positive clearance seals such as labryinth and bushing seals are described in References 19-72 and 152-3. The following sub-topics consider factors which influence gland and seal element design and selection, and present data on specific dynamic seal designs.

6.4.2 Dynamic Seal Classification

Common methods of classifying dynamic seals include type of motion, method of loading, material application, and configuration. Some of these classifications are shown in Table 6.4.2.

6.4.3 Design and Selection Factors

Primary factors which must be considered in dynamic seal design and selection involve relative balance between allowable leakage and permissible wear of the seal and gland. Influencing factors include material properties, interface conditions, compatibility with the sealed media, and environmental effects such as operating temperature and pressure.

6.4.3.1 SEALING INTERFACE. The effectiveness of a dynamic seal design is determined by the capability of the seal interfaces to maintain good mating over the seal operating environment. The mechanisms of sealing described in Detailed Topic 6.3.2.1 are applicable to dynamic seals; however, the extent of deformation at the interface will be less. The contact surface stress is

Table 6.4.2. Dynamic Seal Classifications

Type of Motion
- Sliding
- Reciprocating
- Rotating
- Oscillating

Method of Loading
- Mechanically preloaded
- Pressure-energized
- Positive clearance

Method of Sealing
- Radial
- Face

Material
- Metallic
- Nonmetallic
- Combination

Application
- High pressure
- Vacuum
- High temperature
- Cryogenic

Configuration
- O-ring
- Lip
- Mechanical
- Labyrinth
- Bushing
- Piston ring
- Compression packing
- Molded packing

considerably lower than in a comparable static seal, due to load limitations imposed by wear considerations. Therefore, the effect of gross surface irregularities such as waviness, out-of-roundness, etc., may be the dominant factor in establishing leakage paths. The general subject of surface topography is covered in Detailed Topic 6.3.2.1 under "Static Seals," and is applicable also to dynamic seals. In dynamic seal applications where lubrication is required, gland surface finishes finer than 10 microinches have shown insignificant increase in seal life. In fact, a surface finish which is too smooth (in the range of 2 microinches) cannot support a lubrication film, and premature seal failure may occur (Reference 1-292).

In high pressure dynamic seals, abrasion and tearing of the interface materials are primary reasons for seal failure. The rate and amount of abrasion are difficult to predict in dynamic seal performance, because of changing conditions such as lubrication and friction encountered during operation. These conditions change during the life of the seal. Characteristics which influence the rate of wear include surface finish and hardness, and frictional characteristics at the interface.

Gland Design. In a dynamic seal design installation, all structural members which directly or indirectly influence the performance of the seal element are considered part of the gland. For example, the gland of the sliding seal on a piston will include both the piston and the adjacent cylinder. The primary functions of the gland are to contain the seal element and to provide, either wholly or partially, the contact loading at the seal interface necessary to produce the required sealing stress. In positive clearance type dynamic seals, where there is no relative load between the seal interfaces, the purpose and function of the housing is primarily to contain and support the seal.

Whenever possible, the two surfaces of the gland being sealed should not come in contact; bearing areas should be outside the sealing area. When this is not possible, the part of the gland containing the seal should be a soft bearing material which will not score or mark the part of the gland which moves across the seal.

In dynamic seal applications where the seal mates with a shaft, shaft hardness, smoothness, and material are factors that must be considered. The usual recommendation for shaft hardness is a Rockwell C of at least 50. If the shaft is one of the soft metals, brass or aluminum for example, it is advisable to press a hardened steel ring on the shaft to serve as a seal running surface. Hard, dense chrome plate electro-deposited on the shaft will also serve satisfactorily.

Maximum seal efficiency and life are obtained with a finely finished gland surface, usually in the 10 to 20 microinch range. Polished or ground finishes with concentric marks are preferred in rotary applications. Direction of finishing marks and spiral lead are important; when a finish lead is present, it should be in the direction that guides the sealed media inward.

Friction. The seal friction force which must be overcome in actuating the moving member is a function of the coefficient of friction at the seal interface. Prediction of the coefficient of friction to be expected in actual operation is complicated because of its dependence upon several operating parameters, including rate of movement, the time at rest prior to movement (which influences breakout friction), operating temperature, reaction sensitivity of the surfaces to the contained media, surface geometries, and the amount of wear to be expected.

One of the major factors influencing friction at the seal interface and wear life of the seal components is the relative surface finish of the interfaces. The machinability of metallic seal materials therefore becomes a matter for consideration. Relative surface conditions which can be expected from various manufacturing operations are shown in Table 6.3.2.1c. Other material properties which influence the friction coefficient of seal materials are the relative surface hardness and type of surface film on the seal interfaces. In general, the softer metals exhibit a higher coefficient of friction.

END OF REFERENCE
51

REFERENCE
52

PLASTICS FOR AEROSPACE VEHICLES. PART I. REINFORCED PLASTICS. MIL-HDBK-17A, DEPT. OF DEFENSE, JAN. 1971.

MILITARY HANDBOOK

MIL-HDBK-17A
January 1971

Superseding
MIL-HDBK-17
5 November 1959

PLASTICS FOR AEROSPACE VEHICLES

PART 1. REINFORCED PLASTICS

DEPARTMENT OF DEFENSE

Washington, D.C. 20025

For sale by the Superintendent of Documents, U.S. Government Printing Office, Washington, D.C., 20402 - Price $2.50

CONTENTS

		Page
	Chapter 1 Introduction	
1.1	Purpose and Scope	1-1
1.2	Proprietary Products	1-1
1.3	General Features of Fiber Reinforced Composites	1-2
1.4	Definition of Terms	1-3
1.5	Symbols	1-3
1.6	Test Procedures	1-3
1.7	Applicable Specifications	1-3
	Chapter 2 Materials and Processes	
2.1	Introduction	2-1
2.2	Resins	2-1
2.2.1	Epoxy Resins	2-1
2.2.2	Polyester Resins	2-6
2.2.3	Phenolic Resins	2-7
2.2.4	Silicone Resins	2-9
2.2.5	Polyimide Resins	2-10
2.3	Reinforcements	2-11
2.3.1	Fiberglass	2-11
2.3.2	Boron	2-15
2.3.3	High Modulus Graphite Fibers	2-16
2.3.4	Other Reinforcements	2-16
2.4	Fabrication	2-17
2.4.1	Material Systems	2-17
2.4.2	Fabrication Methods	2-17
2.4.3	Cure and Postcure	2-19
2.4.4	Sandwich Constructions	2-19
2.4.5	Tooling	2-20
	Chapter 3 Design and Analysis of Composites	
3.1	Bases for Analysis	3-1
3.1.1	Preliminary Considerations	3-1
3.1.1.1	Effects of Anistropy	3-3
3.1.1.2	Earlier Design Procedures	3-4
3.1.2	Stress-Strain Relations for Isotropic Materials	3-5
3.1.2.1	Physical Significance of the Elastic Constants	3-5
3.1.2.2	Nomenclature of Stress and Strain	3-8
3.1.2.3	Generalized Hooke's Law for Isotropic Materials	3-9
3.1.2.4	Contracted Notation	3-11
3.1.2.5	Plane Stresses	3-15
3.1.2.6	Stress and Strain Transformations	3-17
3.1.3	Stress-Strain Relations for Anisotropic Materials	3-21
3.1.3.1	Directional Response Characteristics	3-21
3.1.3.2	Generalized Hooke's Law for Anistropic Composites	3-24
3.1.3.3	Transformation Equations for Orthotropic Materials	3-31
3.1.4	Theory of Plates and Shells	3-36
3.1.4.1	Strain-Displacement Equations	3-37

TABLE 2-2 DIELECTRIC CONSTANT AND LOSS TANGENT FOR EPON 828 EPOXY AT X-BAND FREQUENCY

Base Resin *Curing Agent* *Composition*		*Epon 828* *MPDA* *100/14*	*Epon 828* *BF_3MEA* *100/3*
Dielectric Constant, 10 GHz, dry	75F 250F 300F	3.25 3.62 3.70	2.98 3.11 3.19
Loss Tangent, 10 GHz, dry	75F 250F 300F	0.035 0.076 0.072	0.022 0.047 0.055

TABLE 2-3 ELECTRICAL REQUIREMENTS FOR EPOXY AND POLYESTER LAMINATES AT X-BAND FREQUENCY

STANDARD CONDITION			
Epoxy	*Polyester*	*Dielectric Constant*	*Loss Tangent*
Grade A	Class 1	3.6 – 4.0	0.020 (max.)
Grade B	Class 2	4.0 – 4.2	"
Grade C	Class 3	4.2 – 4.4	"
Grade D	Class 4	4.4 – 4.6	"
IMMERSION CONDITION			
Dielectric Constant shall not exceed the standard condition by more than 5%. Loss Tangent 0.025 maximum for all grades and classes.			
HIGH TEMPERATURE			
Dielectric constant shall not vary from standard condition by more than ± 3.0%. Loss Tangent 0.045 maximum for all grades and classes.			

Thermal Stability: The thermal stability of epoxy resins is evaluated by thermogravimetric analysis (TGA), differential thermal analysis (DTA) or other techniques. Conventional epoxy and epoxy novolacs subjected to TGA show rapid decomposition at approximately 572F in vacuum and in oxygen atmosphere. The total decomposition upon reaching 1652F varies with resin type and curing agent, ranging from 50 to 80 percent, with epoxy novolacs showing the lower losses.

Thermal Conductivity: The thermal conductivity of epoxy resins varies with resin type and the amount and type of curing agent. It normally ranges from 0.085 to 0.110 BTU/ft. hr. ^{o}F.

Thermal Expansion: Similarly, the coefficient of thermal expansion depends upon the resin type, curing agent and the amount of curing agent. For temperatures of from -65F to approximately 220F, it varies from 33 to 39 x 10^{-6} in./in./^{o}F.

Flammability: Epoxy resins are not flame retardant and require the addition of chlorinated curing agents or brominated polymers to acquire flame resistant characteristics. Antimony trioxide is usually added to the system in conjunction with these materials. These modifications result in some decrease in mechanical properties, depending on the percentage of additives to the system.

2.2.2 POLYESTER RESINS

2.2.2.1 *Definitions.* Polyesters for reinforced plastics include the unsaturated polyesters and the allyl type resins. The unsaturated polyesters are synthesized by the esterification of dibasic acids with dihydric alcohols and are supplied as monomer solutions of the esterification product. During cure, which requires a catalyst, the monomer reacts with the ester, resulting in a cross-linked, thermoset resin. Allyl resins are homopolymers of diallylphthalate or diallylisophthalate. Final cure may be brought about by reacting the prepolymer with various monomers, or by a continued reaction of residual allylic groups within the polymer chain.

2.2.2.2 *Specifications.* Requirements for polyester resins are covered in MIL-R-7575, Resin, Polyester, Low Pressure Laminating and in MIL-R-25042, Resin, Polyester, High Temperature Resistant, Low Pressure Laminating. Resins for either specification may be qualified as liquid systems or as preimpregnated fiberglass fabrics.

2.2.2.3 *Polyester Formulation.* Most polyesters are polymerized from a mixture of unsaturated and saturated acids (or anhydrides). The unsaturates provide sites for reaction with the monomer, while the saturates control the location of these sites within the polymer molecule. Maleic anhydride and its isomer fumaric acid are the principal unsaturates in polyester synthesis. The common saturates are orthophthalic anhydride and isophthalic acid. The principal dibasic alcohols are propylene, diethylene and ethylene glycols. Monomers for laminating resins include diallylphthalate (DAP), diallylisophthalate (DAIP), triallylcyanurate (TAC), styrene, vinyl toluene, methylmethacrylate, and dichlorostyrene.

2.2.2.4 *Curing Mechanisms.* The usual means of initiating the copolymerization of the polyester with the monomer is by the action of organic peroxide catalysts. The specific catalyst system determines the temperature at which curing takes place. Some catalysts are reactive at room temperatures, while others require the application of varying degrees of heat to initiate reaction. Common catalysts for laminating formulations are benzoyl peroxide and tertiary butylperbenzoate which cure in a temperature range of 235F to 310F. Systems based on methylethylketone peroxide and cobalt naphthenate are used for curing at ambient temperatures. Promoters or accelerators are added to the resin system in specific instances when lower cure temperatures are required. The system may also contain retarders or inhibitors. Retarders serve to reduce peak exotherms, while inhibitors prevent premature polymerization.

The cure rates for the various polyester types depend on the constituent acids and monomers, and to a lesser extent the glycol. For a specific resin system, cure rates and gel times are functions of catalyst and promoter concentration. Inhibitors and retarders have the effect of increasing cure and gel times.

Characteristic of polyester cure is the fact that once the reaction has been initiated it proceeds to completion and cannot be interrupted at an intermediate stage. Completion occurs when approximately 92–95 percent of the unsaturated ester sites have been depleted. With some systems, postcuring may increase the extent of saturation.

2.2.2.5 *Properties of Polyesters*

Effect of Chemical Structure on Mechanical and Physical Properties: The physical and mechanical properties of cured polyesters depend on the acids, glycols and monomers used in preparation of the resin; the proportions of each; and the molecular weight of the initial esterification product.

Equivalent maleic or fumaric based resins show little difference in mechanical properties. Fumaric resins, however, are less susceptible to moisture absorption.

water which appears is from thermal breakdown of hydroxyl groups. From 650F to 1550F the decomposition is composed of several complex reactions resulting in elimination of hydrogen, methane, carbon monoxide, phenol, cresol and xylenol. Degradation by oxidation appears to be a surface phenomenon and can occur during the curing process. Improved stability may be achieved by surface protection and by curing in non-oxidative environments. High temperature postcures also lead to improved stability. Thermograms in air show a rapid onset of degradation beginning at about 600F with 100 percent weight loss at about 1050F. Generally there appear to be no significant differences in the thermochemical behavior of one-step or two-step phenolics, when these resins are compared at equivalent methylene contents.

Flammability: Phenolics, in general, are flame retardant and some formulations are self-extinguishing when evaluated on the basis of Federal Test Method Standard No. 406, Method 2021.

2.2.4 SILICONE RESINS

2.2.4.1 *Definition.* Silicone resins are characterized by a polymeric structure containing alternating silicon and oxygen atoms (siloxane bond) and having two organic groups attached to each silicon. Chain growth and crosslinking reactions take place through the siloxane linkage. The organic groups normally are simple alkyl, aryl or vinyl radicals. The resins for laminating are synthesized from a mixture of monomers and contain both methyl and phenyl groups attached to the silicon.

2.2.4.2 *Available Forms.* Silicone laminating resins are supplied as toluene solutions of partially reacted resins. These varnishes can be dried to tack free solids and are suitable for preimpregnating purposes. Low pressure molding grades can be cured by the usual vacuum or autoclave processes at pressures below 50 psi. High pressure grades are cured at pressures ranging from 300 to 1500 psi.

2.2.4.3 *Specifications.* Requirements for silicones are provided in MIL-R-25506, Resin, Silicone, Low-Pressure Laminating. MIL-R-25506 resins are furnished as general purpose, radio frequency or radar frequency types and may be qualified as liquid or solid resins suitable for impregnation or as preimpregnated fiberglass fabrics.

2.2.4.4 *Curing of Silicones.* The curing of silicones is a condensation reaction involving residual silanol ($-\overset{|}{\underset{|}{Si}} - OH$) groups and resulting in the formation of water. Silicones are capable of self-curing, but the reactions are best controlled by use of catalysts. Amines such as triethanol amine or organometallic salts such as napthenates and octoates of zinc, iron, cobalt and lead are typical catalysts for curing reactions. Cure temperatures range from 350F – 450F and postcuring is generally required to develop optimum high temperature properties.

2.2.4.5 *Properties of Silicone Resins*

Mechanical Properties: The tensile, compressive and flexural strengths of silicone resins and laminates are lower than those for epoxies, polyesters and phenolics. The silicones, however, retain a greater percentage of their initial strengths at elevated temperature and may be exposed for longer periods at these temperatures with less degradation. For example, at 500F after one-half hour exposure, silicone fiberglass laminates retain approximately 40 percent of initial strength. After 25,000 hours at 525F, the laminates retain from 20 to 25 percent of the room temperature flexural strength.

Electrical Properties: Due to an inherent stability and to the fact that no carbon residue is produced, silicone resins exhibit superior electrical properties at elevated temperatures and after exposure for long periods at those temperatures. Representative values for the dielectric constant and loss tangent for silicone fiberglass laminates, tested perpendicular to the laminate at 9.375 GHz, are listed in Table 2-5. Other tests at 1 MHz show little change in dielectric constant or loss tangent after 25,000 hours at 480F.

TABLE 2-5 DIELECTRIC CONSTANT AND LOSS TANGENT FOR DC2106/181 FIBERGLASS SILICONE LAMINATES AT X-BAND FREQUENCY (Ref 2-9)

Temperature °F	*80*	*320*	*560*
25.6% Resin			
D. C.	4.50	4.52	4.45
L. T.	0.0064	0.0063	0.0059
31.0% Resin			
D. C.	4.12	4.14	4.14
L. T.	0.0066	0.0067	0.0072
36.4% Resin			
D. C.	4.11	4.11	4.11
L. T.	0.0064	0.0064	0.0066

Thermal Stability: Silicone resins are relatively stable at elevated temperatures and show lower weight losses compared to other resins. The residue on burning is silicon dioxide. Vacuum pyrolysis indicates a loss of 13 percent by volatilization at 1470F, increasing to 17 percent at 2190F. Comparable results for a phenolic resin are 44 percent and 48 percent, respectively.

2.2.5 POLYIMIDE RESINS

2.2.5.1 *Definition.* Polyimides are formed by the chemical reaction of an aromatic dianhydride with an aromatic diamine. The initial reaction results in a soluble polyamic acid, which is converted to an infusible, insoluble resin by subsequent dehydration and the application of heat. The basic polyimide structure, in generalized form, is shown in which R and R′ are aromatic groups derived from the dianhydride and diamine.

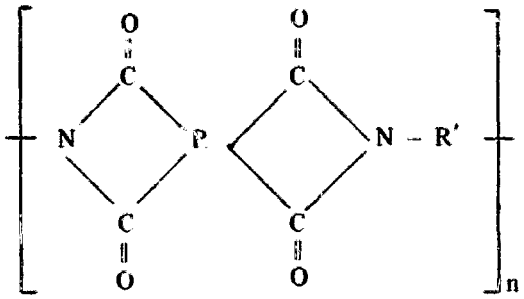

2.2.5.2 *Resin Types.* The dianhydride-diamine reaction produces linear polymers without crosslinking. Modifications in the reactants are required for form resins which can be crosslinked. The commercial resins currently used for laminating purposes are modified types and are crosslinked during the curing process. Other variations in initial reactants result in polymers with amide-imide or ester-imide linkages in the resin structures. These resins, closely related to the polyimides, have been evaluated on an experimental basis, but are not presently used in laminating formulations.

2.2.5.3 *Availability.* Commercial polyimides for lamination are supplied as preimpregnated fabrics or as resin solutions for impregnation.

2.2.5.4 *Processing and Curing.* Polyimides are characterized by high melt temperatures, low solubility and the evolution of volatiles during the curing reactions. The problems in fabricating laminates are attributed to these polymer characteristics. To maintain solubility and allow impregnation of reinforcing fabrics, the polyamic acids are used as laminating varnishes. The initial condensation reaction is interrupted while the resin is still soluble, but is capable of curing to a high molecular weight with minimum volatile by-products. In crosslinked resins, the molecular weight is held at a reduced level by end-blocking the polymer chain, thus producing soluble, lower melting precursors. The crosslinking reaction is relied upon to form a cured high molecular weight resin.

Polyimides can be laminated by conventional vacuum, augmented vacuum and press molding methods using dry layups. Filament winding also requires prepregs and a vacuum cure for best results. Close control of prepreg properties, B-staging, curing and postcuring is necessary to insure production of sound laminates and filament windings. Prepregs undergo a rapid decrease in flow at temperatures of from 250F to 300F, at which time residual solvents are volatilized. Initial cures take place at temperatures of from 300F to 350F. Postcures at 600F to 700F are required to attain optimum properties.

2.2.5.5 *Mechanical Properties of Polyimide Resins.* Current developments in resin formulations and processing techniques indicate that substantial improvements in the mechanical properties of polyimide laminates are being achieved compared to earlier reported data. Information on these newer laminates will be included in Chapter 4 when available.

2.2.5.6 *Thermal Stability:* The polyimides have shown superior heat aging performance in air compared to other heat resistant resins. They are stable for long periods at 600F. Thermograms in nitrogen indicate practically no weight losses to approximately 700F. Above this temperature losses increase, reaching about 40 percent at 1500F. In oxygen, the weight losses again begin at 700F, but at 1500F they are over 90 percent.

2.3 REINFORCEMENTS

2.3.1 FIBERGLASS

2.3.1.1 *Glass Compositions.* E glass and S glass are the principal glass compositions for aerospace reinforcements. E glass, based on lime-alumina-borosilicate, is more common and most woven fabrics are made from this glass. S glass, a silica-alumina-magnesia composition developed for improved tensile properties, is used mainly as roving or other non-woven forms, and to a lesser extent as a woven fabric. Properties of the two glasses are compared in Table 2-6.

2.3.1.2 *Specifications.* Military specifications related to fiberglass reinforcements include:

MIL-Y-1140, Yarn, Cord, Sleeving, Cloth, and Tape-Glass

MIL-C-9084, Cloth, Glass, Finished for Polyester Resin Laminates

MIL-R-60346, Roving, Glass, Fibrous (For Filament Winding Applications)

WS 1028, Roving, Glass, Epoxy Resin, 20 End, Impregnated, Polaris Fleet Ballistic Missile

WS 1126, Roving, Glass Filament, Polaris Fleet Ballistic Missile.

END OF REFERENCE

52

REFERENCE

53

SPACE MATERIALS HANDBOOK. THIRD ED. NASA SP-3051, 1969.

THIS REFERENCE IS MATERIAL THAT IS READILY AVAILABLE AND THEREFORE THE CONTENTS HAVE NOT BEEN REPRODUCED.

END OF REFERENCE

REFERENCE

54

TESTING METHODS AND TECHNIQUES: STRENGTH OF MATERIALS AND COMPONENTS - A COMPILATION. NASA SP-5944(01).

I. Pinkel
(1 copy - SP's only)
MAIL STOP 6-2

NASA SP-5944 (01)

TECHNOLOGY UTILIZATION

TESTING METHODS AND TECHNIQUES: STRENGTH OF MATERIALS AND COMPONENTS

A COMPILATION

RESEARCH CENTER
Safety Research
Data Institute
MAR 1 1972
CLEVELAND, OHIO

LEWIS RESEARCH CENTER
Aerospace Safety Research
and Data Institute
MAR 1 1972
CLEVELAND, OHIO

NATIONAL AERONAUTICS AND SPACE ADMINISTRATION

Foreword

The National Aeronautics and Space Administration and the Atomic Energy Commission have established a Technology Utilization Program for the dissemination of information on technological developments which have potential utility outside the aerospace community. By encouraging multiple application of the results of their research and development, NASA and AEC earn for the public an increased return on the public investment in aerospace and nuclear R&D programs.

The methods, techniques, and devices presented in this compilation are used in testing the mechanical properties of various materials. Although metals and metal alloys are featured prominently, some of the items describe tests on a variety of other materials, from concrete to plastics. Many of the tests described are modifications of standard testing procedures, intended either to adapt them to different materials and conditions, or to make them more rapid and accurate. In either case, the approaches presented can result in considerable cost savings and improved quality control.

The compilation is presented in two sections. The first deals specifically with material strength testing; the second treats the special category of fracture and fatigue testing.

This compilation is not a complete survey of the field of materials testing. Rather, its sampling of many diverse activities is intended for the interest of mechanical engineers and materials testing technicians. At the same time, it may serve as an introduction to the field for those unfamiliar with the principles and practices of materials testing.

Additional technical information on individual devices and techniques can be requested by circling the appropriate number on the Reader Service Card enclosed in this compilation.

Unless otherwise stated, NASA and AEC contemplate no patent action on the technology described.

We appreciate comment by readers and welcome hearing about the relevance and utility of the information in this compilation.

Technology Utilization Office
National Aeronautics and Space Administration

NOTICE • This document was prepared under the sponsorship of the National Aeronautics and Space Administration. Neither the United States Government nor any person acting on behalf of the United States Government assumes any liability resulting from the use of the information contained in this document, or warrants that such use will be free from privately owned rights.

For sale by the National Technical Information Service, Springfield, Virginia 22151 **$1.00**

Table of Contents

SECTION 1. Material Strength Testing — Page

Tensile Tester Accepts Multiple Coupons 1
Portable Tensile Testing Unit 1
Long Coupon Used for Evaluating Organic Material Tensile Properties 2
Frictional Loading Device for Testing Brittle Materials 2
Tensile Testing Grips Ensure Uniform Loading of Tubular Specimens 3
Testing Filamentary Composites 4
Pin-Ended Column Loading Device 5
Tensile Coupon Gage Length Scriber and Elongation Measurement Device 6
Modified Technique for Elongation Measurement of Thin Metal Strips 7
Tensile-Strength Apparatus Applies High Strain-Rate Load with Minimum Shock 7
Problems in High-Velocity Shock Testing Using a Slingshot Shock Machine 8
Flexure Test Apparatus for Electrical Conductors 9
Controlled Hydraulic Loading Device 9
High-Accuracy Flexure Test Fixture 10
Load Cell Calibrator 11
Testing Weld Strength and Mechanical Properties of 2219-T81 Aluminum Alloy 11
Torsion System for Multiple-Stress-Reversal Creep Testing 12
Testing the Room-Temperature Aging Properties of Tens 50 (T4) Aluminum Alloy 12

SECTION 2. Fracture and Fatigue Testing

Fatigue Testing of 1100-H14 Aluminum Alloy 13
Low-Cycle Fatigue Tests on Nickel Alloys 625 and Hastelloy C 13
Fatigue Data Obtained from Programmed Hydraulic Loading System 14
Hydraulic Servo System Increases Fatigue-Testing Accuracy 15
Fatigue Tester with Flex Plates and Bars Gives True Axial Motion 16
Automatic, Nondestructive Monitoring of Fatigue-Crack Growth 16

Fatigue Cracks Detected and Measured
Without Test Interruption 17
Analysis of Flow-Induced Fatigue in Bellows 17
Cryostat Modified for Rotating-Beam Fatigue Test 18
Fatigue in Reinforced Concrete Beams
under Dynamic Load 19
Survey of Fracture Testing Methods 19
Cracks of Known Size Induced in Metal Samples
for Fracture Mechanics Studies 20
Fracture Mechanics Test Method 20
Accelerated Stress Corrosion Test for Steels
and Nickel Alloys 21
Failure Modes in Polytetrafluoroethylene Examined
Using Fractography 21
Stress Crazing of Chlorotrifluoroethylene Polymer
Caused by Halogenated Solvents 22
A Rapid Stress-Corrosion Test for Aluminum Alloys 22
Chemical Milling Reveals Stress Corrosion Cracks
in Titanium Alloys 23

Section 1. Material Strength Testing

TENSILE TESTER ACCEPTS MULTIPLE COUPONS

A novel device permits rapid, sequential testing of up to 6 tensile coupons without interruption for manual alignment between tests. This feature

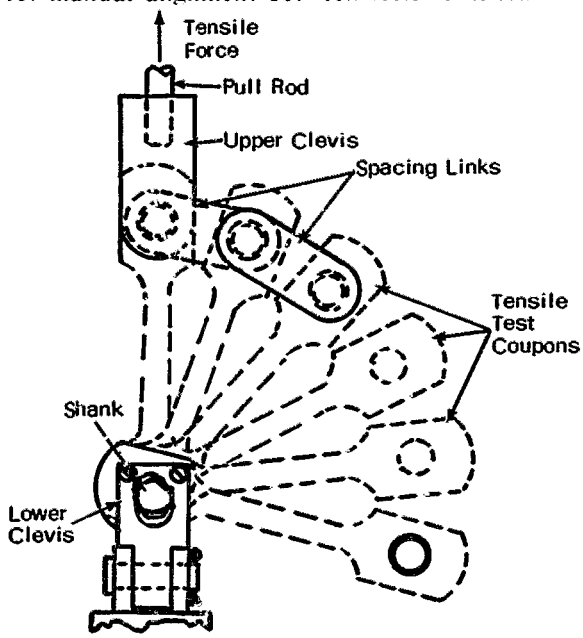

is especially useful when testing is to be performed under controlled environmental conditions, where time would be lost in regaining the proper environment after the interruption.

The device differs from a similar, commercially available system in that it provides positive coupon alignment prior to test, and is much less apt to jam and cause premature failure. As shown in the figure, the device consists of radially arrayed tensile coupons, connected at the upper end by high-strength spacing links (two links per gap) and mounted at the lower end on a special shank. The upper end of the first coupon is attached to the upper mounting clevis, which is attached to the pull-rod of the testing machine. The shank is retained in the lower clevis by keeper plates, and the lower clevis is screwed into the base of the tester. Strain gages are bonded to each specimen, enabling separate stress-strain plots to be made.

As the pull-rod moves upward, the first specimen is stressed to the breaking point. Further vertical movement of the rod causes the linkage connecting the first and second specimens to rotate the lower mounting about the shank and align the second specimen. Tension is then applied to the second coupon across the first pair of spacing links. Progressive rotation of the plate after each failure of a specimen allows complete testing of all specimens.

Source: R. T. Hartunian of
McDonnell Douglas Co.
under contract to
Marshall Space Flight Center
(MFS-2067)

Circle 1 on Reader Service Card.

PORTABLE TENSILE TESTING UNIT

A commercially available, portable, tensile testing unit has been improved by adding an hydraulic accumulator to the tester's hand-pumped load cell. The accumulator allows test loads to be applied at a constant strain rate, thereby improving the accuracy and repeatability of test results obtained.

The addition of the accumulator to the unit provides two separate test systems. The operator can (1) bypass the accumulator and use the hand

pump to apply a predetermined amount of load or strain, or (2) charge the accumulator in advance with sufficient pressure to begin a tensile test and provide a constant rate of strain until specimen failure is achieved.

Source: D. G. Thomann of
North American Rockwell Corp.
under contract to
Marshall Space Flight Center
(MFS-16356)

Circle 2 on Reader Service Card.

LONG COUPON USED FOR EVALUATING ORGANIC MATERIAL TENSILE PROPERTIES

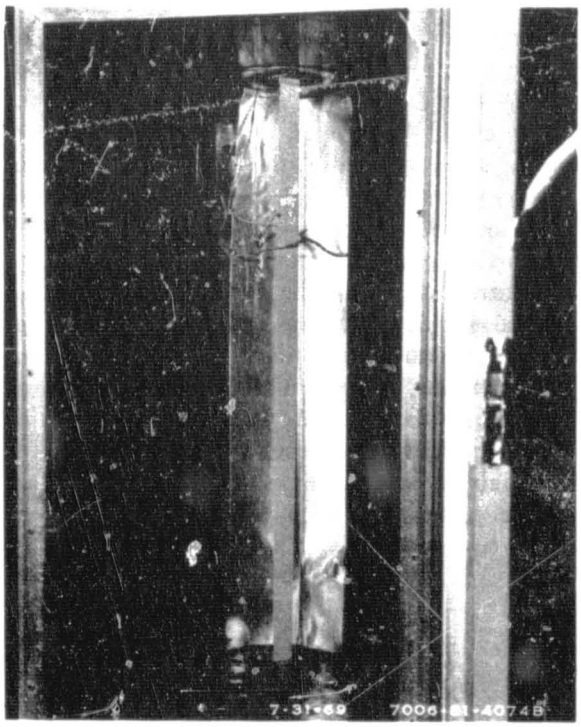

A testing technique for determining the physical properties of organic adhesives uses long tensile specimens made by depositing a controlled thickness of adhesive on giass scrim cloth. The photograph shows one such specimen, mounted for determination of tensile strength.

Previous methods required a specimen formed by bonding two pieces of metal with the adhesive to be tested. However, erroneous results were often produced by such specimens because of the difference in thermal expansion coefficient between metal and adhesive, the quality of the bond, and the variability of adhesive thickness. The new method avoids these problems since it essentially involves only the material being evaluated, and not bonded fixtures.

Source: W. G. Boyd, J. W. Eberhardt,
W. L. Hill, and J. C. Newland of
North American Rockwell Corp.
under contract to
Marshall Space Flight Center
(MFS-16796)

No further documentation is available.

FRICTIONAL LOADING DEVICE FOR TESTING BRITTLE MATERIALS

The illustrated test chamber and insert provide a novel means of avoiding the introduction of bending forces during tensile testing of graphite, beryllium, ceramics, and other brittle materials. This is accomplished by frictional loading of test specimens, ensuring true axial alignment of the specimen in the chamber.

The test chamber consists of a thick-walled

steel cylinder whose diameter and length are consistent with the size of the specimens to be tested. Six equally spaced rows of radially tapped holes are cut into the walls of the cylinder. These holes accept either hydraulic actuators or alignment/reaction bolts. This arrangement permits six-faced loadings of specimens that have a hexagonal cross section.

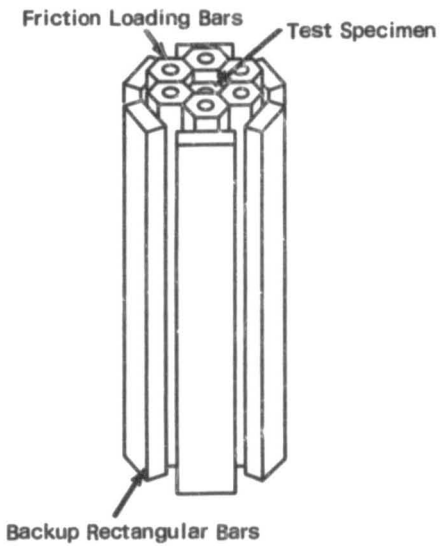

Specimen Assembly

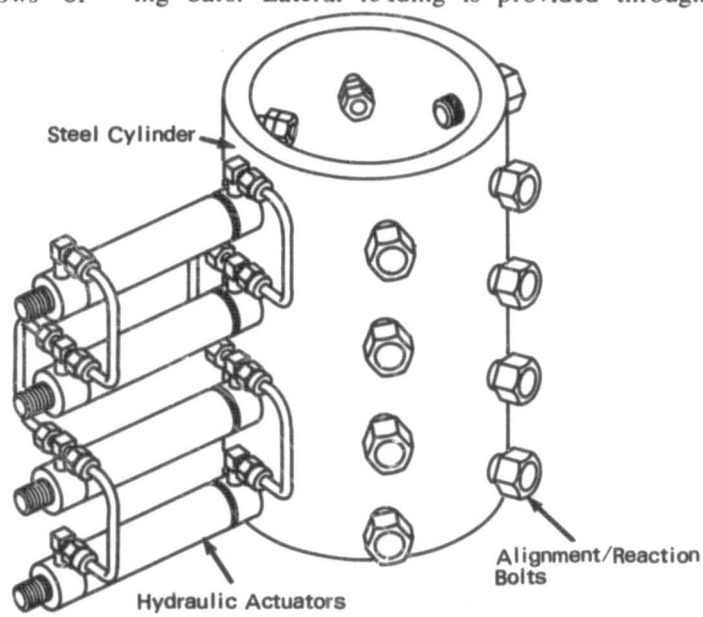

Test Chamber

The test specimen assembly is prepared by surrounding the specimen proper with six frictional loading bars that are slightly longer in length than the test specimen. Backup rectangular bars are added to distribute the lateral loading uniformly. The mating faces of loading bars are machined to provide a small clearance, so that the full lateral load is carried by the test specimen.

The bundled specimen is centered in the test chamber, which is then positioned on a universal testing machine (not shown), with a compression loading block supporting the friction loading bars. Lateral loading is provided through the hydraulic actuators. With a very light lateral pressure applied, the frictional loading bars are compressed by a predetermined amount. The hydraulic actuators are then pressurized to a preset pressure and the compression on the loading bars is released at a uniform rate. As the load is released, the test specimen is placed in tension. Compression release continues until the test specimen fractures.

Source: T. F. Hengstenberg and G. Zibritosky of Westinghouse Astronuclear Laboratory under contract to AEC-NASA Space Nuclear Systems Office (NUC-0051)

No further documentation is available.

TENSILE TESTING GRIPS ENSURE UNIFORM LOADING OF TUBULAR SPECIMENS

A new design, double-grip fixture for attaching tubular specimens to a tensile testing machine solves the problem of unequal stress distribution across the tube cross section.

Standard grips used in the tensile testing of bimetal tube specimens allow tensile loading

to be applied directly only to the outer tube. With such grips, stress is not distributed uniformly to the inner and outer tubes unless they are strongly bonded.

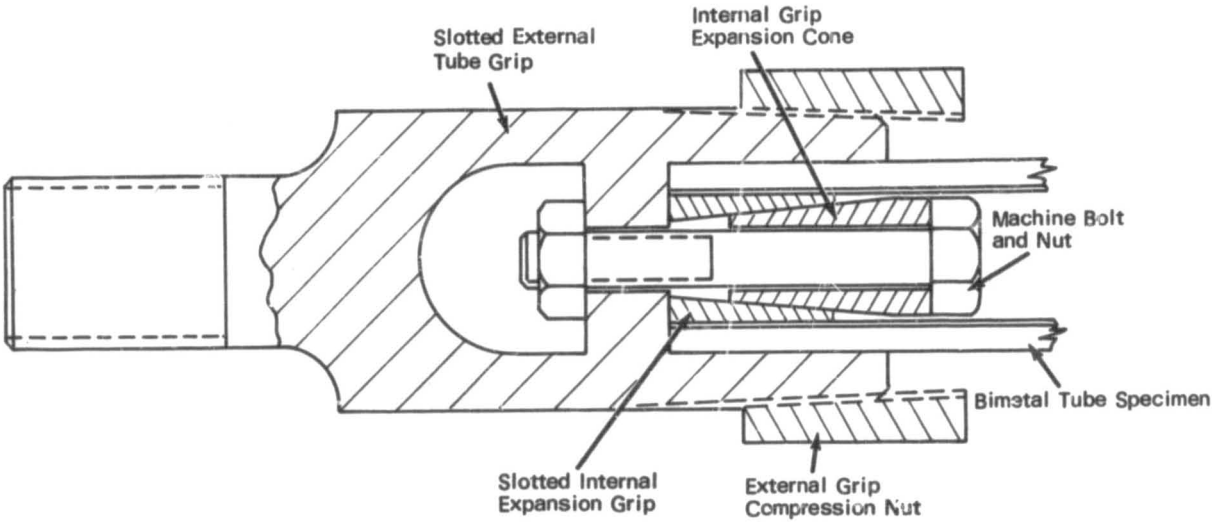

The load distribution problem can be overcome by using tensile testing grips of the design shown in the illustration. Each grip is comprised of (1) a slotted internal expansion grip, (2) an internal grip expansion cone, (3) a standard machine bolt and nut, (4) an external grip compression nut with pipe threads, and (5) a slotted external tube grip with pipe threads at one end and an adapter for attachment to the tensile test machine at the opposite end.

A grip is applied by fitting it to one end of the tube specimen (see fig.). The nut on the machine bolt is tightened to expand the internal tube grip. The external compression nut is then tightened to compress the external grip against the outer surface of the tube specimen. The nut tightening procedure is repeated until the tube specimen is uniformly gripped internally and externally. When the test is completed, the external compression nut is loosened to release the outer grip. Then the internal nut is loosened, allowing the internal grip to contract so that the tube specimen can be slipped free.

Source: V. Hunt and S. D. Driscol of
Aerojet-General Corp.
under contract to
Lewis Research Center
(LEW-10267)

No further documentation is available.

TESTING FILAMENTARY COMPOSITES

Difficulties encountered in tensile testing of filamentary composite materials using the conventional split-dee test (Figure 1) are eased by using a modified test specimen (Figure 2).

The split-dee tensile test has the advantages that the ring-shaped specimen may be readily fabricated by winding, and the test may be performed in a conventional universal testing machine without special fixtures other than the split-dees themselves. However, the test has two disadvantages. First, there is no section across which strain gages may be mounted to measure the stress-strain properties. Second, and more seriously, substantial bending moments are induced in the ring at the split between the two dees. Because membrane stress in the ring causes it to increase in diameter as the load increases, the ring tends to pull away from the

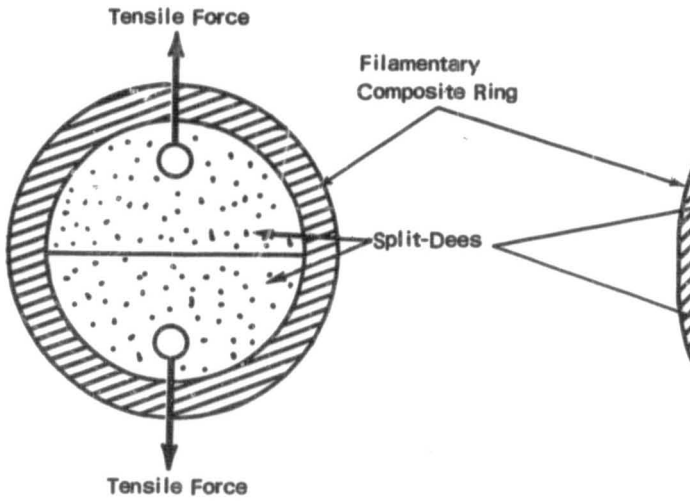

Figure 1. Split-Dee Tensile Test

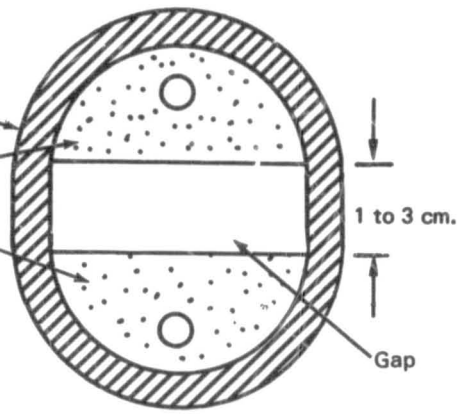

Figure 2 "Racetrack" Filament-Wound Tensile Specimen

corners of the dees. This generates bending moments of a sufficient magnitude to throw doubt on the validity of the test data.

A straight section was added, adjacent to the split in the dees, in an attempt to eliminate the bending moment. Mathematical analysis of the resulting "racetrack" specimen and comparison of test results achieved with it and the ring specimen indicate that, while bending is not eliminated by this addition, it is substantially reduced. Even a relatively short (1 cm) section reduces the bending moment to less than one-half that of the circular ring.

A further advantage of the "racetrack" specimen is that strain gages may be readily attached to the composite material in the center of the straight section.

The following documentation may be obtained from:

National Technical Information Service
Springfield, Virginia 22151
Single document price $3.00
(or microfiche $0.65)

Reference:
NASA-CR-66518 (N68-13926), Design Criteria and Concepts for Fibrous Composites Structures

Source: B. W. Rosen and N. F. Dow of General Electric Co. under contract to NASA Headquarters (HQN-10268)

PIN-ENDED COLUMN LOADING DEVICE

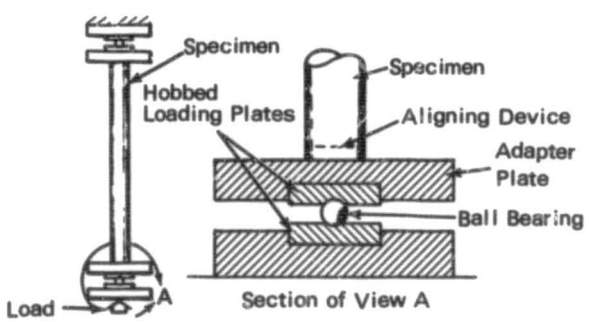

An inexpensive, simple-to-make device can apply a load to a round- or pin-ended column in a universal testing machine and can yield an end-fixture constant near unity. The device allows universal movement, has very low friction under heavy load, and has a maximum end-fixture constant of 1.08.

The device (see fig.) enables a specimen to be loaded between two small steel ball bearings.

The length of the column specimen is considered to be the distance between the centers of the balls. The ball bearing size is selected such that, when the ball is hobbed into the faces of two steel plates and heat treated to a strength of 830–970 MN/m^2 (120 to 140 ksi) for about 1/2 its diameter on each plate, the area of the spherical indentation in the plates will support a slightly greater load than the theoretical load carrying capability of the column specimen. The sets (plate, ball, plate) are kept in matched pairs. One set is used on each end of the specimen. An adapter and a centering device are attached to the plates to accommodate various specimens.

Source: J. F. Sternitzke and M. D. Saslaw of
McDonnell Douglas Corp.
under contract to
Marshall Space Flight Center
(MFS-13468)

Circle 3 on Reader Service Card.

TENSILE COUPON GAGE LENGTH SCRIBER AND ELONGATION MEASUREMENT DEVICE

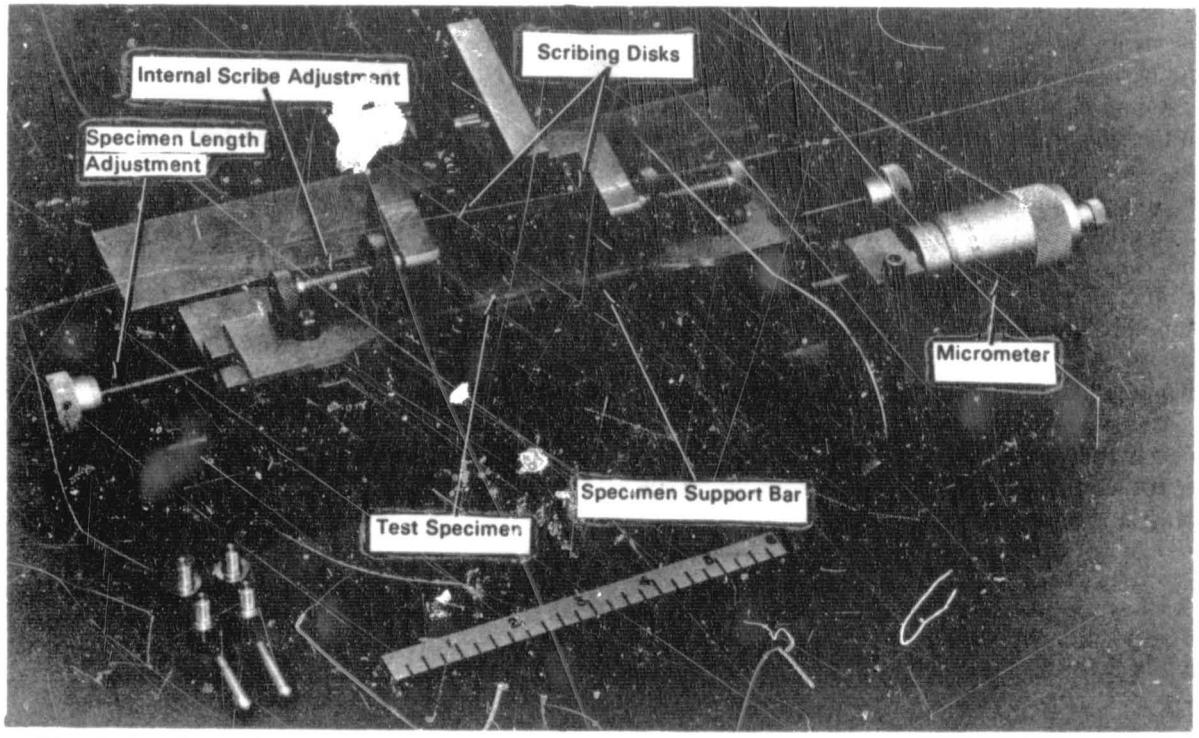

The device shown in the photograph is used to inscribe gage lengths on tensile test coupons, and to measure total elongation after test. Gage lengths are inscribed with adjustable locking knife edges, and the instrument will accept either a round or flat specimen with an overall length between 2.5 and 25 cm.

The elongation is determined by traversing a 40 power magnifier, with cross hairs, from one end of the gage length to the opposite end. The measurement is made with a micrometer.

Source: W. G. Boyd of
North American Rockwell Corp.
under contract to
Marshall Space Flight Center
(MFS-13780)

Circle 4 on Reader Service Card.

MODIFIED TECHNIQUE FOR ELONGATION MEASUREMENT OF THIN METAL STRIPS

The scribing technique discussed in the previous item will not work reliably when very thin specimens are to be tested, because the inscribed marks themselves may act as points of stress concentration in the specimen and cause premature fracture.

A solution to this problem is achieved by applying a thin gold plating to the test coupons before scribing. After test, the specimen may be pieced back together and photographed along with an accurate scale. The specimen should be obliquely lighted in order to reveal the scribe marks in the gold layer.

Source: I. M. Rehn of
Aerojet-General Corp.
under contract to
AEC-NASA Space Nuclear Systems Office
(NUC-10076)

No further documentation is available.

TENSILE-STRENGTH APPARATUS APPLIES HIGH STRAIN-RATE LOAD WITH MINIMUM SHOCK

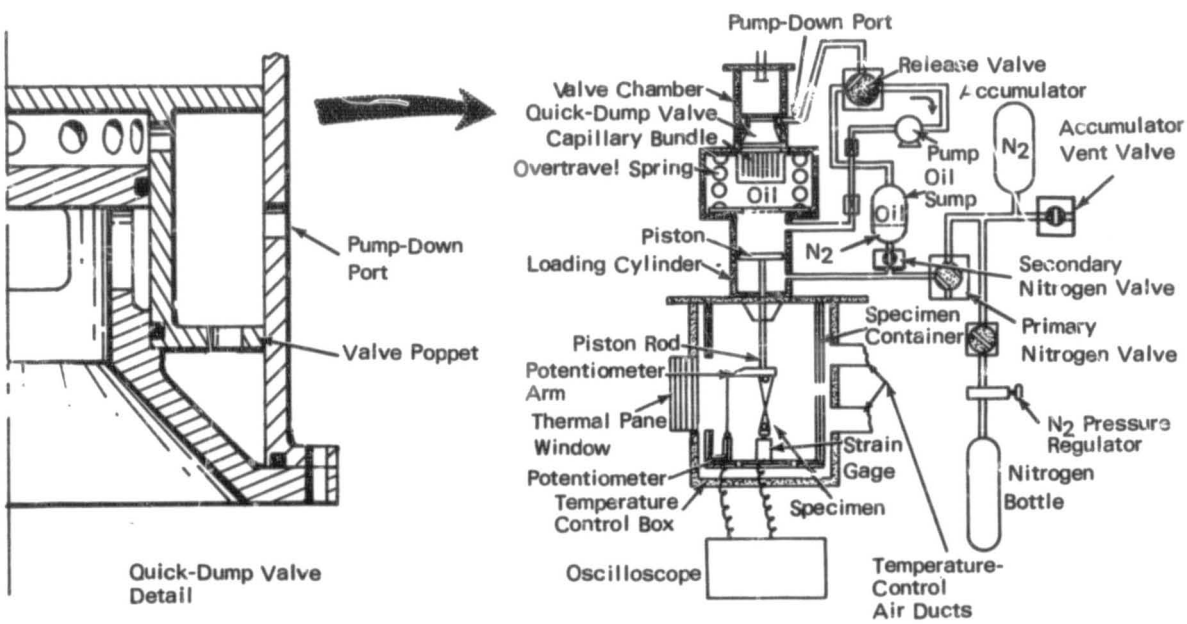

The apparatus shown in the diagram can apply tensile test loads at relatively constant, very high strain rates (up to 8.5 m/s), with minimal shock and vibration to the tensile specimen and apparatus.

The apparatus consists of two primary assemblies, a strain generator and a specimen container, separated by a strain wall. The specimen container is enclosed in a temperature-control box, and the specimen is connected directly to the strain generator through a piston rod.

To ready the system for test, oil is pumped from the pump-down port to the top side of the loading-cylinder piston. This transfer of oil automatically seats the quick-dump valve poppet and also drives the loading-cylinder piston to its lower position. The primary nitrogen valve is opened to pressurize the underside of this piston. The secondary nitrogen valve is then

closed to trap nitrogen pressure in the diaphragmed oil sump. The specimen is attached to the holding devices in the strain box after opening the window in the temperature-control box. When the specimen is in place, the window is closed and the temperature is regulated to the desired degree. The preparations are completed by adjusting an orifice (not illustrated) to provide the desired strain rate.

The test is begun by opening the release valve between the pressurized oil sump and the pump-down port. This action lifts the valve poppet which opens the quick-dump valve and opens a passage for the trapped oil. The nitrogen pressure, acting on the underside of the piston, forces the oil through the capillary bundle and constrains the piston to move upward at a constant rate, applying a constant tensile strain rate to the specimen. An overtravel spring in the spring chamber stops the piston at the top of its travel.

Additional details are contained in U.S. Patent No. 3,404,562, which is available from U.S. Patent Office, price $0.50.

Source: H. E. Cotrill, Jr. and
W. F. MacGlashan, Jr. of
Jet Propulsion Laboratory
under contract to
Department of the Army
(JPL-28 and 29)

PROBLEMS IN HIGH-VELOCITY SHOCK TESTING USING A SLINGSHOT SHOCK MACHINE

The slingshot shock-testing machine diagrammed in the figure is designed for production of high-velocity shocks and is capable of imparting a square-pulse acceleration greater

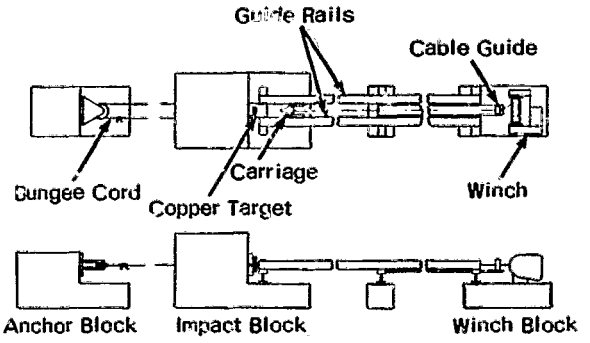

than 196 km/s^2 (20,000 g) with a pulse duration of up to 1.5 ms.

A light tensile load is initially applied to the bungee cord, and the sled is drawn back between two rails to the desired length. The sled is released from a distance which will give it a desired velocity at impact. The tool on the front of the sled impacts into the copper target block to create the desired pulse.

During actual operation, several problems have arisen: (1) The bungee cord is not consistent. Since the cord spring rate changes with each shot, it is difficult to predict impact velocity accurately. (2) Second or third shocks are frequently created due to vibration of the cord. This fatigues the cord, adds to the first problem, and contributes to the failure of instrumentation cabling. (3) Agreement between the various methods of determining the acceleration is not good. (4) Certain limitations on the pulse shape are not clearly defined.

Engineering analysis of these problems has resulted in recommendations for improving the slingshot machine. A more sophisticated, screw-type pretensioning device, in which the bungee cord is terminated with an adjustable shock absorber and no knots are used in the active portion of the cord, could be used to prevent a number of cord difficulties. Motion of the sled after impact could be reduced by mounting a transverse wave suppressor on the rear of the target support. More work should be done on the agreement of the force link and accelerometer readings.

Source: J. W. Shipley of
Caltech/JPL
under contract to
NASA Pasadena Office
(NPO-11193)

Circle 5 on Reader Service Card.

FLEXURE TEST APPARATUS FOR ELECTRICAL CONDUCTORS

A flexure testing machine simultaneously subjects up to four insulated electrical wire specimens to repeated bending stress, and positively indicates failure of the conductor. The wire is repeatedly bent over mandrels at a controlled rate, through a bend angle of $\pm\pi/4$ rad ($\pm 45°$). A relay-actuated control circuit stops the machine upon fracture of any single conductor. Indicator lamps are lighted to reveal the failed specimen. The control and indicator circuitry is needed because many present day insulation materials are capable of bearing the load weights by themselves after conductor fracture.

An alternate mode of operation allows measuring and recording any change in conductor resistance during test. The machine may be programmed to discontinue the test after any resistance value or resistance change ratio is reached.

Source: E. U. Baker of
McDonnell Douglas Corp.
under contract to
Marshall Space Flight Center
(MFS-13572)

Circle 6 on Reader Service Card.

CONTROLLED HYDRAULIC LOADING DEVICE

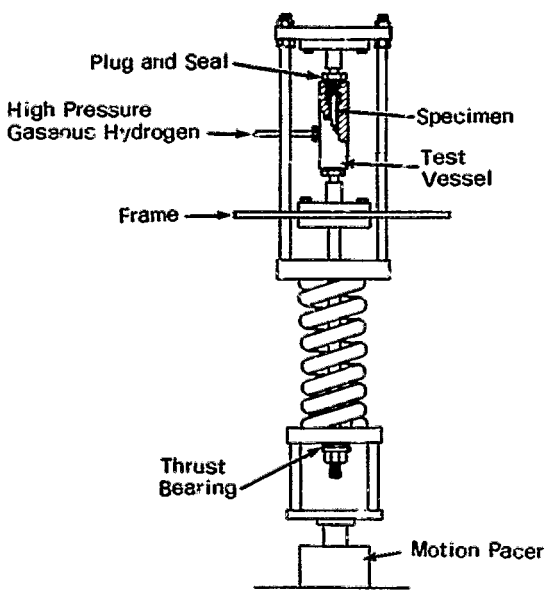

The hydraulic loading device shown in the figure provides either load- or strain-rate control for testing critical tensile specimens. Designed to provide loading at linear strain rates from 0.1 to 0.5 m/m/min, the device effectively paces both load-application and strain-rate from zero to a maximum load of 26.6 kN (6000 lb).

For load-rate control, a commercially available, motion pacer unit is attached to the bottom spring plate of the static loading device. The pacer is used in conjunction with a manual hydraulic flow control valve, which controls the rate at which the hydraulic ram compresses the spring of the static loading device. For specimen strain-rate control, the motion pacer is attached to the top plate of the static loading device. In this mode of operation, cross-head motion is paced.

Source: R. D. Lloyd and G. V. Sneesby of
North American Rockwell Corp.
under contract to
Marshall Space Flight Center
(MFS-2000)

No further documentation is available.

HIGH-ACCURACY FLEXURE TEST FIXTURE

The illustrated flexure test fixture avoids many of the problems encountered with conventional four-point loading fixtures; problems such as inaccuracy in parallelism of the four pins, errors in spacing and centering of the pins, inaccuracy in applying the load at the centerline of the specimen, and difficulties in assuring the perpendicularity of the specimen in relation to the loading pins. Since any error in the measurement of material properties can be detrimental to reliability, elimination of these sources of error is important.

A standard die set normally used for stamping small components forms the basic guide for the fixture. The preloaded linear ball bearings in the die set are reworked to provide a slight clearance. This ensures a fixed spacing and improves the accuracy of the load application point. To further ensure that this point is on the centerline of the specimen, a hardened ball is inserted in the top of the fixture at the precise centerline of the specimen.

To correct the problem of parallelism, the inner load pins are relocated on the base plate in machined V-grooves. The load is applied through hardened balls mounted on the outer span load bar. This arrangement eliminates any twisting action that might be caused either by lack of parallelism in the load application points or by a twisted specimen.

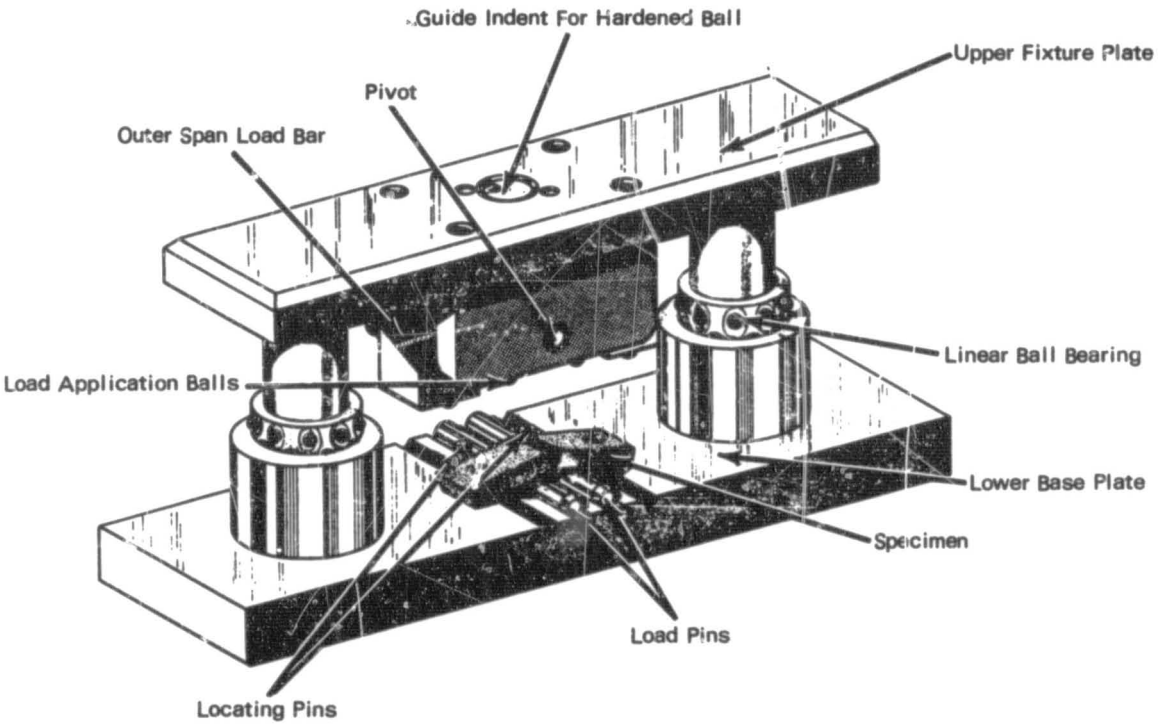

To ensure that the load is applied at the center of the specimen, vertical locating pins position the specimen so that it is perpendicular to the fixed load pins and centered under the moveable loading balls.

Source: G. W. Ellenburg and E. M. Duran of
Westinghouse Astronuclear Laboratory
under contract to
AEC-NASA Space Nuclear Systems Office
(NUC-10246)

Circle 7 on Reader Service Card.

LOAD CELL CALIBRATOR

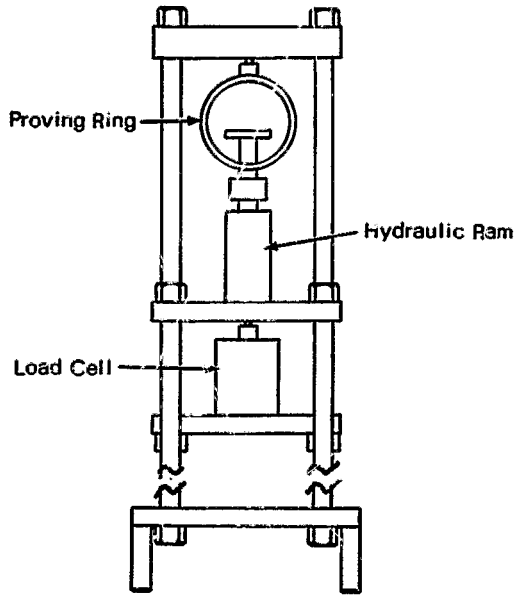

The illustrated device permits the use of a standard proving ring as a calibration transfer device for calibrating load cells of 220 to 2200 N (50 to 500 lb) capacity. Prior to the construction of this device, such low-capacity load cells were calibrated using weights as transfer standards. The device, similar, except in size, to a commercially available force calibrator, is small enough to permit handling low-capacity load cells conveniently.

Source: S. C. Stene and E. R. Lebs of North American Rockwell Corp. under contract to Manned Spacecraft Center (MSC-11865)

Circle 8 on Reader Service Card.

TESTING WELD STRENGTH AND MECHANICAL PROPERTIES OF 2219-T81 ALUMINUM ALLOY

Welding, fracture, tensile-strength, and fatigue tests performed on 2219-T81 aluminum alloy have resulted in improved knowledge of the mechanical properties of this alloy. Among the important results are the following: (1) The yield strength of 2219-T81 sheet and plate decreases significantly when welded. The reduction of yield strength is much greater than the corresponding reduction in ultimate strength. (2) Toughness of base metal 2219-T81 sheet and plate increases with a decrease in temperature. Plane stress and plane strain fracture toughness of the heat-affected zone (HAZ) increases with a decrease in temperature; the HAZ is less tough than the base metal but tougher than any other zone. The weld metal region has the lowest fracture toughness of any of the regions tested. (3) The weld area fracture toughness (plane stress or plane strain) of automatically welded 2219-T81 sheet or plate decreases significantly between 78 and 20 K. (4) The behavior of welded 2219-T81 aluminum plate is quite erratic after three repair welds have been made. The toughness values of repair welded 2219-T81 aluminum can be substantially lower than those of the new welds. (5) Cyclic flaw growth rates are generally higher on the weld metal than on any other region tested. (6) At normal operating stresses, the critical flaw size for 2219-T81 parent metal and welds is quite large, given the standard 2:1 weld land buildup. (7) Due to the very low possible toughness of repair welds, it is recommended that repair welding be kept to a minimum with 2219-T81 aluminum, because serious material property degradation is possible. All repair welds (except for the flaw simulation tests) on this program meet all government specifications for welds. (8) Tungsten inclusions considerably reduce the fracture toughness of the welds. Such inclusions should be removed wherever possible.

The following documentation may be obtained from:

National Technical Information Service
Springfield, Virginia 22151
Single document price $3.00
(or microfiche $0.65)

Reference:
NASA-CR-72097 (N67-17619), A Survey of Welding and Inspection Techniques for 2219-T81 Aluminum Alloy
Source: W. E. Witzell and C. J. Kropp of
General Dynamics/Convair
under contract to
Lewis Research Center
(LEW-10479)

TORSION SYSTEM FOR MULTIPLE-STRESS-REVERSAL CREEP TESTING

A novel torsion system provides exploratory data on accelerated creep due to multiple stress reversals. Conventional creep and relaxation testing is static and offers little information on the creep behavior of metals under cyclic load. Previously, a constant-torque pulley and dead weight system had been used to repeatedly reverse shear stress on tubular specimens, but this proved to be slow and complicated. Push-pull equipment had also been used, but this technique was inherently limited to small strains because of such deformational instabilities as necking and buckling.

Torsional testing of tubular specimens appears best suited for reversed-stress creep tests, since large strains are obtainable while specimen geometry is maintained. Although truly uniform stress distribution is sacrificed, the necking, instability, and nonuniformities in stress and strain encountered in other tests are reduced.

In the test system, torsional loads are measured by using the elastic response of a shaft. The amount of windup, directly proportional to the torque, is measured by a pair of linear variable differential transformers (LVDT's) mounted in a holding fixture. Electronic functions are provided by a load controller. Torque is applied by a hydraulic rotary actuator connected to a torque cell and mounted in a load frame. Fluid flow to the actuator chambers is controlled by a servovalve, and pressure variations at the valve manifold are minimized by an accumulator. The shearing strain is calculated from measurements of the relative angle of rotation of two specimen cross sections.

In system operation, two collars are clamped around the specimen to fasten arms to the sections of interest. These arms are connected to two coaxial cylinders that are free to move (rotate and translate) both about each other and about the bearing race on the torque cell. Relative rotation of the two section clamps is translated into a one-to-one relative rotation of the coaxial cylinders and is measured with a rotary variable differential transformer (RVDT).

Source: P. A. Lilienthal of
University of Illinois
under a grant from
NASA Headquarters
(HQN-10039)

Circle 9 on Reader Service Card.

TESTING THE ROOM-TEMPERATURE AGING PROPERTIES OF TENS 50(T4) ALUMINUM ALLOY

In an attempt to determine the effects of room-temperature aging on the mechanical properties of oil-quenched Tens 50 aluminum alloy, a total of twenty-four 0.63 cm (0.250 in.) diameter tensile test bars were machined from four Tens 50 aluminum alloy "Premium

Strength—Grade 1" castings. The castings were all produced with the same mold design and from the same ladle of metal. The machined test bars were solution heat treated for 12 hours at 865 K and then oil quenched. Two test bars were used for each test. The first two bars were tested after 30 minutes and the last two bars were tested after 24 hours.

The results indicated that room temperature aging of Tens 50 alloy is a slow process, probably requiring several days before minimum strength requirements are met or exceeded.

Source: R. E. Zuech of
North American Rockwell Corp.
under contract to
Marshall Space Flight Center
(MFS-18931)

No further documentation is available.

Section 2. Fracture and Fatigue Testing

FATIGUE TESTING OF 1100-H14 ALUMINUM ALLOY

An investigation of the fatigue properties of pure (1100) aluminum in various gaseous environments has shown that the fatigue life of the metal is greater in vacuum than it is in air, by a factor of about 3:2. The effects of residual concentrations of oxygen, water vapor, and hydrogen on fatigue life have also been investigated.

Fatigue tests were conducted in partial pressure and vacuum environments, using modified ASTM constant stress bend specimens in the cantilever mode of reverse bending. The fatigue life data were plotted as a function of surface strain amplitude calculated from fixed deflection amplitudes. Outer surface stress amplitudes were calculated from the elastic strain levels, assuming negligible fatigue hardening. Preliminary studies have shown that the 1100-H14 aluminum used in this series of fatigue tests exhibits very little strain hardening and maintains an essentially elastic stress-strain response in bending.

Source: M. J. Hordon, M. A. Wright and
M. E. Reed of
National Research Corp.
under contract to
NASA Headquarters
(HQN-10197)

Circle 10 on Reader Service Card.

LOW-CYCLE FATIGUE TESTS ON NICKEL ALLOYS 625 AND HASTELLOY C

Low-temperature, low cycle, flexural fatigue tests have been performed on two prominent nickel alloys to determine short-term deformation and change in load-carrying ability. Flexural reverse-bending fatigue tests were conducted on Alloy 625 and Hastelloy C at speeds up to 30 cycles per minute, with maximum deflections of ±2.41 cm in a total specimen length of 12.7 cm.

For each alloy, two strain gages were cemented to each of two specimens, at 8.1 cm and 3.45 cm from the moving end of the specimen. With the first specimen of each pair, the gages were connected to an X-Y recorder; the second set of gages was connected to an oscilloscope. A standard tensile testing machine was used to deflect each specimen 2.41 cm in tension and in compression.

The conclusions reached were as follows: (1) Alloy 625 strain softened from 0.45% to 0.41% during cycling. Similar post-yield strains were measured at both gages mounted in the constant stress area of the specimen. (2) Hastelloy C strain hardened from 0.52% to 0.72% during cycling. Higher strains were measured near the midlength of the specimen, rather than at the moving end. (3) Greater strain-measuring accuracy was obtained with the X-Y recorder technique than with the oscilloscope.

Source: C. S. Shira of
North American Rockwell Corp.
under contract to
Marshall Space Flight Center
(MFS-18933)

Circle 11 on Reader Service Card.

FATIGUE DATA OBTAINED FROM PROGRAMMED HYDRAULIC LOADING SYSTEM

The servocontrolled hydraulic loading system diagrammed in the figure uses load distribution data obtained from actual case histories as input to a realistic fatigue testing system. Where

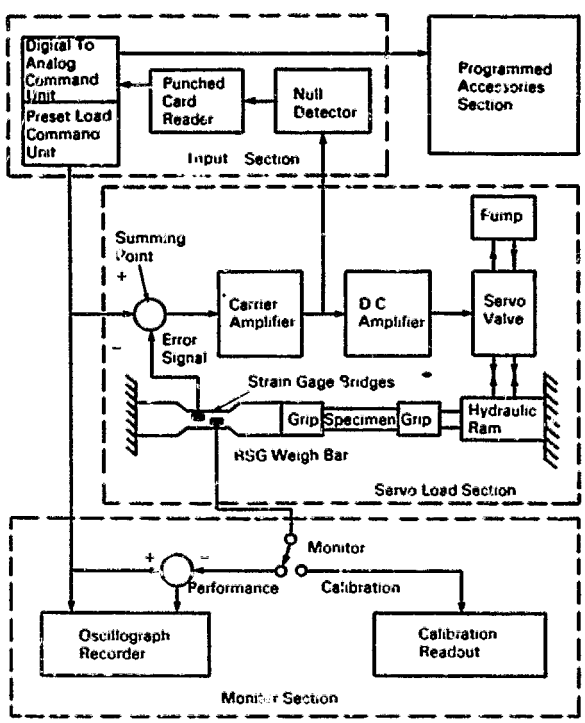

previous fatigue testing methods were generally limited to constant amplitude cyclic loading, this system can apply up to 55 discrete, noncyclic, individually adjustable loads in any desired sequence. The system thus makes available, for the first time, a high-speed test system to obtain accurate material strength data for actual, in-service loading conditions.

As shown, the system comprises four main subsystems, performing the functions of input and command, programmed-accessory control, specimen loading, and monitoring. The input section generates loading command signals, which are introduced at the summing point in the servo load section along with the actual load signal derived from calibrated strain gages. The amplified error signal output from the summing point controls the servo valve, which in turn controls oil flow to the hydraulic ram. The ram-generated force on the test specimen is mechanically coupled back to the strain gages, thus reducing the error signal magnitude. As the error reaches zero, a null detector generates a signal which advances the input section to the next command.

The input section, in addition to selecting load commands, controls the programmed-accessories section. This section comprises a temperature programmer, a recorder programmer, and a load-hold timer. The temperature programmer turns on and turns off an automatic temperature controller, which controls the power to heaters mounted on both sides of the specimen. The recorder programmer supplies power to an oscillograph recorder and a timer that determines record length. The load-hold timer interrupts the cycle, allowing an existing load to be maintained for a preset interval.

In the monitor section, the load command signal is displayed on an oscillograph recorder

and a calibration readout unit, together with the signal from a second strain-gage bridge. The section also includes readout instrumentation needed to calibrate and monitor performance.

Source: W. T. Davis
Langley Research Center
(LAR-10042)

Circle 12 on Reader's Service Card.

HYDRAULIC SERVO SYSTEM INCREASES FATIGUE-TESTING ACCURACY

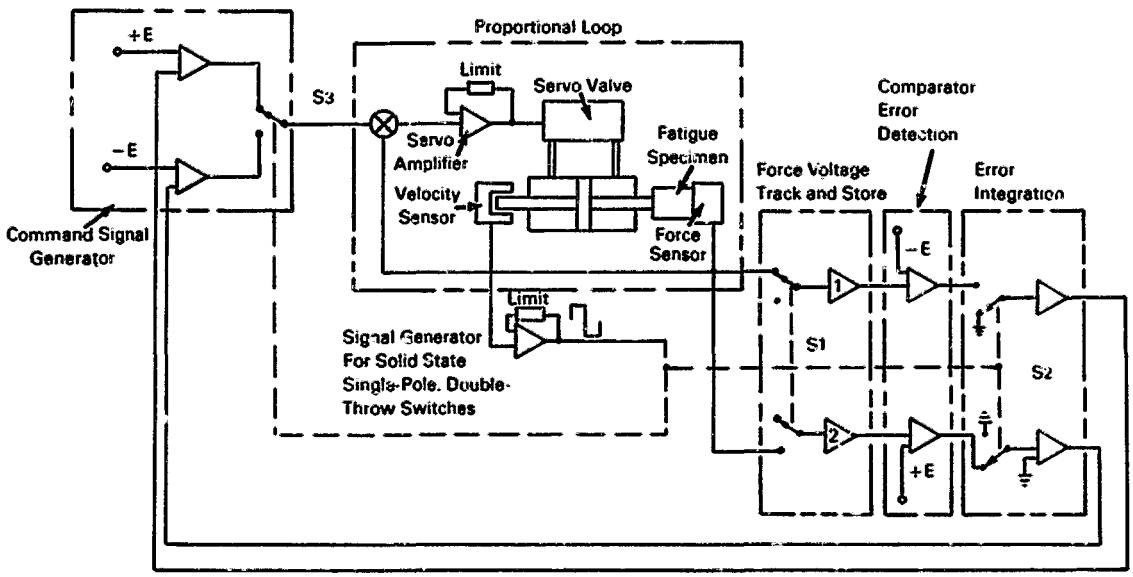

The fatigue testing system shown in the figure has improved the accuracy of loads applied to a standard fatigue specimen. The system consists of a proportional loop hydraulic system and an error-sensing electronic control loop.

The proportional loop contains a servo amplifier with a limit control, a servo valve which drives a piston, a velocity sensor, a force sensor, and the fatigue specimen. Frequency control is obtained by setting the limits on the servo amplifier. This is the normal assembly used for fatigue loading of a specimen.

To increase the accuracy of the system, an error-sensing electronic control loop is added to the proportional loop. This control loop consists of a signal generator, a force voltage tracker and storer, an error detection comparator, an error integrator, SPDT switches, and a command signal generator.

The electronic error sensor tracks and stores the force sensor's output voltage to the point where the velocity changes sign (i.e., the point of maximum force). The stored output voltages are then compared with the desired command reference voltages in the error detection comparator. An error signal generated for each peak is integrated and added to the appropriate command voltage level, and the composite command signal is fed to the proportional loop hydraulic system.

The velocity sensor of the proportional loop system triggers the signal generator which drives the SPDT switches. These switches, S1 and S2, appropriately channel the inputs and outputs of the error sensing electronic control loop to achieve two proper feedback voltages. One of these is selected by switch S3 and fed into the proportional loop.

Source: G. V. Dixon and K. S. Kibler
Langley Research Center
(LAR-217)

No further documentation is available.

FATIGUE TESTER WITH FLEX PLATES AND BARS GIVES TRUE AXIAL MOTION

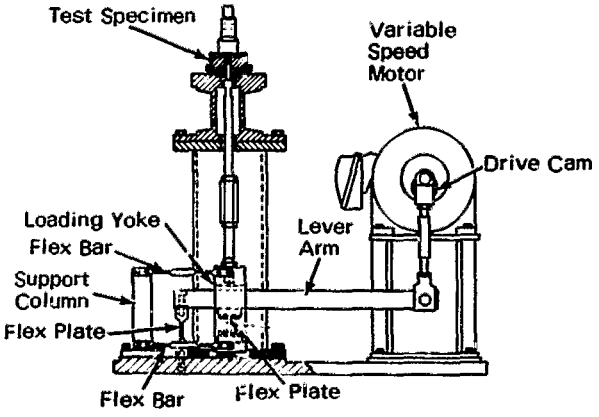

The lever-type load-amplifying fatigue-tester shown in the figure can apply a load to a test specimen, with true axial motion. Operating at speeds from 100 to 900 cycles per minute, the machine can achieve a load amplification ratio of up to 5 to 1.

A variable speed motor and a commercially available cam operate the lever arm. The arm applies an axial load to the specimen under test through two frictionless flex plates, one to take the place of the usual knife blade pivot, and the other to take the place of the usual bearing on the load bar. Parallel flex bars link a loading yoke and the flex plates to a support column, to achieve true axial motion of the load against the test specimen.

Source: C. D. Kurinko and T. F. Hengstenberg of Westinghouse Astronuclear Laboratory under contract to AEC-NASA Space Nuclear Systems Office (NUC-0021)

Circle 13 on Reader Service Card.

AUTOMATIC, NONDESTRUCTIVE MONITORING OF FATIGUE-CRACK GROWTH

An ultrasonic system automatically detects and records the propagation of a fatigue crack in a test specimen. The system employs ultrasonic reflection techniques to monitor the location of the tip of a propagating fatigue crack. A piezoelectric transducer generates an ultrasonic beam, which is coupled through water to a test specimen. The beam is partially reflected from the crack tip, and again from a reference reflector plate that is mounted behind the area containing the fatigue crack. The tranducer's position is adjusted until the two reflected signal amplitudes are equal. Further growth of the fatigue crack causes an imbalance in the reflected signal amplitudes and produces an error voltage. This error voltage activates a servomotor, which moves the transducer across the specimen surface until the reflected signals are again balanced. The distance the transducer moves is equal to the advance of the fatigue crack.

In a typical setup, a 0.318 cm thick aluminum alloy plate, with a 0.396 cm diameter hole in the center to simulate a crack-starting notch, is used as a test specimen. A 0.318 by 1.588 cm reflector plate of the same alloy is clamped to the specimen on one side of the hole. The reflector plate extends across the width of the specimen and is ultrasonically coupled to it by a film of oil. The ultrasonic transducer unit is positioned to face the reflector plate on the opposite side of the hole and aligned to travel parallel to the reflector plate. The transducer unit comprises a 5.0 MHz piezoelectric crystal, a water-filled hollow plastic block, and a servo-drive motor. An O-ring gasket seals the ends of the water column which ultrasonically couples the transducer to the specimen. The transducer is pivot-mounted so that the injection angle of the ultrasonic beam can be varied. A lead screw, coupled to the servo-motor through

a flexible shaft, guides the transducer across the specimen.

Tests were conducted on a specimen into which a slot was being machined to simulate the propagation of a fatigue crack. Increments as small as 0.003 cm were detected and automatically tracked. The repeatability of the system was ±0.013 cm for a number of specimens tested.

Source: F. Hoppe and N. S. Inman of
Fairchild Hiller Corp.
under contract to
Langley Research Center
(LAR-10091)

Circle 14 on Reader Service Card.

FATIGUE CRACKS DETECTED AND MEASURED WITHOUT TEST INTERRUPTION

An ultrasonic flaw detector, involving modified transducers clamped to the specimens, nondestructively detects fatigue cracks. The system provides a permanent, continuous record of cracks encountered throughout fatigue tests, without any need to interrupt or interfere with the tests.

Detecting fatigue cracks by the reflection of ultrasonic energy is similar to detecting distant objects by using radar. Acoustic energy generated by an ultrasonic transducer is transmitted into the test specimen in the form of pulsed envelopes of high-frequency waves. After the pulse is transmitted, the same transducer acts as a receiver for energy reflected from any discontinuity, such as that formed by the metal-air interface of a fatigue crack. The amount of energy reflected from a crack is related to the crack area, the intensity of the incident ultrasonic wave, and the orientation of the crack.

The oscillograph readout is coupled to a gating circuit, permitting a permanent record to be made of signals received from flaws in a selected portion of the specimen while the test is running.

Source: S. J. Klima, D. J. Lesco, and
J. C. Freche
Lewis Research Center
(LEW-266)

Circle 15 on Reader Service Card.

ANALYSIS OF FLOW-INDUCED FATIGUE IN BELLOWS

An investigation of bellows failure caused by flow-induced fatigue has yielded increased understanding of the mechanism of vibration generation and amplification in bellows, and has pointed the way toward a solution to the problem of bellows fatigue.

Fatigue failures are experienced in bellows carrying fluids at high speed. Such failures commonly occur when bellows are subjected to flow speeds around Mach 0.3, but the principles governing this behavior are not well understood. Although a rigorous analysis of this problem is difficult, much insight can be obtained qualitatively.

It can be assumed that flow through a bellows generates random sound waves in the fluid from repeated sources. For example, sound generated by the disturbance in flow past a convolution root will be generated at repeated intervals, corresponding to the convolution spacing, along the bellows. Under these conditions, certain wavelengths of sound will be amplified and others cancelled. Because the sound travels along the bellows in both directions, standing waves can be produced.

Because convolutions are essentially springs, they must be affected to some extent by any varying force such as sound waves. The extent

can be expected to range from zero (if the natural frequency of the bellows structure opposes and cancels the sound frequency) to a very large magnitude (if the natural frequency of the bellows reinforces the sound vibration). This relationship can explain the erratic fatigue results achieved in experiments.

Using the above assumptions, the sonic condition can be examined in a little more detail. Consider first only a single source of sound (one root). An unknown spectrum of wavelengths will be propagated in all directions at the speed of sound in the fluid. Doppler shift will cause the spectrum to be shifted toward longer wavelengths in the direction of flow, and toward shorter wavelengths in the opposite direction.

The amplitude of any given sound wave will decay exponentially as it travels, but if the wave arrives at another source of sound before dying out, its residual amplitude will add to any wave from the new source with which it is in phase. Analysis of this phenomenon, with respect to the constructive interference of waves generated by flow past bellows convolution roots, yields a critical flow speed which coincides with that found by experience to be most prone to cause fatigue failures.

With the general nature of the sound wave established, its effects on the bellows structure can be examined. The standing wave will tend to cause each root to oscillate back and forth π rad out of phase with each neighboring root. The result will be a flexing of each crest. This mode of vibration explains the metallographic observation that the crests of fatigue-failed bellows are heavily cold worked while roots are undisturbed. The natural frequency of the bellows in this type of vibrating motion is therefore critical.

The above analysis appears qualitatively correct. Additional work should be performed to derive a quantitative expression that would show rate of sound amplification. This is suggested because one obvious technique for allowing higher flow velocities would be to introduce a one-half wavelength interruption in the convolutions at an interval just less than the number of convolutions at which the sound intensity would reach a dangerous level. This would cause destructive interference between the two standing waves and would eliminate the vibrations.

Source: R. G. Cron of
North American Rockwell Corp.
under contract to
Marshall Space Flight Center
(MFS-18178)

Circle 16 on Reader Service Card.

CRYOSTAT MODIFIED FOR ROTATING-BEAM FATIGUE TEST

To perform a rotating-beam fatigue test in a cryogenic environment, a stainless steel Dewar is modified by adding extended specimen-supporting members and specially designed rotary seals. Since the test specimen must be rotated at speeds up to 10,000 rpm, successfully sealing the cryogenic environment becomes a critical consideration. This is accomplished by using radially stacked, bellows-mounted graphite seals on opposite sides of the Dewar, with the specimen, in its supporting members, between the seals in the cryogenic environment. The Dewar is supported on a platform that may be adjusted in elevation so that no extraneous weight will

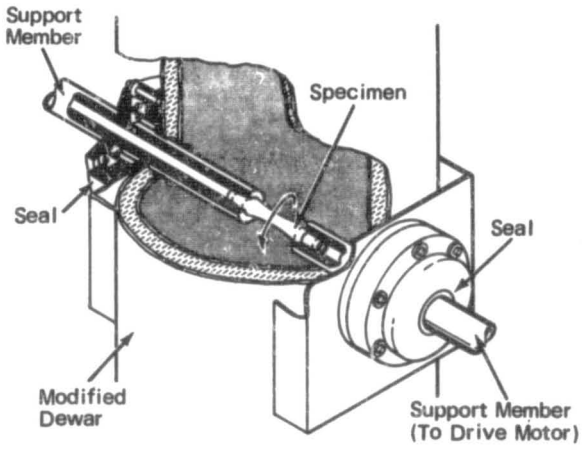

load the specimen during test. Automatic control of liquid level in the Dewar, and a shut-off switch actuated by test specimen failure, permit unattended operation for considerable periods.

Source: T. F. Durham of
North American Rockwell Corp.
under contract to
Marshall Space Flight Center
(MFS-435)

No further documentation is available.

FATIGUE IN REINFORCED CONCRETE BEAMS UNDER DYNAMIC LOAD

Investigation of the strength properties of reinforced concrete beams subjected to vibrational stresses has led to increased knowledge of the dynamic properties of concrete. Such knowledge is needed for the design of buildings frequently subjected to high-intensity vibrations. Buildings located near missile launching pads and jet air fields are obvious examples.

One hundred specially designed, scaled, reinforced concrete beams were tested. Fifteen were tested to determine their static strengths. The remaining beams were tested under sinusoidal and random vibrations to determine their dynamic fatigue characteristics. The beams were mounted, one at a time, on an electromagnetic shaker and were vibrated at their supports. Desired stress levels were maintained by monitoring the input signal to the shaker. The number of vibration cycles was established up to the moment of the specimen's failure. The reinforcing wires imbedded in the concrete beams were also tested by a tensile machine to determine their yield and ultimate tensile strengths and to obtain a better analytical understanding of the strength of the reinforced concrete specimens.

The following documentation may be obtained from:

National Technical Information Service
Springfield, Virginia 22151
Single document price $3.00
(or microfiche $0.65)

Reference:
NASA-CR-79530 (N67-11684) Fatigue of Reinforced Concrete Due to Sinusoidal and Random Loadings

Source: G. C. Chan of
Wyle Laboratories
under contract to
Marshall Space Flight Center
(MFS-14980)

SURVEY OF FRACTURE TESTING METHODS

A comprehensive survey has been prepared on current fracture-toughness testing methods that are based on linear-elastic fracture mechanics. General principles of the basic, two-dimensional crack, stress-field model are discussed in relation to real three-dimensional specimens. The designs and necessary dimensions of specimens for mixed mode and opening mode (plane strain) crack-toughness measurements are considered in detail. Test procedures and instrumentation methods are described, and expressions for the calculation of crack-toughness values are given for the common types of specimens.

Source: J. E. Srawley, M. H. Jones, and
W. F. Brown, Jr.
Lewis Research Center
(LEW-10379)

Circle 17 on Reader Service Card.

CRACKS OF KNOWN SIZE INDUCED IN METAL SAMPLES FOR FRACTURE MECHANICS STUDIES

A technique for inducing controlled cracks in metal test samples for fracture mechanics studies uses standard vibrational fatigue cycling apparatus together with an eddy-current crack-growth monitoring device. Previous methods, that used tensile loading followed by metallographic sectioning of the sample to verify crack size, were much slower and more difficult to control than this new technique.

The parameters of the fatigue tester are adjusted to induce stresses near the yield point of a test sample. The monitor is then used to check crack growth. The measurements may be taken either at intervals during the fatiguing process, or on a continuous basis by directly attaching the device to the sample. In either case, the sample remains installed in the test area, and the final degree of fatigue attained can be controlled within close tolerances.

Source: F. H. Stuckenberg of
North American Rockwell Corp.
under contract to
Marshall Space Flight Center
(MFS-16640)

No further documentation is available.

FRACTURE MECHANICS TEST METHOD

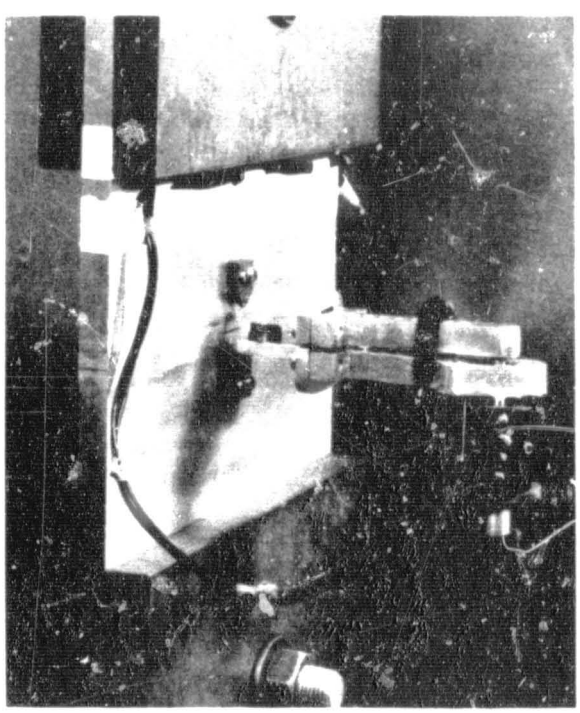

A new experimental technique, using a specially developed crack-opening displacement (COD) gage to monitor crack growth, improves control over the degree of precracking induced in fatigue test specimens. This in turn leads to greater uniformity of test data.

An investigation into the fracture behavior of welds in 2014-T651 aluminum alloy plates utilized precracked specimens with machined, semielliptical cracks extending part way through the weld thickness. Attempts to reduce the data, assuming linear-elastic fracture mechanisms, met with serious difficulties. Extensive and irregular precritical crack growth, and variations attributed to nonhomogeneity, anisotropy, and residual stress gradients, led to the conclusion that simplified proof-test logic was not applicable. An alternate approach, experimentally verifying an established proof-test margin, was complicated by these same irregularity factors. The use of high-magnification extensometers to autographically display compliance behavior during proof-test loading of precracked test specimens provided experimental verification of the source of the problem; i.e., irregular and precritical crack growth.

The illustrated COD gage, shown mounted on a test specimen, consists of a linear variable differential transformer mounted on a bracket. Holders are attached to the specimen surface

spanning the machined crack, and knife-edge clips on the bracket engage the notched arms of the holders. When the precracked joint is placed under load, the gage measures displacements which are primarily due to the behavior of the crack, with the parent metal acting essentially as rigid material.

Source: J. E. Collipriest and D. E. Kizer of North American Rockwell Corp. under contract to Marshall Space Flight Center (MFS-16786)

Circle 18 on Reader Service Card.

ACCELERATED STRESS CORROSION TEST FOR STEELS AND NICKEL ALLOYS

The stress corrosion susceptibility of a wide variety of steels and nickel alloys can be rapidly evaluated using a new laboratory test procedure.

Single-edge-notched specimens are fatigue-cracked, loaded in plane tension, and immersed in 20% by weight NaCl solution at room temperature. A computer program is used to calculate approximate loading parameters, and required testing time is limited to a maximum of 1000 hours. Times as short as 100 hours may be used under some circumstances.

The test can be used to determine: (1) the stress-corrosion susceptibility of many common high-strength alloys; (2) the effects of processing parameters on the susceptibility of these alloys; and (3) the acceptance level for stress corrosion resistance of the alloys. Preliminary seacoast trials have verified the validity of the test.

The same basic approach to the development of a stress-corrosion test has been used before. However, earlier tests were based on the use of fatigue-cracked cantilever bend specimens, which required individual loading fixtures. Using edge-notched tensile specimens allows a large number of specimens to be loaded in series and tested simultaneously in a single, dead-weight, lever-arm loading system.

Source: A. H. Freedman of Northrop Corp. under contract to Marshall Space Flight Center (MFS-13701)

Circle 19 on Reader Service Card.

FAILURE MODES IN POLYTETRAFLUOROETHYLENE EXAMINED USING FRACTOGRAPHY

Fractographic principles, long used in metallurgy, can now be applied to the analysis of the microstructure and fracture characteristics of polytetrafluoroethylene (PTFE). Fractography is a common analytical technique for studying the fracture face of a failed metal by means of both macro- and microphotography. The minute topographical features revealed in the fractographs are then compared with standards prepared from specimens fractured under controlled conditions. Similarity between a standard and a fractograph that represents an actual service failure is used to determine the failure mode.

Notched and unnotched samples of 0.65 cm thick PTFE were tested in tensile and fatigue testing machines, both at room temperature and at the temperature of liquid nitrogen. The test conditions approximated the most extreme stress and cryogenic environments to which the PTFE would be exposed during use. Replicas of the fractured surfaces were prepared by the commonly used, two-stage, acetate replica technique. All fractures were studied in two magnification ranges: the macrorange, from 1 to 10 ×; and the microrange, from 3500 to 15,000 × (with the electron microscope). The various

Card #13

topographic features noted on the fracture faces were defined in terms of observable patterns (chevrons, dimples, tears, ridges, and striations), and then tabulated for all samples.

The results of the study demonstrate that fractography can be used to analyze fractured surfaces of PTFE to determine modes of failure in this material.

Source: B. H. Nerren
Marshall Space Flight Center
(MFS-20294)

No further documentation is available.

STRESS CRAZING OF CHLOROTRIFLUOROETHYLENE POLYMER CAUSED BY HALOGENATED SOLVENTS

Polychlorotrifluoroethylene film, commonly used on seals and bushings in valves, has been found prone to stress crazing under exposure to halogenated solvents.

After ball valve lip seals in service were found in a stress crazed condition, tests were performed to determine the susceptibility of the film to stress crazing. Film samples 3.8 by 6.3 cm in size were stressed by attaching various weights, and exposed to trichloroethylene and trichlorotrifluoroethane solvents. Threshold levels for stress crazing were found to range from 4.1 to 5.5 MN/m^2 (600 to 800 psi) for various combinations of solvent and film thickness.

It was concluded that valves and other components using polychlorotrifluoroethylene seals should never be cleaned with halogenated solvents without disassembly to relieve the seals of stress.

Source: R. E. Cierniak and J. H. Lieb of
North American Rockwell Corp.
under contract to
Marshall Space Flight Center
(MFS-19015)

Circle 20 on Reader Service Card.

A RAPID STRESS-CORROSION TEST FOR ALUMINUM ALLOYS

Continuous immersion in an aqueous sodium chloride-potassium dichromate (1%-NaCl 2%-$K_2Cr_2O_7$) solution has proven to be an effective stress-corrosion test for aluminum alloys which are prone to general corrosion when subjected to standard 3.5% NaCl alternate-immersion testing. Because of the minimal general corrosion of alloys such as 2024, 2014, 2219, and 7075 in this salt-dichromate solution, stress corrosion failures can be readily detected by low-power microscopic examination of the test specimen. The salt-dichromate solution test is particularly well suited to the task of rapidly separating various tempers of 2024, 2219, and 7075 aluminum alloys on the basis of their relative susceptibilities to stress-corrosion cracking.

Stressed alloy specimens, e.g., C-rings, tensile rounds, etc., are immersed in the salt-dichromate solution at a temperature of 333 K ± 1 K. The solution, which is prepared on a weight basis (1%-salt 2%-dichromate) using reagent grade chemicals and distilled water, should exhibit a pH in the range of 3.7 to 4.0. The test solution must be contained in an inert vessel, preferably glass, which will withstand the test temperature.

The recommended immersion period is seven days, but this period may be extended for several weeks without danger of excessive general cor-

rosion of the specimens. Failure of highly stressed susceptible alloys and tempers generally occurs during the first few hours of testing. Therefore, specimens should be inspected at least once during the first four hours' exposure, and twice a day thereafter.

Source: W. J. Helfrich of
Kaiser Aluminum and Chemical Corp.
under contract to
Marshall Space Flight Center
(MFS-20175)

Circle 21 on Reader Service Card.

CHEMICAL MILLING REVEALS STRESS CORROSION CRACKS IN TITANIUM ALLOYS

A solution of the type used for the chemical milling of titanium alloys may be used to reveal stress corrosion cracks, without special surface preparation. The solution consists of 10 parts HF (concentrated), 60 parts H_2O_2 (30% concentration), and 30 parts H_2O, by volume. The surface is simply rinsed in water and dried, swabbed with the solution for 10 to 30 seconds, and rinsed again in water. The cracks can then be observed by the naked eye or at low magnification. The technique is especially useful with large specimens or hardware, where polishing would be impractical. The solution may also be useful in revealing small machining cracks or fatigue cracks, but should not be used when the examination must be totally nondestructive.

Source: D. N. Braski
Langley Research Center
(LAR-10077)

No further documentation is available.

END OF REFERENCE

REFERENCE

55

WEINER, R. S.: BASIC CRITERIA AND DEFINITIONS FOR ZERO LEAKAGE. JPL-TR-32-926, JET PROPULSION LAB. (NASA CR-81189), 1966.

N67-15991

NATIONAL AERONAUTICS AND SPACE ADMINISTRATION

Technical Report No. 32-926

Basic Criteria and Definitions for Zero Fluid Leakage

Richard S. Weiner

LIBRARY COPY

jpl
JET PROPULSION LABORATORY
CALIFORNIA INSTITUTE OF TECHNOLOGY
PASADENA, CALIFORNIA

December 15, 1966

NATIONAL AERONAUTICS AND SPACE ADMINISTRATION

Technical Report No. 32-926

Basic Criteria and Definitions for Zero Fluid Leakage

Richard S. Weiner

Approved by:

Duane F. Dipprey, *Manager*
Liquid Propulsion Section

JET PROPULSION LABORATORY
CALIFORNIA INSTITUTE OF TECHNOLOGY
PASADENA, CALIFORNIA

December 15, 1966

CONTENTS

I. Introduction 1

II. Leak Definitions and Units of Measure 2

III. Zero Liquid Leakage 3

IV. Zero Gas Leakage 10

V. Leak Test Techniques 11

Nomenclature 13

References 14

FIGURES

1. Mechanism of Clogging 3

2. Correlated Liquid and Gas Flow Modes 3

3. Simplified Fluid Flow Conversion Graph 5

4. Fluid Flow Conversion Graph 6

5. Zero Liquid Leakage With Equivalent Test Helium Flow 7

6. Zero Gas Leakage 10

7. Test Methods and Their Test Sensitivities 12

ABSTRACT

This Report defines both liquid and gaseous zero leakage over a pressure range from 1.0 and 0.1 psi, respectively, to 10,000 psi. Graphs are included for clarity and use. The zero liquid leakage graph contains an equivalent gaseous helium test leakage curve. A fluid flow conversion nomograph was constructed from certain applications of the Poiseuille equation and is offered to help simplify efforts of specification writers and test personnel in obtaining equivalent flow rates between fluids, over a wide range of pressures and temperatures. Discussions of leak test methods and test techniques complete the Report. This Report is important to such current programs as *Mariner* and *Surveyor*.

I. INTRODUCTION

As spacecraft missions become more sophisticated, and operate for increasingly greater periods of time, the requirements for improved performance by the systems and components become tighter. One measure of performance is the ability of the fluid flow system, or individual component, to perform satisfactorily under all predicted conditions without failure, which includes without excessive leakage.

Excessive gas or propellant leaks could: (1) affect the performance of an onboard scientific experiment located near the leak exit; (2) require additional attitude control system compensation to create abnormal increase of operating fluid consumption; (3) create a hazardous condition resulting from accumulation in the spacecraft; and 4) decrease the operating fluid's reserve to cause a system's decreased performance, or even a malfunction.

The word *excessive* is relative to the size of the system and to the quantity of the reserve operating fluids. The need for maximizing the payloads is a constant system factor. The resulting propulsion system requirements demand economy of propellants and pressurizing gases. The requirement for extremely small, or no leakage, is fast becoming a prime requisite.

The development of techniques to detect leaking fluids has been painfully slow. The problem has been complicated by the fact that many less-than-satisfactory means of defining the leakage requirements have been attempted for the sake of simplifying design, procurement, and testing specifications. Early definitions of the term *zero leakage* were vague, and did not suggest any leak test procedure as the basis for any definition which could be used by specification writers and test personnel.

II. LEAK DEFINITIONS AND UNITS OF MEASURE

A. Definitions

The confusion that exists over definitions in the field of leak detection demands that certain terms be defined before continuing further.

1. Leak

As noted in Ref. 1: "In vacuum technology a hole, or porosity, in the wall of an enclosure capable of passing gas from one side of the wall to the other under action of a pressure or concentration differential existing across the wall."

For the purpose of this Report the preceding should be amended to:

> a crack, hole, or porosity in the wall of an enclosure capable (contrary to intent) of passing fluid from one side of the wall to the other under action of a pressure or concentration differential existing across the wall.

As a rule, although a leak may be detected during testing, its geometry will remain unknown. Leak testing is mandatory for inspection and rate measurement, because analysis is impossible.

2. Leak Rate and Leakage

In defining the rate of flow of fluids past a leak, the words *leak rate* and *leakage* are used synonymously.

B. Units of Measure

1. Gas Flow

As observed in Ref. 1: "In leak detection practice, *leak rate* is defined as the rate of flow (in pressure-volume units per unit time) through a leak with gas at a specified high pressure (usually atmospheric pressure) on the inlet side, and gas at pressure on the exit side, which is low enough to have negligible effect on the rate of flow."

In this Report, the unit of measure for gas flow, only, shall be standard cubic centimeters per second (std cm^3/sec). The word *standard* is used here to indicate that the flow measurements were converted to standard temperature and pressure (STP) conditions and to show the relationship to mass flow. The following equations are presented for illustration purposes:

$$\dot{W} = \frac{PVM}{RT} \tag{1}$$

as derived from $PV = \frac{W}{M} RT$

2. Liquid Flow

In this Report the liquid flow, *liquid leakage*, is a volumetric unit of measure, cm^3/sec.

III. ZERO LIQUID LEAKAGE

A. Definition

Zero liquid leakage is that value of liquid leak or flow rate at which the surface tension of the liquid has just overcome the pressure acting on the liquid, Fig. 1, and *no* flow occurs – assuming a given pressure and leak diameter. Experiments conducted (Ref. 2) have indicated that generally for liquid there is a range of values at each pressure where the flow rate becomes zero. It is in this range that each liquid has its own zero point at any given pressure.

B. Discussion

Figure 2 shows the two major liquid flow modes: turbulent and laminar. The equation for liquid turbulent flow is (Ref. 2)

$$Q_v = \frac{\pi}{4} d^{5/2} \left(\frac{\Delta P}{2\rho f\zeta} \right)^{1/2} \qquad (2)$$

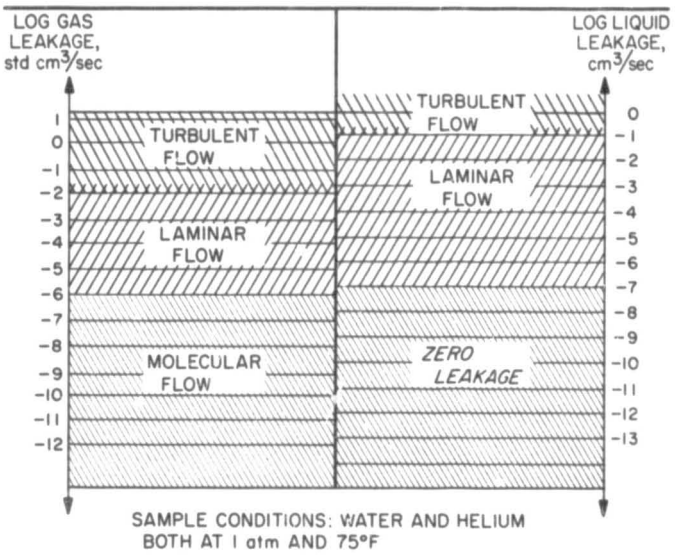

Fig. 2. Correlated Liquid and Gas Flow Modes

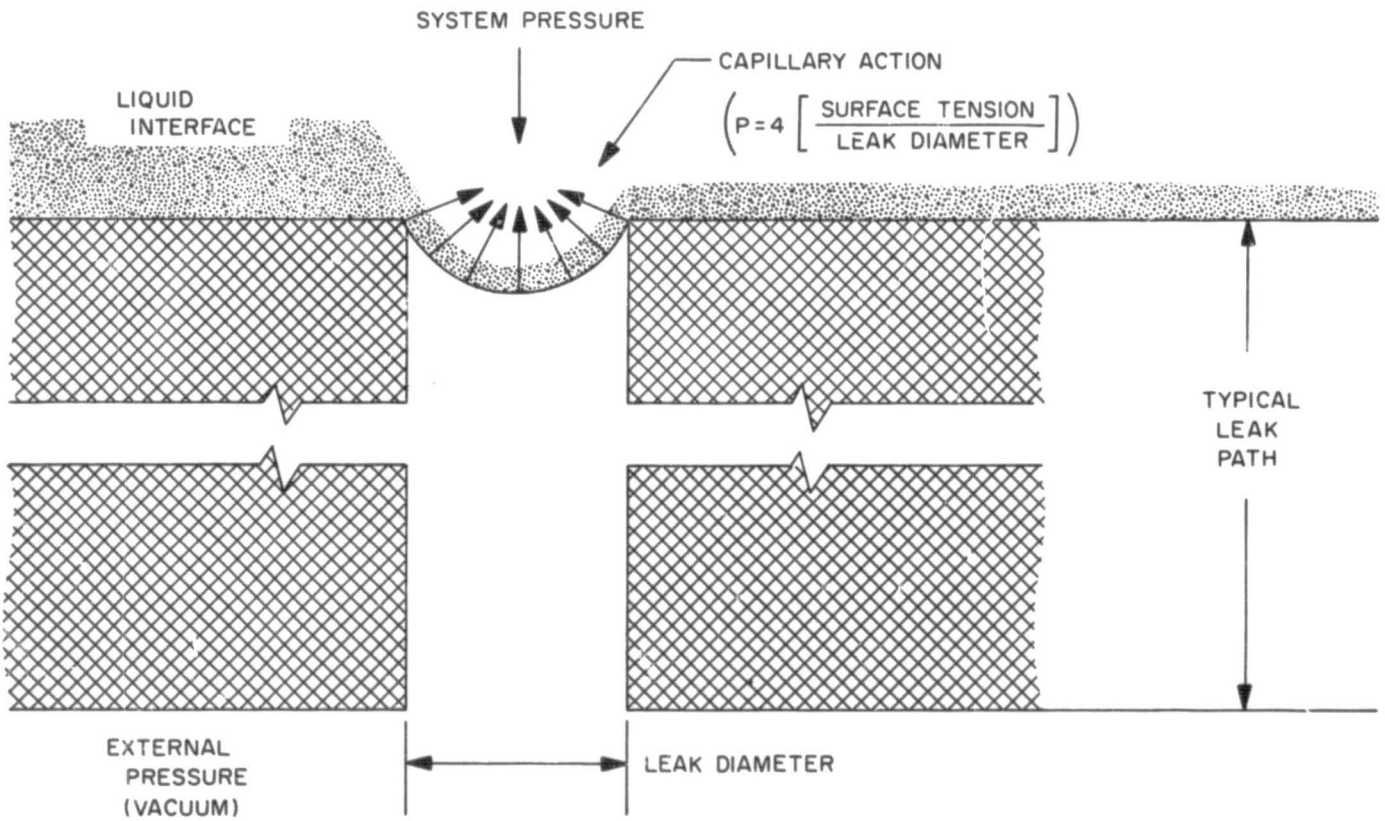

Fig. 1. Mechanism of Clogging

The equation for laminar flow is (Ref. 4)

$$Q = \frac{\pi}{4}\left(\frac{d}{2}\right)^4 \frac{P_2 - P_1}{\eta \zeta} \qquad (3)$$

Flow rate Q is in pressure-volume/time units.

The preceding equations are presented as illustrations only, and are not to be used for calculations.

As the Reynolds Number for laminar flow decreases as a result of increasing viscosity, surface tension becomes the dominant force causing cessation of flow. At this point, zero leakage occurs. However, there is a peculiar set of conditions in which a liquid *wets* the walls of the leak path, thus eliminating the surface tension effects, in turn permitting liquid flow to continue even farther. More work is required to increase knowledge about this effect. It will be shown later that any increased pressure serves to lower the zero leak point for a liquid.

The rate of propellant evaporation through the leak path to a vacuum was examined and found negligible compared with the original liquid leak rate.

Figure 2 shows gaseous helium flow rates directly correlated with liquid flow rates for the same pressure and temperature (75°F, 14.7 psia). This simplified method for correlating liquid and gaseous flow rates was developed at the General Electric Company, Ref. 8, and presented in the form of a nomograph. The nomograph was constructed from the following equation, and is presented here for the reader's interest only.

For gas flow from a high pressure to atmospheric pressure, the Poiseuille equation for viscous flow is

$$Q = \frac{K}{\eta}(P^2 - 1)$$

where pressure units are in atmospheres.

For gas flow from a pressure, generally, but not necessarily atmospheric, to vacuum, the Poiseuille equation becomes

$$Q = \frac{KP^2}{\eta}$$

For essentially incompressible liquid flow with a known pressure differential, the Poiseuille equation becomes

$$Q = \frac{K' \Delta P}{\eta}$$

To construct the nomograph, the preceding three equations, using a common parameter (ΔP), were reduced to the following forms:

$$Q = \frac{K}{\eta}(\Delta P)(\Delta P + 2) \qquad (4)$$

$$Q = \frac{K}{\eta}\Delta P^2 \qquad (5)$$

$$\text{and } Q = \frac{K'}{\eta}\Delta P \qquad (6)$$

Figure 3 shows a simplified version of the nomograph with a sample problem to illustrate its use. The guidelines with a slope of 2:1 and located on the right-hand side represent the gas flow equations; while guidelines having 1:1 slope, and located on the left-hand side, represent the liquid flow equation. Correlating one fluid to the other requires drawing lines parallel to the nomograph guidelines. The discontinuity found between the gas flow and liquid flow guidelines is only the result of the original drawing style. However, a transition between gas and liquid flows is illustrated in the nomograph. The gradual bend represents exhaustion to atmospheric conditions. A sharp, or sudden change from liquid to gas, or vice versa, represents exhaustion to vacuum.

Working the sample problem shown in Fig. 3 will illustrate the application of the nomograph to predict the equivalent liquid propellant leak rate from measured gaseous test helium leakage at a seal.

Assume the following conditions:

1. Gaseous helium leakage past a seal at $S \times 10^{-6}$ std cm^3/sec.
2. Helium test pressure of 1 atmosphere (atm) or 14.7 psia with vacuum on downstream side of the leak, the ΔP across the leak being 14.7 psia.
3. Liquid system flow pressure of 10 atm or 147 psia with vacuum externally, or 147 psia ΔP across the leak.
4. Liquid viscosity of $S \times 10^{-1}$ centipoises (cp).

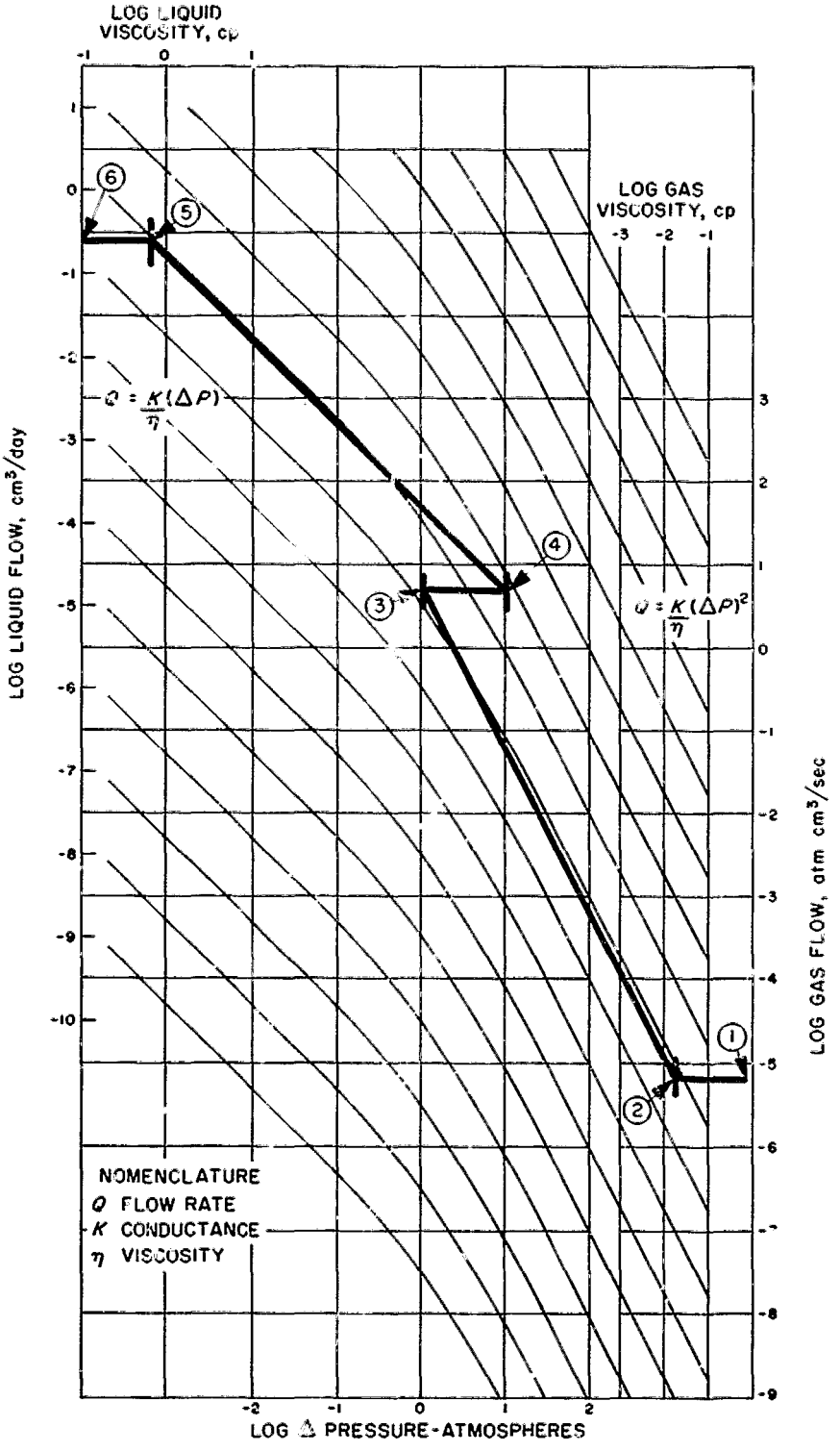

Fig. 3. Simplified Fluid Flow Conversion Graph

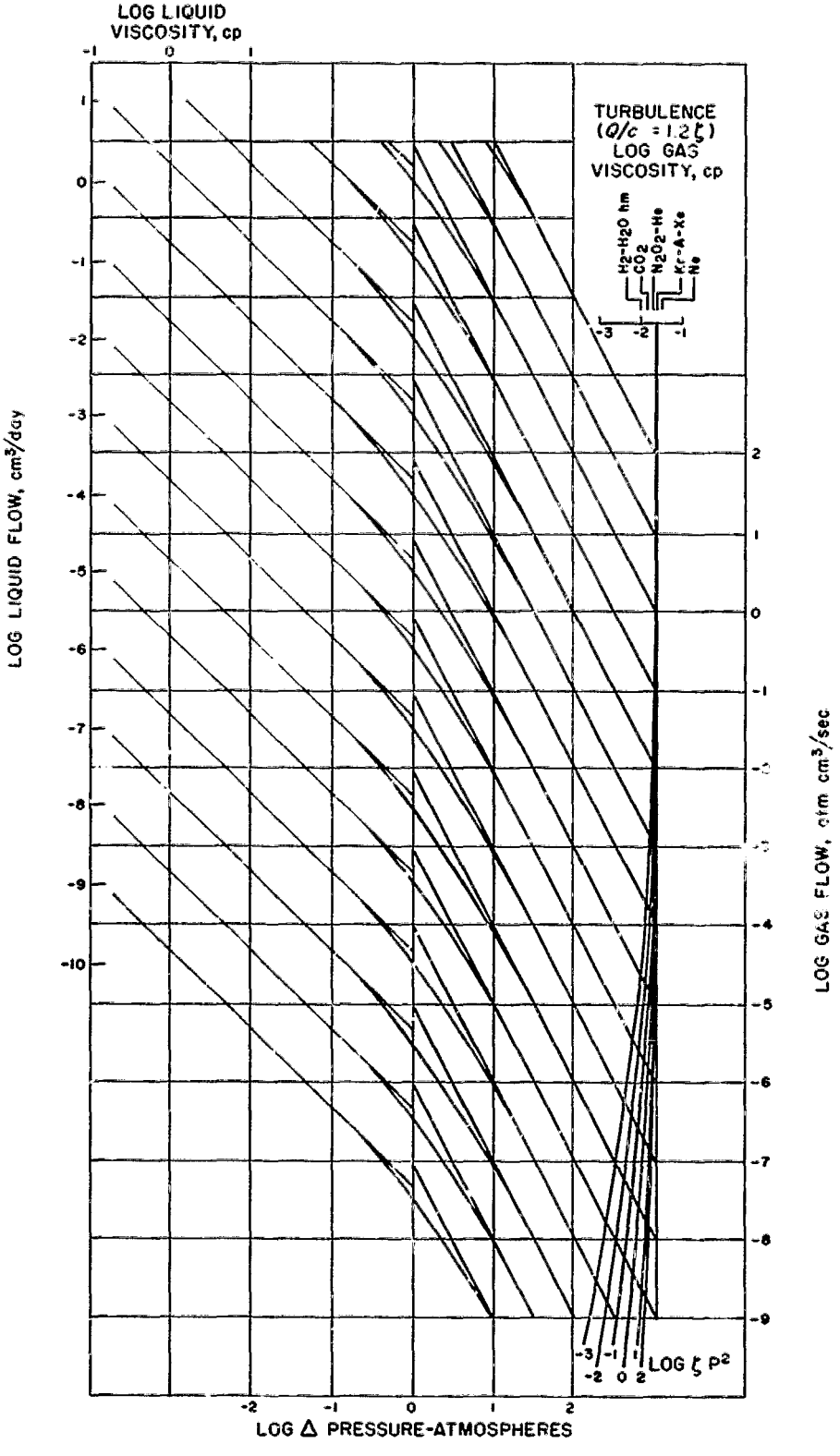

Fig. 4. Fluid Flow Conversion Graph

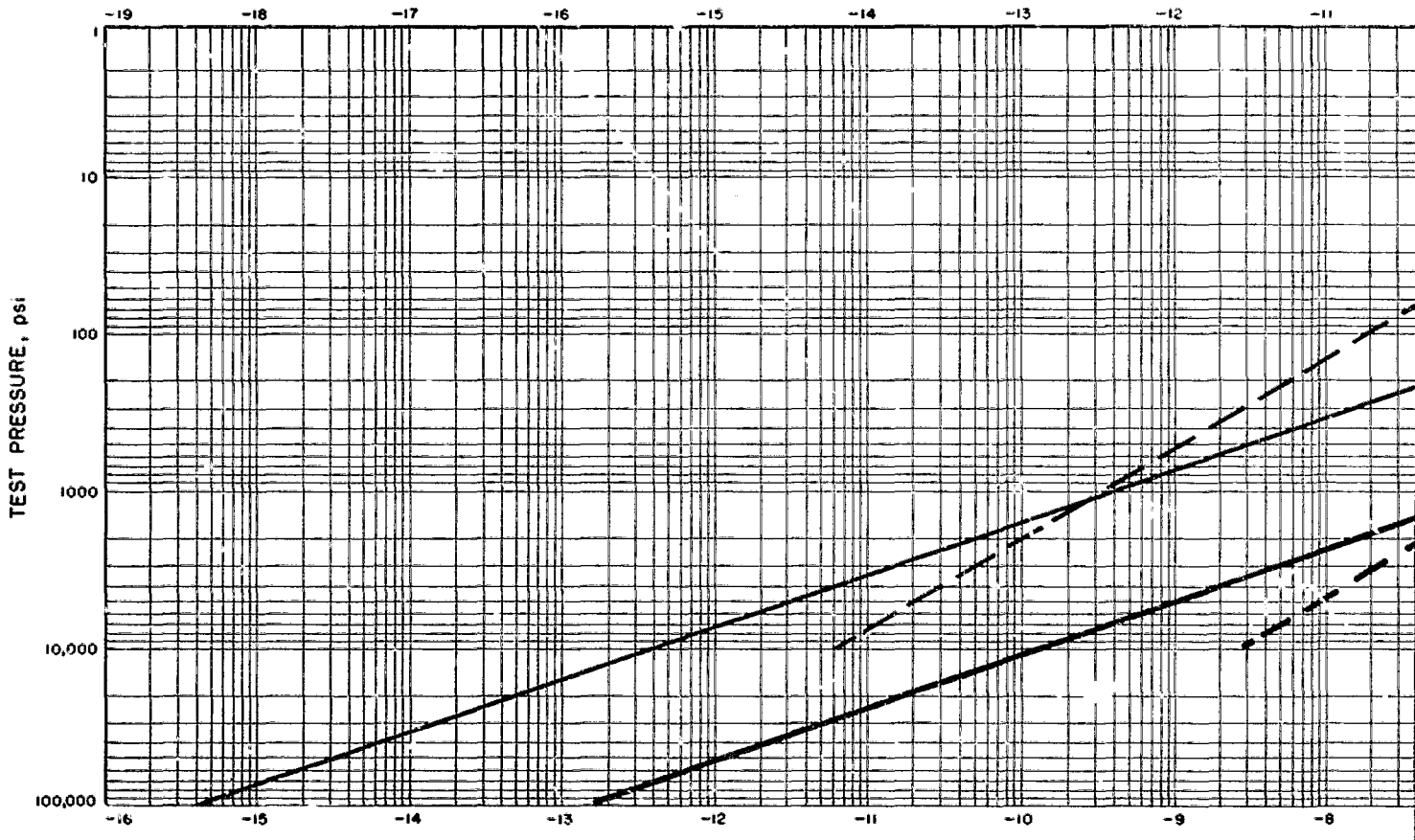
LOG ZERO
-19
-18
-17
-16
-15
-14
-13
-12
-11
1
10
100
1000
10,000
100,000
TEST PRESSURE, psi
-16
-15
-14
-13
-12
-11
-10
-9
-8
LOG EQUIVAL

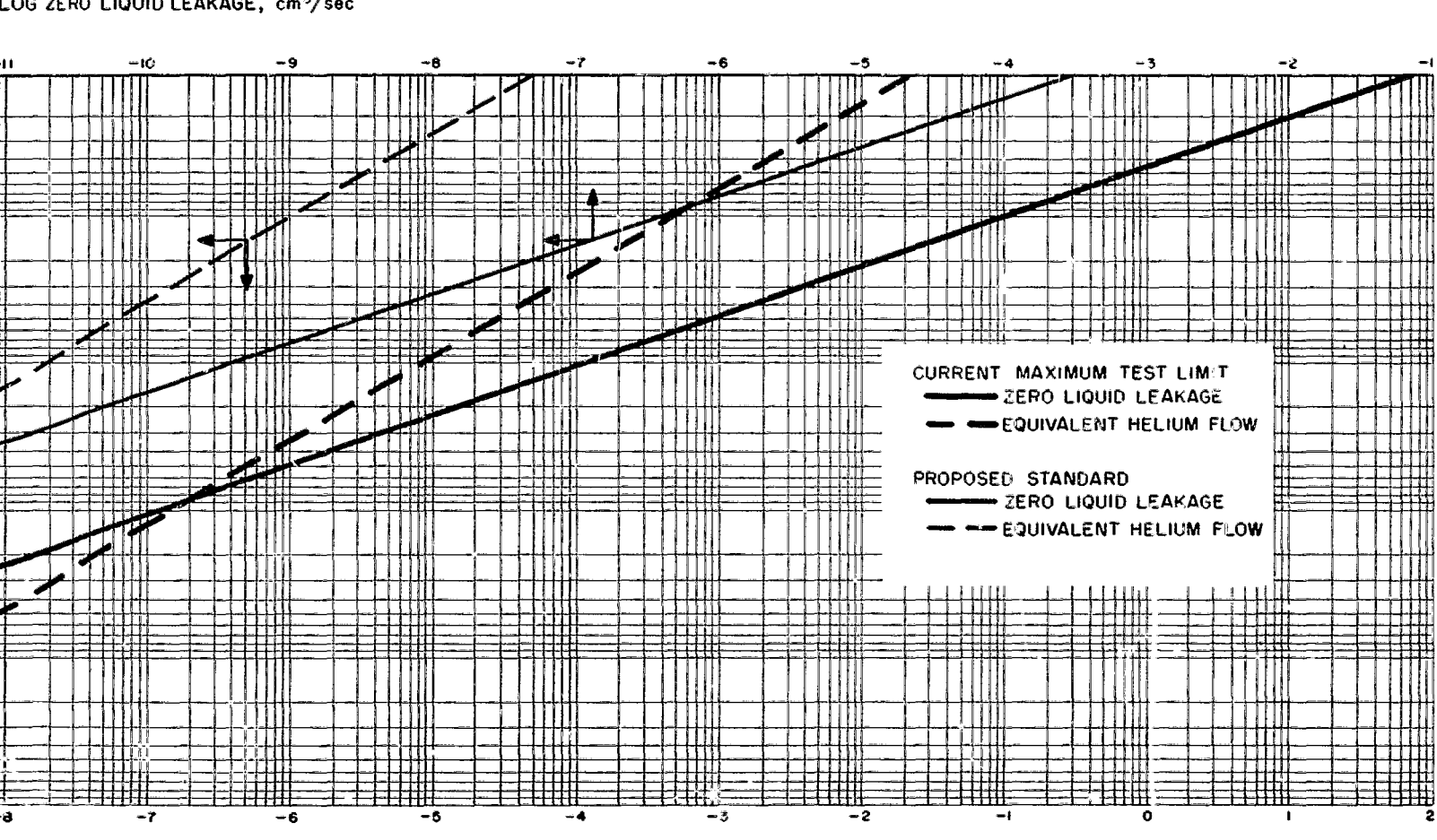

Fig. 5. Zero Liquid Leakage With Equivalent Test Helium Flow

To solve the problem of predicting the equivalent liquid *leak rate* for the known gaseous leakage at the seal, the following plots are made on the nomograph:

1. 8×10^{-6} std cm³/sec helium leakage is located on the right-hand ordinate (log gas flow).
2. A horizontal line is drawn intersecting the helium viscosity value along the abscissa (log gas viscosity).
3. A line parallel with the 2:1 slope is extended from the helium viscosity value until 1 atm pressure is intersected along the Δ pressure abscissa.
4. This pressure point is connected with the liquid system pressure (10 atm) by a horizontal line.
5. A line is drawn parallel with the 1:1 slope graph lines from the previously found liquid pressure value until the intersection is made with the value for the liquid viscosity along the log liquid viscosity abscissa.
6. A horizontal line is drawn from the intersection of liquid flow with liquid viscosity to find the predicted liquid leakage along the log liquid flow ordinate: 3×10^{-1} cm³/day.

While Fig. 2 shows a liquid-gas correlation at 1 atm pressure and 75°F, Fig. 3 provides a graphical solution for correlation at any pressure. Any temperature may be considered merely by selecting that corresponding value of viscosity.

Figure 4 is a complete fluid flow conversion graph. Added to it is a transitional flow component, which includes molecular flow, represented by the ζP^2 factor.

Figure 5 presents two zero liquid leakage models for most liquid propellants and their respective equivalent helium test gas flow rate curves. The upper zero leakage curve indicates the current standard, or maximum limit. It is based on one experimental test point developed earlier by the General Electric Company, whereby, at 1 atm of pressure, the clogging, or zero liquid leakage point for water was in the range of 10^{-6} to 10^{-7} cm³/sec. Assuming the value of 5×10^{-7} cm³/sec as one point on the curve, the following mathematical analysis provides that the required curve pass through the point, for the purpose of extrapolation through the desired pressure range. The equivalent helium flow rate is obtained with the application of the graph, given in Fig. 4, at the same point.

The second, or proposed, standard curve is based on later experimental data provided by Dr. Marr of the General Electric Company. It was shown that at 1 atm of pressure, the clogging, or zero leakage point for water is about 10^{-7} cm³/sec of equivalent helium flow. With this new point available, the new zero liquid leakage curve was obtained by employing the following mathematical analysis. However, as of this writing, the lower leakage curve remains as the proposed standard for further study and consideration. The desired curves are straight lines as shown by Eq. (10) and (13). The slopes of the curves drawn through the selected points are obtained from the following analysis.

For liquid flow to start, the pressure must just exceed the liquid surface tension, Ref. 7, or

$$\Delta P = \frac{4\gamma}{d} \tag{7}$$

which gives,

$$d = \frac{4\gamma}{\Delta P} \tag{8}$$

where γ is surface tension and d is leak diameter. Since from Eq. (3), $Q_{liquid} \propto d^4 (\Delta P)$, then substituting in d

$$Q_{liquid} \propto \frac{(4\gamma)^4}{(\Delta P)^4} (\Delta P) \tag{9}$$

or,

$$Q_{liquid} \propto \frac{(4\gamma)^4}{(\Delta P)^3} \tag{10}$$

Hence, the slope of the *zero liquid leakage* curve with respect to pressure is −3:1.

The equivalent gas flow based on surface tension of the liquid, or rather based on its start of flow because of just overcoming the surface tension γ effect, is found in a like manner.

From Eq. (5),

$$Q_{gas} \propto d^4 (\Delta P)^2 \tag{11}$$

and with the substitution of d, is

$$Q_{gas} \propto \frac{(4\gamma)^4}{(\Delta P)^4} (\Delta P)^2 \tag{12}$$

or finally

$$Q_{gas} \propto \frac{(4\gamma)^4}{(\Delta P)^2} \tag{13}$$

Hence, the slope of the equivalent gas flow curve with respect to pressure is −2:1.

Therefore, from the preceding discussion, it is now possible to specify a *zero liquid leakage* value for liquid propellant systems and components. The curves in Fig. 5 define *zero liquid leakage* in terms of liquid flow rate and also suggest the means of precision testing, an objective stated in the Introduction. Until instruments capable of measuring extremely finite liquid flow rates are developed, the use of helium gas as a detecting medium will provide a precision technique. The helium spectrometer type of leak detector affords the means of detecting the low flows of helium which are equivalent to the required zero leakage, or rather that amount of equivalent gas flow, at any given pressure, where liquid flow ceases. In this manner, the specification writers and the testing personnel now have a practical definition for *zero liquid leakage*.

IV. ZERO GAS LEAKAGE

A. Definition

Zero gas leakage as such does not exist as far as laboratory measurements have thus far been able to determine because of the limitations of laboratory instruments. Therefore an arbitrary curve was constructed as shown in Fig. 6 for use as a specification standard.

B. Discussion

Figure 6 is a straight, sloped curve with a discontinuity at the leakage value of 1×10^{-7} std cm³/sec at which point the line is translated but maintains its original slope.

The lower portion of the curve is based on the basic point of 1 std cm³/yr at 1 atm differential pressure. Other points making up that portion of the curve were obtained from the correlation of the 1 std cm³/yr with equivalent flow rates at the other pressures using the fluid conversion graph. However, the knowledge of future propulsion system requirements dictated that the maximum acceptable equivalent leakage, as originally constructed, was too great at the higher pressures. Hence the arbitrary decision was made to shift a part of the curve upward at 1×10^{-7} std cm³/sec.

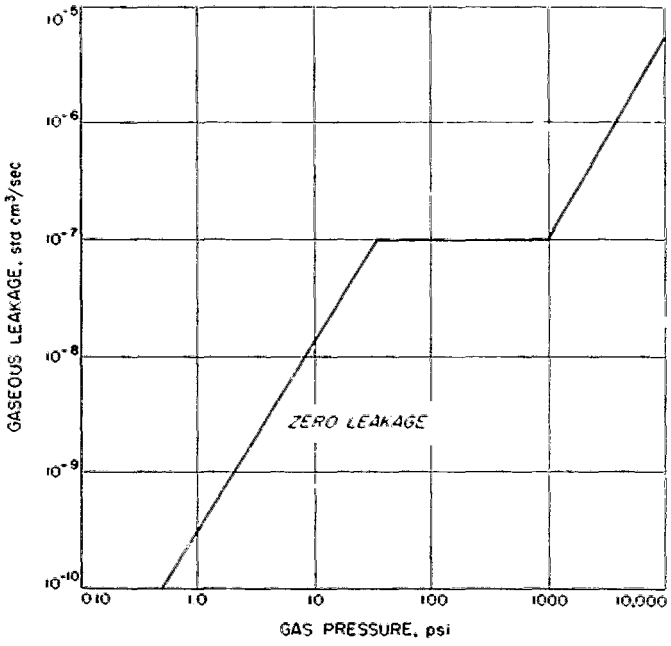

Fig. 6. Zero Gas Leakage

V. LEAK TEST TECHNIQUES

Two types of external leaks exist in most flow systems: (1) permeation through plastic and elastic materials and, (2) viscous flow as through a pinhole. The latter form of leak is the type to permit an equivalent liquid flow. However, the first form (permeation) is detectable during the bell jar type of helium mass spectrometer leak testing and can lead to a false picture when converting the total helium leakage to equivalent propellant leakage. Permeation leakage is the passage or migration rate of atomic helium (by various mechanisms) through the materials, being first adsorbed into the surfaces of the materials under a pressure-type or concentration-gradient driving mechanism and finally desorbed out of the external surface. The basic identifying characteristic of this kind of leak is a gradually increasing rate of change with respect to time. A strip-chart recorder wired to the mass spectrometer target output voltage displays the characteristic whenever it occurs, and also simplifies leak test monitoring. A second identifying characteristic is that at any given pressure, every plastic and elastomer has a helium saturation or leveling-out point past which the leak rate will not increase. This salient feature can be used as a final verification for permeation leakage. If repeated testing is required, and the testing cycle is a matter of only a few hours, the original starting test pressure must be low enough to permit saturation to occur. A convenient rule for increasing test pressure levels during repetitive testing within hours of each other is 2X over the previous value. However, with the removal of helium pressure, the helium concentration will eventually decay from within the plastic or elastomer. The time for helium concentration decay can be calculated. If one can tolerate the long period of time between tests, which may range from an hour to a day, then the test can be repeated at the same pressure as in the original test.

The identifying characteristic of the viscous leak is the relatively constant rate of fluid flow. However, because the leak path can be very tortuous to the flow of a test gas, the time required to traverse the path may take hours, even at pressures greater than 3000 psi. Therefore, precise leak tests should consume at least 3–4 hr of continuous monitoring. When recording the leak characteristic, the sudden change of *leak rate* to a higher but fairly constant value is indicative of additional helium from another viscous leak path.

It is this last type of leak that will produce the liquid propellant leak in a propellant subsystem. Therefore, it is now possible to correlate the leak from gaseous helium in terms of equivalent units of propellant in accordance with the procedure previously described. It is important that initial leak testing should first employ a gas, rather than a liquid, in order not to clog the leak paths.

Experiments have been conducted which show that the *zero leak* condition for liquids is between 10^{-6} and 10^{-7} cm³/sec of liquids with surface tension being the criterion for the exact number. Experiments are currently under way to find the *zero leak* point for liquids, under NASA Contracts No. NAS 7-396 and -434.

Discrepancies appear at times between analytical and empirical leakage data. These may be caused: (1) by the lack of sufficient experimental data to support fully certain analytical techniques; (2) by the actual leak-test methods and techniques; and (3) by the fact that flow systems themselves are **not** designed to include plans concerning future leak checks. While experimental evidence is currently building up in support of the analytical methods used herein, the comparable work in the field is not keeping pace. Not enough work is being accomplished at the system level to improve the accuracy of actual test data; methods that are not amenable to precision continue to be employed because of poor planning and lack of patience in the test execution.

A number of leak-testing techniques, summarized in Fig. 7, have been used for some time. The more common ones are:

1. Soap solution (maximum test sensitivity to 10^{-4} std cm³/sec).
2. Helium mass spectrometer probe or "sniffer." (Maximum test sensitivity quite variable from 10^{-4} to 10^{-6} std cm³/sec.)
3. Bell jar or other such container with a helium mass spectrometer (maximum test sensitivity better than 10^{-9} std cm³/sec).
4. Methods 2 and 3 employ a mixture of nitrogen and helium gases. The helium detection sensitivity is degraded by the volume ratio of the gases in order to use the preceding techniques for detection of gross leaks.

Use of the first two techniques does not assure the operator that he is measuring all of the escaping helium.

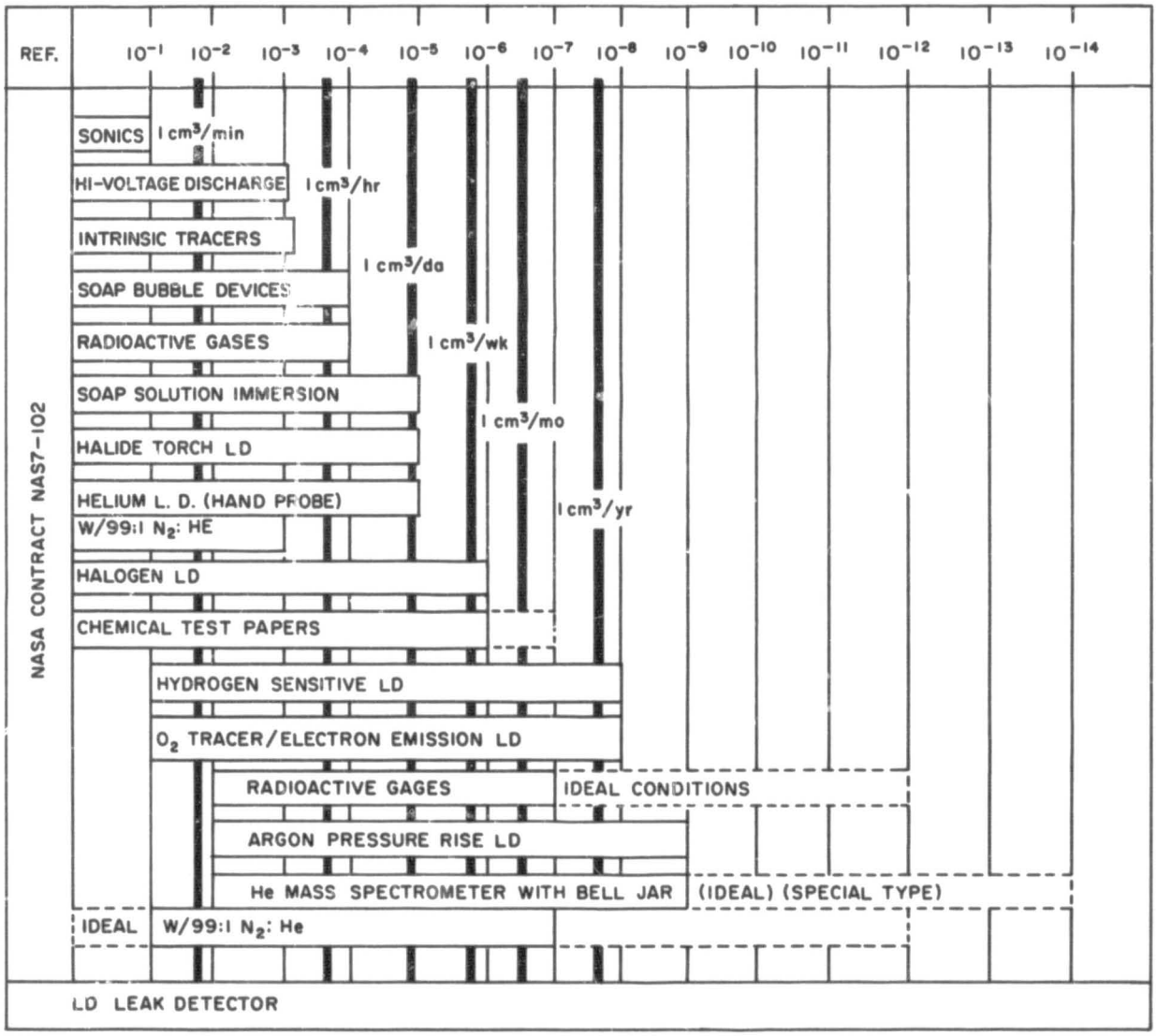

Fig. 7. Test Methods and Their Test Sensitivities

Although the third technique makes the most accurate determination, it is not easily adapted to field use.

Chemical test papers have been the most widely used indication of propellant leakage at the system level in the field. While the test papers may be as sensitive as 10^{-6} to 10^{-7} cm³/sec, the titration of the paper proves somewhat tricky and the results are not always consistent. To date, there is no simple method to measure total liquid propellant leakage; however, some promising techniques have been observed experimentally, Ref. 8.

The importance of temperature effects should always be considered. The leak flow rate changes 1) directly with such geometry alterations as expansion and contraction of cross sections, and 2) inversely with viscosity. The change in viscosity produces the greater effect. Because it can be shown that laminar flow varies inversely with viscosity, a lower temperature requires a greater **equivalent** helium leak for a given liquid propellant leak. Also, for higher temperature operation, a smaller **equivalent** helium leak is required for a given propellant leak.

Gaseous nitrogen may be used in lieu of helium for tests where gross leaks are expected. It is possible to test for propellant leakage in terms of equivalent nitrogen leakage using the fluid flow conversion graph, e.g., Fig. 4. As with helium testing, it is still necessary to capture all of the leaking nitrogen gas, but the vacuum systems of the mass spectrometer are not necessary if the N_2 is passed up a precision-bore glass tube against a low-mass piston, where the rate of ascent equals the leak rate (less the gravitational effects). If leakage is measured in this manner, N_2 is more desirable than helium because it will not permeate through the piston material, e.g., a soap solution film, and because the laminar flow condition is viscosity dependent; therefore this may result in a 10% sensitivity increase.

In the final analysis, some form of total gas leakage measurement technique must be used for correlation with liquid leakage. In light of this, the work previously accomplished at JPL undertakes to fill the lack of such information. The numbers described in this analysis resulted from use of the fluids conversion chart as originated and copyrighted by the General Electric Company.

NOMENCLATURE

d	diameter of leak path
f	friction factor, flow passage
K,K′	conductivity
M	molecular weight
P	pressure
Q	flow rate
R	gas constant
T	absolute temperature
V	volume
W	mass of the gas
γ	surface tension
ζ	length of leak path
η	viscosity
ρ	density
$\propto$	proportionality

Subscripts

1	down stream conditions
2	up stream conditions
v	volume conditions

REFERENCES

1. *Glossary of Terms Used in Vacuum Technology*, Committee on Standards, American Vacuum Society, Inc., May 1958.
2. Marr, J. W., *Study of Static and Dynamic Seals for Liquid Rocket Engines*, Final Report for the Period January 1, 1965 to September 1, 1965, Phase IV, General Electric Company, Advanced Technology Laboratory, Schenectady, New York, November 1965.
3. Marr, J. W., *Study of Static and Dynamic Seals for Liquid Rocket Engines*, Final Report for the Period April 1, 1964 to October 1, 1964, Phase III, General Electric Company, Advanced Technology Laboratory, Schenectady, New York, 1964.
4. Poiseuille, J. M., *Comptes Rendus Hebdomadaires des Seances de l'Academie des Sciences*, Vol. 11, p. 1041, 1840; Vol. 12, p. 112, 1841; Vol. 15, p. 1161, 1842.
5. Hunsaker, J. C., and Ridtmire, B. G., *Engineering Applications of Fluid Mechanics*, Chap. VII, McGraw-Hill Book Company, New York, 1947.
6. Knudsen, M., *Annalen der Physik*, Vol. 28, p. 75, 1909; Vol. 35, p. 389, 1911.
7. Santeler, D. J., and Moller, T. W., "Fluid Flow Conversion in Leaks and Capillaries," *National Symposium on Vacuum Technology Transactions*, pp. 29–36, Chicago, Illinois, October 10–12, 1956.
8. Marr, J. W., *Leak Detection Techniques Manual*, Final Report, General Electric Company, Advanced Technology Laboratory, Schenectady, New York (to be published).

END OF REFERENCE

55

REFERENCE

56

MARR, J. W.: LEAKAGE TESTING HANDBOOK. NASA CR-952, 1968.

NASA CR-952

LEAKAGE TESTING HANDBOOK

By J. William Marr

Distribution of this report is provided in the interest of information exchange. Responsibility for the contents resides in the author or organization that prepared it.

Issued by Originator as Report No. S-67-1014

Prepared under Contract No. NAS 7-396 by
GENERAL ELECTRIC
Schenectady, N.Y.

for Jet Propulsion Laboratory

NATIONAL AERONAUTICS AND SPACE ADMINISTRATIO

For sale by the Clearinghouse for Federal Scientific and Technical Information
Springfield, Virginia 22151 – CFSTI price $3.00

TABLE OF CONTENTS

Section		Page
	FOREWORD	v
1.0.	INTRODUCTION	1
1.0.1.	Summary	2
1.0.1.1.	Part I	2
1.0.1.2.	Part II	3
1.1.	LEAKAGE CATEGORIES	4
1.2.	REASONS FOR LEAKAGE TESTING	5
1.2.1.	Material Loss	5
1.2.2.	Contamination	5
1.2.2.1.	Environmental Damage	5
1.2.2.2.	Personnel Hazard	6
1.2.2.3.	Appearance	6
1.2.3.	Reliability	6
1.2.4.	Sensitivity	7
1.2.4.1.	Optimum Value and Difficulty	8
1.2.4.2.	Cost Considerations	8
1.2.4.3.	Zero Leakage	11
1.3.	FUNDAMENTALS OF TESTING	12
1.3.1.	Leakage Units	12
1.3.1.1.	Dimensions of Leakage Units	12
1.3.1.2.	Conventional Leakage Units	13
1.3.2.	Leakage Conductance	16
1.3.3.	Detector Sensitivity	17
1.3.4.	Leakage Testing Techniques	17
1.3.4.1.	Leakage Measurement	17
1.3.4.1.1.	Static Testing	18
1.3.4.1.2.	Dynamic Testing	21
1.3.4.1.2.1.	Magnitude of Response	21
1.3.4.1.2.2.	System Response Time	22
1.3.4.1.2.3.	Detector Location	28
1.3.4.2.	Leak Location Techniques	28
1.3.4.3.	Sealed Unit Testing	31
1.3.4.3.1.	Unit Sealed With Tracer Gas	31
1.3.4.3.2.	Back-pressurizing Technique	33
1.3.4.3.2.1.	Molecular Flow Leaks	35
1.3.4.3.2.2.	Laminar Flow Leaks	37
1.3.5.	General References	39
1.4	FLOW CHARACTERISTICS	41
1.4.1.	Gas Flow	41
1.4.1.1.	Pneumatic Flows	41
1.4.1.1.1.	Laminar Flow	41
1.4.1.1.2.	Molecular Flow	44
1.4.1.1.3.	Transition Flow	49
1.4.1.1.4.	Turbulent Flow	51

TABLE OF CONTENTS (continued)

Section		Page
1.4.1.1.5.	Choked Flow.	51
1.4.1.1.6.	Distinction Between Modes of Flow.	54
1.4.1.2.	Permeation	55
1.4.2.	Liquid Flow	61
1.4.2.1.	Laminar Flow	61
1.4.2.2.	Turbulent Flow	61
1.4.3.	Correlation Between Flow Types	61
1.4.3.1.	Conversion of Flow Rates for Varying Gases. . .	61
1.4.3.2.	Conversion Between Gases and Liquids.	64
1.4.3.3.	Graphical Correlation	65
1.4.3.3.1.	General Description.	67
1.4.3.3.2.	Corrections For Molecular and Transitional Flow.	67
1.4.3.3.3.	Sample Solutions Incorporating the ℓP^2 Correction.	68
1.4.3.3.4.	Turbulent Flow Limitations	69
1.4.4.	Anomalous Leaks.	69
1.4.4.1.	Check Valve Leaks	69
1.4.4.2.	Geometry Change in Leaks	69
1.4.4.3.	Self-Cleaning Leaks	69
1.4.4.4.	Absorbed or Surface Flow Leaks.	72
1.4.5.	Leak Clogging.	74
1.4.5.1.	Surface Tension and Wetting	74
1.4.5.2.	Pressure Removal and Evaporation.	76
1.4.5.3.	Safety.	78
1.4.6.	General References	81
1.5.	METHODOLOGY OF TESTING	82
1.5.1.	Plan For Testing	82
1.5.1.1.	Accessibility	82
1.5.1.2.	Leaks In Series	82
1.5.1.3.	Component Testing	83
1.5.1.4.	Safety Considerations	86
1.5.1.4.1.	Flammability	86
1.5.1.4.2.	Asphyxiation	88
1.5.1.4.3.	Explosion.	88
1.5.1.4.4.	Implosion.	89
1.5.1.5.	Effects of Gas Properties	89
1.5.1.5.1.	Effect of Tracer Gas Concentration	89
1.5.1.5.2.	Stratification	91
1.5.1.5.3.	Diffusion.	92
1.5.2.	Procedural Techniques.	95
1.5.2.1.	Leakage Measurement	95
1.5.2.1.1.	Hood Testing	95
1.5.2.1.2.	Small Component Testing.	97
1.5.2.1.3.	Weld Testing	101
1.5.2.1.4.	Pipe Testing	104
1.5.2.2.	Leak Location	106
1.5.2.2.1.	General Procedure.	106
1.5.2.2.2.	Design of Probe	107

1.2.4.3. ZERO LEAKAGE

Nothing made by man can be considered to be absolutely leak-tight. Even in the absence of minute porosity, the permeation of certain gases through crystals, polymers, and glasses still occurs. Leak tightness is, therefore, a relative item. It is necessary to establish a practical leakage level for any given component under test. Because leak tightness is a relative term and has no absolute meaning, the sensitivity of the equipment involved is a practical guide. A preliminary decision has to be made concerning the definition of leak tightness for the particular situation. Any increase in sensitivity of a technique brings with it an increase in the expenditure of time and, therefore, an increase in cost. This increase in cost reaches a maximum when the specification reads in one of the following ways:

- No detectable leakage
- No measurable leakage
- No leakage
- Zero leakage

Such a specification is not only expensive, but also very confusing unless the method is precisely described. With specifications such as above, the operator is always working against background instrument noise. He is continually forced to make a decision as to whether the reading he is obtaining is caused by the random fluctuations of his instruments or by the actual detection of specific leakage. It is much easier to discriminate whether a measured leakage is above or below a given standard than to discriminate leakage from random instrument noise. It is therefore suggested that zero leakage be defined as a measurable quantitative value that is insignificant in the operation of the system. Such a procedure carries with it the added advantage that the system or the measurement sensitivity can be compared with a standard, and in that way a qualification of the system can be made during the test operation.

The Jet Propulsion Laboratory, for example, requires that certain components have zero liquid leakage. However, they define this term (Ref. 10) by the operating pressure of the system and the maximum measured gas leakage.

Section 1.4

FLOW CHARACTERISTICS

1.4.1. GAS FLOW

Mass transfer attributed to leakage can occur in two modes: pneumatic flow and permeation. Pneumatic flow occurs when leakage is by passage of fluid through finite holes. Permeation is passage of a fluid into, through, and out of a solid barrier having no holes large enough to permit more than a small fraction of the molecules to pass through any one hole.

1.4.1.1. PNEUMATIC FLOWS

Pneumatic gas flow which occurs in a leak may be placed in four categories: laminar, molecular, turbulent and choked. Table 3 shows the approximate types of flow modes: 10^{-1} to 10^{-6} atm cc/sec for laminar, above 10^{-2} atm cc/sec for turbulent and below 10^{-5} atm cc/sec for molecular type of flow. As may be seen from the table, laminar flow is predominant in the area of leakage interest.

1.4.1.1.1. Laminar Flow

The laminar flow of a fluid in a pipe is defined as a condition where the velocity distribution of the fluid in the cross-section of the pipe is parabolic. Laminar flow is one of the two classes of viscous flow, the other class being turbulent flow. Because turbulent flow is rarely encountered in leaks, the term viscous flow is sometimes incorrectly used to describe laminar flow in leak detection work.

The most familiar laminar flow equation is one developed by Poiseuille (Ref. 27). For the flow through a straight tube of circular cross-section, this equation is:

$$Q = \frac{\pi}{8}\left(\frac{d}{2}\right)^4 \frac{P}{\eta \ell}\left(P_1 - P_2\right) \qquad \text{Equation 1.4-1}$$

where Q = leakage rate
d = diameter of the leak
ℓ = length of the leak
P_1 = upstream pressure, P_2 = downstream pressure
η = viscosity of the gas
P_a = arithmetic mean between P_2 and P_1 $= \frac{P_1 + P_2}{2}$

In the range where this equation is applicable, it has been substantially verified experimentally. The above equation is applicable where the length and diameter of the flow passage are known. This is not the case for most leaks, but the equation may be rewritten in this form:

Table 3

PROPERTIES OF THE VARIOUS FLOWS

	Turbulent*	Choked*	Laminar*	Molecular	Permeation
Leakage region	$>10^{-2}$ atm cc/sec		10^{-1} to 10^{-6} atm cc/sec	$<10^{-5}$ atm cc/sec	Dependent on thickness
Flow-pressure relationship	$Q \propto (P_1^2 - P_2^2)^{\frac{1}{2}}$	$Q \propto P_1$	$Q \propto (P_1^2 - P_2^2)$	$Q \propto (P_1 - P_2)$	$Q \propto (P_1 - P_2)$
Flow-property relationship	$Q \propto \sqrt{\frac{1}{M}}$	$Q \propto \sqrt{\frac{1}{M}\left(\frac{1}{\gamma+1}\right)^{\left(\frac{\gamma+1}{\gamma-1}\right)}}$	$Q \propto \frac{1}{\eta}$	$Q \propto \sqrt{\frac{1}{M}}$	Varies with gas and material

P_1 = Upstream pressure

P_2 = Downstream pressure

* Ideal gas, compressible flow. For turbulent flow, constant friction factor is assumed.

$$Q = K \frac{P_a \left(P_1 - P_2\right)}{\eta} \qquad \text{Equation 1.4-2}$$

where K represents the constants in the above equations and the two geometry factors.

$$K = \frac{\pi}{8} \left(\frac{d}{2}\right)^4 \frac{1}{\ell} \qquad \text{Equation 1.4-3}$$

Laminar flow takes place when the Reynolds' number of flow is lower than a defined critical value. The Reynolds' number is a unitless quantity which defines the flow conditions and is given by:

$$N_{Re} = \frac{d\rho F}{\eta} \qquad \text{Equation 1.4-4}$$

where N_{Re} = Reynolds' number
ρ = fluid density
η = absolute viscosity
F = average flow velocity across a plane in the tube

By substituting the ideal gas equation in the above formula, the expression for the Reynolds' number for an ideal gas becomes:

$$N_{Re} = \frac{Q}{d} \left(\frac{4M}{\pi\eta RT}\right) \qquad \text{Equation 1.4-5}$$

where M = molecular weight
R = gas constant
T = absolute temperature

The critical value of Reynolds' number has been shown to be dependent upon the entrance conditions, roughness of the walls of a tube, and shape of the flow path. In general, for smooth tubes with well-rounded entrances, the critical value is about 1,200. For flow corrections necessitated by turns, constrictions, and surface roughness refer to Ref. 28 and 29.

The kinetic theory states that the viscosity of a gas is given by the relationship (Ref. 30):

$$N = \frac{m\bar{F}}{3\sqrt{2}\pi\sigma^2} \qquad \text{Equation 1.4-6}$$

where $\bar{F}$ = average velocity of the individual molecules
m = molecular mass
σ = molecular diameter

The average velocity of a molecule is:

$$\bar{F} = \left(\frac{8RT}{\pi M}\right)^{1/2} \qquad \text{Equation 1.4-7}$$

the mass of the individual molecules is:

$$m = \frac{M}{A^O} \qquad \text{Equation 1.4-8}$$

where A^O = Avogadro's number: i.e. number of molecules/mole
Substituting Equation 1.4-7 and 1.4-8 in Equation 1.4-6:

$$= \frac{2(MRT)^{1/2}}{3\pi^{3/2}A_O^2} \qquad \text{Equation 1.4-9}$$

This equation shows that the viscosity of a gas is independent of pressure and is proportional to the square root of temperature.

The two most important characteristics of laminar leaks are that the flow is proportional to the difference between the squares of the pressures upstream and downstream of the leak and that the leakage is inversely proportional to the leaking gas viscosity. Table 4 shows the viscosity of most gases is similar. Therefore, a change of gas will not markedly increase the sensitivity of the leak detection method unless this change of gas implies a change of instrument sensitivity. However, as shown on Figure 12, increasing the pressure difference across the leak by a factor of a little over three will increase the flow rate through this leak by a factor of ten. Obviously then, when the leaks to be measured are in the laminar flow range, the simplest method of increasing detection sensitivity is by an increase of pressure across the leak.

1.4.1.1.2. Molecular Flow

Molecular flow is flow through a duct under conditions where the mean free path is greater than the largest dimension of a transverse section of the duct. (Ref. 13) In such a flow, each atom moves independently by random movement. Net flow is from volume of high concentration to one of low concentration.

The mean free path is the average distance that a molecule travels between successive collisions with the other molecules of an ensemble. The mean free path λ is:

$$\lambda = \frac{1}{2\pi n\sigma^2} \qquad \text{Equation 1.4-10}$$

where n = number of molecules in a unit volume
σ = molecular diameter

If $n = gA^O/MV$ Equation 1.4-11

where g = mass of the gas
A^O = Avogadro's number; i.e. number of molecules/mole
M = molecular weight of the gas
V = volume

Table 4

VISCOSITY OF GASES AT 0 C
(Ref. 29)

Gas	Viscosity, Centipoises
Acetylene	0.0092
Air	0.0169
Ammonia	0.0094
Argon	0.0208
Benzene	0.0069
Carbon dioxide	0.0135
Carbon disulfide	0.0089
Carbon monoxide	0.0171
Ethane	0.0085
Ethyl alcohol	0.0082
Ethylene	0.0093
Halogenated hydrocarbon F-11	0.0103
Halogenated hydrocarbon F-12	0.0118
Halogenated hydrocarbon F-21	0.0108
Halogenated hydrocarbon F-22	0.0120
Halogenated hydrocarbon F-113	0.0098
Helium	0.0178
Hydrogen	0.0083
Hydrogen sulfide	0.0118
Methane	0.0100
Nitric oxide	0.0178
Nitrogen	0.0168
Nitrous oxide	0.0133
Oxygen	0.0191
Propane	0.0077
Sulfur dioxide	0.0116
Water	0.0088
Xenon	0.0210

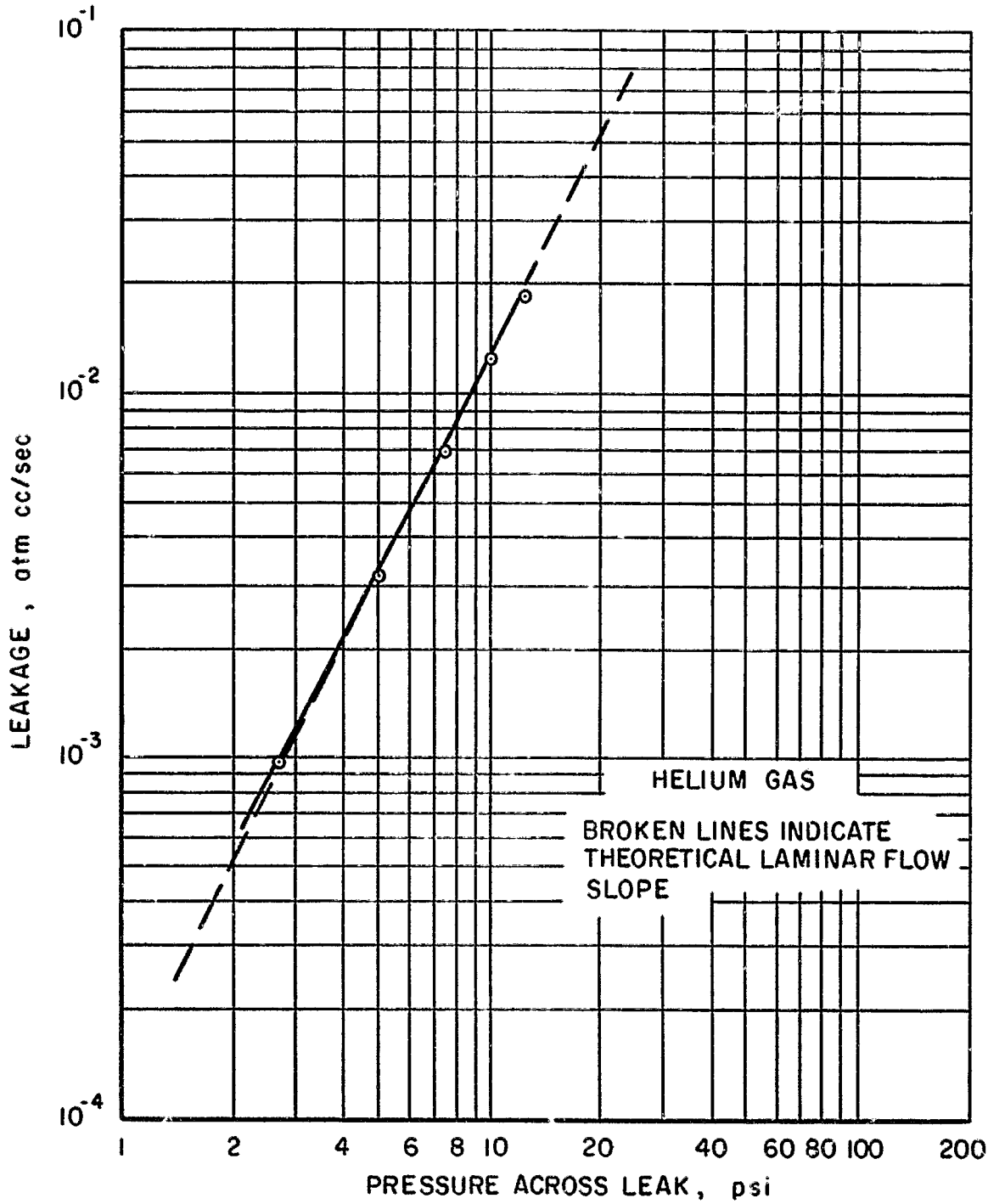

Figure 12. Laminar Flow in a Typical Hardware Leak. (Reprinted from J.W. Marr, Study of Dynamic and Static Seals for Liquid Rocket Engines, Final Report Phase II. Contract NAS 7-102. (Ref. 45))

and replacing V from the ideal gas law with the value in Equation 1.4-11:

$$\lambda = \frac{RT}{\sqrt{2}\pi P A^{o}_{c}{}^{2}} \qquad \text{Equation 1.4-12}$$

Equation 1.4-12 shows that at constant pressure the mean free path is proportional to temperature. However, if the amount of gas in a volume is kept constant, the mean free path is independent of temperature (Equation 1.4-10).

The magnitude of molecular diameters and mean free paths is shown in Table 5. As a convenient calculation guide, the mean free path of air at room temperature is:

$$\lambda \text{ air} = \frac{5 \times 10^{-3}}{P} \text{ centimeters} \qquad \text{Equation 1.4-13}$$

when P is expressed in torr.

The original mathematical derivations of molecular flow are attributed to Knudsen (Ref. 32). The rate of flow in a long pipe is:

$$Q = \frac{\sqrt{2\pi}}{6} \sqrt{\frac{RT}{M}} \frac{d^3}{\ell} (P_1 - P_2) \qquad \text{Equation 1.4-14}$$

where d = diameter of the pipe
ℓ = length of the pipe
P_2 and P_1 = pressures at the two ends

For this formula to apply, the pipe must be of a circular cross-section. For pipes and ducts of a non-circular cross-section the conductance is less than for pipes of circular cross-section and equal area. Equation 1.4-14 applies only if the pipe is much longer than its diameter. Any difficulty experienced by a molecule in entering the pipe must be negligibly small compared to the difficulty in traversing its length. If difficulty is experienced in entering the pipe, the kinetic theory shows that the rate of free molecular escape of gas from the container into a small aperture of area A is:

$$Q = \frac{1}{\sqrt{2\pi}} \sqrt{\frac{RT}{M}} A (P_2 - P_1) \qquad \text{Equation 1.4-15}$$

In the case of an aperture, the opening does not have to be circular to use Equation 1.4-15.

In molecular flow, the conductance of lines and apertures is independent of pressure. Calculations may be made of the effect of turns, apertures, and change in pipe diameter to calculate the overall flow in a leak. Formulas are available in the literature (Ref. 30 and 33) on the effect of structure on the flow rate.

Table 5

MEAN FREE PATHS AND MOLECULAR DIAMETERS
FOR VARIOUS MOLECULES (Ref. 30)

Molecule	Mean Free Path cm x 10^{-3} at 1 Torr and 25 C	Molecular Diameter cm x 10^{-8}
H_2	9.31	2.75
He	14.72	2.18
Ne	10.45	2.60
A	5.31	3.67
O_2	5.40	3.64
CO_2	3.34	4.65
H_2O	3.37	4.68
benzene	1.34	7.65
methane	4.15	4.19
ethane	2.53	5.37
propane	1.82	6.32
n-butane	1.46	7.06
n-pentane	1.19	7.82
n-hexane	1.03	8.42

These equations demonstrate the general form. They are not applicable in most leakage situations, because the leak length and diameter are not known. The molecular flow of a gas mixture is inversely proportional to the square root of their individual masses. Therefore a certain amount of separation takes place through a leak.

Since, in molecular flow the molecules travel independently of each other, it is possible for random molecules to travel from a part of a system at low pressure to another part of the system at a higher pressure. When an ultra-high-vacuum system is being tested by a mass spectrometer leak detector, the mass spectrometer leak detector operates at a pressure of 10^{-7} torr where the ultra-high vacuum system might be operating at a pressure of 10^{-9} torr. When tracer gas enters the ultra-high-vacuum system through a leak, it will eventually arrive from the 10^{-9} torr system to the mass spectrometer operating at 10^{-7} torr by the process of molecular flow. This does not infer that the total flow is from a system at low pressure to one at high pressure, because the mass spectrometer operating at 10^{-7} torr is sending gas molecules into the system at the lower pressure. In the summation of the flows, the total flow is from the high-pressure system to the low-pressure one. The high-pressure system is contributing gas molecules to the ultra-high-vacuum system. Tracer gas flow in the direction opposing the major flow of molecules is possible because of the random mode of molecular flow. The gas molecules, when traveling from one system to the other, do not come in contact with molecules traveling in the other direction.

1.4.1.1.3. Transition Flow

The transition from laminar flow to molecular flow is gradual. The mathematical treatment of this region is extremely difficult. However, a treatment of this region is necessary because a leak from a volume to a vacuum necessarily involves a transition from laminar to molecular flow. Equation 1.4-14 shows that the conductivity of a passage in molecular flow is proportional to the cube of the passage diameter and independent of pressure. Conversely, Equation 1.4-1 shows that the conductivity of the same passage in laminar flow is proportional to the fourth power of the diameter of passage, and proportional to the pressure.

Knudsen (Ref. 32) derived a semiempirical formula for the flow of gases through long tubes in the transition region. This formula is:

$$C = \frac{\pi}{8}\left(\frac{d}{2}\right)^4 \frac{P_a}{\eta \ell} + \frac{1}{6}\,\frac{2\pi RT}{M}\,\frac{d^3}{\ell}\,\frac{1 + \frac{M}{RT}\frac{dP_a}{\eta}}{1 + 1.24\,\frac{M}{RT}\frac{dP_a}{\eta}} \qquad \text{Equation 1.4-16}$$

The formula is valid providing that:

1. The flow is not turbulent in any part of the pipe.

2. The pressure difference between the ends is not so great that the mechanism of the flow (i.e. laminar or molecular) changes along the pipe.

Although the first of these conditions is usually satisfied in the leak, the second generally is not; that is, the transition from laminar to molecular flow does take place. The above equation at low pressures becomes an equation of molecular flow; whereas, at high pressure this equation reduces to one of strictly laminar flow.

Knudsen used the above equation to represent his experimental data. This equation has the effect of molecular flow added to the effect of laminar flow; consequently, it is not an actual representation of the flow mechanism taking place in the leak. The phenomenon is better visualized by realizing that both are occurring at the same time.

Burrows (Ref. 34) combined the equation for laminar flow (Equation 1.4-1) with the one for molecular flow (Equation 1.4-14) to obtain a general equation:

$$Q = \frac{\pi}{8}\left(\frac{d}{2}\right)^4 \frac{P_a}{\eta \ell}(P_1-P_2) + \frac{\sqrt{2\pi}}{6}\sqrt{\frac{RT}{M}}\ \frac{d^3}{\ell}(P_1-P_2) \quad \text{Equation 1.4-17}$$

In a way this equation is an accurate representation of the events occurring in the leak. Both laminar and molecular flow always occur in a leak. However, laminar flow is insignificant at low pressures and the molecular flow mode contributes little to total flow at high pressures.

The above equation is not completely accurate because of a "slipping" of molecules (Ref. 35) in transition flow. In laminar flow, the velocity of the molecular layers is proportional to their distance from the wall, the first layer being stationary. In the transition region slipping of the gas over the walls of the tube occurs; that is, the flow velocity at the walls is not zero. At pressures below the viscous limit, the slip correction becomes an appreciable contribution to the total conductance.

With further reduction in pressure, the dependence of the conductance on pressure becomes more complex. The flow characteristics begin a progressive change from those of viscous slip flow to those of molecular flow, where the conductance becomes independent of the pressure. The complete transition from viscous to molecular flow takes place over roughly two orders of magnitude change in pressure. This effect of slip can change the predicted flow rate by at least 20 percent. Because of this effect, Equation 1.4-16 better represents flow in the transition region. However, it is not capable of handling the total transition region (Ref. 30).

Other authors have (Ref. 34) attempted to derive equations to represent this phenomenon of transition from one type of flow to another. One simple method (Ref. 37) is to calculate laminar flow through one section of the tube, molecular flow through another, and approximate the in-between region.

1.4.1.1.4. Turbulent Flow

In viscous flow above a critical value of the Reynolds' number (about 2100 in the case of circular pipe flow), flow becomes unstable, resulting in innumerable eddies or vortexes in the flow. Any particle in turbulent flow follows a very erratic path, whereas in laminar flow the particle follows a smooth line.

The laws for turbulent flow are quite different from the laws for laminar flow. The equation relating mass flow rate (Q) in units of pressure x volume/time may be written:

$$Q = \pi d^{5/2} \left[\frac{RT(P_1^2 - P_2^2)}{16FM\ell} \right]^{1/2} \qquad \text{Equation 1.4-18}$$

where f, the friction factor, is defined on page 125 of Ref. 28. The friction factor depends on roughness of the channel walls, and can be considered a constant in fully developed turbulent flow.

Turbulent flow, because it requires relatively high velocity, occurs only in rather large leaks.

1.4.1.1.5. Choked Flow

Choked flow, or sonic flow, as it is sometimes called, occurs under certain conditions of geometry and pressure. Assume a passage in the form of an orifice or a venturi, and assume that the pressure upstream is kept constant. If the pressure downstream is gradually lowered, the velocity through the throat or orifice will increase until it reaches the speed of sound through the fluid. The downstream pressure at the time the orifice velocity reaches the speed of sound is called the critical pressure. If the downstream pressure is lowered below this critical pressure, no further increase in orifice velocity can occur, with the consequence that the mass flow rate has reached its maximum. This condition is known as "choked" or "sonic" flow.

Choked flow can occur under the following two conditions. (1) the flow passage must be in the form of an orifice or venturi in which only negligible frictional losses occur upstream of the orifice or throat of the venturi; (2) the ratio of downstream to upstream pressure must be below a certain "critical" value, which is

$$r_c = \frac{2}{\gamma + 1}^{\frac{\gamma}{\gamma - 1}}$$ Equation 1.4-19

The velocity of sound through a gas can be written:

$$F_c = \frac{2\gamma}{\gamma + 1} \frac{RT_1}{M}$$ Equation 1.4-20

where F_c = velocity sound

T_1 = absolute temperature upstream of the orifice where the velocity is low

$\gamma = C_P/C_V$ Equation 1.4-21

where C_P = heat capacity at constant pressure

C_V = heat capacity at constant volume

The mass flow rate under a choked flow condition is:

$$Q = \frac{\pi d^2 P_1 C_0}{4M} \sqrt{RT_1 \gamma \left(\frac{2}{\gamma + 1}\right)^{\frac{\gamma + 1}{\gamma - 1}}}$$ Equation 1.4-22

where d = orifice diameter

P_1 = upstream pressure

C_0 = orifice discharge coefficient

For an ideal monatomic gas, the value of γ is 1.67. For polyatomic molecules, the heat energy supplies is used for increasing not only the kinetic energy of translation, but also the kinetic energy of rotation and vibration. Since the same amount of extra energy is required at both constant pressure and constant volume, γ decreases with molecular complexity. Characteristic values of γ are shown in Table 6. Additional values may be calculated (Ref. 38) or obtained from other references (Ref. 3).

Because of the stringent requirements, choked flow is rarely encountered as the predominant flow mode, except in very large leaks.

Table 6

MOLAR HEAT CAPACITY OF GASES

(in calories per mole at 25 C and 1 atm)

Gas	C_p	C_v	$C_p/C_v = \gamma$
A	4.97	2.98	1.67
He	4.97	2.98	1.67
H_2	6.90	4.91	1.41
O_2	7.05	5.05	1.40
N_2	6.94	4.95	1.40
CO_2	8.96	6.92	1.29
NH_3	8.63	6.57	1.31
ethane	12.71	10.65	1.19
propane	17.60	15.60	1.13

1.4.1.1.6. Distinction Between Modes of Flow

Equations have been presented for the various possible modes of flow that can be encountered in a leak. The following rules may be used to predict the mode most likely to occur. In distinguishing between laminar and molecular flow, the size of the passage and the mean free path are the two important parameters. The distinction may be specified by a dimensionless parameter called the Knudsen number. The Knudsen number is defined as the ratio of the mean free path of the molecule to a characteristic dimension of the channel through which the gas is flowing.

$$N_K = \frac{\lambda}{d} \qquad \text{Equation 1.4-23}$$

where N_K = Knudsen number
λ = mean free path
d = channel diameter

The type of flow encountered in the various Knudsen number ranges is shown in Equation 1.4-24.

$$\frac{\lambda}{d} < 0.01 \text{ laminar flow}$$

$$\frac{\lambda}{d} > 1.00 \text{ molecular flow} \qquad \text{Equation 1.4-24}$$

$$0.01 > \frac{\lambda}{d} > 1.00 \text{ transition flow}$$

Flow in the viscous region is determined by the Reynolds' number which was described in Equation 1.4-5.

$$N_{Re} = \frac{d\rho F}{\eta} = \frac{Q}{d}\,\frac{4M}{\pi\eta RT} \qquad \text{Equation 1.4-5}$$

The distinction between laminar and turbulent flow is shown in Equation 1.4-25

$N_{Re} > 2100$ Turbulent flow

$N_{Re} < 1200$ Viscous flow Equation 1.4-25

$1200 < N_{Re} < 2100$ Either turbulent or viscous depending on duct conditions

Choked flow takes place when the pressure ratio between outlet and inlet reaches a certain minimum value. This, of course, is dependent on other characteristics such as aperture dimension, etc. The formula for the critical pressure ratio is defined by Equation 1.4-26.

$$r = \frac{P_1}{P_2}$$ Equation 1.4-26

The critical ratio below which choked flow takes place is:

$$r_c = \left(\frac{2}{\gamma + 1}\right)^{\gamma/(\gamma-1)}$$ Equation 1.4-19

Choked flow cannot take place when P_1 is so low that molecular flow exists.

1.4.1.2. PERMEATION

Permeation is passage of a fluid into, through, and out of a solid barrier having no holes large enough to permit more than a small fraction of the molecules to pass through any one hole. The process always involves diffusion through a solid and may involve other phenomena such as adsorption, dissociation, migration and desorption.

The general formula for permeation is:

$$q = K_p A \frac{\Delta P}{\ell}$$ Equation 1.4-27

where q = rate of mass flow
K_p = permeation rate constant
A = area normal to flow
ΔP = pressure drop along the flow path
ℓ = length of flow path

The ΔP in this case does not represent absolute pressures, but the difference in partial pressure of the leaking fluid between the two sides of the barrier. The permeation rates for some characteristic materials are shown in Tables 7-10 (Ref. 40). Additional data may be obtained in other tabulations (Ref. 41) and the original references mentioned within.

In these tables, where sufficient data is available to allow calculation, the permeability is given in parametric form:

$$\log_{10} K_p = A - B/T$$ Equation 1.4-28

where the units of K_p are in cc(STP) - mm/cm^2-sec-atm in the case of polymers and glasses and cc(STP) - mm/cm^2-sec$(atm)^{1/2}$ in the case of metals; T is in K. This assumes the Arrhenius type exponential law is followed in termperature and that the permeation rate is proportional to the pressure difference across the membrane in the case of polymers and glasses, and to the difference in the square root of the pressure in the case of metals. Although these assumptions are often safe, there are many exceptions. For convenience in quick comparisons the permeability at 25 C (77 F), P_{25}, is also given in these tables. Note that values for "A" in the tables are given as the sum of two numbers, and that "P" in the tables corresponds to K_p.

Table 7

PERMEABILITY OF POLYMERIC MATERIALS TO H_2, He, N_2, O_2 AND CO_2

P in cc(STP)-mm/cm^2-sec-atm, B in ^oK

MATERIAL	TRADE NAME OR CODE	H_2			He			N_2			O_2			CO_2		
		A	B	$P_{25} \cdot 10^7$	A	B	$P_{25} \cdot 10^7$	A	B	$P_{25} \cdot 10^7$	A	B	$P_{25} \cdot 10^7$	A	B	$P_{25} \cdot 10^7$
Natural Rubber		0.953-1	1908	39	0.146-1	1420	23	0.672-0	2033	6.6	0.903-1	1442	18	0.556-1	1385	102
Rubber Hydrochloride	Pliofilm 140-N$_2$	0.206-3	1228	1.21										0.134-0	2227	0.49
	Pliofilm FM-1							0.386-1	2185	0.7	0.767-2	1838	0.40	0.190-1	1870	0.71
Polybutadiene		0.342-1	1442	32				0.724-1	1702		0.362-1	1551	14.5	0.839-2	1136	105
Polybutadiene hydrogenated	Hydropol				0.241-0	1830	13.0	0.899-1	2447	3.0	0.214-0	2141	6.6	0.946-0	1901	30.8
Polydimethyl butadiene	Methyl rubber	0.669-0	1748	13	0.892-2	1442	11	0.342+2	2906	0.36	0.518+1	2409	1.0	0.892-2	1442	11
Polyisobutylene	Oppanol B-200 (butyl rubber)	0.672-0	2076	4.9	0.544-1	1728	5.6	0.240+1	2979	0.32	0.826-0	2336	0.90	0.191-0	2207	3.8
Polybutadiene-acrylonitrile	Perbunan (Germany)	0.996-1	1739	11.5	0.670-1	1539	8.7	0.841+1	2404	0.69	0.398-0	2054	3.2	0.402-0	1814	23
	Perbunan 18	0.830-2	1395	19.2	0.998-1	1480	12.0	0.542-0	2103	1.92	0.109-0	1879	0.2	0.918-1	1530	48
	Hycar OR 15	0.187-0	1923	5.4	0.304-1	1663	5.2	0.375+2	3910	0.18	0.062-1	2622	0.73	0.453-1	2294	5.2
	Hycar OR 25	0.997-1	1702	8.0	0.392-1	1617	7.5	0.084+1	2688	0.46	0.949-0	2294	1.78	0.750-0	2067	14.1
Polybutadiene-styrene	Buna S, GR-S	0.491-1	1486	30.5	0.114-0	1442	17.5	0.979-0	1901	4.8	0.477-1	1595	13	0.146-0	1240	94
Polychloroprene	Neoprene G	0.954-1	1770	10.3			3.4	0.748-0	2310	0.89	0.732-0	2163	3.0	0.516 0	1857	19.5
Polyvinyl chloride-methylacrylate	Mipolam MP	0.176-0	1945	4.4						0.2	0.505-0	2568	0.20	0.832-0	2141	4.0
Polyalkylpolysulfide	Thiokol B	0.869-0	2310	1.2							0.259+2	2950	0.22	0.839-1	2513	2.4
Polyisteramide-diisocyanate	Vulcaprene A	0.368+0	1987	4.8				0.910+1	2506	0.37	0.955+1	2382	1.15	0.932-1	2054	14.1
Polyethylene (density 0.914)	PE2400 Alathon 14	0.220-0	1921	9.90	0.962-1	1814	3.75	0.524+1	2579	0.74	0.822-0	2229	0.20	0.691-0	2032	9.6
(density 0.960)	Grex	--	--	--	0.144-2	1551	0.67	0.904-1	2076	0.11	0.651-2	1830	0.31	0.718-3	1573	0.28
Polyethylene glycol terephthalate	Mylar A	0.678-4	1201	0.445	0.890-4	1198	0.24	0.995-5	1630	0.0031	0.960-5	1308	0.019	0.5**-4	1359	0.09
Polystyrene	Dow 9041	0.927-5	72	68.5				0.713+2	-18	5.92	0.235-6	-10	18.5	0.178-5	219	277
Polyvinyl chloride + 25% DOP	Geon 101	0.818-5 0.549-5	418 310	3.0 68.7										0.611-7 0.896-6	217 -332	0.062 1839
Polyvinyl chloride 95%, Acetate 5%) + 25% DOP	Bakelite VB1930	0.133-5	476	3.4										0.472-5	299	0.49
		0.074-1	1021	4.3	0.942-2	1574	4.8	0.923+2	2820	0.37	0.933-0	2329	1.4	0.150-0	1931	4.1
Polyvinylidene chloride	Saran 517			0.050			0.011	0.069+1	3071	0.00044	0.932+1	3474	0.0018	0.399-0	2688	0.024
Polycaprolactam	Nylon 6							0.388-0	2447	0.0064	0.995-2	2273	0.023	0.085-1	2120	0.093
Polytetrafluoroethylene	Teflon			18			930			2.4			7.0			
Polychlorotrifluoroethylene) plasticized	Teflene Kel-F	0.998-2	1530	0.74				0.609-0	3060	0.0025	0.890-1	2514	0.028	0.949-4	1513	0.11
		0.160-0	2018	3.4	0.915-1	1485	10.2	0.971-1	3021	0.054	0.399-0	2353	0.31	0.917-1	2346	1.4
Ethyl cellulose (plasticized)	Ethocel 610	0.827-4	751	22.7				0.787-4	1005	5.6	0.602-3	824	18.1	0.524-5	309	32
Cellulose acetate (plasticized)	Celanese P-912	0.220-0	1140	0.7				0.995-4	1429	0.17	0.590-4	1093	0.82	0.925-1	1595	2.0
Cellulose acetate-butyrate	Kodapak II	0.231-3	893	16	0.933-3	1038	10.0	0.765-2	1710	1.1	0.841-3	1330	3.8	0.484-3	921	24
Polypropylene (d = 0.907)								0.111-2	2490	0.33	0.449+1	2401	1.2	0.380-0	1685	5.2
Cellulose nitrate							5.2			0.88			1.6			1.0

*Separated, cells permeable, Vol. II, Glasses, Edition, Physics Data for Researchers, Data Systems in Chapter XIII, Report 1965, NASA, Goddard Program, NSG-398(02), Grant No. CR-53015, Institute of Technical Sciences.

Table 8

PERMEABILITY OF POLYMERIC MATERIALS TO PROPANE AND TO WATER

P in cc (STP)-mm/cm^2-sec-atm, B in ^oK

MATERIAL	TRADE NAME OR CODE	H_2O			PROPANE		
		A	B	$P_{25} \cdot 10^7$	A	B	$P_{25} \cdot 10^7$
Natural Rubber				2600	0.141-1	1202	128
Rubber Hydrochloride	Pliofilm NO	0.0707-0	1726	19			
Poly(butadiene), hydrogenated	Hydropol				0.241+2	2273	41
Poly(isobutylene)	Butyl rubber				0.951-0	2338	1.3
Poly(chloroprene)	Neoprene GN						5.5
Poly(alkylpolysulfide)	Thiokol 3000 ST						1.1
Polyethylene(density 0.922)		0.869-0	1748	68.4			
(density 0.914)	Alathon 14				0.662-1	2447	7.2
(density 0.960)				9.1			
(density 0.964)	Grex				0.459-0	2338	0.41
Polypropylene (d = 0.907)		0.960+1	2207	35.7			
Poly(ethylene glycol terephthalate)	Mylar A	0.508-5	153	98.8			
Polystyrene		0.80-5	0	630			
Poly(vinyl chloride)	Geon 101	0.78-4	514	110			
Poly(vinyl chloride-acetate)	Vinylite VYNWO	0.37-2	874	275			
Poly(vinylidene chloride)	Saran 517	0.941-7	2404	7.5			0.00027
Polyamide	Nylon 6-6			53-516**			
Poly(chlorotrifluoroethylene)	Kel F 300	0.222-1	2050	0.22			
Ethyl cellulose (plasticized)	Ethocell 610	0.995-4	0	9880			
Cellulose acetate		0.621-4	0	4180			
(plus 15% DBP)		0.750-4	0	5620			2.8
Cellulose nitrate				4800			0.0058
Poly(methylmethacrylate)	Lucite			2200			

*Reprinted, with permission, from R. F. Murace, Editor, Design Data for Pressurized Gas Systems (Chapter XII), NAS7-105, 1963, NASA, Session Number N64-18107, Report No. CR 53393. (Office of Technical Services).

**Humidity dependent.

Table 9

PERMEABILITY OF GLASSES

P in cc (STP)-mm/cm^2-sec-atm, B in ^oK

SYSTEM	A	B	P_{25}
H_2-Fused silica	0.398-5	1873	$1.12 \cdot 10^{-12}$
-Vycor (Corning 7900)	0.520-5	1826	$3.9 \cdot 10^{-12}$
He-Fused silica (GE)	0.401-4	1049	$0.76 \cdot 10^{-7}$
-Vycor (Corning 7900)	0.579-4	1049	$1.14 \cdot 10^{-7}$
-Pyrex (Corning 7740)	0.654-4	1398	$0.91 \cdot 10^{-8}$
-Soda lime (Corning 0080)	0.822-4	2403	$5.7 \cdot 10^{-12}$
-X-ray shield (Pittsburgh Plate Glass)	0.662-5	2731	$3.1 \cdot 10^{-14}$
N_2O Fused silica	0.967-4	4820	$6.2 \cdot 10^{-20}$

Table 10

PERMEABILITY OF METALS

P in cc (STP)-mm/cm^2-sec $(atm)^{1/2}$, B in ^oK

SYSTEM	A	B	P_{25}
H_2-Aluminum	0.589-1	3017	$7.5 \cdot 10^{-11}$
Copper	0.621-1	3933	$2.6 \cdot 10^{-14}$
Hastalloy B	0.701-1	3657	$2.7 \cdot 10^{-13}$
Inconel	0.847-1	3649	$4.0 \cdot 10^{-13}$
Iron	0.554-2	1836	$2.6 \cdot 10^{-8}$
Kovar	0.352-1	3497	$4.1 \cdot 10^{-13}$
Monel	0.161-1	2797	$5.9 \cdot 10^{-11}$
Nickel	0.520-1	2885	$6.9 \cdot 10^{-11}$
Niobium	0.749-1	1137	$8.7 \cdot 10^{-5}$
Palladium	0.929-1	2296	$1.7 \cdot 10^{-8}$
Platinum	0.512-1	3936	$2.1 \cdot 10^{-14}$
Steel			
Cold drawn	0.554-2	1879	$1.8 \cdot 10^{-8}$
Low carbon	0.312-2	2288	$4.2 \cdot 10^{-10}$
Stainless 303	0.435-1	3540	$4.6 \cdot 10^{-13}$
304	0.586-1	3715	$1.3 \cdot 10^{-13}$
316, 321	0.273-1	3252	$2.3 \cdot 10^{-12}$
347	0.634-2	3180	$9.2 \cdot 10^{-13}$
410	0.188-1	3260	$5.7 \cdot 10^{-12}$
N_2-Iron	0.093-1	5204	$4.3 \cdot 10^{-19}$
Molybdenum	0.359-0	9837	$4.4 \cdot 10^{-33}$
CO-Iron	0.554-2	4066	$8.1 \cdot 10^{-16}$
O_2-Silver	0.754-1	4941	$1.5 \cdot 10^{-17}$

*Reprinted, with permission, from R. F. Morace, Editor, Design Data for Pressurized Gas Systems (Chapter XII), NAS7-100, 1963, NASA, Session Number N64-18197, Report No. CR 53303, (Office of Technical Services)

If any system is to be relatively leaktight, the materials of construction have to exclude leakage by permeability. As an example, the permeation rate at room temperature of a natural rubber gasket 0.1 inch thick, 0.1 inch wide, and 5 inches in diameter with a one-atmosphere hydrogen pressure differential is 1.6×10^{-5} atm cc/sec. In some uses, this permeation might represent an unacceptable leakage rate.

Permeation presents a problem in leak checking equipment where the construction materials have a high permeability to the tracer gas. For example, if a component containing a rubber diaphragm one millimeter thick and one square inch in surface area is leak checked using helium gas, a leakage of approximately 1×10^{-5} atm cc/sec will be measured across the diaphragm. This leakage is due to permeation of helium through the diaphragm and not any actual holes. It represents the maximum sensitivity of helium leak testing that can be performed on this component. However, if the component is to be used with another fluid to which the membrane is impermeable, the apparent leakage due to permeation measured during leak testing has little meaning under operating conditions.

Another example of this type of false reading is a rubber O-ring. Depending on material, a rubber O-ring usually represents a permeability of approximately 10^{-7} atm cc/sec atm per linear inch of exposed surface. Figure 13 is an example of the permeation rates of O-rings of various materials. This permeability does not have to be taken into consideration during routine leak checking if leakage measurement occurs in a time too short to permit the saturation and mass transfer of helium through the O-ring.

To eliminate permeability as a factor in leakage measurement, three procedures may be used.

1. The leakage measurement may be taken rapidly, not allowing the material to be saturated with gas. This is only possible if the material is relatively thick. For example, a rubber diaphragm will rapidly saturate and almost immediately show leakage. On the other hand, O-rings are relatively thick and will not saturate rapidly enough to give a reading within a reasonable period of time (five minutes). If the diffusivity and solubility of the fluid in the material is known, it is possible to calculate the rate of increase of leakage. This calculation is described by Baer (Ref. 41). However, in many cases (where the leakage path is long) this calculation is not necessary. Rather than calculations, experimental results can determine very quickly if leakage through a thick gasket is inconsequential for short-time periods.

2. The maximum permeability of all components and the resulting mass transfer produced during leak testing may be calculated. Equation 1.4-27 is used for these calculations. In this way, the permeability value will be

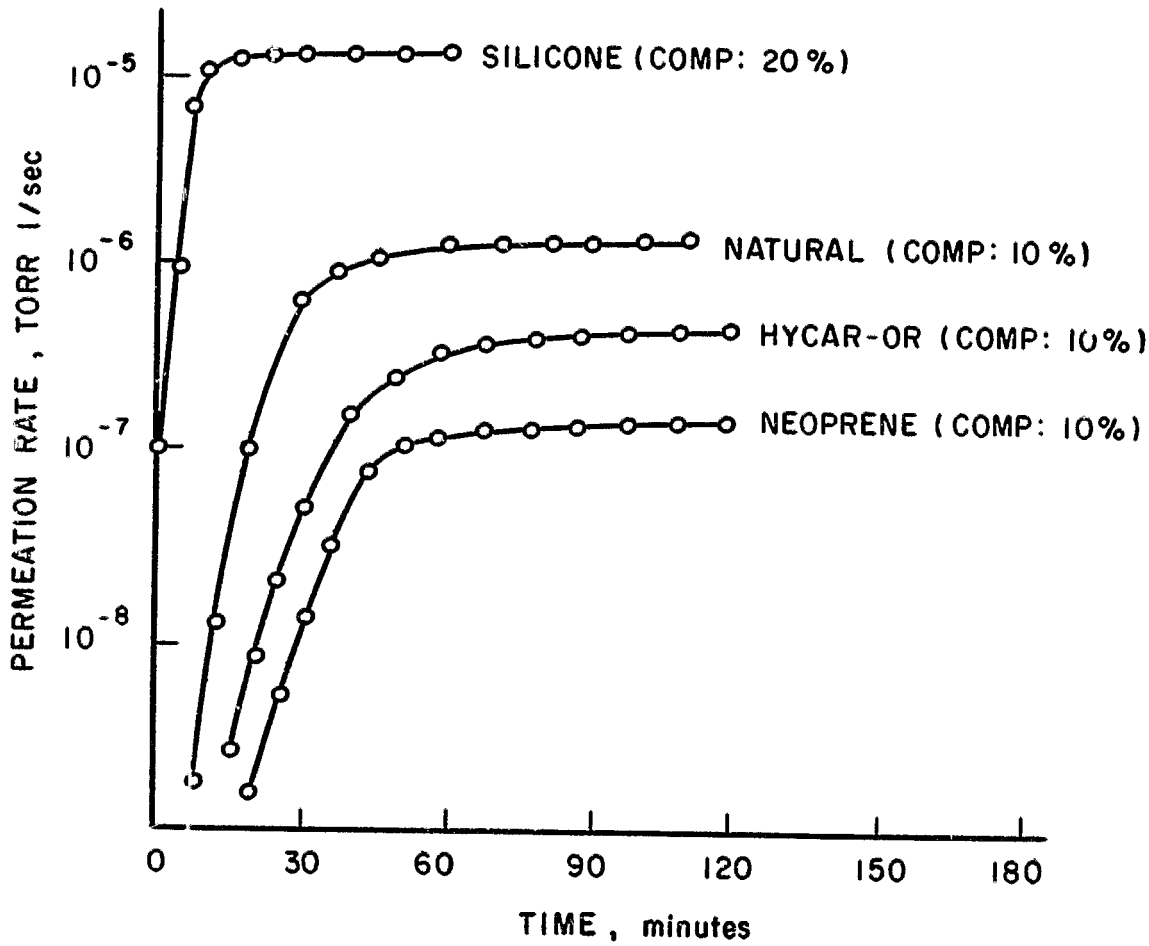

Figure 13. Permeation Rate Versus Time of Rubber Gasket for a 4x4mm Cross Section. (Reprinted with permission from I. Kobayeshi and H. Yada, "Leak Test of Rubber Gaskets," Fundamental Problems in Vacuum Techniques, Vol. I, Pergamon Press, London, 1960, p. 248.)

known and only leakage above this value will be considered as leakage flow.

3. The last method and the most difficult one is to quantitatively measure the leakage at various pressure differentials. Providing the leak being measured is pneumatic (i.e. it is through a hole in the component) and laminar, the flow is proportional to the square of the pressure differential across the leak. However, if the flow is strictly due to permeation, then the flow through the leak will be directly proportional to the difference in concentration across the leak. In this way, the presence of holes in the component can be differentiated from permeation.

1.4.2. LIQUID FLOW

The flow of a liquid through a leak may be one of two modes: laminar or turbulent. The flow characteristics and the requirements for attaining the flow modes are similar for gases and liquids. The criterion is a certain Reynolds' number. The viscous flow equations for gas are different from those for liquids because of the modifications necessary due to gas compressibility.

1.4.2.1. LAMINAR FLOW

Poiseuille's equation for laminar flow leakage is:

$$Q_v = \frac{\pi}{8}\left(\frac{d}{2}\right)^4 \frac{P_1 - P_2}{\eta \ell} \qquad \text{Equation 1.4-29}$$

where Q_v = volume flow in units of volume per unit time.

1.4.2.2. TURBULENT FLOW

Turbulent flow equation for a liquid can be expressed:

$$Q_v = \frac{\pi}{4} d^{5/2} \sqrt{\frac{P_1 - P_2}{2\rho f \ell}} \qquad \text{Equation 1.4-30}$$

Turbulent flow occurs only in very large liquid leaks.

1.4.3. CORRELATION BETWEEN FLOW TYPES

1.4.3.1. CONVERSION OF FLOW RATES FOR VARYING GASES

The equations discussed thus far show the flow relationship in ideal cases. Leaks, however, are not intentional and, therefore, far from ideal. They are not the long straight tubes for which equations are easy to obtain. The general approach to leakage correlation is to predict which flow mode occurs and to predict changes which will occur upon change in conditions within the flow mode.

Table 3 shows the properties of the various flow leaks and how fluid parameters influence the flow rate. This table is derived from the various flow equations presented in the text.

As may be seen from Table 3 the influence of varying the gas is not so great as that of varying the flow mode. Once the flow mode is determined, the conversion to another gas should be relatively easy to make, providing the relationships in the above table are in fact correct. The major difficulty is identifying the predominant flow mode.

The data necessary for the conversion is relatively easy to obtain. For example, the viscosity of many gases is published. Even if the viscosity is not known, approximation should not produce a large error. As shown in Table 4, the viscosity of gases at constant temperature varies by less than half an order of magnitude between the most viscous and the least viscous.

For molecular flow, the molecular weight of the gases is easily available and should cause no problem in the conversion. If choked flow does occur, gamma, necessary for conversion of choked flow leakage, is 1.67 for monatomic gases and rapidly approaches one as the complexity of the gas molecule increases.

Working with a variety of leaks of different sizes and under different conditions, some of the flow modes may readily be eliminated. For example, if the leak rate is small, it is relatively easy to assume that no turbulent flow will take place. If the leak is one going from high pressure to a slightly lower pressure, but not a vacuum, it is likely that molecular flow is not the flow mechanism. In the above case, the flow may be of a laminar nature and therefore conversion to a second flow pressure is relatively easy. Choked flow is rarely encountered in small leaks.

Another example - convert one leakage rate flowing into a vacuum to an anticipated rate for a different pressure into the same vacuum. Calculations described in Ref. 34, show that if the leak is of relatively small size (10^{-5} atm cc/sec or less) molecular flow will play a major role in such a leak. However, should the leak be relatively large (10^{-3} atm cc/sec or greater), the leakage will be predominately of laminar nature. If one can accurately predict the type of flow which will predominate in a leak, one could therefore make accurate conversions to a different set of conditions. Unfortunately, the state-of-the-art is such that these predictions are usually not possible.

Many authors (Ref. 30, 34,37, and 43) have predicted the following predominant flow modes in leaks:

turbulent	$>10^{-2}$ atm cc/sec
laminar	10^{-1} - 10^{-6} atm cc/sec
transition	10^{-4} - 10^{-6} atm cc/sec
molecular	$<10^{-6}$ atm cc/sec

Assuming the flow mode has been identified, the following are sample calculations for correlation of flow rates with the use of different gases and pressure.

This sample calculation is for laminar flow. The general equation for laminar flow is:

$$Q = \frac{\pi}{8} \left(\frac{d}{2}\right)^4 \frac{P_1 + P_2}{\eta \, 2 \, \ell} (P_2 - P_1) \qquad \text{Equation 1.4-1}$$

where Q = leakage (mass flow in units of pressure x (volume/time)
d = average diameter of leak
P_2 = pressure on the entrance side of the leak
P_1 = pressure on the exit side of the leak
η = viscosity and the leaking fluid or fluid mixtures
ℓ = leak length

The dimensions of d and ℓ are usually not known. An apparent conductance K may be calculated by the formula, where this apparent conductance is the product of $\frac{\pi}{8} \frac{d^4}{2} \frac{1}{\ell}$ and any unit conversion factors. From this calculation, an apparent geometry factor can be calculated.

$$K = \frac{\pi}{128} \frac{d^4}{\ell} \qquad \text{Equation 1.4-3}$$

If K is calculated only for conversion from one flow to another, the constant does not have to be in compatible units, providing that the same units are used both in solving for K and using the K in correlation equations.

Using the apparent conductance K calculated above, the flow of any gas at operating pressure may be predicted using Equation 1.4-2.

$$Q = \frac{K}{2\eta} (P_1^2 - P_2^2) \qquad \text{Equation 1.4-2}$$

A similar apparent conductance may be calculated for other flow modes using the equations given earlier in this section. Such calculations are correct only if the flow mode has been correctly chosen.

When there is doubt about the correctness of flow identification, the following procedure is recommended:

1. If pressure is increased, correlate as laminar.

2. If pressure is decreased, correlate as molecular.

3. If gas is changed, correlate as molecular.

Correlation should be performed so that, if an error is made, actual leakage will be no greater than that predicted in the correlation. Correlation of leaks resulting from increased pressure across a leak is not recommended. Reasons for this statement are given in Section 1.4.4.

1.4.3.2. CONVERSION BETWEEN GASES AND LIQUIDS

It is possible to predict liquid leakage from leakage measured under other known conditions. This method is generally applicable on a leak or series of leaks, most of which have a conductance between 1 and 10^{-5} atm cc/sec atm. The procedure consists of calculating an apparent conductance of the leak and, by assuming laminar flow conditions, calculating the expected leakage. The derivation of the equation is as follows.

The equations for flow of gases:

$$Q = \frac{\pi}{8}\left(\frac{d}{2}\right)^4 \frac{P_a}{\eta \ell} \quad (P_1 - P_2) \qquad \text{Equation 1.4-1}$$

and for liquids:

$$Q_v = \frac{\pi}{8}\left(\frac{d}{2}\right)^4 \frac{P_1 - P_2}{\eta \ell} \qquad \text{Equation 1.4-29}$$

both have the similar geometry factor K:

$$K = \frac{\pi}{8}\left(\frac{d}{2}\right)^4 \frac{1}{\ell} \qquad \text{Equation 1.4-3}$$

In substituting the geometry factor, the equations reduce to:

$$Q = \frac{K}{\eta} P_a (P_1 - P_2) \qquad \text{Equation 1.4-2}$$

for gases and:

$$Q_v = \frac{K}{\eta} (P_1 - P_2) \qquad \text{Equation 1.4-31}$$

for liquids. In use, the system leakage is measured and Equation 1.4-2 is solved for K. This calculated K is then used in Equation 1.4-31 so that the liquid leakage may be predicted. Such a procedure will be accurate only in laminar flow leaks. Should the measured leakage be molecular rather than laminar, the error introduced in the calculation will predict a greater liquid leakage than will actually be found. The equation may therefore be used with confidence, since any error will add a margin of safety into the results.

The following restrictions apply to the use of the above method:

1. The leakage is the result of a finite hole or holes and not the result of permeation.

2. The gas flow is laminar, i.e. the flow through the leak is in the range of 1 to 10^{-6} atm cc/sec or is made up of a number of leaks in that flow range.

3. The calculations should at best be considered accurate to only a factor of two. Error in both the measurements and the deviations from the flow equations preclude more accurate solution.

If Equations 1.4-2 and 1.4-31 are combined, the ratio of gas to liquid leakage through the same leak at the same pressure is:

$$\frac{Q}{Q_v} = \frac{\eta_{liq.}\ P_a}{\eta_{gas}} \qquad \text{Equation 1.4-32}$$

This is a convenient method of determining what liquid leakage will exist if the gas leakage is measured at the same pressure.

Experiments were recently performed (Ref. 44) to check the validity of the above correlation. Liquid leakage was measured for leaks with previously measured gas leak rates. It was found that leaks having a gas conductance in the 10^{-3} atm cc/sec range had a liquid leakage approximately one-half that predicted by Equations 1.4-31 or 1.4-32. Leaks in the 10^{-4} atm cc/sec range leaked liquid at a rate approximately one-tenth the rate predicted by theory. Liquid leakage in leaks in the 10^{-5} atm cc/sec atm range were approximately one-twentieth of that predicted by the above equations.

Based on the above, it would appear that the equations for correlation will produce conservative answers, i.e. the actual liquid leakage will always be smaller than that predicted by theory.

It is believed that the liquid flow is lower than calculated for two reasons:

1. No correction was made for any molecular flow component of the measured gas leakage.

2. Physical adsorption completely immobilized a layer of liquid adjacent to the leak wall and therefore reduced the apparent leak diameter.

1.4.3.3. GRAPHICAL CORRELATION

Santeler and Moller (Ref. 43) used the above equations to construct a graph for solution of these correlations. Such a graph is shown on Figure 14. The application of this graphical method is discussed in the following paragraphs.

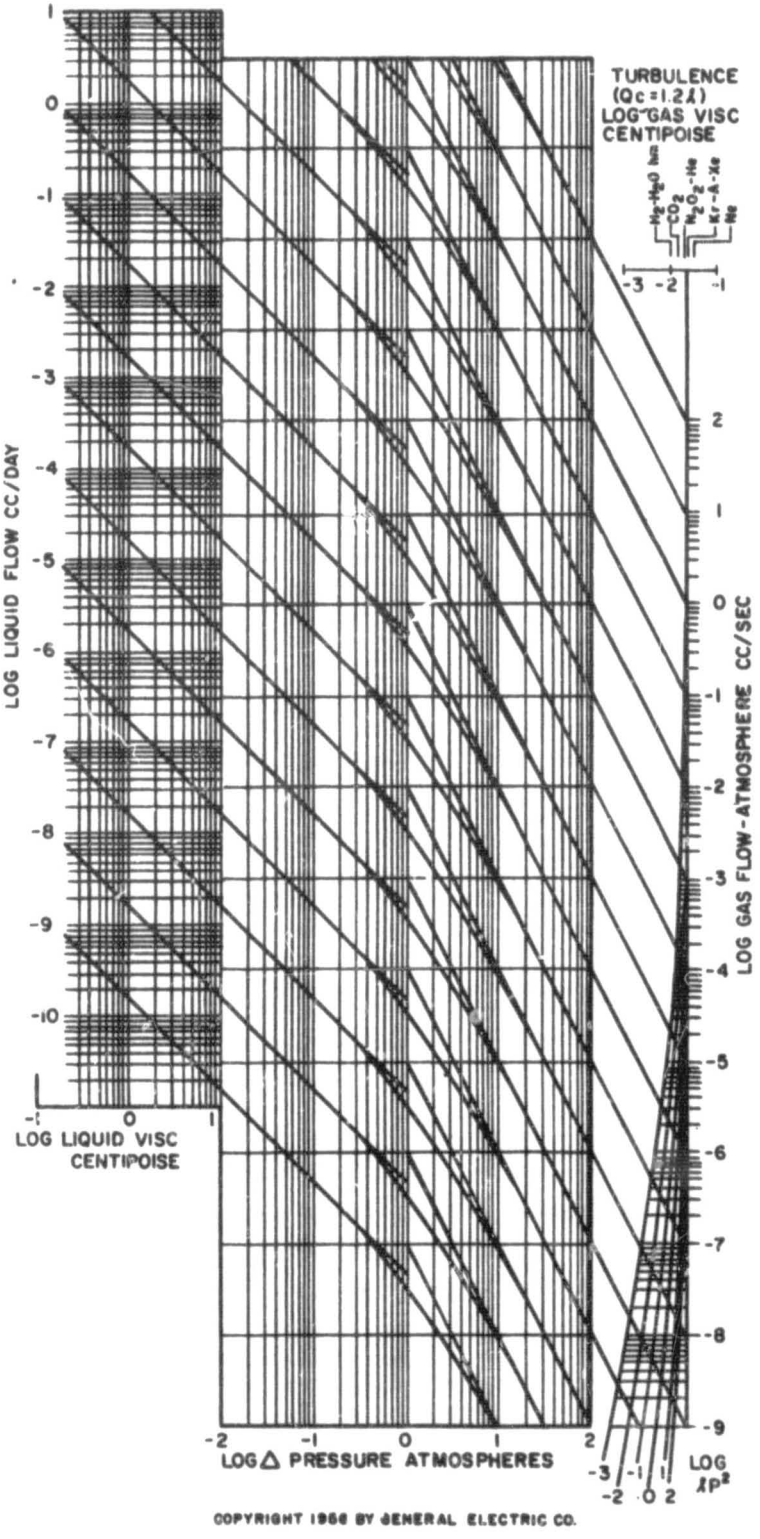

Figure 14. Fluid Flow Conversion Graph

1.4.3.3.1. General Description

Using the equations previously discussed the nomograph (Figure 14) was constructed. In the nomograph, ΔP is plotted on the lower axis. The respective gas and liquid flows are on the right and left margins. The horizontal guide lines are characteristic of a given geometry independent of pressure or type of gas. That is, they represent the K factor in the equations. On the left the diagonal lines are a 45 degree slope which fits the relation $Q = \frac{K}{\eta} \Delta P$ for liquids. On the right side the slope becomes 2:1 which satisfies the relation $Q = \frac{K}{\eta} \Delta P^2$. In order to handle different gases and liquids, two viscosity scales were added to the graph. The scale on the right is for gases while the left scale is for liquids. This liquid viscosity scale has been selected and oriented on the graph so that its decade extensions coincide with the pressure decades. This permits easy extrapolations to higher values of liquid viscosity.

For gaseous flow the units are atm cc/sec while for liquid flow the units are cc/day. Pressure is expressed in atmospheres and length in centimeters. The units used for the viscosity of both liquids and gases are centiposies.

In any use of the graph to make a conversion from one set of pressure and flow conditions for a given gas or liquid to another set of pressure and flow conditions for a new gas or liquid, enter the graph at the right side at the log of the given gas flow or at the left side at the log of the given liquid flow. Move horizontally to the viscosity of the given liquid or to the log ℓP^2 of the given gas. Then move parallel to the diagonal slope lines to the given differential pressure (log ΔP).

In all cases involving liquids, the diagonal movement will be along a straight line, as evidenced by the lines leading from the left side of the graph. Also, diagonal movement is along a straight line for gases if the gas flow is to a vacuum. The curved portions of the diagonal slope lines are used only in cases involving gas differential pressures with no flow to a vacuum.

After the given differential pressure is located by keeping these slope restrictions in mind, move horizontally to the new differential pressure (log ΔP).

Then move parallel to the diagonal slope lines to the log of the new liquid viscosity (i.e., up and to the left along a straight line), or, in the case of a new gas, to the log of ℓP^2 (i.e., down and to the right). Stop at the horizontal line which intersects the new viscosity or the new ℓP^2. The horizontal line is the desired log of the new gas or the new liquid flow rate as determined by the graph.

1.4.3.3.2. Corrections For Molecular and Transitional Flow

Only laminar flow has been considered thus far. Leaks in

size of 10^{-4} atm cc/sec and smaller can be in the transition range between laminar and molecular flow. Very small leaks around 10^{-9} and 10^{-10}, are predominately molecular. The use of a laminar conversion for leaks of either of these types could result in considerable error, since molecular flow is a linear function of pressure rather than the squared function for which the graph is constructed. To make this graph applicable to the conversion of leaks which fall in these two ranges, a correction factor must be applied. It would be desirable if this factor could be applied directly on the basis of the leak size, but unfortunately, this is not the nature of gas flow. It is perfectly feasible for one leak to be in laminar flow while a second leak which passes an identical gas flow under the same pressure conditions could be in molecular flow. With a change in pressure conditions, the flow of gas through the two leaks will become widely different. To apply a correction for molecular flow, either the radius or length of the leak must be estimated. In this handbook, the correction will be based on an assumed length of the leak. The reasons for this selection are two-fold: (1) the length has a linear effect on the equations for both laminar and molecular flow and (2) it is much easier by visual inspection to predict a probable length of leak. Certainly, considerable error might exist in this estimate of length, since the actual flow path may vary from essentially an orifice to a long winding restriction.

A correction on the basis of an assumed length alone is not sufficient. The assumption of a value for the length permits an estimate of the extent to which transition or molecular flow exists, but a pressure correction must then be applied to account for the changed flow condition.

As a parameter for gas flow, the expression ℓP^2 where ℓ is the length in centimeters, and P is the inlet pressure in atmospheres has been chosen. The family of lines on the right side of Figure 14 has been drawn for dry air. The viscosity correction has reduced to a scale in the upper right margin.

1.4.3.3.3. Sample Solutions Incorporating the ℓP^2 Correction

Next, consider how these extra factors are used. Assume that a gas leakage of 10^{-8} has been measured with the conditions of air at one atmosphere to vacuum. It is desired to know what the air leakage would be for pressure conditions of 132 psi gage, or 10 atmospheres absolute, to vacuum. The solution is shown in Figure 14. A value must first be assumed for ℓ, for instance, ℓ = 0.1 cm. The inlet pressure for the test conditions was one atmosphere. Therefore $\ell P^2 = 0.1$. Starting with the flow of 10^{-8} atm cc/sec, move to the line $\log \ell P^2 = -1$, then up to 2:1 sloped line to the pressure of one atmosphere. Here obtain the horizontal characteristic line and move to the new pressure differential condition of 10 atmospheres. Since the low side pressure is still a vacuum, follow down the 2:1 slope. Since the pressure conditions have changed, ℓP^2 has changed to 10 rather than 0.1. By going to the $\log \ell P^2 = 1$ line, the corrected flow of 4×10^{-7} atm cc/sec is obtained. Had the existence of laminar flow been assumed, uncorrected solution would have been obtained. That is, the expected flow would have been 1×10^{-6} atm cc/sec.

1.4.3.3.4. Turbulent Flow Limitations

The graph is developed on the basis of laminar flow and corrected for conditions of transition and molecular flow. There remains only to explore the opposite end of the scale, at high flow rates, to determine under what conditions turbulence can occur.

The point or region of transition from viscous laminar flow to turbulent flow has never been accurately established. In past practice, transition has been considered to begin at a Reynolds' number - defined as $\left(\frac{\rho Fd}{\eta}\right)$ - of approximately 2100. Theoretical considerations of the nature of the flow at this point of transition indicate turbulence should occur when the flow in atm cc/sec exceeds 1.2 times the length of the leak in centimeters. This criterion for incipient turbulence has been included on the conversion graph by the Equation $Q = 1.2\ell$.

1.4.4. ANOMALOUS LEAKS

Four types of leaks were encountered which did not fit in the categories already discussed. These were check valve leaks, surface flow leaks, self-cleaning leaks, and geometry change leaks. The errors in leak measurement due to the presence of these types of leaks could be greater than any errors due to the miscalculation discussed in the flow sections.

1.4.4.1. CHECK VALVE LEAKS

During a study (Ref. 45) of leakage phenomena, examples of check valve and geometry change leaks were found.

Figure 15 is a plot of the leakage-pressure differential obtained on a damaged needle valve. It was observed that although the typical laminar flow curve was obtained at a high pressure differential, below this pressure, the leakage abruptly stopped. Upon increasing the pressure, the leak reappeared. This phenomenon was repeatable.

This type of leak would be particularly hard to detect since the leak cannot be seen below a critical pressure.

1.4.4.2. GEOMETRY CHANGE IN LEAKS

The shape of a leak may change with changes in system pressure. As pressure increases, the expansion of system parts resulting from stresses induced by the increased pressure can cause leakage rates of known leaks to increase beyond the predictions of laminar flow theory. An example of this increase of leak rate with geometry change is shown in Figure 16.

1.4.4.3. SELF-CLEANING LEAKS

In performing work on project NAS 8-4012 (Ref. 46), gaskets under compression are subjected to a high helium pressure and the

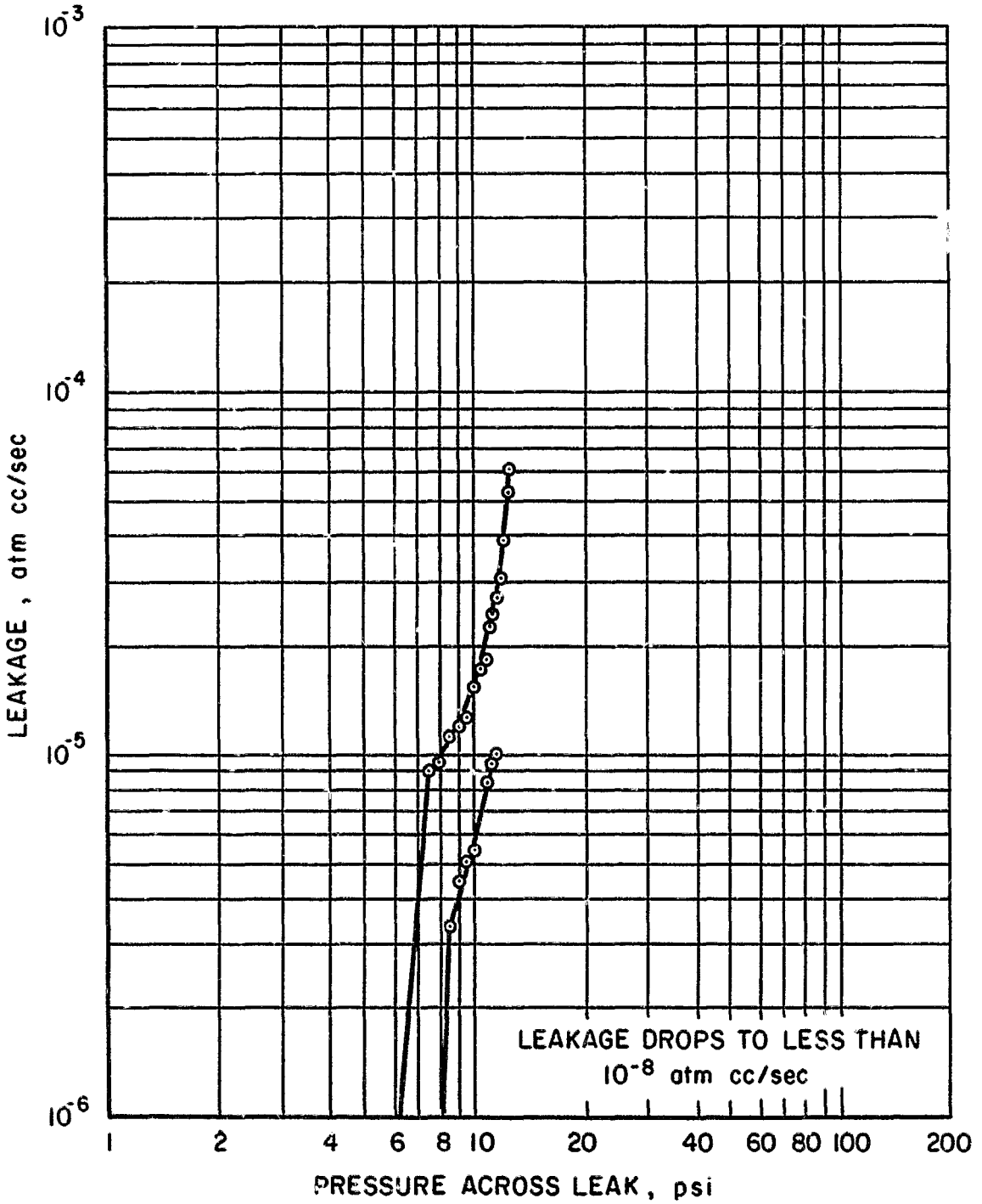

Figure 15. Check-valve Effect in a Hardware Leak. (Reprinted from J.W. Marr. Study of Static and Dynamic Seals in Liquid Rocket Engines. Final Report Phase II. Contract NAS 7-102. (Ref. 45))

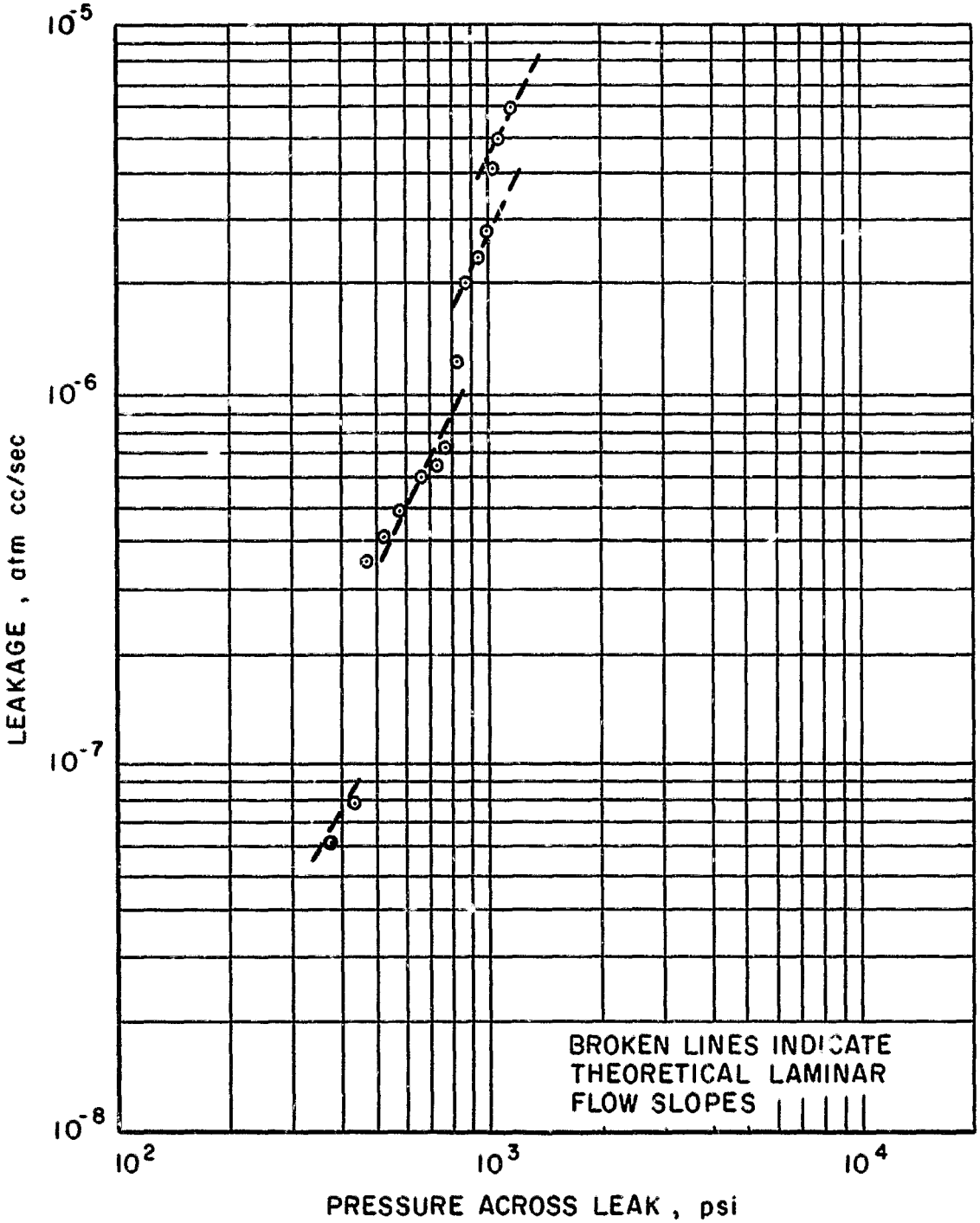

Figure 16. Geometry Change in a Gasket Leak (Reprinted from F. O. Rathbun, Jr., Design Criteria for Zero-leakage Connectors for Launch Vehicles. Report on National Aeronautics and Space Administration Contract NAS 8-4012, for George C. Marshall Space Flight Center, December 1963. (Ref. 46))

leakage quantitatively determined. It was difficult to explain why slope of the pressure-leakage line should be greater than two, since no flow regime would produce such a slope. However, these curves consist of a series of lines with a slope corresponding to that for laminar flow.

Since the increase could result from a permanent deformation of the gasket, an experiment was run using an aluminum gasket too sturdy to be deformed. Figure 17 shows the data obtained during this experiment. During the original increase in pressure, the leakage increased at a rate greater than the square of the pressure increase. However, upon releasing the pressure, the leakage decrease was proportional to the square of the pressure decrease. A second increase in pressure produced an increase which retraced the leakage encountered during the pressure decrease.

It is believed that the original pressure increased cleaned the leakage passages. Further pressure cycling does not effect the maximum leakage. This suggests that whenever possible, leak testing should be done at the proposed operating pressure, in order that potential leaks may be formed and observed.

1.4.4.4. ABSORBED OR SURFACE FLOW LEAKS

The flow of gases and non-condensing vapors through fine capillaries and micropores cannot be dealt with by means of simple methods analogous to those applicable to molecular and laminar flow (Ref. 34). The narrow passages and large surface areas involved cause surface adsorption and surface flow to become important factors. The adsorption may be physical, where only relatively weak van der Waals attractions are involved, or the adsorption may be regarded as chemical, where the surface of the solid provides binding sites for the atoms, and the electronic structure of the solid permits the formation of a chemisorption bond. The nature of the binding sites, the bonds between the gas atoms, and the surface influences the degree of surface migration of the atoms.

The flow along a fine capillary or micropore is assumed to consist of two mechanisms working simultaneously:

1. Molecular flow along the bore of the capillary, whereby molecules are supposed to collide with the wall, re-evaporate, and collide with the wall again without intermolecular collisions, and

2. Surface flow along the wall of the capillary, whereby molecules are adsorbed and diffuse along the surface of the wall.

Both these mechanisms promote gas flow from regions of higher gas concentrations to regions of lower gas concentrations.

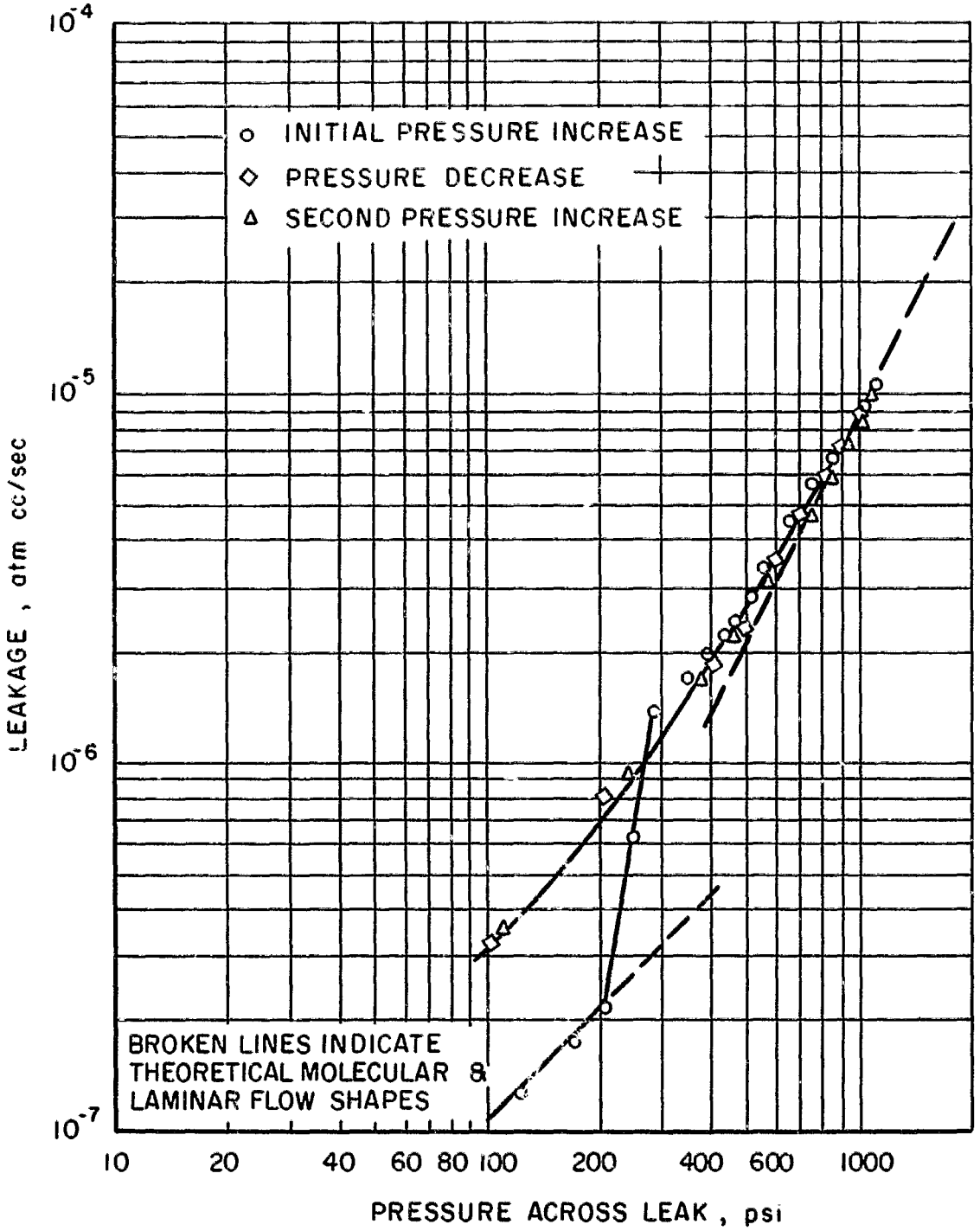

Figure 17. Self-cleaning Effect in Leaks. (Reprinted from F.O. Rathbun, Jr., Design Criteria for Zero-leakage Connectors for Launch Vehicles. Report on National Aeronautics and Space Administration Contract NAS 8-4012, for George C. Marshall Space Flight Center, December 1963. (Ref. 46))

For a given set of conditions, the proportion of molecules that follow the above mechanisms depends on a variety of factors. These factors include:

- The sticking probability (the probability that a molecule striking the surface will become adsorbed)
- The length of time the molecule remains adsorbed (the mean surface lifetime of the molecules
- The coefficient of surface diffusion of the molecules

These features are, in turn, influenced by other characteristics, such as the number of sites occupied by the adsorbed molecules or whether a complete monolayer is involved.

The nearer the properties of a gas approach those of a condensable vapor, the greater the proportion of surface flow. Therefore, a reduction of temperature or an increase of pressure may sometimes promote a total flow in excess of that predicted by the laminar-molecule theory.

Although the final leak rate achieved with a condensable gas will be higher than predicted from flow theory, Hayashi (Ref. 47) predicted that there will be an initial delay of flow due to condensation of the tracer gas on the leak surfaces. This delay is important if a tracer probe technique is used for testing. For example, if butane, a readily condensable gas, is used in a tracer probe, some small leaks will be missed because of the delay caused by the adsorption. Two remedies can be suggested to counter this problem.

1. The use of a non-condensable gas.
2. The use of a detector probe with condensable gases. With use of a detector probe, the gas is continually in contact with the leak and equilibrium is established.

1.4.5. LEAK CLOGGING

1.4.5.1. SURFACE TENSION AND WETTING

Very small holes that may give rise to appreciable leakage rates of gas under high vacuum conditions are sometimes partially or wholly blocked by solid particles having sizes in the micron range, or by liquids as a result of surface tension effects. The blockage may be of a temporary nature and so give rise to misleading test results.

Preferably the system should be kept out of contact with sources that may cause blockage until after proving and rectification have been completed. These ideal conditions cannot always be met in practice. A phenomenon frequently observed is, that if a container to be tested for leaks has at any time after manufacture been in contact with a liquid, no leaks small in size

(i.e., 10^{-7} atm cc/sec or smaller) will be found. The small leaks are clogged with liquid because of surface tension. If water has entered a capillary tube, the pressure necessary to force it out of the tube is given by the following equation (Ref. 48):

$$P = \frac{4\theta}{d} \qquad \text{Equation 1.4-33}$$

where θ = surface tension of the liquid usually expressed in dynes per centimeter
d = tube diameter in centimeters
P = pressure expressed in dynes/cm^2 *

A leak with a diameter of 1 x 10^{-4} centimeter will have a leakage rate for helium approximately 1 x 10^{-6} ℓ atm/sec. If water, with a surface tension of 72 dynes/cm, enters such a leak, the pressure required to force it out is approximately 2.8 atmospheres. Since the pressure differential during leak testing is only 1 atmosphere, this leak is essentially clogged by the use of water. In actual conditions, clogging is more likely to take place than in the above example. Most leaks are neither circular nor regular in diameter. They usually contain constrictions and occasionally consist of slits. The rate of flow in a leak is approximately proportional to the leak cross-sections.

If clogging were to take place, the pressure required to remove a liquid is inversely proportional to the smallest dimension in the cross-section. Therefore, clogging of an orifice or of a slit is more likely to take place than may be assumed from the above example. If the leak in the above example were in fact a slit with the ratio of width to height of 10 to 1, the pressure necessary to remove water from such a slit would be approximately 28 atmospheres. Leakage would be of the same order of magnitude as mentioned in the above example.

Clogging by surface tension can occur in several different ways. As a first breakdown, the clogging can be divided into two forms - with liquid in the system and with gas in the system after it has been in contact with liquid.

With liquid in the system, clogging can occur if the surface of the leak is not wet by the liquid. In that case, no liquid will flow even though a hole exists. On the other hand, if the liquid wets the leak, the equilibrium flow rate through the leak will be that predicted by flow theory. This type of clogging can not be predicted or depended on as a permanent phenomenon, since the wetting properties of the leak might be different from the bulk surface and might change with oxidation, weathering and other treatment.

After the liquid has been removed from the system, clogging can occur from liquid remaining in the leak. It is immaterial

*One atmosphere is equal to 1.063759 x 10^{-6} dynes/cm^2

whether the liquid wets the surface. Clogging as a result of the liquid surface tension occurs in either case.

Unfortunately, clogging is not of a permanent nature. If the temperature of the container is raised, the surface tension of the liquid decreases and quite possibly the liquid inside the leak evaporates.

Leakage much smaller than 10^{-8} atm cc/sec is rarely seen. Such leakages are in the range of detectability, but are a rare phenomenon. They are found on new systems which have never been in contact with liquid. These leaks have to be carefully treated or they will clog during normal handling. It may be calculated that a leak 10^{-8} atm cc/sec has a diameter in the order of 10^{-5} centimeter. To place this number in dimensions of atomic size, its diameter is about 1,000 Angstrom units.* Molecules of contaminants (for example, either hand or machine oil), are in the order of 100 Angstroms in length. Should these molecules be adsorbed in the leak, they would reduce the size of the hole and therefore reduce the leak rate to a point of apparent clogging. According to the equation for molecular flow (Equation 1.4-14), the flow which should predominate in this range is proportional to the cube of the leak diameter. Therefore, a small decrease in leak diameter will produce a drastic decrease in leakage.

1.4.5.2. PRESSURE REMOVAL AND EVAPORATION

A pressurizing test may suffer some restriction in its application to certain types of vacuum equipment, because the design may permit use of only small over-pressures. In these applications the presence of water may easily block a leakage path owing to its high surface tension. For example, when a particular capillary contains water that wets the capillary wall, this capillary will be completely blocked against a gas pressure difference of 1 1/2 atm. A thin mineral oil would be more easily moved in such a capillary, requiring only about 1/2 atm. Even though the applied pressure difference may be sufficient to move the oil, the viscosities of oils are relatively high so that, in practice, an oil may usually be regarded as permanently blocking a capillary of any appreciable length. This is due to the extremely slow rate of flow of oil. Consequently, an oil should never be used for pressure testing before leak testing.

On the other hand, water will evaporate much more readily into a vacuum than would a mineral oil because of the higher vapor pressure of water. The rate of evaporation is accelerated if the temperature is raised. For leak testing evacuated systems, a number of points should be considered.

- A preliminary water pressure test is permissible, but not recommended.

*One centimeter is equal to 10^8 Angstrom units

- Oil should never be used for over-pressure test.

- A compressed air test should never follow a water pressure test before vacuum testing for leaks. This is because the residual water that is held in small capillaries may be forced back by the compressed air into larger voids. Under vacuum conditions, the liquid would evaporate slowly through the capillary restriction.

- Even a preliminary water pressure test is inadvisable for ultra-high vacuum systems. In such a system detection of very small leaks through fine capillaries becomes essential and the time required to ensure clearance of such capillaries (by evaporation of the residual water) may become unduly prolonged.

To summarize, when a liquid is in a capillary, the liquid that has the lower surface tension is more readily moved by a gas-pressure difference, while a liquid that has a higher vapor pressure is more readily evaporated out. As a consequence, capillaries that may be blocked by water under the conditions of an over-pressure test, may often be readily cleared by evaporation of the water into a vacuum. Moreover, apparatus which must undergo a rigorous check for leaks must be dried in a vacuum because small leaks are readily clogged by the water adsorbed on the walls.

Following the general rule, it is preferable that the vessel or component to be leak-tested should be kept out of contact with sources that may cause blockage, until after leak-testing and leak-rectification have been completed.

Solid particles in the millimeter size-range are not, in general, a source of trouble. But solid particles in the micron range may enter and block a capillary temporarily. They may subsequently be displaced, giving rise to an intermittent leak that is difficult to establish and locate. Blockage by solid particles may occur, for example, if the fluid used in connection with magnetic crack-detection work is applied before testing for leaks. Magnetic fluid contains iron particles, of which the greater proportion are usually in the 2 1/2- to-10-micron size-range, and are, therefore, comparable with the cross-sectional dimensions of the capillaries considered here.

One of the disadvantages of porosity will be understood by considering the effect of a hypothetical condition of a thousand capillaries 1/4 inch long situated close together in parallel, each having a radius of 10^{-5} centimeter. The total leak rate through this assembly would be approximately 1.3×10^{-7} torr liter/sec-- that is, about the same order of leakage as a single capillary of 10^{-4} centimeter radius. However, if water has access to the porous assembly, the pressure difference required to remove it from the capillaries would be (from Equation 1.4-33)

$$\frac{2 \times 72}{1 \times 10^{-5}} = 14 \text{ atm or } 210 \text{ lb/in.}^2, \qquad \text{Equation 1.4-34}$$

that is, ten times the pressure difference needed to remove such blockage from a capillary of 10^{-4} centimeter radius.

Small holes in mild steel vessels or components may become permanently blocked by "rusting-up" caused by moisture. In practice it is usually impossible to prevent atmospheric moisture from entering capillaries. Most metals are attacked, more or less, by water in the presence of air. This action gives rise to an oxide film that has a greater specific volume than the metal. This effect applies particularly to mild steel, where the oxide film has a specific volume about seven times greater than that of the parent metal. Consequently, the smaller capillaries, which have the greater tendency to retain water, readily "rust-up." Stainless steel is less likely to be affected in this way.

When a liquid blocks a capillary its removal from the capillary may be influenced by any one, or a combination, of the following factors:

- Wetting combined with surface tension, which resists motion.
- Viscosity, which controls the tendency to flow.
- Vapor pressure, which controls the tendency to evaporate.

Thus, a thin mineral oil in a capillary can be moved with a smaller pressure difference than when water is present, owing to the lower surface tension of the oil. Under similar conditions, a very much longer time would be taken by the oil to pass out of the capillary, because of its greater viscosity compared with water. Burrows (Ref. 34) states the equation needed to calculate the evaporation rate and liquid flow in a capillary.

1.4.5.3. SAFETY

Although the prevention of clogged leaks dictates leak testing be done prior to contact of the system with liquid, the need for safety might overrule this procedure. Pressurizing a system with a liquid does not create the explosion hazard involved with gases under high pressure. Therefore, safety requirements may dictate pressure-testing of a system with a liquid before gases are introduced for leak-testing.

The amount of energy stored in a pressurized tank is a function of the quantity of gas contained in the vessel. Because of this, a high-volume, low-pressure vessel can contain the same stored energy as a low-volume, high-pressure vessel and, therefore, present a hazard of similar magnitude. Because of the similarity in explosive effect, it was decided to equate the

energy available in the tank to that in a quantity of TNT (Ref. 49).

The hazard potential or TNT equivalent of a pressurized vessel is determined by the calculation of the amount of energy available from the explosive expansion of a volume of compressed gas (Ref. 50).

$$E = 454 \left[\frac{V \left(\frac{P_1}{P_2} \right) \left(\frac{T_1}{T_2} \right)}{359} \right] RT \ln \left(\frac{P_1}{P_2} \right) \qquad \text{Equation 1.4-35}$$

where E = energy (calories),
P_1 = original (absolute) pressure of the compressed gas,
P_2 = final or atmospheric pressure,
R = molar gas constant (1.987 cal/gm-mole ^{o}K for an ideal gas),
V = pressure vessel volume (ft^3),
T_1 = ambient air temperature (^{o}K),
T_2 = temperature of the compressed gas (^{o}K).

The standard for energy release is set at 1,000,000,000 cal/ton of TNT or 1,140 cal/gm.

Once the energy equivalent has been established, minimum safe distance for non-operating personnel can be computed, using over-pressure data from reference TNT explosions (Figure 18).

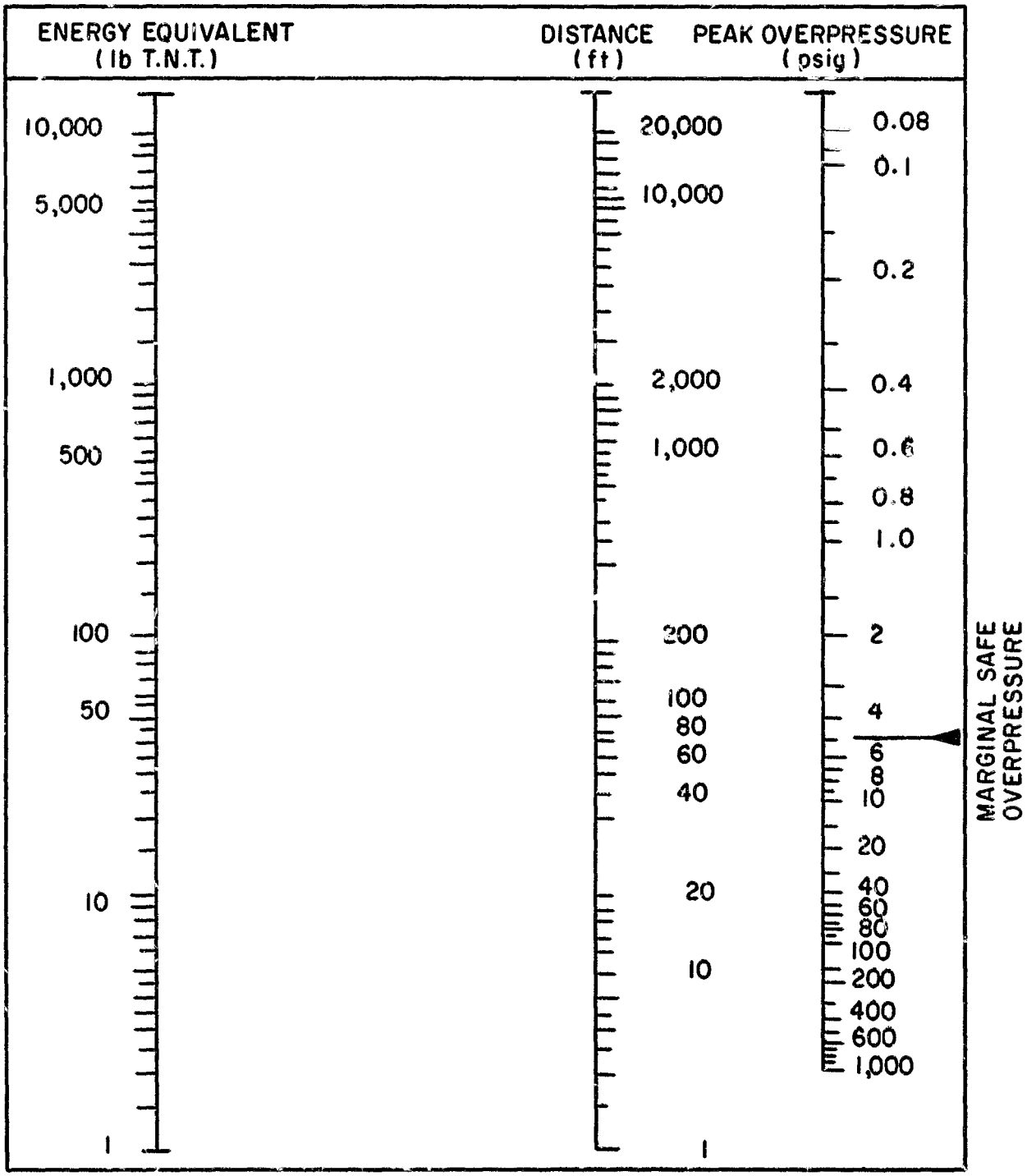

Figure 18. Nomograph for Calculating Magnitude of Blast Hazard from Equivalent Weights of TNT. (Reprinted with permission from R.E. Olson, "Safety Hazards of High Pressure Leak Checks", paper Presented at 56th. Air Force Industry Conference on Missile Leaks and Spil's. Los Angeles, Calif.)

1.4.6. GENERAL REFERENCES

1. Burrows, F., "Flow Through and Blockage of Capillary Leaks", Trans. Inst. Chem. Engrs., Vol. 39, 1961, p. 55.

2. Dushman, S., Scientific Foundations of Vacuum Techniques, Chapter II, John Wiley and Sons, Inc., New York City, 1962.

3. Kobayashi, I., and Yada, H., "Leak Test of Rubber Gaskets", Fundamental Problems in Vacuum Techniques, Vol. 1, Pergamon Press, London, 1960, p. 248.

4. Marr, J.W., Study of Dynamic and Static Seals For Liquid Rocket Engines, Final Report Phase IV on Contract NAS 7-102, September 1965, Report to Chief, Liquid Propulsion Technology, RPL, National Aeronautics and Space Administration, Washington, D.C.

5. Olson, R.E., "Safety Hazards of High Pressure Leak Checks". Paper presented at 56th Air Force/Industry Conference on Missile Leaks and Spills, Los Angeles, 1965.

6. Santeler, D.J., and Moller, T.W., "Fluid Flow Conversion in Leaks and Capillaries", Vacuum Symposium Transactions, 1956, p. 29, also General Electric Company Report R56GL261.

END OF REFERENCE

56

REFERENCE

57

MAY, W. D.: TECHNOLOGY SURVEY ADVANCED VALVE TECHNOLOGY. NASA SP-5019, 1965.

NASA SP-5019

TECHNOLOGY SURVEY

Technology Utilization Division

ADVANCED VALVE TECHNOLOGY

CLEVELAND

NATIONAL AERONAUTICS AND SPACE ADMINISTRATION

NASA SP-5019

TECHNOLOGY SURVEY

Technology Utilitization Division

ADVANCED VALVE TECHNOLOGY

By KENNETH D. MAY

Prepared under contract for NASA
by Midwest Research Institute
Kansas City, Missouri

NATIONAL AERONAUTICS AND SPACE ADMINISTRATION

Washington, D. C. *February 1965*

NOTICE

This document was prepared under the sponsorship of the National Aeronautics and Space Administration. Neither the United States Government, nor NASA, nor any person acting in behalf of NASA: (A) makes any warranty or representation, express or implied with respect to the accuracy, completeness, or usefulness of the information contained in this document, or that the use of any information, apparatus, method, or process disclosed in this document may not infringe privately owned rights; or (B) assumes any liabilities with respect to the use of, or damages resulting from the use of, any information, apparatus, method, or process disclosed in this document.

For sale by the Clearinghouse for Federal Scientific and Technical Information, Springfield, Va. 22151--Price $5.00

TABLE OF CONTENTS

Chapter		Page No.
	BACKGROUND	1
1	Introduction	3
	Purpose of Book	4
	Determine State-of-the-Art	4
	Identify New Advancements	4
	Report New Technology	4
	Sources of Information	5
	Literature	5
	Industry	5
	NASA Centers	5
	Bibliography	6
2	Identification of Newer Problem Areas	7
	Specific Problem Areas	7
	Leakage	7
	Materials	7
	Compatibility	8
	Wear	8
	Design Tolerances	8
	Reliability	8
	Response Time	8
	Repeatability	9
	Radiation	9
	Acceleration, Vibration, and Zero-Gravity	9
	Weight and Size Reduction	9
	Vacuum	9
	Summary	9
	Bibliography	10
	NEW TRENDS AND TECHNIQUES	11
3	Leakage	13
	Definition of Leakage	13
	Definition of Zero-Leakage	14
	General Approaches	14
	Seals	14
	Seats	15
	Packings	15
	Housings	16
	Special Developments	16
	Wet Seals and Cold Welding	16
	Labyrinth Type Seal	18
	Inflatable and Large Valve Seals	20
	Flange Seals	20

DEFINITION OF ZERO-LEAKAGE

In references where "zero-leakage" or "no leakage" is stated, it is not known precisely what is meant because of the lack of an accepted definition for this term. In general, the zero-leakage specification is an indication to use polymeric seats and seals. Metal-to-metal seals usually fail to fulfill this requirement, except for one-time seal applications where metal can be deformed to obtain a leakage of less than 10^{-8} atmospheric cc/sec helium.

In an extensive study by Advanced Technology Laboratories, General Electric Company, Schenectady, New York, zero-leakage has been defined to be a leakage of less than 10^{-8} atmospheric cc/sec helium. Another industrial source indicates that, while zero-leakage has no meaning, it may be considered to be in the range of 10^{-4} to 10^{-8} atmospheric cc/sec helium. At NASA's Manned Spacecraft Center in Houston, Texas, zero-leakage is defined as no more than 1.4×10^{-3} standard cc/sec GN_2 at 300 psig and at ambient temperature. Leakage requirements and specifications for valves for unmanned missions, obtained from interviews with the prime manufacturers, varied from 1.15×10^{-5} standard cc/sec to 0 for N_2O_4, and from 8.3×10^{-3} standard cc/sec to 1.4×10^{-4} standard cc/sec for other gases.

GENERAL APPROACHES

Seals

The major problems encountered with valve seals result from the extremes in temperature, pressure, and vibrational environment in which seals must function reliably. Generally the static seals, as used to seal flanges, employ either the "O"-ring or the self-loading principle. In both cases, an increase in fluid pressure causes an increase in tightness of the seal. This also applies to dynamic seals, such as those used in a piston ring, but the design of this type seal is quite different. Mechanical seals used on high speed rotating shafts are pressure balanced so that the unit load on the face is nearly constant over the fluid pressure range for which it is designed to operate. The secondary seal in such a mechanical sealing arrangement is usually a plastic material, but a welded metal bellows is often used for a more positive secondary seal. Plastic materials usually used for "O"-ring type application are the fluorocarbon plastics (Teflon and Kel-F)* because of: (1) the wide temperature range over which they can work efficiently; (2) their chemical inertness; and (3) their excellent wear properties.

* Teflon: Trademark for tetrafluoroethylene (TFE) fluorocarbon resin, E. I. du Pont de Nemours and Company, Inc.
Kel-F: Trade name for a line of fluorocarbon products, Minnesota Mining and Manufacturing Company, Chemical Division.

END OF REFERENCE
57

REFERENCE

58

SEVENTH CONFERENCE ON SPACE SIMULATION. NASA SP-336, 1973.

NASA SP-336

SEVENTH CONFERENCE ON

SPACE SIMULATION

A symposium held in

LOS ANGELES, CALIFORNIA

November 12-14, 1973

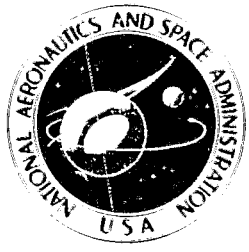

NATIONAL AERONAUTICS AND SPACE ADMINISTRATION

NASA SP-336

SPACE SIMULATION

The proceedings of a symposium held November 12–14, 1973,
at the International Hotel, Los Angeles, California

Sponsored by

The American Institute of Aeronautics and Astronautics
The American Society for Testing and Materials
Institute of Environmental Sciences
and the National Aeronautics and Space Administration

Prepared at Goddard Space Flight Center

Scientific and Technical Information Office 1973
NATIONAL AERONAUTICS AND SPACE ADMINISTRATION
Washington, D.C.

Paper No. 26

LEAK TESTING OF HIGH PRESSURE OXYGEN AND NITROGEN TANK SYSTEMS FOR THE SKYLAB AIRLOCK*

R. A. Dutton, G. L. Adlon and R. K. Weinberger,
McDonnell Aircraft Company, St. Louis, Missouri
R. G. Morris, Jr., *McDonnell Douglas Astronautics Company, Eastern Division, St. Louis, Missouri*

ABSTRACT

An existing Propulsion Test Facility was modified for use as a leak test facility for acceptance testing of the 3000 psig oxygen and nitrogen gas storage tank systems used on the Skylab Airlock U-1 and U-2 Vehicles. Leak rates in the range of 10^{-2} to 10^{-5} standard cc/sec of helium were measured remotely from an explosion containment test cell. Selection of the test site was based on consideration of techniques, equipment, potential test hazards, leak measurement methods, and the availability of existing applicable equipment from prior test programs. Facility design, operating experience, and test results are discussed.

INTRODUCTION

The life support atmosphere of the Skylab Orbital Workshop is supplied by six oxygen and six nitrogen tank assemblies mounted on the Airlock. Each tank is pressurized to 3000 psig with gas prior to launch. The maximum allowable equivalent helium leak rate at 3000 psig for each tank assembly, including its valve package, is 10^{-2} standard cc/sec.

Although the tanks themselves were leak checked by their suppliers prior to delivery to MDC, additional hydrostatic and leak testing was required after installation of the valve packages and associated pressure transducers at MDC. The tanks were received at MDAC-E and the valve package attached by brazing. The brazed joint connection was designed to permit replacement of a defective valve package without danger of damaging the tank or valve package. The leak test program was designed to assure that the entire tank assembly, including its valve package, was ready for installation on the Airlock vehicle without the necessity for subsequent leak checking.

*This paper is related to work performed under NASA Contract NAS 9-6555.

Although numerous smaller high pressure tanks had been pressure and leak tested in previous programs, none of them presented as much damage potential in the event of tank or valve package failure. Therefore, special precautions were taken to reduce the risk of harm to personnel and facilities.

TEST SPECIMEN DESCRIPTION AND SAFETY CONSIDERATIONS

The oxygen tanks are constructed with a 321 stainless steel liner reinforced by a filament wound fiberglass-epoxy shell bonded to the liner. The nominal external dimensions are 45 in. diameter and 90 in. long. Minimum internal volume is 57 ft^3. The tank assembly weight does not exceed 2500 pounds. Nitrogen tanks are fabricated from titanium hemispheres welded together at their circumference. The nominal external diameter of each spherical nitrogen tank is 41 in., and the minimum internal volume is 19.28 ft^3; tank assembly weight did not exceed 393 pounds. The tanks and their control valve packages were hydrostatically tested, prior to leak measurement, with Freon PCA (Precision Cleaning Agent) to 1.50 times the 3000 psig working pressure (or approximately 4500 psig). The nitrogen tank design pressure considerations were 3000 psig working, 5000 psig proof, and 6660 psig burst at 70°F. The oxygen tank assembly design pressure considerations were 4500 psig working, 7530 psig proof and 10,000 psig burst.

Freon PCA was used for three reasons: (1) to avoid potential tank weakening which can occur if, for example, methyl alcohol is used to hydrostatically test titanium tanks at high pressure, (2) to avoid potential corrosion problems of valve packages when water is used, and (3) to permit thorough removal of the hydrostatic test fluid after testing. The nitrogen tanks have an operating temperature range of -20 to 160°F. The oxygen tanks have a similar temperature restriction but with an additional requirement to avoid temperature changes in the liner of 1°F per minute or more, which might cause debonding of the tank liner from its reinforcing filament wound fiberglass-epoxy reinforcement.

An initial examination of the potential hazards of leak testing large high pressure tanks revealed that it would be unwise to conduct the work in a conventional building. The types of tanks to be tested had exhibited excellent safety records in previous programs and the likelihood of tank rupture was considered very slight. However, tank rupture due to flaws, human error, or any other cause could produce catastrophic results in a conventional laboratory. For example, calculations indicated that the 19.28 ft^3 nitrogen tank at 3000 psig contained potential energy equivalent to 14.0 pounds of TNT. The 57 ft^3 oxygen tank at 3000 psig contained the energy of approximately 41.0 pounds of TNT, although, due to the type of tank construction, the energy might be released at a slightly less explosive rate.

The need to perform the leak tests in a remote safe facility became evident. A high pressure fuel test facility with a 7 ft diameter vacuum chamber became available from another program. The chamber was located in a test cell designed for explosion containment. Cell operations could be monitored and controlled from an adjacent control room. A study showed that the facility could be modified economically within the available schedule time.

The test cell chosen had been designed to withstand an internal pressure 225 psi above normal atmospheric pressure without rupturing the walls and without forcing the doors open. Calculations indicated the possibility that in the event of a tank failure, shrapnel could acquire enough energy to damage but not penetrate the foot-thick cell walls which were constructed of concrete with two independent grids of 1-1/4 in. diameter steel rods on 9 in. centers. The cell doors, made of steel I-beams with welded steel facing plates and filled with concrete, were secured with massive locking plates at their top and bottom. Part of the control cell was separated from the test cell by two reinforced concrete walls, one on each side of an access hallway. The most conservative calculations indicated the possibility that impact of large pieces of shrapnel with the inside surface of the test cell wall might cause spalling of concrete from the opposite side of the wall. Therefore, a barrier of sand bags was erected parallel to the single wall separating a portion of the test cell from the control cell.

SURVEY OF LEAK TEST METHODS

Various ways were considered to measure leak rates of the tank systems. The chamber rate of pressure rise method with the chamber vacuum pump operating was found to be too insensitive and unsteady to measure 10^{-3} standard cc/sec of gas leakage over any reasonable time span. Chamber leakage, chamber outgassing, test article outgassing, chamber temperature changes, and tank system temperature changes (principally heating during the filling process) would have obscured the measurement of the small allowable leakage.

Comparison of tank leakage into a chamber with leakage from a reference manometer was found to be theoretically sensitive enough, but would have been subject to some of the same uncertainties as for the chamber rate of rise method. In both cases, the source of the gas could not be determined to be actual tank system leakage instead of a combination of leakage and outgassing.

A variation of the chamber rate of pressure rise was considered in which the chamber would be evacuated and then sealed off from its pump. Its rate of rise due to leakage, outgassing, etc., would be measured and plotted as a function of time. Then the tank system would be pressurized and the new chamber rate of pressure rise would be plotted. The difference in the slopes of the curves would be interpreted as tank system leakage. This

method would not distinguish accurately between actual tank leakage and outgassing due to tank heating.

Various techniques of bagging the tank system to collect helium leaking from the tank system were considered, but were found to be too insensitive and uncertain for good quantitative results. Helium permeation through the bag and helium nonuniformities within the bag would have been difficult to determine.

A technique was considered in which the tank system would be enclosed within an inner chamber containing its own ion gauge. The inner chamber would be within a conventional space chamber with its ion gauge. The inner chamber would have a gas inleak system and a solenoid valve between the inner and outer chambers. During initial evacuation the solenoid valve would be open to equalize pressures in both chambers; then the solenoid valve would be closed. During a leak test, the rate of rise of the inner chamber relative to the outer chamber would be a measure of the tank system leakage. A measured flow of gas from the inleak system would be used for reference purposes to calibrate the leak rate.

A somewhat similar system using two ion gauges in series, with a passage of known conductance between them, could be used to measure the gas flow from a test article in the inner chamber to the outer chamber. This principle is used in calibrating ultrahigh vacuum gauges by extrapolation of the response of two standard gauges operating within their normal ranges.

All of the methods mentioned above in this section have various drawbacks, particularly the inability to distinguish between true tank system leakage and gas flow from other sources such as outgassing of tank and chamber materials.

The method selected for the leak test program was that of placing the tank system in a vacuum chamber, pressurizing the tank with a mixture of 10% helium and 90% nitrogen, and then measuring the helium leaking into the chamber.

A further description of various leak detection methods used in the Space Systems Laboratory at MSC has been presented elsewhere.[1]

FACILITY DESIGN REQUIREMENTS AND ASSEMBLY

A portion of the propulsion test facility which was available for modification for leak testing is shown in plan view in Figure 1. The 7 ft diameter vacuum chamber in Cell 6, normally evacuated only by the mechanical pumps and blowers in the adjacent vacuum system room, was modified to provide high vacuum and leak measurement capability.

The tank system specifications required that each tank, including valve package and pressure and temperature transducers, have an equivalent helium leak rate no greater than 10^{-2} standard cc/sec. With the concurrence of the Airlock Project, a mixture of helium and nitrogen was chosen for leak testing; this was considered acceptable provided that the total gas pressure was 3000 psig and that proper allowance was made for the ratio of helium to nitrogen. Since actual leakage through passages of fixed

END OF REFERENCE

58

REFERENCE

59

BURROWS, G.: FLOW THROUGH AND BLOCKAGE OF CAPILLARY LEAKS. TRANS. INST. CHEM. ENGRS., VOL. 39, 1961.

1.5-0-0

FLOW THROUGH AND BLOCKAGE OF CAPILLARY LEAKS

By G. BURROWS, A.M.I.Mech.E. (ASSOCIATE MEMBER)*

SUMMARY

To help in understanding the behaviour of small leaks in vacuum equipment, the various types of gas flow that can occur through small-bore capillaries are considered, and some formulae are derived that represent flow rates under different conditions. The factors that control the flow of liquids through capillaries are reviewed, together with the behaviour to be expected when a volatile liquid evaporates from a capillary into a vacuum. The limitations imposed by porosities are examined, taking into account the special features of adsorbed flow. Some causes of capillary blockage are investigated, including surface tension and surface adhesion effects, and the conditions under which the influence of viscosity exerts a significant restriction. The removal of such blockage by a pressure difference and by evaporation is discussed.

Introduction

Vessels and components that are intended for use under high vacuum must be tested for leakage before being put into service. The very small holes that can cause appreciable leakage may be temporarily blocked during the test, and so give rise to misleading results. Attention will first be drawn to some simple relationships that govern leakage rates through small holes or capillaries. The causes of blockage will then be discussed and, in certain instances, methods of removing blockage will be considered. Although some aspects of these subjects have been previously reviewed by Jean[1] and by de Bersuder,[2] the present paper shows how the viscosities of liquids and vapours influence their flow, either separately or together, through small leakage paths, and how the total flow of gases may be regarded as the sum of their laminar and molecular flows.

Gas Leakage Rate for a Given Size of Hole

The rate of flow of a gas or vapour may be expressed in the form (p . V) per second for a given gas at a given temperature, where p is in pressure units and V is in volumetric units. The values of leak rates applicable to vacuum equipment can be stated in torr-litre per second. That is, the volumetric flow is stated in litres per second, the corresponding pressure being expressed in torr, noting that 1 torr = 1 mm of mercury, and that 760 mm of mercury is equivalent to 1 atmosphere.

It is necessary carefully to distinguish between the term micron as applied to units of size, and micron as applied to units of pressure. Confusion sometimes arises when a dimension, such as the radius of a small hole, is expressed in microns in association with a pressure which is also given in similar units. The present discussion will, therefore, use centimetres (cm) to represent linear dimensions, while pressures will be measured from zero and stated in torr.† Thus the product (p . V) may be expressed either as torr litre or as 10^{-3} torr cm³. It may be noted that the rate of flow, when represented in the form torr cm³/s, is identical in numerical value with litre-micron/s (usually abbreviated to lusecs by the vacuum technician), where 1 μ = 1 micron = 10^{-3} torr.

It is assumed that all gross leaks have been eliminated, and that any remaining leaks are individually not much greater than would be represented by an air flow rate, at 20° C, of 10^{-2} torr-l./s. The smallest leaks that can be detected depend on the sensitivity of the method used, and may be as low as 10^{-10} torr-l./s. Leakage may occur through a single hole, regarded as a capillary, or by way of a porous condition, which, in effect, consists of a number of fine capillaries in parallel.

Types of flow

At low pressures, and with capillaries of small bore, molecular flow occurs, the simplifying assumption being made that molecules never collide with other molecules but only with the capillary wall. At higher pressures, and with capillaries of larger bore, the molecules collide more frequently with each other than with the capillary wall. This causes laminar flow, characterized by the assumption of zero flow of gas at the capillary wall with maximum flow along the axis, the intermediate layers being imagined as sliding over each other. Under these conditions, the moving gas possesses another attribute, viscosity, which is absent in molecular flow. Where very fine capillaries and micropores are concerned, the narrow passages and large surface areas cause surface adsorption and surface flow to become important. As the surface flow of gas is sensitive to the kind of surface and its condition, flow rates for different gases through porosities cannot readily be derived by calculation. The following treatment is therefore confined quantitatively to single capillaries in the range in which surface flow forms a negligible proportion of the total. This implies that, under the conditions postulated, the capillary radius cannot be much less than 10^{-6} cm. On this basis, the flow of gases through capillaries between the extremes of fully molecular flow and fully laminar flow may be regarded[3] as the sum of the molecular and laminar flows. As a point of interest, it may be deduced that, with reference to the supposed slip at the capillary wall which is usually associated with laminar flow, the value of the slip at all pressures is equivalent, in the present discussion, to the molecular flow at zero pressure.

* Research Department, Associated Electrical Industries (Manchester) Ltd., Manchester, 17.

† *cf.* British Standard 2951 : 1958.

The method of integrating short segments of tube adopted by Loevinger and Guthrie[4] appears to be inadmissible, because the constants in their segment equation, derived and introduced by Knudsen,[5] apply only to tubes that are long in proportion to their diameter. It is evident from Knudsen's original paper that his equation, which is the result of integrating the tube length from 0 to ∞, was not intended for further integration.

If Knudsen's equation for mixed flow through a long tube is used to calculate the specific flow $Q/\Delta p$, and if the values so derived are plotted against the corresponding mean pressure $\bar{p}$, it will be found that, starting from near-zero pressure, the resultant curve passes through a minimum value and then increases with rise of pressure towards the straight line that represents the fully laminar form of flow. The dip in the curve is believed to be due to the increasing obstruction suffered by those molecules that take long diffusion paths along the tube in a mainly axial direction. This minimum is not so clearly defined in the case of an irregular capillary or porous medium, because in such circumstances free paths much longer than the mean radius are not likely to occur.

The variation in the specific flow represented by the dip in the curve is often small enough to be ignored, with the result that the inclined straight line that represents laminar flow can be extrapolated back to intercept the ordinate at zero mean pressure. The total specific flow within the defined range, corresponding to any mean pressure, may then be found from the appropriate point on the inclined straight line that starts from this intercept. For present purposes, the intercept represents the molecular flow component, independent of the mean pressure. The slip flow, associated with laminar flow through a single capillary, is in fact slightly less than the theoretical molecular flow, but the difference is not sufficient to affect this discussion.

Based on the simplifying assumptions made here, the total flow rate Q, consisting of the sum of the molecular and laminar flows, for a gas of molecular weight M through a capillary of radius r and length L where L is at least $50\,r$, is given very nearly by the expression:[3]

$$Q = 30{\cdot}4\,\Delta p_t \frac{r^3}{L}\left[1{\cdot}71 \times 10^{-3}\frac{r \cdot \bar{p}_t}{\eta} + \sqrt{\frac{T}{M}}\right] \text{ torr-l./s} \quad . \quad (1)$$

where Δp_t = pressure difference $(p_1 - p_2)$ across ends of capillary (torr).

$\bar{p}_t$ = mean pressure, $\frac{p_1 + p_2}{2}$ (torr).

$T = (273 + t^0)$, where t^0 = temperature (°C).

η = viscosity of gas (poise), at absolute temperature T.

If one end of the capillary is at atmospheric pressure of gas and the other end opens into a high vacuum (zero pressure) then Δp_t is 760 torr and $\bar{p}_t$ is 380 torr, so that equation (1) reduces to:

$$Q = 2{\cdot}31 \times 10^4 \frac{r^3}{L}\left[\left(6{\cdot}5 \times \frac{r}{\eta}\right) + \sqrt{\frac{T}{M}}\right] \text{ torr-l./s} \quad . \quad (2)$$

The term $6{\cdot}5 \times r/\eta$ within the square brackets represents the proportion of laminar flow, and the term $\sqrt{(T/M)}$ the proportion of molecular flow.

Thus for air at 20° C equation (2) becomes:

$$Q = 2{\cdot}31 \times 10^4 \frac{r^3}{L}[3{\cdot}55 \times 10^4\, r + 3{\cdot}18] \text{ torr-l./s} \quad . \quad (3)$$

from which we deduce that, under the stated pressure difference, for a capillary radius of 8×10^{-4} cm the gas flow will be about 90% laminar, while for a radius of 10^{-5} cm the gas flow will be about 90% molecular.

Also, from equation (3), the flow rate for the larger bore capillary that gives 90% laminar flow is $3{\cdot}7 \times 10^{-1}/L$ torr-l./s; that is, $3{\cdot}7 \times 10^{-1}$ torr-l./s for a capillary 1 cm long or $3{\cdot}7 \times 10^{-2}$ torr-l./s for a capillary 1 mm long, these leak rates being quite appreciable. For the smaller bore capillary that gives 90% molecular flow, the flow rate is found to be $8{\cdot}2 \times 10^{-11}/L$ torr-l./s which corresponds to $8{\cdot}2 \times 10^{-11}$ torr-l./s for a capillary 1 cm long or $8{\cdot}2 \times 10^{-10}$ torr-l./s for a capillary 1 mm long, these leak rates being very small. It follows therefore that, for a single capillary, small leak rates may usually be regarded as a mixture of laminar and molecular flow, where leakage occurs from the external atmosphere into a vacuum.

The general behaviour of air flow through a capillary will be understood by reference to Fig. 1, where the product $Q \cdot L$ is plotted against the capillary radius, r, the leakage of atmospheric air at 20° C being shown by the full black line. The dotted lines refer to liquid air and will be explained later.

Suppose that test results show an air leak rate of 10^{-5} torr-l./s at 20° C from atmosphere into a vacuum. If it is assumed that the leak is caused by a single hole then, from Fig. 1, it will be seen that the flow may be due to a capillary having a length of 1 cm and a radius of $3{\cdot}2 \times 10^{-4}$ cm, or alternatively by a capillary having a length of (say) 0·1 cm and a radius of $1{\cdot}7 \times 10^{-4}$ cm. The actual length and radius of the capillary are, of course, unknown.

The values deduced from Fig. 1 may be used in the following way to estimate the flow rate of another gas through the same leak at a selected temperature. If, for example, it is required to estimate the flow rate of hydrogen at 0° C through a hole that leaks air at a rate of 10^{-5} torr-l./s at 20° C, then, with reference to equation (2):

$\eta = 0{\cdot}86 \times 10^{-4}$ poise, $T = 273°$ K, and $M = 2$.

Using one pair of capillary dimensions deduced for the air leak rate, namely, $L = 1$ cm and $r = 3{\cdot}2 \times 10^{-4}$ cm, then for hydrogen:

$$Q = 2{\cdot}31 \times 10^4 \frac{(3{\cdot}2 \times 10^{-4})^3}{1}\left[6{\cdot}5 \times \frac{3{\cdot}2 \times 10^{-4}}{0{\cdot}86 \times 10^{-4}} + \sqrt{\frac{273}{2}}\right]$$
$$= 2{\cdot}7 \times 10^{-5} \text{ torr-l./s.}$$

Using the alternative capillary dimensions $L = 0{\cdot}1$ cm and $r = 1{\cdot}7 \times 10^{-4}$ cm, then,

$$Q = 2{\cdot}31 \times 10^4 \frac{(1{\cdot}7 \times 10^{-4})^3}{0{\cdot}1}\left[6{\cdot}5 \times \frac{1{\cdot}7 \times 10^{-4}}{0{\cdot}86 \times 10^{-4}} + \sqrt{\frac{273}{2}}\right]$$
$$= 2{\cdot}8 \times 10^{-5} \text{ torr-l./s.}$$

These two results indicate that, in this example, the expected leak rate for hydrogen would be about 2½ times that for air.

It will have been noted that, for different gases, leak rates in the laminar flow region are dependent on viscosities, while leak rates under molecular flow conditions are dependent on molecular weights. These features cause variations in the relative leak rates for different gases, as indicated in Table I.

TABLE I.—*Relative Leak Rates for Different Gases Compared with that for Air at 20° C*

(From atmospheric pressure into a vacuum)

Radius of capillary	10^{-5} cm	10^{-4} cm	10^{-3} cm
Kind of flow (for air) at mean pressure	Approaching laminar flow	Approx. 50% laminar-molec. flow	Approaching molecular flow
* Flow rate for air: product QL, according to equation (2)	$0{\cdot}89\times10^{-9}$	$1{\cdot}6\times10^{-7}$	$8{\cdot}2\times10^{-11}$
Relative leak rates			
Air	1·0	1·0	1·0
Argon	0·83	0·84	0·85
Carbon dioxide	1·20	1·04	0·85
Helium	1·09	1·77	2·51
Hydrogen	2·22	2·90	3·62

* Q = air flow (torr L/s).
L = length of capillary (cm).

Equation (2) was used to calculate the flow rates for each gas through a capillary of the appropriate radius and under the conditions specified, the viscosities at 20° C being taken from published values. The rates thus derived are listed in Table I as ratios compared with air flow rates.*

As will be discussed later, in very small capillaries and for substances in the gaseous phase that have critical temperatures above the prevailing temperature, there is a greatly increased risk that adsorption with partial condensation may occur, these conditions giving rise to surface effects that may cause the net total flow to be greater or less than that predicted by formulae based solely on laminar-molecular flow.

Liquid Leakage Rate for a Given Size of Hole

Flow of involatile liquids

The behaviour of a liquid when leaking into a vacuum through a capillary from a bulk source at a given pressure depends on the properties of the liquid at the prevailing temperature and, in certain cases, on whether wetting occurs; that is on whether the attractive forces exerted by the capillary wall on the liquid molecules are greater than the forces between the liquid molecules themselves.

For present purposes the vacuum will be regarded as equivalent to zero pressure. The simplest case of liquid flow occurs when there is a steady flow of degassed liquid through the capillary and the vapour pressure of the liquid is so low that there is negligible evaporation of the liquid into the vacuum. Since liquids may be regarded as incompressible compared with gases, it is convenient to express the liquid flow in volumetric units. The volume flowing per second is then given by the basic equation for the laminar flow of liquids, namely:

$$\frac{V}{t} = \pi r^2 \cdot v = \frac{\Delta p \cdot \pi \cdot r^4}{8 \cdot L \cdot \eta_L} \text{ cm}^3/\text{s} \quad . \quad . \quad . \quad (4)$$

where v = mean velocity (cm/s).
Δp = pressure difference [dyn/cm² (1 atms = 10^6 dyn/cm²)].
η_L = viscosity of liquid at prevailing temperature (poise).
r and L = radius and length of capillary (cm).

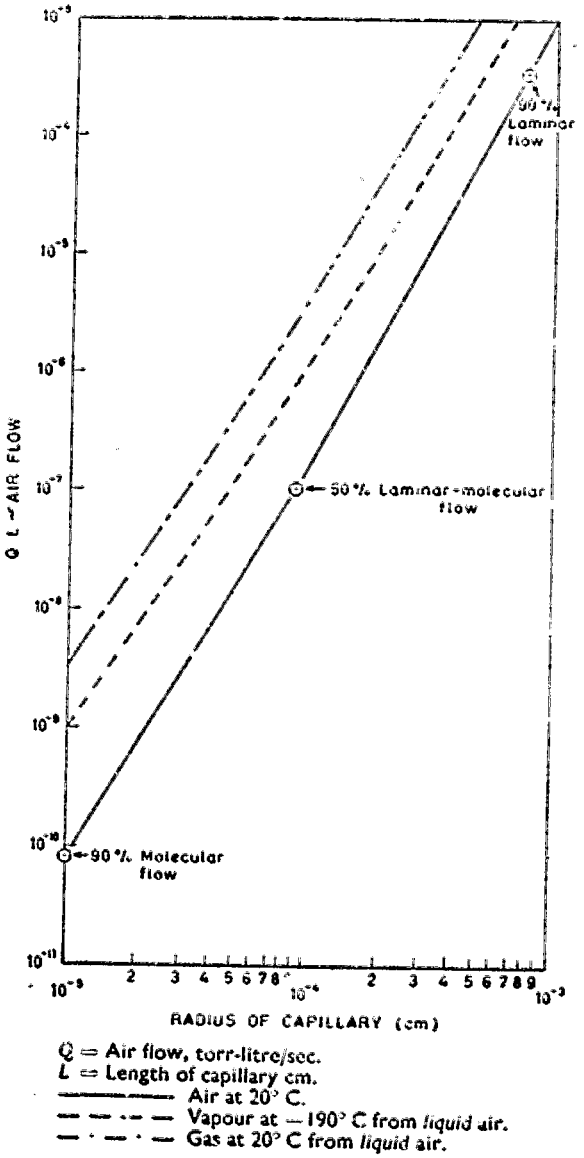

Fig. 1.—Air flow through a capillary from atmospheric pressure into a vacuum

Capillary pressure

When the liquid does not occupy the full length of the capillary, then the capillary pressure exerted by the surface tension of the liquid must be taken into consideration in conjunction with the degree of wetting of the capillary wall

* Since this paper was written, particulars have been reported by Ash and Grove (*Trans. Faraday Soc.*, 56, 1960, 1357) of low-pressure gas flow through a porous ceramic having an average pore radius of the order of 10^{-4} cm. Their experiments were carried out at various pressures that enabled flow rates under laminar and molecular conditions to be determined independently. The Poiseuille (laminar) permeabilities K_P, and also the Knudsen (molecular) permeabilities K_K are tabulated by Ash and Grove for various gases. The ratios of the laminar permeabilities K_P of the different gases agree reasonably closely with the corresponding ratios in Table I under the column heading "Approaching laminar flow". Similar agreement is also shown between the ratios of molecular permeabilities K_K of Ash and Grove with the ratios in Table I under the column heading "Approaching molecular flow".

by the liquid. These conditions are illustrated diagrammatically in Fig. 2. The value of the contact angle ϕ is a measure of the degree of wetting of the solid by the liquid, and indicates the relative strengths of the attractive forces exerted by the capillary wall on the liquid molecules, compared with the attractive forces between the liquid molecules themselves.

Referring to Fig. 2 and ignoring the effect of gravity—the action is similar if the diagram is turned sideways—the pull of surface tension acting round the edge of the meniscus is balanced by the gas pressure in the capillary. When equilibrium has become established, then

$$\pi r^2 p_v = 2\pi r \cdot \sigma \cdot \cos\phi \qquad (5)$$

where r = radius of capillary (cm).
σ = surface tension (dyn/cm).
p_v = gas pressure (dyn/cm²).
ϕ = contact angle.

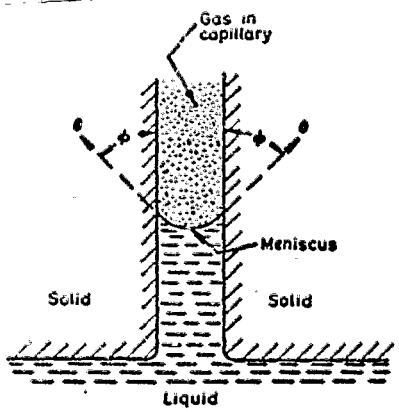

Fig. 2.—*Effect of surface tension on a liquid in a capillary*

The gas pressure, p_v, is the "holding pressure". This pressure will hold the liquid stationary at any point, assuming a straight uniform capillary. If the actual gas pressure is less then p_v the liquid will travel along the capillary, the rate of travel increasing with reduction of pressure. A pressure greater than p_v will force the liquid in the capillary back towards the bulk liquid.

When the effect of surface tension is a maximum, that is, when $\cos\phi = 1$, then from equation (5),

$$p_v = \frac{2\sigma}{r} \qquad (6)$$

If the liquid is in the form of a thread of length, l, having both ends contained within a capillary of greater length, and if the liquid completely wets the capillary wall, then the end effects of surface tension become equal and opposite in direction. In these circumstances the movement of the thread of liquid under the influence of a pressure difference Δp is given approximately by equation (4) in which L is replaced by the length l of the thread, the only force opposing motion being that due to the viscosity of the liquid. In practice, the movement of the thread may give rise to different values of the "advancing" and "receding" contact angles, but this effect is of little importance to the present discussion. When the liquid thread reaches the end of the capillary, the surface tension effect at the capillary outlet disappears, but that at the opposite end of the thread remains.

It may be inferred from equation (4) that the time, t, taken by a thread of liquid of length l, situated at the end of a capillary, to be pushed out of the capillary is given by

$$t = \frac{4 \cdot \eta \cdot l^2}{\Delta p \cdot r^2} \text{ s} \qquad (7)$$

where Δp in dyn/cm² is the constant pressure difference across the ends of the thread required to overcome viscosity. The extra pressure p_v required to overcome surface tension is independent of Δp.

Flow of volatile liquids

When the liquid has an appreciable vapour pressure P_v at the prevailing temperature, the liquid evaporates into the vacuum towards the exit end of the capillary. As examples of such liquids we may cite water at room temperature, or liquid air at its boiling point.

The action that occurs may be visualized in the following way. The volatile liquid penetrates into the capillary, the combined effects of liquid head h and atmospheric pressure P_A pushing it in, and also, if the liquid wets the capillary wall, the surface tension σ draws the liquid into the capillary. The liquid evaporates at vapour pressure P_v while travelling down the capillary, the resultant vapour passing along the remaining length of the capillary into the vacuum. Under steady conditions, the interface between the liquid and its vapour takes up a fixed position somewhere along the length of the capillary. We may therefore divide the length L of the capillary into two parts, one part of length x containing the vapour, and the other of length $(L - x)$ containing the liquid.

For simplicity, the following assumptions are made:

(i) that the liquid wets the capillary and that therefore the contact angle $\phi = 0$ and $\cos\phi = 1$,

(ii) that the temperature along the length of the capillary is the same as that of the liquid that enters it,

(iii) that the effect of the curvature of the liquid meniscus in the capillary on the vapour pressure of the liquid compared with a plane surface is negligible, which implies that the capillary radius cannot be much less than 10^{-6} cm.,

(iv) that the vapour exerts a back pressure on the liquid surface in the capillary equal to the saturation vapour pressure at the prevailing temperature,

(v) that the mass flow of fluid (g/s) is the same at all cross-sections along the length of the capillary.

Considering first the mass flow of vapour G_v along the part x of the capillary length, we make use of equation (1), but as the length x may not be large compared with the radius r, we substitute L in equation (1) by

$$\left(x + \frac{8}{3}r\right)$$

where $\frac{8}{3}r$ helps to compensate for the end effect. If, in equation (1), the total flow rate is now converted from torr litres per second to grams per second there results:

$$G_v = \frac{0{\cdot}486\,P_v r^3}{\left(x + \frac{8}{3}r\right)} \cdot \frac{M}{T}\left[\frac{8{\cdot}55 \times 10^{-3} r P_v}{\eta_v} + \sqrt{\frac{T}{M}}\right] \text{ g/s} \qquad (8)$$

where the vapour pressure P_v is in torrs, the vapour viscosity η_v is in poises, and the temperature is T °K.

The vapour flow rate for a given substance at a given temperature according to equation (8) may be written in abbreviated form as:

$$G_v = \frac{f(r)_v}{\left(x + \frac{8}{3}r\right)} \text{ g/s} \quad . \quad . \quad . \quad (9)$$

For the liquid, the mass flow G_L along the part $(L - x)$ of the capillary may be derived with the help of equation (4). In the present instance the pressure difference Δp consists of:

$$\Delta p = \left[1{\cdot}33 \times 10^3 (P_A + h - P_v) + \frac{2\sigma}{r}\right] \text{ dyn/cm}^2 . \quad (10)$$

where the atmospheric pressure P_A, the liquid head h, and the vapour pressure P_v are all in torrs, the surface tension σ being in dynes per centimeter. Thus equation (4) now becomes:

$$G_L = \frac{\left[1{\cdot}33 \times 10^3 (760 + h - P_v) + \frac{2\sigma}{r}\right] \pi r^4 \rho_L}{8(L - x)\eta_L} \text{ g/s} \quad . \quad (11)$$

where ρ_L is the density of the liquid (g/cm³).

The liquid flow rate for a given substance at a given temperature according to equation (11) may be written in abbreviated form as:

$$G_L = \frac{f(r)_L}{(L - x)} \text{ g/s} \quad . \quad . \quad . \quad (12)$$

From equation (9) we find:

$$x = \frac{f(r)_v}{G_v} - \frac{8}{3}r \quad . \quad . \quad . \quad (13)$$

and from equation (12) we find:

$$x = L - \frac{f(r)_L}{G_L} \quad . \quad . \quad . \quad (14)$$

Under steady conditions, the vapour mass flow rate G_v is equal to the liquid mass flow rate G_L and therefore, from equations (13) and (14):

$$G_v L = f(r)_v + f(r)_L \text{ g/s} \quad . \quad . \quad (15)$$

where $\frac{8}{3}r$ is neglected in comparison with the total length L,

and where

$$f(r)_v = 0{\cdot}486 P_v \cdot r^3 \frac{M}{T}\left[\frac{8{\cdot}55 \times 10^{-3} r \cdot P_v}{\eta_v} + \sqrt{\frac{T}{M}}\right] \quad (16)$$

and

$$f(r)_L = \frac{\left[1{\cdot}33 \times 10^3 (760 + h - P_v) + \frac{2\sigma}{r}\right] \pi r^4 \rho_L}{8\eta_L} \quad . \quad (17)$$

As an example of the use of equation (15), (16), and (17), we consider the flow to be expected through a capillary when one end is open to liquid air at about $-190°$ C, and the other end opens into a vacuum (zero pressure). Because liquid nitrogen and liquid oxygen have different volatilities, some fractionation of the mixture will occur. For the purpose of this example, the following representative values are adopted for liquid air:

$P_v = 760$ torr
$\eta_L = 1{\cdot}72 \times 10^{-3}$ poise
$\sigma = 12$ dyn/cm
$h = 15$ cm of liquid (assumed), say 10 torr
$M = 28{\cdot}9$
$T = 83°$ K
$\eta_v = 0{\cdot}60 \times 10^{-4}$ poise
$\rho_L = 0{\cdot}9$ g/cm³

When the foregoing values are substituted and the mass flow G_v is converted into torr litre per second at $-190°$ C and torr litre per second at 20° C respectively, the corresponding curves for the product $Q \cdot L$ may be plotted for different values of the capillary radius r as indicated on the graph Fig. 1, where the broken line relates to the air flow at $-190°$ C, and the dash-dot line to the air flow at 20° C.

It will be noted that, for a capillary of radius $r = 10^{-6}$ cm which, for atmospheric air, would give rise to small leaks in the molecular flow region, the leakage in torr litre per second at 20° C from liquid air would be about 40 times* the leakage of atmospheric air, while for capillaries approaching 10^{-4} cm radius that give relatively large leaks in the laminar flow region, the leakage at 20° C from liquid air would be about 15 times the leakage of atmospheric air.

Adsorbed or Surface Flow

The flow of gases and non-condensing vapours through fine capillaries and micropores cannot be dealt with by means of simple methods analogous to those applicable to molecular and laminar flow. The narrow passages and large surface areas involved cause surface adsorption and surface flow to become important factors. The adsorption may be physical, where only relatively weak van der Waals attractions are involved, or the adsorption may be regarded as chemical, where the surface of the solid provides binding sites for the atoms, and the electronic structure of the solid permits the formation of a chemisorption bond. The nature of the binding sites and the bonds between the gas atoms and the surface influences the degree of surface migration of the atoms.

In practice, the flow along a fine capillary or micropore is assumed to consist of two mechanisms working simultaneously, namely, (i) molecular flow along the bore of the capillary, whereby molecules are supposed to collide with the wall, re-evaporate, and collide with the wall again without inter-molecular collisions, and (ii) surface flow along the wall of the capillary, whereby molecules are adsorbed and diffuse along the surface of the wall. Both these mechanisms promote gas flow from regions of higher gas concentrations to regions of lower gas concentrations.

For a given set of conditions, the proportion of molecules that conform to mechanism (i) compared with mechanism (ii) depends on a variety of factors that include, (*a*) the sticking probability, that is, the probability that a molecule striking the surface will become adsorbed, (*b*) the length of time the molecule remains adsorbed, that is, the mean surface lifetime of the molecule, and (*c*) the coefficient of surface diffusion of the molecules. These features are, in turn, influenced by other characteristics, such as the number of sites occupied by the adsorbed molecules, or whether a complete monolayer is involved.

It will be understood therefore that, for a stated pressure

*The author has been advised by Mr. W. Steckelmacher of Edwards High Vacuum Ltd., that this deduced factor of 40 for small leaks is of the same order as that found in practice.

and temperature, the total flow rate of a gas through a given fine capillary or pore, depends not only on the nature of the gas, but also on the material and condition of the surface of the capillary. As examples of some typical interactions between gases and solids, we may note that there is little or no chemisorption of hydrogen on aluminium, silver, gold, tin, or lead, whereas hydrogen can be rapidly chemisorbed on nickel, iron, and tungsten.

In general, through micropores, the contribution of surface flow to molecular flow is relatively negligible for an inert gas such as helium, but may become appreciable for a diatomic gas such as hydrogen or nitrogen. Surface diffusion tends to be more marked with larger and heavier molecules, since these are more easily condensed and adsorbed, but variations may occur even with substances having the same molecular weight: Kammermayer and Wyrick[6] have described how, with a mixture of propane and carbon dioxide, both having a molecular weight of 44, propane passes through porous glass at a faster rate than carbon dioxide.

The extent to which an easily-condensable gas or vapour is likely to be adsorbed can often be inferred from the critical temperature of the substance, this property acting as a guide to the intermolecular potential. Thus, the higher the critical temperature of a substance the greater its tendency to be adsorbed and to show evidence of surface flow, provided, of course, that complete condensation does not occur.

With this proviso, the nearer the properties of a gas approach those of a condensable vapour, the greater the proportion of surface flow, and, therefore, a reduction of temperature or an increase of pressure may sometimes promote a total flow in excess of that predicted by the laminar-molecular theory.

As an example of the influence of the critical temperature of a substance, we deduce that, under similar conditions, the proportions of surface flow through fine capillaries should, for the following gases, increase in the order given, namely, carbon dioxide (critical temperature: 31·1° C), propane (critical temperature: 96·8° C) and sulphur dioxide (critical temperature: 157·2° C); the available experimental evidence indicates that, in appropriate circumstances, there is a tendency for these gases to behave relatively in the way suggested.

For a gas which is adsorbed, the surface concentration gradient through a porosity may take an appreciable time—minutes or hours—to become steady, as shown by a constant flow rate. It has been pointed out by Carman and Malherbe[7] that, owing to adsorption, the apparent initial flow rate of gas through micropores may, in some cases, be as much as ten times the final value.

In view of the difficulty of interpreting the results of leak-rate tests through micropores, it is important that all precautions should be taken to avoid the occurrence of porosities when constructing apparatus that is intended for operation under high vacuum conditions. This recommendation applies more particularly in cases where the equipment is required to conform to a specified degree of vacuum-tightness. Should porosities be present, then comparative results will be more consistent if helium is used as the search gas for leak-testing, because its relatively inert nature gives rise to very little adsorption. For less inert gases, the proportion of surface flow is sensitive to the kind of surface and its condition.

Where readily-condensable gases are concerned, a system of multilayer condensation may be built up on the capillary walls, the resulting layers conforming more to the properties of a liquid film. In these circumstances, the presence of an adsorbed liquid layer of thickness δ at the wall will cause the effective radius of the capillary to be reduced to a value $(r - \delta)$. Owing to the incompressibility of liquids, the surface concentration gradient, which contributes to the flow of non-condensing gases through porosities, is absent. On the contrary, the stationary adsorbed liquid surface layers reduce the effective bore of the pores, and may tend to reduce the gas flow, under steady conditions.

A further complication may arise when other less-condensable gases flow through porosities lined with a liquid layer. These less-condensable gases may have different solubilities in such a liquid film, and may therefore be subjected to different degrees of retardation in their flow through the pores, in a manner analogous to the different "retention times" experienced in gas chromatography. It is apparent, therefore, that flow rates for different gases and vapours through porosities having undetermined properties cannot readily be predicted by calculation.

Causes of Capillary Blockage

Small holes, that may give rise to appreciable leakage of gas under high vacuum, can be partially or wholly blocked by solid particles having sizes in the micron range, or by liquids as a result of surface tension effects. The blockage may be of a temporary nature and so give rise to misleading test results.

Following the general rule, it is preferable that the vessel or component to be leak-tested should be kept out of contact with sources that may cause blockage until after leak-testing and leak-rectification have been completed. These ideal conditions cannot always be met in practice, and it is the purpose of this and the following sections to discuss some causes of blockage, and in certain instances to indicate briefly how such blockage may be removed.

Solid particles in the millimetre size-range are not, in general, a source of trouble, but solid particles in the micron range may enter and block a capillary temporarily, and may subsequently be displaced, giving rise to an intermittent leak that is difficult to establish and locate. Blockage by solid particles may occur, for example, if the fluid used in connection with magnetic crack-detection work is applied before testing for vacuum leaks. The magnetic fluid used contains iron particles, of which the greater proportion are usually in the 2½ to 10 micron size range, and are, therefore, comparable with the cross-sectional dimensions of part of the range of sizes of capillaries considered here.

Small holes in mild steel vessels or components may become permanently blocked by a process of "rusting-up" caused by moisture. In practice it is usually impossible to prevent atmospheric moisture from entering capillaries. Most metals are attacked, more or less, by water in the presence of air. This action gives rise to an oxide film that has a greater specific volume than the metal. This effect applies particularly to mild steel, where the oxide film has a specific volume about seven times greater than that of the parent metal. Consequently, the smaller capillaries, which have the greater tendency to retain water, readily "rust-up". Stainless steel is less likely to be affected in this way.

When a liquid blocks a capillary, its removal from the capillary may be influenced by any one, or a combination, of the following factors:

(i) wetting combined with surface tension, which resists motion;

(ii) viscosity, which controls the tendency to flow;

(iii) vapour pressure, which controls the tendency to evaporate.

With reference to item (ii), the greater the surface tension of the liquid and the smaller the radius of the capillary, the greater the pull that draws the liquid into the capillary, this effect being dependent also on the degree of wetting of the capillary wall by the liquid. Providing that sufficient force—gas pressure—is available to overcome the net effect of surface tension, then, considering item (iii), the viscosity of the liquid determines the time required for the removal of a thread of liquid from the capillary, under the influence of the excess gas pressure. If the vessel under test is subjected to a vacuum, either internally or externally, then, regarding item (iii), any liquid held in the capillary by surface tension will evaporate into the vacuum, the rate of evaporation being dependent on the vapour pressure of the liquid. If the temperature is raised, the rate of evaporation will be increased. It is assumed that the capillary is sufficiently small, so that the amount of cooling by evaporation is negligible.

The process of leak-testing a vessel or component is usually carried out by creating a pressure difference of gas across the possible source of leakage. This may be done by maintaining atmospheric pressure of gas at one end of the leakage path and causing the other end to be maintained at either:

(*a*) a pressure of gas above atmospheric, this being usually designated as an over-pressure test, or

(*b*) at some pressure below atmospheric. If this lower pressure is maintained at some value less than about 1 torr, then variations of the lower pressure will have a negligible influence on the flow rate of gas through the leak, and evaporation of any liquid that may be present in the capillaries will be facilitated.

In the next section we shall examine some factors that concern the removal of liquids from capillaries by the application of a pressure difference, and this will be followed by a Section in which the removal of such blockage by evaporation will be considered.

Removal of Capillary Blockage by Pressure Difference

If it is assumed that the liquid wets the capillary wall, then the presence of water may easily block a leakage path because of its high surface tension. Consider, for example, a capillary of radius 10^{-4} cm which would, according to equation (3), give rise to an air leak at 20° C of 2×10^{-7} torr l./s if $\frac{1}{4}$ in. long. If this capillary contained water that wet the capillary wall, then, according to equation (6), the pressure p_0 needed to overcome the effect of surface tension, or surface adhesion, would be

$$\frac{2 \times 72}{1 \times 10^{-4}} = 1{\cdot}4 \times 10^6 \text{ dyn/cm}^2$$

or 1·4 atm, say 21 lb/in², and therefore a pressure difference in excess of this value would be needed to remove the blockage caused by the presence of the water. A thin mineral oil would be more easily moved in such a capillary as, owing to its lower surface tension, it would require a smaller pressure difference of

$$\frac{2 \times 27}{1 \times 10^{-4}} = 0{\cdot}54 \times 10^6 \text{ dyn/cm}^2$$

or 0·54 atm, say 8 lb/in².

One of the disadvantages of porosity will be understood by considering the effect of a hypothetical condition consisting of a thousand capillaries $\frac{1}{4}$ in. long situated close together in parallel each having a radius of 10^{-6} cm. The total leak rate through this assembly would be approximately $1{\cdot}3 \times 10^{-7}$ torr l./s as derived by means of equation (3), that is, about the same order of leakage as a single capillary of 10^{-4} cm radius. However, if water had access to the porous assembly, the pressure difference required to remove it from the capillaries would be

$$\frac{2 \times 72}{1 \times 10^{-6}} = 14 \text{ atm or } 210 \text{ lb/in}^2,$$

that is, ten times the pressure difference needed to remove such blockage from a 10^{-4} cm radius capillary.

The effect of surface wetting becomes of importance when using the bubble test for leaks. This method of leak location consists of pressurising the vessel with a gas which, on leaking out, causes bubbles to form in the surrounding liquid. In one version, a solution of soap and water is brushed over the suspected areas, but, as a soap solution promotes surface wetting, water is thereby encouraged to enter and block very small leaks. This tendency may be reduced, however, if the vessel is always pressurised with gas before covering the area under test with any liquid.

It is of interest to examine also the features that control the rate at which a non-evaporating liquid that blocks a capillary may be removed, provided that an excess pressure is available to overcome viscosity in addition to the pressure required to overcome surface tension. For this purpose we make use of equation (7) to calculate the times taken to push water at room temperature out of the porous assembly, and also out of the single capillary previously considered, assuming that a thread of liquid $\frac{1}{4}$ in. long is to be removed under an excess pressure difference Δp of 1 atm.

For the porous assembly comprising 10^{-6} cm radius capillaries we have:

$$t = \frac{4 \times 0{\cdot}01 \times (0{\cdot}635)^2}{10^6 \times (10^{-6})^2} = 160 \text{ s}$$

while for the single capillary of 10^{-4} cm radius the time would be:

$$t = \frac{4 \times 0{\cdot}01 \times (0{\cdot}635)^2}{10^6 \times (10^{-4})^2} = 1{\cdot}6 \text{ s}$$

The foregoing comparison serves as another instance of the unfavourable conditions imposed by porosities. We may note also that if, instead of water, the capillaries contained a thin mineral oil having a viscosity of 1 poise at room temperature, the respective times would be 1o 000 s for the porous assembly and 160 s for the single capillary.

Thus, a thin mineral oil in a capillary can be moved with a smaller pressure difference than when water is present owing to the lower surface tension of the oil, but, under similar conditions, a very much longer time would be taken by the oil to pass out of the capillary, because of its greater viscosity compared with that of water.

Removal of Capillary Blockage by Evaporation

The preceding section assumes that no evaporation of the liquid occurs. We shall now discuss the process of removal of liquids from capillaries by evaporation.

For the general case, the vessel is evacuated so that, in effect, one end of the capillary is maintained at zero pressure while atmospheric pressure is applied to the other end. This atmospheric pressure is supposed to be insufficient to overcome the surface adhesion of a thread of liquid in the capillary, and therefore, in the absence of any additional excess pressure, the only way of clearing the capillary is by evaporation of the liquid into the vacuum. It follows from equation

(6) that, under the conditions postulated, the maximum radius of the capillary is, for water,

$$2 \times 73 \times 10^{-6} = 1{\cdot}5 \times 10^{-4} \text{ cm at } 20^\circ \text{ C}$$

and

$$2 \times 59 \times 10^{-6} = 1{\cdot}2 \times 10^{-4} \text{ cm at } 100^\circ \text{ C},$$

or, for a thin mineral oil,

$$2 \times 28 \times 10^{-6} = 5{\cdot}6 \times 10^{-5} \text{ cm at } 20^\circ \text{ C}$$

and

$$2 \times 23 \times 10^{-6} = 4{\cdot}6 \times 10^{-5} \text{ cm at } 100^\circ \text{ C}.$$

Suppose that in a short time $\delta\tau$, a mass of liquid is evaporated from a capillary, this quantity corresponding to a short length δx of liquid measured along the length of the capillary. Then, if G_v is the instantaneous rate of evaporation in gram per second, and ρ is the density of the liquid in gram per cubic centimetre we have:

$$\frac{G_v}{\rho}\,\mathrm{d}\tau = \pi r^2\,\mathrm{d}x \quad . \quad . \quad . \quad (18)$$

where r is the radius of the capillary.

If equation (18) is rearranged with G_v substituted from equation (8) and then integrated between the limits 0 and t for the time, and between l_1 and l_2 for the thread of liquid in the capillary, where l_1 and l_2 are both measured from the open end of the capillary and $(l_2 - l_1)$ is the initial length of the liquid thread, we obtain:

$$\int_0^t \mathrm{d}\tau = \int_{l_1}^{l_2} \frac{\rho}{G_v} \cdot \pi r^2\,\mathrm{d}x$$

$$= \int_{l_1}^{l_2} \frac{\rho\pi r^2}{0{\cdot}486\,P_v r^3 \dfrac{M}{T}\left[\dfrac{8{\cdot}55 \times 10^{-3}\,r\,P_v}{\eta_v} + \sqrt{\dfrac{T}{M}}\right]} \left(x + \frac{8}{3}r\right)\mathrm{d}x$$

$$= \frac{\rho}{5{\cdot}83 \times 10^{-3} P_v \left[\dfrac{8{\cdot}55 \times 10^{-3}\,r\,P_v M}{\eta_v T} + \sqrt{\dfrac{M}{T}}\right]} \int_{l_1}^{l_2} \left(\frac{3x}{8r} + 1\right)\mathrm{d}x \quad . \quad (19)$$

On performing the integration indicated as part of equation (19), we obtain the result:

$$t = \left[\frac{3}{16r}(l_2 + l_1) + 1\right](l_2 - l_1) \quad . \quad . \quad (20)$$

If it is assumed that the liquid fills the capillary, then l_1 is zero and equation (20) becomes:

$$t = \left[\frac{3}{16} \cdot \frac{l_2^2}{r} + l_2\right] \quad . \quad . \quad . \quad (21)$$

In equation (21), if r is small, as in the case under consideration, then l_2 can be neglected in comparison with

$$\frac{3}{16} \cdot \frac{l_2^2}{r},$$

and the latter factor may be substituted for the integrated part of equation (19), giving the simplified form:

$$t = \frac{3{\cdot}22\,l^2\rho}{r\,P_v\left[\dfrac{8{\cdot}55 \times 10^{-3}\,r\,P_v M}{\eta_v T} + \sqrt{\dfrac{M}{T}}\right]} \text{ s} \quad . \quad (22)$$

where l is the initial length of liquid thread in the filled capillary, P_v is the vapour pressure in torr of the liquid and ρ its density, both at temperature T° K, η_v is the viscosity of the vapour, and M is the molecular weight of the substance.

Equation (22) applies only where the radius r is small compared with the length l, and therefore any limitation imposed by sonic velocity, to which the vapour may be subjected at the outlet end of the capillary, will form a negligibly small part of the process of evaporation. For very small capillaries and low vapour pressures the laminar flow component may become sufficiently small to be ignored, with the result that the molecular flow component $\sqrt{(M/T)}$ controls the process and equation (19) with equation (20) or (21) can be used to represent the vapour flow even though the lengths are not necessarily large compared with r.

If, in equation (22), l^2 is brought over to the left-hand side, then values of t/l^2 for capillaries of different radii r may be calculated with the aid of equation (22) using values of vapour pressure P_v and vapour viscosity η_v suitable for various values of the corresponding absolute temperature T. This has been done for water, the results being depicted in the graph Fig. 3, where t/l^2 is plotted against the appropriate temperature in degrees Centigrade. For simplicity, the length l of the capillary, initially filled with water, may be assumed to be 1 cm, when the values measured along the ordinates represent the time t in seconds required to empty the capillary by evaporation of the water into a vacuum.

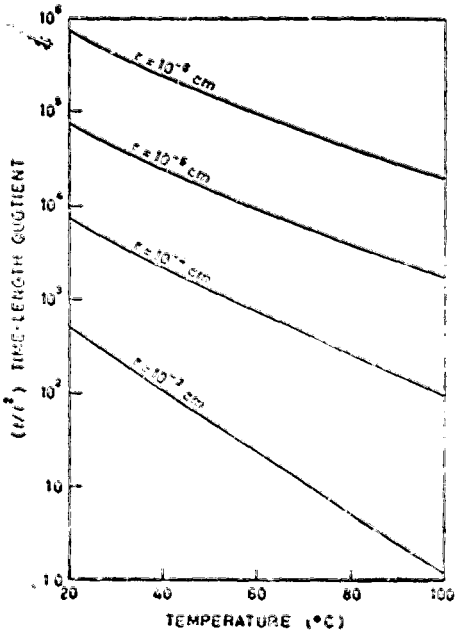

t = time for evaporation, (s)
l = length of capillary, (cm)
r = radius of capillary

Fig. 3.—*Evaporation of water from a filled capillary into a vacuum*

Reference to Fig. 3 shows that a capillary 10^{-4} cm radius by 1 cm long when filled with water and held at 60° C would empty itself by evaporation in about 12 minutes, but that

evaporation of water from a 10^{-5} cm radius capillary of similar length at the same temperature would take about 2½ hours.

The elimination of oil from capillaries by evaporation is in most cases impossible because of the comparatively low vapour pressures of oils. Consider, for example, a thin mineral oil that has an average molecular weight of 200, with a density of 0·83 g/cm³ and an effective vapour pressure of 10^{-2} torr at 60° C, these values being typical and not representative of any particular oil. Viscosities of organic vapours are usually of the order of 10^{-4} poise, and if these typical values for an oil at 60° C are substituted in equation (22) it will be found that, even for capillaries of 10^{-4} cm radius, the term $\sqrt{(M/T)}$ within the square brackets, which represents the proportion of molecular flow of vapour, is greatly in excess of the other term and therefore the proportion of laminar flow is negligible for oil vapour in capillaries of the size under consideration.

The value of t/l^2 for a capillary of 10^{-4} cm radius as deduced by substitution of the assumed physical quantities in equation (22) is $5{\cdot}45 \times 10^8$, which means that, theoretically, the oil would take nearly 1000 hours at 60° C to evaporate out of the capillary if 1 cm long.

Conclusions

We have seen how the gas flow for small leaks may be regarded as a mixture of laminar and molecular components, tending towards fully laminar flow for capillaries of larger radius and at higher pressures, and towards fully molecular flow for capillaries of smaller radius and at lower pressures.

The formulae that represent the combined effects of laminar and molecular flow should not be applied to capillaries having radii much less than 10^{-6} cm, because in these smaller sizes the effect of the internal surface area of the wall of the capillary becomes large compared with its cross-sectional area, with the result that surface flow may form a significant part of the total flow from atmospheric pressure into a vacuum. The amount of surface flow is influenced largely by the type of gas molecule and the nature of the surface of the capillary wall, consequently the flow rates of different gases through very small capillaries—and more especially through porosities—in different materials cannot generally be predicted, owing to the absence of data concerning surface adsorption and surface diffusion. The more inert types of gas are less readily adsorbed, and therefore helium gas is most likely to give reliable and reproducible flows when measuring leak rates through porosities.

When a liquid is contained in a capillary that has one end open to an evacuated space, then the liquid in the capillary will evaporate into the vacuum, the rate of evaporation being dependent on the vapour pressure of the liquid. An example of this kind of behaviour is shown by a cold trap which contains liquid air that leaks into a vacuum. Calculations indicate that, if the leakage path is regarded as a capillary, the rate of small leaks of liquid air in the molecular flow region would be about 40 times the leakage of atmospheric air at 20° C, while for larger leaks in the laminar flow region, the liquid air leak rate would be about 15 times the leakage of atmospheric air.

For liquids of low vapour pressure, the rate of evaporation may be so small that the capillary may be regarded as permanently blocked by the liquid, unless some alternative method of removal is adopted, such as a pressure difference across the ends of the capillary. This alternative necessitates, however, that the applied pressure must be sufficient to overcome surface tension and surface adhesion effects, which vary according to the kind of liquid and the extent to which it wets the capillary wall. Even though the applied pressure difference is sufficient to move the liquid, the viscosity of the liquid may be such that the time required for its removal may become excessive.

In practice, the removal of water from capillaries is most readily accomplished by reduction of pressure, preferably accompanied by the application of heat. This procedure causes the water to be vaporized, when it can be pumped away as a gas, eliminating surface tension effects. Oils possess relatively low vapour pressures and high viscosities compared with water, and therefore the removal of oil from capillaries may frequently be impossible by means of normal methods. For this reason it is important that all surfaces which may be the source of leakage paths should be kept free from oil until after testing for leaks.

The foregoing discussion leads to the conclusion that a preliminary water pressure test is sometimes permissible, but the use of oil for pressure testing before leak testing should be prohibited. It should also be mentioned that a compressed air test should never follow a water pressure test before vacuum testing for leaks, because the residual water that is held in small capillaries may be forced back by the compressed air into larger voids from which, under vacuum conditions, the liquid would evaporate only slowly through the capillary restriction. For apparatus that is required to operate at very low pressures, or where it is important to reduce leakage to the smallest practicable value, even a preliminary water pressure test may sometimes be inadvisable because the detection of very small leaks through fine capillaries then become essential, and the time required to ensure clearance of such capillaries, by evaporation of the residual water when vacuum testing, may become unduly prolonged.

Acknowledgment

The author wishes to thank Sir Willis Jackson, F.R.S., Director of Research and Education, Associated Electrical Industries (Manchester) Ltd., for permission to publish this paper.

References

[1] Jean, R., *Le Vide*, July–August, 1958, 188
[2] Bersuder, L. de, *Le Vide*, January–February, 1959, 23.
[3] Burrows, G., *Jnl. Appl. Chem.*, 1957, 7, 375.
[4] Loevinger, R. and Guthrie, A. in Guthrie, A. and Wakerling, R. K. (Eds.). *Vacuum Equipment and Techniques*, 1949 (New York: McGraw Hill Book Co.)
[5] Knudsden M. *Ann. Phys.*, 1908, 28, 75.
[6] Kammermayer, K., and Wyrick, D. D., *Ind. & Engng Chem.*, 1958, 50, 1309.
[7] Carman, P. C., and Malherbe, P. R., *Proc. Roy. Soc.*, 1950, A203, 165.

The manuscript of this paper was received on 27 July, 1960.

END OF REFERENCE

Card #14

REFERENCE

60

KELLY, J. H.; ET AL: PERMEABILITY DATA FOR AEROSPACE APPLICATIONS. IIT RESEARCH INSTITUTE (NASA CR-95393), 1968.

0
2 Put these two on our shelf

N69-14111

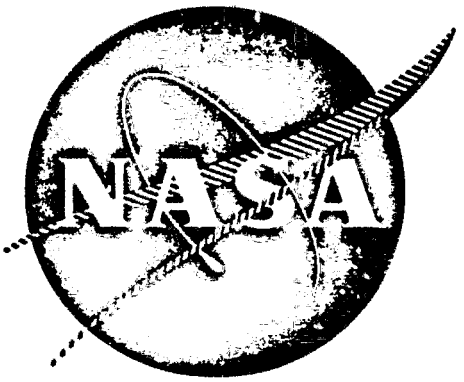

PERMEABILITY DATA FOR AEROSPACE APPLICATIONS

PREPARED FOR

NATIONAL AERONAUTICS AND SPACE ADMINISTRATION

CONTRACT NAS7-388

MARCH 1968

IITRI

IIT RESEARCH INSTITUTE

CHICAGO, ILLINOIS

I-1 INTRODUCTION

The primary purpose of this book is to present a compilation of available information on the permeation of propellants and pressurant gases through metals, non-metals, and composite materials, in a form suitable for use by the designers of spacecraft liquid propulsion systems. It is intended that the information contained in this handbook be used in conjuction with the various methodologies currently employed to select component and material combinations and to establish the design details of suitable liquid propulsion systems.

The sections of this guidebook are established in the following order:

Section I, "Introduction" includes directions for use of the data and indices, a discussion of the units in which permeation data were reported, and unit conversion tables.

Section II, "Test Methods" describes the various methods used to measure permeation rates, compare their reliability and validity, and evaluate their utility.

Section III, "Mechanisms of Permeation" defines permeation and describes the mechanism thereof in engineering terms, with a discussion of the theories relating to permeation, and sample analyses and calculations.

Sections IV and V, "Data" present data collected from the literature and the aerospace industry. Factors affecting permeation, such as temperature, diffusivity, solubility, etc., are reported concurrent with permeation data. The data included

in these sections have been evaluated with respect to the literature -- they have not been verified by an experimental program under this contract.

The data are presented in two sections. Data for materials and fluids of primary spacecraft applications have been grouped in Section IV. Section V contains data for the systems which are not presently of primary application. The entire handbook is in looseleaf form to provide a capability for updating.

Section VI, "Coordinate Index" consists of an index to the data in coordinate form, and includes trade names and types as well as chemical nomenclature. The location of data for any permeant-material systems included in the handbook can be found rapidly by use of this index.

Section VII, "References" contains two listings of references used in the preparation of the handbook. The first list is arranged by arbitrarily assigned reference numbers and consists of authors and titles. The second list is arranged alphabetically by author's last name and contains complete bibliographic information.

I-2 HANDBOOK DATA ORGANIZATION

The data in each of the two data sections are ordered alphabetically by permeant and within each permeant group alphabetically by material.

The data for each permeant-material system are presented in the following format:

A. Column 1 - Type or trade name. For example, polychlorotrifluoroethylene may be called Kel F or Trithene. Common trade names, such as Mylar, Lexan, etc., are also referenced in the coordinate index. Data for each type or trade name within a permeant-material system are grouped.

B. Column 2 - Temperature in degrees Celsius. This is the secondary order of each group, by ascending order of temperature.

C. Column 3 - Permeability Rate, in scc cm/cm^2 sec Bar, with the understanding that each value is to be multiplied by 10^{-8}, e.g., the appearance of 3.46 in this column means that the permeability rate is 3.46×10^{-8} scc cm/cm^2 sec Bar. Use of the constant factor and units permits direct comparison between systems.

D. Column 4 - Permeability rate as reported. This is merely a transcription of the data found in the literature.

E. Column 5 - Units reported. This number is an arbitrarily chosen integer that refers to the unit system in which the given datum was reported. A complete list of units and their conversion factors to the standard is given in section I-3.

F. Column 6 - Reference. This number refers to the reference(s) in which the datum was found. The references are listed by number in section VI.

G. Column 7 - Solubility. This column gives the solubility in scc/cc Bar, if this datum was available for the system.

H. Column 8 - Diffusivity. This column gives the diffusivity in cm^2/sec, if this datum was available for the system.

I. Column 9 - Comments. Any relevant comments as to membrane composition, thickness, pressures, etc., are given here.

Type or Trade Name	Temp. °C	Permeability Std. Units$_8$ (Value x 10^{-8})	Permeability as Reported	Units Rptd.	Ref.	Solubility scc/cc Bar	Diffusivity cm^2/sec	Comments
	25	12.8	13×10^{-7}	6	378			

References Reporting: 378

PERMEANT: Oxygen O_2

MATERIAL: Buna S

PERMEANT: Oxygen O_2

MATERIAL: Butadiene-Acrylonitrile Copolymer

Type or Trade Name	Temp. °C	Permeability Std. Units$_8$ (Value x 10^{-8})	Permeability as Reported	Units Rptd.	Ref.	Solubility scc/cc Bar	Diffusivity cm^2/sec	Comments
Perbunan 18	25	6.1	6.2×10^{-7}	6	378			
Perbunan 18	25	6.15	6.23×10^{-8}	8	390	.077	$.79 \times 10^{-6}$	
Perbunan 18	50	18.9	19.1×10^{-8}	8	390	.083	2.30×10^{-6}	
German Perbunan	25	3.2	3.2×10^{-7}	6	378			
German Perbunan	25	2.90	2.94×10^{-8}	8	390	.067	$.43 \times 10^{-6}$	
German Perbunan	50	10.4	10.5×10^{-8}	8	390	.072	1.44×10^{-6}	
Hycar-OR-15	25	.72	$.73 \times 10^{-7}$	6	378			
Hycar-OR-15	25	.72	$.73 \times 10^{-8}$	8	390	.053	$.136 \times 10^{-6}$	
Hycar-OR-15	30	.72	9.6×10^{-10}	3	325			
Hycar-OR-15	50	3.45	3.50×10^{-3}	8	390	.061	$.565 \times 10^{-6}$	

Type or Trade Name	Temp. °C	Permeability Std. Units ($\times 10^{-8}$)	Permeability as Reported	Units Rptd.	Ref.	Solubility scc/cc Bar	Diffusivity cm^2/sec	Comments
Hycar-OR-25	25	1.76	1.78×10^{-7}	8	378			
Hycar-OR-25	25	1.76	1.78×10^{-8}	6	390	.063	$.28 \times 10^{-6}$	
Hycar-OR-25	50	6.99	7.08×10^{-8}	8	390	.065	1.08×10^{-6}	

References Reporting: 325, 378, 390

PERMEANT: Oxygen O_2

MATERIAL: Butadiene-Acrylontrile Copolymer

PERMEANT: Oxygen O_2

MATERIAL: Cellophane-Aluminum-Saran Laminate

Type or Trade Name	Temp. C	Permeability Std. Units ($\times 10^{-8}$)	Permeability as Reported	Units Rptd.	Ref.	Solubility scc/cc Bar	Diffusivity cm^2/sec	Comments
	NG	.0008	11×10^{-13}	3	275			

References Reporting: 275

Type or Trade Name	Temp. °C	Permeability Std. Units ($\times 10^{-8}$)	Permeability as Reported	Units Rptd.	Ref.	Solubility scc/cc Bar	Diffusivity cm^2/sec	Comments
	NG	.6	$.08 \times 10^{-9}$	1	203			
	20-30	.3 to .59	.4 to .78 $\times 10^{-9}$	3	210			
	23	.102	$.0136 \times 10^{-9}$	1	207			.001 in. thick
	30	.53	7.0×10^{-10}	3	311			
Lumarith P-912	-25	.17	2.30×10^{-10}	3	242			
Lumarith P-912	0	.405	5.40×10^{-10}	3	242			
Lumarith P-912	30	.59	7.8×10^{-10}	3	240 325			
Lumarith P-912	60	2.07	27.6×10^{-10}	3	242			
Celanese P-912	25	.81	$.82 \times 10^{-7}$	6	378			

References Reporting: 203, 207, 210, 240, 242, 311, 325, 373

PERMEANT: Oxygen O_2

MATERIAL: Cellulose Acetate

PERMEANT: Oxygen O_2

MATERIAL: Cellulose Acetate Butyrate

Type or Trade Name	Temp. °C	Permeability Std. Units ($\times 10^{-8}$)	Permeability as Reported	Units Rptd.	Ref.	Solubility scc/cc Bar	Diffusivity cm^2/sec	Comments
	29	4.2	$.56 \times 10^{-9}$	1	208			.0026 cm thick
Kodapak II	25	2.8	2.8×10^{-7}	6	378			

References Reporting: 208, 378

Type or Trade Name	Temp. °C	Permeability Std. Units (8) (Value x 10^{-8})	Permeability as Reported	Units Rptd.	Ref.	Solubility scc/cc Bar	Diffusivity cm^2/sec	Comments
	25	1.48	1.5×10^{-7}	6	378			

References Reporting: 378

PERMEANT: Oxygen O_2

MATERIAL: Cellulose Nitrate

PERMEANT: Oxygen O_2

MATERIAL: Chlorinated Polyether

Type or Trade Name	Temp. °C	Permeability Std. Units ($_{-8}$) (Value x 10^{-8})	Permeability as Reported	Units Rptd.	Ref.	Solubility scc/cc Bar	Diffusivity cm^2/sec	Comments
Penton	24	.054	.0072 x 10^{-9}	1	208			.00183 cm thick

References Reporting: 208

Type or Trade Name	Temp. °C	Permeability Std. Units ($\times 10^{-8}$)	Permeability as Reported	Units Rptd.	Ref.	Solubility scc/cc Bar	Diffusivity cm^2/sec	Comments
2804	Room	360	48×10^{-9}	1	203 206 241			
3010	Room	158	21×10^{-9}	1	203 206 241			

References Reporting: 203, 206, 241

PERMEANT: Oxygen O_2

MATERIAL: COHR-Coated Glass Fabric

PERMEANT: Oxygen O_2

MATERIAL: Delrin (acetal)

Type or Trade Name	Temp. C	Permeability Std. Units ($\times 10^{-8}$)	Permeability as Reported	Units Rptd.	Ref.	Solubility scc/cc Bar	Diffusivity cm^2/sec	Comments
	30	.29	$.038 \times 10^{-9}$	1	208			.024 cm thick

References Reporting: 208

Type or Trade Name	Temp. °C	Permeability Std. Units ($\times 10^{-8}$)	Permeability as Reported	Units Rptd.	Ref.	Solubility scc/cc Bar	Diffusivity cm^2/sec	Comments
	20-30	.04 to 1.2	.049 to 1.6 x 10-9	3	210			
Epon-1001	29	.04	$.0049 \times 10^{-9}$	1	208			.0022 cm thick
Hysol	31	1.2	$.16 \times 10^{-9}$	1	208			.026 cm thick

References Reporting: 208, 210

PERMEANT: Oxygen O_2

MATERIAL: Epoxy

PERMEANT: Oxygen O_2

MATERIAL: Ethyl Cellulose

Type or Trade Name	Temp. C	Permeability Std. Units ($\times 10^{-8}$)	Permeability as Reported	Units Rptd.	Ref.	Solubility scc/cc Bar	Diffusivity cm^2/sec	Comments
	NG	8.4	6.6	5	346			
	20-30	19.9	26.5×10^{-9}	3,1	210 241 385			
	Room	15.8	2.1×10^{-9}	1	203 206			
	25	13.8	1.84×10^{-9}	1	243			Average of 4 samples
Plasticized	30	19.9	265×10^{-10}	3	240 325			
Ethocel	20	16.1	2.15×10^{-9}	1	243			
Ethocel	30	19.9	2.65×10^{-9}	1	243			
Ethocel	40	25.5	3.40×10^{-9}	1	243			
Ethocel 610	25	17.9	18.1×10^{-7}	6	378			
Ethanol-cast	28	6.0	$.80 \times 10^{-9}$	1	208			.00241 cm thick

Type or Trade Name	Temp. C	Permeability Std. Units ($\times 10^{-8}$)	Permeability as Reported	Units Rptd.	Ref.	Solubility scc/cc Bar	Diffusivity cm^2/sec	Comments
THF-cast	28	6.5	$.87 \times 10^{-9}$	1	208			.00254 cm thick

References Reporting: 203, 206, 208, 210, 240, 241, 243, 325, 346, 378, 385

PERMEANT: Oxygen O_2

MATERIAL: Ethyl Cellulose

PERMEANT: Oxygen O_2

MATERIAL: Ethylene-Propylene (florinated)

Type or Trade Name	Temp. °C	Permeability Std. Units ($\times 10^{-8}$)	Permeability as Reported	Units Rptd.	Ref.	Solubility scc/cc Bar	Diffusivity cm^2/sec	Comments
	20-30	4.4	5.9×10^{-9}	3	210			

References Reporting: 210

Type or Trade Name	Temp. °C	Permeability Std. Units ($\times 10^{-8}$)	Permeability as Reported	Units Rptd.	Ref.	Solubility scc/cc Bar	Diffusivity cm^2/sec	Comments
	25	8.5	$.86 \times 10^{-7}$	8,6	225 378		12.0×10^{-7}	
	25				222	.102		

References Reporting: 222, 225, 378

PERMEANT: Oxygen O_2

MATERIAL: Hydropol

PERMEANT: Oxygen O_2

MATERIAL: Isoprene-Acrylonitrile Copolymer

Type or Trade Name	Temp. °C	Permeability Std. Units ($\times 10^{-8}$)	Permeability as Reported	Units Rptd.	Ref.	Solubility scc/cc Bar	Diffusivity cm^2/sec	Comments
	25	.64	$.65 \times 10^{-8}$	8	390	.070	$.092 \times 10^{-6}$	
	50	3.39	3.43×10^{-8}	8	390	.075	$.45 \times 10^{-6}$	

References Reporting: 390

Type or Trade Name	Temp. °C	Permeability Std. Units ($\times 10^{-8}$)	Permeability as Reported	Units Rptd.	Ref.	Solubility scc/cc Bar	Diffusivity cm^2/sec	Comments
	25	1.77	1.79×10^{-8}	8	390	.074	$.24 \times 10^{-6}$	
	50	7.42	7.52×10^{-8}	8	390	.090	$.83 \times 10^{-6}$	

References Reporting: 390

PERMEANT: Oxygen O_2

MATERIAL: Isoprene-Methacrylonitrile Copolymer

PERMEANT: Oxygen O_2

MATERIAL: Methyl Cellulose

Type or Trade Name	Temp. °C	Permeability Std. Units ($\times 10^{-8}$)	Permeability as Reported	Units Rptd.	Ref.	Solubility scc/cc Bar	Diffusivity cm^2/sec	Comments
	23	.379	$.0505 \times 10^{-9}$	1	207			.00254 cm thick
	Room	.525	$.07 \times 10^{-9}$	1	203 206			

References Reporting: 203, 206, 207

Type or Trade Name	Temp. C	Permeability Std. Units ($\times 10^{-8}$)	Permeability as Reported	Units Rptd.	Ref.	Solubility scc/cc Bar	Diffusivity cm^2/sec	Comments
	25	.69	$.70 \times 10^{-7}$	6	378			

References Reporting: 378

PERMEANTL Oxygen O_2

MATERIAL: Mipolam HP

PERMEANT: Oxygen O_2

MATERIAL: Neoprene

Type or Trade Name	Temp. °C	Permeability Std. Units ($\times 10^{-8}$)	Permeability as Reported	Units Rptd.	Ref.	Solubility scc/cc Bar	Diffusivity cm^2/sec	Comments
	23	3.1	4.12×10^{-11}	2	418			
G	25	3.0	3.0×10^{-7}	6	266 378 425			

References Reporting: 266, 378, 418, 425

Type or Trade Name	Temp. °C	Permeability Std. Units ($\times 10^{-8}$)	Permeability as Reported	Units Rptd.	Ref.	Solubility scc/cc Bar	Diffusivity cm^2/sec	Comments
6	0	.0071	$.095 \times 10^{-10}$	3	242			
6	25	.023	$.023 \times 10^{-7}$	6	378			
6	26	.03	$.004 \times 10^{-9}$	1	208			
6	30	.029	$.38 \times 10^{-10}$	3	210,240 311,325			
6	60	.147	1.96×10^{-10}	3	210,240 311,325			
6	80	.411	5.48×10^{-10}	3	210,240 311,325			
6	90	.637	8.49×10^{-10}	3	210,240 311,325			

References Reporting: 208, 210, 240, 242, 311, 325, 378

PERMEANT: Oxygen O_2

MATERIAL: Nylon

PERMEANT: Oxygen O_2

MATERIAL: Polybutadiene

Type or Trade Name	Temp. °C	Permeability Std. Units ($\times 10^{-8}$)	Permeability as Reported	Units Rptd.	Ref.	Solubility scc/cc Bar	Diffusivity cm^2/sec	Comments
	20-30	14.3	19.1×10^{-9}	3	210			
	Room	14.3	1.9×10^{-9}	1	241 385			
	25	14.3	14.5×10^{-7}	6	378			
	25	14.3	14.5×10^{-8}	8	390	.096	1.5×10^{-6}	
	30	14.3	191×10^{-10}	3	325			
	50	35.5	36×10^{-8}	8	390	.096	3.7×10^{-6}	

References Reporting: 210, 241, 325, 378, 385, 390

Type or Trade Name	Temp. °C	Permeability Std. Units ($\times 10^{-8}$)	Permeability as Reported	Units Rptd.	Ref.	Solubility scc/cc Bar	Diffusivity cm^2/sec	Comments
	20-30	.72 to 6.2	.96 to 8.2 $\times 10^{-9}$	3	210			

References Reporting: 210

PERMEANT: Oxygen O_2

MATERIAL: Polybutadiene-Acrylonitrile

PERMEANT: Oxygen O_2

MATERIAL: Polybutadiene-Styrene

Type or Trade Name	Temp. °C	Permeability Std. Units ($\times 10^{-8}$)	Permeability as Reported	Units Rptd.	Ref.	Solubility scc/cc Bar	Diffusivity cm^2/sec	Comments
	20-30	12.9	17.2×10^{-9}	3	210			

References Reporting: 210

Type or Trade Name	Temp. °C	Permeability Std. Units ($\times 10^{-8}$)	Permeability as Reported	Units Rptd.	Ref.	Solubility scc/cc Bar	Diffusivity cm^2/sec	Comments
	20-30	1.5	2.0×10^{-9}	3	210		6.7×10^{-9}	
Lexan	0	.50	6.7×10^{-10}	3	388			
Lexan	25	1.1	1.4×10^{-9}	3	388	.50	2.1×10^{-8}	
Lexan	28	1.5	$.20 \times 10^{-9}$	1	208			
Lexan	50	1.95	2.6×10^{-9}	3	388		5.4×10^{-8}	
Lexan	75	3.4	4.5×10^{-9}	3	388		1.3×10^{-7}	
Lexan	100	5.1	6.8×10^{-9}	3	388		2.4×10^{-7}	
Lexan	125	7.5	1.0×10^{-8}	3	388			
Lexan	150	13.5	1.8×10^{-8}	3	388			
Lexan	175	22.5	3.0×10^{-8}	3	388			

PERMEANT: Oxygen O_2

MATERIAL: Polycarbonate

PERMEANT: Oxygen O_2

MATERIAL: Polycarbonate

Type or Trade Name	Temp. C	Permeability Std. Units ($\times 10^{-8}$)	Permeability as Reported	Units Rptd.	Ref.	Solubility scc/cc Bar	Diffusivity cm^2/sec	Comments
BPA	Room	1.2	$.16 \times 10^{-9}$	1	203 206			
Mobay	31	2.0	$.26 \times 10^{-9}$	1	208			.0042 cm thick

References Reporting: 203, 206, 208, 210, 388

Type or Trade Name	Temp. °C	Permeability Std. Units$_8$ (Value x 10^{-8})	Permeability as Reported	Units Rptd.	Ref.	Solubility scc/cc Bar	Diffusivity cm^2/sec	Comments
	30	.0075	$.10 \times 10^{-10}$	3	240			
Kel-F	25	.0075	$.001 \times 10^{-9}$	1	208			Unplasticized
Kel-F	25	.028	$.028 \times 10^{-7}$	6	378			
Kel-F	30	.038	$.05 \times 10^{-9}$	3	340 374			30% Crystallinity
Kel-F	30	.0098	$.013 \times 10^{-9}$	3	340 374			80% Crystallinity
Kel-F-300	0	.0053	$.07 \times 10^{-10}$	3	311			30% Crystallinity
Kel-F-300	0	.082	1.1×10^{-10}	3	311			Plasticized
Kel-F-300	0	.003	$.04 \times 10^{-10}$	3	311			Unplasticized
Kel-F-300	25	.03	$.40 \times 10^{-10}$	3	311			30% Crystallinity
Kel-F-300	30	.039	$.52 \times 10^{-10}$	3	311			Unplasticized

PERMEANT: Oxygen O_2

MATERIAL: Polychlorotrifluoroethylene

PERMEANT: Oxygen O_2

MATERIAL: Polychlorotrifluoroethylene

Type or Trade Name	Temp. C	Permeability Std. Units ($\times 10^{-8}$)	Permeability as Reported	Units Rptd.	Ref.	Solubility scc/cc Bar	Diffusivity cm^2/sec	Comments
Kel-F-300	30	.42	5.6×10^{-10}	3	311 325			Plasticized
Kel-F-300	40	.069	$.92 \times 10^{-10}$	3	311			30% Crystallinity
Kel-F-300	40	.019	$.25 \times 10^{-10}$	3	311			80% Crystallinity
Kel-F-300	50	.032	$.43 \times 10^{-10}$	3	311			80% Crystallinity
Kel-F-300	50	.108	1.44×10^{-10}	3	311			30% Crystallinity
Kel-F-300	60	.051	$.68 \times 10^{-10}$	3	311			80% Crystallinity
Kel-F-300	60	.218	2.90×10^{-10}	3	311			Unplasticized
Kel-F-300	60	2.1	28×10^{-10}	3	311 325			Plasticized
Kel-F-300	75	.431	5.74×10^{-10}	3	311			30% Crystallinity
Kel-F-300	80	.139	1.85×10^{-10}	3	311			80% Crystallinity

Type or Trade Name	Temp. C	Permeability Std. Units ($\times 10^{-8}$)	Permeability as Reported	Units Rptd.	Ref.	Solubility scc/cc Bar	Diffusivity cm^2/sec	Comments
Trithene B	-25	.015	$.20 \times 10^{-10}$	3	242			
Trithene B	0	.83	1.1×10^{-10}	3	242			
Trithene B	30	.42	5.6×10^{-10}	3	242			
Trithene B	60	2.1	28.0×10^{-10}	3	242			
Trithene	23	.0038	13	23	399			Concentration varying test
Trithene	23	.0052	18	23	399			Volume varying test
Trithene	23	.0067	23	23	399			Pressure varying test

References Reporting: 208,240,242, 311,325,340, 374,378,399

PERMEANT: Oxygen O_2

MATERIAL: Polychlorotrifluororthylene

PERMEANT: Oxygen O_2

MATERIAL: Polydimethyl-Butadiene

Type or Trade Name	Temp. C	Permeability Std. Units$_8$ (Value x 10^{-8})	Permeability as Reported	Units Rptd.	Ref.	Solubility scc/cc Bar	Diffusivity cm^2/sec	Comments
	20-30	1.6	2.1×10^{-9}	3	210			

References Reporting: 210

Type or Trade Name	Temp. °C	Permeability Std. Units ($\times 10^{-8}$)	Permeability as Reported	Units Rptd.	Ref.	Solubility scc/cc Bar	Diffusivity cm^2/sec	Comments
Alathon 14	25	1.65	2.20×10^{-7}	6	378			
Alathon 14	25	1.65	$.220 \times 10^{-7}$	8	225		4.6×10^{-7}	
Alathon 15	0	1.2	1.6×10^{-10}	1	209 223			
Alathon 15	0	.75	1.0×10^{-10}	1	223			Variable volume test
Alathon 15	0	.50	6.7×10^{-11}	1	223			Variable pressure test
Alathon 15	15	2.85	3.8×10^{-10}	1	223			
Alathon 15	30	6.75	9.0×10^{-10}	1	209 223			
Alathon 15	30	4.5	6.0×10^{-10}	1	223			Variable volume test
Alathon 15	30	3.6	4.8×10^{-10}	1	223			Variable pressure test
Alathon 15	50	15.0	2.0×10^{-9}	1	209 223			

PERMEANT: Oxygen O_2

MATERIAL: Polyethylene

PERMEANT: Oxygen O_2

MATERIAL: Polyethylene

Type or Trade Name	Temp. °C	Permeability Std. Units ($_{-8}$) (Value x 10^{-8})	Permeability as Reported	Units Rptd.	Ref.	Solubility scc/cc Bar	Diffusivity cm^2/sec	Comments
Alathon 15	50	12.4	1.65×10^{-9}	1	223			Variable volume test
Alathon 15	50	10.9	1.45×10^{-9}	1	223			Variable volume test
	25				222	.0769		
	30	4.1	5.5×10^{-9}	3	374			60% Crystallinity
	30	1.6	2.1×10^{-9}	3	374			69% Crystallinity
	30	.83	1.1×10^{-9}	3	374			78% Crystallinity
	30	.795	1.06×10^{-9}	3	374			81% Crystallinity
	30	.38	$.5 \times 10^{-9}$	3	374			83% Crystallinity
Hypalon	20-30	2.1	2.8×10^{-9}	3	210			
Hypalon	30	2.5	$.33 \times 10^{-9}$	1	208			.0069 cm thick

Type or Trade Name	Temp. C	Permeability Std. Units ($\times 10^{-8}$)	Permeability as Reported	Units Rptd.	Ref.	Solubility scc/cc Bar	Diffusivity cm^2/sec	Comments
L-film	26	3.5	$.47 \times 10^{-9}$	1	208			.0024 cm thick
Monaxially Orientated	32	3.5	$.46 \times 10^{-9}$	1	208			.00483 cm thick
Biaxially Orientated	27	1.8	$.24 \times 10^{-9}$	1	208			.00254 cm thick
DE 2400	0	.581	$.0774 \times 10^{-9}$	1	211			.0013 in. thick
DE 2400	0	.431	$.0575 \times 10^{-9}$	1	211			.00156 in. thick
DE 2400	25	2.63	$.350 \times 10^{-9}$	1	211			.0013 in. thick
DE 2400	25	2.09	$.278 \times 10^{-9}$	1	211			.00156 in. thick
DE 2400	50	9.45	1.26×10^{-9}	1	211			.0013 in. thick
DE 2400	50	7.95	1.06×10^{-9}	1	211			.00156 in. thick
DE 2500	0	.521	$.0695 \times 10^{-9}$	1	211			.0015 in. thick

PERMEANT: Oxygen O_2

MATERIAL: Polyethylene

PERMEANT: Oxygen O_2

MATERIAL: Polyethylene

Type or Trade Name	Temp. °C	Permeability Std. Units ($\times 10^{-8}$)	Permeability as Reported	Units Rptd.	Ref.	Solubility scc/cc Bar	Diffusivity cm^2/sec	Comments
DE 2500	25	2.30	$.306 \times 10^{-9}$	1	211			.0015 in. thick
DE 2500	50	8.03	1.07×10^{-9}	1	211			.0015 in. thick
.917g/cc	23	.7839	$.1045 \times 10^{-9}$	1	207			.00254 cm thick
.922g/cc	30	4.13	55×10^{-10}	3	240			
.922g/cc	30	5.2	69×10^{-10}	3	311			
.929g/cc	32	.83	$.11 \times 10^{-9}$	1	208			.0023 cm thick
.938g/cc	30	1.6	21×10^{-10}	3	311			
.950g/cc	23	.50	$.066 \times 10^{-10}$	1	207			.00254 cm thick
.953g/cc	30	.83	11×10^{-10}	3	311			
.960g/cc	30	.47	$.062 \times 10^{-9}$	1	207			

PERMEANT:

MATERIAL:

Type or Trade Name	Temp. °C	Permeability Std. Units$_8$ (Value x 10^{-8})	Permeability as Reported	Units Rptd.	Ref.	Solubility scc/cc Bar	Diffusivity cm^2/sec	Comments
.961g/cc	27	2.2	.29 x 10^{-9}	1	208			.0018 cm thick
.964g/cc	25	.31	.31 x 10^{-7}	6	378			
.960g/cc	30	.80	10.6 x 10^{-10}	3	240			
Alathon 14	25				237	.0395		
Alathon 34	25				237	.031		
Grex	25				237	.022		

References Reporting: 207,208,209, 210,211,222, 223,225,237, 240,311,374, 378

PERMEANT: Oxygen O_2

MATERIAL: Polyethylene

PERMEANT: Oxygen O_2

MATERIAL: Polyethylene Terephthalate

Type or Trade Name	Temp. °C	Permeability Std. Units$_8$ (Value x 10^{-8})	Permeability as Reported	Units Rptd	Ref.	Solubility scc/cc Bar	Diffusivity cm^2/sec	Comments
	20-30	.023	.03 x 10^{-9}	3	210			
	23	.014	.0019 x 10^{-9}	1	203, 207			.001 in. thick
	NG	.023	.30 x 10^{-10}	3	275			Average of 3 samples
Mylar A	-25	.0035	.046 x 10^{-10}	3	242			
Mylar A	0	.0098	.13 x 10^{-10}	3	242			
Mylar A	23	.017	59	23	399			Concentration varying test
Mylar A	23	.017	59	23	399			Volume varying test
Mylar A	23	.014	48	.23	399			
Mylar A	25	.019	.019 x 10^{-7}	6	378			
Mylar A	30	.034	.45 x 10^{-10}	3	242			

Type or Trade Name	Temp. °C	Permeability Std. Units ($_{8}$) (Value x 10^{-8})	Permeability as Reported	Units Rptd.	Ref.	Solubility scc/cc Bar	Diffusivity cm^2/sec	Comments
Mylar A	30	.017	$.22 \times 10^{-10}$	3	240 311 325			
Mylar A	60	.083	1.1×10^{-10}	3	242			
Mylar 25-V-200	50	Very low			211			
	25				224	.075		

References Reporting: 203,207,210
211,224,240
242,275,311
325,378,399

PERMEANT: Oxygen O_2

MATERIAL: Polyethylene Terephthalate

PERMEANT: Oxygen O_2

MATERIAL: Polyformaldehyde (acetal)

Type or Trade Name	Temp. C	Permeability Std. Units ($\times 10^{-8}$)	Permeability as Reported	Units Rptd.	Ref.	Solubility scc/cc Bar	Diffusivity cm^2/sec	Comments
	20-30	.029	$.038 \times 10^{-9}$	3	210			

References Reporting: 210

Type or Trade Name	Temp. °C	Permeability Std. Units ($\text{Value} \times 10^{-8}$)	Permeability as Reported	Units Rptd.	Ref.	Solubility scc/cc Bar	Diffusivity cm^2/sec	Comments
	20-30	.98	1.3×10^{-9}	3	210			

References Reporting: 210

PERMEANT: Oxygen O_2

MATERIAL: Polyisobutylene-Isoprene

PERMEANT: Oxygen O_2

MATERIAL: Polymethylpentadiene

Type or Trade Name	Temp. °C	Permeability Std. Units ($\times 10^{-8}$)	Permeability as Reported	Units Rptd.	Ref.	Solubility scc/cc Bar	Diffusivity cm^2/sec	Comments
	25	7.52	7.62×10^{-8}	8	390	.136	$.55 \times 10^{-6}$	
	50	25.6	25.9×10^{-8}	8	390	.129	1.98×10^{-6}	

References Reporting: 390

Type or Trade Name	Temp. °C	Permeability Std. Units ($\times 10^{-8}$)	Permeability as Reported	Units Rptd.	Ref.	Solubility scc/cc Bar	Diffusivity cm^2/sec	Comments
	20-30	1.7	2.3×10^{-9}	3	210			
	23	.702	2420	23	399			Volume varying test
	23	.720	2483	23	399			Concentration test
	23	.673	2320	23	399			Pressure varying test
	25	1.2	1.2×10^{-7}	6	378			
	30	.6	2.1×10^{-9}	3	374			
Profax	28	1.05	$.14 \times 10^{-9}$	1	208			.0015 cm thick
Cryovac	30	.83	$.11 \times 10^{-9}$	1	208			.0015 cm thick
Escon	27	1.05	$.14 \times 10^{-9}$	1	208			Monaxial
Escon	27	.58	$.077 \times 10^{-9}$	1	208			Biaxial

PERMEANT: Oxygen O_2

MATERIAL: Polypropylene

PERMEANT: Oxygen O_2

MATERIAL: Polypropylene

Type or Trade Name	Temp. °C	Permeability Std. Units ($\times 10^{-8}$)	Permeability as Reported	Units Rptd.	Ref.	Solubility scc/cc Bar	Diffusivity cm^2/sec	Comments
.907g/cc	30	1.72	2.29×10^{-9}	3	385			

References Reporting: 208,210,374, 378,385,399

Type or Trade Name	Temp. °C	Permeability Std. Units ($\times 10^{-8}$)	Permeability as Reported	Units Rptd.	Ref.	Solubility scc/cc Bar	Diffusivity cm^2/sec	Comments
	NG	5.6	4.4	5	346			
	Room	18	2.40×10^{-9}	1	241 385			
	Room	.9	$.12 \times 10^{-9}$	1	208			
	20	1.3	$.174 \times 10^{-9}$	1	207			.001 in. thick
	20	18.2	2.42×10^{-9}	1	243			
	20-30	1.13 to 18.8	1.5 to 25 $\times 10^{-9}$	3	210			
	23	.213	745	23	399			Concentration varying test
	23	.294	1015	23	399			Volume varying test
	23	.272	937	23	399			Pressure varying test
	30	.83	11×10^{-10}	3	240 311			

PERMEANT: Oxygen O_2

MATERIAL: Polystyrene

PERMEANT: Oxygen O_2

MATERIAL: Polystyrene

Type or Trade Name	Temp. °C	Permeability Std. Units$_8$ (Value x 10^{-8})	Permeability as Reported	Units Rptd.	Ref.	Solubility scc/cc Bar	Diffusivity cm^2/sec	Comments
	30	18.0	2.40×10^{-9}	1	243			
	40	17.6	2.35×10^{-9}	1	243			
Polyflex	25	1.6	$.21 \times 10^{-9}$	1	208			.00303 cm thick
DOW 0641	25	18.3	18.5×10^{-7}	6	378			

References Reporting: 203, 207, 208, 210, 240, 241, 243, 311, 346, 378, 385, 399

Type or Trade Name	Temp. °C	Permeability Std. Units ($\times 10^{-8}$)	Permeability as Reported	Units Rptd.	Ref.	Solubility scc/cc Bar	Diffusivity cm^2/sec	Comments
	20-30	.26	$.34 \times 10^{-9}$	3	210			

References Reporting: 210

PERMEANT: Oxygen O_2

MATERIAL: Polystyrene-Acrylonitrile

PERMEANT: Oxygen O_2

MATERIAL: Polystyrene-Methacrylonitrile

Type or Trade Name	Temp. °C	Permeability Std. Units ($\times 10^{-8}$)	Permeability as Reported	Units Rptd.	Ref.	Solubility scc/cc Bar	Diffusivity cm^2/sec	Comments
	20-30	.12	$.16 \times 10^{-9}$	3	210			

References Reporting: 210

Type or Trade Name	Temp. °C	Permeability Std. Units$_8$ (Value x 10^{-8})	Permeability as Reported	Units Rptd.	Ref.	Solubility scc/cc Bar	Diffusivity cm^2/sec	Comments
	20-30	1.14 to 3.6	1.52 to 4.8 x 10^{-9}	3	210			
Estane	32	1.3	.17 x 10^{-9}	1	208			.0025 cm thick
Adiprene	29	3.6	.48 x 10^{-9}	1	208			.0021 cm thick
PC-6	30	1.6	.21 x 10^{-9}	1	208			.010 cm thick

References Reporting: 208, 210

PERMEANT: Oxygen O_2

MATERIAL: Polyurethane

PERMEANT: Oxygen O_2

MATERIAL: Polyvinyl Butyral

Type or Trade Name	Temp. °C	Permeability Std. Units ($\times 10^{-8}$)	Permeability as Reported	Units Rptd.	Ref.	Solubility scc/cc Bar	Diffusivity cm^2/sec	Comments
Butbar B76	27	18.2	2.42×10^{-9}	1	208			.00094 cm thick

References Reporting: 208

Type or Trade Name	Temp. °C	Permeability Std. Units ($\times 10^{-8}$)	Permeability as Reported	Units Rptd.	Ref.	Solubility scc/cc Bar	Diffusivity cm^2/sec	Comments
	NG	.105	$.014 \times 10^{-9}$	1	203			
	28	1.88	$.25 \times 10^{-9}$	1	208			
	20-30	.09 to 4.5	.12 to .6 $\times 10^{-9}$	3	210			
	30	.09	1.2×10^{-10}	3	240 311			
Plasticized	23	.066	226	23	399			Concentration varying test
Plasticized	23	.064	219	23	399			Volume varying test
Plasticized	23	.062	212	23	399			Pressure varying test
Plasticized	23	.056 to .9	.0074 to .120 $\times 10^{-9}$	1	207			
Rigid	23	.035	$.0047 \times 10^{-9}$	1	207			
THF Cast Unplasticized	32	.26	$.034 \times 10^{-9}$	1	208			.00508 cm thick

PERMEANT: Oxygen O_2

MATERIAL: Polyvinyl Chloride

Type or Trade Name	Temp. °C	Permeability Std. Units ($\times 10^{-8}$)	Permeability as Reported	Units Rptd.	Ref.	Solubility scc/cc Bar	Diffusivity cm^2/sec	Comments
THF Cast 16.8% Plasticized	31	.75	$.10 \times 10^{-9}$	1	208			.00788 cm thick
THF Cast 19.3% Plasticized	31	1.35	$.18 \times 10^{-9}$	1	208			.00457 cm thick

References Reporting: 203, 207, 208, 210, 240, 311, 399

Type or Trade Name	Temp. °C	Permeability Std. Units$_8$ (Value x 10^{-8})	Permeability as Reported	Units Rptd.	Ref.	Solubility scc/cc Bar	Diffusivity cm^2/sec	Comments
Fluorinax	28	6.98	$.93 \times 10^{-9}$	1	208			.00256 thick

References Reporting: 208

PERMEANT: Oxygen O_2

MATERIAL: Polyvinyl Chloride (fluorinated)

PERMEANT: Oxygen O_2

MATERIAL: Polyvinyl Chloride-Polyvinyl Acetate

Type or Trade Name	Temp. °C	Permeability Std. Units ($\times 10^{-8}$)	Permeability as Reported	Units Rptd.	Ref.	Solubility scc/cc Bar	Diffusivity cm^2/sec	Comments
	0	.46	$.061 \times 10^{-9}$	1	211 219			
VYHH	2				221		1.74×10^{-4}	
VYHH	11				221		6.12×10^{-4}	
VYHH	14				221		9.50×10^{-4}	
	22	.96	8300	23	399			Concentration varying test
	23	.43	1470	23	399			Volume varying test
	23	.46	1590	23	399			Pressure varying test
	Room	2.3	$.3 \times 10^{-9}$	1	241 385			
VYHH	24				221		12.6×10^{-4}	
	25	2.0	$.27 \times 10^{-9}$	1	211 219			

Type or Trade Name	Temp. °C	Permeability Std. Units ($\times 10^{-8}$)	Permeability as Reported	Units Rptd.	Ref.	Solubility scc/cc Bar	Diffusivity cm^2/sec	Comments
	50	7.1	$.95 \times 10^{-9}$	1	221			
VYHH	54				221		75.5×10^{-4}	
VYHH	66						129.5×10^{-4}	
VYHH	88				221		291.8×10^{-4}	

References Reporting: 211,219,221, 241,385,399

PERMEANT: Oxygen O_2

MATERIAL: Polyvinyl Chloride-Polyvinyl Acetate

PERMEANT: Oxygen O_2

MATERIAL: Polyvinyl Fluoride

Type or Trade Name	Temp. °C	Permeability Std. Units ($\times 10^{-8}$)	Permeability as Reported	Units Rptd.	Ref.	Solubility scc/cc Bar	Diffusivity cm^2/sec	Comments
	23	.013	44	23	399			Concentration varying test
	23	.014	47	23	399			Volume varying test
	23	.015	52	23	399			Pressure varying test
	20-30	.015	$.02 \times 10^{-9}$	3	210			

References Reporting: 210, 399

Type or Trade Name	Temp. °C	Permeability Std. Units ($\times 10^{-8}$)	Permeability as Reported	Units Rptd.	Ref.	Solubility scc/cc Bar	Diffusivity cm^2/sec	Comments
	Room	.023	$.003 \times 10^{-9}$	1	203			
	20-30	.004	$.005 \times 10^{-9}$	3	210			
	30	.004	$.053 \times 10^{-10}$	3	240 311 325			
Saran	NG	.0025	.56	7	389			
Saran	23	.0045	$.0006 \times 10^{-9}$	1	207			.001 in. thick
Saran	31	.0083	$.0011 \times 10^{-9}$	1	208			.001 in. thick
Saran 517	0	.0012	$.016 \times 10^{-10}$	3	242			
Saran 517	25	.0018	$.0018 \times 10^{-7}$	6	378			
Saran 517	30	.004	$.051 \times 10^{-10}$	3	242			
Saran 517	60	.49	$.65 \times 10^{-10}$	3	242			

PERMEANT: Oxygen, O_2

MATERIAL: Polyvinylidene Chloride

PERMEANT: Oxygen O_2

MATERIAL: Polyvinylidene Chloride

Type or Trade Name	Temp. °C	Permeability Std. Units ($\times 10^{-8}$)	Permeability as Reported	Units Rptd.	Ref.	Solubility scc/cc Bar	Diffusivity cm^2/sec	Comments
Saran 517	90	.30	4.0×10^{-10}	3	242			

References Reporting: 203, 207, 208, 240, 242, 311, 325, 378, 389

Type or Trade Name	Temp. °C	Permeability Std. Units$_8$ (Value x 10^{-8})	Permeability as Reported	Units Rptd.	Ref.	Solubility scc/cc Bar	Diffusivity cm^2/sec	Comments
	20-30	1.1	1.5×10^{-9}	3	210			
Viton A	26	1.7	$.22 \times 10^{-9}$	1	208			.02 cm thick

References Reporting: 208, 210

PERMEANT: Oxygen O_2

MATERIAL: Polyvinylidene Fluoride-Hexafluoropropylene

PERMEANT: Oxygen O_2

MATERIAL: Polyvinyl Toluene

Type or Trade Name	Temp. °C	Permeability Std. Units$_8$ (Value x 10^{-8})	Permeability as Reported	Units Rptd.	Ref.	Solubility scc/cc Bar	Diffusivity cm^2/sec	Comments
	23	1.66	$.221 \times 10^{-9}$	1	207			.00254 cm thick

References Reporting: 207

Type or Trade Name	Temp. °C	Permeability Std. Units$_8$ (Value x 10^{-8})	Permeability as Reported	Units Rptd.	Ref.	Solubility scc/cc Bar	Diffusivity cm^2/sec	Comments
	Room	1.05	$.14 \times 10^{-9}$	1	203			
	25	.977	$.99 \times 10^{-8}$	8	390	.121	$.081 \times 10^{-6}$	
	26	4.2	$.56 \times 10^{-9}$	1	208			.034 cm thick
	30	.98	13.0×10^{-10}	3	240 311 325			
	50	3.98	4.03×10^{-8}	8	390	.104	$.384 \times 10^{-6}$	
Oppanol B-200	25	.89	$.90 \times 10^{-7}$	6	378			

References Reporting: 203,208,240, 311,325,378, 390

PERMEANT: Oxygen O_2

MATERIAL: Rubber, Butyl

PERMEANT: Oxygen O_2

MATERIAL: Rubber, Dimethylsilicone

Type or Trade Name	Temp. °C	Permeability Std. Units ($\times 10^{-8}$)	Permeability as Reported	Units Rptd.	Ref.	Solubility scc/cc Bar	Diffusivity cm^2/sec	Comments
	Room	450	60×10^{-3}	1	203 206 297			

IV-8.60

References Reporting: 203, 206, 297

Type or Trade Name	Temp. °C	Permeability Std. Units ($_{8}$) (Value x 10^{-8})	Permeability as Reported	Units Rptd.	Ref.	Solubility scc/cc Bar	Diffusivity cm^2/sec	Comments
	Room	82.5	11×10^{-9}	1	203 206			

References Reporting: 203, 206

PERMEANT: Oxygen O_2

MATERIAL: Rubber, Fluorosilicone

PERMEANT: Oxygen O_2

MATERIAL: Rubber Hydrochloride

Type or Trade Name	Temp. °C	Permeability Std. Units ($\times 10^{-8}$)	Permeability as Reported	Units Rptd.	Ref.	Solubility scc/cc Bar	Diffusivity cm^2/sec	Comments
Pliofilm	27	1.9	$.25 \times 10^{-9}$	1	208			.0183 cm thick
Pliofilm FM-1	-25	.026	$.34 \times 10^{-10}$	3	242			
Pliofilm FM-1	0	.16	2.1×10^{-10}	3	242			
Pliofilm FM-1	25	.40	$.40 \times 10^{-7}$	6	378			
Pliofilm FM-1	30	.41	5.4×10^{-10}	3	242			
Pliofilm FM-1	60	1.9	25.0×10^{-10}	3	242			
Pliofilm FM	30	.41	5.4×10^{-10}	3	325			
	23	.113	$.0151 \times 10^{-9}$	1	207			.001 in. thick
	20-30	.019 to .41	.025 to $.54 \times 10^{-9}$	3	210			
Pliofilm NO	30	.023	$.30 \times 10^{-10}$	3	240			

Type or Trade Name	Temp. °C	Permeability Std. Units ($\times 10^{-8}$)	Permeability as Reported	Units Rptd.	Ref.	Solubility scc/cc Bar	Diffusivity cm^2/sec	Comments
Pliofilm P4	30	1.8	24×10^{-10}	3	311			

References Reporting: 207, 208, 210, 240, 242, 311, 325, 378

PERMEANT: Oxygen O_2

MATERIAL: Rubber Hydrochloride

PERMEANT: Oxygen O_2

MATERIAL: Rubber, Methyl

Type or Trade Name	Temp. °C	Permeability Std. Units ($\times 10^{-8}$)	Permeability as Reported	Units Rptd.	Ref.	Solubility scc/cc Bar	Diffusivity cm^2/sec	Comments
	25	1.6	1.6×10^{-7}	6	378			
	25	1.6	1.6×10^{-8}	8	390	.113	$.14 \times 10^{-6}$	
	30	1.58	21.1×10^{-10}	3	325			
	50	7.0	7.1×10^{-8}	8	390	.115	$.61 \times 10^{-6}$	

References Reporting: 325, 378, 390

Type or Trade Name	Temp. °C	Permeability Std. Units ($\times 10^{-8}$)	Permeability as Reported	Units Rptd.	Ref.	Solubility scc/cc Bar	Diffusivity cm^2/sec	Comments
	Room	17.3	2.3×10^{-9}	1	241 385			
	Room	18.0	2.4×10^{-9}	1	203 206			
	20-30	17.3	23.0×10^{-9}	3	210			
	25	17.8	1.8×10^{-6}	6	266 378 425			
	25	17.57	1.78×10^{-7}	8	225		17.3×10^{-7}	
	25				222	.10		
	25	17.5	17.7×10^{-8}	8	390	.111	1.58×10^{-6}	
	30	17.48	233×10^{-10}	3	240 325			
	50	46.4	47.0×10^{-8}	8	390	.099	4.70×10^{-6}	

References Reporting: 203, 206, 210, 222, 225, 240, 241, 266, 325, 378, 385, 390, 425

PERMEANT: Oxygen O_2

MATERIAL: Rubber, Natural

PERMEANT: Oxygen O_2

MATERIAL: Rubber, Nitrile Silicone

Type or Trade Name	Temp. °C	Permeability Std. Units$_8$ (Value x 10^{-8})	Permeability as Reported	Units Rptd.	Ref.	Solubility scc/cc Bar	Diffusivity cm^2/sec	Comments
	Room	63.8	8.5×10^{-9}	1	203 206			
	31	218	29×10^{-9}	1	208			Cured 16 hr
	31	225	30×10^{-9}	1	208			Cured 1 hr

References Reporting: 203, 206, 208

Type or Trade Name	Temp. °C	Permeability Std. Units$_8$ (Value x 10^{-8})	Permeability as Reported	Units Rptd.	Ref.	Solubility scc/cc Bar	Diffusivity cm^2/sec	Comments
Thiokol ZR-300	23	5.78	$.77 \times 10^{-9}$	1	208			.2 cm thick
Thiokol B	25	.22	$.22 \times 10^{-7}$	6	378			

References Reporting: 208, 378

PERMEANT: Oxygen O_2

MATERIAL: Rubber, Polysulfide

PERMEANT: Oxygen O_2

MATERIAL: Rubber, Silicone

Type or Trade Name	Temp. °C	Permeability Std. Units ($\times 10^{-8}$)	Permeability as Reported	Units Rptd.	Ref.	Solubility scc/cc Bar	Diffusivity cm^2/sec	Comments
	NG	269	3.59×10^{-8}	1	223			
	Room	195	26×10^{-9}	1	385			
	20-30	75 to 450	100 to 600×10^{-9}	3	210			
Coated on fabric	Room	158 to 360	21 to 48×10^{-9}	1	385			
RTV-11	29	380	50.6×10^{-9}	1	409			
RTV-11	33	386	51.4×10^{-9}	1	409			
RTV-11	44	428	57.1×10^{-9}	1	409			
RTV-20	29	299	39.9×10^{-9}	1	409			
RTV-20	33	308	41.0×10^{-9}	1	409			
RTV-20	43	342	45.6×10^{-9}	1	409			

Type or Trade Name	Temp. °C	Permeability Std. Units ($\times 10^{-8}$)	Permeability as Reported	Units Rptd.	Ref.	Solubility scc/cc Bar	Diffusivity cm^2/sec	Comments
RTV-40	24	320	42.6×10^{-9}	1	409			
RTV-40	34	344	45.8×10^{-9}	1	409			
RTV-40	43	351	46.8×10^{-9}	1	409			
RTV-90	23	398	53×10^{-9}	1	208			.031 cm in.
RTV-501	23	404	53.8×10^{-9}	1	409			
RTV-501	33	445	59.3×10^{-9}	1	409			
RTV-501	43	493	65.7×10^{-9}	1	409			
RTV-501	6	319	42.5×10^{-9}	1	409			
RTV-502	11	344	45.9×10^{-9}	1	409			
RTV-502	24	270	36×10^{-9}	1	208			.0141 cm thick

PERMEANT: Oxygen O_2
MATERIAL: Rubber, Silicone

PERMEANT: Oxygen O_2

MATERIAL: Rubber, Silicone

Type or Trade Name	Temp. °C	Permeability Std. Units$_8$ (Value x 10^{-8})	Permeability as Reported	Units Rptd.	Ref.	Solubility scc/cc Bar	Diffusivity cm^2/sec	Comments
RTV-502	23	415	55.3×10^{-9}	1	409			
RTV-502	33	453	60.4×10^{-9}	1	409			
RTV-502	43	497	66.3×10^{-9}	1	409			
RTV-601	33	567	75.6×10^{-9}	1	409			
RTV-601	43	583	77.7×10^{-9}	1	409			
Eccosil 4712	21	210	28.0×10^{-9}	1	409			
Eccosil 4712	32	234	31.2×10^{-9}	1	409			
Eccosil 4712	44	257	34.3×10^{-9}	1	409			
Sylgard 182	21	300	40.0×10^{-9}	1	409			
Sylgard 182	34	346	46.1×10^{-9}	1	409			

Type or Trade Name	Temp. °C	Permeability Std. Units ($\times 10^{-8}$)	Permeability as Reported	Units Rptd.	Ref.	Solubility scc/cc Bar	Diffusivity cm^2/sec	Comments
Sylgard 182	44	384	51.2×10^{-9}	1	409			
G.E. SE450	Room	443	59×10^{-9}	1	203 206			
Silastic-50	Room	195	26×10^{-9}	1	203 206 241			
Silastic	25	443	59×10^{-9}	1	208			.0136 cm thick
Silastic LS-63	26	78	10.4×10^{-9}	1	208			.23 cm thick

References Reporting: 203, 206, 208, 210, 223, 241, 385, 409

PERMEANT: Oxygen O_2

MATERIAL: Rubber, Silicone

PERMEANT: Oxygen O_2

MATERIAL: Silver

Type or Trade Name	Temp. °C	Permeability Std. Units$_8$ (Value x 10^{-8})	Permeability as Reported	Units Rptd.	Ref.	Solubility scc/cc Bar	Diffusivity cm^2/sec	Comments
	25	NC	1.5×10^{-17}	13	378			

References Reporting: 378

Type or Trade Name	Temp. °C	Permeability Std. Units ($\times 10^{-8}$)	Permeability as Reported	Units Rptd.	Ref.	Solubility scc/cc Bar	Diffusivity cm^2/sec	Comments
	23	.262	$.0349 \times 10^{-9}$	1	207			.00254 cm

References Reporting: 207

PERMEANT: Oxygen O_2

MATERIAL: Styrene-Acrylonitrile

PERMEANT: Oxygen O_2

MATERIAL: Teflon

Type or Trade Name	Temp. °C	Permeability Std. Units ($\times 10^{-8}$)	Permeability as Reported	Units Rptd.	Ref.	Solubility scc/cc Bar	Diffusivity cm^2/sec	Comments
	Room	.003	$.0004 \times 10^{+9}$	1	203 206			
TFE	25	7.5	7.6×10^{-7}	6	378			
FEP	23	NC	.39	24	333			
FEP	25	3.37	750	7	334			
FEP	50	9.22	2050	7	334			
FEP	75	17.99	4000	7	334			
FEP	100	31.48	7000	7	334			

References Reporting: 203,206,333, 334,378

Type or Trade Name	Temp. °C	Permeability Std. Units ($\times 10^{-8}$)	Permeability as Reported	Units Rptd.	Ref.	Solubility scc/cc Bar	Diffusivity cm^2/sec	Comments
Arc-cast	2100	NC	.10	15	432			
Arc-cast	2200	NC	.15	15	432			
Arc-cast	2300	NC	.14	15	432			
Arc-cast	2600	NC	.12	15	432			

References Reporting: 432

PERMEANT: Oxygen O_2

MATERIAL: Tungsten

PERMEANT: Oxygen O_2

MATERIAL: Vinylidene-Acrylonitrile

Type or Trade Name	Temp. °C	Permeability Std. Units ($\times 10^{-8}$)	Permeability as Reported	Units Rptd.	Ref.	Solubility scc/cc Bar	Diffusivity cm^2/sec	Comments
F218	NG	.0032	.710	7	389			
F220	NG	.0154	3.42	7	389			

References Reporting: 389

Type or Trade Name	Temp. °C	Permeability Std. Units (10^{-8}) (Value x 10^{-8})	Permeability as Reported	Units Rptd.	Ref.	Solubility scc/cc Bar	Diffusivity cm^2/sec	Comments
	Room	.0038	.0005 x 10^{-9}	1	203 206			

References Reporting: 203, 206

PERMEANT: Oxygen O_2

MATERIAL: Vinylidene Chiiride-Vinylchloride

PERMEANT: Oxygen O_2

MATERIAL: Vinylidene Fluoride-Chlorotrifluoroethylene

Type or Trade Name	Temp. °C	Permeability Std. Units ($\times 10^{-8}$)	Permeability as Reported	Units Rptd.	Ref.	Solubility scc/cc Bar	Diffusivity cm^2/sec	Comments
X-500	25	.015	$.20 \times 10^{-10}$	3	311			
X-500	40	.089	1.18×10^{-10}	3	311			
X-500	50	.154	2.05×10^{-10}	3	311			
X-500	75	.580	7.73×10^{-10}	3	311			
X-5500	0	.083	1.11×10^{-10}	3	311			
X-5500	13	.281	3.74×10^{-10}	3	311			
X-5500	25	.701	9.34×10^{-10}	3	311			
X-5500	50	3.79	50.5×10^{-10}	3	311			
X-3700	0	.047	$.62 \times 10^{-10}$	3	311			
X-3700	25	.410	5.46×10^{-10}	3	311			

Type or Trade Name	Temp. °C	Permeability Std. Units ($\times 10^{-6}$)	Permeability as Reported	Units Rptd.	Ref.	Solubility scc/cc Bar	Diffusivity cm^2/sec	Comments
X-3700	50	2.56	34.1×10^{-10}	3	311			
X-3700	75	8.33	111×10^{-10}	3	311			

References Reporting: 311

PERMEANT: Oxygen O_2

MATERIAL: Vinylidene Fluoride-Chlorotrifluoroethylene

PERMEANT: Oxygen O_2

MATERIAL: Visqueen

Type or Trade Name	Temp. °C	Permeability Std. Units$_8$ (Value x 10^{-8})	Permeability as Reported	Units Rptd.	Ref.	Solubility scc/cc Bar	Diffusivity cm^2/sec	Comments
	20	2.44	$.325 \times 10^{-9}$	1	243			
	30	4.13	$.55 \times 10^{-9}$	1	243			
	40	6.9	$.92 \times 10^{-9}$	1	243			

References Reporting: 243

Type or Trade Name	Temp. °C	Permeability Std. Units$_8$ (Value x 10^{-8})	Permeability as Reported	Units Rptd.	Ref.	Solubility scc/cc Bar	Diffusivity cm^2/sec	Comments
	30	1.13	15.1×10^{-10}	3	325			
A	25	1.13	1.15×10^{-7}	6	378			
A	25	1.13	1.15×10^{-8}	8	390	.047	$.24 \times 10^{-6}$	
A	50	4.73	4.79×10^{-8}	8	390	.051	$.92 \times 10^{-6}$	

References Reporting: 325,378,390

PERMEANT: Oxygen O_2

MATERIAL: Vulcaprene

Authors and Titles of References

Arranged by IITRI Reference Number

A complete bibliography follows this section. It is printed on blue paper, and is arranged alphabetically by author's last name. Thus to obtain bibliographic information, first look up reference number in this section, get author's name and title of the paper, and then look in the blue section for the complete citation.

200. Muraca, R. W., "Development of Techniques to Improve Bladder Materials and Test Methods."

201. Weiner, R. S., "Basic Criteria and Definitions for Zero Fluid Leakage."

202. Hollywood, L. P., Metz, T. R. and Porter, R. N., "Storage Tests of Nitrogen Tetroxide and Hydrazine in Aluminum Containers."

203. Robb, W. L., "Thin Silicone Membranes--Their Permeation Properties and Some Applications."

204. Levine, N. B. and Krainman, H., "Nitroso Rubber Expulsion Bladders for Nitrogen Tetroxide Application."

205. Buckley, D. J. and Berger, M., "Swelling of Polymer Systems in Solvents. II. Mathematics of Diffusion."

206. Anon. "Permselective Membrane."

207. Brown, W. E. and Sauber, W. J., "Gas Transmission by Plastics Films."

208. Major, C. J. and Kammermeyer, K., "Gas Permeability of Plastics."

209. Stern, S. A., Sinclair, T. F. and Gareis, P. J., "Improved Permeability Apparatus of the Variable-Volume Type."

210. Lebovits, A., "Permeability of Polymers to Gases, Vapors, and Liquids."

211. Brubaker, D. W. and Kammermeyer, K., "Flow of Gases Through Plastic Membranes."

212. Norton, F. J., "Permeation of Gases Through Solids."

213. Rogers, C. E., Stannett, V. and Szwarc, M., "Permeability Valves - Permeability of Gases and Vapors Through Composite Membranes."

214. Stern, S. A., et al. "Helium Recovery by Permeation."

215. Li, N. N., Long, R. B. and Henley, E. J., "Membrane Separation Processes."

216. Myers, A. W., et al. "The Gas and Vapor Permeability of Plastic Films and Coated Papers. IV. The Permeation of Water Vapor."

217. Lakshminarayanaiah, N., "Transport Phenomena in Artificial Membranes."

218. Anon. "Teflon Sandwich Permeability Studies."

219. Tuwiner, S., "Diffusion and Membrane Technology - Permeation of Membranes by Gases and Vapors."

220. McCall, D. W., Ambrose, J. F. and Lanza, V. L., "Diffusion in Ethylene Polymers. II. Desorption of Water."

221. Kumins, C. A. and Roteman, J., "Diffusion of Gases and Vapors Through Polyvinyl Chloride-Polyvinyl Acetate Copolymer Films. I. Glass Transition Effect. II. Effect of Polymer Segment Mobility."

222. Michaels, A. S. and Bixler, H. J., "Solubility of Gases in Polyethylene."

223. Stern, S. A., et al. "Performance of a Versatile Variable-Volume Permeability Cell. Comparison of Gas Permeability Measurements by the Variable-Volume and Variable-Pressure Methods."

224. Vieth, W. R., Alcalay, H. H. and Frabetti, A. J., "Solution of Gases in Oriented Poly (ethylene terephthalate)."

225. Michaels, A. S. and Bixler, H. J., "Flow of Gases Through Polyethylene."

226. Bearman, M. Y. and Bearman, R. J., "Isothermal Permeabilities from Thermo-osmosis Experiments."

227. Yasuda, H. and Stannett, V., "Permeation, Solution, and Diffusion of Water in Some High Polymers."

228. Anon. "Storable Liquid Propellants for Titan II."

229. Luzzi, T., "A Review of the Physics of Gas Adsorption on Solid Surfaces."

230. Passmore, E. M., et al. "Investigation of Diffusion Barriers for Refractory Metals."

231. Peterson, N. L., "Diffusion in Refractory Metals."

232. Bailey, C. C., Holland, W. D. and Hulsebos, J., "Hydrogen Permeation Measurements on Vapor Barrier Materials for Cryogenic Insulations."

233. Riley, M. W. and Peckner, D., "Metals vs. Plastics: Performance - The Key to Selection."

234. Walker, R. E. and Westenberg, A. A., "Molecular Diffusion Studies in Gases at High Temperature: Results and Interpretation of the CO_2-O_2, CH_4-O_2, H_2-O_2, CO-O_2, and H_2O-O_2 Systems."

235. Weber, T. "Evaluation of Gaseous and Particulate Components in Manned Space Stations."

236. Walker, R. E. and Westenberg, A. A., "Molecular Diffusion Studies in Gases at High Temperature: Results and Interpretation of the He-A System."

237. Michaels, A. S. and Parker, R. B., "The Determination of Solubility Constants for Gases in Polymers."

238. Long, R. B., "Liquid Permeation Through Plastic Films."

239. Michaels, A. S., et al. "Conditioned Polyethylene as a Permselective Membrane."

240. Myers, A. W., et al. "Permeability of Polyethylene to Gases and Vapors."

241. Kammermeyer, K. "Silicone Rubber as a Selective Barrier - Gas and Vapor Transfer."

242. Waack, R., et al. "Permeability of Polymer Films to Gases and Vapors."

243. Brubaker, D. W. and Kammermeyer, K., "Separation of Gases by Means of Permeable Membranes - Permeability of Plastic Membranes to Gases."

244. Collins, J. J. "A Report on Acid-Resistant Molecular Sieve - Types AW-300 and AW-500."

245. Meares, P. "Transient Permeation of Organic Vapors Through Polymer Membranes."

246. Miller, G. H. and Parcell, L. J., "Para-Ortho Hydrogen Conversion."

247. Walters, W. H. "Summary Report on the Investigations to Date of Permeation of Propellants Through Bladders."

248. Olewinski, W. J., et al. "Investigation of Toxic Properties of Materials Used in Space Vehicles."

249. Klute, C. H. "Diffusion of Small Molecules in Semi-crystalline Polymers: Water in Polyethylene."

250. Klute, C. H. "Diffusion of Small Molecules in Semi-crystalline Polymers. II. Permeability of Unoriented Polymer Films."

251. Lohr, J. E. and Scholz, J. J., "Physical Adsorption on Poly (methyl - methacrylate)."

252. Van Amerongen, G. J. "The Permeability of Different Rubbers to Gases and Its Relation to Diffusivity and Solubility."

253. Fehlner, F. P. "Adsorption of Oxygen on Ultra-Thin Titanium Films."

254. Harrington, W. L., Skogerboe, R. K. and Morrison, G. H., "Determination of Trace Amounts of Carbon, Oxygen, and Nitrogen in Metals by Spark Source Mass Spectrometry."

255. Levine, N. B., Krainman, H. and Green, J., "Positive Expulsion Bladders for Storable Propellants."

256. Stansfield, O. M. "The Influence of Tensile Stress on Gaseous Permeation in Glassy-State and Complex Ceramics."

257. Mathews, A. J. "Evaluation of Porous Materials as Molecular Leaks."

258. Picking, J. W. "Sunflower Power Conversion System."

259. Walter, R. J. "Evaluation of the Effects of High Pressure Hydrogen on Storage Vessel Materials."

260. Rommel, M. Internal Letter - Permeability of Teflon by NTO.

261. Settle, J. P. and Schuler, F. T., "Gemini Oxidizer Expulsion Bladder Materials at Temperatures in the Range 15-165F."

262. Walter, R. J. "Compatibility of Tantalum and Columbium Alloys with Hydrogen."

263. Lee, J. Private Communication between Mr. Peter Schipma (IITRI) and Mr. John Lee, Rocketdyne, May 16, 1967.

264. Lee, J. Private Communication between Mr. Peter Schipma (IITRI) and Mr. John Lee, Rocketdyne, May 16, 1967.

265. Jackson, J. D. "Permeability of Titanium to Hydrogen."

266. Elwell, R. C., et al. "Study of Dynamic and Static Seals for Liquid Rocket Engines. Volume 2: Studies on Special Topics in Sealing."

267. Corridan, R. E. "Research on Diffusion of Hydrogen Through Palladium."

268. Egger, C. T., et al. "Permeation of Adhesively Bonded Joints by Gaseous and Liquid Hydrogen."

269. Anon. "Study of Static and Dynamic Seals for Liquid Rocket Engines."

270. Loats, H. L., et al. "Space Station Connection and Seal Study."

271. Krusos, J. N., et al. "Design Criteria and Quality Control Studies for Teflon Expulsion Bladders."

272. Anon. "Study of Static and Dynamic Seals for Liquid Rocket Engines."

273. Prins, W. and Hermans, J. J., "Theory of Permeation Through Metal Coated Polymer Films."

274. Rudd, B. D., Vose, D. W. and Johnson, S., "The Permeability of Niobium to Hydrogen."

275. Huldy, H. J. "Gas Permeability Apparatus for Films and Sheets."

276. Glyde, H. R. and Mayne, K. I., "Helium Diffusion in Aluminum."

277. Efros, D. A. "Permeability of Porous Media During the Filtration of a Gassed Liquid."

278. Brandt, W. W. and Anyas, G. A., "Diffusion of Gases in Fluorocarbon Polymers."

279. Stannett, V. and Yasuda, H., "Liquid versus Vapor Permeation Through Polymer Films."

280. Huffine, C. L. and Williams, J. M., "Hydrogen Permeation Through Metals, Alloys, and Oxides at Elevated Temperatures."

281. Crank, J. "Diffusion in Media with Variable Properties. III. Diffusion Coefficients which vary Discontinuously with Concentration."

282. Gorman, J. K. and Nardella, W. R., "Hydrogen Permeation Through Metals."

283. Heinrich, R. R., Johnson, C. E. and Crouthamel, C. E., "Hydrogen Permeation Studies. I. Armco Iron and Iron-Molybdenum Alloys."

284. Barrer, R. M., Barrie, J. A. and Raman, N. K., "Solution and Diffusion in Silicone Rubber. I. A Comparison with Natural Rubber."

285. Barrer, R. M., Barrie, J. A. and Raman, N. K., "Solution and Diffusion in Silicone Rubber. II. The Influence of Filters."

286. Li, N. N. and Henley, E. J., "Permeation of Gases Through Polyethylene Films at Elevated Pressures."

287. Weiss, H. G., et al. "Modification of the Hydrazine-Nitrogen Tetroxide Ignition Delay."

288. Steigerwald, E. A. "The Permeation of Hydrogen Through Metals and Metal-plus-Oxide Systems."

289. Anon. "Research in the Chemical, Physical and Metallurgical Sciences."

290. Pierce, C. M. "The Diffusion of Hydrogen and Other Light Gases Through Membranes, Porous Media, and Thin Plates: An Annotated Bibliography."

291. Anon. "Elastomeric and Compliant Materials for Liquid Rocket Fuel and Oxidizer Application. Part 1."

292. Johnson, R. L. Private Communication between Mr. Peter Schipma (IITRI) and Dr. Robert L. Johnson, TRW.

293. Levine, N. B. Private Communication between Mr. Peter Schipma (IITRI) and Mr. N. B. Levine, Thiokol, April 25, 1967.

294. Block, F. G. and O'Grady, J. J., "The Development of a Low Temperature Vapor Filled Thermionic Converter."

295. Steigerwald, E. A. "The Permeation of Hydrogen Through Materials for the Sunflower System."

296. Bauman, A. J. and Stembridge, C. W., "A Continuous Recording Automatic Permeameter, with Application to the Permeation of Nitrogen Tetroxide Through Teflon."

297. Robb, W. "A Summary of Some Room Temperature Permeation Rates for Dimethyl Silicone Rubber."

298. Anon. Space Programs Summary No. 37-34, Volume IV, June 1, 1965 - July 31, 1965.

299. Vango, S. P. "Determination of Permeability of Cast Teflon Sheet to Nitrogen Tetroxide and Hydrazine."

300. Anon. "Pressurization Design Guide. Vol. II."

301. Sanger, M. J., Molho, R. and Morris, E. E., "Stainless Steel Lined Glass Wound Tank."

302. Greenspan, H. J. and Curtis, D. L., "Cabin Sealing of Aerospacecraft."

303. Darms, F. J., Molho, R. and Morris, E. F., "Stainless Steel Lined, Glass Filament Wound Tanks for Long-Term Storage of Nitrogen Tetroxide and Other Propellants."

304. Bruman, A. J. "Some Design Considerations, Large Expulsion Bladders for Nitrogen Tetroxide and Hydrazine."

305. Eisemann, J. L. "Purification of Organic Compounds by Membrane Permeation."

306. Smetana, F. O. "A Theoretical and Experimental Study of Gas Flow Through Cloth over a Range of Pressures and Temperatures."

307. Wiseman, J. R., Sawyer, R. and Cheetham, C., "Propellant Feed System Analog - A Valuable Tool for Establishing the Effects of Upstream Dynamics on Reaction Control Rocket Motor Performance."

308. Anon. "Pressurization Design Guide. Vol. I."

309. Marr, W. J. "Leakage Testing Handbook."

310. Bialous, A. J. "Characteristics and Sources of Commercially Available Leak Detectors."

311. Myers, W., et al. (Syracuse Univ., Syracuse, N. Y.). Modern Plastics 37, No. 10, 139-40, 142, 145, 211, June 1960.

312. Frisch, H. L. "Factorization of the Activation Energies of Permeation and Diffusion of Gases in Polymers."

313. Stannett, V. and Yasuda, H. "Liquid versus Vapor Permeation Through Polymer Films."

314. Michaels, A. S., Vieth, W. R. and Bixler, H. J., "The Measurement of Diffusion Constants of Gases in Polymers by Sorption Techniques."

315. Sivadjian, J. and Corral, F., "Hygrophotographic Studies on the Permeability to Water and Moisture of Packaging Materials."

316. Sivadjian, J. and Riberio, D., "Permeability to Water and Water Vapor of Plastic Materials by the Hygrophotographic Technique."

317. Meares, P. "The Diffusion of Gases Through Polyvinyl Acetate."

318. Jolley, J. E. and Hildebrand, J. H., "Solubility, Entropy, and Partial Molal Volumes in Solutions of Gases in Non-polar Solvents."

319. McCall, D. W. and Slichter, W. P., "Diffusion in Ethylene Polymers. III. Effects of Temperature and Pressure."

320. Meares, P. "Second-Order Transition of Poly(vinyl acetate)."

321. Barrer, R. M., Barrie, J. A. and Slater, J., "Informal Discussion on Diffusion with Special Reference to High Polymers. Comparison of Ethylcellulose and Rubber as Diffusion and Sorption Media."

322. Crank, J. "Diffusion with Rapid Irreversible Immobilization."

323. Meares, P. "Solubilities of Gases in Poly(vinyl acetate)."

324. Barrer, R. M. and Fergusson, R. R., "Diffusion of Benzene in Rubber and Polythene."

325. Stannett, V. and Szwarc, M., "The Permeability of Polymer Films to Gases - A Simple Relationship."

326. Bent, H. A. "Permeability of Liquids of Polyethylene and Irradiated Polyethylene."

327. Barrie, J. A. and Platt, B., "Sorption and Diffusion in Crystalline Elastomers. I. Solubility of Isomeric Hydrocarbons in Stretched Rubber."

328. Frisch, H. L. "Association Studies in Polymer Solutions."

329. Klute, C. H. and Franklin, P. J., "Permeation of Water Vapor Through Polyethylene."

330. Lasoski, S. W., Jr. and Cobbs, W. H., Jr., "Moisture Permeability of Polymers. I. Role of Crystallinity and Orientation."

331. Steigerwald, E. A. "The Permeation of Hydrogen Through Constructional Materials."

332. Bottorff, M. R. "An Evaluation of Composite Teflon-Aluminum Foil Bladders for Surveyor Vernier Propulsion System."

333. Anon. "Reviewing the Chemical Properties of Teflon Resins."

334. Anon. "Chemical Properties - Resistance to Chemical and Solvent Attack."

335. Sperati, C. A. and Starkweather, H. W., Jr., "Fluorine-Containing Polymers. II. Polytetrafluoroethylene."

336. Anon. "Structural Adhesive Bonding Conference."

337. Anon. Notice of Conference on Properties of Polymers at Cryogenic Temperatures."

338. Muraca, R. F. "Development of Techniques to Improve Bladder Materials and Test Methods."

339. Zimm, B. H. and Lundberg, J. L. (General Electric Co., Schenectady, N. Y.). J. Phys. Chem. 60, 425-8, 2956.

340. Myers, A. W., et al. "The Gas and Vapor Permeability of Plastic Films and Coated Papers. V. Effect of Crystallinity."

341. Rogers, C. E., Stannett, V. and Szwarc, M., "The Gas and Vapor Permeability of Plastic Films and Coated Papers. VII. The Permeation of Organic Vapors."

342. Bearman, R. J., "The Thermoosmosis of the Rare Gases Through a Rubber Membrane."

343. Crank, J. "A Diffusion Problem in which the Amount of Diffusing Substance is Finite. II. Diffusion with Non-linear Adsorption."

Card #15

344. Denbigh, K. G.,and Raumann, G., "The Thermoosmosis of Gases Through a Membrane. I. Theoretical."

345. Denbigh, D. G., and Raumann, G., "The Thermoosmosis of Gases Through a Membrane. II. Experimental."

346. Weller, S. and Steiner, W. A., "Engineering Aspects of Separation of Gases. Fractional Permeation Through Membranes."

347. Lundberg, J. L., Wilk, M. B. and Huyett, M. J., "Sorption Studies Using Automation and Computation."

348. Norton, F. J. "Rare Gas Permeation Through Polymers."

349. Tung, L. H. and Buckser, S. (Dow Chem. Co., Midland, Mich.). J. Phys. Chem. 62, 1530-4, 1958.

350. Weller, S. W. and Steiner, W. A., "Separation of Oxygen from Gas Mixture."

351. Kumins, C. A., Rolle, C. J. and Roteman, J., "Water-Vapor Diffusion Through Vinyl Chloride-Vinyl Acetate Copolymer."

352. Griskey, R. G. and Waldman, N., "Thermodynamic Properties of Polymers - Part I."

353. Griskey, R. G. and Waldman, N., "Thermodynamic Properties of Polymers - Part II. High Density Polyethylene."

354. Shore, J. J. "The Effect of Nitrogen Tetroxide on Some Halogenated Plastics."

355. Johnson, R. L. "A Study to Analyze the Permeation of High Density Gases and Propellant Vapors Through Single Layer Teflon or Teflon Structure Materials and Laminates."

356. Johnson, R. L. "A Study to Analyze the Permeation of High Density Gases and Propellant Vapors Through Single Layer Teflon or Teflon Structure Materials and Laminations." Quarterly Progress Report No. 2.

357. Johnson, R. L. "A Study to Analyze the Permeation of High Density Gases and Propellant Vapors Through Single Layer Teflon or Teflon Structure Materials and Laminates." Quarterly Progress Report No. 3.

358. Johnson, R. L. "A Study to Analyze the Permeation of High Density Gases and Propellant Vapors Through Single Layer Teflon or Teflon Structure Materials and Laminations." Quarterly Progress Report No. 4.

359. Anon. "Annotated Bibliography: The James Forrestal Campus Library Acquisition."

360. Frisch, H. L., "Gas Permeation Through Membranes due to Simultaneous Diffusion and Convection."

361. Frisch, H. L., "The Time Lag in Diffusion."

362. Frisch, H. L., "The Time Lag in Diffusion. II."

363. Pollak, H. O. and Frisch, H. L., "The Time Lag in Diffusion. III."

364. Frisch, H. L. "The Time Lag in Diffusion. IV."

365. Ticknor, L. B., "On the Permeation of Cellophane Membranes by Diffusion."

366. Stamm, A. J. "Diffusion of Water into Uncoated Cellophane. I. From Rates of Water Vapor Adsorption, and Liquid Water Absorption."

367. Sivadjian, J. "Measure of Permeability of Plastic Material, Leather, and Similar Substances Against Moistness and Water by the Hygrophotographic Method."

368. Rosen, B. and Singleton, J. H., "Automatic Recording, Gas/Polymer-Film Permeameter."

369. Pilar, F. L. "The Flow of Gases Through High Polymer Films in Equilibrium with Sorbed Vapors."

370. Buckley, D. J., Berger, M. and Poller, C., "The Swelling of Polymer Systems in Solvents. I. Method for Obtaining Complete Swelling-Time Curves."

371. Rogers, C., et al. "Studies in the Gas and Vapor Permeability of Plastic Films and Coated Papers. Part I. Determination of the Permeability Constant."

372. Rogers, C., et al. "Studies in the Gas and Vapor Permeability of Plastic Films and Coated Papers. Part II. Some Factors Affecting the Permeability Constant."

373. Meyer, J. A., et al. "Studies in the Gas and Vapor Permeability of Plastic Films and Coated Papers. Part III. The Permeation of Mixed Gases and Vapors."

374. Rodgers, C. E. "Permeability and Chemical Resistance."

375. Lindstrom, J. "Membrane Separation."

376. Marcus, J. P., Day, W. A. and Jelinek, J. G., "Design and Development of an Elastomer Seal for Long Term Hazardous Propellant Storage."

377. Peters, P. Private Communication between Mr. Peter Schipma (IITRI) and Dr. Philip Peters (General Electric Co., Schenectady, N. Y.), June 15, 1967.

378. Muraca, R. F. Private communication between Mr. Peter Schipma (IITRI) and Dr. Ralph Muraca, Stanford, June 15, 1967.

379. Johnson, R. and Van Nice, L. Private communication between Mr. Peter Schipma (IITRI) and Dr. R. Johnson and Mr. L. Van Nice, TRW, May 17, 1967.

380. Lupakov, I. S., Kuz'michev, Yu, S., "Determination of the Permeability of Tube Walls for Helium."

381 Lupakov, I. S., Kuz'michev, Yu, S., "The Permeability of Metallic Tube Walls for Helium."

382. Erdmann-Jesnitzer, F., "Permeability of Electrolytic Nickel to Hydrogen and Sorption of it at Room Temperature."

383. Brauniegl, H. and Lenhart, H., "The Permeability of Films of Synthetic Resins and Hydrated Cellulose for Hydrogen Sulfide and Ammonia."

384. Drinberg, A., Ya., "Gas Permeability of Films of Some Lyophilic Colloids."

385. Kammermeyer, K. "Separation of Gases by Diffusion Through Silicone Rubber."

386. Binning, R. C., Jennings, J. F. and Martin, E. C., "Separation of Liquids by Permeation Through a Membrane."

387. Michaels, A. S., Vieth, W. R. and Bixler, H. J., "Gas Permeability of Highly Oriented Dibutyl Maleate-ethylene Copolymer Films."

388. Norton, F. J. "Gas Permeation Through Lexan Polycarbonate Resin."

389. Bennett, B., Cooper, C. W. and Luttinger, M., "Preparation and Gas Permeability of Vinylidene Chloride Copolymer Films."

390. Van Amerogen, G. J. "Influence of Structure of Elastomers on Their Permeability to Gases."

391. Watson, E. C. "An Experimental Investigation at Mach Numbers from 2.1 to 3.0 of Circular Internal-Compression Inlets Having Translatable Centerbodies and Provisions for Boundary-Layer Removal."

392. Kumins, C. A. and Roteman, J., "Effect of Solid-Polymer Interaction on Transition Temperature and Diffusion Coefficients."

393. Barrer, R. M., Barrie, J. A and Slater, J., "Sorption and Diffusion in Ethyl-cellulose. I. History Dependence of Sorption Isotherms and Permeation rates. II. Quantitative examination of Settled Isotherms and Permeation Rates."

394. Barrer, R. M. and Barrie, J. A., "Scrption and Diffusion in Ethylcellulose. IV. Water in Ethylcellulose."

395. Davis, O. H. and Mitchell, G. A., "Performance of a Mach Number 3.0 Design Axisymmetric Doublecone External-Compression Inlet in the Mach Number Range 1.97 to 0.79."

396. Stitt, L. E. and Salmi, R. J., "Performance of a Mach 3.0 External-Internal-Compression Axisymmetric Inlet at Mach Numbers from 2.0 to 3.5."

397. Abbott, H. M. "Adhesives, Seals, Gaskets and Polymeric Materials for Aerospace Applications: An Annotated Bibliography."

398. Smith, T. "Kinetics and Mechanism of Hydrogen Permeation of Oxide Films on Zirconium."

399. Taylors, E. A., Karel, M. and Proctor, B. E., "Measurement of Oxygen Permeability."

400. Barrer, R. M. and Grove, D. M., "Flow of gases and vapors in a porous medium and its bearing on adsorption problems."

401. Barrer, R. M., "Permeation, diffusion and solution of gases in organic polymers."

402. Anon. "Teflon 100, 110, and 120."

403. Webb, R. W., "Permeation of hydrogen through metals."

404. Studt, P. L., "Mechanisms of gaseous permeation through glass, single-crystal silicon, and germanium; and stress-enhanced gaseous permeation through alumina bodies."

405. Gilbert, L. L., "Materials problems in chemical liquid-propellant rocket systems."

406. Chinberg, V. L. and Perkins, H., "Preliminary studies of liquid oxygen expulsion bladders."

407. Bruner, L. J., "The electrical properties of semipermeable membranes."

408. Rhyne, J. W., "Silver-cadmium battery development program."

409. Coleman, M. J., "Investigation of unique gas permeability cell system to remove CO_2 and other noxious gases from spacecraft cabins."

410. Anon. "Teflon 30, 30B, 42."

411. Anon. "TFE - Fluorocarbon resin dispersions - properties and processing techniques."

412. Andreopoulos, T. C., "MPU bladder development."

413. Fick, H. J.,"Evaluation of the compatibility of polyvinylidene fluoride (KYNAR) with storable liquid propellants (nitrogen tetroxide and hydrazine)."

414. Podall, H. E., et al. "Development of improved polymeric materials for cryogenic propellant tank liners and positive expulsion bladders."

415. Muraca, R. F.,"Investigation of the space storability of pressurizing gases."

416. Krusos, J. N. Private communication between Mr. Peter Schipma (IITRI) and Mr. James Krusos (BAC), June 15, 1967.

417. Jones, P. M. S., Gibson, R. and Evans, J. A., "The permeation and diffusion of hydrogen isotopes through steels."

418. Saalfeld, F. E. and McDowell, M. V., "A mass spectrometric method for the determination of permeability coefficients."

419. Anon. "Pressurization design guide III."

420. Vango, S. P. and Krasinsky, J. B., "Continued effort in metal plating of teflon sheet as a means of reducing permeation."

421. Vango, S. P. and Krasinsky, J. B., "Additional results on metal plating of teflon sheet."

422. Vango, S. P. and Krasinsky, J. B., "Metal plating of teflon sheet as a means of reducing permeation."

423. Hsieh, P. Y., "A study of the encapsulation applicable to liquid rocket fuel."

424. Myers, A. W., Stannett, V. T. and Szwarc, M., "The permeability of polypropylene to gases and vapors."

425. Sneck, H. J., "Apperdix A - A survey of gas permeation through metals and polymers."

426. Bachmann, R. C., "Research on diffusion of hydrogen through palladium-silver alloy."

427. Pemsler, J. P., Anderson, R. W. and Rapperport, E. J., "Solubility and diffusion of gases in beryllium."

428. Stanford, H. B., "The measured permeability to nitrogen tetroxide of some potential bladder materials."

429. Jones, P. M. S., Gibson, R. and Evans, J. A., "The permeation and diffusion of hydrogen in molybdenum."

430. Jones, P. M. S., Gibson, R. and Evans, J. A., "The Permeation and diffusion of hydrogen isotopes through stainless steels. Part 2."

431. Gibson, R., Jones, P. M. S. and Evans, J. A., "The permeation and diffusion of hydrogen isotopes through stainless steels. Part 1."

432. Aitken, E. A., et al. "Measurement of the permeability of tungsten to hydrogen and to oxygen."

433. Hewitt, G. F., Moore, M. J. C. and Sharratt, E. W., "The permeability of nuclear grade graphite to a variety of gases."

434. Lare, P. J., et al. "Investigation of the effects of mechanical stress on the permeability of engineering materials to certain cryogenic and storable propellants used in launch vehicles."

435. Sage, B. H., "Some properties of nitric acid, nitrogen dioxide, nitric oxide, water and their mixtures."

436. Fish, W. R., "Storable liquid propellants, nitrogen tetroxide/aerozine 50."

437. Keller, O. F. and Toth, L. R., "ALPS generant tank and cell assembly."

438. Porter, R. N., "The fabrication of seamless teflon propellant expulsion bladders."

439. Edwards, R. H., "Permeation of monatomic gases through aluminum oxide."

440. Van Raaij, P. T. and Winkel, P., "The permeability of plastic films and foils to gases, vapors and liquids."

441. Anon. "Handling and storage of nitrogen tetroxide."

442. Chipchak, D., et al. "Development of expulsion and orientation systems for advanced liquid rocket propulsion systems."

443. Vargo, E. J. and Cooper, D. B., "An investigation of the corrosion resistance of metallic materials to molten lithium hydride at cyclic elevated temperature."

Bibliography

Arranged Alphabetically by Author's Last Name

REFERENCES

Anon. (Aerojet-General Corp., Sacramento, Calif.). Storable liquid propellants for Titan II. Report No. LRP 198, 41 pp., June 1, 1962, AD 445 780 (IITRI ref. 228).

Anon. (Aerojet-General Corp., Von Karmen Center, Azusa, Calif.). Pressurization design guide. Vol. I. Contract No. NAS7-169, Sept. 1964 (IITRI ref. 308).

Anon. (Aerojet-General Corp., Von Karmen Center, Azusa, Calif.). Pressurization design guide. Vol. II. Contract No. NAS7-169, Sept. 1964 (IITRI ref. 300).

Anon. (Aerojet-General Corp., Von Karmen Center, Azusa, Calif.). Pressurization design guide. Vol. III. Contract No. NAS7-169, Sept. 1964 (IITRI ref. 419).

Anon. (Army Chem. Center, Edgewood, Md.). Handling and storage of nitrogen tetroxide. Contract No. AF 33(616)60-20. Final Report, 106 pp., May 1963 (IITRI ref. 441).

Anon. (Jet Propulsion Lab., Pasadena, Calif.). Space Programs Summary No. 37-34, Volume IV, June 1, 1965-July 31, 1965, 307 pp., Aug. 31, 1965 (IITRI ref. 298).

Anon. (E. I. duPont de Nemours and Co., Fluorocarbons Div., Wilmington, Del.). Chemical properties - resistance to chemical and solvent attack. Bull. T-3B - duPont Teflon FEP fluorocarbon film, 2 pp. (IITRI ref. 334).

Anon. (E. I. duPont de Nemours and Co., Wilmington, Del.). Reviewing the chemical properties of "Teflon" resins. J. of Teflon, Reprint No. 22, 5 pp., Dec. 1964 (IITRI ref. 333).

Anon. (E. I. duPont de Nemours and Co., Wilmington, Del.). Teflon 100, 110, and 120. Bull. No. A-21458, 5 pp., Aug. 1961 (IITRI ref. 402).

Anon. (E. I. duPont de Nemours and Co., Wilmington, Del.). TFE - Fluorocarbon resin dispersions - properties and processing techniques. Info. Bull. X-50e, 6 pp. (IITRI ref. 411).

Anon. (E. I. duPont de Nemours and Co., Wilmington, Del.). Teflon 30, 30B, 42. Bull No. A-25040, 3 pp. (IITRI ref. 410).

Anon. (General Electric Co., Advanced Technol. Lab., Schenectady, N.Y.). Study of static and dynamic seals for liquid rocket engines. Contract No. NAS7-102, Final Report, Jan. 1 1965-Sept. 1, 1965, 407 pp., Nov. 1965 (IITRI ref. 272).

Anon. (General Electric Co., Advanced Technol. Lab., Schenectady, N.Y.). Study of static and dynamic seals for liquid rocket engines. Contract No. NAS7-102, Final Report, Apr. 1, 1964-Oct. 1, 1964, 39 pp., 1964 (IITRI ref. 269).

Anon. (General Electric Co., Res. and Dev. Center, Schenectady, N.Y.). Permselective membrane. 6 pp. (IITRI ref. 206)

Anon. (NASA, George C. Marshall, Space Flight Center, Huntsville, Ala.). Structural Adhesive Bonding Conference. NASA George C. Marshall Space and Flight Center, Huntsville, Ala. Mar. 15-16, 1966 (IITRI ref. 336).

Anon. (NASA, Lewis Res. Center and Case Inst. of Technol., Cleveland, Ohio). Notice of Conference on Properties of Polymers at Cryogenic Temperatures. NASA Lewis Res. Center, Cleveland, Ohio. Apr. 25-27, 1967, 12 pp., 1967 (IITRI ref. 337).

Anon. (North American Aviation, Inc., Rocketdyne Div., Canoga Park, Calif.). Research in the chemical, physical, and metallurgical sciences. Contract No. AF04(611)-8502, Report No. RTD-TDR-64-21. 128 pp., Feb. 1964 (IITRI ref. 289).

Anon. (Princeton Univ., Princeton, N.J.). Annotated Bibliography - The James Forrestal Campus Library acquisition. 117 pp., July 5, 1967 (IITRI ref. 359).

Anon. (Redel Inc., Scientific Res. and Dev., Anaheim, Calif.). Teflon sandwich permeability studies. Final Report P.O. 2478-6004, 56 pp., Oct. 14, 1963. 26 refs. (IITRI ref. 218)

Anon. (Thiokol Chem. Corp., Reaction Motors Div., Denville, N.J.). Elastomeric and compliant materials for liquid rocket fuel and oxidizer application. Part 1. Contract No. AF33(657)-11093, Mar. 1964 (IITRI ref. 291).

Abbott, H. M. (Lockheed Missile and Space Co., Sunnyvale, Calif.). Adhesives, seals, gaskets and polymeric materials for aerospace applications: An annotated bibliography. Contract No. AF33(657)-10107, Report No. 3-06-63-2, 202 pp., Nov. 1963, AD 443 256 (IITRI ref. 397).

Aitken, E. A., et al. (General Electric Co., Nuclear Materials and Propulsion Operation, Cincinnati, Ohio). Measurement of the permeability of tungsten to hydrogen and to oxygen. Contract No. NAS3-6216, Final Report, 53 pp., May 1966 (IITRI ref. 432).

Andreopoulos, T. C. (Radio Corp. of America, Aerospace Systems Div., Burlington, Mass.). MPU bladder development. Contract No. AF 04(695)-273, 211 pp., Nov. 4, 1963 (IITRI ref. 412).

Bachmann, R. C. (Advanced Technol. Labs., Mountain View, Calif.). Research on diffusion of hydrogen through palladium-silver alloy. Phase 3. Contract NAS7-118, Final Report, Apr. 1964-May 1965, 96 pp., May 1965 (IITRI ref. 426).

Bailey, C. C., Holland, W. D. and Hulsebos, J. (Lockheed-Georgia Co., Div. of Lockheed Aircraft Corp., Marietta, Ga.). Hydrogen permeation measurements on vapor barrier materials for cryogenic insulations, 5 pp., 1963. Society of Automotive Engineers, National Aeronautic and Space Engineering and Manufacturing meeting, Los Angeles, Calif., Sept. 23-27, 1963 (IITRI ref. 232).

Barrer, R. M. and Barrie, J. A. (Imperial Coll., London, Engl.). Sorption and diffusion in ethylcellulose. IV. Water in ethylcellulose. J. Polymer Sci. 28, 377-86, 1958 (IITRI ref. 394).

Barrer, R. M., Barrie, J. A. and Slater, J. (Imperial Coll., London, Engl.). Informal discussion on diffusion with special reference to high polymers. Comparison of ethylcellulose and rubber as diffusion and sorption media. Trans. Faraday Soc. 53, p. 1145, 1957 (IITRI ref. 321).

Barrer, R. M. and Fergusson, R. R. (Imperial Coll., London, Engl.). Diffusion of benzene in rubber and polythene. Trans. Faraday Soc. 54, 989-1000, 1958 (IITRI ref. 324).

Barrer, R. M., Barrie, J. A. and Slater, J. (Imperial Coll. Sci. Technol., London, Engl.). Sorption and diffusion in ethylcellulose. I. History dependence of sorption isotherms and permeation rates. II. Quantitative examination of settled isotherms and permeation rates. J. Polymer Sci. 23, 315-44, 1957 (IITRI ref. 393).

Barrer, R. M. and Grove, D. M. (Univ. of Aberdeen, Marischal Coll., Engl.). Flow of gases and vapors in a porous medium and its bearing on adsorption problems. Part I. The steady state of flow. Trans. Faraday Soc. 47, 826-837, Aug. 1951 (IITRI ref. 400).

Barrer, R. M. (Univ. of Cambridge, Dept. of Colloid Sci., Cambridge, Engl.). Permeation, diffusion and solution of gases in organic polymers. Trans. Faraday Soc. 35, 628-43, 1939 (IITRI ref. 401).

Barrer, R. M., Barrie, J. A. and Raman, N. K. (Imperial Coll., Physical Chem. Lab., South Kensington, London, Engl.). Solution and diffusion in silicone rubber. I. A Comparison with natural rubber. Polymer 3, 595-603, 1962 (IITRI ref. 284).

Barrer, R. M., Barrie, J. A. and Raman, N. K. (Imperial Coll., Physical Chem. Lab., South Kensington, London, Engl.). Solution and diffusion in silicone rubber. II. The influence of fillers. Polymer 3, 604-14, 1962 (IITRI ref. 285).

Barrie, J. A. and Platt, B. (Imperial Coll., London, Engl.). Sorption and diffusion in crystalline elastomers. I. Solubility of isomeric hydrocarbons in stretched rubber. J. Polymer Sci. 49, 479-93, 1961 (IITRI ref. 327).

Bauman, A. J. and Stembridge, C. W. (Jet Propulsion Lab., Pasadena, Calif.). A continuous recording automatic permeameter, with application to the permeation of nitrogen tetroxide through Teflon. Programs Summary No. 37-30, 4, 206-208, Dec. 31, 1964 (IITRI ref. 296).

Bearman, R. J. (Stanford Univ., Stanford, Calif.). The thermo-osmosis of the rare gases through a rubber membrane. J. Phys. Chem. 61, 708-13, 1957 (IITRI ref. 342).

Bearman, M. Y. and Bearman, R. J. (Univ. of Kansas, Lawrence, Ka.). Isothermal permeabilities from thermo-osmosis experiments. J Appl. Polymer Sci. 10, No. 5, 773-86, 1966 (IITRI ref. 226).

Bennett, B., Cooper, C. W. and Luttinger, M. (Battelle Mem. Inst., Columbus, Ohio). Preparation and gas permeability of vinylidene chloride copolymer films. J. Appl. Polymer Sci. 6, S23-S24, 1962 (IITRI ref. 389).

Bert, H. A. (Univ. of Minn., Minneapolis, Minn.). Permeability to liquids of polyethylene and irradiated polyethylene. J. Polymer Sci. 24, 387-400, 1957 (IITRI ref. 326).

Bialous, A. J. (General Electric Res. and Dev. Center, Schenectady, N.Y.) Characteristics and sources of commercially available leak detectors. Contract No. NAS7-396, Report No. S 67 1013, 158 pp., June 1967 (IITRI ref. 310).

Block, F. G. and O'Grady, J. J. (Radio Corp. of America, Lancaster, Penn.). The development of a low temperature vapor filled thermionic converter. Contract No. AF33(616)-7903, Report No. TDR-62-324, 168 pp., June 1962, AD 278 810 (IITRI ref. 294).

Binning, R. C., Jennings, J. F. and Martin, E. C. (Standard Oil Co., Chicago, Ill.). Separation of liquids by permeation through a membrane. U.S. Patent 2,985,588, May 23, 1961 (IITRI ref. 386).

Bottorff, M. R. (Hughes Aircraft Co., Culver City, Calif.) An evaluation of composite teflon-aluminum foil bladders for surveyor vernier propulsion system. Contract No. NAS7-100, JPL Contract No. 950056, 70 pp., Mar. 2, 1967 (IITRI ref. 332).

Brandt, W. W. and Anyas, G. A. (Ill. Inst. of Technol., Dept. of Chem., Chicago, Ill.). Diffusion of gases in fluorocarbon polymers. J. Appl. Polymer Sci. 7, 1919-31, 1963 (IITRI ref. 278).

Braunisch, H. and Lenhart, H. (KALLE akt.-Ges., Weisbaden, Ger.). The permeability of films of synthetic resins and hydrated cellulose for hydrocarbon sulfide and ammonia. Kolloid-Z. 177, 24-9, 1961 (IITRI ref. 383).

Brown, W. E. and Sauber, W. J. Gas transmission by plastics films. Modern Plastics 36, No. 12, 107, 110, 112-14, 116, 190, Aug. 1959 (IITRI ref. 207).

Brubaker, D. W. and Kammermeyer, K. (State Univ. of Iowa, Iowa City, Ia.). Flow of gases through plastic membranes. Ind. Eng. Chem. 45, 1148-52, 1953 (IITRI ref. 211).

Brubaker, D. W. and Kammermeyer, K. (State Univ. of Iowa, Iowa City, Ia.). Separation of gases by means of permeable membranes - permeability of plastic membranes to gases. Ind. Eng. Chem. 44, 1465-74, June 1952 (IITRI ref. 243).

Bruman, A. J. (Jet Propulsion Lab., Pasadena, Calif.). Some design considerations, large expulsion bladders for nitrogen tetroxide and hydrazine. Contract No. NAS7-100, JPL-TR-32-862, 38 pp., Jan. 15, 1966 (IITRI ref. 304).

Bruner, L. J. (Univ. of Calif., Dept. of Phys., Riverside, Calif.). The electrical properties of semipermeable membranes. Contract No. Nonr-4442(00), Annual Summary Report, Jan. 1-Dec. 31, 1964, 32 pp., Oct. 1964 (IITRI ref. 407).

Buckley, D. J. and Berger, M. (Esso Res. and Eng. Co., Central Basic Res. Lab., Linden, N.J.). Swelling of polymer systems in solvents. II. Mathematics of diffusion. J. Polymer Sci. 56, 175-88, 1962 (IITRI ref. 205).

Buckley, D. J., Berger, M. and Poller, C. (Esso Res. and Eng. Co., Central Basic Res. Lab., Linden, N.J.). The swelling of polymer systems in solvents. I. Method for obtaining complete swelling-time curves. J. Polymer Sci. 56, 163-74, 1962 (IITRI ref. 370).

Chinberg, V. L. and Perkins, H. (NASA George C. Marshall Space Flight Center, Huntsville, Ala.). Preliminary studies of liquid oxygen expulsion bladders. NASA Tech. Memorandum X-53005, 27 pp., Oct. 12, 1964 (IITRI ref. 406).

Chipchak, D., et al. (Bell Aerosystems Co., Buffalo, N.Y.). Development of expulsion and orientation systems for advanced liquid rocket propulsion systems. Contract No. AF 04(611)-8200. Final Report, Oct. 15, 1962-Mar. 31, 1963. 263 pp., July 1963 (IITRI ref. 442).

Coleman, M. J. (Iowa State Univ. of Sci. and Technol., Dept. of Chem. Eng., Ames, Io.). Investigation of unique gas permeability cell system to remove CO_2 and other noxious gases from spacecraft cabins. Contract No. NASr-73. Final Report period ending Mar. 31, 1965. 110 pp., 1965 (IITRI ref. 409).

Collins, J. J. (Union Carbide Corp., Linde Div., New York, N.Y.) A report on acid-resistant molecular sieve - types AW-300 and AW-500. Union Carbide Corp. Bull. No. F-84-1454, Nov. 15, 1961 (IITRI ref. 244).

Corriden, R. E. (Advanced Technol. Labs. Div. of American-Standard, Mountain View, Calif.) Research on diffusion of hydrogen through palladium. Contract No. NAS7-118. Quarterly Progress Report, Jan.-Apr. 1962. 14 pp., 1962. 3 refs. (IITRI ref. 267).

Crank, J. (Courtaulds, Ltd., Maidenhead, Berks, Engl.). Diffusion in media with variable properties. III. Diffusion coefficients which vary discontinuously with concentration. Trans. Faraday Soc. 47, 450-61, 1951 (IITRI ref. 281).

Crank, J. (Courtaulds, Ltd., Maidenhead, Berks, Engl.). Diffusion with rapid irreversible immobilization. Trans. Faraday Soc. 53, 1083-91, 1957 (IITRI ref. 322).

Crank, J. (Courtaulds, Ltd., Maidenhead, Berks, Engl.). A diffusion problem in which the amount of diffusing substance is finite. II. Diffusion with nonlinear adsorption. Phil. Mag. 39, 140-9, 1948 (IITRI ref. 343).

Darms, F. J., Molho, R. and Morris, E. F. (Aerojet-General Corp., Chem. and Structural Products, Von Karman Center, Azusa, Calif.). Stainless-steel-lined, glass-filament-wound tanks for long-term storage of nitrogen tetroxide and other propellants. Contract No. AF 33(615)-3619. Report No. 1014-01-1. Jan. 1-Mar. 31, 1966. 35 pp., Apr. 1966 (IITRI ref. 303).

Davis, O. H. and Mitchell, G. A. (Imperial Coll., Physical Chem. Labs., London, Engl.). Performance of a mach number 3.0 design axisymmetric doublecone external-compression inlet in the mach number range 1.97 to 0.79. Tech. Memorandum X-154, 29 pp., Apr. 1960 (IITRI ref. 395).

Denbigh, K. G. (Univ. of Cambridge, Chem. Eng. Lab., Cambridge, Engl.), and Raumann, G. (I.C.I., Ltd., Butterwick Res. Lab., Welwyn, U.K.). The thermo-osmosis of gases through a membrane. I. Theoretical. Proc. Royal Soc. (London) A210, 377-87, 1952 (IITRI ref. 344).

Denbigh, K. G. (Univ. of Cambridge, Chem. Eng. Lab., Cambridge, Engl.), and Raumann, G. (I.C.I., Ltd., Butterwick Res. Lab., Welwyn, U.K.). The thermo-osmosis of gases through a membrane. II. Experimental. Proc. Royal Soc. (London) A210, 518-33, 1952 (IITRI ref. 345).

Drinberg, A., Ya. Gas permeability of films of some lyophilic colloids. J. Phys. Chem. 6, 870-882. 1935 (IITRI ref. 384).

Edwards, R. H. (Univ. of Calif., Lawrence Radiation Lab., Berkeley, Calif.). Permeation of monatomic gases through aluminum oxide. AEC Contract No. W-7405-ENG-48. 47 pp., Aug. 25, 1966 (IITRI ref. 439).

Efros, D. A. (All-Union Petroleum Gas Sci. Res. Inst.). Permeability of porous media during the filtration of a gassed liquid. USSR, AN, Doklady. 132, pp. 311-4. May 1960. Transl. Sov. Phys. - Doklady, 5, pp. 493-6. Nov.-Dec. 1960. 17 refs. (IITRI ref. 277).

Egger, C. T., et al. (NASA, George C. Marshall Space Flight Center, Huntsville, Ala.). Permeation of adhesively bonded joints by gaseous and liquid hydrogen. Report No. NASA-TM-X-53066, 39 pp., June 19, 1964 (IITRI ref. 268).

Eisemann, J. L. (Ionics, Inc., Cambridge, Mass.). Purification of organic compounds by membrane permeation. Contract No. DA-18-108-Cml-6626, 78 pp., Apr. 18, 1963, AD 408 670 (IITRI ref. 305).

Elwell, R. C., et al. (General Electric Co., Advanced Technol. Labs., Schenectady, N.Y.). Study of dynamic and static seals for liquid rocket engines. Volume 2: Studies on special topics in sealing. Contract No. NAS7-102. Final Report, Feb. 26, 1962-Feb. 25, 1963, 163 pp., Mar. 29, 1963 (IITRI ref. 266).

Erdmann-Jesnitzer, F. Permeability of electrolytic nickel to hydrogen and sorption of it at room temperature. Bergakademie 13, 8-16, 1961 (IITRI ref. 382).

Fehlner, F. P. Adsorption of oxygen on ultra-thin titanium films. Nature 210, 1035-6, June 4, 1966 (IITRI ref. 253).

Fick, H. J. (Schjeldahl (G.T.) Co., Northfield, Minn.). Evaluation of the compatibility of polyvinylidene fluoride (KYNAR) with storable liquid propellants (Nitrogen tetroxide and hydrazine). JPL Contract NI-120421. Contract NAS7-100, 23 pp., Jan. 30, 1963 (IITRI ref. 413).

Fish, W. R. (Aerojet-General Corp., Sacramento, Calif.). Storable liquid propellants, nitrogen tetroxide/aerozine 50. Report No. LRP 198, 384 pp., 1962 (IITRI ref. 436).

Frisch, H. L. (Univ. of Southern Calif., Dept. of Chem., Los Angeles, Calif.). Association studies in polymer solutions. J. Polymer Sci. 18, 299-302, 1955 (IITRI ref. 328).

Frisch, H. L. (Univ. of Southern Calif., Dept. of Chem., Los Angeles, Calif.). Gas permeation through membranes due to simultaneous diffusion and convection. J. Phy. Chem. 60, 1177-1181, Sept. 1956 (IITRI ref. 360).

Frisch, H. L. (Univ. of Southern Calif., Dept. of Chem., Los Angeles, Calif.). The time lag in diffusion. J. Phy. Chem. 61, 93-95, Jan. 1957 (IITRI ref. 361).

Frisch, H. L. (Bell Telephone Lab., Murray Hill, N.J.). The time lag in diffusion. II. J. Phys. Chem. 62, 401-404, Apr. 1958 (IITRI ref. 362).

Frisch, H. L. (Bell Telephone Labs., Murray Hill, N.J.). The time lag in diffusion. IV. J. Phy. Chem. 63, 1249-59, Aug. 1959 (IITRI ref. 364).

Frisch, H. L. (Bell Telephone Labs., Murray Hill, N.J.). Factorization of the activation energies of permeation and diffusion of gases in polymers. J. Polymer Sci. Pt.B 1, No. 11, 581-6, 1963 (IITRI ref. 312).

Gibson, R., Jones, P. M. S. and Evans, J. A. (Atomic Weapons Res. Establishment, Aldermaston, Engl.). The permeation and diffusion of hydrogen isotopes through stainless steels. Part 1: Niobium stabilized S110 steel. AWRE Report 0-47/65, 32 pp., Sept. 1965 (IITRI ref. 431).

Gilbert, L. L. (Aerojet-General Corp., Azusa, Calif.). Materials problems in chemical liquid-propellant rocket systems. Tech. Memorandum 89, 41 pp., Aug. 1959 (IITRI ref. 405).

Glyde, H. R. and Mayne, K. I. (Clarendon Lab., Oxford, Engl.). Helium diffusion in aluminum. Phil. Mag.(GB), 12, 997-1003, Nov. 1965 (IITRI ref. 276).

Gorman, J. K. and Nardella, W. R. (Sperry Gyroscope Co., Electric Tube Div., Great Neck, N.Y.). Hydrogen permeation through metals. Vacuum 12, 6 pp., Jan.-Feb. 1962 (IITRI ref. 282).

Greenspan, H. J. and Curtis, D. L. (Litton Systems, Inc., Space Sci. Lab., Beverly Hills, Calif.). Cabin sealing of aerospacecraft. Contract No. AF33(616)-8166, Tech. Doc. Report ASD-TDR-62-661, 73 pp., Feb. 1963 (IITRI ref. 302).

Griskey, R. G. and Waldman, N. (Virginia Polytechnic Inst., Chem. Eng. Dept., Blacksburg, Va.). Thermodynamic properties of polymers - Part I. Modern Plastics 43, No. 7, pp. 119-120, 177, Mar. 1966 (IITRI ref. 352).

Griskey, R. G. and Waldman, N. (Virginia Polytechnic Inst., Chem. Eng. Dept., Blacksburg, Va.). Thermodynamic properties of polymers - Part II. High density polyethylene. Modern Plastics 43, No. 7, 121-123, Mar. 1966 (IITRI ref. 353).

Harrington, W. L., Skogerboe, R. K. and Morrison, G. H. (Cornell Univ., Dept. of Chem., Ithaca, N.Y.). Determination of trace amounts of carbon, oxygen, and nitrogen in metals by spark source mass spectrometry. Analyt. Chem. 38, No. 7, 821-8, June 1966 (IITRI ref. 254).

Heinrich, R. R., Johnson, C. E. and Crouthamel, C. E. (Argonne Natl. Lab., Chem. Eng. Div., Argonne, Ill.). Hydrogen permeation studies. I. Armco iron and iron-molybdenum alloys. J. Electrochem. Soc.(USA), 112, No. 11, 1067-70, Nov. 1965 (IITRI ref. 283).

Hewitt, G. F., Morre, M. J. C. and Sharratt, E. W. (U. K. Atomic Energy Authority, Harwell, Engl.). The permeability of nuclear grade graphite to a variety of gases. AWRE Report No. R-3994, 28 pp., Sept. 1966 (IITRI ref. 433).

Hollywood, L. P., Metz, T. R. and Porter, R. N. (Jet Propulsion Lab., Pasadena, Calif.). Storage tests of nitrogen tetroxide and hydrazine in aluminum containers. Contract No. NAS7 100 Tech. Report No. 32-1039, 21 pp., Jan. 15, 1967 (IITRI ref. 202).

Hsieh, P. Y. (National Cash Register Co., Fundamental Res Dept., Dayton, Ohio). A study of the encapsulation applicable to liquid rocket fuel. Contract No. Nonr-2848(00). Interim Report No. 4. July 1, 1961-June 30, 1962, 54 pp., July 1962 (IITRI ref. 423)

Huffine, C. L. and Williams, J. M. (General Electric Aircraft Nuclear Propulsion Dept., Cincinnati, Ohio). Hydrogen permeation through metals, alloys, and oxides at elevated temperatures. Corrosion 16, p. 430, 1960 (IITRI ref. 280).

Huldy, H. J. (Appl. Natl. Sci. Res., Central Lab., Delft, Neth.). Gas permeability apparatus for films and sheets. J. Appl. Polymer Sci. 8, No. 6, 2883-98, 1964 (IITRI ref. 275).

Jackson, J. D. (Battelle Mem. Inst., Defense Metals Info. Center, Columbus, Ohio). Permeability of titanium to hydrogen. DMIC Technical note, 3 pp., July 29, 1964 (IITRI ref. 265).

Johnson, R. L. (Thompson Ramo Wooldridge, Inc., TRW Systems Group, Redondo Beach, Calif.). Private communication between Mr. Peter Schipma (IITRI) and Dr. Robert L. Johnson (TRW). May 17, 1967 (IITRI ref. 292).

Johnson, R., Ph.D. and Van Nice, L. (Thompson Ramo Wooldridge, Inc., TRW Systems Group, Cleveland, Ohio). Private communication between Mr. Peter Schipma (IITRI), Dr. R. Johnson and Mr. L. Van Nice (TRW), May 17, 1967 (IITRI ref. 379).

Johnson, R. L. (Thompson Ramo Wooldridge, Inc., TRW Systems Group, Redondo Beach, Calif.). A study to analyze the permeation of high density gases and propellant vapors through single layer teflon or teflon structure materials and laminates. Contract No. NAS7-505, Quarterly Progress Report No. 1, July 5-Oct. 5, 1966, 9 pp., Oct. 5, 1966 (IITRI ref. 355).

Johnson, R. L. (Thompson Ramo Wooldridge, Inc., TRW Systems Group, Redondo Beach, Calif.). A study to analyze the permeation of high density gases and propellant vapors through single layer teflon or teflon structure materials and laminations. Contract No. NAS7-505, Quarterly Progress Report No. 2. Oct. 5-Jan. 5, 1967, 22 pp., January 4, 1967 (IITRI ref. 356).

Johnson, R. L. (Thompson Ramo Wooldridge, Inc., TRW Systems Group, Redondo Beach, Calif.). A study to analyze the permeation of high density gases and propellant vapors through single layer teflon or teflon structure materials and laminations. Contract No. NAS7-505, Quarterly Progress Report No. 3. Jan. 5-Apr. 15, 1967, 9 pp., Apr. 3, 1967 (IITRI ref. 357).

Johnson, R. L. (Thompson Ramo Wooldridge, Inc., TRW Systems Group, Redondo Beach, Calif.). A study to analyze the permeation of high density gases and propellant vapors through single layer teflon or teflon structure materials and laminations. Contract No. NAS7-505, Quarterly Progress Report No. 4. Apr. 5-July 5, 1967, 12 pp., July 10, 1967 (IITRI ref. 358).

Jolley, J. R. and Hildebrand, J. H. (Univ. of Calif., Berkeley, Calif.). Solubility, entropy, and partial molal volumes in solutions of gases in nonpolar solvents. J. Am. Chem. Soc. 80, 1050-4, 1958 (IITRI ref. 318).

Jones, P. M. S., Gibson, R. and Evans, J. A. (Atomic Weapons Res. Establishment, Aldermaston, Engl.). The permeation and diffusion of hydrogen isotopes through steels. Part 3: Maraging steel. AWRE Report No. 0-16/66, 22 pp., Apr. 1966 (IITRI ref. 417).

Jones, P. M. S., Gibson, R. and Evans, J. A. (Atomic Weapons Res. Establishment, Aldermaston, Engl.). The permeation and diffusion of hydrogen in molybdenum. AWRE Report No. 0-16/66. 14 pp., Feb. 1966 (IITRI ref. 429).

Jones, P. M. S., Gibson, R. and Evans, J. A. (Atomic Weapons Res. Establishment, Aldermaston, Engl.). The permeation and diffusion of hydrogen isotopes through stainless steels. Part 2: EN58B low carbon steel. AWRE Report No. 0-90/65. 25 pp., Nov. 1965 (IITRI ref. 430).

Kammermeyer, K. (State Univ. of Iowa, Dept. of Chem. Eng., Iowa City, Ia.). Silicone rubber as a selective barrier-gas and vapor transfer. Ind. Eng. Chem. 49, 1685-6, Oct. 1957 (IITRI ref. 241).

Kammermeyer, K. (Selas Corp. of America, Penn.). Separation of gases by diffusion through silicone rubber. U.S. Patent 2,966,235, Dec. 27, 1960 (IITRI ref. 385).

Keller, O. F. and Toth, L. R. (Jet Propulsion Lab., Pasadena, Calif.). ALPS generant tank and cell assembly. Contract No. NAS7-100, Tech. Report No. 32-865, 53 pp., Feb. 28, 1966 (IITRI ref. 437).

Klute, C. H. (Diamond Ordnance Fuze Labs., Washington, D.C.) Diffusion of small molecules in semicrystalline polymers. II. Permeability of unoriented polymer films. J. Polymer Sci. 41, 307-17, 1959 (IITRI ref. 250).

Klute, C. H. (Diamond Ordnance Fuze Labs., Washington, D.C.). Diffusion of small molecules in semicrystalline polymers: water in polyethylene. J. Appl. Polymer Sci. 1, 340-50, 1959 (IITRI ref. 249).

Klute, C. H. and Franklin, P. J. (Diamond Ordnance Fuze Labs., Washington, D.C.). Permeation of water vapor through polyethylene. J. Polymer Sci. 32, 161-76, 1958 (IITRI ref. 329).

Krusos, J. N., et al. (Bell Aerosystems Co., Div. of Bell Aerospace Corp., Buffalo, N.Y.). Design criteria and quality control studies for teflon expulsion bladders. Bell Report No. 8460-933012, Contract No. NASw-1317, Mar. 1967 (IITRI ref. 271).

Krusos, J. N. (Bell Aerosystems Co., Div. of Bell Aerospace Corp., Buffalo, N.Y.). Private communication between Mr. Peter Schipma (IITRI) and Mr. James Krusos (BAC), June 15, 1967 (IITRI ref. 416).

Kumins, C. A. and Roteman, J. (Interchemical Corp., Central Res. Labs., New York, N.Y.). Diffusion of gases and vapors through polyvinyl chloride-polyvinyl acetate copolymer films. I. Glass transition effect. II. Effect of polymer segment mobility. J. Polymer Sci. 55, 683-711, 1961 (IITRI ref. 221).

Kumins, C. A., Rolle, C. J and Roteman, J. (Interchemical Corp., New York, N.Y.). Water-vapor diffusion through vinyl chloride-vinyl acetate copolymer. J. Phys. Chem. 61, 1290-6, 1957 (IITRI ref. 351).

Kumins, C. A. and Roteman, J. (Interchemical Corp., Central Res. Lab., New York, N.Y.). Effect of solid-polymer interaction on transition temperature and diffusion coefficients. J. Polymer Sci. Pt. A 1, No. 1, 527-40, 1963 (IITRI ref. 392).

Lakshminarayanaiah, N. (Univ. of Penn., Philadelphia, Penn.). Transport phenomena in artificial membranes. Chem. Rev. 65, No. 5, 491-565, 1965. 609 refs. (IITRI ref. 217).

Lare, P. J., et al (Melpar, Inc., Falls Church, Va.). Investigation of the effects of mechanical stress on the permeability of engineering materials to certain cryogenic and storable propellants used in launch vehicles. Contract No. NAS8-11322. Annual Summary Report, June 30, 1964-June 30, 1965, 143 pp., Sept. 1965 (IITRI ref. 434).

Lasoski, S. W., Jr. and Cobbs, W. H., Jr. (E. I. duPont de Nemours and Co., Buffalo, N.Y.). Moisture permeability of polymers. I. Role of crystallinity and orientation. J. Polymer Sci. 36, 21-33, 1959 (IITRI ref. 330).

Lebovits, A. (U.S. Naval Appl. Sci. Lab., Brooklyn, N.Y.). Permeability of polymers to gases, vapors, and liquids. Modern Plastics 43, No. 7, 139-42, Mar. 1966 (IITRI ref. 210).

Lee, J. (North American Aviation, Inc., Rocketdyne Div., Canoga Park, Calif.). Private communication with Mr. John Lee, Rocketdyne. May 16, 1967 (IITRI ref. 264).

Lee, J. (North American Aviation, Inc., Rocketdyne Div., Canoga Park, Calif.). Private communication between Mr. Peter Schipma (IITRI) and Mr. John Lee (Rocketdyne), May 16, 1967 (IITRI ref. 263).

Levine, N. B. and Krainman, H. (Thiokol Chemical Corp., Reaction Motors Div., Denville, N.J.). Nitroso rubber expulsion bladders for nitrogen tetroxide application. Contract No. AF33(615)-5311, Report No. RMD 5094-Q3, Dec. 1, 1966-Feb. 28, 1967, 23 pp., Apr. 1967 (IITRI ref. 204).

Levine, N. B., Krainman, H. and Green, J. (Thiokol Chem. Corp., Reaction Motors Div., Denville, N.J.). Positive expulsion bladders for storable propellants. Contract No. AF33(615)-1661, Tech. Report No. AFML-TR-65-379, 42 pp., Jan. 1966 (IITRI ref. 255).

Levine, N. B. (Thiokol Chem. Corp., Reaction Motors Div., Denville, N.J.). Private communication between Mr. Peter Schipma (IITRI) and Mr. N. B. Levine (Thiokol), Apr. 25, 1967 (IITRI ref. 293).

Li, N. N. and Henley, E. J. (Stevens Inst. of Technol., Hoboken, N. J.). Permeation of gases through polyethylene films at elevated pressures. J. of AICE 10, No. 5, 666-70, 1964 (IITRI ref. 286).

Li, N. N., Long, R. B (Esso Res. and Eng. Co., Process Res. Div., Linden, N.J.). and Henley, E. J. (Stevens Inst., Hoboken, N.J.). Membrane separation processes. Ind. Eng. Chem. 57, No. 3, 18-29, Mar. 1965 (IITRI ref. 215).

Lindstrom, J. (Stanford Univ. School of Med., Instr. Res. Lab., Palo Alto, Calif.). Membrane separation. NASA Grant NsE 81-60, Tech. Report IRL-1046, 54 pp., Apr. 1966 (IITRI ref. 375).

Loats, H. L., et al. (Environmental Res. Assoc., Randallstown, Md.). Space station connection and seal study. Contract No. NAS1-2164, 149 pp., Oct. 1962. 59 ref. (IITRI ref. 270)

Lohr, J. E. and Scholz, J. J. (Univ. of Nebraska, Avery Chem. Lab., Lincoln, Neb.). Physical adsorption on poly(methyl methacrylate). J. Colloid Sci. 20, No. 8, 846-56, Oct. 1965 (IITRI ref. 251).

Long, R. B. (Esso Res. and Eng. Co., Central Basic Res. Lab., Linden, N.J.). Liquid permeation through plastic films. I&EC Process Design and Development 4, No. 4, 445-51, Nov. 1965 (IITRI ref. 238).

Lundberg, J. L., Wilk, M. B. and Huyett, M. J. (Bell Telephone Lab., Inc., Murray Hill, N.J.). Sorption studies using automation and computation. Ind. Eng. Chem., Fundamentals 2, 37-43, 1963 (IITRI ref. 347).

Lupakov, I. S., Kuz'michev, Yu., S. Determination of the permeability of tube walls for helium. Atomic Energy (USSR) 15, No. 1, 79-80, 1963 (IITRI ref. 380).

Lupakov, I. S., Kuz'michev, Yu., S. The permeability of metallic tube walls for helium. Atomic Energy (USSR) 17, No. 1, 49-52, 1964 (IITRI ref. 381).

Luzzi, T. (Grumman Aircraft Engineering Corp., Res. Dept., Bethpage, N.Y.). A review of the physics of gas adsorption on solid surfaces. RE-185, 46 pp., Oct. 1964. 34 refs. (IITRI ref. 229).

Major, C. J. and Kammermeyer, K. (State Univ. of Iowa, Iowa City, Ia.). Gas permeability of plastics. Modern Plastics 39, No. 11, 135, 138, 140, 142, 145-6, 179-80, July 1962 (IITRI ref. 208).

Marcus, J. P., Day, W. A. (Martin Co., Denver, Colo.) and Jelinek, J. G. (Parker Seal Co., Culver City, Calif.). Design and development of an elastomer seal for long term hazardous propellant storage. Proc. of the Conference on the Design of Leak-Tight Fluid Connectors. NASA. George C. Marshall Space Flight Center, 129-44, 1965 (IITRI ref. 376).

Marr, W. J. (General Electric Res. and Dev. Center, Schenectady, N.Y.). Leakage testing handbook. Contract No. NAS7-396. 392 pp., June 1967 (IITRI ref. 309).

Mathews, A. J. (ARO, Inc., Aerospace Environmental Facility, Arnold Air Force Station, Tenn.). Evaluation of porous materials as molecular leaks. Contract No. AF40(600)-1000, 31 pp., July 1964 (IITRI ref. 257).

McCall, D. W. and Slichter, W. P. (Bell Telephone Labs., Murray Hill, N.J.). Diffusion in ethylene polymers. III. Effects of temperature and pressure. J. A. Chem. Soc. 80, 1861-8, 1958 (IITRI ref. 319).

McCall, D. W., Ambrose, J. F. and Lanza, V. L. (Bell Telephone Labs., Murray Hill, N.J.). Diffusion in ethylene polymers. II. Desorption of water. J. Polymer Sci. 26, 165-169, 1957 (IITRI ref. 220).

Meares, P. (Univ. Old Aberdeen, Dept. of Chem., Scot.). Transient permeation of organic vapors through polymer membranes. J. Appl. Polymer Sci. 9, No. 3, 917-32, 1965 (IITRI ref. 245).

Meares, P. (Univ. Old Aberdeen, Scot.). Second-order transition of poly(vinyl acetate). Trans. Faraday Soc. 53, 31-40, 1957 (IITRI ref. 320).

Meares, P. (Univ. Old Aberdeen, Scot.). Solubilities of gases in poly(vinyl acetate). Trans. Faraday Soc. 54, 40-6, 1958 (IITRI ref. 323).

Meares, P. (Univ. Old Aberdeen, Scot.). The diffusion of gases through polyvinyl acetate. J. Am. Chem. Soc. 70, 3415-22, 1954 (IITRI ref. 317).

Meyer, J. A., et al. (Syracuse Univ., State Coll. of Forestry, Syracuse, N.Y.). Studies in the gas and vapor permeability of plastic films and coated papers. III. The permeation of mixed gases and vapors. Tappi 40, No. 3, 142-46, Mar. 1957 (IITPI ref. 373).

Michaels, A. S. and Parker, R. B. (Mass. Inst. of Technol., Dept. of Chem. Eng., Cambridge, Mass.). The determination of solubility constants for gases in polymers. J. Phys. Chem. 62, p. 1604, Dec. 1958 (IITRI ref. 237).

Michaels, A. S., et al. (Mass. Inst. of Technol., Dept of Chem. Eng., Cambridge, Mass.). Conditioned polyethylene as a permselective membrane. I&EC Process and Development 1, No. 1, 14-25, Jan. 1962 (IITRI ref. 239).

Michaels, A. S. and Bixler, H. J. (Mass. Inst. of Technol., Dept. of Chem. Eng., Cambridge, Mass.). Flow of gases through polyethylene. J. Polymer Sci. 50, 413-39, 1961 (IITRI ref. 225).

Michaels, A. S. and Bixler, H. J. (Mass. Inst. of Technol., Dept. of Chem. Eng., Cambridge, Mass.). Solubility of gases in polyethylene. J. Polymer Sci. 50, 393-412, 1961 (IITRI ref. 222).

Michaels, A. S., Vieth, W. R. and Bixler, H. J. (Mass. Inst. of Technol., Cambridge, Mass.). The measurement of diffusion constants of gases in polymers by sorption techniques. J. Polymer Sci. Pt. B 1, 19-23, 1963 (IITRI ref. 314).

Michaels, A. S., Vieth, W. R. and Bixler, H. J. (Mass. Inst. of Technol., Cambridge, Mass.). Gas permeability of highly oriented dibutyl maleate-ethylene copolymer films. J. Appl. Polymer Sci. 8, No. 6, 2735-50, 1964 (IITRI ref. 387).

Miller, G. H. and Parcell, L. J. (Texaco Experiment, Inc., Richmond, Va.). Para-ortho hydrogen conversion. Quarterly Progress Report No. 5, June-Aug. 1964. Contract No. AF33(657)-11123, 20 pp., Sept. 15, 1964, AD 461 007 (IITRI ref. 246).

Muraca, R. W. (Stanford Res. Inst., Menlo Park, Calif.). Development of techniques to improve bladder materials and test methods. JPL Contract No. 951484, Contract No. NAS7-100. Interim Report No. 1, May 18, 1966-May 17, 1967, 66 pp., June 17, 1967 (IITRI ref. 200).

Muraca, R. F. (Stanford Res. Inst., Menlo Park, Calif.). Development of techniques to improve bladder materials and test methods. Contract No. NAS7-100, JPL Contract No. 951484, Monthly Progress Report No. 14, June 18-July 17, 1967, 11 pp., Aug. 1, 1967 (IITRI ref. 338).

Muraca, R. F., Ph. D. (Stanford Res. Inst., Menlo Park, Calif.). Private communication between Mr. Peter Schipma (IITRI) and Dr. Ralph F. Muraca (SRI), June 15, 1967 (IITRI ref. 378).

Muraca, R. F. (Stanford Res. Inst., Menlo Park, Calif.). Investigation of the space storability of pressurizing gases. Contract No. NAS7-105, Final Summary Report Feb. 18, 1962-Dec. 31, 1963, 15 pp., Dec. 31, 1963 (IITRI ref. 415).

Myers, A. W., et al. (Syracuse Univ., State Coll. of Forestry, Syracuse, N.Y.). Permeability of polyethylene to gases and vapors. Modern Plastics 34, No. 9, 157-8, 160, 162, 164-5, May 1957 (IITRI ref. 240).

Myers, A. W., et al. (Syracuse Univ., State Coll. of Forestry, Syracuse, N.Y.). The gas and vapor permeability of plastic films and coated papers. VI. The permeation of water vapor. Tappi 44, No. 1, 58-64, Jan. 1961 (IITRI ref. 216).

Myers, A. W., Stannett, V. T. and Szwarc, M. (Syracuse Univ., State Coll. of Forestry, Syracuse, N.Y.). The permeability of polypropylene to gases and vapors. J. Polymer Sci. 35, 285-8, 1959 (IITRI ref. 424).

Myers, A. W., et al. (Syracuse Univ., State Coll. of Forestry, Syracuse, N.Y.). The gas and vapor permeability of plastic films and coated papers. V. Effect of crystallinity. Tappi 41, 716-20, 1958 (IITRI ref. 340).

Myers, W., et al. (Syracuse Univ., Syracuse, N.Y.). Modern Plastics 37, No. 10, 139-40, 142, 145, 211, June 1960 (IITRI ref 311).

Norton, F. J. (General Elec. Res. Lab., Schenectady, N.Y.). Permeation of gases through solids. Appl. Phys. 28, 34-39, Jan. 1957 (IITRI ref. 212).

Norton, F. J. (General Elec. Co., Schenectady, N.Y). Rare gas permeation through polymers. J. Chem. Phys. 22, 1145, 1954 (IITRI ref. 348).

Norton, F. J. (General Electric Lab., Schenectady, N.Y.). Gas permeation through Lexan polycarbonate resin. J. Appl. Polymer Sci. 7, No. 5, 1649-59, 1963 (IITRI ref. 388).

Olewinski, W. J., et al. (General Elec. Co., Missile and Space Div., Philadelphia, Penn.). Investigation of toxic properties of materials used in space vehicles. Contract No. AF 33(657)-8029. Tech. Doc. Report No. AMRL-TDR-63-99. Mar. 1962-Jan. 1963. 162 pp., Dec. 1963 (IITRI ref. 248).

Passmore, E. M., et al. Investigation of diffusion barriers for refractory metals. WADD TR 60-343, 58 pp., Aug. 1960. 14 refs. (IITRI ref. 230)

Pemsler, J. P., Anderson, R. W. and Rapperport, E. J. (Nuclear Metals, Inc., Concord, Mass.). Solubility and diffusion of gases in beryllium. Contract No. AF 33(616)-7665, Final Report, Nov. 1960-Oct. 1961, 32 pp., Feb. 1963. 8 ref. (IITRI ref. 427)

Peters, P., Ph.D. (General Electric Res. Lab., Schenectady, N.Y.). Private communication between Mr. Peter Schipma (IITRI), and Dr. Phil Peters (GE), June 15, 1967 (IITRI ref. 377).

Peterson, N. L. Diffusion in refractory metals. USAF, WADD TR 60-793, 176 pp., Mar. 1961. 193 refs. (IITRI ref. 231)

Picking, J. W. (Thompson Ramo Wooldridge, Inc., Tapco Div., Cleveland, Ohio). Sunflower power conversion system. 14th Quarterly Report, June-Aug. 1963, 27 pp., 1963 (IITRI ref. 258).

Pierce, C. M. (Lockheed Missiles and Space Co., Sunnyvale, Calif.). The diffusion of hydrogen and other light gases through membranes, porous media, and thin plates: an annotated bibliography. AD 418 234, 13 pp., Oct. 1962 (IITRI ref. 290).

Pilar, F. L. (Univ. of Concinnati, Appl. Sci. Res. Lab., Cincinnati, Ohio). The flow of gases through high polymer films in equilibrium with sorbed vapors. J. Polymer Sci. 45, 205-15, 1960 (IITRI ref. 369).

Podall, H. E., et al. (Melpar, Inc., Falls Church, Va.). Development of improved polymeric materials for cryogenic propellant tank liners and positive expulsion bladders. Contract No. NAS3-4183. Final Report, May 1, 1964-Apr. 30, 1965, 176 pp., June 1965 (IITRI ref. 414).

Pollak, H. O. and Frisch, H. L. (Bell Telephone Labs., Inc., Murray Hill, N.J.). The time lag in diffusion. III. J. Phy. Chem. 63, p. 1022, 1959 (IITRI ref. 363).

Porter, R. N. (Jet Propulsion Lab., Pasadena, Calif.). The fabrication of seamless teflon propellant expulsion bladders. Contract No. NAS7-100, Tech. Report 32-914, 23 pp., June 15, 1966 (IITRI ref. 438).

Prins, W. and Hermans, J. J. (Syracuse Univ., State Univ. Coll. of Forestry, Cellulose Res. Inst., Syracuse, N.Y.). Theory of permeation through metal coated polymer films. J. Phys. Chem. 63, 716-19, 1959 (IITRI ref. 273).

Riley, M. W. and Peckner, D. Metals vs. plastics: performance-the key to selection. Preprint 381B, 8 pp., SAE, Summer Mtg., St. Louis, Mo., June 5-9, 1961 (IITRI ref. 233).

Robb, W. (General Electric Co., Schenectady, N.Y.). A summary of some room temperature permeation rates for dimethyl silicone rubber, p. 16 (IITRI ref. 297).

Robb, W. L. (General Electric Res. and Dev. Center, Schenectady, N.Y.). Thin silicone membranes -- their permeation properties and some applications. Report No. 65-C-031, 23 pp., Oct. 1965 (IITRI ref. 203).

Rodgers, C. E. (Bell Telephone Labs., Inc., Murray Hill, N.J.). Permeability and chemical resistance. Chapter 9, pp. 609-688. Baer, E. Engineering Design of Plastics. Reinhold, New York, N.Y., 1964 (IITRI ref. 374).

Rogers, C. E., Stannett, V. and Szwarc, M. (Syracuse Univ., State Coll. of Forestry, Chem. Dept., Syracuse, N.Y.). Permeability valves - permeability of gases and vapors through composite membranes. Ind. Eng. Chem. 49, 1933-6, Nov. 1957 (IITRI ref. 213).

Rogers, C., et al. (Syracuse Univ., State Coll. of Forestry, Syracuse, N.Y.). Studies in the gas and vapor permeability of plastic films and coated papers. Part II. Some factors affecting the permeability constant. Tappi 39, No. 11, 741-47, Nov. 1956 (IITRI ref. 372).

Rogers, C., et al. (Syracuse Univ., State Coll. of Forestry, Syracuse, N.Y.). Studies in the gas and vapor permeability of plastic films and coated papers. Part I. Determination of the permeability constant. Tappi 39, No. 11, 737-41, Nov. 1965 (IITRI ref. 371).

Rogers, C. E., Stannett, V. and Szwarc, M. (Syracuse Univ., State Coll. of Forestry, Syracuse, N.Y.). The gas and vapor permeability of plastic films and coated papers. VII. The permeation of organic vapors. Tappi 44, 715-25, 1961 (IITRI ref. 341).

Rommel, M. (North American Aviation, Inc., Rocketdyne Div., Canoga Park, Calif.). Internal letter - Permeability of teflon by NTO. 2 pp., Oct. 14, 1965 (IITRI ref. 260).

Rosen, B. and Singleton, J. H. (Westinghouse Res. Labs., Chem. Dept., Pittsburgh, Penn.). Automatic recording, gas/polymer-film permeameter. J. Polymer Sci. 25, 225-28, 1957 (IITRI ref. 368).

Rhyne, J. W. (Telecomputing Corp., Power Sources Div., Denver, Colo.). Silver-cadmium battery development program. Contract No. NAS5-1431, Quarterly Tech. Progress Report for Fourth Quarter, ending Aug. 20, 1962, 13 pp., Sept. 1962 (IITRI ref. 408).

Rudd, B. D., Vose, D. W. and Johnson, S. (Metal Hydride Inc., Res. and Dev. Labs., Beverly, Mass.). The permeability of niobium to hydrogen. J. Phys. Chem. 66, 351-3, Feb. 1962 (IITRI ref. 274).

Saalfeld, F. E. and McDowell, M. V. (Naval Res. Lab., Chem. Div., Washington, D.C.). A mass spectrometric method for the determination of permeability coefficients. NRL Report No. 6182. 11 pp., Dec. 30, 1964 (IITRI ref. 418).

Sage, B. H. (Jet Propulsion Lab., Pasadena, Calif.). Some properties of nitric acid, nitrogen dioxide, nitric oxide, water and their mixtures. Contract No. DA-04-495-Ord 18. JPL Report 20-107, 145 pp., Oct. 15, 1957 (IITRI ref. 435).

Sanger, M. J., Nolho, R. and Morris, E. E. (Aerojet-General Corp., Chem. and Structural Products Div., Von Karman Center, Azusa, Calif.). Stainless steel lined glass wound tank. Contract No. AF33(615)-3619, Tech. Report Jan.-July 1966, 50 pp., Dec. 1966 (IITRI ref. 301).

Settle, J. P. and Schuler, F. T. (Wright Patterson AFB, Materials Lab., Ohio). Permeation tests of candidate Gemini oxidizer expulation bladder materials at temperatures in the range 15-165F. Materials & Processes Report No. 3-253-020, 43 pp., Feb. 18, 1963 (IITRI ref. 261).

Shore, J. J. (Aerojet-General Corp., Liquid Rocket Plant, Eng. Div., Sacramento, Calif.). The effect of nitrogen tetroxide on some halogenated plastics. Report No. NM-28-B-1, 4 pp., Apr. 1959 (IITRI ref. 354).

Sivadjian, J. and Riberio, D. (Inst. Pasteur, Paris, Fr.). Permeability to water and water vapor of plastic materials by the hygrophotographic technique. J. Appl. Polymer Sci. 8, No. 3, 1403-13, 1964 (IITRI ref. 316).

Sivadjian, J. and Corral, F. (Inst. Pasteur, Paris, Fr.). Hygrophotographic studies on the permeability to water and moisture of packaging materials. J. Appl. Polymer Sci. 6, 561-70, 1962 (IITRI ref. 315).

Sivadjian, J. (Pasteur Inst., Paris, Fr.). Measure of permeability of plastic material, leather, and similar substances against moistness and water by the hygrophotographic method. J. Polymer Sci. 24, 63-66, 1957 (IITRI ref. 367).

Smetana, F. O. (Univ. of Southern Calif., Eng. Center, Los Angeles, Calif.). A theoretical and experimental study of gas flow through cloth over a range of pressures and temperatures. Contract AF33(616)-7102, Report No. USAF-RW-TR-61-192, 124 pp., Sept. 1961 (IITRI ref. 306).

Smith, T. (North American Aviation Sci. Center, Thousand Oaks, Calif.). Kinetics and mechanism of hydrogen permeation of oxide films on zirconium. J. Nucl. Mater. 18, No. 3, 323-336, Mar. 1966 (IITRI ref. 398).

Sneck, H. J. (General Electric Co., Bearing and Lubrication Center, General Eng. Lab., Schenectady, N.Y.). Appendix A - A survey of gas permeation through metals and polymers. pp. 4-13, Aug. 28, 1962 (IITRI ref. 425).

Sperati, C. A. and Starkweather, H. W., Jr. (E. I. duPont de Nemours and Co., Du Pont Experimental Station, Wilmington, Del.). Fluorine-containing polymers. II. Polytetrafluoroethylene. Advances in Polymer Sci. 1m 75-113, 1958.

Stamm, A. J. (U.S. Dept. of Agriculture, Forest Ser., Forest Product Lab., Madison, Wis.). Diffusion of water into uncoated cellophane. I. From rates of water vapor adsorption, and liquid water absorption. J. Phys. Chem. 60, 76-82, Jan. 1956 (IITRI ref. 366).

Stanford, H. B. (Jet Propulsion Lab., Pasadena, Calif.). The measured permeability to nitrogen tetroxide of some potential bladder materials. Contract No. NAS7-100, Tech. Memorandum 33-123, 14 pp., Mar. 24, 1963 (IITRI ref. 428).

Stannett, V. and Yasuda, H. (Res. Triangle Inst., Durham, N. Carolina). Liquid versus vapor permeation through polymer films. J. Polymer Sci. 289-93, 1963 (IITRI ref. 313).

Stannett, V. and Yasuda, H. (Res. Triangle Inst., Camille Dreyfus Lab., Durham, N. Carolina). Liquid versus vapor permeation through polymer films. J. Polymer Sci. Pt.B, 1, No. 6, 289-93, 1963 (IITRI ref. 279).

Stannett, V. and Szwarc, M. (State Univ. of New York, Syracuse, N.Y.). The permeability of polymer films to gases - a simple relationship. J. Polymer Sci. 16, 89-91, 1955 (IITRI ref. 325).

Stansfield, O. M. (Univ. of Calif., Lawrence Radiation Lab., Berkeley, Calif.). The influence of tensile stress on gaseous permeation in glassy-state and complex ceramics. Contract No. W-7405-eng-48, 78 pp., Apr. 2, 1963. 24 refs. (IITRI ref. 256).

Steigerwald, E. A. (Thompson Ramo Wooldridge Inc., Tapco Div., Cleveland, Ohio). The permeation of hydrogen through metals and metal-plus-oxide systems. Project No. 512-278131-08, TM 2865-67, 12 pp., Mar. 31, 1961 (IITRI ref. 288).

Steigerwald, E. A. (Thompson Ramo Wooldridge, Inc., TRW Electromechanical Div., Cleveland, Ohio). The permeation of hydrogen through materials for the sunflower system. Contract No. NAS5-462, 91 pp., Nov. 1963 (IITRI ref. 295).

Steigerwald, E. A. (Thompson Ramo Wooldridge, Inc., Tapco Div., Cleveland, Ohio). The permeation of hydrogen through constructional materials. Contract No. NAS5-462, June 1962. Topical Report, Feb. 1, 1961-Nov. 30, 1961. Project No. 512-278131-08, 55 pp., Nov. 30, 1961 (IITRI ref. 331).

Stern, S. A., et al. (Union Carbide Corp., Linde Div., Tonawanda, N.Y.). Helium recovery by permeation. Ind. Eng. Chem. 57, No. 2, pp. 49-60, Feb. 1965 (IITRI ref. 214).

Stern, S. A., et al. (Union Carbide Corp., Linde Div., Tonawanda, N.Y.). Performance of a versatile variable-volume permeability cell. Comparison of gas permeability measurements by the variable-volume and variable-pressure methods. J. Appl. Polymer Sci. 7, No. 6, 2035-51, 1963 (IITRI ref. 223).

Stern, S. A., Sinclair, T. F. and Gareis, P. J. (Union Carbide Corp., Tonawanda, N.Y.). Improved permeability apparatus of the variable-volume type. Modern Plastics 42, No. 2, pp. 154, 156, 158, 204, 206, Oct. 1964 (IITRI ref. 209).

Stitt, L. E. and Salmi, R. J. (NASA Lewis Res. Center, Cleveland, Ohio). Performance of a Mach 3.0 external-internal-compression axisymmetric inlet at Mach numbers from 2.0 to 3.5. Tech. Memorandum X-145, 20 pp., Jan. 1960 (IITRI ref. 396).

Studt, P. L. (Univ. of Calif., Lawrence Radiation Lab., Berkeley, Calif.). Mechanisms of gaseous permeation through glass, single-crystal silicon, and germanium; and stress enhanced gaseous permeation through alumina bodies. Contract No. W-7405-eng-48, 141 pp., Sept. 1962. 65 refs. (IITRI ref. 404).

Taylors, E. A., Karel, M. and Proctor, B. E. Measurement of oxygen permeability. Modern Packaging 33, No. 10, p. 131, 1960 (IITRI ref. 399).

Ticknor, L. B. (American Visose Corp., Res. and Dev. Div., Marcus Hook, Pa.). On the permeation of cellophane membranes by diffusion. J. Phys. Chem. 62, 1483-1485, Dec. 1958 (IITRI ref. 365).

Tung, L. H. and Buckser, S. (Dow Chem. Co., Midland, Mich.). J. Phys. Chem. 62, 1530-4, 1958 (IITRI ref. 349).

Tuwiner, S. Diffusion and membrane Technology - Permeation of membranes by gases and vapors. Chapter 12, pp. 215-234, Reinhold Publn. Corp., New York, 1962 (IITRI ref. 219).

Van Amerongen, G. J. (Rubber-Foundation, Delft, Holland). The permeability of different rubbers to gases and its relation to diffusivity and solubility. J. Appl. Phys. 17, p. 972, 1946 (IITRI ref. 252).

Van Amerogen, G. J. (Rubber Foundation, Delft, Neth.). Influence of structure of elastomers on their permeability to gases. J. Polymer Sci. 5, 307-32, 1950 (IITRI ref. 390).

Vango, S. P. (Jet Propulsion Lab., Pasadena, Calif.). Determination of permeability of cast teflon sheet to nitrogen tetroxide and hydrazine. Contract No. NASw-6, TM 33-55, 14 pp., Aug. 25, 1964 (IITRI ref. 299).

Vango, S. P. and Krasinsky, J. B. (Jet Propulsion Lab., Pasadena, Calif.). Metal plating of teflon sheet as a means of reducing permeation. Space Programs Summary No. 37-21, Vol. IV, Apr. 1, 1963-May 31, 1963, 271 pp., June 30, 1963 (IITRI ref. 422).

Vango, S. P. and Krasinsky, J. B. (Calif. Inst. of Technol., Jet Propulsion Lab., Pasadena, Calif.). Additional results on metal plating of teflon sheet. Space Programs Summary No. 37-26, Aug. 1, 1963-Sept. 30, 1963, 319 pp., Oct. 31, 1963 (IITRI ref. 421).

Vango, S. P. and Krasinsky, J. B. (Calif. Inst. of Technol., Jet Propulsion Lab., Pasadena, Calif.). Continued effort in metal plating of teflon sheet as a means of reducing permeation. Space Programs Summary No. 37-23, Volume IV, 319 pp., Oct. 31, 1963 (IITRI ref. 420).

Van Raaij, P. T. and Winkel, P. (RV)-TNO, Chem. Lab., Rijswijk. Neth.). The permeability of plastic films and foils to gases, vapors and liquids. Report No. 1966-16, 33 pp., 1966 (IITRI ref. 440).

Vargo, E. J. and Cooper, D. B. (Thompson Ramo Wooldridge, Inc., Tapco Div., Cleveland, Ohio). An investigation of the corrosion resistance of metallic materials to molten lithium hydride at cyclic elevated temperature. Contract No. NAS5-462, 142 pp., Feb. 1962 (IITRI ref. 443).

Vieth, W. R., Alcalay, H. H. and Frabetti, A. J. (Mass. Inst. Technol., Dept. of Chem. Eng., Cambridge, Mass.). Solution of gases in oriented poly(ethylene terephthalate). J. Appl. Polymer Sci. 8, No. 5, 2125-38, 1964 (IITRI ref. 224).

Waack, R., et al. (Syracuse Univ., State Coll. of Forestry, Dept. of Chem., Syracuse, N.Y.). Permeability of polymer films to gases and vapors. Ind. Eng. Chem. 47, 2524-7, 1955 (IITRI ref. 242).

Walker, R. E. and Westenberg, A. A. (John Hopkins Univ., Appl. Phys. Lab., Silver Springs, Md.). Molecular diffusion studies in gases at high temperature: results and interpretation of the CO_2-O_2, CH_4-O , H_2-O_2, CO-O_2, and H_2O-O_2 systems. CM-959, 31 pp., Aug. 1959 (IITRI ref. 234).

Walker, R. E. and Westenberg, A. A. (John Hopkins Univ., Appl. Phys. Lab., Silver Springs, Md.). Molecular diffusion studies in gases at high temperature: results and interpretation of the He-A system. CM-958, 20 pp., Aug. 1959 (IITRI ref. 236).

Walter, R. J. (North American Aviation, Inc., Rocketdyne Div., Canoga Park, Calif.). Compatibility of tantalum and columbium alloys with hydrogen. Res. Report No. 65-3, 80 pp., Feb. 1965 (IITRI ref. 262).

Walter, R. J. (North American Aviation, Inc., Rocketdyne Div., Metallic Materials Res., Canoga Park, Calif.). Evaluation of the effects of high pressure hydrogen on storage vessel materials. RM-1152-354, 12 pp., May 12, 1965 (IITRI ref. 259).

Walters, W. H. (Bell Aerosystems Co., Buffalo, N.Y.). Summary report on the investigations to date of permeation of propellants through bladders. Report No. 8500-950-001, Rev. B, 50 pp., Oct. 1962 (IITRI ref. 247).

Watson, E. C. (NASA, Ames Res. Center, Moffett Field, Calif.). An experimental investigation at Mach numbers from 2.1 to 3.0 of circular internal-compression inlets having translatable centerbodies and provisions for boundary-layer removal. Tech. Memorandum X-156, 26 pp., Jan. 1960 (IITRI ref. 391).

Webb, R. W. (Atomics International, Canoga Park, Calif.). Permeation of hydrogen through metals. Contract No. AT(11-1)-GEN-8, 24 pp., July 1965. 24 refs. (IITRI ref. 403).

Weber, T. (Aerospace Med. Div., School of Aerospace Med., Brooks AFB, Tex.; and Beckman Instr., Inc., Fullerton, Calif.). Evaluation of gaseous and particulate components in manned space stations. Paper 63-258, 8 pp, Am. Inst. Aeronaut. and Astronautics, summer meeting, Los Angeles, Calif., June 17-20, 1963 (IITRI ref. 235).

Weiner, R. S. (Jet Propulsion Lab., Calif. Inst. of Tech., Pasadena, Calif.). Basic criteria and definitions for zero fluid leakage. JPL Contract No. NAS7-100. Technical Report No. 32-926, 14 pp., Dec. 15, 1966 (IITRI ref. 201).

Weiss, H. G., et al. (Dynamic Science Corp., South Pasadena, Calif.). Modification of the hydrazine-nitrogen tetroxide ignition delay. J. of AIAA 2, No. 12, 2222-2223, Dec. 1964 (IITRI ref. 287).

Weller, S. W. and Steiner, W. A. (to the United States of America, as represented by the Secy. of the Interior). Separation of oxygen from gas mixture. U.S. Patent 2,540,151, Feb. 6, 1951 (IITRI ref. 350).

Weller, S. and Steiner, W. A. (U.S. Bur. of Mines, Pittsburgh, Pa.). Engineering aspects of separation of gases. Fractional permeation through membranes. Chem. Eng. Progress 46, 585-90, 1950 (IITRI ref. 346).

Wiseman, J. R., Sawyer, R. and Cheetham, C. (Thiokol Chem. Corp., Reaction Motors Div., Denville, N.J.). Propellant feed system analog - a valuable tool for establishing the effects of upstream dynamics on reaction control rocket motor performance. Chemical Propulsion Information Agency, CPIA 121, Vol. II: 8th Liquid Propulsion Symposium, Cleveland, pp. 87-115, Nov. 1966 (IITRI ref. 307).

Yasuda, H. and Stannett, V. (Syracuse Univ., State Coll. of Forestry, Chem. Dept., Syracuse, N.Y.). Permeation, solution, and diffusion of water in some high polymers. J. Polymer Sci. 57, 907-923, 1962 (IITRI ref. 227).

Zimm, B. H. and Lundberg, J. L. (General Electric Co., Schenectady, N.Y.). J. Phys. Chem. 60, 425-8, 1956 (IITRI ref. 339).

END OF REFERENCE

REFERENCE

61

DESIGN DATA FOR PRESSURIZED GAS SYSTEMS. STANFORD RESEARCH INSTITUTE, NOV. 1963.

RETURN TO
SRI LIBRARY-REPORTS
G-037

LOAN COPY
DO NOT
DESTROY OR DAMAGE

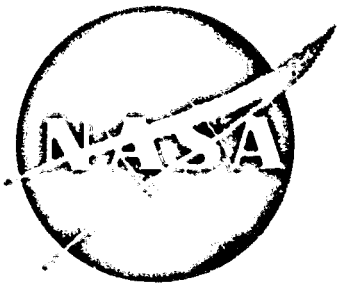

DESIGN DATA FOR PRESSURIZED GAS SYSTEMS

Prepared for

NATIONAL AERONAUTICS AND SPACE ADMINISTRATION

Contract NAS7-105

NOVEMBER 1963

STANFORD RESEARCH INSTITUTE

MENLO PARK, CALIFORNIA

Acc. No. 11237
#2

I INTRODUCTION

The primary purpose of this book is to present concise summaries of available information on the fundamental parameters governing the design of pressurized-gas systems for spacecrafts. It is intended that the information contained in this book be used in conjunction with the various methodologies currently employed to select component combinations and to establish the design details of suitable pressurized-gas systems. Sufficient room is available in the binder to provide for future expansion of the various sections and to enable the user to incorporate additional pages of information.

The section on "Space Environment" summarizes the available information on the composition of the upper atmosphere, the distribution of meteoroids, and on the various types of radiations encountered by spacecrafts.

The section entitled "Attitude Control Theory" consists of a very brief presentation of the salient principles underlying the design of pressurized-gas attitude-control systems.

The behavior of liquids in essentially gravitationally-free systems (zero-g) is summarized under the heading "Zero-Gravity Considerations." Only those aspects related to pressurized-gas systems are discussed.

A section entitled "Nozzle Performance" summarizes the computation of the performance of fluids expanding through nozzles; it includes condensable as well as noncondensable gases.

A very brief discussion of the aspects of defining the storage efficiency of gases from the viewpoint of weight, performance, reliability, etc. is given in the section "Storage Efficiency."

The section on "Pressure Vessels" indicates some of the newer computational methods for the design of vessels subjected to thermal as well as pressure stresses.

A brief review and summary of the principles of statistical relationships as applied to test programs is presented in the section entitled "Reliability," and is intended to provide guidelines for the engineer.

Brief collections of data on the physical properties of the metals most frequently used to construct pressurized-gas systems are contained in the section entitled "Materials"; synoptic data on the compatibility of these materials with selected gases and liquids are also included.

The fundamental aspects of diffusion and permeability theory are given in the section entitled "Permeability Theory," together with data on the permeability of various polymers and elastomers.

The section on "Rings and Seals" includes data on the effect of the space environment on materials used to effect tight junctures in pressurized-gas systems.

The section "Properties of Gases" consists of an extensive tabular and graphic compilation of the physical and thermodynamic properties of the gases or liquids which may be used in pressurized-gas systems. The data in this section are the most accurate available at this time and may be used freely to compute or estimate pressurized-gas performance.

Sections on "Valves" and "Pressurization Systems" include no information; it is anticipated that material selected for inclusion in these sections will be made available in the future.

XII-4 PERMEABILITY OF MATERIALS TO GASES

Tables XII-4-1 and XII-4-2 give selected permeabilities of various polymeric materials to H_2, He, N_2, O_2, CO_2, H_2O, and C_3H_8. Values for H_2 and He (plus one value for N_2) and typical glasses are give. in Table XII-4-3. It will be recalled from Section VIII that the permeability of glasses drops off sharply at a molecular diameter of the permeant over about 2.5 Å and that it is also decreased as the content of glass formers, SiO_2, B_2O_3, and P_2O_5, is decreased. In Table XII-4-4, permeability data for various gases through metals are collected.

In all the tables, where there are sufficient data to allow calculation, the permeability is given in parametric form:

$$\log_{10} P = A - B/T$$

where the units of P are in cc (STP)-mm/cm^2-sec-atm in the case of polymers and glasses and cc (STP)-mm/cm^2-sec-(atm)$^{1/2}$ in the case of metals, B is in °K in all cases. This assumes the Arrhenius type exponential law is followed in temperature and that the permeation rate is proportional to the pressure difference across the membrane in the case of polymers and glasses and to the difference in the square root of the pressure in the case of metals. Although these assumptions are often safe, there are many exceptions, as discussed in Section VIII. For convenience in quick comparisons the permeability at 25°C (77°F), P_{25}, is also given in the tables.

REFERENCE 61

PAGE XII-4.2 BLANK

Table XII-4-1

PERMEABILITY OF POLYMERIC MATERIALS TO H_2, He, N_2, O_2 AND CO_2

P in cc(STP)-mm/cm^2-sec-atm, B in °K

MATERIAL	TRADE NAME OR CODE	H_2			He			N_2			O_2			CO_2			REF.
		A	B	$P_{25} \times 10^7$	A	B	$P_{25} \times 10^7$	A	B	$P_{25} \times 10^7$	A	B	$P_{25} \times 10^7$	A	B	$P_{25} \times 10^7$	
Natural Rubber		0.663-1	1508	39	0.146-1	1420	23	0.672-0	2032	6.6	0.903-1	1442	18	0.556-1	1355	102	29
Rubber Hydrochloride	Pliofilm 140-N_2	0.206-3	1223	1.21										0.134-0	2227	0.49	
	Pliofilm RM-1							0.386-1	2185	0.11	0.767-2	1836	0.40	0.160-1	1879	0.71	31
Poly(butadiene)		0.342-1	1442	32				0.724-1	1792	4.9	0.362-1	1551	14.5	0.839-2	1136	105	29
Poly(butadiene), hydrogenated	Hydropol				0.241-0	1836	12.0	0.695-1	2447	3.0	0.214-0	2141	8.6	0.946-0	1901	36.8	16
Poly(dimethyl butadiene)	Methyl rubber	0.000-0	1748	13	0.892-2	1442	11	0.342+2	2906	0.36	0.518+1	2469	1.6	0.892-2	1442	11	29
Poly(isobutylene)	Oppanol B-200 (butyl rubber)	0.672-0	2076	4.9	0.544-1	1726	5.6	0.740+1	2797	0.22	0.820-0	2333	0.90	0.991-0	2207	3.8	29
Poly(butadiene-acrylonitrile)	Perbunan (German)	0.996-1	1770	11.5	0.079-1	1530	8.7	0.041+1	2404	0.89	0.398-0	2054	3.2	0.462-0	1814	23	29
	Perbunan 18	0.830-2	1355	19.2	0.098-1	1486	12.9	0.542-0	2163	1.92	0.100-0	1879	6.2	0.818-1	1530	48	30
	Hycar OR 15	0.187-0	1923	5.4	0.364-1	1683	5.2	0.375+2	3016	0.18	0.662+1	2622	0.73	0.453+1	2294	5.7	30
	Hycar OR 25	0.967-1	1792	9.0	0.302-1	1617	7.5	0.684+1	2688	0.46	0.949-0	2294	1.78	0.750-0	1967	14.1	30
Poly(butadiene-styrene)	Buna S, GR-S	0.491-1	1486	30.5	0.114-0	1442	17.5	0.079-0	1901	4.8	0.477-1	1595	13	0.146-0	1246	94	29
Poly(chloroprene)	Neoprene G	0.954-1	1770	10.3			3.4	0.748-0	2316	0.89	0.732-0	2163	3.0	0.518-0	1857	15.5	29
Poly(vinyl chloride-methylacrylate)	Mipolan MP	0.176-0	1945	4.4						0.2	0.505-0	2568	0.70	0.832-0	2141	4.0	29
Poly(alkylpolysulfide)	Thiokol B	0.869-0	2316	1.2							0.255+2	2950	0.22	0.839+1	2513	2.4	29
Poly(esteramide-diisocyanate)	Valcaprene A	0.280-0	1967	4.8				0.519+1	2666	0.37	0.055+1	2382	1.15	0.042+1	2054	14.1	30
Polyethylene (density 0.914)	DE2400 Alathon 14	0.220-0	1921	5.96	0.662-1	1814	3.75	0.524+1	2579	0.74	0.822-0	2229	2.20	0.801-0	2032	9.6	8,16
(density 0.964)	Grex	--	--	--	0.144-2	1551	0.87	0.004-1	2076	0.11	0.651-2	1836	0.31	0.718-3	1573	0.28	16
Poly(ethylene glycol terephthalate)	Mylar A	0.678-4	1201	0.445	0.890-4	1198	0.74	0.995-5	1639	0.0031	0.960-5	1398	0.019	0.509-4	1356	0.90	8,31
Polystyrene	Dow 0641	0.077-5	72	68.5				0.713-7	-18	5.92	0.235-6	-10	18.5	0.178-5	219	277	7
Polyvinyl chloride	Geon 101	0.818-6	418	2.6										0.611-7	217	0.762	7
+ 20% DOP		0.549-5	216	66.7										0.896-6	-332	1025	7
Polyvinyl (chloride 95%, Acetate 5%) + 25% DOP	Bakelite VB1930	0.133-5	478	3.4										0.472-5	799	0.49	7
		0.074-1	1621	4.3	0.942-2	1570	4.8	0.023+2	2820	0.37	0.933-0	2320	1.4	0.150-0	1931	4.1	7
Polyvinylidene chloride	Saran 517			0.050			0.011	0.960+1	3671	0.00044	0.922+1	3474	0.0018	0.399-0	2688	0.024	26,31
Poly(caprolactam)	Nylon 6							0.386-1	2447	0.0064	0.995-2	2273	0.023	0.085-1	2120	0.093	31
Poly(tetrafluoroethylene)	Teflon			18			530			2.4			7.6				5
Poly(chlorotrifluoro-ethylene)	Trithene, Kel-F	0.008-2	1535	0.74				0.608-0	3060	0.0025	0.890-1	2514	0.028	0.940-4	1513	0.11	19,31
plasticized		0.160-0	2018	2.4	0.015-1	1485	10.7	0.971+1	3021	0.054	0.390-0	2353	0.31	0.017+1	2346	1.4	19,31
Ethyl cellulose (plasticized)	Ethocel 610	0.877-4	751	22.7				0.787-4	909	6	0.022-3	824	18.1	0.524-5	305	52	7,31
Cellulose acetate (plasticized)	Celanese P-912	0.220-0	1149	6.7				0.995-4	1420	0.17	0.580-4	1093	0.62	0.075-1	1556	7.0	8,31
Cellulose acetate-butyrate	Kodapak II	0.231-3	893	16	0.533-3	1038	10.9	0.765-2	1710	1.1	0.041-2	1370	2.8	0.484-3	921	24	8
Polypropylene (d = 0.907)								0.111+2	2906	0.23	0.449+1	2491	1.2	0.386-0	1988	5.2	18
Cellulose nitrate							5.2			0.33			1.5			1.6	14

Table XII-4-2

PERMEABILITY OF POLYMERIC MATERIALS TO PROPANE AND TO WATER

P in cc (STP)-mm/cm^2-sec-atm, B in °K

MATERIAL	TRADE NAME OR CODE	H_2O			PROPANE			REF.
		A	B	$P_{25} \times 10^7$	A	B	$P_{25} \times 10^7$	
Natural Rubber				2600	0.141-1	1202	128	13,16
Rubber Hydrochloride	Pliofilm NO	0.0707-0	1726	19				17
Poly(butadiene), hydrogenated	Hydropol				0.241+2	2273	41	16
Poly(isobutylene)	Butyl rubber				0.951-0	2338	1.3	4
Poly(chloroprene)	Neoprene GN						5.5	28
Poly(alkylpolysulfide)	Thiokol 3000 ST						1.1	28
Polyethylene(density 0.922)		0.869-0	1748	68.4				17
(density 0.914)	Alathon 14				0.662-1	2447	7.2	16
(density 0.960)				9.1				17
(density 0.964)	Grex				0.459-0	2338	0.41	16
Polypropylene (d = 0.907)		0.960+1	2207	35.7				18
Poly(ethylene glycol terephthalate)	Mylar A	0.508-5	153	96.8				17
Polystyrene		2.80-5	0	630				4
Poly(vinyl chloride)	Geon 101	0.78-4	514	110				4
Poly(vinyl chloride-acetate)	Vinylite VYNW	0.37-2	874	275				4
Poly(vinylidene chloride)	Saran 517	0.941-7	2404	7.5			0.00027	17,26
Polyamide	Nylon 6-6			53-516*				17
Poly(chlorotrifluoroethylene)	Kel F 300	0.222-1	2050	0.22				19,31
Ethyl cellulose (plasticized)	Ethocell 610	0.995-4	0	9880				17
Cellulose acetate		0.625-4	0	4180				17
(plus 15% DBP)		0.750-4	0	5620			2.8	14,17
Cellulose nitrate				4800			0.0058	13,17
Poly(methylmethacrylate)	Lucite			2200				13

* Humidity dependent.

Table XII-4-3

PERMEABILITY OF GLASSES

P in cc (STP)-mm/cm^2-sec-atm, B in °K

SYSTEM	A	B	P_{25}	REFERENCE
H_2-Fused silica	0.398-5	1872	1.12×10^{-12}	1
-Vycor (Corning 7900)	0.520-5	1826	3.9×10^{-12}	1
He-Fused silica (GE)	0.401-4	1049	0.76×10^{-7}	1
-Vycor (Corning 7900)	0.579-4	1049	1.14×10^{-7}	1
-Pyrex (Corning 7740)	0.654-4	1398	0.91×10^{-8}	20
-Soda lime (Corning 0080)	0.822-4	2403	5.7×10^{-12}	20
-X-ray shield (Pittsburgh Plate Glass)	0.662-5	2731	3.1×10^{-14}	20
N_2-Fused silica	0.967-4	4820	6.2×10^{-20}	2

Table XII-4-4

PERMEABILITY OF METALS

P in cc (STP)-mm/cm^2-sec (atm)$^{\frac{1}{2}}$, B in °K

SYSTEM	A	B	P_{25}	REFERENCE
H_2-Aluminum	0.589-1	3017	7.5×10^{-11}	27
Copper	0.621-1	3933	2.6×10^{-14}	6
Hastelloy B	0.701-1	3657	2.7×10^{-13}	23
Inconel	0.847-1	3649	4.0×10^{-13}	6
Iron	0.554-2	1836	2.6×10^{-8}	6
Kovar	0.352-1	3497	4.1×10^{-13}	6
Monel	0.161-1	2797	5.9×10^{-11}	6
Nickel	0.520-1	2885	6.9×10^{-11}	6
Niobium	0.749-1	1137	8.7×10^{-5}	24
Palladium	0.929-1	2296	1.7×10^{-8}	3
Platinum	0.512-1	3936	2.1×10^{-14}	12
Steel				
Cold drawn	0.554-2	1879	1.8×10^{-8}	6
low carbon	0.312-2	2288	4.2×10^{-10}	22
Stainless 303	0.435-1	3540	4.6×10^{-13}	6
304	0.586-1	3715	1.3×10^{-13}	6
316, 321	0.273-1	3252	2.3×10^{-12}	11
347	0.634-2	3180	9.2×10^{-13}	11
410	0.188-1	3260	5.7×10^{-12}	11
N_2-Iron	0.093-1	5204	4.3×10^{-19}	25
Molybdenum	0.359-0	9837	4.4×10^{-33}	27
CO-Iron	0.554-2	4066	8.1×10^{-16}	25
O_2-Silver	0.754-1	4941	1.5×10^{-17}	15

XII-4. REFERENCES

1. Altemose, V. O., *J. Appl. Phys.*, **32**, 1309 (1961).
2. Barrer, R. M., *J. Chem. Soc.*, **1934**, 378.
3. Barrer, R. M., *Trans. Faraday Soc.*, **36**, 1235 (1940).
4. Barrer, R. M., and Skirrow, G., *J. Polymer Sci.*, **3**, 549 (1948).
5. Barton, R. S., *AERE-M599* (1960).
6. Borman, J. K., and Nardella, W. R., *Vacuum*, **12** 19 (June, 1962).
7. Brubaker, D. W., and Kammermeyer, K., *Ind. Eng. Chem.*, **44** 1465 (1952).
8. Brubaker, D. W., and Kammermeyer, K., *ibid.*, **45**, 1148 (1953).
9. Brubaker, D. W., and Kammermeyer, K., *ibid.*, **46**, 733 (1954).
10. Doty, P. M., Aiken, W. H., and Mark, H., *ibid.*, **38**, 788 (1946).
11. Flint, P. S., *KAPL-659* (1951).
12. Hamm, W. R., *J. Chem. Phys.*, **1**, 476 (1933).
13. Hare, E. F., Contract No. NOnr 2848(00), *Interim Report No. 1* (July, 1960).
14. Hsieh, P. Y., Contract No. NOnr 2848(00), *Interim Report No. 2* (January, 1961).
15. Johnson, F. M. G., and Larose, P., *J. Am. Chem. Soc.*, **46**, 1377 (1924); **49**, 312 (1927).
16. Michaels, A. S., and Bixler, H. J., *J. Polymer Sci.* **50** 413 (1961).
17. Myers, A. W., Meyer, J. A., Rogers, C. E., Stannett, V., and Szwarc, M., *TAPPI*, **44**, 58 (1961).
18. Myers, A. W., Stannett, V., and Szwarc, M., *J. Polymer Sci.*, **35**, 285 (1959).
19. Myers, A. W., Tammela, V., Stannett, V., and Szwarc, M., *Modern Plastics*, **37**, 139 (June, 1960).
20. Norton, F. J., *J. Am. Ceramic Soc.*, **36**, 90 (March, 1953).
21. Norton, F. J., *J. Chem. Phys.*, **22**, 1145 (1954).
22. Norton, F. J., quoted in Ref. 11.
23. Rudd, R. W., and Vetrano, J. B., *NAA-SR-4898 Rev.*, (1961).
24. Rudd, R. W., Vose, D. W., and Johnson, S., *J. Phys. Chem.*, **65**, 1018 (1961).
25. Ryder, H. M., *Elect. J.*, **17**, 161 (1920).
26. Sarge, T. W., *Anal. Chem.*, **19**, 396 (1947).
27. Smithells, C. J., and Ransley, C. E., *Proc. Royal Soc. (London)*, **A150**, 172 (1935).
28. Stout, L. E., Geisman, R., and Mozley, J. M., Jr., *Chem. Eng. Progress*, **44**, 219 (1948).
29. Van Amerongen, G. J., *J. Appl. Phys.*, **17**, 972 (1946).
30. Van Amerongen, G. J., *J. Polymer Sci.*, **5**, 307 (1950).
31. Wook, H., Alex, N. H., Frisch, H. L., Stannett, V., and Szwarc, M., *Ind. Eng. Chem.*, **47**, 2524 (1955).

END OF REFERENCE

61

REFERENCE

62

EROSION BY CAVITATION OR IMPINGEMENT. STP-408, AMERICAN SOCIETY FOR TESTING & MATERIALS, 1966.

THIS REFERENCE IS COPYRIGHTED MATERIAL AND THEREFORE THE CONTENTS HAVE NOT BEEN REPRODUCED FROM THE TEXT.

END OF REFERENCE

REFERENCE

63

GLENN, H. L.; AND O'NEAL, G.: WATCH THOSE DENTS.
AEROSP. SAFETY, VOL. 27, NO. 8, AUG. 1971.

THIS MATERIAL HAS BEEN APPROVED FOR PUBLICATION PER
LETTER FROM JOHN D. MIELKE, MAJOR, USAF, EDITOR, AEROSPACE
SAFETY MAGAZINE TO JOANNE FOLK DATED AUG. 22, 1974.

watch those dents

HARVIE L. GLENN/GARY O'NEAL
Engine IM Division
OCAMA, Tinker AFB, Okla.

Investigation of a J57 high pressure fuel tube removed from service because of fuel leakage from a small pin hole revealed that the hole was caused by cavitation erosion. In this case the erosion was attributed to a dent in the tube upstream from the hole.

Cavitation erosion is caused by relative motion between a metal surface and a liquid—in this case the inside wall of the tube and JP4. The cavitation is the result of voids (cavities) forming in the liquid then collapsing against the metal surface. In this failure the dent caused voids to form in the JP4 and then collapse downstream against the inner wall of the tube. Collapse of cavitation voids can produce impact pressures by implosion exceeding the yield strength of most metals.

When the voids collapse, the surface of the metal is subjected to repeated local plastic deformations that result in ultimate fracture and disintegration.

Maintenance activities should keep a sharp lookout for dents in high pressure fuel tubes exceeding TO limits. OCAMA (MMTTJB) is presently working to develop better methods (NDI) for inspecting fuel tubes and expects to have a procedure available by the end of 1971. ★

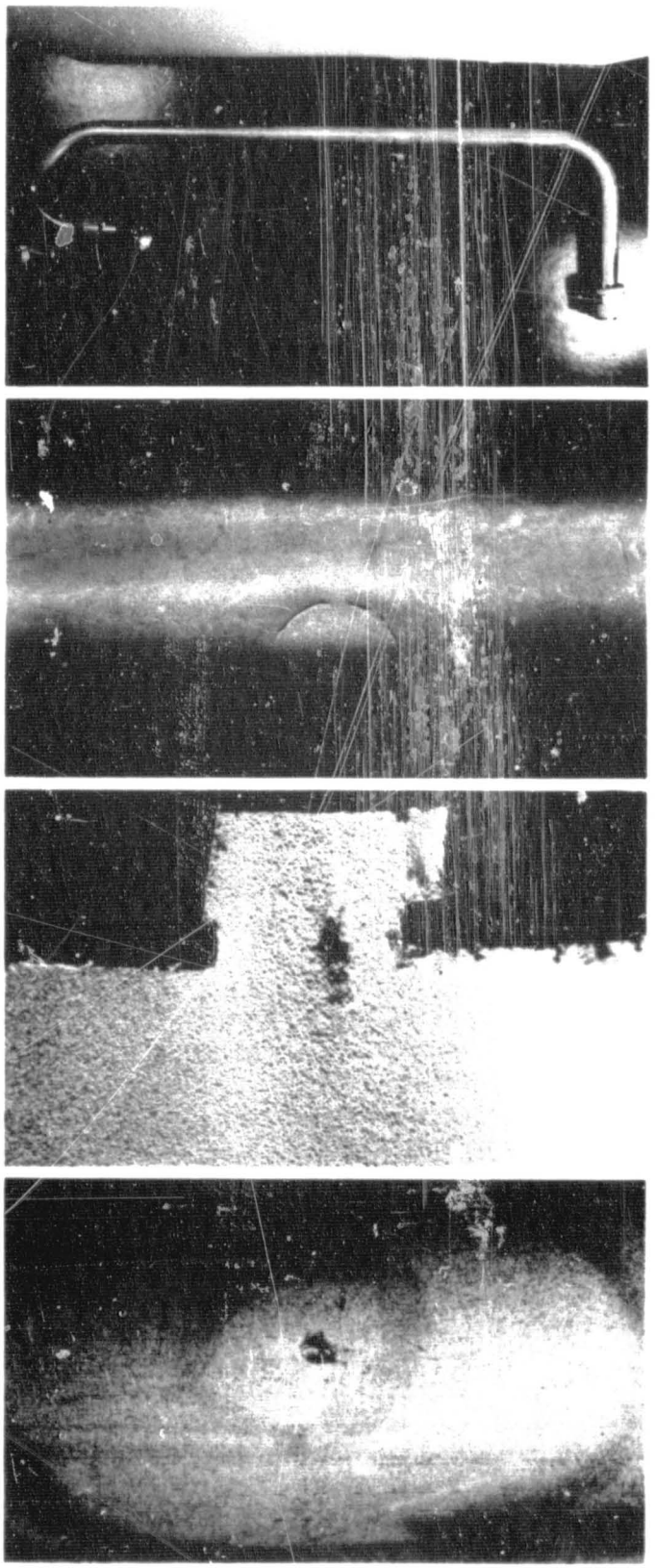

Top to bottom—High pressure fuel tube, dent in tube, cutaway showing hole and interior erosion of tube, exterior view of the hole.

END OF REFERENCE

REFERENCE

64

BAUM, J. V.; GOOBICH, B.; AND TRAINER, T. M.: AN EVALUATION OF HIGH-PRESSURE OXYGEN SYSTEMS. AMRL-TDR-62-102, AEROSPACE MEDICAL RESEARCH LAB., SEPT. 1962.

1.3-9-1
1.4-7-1
CDC K-3011

AMRL-TDR-62-102

AN EVALUATION OF HIGH-PRESSURE OXYGEN SYSTEMS

TECHNICAL DOCUMENTARY REPORT NO. AMRL-TDR-62-102

September 1962

Life Support Systems Laboratory
6570th Aerospace Medical Research Laboratories
Aerospace Medical Division
Air Force Systems Command
Wright-Patterson Air Force Base, Ohio

LIBRARY COPY

LEWIS LIBRARY, NASA
CLEVELAND, OHIO

Contract Monitor: Irving H. Lantz
Project No. 6373, Task No. 637302

[Prepared under Contract No. AF 33(616)-8267
by
J. V. Baum
B. Goobich
T. M. Trainer
Battelle Memorial Institute, Columbus, Ohio]

ABSTRACT

A research program was conducted to investigate the relative safety of 7500-psi gaseous oxygen systems when used as a source of breathing oxygen in aerospace vehicles. Experiments were performed to investigate the effects on the system of temperature, vibration, shock, extended storage, and contamination. Also studied were the effects of high pressure, high-velocity flow, and heating due to rapid compression. Evaluation of the results of this program indicates that 7500-psi gaseous oxygen systems can be comparatively safe if proper safety precautions are taken. Under controlled operations, the hazard of explosion because of contamination can be overcome. Stainless steel and Monel alloys were found to be acceptable materials of construction. Teflon and Kel-F compounds appear to be suitable for seals. Hydrocarbons in minute concentrations were found not to be dangerously reactive. Electrostatic charges due to high-velocity flow were small, but there was evidence that erosion could be a serious problem. Although no appreciable chemical reactions occurred during the normal experimental program, it must be realized that controlled laboratory procedures are not widely prevalent. High-pressure oxygen systems must be treated as "new" and representing dangerous, explosive possibilities. It is recommended that further detailed studies of the combustion process be performed. Spontaneous ignition temperatures for the materials and contaminants considered in this research should be investigated under both static and dynamic conditions. It is recommended that, before high-pressure gaseous oxygen systems be used extensively as are systems at lower pressures, reliability of the system and equipment used for handling the gas be increased through improved equipment design.

PUBLICATION REVIEW

This technical documentary report has been reviewed and is approved.

Wayne H. McCandless

WAYNE H. McCANDLESS
Chief, Life Support Systems
Laboratory

was evacuated by vacuum pump (G) and the gas from (D) was allowed to expand into the evacuated system. Valve (C) was then closed and the system evacuated again. The gas remaining in (D) was allowed to expand again. This process was repeated until vacuum gage (E) indicated an absolute pressure reading in reactor (J) of from 1/2 to 3 inches of mercury, depending on the concentration required. Valve (H) was then closed and the test reactor (J) removed. Reactor (J) was then connected to the apparatus being used for the actual experiment and charged with 7500-psi oxygen. This technique was used for all experiments in which hydrocarbon gases were evaluated.

In the second storage experiment, five reactors of stainless steel were charged with 7500-psi oxygen at 260 F. This experiment lasted for 500 hours. The 260 F temperature was maintained throughout the experiment. The specimens tested in this second storage experiment were different from those used in the first experiment. Included in the second series of reactors were tensile specimens of Kel-F and Teflon, deposits of carbon dust, and strands of steel wool. Another condition of this experiment was the use of welded and brazed tubing connections.

Initially all of the reactors were constantly vibrated at 35,800 cycles per minute to simulate dynamic conditions. However, after only 94 hours, two valve connections began to loosen and the pressure in the respective reactors dropped below 2500 psi. For the remainder of the experiment, the reactors were not vibrated and only three of the original five reactors retained the 7500-psi pressure. Figure 12 shows the arrangement of the reactors and the special steel box constructed to house them.

Flow

One objective of the flow experiments was to determine erosion effects for different materials. A second objective was to measure the amount of electrostatic charge generated by the high-pressure high-velocity gas as it expanded through an orifice. The major difficulty encountered in these experiments was the shortness of the flow duration with each charge of high-pressure oxygen. Only a maximum of 45 milliliters of gas could be generated at one time and only 15 to 30 milliliters could be stored.

The arrangement used for the flow experiments is shown in Figure 13. Figure 14 includes details of the retainer assembly and the orifice.

The high-pressure gas was first generated in cylinder (A) where pressures as high as 12,000 psi were generated to permit longer blowdown periods. Valve (C) was then opened and high-pressure high-velocity gas flowed through the retainer-orifice assembly (E) and expanded to atmospheric pressure.

The blowdown period was measured from the time valve (C) was opened until pressure gage (B) indicated 1000 psi. Diameters of the orifices ranged from 0.005 to 0.013 inches. A 0.005-inch-diameter orifice allowed a total blowdown period of 1 minute for each charge. The blowdown period with the 0.013-inch-diameter orifice was only 20 seconds per charge. During a normal 8-hour day, a maximum of eight or nine charges were generated.

Electrostatic charges were measured as shown in Figure 13. Probes of different materials and geometries were inserted into the retainer assembly and placed about 1/8 inch behind the orifice exit. The static charge was picked up by the probe, measured by the Sweeney gage, and transcribed into a visual plot by the oscillograph recorder.

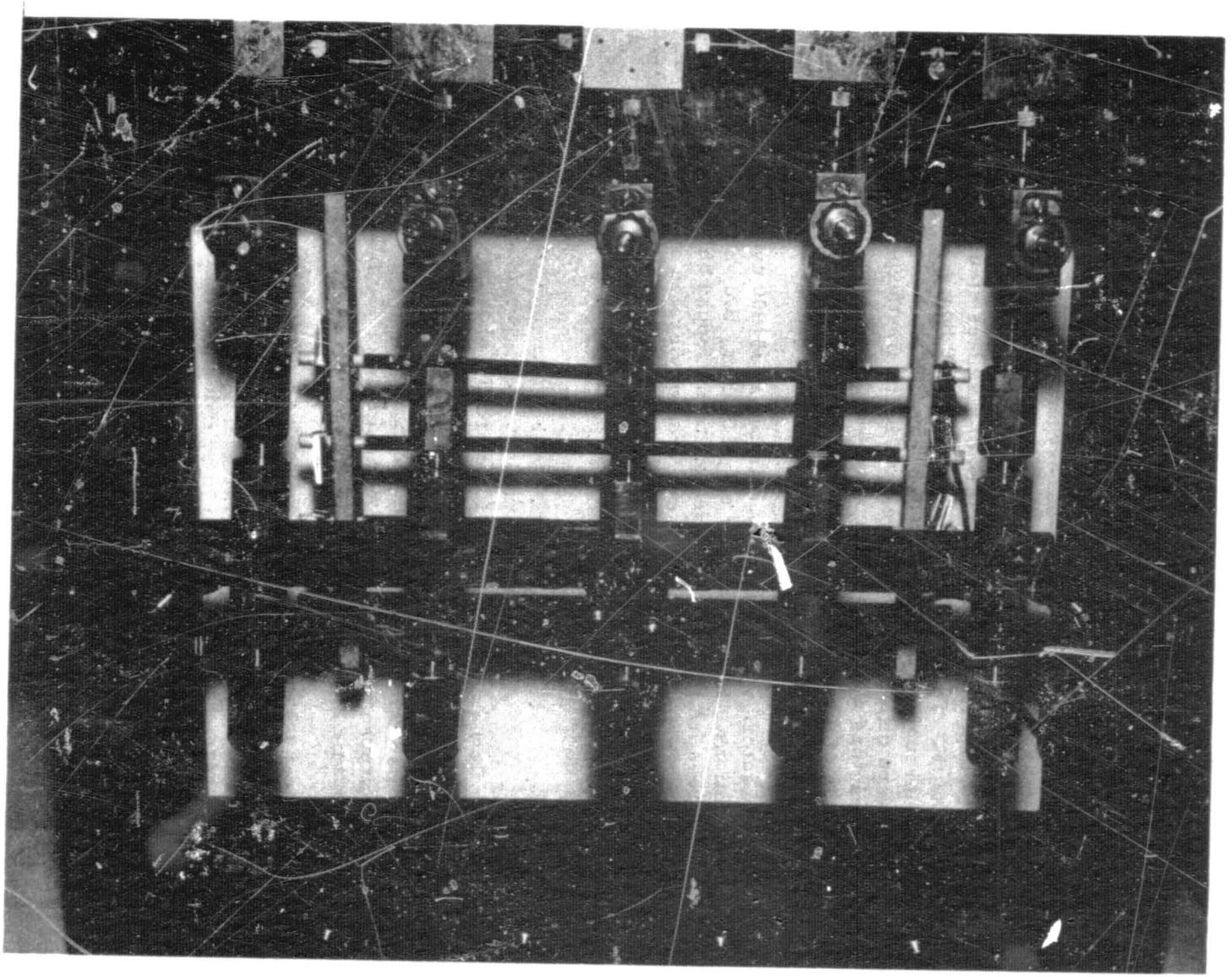

FIGURE 12. REACTORS ASSEMBLED FOR 500-HOUR DYNAMIC STORAGE. EXPERIMENTS '26 THROUGH 130

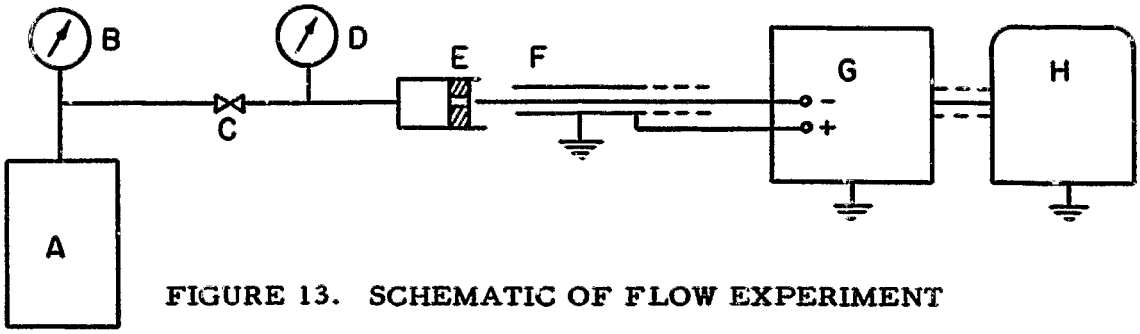

FIGURE 13. SCHEMATIC OF FLOW EXPERIMENT

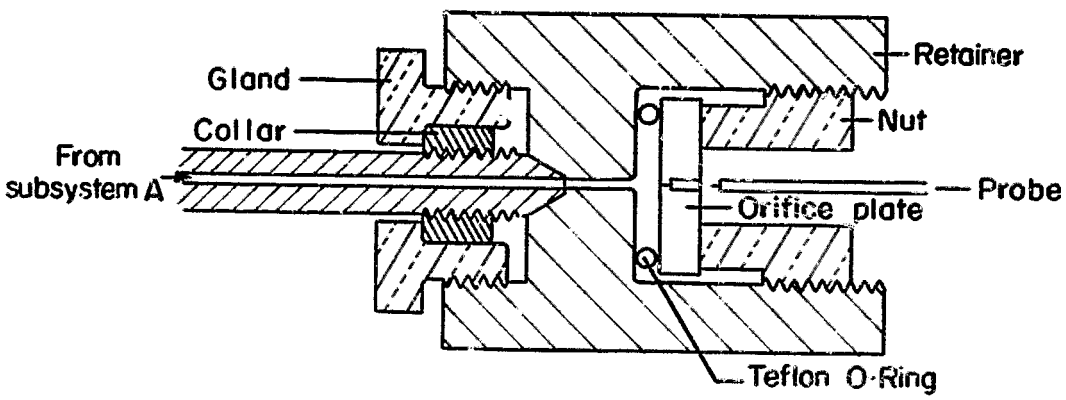

FIGURE 14. DETAILS OF ORIFICE AND RETAINER

Figure 15 shows the actual curve plotted during Experiment 93 when the static voltage was recorded as +0.20 volt. In Appendix IV, Table 16, specific details of experimental conditions, probes used, and voltages recorded are tabulated for all the flow experiments.

Surge

The primary aim in performing the surge experiments was to determine the temperature rise caused by rapid compression. A stainless steel receiver of 3.5-milliliter volume was used for these experiments. As shown in Figure 16, the receiver was immersed in an ice bath (E) to assure a constant reference temperature and to permit better measurement of the resulting rise in temperature.

The receiver (D) was charged to high pressure levels in one rapid charging cycle. Pressures ranging from 10,000 to 16,000 psi were generated in cylinder (A). Hand valve (C) was then opened rapidly and the gas was allowed to expand into the receiver. Depending upon the initial upstream pressure, the instantaneous pressures recorded in the receiver ranged from 5000 to 8300 psi. Simultaneously, the rise in temperature was measured by thermocouple (F) and was recorded on oscillograph (G).

An iron-constantin pencil thermocouple with a 1/8-inch stainless steel tubular sheath was used. The thermocouple wires were brought through the tube and welded at the tip, permitting direct measurement of the temperature fluctuation inside the receiver. The temperature rise measured was that of the gaseous contents of the receiver.

EVALUATION OF EXPERIMENTAL RESULTS

The discussion of experimental results is divided into seven sections. Presented in each section is a discussion of the materials investigated, the experiments performed, the results obtained, and the conclusions derived. The seven sections are:

- Materials Compatibility
- Hydrocarbon Contaminants
- Solid-Particle Contaminants
- Materials of Construction
- Electrostatic Charges
- Adiabatic Heating
- Experimental Equipment Evaluation.

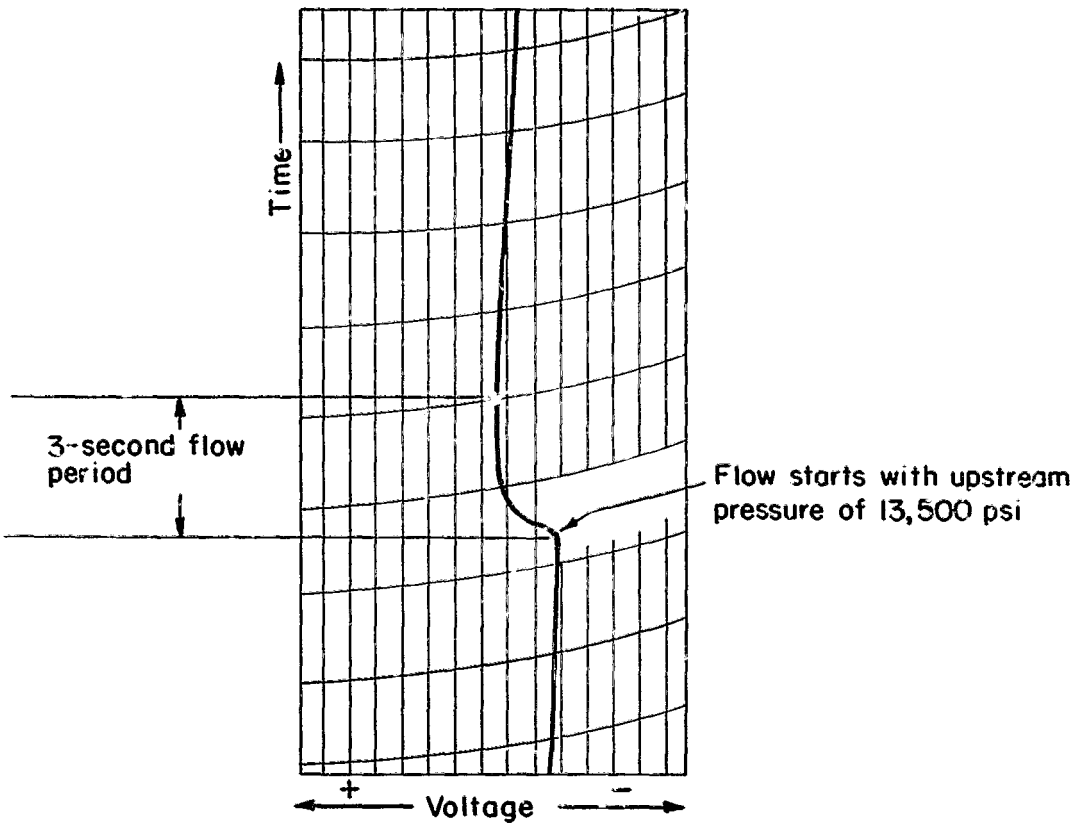

FIGURE 15. ELECTROSTATIC VOLTAGE RECORDED DURING EXPERIMENT 93

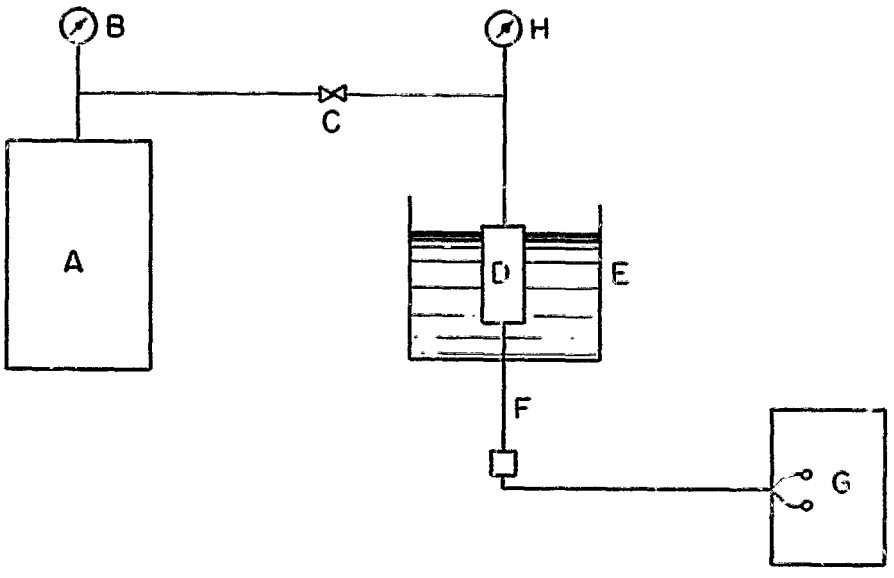

FIGURE 16. SYSTEM USED FOR SURGE EXPERIMENTS

Materials Compatibility

Materials Investigated

Investigations of materials compatibility were conducted for five polymers: Teflon, Kel-F, Viton, neoprene, and nylon. These were chosen because of their possible application as static or dynamic seals or bearings. The following experiments were performed:

(1) Thermal and vibration tests were performed with Teflon, Kel-F, Viton, and neoprene O-rings when compressed as static seals and also when unconfined.

(2) Thermal and storage tests were performed with Teflon, Kel-F, and nylon dumbbells to determine what changes in elastic properties result from different conditions and periods of exposure.

(3) Flow experiments were performed with Teflon and Kel-F orifices to determine erosion resistance of these materials. The orifices were made from disks 3/16-inch thick and 3/4-inch diameter, with a 0.006-inch-diameter hole through the center.

(4) Storage experiments were performed with shredded pieces of Kel-F, Teflon, and neoprene to determine whether frayed and ragged edges are more susceptible to chemical reaction than the smooth surface normally provided with gaskets and O-rings.

Evaluation of Results

During the experiments no spontaneous changes in pressure or temperature were recorded. This indicated that no gross chemical reaction such as combustion or detonation occurred. Mass spectroscopic analysis of the residual gases also indicated no combustion. However, tensile-test analysis and visual inspection of the specimens indicated that nylon, Viton, and neoprene suffered appreciable chemical change and deterioration of physical properties. Nylon especially deteriorated so badly that tensile tests were not possible.

The extent of the oxidation effect is shown in Table 1 by the changes in tensile strength and ductility as indicated by per cent elongation of standard O-rings. Teflon seems to be an exception in that both the strength and ductility of the O-rings increased slightly. Teflon O-rings increased 1.3 per cent in strength and 8 per cent in ductility. Kel-F decreased 5.5 per cent in strength, but ductility remained the same. Viton and neoprene showed decreases of 23.5 and 58 per cent in strength and decreases of 8.5 and 28.5 per cent in ductility. These results, of course, reflect only a small sampling and a more accurate and reliable comparison would be dependent upon a broader analysis.

In addition to loss of strength, neoprene and Viton O-rings exhibited a high degree of oxygen absorption. O-rings of both polymers when removed from the test reactor had swelled to almost twice their original size and surface blisters were observed. This effect was apparently caused by the absorption of high-pressure oxygen gas. After

remaining at ambient pressure for a short period, the O-rings returned to their original size. In some cases the blisters popped like over-inflated balloons. In all likelihood, seals made of these polymers would be inadequate for extended use because of oxygen embrittlement and high porosity of the polymer.

Teflon dumbbells exposed to high-pressure oxygen for 48 hours at 260 F showed an average change in tensile strength of -2 per cent and an average change in elongation of +10.7 per cent (Table 2). Kel-F dumbbells exposed for an equal period under identical conditions showed average changes of -10.2 per cent in strength and -30.0 per cent in elongation. The Teflon dumbbell exposed for 94 hours in Experiment 126 failed at a machining flaw when subjected to a tensile test. Therefore, the maximum elongation of 1.16 inches is not a true value.

The Teflon specimen exposed for 500 hours in Experiment 127 had exactly the same strength and ductility as the standard specimen. In the light of the demonstrated tendency of Teflon to increase in strength and ductility when exposed for short periods, the results of Experiment 127, if typical, can be interpreted to mean that the crossover point had been surpassed between 48 and 500 hours of exposure and further exposure may result in decreased strength and ductility.

The Kel-F specimen exposed in Experiment 128 demonstrated significant reduction of ductility (81.5 per cent). Corresponding loss in strength was 14.5 per cent. Furthermore, many compression shear failure cracks were visible below the surface of the Kel-F bar after exposure and probably one of these cracks caused the bar to fail prematurely.

Samples of these same materials were also exposed to 260 F for 48 hours in air at normal atmospheric pressure. The Teflon specimen exposed to air at atmospheric pressure increased in ductility appreciably more than the specimens that had been exposed to high-pressure oxygen. Even the strength of the Teflon bar increased by 6 per cent. Kel-F showed decreases of only 2.7 per cent in strength and 44.4 per cent in ductility. The appearance of the Kel-F specimen indicates that failure occurred prematurely because of a machining flaw. The sizable loss in ductility is attributed to this.

Flow experiments were performed to determine erosion resistance of Teflon and Kel-F. The area in the center of the Teflon orifice plate collapsed as shown in Figure 17 when first exposed to 10,000-psi oxygen. This plate was a 3/16-inch-thick disk with a 1/2-inch-diameter unsupported area in the center. It had a 0.006-inch-diameter hole. A second orifice with an unsupported area of 1/16-inch diameter and a 0.006-inch-diameter hole was then exposed to 10,000-psi oxygen. After only 2-1/2 minutes of oxygen flow, the hole was plugged. The oxygen gas, still under high pressure, was forced to escape around the periphery of the disk causing the Teflon to cold flow and to be extruded into the clearance space around the peripheral edge of the steel back-up disk.

The Kel-F disk, also with an unsupported area of 1/2-inch diameter, had sufficient strength to prevent the collapse encountered with Teflon. The Kel-F did not tend to cold flow; however, after 15 minutes of flow, the Kel-F disk showed appreciable concaving. Although the disk did not collapse, it appeared that collapse could have occurred momentarily.

TABLE 1. TENSILE-TEST RESULTS FOR TEFLON, KEL-F, VITON, AND NEOPRENE O-RINGS

Experiment	Maximum Pull, pounds				Maximum Elongation, inches			
	Teflon	Kel-F	Viton	Neoprene	Teflon	Kel-F	Viton	Neoprene
Standard	19.5	65.7	15	17.5	1.12	0.147	1.29	1.39
11	18.5	--	6.5	--	1.12	--	0.92	--
13	20.0	--	12	--	1.26	--	1.28	--
14	--	58	--	8	--	0.13	--	1.24
15	--	53	--	5	--	0.18	--	1.18
18	19.5	59	13.5	10.0 11.5	1.16	0.16	1.30	1.14 1.20
19	21.0	--	14	--	1.30	--	1.22	--
20	--	78	--	1.5	--	0.13	--	0.40
21	--	62	--	8.5	--	0.14	--	0.80

TABLE 2. TEST CONDITIONS AND TENSILE-TEST RESULTS FOR TEFLON, KEL-F, AND NYLON DUMBBELLS

Experiment	Material	Pressure, psi	Temperature, F	Elapsed Time, hours	Results	
					Max Pull, pounds	Max Elongation, inches
--	Teflon (standard)	--	--	--	50	2.05
103	Teflon	15[a]	260	48	53	2.67
100	Teflon	7800/8000	260	48	50	2.34
100	Teflon	7800/8000	260	48	48	2.20
126	Teflon	7500	260	94	53	1.16[b]
127	Teflon	7500	260	500	50	2.00
--	Kel-F (standard)	--	--	--	187	0.54
102	Kel-F	15[a]	260	48	182	0.30[b]
101	Kel-F	7800	260	48	166	0.42
101	Kel-F	7800	260	48	170	0.34
128	Kel-F	7500	260	500	160	0.10
109	Nylon	5500/8500	260	47	Tensile test not possible because of embrittlement and specimen deterioration	
110	Nylon	5500/8500	70	46		

(a) Conducted in air.

(b) Early failure caused by machining flaw in sample.

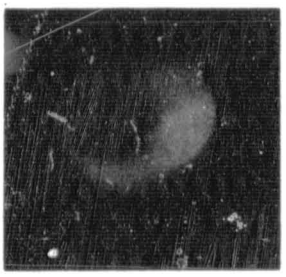

a. Front View

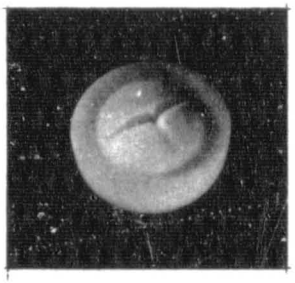

b. Back View

FIGURE 17. TEFLON ORIFICE DISK AFTER EXPOSURE TO 10,000-PSI OXYGEN

Photomicrographs of the Kel-F disk (Figure 18) indicate that peripheral edge deterioration is appreciable. Deep gouges and scratches appear along the entire edge. The cross-sectional view shows how badly the leading edge has been rounded off. Also, it appears that the force exerted on the diametral surface has caused the Kel-F material to "melt" and flow in the same direction of the gas stream. This appears to be similar to the cold flow of the Teflon disk.

In the static 616-hour storage experiment, shredded specimens of Viton, Kel-F, and Teflon were subjected to continuous exposure to oxygen at 7500 psi. The mass spectroscopic analyses made of the residual gases showed no evidence of chemical reaction and there appeared to be no visual evidence of physical deterioration. Emission spectrographic analysis indicated no change in the Teflon.

Conclusions

Teflon and Kel-F are both compatible with high-pressure oxygen systems with regard to chemical reactivity, and they manifest a high degree of stability. Viton, however, shows questionable compatibility although an insufficient number of samples were tested in this program to draw firm conclusions. AiResearch also reports some failures with Viton O-rings but nevertheless they are using them as seals in the Mercury control equipment.[10] In any case, neoprene seals were found to be incompatible with high-pressure oxygen.

Pure Teflon suffers from certain physical weaknesses. It tends to cold flow very easily, and because of its high ductility and lubricity, it is easily extruded out of shape when unconfined. Neither does a thin, unsupported Teflon disk have sufficient strength to prevent collapse when high-pressure forces are applied.

Kel-F has sufficient strength and rigidity to partially overcome the cold-flow problem for short periods and it can withstand instantaneous impacts from flow that would cause Teflon to collapse or extrude. However, Kel-F does not appear to be sufficiently ductile for seal use, nor does it provide the lubricity of Teflon. A possible solution, aside from the conventional compounding of Teflon with ceramic, glass fiber, and asbestos cloth, is use of a new compound of Teflon and Kel-F. This compound consists of 80 parts Kel-F and 20 parts Teflon. According to the developer, Minnesota Mining and Manufacturing Corporation, it is sufficiently strong to resist cold flow, is more

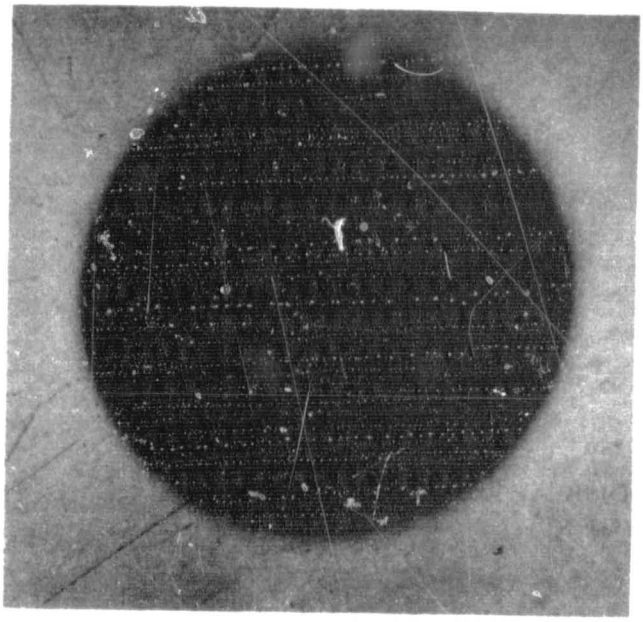

a. Face View Before Exposure

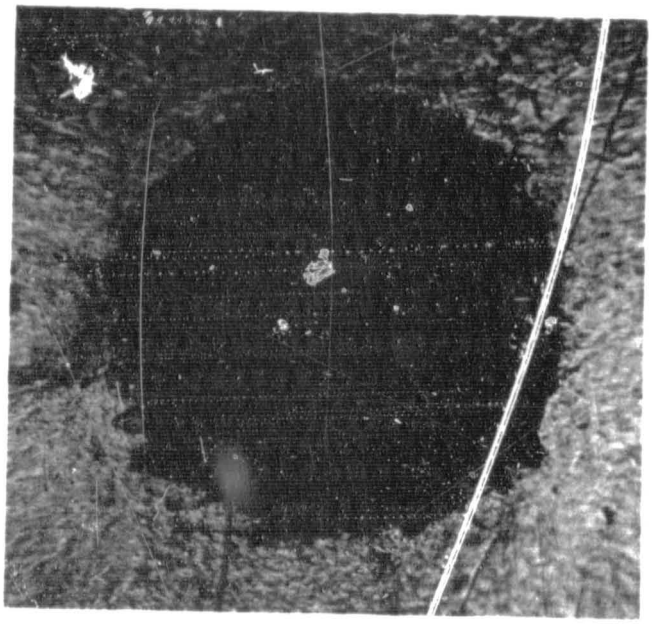

b. Face View After 15 Min of Flow

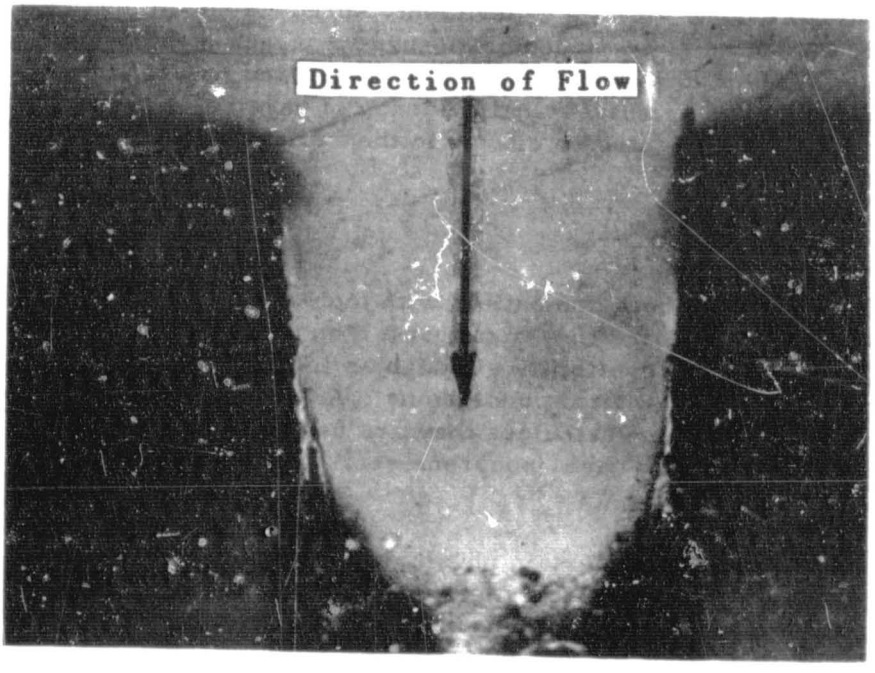

c. Cross-Sectional View After 15 Min of Flow

FIGURE 18. FACE AND CROSS-SECTIONAL VIEWS OF 0.006-INCH DIAMETER KEL-F ORIFICE

ductile than pure Kel-F, and retains the lubricity of Teflon. However, both Kel-F and Teflon should be employed as seals only when closely confined (like O-rings) to prevent possible collapse or cold flow.

Hydrocarbon Contaminants

Determination of the effects of various hydrocarbon contaminants was based on the acceptable limits imposed by Aeronautical Systems Division on aviators' breathing oxygen. These limits are given in Table 3.

TABLE 3. ACCEPTABLE LIMITS OF HYDROCARBON CONTAMINANTS

Contaminant	Symbol	PPM, vol
Methane	CH_4	15.00
Acetylene	C_2H_2	0.05
Ethylene	C_2H_4	1.00
Propane	C_3H_8	1.00
Butane	C_4H_{10}	1.00
Pentane	C_5H_{12}	0.20
Hexane	C_6H_{14}	0.02
Decane	$C_{10}H_{22}$	10.05

Experiments Performed

Four types of experiments were performed: (1) vibration, (2) shock, (3) storage for 616 hours at static conditions, and (4) exposure for short periods at temperatures as high as 400 F.

All of the hydrocarbons listed in Table 3 were investigated. Because of the rather minute concentrations required and the small volumes of gases involved, it was necessary to estimate the mixtures in each charge.* The method by which the reactors were charged with the gaseous hydrocarbon is described on page 17. Liquid hydrocarbon concentrations were determined by the amount of liquid released from a medicine dropper. After each experiment, a sample of the residual gas was analyzed by mass spectroscopy, and by this means the actual concentrations of various gases were determined. It also served to show by CO_2 and CO concentrations whether a chemical reaction had occurred. Table 4 lists the hydrocarbons investigated, the maximum temperature imposed, the original hydrocarbon charge used, and the amount of hydrocarbon found in the residual gas of each experiment.

*See Appendix V.

END OF REFERENCE

REFERENCE

65

MURPHY, D. W.: AN EXPERIMENTAL INVESTIGATION OF GEYSERING IN VERTICAL TUBES. ADVANCES IN CRYOGENIC ENGINEERING, VOL. 10, K. D. TIMMERHAUS, ED., PLENUM PRESS, 1964.

REFERENCE

A Cryogenic Engineering Conference Publication

LEWIS RESEARCH CENTER
Aerospace Safety Research
and Data Institute

Advances in Cryogenic Engineering

VOLUME 10

Proceedings of the 1964
Cryogenic Engineering Conference
(Sections A-L)

K. D. TIMMERHAUS, *Editor*
Engineering Research Center
University of Colorado
Boulder, Colorado

LIBRARY COPY
RETURN TO
LEWIS LIBRARY
CLEVELAND, OHIO

Distributed by
PLENUM PRESS
NEW YORK
1965

I–7

AN EXPERIMENTAL INVESTIGATION OF GEYSERING IN VERTICAL TUBES*

D. W. Murphy

Martin Company
Denver, Colorado

INTRODUCTION

The phenomenon termed geysering can be described as the rapid expulsion of a boiling liquid and its vapor from a vertical tube. The primary engineering interest in geysers is in the missile industry since many rocket vehicles use cryogenic fluids as the vehicle propellants. The geyser problem arises in the design of propellant feed systems, which typically use long lines to connect the propellant tank to the engine. Because the propellants are cryogenic, the atmosphere heats the propellant in the feed line during the time period following missile fueling and prior to launch. If a geyser occurs during this period and the line is emptied of liquid, the liquid, in refilling, can cause impact loads at the bottom of the line high enough to seriously damage the vehicle. In addition, if the feed line is damaged, the propellant in the missile tank may drain out, creating a safety hazard throughout the launch area. If sufficient information concerning the factors which produce geysering were available during the initial design of the propellant feed system, the geyser problem might possibly be eliminated by appropriate design.

This study was initiated to develop a method for the prediction of geysering and non-geyser combinations of system geometry, fluid properties, and heating rate. An experimental program, based upon work done by others [1–2] in conjunction with free convection cooling of turbine blades, was conducted, which resulted in an empirical correlation for the prediction of geysering. This correlation was based on the results of 114 geyser tests using water, Freon 113, liquid nitrogen, and liquid hydrogen as test fluids. Geyser tubes of 4, 6, 8, and 13 in. diameter were used. The heat flux range was between 50 and 1900 Btu/ft²-hr.

DISCUSSION

When a long vertical tube with a reservoir at the top and closed at the bottom is filled with liquid and heated along the tube wall, the heat will be transferred to the liquid surface by means of free convection. This convection process, shown schematically in Fig. 1, establishes fluid circulation within the tube by which heated fluid rises and cool fluid from the reservoir descends in the tube. A portion of the heat entering at the tube wall will be liberated at the liquid surface in the reservoir by evaporation and the remainder will result in a sensible heat gain by the liquid.

As the heating process continues, the fluid bulk temperature is increased until the fluid in approximately the upper ¼ of the tube becomes saturated. Once the fluid becomes saturated, additional heat input to the liquid results in bubble production. The bubbles are formed on the wall, detach, start to rise in the liquid, and begin to coalesce. In coalescing they form a larger bubble called a Taylor bubble (see Fig. 2). The formation of a large

* Work supported by NASA George C. Marshall Space Flight Center under Contract NAS8-5418.

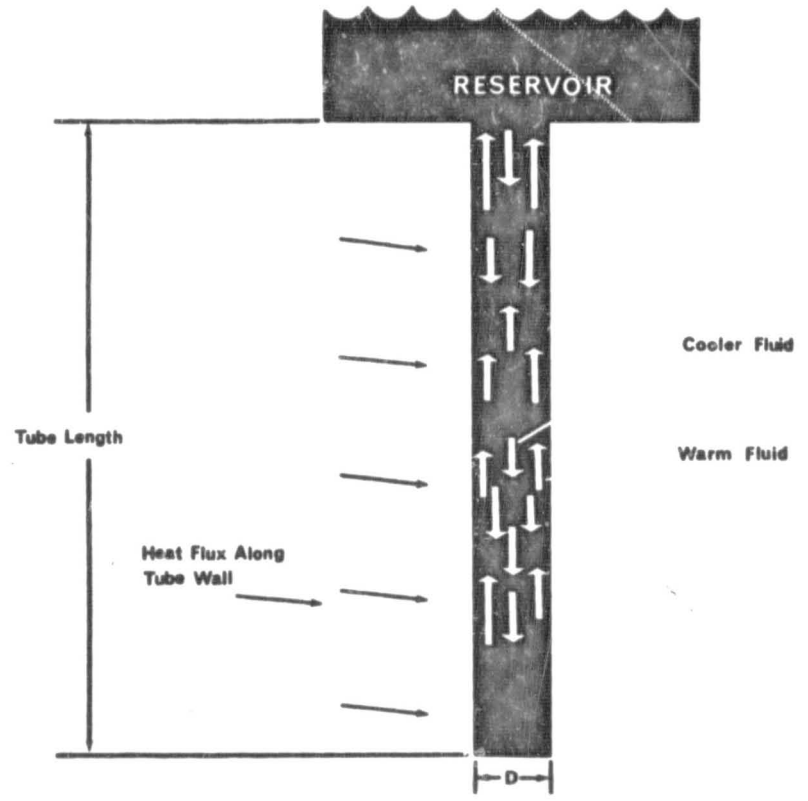

Fig. 1. Fluid circulation in a geyser tube.

bubble results in a pressure reduction below the bubble. Since the liquid below the bubble was at its saturation temperature, the reduction in pressure causes a portion of the liquid to vaporize, thereby forming more bubbles. As new bubbles are formed the pressure is again reduced, permitting more liquid to vaporize. This self-sustaining reaction occurs rapidly and forms vapor at a rate considerably greater than can be removed from the tube. The consequence of this difference in these rates is the explosive expulsion of the liquid from the tube. As the tube is refilled with fluid from the reservoir, the resulting impact or "water hammer" force may cause structural damage to the system.

This paper is concerned mainly with the breakdown in the natural convection heat transfer process which brings about the conditions for geysering. Free convection in vertical tubes has been studied extensively in the past [1–4]. These studies have included investigations of free convection cooling of gas turbine blades by means of drilled passages in the blades and a coolant reservoir in the hub.

These studies have resulted in correlations for the heat transfer rate in terms of the Nusselt number, the Rayleigh number, and the L/D ratio. Because these investigations were concerned only with single-phase, steady-state heat transfer, the results were not directly applicable to the problem of geysering. However, they did provide a good starting point for an experimental program to develop a method of predicting geysering.

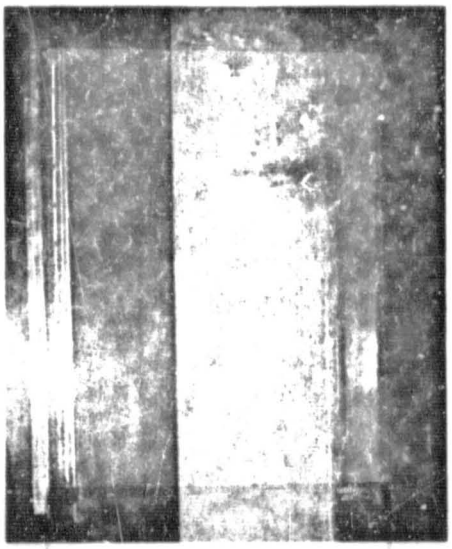

Fig. 2. Taylor bubble formation in water in a 4-in. pyrex tube.

EXPERIMENTAL PROGRAM

The experimental program consisted of a series of 114 tests in which vertical tubes containing different fluids were heated at controlled rates to determine if geysering would occur. The test fluids used were water, Freon 113, liquid nitrogen, and liquid hydrogen. Five tube diameters were tested ranging from 4 to 13 in. Tube L/D ratios were varied between 1.5 and 30. The heat flux range studied was between 50 and 1980 Btu/ft^2-hr.

The general geyser tube configuration used in all geyser tests consisted simply of a cylindrical reservoir mounted on top of the vertical tube (see Fig. 1). Pressure taps and fill connections were installed at the bottom of each geyser tube for monitoring the hydrostatic pressure during geysering and for filling the tube. Table I presents a summary of the geyser tubes used, and the conditions investigated during the program. In addition, Table I also presents the geyser tube material, and the test fluids used in each tube.

General Electric T-3 infrared heating lamps were used for tubes A and B with water and Freon. Figure 3 shows geyser tube A with the infrared heating system installed in the test cell. The lamps are approximately 12 in. in length, and are capable of producing 1000 W when operated on 220 V. The system contained 11 rows (covering approximately 12 ft of tube length) consisting of 8 equally spaced lamps in each row. The lamps were mounted in aluminum channel sections which served as reflectors to direct the radiation and provide

Table I. Summary of Test Conditions

Tube designation	Tube diameter, in. ID	Tube diameter, in. OD	Tube length tested, ft	Heat flux range, Btu/ft^2-hr	Number of tests	Tube material	Test fluid
A	4.22	4.75	2 → 9	120 → 410	26	Pyrex	H_2O
B	4.00	4.50	2 → 10	40 → 770	68	Aluminum	H_2O, Freon-113, LN_2, LH_2
C	5.75	6.00	8	28 → 84	3	Aluminum	LN_2
D	7.75	8.00	9 → 14	48 → 1980	15	Aluminum	H_2O, LN_2
E	13.00	13.50	28.3	14.7 → 44	2	Aluminum	LN_2

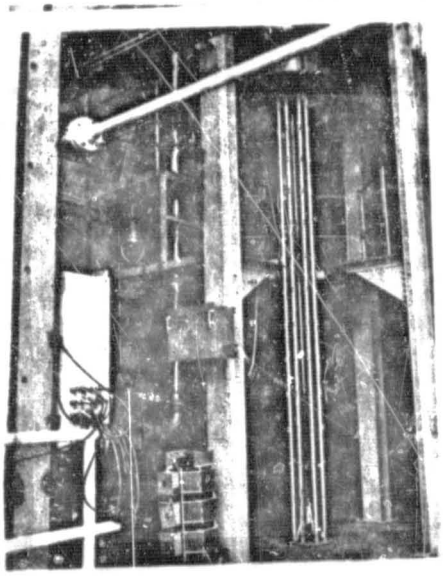

Fig. 3. Geyser tube A installed in test cell.

uniform heating of the tube surface. Voltage across the lamps was controlled by means of a 220-V three-phase Variac. Each of the rows was wired through a toggle switch for individual control. This arrangement permitted operation of any desired combination of rows at one time. By energizing the desired number of rows from the top of the tube, the effective tube length could be varied without modification of the glass tube. Glass was selected because the low thermal conductivity prevented heating of the liquid below the last row of energized lamps and also to permit observation of the geyser process.

In order to simulate a missile line, the water must be heated by convection from the hot tube wall. Because the heating was by radiation, it was necessary to increase the absorptivity of the pyrex tube from a value of about 0.60 to near 1.0 to prevent direct heating of the water by the radiant energy. The higher absorptivity was achieved by painting the pyrex tube with a solution of carbon black and lacquer. The lacquer evaporated leaving the carbon black on the surface, thereby providing the desired absorptivity.

The heating system used on geyser tube D for the water tests consisted of a series of electric blanket heaters 12 in. wide and 25 in. long. This heating system was used because the radiation heating system was found to have insufficient power available. The blanket heaters were wrapped around the tube, and covered with a 1-in. layer of polyurethane insulation to minimize the losses to the surroundings. The heaters were energized by means of the 220-V Variac previously described. The heat flux was determined by measuring the power input to the heaters and subtracting the heat losses through the foam insulation (calculated using the steady-state conduction equation). The temperature difference across the foam was determined from thermocouple measurements.

The tests employing liquid nitrogen and liquid hydrogen did not require the use of an external heating system. Instead, the heat flux was readily controlled by insulating the geyser tube with various thicknesses of polyurethane foam. Insulation thicknesses of 0, $\frac{1}{4}$, $\frac{1}{2}$, and 1 in. were used for the liquid-nitrogen tests. The thicknesses used in the liquid hydrogen tests were 7, 4, and $\frac{1}{4}$ in. A helium gas atmosphere was provided around the foam insulation in the hydrogen tests to prevent the condensation of air in the insulation.

The heat flux for the foam insulated tubes was calculated by means of the one-dimension, steady-state conduction equation in cylindrical coordinates. The temperature difference across the foam was measured with copper–constantan thermocouples. The thermal conductivity of the foam for the liquid-nitrogen tests was obtained from the work of Hertz [5].

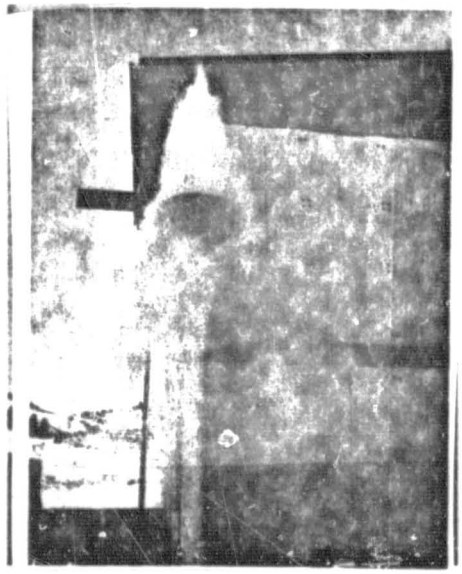

Fig. 4. Geyser tube D during a liquid-nitrogen geyser.

Heat flux for the liquid-hydrogen tests was calculated using the thermal conductivity of helium [6] because of the helium purge around the open cell type foam. The heat flux for the liquid-nitrogen tests without insulation could not be calculated readily because of the effects of small quantities of air condensing on the tube. Instead, the work of Ruccia and Mohr [7] on heat transfer to uninsulated liquid-oxygen tanks was used as a basis for estimating the heat transfer to the uninsulated liquid-nitrogen tubes. A value of 700 Btu/ft²-hr (approximately 25 % greater than the reported heat flux for the uninsulated liquid-oxygen line) was selected as being a close approximation of the actual heat flux. Figure 4 shows geyser tube D during a liquid-nitrogen geyser.

RESULTS

The initial attempt to obtain a correlation that would predict geyser *vs.* nongeyser conditions as a function of heat flux, tube geometry, and fluid properties was based upon the work of Lighthill [1] and Martin [2] on the cooling of turbine blades. The data taken at the onset of geysering with geyser tubes A and B were plotted in the form of the Nusselt number *vs.* the Rayleigh number. The fluid properties were evaluated at the arithmetic mean temperature between the top fluid centerline and the bottom inside wall temperatures. The inside wall temperature could not be measured, but it was estimated with adequate accuracy from a measured outside wall temperature. The plotted data were found to correlate well with that of Lighthill and Martin's, but it did not provide a means of distinguishing between the geysering and nongeysering regimes.

Since the geyser process is strongly time-dependent, and the attainment of liquid saturation is a prerequisite for geysering, the time required for all the fluid in the tube to attain saturation seemed to be a significant variable upon which to attempt a correlation. Therefore, the second correlation attempt included the Fourier number (N_{Fo}) as a time parameter. Time-zero was taken at the time the fluid in the tube was at a uniform temperature equal to the saturation temperature at the top of the tube.

A correlation of the test data from geyser tubes A and B was attempted by plotting the Nusselt number as a function of the Rayleigh–Fourier number product. This attempt also failed to yield the desired separation between geysering and nongeysering.

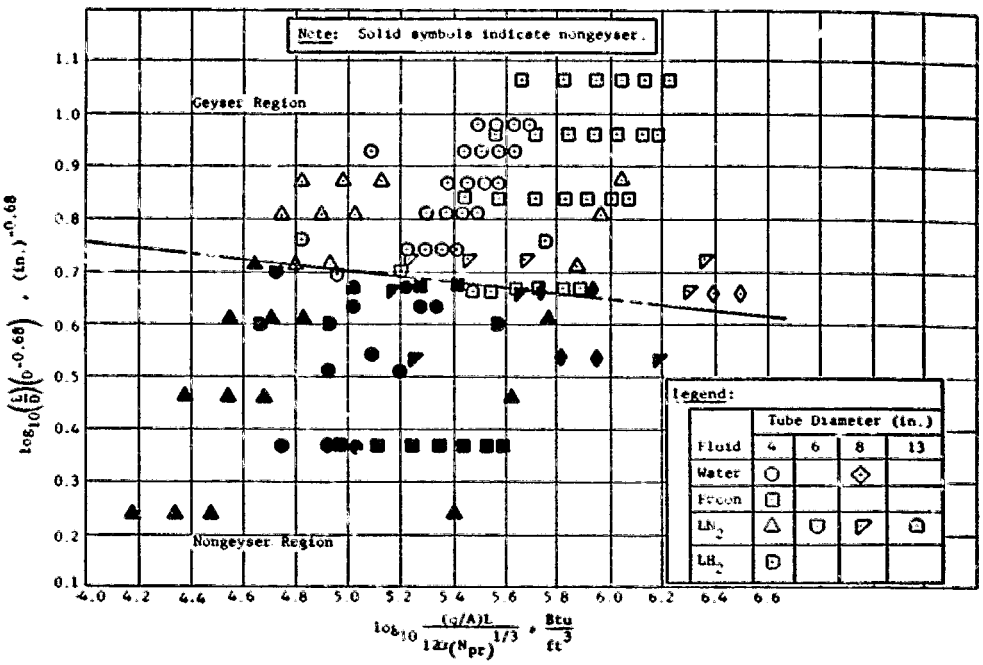

Fig. 5. Geyser–nongeyser correlation.

These data were then cross-plotted and adjusted by means of a series of trial and error approaches until a plot of the dimensionless tube geometry ratio (the heated tube length divided by the tube inside diameter) as a function of a parameter Z was attained, where Z is defined as

$$Z = \frac{(q/A)L}{12\alpha(N_{Pr})^{1/3}} \tag{1}$$

This method yielded the desired separation between the geyser and nongeyser regimes for the data obtained from geyser tubes A and B. Tests were then conducted on geyser tubes C, D, and E to verify the correlation for other diameters. The results of these tests showed that a correlation of L/D vs. Z was not sufficient to describe geysering as a function of tube diameter. Examining the test data from tubes C, D, and E showed that replacing the term L/D by $(L/D)\ D^{-0.68}$ resulted in a geyser–nongeyser correlation valid for all tube diameters and fluid properties. This final correlation is presented in Fig. 5.

The correlation presented in Fig. 5 is an empirical correlation which adequately describes the conditions that produce geysering. The fluid properties contained in Fig. 5 were evaluated at the temperature corresponding to fluid saturation at standard atmospheric pressure (14.7 psia). The same separation line was attained when the fluid properties were evaluated at saturation temperature corresponding to both 25 and 50 psia.

In the tests conducted in this study, the pressure at the top of the geyser tube was atmospheric (12 psia). In the case of an actual missile system, the pressure at the top of the propellant feed line will be considerably above atmospheric (as great as 2.5 atm), depending upon the ullage pressure and depth of liquid in the missile propellant tank. Griffith [8] has shown that the tendency of a tube to geyser is essentially independent of the pressure at the top of the tube. In his investigation, Griffith conducted geyser tests on various tubes and fluids with the pressure at the top of the tube ranging from 1 to 2.5 atm. His conclusions were that while increasing the pressure retards the bubble formation rate and consequently lowers the geyser frequency, the tube would still geyser. The importance of this correlation

is its value as a design tool. For instance, a propellant feed line for a missile can be designed in the normal manner and then the design checked with this correlation to determine if geysering will occur. If it is determined that the line will geyser, it may then be possible to modify the design in such a way as to preclude geysering. Since this investigation is concerned only with determining if a tube will or will not geyser, and not the geyser frequency, this correlation should adequately describe the combinations of fluid properties, heating rates, and system geometry that will produce geysering.

CONCLUSIONS

A satisfactory correlation has been developed for the prediction of geysering in terms of heating rate, system geometry, and fluid properties. The correlation was developed for a range of variables encountered in missile design. This correlation can be used in the design of missile suction lines to prevent geysering or assist in eliminating geysering in existing systems.

NOTATION

A = heat transfer area of pipe
D = pipe diameter
L = heated pipe length
N_{Pr} = Prandtl number
q = heat transfer rate
α = thermal diffusivity
Z = defined by (1)

REFERENCES

1. M. J. Lighthill, *Quart. J. Mech. Applied Math.* **6**, Pt. 4, 398 (1953).
2. B. W. Martin, *Proc. Roy. Soc.* (London), *Ser. A* **231**, 502 (1955).
3. E. R. G. Eckert and T. W. Jackson, "Analytical Investigation of Flow and Heat Transfer in Coolant Passages of Free Convection Liquid Cooled Turbines," NACA TN 2207 (1950).
4. S. Ostrach and P. R. Thornton, *Trans. ASME* 363 (February 1958).
5. J. F. Haskins and J. Hertz, in *Advances in Cryogenic Engineering*, *Vol. 7*, Plenum Press, New York (1962), p. 353.
6. R. B. Scott, *Cryogenic Engineering*, D. van Nostrand Company, Princeton, New Jersey (1959).
7. F. E. Ruccia and C. M. Mohr, in *Advances in Cryogenic Engineering*, *Vol. 4*, Plenum Press, New York (1960), p. 307.
8. P. Griffith, "Geysering in Liquid Filled Lines," Paper presented at the ASME-AICHE Heat Transfer Conference, Houston, Texas, (August 5–8, 1962).

DISCUSSION

Question by V. Smith, The Boeing Company: Based on the results of your investigation, which parameters have the greatest effect on geysering?

Answer by Author: The most significant parameters are the length of the tube and the length-to-diameter ratio. The heat flux seems to have only a minor effect.

END OF REFERENCE

REFERENCE

66

PROTECTIVE FINISHING SYSTEMS FOR ROCKETS, GUIDED MISSILES, SUPPORT EQUIPMENT AND RELATED MATERIALS. MIL-STD-186C (MI), DEPT. ARMY, OCT. 31, 1971.

MIL-STD-186C (MI)
31 October 1971
SUPERSEDING
MIL-STD-186B (MI)
30 March 1964

MILITARY STANDARD

PROTECTIVE FINISHING FOR ARMY MISSILE WEAPON SYSTEMS

FSC MFFP

FOREWORD

The purpose of this standard is to establish minimum requirements for the protective finishing systems of rockets, guided missiles, all support equipment and related materials.

For convenience in referencing, all procedures, whether they merely clean a surface, deposit a film, or perform some other desirable function, are regarded as "Finishes".

Examples of use of this document are: Assume a part is to be finished with chromated cadmium plate, 0.0003 inch thick. Turning to Table III, Metallic Coatings, find the designation for this finish to be Code 305. The instructions on the drawing would be: "Code 305 MIL-STD-186". It is unnecessary to mention any preliminary steps such as cleaning, because Specification QQ-P-416, Plating, Cadmium (Electrodeposited), referenced in Code 305, provides for this.

Assume that an aluminum item is to be finished with olive drab semigloss enamel. According to Table IV, Organic Finishes, this finish is Code 407. Assume the preparation for painting to be wash primer, Code 401, and primer to be Code 402. In this case, cleaning, Code 106, Table I, Cleaning Methods, of the part will be specified by the drawing. The drawing instruction would read: "Finish Codes: 106/401/402/407, in accordance with MIL-STD-186".

If circumstances require that parts of an assembly be primed separately and be given final coats after assembly, the instruction might read:

"Finish Codes: 106/401/402/407, MIL-STD-186, prime before assembly."

Compliance with this standard will promote uniformity in the protective finishing of rockets, guided missiles, all support equipment and related materials. Compliance with the standard does not relieve the supplier of his responsibility to assure satisfactory operation after storage as specified in his contract.

CONTENTS

		Page
1.	SCOPE	1
1.1	Scope	1
1.2	Selection of finishing system	1
2.	APPLICABLE DOCUMENTS	1
2.1	Government documents	1
2.2	Other publications	7
3.	DEFINITIONS	8
3.1	Definitions	8
3.2	Exterior surfaces	8
3.3	Hermetically sealed	8
3.4	Supplier	8
3.5	Nonreparable	8
4.	GENERAL REQUIREMENTS	9
4.1	Applicability of requirements	9
4.2	Design usage	9
4.3	Materials	9
4.4	Finishing requirements	9
4.5	Surfaces	9
4.6	Cleaning of surfaces	9
4.7	Organic soil removal	10
4.8	Painting	10
4.9	Plating	10
5.	DETAIL REQUIREMENTS	10
5.1	Cleaning requirements	10
5.1.1	General	10
5.1.1.1	Corrosion and heat resisting metals	10
5.1.1.2	Flux removal	10
5.1.1.3	Rinsing	11
5.1.2	Aluminum and its alloys	11
5.1.3	High-hardness steels	11
5.1.4	Low-hardness steels	11
5.1.5	Magnesium and its alloys	11
5.1.6	Titanium and its alloys	11
5.1.7	Copper, Brass, Cadmium, Tin	11
5.1.8	Wood	11
5.2	Surface treatments	12
5.2.1	Aluminum and aluminum alloys	12
5.2.1.1	Electrically conductive surfaces	12
5.2.1.2	Surface treatment of assemblies	12
5.2.1.3	Touch-up	12
5.2.2	Magnesium alloys	12
5.2.2.1	Method	12
5.2.2.2	Touch-up	13
5.2.3	Iron and Steel	13
5.2.4	Corrosion and heat resistant alloys	13

CONTENTS CONTINUED

5.2.5	Cadmium	13
5.2.6	Copper and copper alloys	13
5.2.7	Tin	13
5.2.8	Wood	14
5.3	Metallic coatings	14
5.3.1	Cadmium plating	14
5.3.2	Vacuum deposited cadmium	14
5.3.3	Chromium plating	14
5.3.4	Black chromium plate	15
5.3.5	Porous chromium plate	15
5.3.6	Gray chromium plate	15
5.3.7	Nickel plating	15
5.3.8	Electroless nickel coating	15
5.3.9	Black nickel plating	15
5.3.10	Tin plating	15
5.3.11	Hot-dip coatings	16
5.3.12	Silver plating	16
5.3.13	Gold plating	16
5.3.14	Rhodium plating	16
5.3.15	Palladium plating	16
5.3.16	Copper plating	16
5.4	Nonmetallic coatings	16
5.4.1	Phosphate treatments	16
5.4.2	Black oxide treatments	16
5.4.3	Hard anodic coatings for aluminum and its alloys	16
5.4.4	Metallo-ceramic and ceramic coatings	16
5.5	Organic coatings	17
5.5.1	General priming and painting of surfaces	17
5.5.2	Equipment and facilities	17
5.5.2.1	General	17
5.5.2.2	Spray equipment	18
5.5.2.3	Personnel safety requirements	18
5.5.2.4	Electrical grounding	18
5.5.2.5	Infrared lamps	18
5.5.3	Preparation of surface	18
5.5.3.1	Cleaning, general	18
5.5.3.2	Tests for surface condition before painting	19
5.5.3.2.1	Reaction of surface	19
5.5.3.2.2	Water-break test	19
5.5.3.2.3	Water-break procedure	20
5.5.3.2.4	Special precautions	20
5.5.4	Application of paint type materials	20
5.5.4.1	General	20
5.5.4.2	Production spray test panels	20
5.5.4.3	Air and weather conditions	21
5.5.4.3.1	Lacquer	22

CONTENTS CONTINUED

5.5.4.3.2	Enamel	22
5.5.4.4	Time of application of paint-type materials	22
5.5.4.4.1	First coat	22
5.5.4.4.2	System	22
5.5.4.4.3	Drying time (wash primer)	23
5.5.4.4.4	Drying time (primer)	23
5.5.4.4.5	Top coating	23
5.5.4.5	Spraying over bare metal	24
5.5.4.6	Thickness of finish (dry thickness)	24
5.5.4.7	Application of lacquer	24
5.5.4.8	Application of enamel	24
5.5.4.9	Application of insignia and markings	25
5.5.4.10	Use of masking tape	25
5.5.4.11	Use of sanding surfacer	25
5.5.4.12	Miscellaneous requirements	26
5.5.4.12.1	Tack-ragging	26
5.5.4.12.2	Cloths, tack-rags	26
5.5.4.12.3	Touch-up	26
5.5.4.12.4	Smoothness of wash primer and primer coats	26
5.5.4.12.5	Final dry of the finish	27
6.	INSPECTION	27
6.1	Responsibility for inspection	27
6.2	General inspection requirements	27
6.2.1	Tests	28
6.3	Paint application	28
6.3.1	General	28
6.3.2	Cleanliness	28
6.3.3	Hiding power, gloss, and smoothness	28
6.3.4	Adhesion	28
6.3.5	Film thickness	29
6.3.6	Sampling frequency	29
6.3.7	Laundering of shop cloths	30

TABLES

I	Cleaning Methods	31
II	Surface Treatments	32
III	Metallic Coatings	34
IV	Organic Coatings	38
V	Sealing and Bonding	44
VI	Encapsulants and Potting Compounds	46
VII	Lubrication and Preservation	47
VIII	Miscellaneous	48

MILITARY STANDARD

PROTECTIVE FINISHING FOR ARMY MISSILE WEAPON SYSTEMS

1. SCOPE

1.1 Scope - This standard establishes the minimum requirements for procedures, materials, and systems for cleaning, plating, painting and finishing metals, wood, electronic materials, parts and assemblies for rockets, guided missiles and components to protect them from deterioration.

1.2 Selection of finishing system - Unless otherwise specified the responsibility for selecting the cleaning method, surface treatment, metal coating, paint system or other finish shall rest with the activity responsible for the end item. The materials treatment and finishes shall be selected from those listed herein and shall be referenced on drawings, in contracts, and item specifications by the appropriate finish numbers of MIL-STD-186. This does not preclude the acceptance of a proven commercial finish selected by the manufacturer, supplier or contractor and which is concurred in by the procuring activity. Numerous finish codes are contained in tables that are not referenced in the requirement sections i.e. sealants, conformal coatings, lubricants, adhesives, that are satisfactory for use. Where the finish or corrosion protection processes are not adequately defined, the problem shall be brought to the attention of the procuring activity.

CODE NUMBER SYSTEM

Cleaning Methods	100 Numbers
Surface Treatment	200 Numbers
Metallic Coatings	300 Numbers
Organic Coatings	400 Numbers
Sealing and Bonding	500 Numbers
Encapsulants & Potting	600 Numbers
Lubrication & Preservation	700 Numbers
Miscellaneous	800 Numbers

2. APPLICABLE DOCUMENTS

2.1 Government documents - Issues of the following documents in effect on the date of invitation for bids form a part of the standard to the extent specified herein.

SPECIFICATIONS

FEDERAL

O-T-236	Tetrachloroethylene (Perchloroethylene) Technical Grade
P-C-436	Cleaning Compound, Alkali, Boiling Vat (Soak) or Hydrosteam
QQ-C-320	Chromium Plating (Electrodeposited)
QQ-N-290	Nickel Plating (Electrodeposited)
QQ-P-416	Plating, ium (Electrodeposited)
TT-C-490	Cleaning and Pretreatment of Ferrous Surfaces for
TT-E-527	Enamel, Alkyd, Lustreless
TT-E-529	Enamel, Alkyd, Semi-Gloss
TT-E-776	Ethylene Glycol Monobutyl Ether (For use in organic coatings)
TT-I-558	Ink, Marking Stencil, Opaque, for Nonporous Surfaces (Metals, Glass, etc.)
TT-I-735	Isopropyl Alcohol
TT-L-54	Lacquer, Spraying, Acid Resistant (For Aluminum Surfaces Around Storage Batteries)
TT-T-266	Thinner, Dope And Lacquer (Cellulose-Nitrate)
TT-W-571	Wood Preservation, Treating Practices
TT-W-572	Wood Preservative, Water-Repellant
UU-T-106	Tape, Pressure-Sensitive Adhesive, Masking, Paper
VV-L-800	Lubricating Oil, General Purpose, Preservative (Water Displacing Low Temperature)
DDD-T-539	Towels, Machinery Wiping (Laundered)
MMM-A-121	Adhesive, Bonding Vulcanized Synthetic Rubber To Steel

MMM-A-132	Adhesive, Heat Resistant, Airframe Structural Metal to Metal
RIPARED-636	Coating, Protective, Thermally fused Epoxy Plastic (For Metal Surfaces)

MILITARY

MIL-T-152	Treatment, Moisture and Fungus Resistant, of Communications, Electronic, and Associated Electrical Equipment
MIL-V-173	Varnish, Moisture-and-Fungus Resistant (For the Treatment of Communications, Electronic and Associated Electrical Equipment)
MIL-E-463	Ethyl Alcohol, (For Ordnance Use)
MIL-F-495	Finish, Chemical, Black for Copper Alloys
MIL-S-974	Surfacer, Sanding
MIL-L-3150	Lubricating Oil, Preservative, Medium
MIL-M-3171	Magnesium Alloy, Processes for Corrosion Protection of
MIL-A-3920	Adhesive, Optical, Thermosetting
MIL-S-4383	Sealing Compound, Topcoat, Fuel Tank, Buna-N Type
MIL-A-5092	Adhesive, Rubber Base, General Purpose
MIL-A-5540	Adhesive, Polychloroprene
MIL-C-5541	Chemical Films for Aluminum and Aluminum Alloys
MIL-A-6091	Alcohol, Ethyl, Specially Denatured, Aircraft
MIL-P-6808	Primer Coating, Zinc Chromate, for Aircraft and Missile Applications, Application of
MIL-I-6869	Impregnants for Aluminum Alloy and Magnesium Alloy Castings
MIL-S-7502	Sealing Compound, Integral Fuel Tanks and Fuel Cell Cavities, High Adhesion, Accelerator Required

MIL-T-7003	Trichlorethylene, Stabilized Degreasing
MIL-P-8116	Putty, Zinc Chromate, General Purpose
MIL-C-8507	Coating, Wash Primer (Pretreatment) for Metals, Application of (For Aeronautical Use)
MIL-I-8574	Inhibitors, Corrosion, Volatile, Utilization of
MIL-A-8576	Adhesive, Acrylic Base, for Acrylic Plastic
MIL-P-8585	Primer Coating, Zinc Chromate, Low-Moisture Sensitivity
MIL-A-8623	Adhesive, Epoxy Resin, Metal
MIL-A-8625	Anodic Coatings, for Aluminum and Aluminum Alloys
MIL-S-8802	Sealing Compound, Temperature Resistant, Integral Fuel Tanks and Fuel Cell Cavities, High-Adhesion
MIL-C-8837	Coating, Cadmium (Vacuum Deposited)
MIL-A-9067	Adhesive Bonding, Process and Inspection Requirements for
MIL-M-10578	Metal Conditioner and Rust Remover (Phosphoric Acid Base)
MIL-T-10727	Tin Plating; Electrodeposited or Hot-dipped, for Ferrous and Non Ferrous Metals
MIL-G-10925	Grease, Automotive and Artillery
MIL-S-11030	Sealing Compound, Non-curing, Polysulfide Base
MIL-P-11414	Primer, Lacquer, Rust-Inhibiting
MIL-C-11436	Chromium, Gray Plated
MIL-C-13924	Coating, Oxide, Black, for Ferrous Metals
MIL-C-14460	Corrosion Removing Compound, Sodium Hydroxide Base, for Electrolytic or Immersion Application
MIL-C-14538	Plating, Black Chromium (Electrodeposited)
MIL-C-14550	Copper Plating (Electrodeposited)
MIL-C-15328	Primer, (Wash), Pretreatment, Blue, (Formula No. 117-B for Metals)

MIL-S-15847	Spray Gun And Accessories, Paint And Dope, Aircraft Use
MIL-C-16173	Corrosion Preventive Compound, Solvent Cutback, Cold Application
MIL-E-16738	Enamel, Exterior, White, Vinyl-Alkyd (Formula No. 122-82)
MIL-I-16923	Insulating Compound, Electrical, Embedding
MIL-P-18317	Plating, Black Nickel (Electrodeposited) on Brass, Bronze or Steel
MIL-S-18718	Cleaning Compound, Solvent
MIL-C-20218	Chromium Plating, Electrodeposited, Porous
MIL-I-22110	Inhibitors, Corrosion, Volatile, Crystalline
MIL-S-22473	Sealing, Locking & Retaining Compounds, Single-Component
MIL-C-22750	Coating, Epoxy-Polyamide
MIL-T-23142	Tape, Pressure-Sensitive Adhesive, for Dissimilar Metal Separation
MIL-P-23377	Primer Coating, Epoxy-Polyamide, Chemical And Solvent Resistant
MIL-C-23411	Corrosion Preventive Compound Clear
MIL-S-23586	Silicone Rubber Compound, Room Temperature Vulcanizing
MIL-A-25457	Adhesive, Air-Drying, Silicone Rubber
MIL-A-25463	Adhesive, Metallic Structural Sandwich Construction
MIL-C-26074	Coating, Nickel-Phosphorous, Electroless Nickel, Requirements for
MIL-I-43553	Ink, Marking, Epoxy Base
MIL-S-45180	Sealing Compound, Gasket, Hydrocarbon Fluid, Water Resistant

MIL-M-45202	Magnesium Alloys, Anodic Treatment Of
MIL-G-45204	Gold Plating, Electrode Deposited
MIL-P-45209	Palladium Plating (Electrodeposited)
MIL-L-46002	Lubricating Oil, Contact And Volatile Corrosion Inhibited
MIL-L-46010	Lubricant, Solid Film, Heat Cured, Corrosion Inhibiting
MIL-I-46058	Insulating Compound, Electrical (For Coating Printed Circuit Assemblies)
MIL-P-46076	Plastic, Polyurethane, Flexible, Potting And Molding Compound
MIL-R-46085	Rhodium Plating, Electrodeposited
MIL-S-46090	Silicone, Foam, Low-Density, Room Temperature Vulcanizing
MIL-A-46106	Adhesive-Sealant, Silicone RTV, General Purpose (For Electrical And Mechanical Sealing)
MIL-E-46117	Enamel, Alkyd, Lustreless, Solar Heat Reflecting, Olive Drab
MIL-P-46127	Coating, Gray, Undercoat, (Solar Heat Reflecting)
MIL-E-46136	Enamel, Semi-Gloss, Alkyd, Solar Heat Reflecting, Olive Drab
MIL-P-46843	Printed Circuit Assemblies, Design And Production Of
MIL-S-46844	Solder Bath Soldering of Printed Wiring Assy, Automatic Machine Type
MIL-L-46147	Lubricant, Solid-Film, Air-cured (Corrosion Inhibiting)
MIL-P-46847	Plastic Material, Foamed Polyurethane For Encapsulating Electronic Components
MIL-P-46856	Primer, Coating, Epoxy, Process For Application

MIL-D-50000	Dioctyl-P-Phenylendiamine (Antiozonant)
MIL-L-52043	Lacquer, Semigloss
MIL-P-52192	Primer, Epoxy
MIL-E-52227	Enamel, Semigloss
MIL-A-81236	Adhesive, Epoxy Resin With Polyamide Curing Agent
MIL-C-81302	Cleaning Compound, Solvent, Trichlorotrifluoroethane
MIL-C-81309	Compound, Corrosion Preventive, Water Displacing, Ultra-Thin Compound
MIL-T-81533	Trichlorethane, 1,1,1 (Methyl Chloroform) Inhibited, Vapor Degreasing

STANDARDS

FEDERAL

Fed Std No. 595 Colors

Fed Test, Method STD No. 141, Paint, Varnish, Lacquer, And Related Materials; Methods of Inspection, Sampling And Testing

MILITARY

MIL-STD-1250	Corrosion Prevention And Deterioration Control In Electronic Components And Assemblies
MIL-STD-276	Impregnation Of Porous Nonferrous Metal Castings

(Copies of specifications, standards, drawings, and publications required by suppliers in connection with specific procurement functions should be obtained from the procuring activity or as directed by the contracting officer).

2.2 Other publications - The following documents form a part of this standard to the extent specified herein. Unless otherwise indicated, the issue in effect on date of invitation for bids or request for proposal shall apply.

ASTM B 253 Preparation of and Electroplating Aluminum Alloys (Application for copies should be addressed to American Society for Testing and Materials, 1916 Race Street, Philadelphia, Pa. 19103).

NFPA No. 30 Storing
NFPA No. 33 Spray Finishing
NFPA No. 34 Dip Tank

(Application for copies should be addressed to the National Fire Protection Association, 60 Batterymarch Street, Boston, Mass. 02110.

3. DEFINITIONS

3.1 Definitions - For the purposes of this standard, the following definitions apply.

3.2 Exterior surfaces - The outward or exposed surfaces of the weapon and ground support equipment after all doors, hatches, and access ports are closed shall be considered as exterior surfaces.

3.3 Hermetically sealed - A hermetically sealed system is one that is purged and filled with a dry, inert gas medium, or one where humidity is properly controlled to less than 10 percent relative humidity before sealing. Hermetic sealing shall also be defined as sealed to the extent that there shall be no moisture-laden air or water introduced into the sealed unit or component when subjected to combination of the following:

(a) Moisture resistance testing for 15 days, moisture to be maintained at 95 percent relative humidity and temperature to be cycled at a constant rate between -65°F and 155°F during each twenty-four hour period.

(b) Leak testing either at a vacuum of 5 pounds per square inch absolute (psia) or at an external pressure of 20 psia for not less than 2 hours. Unit of measurement for leaks shall be, atmospheric cubic centimeters per second (Atm cc/sec) allowable limit for leaks shall be 10^{-8} Atm cc/sec to 10^{-5} Atm cc/sec.

3.4 Supplier - The supplier is that contractor who has accepted an order from the Government or who has entered into a contract with the Government for the purpose of furnishing parts, components, and assemblies complying with the requirements of this standard.

3.5 Nonreparable - Nonreparable is defined as a characteristic of assemblies or components that can only be repaired at the maintenance echelon where purging, evacuation, or pressurization described in 3.2 can be accomplished.

4. GENERAL REQUIREMENTS

4.1 Applicability of requirements - The requirements specified herein shall be applicable to all parts of the weapon system except parts which are encapsulated or enclosed in hermetically sealed containers.

4.2 Design usage - Reference to this standard (MIL-STD-186) and callouts of the code numbers on engineering drawings are mandatory. This is required to simplify preparation of drawings and facilitate in updating drawings affected by a major finishing change.

4.3 Materials - Materials shall conform to applicable specifications as specified herein. Materials not covered by applicable specifications shall not be used unless approved by the procuring authority.

4.4 Finishing requirements - Unless otherwise specified, all fabrication operations, such as cutting, drilling, punching, forming, grinding, honing, welding, joining, and any other operations which will affect the finish of the item as well as cleaning (see 4.6), shall be completed prior to the application of any surface treatments, metallic and nonmetallic coatings required for finishing of the metals and alloys.

4.5 Surfaces - Unless otherwise specified, parts shall conform to specified dimensions, surface roughness and condition prior to cleaning, surface treatment and plating. In the case of metals which may respond in a nonuniform manner when metal removal is accomplished with mechanical, chemical, electrochemical methods, appropriate inspection procedures shall be established and used to insure that each part has a uniform surface, including freedom from pits, intergranular attack and significant etching. Where etching has occurred, the degree found shall be demonstrated not to affect the serviceability of the parts.

4.6 Cleaning of surfaces - Prior to application of the surface treatments and metallic coatings covered by this specification cleaning shall be as specified herein, using materials and processes which have no damaging effect on the metal, including freedom from pits, intergranular attack and significant etching. Appropriate inspection procedures shall be established and used. After cleaning, all parts shall be completely free of corrosion products, scale, paint, grease, oil, flux, and other foreign materials including other metals, and shall be given the specified treatment as soon as practicable after cleaning. Particular care shall be exercised in the handling of

parts to assure that foreign metals are not inadvertently transferred to the clean surfaces as may occur when steel is allowed to come into contact with zinc surfaces. Parts having high residual tensile stresses, which are to be cleaned by chemical or electrochemical methods, shall be stress relieved prior to cleaning. Parts which may have high sustained tensile stresses as the result of assembly, or crevices which can retain cleaning solutions, shall be cleaned prior to assembly.

4.7 Organic soil removal - Vapor degreasing shall be done with trichloroethylene conforming to MIL-T-7003 or perchloroethylene conforming to O-T-236, or trichloroethane 1,1,1 conforming to MIL-T-81533. Carbon tetrachloride shall not be used for degreasing. The use of alcohol and Freon are permitted for cleaning electronic assemblies.

4.8 Painting - Unless otherwise specified herein, interior and exterior surfaces of the weapon system shall be primed and painted.

4.9 Plating - All plating with the exception of nickel, chromium, gold, palladium, platinum, and rhodium shall receive a supplementary treatment such as phosphate, chromate, wash primer, varnish or conformal coating.

5. DETAIL REQUIREMENTS

5.1 Cleaning requirements

5.1.1 General

5.1.1.1 Corrosion and heat resisting metals - Corrosion and heat resisting metals and alloys shall be cleaned by suitable chemical or mechanical processes, or combinations thereof; except materials that are sensitive to deleterious constituents such as hydrogen, oxygen, nitrogen and chemical reactions such as hydrogen embrittlement, oxidation, or hardening. These materials shall be cleaned by mechanical processes only.

5.1.1.2 Flux removal - Soldering, welding, and brazing fluxes shall be completely removed. Washing with hot water, alcohol, (ethyl alcohol per MIL-A-6091 or MIL-E-463, or isopropyl alcohol per TT-I-735), MIL-C-81302 or solvent, blend of MIL-C-81302 plus 35% isopropyl alcohol per TT-I-735 or a solvent conforming to MIL-T-7003 shall be used. Methyl or wood alcohol (methanol) shall not be used unless approved by the procuring activity.

5.1.1.3 Rinsing - Where materials are employed that show an acid or alkaline reaction, the cleaned parts shall be given a through water rinse to remove all acid or alkali prior to further treatment. (See paragraph 5.5.3)

5.1.2 Aluminum and its alloys - Aluminum and its alloys shall be either chemically or mechanically cleaned. The use of uninhibited alkaline materials, such as sodium hydroxide solutions, and of abrasives containing iron, steel wool, copper wool, iron oxide rouge, and steel wire, which may become embedded and accelerate corrosion of aluminum alloys is prohibited. Materials conforming to P-C-436 shall be used for chemical cleaning. Sheet stock surfaces to receive anodic conversion coating treatment, sand castings, forging and heat treated stock shall be deoxidized (all oxide film removed with a suitable etchant) after cleaning. Other materials or methods may be approved for use by the procuring activity. For this approval, data proving freedom from damage due to etching, pitting, and stress corrosion cracking, shall be submitted to that activity.

5.1.3 High-hardness steels - Steels of Rockwell hardness C40 or over, including carburized and steel surfaces hardened by using other methods, shall be either sand, abrasive grit, steel shot, grit or glass bead blasted for rust or scale removal. Acid pickling or other hydrogen producing processes shall not be used.

5.1.4 Low-hardness steels - Steels of Rockwell hardness less than C40 shall be cleaned in accordance with TT-C-490 or acid pickling as specified in Table I.

5.1.5 Magnesium and its alloys - Magnesium and its alloys shall be cleaned in accordance with MIL-M-3171 or MIL-M-45202.

5.1.6 Titanium and its alloys - For titanium and titanium alloys, vapor degreasing shall not be used, unless approved by the procuring activity. When permitted, the titanium parts shall be pickled after vapor degreasing. Where vapor degreasing is not permitted, a mild alkaline cleaner conforming to P-C-436b shall be used for soil removal from titanium and its alloys. For removal of contamination other than organic soil, titanium and its alloys shall be mechanically cleaned. Other cleaning methods shall not be used, unless approved by the procuring activity.

5.1.7 Copper, Brass, Cadmium, Tin - Cleaning shall be accomplished by any method of Table I, or as specified.

5.1.8 Wood - Wood surfaces shall be sanded or otherwise mechanically prepared to provide a clean, smooth surface free of waxes, oils or greases.

5.2 Surface treatments - Codes for surface treatments are enumerated in Table II.

5.2.1 Aluminum and aluminum alloys - All aluminum and aluminum alloys, including clad aluminum alloy surfaces, shall be anodized to produce coatings conforming to MIL-A-8625, either Type I, Type II or Type III. When paint finishing systems are to be applied, chemical films per MIL-C-5541 or wash primer, MIL-C-15328, may be substituted for anodic coatings.

5.2.1.1 Electrically conductive surfaces - Anodic coatings shall be omitted from surfaces which require high electrical conductivity at relatively high impedance and high frequencies (RF). These areas shall be coated with an inherent corrosion resistant metal such as nickel. Chemical films conforming to MIL-C-5541 are prohibited.

5.2.1.2 Surface treatment of assemblies - Surface treatment shall be applied to assemblies and detail parts prior to assembly, except where surface treatment will interfere with the joining processes such as brazing or welding. The assemblies, or parts, shall not contain cavities or crevices where the process solutions can be retained.

5.2.1.3 Touch-up - When paint finish systems are to be applied, all surfaces which have the anodic coating removed or damaged shall be touched up with MIL-C-5541 materials approved for Class 2 treatment by Grade B application (brush or swab) and the application shall be confined to the area of damage. Chemical film materials suitable for Class 1 treatment by Grade B application shall be used for touch-up if the surface film is not to be further treated by painting. This operation is required for drilled, punched or countersunk holes located on exterior surfaces, unless other methods of corrosion protection are used and approved by the procuring activity.

5.2.2 Magnesium alloys -

5.2.2.1 Method - All magnesium alloys shall receive an anodic coating in accordance with MIL-M-45202, Type I, or Type II, Class A. Anodic coating applied in accordance with MIL-M-45202 shall be used for parts subject to abrasion, erosion, or wear. Note: MIL-M-3171 treatments shall only be used for temporary protection or as a paint base.

5.2.2.2 Touch-up - All surfaces which have the anodic coating removed or damaged shall be touched up, using either the Type I or Type VI process of MIL-M-3171. Touched-up or damaged magnesium surfaces, anodic coated in accordance with MIL-A-45202, may be reanodized.

5.2.3 Iron and steel - Immediately following cleaning and before the surfaces show any evidence of rusting or other soiling, all iron and steel surfaces shall be zinc base phosphate treated in accordance with TT-C-490, Type I. Iron base phosphate treatment, TT-C-490, Type II shall be used if the paint system to be applied requires baking at temperatures exceeding 375°F or if the part is to be formed or shaped after phosphating. In the event that phosphating cannot be applied, the clean surfaces shall be coated with wash primer conforming to MIL-C-15328, as called for TT-C-490, Type III.

5.2.4 Corrosion and heat resistant alloys - The 200, 300, 400 and precipitation hardenings stainless steels shall be passivated by immersion for 30 minutes in a hot (120 to 130°F) aqueous solution containing 20 percent by volume nitric acid (Specific Gravity 1.42) and 2 percent by weight of sodium dichromate, rinsed in clean hot water and then thoroughly dried. This is normally the final finish requirement for the 300 grade stainless steel. 400 series stainless steel will not accept passivation unless fully hardened. The remainder of the stainless steels will require additional protective finishes. Nitrided surfaces shall not be passivated. Monel, Inconel, Hastelloys and Titanium do not normally require further treatment after cleaning. Surfaces to be painted shall be coated with wash primer, MIL-C-15328.

5.2.5 Cadmium - Cleaned surfaces shall be kept free of finger marks, dirt, and dust or other contaminants and before corrosion occurs they shall be chromate treated according to QQ-P-416, Type II. In the event that chromate treatments cannot be used, the surfaces shall be treated with wash primer, MIL-C-15328 or treated in accordance with QQ-P-416, Type II, prior to applying a paint system.

5.2.6 Copper and copper alloys - Surfaces shall be given a black oxide coating according to MIL-F-495. Black oxide surfaces shall be protected from all contamination prior to application of a paint system.

5.2.7 Tin - Tin surfaces shall receive a supplementary treatment of organic coating, varnish MIL-V-173, or wash primer MIL-P-15328, conformal coating MIL-I-46058, or a paint system to prevent corrosion. Tin surfaces shall be coated with wash primer MIL-P-15328 prior to receiving a paint system.

5.2.8 Wood - Wood surfaces shall be treated with wood preservative conforming to Type III composition B of TT-W-572, using the vacuum-pressure or vacuum-soak treating method, immersion treatment, or brush treatment.

5.3 Metallic coatings - Codes for metallic coatings are enumerated in Table III. Metallic coatings shall be applied by electrodeposition, electroless deposition, spray metallized, or vacuum-deposited methods in conformance with applicable specifications listed herein. Other processes may be used, subject to approval by the procuring activity. Necessary process and quality control requirements shall be established and technical data developed which shall be submitted to the procuring activity substantiating that the proposed coatings are equivalent to the coatings they are intended to replace relative to corrosion resistance, wear, and other functional characteristics and effect on static and dynamic properties of the metals and alloys to which they are applied. The surface roughness of the surface to be plated shall be as specified on the applicable drawing. All sharp edges shall be broken and all burrs shall be removed before coating.

5.3.1 Cadmium plating - Cadmium plating shall be in accordance with QQ-P-416. Supplementary treatments are required to provide corrosion resistance. Cadmium plating shall not be used in the following applications:

(a) Parts of hydraulic equipment which may be in contact with hydraulic fluid.

(b) Parts in frictional contact where gouging or binding may be a factor, or where corrosion would interfere with normal functioning.

(c) In confined spaces, in the presence of organic materials which give off corrosive and damaging vapors.

5.3.2 Vacuum deposited cadmium - Parts which cannot be thoroughly cleaned to insure removal of the plating solution shall be vacuum coated with cadmium in accordance with MIL-C-8837. Vacuum deposited cadmium shall be used for high hardness (Rockwell C-40 or above) subject to the deleterious effects of hydrogen embrittlement.

5.3.3 Chromium plating - Chromium plating shall be used for surfaces subject to wear, abrasion or erosion, except where other surface hardening processes are used such as nitriding and carburizing, or where other wear and abrasion resistant coatings are specified. Chromium plating shall be in accordance with QQ-C-320.

5.3.4 Black chromium plating - Black chromium plating shall be used where a non-reflective surface abrasion and corrosion resistance are required. Black chromium plating shall be in accordance with MIL-C-14538.

5.3.5 Porous chromium plate - Porous chromium plate is another form of engineering chromium. The process produces etched channels or pores in the surface of the plating to retain miniature pools of lubricating oils. Porous chromium plate shall be in accordance with MIL-C-20218.

5.3.6 Gray chromium plate - Gray chromium plate is a durable, protective camouflage finish used on aluminum, copper alloys and steel, such as rotary dials and knobs for improved durability under frictional contact. Gray chromium plate shall be in accordance with MIL-C-11436.

5.3.7 Nickel plating - Nickel plating shall be used for the following applications only:

(a) Where temperatures do not exceed 1000°F and other coatings would not be suitable.

(b) To minimize the effects of such dissimilar metal contacts, such as mild steel with unplated corrosion-resisting steel or stainless steel in contact with other stainless steel.

(c) As an undercoat for other functional coatings.

(d) As a protective finish on metals without further supplementary treatment.

Nickel plating of parts and surfaces shall be in accordance with QQ-N-290.

5.3.8 Electroless nickel coating - Where specified, electroless nickel coating shall be in accordance with MIL-C-26074. Type II shall be specified where the combination of high hardness and corrosion resistance are required.

5.3.9 Black nickel plating - Black nickel plating shall be in accordance with MIL-P-18317.

5.3.10 Tin Plating - Tin plating shall be used only where the properties of this material present distinct advantages in comparison with cadmium. A plating of tin may be used in lieu of cadmium on parts

that are subsequently soldered. Where tin plating is specified, it shall be applied in accordance with MIL-T-10727. Caution: Tin plating per MIL-T-10727, Type I, shall not be used where electrical or electronic circuits are involved.

5.3.11 Hot-dip coatings - Hot-dip coatings are preferred where tin-lead and tin plating are required. Hot-dip tin shall be in accordance with MIL-T-10727, Type II.

5.3.12 Silver plating - Silver plating shall be in accordance with QQ-S-365.

5.3.13 Gold plating - Gold plating shall be in accordance with MIL-G-45204. It shall be used only where its electrical and corrosion resistance characteristics are required. Precautions for electrical use are outlined in MIL-STD-1250 and shall be observed.

5.3.14 Rhodium-plating - Rhodium plating shall be in accordance with MIL-R-46085.

5.3.15 Palladium plating - Palladium plating shall be in accordance with MIL-P-45209.

5.3.16 Copper plating - Copper plating shall be in accordance with MIL-C-14550.

5.4 Nonmetallic coatings - Codes for nonmetallic coatings are enumerated in Table II.

5.4.1 Phosphate treatments - Phosphate treatments for ferrous parts, which are subsequently to be painted, shall conform to Type I of TT-C-490.

5.4.2 Black oxide treatments - Black oxide treatments, conforming to MIL-C-13924 and MIL-F-495 shall be used only on surfaces continually coated with oil and not exposed to severe corrosive conditions. Black oxide treatments shall be used only for close tolerance parts where more protective type coatings cannot be employed due to dimensional changes.

5.4.3 Hard Anodic coatings for aluminum and its alloys - Where hard anodic coatings are specified, they shall conform to Type III of MIL-A-8625.

5.4.4 Metallo-ceramic and ceramic coatings - Metallo-ceramic and ceramic coatings shall not be used prior to approval by the

procuring activity. Necessary process and quality control requirements shall be established, and technical data developed which shall be submitted to the procuring activity substantiating that the proposed coatings are entirely satisfactory for the intended use.

5.5 Organic coatings - Codes for organic coatings are enumerated in Table IV.

5.5.1 General priming and painting of surfaces - Interior and exterior surfaces of the weapon system shall be painted with the materials specified herein. The painting sequence for all metals shall be wash primer, primer, and top coats. The requirement for wash primer may have already been specified in the surface treatment paragraphs on the metal surfaces. The use of wash primer on high hardness RC 40 steels is prohibited. High hardness Rockwell C 40 steels should be cleaned, primed and top coated.

5.5.2 Equipment and facilities -

5.5.2.1 General - The equipment and facilities used in applying surface finishes shall be suitable and adequate for the purpose and shall be subject to approval of the procuring activity. All safety precautions contained in Standard NFPA Nos. 30, 33, and 34 shall be observed. Painting shall be conducted in properly ventilated spray rooms or areas. Paint spray rooms shall be ventilated by means of a forced draft, effecting at least three complete changes of air every hour. Doors and windows shall be kept closed to exclude dirt and dust. The air shall be introduced into the room in such manner as not to cause turbulence or excessive air currents which would have the effect of causing orange peel in the paint film. Sufficient ventilation shall, however, be maintained to keep dried overspray from settling on surfaces which have already been painted and are still tacky. Where practicable, water-washed exhaust systems or grilled flooring over flowing water should be used. Humidity and temperature indicators shall be installed and in proper operation. Controls shall be employed for humidity and temperature or for temperature alone if a satisfactory ratio of temperature and humidity can be maintained, as defined herein. To insure that dirt and dust are kept to a minimum, all air entering spray booths or rooms shall be filtered; spray areas are to be kept clean; lint-bearing rags shall not be allowed in such areas; a positive air pressure shall be maintained in the spray booth or room. Lighting conditions shall be in accordance with the 1968 Illuminating Engineering Society Handbook. Lights in the floor, as well as coatings of high light reflectance, shall be used where required to increase lighting efficiency. The paint spray room floors shall be cleaned as frequently as required in insure good housekeeping.

Card #16

5.5.2.2 Spray equipment - Spray guns and accessories shall conform to MIL-S-15847. All lines shall be kept free from condensation of oil and water by filtering the lines as necessary. It is essential that good housekeeping be practiced. Paint lines shall be cleaned with the same solvent used for thinning the particular paint, at the end of each working day and before changing color or type of paint. Traps shall be included in all air lines used with spray painting equipment in order to entrap any condensed moisture, oil, or foreign materials. Paint pressure pots shall be thoroughly cleaned at least once each week.

5.5.2.3 Personnel safety requirements - All requisite safety precautions shall be taken by painting personnel, under supervision of the Safety Engineer and the Industrial Health Officers, with regard to toxicity or industrial health hazards in accordance with existing instructions and regulations. Adequate paint spray respirators, non-sparking shoes, and other safety devices, shall be made available for and utilized by painting personnel.

5.5.2.4 Electrical grounding - All safety precautions contained in Standard NFPA No. 33 regarding storage of finishing materials and thinners, fire-prevention, non-sparking floors and equipment, vapor and explosion-proof requirements, are hereby applicable. The above should not be construed as covering all the requirements, but are illustrative of general safety requirements.

5.5.2.5 Infrared lamps - In the use of infrared lamps, the size of the lamps and their number and spacing shall be such as to effect a distribution of heat as evenly as possible over the painted surface. Adequate precautions shall be taken to avoid concentration of flammable vapors in the immediate area of the infrared lamps and the parts being painted. In addition, wire mesh screen with suitable opening approximately 2 inches wide shall be rigidly fixed about 3 or 4 inches above the lamps to prevent their breakage by falling objects. The individual lamps shall be tightened at frequent intervals to prevent arcing in the sockets.

5.5.3 Preparation of surface -

5.5.3.1 Cleaning, general - All metal surfaces shall be thoroughly clean and dry at the time of application of any paint-type coating. Meticulous cleaning prior to all painting operations cannot be overemphasized since this factor is of prime importance in obtaining a satisfactory paint finish. Reclaimed paint thinner or other reclaimed thinners shall not be used for cleaning purposes, since these materials

may leave a grease film which will cause poor adhesion of the next coat. All abrasive or foreign particles and rough edges shall be removed after sanding or cutting operations before application of paint-type materials. Cleaning shall be accomplished with solvents, detergents, and processes which have no deleterious effect on the surface and which produce surfaces satisfactory for receiving subsequent finishes. After general cleaning to remove the major contaminants, such as paints, oil, soil, grease, etc., the following procedures have been employed successfully. Immediately prior to painting, to obtain a surface capable of supporting an unbroken film of water:

(a) Swab on MIL-S-18718 solvent, disbursed from plunger-type safety cans, using clean cloths complying with the requirements of 5.5.4.12.2. Do not dip the cloths in the container of solvent, as this would contaminate the bulk of the solvent and result in transfer of the contaminate to the surface being prepared for painting.

(b) Next check the surface with red litmus paper moistened with distilled water, which should not turn blue. If the litmus paper turns blue, it will be necessary to apply a 0.20 to 0.25 percent chromic acid solution to achieve a neutral or slightly acid surface, in accordance with the procedure specified in 5.5.3.2.1.

(c) Finally, check the surface for absence of water-break, employing the test procedure described in 5.5.3.2.3.

5.5.3.2 Tests for surface condition before painting - The following tests shall be conducted before the actual painting:

5.5.3.2.1 Reaction of surface - The surface shall have a neutral or slightly acid reaction. Moistened red litmus paper when applied to the surface shall not turn blue, otherwise a 0.20 to 0.25 percent chromic acid solution shall be applied to achieve a neutral or slightly acid surface. The chromic acid solution shall be permitted to remain on the surface for 2 to 5 minutes followed by a water rinse, and the surface then wiped dry with clean, lint-free cloths meeting the requirements of 5.5.4.12.2.

5.5.3.2.2 Water-break test - Representative areas of the surface to be painted shall be tested by the procedure described in 5.5.3.2.3 for ability to support an unbroken film of distilled water.

5.5.3.2.3 Water-break test procedure - A mist of distilled water shall be atomized on the surface under test, representative of the large surface being tested, employing any convenient atomizing device. Should the water gather into discrete droplets within 25 seconds, then the surface shows a "water-break" and it shall be considered presumption of the presence of an impurity on the surface, such as free alkali, residual detergent, etc., and the surface shall be considered as also having failed the test. The surface shall have passed the water-break test when the water droplets do not flash-out suddenly, but coalesce into a continuous film of water.

5.5.3.2.4 Special precautions - Solvent cleaning of the surface is a requirement if there is a break in the painting sequence of overnight or longer. A final hand wipe-down shall be performed immediately before painting to insure scrupulous cleanliness and a proper paintable surface. After cleaning, particularly after stripping operations or steam cleaning, special precautions shall be taken to assure thorough draining of all liquids from between faying surfaces, crevices, inspection doors, pockets, preferably by permitting the part to stand for a sufficient time to permit such drainage, after which the affected area should be recleaned as necessary. It will be found advantageous to seal crevices, joints, seams, etc., with a plastic composition which will resist the action of paint stripper and cleaners and which subsequently can be easily removed.

5.5.4 Application of paint type materials -

5.5.4.1 General - Unless otherwise specified herein or in the detail process specifications, paint-type protective coatings may be applied by spraying, brushing, tumbling, roller coating, flow-coating, or any other approved method which will insure the application of a smooth, continuous film that is free of imperfections, such as dried overspray, runs, sags, blisters, or orange peel. The use of dipping is subject to such hazards to the quality of the finish that the use of dip coating is strongly discouraged. If, however, dipping of primer is employed, the precautions stated in the applicable specification shall be observed. PRIOR TO SPRAYING OF SPRAYING OF PAINT, THE SAFETY PRECAUTIONS WITH REGARD TO GROUNDING, AS PRESCRIBED BY 5.5.2.4 SHALL BE STRICTLY ENFORCED.

5.5.4.2 Production spray test panels - Prior to the spraying operation, the suitability of materials for the entire system shall be determined experimentally on panels approximately 4 by 7 inches in

size of the same materials to be used for the finished item. The panel shall be coated under prevailing conditions with the finish system that is to be applied. If the finish system applied to the experimental panel is satisfactory, then full scale operations may begin. Defects found in the experimental application, such as blushing, incorrect thickness, excessive orange peel, sagging, shall be corrected prior to large scale application.

5.5.4.3 Air and weather conditions - Coatings shall not be applied under unfavorable atmospheric conditions, such as high humidity, strong drafts, or low temperatures. In the event the following conditions cannot be met, painting operations shall be suspended until acceptable conditions are re-established. Data for thinning materials for spray application at other than standard room temperature and humidity conditions shall be as specified in the applicable process specifications, or shall be determined experimentally by the applicator. For cold spraying of lacquer thinned with TT-T-266 for thinner, blushing generally can be avoided by observing the following humidity schedule:

Permissible atmospheric conditions for spraying lacquer containing no added blush-retardant thinner

Dry bulb temperature °F	Percent relative humidity (maximum)
90	56
85	59
80	63
75	68
70	74
65	80
60	85

Under conditions of high temperature 26.6 to 35 degrees C. (80 to 90 degrees F.) and low relative humidity (less than 20 percent), dry spray may be encountered. Hence, under such conditions, blush-retardent thinner shall be used. If blushing of lacquer top coat is observed on the test panel specified in 5.5.4.2, blush-retardant thinner shall be used. A blush-retardant thinner is available, Federal Specification TT-E-776, but it should be used with caution because of the slow release from the film. The use of this blush-retardant thinner is as follows:

Specification TT-E-776:

For each gallon of TT-T-266 thinner, replace up to 1½ pints with ethylene glycol monobutyl ether conforming to TT-E-776. Only the

minimum amount necessary to alleviate blushing should be used since sagging may result. Also, drying may be retarded as much as 10 minutes if ambient temperatures are low.

Permissible atmospheric conditions for spraying lacquer containing blush-retardant thinner

Dry bulb temperature °F	Percent relative humidity (maximum)
90	60
85	64
80	69
75	75
70	81
65	87
60	90

Dry bulb temperature - When humidity control is not available, the relative humidity may be lowered by raising the dry bulb temperature proportionately, but not to exceed 32.2 degrees C. (90 degrees F.) for normal operation (unless TT-E-776 blush-retardant thinner is added).

Safe limits for enamel - Enamel can safely be applied at higher relative humidities than lacquers without encountering blushing.

5.5.4.3.1 Lacquer - Air temperatures shall not be less than 15.5 degrees C. (60 degrees F) nor greater than 32.2 degrees C. (90 degrees F.) and the relative humidity shall not be greater than 85 percent except in the case where lacquer is used with blush-retardant thinner, then 90 percent is permissible, per paragraph 5.5.4.3.

5.5.4.3.2 Enamel - For enamel topcoats, epoxy primer, wash primer and epoxy topcoats, air temperatures shall not be less than 15.5 degrees C. (60 degrees F.) nor greater than 37.7 degrees C. (100 degrees F.) and the relative humidity shall not be greater than 90 percent.

5.5.4.4 Time of application of paint-type materials -

5.5.4.4.1 First coat - Surfaces shall receive the wash primer coating, or where wash primer is not prescribed, the first primer coat shall be applied within a 2-hour maximum period after final cleaning.

5.5.4.4.2 System - Surface coatings shall be applied as follows:

Wash primer plus primer plus first lacquer coat or enamel coat shall be applied on the exterior surfaces within 24 hours. Where production operations are suspended for short periods, e.g., over week-ends,

holidays, etc., this time may be extended as necessary, but not to exceed 72 hours, provided the adhesion is unaffected threby, as determined by the wet tape scratch adhesion inspection test described in 6.3.4 OUTDOOR STORAGE OF PRIMED PARTS BEFORE SUBSEQUENT FINISHING OPERATIONS IS PROHIBITED.

5.5.4.4.3 Dry time (wash primer) - When MIL-P-8585, zinc chromate, primer or MIL-P-52192, epoxy primer, is used, the minimum and maximum drying times shall be those prescribed by MIL-P-6808 or MIL-P-46856 respectively. The minimum drying time for lacquer-type primer, under ideal atmospheric conditions shall be at least 1 hour. Under other conditions, the drying time of the lacquer-type primer shall be extended as necessary to avoid lifting, embrittlement, and adhesion difficulties induced by the high solvency thinners in the topcoats. The precautions outlined in MIL-P-6808 to avoid degradation of the primer prior to topcoating, as a result of outdoor exposure, especially in sunlight, shall be scrupulously observed.

5.5.4.4.4 Drying time (primer) - When Specification MIL-P-8585 zinc chromate primer or MIL-P-52192, epoxy primer is used, the minimum and maximum drying times shall be those prescribed by Specification MIL-P-6808 or MIL-P-46856 respectively. The minimum drying time for lacquer-type primer, under ideal atmospheric conditions shall be at least 1 hour. Under other conditions, the drying time of the lacquer-type primer shall be extended as necessary to avoid lifting, embrittlement, and adhesion difficulties induced by the high solvency thinners in the topcoats. The precautions outlined in Specification MIL-P-6808 to avoid degradation of the primer prior to topcoating, as a result of outdoor exposure, especially in sunlight, shall be scrupulously observed.

5.5.4.4.5 Topcoating - The first coat of lacquer shall be dried at least 45 minutes before sanding, tack-ragging, or application of the second coat. The second coat of lacquer may be applied at the convenience of the manufacturer but not to exceed 96 hours after application of the first coat provided, in cases where a delay occurs before application of the second coat, suitable prior cleaning and light scuff sanding is performed on the first lacquer coat to assure adequate adhesion of the second coat. A solvent wipe-down is mandatory if there is an overnight delay or longer in the painting sequence.

5.5.4.5 Spraying over bare metal - Wash primer shall be applied in accordance with MIL-C-3507. Zinc chromate primer shall be applied over the wash primer in accordance with MIL-P-6808. Epoxy primer shall be applied in accordance with MIL-P-46856.

5.5.4.6 Thickness of finish (dry thickness) - The film thickness of each single dried coat of paint-type material shall be controlled within the following limits: 0.0003 to 0.0005 inch for wash primer, 0.0006 inch for one coat of zinc chromate primer, 0.0005 to 0.0008 inch for one coat of lacquer, and 0.0008 to 0.0012 inch for one mist plus one wet coat of enamel or varnish, or as specified in the applicable finishing specification. The thickness of two coats of zinc chromate primer shall not exceed 0.0007 inch on surfaces which are to be topcoated. Because of the greatly reduced corrosion-inhibiting effectiveness and coverage in dried film thickness of less than 0.0003 inch, solitary zinc chromate primer films below this thickness should be avoided. The general finish shall be maintained below the maximum thickness specified to avoid cracking, flaking, and checking of the paint finish. Where sanding surfacer is used, which is permitted only on limited areas, and subject to the restrictions contained in 5.5.4.11 the thickness of the finish may be increased in these areas by 0.0006 inch. Where insignia and markings are added by painting, the total thickness of finish on these areas may be increased by approximately 0.001 inch. Where decalcomanias are used, the additional thickness is controlled by the decalcomania specification.

5.5.4.7 Application of lacquer - Lacquer is normally applied by the cold spray process. In the cold spray process, in general, two full wet consecutive passes of the spray gun. One coat shall be applied by one double or cross pass of the gun, followed by a second similar application after the first coat has set up. A minimum of 45 minutes' drying time shall be allowed between lacquer coats. If insufficient time is allowed for drying of the first coat and evaporation of the major portion of the thinner, the thinner in the second coat, may, when added to the unevaporated thinner remaining in the first coat, cause sags and runs. The force of the air from the spray gun could also disbrub the softened first coat and produce considerable orange peel.

5.5.4.8 Application of enamel - A thin coat or "tack" of enamel shall be applied with a light pass of the gun, and while it is still tacky, followed with one full wet coat. No mist coat shall be used after application of the wet enamel coat.

5.5.4.9 Application of insignia and markings - Paint used for the application of insignia and markings shall be of the same specification as the background material. On bare metal the insignia shall be applied by means of a complete wash primer plus primer plus topcoat finish scheme. On painted surfaces coated with a complete finish scheme only the topcoat material is required for marking. The additional thickness of finish resulting from the application of insignia and marking shall be within the limits prescribed in 5.5.4.6. Workmanship shall be of high quality with clear, sharp outlines of characters. Any method that causes ridges in the application of insignia and markings shall be avoided as much as possible, and the use of a knife or any metal blade on the part in the application procedure is prohibited. Masking tape used in the application of insignia and markings shall be removed as soon as practicable to avoid staining of the painted surfaces.

5.5.4.10 Use of masking tape - Masking tape used in the application of insignia and markings shall be such as not to impair the properties of, or discolor, the paint film when such tape is used in the particular painting process employed. Absence of these defects shall be verified by examining the painted surface after the tape has been removed and the surface exposed to sunlight for a minimum of 48 hours.

5.5.4.11 Use of sanding surfacer - In small areas on exterior surfaces that are severely scratched or abraided, or where otherwise considered necessary to obtain an aerodynamically smooth exterior surface on limited areas, one coat of MIL-S-974 sanding surfacer will be permitted but the material shall not be applied to the entire part, and its use shall be held to an absolute minimum. Only a minimum thickness of surfacer shall be applied. The material shall be sprayed on after the primer coat and immediately under lacquer or enamel topcoats. Surfacer must not be used for purposes of concealing rivet or screw heads. Allow the surfacer to air-dry at least 16 hours, and then water-sand very smooth with Nr. 400 wet or dry sandpaper to a thickness of 0.0006 inch. For emergency use, 4 hours air-dry before sanding will be acceptable, provided extreme care is exercised to prevent scratching of the surfaces. Sanding may extend through to the primer coat in spots but care must be exercised to avoid either sanding through to expose bare metal or removing appreciable amounts of the primer coat. After the sanding operation, the part shall be washed with water to remove grit and foreign matter and allowed to dry thoroughly. The quantity of sanding surfacer shall not exceed 1 quart, diluted for application, per 2,500 square feet of exterior surface.

5.5.4.12 Miscellaneous requirements -

5.5.4.12.1 Tack-ragging - To insure that all areas to be painted are free from foreign matter, they shall be "tack-ragged" immediately before painting. The "tack-ragging" shall be accomplished on each area to be finished immediately prior to the application of finishing material to that area. "Tack-ragging" is more applicable to those surfaces requiring sanding to obtain aerodynamically smooth properties.

5.5.4.12.2 Cloths, tack-rags - Only clean, soft, dry, contaminant-free, lint-free, desized, wiping cloths shall be employed in all steps of surface preparation, chemical surface treatment, cleaning, tack-ragging, and painting operations. Use of commercial rental wiping cloths is prohibited. Laundered shop cloths are permitted when the following conditions are met:

(a) The cloths returned from laundering shall be only those originally sent to the laundry by the paint shops of the contractor or overhaul station. Suitable marking by permanent marking inks or dyes shall be employed to insure segregation and return of cloths used for paint shop purposes.

(b) The laundered cloths shall comply with DDD-T-539, plus the following additional requirements: Complete absence of any trace of silicone-type material as determined by laboratory tests, including Soxhlet extraction.

5.5.4.12.3 Touch-up - The use of aerosol spray-cans of finishing materials is permitted for touch-up of scratches and heads of fastenings, as well as small areas not exceeding 4 square inches. When necessary to touch-up or refinish a bare spot on an assembly, the edges of the finish adjacent to the bare spot shall be tapered by sanding. The wash primer should then be spotted in over the bare area and feathered over the old finish. The wash primer will adhere to an acceptable degree to the adjacent finish but the adhesion will not be as outstanding at these edges as it is to bare metal. The wash primer may be omitted if thin scratches or small areas are involved.

5.5.4.12.4 Smoothness of wash primer and primer coats - The wash primer should be dry scuffed with kraft paper in accordance with MIL-C-8507. The primer should be applied as smoothly as possible, since specks and occlusions will carry through to the topcoat and impart undesirable roughness to the final finish. In spraying primer, proper spray techniques are necessary to avoid dry overspray which results in excessive roughness. A properly applied primer film should be free from streaks, blisters, seeds, excessive silkings, or other irregularities of surface. Dry scuff sanding by hand, using No. 400 or

No. 320 sandpaper should be employed, as necessary, to remove specks of roughness that might carry through to the topcoats, but extreme care should be exercised to avoid removing the primer down to wash primer. Great caution is necessary to avoid gouging the surface of rivets and other protuberances and edges of faying surfaces with the sandpaper, and thus remove the primer to bare metal, which results in subsequent susceptibility to corrosion. Should this be, normal touch-up with primer should be accomplished. Areas where primer presents a distinctly rough appearance not removable by sanding should be stripped and new primer applied to the area involved. If bubbling of the wash primer and subsequent coatings are encountered on magnesium, it may be taken as evidence of inadequate surface treatment of the magnesium. Such bubbled coatings should be removed immediately and the surface given a manually applied chemical surface treatment, followed by wash primer.

5.5.4.12.5 Final dry of the finish - The parts, after painting, shall be permitted to dry in a dust-free atmosphere for a sufficient time prior to moving to insure that the paint is adequately dry and to avoid damage of the finish. Painted parts shall also be protected from condensing moisture and rain during the first 24 hours after painting. This time may vary somewhat depending on the temperature and type of paint used.

6. INSPECTION

6.1 Responsibility for inspection - Unless otherwise specified in the contract or purchase order, the supplier is responsible for the performance of all inspection as specified herein. Except as otherwise specified, the supplier may utilize his own facilities or any commercial laboratory acceptable to the Government. The Government reserves the right to perform any of the inspections set forth in this standard where such inspections are deemed necessary to assure supplies and services conform to prescribed requirements.

6.2 General inspection requirements - All equipment being processed shall be inspected at the various stages of cleaning, surface treating, electroplating, and application of other types of finishes and coatings, to ascertain that each process is done in strict accordance with this standard and individual specifications. The inspections and tests covered in this section shall not be considered restrictive. Any condition not in full accord with the applicable drawings and specifications shall be regarded as defective.

6.2.1 Tests - Materials, prior to their use, shall be inspected, sampled and tested in accordance with the applicable specification and standard to determine compliance with the requirements of the particular specification.

6.3 Paint application -

6.3.1 General - Inspectors shall conduct frequent and regular checks to assure compliance with the requirements of this standard. The items specifically detailed below shall receive the most scrupulous attention by Inspectors and Quality Control personnel.

6.3.2 Cleanliness - Inspectors shall conduct tests just prior to application of paint-type coatings to assure that the surface is thoroughly clean and free from contaminants. The water break test described in 5.5.3.2 and the litmus paper test described in 5.5.3.2.1 shall be applied to questionable surfaces to assure that adequate cleaning and rinsing procedures have been employed and to check for freedom from residual steam-cleaning compound and other cleaning materials residues. If representative test areas fail these tests, the parts shall be returned to the cleaning process and recleaning accomplished.

6.3.3 Hiding power, gloss, and smoothness - Inspectors shall conduct regular and frequent inspection tests to insure smoothness of finish system. Regardless of whether the finish is high gloss or low gloss, specks and bumps detected visually or by drawing the finger tips across the sanded or rubbed finish in various directions shall be removed; there shall be no seediness or roughness caused by dried overspray, improper thinning, or improper gun adjustment. The painted surfaces (when dry) shall be checked visually for hiding power and gloss by comparison with an approved sample.

6.3.4 Adhesion - Inspectors shall conduct regular and frequent wet tape adhesion tests on the exterior finish after drying for a period of at least 48 hours for a lacquer system and 72 hours for an enamel system, the test to be conducted on a sufficient number of samples to assure maintenance of a satisfactory level of adhesion on full production. In performing this test, it is suggested that a piece of cloth or plastic be taped on the area under inspection. The test area shall be kept soaked 24 hours minimum with tap or distilled water. The test areas shall have a minimum diameter of 3 inches. Remove the wet cloth and blot up the surface water. Immediately thereafter, apply a 1-inch strip of tape, UU-T-106 (only newly manufactured tape shall be used), adhesive down. Press the tape down, using two passes of a 2½ pound

rubber covered roller or employ firm pressure with the thumb. In general the tape shall not be applied over rivets, skin laps, holes, slots, or screw heads. Repeated application of the tape on one area is not necessary. Remove the tape in one abrupt motion and examine the tested area for any paint damage, such as removal of paint at one of the layers of the finish system or removal of the entire system from metal. Test panels shall be sprayed with the complete finish, along with production items, and scratch wet tape adhesion tests per method 6301.1 of Fed-Std Test Method 141 conducted on these panels after a 24-hour soaking period in distilled water, the test to be conducted immediately after removal from the water. Suitable adjustments shall be made in the materials and processes, based on the results of these tests.

6.3.5 Film thickness - Contractors, inspectors, and painters shall exercise constant diligence to maintain careful control of the thickness of paint finish during the production process to insure continual adherence to the established thickness limits as specified in 5.5.4.6. Inspectors shall conduct regular and frequent paint thickness measurements on the production parts with a suitable measuring device on a sufficient number of selected areas to assure maintenance of the overall thickness of the finish below the maxima detailed in 5.5.4.6. The thickness measurement of the paint film shall be taken after all scuffing and sanding operations are completed on the paint coat being measured. When the painter has the gun adjusted and is ready to start spray painting, he shall first spray paint test panels as prescribed in 5.5.4.2. The thickness of the paint should then be measured on the panels with a micrometer or an Ames Thickness Gauge or equivalent, allowing 0.0001 to 0.0002 inch for further contraction in thickness to be expected during the drying of the paint. If the film thickness exceeds the allowable maximum, as specified above, necessary adjustments shall be made of the spray gun, paint viscosity, etc., and the trail spraying repeated until proper thickness is obtained. Then the painters may proceed with painting. The approved sprayed test panels may also be utilized for verifying the process for quality control and qualifying the individual painters.

6.3.6 Sampling frequency - Sampling for the inspection tests of Section 6 shall be accomplished: (a) When a new supplier furnishes materials used in the production process, (b) When evidence occurs of deterioration in the quality of the finish, (c) When a change of process or sequence is affected, and (d) A minimum of one inspection a week for those weeks when painting facilities are used. The quality control tests of 6.3.2, 6.3.3, 6.3.4 and 6.3.5 of this standard shall be conducted at least once a week in the production painting of parts,

as a minimum requirement. The results of the inspection tests shall be reviewed by the Government Inspector for conformance with established quality criteria.

6.3.7 Laundering of shop cloths - When laundered shop cloths are employed, Inspectors shall conduct regular and frequent inspection tests at the laundry or after return of the laundered cloths, or both; and spot-tests of the cloths just prior to actual usage in the shop, in sufficient numbers to assure compliance with the provisions of 5.5.4.12.2 herein.

Patent Notice - When Government drawings, specifications, or other data are used for any purpose other than in connection with a definitely related Government procurement operating the United States Government thereby incurs no responsibility nor any obligation whatsoever; and the fact that the Government may have formulated, furnished, or in any way supplied the said drawings, otherwise as in any other manner licensing the holder or any other person or corporation, or conveying any rights or permission to manufacture, use, or sell any patented invention that may be any way be related thereto.

CUSTODIAN:
Army - MI
Navy
Air Force

REVIEW
Army - ME,MI,MR,SL
Navy
Air Force

USER
Army -
Navy
Air Force

PREPARING ACTIVITY
Army Missile Command
Redstone Arsenal, Alabama
Project No. MFFP-A024

END OF REFERENCE

66

REFERENCE

67

SATURN FLIGHT MANUAL SA 506. MSFC-MAN-506, NASA MARSHALL SPACE FLIGHT CENTER, FEB. 1969.

THIS REFERENCE HAS A LIMITED DISTRIBUTION AND MAY NOT BE REPRODUCED.

END OF REFERENCE

REFERENCE

68

METALLIC MATERIALS AND ELEMENTS FOR AEROSPACE VEHICLE STRUCTURES. MIL-HDBK-5A, DEPT. DEFENSE, FEBRUARY 8, 1966.

THIS REFERENCE IS MATERIAL THAT IS READILY AVAILABLE AND THEREFORE THE CONTENTS HAVE NOT BEEN REPRODUCED.

END OF REFERENCE

68

REFERENCE

69

AEROSPACE STRUCTURAL METALS HANDBOOK. AFML-TR-68-115, MECHANICAL PROPERTIES DATA CENTER, BELFOUR STULEN, INC., 1971.

THIS REFERENCE IS MATERIAL THAT IS READILY AVAILABLE AND THEREFORE THE CONTENTS HAVE NOT BEEN REPRODUCED.

END OF REFERENCE

REFERENCE

70

HUZEL, D. K.; AND HUANG, D. H.: DESIGN OF LIQUID PROPELLANT ROCKET ENGINES. NASA SP-125, 1971.

REFERENCE

LEWIS RESEARCH CENTER
Aerospace Safety Research
and Data Institute
JUL 7 1971
CLEVELAND, OHIO

N70-26065
NASA SP-125

COPY 1

DESIGN OF LIQUID PROPELLANT ROCKET ENGINES

SECOND EDITION

HUZEL and HUANG

NATIONAL AERONAUTICS AND SPACE ADMINISTRATION

N70-26065
NASA SP-125

DESIGN OF LIQUID PROPELLANT ROCKET ENGINES

SECOND EDITION

Dieter K. Huzel and David H. Huang
Rocketdyne Division, North American Rockwell, Inc.

Scientific and Technical Information Office 1971
NATIONAL AERONAUTICS AND SPACE ADMINISTRATION
Washington, D.C.

PREFACE

This book intends to build a bridge for the student and the young engineer: to link the rocket propulsion fundamentals and elements (which are well covered in the literature) with the actual rocket engine design and development work as it is carried out in industry (which is very little, if at all covered in literature). The book attempts to further the understanding of the realistic application of liquid rocket propulsion theories, and to help avoid or at least reduce time and money consuming errors and disappointments. In so doing, it also attempts to digest and consolidate numerous closely related subjects, hitherto often treated as separate, bringing them up to date at the same time.

The book was written "on the job" for use by those active in all phases of engine systems design, development, and application, in industry as well as government agencies. Since it addresses itself to human beings set out to create new machines, rather than describing machines about to dominate man, the language chosen may not always be "functional" in the strict sense of the word.

The book presents sufficient detail to familiarize and educate thoroughly those responsible for various aspects of liquid propellant rocketry including engine systems design, engine development, and flight vehicle application. It should enable the rocket engineer to conduct, independently, complete or partial engine systems preliminary detail designs and to understand and judge the activities in, and the problems, limitations, and "facts of life" of the various subsystems making up a complete engine system. It also attempts to educate those ultimately interested in specialized subsystems and component design (thrust chamber, turbopump, control valves, etc.) about their own as well as neighboring subsystems and about the complete engine system. This should enable the student to prepare realistic analytical calculations and design layouts with a long headstart toward the final specialized designs for subsystem production release.

Special emphasis has been placed on engine flight application to stimulate engine systems and subsystem designers to think in these terms from the outset. The book is intended as a textbook, with specific consideration of the teacher without industry experience. We hope it will stimulate those desiring to specialize in the area of a rocket engine subsystem by supplying adequate information to enable them to benefit fully from the specialized literature. Thus it provides a realistic expert introduction for those joining the liquid propellant rocket engine field.

We gratefully acknowledge the most valuable assistance by members of the Rocketdyne and the Space Divisions of North American Rockwell, Inc., Los Angeles. We are particularly indebted to R. E. Grate, C. A. MacGregor, H. M. Alexander, S. B. Macaluso and T. Holwager of Rocketdyne Division, and to R. E. G. Epple, R. W. Westrup, R. D. Hammond, and D. A. Engels of Space Division, who reviewed the various chapters of the manuscript and contributed valuable ideas.

Special recognition goes to R. F. Strauss of Astrosystems International, New Jersey, who inspired the manuscript and rendered valuable assistance during the various phases of its preparation.

In particular, the authors are indebted to the manifold support they received from North American Rockwell, Inc., and its divisions. Rocketdyne's engine technology has provided a major foundation for the book.

Dieter K. Huzel
David H. Huang

Impeller design relative outlet flow angle:

$$\tan \beta_2' = \frac{c_{m2}}{(u_2 - c_{u2}')} = \frac{52.5}{205} = 0.256; \quad \beta_2' = 14°22'$$

Referring to figure 6-38a, and to equation (6-42), the width of the impeller at the vane inlet

$$b_1 = \frac{Q_{imp}}{3.12 \pi d_1 c_{m1} \epsilon_1}$$

$$= \frac{12\,855}{3.12 \times \pi \times 8.45 \times 53.1 \times 0.82} = 3.56 \text{ in}$$

From equation (6-43), the width of the impeller at the discharge

$$b_2 = \frac{Q_{imp}}{3.12 \pi d_2 c_{m2} \epsilon_2}$$

$$= \frac{12\,855}{3.12 \times \pi \times 14.8 \times 52.5 \times 0.88} = 1.91 \text{ in}$$

From equation (6-5) the overall pump flow coefficient

$$\phi = \frac{c_{m2}}{u_2} = \frac{52.5}{453} = 0.116$$

A-1 Stage Engine Oxidizer Pump Impeller Design Summary

Required impeller developed head and ΔH_{imp} = 3252 ft, Q_{imp} = 12 855 gpm flow capacity

Inlet velocity diagram (at mean inlet effective diameter d_1)
- $\alpha_1' = 61°13'$, $\beta_1' = 13°3'$
- $u_1 = 258.5$ ft/sec, $v_1' = 235$ ft/sec
- $c_1' = 60.5$ ft/sec, $c_{u1}' = 29.2$ ft/sec, $c_{m1} = 53.1$ ft/sec

Outlet velocity diagram (at outlet diameter d_2)
- $\alpha_2' = 11°58'$, $\beta_2' = 14°22'$
- $u_2 = 453$ ft/sec, $v_2' = 211.6$ ft/sec
- $c_2' = 253.4$ ft/sec, $c_{u2}' = 248$ ft/sec, $c_{m2} = 52.5$ ft/sec

Inlet dimensions
- inlet eye diameter = $d_{1t} = 11.05$ in
- inlet hub diameter = $d_{1h} = 4.65$ in
- inlet mean effective diameter = $d_1 = 8.45$ in
- inlet vane angle at diameter $d_1 = \beta_1 = 13°3'$
- inlet vane width $b_1 = 3.56$ in

Outlet dimensions
- outside diameter $d_2 = 14.8$ in
- discharge vane angle $\beta_2 = 24°$
- impeller outlet width $b_2 = 1.91$ in

Number of impeller vanes (eq. 6-44) $z_i = \beta_2/3 = 24/3 = 8$

Design of Casings

The main function of a pump casing is to convert the kinetic energy of high flow velocity at the impeller discharge into pressure. It does not contribute to the generation of head. The construction of a typical centrifugal pump casing is shown in figure 6-5. The front section of the casing, which provides the pump inlet and houses the inducer, is called the suction nozzle. The rear section of the casing, which collects the fluid from the impeller and converts the velocity head into pressure prior to discharge, is called the volute.

Since the flow path in a suction nozzle is short and the flow velocities are relatively low, the head loss in a suction nozzle due to friction is very small. The contour of the suction nozzle is designed to suit the inducer configuration. A tapered suction nozzle (as shown in fig. 6-14), also known as an end suction nozzle, together with a tapered inducer, yields best results in most respects. This nozzle, the area of which gradually decreases toward the impeller eye, greatly steadies the flow and assures uniform feed to the impeller. In liquid oxygen pumps, frequently a liner made of a material such as Kel-F is inserted between inducer and suction nozzle wall. This eliminates the possibility of metal-to-metal rubbing in the presence of narrow inducer tip clearances. Rubbing in liquid oxygen pumps may cause dangerous explosions. In turbopumps of the single-shaft type (fig. 6-18), the fuel is introduced to the fuel pump in a radial direction. Special guide devices are required in the inlet to minimize pressure drops because of the need of turning the flow axially into the inducer.

Two types of volute casing are used in rocket centrifugal pumps, the plain volute and the diffusing vane volute (see fig. 6-43). In the first, the impeller discharges into a single volute channel of gradually increasing area. Here, the

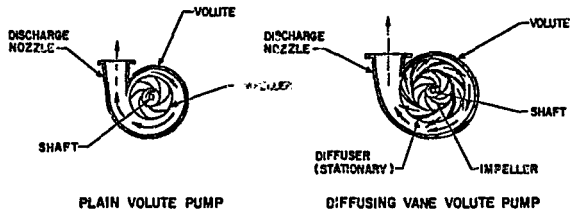

Figure 6-43.–Plain volute and diffusing vane volute centrifugal pump casings.

major part of the conversion of velocity to pressure takes place in the conical pump discharge nozzle. In the latter, the impeller first discharges into a diffuser provided with vanes. A major portion of the conversion takes place in the channels between the diffusing vanes before the fluid reaches the volute channel. The main advantage of the plain volute is its simplicity. However, the diffusing volute is more efficient. Head losses in pump volutes are relatively high. Approximately 70 to 90 percent of the flow kinetic energy is converted into pressure head in either volute type.

The hydraulic characteristics of a plain volute are determined by several design parameters which include: volute throat area a_v and flow areas a_θ, included angle θ_S between volute side walls (fig. 6-44), volute tongue angle α_v, radius r_t at which the volute tongue starts, and volute width b_3. Their design values are somewhat influenced by the pump specific speed N_S and are established experimentally for best performance.

All of the pump flow Q passes through the volute throat section a_v, but only part of it passes through any other section, the amount depending on the location away from the volute tongue. One design approach is to keep a constant average flow velocity c_3' at all sections of the volute. Thus

$$c_3' = \frac{Q}{3.12\,a_v}\,\frac{1}{3.12}\,\frac{\theta}{360}\,\frac{Q}{a_\theta} \qquad (6\text{-}69)$$

where

c_3' = average flow velocity in the volute, ft/sec
Q = rated design pump flow rate, gpm
a_v = area of the volute throat section, in^2
a_θ = area of a volute section (in^2), at an angular location θ (degrees) from the tongue

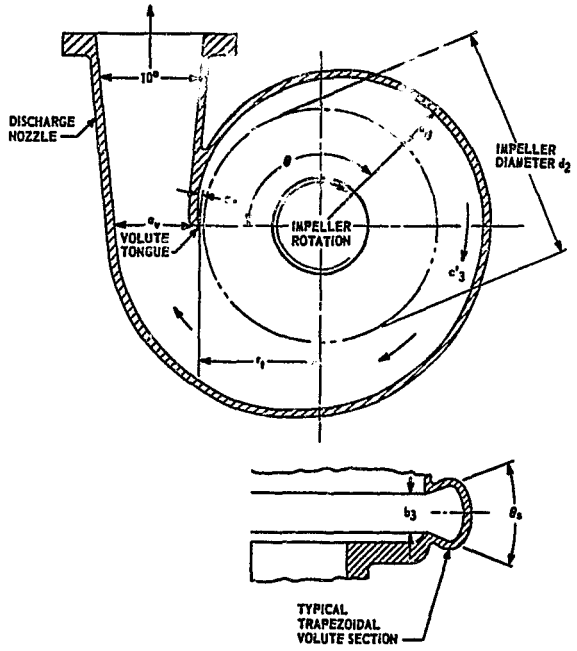

Figure 6-44.–Plain volute casing of a centrifugal pump.

The design value of the average volute flow velocity c_3' may be determined experimentally from the correlation

$$c_3' = K_v\sqrt{2g\Delta H} \qquad (6\text{-}70)$$

where

K_v = experimental design factor; typical values range from 0.15 to 0.55. K_v is lower for higher specific speed pumps
ΔH = rated design pump developed head, ft
g = gravitational constant, 32.2 ft/sec^2

In order to avoid impact shocks and separation losses at the volute tongue, the volute angle α_v is designed to correspond to the direction of the absolute velocity vector at the impeller discharge: $\alpha_v \cong \alpha_2'$. Higher specific speed pumps have higher values of α_2' and thus require higher α_v. The radius r_t at which the tongue starts should be 5 to 10 percent larger than the outside radius of the impeller to suppress turbulence and to provide an opportunity for the flow leaving the impeller to equalize before coming into contact with the tongue.

The dimension b_3 at the bottom of a trapezoidal volute cross section is chosen to minimize losses due to friction between impeller

discharge flow and volute side walls. For small pumps of lower specific speeds, $b_3 = 2.0\,b_2$, where b_2 is the impeller width at the discharge, in. For higher specific speed pumps, $b_3 = 1.6$ to $1.75\,b_2$. The maximum included angle θ_S between the volute side walls should be about 60°. For higher specific speed pumps, or for higher impeller discharge flow angles α_2', the value of θ_S should be made smaller.

The pressure in the volute cannot always be kept uniform, especially under off-design operating conditions. This results in a radial thrust on the impeller shaft. To eliminate or reduce the radial thrust, double-volute casings have been frequently used (fig. 6-45). Here, the flow is divided into two equal streams by two tongues set 180° apart. Although the volute pressure unbalances may be the same as in a single-volute casing, the resultant of all radial forces may be reduced to a reasonably low value, owing to symmetry.

The diffusing vane volute has essentially the same shape as a plain volute, except that a number of passages are used rather than one. This permits the conversion of kinetic energy to pressure in a much smaller space. The radial clearance between impeller and diffuser inlet vane tips should be narrow for best efficiency. Typical values range from 0.03 to 0.12 inch, depending upon impeller size. The width of the diffuser at its inlet can be approximated in a manner similar to that used for the width of a plain volute (i.e., 1.6 to 2.0 impeller width b_2). A typical diffuser layout is shown in figure 6-46. The vane inlet angle α_3 should be made equal or close to the absolute impeller discharge flow angle α_2'. The design value of the average flow velocity at the diffuser throat c_3' may be approximated by

$$c_3' = \frac{d_2}{d_3} c_2' \qquad (6\text{-}71)$$

where

c_3' = average flow velocity at the diffuser throat, ft/sec
d_2 = impeller discharge diameter, in
d_3 = pitch diameter of the diffuser throats, in
c_2' = absolute flow velocity at impeller discharge, ft/sec

Since each vane passage is assumed to carry an equal fraction of the total flow Q, the following correlation may be established:

$$b_3 h_3 z = \frac{Q}{3.12\,c_3'} \qquad (6\text{-}72)$$

where

b_3 = width of the diffuser at the throat, in
h_3 = diffuser throat height, in
z = number of diffuser vanes
Q = rated design pump flow rate, gpm

The number of diffuser vanes z should be minimum, consistent with good performance, and should have no common factor with the number of impeller vanes to avoid resonances. If possible,

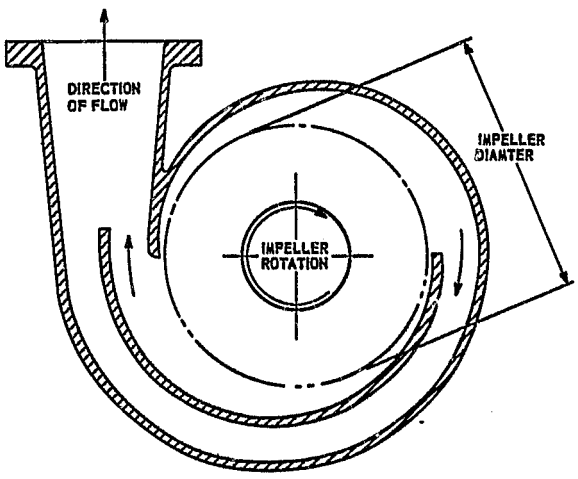

Figure 6-45.–Typical single discharge, 180° opposed double-volute casing of a centrifugal pump.

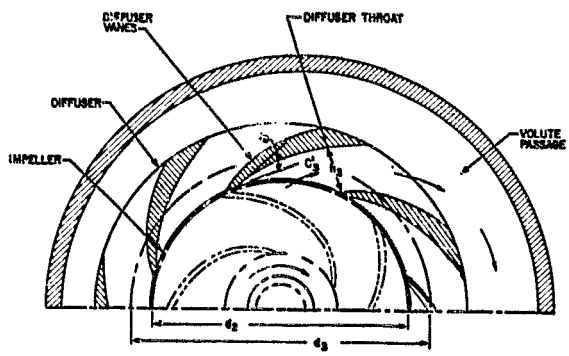

Figure 6-46.–Typical layout of the diffuser for a centrifugal pump volute casing.

the cross section of the passages in the diffuser are made nearly square; i.e., $b_3 = h_3$. The shape of the passage below the throat should be diverging, with an angle between 10° to 12°. The velocity of the flow leaving the diffuser is kept slightly higher than the velocity in the pump discharge line.

Rocket pump casings are frequently made of high-quality aluminum-alloy castings. In low-pressure pumps, the casing wall thickness is held as thin as is consistent with good foundry practice. Owing to the intricate shape of the castings, stress calculations are usually based upon prior experience and test data. For a rough check, the hoop stress at a casing section may be estimated as

$$S_t = p\frac{a}{a'} \qquad (6\text{-}73)$$

where

S_t = hoop tensile stress, lb/in^2
p = local casing internal pressure, psia (or pressure difference across the casing wall, psi)
a = projected area on which the pressure acts, in^2
a' = area of casing material resisting the force pa, in^2

The actual stress will be higher, because of bending stresses as a result of discontinuities and deformation of the walls, and thermal stresses from temperature gradients across the wall.

Sample Calculation (6-8)

The flow conditions at the outlet of the A-1 stage engine oxidizer pump impeller were derived in sample calculation (6-7). Calculate and design a double-volute (spaced 180°), single-discharge-type casing (as shown in fig. 6-45) for the same pump, assuming a design factor K_v of 0.337.

Solution

From equation (6-70), the average volute flow velocity may be calculated as

$$c_3' = K_v\sqrt{2g\Delta H} = 0.337\times\sqrt{2\times32.2\times2930} = 146 \text{ ft/sec}$$

Referring to figures 6-44 and 6-45, and from equation (6-69), the required volute flow area at any section from 0° to 180° away from the volute tongue may be calculated for both volutes as

$$a_\theta = \frac{\theta Q}{3.12\times360\times c_3'} = \frac{12420}{3.12\times360\times146}\theta = 0.076\theta$$

At $\theta = 45°$, $a_{45} = 3.42$ in^2; at $\theta = 90°$, $a_{90} = 6.84$ in^2; at $\theta = 135°$, $a_{135} = 10.26$ in^2; and at $\theta = 180°$, $a_{180} = 13.68$ in^2.

Total volute throat area at the entrance to the discharge nozzle

$$a_v = 2\times13.68 = 27.36 \text{ in}^2$$

The volute angle α_v can be approximated as

$$\alpha_v = \alpha_2' = 11°58', \text{ say } 12°$$

The radius r_t at which the volute tongues start can be approximated as (assuming 5 percent clearance)

$$r_t = \frac{d_2}{2}\times1.05 = \frac{14.8}{2}\times1.05 = 7.77 \text{ in}$$

The width at the bottom of the trapezoidal volute section shall be

$$b_3 = 1.75b_2 = 1.75\times1.91 \text{ in} = 3.34 \text{ in}$$

Allowing for a transition from the shape of the volute to round, we use a diameter of 6.25 inches, or an area of 30.68 in^2, for the entrance to the discharge nozzle. With a 10° included taper angle and a nozzle length of 10 inches, the exit diameter of the discharge nozzle can be determined as

$$d_e = 6.25 + 2\times10\times\tan 5°$$
$$= 6.25 + 2\times10\times0.0875 = 6.25 + 1.75$$
$$= 8 \text{ in (or an area of } 50.26 \text{ in}^2)$$

Flow velocity at the nozzle inlet:

$$\frac{12420}{3.12\times30.68} = 130 \text{ ft/sec}$$

Flow velocity at the nozzle exit:

$$\frac{12420}{3.12\times50.26} = 79.4 \text{ ft/sec}$$

Balancing the Axial Thrust of Centrifugal Pumps

Unbalanced axial loads acting on the inducer-impeller assembly of centrifugal pumps are primarily the result of changes in axial momentum, and of variations in pressure distribution at the periphery of the assembly. These unbalanced forces can be reduced by mounting two propellant pumps back to back, as shown in figures 6-14 and 6-18. More subtle balancing of the axial loads can be accomplished by judicious design detail, which is especially important in high-pressure and high-speed pump applications. Either one of the following two methods is frequently used.

With the first method (as shown in fig. 6-47), a balance chamber is provided at the back shroud of the impeller, between back wearing ring diameter d_{br} and shaft seal diameter d_s. Balancing of axial loads is effected by proper selection of the projected chamber area and of the admitted fluid pressure. The pressure level p_c in a balance chamber can be controlled by careful adjustment of the clearances and leakages of the back wearing ring and the shaft seals. The required p_c may be determined by the following correlation:

$$p_c\pi(d_{br}^2 - d_s^2) = p_v\pi(d_{br}^2 - d_{fr}^2) + p_1\pi(d_{fr}^2 - d_t^2) + p_0\pi d_h^2 + \frac{4\dot{w}_i c_{m0}}{g} \pm T_e \quad (6\text{-}74)$$

where

p_c = balance chamber pressure, psia
p_v = average net pressure in the space between impeller shrouds and casing walls, psia
p_1 = static pressure at the inducer outlet, psia
p_0 = static pressure at the inducer inlet, psia
d_s = effective shaft seal diameter, in
d_h = hub diameter at the inducer inlet, in
d_t = inducer tip diameter = eye diameter at the impeller inlet, in
d_{fr} = front wearing ring diameter, in
d_{br} = back wearing ring diameter, in
$\dot{w}_i$ = inducer weight flow rate, lb/sec
c_{m0} = axial flow velocity at the inducer inlet, ft/sec (converts to radial)
g = gravitational constant, 32.2 ft/sec^2
T_e = external axial thrust due to unbalanced axial loads of the other propellant and/or the turbine; lb. A positive sign indicates a force which tends to pull the impeller away from the suction side, a negative sign indicates the opposite.

The static pressure at the inducer outlet, p_1, can be either measured in actual tests, or approximated by

$$p_1 = k_i p_0 \quad (6\text{-}75)$$

where

k_i = design factor based on experimental data (ranging from 1.1 to 1.8)
p_0 = static pressure at the inducer inlet, psia

The average pressure in the space between impeller shrouds and casing side walls, p_v, may be approximated by

$$p_v = p_1 + \frac{3}{576}\frac{u_2^2 - u_1^2}{2g}\rho \quad (6\text{-}76)$$

where

u_2 = peripheral speed at the impeller outside diameter d_2, ft/sec
u_1 = peripheral speed at the impeller inlet mean effective diameter d_1, ft/sec
ρ = density of the pumped medium, lb/ft^3

The main advantage of the balance chamber method is flexibility. The final balancing of the turbopump bearing axial loads can be accomplished in component tests by changing the value of p_c through adjustment of the clearances at the wearing ring and shaft seals. However, this tends to increase leakage losses.

In the second method (as shown in fig. 6-48), straight radial ribs are provided at the back shroud of the impeller to reduce the static pressure between the impeller back shroud and casing wall through partial conversion into kinetic energy. This reduction of axial forces acting on the back shroud of the impeller may be approximated by the following correlation:

$$F_a = \frac{3\pi}{4608}(d_r^2 - d_s^2)\frac{(u_r^2 - u_s^2)}{2g}\rho\frac{(s+t)}{2s} \quad (6\text{-}77)$$

where

F_a = reduction of the axial forces acting on the back shroud of impeller, lb
d_r = outside diameter of the radial ribs, in

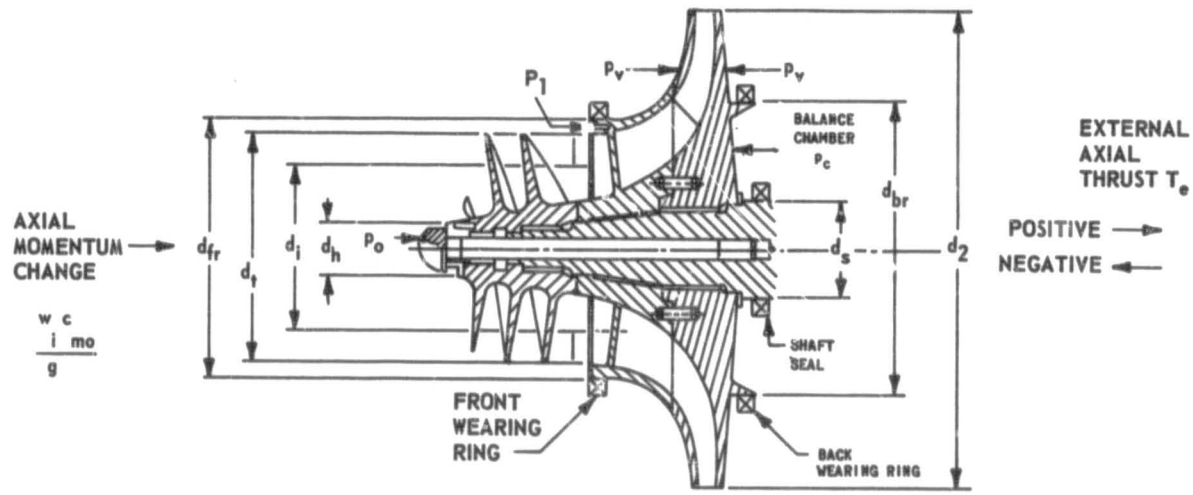

Figure 6-47.–Balancing axial thrusts of a centrifugal pump by the balance chamber method.

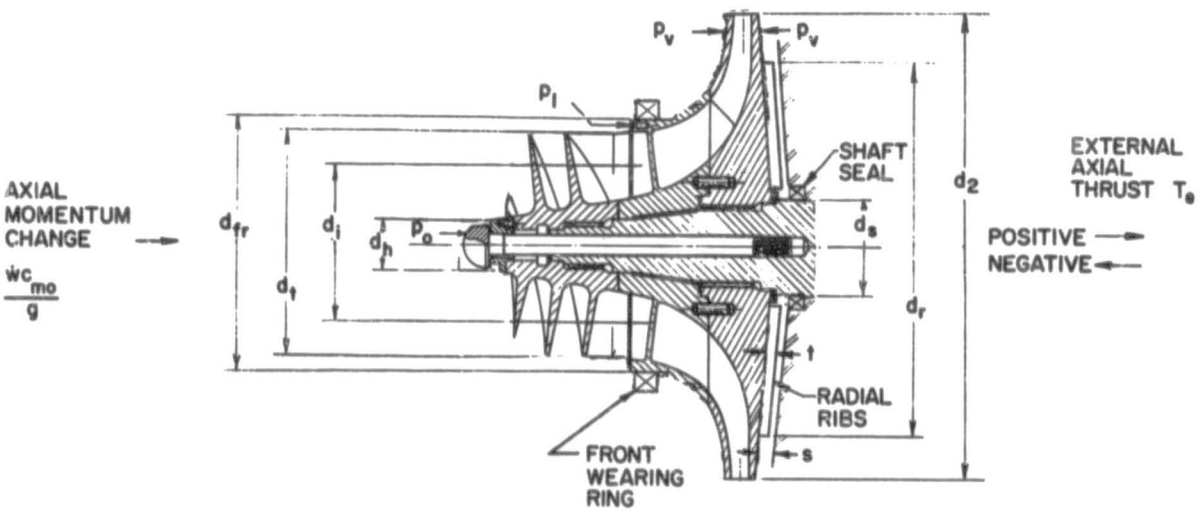

Figure 6-48.–Balancing axial thrusts of a centrifugal pump by the radial rib method.

d_s = effective shaft seal diameter $\cong$ inside diameter of the radial ribs, in
u_r = peripheral speed at diameter d_r, ft/sec
u_s = peripheral speed at diameter d_s, ft/sec
g = gravitational constant, 32.2 ft/sec^2
ρ = density of the pumped medium, lb/ft^3
t = height or thickness of the radial ribs, in
s = average distance between casing wall and impeller back shroud, in

The required F_a may be determined by the following correlation:

$$p_v\pi(d_{fr}^2 - d_s^2) - 4F_a = p_1\pi(d_{fr}^2 - d_t^2) + p_0\pi d_h^2 + \frac{4\dot{w}c_{mo}}{g} \pm T_e \quad (6\text{-}78)$$

The pressures p_1 and p_v may be approximated by equations (6-75) and (6-76). See equation (6-74) for other terms.

Sample Calculation (6-9)

Radial ribs (similar to those in fig. 6-48) are used on the back shroud of the A-1 stage engine

oxidizer pump impeller, with the following dimensions:

Outside diameter of the radial ribs, $d_r = 14.8$ in (equal to d_2)
Inside diameter of the radial ribs, $d_s = 4.8$ in
Height of the radial ribs, $t = 0.21$ in
Width of the radial ribs, $w = 0.25$ in (not critical)
Average distance between the casing wall and impeller back shroud, $s = 0.25$ in

Estimate the reduction of the axial forces acting on the back shroud of the impeller, due to the radial ribs.

Solution

The peripheral speed at diameter d_r

$$u_r = \frac{\pi N}{720} d_r = \frac{\pi \times 7000}{720} \times 14.8 = 452 \text{ ft/sec}$$

The peripheral speed at the diameter d_s

$$u_s = \frac{\pi N}{720} d_s = \frac{\pi \times 7000}{720} \times 4.8 = 147 \text{ ft/sec}$$

From equation (6-77), the reduction of the axial forces

$$F_a = \frac{3\pi}{4608}(219.04 - 23.04)\frac{(204\,304 - 21\,609)}{2 \times 32.2} \times 71.38 \times \frac{(0.25 + 0.21)}{2 \times 0.25} = 74\,680 \text{ lb}$$

6.4 DESIGN OF AXIAL-FLOW PUMPS

Except when used as inducers, application of axial-flow pumps in rocket engines is essentially limited to liquid hydrogen systems in a multistage configuration. Thus, the following discussions are applicable to axial-flow hydrogen pumps only. Multistage axial-flow hydrogen pumps are applied in regions which are beyond the capability of a single-stage centrifugal pump, since their construction is comparatively simple (fig. 6-4). As can be seen in figure 6-6, the fluid in an axial-flow pump flows from one stage to the next with a minimum of connecting passages.

The head rise of a typical single-stage centrifugal hydrogen pump is limited to about 65 000 ft (2000 psi). Beyond this point, a multistage axial-flow pump is selected. For each stage of an axial-flow pump, head rises of 5000 to 9000 feet can be obtained.

The capacity of an axial-flow hydrogen pump is usually limited to about 5500 gpm as a minimum. This is due to the minimum practical height h_v of the vanes (fig. 6-49). For heights below 0.5 inch, the tip clearance required for efficient performance becomes critical, causing manufacturing problems. A reduction in rotor diameter below certain values is not practical either, because of the high rpm required for proper blade speed.

Figure 6-50 presents typical operating regions of various liquid hydrogen pump types. These include centrifugal pumps of $(N_S)_1 = 500$ per

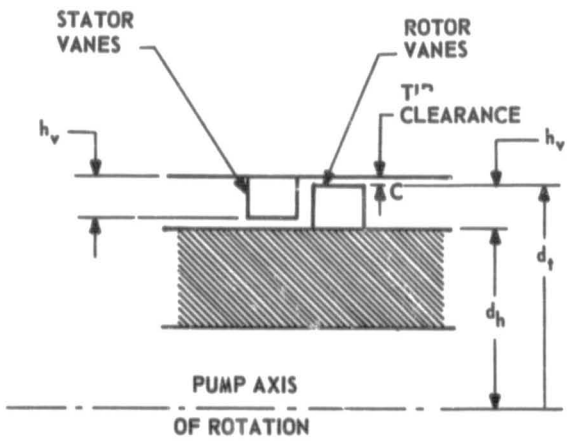

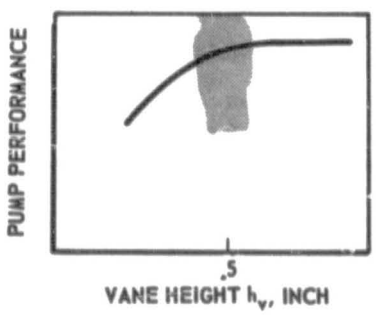

Figure 6-49.—Effect of vane height on the performance of an axial-flow pump.

$$\eta_{nb} = \frac{U(C_1 \cos \alpha_1 + C_2 \cos \alpha_2 + C_3 \cos \alpha_3 + C_4 \cos \alpha_4)}{gJ\Delta H}$$

$$= \frac{1308(2880 \times 0.906 + 1070 \times 0.058 + 2880 \times 0.906 + 1070 \times 0.058)}{32.2 \times 778 \times 359}$$

$$= 0.78$$

The turbine machine efficiency is assumed to be the same as that used in design (a):

$$\eta_m = 0.852$$

From equation (6-148), the overall turbine efficiency

$$\eta_t = \eta_{nb}\eta_m = 0.78 \times 0.852 = 0.664$$

A-1 Stage Engine Alternate Turbine Design Summary (Two-Stage, Two-Rotor, Pressure-Compounded, Impulse Type)

For velocity diagrams at mean diameter d_m, see figure 6-59.

$U = 1308$ fps:

$\alpha_1 = 25°$; $\beta_1 = 43°8'$; $C_1 = 2880$ fps; $V_1 = 1784$ fps; $\alpha_2 = 86°40'$; $\beta_2 = 38°$; $C_2 = 1070$ fps; $V_2 = 1736$ fps; $\alpha_3 = 25°$; $\beta_3 = 43°8'$; $C_3 = 2880$ fps; $V_3 = 1784$ fps; $\alpha_4 = 86°40'$; $\beta_4 = 38°$; $C_4 = 1070$ fps; $V_4 = 1736$ fps

Isentropic enthalpy drops:

First-stage nozzles, $\Delta H_{0\text{-}1'} = 179.5$ Btu/lb

First-stage rotor blades, $\Delta H_{1\text{-}2'} = 10.75$ Btu/lb

Second-stage nozzles, $\Delta H_{2\text{-}3'} = 158$ Btu/lb

Second-stage rotor blades, $\Delta H_{3\text{-}4'} = 10.75$ Btu/lb

Working efficiencies:

$\eta_t = 66.4\%$; $\eta_n = 92\%$; $\eta_{nb} = 78\%$; $\eta_m = 85.2\%$

Mean diameter of nozzles and blades:

$d_m = 42.7$ in

Comment: The overall efficiency of the pressure compounded turbine is higher than that of design (a). However, a relatively large d_m is required (weight, size).

6.6 DESIGN OF TURBOPUMP BEARINGS, SEALS, AND GEARS

Turbopump Bearing Design

A turbopump shaft is supported by two or more bearings. The loads on the bearings are the result of forces which act on the shaft or on the parts supported by the shaft. These forces may be divided into two classes: those which act at right angles to the shaft axis (radial forces), and those which act parallel to the shaft axis (thrust loads).

Radial loads on turbopump bearings may result from one or more of the following sources:

(1) Weights of parts such as shafts, pump impellers, turbine rotors, gears
(2) Centrifugal forces due to unbalance of these rotating parts
(3) Forces due to inertia, resulting from rapid acceleration
(4) Resultant radial forces on the impeller due to nonuniform pressure distribution in the discharge volute of the pump
(5) Tangential or torque forces induced by the gears

Thrust loads on turbopump bearings may result from one or more of the following sources:

(1) Weight of rotating parts mounted on a vertical shaft
(2) Unbalanced axial thrust of the pumps
(3) Resultant axial thrust on the turbine rotor blades

For the turbopumps of liquid rocket engines, high-speed ball and roller bearings are used almost exclusively. A typical two-bearing design is shown in figure 6-7. A ball bearing carries both radial and thrust loads. It is paired with a roller bearing which carries only radial loads, however, of a higher magnitude. A typical three-bearing arrangement is shown in figure 6-63. The shaft radial loads are carried by a single roller bearing at the turbine end and by a roller and a ball bearing on the pump side. The ball bearing also absorbs the thrust loads. As a rule, the shaft thrust loads in a turbopump are carried by a single or dual bearing located at one end of the shaft. Thus loads from thermal expansion or contraction of the shaft are avoided.

Bearing design data with regard to load-carrying capacity, operating speed, and service life are usually furnished by the manufacturers. The useful life of a bearing is dependent upon its speed and load, and may be expressed by the correlation:

$$\text{Life, hours} = K_b\left(\frac{\text{Rated speed, rpm}}{\text{Actual operating speed, rpm}}\right) \times\left(\frac{\text{Rated capacity, lb}}{\text{Actual working load, lb}}\right)^4 \quad (6\text{-}153)$$

where K_b = design factor usually furnished by manufacturer.

If a bearing is subjected to both thrust and radial loads, the two can be combined into a single equivalent radial load:

$$P = R + xA \quad (6\text{-}154)$$

where

P = equivalent radial load used for bearing selection, lb
R = actual radial load, lb
A = actual thrust load, lb
x = design coefficient usually furnished by manufacturer

Rocket turbopump bearings quite commonly are cooled and lubricated by the propellants pumped. They are usually operated at very high "*DN*" values, a parameter which is the product of the bearing bore D (millimeters), and the bearing rotative speed N (rpm).

Propellant lubrication has the advantage of eliminating an additional lubricant supply system, and of simplifying bearing sealing problems. The following are important design considerations for propellant-lubricated bearings:

(1) Characteristics of the propellants, such as thermal stability, operating temperature, chemical inertness, viscosity.
(2) Compatibility of the bearing materials with the propellants. The application of certain high-strength alloys is sometimes limited by the propellants used.

The "*DN*" rating is convenient when selecting high-speed ball or roller bearings. As the rotative speed of a bearing increases, contact fatigue of the outer race caused by centrifugal loads of the balls or rollers may cause failures. In addition, bearing contact speeds will result in nonrolling phenomena with attendant failures caused by overheating. Through proper selection of the bearing geometry, these problems can be minimized, and the *DN* rating increased. Note that for a given horsepower rating, the shaft size based on allowable stress does not decrease proportionally with the increase of shaft design speed. Thus the required bearing *DN* value rapidly increases for high-speed turbopumps. As a result, especially for liquid hydrogen application, the turbopump rpm is often determined by the *DN* limits of the bearings.

A most important bearing design consideration is the expected operating life of the rocket engine. The bearings must have adequate statistical probability of conforming with this requirement. A generally accepted life rating for ball and roller bearings is the "B-10 life." The term denotes the operating life (hours) of a "population" of bearings at a given load and speed, at the expiration of which statistically 10 percent of them will have failed. Of course, in actual rocket engine operation, component reliability must be much higher. Bearing life at a given load and speed varies inversely with reliability. For instance, the B-1 life (99 percent reliability) is one-tenth of the B-10 life (90 percent reliability), or one-fiftieth of the B-50 life (50 percent reliability). Therefore, turbopump bearings are generally designed for a B-10 life of at least 100 hours. This corresponds to a B-1 life of 10 hours, or a B-0.1 life (99.9 percent reliability) of 1 hour, the latter by order of magnitude being the life the bearing most likely will actually see. For critical applications, an even higher life rating may be selected.

Figure 6-61 presents the centrifugal load *DN* limits in terms of 10, 100, and 1000 hours of B-10 life for a typical ball bearing design (extra-light series).

The stress-limiting *DN* values of roller bearings are much higher than for ball bearings; however, it is extremely difficult to control the temperature rise in a roller bearing, if the *DN* value is above 1.5×10^6, due to excessive cage slip. Generally, rocket turbopump bearings have been successfully operated at *DN* values up to 1.5×10^6. Limited test information indicates possible satisfactory operation at 2.0×10^6 *DN*.

Dynamic Seal Design

The principal dynamic, i.e., rotating seal types used in liquid rocket turbopumps are the labyrinth, face-riding, and shaft-riding seals. Satisfactory seal operation depends upon good design which considers many factors, including

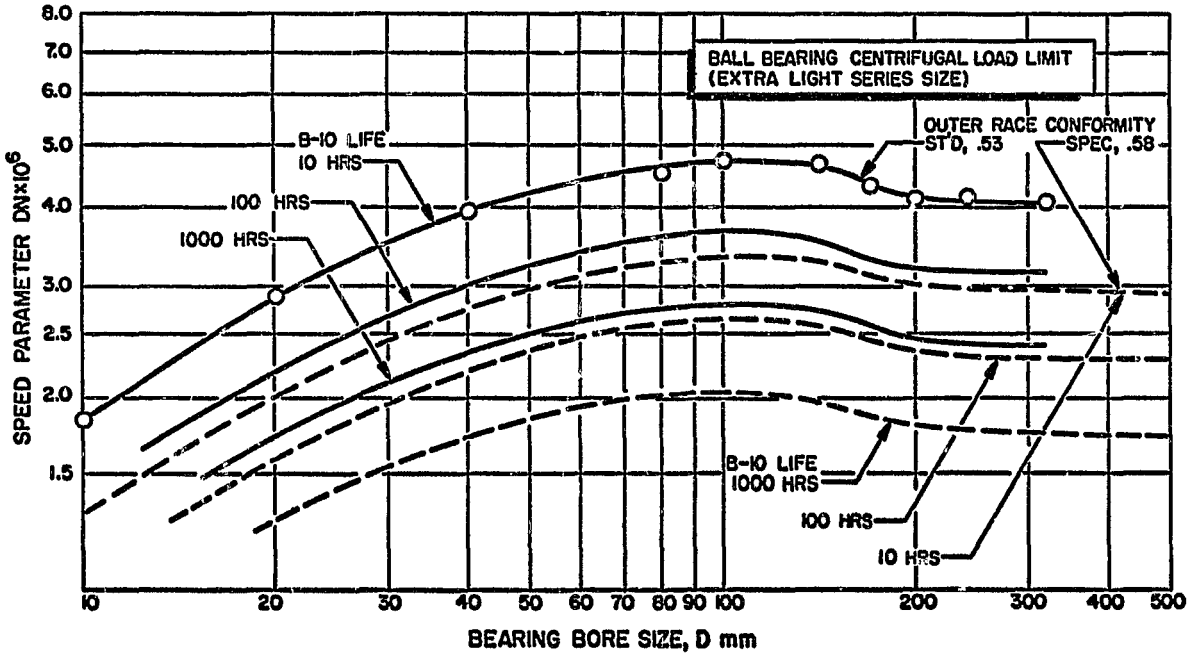

Figure 6-61.–Ball bearing centrifugal load DN limits.

fluid pressure surges, vibration, expansion and contraction of sealing components, contact pressure between sealing surfaces, rubbing velocities of the sealing surfaces, smooth and friction-free operation of internal sealing parts, and on squareness of the sealing surfaces. Any influence which directly or indirectly subsequently alters these factors can cause improper operation of the seal.

As shown in figure 6-62, the labyrinth seal is a clearance-type seal. The fluid tending to pass through the sealing interface is throttled many times and is forced to follow a devious path. The function of a labyrinth seal is not to prevent fluid leakage entirely, but rather to reduce leakage to a reasonable level at a minimum of friction and wear. The amount of leakage through a labyrinth seal can be estimated by the correlation

$$Q_e = C_S A_C \sqrt{24 g \Delta p_S / \rho} \qquad (6\text{-}155)$$

where

Q_e = leakage rate, in^3/sec
A_C = seal clearance area, in^2
Δp_S = pressure differential across the seal, lb/in^2
ρ = density of the fluid lb/in^3
C_S = seal leakage coefficient, established experimentally

Labyrinth seals are used for the wearing rings of pump impellers, as well as for the rotating seals attached to the sealing diaphragm between two turbine stages.

In a face-riding-type seal the sealing is accomplished through rubbing contact between the precision-lapped faces of a floating seal washer and a shoulder ring. The mating faces are at a right angle to the axis of rotation. As shown in figure 6-62, the floating seal washer is attached to a metal bellows. The bellows, in turn, is welded to a stationary seal housing which is secured and statically sealed to the casing. The bellows provides flexibility and spring force to the contact face, permitting it to follow axial and angular movement without leakage. Sometimes a lip seal is used in conjunction with a spring-loaded floating washer, instead of a bellows.

The shaft-riding seal (fig. 6-62) consists of a seal housing, a seal retaining plate, and several seal segments. The segments form a ring around the shaft and are held against it by garter springs.

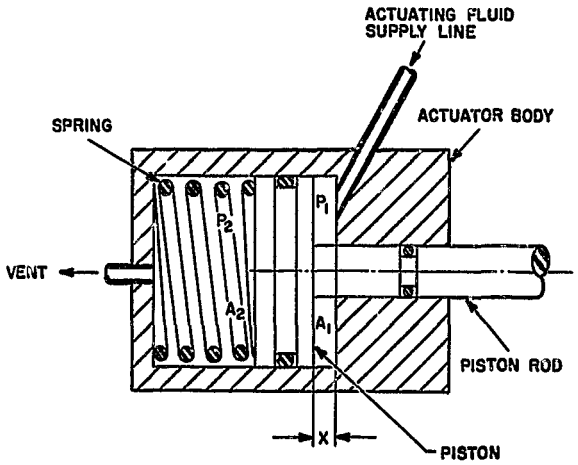

Figure 7-23.—Schematic of a typical piston-type actuator.

a_p = acceleration of the piston, ft/sec^2
A_1 = area of the piston actuating side, in^2
A_2 = area of the piston vent side, in^2
p_1 = actuating pressure, psia. This is the pressure at the actuating fluid source, less the supply-line pressure drop which depends on the flow rate (a function of acceleration a_p)
p_2 = vent pressure, psia. This is the ambient pressure, plus the vent-line pressure drop which also depends on flow rate (again a function of acceleration a_p)
F_r = resistance force of the control function, lb, which also may be a function of acceleration a_p
F_f = friction forces (seals, sliding surfaces, etc.), lb
F_S = initial spring force, lb (at $x = 0$)
C = spring rate, lb/in
x = distance traveled by the piston from its initial position, in

Since the relations between p_1, p_2, F_r, and a_p are not linear, equation (7-10) may become complex and require a high-speed computer for solution.

7.7 DESIGN OF DYNAMIC SEALS FOR FLUID-FLOW-CONTROL COMPONENTS

Apart from the static seals, which will be treated in chapter IX, two basic types of dynamic seals are required for fluid-flow-control components: seals for moving (reciprocating and rotating) cylindrical elements such as actuator pistons, shafts, and rods; and seals for valve seats. Here, too, temperature is one of the most important design considerations. Seals can be classified into those for medium-temperature service (−60° to 400° F), low-temperature service (−60° to −425° F), and high-temperature service (400° F and up). The selection of the configurations and the materials for these seals is based to a large extent on service conditions and type of fluid involved. Generally, soft nonmetallic or elastomeric seals are used wherever possible. The outstanding advantage of these seals is that they function satisfactorily despite minor imperfections in the seal or the mating part.

Design of Dynamic Seals for Medium-Temperature Services

Elastomeric O-rings have been widely applied as dynamic seals for moving cylindrical parts as well as for valve seats. However, proper design techniques must be observed to assure success. Figure 7-24 and table 7-5 represent recommended design practices for diametral-squeeze-type O-ring seals for typical dynamic and static applications. Figure 7-26 shows a typical O-ring seal used for a valve seat. Important design considerations for dynamic O-ring seals are summarized as follows:

1. *Design correlations between fluid pressure, O-ring compound hardness and diametral clearance.*—A frequent cause of seal failure is the extrusion of diametral-squeeze-type O-rings into the clearance gap adjacent to the O-ring groove (when under pressure) (fig. 7-25), leaving a permanent deformation after the pressure is reduced. Fluid pressure influences O-ring seal design because it affects the choice of compound hardness. The combination of fluid pressure and chosen hardness will determine the maximum clearance E that can be tolerated safely. A proper combination of clearance and O-ring hardness may prevent O-ring extrusion (table 7-5). In general, the O-ring nominal section diameter is chosen as large as space and installation considerations will permit. Past designs usually will provide a useful guide. In addition, Teflon backup rings as shown in figure 7-25 are recommended for dynamic O-ring seals at sealing pressures over 800 psi and for static O-ring seals at pressures above 1500 psi.

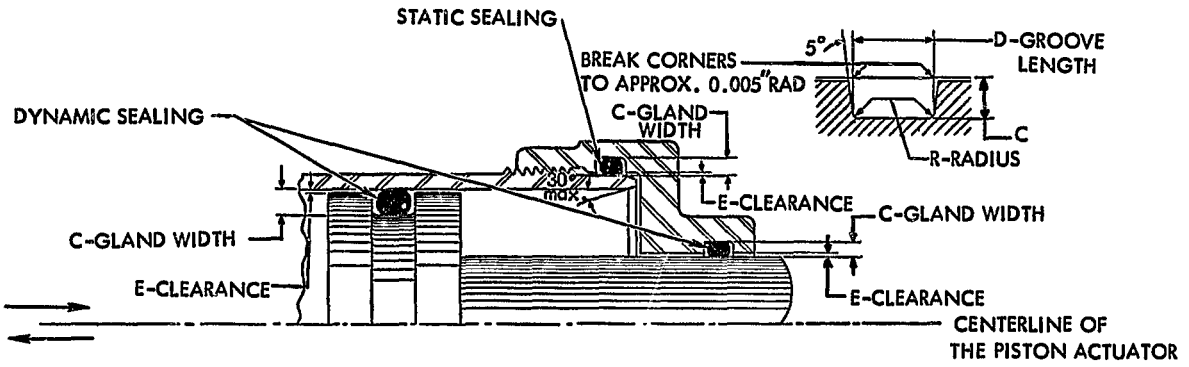

Figure 7-24.–Diametral-squeeze-type O-ring seals in typical dynamic and static applications.

2. *Surface finish requirements.*–The finish of the sliding surfaces in contact with dynamic O-ring seals should be as smooth as possible. They should be ground, honed, or polished to a microinch finish of 8 to 10 rms. It has been found that a finish within this range yields a longer life than either rougher or smoother finishes. Codirectional patterns, as produced by honing, have been proven to be the best surface finish for any type of dynamic sliding seal. For still better results, after an initial finishing, the surface could be hard chrome or nickel plated and again finished. The plating provides a hard, slippery surface that resists corrosion, wear, and scratching. A microinch finish of 60 rms or better is recommended for surfaces in contact with static diametral-squeeze-type O-ring seals.

3. *Friction of dynamic O-ring seals.*–The breakaway friction of a dynamic O-ring seal is usually about three times the running friction. Breakaway and running frictions increase with fluid pressure, O-ring hardness, diametral squeeze, and decrease of temperature. Accurate values of O-ring frictions can only be obtained experimentally for a given design.

4. *Selection of O-ring compounds.*–A great variety of O-ring elastomer compounds is available, with trade names such as Silicone rubber, Buna N, Butyl, Viton, Teflon, and Kel-F. The selection of an O-ring compound and its physical

TABLE 7-5.–*Recommended Design Practice for Diametral-Squeeze-Type O-Ring Seals*

[See fig. 7-15 for explanation of dimensions; all dimensions in inches]

O-ring nominal section diameter	O-ring section diameter	Diametral squeeze, min		C–gland width		D–groove length	R–radius, min	2×E–diametral clearance, max
		Dynamic	Static	[a]Dynamic	[b]Static			
1/16	0.070 ±0.003	0.010	0.015	0.057	0.052	3/32	1/64	0.005
3/32	0.103 ±0.003	.010	.017	.090	.083	9/64	1/64	.005
1/8	0.139 ±0.004	.012	.022	.123	.113	3/16	1/32	.006
3/16	0.210 ±0.005	.017	.032	.188	.173	9/32	3/64	.007
1/4	0.275 ±0.006	.029	.049	.240	.220	3/8	1/16	.008

Fluid pressure	O-ring compound hardness
0-1000 psi	70 Shore "A" Durometer
1000-2000 psi	80 Shore "A" Durometer
2000 psi and higher	90 Shore "A" Durometer

[a]Tolerance = +0.000, -0.001.
[b]Tolerance = +0.000, -0.005.

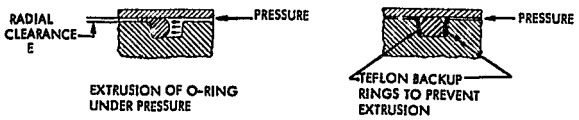

Figure 7-25.–Extrusion of the diametral-squeeze-type O-ring under pressure and the application of backup rings.

properties (furnished by the producer) is based on operating conditions such as type of fluid or propellant, pressure, temperature, and type of seal (dynamic or static).

5. *Installation of diametral-squeeze-type O-ring seals.*–Proper installation of O-rings during component assembly is extremely important to assure an effective seal. Generous chamfers or radii should be provided on all edges and corners in contact with O-rings to minimize the possibility of cutting or scratching during the assembly process.

6. *O-ring seals for valve seats.*–O-rings can be applied effectively as seals for valve seats (fig. 7-26). The resiliency of the O-ring absorbs shock loads and seals tightly at all pressures, even when some dirt and grit are present in the system. One design problem is to prevent the O-ring from being blown out of the groove. This can be prevented by providing a dovetail O-ring groove in a two-piece valve poppet (see fig. 7-26).

Design of Dynamic Seals for Low-Temperature Services

For cryogenic or low-temperature services, lip-type seals made of elastomer sheets (figs. 7-27, 7-28, and 7-29) are used effectively as dynamic seals for moving cylindrical parts and valve seats. This type of seal has been applied successfully at sealing pressures over 2000 psi, and at temperatures as low as −425° F. They are also reasonably effective when sealing low-molecular-weight gases such as helium and hydrogen.

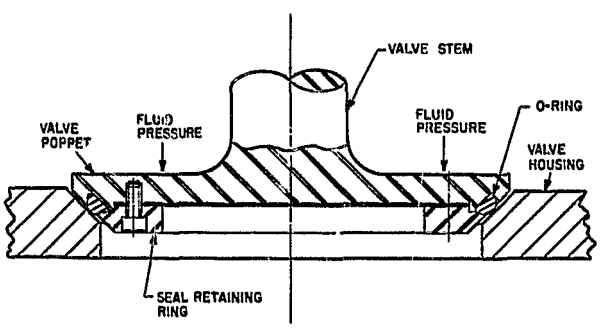

Figure 7-26.–Typical valve seat O-ring seal design for poppet-type valves.

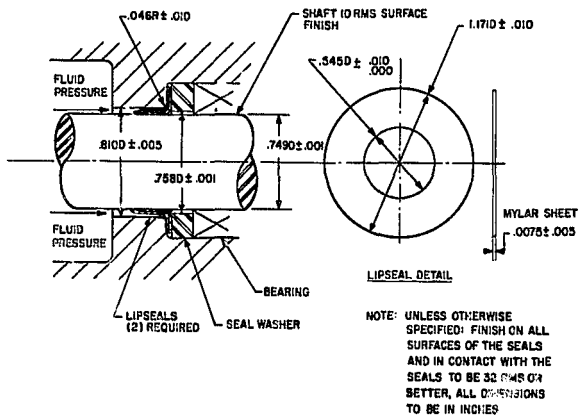

Figure 7-27.–Typical rotating lip-seal design for valve actuator shaft.

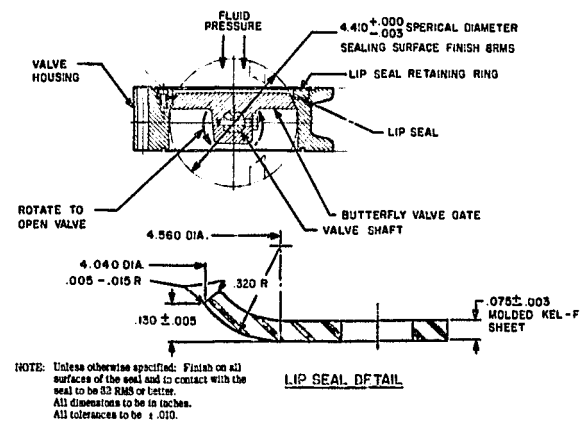

Figure 7-28.–Typical valve seat lip-seal design for butterfly-type valves.

The basic design principle of lip seals is to employ the fluid pressure to increase the contact pressure at the sealing surfaces. Due to their lip configuration, the resilience of these seals is maintained even at very low temperatures. Design considerations for lip seals are similar

to those for O-ring seals. The design approaches can best be illustrated by examples. Figure 7-27 shows a typical valve shaft rotating lip seal arrangement, including dimensions and surface finishes, for liquid oxygen and hydrogen service. Figure 7-28 presents the valve seat lip seal of a butterfly valve for use with the same liquids. Valve seat O-ring seals (fig. 7-26) made of Kel-F have also been successfully applied in poppet-type valves for liquid oxygen. The design of lip seals for piston-type actuators using low-temperature helium gas as the actuating fluid is shown in figure 7-29.

In liquid hydrogen service, metallic bellows (as shown in fig. 7-30) have been used to a great extent to achieve positive dynamic sealing. However, pressure levels and available space impose limitations on their application.

Design of Dynamic Seals for High-Temperature Services

The metallic bellows (fig. 7-30) is most frequently used as reciprocating-type dynamic seals for high-temperature services. Two types of metallic bellows are distinguished: the hydraulic-formed and the multidisk welded type. The former is made of one to three plys of sheet metal and is designed for all pressure ranges. The latter is for relatively low-pressure services and for high flexibility.

A metallic bellows of any type behaves, in part, like a helical spring. The spring rate (lb/in of movement) is a direct function of the

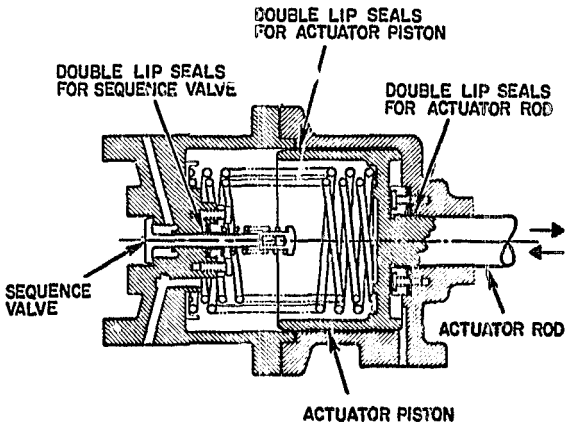

Figure 7-29.–Lip seals for piston-type actuators. Double lip seals seal pressures both ways.

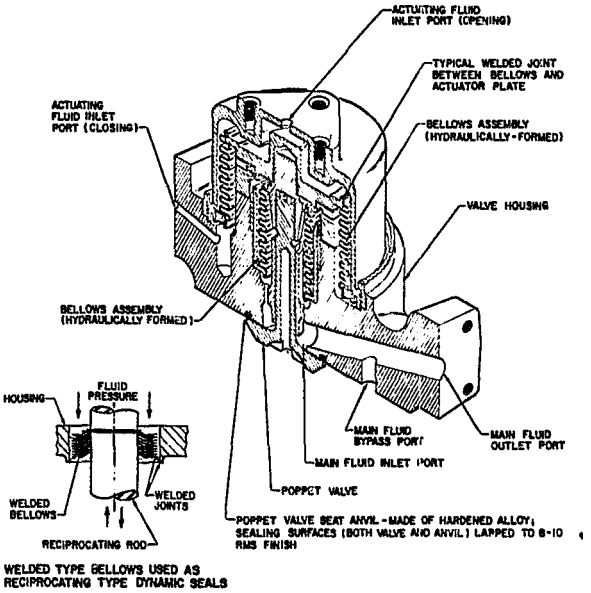

Figure 7-30.–Metallic bellows used as reciprocating-type dynamic seals in a typical poppet valve for high- and low-temperature services.

elastic modulus, and of approximately the square of the thickness of the material. It is also a function of the outside-inside diameters and of the number of convolutions and their curvature. For maximum flexibility (inches of stroke/lb of load), a minimum inside diameter combined with a maximum outside diameter should be used. Also, material thickness (within stress limitations) and modulus of elasticity should be minimum.

Generally, bellows design data, such as stock size, allowable working pressure, spring rate, materials and service temperature, are supplied by the manufacturers. Important design considerations are discussed in the following:

1. *Application of pressure.*–When a bellows is subjected to a differential pressure between interior and exterior, it is preferable to apply the higher pressure to the exterior. This reduces stress, and permits higher pressures and longer life for a given design.

2. *Provision of mechanical stops.*–These should always be provided to prevent extension of the bellows beyond its permissible extended length and compression beyond its "bottomed" height.

Chapter VIII

Design of Propellant Tanks

Liquid propellant rocket engines and the tanks feeding them, together with certain auxiliary systems such as pressurization, form the propulsion system. For reasons set forth in section 1.5, a discussion of tank design is included here. The need for close coordination between engine and tank designer is reemphasized, particularly if they are members of different contractors.

8.1 BASIC DESIGN CONFIGURATIONS OF PROPELLANT TANKS

The configuration of propellant tanks depends largely on vehicle mission and size. In most modern designs, the tanks form an integral part of the vehicle structure. Propellant tanks can be categorized, according to vehicle application, as follows:

(1) Prepackaged storable liquid systems
(2) Booster stage systems
(3) Upper stage systems

Propellant Tanks for Prepackaged Storable Liquid Systems

Figure 8-1 presents the configuration of a typical prepackaged storable liquid propulsion system. The tanks are arranged in tandem, with a common bulkhead between. This system is designed for long storage periods, perhaps 5 to 10 years. A main characteristic of these systems is that the propellants are factory loaded and are hermetically sealed in the tanks by burst diaphragms. Both tank and diaphragm construction materials must be compatible with the propellants for the storage duration. In the example, the propellants are expelled by pressurized gases produced by a solid propellant gas generator. The tank walls form an integral part of the vehicle structure and are designed to withstand the internal pressure loads as well as the vehicle dynamic loads. In some designs the tanks are further stabilized by the internal pressure against buckling; i.e., the walls are always kept under tension loads by a specified pressure level maintained during storage and handling. In smaller units, the walls are usually capable of taking external loads without being pressurized internally. Operational tank pressures for these range from 400 to 2000 psia.

Prepackaged storable liquid systems are usually employed to relatively short-duration, low-thrust applications. Since the tanks form an integral part of the propulsion system, they are designed and furnished by the engine builder. In one design, the thrust chamber is located inside the aft tank and welded directly to the tank bulkhead.

Propellant Tanks for Booster Stage Systems

Figure 8-2 presents the propellant tank design configuration of a typical propulsion system as used in the booster stages of a large launch vehicle such as the Saturn V. The system shown can be used for either storable or cryogenic propellants. The tanks are arranged in tandem; their walls form an integral part of the vehicle structure. For booster application, overall vehicle systems optimization usually dictates use of a turbopump-fed engine system. This permits relatively low operational tank pressures, ranging from 30 to 100 psia.

Since the tanks represent a large percentage of the vehicle structural (inert) weight, advantage is taken of the low-pressure levels by constructing the tanks with extremely thin-wall thicknesses. However, the often huge tank structures thus become sensitive to external buckling loads. To stabilize the tank structures of large booster stage systems, two basic design avenues are open: pressure-stabilization and self-supporting structures. In the pressure-stabilized systems, such as the Atlas ICBM, the

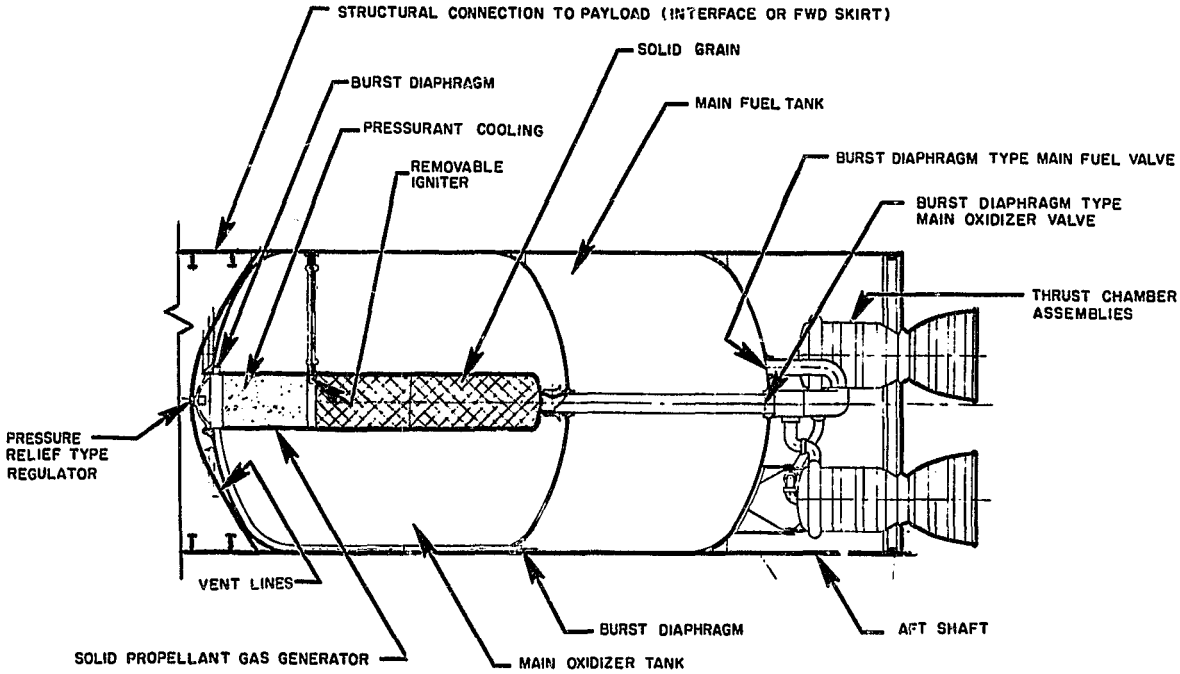

Figure 8-1.–Propellant tank design configuration of a typical prepackaged storable liquid propulsion system.

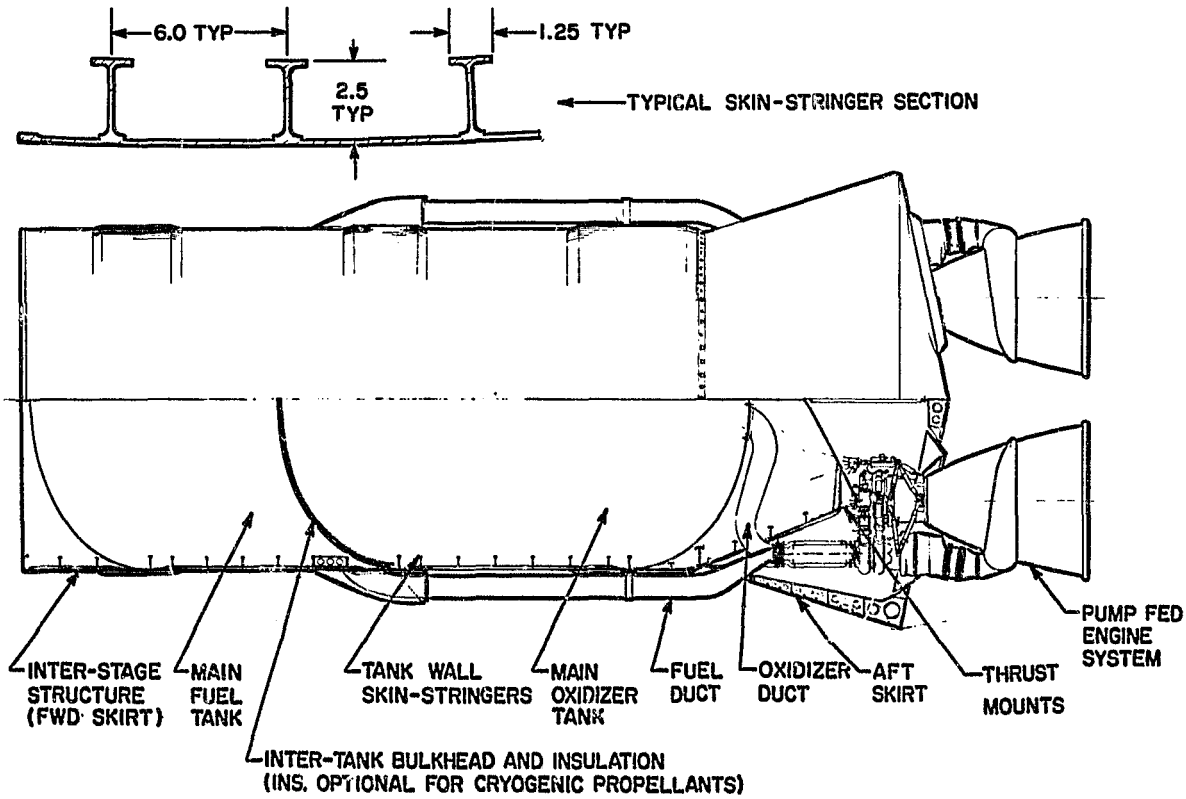

Figure 8-2.–Propellant tank design configuration of a typical booster stage propulsion system.

tank pressures must be constantly maintained above a specified minimum by elaborate controls. This tank structure basically is a thin-wall monocoque, requiring special handling procedures. In most booster-stage systems, the propellant tanks are self-supporting types, the tank walls being reinforced by skin stringers (fig. 8-2), or by other structural means, such as waffle grid patterns.

When cryogenic propellants are used, tank insulation may be required. Insulation is mandatory in liquid hydrogen system to prevent ambient air liquefaction which causes high heat transfer rates with attendant high boiloff rates, and safety hazards.

Propellant Tanks for Upper Stage Systems

Figure 8-3 presents the propellant tank design configuration of a typical pressure-fed, upper stage propulsion system. Here, the tanks are contained within an outer cylindrical shell, through which thrust is transmitted to the payload. The shell is designed to withstand all anticipated boost and flight loads. The propellant tankage consists of two individual units. The main fuel tank is located forward, and the main oxidizer tank near the aft end. The two welded aluminum-alloy tanks are modified spheres, faired into conical sections at the bottom, for propellant discharge. The tanks are bolted to the shell structure around their support ring. The thrust chamber assembly is located just below, and closely coupled to, the oxidizer tank. Thrust is transmitted to the outer shell through the aft half of the oxidizer tank. Both tanks may be insulated independently, for cryogenic propellant service.

Many upper-stage vehicles employ a pressurized gas feed propulsion system. Tank pressures range from 100 to 400 psia. The system shown in figure 8-3 uses stored helium gas for

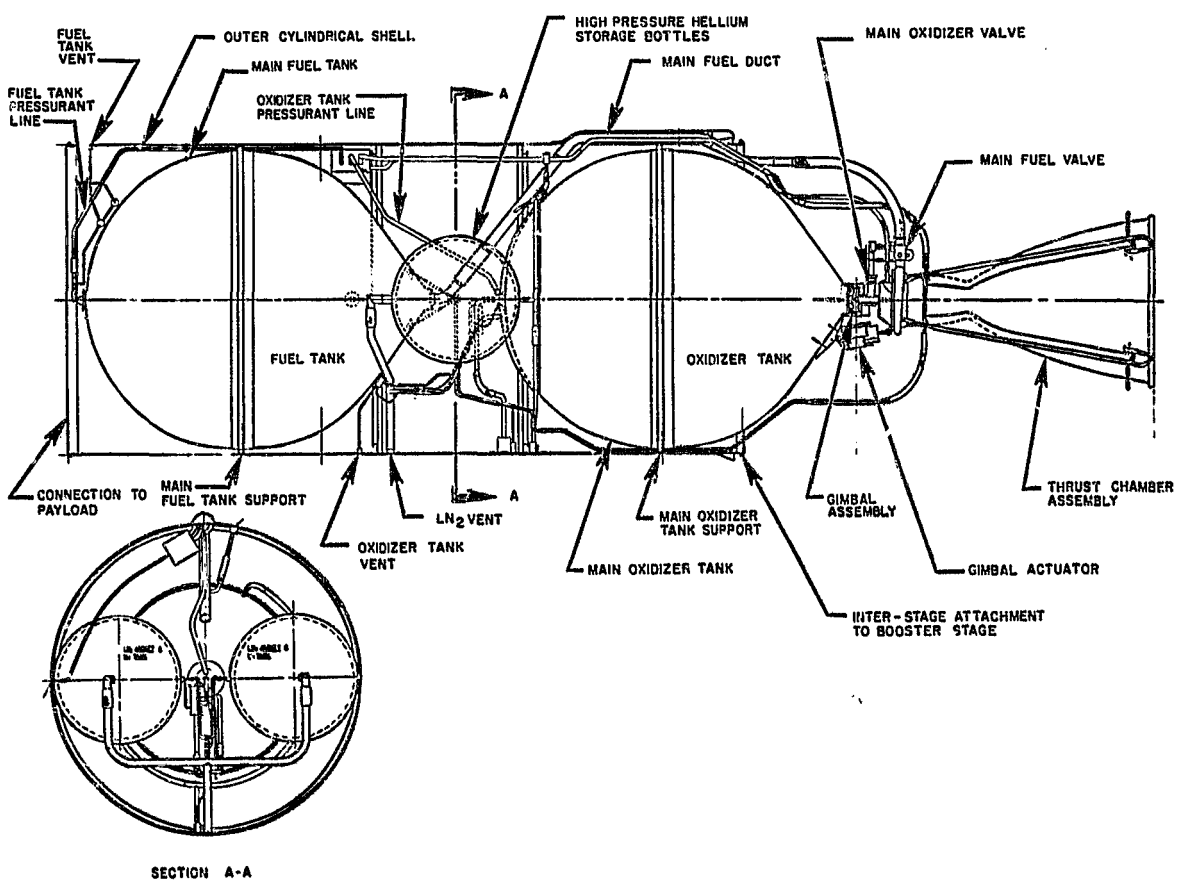

Figure 8-3.—Propellant tank design configuration of a typical upper stage propulsion system.

pressurization. The gas is stored at an initial pressure level from 4500 to 5500 psia at -300° F in two liquid-nitrogen-jacketed, high-pressure spherical bottles located between the two main propellant tanks.

It is for upper stage propulsion systems that the engine designer may most likely also design the tankage. The following discussions, therefore, will confine themselves to these systems. By contrast, the design of booster tanks will probably always be made by an independent group. However, many of the design principles presented here are equally applicable to booster tanks and may thus further the understanding of their design problems.

8.2 GENERAL DESIGN CONSIDERATIONS FOR PROPELLANT TANKS

The tank design is greatly influenced by systems optimization within the overall vehicle design. A principal design objective is for the vehicle to yield the highest payload and/or velocity increment with maximum possible reliability. Design details depend largely upon type of propellants, vehicle mission requirement and configuration, propulsion system design, and available construction materials and fabrication techniques. Some of the most important considerations follow.

Propellant Properties

Propellants affect tank design mainly by their physical and chemical characteristics. The boiling point or storage temperature of a propellant determines the operating temperature range of the tank assembly. Cryogenic propellants cause tank design problems from thermal gradients, from the need for insulation and from the need for construction materials capable of remaining ductile at very low temperatures. The very low density of some propellants, such as liquid hydrogen, requires tanks of considerable volume. The highly corrosive and reactive properties of other propellants severely limit the selection of tank materials.

Shape and Size of Propellant Tanks

Propellant tanks are pressure vessels. Disregarding other factors, the lightest pressure vessel for a given volume is a spherical shell, since it has the smallest surface to volume ratio. It also has the smallest shell stress for a given internal pressure. While a sphere may be the lightest pressure vessel, the combination of several spheres into the generally cylindrical envelope typical for most rocket vehicles would cause a sizable volume penalty. Furthermore, a sphere would preclude the use of the tank wall as a load-carrying member of the vehicle structure (figs. 8-1 and 8-2), resulting in further weight and volume penalties.

Thus both vehicle configuration and tank pressure level will determine the shape of propellant tanks. For vehicles of relatively large length-to-diameter ratios and of limited space envelopes, cylindrically shaped tanks are used. For relatively high tank pressures and less stringent space conditions, spherical tanks may be employed to best advantage (fig. 8-3). The ends of cylindrical tanks can have either spherical or ellipsoidal shapes. The basic cylindrical tank with spherical ends is lighter than one with ellipsoidal ends. However, the overall weight of an ellipsoidally ended tank may be less when the shorter interstage structure required is considered. In some designs the propellant tank aft ends are faired into conical or other special shapes to accommodate the thrust loads from engine assemblies as well as to minimize trapped propellants.

The required size or volume of a propellant tank is the sum of usable propellant volume and other volume requirements:

$$V_t = V + T + B + U \qquad (8\text{-}1)$$

where

V_t = propellant tank design volume, ft^3

V = usable propellant volume calculated from propulsion system requirements, ft^3 (may include a "usable residual" term representing design reserves, mixture ratio shift effects, etc.)

T = trapped propellant volume. This is a function of system design configuration and includes propellants trapped in tank, ducts, thrust chamber cooling jacket, etc., ft^3

B = boiled-off propellant volume (applicable only to cryogenic propellants), ft^3

U = tank ullage volume, ft^3

The calculation of propellant volume is based on the propellant density at specific temperatures. A standard temperature of 68° F is used for storable propellants. Boiling point conditions at ambient pressure are used for the cryogenic propellants. The tank ullage-volume calculations should allow for propellant volume changes due to temperature change of the tanked propellant, and for tank deformation when pressurized. This is especially important for prepackaged storable liquid systems to prevent excessive tank ullage pressures when the system is exposed to a specified upper temperature limit during storage. Adequate ullage volume is also required to maintain tank pressure at starting when the relative ullage volume increase is large and may tax the response of the pressurization system.

Sample Calculation (8-1)

The following data are given for the A-4 stage propulsion system, including two engines:

Oxidizer (N_2O_4) density, 90.12 lb/ft^3
Oxidizer weight flow rates, 12.78 lb/sec/engine
Fuel (N_2H_4) density, 63.17 lb/ft^3
Fuel weight flow rate, 10.65 lb/sec/engine
Nominal engine firing duration at full thrust, 410 sec
Trapped oxidizer volume, $T_o = 0.9$ ft^3
Trapped fuel volume, $T_f = 1.8$ ft^3
Tank ullage volume, $U = 2.5\%$ of propellant volume

Determine the volume of the propellant tanks.

Solution

The required usable oxidizer volume

$$V_o = \frac{12.78 \times 2 \times 410}{90.12} = 116.2 \text{ ft}^3$$

The oxidizer tank ullage volume

$$U_o = (V_o + T_o) \times 0.025 = 117.1 \times 0.025 = 2.9 \text{ ft}^3$$

From equation (8-1), the required design volume of the oxidizer tank

$$V_{to} = V_o + T_o + U_o = 116.2 + 0.9 + 2.9 = 120 \text{ ft}^3$$

The required usable fuel volume

$$V_f = \frac{10.65 \times 2 \times 410}{63.17} = 138.2 \text{ ft}^3$$

The fuel tank ullage volume

$$U_f = (V_f + T_f) \times 0.025 = 140 \times 0.025 = 3.5 \text{ ft}^3$$

From equation (8-1), the required design volume of the fuel tank

$$V_{tf} = V_f + T_f + U_f = 138.2 + 1.8 + 3.5 = 143.5 \text{ ft}^3$$

Propellant Tank Arrangement

In most vehicle systems, the propellant tanks are arranged in tandem. Other arrangements are used for specific design reasons. Figure 8-4

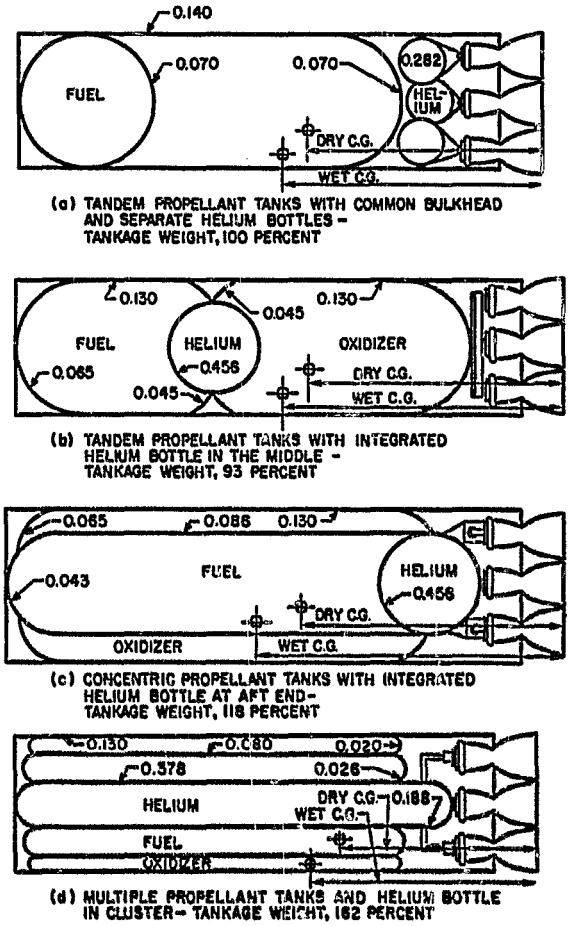

(a) TANDEM PROPELLANT TANKS WITH COMMON BULKHEAD AND SEPARATE HELIUM BOTTLES – TANKAGE WEIGHT, 100 PERCENT

(b) TANDEM PROPELLANT TANKS WITH INTEGRATED HELIUM BOTTLE IN THE MIDDLE – TANKAGE WEIGHT, 93 PERCENT

(c) CONCENTRIC PROPELLANT TANKS WITH INTEGRATED HELIUM BOTTLE AT AFT END – TANKAGE WEIGHT, 118 PERCENT

(d) MULTIPLE PROPELLANT TANKS AND HELIUM BOTTLE IN CLUSTER – TANKAGE WEIGHT, 162 PERCENT

Figure 8-4.–Various propellant tank arrangements of a typical vehicle system.

SP 125

presents various propellant tank configurations for a typical vehicle system using helium for tank pressurization. A design analysis will determine the best solution for a given propellant storage volume and vehicle space envelope. General considerations are:

(1) Minimum overall weight
(2) Maximum storage volume in a given envelope
(3) Least possibility of propellant mixing
(4) Clean aerodynamic vehicle shape
(5) Ease of installation of ducts and lines
(6) Ease of insulation
(7) Ease of fabrication and handling
(8) Minimum trapped (unusable) propellants

Arrangement (a) is taken as standard. Arrangement (b), combining tandem propellant tanks with an integrated helium bottle in between, results in lowest weight; however, it poses design problems in the routing of pneumatic lines and controls. Arrangement (c) with concentric tanks eases the installation of propellant ducts, but has the possibility of simultaneous puncture of both tanks (by bullets or from other causes), and subsequent mixing of the propellants. Arrangement (d) with multiple tanks has the highest weight, but is easier to fabricate and handle especially for very large vehicles.

Working Loads

The propellant tanks are structural members which must be designed to withstand a combination of the following probable working loads:

(1) Internal pressure loads and their dynamic effects
(2) Axial thrust loads and their dynamic effects
(3) Bending moments due to vehicle transverse accelerations, wind loads, and shifting of the center of gravity
(4) Aerodynamic forces
(5) Thrust vector control forces
(6) Vibration loads
(7) Loads produced by mounting arrangement
(8) Loads caused by thermal transients and gradients
(9) Loads produced during ground handling

In most vehicle systems, internal tank pressure loads and axial thrust loads are the principal ones. Other loads require careful evaluation, including model tests or full-size experiments.

Safety Factors for Propellant Tank Designs

The recommended criteria for working loads presented in chapter II (eqs. 2-8 through 2-11) are generally applicable to propellant tank designs. However, when calculating allowable working stresses from tank internal pressure, the following correlations are recommended for various situations:

(1) No hazard to personnel or vital equipment:

$$S_w = F_y \tag{8-2}$$

or

$$S_w = \frac{F_u}{1.25} \tag{8-3}$$

(2) Special safety devices are provided for personnel (example: the booster for a manned upper stage which has an ejection device with an exceptionally high degree of reliability):

$$S_w = \frac{F_y}{1.1} \tag{8-4}$$

or

$$S_w = \frac{F_u}{1.35} \tag{8-5}$$

(3) Hazard to personnel or vital equipment:

$$S_w = \frac{F_y}{1.33} \tag{8-6}$$

or

$$S_w = \frac{F_u}{1.65} \tag{8-7}$$

where

S_w = maximum allowable working stress, psi; i.e., the stress due to maximum tank working pressure under normal transient and steady operating conditions

F_y = yield strength, psi, of the tank construction material, at operating temperature conditions

F_u = ultimate strength, psi, of the tank construction material under operating temperature conditions

S_w is calculated for both F_y and F_u. The lower value should then be used. All propellant tanks are subjected to hydrostatic pressure tests prior to acceptance. For case (1), the proof test pressure equals maximum tank working pressure.

SP125

For case (2) and (3), the proof test pressures should be 110 percent of the maximum tank working pressure. For high-pressure inert gas, long-duration storage bottles, the following correlations are recommended:

No hazard to personnel:

$$S_w = \frac{F_y}{1.33} \qquad (8\text{-}8)$$

Hazard to personnel:

$$S_w = \frac{F_y}{1.67} \qquad (8\text{-}9)$$

Sample Calculation (8-2)

The start transient of a prepackaged storable liquid propulsion system for an aircraft-launched missile is programed not to reach main-stage level until the missile is at a specific distance from the aircraft.

Calculate the maximum allowable working stresses for the propellant tanks, if they are made of–

(a) Aluminum alloy 6061-T6, $F_y = 35\,000$ psi, $F_u = 45\,000$ psi

(b) Aluminum alloy 6066-T6, $F_y = 50\,000$ psi, $F_u = 57\,000$ psi

Solution

(a) *Tank made of aluminum alloy 6061-T6.*– Since the system involves personnel safety during start transient, equations (8-6) and (8-7) will be applied.

$$S_w = \frac{F_y}{1.33} = \frac{35\,000}{1.33} = 26\,300 \text{ psi}$$

or

$$S_w = \frac{F_u}{1.65} = \frac{45\,000}{1.65} = 27\,260 \text{ psi}$$

Thus, the maximum allowable working stress during start transient = 26 300 psi.

During mainstage operation, personnel are considered safe and equations (8-4) and (8-5) can be used:

$$S_w = \frac{F_y}{1.1} = \frac{35\,000}{1.1} = 31\,800 \text{ psi}$$

or

$$S_w = \frac{F_u}{1.35} = \frac{45\,000}{1.35} = 33\,360 \text{ psi}$$

The maximum allowable working stress for mainstage = 31 800 psi.

(b) *Tank made of aluminum alloy 6066-T6.*– During start transient

$$S_w = \frac{F_y}{1.33} = \frac{50\,000}{1.33} = 37\,600 \text{ psi}$$

or

$$S_w = \frac{F_u}{1.33} = \frac{57\,000}{1.65} = 34\,560 \text{ psi}$$

The maximum allowable working stress during start transient = 34 560 psi.

During mainstage operation

$$S_w = \frac{F_y}{1.1} = \frac{50\,000}{1.1} = 45\,400 \text{ psi}$$

or

$$S_w = \frac{F_u}{1.35} = \frac{57\,000}{1.35} = 42\,200 \text{ psi}$$

The maximum allowable working stress during mainstage = 42 200 psi.

Material and Fabrication Considerations in Propellant Tank Design

In addition to considerations of propellant compatibility and operational temperature ranges, selection of construction materials for propellant tanks is based on their strength-to-density ratio at a given temperature and on their ductility. For a given working pressure, the lightest tank structure will be the one made of the material with the highest ratio of ultimate strength to density. Most frequently used construction materials for propellant tanks are:

(1) Aluminum alloys, such as 6061-T6, 6066-T6, and 2014-T6. Room temperature properties: Average density $\rho = 0.1$ lb/in^3, F_y up to 60 000 psi, F_u up to 70 000 psi, $F_u/\rho = 70 \times 10^4$

(2) Stainless steels, such as AISI 347 (for low-pressure tanks only), 17-7 PH and PH 15-7 Mo. Room temperature properties: Average density $\rho = 0.285$ lb/in^3, F_y up to 200 000 psi. F_u up to 220 000 psi. $F_u/\rho = 77.2 \times 10^4$

(3) Fiber glass, filament wound with an aluminum-alloy liner. Room temperature properties (fiber glass only): Average density $\rho = 0.08$ lb/in^3, $F_u = 120\,000$ psi. $F_u/\rho = 150 \times 10^4$

Aluminum alloys are compatible with most storable and cryogenic propellants, and may be used for working temperatures up to 350° F. Stainless steels are suitable for storable (limited duration) and cryogenic propellants, and are suitable for higher temperatures (800° F maximum). Fiber glass is limited to moderate temperature conditions (−60° to 160° F).

Fabrication methods for propellant tanks depend largely upon the type of material used. Most important considerations for tank fabrication are dimension control, heat treating, and welding. The lowest recommended wall-stock size for propellant tanks is about 0.010 inch for stainless steels and 0.020 for aluminum alloys. While tank stress calculations must consider the lower limit of wall-thickness variation, the upper limit is used for tank-weight calculation. The strength of a metal may fall into a band, too, the width of which depends on the heat-treating process. Stress calculation will be based on the minimum expected strength. The quality of the welding process or the efficiency of a welded joint may require extra stock added to the wall thickness as calculated from other working stresses. An assumed weld efficiency of 85 to 95 percent is a reasonable value for steels (50 to 65 percent for aluminum). To minimize weight penalties, build-up lands may be used at the welds (fig. 8-9) for an equivalent 100 percent weld efficiency. Figure 8-5 presents the construction of a welded propellant tank. Note the segmented tank end which is typical for large-size tanks.

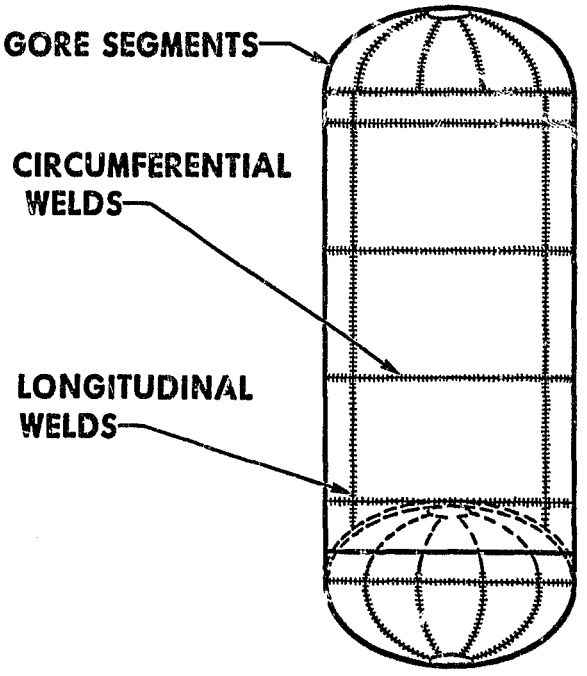

Figure 8-5.—Typical welded propellant tank construction. S P 1 2 5

Other Propellant Tank Design Problems

Many other design and analysis problems will have to be carefully considered before a successful propellant tankage can be produced. The relatively thin, highly stressed shells make it difficult to attach concentrated loads. The loads must be spread out in a suitable way to prevent localized overstresses. Cryogenic propellants may create thermal transient and gradient problems. While the empty portion of a tank may be subject to aerodynamic heating, the filled portion may be at a very low temperature. Additional thermal problems may arise in outer space, from solar heating of one tank side and radiation cooling of the other.

Also partly the tank designer's responsibility is the solution of certain problems associated with the management of the propellants within the tanks, such as:

(1) Uniform dispersion of the entering tank pressurant
(2) Sensing of propellant quantities (PU)
(3) Prevention of propellant sloshing
(4) Expulsion of the propellants under adverse conditions
(5) Fill, drain, vent and pressure relief of the propellant tanks

8.3 STRUCTURAL DESIGN OF PROPELLANT TANKS

As a rule, the wall thickness of propellant tanks is first calculated from stresses caused by internal pressure loads and discontinuities. Then the design is checked for other loads. If the wall thickness of a pressure vessel is small compared to the radii of wall curvature ($t/r \leq 1/15$),

and offers no resistance to bending, the wall is subjected only to direct or hoop-membrane stresses, assumed to be uniformly distributed over the thickness. However, if any discontinuity is present along the wall, such as an abrupt change in radius of curvature or wall thickness, discontinuity and bending stresses are added. At a sufficient distance from the juncture between tank ends (sphere or ellipsoid) and cylindrical shell (where interaction does not occur), the maximum stress in the tank wall due to internal pressure is calculated using the hoop-membrane stress formula only.

Figure 8-6 identifies the major tank elements. In an optimum tank design, the wall thickness varies according to a combination of local membrane, bending, and discontinuity stresses. This is especially true for the spherical and ellipsoidal tank ends. The structural calculation methods for volume, wall thickness, wall surface area, and weight of various tank shapes will now be discussed. The following general terminology is used:

p_t = maximum tank working pressure, psig
S_w = maximum allowable working stress of the tank construction material, psi
ρ = density of the tank construction material, lb/in^3
E = modulus of elasticity, psi
ν = Poisson's ratio
e_w = weld efficiency

Spherical Tanks

(1) Volume, in^3:

$$V_S = \frac{4\pi a^3}{3} \tag{8-10}$$

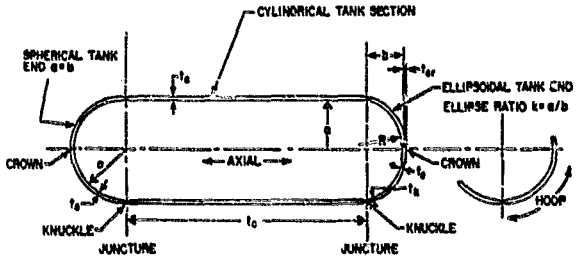

Figure 8-6.—Nomenclature of principal tank elements.

where a = nominal radius of the tank, in

(2) Wall thickness, in, required to withstand membrane stresses from internal tank pressure:

$$t_S = \frac{p_t a}{2 S_w e_w} \tag{8-11}$$

(3) Wall surface area, in^2:

$$A_S = 4\pi a^2 \tag{8-12}$$

(4) Weight, lb:

$$W_S = 4\pi a^2 t_S \rho \tag{8-13}$$

(5) Critical pressure due to external loading, psi. When the external pressure is higher than the internal tank pressure, the pressure differential across the tank wall may cause the tank to buckle.

$$p_{cr} = \frac{2Et_S^2}{a^2}\sqrt{3(1-\nu^2)} \tag{8-14}$$

Ellipsoidal and Spherical Tank Ends (fig. 8-6)

Note that the spherical end is a special case of ellipsoidal end, in which the major half-diameter, a, equals the minor half-diameter, b.

(1) Volume:

Ellipsoidal tank end volume, in^3:

$$V_e = \frac{2\pi a^2 b}{3} \tag{8-15}$$

Spherical tank end volume, in^3:

$$V_S = \frac{2\pi a^3}{3} \tag{8-16}$$

where

a = elliptical tank end major half-diameter, in
= radius of the cylindrical tank section
b = elliptical tank end minor half-diameter, in

(2) Wall thicknesses considering combined membrane, discontinuity, and local bending stresses caused by internal tank pressure p_t. An equivalent wall thickness, which is an average value of knuckle-and-crown thickness, may be

used to calculate the weight of the tank ends.

$$t_k = \frac{K p_t a}{S_w e_w} \tag{8-17}$$

$$t_{cr} = \frac{p_t R}{2 S_w e_w} \tag{8-18}$$

$$t_e = \frac{(t_k + t_{cr})}{2} = \frac{p_t a \left(K + \frac{k}{2}\right)}{2 S_w} \tag{8-19}$$

$$t_S = \frac{p_t a (K + \frac{1}{2})}{2 S_w} \tag{8-20}$$

$$\frac{t_e}{t_S} = \frac{\left(K + \frac{k}{2}\right)}{(K + \frac{1}{2})} \tag{8-21}$$

$$\frac{t_e}{t_c} = \frac{\left(K + \frac{k}{2}\right)}{2} \tag{8-22}$$

where

k = tank end ellipse ratio = a/b; $k = 1$ for a spherical end

R = tank end crown radius, in = ka; $R = a$ for a spherical end

K = stress factor, a function of the ellipse ratio k. Figure 8-7 presents a K versus k curve for combined membrane, discontinuity, and local bending stresses

t_k = wall thickness at the knuckle, in

t_{cr} = wall thickness at the crown, in

t_e = equivalent wall thickness of an ellipsoidal tank end, in

t_S = equivalent wall thickness of a spherical tank end, in

t_c = wall thickness of a cylindrical tank section, in

(3) Wall surface area:

Ellipsoidal tank end surface area, in^2:

$$A_e = a^2 + \frac{\pi b^2 \ln\left[\frac{(1+e)}{(1-e)}\right]}{2e} \tag{8-23}$$

Spherical tank end surface area, in^2:

$$A_S = 2\pi a^2 \tag{8-24}$$

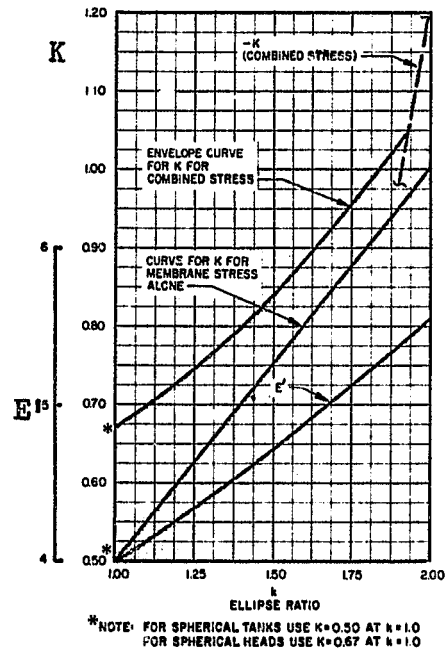

Figure 8-7.—Ellipse ratio k versus knuckle stress factor K, compression stress -K, and parameter E'. (From ARS paper, "Design Criteria and Analyses for Thin-Walled Pressurized Vessels and Interstage Structures," by T. J. Hart.)

where

e = eccentricity = $\frac{\sqrt{a^2 - b^2}}{a} = \sqrt{1 - \frac{1}{k^2}}$

(4) Weight:

Ellipsoidal tank end weight, lb:

$$W_e = \frac{\pi a^2 t_e E' \rho}{2k} \tag{8-25}$$

Spherical tank end weight, lb:

$$W_S = 2\pi a^2 t_S \rho \tag{8-26}$$

where

E' = design factor = $2k + \frac{1}{\sqrt{k^2 - 1}} \ln \frac{k + \sqrt{k^2 - 1}}{k - \sqrt{k^2 - 1}}$ (see fig. 8-7)

(5) Critical pressure due to external loading, psi:

For an ellipsoidal tank end, it may be approximated as

$$p_{cre} = \frac{C_b 2 E t_e^2}{R^2} \qquad (8\text{-}27)$$

For a spherical tank end

$$p_{crs} = \frac{0.342\, E t_s^2}{a^2} \text{ (approximately)} \qquad (8\text{-}28)$$

where

C_b = buckling coefficient, a function of R/t_e, ranging from 0.05 to 0.10

Cylindrical Tank Section

(1) Volume, in^3:

$$V_c = \pi a^2 l_c \qquad (8\text{-}29)$$

where

a = radius, in

l_c = length, in

(2) Wall thickness, in, required to withstand membrane stresses due to internal tank pressure:

$$t_c = \frac{p_t a}{S_w e_w} \qquad (8\text{-}30)$$

(3) *Discontinuity stresses.*—The discontinuity at the juncture between the cylindrical tank section and the tank ends will cause bending and shear loads along the cylindrical circumference at the juncture, and the adjacent areas. These discontinuity stresses are superimposed upon the membrane stresses and comprise: (a) axial bending stress; (b) hoop bending stress; (c) additional hoop stress due to the shear load; (d) shear stress. Discontinuity stresses fade out rapidly, so that they become negligibly small a short distance from the juncture. Detail analyses of discontinuity stresses can be found in standard textbooks. In general, buildup of wall thickness of less than $0.5\, t_c$, near the juncture, will suffice for most designs, with only small weight penalty.

(4) Wall surface area, in^2:

$$A_c = 2\pi a l_c \qquad (8\text{-}31)$$

(5) Weight, lb:

$$W_c = 2\pi a l_c t_c \rho \qquad (8\text{-}32)$$

(6) External loading critical pressure, psi:

For a short tank (i.e., $l_c < 4.9\, a\sqrt{a/t_c}$):

$$p_{crc} = 0.807 \frac{E t_c^2}{l_c a} \sqrt[4]{\left(\frac{1}{1-\nu^2}\right)^3 \frac{t_c^2}{a^2}} \qquad (8\text{-}33)$$

For long tanks (i.e., $l_c \geq 4.9\, a\sqrt{a/t_c}$):

$$p_{crc} = \frac{E t_c^3}{4(1-\nu^2) a^3} \qquad (8\text{-}34)$$

where E = modulus of elasticity.

Sample Calculation (8-3)

The following design data are specified for the A-4 stage propulsion system, which employs a cylindrical propellant tank section with ellipsoidal ends (preliminary layout shown in fig. 3-10).

Required design volume of the oxidizer tank, $V_{to} = 120$ ft^3

Maximum oxidizer tank working pressure, $p_{to} = 180$ psia

Required design volume of the fuel tank, $V_{tf} = 143.5$ ft^3

Maximum fuel tank working pressure, $p_{tf} = 170$ psia

Internal radius of the cylindrical tank section, $a = 41$ in

Tank construction material, aluminum alloy 6066-T6: $F_y = 50\,000$ psi; $F_u = 57\,000$ psi; $\rho = 0.101$ lb/in^3; $E = 10.4 \times 10^6$ psi; $\nu = 0.36$

Weld efficiency, $e_w = 100$ percent.

Determine the following:

(a) Required internal tank dimensions

(b) Required thickness of the tank walls at various sections, considering internal pressure loads, discontinuity, and local bending stresses

(c) Approximate weight of the tankage

(d) Critical external loading pressures, using a buckling coefficient, $C_b = 0.10$ for the tank ends

Solution

(a) Since the oxidizer tank consists of two ellipsoidal ends without a cylindrical section, equation (8-15) may be applied:

$$V_{to}=\frac{2\times 2\pi a^2 b}{3}$$

We rearrange to obtain the minor elliptical half-diameter of the tank ends:

$$b=\frac{3\times V_{to}}{2\times 2\pi a^2}=\frac{3\times 120\times 1728}{4\times\pi\times(41)^2}=29.4 \text{ in}$$

The tank end ellipse ratio:

$$k=\frac{a}{b}=\frac{41}{29.4}=1.395$$

Since we use an ellipsoidal end of the same proportion at the fuel tank top, the fuel tank volume may be treated as the volume of a cylindrical tank section with the length l_c. From equation (8-29), the volume of the fuel tank:

$$V_{tf}=\pi a^2 l_c$$

$$l_c=\frac{V_{tf}}{\pi a^2}=\frac{143.5\times 1728}{\pi\times(41)^2}=46.9 \text{ in}$$

To summarize the internal dimensions of the tankage:

$$a=41 \text{ in},\quad b=29.4 \text{ in},\quad k=1.395,\quad l_c=46.9 \text{ in}$$

(b) We assume that certain missions of the A-4 vehicle require it to be man rated. From equations (8-6) and (8-7), the maximum allowable working stresses are derived:

$$S_w=\frac{F_y}{1.33}=\frac{50\,000}{1.33}=37\,600 \text{ psi}$$

$$S_w=\frac{F_u}{1.65}=\frac{57\,000}{1.65}=34\,560 \text{ psi}$$

We use the lower value of 34 560 psi.

From figure 8-6, the tank end stress factor K of the combined stresses is 0.80 for an ellipse ratio k of 1.395. From equation (8-17), the required wall thickness at the knuckle of the oxidizer tank end

$$t_{ko}=\frac{Kp_{to}a}{S_w}=\frac{0.80\times 180\times 41}{34\,560}=0.171 \text{ in}$$

From equation (8-18), the required wall thickness at the crown of the oxidizer tank end

$$t_{cro}=\frac{p_{to}R}{2S_w}=\frac{180\times 1.395\times 41}{2\times 34\,560}=0.149 \text{ in}$$

From equation (8-19), the equivalent wall thickness of the oxidizer tank end

$$t_{eo}=\frac{(t_{ko}+t_{cro})}{2}=\frac{(0.171+0.149)}{2}=0.16 \text{ in}$$

NOTE: In some designs, weight has been saved by taking advantage of the fact that the bulkhead common to both tanks is subject to a relatively small differential pressure in operation. Such systems, however, require more elaborate pressurization and loading systems including interlocks. In case of malfunction, the common bulkhead may suffer serious damage.

The required wall thickness at the knuckle of the fuel tank end:

$$t_{kf}=\frac{t_{ko}p_{tf}}{p_{to}}=\frac{0.171\times 170}{180}=0.162 \text{ in}$$

The required wall thickness at the crown of the fuel tank end:

$$t_{crf}=\frac{t_{cro}p_{tf}}{p_{to}}=\frac{0.149\times 170}{180}=0.141 \text{ in}$$

The equivalent wall thickness of the fuel tank end:

$$t_{ef}=\frac{(t_{kf}+t_{crf})}{2}=\frac{(0.162+0.141)}{2}=0.152$$

From equation (8-30), the required wall thickness of the cylindrical tank section:

$$t_c=\frac{p_{tf}a}{S_w}=\frac{170\times 41}{34\,560}=0.202 \text{ in}$$

Provide a buildup of $0.4\,t_c$ on the cylindrical tank section wall near the juncture to allow for discontinuity stresses:

$t_{cj} = t_c + 0.4\,t = 0.202 + 0.4 \times 0.202 = 0.283$ in

To summarize:

$t_{ko} = 0.171$ in, $t_{cro} = 0.149$ in, $t_{eo} = 0.16$ in
$t_{kf} = 0.162$ in, $t_{crf} = 0.141$, $t_{ef} = 0.152$ in
$t_c = 0.202$ in, $t_{cj} = 0.283$ in

(c) From equation (8-25), the weight of the oxidizer tank end:

$$W_{eo} = \frac{\pi a^2 t_{eo} E' \rho}{2k}$$

From figure 8-7, E' is 4.56, for $k = 1.395$:

$$W_{eo} = \frac{\pi(41)^2 \times 0.16 \times 4.56 \times 0.101}{2 \times 1.395} = 139.5 \text{ lb}$$

The weight of the fuel tank end:

$$W_{ef} = \frac{W_{eo} t_{ef}}{t_{eo}} = \frac{139.5 \times 0.152}{0.16} = 132.8 \text{ lb}$$

From equation (8-32), the weight of the cylindrical tank section:

$$W_c = 2\pi a l_c t_c \rho = 2 \times 41 \times 46.9 \times 0.202 \times 0.101 = 246.4 \text{ lb}$$

Add 4 percent of overall tankage weight for local wall thickness buildups, to allow for welded joints, discontinuity stresses, etc., and for tolerances during fabrication.

Approximate overall weight of the tankage (less accessories):

$$W_t = 1.04(2 \times W_{eo} + W_{ef} + W_c)$$
$$= 1.04(2 \times 139.5 + 132.8 + 246.4) = 685 \text{ lb}$$

(d) From equation (8-27), the critical external loading pressure for the oxidizer ends

$$p_{ereo} = \frac{C_b 2 E t_{eo}^2}{R^2} = \frac{0.10 \times 2 \times 10.4 \times 10^6 \times (0.16)^2}{(1.395 \times 41)^2}$$
$$= 16.3 \text{ psi}$$

The critical external loading pressure for the fuel tank end:

$$p_{eref} = \frac{C_b 2 E t_{ef}^2}{R^2} = \frac{0.10 \times 2 \times 10.4 \times 10^6 \times (0.152)^2}{(1.395 \times 41)^2}$$
$$= 14.7 \text{ psi}$$

We find that $l_c < 4.9a\sqrt{a/t_c}$. Thus equation (8-33) applies, yielding an external loading critical pressure for the cylindrical tank section

$$p_{erc} = \frac{0.807 \times 10.4 \times 10^6 \times (0.202)^2}{46.9 \times 41} \times \sqrt[4]{\left(\frac{1}{1-(0.36)^2}\right)^3 \left(\frac{0.202}{41}\right)^2}$$
$$= 13.9 \text{ psi}$$

Axial Compressive Loading on the Cylindrical Tank Section

In integrated propellant tank designs (figs. 8-2 and 8-3), the cylindrical tank section must withstand large axial compressive loads during vehicle handling and operation. If the tank is not pressurized, i.e., if tank pressure = ambient pressure, the critical axial compressive stress for an unstiffened cylindrical tank may be calculated as

$$S_c = \left[9\left(\frac{t_c}{a}\right)^{1.6} + 0.16\left(\frac{t_c}{l_c}\right)^{1.3}\right] E \qquad (8\text{-}35)$$

where S_c = critical axial compressive stress, psi. This is the axial compressive stress that will cause the tank to buckle

One method of increasing the axial load-carrying ability of a cylindrical tank section with minimum weight penalty is to pressurize the tank. This is known as pressure stabilization. Internal pressure will raise the critical buckling stress of a tank; or it may be used to counterbalance an axial compressive load F_a, lb, where

$$F_a = \pi a^2 p_t \qquad (8\text{-}36)$$

Pressurization will also reduce tank failures from very large bending loads. However, if the pressure is ever permitted to drop below a value necessary to carry the axial and bending loads, the tank will collapse and the vehicle will probably be damaged beyond repair.

An alternative method of increasing the external load-carrying ability of a cylindrical tank is to make it self-supporting. This involves stiffening the cylindrical skin by means of longitudinal and circumferential members, or honeycomb structures. The members may be either separate stiffeners welded to the tank wall, or may be made integral with the wall by machining or chemically milling a thicker sheet.

Sample Calculation (8-4)

For the A-4 stage tankage, calculate:

(a) Critical axial compressive load of the cylindrical tank section with no internal pressure.

(b) Required internal tank pressure to offset an axial compressive load of 100 000 pounds with no compressive stress on the cylindrical tank section.

Solution

(a) From equation (8-35), the critical compressive stress of the cylindrical tank section:

$$S_c = \left[9\left(\frac{0.202}{41}\right)^{1.6} + 0.16\left(\frac{0.202}{46.9}\right)^{.3}\right] \times 10.4 \times 10^6$$

$$= 20\,360 \text{ psi}$$

The critical axial compressive load of the cylindrical tank section:

$$F_c = S_c \times 2\pi a t_c = 20\,360 \times 2\pi \times 41 \times 0.202$$

$$= 1\,060\,000 \text{ lb}$$

From the results it is obvious that the A-4 stage tankage is capable of withstanding a substantial axial compressive load without internal pressurization.

(b) From equation (8-36), the required internal tank pressure:

$$p_t = \frac{F_a}{\pi a^2} = \frac{100\,000}{\pi \times (41)^2} = 18.95 \text{ psi}$$

Water Hammer Effects Due to Impact

When a loaded propellant tank is subject to an impact force, a water-hammer effect occurs within the tank. This effect produces a surge of the tank internal pressure. For very short impacting times (less than 1.2×10^{-3} sec), the following correlations are established for cylindrically shaped propellant tanks:

$$p_S = \frac{c\dot{w}}{\pi a^2 g} \tag{8-37}$$

$$c = \frac{c'}{\sqrt{1 + \left[\dfrac{2.5\,E_p a(1 - 0.8\,\nu)}{E t_c}\right]}} \tag{8-38}$$

where

p_S = pressure surge due to the impact, psi
$\dot{w}$ = equivalent flow rate of the propellant due to the impact, lb/sec
a = radius of the cylindrical tank, in
t_c = wall thickness of the cylindrical tank, in
g = gravitational constant, 32.2 ft/sec^2
c = acoustic velocity of the restrained propellant, in/sec
c' = free acoustic velocity of the propellant, in/sec
E_p = compressive modulus of elasticity of the propellant, psi
E = modulus of elasticity of the tank construction material, psi
ν = Poisson's ratio of the tank construction material

In many prepackaged liquid applications, the propellant tankage is required to withstand certain impact loads, as specified by the height of the drop tests. The details of estimating tank pressure surges from a free-fall impact are illustrated by sample calculation (8-5).

Sample Calculation (8-5)

The following data are given for the cylindrical fuel tank of a prepackaged storable liquid propulsion system:

Fuel, N_2H_4
Fuel density, $\rho_p = 63.17$ lb/ft^3
Compressive modulus of elasticity of the fuel, $E_p = 6.06 \times 10^5$
Free acoustic velocity of the fuel, $c' = 80\,100$ in/sec
Tank construction material, aluminum alloy 6066-T6
Modulus of elasticity of the tank construction material, $E = 10.4 \times 10^6$

Poisson's ratio of the tank construction material, $v = 0.36$
Radius of the cylindrical tank, $a = 4$ in
Length of the cylindrical tank, $l_c = 50$ in
Wall thickness of the cylindrical tank, $t_c = 0.167$ in
For a tank falling in direction of its longitudinal axis, estimate:
(a) Tank pressure surge due to the impact after a 6-foot free drop
(b) Tank pressure surge due to the impact after a 20-foot free drop

Solution

(a) For a 6-foot free drop the final velocity at impact:

$$V = \sqrt{2gh} = \sqrt{2 \times 32.2 \times 6} = 19.65 \text{ fps}$$

This yields an equivalent propellant flow rate due to impact of

$$\dot{w} = \rho_p \pi a^2 V = 63.17 \times \pi \times \left(\frac{4}{12}\right)^2 \times 19.65 = 434.5 \text{ lb/sec}$$

From equation (8-38), the acoustic velocity of the restrained fuel

$$c = \frac{80\,100}{\sqrt{1 + \left[\dfrac{2.5 \times 6.06 \times 10^5 \times 4(1 - 0.8 \times 0.36)}{10.4 \times 10^6 \times 0.167}\right]}}$$

$$= 43\,100 \text{ in/sec}$$

Impact time delay in the tank:

$$\frac{l_c}{c} = \frac{50}{43\,100} = 1.16 \times 10^{-3} \text{ sec (i.e., } < 1.2 \times 10^{-3} \text{ sec)}$$

Using equation (8-37), we obtain the tank pressure surge due to impact after a 6-foot free drop:

$$p_S = \frac{c\dot{w}}{\pi a^2 g} = \frac{43\,100 \times 434.5}{\pi \times (4)^2 \times 386} = 964 \text{ psi}$$

(b) After a 20-foot free drop, the final velocity at impact is

$$V = \sqrt{2gh} = \sqrt{2 \times 32.2 \times 20} = 35.9 \text{ fps}$$

The equivalent propellant flow rate due to impact:

$$\dot{w} = \rho_p \pi a^2 V = 63.25 \times \pi \times \left(\frac{4}{12}\right)^2 \times 35.9 = 792.5 \text{ lb/sec}$$

The tank pressure surge due to impact after a 20-foot free drop:

$$p_S = \frac{c\dot{w}}{\pi a^2 g} = \frac{43\,100 \times 792.5}{\pi \times (4)^2 \times 386} = 1765 \text{ psi}$$

8.4 DESIGN OF STORABLE LIQUID PROPELLANT TANKS

The design of tanks for storable liquid propellants uses the same general design practices applied to other propellant tanks, except in the area of compatibility. Most storable propellants will remain stable for long periods of time if stored in tanks constructed of materials compatible with the propellants. To minimize propellant decomposition and tank material corrosion, the surface of tank walls in contact with the propellants must be smooth and clean.

Tank Material Compatibility

Prior to final selection, a detail study is required to determine the compatibility of potential tank construction materials with the propellant combination involved. In this study, two major considerations should be kept in mind: (1) the expected storage life of the propulsion system, and (2) the credibility of the available data. For a required storage period of less than 3 years, the compatibility data for many materials with various propellants are generally reliable. However, for longer periods, such as a 10-year storage requirement, the design data are usually extrapolated from the results of relatively short-term testing. Figure 8-8 illustrates the typical extrapolated corrosion and passivity rate of aluminum alloy 6066-T6 exposed to the liquid phase of inhibited red fuming nitric acid (IRFNA).

Much of the available compatibility test data tend to contradict each other. This is the result of differing test methods, conditions, and criteria. It involves the risk that although a material may be acceptable for a relatively short exposure, it may fail when the exposure time to a particular

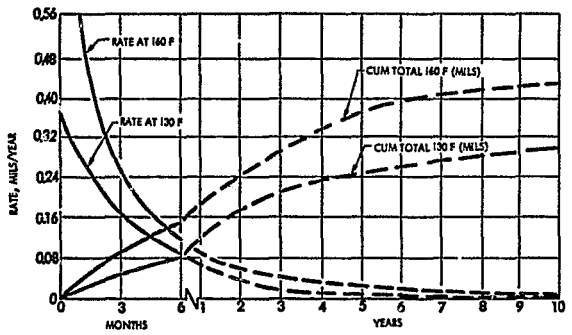

Figure 8-8.–Typical extrapolated corrosion and passivity rate of aluminum alloy 6066-T6 exposed to the liquid phase of IRFNA.

environment is increased. Whenever a discrepancy of material compatibility is observed, thorough verification of the test conditions is indicated. For most of the long-term storable propellant tankage, the aluminum alloys are used for best results. Austenitic and semiaustenitic stainless steels should be used only for rather short-term storage.

Tank Construction

One of the prime design objectives of storable propellant tankage is the elimination of maintenance during storage and prefiring activities. This may be accomplished by an all-welded, hermetically sealed construction. To achieve hermetic sealing, leakproof burst diaphragms are installed throughout the inlets and outlets of the tankage. Propellant fill ports are welded shut after tanking. Tandem tanks are favored over concentric tanks, since propellants are more positively separated during storage, transportation, and other adverse conditions. In some applications, the common bulkhead between two propellant tanks is designed to withstand a differential pressure in either direction that may result from inconsistent burst diaphragms. However, the burst diaphragm at the pressurant inlet to the oxidizer tank of the A-4 system is designed to a lower burst pressure than that of the pressurant inlet diaphragm for the fuel tank. This insures that the oxidizer tank pressure is always the higher.

Full-penetration welds should be used in the construction of all propellant tanks. This is especially important for storable propellants. A full-penetration "100 percent" weld is one where complete fusion has taken place to the root of the joint. Unfused edges, oxide notch, or any concavity at the root indicate lack of full penetration. All full-penetration welds which cannot be visually examined on the reverse side must be X-rayed to assure full penetration. Figure 8-9 presents the design detail of a typical full-penetration, single-welded butt joint.

If possible, interpropellant welding (i.e., the fuel and oxidizer are separated by only one welded joint) should be avoided in tank designs. A double-weld design will prevent the mixing of propellants due to a single failure of welded joints. Figure 8-10 presents the design of a typical storable propellant tank with a forged one-piece common bulkhead. A double-weld design is used on the center-hold joint for the oxidizer duct.

Tank Wall Surface Requirements

The inner surfaces of the storable propellant tank wall must be relatively free of rust deposits

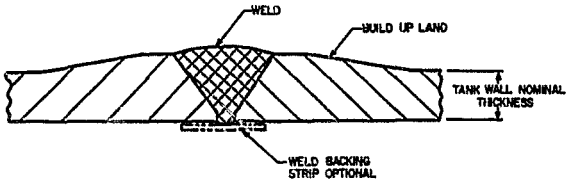

Figure 8-9.–Design detail of a typical full-penetration, single-welded butt joint for propellant tanks.

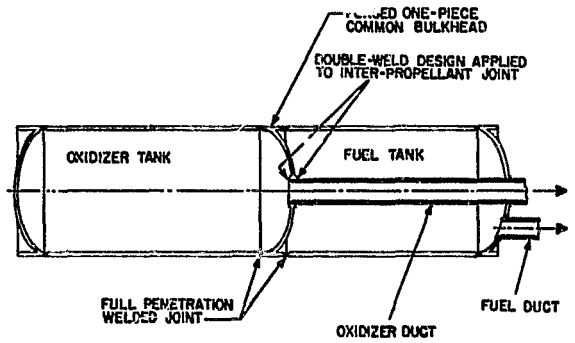

Figure 8-10.–Design of a typical storable propellant tank with a forged one-piece common bulkhead.

and tool marks. All welded joints should be ground to achieve a smooth dent-free contour. If an aluminum alloy is used for tank construction, anodizing of the inner surfaces is recommended. The tank should be cleaned and treated before use. The process rendering the surfaces inactive is known as passivation. Basically, passivation involves the cleaning of tank interior with solvents and, in some cases, the treatment with alkaline or acid solution. Passivation differs from conditioning or stability testing of a tank. Stability testing of a tank involves the application of a propellant rinse prior to propellant tanking.

8.5 DESIGN OF CRYOGENIC LIQUID PROPELLANT TANKS AND THEIR INSULATION

In the design of cryogenic propellant tanks, there are several potential problem areas which may affect proper functioning and reliability:

(1) Properties of the tank construction materials at the cryogenic propellant service temperature range
(2) Thermal stresses induced in the tank structure by temperature gradients
(3) The relief of tank pressure caused by boiloff of the cryogenic propellants
(4) Thermal insulation of the tank walls

The knowledge of the precise strength characteristics, degree of brittleness, and notch sensitivity of the tank construction materials at cryogenic temperatures (as low as -423° F for liquid hydrogen service) is a prerequisite for their selection. In general, most of the aluminum alloys, the austenitic and semiaustenitic stainless steels, possess good mechanical properties at cryogenic temperatures (also see ch. II). The thermal stresses can be analyzed by determining the temperature profile at various regions of the tank and may be minimized by discrete design approaches. The capacity of the tank relief valve should be based on the maximum anticipated propellant boiloff rate during ground hold and actual operation of the vehicle systems.

Among the cryogenic propellants, liquid hydrogen imposes the most serious tank design problems. This is mainly due to its very low service temperature and its relatively large specific volume. Design problems are especially acute with the hydrogen tank insulation. It often becomes one of the most critical design factors in a hydrogen-fueled vehicle system. The difficulties arising in hydrogen systems in connection with heat transfer may be dramatically illustrated as follows:

Assume two tanks of equal size, subject to the same heat influx per unit time. One is filled with liquid oxygen, the other with liquid hydrogen. The ratio of heat of vaporization per unit weight $O/H = 0.48$, but the density ratio is $O/H = 14.3$. Thus the volume rate of vaporization in the hydrogen tank is 6.85 times faster than in oxygen. In reality, the heat influxes would not be equal for two uninsulated tanks, because of the higher temperature differential across the wall, and especially because of the greatly increased heat-transfer rate from air liquefaction on the hydrogen tank surface. This may further accelerate the hydrogen volume boiloff rate to approximately 70 times that of oxygen. In an actual oxygen/hydrogen system, operating at a weight mixture ratio $O/H = 5$, the tanked mixture ratio by volume is $H/O = 3.23$. Depending on the shape of the tanks (surface ratio), this may again double or triple the relative boiloff rate of hydrogen. The absolute necessity for insulation to drastically reduce heat influx into a hydrogen system becomes apparent.

Boiloff rates are not the only problem caused by the physical properties of hydrogen. Near the ambient boiling temperature, the gradient of vapor pressure is 2.4 psi/°R, as compared to 0.78 psi/°R for liquid oxygen. Moreover, this gradient increases rapidly with increasing temperature, which would be experienced following tank pressurization. Figures 8-11 and 8-12 show the trend for both liquid oxygen and hydrogen. The data have great significance to pump NPSH. As may be seen, just one degree of liquid-hydrogen-temperature rise requires a 3-psi increase in tank pressure to maintain proper NPSH. In a large vehicle, the required increase in tank-wall thickness may affect payload capability noticeably. The situation is further aggravated by the high heat influx into hydrogen, for reasons mentioned in connection with boiloff. Even for relatively short boost periods, rapid warmup may create a problem more severe than boiloff, and places further emphasis on adequate insulation. The following discussion of tank insulations,

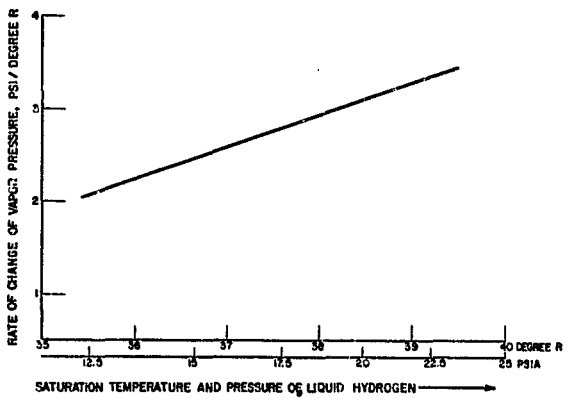

Figure 8-11.–Rate of change of saturation vapor pressure to temperature for liquid hydrogen.

therefore, is specially slanted to hydrogen service.

Insulation Requirements for the Cryogenic Propellant Tanks

Most vehicle missions include three distinct phases during which effective insulation for the cryogenic propellant tanks is essential: ground hold period, the boost phase, and coast flight in space. The propellant tank insulation design will primarily be based on flight performance criteria. However, propellant evaporative losses during long hold periods on the ground requiring continuous topping may also become a significant cost item. If long hold periods with a filled tank are anticipated, it may be indeed economical

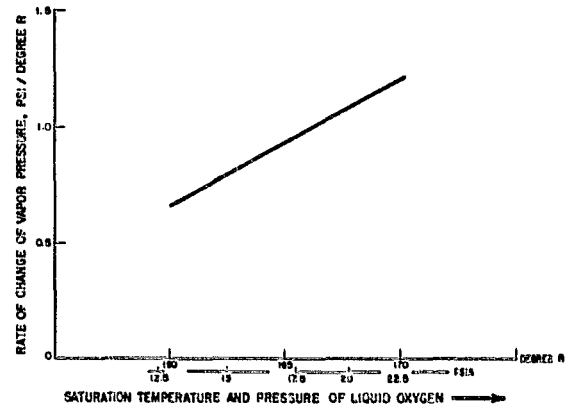

Figure 8-12.–Rate of change of saturation vapor pressure to temperature for liquid oxygen.

to provide an insulating blanket on the tanks, which is remotely removed just prior to liftoff. During the boost phase, high temperatures from aerodynamic heating, and large aerodynamic forces are encountered. Although of short duration, this phase dictates the structural elements of the insulation. During coast flight in space, the principal source of thermal energy is radiation from the Sun and the planets. By the use of radiation shields surrounding the basic tank insulation, the heat flux across the tank wall can be effectively controlled. The properties of the materials used in a solar shield are very important, such as the absorptivity and emissivity of the surface when subjected to various types of radiation and body temperatures. Magnesium oxide and silver are two materials showing promise for use in solar shields. These materials may be applied as coatings onto a lighter base material such as aluminum. The amount of shielding required depends on the duration of the coast flight and on optimization of shield weight versus propellant boiloff weight.

Basic Insulation Types

Major desirable design features of an insulation include: light weight, uniform and repeatable insulation characteristics, ease of application, low cost, low hazard, reasonable ruggedness, ease of repair, good reliability, and above all, low heat conductivity.

Excellent results can be achieved with a laminated-type insulation. This employs an aluminum foil and fiber-glass structure, often in multiple layers. The aluminum foils act as reflectors, effectively rejecting radiative heat, while the evacuated space in between prevents conductive heat transfer. This insulation can be applied to single-curved and to large-diameter, double-curved surfaces. The laminar insulation is sensitive to damage, however, possibly resulting in loss of vacuum due to cracks and to infiltration of leak gases. Application to airborne system thus has been infrequent.

For the latter, honeycomb-supported structures are finding wide application. Figure 8-13 shows the typical example of an externally applied hydrogen tank insulation of this type. A ½- to ¾-inch nominal-size plastic honeycomb is installed between an inner and outer facing

SP 125

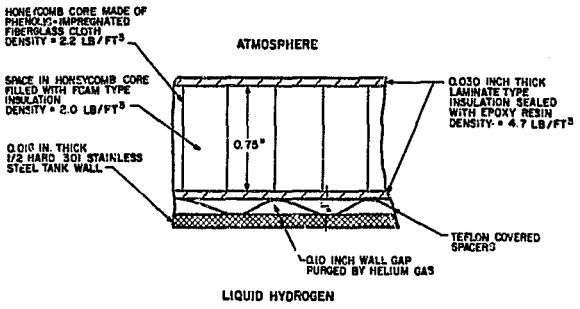

Figure 8-13.–Construction elements of a typical liquid hydrogen tank insulation design (external type).

sheet. The cells may or may not (weight!) be filled with an isocyanate-type foam. The foam bubbles or the properly sealed cells will form individual vacuum spaces when cold (cryopumping). However, because of the possibility of vacuum degradation by infiltration of air (outer insulation), or hydrogen (inside insulation), it is often preferred to purge the cells with helium, for which lateral passage ways must be provided. The purge also serves as a leak-detection device, in conjunction with gas analyzers, to detect contamination of the helium from leaks. In figure 8-13, a separate gap is purged with helium, rather than the honeycomb cells.

The thermal conductivity of the insulation shown is about 3.8×10^{-7} Btu-in/in^2-sec-°F (0.2 Btu-in/ft^2-hr-°F).

Thermal conductivities of various types of insulation vary from 0.05×10^{-7} to 6.0×10^{-7} Btu-in/in^2-sec-°F. Their densities range from 2.0 to 20 lb/ft^3. Since the quality of an insulation will affect cost and weight, an optimization study will have to be made, based on mission characteristics.

Sample Calculation (8-6)

Determine the heat-transfer rates in Btu/in^2-sec across the tank insulation shown in figure 8-13 during–

(a) *Ground hold.*–The temperature of the insulation surface near the tank wall is around -360° F and the outer surface is 70° F.

(b) *Boost phase.*–The inner insulation surface temperature reaches -210° F and the outer insulation temperature reaches 800° F.

SP 125

Solution

(a) During ground hold, the temperature differential across the insulation $\Delta T = 70-(-360) = 430°$ F. The overall thickness of the insulation $t = 2\times0.03+0.75 = 0.81$ in. From equation (4-19), the heat transfer rate

$$q=\left(\frac{k}{t}\right)\Delta T=\left(\frac{3.8\times10^{-7}}{0.81}\right)\times430$$

$$=2.02\times10^{-4}\ \text{Btu/in}^2\text{-sec}$$

(b) During the boost phase, $\Delta T = 800-(-210) = 1010°$ F. The heat-transfer rate

$$q=\left(\frac{k}{t}\right)\Delta T=\left(\frac{3.8\times10^{-7}}{0.81}\right)\times1010$$

$$=4.74\times10^{-4}\ \text{Btu/in}^2\text{-sec}$$

Selection of Tank Insulation Designs

Many factors will influence the selection of a tank insulation design. The insulation may be located internal or external to the tank wall; it can be integral, or disposable during boost; i.e., it can be bonded in place or mechanically retained. Basically, any insulation applied to a tank must be justified with respect to advantages of performance and/or economy.

Locating the insulation inside of the propellant tank has the obvious advantage of protecting the insulation from handling damage. The tank structure is isolated from the severest low-temperature effects of the propellant and is thus subjected to only moderate thermal cycling from its source. Internal insulation also minimizes propellant loss when chilling the tank during filling. However, if a crack or leak should occur in internal insulation of a hydrogen tank, gaseous hydrogen would enter the crack and gradually increase the heat transfer. Other undesirable features of internal insulation are apparent, such as: difficulties in installation; in locating and repairing of leaks; and in cleaning the tank. Internal insulation is also subject to higher pressures and more severe temperature effects which tend to impair the insulation sealing.

External insulation has the advantage of isolating the tank structure from the extreme temperature of aerodynamic heating during boost. Installation, repair, and sealing of the external

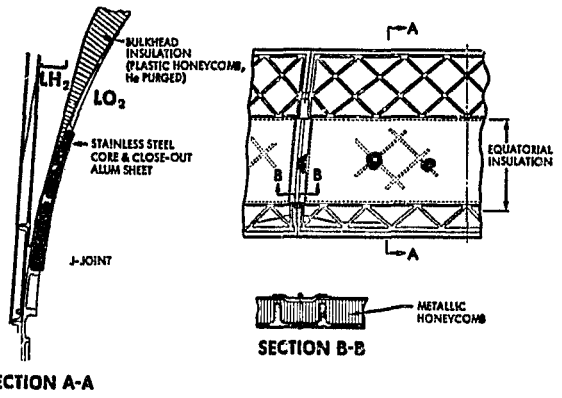

Figure 8-14.–Design of a typical insulated common bulkhead separating LH_2 and LO_2 tanks.

insulation can all be done without special consideration of access, ventilation, and curing techniques in closed areas. However, special consideration will be required for tank leak detection, especially with integrally insulated areas. If a crack does occur in the external insulation, liquefaction of air and cryopumping will occur resulting in a significant rise in heat transfer.

Insulation for Common Bulkheads

When a common bulkhead is used between propellant tanks and cryogenics are involved, insulation is required to prevent freezing of the propellant with the higher boiling point. Figure 8-14 shows the equatorial area of a typical insulated common bulkhead. A fiber-glass honeycomb is located between a forward and an aft facing sheet. In the equatorial area, where the facing sheets have to be faired into the cylindrical tank portion, they are reinforced by waffle grid ribs. This design also requires special insulation on the inside of the LOX tank in the equatorial region. No foam filler was used in this particular example.

8.6 DESIGN OF FIBER-GLASS FILAMENT-WOUND LIQUID PROPELLANT TANKS

Most of the pressure vessels which possess surfaces of revolution can be fabricated conveniently by the technique of filament winding. By this method a lightweight structural member can be produced with mechanical precision and versatility of construction and materials. A strength-to-density ratio, F_u/ρ, can be obtained by filament winding and impregnating the fiber-glass roving with a suitable resin, which is higher than can be achieved by any other method or material. For instance, the strength-to-density ratio of a fiber-glass filament-would resin-bonded structure (average $\rho = 0.08$ lb/in^3, $F_u = 120\,000$, $F_u/\rho = 150 \times 10^4$) is about twice that of high-strength alloy steels.

Good reliability and close dimensional control of filament-wound pressure vessels is assured through the use of calibrated winding machines which orient the reinforcing fibers precisely. However, most of the liquid propellants are not compatible with resin-impregnated, fiber-glass structures. Therefore, an aluminum tank liner which is compatible with both propellants, must be used to separate the fiber glass from the liquid. It also provides a positive sealing barrier, since the resin-bonded fiber-glass material is pervious to both liquid and vapor over extended periods. Figure 8-15 presents a typical aluminum-lined, fiber-glass filament-wound liquid propellant tank.

Design and fabrication of fiber-glass filament-wound tanks with a thin aluminum liner is basically simple. However, a key problem arises from the fact that the modulus of elasticity of fiber-glass resin-bonded materials is about 5×10^6 psi, while that of aluminum is about 10×10^6 psi, and that the strength of the aluminum is usually no more than a third of that of the fiber glass. Since the geometry of the tanks usually imposes equal strain on aluminum liner and fiber glass as the tank is pressurized, the aluminum becomes loaded to its elastic limit long before the fiber glass reaches the level of its high-strength capability. Consequently, with a plain liner configuration, the aluminum is stretched far beyond its elastic limit and forced back to its original shape each time the tank is pressure cycled. Thus, the liner may experience fatigue failure after a small number of pressure cycles. The pressure-cycle life of a plain liner depends on amount of stretch beyond the elastic limit, type of aluminum, bonding between lines and fiber glass, weld joints, variation in thickness and contours, etc. A well-designed, plain-type tank liner should have a life of about 10 to 20 pressure cycles.

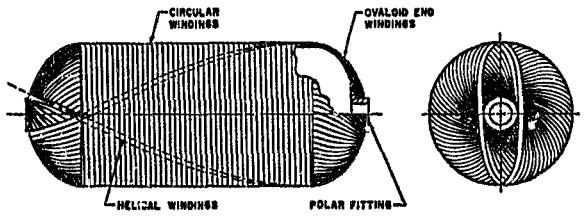

Figure 8-15.—A typical aluminum-lined, fiberglass, filament-wound liquid propellant tank.

One design approach to extend cycle life is to use a corrugated liner. The corrugations have an effect equivalent to reducing the modulus of elasticity of the aluminum liner to a value less than that of the fiber glass. For instance, if the fiber glass is stressed to 100 000 psi and has a modulus of elasticity of 5×10^6, its extension will be 2 percent. The corrugations of the liner then should be designed to permit the 2-percent extension so that the aluminum will not be stressed beyond its elastic limit.

8.7 DESIGN OF PROPELLANT TANK PRESSURANT DIFFUSERS

The main function of a pressurant diffuser is to introduce the pressurant gases evenly into the propellant tank at a desired direction and velocity. The gases are usually injected in a plane near the tank forward end, at a right angle to the tank and vehicle axes. This will minimize disturbances at the pressurant-propellant interface. Figure 8-16 presents some typical propellant tank pressurant diffuser designs. A radial-type diffuser, located at the tank axis, is used for the fuel tank. This arrangement permits a simple, lightweight diffuser design. However, the reversed ellipsoidal common bulkhead at the forward end of the oxidizer tank requires a ring-type diffuser, consisting of many individual diffusing nozzles located at the circumference of the tank.

The pressurant enters the tank at a temperature level depending on the source, such as a LOX heat exchanger. In some cases, this may not be the optimum temperature for critical structural members. In these cases, a separation tube (Hilsch tube) may be combined with the diffuser. Without moving parts, it operates on the principle of separating the higher energy molecules from those with lower energy. Temperature spreads of 100° F or more can be obtained, depending on construction and available pressure drop. Advanced configurations have been developed by the AiResearch Manufacturing Co. In a LOX/hydrogen system with common bulkhead, the device may be used to direct the cold stream toward the bulkhead, thus lowering the temperature differential and resultant heat transfer across it.

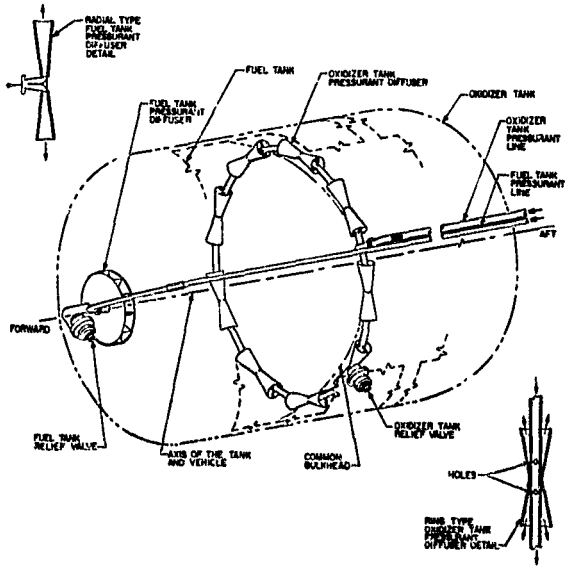

Figure 8-16.—Typical designs of propellant tank pressurant diffusers.

8.8 PROPELLANT EXPULSION UNDER ZERO GRAVITY OR OSCILLATORY G-LOADING CONDITIONS

Under zero or oscillatory g-loading conditions typical for many vehicle trajectories, fluid location in a propellant tank becomes uncertain and requires means to prevent gas pockets from interfering with propellant expulsion. The propellants must be either subjected to an acceleration force for settling immediately prior to usage, or they must be continuously confined in the tank. The two approaches can be defined as impulse settling and positive expulsion.

Impulse Settling

This method employs a small propulsive force directed axially, parallel to the vehicle centerline of thrust. This acceleration forces the propellant to cover the tank outlet prior to initiation of main engine operation. This approach is especially suitable for most space vehicles, because their low-thrust reaction control units can be used to perform the auxiliary function of providing the thrust required for propellant settling.

Although this method would eliminate the need for positive expulsion devices for the main propellant tanks, it would necessitate separate positive-expulsion propellant tank or tanks for the sole use of the reaction control system. The possible disadvantages of this impulse-settling method are (1) no control of vehicle center-of-gravity shifts, and (2) low thrust-to-weight ratio under these conditions, which may increase response times beyond tolerable limits.

For single-start upper stages, jettisonable short-duration solid settling rockets may also be applied to advantage.

Positive Expulsion

The other method of achieving proper fluid orientation within the propellant tanks is by continuously confining the propellant to the vicinity of the tank outlet. A positive expulsion propellant tank assembly usually consists of an outer tank shell and an inner movable expulsion device. Frequently used positive expulsion devices are: (1) metallic diaphragms, (2) elastomer diaphragms, and (3) moveable pistons. The design of the expulsion devices depends upon a number of considerations. Primary among these is the design configuration of the propellant tank. Another is the allowable shift of vehicle center of gravity during expulsion, which in many vehicle applications must be minimized to avoid instabilities induced by a pitch or yaw maneuver. A choice of construction materials capable of sustained contact with the pressurants and propellants must also be made.

Metal Expulsion Diaphragms

Metal expulsion diaphragms made of 1100-0 aluminum (0.010 to 0.020 inch thick) are desirable for long-term storage contact with storable propellants and higher temperature pressurant gases. Figure 8-17 presents a concentric-circular, convoluted metal positive expulsion diaphragm used in a spherical tank. This system is unique for bipropellant systems because it allows both propellants to be stored in the same tank, as long as the volumetric mixture ratio does not deviate appreciably from unity. An expulsion efficiency above 97 percent (i.e., the percentage of the propellant which can be expelled from the tank) may be expected. This design also minimizes shift of center of gravity during the entire process of expulsion.

Figure 8-18 presents the corrugated metal positive expulsion diaphragm applied to a cylindrical tank. A center post is provided to support the diaphragm. The diaphragm is formed into a lobed corrugation capable of performing the required mechanical expansion. Transition sections are provided at both ends of the diaphragm for attachment to the tank ends. An expulsion efficiency of 97 to 98 percent may be achieved with this design. However, the utilization of

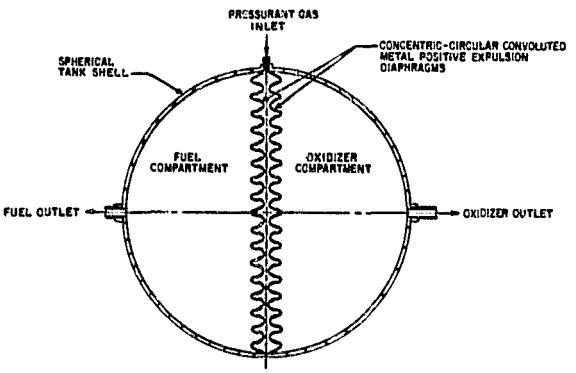

Figure 8-17.—Concentric-circular convoluted metal positive expulsion diaphragms used in a spherical-shape propellant tank.

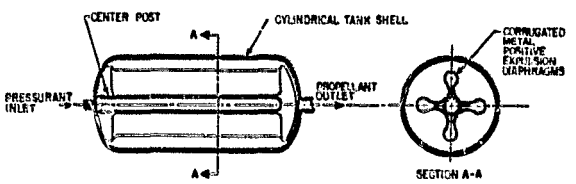

Figure 8-18.—Corrugated metal positive expulsion diaphragm used in a cylindrically shaped propellant tank.

tank volume is less efficient due to dimensional limitations (i.e., size of the center post compared to tank diameter). This design, too, minimizes shift of center of gravity.

One disadvantage of the metal diaphragms is that only one complete expulsion cycle is possible, because the metal probably will be cold worked. The cold working not only changes metal elastic properties and the Δp required for expulsion, but may cause fatigue failure.

Elastomer Expulsion Diaphragms

Elastomer-type diaphragms are applicable to most tank configurations and often offer a more efficient utilization of tank volume. One design approach takes advantage of the stretching properties of pure elastomer and uses the diaphragm as a bladder. Figure 8-19 presents the bladder-type elastomer positive expulsion diaphragm used in a spherical tank. As the bladder is pressurized and inflates, the propellant is displaced and positively expelled and uniformly confined during all phases of expulsion. By positioning the bladder in the geometric center of the tank, center-of-gravity shift during expulsion is virtually eliminated.

The initial unpressurized volume within the bladder can be utilized as the ullage volume. The elastomer diaphragm will produce an expulsion efficiency of up to 99 percent in many tank configurations. In addition, it is capable of many expulsion and refill cycles. An inherent disadvantage of pure elastomers in storage contact with many storable propellants is tensile-strength degradation as a function of time. They are also incompatible with hot pressurant gases produced by gas generators.

Positive Expulsion By Movable Pistons

An alternate method of obtaining positive expulsion in cylindrical tanks is a movable piston actuated by pressurant gas. Positive attachment is required during storage to keep the piston in the proper position. To prevent leakage during operation, seals will be required. The seals may be piston-type rings or some type of metallic wiper seal. In either case, the dimension and surface finish of the tank inside diameter should be maintained relatively accurate and smooth. In some designs a concentric center post is utilized to guide the piston, requiring an additional seal. Figure 8-20 presents the design of a movable piston guided by a center post.

The pressure differential across the movable piston required to overcome friction during operation increases the required pressurant pressure and the tank structural pressure loads for a given propellant pressure at the tank outlet. It may be estimated by

$$\Delta p A_p = f_S F_n L_S \qquad (8\text{-}39)$$

where

Δp = pressure differential across the piston, psi

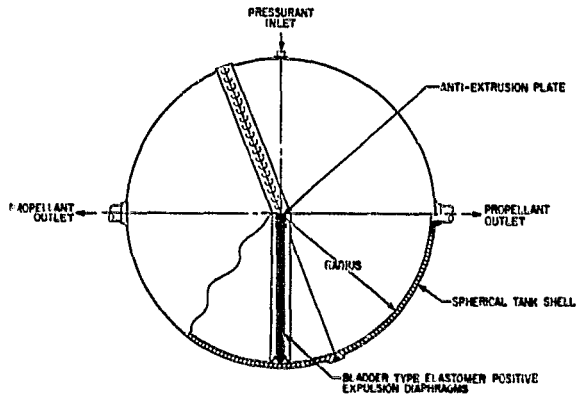

Figure 8-19.—Bladder-type elastomer positive expulsion diaphragms used in a spherically shaped propellant tank.

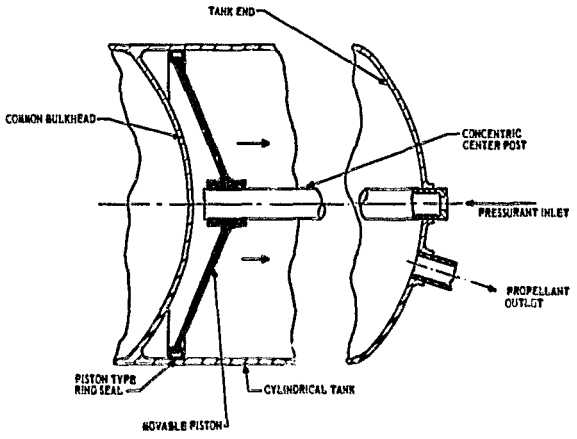

Figure 8-20.—Movable piston used in a cylindrical propellant tank for positive expulsion.

A_p = cross-sectional area of the piston, in^2
f_S = coefficient of friction of the piston seals
F_n = unit normal force reacted by the piston seals on tank wall and guide post, lb/in of seal
L_S = total length of all piston seals, in

Sample Calculation (8-7)

The following data are given for a cylindrical positive expulsion tank with a movable piston as shown in figure 8-20:

Inside diameter of the tank, 20 in
Diameter of the guide post, 1.5 in
Coefficient of friction of the piston seals, $f_S = 0.1$
Unit normal force reacted by the seals, $F_n = 500$ lb/in

Estimate the pressure differential across the movable piston.

Solution

The cross-sectional area of the piston

$$A_p = \frac{\pi \times (20)^2}{4} - \frac{\pi \times (1.5)^2}{4} = 314.16 - 1.76 = 312.4 \text{ in}^2$$

The total length of piston seals:

$$L_S = \pi \times (20 + 1.5) = 67.54 \text{ in}$$

Substitute this into equation (8-39); the pressure differential across the piston

$$\Delta p = \frac{f_S F_n L_S}{A_p} = \frac{0.1 \times 500 \times 67.54}{312.4} = 10.8 \text{ psi}$$

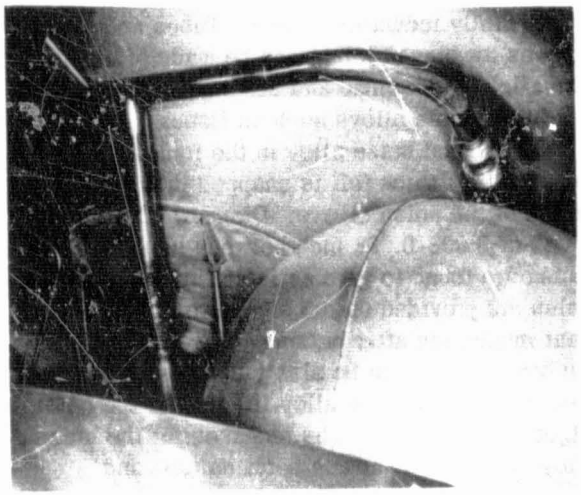

Figure 9-17.–In-place brazed joints applied in an upper stage propulsion system.

9.5 DESIGN OF DUCTS FOR ROCKET ENGINES

Basic Design Considerations

Primary design considerations for various ducts used on rocket engines are:

1. *Fluid flow rate and system pressure drop.*–The size of the duct is determined largely by the required flow rate and permissible pressure drop of the flow system. An optimization must be made considering duct weight, pressure drop, and space, before finalizing the duct size.

2. *Working temperature and pressure of the fluid.*–The selection of construction materials and structural design for ducts depends mainly on the working temperature and pressure level of the fluid, but also on chemical compatibility. Temperature also influences line flexibility and duct geometry.

3. *Duct joints.*–The number and type of joints in a duct system are usually determined by system assembly and servicing requirements. All mechanically sealed joints should be reviewed, at various engine design and development phases, for their possible elimination or replacement by in-place, induction-brazed or welded joints. (See secs. 9.3 and 9.4.)

4. *Line flexibility and geometry.*–The required degree of flexibility in a duct system is dictated by component tolerance buildups, misalinements, and required freedom of movement to allow for temperature changes, dynamic loads, and engine gimbal effects, if any. This often determines the line geometry. In general, however, lines should be as short and straight as possible.

5. *Structural integrity.*–The structural design of a duct system may involve a number of complex problems. This is especially true with ducts for elevated or very low temperatures, and requiring a high degree of flexibility. The design and fabrication of metal bellows for application in ducts is a highly specialized technology.

Duct Design for Minimum Pressure Drop

Techniques for fluid-flow pressure drop determination have been discussed in chapter VII. Equation (7-7) may be used to estimate the pressure drop of a straight duct section. Either equation (7-7) or (7-9) can be utilized to predict the pressure drops of other shapes, for which some experimental data are available.

Besides avoiding excessive flow velocities at various sections of a duct system, basic requirements for minimum pressure drop are: constant flow area, smooth flow surfaces and path, minimum length, and few turns. In most duct designs, a certain number of turns is unavoidable. The design of these turns affects considerably the overall pressure drop of a duct system.

A turn may offer a large resistance to the flow if not carefully designed. Investigations show that the flow resistance in a bend with constant cross section is affected directly by its turning radius ratio R/D (where R = radius of curvature of the axis of the duct, D = diameter or width of the duct) (see fig. 7-21). By increasing the turning radius ratio, large reductions in pressure drop are possible. Bends with a circular section are better than those with a square section. However, the square section may be much improved by changing it to a rectangle, so that the turn is made on the short side; that is, the loss can be decreased by increasing the rectangle aspect ratio W/D (where W = width of the long side, D = width of the short side). For a duct with a rectangular section, therefore, a very efficient corner may be produced if the values of both the radius ratio and the aspect ratio are kept large.

This consideration should be applied in all cases where a sharp turning corner is unavoidable, such as the elbow-type turbopump inlet ducts shown in figure 6-15. Here, the loss around the sharp corner is due largely to the zero radius ratio. To reduce this pressure drop, guide vanes can be very effectively used. If the junctions of the duct walls on the diagonal are smoothed out and vanes added as shown in figure 9-18, the compartments so formed may be made to have a good radius ratio and a high aspect ratio. Since in most cases only a few vanes need to be added for high aspect ratios, the remaining problem is one of securing a good radius ratio.

The radius and aspect ratios of each compartment are increased as the gap/chord ratio S/C is reduced (fig. 9-18). Theoretically, then, the corner pressure drop will decrease as the ratio S/C is decreased. However, each additional vane adds more surface area and blockage, and consequently tends to increase losses. The S/C ratio can be optimized in tests and ranges from 0.25 to 0.45. Well-designed elbow-type sharp turns with guide vanes may have resistance coefficients K as low as 0.1 to 0.2 (see eq. 7-9).

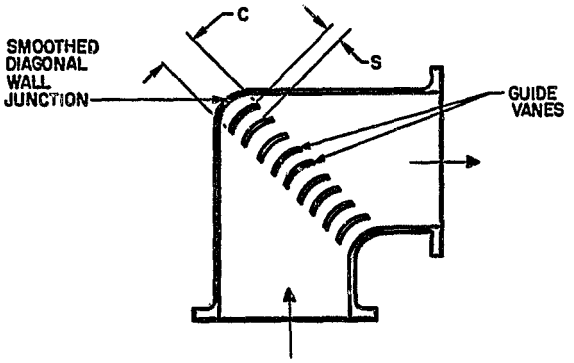

Figure 9-18.–Elbow-type sharp turning duct with guide vanes.

Duct Design for Flexibility

For most interconnecting ducts between two engine components, the required flexibility such as for misalinements and temperature changes can be achieved by placing one or two bellows sections in the line (figs. 9-4 and 9-5). These may be either restrained or unrestrained, depending on structural loading considerations. In ducts connecting two components involving large relative movements, a minimum of three flexible sections is required. The longitudinal axis of at least two of the bellows sections should be positioned at a right angle to one another. Restrained bellows are preferred.

The duct systems shown in figure 9-3 illustrate a basic three-bellows arrangement as applied to gimbaled clustered engines. Figure 9-19 presents one of the frequently used design approaches for a relatively short duct system to facilitate large movements during gimbaling of an engine system. The three flexible sections are kept in the plane of the engine gimbal point. This results in minimum displacements of the sections for a given engine movement. Bellows-type universal joints (fig. 9-20) may be conveniently incorporated into this duct system by welding. These joints are made of stainless steel and will operate at cryogenic and elevated temperatures (up to 1000° F). The internal restraining mechanism is designed to give a smooth flow passage for low-pressure drop.

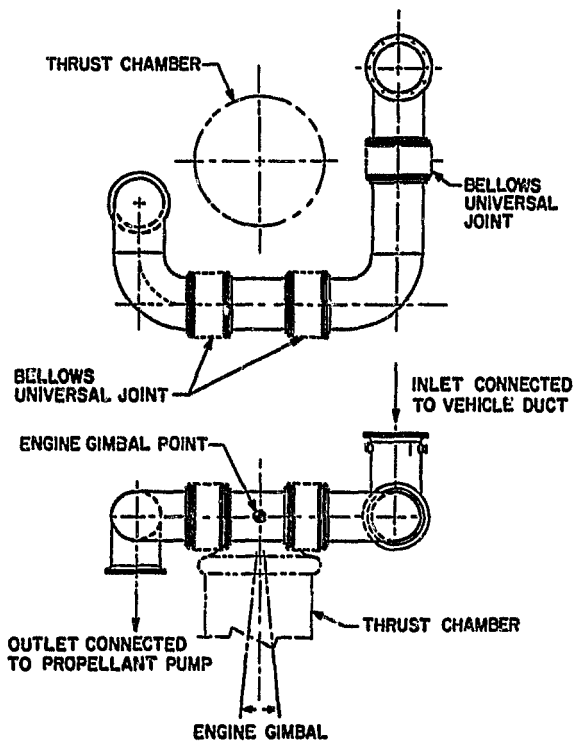

Figure 9-19.–Typical propellant supply duct designed for the flexibility required for engine gimbaling.

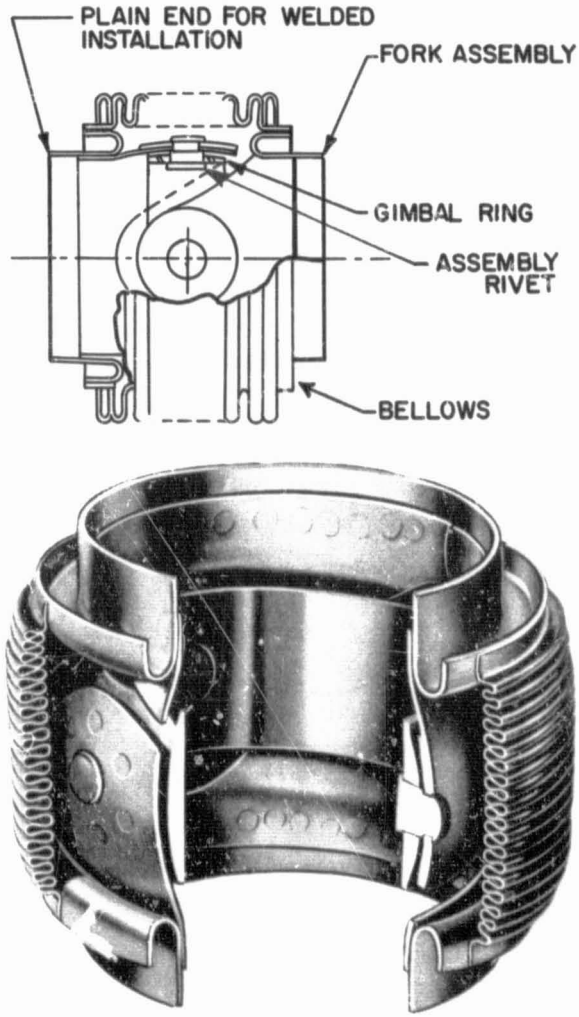

Figure 9-20.–Typical gimbal-ring-type bellows universal joint designed and manufactured by Marman Division of Aeroquip Corp.

For higher pressure applications (over 200 psi), external wire braids or links may be used to restrain the bellows section. The braids can be made of stranded stainless-steel wires, about 0.012-inch diameter. In extreme cases, more than one layer of braid should be used with regard to the high separation loads.

Structural Design of Bellows For Flexible Ducts

Most of the bellows used for flexible ducts in rocket engines are hydraulically formed by radially expanding thin-wall tubing, at spaced intervals along its axis, coincident with an axial compression, to a configuration as shown in figure 9-21. Our discussion will be confined to this type of bellows. The various structural characteristics and design correlations of bellows are presented using the following nomenclature (see figs. 9-21 and 9-22):

C_t = bellows wall-thinning correction factor
C_p = ply interreaction factor (1.00 for 1-ply bellows, 0.90 for 2-ply bellows, and 0.85 for 3-ply-or-more bellows)
d_0 = outside diameter of the bellows, in
d_i = outside diameter of the convolution root of the bellows, in
$d_m = \sqrt{(d_i^2 + d_0^2)/2}$ = root-mean-square diameter of the bellows, in
d_d = mean duct diameter, in
E = modulus of elasticity of the bellows material, psi
e_a = axial deflection of the bellows, in
e_b = equivalent axial deflection of the bellows due to pure bending, in
e_p = equivalent axial deflection of the bellows due to parallel offset, in
e_s = equivalent axial deflection of the bellows due to pure shear, in
F_s = shear load, lb
F_p = pressure separating load, lb
G = shear modulus of elasticity of the bellows material, psi
$h = (d_0 - d_i)/2$ = mean convolution height, in
L = pitch of the bellows (axial length of a convolution), in
$L_a = (N_c - 0.5)L + N_p t$ = free axial length of the bellows, in
N_c = number of bellows convolutions
N_p = number of bellows plys
t = thickness of the bellows wall, in
L_b = axial length of the rigid duct section, in
M = bending moment, in-lb
p = internal (or external) fluid pressure, psi
p_{cr} = critical stability pressure of the bellows, psi
R_a = axial spring rate of the bellows, lb/in
R_b = bending spring rate of the bellows, lb-in/degree
R_p = parallel offset spring rate of the bellows, lb/in
R_s = shear spring rate of the bellows, lb/in

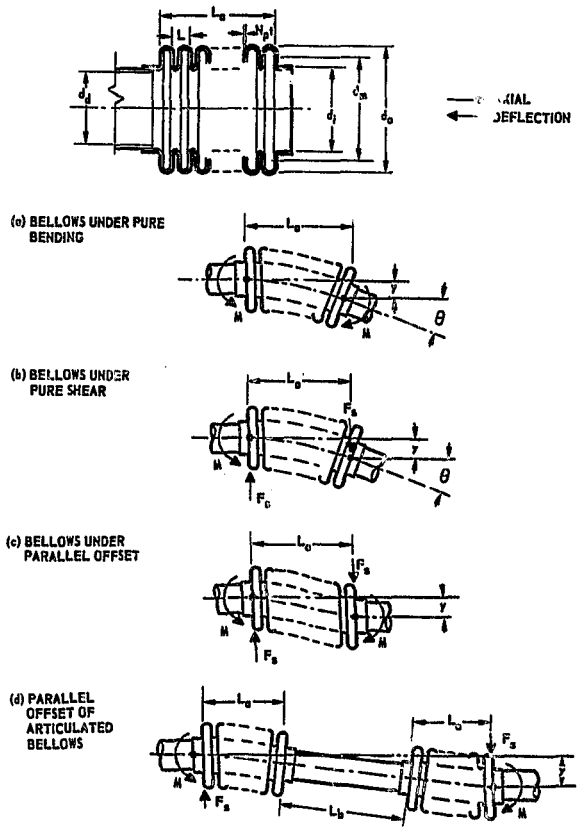

Figure 9-21.–Elements and various motions of bellows.

R_t = torsional spring rate of the bellows, lb-in/degree
S_b = bellows bulging stress, psi
S_h = bellows hoop stress, psi
S_m = bellows motion stress, psi
S_s = bellows shear stress, psi
S_t = bellows torsion stress, psi
T = torsional moment, in-lb
T_{cr} = critical stability torque of the bellows, psi
v = Poisson's ratio of the bellows material, in
y = transverse deflection of the bellows, in
θ = bending angle of rotation, degrees
ϕ = torsional angle of rotation, degrees

1. *Thinning of the bellows wall.*–Hydraulic-formed bellows are usually made by starting with tubes of the same diameter as the bellows diameter at the root of convolution, d_i. The typical thinning profile of a bellows wall starts with the original material thickness at the root of the convolution, and tapers approximately linearly to the minimum thickness at the convolution outside diameter (fig. 9-22). Amounts of thinning range from 10 to 40 percent. Effects of thinning are considered by applying the thinning correction factor C_t (fig. 9-22) to the bellows design.

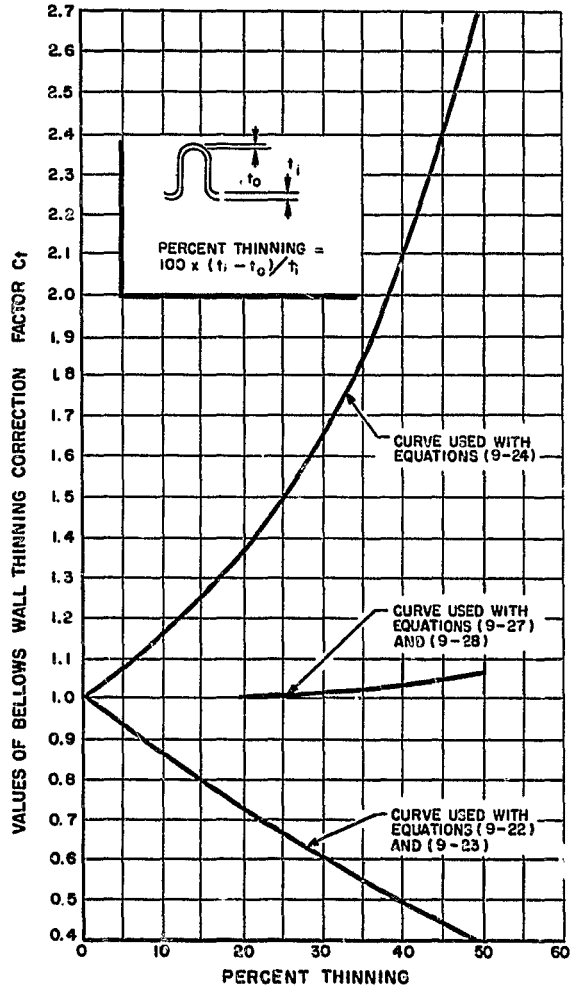

Figure 9-22.–Bellows wall thinning correction factor C_t versus percent thinning.

2. *Bellows axial spring rate:*

$$R_a = \frac{1.49\, C_t C_p N_p E d_i t^3}{N_c h^3}, \text{ lb/in}$$

(steel and nickel alloys) (9-22)

$$R_a = \frac{1.23\, C_t C_p N_p E d_i t^3}{N_c h^3}, \text{ lb/in}$$

(aluminum alloys) (9-23)

3. *Bulging stresses.*—These are the radial bending stresses induced in the side walls of the bellows, by internal or external pressure. Bulging stresses should be kept below those listed in table 9-9:

$$S_b = \frac{C_t p h^2}{2 N_p t^2}, \text{ psi} \qquad (9\text{-}24)$$

4. *Separating loads.*—Bellows are pressure loaded so that they experience a separating load, in addition to the normal duct axial force:

$$F_p = \frac{p(d_m^2 - d_d^2)\pi}{4}, \text{ lb} \qquad (9\text{-}25)$$

5. *Hoop stresses.*—The bellows hoop stresses are calculated by using the total area per inch of bellows axial length of a tube of equivalent wall thickness. Hoop stresses should always be kept lower than the yield and ultimate strength of the bellows materials by a specified margin.

$$S_h = \frac{p d_m}{2 N_p t}\left[0.57 + \left(\frac{2h}{L}\right)\right], \text{ psi} \qquad (9\text{-}26)$$

6. *Motion stresses due to axial deflections of the bellows.*—These are due to bending of the bellows side walls. Allowable motion stresses for bellows materials, with respect to design cycle life, are given in table 9-9:

$$S_m = \frac{1.40\, C_t E t e_a}{N_c h^2}, \text{ psi}$$

(steel and nickel alloys) (9-27)

$$S_m = \frac{1.78\, C_t E t e_a}{N_c h^2}, \text{ psi}$$

(aluminum alloys) (9-28)

All other types of bellows motions, such as angular and parallel offset, can be converted into an equivalent bellows axial deflection, and applied to equations (9-27) and (9-28) to calculate the corresponding motion stresses.

7. *Bellows under pure bending* (fig. 9-21a):

$$R_b = \frac{M}{\theta} = \frac{d_m^2 R_a}{458.4}, \text{ lb-in/degree} \qquad (9\text{-}29)$$

$$e_b = \frac{d_m \sin\theta}{2}, \text{ in} \qquad (9\text{-}30)$$

Motion stresses due to pure bending can be calculated by substituting e_b for e_a in equations (9-27) and (9-28).

8. *Bellows under pure shear* (fig. 9-21b):

$$R_S = \frac{F_S}{y} = \frac{3 d_m^3 R_a}{8 L_a^2}, \text{ lb/in} \qquad (9\text{-}31)$$

$$\theta = \frac{229.2\, F_S L_a}{R_a d_m^2}, \text{ degrees} \qquad (9\text{-}32)$$

$$e_S = \frac{3 d_m y}{2 L_a}, \text{ in} \qquad (9\text{-}33)$$

Motion stresses due to pure shear can be calculated by substituting e_S for e_a in equations (9-27) and (9-28).

9. *Bellows under parallel offset* (fig. 9-21c):

TABLE 9-9.—*Yield Strength, Limiting Bulging Stresses, and Allowable Motion Stresses of Frequently Used Bellows Materials*

Material	Yield strength, psi	Limiting bulging stresses, psi		Allowable motion stresses, psi		
		$t \leq 0.012$ in	$t \geq 0.013$ in	1000 cycles	10 000 cycles	100 000 cycles
321 and 347 stainless steels	39 000	140 000	120 000	208 000	150 000	92 000
19-9DL	88 000	140 000	120 000	208 000	150 000	92 000
A-286	180 000	190 000	150 000	160 000	150 000	138 000
Inco 718	170 000	190 000	150 000	160 000	150 000	138 000
Inconel X	98 000	190 000	150 000	160 000	150 000	138 000
6061-T6 aluminum alloy	40 000	65 000		106 000	68 000	28 000

$$R_p=\frac{F_s}{y}=\frac{3\,d_m{}^2R_a}{2\,L_a{}^2}, \text{ lb/in} \qquad (9\text{-}34)$$

$$M=\pm\frac{F_sL_a}{2}=\pm\frac{3\,d_m{}^2yR_a}{4\,L_a{}^2}, \text{ in-lb} \qquad (9\text{-}35)$$

$$e_p=\frac{3\,d_my}{L_a}, \text{ in} \qquad (9\text{-}36)$$

Motion stresses due to parallel offset can be calculated by substituting e_p for e_a in equations (9-27) and (9-28).

10. *Parallel offset of articulated bellows* (fig. 9-21d):

$$R_p=\frac{F_s}{y}=\frac{3\,d_m{}^2R_a}{2}$$

$$[4\,L_a{}^2+6\,L_aL_b+3\,L_b{}^2], \text{ lb/in} \qquad (9\text{-}37)$$

$$M=\pm\frac{F_s(2\,L_a+L_b)}{2}$$

$$=\frac{3\,d_m{}^2(2\,L_a+L_b)yR_a}{4(4\,L_a{}^2+6\,L_aL_b+3\,L_b{}^2)}, \text{ in-lb} \qquad (9\text{-}38)$$

$$e_p=\frac{3\,d_m(2\,L_a+L_b)y}{(4\,L^2+6\,L_aL_b+3\,L_b{}^2)}, \text{ in} \qquad (9\text{-}39)$$

e_p can be substituted for e_a in equations (9-27) and (9-28) to calculate motion stresses.

11. *Bellows torsion.*—The stress due to bellows torsion is given by the twist of a thin tube:

$$S_t=\frac{2\,T}{N_p\pi d_i{}^2t}, \text{ psi} \qquad (9\text{-}40)$$

$$R_t=\frac{T}{\phi}=\frac{1.37\times10^{-2}\,Gd_itN_p}{(2\,h+0.57\,L)N_c}, \text{ lb-in/degree} \qquad (9\text{-}41)$$

12. *Bellows squirm due to internal pressure.*—When a restrained bellows is pressurized internally beyond a critical level, it experiences a stability failure of the same type as a buckling column:

$$p_{cr}=\frac{5.02\,R_a}{L_a\left(\frac{d_o}{d_i}\right)}, \text{ psi} \qquad (9\text{-}42)$$

13. *Bellows buckling due to external pressure.*—When a bellows is pressurized externally, it buckles in same manner as a thin cylinder:

$$p_{cr}=\frac{4\,EtN_ph^3}{(1-\nu^2)d_m{}^3p_b}, \text{ psi} \qquad (9\text{-}43)$$

14. *Bellows squirm due to torsion.*—When a bellows is loaded by pure torsion, it tends to buckle in some manner as with internal pressure squirm:

$$T_{cr}=\frac{\pi d_m{}^2R_a}{2}, \text{ in-lb} \qquad (9\text{-}44)$$

The values for p_{cr} and T_{cr} of bellows under angular and offset deflections will be reduced considerably. A correction factor which ranges from 0.2 to 0.9, as determined by experiments, should be applied.

15. *Allowable working stresses for bellows materials.*—Bellows generally operate in the plastic range. However, it has been the practice to calculate stresses on the basis of elastic deformation, and correlate the data on that basis. In reality, the calculated stresses are only index stresses, which define the plastic conditions of the bellows, under the influence of pressure and motion loading. The yield strength, limiting bulging stresses, and allowable stresses of frequently used bellows materials are presented in table 9-9.

16. *Bellows used at elevated temperatures.*—For applications at elevated temperatures allowable working stresses for bellows materials must be adjusted accordingly. Generally, an internal liner should be provided to protect the bellows against high-velocity, hot-gas flows.

17. *Bellows forming limits.*—Bellows designs are limited by how severely the material can be worked during forming. Generally, the following geometric limits should be used for bellows up to three plys:

$$\text{Maximum: } \frac{d_o}{d_i}=1.35 \qquad (9\text{-}45)$$

$$\text{Minimum: } L=(8+2\,N_p)t, \text{ in} \qquad (9\text{-}46)$$

Sample Calculation (9-4)

Design a bellows, as shown in figure 9-4, for the oxidizer pump discharge flexible duct of the A-1 stage engine, with the following data and requirements, in addition to those given in sample calculations (9-1) and (9-2).

Bellows material, Inco 718
Thinning of bellows wall, 20 percent
Outside diameter of the convolution root of the bellows, $d_i = 8$ in
Free axial length of the bellows, $L_a = 7$ in maximum
Required angular movement, $\theta = \pm 3°$
Life, 10 000 cycles

In addition, determine the following:

Bellows axial spring rate, R_a
Bending or angular spring rate of the bellows, R_b
Bending moments of the duct at 3° angular motion, M
Required restraining link load at maximum working pressure

Solution

We will first use the limiting bulging stress of the bellows material to establish the ratio of convolution height h to wall thickness t. From figure 9-22, wall-thinning correction factor $C_t = 1.36$, for 20 percent thinning. From table 9-9, the limiting bulging stress for Inco 718 at $t > 0.013$ inch is 150 000 psi. From sample calculation (9-2) the design limit pressure of the duct is 1925 psi. Substitute all these into equation (9-24) for a three-ply bellows:

$$S_b = \frac{C_t p h^2}{2 N_p t^2}$$

$$\frac{h}{t} = \sqrt{\frac{2 N_p S_b}{C_t p}} = \sqrt{\frac{2 \times 3 \times 150\,000}{1.36 \times 1925}} = 18.5$$

For a reasonable value of h, in a bellows of this size, we arrive at a wall thickness t of 0.022 in (after several tries):

$$h = 18.5 \times 0.022 = 0.407 \text{ in, say } 0.410 \text{ in}$$

The bellows root-mean-square diameter and the equivalent axial deflection due to 3° angulation can now be found:

$$d_o = d_i + 2h = 8 + 2 \times 0.410 = 8.820 \text{ in}$$

$$d_m = \sqrt{\frac{(d_i^2 + d_o^2)}{2}} = \sqrt{\frac{(8^2 + 8.82^2)}{2}} = 8.42 \text{ in}$$

From equation (9-30), the equivalent axial deflection of a bellows, due to pure bending or angulation:

$$e_b = \frac{d_m \sin \theta}{2} = \frac{8.42 \times \sin 3°}{2} = 0.22 \text{ in}$$

Table 9-9 lists, for Inco 718 and a life of 10 000 cycles, an allowable motion stress of 150 000 psi. It is good practice, however, to use a lower value for high-pressure bellows designed for improved stability. In our design, we use a value of 0.36 times the limiting bulging stress. Thus, the motion stress = $0.36 \times 150\,000 = 54\,000$ psi. Substitute this and e_b into equation (9-27):

$$S_m = \frac{1.40 C_t E t e_b}{N_c h^2}$$

$$N_c = \frac{1.40 C_t E t e_b}{S_m h^2} \text{ (from fig. 9-22, } C_t = 1 \text{ for 20 percent thinning)}$$

$$= \frac{1.40 \times 1 \times 29.6 \times 10^6 \times 0.022 \times 0.22}{54\,000 \times (0.410)^2} = 22.1, \text{ say } 22$$

From equation (9-46), the pitch of the bellows

$$L = (8 + 2N_p)t = (8 + 2 \times 3) \times 0.022 = 0.308, \text{ say } 0.310 \text{ in}$$

Free axial length of the bellows:

$$L_a = (N_c - 0.5)L + N_p t$$
$$= (22 - 0.5) \times 0.310 + 3 \times 0.022$$
$$= 6.66 + 0.066 = 6.726 \text{ in (i.e., less than 7 in)}$$

From figure 9-22, the correction factor C_t for the axial spring rate at 20 percent thinning is 0.72. Substitute this into equation (9-22) to obtain the axial spring rate of the bellows:

$$R_a = \frac{1.49 C_t C_p N_p E d_i t^3}{N_c h^3}$$

$$= \frac{1.49 \times 0.72 \times 0.85 \times 3 \times 29.6 \times 10^6 \times 8 \times (0.022)^3}{22 \times (0.410)^3}$$

$$= 4550 \text{ lb/in}$$

From equation (9-42), the critical internal stability pressure for bellows without angulation:

$$p_{cr}=\frac{5.02\times R_a}{L_a\left(\frac{d_0}{d_i}\right)}=\frac{5.02\times 4550}{6.726\left(\frac{8.82}{8}\right)}=3080 \text{ psi}$$

Comparing this with the maximum working pressure of 1750 psi, a safety factor of 3080/1750 = 1.76 remains to allow for bellows stability under conditions of angulation.

From sample calculation (9-2), the yield pressure = 2117 psi, and the ultimate pressure = 2887 psi. Substitute these into equation (9-26), to obtain the yield hoop stress of the bellows:

$$S_h=\frac{pd_m}{2N_pt}\left[0.57+\left(\frac{2h}{L}\right)\right]$$

$$=\frac{2117\times 8.42}{2\times 3\times 0.022}\times\left[0.57+\left(\frac{2\times 0.41}{0.31}\right)\right]$$

$$=42\,000 \text{ psi (less than } 170\,000 \text{ psi)}$$

The ultimate hoop stress of the bellows:

$$S_h=\frac{42\,000\times 2887}{2117}=57\,300 \text{ psi (less than } 200\,000 \text{ psi)}$$

The bellows design configuration is now established:

$d_i = 8$ in	$d_0 = 8.82$ in	$d_m = 8.42$ in
$t = 0.022$ in	$N_p = 3$	$h = 0.41$ in
$N_c = 22$	$L = 0.31$ in	$L_a = 6.726$ in
$R_a = 4550$ lb/in		

From equation (9-29), the angular spring rate of the bellows

$$R_b=\frac{d_m^2R_a}{458.4}=\frac{(8.42)^2\times 4550}{458.4}=705 \text{ in-lb/degree}$$

The bending moment on the duct at 3° angulation

$$M=R_b\theta=705\times 3=2115 \text{ in-lb}$$

From equation (9-25), the bellows pressure separating load

$$F_p=\frac{p(d_m^2-d_d^2)\pi}{4}$$

The required restraining link load at maximum working pressure, considering the normal axial force

$$F=F_p+\frac{pd_d^2\pi}{4}=\frac{pd_m^2\pi}{4}=\frac{1750\times(8.42)^2\times\pi}{4}$$

$$=97\,500 \text{ lb}$$

9.6 DESIGN OF GIMBAL MOUNTS

Gimbal Design Considerations

Primary design considerations for gimbal mounts are:

1. *Required pivotal movement of engine assembly or thrust chamber for thrust vector control.*—Generally ranging from ±4° to ±10°.
2. Required adjustment for thrust alinement and positioning.
3. *Thrust level.*—This determines the structural and bearing design of the gimbal mounts.
4. *Required operational life.*—Generally 1000 cycles minimum.
5. Minimum deformation of the bearing surface, prevention of bearing surface galling.
6. *Propellant duct installation.*—Some designs require flow of one of the propellants through the center of the gimbal mount.
7. *Maintenance of the gimbal mount.*—This is largely affected by the lubrication requirement of the bearing surfaces. If possible, a gimbal boot should be provided to protect the bearing surfaces from dust, water, and foreign materials.
8. *Lightweight.*—High strength-to-weight materials should be used.

Ring-Type Gimbal Mounts

Figure 9-23 presents a typical gimbal mount designed for low-thrust, upper stage engine applications up to 20 000 pounds. The design is a closed-yoke, flowthrough-ring type gimbal, utilizing plain bearing pivot joints. This configuration provides for the main oxidizer duct to pass through the assembly in the longitudinal axis to the thrust chamber dome. The gimbal mount is designed to connect the vehicle main oxidizer

END OF REFERENCE

70

REFERENCE

71

LIQUID ROCKET TANKS AND COMPONENTS. NASA SP-8088, 1974.

NASA
SPACE VEHICLE
DESIGN CRITERIA
(CHEMICAL PROPULSION)

NASA SP-8038

LEWIS RESEARCH CENTER
Aerospace Safety Research
and Data Institute
DEC 06 1974
CLEVELAND, OHIO

LIQUID ROCKET METAL TANKS AND TANK COMPONENTS

MAY 1974

NATIONAL AERONAUTICS AND SPACE ADMINISTRATION

GUIDE TO THE USE OF THIS MONOGRAPH

The purpose of this monograph is to organize and present, for effective use in design, the significant experience and knowledge accumulated in development and operational programs to date. It reviews and assesses current design practices, and from them establishes firm guidance for achieving greater consistency in design, increased reliability in the end product, and greater efficiency in the design effort. The monograph is organized into two major sections that are preceded by a brief introduction and complemented by a set of references.

The State of the Art, section 2, reviews and discusses the total design problem, and identifies which design elements are involved in successful design. It describes succinctly the current technology pertaining to these elements. When detailed information is required, the best available references are cited. This section serves as a survey of the subject that provides background material and prepares a proper technological base for the *Design Criteria* and Recommended Practices.

The *Design Criteria*, shown in italics in section 3, state clearly and briefly what rule, guide, limitation, or standard must be imposed on each essential design element to assure successful design. The *Design Criteria* can serve effectively as a checklist of rules for the project manager to use in guiding a design or in assessing its adequacy.

The Recommended Practices, also in section 3, state how to satisfy each of the criteria. Whenever possible, the best procedure is described; when this cannot be done concisely, appropriate references are provided. The Recommended Practices, in conjunction with the *Design Criteria*, provide positive guidance to the practicing designer on how to achieve successful design.

Both sections have been organized into decimally numbered subsections so that the subjects within similarly numbered subsections correspond from section to section. The format for the Contents displays this continuity of subject in such a way that a particular aspect of design can be followed through both sections as a discrete subject.

The design criteria monograph is not intended to be a design handbook, a set of specifications, or a design manual. It is a summary and a systematic ordering of the large and loosely organized body of existing successful design techniques and practices. Its value and its merit should be judged on how effectively it makes that material available to and useful to the designer.

CONTENTS

	Page
1. INTRODUCTION	1
2. STATE OF THE ART	3
3. DESIGN CRITERIA and Recommended Practices	93
APPENDIX A - Conversion of U.S. Customary Units to SI Units	127
APPENDIX B - Glossary	129
REFERENCES	139
NASA Space Vehicle Design Criteria Monographs Issued to Date	151

SUBJECT	STATE OF THE ART		DESIGN CRITERIA	
TANK CONFIGURATION	*2.1*	13	*3.1*	93
Vehicle-Tank Optimization	*2.1.1*	13	*3.1.1*	93
Subsystem-Tank Optimization	*2.1.2*	14	*3.1.2*	93
TANK MATERIAL	*2.2*	16	*3.2*	94
Mechanical Properties	*2.2.1*	17	*3.2.1*	94
Temperature Effects on Properties	*2.2.1.1*	18	*3.2.1.1*	94
Fatigue Strength	*2.2.1.2*	19	*3.2.1.2*	95
Creep	*2.2.1.3*	19	*3.2.1.3*	95
Biaxial-Stress Properties	*2.2.1.4*	20	*3.2.1.4*	95
Fabrication Considerations	*2.2.2*	21	*3.2.2*	96
Shaping and Forming	*2.2.2.1*	21	*3.2.2.1*	96
Welding	*2.2.2.2*	23	*3.2.2.2*	97
Thermal Processing	*2.2.2.3*	24	*3.2.2.3*	97
Material Compatibility with Environments	*2.2.3*	28	*3.2.3*	98
Sources of Material/Fluid Reactions	*2.2.3.1*	30	*3.2.3.1*	99

SUBJECT	STATE OF THE ART		DESIGN CRITERIA	
Manufacturing Fluids and Process	*2.2.3.1.1*	30	*3.2.3.1.1*	99
Testing Fluids	*2.2.3.1.2*	31	*3.2.3.1.2*	100
Stored Fluids	*2.2.3.1.3*	31	*3.2.3.1.3*	100
Atmospheric and Environmental Corrosion	*2.2.3.1.4*	32	*3.2.3.1.4*	100
Types of Material/Fluid Reactions	*2.2.3.2*	33	*3.2.3.2*	101
Stress-Corrosion Cracking	*2.2.3.2.1*	33	*3.2.3.2.1*	101
Galvanic Corrosion	*2.2.3.2.2*	37	*3.2.3.2.2*	102
Hydrogen-Environment Embrittlement	*2.2.3.2.3*	38	*3.2.3.2.3*	102
Material Ignition	*2.2.3.2.4*	39	*3.2.3.2.4*	102
Fracture Control	*2.2.4*	40	*3.2.4*	103
Material Fracture Toughness	*2.2.4.1*	43	*3.2.4.1*	104
Safe-Life Analysis	*2.2.4.2*	47	*3.2.4.2*	105
Additional Elements in a Fracture-Control Program	*2.2.4.3*	48	*3.2.4.3*	105
TANK STRUCTURAL DESIGN	*2.3*	49	*3.3*	106
Safety Factor	*2.3.1*	50	*3.3.1*	106
Loads Analysis	*2.3.2*	52	*3.3.2*	107
Tank Sidewall	*2.3.2.1*	52	*3.3.2.1*	107
End Closure	*2.3.2.2*	52	*3.3.2.2*	107
Intertank Bulkhead	*2.3.2.3*	52	*3.3.2.3*	108
Attachment	*2.3.2.4*	53	*3.3.2.4*	108
Membrane Thickness	*2.3.3*	53	*3.3.3*	108
Sidewall	*2.3.4*	54	*3.3.4*	109
Skin-Stringer-Frame	*2.3.4.1*	54	*3.3.4.1*	109
Waffle	*2.3.4.2*	55	*3.3.4.2*	109
Monocoque	*2.3.4.3*	58	*3.3.4.3*	111
End Closure	*2.3.5*	58	*3.3.5*	111
Forward Bulkhead	*2.3.5.1*	61	*3.3.5.1*	111
Aft Bulkhead	*2.3.5.2*	62	*3.3.5.2*	112
Intertank Bulkhead	*2.3.5.3*	64	*3.3.5.3*	112
Sandwich Construction			*3.3.5.3.1*	113

SUBJECT	STATE OF THE ART		DESIGN CRITERIA	
Attachment Junctures	*2.3.6*	65	*3.3.6*	113
Weld Joints	*2.3.6.1*	65	*3.3.6.1*	113
Bulkhead/Sidewall Juncture	*2.3.6.2*	67	*3.3.6.2*	115
Bosses and Support Provisions	*2.3.6.3*	69	*3.3.6.3*	115
Openings and Access Doors	*2.3.7*	71	*3.3.7*	116
TANK COMPONENTS	*2.4*	72	*3.4*	118
Propellant Slosh and Vortex Suppression Devices	*2.4.1*	72	*3.4.1*	118
Propellant Positioning Devices	*2.4.2*	72	*3.4.2*	118
Propellant Expulsion Devices	*2.4.3*	74	*3.4.3*	119
Expulsion Efficiency	*2.4.3.1*	76	*3.4.3.1*	119
Material	*2.4.3.2*	77	*3.4.3.2*	120
Design Margin	*2.4.3.3*	79	*3.4.3.3*	120
Tank Insulation	*2.4.4*	82	*3.4.4*	121
TANK DESIGN ANALYSIS	*2.5*	82	*3.5*	121
Strength Analysis	*2.5.1*	85	*3.5.1*	121
Tension-Loaded Structure	*2.5.1.1*	86	*3.5.1.1*	122
Compression-Loaded Structure	*2.5.1.2*	87	*3.5.1.2*	122
Major Junctures	*2.5.1.3*	87	*3.5.1.3*	122
Local Attachments and Openings	*2.5.1.4*	88	*3.5.1.4*	123
Structural Dynamics	*2.5.2*	88	*3.5.2*	123
Bending Frequency	*2.5.2.1*	89	*3.5.2.1*	124
External Dynamic Environment	*2.5.2.2*	89	*3.5.2.2*	124
TANK FABRICATION	*2.6*	89	*3.6*	125
TESTING AND INSPECTION	*2.7*	90	*3.7*	125

efficiency of materials for a compressively loaded structure, it is usually necessary to utilize a structural index that represents the structural configuration and the loading anticipated. This subject is treated in references 6 and 7.

2.2.1 Mechanical Properties

The mechanical properties of concern in the design and analysis of propulsion-system tanks are ultimate tensile strength (F_{tu}), which governs ultimate burst pressure under ductile failure conditions; tensile yield strength (F_{ty}), because of the requirement that there be no yielding either at limit load conditions or during proof testing; compressive yield strength (F_{cy}) for compression critical structures; and the material elastic properties (E, G, and ν). Shear and bearing strength properties (F_{su}, F_{bru}, and F_{bry}) apply to design details such as mechanical attachments and are not normally important factors in the selection of materials.

High-cycle, low-stress fatigue data sometimes are required to evaluate the effects of structural vibration or severe acoustic environment. Low-cycle, high-stress fatigue data often are used to evaluate the effects of multiple pressurization cycles. The material properties utilized in fracture-mechanics analyses are discussed in section 2.2.4.

The effects of a number of important variables on mechanical properties must be considered. These variables include temperature, thermal exposure, duration of loading, biaxiality and triaxiality of loading, rate of loading, and unusual environments such as corrosive fluids and radiation. Design properties are determined for base metal and welds and sometimes for weld heat-affected zones. The effects of loading direction with respect to base-metal grain orientation are considered. Properties along the direction of the weld bead as well as across the weld are evaluated. The effects of all processing, forming, and heat treatments on material design properties are evaluated.

Whenever possible, the precise values of the material mechanical properties used in design and analysis (the "design allowables") are determined by methods that result in consistent levels of reliability for all materials and conditions of application and service. The military handbooks, MIL-HDBK-5B (ref. 8) for metals and MIL-HDBK-17A (ref. 9) for plastics, contain considerable design property data. Nearly all other sources of materials properties data, unless explicity stated otherwise, contain only typical values that are not suitable *per se* as design values.

The methods used to compute design allowable strengths of unflawed materials for MIL-HDBK-5B are covered in MIL-HDBK-5B Guidelines for the Presentation of Data (ref. 8, ch. 9). Two reliability levels are observed, "A" values, which must be met or exceeded by the product 99 percent of the time, and "B" values, which must be met or exceeded 90

percent of the time. In both values, a statistical confidence level of 95 percent is observed. "A" allowables are used for single-load-path structures such as pressure vessels.

The determination of design property values for welds presents some special problems. Design values are not currently available in reference 8 for welded alloys of interest for aerospace pressure vessels. Weld test data that are available in the literature can be used only as a guide to the values that might be reliably obtained in any given welding setup. The many variables that affect weld quality and strength are discussed further in section 2.2.2.2 of this monograph and treated in detail in reference 10; methods for determining weld allowables are also discussed in the same reference.

The basic approach for determining weld allowables that is described in reference 10 is similar to the approach recommended in the MIL-HDBK-5B Guidelines (ref. 8, ch. 9) for metals in general (assuming that process control is exercised over all of the significant welding variables) with but one important exception: the minimum weld strength determined by statistical analysis of test data on weld coupons may be given a further reduction to account for differences between the behavior of coupons and welded structures. This reduction factor has been termed a "coupon/structure ratio" (ref. 10, p. 71) and is evaluated by comparative tests of coupons and representative structures such as subscale tanks. Values of this ratio used to establish allowable weld strengths for tanks and other structures on the Apollo spacecraft and Saturn S-II stage have been in the range of 0.80 to 0.90 (10 to 20 percent reduction in strength).

2.2.1.1 TEMPERATURE EFFECTS ON PROPERTIES

Reduced temperatures tend to increase material mechanical strength properties, but often decrease material ductility and toughness values. Such strength increases sometimes are utilized in the design and analysis of tanks intended for the containment of cryogens when a significant weight saving can be realized. However, it is then necessary to ensure that the fracture toughness of the material is adequate for the anticipated operational and proof-testing conditions; this subject is treated in detail in section 2.2.4. It is also necessary to ensure that room-temperature tank pressurizations can be limited to values that are consistent with the lower room-temperature mechanical properties.

Elevated temperatures tend to reduce material mechanical properties. For some materials (e.g., titanium alloys), even a small increase in temperature above room temperature results in a significant reduction in strength (approximately 10 percent at 200° F). Temperature increases on this order can result from compression heating during pressurization of high-pressure gas containers when a proper heat exchanger is not used. If such effects are not considered, yielding may occur in tanks fabricated from titanium and other alloys that are sensitive to temperature.

2.3.2 Loads Analysis

Vehicle-tank structure must be adequate not only to withstand the loads from vibration, thermal shock, propellant slosh, and tank internal pressure, but also to provide the main load path for vehicle body loads. Thus, it is necessary to consider all conditions of loading during the design phase, because the type of loads can influence the selection of tank construction: compressive loads may dictate semi-monocoque construction, whereas pure pressure loads may dictate membrane-type construction. Vehicle-tank subassemblies are subjected to different types of loading conditions and therefore must be examined separately.

2.3.2.1 TANK SIDEWALL

Vehicle-tank sidewalls are subjected to pressure, propellant inertial forces axial load, and bending moments. Loads in the hoop direction are determined by combining the tank ullage head pressures and load pressure with the propellant inertia forces. The longitudinal loads result from a combination of ullage pressure, tank axial load, and bending moment. Methods for combining these loads are shown in reference 96.

2.3.2.2 END CLOSURE

Loads imposed on the end closures of vehicle tanks are the result of the tank ullage pressure and acceleration forces on the propellants. During boost, aft bulkheads have a maximum pressure at the apex, whereas forward bulkheads have minimum pressure at the apex. To establish the load at a specific location on the end closure, both pressure and closure geometry must be considered. Methods for determining these loads are described in reference 97.

2.3.2.3 INTERTANK BULKHEAD

Where there are separate and individual bulkheads on two adjoining tanks, the load on each is determined as described above for tank end closures. The single "common bulkhead", however, is subjected to either burst or collapse loads and to temperature gradients through its thickness. Applied loads (pressure) at any given point are calculated in the manner described for tank end closures, except that the bulkhead "feels" only the difference between the forward and aft pressures at any given point. To maintain stability under collapsing pressure loads, the bulkhead is designed to have a large bending stiffness (as compared with a membrane bulkhead). Consequently, the resulting design (stiffened skin or sandwich) requires a more sophisticated internal-loads analysis. This generally is

accomplished by a multilayered shell-of-revolution program (refs. 98 and 99) that takes into account the extensional, shear, and bending stiffnesses in both the hoop and meridional directions of both facing sheets and core. A membrane bulkhead is satisfactory if caution is exercised in maintaining a positive Δp in the right direction.

2.3.2.4 ATTACHMENT

Loads are imposed on a tank at the points where other portions of the system are mated to the tank. The magnitude and direction of the loads generally are a function of the weight of the attached component or subsystem multiplied by the established amplication factor for acceleration and vibration forces. Only the attachment bolts and the most immediate structure feel these loads in full magnitude. To a great extent, experience and judgment are used to determine the magnitude of load on the adjoining structure by making due allowance for the damping that occurs as the force progresses from the point of excitation. Axial growth of vehicle tanks poses no restraint on tank function, but attachment of subsystem tanks must be analyzed carefully to allow for the loads generated at the attachment points by changing pressure and temperature.

2.3.3 Membrane Thickness

Except in rare cases, liquid rocket propulsion system tanks are thin-wall structures, i.e., the wall thickness is less than about one-tenth the tank radius (ref. 100, p. 293). This permits the use of simple stress formulas in the trade studies of simple geometrical shapes such as spheres and cylinders. Tentative material selections and corresponding membrane thicknesses and operational stress levels are obtained by using only mechanical-property data in conjunction with arbitrarily selected factors of safety. Practical considerations of producibility, handling, and stiffness are evaluated to validate these preliminary selections.

Before material is selected, working stress level, membrane thickness, and fracture-control consideration must be taken into account. The material must possess suitable levels of toughness and resistance to subcritical flaw growth to ensure compliance with intended tank service life. Material selection is followed by definition of the proof-test stress, operational stress, and NDI requirements consistent with mission performance requirements, as discussed in section 2.2.4.2. In the determination of membrane thickness, the most restrictive condition (e.g., safety factor, fracture-control criteria, producibility, or handling) must be identified and employed.

Because of its strength/density ratio, a certain material may provide a weight advantage analytically that is negated by further investigation. In trade studies made for the propulsion-system tanks for the Apollo Service Module, it was determined that fiberglass

provided the lightest weight tank. However, the addition of reinforcements for reaction of the support loads, tank membrane penetrations, and attachment of closeout doors negated the weight advantage, and 6Al-4V titanium alloy ultimately was used. Sometimes the analytically permissible thinness of the tank membrane may be outside the limits of proven fabrication techniques, or it may result in extremely fragile tanks. For example, the shells for the positive expulsion tanks in the Apo[illegible] Service Module required a hemispherical membrane thickness (6Al-4V titanium) of 0.011 in. based on pressure considerations only, but manufacturing and handling considerations dictated the 0.023-in. thickness that presently is used.

In the case of vehicle tanks, for which material is selected during configuration optimization, the designer proceeds directly to establish membrane thickness. The membrane thickness for a vehicle-tank sidewall is dictated by the product of hoop tension load under the maximum anticipated internal pressure times the factor of safety. The sidewall membrane usually is stiffened against buckling by various means such as stringers, frames, or ribs spaced in a waffle pattern. In some cases (e.g., the Atlas and Centaur vehicles), additional membrane rigidity is attained through the internal working pressure within the tank.

2.3.4 Sidewall

Sidewall design is especially important in the design of large vehicle tanks, which generally not only contain the vehicle propellants but transmit vehicle body loads as discussed in section 2.3.2.1. The principal sidewall designs for pressurized vehicle tanks are skin-stringer-frame, waffle, and monocoque construction. Selection of the optimum type of structure is dependent on the magnitude of the externally applied body loads and the type of propellants to be contained. Highly loaded sidewalls generally are designed with skin-stringer-frame construction, whereas lightly loaded sidewalls are waffle construction. Very lightly loaded sidewalls can be monocoque construction but usually must be pressurized for stability.

2.3.4.1 SKIN-STRINGER-FRAME

Integral stiffening is the form of skin-stringer construction that is best suited for propellant tanks. This design eliminates the thousands of potential leaks associated with the mechanical attachments between the skin and the stringers and frames of conventional construction. Two configurations of skin-stringer design shown in figure 5 consist of (a) panels in which the skin, "blade" stringers, and horizontal ribs are machined as an integral unit, frames being attached mechanically to the horizontal ribs after the panels are formed; and (b) panels in which only skin and "T" stringers are machined, and frames are added after forming by

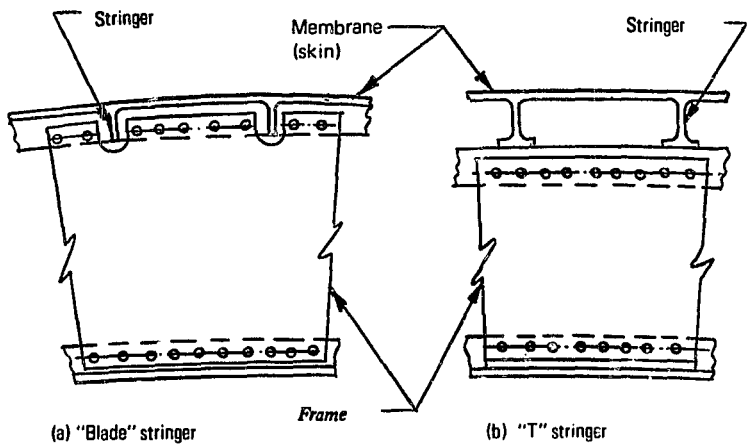

Figure 5. – Two kinds of skin-stringer-frame construction.

mecha ical attachment to the inboard flanges of the T stringers. The blade design is lighter in the lower load regime, whereas the T-stringer desig is lighter at higher load levels. Membrane thicknesses are based on the hoop tension loads under maximum expected internal t k pressure. Stringer spacing is dictated by local stability requirements. Stringer configuration and frame spacing for minimum-weight structure are based on general stability requirements under critical (varies with temperature) axial compression loads in combination with internal pressures. The material used must be readily machinable and have good forming and welding characteristics. Welded joints are highly desirable as a means to avoid propellant leakage. Since tensile design allowables for a weld are lower than those for the parent material, compensation is made by an appropriate increase in thickness at the weld joints. It is desirable to design so that the skin does not buckle at the design load. Skin buckling also impairs the reliability of any external insulation and causes sudden changes in the flexural stiffness of the vehicle stage. The stiffener spacing required to keep the skin unbuckled at limit load is determined from curved-panel buckling data, due account being given the stabilizing influence of tank internal working pressure. Once skin thickness and stringer spacing have been fixed, computer programs (ref. 101) can readily optimize the stringer and frame configuration to provide the load-carrying capability that meets the required column buckling and general stability requirements. Figure 6 shows a typical sidewall construction successfully used on the LH_2 tank for the Saturn S-II stage.

2.3.4.2 WAFFLE

A tank membrane stiffened by integral ribs that are arranged in a "waffle" pattern is a form of construction that not only is efficient in the usual loading range but also possesses many

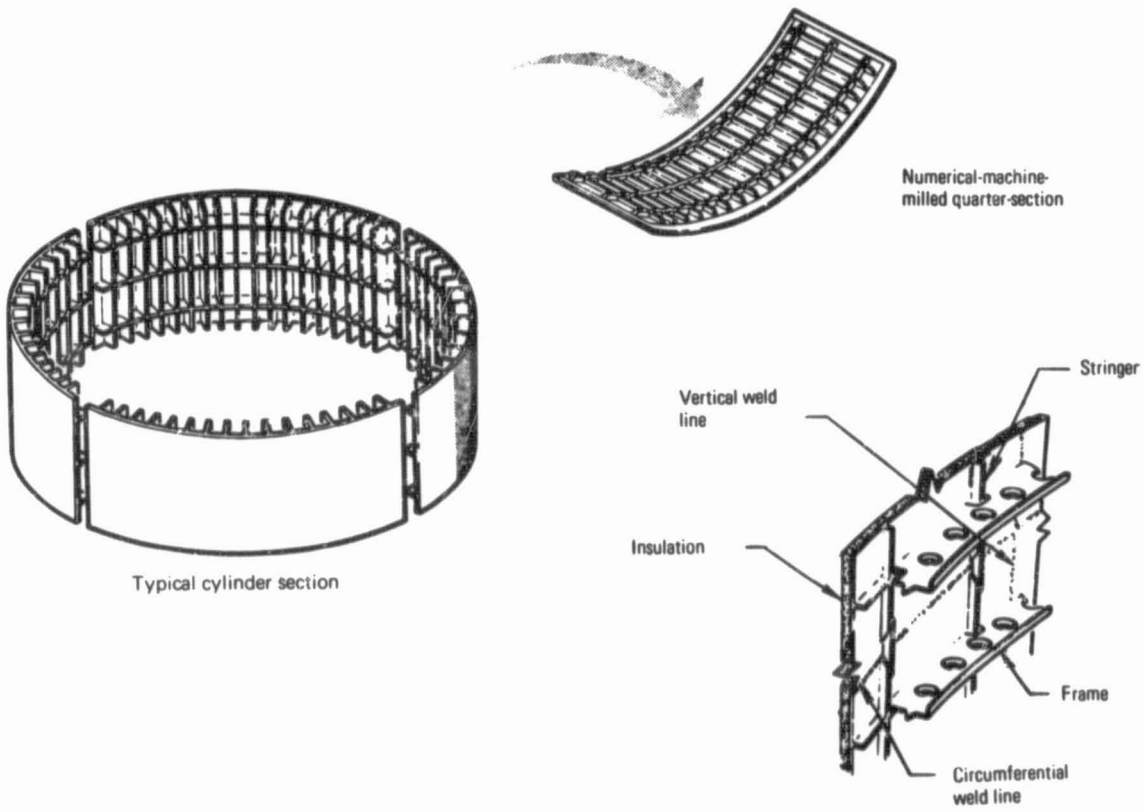

Figure 6. – Sidewall construction on LH_2 tank for Saturn S-II stage.

manufacturing advantages. Waffle construction is utilized in the design of the Saturn S-IV-B stage. The integral rib stiffeners usually are formed by mechanical or chemical milling of the waffle pattern in a thick plate; mechanical milling is the more efficient method. Design of the waffle structure usually is dictated by primary shell stability requirements; therefore, a low density material is advantageous. The plate material usually is easy to machine, and fabrication is economical. Because of these two considerations, aluminum-alloy plate is a prime candidate for the waffle plate material. Figure 7 shows two kinds of waffle configuration, square and isogrid.

In the widely-used square pattern (fig. 7(a)), the rib spacing is such that the individual skin panels will buckle under the same load that will cause a general instability or failure of the entire vehicle tank cylindrical structure. The general instability mode of failure is

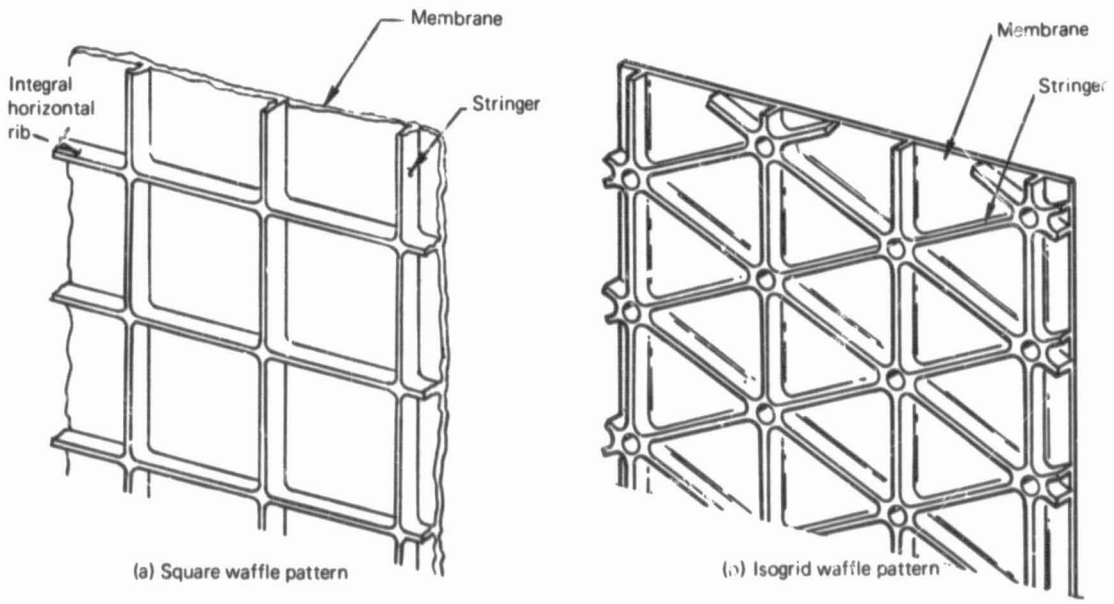

Figure 7. – Two basic waffle configurations.

determined as the critical buckling load of an equivalent isotropic cylinder. The waffle efficiency theoretically increases with increasing plate thickness and decreasing skin and rib thickness; however, minimum skin thickness is dictated by the hoop tension requirements. The rib spacing and height are optimized on the basis of this fixed skin thickness. Where the continuity of stiffening ribs is interrupted, weld lands are sufficiently thick to maintain shell stability. This construction constitutes a fabrication advantage in that all mechanical and individual rib splices are eliminated.

Another waffle design that has shown excellent promise is the isogrid configuration. Isogrid is a pattern of integral stiffening consisting of a gridwork of equilateral triangles, as shown in figure 7(b). This structural arrangement, currently used on the tankage on the Delta vehicle, has the following properties:

(1) The bending and extensional stiffnesses are independent of the grid orientation.

(2) No coupling between the grid and the skin due to Poisson-ratio effects exists for material with $\nu = 1/3$. This condition implies that strength calculations for inside or outside stiffening are identical.

(3) Because of properties (1) and (2), isogrid shell analysis is equivalent to that for monocoque when the proper equivalent thickness and equivalent modulus of elasticity are used. Because of the simplicity of the analysis, it is comparatively easy to optimize and design isogrid structure.

Analytical weight comparisons of rectangular waffle grid patterns and isogrid patterns have shown the isogrid pattern to be lighter. In addition, tests have shown that with isogrid construction, in comparison with rectangular patterns, appreciably higher stresses can be developed prior to buckling.

Waffle construction offers several other practical advantages: manufacturing is simple because of the elimination of internal structure; reinforced areas in the milling pattern for cutouts or attachment provisions are easily incorporated; and the fact that the skin will remain smooth and unbuckled precludes problems of debonding of, and damage to, external insulation.

2.3.4.3 MONOCOQUE

In general, pressure-stabilized monocoque construction results in the lowest structural weight. A material with a high tensile yield strength is necessary. Pressure-stabilized structures such as the Atlas and Centaur vehicles require extreme care during fabrication and transportation to preclude handling damage. Prevention of buckling in a pressure-stabilized monocoque structure requires that the meridional pressure stress be greater than the compressive meriodional stress created by external loads.

2.3.5 End Closure

End closures significantly affect cylindrical tankage length, and the basic end-closure configurations are established during the vehicle configuration optimization phase as described in section 2.1. Not only is the end-closure shape a consideration, but the closure between two tanks must be optimized; a selection must be made in favor of two separate bulkheads or one common bulkhead.

Theoretically, there are an infinite number of shapes from which to select. In actual practice, however, closure shapes usually represent a familiar geometric figure or minor variation thereof. For example, the Titan and Saturn S-IV tanks are designed with hemispherical end closures, Saturn S-II end closures are oblate spheroids, and the Atlas, Saturn IC, and Centaur tanks employ ellipsoidal end closures. Such standard geometric shapes facilitate weight analysis through computer subroutines as presented in reference 5. Figure 8 depicts some of the surfaces of revolution that have been analyzed by computer subroutines.

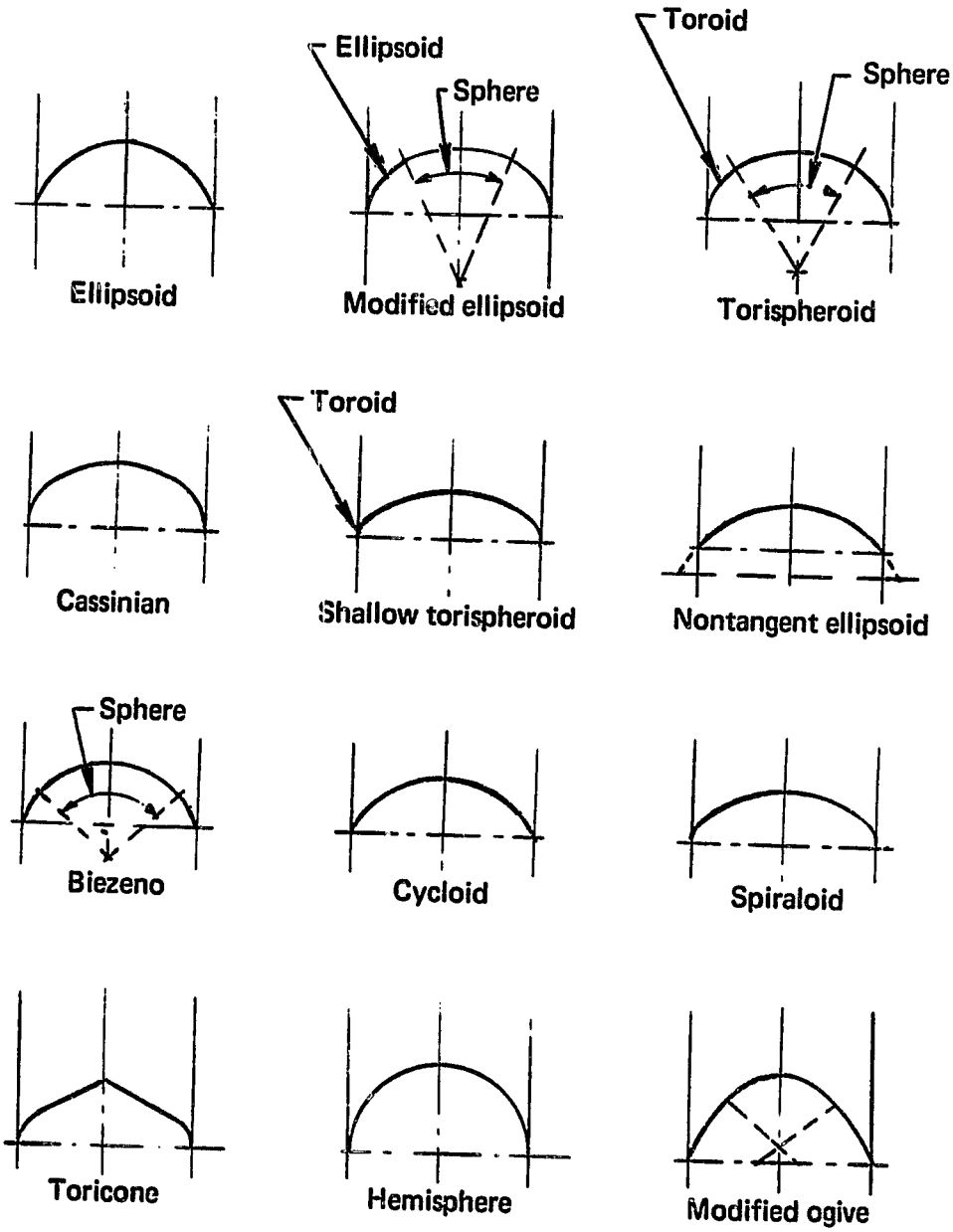

Figure 8. – Some surfaces of revolution that have been analyzed by computer subroutines.

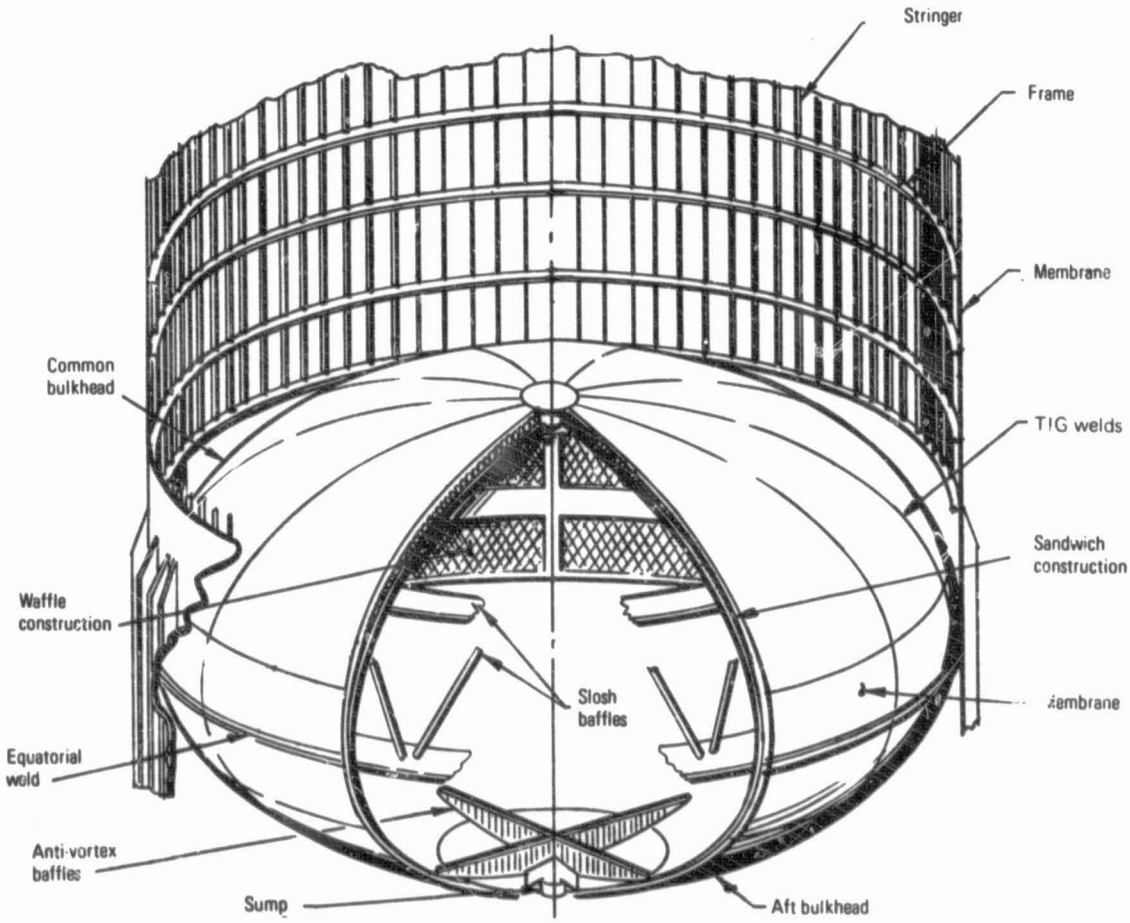

Figure 9. -- Cutaway drawing of the LOX/LH_2 tanks in the Saturn S-II stage.

Figure 9 shows the end closures used in the LOX tank of the Saturn S-II stage. Sandwich construction is employed to resist buckling where compressive loads exist, whereas a simple membrane construction is adequate for the areas loaded only in tension.

An example of honeycomb sandwich structure is shown in figure 10. For given facing materials and thicknesses, the core depth and density are dictated by the requirement for preventing primary instability and "face wrinkling" of the facing sheets. The variation of unit weight of the composite sandwich structure with the ratio of thickness of the two facings is investigated, and the optimum arrangement is determined.

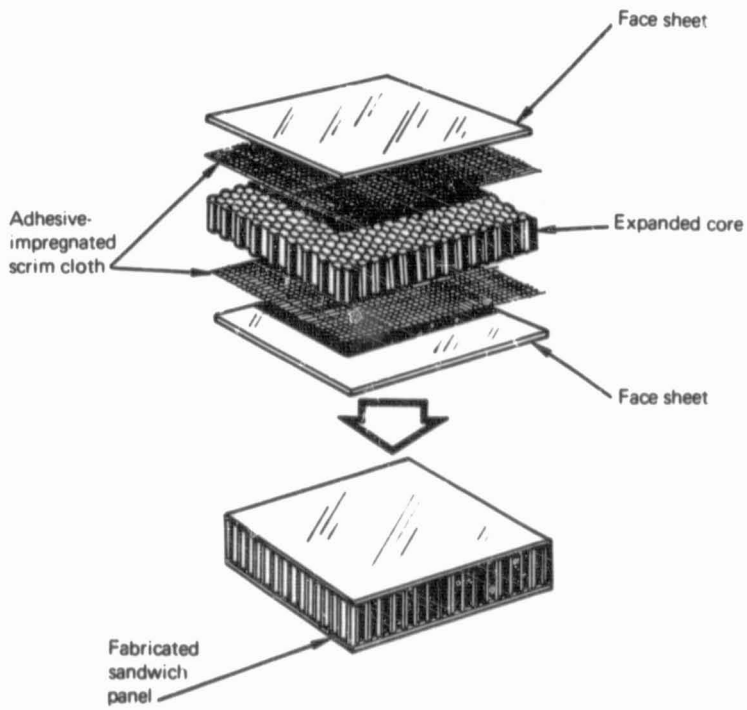

Figure 10. – Example of honeycomb sandwich structure.

The use of sandwich construction for the intertank bulkhead of booster tanks offers the possibility of significant weight savings. When tank internal pressures are low and shell instability is the critical problem, the facing sheets can be designed to operate at stresses close to the material compression yield stress. The total facing thickness is dependent on stresses associated with maximum tank pressure. The facings may be critical either under ultimate strength requirements in which the hoop tension stresses due to tank pressure are of primary importance or under yield requirements in which the combination of thermal and pressure stresses is of significance. Reference 102 presents typical methods used in selecting honeycomb sandwich structure.

2.3.5.1 FORWARD BULKHEAD

This bulkhead generally is convex (external surface), loaded primarily by bursting pressure; a thin sheet or "membrane" is the usual design approach. In a thin-shell design, the

head-depth-to-diameter relation must be analyzed to determine compressive stresses in the knuckle radii to ensure that no circumferential buckling pattern occurs. These analyses generally must be confirmed by tests, since information on buckling of heads due to internal pressure is meager.

To achieve minimum weight, the shell thickness is tapered so that the entire bulkhead is operating at the maximum allowable stress level in the meridional direction, regardless of shape. For minimum cost, however, a constant-thickness bulkhead is more desirable. Although a single-piece bulkhead is preferred, material size and current forming methods such as spin-forming, stretch-forming, hydroforming, or explosive-forming make this impossible. Generally, therefore, the bulkhead is designed to be fabricated by welding together a single central "dollar" section to a welded subassembly consisting of a number of gore segments. This practice avoids the juncture of the multiple welds where the gore sections meet at a common point. Hoop compressive stresses usually are avoided, the result being certain restrictions on bulkhead local radii of curvature, which in turn results in height-to-radius limitations.

Figure 11 shows a typical weight optimization curve for the Saturn S-II stage generated by the subroutine of reference 5. The curves show graphically the weight variations of tank sidewall, skirt, and bulkhead as the configuration of the bulkhead is varied. For the loading condition of the Saturn S-II LH_2 tank, the hemispherical bulkhead results in the heaviest structure, because of the necessity for a long skirt length.

2.3.5.2 AFT BULKHEAD

Aft bulkheads differ from forward bulkheads only in that hoop compressive forces may develop under certain conditions of loading. The region from the equator to the liquid level always will be in hoop compression during filling (assuming no ullage pressure), and compressive stresses also may occur during flight as a function of bulkhead local curvatures and the ratio of ullage pressure to acceleration-induced forces.

Aft bulkheads generally require waffle or sandwich construction or other kind of circumferentially stiffened structure in the upper portion. Minimum-weight design generally will dictate a shell of revolution with changing curvature and varying geometry. There are no reliable techniques for the stability analysis for this type of structure under the varying biaxial load conditions encountered. It is, therefore, mandatory that the analysis be conservative and that it be complemented with stringent verification testing. An additional significant consideration is that aft bulkheads must provide for engine feedlines. A central location is the preferable choice for a single engine.

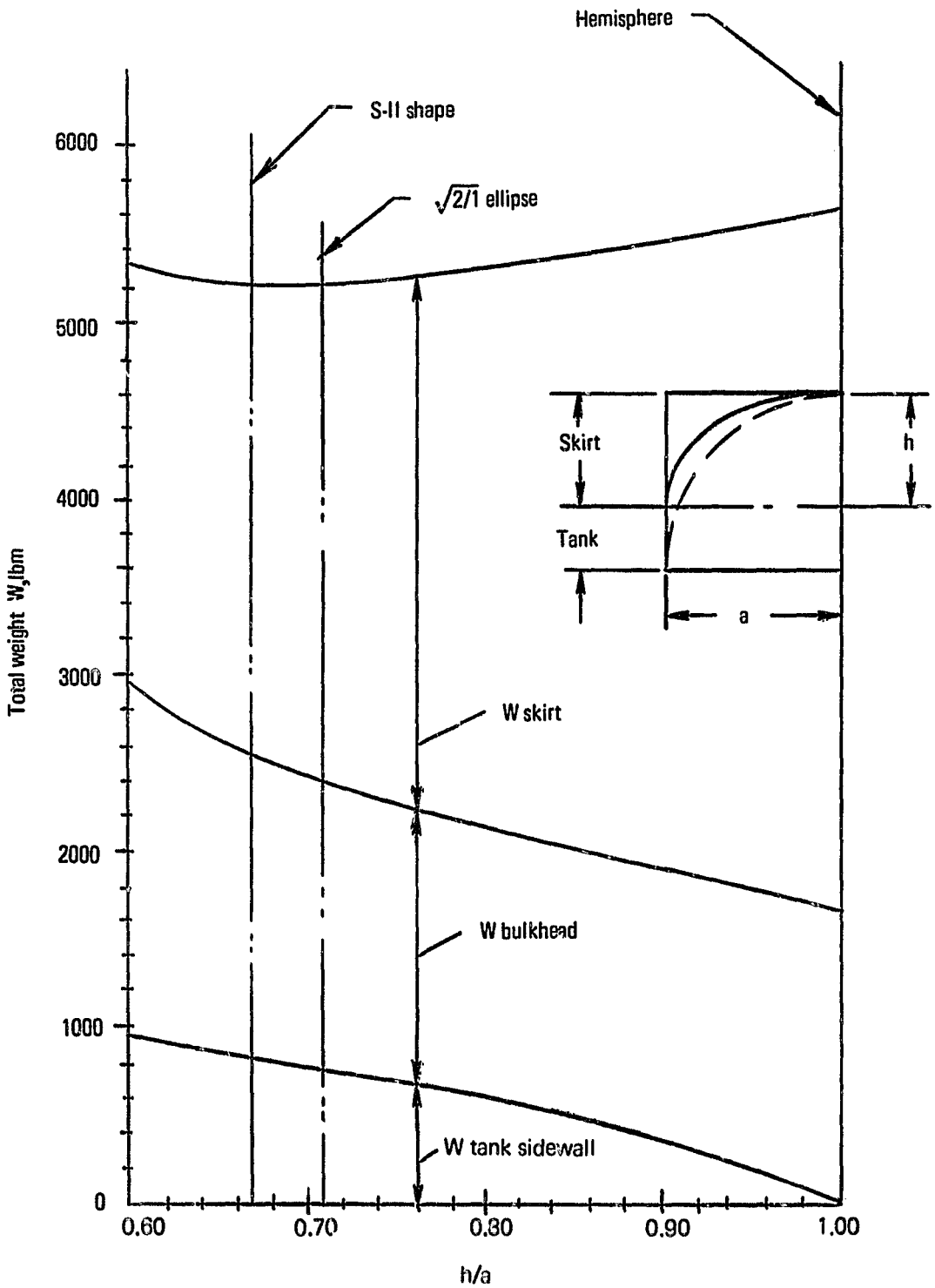

Figure 11. -- Variation of tank weight with variation of end-closure configuration (LH_2 tanks for S-II stage).

2.3.5.3 INTERTANK BULKHEAD

The fluids in a bipropellant vehicle are separated physically (and possibly thermally) either by two separate membrane bulkheads or by a common bulkhead. Figure 12 shows the two bulkhead concepts.

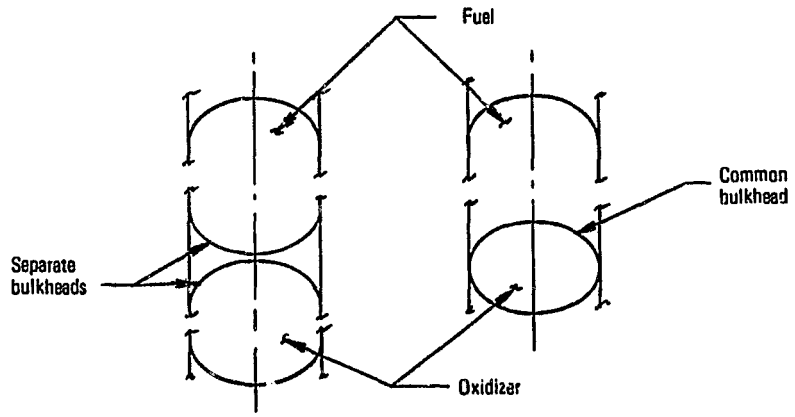

Figure 12. – Sketches of two basic types of intertank bulkheads.

The common bulkhead may be either self-supporting or pressure-stabilized. One feature of dual separate membranes is that space for and access to the fluid lines coming from the bottom of the forward tank is provided. Consideration must be given to the special problems involved in routing these lines either through or around the forward bulkhead of the lower tank.

There are several unique features in the self-supporting type of common bulkhead that make a determination of bulkhead weight versus bulkhead height somewhat more complex. The bulkhead must be designed for both bursting and collapsing pressures. The bulkhead therefore is of waffle or sandwich construction to provide stability under collapsing pressure. If insulation also is a requirement, sandwich construction usually is the most efficient, but consideration then must be given to both thermal and pressure stresses. Convex-vs-concave bulkhead (forward surface) attitudes are evaluated in connection with the relative magnitude of the burst-vs-collapse pressures. In general, consideration of the routing of the forward-tank propellant lines makes the convex (forward surface) attitude more desirable. Trapped residuals in the forward tank are minimized by the use of low-density filler material in the volume below the propellant outlets.

2.3.6 Attachment Junctures

2.3.6.1 WELD JOINTS

Weld-joint design is one of the most critical requirements of sound vehicle tankage structure. Since weld strength is less than that of the parent material, adequate load capacity must be achieved by increasing material thickness at the weld joint. Ideally, the thicker weld land would be made symmetrical about the membrane material. However, the expense of milling both sides and the desirability of maintaining a smooth exterior surface for aerodynamic reasons are overriding considerations that lead to the eccentric weld land configuration usually employed on booster tanks. Effective weld-joint strength can in some cases be improved by shaving the bead; this practice reduces stress raisers, removes the area most apt to contain flaws, and improves weld-joint ductility.

Optimum joint configuration can be achieved only by an extensive test program for determining the proper dimensions for the weld-land geometry for each material. Figure 13

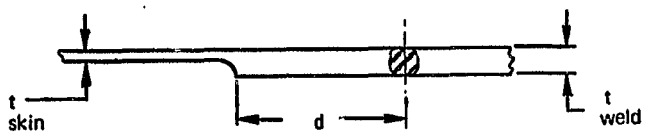

(a) Abrupt termination of weld land

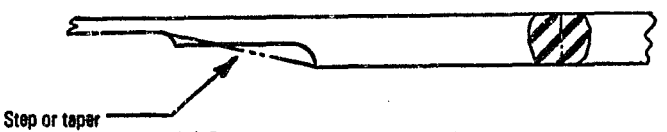

(b) Stepped or tapered termination of weld land

Figure 13. – Weld-joint configurations for vehicle tanks.

displays two weld-land designs for 2014-T6 and 2219-T87, two aluminum alloys commonly used in current vehicle tankage. Weld-land thicknesses range from 2 to 2¼ times the basic membrane thickness, and weld-land widths range from 1.25 to 2.00 in. The 1.25-in. width is the minimum required to prevent the heat-affected zone HAZ and the resultant strength reduction therein from reaching the fully stressed basic membrane. Weld-land thicknesses in excess of 2¼ to 2½ times the basic membrane thickness with abrupt terminations (fig. 13(a)) introduce bending stresses and some reduction in joint strength at the point where

the basic membrane meets the weld land. This concentrated strength reduction is avoided by introducing a stepped or tapered section between the skin and weld land as shown in figure 13(b).

In the typical subsystem tank, the weld joint for assembling tank sections is potentially the predominant structural discontinuity. The designer's task is to minimize the structural discontinuity across this joint. Underdesign results in premature tank failure in the weld joint. Overdesign results in a ring or span of material that is much more rigid than the tank membrane; the resultant difference in deflection while the tank is under load causes flexure in the tank membrane and possibly lower cyclic life. Figure 14 depicts some commonly used preweld joint preparations that have proven highly satisfactory in tank development programs to date.

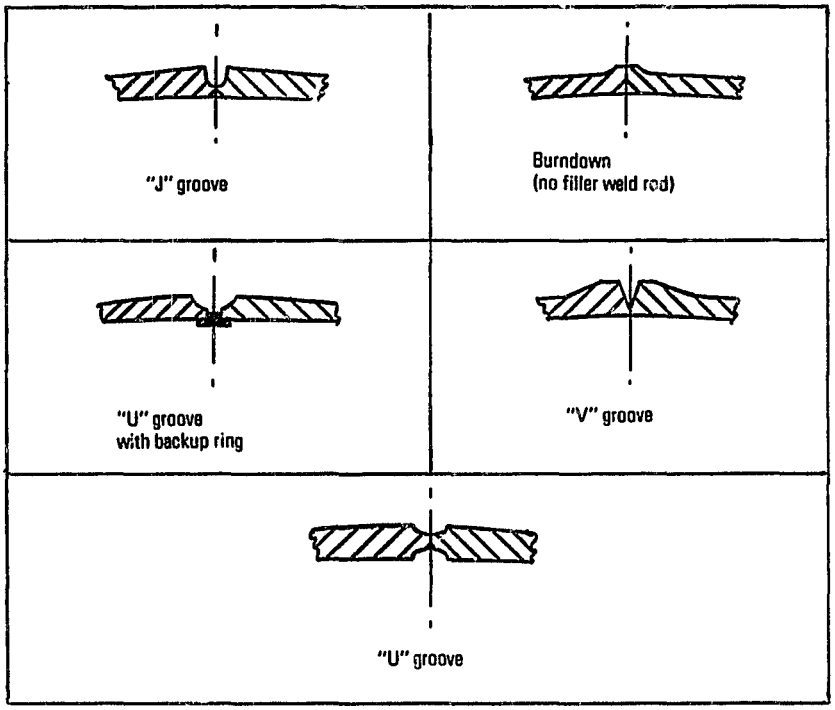

Figure 14. – Weld-joint configurations for subsystem tanks.

Since weld joints inherently are subject to variations in production, the experienced designer strives to minimize the linear length of weld joints in his tank designs. When possible, tank cylindrical sections are made by spin forging, thus eliminating longitudinal welds.

The probable introduction of distortion and oxidation, plus the need for elaborate equipment, preclude heat treatment of subsystem tank assemblies following welding. Postweld processing usually is limited to tank aging to relieve internal stresses caused by welding. The designer, as in vehicle-tank design, therefore increases the material thickness in the HAZ to compensate for the reduction in material strength that occurs as a result of annealing at and adjacent to the weld. Ideally, the gradations in loss of material strength would be precisely balanced by increased material thickness through a precisely contoured joint transition. From the practical standpoint, however, the additional joint efficiency and weight reduction frequently do not justify the attendant analysis and machine contouring effort, and a straight-taper joint transition is used.

Use of sophisticated chemicals and high-performance components in liquid rocket systems has emphasized the necessity for fluid cleanliness and for tanks that are cleanable. It may be noted in figure 14 that, except for the joint with a backup ring, the joints will be readily cleanable. In tanks with small ports, where interior access subsequent to welding is limited, it is mandatory that the weld-joint design require negligible cleanup following weld.

2.3.6.2 BULKHEAD/SIDEWALL JUNCTURE

A critical item in the design of liquid rocket tanks is the method of joining the major structural components (e.g., bulkhead to tank sidewall and skirt to tank sidewall). These junctures normally occur at a common location and almost always are accomplished with an appropriate fitting. A widely used fitting is a "Y" ring, so named because of its cross-sectional appearance. Examples of Y-rings, as used on the Saturn IC and the Titan II, are shown in figure 15. A different method, used on the Centaur, provides an angle for mechanical attachment of the skirt (fig. 16).

The Y-ring type of joint serves the following functions:

- Provides a structural load path from bulkhead to tank and from skirt to tank.
- Provides a leak-proof container.
- Provides easy inspectability and weld repair prior to skirt installation.
- Provides for mechanical attachment of skirt.
- When properly designed, creates low hoop stresses in the difficult meridian welds (three in Saturn IC tank) that splice the Y-ring segments.

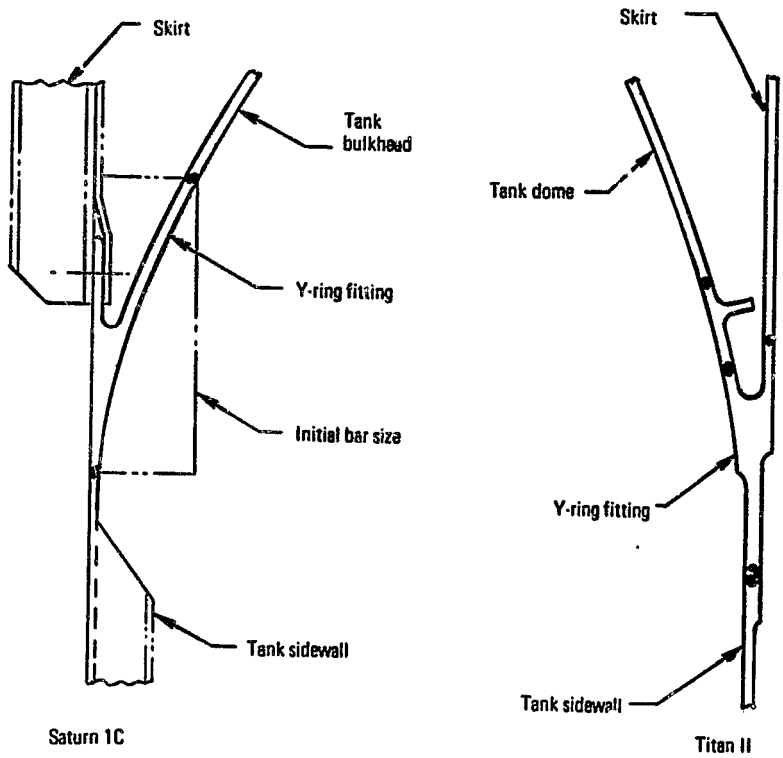

Figure 15. – Examples of Y-ring bulkhead/sidewall junctures.

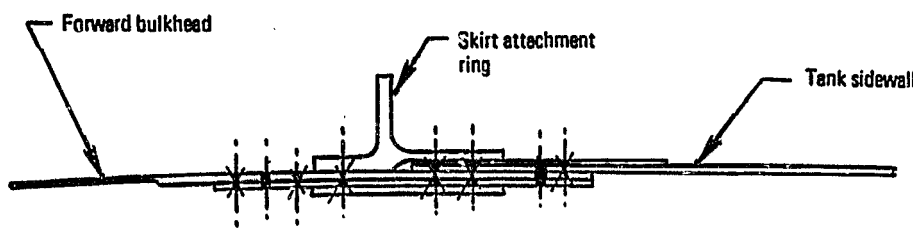

Figure 16. – Example of bulkhead/sidewall juncture used in Centaur.

A principal disadvantage associated with this type of joint is the difficulty associated with making the ring-splice meridian welds. This welding usually is accomplished in one of two ways:

(1) The initial bar stock is rolled to tank contour, the weld joint is prepared, and the entire cross section of the bar is welded by an extremely large number of passes. The desired cross section then is machined from the completed bar ring.

(2) The bar stock is machined to the desired cross section and formed to the required contour. The circumferential splices then are made by one or two welding passes along each leg and stem of the "Y".

The completed Y-ring then is mated to the bulkhead and tank sidewall by a circumferential weld and is mechanically spliced to the skirt.

The splice-joint buildup used on the Centaur tanks employs simple flat sheets for stiffening the membrane in the area of the skirt attachment ring.The ring (T-section) is machined from a circular forging, thereby eliminating welding of ring segments.

This method has the following advantages:

(1) It avoids expensive forgings, machining, and associated tooling.

(2) The bolting ring works with a variety of configurations, and mating of adjacent structure is comparatively simple.

(3) Weld discrepancies are easily repaired.

It has the following disadvantages:

(1) The method requires spot welding through as many as five layers of skin.

(2) The thin sheets require stringent control of weld schedules.

(3) Vehicle separation requires a circumferential shaped charge to fracture the ring.

2.3.6.3 BOSSES AND SUPPORT PROVISIONS

Attachment of system components and tank mounting structure generally is accomplished by providing local support points or bosses in tank structure. To avoid tank penetration, the bosses are made deep enough to accommodate mechanical fasteners. When the basic structure is made from a stock size of sufficient thickness, these bosses are integrally milled

Card #17

with the basic structure. This process creates "hard spots" that remain flat during forming and force the adjoining structure to do additional straining during both forming and subsequent tank tension loading. Additional local reinforcing is provided to minimize this excess straining by distributing the strain over a larger area. The reduced eccentricity and increased distance from the basic thickness to the hard-spot thickness minimize bending stresses at the discontinuity.

When system attachments are made to thin-shell structure such as a membrane bulkhead, the use of integral bosses requires a much larger initial material thickness and more extensive milling. Fabrication of attach bosses also can be accomplished by welding a circular machined ring (containing the boss) to the bulkhead; however, residual stresses from the welding can cause severe warpage in thin, compound-curvature bulkheads (less severe for flat or hemispherical shapes). This warpage can be minimized by the use of hard tooling and close tolerance parts and by shrink-fitting fitup procedures before welding. However, scrappage rate is high because of the limited repairability of this type of weld.

The nonintegral support provisions involve welding machined fittings (ports, flanges, support pads) to the tank membrane. This practice requires either providing a ring of thicker material in the tank membrane to compensate for the strength loss from welding or lowering the permissible tank operating pressure. In addition to structural analysis of the designs, the designer must consider both accessibility for tank cleaning following welding and distortion of the tank membrane due to weld heat. An advantage of nonintegral fittings is that the tank designer has more latitude in the method of fabrication of the tank membranes.

Although the integral fittings complicate membrane forging and machining, experience has shown that they are superior to welded fittings because of the absence of heat distortion, strength reduction, weld-induced contamination, and uncertainty about weld integrity that attend welded joints. To minimize the effect of integral-fitting discontinuities on the tankshell, however, the tank designer strives to minimize the number of fittings. Frequently, in gas-pressurant tanks, the fluid ports and tank supports are combined into a common boss. In liquid propellant tanks, the single access opening is attained by use of a closeout cover that contains both the inlet and outlet lines. When multiple tanks are used in series, the inlets usually are connected to standpipes within the tanks to preclude reverse migration of the fluids and to ensure series feedout.

Internal standpipes and stillwells in liquid-carrying tanks usually require end supports to withstand liquid slosh impact and to alter vibrational response. These internal supports most commonly utilize a slip joint to allow for longitudinal expansion and contraction of the tank but provide support to the standpipe and stillwells against side loads.

2.3.7 Openings and Access Doors

For purposes of this monograph, the term "openings" applies to all types of ports and access openings in the tank membrane. Openings and access doors are treated together because they represent similar design problems in membrane discontinuity. Ideally, the tank membrane would have no openings or access doors; realistically, of course, these provisions are required. Tank openings and access doors for propellant tankage generally are located at or near the apex of the bulkheads. This location has the advantage of being relatively easy to fabricate and simple to analyze, and it facilitates entry into the tank interior. The primary design objective is to prevent leakage throughout the entire life cycle. Two methods that employ integral bolting rings are illustrated in figures 17(a) and (b); the method employed on the Centaur for the forward door is shown in figure 17(c).

A bearing lip and oversize holes (fig. 17(a)) will reduce joint rotation due to eccentric bolt shear loading, whereas a large cross-sectional area in the bulkhead boss (fig 17(b)) will accomplish the same purpose by forcing most of the load to remain in the bolting ring and

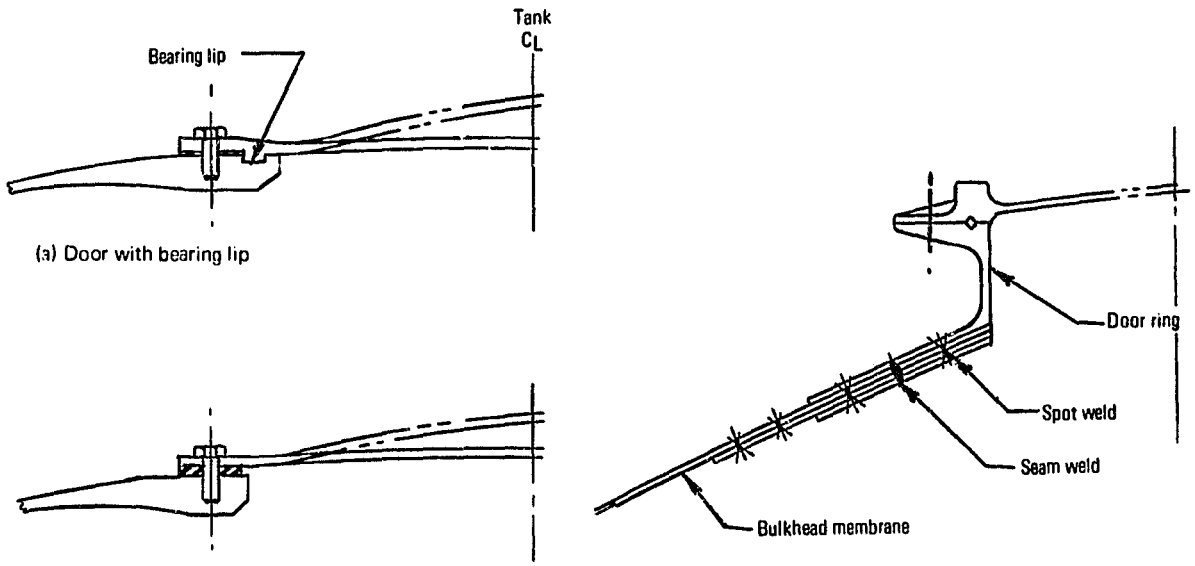

(a) Door with bearing lip

(b) Bulkhead boss with large cross-sectional area

(c) Centaur forward door

Figure 17. – Three designs for a tank access door.

not go through the door. Either design can incorporate a door of smaller radius of curvature than that of the adjoining structure in order to further reduce loads in the door, boss, and across the joint (dashed-line configuration).

Experience has also shown that in the design for a radial sealing gasket the final gap requirements between the door flange and the ring flange must be considered, since a local bending moment is induced as the torque is applied to the assembly bolts. It is desirable to select bolt spacing and seal and flange designs that minimize the final bending moment of the bolt joint.

Tank openings for system installations create local discontinuities at the attach points. The subject is discussed in section 2.3.6.3.

2.4 TANK COMPONENTS

2.4.1 Propellant Slosh and Vortex Suppression Devices

Sloshing of propellants can adversely affect vehicle stability and the integrity of the tank structure. Baffles are therefore provided to damp liquid motion. In cylindrical tanks, baffles generally take the form of flat rings attached to the structural shell as shown in figure 1; here they serve the double purpose of providing fluid damping as well as shell stability. For oblate spheroidal tanks, baffles may take the form of a truncated cone either perforated or open trussed. These cones generally are supported at the equatorial region and provide for liquid motion inhibition at the surface level only or throughout its height. A clear understanding of slosh and methods of counteracting it in large tanks may be obtained from the material in reference 103.

Fluid vortexing occurs at engine feed-line outlets; it is most severe at outlets in tank aft bulkheads, especially at central locations. Antivortex baffles generally take the shape of radial vanes either attached directly to the bulkhead skins or cantilevered outward from a central attachment. Figure 1 shows a method used for multiple outlets and figure 9 depicts a method employed for a centrally located fluid outlet.

2.4.2 Propellant Positioning Devices

A major problem in designing for a space environment is to provide a supply of gas-free propellant to the engine at the start of each firing cycle. In the near-zero-"g" operational environment of orbital spacecraft, gravitational forces are negligible, and capillary forces

END F REFERENCE

REFERENCE

72

TECHNICAL MANUAL OF OXYGEN/NITROGEN CRYOGENIC SYSTEMS. NAVAIR 06-30-501, NAVAL AIR SYSTEMS COMMAND, MAR. 1971.

THIS MATERIAL HAS BEEN APPROVED FOR PUBLICATION BY S. J. WALLER, NAVAL AIR SYSTEMS COMMAND, AUG. 23, 1974.

NAVAIR 06 - 30 - 501

Technical Manual
of
OXYGEN / NITROGEN
CRYOGENIC SYSTEMS

THIS PUBLICATION SUPERSEDES NAVAIR 06–30–501
DATED 1 JULY 1968

PUBLISHED BY DIRECTION OF
THE COMMANDER OF THE NAVAL AIR SYSTEMS COMMAND

1 MARCH 1971

Reproduction for non-military use of the information or illustrations contained in this publication is not permitted without specific approval of the issuing service (NAVAIR or USAF). The policy for use of Classified Publications is established for the Air Force in AFR 205-1 and for the Navy in Navy Regulations, Article 1509.

LIST OF CHANGED PAGES ISSUED

INSERT LATEST CHANGED PAGES. DESTROY SUPERSEDED PAGES.

NOTE: The portion of the text affected by the current change is indicated by a vertical line in the outer margins of the page.

* The asterisk indicates pages changed, added or deleted by the current change.

ADDITIONAL COPIES OF THIS PUBLICATION MAY BE OBTAINED AS FOLLOWS: NAVAIR

USAF ACTIVITIES—In accordance with Technical Order No. 00-5-2.

NAVY ACTIVITIES—Use DD FORM 1348 and submit in accordance with the instructions contained in NAVSUP PUBLICATION 437—Military Standard Requisitioning and Issue Procedures.

For information on other available material and details of distribution refer to NAVSUP PUBLICATION 2002, SECTION VIII, PART C and NAVAIR 00-500A.

TABLE OF CONTENTS

Chapter Page

LIST OF ILLUSTRATIONS vi

LIST OF TABLES. xi

INTRODUCTION xiii

1. AIR SEPARATION AND GAS LIQUEFACTION PROCESSES 1-1

Refrigeration and Liquefaction. 1-2
Ideal liquefaction system 1-2
Liquid expansion. 1-3
Joule-Thomson expansion 1-5
Engine expansion 1-8

Heat Exchangers 1-12

Regenerators 1-14

Rectification 1-17
Principles of rectification. 1-17
Rectification column. 1-18

Air Separation Systems 1-22
Linde single-column system 1-22
Linde double-column system 1-22
Other systems 1-26
Portable parallel-column plant 1-26

Purification. 1-30

2. BASIC ENGINEERING DESIGN PRINCIPLES 2-1

Insulation Systems 2-1
No insulation. 2-2
Nonevacuated insulations 2-3
vapor barriers 2-3
foams 2-5
fibers 2-6
powders 2-7

Chapter Page

Evacuated insulations 2-8
foams 2-8
fibers 2-9
powders 2-10
multiple-layer 2-13
high vacuum 2-19
condensing vacuum 2-20
comparison of insulations 2-22

Storage and Transport Vessels 2-23
Small dewars 2-23
Medium capacity dewars (50-2000 gallons) 2-25
vessel configuration and capacity 2-25
structural design 2-28
suspension system 2-30
piping 2-35
dewar appurtenances (manways, baffles) 2-42

Converters 2-44
Low loss closed-loop transfer system 2-45

Vaporizers 2-51

Pumps 2-54
High pressure pumps 2-55
Medium pressure pumps 2-58
Low pressure pumps 2-60

Transfer Lines 2-60

Valves 2-70

3. INSTRUMENTATION 3-1

Temperature 3-1
Thermocouples 3-2
thermocouple extension wires 3-5
spurious or parasitic emf's 3-5
thermopiles 3-6
thermocouple materials 3-7
polarity 3-10
reference tables 3-11
calibration 3-12
Resistance thermometers 3-12
metallic resistance thermometers 3-12
nonmetallic semiconductor resistance thermometers 3-16

CHAPTER 2

BASIC ENGINEERING DESIGN PRINCIPLES

In this chapter, equipment used for the storage, transport and transfer of cryogenic fluids (particularly liquid oxygen and liquid nitrogen) is discussed along with design features and criteria which are uniquely cryogenic. Elements of design that are not peculiar to low temperature systems are not discussed here, since they are beyond the scope of this work and may easily be found elsewhere.

The chapter is divided into sections on insulation systems, storage tanks, converters, vaporizers, pumps, transfer lines, and valves. Although each is a topic in itself and stands as such, an interrelation exists that soon becomes apparent. The endeavor in each section is to present the engineering rationale of cryogenic design as it applies to the various items of low temperature equipment.

INSULATION SYSTEMS

Underlying the effective and efficient use of most cryogenic equipment is the associated thermal insulation system. Taking a common household refrigerator as one example, if some of the insulation were removed from the walls, electrical power costs would increase because of the greater length of time required for compressor operation; this increased running time is due to a longer refrigeration duty cycle which would be necessary to keep the food as cold as it had been before loss of insulation. If all of the insulation were removed, a much larger and more expensive refrigeration system would be needed and again the power costs would go up, resulting in an unnecessarily expensive operation. As another example, the summertime air conditioning costs for an uninsulated or poorly insulated house can wreck an otherwise manageable budget, making it soon apparent that something should be done to correct the condition. If a choice is made to insulate (rather than sell it or live with it unhappily or uncomfortably), the stage is set for other more specific decisions that must follow concerning: type of material and thermal efficiency, quantity, durability, application, maintenance, cost, etc. Each is important and one bears on the other.

It does not necessarily follow from the above examples that the more insulation there is, the better the situation becomes — not when cost is a factor. As will be seen later in this chapter, an optimum amount or degree of insulation exists for any given case, and this optimum varies from no insulation at all to as much as can be fitted into a reasonable-sized enclosure. Within the bounds of poor

insulation and good insulation, there exist the categories of nonevacuated (gas-filled) and evacuated insulations and an even further classification of material groups below this, as illustrated in figure 2-1. The figure plots type of insulation against thermal conductivity (which will be shown in Chapter 6 to be a measure of effectiveness or efficiency of a thermal insulation system); for certain applications where weight also is of concern, the product $k\rho$ (thermal conductivity times density) is sometimes additionally provided — this product frequently is referred to as a 'figure of merit'.

To cover thermal insulation systems in more specific detail, each of the major categories is discussed in the following sub-sections.

NO INSULATION

For short term experiments or unusual circumstances where available piping and tanks have to be used quickly and without particular regard for efficiency or cost of liquids, it is sometimes possible to use bare, uninsulated components to accomplish a job. Actually, in such cases, the bare (cryogen containing) walls under most atmospheric conditions do not remain bare very long, nor are they entirely without insulation since water vapor from the ambient air condenses on the cold surfaces, forming frost. The tenacity of this frost is small, as it is easily jiggled or blown off under relatively mild conditions of vibration or wind (figure 2-2); however it does furnish some insulation value, with heat transfer rates to the liquid being reduced by a factor of two in certain instances after the frost has been produced. Because of the uncertain constitution of water vapor in the air and the unpredictability of wind and vibration, any beneficial thermal insulating qualities of frost are undependable and they should only be looked upon as a bonus at best. Also, in the process of frost formation, the condensation taking place liberates heat at the condensing surface, some portion of which ultimately and undesirably is passed on to the cryogen, causing additional liquid to be evaporated and wasted.

Before leaving the subject of frost, mention should be made of the fact that while it does form on bare liquid oxygen equipment and some pieces containing liquid nitrogen, at temperatures near and below the normal boiling point of nitrogen air liquefies and continually bathes or washes off these colder surfaces. Not only does the heat of condensation of the air augment heat transfer through these surfaces to the cryogen (which in itself is undesirable), but the possibility that liquid air may be dripping on some non-compatible (with the liquid oxygen component of liquid air) material creates a potential safety hazard. Also, the liquid air is very cold which, if it is permitted to drip on non-cryogenic materials of construction, can be a cause of low temperature embrittlement.

Finally, while bare uninsulated equipment may be utilized for certain unusual, non-repetitive operations, the consequences can be costly in terms of fluid consumption and safety requirements, and should be considered carefully.

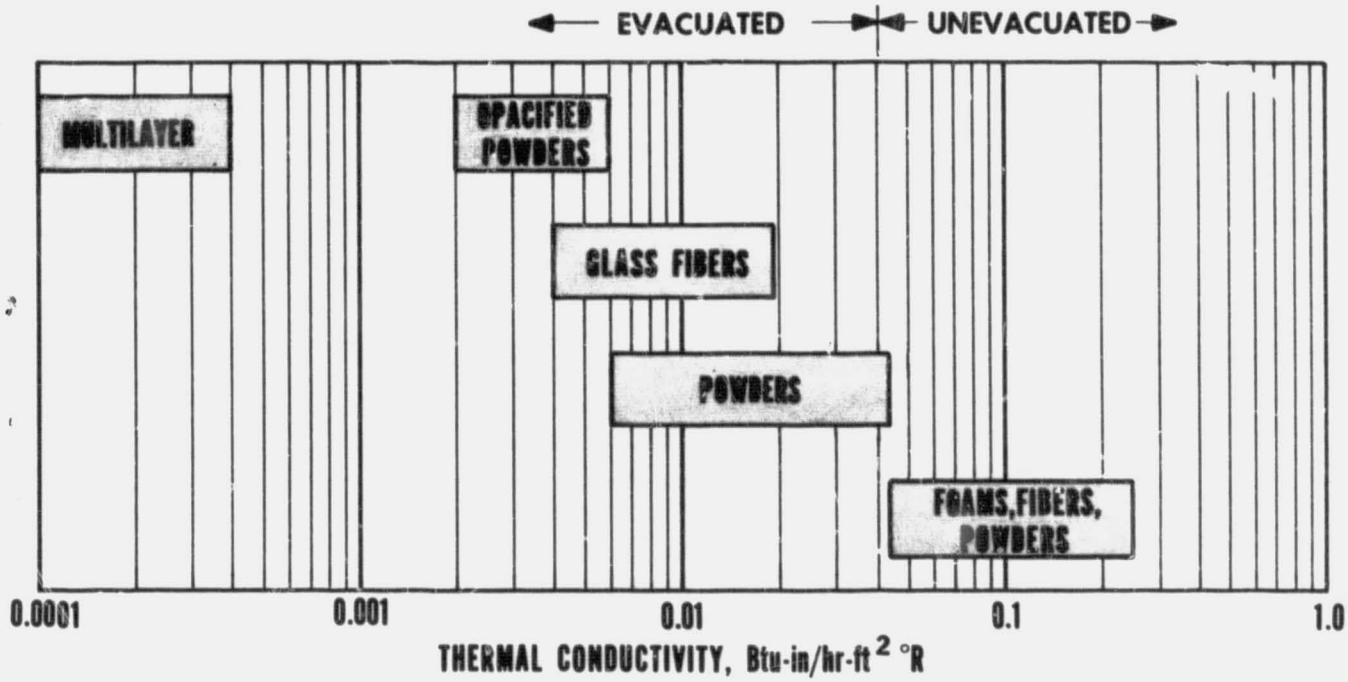

Figure 2-1. Comparison of thermal insulation materials for cryogenic systems between the temperatures of 540 °R and 140 °R (2 to 5 lb/ft^3 density range).

NONEVACUATED INSULATIONS

In those cases where some insulation is clearly required but the expense and complexity of evacuated insulation systems are unwarranted, a reasonably good selection of materials may be made from plastic foams, glass fibers, foam-fiber composites, and powders. Advantages and disadvantages peculiar to the application and use of each type are discussed below after a preliminary note on the subject of vapor barriers.

Vapor barriers

In order to maintain as-installed efficiency of a cryogenic insulation system, it is generally necessary to use a vapor-proof covering, or vapor barrier, on the warm surface of the insulation. Reason for concern here is that without such an enclosure, atmospheric moisture, air, etc. are free to migrate through the somewhat porous insulating materials until a region cold enough for condensation or freezing to occur is encountered. When this happens and if it is sufficiently

Figure 2-2. Frost formation on bare liquid oxygen tank.

cold, moisture solidifies, air liquefies, and the effective or apparent thermal conductivity of insulation increases because of the additional higher conductivity constituents now embedded in the previously gas-filled pores. Also, in some relatively open, high void-to-solid material composition insulations on liquid nitrogen equipment, a reflux action occurs; air first permeates the insulation, then condenses on or near the cold equipment surface and drips off into a warmer region where it evaporates, after which the cycle repeats itself again and again. This not only increases heat input to the cryogen because of a continual liberation of the heat of condensation of the air liquefying on the cold surface as in the earlier uninsulated case, but it also establishes a previously described safety problem if the insulation is incompatible with oxygen, since an appreciable fraction of liquid air is liquid oxygen after refluxing.

Choice of vapor barrier depends upon the type of insulation being used, environmental conditions, permanence of the installation, and budget. If the insulation is rigid enough to provide adequate support, a flexible metal foil or plastic film may be employed. If a rugged, sturdy cover is required because of the use of non-rigid insulation (powder, for example), extreme weather conditions, abusive external conditions, long-term maintenance-free requirements, or any combination of these, a heavier metallic sheath is desirable. In any case, a gas-tight installation requires an appropriate sealant at all joints as well as a puncture-free covering. For some applications where the insulated surfaces are of such complex shape as to make impossible the achievement of a gas-tight barrier, a non-condensable gas like helium may be bled into the insulation beneath the covering in such a way as to maintain a slight positive gage pressure in that space — thereby preventing the infiltration of air and moisture and the problems that go with them. Initial cost of the latter system is minimal when compared to one which is vapor-tight, but a continuing need for bleed gas may soon offset this particular advantage. Also, if helium is used for such a purpose, the thermal conductance of the system increases due to the high conductivity of this gas.

Foams

Polyurethane and polystyrene plastic foams are the ones most commonly used in low temperature work, with variations in these two types available as to density, strength, thermal conductivity, intercellular gas composition, rigid or flexible structure, open or closed cells, application method (preformed, foam-in-place, spray-on), etc. Due to the large selection of physical properties and characteristics, foam insulations can be tailored to many situations requiring rather modest thermal protection qualities. One major drawback in the use of such material relates to the large thermal expansivity of plastics and plastic foam — often a factor of five or ten greater than metals like steel and aluminum. On cool-down to cryogenic temperatures, the considerable contraction that occurs generates thermal stresses which in turn cause cracks to develop in many of these foams. Certain flexible foams seem to better accommodate this type of stress than the more rigid formulations; however this is not meant to be taken as a generalization.

Several things can be done to reduce this problem, including the use of interspersed fibers, threads, or honeycomb as reinforcement materials and the deliberate employment of precracked foams (slabs) in such a way as to permit whatever contraction or expansion must take place to occur at the slab edges (the reasoning here is similar to that behind the placement of expansion cracks in sidewalks). With this latter technique, the fact that unsealed joints are present requires that a liner be used if the application is internal, or a vapor barrier for external utilization — see figure 2-3. Shiplapped joints are reasonably good here but care must be taken that the liner not be destructively pinched between the joints; this often is quite difficult to do. 1/4, 1/2, and 1 mil thick polyester plastic films have been used successfully as liner material, sometimes in multiple sets of two and three in case one accidentally is punctured or leaks.

Attachment methods to tank and pipe walls may involve banding (cinch bands for external placement or expansion bands internally), special low temperature adhesives, or a foamed-in-place installation which adheres to adjacent surfaces. Unprotected rigid foams can be rather easily damaged so care should be taken working with and around them. Even without damage, the insulating properties of these materials may change with time. This is due to the fact that the overall thermal conductance of the foam has two main components — conduction through the solid plastic cell walls and conduction through the cellular gas. When the foam is being made, reaction between chemicals involved in the process liberates gas which remains in the cells or voids for some time. If, however, the foam is not used soon after manufacture but stored in contact with air instead, the original gas gradually diffuses out of the cells and is replaced with ambient air. For some of the more efficient materials this exchange can account for an increase in conductivity of 50 percent, and if for some reason (purging, inerting, etc.) helium became the replacement gas, the conductivity would rise to many times its original value.

Fibers

Glass fibers (either in bulk or batt form) are used occasionally to insulate cryogenic vessels and transfer lines in cases where shock and vibration loading might otherwise be serious. The fibers resist settling and, of course, cracking under mechanical and thermal abuse, and they are chemically inert to hazardous environments if used without organic binders which are incompatible with oxygen. Rock wool, a fibrous insulation, has been used in cold boxes[1] for many years; the advantage here is low cost coupled with ease of removal in the event that repairs or maintenance become necessary within the box. Insulating qualities of this type of insulation are achieved by virtue of the submicron diameter fibers being ran-

[1] The term 'cold box' is used to designate an insulated enclosure surrounding cryogenic components such as heat exchangers, purifiers, valves, etc. of generally irregular shape. In order to provide a simple method of thermal protection for these items, a box or shell is built around them and insulation is subsequently poured or stuffed into the voids — being held in place by the containing walls.

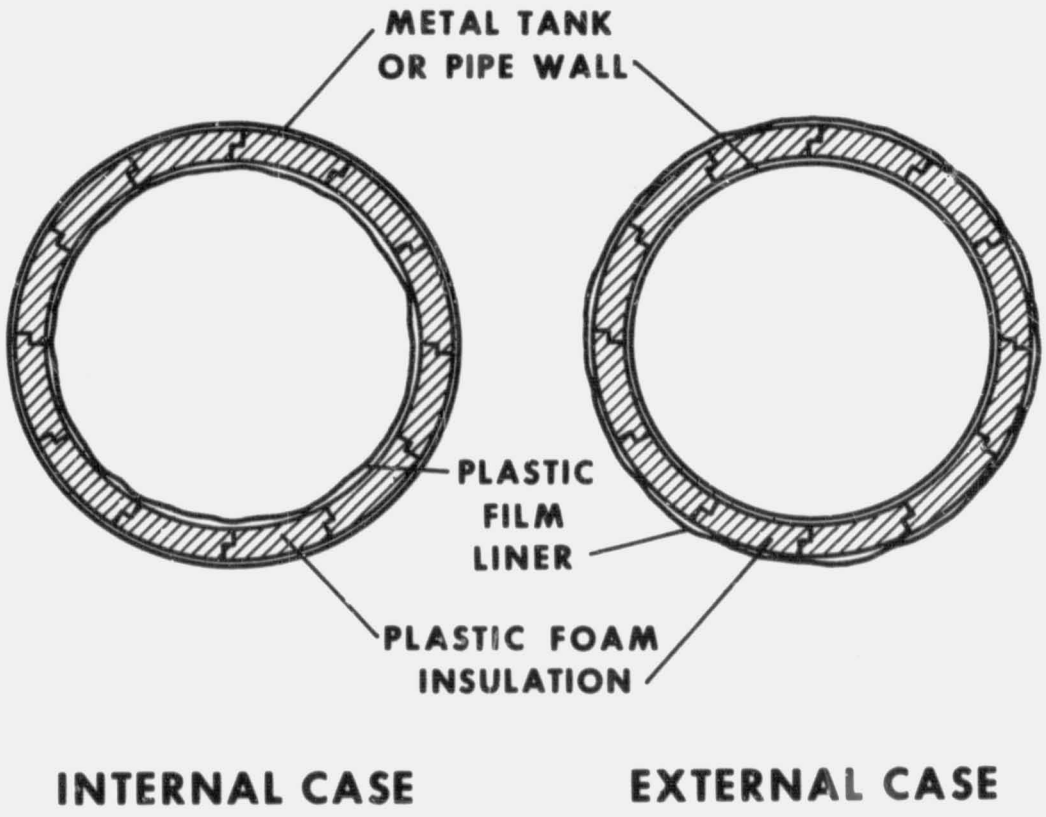

Figure 2-3. Jointed plastic foam insulation and liner.

domly oriented, furnishing a multitude of poorly conducting points of contact between individual fibers.

Powders

Perlite and silica gel are two of the most frequently used powders for cryogenic insulation, with perlite favored in many applications because of its great cost advantage — about ten to one over silica gel. Although the apparent thermal conductivity of a powder is roughly of the same order as the conductivity of the gas contained in its pores, indicating that very little heat actually is being transmitted through the particles themselves, this is still an improvement over no powder at all,since total heat transfer to a cold surface surrounded by gas (air, for example) involves not only conduction but also convection and radiation; powder reduces convection by providing only very small gas pockets which are not conducive to this type of heat transfer, and it has an obvious radiation inhibiting effect because of the many solid particles involved.

Since powders must be totally contained in order to remain in place properly, they require their own at least partially effective vapor barrier in the form of a retaining wall. Even though a weight and cost penalty is paid for this necessary enclosure, it does provide a relatively easy means of insulation application; the powder simply is poured into a filling port located at a high point of the item being insulated and when full, the port is sealed. This access point also may be used as a visual observation port to detect any change that might occur in the level of powder with time, as all powders tend to settle or pack if used in mobile equipment. Upon settling, higher boiloff occurs and cold spots usually are noted at the insulation-deficient region; additional powder should be supplied to correct this situation when it is observed (following warm-up). Vessels that do not have hermetically sealed outer shells occasionally are designed to vent through the insulation space in order to maintain a positive gas pressure in that region preventing any infiltration of moisture-laden air.

EVACUATED INSULATIONS

Where the ultimate in insulation is required, figure 2-4 illustrates the value of evacuation, or reduction of pressure below atmospheric, on the system. More than one, and often several, orders of magnitude (factors of ten) decrease in thermal conduction are achieved by drawing a vacuum on the insulation and, as is seen on the graph, the amount by which the pressure is reduced has a direct bearing on the excellence of the insulation to a point. All of the previously described insulations are improved in a vacuum environment, and additionally, several others may now be considered — multiple-layer and high vacuum.

A disadvantage in the use of such an insulation scheme lies in the high cost of obtaining and then maintaining vacuum-tight systems. Considerable care and craftsmanship are necessary in such construction and cleanliness is essential. More will be said of this in a later section on storage and transport vessel design, however.

Covering the various insulations in order of decreasing thermal conductivity (or increasing insulating effectiveness), the following discussions now apply to evacuated materials rather than the unevacuated types previously examined.

Foams

It has been found that most plastic foams (even closed-cell) can be evacuated, with subsequent reduction in thermal conductivity to one-half or less of the original conductivity. In the case of closed-cell foams, the rate of liberation of confined gases is quite slow and long pumping times are necessary — occasionally on the order of weeks — depending on the size of the pump, thickness and type of insulation, and distribution of evacuation ports. The inclusion of evacuated foams in this manual is not meant to recommend them for immediate application, since additional research on the attainment and retention of vacuum in practical

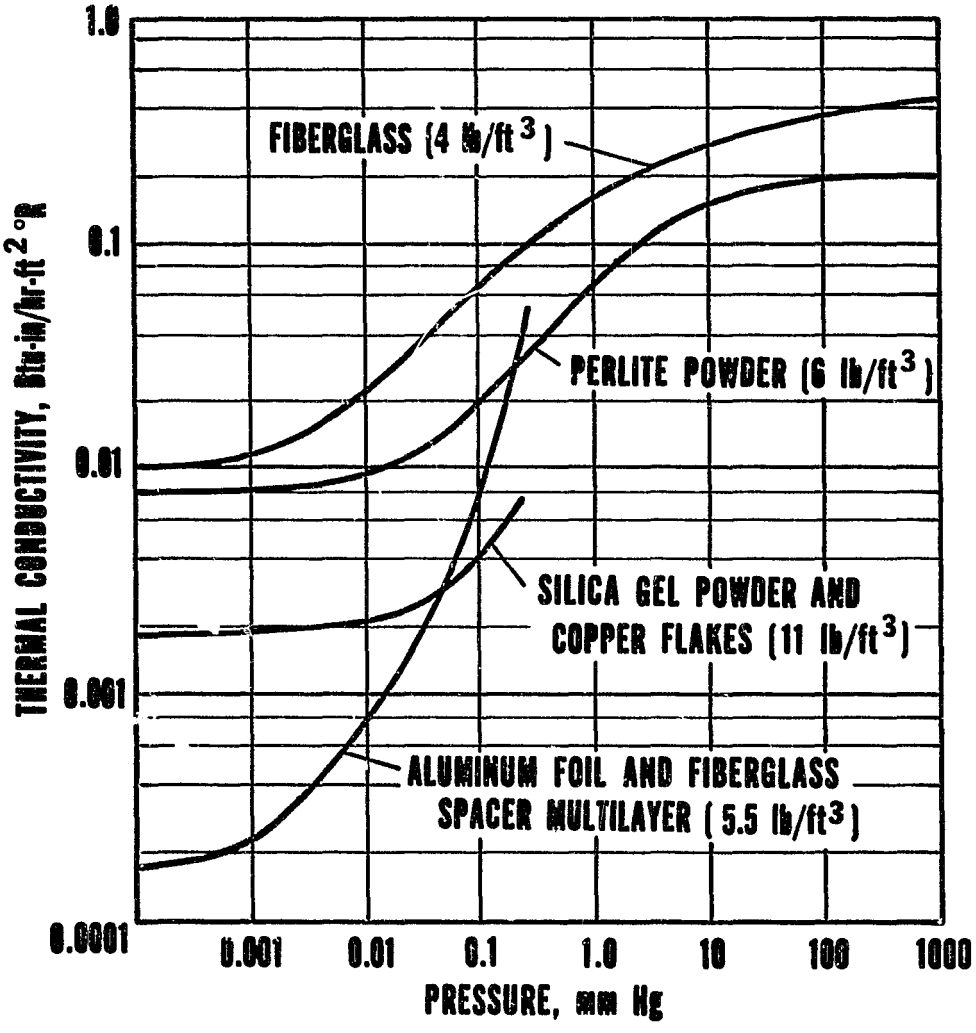

Figure 2-4. Effect of gas pressure on thermal conductivities of various cryogenic insulations.

situations still must be done; the primary purpose in listing here is to offer only one of a series of examples on improvement of insulating materials by currently available vacuum pumping techniques.

Fibers

As seen in figure 2-1, fibers fall in somewhat of an intermediate position between plain powders and opacified powders (of which more will be said shortly). To avoid breaking up the discussion on powders, the use of evacuated fibers will be pursued briefly at this point.

In the use of evacuated fibers (again in batt or bulk form), it becomes necessary to employ only those materials, usually glass, without binders or lubricants, since these additives have the particularly adverse effect of outgassing and therefore slowly destroying the vacuum in the insulation enclosure. Recalling the benefits of unevacuated fiber application, advantages again appear in the usually difficult environments of shock and vibration — only now with the conductivity reduced by a factor of ten or so below the unevacuated case.

Powders

In measuring the heat transfer through powders having high volume ratios of gas-filled voids to solid particles, it has been noted that the apparent thermal conductivity is essentially that of the gas alone. This means that whatever small difference remains may be attributed to conduction through the solid minus the powder-effected combined reductions in convective and radiant heat transmission. If the interstices are now evacuated, results similar to those shown in figure 2-4 are obtained which are plotted in what characteristically may be termed S-curves. This shape of curve is due to the fact that heat transfer through the powder is practically pressure-independent at both high and low pressures, but at some intermediate value, depending on the gas present, a very large drop in conductivity takes place. Theoretically such an occurrence may be explained by the fact that at these pressures where the conductivity drastically decreases, the molecular mean free path (or distance between molecular collisions) of the gas is roughly comparable to the average dimension of the interstitial space. Actually this reduction should continue as the pressure decreases, but it is practically limited by residual solid conduction through the powder and internal radiant heat transfer from particle to particle.

A rather interesting approach was taken once thermal radiation was finally recognized as a contributing factor to heat transport through powders (a condition previously thought to be non-existent or extremely small because of the visual opaqueness of the material). It was reasoned that perhaps little radiation shields (opacifiers) in the form of highly reflective metallic powders or flakes could be added to the insulating powders in such a manner and in such quantities as to decrease the radiation loss while hopefully not increasing the conductive loss very much because of the new metallic additive. Research resulting from the above considerations, which was conducted on a select group of powders and opacifiers, indicated that the lowest apparent conductivities were achieved by adding as little as 15 weight percent metal to some of the powders — significantly improving their insulating qualities (figure 2-5).

Certain disadvantages unfortunately are inherent in the use of these so-called opacified powders. The cost is increased because of the expense associated with (1) furnishing the metallic elements and then (2) mixing them thoroughly with the perlite, silica gel, or whatever is being used as the primary insulant. In mobile equipment, the metallic additive sometimes settles with time — lowering

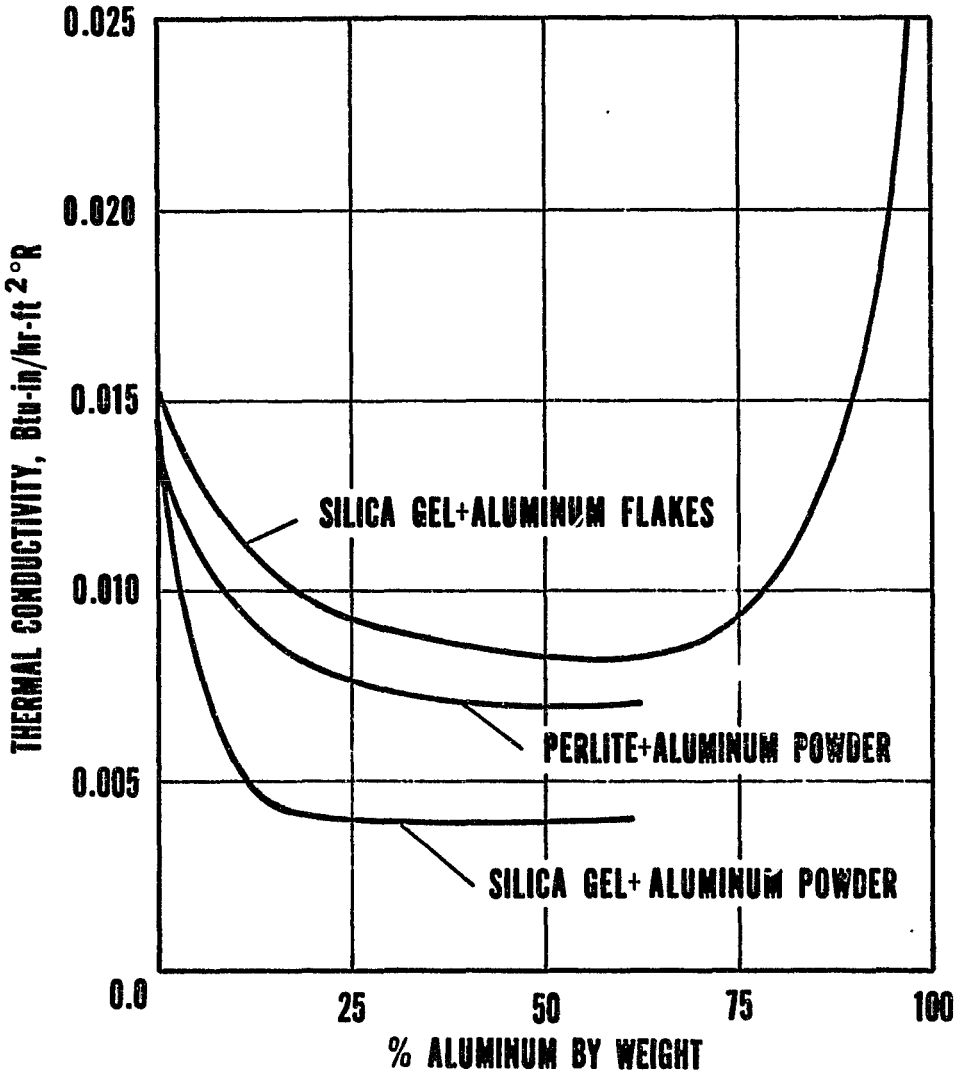

Figure 2-5. Effect of metallic additives on apparent thermal conductivities of evacuated powder insulations between 540°R and 140°R.

the insulation value where the metal is depleted because of increased radiation loss, and also lowering it where the metal is more abundant because of increased conduction loss through the highly conductive metal; this then requires remixing with attendant cost of labor and downtime of equipment. Finally the incorporation of metallic particles into insulation for oxygen equipment may be considered hazardous due to the flammability of such mixtures under certain conditions; tests have indicated no ignition for 20 percent aluminum powder in perlite in an oxygen atmosphere, but as pointed out earlier, settling can occur to inadvertently in-

crease the initial metal concentration. Opacified powders never should be dried at high temperatures after mixing because many of them are highly combustible.

A major consideration in the design of evacuated powder insulated vessels involves the associated evacuation system. First, the size of the smallest powder particle must be known so that a properly rated filter can be installed to keep powder out of the vacuum pump; if adequate filtration is not accomplished, the pump can be quickly ruined by abrasive action of the powder on rotating parts. Next, a pumping conduit made of perforated tubing, wrapped with fiberglass and encased in wire mesh or screen, is run from one end of the vessel to the other in several manifolded locations to more easily permit evacuation of the insulation space. If only one filter-protected pumpout hole or port were provided, pump-down time would be excessively long since powder greatly impedes the flow of gas through it; while the vacuum reading at the pumpout location might be similar to that at the pump, the reading at a remote end of the vessel might be orders of magnitude greater. With the manifolded arrangement, a better equalized pressure reduction occurs.

Powder should be dry at the time of its introduction to the insulating enclosure. Most powders are hygroscopic (capable of attracting and absorbing water vapor from the air) and moisture is one thing that is not wanted in the insulation, since it freezes when the equipment goes into service and forms a highly conductive constituent within the powder interstices. In the case of perlite it is best to obtain the powder directly from the manufacturer in freshly made condition where it has not had an opportunity to take on water; it then should be used immediately and sealed up. If this is not possible, the next best approach is procurement in bags of low moisture permeability followed by use as soon as possible. In some cases it may be found necessary to dry the powder prior to use because of an unduly wet condition. If these precautions are not taken, the moisture will have to be removed during the pumpout process and additional days or even weeks could be consumed for just this reason. Generally speaking, moist powder cannot be adequately evacuated; the best procedure is to remove and replace it with fresh dry powder.

On the subject of pumpout, an obvious question arises as to just how low must the vacuum be before the system can be sealed off. Referring back to figure 2-4, it is seen that evacuation below 1 micron has very little, if any, effect on the apparent thermal conductivity of powders and 10 microns is almost as good. In addition to this, we know that if the insulation enclosure does not leak and moisture has been kept out of the system, cooldown of the vessel during the tanking process has a desirable effect of reducing the insulation pressure even further due to condensation and solidification of certain interstitial gas constituents and contraction of the residual gas by cooling. It is not possible to say just how much reduction in pressure can be achieved by these latter mechanisms, since they are directly related to the makeup of the system itself, but at times it can be as much as an order of magnitude — say a drop from 0.200 to 0.020 mm Hg (200 to 20 microns).

Although heat flow through the insulation is only part of the total picture (supports and piping accounting for additional losses as will be explained later), it is essential that the S-curve concept of figure 2-4 be held in mind with the rather drastic upward departure from a low thermal conductivity plateau at 5 to 10 microns. The penalty paid for increasing the pressure beyond this point can be easily visualized and understood when this figure is recalled.

Should it become necessary to leak-check or repair equipment already filled with powder, it is sometimes essential to remove the insulation. Emptying ports on the underside of equipment facilitate this to a considerable extent, but in the event that these are not available, clean industrial vacuum cleaners with extension nozzles may be used to suck out the powder, after which it should be packaged in vapor tight bags or containers until reuse. The relative ease of filling and draining powder insulation in small and moderately-sized systems is one of the advantages of this type of material; in much bigger systems (fixed-plant cold boxes and large storage vessels), it is a disadvantage since the required external powder storage volume becomes appreciable.

"Keep the powder dry" is a key phrase that must be recalled and understood in all fill, drain, and repair operations involving this form of insulation. If it is wet it will not pump down until all moisture is removed; if it does not pump down, uncertainty will persist as to whether water actually is the problem or whether the enclosure leaks. This may then turn into a time consuming evaluation problem.

Multiple-layer

These are variously called multilayer, laminar and super insulations and have been found to be the most effective of all — also the most expensive. Historically, development stems from the knowledge that there are three different modes or mechanisms of heat transfer — conduction, convection and radiation — and if the space between two boundaries such as the inner and outer walls of dewars and transfer lines is sufficiently evacuated, (disregarding extraneous conduction effects of supports and piping) gas conduction and convection are eliminated and radiation is all that remains. By placing a highly reflective wall or shield between the two original walls, radiation transfer theoretically may be decreased to 1/2 of the initial value; two shields can result in 1/3 of the value; 3 in 1/4; etc.; for a large number of shields, radiant transmission can be decreased by a value approximating 1/(number of shields involved). One difficulty in achieving this ideal situation is that each shield must be in complete thermal isolation (no contact between shields whatsoever). This is impossible in any practical situation so ideal radiation shield behavior is unattainable.

Multilayer insulations are the next best thing, however, and they are practicable. Two major types have evolved in recent years, and both have had sufficient usage to make reasonable judgment of their qualities. One shown in figure 2-6 is an interleaved construction of metal (usually aluminum) foil and fiber

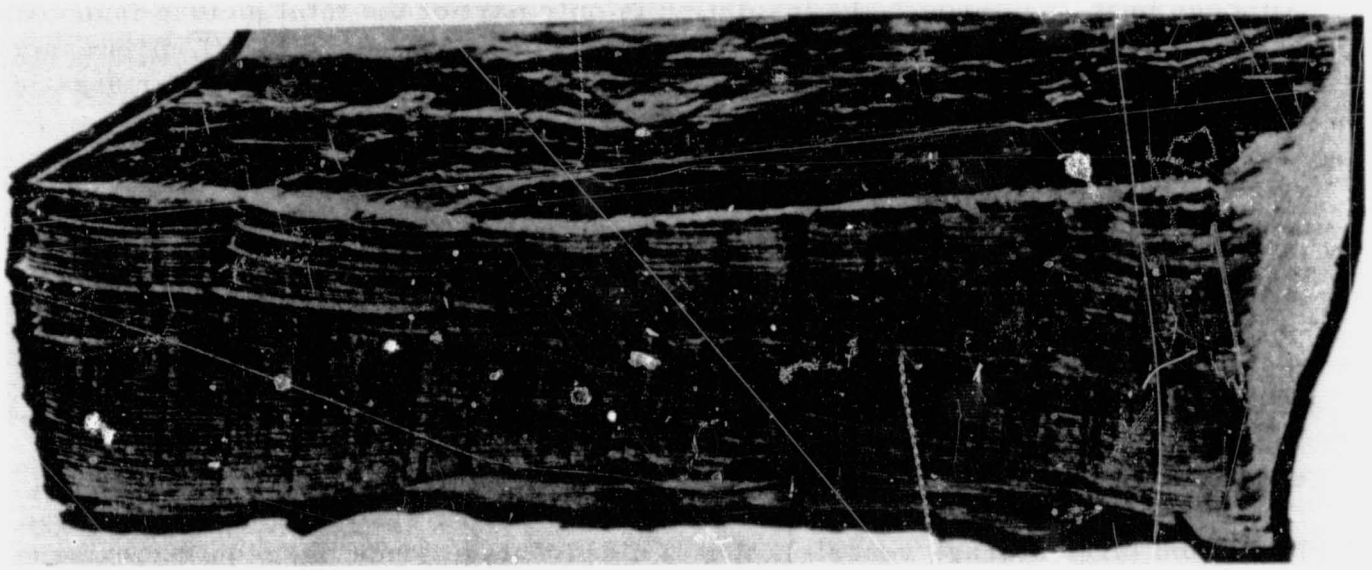

Figure 2-6. Multiple-layer insulation.

(usually glass) mesh or paper — aluminum being the radiation shield and fiberglass being the low conductivity spacer. The other is plastic (usually polyester) film which has been metallized (usually vapor-deposited aluminum) on one side and then crinkled or dimpled to provide only small contact areas between the alternately metallized and non-metallized sides of the plastic — aluminum again being the radiation shield carried now on a plastic film base for both strength and low conductivity support.

Since this form of insulation is applied to regular cylindrical surfaces such as tanks and transfer lines in a spiral fashion, it is recognized that the true multiple radiation shield concept has been modified; instead of separate concentric shields, there is now one continuous wrap. The shield thickness generally varies between a quarter mil (for metallized layers) and several mils (for metal foils), and the ratio of thermal conductance along the spiral path to that which is perpendicular to, or across, the layers ranges from about 1,000 for metallized films to 1,000,000 for the heavier foils. This spiral conduction then, plus the effect of thermally conductive spacers between the shields, prevents attainment of the concentric, individually isolated shield arrangement and performance in any real manner; however it is as close to it as the present state of the art permits and actually is quite good.

Experimental curves similar to the one presented in figure 2-7 have been developed for most multi-shield/spacer combinations. Such information facilitates optimum selection of materials; for the case shown, 70 layers per inch is

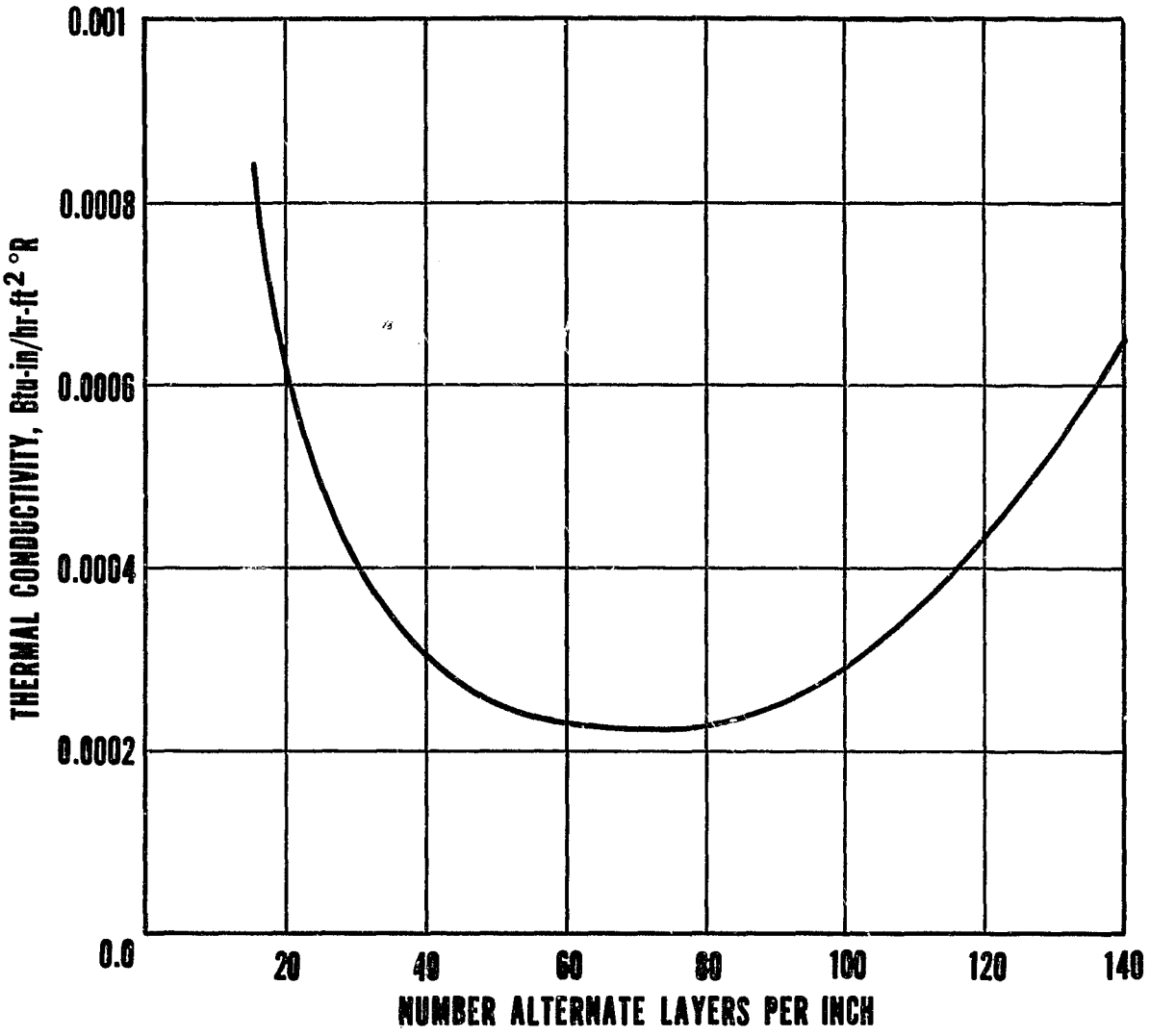

Figure 2-7. Thermal conductivity versus number of alternate layers of glass fiber paper and aluminum foil per inch thickness of insulation between 540°R and 140°R.

the most efficient choice possible and 60 layers is just about as good. High thermal losses (at least double the optimum, for example, at densities lower than 30 layers per inch or higher than 120 layers per inch) accrue by departing appreciably from this optimum, and of course weight penalties are paid at unnecessarily high (over 70 layers per inch) packing densities. Returning to the discussion on the original concept of multiple shields made in the introductory paragraph of this section, increasing the number of shields should decrease any thermal loss due to radiation. Ideally this happens, but with spacer materials now also involved, compaction beyond a certain point increases the shield-to-spacer contact enough to

cause heat to be transmitted by conduction at a greater rate then it is impeded by blocking radiation. This is exactly what occurs in figure 2-7 as the curve proceeds upward and to the right from its minimum conductivity value.

One of the most serious problems encountered in the application of multilayer insulations has to do with the effect of penetrations on thermal performance. These penetrations are created by piping, supports and various structural elements within the insulation space and, depending on the manner in which they are made, can alter drastically the efficiency of the insulation. If the shields are thermally shorted (in direct contact) with the penetrating element as in figure 2-8a, heat flow through the element into the metallic layers can harmfully modify the temperature field that otherwise would have been established through the insulation in the absence of the penetration. A reason for this thermal upset lies in the statement made earlier that anywhere from a thousand to a million times more heat may be conducted along, rather than across, a single multilayer shield/spacer combination, and therefore any heat supplied by a penetrating element in contact with the individual metallic shields can move deeply into the insulation in a direction parallel to the layers. To obstruct this undesirable conduction path, a poorly conducting buffer material such as plastic foam or fiberglass often is used as shown in figure 2-8b, thermally isolating the multilayer from the intruding element without creating a gap through which radiation can pass.

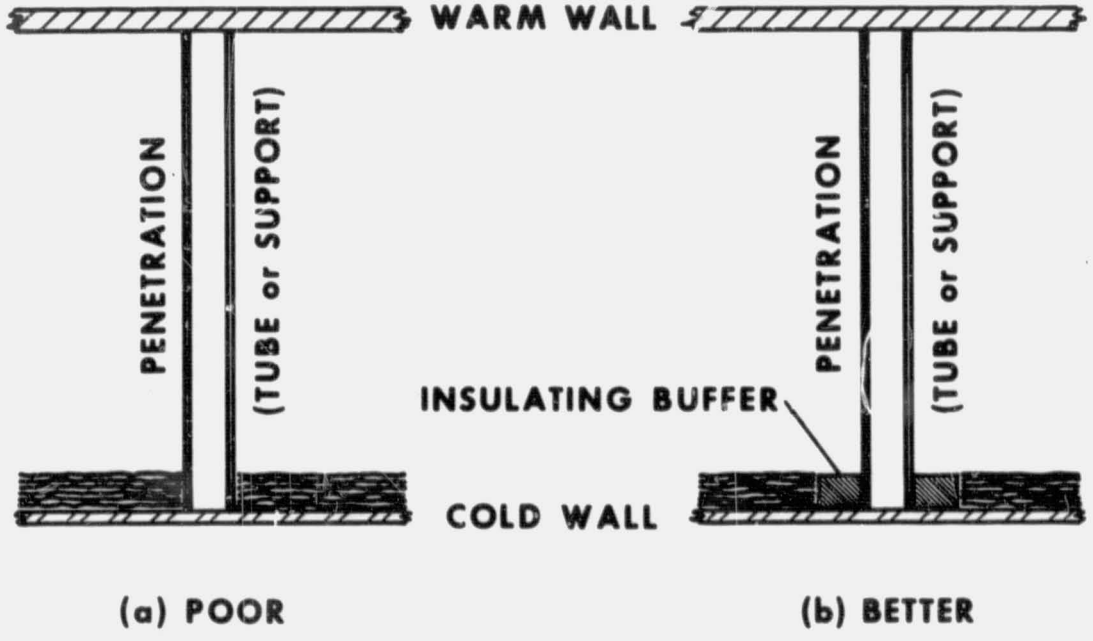

Figure 2-8. Penetration design schematic.

This last topic is an important one as will be attested by most fabricators of multilayer insulation systems. The apparent thermal conductivities shown by several of the graphs included in this section have been derived from actual laboratory experiments on small representative samples. However, when application is made to large equipment, it is found sometimes that a manyfold increase in heat transmission occurs over that which has been estimated by laboratory evaluation. On careful analysis, the discrepancy frequently is seen to be caused by poor installation techniques resulting in so-called 'radiation gaps'.

It has been pointed out that thermal shorts to penetrations have a degrading effect on the performance of multilayers, but an equally serious problem occurs if abutting segments of insulation are not mated properly — that is, if they are not brought together in a thermally satisfactory fashion at all joints. Referring to figure 2-9, sufficient precision cannot be achieved in wrapping these insulations to assure that, for example, layer 33 only touches abutting layer 33, 54 only touches 54, etc., etc. Should layers of dissimilar numerical designation touch each other, a disturbance of the equilibrium temperature distribution through the insulation results and the overall thermal efficiency is lowered. On the other hand, if a gap is created to discourage the thermal shorting condition, radiation transfer occurs through the gap and the situation is again bad. A solution to this problem is gained by careful, time-consuming piecework where individual layers are matched and fitted together one at a time during the wrapping process. Appropriate attention must also be given to the prevention of movement or shifting of the insulation segments with respect to one another in service; if this is not assured, all benefit of good joint preparation can be lost.

As with all materials discussed earlier, care should be taken to keep moisture out of the insulation during prefabrication storage and actual assembly, primarily because of the excessively long pumpdown times otherwise required for evacuation. Multilayers are especially difficult in this respect, even without the additional complication of water vapor, since such long distances must be travelled by each gas molecule before escaping its closely spaced (between layers) region of confinement. Because most of the gas molecules must be removed to achieve the very low pressure environment necessary for efficient use of this type of insulation (10^{-4} mm Hg or better), more than just casual attention should be given to this design problem.

Two rather descriptive terms have been used to depict the evacuation techniques that apply to multilayer insulations: edge pumping and broadside pumping (figure 2-10).

The first of these occurs when pumping is attempted through the edge or side of a laminar insulation. This is not a good method from the standpoint of time, since for one 100 layer per inch sample of insulation it has been determined that two weeks of pumping removes only one molecular layer of gas from all exposed surfaces. Further, to provide a means for edge pumping, the edge must

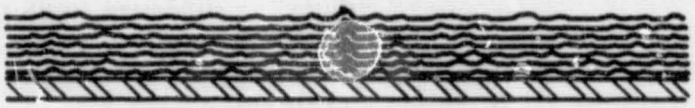

(a) ABUTTING JOINT

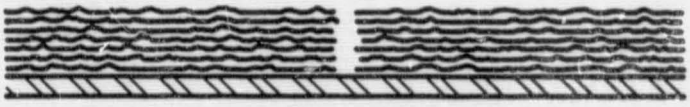

(b) GAPPED JOINT

(c) INTERLEAVED JOINT

Figure 2-9. Multiple-layer insulation joints.

be exposed to permit the gas to flow from the insulation to the vacuum pump; such exposure allows thermal radiation penetration which previously was shown to be detrimental.

An alternative is broadside pumping through perforated layers of radiation shielding. Many small holes are preferred over an equivalent area of fewer large holes, and a 10 percent perforation (10 percent of the area is removed) has been found to increase the gas removal at a rate roughly a thousand times greater than

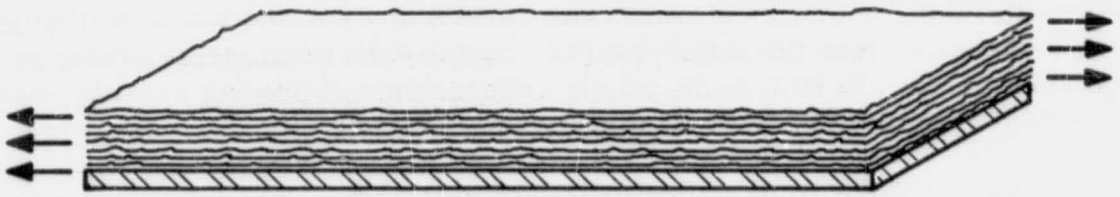

(a) EDGE PUMPING

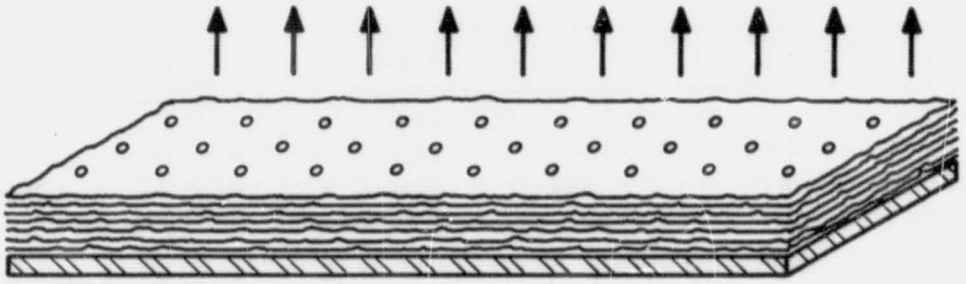

(b) BROADSIDE PUMPING

Figure 2-10. Multiple-layer insulation pumping schemes.

that possible with edge pumping. Unfortunately, the greater the perforated area becomes, the less effective are the radiation shields since the perforating process naturally removes a certain amount of radiation blocking reflective material; a compromise is required therefore between pumping speed and insulating efficiency.

High vacuum

Last but by no means least of the more efficient insulations is one which has been utilized most successfully in the common thermos bottle — an evacuated enclosure bounded by silvered glass walls. High vacuum is essential here but in order to achieve further improvement, highly reflective facing surfaces generally are used in conjunction with it.

Taking cryogenic storage vessels and transfer lines as representative examples of double-walled (for insulating purposes) construction and once again returning to the three basic modes of heat transfer, if the space between walls is evacuated to 10^{-6} mm Hg or better, heat transmission in this space by gaseous

conduction and convection is reduced practically to zero — leaving only radiation between walls and conduction through any solid supports and tubes that might be present. Assuming that the latter conduction losses are made as small as possible through good cryogenic design practices covered in a following section, reduction of the radiant transfer becomes of major concern.

In Chapter 6 the importance of highly reflective, low emittance surfaces will be explained in the above context. Now, certain generalizations may be made to assist in understanding and improving the tasks of materials selection and surface treatment and preparation:

1) The best reflectors are also the best electrical conductors (copper, silver, gold, aluminum).

2) Emittance of a surface decreases (reflectance increases) with decreasing temperature, and increases with surface contamination (fingerprints, oils, greases), alloying elements, and mechanical polishing (which work hardens the surface).

3) Visual appearance is not a reliable indicator of reflectance since dull, matte finishes are sometimes more reflective than bright, polished surfaces.

Table 2-1 provides a listing of the emittances of various metal surfaces which illustrates the effects of surface selection, treatment and preparation just discussed.

It follows that the art of creating a good high vacuum insulation system involves not only the design and construction of a vacuum-tight enclosure capable of achieving and retaining an absolute pressure no greater than 10^{-6} mm Hg but also the use of low emittance materials which are compatible with low temperature service. Advantages in such an insulating scheme are that no actual insulating material or significant amount of space is required (with accompanying additional weight, cooldown loss and extra volume) as in the bulk insulating systems previously mentioned. However much better vacuums are necessary, and the wall surface preparation demands great care and effort.

Condensing vacuum

A variation of the classic high vacuum insulation just described has been experimentally investigated for use in transfer lines and appropriately termed condensing vacuum insulation. Because of the gradual loss of vacuum with time and subsequent repumping requirement associated with many pieces of vacuum equipment, a clever scheme was developed to extend appreciably the service life of equipment in only occasional use — that is, items which are frequently warm and without cryogen.

By filling the insulation space of an otherwise vacuum-insulated transfer line with a pure gas, which is condensable and has very low vapor pressure at the

Table 2-1. Minimum values of emittances for selected metal surfaces

Material[1]	Emittance[2]
Aluminum, 0.001" & 0.0015" household foil	0.02
Aluminum, vapor deposited on polyester film	0.04
Brass, yellow 0.001" shim stock	0.03
Cadmium, mossy plate	0.03
Chromium, electroplate	0.08
Copper, electrolytic, careful polish	0.02
Copper, pure, carefully prepared	0.01
Gold, 0.0015" foil	0.01
Gold, vapor deposited on polyester film	0.02
Lead, 0.004" foil	0.04
Nickel, 0.004" foil	0.02
Platinum	0.02
Silver	0.01
Stainless steel, type 302	0.05
Tin, 0.001" foil	0.01
Zinc, 0.0065" foil	0.03
Solder, 50-50	0.03

[1] all materials solvent cleaned unless otherwise stated

[2] for surface at 140°R from radiation source at 540°R

temperature of the cryogen it is to be used with, to a pressure above atmospheric, the following benefit is gained: When the line is warm, any slight leakage only results in loss of some gas which is at a pressure above its surroundings. When the line is cold, the gas condenses and creates a good insulating vacuum; during this cold period any small leakage does go into the system but this normally would be the case in all high vacuum insulated equipment. The achievement here is that no insulation destroying leakage is able to occur inward when the item is not being used, and any outward loss that does take place is insignificant when compared with the amount of condensable gas present (or available to leak).

Pure carbon dioxide has been used successfully for this purpose. Since the particles of solid CO_2 that condense on the cold surfaces are of the form of snow, it is necessary to wrap the cold surface with a thin blanket of loosely packed fiberglass covered with a perforated aluminum foil radiation shield; this furnishes a porous nesting place for the solid CO_2, preventing it from becoming dislodged by movement or vibration which would cause the particles to evaporate on hitting a warmer surface, degrade the vacuum and thereby increase the heat gain due to gaseous conduction and subsequent recondensation.

In order to utilize effectively this scheme of insulation, emphasis must be placed on the purity of the condensable gas. If it is not pure, residual constituents in a gaseous (non-condensed) state can prevent attainment of a good vacuum and the method is useless. Also, if the equipment is going to be in cold service during the greater part of its lifetime, the scheme is impractical as the value derives only from the warm periods of inactivity.

Comparison of insulations

Table 2-2 offers a comparison of several cryogenic insulations discussed earlier in this section. The listing is made in order of increasing insulating value

Table 2-2. Comparison of insulations

Type of Insulation [Boundary temperatures: 540°R - 140°R]	Heat Flow/6" thickness [Btu/hr-ft^2]
Helium-filled perlite powder (5 to 6 lb/ft^3) at atmospheric pressure	58
Helium gas at atmospheric pressure	53
Polystyrene plastic foam (2 lb/ft^3)	15
High vacuum, 10^{-6} mm Hg, wall emittances $\approx$0.02	3
Evacuated perlite powder (5 to 6 lb/ft^3)	0.5
Opacified silica gel powder with copper flakes	0.1
Multilayer insulation	0.01

for an arbitrary 6 inch thickness of material between an outside temperature of 540°R and the temperature of liquid nitrogen, 140°R. As implied in the preceding discussions, insulating efficiency alone does not determine the material to be used. Cost, weight, ease of application, and maintenance all have a bearing on the final selection, and a good knowledge of characteristic properties and behavior along with the inherent advantages and disadvantages are essential to a proper choice.

STORAGE AND TRANSPORT VESSELS

As now may be appreciated, one of the major applications for low temperature insulations is in the thermal protection of cryogenic storage and transport vessels. After the air separation process and accompanying liquefaction of atmospheric gases have been accomplished, equipment must be available to store and subsequently transfer the fluids to wherever they are to be used. Vessels that are designed for such purposes vary in size from as little as a quart to capacities approaching a million gallons, with the larger tanks (over 28,000 gallons) being fixed, non-movable storage containers. Few Navy requirements involve anything over 2000 gallons so while the design features and practices described here generally apply to all cryogenic vessels, the main emphasis is on smaller tankage.

SMALL DEWARS

An appropriate introduction to this subject requires that mention be made of the fact that the first vacuum-insulated, double-walled glass vessel for cryogenic liquids was invented by Sir James Dewar in 1892. The designation "dewar" or "dewar vessel" has been applied to all shapes and sizes of vacuum-insulated containers and is as common to the scientist and engineer in the low temperature field as "thermos" is to the lunch-carrying man on the street.

Craftsmanship is a distinct and basic feature of dewar construction, with great care being required for vacuum-tight closures and reflective surface preparation. Materials used in the fabrication of these small containers vary with style — the inner and outer walls of figure 2-11a being glass, the spheres of 2-11b being copper with soft-soldered joints, and the concentric cylinders of 2-11c being stainless steel, either deep drawn or with welded heads. All internal vacuum facing surfaces are highly reflective to minimize radiant heat transfer across the vacuum space to the inner container, and the vertical cylindrical supporting members for all cases are of low thermal conductivity materials: glass in figure 2-11a, stainless steel in 2-11c, and either stainless steel or reinforced plastic in 2-11b.

Activated charcoal frequently is used in these and larger dewars to gather and retain gases in the insulating vacuum space — both residual (those that have not been removed by pumping) and those entrapped in the materials of construction

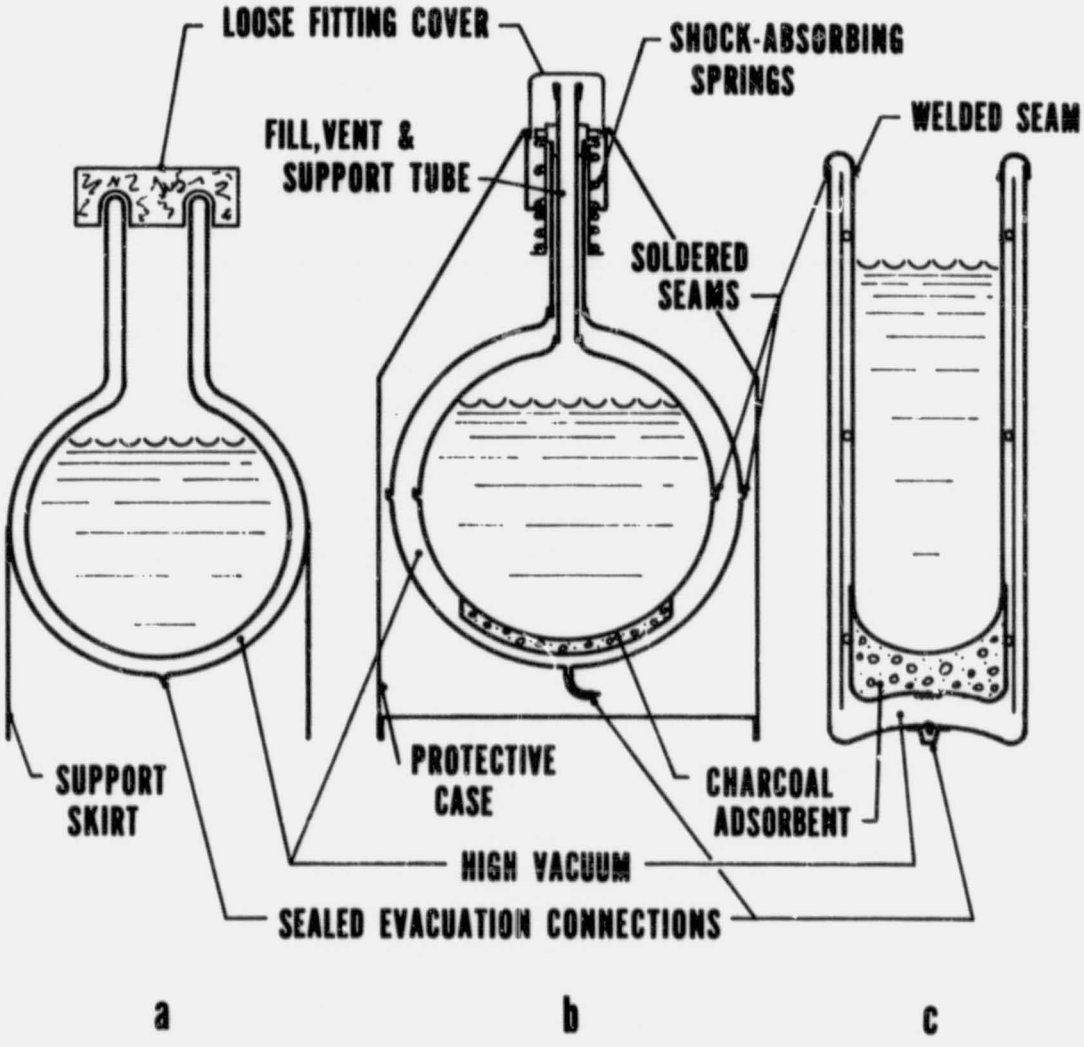

Figure 2-11. Small vacuum-insulated dewar vessels.

(which slowly evolve or outgas and tend to spoil the vacuum). An adsorbent like charcoal is not effective when warm; however the colder it gets, the greater becomes its capacity to collect gas. In a good design, the adsorbent holder is attached to the vacuum side of the coldest part of a dewar where it will remain cold for the longest possible time — this is the bottom of the inner shell as shown in figure 2-11b and 2-11c, which stays cold until the last drop of cryogen boils away or is withdrawn.

MEDIUM CAPACITY DEWARS (50 - 2000 gallons)

As the requirement for increased capacity storage and transportation of cryogenic fluids is established, different design concepts are developed to accommodate heavier loads and acceleration forces. The comparatively simple, smaller configurations now become impractical and are replaced by vessels resembling the general design shown in figure 2-12. Many different modifications of this basic dewar are possible but the primary elements of construction illustrated here are for the most part common to all designs. Each of these elements will be touched upon in subsequent discussion.

Vessel configuration and capacity

Although each manufacturer of cryogenic containers has his own line of standard sizes, the capacity range and style of equipment varies among companies. Selection possibilities are practically unlimited since the industry was founded on a custom-building business and prototype development still is very strong. Usually the buyer has the responsibility of specifying capacity, efficiency and configuration of tankage, and to do this he must be aware of anticipated supply and demand of the cryogens to be handled, space limitations, safety regulations and numerous incidental items.

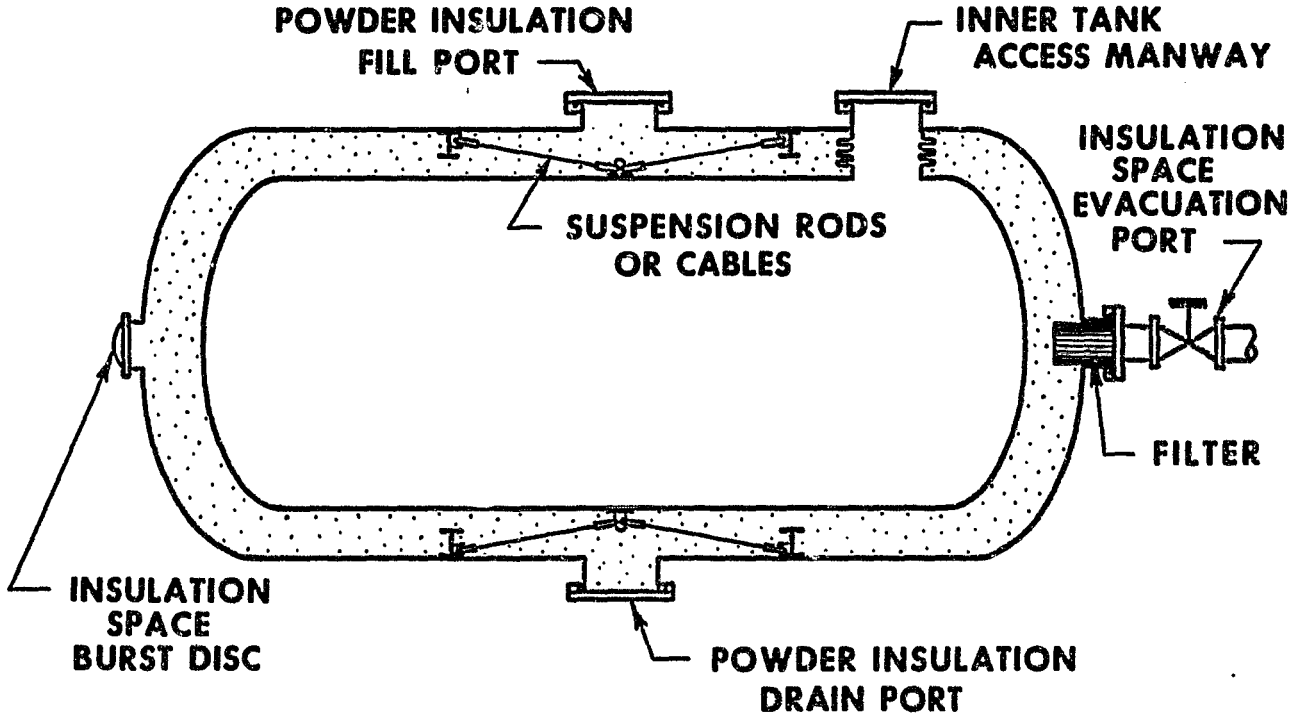

Figure 2-12. Basic dewar vessel construction (minus piping).

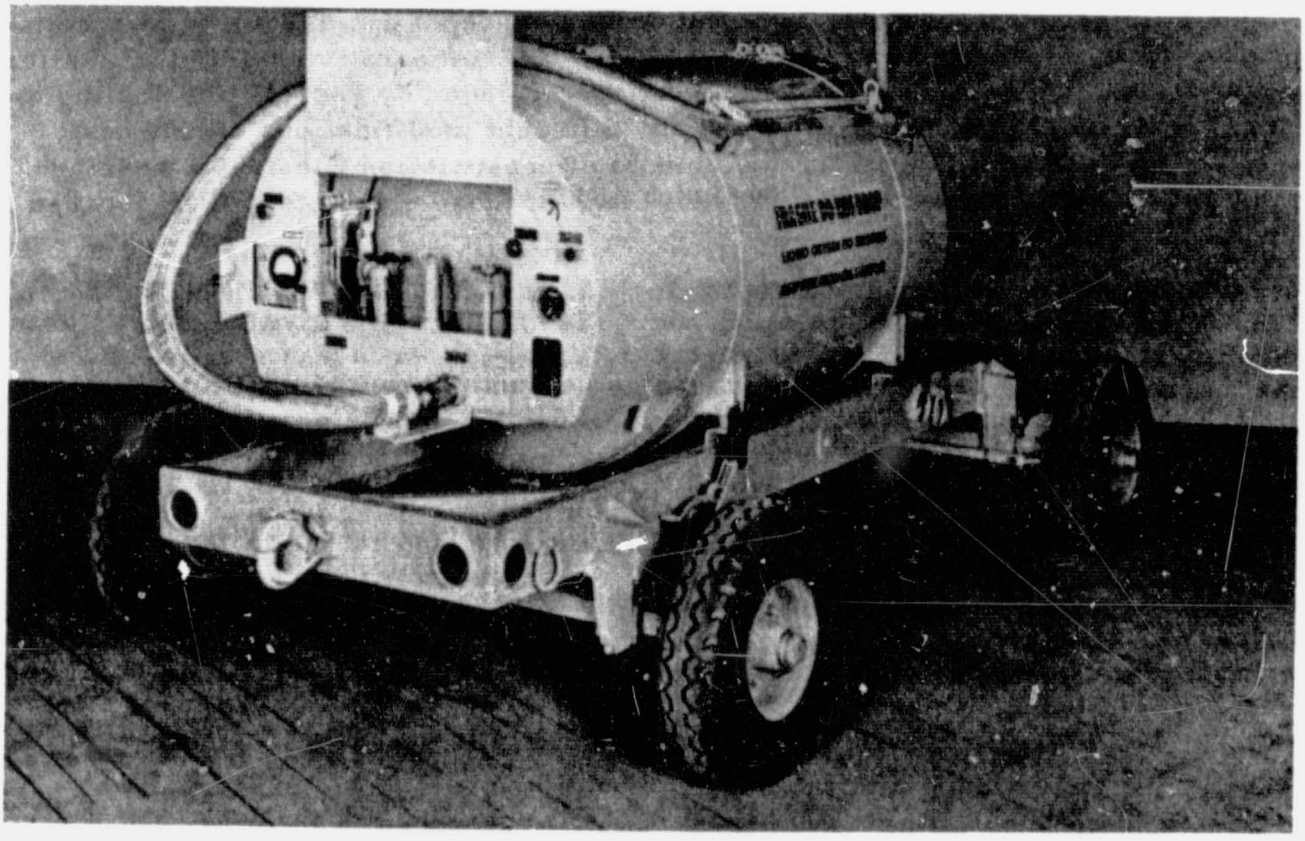

Figure 2-12a. Typical 50 gallon liquid oxygen servicing trailer.

Due consideration must be given to the shape of a cryogenic vessel if good thermal performance is desired. A spherical container is optimum in this respect since the surface area of a sphere is smaller than that of any other shape per unit volume of stored liquid. Less surface area means less heat gained by the fluid since the heat transfer is a function of area as well as thermal conductivity, thickness, and temperature difference across the tank insulation. Furthermore, less weight is involved — not only because of a smaller shell area, but also because spherical shells are stronger and therefore can be thinner than other shapes for a given pressure rating.

If a sphere is impractical or impossible to use, the next most efficient configuration is cylindrical (either horizontal or vertical) with length roughly

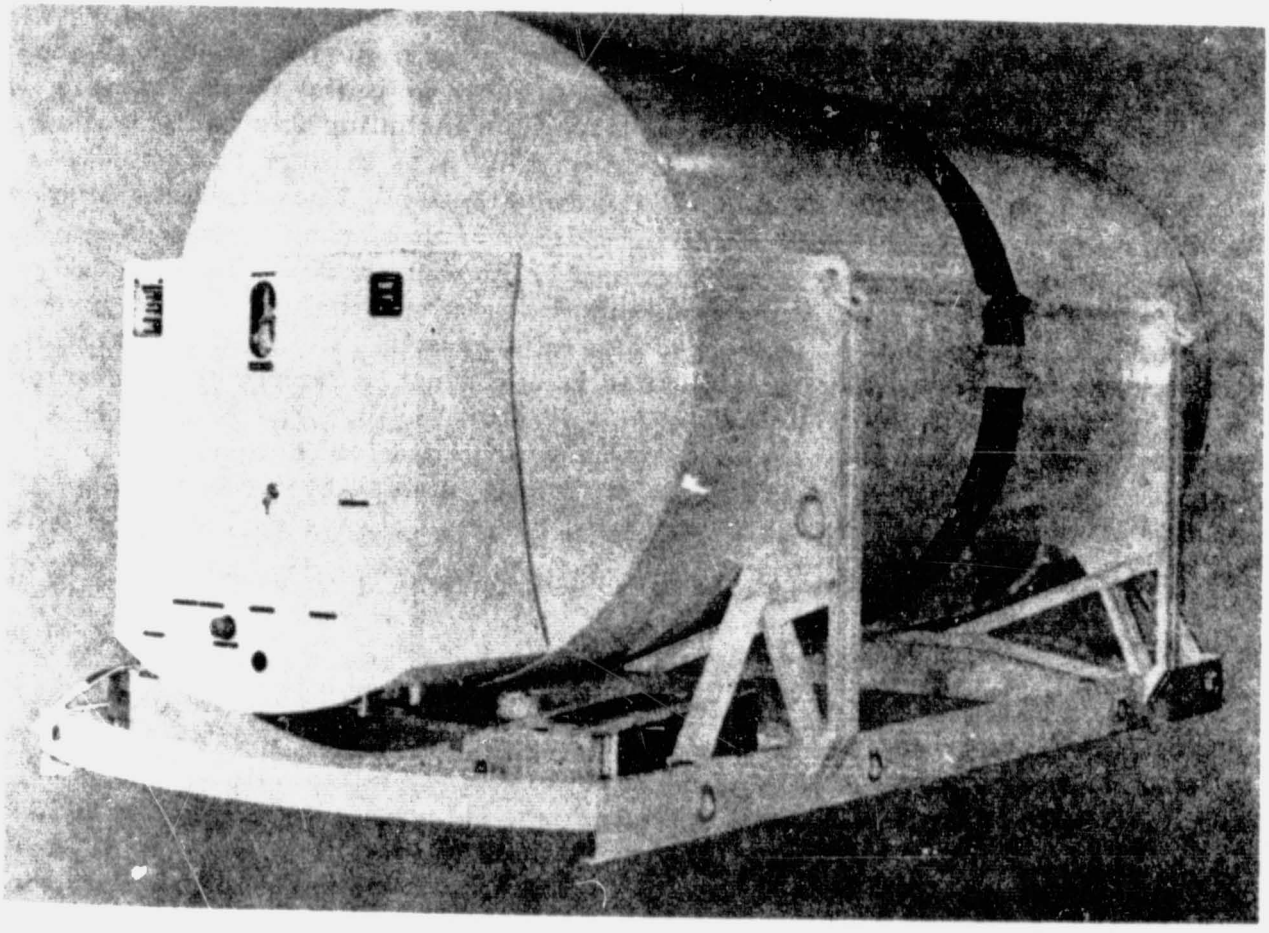

Figure 2-12b. Typical 2000 gallon liquid oxygen storage tank.

equal to diameter; this shape very crudely approximates a sphere with some of the previously wasted space now filled in and useable. As the size of such a dewar increases, however, and if it is to be used for transport, it may be that in attempting to retain this 1 to 1 dimensional relationship the permissible width for air, road or rail travel is reached beyond which the vessel diameter cannot increase; it must then grow longitudinally with resulting loss in good thermal performance. Little can be done but to accept this penalty after first assuring that reasonable thought has been given to the best choice of insulation for this application. It should be of high thermal efficiency to minimize the installed thickness, permitting the inner tank diameter to be as large as possible within the specified or necessary limiting confines of the outer vacuum jacket.

The designated size of a vessel usually is given in actual liquid capacity — that is, a 500 gallon dewar holds 500 gallons of liquid saturated, or under equilibrium conditions, at 1 atmosphere pressure. The measured volume of most cryogenic tanks, however, is about 10 percent greater, or in the above example, 550 gallons. Although various reasons are given for including this additional capacity, the main purpose is to contain (without overflow loss through the vent pipe) the liquid as it warms up and expands upon pressurization. Pressurized transfer of liquid cryogens will be covered shortly, but the result of such a process can be observed on any vapor pressure graph in Chapter 7 — an increase in pressure requires an increase in temperature for saturated, or equilibrium, conditions in a liquid volume. Then, just as in the radiator of an automobile or in a teakettle, if sufficient room for expansion of the heated liquid is not provided, the containers will overflow at some higher (than filling) temperature point. The 10 percent (sometimes more, sometimes less) extra space furnished for this purpose is termed ullage volume, and unless loss through the vent is acceptable when the vessel is both full and undergoing pressurization, its provision always should be considered.

Structural Design

Where the matter of public safety arises in the use of cryogenic tankage, the vessels are constructed and tested in accordance with applicable structural codes (e.g., ASME Boiler and Pressure Vessel Code - Section VIII: Unfired Pressure Vessels); for some transport equipment, Department of Transportation regulations apply as well. It is not meant to be the purpose here to detail all aspects of conventional vessel design; rather it is the intent to point out the additional requirements for low temperature application.

In order to be acceptable for such service, a material must not only possess suitable physical properties at very low temperatures, but also it must be compatible with the fluid it is carrying. Nitrogen offers no problem in this latter respect, but oxygen is not as easy to work with. More will be said of oxygen compatibility in Chapter 4; for now it will be disregarded. Copper, aluminum and austenitic stainless steels are the metals most commonly used for cryogenic tankage, with copper more often used in small containers and the latter in larger vessels. Property values for each of these are presented in Chapter 7. It is immediately seen from the mechanical property data that the strength of these particular materials increases with decreasing temperature — some by a factor of two or more — and this is a welcome advantage to low temperature work. A disadvantage is that these materials are expensive when compared to the carbon and low-alloy steels usually employed in non-cryogenic vessels and in the warm outer shells of cryogenic tanks.

It may be argued that good use could be made of the low temperature increase of strength; thinner wall thicknesses and therefore less material at less cost could directly help in counteracting the high cost per pound of metal and

perhaps go far in attempting to equate the financial discrepancy between materials for low and moderate temperature application. If one could be assured that the construction materials with desirable low temperature properties will always be at low temperature when in service, then design to the higher strength values might be in order. This is not the case, however, since a dewar often is only partly full for days or even weeks and in such a state the upper portions out of the liquid become warm — occasionally as much as several hundred degrees above the temperature of the cryogen in poorly conducting stainless steel vessels. Thus, the warm metal no longer has its increased low temperature strength and any design incorporating such characteristic properties might easily fail in service.

Related to the subject of shell thickness are not only the pressure capability and total weight of the vessel but also thermal losses due to the necessary ruggedness of the suspension system and cooldown of the metal. In the following section on support techniques it will be noted that one of the several factors in good suspension system design has to do with minimizing the cross-sectional area of the support members. By reducing the weight of the liquid-carrying inner shell, it follows that less strength and therefore fewer or smaller diameter members are required and the performance is improved. Also by keeping the wall of the inner shell as thin as possible, the amount of liquid boiled off in cooling the metal tank down to the temperature of the stored cryogen is minimized; more is said of this in a forthcoming section on cooldown losses.

Although much of this discussion on structural design is concerned with the cryogenic inner tank, the warm outer shell is equally important. As a low pressure rated enclosure with vacuum on one side and atmospheric pressure on the other, it would seem that not much is required in the way of strength, etc. This is generally true of perfectly formed (exactly round) cylinders and spheres with no concentrated support loading and no possible internal pressure rise, but it is not the case for a real outer dewar shell. Supports are attached to the outer tank walls, and pads and stiffening rings usually are used at the attachment points to spread the load effects out over an appropriately large area. Rings also improve the stability of a shell, maintaining it in a circular condition to prevent any tendency to collapse or buckle because of out-of-round distortion. The end closures of a vessel, consisting of dished or spherical heads, also assist in stiffening and maintaining circularity and are of definite importance in any overall strength consideration. As we will see in the piping discussion, care must be taken that cold pipes, or dripping liquid air from these pipes, do not contact the warm shell in any manner; since non-cryogenic materials of construction such as carbon steel often are used for outer tank walls, any decrease in temperature could have disasterous consequences because of cold embrittlement and loss of strength. Along the same line, cold gas relief and vent ports should not be situated in such a way that will permit impingement of cold fluid on the warm shell.

The possibility of internal pressure rise also has been mentioned as a design consideration. If the inner tank or connecting piping between shells should rupture or simply spring a leak, any internal pressure within the tank plus that which is created additionally by vaporizing cryogen in the warmer insulation space, not only ruins or degrades the quality of the insulation, but also may impose an excessive pressure (and therefore stress) on the outer shell. As insurance against such a hazardous situation, burst discs or spring-loaded vacuum-tight relief devices are made an integral part of the outer tank wall and are set to relieve at least several psi above atmospheric pressure.

Suspension System

Of major concern in the design of a low heat conducting internal support structure for dewars is the shock or acceleration loading it must withstand under both anticipated ordinary and possible extraordinary service conditions. For a stationary storage vessel acted upon by gravity only, the design is rather simple and straightforward. However, if one must contend also with earthquakes, ordnance blast effects, or acceleration/deceleration forces encountered during transport by highway, rail or air, the situation becomes more complex. Table 2-3 lists acceleration forces commonly used as design criteria, where the loadings are given in multiples of the local acceleration of gravity — 3 g denotes an acceleration force of 3 times the weight of the body being acted upon. Considering the effect of 3 g's on a particular dewar suspension system, the weight of a full inner container (say a 500 gallon tank of liquid oxygen weighing 5000 pounds) would be multiplied by 3, and the supports would necessarily have to be engineered to hold 5000 pounds x 3, or 15,000 pounds.

For certain applications, the load-bearing properties of powder insulations have been utilized in conjunction with supports to permit load sharing between the

Table 2-3. Minimum acceleration forces for cryogenic vessel design

Type of Vessel	Vertical Down g	Vertical Up g	Longitudinal g	Lateral g
Stationary (empty)	3	0.5	3	0.5
Stationary (full)	1.5	0.5	0.5	0.5
Air transport (full)	4.5	3.5	8	3
Road transport (full)	2	1	1	1
Small portable (full)	5	4	4	4

supports and the powder during periods of high-dynamic loading (shock, for example); this lowers the strength requirement of the supports and therefore allows incorporation of a less thermally conductive structure for inner shell suspension. Pertinent powder dynamic load characteristic information, combined with appropriate computational procedures, must be used here to assure no overstressing of the supports at maximum load conditions — that is, to assure that the powder does, in fact, take its share of the applied load.

While on the topic of load-bearing qualities of powder insulations as related to support systems, it also should be mentioned that powders are capable of applying loads to such structures as well as relieving them. As illustrated by figure 2-13, when a dewar is filled with a cryogen its inner shell contracts because of the cooling and its outer shell remains warm and dimensionally fixed. By contracting, the cold shell creates a void around it which is soon filled by adjacent powder with resulting loss of insulation in an upper region of the tank. At some later time, then, when the vessel is warmed up after complete withdrawal of cryogen (for purging or some other reason), the inner shell expands and packs the powder which previously had fallen into its contraction gap. Depending on the type of powder used, the configuration of the vessel, and the number of cooling/heating cycles undergone by the equipment, it is known that a situation can develop wherein the packing or compaction of powder generates sufficient pressure to distort or even break certain vulnerable support systems. The incidence of reported failures from this cause is small, but nevertheless it is a problem which can be alleviated by intelligent design. The most common remedy involves application of a fiberglass insulating blanket around the inner tank wall, as shown in the bottom part of figure 2-13, in such a manner that it is compressed when the container is warm and expands to fill the void created as the inner shell cools and contracts. Any powder which would have moved otherwise now is constrained.

As to the design of the support member itself, numerous schemes have been used successfully (some not so successfully), and almost unlimited possibilities exist, depending on cost, complexity of application, and ultimately the ingenuity of the designer. Looking at the Fourier equation which computes conduction heat transfer through any material (of which more will be said in Chapter 6),

$$q = kA\frac{\Delta T}{\Delta \ell} ,$$

it is evident that heat (q) transferred through a support element would be decreased by decreasing the thermal conductivity (k) or the cross-sectional area (A) of the element or by increasing its length ($\Delta \ell$); the temperature difference (ΔT) between warm and cold shells is assumed constant for most practical cases. The key to good cryogenic support design, then, is to use a material of poor thermal conductivity with sufficient strength to minimize its required cross-sectional area — making it as long as possible consistent with stability and vessel geometry. Stainless steel rods, tubes, and cables have been used in such service as well as cer-

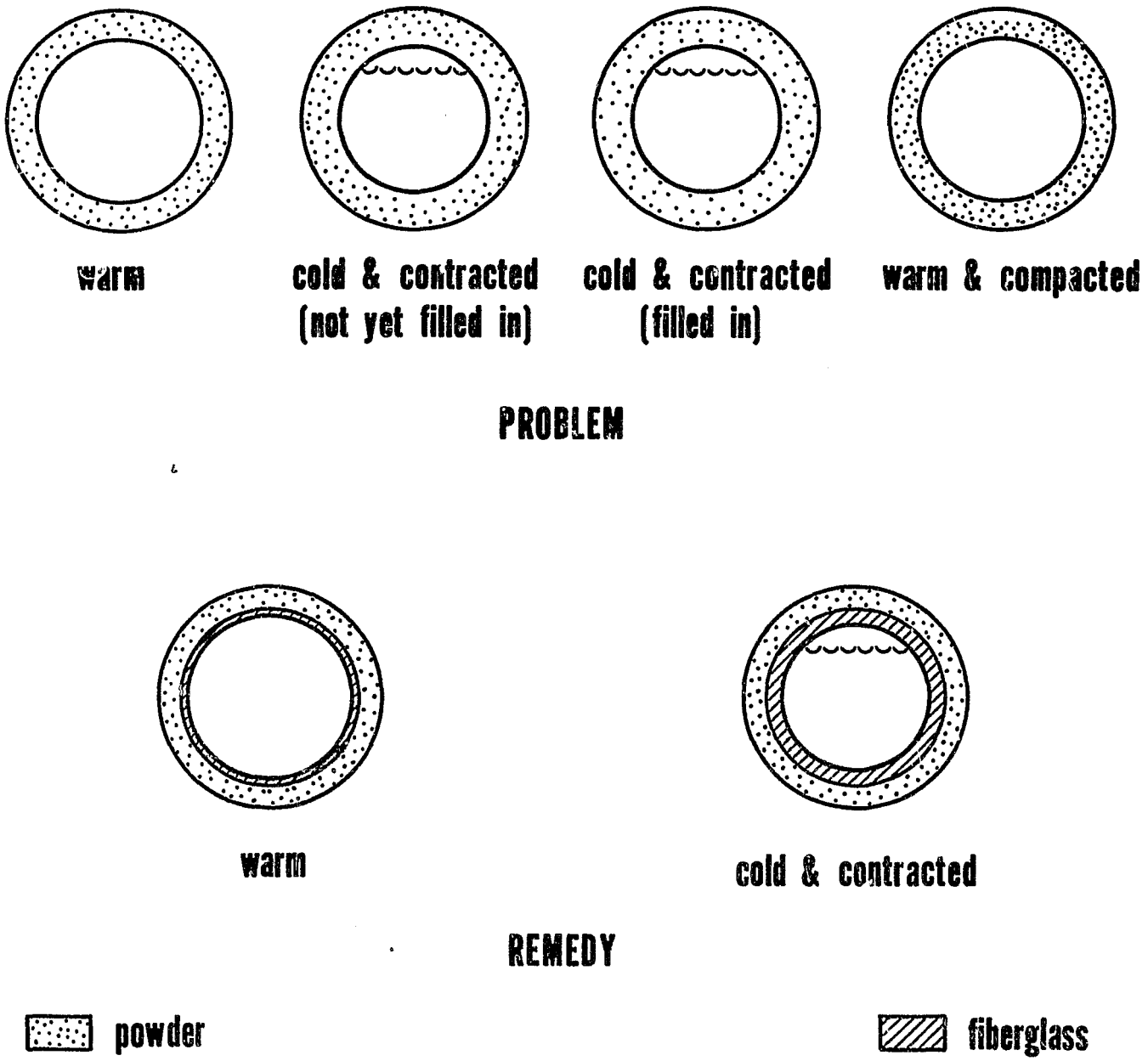

Figure 2-13. Powder insulation compaction (cause and remedy).

tain reinforced plastics and fibers. Figure 2-14 illustrates some of the methods employed in dewar suspension systems. Springs, conical washers or slotted end fittings generally are required to accommodate whatever thermal contractions and expansions occur in the total suspension system.

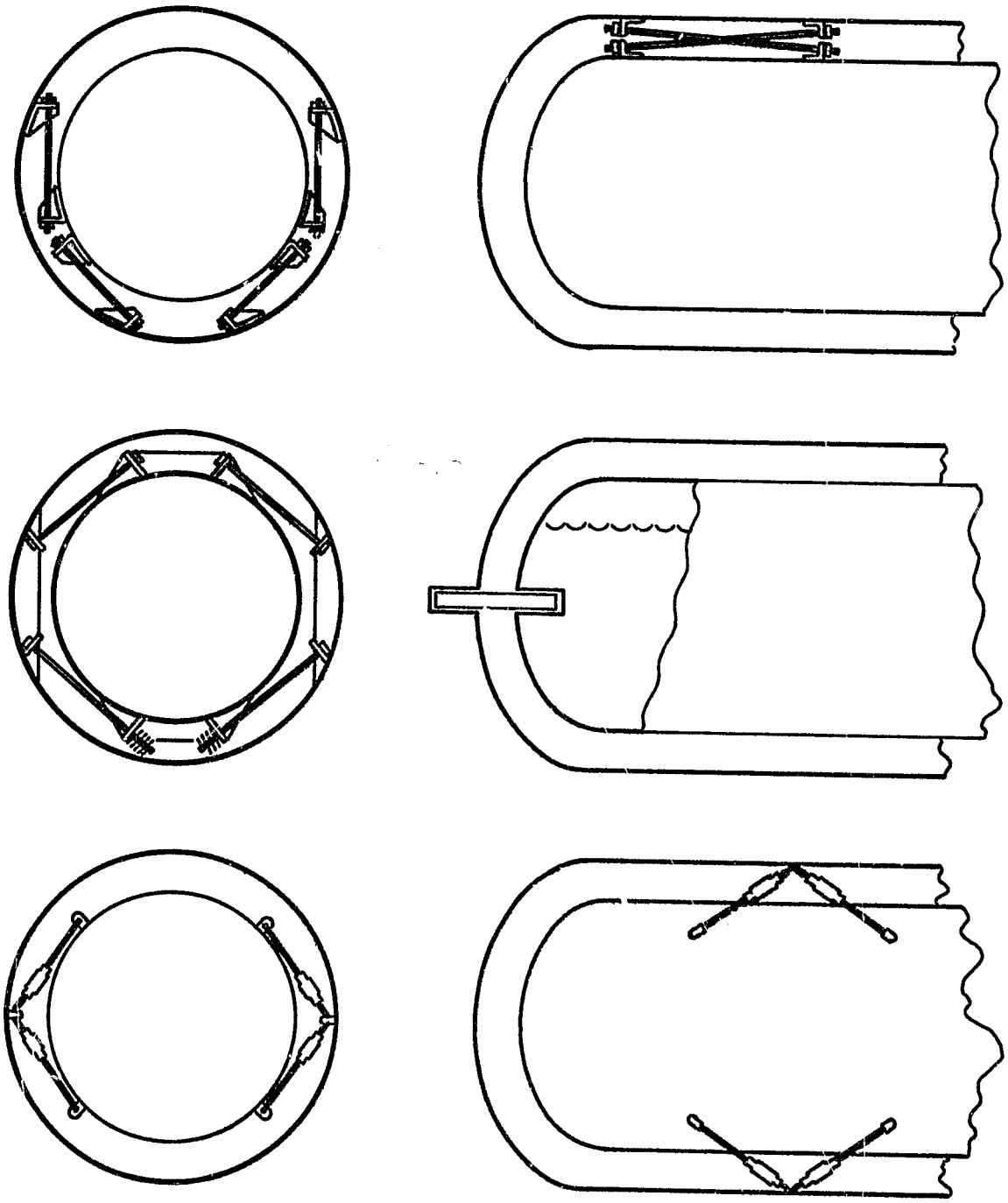

Figure 2-14. Dewar suspension systems.

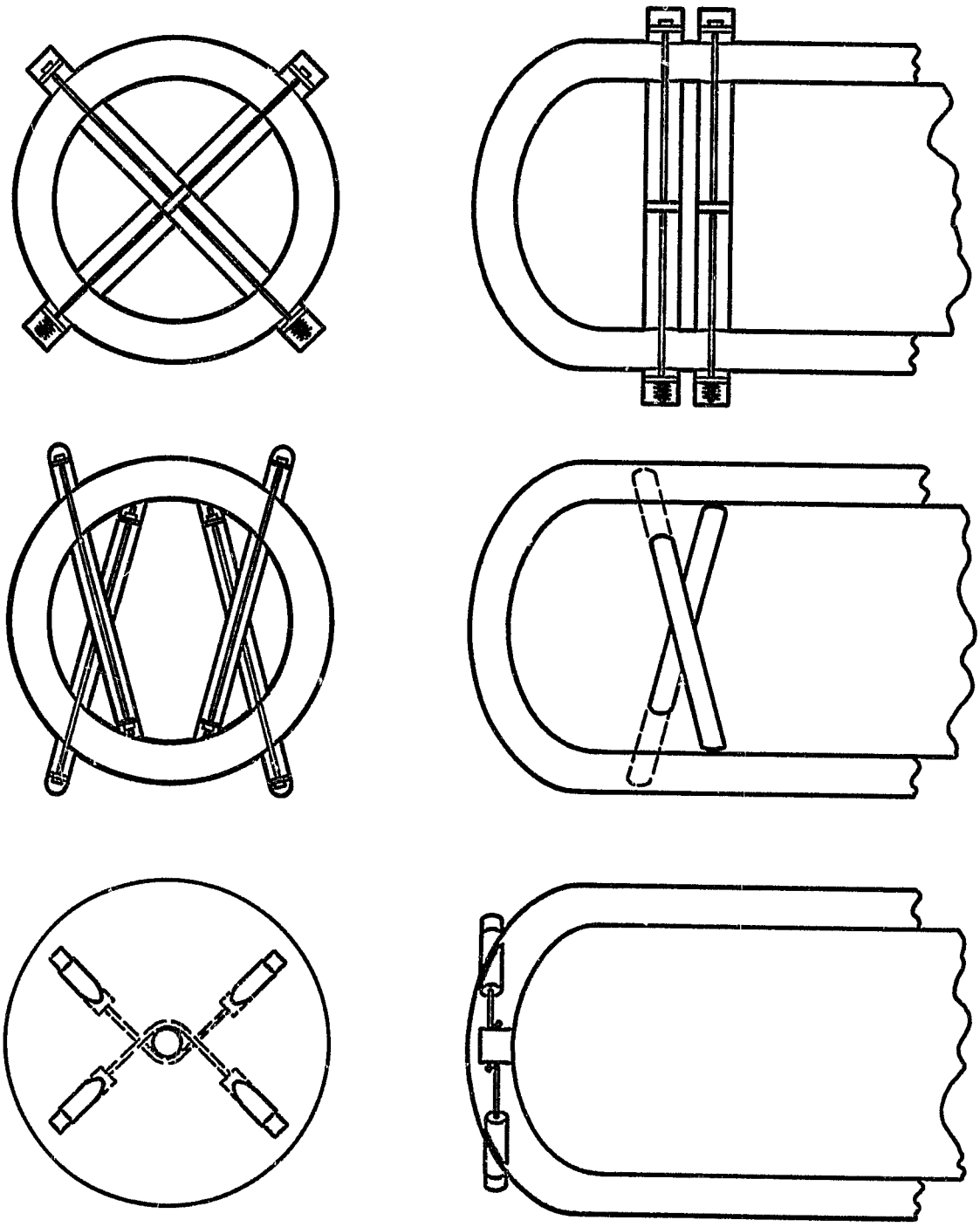

Figure 2-14. Dewar suspension systems. (con't.)

As a help in the selection of materials to be used as supports, the ratio of allowable yield strength to thermal conductivity generally is considered an important criterion. The larger this ratio is for any given support member, the better the situation becomes from a standpoint of minimizing heat input through this support to the cryogen. Again, complexity of application and cost enter into the picture, but the ratio described above is useful in the selection of dewar suspension systems. Stainless steel, which has been used extensively, is quite good (has a high ratio value) in this respect; however, polyester fibers in the form of webbing or cording are even better by an order of magnitude or so. Unfortunately, the application of this fiber material is somewhat difficult.

Piping

In order to fill and empty a dewar, vent it, measure pressure and liquid level, and generally provide means to accomplish many different requirements, it becomes necessary to run tubes or pipes from the inner container through the outer vacuum jacket or shell. However, any means of connection between the cryogen and its much warmer external environment furnishes a path for heat conduction through the connecting material similar to that encountered with supports and suspension systems; it follows that more than superficial consideration must be given to this aspect of tank design and construction.

Recalling the basic heat conduction equation again, it is evident that heat transfer from warm to cold end of the piping will be minimized by using a poorly conducting material such as stainless steel, by keeping the cross-sectional area of the pipe or tube minimal either through the use of small diameter or thin walls (or both), and by using as long lengths as possible consistent with common sense and configuration restrictions.

Examining these one at a time, stainless steel is almost always a good choice of low conductivity material for this purpose, having but one major drawback when used in aluminum tank construction. Stainless and aluminum are difficult to join hermetically and since vacuum-tight joints are required where piping penetrates each wall, this combination of materials can present a serious problem. Fortunately, several different types of transition (bi-metallic) couplings have been developed to improve this situation and the difficulty has been alleviated appreciably. Transition couplings for cryogenic service are part aluminum/part stainless steel joints made in such a way that the aluminum member is outermost, since it contracts more on cooling than the steel and makes the joint even tighter in low temperature service. Several different manufacturing methods for this type of coupling are shown in figure 2-15.

Inasmuch as thin-wall stainless steel tubing is available in practically any desired length, little difficulty is experienced on this account. Pressure rating of the dewar generally dictates tube wall thickness, although for very small diameter instrumentation tubing, designing to this criterion may lead to impractically thin

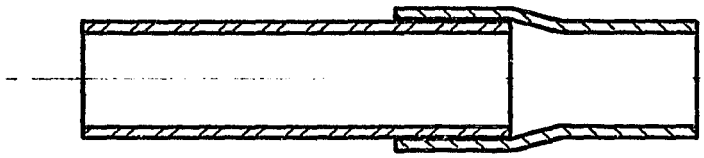

(a) PRE-TINNED OR PLATED, SOFT-SOLDER FILLED TUBULAR LAP JOINT

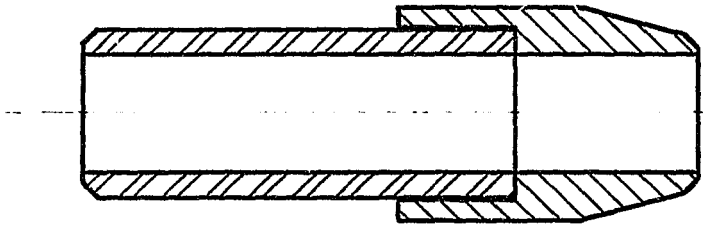

(b) CAST MOLECULAR BOND OR BI-METAL BRAZE JOINT

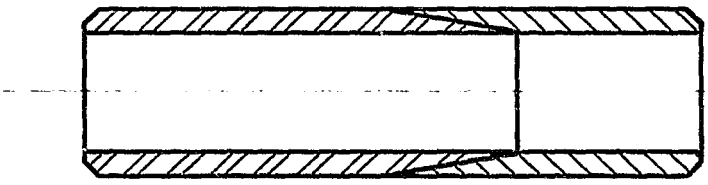

(c) HOT DIFFUSION-BONDED, HIGH PRESSURE EXTRUSION JOINT

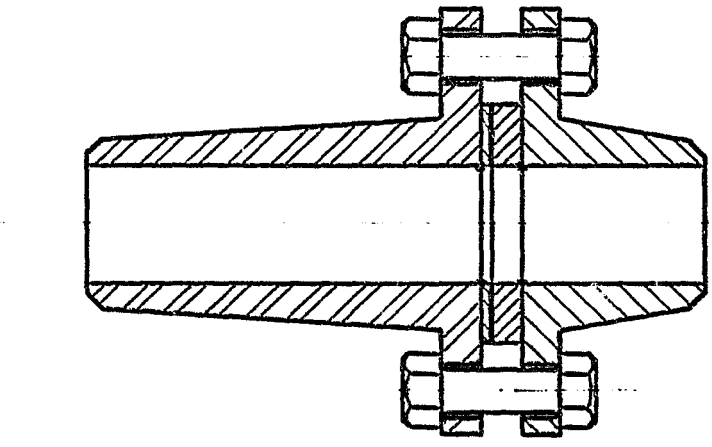

(d) COLD PRESSURE-WELDED RING J OINT

Figure 2-15. Aluminum-to-stainless steel transition (bi-metallic) couplings.

walls which could be subject to abuse and damage on installation or in use; to reduce this problem, the tube wall thickness specification would be increased to a more practical value than that required solely for pressure capability.

Various methods are used to run tubing or piping between and through the inner and outer tank walls, and these are best described by looking at figure 2-16. Assuming the most popular dewar configuration involving horizontal cylindrical tanks, available space and ease of fabrication usually prescribe how the piping is to be placed. If a small insulation thickness (and therefore a short distance) between the cold and warm tank shells is necessary, straight-through piping similar to that shown in figure 2-16f often is used, requiring no bending of the pipe but involving an external expansion bellows to accommodate any dimensional change when the tank and pipe are cooled to service conditions. An internally placed bellows such as the one illustrated in 2-16b is not recommended since it is more likely to fail than any other element of the piping scheme; a better location is outside of the system where it can be examined and repaired. Lack of any provision for contraction or expansion remove 2-16c and 2-16e from further useful consideration, whereas the 'goosenecked' configuration of 2-16g, the long vertical riser of 2-16d, and the flexible small diameter instrumentation tube of 2-16a are acceptable in many designs.

It may have been noted that six of the illustrated seven outer shell tube penetrations are made through cylindrical standoffs or pant-legs; the purpose here is to isolate the warm vessel wall from cold liquid or gas bearing tubes (fill, empty or vent) through the use of poorly conducting (usually stainless steel) connections to that wall. If the outer tank shell is made of aluminum, a flanged O-ring sealed design such as the one shown in 2-16g may be arranged to make a separable aluminum-to-stainless steel transition rather than using the bi-metallic couplings of figure 2-15. Instrumentation tube 2-16a remains without a standoff since the gas it contains is always warm at the outer wall position (no flow occurs as the external extremity is plugged by a pressure gage or some other form of closure). The scheme of 2-16e is bad for a number of reasons: the distance between wall attachments is quite short, permitting excessive heat transfer to the cryogen; no expansion or contraction mechanism is incorporated in the design; and considerable refluxing[2] can occur in the tube (e.g., it is possible for vapor to condense on the inner wall of the cold tube surrounded by liquid; the condensate then flows toward the warm end of the tube where it vaporizes, and the process repeats).

In summary, figure 2-16 is meant to illustrate both good and bad features of cryogenic liquid and gas piping design, and the acceptable schemes of pipe runs, expansion techniques, attachment methods and standoffs are to be intermingled in

[2] Refluxing is a repetitive process wherein heating occurs, creating vapor from a liquid which then recondenses on a cooled surface and flows back to be heated once again.

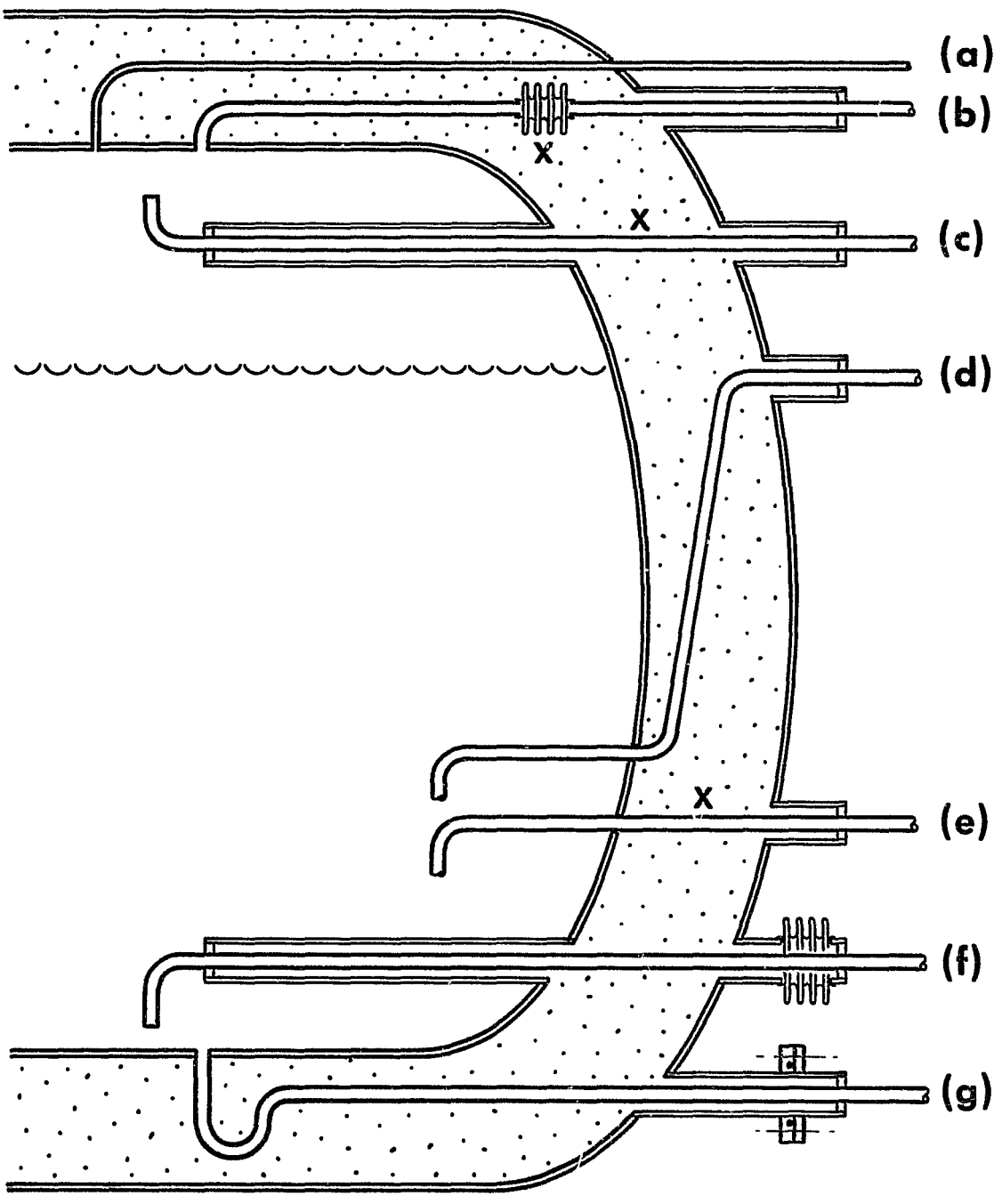

Figure 2-16. Dewar piping details.

the designers (or readers) bag of tricks — to be retrieved selectively as the occasion demands. For example, the geometry of 2-16g may be the perfect answer for an application involving a large insulating annulus, whereas something like 2-16d will work equally well at the end of a tank if the annulus is small and crowded.

As seen in figure 2-17, liquid piping not only is used to fill and empty a dewar (sometimes one line performs both duties) but in many cases a pipe may also supply liquid to an ambient air heat exchanger where it is vaporized and used in pressurizing the dewar. From the standpoint of simplicity, low heat input, and

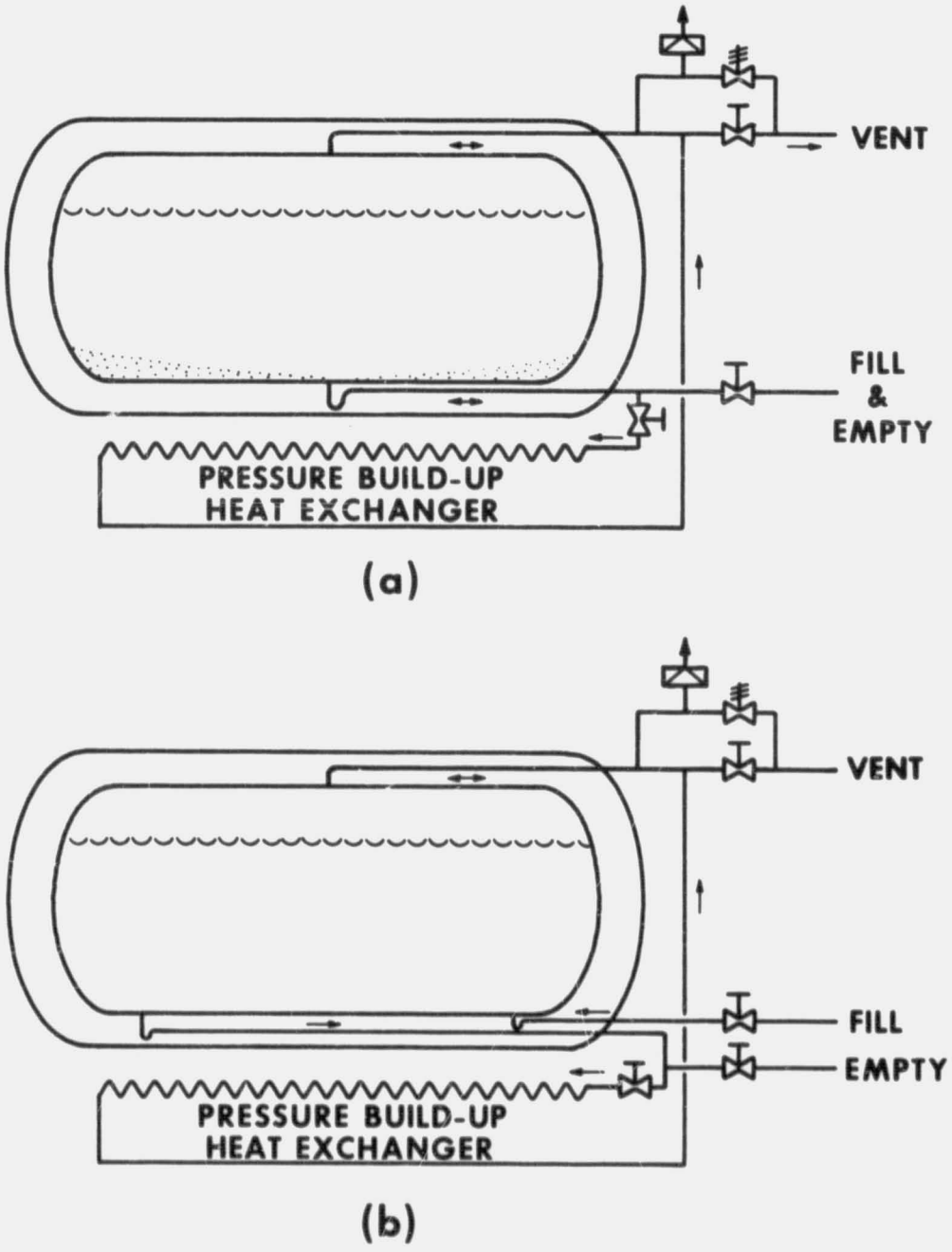

Figure 2-17. Dewar piping schematics.

minimum cost, one internal pipe could be used to satisfy all three liquid functions in the manner shown schematically by figure 2-17a. This precludes simultaneous filling and emptying, however, and therefore wouldn't work if a requirement existed to be able to fill a storage dewar from a generating plant while at the same time dispensing liquid from the same dewar. Also, in the case of an oxygen vessel, there is reason to believe that one multipurpose pipe connection does not induce sufficient mixing within the liquid space to avoid a build-up of contaminants. As one solution, two widely separated lines may be used to permit simultaneous filling and withdrawal as well as to establish flow patterns more conducive to sweeping the tank bottom between entrance and exit, moving whatever contamination enters the tank through it and hopefully out again.

Additionally, a sump or well may be built into the bottom of a liquid container in such a fashion that heavy contaminants tend to migrate towards this low point of the system while the lighter particles float on the surface of the cryogen. If solids are undesirable in the withdrawal product, establishment of the withdrawal pipe inlet some distance above the sump but below the minimum permissible liquid level theoretically furnishes the user with pure liquid. Provision must be made, however, to periodically drain and purge such a system since the concentration of contaminants will build up with time — eventually to some unacceptable level of impurity. As an alternative, if a certain amount of heavy contaminant is acceptable in the withdrawal product, the sump can again be used — only this time with the withdrawal pipe inlet right at the bottom of the sump. In such a situation, the particles continuously migrate to the low point (as before) but are withdrawn almost as fast as they accumulate. This avoids an increasing concentration of heavy contaminants with time and only leaves the lighter floating solids, requiring perhaps fewer periodic tank purges than the previous method. Emphasis must be placed on the requirements and demands of the user, however, and if liquid with essentially zero contamination is specified, the latter scheme is out and the one preceding it should be used. If longer time intervals between tank purging is of prime importance, and purity is of secondary concern (within reasonable limits), the latter technique may be worth considering.

One final point should be made on the above sump discussion. If, for some reason, the particles do not behave as predicted and do not move to the sump or float on the surface (perhaps they develop electrostatic charges which cause them to adhere to their containing tank walls), these schemes are then of small value — providing a false sense of security which could be hazardous. We do not know enough about this today to make any positive statement concerning the matter, but we do know that application of good engineering design principles and intelligence can only improve the situation.

For oxygen systems in particular, then, where contaminants can be both hazardous and undesirable (e.g., in a pilots breathing oxygen where foreign odors in the vaporized gas may be annoying or even sickening), considerable attention must be given to the piping design in and related to the storage container; if dead

ends or dead spaces are permitted to exist, allowing the accumulation of contaminants or other particulate material, one result could be disaster in the form of explosion or death from breathing toxic vapors.

Gas or vapor phase piping is also a necessary part of any cryogenic storage or transport vessel. Looking back at figure 2-17, it is evident that the vapor space or ullage above the liquid surface may be vented through several different types of valves or other devices — a hand-operated or manual valve, a relief valve, and a burst or rupture disc. If the tank is being pressurized (either through the ambient air heat exchanger or by self-heating and subsequent vaporization of the contained fluid), the manual valve must be shut. However, to avoid accidental overpressurization beyond the maximum allowable working pressure of the equipment, the relief valve is set to open at about 1.1 times the working pressure; in the event this valve sticks closed or otherwise malfunctions, a burst disc is included to rupture at a pressure slightly greater than the setting of the relief valve.

The dewar pressurization system, again shown in figure 2-17, involves a combination of both gas and liquid piping and valving. By opening the heat exchanger valve and closing the vent, fluid enters the exchanger in a liquid state, vaporizes and returns to the tank as a gas. The driving potential for such a process is the pressure head of liquid above the tank outlet to the heat exchanger; as the amount of liquid in the tank is depleted, less head is available to force the liquid into its vaporizer and more ullage space is available to be pressurized — each of these conditions having the effect of slowing down the rate of pressurization. Understandably, the fuller the tank, the faster the rate of pressurizing (this applies both to external vaporization through a heat exchange tube and to internal vaporization due to self-heating via normal heat input through the insulation). In some equipment, diffusers are attached to the pressurizing tube outlet in the tank to more evenly distribute the incoming gas throughout the vapor space; these devices reduce the velocity of the pressurizing gas and also decrease any impingement effect of gas jetting on the surface of the liquid. The attempt here is to cut down on the condensation of incoming gas as it is forcibly mingled with the cold liquid (if condensation is reduced, less gas is required to achieve a given level of pressurization), but there has been some evidence, for certain systems at least, that a net vaporization rather than condensation occurs in such jet impingement circumstances. Therefore, at this time, no clear cut recommendation can be made on whether or not the additional expense of a diffuser is warranted.

One final comment should be made before leaving the subject of piping. It is essential that pipe runs be designed to avoid any possibility of liquid flowing (during periods of no intentional transfer) from its container toward a warmer region where it can only evaporate and be wasted. For stationary storage vessels this is simple to accomplish, but additional thought must be given to transport dewars going up and down hills in transit and to any tanks located in aircraft subject to odd maneuvers or motions. If the maximum vessel inclination is known, piping configuration can be adjusted accordingly. If it is unknown, the designers

intuition and good judgment must be relied upon — e. g., the loop of figure 3-13a might be a reasonable choice to accommodate most eventualities.

Dewar appurtenances (manways, baffles)

Depending on the conditions of use, cryogenic fluid vessels are occasionally equipped with additional features to solve specific problems.

Access ports or manways sometimes are built into the upper tank walls, as shown in figure 2-18, to permit inspection and cleaning of the inner container, or in the case of experimental vessels, to permit placement of research instrumentation and equipment in the cryogen space. The ports may be constructed in several ways, two of which are illustrated by figures 2-18a and 2-18b, and each has its own advantages and disadvantages. 2-18a is not penalized by additional heat transfer to the cryogen since insulation between the ports and therefore between the shells is not disturbed by additional conduction paths or degraded insulation, as is the case in 2-18b where expansion bellows and non-evacuated insulation separate the inner and outer ports. On the other hand, any leak at the difficult-to-make-and-keep low temperature inner shell cover seal destroys the insulating vacuum of the entire vessel in 2-18a,whereas it only adds a little gas to the volume enclosed by the bellows in 2-18b. Also, the insulating vacuum must be broken each time access is gained to the inner tank of 2-18a, requiring a time-consuming pump-down when the vessel is being readied for service once again,which might be further lengthened by moisture absorption of the insulation which was necessarily exposed during the access period.

In the design of large transport dewars, it becomes necessary to consider the use of baffles in the liquid compartment. During one road test, it was found that a typical cryogenic tank on a 30-hour trip underwent roughly 1600 accelerations and decelerations due to starts, stops and speed changes. Depending on severity of these velocity changes, tank geometry, weight of fluid involved, and perhaps several other lesser items, various effects occur in and on the total tank system that are both bad and good. In the bad category, sloshing liquid or liquid that moves against its containing walls by virtue of any change in velocity of the container applies additional forces to those walls which must be accounted for in the tank design stress analysis. In the process of moving along or against the shell, energy gained by the liquid eventually converts to heat by friction which consequently vaporizes and wastes liquid. Such losses may be significant for low heat-of-vaporization liquids like helium and hydrogen but they are relatively unimportant for nitrogen and oxygen. The stress problem may be another matter, however, and handling difficulties by drivers of road transports certainly should be taken into account as well. In order to decrease the amount of sloshing that might occur under transport conditions, baffles or slosh plates are installed with openings at the bottom and occasionally at other locations to equalize the liquid level throughout the tank. Although the problem of longitudinal sloshing is most important, lateral effects must also be examined in certain cases. Aside from

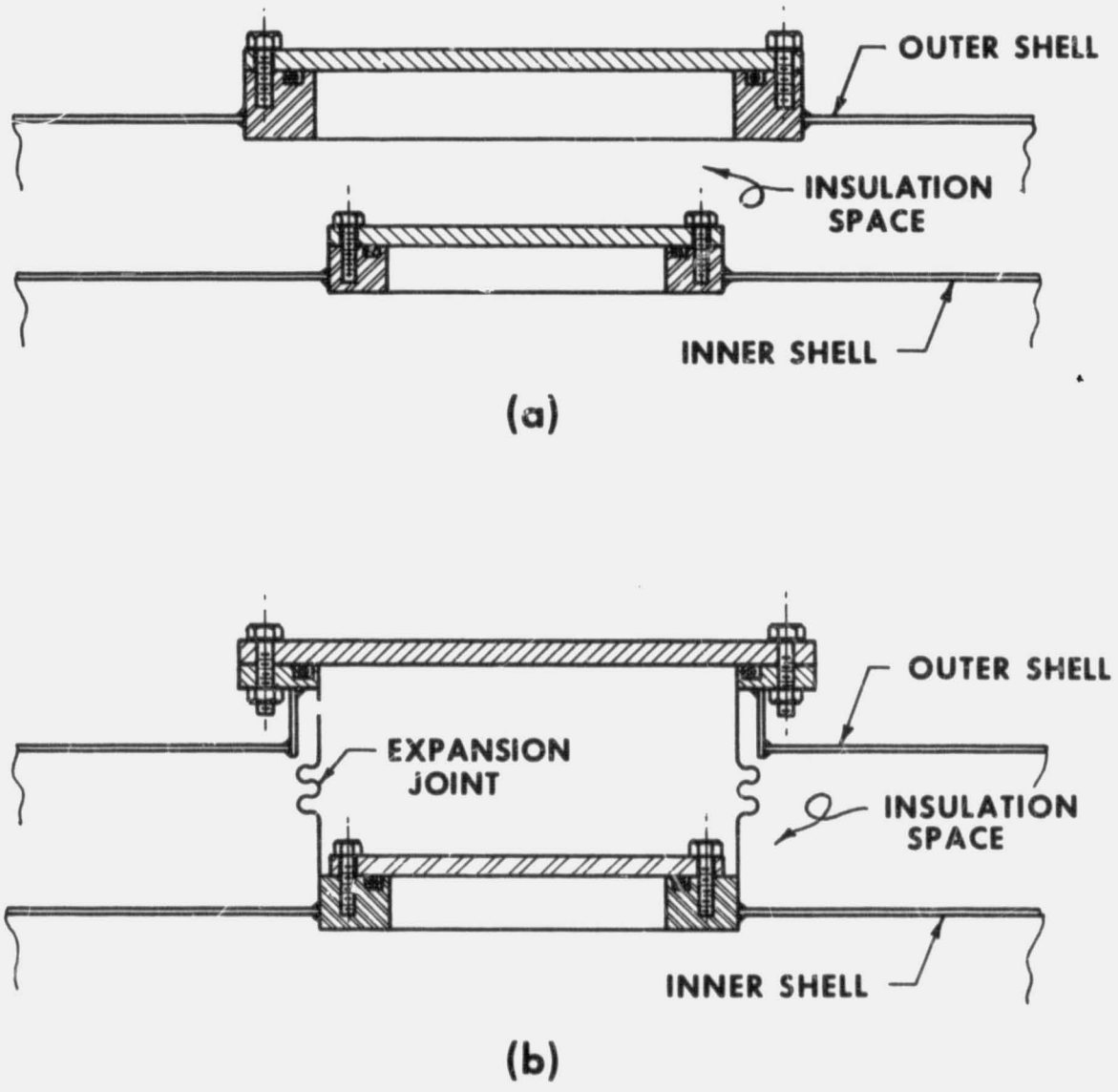

Figure 2-18. Dewar access ports or manways.

the increase in weight of the vessel, baffles tend to reduce the amount of agitation and therefore mixing of the liquid which normally occurs in transit; such mixing is useful for the reduction of thermal stratification in the liquid and the decrease in mixing is a penalty one pays to accomplish something else. To help in this respect, if the baffles are constructed of heavy gage materials of high thermal conductivity such as aluminum or copper, vertical equalization of liquid temperature in the tank is enhanced and stratification may be reduced.

END OF REFERENCE

REFERENCE

73

ASME BOILER AND PRESSURE VESSEL CODE, SECTION VIII, PRESSURE VESSELS, DIVISION 1. ASME, 1968.

THIS REFERENCE IS COPYRIGHTED MATERIAL AND THEREFORE THE CONTENTS HAVE NOT BEEN REPRODUCED FROM THE TEXT.

END OF REFERENCE

REFERENCE

74

ASME BOILER AND PRESSURE VESSEL CODE, SECTION VIII, PRESSURE VESSELS, DIVISION 2 - ALTERNATIVE RULES. ASME, 1971.

THIS REFERENCE IS COPYRIGHTED MATERIAL AND THEREFORE THE CONTENTS HAVE NOT BEEN REPRODUCED FROM THE TEXT.

END OF REFERENCE

74

REFERENCE
75

ASME BOILER AND PRESSURE VESSEL CODE, SECTION IX, WELDING QUALIFICATIONS. ASME, 1971.

THIS REFERENCE IS COPYRIGHTED MATERIAL AND THEREFORE THE CONTENTS HAVE NOT BEEN REPRODUCED FROM THE TEXT.

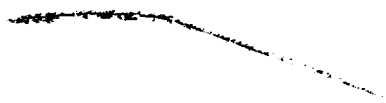

END OF REFERENCE

75

REFERENCE

76

WELDING HIGH PRESSURE SYSTEMS AND CRYOGENIC SYSTEMS. TECH. ORDER 00-25-224, AIR FORCE, AUG. 30, 1965.

THIS REFERENCE HAS A LIMITED DISTRIBUTION AND MAY NOT BE REPRODUCED.

END OF REFERENCE

76

REFERENCE

77

RECOMMENDED RULES FOR DESIGN AND CONSTRUCTION OF LARGE, WELDED, LOW-PRESSURE STORAGE TANKS. API STANDARD 620, AM. PETROLEUM INST., FOURTH ED., FEB. 1970; SUPPLEMENT, APR. 1971.

THIS REFERENCE IS COPYRIGHTED MATERIAL AND THEREFORE THE CONTENTS HAVE NOT BEEN REPRODUCED FROM THE TEXT.

END OF REFERENCE

77

REFERENCE

78

TENTATIVE STANDARD - INSULATED TANK TRUCK SPECIFICATION. CGA-341, COMPRESSED GAS ASSOCIATION, 1970.

THIS REFERENCE IS MATERIAL THAT IS READILY AVAILABLE AND THEREFORE THE CONTENTS HAVE NOT BEEN REPRODUCED.

END OF REFERENCE

78

REFERENCE

79

TRANSPORTATION. CODE OF FEDERAL REGULATIONS, TITLE 49, PTS. 100-199, SUP. DOCS., JAN. 1, 1972.

THIS REFERENCE IS MATERIAL THAT IS READILY AVAILABLE AND THEREFORE THE CONTENTS HAVE NOT BEEN REPRODUCED.

END OF REFERENCE

79

NASA
SPACE VEHICLE
DESIGN CRITERIA
(STRUCTURES)

NASA SP-8040

FRACTURE CONTROL OF METALLIC PRESSURE VESSELS

CASE FILE
COPY

MAY 1970

NATIONAL AERONAUTICS AND SPACE ADMINISTRATION

FOREWORD

NASA experience has indicated a need for uniform criteria for the design of space vehicles. Accordingly, criteria are being developed in the following areas of technology:

Environment
Structures
Guidance and Control
Chemical Propulsion

Individual components of this work will be issued as separate monographs as soon as they are completed. A list of all previously issued monographs in this series can be found at the end of this document.

These monographs are to be regarded as guides to design and not as NASA requirements, except as may be specified in formal project specifications. It is expected, however, that the criteria sections of these documents, revised as experience may indicate to be desirable, eventually will become uniform design requirements for NASA space vehicles.

This monograph was prepared under the cognizance of the Langley Research Center. The Task Manager was W. C. Thornton. The author was C. F. Tiffany of The Boeing Company. A number of other individuals assisted in developing the material and reviewing the drafts. In particular, the significant contributions made by C. P. Berry and R. A. Rawe of McDonnell Douglas Corporation; D. W. Hoeppner of Lockheed-California Company; R. L. Johnston of NASA Manned Spacecraft Center; G. F. Kappelt of Bell Aerosystems Company; J. M. Krafft of the U. S. Naval Research Laboratory; G. T. Smith of Lewis Research Center; H. G. McComb, Jr., of Langley of Grumman Aircraft Engineering Corporation; J. C. Lewis of Jet Propulsion Laboratory; G. T. Smith of Lewis Research Center; H. G. McComb, Jr. of Langley Research Center; and C. D. Crockett of NASA George C. Marshall Space Flight Center are hereby acknowledged.

May 1970

CONTENTS

1. INTRODUCTION 1

2. STATE OF THE ART 3

2.1 Critical Flaw Sizes 5
2.2 Initial Flaw Size 10
2.2.1 Nondestructive Inspection 10
2.2.2 Proof Test 12
2.2.2.1 Effect of Applied Stress Levels 13
2.2.2.2 Effect of Wall Thickness 14
2.2.2.3 Effect of Proof-Test Temperature 14
2.2.2.4 Effect of Test Fluids 14
2.2.2.5 Effect of Test Duration and Pressurization/Depressurization Rate 16
2.2.2.6 Effect of Multiple Proof Tests 16
2.2.2.7 Need for Postproof-Test Inspection 17
2.2.2.8 Need for Combined-Load Proof Tests 17
2.3 Subcritical Flaw Growth 18
2.3.1 Sustained-Stress Flaw Growth 19
2.3.2 Combined Cyclic and Sustained-Stress Flaw Growth 23

3. CRITERIA 25

3.1 Design Conditions 25
3.2 Materials 26
3.3 Critical Flaw Sizes 27
3.4 Initial Flaw Size 27
3.5 Allowable Stress-Intensity Ratio 27
3.6 Proof Test 28

4. RECOMMENDED PRACTICES 28

4.1 Design Conditions 29
4.2 Materials 30
4.3 Critical Flaw Sizes 32
4.4 Initial Flaw Size 34
4.5 Allowable Stress-Intensity Ratio 35
4.6 Proof Test 36

APPENDIX A Design Trade – Illustrative Example 39

APPENDIX B Allowable Stress-Intensity Ratio – Illustrative Examples 43

B.1 Thick-Walled Pressure Vessel 43
B.2 Thin-Walled Pressure Vessel 46

REFERENCES 51

SYMBOLS 55

NASA SPACE VEHICLE DESIGN CRITERIA MONOGRAPHS ISSUED TO DATE 57

FRACTURE CONTROL OF METALLIC PRESSURE VESSELS

1. INTRODUCTION

Pressure vessels often contain small flaws or defects that are inherent in the materials or introduced during a fabrication process. These defects can, in many cases, cause severe reduction in the load-carrying capability and the operational life of pressure vessels. If the flaws are large in comparison to those causing failure at the proof-pressure stress levels, failure of the vessels will occur during initial pressurization. If the initial flaws are small, the vessels may withstand several operational pressure cycles and a number of hours of sustained-pressure loading before the flaws grow to a size that will result in failure. From an economic standpoint, it is important to minimize the possibility of failure of space vehicle pressure vessels during proof testing. From the standpoint of economics and personnel safety, it is imperative to prevent mission or operational failures.

During the past several years there have been costly proof-test failures directly attributable to small, preexisting flaws. In one example, a large steel rocket motor case failed at a stress less than 50 percent of the material yield strength. This failure originated at a small internal flaw having a depth less than one fifth of the material thickness. Other proof-test failures occurred in large propellant tanks and smaller auxiliary tanks used in the Apollo program.

Other failures have occurred after proof testing during the preflight checkout and/or storage of pressure vessels. One such failure occurred when a high-pressure helium tank, used in a defensive missile system, ruptured after 21 hours of sustained pressurization. This failure originated at an inclusion in the parent metal. The initial flaw increased approximately 50 percent in size during the time the tank was pressurized, and failure resulted. Although this is an example of failure resulting from flaw growth under sustained stress in a relatively inert environment, many more failures have occurred in which the environment played the dominant role. A number of titanium pressure vessels failed in N_2O_4 and methanol environments, and high-strength steel vessels failed in water environments. In these cases, the initial flaw sizes were often small (i.e., less than 10 percent of the size required to cause failure) and could not have been detected by nondestructive inspection. However, with the vessels at pressure for a time, the

environment induced significant amounts of stable flaw growth and the vessels eventually failed.

The purpose of this monograph is to present criteria and recommend practices that aid in the design of metallic pressure vessels by minimizing the occurrence of proof-test failures resulting from cracks and assuring against preflight and flight failures. The criteria and recommended practices permit wide latitude in the selection of materials and operational stress levels, detail design, analysis, and test to allow minimization of weight and/or cost as may be dictated by specific vehicle and mission requirements. This monograph is applicable to metallic pressure vessels whose design is primarily controlled by internal pressure requirements. These vessels include high-pressure gas bottles, solid-propellant motor cases, and storable and cryogenic liquid-propellant tanks – both integral and removable. Criteria and recommended practices for the design of pressurized cabins, inflatable structures, and vessels fabricated from composite materials will be presented in other monographs planned for this series.

To minimize proof test and prevent service failures of metallic pressure vessels, the three basic considerations are (1) the initial flaw sizes, (2) the critical flaw sizes (i.e., the sizes required to cause fracture at a given stress level), and (3) the subcritical flaw-growth characteristics. To prevent proof-test failures, the actual initial flaw sizes must be less than the critical flaw sizes at the proof-stress level. To guarantee that the vessel will not fail in service, it must be shown that the largest possible initial flaw in the vessel cannot grow to critical size during the required life span of the vessel. The basic parameters affecting critical flaw sizes are the applied stress levels, the material fracture toughness values, the pressure-vessel wall thickness, and the location and orientation of flaws. The determination of actual initial flaw sizes is limited by the capabilities of the available nondestructive inspection procedures; however, this limitation can often be partially circumvented by using information obtained from a successful proof test. A proof test in which the vessel does not fail provides information on the maximum possible initial-to-critical stress-intensity ratio within the vessel which, in turn, allows the size of the maximum possible initial flaw to be estimated. Subcritical flaw growth depends on several factors including the stress level, initial flaw size, environment, material, and pressure/time history of the particular pressure vessel.

Because many factors are involved, it is unlikely that the problem of premature fracture of pressure vessels will be completely resolved in the immediate future. During the past 10 to 15 years, however, significant progress has been made in several different areas (i.e., mechanics, metallurgy, inspection, etc.); accomplishments in the field of fracture mechanics have been particularly significant. Linear-elastic fracture mechanics has provided a basic framework and engineering language for describing the fracture of materials under static, cyclic, and sustained-stress loading, and is the basis for the criteria and recommended practices presented in this monograph.

The related problems of stress corrosion, fatigue, and discontinuities in pressure-vessel design will not be treated herein, but will be covered in other monographs now in preparation.

2. STATE OF THE ART

The problem of premature fracture of metallic structures is not new (e.g., the large molasses tank failure in 1919, the methane storage tank failure in 1944, the 25-percent failure rate of Liberty ships during World War II, and the Polaris motor case failures during the 1950's). Even today there is a general lack of specific guides in industry and government manuals, specifications, and codes for the control of fracture of metallic pressure vessels. This results from the complexity and interdisciplinary nature of the problem, the lengthy time required to develop and verify experimentally the technical approaches, and the differing opinions on technical approach. The design of metallic pressure vessels generally has been (and to some extent, is still) based on the following principles:

1. The gross stress levels at the proof and operating conditions should be kept below the yield strength of the material to prevent large-scale deformations.

2. The fracture strength will be greater than the yield strength and equal to or greater than the minimum guaranteed ultimate tensile strength of the material.

3. Local yielding may occur around discontinuities, but the overall structural integrity will be maintained by load relief and redistribution.

4. The factor of safety provides for uncertainties in stress analysis, fabrication, and applied loads, and allows for possible degradation in strength with service life.

5. Selection of factors of safety should be based primarily on experience, a qualitative assessment of the uncertainties associated with a specific design, and the reliability requirements.

6. Sharp-edged flaws or defects will not be allowed and, if any occur, they will be detected by nondestructive inspection and subsequently repaired.

Although many apparently successful pressure vessels have been designed according to the above principles, there have been many costly failures at gross stress levels well below the yield strength. In many of these cases, local yielding did not occur, sharp-edged flaws were missed by inspection, and the past experiences used in selection of the factors of safety were not applicable.

Various approaches have been suggested for use in the control of premature fracture. In reference 1, E. T. Wessel and his coworkers compare and appraise a number of these approaches, primarily on the basis of their applicability to engineering design and material evaluation. They classify the approaches into the two general categories of transition temperature and stress analysis. The lack of an abrupt ductile-to-brittle transition in high-strength steel, aluminum, and titanium alloys combined with a lack of quantitativeness eliminated the transition temperature approaches from consideration. The various stress analysis approaches, based on either stress or strain criteria of fracture, had not been developed sufficiently, lacked quantitativeness, or could not handle the fracture control problem with the desired degree of completeness. It was concluded from this study that linear-elastic fracture mechanics was the approach best suited to design application. The same conclusion was reached by other investigators, both before and after the study.

The primary limitation of linear-elastic fracture mechanics to date is that at stress levels above the yield strength of the material, fracture cannot be described by the critical stress-intensity parameter, K_{Ic}, and subcritical flaw growth cannot be described as a function of the crack-tip stress-intensity factor, K_I. From the standpoint of application, this means that at stress levels above the yield strength, critical flaw size and subcritical flaw-growth data must be obtained empirically over a range of flaw sizes for the specific material and thickness of interest. Also, from the standpoint of fracture testing, it means that extremely thick test specimens are required to cause fracture prior to general yielding and thus obtain K_{Ic} values for materials with a high fracture resistance (refs. 2 and 3). Another limitation is the relatively small quantity of fracture toughness and subcritical flaw-growth data that is generally available.

A less important limitation of fracture mechanics is that stress-intensity solutions, to describe accurately the functional relationship between flaw size and stress level for various flaw shapes and boundary stress conditions, are still under development. Upon completion, these solutions should improve the accuracy of critical flaw-size estimates and pressure-vessel life predictions. However, at the present state of development, fracture specimen test data and fracture mechanics analysis can be used to predict critical flaw sizes and failure modes, to estimate minimum structural life, to establish proof-test factors and proof-testing procedures, to provide a basis for establishing nondestructive inspection flaw acceptance limits, to compare candidate materials, to assist in basic alloy development, to perform failure analyses, and finally (and perhaps

most importantly), to provide a framework for understanding the interrelationships between the various factors that affect the flightworthiness and weight of metallic pressure vessels.

2.1 Critical Flaw Sizes

Flaw types that often go undetected in metallic pressure vessels are the surface and embedded flaws. The flaw size required to cause fracture at a given applied stress level is called the critical size. If the vessel contains an initial flaw which exceeds the critical size at the proof-stress level, catastrophic failure can be expected during proof testing. Failure during service operation will occur when the initial flaw is less than the critical size at the proof-stress level, but grows with service usage until it reaches the critical size at the operating stress level. Pressure vessel leakage occurs when an initial flaw grows through the thickness of the vessel wall prior to reaching critical size.

In elastic stress fields, the critical sizes for surface and internal flaws depend on the plane-strain critical stress-intensity or fracture toughness values (K_{Ic}) of the vessel materials, and the applied stress levels. If the critical flaw sizes are small with respect to the wall thickness of the pressure vessel, the vessel is termed "thick walled." If the critical sizes approach or exceed the wall thickness, the vessel is termed "thin walled."

The critical flaw sizes for surface flaws in uniformly stressed thick-walled vessels can be calculated using the following expression:

$$(a/Q)_{cr} = \frac{1}{1.21\pi}\left(\frac{K_{Ic}}{\sigma}\right)^2 \qquad (1)$$

For small internal flaws the same expression can be used except the 1.21 coefficient is decreased to unity.

Figure 1 shows the relationship between the flaw-shape parameter, Q, and the flaw depth-to-length ratio; figure 2 is a graphical representation of equation (1).

To predict critical flaw sizes (as well as failure modes and operational life) of thin-walled pressure vessels, it is necessary to know the stress intensity for flaws that become very deep with respect to the wall thickness. The stress-intensity solution shown in equation (1) for the semielliptical surface flaw was derived by Irwin (ref. 4) and was found to be reasonably accurate for flaw depths up to about 50 percent of the material thickness. At greater depths, the applied stress intensity is magnified by the effect of the free surface near the flaw tip. This means that in thin-walled vessels, the flaw-tip stress intensity can attain the critical value (i.e., the K_{Ic} value) at a flaw size significantly smaller than that which would be predicted using equation (1).

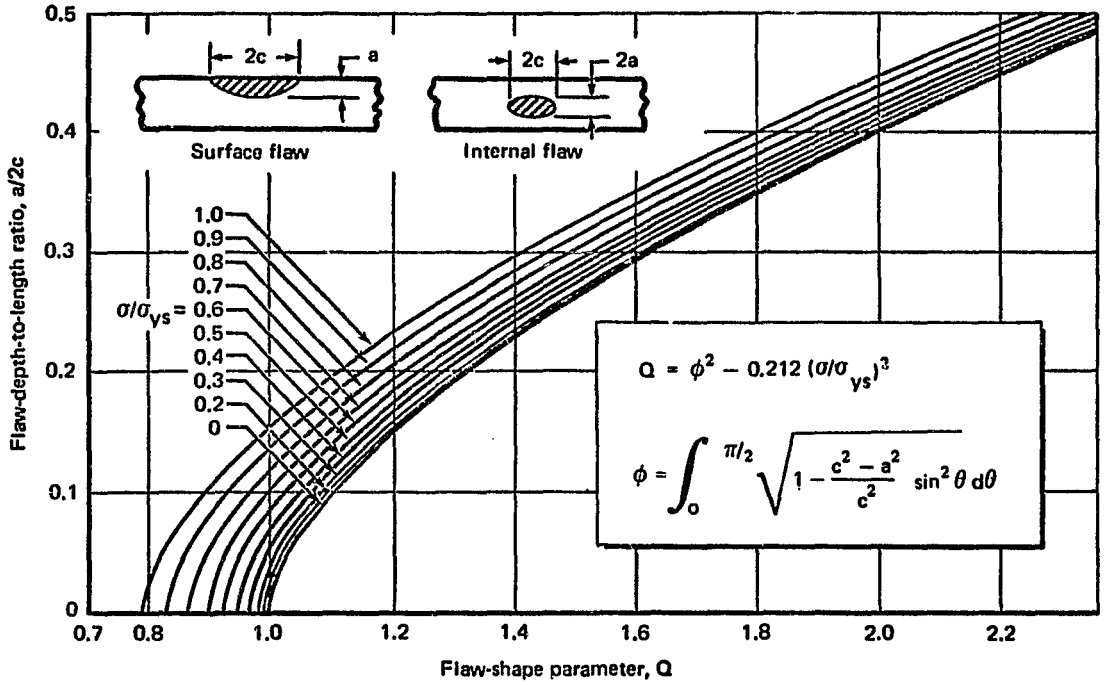

Figure 1 – Flaw-shape parameter curves

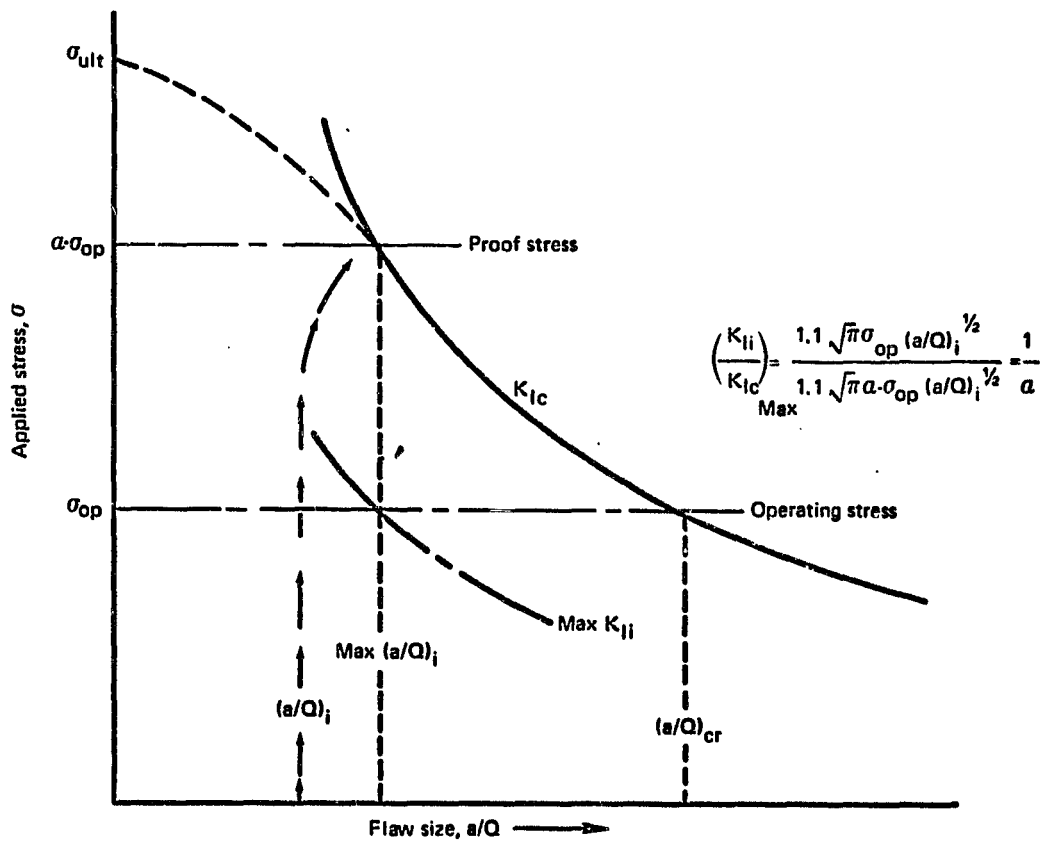

Figure 2. – Applied stress vs critical flaw size.

Kobayashi and Smith developed approximate solutions for deep surface flaws that are very long with respect to their depth (i.e., small a/2c values) and for semicircular surface flaws (i.e., a/2c = 0.5), respectively (refs. 5 and 6). Results of their solutions are shown in terms of a stress-intensity magnification factor, M_K, versus a/t in figure 3. Reference 7 shows an estimate made by NASA/MSC of how M_K varies as a function of a/2c between values of a 2c of 0 and 0.5. The M_K factor is applied to the original Irwin equation to obtain the stress intensity for deep surface flaws. The magnification reaches a maximum value of less than 10 percent for semicircular flaws, whereas there is an increase of about 60 percent for flaws having smaller values of a/2c.

Experimental data obtained on several materials with varying flaw sizes and flaw shapes appear to provide a fair degree of substantiation of the available approximate solutions (ref. 8). An exact numerical solution for deep, semielliptical, surface flaws with varying values of a/2c is under development, and additional experimental investigations are being performed.

To illustrate the effect of the deep-flaw stress-intensity magnification on predicted critical flaw sizes, it is convenient to assume that the vessel contains flaws which are long with respect to their depth. When the flaw-shape parameter, Q, is approximately equal to unity (i.e., for long flaws), the flaw size can be described in terms of the flaw depth, a. A predicted critical flaw-size curve (obtained using Kobayashi's M_K curve) for

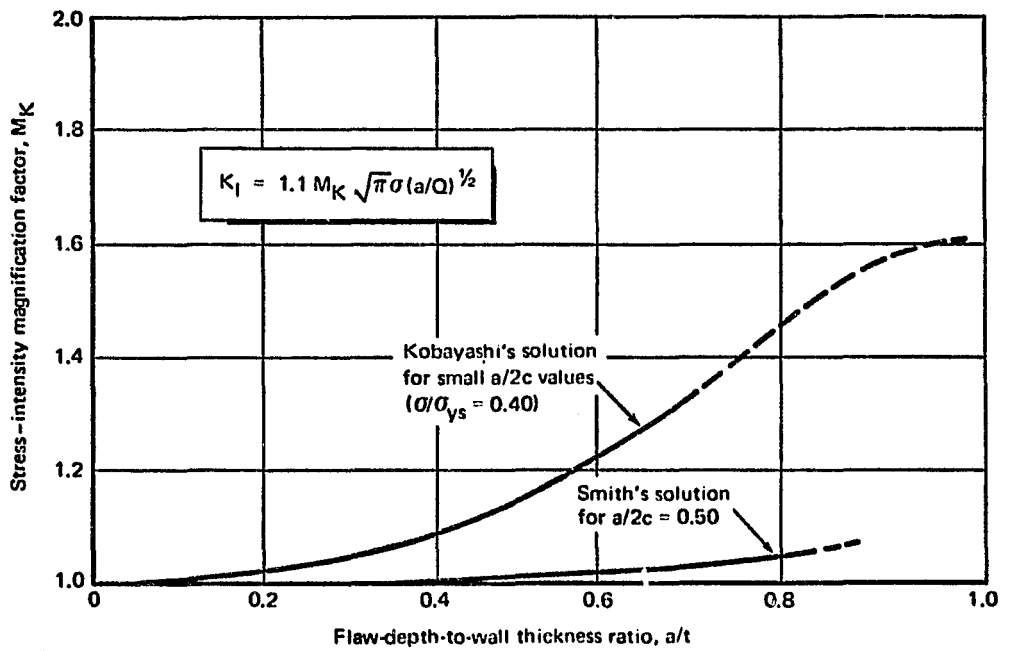

Figure 3. -- Stress-intensity magnification factors for deep surface flaws.

a typical tank material and wall thickness is shown in figure 4. Also shown for comparison is the critical flaw-size curve for the same material in a thick-walled vessel. The curve for the thin-walled vessel is characterized by a significant reduction in failing stress at a given flaw size as compared to that for the thick-walled vessel. The life and potential failure modes of these thin-walled vessels are schematically illustrated in figure 5. The failure mode for thin-walled vessels can be complete fracture if the critical flaw depth is less than the wall thickness at the operating stress level (figure 5A). Figure 5B illustrates the case where the critical flaw depth is greater than the wall thickness at the operating stress level and the resulting failure mode is leakage.

From equation (1) it is apparent that to predict the critical sizes for surface and internal flaws it is necessary to know the plane-strain fracture toughness (K_{Ic}) values for the vessel materials (i.e., parent metal, welds, etc.). In heavy-gage, high-strength materials or in thin-gage materials that are relatively brittle, it is generally a straightforward task to obtain K_{Ic} values from laboratory tests. Several types of test specimens are used to measure K_{Ic}values. These include fatigue-cracked bend specimens, surface-flawed specimens, crack-line loaded specimens, center-cracked and edge-cracked sheet specimens, and fatigue-cracked round notched-bar specimens. Testing requirements, limitations, advantages, and disadvantages of these various types of test specimens are discussed in considerable detail in references 2 and 3.

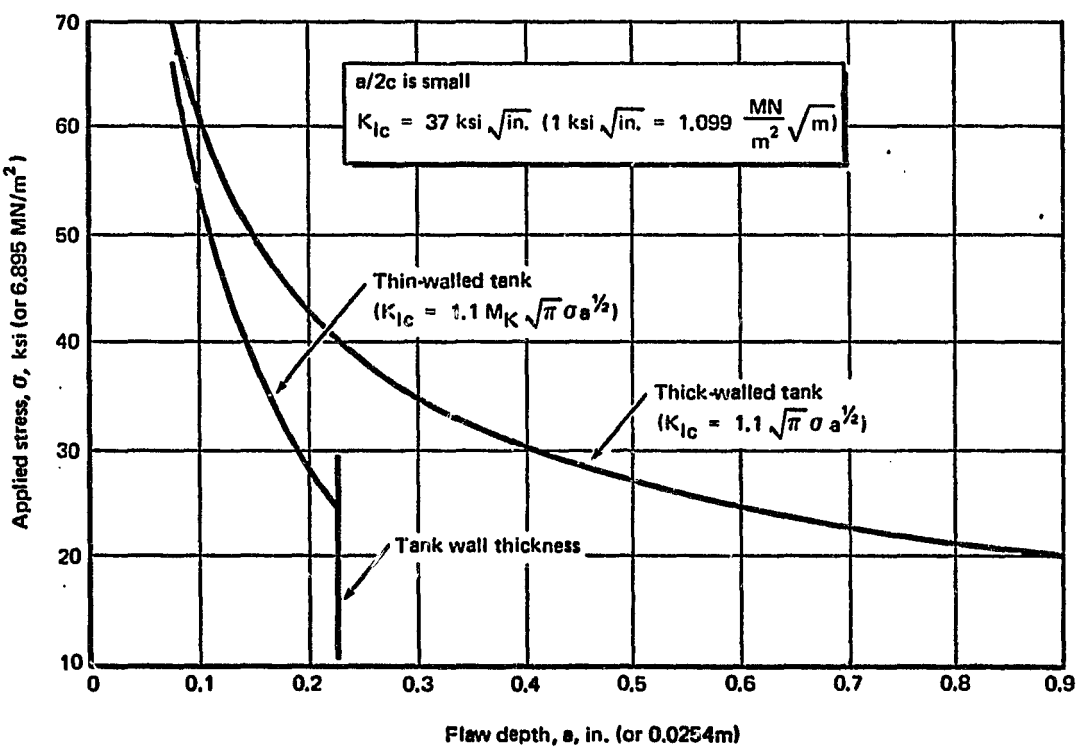

Figure 4. – Critical flaw-size curves at LO_2 temperature for 2219-T87 aluminum

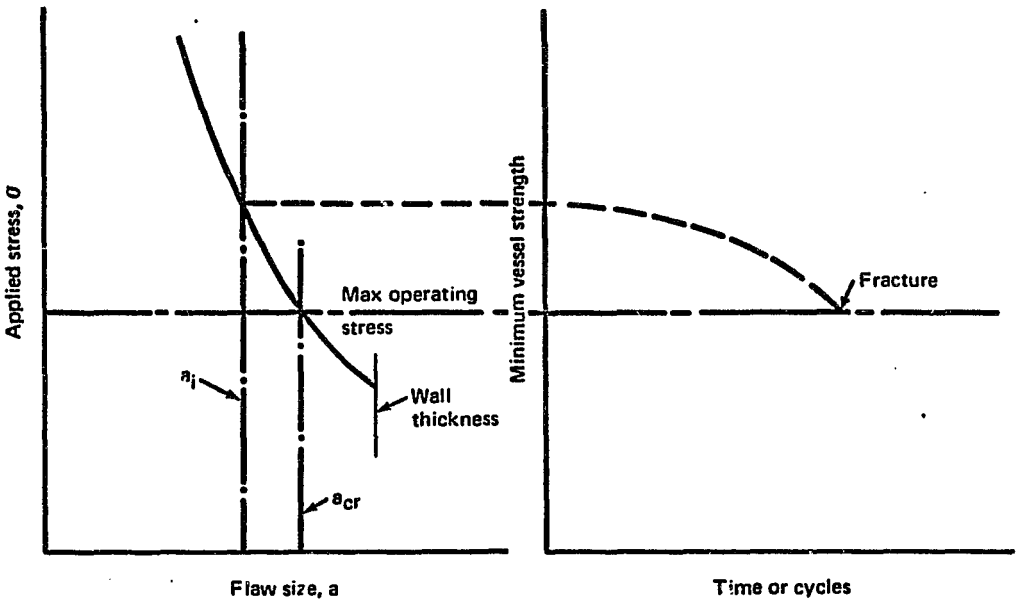

A. Failure mode = fracture

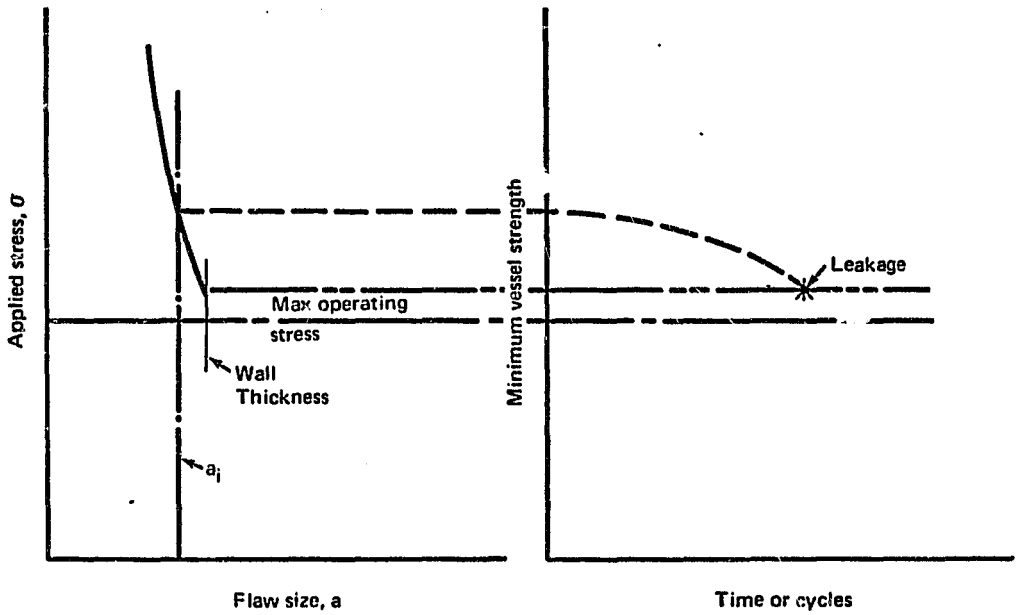

B. Failure mode = leakage

Figure 5. – Schematic representation of thin-walled vessel life.

For predicting critical flaw sizes in aerospace pressure vessels, the surface-flawed specimen has probably been the most widely used. However, the fatigue-cracked bend specimen has the distinct advantage of being the only test specimen for which a detailed proposed recommended practice has been published by the American Society for Testing Materials (ref. 9).

In thin-gaged materials with moderate-to-high toughness, as well as all other situations where the fracture stress levels exceed the yield strength, it is necessary to obtain critical flaw-size data empirically. This was generally accomplished by testing a series of surface-flawed specimens with thickness equal to the pressure-vessel wall thickness and having various initial flaw sizes. Examples of such specimen tests are included in references 10 and 11. Also, an example of such test data is shown in figure 6. These data were obtained from reference 12.

2.2 Initial Flaw Size

To prevent failure, either the actual initial flaw sizes or the maximum possible initial flaw sizes (or initial stress-intensity factors) of pressure vessels must be known. Nondestructive inspection is the only means of determining actual initial flaw sizes. A successful proof test can provide a measure of the maximum possible initial-to-critical stress-intensity ratio, and in turn allows the maximum possible initial flaw size to be estimated.

2.2.1 Nondestructive Inspection

The more common inspection techniques for inspection of aerospace pressure vessels are radiographic, ultrasonic, penetrant, and magnetic particle. Other techniques investigated for potential production usage include eddy current and infrared (ref. 13). Several studies have been performed during the past several years to evaluate the capabilities of these various techniques to detect the different types of flaws found in pressure vessels (refs. 13 and 14). Results of these studies, combined with actual pressure-vessel inspection experience, lead to the following general conclusions:

1. With the use of multiple inspection systems (e.g., X-ray, ultrasound, and penetrant), most surface and internal flaws encountered in pressure vessels can be, and generally are, detected. However, it is unsafe to assume that all potentially dangerous flaws will be found at all times (e.g., tight cracks are particularly difficult to detect).

2. The lower limits of inspection detection capability (i.e., the largest initial flaw sizes which can escape detection) cannot be confidently established.

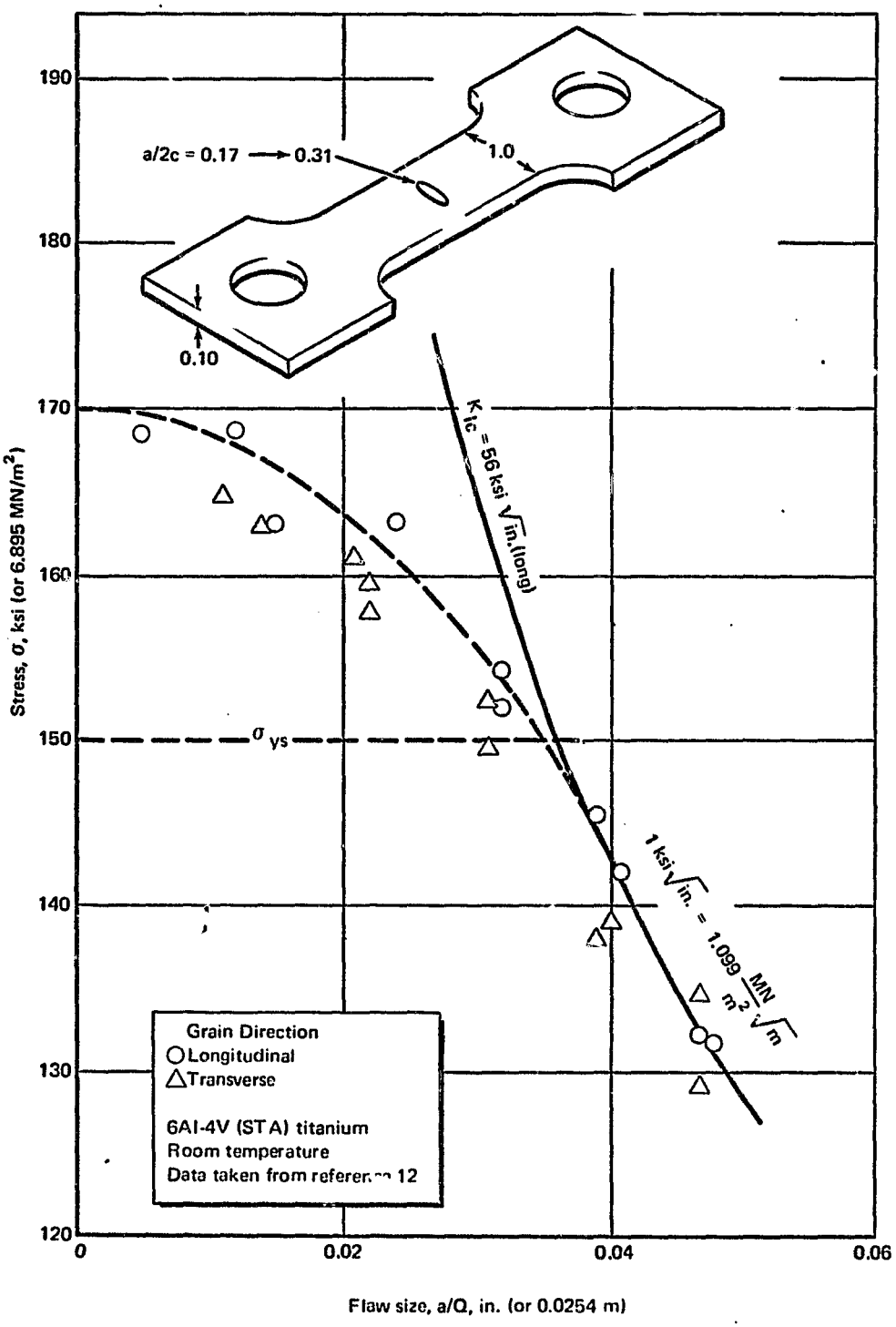

Figure 6. – Empirical critical flaw size data

3. The inspection procedures commonly used do not provide the precise measure of initial flaw sizes (i.e., length and depth) necessary for use in a fracture mechanics analysis.

4. Regardless of the limitations of the techniques, there is no practical alternative but to rely on nondestructive inspection to prevent proof-test failures of most high-strength pressure vessels.

2.2.2 Proof Test

For many years, it was normal practice to perform proof-pressure tests on pressure vessels; these tests, in effect, have served at least as one of the final inspections prior to service usage of the vessels. However, prior to about 1960, very little was understood regarding the determination of proof-test factors and proof-test procedures to minimize potential damaging effects of the test, yet ensure adequate subsequent service performance. During the past ten years, it has become apparent from the results of fracture mechanics studies and aerospace pressure-vessel experience that a properly designed and successfully executed proof-pressure test is probably the most reliable nondestructive inspection technique available for insuring that there are no initial flaws of sufficient size to cause failure under operating conditions.

It was originally pointed out in reference 15 and illustrated in figure 2 of this document, that a successful proof test to a pressure of α times the maximum operating pressure indicates that the maximum possible K_{Ii}/K_{Ic} at the maximum operating pressure is equal to $1/\alpha$ and that this value could be used with subcritical flaw-growth data to estimate the minimum life of the pressure vessel. Additionally, it is generally true that the validity of the minimum life predictions do not depend upon accurate values of either the actual applied stress levels or the fracture toughness (K_{Ic}), both of which vary throughout a given vessel. However, it should be noted that to estimate the maximum possible initial flaw sizes in any specific area of the vessel, it is necessary to know the accurate applied stress levels and the K_{Ic} values.

From the standpoint of initial design, the minimum required proof-test factor for a pressure vessel is $\alpha = 1 \div$ allowable K_{Ii}/K_{Ic}. The allowable value of K_{Ii}/K_{Ic} depends on the required service life of the vessel and the subcritical flaw-growth characteristics of the vessel materials and, ideally, should be a statistically meaningful value obtained from laboratory test data.

Since the introduction of the proof-test concept, based on fracture mechanics, concern has been expressed about possible damaging effects of the proof test; there has been speculation that the test could cause the operational failure of a vessel that might have

performed satisfactorily had a proof test not been performed. Subcritical flaw growth can, and often does, occur in relatively inert environments. Therefore, it is likely that during the time required to perform a proof test, initial flaws or defects in the vessel that are evident can increase in size or possibly flaws which were not evident could be opened up. In fact, if the proof test is not properly designed (e.g., if a is $< 1 \div$ allowable K_{Ii}/K_{Ic}, depressurization rates are too slow, or the test is conducted with an aggressive test fluid), the flaw growth occurring during the test could be sufficient to cause an operational failure.

During the past several years there have been numerous questions about the value of the proof test with regard to the effects of applied stress levels and pressure-vessel wall thickness, selection of the test temperature, test fluids, pressurization and depressurization rates, time at maximum pressure, multiple proof-test cycles, the need for postproof inspection, and the need to simulate service loads other than internal pressure. At present, there does not appear to be unanimity of opinion throughout industry on the effects of these items. However, based on the premise that most pressure-vessel failures result from the existence and growth of flaws, several observations and analyses can and have been made. These are summarized in the following paragraphs.

2.2.2.1 Effect of Applied Stress Levels

To prevent general yielding during proof testing, pressure-vessel membrane stresses are normally limited to a value equal to or less than the yield strength of the material. However, in practice, local stress levels often exceed the yield strength as a result of design or manufacturing discontinuities and/or residual stresses. Also, in some cases (e.g., cryoformed stainless steel vessels), the entire vessel may be purposely subjected to stress levels well above the yield strength.

As shown in figure 2, when the applied stress approaches and exceeds the yield strength of the material, the critical flaw-size curve deviates from the theoretical curve based on a constant K_{Ic} so that critical flaw sizes are smaller than those predicted by linear-elastic fracture mechanics. If the applied stresses in a pressure vessel at proof pressure exceed the yield strength, and if the vessel passes the proof test, the maximum possible K_{Ii}/K_{Ic} proven by the test is smaller than $1/a$. The minimum operational life of the vessel then should exceed the required life, which was used to determine a originally. A potentially beneficial effect of high proof-stress levels is that flaws may tend to be blunted and, as a result, the subcritical flaw growth during operational use of the vessel could be retarded. An apparent disadvantage is that at high proof-stress levels the critical flaw sizes may be very small compared to those that can normally be detected; thus the proof-test failure rate may be quite high.

2.2.2.2 Effect of Wall Thickness

It has been shown by analysis that regardless of the pressure-vessel wall thickness, the required minimum proof-test factor a is $1 \div$ allowable K_{Ii}/K_{Ic}. However, the value of the proof test in providing assurance against service failure changes with decreasing wall thickness and/or increasing fracture toughness, K_{Ic}, the same as occurs with the predicted pressure-vessel failure mode. This is discussed in more detail in reference 16 and illustrated in figure 7.

2.2.2.3 Effect of Proof-Test Temperature

If the proof test is performed at a different temperature than service operating temperature, the required minimum proof-test factor a is as follows:

$$a = \frac{1}{\text{Allowable } K_{Ii}/K_{Ic} \text{ at operating temperature}} \times \frac{K_{Ic} \text{ at proof-test temperature}}{K_{Ic} \text{ at operating temperature}} \qquad (2)$$

The advantages of testing at a temperature where the value of K_{Ic} is lower than it is at the operational temperature are as follows: (1) a lower proof-test factor can be used to guarantee the same operational life as guaranteed by the corresponding higher proof-test factor at the operational temperature, and (2) a larger operational life can be assured by using the same proof-test factor as the one at operational temperature. The disadvantage is the need to know accurately how K_{Ic} varies with temperature for all of the materials in the vessel as well as the statistical variation in K_{Ic} for each material. Also possible increased risk of proof-test failures is associated with the second case.

2.2.2.4 Effect of Test Fluids

During the late 1950's it became apparent that the test fluid was often a major factor contributing to the many proof-test failures that were being experienced. At that time considerable emphasis was placed on the use of high-strength steel alloys in solid-propellant motor cases, and it was common practice to perform the proof test using water as the test fluid. One of the first systematic studies on the detrimental effects of water on high-strength steel motor cases was performed by Shank *et al.* (ref. 17). In this study it was shown that by the mechanism of hydrogen cracking, the water was promoting slow flaw growth that eventually resulted in failure of the motor cases. With the use of oil as the proof-test fluid, the problem was overcome. Similar results were obtained by researchers in other studies.

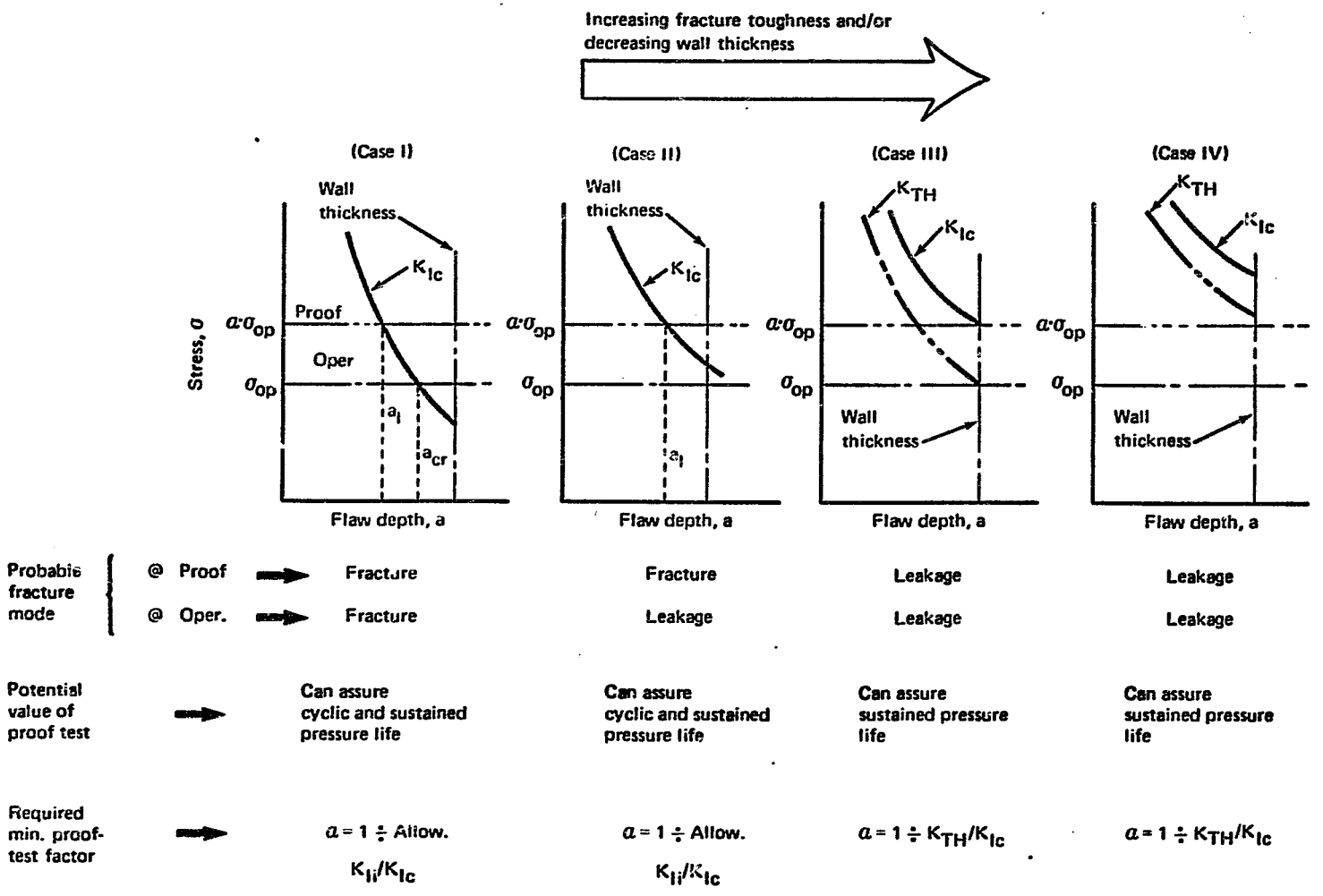

Figure 7. – The effect of wall thickness on value of proof test.

As the heat treat strength levels of steel alloys are reduced, they seem to become less and less susceptible to water-induced flaw growth [e.g., water is often used as a proof-test fluid for steel alloys having a yield strength below about 180 to 200 ksi (1 ksi = 6.895 MN/m^2)]. Corrosion inhibitors, such as sodium dichromate, are often used in the water; distilled water is sometimes used; and some pressure-vessel fabricators use demineralized water. While these measures may be quite effective in inhibiting general pitting corrosion, there appears to be little or no evidence that they will inhibit flaw growth under sustained stress if a flaw is present.

The selection of the proper proof-test fluid is an important consideration for all alloys. With precracked tensile specimens tested under sustained stress in the intended test fluid, it is possible to obtain a measure of the adequacy of the fluid for use in the proof test. (See sections 2.3 and 4.)

2.2.2.5 Effect of Test Duration and Pressurization/Depressurization Rate

If the vessel is pressurized slowly, or if the proof pressure is sustained for a long period of time, the probability of a proof-test failure is increased because of possible slow flaw growth. However, after a successful test it can still be said that the maximum possible K_{Ii}/K_{Ic} at the operating pressure is equal to $1/a$. On the other hand, if the vessel is depressurized slowly so that the flaw that was just smaller than the critical size at the proof-stress level continues to grow, the maximum possible K_{Ii}/K_{Ic} after the test will be greater than $1/a$. In fact, it appears that if the rate of increase in stress intensity caused by flaw growth is greater than the rate of decrease in stress intensity caused by reduction in stress, the vessel could even fail during depressurization.

The amount of flaw growth that will occur during depressurization depends upon the actual K_{Ii}/K_{Ic} ratio (or initial flaw size) at the start of depressurization, the depressurization rate, and the flaw-growth characteristics of the vessel materials under sustained stress in the proof-test fluid. If it is assumed that the K_{Ii}/K_{Ic} ratio approaches unity (i.e., the vessel is just about to fail) at the start of depressurization, and if sustained-stress flaw growth-rate data for the material in the test fluid are available, it is possible to determine the maximum possible K_{Ii}/K_{Ic} at the start of the vessel's operational life as a function of depressurization time. This has been done for some specific material and test fluid combinations in reference 7.

2.2.2.6 Effect of Multiple Proof Tests

In general, it appears that very little can be gained by performing multiple-cycle proof tests. Even after the last cycle, all that can be said is that the maximum possible $K_{Ii}/K_{Ic} = 1/a$, and that the cycles performed after the first cycle could have done some

needless damage to the vessel because of cyclic flaw growth. However, special circumstances occasionally dictate the need, or make it desirable, to conduct more than one proof test. The majority of the vessels used in the Apollo program use a single-cycle proof test.

2.2.2.7 Need for Postproof-Test Inspection

Current practice in industry regarding inspection after proof testing is divided, and there have been arguments made both for and against this inspection. There is general agreement that postproof-test nondestructive inspection can in some cases detect flaws which were previously missed (perhaps because the flaws were too tight) and detect flaw enlargement that may have occurred as a result of the proof test. Also, inspection after proof test can potentially point to areas of the vessel requiring process or design improvement. Considering this to be the case, the postproof inspection of at least the initial vessels fabricated from a new design appears desirable.

However, the discovery of flaws following a proof test can create a dilemma concerning the action required. If the flaws are repaired, another proof-test and postproof-test inspection are generally required. This cycle could conceivably be repeated several times before the vessel is (or appears to be) free of flaws. Furthermore, it is argued (and many times correctly so) that the multiple repairs can be more detrimental than the original flaws.

From the standpoint of fracture mechanics, there seems to be no particular need for postproof-test inspection if the proof test is properly designed and successfully executed. Any flaws that may be present after the test should not be of sufficient size to cause operational failure of the pressure vessel.

Based on pressure-vessel experience, there appears to be no strong arguments either for or against postproof-test inspection. Because the inspection in itself is not harmful, there is no reason to say that it should not be performed. However, it does appear that caution should be exercised to avoid over repair and reproof.

2.2.2.8 Need for Combined-Load Proof Tests

In most proof tests of pressure vessels, internal pressure is the only applied load. However, in some cases, vessels are critical for internal pressure combined with flight loads, and it is not possible to represent the operational stress levels in the vessel by internal pressure alone. In such cases, it generally appears desirable to include provisions in the test setup to apply representative flight loads combined with internal pressure. This has been done for some aerospace pressure vessels.

2.3 Subcritical Flaw Growth

Subcritical flaw growth can occur as a result of cyclic loading, sustained-stress loading, and combined sustained-stress and cyclic loading. When the sustained-stress flaw growth is environmentally induced, it is often termed stress corrosion; combined cyclic and sustained-stress growth is called corrosion fatigue when environmentally induced. Because of the potentially high rates of flaw growth, the problems of sustained-stress and combined cyclic and sustained-stress flaw growth are particularly important in the design of aerospace pressure vessels.

Data from fracture specimen tests can be used in a fracture mechanics analysis to predict the number of cycles or the time the vessel must be under sustained pressure for an initial flaw to grow to critical size. It has been shown (refs. 19 to 23) that for a given environment and cyclic loading profile, the time or cycles to failure depends primarily upon the magnitude of the initial stress intensity, K_{Ii}, as compared to the critical stress intensity, K_{Ic} [i.e., cycles or time to failure = $f(K_{Ii}/K_{Ic})$]. This is particularly significant, because, as pointed out in the previous section, the proof test provides a measure of the maximum possible K_{Ii}/K_{Ic} in the vessel.

During the past several years, cyclic and sustained-stress flaw-growth data have been obtained for a large number of different pressure vessel materials in a wide variety of environments. Although there are several methods of graphically presenting such data, probably the simplest and most useful are plots of K_{Ii}/K_{Ic} versus cycles to failure and K_{Ii}/K_{Ic} versus time to failure. Figure 8 shows typical K_{Ii}/K_{Ic} versus cycle data for

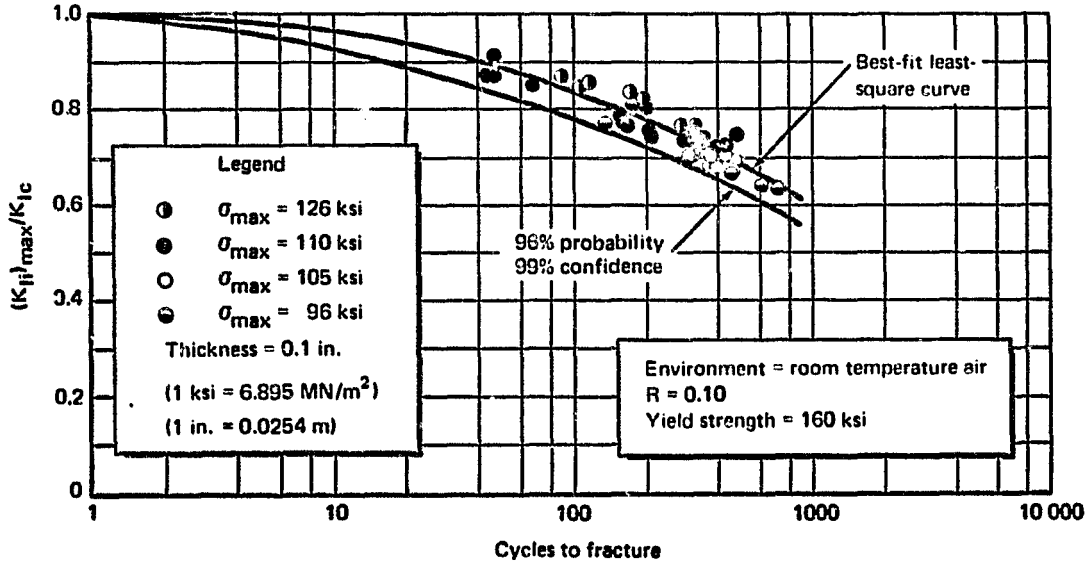

Figure 8. – Cyclic flaw-growth data for heat-treated 6Al-4V titanium.

6Al-4V titanium at room temperature. Both the best-fit curve and the 96-percent probability and 99-percent confidence-level curve are shown. Figure 9 shows K_{Ii}/K_{Ic} versus time data for 6Al-4V titanium in two different liquid environments. Experimental procedures used to obtain such cyclic and sustained-stress flaw-growth data are described in several references including references 18 to 23.

Several different types of test specimens have been used to obtain subcritical flaw-growth data. These include round notched bars, surface-flawed specimens, center-cracked panels, single-edge notched specimens, crack-line loaded specimens, and notched-bend specimens. Of major interest to the pressure-vessel designer is the growth of flaws under plane-strain conditions. Specimens containing through-cracks must be relatively thick, for most materials, to develop plane-strain conditions at the tip of the crack. This requirement has restricted the use of such specimens for the thin-walled pressure-vessel life prediction problem. On the other hand, such specimens have the advantage of permitting the observation and measurement of crack growth during the course of the test. Acquisition of these data has not been limited to any one type of specimen; however, the majority of the data on aerospace pressure vessel materials has been obtained with the surface-flawed specimen.

2.3.1 Sustained-Stress Flaw Growth

The most important characteristic observed in all sustained-stress flaw-growth experiments performed to date is the existence of a threshold stress-intensity level for a given material in a given environment. The observation has been that below a given

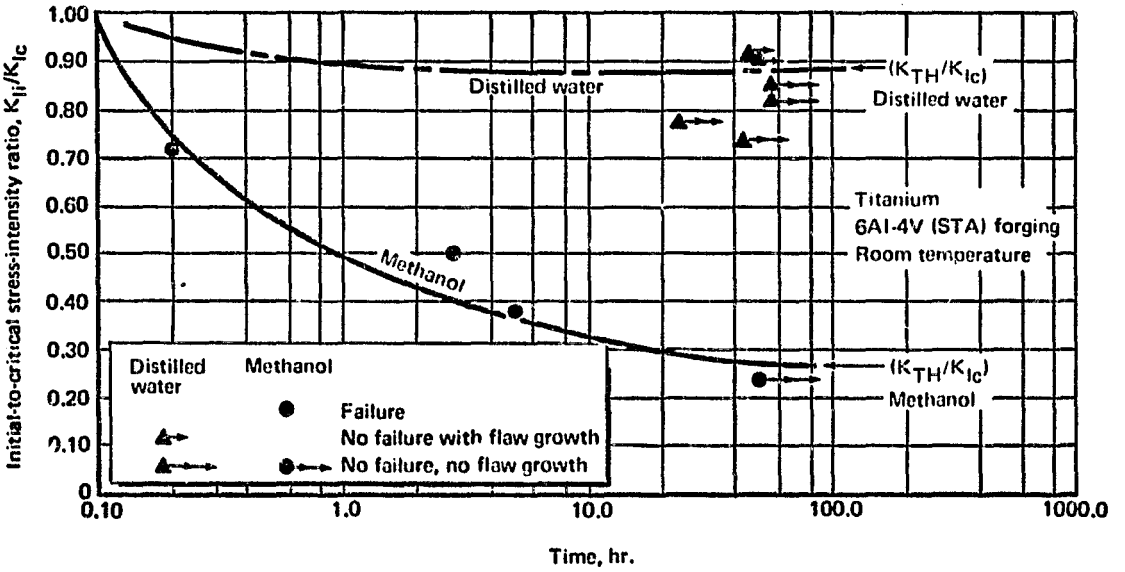

Figure 9. – Sustained-load flaw-growth data.

value of stress intensity, or K_{Ii}/K_{Ic} ratio, flaw growth has not been detected; above this value, growth does occur and can result in fracture. This stress intensity has been designated as K_{TH} and is shown in figure 9.

The discovery of a unique K_{TH} for a given material and environment is the key to the design of safe pressure vessels subjected to sustained loading. While K_{TH} can be 80 percent of K_{Ic}, or higher, in relatively inert environments, hostile media can reduce its value to less than one-half of K_{Ic} (fig. 9). In general, it has been found that K_{TH} values decrease with increasing yield strength in steel alloys (refs. 24 and 25) Also, there is considerable evidence indicating that sustained-load flaw growth is most severe under conditions of plane strain (ref. 26). Reference 27 shows that K_{TH} values, determined from tests of through-the-thickness cracked specimens, increase with decrease in specimen thickness.

Studies of flaw growth and stress intensity for materials in aggressive environments (refs. 25 to 31) indicate an ever increasing flaw-growth rate with increasing stress intensity; however, as shown in reference 7, the growth rate may be relatively constant over an appreciable range of stress intensities. In tests for K_{TH}, wide scatter is often encountered in the data. Also encountered are abnormally short times to failure and very marked dependence on environmental characteristics (media and temperature). Even minor changes in the chemical composition of the environment can significantly affect the K_{TH} value (refs. 21 and 22).

In chemically inert environments, the crack growth rate initially decreases with increasing stress intensity. If the initial-stress intensity is sufficiently low, the crack may halt. At higher stress intensities, the crack growth rate passes through a minimum value and then increases steadily until the crack becomes unstable. This flaw-growth behavior is reported by Johnson (ref. 24) for AM 350 steel in a purified argon environment.

This behavior is also noted in reference 20, where two threshold stress intensities were defined for 5 Al-2.5 Sn (ELI) titanium and 2219-T87 aluminum in the environments of room air, liquid nitrogen, and liquid hydrogen. One threshold stress intensity was defined as that value above which flaw growth to failure could be expected, and the other as the value below which there is no flaw growth. In between these two threshold stress intensities, small amounts of flaw growth can occur; however, the growth apparently arrests after a short time at load.

From these remarks, it is apparent that the service conditions must be carefully simulated when developing K_{TH} data for pressure vessel design. Some examples of experimentally determined K_{TH}/K_{Ic} ratios are shown in table I.

TABLE I. – TYPICAL THRESHOLD STRESS-INTENSITY DATA FOR VARIOUS MATERIAL/ENVIRONMENT COMBINATIONS

Material	Temp., °F [a]	σ_{ys}, ksi [b]	Fluid environment	$\frac{K_{TH}}{K_{Ic}}$	Ref.
6Al-4V (STA) titanium forging	RT [c]	160	Methanol	0.24	21
	RT	160	Freon M.F.	0.58	21
	RT	160	N_2O_4 (.30 % NO)	0.74	22
	RT	160	N_2O_4 (.60 % NO)	0.83	22
	RT	160	H_2O + sodium chromate	0.82	21
	RT	160	H_2O	0.86	21
	RT	160	Helium, air, or GOX	0.90	21
	RT	160	Aerozine 50	0.82	21
	90	160	N_2O_4 (.30 % NO)	0.71	22
	90	160	N_2O_4 (.60 % NO)	0.75	22
	105	160	Monomethyl-hydrazine	0.75	21
	110	160	Aerozine 50	0.75	21
6Al-4V titanium weldments (heat-affected zones)	RT	126	Methanol	0.28	21
	RT	126	Freon M.F.	0.40	21
	RT	126	H_2O	0.83	21
	RT	126	H_2O + sodium chromate	0.82	21
5Al-2.5 Sn (ELI) titanium plate	-320	180	LN_2 ($\sigma <$ proportional limit)	>0.90	20
	-320	180	LN_2 ($\sigma >$ proportional limit)	0.82	20
	-423	210	LH_2	>0.90	20
2219-T87 aluminum plate	RT	58	Air	0.90 [d]	20
	-320	66	LN_2	0.82 [d]	20
	-423	72	LH_2	>0.85 [d]	20
4330 steel	RT	205	Water	0.24	24
4340 steel	RT	>200	Salt water	<0.20	32
GTA welds:					
18Ni (200) steel	RT	200	Salt water spray	>0.70	33
18Ni (250) steel	RT	235	Salt water spray	>0.70	33
12Ni-5Cr-3 Mo steel	RT	170	Salt water spray	>0.70	33
9Ni-4Co-2.5C steel	RT	170	Salt water spray	>0.70	33
Inconel 718	RT	165	Gaseous hydrogen at 5000 psig	<0.25	34

[a] $^{\circ}K = (5/9)(^{\circ}F + 459.67)$.

[b] 1 ksi = 6.895 MN/m^2.

[c] Room temperature.

[d] No failure K_{TH}, some growth observed at lower values (ref. 10).

Probably the most convincing evidence that the stress-intensity factor, K, is the controlling mechanical parameter in sustained-stress flaw growth are the strong correlations obtained between various types of fracture test specimens and between test specimens and actual pressure vessels.

Beachem and Brown (ref. 35) explored this consistency using three different test specimen types:

1. The center-cracked plate.
2. The urface-flawed plate.
3. The precracked cantilever beam.

Using 4340 steel in a dilute NaCl solution, the same K_{TH} value was obtained for all three types of test specimens. The work of Smith, Piper, and Downey (ref. 28) provides additional evidence. They used center-cracked specimens to determine the threshold stress intensity for crack initiation with end loading, and crack arrest with wedge-force loading. For Ti-8Al-1Mo-1V alloy in 3½ percent salt solution, the threshold stress intensity for crack initiation was 20 to 25 ksi$\sqrt{\text{in.}}$ (1 ksi$\sqrt{\text{in.}}$ = 1.099 $\frac{\text{MN}}{\text{m}^2}\sqrt{\text{m}}$) and for crack arrest 20 to 22 ksi$\sqrt{\text{in.}}$ For end-loaded test specimens under constant load, both the stress-intensity factor and net section stress increase with increasing crack length; with wedge-force loading, the net section stresses increase whereas the stress intensity decreases with increasing crack length. The excellent agreement between initiation and arrest values of K_{TH} clearly shows that it is the stress-intensity parameter and not net section stress that is the controlling parameter in sustained-stress crack growth. Correlations between sustained-stress flaw growth in surface-flawed fracture test specimens and pressure vessels subjected to sustained pressurization are shown in references 10, 20, and 34.

In addition to comparisons of laboratory test specimen data to pressure-vessel data, there have been several instances where data from sustained-stress fracture-test specimens and fracture-mechanics analyses have been used to describe conditions leading up to service failures and to arrive at corrective actions. Examples of service failure analyses include: a 4330-steel hydraulic actuator that failed in a water environment as shown in references 2 and 32; titanium pressure-vessel failures in a N_2O_4 propellant environment shown in reference 36; and titanium pressure-vessel failures in a methanol environment shown in reference 21.

2.3.2 Combined Cyclic and Sustained-Stress Flaw Growth

The use of K_{Ii}/K_{Ic} versus cycle data to predict the life of thick-walled pressure vessels was first reported in the literature in reference 15. It indicated that if the maximum possible K_{Ii}/K_{Ic} in the vessel were known (i.e., from a successful proof test), the ordinate of a K_{Ii}/K_{Ic} versus cycles plot, such as that shown in figure 8, could be entered at the appropriate value of K_{Ii}/K_{Ic} and the predicted minimum number of cycles to fracture read from the abscissa. Experimental substantiation of this approach, based on tests of actual preflawed pressure vessels, was subsequently presented in references 10, 18, and 19. However, this approach was based on the assumption that the pressure vessel was cycled at a speed comparable to that used in generating the test specimen data or that cyclic speed was not important. In reference 2, it was hypothesized that for values of initial-stress intensity (K_{Ii}) below the sustained-stress, threshold-stress intensity value (K_{TH}), cyclic speed (or hold time at maximum load) probably would not affect the cyclic growth rate of flaws; but for values of K_{Ii} above K_{TH}, it could have a significant effect. In other words, the minimum cyclic life was limited by the number of cycles required to increase the value of K_{Ii} to the K_{TH} value, and above the K_{TH} level, failure could occur in one additional cycle if the hold time was sufficiently long. On a curve of K_{Ii}/K_{Ic} versus log cycles to fracture, this cyclic life is represented by the difference between the number of cycles at the ordinates of K_{Ii}/K_{Ic} and K_{TH}/K_{Ic}.

To date there are limited experimental data to substantiate this hypothesis. These data were developed for 2219-T87 aluminum and 5Al-2.5Sn(ELI) titanium in the relatively inert environment of liquid nitrogen and are shown in reference 20. When materials are subjected to more aggressive environments (i.e., those resulting in low K_{TH}/K_{Ic} values) there is considerable doubt regarding the general validity of the hypothesis. There are some data on 8Al-1Mo-1V titanium in a salt-water environment that indicate cyclic frequency has no significant effect on flaw-growth rate at stress-intensity levels below K_{TH}. These data are shown in reference 37. On the other hand, recent investigations by Barsom (ref. 38) and Wei (ref. 37) have shown that for some material-environment combinations, both the environment and the cyclic frequency can affect the flaw-growth rates at values of stress-intensity below K_{TH}. For example, Barsom has shown that, for 12Ni steel in a salt water environment, cyclic growth rates of flaws are higher than in a dry environment and progressively increase with decreasing cyclic frequency (i.e., from 10 Hz to 0.1 Hz) at stress-intensity (K_{max}) levels less than K_{TH}. A complete explanation of this type of behavior has not been obtained; however, it is apparent that additional research on environmentally enhanced fatigue growth (i.e., corrosion fatigue) is required.

If it is necessary to use materials having low-threshold, stress-intensity values (less than 70- to 80-percent K_{Ic}) in the expected operating environment, it appears that the effect of environment and cyclic frequency on cyclic growth rates of flaws should be determined and the appropriate rates used to estimate the life of the pressure vessel. As previously mentioned, the minimum allowable cyclic life is limited to the number of cycles required to increase the value of the initial stress intensity K_{Ii} to the K_{TH} value.

The technique for using data on K_{Ii}/K_{Ic} versus cycles to fracture to estimate pressure-vessel life also depends on pressure-vessel wall thickness. For thick-walled vessels, the K_{Ii}/K_{Ic} curves can be used directly, as previously indicated. For thin-walled vessels, the task is somewhat more complicated. When the depth of a surface flaw becomes large with respect to the wall thickness of the vessel, the stress intensity is higher than that predicted by the original Irwin surface-flaw equation (ref. 4), and as a resul , the subcritical flaw-growth rates will be higher and the total vessel life shorter than that obtained from K_{Ii}/K_{Ic} curves of the type shown in figure 8. (It should be noted that shallow surface-flaw test specimens were used in generating the basic K_{Ii}/K_{Ic} data.) The increase in stress intensity for long surface flaws and for semicircular surface flaws, which become deep with respect to the vessel's wall thickness, has been approximated by Kobayashi and Smith, respectively (Sec. 2.1). As indicated in reference 8 and shown in the example in Appendix B, for thin-walled vessels, it is necessary to use flaw growth-rate data and to account for the stress-intensity magnification of deep flaws when making estimates of vessel life. Curves of flaw-growth rate can be obtained by differentiating the curves of K_{Ii}/K_{Ic} versus cycle. For a given vessel design, the flaw growth-rate curves can then be arithmetically integrated using the Kobayashi approximation to account for the increase in stress intensity as the flaw approaches the free surface of the pressure-vessel wall. A relatively simple procedure is shown in reference 8. Like thick-walled vessels subjected to long hold times at maximum pressure, the cyclic life of thin-walled vessels is the number of cycles required to increase the stress intensity from some known or maximum possible initial value to the threshold value for sustained stress flaw growth.

In the analysis of thin-walled vessels, if it is found that the flaw gets very deep (i.e., approximately one plastic zone size from the back surface of the vessel wall) prior to attaining the threshold-stress intensity, it appears wise to experimentally determine cyclic flaw-growth rates with preflawed test specimens having the same thickness as the actual vessel wall. The plane-strain plastic zone size can be approximated by

$$\frac{\pi}{16}\left(\frac{K_I}{\sigma_{ys}}\right)^2 \qquad (3)$$

Recent studies (ref. 39) have shown that in this situation the flaw-growth rates at a given stress-intensity level may be higher than those predicted from the results of shallow-flaw, thick-specimen test data.

The design objective is to assure that the minimum acceptable pressure-vessel life will be attained, rather than to estimate life per se. This can be accomplished from an accurate prediction of the service life by using laboratory cyclic and sustained-stress flaw-growth data to establish allowable K_{Ii}/K_{Ic} ratios, and by determining from these ratios the required proof-test factors and maximum permissible initial flaw sizes.

3. CRITERIA

Metallic pressure vessels for space vehicles shall be designed to avoid service failure caused by flaws and to ensure that the probability of catastrophic failure resulting from flaws during proof tests is remote. The pressures, temperatures, environments, and stresses from sources other than internal pressure to which the pressure vessels will be exposed shall be accounted for. The materials selected for pressure vessels shall possess appropriate fracture- and flaw-growth characteristics; and, all material properties or characteristics used in design and analysis shall be taken from reliable sources of data or adequately substantiated by tests. Critical flaw sizes for stress levels of interest shall be determined by analysis or test as appropriate. Where possible, the maximum size of initial flaws permitted in pressure vessels shall be sufficient to have a high probability of detection by nondestructive inspection but not sufficient to attain the critical flaw size during the pressure vessel's service life. In addition, the permissible initial flaw size shall be less than the critical flaw size at the proof-pressure stress level. The initial stress-intensity ratio permitted in pressure vessels shall be selected to ensure that the critical stress-intensity ratio is not attained during the design life of the vessel. Each pressure vessel shall be proof tested. The proof-pressure level shall be selected to demonstrate that the pressure vessel is free of flaws larger than the permissible initial flaw size or that the actual initial stress-intensity ratio is less than the permissible initial stress-intensity ratio. Account shall be taken of differences between the proof test and service temperatures, and of the time required to pressurize and depressurize the vessel during the proof test.

3.1 Design Conditions

The maximum operating pressure shall be determined for each pressure vessel, and the probability of exceeding this pressure during test (except proof test) and service usage

Card #18

shall be sufficiently low to be consistent with the overall vehicle flightworthiness requirements.

The internal pressure-time-temperature history for the vessel during test, storage, and service use shall be determined.

The internal and external liquid and gaseous environments to which the vessel will be exposed during test, storage, and service use shall be determined.

Temperature gradients associated with all critical ground and flight conditions shall be determined and accounted for in the design and test of each metallic pressure vessel.

Stresses resulting from flight and ground loads shall be determined analytically and/or experimentally; if they occur simultaneously with and are additive to internal pressure stresses, they shall be accounted for in the design and simulated during the proof test of the vessel.

Local yielding caused by stresses resulting from design discontinuities and manufacturing discontinuities shall be permitted at the proof-test pressure level if empirical flaw size versus stress data have been obtained for the particular discontinuities in question (e.g., asymmetrical weld lands, mismatch, etc.) and if it has been demonstrated that at the proof-test pressure the flaw size required to cause fracture either exceeds the local material thickness or is of sufficient size to result in a high probability of detection. This procedure is necessary to minimize the probability of proof-test failure. General yielding shall not be permitted at the proof-pressure level unless the pressure vessel is designed to accommodate it.

3.2 Materials

The fracture and subcritical flaw-growth characteristics of the pressure vessel materials shall be determined for all critical environmental conditions.

Materials with low sustained-stress, threshold-stress intensity values in the anticipated service environment shall not be used in metallic pressure vessels unless adequate protection from the service environment can be demonstrated by test.

Material properties used in the design of metallic pressure vessels shall be the "A" values of MIL-HDBK-5 for unflawed parent metal or obtained in the same manner as those values.

Material properties of weldments and repaired weldments shall be obtained by tests based on the same procedure used in obtaining the "A" values of MIL-HDBK-5 for unflawed parent metal.

3.3 Critical Flaw Sizes

When the proof and maximum-operating stress levels are less than the tensile yield strength of the pressure-vessel material, the critical flaw sizes shall be calculated and based on the appropriate stress-intensity equations, the applied stress, and the measured plane-strain fracture toughness of the material.

When the applied stress (proof or operating) exceeds the tensile yield strength of the material, the critical flaw sizes shall be empirically determined using test specimens that contain flaws simulating those that could be encountered in the actual pressure vessel.

3.4 Initial Flaw Size

The maximum permissible initial flaw size in metallic pressure vessels shall be the largest flaw which cannot attain the critical flaw size within the required life span of the vessel, and shall be smaller than the critical flaw at the proof-stress level.

Pressure-vessel joints having the permissible radial and/or angular mismatch and containing the maximum permissible initial surface-flaw size on the high tension-stressed surface shall be capable of withstanding the proof stress without failure.

3.5 Allowable Stress-Intensity Ratio

The allowable initial-to-critical stress-intensity ratio for a metallic pressure vessel shall be the largest value which cannot attain unity within the required life span of the vessel.

The allowable initial-to-critical stress-intensity ratio shall be no higher than the value obtained from an analysis of the subcritical flaw-growth tests of the pressure-vessel materials in the anticipated service environments.

The allowable initial-to-critical stress-intensity ratio for metallic pressure vessels subject to short-time pressurization shall be allowed to exceed the threshold-to-critical stress-intensity ratio only if it can be shown by test that the allowable ratio cannot attain unity during the operational life of the vessel.

3.6 Proof Test

Each pressure vessel shall be subjected to a proof test. The proof-test factor shall be equal to, or greater than, one divided by the allowable initial-to-critical stress-intensity ratio.

When it has been shown by test that the pressure-vessel materials exhibit a decreasing fracture resistance with decreasing temperature, the proof test shall be conducted at a temperature equal to, or less than, the lowest expected operating temperature.

The pressurization time and hold time at the proof-pressure level shall be the minimum practical, consistent with possible test-system limitations. Emphasis shall be placed on minimizing depressurization time.

Analytical and experimental verification that the probable service failure mode is leakage rather than catastrophic fracture shall be required when assurance of safe operational life cannot be provided by proof test.

4. RECOMMENDED PRACTICES

From the discussion in Section 2 it is apparent that to prevent proof-test failures, low proof-stress levels and materials having high fracture-toughness values should be used so that the critical flaw sizes are large and hopefully exceed the thickness of the pressure-vessel wall. In this case the worst that could happen during proof testing is that the vessel would leak and require repair. Also, it is apparent that to obtain maximum assurance of safe operational performance it would be preferable to use large proof-test factors, low operational-stress levels, and materials with low flaw-growth rates under cyclic loads and high values of K_{TH} in the expected service environment. However, the use of high proof-test factors, low proof-stress levels, low operating-stress levels, and materials having very high fracture-toughness values (often associated with low tensile strengths) generally leads to excessively high pressure-vessel weight. With the possible exception of some first-stage launch-vehicle tankage, these vessels are generally not cost effective in terms of the delivery cost in dollars-per-pound of payload in orbit.

Tradeoffs can and should be made to arrive at an optimum design for a given pressure vessel application. The interrelations between materials, the required service life of the vessel, the required proof-test factor, the allowable flaw sizes, the probability of proof-test failure, and the weight of the pressure vessel should be understood and carefully assessed. These interrelations are illustrated in a simplified example in Appendix A. Tradeoffs, however, must be made within the constraints provided by the design criteria of the previous section.

4.1 Design Conditions

To prevent premature service failure of metallic pressure vessels, it is extremely important to consider the entire anticipated pressure-time-temperature history of the vessel and the environments to which it will be exposed.

The value of maximum operating pressure used in the design of liquid propellant tanks and gas bottles should equal the maximum nominal-operating pressure plus the upper tolerance of the pressure-limiting device. This device should have a reliability consistent with the overall vehicle flightworthiness requirements.

The predicted pressure-vessel history should include pressures, times, temperatures, and fluid and gaseous environments for all of the anticipated cycles, starting with the initial proof-pressure test and ending with the last service-pressure cycle. Also, it is important to include pressurization rates, depressurization rates, and hold times. In those cases where the life history of the vessel cannot be accurately predicted, a design life envelope should be established and the appropriate operational limitations placed upon the completed vessel.

Loads other than internal pressure, such as slosh, sonic, vibration, handling, and transportation loads, should be determined in accordance with applicable NASA monographs. Effort should be made to minimize high stresses resulting from flight and ground loads by careful detailed design and by using antislosh, damping, and antishock devices. Stresses resulting from external flight and ground loads should be determined analytically and/or experimentally, and accounted for in the design of the pressure vessel. Temperature gradients (and resulting thermal stresses) should be determined for all critical ground and flight conditions. If the stresses are of sufficient magnitude to affect the basic vessel design, an effort should be made to minimize or eliminate these stresses using thermal insulation, controlled fill rates of cryogens, etc.

Wherever possible, the objective should be to eliminate residual stresses by stress relief treatments. If this is not practical, residual stresses should be minimized by careful design and controlled welding procedures.

A stress analysis should be performed for every vessel and include stresses resulting from internal pressure, ground and flight loads, and thermal gradients. The analysis of stresses resulting from internal pressure should include primary membrane stresses and secondary bending and membrane stresses that result from design discontinuities and allowable design deviations.

General yielding should be avoided during pressure testing except for those vessels that are specifically designed to accommodate it (e.g., cryoformed stainless-steel vessels). To

avoid general yielding during proof-pressure testing, the minimum design ultimate factor of safety, $(F.S.)_{MDU}$, should be as follows:

$$(F.S.)_{MDU} = a \times \frac{\text{Parent metal ultimate strength}}{\text{Parent metal yield strength}} \quad (4)$$

Where

a = Proof factor = $1 \div (\text{Allowable } K_{Ii}/K_{Ic})$

The factors previously specified are minimum values for all metallic pressure vessels used on both manned and unmanned vehicles. Uncertainties in loads, pressures, service environments, and/or service requirements may make it necessary to use higher factors; however, in no case should lower factors be used.

4.2 Materials

The following fracture and subcritical flaw-growth characteristics should be obtained for materials intended for use in metallic pressure vessels:

1. The plane-strain fracture toughness values (i.e., K_{Ic} values) for the parent metal, weldments, and heat-affected zones at the operating- and proof-test temperatures, and in the principal directions of loadings.

2. The threshold stress-intensity (K_{TH}) values for the parent metal, weldments, and heat-affected zones in simulated service environments.

3. The cyclic flaw-growth data (curves of K_{Ii}/K_{Ic} versus cycles or $\frac{d(\frac{a}{Q})}{dN}$ versus K) for the parent metal, weldments, and heat-affected zones.

In addition, the effects of material processing on these fracture characteristics should be determined. A quality control program should be established to determine that large variations in values of toughness or threshold stress-intensity ratios do not occur from one batch, or heat, of material to another. Also, each manufacturing process that might adversely affect the strength, toughness, and threshold stress-intensity values of the end product (e.g., welding and heat treating) should be certified by performing specimen tests. Test specimens should have the same shape, be made from the same materials, and use the processes planned for production hardware.

The quantity of fracture test data obtained should be determined on the basis of the impact a failure would have on the mission, schedules, and costs.

To comply with the criteria in this monograph, it is unnecessary to limit the determination of fracture toughness values to any particular type of test specimen. However, it does appear that the curves of predicted critical flaw size (based on the measured K_{Ic} values) for the pressure-vessel parent metal, weldments, and heat-affected zones should be verified by data from a series of surface-flawed specimen tests. The test specimens should be the same thickness, processed in the same manner as the vessel, and each should contain a different size flaw. Procedures for specimen fabrication and test are discussed in reference 19. To eliminate the effects of inplane bending and specimen width, the test-specimen width should be about five times the surface-flaw length (i.e., the 2c dimension).

Likewise, the acquisition of threshold stress-intensity (K_{TH}) data and cyclic flaw-growth data should not be limited to the use of any one type of test specimen. However, the surface-flawed specimen has been used to obtain the majority of such data to date (Sec. 2).

The recommended experimental approaches for using surface-flawed test specimens to obtain data on K_{Ii}/K_{Ic} versus cycles, and K_{Ii}/K_{Ic} versus time are described in references 19 to 23; therefore, it is unnecessary to repeat the approaches in detail in this monograph, however, the following deserve particular attention.

Data on cyclic and sustained-stress flaw growth should be obtained for parent metal, weldments, and heat-affected zones. The test specimens should be of sufficient width to prevent inplane bending effects; for the cyclic tests, it is particularly important that the test specimen be sufficiently thick to ensure that the flaw attains the critical size before growing more than half way through the thickness of the specimen. It is also recommended that cyclic tests be performed in the anticipated service environment and that the effect of cyclic frequency be evaluated. In most cases, a cyclic frequency of about 0.0167 to 0.0833 Hz (1 to 5 cpm) is considered suitable. For the sustained-stress tests accurate simulation of the anticipated service environment should be emphasized. A complete set of data on K_{Ii}/K_{Ic} versus cycle should be obtained for each of the anticipated service-loading profiles (i.e., R values). It is conceivable that in some cases prior load, temperature, and environment histories could have a detrimental effect on cyclic- and sustained-stress, flaw-growth characteristics. If this is suspected, the effects should be determined experimentally.

The required fracture-toughness and subcritical flaw-growth characteristics of materials to be used in metallic pressure vessels cannot be specified in terms of specific minimum or maximum allowable values because of the many factors involved. However, in general, it is recommended that the material have sufficient fracture toughness so that the predicted critical flaw sizes at the applied proof stress are sufficiently large so that there is a high probability of their being detected prior to the test. Also, materials that

exhibit a low-threshold stress intensity in the anticipated service environment should be avoided. If the material has a K_{TH} value below about 70 percent of K_{Ic}, the possible use of alternate materials should be investigated.

Use of the improvements in allowable uniaxial ultimate and yield strengths caused by biaxial stress fields results in increased operational and proof stresses as well as lighter weight pressure vessels. The higher stresses reduce the critical flaw sizes, however, and increase the chances of premature failure of the pressure vessel. Therefore, increases in the allowable uniaxial tensile yield and ultimate strengths of parent metal caused by biaxial stress should be taken into account only if

1. The critical flaw sizes associated with the increased proof-stress level are large (high probability of being detected prior to the test).

2. Sufficient experimental data are available to allow a reliable determination of the biaxial improvement factor.

Because of the high probability of the occurrence of defects and the complexities in stress fields introduced by design and manufacturing discontinuities, biaxial strength elevation should not be used to establish allowable ultimate strengths of welded joints.

In cases where the effect of the biaxial stress field reduces the uniaxial tensile strength, the amount of the reduction should be determined experimentally and used to establish allowable strengths.

4.3 Critical Flaw Sizes

Prevention of proof-test failure requires knowledge of the critical flaw sizes at proof-stress levels, knowledge of possible flaw growth during proof test, and detection and repair of all flaws that exceed or could attain the critical size during proof test. Prediction of accurate critical flaw sizes is not always an easy task; however, it is a necessary goal.

The concept of critical flaw sizes and the equations for determining these sizes for surface flaws in thick- and thin-walled vessels were introduced in section 2. These equations apply, however, only when the gross stress levels of the pressure vessel are below the yield strength of the pressure-vessel material and when the stresses are uniform through the thickness of the vessel wall. When this is the case (as in areas of a vessel that are under membrane stress), it must be recognized that the accuracy of the calculated critical flaw size depends directly on how accurately the material's fracture toughness (K_{Ic}) and the applied stress levels are known. When calculating critical flaw

sizes for these areas of uniform elastic stress, the value of K_{Ic} selected for design and the maximum possible applied stress level (i.e., that corresponding to the minimum material gage) should be used. In addition, it is a conservative viewpoint to assume that the flaws are surface (or just subsurface) flaws and that they are long in relation to their depth so that $Q \approx 1.0$. The resulting predicted critical flaw size is thus described by the single dimension, a (i.e., the depth). When this depth is large with respect to the wall thickness (i.e., greater than about half the thickness), the effect of deep-flaw stress-intensity magnification should be accounted for. The equation shown in figure 3 attempts to do this by the addition of the M_K factor. A reasonable estimate for M_K is the approximate Kobayashi solution shown in figure 3. While recent data (ref. 39) indicate that its use can result in somewhat conservative answers for the more ductile materials and perhaps slightly unconservative answers for the brittle materials, it is recommended that the figure 3 curve be used until improved solutions are obtained. Since the equation shown in figure 3 is not explicit in terms of the critical flaw size, various critical depths (a_{cr}) should be assumed for the long surface flaw, the M_K values determined from the Kobayashi curve, and the failure stresses calculated. The curve of σ versus a_{cr} can then be plotted. If the a_{cr} at the proof- (or operating-) stress level is larger than the wall thickness, the expected failure mode for the vessel at proof- (or operating-) pressure would be leakage. However, this can be predicted with confidence only if there are no higher stressed areas in the vessel where the critical flaw depth would be smaller, or if the value calculated for a_{cr} exceeds the wall thickness by a significant amount.

In most vessels there are areas where the stresses are not uniform through the thickness of the wall (i.e., at mismatched weld joints, asymmetrical weld lands, changes of contour, etc.) and many times it is known that at the proof pressure the total applied stresses in these local areas exceed the yield strength of the material. If it is known that the stresses approach or exceed the material yield strength, an estimate of the critical flaw sizes (for long surface flaws) may be made by test. For these cases, the critical flaw-size data should be obtained by testing a series of surface-flawed specimens (with various size flaws) that model the actual hardware. It is further recommended that the flaws be made long in relation to their depth (i.e., small a/2c ratios) and that the specimen width be about five times the flaw length.

In areas of nonuniform stress (e.g., combined bending plus tension) where the stresses are within the elastic range, it is possible to make reasonably accurate estimates of the critical flaw sizes by analysis. References 6 and 40 present both approximate and numerically exact stress-intensity solutions for nonuniform stress fields. Also, there are often special situations (particularly during the failure analysis studies or Material Review Board type actions) where it is of interest to predict critical sizes (or failure stresses) for flaws of shapes, locations, or orientations other than those previously

discussed. For example, corner flaws, near-surface internal flaws, coplanar-internal flaws, and sharp-tailed porosity may all be encountered. Again, for most of these situations, reasonably accurate analytical estimates can be made (providing the stress field is elastic) using various available stress-intensity solutions. Some such solutions are included in references 2, 6, 41, and 42. Others are currently being developed.

4.4 Initial Flaw Size

The two distinct areas of concern regarding initial flaw sizes are as follows:

1. The determination of either actual or maximum possible initial flaw sizes in the vessel as initially fabricated, and before and after the proof test.

2. The determination of maximum permissible initial flaw sizes (i.e., the allowable initial flaw sizes) before the proof test.

Nondestructive inspection (i.e., X-ray, ultrasonic, etc.) is the only means for determining actual initial flaw sizes before the proof test (Sec. 2), consequently, such inspections should be used to minimize the possibility of proof-test failure. The extent of nondestructive inspection should be determined on an individual basis, taking into consideration the consequences of a proof-test failure, the capabilities of the available inspection techniques, and the sizes of initial flaws that must be detected (i.e., the allowable initial flaw sizes).

The successful proof test provides a direct measure of the maximum possible initial-to-critical stress-intensity ratio to predict the specific maximum possible initial flaw sizes that may exist in the vessel after the proof test and before the service usage. (Due to possible flaw growth during the proof test, the initial flaw sizes before and after the proof test may not be the same). If the proof test is properly designed and successfully executed, the maximum possible initial flaw sizes after the proof test are equal to the predicted critical flaw sizes at the proof-stress level. However, since the proof test itself provides assurance against operational failure, the prevention of such failure does not require the prediction of allowable initial flaw size.

Allowable initial flaw sizes should be determined for the following specific purposes:

1. Assessing the adequacy of the nondestructive inspection procedures.

2. Assessing the adequacy of the flaw or defect acceptance limits.

3. Assessing the probability of a proof-test failure.

These require that the allowable initial flaw sizes be established for all high-stressed areas of the vessel, including the parent metal, weldments, and heat-affected zones.

The allowable initial flaw sizes should be established using the allowable initial-to-critical stress-intensity ratios determined from subcritical flaw-growth test data (Sec. 4.5); the measured K_{Ic} values for the parent metal, welds, and heat-affected zones; experimental measurements of possible flaw growth that could occur during proof test; and the appropriate stress-intensity equations for various flaw-geometry and boundary-stress conditions. The same stress-intensity equations used in predicting critical flaw sizes (Sec. 4.3) should be used to establish allowable initial flaw sizes except to substitute the allowable value of K_{Ii} for K_{Ic}.

4.5 Allowable Stress-Intensity Ratio

The allowable initial-to-critical stress-intensity ratio (i.e., allowable K_{Ii}/K_{Ic} ratio) is an important element in the control of fracture of metallic pressure vessels. Consequently, extreme care should be exercised in selecting the values of this ratio to be used in establishing the proof-test factor and the allowable initial flaw sizes. The allowable K_{Ii}/K_{Ic} ratio to be used in determining the proof-test factor (Secs. 3.2 and 4.1) should be a statistically meaningful value obtained from an analysis of the subcritical flaw-growth test data in the various anticipated service environments for the parent metal, welds, and heat-affected zones. When allowable K_{Ii}/K_{Ic} ratios are used to establish allowable initial flaw sizes, the value of K_{Ii}/K_{Ic} for the specific area of interest of the vessel should be used. Also, the selected design value of K_{Ic} should be used.

The allowable K_{Ii}/K_{Ic} ratio should be determined, using statistically meaningful curves of subcritical flaw growth (i.e., K_{Ii}/K_{Ic} versus cycle and K_{Ii}/K_{Ic} versus time) and the most severe service history anticipated for the vessel (Sec. 4.1).

The flaw-growth curves should take into account possible heat-to-heat variations in the values of K_{TH} and K_{Ic} and the scatter in these values within a given heat. References 22 and 43 present discussions on the effects of data scatter and heat-to-heat variations.

Complexity of the analysis required to determine allowable K_{Ii}/K_{Ic} ratios depends upon the pressure-vessel design and the complexity of the anticipated service history. A recommended procedure for performing this analysis can best be illustrated by specific examples for thick- and thin-walled vessels. These examples are presented in Appendix B.

4.6 Proof Test

Every pressure vessel should be proof tested to a stress level equal to or greater than the maximum operating stress times a (a = 1 ÷ allowable K_{Ii}/K_{Ic}). If the vessel is proof tested at a temperature other than the operating or service temperature, the minimum proof-test factor, a, should be determined by equation (2) in Section 2.

In this case, it is important that the values of K_{Ic} are known for all areas of the vessel and that it is known how they vary as a function of temperature. Also, it is important to know the probable scatter in values of K_{Ic} at both the operating and proof-test temperature. To ensure that the proof-test factor obtained will be adequate, the upper statistical value of the K_{Ic} scatter band at the proof-test temperature and the lower statistical value at the operating temperature should be used.

The proof test should be conducted with a test fluid that will neither induce general corrosion pitting nor severe stress-corrosion cracking. The values of K_{TH} for the vessel materials should be obtained from sustained-stress fracture tests performed in the test fluid at the proof-test temperature. If the values of K_{TH} are low, either an alternate fluid should be selected or, if this is not practical, methods of protecting the vessel or inhibiting the action of the test fluid should be investigated.

Slow flaw growth during pressurization and elapsed time at proof pressure should be minimized by rapid pressurization rates and short hold times. The pressurization time should be the minimum possible, consistent with the capabilities of the test equipment. A maximum hold time of about 15 seconds is considered to be reasonable.

It is extremely important to minimize the time necessary to depressurize from the proof pressure to a pressure equal to K_{TH}/K_{Ic} times the proof pressure. If this cannot be accomplished in a few seconds because of test-system limitations or the pressure-vessel design, the potential detrimental effects of the slower depressurization should be determined by analysis. An illustrative example of a recommended analysis procedure is shown in reference 7.

Proof testing of metallic pressure vessels should be limited to a single pressure cycle unless there are special circumstances indicating the need for additional cycles. Special circumstances include the following cases:

1. A single proof test cannot be designed to envelop the critical operational pressure, temperature, and external loading combinations.

2. The vessel was modified or repaired after the initial proof test and the modified or repaired areas of the vessel need to be proof tested.

3. It is desired to recertify the vessel for additional service usage after it has been in service for a period of time.

4. From an economical standpoint, it is desired to test components (e.g., bulkheads) of the vessel prior to final assembly.

5. It has been shown by laboratory experiments on preflawed simulated parts or specimens that a prior test at a higher temperature is advantageous to minimuze the risk of failure at the design temperature.

A failure-mode analysis should be performed for each completed pressure-vessel design. The predicted failure mode (i.e., leakage or complete fracture) should be determined at the proof and maximum operating conditions.

Analytical and experimental verification that the probable failure mode is leakage rather than complete fracture should be obtained in cases where assurance of operational life is not provided by the proof test.

For those pressure vessels which are critical for internal pressure combined with flight loads, it may not be possible to represent the operational stress levels in the vessel by internal pressure alone. In such cases, the proof test should include provisions to apply representative flight loads combined with internal pressure.

REFERENCE 80
PAGE 38 BLANK

APPENDIX A

DESIGN TRADE-ILLUSTRATIVE EXAMPLE

Figure A-1 illustrates how the various factors affecting reliability and weight are interrelated for pressure vessels designed to contain liquid hydrogen. In the upper portion of the figure, the cyclic lives of two materials are shown as a function of the inverse of the stress-intensity ratio (K_{Ii}/K_{Ic}). The cyclic growth of initial defects or flaws in a vessel is primarily a function of this ratio. Also, it can be shown that the maximum possible K_{Ii}/K_{Ic} ratio in a pressure vessel after a successful proof test is equal to 1 divided by the proof-test factor, a, or $K_{Ic}/K_{Ii} = a$. The solid lines are based on the assumption of rapid pressure cycling where the sustained-stress flaw growth above K_{TH} is negligible. The dashed lines are based on the assumption that there are long-duration hold times at maximum pressure; and, consequently, the life is the number of cycles required for the applied stress intensity to reach K_{TH}.

In the center portion of the figure, constant flaw-size lines are shown as a function of the proof-test factor and the square of the ratio of the plane-strain fracture toughness, K_{Ic}, and the operational stress level σ_{op}. These curves were obtained as follows:

$$K_{Ic} = 1.95\, \sigma_{proof}\, (a/Q)^{\frac{1}{2}}_{cr_{proof}} \qquad \text{(A-1)}$$

however:

$$\sigma_{proof} = a\, \sigma_{op}$$

$$\max (a/Q)_{i_{op}} = (a/Q)_{cr_{proof}}$$

substituting:

$$K_{Ic} = 1.95\, a\, \sigma_{op}\, (a/Q)^{\frac{1}{2}}_{i}$$

$$\left(\frac{K_{Ic}}{\sigma_{op}}\right)^2 = 3.8\, a^2\, (a/Q)_i \qquad \text{(A-2)}$$

With $(a/Q)_i$ held as a constant, the equation can be solved and plotted in terms of $(K_{Ic}/\sigma_{op})^2$ vs a.

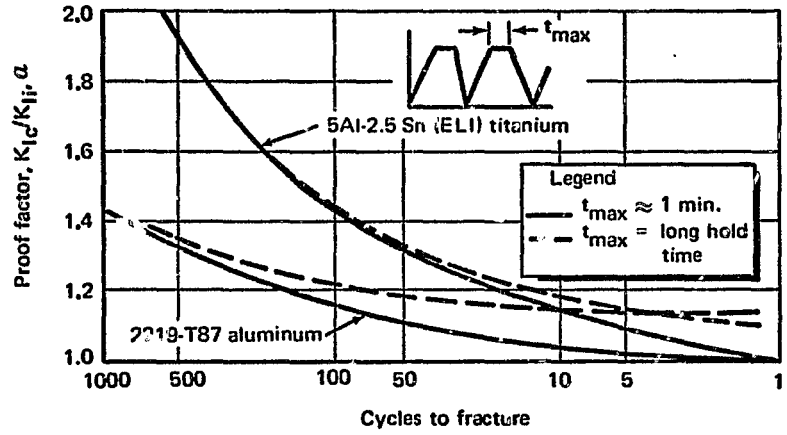

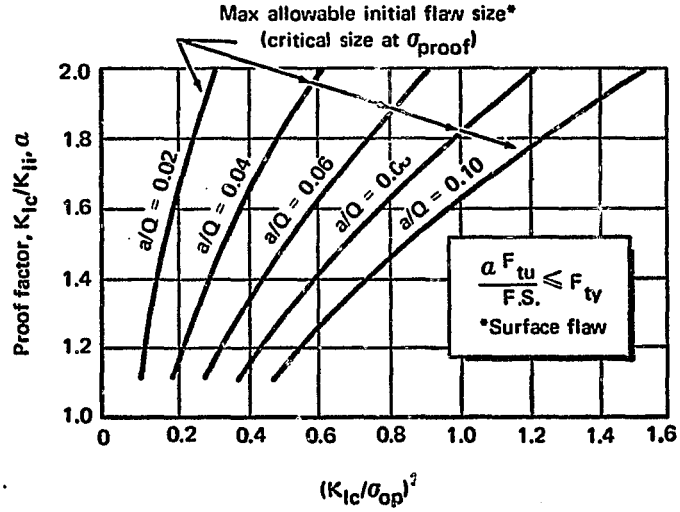

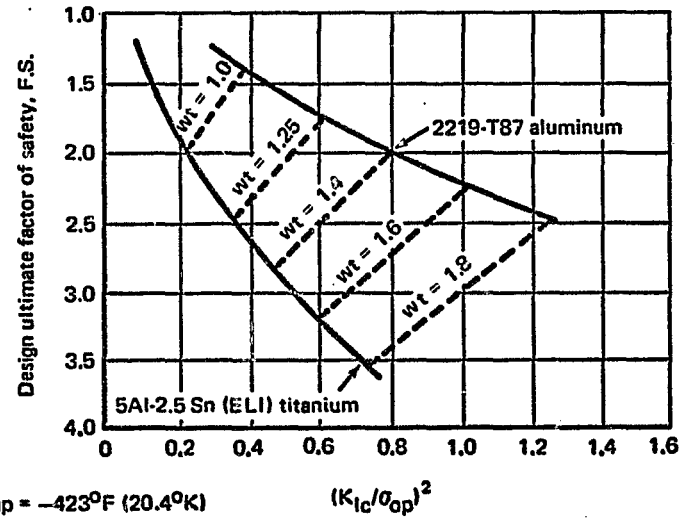

Design temp = −423°F (20.4°K)

Figure A-1. — Interrelated factors affecting the weight and reliability of thick-walled LH_2 pressure vessels.

The lower portion of the figure shows the relationship between the design ultimate factor of safety (F.S.) and $(K_{Ic}/\sigma_{op})^2$ for the two materials, obtained from the following relationship:

$$\left(\frac{K_{Ic}}{\sigma_{op}}\right)^2 = \left(\frac{K_{Ic}}{\frac{\sigma_{ult.}}{F.S.}}\right)^2 = (F.S.)^2 \left(\frac{K_{Ic}}{\sigma_{ult.}}\right)^2 \qquad \text{(A-3)}$$

Points of equal pressure-vessel weight were computed for the aluminum and titanium, and connected by dashed lines with the relative weight indicated.

Consider a typical design problem: suppose it were desired to design a high-pressure helium vessel to be contained within a larger LH_2 propellant tank and have a required minimum life of 500 pressure cycles. From the upper portion of the figure it can be seen that a successful proof test to 1.95 times the maximum operating pressure would be required to assure this life using the titanium alloy, and 1.35 times the maximum operating pressure using the aluminum alloy. It should be noted that the 1.95 factor is somewhat higher than the conventional proof factor usually specified for high-pressure gas bottles and the 1.35 factor is lower than that usually specified. Suppose it were decided to use a conventional ultimate factor of safety of 2.5, commonly used for high-pressure bottles. From the lower portion of the figure it can be seen that $(K_{Ic}/\sigma_{op})^2$ equals 0.35 for the titanium and 1.25 for the aluminum. Also, it is seen that the weight of the aluminum vessel will be 1.8/1.25 or 1.44 times the weight of the titanium vessel. In the center portion of the figure, the flaw sizes that will cause failure during proof test can be determined. For the titanium vessel this is slightly greater than 0.02 in. (1 in. = 0.0254 m) (i.e., the depth of a long surface flaw) and for the aluminum vessel it is $>>$ 0.10 in.

It is doubtful if the titanium tank could successfully pass the proof test because of the difficulty in detecting an initial flaw size as small as the critical flaw size at the proof stress. On the other hand, this does not appear to be a problem with the aluminum tank. The use of the conventional factor of safety of 2.5 seems to unduly penalize the aluminum tank (i.e., causes it to be excessively heavy), and yet it is marginally adequate for the titanium tank.

If an aluminum tank were designed with an ultimate factor of safety of about 1.75, its weight would be equal to that of the titanium tank designed with an ultimate factor of safety of 2.5, and the critical flaw size at the proof-stress level (1.35 times σ_{op}) would be about 0.09 in. This flaw is still about four times larger than that for the titanium vessel and is sufficiently large to create some degree of confidence that all initial flaws,

equal to or greater than this size, will be detected by nondestructive inspection. As a result, proof-test failures (and the resulting high costs) should not be as probable as with the titanium vessel.

From the foregoing example it is apparent that using standardized design factors does not assure optimum (nor in some cases even adequate) designs. To preclude the possibility of failure of hazardous vessels, high factors of safety have often been specified. However, to save weight (caused by the high factors of safety) the designer has been forced to use higher strength (and generally lower toughness) materials. As a result, the risk of failure has often been increased rather than reduced.

While it can be argued that standardized factors of safety have been adequate for many past applications, the designer must concern himself not with average behavior, but with the exception which can result in failure. During recent years there have been costly exceptions.

APPENDIX B
ALLOWABLE STRESS-INTENSITY RATIO - ILLUSTRATIVE EXAMPLES

B.1 Thick-Walled Pressure Vessel

Suppose it is anticipated that a thick-walled 6Al-4V titanium helium tank will go through the preflight service history shown in figure B-1. The maximum design operating stress is σ_{op} and R is the ratio of minimum-to-maximum stress during a cycle. The following is a tabulation of the preflight history:

1. 200 loading cycles with the maximum stress = 90 percent of σ_{op} and R = 0.1.

2. 4300 loading cycles with the maximum stress = σ_{op} and R = 0.7.

3. 260 loading cycles with the maximum stress = 95 percent of σ_{op} and R = 0.4.

4. 60 loading cycles with the maximum stress = σ_{op} and R = 0.1.

5. A long-duration flight cycle with the maximum stress = σ_{op}.

To design an adequate proof test for this vessel, it is necessary to determine the maximum allowable K_{Ii}/K_{Ic} ratio and then to calculate the minimum proof-test factor.

The cyclic life curves for 6Al-4V titanium (STA) are reproduced in figure B-2 for R = 0.1 and R = 0.4, and R = 0.7 from reference 22. The change in K_{Ii}/K_{Ic} throughout the life of the titanium tank is graphically illustrated in figure B-2 and determined by the following procedure.

Because the value of threshold stress intensity for sustained-stress flaw growth is 90 percent of K_{Ic} (table I), the allowable value of K_{Ii}/K_{Ic} at the beginning of the long-duration flight cycle at σ_{op} is 0.90. This requirement is illustrated by point A in figure B-2.

The 60 loading cycles at σ_{op} and R = 0.1 change the K_{Ii}/K_{Ic} ratio from point A to point B in figure B-2. Point B is 60 cycles to the right of point A, with the cycles being measured along the abscissa of the plot of R = 0.1. Hence, the allowable K_{Ii}/K_{Ic} ratio at the beginning of the 60 cycles (point B in figures B-1 and B-2) is 0.84.

APPENDIX B

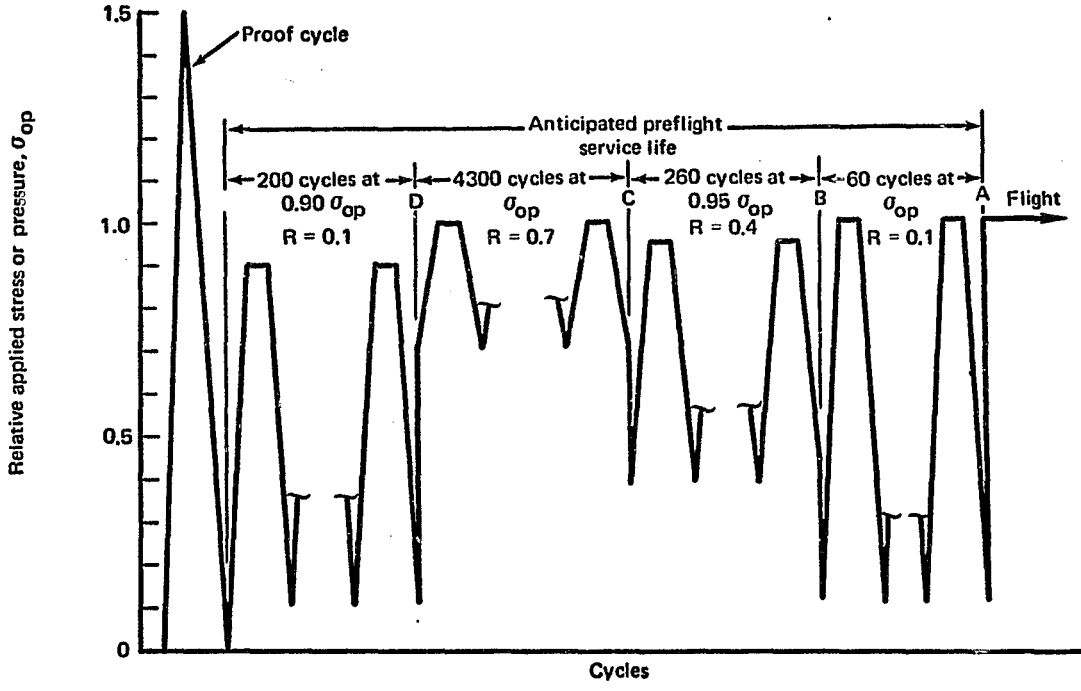

Figure B-1. – History of cyclic stresses of a thick-walled vessel.

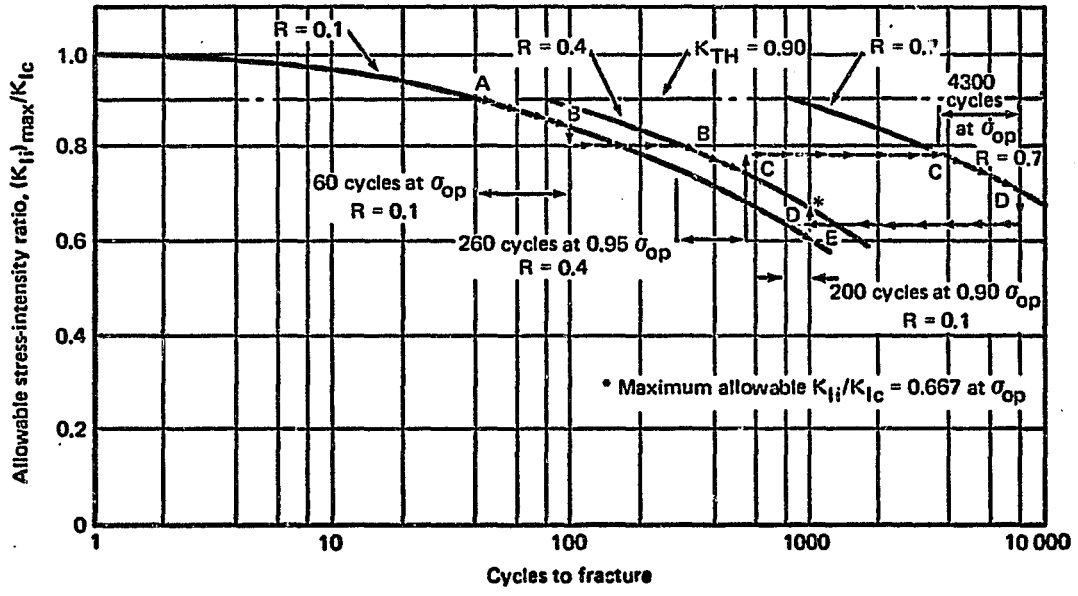

Figure B-2. – Determination of allowable stress-intensity ratio for a thick-walled vessel.

APPENDIX B

K_{Ii}/K_{Ic} is proportioned to the stress level (σ) because

$$K_{Ii}/K_{Ic} = \frac{1.1\sqrt{\pi}\ \sigma\ (a/Q)^{\frac{1}{2}}}{K_{Ic}} \qquad \text{(B-1)}$$

The stress level is 5 percent lower at the end of the 260 cycles than at the beginning of the 60 cycles, and since the flaw size is the same for both stress levels at that point (point B in figure B-1), then the allowable value of K_{Ii}/K_{Ic} at the end of the 260 loading cycles is (0.95/1.00) times 0.84 = 0.798. This K_{Ii}/K_{Ic} ratio is given by point B in figure B-2 on the R = 0.4 curve.

The 260 loading cycles with the maximum stress = 0.95 σ_{op} and R = 0.4 change the K_{Ii}/K_{Ic} ratio from that given by point B to that given by point C in figure B-2. Point C is 260 cycles to the right of point B on the plot of R = 0.4. Hence, the allowable K_{Ii}/K_{Ic} ratio at the beginning of the 260 cycles (point C in figures B-1 and B-2) is 0.74.

The stress level is 5 percent higher at the end of the 4300 cycles than at the beginning of the 260 cycles and, by the same reasoning given above, the allowable value of K_{Ii}/K_{Ic} at the end of 4300 cycles is (1/0.95) times 0.74 = 0.78. This K_{Ii}/K_{Ic} ratio is given by point C in figure B-2 on the R = 0.7 curve.

The 4300 loading cycles at σ_{op} and R = 0.7 change the K_{Ii}/K_{Ic} ratio from point C to point D in figure B-2. Point D is 4300 cycles to the right of point C on the plot of R = 0.7. Hence, the allowable K_{Ii}/K_{Ic} ratio at the beginning of the 4300 cycles (point D in figs. B-1 and B-2) is 0.70.

The stress level is 10 percent lower at the end of the 200 cycles than at the beginning of the 4300 cycles and therefore the allowable value of K_{Ii}/K_{Ic} at the end of the 200 cycles is (0.90/1.00) times 0.70 = 0.63. This K_{Ii}/K_{Ic} ratio is given by point D in figure B-2 on the R = 0.1 curve.

The 200 loading cycles with the maximum stress at 0.90 σ_{op} and R = 0.1 change the K_{Ii}/K_{Ic} ratio from that given by point D to that given by point E in figure B-2. Hence, the allowable K_{Ii}/K_{Ic} ratio at the beginning of the 200 cycles (point E in figs. B-1 and B-2) is 0.6. The operating stress is 10 percent higher than the stress at the beginning of the 200 cycles so that the allowable value of K_{Ii}/K_{Ic} at the operating stress is (1.0/0.9) times 0.6 = 0.667. This is shown by the asterisk in figure B-2.

Thus, for the pressure vessel subjected to the anticipated service history given, the maximum allowable K_{Ii}/K_{Ic} ratio at the end of the proof cycle is 0.667 and the minimum required proof-test factor is $a = 1/0.667 = 1.5$. This indirectly imposes a restriction on the maximum allowable operating stress because the proof stress should not exceed the yield strength of the material. Hence, the maximum allowable operating stress is 0.667 times σ_{ys}.

B.2 Thin-Walled Pressure Vessel

Suppose a thin-walled 6Al-4V (STA) titanium propellant tank designed to contain N_2O_4 at room temperature is expected to withstand a preflight service history, graphically shown in figure B-3, and tabulated as follows:

1. 20 loading cycles with maximum stress = 95 percent of the maximum design operating stress, σ_{op}.
2. 9 loading cycles with maximum stress = σ_{op}.
3. 20 loading cycles with maximum stress = 89 percent of σ_{op}.
4. A long-duration flight cycle with maximum stress = σ_{op}.

In the thin-walled tank, the flaw depth becomes deep with respect to the wall thickness of the tank before reaching the critical size. Hence, the stress-intensity factor must be corrected for the a/t ratio according to figure 3. Suppose the thickness of the tank wall is 0.022 in. (1 in. = 0.0254 m) and the maximum design operating stress, σ_{op} is 84.4 ksi (1 ksi = 6.895 MN/m^2). Under the specified environmental conditions, the material of this gage has a minimum fracture toughness of 37 ksi $\sqrt{in.}$ (1 ksi $\sqrt{in.}$ = 1.099 $\frac{MN}{m^2}\sqrt{m}$) and a threshold stress intensity of 80 percent of K_{Ic}. The plot of flaw-growth rate versus K_{Ii}/K_{Ic} for the material is shown in figure B-4 for σ = 105 ksi (1 ksi = 6.895 MN/m^2). The effect of the stress level on the growth rate is indicated by the equation on the plot. Taking this effect into consideration, the curve is arithmetically integrated, according to the method outlined in reference 8, for three stress levels. These integrated plots (flaw depth versus cycles to fracture) are shown in figure B-5. In the calculations, it was assumed that the value of Q is unity (i.e., the flaws are relatively long with respect to their depth).

APPENDIX B

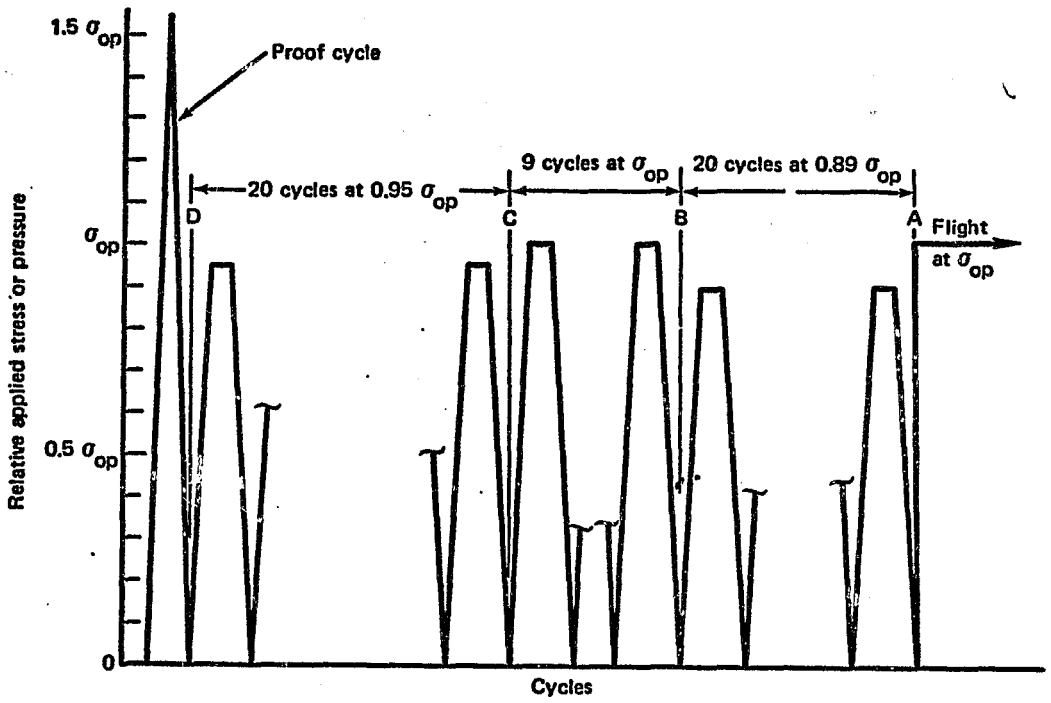

Figure B-3. History of cyclic stresses of a thin-walled vessel.

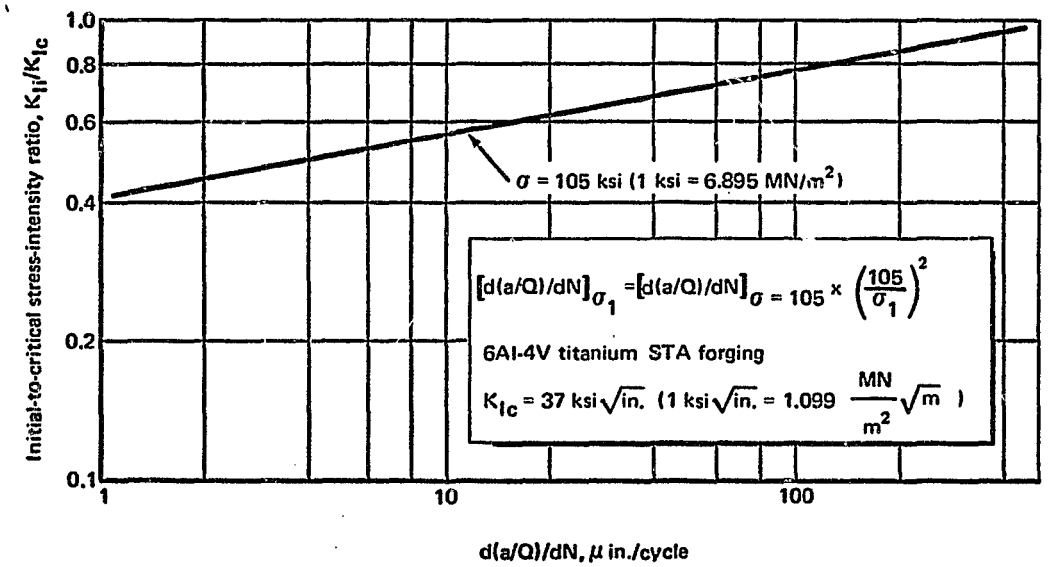

Figure B-4. – Cyclic flaw-growth curve.

Because the threshold stress intensity is 0.80 K_{Ic}, the allowable value of K_{Ii}/K_{Ic} at the beginning of the long-duration flight cycle is 0.80. This requirement is illustrated by point A on the curve of σ_{op} in figure B-5.

The tank-wall stress increases by 11 percent at the end of 20 loading cycles with the maximum stress = 0.89 σ_{op}; however, the flaw size remains the same during the stress increase. This is shown by point A on the plot of 0.89 σ_{op} in figure B-5.

The 20 loading cycles with the maximum stress = 0.89 σ_{op} changes the flaw depth (a) from point A to point B on the plot of 0.89 σ_{op} in figure B-5. Point B is 20 cycles to the right of point A with the cycles being measured along the abscissa of the plot.

The stress decreases by 11 percent at the end of 9 cycles with the maximum stress = σ_{op}. This is shown by point B on the plot of σ_{op} in figure B-5.

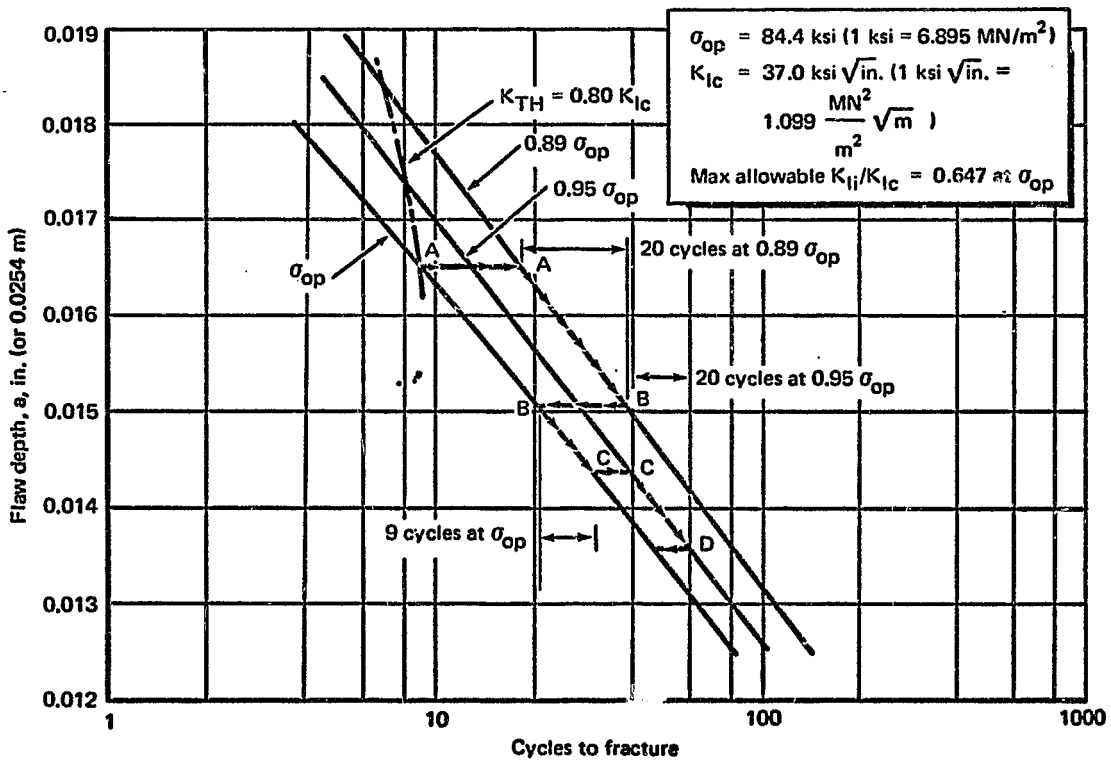

Figure B-5. – Determination of allowable stress-intensity ratio for a thin-walled vessel.

APPENDIX B

The 9 loading cycles with the maximum stress = σ_{op} changes flaw depth (a) from point B to point C on the plot of σ_{op}. Point C is 9 cycles to the right of point B.

The tank-wall stress increases by 5 percent at the end of 20 loading cycles with the maximum stress = 0.95 σ_{op}. This is shown by point C on the plot of 0.95 σ_{op} in figure B-5.

The 20 loading cycles at 0.95 σ_{op} changes flaw depth (a) from point C to point D on the plot of 0.95 σ_{op}. Point D is 20 cycles to the right of point C. The value of the flaw depth at point D is 0.01356 in. (1 in. = 0.0254 m).

The maximum allowable value of K_{Ii}/K_{Ic} at the end of the proof-test cycle then is given by

$$\frac{K_{Ii}}{K_{Ic}} = \frac{1.1\, M_K \sqrt{\pi a}\ \sigma_{op}}{37.0} \qquad \text{(B-2)}$$

σ_{op} = 84.4 ksi (1 ksi = 6.895 MN/m^2), a/t = 0.01356/0.022 = 0.615, and M_K from figure 3 is 1.25.

Hence, the maximum allowable K_{Ii}/K_{Ic} ratio is 0.647, and the proof factor is a = 1/0.647 = 1.55.

REFERENCE 80

PAGE 50 BLANK

REFERENCES

1. Wessel, E. T.; Clark, W. G.; and Wilson, W. K.: Engineering Methods for the Design and Selection of Materials Against Fracture. U.S. Army Tank and Automotive Center Report, Contract No. DA-30-069-AMC-602(T), 1966.

2. Tiffany, C. F.; and Masters, J.N.: Applied Fracture Mechanics. Fracture Toughness Testing and its Applications. ASTM Spec. Tech. Publication No. 381, 1965, pp. 249-277.

3. Brown, W. F., Jr.; and Srawley, J. E.: Plane Strain Crack Toughness Testing of High Strength Metallic Materials. ASTM Spec. Tech. Publication No. 410, 1966.

4. Irwin, G. R.: Crack Extension Force for a Part-Through Crack in a Plate. Trans. ASME, J. Appl. Mech., Series E, vol. 29, no. 4, Dec. 1962, pp. 651-654.

5. Kobayashi, A. S.: On the Magnification Factors of Deep Surface Flaws. Structural Development Research Memorandum No. 16, The Boeing Co., Dec. 1965.

6. Smith, F. W.: Stress Intensity Factor for a Semi-Elliptical Flaw. Structural Development Research Memorandum No. 17, The Boeing Co., Aug. 1966.

7. Tiffany, C. F.; Masters, J. N.; and Bixler, W. D.: Flaw Growth of 6Al-4V Titanium in a Freon T.F. Environment. NASA CR-99632, 1969.

8. Tiffany, C. F.; Masters, J. N.; and Pall, F. A.: Some Fracture Considerations in the Design and Analysis of Spacecraft Pressure Vessels. Paper presented at the ASM National Metals Congress (Chicago), Oct. 1966.

9. Anon.: ASTM Recommended Practice for Plane-Strain Fracture Toughness Testing of High Strength Metallic Materials Using a Fatigue Cracked Bend Specimen. ASTM Standards, Part 31, May 1969, pp. 1099-1114.

10. Tiffany, C. F.: Investigation of Preflawed 2219 Aluminum Tanks. Rept. D5-13663, The Boeing Co., Aug. 1966.

11. Hall, L. R.; and Tiffany, C. F.: Fracture and Flaw Growth Investigation for 2014-T6 Aluminum Weldments Used in Saturn II LH_2 Tanks. Rept. D5-15737, The Boeing Co., Nov. 1967.

12. Smith, A. B.: Missile Motor Cases. Metals Engineering Quarterly, vol. 3, no. 4, Nov. 1963, pp. 55-63.

13. Johnson, H. A.; et al.: Large Motor Case Evaluation. Annual Progress Report, Vol. II, USAF Contract AF33(615)-1623, June 1965.

14. Srawley, J. E.; and Esgar, J. B.: Investigation of Hydrotest Failure of Thiokol Chemical Corporation 260-inch Diameter SL-1 Motor Case. NASA TM X-1194, 1966.

15. ASTM Special Committee on Fracture Testing of High-Strength Metallic Materials: Progress in the Measurement of Fracture Toughness and the Application of Fracture Mechanics to Engineering Problems. Materials Research and Standards, vol. 4, no. 3, Mar. 1964, pp. 107-119.

16. Shah, R. C.: Fracture Mechanics Assessment of Apollo Launch Vehicle & Spacecraft Pressure Vessels. Vol. 1. Rept. D2-114248-1, The Boeing Co., Nov. 1968.

17. Shank, M. E.; Spaeth, C. E.; Cook, V. W.; and Coyne, J. E.: Solid Fuel Rocket Chambers for Operation at 240,000 psi and Above. Metal Progress, vol. 76, no. 5, Nov. 1959, pp. 74-81 (part I), and vol. 76, no. 6, Dec. 1959, pp. 84-92 (part II).

18. Tiffany, C. F.; and Lorenz, P. M.: An Investigation of Low-Cycle Fatigue Failures Using Applied Fracture Mechanics. Rept. ML-TDR-64-53, Battelle Memorial Institute, May 1964.

19. Tiffany, C. F.; Lorenz, P. M.; and Hall, L. R.: Investigation of Plane Strain Flaw Growth in Thick-Walled Tanks. NASA CR-54837, 1966.

20. Tiffany, C. F.; Lorenz, P. M.; and Shah, R. C.: Extended Loading of Cryogenic Tanks. NASA CR-72252, 1967.

21. Tiffany, C. F.; and Masters, J. N.: Investigation of the Flaw Growth Characteristics of 6Al-4V Titanium Used in Apollo Spacecraft Pressure Vessels. NASA CR-65586, 1967.

22. Masters, J. N.: Cyclic and Sustained Load Flaw Growth Characteristics of 6Al-4V Titanium. NASA CR-92231, 1968.

23. Hall, L. R.: Plain Strain Cyclic Flaw Growth in 2014-T62 Aluminum and 6Al-4V (ELI) Titanium. NASA CR-72396, 1968.

24. Johnson, H. H.; and Paris, P. C.: Subcritical Flaw Growth. Engineering Fracture Mechanics, vol. 1, no. 1, June 1968, pp. 3-45.

25. Peterson, M. H.; Brown, B. F.; Newbegin, R. L.; and Grover, R. E.: Stress Corrosion Cracking of High Strength Steel and Titanium Alloys in Chloride Solutions at Ambient Temperature. Corrosion, vol. 23, no. 5, May 1969, pp. 142-148.

26. Brown, B. F.: A New Stress Corrosion Cracking Test Procedure for High Strength Alloys. Paper presented at the ASTM Arsenal Meeting at Purdue University (Lafayette, Ind.), June 13-18, 1965.

27. Piper, D. E.; Smith, S. H.; and Carter, R. V.: Corrosion Fatigue and Stress Corrosion Cracking in Aqueous Environments. Metals Engineering Quarterly, vol. 8, Aug. 1968, pp. 50-63.

28. Smith, H. R.; Piper, D. E.; and Downey, F. K.: A Study of Stress Corrosion Cracking by Wedge Force Loading. Engineering Fracture Mechanics, vol. 1, no. 1, June 1968, pp. 123-128.

29. Johnson, H. H.; and Willner, A. M.: Moisture and Stable Crack Growth in a High Strength Steel. Applied Materials Research, vol. 4, no. 1, Jan. 1965, pp. 34-40.

30. Steigerwald, E. A.; and Benjamin, W. D.: Stress Corrosion Cracking Mechanisms in Martinistic High Strength Steels. Third Quarterly Progress Report, Contract AF 33(615)-3651, Air Force Materials Laboratory, 1967.

31. Irwin, C. R.: Moisture Assisted Slow Crack Extension in Glass Plate. Memorandum Report 1678, Naval Research Laboratory, 1966.

32. Koetje, E. L.: Report on Failure of T. E. Actuator. Rept. D2-16676-1, The Boeing Co., July 1965.

33. Tiffany, C. F.; Masters, J. N.; and Regan, R. E.: Large Motor Case Technology Evaluation. Rept. AFML-TR-67-190, Air Force Materials Laboratory, Aug. 1967.

34. Lorenz, P. M.: Fracture Toughness and Sustained Flaw Growth Characteristics of Inconel 718 in the Environment of Pressurized Gaseous Hydrogen. Rept. D2-114404-1, The Boeing Co., Oct. 1968.

35. Beachem, C. D.; and Brown, B. F.: A Comparison of Three Specimens for Evaluating the Susceptibility of High Strength Steel to Stress Corrosion Cracking. Internal Report, U.S. Naval Research Laboratory, 1967.

36. Haese, W. P.: Investigation of Fracture of 6Al-4V Titanium in N_2O_4. Rept. D2-24057-1, The Boeing Co., Dec. 1965.

37. Wei, R. P.: Some Aspects of Environment-Enhanced Fatigue Crack Growth. Paper presented at ASTM Fall Meeting (Atlanta, Ga.), Oct. 3, 1968.

38. Barsom, J. M.: Corrosion-Fatigue Crack Propagation Below K_{ISCC}. Paper presented at the National Symposium on Fracture Mechanics at Lehigh University (Bethlehem, Pa.), Aug. 26, 1969.

39. Masters, J. N.; Haese, W. P.; and Finger, R. W.: Investigation of Deep Flaws in Thin Walled Tanks. NASA CR-72606, 1969.

40. Shah, R. C.; and Kobayashi, A. S.: Stress Intensity Factor for an Elliptical Crack Under Arbitrary Normal Loading. Paper presented at the Second National Symposium on Fracture Mechanics at Lehigh University (Bethlehem, Pa.), June 17-19, 1968.

41. Kobayashi, A. S.; Ziv, M.; and Hall, L. R.: Approximate Stress Intensity Factor for an Embedded Elliptical Crack Near Two Parallel Free Surfaces. Int. J. of Fracture Mechanics, vol. 1, no. 2, June 1965, pp. 81-95.

42. Shah, R. C.; and Kobayashi, A. S.: On the Parabolic Crack in an Elastic Solid. Engr. Fracture Mech., vol. 1, no. 2, Aug. 1968, pp. 309-325.

43. Lorenz, P. M.: Compatibility of Tankage Materials with Liquid Propellants. Rept. AFML-TR-69-99, Air Force Materials Laboratory, May 1969.

SYMBOLS

a	semiminor axis of the ellipse $x^2/c^2 + y^2/a^2 = 1$ or crack depth of the semielliptical surface flaw, in. (1 in. = 0.0254 m)
$2c$	crack length of the semielliptical surface flaw, in.
K_I	plane-strain stress-intensity factor, ksi$\sqrt{\text{in.}}$ (1 ksi$\sqrt{\text{in.}}$ = 1.099 $\frac{\text{MN}}{\text{m}^2}\sqrt{\text{m}}$)
K_{Ic}	plane-strain critical stress-intensity factor or fracture toughness of the material, ksi$\sqrt{\text{in.}}$
K_{Ii}	plane-strain stress-intensity factor at initial conditions, ksi$\sqrt{\text{in.}}$
K_{TH}	plane-strain threshold stress-intensity level, ksi$\sqrt{\text{in.}}$
M_K	stress-intensity magnification factor for deep surface flaws based on Kobayashi's solution
N	number of cycles
Q	flaw-shape parameter = $\phi^2 - 0.212\,(\sigma/\sigma_{ys})^2$
R	ratio of minimum to maximum stress during a cycle
T	time, hr
t	thickness of plate (specimen), in.
α	proof-test factor
θ	angle of integration
σ	uniform gross stress applied at infinity and perpendicular to plane of crack, ksi (1 ksi = 6.895 MN/m^2)
σ_{op}	maximum design operating stress, ksi
σ_{ult}	ultimate strength of the material, ksi
σ_{ys}	uniaxial tensile yield strength of the material, ksi
ϕ	complete elliptical integral of the second kind having modulus k defined as $k = (1 - a^2/c^2)^{\frac{1}{2}}$

SUBSCRIPTS

cr	at critical conditions
i	at initial condition
op	operational

END OF REFERENCE

REFERENCE

81

JOHNSON, R. E.: APOLLO EXPERIENCE REPORT - THE PROBLEM OF STRESS-CORROSION CRACKING. NASA TN D-7111, 1973.

NASA TECHNICAL NOTE

NASA TN D-7111

NASA TN D-7111

APOLLO EXPERIENCE REPORT - THE PROBLEM OF STRESS-CORROSION CRACKING

by Robert E. Johnson

Manned Spacecraft Center
Houston, Texas 77058

NATIONAL AERONAUTICS AND SPACE ADMINISTRATION • WASHINGTON, D. C. • MARCH 1973

1. Report No.	2. Government Accession No.	3. Recipient's Catalog No.
NASA TN D-7111		

4. Title and Subtitle	5. Report Date
APOLLO EXPERIENCE REPORT THE PROBLEM OF STRESS-CORROSION CRACKING	March 1973
	6. Performing Organization Code

7. Author(s)	8. Performing Organization Report No.
Robert E. Johnson, MSC	MSC S-344
	10. Work Unit No.
9. Performing Organization Name and Address	914-13-20-06-72
Manned Spacecraft Center Houston, Texas 77058	11. Contract or Grant No.
	13. Type of Report and Period Covered
12. Sponsoring Agency Name and Address	Technical Note
National Aeronautics and Space Administration Washington, D.C. 20546	14. Sponsoring Agency Code

15. Supplementary Notes

The MSC Director waived the use of the International System of Units (SI) for this Apollo Experience Report because, in his judgment, the use of SI Units would impair the usefulness of the report or result in excessive cost.

16. Abstract

Stress-corrosion cracking has been the most common cause of structural-material failures in the Apollo Program. The frequency of stress-corrosion cracking has been high and the magnitude of the problem, in terms of hardware lost and time and money expended, has been significant. In this report, the significant Apollo Program experiences with stress-corrosion cracking are discussed. The causes of stress-corrosion cracking and the corrective actions are discussed, in terminology familiar to design engineers and management personnel, to show how stress-corrosion cracking can be prevented.

17. Key Words (Suggested by Author(s))	18. Distribution Statement
*Stress Corrosion *Aluminum Alloys *Titanium Alloys	

19. Security Classif. (of this report)	20. Security Classif. (of this page)	21. No. of Pages	22. Price
None	None	20	$3.00

* For sale by the National Technical Information Service, Springfield, Virginia 22151

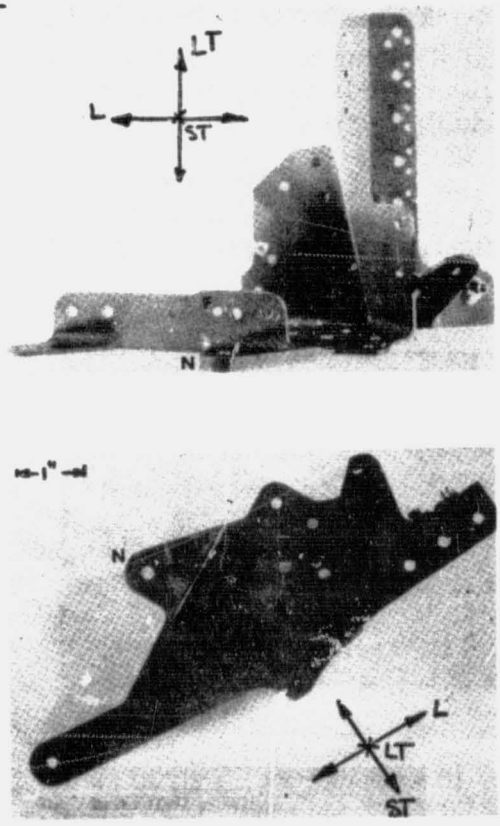

Figure 17. - Cracking on a machined part. (Note the relationship of the crack to the alloy grain direction.)

Over 130 parts in the LM program were found to be cracked as a result of stress corrosion. Many corrective actions were instituted. Among the solutions were component redesign, heat treatment to make the components less susceptible, shimming or otherwise relieving fabrication stresses, addition of corrosion-protection coatings to preclude as much of the corrosive environment as possible, and shot peening to introduce compressive surface stresses.

Pressure-Vessel Stress Corrosion

The problem of stress-corrosion cracking in pressure vessels is especially serious because the occurrence of this problem usually results in catastrophic failure of the vessel and associated damage to other hardware near the pressure vessel. Some of the significant Apollo Program pressure-vessel failures are described individually in the following sections.

Nitrogen tetroxide in titanium-alloy pressure vessels. - In all of the Apollo spacecraft propulsion systems, nitrogen tetroxide is used as the oxidizer. The storage of nitrogen tetroxide under pressure in titanium-alloy pressure vessels was a subject of concern because of known reactions between titanium and other oxidizers. Extensive test programs were conducted before 1964 to approve the use of type 6Al-4V titanium alloy as the standard Apollo spacecraft pressure-vessel material for this application. In 1964, qualification tests on the Apollo spacecraft main propellant tanks were completed. The tests included 30-day exposures of the pressure vessels to nitrogen tetroxide under the maximum wall stress of approximately 100 ksi.

In 1965, a stress-corrosion failure of an Apollo reaction control system pressure vessel occurred. This failure could only have been caused by the nitrogen tetroxide reacting with the titanium-alloy pressure vessel. The failure analysis (refs. 2 and 3) showed that a change in the nitrogen tetroxide composition, within the limits of the procurement specification for the oxidizer, had eliminated one oxide of nitrogen and created a fluid that was causing serious stress-corrosion cracking of the titanium alloy. Details of the failed hardware are shown in figure 18.

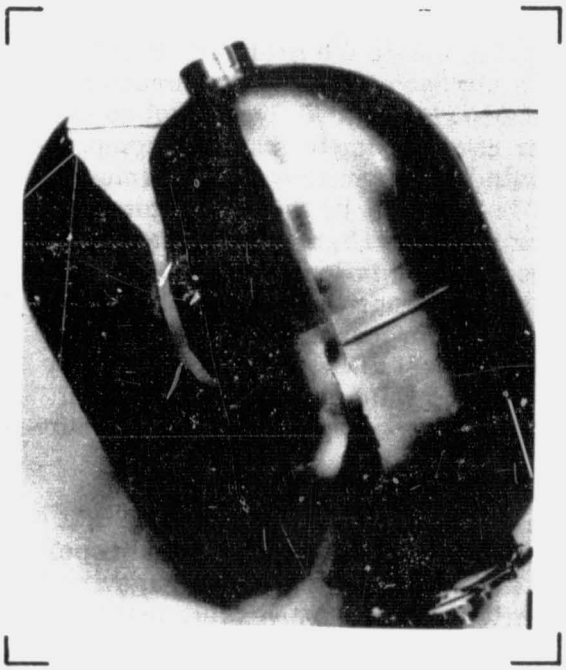

(a) Failed pressure vessel.

(b) Magnified view of the inside surface showing cracks.

(c) Transgranular cracks.

(d) Electron fractograph of the failed surface.

Figure 18. - Stress corrosion of type 6Al-4V titanium alloy from a failed nitrogen tetroxide pressure vessel.

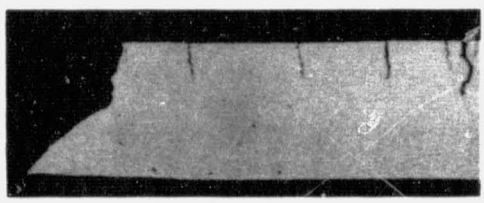

(e) Cross section of the pressure-vessel wall showing a flat fracture with a shear lip.

Figure 18. - Concluded.

To eliminate the problem, NASA generated a nitrogen tetroxide procurement specification that carefully controlled the oxidizer composition to maintain compatibility with the pressure-vessel titanium alloy. In addition, by taking samples of the oxidizer from the flight supply system before the oxidizer is loaded into the spacecraft and by testing the oxidizer in contact with stressed precracked samples of the pressure-vessel alloy, NASA continues to ensure that no fluid change has occurred that could cause aggressive reactions during a flight.

Methanol in titanium-alloy pressure vessels. - The most damaging failure of a pressure vessel in the Apollo Program occurred in October 1966 when a main propellant tank ruptured inside an Apollo service module and caused extensive damage and serious loss of hardware. The failure occurred while the pressure vessel, made of titanium alloy 6Al-4V, was filled with methanol and was pressurized. The failure mode was stress-corrosion cracking.

In this instance, methanol was used for safety reasons in the system checkout instead of the toxic propellant. Methanol was selected for its physical similarity (density, viscosity) to the propellant and because it could be removed from the system easily without leaving a residue or other contamination. The approval for the use of methanol was based on a literature search, which uncovered no data to indicate a potential problem. After the failure of the Apollo spacecraft hardware, numerous programs were initiated to investigate the problem, and the seriousness of the problem was defined in several technical papers (ref. 4). Examples of the metallography from the failed material are shown in figure 19. Additional information concerning the failure analysis is contained in references 3 and 5.

In retrospect, the lack of a test program to approve pressure-test fluids before they were used and a continuing check against contaminants during use caused a serious program problem. The Manned Spacecraft Center has corrected this situation by requiring compatibility testing before a new pressure-vessel material or a new test environment can be used in the Apollo Program.

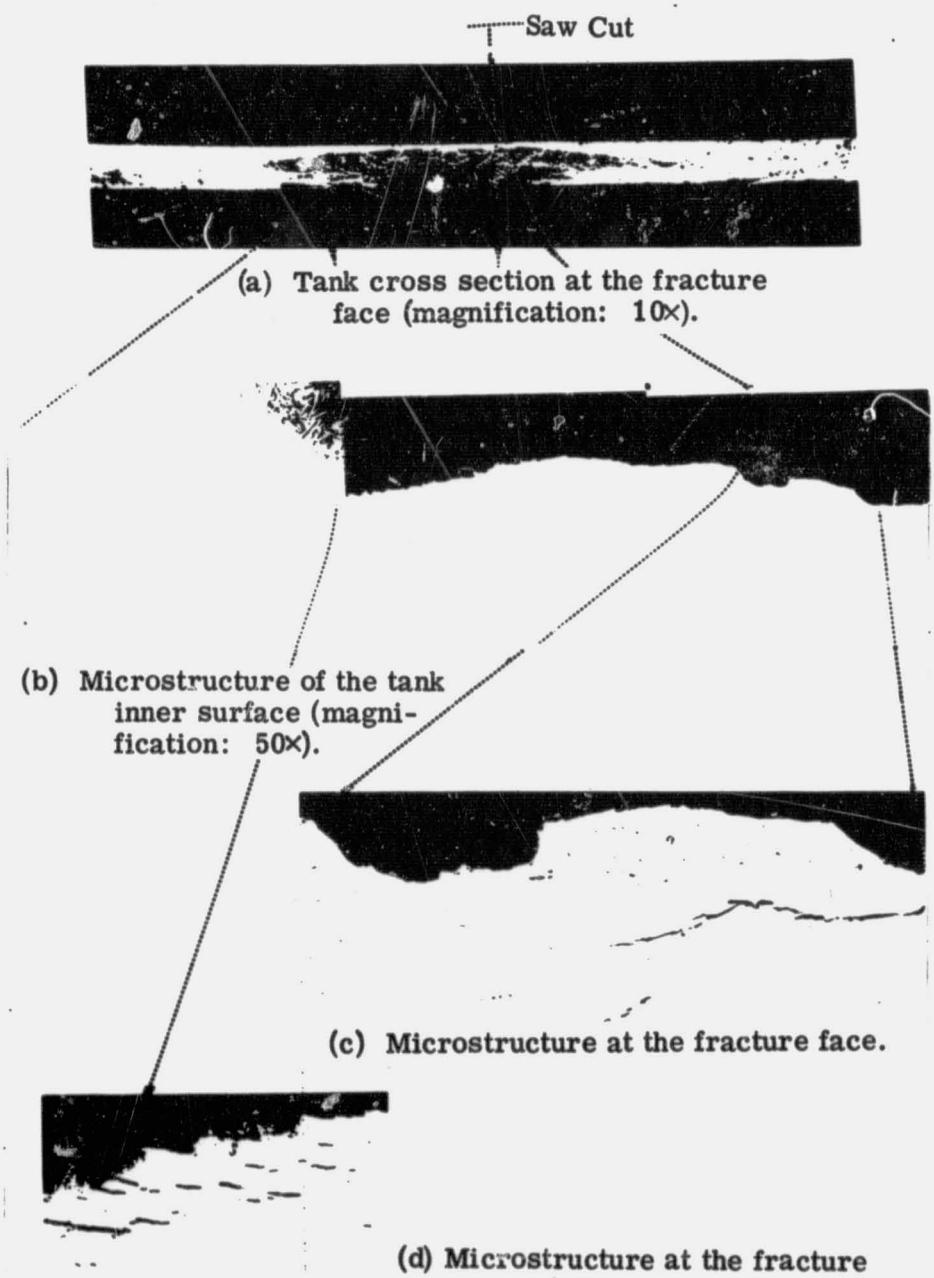

Figure 19. - Origin of the failure that resulted from methanol in a type 6Al-4V titanium-alloy pressure vessel.

Solid-fuel-rocket motor case made of type 4335V steel alloy. - Type 4335V steel alloy was heat treated to a minimum tensile strength of 210 000 psi. During hydrostatic acceptance testing, stress-corrosion cracking occurred that resulted in the rupture of

two motor cases. The test fluid was water, and failure analysis showed that stress-corrosion cracking would occur if defects existed in the stressed alloy when it was brought into contact with water. The defects in the motor cases were identified as tight cracks that had resulted from the welding operation and that could not be detected by the postweld inspection. The corrective action for the problem was to change to a compatible test fluid, hydraulic fluid, and to make the inspection and quality-control procedures of the welding operation more thorough.

Oxygen-storage vessel made of type D6AC steel alloy. - Type D6AC steel alloy was heat treated to the 220 000- to 240 000-psi tensile-strength range and was used to store gaseous oxygen under pressure. The failure of one pressure vessel because of stress-corrosion cracking was caused by a small defect on the exterior surface of the pressure sphere. The corrosive medium was listed as water because the test consisted of immersing the vessel under water during hydrostatic testing. The vessel was nickel plated and the defect was found to contain nickel, which indicated the presence of the flaw before nickel plating. The corrective action taken was to change the test fluid to oil and to discontinue the immersion of the tank during pressure testing. Also, inspection procedures were tightened to enable detection of pressure-vessel defects before testing.

CONCLUSIONS

The Apollo spacecraft is constructed of high-strength alloys and is designed and fabricated to be a highly efficient, low-weight vehicle. Stress corrosion has been a serious problem in the Apollo Program and reflects the type of problem that can occur in a program requiring these characteristics. To illustrate the type of problem encountered, several examples are examined.

The examples discussed in this report are typical ones and do not represent all of the stress-corrosion cracking failures experienced in the Apollo Program. However, the examples discussed do represent the most significant problems encountered in the Apollo Program and allow the following general conclusions to be drawn concerning improvements that are needed to prevent the recurrence of similar problems in future programs.

1. With the exception of two environments, information on the stress-corrosion cracking behavior of the alloys used in Apollo spacecraft hardware was available and could have been used to avoid many of the stress-corrosion cracking failures if the information had been applied correctly during the design, fabrication, and test phases.

2. Without proper consideration of stress-corrosion cracking, such design changes as those for vehicle weight reduction can seriously affect the stress-corrosion sensitivity of the vehicle hardware by changing fabrication techniques, raw-material mill forms, and stress levels, and by eliminating corrosion-protection systems.

3. Specific alloys and alloys subjected to certain heat-treatment procedures are very susceptible to stress-corrosion cracking, and their use should be avoided wherever possible. Control should be exercised by the contractors and NASA over the use

of these alloys to ensure that adequate consideration of stress-corrosion cracking has been given to those applications in which the use of these materials is required.

4. New environment/alloy combinations must be examined experimentally before they are used in a program. The use of material forms, heat treatments, stresses, potential stress concentrations, and environments must be simulated if meaningful service data are to be obtained and program problems are to be avoided.

Manned Spacecraft Center
National Aeronautics and Space Administration
Houston, Texas, July 10, 1972
914-13-20-06-72

REFERENCES

1. Godard, Hugh P.; Jepson, W. B.; Bothwell, M. R.; and Kane, Robert L.: The Corrosion of Light Metals. John Wiley and Sons, Inc., 1967.

2. Johnson, Robert E.; Kappelt, George F.; and Korb, Larry J.: A Case History of Titanium Stress Corrosion in Nitrogen Tetroxide. Paper presented at 1966 Natl. Metals Congress Chicago, 1966. Also available as NASA TM X-59615.

3. Brownfield, C. D.: The Stress Corrosion of Titanium in Nitrogen Tetroxide, Methyl Alcohol, and Other Fluids. SD 67-213A, revised ed., North American Rockwell Rept., June 1968.

4. Anon.: Accelerated Crack Propagation of Titanium by Methanol, Halogenated Hydrocarbons, and Other Solutions. Defense Metals Information Center Memorandum 228, Mar. 6, 1967.

5. Johnston, Robert L.; Johnson, Robert E.; Ecord, Glenn M.; and Castner, Willard L.: Stress-Corrosion Cracking of Ti-6Al-4V Alloy in Methanol. NASA TN D-3868, 1967.

END OF REFERENCE

81

REFERENCE

82

CAMPBELL, J. E.; BERRY, W. E.; AND FEDDERSEN, C. E.: DAMAGE TOLERANT DESIGN HANDBOOK. MCIC-HB-01, METALS AND CERAMICS INFORMATION CENTER, BATTELLE MEMORIAL INST., 1972.

THIS REFERENCE IS MATERIAL THAT IS READILY AVAILABLE AND THEREFORE THE CONTENTS HAVE NOT BEEN REPRODUCED.

END OF REFERENCE

82

REFERENCE

83

HOOD, D. W.; EICHENBERGER, T. W.; AND LOVELL, D. T.: AN INVESTIGATION OF THE GENERATION AND UTILIZATION OF ENGINEERING DATA ON WELDMENTS. AFML-TR-68-268, AIR FORCE MATERIALS LAB. (AD-851938), 1968.

43,835

AD-851 938
AFML-TR-68-268

AFML TECHNICAL LIBRARY
OFFICIAL FILE COPY

AN INVESTIGATION OF THE GENERATION AND UTILIZATION OF ENGINEERING DATA ON WELDMENTS

D. W. Hood
T. W. Eichenberger
D. T. Lovell
The Boeing Company

TECHNICAL REPORT AFML-TR-68-268
OCTOBER 1968

DISTRIBUTION LIMITATION NOW REMOVED, GOVERNMENT REPORTS ANNOUNCEMENTS, VOL.72,NO.21,P.140, 11-10-72.

This document is subject to special export controls and each transmittal to foreign governments or foreign nationals may be made only with prior approval of the Air Force Materials Laboratory (MAAM), Wright-Patterson Air Force Base, Ohio 45433.

Air Force Materials Laboratory
Air Force Systems Command
Wright-Patterson Air Force Base, Ohio

AN INVESTIGATION OF THE GENERATION AND UTILIZATION OF ENGINEERING DATA ON WELDMENTS

D. W. Hood
T. W. Eichenberger
D. T. Lovell

DISTRIBUTION LIMITATION NOW REMOVED, GOVERNMENT REPORTS ANNOUNCEMENTS, VOL.72,NO.21,P.140, 11-10-72.

This document is subject to special export controls and each transmittal to foreign governments or foreign nationals may be made only with prior approval of the Air Force Materials Laboratory (MAAM), Wright-Patterson Air Force Base, Ohio 45433.

NOTICES

When government drawings, specifications, or other data are used for any purpose other than in connection with a definitely related government procurement operation, the United States government thereby incurs no responsibility nor any obligation whatsoever; and the fact that the government may have formulated, furnished, or in any way supplied the said drawings, specifications, or other data, is not to be regarded by implication or otherwise as in any manner licensing the holder or any other person or corporation, or conveying any rights or permission to manufacture, use, or sell any patented invention that may in any way be related thereto.

This document is subject to special export controls and each transmittal to foreign governments or foreign nationals may be made only with prior approval of MAAM, Air Force Materials Laboratory.

Information in this report is embargoed under the Department of State ITIAR. This report may be released to foreign governments by department or agencies of the U.S. government subject to approval of Air Force Materials Laboratory, Materials Applications Division, or higher authority within the Air Force. Private individuals or firms require a Department of State export license.

Copies of this report should not be returned unless return is required by security considerations, contractual obligations, or notice on a specific document.

ABSTRACT

Present industry methods of obtaining engineering data on weldments were reviewed through literature and industrial surveys. Serious lack of uniformity was found within the aerospace industry in the development and use of engineering design data. Difficulties in defining weldment characterization, primarily due to the absence of adequate government or industry-wide welding process specifications, were the major factors limiting industry-wide generation and the use of weldment design data. The determination of weldment design strengths from coupon-derived data, structural data, and other factors has resulted in many differences in design values. It was concluded from the literature and industrial surveys that properly characterized coupon-derived weldment design data was the most meaningful approach in establishing and presenting data that would have industry-wide usefulness. It was also evident that in using coupon-derived weldment design data, a correlation factor must be established for each specific structural component. Guidelines for the generation and presentation of weldment design data were developed. These guidelines were used in a model test program in which design data on 6061 aluminum and Ti-6Al-4V titanium alloy weldments were obtained. Coupon-derived data was statistically treated to determine the minimum weld strength for the two alloys. Significant welding variables and conditions were identified. Manual repair welding was the most significant variable which affected the weldment design strength. The correlation between coupon data and structure was demonstrated by testing welded tubes and pressure vessels. The test program effectively demonstrated the validity of the guidelines.

Based on the surveys and the weldment data obtained in this program, recommendations are made to include the guidelines for the generation and utilization of engineering data on weldments in *Mil-Hdbk-5---Guidelines for Presentation of Data*, AFML-TR-66-386, February, 1967.

(This abstract is subject to special export controls, and each transmittal to foreign governments or foreign nationals may be made only with prior approval of the Air Force Materials Laboratory (MAAM), Wright-Patterson Air Force Base, Ohio 45433.)

(186 pp) (28 fig.) (47 tbls..) (33 ref.)

SECTION VI

RECOMMENDED GUIDELINES

Guidelines have been developed for establishment of engineering data on weldments. The purpose of these guidelines is to provide a uniform procedure by which meaningful engineering data can be developed for use within the aerospace industry.

These guidelines generally reflect the procedures currently used within the aerospace industry. They are applicable to all types of weldable materials and welding processes. However, recommended test coupon configurations and testing methods have been limited to the evaluation of butt-type joints.

In developing these guidelines, a deliberate attempt was made to provide a procedure by which data on weldments could be generated in a manner similar to that of base metals in Mil-Hdbk-5. The guidelines contain procedures that deal with definitions, population definition, data generation, data treatment, and data presentation.

The guidelines have been prepared such that they can be utilized without reference to the remainder of this report.

The intent of these guidelines is to set forth procedures for generation and presentation of engineering data on weldments. These procedures are applicable to the aircraft and aerospace industry and concern all materials joined by welding processes.

A distinction is made in properties of weldments between those applicable to design and those used for welding development and process control. These guidelines are concerned with those properties applicable to design.

The approach followed establishes coupon-derived design properties for weldments produced under known and defined conditions. Appropriate analysis must be conducted to adapt the coupon-derived data to design of the structure being considered. This is accomplished by determining the state of stress for the component joint and/or by relating structural hardware test results to the coupon-derived design properties. The sequential steps of these procedures are summarized in Figure 11. This approach is consistent with the techniques used to obtain design data for Mil-Hdbk-5 [1], as defined in Reference 26.

These procedures require detailed definition of the welding conditions which the design strengths represent. Current military welding specifications do not contain adequate requirements for defining a meaningful population of weldments. Due to this lack of applicable industry-wide specifications, the necessary information must be presented with the coupon-derived weldment design data.

These guidelines establish procedures for the orderly generation and presentation of design data for weldments and consist of sections covering definitions, population definition, data generation, data treatment, and data presentation. These sections are presented below.

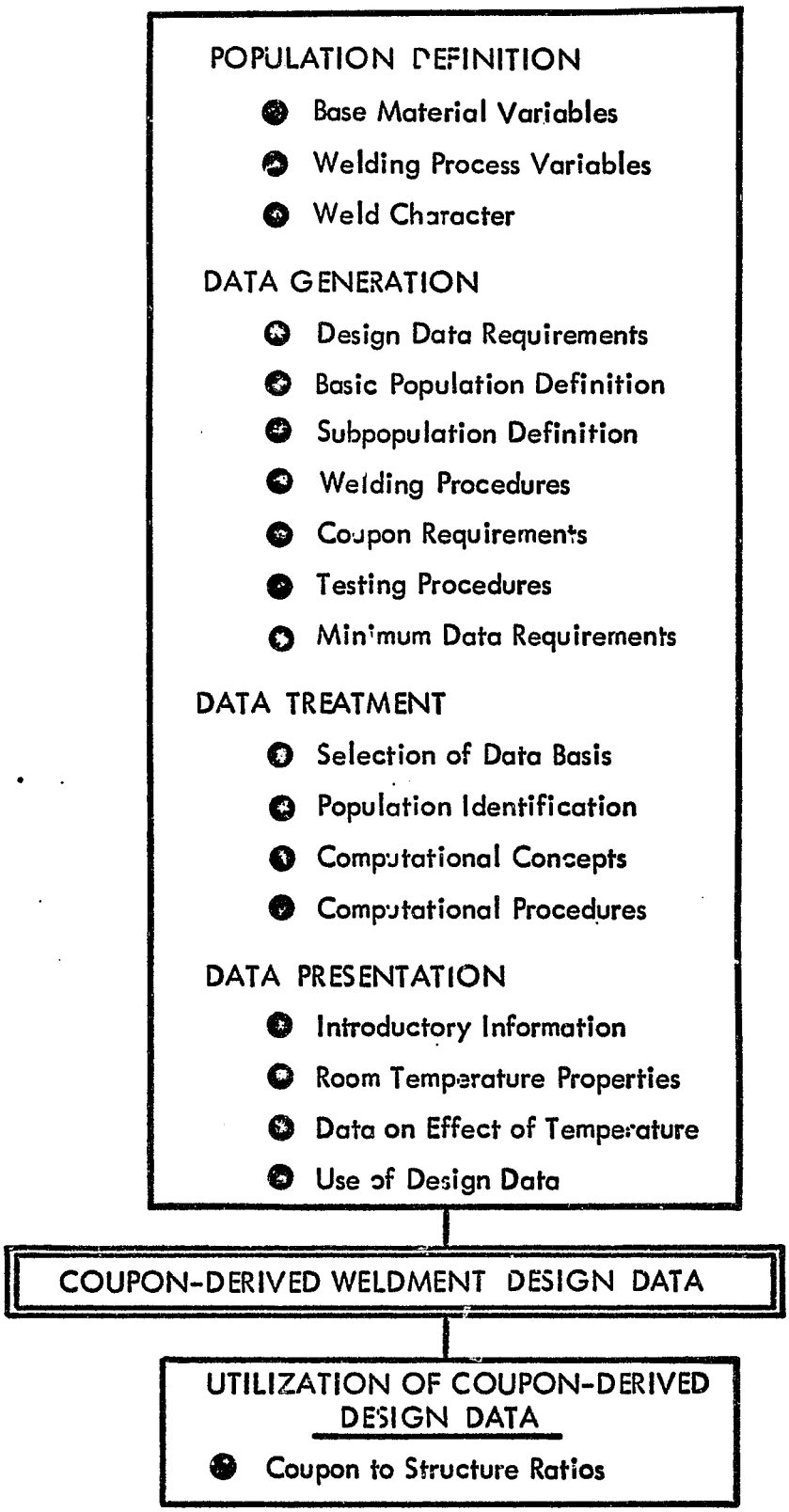

Figure 11: GUIDELINE PROCEDURES FOR COUPON-DERIVED WELDMENT DESIGN DATA

DEFINITIONS

Throughout the guidelines and in the preparation of data, definitions of the American Welding Society [33] will be used for terms relating to welding.

The definitions utilized in References 1 and 26 will be used for other terms relating to material properties and statistical treatment of data.

POPULATION DEFINITION

Determination and presentation of industry-wide properties of weldments requires adequate definition of pertinent welding parameters, including a description of base materials, welding process variables, and weld character. In the case of general metallic material properties, reference to industry-accepted material procurement specifications provides this basis for definition. For weldments, current military process specifications are not sufficiently detailed to adequately describe a given population of weldments. Present industry practice involves the stipulation of requirements and conditions in addition to those of the military specifications in order to obtain consistent, high-quality weldments meeting the requirements of industry. Therefore, at the present time, the procedure of stipulating requirements must be utilized in establishing industry-wide design data in lieu of a referenceable welding specification.

The most significant variables to be considered in weldment characterization (population definition) are divided into three basic categories: base materials, welding process variables, and weld character (see Figure 12). The variables listed are the minimum that must be identified and recorded during the initial portion of the program.

Base Materials

Initial consideration must be given to the base materials. This classification includes appropriate stipulation of alloy, composition, form, preweld and postweld heat-treat condition, filler material, and material thickness. Selection, specification, and control of these variables are generally straightforward, following the same procedures as would be used in base metal design data determination.

Welding Process Variables

The most difficult aspect of weldment characterization is establishment of welding variables. These variables must be sufficiently detailed to represent the population of weldments produced, as well as to allow later reproduction of welds within this population. The appropriate selection of variables to be stipulated must be based on an interpretation of their effect on weldment properties and the desirability of control. Using the variable of thermal-control tooling as an example, it may be found that various types of tooling influence tensile properties of a weld joint by their effect on cooling rate. However, the difficulty in adequately describing thermal-control tooling for more than a single application makes it desirable to treat tooling as a random and uncontrolled variable. This same judgment of effect on properties and desirability of control must be made for each of the welding process variables.

BASE MATERIAL

Alloy, Composition, Form, Pre-and Post-Weld Heat Treat Condition, Material Thickness, Filler Material

WELDING PROCESS VARIABLES

Joint Preparation	Tooling	Welding Conditions	Weld Repair
Joint Type	Alignment	Welding Process	Number of Repairs
Edge Preparation	Restraint	Welding Method	Type of Repair
Cleaning	Thermal Control	Welding Position	
		Heat Input (Weld Setting)	
		Preheat	
		Interpass Temperature	
		Shielding Gas	

WELD CHARACTER

Inspection Methods

- NDT
  - Visual
  - Radiographic
  - Penetrant
  - Magnetic Particle
  - Ultrasonic
- DT
  - Transverse Tensile Test

Acceptance Levels

- External
  - Underfill and Undercut
  - Cracks
  - Pores
  - Reinforcements
- Internal
  - Pores
  - Inclusions
  - Cracks
  - Lack of Fusion
- Tensile Properties
  - Minimum & Minimum Average

Figure 12: SUMMARY OF POPULATION DEFINITION CONSIDERATIONS

Weld Character

The third grouping of welding conditions is weld character, which is viewed from two aspects: actual character, and means of determining character. Appropriate levels of weld character must be prescribed in order to define a population of weldments. This includes a description of internal and external quality levels as well as a minimum joint strength requirement. In most specifications there are several weld classes that serve to identify in detail the quality level requirements. However, in lieu of reference to a specific class in an industry-wide specification, detailed quality levels must be given. In addition, the means of determining these weldment characteristics must be established. This involves stipulation of both nondestructive and destructive test methods.

In summary, the primary concern of population definition for weldments is to describe welding conditions in a manner that will allow reproduction of this same population and be sufficiently detailed to allow proper data analysis.

DATA GENERATION

Data generation concerns the development of a testing program based upon considerations of design data requirements, population definition, subpopulation definition, welding procedures, testing procedures, and minimum data requirements. A graphic summary of each of these elements is shown in Figure 13 and is discussed in the following paragraphs.

Design Data Requirements

Initially the type of data required and the general welding conditions of interest must be established based upon anticipated use of the data. This includes the type of property needed (e.g., tensile, fatigue), the type of data required (statistical or average), and the general welding conditions for which the data will be generated.

Basic Population Definition

The next step is selection of a basic population definition satisfying the general welding conditions previously established. The procedures outlined previously for population definition require a detailed review of applicable welding conditions in order to select a single population which will provide data consistent with the requirements for data treatment. The example shown in Table IV for 6061 aluminum weldments would be typical of a basic population definition. In this example, tooling and heat input have not been specified. It is recognized that these variables have a potential influence upon weldment properties and may require a redefinition of the original population as a result of later data analysis.

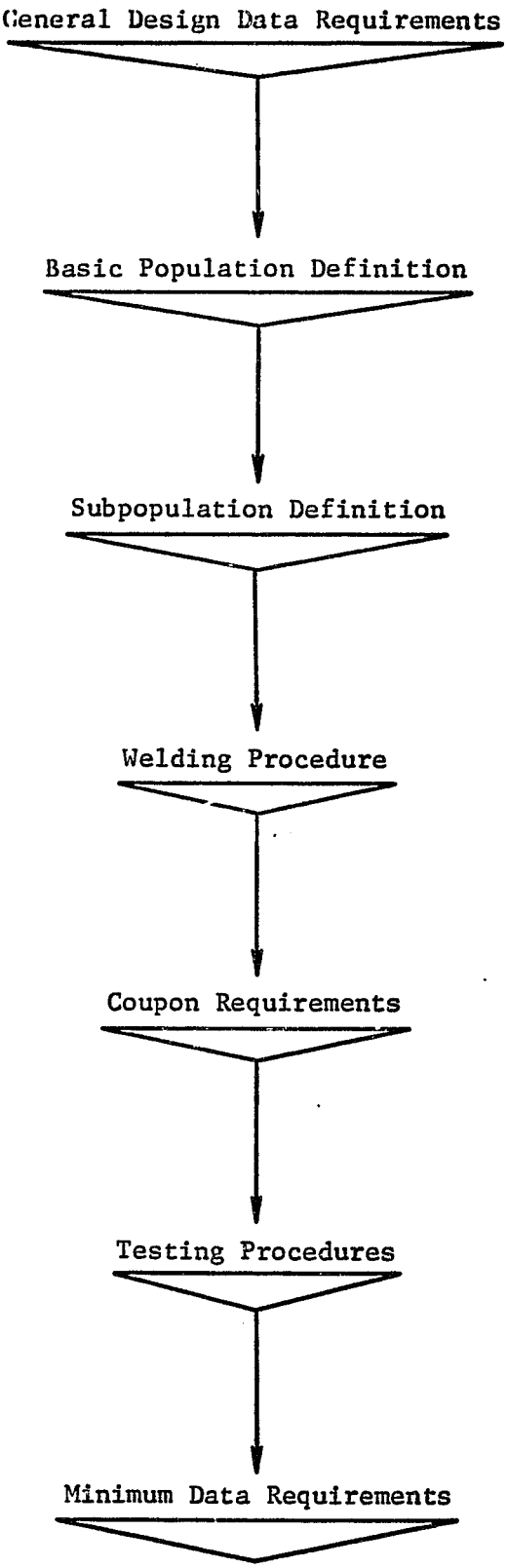

Figure 13: TESTING PROGRAM CONSIDERATIONS

Table IV: EXAMPLE POPULATION DEFINITION

BASE MATERIALS

- Alloy: 6061 Aluminum per QQ-A-250/11
- Form: Sheet
- Preweld Heat Treat Condition: T4 or T6
- Postweld Heat Treat Condition: As-Welded
- Material Thickness: 0.09 inch
- Filler Material: 4043 per QQ-B-655

WELDING VARIABLES

- Joint Preparation
  - Joint Type: Butt
  - Edge Preparation: Square Groove
  - Cleaning: Deoxidize, solvent wipe and hand scrape
- Tooling: None Specified
- Welding Conditions
  - Process: Mechanized GTA
  - Sequence: Single Pass
  - Position: Flat
  - Heat Input: Not Specified
  - Weld Repair: None

WELDMENT QUALITY

- Inspection Methods
  - Visual
  - Radiographic, Mil-Std-453
  - Penetrant, Mil-I-6866
- Acceptance Levels
  - External
    - Weld Beads: Removed Flush
    - Underfill and Undercut: None Allowed
    - Cracks: None Allowed
    - Pores: *Maximum size 0.02-inch, one per inch
    - Mismatch: 10% of Thickness Maximum
  - Internal
    - Pores and Inclusions: *Maximum Size 50% T or 0.12 inch whichever is lesser. Maximum accumulated amount less than 2% of cross section area
    - Cracks: None Allowed
    - Lack of Fusion: None Allowed

*Sharp-tailed or crack-like indications not allowed, appropriate acceptance levels will be added.

Subpopulation Definition

Selection of appropriate subpopulations is the next step in test program planning. Obvious subpopulations or associated populations of the previous example would be alternative weld/heat-treating sequences, filler materials, welding processes, weld repair, joint thickness, and weld classes (quality level). The selection of these preplanned subpopulations is dependent upon previous knowledge of their potential effect on weldment properties. However, those mentioned are the most frequently encountered subpopulations required.

Welding Procedure

The variables defining the selected basic and subpopulations must be controlled within their prescribed ranges during test program welding. This requires welding in accordance with a referenced specification and any additional requirements which may limit the population. *The generation of this data requires that welding be conducted under production conditions rather than closely controlled laboratory conditions.* In addition, data for development of design properties must adequately represent the variation allowed in the referenced specification and/or supplemental requirements for each variable.

Weldments from which data are generated should represent the product of several welders, welding machines, and weld setups. It is advisable to select test samples from weldments produced at different times by different operators guided only by the specified requirements. Weldment characterization must be representative of final products rather than the idealized characterization used in many weld development studies.

Coupon Requirements

Considerable variation in actual coupon dimensions used within the aerospace industry has resulted in difficulties in obtaining comparative data. To provide the necessary uniform basis for obtaining weldment data, recommended configurations are presented in the following discussion.

Transverse-Weld Tensile Coupons---Two types of transverse-weld tensile coupon configurations are recommended. Flat coupons are to be used for materials up to 0.5-inch thickness. For weld joint thicknesses greater than 0.5 inch, round coupons are recommended. These two configurations are shown in Figures 14 and 15, respectively. Exact specimen dimensions are dependent on the thickness of the weldment being evaluated, but geometric similitude is maintained within each type of specimen. Appropriate dimensions are given for the reduced test section of each coupon. The dimensions of the gripping areas at each end are optional and may be modified to accommodate standard test fixtures.

The weld beads should be removed from all flat coupons since industry standards have not been established regarding weld reinforcement configuration. This requirement provides a more uniform base on which data from several sources may be combined. When data is required for welds with reinforcements intact, their configuration must be specified.

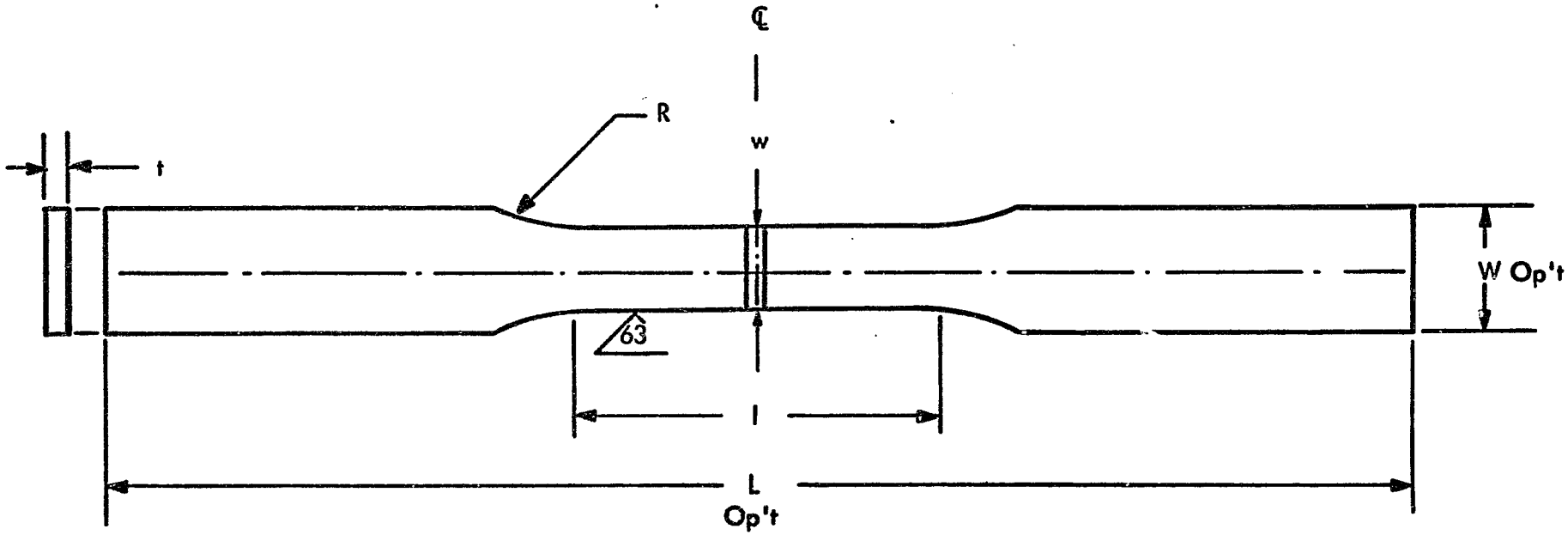

t	w	l	R
<.188	0.5	2.25	1 min.
0.188 to 0.25	0.75	3.0	1.5 min.
0.25 to 0.5	1.0	4.0	2 min.

NOTES:

1. Dimension "W" and "L" optional.
2. Weld bead on or off optional.
3. Fillet radii must fair smoothly into reduced section.
4. Material and grain direction per test requirements.
5. Specimens warped from welding or heat treatment shall not be straightened.
6. Reduced section machined surfaces 63 .
7. The reduced section and grip ends must be symmetrical about the longitudinal ℄ within ± 0.01.
8. Tolerances except otherwise noted: Linear ± 0.03, Angular ±1°.

Figure 14: FLAT TRANSVERSE-WELD TENSILE COUPON

63

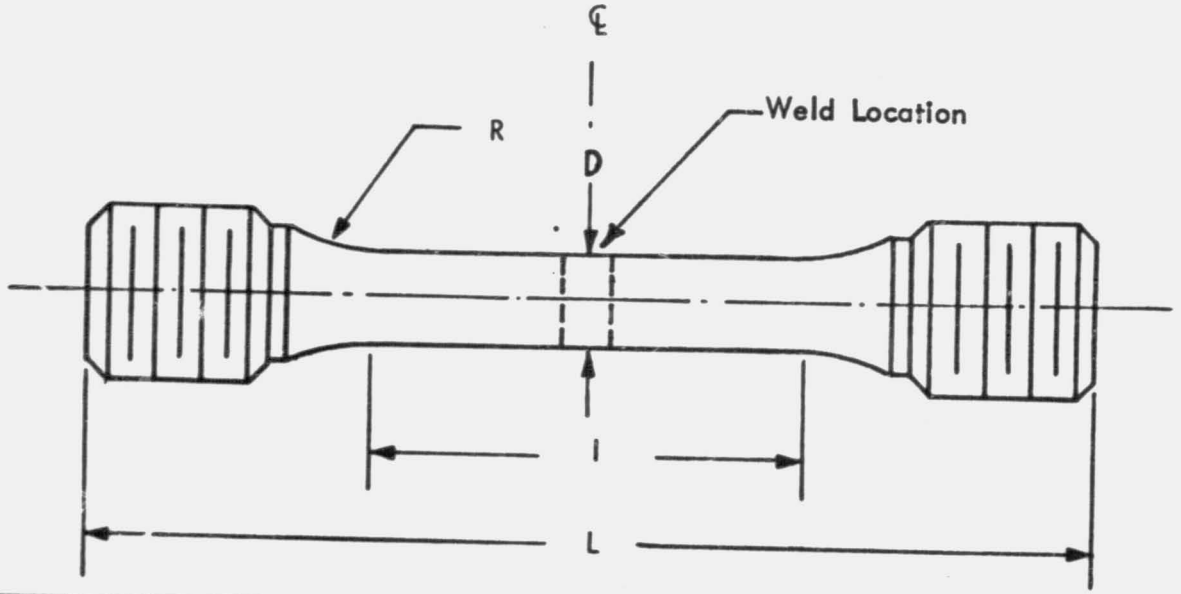

D	l	R
0.250	1.25	0.250
0.505	2.0	0.50

NOTES:

1. Dimension "L" and thread size optional.
2. Fillet radii must fair smoothly into reduced section.
3. Reduced section machined surface 32
4. Heat treatment to be performed prior to finish machining.
5. The reduced section and grip ends must be symmetrical about the longitudinal ℄ within ± 0.01.
6. Tolerances except otherwise noted: Linear ± 0.03, Angular ±1°.

Figure 15: ROUND TRANSVERSE-WELD TENSILE COUPON

When round coupons are used in thick weldments, location within the weldment becomes an additional variable which must be described and associated with the data.

Other Weldment Coupons---At present, coupon configuration requirements for the evaluation of properties other than transverse tensile have not been sufficiently defined to be utilized on an industry-wide basis.

Due to the nature of fatigue testing, no specific test configurations are recommended. Configurations selected according to standard base metal practices have been used which may be satisfactory. Weld reinforcements are of particular significance in fatigue testing and should be removed or specified in detail along with a description of the coupon used.

Fracture toughness coupons should conform to the latest requirements defined by the ASTM recommended practice. Crack location with respect to the weldment is of particular importance, and the criteria for validity of the specimen must be met.

The coupons used for evaluation of other weldment properties, such as fillet-weld shear strength and creep or stress rupture, also require definition in order to be used for industy-wide design strengths.

Testing Procedures

The availability of accepted test methods for base metal evaluation, as evidenced by federal and ASTM standards, has resulted in their general application to testing of weldments. Tensile testing per Federal Test Method Standard 151 is recommended. These standards control test equipment, data accuracy, and loading rates. Reference to existing base metal test methods are generally considered satisfactory for mechanical property testing of weldments except for the configuration definition. The testing practice and any deviations should be reported when data samples are generated. In no case may a test result be discarded on the basis of a defect found after final inspection---for example, during posttest examination of the fractured surfaces.

Minimum Data Requirements

The quantity of data that must be collected or generated depends upon the population definition and the basis on which it is to be analyzed. The bases fall into two categories: data to be statistically analyzed, and data to be presented on an average basis as defined under "Data Treatment."

Statistical Sample Requirements---The data sample must be adequate to determine the form and distribution of the population from which it was drawn. If the weldment population definition is broad and allows considerable latitude in the range of parameters defined, it is obvious that larger sample sizes will be required. Certain minimum requirements can be stated, however, based on statistical considerations.

For data to be directly analyzed on a statistical basis, a typical weldment population exhibiting nearly normal distribution characteristics should

be represented by a sample containing a minimum of 100 observations. These observations should include at least 10 subsamples representing random variables such as base material lots, filler material lots, weld processing variables, and weld machine operators and setups.

Direct analysis of a data sample that is not normally distributed requires at least 300 tests to adequately define minimum strengths. As in the previous case, these observations should be representative of the total population.

Where subpopulations are defined, the above minimum data requirements apply to each subpopulation which shows a significant difference in properties.

At least 10 pairs of measurements should be used for an indirect analysis based on derived ratios. These paired observations should represent the range of variables in the specified population. If broad ranges in parameters are involved, additional observations may be required.

Average Sample Requirements---No specific data requirements have been established for properties presented on an average basis, but some general considerations are given.

Due to the number of variables inherent in a welding process, it is advisable to make as broad a sampling as practicable within the population definition. The range of material and processing parameters included in the sample will obviously influence the sample size. The total number of observations should be sufficient to identify factors that may be significant within the population such as joint thickness, weld repair, filler material, and heat-treat condition.

DATA TREATMENT

The procedures used in the analysis of test data should be based on uniform techniques that lend themselves to obtaining meaningful results while permitting some variation in approach based on decisions which are not completely arbitrary. Certain concepts have been used in this framework for base metal analyses which lend themselves to analysis techniques for weldments. The guidelines established for analysis of data for inclusion in Reference 1, as presented in Reference 26, are used as a basis for the development of analysis techniques applicable to mechanical property data for weldments.

The exact procedures used for the analysis of test data may vary from one sample to another depending on the type and quantity of data. Selection of the appropriate procedure requires a number of decisions that can best be illustrated by the flow chart shown in Figure 16. These decisions fall into the following categories:

1) Determine the basis on which the data will be presented;

2) Establish the population to which the properties apply;

3) Determine the procedure for computations;

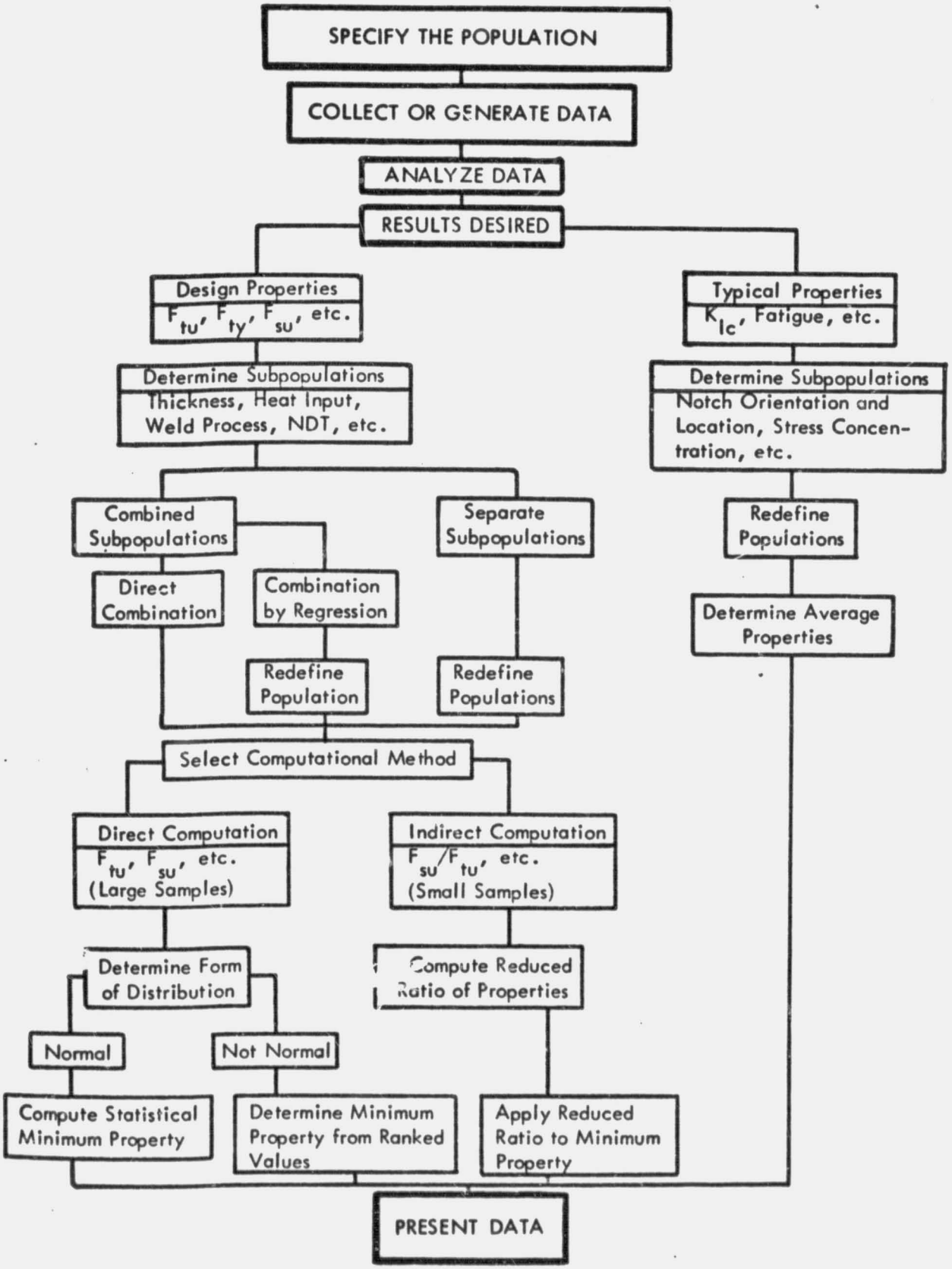

Figure 16: FLOW OF DATA FOR ANALYSIS

4) Perform the computations.

These items are described in greater detail in the following sections.

Selection of Data Basis

The end results desired and the type and quantity of data available are the major factors in selecting the data basis. Certain properties, such as fracture toughness and fatigue, are usually presented on an average basis. For tensile ultimate strength properties, minimum design strengths at stated reliability levels are desired.

The selection of the data basis must be consistent with the quantity of data available and the manner in which it represents the specified population. Calculation of statistical minimum values from a sample that does not adequately represent all of the parameters allowed in the specified population may result in values which are not valid for the intended basis.

To provide weldment data for aerospace applications consistent with the assurance levels associated with design strengths in Mil-Hdbk-5, all data should be presented on one of the following bases:

A Basis---The value above which at least 99% of the population of values is expected to fall, with a confidence of 95%.

B Basis---The value above which at least 90% of the population of values is expected to fall, with a confidence of 95%.

S Basis---The minimum value specified by the governing specification. The statistical assurance associated with this value will depend on the quality control requirements of the specification.

Average Basis---The property is an average value. No statistical assurance is associated with this value.

Population Identification

For computational purposes, the population definition must be restrictive enough to ensure that the computed properties are realistic and useful. This requires the establishment of the range of conditions for which the mechanical property can be characterized by a single distribution. The general procedure for specifying a population has been previously given; however, the analysis of data may indicate that further refinement is necessary.

The specified population will include the more obvious factors such as base material, filler material, heat-treat condition, and weld process; but less obvious factors such as joint thickness, heat input, and welding position may require further evaluation. When previously unspecified parameters or parameters that have a broad range appear to be significant, the data should be grouped in appropriate subpopulations prior to further analysis. For data to be presented on an average basis, the apparent subpopulations should be defined and presented with the data. To resolve the significance of these

subpopulations in a sample to be analyzed for minimum properties, appropriate statistical tests of significance should be performed on the respective groups of data.

The statistical tests of significance are conducted for specific confidence levels and provide a sound basis for decision-making. Data groups showing no significant differences may be combined for further analysis. If differences exist, the subpopulations representing the data groups should be defined and the groups analyzed separately. The minimum strength representing the total population is determined from the subpopulation exhibiting the lowest strength.

In some cases, properties may vary continuously with some characteristic such as thickness. A correlation may be established between the property and the characteristic through regression analysis. The use of regression analysis provides a tool whereby the data groups may be recombined for further analysis.

Computational Concepts

The development of average property values requires only the calculation of the average property. If the range of values for the property varies more than ±5% from the average value, it is advisable to report the range as well. No statistical confidence is associated with this value.

Two statistical concepts may be logically applied to the analysis of weldment data. The first concept requires a direct statistical analysis of data to arrive at design properties of stated reliability. The second concept uses an indirect computational method whereby the properties of interest are established through their relationship to a property for which direct calculations are available. The statistical regression analysis is usable with either of these concepts.

Direct analysis requires relatively large amounts of data. This technique requires sufficient data to describe the form of the distribution as well as its dispersion characteristics. The form of the distribution is determined on a statistical basis by applying the chi-squared test for normality. For populations exhibiting nearly normal behavior, the computational procedures for the normal distribution are used. If the distribution is not normal, a nonparametric analysis is used which assumes a random selection of data points and uses a ranking of the individual values to arrive at the required minimum value.

The indirect analysis operates on ratios of paired properties. This procedure requires the pairing of values determined for the property being evaluated with a corresponding property for which a direct statistical distribution is known. A statistical analysis is performed on ratios of the paired observations to arrive at a reduced ratio at a stated confidence level. This reduced ratio is applied to the minimum value for the known property to derive the appropriate minimum value for the required property. Proper selection of confidence limits gives derived property values of approximately the same assurance levels as for the direct property. This procedure is applicable for relatively small data samples. As few as 10 pairs of measurements may be used if the data adequately covers the range of parameters inferred in the population definition.

The large data samples required for direct statistical analysis will usually limit its use to tensile ultimate strength of weldment coupons. The indirect analysis may be used to derive other properties of interest using smaller samples. One example would be to derive the minimum shear strength for the cases where only the tensile distribution is known; one would operate on the ratio SUS/TUS in this case.

The indirect computation method also provides a tool for rational development of weld factors to be used in translating coupon-derived minimum properties to hardware design. In this case, the ratio of hardware failure stress to control coupon failure stress is used as discussed under use of design data.

Computational Procedures

The computational procedures used for the development of minimum design strengths for weldments in aerospace structure should result in values consistent with the assurance levels associated with design strength values in Reference 1. As such, the computational procedures and statistical assurance limits required are consistent with those presented in Reference 26. Reference to AFML-TR-66-386 will provide examples in the use of the various computational forms and values for the statistical factors needed for the computations of: (1) direct computation for the normal distribution; (2) direct computation for the unknown distribution; and (3) indirect computation of property values.

DATA PRESENTATION

The presentation of data on weldments is complicated by the lack of welding specifications suitable for reference. In lieu of these specifications, a description of the pertinent welding conditions must be given in association with the property data. This may be cumbersome in some regards; however, it is necessary in order to provide meaningful and useful engineering data.

A minimum number of welding conditions should be shown in the data presentation for each basic population of weldments considered. These would include the conditions of major significance to the potential users of the data. In the population definition discussion, the many potential welding variables were discussed. Among these many variables, the following variables are the minimum that should always be specified where applicable:

1) Alloys,
2) Weld heat-treat conditions,
3) Filler materials,
4) Welding processes,
5) Weld repairs,
6) Joint thicknesses,
7) Joint types,
8) Weld quality levels,
9) Welding method, i.e., manual or mechanized.

Since the data presented are based on coupon-derived results, it is also necessary to provide comments on use of the data in structural design.

Introductory Information

When weldment data is presented it should include introductory comments to aid designers in selecting appropriate welding processes or conditions. In addition, comments alerting a designer to possible fabrication problems or environmental effects should be included. These may include: (1) potential weld heat-treating sequences for the alloy; (2) applicable welding methods; (3) comments on weldment properties; (4) discussion of pertinent welding process variables such as heat input sensitivity or restrictions, preheat requirements, atmospheric contamination, and significant metallurgical phenomena.

Room Temperature Properties

Data on room temperature properties of weldments are presented in tabular form as illustrated in Table V. The table describes base material, welding variables, and weld character conditions that the data represents, as well as the properties of interest. As footnotes to this table, the additional information required to describe these conditions is presented. Precautionary notes for use of the data in design also must be given, and are discussed below.

Data on Effect of Temperature

A typical effect-of-temperature curve of weldment properties is shown in Figure 17. This type of curve would be presented in conjunction with room temperature properties and would reference the welding conditions and precautionary notes of the room temperature case.

Use of Design Data

As a footnote to the coupon-derived design data, it is necessary to present precautionary notes on the use of the data in structural design. It is recognized that coupons may not fail under load in the same manner as a structure. This lack of one-to-one correlation may be due to either differences in weldment character resulting from the potentially higher variability of production welding or state of stress. Coupon-structure ratios are used to account for these differences.

Correlations developed using the ratioing techniques described in the computational concepts discussion may be used to determine appropriate ratios. The determination of an adequate design requires the application of the appropriate structure-coupon ratio to the coupon-derived property.

Table V: TYPICAL FORMAT FOR PRESENTATION OF ROOM TEMPERATURE PROPERTIES OF WELDMENTS

Material	Material Thickness	Weld Joint Type	Filler Wire Alloy	Heat Treat After Welding	Properties [1]				
					F_{tu} [2]		F_{tu} [3]		Other Properties or → → Welding Conditions
					A	B	A	B	
6061-T4	Up to 0.30 Above 0.30	Sq. Butt Groove	4043 4043	Aged to T6					
6061-T4 6061-T6	Up to 0.30 Above 0.30	Sq. Butt Groove	4043 4043	As-Welded					
6061-F	Up to 0.30 Above 0.30	Sq. Butt Groove	4043 4043	Sol. HT and Age to T6					

[1] These coupon-derived properties are subject to the usage limitations discussed under "Use of Design Data."

[2] For the following welding conditions - - - - - -

[3] For the following welding conditions - - - - - -

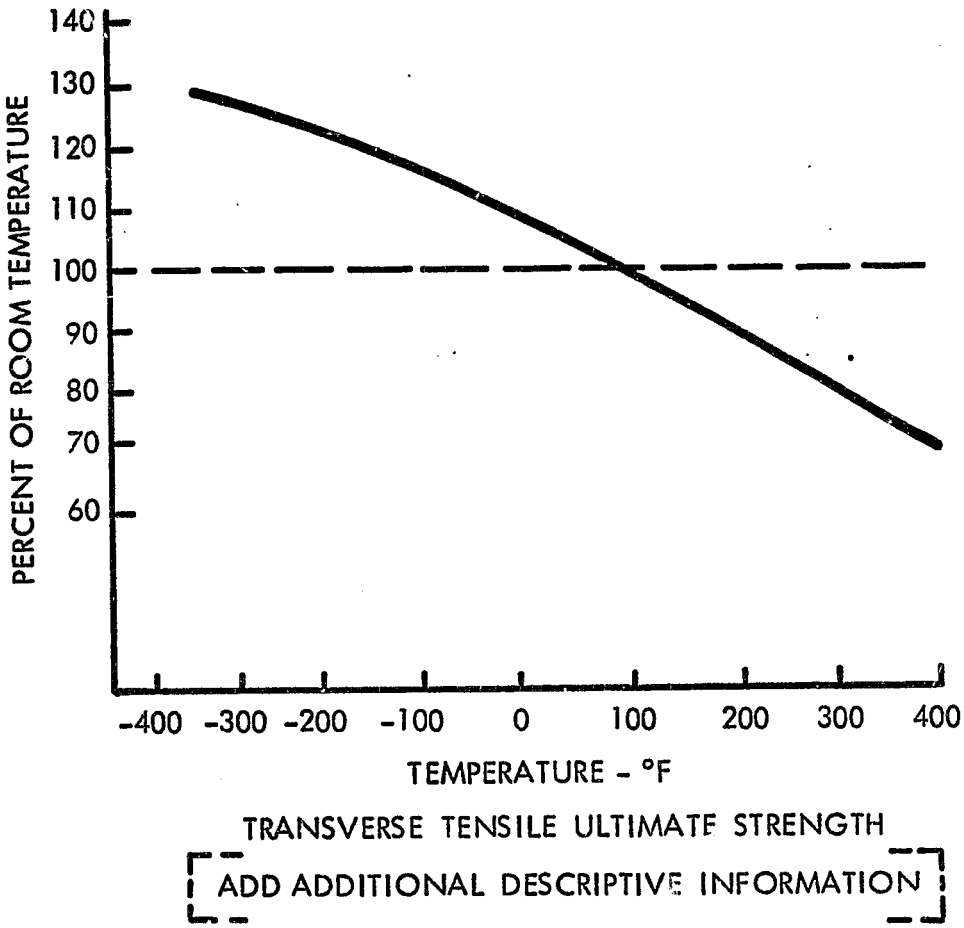

Figure 17: TYPICAL EFFECT OF TEMPERATURE PRESENTATION

END OF REFERENCE

83

REFERENCE

84

ARNETT, R. W.; WARREN, K. A.; AND MULLEN, L. O.: OPTIMUM DESIGN OF LIQUID OXYGEN CONTAINERS. WADC REP. TR 59-62, WRIGHT-PATTERSON A. F. BASE, (PB-181108), 1961.

ASAPRL
63, 152

TECHNICAL REPORT 59-62

DO NOT DESTROY
RETURN TO
TECHNICAL INFORMATION LIBRARY
ASAPRL

FILE COP

OPTIMUM DESIGN OF LIQUID OXYGEN CONTAINERS

ROBERT W. ARNETT
KEITH A. WARREN
LEWIS O. MULLEN

CRYOGENIC ENGINEERING LABORATORY
NATIONAL BUREAU OF STANDARDS

Wright-Patterson
Technical Library
Dayton, Ohio

AUGUST 1961

AERONAUTICAL SYSTEMS DIVISION

NOTICES

When Government drawings, specifications, or other data are used for any purpose other than in connection with a definitely related Government procurement operation, the United States Government thereby incurs no responsibility nor any obligation whatsoever; and the fact that the Government may have formulated, furnished, or in any way supplied the said drawings, specifications, or other data, is not to be regarded by implication or otherwise as in any manner licensing the holder or any other person or corporation, or conveying any rights or permission to manufacture, use, or sell any patented invention that may in any way be related thereto.

Qualified requesters may obtain copies of this report from the Armed Services Technical Information Agency, (ASTIA), Arlington Hall Station, Arlington 12, Virginia.

This report has been released to the Office of Technical Services, U. S. Department of Commerce, Washington 25, D. C., for sale to the general public.

Copies of ASD Technical Reports and Technical Notes should not be returned to the Aeronautical Systems Division unless return is required by security considerations, contractual obligations, or notice on a specific document.

WADC TECHNICAL REPORT 59-62

OPTIMUM DESIGN OF LIQUID OXYGEN CONTAINERS

ROBERT W. ARNETT
KEITH A. WARREN
LEWIS O. MULLEN

CRYOGENIC ENGINEERING LABORATORY
NATIONAL BUREAU OF STANDARDS

AUGUST 1961

DIRECTORATE OF AEROSPACE GROUND EQP ENGR
AF DELIVERY ORDER 33(616)56-15
PROJECT No. 8610

AERONAUTICAL SYSTEMS DIVISION
AIR FORCE SYSTEMS COMMAND
UNITED STATES AIR FORCE
WRIGHT-PATTERSON AIR FORCE BASE, OHIO

McGregor & Werner, Inc., Dayton, O.
500 - November 1961 - 9-283

ABSTRACT

The basic parameters influencing the design of liquid oxygen containers are considered and their design interrelation evaluated. Factors considered include materials, configuration, insulation, support members, instrumentation, valves, piping, weight, evaporation loss, and accessory items such as vacuum pumps and transfer hoses. Means for evaluating and optimizing the combination of the various factors are presented together with experimental work conducted in areas where information was lacking. Description of the design and construction of a liquid oxygen container together with the thermal test results on the container is included.

PUBLICATION REVIEW

This report has been reviewed and is approved.

FOR THE COMMANDER:

Allen M. Paulson

ALLEN M. PAULSON
Chief, Gas Servicing Branch
Servicing Equipment Division
Directorate of Aerospace Ground Eqp Engr

While the polystyrene and resin epoxy foams did not reach a minimum until the end of the indicated pumping period virtually all of the improvement in the isocyanates was realized in 3 to 5 days. This result is logical since the isocyanates were each sold as open-celled foams while the other two were of the closed cell variety. These tests were conducted with a dynamic vacuum and it is probable that a pressure increase would result under static vacuum conditions.

Another factor which affects the use of foams in LOX vessels is the combustion hazard since saturation with oxygen gas and/or liquid oxygen may occur. A sample of the rigid isocyanate, when tested in the same apparatus as the perlite-aluminum powder mixtures (Figure 48), ignited immediately and completely in an explosive manner.

Results of these tests show the foams tested to be unsuitable for use with LOX and of limited value for insulation of other liquefied gas containers.

PROPERTIES OF EVACUATED PERLITE

Perlite-Aluminum Powder Mixtures

Work down in the laboratory here has established the desirability of adding aluminum powder to evacuated powders to achieve a reduction in mean thermal conductivity. The possibility of leaking oxygen saturating the insulating medium raises the danger of combustibility of such a mixture.

To determine the extent of this danger the apparatus shown in Figure 48 was used. In this equipment the mixture being tested (C) is supported on a bed of +30 mesh perlite (D) which is in turn supported on a glass fiber cloth (E) and 100 mesh Monel screen (F). The test chamber is sealed to the walls with an asbestos packing (H). Pure oxygen gas is introduced through tube (G) and passes up through the sample and support medium. Sufficient time is allowed to permit oxygen to permeate the sample (10 minutes or more) at which time a hot nichrome wire (A) is lowered into contact with the sample. This wire is made of 18 turns of No. 22 gauge helically wound nichrome heater wire. Fifty watts of electric power is dissipated in the coil heating it to a point just below the melting point of the wire. Results are shown in Table 10. The term "some" in the combustion column indicates local burning in close proximity to the wire while "complete" indicates that burning initiated by the coil propagated throughout the body of the sample.

Minimum values for conductivity for some powder mixtures are closely approached for concentrations of 20% aluminum powder by weight

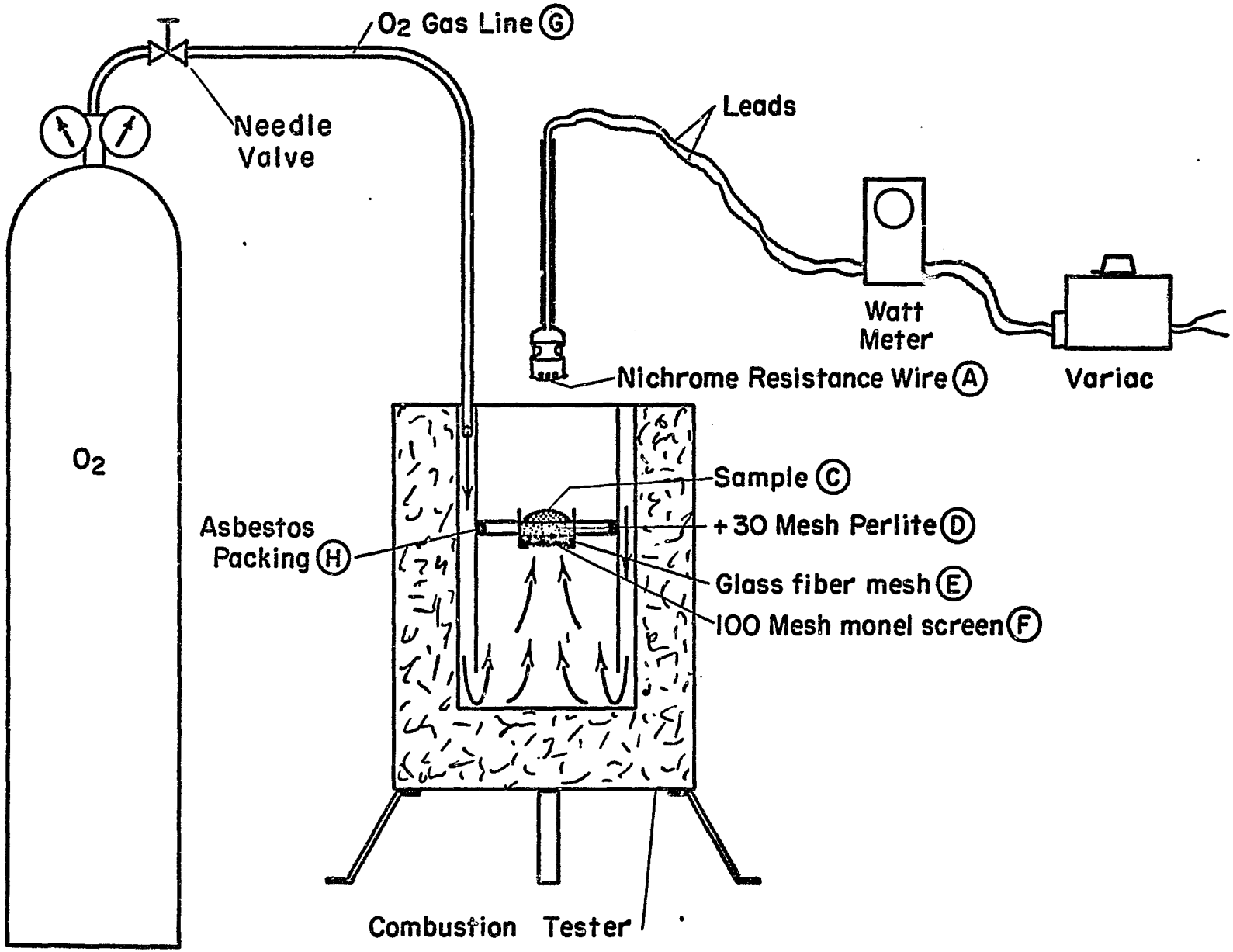

Figure 48. Combustion Test Apparatus

Table 10

Test No.	Mixture	Combustion	Comment
1.	10% Baker Al.[1] 90% perlite[2]	None	Wattage increased till nichrome wire element failed.
2.	15% Baker Al. 85% perlite	None	element failed
3.	20% Baker Al. 80% perlite	None	element failed
4.	25% Baker Al. 75% perlite	Some	element failed
5.	30% Baker Al. 70% perlite	Complete	
6.	35% Baker Al. 65% perlite	Complete	
7.	30% Baker Al. 70% perlite	Complete	
8.	25% Baker Al. 75% perlite	Some	element failed
9.	30% Alcoa Al.[3] 70% perlite	None	element failed
10.	50% Alcoa Al. 50% perlite	None	element failed
11.	75% Alcoa Al. 25% perlite	Complete	Propagated slowly but completely.

(1) Baker USP aluminum powder, lot 4776, (cleaned)
(2) -30 mesh perlite from Persolite Product, Inc.
(3) Alcoa aluminum pigment No. 123.

or less. As seen in Table 10 this appears to be safely below the combustion point.

From the above results it is concluded that no combustion danger exists if suitable mixtures are utilized. A low aluminum percentage is also desirable from the viewpoint of insulation weight.

Load Carrying Ability

One of the major sources of heat leak into a liquefied gas storage vessel is that due to heat conduction along the supporting members. Two of the most obvious methods for reducing this heat leak are, (1) Use of a material with reduced thermal conductivity, and (2) reduction of the area of heat path. The first of these methods is discussed in a presentation on possible support member materials appearing elsewhere in this report. The second method is more difficult to achieve, particularly when high shock load conditions are to be encountered.

One method which appears promising in vessels which utilize evacuated powder type of insulation is to use the powder as a load carrying medium. Evaluation of the load carrying ability of evacuated perlite was therefore undertaken.

Apparatus

Determination of the load carrying ability of evacuated perlite was made with the apparatus shown in Figures 49 and 50. The chamber (A) is an 8 inch I. D., 1/4 inch wall brass tube closed on one end with a soldered plate and provided with an O-ring flange on the other, a 3/4 inch diameter opening closed with a rubber stopper and protective cap in provided in the wall near the bottom for filling the chamber with powder. A 2 1/4 inch diameter cylinder is soldered through the center of the top cover plate. Through the cover plate, to the side of cylinder, is a 3/4 inch diameter vacuum pump connection fitted on the underside with a screen and glass wool filter.

An O-ring sealed piston with extension shafts to fit the cylinder was made from one piece of brass. The lower shaft passes through a Teflon packed wiper gland in the bottom of the cylinder. Another O-ring seal is used through the removable cylinder cap which is screwed to the cylinder and sealed with a flat neoprene gasket. The end of the top extension shaft is fitted with an adjustable button. Four 3/8 inch tubes pass through the cylinder cap. One of these is used to transmit the pressure existing on the top of the piston to a calibrated absolute pressure gauge. The other three tubes are connected through a 1 inch ball type quick opening valve (C)

END OF REFERENCE

84

REFERENCE

85

OLSON, R. E.: SAFETY AND DESIGN CONSIDERATIONS FOR GAS STORAGE VESSELS. M-64-137, MARTIN CO., AUG. 1964.

M-64-137

Copy No. 55

SAFETY AND DESIGN CONSIDERATIONS FOR GAS STORAGE VESSELS

330 EV
16 2 SB
82 8 PR

Authors

Richard E. Olson, Senior Design Engineer

Albert J. Finger, Product Safety Specialist

MARTIN COMPANY
Denver, Colorado
Aerospace Division of Martin-Marietta Corporation

CONTENTS

	Page
Contents	ii and iii
Introduction	1
I. Stored Energy	2
II. Fragmentation	6
III. Physiological Damage	7
IV. Design Considerations	9
V. Safety Considerations	10
References	14
Bibliography	14
Distribution	

Figure

1	High-Volume Low-Pressure Tank Failure Showing Tearing and Shredding Effect of Stored Energy Release	3
2	Top Half of 10-cu ft Sphere: Stored Energy Caused this Portion to Travel 250 ft in Air and 150 yd after Deforming Heavy Structural I-Beam on Facility Roof	6
3	Test Facility Damage from Shock Overpressure Caused by Weld Failure on 10-cu ft Sphere at Approximately 6000 psi: Sphere Broke in Two Halves with Little or No Fragmentation	10

Table

1	Nomogram for Demonstrating Magnitude of Blast Hazard from Equivalent Weights of TNT	5
2	Probability of Fatality and Injury from Shock Overpressure	7
3	Energy Equivalent Table	12
4	Pressure and Volume Conversions	13

INTRODUCTION

Pressurized gas storage tanks have been recognized for some time to represent a large energy potential.

The arrival of the missile and the space age brought with it the need for tanks with lightweight structure and necessarily lower safety factors. An increased safety hazard came with the lower safety factors.

The fact that these vessels represent a "Big Bomb" is not sufficient information to establish safe operating procedures for testing. First, the magnitude of the hazard must be defined.

The purpose of this report is to establish a simplified method for determining the potential hazard. Design and safety considerations will also be presented.

I. STORED ENERGY

Pressure storage vessels of low safety factor, as used in airborne missile and space vehicle pressure systems, present an extreme safety hazard. Because of the necessary lightweight characteristics of the vessel structure, any damage to the thin skin can cause the pressurized vessel to disintegrate with a large energy release. This energy release can create a shock overpressure similar to that created by a chemical explosion, although no chemical reaction takes place.

The amount of energy release is a function of the quantity of gas contained in the vessel. Because of this, a high-volume low-pressure vessel can contain an equal amount of energy as a low-volume high-pressure vessel (Fig. 1). The potential energy available in a pressurized vessel can be equated to the energy constant of TNT. As an example: a 1940-cu ft vessel at 10 psi will contain the same amount of energy as a 2-cu ft vessel at a pressure of 3000 psi (3.5 lb of TNT).

The rapidity with which the energy release takes place is an important consideration. This can vary with vessel size, shape, wall thickness, and fabrication methods. For the purpose of illustrating the magnitude of the hazard, the extreme case of instant and total removal of gas confinement will be used. The sudden release of energy is transmitted through the air in the form of a shock wave, formed by the sudden displacement of the air surrounding the vessel. The shock wave carries with it a measurable overpressure varying with the intensity of the initial displacement. The shock overpressure diminishes rapidly as the distance from the point of generation increases, and will degenerate into a sound wave as the overpressure approaches zero. The effect is similar to that of a chemical explosion. A large leak would dissipate the same amount of energy, but without the explosive effect.

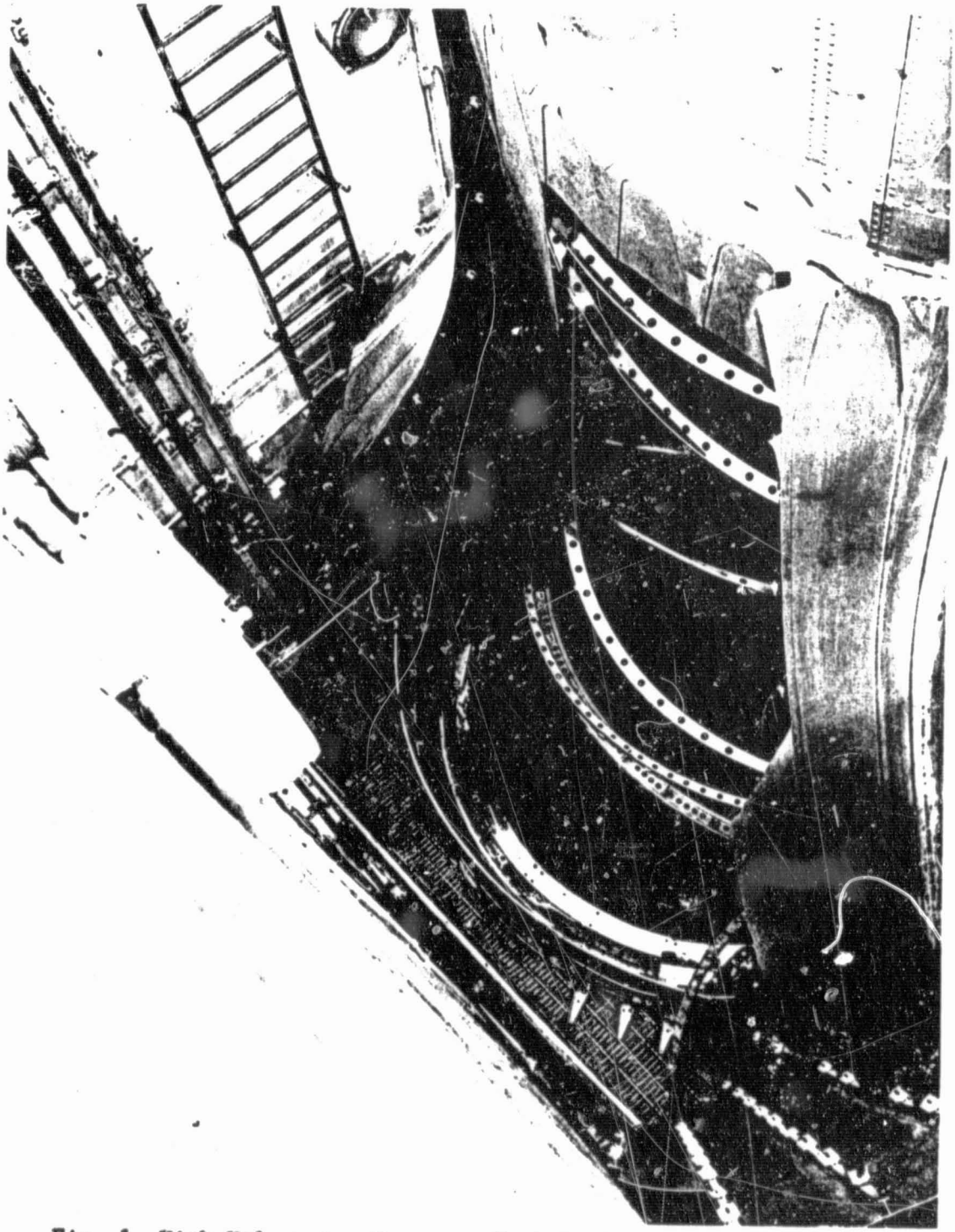

Fig. 1 High-Volume Low-Pressure Tank Failure Showing Tearing and Shredding Effect of Stored Energy Release

The hazard potential or TNT equivalency of a pressurized vessel is determined by the calculation of the amount of energy available from the explosive expansion of a volume of compressed gas:

$$E = 454 \left[\frac{V\left(\frac{P_1}{P_2}\right)\left(\frac{T_1}{T_2}\right)}{359}\right] RT \ln\left(\frac{P_1}{P_2}\right),$$

where

E = energy (calories),

P_1 = the original (absolute) pressure of the compressed gas,

P_2 = final or atmospheric pressure,

R = molar gas constant (1.987 cal/gm-mole °K for an ideal gas),

V = pressure vessel volume,

T_1 = ambient air temperature (°K),

T_2 = temperature of the compressed gas (°K).

The standard for energy release is set at 1,000,000,000 cal/ton of TNT or 1,140 cal/gm.

Once the energy equivalent has been established, minimum safe distance for nonoperating personnel can be computed, using overpressure data from reference TNT explosions (Table 1).

E- 8033

Fig. 5-9. Nomogram for Magnitude of Blast Hazard from Equivalent Weights of TNT * (Ref. 107, p. 5)

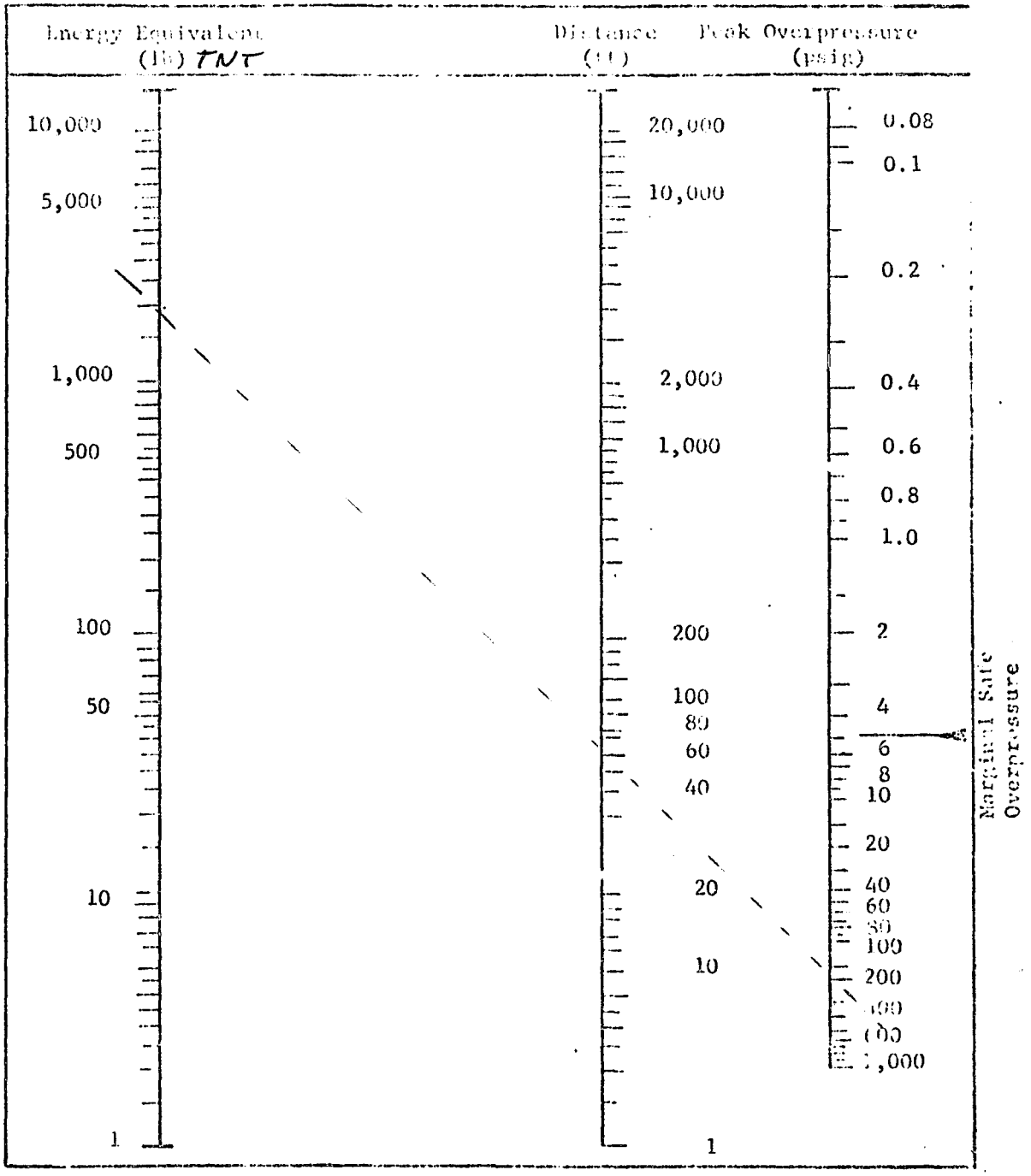

* A missing factor (energy equivalent, distance, or peak overpressure) can be determined by locating the two known factors on the scales. Connect these points with a straight line. The point of intersection of this line and the third scale determines the missing factor.

II. FRAGMENTATION

Very little data exist on fragmentation as associated with exploding pressure vessels.

In an analysis of an actual explosion (Ref 1), it was estimated that approximately 10% of the available energy is used in deforming the tank structure and imparting a velocity to the resulting fragments. The initial velocity of a given fragment can be estimated from this information. However, since the behavior of the particles will vary with vessel, size, shape, wall thickness, method of construction (Fig. 2), and to some degree, atmospheric conditions, the fragmentation hazard magnitude is entirely unpredictable. Because of this, adequate protection for personnel and operating equipment must be provided.

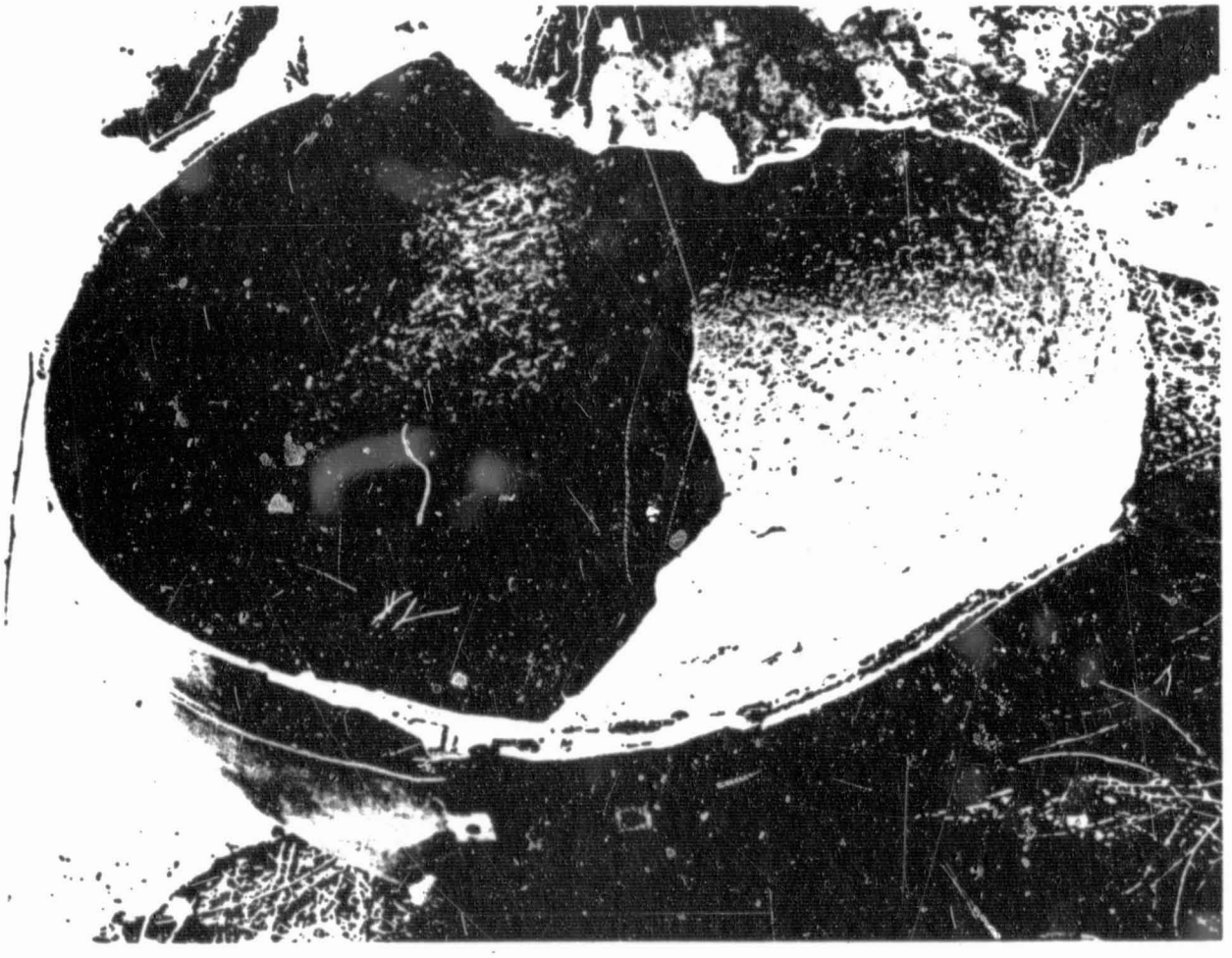

Fig. 2 Top Half of 10-cu ft Sphere: Stored Energy Caused this Portion to Travel 250 ft in Air and 150 yd after Deforming Heavy Structural I-Beam on Facility Roof

III. PHYSIOLOGICAL DAMAGE

Laboratory tests and field studies have established that the maximum allowable shock overpressures a human can safely be subjected to is a 5-psi stagnation overpressure. These studies have also indicated that when the pressure rises rapidly, a peak overpressure as low as 35 psi with a duration of 400 msec could cause death in human beings. Damage to lungs can occur as low as 6 to 7 psi and eardrum rupture will occur with a 50% probability between 20 to 30 psi. Damage to eardrums can occur as low as 6 psi. Probability of fatality and injury from shock overpressure are shown in Table 2.

Table 2 Probability of Fatality and Injury from Shock Overpressure

Blast Effect	Limiting Criteria	Threshold Overpressure (psi)
Primary	99% Probability of Fatality	55 to 65
	50% Probability of Fatality	45 to 55
	1% Probability of Fatality	35 to 45
	Lung Damage	15
	Eardrum Rupture	5
Secondary	Penetration into Abdomen	115 fps for a 10-gm Glass Missile
	Nonpenetrative Skull Fracture	10 fps for a 10-lb Masonry Missile
Tertiary	Skull Fracture from Impact	10 fps for Displacement of a 160-lb Man

*The minimum overpressure at which a 160-lb man can attain a velocity of 10 fps has been determined to be 3 psi for a man standing face-on and 5 psi for a man standing side-on (Ref 2).

Primary effects include injuries resulting from air pressure changes caused by primary pressure release and its reflections from stationary objects.

Secondary effects include injuries that follow the impact of penetrating and nonpenetrating missiles energized by the pressure release.

Tertiary effects stem from the physical displacement of a man by the blast and subsequent impact on stationary objects.

Damage as a result of the impact of a large fragment on a man occurs at velocities of 10 fps. Damage from small fragments is encountered in areas where these fragments can attain velocities over 115 fps.

IV. DESIGN CONSIDERATIONS

The safe operation of any system begins with the designer. Several basic considerations the designer must make if he is to achieve this goal are:

1) Not specify leak checks or other operations in which personnel are involved when pressures are at a level greater than operating pressure or one-half design burst pressure, whichever is lesser;

2) Specify proof pressure checks to a value no less than 150% of maximum expected operating pressure when work near a pressurized vessel is necessary;

3) Not specify proof checks using gas as a pressure medium;

4) Provide protection that will enable pressure relief at a value not to exceed 10% of the maximum expected operating pressure when supply pressure is capable of exceeding the proof pressure of the vessel.

V. SAFETY CONSIDERATIONS

The high energy potential of airborne pressure vessels present a safety hazard that is difficult to define. Because of the thin skin and low factor of safety designed into these vessels, any damage incurred while under pressure may cause explosive disintegration (Fig. 3).

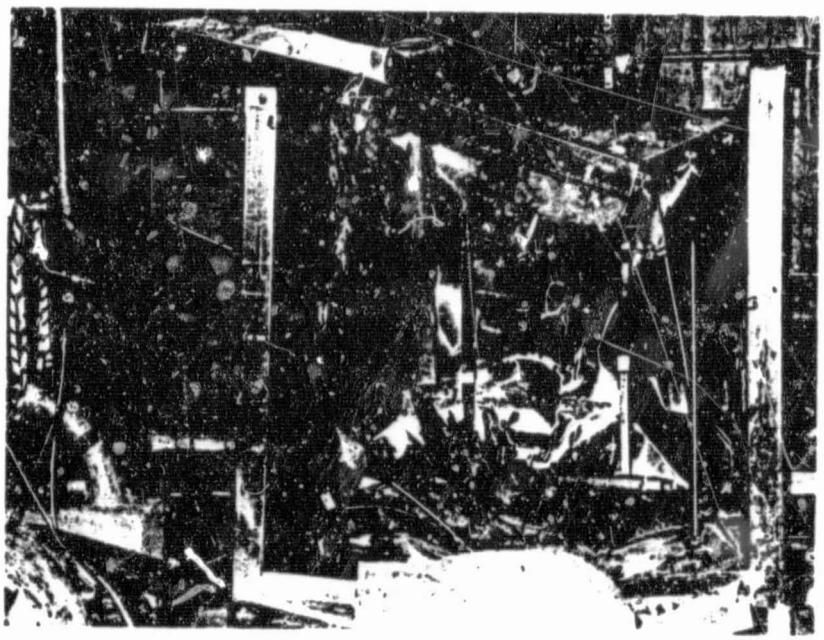

Fig. 3 Test Facility Damage from Shock Overpressure Caused by Weld Failure on 10-cu ft Sphere at Approximately 6000 psi: Sphere Broke in Two Halves with Little or No Fragmentation

Because of the necessity of testing in the operating range, strict safety requirements must be established to minimize the possibility of this occurring:

1) Under no circumstances should the maximum design operating pressure be exceeded when gas pressure testing.

2) No tests at operating pressure should be conducted until the vessel has been successfully proof tested to not less than 150% of the maximum design operating pressure. Proof testing with gas should not be specified in lieu of hydrostatic testing without complete analysis of the hazard magnitude.

3) Before proof pressure tests, no pressurization to a value greater than 12% of the intended proof pressure should be conducted. At no time should it be permissible to exceed this value in an area not specifically designated for pressure testing. Areas where access control is difficult, where minimum safe distance cannot be enforced, or where personnel congestion may exist, should not be designated for pressure testing.

4) Before gas pressure testing, a controlled area should be set up using data from Tables 2, 3, and 4. No access to controlled areas should be permitted from the time vessel pressurization begins until pressure has stabilized. The minimum stabilization time should be 10 min from the time test pressure is reached.

5) The controlled area should extend to the minimum safe distance from the outer skin of the vessel under test. If the vessel is contained within a structure, the minimum safe distance should be measured horizontally from the nearest point on that structure to the edge of the controlled area. No tools other than those necessary for testing are allowed in this area.

6) Whenever the safety factor is less than 1.5:1, no personnel access to the controlled area should be allowed until pressure has been reduced to an acceptable level. An acceptable level will be no greater than two-thirds of proven pressure capability.

7) No corrosive or hazardous liquid should be used in a pressure vessel until the vessel has been successfully tested to 150% of its designed test or operating pressure. Corrosive or flammable liquids should not be used for hydrostatic testing.

The personnel hazard is increased as the safety factor is increased. The hazard is at its minimum where a factor of safety of 4:1 or greater can be maintained. It is not necessary to restrict personnel access at this level.

Table 3 Energy Equivalent Table

Tank Pressure (psig)	Energy Equivalent per Cubic Foot of Tank Volume
10	0.001238
20	0.002711
30	0.004591
40	0.00748
50	0.00936
60	0.01277
70	0.01458
80	0.01729
90	0.0203
100	0.0230
200	0.0566
300	0.09418
400	0.1340
500	0.1787
600	0.2252
700	0.2719
800	0.3211
900	0.3710
1000	0.4150
2000	0.4937
3000	1.043
4000	2.218
5000	2.960
6000	3.650
7000	4.326
8000	5.05
9000	5.79
10000	7.53
20000	15.29
30000	22.53

Note: To obtain the pressure vessel energy equivalent, multiply the energy equivalent per cubic foot by the vessel volume in cubic feet.

Table 4 Pressure and Volume Conversions

Pressure Conversion Table					
Pounds per Square Inch (Absolute)	Pounds per Square Foot (Absolute)	Inches of Mercury	Inches of Water	Atmospheres	Kilograms per Square Centimeter
1	144	2.036	27.70	0.06804	0.07031
0.00695	1	0.01414	0.1924	0.4725×10^{4}	0.4882×10^{-4}
0.4912	70.73	1	13.61	0.03342	0.03453
0.03610	5.2023	0.07349	1	0.002538	0.002456
14.70	2116.3	29.92	407.2	1	1.0333
14.22	2048	28.96	394.0	0.9678	1

Volume Conversion Table					
Cubic Inches	Cubic Feet	Cubic Yards	U.S. Gallons	Liters	Cubic Centimeters
1	0.5787×10^{-4}	0.2143×10^{-5}	0.004329	0.01639	16.39
1,728	1	0.03704	7.481	28.32	28,320
46,656	27	1	202.0	764.6	764,600
231	0.1337	0.004951	1	3.785	3,785
6,102	0.03531	0.001308	0.2642	1	1,000

REFERENCES

1. "Effects of Gaseous Detonation Upon Vessels and Piping." Chemical Engineering Progress, Chap. 1, Sec VIII, December 1957.

2. Safety and Design Considerations for Static Test and Launch of Large Space Vehicles. Joint Air Force-NASA Hazard Analysis Board, 1 June 1962.

BIBLIOGRAPHY

Bate, L. F., Jr. and Dunkie, C. G.: Safe Distances Based on 10% and 1% TNT Equivalent Blast Effects of a Hypergolic Propellant Mixing Reaction. Report No. LV-146. Martin Company, Denver Colorado, 17 December 1962.

Kinney, G. F.: Explosive Shocks in Air.

Preliminary Analysis of Early Flight Hazards, Saturn C-5 and NOVA Vehicles. SSTG Report No. SS31.246.

Suarez, E., Fonso, A., Chambers, A. E., and Hatz, D. J.: Research on Hazard Classification of New Liquid Rocket Propellants. Vol 1. Rocketdyne Division, North American Aviation, Inc, October 1961.

END OF REFERENCE

Card #19

REFERENCE

86

LETSON, A. J.: RL10A-3-3, ROCKET ENGINE OXIDIZER PUMP DEVELOPMENT PROGRAM. REP. PWA FR-1890, PRATT & WHITNEY AIRCRAFT, 1966.

THIS REFERENCE IS MATERIAL THAT IS READILY AVAILABLE AND THEREFORE THE CONTENTS HAVE NOT BEEN REPRODUCED.

END OF REFERENCE

86

REFERENCE

87

LIQUID ROCKET ENGINE CENTRIFUGAL FLOW TURBOPUMPS,
NASA SPACE VEHICLE DESIGN CRITERIA (CHEMICAL PROPULSION).
NASA SP-8109, 1973.

NASA
SPACE VEHICLE
DESIGN CRITERIA
(CHEMICAL PROPULSION)

NASA SP-8109

LIQUID ROCKET ENGINE CENTRIFUGAL FLOW TURBOPUMPS

DECEMBER 1973

NATIONAL AERONAUTICS AND SPACE ADMINISTRATION

GUIDE TO THE USE OF THIS MONOGRAPH

The purpose of this monograph is to organize and present, for effective use in design, the significant experience and knowledge accumulated in development and operational programs to date. It reviews and assesses current design practices, and from them establishes firm guidance for achieving greater consistency in design, increased reliability in the end product, and greater efficiency in the design effort. The monograph is organized into two major sections that are preceded by a brief introduction and complemented by a set of references.

The State of the Art, section 2, reviews and discusses the total design problem, and identifies which design elements are involved in successful design. It describes succinctly the current technology pertaining to these elements. When detailed information is required, the best available references are cited. This section serves as a survey of the subject that provides background material and prepares a proper technological base for the *Design Criteria* and Recommended Practices.

The *Design Criteria*, shown in italics in section 3, state clearly and briefly what rule, guide, limitation, or standard must be imposed on each essential design element to assure successful design. The *Design Criteria* can serve effectively as a checklist of rules for the project manager to use in guiding a design or in assessing its adequacy.

The Recommended Practices, also in section 3, state how to satisfy each of the criteria. Whenever possible, the best procedure is described; when this cannot be done concisely, appropriate references are provided. The Recommended Practices, in conjunction with the *Design Criteria*, provide positive guidance to the practicing designer on how to achieve successful design.

Both sections have been organized into decimally numbered subsections so that the subjects within similarly numbered subsections correspond from section to section. The format for the Contents displays this continuity of subject in such a way that a particular aspect of design can be followed through both sections as a discrete subject.

The design criteria monograph is not intended to be a design handbook, a set of specifications, or a design manual. It is a summary and a systematic ordering of the large and loosely organized body of existing successful design techniques and practices. Its value and its merit should be judged on how effectively it makes that material available to and useful to the designer.

$$\eta_m = \frac{P_a}{P_{sh}} = \frac{\text{power available for hydrodynamic work}}{\text{shaft horsepower}} \quad (6)$$

where

P_a = shaft horsepower minus mechanical losses

The mechanical losses for pumps with impellers 10 in. in diameter or larger are very small and may be neglected. For pumps with impellers as small as 1.0 in. in diameter, the mechanical losses (seal and bearing power) may be as high as 20 percent of the shaft power.

Head coefficient ψ is a measure of headrise related to impeller discharge tip speed u_{t2}:

$$\psi = \frac{gH}{u_{t2}^2} \quad (7)$$

where

g = acceleration due to gravity

u_{t2} = impeller discharge tip speed

Figure 3 is a representative $N_s - D_s$ diagram relating N_s, D_s, η, and ψ for both centrifugal and axial flow turbopumps; additional information of this kind is presented in references 4 and 5.

2.2.1.1 CRITICAL SPEED

A basic objective in the design of rotating machinery is to avoid operation at a critical speed, i.e., a shaft rotative speed at which a rotor/stator system natural frequency coincides with a possible forcing frequency. Three important critical speeds usually are associated with a turbopump that has a shaft support system with two radial bearings: the shaft bending critical speed, and two speeds that are a function of the nonrigid bearing supports (refs. 6 through 32).

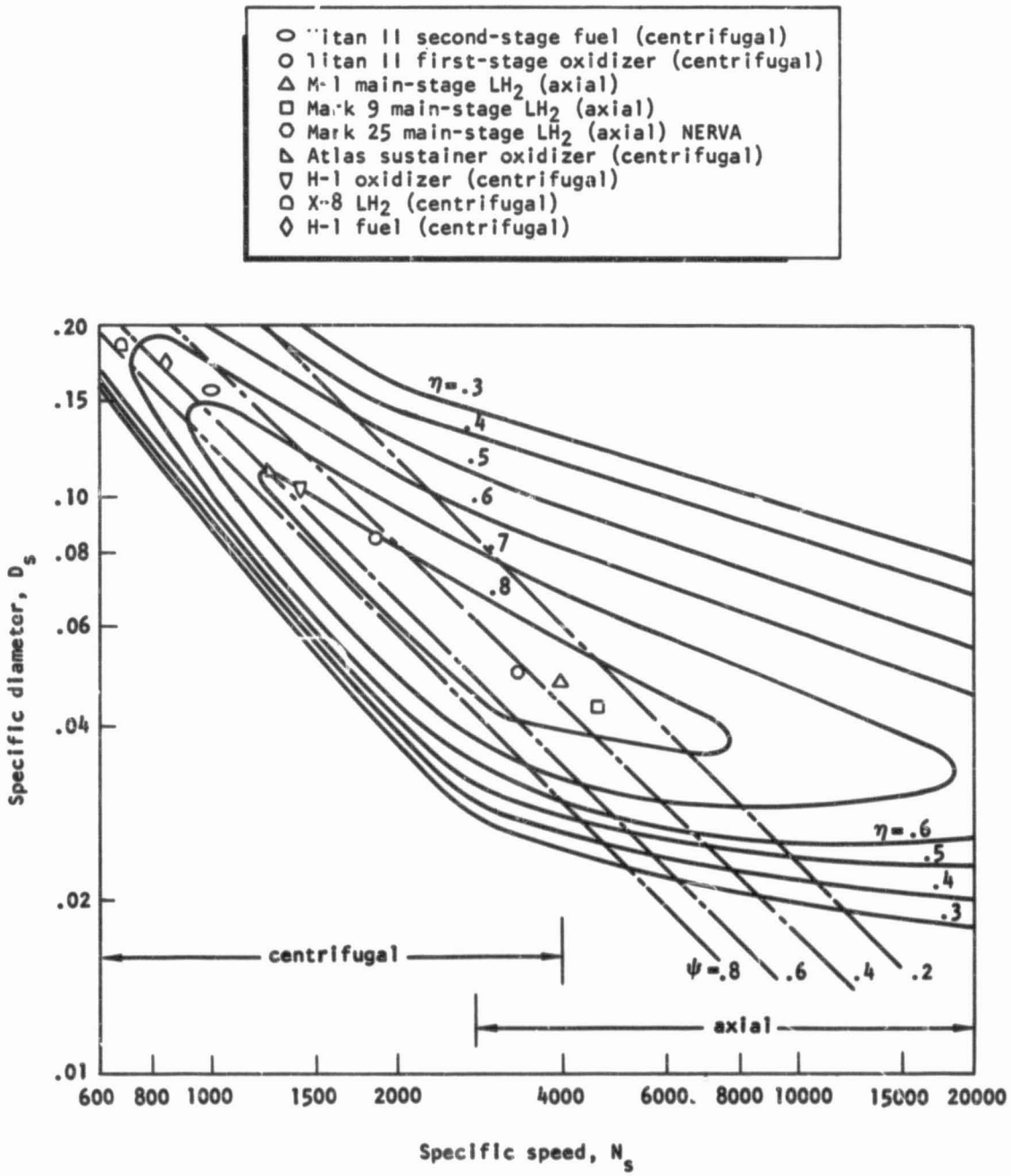

Figure 3. – Representative $N_s - D_s$ diagram for centrifugal and axial flow turbopumps.

There are two distinct design philosophies currently applied in the design of rocket engine turbopumps. In one (ref. 6), the bearing-and-shaft system is designed with all of the turbopump operating speeds kept below the first rigid-body whirl critical speed. To achieve this condition, high bearing spring rates are required. Therefore, roller bearings are often used at both ends of the shaft along with ball bearings if needed for axial thrust.

The other design philosophy (ref. 30) calls for normal pump operation above the first and second whirl critical speeds, but below any mode wherein significant shaft bending occurs. This practice requires lower bearing or bearing-support spring rates and a minimal internal looseness of the bearings. Consequently, only preloaded ball bearings are used. Duplex ball bearings are often used to increase the bearing radial-load capacity.

In both design approaches, a margin of approximately 20 percent is allowed between the shaft operating speed and the nearest calculated whirl critical speed. The disadvantages of operating liquid-hydrogen pumps below the first rigid-body whirl critical speed are the necessary high bearing spring rates and high bearing DN values; as a consequence, when the hydrogen-pump shaft transmits torque through the bearing, the bearing stresses and bearing wear tendencies generally are higher than the acceptable values. The disadvantage of operating above the first rigid-body whirl critical speed is the possibility that subsynchronous whirling instabilities will occur; in addition, machines that operate above the first or second critical speeds of the shaft can incur excessive bearing dynamic loads during partial-speed operation unless sufficient damping is provided (ref. 31).

Nearly all dense-fluid turbopumps operate below the first critical speed. Liquid-hydrogen pumps often operate between two critical speeds, and throttleable pumps may operate at a critical speed for a limited time during start transients or during test. The designer can ease critical-speed difficulties by employing light hardware that is carefully balanced. Axial dimensions are kept short, and the flow passages are shaped to yield optimum bearing spans. Reference 28 presents the important analytical procedures and considerations. For pumps that must operate over a wide speed range, it is necessary to determine whether all operation will be below the first critical speed or between two widely separated critical speeds, or whether some operation at a critical speed will be necessary. Operation below the first critical speed requires a lower maximum design speed. The degree of damping and the energy input, usually set by rotor imbalance, determine the maximum amplitude that will occur at resonance. For many designs, operation through a resonant speed on startup and shutdown transients is acceptable; however, sustained operation during rocket engine mainstage at speeds between 80 and 120 percent of a shaft critical speed set by bearing spring rate is avoided. Limited operation during development tests designed to evaluate amplitudes at critical speed is allowable.

must be made for manufacturing and assembly errors that result in offset of rotors from true center. Normality control and piloting influence the rotor rotating center after assembly. Provisions for final balance after assembly can be used to minimize imbalance in very-high-speed machines.

In the assembly of built-up rotors, the possibility of misassembly exists whenever a part can be mounted in more than one position. Various practices are used to preclude the possibility of misassembly. These usually take the form of minor modifications to the hardware that prevent mating the parts when they are not in the correct position.

All the various components of a rotating assembly obviously must be designed for the same direction of rotation. It is an established practice to coordinate design efforts and avoid problems of mismatched direction of rotation by making a preliminary axonometric projection of the assembly that shows clearly the direction of rotation. Copies are furnished to all designers on the job.

High-speed impellers are proof tested by prespinning each part during the fabrication process to provide partial quality assurance. Prespinning each impeller has additional benefits in that local yielding occurs at areas of high strain concentration such as bolt holes, splines, and keyways. This yielding produces favorable residual stresses that effectively prestress the part and prevents the occurrence of yielding during operation.

2.3.4 Materials

Impeller materials that have been used successfully with rocket propellants are shown in table II. Materials that are not listed as cast were forged. The materials are chemically compatible with the pumped fluid, have satisfactory strength and ductility at the operating temperatures, and can be used to fabricate impellers with existing technology.

2.4 HOUSING

The pump housing is the physical structure that forms the containing envelope for the pump. It consists of the casing (the part of the pump that surrounds the impeller), the diffusing system and volute for single-stage pumps, and the crossover system for multistage pumps. The diffusing system may include vaned or vaneless diffusers upstream of the volute and a conical diffuser or duffusers downstream of the volute. In addition, the housing contains and mounts the bearings that support the rotating assembly and the seals that prevent leakage of the pumped fluid. Consideration is given to both the mechanical and hydraulic factors in selecting a particular housing configuration, because the housing not

Table II. - Materials Successfully Used for Impellers

Impeller material	Pumped fluid						
	LH_2, CH_4	IRFNA, N_2O_4	LOX	LF_2	FLOX	RP-1	N_2H_4, UDMH, or 50/50 mixture
Aluminum							
A356 (cast)		X	X				X
A357 (cast)			X		X	X	
2014-T6	X						
6061-T6			X			X	X
7075-T73	X	X	X			X	X
7079			X				
Steel							
AM 350		X					X
304L (cast)		X	X				
304L		X					X
310			X			X	
347 (cast)			X				
Inconel 718 (cast)			X	X	X		
"K" Monel			X				
Ti-5Al-2.5Sn	X					X	

Note: X indicates that the material was used successfully with the fluid shown; absence of X means either that no data on the use are available or that the material was incompatible with the fluid. Materials not shown as cast were forged.

only represents the major segment of pump weight but has a most significant effect upon pump efficiency. It is commonly accepted that the housing determines the operating point where the best efficiency occurs (refs. 63 and 64).

Housings have been successfully fabricated using two basic processes: casting in one or more pieces, or welding together forged, formed, cast, or machined elements. Materials have included cast aluminum alloys, cast stainless steels, and high-strength wrought aluminum alloys and steels. Sometimes, separate liners are used to provide an inert material as an interface with the impeller to achieve configuration flexibility or to simplify fabrication.

Duffuser vanes can be integral or separate. Reinforcing bolts through diffuser or guide vanes have provided structural aid.

Housing structures must be designed to sustain mounting loads as well as internal pressure loads. External loads on parts such as the volute may be minimized by incorporating flexible ducts that minimize bending loads.

2.4.1 Hydrodynamic Design

The hydrodynamic design of the housing components is based on a combination of theoretical and empirical considerations. A systematic experimental background similar to that for axial pump and compressor cascades is not available, because the greater geometric and analytical complexity of the centrifugal pump makes the experimental task more difficult and because to date there has been less emphasis on this approach.

2.4.1.1 CASING

Major considerations in the design of the casing involve the shape and smoothness of the interior walls that form the flow path from the inlet to the diffiuser (fig. 1). The shape must follow closely the exact contour of the impeller, particularly for an open-face impeller where this wall contour establishes the size and uniformity of the tip clearance. The roughness of the casing inner wall – due either to surface finish or to fasteners and attachment points – influences the radial pressure gradient and thereby the axial thrust balance. Furthermore, increasing roughness of the wall increases the impeller disk friction loss. Current practice is to achieve a surface finish of about 63 μ in./in.; necessary fasteners and attachment points are located as close as possible to the pump center line where the impeller relative velocity and therefore fluid velocity – is at its lowest.

2.4.1.2 DIFFUSION SYSTEM

The pump diffusion systems of interest for both single and multistage pumps are the vaneless and vaned diffuser upstream of the volute and the conical diffuser downstream of the volute. For multistage pumps, the diffusing system between stages may consist of a vaned diffuser followed by an internal crossover passage with no volute, or a volute followed by external crossover tubes.

2.4.1.2.1 Vaneless Diffuser

The gap between the impeller discharge and the vaned diffuser inlet or the volute tongue (referred to as a vaneless diffuser) acts as a mixing zone for the impeller blade wakes; this

mixing can significantly suppress pressure-perturbation effects (ref. 65). Figure 24 shows this gap expressed as the ratio of diametral clearance to impeller diameter plotted against impeller discharge flow angle. The available mixing length is approximately the radial clearance divided by the sine of the impeller discharge flow angle. Current practice is to maintain a constant ratio of mixing length to impeller diameter by increasing the spacing as the impeller discharge flow angle increases.

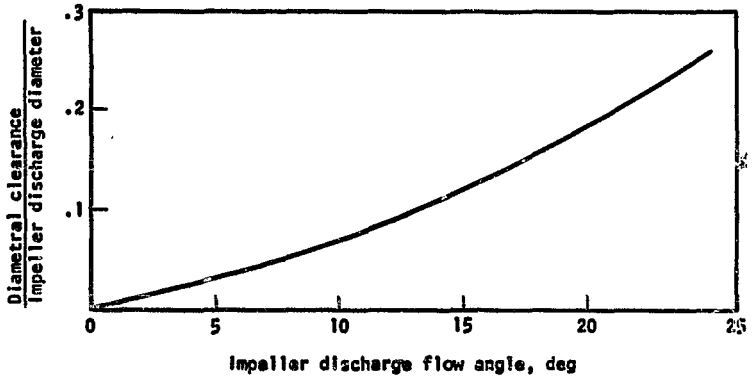

Figure 24. – Impeller-to-stator spacing as a function of discharge flow angle.

As an example of the influence of this gap size, a gain of 1.8 percent in the efficiency of the NERVA pump (at a specific speed of 980) was obtained by trimming the impeller and thereby increasing the ratio of diametral clearance to impeller diameter from 0.03 to 0.06.

It should be noted that any increase in gap size above the minimum values necessary for suppression of pressure perturbations (fig. 24) reduces efficiency and increases weight. In addition, pressure losses in the vaneless diffuser increase as pump specific speed decreases; these pressure losses may be calculated by procedures presented in reference 66. The required radial clearance may be reduced by design of the impeller to produce a minimum thickness of the boundary layer.

2.4.1.2.2 Vaned Diffuser

A vaned diffuser provides volute flow-matching over a wide flow range and also a lower volute velocity that reduces the pressure differences caused by manufacturing variations.

Both the volute flow-matching and reduced volute velocity reduce impeller radial loads. Vaned diffusers are also used to obtain maximum pump efficiency. The reduced volute velocity results in a 3-percent increase in pump efficiency at a specific speed of 1200 and greater improvement as specific speeds are decreased (ref. 4). However, vaned diffusers designed for radial-vaned impellers in low-specific-speed pumps have exhibited discontinuities in the head/capacity curve at flow rates of 45 to 50 percent of the best-efficiency operating point (fig. 13). Operation at or near this region of head discontinuity (diffuser stall) usually is unstable and is avoided. The design-point efficiency of pumps with vaned diffusers generally is higher and remains higher with decreasing flow, but falls more rapidly with increasing flow than that for pumps with a vaneless volute.

Most investigators (refs. 63, 64, 67, and 68) agree that the diffuser throat area is the most important parameter for determining a match with the impeller discharge flow. Figure 25

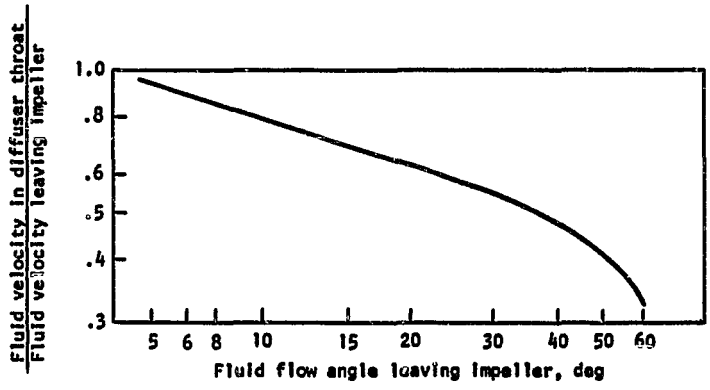

Figure 25. – Relative velocities in diffuser throat and at impeller discharge as a function of fluid flow angle.

presents the ratio of diffuser throat velocity to impeller discharge velocity that may be used to calculate the diffuser throat area. The diffuser inlet angle and shape also influence the slope of the characteristic curves; however, systematic design information is not available.

The rate of diffusion described by the effective cone angle of the vaned diffuser strongly influences the number of diffuser vanes required. Eckert and Schnell (ref. 66) present an equation that relates the required number of circular arc diffuser vanes to the diffuser equivalent cone angle θ, radius ratio R_4/R_3, discharge-to-inlet area ratio A_4/A_3 of the vaned diffuser, and vane inlet angle β_3. The results of calculations for several area ratios are presented in figure 26; the equivalent cone angle used in the calculations was 8°. A small number of diffuser vanes minimizes blockage, and so each diffuser passage is fed by more than one impeller passage (ref. 69).

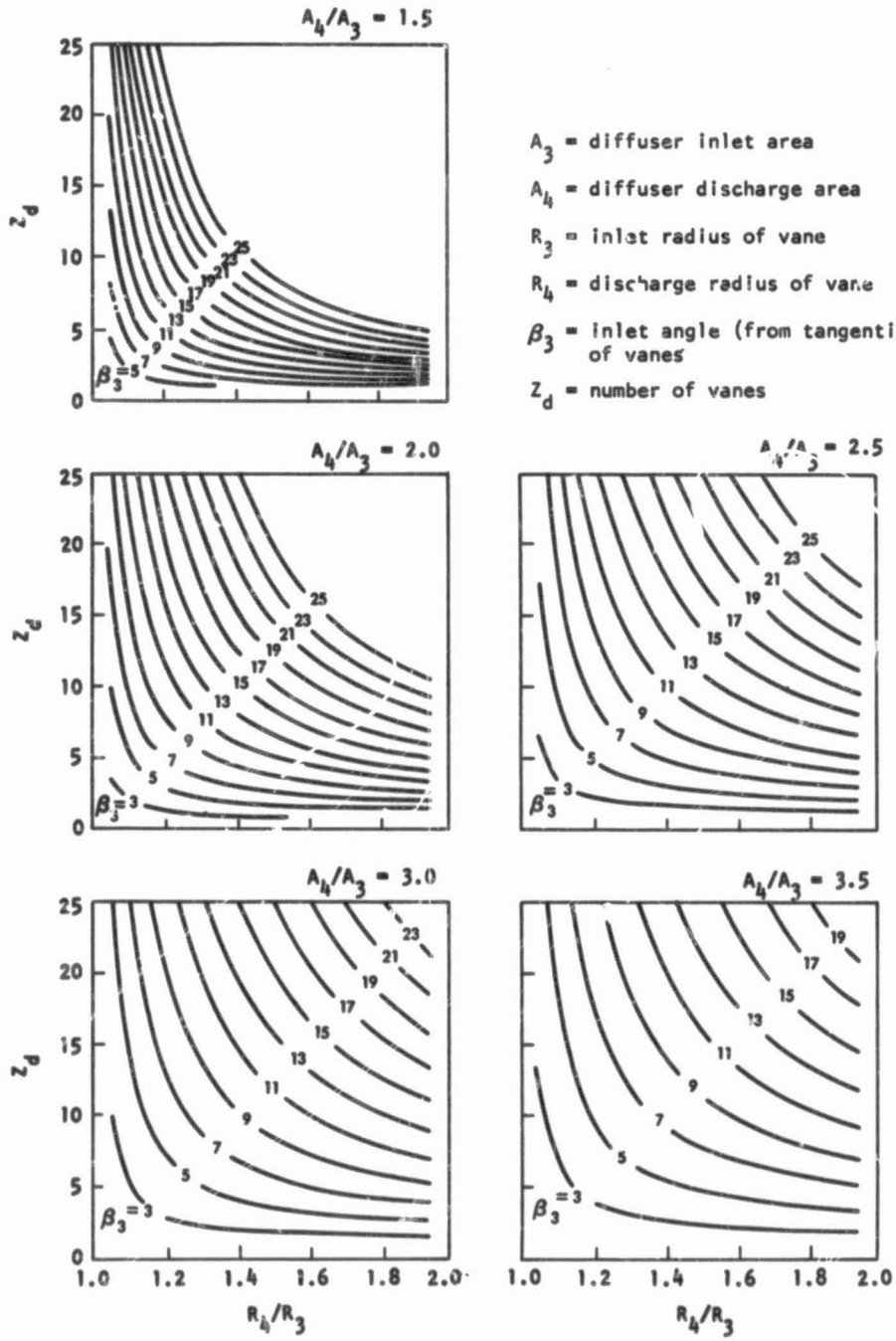

Figure 26. — Required number of circular arc diffuser vanes Z_d as a function of R_4/R_3, A_4/A_3, and β_3 for $\theta = 8°$.

For minimum losses, the diffuser vane inlet angle, β_3, is designed to match the entering fluid flow angle at the design flow rate. If the pump is required to operate at reduced flow rates (as in a throttled engine), the diffuser vane inlet angle may be designed to match the inlet flow angle at a flow coefficient as low as 80 percent of the nominal value for maximum engine thrust.

The influence of various diffuser area distributions may be evaluated by means of a computer program such as that presented in reference 70; this evaluation permits comparison of velocity gradients with previously tested successful diffusers.

When diffusers are required to carry casing structural forces, a vane island type of diffuser (fig. 27(a)) may be used. The inlet angle and throat area requirements for the vane island diffuser are the same as those for vaned diffusers (fig. 27(b)). The relation between throat area and discharge area is described by the cone angle, which normally is 7° to 10° (ref. 71).

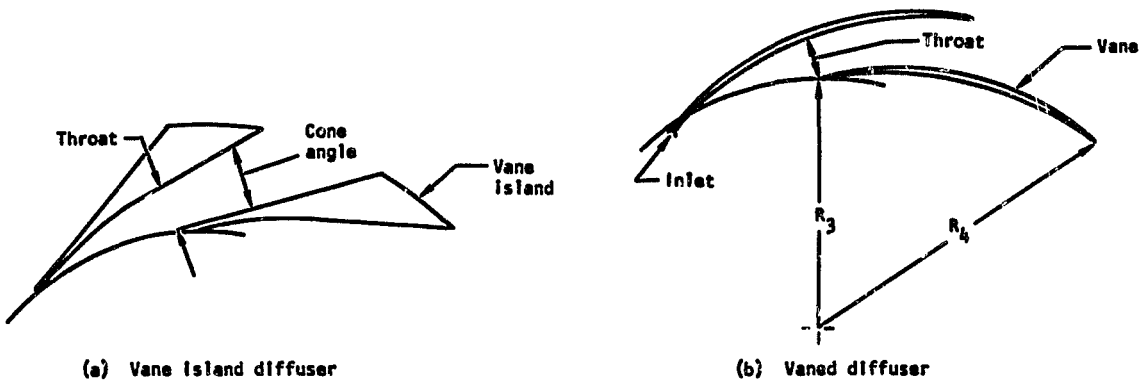

Figure 27. – Vaned diffuser designs.

For all types of diffusers, the diffusion factor D for a single stage of diffusion is maintained less than or equal to 0.6. D can be expressed as

$$D = \frac{P_{s3} - P_{s\,min}}{P_{t3} - P_{s\,min}} \tag{18}$$

where

P_{s3} = static pressure at diffuser inlet

$P_{s\,min}$ = minimum pressure in diffuser

P_{t3} = total pressure at diffuser inlet

The width of a diffuser vane b_3 is made approximately equal to the impeller tip width b_{t2}, i.e.,

$$b_3 = (.9 \text{ to } 1.0)\, b_{t2} \tag{19}$$

and the side walls are rounded or faired. These practices minimize flow separation even under conditions of axial misalignment with the impeller and produce an efficient energy conversion in the diffuser.

2.4.1.2.3 Interstage Flow Passage

Interstage flow passages (fig. 11) are required in multistage pumps to guide the fluid from the discharge of one stage to the inlet of the next stage and to provide velocity matching. Limited design information is available for multistage rocket pumps because only a few have been designed and tested. Examples are the J-2S fuel pump, which has vaned interstage passages, and the breadboard liquid-hydrogen pump (ref. 62), which had a double-discharge volute with two external crossover tubes. Some of the concepts and practices for the design of interstage flow passages used in the commercial pump and compressor industry are presented in references 66 and 72.

An additional objective when using a vaned diffuser with a volute is to avoid the possibility of wave reinforcement of the pressure waves that result from the interaction of the impeller blade wakes with the diffuser vanes. The impeller discharge blade number Z_2, diffuser vane number Z_d, and volute flow-path length πD_v are important design parameters. Superposition of pressure waves can result in large amplitude oscillations in discharge pressure. This superposition, or reinforcement, of waves is avoided by proper matching of the number of impeller blades and the number of diffuser vanes. Reinforcement of the j^{th} harmonic of the waves will occur whenever the reinforcement index m is an integer, where m is given by the expressions (refs. 65 and 73)

$$m = j\,\frac{Z_2}{Z_d}\left\{\frac{Z_d - Z_2}{Z_2} + \frac{\pi D_v N}{(a+W)}\right\} \quad \text{if } Z_2 > Z_d \tag{20}$$

and

$$m = j\,\frac{Z_2}{Z_d}\left\{\frac{Z_d - Z_2}{Z_2} - \frac{\pi D_v N}{(a+W)}\right\} \quad \text{if } Z_d > Z_2 \tag{21}$$

where

- j = order of the harmonic of the fundamental wave frequency
- D_v = average distance from center of pump to center of volute passage
- a = velocity of sound in liquid
- W = average relative velocity of fluid in volute passage

2.4.1.3 VOLUTE

The object of volute design is to provide a distribution of cross-sectional area with respect to wrap angle that will yield a constant impeller discharge static pressure at the design point of the pump; the radial load on the shaft and the impeller vibrations are thereby minimized. An asymmetric volute cross section is preferred because it produces a single vortex that is stable and that improves the efficiency of the conical diffuser at the exit (refs. 66 and 71). The conical diffuser at the volute exit will operate efficiently when the included angle for circular cross sections is between 7° and 9°; for square cross sections, 6°; and for two parallel walls, 11°.

The inlet angle of the volute tongue is designed for zero incidence angle at the design flow in order to reduce the losses associated with the volute, to minimize local pressure differences, and to reduce the amplitude of the pressure oscillations in the pump discharge. If a vaned diffuser precedes the volute, the transition from the vaned diffuser to the volute tongue must be designed to avoid an interaction that would lead to an unstable (e.g., bi-stable) pump head-versus-flow characteristic. Stable flow is achieved by fairing one diffuser vane into the volute tongue or by leaving a large clearance between the vane discharge and the tongue.

2.4.1.3.1 Cross-Sectional Area

Two methods are in use for sizing the volute cross-sectional area: constant moment of momentum, and constant mean velocity.

Constant moment of momentum. – The fluid tangential velocity is assumed to be inversely proportional to the radius. After the volute shape has been established, the volute cross-sectional area satisfying the given flow requirement is determined at each circumferential station. The constant-moment-of-momentum method was applied to the design of Titan I and Titan II pump housings; corrected for friction losses (ref. 74), the method was used in the design of the J-2S Mark 29 fuel pump, which experienced very light radial bearing loads.

Constant mean velocity. – The velocity is assumed to be constant, and therefore the cross-sectional area is increased proportionally as the central volute wrap angle increases. The method was developed as a simplification in volute design.

Although there are only minor differences in pump efficiency between the two methods (ref. 64), the unsymmetrical pressure (with its associated radial hydraulic forces upon the impeller) around the volute passage has been found to be higher in designs based on the constant-mean-velocity method (ref. 63).

2.4.1.3.2 Off-Design Radial Load

Splitter vanes or multiple tongues and vaned diffusers in the volute housing or double-outlet volutes (fig. 28) are used to reduce radial thrust over a wide flow range and to provide structural support to the housing. The greater the number of symmetrically located splitter vanes, the better is the balance of radial thrust. This is an advantage of the multiple-tongue volute. Vaned diffusers reduce the velocity of the fluid and control the flow angle at the entrance to the volute tongue and therefore produce a uniform impeller discharge pressure with a resultant low radial load. The impeller discharge pressure as a function of angular distance from the tongue is presented for three types of volutes and a range of flowrates in figure 29 (ref. 75).

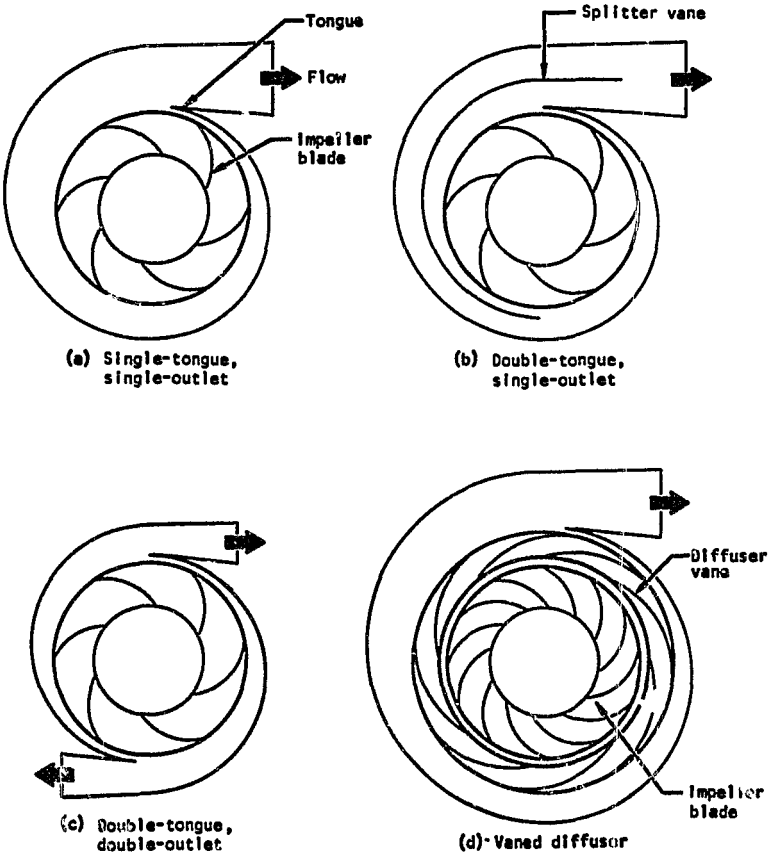

Figure 28. – Volute configurations.

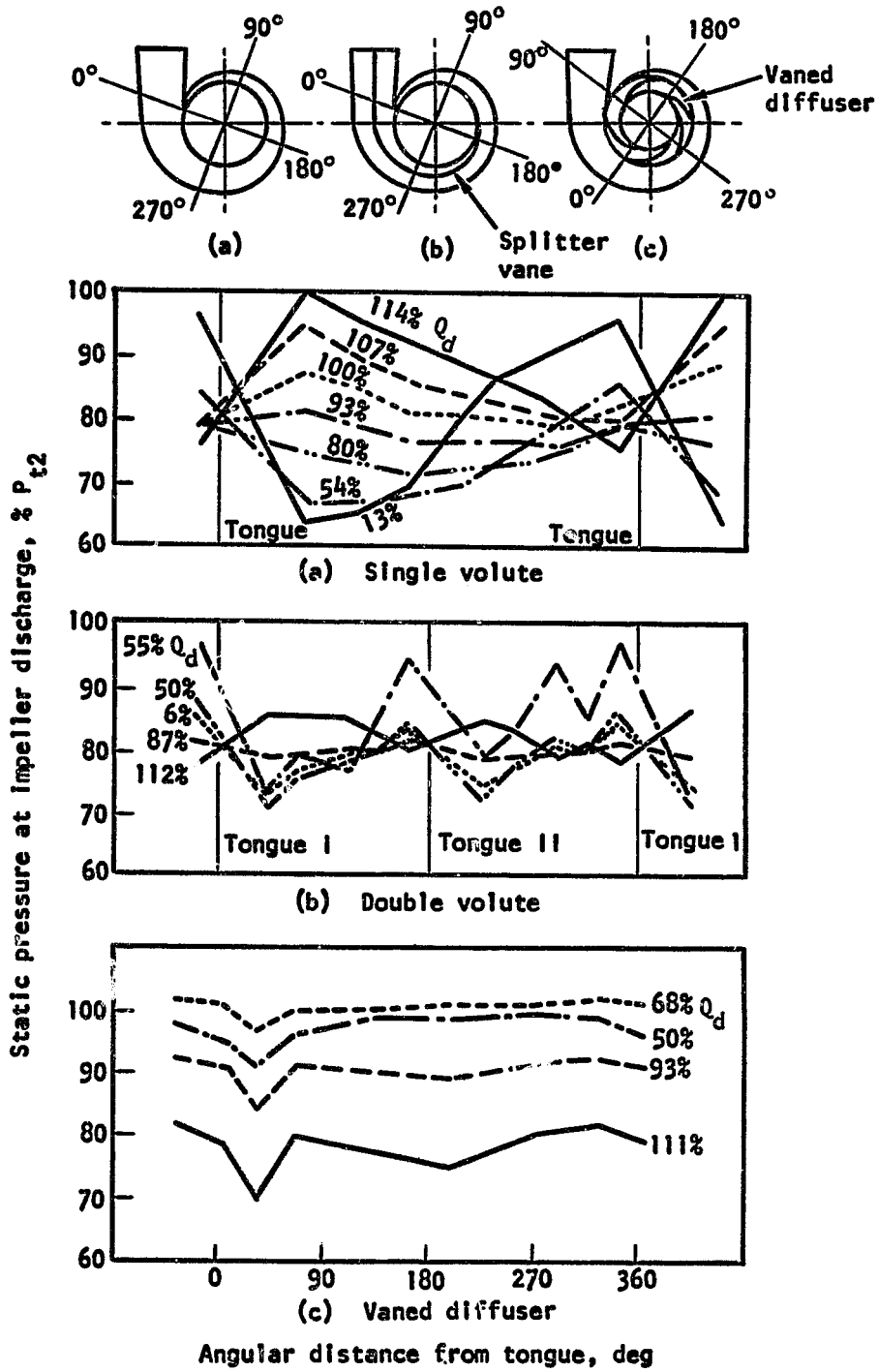

Figure 29. – Impeller discharge pressure as a function of volute design and percent design flowrate.

2.4.2 Structural Design

The housing structure must be capable of withstanding external mounting loads as well as loads due to internal pressures, and deformation must be limited so that sealing surfaces will remain effective and bearing supports will not be distorted. The housing structure must be adequate to accommodate access for instrumentation.

A major concern in housing design is the integrity of the volute tongue that withstands a large volute-separating load. The tongue must be ductile; when the volute is cast of aluminum, provisions are made to chill the tongue region rapidly during casting to provide both high ductility and strength. The volute structure is proof-pressure tested to produce tongue yielding. This practice results in lower tongue stress and improved fatigue life during normal pump operation. Figure 30 presents several successful structural design solutions.

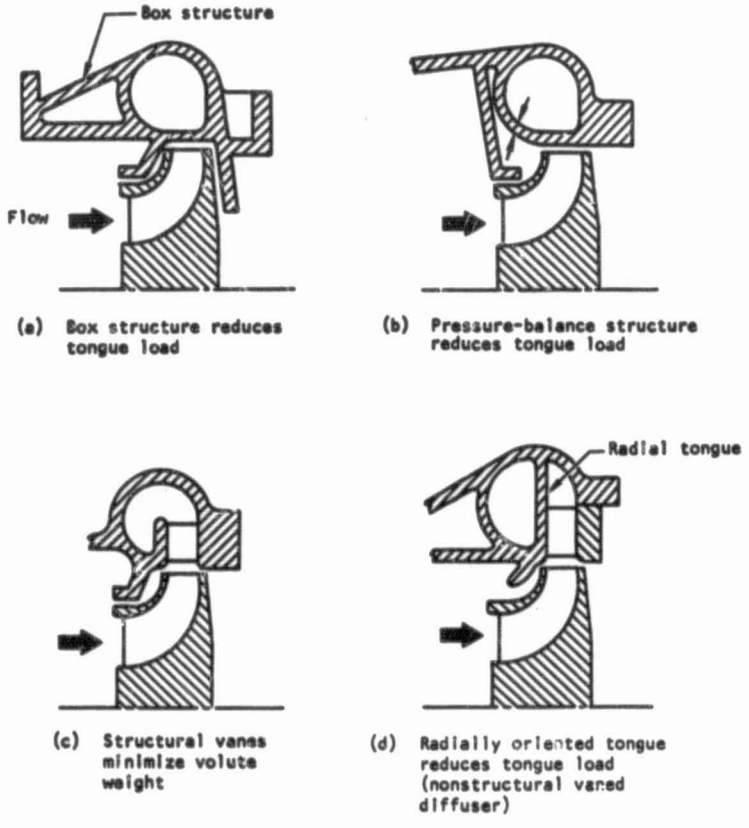

Figure 30. – Volute structural geometries.

Figure 30(a) utilizes a box structure to minimize the volute tongue deformation. The design in figure 30(b) pressure balances much of the volute to minimize tongue deformation. In figure 30(c), structural diffuser vanes support volute separating forces and thereby minimize weight. The design of figure 30(d) utilizes a long radially oriented tongue in conjunction with nonstructural diffuser vanes in a folded volute; the long radial tongue is loaded in bending rather than in tension so that the loads are minimized.

In order to minimize external forces upon the pump housing, the inlet and discharge ducting may be connected to the engine by flexible bellows. Another method for keeping external loads low is to utilize the discharge duct as part of the mounting structure to the engine in conjunction with hinged mounting points on the housing. This design requires the use of only a low-pressure bellows at the pump inlet and so is adaptable to high pump-discharge pressures. For minimum volute separating forces, a circular cross section is used. Housing stresses and deflection may be calculated by procedures presented in references 61 and 76. The steady state and dynamic stresses calculated for the pump housing are evaluated by means of a modified Goodman diagram (fig. 23) in order to establish the capability of the design to meet the required life. Safety factors are applied to compensate for uncertainties in material properties and analytical techniques. The values of the safety factors vary with the type of material control, quality control, and structural development program and with the expected application. Current practices in the use of structural design safety factors are summarized in table III.

2.4.3 Mechanical Design

The mechanical design of the pump housing must satisfy the hydrodynamic requirements and in addition provide reliable structure, leak-free joints and static seals, reliable fasteners and attachments, materials compatible with the propellants, and fabrication feasibility. Provision for anticipated special instrumentation is made during the design phase to ensure access and structural reliability.

2.4.3.1 JOINTS AND STATIC SEALS

Joints serve to connect housing components and to carry loads. A joint also may be required to prevent a leak from a region of high pressure to one of lower pressure internally or to the environment surrounding the pump.

Bolt and stud-nut and clamp-type flange configurations have been used successfully. For high-pressure pumps (>1000 psi), bolts or studs with nuts to connect mating flange joints have been used. Face-to-face contact is preferred in order to control contact loads, minimize relative motion and so avoid fretting, and provide reliable dimensional control. The joint

Table III. - Current Practices in Structural Design

Basic safety factors	Practice
Minimum yield factor of safety	≥ 1.1
Minimum ultimate factor of safety	≥ 1.4
Design loads	Most critical combined conditions
Material properties	Minimum guaranteed, based on maximum operating temperature, environment, and service life
Primary stresses	Maintain yield and ultimate safety factors
Secondary stresses	Local yielding allowed; maintain ultimate safety factor on total strain
Fatigue factors	
Low-cycle fatigue	4X predicted cycles
High-cycle fatigue	10X predicted cycles
Accumulation damage	Sum of 4X low-cycle fatigue damage + 4X creep damage + 10X high-cycle fatigue damage ≤ 1.0
Service life	Consider operating condition profile for total design life
Special pressure vessel factors	
Verification pressures	
Proof pressure	Proof factor X limit pressure at design temperature
Burst pressure	1.5X limit pressure at design temperature
Limit pressure	Maximum expected operating pressure including surges, accelerations, and oscillations
Proof factor	Value established by fracture mechanics analysis, or 1.2, whichever is greater
Checkout pressures	
Proof pressure	1.5X checkout pressure
Burst pressure	2.0X checkout pressure
Checkout pressure	System checkout pressure permitted with personnel present

design is influenced by the static-seal configuration and by assembly and installation requirements. Flange static seals that have been successfully used are O-rings, spring-loaded O-rings, K-seals, and conoseals (ref. 77). The welded seal is of particular interest for very low leakage and light weight. With welded seals, lightweight flexible lips are sealed by welding at assembly; load transmission is provided by bolted flanges.

Static-seal mating surfaces in the housing must be free from distortions that exceed the seal capability for conformance. The seal materials must be capable of maintaining an effective seal after a long shelf life. Materials that relax under prolonged load are not satisfactory seal

materials, because they may not be able to conform to joint deformation after lengthy storage periods. The pressure differential to which external seals are subjected normally are minimized by the use of a double-seal arrangement with a drain to a low-pressure point provided between the two seals. Further information on the design of static seals may be found in reference 77.

2.4.3.2 FASTENERS AND ATTACHMENTS

Fasteners and attachments used in housings are almost always of special design because of the chemical or thermal unsuitability of most materials available commercially. Although these special designs are custom made, the cost usually remains competitive because of the detailed stress analysis, chemical compatibility and strength certification, material and fabrication traceability, and configuration control that must be applied to all fasteners and attachments. The use of special designs can avoid the inadvertent substitution of a different material or the same material with a different heat treatment. Fasteners are designed to permit repeated assembly and disassembly without damage. Sufficient material allowances are made to allow repair by installation of thread inserts or use of oversized studs. Fastener and attachments are designed so that thorough cleaning is possible.

Positive locking devices are provided for all fasteners and attachments to prevent loosening by vibration; snap rings are avoided unless positive retention can be ensured.

Fastener preload is controlled carefully in order to minimize fretting and to maintain consistent housing-assembly spring rates.

2.4.3.3 ASSEMBLY PROVISIONS

Certain provisions are made in design to ensure that assembly of the housing does not introduce problems and difficulties. For example, housing liners used to minimize the explosion hazard due to inadvertent rubbing with adjacent rotating components are vented to low-pressure regions to eliminate the possibility that the liner may deviate from the housing contour and rub a rotating component.

Also, the dimensions and significant characteristics of all parts and components are carefully controlled. Detailed logs are kept so that measurements and checks can be repeated exactly as specified.

Finally, provisions are made to minimize any possibility of misassembly of parts. As in the case of the impeller, these provisions usually take the form of minor changes to the hardware that preclude incorrect mating of parts.

2.5 THRUST BALANCE SYSTEM

The thrust balance system of a turbopump balances the forces resulting from fluid pressure and fluid momentum changes originating in the turbine and the pump. The forces must be balanced to a residual value that can be reliably sustained by the turbopump bearings (ref. 43).

Devices for balancing axial thrust include impeller balance ribs, impeller seals, anti-vortex ribs, self-compensating balance pistons, and thrust bearings (figs. 31 and 32). In most cases, combinations of devices have been used. A large effort in pump development programs has

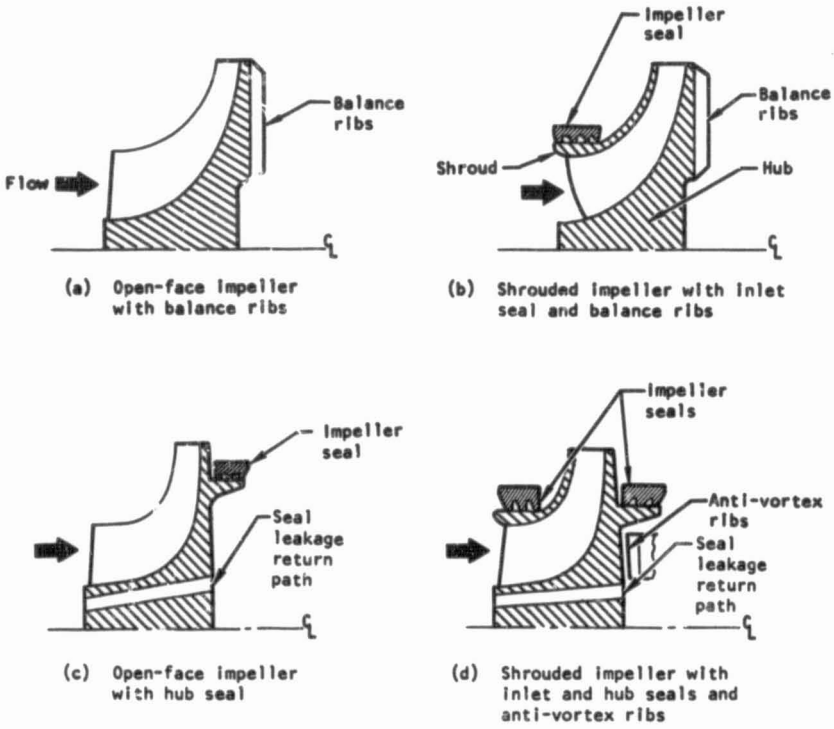

Figure 31. – Methods for balancing axial thrust.

been directed to solving axial-thrust problems. The chief difficulty lies not in designing systems for balancing thrust, but in predicting accurately the magnitude of the unbalanced forces. The usual approach is to utilize the initial analytical results to design test setups for measuring pressures and forces and operating clearances accurately. Then the design is refined on the basis of the test results.

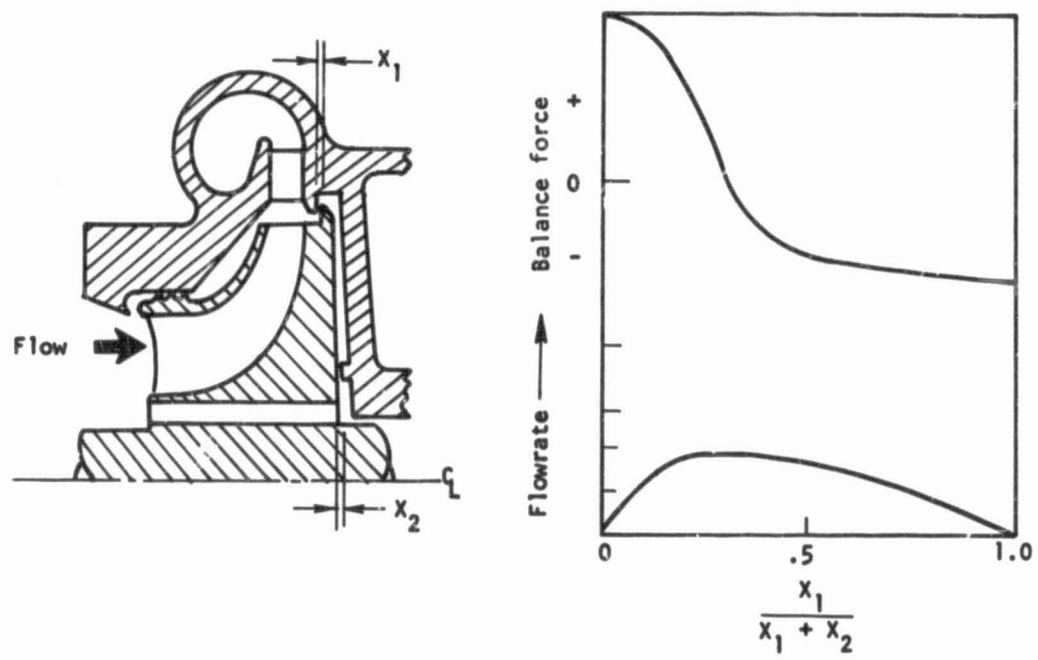

(a) Integral series-flow balance piston

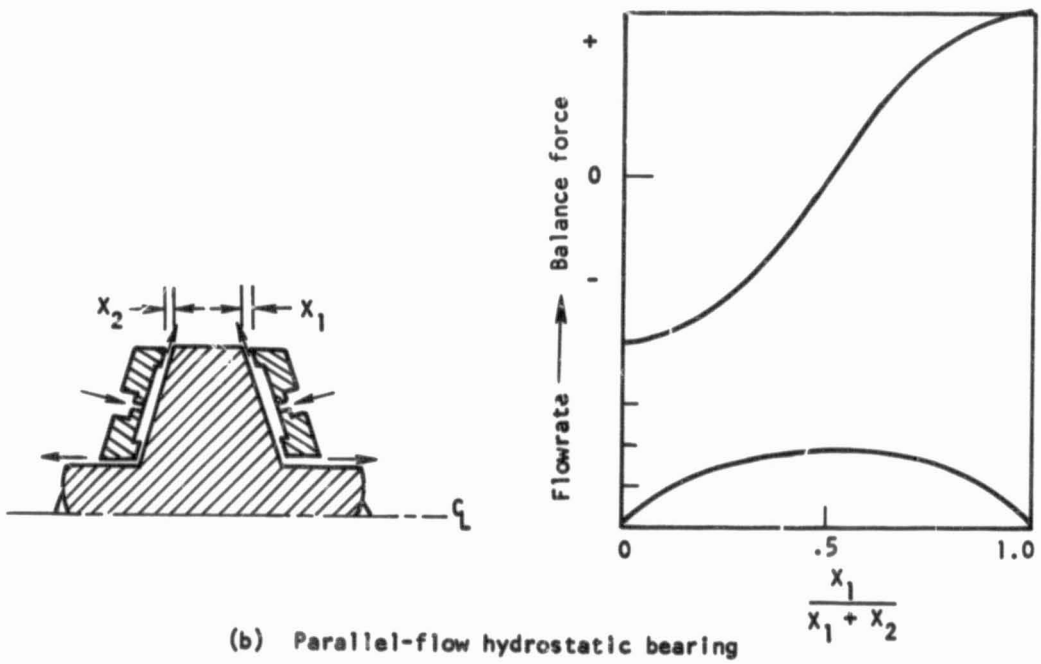

(b) Parallel-flow hydrostatic bearing

Figure 32. – Schematics and force diagrams for typical balance piston and hydrostatic bearing.

2.5.1 Unbalanced Forces

Turbine forces are balanced by the pump axial-thrust system in state-of-the-art turbopumps. Procedures for calculating turbine pressures and axial forces are presented in reference 42. Model turbine tests are used to measure internal pressures so that thrust balance forces may be more accurately estimated. Since nozzle spouting velocities are very high, flow steps in the stream can produce large axial forces on rotors. Rotor/stator alignment and the shape of the turbine rotor downstream of the nozzle are controlled to maintain these forces within the capability of the hardware.

In the pump, pressure gradients occur on the smooth nonpumping impeller hub and shroud surfaces as well as on the open faces of impellers. The pressure gradients on the nonpumping surfaces caused by viscous forces may be calculated by the procedures presented in reference 79. The pressures on the face of an open impeller may be calculated by procedures presented in references 53, 54, and 80.

2.5.2 Methods of Thrust Balance

2.5.2.1 IMPELLER WEAR RINGS

Impeller wear rings, also called impeller seals, are used on the front shroud and hub of shrouded impellers for control of axial thrust (figs. 31(b) and (d)). The area at a diameter smaller than the hub wear ring is held at a pressure slightly above the impeller inlet value by directing the leakage flow from the wear ring to the impeller inlet through holes in the impeller or through external passages. The relative diameters of the two wear rings are sized to produce the required balance force. The J-2 oxidizer pump, which is thrust balanced by use of wear rings, utilizes anti-vortex ribs at a diameter smaller than the hub wear ring to influence the radial pressure gradient in that area. Control of the pressure gradient in that region by trimming the ribs permits adjusting the axial thrust of the impeller without changing the diameters of the impeller wear rings.

The fuel turbopump in the F-1 engine had lead-plated impeller wear rings. When the wear ring rubbed during operation, the relatively soft lead "rolled up" and caused wear on the back disk of the impeller and shroud. The problem was minimized by improving the bond of the lead to the base metal and by enlarging the clearances to reduce the degree of rubbing.

2.5.2.2 IMPELLER BALANCE RIBS

Impeller balance ribs are blades located on the back of the impeller hub (fig. 31(a)). They form a low- or zero-flow impeller that provides a large pressure gradient where they are

located. The rib pumping action reduces the pressure at the smaller diameter to counteract the low pressure at the impeller inlet. Holes may be provided through the impeller into the inside diameter region of the balance ribs to vent that region statically and to provide a positive coolant flow into the balance ribs to prevent cavitation caused by fluid heating that results from the pumping work of the balance rib. Balance ribs have been used on many successful turbopumps; however, usually more development work is required to obtain a configuration that is as effective as wear rings.

The gear-driven Titan pumps utilized open-face impellers with balance ribs on the impeller hub that reduced the axial force to a value that could be sustained by a split-inner-race ball bearing. The F-1 turbopump had shrouded impellers; for control of axial thrust, the oxidizer pump impeller incorporated an inlet wear ring and balance ribs, while the fuel pump impeller incorporated inlet and hub wear rings. The pump forces balanced the direct-drive turbine forces such that tandem split-inner-race ball bearings could sustain the unbalanced axial force.

2.5.2.3 BALANCE PISTONS AND HYDROSTATIC BEARINGS

When pumps operate at very high speeds, ball bearings are not capable of sustaining the normal operating unbalanced axial forces. For these applications, balance pistons and hydrostatic bearings are used. The two types that have been used for rocket engine centrifugal pumps are the series-flow balance piston integral with the impeller (fig. 32(a)) and the separate parallel-flow hydrostatic bearing (ref. 45 and fig. 32(b)). Both types are self-compensating bearings that seek an operating clearance such that the bearings that radially locate the rotor operate with an acceptable axial force. These bearings are designed to operate with a sufficient effective spring rate to avoid axial resonances of the rotating assembly. The design of balance pistons and hydrostatic bearings usually is based on procedures like those presented in reference 81.

The J-2S fuel pump incorporated a series-flow balance piston integral with the hub of the second-stage impeller, his piston reduced the axial load to values that could be sustained by ball bearings that were axially located by springs. The ball bearings positioned the rotating assembly and sustained the spring-limited axial forces until pump pressures increased to values allowing the balance piston to sustain the axial loads. The first stage, an integral-inducer mixed-flow impeller, provided the axial force to balance the turbine force. The balance piston used a rub ring of fiberglas-reinforced Teflon to minimize possible galling of the orifices. The material delaminated, and the orifices opened up. The problem was solved by using lead-filled porous bronze for the rub rings. The J-2 axial fuel pump initially used carbon rub rings; the rings cracked, causing the orifices to open up. The problem also was solved by use of lead-filled porous bronze rub rings.

The breadboard liquid-hydrogen pump (ref. 45) used back-to-back open-face impellers of different diameters to react the turbine thrust, with a pump-discharge-fed, double-acting hydrostatic bearing for axial force balance. The pump roller bearings could support only radial loads.

2.5.2.4 BALL BEARINGS

When the density of the pumped fluid exceeds that of water, ball bearings frequently are the preferred method for sustaining unbalanced loads. The higher fluid density results in lower required pump speeds and lower impeller disk areas for a given pressure rise. The lower speed allows use of larger bearings, and the lower impeller disk area results in lower forces. Both factors permit ball bearings to sustain the resulting unbalanced loads. When bearing DN values are sufficiently low, single or multiple ball bearings can carry substantial loads when adequately cooled. Split-inner-race and angular-contact bearings are capable of sustaining larger axial loads than are deep-groove bearings. Bearing applications are discussed in reference 43.

2.5.3 Materials

Materials for thrust balance systems (table V) are selected for compatibility with the propellant, adequate strength at the required rotating speed, and minimum explosion hazard

Table V. - Materials for Thrust Balance Systems

Component	Material				
Balance ribs	Same material as impeller				
Anti-vortex vanes	Same material as housing				
Impeller seals	KEL-F*, stainless steels*, fiberglas-reinforced Teflon, silver*, leaded bronze, impeller materials, housing materials				
Balance piston	Al 2024 anodized	Al 7075-T73	Inconel 718*	"K" Monel*	Ti-5Al-2.5Sn
Balance-piston orifice	Flame-plated tungsten carbide on 310 stainless	304 stainless	Silver-plated 310 stainless; silver	Leaded bronze	Leaded bronze

*Material suitable for use with LOX.

in the event of an inadvertent rub. Plastic materials such as Kel-F, Teflon, and fluorinated polyvinyl chloride resist burning if rubbed on the impeller in liquid-oxygen pumps and therefore are safe stationary sealing materials when the seal pressure differential is not excessive. The same materials are also satisfactory in liquid-hydrogen pump service.

Materials for the balance-piston orifice are selected to resist galling if rubbed against balance piston rotor or impeller materials. To date, balance piston experience has been almost solely limited to hydrogen pumps. Future oxygen-pumps with balance pistons must limit orifice materials to those that can be LOX-cleaned, resist explosion or ignition upon impact, and are chemically and physically stable in liquid oxygen.

3.4 HOUSING

3.4.1 Hydrodynamic Design

3.4.1.1 CASING

The casing interior wall shall not adversely affect pump efficiency or impeller axial thrust.

The casing interior contour should follow closely the exact contour of the impeller; this relation is particularly important for open-face impellers, since the casing wall establishes the tip clearance. The wall surface finish should be about 63 μ in./in. and free from fasteners, attachment points, and any surface protuberances; necessary fasteners should be located close to the pump centerline.

If recommended conditions of contour and smoothness cannot be met, tests should be made to evaluate the influence of surface roughness on the radial pressure gradient and thereby on axial thrust.

3.4.1.2 DIFFUSION SYSTEM

3.4.1.2.1 Vaneless Diffuser

The length of a vaneless diffuser (the impeller-to-stator spacing) shall result in the highest efficiency attainable without producing unacceptable discharge-pressure oscillations.

The empirical curve in figure 24 should be used as a guide to achieve high performance with acceptable oscillations in pump discharge pressure. Reference 65 presents the influence of impeller diffusion and clearance. Pressure losses in the vaneless diffuser can be calculated by the procedures given in reference 66.

3.4.1.2.2 Vaned Diffuser

A vaned diffuser shall minimize impeller radial loads over wide flow ranges and maximize pump efficiency at low specific speed.

For minimum radial loads, the vaned diffuser discharge velocity should match the volute velocity and the flow angle should match the volute tongue angle.

For maximum flow range, design the vaned diffuser so the efficiency at maximum flow rate is equivalent to that with the impeller discharging directly into a volute. Design the diffuser vane width equal to or smaller than the impeller tip width (100 percent to 90 percent) and provide well-rounded or faired side walls to permit misalignment without flow separation. Allow for wear-ring leakage flow with shrouded impellers, because the leakage reduces the width of the flow sheet entering the diffuser.

Good proportions for the diffuser channel should be established by an iteration between a minimum hydraulic radius for the required area and the number of diffuser vanes (usually, the prime number nearest to the number of impeller blades). The diffuser throat dimensions for the pump best-efficiency operating point should provide an area adequate for the passage flowrate and for the velocity at the diffuser throat mean radius, calculated by the conservation-of-momentum method from the velocity at the impeller discharge radius (fig. 25).

If a conical diffuser is used downstream, the vaned diffuser and volute tongue should be separated by a radius ratio greater than 1.05 or the tongue should virtually touch the diffuser; otherwise, pump discharge pressures may become unstable and degrade engine performance by introducing fluctuations in thrust.

Use vaned diffusers to reduce the velocity in the volute when the pump overall head coefficient is greater than 0.5, when $N_s < 1000$, and when maximum efficiency or low weight is important.

Select the number of diffuser vanes to diffuse efficiently when the requirements for inlet flow angle, radius ratio, and velocity ratio are satisfied; the number should be compatible with the number of impeller vanes. The diffuser should not exceed the equivalent-cone-angle diffusion rates indicated by figure 26; the diffusion factor for a single stage should not exceed 0.6.

Avoid boundary-layer growth, which limits further diffusion. The exit radius of a ring of diffuser vanes should not be greater than 1.4 times the inlet radius. If necessary, use more than one ring to achieve the required velocity ratio.

3.4.1.2.3 Interstage Flow Passage

The inlet of an interstage flow passage shall accept the impeller discharge flow, and the outlet of the passage shall provide the flow necessary for the following impeller – all without unacceptable pressure or flow oscillations.

The practices discussed in references 66 and 72 should be observed in designing interstage flow passages. When a vaned radial diffuser is followed by a volute, equation (20) or (21)

should be used to establish the parameters so that reinforcement of pressure waves generated by the impeller blade wakes is precluded.

To avoid excessive diffusion in any one stage, use staged diffusion (e.g., a vaned diffuser followed by a multiple-outlet volute with conical exit diffusers, or vaned radial diffusers followed by axial diffusers and crossover passages) between stages of a multiple-stage pump. It is recommended that external high-pressure flange joints be avoided.

3.4.1.3 VOLUTE

The volute shall enhance maximum downstream conical diffuser efficiency and prevent bi-stable pump head/flow characteristics.

The volute cross section should be asymmetrical so that it produces a single vortex, which improves conical diffuser performance. Use the asymmetrical volute to provide a stable pump characteristic. With a vaned diffuser, provide a stable characteristic by fairing one diffuser vane into the volute tongue or by leaving a large clearance between the vane discharge and the tongue. Both means avoid interaction with the volute-exit conical diffuser.

The divergence angle of volute-exit conical diffusers, expressed as included angle, should be as follows (ref. 71): for circular cross sections, 7° to 9°; for square cross sections, 6°; and for two parallel walls, 11°.

3.4.1.3.1 Cross-Sectional Area

The volute cross-sectional area shall result in minimum impeller radial load at the design point.

The constant-moment-of-momentum method adjusted for friction loss will produce minimum design-point impeller radial loads. The procedures presented in reference 74 may be followed for this analysis.

3.4.1.3.2 Off-Design Radial Load

In variable-flow pumps, the volute shall not impose additional radial loads on the impeller.

Any of several methods of radial-load control that have proven effective over a wide flow range of a pump may be used: multiple-tongue volute, vaned diffuser, double-outlet volute, and combinations of these (figs. 28(b), (c), and (d)).

To minimize radial thrust loads, particularly at off-design flow conditions, employ double-outlet volutes without vaned diffusers. When single outlets are required, use vaned diffusers to minimize the radial loads caused by nonuniform circumferential static pressures. It is recommended that the design of the pump discharge housing be similar to an existing design that produces minimum radial thrust over the flow range desired and that potential-flow analysis be used to estimate the radial thrust.

3.4.2 Structural Design

The housing shall withstand all predicted loads and stresses without rupture or unacceptable amounts of deflection.

Housing stresses and deflections may be calculated by procedures presented in references 61 and 76. Stress levels and deflections should be compatible with the selected materials. The factors of safety used for the housing design should be consistent with the material-control procedures and the accuracy of the calculated or measured stress levels.

Critical-speed effects, in terms of housing stiffness, should be evaluated as part of the housing analysis to ensure adequate spring rate of bearing supports.

It is recommended that machined integral-diffuser vanes serve as main structural members of high-pressure volutes and that the volute assembly reduce the influence of pressure- and line-load-induced deflections on critical clearances. Housing pressure loads should not pass through the leading edges of a vaned diffuser.

The volute tongue forms a stiff, highly loaded point in a flexible system. For this reason the tongue leading edge should be smoothly finished and shot peened if required to improve fatigue life. The ratio of volute fillet radius to web thickness should be as large as possible; a ratio greater than 1.0 will result in a minimum stress concentration.

It is recommended that volutes be sized to maintain safety factors as shown in table III when material properties are compared with primary effective stresses.

If the calculated elastic peak stress and corresponding peak strain is greater than twice the elastic limit strain, then cyclic plastic strain will occur. The volute must then be checked to ensure adequate safety factor against low-cycle fatigue failure. The low-cycle fatigue safety factor should be based on cycles to failure and should be no less than 4, i.e., the number of cycles to failure should be 4 times the number of predicted operating cycles.

Mounting loads should be minimized by designing the structure to prevent distortions of the mount points on the engine from inducing pump loads. Use hinged mounts and flexible duct

connections as required. Provide volute and housing strength to accept mounting loads.

Minimize volute and housing deflections to maintain running clearance and bearing loads within allowable limts. It is recommended that shear webs (box structure) be employed to reduce housing deflections, and that the pressure-induced loads be balanced to reduce the forces. It is also recommended that axial ties, across the volute, be incorporated to reduce these deflections. Diffuser vanes, through-bolts, and flow splitters can be used for this purpose.

Provide adequate wall thickness and space for instrumentation bosses, probes, line routing, terminals, and brackets, along with a capability for replacing such hardware during testing.

3.4.3 Mechanical Design

3.4.3.1 JOINTS AND STATIC SEALS

Joints and static seals shall be free from unacceptable leakage during storage and operation, including repeated operation.

Minimize the number of external joints. Each joint should be evaluated for effect upon assembly sequence and reliability, manufacturing ease and cost, material availability, and inspectability.

Joints and static seals should be free from yielding under load and should not relax to a permanently deformed shape under prolonged storage. A static seal should operate in its elastic range over all conditions. Joint deflections should not exceed the conformance capability of the mating static seals.

Avoid the use of materials or designs for static seals that lead to loss of ability to seal after prolonged periods of storage. Use metallic seals or composite seals in which the metal provides the spring force. Manufacturer's claims of static-seal performance should be carefully evaluated against the specific application. Tests in the correct environment prior to design commitment are recommended.

Seal surfaces should be hard, so that they will not be marred by mating surfaces under load; hard surface coatings or hard materials may be used. Design so that external seal surfaces are not easily damaged in handling; use protruding rings, studs, or other devices that prevent accidental contact of seal surfaces with tables, floors, or wrenches.

Welded joints and dual seals with inert-buffer-fluid pressurization or leakage bleed-off should be considered for zero-leakage joints. All high-pressure dual seals should be vented to internal low-pressure cavities.

For a flanged joint, verify that under thermal, mechanical, or pressure loads

(1) Flange alignment is maintained by piloting.

(2) The flange does not rotate.

(3) The joint is not distorted or opened.

(4) There is no unacceptable change in radial or axial fit.

It is recommended that flange deflection or rotation analyses be based on maximum operating pressures and the most severe interface thermal gradients established by a finite-element heat-transfer program. Through-holes and nuts or oversize high-strength inserts are recommended if stresses in the flange are excessive. The elastic deformation of the joint elements should be included in the analysis.

Thin flange joints with many small, closely-spaced bolts are superior to thicker flanges with few large bolts. Bolt-and-nut flange attachments are preferred over threaded-hole flanges. Provide adequate space for wrenches in the design of flanges and joints to avoid the possibility of easy stud-bolt damage.

Control of the configuration by an interface control drawing with a check of mating faces is recommended.

3.4.3.2 FASTENERS AND ATTACHMENTS

Fasteners and attachments for centrifugal pump assembly

- *Shall maintain critical fits and clearances, with controlled preload.*
- *Shall withstand repeated use.*
- *Shall have positive locking devices.*
- *Shall not contaminate the system or react with the service or test fluid.*

Conduct a thermal analysis based upon predicted duty cycles and test conditions. Then, superimpose these thermal conditions on a stress analysis that includes deflections induced by operating dynamics. Thus, the adequacy of fits and attachments can be assessed upon the basis of combined effects. A special configuration, or revised duty cycle, or test procedures may be required. Good fastener design practice (e.g., control of load and preload, avoidance of stress raisers, smooth transition, and proper material selection) is recommended.

A direct determination of preload is recommended. This should be done by measuring the increase in depth of a longitudinal hole in the bolt and comparing it with the desired preload expressed as strain or by measuring the force required to obtain the preload.

It is recommended that wrench clearances provide space for accurate determination of torque values; therefore, accessibility and non-awkward positioning for standard wrenches are necessary.

Materials for fasteners and attachments should be those that resist galling. Sufficient material should be present in the housing to permit repair by installation of thread inserts or oversize studs.

Tab washers, cup washers, and lock-wire are preferred locking devices; however, lock-wire is not recommended for rotating attachments. When lock-wire is used, take special care to avoid failure of the wire or contamination by the ends cut off during assembly. Tab-on-tong or cup-on-slot lockwashers are recommended for critical attachments.

Provide a large safety margin on tab stress so that the tabs retaining the washer to the stationary part will not be sheared. It is recommended that the face of the bolt or nut be relieved to prevent axial contact, false torque, or damage of the bolt or nut face by the sharp-edge washer tabs. Ductile washer material should be used.

If snap rings are mandatory, careful evaluation of groove detail, installation procedure, material selection, and loading is necessary; positive locking against creepout is required.

Fastener and attachments should be designed to permit thorough cleaning; blind holes should be avoided wherever possible. Material surfaces should resist fretting, which can cause contamination. Propellant-compatible coatings may be used to eliminate base-material fretting.

Thread lubricants for liquid-oxygen service should be tested for compatibility with the propellant (ref. 84).

3.4.3.3 ASSEMBLY PROVISIONS

3.4.3.3.1 Housing Liners

Housing liners shall not be damaged by pressure behind the liner.

Pressure relief holes should be used to vent the liner/housing cavity to the main stream to prevent distortion and damage.

END OF REFERENCE

87

REFERENCE

88

WISLICENUS, F.: FLUID MECHANICS OF TURBOMACHINERY, VOLS. 1 AND 2. DOVER PUBLICATIONS, INC., NEW YORK, 1965.

THIS REFERENCE IS COPYRIGHTED MATERIAL AND THEREFORE THE CONTENTS HAVE NOT BEEN REPRODUCED FROM THE TEXT.

END OF REFERENCE

88

REFERENCE

89

STEPHANOFF, A. J.: CENTRIFUGAL AND AXIAL FLOW PUMPS, SECOND ED. JOHN WILEY & SONS, INC., 1957.

THIS REFERENCE IS COPYRIGHTED MATERIAL AND THEREFORE THE CONTENTS HAVE NOT BEEN REPRODUCED FROM THE TEXT.

END OF REFERENCE

89

REFERENCE

90

LIQUID ROCKET ENGINE TURBOPUMP INDUCERS. NASA SP-8052, 1971.

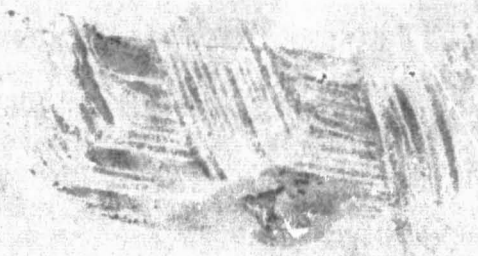

NASA SP-8052

NASA
SPACE VEHICLE
DESIGN CRITERIA
(CHEMICAL PROPULSION)

LIQUID ROCKET ENGINE TURBOPUMP INDUCERS

MAY 1971

NATIONAL AERONAUTICS AND SPACE ADMINISTRATION

FOREWORD

NASA experience has indicated a need for uniform criteria for the design of space vehicles. Accordingly, criteria are being developed in the following areas of technology:

Environment
Structures
Guidance and Control
Chemical Propulsion

Individual components of this work will be issued as separate monographs as soon as they are completed. This document, part of the series on Chemical Propulsion, is one such monograph. A list of all monographs issued prior to this one can be found on the last page of this document.

These monographs are to be regarded as guides to design and not as NASA requirements, except as may be specified in formal project specifications. It is expected, however, that these documents, revised as experience may indicate to be desirable, eventually will provide uniform design practices for NASA space vehicles.

This monograph, "Rocket Engine Turbopump Inducers," was prepared under the direction of Howard W. Douglass, Chief, Design Criteria Office, Lewis Research Center; project management was by Harold W. Schmidt and Lionel Levinson. The monograph was written by Jakob K. Jakobsen of Rocketdyne Division, North American Rockwell Corporation, and was edited by Russell B. Keller, Jr. of Lewis. To assure technical accuracy of this document, scientists and engineers throughout the technical community participated in interviews, consultations, and critical review of the text. In particular, J. Farquhar III of Aerojet-General Corporation, W. E. Young of Pratt Whitney Aircraft Division, United Aircraft Corporation, and M. J. Hartmann and C. H. Hauser of the Lewis Research Center individually and collectively reviewed the text in detail.

Comments concerning the technical content of this monograph will be welcomed by the National Aeronautics and Space Administration, Lewis Research Center (Design Criteria Office), Cleveland, Ohio 44135.

May 1971

GUIDE TO THE USE OF THIS MONOGRAPH

The purpose of this monograph is to organize and present, for effective use in design, the significant experience and knowledge accumulated in development and operational programs to date. It reviews and assesses current design practices, and from them establishes firm guidance for achieving greater consistency in design, increased reliability in the end product, and greater efficiency in the design effort. The monograph is organized into two major sections that are preceded by a brief introduction and complemented by a set of references.

The State of the Art, section 2, reviews and discusses the total design problem, and identifies which design elements are involved in successful design. It describes succinctly the current technology pertaining to these elements. When detailed information is required, the best available references are cited. This section serves as a survey of the subject that provides background material and prepares a proper technological base for the *Design Criteria* and Recommended Practices.

The *Design Criteria,* shown in italic in section 3, state clearly and briefly what rule, guide, limitation, or standard must be imposed on each essential design element to assure successful design. The *Design Criteria* can serve effectively as a checklist of rules for the project manager to use in guiding a design or in assessing its adequacy.

The Recommended Practices, also in section 3, state how to satisfy each of the criteria. Whenever possible, the best procedure is described; when this cannot be done concisely, appropriate references are provided. The Recommended Practices, in conjunction with the *Design Criteria,* provide positive guidance to the practicing designer on how to achieve successful design.

Both sections have been organized into decimally numbered subsections so that the subjects within similarly numbered subsections correspond from section to section. The format for the Contents displays this continuity of subject in such a way that a particular aspect of design can be followed through both sections as a discrete subject.

The design criteria monograph is not intended to be a design handbook, a set of specifications, or a design manual. It is a summary and a systematic ordering of the large and loosely organized body of existing successful design techniques and practices. Its value and its merit should be judged on how effectively it makes that material available to and useful to the designer.

CONTENTS

	Page
1. INTRODUCTION	1
2. STATE OF THE ART	3
3. DESIGN CRITERIA and Recommended Practices	49
REFERENCES	87
GLOSSARY	92
NASA Space Vehicle Design Criteria Monographs Issued to Date	98

SUBJECT	STATE OF THE ART		DESIGN CRITERIA	
HEAD-RISE CAPABILITY	—	—	*3.0*	49
INDUCER INLET-EYE AND LEADING-EDGE GEOMETRY	*2.1*	7	*3.1*	49
Inlet Casing	*2.1.1*	7	*3.1.1*	49
Hub Size and Shape	*2.1.2*	11	*3.1.2*	50
Inlet Tip Diameter and Contour	*2.1.3*	12	*3.1.3*	50
Fluid Thermodynamic Effects	*2.1.4*	13	*3.1.4*	54
Blade Profile	*2.1.5*	17	*3.1.5*	55
Blade Leading-Edge Sharpness	*2.1.6*	21	*3.1.6*	56
Blade Sweep	*2.1.7*	21	*3.1.7*	56
Blade Cant	*2.1.8*	21	*3.1.8*	56
Blade Angle	*2.1.9*	21	*3.1.9*	57
Blade Lead	*2.1.10*	22	*3.1.10*	57
Blade Thickness	*2.1.11*	22	*3.1.11*	57
Blade Camber	*2.1.12*	22	*3.1.12*	58
Blade Surface Finish	*2.1.13*	23	*3.1.13*	58
Blade Number	*2.1.14*	23	*3.1.14*	59
Cascade Solidity	*2.1.15*	24	*3.1.15*	59

SUBJECT	STATE OF THE ART		DESIGN CRITERIA	
INDUCER FLOW-CHANNEL AND BLADE GEOMETRY	*2.2*	24	*3.2*	59
Channel Flow	*2.2.1*	24	*3.2.1*	59
Discharge Flow	*2.2.2*	26	*3.2.2*	60
Impeller-Inducer Matching	*2.2.3*	27	*3.2.3*	60
Trailing-Edge Sharpness	*2.2.4*	28	*3.2.4*	61
Trailing-Edge Contour	*2.2.5*	28	*3.2.5*	61
Discharge Angle	*2.2.6*	28	*3.2.6*	62
Deviation Angle	*2.2.7*	28	*3.2.7*	62
Clearance Losses	*2.2.8*	30	*3.2.8*	62
Shrouding	*2.2.9*	30	*3.2.9*	63
Blade Geometry Description	*2.2.10*	31	*3.2.10*	63
INDUCER INLET LINE	*2.3*	31	*3.3*	64
Inlet-Line Configuration	*2.3.1*	32	*3.3.1*	64
Inlet-Line Fluid Velocity	*2.3.2*	32	*3.3.2*	64
Inlet-Line Heat Transfer	*2.3.3*	32	*3.3.3*	65
Bypass Flow	*2.3.4*	33	*3.3.4*	65
Backflow and Prewhirl	*2.3.5*	33	—	—
MECHANICAL DESIGN AND ASSEMBLY	*2.4*	34	*3.4*	65
Hub Configuration	*2.4.1*	34	*3.4.1*	65
Blade Root Juncture	*2.4.2*	35	*3.4.2*	66
Shaft Dimensions	*2.4.3*	35	*3.4.3*	67
Piloting	*2.4.4*	35	*3.4.4*	67
Axial Retention	*2.4.5*	36	*3.4.5*	68
Clearance Effects	*2.4.6*	36	*3.4.6*	70
Shroud	*2.4.7*	37	*3.4.7*	72
Misassembly	*2.4.8*	37	*3.4.8*	72
Rotation Direction	*2.4.9*	37	*3.4.9*	72
Inducer Balancing	*2.4.10*	39	*3.4.10*	73
Cavitation-Induced Oscillations	*2.4.11*	39	—	—

SUBJECT	STATE OF THE ART		DESIGN CRITERIA	
MATERIAL SELECTION	*2.5*	40	*3.5*	73
Strength	*2.5.1*	40	*3.5.1*	73
Chemical Reactivity	*2.5.2*	40	*3.5.2*	74
Special Properties	*2.5.3*	41	*3.5.3*	75
VIBRATION CONSIDERATIONS	*2.6*	43	*3.6*	76
High-Frequency Fatigue	*2.6.1*	43	*3.6.1*	76
Resonance	*2.6.2*	43	*3.6.2*	76
Self-Induced Vibration	*2.6.3*	44	*3.6.3*	77
Determination of Blade Natural Frequencies	*2.6.4*	44	*3.6.4*	77
STRUCTURAL CONSIDERATIONS	*2.7*	45	*3.7*	79
Blade Loading	*2.7.1*	45	*3.7.1*	79
Blade Stress	*2.7.2*	46	*3.7.2*	80
Hub Strength	*2.7.3*	47	*3.7.3*	80
Shaft Shear Section Strength	*2.7.4*	47	*3.7.4*	83
Safety Factors	*2.7.5*	48	*3.7.5*	84
Hub Stress Verification	*2.7.6*	48	*3.7.6*	86
Inducer Proof Test	*2.7.7*	48	*3.7.7*	86

LIST OF FIGURES AND TABLES

Figure	Title	Page
1	Basic inducer types	5
2	Hubless inducer	6
3	Inlet elbow	8
4	Dual inlet	8
5	Arrangement of inlet casings	9
6	Dual inlet casing	10
7	Inlet elbow development	11
8	Cascade and flow parameters	18
9	Blade in cavity	20
10	Backflow deflector configuration	33
11	Conventional low-head inducer hub	35
12	High-head inducer hub	35
13	Axial retention arrangement	36
14	Turbopump flow pattern	38
15	S'_s-D'_s chart (zero pre-rotation) high-speed range	52
16	S'_s-D'_s chart (zero pre-rotation) low-speed range	53
17	Wedge angle	55
18	Hub profile	66
19	External piloting	68
20	Liquid-oxygen inducer, reduced tip clearance	71
21	Burst factor vs. elongation for various design factors	82
22	Shear section	83
23	Goodman diagram	85

Table	Title	Page
I	Basic Inducer Types: Design and Performance Summary	4

LIQUID ROCKET ENGINE TURBOPUMP INDUCERS

1. INTRODUCTION

The inducer is the axial inlet portion of the turbopump rotor whose function is to raise the inlet head by an amount sufficient to preclude cavitation in the following stage. The inducer may be an integral part of the pump rotor or it may be mounted separately on the pump shaft upstream of the impeller. The principal objective in the design of an inducer is the attainment of high suction performance, but the achievement of maximum performance is limited by structural design considerations. The optimum design, therefore, is a compromise that provides adequate suction performance while maintaining structural integrity under all operating conditions. Such a design depends on simultaneous satisfactory solutions of hydrodynamic and mechanical problems.

The hydrodynamic problems involve obtaining the required suction specific speed and head rise of the inducer without introducing undesirable cavitation. Much work has been done on the theoretical hydrodynamic design of the inducer for an ideal fluid, which normally is assumed to resemble cold water in its effect on suction performance. However, it has not yet been possible to use test results on inducer performance with cold water to predict actual performance with the intended pump fluid. Other major unsolved problems involve obtaining satisfactory theoretical treatments for (1) three-dimensional effects, (2) the suction performance of inducer cascades with curved blades, (3) the effects of blade leading-edge sweep, and (4) the effects of tip clearance. In the absence of a satisfactory analytical basis for design, these hydrodynamic problems are solved empirically by utilizing experience with previous successful designs.

The mechanical problems involve maintaining the structural integrity of the blade leading edge and providing for blade and hub stresses due to blade loading, flow instabilities, and centrifugal forces. They include also proper choice of material, which must be compatible with both the pump operating fluid and the pump test fluid, and selection of the best way to assemble the inducer in the pump during fabrication. The achievement of an optimum inducer design requires a systematic survey of all mechanical design factors. This survey is based on a combination of fundamental theory and practical experience related to previously proven inducer designs and enables the designer to identify the effect of design variants on the overall performance, on ease of manufacture, on simplicity and reliability of assembly, and on strength and reliability of the chosen design.

In keeping with this approach, this monograph is based on a critical evaluation of available information on the hydrodynamics, mechanical design, development, and testing of pump inducers. Its purpose is to furnish well-established, specific design practices for pump inducers based on the present state-of-the-art technology. These practices are presented in a form matched to the needs of the design team, along lines following the natural and logical progression of the design effort. The material is arranged to reflect both the natural organization of work and the corresponding division of the design team to deal with hydrodynamics, mechanical design, material selection, and vibration and stress problems.

The design philosophy in the monograph is to seek an optimization of the hydrodynamic parameters to obtain the highest suction specific speed possible without violating structural and mechanical design constraints. The approach is to design for the maximum acceptable tip cavitation number by a mathematical optimization process. This establishes an optimum value for the flow coefficient and the corresponding fluid angle. To achieve a certain margin of operation, the blade suction surface is kept within the cavity boundary up to a flowrate somewhat higher than design requirements. The blade thickness, as given by the wedge angle between the pressure and the suction sides of the blade at the leading edge, increases with the ratio of incidence angle to blade angle. The bending stresses in the leading edge then decrease, even though the increased incidence angle raises the hydrodynamic load. Root bending stresses are lowered by the increase in wedge angle possible at the root section. Since the head rise obtained with flat-plate inducers is low, a simple radial-equilibrium check of the flow distribution is sufficient to verify that there is no backflow in the blade channel at the design point. By this approach, inducer design can achieve the most effective combination of hydrodynamic and mechanical factors.

2. STATE OF THE ART

Inducers are classified according to head-rise capability and also according to the shape of the meridional flow path. They are divided by head-rise capability into low head (head coefficent $\psi \leq 0.15$)[1] and high head ($\psi > 0.15$). The head-rise capability is a function of blade geometry (i.e., flat-plate, modified-helix, or vortex type). The low-head inducer blading is either flat-plate or flat-plate plus modified-helix, depending on hub-tip contours and ψ value. The high-head inducer blading is a combination of flat-plate, modified-helix, and vortex-type blading with splitter vanes. The high-head inducer may be divided into the inducer proper and the discharge blade section; it is actually an axial-flow impeller with an integral inducer covering a solidity between 2.0 and 2.50. When inducers are classified according to meridional cross section, they are divided into four basic types: (1) cylindrical tip and hub; (2) cylindrical tip, tapered hub; (3) tapered tip and hub; and (4) shrouded with or without a hub.

Figure 1 gives six characteristic examples of the basic inducer types taken from actual practice. Examples (a) to (d) are low-head inducers, and (e) and (f) are high-head inducers. Notice that all the inducers with the exception of (c) maintain a constant tip diameter at the inlet for an axial length corresponding to a solidity of 1 or higher. This design practice benefits the suction performance by maintaining optimum conditions until the blade cavity has collapsed (type (c) was designed before this practice was established). Table I summarizes design and performance parameters of these inducers.

The shrouded inducer with a large forward sweep of the blade is also known as the hubless inducer because of its appearance (fig. 2). The blading is thus supported by the shroud, which in turn is supported and driven either through the rear portion of the inducer blading by the inducer short hub or, in the case of a truly hubless design, by attachment to the impeller shroud. The front hubless portion and the rear hub portion of the inducer are machined separately and joined by welding.

Thus, the hubless inducer differs from the conventional inducer in that its blading is supported by the shroud instead of by the hub; also, if the conventional inducer is considered a screw, then the hubless inducer must be considered a nut. The hubless inducer concept is associated with several assumed advantages: (1) it eliminates tip vortex cavitation; (2) it centrifuges eventual bubbles toward the center, where they may collapse harmlessly; and (3) it offers the possibility of using an extremely large forward sweep of the vanes to obtain a sweptwing effect similar to that of supersonic plane design.

[1]Symbols, subscripts, and abbreviations are defined in the Glossary.

Table I.—Basic Inducer Types: Design and Performance Summary

Rocket engine	Thor	J-2	X-8	X-8	J-2	J-2
Pump designation	Mark 3	Mark 15	Mark 19	Mark 19	Mark 15	Mark 15
Example in fig. 1	(a)	(b)	(c)	(d)	(e)	(f)
Pump fluid	Liquid oxygen	Liquid oxygen	Liquid oxygen	Liquid oxygen	Liquid hydrogen	Liquid hydrogen
Head type	Low	Low	Low	Low	High	High
Cross-sectional profile or geometry	Cylindrical tip and hub	Cylindrical tip, tapered hub	Tapered tip and hub	Shrouded	Cylindrical tip, tapered hub	Tapered tip and hub
Design flow coefficient ϕ_d(1)	0.116	0.109	0.106	0.05	0.0942	0.0735
Design head coefficient ψ_d(1)	0.075	0.11	0.10	0.063	0.21	0.20
Inlet tip blade angle β	14.15°	9.75°	9.8°	5.0°	7.9°	7.35°
Suction specific speed S_s in water(2)	28,500	34,300	31,200	58,000	43,200	44,200
Hub-tip ratio ν at inlet	0.31	0.20	0.23	0.19	0.42	0.38
Number of blades	4	3	3	2	4 + 4	4 + 4
Leading-edge sweep	Radial with rounded tips	Sweptback	Sweptback	Sweptforward	Sweptback	Sweptback

(1) Based on inlet tip blade speed.
(2) At 10% head dropoff from noncavitating head.

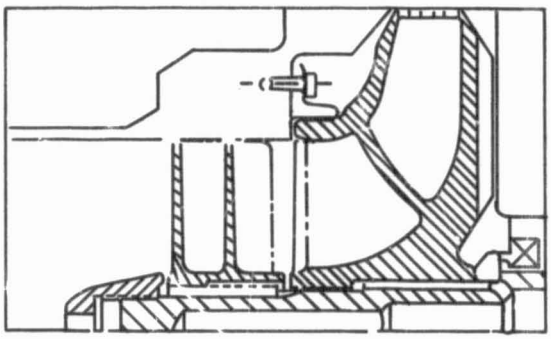

(a) Low-head inducer with cylindrical tip and hub

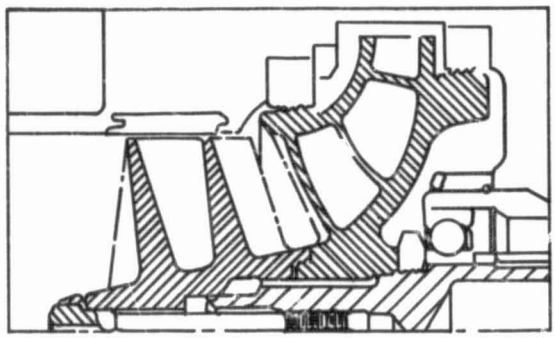

(b) Low-head inducer with cylindrical tip, tapered hub

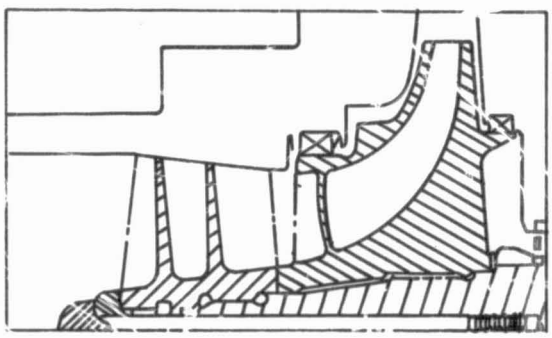

(c) Low-head inducer with tapered tip and hub

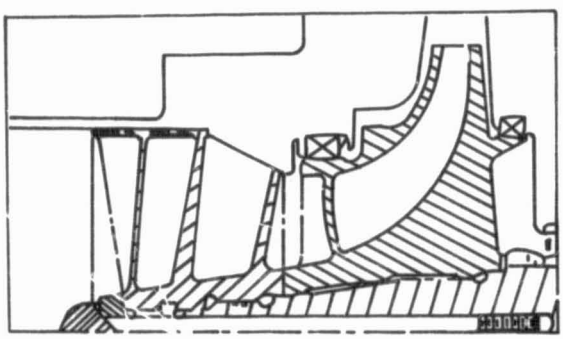

(d) Low-head inducer, shrouded

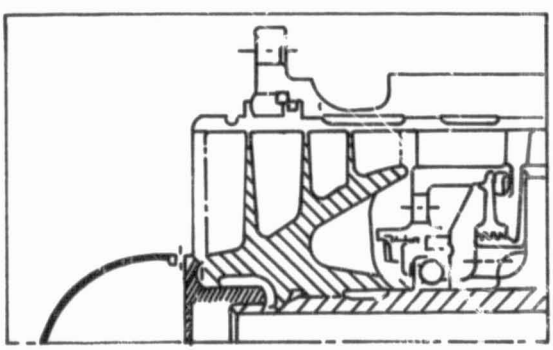

(e) High-head inducer with cylindrical tip, tapered hub

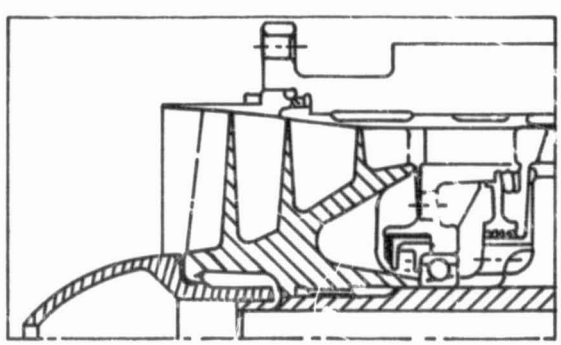

(f) High-head inducer with tapered tip and hub

Figure 1.—Basic inducer types.

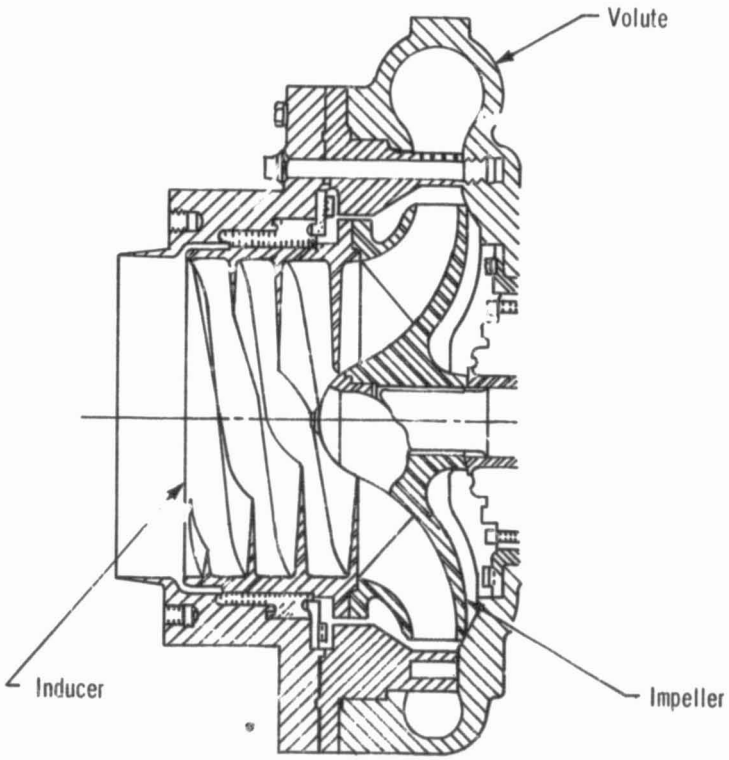

Figure 2.—Hubless inducer.

The concept, however, also has serious disadvantages: (1) the hubless inducer is difficult to manufacture, and the vanes cannot be properly machined to obtain the desired accuracy and surface finish; and (2) structurally the free floating ring of the shroud cannot carry high-speed centrifugal forces, and the inducer is reduced to a low-speed device.

Experimentally the hubless inducer has shown suction performance about equal to that of the conventional type, but somewhat worse efficiency and head coefficient. As a consequence of the performance limitations, manufacturing problems, and space requirements, the hubless inducer is not a serious contender to the conventional hub-type inducer and cannot be considered a state-of-the-art item.

2.1 Inducer Inlet-Eye and Leading-Edge Geometry

The inducer design is optimized with respect to system considerations. Suction specific speed S_s and suction specific diameter D_s are the characteristic parameters that describe the inducer suction performance in terms of shaft rotative speed n, flowrate Q, inducer inlet tip diameter D, and critical or required net positive suction head NPSH:

$$S_s = n\,Q^{1/2}\,(\mathrm{NPSH})^{-3/4} \tag{1a}$$

$$D_s = D\,Q^{-1/2}\,(\mathrm{NPSH})^{1/4} \tag{1b}$$

Details involved in determining the values of n, Q, and NPSH are provided in the design criteria monograph "Turbopump Systems for Liquid Rocket Engines."

In general, the flowrate is fixed by the engine specific impulse and thrust level. The available NPSH is a function of structural considerations that involve tank pressure and the minimum needs of the pump suction performance. The shaft speed is limited by various system considerations concerning the turbopump design. To minimize the weight of the turbopump, the shaft speed is generally chosen as high as is permitted by considerations of mechanical design of the turbopump unit and the swallowing capacity of the inducer. This swallowing capacity is limited by the vapor cavitation or by combined vapor–dissolved gas cavitation that takes place in the liquid adjacent to the suction side of the inducer blades at the leading edge. The cavitation is most severe at the blade tip, where blade speed is highest. As blade speed increases, the cavity at the leading edge becomes larger and increasingly blocks the flow. When the blade speed exceeds the value associated with the maximum obtainable suction specific speed, head rise is lost. The solution to this cavitation problem lies in careful attention to the design of the inducer inlet configuration, with special emphasis on the hydrodynamic aspects of the blade leading-edge geometry that determine the suction performance of the inducer.

2.1.1 Inlet Casing

The configuration of the inducer inlet casing is dictated by systems considerations. The preferred shape is the axial inlet in line with the inlet duct (fig. 1). This arrangement provides unobstructed flow into the inducer; it requires an overhung impeller driven from the rear through the pump scroll.

Space and systems limitations may require a 90° bend that features either single or dual inlets on opposite sides of the casing; this requirement also exists when the pump is driven from the front end (figs. 3 and 4).

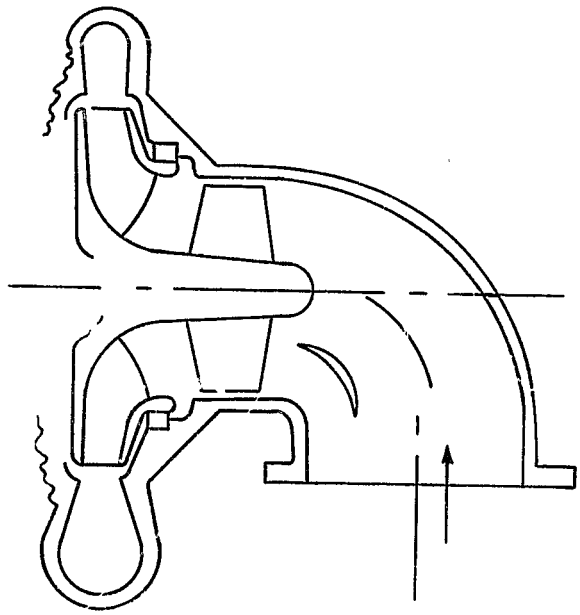

Figure 3.—Inlet elbow.

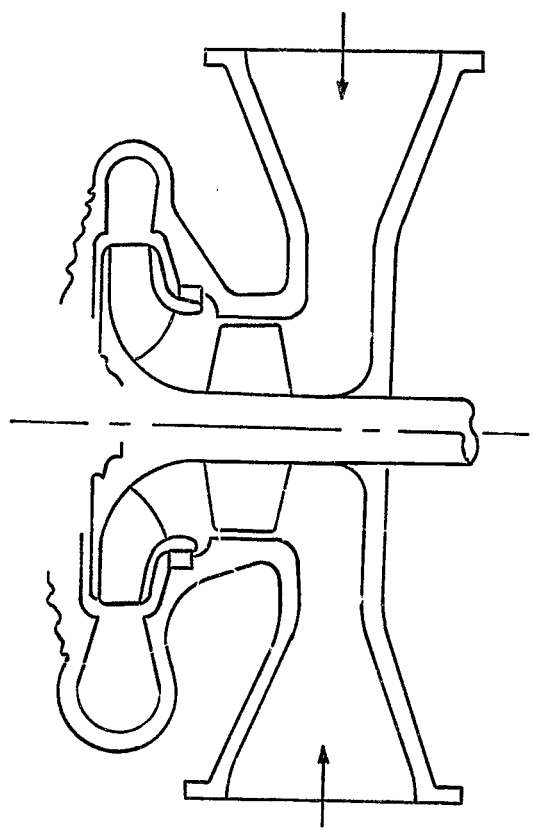

Figure 4.—Dual inlet.

The arrangement of the inlet casings for a propellant pump with fuel and oxidizer pumps back-to-back, driven through an intermediate reduction gear from an offset turbine, is shown in figure 5. Notice the combination of a mitered bend and a cascade of turning vanes to obtain a compact and efficient elbow.

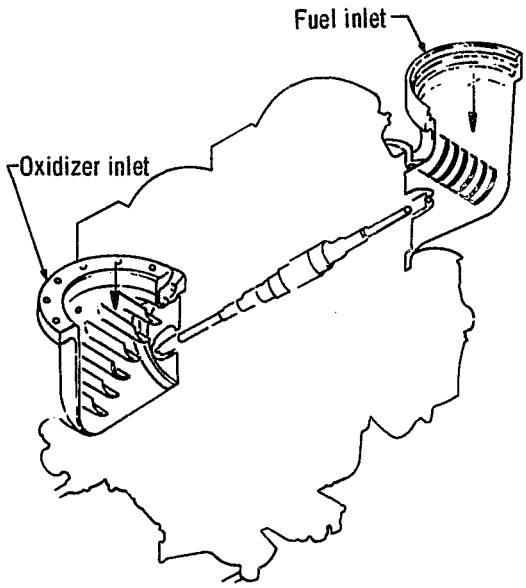

Figure 5.—Arrangement of inlet casings.

The use of vanes to obtain a uniform circumferential flow distribution for a dual inlet pump is shown in figure 6.

Development of an inlet elbow is shown in figure 7, which compares the original, unsatisfactory configuration with the final, improved configuration. The original configuration, without vanes, had unstable flow and backflow at the inner radius of the elbow. Addition of two turning vanes alone did not stabilize flow because of the abrupt turning at the original inner radius. The elbow was redesigned with an extended turning region aided by three turning vanes. The final design shown in figure 7 was effective in producing stable flow. This inlet elbow is used with the dual inlet casing of figure 6.

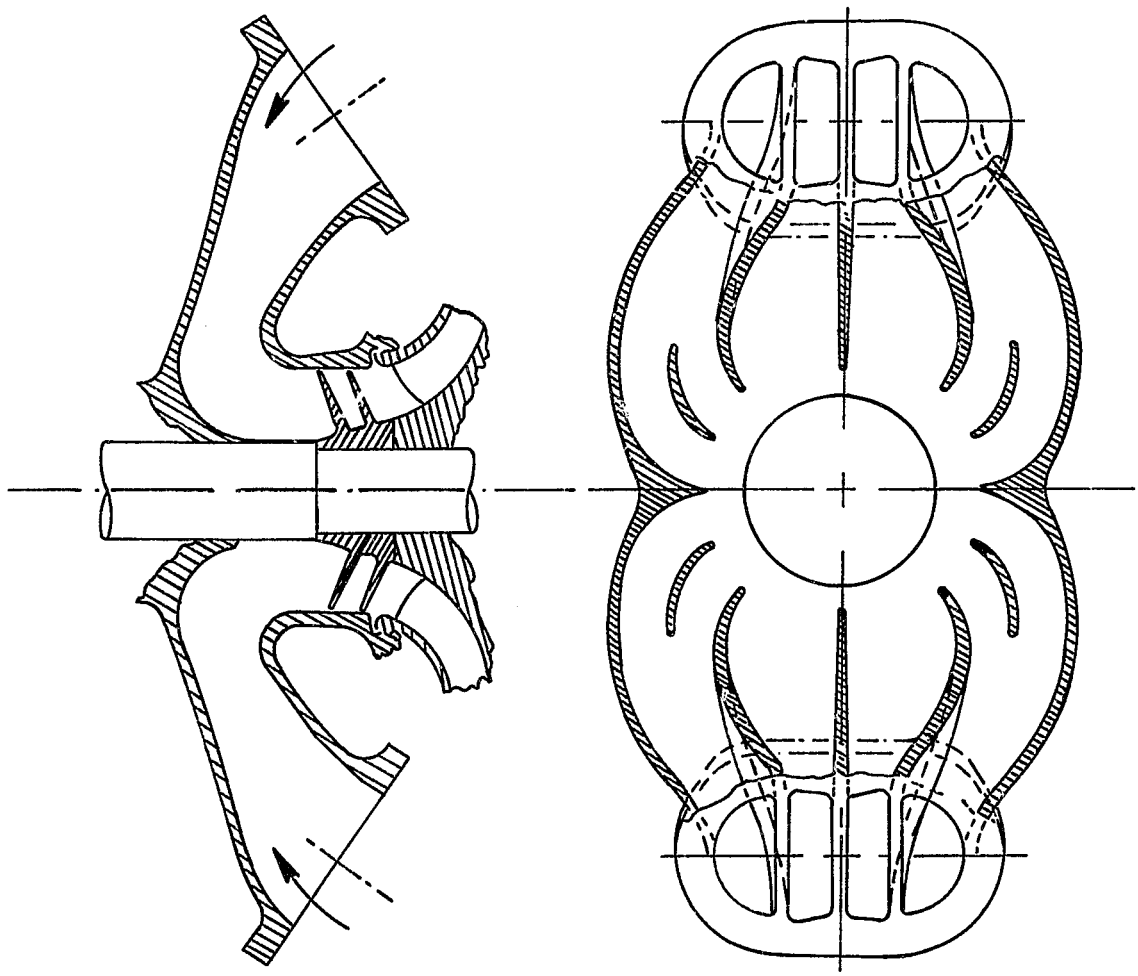

Figure 6.—Dual inlet casing.

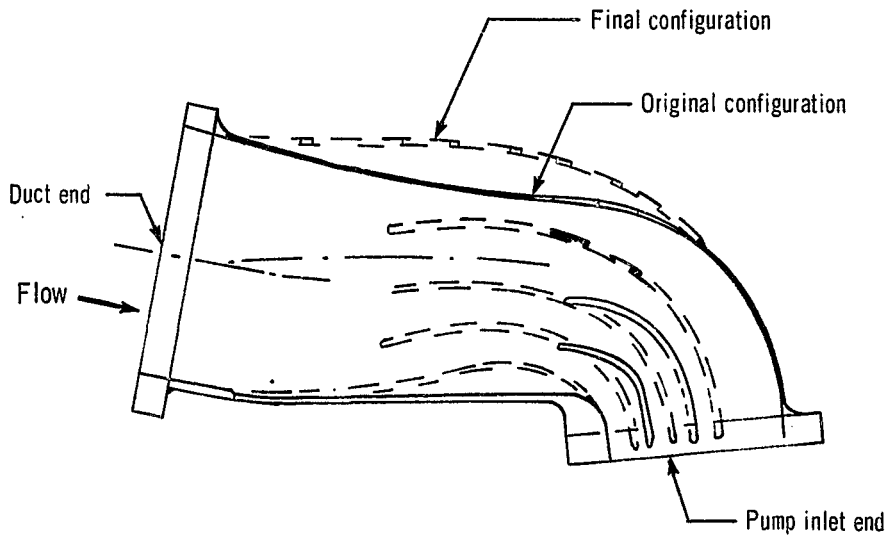

Figure 7.—Inlet elbow development.

2.1.2 Hub Size and Shape

The inducer hub diameter on the inlet end is determined primarily by the structural requirement that the hub withstand the loads from torque transmittal and the loads from the combined fluid and mass forces acting on the blades (and possibly on the hub itself in high-head inducers). In addition, the final size selected for the hub must allow for the installation and use of a spinner nut or axial bolt large enough for axial retention of the inducer.

When the pump is driven from the rear, the inducer hub diameter on the inlet end can be kept small; normally the hub-to-tip diameter ratio ν is in the range $\nu = 0.2$ to 0.4. When the pump is driven from the inlet end, the full pump torque must be transmitted through the inducer hub. In this case, the hub-to-tip diameter ratio falls normally in the range $\nu = 0.5$ to 0.6.

The contour of the inducer hub depends on the hub inlet and outlet diameters. The inlet diameter normally is chosen as small as possible consistent with structural considerations discussed in section 2.7.3. The outlet diameter is chosen to match the component following the inducer; for low-head inducers this is the impeller eye, and for high-head inducers it is an axial stage. The resulting hub contour for a low-head inducer normally is a straight taper of 8° to 12°. High-head inducers combine a low-head inducer section with a mixed-flow integral or separate section that generates additional head and matches the axial stage following it. The hub contour in this case consists of a straight taper for the inducer section, with a curved, smooth transition between this taper and the discharge diameter and slope of the mixed-flow section.

2.1.3 Inlet Tip Diameter and Contour

The most suitable inlet tip diameter D is derived from the relationship between suction specific speed S_s, blade tip cavitation number K, and flow coefficient ϕ by mathematical consideration of optimum flow conditions for maximum suction performance. For an inducer with zero prewhirl, these relationships are given by the following equations:

$$\tau = K + K\phi^2 + \phi^2 \tag{2}$$

$$S'_s = 8147\,\phi^{1/2}\,\tau^{-3/4} \tag{3}$$

$$S_s = S'_s(1 - \nu^2)^{1/2} \tag{4}$$

where S'_s is the corrected suction specific speed obtainable for zero hub-to-tip radius ratio ν and $\tau = 2g(\text{NPSH})/u^2$ is the cavitation parameter. For an inducer with zero prewhirl and a fixed hub-to-tip radius ratio the consideration of optimum flow conditions leads to the so-called Brumfield criterion (refs. 2-5) for the optimum flow coefficient ϕ_{opt}:

$$K = \frac{2\,\phi^2_{opt}}{1 - 2\,\phi^2_{opt}} \tag{5}$$

which solved for ϕ_{opt} in terms of K gives

$$\phi_{opt} = \sqrt{\frac{K}{2(1 + K)}} \tag{6}$$

The corresponding suction specific speed then is a mathematical maximum given by

$$\max S'_s = \frac{5055}{(1 + K)^{1/4}\,K^{1/2}} \tag{7}$$

showing that theoretically the suction specific speed is limited only by the minimum cavitation number K^* at which the blade will operate. Values of K^* as low as 0.01 to 0.006 have been obtained experimentally for very thin blades and small blade and wedge angles ($\beta \cong 5°$, $\alpha_w \cong 2°$).

The inducer inlet tip diameter D follows from the definition of the flow coefficient $\phi = c_m/u$, where $c_m = Q/A$ when inlet flow area A and blade tip speed u are expressed in terms of D. With proper consideration of units, there results

$$D = 0.37843\left[\frac{Q}{(1 - \nu^2)n\,\phi}\right]^{1/3}, \text{ ft} \tag{8}$$

where

Q = flow, gpm

n = shaft speed, rpm

The optimum value for D follows from equation (8) by using the optimum value for ϕ from equation (6).

To obtain the maximum suction performance, the inlet tip diameter must be held constant and equal to its optimum value at the inlet (as determined above) for an axial distance equal to one axial blade spacing downstream of the leading edge. This design practice leaves the partial cavity on the blade undisturbed until the channel section is reached.

To ensure the uniform inlet velocity assumed in the optimization, the diameter of the duct or housing upstream of the leading edge is held constant for a length equal to at least one axial spacing. Thus, the housing diameters both downstream and upstream of the blade leading edge are held constant. In most cases, these diameters are the same; but they may differ because of special considerations such as the effects of leakage flow or the use of a shroud.

The design approach outlined in this section must be modified for the hubless inducer because a nonuniform velocity distribution is induced at the blade leading edge by the strong forward sweep of the blading featured in the hubless inducer. No state-of-the-art design approach is known at present. A cross section of an actual design of an experimental hubless inducer is shown in reference 1, but no design approach is indicated.

2.1.4 Fluid Thermodynamic Effects

For an ideal fluid, which is as approximated by cold water, hydrocarbon and amine fuels, and other low-vapor-pressure fluids, the limitation on suction performance is always leading-edge cavitation in the inducer. With certain fluids there is observed a thermodynamic suppression head (TSH) that acts to decrease the critical NPSH requirements of the inducer (refs. 1, 6-25). Among the fluids known to exhibit this effect are liquid hydrogen, liquid oxygen, storable oxidizers such as N_2O_4, and hot (over 200° F) water. For liquid hydrogen this effect may be so strong that the swallowing capacity is limited only by cavitation in the inlet duct; i.e., by $c_m^2/2g = (NPSH)_{tank}$, where c_m is the meridional velocity, calculated for single-phase flow and $(NPSH)_{tank}$ is the minimum available net positive suction head in the tank at operating conditions.

Thermodynamic suppression head is an effect brought about by the decrease in fluid vapor pressure and additionally, in the case of two-phase flow, by the decrease in fluid density. The phenomenon of TSH is best defined and understood in the following mathematical formulations.

The basic condition for pump suction performance is that

$$(\text{NPSH})_{\text{required}} \leqq (\text{NPSH})_{\text{available}} \tag{9}$$

The $(\text{NPSH})_{\text{required}}$ is determined by the characteristic pump suction specific speed $S'_s{}^*$, which is obtained from pump performance with an ideal fluid (approximated in practice by cold water). From equations (1) and (4), with Q' as defined in equation (24)

$$(\text{NPSH})_{\text{required}} = (n\, Q'^{1/2}/S'_s{}^*)^{4/3} \tag{10}$$

assuming that the pump characteristic suction performance is independent of the pump fluid.

By definition, the net positive suction head is the excess of fluid total pressure p_{total} above vapor pressure p_v divided by the fluid density ρ_F at the prevailing local conditions. It follows then that the pump sees the value

$$(\text{NPSH})_{\text{available}} = \left(\frac{p_{\text{total}} - p_v}{\rho_F} \right)_{\text{at inducer leading edge}} \tag{11}$$

where p_{total}, p_v, and ρ_F are the local values measured at the inducer inlet; they are different from the values at the tank and depend on the flow conditions.

For the hypothetical ideal fluid, the NPSH value is of constant magnitude (except for line friction loss) throughout the inlet system from tank to inducer inlet under all flow conditions; i.e.,

$$(\text{NPSH})_{\text{ideal fluid}} = \left(\frac{p_{\text{total}} - p_v}{\rho_F} \right)_{\text{tank}} - H_{\text{loss}} \tag{12}$$

where p_{total}, p_v, and ρ_F are the values in the tank at its outlet, and where H_{loss} is the line head loss due to friction.

By definition, the thermodynamic suppression head is determined by the following equation:

$$(\text{NPSH})_{\text{available}} = (\text{NPSH})_{\text{ideal fluid}} + \text{TSH}, \quad \text{or TSH} = (\text{NPSH})_{\text{a}} - (\text{NPSH})_{\text{if}} \tag{13}$$

In practice, $(\text{NPSH})_{\text{available}}$ has never been measured directly, but its value has been inferred from the measured pump suction performance with various liquids by assuming that the equal sign applies in equation (9) when head breakdown occurs.

Various semiempirical correlations of TSH with fluid properties and pump parameters have been attempted (refs. 24 through 27). These correlations are based on a relationship between the thermal cavitation parameter α, the thermal diffusivity of the liquid $\mathbf{K}_L$, and the size and speed of the pump.

The thermal cavitation parameter and diffusivity are functions of the fluid properties only; i.e.,

$$\alpha = \frac{J L^2}{T c_L \frac{\rho_L}{\rho_v} \left(\frac{\rho_L}{\rho_v} - 1 \right)} \tag{14}$$

and

$$\mathbf{K}_L = \frac{k_L}{\rho_L c_L} \tag{15}$$

where

J = energy conversion factor, 778.2 ft-lb/Btu
L = latent heat, Btu/lb
c_L = specific heat of liquid, Btu/lb-°R
T = fluid bulk temperature, °R
ρ_L = liquid density, lb/ft^3
ρ_v = vapor density, lb/ft^3
k_L = thermal conductivity of liquid, Btu/(sec-ft-°R)
$\mathbf{K}_L$ = thermal diffusivity of liquid, ft^2/sec
α = thermal cavitation parameter, ft

Holl (ref. 22) combined the parameters α and $\mathbf{K}_L$ to form the thermal factor β:

$$\beta = \frac{\alpha}{\sqrt{\mathbf{K}_L}}, \text{ sec}^{1/2} \tag{16}$$

By hypothesis, TSH is a function of the fluid thermodynamic cavitation properties, the fluid velocity U_c on the cavity boundary, and the length L_c of the cavity. The variables TSH, α, $\mathbf{K}_L$, U_c, and L_c form a set of three independent, physically significant, dimensionless groups through which the functional relationship is expressible. One set of three basic groups includes (TSH/α), (L_c/α), and ($U_c L_c/\mathbf{K}_L$), from which other sets are formed by combination, e.g., (TSH/L_c), (L_c/α), and ($\beta^2 U_c/L_c$). The application of dimensionless groups to the analysis of pump performance studies requires a relation between a set of basic groups, e.g.,

$$\frac{(\text{TSH})}{L_c} = C (L_c/\alpha)^{m1} (\alpha U_c/\mathbf{K}_L)^{m2} (L_c/S)^{m3} \tag{17}$$

where the constant C and the exponents $m1$, $m2$, and $m3$ are determined by tests on similar pumps, S is the blade spacing, and U_c is a function of the blade tip speed u. So far, no such relationship with well-established values for the constants and exponents has been found.

A cavitation number K_c, based on the cavity pressure instead of the liquid bulk vapor pressure, has been defined (refs. 24 through 27):

$$K_c = \frac{p_s - p_c}{\rho_F w^2/2g} \tag{18}$$

where

p_s = fluid static pressure, lb/ft^2
p_c = fluid vapor pressure in cavity at leading edge, lb/ft^2
ρ_F = fluid density, lb/ft^3
w = fluid velocity relative to blade at tip, ft/sec
g = gravitational constant, 32.174 ft/sec^2

Venturi cavitation studies show that K_c is approximately constant while the conventional cavitation number K varies when both are measured over a large range of liquids, temperatures, velocities, and venturi sizes, provided the geometric similarity of the cavitated region is maintained (i.e., the ratio of cavity length to diameter, L_c/D_c, is constant). The studies on venturi cavitation have produced information useful in understanding the problem of thermal suppression head in pumps. On the basis of these studies, attempts have been made to predict actual values for TSH for various fluids used in pumps (ref. 25). The correlations obtained, however, do not allow successful prediction of pump performance without the availability of reference data, i.e., data on the actual performance of the pump with a liquid having TSH effects.

Fluid thermodynamic effects on suction performance are considered in the design phase by a correction on the available NPSH value. An empirical allowance for TSH is added to the tank NPSH value (less the inlet line head loss). The assumed TSH value is based on previous experience with the fluid. No theoretical prediction is attempted at present. Presently established empirical values for the Mark 10 (F-1 engine) liquid-oxygen pump (inducer tip speed: 300 ft/sec) and the Mark 15 (J-2 engine) liquid-hydrogen pump (inducer tip speed: 900 ft/sec) are as follows:

Mark 10-0: TSH = 11 ft, at 163° R
Mark 15-F: TSH = 250 ft, at 38° R

These values are used with considerable reservation, however, when applied to other pumps, because the occurrence of thermodynamic suppression head is not well understood and the effect of a change in the characteristic parameters is not known. The TSH value of a fluid increases with temperature almost as a linear function of vapor pressure (ref. 20). Tests also indicate the existence of a speed and fluid velocity effect increasing the TSH with speed (rpm) at fixed flow coefficients (refs. 28 and 29).

Another common practice to allow for the fluid thermodynamic effect empirically in the design phase is to assume a value (based on experience) for an NPSH factor Z, defined by

$$Z = \frac{2g(\text{NPSH})_{\text{tank}}}{c_m^2} \tag{19}$$

which corresponds to a TSH correction of

$$(\text{TSH}) = \frac{(Z_{\text{opt}} - Z)c_m^2}{2g} \tag{20}$$

giving the total required NPSH value

$$(\text{NPSH})_{\text{required}} = (\text{NPSH})_{\text{tank}} + (\text{TSH}) = \frac{Z_{\text{opt}}\, c_m^2}{2g} \tag{21}$$

where

$$Z_{\text{opt}} = 3(1 - 2\phi^2_{\text{opt}}) \cong 3 \tag{22}$$

for small ϕ_{opt}.

Present liquid-hydrogen pumps are able to pump two-phase hydrogen at pump-inlet vapor volume fractions up to 20 percent at design liquid flow coefficient. The basic limit to pumping two-phase hydrogen occurs when, at high flow coefficients, the flow area within the inducer blade passages becomes less than upstream flow area. When this occurs, both two-phase flow and pure saturated liquid flow will choke (ref. 30). Further experimental investigations aimed at establishing proper criteria for two-phase flow are in progress.

2.1.5 Blade Profile

In a well-designed inducer cascade, the blade profile does not interfere with the free-streamline boundary of the cavitating flow at the blade leading edge.

If so-called real fluid effects due to viscosity of the fluid and surface roughness of the blade are neglected, the flow in cavitating inducers may be adequately described by potential flow models with a simplified geometry. These models all are based on the assumption of a two-dimensional, irrotational, steady flow of an incompressible, inviscid fluid through a two-dimensional cascade of blades. The cascade and flow conditions represent those of the actual inducer at some fixed radial station.

A set of physically significant, characteristic parameters relating to the state of the fluid, the entering and leaving flows, and the geometry of the cascade is illustrated in figure 8.

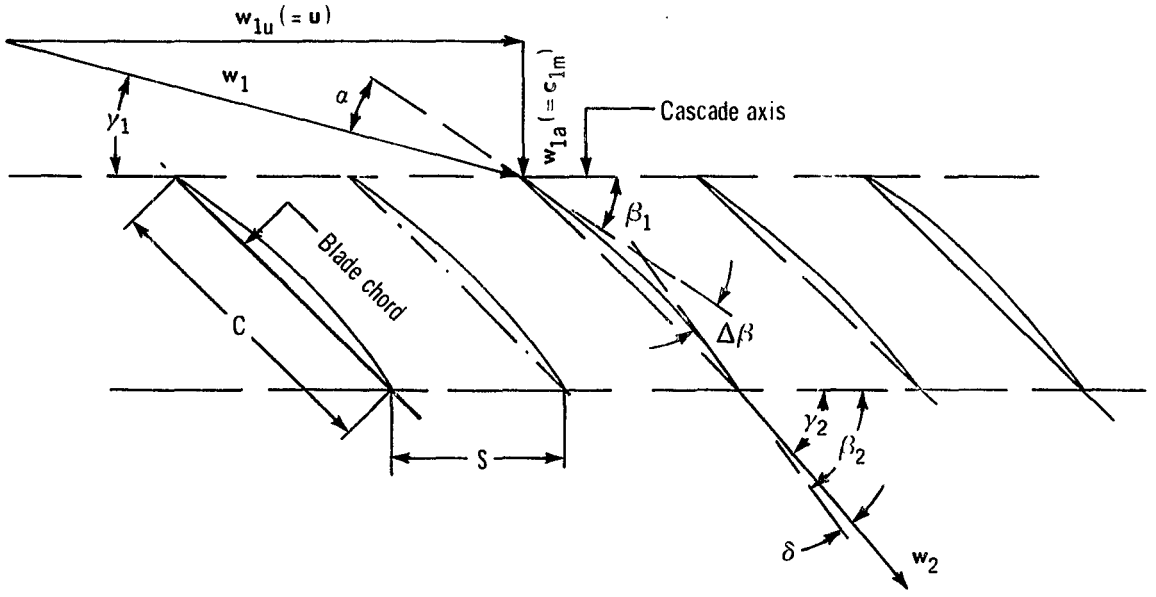

Figure 8.—Cascade and flow parameters.

The cascade geometry parameters are blade angle β, blade camber $\Delta\beta$, chord length C, and cascade spacing S. Subscripts 1 and 2 or, occasionally and more distinctly, LE and TE denote the leading and trailing edges, respectively. The entering and leaving flows are characterized by the relative velocities w_1 and w_2 and the angles γ_1 and γ_2 of these flows with the cascade axis. The velocity components normal and parallel to the cascade axis are w_m (or w_a) and w_u, respectively. These two components commonly are designated meridional and tangential components, referring to the equivalent usage for inducer flow. The meridional flow may or may not be axial but, by common usage, is always referred to as meridional because the cascade represents the meridional flow picture of the inducer. The cascade velocity w_1 is the vector sum of the two components represented by the blade velocity u and the fluid meridional velocity c_m at the inducer inlet. The inlet velocity c_m is assumed uniform over the inlet area; hence

$$c_m = \frac{4Q'}{\pi D^2} \tag{23}$$

where Q' is a corrected flowrate expressed by

$$Q' = \frac{Q}{(1 - \nu^2)} \tag{24}$$

giving the equivalent swallowing capacity of a hubless inducer.

Various models for the flow in flat-plate cascades with cavitating flow have been proposed and studied. These models differ essentially in the manner of cavity closure. There is no unique solution for a constant-pressure cavity of finite length, because the cavity can be terminated in a variety of ways. Among these cavity models are a re-entrant jet, an image plate on which the free streamline collapses, and the free-streamline wake model where the flow gradually recovers pressure on a solid boundary that resembles a wake. Experimental and visual observations indicate that, of all these models, the free-streamline wake model (wake model, for short) simulates to some extent the actual wake downstream of the cavity terminus, where intense mixing may be seen. The wake model of the flat-plate cascade with semi-infinite blades yields the simplest possible simulation of the important flow features of a cavitating inducer with partial cavitation. The theory is described and derived in detail in reference 31. For supercavitating flow with an infinite cavity, existing solutions (refs. 32 and 33) treat cascades with a finite chord length and arbitrary camber.

The wake model gives a good approximation to the cavitating flow in the inducer and is a useful tool for the inducer designer in calculating the cavity boundary. The main difficulty lies in the evaluation of the free-streamline theory as a function of cavitation number and angle of incidence of the inducer flow; the analysis involves the numerical evaluation of some complex variable relationships for the cavity shape. A computer program written to accomplish these objectives for any given inducer blade is available (ref. 34).

The cavity velocity w_c follows from Bernoulli's law and the definition of the cavitation number, giving

$$w_c = w_1 \sqrt{1 + K} \tag{25}$$

Similarly, combining this with the stagnation point condition for the velocity ratios results in

$$w_2 = \frac{w_c}{F + (F^2 - 1)^{1/2}} \tag{26}$$

where F stands for the expression

$$F = \frac{(1 + K)^{1/2} \sin \beta + (1 + K)^{-1/2} \sin (\beta - 2\alpha)}{2 \sin (\beta - \alpha)} \tag{27}$$

The wake or cavity height h_c is found from

$$\frac{h_c}{S} = \sin \beta - (w_1/w_2) \sin (\beta - \alpha) \tag{28}$$

which determines the maximum blade thickness that may be contained in the cavity with proper shaping of the leading edge (fig. 9).

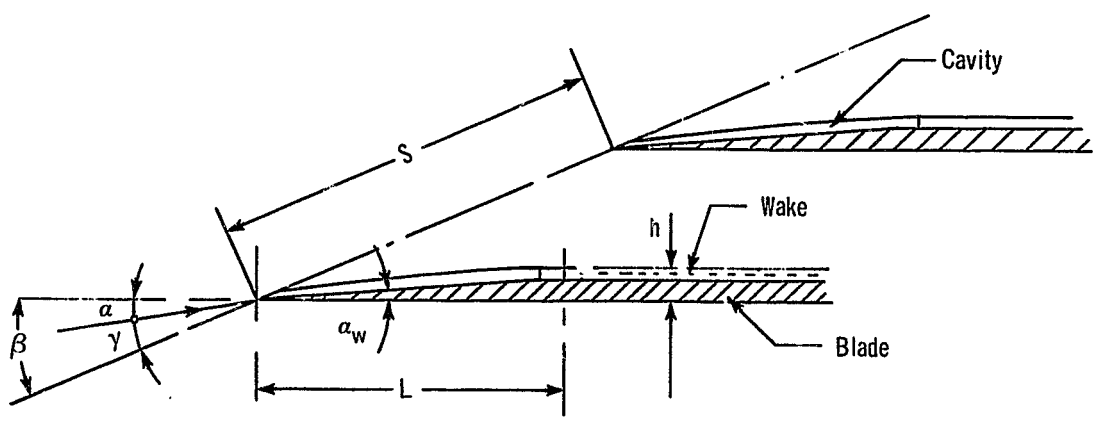

Figure 9.—Blade in cavity.

For the extreme case of supercavitation, the free streamline approaches a wedge shape at the leading edge with an angle equal to the angle of incidence α.

The cavitation number K attains its minimum value at supercavitation:

$$K_{min} = \frac{2 \sin \alpha \sin (\beta - \alpha)}{1 + \cos \beta} \tag{29}$$

When $\alpha = 0$ or $\alpha = \beta$, then $K_{min} = 0$; but these values are not realistic, because in the first case there is no deflection of the flow and in the second case there is no throughflow in the cascade. The equation does bring out clearly that, to obtain small cavitation numbers, the blade angle should be small.

At $\alpha = \beta/2$ a maximum value of K_{min} is obtained:

$$\max K_{min} = \tan^2 \frac{\beta}{2} \tag{30}$$

which also shows the need for small blade angles β to get small values of K. Because of blade thickness and boundary-layer blockage, in actual operation with a real fluid the attained values of K are approximately two to three times greater than the maximum values of K_{min}.

2.1.6 Blade Leading-Edge Sharpness

The radius of curvature of the free streamline r_{FSL} at the leading edge constitutes an upper limit for the permissible nose radius of the blade profile. In practice this radius is very small and, in case of supercavitation, $r_{FSL} = 0$. This means that the blade should be knife-sharp at the leading edge, in agreement with experimental evidence. When ultimate suction performance is required, the leading edge is made knife-sharp. However, a practical limit on the radius of the leading edge is the value $t/100$, where t is the maximum thickness of the blade profile. For large inducers (e.g., those used in the J-2 and F-1 engines), common practice is to leave the edge 0.005 to 0.010 in. thick.

2.1.7 Blade Sweep

The radial shape of the leading edge affects both the suction performance and the blade load and bending stress. Sweeping back and rounding off the radial contour of the leading edge has resulted in increases of 10 to 25 percent in suction specific speed (refs. 35 and 36). Structurally, the sweepback removes the corner flap and redistributes the blade load, thus reducing the possibility of failure. The blade wrap is reduced, but the reduction can be allowed for in the design by a slight increase in axial length. On shrouded inducers, the leading edge is usually swept forward to avoid sharp corners and to provide fillets where the blade meets the shroud.

2.1.8 Blade Cant

Canting of the blade is done for mechanical reasons only. At high blade loadings, the blade is canted forward to partially counterbalance hydrodynamic and centrifugal bending forces; also, canting produces a double curvature, which makes the blade stiffer and stronger. The backward or forward sweep of the leading edge is obtained by a face cut on the inducer blading such that forward canting of the blade results in a sweepback of the leading edge and a backward cant angle results in a forward-swept leading edge. Machining of the blade space is easier when the blade is perpendicular to the hub taper.

2.1.9 Blade Angle

The inducer suction performance is a function of the blade angle β at the leading edge.

The flow incidence angle α is chosen to minimize blade blockage. Experience indicates that for design purposes the ratio α/β is a characteristic parameter that varies with blade thickness as necessary to keep the blade inside the cavity. Values for this ratio range from a low of 0.35 for thin blades to a high of 0.50 for thick blades; the mean of 0.425 is a common design value.

2.1.10 Blade Lead

For an inducer, the best inlet configuration is the so-called flat-plate inducer, which has constant lead both radially and axially. The lead of the blade is given by

$$\Lambda = 2\pi r \tan \beta \tag{31}$$

where r is the radial coordinate on the blade.

The fluid velocity relative to the blade w varies along the radius according to the velocity diagram based on the flow coefficient at the blade tip and the inlet velocity c_m. The blade angle must vary correspondingly along the radius to maintain optimum values of α/β. For a uniform flow with zero prewhirl and small blade angles, this variation agrees well with the commonly used flat-plate inducer blade-angle variation with radius (i.e., $r \tan \beta = \text{constant}$), which is easy to manufacture.

2.1.11 Blade Thickness

The blade thickness t is determined from a combination of hydrodynamic and structural design considerations.

Hydrodynamically, the blade thickness is designed to lie inside the cavity (ref. 4) and wake of the cavitating flow at design NPSH and at 10 to 20 percent over design flow. Structurally, the blade is designed to resist the worst combination of centrifugal and pressure forces. To reduce stress concentrations at the root section, a generous fillet is provided at the hub juncture.

The result is a blade that tapers along its length from a maximum thickness at the hub to a minimum thickness at the tip.

2.1.12 Blade Camber

The head-rise capability of the flat-plate inducer is fixed at about $\psi \cong 0.075$ by the limited fluid turning angle of a straight cascade. For higher head coefficients, a cambered blade profile is required. Experiments have shown that suction performance may be maintained with a cambered blade when the blade angle at the leading edge

β_{LE} is the same as for the flat-plate cascade. In order to maintain the same cavity development, the cambered blade starts with zero curvature, and the camber gradually increases from zero at the inlet to the required amount at the discharge. The variation of the curvature follows a smooth monotone curve from zero at the leading edge to a maximum at the trailing edge. The simplest distribution of camber is given by the circular arc with the blade angle increasing steadily from β_1 to β_2 and constant curvature from inlet to outlet. A circular-arc blade has been used for small amounts of camber (i.e., a few degrees); but this blade does not satisfy the recommended variation of curvature from zero at the inlet to a maximum at the outlet, and there is some loss of suction performance. It is common practice to assume some distribution of camber on the rms (root-mean-square) diameter and calculate the corresponding head-rise distribution as a check.

2.1.13 Blade Surface Finish

A considerable amount of research (refs. 37 and 38) has been carried out on the effect of surface roughness on cavitation inception and hydraulic efficiency. It has been found, for example, that, when the measured efficiency of a hydraulically smooth specimen with a 2 μ in. surface finish (ASA) was compared with the measured efficiency of specimens that had 160 μ in. finishes, efficiency was reduced 5.9 percent with chordwise striations and 7.2 percent with spanwise striations (ref. 37). Early occurrence of incipient cavitation as an effect of surface roughness has also been observed.

2.1.14 Blade Number

When high-density fluids are pumped, the hydraulic loads on the blades require large blade chords to provide adequate bending strength. In addition, the hydrodynamic requirement for a small ratio of blade thickness to blade spacing to accommodate the blade thickness inside the cavity makes a large spacing necessary. These requirements for long chord length and large blade spacing are equivalent to a requirement for low blade numbers.

The choice of blade number affects the axial length of the inducer, which is proportional to the blade chord length. The possibility of alternate blade cavitation makes an odd number of blades desirable (ref. 39). Alternate blade cavitation is one of several possible cavitation patterns.

One-bladed inducer designs have been considered, but were given up because of balancing problems. The best suction performance is obtained with a small number of blades, normally between two and five. A three-bladed inducer is the preferred design if design considerations such as solidity, aspect ratio, and axial length permit. The blade number N is chosen with matching requirements of the impeller in

mind. Preferably, the impeller blade number is made a multiple of N to promote symmetry of flow. When the impeller blade number is a prime, however, no such choice is possible.

2.1.15 Cascade Solidity

The solidity of the inducer cascade σ affects the suction performance through its effect on blade loading and deviation angle (refs. 40 and 41). Solidity is given by

$$\sigma = \frac{C}{S} \cong \frac{L_{ax}}{\Lambda} \tag{32}$$

as a function of chord length C and blade spacing S and also as a function of blade axial length L_{ax} and blade lead Λ. For a flat-plate inducer, the solidity stays essentially constant over radius except for effects of blade sweepback. A high solidity improves the suction performance and tends to counteract cavitation-induced oscillations. For best suction performance, current practice requires $\sigma \geq 2.0$ to 2.5 at all blade sections from tip to hub, and low values for blade loading and deviation angle. This condition gives the leading-edge cavity sufficient time to collapse undisturbed by pressure fields from channel loading of the blade. By experience, any infringement on this condition has resulted in unsatisfactory performance. For instance, the employment of splitter vanes or increased camber to gain additional head rise in this inlet region has been unsuccessful.

2.2 Inducer Flow-Channel and Blade Geometry

The head rise and efficiency of the inducer depend to a great extent on the flow conditions in the channel region of the blading, i.e., the region where the blades overlap. The special problems of pump inducers with high head rise require careful design of the channel region of the blade. The blade geometry and the contours of the meridional flow passage constitute special problems for efficient design.

2.2.1 Channel Flow

The flow conditions in the channel region may be estimated for an incompressible fluid by an approximate calculation based on four assumptions:

(1) Constant radial lead,

$$\lambda = r \tan \beta = \text{constant} \tag{33}$$

(2) Simple radial equilibrium,

$$\frac{dh}{dr} = \frac{c_u^2}{r\,g} \tag{34}$$

where h is fluid static head.

(3) Perfect guidance (fluid follows blade),

$$\gamma = \beta \tag{35}$$

(4) Zero loss (100-percent efficiency),

$$H = h + \frac{c^2}{2g} = H_1 + \frac{u\,c_u}{g} \tag{36}$$

where H is the total head and H_1 is the total head at station 1.

The blade cant angle is assumed to be zero or small. Under these assumptions, the flow at an arbitrary axial station l is given by the equation for the local head coefficient,

$$\frac{d\,\psi_l}{\psi_l} + \frac{2r\,dr}{r^2 + \lambda^2} = 0 \tag{37}$$

with the solution

$$\psi_l = \frac{C_\psi}{r^2 + \lambda^2} = \frac{C_\psi}{\lambda^2}\sin^2\beta = \frac{C_\psi}{r^2}\cos^2\beta \tag{38}$$

where C_ψ denotes a constant of integration that must satisfy the continuity condition. The local velocities are given by

$$c_a = (1 - \psi_l)\lambda\omega \tag{39}$$

$$c_u = \psi_l r\omega \tag{40}$$

where ω is the angular velocity of the inducer and $\lambda\omega$ and $r\omega$ are, respectively, lead velocity and blade velocity of the inducer.

The parameters λ and C_ψ may vary with the axial station. The local total head-rise ΔH is

$$\Delta H = C_\psi\,\omega^2\,\frac{\cos^2\beta}{g} = \Delta H_{ms}\,\frac{\cos^2\beta}{\cos^2\beta_{ms}} \tag{41}$$

where ΔH_{ms} is the headrise at some convenient radial reference station, preferably the rms radius. The constant C_ψ depends on the blade blockage at the axial station considered. For a tapered blade, the integrations can be performed and the constant expressed in closed form. The local blade thickness is given by

$$t_1 = a - br \tag{42}$$

where

$$b = \frac{t_H - t_I}{r_T - r_H} \tag{42a}$$

and

$$a = t_H + b\, r_H \tag{42b}$$

Then, for an inducer with blade number = j, the constant is given by

$$C_\psi = \frac{I_{A1} - j\, I_{B1} - (Q/\lambda\omega)}{I_{A2} - j\, I_{B2}} \tag{43}$$

where I_{A1}, I_{A2}, I_{B1}, and I_{B2} are given by

$$I_{A1} = \pi (r_T^2 - r_H^2) \tag{43a}$$

$$I_{A2} = 2\pi \ln \frac{\sin \beta_H}{\sin \beta_T} \tag{43b}$$

$$I_{B1} = \frac{a\lambda}{2} \left[\frac{\cos \beta}{\sin^2 \beta} - \ln \left(\tan \frac{\beta}{2} \right) \right]_H^T - \frac{b\lambda^2}{3} \left[\sin^{-3} \beta \right]_H^T \tag{43c}$$

$$I_{B2} = - \left[\frac{a}{\lambda} \ln \left(\tan \frac{\beta}{2} \right) + b \frac{1}{\sin \beta} \right]_H^T \tag{43d}$$

The subscripts T and H denote tip and hub, respectively, and

$$\left[f(\beta) \right]_H^T = f(\beta_T) - f(\beta_H) \tag{44}$$

2.2.2 Discharge Flow

The normal low-head inducer design is used as the inlet portion of the pump impeller, which may be radial, axial, or mixed-flow type. The flow passes directly from one rotating component to another without intervening stators. As a result, no matching problems are encountered except, possibly, that of finding an optimum relative location of the two sets of blades that will prevent wakes from blades in

the upstream rotor from hitting blades in the downstream rotor. However, this normal low-head inducer design may be combined with a high head-rise channel region following the inducer proper to form a so-called high-head inducer. The matching of this combination with the following component, a stator, presents a problem, because the stator needs a radially constant head across the passage in order to operate efficiently. For this condition to exist, the inducer discharge must be a free vortex flow with a rotation that is given by the expression

$$r\,c_u = \text{constant} \tag{45}$$

This condition is difficult to obtain physically with the inducer blades, because the rotation of a helical inducer is given by

$$\frac{r + \lambda^2}{r\,c_u} = \text{constant}\ (=\omega C_\psi) \tag{46}$$

For free-vortex-flow blading, the hub angle becomes greater and the tip angle smaller than for a helix with a radially constant lead. This configuration results in different wrap angles for hub and tip and a corresponding manufacturing problem. One solution to this problem is to divide the inducer into two or more parts, with the front part consisting of the actual inducer and an extended channel region and the other parts consisting of axially interrupted blading. These inducer parts may either be on separate hubs or be machined on the same hub. If separate pieces, they must be fastened together or fastened separately to the shaft. The head is calculated for a number of streamlines, assuming simple radial equilibrium; this method has been shown to give close agreement (refs. 42 and 43) with measured values for the axial velocities. The axisymmetric blade-to-blade solutions are more accurate but are seldom used for axial flow because of their complexity.

2.2.3 Impeller-Inducer Matching

The inducer discharge dimensions must match those of the impeller eye. The requirements for the impeller eye diameter and the inducer discharge diameter may be conflicting because of head-rise limitations, in that an increase in the impeller eye diameter will decrease the impeller head but an increase in inducer discharge diameter will increase the inducer head, and vice versa. For these reasons, the exact matching of inducer discharge diameters and impeller inlet eye diameters may be impractical. With sufficient axial clearance between the two components, however, a reasonably smooth boundary of the flow passage may be drawn.

The axial clearance distance (inducer-impeller or inducer-stator) is dictated mainly by mechanical design considerations such as minimum length and weight of pump and rotor and assembly requirements. However, for inducer-stator combinations (as in axial-flow pumps), the minimum permissible clearance for safe running must be maintained. The magnitude of the permissible axial clearance depends on the stiffness of the rotor and the casing, on the rigidity of the bearings, on the differential

thermal expansion of rotor and stator, and possibly on distortions due to load and temperature. Hydrodynamic matching between inducer and impeller also requires a certain minimum clearance of the magnitude of the blade gap, which equals L_{ax}/σ. For good suction performance, the axial spacing between inducer and impeller blades is kept at least as large as this blade gap.

2.2.4 Trailing-Edge Sharpness

Sharpening of the trailing edges is not critical. Trailing-edge sharpening is used particularly in applications where it is important that the blade wake and drag of the inducer be minimized. The trailing-edge sharpening increases the head rise and improves the efficiency of the inducer. The preferred blade sharpening is centerline faired.

2.2.5 Trailing-Edge Contour

The trailing-edge contour normally is not critical and often is left straight radial. The major consideration in contouring the trailing edge is the proximity of stators, coupled with the possibility of blade flutter. The structural integrity of the blade is improved by cutting off the outer corner of the blade at the sacrifice of some solidity.

2.2.6 Discharge Angle

The fluid turning angle $\Delta\gamma$ along a streamline follows from the Euler equation for the head rise

$$g\,\Delta H_{net} = \Delta\,(u\,c_u)\,\eta_{bl} \tag{47}$$

The equation is solved for the tangential velocity component at the discharge c_{u2}, to determine the velocity triangle and the fluid discharge angle γ_2. The blade efficiency η_{bl} is assumed to be 0.85.

For low-head inducers it is satisfactory to determine the lead of the inducer based on the rms station only. For high-head inducers with free vortex flow, the lead of the inducer is determined for a minimum of two radial stations, one close to the hub and the other close to the tip, to define the blade completely.

2.2.7 Deviation Angle

The blade angle varies along radius according to $\lambda = r \tan \beta$, where the lead ($\Lambda = 2\pi\lambda$) should be determined for the mean (i.e., rms) diameter D_{ms} from the

required headrise. The discharge blade angle $\beta_{ms,TE}$ is the sum of the fluid angle $\gamma_{ms,TE}$ and the deviation angle δ at this station. The deviation angle δ is an expression of how well the blading guides the fluid. The value of δ may be estimated from rules developed for compressor blades by Carter (ref. 44) and by other investigators (refs. 45 and 46). None of the studies on deviation angle was made for inducers, but Carter's rule has given reasonably good results when modified to allow for the different flow conditions in inducers and compressors. Carter's rule is

$$\delta = M(\beta_{TE} - \beta_{LE})/\sigma^b \tag{48}$$

where

σ = solidity
b = exponent, a function of inlet blade angle β_{LE} with values in the range from 0.5 to 1.0; approximate value of b for inducers is 0.5
M = coefficient, a function of stagger angle and the location of maximum thickness; approximate values of M for inducers are 0.25 to 0.35

Carter's rule is derived from an empirical correlation between cascade parameters and experimental deviation angles for purely two-dimensional flow with constant blade height and the incidence angle of impact-free entry, essentially zero for thin blades. Sometimes a modified form of the rule, based on fluid turning angle $\Delta\gamma$, is used for flat-plate inducers with

$$\delta = 0.10 \text{ to } 0.20\,\Delta\gamma \tag{49}$$

However, because the flow is not two-dimensional and because the flow area and blade height of inducers vary from inlet to discharge, the application of Carter's rule to inducer blades involves various corrections. The blade camber usually is referred to a zero-action blade camber $\Delta\beta_0$, such that the active blade camber is given by

$$\Delta\beta_{active} = \Delta\beta - \Delta\beta_0 = \beta_{1E} - \beta_{TE,0} \tag{50}$$

Also, the incidence angle α is included with the blade camber, so that the deviation angle is found from

$$\delta = \frac{M(\alpha + \Delta\beta_{active})}{\sqrt{\sigma}} \tag{51}$$

where

$$\Delta\beta = \beta_{TE} - \beta_{LE} \tag{52}$$

and, with approximation,

$$\Delta\beta_0 = \beta_{TE,0} - \beta_{LE} \cong \left[\frac{A_1}{A_2} \left(\frac{r_1}{r_2} \right)_s - 1 \right] \beta_{LE} \tag{53}$$

which follows from continuity of flow for a helical inducer. The ratios (A_1/A_2) and $(r_1/r_2)_s$ are, respectively, the ratio of inducer inlet area to discharge area and the ratio of the radii at inlet and discharge of a stream surface s containing the blade section, e.g., at tip, hub, and rms stations.

On high-head inducers, Carter's rule is used to find the deviation angle of the vortex-type blading constituting the channel region of the inducer, such that the required camber angle of this part of the inducer blading can be established.

2.2.8 Clearance Losses

The inducer performance is strongly dependent on the effect of clearance losses. The leakage flow through the clearance has a disturbing effect on the main flow entering the blading, tending to cause early separation. It is the source of the first visual occurrence of cavitation and lowers the suction performance correspondingly at partial head dropoff, but not at supercavitation.

The clearance losses are a function of the ratio c/L of radial clearance to blade length or, preferably and more precisely, of the ratio of clearance to passage height $(D - d)/2$. This latter expression is particularly appropriate in extreme cases where the clearances are large. A study of inducers with cylindrical tip contour indicates that the loss in performance may be estimated from the following empirical relationships:

The effect on S_s follows from

$$S_s = S_{s,0}(1 - k_s \sqrt{c/L}) \tag{54}$$

and the effect on ψ follows from

$$\psi = \psi_0(1 - k_\psi \sqrt{c/L}) \tag{55}$$

where (from experiments) $k_s = 0.50$ to 0.65 and $k_\psi = 1.0$. The subscript 0 refers to zero clearance.

The clearance effect is compensated for in design by additional blade length and work input.

2.2.9 Shrouding

Shrouding of inducers serves three principal functions: control of clearance; reinforcement of structure; and protection of blades, liner, and housing from erosion or cavitation damage.

(1) Clearance control.—By use of a shroud, the blading may be run with zero clearance losses except for the leakage past the shroud; this leakage is controlled by using close-clearance wearing rings of a suitable material with good rubbing and wearing qualities, e.g., polychlorotrifluoroethylene (Kel-F).

(2) Structural reinforcement.—By proper design, the shroud can be made to distribute the blade forces more uniformly, both among the blades and over the axial extent of the blading. Also, the shroud absorbs some of the bending load that otherwise would have to be carried by the blade root. With cambered blades, the stiffening effect of a shroud is especially strong; blade vibrations are prevented or dampened, and the stress level due to bending is reduced.

(3) Erosion or cavitation damage protection.—In certain cases the flow around the end of the blades, in the clearance space, has produced cavitation erosion of a nonmetallic lining (e.g., Kel-F) used to improve rubbing characteristics of the blading. Cavitation erosion will destroy such a soft liner in a very short time. The only solution then is to use a shrouded rotor. Shrouding of inducers occasionally is used as a fix for design shortcomings discovered in the development period. Tests on similar inducers with and without shrouds have shown the shrouded inducer to have slightly worse performance (refs. 47-49). The shroud may or may not cover the full axial length of the blading (see sec. 2.4.7).

2.2.10 Blade Geometry Description

For fabrication of an inducer with the desired blade geometry, the geometry must be expressed in terms suitable for manufacturing and inspection purposes, i.e., the blade shape must be described by coordinates that can be obtained by direct measurements on the inducer. It is common practice to convert the blade description in terms of blade angles, blade thickness variation, and leading- and trailing-edge geometry into a set of coordinates for both pressure and suction sides of the blade. This conversion ordinarily is done by a manufacturing division department for master dimensions; a special computer program is used. It may be done on the drafting board by making an accurate layout of the blading. A tolerance band is always specified for the theoretical coordinates to ensure repeatable performance of the inducers.

2.3 Inducer Inlet Line

Inducer cavitation performance is dependent on the inlet flow conditions that in turn are dependent on the inlet-line configuration and the inducer operating point. These relationships are discussed in the sections below.

2.3.1 Inlet-Line Configuration

Any configuration that causes a loss in NPSH or creates a nonuniform flow distribution will be detrimental to the inducer suction performance. To obtain smooth flow into the inducer eye, the inlet-line area is blended smoothly into the inducer inlet area without any sudden diameter changes or breaks in the wall contour. Any projection of a rib or stud into the inlet flow or imperfect matching of duct and inducer inlet-casing diameters has a detrimental effect on the suction performance and smooth operation of the inducer. Sudden expansion and contraction sections of the inlet line are avoided because of the high loss coefficients involved and the strong turbulence created. When turbopump installation in the engine system requires a bend in the line, a vaned elbow or a large-radius elbow with a low loss coefficient and a uniform exit-flow distribution is used, depending on space limitations (see also sec. 2.1.1.1).

2.3.2 Inlet-Line Fluid Velocity

It is important that no cavitation occur anywhere in the inlet line. To achieve this objective, the velocity of the fluid at any point in the line is kept below its velocity at the inducer inlet. Even fluids with large fluid thermodynamic effects, such as liquid hydrogen, are kept well below the maximum obtainable cavitating velocity of

$$c_{m,\,max} = \sqrt{2g\,(NPSH)_{tank}} \tag{56}$$

at which the static pressure equals the vapor pressure. Fluids that do not exhibit fluid thermodynamic effects do not exceed the value

$$c_m = \sqrt{\frac{2g\,(NPSH)_{tank}}{3}} \tag{57}$$

2.3.3 Inlet-Line Heat Transfer

For cryogenic propellants, heat transfer from the atmosphere to the tank and the inlet line may raise the temperature of the fluid by an amount that significantly lowers the NPSH available to the inducer. An uninsulated liquid-oxygen line exposed to the atmosphere builds up an insulating layer of ice from the moisture in the air. Apart from the benefit derived from this effect, liquid-oxygen lines often carry thermal insulation to protect them against thermal radiation and convection heating in space. An uninsulated liquid-hydrogen line exposed to the atmosphere does not develop an ice layer but acts as a condenser, liquefying the air around it. Thus, it has a high rate of heat transfer, and the duct fluid experiences a rise in temperature of several degrees.

It is common practice to reduce such heating of hydrogen by using a vacuum-jacketed inlet line. The line, including bellows, is a double-wall design.

2.3.4 Bypass Flow

The balance piston bypass flow of axial-flow liquid-hydrogen pumps can create undesirable effects if not reintroduced in a careful manner. Whenever the geometry of the inducer and the relative pressure level of the bypass fluid permit, this fluid is discharged behind the inducer. Otherwise, it is reintroduced into the main flow either through a hollow inducer shaft and spinner into the center of the inlet duct or through a duct back to the inlet duct in a manner that causes a minimum of disturbance to the main flow.

2.3.5 Backflow and Prewhirl

Backflow occurs at low flow (about 90 percent or less of design value) as a result of local head breakdown in the tip region. The detailed effects of backflow on inducer performance have not yet been established. Since backflow is a phenomenon of uncontrolled flow, it is desirable to attempt to reduce it or to control its effects.

Incorporating a backflow deflector in the inlet line (fig. 10) may improve the suction performance at low flow (refs. 50-52). Below nominal flow (i.e., between 20 and 90 percent of design flow) where backflow becomes significant, the deflector results in increased head, reduced critical NPSH, and lower amplitudes of low frequency oscillations. Above nominal flow, the deflector has a detrimental effect.

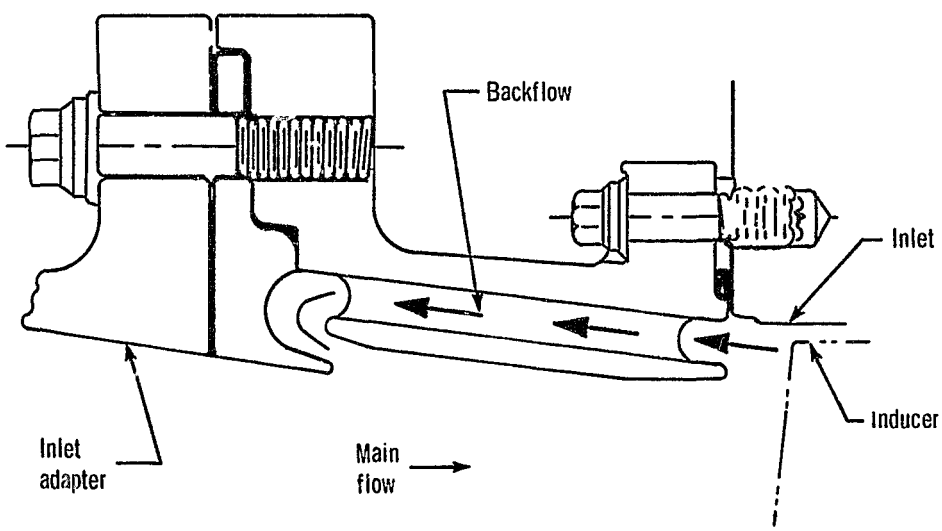

Figure 10.—Backflow deflector configuration.

Data using the backflow deflector are limited, however, and further development work is needed on deflector design and operation.

Backflow at the inducer inlet may cause erroneous inlet pressure readings if the data station location is close to the inducer inlet. In this event, it is difficult to obtain reliable NPSH values in suction performance tests. To get inlet pressure readings that are not influenced by upstream flow disturbances caused by the inducer, the data station is located, when possible, at least 20 diameters upstream of the inducer. The accuracy of the NPSH values is also improved by the use of an inlet section having a locally enlarged area that muffles the backflow generated by the inducer at low flows and low NPSH. This design is purely a device for improving pressure measurement. It does not improve flow conditions in general and, in fact, may cause a slightly increased head loss of the flow. The design is incorporated only for measurement purposes and is removed when no longer required.

Prewhirl of the inlet flow may be generated through momentum transfer by mixing the inlet flow with high-velocity fluid taken from the pump discharge and injected through a ring of orifices in a tangential direction upstream of the inducer. Prewhirl introduced in this manner has improved flow distribution and reduced flow instabilities that occur when the pump is throttled. At throttled conditions, the suction performance was increased a maximum of 50 percent with the use of about 10-percent recirculation (refs. 53-55). The use of prewhirl by mixing is still an experimental feature and has not yet become an established design practice. When pumping liquid hydrogen, heating of the pump fluid due to recirculation may become a limiting factor, but no data to that effect are available.

2.4 Mechanical Design and Assembly

All the fundamental considerations for performance, structural integrity, and manufacturing must be coordinated into a complete and unified layout providing all the information needed for the manufacturing process. Mechanical design and assembly constitute the backbone of inducer design.

2.4.1 Hub Configuration

Figures 11 and 12 show the typical hub configuration for low-head, low-speed applications and high-head, high-speed applications. Hydrodynamically, the hub diameter should be small on the inlet end and should match the fluid passage of the downstream component (impeller, axial flow blade, etc.) on the discharge end. Structurally, however, the hub must be sized to sustain the loads imposed, i.e., the hub radial thickness must provide a foundation capable of developing the necessary centrifugal and bending strength of the blades along the blade-hub junction. The hub normally is made somewhat longer than the blade plus the fillets to allow room for machining and tool runout.

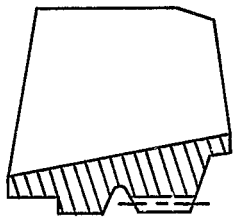

Figure 11.—Conventional low-head inducer hub.

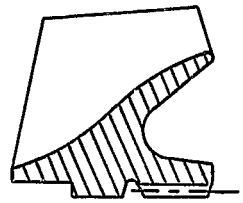

Figure 12.—High-head inducer hub.

2.4.2 Blade Root Juncture

The fillet at the blade root is a purely structural means to avoid or reduce stress concentrations (ref. 56), improving fatigue life correspondingly. Hydrodynamically the fillet represents a deviation from the true blade profile desired; it protrudes through the cavity and disturbs the flow. Where stress concentrations cannot be avoided, their effect may be minimized by polishing or shot peening (ref. 57) the blade surface.

2.4.3 Shaft Dimensions

The pump shaft is part of the general pump design, but the inducer end of the shaft is determined by the inducer designer to fit the requirements of the inducer drive and attachment. These requirements include adequate splines or keyways to drive the inducer, means for axial retention (spinner nut or bolt), possibly a hollow shaft to provide for return flow, and any special provisions for assembly and retention of rotating parts.

The impeller torque normally is much greater than that of the inducer, which means that the shaft and hub under the impeller must be larger than those under the inducer. The torque load is strongly dependent on pump speed and flowrate, and may have cyclic variations during periods of flow instabilities. The inducer power torque load can be transmitted to the hub from the driving shaft by several methods. Shear pins or keys are normally used for low-torque applications, and splines are used for high-torque applications.

2.4.4 Piloting

Radial piloting is a major concern in high-speed rotating hardware where rotor balancing and critical speeds are of importance. Positive piloting even under maximum operating conditions constitutes an established practice.

2.4.5 Axial Retention

Studs and bolts used for axial retention of inducer rotating parts are highly loaded to provide the clamping force necessary to withstand the maximum inducer axial forces that occur during operation. Great care is taken not to overstress fasteners during assembly; precalculated amounts of stretch are used as a measure of the actual preload.

The axial retention of the inducer is the major factor in preventing any relative motion between two parts that can cause fretting corrosion at the interface. Relative motion is particularly critical for oxidizer pumps, where the heat generated might initiate an explosion. To prevent any relative motion, the axial preload is kept high enough to provide positive axial piloting at all times, and the method of applying the preload is controlled accurately. When this procedure is not possible, fretting is minimized by the use of various types of surface treatments such as plating or the use of a dry-film lubricant with the oxidizer.

An example of an arrangement for axial retention is shown in figure 13.

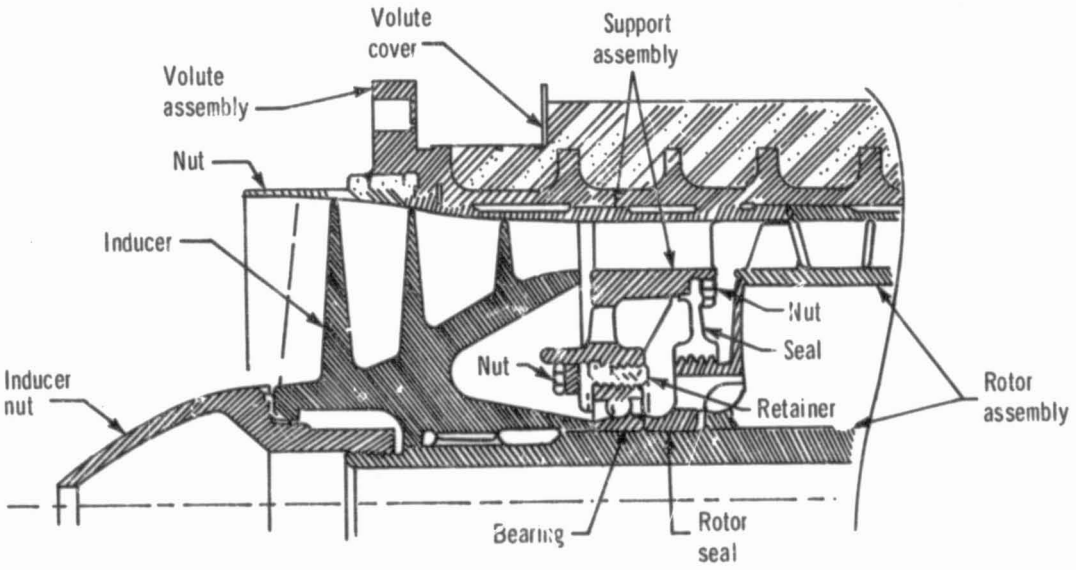

Figure 13.—Axial retention arrangement.

2.4.6 Clearance Effects

The blade tip clearance, the gap between the inducer blade tip and the pump inlet-tunnel inner surface, is a critical parameter (sec. 2.2.8). When the clearance is inadequate, shaft loads may cause inducer deflections such that interference with the housing will occur. The resultant interference may induce loads of such a magnitude that blade failures occur or sufficient heat is generated to cause chemical reactions or explosions in the case of oxidizer pumps. The effect of blade rubbing

is strongly dependent on the blade and housing material and the fluid environment. For instance, high-speed rubbing of titanium blade tips against the steel housing in fuel inducers has not produced unusual wear or galling.

The dimensions of the matching components, rotor and housing, where rubbing might occur are of critical importance in the estimation of the effect of stress and strain and of thermal expansions and distortions on the running clearances. A detailed study of these effects precedes the final determination of the blueprint dimensions of rotor and housing.

Cryogenic pumps often are tested initially in water. In this test condition, the rotor assembly runs at a temperature much different from that of the pump operating conditions, with a large effect on running clearance. Therefore, great care is taken to identify, calculate, and account for all possible deflections, displacements, and thermal expansions and distortions so that the effective clearances are at all times within the operational design allowables.

2.4.7 Shroud

As discussed in section 2.2.9, a shroud is often used to obtain clearance control. However, in high-speed inducers, a shroud cannot support itself as a free-floating ring but must be carried by the blades. This limitation restricts the use of a hubless inducer to low-speed applications. Present manufacturing practices allow the shroud to be welded or brazed onto the blade tips or allow the inducer to be cast as one piece. Inducers can be cast with very little machining or cleanup required except for the leading-edge and trailing-edge fairing, which should be kept smooth. The leading edge is usually swept forward on shrouded inducers to avoid sharp corners and to provide fillets at the shroud-to-blade junctures. The shroud may or may not cover the full axial length of the blading.

2.4.8 Misassembly

In the assembly of built-up rotors, the possibility of misassembly exists whenever a part can be mounted in more than one position. Various practices are used to preclude the possibility of misassembly. These usually take the form of minor modifications to the hardware that prevent mating the parts when they are not in the correct position.

2.4.9 Rotation Direction

All the various components of a rotating assembly obviously must be designed for the same direction of rotation. It is an established practice to coordinate design efforts and avoid problems of mismatched direction of rotation by making a preliminary axonometric projection of the assembly that shows clearly the direction of rotation (fig. 14). Copies are furnished to all designers on the job.

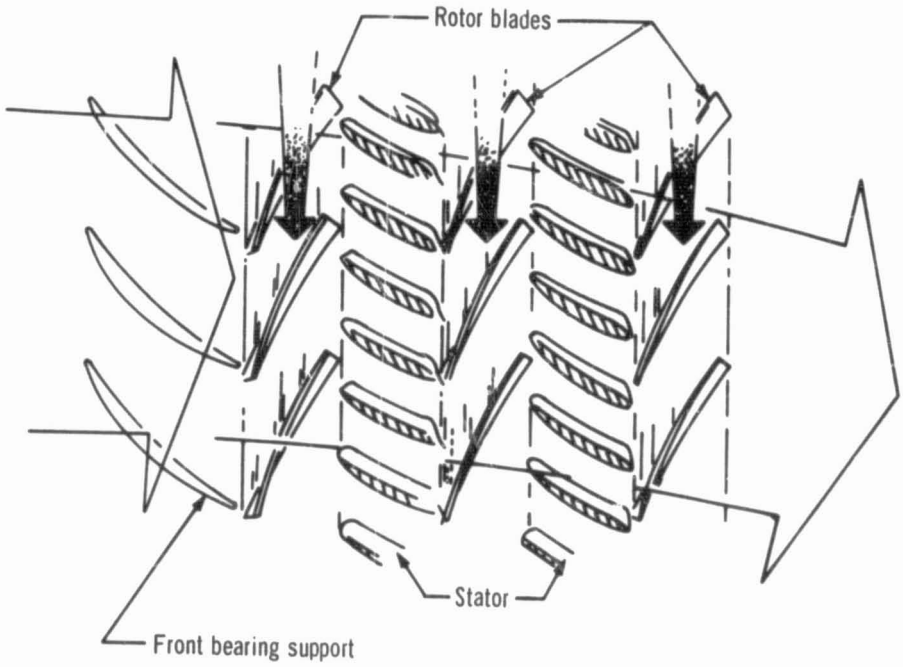

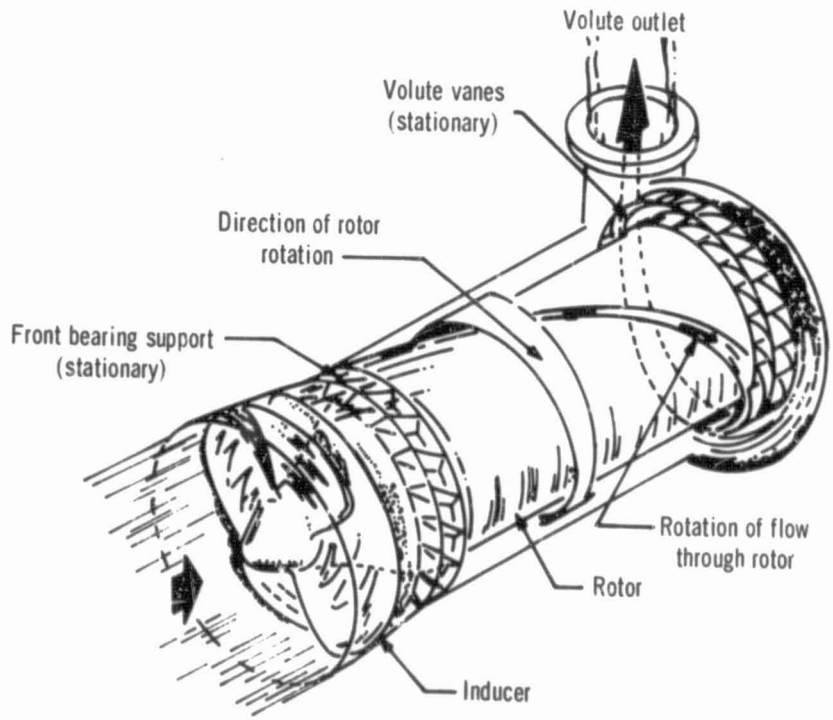

Figure 14.—Turbopump flow pattern.

2.4.10 Inducer Balancing

Because the inducer is part of a high-speed rotor system, it must be well balanced to obtain stable running. Inducer components are balanced separately to specified limits, depending on pump size and speed, mainly by removal of material. Material is removed either by drilling holes in the hub parallel to the axis or by thinning and fairing the blade tip. The conventional way of balancing is to remove material from the heavy side of the part. In aerospace designs, however, space and weight limitations often do not provide sufficient material to allow removal for balancing. Sometimes weighting must be used instead. For instance, for aluminum parts, the addition of lead plugs can increase the possible amount of correction by a factor of 3 to 4.

For oxidizer pumps the danger of entrapping contamination always exists. For that reason, holes or crevices in the inducer (such as tapped holes for the addition of screws) are undesirable because contaminants may collect there. Only metal removal is used as the method for balancing these pumps. Although with hydrocarbon fuels and hydrogen there is little or no concern with respect to chemical compatibility of the propellant with contaminants, there is a potential for the reaction of hydrazine base fuels with contaminants such as iron or rust (ref. 58). These materials can catalyze the decomposition of monomethylhydrazine, and the resultant gases can cause cavitation in turbomachinery.

2.4.11 Cavitation-Induced Oscillations

In most inducers, pressure and flow oscillations occur over some region of the operating NPSH and flow range. The oscillations of concern are in the low-frequency range, 5 to 40 Hz, and are the direct result of the hydrodynamic coupling of the inducer with the flow system of which it is a part. These oscillations can be of sufficient magnitude to impair the inducer performance in a pumping system. No specific criteria for absolute stability are known. Although there have been observations on trends or effects that are considered beneficial (refs. 59-67), the understanding and successful prediction of these cavitation-induced oscillations require further research.

Three methods, none of them a proven and consistent success, have been tried (refs. 59-67) to eliminate or reduce the inducer-generated pressure oscillations:

(1) Drilling holes in the blades.—The holes tend to stabilize the cavity and thus eliminate oscillation. Hole drilling is still very much an art in that there is little knowledge of how cavity behavior is affected by holes. Inducers of different designs do not act alike, and the required hole pattern is unpredictable from one inducer design to another. Rebalancing of the inducer is required if holes are drilled.

(2) Physically attaching wedges to the inducer blade.—These wedges are attached to the suction side of each blade near the tip. The purpose of the wedge

is to provide a solid surface upon which the blade cavity can close, thus stabilizing its position. This practice may be harmful to the suction performance. Rebalancing of the inducer is required if wedges are attached.

(3) Increasing the tip clearance.—This practice is the most ineffective and most harmful. It degrades the suction performance (NPSH) and, in most cases, does not change the pressure oscillation pattern.

2.5 Material Selection

The material selected for pump inducers must possess a combination of strength, chemical reactivity, and special properties suitable for the intended use.

The use of given values for the strength properties of the inducer material must take into account the effect of random variations in materials composition, the effect of variations in treatment from batch to batch, and the spread of test results. To put the design procedure on a firm basis in this respect, it has become an established practice to base the design stress level on the minimum guaranteed properties in accordance with principles stated in reference 68 (par. 1.4.1.1, Basis A).

2.5.1 Strength

Inducer materials normally are selected from the alloys of stainless steel, titanium, and aluminum. The respective specific densities of these preferred alloys are approximately 8.0, 4.5, and 2.7; they therefore represent a wide spectrum of material densities. The strengths of these materials vary somewhat in the same order as the densities. For applications involving inertia loading, the strength-to-density ratio (often somewhat misleadingly called strength-to-weight ratio) is an important parameter for material selection; for other types of loading (e.g., hydrodynamic, static preload in assembly, thrust forces), the strength itself is the important parameter. In particular cases where minimum blade thickness is of overriding concern for high suction performance and where the hydrodynamic loading causes large bending moments, the material with the highest strength is preferred.

The selection of a specific material from those listed above is further limited by considerations of chemical reactivity, cavitation erosion, and the need for special properties such as ductility, notch toughness, etc.

2.5.2 Chemical Reactivity

Material selection for pump inducers is governed by considerations of compatibility with the pump fluid and operation. Of special concern are the explosion hazard for oxidizer pumps, hydrogen embrittlement for liquid-hydrogen pumps, and general corrosion effects.

Titanium alloys are preferred for fuel inducers because of their high strength-to-density ratio and superb resistance to cavitation erosion. They are not used for oxidizer pump applications because of chemical reactivity; they propagate fire violently or show rapid reaction when ignited by high-temperature friction conditions.

Titanium alloys offer no problem with hydrazine, UDMH, and water (refs. 69 through 73), but they are not compatible with liquid fluorine or liquid oxygen or with a mixture of these fluids (FLOX). Ignition has been observed at different impact levels on titanium alloys tested in liquid fluorine; similar tests on titanium samples in oxygen have shown that ignition in liquid oxygen is even more severe than in liquid fluorine. In all tests with fluorine, even though the reaction was initiated, it failed to propagate itself; whereas in oxygen (in 1 test out of 26) the ignition became general and the sample was burned completely (ref. 74).

IRFNA causes rapid intergranular corrosion of titanium alloys. The corrosion products are pyrophoric and present an extremely dangerous explosive hazard. Titanium alloys used with uninhibited nitrogen tetroxide (brown N_2O_4) undergo stress corrosion cracking. In addition, titanium alloys are not compatible with N_2O_4 when used in rotating components where rubbing or fretting can occur. High-speed rubbing in N_2O_4 has caused ignition of the titanium alloy; however, unlike the pyrophoric reaction with oxygen, the fire does not propagate once the rubbing ceases.

Aluminum alloys are compatible with the cryogenic liquids: hydrogen, oxygen, nitrogen, FLOX, and fluorine. At room temperature they are satisfactory with water, IRFNA, UDMH, and N_2O_4. One aluminum alloy (7075-T73) is free of stress corrosion cracking and is selected where residual stresses have been imposed on the part. However, aluminum alloys are susceptible to cavitation erosion.

K-Monel and Inconel 718 are often used in inducers for low-speed, cavitating oxidizer pumps. The blades can be thinner than those of aluminum, and the resistance to cavitation erosion is much higher.

Steel inducers used for development testing in the water test facility tend to deteriorate quite rapidly because of rusting. To protect the shiny surface that facilitates the visual observation of the cavitating flow in the inducer, some form of rust protection may be used. This protection also helps maintain the shape and sharpness of the leading edge.

Titanium and aluminum alloys may be quite sensitive to exposure to certain chemical cleaning fluids or solvents that can cause stress corrosion, with correspondingly impaired fatigue strength for later application. Use of such fluids and solvents is avoided.

2.5.3 Special Properties

The thermal environment in cryogenic pumps creates problems of brittleness and

loss of elongation in materials otherwise acceptable for use in inducers. The content of interstitial elements such as oxygen, hydrogen, and nitrogen adversely affects the ductility and notch and fracture toughness of titanium alloys at cryogenic temperatures. Therefore, there has been established an extra-low-interstitial (ELI) grade of the Ti-5Al-2.5Sn alloy (and also the Ti-6Al-4V alloy) in which the interstitial elements oxygen, nitrogen, and hydrogen and the substitutional element iron are controlled at lower-than-normal contents. Ti-5Al-2.5Sn ELI alloy forgings are employed for pumping liquid hydrogen in several experimental fuel pumps. The Ti-5Al-2.5Sn ELI alloy was selected because of its high strength-to-density ratio at the temperature of liquid hydrogen (−423° F); notch toughness and ductility remain at acceptable levels down to −423° F.

The resistance to cavitation damage is an important consideration in material selection for high-suction-specific-speed inducers. However, because of the short operating time of rocket engine turbopumps, it is more of a problem in the development stage than in the actual mission.

Inducers made from annealed Ti-6Al-4V forgings are used to pump RP-1. The Ti-6Al-4V alloy replaced an aluminum alloy inducer of the same design because of its greater strength and significantly greater resistance to cavitation erosion. Because the inducer operates at ambient temperatures, Ti-6Al-4V of normal interstitial content is used in this application.

The finished surface of aluminum inducers is no harder than Rockwell B88 and requires some surface protection to reduce handling damage and cavitation erosion. Aluminum inducers normally are protected with an anodic coating. When the inducer is operated in fluorine or in any of the storable propellants IRFNA, N_2O_4, and UDMH, the coating will dissolve slowly. This dissolution does not present a problem in normal operational use, but when the inducer is used repeatedly, as in development programs, the coating is renewed after use to maintain surface protection.

After the critical requirements of strength, ductility, and erosion resistance have been satisfied, there remain the manufacturing considerations. Here, ease of machining, forging and casting characteristics, and weldability dictate the choice of material. Titanium alloy machining is similar to that of stainless steel. However, relatively high tool pressures are required for cutting titanium and, as a result, cutting tool must have quite rigid supports. Furthermore, the elastic modulus of titanium alloys (16.5×10^6 psi) is nearly one-half that of iron- and nickel-base alloys. Titanium alloy workpieces thus are more likely to flex under high tool pressures. On this account, tooling fixtures must hold the workpiece rigidly and the cutting tools must have rigid support. The combination of high tool pressures and high flexibility of the workpiece can make the machining of complex passageways and of cantilevered blades extremely difficult. Machining costs for parts made from titanium alloys are much greater than for comparable parts made from aluminum alloys. However, titanium alloys are considered much easier to machine than such alloys as Inconel 718 or Rene' 41. Titanium alloys have a much smaller degree of work hardening than do austenitic stainless steels and a much lower surface hardness (e.g., R_c 36 vs. 50) than do high-strength steels (e.g., 4340) of comparable strength-to-density

ratios. Forging titanium alloys is more difficult than forging aluminum alloys and most steels. Titanium alloys are readily weldable by gas, tungsten arc, or electron beam processes. Titanium casting is not yet an established, state-of-the-art practice.

2.6 Vibration Considerations

The typical inducer is exposed to oscillatory pressure loading during operation. The oscillating pressures are induced by flutter, cavitation, upstream obstructions, or other pressure-wave generators that exist in the pumping system. Because inducer blade failures are typically fatigue-oriented, effort to prevent resonant vibration of the blade is warranted. Designs relying on built-in damping due to shrouds have not been too successful. The typical high-head inducer blades, which are designed for high-speed operation, normally are rigid enough to place their natural frequencies well above the cavitation-induced, high-amplitude, low-frequency pressure oscillations (1 to 100 Hz).

A vibration analysis of an inducer design is difficult because of the uncertain knowledge of the amplitude and frequency of the exciting forces and the complexity of the mathematical analysis required to determine the response of the elastic structure in terms of resonant frequencies and damping properties. Despite the difficulties, a vibration analysis is essential to achieving a design that minimizes the probability of inducer blade failures due to high-frequency fatigue.

2.6.1 High-Frequency Fatigue

The most common cause of blade failure in turbomachinery is fatigue fracture induced by high-frequency alternating stresses, which are proportional to the vibration amplitude of the blade. To prevent fatigue failure, the oscillatory stresses are kept below the endurance limit (level of stress at which the material can endure an unlimited number of cycles). Ideally, the blade frequency and response to a forcing function should be predicted by analytical means, and the stress level and fatigue life calculated on this basis. As noted, this analysis usually is not possible for inducer blades because of the complexity of the analysis and the unknown nature of the forcing function (refs. 75 and 76). However, inducer fatigue or vibration failures have been few; in general, the main part of canted inducer blades has proven much too rigid to be prone to vibration failure (ref. 77). The critical parts of the blade in this respect are the leading-edge and trailing-edge regions (ref. 78).

2.6.2 Resonance

Because of the uncertainties involved in determining the oscillatory stress levels in inducer blades, it is common practice to avoid operation at resonant frequencies. This is done by modifying either the forcing frequencies or the blade natural frequencies by various means such as changing the number of wake generators (ribs,

vanes, etc.), changing the shaft speed, or making the blade stiffer. By experience, only first- and second-order harmonics have proven critical in inducer operation.

2.6.3 Self-Induced Vibration

Another source of vibration failure is self-induced vibration that causes blade flutter at the inlet corner of the blade. This flutter has not been a serious problem, but it is best avoided or minimized by trimming back the blade to remove the corner portion that is susceptible to flap. Blade flutter at the trailing edge has not been a problem in inducer-impeller combinations, but it is a consideration in inducer-stator combinations.

2.6.4 Determination of Blade Natural Frequencies

Theoretically, the blade natural frequencies are determined by the blade geometry and material. In practice, however, certain corrections and modifications are applied to the theoretical or nominal values to account for the effect of blade dimensional tolerances, the stiffening effect of the centrifugal force, variations in material elastic properties with temperature, and virtual-mass effects caused by the surrounding medium.

Variations in blade geometry due to dimensional tolerances affect the blade natural frequencies and produce frequency bands. The frequency increases when the root has maximum thickness and the tip minimum thickness, and decreases when the converse is the case. Therefore, the blade frequency may have any value inside the band of frequencies corresponding to the blade tolerance band.

The centrifugal force on the blade has a restoring component that adds to the elastic force, resulting in a stiffer blade. As a consequence, natural frequencies tend to increase as speed is increased.

The material elastic properties vary with temperature, and at operating temperatures these properties may be quite different from those at ambient conditions. The effect of the change on the blade natural frequency is considered when the results of vibration tests in air are reduced to inducer operating conditions.

The blade resonant frequency is directly proportional to the square root of the blade stiffness and inversely proportional to the square root of the mass in motion. When the blade vibrates, the mass in motion consists of the mass of the blade and the mass of some fluid in a space near the blade (i.e., the virtual mass). Because of the effect of the virtual mass vibrating with the blade, the blade frequency changes when the temperature (and therefore the material modulus of elasticity E) changes as well as when the fluid density (and therefore the mass in motion) changes. Calculating the mass of the blade is trivial, but no method exists for calculating the

virtual mass. The virtual-mass effect is estimated from the results of vibration experiments normally conducted in a convenient test fluid (for instance, water, if cryogenic applications are involved). The data are interpreted for the actual pump fluid by scaling the experimental results to account for the differences in fluid densities relative to the density of the blade material.

Analytical methods for calculating inducer blade frequency are complex. The exact solution of the partial differential equations governing the displacements and stresses due to time-dependent excitation forces usually cannot be obtained. Results obtained from numerical methods are limited and at best approximate. Therefore, the natural frequencies are always determined or verified by experimental methods.

2.7 Structural Considerations

The design of an inducer for maximum hydrodynamic performance must be tempered by structural design considerations. This section summarizes the critical considerations and methods involved in the structural analysis of the inducer design.

2.7.1 Blade Loading

The inducer blade loading analysis involves two distinct areas: leading-edge loading and channel loading. In low-head inducers, most of the head is developed in the leading-edge region; the remaining part of the blade is lightly loaded, and only the leading-edge loading need be considered. For high-head requirements, a large part of the head is developed in the channel region; the blade loading in that part of the inducer becomes large, and the channel loading must be included in the structural analysis. The leading-edge loading is calculated by a computer program such as that provided in reference 79. The channel loading is calculated by computer programs based on an axisymmetric or blade-to-blade solution of the noncavitating inducer flow. Another approach for determining the channel loading is to use the theory of simple radial equilibrium to calculate the pressure distribution on the blades (sec. 2.2.1).

The blade loading consists of both steady-state and alternating loads. Both kinds of loads arise from the same sources: inertia and fluid effects. High-performance inducers are designed to operate under partial cavitation. During part of component testing, the inducer is operated in deep cavitation with pressure forces approaching zero. To allow for this condition, the blade is also analyzed for centrifugal loads alone. Alternating (periodic and random) blade loads are induced by flow oscillations and instabilities. In addition, wakes and reflected pressure pulses from an obstruction (a bearing support or stator) can cause cyclic blade loading.

Because analytical values of the dynamic pressure loads are not available, a percentage of steady-state load normally is assumed to provide a margin of safety against high-frequency fatigue failure; the assumed value of 20 percent has given satisfactory results.

The inducer thrust, of concern for shaft and bearing design, is calculated from the flow conditions and the inducer layout. Unsymmetric flow in inducers has produced radial forces equal in magnitude to 30 percent of the axial thrust. The hydrodynamic blade loading depends on the density and the cavitation properties of the fluid. The temperature of the fluid is an important parameter in respect to material properties. Development tests of an inducer often are performed in a test fluid different from the pump design fluid. The effect on structural design may change stress levels and operating temperatures enough to make it desirable to use a different material for the development test model.

2.7.2 Blade Stress

Three methods to calculate the critical stresses in the inducer blade are available.

One method simplifies the analysis by dividing the blade into a series of independent pie-shaped beams, cantilevered from the inducer hub. Shell continuity is taken into account by an averaging technique and a plate correction factor. The beam loading is determined from the pressure profile for each segment. To correct for angular difference at hub and tip caused by blade twist, the effective center of curvature based on the hub and tip length for the blade is found for each segment. The pressure loading and bending moments are then calculated for an effective pie shape with center at the center of curvature. This analysis ignores tangential stress and circumferential beam action and tends to overestimate the bending moment at the hub.

The second method models the inducer as an axisymmetric shell of revolution (a canted blade being modeled by one or more conical shells for the critical sections) from which moments and stresses are obtained.

The third method is the most accurate, but also the most time-consuming. In this method the blade is divided into a number of finite triangular plate elements, for which a stiffness matrix is set up and solved for the displacement (refs. 80-82). The basic steps in the finite-element technique are as follows: The structure is divided into many elastic elements, which are connected to each other at their corners (called nodes). In general there are three displacements and three rotations and corresponding forces at each node. A square symmetric element stiffness matrix k_i is then determined. This matrix relates the column matrix of nodal forces f_i to a column matrix of nodal deflections δ_i by the matrix equation

$$f_i = k_i \, \delta_i \tag{58}$$

which expresses the equilibrium conditions for the ith element.

The particular method selected depends on cost and availability of computer facilities. To save cost and time, a simple beam or axisymmetric-type analysis is used to rough-size the blade. When the final design has been established, the stress analysis is refined by the finite-element method.

Regardless of the analytical technique used, the calculated stresses at the blade ends, where it joins hub or shroud, are amplified with a stress-concentration factor. This practice allows for stress concentrations at the blade root that have caused fatigue failures.

2.7.3 Hub Strength

Critical stress regions exist in the inducer hub at various locations. One critical area is in the vicinity of the blade root, where failures have occurred because of insufficient strength of the hub wall. Another critical area is the undercut or hollowed-out hub profile at the discharge end of high-head inducers. Stress concentrations here have caused fatigue failures in the hub as a result of discontinuities at the blade juncture or at holes and splines in the hub.

In general, little information on inducer burst speed is available. Thus, the only approach is to utilize data from disc testing together with parameters for material ductility and ultimate strength. The present state of the art of disc design is based on the experimental observation that the average tangential disc stress σ_{AT} is more characteristic of disc failure than the maximum calculated disc stresses. Essentially, failure occurs when the average tangential stress exceeds a certain fraction f_b of the ultimate tensile strength F_{tu} of the material. The value of f_b, which is called the burst factor, is determined experimentally as a function of the elongation of the material and a design factor f_d equal to the average tangential stress divided by the maximum tangential stress. Various configurations of discs classified by the design factor f_d have been tested and the experimental data plotted (ref. 83); the results are given in figure 21 (presented in sec. 3.7.3).

The average tangential stress is defined as the centrifugal force on one-half the disc divided by the cross-sectional area carrying this force. It may be obtained from the calculated elastic stress distribution by

$$\sigma_{AT} = \frac{1}{A_H} \int \sigma_t \, dA_H \tag{59}$$

where A_H is the area of the inducer-hub meridional cross section over which the integral is taken and σ_t is the local tangential stress. The speed at which the inducer hub would rupture or yield excessively because of centrifugal stresses is called the burst speed or yield speed, respectively.

2.7.4 Shaft Shear Section Strength

The inducer shaft shear section transmits the inducer torque. It is sized with consideration to the steady-state power torque, the alternating power torque, and the axial stress at the shear section (refs. 56, 68, and 84). Because the rotor alternating torque

is unknown, a rotor alternating shear stress equal to 5 percent of the steady-state shear stress was assumed for the Phoebus engine (Mark 9) and J-2 engine (Mark 15-F) axial-flow hydrogen pumps. This approximation has provided adequate reliability for these pumps.

2.7.5 Safety Factors

The structural integrity of a part customarily is ensured by establishment of a value greater than unity for the ratio of the stress capability of the part material to the calculated stress on the part. In specifying this ratio, or safety factor, it is the practice to consider only the minimum guaranteed values for material properties; these values are established by military standards or by equivalent statistical tests.

Some uncertainty exists concerning fatigue data. Before construction of the Goodman diagram (ref. 56), fatigue data obtained from polished laboratory specimens are modified to account for the effects of surface finish, temperature, erosive or corrosive environment, material grain size, surface residual stress from machining, and type of loading (tension-tension vs. bending).

Safety factors obtained for a particular design are dependent on the technique used in the stress analysis. Care must be exercised in comparing safety-factor values obtained from different sources.

2.7.6 Hub Stress Verification

Because the analytical methods for stress analysis and failure prediction are approximate in nature, an experimental verification is performed for highly stressed, complex components such as the inducer hub. The burst speed is determined by spin testing to failure an inducer provided with suitable instrumentation.

2.7.7 Inducer Proof Test

High-speed inducers are proof-tested by prespinning each part during the fabrication process to provide partial quality assurance. Prespinning each inducer has additional benefits in that local yielding occurs at areas of high strain concentration such as bolt holes, splines, and keyways. This yielding produces favorable residual stresses that effectively prestress the part and prevent the occurrence of yielding during operation.

Card #20

3. DESIGN CRITERIA and Recommended Practices

3.0 Head-Rise Capability

The inducer shall generate sufficient head to prevent cavitation from impairing the suction performance of the impeller or stator following it.

For design purposes, an estimate of the NPSH requirement should be made by using either of two essentially different approaches: (1) the NPSH may be calculated from values of the suction specific speed previously measured for impellers of similar design, or (2) the NPSH may be based on an estimate of the cavitation number requirements for hydrofoils similar in form and profile nose radius to the actual impeller blades. A good way to make this latter estimate is to let

$$1 + K = C_p \tag{60}$$

where C_p is the pressure coefficient of a similarly shaped airfoil, which may be obtained from any collection of airfoil data (e.g., ref. 85). Then, use the energy equation to get

$$1 + \tau = (1 + K)(1 + \phi^2) = C_p\,(1 + \phi^2) \tag{61}$$

An approximate value of C_p for an uncambered airfoil is between 1.3 and 1.5. To estimate K, the single airfoil C_p should be corrected for blockage effects by increasing it in the ratio of the blockage factor squared.

The head generated by the inducer at a given speed is a function of the flow-channel and blade geometry. These subjects are treated in detail in sections 2.2 and 3.2.

3.1 Inducer Inlet-Eye and Leading-Edge Geometry

3.1.1 Inlet Casing

The inducer inlet casing shall provide free, uniform, and undisturbed axial flow into the inducer.

It is recommended that an axial inlet be provided by mounting the inducer on the end of the pump shaft, the inducer being driven from the rear through the scroll of the pump. If engine arrangement or space limitations prohibit the use of a straight axial inlet from the tank or at least several diameters of straight ducting to reduce flow distortions, the alternate solution is to use a dual inlet casing or a vaned elbow. The

casing should be carefully tailored, with smoothly contoured flow passages that match flow areas to local flow requirements so that velocity changes are reduced while the flow is gradually turned into the axial direction.

3.1.2 Hub Size and Shape

The inducer hub shall be as small as possible consistent with structural requirements, and its outlet end shall match the hub of the following stage.

To reduce blockage area for the flow and provide for best suction performance, it is recommended that the hub-to-tip diameter ratio be kept between 0.2 and 0.4 for rear drive and between 0.5 and 0.6 for front drive. Structural and mechanical suitability must be verified by analysis. The hub should be contoured from inlet to outlet so that the hub taper joins smoothly with the impeller hub taper and the hub diameters match. High-head inducers featuring an additional mixed-flow section should provide smooth transition between the taper of the inducer section and the taper of the stator section. Subsequent calculations of hydrodynamic blade loading may show a need for minor modifications of the hub contour.

3.1.3 Inlet Tip Diameter and Contour

3.1.3.1 Tip Diameter

The inlet tip diameter shall be derived from mathematical consideration of optimum flow conditions for maximum suction performance.

The inlet tip diameter should be obtained mathematically from the relationship between suction specific speed S_s, blade tip cavitation number K, and flow coefficient ϕ as follows:

(A) When the suction performance is specified in terms of Q, n, and NPSH, the blades must operate at the highest possible value (K_d) of the cavitation number K.

For an inducer with a fixed hub-to-tip radius ratio and no prewhirl, this condition leads to Brumfield's criterion (ref. 2) for the optimum flow coefficient, which, expressed in terms of the corrected suction speed of the inducer, gives the (cubic) equation in ($2\,\phi^2_{opt}$):

$$\frac{2\,\phi^2_{opt}}{(1 - 2\,\phi^2_{opt})^{3/2}} = \left(\frac{5055}{S'_s}\right)^2 \tag{62}$$

With good approximation, the solution may be expressed by S'_s as

$$\phi_{opt} = \frac{3574/S'}{(1 + \sqrt{1 + 6(3574/S'_s)^2})/2} \tag{63}$$

For the small values of ϕ_{opt} (about 0.10 or less) encountered in inducer design, the divisor approaches unity.

From equation (5),

$$K_d = \frac{2\phi^2_{opt}}{1 - 2\phi^2_{opt}} \tag{64}$$

From equation (8),

$$D_{opt} = 0.37843 \left(\frac{Q}{(1 - \nu^2) n \phi_{opt}} \right)^{1/3}, \text{ ft} \tag{65}$$

This procedure solves the problem of finding optimum operating conditions and the corresponding maximum operating cavitation number K_d for an inducer with a design point specified by Q, n, and NPSH.

(B) When only two of the three performance parameters—Q, n, and NPSH—are given, maximize the suction specific speed while assuming a certain blade cavitation number K^*.

This practice leads again to Brumfield's criterion, from which

$$\phi_{opt} = \sqrt{\frac{K^*}{2(1 + K^*)}} \tag{66}$$

which determines the inlet diameter, and

$$S'_{s,\,max} = \frac{5055}{K^{*1/2}(1 + K^*)^{1/4}} \tag{67}$$

showing that the suction specific speed is limited only by the K^* value, which should be as small as possible. The actual K^* value used is an empirical number and must be based on previous experience with similar designs.

The relationship between the important parameters K, ϕ, Z (secs. 2.1.4 and 3.1.4), and S', characteristic for suction performance may be presented in a very convenient manner by an S'_s-D'_s chart, where D'_s is the corrected suction specific diameter. Figures 15 and 16 show S'_s-D'_s diagrams covering the whole range of practical pump operation. The values satisfying the Brumfield criterion are plotted in the curve for optimum D'_s.

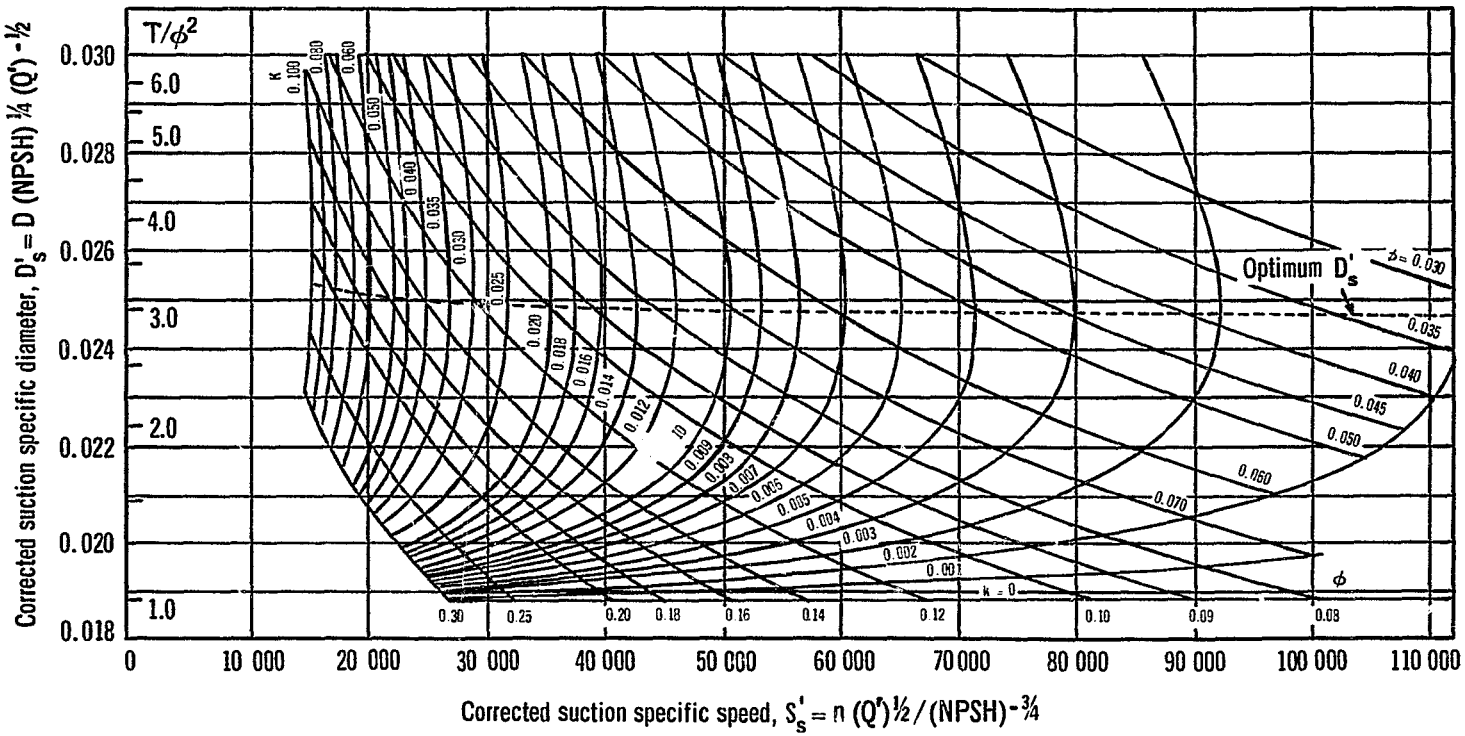

Figure 15.—S'_s-D'_s chart (zero pre-rotation), high-speed range.

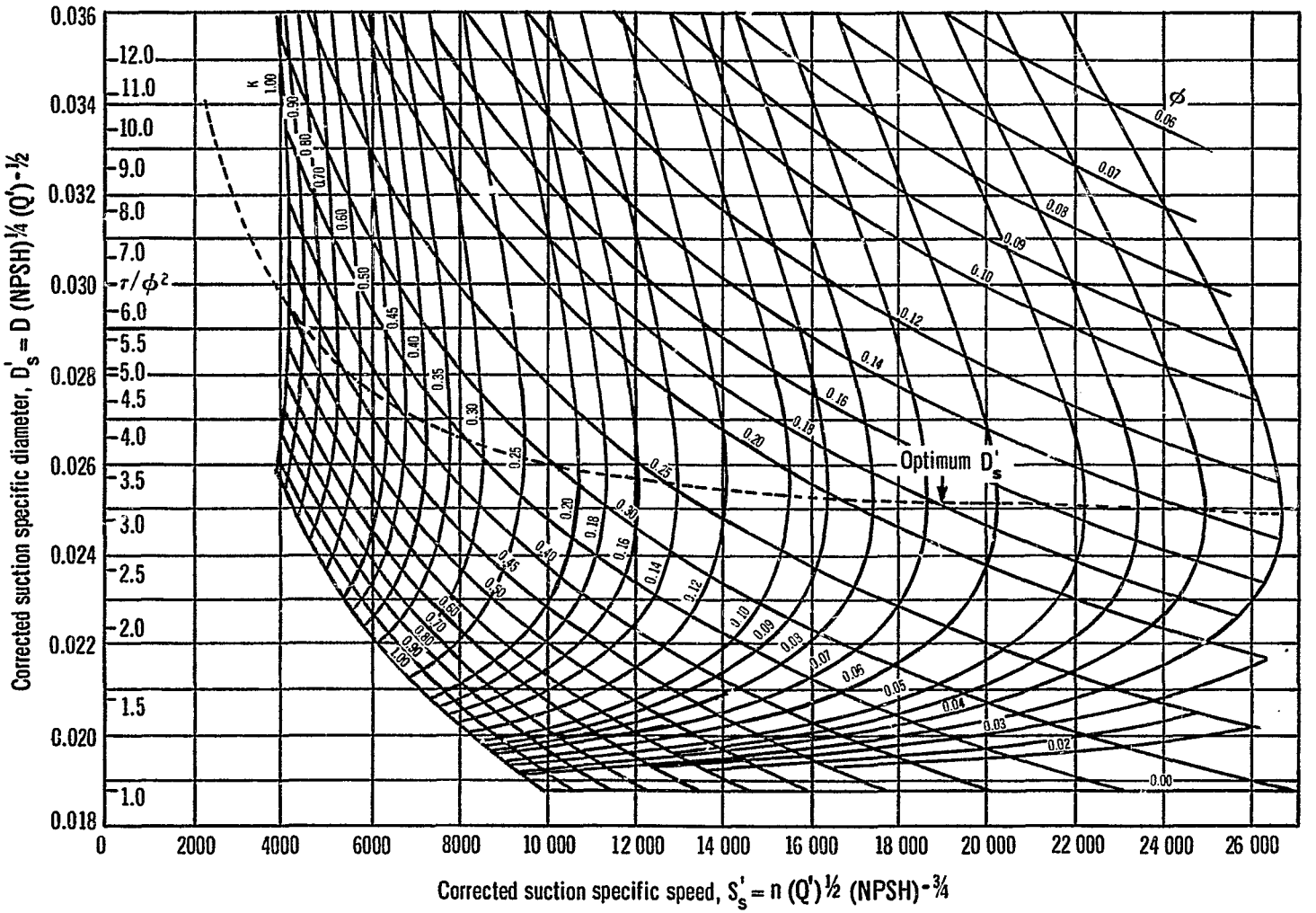

Figure 16.—S'_s-D'_s chart (zero pre-rotation), low-speed range.

The S'_s-D'_s diagram may be used in the following ways:

(1) To check the suitability of an existing design for suction performance at various operating points.
(2) To determine the effect on suction specific speed of changing the pump fluid for different values of Z.
(3) To determine optimum flow coefficient and inlet diameter required to meet suction performance specified in terms of the parameters n, Q, and NPSH.

3.1.3.2 Tip Contour

The inducer tip contour shall maintain the optimum flow conditions on the blade until the channel section is reached.

The tip contour should be held cylindrical at its optimum value at the inlet for an axial length at least equal to an axial blade spacing ($= \pi D/N \sin \beta$) and the inlet duct should be constant diameter on this length, both downstream and upstream of the leading edge for an inducer with a straight inlet. For an inducer with an elbow in the inlet, the upstream cylindrical length should at least be doubled for optimum suction performance.

3.1.4 Fluid Thermodynamic Effects

Fluids with high vapor head shall not produce unexpected fluid thermodynamic effects on suction performance.

Fluid thermodynamic effects, important for cryogenic fluids, should be accounted for by applying a TSH correction to the tank NPSH, then subtracting friction loss in inlet line to obtain the available NPSH at the inducer inlet:

$$(\text{NPSH})_{\text{available}} = (\text{NPSH})_{\text{tank}} + \text{TSH} - H_{\text{loss}} \tag{68}$$

The value of TSH cannot be predicted for an arbitrary inducer design and condition of operation; however, semiempirical correlations of TSH with fluid properties and pump parameters have been made. Tests of experimental inducers have shown that the fluid thermodynamic effects vary appreciably with the liquid, liquid temperature, rotative speed, flowrate, and inducer design. It is recommended that reference be made to recent technical literature to obtain experimental values of TSH for an inducer similar in design to the one being considered.

3.1.5 Blade Profile

The blade profile shall not interfere with the free-streamline boundary of the cavitation flow; that is, the blade must stay inside the cavity and wake at operating conditions.

It is recommended that the blade wedge angle α_w (fig. 17) be determined from

$$\alpha_w = \beta - \beta_w \tag{69}$$

where β is the blade angle and

$$\beta_w = \text{arc tan } (1.10\,\phi_d) \tag{70}$$

ϕ_d being the design flow coefficient. The numerical factor 1.10 in the equation means that the inducer blade will be inside the cavity for up to 110 percent of design flow and will present no additional blockage near the leading edge beyond that of the cavity.

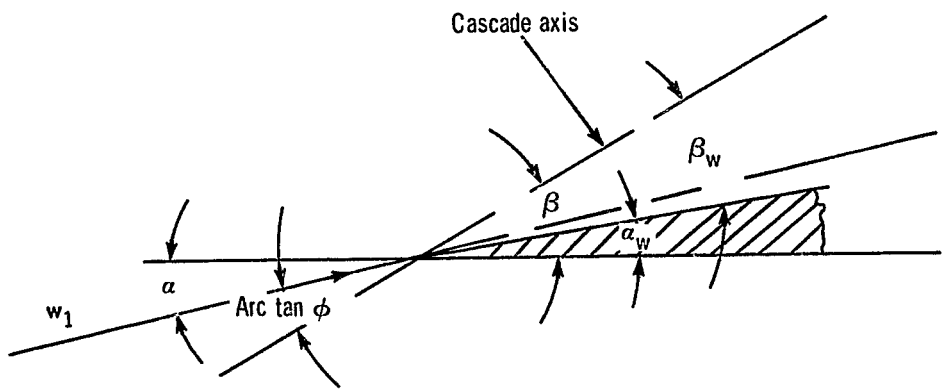

Figure 17.—Wedge angle.

If this factor is chosen larger than 1.10, the operating range becomes wider but the blade becomes very thin and may present a stress problem. The blade sharpening described is the so-called suction-side fairing of the blade (ref. 86). When stress conditions are severe and some suction performance may be sacrificed, the blade fairing may be modified by combining the suction-side fairing with a similar amount of sharpening on the pressure side to obtain centerline fairing. All sharpening should blend smoothly into the blade thickness. This simplified approach to leading-edge design has given good results. However, when very high suction performance and blade loading are required (over 40,000 S_s), the blade should be designed to match exactly the free-streamline boundary of the cavity at the highest flow (110 percent) so that the best guidance for the flow and the strongest leading edge may be obtained.

3.1.6 Blade Leading-Edge Sharpness

The blade leading edge shall be as sharp as consistent with practical limitations of strength and manufacturing considerations.

A practical measure for the sharpness of the blade is the maximum permissible leading-edge radius R_{LE} of the blade profile. It is recommended that the practical limit on leading-edge radius be

$$R_{LE} \leqq 0.01\, t \tag{71}$$

where t is the thickness of the blade profile at the particular radial station.

3.1.7 Blade Sweep

The leading-edge radial shape or contour shall improve suction performance and increase the mechanical strength of the blade.

The leading-edge radial shape or contour should be swept back for an unshrouded inducer and swept forward for a shrouded inducer. For structural reasons, the cutback in wrap angle at the tip for a sweptback leading edge should be equal to or greater than the wrap angle of the blade fairing at the hub. Then the blade will have reached its full thickness at the root when the leading-edge contour reaches the tip diameter and the blade forces attain their full value. The loss in solidity due to the cutback at the tip should be compensated for with a corresponding increase in axial length such that the solidity is maintained at its full value.

It is recommended that the leading-edge sweepback be an arc with a radius not less than the length of the blade fairing l_w. The outer part of the arc may be tangent to the inducer circumference for a minimum size sweepback (of radius l_w). The inner part of the arc should be radial, i.e., the leading edge should be radial next to the hub to provide room for the blade fairing.

3.1.8 Blade Cant

The cant angle shall be a compromise of its effects on blade bending stress, machining of the blade, and the leading- and trailing-edge geometry.

The inducer-blade cant angle should counterbalance pressure load and centrifugal force on the blade. For ease of machining, the blade should be perpendicular to the hub taper. The leading-edge sweepback at the blade tip,

$$\theta = r\Sigma\,, \text{ radians} \tag{72}$$

due to the canting of the blade, should be modified by the use of a conical face cut, according to the relationship

$$\Sigma = \frac{(1 - \nu)\,(\tan \alpha_{cone} + \tan \alpha_{cant})}{\lambda} \tag{73}$$

to obtain the desired amount of sweepback with the chosen cant angle α_{cant}. The cone angle α_{cone} is measured in the opposite direction of α_{cant}.

3.1.9 Blade Angle

The leading-edge blade angle β shall minimize blade blockage at optimum flow coefficient by meeting criterion 3.1.5.

Use the ratio of incidence angle to blade angle as a characteristic parameter α/β for design purposes. The ratio should be chosen in the range from a low value of 0.35 for thin blades to a high of 0.50 for thick blades. A mean value, 0.425, has gained preference. However, if a wide range of flow is required, the design value of α/β should be greater than the (optimum) 0.425 value to avoid blade blockage.

3.1.10 Blade Lead

The radial variation of the inducer leading-edge blade angle shall match the radial variation of the inlet velocity diagrams.

It is recommended that the inducer be designed as a flat-plate cascade at the blade inlet; i.e., at the leading edge, the blade pressure side should be part of the surface of a constant-lead helix $\lambda = r \tan \beta$, where $\Lambda = 2\pi\lambda$ is the lead of the helix and β is the local blade angle. This design produces optimum cavitation performance, essentially uniform over radius, and provides ease of manufacture. Its main disadvantages are high leading-edge loading and a low head rise (maximum $\psi \cong 0.075$).

3.1.11 Blade Thickness

The blade thickness variation shall be consistent with the radial variation of the cavity wake height so that the blade is entirely within the cavity at design conditions of speed, flow, and NPSH.

The blade thickness is determined almost entirely by mechanical considerations in regard to stress and vibration. The blade should be made thicker at the hub than at the tip. Usually the blade radial sections are formed by straight lines from the hub to the tip on both pressure and suction sides. They need not be straight lines, but

these are usually easier to define and to manufacture. However, for best hydrodynamic performance the blade thickness variation should match the variation of the cavity wake height at the critical NPSH design condition and 110 percent flow, calculated from the free-streamline wake theory. The blade root fillet (sec. 3.4.2) must also be taken into account as a factor in the thickness variation with an effect on flow.

3.1.12 Blade Camber

The blade camber shall produce the turning angle needed for the head-rise requirement while maintaining the suction performance of the flat-plate inducer.

For head coefficients beyond the capability of the flat-plate inducer ($\psi \approx 0.075$), a certain amount of blade camber ($\beta_2 - \beta_1$) is needed. The result is a modified, variable lead helical inducer, which starts out as a flat-plate inducer but whose camber gradually increases from zero at the leading edge to the required camber at the trailing edge. The variation of the blade curvature should follow a smooth, monotone curve from zero at the leading edge to a maximum at the trailing edge. Then the suction performance will be unaffected by the blade camber. The simplest distribution satisfying this condition is given by a linear variation of the curvature from inlet to outlet. The corresponding blade-angle variation is given approximately by a parabolic relationship:

$$\beta = \beta_1 + (\beta_2 - \beta_1)\,(z/L_{ax})^2 \tag{74}$$

where z is the axial coordinate and L_{ax} the axial length of the blade. It is common practice to specify the blade-angle distributions for the rms radius. The distribution of the blade angle along some meridional curve, contour, or streamline is related to the blade wrap angle θ through the slope equation

$$dz = \tan\beta\, d(r\theta) = \frac{\Lambda}{2\pi r}\, d(r\theta) \tag{75}$$

where Λ is the local lead and dz the change in axial coordinate for the infinitesimal change in blade wrap $d(r\theta)$. The corresponding wrap angle θ may be found by numerical methods from this first-order nonlinear differential equation between θ, z, β, and r such that the blade layout can be completed.

3.1.13 Blade Surface Finish

The blade surface finish shall be hydraulically smooth.

The required degree of surface finish cannot be attained by machining only. It is recommended that the blade be polished after machining to a finish of at least 25 μ-in. rms.

3.1.14 Blade Number

The number of inducer blades shall be as small as considerations of solidity and axial space permit.

The number of blades should be not less than two nor more than five, with three or four being preferred. An odd number of blades prevents alternate cavitation from occurring; three is therefore a preferred choice if other, more critical considerations permit. It is recommended that whenever possible the blade number N be selected so that the impeller blade number is a multiple of N. This relationship promotes symmetry of flow into the impeller.

3.1.15 Cascade Solidity

The solidity of the inducer shall be large enough to satisfy high suction performance and fluid turning requirements, without exceeding a suitable angle of deviation or introducing manufacturing problems due to small blade spacing.

For a low-head inducer, the solidity σ should be 2.5 for the inducer proper. For a high-head inducer, consisting of an inlet region featuring a flat-plate inducer of solidity 2.0 to 2.5 and an outlet region with increased camber featuring vortex-type blading with splitter vanes, the solidity of the outlet region or transition stage should be treated separately and may require consideration of the effects of deviation angle (sec. 3.2.7).

3.2 Inducer Flow-Channel and Blade Geometry

3.2.1 Channel Flow

The inducer shall provide a monotone increase in head along any streamline through the inducer without backflow at any station.

The head distribution should be calculated assuming simple radial equilibrium and perfect guidance of the fluid by the blades (eqs. (34) and (35)). In the application of this analysis to the actual inducer blade, a few modifications should be made to account for the effect of these assumptions. To account for the assumption of perfect guidance, one may assume that the deviation angle is distributed along the arc length of the blade, and then apply a correction factor to the axial distribution of the lead of the inducer helix. The calculated head distributed may be corrected by multiplication with an assumed value of the blade efficiency. The head distribution in the cavitating region of the blade should be calculated from the cavity theory, wake model (ref. 31). The transition between the two regions is not well understood, and there is a lack of experimental and analytical evidence of the flow conditions in the transition region.

It may be postulated without evidence that the blading should reach a solidity of $\sigma = 2$ or higher before any essential amount of blade camber is introduced, so that the cavity-collapse process behind the leading edge may progress undisturbed.

In interpreting the results obtained in calculating the flow distribution, it should be noted that $c_a = 0$ for $\psi = 1$; i.e., to avoid backflow, the local head coefficient ψ should be less than 1 at all stations. To alleviate any backflow problem discovered in the calculation, the blade camber should be modified and a new check performed. A simplified approach is permissible for low-head inducers, which are essentially flat-plate inducers with zero or very small channel loading. In this case, a one-dimensional check should be made of the flow at the rms diameter, checking the blade angle against the fluid angle at axial intervals through the inducer to correct for blockage effects due to tip and hub contour variations as well as blade blockage. The corresponding c_u values should also be calculated to ensure a monotone head rise throughout the length of the inducer.

3.2.2 Discharge Flow

The inducer discharge head and flow distribution shall satisfy the requirements of the impeller or high-head inducer following it.

In general, this requirement is no problem for low-head inducers used in conjunction with centrifugal impellers. However, there is a requirement for a uniform head-rise distribution at the discharge from the inducer that must be met when the inducer is used in a multistage axial pump with repeating stages.

The requirement of uniform head rise for high-head inducers results in the so-called free-vortex-flow type of rotation (eq. (45)). A deviation from the free vortex flow of about ± 5 percent is acceptable. To match the free-vortex-flow requirement, the inducer blade should be twisted at the discharge; i.e., it should be a double-definition blade with different leads at root and tip sections. Excessive twist, however, introduces stresses that must be analyzed and provided for. To avoid excessive twist of the long inducer blades, the blading should be divided into axial sections, thus simplifying both stress and manufacturing problems. The solidity should be increased by the addition of partial blades between the main blades.

3.2.3 Impeller-Inducer Matching

3.2.3.1 Basic Requirements

The inducer-impeller combination shall present a smooth meridional flow passage with an axial spacing consistent with hydrodynamic and mechanical requirements.

The inducer discharge hub and tip diameters should match the impeller inlet-eye dimensions closely enough that a smooth contour may be drawn. For easy clearance

control on unshrouded blading, the tip contour should be cylindrical if head-rise requirements of inducer and impeller permit.

3.2.3.2 Axial Clearance

Hydrodynamic matching between inducer and impeller shall include a minimum axial clearance of the same magnitude as the blade gap.

The minimum clearance should be of the maginitude of

$$\Delta z = \frac{2\pi r}{N} \sin \beta_{TE} \tag{76}$$

which for a flat-plate inducer reduces to

$$\Delta z = \frac{L_{ax}}{\sigma} \cong \frac{\text{lead}}{\text{blade number}} = \frac{\Lambda}{N} \tag{77}$$

3.2.4 Trailing-Edge Sharpness

The blade trailing edge shall be as thin as possible consistent with structural and manufacturing considerations.

A thin trailing edge is desirable for optimum performance, but not critical. A recommended value giving low drag for the trailing-edge radius R_{TE} is

$$R_{TE} = 0.02\, t \tag{78}$$

where t is thickness of the blade profile at the particular radial station.

The trailing edge normally is sharpened to $R_{TE} = 0.025$ to 0.050 in. The trailing edge should be centerline faired as designed but should be modified as necessary during the development stage to correct for an insufficient head rise. The length of the trailing-edge fairing is not critical, but the transition from the blade must be smooth with a gradual change in thickness.

3.2.5 Trailing-Edge Contour

The contour of the trailing edge shall be free of corners that are structurally inadequate and prone to blade flutter or oscillation.

Minimize the tendency of the trailing edge to flutter by using forward-swept fairings of 20° to 40° wrap angle. It is good practice to have the blade reach its full thickness

at the hub before the full radial blade height is reached. When the blade edges are contoured and faired, the inducer axial length should be increased to maintain the required solidity.

3.2.6 Discharge Angle

The fluid turning angle shall be based on the head-rise requirements of the inducer, allowing for blade losses.

For low-head inducers the turning angle $\Delta\gamma$ should be determined for the rms station such that the Euler head multiplied by an assumed blade efficiency of about 85 percent equals the required head rise.

For high-head inducers with free vortex flow, the turning angle should also be determined at both the root and the tip section so that a double-definition blade may be specified.

3.2.7 Deviation Angle

The trailing-edge angle $\beta_{ms,TE}$ shall minimize deficiencies in head rise.

The discharge blade angle should include a correction for the effect of an imperfect guidance in the form of a deviation angle δ, which may be estimated from Carter's rule (sec. 2.2.7) or from other sources (refs. 45 and 46) by a trial-and-error method. A normal target tolerance is 5 percent of design values. In regard to the discharge blade angle, this correction means that $\beta_{ms,TE}$ should be given by

$$\beta_{ms,TE} = \gamma_{ms,TE} + \delta_{ms} + 0.05\,\Delta\gamma_{ms} \tag{79}$$

where $\Delta\gamma_{ms} = \gamma_{ms,TE} = \gamma_{ms,LE}$ is the turning angle of the fluid at the rms station, ms. The customary tolerance on the blade angle is 1/2°. In some cases, limiting the deviation angle to 2° may produce more stable flow.

3.2.8 Clearance Losses

The effect of blade tip clearance on inducer performance shall be as small as possible.

For good suction performance, the blade tip clearance at the inlet should be as small as possible for a distance of at least one axial blade spacing. The clearance area should never exceed 3 percent of the flow area. For comparison purposes, clearance areas of 1 to 1.5 percent of the flow area are common practice.

The gain in performance from close clearances should be weighed against the difficulties encountered in maintaining such clearances. Recommended values of the ratio of radial clearance to blade length depend on the application and the actual design and materials used. Minimum practical values reached for fuel and oxidizer pumps are 0.005 and 0.020, respectively. Frequently, nonmetallic liners are used in the housings of inducers running in liquid oxygen so that close running clearances may be maintained without danger of sparking.

3.2.9 Shrouding

A shroud on the inducer, used when mechanical reasons so dictate, shall provide clearance control, structural reinforcement, or erosion damage protection.

When possible, a shroud should be made integral with the blading. When it cannot be made integral, it should be welded or brazed to the blading, and care should be taken to obtain a strong joint. Brazing is not recommended for high-operating-stress regions or for cryogenic applications.

When a shroud is used, the wearing-ring seal should maintain close clearances to preserve efficiency and suction performance. The inner diameter of the shroud should be flush with the inlet line outer diameter to minimize flow disturbances.

3.2.10 Blade Geometry Description

3.2.10.1 Specification Form

Final specification of the blade shape shall be suitable for fabrication and inspection purposes.

Give blade descriptions by coordinates to both blade surfaces rather than by blade angle and thickness distribution. Specify these coordinates at two parallel positions or cuts: one next to the hub but above the fillet, and the other near the tip.

Blade thicknesses are established at the two positions; all other thicknesses are a function of a straight-line tool cut between the two blade definitions. The inducer blade angles β should be defined initially at intervals along either one or two cylindrical or conical sections, according to the hydrodynamic design. A blade angle distribution called out at two stations implicitly defines a variable blade cant angle. From these definitions and from the blade fairing and the hub and tip geometry, the blade surface coordinates and the tool positions for both sides of the blade should be derived by computing and layout procedures. The coordinates and tool positions may be defined along either conical or cylindrical cuts as preferred by the manufacturer.

REFERENCE 90
PAGE 64 BLANK

3.3.3 Inlet-Line Heat Transfer

Heat transfer to the fluid in the inlet line shall not reduce the available NPSH for the inducer below acceptable levels.

It is recommended that heat transfer to both the tank and the inlet line be investigated carefully. The amount of line insulation required to reduce the fluid temperature rise to allowable levels should be determined before final design specifications for the pump and inducer are made.

3.3.4 Bypass Flow

The reintroduction of leakage or bypass flows from bearings or balance-piston operation shall cause a minimum of disturbance to the main flow.

If possible, all bypass flows should be reintroduced after the inducer. Otherwise they may be fed through a hollow shaft and spinner into the center of the inlet line, where they cause the least disturbance.

3.4 Mechanical Design and Assembly

3.4.1 Hub Configuration

3.4.1.1 Wall Thickness

The hub wall shall be adequate to absorb the blade bending moments and the blade centrifugal pull, and shall have adequate hoop capability to carry the centrifugal force induced by its own mass.

The hub radial thickness should be at least $\sqrt{1/2}$ times the blade thickness to carry the blade bending moments. If the hub has a center hole with a diameter approaching the hub diameter, it is recommended that the hub radial thickness be equal to or greater than the blade thickness to accommodate both the bending moments and the centrifugal forces.

3.4.1.2 Diameter

The hub shall be of sufficient diameter and thickness to hold the shaft and transmit the shear load from the keys or splines.

The hoop discontinuity and stress concentration effects caused by the key way or spline teeth on the hub inner diameter must be considered when the hub is sized

in accordance with procedures set forth in the design criteria monograph "Liquid Rocket Engine Turbopump Shafts and Couplings."

3.4.1.3 Wall Contour

If the discharge diameter is greater than required by structural considerations, the hub configuration shall minimize the weight.

If the hub discharge diameter is large (with or without the center hole), the hub should be profiled and hollowed out as shown in figure 18 to minimize weight while maintaining an adequate margin on the burst speed.

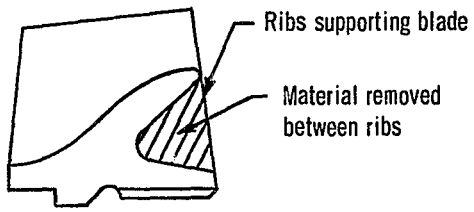

Figure 18.—Hub profile.

3.4.1.4 Axial Length

The inducer hub axial length shall be sufficient to permit full runout of the blade-to-hub fillet radius at leading and trailing edges during machining.

It is recommended that at each end of the hub an axial length equal to at least twice the fillet radius be added to the axial length of the blading.

3.4.2 Blade Root Juncture

The fillet at the blade root-to-hub juncture shall satisfy structural requirements but have minimum effect on the hydrodynamic performance of the blade.

The blade fillet should be a compromise among structural, hydrodynamic, and manufacturing considerations. A practical compromise is a circular fillet of radius equal to the blade thickness t. Better still in both structural and hydrodynamic respects, but more complicated to make, is an elliptical fillet with the radius joining the blade equal to t and the radius joining the hub equal to $t/2$.

When hydrodynamic requirements limit the fillet size, the fillet should be shot peened to improve fatigue resistance. Shot peening should also be used as a development tool to improve the fatigue resistance of inducers that experimentally have shown a tendency to fail by fatigue of the blade junctions.

3.4.3 Shaft Dimensions

3.4.3.1 Size

The inducer shaft size shall be adequate to carry the torque, preload, shear, and bending loads imposed on it at the worst operating condition.

Shaft size should be established in accordance with procedures set forth in the design criteria monograph "Liquid Rocket Engine Turbopump Shafts and Couplings." When sizing the shaft, allow for possible later modifications of the inducer design by adding 10 to 15 percent to the diameter required by structural analysis.

3.4.3.2 Torque Transmission

The torque transmission device shall be sized for the maximum torque load, considering potential cyclic variations.

Shear pins or keys normally are limited to low-torque applications. Splines are recommended for high-torque applications. Preferably, the arrangement of keys or splines should allow assembly in only one position so that proper balancing is maintained after reassembly.

3.4.4 Piloting

The inducer shall be piloted radially in the pump rotor assembly at all operating conditions.

When the design involves centrifugal stresses large enough to cause the inducer to come loose on the shaft, an inverted or external type of piloting is recommended. In this design, the inducer is piloted inside a groove or in a hole in the center of the shaft (fig. 19).

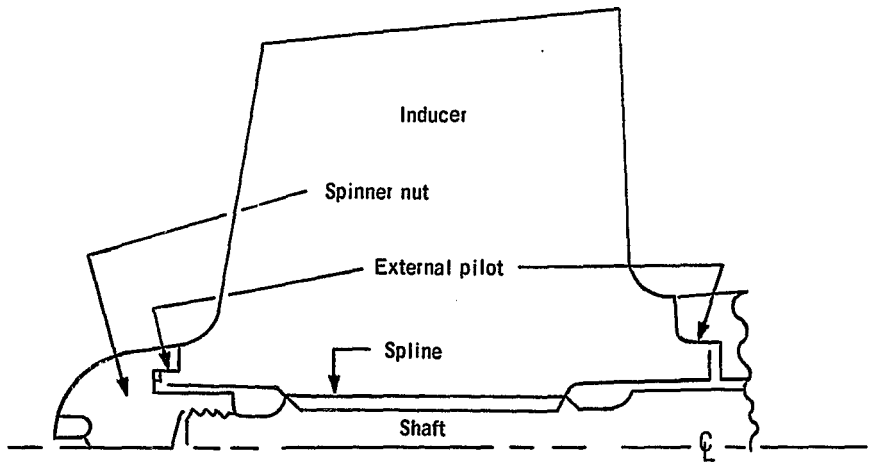

Figure 19.—External piloting.

3.4.5 Axial Retention

3.4.5.1 Axial Preload

The axial preload at assembly shall be adequate to withstand maximum hydrodynamic forces including dynamic forces, thermal contraction, centrifugal contractions including "Poisson's" contractions, and unbalance.

Dynamic forces cannot be known in advance; they may be estimated to be 30 percent of the steady hydrodynamic forces. Thermal contractions should be calculated on the basis of a slow chilldown period and should include the effects of differential expansion or contraction due to differences in thermal expansion coefficients. In the event of a fast chilldown, thermal effects due to different rates of cooling should be considered and evaluated.

Radial stresses due to centrifugal loads produce a radial elongation of the material with an accompanying contraction in the axial direction (the Poisson effect). These dimensional changes should be determined from the general stress condition by using the Poisson ratio of the material (this ratio has the approximate value of 0.3 for most materials of construction). The Poisson effect may produce loose fits that otherwise would not be expected, and it therefore must be carefully evaluated for the materials and stresses involved (ref. 87).

Unbalance should be identified by dynamic balancing, and then compensated.

3.4.5.2 Fastener Unloading

Bolts and studs in rotating assemblies shall not yield or unload under operating conditions.

Avoid any permanent deformation that would cause the assembly to come loose. Bolts and studs should be installed by measured amounts of stretch wherever practical. Three general methods may be employed:

(1) If both ends of a bolt are accessible, it may be measured with large outside micrometers. Usually the rotor parts being clamped undergo measurable compression, and therefore individual bolts in bolt circles must be progressively stretched.
(2) Stud stretch is generally measured by determining the change in length of a concentric center hole. This hole must pass through the entire working length of the stud.
(3) If measurement along a center hole is not practical, the increased protrusion of the nut end may be measured. Compression of the clamped parts must then be accounted for, or determined to be negligible.

The effect of chilling of parts by cryogenic propellants must be analyzed, and the combined effect of the axial shortening of rotating parts due to Poisson's effect coupled with radial growth due to centrifugal force must be accounted for. Such effects are particularly important when assemblies are composed of various materials with different coefficients of thermal contraction and different moduli of elasticity.

3.4.5.3 Preload Control

The inducer axial retention preloads at assembly shall be sufficient to preclude separation and fretting during operation and shall be accurately controlled.

To achieve uniform axial preloading of through-bolts, measure the bolt elongation or the nut rotation. The use of bolt torque measurements in critical load applications is not recommended because the variation in friction coefficient makes this method an unreliable index to preloading.

3.4.5.4 Galling, Fretting, and Seizing

Parts in rotating assemblies shall not experience galling, fretting, or seizing.

It is recommended that threaded joints and mating surfaces be coated with a suitable lubricant (ref. 88) or that they be silver plated. The tendency of titanium to

gall and seize has not yet proved to be a problem in inducer applications; however, whenever possible, a dry-film lubricant that is chemically compatible with the propellant should be used.

To eliminate or reduce fretting of the shaft and hub splines, a spline drive should have interference-fit pilot diameters at each end of the spline, or the spline teeth should have an interference fit under all operating conditions. For oxidizer applications, it is recommended that the radial pilot surfaces be coated with an acceptable lubricant (ref. 88) or that they be silver plated. When the radial stack interference fit requirements are evaluated, the relative thermal contractions, the centrifugal deflections, and the steady-state and oscillatory hydrodynamic loading extremes should be identified and included in the calculations.

3.4.6 Clearance Effects

The blade tip or shroud radial and axial clearances shall be as small as possible, but always sufficient to preclude detrimental rubbing between inducer and housing under any operating condition.

Pump rotating parts must not be allowed to rub metal-to-metal in oxidizer pumps.

Practically attained minimum values of the inducer clearance-to-blade length ratio are 0.5 percent for fuel and 2.0 percent for oxidizer applications. When closer clearances are required for oxidizer applications, a Kel-F liner or its equivalent should be used for the inducer casing. Since Kel-F has poor wearing properties at room temperature, it should not be used for water tests. The use of a Kel-F coating is shown in figure 20.

For pumps in which efficiency is not important, a large clearance can be used to prevent rubbing. For most rocket pumps, however, efficiency and suction performance are important enough to justify a more sophisticated design. The preferred practice is to house open impellers or inducers in a nonmetallic "tunnel"; with this arrangement, slight rubbing can be allowed. For shrouded impellers or inducers where nonmetallic wearing rings are used, multiple lands should be provided in the wearing rings to sustain rubbing with the lowest resisting torque.

The calculation of minimum required clearances must consider (1) manufacturing tolerances; (2) differential thermal expansion of inducer and housing including possible distortions occurring during chilldown and operation; (3) change in dimensions produced by operating conditions (e.g., centrifugal strain of blade and hub and deflections due to bending of the blade); (4) potential radial shaft and bearing deflections resulting from unbalanced inertia forces and radial hydrodynamic loads; and (5) potential axial displacements resulting from thermal and mechanical causes, if the inducer tip contour is not cylindrical.

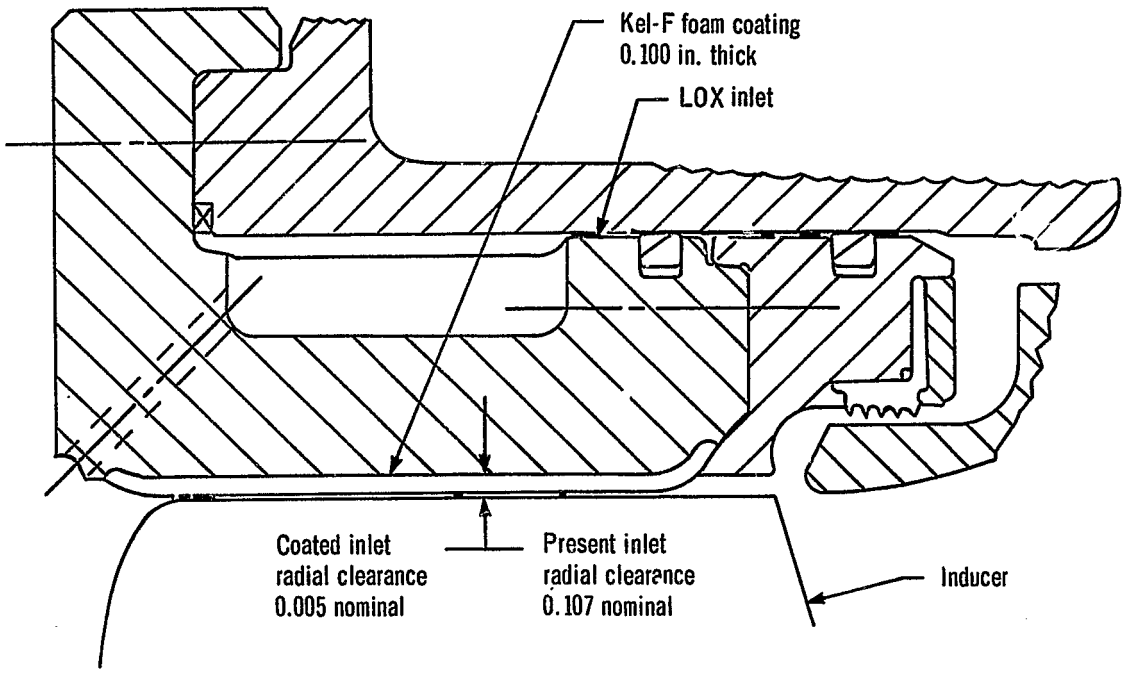

Figure 20.—Liquid-oxygen inducer, reduced tip clearance.

The maximum hydrodynamic loads should be considered in selecting the inducer tip clearances. The radial load should be considered equal to 30 percent of the inducer axial thrust unless better values are available. The following practices are recommended to minimize the possibility of interference rubbing:

(1) Provide adequate running clearances for steady-state operation.
(2) Design to minimize housing deflections.
(3) Account for all extremes of thermal deflections.
(4) Account for loads induced by engine malfunction, such as discharge valves not opening or closing in programmed sequence.

If models of cryogenic pumps are to be tested in other fluids, make proper allowance for different stackups, fits, and clearances. To get comparable test results, the design should be modified to maintain the clearance-to-blade length ratio c/L while running in the test fluid.

3.4.7 Shroud

The thickness of the shroud and its attachment to the blades shall be adequate for centrifugal loading effects from the shroud's mass and for the effect of the blades.

The inducer shroud thickness should be the minimum consistent with the centrifugal forces and the loads at the shroud-blade junction, as determined by a detailed stress analysis of the compound stress conditions in the shroud-blade structure combined with a knowledge of material properties.

The method of attachment of the shroud to the blading must be such that all junction loading can be adequately transferred to the blade. Integrally machined or cast shrouds are recommended. Attaching the shroud by welding is acceptable when the weld is inspected carefully by X-ray or other means. Brazing is not recommended for high-operating-stress regions or for cryogenic applications.

3.4.8 Misassembly

The design of rotating assemblies (rotors, turbine discs, blading, spacers and other symmetrical or near-symmetrical parts) shall preclude backward installation.

When only one orientation for a part is permissible, preclude misassembly in one of the following ways:

(1) Stepped land sizes on studs.
(2) Missing tooth (and mating space) on splines.
(3) Nonsymmetrical hole patterns for multiple bolt or stud fastening.
(4) Fixed dowel pins or keys (used mostly for stationary parts or lightly loaded rotary parts).

3.4.9 Rotation Direction

The direction of inducer rotation shall be consistent with the direction of rotation of the pump rotor assembly.

To avoid any inadvertent mismatch of the direction of rotation for the various components of a turbopump, preparation of an axonometric schematic of the complete rotor assembly, showing direction of rotation, should be the first order of business for the layout designer. Provide copies to all those involved with design and assembly.

3.4.10 Inducer Balancing

Inducer dynamic balance shall satisfy requirements imposed by the pumping system.

A two-plane dynamic balancing should be performed on a balancing machine of suitable size. Further balancing of the entire pump or turbopump assembly should be done as required.

Typical turbopump practice for speeds of around 30,000 rpm is to balance to within 0.01 oz-in. per balance plane for a two-plane balance on a part weighing 10 to 15 lb.

For oxidizer pumps, balancing should be accomplished through metal removal only; holes or grooves for weight addition should not be used.

Metal removal on hydrodynamic surfaces should be within the tolerance band of the surface. The cut must be faired smoothly into the blade surface.

3.5 Material Selection

Material strength properties used in material selection shall be the minimum guaranteed properties.

The minimum guaranteed material properties are established as military standards. Because of the statistical nature of the distribution of test results for material properties, a one-sided tolerance factor for evaluating compliance of test data with specifications should be used. Values of 99 percent for conformance or probability and 95 percent for confidence level are recommended (ref. 68, par. 1.4.1.1, Basis A). All materials should be compared on the basis of the minimum guaranteed properties in accordance with these recommended values for statistical significance.

3.5.1 Strength

The inducer material shall possess the best strength-to-density ratio for the particular inducer needs, provided it meets all the criteria in sections 3.5.2 *and* 3.5.3.

The strength properties should include the ultimate, yield, elongation, and endurance limits of the material. In the choice of material, the relative importance of these limits for the application in question should be considered. Aluminum and titanium forgings are the preferred inducer material choices for minimum weight but are subject to limitations noted in sections 3.5.2 and 3.5.3.

REFERENCE 90
PAGE 74 BLANK

3.5.2.2 Stress Corrosion

The inducer material shall possess acceptable resistance to stress corrosion.

When residual stresses are imposed by the manufacturing method or by assembly, the 7075-T73 aluminum alloy should be preferred to the 2014-T6 aluminum alloy, which has a low stress-corrosion threshold. Similarly, titanium alloys should not be used in brown N_2O_4 (i.e., uninhibited nitrogen tetroxide containing over 1.00 percent nitric oxide).

3.5.2.3 Degradation by Fluids

Inducer materials such as titanium and aluminum alloys shall not experience degradation from fluids or solvents used during cleaning, processing, or operation.

Cleanliness of the parts is of the utmost importance prior to any welding or thermal treatment of titanium; however, halogenated solvents should never be used prior to any welding or thermal treatment. Methanol causes stress corrosion in titanium alloys at room temperature; it should never be employed for any processing, testing, or operational service in contact with titanium alloys.

3.5.3 Special Properties

3.5.3.1 Cavitation

The resistance of the inducer material to cavitation damage shall be adequate for the intended use.

A steel alloy such as K-Monel or Inconel 718 is recommended for low-speed, cavitating oxidizer inducers. A titanium alloy is recommended for cavitating fuel inducers. Aluminum alloys should be avoided wherever cavitation erosion may affect the useful life and performance. When aluminum alloys are used, they should be protected with anodic coatings as described in section 3.5.2.1.

3.5.3.2 Thermal Environment

The material shall withstand the thermal environment at operating conditions without excessive degradation.

Excessive brittleness at low temperatures must be avoided for cryogenic applications. The titanium alloy Ti-5Al-2.5Sn ELI is recommended for liquid-hydrogen temperature (−423° F). Both Ti-5Al-2.5Sn ELI and Ti-6Al-4V ELI are recommended

at liquid-nitrogen temperature (−320° F). All the recommended aluminum alloys are satisfactory for operation from room temperature down to liquid-hydrogen temperature. If they are made of the recommended alloys, parts that are of suitable strength at ambient temperatures are still stronger at cryogenic temperatures.

3.5.3.3 Fabrication

The material shall be suitable for the intended manufacturing and fabrication method.

A cast-aluminum inducer would be the proper choice for low-stress applications when low cost is important. Aluminum is easy to forge and machine, but welding or brazing this material is not practicable.

Titanium alloy parts are more expensive to machine than comparable parts of aluminum alloys but are less expensive than alloys such as Inconel 718 or Rene' 41. The recommended titanium alloys can be welded readily by either gas-tungsten arc or electron-beam processes. Proper welding procedures should be observed for titanium alloys.

3.6 Vibration Considerations

3.6.1 High-Frequency Fatigue

The inducer blades shall not experience vibration amplitudes above the fatigue limit.

Design the inducer initially from strength considerations alone and then analyze (ref. 69) the vibration behavior of known problem areas of the blade, such as leading- and trailing-edge corner flap and flutter. To prevent fatigue failure, the blade should be sized so that oscillatory stresses are kept below the endurance limit.

3.6.2 Resonance

The blades shall not experience resonant vibration produced by fixed-wake forcing frequencies.

It is recommended that at least a 15-percent margin between blade frequency and wake frequency be maintained in the operating speed range. It is, however, sometimes difficult to achieve this margin. It is established practice to consider only first- and second-order harmonic vibration for inducer blades. Both upstream and downstream wakes should be considered as the source of forcing frequencies. The blade natural frequencies and fixed-wake forcing frequencies should be compared on

a Campbell diagram (ref. 89) to determine the critical speeds at which resonant vibration will occur. Where possible, obtain the recommended margin by changing the obstacle producing the wake. Otherwise, modify the blade to change its natural frequency.

3.6.3 Self-Induced Vibration

The blades shall not experience flutter resulting from self-induced oscillations.

Blade flutter should be alleviated by trimming back the leading or trailing edges or by adding a shroud to the inducer. The recommended trimming angles are 60° to 140° wrap for the leading edge and 20° to 40° for the trailing edge. If the blades are trimmed back, the axial length of the inducer should be increased to maintain adequate solidity of the blading.

3.6.4 Determination of Blade Natural Frequencies

The blade natural frequencies shall be determined by vibration analysis and by testing.

The initial vibration analysis should establish nominal values for blade frequencies based on blade geometry and material and nominal operating conditions. The effects of blade manufacture and actual conditions of use on the nominal values should be accounted for by following the practices set forth in sections 3.6.4.1 through 3.6.4.4. Because present analytical techniques give only approximate results, the values for blade frequencies must be verified by testing a prototype inducer as required in section 3.6.4.5.

3.6.4.1 Tolerance Bands

In the determination of the natural frequency bands, the vibration analysis of the blade shall take into account the blade dimensional tolerance bands.

The blade should be analyzed for the maximum root–minimum tip thickness and minimum root–maximum tip thickness to determine the natural frequency bands.

3.6.4.2 Centrifugal Stiffening

The vibration analysis shall consider the effect of centrifugal stiffening on the blade natural frequencies.

The restoring component of the centrifugal force should be added to the restoring force due to the blade elastic bending properties.

3.6.4.3 Temperature Effects

The vibration analysis shall account for the effect of the operating temperatures on the elastic properties of the material.

The effect of cryogenic temperatures on the elastic modulus of the material is to raise the natural frequency. If operation with a test fluid different from the design fluid is contemplated, the resulting frequency bands should be corrected by use of the relationship

$$\frac{n_{op}}{n_{test}} = \sqrt{\frac{E_{op}}{E_{test}}} \tag{80}$$

where n_{op} and n_{test} are frequencies under operating and test conditions, respectively, and E_{op} and E_{test} are the corresponding values for the material elastic modulus.

3.6.4.4 Virtual Mass Effect

The vibration analysis shall include the effects of the virtual mass of fluid moving with the blade under operating conditions.

The reduction in blade natural frequencies should be determined or verified by prototype testing. The following reductions (ref. 90) should be taken as order-of-magnitude values giving estimates of the effect: a 4-percent reduction of the fundamental frequency in liquid hydrogen, and a 24- to 31-percent reduction (two different designs) in liquid oxygen. The effect of the virtual mass may be estimated by the approximate relationship

$$n_F = \frac{n_0}{\sqrt{1 + K(\rho_F/\rho_{bl})}} \tag{81}$$

where n_F and n_0 are frequency with and without fluid, respectively, K is a constant factor characteristic of the blading considered, and ρ_F and ρ_{bl} are densities of fluid and blade material, respectively. The value of K should be determined in each case from test results. No analytical approach is recommended at present. The effect should be allowed for when the results of blade vibration tests in air are reduced to inducer operating conditions.

3.6.4.5 Natural Frequencies

Vibration tests on each prototype inducer design shall verify and accurately determine the blade natural frequencies.

The vibration tests should include excitation in air and in the pumping fluid medium if possible. The modes of vibration can be determined by fuller's earth, stroboscopic films, strain gages, or accelerometers during the shake test.

3.7 Structural Considerations

3.7.1 Blade Loading

The load analysis shall determine critical loads on blades for both steady-state and alternating conditions, encompassing all anticipated hydrodynamic and inertia loads in the operating and test range.

It is recommended that all loads and forces be calculated on the basis of a mechanical design speed that is 110 percent of the maximum speed or 120 percent of nominal speed, whichever is higher. The critical blade loadings should be based on the worst flow/NPSH/speed conditions that can occur during operation or testing. Particular attention should be paid to situations where test conditions differ from the design conditions.

The minimum flow–maximum NPSH condition should be used to define the leading edge loading of the blades, and the minimum flow–minimum NPSH condition should be used to define blade loadings in the channel section of the blade. Use a computer program like that provided in reference 79 to calculate the leading-edge loading. The channel loading may be calculated by a computer program based on an axisymmetric or blade-to-blade solution of the noncavitating inducer flow, or it may be determined by using the theory of simple radial equilibrium to calculate the pressure distribution on the blades.

The study of oscillatory blade loads should include the effects of periodic flow fluctuations, circumferential nonuniformities of flow and pressure wakes from ribs or stator blades, and random vibrations. Since these effects are not predictable at the design phase, assume an alternating load equal to 20 to 30 percent of the steady-state hydrodynamic loads. Use accurate values for the important fluid properties that affect the structural analysis: density, temperature, pressure, and vapor pressure. These determine hydrodynamic forces and affect material properties and NPSH values.

If models of cryogenic pumps are to be tested in other fluids, attention should be directed to the change in stress level that results from the change in fluid density and pump speed. A stronger material may have to be used, or one of lower stress capability may be satisfactory for the model, depending on strength and cost considerations.

3.7.2 Blade Stress

The stress analysis shall determine critical values of stress and strain for both steady-state and alternating conditions, based on the established critical loads and inducer geometry with proper allowance for manufacturing tolerances.

It is recommended that the critical stress regions corresponding to potential failure lines be found by plotting the stress level at various locations on the blade. These stresses may be found by the methods described in section 2.7.2. Critical sections are normally at the root junction or close to it, or on bending lines for a blade corner. Blade corners may be rounded off to reduce bending stresses. The effect of manufacturing tolerances on blade dimensions should be evaluated by using minimum root thickness and maximum tip thickness.

3.7.2.1 Discontinuities

The stress analysis shall include the effect of stress concentrations due to discontinuities at bolt holes and keyways or splines in the inducer hub and at the blade-hub and blade-shroud junctions.

It is recommended that the stress-concentration factor for blade root fillets or other discontinuities be applied to the blade alternating stress before the Goodman diagram is used to determine the blade structural adequacy. The endurance limit is reduced by stress-concentration effects on the alternating stress but not by its effects on the mean stress for ductile materials. The full theoretical stress-concentration factor K_t should be used if actual stress-concentration factors K_{tf} are not available.

3.7.2.2 Load Concentrations

The stress analysis shall identify and analyze peak stress regions associated with hub-profile load concentrations.

The blade centrifugal pullout of the hub and reversals in the hub profile, together with discontinuities due to splines, keyways, and eccentric bolt holes, should be considered potential failure areas (refs. 83, 91-96). A special study of these local problem areas is recommended.

3.7.3 Hub Strength

Stress analysis shall verify that the disc burst speed for the inducer hub is at the level required.

The disc burst speed for the inducer hub should be determined from the relationship

$$n_{\text{burst}} = n\sqrt{\frac{\sigma_{\text{AT, burst}}}{\sigma_{\text{AT}}}} \tag{82}$$

where σ_{AT} is the average tangential stress in the disc at the speed n and $\sigma_{\text{AT, burst}}$ is the average tangential stress at the burst speed n_{burst}. The average tangential stress must be calculated for the weakest cross section of the disc according to equation (59):

$$\sigma_{\text{AT}} = \frac{1}{A'_H}\int \sigma_t \, dA_H$$

where A'_H is the meridional cross-sectional area of the disc (or hub) at its weakest section (i.e., allowing for bolt holes, splines, etc.), and the integral represents the total centrifugal force acting on one-half the disc (or hub); σ_t is the tangential stress at the speed considered acting on the area element dA_H.

The average tangential stress at burst $\sigma_{\text{AT, burst}}$ is obtained from the empirical relationship

$$\sigma_{\text{AT, burst}} = f_b F_{tu} \tag{83}$$

where F_{tu} is the material ultimate tensile strength from the guaranteed minimum properties and f_b is a so-called burst factor. The factor f_b has been established experimentally as a function of a disc design factor f_d, which represents the nonuniformity of the stress distribution existing in the disc in the unyielded state, and also as a function of the material's capability to yield; specifically, the elongation e measured on a test rod over a length equal to 4 diameters of the rod. This combined functional relationship is presented in figure 21. This relationship must be used to determine f_b from a knowledge of f_d for the disc in question.

The design factor f_d is defined by the ratio

$$f_d = \frac{\sigma_{\text{AT}}}{\sigma^*_{\text{MT}}} \tag{84}$$

calculated at some speed n, where σ^*_{MT} is the maximum tangential stress in the disc including stress-concentration effects at eccentric bolt holes and at the base of spline teeth in a central hole, i.e.,

$\sigma^*_{\text{MT}} = \sigma_{\text{MT}}$ times stress-concentration factor
σ_{MT} = maximum tangential stress obtained from the basic stress analysis for elastic deformation

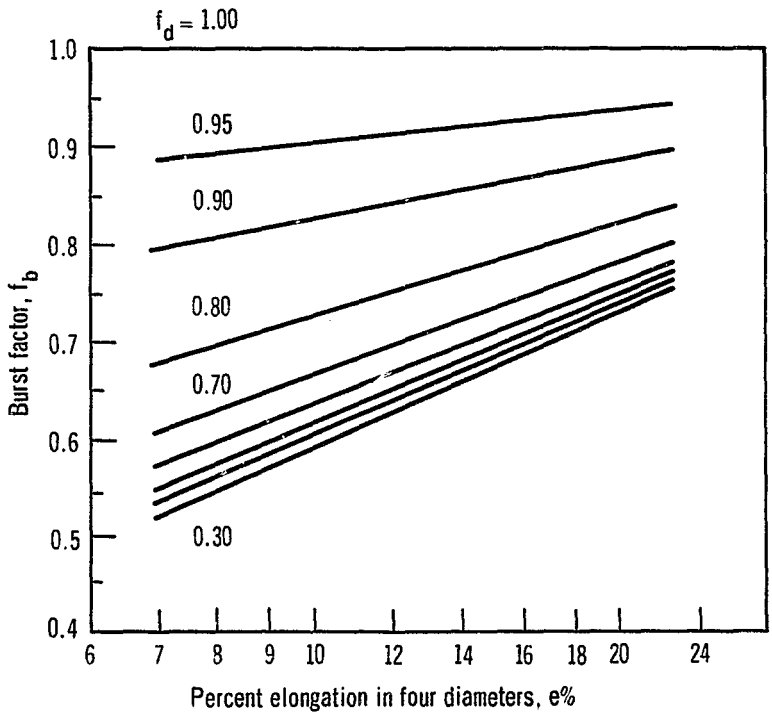

Figure 21.--Burst factor vs. elongation for various design factors.

3.7.3.2 Yield Speed

Stress analysis shall verify that the disc yield speed is at the level required.

The disc yield speed should be calculated from

$$n_{\text{yield}} = n\sqrt{\frac{F_{ty}}{\sigma_{AT}}} \tag{85}$$

where F_{ty} is the yield strength of the material. The calculation of σ_{AT} is described above. The value for n_{yield} is straightforward, as shown.

3.7.3.3 Safety Factors on Hub Speeds

The inducer burst speed and yield speed shall provide adequate safety factors relative to the mechanical design speed.

Recommended values of these safety factors are 1.20 for the inducer burst speed and 1.05 for the inducer yield speed. These values give the ratio of inducer burst speed or yield speed to mechanical design speed (sec. 3.7.1).

3.7.4 Shaft Shear Section Strength

The rotor shaft shear section shall be sized on the basis of the allowable shear stress for the compound stress condition.

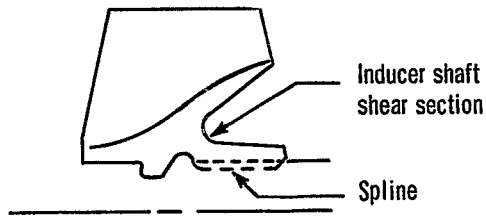

Figure 22.—Shear section.

The inducer shaft shear section (fig. 22) should be sized according to the following relationship (adapted from eq. (37) in ref. 56) for the allowable shear stress:

$$\tau_0 = \left(\frac{L_s F_{ty}}{n_{ult} \sqrt{3}} \right) \frac{\sqrt{1 - \left(\frac{n_{ult}\, \sigma_{ax}}{L_b F_{ty}} \right)^2}}{1 + \left(\frac{K_{tsf} L_s F_{ty}}{F_e} \right) \left(\frac{\tau_{alt}}{\tau_0} \right)} \tag{86}$$

where

$$L_b = (4/\pi) L_s \tag{86a}$$

$$L_s = 4/3\, [1 - (d_i/d_o)^3]/[1 - (d_i/d_o)^4] \tag{86b}$$

and

n_{ult} = safety factor against ultimate failure
K_{tsf} = fatigue notch factor for shear stress
F_e = material endurance strength, $lb_f/in.^2$
τ_0 = allowable shear stress, $lb_f/in.^2$
τ_{alt} = alternating shear stress, $lb_f/in.^2$
σ_{ax} = axial stress, $lb_f/in.^2$
d_i and d_o = inside and outside diameters of hub shear section, in.

Note: $L_b F_{ty}$ < material ultimate strength. Allowance for alternating shear should be made by assuming $\tau_{alt}/\tau_0 = 0.05$.

3.7.5 Safety Factors

Safety factors shall be based on the guaranteed minimum material properties at the operating condition.

The endurance limit, ultimate, and yield data should be modified to represent actual blade conditions considering the effects of temperature, surface finish, residual stress from the manufacturing processes, material grain size, heat treatment, and type of loading.

3.7.5.1 Fatigue Failure

The safety factor against fatigue failure shall be based on a Goodman diagram constructed from experimental values for material fatigue strength.

Because the nature of the blade alternating stress cycle generally is unknown, it is recommended that the endurance limit strength values be used in constructing the Goodman diagram (ref. 68), figure 23. In using the Goodman diagram, the stress-concentration factor should be applied for the alternating stress only. Peak stress points should be considered at all radii. In general, the blade root fillet tangent plane is most critical.

3.7.5.2 Ultimate Failure and Yielding

Safety factors against ultimate failure and yielding shall be based on the peak stress $(\sigma_{mean} + \sigma_{alt})$ *that includes the stress-concentration effects caused by discontinuities.*

The magnitude of the stress-concentration factor should be based on the ability of the material to yield. For brittle materials with low ductility and notched strength less than unnotched strength, the full theoretical value of the stress-concentration factor should be used in determining the peak stress. For materials with high ductility and notched strength greater than unnotched strength, the stress-concentration factor approaches 1 as yielding occurs and therefore can be neglected in the prediction of the peak stress.

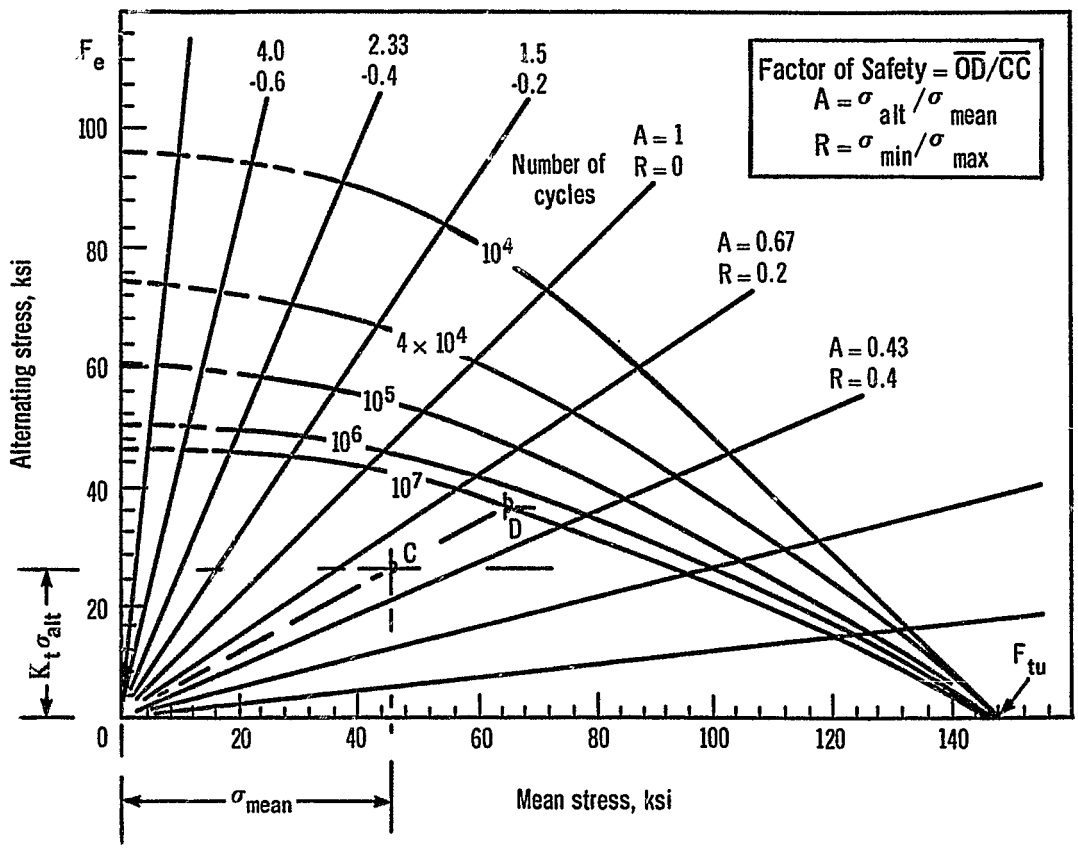

Figure 23.—Goodman diagram.

3.7.5.3 Values for Safety Factors

The safety factors on yield, ultimate, and fatigue strength shall be adequate for all stress conditions and shall be consistent with well-established design practice.

Experience indicates that the following safety factors have been adequate for successful inducer design:

Fatigue, $n_f = 1.5$
Ultimate, $n_{ult} = 1.5$
Yield, $n_y = 1.1$

These safety factors are based on stress levels obtained at the mechanical design speed.

If the alternating stress component is accurately determined, the fatigue safety factor could justifiably be reduced. The safety factors are highly dependent on strict quality control practices.

3.7.6 Hub Stress Verification

For high-speed inducer designs, the inducer spin test shall verify the predicted hub stress.

When centrifugal stresses govern the design, a prototype inducer should be run to destruction. Adequate instrumentation should be provided such that the stress distribution and critical deflections can be obtained to verify the calculations.

3.7.7 Inducer Proof Test

The inducer spin proof test shall verify the predicted structural capability of the inducer.

Spin testing is recommended when the mechanical design speed exceeds 60 percent of the burst speed in the operating environment. The proof-test spin speed should subject the inducer material to strains equal to or greater than the centrifugal strains it will experience during operation, and should demonstrate the same maximum centrifugal stress-to-available-strength ratio as that which will occur at the mechanical design operating conditions. The spin speed should not exceed the speed at which gross yielding will occur or induce partial failure by approaching the room-temperature burst speed. It is recommended that the spin speed have no less than 10-percent margin on the room-temperature burst speed. A spin duration of no less than 2 minutes is recommended.

REFERENCES

1. Gross, L. A.; and Miller, C. D.: A Performance Investigation of an Eight-Inch Hubless Pump Inducer in Water and Liquid Nitrogen. NASA TN D-3807, 1967.
2. Brumfield, R. G.: Optimum Design for Resistance to Cavitation in Centrifugal Pumps. P-10 Propulsion Memorandum, U. S. Naval Ordnance Test Station, Feb. 1948.
3. Ross, C. C.; and Banerian, G.: Some Aspects of High-Suction Specific Speed Pump Inducers. Trans. ASME, vol. 78, Nov. 1956, pp. 1715-1721.
4. Stripling, L. B.: Cavitation in Turbopumps—Part 2. J. Basic Eng., vol. 84, Sept. 1962, pp. 339-350.
5. Wislicenus, G. F.: Critical Considerations on Cavitation Limits of Centrifugal and Axial-Flow Pumps. Trans. ASME, vol. 78, Nov. 1956, pp. 1707-1714.
6. Lewis, G. W., Jr.; Sandercock, D. M.; and Tysle, E. R.: Cavitation Performance of an 83° Helical Inducer Operated in Liquid Hydrogen. NASA TM X-419, 1961.
7. Osborne, W. M.: Investigation of a Liquid-Fluorine Inducer and Main-Stage Pump Combination Designed for a Suction Specific Speed of 20,000. NASA TM X-1070, 1965.
8. Salemann, V.: Cavitation and NPSH Requirements of Various Liquids. J. Basic Eng., vol. 81, June 1959, pp. 167-180.
9. Stepanoff, A. J.: Cavitation Properties of Liquids. J. Eng. Power, vol. 86, Apr. 1964, pp. 195-200.
10. *Anon.: Evaluation of NPSH Performance of the Model Mark 3 LOX Turbopump Used in the Thor MB-3 Propulsion System. R-3995, Rocketdyne Div., North American Rockwell Corp. Unpublished, Apr. 1967.
11. *Iura, T.: Cavitation Performance of Pump With Inducer in Liquid Oxygen and Liquid Nitrogen. DDR 512-114, Rocketdyne Div., North American Rockwell Corp. Unpublished, Jan. 1956.
12. *Stremel, R. L.: Water Versus "Cold LOX" Performance Comparison Study for the Various Mark 4 LOX Pump Configurations. CEM 0125-15, Rocketdyne Div., North American Rockwell Corp. Unpublished, Apr. 1960.
13. *Walsh, J. K.: Mark 15 LOX Pump Calibration. TAMM 6115-50, Rocketdyne Div., North American Rockwell Corp. Unpublished, Aug. 1966.
14. *DiCristina, H.: Water, Alcohol, and JP-5 Tests of a Phase 5 Fuel Pump. PED 55-5807, Rocketdyne Div., North American Rockwell Corp. Unpublished, Dec. 1955.
15. Hammitt, F. G.: Observation of Cavitation Scale and Thermodynamic Effects in Stationary and Rotating Components. J. Basic Eng., vol. 35, Mar. 1963, pp. 1-16.
16. Jacobs, R. B.; Martin, K. A.; and Hardy, R. J.: Direct Measurement of Net Positive Suction Head. J. Basic Eng., vol. 81, June 1959, pp. 147-154.
17. Grindell, A. G.: Correlation of Cavitation Inception Data for a Centrifugal Pump Operating in Water and in Sodium-Potassium Alloy (NaK). J. Basic Eng., vol. 82, Dec. 1960, pp. 821-828.
18. Hollander, A.: Thermodynamic Aspects of Cavitation in Centrifugal Pumps. ARS J., vol. 32, no. 10, Oct. 1962, pp. 1594-1595.
19. Stahl, H. A.; and Stepanoff, A. J.: Thermodynamic Aspects of Cavitation in Centrifugal Pumps. Trans. ASME, Series D, vol. 78, Nov. 1956, pp. 1691-1693.
20. Jakobsen, J. K.: On the Mechanism of Head Breakdown in Cavitating Inducers. J. Basic Eng., vol. 86, June 1964, pp. 291-305.

*Dossier for design criteria monograph "Liquid Rocket Engine Turbopump Inducers." Unpublished, 1968. Collected source material available for inspection at NASA Lewis Research Center, Cleveland, Ohio.

21. Jacobs, R. B.; and Martin, K. B.: Cavitation Problems in Cryogenics. Technical Briefs, J. Basic Eng., vol. 82, Sept. 1960, pp. 756-757.

*22. Holl, J. W.: The Influence of Temperature, Size and Speed on NPSH. TSM 7115-2077, Rocketdyne Div., North American Rockwell Corp. Unpublished, Aug. 1967.

23. Ruggeri, R. S.; Moore, R. D.; and Gelder, T. F.: Method for Predicting Pump Cavitation Performance. NASA TM X-52316, 1967.

24. Moore, R. D.; and Ruggeri, R. S.: Prediction of Thermodynamic Effects of Developed Cavitation Based on Liquid-Hydrogen and Freon-114 Data in Scaled Venturis. NASA TN D-4899, 1968.

25. Ruggeri, R. S.; and Moore, R. D.: Method for Prediction of Pump Cavitation Performance for Various Liquids, Liquid Temperatures, and Rotative Speeds. NASA TN D-5292, 1969.

26. Gelder, T. F.; Ruggeri, R. S., and Moore, R. D.: Cavitation Similarity Considerations Based on Measured Pressure and Temperature Depressions in Cavitated Regions of Freon-114. NASA TN D-3509, 1966.

27. Moore, R. D.; and Ruggeri, R. S.: Venturi Scaling Studies on Thermodynamic Effects on Developed Cavitation of Freon-114. NASA TN D-4387, 1968.

28. Meng, P. R.; and Moore, R. D.: Hydrogen Cavitation Performance of 80.6° Helical Inducer Mounted in Line with Stationary Centerbody. NASA TM X-1935, 1970.

29. Moore, R. D.; and Meng, P. R.: Thermodynamic Effects of Cavitation of an 80.6° Helical Inducer Operated in Hydrogen. NASA TN D-5614, 1970.

30. Bissell, W. R.; Wong, G. S.; and Winstead, T. W.: An Analysis of Two-Phase Flow in LH_2 Pumps for O_2/H_2 Rocket Engines. AIAA Paper No. 69-549, AIAA 5th Propulsion Joint Specialist Conference (U.S. Air Force Academy, Col.), June 1969.

31. Stripling, L. B.; and Acosta, A. J.: Cavitation in Turbopumps—Part 1. J. Basic Eng., vol. 84, Sept. 1962, pp. 326-338.

32. Wade, R. B.; and Acosta, A. J.: Investigation of Cavitating Cascades. J. Basic Eng., vol. 89, Dec. 1967, pp. 693-706.

33. Jakobsen, J. K.: Supercavitating Cascade Flow Analysis. J. Basic Eng., vol. 86, Dec. 1964, pp. 805-814.

34. Jakobsen, J. K.: Computer Program To Calculate Cavity on Inducer Blade. NASA Tech Brief, NAR 53852, 1968.

*35. King, W. S.: The Effect of Sweeping Back the Leading Edges of a 5.5 Inch Inducer. DDR 712-3003, Rocketdyne Div., North American Rockwell Corp. Unpublished, Oct. 1957.

*36. Iura, T.: Effect of Blade Leading Edge Modification on the Cavitation Performance of a Straight-Milled Inducer. DDR 512-61, Rocketdyne Div., North American Rockwell Corp. Unpublished, Sept. 1955.

37. Numachi, F.: Effect of Surface Roughness on Cavitation Performance of Hydrofoils—Part 3. J. Basic Eng., vol. 89, Mar. 1967, pp. 201-209.

38. Holl, J. W.: The Inception of Cavitation on Isolated Surface Irregularities. J. Basic Eng., vol. 82, Mar. 1960, pp. 169-183.

39. Acosta, A. J.: An Experimental Study of Cavitating Inducers. ACR 38, Second Symposium, Naval Hydrodynamics, Office of Naval Hydrodynamics, Office of Naval Research, 1958; Discussion by Toru Iura, p. 554.

*40. Rosenmann, W.: Results of Testing Three Experimental Model 17-Inch Mark 10 LOX Inducers at the CTL-I Water Tunnel Facility. TAMM 6115-54, Rocketdyne Div., North American Rockwell Corp. Unpublished, Aug. 1966.

*Dossier for design criteria monograph "Liquid Rocket Engine Turbopump Inducers." Unpublished, 1968. Collected source material available for inspection at NASA Lewis Research Center, Cleveland, Ohio.

*41. King, W. S.: Effect of Partial Blading on 5.5-Inch Inducer. DDM 712-3022, Rocketdyne Div., North American Rockwell Corp. Unpublished, Oct. 1957.

42. Montgomery, John C.: Analytic Performance Characteristics and Outlet Flow Conditions of Constant and Variable Lead Helical Inducers for Cryogenic Pumps. NASA TN D-583, 1961.

43. Sandercock, D. M.; Soltis, R. F.; and Anderson, D. A.: Cavitation and Non-Cavitation Performance of an 80.6° Flat-Plate Helical Inducer at Three Rotational Speeds. NASA TN D-1439, 1962.

44. Carter, A. D. S.; and Hughes, H. P.: A Theoretical Investigation Into the Effect of Profile Shape in the Performance of Aerofoils in Cascade. R&M 2384, British A.R.C., 1946.

45. Lieblein, S.: Incidence and Deviation Angle Corrections for Compressor Cascades. J. Basic Eng., vol. 82, Sept. 1960, pp. 575-587.

46. Lieblein, S.: Experimental Flow in Two-Dimensional Cascades; Chapter VI, Aerodynamic Design of Axial Flow Compressors. NASA SP-36, pp. 183-226.

*47. Rosenmann, W.: Mark 15 LOX Shrouded Inducer Test Report. TAMM 5115-103, Rocketdyne Div., North American Rockwell Corp. Unpublished, Dec. 1965.

*48. Schaffer, R. J.: Mark 10 Model LOX Inducer Performance With Shroud. CEM 0125-90, Rocketdyne Div., North American Rockwell Corp. Unpublished, Nov. 1960.

49. Wood, G. M.; Welna, H.; and Lamers, R. P.: Tip-Clearance Effects in Centrifugal Pumps. J. Basic Eng., vol. 87, Dec. 1965, pp. 932-940.

*50. Goff, L. R.: Backflow Deflector Influence on the Mark 10 LOX Pump Suction Performance Tests Conducted on CTL-V. TAMM 4115-86, Rocketdyne Div., North American Rockwell Corp. Unpublished, July 1964.

*51. Nielson, C. E.; and Fishburn, F. R.: The Effects of a Backflow Deflector Upon Mark 10 FRT Oxidizer Pump Head-Flow and Suction Performance and Pressure Oscillation at Bravo 2A. TAMM 6115-15, Rocketdyne Div., North American Rockwell Corp. Unpublished, Mar. 1966.

*52. Jackson, E.; and Goff, L.: Mark 10 LOX Pump Performance As Influenced by Inducer Diameter and by the Vaned Backflow Deflector. TAMM 5115-88, Rocketdyne Div., North American Rockwell Corp., Unpublished, Oct. 19, 1966.

*53. Hoshide, R. K.: Prewhirl Test Results on the Model Mark 10 LOX Pump. TAMM 2115-5, Rocketdyne Div., North American Rockwell Corp. Unpublished, Feb. 1962.

*54. Hoshide, R. K.: Test Results of the X-8 Pump Utilizing Prewhirl. TAMM 3115-2054, Rocketdyne Div., North American Rockwell Corp. Unpublished, Oct. 1963.

55. Wong, G. S.; MacGregor, C. A.; and Hoshide, R. K.: Suppression of Cavitation and Unstable Flow in Throttle Turbopumps. J. Spacecraft Rockets, vol. 2, no. 1, Jan.-Feb. 1965, pp. 73-80.

56. Peterson, R. E.: Stress Concentration Design Factors. John Wiley & Sons, Inc., 1962.

*57. Non-Ferrous Metallurgy Unit: Evaluation of Shot Peening as a Means of Increasing Life of F-1 Tens-50-T60 LOX Impellers at Cryogenic Temperatures. MPR 4-252-138, Rocketdyne Div., North American Rockwell Corp. Unpublished, June 1964.

58. Anon.: Compatibility of Materials With Rocket Propellants and Oxidizers. Memorandum 201, Defense Metals Information Center, Battelle Memorial Institute (Columbus, Ohio), Jan. 1965, pp. 5, 6, 17.

*59. Goff, L.; and Jackson, E.: Effect of Increased Inducer Radial Clearance on Low Frequency Pump Inlet Oscillations, H-Q and Suction Performance for the Mark 10 Fuel Pump. TAMM 6115-34, Rocketdyne Div., North American Rockwell Corp. Unpublished, June 1966.

*Dossier for design criteria monograph "Liquid Rocket Engine Turbopump Inducers." Unpublished, 1968. Collected source material available for inspection at NASA Lewis Research Center, Cleveland, Ohio.

*60. Jackson, E. D.: Mark 10 Quieting Program—Oscillation Reduction by Holes in the Inducer Blades. Phase I—Water Tunnel Study Using Mk 4 Inducers. TAMM 5115-23, Rocketdyne Div., North American Rockwell Corp. Unpublished, Feb. 1965.

*61. Jackson, E. D.; and Fishburn, F. R.: Test Results for the Model Mark 10 Fuel Pump With the 20-Inch Model Turbine Fuel Inlet Manifold, 6+6 Impeller and Tapered Inducer With and Without Holes. Unpublished, TAMM 5115-78, Rocketdyne Div., North American Rockwell Corp. Oct. 1965.

*62. Jackson, E. D.: Oscillation and Suction Performance Results of Test With Mark 10 Fuel Inducer and Modifications in Water Tunnel. TAMM 5115-80, Rocketdyne Div., North American Rockwell Corp. Unpublished, Sept. 1965.

*63. Stremel, R. L.: Elimination of Pressure Surges Occurring in the Mark 3 LOX Pump. CEM/FGD/925-2039, Rocketdyne Div., North American Rockwell Corp. Unpublished, May 1959.

*64. Jackson, E. D.: Oscillation and Suction Performance Results of Tests With Mark 10 LOX Inducers With and Without Holes in the Water Tunnel. TAMM 5115-91, Rocketdyne Div., North American Rockwell Corp. Unpublished, Nov. 1965.

*65. Rosenmann, W.: Results of Testing Gas Injection in Mark 10 Fuel Inducer. TAMM 5115-76, Rocketdyne Div., North American Rockwell Corp. Unpublished, Sept. 1965.

*66. Nielson, C.; and Fishburn, F.: POGO J-2 Oxidizer Pump Test Results—(a) Head Capacity and Suction Performance, (b) Gaseous Helium Injection, (c) LOX Warming. TAMM 5155-77, Rocketdyne Div., North American Rockwell Corp. Unpublished, Nov. 1965.

67. Jackson, E. D.: Final Report, Study of Pump Discharge Pressure Oscillations. NASA CR-80153, 1966.

68. Anon.: Metallic Materials and Elements for Aerospace Vehicle Structures. MIL-HDBK-5A, Department of Defense, Feb. 8, 1966.

69. Agricola, K. R.: The Usefulness of Materials Used in Booster Structures. Paper presented at the Symposium, The Application and Properties of Materials Used in Aerospace Vehicle Design, sponsored by The Martin Company (Denver, Colo.), May 4-6, 1960.

70. Anon.: 6000 Pound Thrust Jet Propulsion Unit; Part II, Materials Corrosion Data. Rep. SPD 121, Contract AF W33(038)-ac-13916, M. W. Kellogg Company, Mar. 1948.

71. Nelson, G. A.: Corrosion Data Survey. Shell Development Company (Emeryville, Calif.), 1960.

72. Ordin, P. M.; Miller, R. O.; and Diehl, J. M.: Preliminary Investigation of Hydrazine As a Rocket Fuel. NACA Rep. E7H21, May 1948.

73. Liberto, R. R.: Research and Development on the Basic Design of Storable High-Energy Propellant Systems and Components. Final Rep. TR 60-61, Contract AF 33(616)-6689, Bell Aerosystems Co. (Buffalo, N. Y.), May 1961.

74. Schmidt, H.: Fluorine and Fluorine-Oxygen Mixtures in Rocket Systems. NASA SP-3037, 1967.

75. Young, J. O.; and Holl, J. W.: Effects of Cavitation on Periodic Wakes Behind Symmetric Wedges. J. Basic Eng., vol. 88, Mar. 1966, pp. 163-176.

76. Yeh, H.; and Eisenhuth, J. W.: The Unsteady Wake Interaction in Turbomachinery and Its Effect on Cavitation. J. Basic Eng., vol. 81, June 1959, pp. 181-189.

*77. Lambert, R. B.: Vibration Tests of Mark 10 LOX Inducer. SM 4111-8057, Rocketdyne Div., North American Rockwell Corp. Unpublished, Dec. 1964.

*78. King, W. S.: Investigation of the Blade Failure on the Mark 6 Model Oxidizer Inducer. DDM 812-3025, Rocketdyne Div., North American Rockwell Corp. Unpublished, Mar. 1958.

*Dossier for design criteria monograph "Liquid Rocket Engine Turbopump Inducers." Unpublished, 1968. Collected source material available for inspection at NASA Lewis Research Center, Cleveland, Ohio.

*79. Stripling, L. B.: Digital Computer Program—Flat Plate Blade Loading Analysis. Free-Streamline-Wake Theory. IR 220, Rocketdyne Div., North American Rockwell Corp. Unpublished, 1962.

80. Herman, L. R.: Bending Analysis for Plates. Proceedings of the Conference on Matrix Methods in Structural Mechanics, Wright-Patterson AFB (Dayton, Ohio), Oct. 1965, AFFDL TR 66-80 (AD 646300), Nov. 1966, pp. 577-602.

81. Becker, E.; and Brisbane, J.: Application of the Finite Element Method to Stress Analysis of Solid Propellant Rocket Grains. Rep. S-76, Rohm & Haas Co., vol. I (AD 474031), Nov. 1965; vol. II, part 1 (AD 476515); vol. II, part 2 (AD 476735), Jan. 1966.

82. Lang, T. E.: Summary of the Functions and Capabilities of the Structural Analysis and Matrix Interpretive System Computer Program (SAMIS). Tech. Rep. 32-1075, Jet Propulsion Lab., NASA CR-83742, Apr. 1967.

83. Holms, A. G.; and Repko, A. J.: Correlation of Tensile Strength, Tensile Ductility, and Notch Tensile Strength With the Strength of Rotating Disks of Several Designs in the Range of Low and Intermediate Ductility. NACA TN 2791, 1952.

84. Rosenmann, W.: Experimental Investigations of Hydrodynamically Induced Shaft Forces With a Three Bladed Inducer. Symposium on Cavitation in Fluid Machinery, ASME Winter Annual Meeting (Chicago, Ill.), Nov. 1965, pp. 172-195.

85. Abbott, I. H.; and Von Doenhoff, A. E.: Theory of Wing Sections. Dover Pub., Inc., 1960.

*86. Goff, L. R.; and Gulbrandsen, N. C.: Results of the Suction Side Refaired Mark 10 LOX Pump Inducer Tests Conducted at CTL-V, Cell 4A and Bravo 2. TAMM 4115-138, Rocketdyne Div., North American Rockwell Corp. Unpublished, Nov. 1964.

*87. Dolony, J. F.: Axial Stack-up Analysis and Prestressed Bolts. Stress Note No. 15, Rocketdyne Div., North American Rockwell Corp. Unpublished, Oct. 1964.

88. Campbell, M.; Thompson, M. B.; and Hopkins, V.: Solid Lubricant Handbook for Use in the Space Industry. Contract NAS8-1540, Control No. TP85-137, Midwest Research Institute (Kansas City, Mo.), 1968.

89. Campbell, W.: The Protection of Steam Turbine Disc Wheels From Axial Vibration. Trans. ASME, vol. 46, 1924, pp. 31-140; Discussion, pp. 140-160.

*90. Turner, J. D.: The Effect of Fluid Density on Stator Blade Resonant Frequency. SM 3111-8073A, Rocketdyne Div., North American Rockwell Corp. Unpublished, Dec. 1963.

91. Anderson, R. G.: How To Design High Speed Rotating Parts for Maximum Burst Resistance. Mach. Design, vol. 29, no. 21, Oct. 17, 1957, pp. 148-156.

92. Holms, A. G.; Jenkins, J. E.; and Repko, A. J.: Influence of Tensile Strength and Ductility on Strengths of Rotating Disks in Presence of Material and Fabrication Defects of Several Types. NACA TN 2397, 1951.

93. Holms, A. G.; and Jenkins, J. E.: Effect of Strength and Ductility on Burst Characteristics of Rotating Disks. NASA TN 1667, 1948.

94. Winne, D. H.; and Wundt, B. M.: Application of the Griffith-Irwin Theory of Crack Propagation to the Bursting Behavior of Discs, Including Analytical and Experimental Studies. Trans. ASME, vol. 80, Nov. 1958, pp. 1643-1658.

95. Anon.: Mechanical Design Aspects of Centrifugal Impellers With High Tip Speed Capability (U). Rep. 7446-01F, Contract AF 04(611)-7446, Aerojet-General Corp. (AD 350716), Mar. 1963. Confidential.

96. Anon.: Mechanical Design Aspects of Centrifugal Impellers With High Tip Speed Capability: The Results of Experimental Program (U). Report Phase II Final. Rep. 7446-01F, Aerojet-General Corporation (AD 340146), Aug. 1963. Confidential.

*Dossier for design criteria monograph "Liquid Rocket Engine Turbopump Inducers." Unpublished, 1968. Collected source material available for inspection at NASA Lewis Research Center, Cleveland, Ohio.

REFERENCE 90

PAGE 92 BLANK

GLOSSARY

Symbol	Definition	Remarks
A	inducer inlet flow area, ft^2	$\pi/4\ (D^2 - d^2)$
A_H	meridional cross-sectional area of inducer hub, in.^{2}	
a	mathematical expression, eq. (42)	defined in eq. (42b)
b	mathematical expression, eq. (42)	defined in eq. (42a)
b	exponent in eq. (48)	approx. value = 0.5
C	blade chord length, ft	
C	empirical constant, eq. (17)	
C_p	pressure coefficient, eq. (61)	defined in eq. (60)
C_ψ	constant of integration, eqs. (38) and (41)	defined in eq. (43)
c	absolute fluid velocity, ft/sec	
c	radial clearance, ft	eqs. (54) and (55)
c_L	specific heat of liquid, Btu/(lb-°R)	
$c_{m,max}$	maximum obtainable meridional fluid velocity, ft/sec	
D	inducer inlet tip diameter, ft	
D_c	cavity diameter, ft	
D_s	suction specific diameter	$D\,(\mathrm{NPSH})^{1/4}/Q^{1/2}$
D'_s	corrected value of D_s (zero hub blockage)	fig. 1 $(1 - \nu^2)^{1/2} D_s$
d	inducer inlet hub diameter, ft	
d_i, d_o	inside and outside diameters of hub shear section, in.	
E	material modulus of elasticity	
ELI	extra-low-interstitial (content of interstitial elements)	
e	elongation in 4-diameter length of test rod	
F	mathematical expression, eq. (26)	defined in eq. (27)
F_e	material endurance limit strength, lb/in.^{2}	
F_{tu}	material ultimate tensile strength, lb/in.^{2}	
F_{ty}	material yield strength, lb/in.^{2}	

Symbol	Definition	Remarks
FLOX	mixture of liquid oxygen and fluorine	
f_b	disc burst factor	
f_d	disc design factor	
f_i	column matrix of nodal forces	
g	acceleration of gravity, 32.174 ft/sec^2	
H	total head, ft	
H_{loss}	line friction head loss, ft	
ΔH	local total head rise, ft	
ΔH_{net}	net total head rise per stage, ft	
Hz	Hertz, cps	
h	static head, ft	p_s/ρ
h_c	cavity height, ft	
I_{A1}	expression for integral, eq. (43)	defined in eq. (43a)
I_{A2}	expression for integral, eq. (43)	defined in eq. (43b)
I_{B1}	expression for integral, eq. (43)	defined in eq. (43c)
I_{B2}	expression for integral, eq. (43)	defined in eq. (43d)
IRFNA	inhibited red fuming nitric acid	
J	energy conversion factor	778.2 ft-lb/Btu
j	symbol for blade number in eq. (43)	
K	blade tip cavitation number	$\frac{p_s - p_v}{\frac{1}{2}\rho w_1^2/g}$
K	empirical constant, eq. (81)	
K^*	minimum value of cavitation number K at which blade will operate	
K_c	cavitation number based on cavity pressure p_c instead of fluid bulk vapor pressure p_v	$\frac{p_s - p_c}{\frac{1}{2}\rho w_1^2/g}$
K_{min}	cavitation number at supercavitation	
K_t	theoretical stress concentration factor	
K_{tf}	actual stress concentration factor	
K_{tsf}	fatigue notch factor for shear stress	
k	thermal conductivity, Btu/(sec-ft-°R)	
k_i	square symmetric element stiffness matrix	

Symbol	Definition	Remarks
k_s	empirical coefficient, eq. (54)	$k_s = 0.50$ to 0.65 experimentally
k_ψ	empirical coefficient, eq. (55)	$k_\psi = 1.0$
L	latent heat, Btu/lb, eq. (14)	
L	blade radial length, ft	
L_{ax}	axial length of blade, ft	
L_b	mathematical expression, eq. (86)	defined in eq. (87)
L_c	cavity length, ft	
L_s	mathematical expression, eq. (86)	defined in eq. (88)
l_w	length of blade wedge, ft	
M	coefficient, eq. (48)	has value $\approx$ 0.25 to 0.35
ms	mean or rms station	
$m1, m2, m3$	empirical exponents, eq. (17)	
N	blade number	
NPSH	net positive suction head, ft	$(p_{total} - p_v)/\rho_F$
$NPSH_{tank}$	minimum net positive suction head in tank at operating conditions, ft	
n	shaft or hub speed, rpm	
n	natural frequency of blade, Hz	measured at condition shown by subscript
n_f	safety factor for fatigue	
n_{ult}	safety factor against ultimate failure	
n_y	safety factor against yield failure	
n_0	natural frequency of blade in vacuum (or in atmosphere), Hz	
p_c	fluid vapor pressure in cavity at leading, edge, lb/ft^2	
p_s	fluid static pressure, lb/ft^2	
p_{total}	total fluid pressure at any point, lb/ft^2	$p_s + 1/2\rho_F c^2$
p_v	fluid bulk vapor pressure, lb/ft^2	
Q	flowrate, gpm	
Q'	corrected flowrate	$Q/(1 - v^2)$
R	radius of blade edge, in.	
R_C	Rockwell hardness C	

Symbol	Definition	Remarks
r	radial coordinate, ft	
r_{FSL}	radius of curvature of free streamline, in.	
rms	root mean square	$X_{rms} = \sqrt{\frac{X_1^2 + X_2^2 + \cdots + X_n^2}{n}}$
$r\theta$	blade wrap, ft	
$r\omega$	blade velocity, ft/sec	
S	blade or cascade spacing, ft	$\pi D/N$
S_s	suction specific speed	$nQ^{1/2}$ (NPSH)$^{-3/4}$
$S_{s,0}$	suction specific speed for zero clearance	
S'_s	corrected suction specific speed	$S_s/(1 - v^2)^{1/2}$
S'^*_s	characteristic suction specific speed (determined in cold water)	
$S'_{s,max}$	maximum suction specific speed obtainable with K^*	
T	fluid bulk temperature, °R	
TSH	thermal suppression head, ft	
t	blade thickness, in.	
U_c	fluid velocity on cavity boundary, ft/sec	
UDMH	unsymmetric dimethyl hydrazine	
u	blade tip speed, ft/sec	$\pi D\, n/60$
w	fluid velocity relative to blade at tip, ft/sec	$\sqrt{u^2 + c_m^2}$
w_c	fluid velocity on cavity boundary, ft/sec	
Z	NPSH factor	$2g\ (\text{NPSH})_{\text{tank}}/c_m^2$
z	axial coordinate, ft	
dz	change in z with change in $r\theta$, ft	
Δz	axial blade clearance, ft	
α	incidence angle of flow at blade leading edge, deg	
α	thermal cavitation parameter	defined in eq. (14), used in eq. (17)
α_{cant}	blade cant angle, deg	
α_{cone}	blade cone angle, deg	
α_w	wedge angle of blade, deg	

Symbol	Definition	Remarks
β	thermal factor, $sec^{1/2}$	defined in eq. (16)
β	blade angle, deg	
$\Delta\beta$	blade camber, deg	
β_w	blade angle measured to suction side of wedge, deg	
γ	fluid angle, deg	
$\Delta\gamma$	fluid turning angle, deg	
δ	deviation angle, deg	
δ_i	column matrix of modal deflections	
η	hydraulic efficiency	
θ	blade wrap angle (leading-edge sweep), rad	
K	thermal diffusivity, ft^2/sec	defined in eq. (15), used in eqs. (16) and (17)
Λ	blade lead, ft	
λ	blade lead per radian, ft/rad	
$\lambda\omega$	blade lead velocity, ft/sec	
ν	hub-to-tip diameter ratio	d/D
ρ	density, lb/ft^3	
Σ	mathematical expression, eq. (72)	defined in eq. (73)
σ	cascade solidity	
σ_{alt}	alternating stress, $lb/in.^2$	$(\sigma_{max} - \sigma_{min})/2$
σ_{AT}	average tangential stress at speed N, $lb/in.^2$	
$\sigma_{AT,\ burst}$	average tangential stress at burst speed, N_{burst}, $lb/in.^2$	
σ_{ax}	axial stress, $lb/in.^2$	
σ_{MT}	maximum tangential stress from basic stress analysis, $lb/in.^2$	
σ^*_{MT}	maximum tangential stress in disc including stress concentration effects, $lb/in.^2$	
σ_{mean}	average stress, $lb/in.^2$	$(\sigma_{max} + \sigma_{min})/2$
σ_t	local tangential stress, $lb/in.^2$	
τ	cavitation parameter	$(NPSH)/(u^2/2g)$
τ_{alt}	alternating shear stress, $lb/in.^2$	eq. (86)

Symbol	Definition	Remarks
τ_0	allowable shear stress, lb/in.^{2}	eq. (86)
ϕ	flow coefficient, ref. to inlet tip blade speed	c_m/u
ψ	head coefficient, ref. to inlet tip blade speed	$H/(u^2/g)$
ψ_l	head coefficient, local value at radius r	c_u/u
ψ_0	head coefficient for zero clearance	
ω	angular velocity, rad/sec	

Subscripts

1	inlet	*m*	meridional
2	outlet	ms	mean or rms station
a	axial component	op	operating conditions
bl	blade	opt	optimum
burst	burst speed	*T*	tip
d	design value	TE	trailing edge
F	fluid	test	test conditions
H	hub	*u*	tangential component
L	liquid	*v*	vapor
LE	leading edge	yield	yield speed
l	local station		

NASA SPACE VEHICLE DESIGN CRITERIA
MONOGRAPHS ISSUED TO DATE

ENVIRONMENT

SP-8005	Solar Electromagnetic Radiation, June 1965
SP-8010	Models of Mars Atmosphere (1967), May 1968
SP-8011	Models of Venus Atmosphere (1968), December 1968
SP-8013	Meteoroid Environment Model—1969 (Near Earth to Lunar Surface), March 1969
SP-8017	Magnetic Fields—Earth and Extraterrestrial, March 1969
SP-8020	Mars Surface Models (1968), May 1969
SP-8021	Models of Earth's Atmosphere (120 to 1000 km), May 1969
SP-8023	Lunar Surface Models, May 1969
SP-8037	Assessment and Control of Spacecraft Magnetic Fields, September 1970
SP-8038	Meteoroid Environment Model—1970 (Interplanetary and Planetary), October 1970

STRUCTURES

SP-8001	Buffeting During Atmospheric Ascent, revised November 1970
SP-8002	Flight-Loads Measurements During Launch and Exit, December 1964
SP-8003	Flutter, Buzz, and Divergence, July 1964
SP-8004	Panel Flutter, July 1964
SP-8006	Local Steady Aerodynamic Loads During Launch and Exit, May 1965
SP-8007	Buckling of Thin-Walled Circular Cylinders, revised August 1968
SP-8008	Prelaunch Ground Wind Loads, November 1965
SP-8009	Propellant Slosh Loads, August 1968
SP-8012	Natural Vibration Modal Analysis, September 1968
SP-8014	Entry Thermal Protection, August 1968
SP-8019	Buckling of Thin-Walled Truncated Cones, September 1968
SP-8022	Staging Loads, February 1969

SP-8029	Aerodynamic and Rocket-Exhaust Heating During Launch and Ascent, May 1969
SP-8031	Slosh Suppression, May 1969
SP-8032	Buckling of Thin-Walled Doubly Curved Shells, August 1969
SP-8035	Wind Loads During Ascent, June 1970
SP-8040	Fracture Control of Metallic Pressure Vessels, May 1970
SP-8046	Landing Impact Attenuation For Non-Surface-Planing Landers, April 1970
SP-8050	Structural Vibration Prediction, June 1970

GUIDANCE AND CONTROL

SP-8015	Guidance and Navigation for Entry Vehicles, November 1968
SP-8016	Effects of Structural Flexibility on Spacecrafe Control Systems, April 1969
SP-8018	Spacecraft Magnetic Torques, March 1969
SP-8024	Spacecraft Gravitational Torques, May 1969
SP-8026	Spacecraft Star Trackers, July 1970
SP-8027	Spacecraft Radiation Torques, October 1969
SP-8028	Entry Vehicle Control, November 1969
SP-8033	Spacecraft Earth Horizon Sensors, December 1969
SP-8034	Spacecraft Mass Expulsion Torques, December 1969
SP-8036	Effects of Structural Flexibility on Launch Vehicle Control Systems, February 1970
SP-8047	Spacecraft Sun Sensors, June 1970
SP-8058	Spacecraft Aerodynamic Torques, January 1971
SP-8059	Spcecraft Attitude Control During Thrusting Maneuvers, February 1971

CHEMICAL PROPULSION

SP-8025	Solid Rocket Motor Metal Cases, April 1970
SP-8041	Captive-Fired Testing of Solid Rocket Motors, March 1971
SP-8048	Liquid Rocket Engine Turbopump Bearings, March 1971
SP-8051	Solid Rocket Motor Igniters, March 1971

NASA-Langley, 1971 —— 28

END OF REFERENCE

90

REFERENCE

91

ROCKET ENGINE TURBOPUMP SHAFTS AND COUPLINGS. NASA SPACE VEHICLE DESIGN CRITERIA (CHEMICAL PROPULSION). NASA SP-8101, 1970.

NASA
SPACE VEHICLE
DESIGN CRITERIA
(CHEMICAL PROPULSION)

LEWIS RESEARCH CENTER
Aerospace Safety Research
and Data Institute
JAN 2 1974
CLEVELAND, OHIO

NASA SP-8101

LIQUID ROCKET ENGINE TURBOPUMP SHAFTS AND COUPLINGS

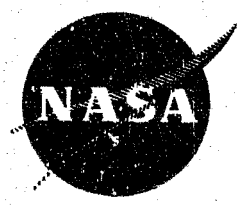

SEPTEMBER 1972

NATIONAL AERONAUTICS AND SPACE ADMINISTRATION

GUIDE TO THE USE OF THIS MONOGRAPH

The purpose of this monograph is to organize and present, for effective use in design, the significant experience and knowledge accumulated in development and operational programs to date. It reviews and assesses current design practices, and from them establishes firm guidance for achieving greater consistency in design, increased reliability in the end product, and greater efficiency in the design effort. The monograph is organized into two major sections that are preceded by a brief introduction and complemented by a set of references.

The State of the Art, section 2, reviews and discusses the total design problem, and identifies which design elements are involved in successful design. It describes succinctly the current technology pertaining to these elements. When detailed information is required, the best available references are cited. This section serves as a survey of the subject that provides background material and prepares a proper technological base for the *Design Criteria* and Recommended Practices.

The *Design Criteria*, shown in italics in section 3, state clearly and briefly what rule, guide, limitation, or standard must be imposed on each essential design element to assure successful design. The *Design Criteria* can serve effectively as a checklist of rules for the project manager to use in guiding a design or in assessing its adequacy.

The Recommended Practices, also in section 3, state how to satisfy each of the criteria. Whenever possible, the best procedure is described; when this cannot be done concisely, appropriate references are provided. The Recommended Practices, in conjunction with the *Design Criteria*, provide positive guidance to the practicing designer on how to achieve successful design.

Both sections have been organized into decimally numbered subsections so that the subjects within similarly numbered subsections correspond from section to section. The format for the Contents displays this continuity of subject in such a way that a particular aspect of design can be followed through both sections as a discrete subject.

The design criteria monograph is not intended to be a design handbook, a set of specifications, or a design manual. It is a summary and a systematic ordering of the large and loosely organized body of existing successful design techniques and practices. Its value and its merit should be judged on how effectively it makes that material available to and useful to the designer.

CONTENTS

	Page
1. INTRODUCTION	1
2. STATE OF THE ART	3
3. DESIGN CRITERIA and Recommended Practices	60
REFERENCES	97
GLOSSARY	109
NASA Space Vehicle Design Criteria Monographs Issued to Date	117

SUBJECT	STATE OF THE ART		DESIGN CRITERIA	
SHAFT DESIGN	*2.1*	3	*3.1*	60
Design Parameters	*2.1.1*	4	*3.1.1*	60
Shaft Speed	*2.1.1.1*	4	*3.1.1.1*	60
Optimization	–	–	*3.1.1.1.1*	60
Transient Dwells and Overshoots	–	–	*3.1.1.1.2*	60
Steady-State Operation	–	–	*3.1.1.1.3*	61
Bearing and Seal Locations	*2.1.1.2*	5	*3.1.1.2*	61
Shaft Size	*2.1.1.3*	6	*3.1.1.3*	62
Shaft Discontinuities and Transitions	*2.1.1.4*	7	*3.1.1.4*	62
Service Environment	*2.1.1.5*	8	*3.1.1.5*	64
Thermal Environment	–	–	*3.1.1.5.1*	64
High-Pressure Gaseous-Hydrogen Environment	–	–	*3.1.1.5.2*	65
Corrosive Environments	–	–	*3.1.1.5.3*	65
Hard Vacuum	–	–	*3.1.1.5.4*	66
Material Selection	*2.1.2*	9	*3.1.2*	66
Mechanical Properties	–	–	*3.1.2.1*	66
Thermal Properties	–	–	*3.1.2.2*	67

SUBJECT	STATE OF THE ART		DESIGN CRITERIA	
Stress Corrosion and Hydrogen Embrittlement	–	–	*3.1.2.3*	67
Low-Temperature Embrittlement	–	–	*3.1.2.4*	67
Surface Condition	–	–	*3.1.2.5*	68
Structural Analysis	*2.1.3*	11	*3.1.3*	68
Loads	*2.1.3.1*	11	*3.1.3.1*	68
Safety Factors	*2.1.3.2*	12	*3.1.3.2*	70
Analytical Methods	*2.1.3.3*	13	*3.1.3.3*	70
Assembly and Operation	*2.1.4*	13	*3.1.4*	72
Dimensions and Fits	*2.1.4.1*	13	*3.1.4.1*	72
Datums	–	–	*3.1.4.1.1*	72
Dimensional Inspection	–	–	*3.1.4.1.2*	72
Bearing Clearances	–	–	*3.1.4.1.3*	72
Tolerance Limits	–	–	*3.1.4.1.4*	72
Piloting	–	–	*3.1.4.1.5*	73
Component Running Positions and Clearances	*2.1.4.2*	15	*3.1.4.2*	74
Retaining Bolts and Locking Devices	*2.1.4.3*	15	*3.1.4.3*	75
Bolt Mechanical Strength	–	–	*3.1.4.3.1*	75
Bolt Preload	–	–	*3.1.4.3.2*	75
Vibration	–	–	*3.1.4.3.3*	76
Bolt Arrangement and Fit	–	–	*3.1.4.3.4*	76
Galling, Seizing, and Fretting	–	–	*3.1.4.3.5*	76
Locking Device Action	–	–	*3.1.4.3.6*	77
Assembly Aids	*2.1.4.4*	17	*3.1.4.4*	77
Quality Control	*2.1.5*	17	*3.1.5*	77
Inspection Method	–	–	*3.1.5.1*	77
Component Contamination	–	–	*3.1.5.2*	78
Spline Inspection	–	–	*3.1.5.3*	78
Curvic Coupling Inspection	–	–	*3.1.5.4*	78

SUBJECT	STATE OF THE ART		DESIGN CRITERIA	
SHAFT DYNAMICS	*2.2*	19	*3.2*	79
Dynamic Behavior	*2.2.1*	19	*3.2.1*	79
Whirl Motions	*2.2.1.1*	19	*3.2.1.1*	79
Forced Whirls and Critical Speeds	*2.2.1.2*	19	*3.2.1.2*	79
Steady-State Operating Speed Limitations	–	–	*3.2.1.2.1*	79
Assessing Importance of Critical Speeds	–	–	*3.2.1.2.2*	80
Self-Excited Whirls and Instabilities	*2.2.1.3*	27	*3.2.1.3*	80
Aerodynamic-Induced Instability	*2.2.1.3.1*	27	–	–
Instability Caused by Internal Friction	*2.2.1.3.2*	29	–	–
Whirl Induced by Dry Friction	*2.2.1.3.3*	29	–	–
Whirl Induced by Fluid-Film Bearing	*2.2.1.3.4*	30	–	–
Torsional Critical Speeds	*2.2.1.4*	30	*3.2.1.4*	81
Thin-Wall Hollow-Shaft Vibrations	*2.2.1.5*	30	*3.2.1.5*	82
Analysis of Shaft Dynamic Behavior	*2.2.2*	31	*3.2.2*	82
Modeling for Theoretical Analyses	*2.2.2.1*	31	*3.2.2.1*	82
Mass and Stiffness Distributions	*2.2.2.1.1*	31	*3.2.2.1.1*	82
Mechanical Joints, Shaft-Riding Elements, and Abrupt Changes in Shaft or Casing Cross Sections	*2.2.2.1.2*	34	*3.2.2.1.2*	83
Casing and Machine Mount Effects	*2.2.2.1.3*	36	*3.2.2.1.3*	84
Bearing Spring and Damping Forces	*2.2.2.1.4*	38	*3.2.2.1.4*	84
Rotor Imbalance Forcing Functions	*2.2.2.1.5*	40	*3.2.2.1.5*	85
Virtual Mass and Damping	*2.2.2.1.6*	43	*3.2.2.1.6*	86
Mathematical Methods and Computer Solutions	*2.2.2.2*	43	*3.2.2.2*	86
Analysis of Rotors Supported by Fluid-Film Bearings	*2.2.2.2.1*	43	–	–
Analysis of Rotors Supported by Rolling-Contact Bearings	*2.2.2.2.2*	44	–	–
Analysis of Shaft Systems with Unsymmetric Supports	*2.2.2.2.3*	45	–	–

SUBJECT	STATE OF THE ART		DESIGN CRITERIA	
Prediction Accuracy	*2.2.2.3*	45	*3.2.2.3*	87
Adjustment of Critical Speeds and Response Levels	*2.2.3*	47	*3.2.3*	87
Balancing	*2.2.4*	48	*3.2.4*	88
COUPLING DESIGN	*2.3*	49	*3.3*	89
Splines	*2.3.1*	49	*3.3.1*	89
Size and Configuration	–	–	*3.3.1.1*	89
Teeth in Contact	–	–	*3.3.1.2*	90
Curvic Couplings	*2.3.2*	50	*3.3.2*	91
Proportions for Joint Stiffness	–	–	*3.3.2.1*	91
Size and Configuration	–	–	*3.3.2.2*	91
Parallel-Sided Face Couplings	*2.3.3*	53	*3.3.3*	92
DESIGN CONFIRMATION TESTS	*2.4*	54	*3.4*	92
Nonrotating Tests	*2.4.1*	54	*3.4.1*	93
Data Correlation	–	–	*3.4.1.1*	93
Rotating System Tests	*2.4.2*	58	*3.4.2*	94
Instrumentation	*2.4.2.1*	58	*3.4.2.1*	94
Type of Instrumentation	–	–	*3.4.2.1.1*	94
Instrumentation Location	–	–	*3.4.2.1.2*	95
Interpretation of Data	*2.4.2.2*	59	*3.4.2.2*	95
Special Tests	*2.4.3*	59	*3.4.3*	96

The magnitudes of most of the identified loads on a shaft are evaluated by computation during the design phase. Loads that do not lend themselves to this computational analysis (i.e., vibratory and malfunctioning loads) are given appropriate consideration by designing to minimize the magnitude of such loads.

The load predictions in some cases have been inaccurate. Radial loads due to rotor dynamics have sometimes been twice as large as the loads calculated in response analyses. Also, radial loads due to nonsymmetrical pressure distributions resulting from pump-housing discharge ports, in-flow obstructions, etc., do not lend themselves to accurate predictions of magnitude. Calculation of net pump or rotor axial thrust, which is the algebraic sum of large thrust component forces, has given values substantially different from the subsequently experimentally determined ones.

2.1.3.2 SAFETY FACTORS

Usually, the safety factors for static stresses are specified to the designer. Table III displays some examples of safety factors that have been used in turbopump shaft design.

Table III – Typical Safety Factors Used in Shaft Design

Rocket engine	Yield safety factor	Ultimate safety factor
XLR-87-AJ-3/5 and XLR-91-AJ-3/5	1.0	1.25
M-1	1.0	1.5
XLR-87/91-AJ-9	1.0	1.4
J-2 and F-1	1.1	1.5
ARES	1.2	1.6
RL 10	1.2	1.5

Generally, the fatigue safety factors are not specified. Values of 1.25 and 1.33 have been used.

Selecting safety factors in accordance with the desired reliability rather than more or less arbitrarily choosing them has become the desired engineering approach. The goal is to account for variations in material properties; effects of size; effects of machining and processing operations on properties; accuracy in predicting environments and loads; accuracy of stress analysis models; etc., by use of probabilistic mathematics (refs. 40

2.2 Shaft Dynamics

A vast amount of material has been published on the subject of shaft dynamics. The more complete treatments, which cover important aspects not usually covered in standard textbooks, are given in references 54 through 70. The treatment herein is restricted to those aspects of shaft dynamics that must be taken into account in the design of the shaft and coupling.

2.2.1 Dynamic Behavior

2.2.1.1 WHIRL MOTIONS

Shaft whirling usually is described in terms of shaft motion about an external longitudinal axis; whether this motion is forced or self-excited is noted also. Motions of the shaft during whirling normally are described by the type of whirl path or orbit and by the direction and speed of the whirl relative to the shaft rotation. Some of the basic classifications of shaft motion are illustrated in figure 3. In the examples shown, when shaft speed Ω equals the magnitude of whirl velocity ω, the motion is called synchronous. Shaft motions can become highly complex as illustrated in figure 3(f) and as discussed in references 58, 71, and 72.

2.2.1.2 FORCED WHIRLS AND CRITICAL SPEEDS

Types of forced whirls and their causes identified by Yamamoto from his work with rolling-contact bearings (refs. 58 through 61) are presented in table V. Other causes of forced whirls are associated with trapped fluids (ref. 73), bearing clearances (refs. 72, 74, and 75), bearing-noise vibrations (ref. 76), gear-meshing excitations, and rotating-stall excitations at a frequency approximately half the shaft speed (ref. 77). Shaft torque and thrust misalignment between coupled shafts can induce lateral and torsional vibrations.

A critical speed is defined as a shaft rotative speed at which a rotor-stator system natural frequency coincides with a possible forcing frequency. If all the possible system critical speeds of a given machine are considered as speeds at which operation is untenable, then the operating speed zones are severely limited. For example, figure 4, a plot similar to those of Yamamoto (refs. 58 through 61), shows numerous critical speeds for a shaft supported in rolling-contact bearings. Here the natural frequencies of various shaft modes of vibration are plotted as a function of shaft speed. "Rays" emanating from the zero point of the curve show corresponding forcing functions (e.g., impeller vane-to-housing frequency and bearing-ball translation frequency). Theoretically, the intersection of each ray with a natural frequency is a critical speed; however, experience has shown that many of these critical speeds have negligible practical importance.

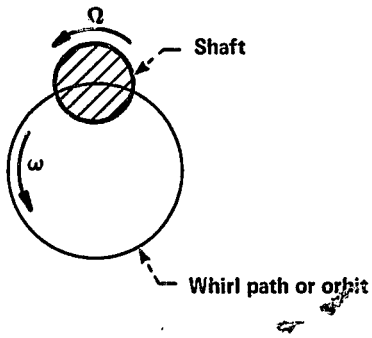

(a) Forward circular whirl

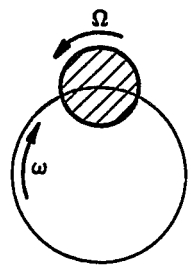

(b) Reverse or backward circular whirl

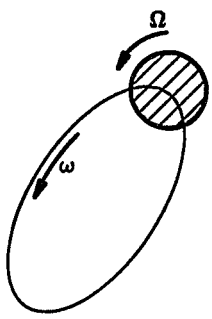

(c) Forward elliptical whirl

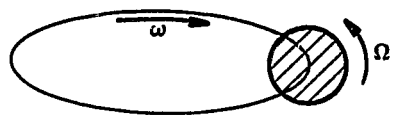

(d) Reverse elliptical whirl

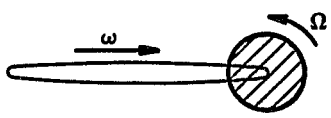

(e) Lateral vibration

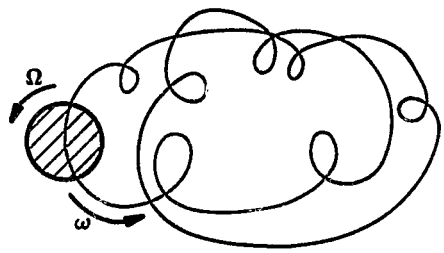

(f) Complex whirl

Figure 3. – Basic classifications of shaft motion

Table V – Types and Causes of Forced Whirling Identified by Yamamoto (refs. 58 through 61)

Type	Cause
Forward circular precession, $\omega = \Omega$	Rotor imbalance
Backward circular precession, $\omega = \Omega$	Unequal bearing stiffness in different radial directions
Noncircular precessions, $\omega = \pm \Omega$	Unequal bearing stiffnesses in different radial directions, or Transient changes in Ω, or Externally applied rectilinear vibrations
Shaft whipping caused by guard ring or shroud rub	When the shroud rubs, more stiffness is added to the shaft; and thus the critical speed is driven up ahead of the operating speed
Nonsynchronous motions, $\omega = (0.4 \text{ to } 0.5)\ \Omega$	One oversized or undersized ball or roller in bearing; thus motion is excited at cage rotational speed
Nonsynchronous motions, $\omega = 2\Omega, 3\Omega, 4\Omega, \ldots\ldots$	Bearing defects, such as oval inner or outer races
"Sum and difference" critical speeds, $\omega_i \pm \omega_j = \Omega$	Nonlinear, nonsymmetrical spring characteristics
Subharmonic precession, $\omega = \frac{\Omega}{2}, \frac{\Omega}{3}, \ldots\ldots\ldots$	Nonlinear, nonsymmetrical shaft stiffness
Unexpected jumps in response	Nonlinearity in shaft system stiffness or forcing functions

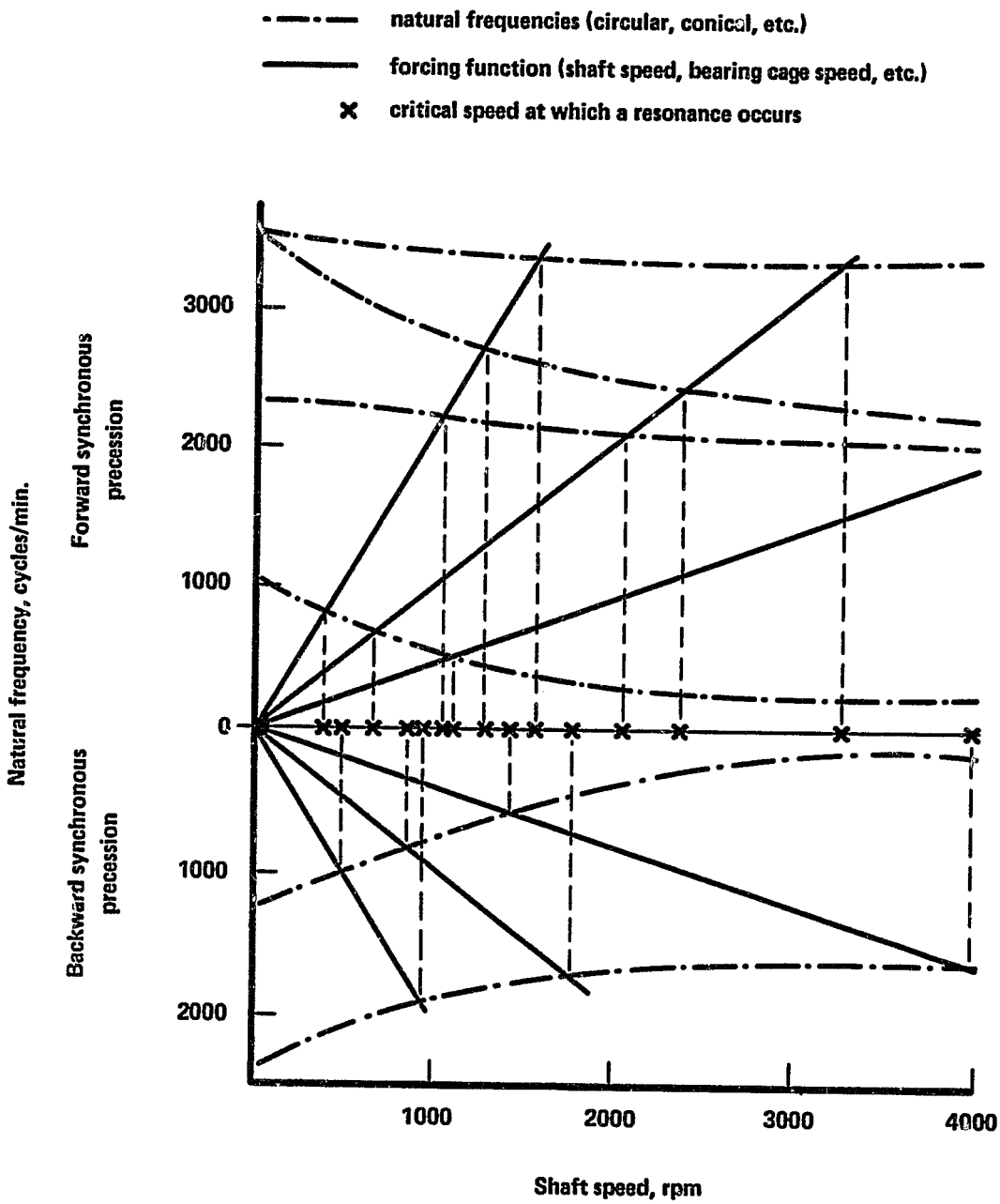

Figure 4. – Typical plot of shaft speed vs natural frequency (showing many secondary critical speeds for a shaft supported in rolling-contact bearings)

Usually, critical speeds associated with synchronous forward forced motions or precessions that are excited easily by rotor imbalance are considered as the most important. These synchronous-forward-precession critical speeds, whose values are governed primarily by the rotor mass and the combined or individual stiffnesses of the rotor, bearings, or bearing supports, are herein referred to as "major" critical speeds. "Secondary" critical speeds or resonances refer to all other critical speeds not classified as major. Thus, secondary critical speeds include the nonsynchronous criticals identified by Yamamoto, rotor/bearing/casing system criticals that are controlled primarily by the casing dynamics, and backward-whirl criticals. It is common practice to ignore the secondary critical speeds and consider only major critical speeds when designing a new turbopump, even though it is recognized that the nonsynchronous whirls described by Yamamoto can occur and can be troublesome. Accordingly, experimental evaluation after the machine is built usually is appropriate.

Parts (a), (b), and (c) of figure 5 show shaft motion of the Titan III (87-9) turbine shaft as measured by distance detectors mounted at right angles to each other and perpendicular to the shaft axis. These plots display some secondary resonances when increasing amounts of imbalance weight are added to the rotor. The secondary criticals, which were coupled system modes, were governed primarily by the casing dynamic characteristics. Note that the shaft orbit amplitudes were magnified dynamically by factors of only 2 or 3. The secondary criticals did not result in significant resonant buildup; with a well-balanced rotor, these secondary resonances were difficult to detect experimentally.

The casing local to the turbine bearings had a complex, irregular, asymmetric configuration. Tests showed both a generally soft radial direction and a stiff radial direction with intermediate local stiffness perturbations. These stiffness variations were responsible for a lateral vibration that was indicated by one distance detector peaking at the same time that a second detector decreased.

Other phenomena found experimentally are as follows:

(1) Unstable, sharply fluctuating response (fig. 5(d)) occurred when loose fits existed between the bearing outer race and the bearing sleeve and housing. During this unstable motion, the turbine gave off a "growling" noise.

(2) Tests with tight fits and very small bearing internal play showed very smooth response (fig. 5(e)).

(3) Tests with tight fits and nominal bearing internal play (0.001 in. [25μm] TIR) sometimes showed secondary unstable very-low-amplitude vibration throughout almost the entire zero- to full-speed range when rotors were well balanced. Adding imbalance stabilized the motion.

(4) The location of some of the secondary criticals shifted as much as 10 percent as a result of loose fits.

Sometimes it is difficult during the design phase to establish whether a particular rotor/bearing/casing critical should be considered as a major or secondary critical speed.

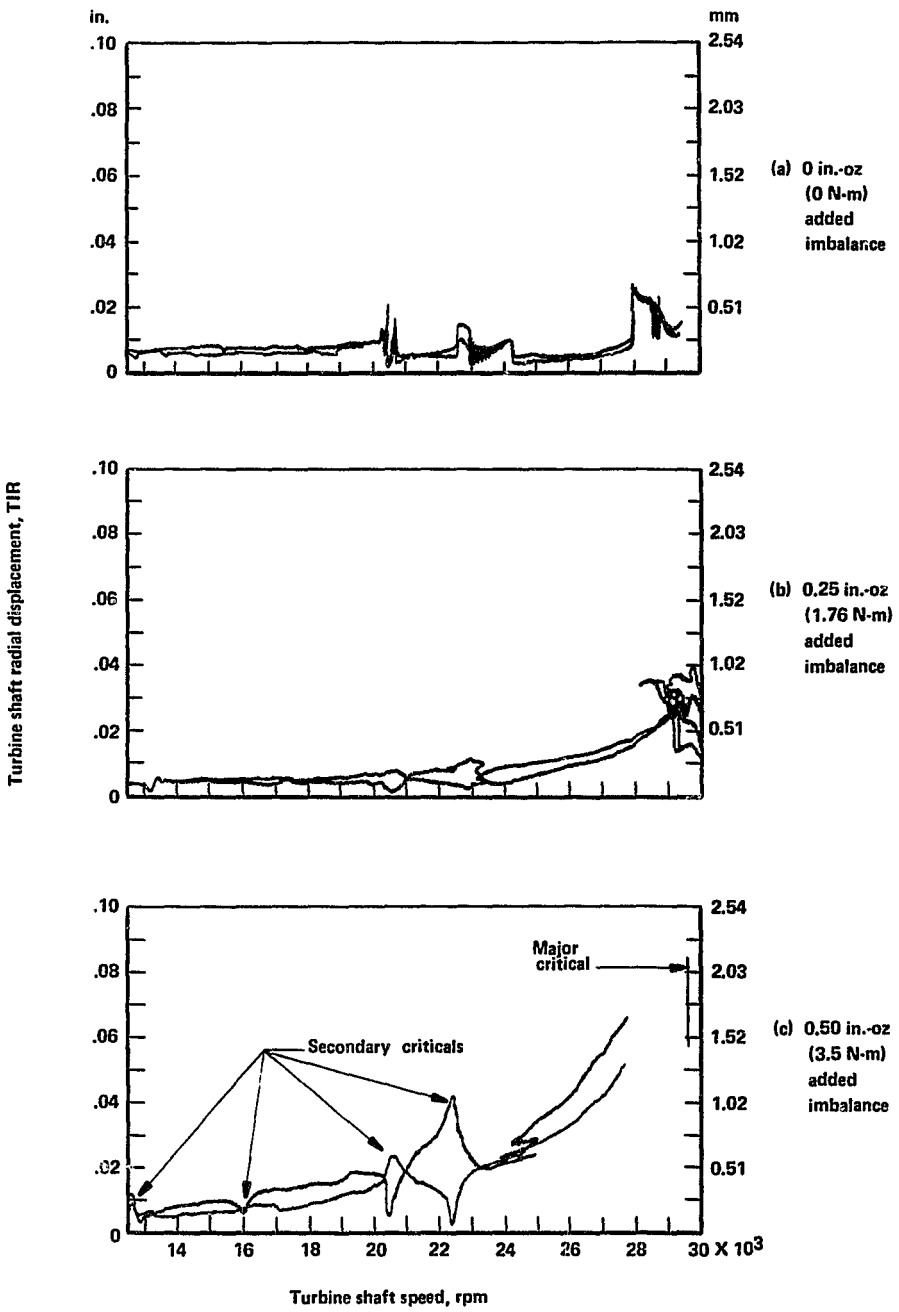

Figure 5. – Spin test data for Titan III XLR-87-AJ-9 turbine

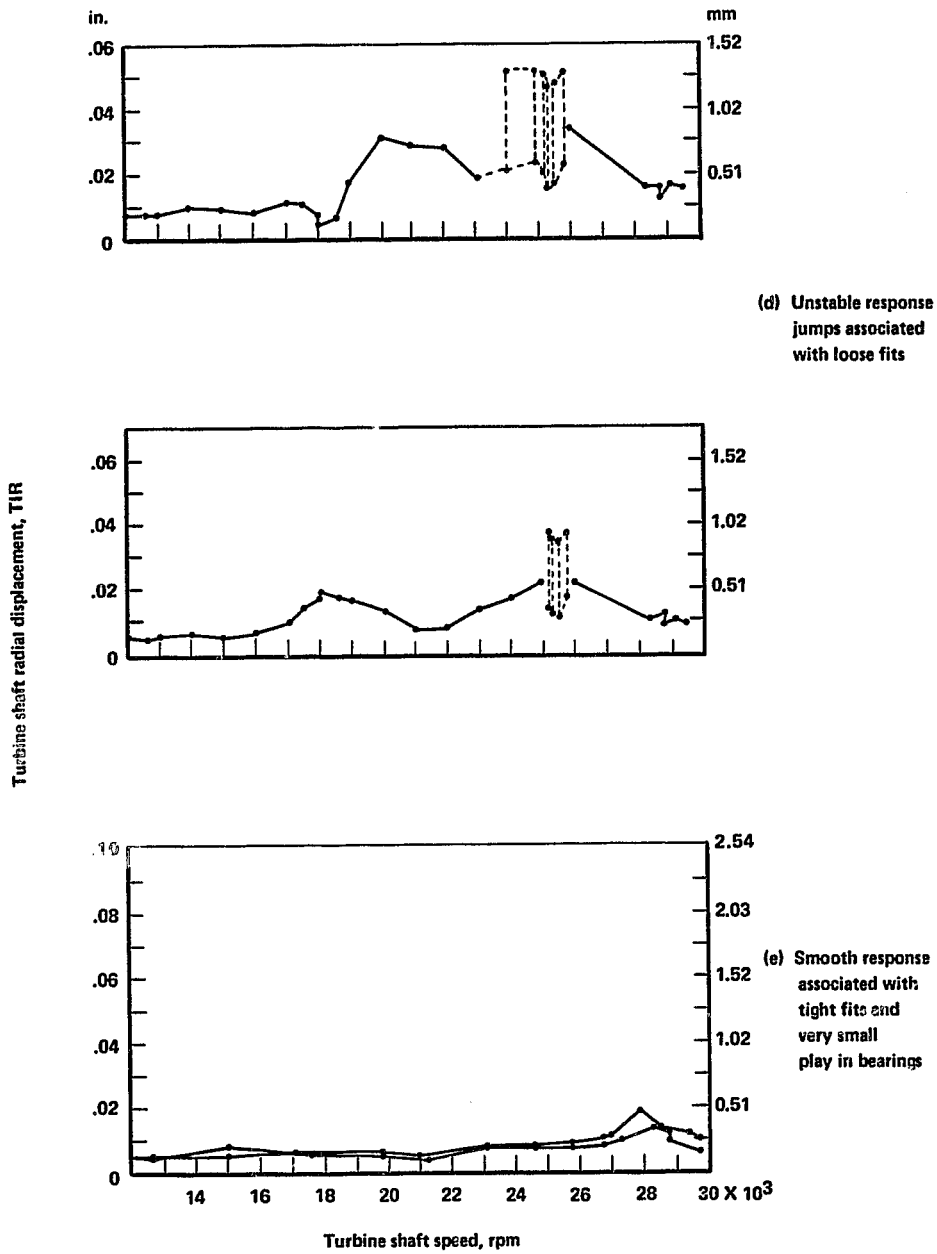

Figure 5. – Concluded

However, computed mode shapes for such system criticals frequently have been sufficient basis for judgment. For example, when the casing mass is much greater than the rotor mass and inspection of a mode shape shows most of the vibrational amplitudes to be in the casing, a good possibility exists that the associated critical speed rotor amplitude buildup will be limited to tenable levels, because casings usually can dissipate considerable vibrational energy. However, if the vibrational amplitudes are controlled only by bearing or bearing support displacements while the rotor and casing are acting essentially as rigid bodies, then untenable vibration amplitude buildup is probable if the shaft operates a sufficient time at the critical speed.

Inspection of only the mode shapes is not always adequate. The amount of energy dissipated each cycle is approximately equal to the product of the logarithm of the damping decrement and the vibrational kinetic energy of the structure. Some modes show little amplitude in the casing, and inspection alone would indicate large rotor amplitudes at the associated critical speed. When the system distribution of kinetic energy is evaluated, a large percentage of the vibrational energy may be found in the casing. This distribution is possible because of the relatively large mass of the casing, even though casing amplitudes are relatively small when compared with those of the rotor. Experience has shown that passing through or running at the system critical speeds that show most of the motion in the casing is practical as long as fatigue failures of the casing components do not develop. However, if the casing does not contain a large part of the vibrational energy, high bearing loads and attendant damage may occur. Durability of the casing is demonstrated by analysis and test.

Sometimes the mode shapes at the second and higher shaft-bending critical speeds are considerably different from those predicted by theory. It has been found experimentally that both second and third criticals have modes that consist of the usually predicted shapes super imposed with the first-mode shape (fig. 28.9 of ref. 78).

If a rotor, its bearings, and the casing have essentially symmetric mass and stiffness properties about the shaft axis, the most probable orbital motion is circular. For asymmetrical properties, the usual orbital motion is elliptical and, at the criticals, approaches lateral vibration. The Titan II (87-5) shaft, which utilized angular-contact bearings and was a built-up shaft with many joints, was supported in a casing that was highly asymmetric in both stiffness and mass. Shake tests of the rotor supported in "rigid" bearing mounts yielded fundamental bending frequencies ranging from 315 to 365 cps, the value depending on excitation amplitude. When the rotor was assembled in the casing, the lateral-vibration natural frequencies dropped a small amount in magnitude and assumed some directional dependency. When the shaft was spin tested in the assembled casing, dual resonant peaks were found at approximately 290 and 340 rps. Normally, a spinning-shaft natural frequency (critical speed) is expected to be somewhat higher than the lateral-vibration natural frequency because the disk gyroscopic moment stiffens the shaft. However, the dual resonance peaks corresponded to lateral-vibration shaft motions in planes at right angles to each other. As the motions were lateral rather than circular, the disk gyroscopic stiffening moments associated with forward circular orbits vanished.

Response predictions usually are accomplished during the design analysis phase to obtain such data as bearing reactions, whirl orbits, shaft shear and bending moments, and sensitivity to locations of imbalance. These data then are compared with bearing capacities, rotor tip clearances, joint and bolt preload and stiffness capabilities, and the planes of balancing, respectively.

Gear teeth, misaligned crowned splines, and flexible couplings have been known to couple shaft lateral and torsional motions. Rotor blades that had a natural frequency close to a shaft critical suffered fatigue cracking failure. Thus, comparison of the critical speed to other known resonant speeds is useful.

When fluid-film bearings are used, in most instances the undamped-critical-speed calculations wherein bearing stiffness is considered but damping is neglected are insufficient. Often, undamped critical speeds do not correspond to the speed of maximum rotor imbalance response (ref. 79). Thus, response computations usually are used to evaluate the effect of bearing damping on locations of critical speeds; vibration amplitudes at critical speeds; and response of the rotor, throughout the operating speed range, resulting from the amount and distribution of imbalance.

2.2.1.3 SELF-EXCITED WHIRLS AND INSTABILITIES

Self-excited whirls of shafts supported in rolling-contact bearings have been linked with aerodynamic excitation forces, internal rotor friction attributable to causes such as shrink fits and builtup rotors, and dry friction. Shafts using fluid-film bearings can develop hydrodynamic-excited whirls.

Self-excited whirls and instabilities of shafts operating supercritical still do not lend themselves to accurate computational evaluation. Only for the simplest machines can the whirl threshold speed be accurately predicted, and whirl amplitudes are not predictable for any machine. The present practice for supercritical designs is to minimize those design factors that promote instabilities (e.g., shrink fits, builtup shafts, and rotor flexibility), build the machine, and experimentally confirm its stability or develop it into a stable operating machine.

2.2.1.3.1 Aerodynamic-Induced Instability

The E-blade Mark 9 axial-flow turbopump exhibited strong nonsynchronous whirl motion under certain operating conditions. The exact cause, or the mechanism that initiated this behavior, was not established conclusively. However, the instability appears to have been a hydrodynamic effect created by a circumferential variation in the pump pressure distribution. One E-blade Mark 9 pump failed catastrophically; self-excited whirl was strong among the possible causes identified by failure analysis reported in reference 80. Figure 6 (from ref. 80) illustrates the typical rotor motions arising from aerodynamic-induced instability.

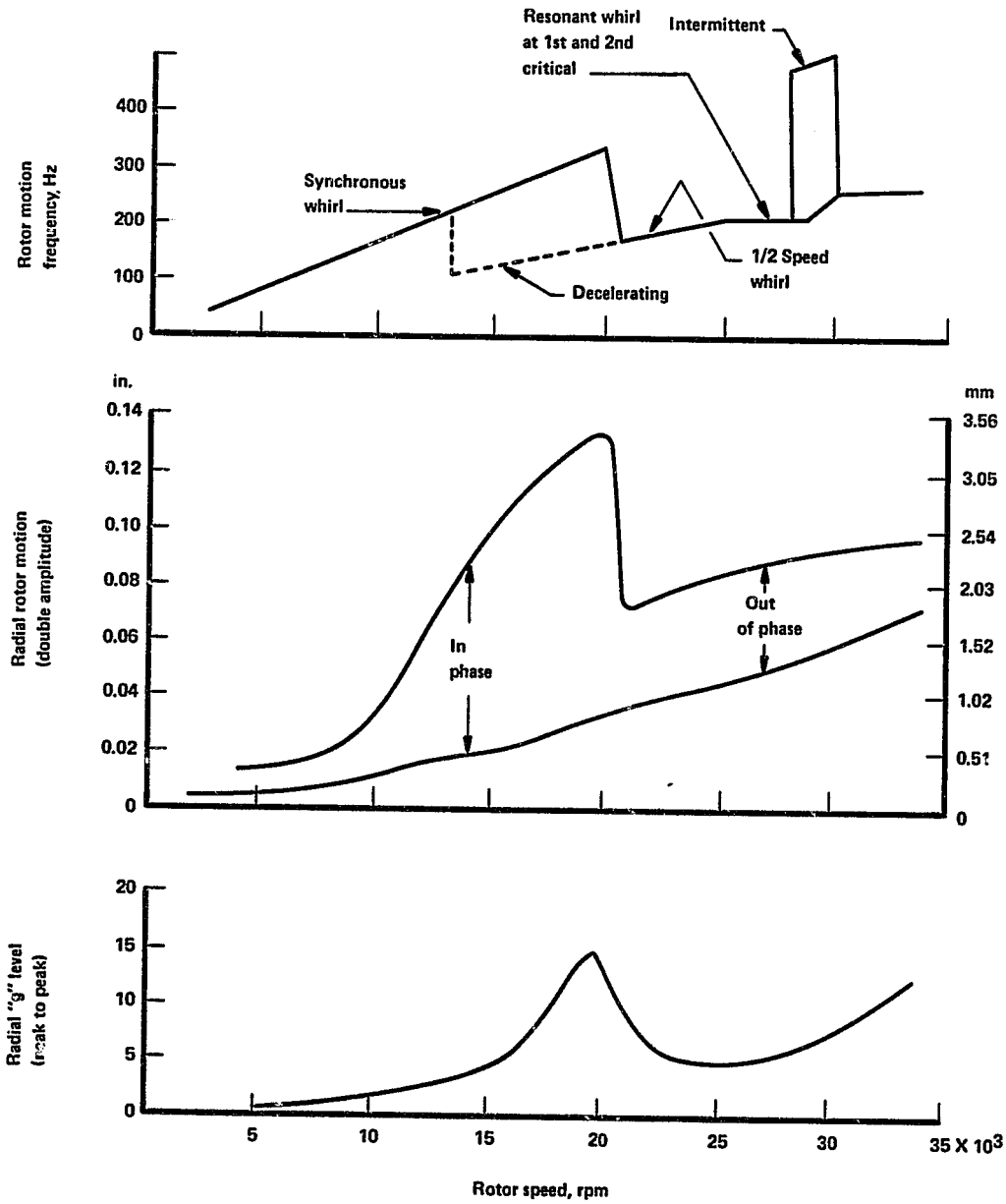

Figure 6. – Typical rotor motions due to aerodynamic–induced instabilities (ref. 80)

The Mark 25 axial-flow pump exhibited subsynchronous whirl (ref. 81). However, no known hardware damage occurred during the many system tests conducted, even though the resulting vibration levels were undesirable. An experimental liquid-hydrogen turbopump experienced nonsynchronous whirl caused by either hydraulic instability or loose fits (ref. 82).

Severe aerodynamic-excited whirl of several jet-engine axial compressors and turbines resulted from two causes (ref. 83): (1) the circumferential variation of static pressure acting on the cylindrical surface of the rotor, particularly within the labyrinth seals; and (2) the eccentricity of the rotor causing circumferential variation of the blade-tip clearance and a corresponding variation in local efficiency and imbalance torque. Several different designs exhibited whirling. All rotors that whirled had relatively large rotor flexibility, which was demonstrated by the low critical speed of the rotor and support system. In almost every instance, stability was achieved by increasing the stiffness of the rotor or that of the rotor support or both. The whirl speed was approximately 40 to 50 percent of the rotation speed. Reference 83 states that damper bearings providing friction relative to fixed axes effectively help protect against shaft whip and whirl. Self-excited whirl caused by pressure changes associated with varying clearances around the labyrinth seals also is mentioned in reference 84.

Fluid-film thrust bearings sometimes are used in conjunction with rolling-contact radial-load bearings. If the fluid has sufficient viscosity, these thrust bearings may develop damping forces in the direction normal to the shaft axis and thus tend to inhibit self-excited whirl. A reduction of thrust, however, could reduce the damping enough to permit whirl; such a possibility was mentioned in association with the removal of the gravity field from a vertically mounted rotor (ref. 85). Film thrust bearings used in liquid hydrogen are not expected to produce much damping.

2.2.1.3.2 Instability Caused by Internal Friction

Whereas external frictional forces usually aid in damping the oscillations, the internal frictional forces can, under certain circumstances, cause unstable whirl buildup if the shaft is operating above its first critical speed. Sources of internal friction found to be significant are builtup shafts and joints or disks shrunk or firmly bolted onto the shaft. Hysteresis forces in the shaft material have been identified as a possible source of internal-friction-induced instability, but no instabilities attributable to this cause have been reported. Most of the available information on effects of internal friction on the stability of high-speed rotors is summarized in reference 86.

2.2.1.3.3 Whirl Induced by Dry Friction

The phenomenon of a violent shaft backward whirl or whip caused by friction in a dry-clearance bearing (i.e., the clearance between outer race and housing is not lubricated) or by the shaft striking a rough or unlubricated guide is described on page 292 of reference 84.

A recent study (ref. 87) shows how the occurrence of slip between the shaft and the bearing can contribute to the violence of the whirl and can cause it to develop into near-resonant motion over a large range of speeds. This whirl motion and instability buildup can occur also when the shaft is operating below the system first critical speed. This kind of problem is relieved by tightening the bearing fit, or by pinning the bearing to prevent rotation, or, in extreme cases, by making the inner bearing race integral with the shaft.

2.2.1.3.4 Whirl Induced by Fluid-Film Bearing

Subsynchronous whirls sometimes are referred to as oil whip, resonant whip, half-frequency whirl, or just nonsynchronous whirl. Such whirls caused by the characteristics of fluid-film bearings are again becoming of concern in the design of rocket engine turbopump shafts. Most recent turbopump shaft designs utilized rolling-contact bearings. However, the needs for increased performance, higher speed, and longer life have resulted in the serious consideration of fluid-film hydrostatic bearings. Rolling-contact bearings have DN and life limitations related directly to shaft size and speed, whereas fluid-film bearings apparently do not. Thus a shaft with rolling-contact bearings is more restricted in diameter than a shaft with fluid-film bearings, the result being a shaft with less stiffness and lower shaft bending critical speeds.

Within the last few years, the state of the art has been enlarged greatly in regard to the mathematical modeling of the fluid-film bearings and accuracy of the analysis of the influence of these bearings upon shaft stability and response to imbalance force (refs. 63 through 65, 68, and 79). The improved dynamic analyses give good predictions of actual operating characteristics.

2.2.1.4 TORSIONAL CRITICAL SPEEDS

The torsional vibrational modes in rocket engine turbopump shafts have not limited or controlled design. Often, torsional critical speeds are not even calculated; but, when they are, the calculated values usually are compared with the possible forcing frequencies of (1) gear teeth meshing (when gears are used), (2) low orders of rotational speed (i.e. speeds equal to rotor speed or low multiples thereof) caused by shaft imbalance or misalignments of couplings, and (3) impeller-vane and stator-vane passing frequencies.

In addition, these calculated torsional natural frequencies are compared with other system natural frequencies (e.g., shaft whirl or lateral vibration, turbine blades, and impeller vanes) to ascertain whether any possible coupling or energy transfer is likely.

2.2.1.5 THIN-WALL HOLLOW-SHAFT VIBRATIONS

Thin-wall, cylindrical, drum-type shafts, which are characteristic of axial-flow pumps, have experienced critical-speed problems and fatigue cracking associated with nodal-circle and

nodal-diameter vibrations of the type shown in figure 7. The usual design modification is to change the environment acoustics to reduce the magnitude of excitation, change the driving frequencies, or change the shaft vibration natural frequencies.

2.2.2 Analysis of Shaft Dynamic Behavior

2.2.2.1 MODELING FOR THEORETICAL ANALYSES

Even though simple models have been adequate in some cases, experience has shown that the classical models for predicting shaft whirl critical speeds and response usually yield very crude estimates. This has been attributable primarily to the exclusion of, or improper account for, the effects of influential items: rotor mass and stiffness distributions, mechanical joints, shaft-riding elements, abrupt changes in shaft cross section, casing and machine mount effects, bearing spring and damping forces, shear deformation, gyroscopic and rotary inertia moments, rotor imbalance forces, and virtual mass and damping associated with operating in dense fluids. Details of current techniques for modeling and analyzing these critical items are presented in the sections that follow.

The technology of modeling for torsional critical speeds is adequately set forth in references 88 through 90. Reference 88 covers modeling procedures and summarizes many formulas and charts for modeling common shaft components to obtain equivalent mass and stiffness distributions. Consideration is given to the hollow circular shaft with an eccentric bore; the solid shaft with a linear taper (a gradual change in cross section); the abrupt-step shaft; the shaft with a keyway; the splined shaft; the shaft with a flat side; a branched system running at different speeds; torsional stiffness of spur and bevel gears, spiral gears, helical gears, couplings, and clutches; and other significant conditions. No further discussion of torsional critical speeds will be presented herein.

2.2.2.1.1 Mass and Stiffness Distributions

Significantly improved models for shaft-dynamics analyses have been developed over the past decade (refs. 6, 54, 79, and 91 through 93). Figure 8 illustrates two of the typical improved shaft dynamic models. In figure 8(a) (ref.6) K^L represents the lateral spring constants of the casing mounts and bearings, and K^T symbolizes the torsional spring constant at the shaft/rotor splines; C^L and C^T represent corresponding damping coefficients for use with the indicated spring constants. In figure 8(b) (ref. 92), the bearing lateral spring constant K is subscripted p or t to identify the bearings at the pump or turbine end, respectively.

Tradeoffs between model and analysis complexities have resulted in the Myklestad lumped-mass model or an extension thereof being the one most commonly used. In its simplest form, this model consists of the rotor masses lumped at stations along the rotor and connected by massless elastic beams and linear support springs (refs. 94 through 96). The usual refinements to this model include the addition of shear deformation to the beam and

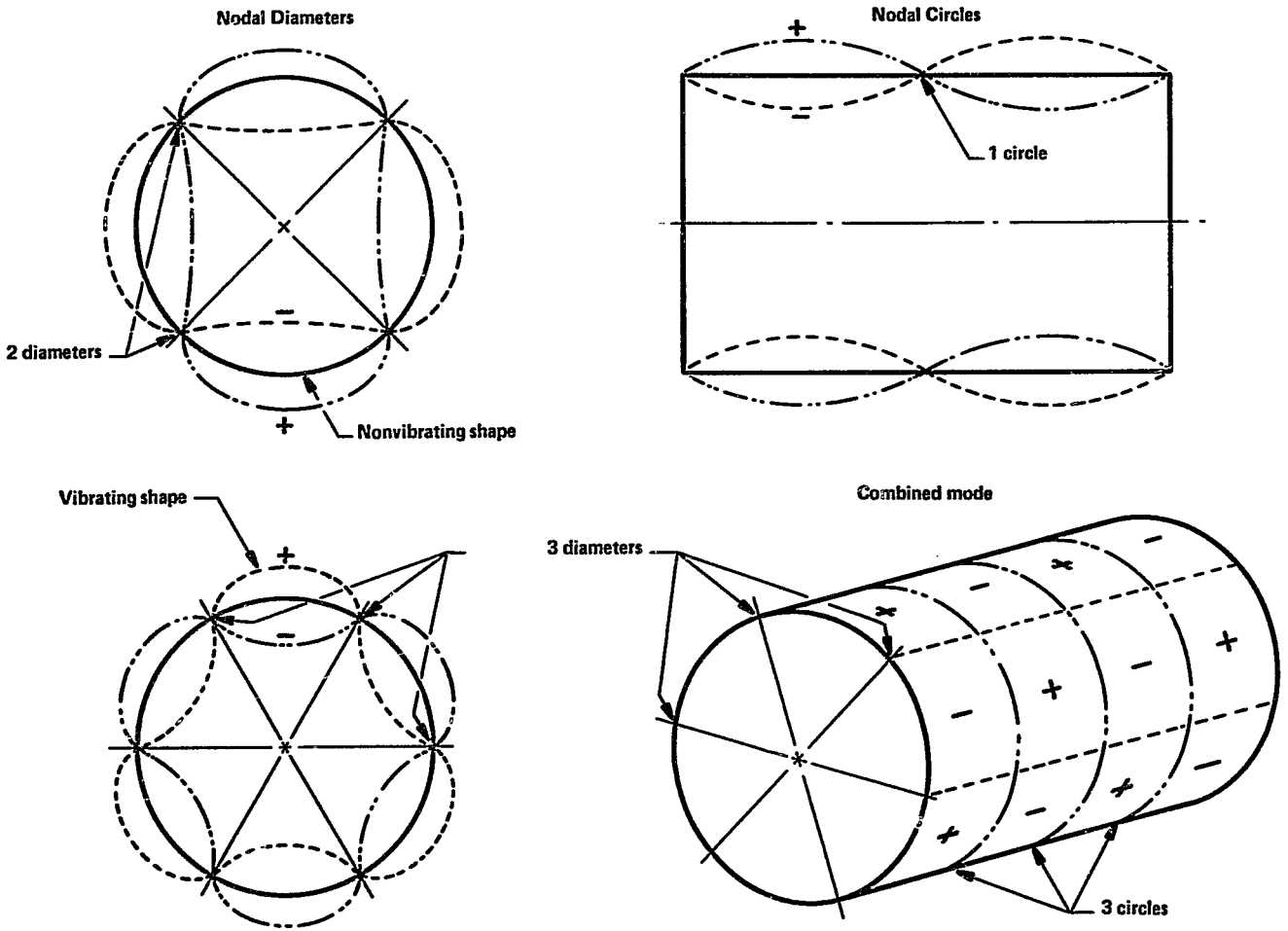

Figure 7. – Nodal-circle and nodal-diameter vibrations in a thin-wall hollow shaft

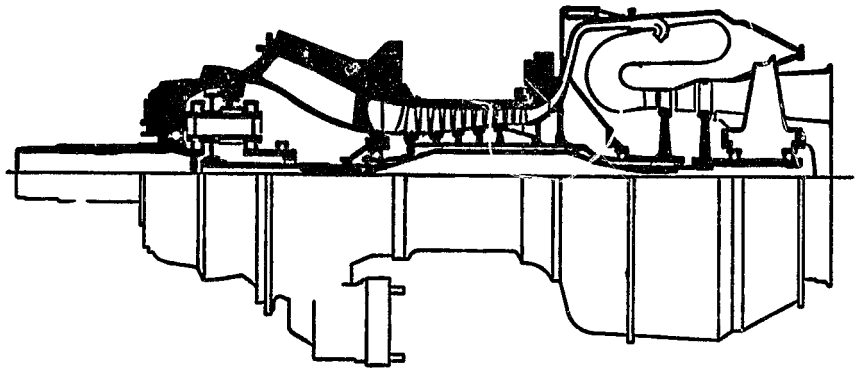

(T53 turboprop engine)

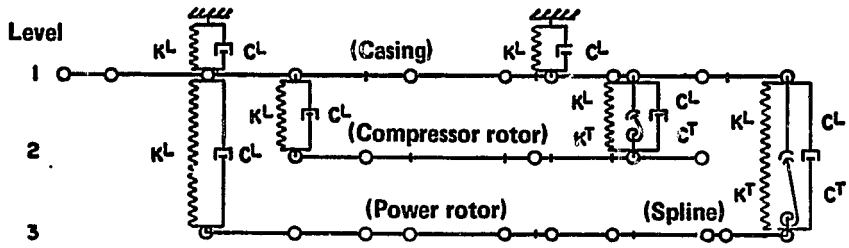

(T53 equivalent dynamic system used in connection with the vibration analysis)

(a) T53 turboprop engine (ref. 6)

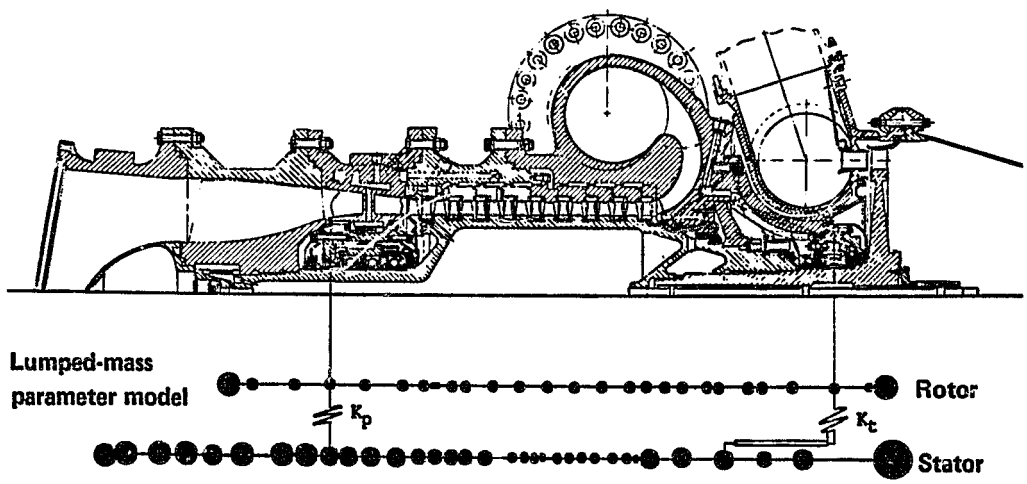

(b) M-1 fuel turbopump (ref. 92)

Figure 8. – Typical models for shaft dynamics analysis

gyroscopic moments (ref. 97). Further refinements have included the use of uniform continuous-mass beams instead of massless beams (refs. 54, 79, and 88), unsymmetrical bearing stiffness and damping models for fluid-film bearings (refs. 54, 79, and 91), nonlinear bearing stiffness for rolling-contact bearings (ref. 92), gyroscopic representation for nonsynchronous whirl (ref. 98), and coupled rotor/casing multiple-beam models (refs. 6, 92, 93, and 97).

2.2.2.1.2 Mechanical Joints, Shaft-Riding Elements, and Abrupt Changes in Shaft or Casing Cross Sections

The stiffness of a builtup rotor usually is far less than that of a one-piece rotor even when the joints are preloaded at assembly. If the forces applied to the joint during operation exceed the preload, the joint can open up and cause a loss in overall stiffness. Figure 9

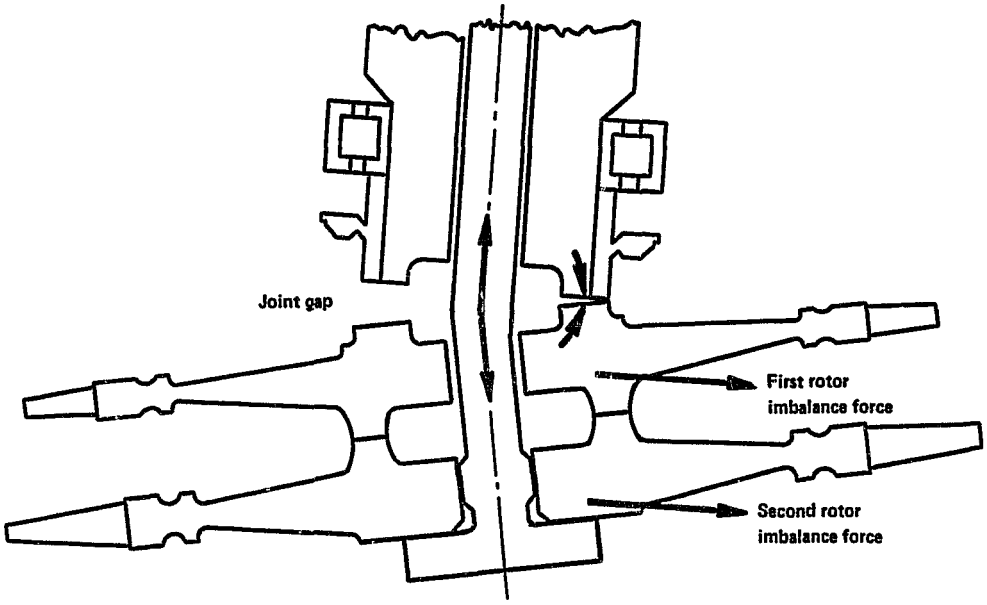

Figure 9. – Curvic coupling joint loosening under load

depicts the condition wherein the centrifugal forces of the turbine wheels imposed sufficient moment to overcome the joint preload and cause a great increase in joint flexibility. Even properly preloaded joints do not ensure that a builtup rotor will develop stiffnesses approaching that of one-piece construction. Curvic couplings with full preload are inherently a local flexibility in comparison with welded joints of similar size. However, if the coupling is placed in a position of low shaft bending moment, the local softness may not result in a significant reduction in rotor stiffness and natural frequencies. Couplings used as shown in figure 10 have exhibited additional flexibilities.

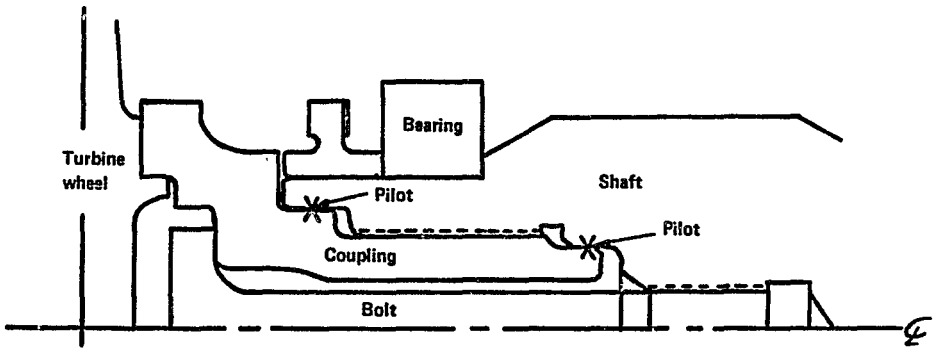

Figure 10. – Coupling between shaft and turbine that results in additional flexibilities

Shaft-mounted components (e.g., shrunk-on impellers, shaft sleeves, and bearing races) usually result in stiffening of the shaft; however, the degree of stiffening may be influenced by axial preloading. Long stackups of shaft-riding elements sometimes do not obtain good axial preloading when each piece is put on the shaft with interference fits. Gaps as shown in figure 11 cause a reduction in shaft stiffness. Any abrupt changes in shaft cross sections, such as the transition in a hollow shaft from a small to a large diameter, produce local flexibilities as indicated in figure 12.

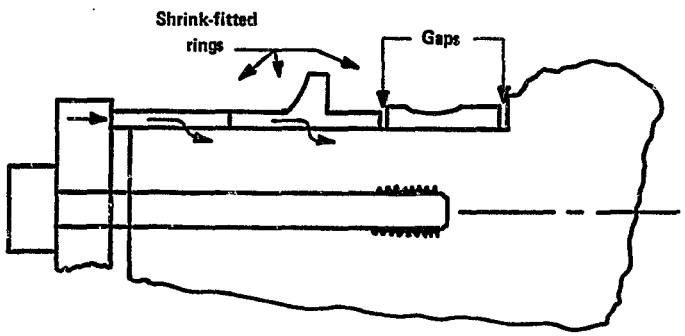

Figure 11. – Gaps on shaft-mounted components that affect overall shaft stiffness

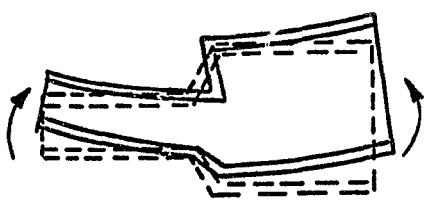

Figure 12. – Local flexibility of hollow shaft at transition from large to small diameter

2.2.2.1.3 Casing and Machine Mount Effects

Bearing-support flexibility can exert significant influence on critical speeds (refs. 6, 7, 54, 55, 93, and 99 through 102). The following are the four major considerations regarding casing and machine mount effects:

(1) Gross trends in casing mass and mount stiffness
(2) Dynamic coupling with the rotor
(3) Casing stiffness local to the bearings and near locations where loads are concentrated (e.g., struts)
(4) Symmetry of the casing mass and stiffness about the shaft axis

Analysis of the simple 2-degree-of-freedom system (ref. 99) provides some insight into the first major consideration. Figure 13 shows the general solution. Here M_1, K_1, M_2, K_2

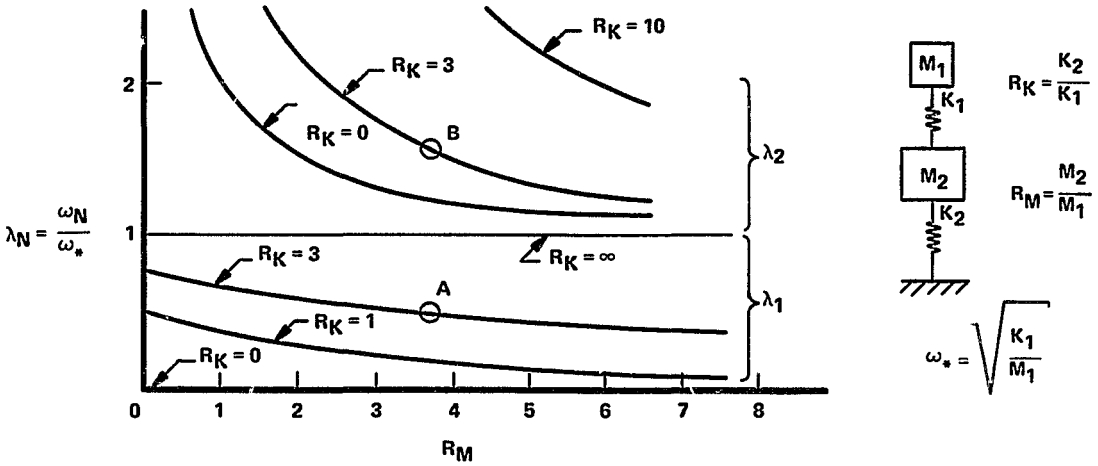

Figure 13. – General solution for simple 2-degree-of-freedom system

represent the rotor mass, rotor and bearing stiffness spring constant, casing mass, and casing mount stiffness spring constant, respectively; ω represents the whirl frequency, subscript i (i = 1 or 2) denoting the first or second system natural frequency and * denoting the simple rotor/bearing natural frequency. The symbols R_K and R_M are ratios of the casing-to-rotor spring constants and casing-to-rotor masses; λ_i is the ratio of shaft system natural frequency to the simple 1-degree-of-freedom rotor/bearing natural frequency.

If the casing mass M_2 is much larger than the rotor mass M_1 (i.e., R_M is relatively large) and the casing mount stiffness spring constant K_2 is relatively small, a system natural frequency less than ω_* will exist. This frequency, corresponding to point A, will be substantially lower than the rotor/bearing natural frequency $\sqrt{K_1/M_1}$ indicated by $\lambda_1 = 1.0$, analogous to K_2 and

therefore R_K tending toward infinity. A second system natural frequency such as point B will exist above the simple rotor/bearing natural frequency.

This analogy suggests that if proper mass and stiffness proportions are used in the design of the machine housing and mounting, two results will follow:

First: There will be low natural frequencies whose modes consist of the entire machine vibrating in a rigid-body fashion on the mounting springs with very little relative motion between the rotor and its casing. The shaft speeds that excite these vibrations will be equal to the low natural frequencies. Damping could easily be supplied to limit the amplitudes of these vibrations.

Second: The first significant shaft whirl critical speed will be equal to or above that of the rotor/bearing model.

Experience with rocket engine turbopumps has shown the first expected condition to be an accurate prediction. Usually, the low rigid-body modes occur at approximately 5 to 10 percent of the nominal shaft speed. Thus, no loss in accuracy occurs in predicting high-speed shaft response as a result of omitting the mounting stiffness in the analytical model. However, the second consequence indicated often is not valid because of the effects of dynamic coupling of the casing with the rotor and because of the effects of casing stiffness local to the bearings.

Dynamic coupling of the casing with the rotor has been found to be very influential in machines using rolling-contact bearings in conjunction with flightweight casings (refs. 6, 103, and 104). Use of a variable-property beam to model the casing in a manner similar to that for modeling the rotor has given good results.

A flexible tie between the rotor and casing (e.g., a low-stiffness hydrodynamic oil journal bearing or a flexible housing supporting the bearing) can, if it has an appropriate amount of flexibility, effectively decouple the casing from the rotor dynamics. In this case, a model considering the casing as ground yields good predictions.

Casing flexibility local to the bearing is undesirable when the shaft is designed to operate below the first system critical speed. This local flexibility, which is typical of an overhung turbine with rolling-contact bearings, usually occurs in the housing between the bearing outer race and the larger diameter pump casing. An M-1 turbopump bearing-support housing that exhibited flexibility was evaluated both analytically and experimentally for static spring rate (ref. 92). The analytical evaluation utilized two methods: an approximate-beam solution, and a finite-element solution (ref. 105); the experimental evaluation consisted of testing scaled aluminum models. The major findings were as follows:

(1) Shear deformation and warping of the end circular cross section into an oval pattern were the major flexibility sources.

(2) The stiffness computed by the approximate-beam method was 2½ times greater than the actual value.

(3) The stiffness values computed by the finite-element method were within 4 percent of the model test data.

The degree of symmetry of the casing mass and stiffness about the shaft axis influences the critical speeds. When symmetry exists, the shaft usually executes forward synchronous circular whirls as a result of imbalance. The critical speeds then are predicted on the assumption that disk gyroscopic stiffening is operative. When asymmetry in casing mass and stiffness exists, the shaft starts to execute elliptical whirl as it approaches a critical speed, and the whirl will become a lateral vibration. Where a symmetrical casing normally would have a single critical, the asymmetry causes two criticals to occur. Further, the criticals can occur at much lower speeds because the lateral motion causes the disk gyroscopic stiffening effects to vanish and disk rotary inertia softening to occur (ref. 106).

2.2.2.1.4 Bearing Spring and Damping Forces

Cylindrical roller and angular-contact ball bearings are the only types of rolling-contact bearings that have been used extensively for radial support in rocket engine turbopumps. Since internal damping of a rolling-contact bearing is negligibly small, stiffness is the important bearing characteristic that influences shaft dynamics. Approximate values of spring rate can be computed using the Palmgren formulas (refs. 107 and 108). Methods for more accurately determining spring rates are available in references 108 through 112. Reference 1 presents additional material on bearing load characteristics.

Usually, the shaft whirl is assumed to be circular. When unidirectional radial bearing reactions are small compared with the expected rotating radial bearing reactions associated with whirling, the spring-rate value K has been taken as the secant rather than the tangent value, i.e., $K = R/\delta$ instead of $K = dR/d\delta$, where R is the radial load and δ is radial displacement (refs. 72 and 92).

The bearing spring rate usually is nonlinear. The cylindrical roller bearing, which is a load-stiffening system, is well represented by an exponential function relating radial load R to radial displacement δ, e.g., $R = A\delta^B$ where A and B are constants, and $K = R/\delta = A\delta^{B-1}$. The spring-rate behavior of the angular-contact bearing can vary from almost linear to highly nonlinear, depending on the preload, applied load, and rotational speed. Stiffness characteristic ($K = dR/d\delta$) curves that have been published (ref. 56) were developed with equations that account for preload, applied load, and change in contact angle but exclude the effects of ball centrifugal and gyroscopic loads that are important at high rotational speeds (ref. 113). However, mathematical formulations described in reference 112 include all the effects associated with high rotational speed. A computer program based on these formulations was applied (ref. 114) to 40mm, 15° angular-contact bearings; the spring-rate characteristics shown in figure 14 resulted.

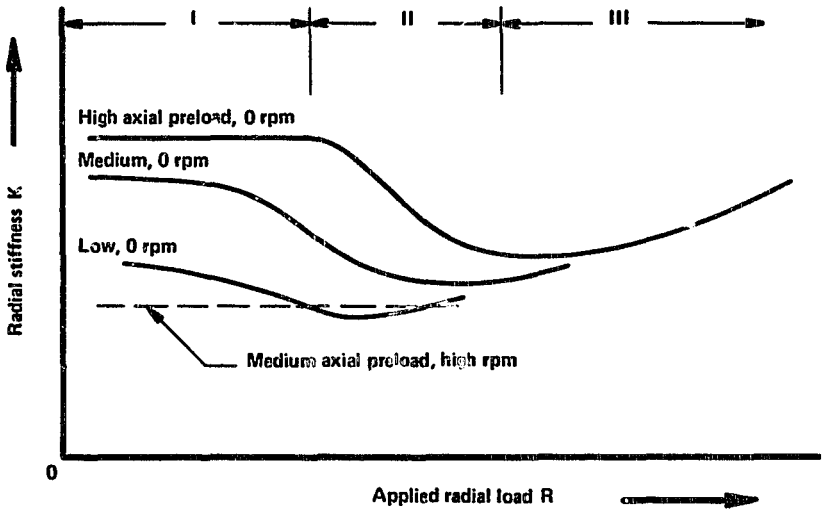

Figure 14. – Typical stiffness characteristics calculated for angular-contact bearings (ref. 114)

Neglecting speed effects, the charateristics are identical to those given in reference 56. There are three basic regions: the first (I) shows almost constant stiffness, the second (II) shows a decrease to a minimum stiff and the third (III) shows increasing stiffness. Region I is typified by sufficient axial p d to hold the stiffness high and constant. In region II, the magnitude of radial load approaches the axial preload and fewer balls are in contact, the result being a decrease in stiffness. In region III, the axial preload is no longer effective and, as the radial load increases, the stiffness starts to increase because the ball contact areas are increasing rapidly. Most importantly, when the speed effects were included in the analysis, it was found that the stiffness dropped approximately 50 percent in the regions of low applied radial load. Thus, it appears that the speed effects negated the expected beneficial effects of axial preload on radial stiffness. This effect is shown in other published works (refs. 80 and 115).

Cylindrical roller bearings develop radial resistance to radial motion only. However, angular-contact ball bearings can develop both radial and axial reactions. The radial reaction for a rad l displacement is, by far, the primary resistance. However, in cases where the bearing stiffness controls the shaft dynamics at operating conditions, all resistances may have to be included to achieve good predictions.

Some analysts have attempted to account for the moment resistance in angular-contact bearings by using a radial spring located at an "effective bearing center" instead of at its actual location on the shaft, as shown in figure 15.

The effective-b ring-center location has in the past been taken incorrectly as point CP. One investigator (ref. 116) considered this condition and concluded that the location lies approximately halfway between points CP and BL. Experience has shown that, with shafts

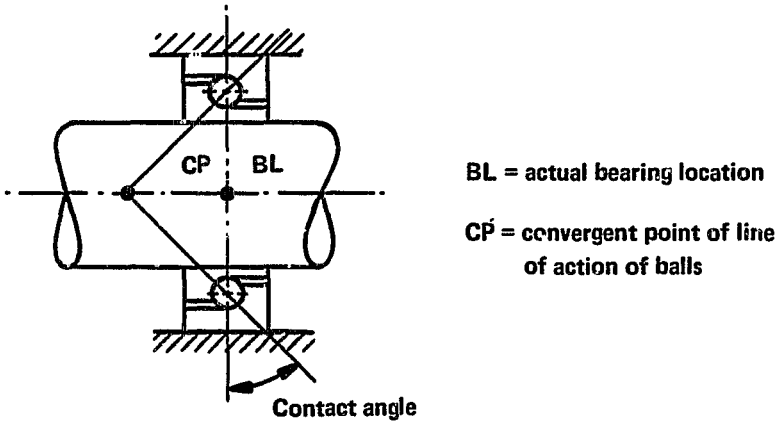

Figure 15. – Model for locating effective bearing center for angular-contact bearings

supported by angular-contact bearings, often only the radial resistance represented by a nonlinear spring located at the actual bearing center is necessary to obtain good predictions of shaft dynamics.

The representation of all-fluid-film journal bearings by linearized equations has produced good design information (refs. 54, 57, 79, 117, and 118). Eight coefficients representing both spring and damping forces are used. These coefficients are calculated from lubrication theory and the properties of the particular bearing. Moreover, coefficients have been published for many of the types of fluid-film bearings (refs. 57, 119, and 120).

2.2.2.1.5 Rotor-Imbalance Forcing Functions

A shaft usually exhibits synchronous whirl during operation because of the centrifugal forces associated with rotor imbalance. The amplitude of this whirl is related to the rotor-imbalance forcing functions. Actual rotor imbalance in rocket turbopump shafts rarely is equal to the balancing limits specified by the engineering drawings. This difference results from the shaft usually being balanced initially by subcomponents and then as an assembled rotor on a balancing machine (ref. 121), disassembled, and then reassembled in the turbopump. Misalignments allowed by factors such as pilot tolerances, runouts, parallelism, and perpendicularities can alter the very fine balance attained with the balancing machine (refs. 122 and 123).

Fits shift during operation as a result of effects such as thermal expansion differences between adjacent parts and mechanical deformations attributable to centrifugal forces. Sometimes these fit shifts allow eccentric shifting of adjacent rotor parts and thereby produce rotor imbalance. Furthermore, when roller bearings are used to support the shaft, the internal play in these bearings can allow the shaft to excite cylindrical or conical whirl modes of motion; this is especially true if the magnitudes of unidirectional radial loads from sources other than whirling are small relative to the potential whirl forces. This whirling associated with bearing internal play (fig. 16) can develop centrifugal loads that reach an

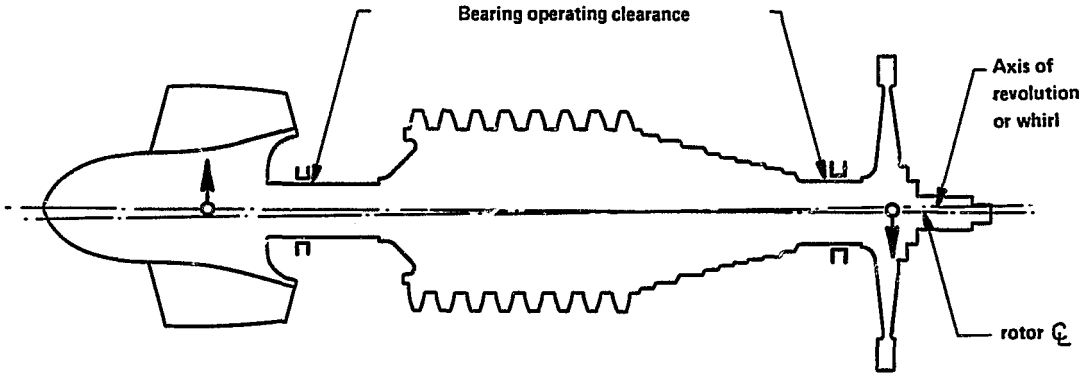

Figure 16. – Conical whirl associated with bearing internal play

order of magnitude greater than those resulting from the specified balance limits (refs. 92, 124, and 125). The effects of clearance between the outer race and the casing for an axially preloaded ball bearing are best determined experimentally; analytical treatments of possible effects are discussed in references 72 and 74 through 76.

The following examples indicate the possible magnitudes of imbalance and its influence on shaft response:

In the XLR-87-5 engine, the high-speed shaft weighed approximately 25 lb (11.3 kg); it was balanced to a specified value of 0.01-in.-oz (0.071 N-mm) static and 0.05-in.^{2}-oz (9.0 N-mm^2) dynamic imbalance. Blueprint tolerances allowed 0.001-in. (25μm) looseness between the pilot diameters at the two joints holding the two overhung turbine rotors and shaft together. Disassembly after balancing was necessary. Based on the pilot tolerances, reassembly static imbalance could be on the order of 0.4 in.-oz (2.8 N-mm), which is 40 times the specified requirement. Checks made on the balance machine verified that loosening of the turbine rotor bolts and radial shifting of the rotors could induce the above stated limits (ref. 123). Eventually the entire shaft was redesigned to eliminate this problem and others that had developed.

In another case (ref. 122), a gas-turbine rotor was to be balanced to an error of 0.02 in.-oz (0.141 N-mm). However, in production, runouts could not be held to better than 0.001 TIR, which was equivalent to 0.10 in.-oz (0.71 N-mm). Also, the rolling-contact inner race runout tolerance of 0.002 TIR added another 0.02 in.-oz (0.141 N-mm). Thus, imbalance six times greater than the balance error was possible. The problem was solved by redesigning the bearing system, replacing rolling-contact bearings with fluid-film bearings.

As a final example, figure 17 shows the source and magnitude of residual imbalances in the M-1 fuel turbopump rotor (ref. 92).

Component	Weight		Specified balance limits	
	lb	kg	in.-oz	N-mm
Rotor and blades	380.0	172.4	0.141	0.02
1st-stage inducer	82.0	37.2	.141	.02
2nd-stage inducer	9.3	4.2	.141	.02
Thrust balance disk	19.3	8.8	.072	.01
Turbine rotor	215.0	97.5	.353	.05
Balance plane I:	.35 in.-oz (2.47 N-mm) spec.; .25 in.-oz (1.76 N-mm) actual			
Balance plane II:	.75 in.-oz (5.29 N-mm) spec.; .48 in.-oz (3.39 N-mm) actual			

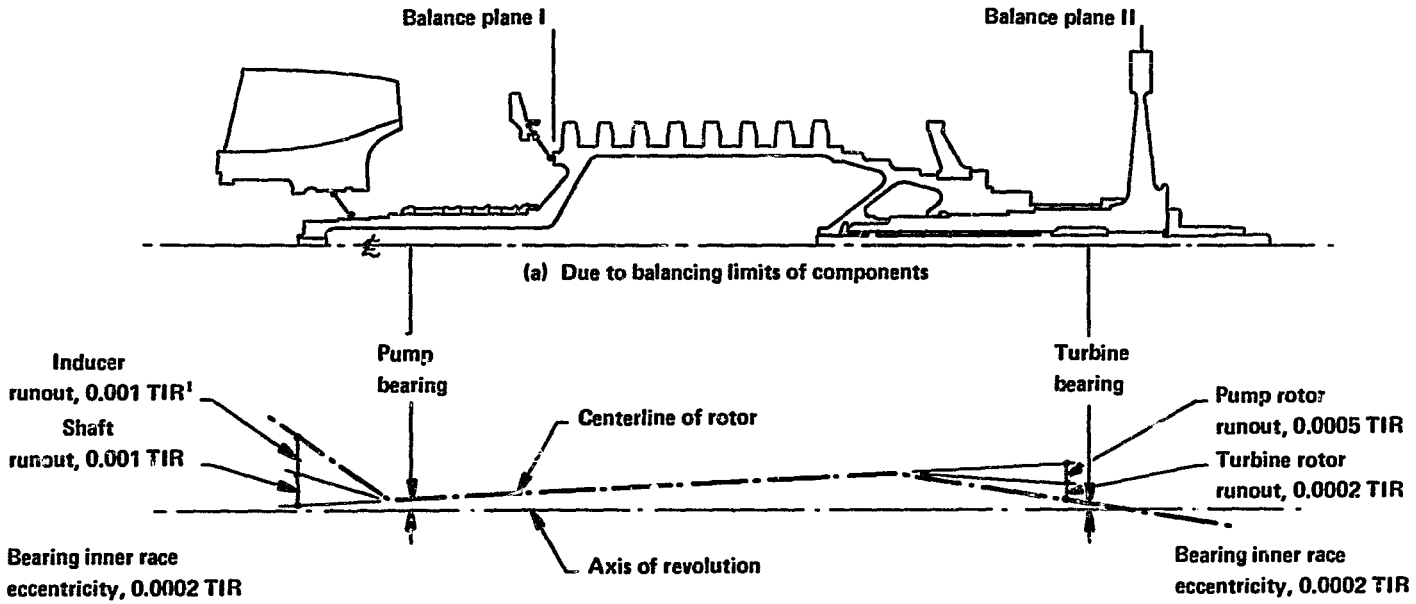

[1] TIR units are in inches (.001 in. = 25.4 μm).

Figure 17. – Residual imbalances, M-1 fuel turbopump rotor (ref. 92)

2.2.2.1.6 Virtual Mass and Damping

Virtual mass and damping associated with operation in dense fluids can have significant effects on the shaft dynamics. Unfortunately, a good quantitative analysis to evaluate these effects does not exist at the present time.

A study of the effect of gear restraint on the whirl of a pinion shaft (ref. 126) found that (1) whirl amplitude was reduced by frictional damping; (2) the resonant frequency was reduced, presumably by the inertia effects of the gear; (3) subharmonic as well as superharmonic resonances appeared in some of the tests because the vibration system was nonlinear; and (4) a self-sustained whirl frequency occurred.

2.2.2.2 MATHEMATICAL METHODS AND COMPUTER SOLUTIONS

Most of the digital computer programs suitable for calculating the natural frequencies, mode shapes, and imbalance response are based on or are extensions of the techniques given in references 96, 127, and 128. Good discussions of these methods are available in references 97 and 129.

References 88, 89, and 90 describe the appropriate methods for calculating torsional critical speeds. In addition, reference 88 provides a computer program in FORTRAN.

2.2.2.2.1 Analysis of Rotors Supported by Fluid-Film Bearings

Reference 65 includes program descriptions, a user's manual, and FORTRAN listings; it is available to qualified users from the U.S. Defense Documentation Center, Alexandria, VA.

Two programs are outlined in the reference:

(1) Imbalance response of a rotor in fluid-film bearings

(2) Stability of a rotor in fluid-film bearings

Program (1) is very general; it calculates the rotor whirl amplitude and the force transmitted to the base as the result of a given rotor imbalance. The rotor is flexible and can have any arbitrary geometry. Also, there can be splined couplings in the rotor, and several bearings. The bearing pedestals can be assigned both flexibility and damping. Because the bearing film forces are not the same in all directions, the whirl motion of the rotor is treated as two-dimensional in such a way that it becomes an orbit around the equilibrium position. The orbit is elliptical, and its dimension as well as orientation vary along the length of the rotor. The computer program calculates the whirl orbits for a number of points along the rotor and also gives the components of the force transmitted to the foundations.

Program (2) applies to an arbitrary rotor geometry. There can be several bearings, and the stiffness as well as damping of the bearing pedestals can be included. The program calculates the speed at the onset of instability (the threshold speed) and the corresponding whirl frequency.

In both programs, the dynamic properties of a fluid-film bearing are expressed in terms of eight coefficients: four spring coefficients, and four damping coefficients. The values for these coefficients depend on the bearing type, the bearing dimensions, the viscosity of the lubricant, the bearing load, and the rotor speed. The rotor mass and elastic properties are represented by lumped masses connected by elastic beam elements typical of the Myklestad model. A special treatment of the gyroscopic moment is used to account for the elliptical orbit motion.

2.2.2.2.2 Analysis of Rotors Supported by Rolling-Contact Bearings

A preferred program for this analysis is presented in reference 92. This program is available from COSMIC, University of Georgia, Athens, GA.

Basically, this program is an analysis of the forced undamped vibrations of two elastically coupled, lumped-parameter beams. The whirl analysis of a rotor/bearing/casing system is facilitated by the assumptions that the rotor, casing, and bearing stiffness characteristics are axially symmetric and that the shaft executes circular orbits. Bearing nonlinearities, casing as well as rotor distributed mass and elasticity, rotor imbalance forcing functions, gyroscopic and rotary inertia moments, and shear and flexural deformations are included in the system-dynamics analysis.

The analysis is based on a lumped-parameter model using a modified Myklestad-Thomson transfer-matrix technique. Bearings are characterized as springs that can have constant spring rates or load-dependent values defined by $K = A \cdot L^B$ or by a table of L vs K points, where A and B are constants. L is the load transmitted through the spring, and K is the spring rate. The bearings have nonlinear load displacement characteristics, and therefore the solution is achieved by iteration. Rotor imbalances allowed by factors such as pilot tolerances and runouts as well as bearing clearances (which allow conical or cylindrical whirl) determine the forcing-function magnitudes. The computer programs first obtain a solution wherein the bearings are treated as linear springs of given spring rates. Then, based on the computed bearing reactions, new spring rates are predicted, and another solution of the modified system is made. The iteration is continued until the changes to bearing spring rates and bearing reactions become negligibly small.

If the machine operating speed is near a critical speed, the magnified bearing reaction is of interest for comparison with the bearing capacity. The nonlinear treatment of the bearings by this method shows that the predicted bearing reactions based on a linear representation of the bearings can be lower than the actual values.

2.2.2.2.3 Analysis of Shaft Systems with Unsymmetric Supports

Reference 88 includes a program description, a user's manual, and FORTRAN listings. It is available to qualified users from the U.S. Defense Documentation Center.

The lateral undamped natural frequencies and mode shapes of shaft systems with unsymmetric supports can be obtained with this program. The rotor is modeled with both continuous and lumped mass elements. The elasticity elements utilize beam theory; flexural deformations are included, but shear deformation is excluded. Moreover, this program does not include any treatment of the casing. Many designs purposely utilize a flexible housing between the rolling-contact bearing and the main machine casing in order to obtain low values for the first two critical speeds. In these cases, the casing is effectively decoupled from the rotor, and a dynamic model of the rotor supported on springs that are tied to ground is sufficient for good predictions.

2.2.2.3 PREDICTION ACCURACY

Locations of operating whirl critical speeds that are governed mainly by the rotor mass and the combined or individual stiffness of the rotor, bearing, or bearing support mount usually can be predicted within ± 5 percent. When the casing dynamics couple with the rotor sufficiently to require a system rotor/bearing/casing model for analysis, the prediction accuracy of critical-speed locations is approximately ± 10 percent provided that the conditions listed in section 3.2.2.1 are met. When these conditions are not satisfied, errors in predictions of criticals can easily be ± 20 percent and sometimes as great as ± 50 percent.

The prediction of response levels in general has been even more inaccurate. It is not uncommon for measured data to differ by a factor of 2 or 3 from the predicted data. These large discrepancies arise because values of imbalance are hard to predict accurately, and most turbopump operating speeds usually come within 15 to 20 percent of a major critical speed or closer to a secondary critical. A small error in predicting the locations of these criticals can result in significant error in predicting the response level (fig. 18).

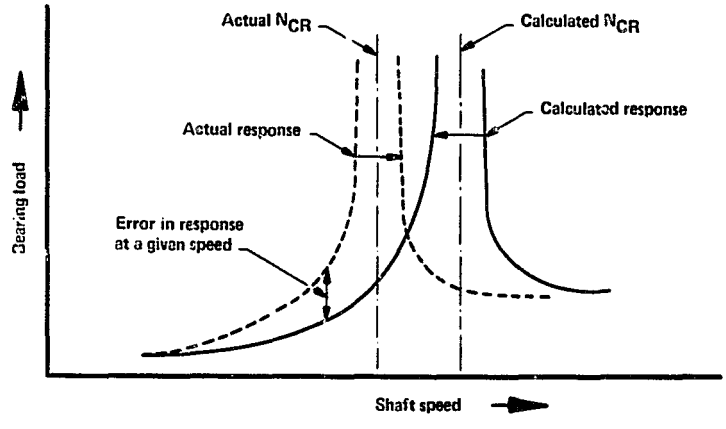

Figure 18. – Error in prediction of response resulting from a small error in prediction of critical speed N_{CR}

Table VII shows a typical comparison of calculated and experimental natural frequencies and the associated kinetic energy distribution. Additional information on prediction accuracy is available in the literature (e.g., refs. 6, 8, 54, 78, and 79).

2.2.3 Adjustment of Critical Speeds and Response Levels

The following major factors influence critical speeds:

(1) Shaft mass and stiffness magnitude and distribution

(2) Bearing and seal location, stiffness, and damping

(3) Bearing mount stiffness

(4) Casing mass and stiffness magnitude and distribution

The first factor, although obvious to most shaft designers, has often been overlooked. Stiffness of a shaft that has shaft-mounted components such as shrunk-on impellers, shaft sleeves, and bearing races can be changed markedly by changing the fits and the axial preloading. Furthermore, curvic couplings and other mechanical joints not maintained in compression will allow considerable flexibility.

Critical speeds can be influenced significantly by the flexibilities of the bearings, the bearing mounts, and the machine casing (refs. 7 and 93). Advantage has been taken of the support effects to effectively adjust or tune the critical speeds to the desired values (refs. 130 through 132). Flexible bearing mounts, as indicated in figure 19, have been used to produce low first and second criticals, which are rigid-body translation and rotation modes, as well as to yield a large available speed range for operation between the second and third criticals, the third critical being basically the first shaft bending mode.

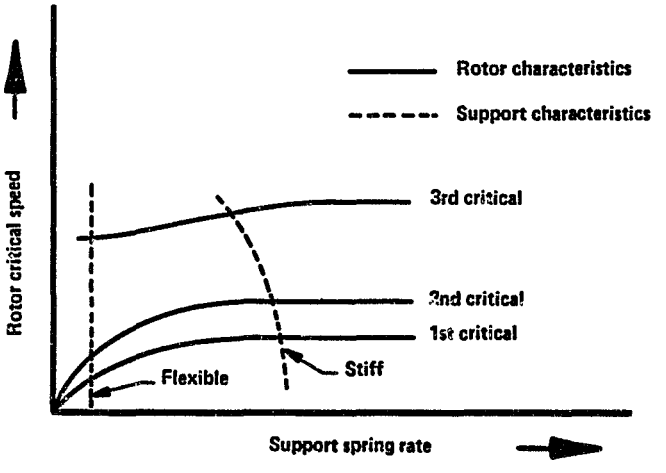

Figure 19. – Effect of support spring rate on rotor critical speed

TABLE VI – Summary of Calculated and Experimental Natural Frequencies for the XLR-87-AJ-9 Turbine Shaft

(a) Calculated natural frequencies, Hz

Rotor/bearing model[1]		Rotor/bearing/casing models			
		Dynamic stiffness method		Refined double-beam model[2]	
Lateral vibration	Forward Circular Whirl	Lateral vibration	Forward circular whirl	Lateral vibration	Forward circular whirl
—	—	—	—	198/220	200/220
—	—	265	265	327/372	328/374
—	—	400	440	403/480	456/530
517	630	590	650	635/671	> 650

[1] Model not valid for lower frequencies

[2] First value corresponds to min. stiffness casing model, and second corresponds to max. stiffness casing model.

(b) Experimental data

Spin tests. – Speeds of vibration buildup, rps				Shake tests. – Natural frequencies, Hz	
Tight fits and small bearing clearances		Loose fits and large bearing clearances			
Elliptical whirls	Circular whirls	Elliptical whirls	Circular whirls	Casing without rotor	Rotor/bearing (rigid mounting)
200-215/260-270	not meas.	200-215/235-250	not meas.	195-200	not meas.
330-343/372-390	" "	300/350	" "	230-250/300	" "
407 /440-450	470-485	not meas.	427-440	480	" "
>500	>500	>550	>550	not meas.	540

(c) Kinetic energy distribution for various natural frequencies, calculated on the basis of the associated rotor/casing system mode shapes

Natural frequency, Hz	Kinetic energy distribution, %	
	Rotor	Casing
198/220	7	93
327/372	13	87
403/480	4	96
456/530	74	26
635/671	95	5

Seals and wear rings can act as fluid-film bearings and produce stiffness and damping, and thus affect critical speed locations as well as rotor stability (ref. 133).

A significant reduction in response levels has been accomplished by using improved balance techniques. The use of squeeze-film dampers for adding or increasing damping to reduce response is gaining considerable interest among designers of shafts for aircraft engines. Both hydraulically mounted rolling-contact bearings (refs. 134 and 135) and squeeze-film dampers between two nonrotating parts in parallel with a flexible bearing support (refs. 130, 131, and 136) have been used. Although damper bearings of the Coulomb-friction type have been used successfully in jet engines (ref. 83), squeeze-film dampers have not yet been used successfully in rocket engine turbomachinery. Providing nonlinear stiffness properties to the bearing support also has been used to limit resonant-amplitude buildups (ref. 132). Nonlinearity without any added damping has the advantage over the damped, flex-mounted technique (ref. 130) in that lower force is transmitted at supercritical speeds. However, care must be taken to preclude "superwhirling" (refs. 72 and 75) and delayed resonances.

2.2.4 Balancing

References 54, 84, 121, and 137 through 142 represent a good survey of the major literature on balancing. There are two main classes of rotor balancing: the rigid rotor, and the flexible rotor. The object of rigid-rotor balancing is to ensure that the center of mass of the rotor lies in the centerline of the bearings and that no couple is transmitted to the bearings. At low balance speeds, the imbalance is independent of speed. Conversely, a flexible rotor balanced in one mode is not necessarily balanced in another mode. Rotors that have only two correction planes available generally operate below the first bending critical speed. Imbalance usually is measured by radial runout.

Balancing of the complete assembly has been sufficient for low speeds, but separate balancing of components has been the practice for higher speeds. The advantage of component balancing is that it allows for the interchangeability of parts and reduces internal shaft moments. Eccentricity tolerances result in imbalance at assembly. Modal balancing is a step-by-step method for balancing at successive critical speeds with corrections made so that the balance at the previous modes is unaffected. Modal balancing is preferred for shafts operating steady-state at critical speeds, but it is very costly.

Balancing capability has not been a limiting factor for turbopump rotors operating below the first bending critical speed. In some cases, a known imbalance has been added to create a bearing radial load and prevent ball or roller skidding.

The procedure for rotor assembly balancing has varied. Either the rotating assembly is balanced by removing material in specified planes or it is balanced by relocating previously balanced components rotationally with respect to each other. The latter method is used when the components are joined by curvic couplings, and it is merely a matter of remating the curvics in a different radial position. Even with a carefully balanced shaft, however,

imbalance has occurred when a curvic coupling joint that was tight at assembly became loose during operation because vibrations relieved the frictional binding. Imbalance also has occurred when the coupling was misaligned as a result of foreign material lodged between the teeth.

2.3 Coupling Design

The types of couplings most commonly used for liquid rocket engine turbopumps are the involute spline, curvic coupling, and parallel-sided face coupling; fitted-bolt, friction-bolted-flange, and ball-spline couplings are very rarely used. The involute spline, curvic coupling, and parallel-sided face coupling are discussed in detail in the three sections that follow. The design requirements of the fitted-bolt and friction-bolted flange are comparatively simple and are not discussed herein.

2.3.1 Splines

Splines have been used more than any other coupling because of large load-carrying capacity, low cost, and reliability. Splines require a change in shaft diameter. Most turbopump splines have an involute profile similar to gear teeth in that they can be cut and measured with the same machines used for gear teeth. However, splines differ from gears in that they have no rolling action and 25 percent or more of the teeth contact at once. Splines seldom pit or break at the root, although they do fail by shear, fretting, corrosion, and fatigue. Fixed splines permit no relative or rocking motion between internal and external teeth. The fit between mating parts can be either tight or loose. Flexible splines are vulnerable to wear because they permit some rocking motion, and under torque the teeth slip axially to accommodate axial expansion or runout. Fully crowned splines have been successful with as much as a 3° misalignment. Various splines (e.g., aligned, misaligned, and precision) have been used with various types of fits such as major diameter, side, interference, loose side, and combination with stepped pilot diameters at each end. Minor-diameter fits are not used because of the relatively small contact surface area on which to provide good positioning and because large root stresses are induced in the weaker member of the coupling. Fretting in the splines of inducers or impellers of oxidizer or monopropellant pumps is a potential source of ignition. This fretting can be controlled by using a tight axial clamp-up in the assembly and by setting tight fits on the radial positioning surfaces. After test, minor contact marks usually are acceptable for the splines of oxidizer and monopropellant pumping elements, but clearly defined fretting normally is not allowed.

Most fixed splines have been of the 30°-involute stubbed-tooth configuration. When the splines are used as a flexible coupling, the tooth form usually is special, tending toward (1) a lower contact angle (14.5°) to minimize runout effects on balance and (2) a longer addendum to provide larger contact areas.

The current trend is to design splines so that an increased percentage of the teeth make contact. Special tolerances and inspection techniques are required when over 25 percent of the teeth make contact. For fixed splines with a width one-third the pitch diameter, the

(1) Eliminate the dangerous tensile stresses.

(2) Remove the corrosive environment or render it less harmful by using protective barriers (coatings, platings, material processing, etc.).

(3) Replace the metal in the particular application with another material that does not fail in the specific environment.

Steel alloys that should be avoided because of very low resistance to stress-corrosion cracking (ref. 159) are the following:

Alloy	Temper
17-4 PH	All tempers
17-7 PH	All except CH 900
PH15-7 Mo	All except CH 900
AM 355	<SCT900 FH
H-11	All tempers
Vascojet 1000	All tempers
Low-alloy	>180 ksi (1.24 GN/m^2) yield strength

3.1.1.5.4 Hard Vacuum

The shaft and coupling properties shall not be degraded below acceptable limits by cold-welding or adhesion, evaporation, decomposition, or sublimation in prolonged hard vacuum.

Use aluminum coatings in place of cadmium, zinc, or magnesium in a prolonged hard vacuum. Special lubricants (refs. 52 and 53) that do not evaporate, sublime, or decompose must be used.

3.1.2 Material Selection

3.1.2.1 MECHANICAL PROPERTIES

The minimum mechanical properties of the shaft and coupling material shall not be less than those required to satisfy the critical operating loading and environmental conditions.

The main mechanical properties to consider in choosing the material are the tensile yield and ultimate strengths, creep strength, ductility as measured by reduction in area and fracture toughness (ref. 160), fatigue strength, thermal expansion or contraction

coefficients, and modulus of elasticity. The material strengths and other physical properties should be evaluated for the entire range of operating and nonoperating environments. Property values should be selected from authoritative sources such as MIL-HDBK-5A (ref. 161), Department of Defense reports, or documented test values when appropriate. Property values should be based on statistical evaluation of the test data, and the values used for design should be those for which the probability is 95 percent that 99 percent of the samples exceed the design values (e.g., "A" values in ref. 161).

A material that has good low-cycle fatigue (LCF) strength does not necessarily have good high-cycle fatigue (HCF) strength (ref. 48). For good HCF life, a material with high tensile strength is best, whereas for LCF a material with lower tensile strength but high ductility is best (fig. 5). Furthermore, for long life in high-temperature use, good creep-rupture strength also is necessary (refs. 162 and 163).

3.1.2.2 THERMAL PROPERTIES

Differential thermal expansion or contraction of the shaft and bearing-race materials shall not result in race fracture or loose fits.

The thermal-expansion properties of the shaft and the bearing materials at operating temperature should be matched as closely as possible. The effect of differential expansion on bearing clearance and bearing race-to-shaft fit should be calculated for conditions of assembly, nonoperating chilldown, and transient and steady-state operation as appropriate. For critical applications, the available material thermal-expansion data may not be accurate enough; in such cases, conduct special thermal-expansion tests.

3.1.2.3 STRESS CORROSION AND HYDROGEN EMBRITTLEMENT

The shaft and coupling material shall not suffer deleterious effects of stress-corrosion cracking or hydrogen embrittlement.

The material selected should be compatible with the propellant and environment. When there is potential exposure to high-pressure gaseous hydrogen, avoid the use of materials that become brittle in that environment. Refer to section 3.1.1.5 for a more complete discussion of stress corrosion and hydrogen embrittlement.

3.1.2.4 LOW-TEMPERATURE EMBRITTLEMENT

The shaft and coupling materials shall not be susceptible to brittle fracture due to low-temperature embrittlement.

The material should have at least 5-percent reduction-in-area ductility, more than 15 lb-ft (20.3 N-m) of Charpy V-notch impact energy, and adequate fracture toughness (ref. 160) at the operating temperature. In establishing the minimum fracture-toughness requirements, consideration should be given to the size of fabrication flaws and cracks that may go undetected during NDT inspection, the operating stress levels, and the desired life (ref. 49).

Low-alloy steels such as 9310, 4340, 440C, and AM-350 should not be used at cryogenic temperatures.

3.1.2.5 SURFACE CONDITION

The shaft and coupling shall not suffer surface wear, fretting, or galling of sufficient magnitude to cause shaft, coupling, or associated parts to fail.

The shaft or coupling material should be selected with due account for the possible need to heat treat, case harden, or coat the surfaces. These surface treatments and the materials for mating parts should be evaluated for the effects on the material tensile and fatigue strength as well as effects on wear, fretting, or galling. Typical past solutions are described in section 2.1.2 and in reference '64.

3.1.3 Structural Analysis

3.1.3.1 LOADS

The structural analysis of the shaft and coupling shall evaluate the critical combinations of radial, axial, and torsional loads, both steady and alternating, encompassing all anticipated conditions in the operating and test range.

"Worst-case" design operating conditions should be used in evaluating each load, and the loads should be combined vectorially to yield the "worst-case" combined loads.

Probable accuracy of computed loads should be assessed and, if applicable, calculated values modified to obtain conservative worst-condition predictions. For example, small percentage variations in large pressure forces on the impeller front and back faces always result in considerable variations in magnitudes of net thrust.

The following kinds of loads should be evaluated as indicated:

Radial

Rotor dynamics. – Rotating imbalance and self-excited whirl forces. An analysis of shaft response to imbalance forces should be accomplished as outlined in section 3.2.2.1.4. For fail-safe considerations, include in rotor dynamic loads the loads induced

by rotor imbalance caused by failure of one blade and assume that these loads will act over the entire engine operating period required for the mission.

Rotor pressure loading. – Unequal pressure around impeller shrouds, discharge outlets, etc. The pressure profiles should be integrated for load magnitudes.

Vehicle accelerations. – Longitudinal and lateral flight motion; engine gimbal snubbing; gyroscopic action of rotor, vehicle rotation, or engine gimbaling. Engine and vehicle specifications should be reviewed for acceleration, gimbaling, and maneuver requirements.

Gear and bearing reactions due to shaft power torque.

Constraint of thermal expansions or contractions. – Conduct a heat-transfer analysis to obtain the thermal profiles of the assembly. Then calculate thermally-induced loads and their interaction with assembly loads.

Axial

Rotor axial vibrations. – The natural frequency of the rotor/bearing system treated as a rigid rotor mass on a simple spring should not coincide with the shaft operating speed (or multiples of 2 or 3 thereof) unless a response analysis or test demonstrates that no adverse effect occurs. For preliminary design, axial vibration loads may be considered to have amplitudes about 5 percent of the bearing thrust loads. If testing shows that these vibrations are significant, then experimental evaluation is recommended.

Rotor pressure loading. – Unbalance thrust across impellers, turbine wheels, balance pistons, and thrust bearings should be integrated for load magnitudes.

Vehicle accelerations. – Same sources listed above for radial.

Gear reactions to shaft power torque. – Helical gears, misaligned splines.

Assembly axial preload. – Built-up shafts, turbine and impeller retaining bolts.

Self-constrained or bearing-constrained shaft thermal expansions or contractions. – Evaluate as above for radial.

Torsional

Shaft power torque.

Torsional vibration inertia forces. – For preliminary design, torsional vibration loads may be considered to have amplitudes of about 5 percent of the nominal power torque load. If operation shows these vibrations to be more significant, then experimental evaluation is recommended.

3.1.3.2 SAFETY FACTORS

The shaft and coupling design safety factors shall be adequate to achieve the specified reliability.

Safety factors applied to limit loads should be equal to or larger than 1.1, 1.3, and 1.25 for yield, ultimate, and fatigue strengths, respectively. The preferred values are 1.1, 1.4, and 1.33. If sufficient statistical data are available for a particular application to justify the use of probabilistic-reliability methods (refs. 40 through 45), then the statistically determined values for safety factor should be used.

3.1.3.3 ANALYTICAL METHODS

Structural analysis shall verify that the shaft and coupling have adequate strength throughout service life to preclude structural failure due to deformation or collapse, fracture, or wear.

The shaft should be analyzed for all critical loading conditions defined in 3.1.3.1, due account being given to stress concentrations, environmental considerations, material strength properties, required safety factors, and clearances between the stationary and rotating parts. Adverse deformation or collapse failure margins should be calculated, consideration being given to potential elastic, plastic, or creep deflections or buckling. Specific details of such analyses can be found in almost any book treating machine design or strength of materials.

Fracture-failure margins should be evaluated for both time-dependent and time-independent failure mechanisms. Time-independent mechanisms include the well-understood simple ductile overload and the much-less-understood, complicated, and less-predictable brittle rupture. Factors that may contribute to brittle rupture are low material ductility and low fracture toughness, fabrication flaws, weld defects, design notches and stress raisers, degree of stress triaxiality, high strain rates, low temperature, hostile environments (chemical or physical), and improper material heat treatment. The most promising engineering approach for assessing sensitivity to brittle fracture is the use of the principles of linear elastic fracture mechanics (refs. 165 and 166).

Time-dependent fracture mechanisms encompass both static and cyclic loads. The possibility of delayed fracture under static loads due to creep rupture, stress-corrosion cracking, or hydrogen embrittlement should be assessed. The shaft design should be analyzed for fracture potential due to fatigue induced by cyclic or combined static and cyclic loads; the analysis should include thermal stress that may induce low-cycle fatigue or large residual mean tensile stresses that reduce the alternating stress capability.

Card #21

In the evaluation of high-cycle fatigue, the critical effective stress levels should be determined by use of the distortion-energy (i.e., Von Mises-Hencky theory) definition of effective stress for multiaxial stress states (refs. 11 and 12). The shaft-material fatigue endurance strength should be established by using existing guidelines (refs. 12, pp. 166-176 and 46, pp. 221-229) and by reducing the smooth-bar material-specimen fatigue strength to allow for the modifying effects of surface finish, size, temperature, notch sensitivity, residual stresses, material directional effects, corrosion, plating, and reliability. For combined alternating and steady stress levels, use experimentally determined stress-range diagrams or modified Goodman diagrams (refs. 167 and 168). To assess the combination of multilevel magnitudes of cyclic stress, the Miner theory of linear cumulative damage (ref. 169) may be used to predict fracture with a usage factor of 0.70 (refs. 169 through 172). However, the accuracy of any cumulative-damage theory suffers under certain conditions, and the designer should be acquainted with the limitations as presented in the cited references.

All shaft components should be stress analyzed with sufficient depth to identify peak stress levels associated with all the applicable load sources previously identified. For long life and multiple reuse applications, special emphasis should be given to the evaluation of thermal and geometrical discontinuity stresses, as they are common causes of fatigue. Critical buckling stress levels of hollow thin-wall shafts also must be evaluated, and a margin to preclude buckling must be provided.

The critical effective stress and strain levels that govern cyclic fatigue life must be kept below the endurance limit of the material for the required number of duty cycles times an appropriate safety factor. Stress concentrations should be minimized by using maximum radii in fillets, optimizing transition sections, locating mechanical and weld joints in low-nominal-stress areas, and undercutting and placing relief holes to smooth out the distribution of stress. Analytical determination of the stress levels by comprehensive digital-computer structural-analysis programs and experimental-stress-analysis techniques, where applicable, may be necessary to determine locations and magnitudes of critical effective stress levels. The methods for predicting low-cycle fatigue life are continually being modified and improved; the present recommended methods are those described in references 173 through 176.

(Wear failures of the adhesive type such as galling or scoring are caused primarily by a lack of separating film; many times these failures can be precluded simply by use of a lubricant. Abrasive wear failure due to shaft rubs should be minimized by providing clearances adequate to preclude rubbing. Fretting-corrosion wear, which is caused by the relative oscillatory motion of two surfaces under normal force such as in press fits, can be overcome by using tight fits, inducing residual surface compressive stresses, and reducing the vibration level).

3.2 Shaft Dynamics

3.2.1 Dynamic Behavior

3.2.1.1 WHIRL MOTIONS

Shaft dynamic analyses shall be appropriate to the type of whirl motion.

For all designs, forward synchronous circular whirl motion should be assumed for calculations of critical speeds and shaft response. If the casing or bearing mount is asymmetrical about the shaft axis in either mass or stiffness, the forward synchronous elliptical and lateral vibration motion also should be analyzed for critical speeds and shaft response.

3.2.1.2 FORCED WHIRLS AND CRITICAL SPEEDS

3.2.1.2.1 Steady-State Operating Speed Limitations

There shall be no steady-state shaft operation near a major critical speed if bearing failure, rotor-tip rubbing, or other undesirable associated phenomenon can occur.

The lowest major critical speed whose mode shows a preponderance of the system potential energy to be due to rotor bending as compared with stator or bearing deformations should be no lower than 125 percent of the normal operating speed or 115 percent of the maximum overspeed, whichever is greater. The maximum bearing reactions at any steady-state speed should be compared with the bearing capacities, due regard being given to the required life, reliability, and applied bearing loads from sources other than shaft dynamics. Likewise, it is recommended that rotor whirl orbit amplitudes be computed and compared with available operating clearances (ref. 183).

Major critical speeds that involve appreciable stator or bearing deformation and that are lower than the operating speed are permissible when they comply with the following restrictions:

(1) The speed is no higher than 85 percent of the lowest steady-state operating speed.

(2) The speed is the lowest possible speed consistent with other design requirements (e.g., rotor running positions and displacements under worst loading should not exceed tip clearances).

(3) The rate of change in shaft speed while passing through the criticals is sufficient to preclude excessive response. Calculations (refs. 184 through 190) of possible response magnitudes should be made during the design phase.

(4) Self-excited whirls do not develop into untenable response levels.

If calculated critical speeds of the type discussed above are closer to the operating speed range than allowed by the restrictions given, and if the speeds cannot be moved appreciably without compromise of other design requirements, approval of the design regarding critical speeds should be based on comprehensive vibration tests of the complete rotor/stator assembly and on the comparison of experimentally determined operating clearances and bearing loads with the design allowables.

Tracking shaft motion with proximity probes (sec. 3.4.2) is especially recommended for initial testing of machines that operate above the first system major critical speed. This procedure allows evaluation of the potential of the rotor for self-excited whirling.

3.2.1.2.2 Assessing Importance of Critical Speeds

Analyses during the design phase shall define the major critical speeds.

To facilitate assessing the importance of various critical speeds, conduct analyses as described in section 2.2.1.2 so that the following information is obtained:

(1) Location of critical speeds relative to the operating speeds

(2) Mode shapes and kinetic energy distribution

(3) Response predictions: bearing reactions, whirl orbits, and sensitivity to imbalance

(4) Closeness of the critical to other identified resonant speeds

(5) Type of motion: synchronous or nonsynchronous, forward or backward, forced or self-excited, circular or noncircular

(6) Effort required to change critical speed or modify response level by design changes

Secondary critical speeds should be computed and listed for future reference as possible diagnostic aids in the event of failure preceded by peculiar shaft dynamic characteristics such as nonsynchronous vibrations, beats in response level, or other behavior described in references 58 through 61.

3.2.1.3 SELF-EXCITED WHIRLS AND INSTABILITIES

Shafts designed to operate above the first system critical speed shall not experience damaging effects of self-excited nonsynchronous whirls.

Rotors supported in rolling-contact bearings should be analyzed for self-excited whirl potentials by the methods presented in reference 83. This reference covers aerodynamic-induced instabilities and provides practical solutions to such problems.

Built-up shafts and rotors using press- or shrink-fitted items (e.g., sleeves and collars) should not be run above the system major critical speed whose mode has significant shaft bending, and damping is insufficient to preclude shaft rubbing, bearing overload, or shaft, coupling, or stator overstress. Reference 86 provides a detailed summary of additional causes and ways of eliminating harmful whirls induced by internal friction.

Operating a shaft with a dry-clearance bearing or a shaft rubbing on an unlubricated guard should be avoided throughout the entire speed range. If dry rubbing occurs, reverse whirl can become a near-resonant whirl over a large range of shaft speeds including speeds below the first system critical speed. To obtain the broadest band of whip-free rubbing, the rotor and stator natural frequencies should be kept dissimilar, and the rotor and stator dampings made close to one another (ref. 191). Other ways of mitigating whirls induced by dry friction, if they occur, are to (1) change the design by increasing operating clearances, (2) raise the rotor/stator system natural frequencies, (3) improve the rotor balance, or (4) coat the rubbing area with a low-friction-surface material.

Asymmetry in the stiffness of rotor casing or foundation should also be considered as a means of increasing the threshold speed of nonsynchronous self-excited whirls (ref. 192). Rotors using fluid-film bearings can be evaluated for stability by the methods described in references 54, 65, 68, and 83.

3.2.1.4 TORSIONAL CRITICAL SPEEDS

Shaft systems that have flexible couplings or that are part of a gearbox shall be free of harmful torsional critical speeds.

The torsional natural frequencies should be computed by appropriate methods such as those in references 88 through 90. To identify the shaft speeds that may be critical, the natural frequencies and the potential excitation frequencies should be cross plotted against shaft speed as shown in figure 4. Intersections determine critical speeds. Consult section 2.2.3 and references 63, 89, and 90 for sources of excitation. Steady-state shaft operating speeds should not coincide with the first system natural frequency or one-half or one-third of it. If the product of the number of gear teeth, or the number of impeller vanes, or the number of stator vanes multiplied by the rotational speed matches a natural frequency, operation at that speed is not recommended unless it can be shown by response computations or by test that adverse vibrations do not occur.

3.2.1.5 THIN-WALL HOLLOW-SHAFT VIBRATIONS

A thin-wall hollow shaft shall be free of harmful nodal-circle and nodal-diameter vibration critical speeds.

The methods and considerations of reference 193 should be used for analysis of potential nodal-circle and nodal-diameter vibration critical speed of hollow-drum-type shafts. If harmful vibration is predicted by analysis or develops in testing, the design thickness or excitation characteristics should be changed to detune the resonance.

3.2.2 Analysis of Shaft Dynamic Behavior

3.2.2.1 MODELING FOR THEORETICAL ANALYSES

3.2.2.1.1 Mass and Stiffness Distributions

The model shall simulate accurately variations of mass and stiffness throughout the entire rotor/bearing/casing system, include both flexural and shear deformation elements, and account for gyroscopic and inertia moments.

For the analysis of rotor/bearing/casing systems with rolling-contact bearings, multilevel lumped- or continuous-mass models are recommended; a typical model is shown in figure 30. For a lumped-mass model, the number of mass stations per level should exceed by a factor of four or five the number of that critical speed that follows after the upper limit of the operating speed. For all levels, a total of approximately 20 to 40 stations should be used.

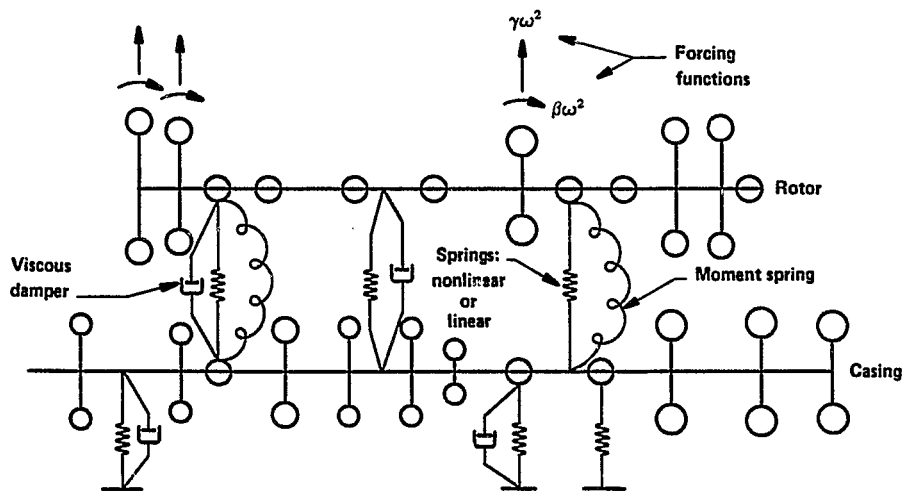

Figure 30. – Typical lumped-mass rotor/casing model

For systems with fluid-film bearings that are relatively soft as compared with the rotor stiffness or systems with flexibly mounted bearings, the single-level lumped- or continuous-mass models can be used.

Model basic elements of the Myklestad lumped-mass type (refs. 6, 92, 97, and 98) or the continuous-mass type (refs. 79 and 88) are recommended.

Gyroscopic-moment treatments for circular whirl and lateral vibration (refs. 98 and 183) are recommended for shafts supported by rolling-contact bearings. The treatment accounting for elliptical whirl motions (ref. 65) is recommended for shafts supported by fluid-film bearings.

When the accuracy of calculated model properties, (e.g., stiffness of a bearing support housing and bearing stiffness) is questionable and the parametric analyses show that these properties significantly influence the critical-speed characteristics, tests should be conducted to allow experimental determination of the proper model properties. See section 3.4 for recommended tests.

3.2.2.1.2 Mechanical Joints, Shaft-Riding Elements, and Abrupt Changes in Shaft or Casing Cross Section

The model shall simulate the actual stiffness influences associated with mechanical joints, shaft-riding elements, and abrupt changes in shaft or casing cross section.

"Equivalent-beam" sections or influence coefficients are recommended for representing the actual stiffnesses associated with the curvic coupling or similar joints, shaft-riding elements, and abrupt changes in shaft or casing cross section. Axial and moment load-deflection data obtained from tests of the actual joints or of similar previous designs are best for determining the equivalent system properties. For preliminary design, when applicable test data or good experience does not exist, it is recommended that curvic-coupling equivalent-beam sections be assumed to have a wall thickness of 1 to 3 percent of the tooth face width (i.e., $t_o/F = 0.01$ to 0.03) for a length equal to the whole depth of the teeth (fig. 31).

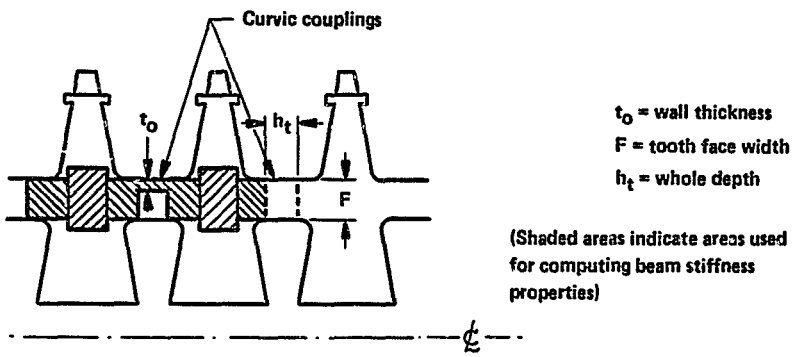

Figure 31. – Curvic coupling equivalent beam sections

The experimental data presented in figure 8.5 of reference 132 should be consulted for determining the stiffening effects of such items as shrunk-on hubs and shrunk-on shaft sleeves. Flexibility effects of conical transition sections or abrupt changes of diameter in the casing or in hollow shafts should be evaluated analytically using a digital computer program for a shell of revolution subjected to non-axisymmetrical loads (refs. 194 through 196).

3.2.2.1.3 Casing and Machine Mount Effects

The model shall accurately simulate the influences of the bearing mounts and casing.

The bearing mounts and casing should be represented by distributed-mass and variable-stiffness models similar to those used for the rotor unless the bearing mount is purposely designed to be flexible, or unless relatively soft fluid-film bearings are used. For these cases, only the bearing-mount stiffness need be modeled, and the casing can be considered as ground.

3.2.2.1.4 Bearing Spring and Damping Forces

The model shall include bearing spring and damping forces as appropriate.

Effects of preload, high-speed centrifugal and gyroscopic loads, and nonlinear load-deflection characteristics should be included in the analyses of angular-contact-bearing stiffness. Analyses of roller-bearing stiffness should include the effects of bearing internal play, shaft misalignment, and the load-deflection nonlinearities. It is recommended that spring rates of rolling-contact bearings be determined by the methods presented in reference 112. Models for rolling-contact bearings need not include damping forces unless special damping mechanisms are part of the design.

Fluid-film bearings must be represented by spring and damping forces that are defined as a function of shaft speed. As labyrinth seals and wear rings also can act like fluid-film bearings to produce stiffness and damping and affect the rotor stability, they should be given proper consideration in the shaft dynamics model. Fluid-film bearings may be characterized and evaluated by techniques given in the references cited in section 2.2.2.1.4.

3.2.2.1.5 Rotor Imbalance Forcing Functions

The model shall include imbalance forcing functions that will enable response evaluation.

Imbalance forcing functions should account for the residual imbalance after balancing, possible imbalance upon reassembly caused by such factors as pilot fits and runouts, possible balance change during operation resulting from load and thermal distortions, and conical or cylindrical whirl forces allowed by roller-bearing internal clearances.

Rotor imbalances that induce circular whirl motion may be represented by the expressions

$$F_s = (Ch_s \pm eW/g)\,\Omega^2 = \gamma\Omega^2$$

$$= (h_s \pm eM)\,\Omega^2 = \gamma\Omega^2 \qquad \text{(SI units)}$$

$$F_d = (Ch_d \pm \theta\, I_d/g)\,\Omega^2 = \beta\Omega^2$$

$$= (h_d \pm \theta\, I_d{}^1)\,\Omega^2 = \beta\Omega^2 \qquad \text{(SI units)}$$

where

F_s = static imbalance, lb (kg)

C = 1.62×10^{-4} lb-sec^2/in. = (lb/16 oz) x (1/g)

h_s = static balance error attained on balance machine, in.-oz (m-kg)

W = component weight, lb

g = acceleration due to gravity, 386 in./sec^2

e = radial eccentricity caused by fit changes, bearing internal play, runouts, etc. that are not corrected for by balancing, in. (m)

Ω = rotational speed, radians/sec

γ = static imbalance forcing function, lb/(rad/sec)^2 (kg/(rad/sec)^2)

M = component weight, kg

F_d = dynamic imbalance, in.-lb (m-kg)

h_d = dynamic balance error, in.^{2}-oz (m^2-kg)

I_d = component diametral moment of inertia, lb-in.^{2}

θ = angular eccentricity, rad.

β = dynamic imbalance forcing function, in.-lb/(rad/sec)^2 (m-kg/(rad/sec)^2)

I_d^1 = component diametral moment of inertia, (kg-m^2)

The ± sign in the equations are used to imply that, strictly speaking, the two quantities in the parentheses do not combine algebraically, but vectorially. However, as the actual vector orientation is unknown, these quantities usually are assumed to be algebraically additive.

For elliptical whirl motion, the forcing functions in reference 57 should be used.

3.2.2.1.6 Virtual Mass and Damping

When necessary, the model shall include the virtual mass and damping associated with shaft operation in a dense fluid or a geared system.

Virtual mass and damping effects of dense fluids (i.e., density of water or greater) can significantly affect critical speeds and shaft response. However, as adequate quantitative theoretical treatments are not available, experimental determinations of the proper model properties should be made. The gear restraint imposed on a pinioned shaft should be accounted for in the model by the technique given in reference 126.

3.2.2.2 MATHEMATICAL METHODS AND COMPUTER SOLUTIONS

Mathematical formulations and resulting computer programs shall be capable of accounting for all the applicable characteristics of the analytical model.

The types of computer programs recommended for the analysis of rotors supported on fluid-film bearings are those presented in references 65, 79, and 91. The types of computer programs recommended for the analysis of rotors supported by rolling-contact bearings are those presented in references 6, 88, 92, and 183. As noted earlier, the computer programs in references 65, 88, and 92 are generally available.

In utilizing any of the available computer programs, the following factors, which are not included in the programs, should be considered:

(1) Fluid-film bearings are not always soft enough relative to the casing to decouple the casing effectively from the rotor/bearing dynamics. The program in reference 65 is limited to a simple lumped mass at each bearing to represent the casing. However, this computer program for rotor/bearing dynamics could, if necessary, be expanded to include a continuous-mass beam model to represent the casing as well as the rotor.

(2) Angular-contact ball bearings can have highly nonlinear spring characteristics that are dependent on axial as well as radial and moment loads on the bearings. To account more accurately for the ball-bearing characteristics, the equations of reference 112 or 113 are incorporated into the rotor/bearing computer programs. This step allows inclusion of the effects of the bearing nonlinear spring characteristics, as influenced by thrust and imbalance, on the critical speeds.

3.2.2.3 PREDICTION ACCURACY

The expected accuracy of the theoretical predictions of critical speeds and response magnitudes shall be known.

Prediction accuracy determined experimentally on previous machines of similar configuration is the best basis for assessing expected accuracy for new machines. In addition, those factors that affect prediction accuracy (sec. 2.2.2.3) should be included in the assessment. Moreover, calculated critical speeds should never be considered more accurate than the predicted value ± 5 percent. The response magnitudes (shaft deflections, bearing loads, etc.) should be considered to be fairly unpredictable; they may be two or three times the calculated values.

3.2.3 Adjustment of Critical Speeds and Response Levels

A design change to adjust critical speeds and response levels shall be based on theoretical or experimental analyses that predict the magnitude of adjustment that can be expected and the impact of the design change on other design considerations such as strength, fabrication complexity, and cost.

Analytical evaluation of the influence of the various parameters affecting critical-speed locations and responses should be the basis for design selection or modification. Experimental confirmation using the techniques recommended in section 3.4 should be accomplished. Short of major shaft redesign, the following techniques should be considered for adjusting critical-speed locations:

(1) Change bearing stiffness by increasing the axial preload of angular-contact bearings, by replacing angular-contact with roller bearings, or by replacing each angular-contact bearing with duplex-bearing sets mounted back-to-back.

(2) Change bearing mount or casing stiffness.

(3) Change fits and axial preloading of shaft-mounted elements such as shrunk-on impellers, bearing races, and sleeves.

(4) Change axial preload of joint-retaining bolts.

Recommended techniques that should be considered for adjusting response levels are the following:

(1) Improve rotor balance by reducing the amount of residual imbalance, by increasing the quality of the balance with multiplane corrections and high-speed techniques, and by minimizing the potential for imbalance developing on reassembly in the turbopump.

(2) Change operating speed or critical speeds to detune shaft.

(3) Reduce internal clearance of roller bearings, and add or increase damping.

(4) Increase the rate of passing through the critical speed directly before the region of resonance, and reduce the acceleration just above the critical speed (ref. 67).

3.2.4 Balancing

The method of balancing and required balance accuracy shall be consistent with (1) mass and shape of the rotor, (2) shaft operating speeds and their relations to the critical speeds, and (3) required turbopump life.

Static balance may be used for rotors of large mass, large mass-moment-of-inertia, and small axial thickness. Dynamic low-speed balancing may be used for rotors operating below the first bending critical. Dynamic high-speed balancing is required when rotors operate above the first bending critical. If n is the number of shaft bending criticals through which the shaft is operated, then the rotor should be balanced in a minimum of n+2 planes (ref. 137).

As a general guide, the rotor should be balanced to an eccentricity of about 50 to 100μ in. (1.27 to 2.54μm). Separate balance of rotor components is advisable when the component is of large mass, large mass-moment-of-inertia, and appreciable axial length. The shaft or component should be supported at the same surfaces that determine the axis of rotation during turbopump operation.

The material for balancing should be added or removed where the diameter is large, so that the relative amount of material change is small. For components that will be used with liquid oxygen, grind material away rather than drill holes, because contaminants may collect in the holes.

Tie bolts should be piloted to maintain concentricity. To minimize required balance corrections, locate fasteners, slots, wrench flats, etc. symmetrically on the shaft.

3.3 Coupling Design

The coupling type shall satisfy applied loads, required alignment, and envelope limits.

Splines are recommended as the coupling to be used where there is torque load but no axial or thrust load and where there is sufficient space for separate piloting. Curvic couplings are recommended for use in highly loaded applications where there is both axial and torque loading and where precision piloting is needed. Parallel-sided face couplings are recommended for lightly loaded applications (both axial and torque) and for applications where space permits separate piloting.

3.3.1 Splines

3.3.1.1 SIZE AND CONFIGURATION

The spline design shall conform to the ASA standard ANSI B 92.1[1] *except when modifications will improve the performance.*

A circular-arc space width equal to one-half the circular pitch should be used for the internal member with tolerance in the plus direction. The clearance then establishes the maximum tooth width of the external member with tolerance on the minus side. If a side bearing fit is desired, the clearance should be in the order of 0.0001 in. (2.54 μ m). If a corrective helix angle is used, the hand of the helix angle should be that which tends to unwind the helix of the external toothed member under torque load.

Inducers and impellers of oxidizer or monopropellant pumps should be driven by splines that are straddled by centering pilots. For these applications, the splines should have the relatively loose Class 1 side-fit dimensions, while the pilots should be tight at operating temperature. The fits to be used at the pilots will vary with rotor design and materials. It should be an interference fit at operating temperatures. For example, a recommended maximum interference for an aluminum pumping element mounted on an Inconel X750

[1] Reference 182

shaft is approximately 0.001-in. (25.4μm) interference for each inch (2.54 cm) of pilot diameter in the size range from 1 to 3 in. (2.54 to 7.62 cm); the minimum interference should be about 0.0009 in. (23μm) less than the maximum. Tests should be performed to ensure that the fit is tight enough to prevent any clearly defined fretting in the spline or other mating surfaces.

The use of side-fit splines with straddling pilot diameters is recommended for other main drives; however, a major-diameter-fit spline without pilots is an acceptable alternate for splines operating at moderate temperatures. The major-diameter-fit spline is to be preferred for appropriate applications where it allows the rotor length to be decreased as a result of eliminating the pilots.

When involute splines are used in a hot-turbine environment, the Class 1 side-fit spline with straddling pilot diameters is recommended. In this case, because of the temperature transients, the pilots should be tight at all temperatures if the centering of the turbine wheel is fixed by the pilots.

Main-drive splines should be 14½°, 30-percent stub tooth. An even number of teeth should be used. The full-fillet radii should be used whenever possible, and the dimensions on the drawing should control the upper and lower limit of the diametral pitch. When space does not permit both members to have fillet root, it should be on the external teeth because they are generally weaker in root tensile strength.

A crowned spline is suitable for misalignments in the range of 0.25° to 3°.

Accessory drive splines should be 30°, 50-percent stub tooth.

3.3.1.2 TEETH IN CONTACT

The number of teeth assumed to be in contact shall be based on the tolerances required and the degree of final inspection.

For lightly loaded splines, 25 percent of the teeth should be assumed to be in contact. A spline length of two-thirds to one shaft diameter is recommended. For highly loaded splines, 50 percent of the teeth may be assumed in contact provided that the tolerances are tightly controlled and finished parts are closely inspected. This inspection should include tooth thickness, form, spacing, and interference as well as inspection by gages to ensure interchangeability.

3.3.2 Curvic Couplings

3.3.2.1 PROPORTIONS FOR JOINT STIFFNESS

The ratio of the rotor disk diameter to the coupling outer diameter shall be as small as possible.

The ratio of the disk diameter to the curvic outer diameter (fig. 22) should not exceed 4 for maximum joint rigidity and stability.

3.3.2.2 SIZE AND CONFIGURATION

The coupling size and configuration shall satisfy the requirements imposed by critical loading conditions, necessary safety factors, and specified reliability.

For initial sizing, approximate analysis may be used. A useful formula (ref. 143), based on a face length of 12.5 percent of the coupling diameter and an ultimate strength of 150,000 psi (1.03 GN/m^2), gives the required curvic coupling outside diameter in inches as equal to the cube root of T/1310,where T is the shaft torque in in.-lbf. (In meters, the OD is equal to the cube root of $T/(9.03 \times 10^6)$, where T is the shaft torque in N-m).

For final sizing, detailed stress analysis should be used. The stress analysis should include tooth shear, contact surface stress, transverse shear, and tension across the tooth at the root. Effects of fretting on tooth cracking also should be considered (ref. 197). The axial force used for the analysis in conjunction with the power torque load should account for the retaining bolt preload of 1.5 to 2 times the separating force and its tolerance plus other operational applied loads (sec. 3.1.3). The coupling may be subjected to a higher-than-normal load at initial assembly in order to increase the contact area.

When standard tooth proportions are used, the contact surface area and shear area remain constant for a given coupling diameter regardless of the number of teeth. The tooth proportions, diametral pitch, and stress limits of reference 143 should be used for long-life, high-reliability applications. However, the reference 143 values are conservative for short-life applications (1 hour or less); hence, stress limits twice those of the reference may be used in short-life designs. Higher stress limits may be tolerated if joint strength is verified experimentally. A tooth contact angle of 30° is recommended. For highly loaded couplings, the surface contact area should be controlled by using close tolerances and rigid inspection.

The detail design should always be directed to eliminating stress raisers or reducing their effect. Typical means of accomplishing this are to avoid bolt holes in curvic coupling teeth and to follow the recommendations in section 3.1.1.4.

For multiple-reuse and long-life applications, an analysis of both high- and low-cycle fatigue should be made (sec. 3.1.3.3).

3.3.3 Parallel-Sided Face Couplings

Parallel-sided face couplings shall not be subject to heavy loads or critical piloting.

Structural analysis of the teeth, retaining bolt, and pilot should be accomplished to ensure that the coupling design has adequate strength to withstand the loads and intended environmental use. Particular attention should be given to tooth tolerances, clearances, and plastic deformation that may be necessary to develop significant tooth-to-tooth load sharing. With one tooth in contact, the pilot is subjected to a transverse load that may result in shaft misalignment due to pilot deflection.

3.4 Design Confirmation Tests

Tests shall provide confirmation of the rotor design adequacy.

Tests should be made to confirm all questionable assumptions used in the design analyses when it is expected that deviations from the assumptions seriously affect design adequacy. These tests should include shake and rotating system tests as well as special stiffness and strength tests as appropriate. The tests should evaluate

(1) Critical speeds, whirl deflection shapes and orbit magnitudes, and bearing reactions.

(2) Any unknown significant shaft dynamic characteristics such as self-excited whirls at supercritical speeds.

(3) The effects on shaft performance of tie-bolt preload, bearing clearances, amounts and locations of imbalance, and static forces applied to the shaft.

(4) The effects of acceleration rate and flexible-mount stiffness on the ease of passing through critical speeds.

(5) Curvic-coupling stiffness under axial and moment loads.

(6) Bolt preload as a function of bolt stretch and pretorque.

(7) Bearing-mount stiffness.

(8) Shaft and coupling ultimate static and fatigue strengths.

3.4.1 Nonrotating Tests

Nonrotating (shake) tests shall provide data suitable for evaluating the dynamic characteristics of the rotor/bearing subsystem.

The test data should be used primarily for built-up shafts to confirm the accuracy of the analytical model used for the rotor and bearings (sec. 3.2.2.1).

The first shake tests of the rotor system should be with the rotor supported by flexible wire to simulate a free-free bearing support condition. These tests should be used to give data regarding tie-bolt preload requirements, effective stiffness of joints and shaft-riding elements, and rotor-only free-free bending natural frequencies and mode shapes. These data provide an excellent check on the accuracy of the model used for the rotor in the analysis of rotor/bearing/casing system dynamics.

A second series of shake tests is recommended mainly if the rotor bearing system supports are purposely designed as flexible mounts. Then, a number of different flexible-mount configurations should be used to provide data for selecting the appropriate mount configuration that will "tune" the rotor to the desired dynamic characteristics. These tests also provide additional data on tie-bolt preload and rotor stiffness effects.

The instrumentation used in this series of tests may be any of the standard vibration-laboratory instrumentation that will yield the type of data desired.

3.4.1.1 DATA CORRELATION

The evaluation of findings from shake tests shall be consistent with the differences that exist between the shake test and the actual rotating test hardware and environment.

The following should be evaluated for differences:

(1) Levels of excitation.– A very low, constant-level excitation usually is used in shake tests, whereas excitation from a rotating imbalance force increases in proportion to the square of the rotational frequency.

(2) Gyroscopic and rotary inertia effects.– Natural frequencies during shake tests are lowered because of rotary inertia of the disks, whereas in forward circular whirl rotation the disks produce gyroscopic stiffening that raises the natural frequencies.

(3) Bearing clearances and effective stiffness.

(4) Damping.

(5) Rotor stiffness developed by shaft-riding elements, and rotor stiffness at the joints and couplings.

(6) The housing, casing, or support mount dynamic stiffness characteristics.– Shake tests usually involve something other than the actual machine casing.

3.4.2 Rotating System Tests

During design or initial development stages, turbopump rotating tests shall provide system-dynamics data suitable for evaluating system characteristics.

Critical-Speed spin-rig tests.– This test series should consist of many spin tests with selected different bearing-mount configurations. The spin-rig rotor and bearing hardware should be sufficiently close to actual detail design configuration to simulate fully the actual mass and stiffness magnitudes and distribution. The casing need only be crudely simulated if the mount dynamically decouples the rotor/bearing-mount system from the turbopump casing.

This series of tests should be the main tool for achieving the overall test objectives for the rotor-dynamics design program. However, as the rig will not simulate all fluid dynamic properties or the clearances between rotor and stator parts of the prototype, the assurance that self-excited subsynchronous whirls will not occur or will not be damaging must await the full-scale prototype tests.

Full-Scale prototype rotating system tests.– These tests should consist of the normal development tests planned for the turbopumps. Rotor dynamic data should be obtained by using appropriate instrumentation to monitor shaft motion and general turbopump vibration level. Accelerometers, velocity probes, and distance detectors should be placed at locations known from the prior system-dynamics analyses and tests to be sensitive indicators of vibration levels. Data from this series of tests should confirm findings from the earlier test series and identify any new characteristics associated with the prototype hardware that was not evidenced at the lower level of simulation of the spin-rig test series. These spin tests should be accomplished early enough to allow a redesign cycle if necessary.

3.4.2.1 INSTRUMENTATION

3.4.2.1.1 Type of Instrumentation

The test instrumentation shall be appropriate for the dynamics data desired and for the test conditions.

As applicable, the following should be considered:

(1) Distance detectors to monitor shaft motion; because of their sensitivity to temperature, the distance detectors should be calibrated.

(2) Velocity probes for frequencies up to 1000 Hz; accelerometers for frequencies above 1000 Hz.

(3) Output signal filtered to isolate the frequency of interest.

(4) An oscilloscope to monitor visually the wave form and amplitude.

(5) Instrumentation system frequency response substantially higher than the maximum frequency of interest.

(6) Instrumentation capabilities compatible with the environment.

(7) A tracking filter for variable speed tests.

(8) Rokide or plasma spray to bond strain gages to high-temperature (>1500° F (1089 K)) rotating parts.

(9) Readings clearly representative of shaft motion and not unduly influenced by the mount response.

(10) Instrumentation that does not alter the response of the shaft by mass loading or aerodynamic interference.

3.4.2.1.2 Instrumentation Location

Instrumentation locations shall be adequate to monitor general vibration levels.

Instrumentation should be placed at locations known from prior system dynamic tests to be the best locations for indicating overall vibration levels. Usually, accelerometers and velocity probes placed near bearing locations serve well. Place the distance detectors in 90°-displaced pairs at various locations along the shaft, preferably where nodes are not expected; both lateral and axial shaft motion should be measured. Distance detectors measure relative motion between the shaft and the distance detector mount only; therefore, it may be necessary to place accelerometers or velocity probes on these mounts to measure the mount absolute motions.

3.4.2.2 INTERPRETATION OF DATA

The interpretation of vibration data shall be adequate to determine normal levels of vibrations and to identify abnormal conditions.

The following techniques should be considered, as applicable, to aid in data interpretation:

- View unfiltered vibration wave form.
- Plot first-order vibration amplitudes versus shaft speed.
- View the Lissajous pattern at the various speeds of interest.
- Analyze data using narrow-bandwidth filters to produce a plot of vibration intensity versus frequency (i.e., power spectral density analyses) for a constant shaft speed.

Vibrations with frequency equal to shaft speed are called first-order vibrations. Typical causes of various-order vibrations are as follows:

(1) Half order: Self-excited whirl, cage rotational frequency.

(2) First order: Rotor imbalance.

(3) Second order: Bearing misalignment, assembly looseness, and impending coupling failure.

(4) Higher order: Blade passing, gear mesh, bearing noise, torque pulsations, and background vibrations.

3.4.3 Special Tests

Special tests shall evaluate critical design factors that cannot be determined accurately by other means.

When rotor or stator component or assembly characteristics are difficult to calculate accurately, and when the characteristics can cause a significant influence on the proper functioning of the shaft, experimental analysis using models or the actual component should be employed. As applicable, bearing and bearing-support-housing static and dynamic load deflection tests should be used for stiffness evaluations. Retaining bolts holding turbine or pump parts to the shaft should be calibration tested for preload. With this information, the required assembly technique to ensure that the desired preload is achieved during assembly can be established.

END OF REFERENCE

91

REFERENCE

92

PROHL, M. A.: A GENERAL METHOD OF CALCULATING CRITICAL SPEEDS OF FLEXIBLE ROTORS. J. APPL. MECH., VOL. 12, SEPT. 1945.

A General Method for Calculating Critical Speeds of Flexible Rotors

By M. A. PROHL,[1] WEST LYNN, MASS.

The existing methods for determining critical speeds are subject to the following limitations: On the one hand the methods that are general, i.e., that permit the calculation of higher critical speeds as well as the fundamental, involve computations so complicated as to be impractical for any but the simplest of rotors. On the other hand, the methods for which the computations are comparatively simple, such as the familiar methods of Rayleigh and Stodola, lack generality in that critical speeds other than the fundamental cannot be definitely determined (1).[2] The calculation method presented in this paper combines generality with comparative simplicity. Any critical speed—first, second, or higher—may be calculated with equal ease. The rotor may have any number of spans and its cross section may vary in any prescribed manner provided circular symmetry is maintained. Any number of disks or symmetrical masses may be attached. The shaft journals may be considered to be elastically supported in the bearing with respect to both deflection and tilting of the journals; the elastic constants must, however, be symmetrical. The so-called "gyroscopic effect" associated with the moment of inertia of the disks on the rotor may be readily taken into account.

Nomenclature

The following nomenclature is used in the paper:

- A = mass moment of inertia of disk about its axis of symmetry, lb-in-sec^2
- B = mass moment of inertia of disk about axis through center of gravity and normal to axis of symmetry, lb-in-sec^2
- C = bearing stiffness factor for resistance to tilting of shaft, lb-in.
- D = diameter of disk, in.
- E = modulus of elasticity, psi
- H = angular momentum, lb-in-sec
- h = thickness of disk, in.
- I = diametral moment of inertia of shaft cross section, in.^{4}
- K = bearing stiffness factor for resistance to deflection of shaft, lb per in.
- M = bending moment, lb-in.
- m = mass, lb-sec^2/in.
- t = time, sec
- V = shearing force, lb
- x = distance along shaft, in.
- y = deflection of shaft, in.
- β = shaft-section flexibility constant (1/lb-in.)
- θ = slope of shaft (nondin ensional)
- μ = mass per unit length, lb-sec^2/in.^{2}
- ρ = mass density lb-sec^2/in.^{4}
- ϕ = angle, radians
- ω = speed of rotation or frequency of vibration, radians per sec

General Considerations

For a balanced shaft of variable diameter which is rotating or "whirling" steadily at a critical speed ω with its central axis in a bowed shape, the following differential equation applies (2, 3)

$$\frac{d^2}{dx^2}\left(EI\frac{d^2y}{dx^2}\right) = \mu\omega^2 y \quad [1]$$

From the elementary beam theory

$$EI\frac{d^2y}{dx^2} = M \quad [2]$$

Equation [1] becomes

$$\frac{d^2M}{dx^2} = \mu\omega^2 y \quad [3]$$

Equation [1] is a fourth-order differential equation, and hence there are four boundary conditions to be satisfied. Any speed of rotation for which it is possible to effect a solution of this equation which satisfies these four boundary conditions constitutes a critical speed. Equations [2] and [3] form the basis for making such a solution by a simultaneous construction of the bending-moment and deflection diagrams using a step-by-step integration process. Let the shaft be divided into a series of appropriate sections. Equations [2] and [3] may be rewritten as follows

$$\Delta\left(\frac{dy}{dx}\right) = \left(\frac{\Delta x}{EI}\right)M_{avg} \quad [4]$$

$$\Delta\left(\frac{dM}{dx}\right) = (\mu\omega^2\Delta x)y_{avg} \quad [5]$$

where Δx is the length of a given section and M_{avg} and y_{avg} are the average values of bending moment and deflection for that section.

Equation [4] states that the change in slope of the deflection curve which occurs at the given section is proportional to the average bending moment, the proportionality factor being the flexibility constant $\left(\frac{\Delta x}{EI}\right)$. Equation [5] states that the change in slope of the bending-moment diagram, which occurs at the given section, is proportional to the average deflection, the proportionality factor being the inertia force of the section mass per unit of deflection ($\mu\omega^2\Delta x$).

Dr. H. Poritsky of the Engineering General Division of the author's company has proposed a graphical method of solution in which the bending moment and deflection diagrams are represented by a series of straight-line segments, the finite changes in

---

[1] Turbine Engineering Division, General Electric Company. Jun. A.S.M.E.

[2] Numbers in parentheses refer to the Bibliography at the end of the paper.

Contributed by the Applied Mechanics Division and presented at the Annual Meeting, New York, N. Y., Nov. 27–Dec. 1, 1944, of The American Society of Mechanical Engineers.

Discussion of this paper should be addressed to the Secretary, A.S.M.E., 29 West 39th Street, New York, N. Y., and will be accepted until Oct. 10, 1945, for publication at a later date. Discussion received after the closing date will be returned.

Note: Statements and opinions advanced in papers are to be understood as individual expressions of their authors and not those of the Society.

slope between adjacent segments being given by Equations [4] and [5].

The calculation method presented in this paper is on a numerical rather than a graphical basis, and the integration procedure is somewhat more elaborate than that indicated in the foregoing equations. A tabular form has been prepared to assist the calculator.

In general, for any assumed speed of rotation, bending-moment and deflection diagrams can be constructed which satisfy three of the four required boundary conditions. Only if the assumed speed of rotation is exactly equal to a critical speed can the fourth boundary condition also be satisfied. Hence by plotting the discrepancy in the fourth boundary condition as a function of the assumed speed, and noting where the discrepancy becomes zero, the various critical speeds can be obtained. In plotting such a curve, it is necessary to select some arbitrary boundary condition and hold it constant. Such a condition might be, for example, the slope of the deflection curve at a shaft end simply supported in a bearing.

The numerical method of this paper is analogous to Holzer's method (4) for calculating natural frequencies of torsional vibration. However, the problem of calculating critical speeds is inherently more complicated since four integrations are involved instead of two, and additional complications arise in dealing with the boundary conditions.

It should be noted that the foregoing type of analysis applies equally well to the determination of the natural frequencies of transverse vibration of a beam of variable cross section since Equation [1] is also the differential equation for this case.[3]

The Calculation Method

In order to apply the numerical-calculation method of this paper, the actual rotor must be transformed into an idealized equivalent system consisting of a series of disks connected by sections of elastic but massless shaft. The mass of these disks and their spacing are chosen so as to approximate the distribution of mass in the actual rotor. Likewise, the bending flexibility of the connecting sections of shaft is taken so as to correspond to the actual flexibility of the rotor. In the discussion which immediately follows, it will be assumed that the moment of inertia of the disks is negligible so that the disks may be treated as mass points.

In Fig. 1, a portion of an idealized system is shown together with the shearing force, bending moment, and deflection diagrams. Assume that this system is whirling in the deflected position at some speed ω. Since each section of shaft is massless, the shearing force is constant between any two masses, and hence the bending-moment diagram has a constant slope directly equal to the shearing force (5)

$$\frac{dM}{dx} = V \qquad [6]$$

A finite change in shearing force occurs at each mass, which is equal to the inertia force of the mass

$$\Delta V = m\omega^2 y \qquad [7]$$

This finite change in shearing force results in a finite change in slope of the moment diagram at each mass. Because of the continuity of the shaft, the deflection diagram is a smooth curve with no breaks or discontinuities. The equation for the variable slope of the deflection curve for each section will be a quadratic, and the equation for the deflection curve will be a cubic.

Assume that the following quantities are known at the left-hand end of the system in Fig. 1:

V_0 = shearing force (due to bearing reaction)
M_0 = bending moment (due to bearing reaction)
θ_0 = slope of deflection curve
y_0 = deflection

There will be a change in shearing force at point 0 due to the inertia force of the mass m_0 according to Equation [7], and hence the shearing force V_1 for the section of shaft between point 0 and point 1 (section 1) is

$$V_1 = V_0 + m_0\omega^2 y_0 \qquad [8]$$

The bending moment M_1 at point 1 is

$$M_1 = M_0 + V_1(\Delta x)_1 \qquad [9]$$

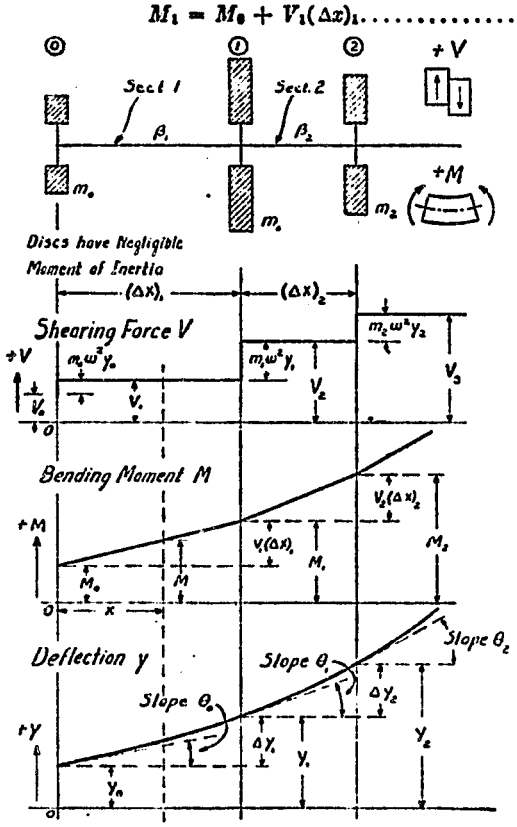

FIG. 1 SHEARING-FORCE, BENDING-MOMENT, AND DEFLECTION DIAGRAMS FOR AN IDEALIZED SYSTEM

The bending moment M at any distance x from the left-hand end of section 1 is

$$M = M_0 + \frac{M_1 - M_0}{(\Delta x)_1} x \qquad [10]$$

The slope θ of the deflection diagram for the first section is obtained as follows

$$\theta = \frac{1}{(EI)_1}\int_0^x M dx + c \qquad [11]$$

where c is a constant of integration.

Substituting Equation [10] in [11] and integrating gives

$$\theta = \frac{1}{(EI)_1}\left[M_0 x + \frac{M_1 - M_0}{(\Delta x)_1}\frac{x^2}{2}\right] + \theta_0 \qquad [12]$$

[3] After this paper had been submitted, the author's attention was drawn to a recently published paper by N. O. Myklestad in which a method for calculating natural frequencies of transverse beam vibration is presented that is fundamentally the same as the method of this paper although quite different in its application. See reference (6) in the Bibliography.

The deflection y is obtained as follows

$$y = \int_0^x \theta dx + c' \quad [13]$$

where c' is a constant of integration.

Substituting Equation [12] in [13] and integrating gives

$$y = \frac{1}{(EI)_1}\left[M_0 \frac{x^2}{2} + \frac{M_1 - M_0}{(\Delta x)_1}\frac{x^3}{6}\right] + \theta_0 x + y_0 \quad [14]$$

It is only necessary to know the slope θ and the deflection y at the end of the section (i.e., point 1). Substituting $(\Delta x)_1$ for x and β_1 for $\left(\frac{\Delta x}{EI}\right)_1$ in Equations [12] and [14] gives

$$\theta_1 = \beta_1\left(\frac{M_0}{2} + \frac{M_1}{2}\right) + \theta_0 \quad [15]$$

$$y_1 = \beta_1\left(\frac{M_0}{3} + \frac{M_1}{6}\right)(\Delta x)_1 + \theta_0(\Delta x)_1 + y_0 \quad [16]$$

From the value of the deflection at point 1, as given by Equation [16], it is now possible to evaluate the change in shearing force at point 1, and hence the shearing force V_2 in shaft section 2.

$$V_2 = V_1 + m_1\omega^2 y_1 \quad [17]$$

The bending moment M_2 at point 2 is

$$M_2 = M_1 + V_2(\Delta x)_2 \quad [18]$$

The bending moment in shaft section 2 is now completely specified, and the slope θ_2 and the deflection y_2 at point 2 may be evaluated by equations similar to Equations [15] and [16]. By repeating this process for successive sections, the bending moment and deflection diagrams for the remainder of the span may be calculated.

The equations for the nth section and point are listed as follows

$$V_n = V_{n-1} + m_{n-1}\omega^2 y_{n-1} \quad [19]$$

$$M_n = M_{n-1} + V_n(\Delta x)_n \quad [20]$$

$$\theta_n = \beta_n\left[\frac{M_{n-1}}{2} + \frac{M_n}{2}\right] + \theta_{n-1} \quad [21]$$

$$y_n = \beta_n\left[\frac{M_{n-1}}{3} + \frac{M_n}{6}\right](\Delta x)_n + \theta_{n-1}(\Delta x)_n + y_{n-1} \quad [22]$$

where

β_n = flexibility constant $= \left(\frac{\Delta x}{EI}\right)_n$

It is convenient in carrying out these calculations in tabular form to introduce two auxiliary quantities; let

$$M_n' = \frac{M_{n-1}}{3} + \frac{M_n}{6} \quad [23]$$

$$M_n'' = \frac{M_{n-1}}{6} + \frac{M_n}{3} \quad [24]$$

Equations [21] and [22] may be expressed in terms of these auxiliary quantities as follows

$$\theta_n = \sum_{n=1}^{n} [\beta_n M_n' + \beta_n M_n''] + \theta_0 \quad [25]$$

TABLE 1 SAMPLE CALCULATION AT ASSUMED SPEED OF 5000 RPM

(ω = 523.6 radians per sec. for span 1 of rotor shown in Fig. 2.)

	(1) n	(2) ΔV	(3) V	(4) ΔX	(5) ΔM	(6) M	(7) $\frac{1}{3}M$	(8) $\frac{1}{6}M$	(9) $M' + M''$	(10) $\beta \cdot 10^7$	(11) $\beta M' + \beta M''$	(12) $\frac{\Delta y'}{\Delta x}$	(13) Δx	(14) $\Delta y'$	(15) $\Delta y''$	(16) y	(17) $m\omega^2$	(18) θ	(19) $A \cdot \beta\omega^2$	(20) n
											x 10⁷	x 10⁷		x 10⁷		x 10⁷		x 10⁷		
I	0	0	1.000			0	0	0								0	880	0		0
	1	.0018	1.000	4,063	4,063	4,063	1,354	677	2,031	3.80	2.57	2.57	4,063	10.43	0	10.43	1760			1
	2	.0176	1.0018	4,063	4,067	8,133	2,711	1,355	4,066	3.80	10.09 / 12.87	18.01	4,063	73.2	0	83.6	2100			2
	3	.2083	1.0194	3,625	3,695	11,828	3,943	1,971	5,914	1.421	6.45 / 7.53	37.53	3,625	136.0	0	219.6	9490			3
	4	1.311	1.2277	5,188	6,37	18,20	6,067	3,033	9,100	1.210	8.44 / 9.72	53.50	5,188	277.6	0	497.2	26350			4
	5	4.557	2.539	6,875	17.45	35.65	11.883	5.942	17,825	0.833	.52 / .64	63.74	6,875	438.	0	935.	48700			5
	6	2.988	7.096	6,000	42.6	78.2	26.07	13.04	39,11	0.377	.94 / 1.21	65.32	6,000	392.0	0	1327.	22500			6
	7	1.984	10.084	4,250	42.9	121.1	40.37	20.18	60,55	.990	45.8 / 52.9	112.3	4250	477.	0	1804.	10990			7
	8	2.258	12.068	1,000	12.07	133.2	44.40	22.20	66,60	0.1123	.7 / .7	165.9	1,000	166.0	0	1970.	11460			8
	9	1.203	14,326	6,125	87.7	220.9	73.63	36.82	110,45	1.879	152.6	319.2	6,125	1955.	0	3925.	3065			9
	10	1.158	15,529	2,375	36.88	257.8	85.93	42.96	128,89	1.043	160.0 / 121.6	620.8	2,375	1475.	0	5400.	2145			10
	11		16.687	3,688	61.5	319.3	106.43	53.22	159,65	1.131	128.0 / 157.4	906.2	3,688	3342.	0	8742.		1075.2		11
											169.0 / 1075.2									
II	0	0	0	4,063	0	0	0	0	0	3.80	0	0	4,063	0	4,063	0	880	1.000		0
	1	7150	7150	4,063	29050	29050	9680	4840	14520	3.80	.00184	.00184	4,063	.007	4,063	4,063	1760			1
	2	17080	24230	3,625	87800	116850	38950	19480	58430	1.421	.00368 / .00414	.00966	3,625	.035	3,625	8,133	2100			2
	3	111,900	136,130	5,188	706,000	822,800	274,300	137,150	411,450	1.210	.00622 / .02131	.03719	5,188	.193	5,188	17,793	9490			3
	4	453,000	589,100	6,875	4050,000	4872,800	1624,300	812,150	2436,450	0.833	.03355 / .00470	.07744	6,875	.532	6,875	24,581	26350			4
	5	1198,000	1787,100	6,000	10720,000	15593,600	5198,080	2599,000	7797,080	0.377	.00763 / .01592	.00993	6,000	.606	6,000	31,187	22500			5
	6	702,000	2489,100	4,250	14580,000	30173,600	8724,000	4362,000	13086,000	.990	.02266 / .946	1.070	4,250	4,547	4,250	39,984	10990			6
	7	440,000	2929,100	1,000	2929,000	29102,000	9701,000	4850,000	14551,000	0.1123	1.121 / .015	2,206	1,000	2,206	1,000	43,190	11460			7
	8	495,000	3424,100	6,125	20950,000	58052,000	16683,000	8342,000	25025,000	1.879	.016 / 3.390	5,612	6,125	34,37	6,125	83,69	3065			8
	9	256,500	3680,600	2,375	8740,000	58792,000	19597,000	9798,000	29395,000	1.043	4.067 / 2.763	12,422	2,375	29,50	2,375	115,56	2145			9
	10	248,000	3928,600	3,688	14480,000	73270,000	24423,000	12211,000	36634,000	1.131	2.915 / 3.598 / 3.871 / 22,886	18,935	3,688	69,8	3,688	189,0		23,886		10
	11																			11

$$y_n = \left\{\beta_n M_n' + \sum_{n=1}^{n-1}[\beta_n M_n' + \beta_n M_n'']\right\}(\Delta x)_n + \theta_0(\Delta x)_n + y_{n-1} \quad [26]$$

The form shown in Table 1 involves the use of Equations [19], [20], [25], and [26], together with the equations for the following auxiliary quantities:

$$(\Delta V)_n = m_n\omega^2 y_n \quad [27]$$

$$(\Delta M)_n = V_n(\Delta x)_n \quad [28]$$

$$(\Delta y')_n = \left\{\beta_n M_n' + \sum_{n=1}^{n-1}[\beta_n M_n' + \beta_n M_n'']\right\}(\Delta x)_n \quad [29]$$

$$(\Delta y'')_n = \theta_0(\Delta x)_n \quad [30]$$

$$(\Delta y)_n = (\Delta y')_n + (\Delta y'')_n = y_n - y_{n-1} \quad [31]$$

From the foregoing equations, it can be demonstrated that the shearing force, bending moment, slope, and deflection at any point in the span will be linear functions of the four assumed quantities at the left-hand end of the span, i.e., at point 0. Hence, the deflection, for example, at point n may be expressed by the following equation

$$y_n = A_n V_0 + B_n M_0 + C_n\theta_0 + D_n y_0 \quad [32]$$

where A_n, B_n, C_n, and D_n represent numerical coefficients which may be determined by using the tabular form. Actually it is not necessary to determine all four coefficients. Since two boundary conditions must always be known at the end of the system from which the calculations originate, two of the terms in Equation [32] can be eliminated. Thus only two coefficients need to be evaluated and this is done in two parts on the tabular form.

The boundary conditions at the left-hand end of the system may be specified in general form as follows

$$Ky_0 = -V_0 \quad [33]$$

$$C\theta_0 = M_0 \quad [34]$$

The minus sign in Equation [33] arises from the conventions employed. Terms K and C are stiffness constants which specify the elastic restraint exerted on the shaft by the supporting bearing. It is assumed that these stiffness constants are symmetrical, i.e., of the same magnitude for all directions normal to the shaft.

The boundary conditions take the following form for certain limiting cases:

Fixed End. The bearing is infinitely stiff against both displacement and rotation or tilting of the shaft, i.e., $K = C = \infty$. Hence from Equations [33] and [34], the following conditions must apply if the shearing force and bending moment are to be finite: $y_0 = 0$ and $\theta_0 = 0$.

Simply Supported End. The bearing is infinitely stiff against displacement but offers no restraint to tilting of the shaft, i.e., $K = \infty, C = 0$. Hence $y_0 = 0$ and $M_0 = 0$.

Free End. The shaft end is completely free, i.e., $K = C = 0$; hence $V_0 = 0$, and $M_0 = 0$.

The boundary conditions that apply at a common point between two spans of a multispan rotor are specified in the following manner: Let k denote the common point between span 1 and span 2. By reason of the continuity of the shaft

$$(\theta_k)_{\text{span 2}} = (\theta_k)_{\text{span 1}} \quad [35]$$

$$(y_k)_{\text{span 2}} = (y_k)_{\text{span 1}} \quad [36]$$

The bearing reactions are treated by equations similar to Equations [33] and [34]

$$Ky_k = -\{(V_k)_{\text{span 2}} - (V_k)_{\text{span 1}}\} \quad [37]$$

$$C\theta_k = \{(M_k)_{\text{span 2}} - (M_k)_{\text{span 1}}\} \quad [38]$$

Sample Calculation

The drawing of the rotor used for this calculation is given in Fig. 2. The rotor has two spans, span 1 being supported between two bearings, and span 2 being overhung. Also shown in Fig. 2 is a diagrammatic representation of the idealized system. This idealized system is obtained by dividing the shaft of the rotor into sections of constant diameter. The total mass existing within a given section is divided into two parts which are concentrated at the ends of the section, this division of mass being such that the center of gravity of the section mass remains unchanged. The flexibility constants are evaluated using the actual physical dimensions of the shaft sections. While this method of constructing the idealized system is somewhat arbitrary, it should be sufficiently accurate for all practical purposes provided enough sections are used.

In Table 1, the calculations for span 1 are given in tabular form for an assumed speed of 5000 rpm (ω = 523.6 radians per sec). The values for the section lengths Δx, disk masses m, and shaft-flexibility constants β for the idealized system, as shown in Fig. 2, are listed directly on the tabular form in the proper columns (the values of the masses being multiplied by ω^2 to give the inertia force constants $m\omega^2$). In so far as the calculation is concerned, the rotor is completely specified by these three groups of quantities. (It is assumed that the disks on the rotor have negligible moment of inertia, i.e., there is no gyroscopic effect.)

The assumption is made that the shaft is simply supported in its bearings. From Equations [33] and [34], the following boundary conditions are obtained for the left-hand end of span 1 (point 0)

$$y_0 = 0$$

$$M_0 = 0$$

The shearing force V_0 and the slope of the deflection curve θ_0 are carried in the calculation as unknowns. On the tabular form this is done by making the calculation in two parts with the following initial conditions (note the encircled figures in Table 1)

$$\text{I}\begin{cases} V_0 = 1.000 \\ \theta_0 = y_0 = M_0 = 0 \end{cases} \qquad \text{II}\begin{cases} V_0 = y_0 = M_0 = 0 \\ \theta_0 = 1.000 \end{cases}$$

With the initial conditions specified the calculation proceeds across the table from left to right, the figures on one horizontal line being completed before proceeding to the next line. Although the general equations given in the preceding section of the paper define all of the operations on the form, several features may need further explanation. Values pertaining to the mass points are entered on the horizontal lines. Values pertaining to the shaft sections are entered in the spaces between the lines. The auxiliary quantities M' and M'' in column 8 are each obtained by adding together one value from column 6 and one value from column 7. The manner in which this addition is made is indicated by the arrows inserted on the form. The quantity $\left(\frac{\Delta y'}{\Delta x}\right)$ in column 11 is obtained by a summation of the values in column 10 proceeding from the top of the column down to but not including the second of the two values for the last section involved in the particular summation. The broken lines drawn on the form in columns 10 and 11 indicate the values involved in successive summations. The slope θ in column 17 is obtained by summing the values in column 10 from the top down to the point for which the slope is desired.

From the calculations in Table 1, the following equations are

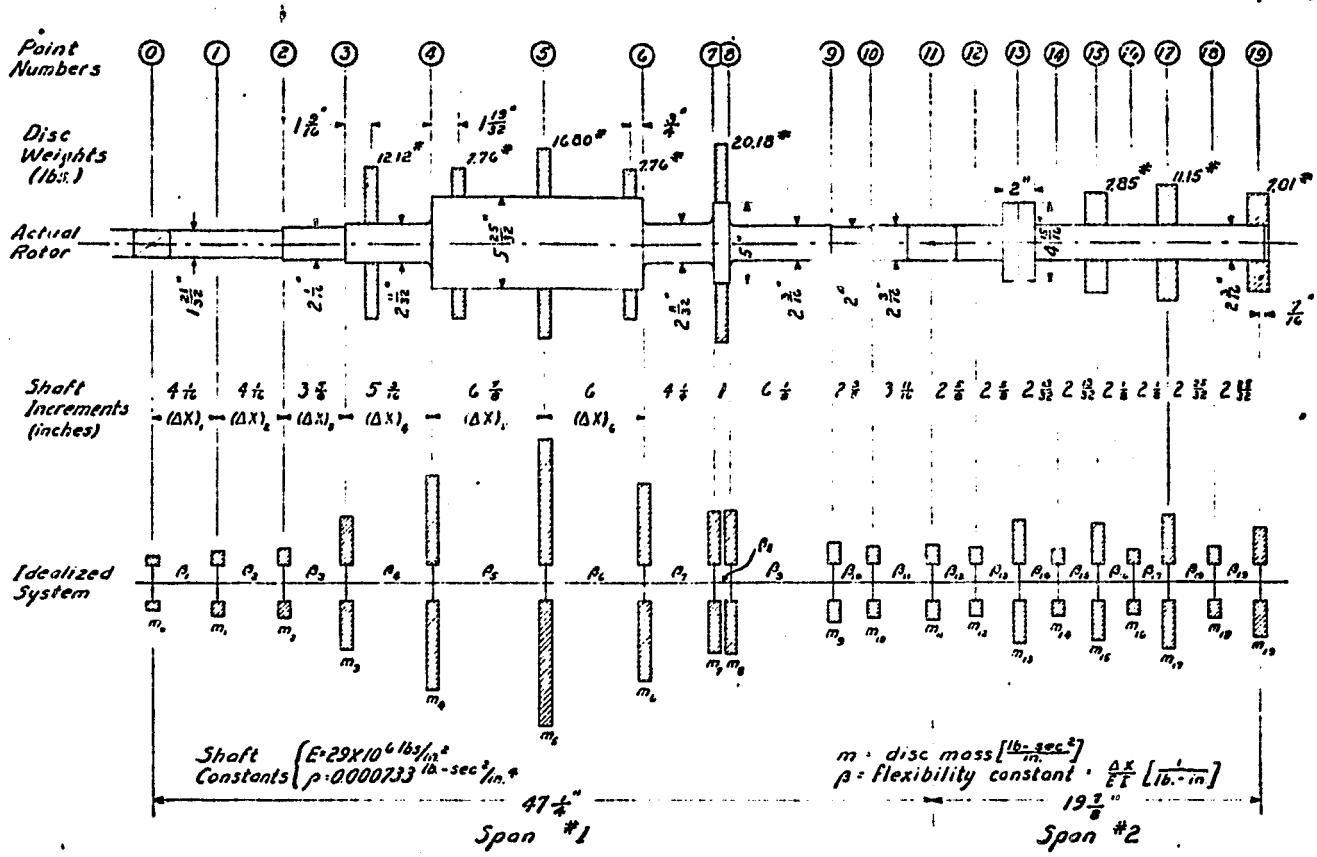

FIG. 2 ROTOR USED FOR SAMPLE CALCULATION

obtained for the slope, deflection, and bending moment at point 11 (the common point between span 1 and span 2)

$$\theta_{11} = 0.00010752\ V_0 + 23.806\,\theta_0 \quad \text{[39]}$$

$$y_{11} = 0.0008742\ V_0 + 189.0\,\theta_0 \quad \text{[40]}$$

$$M_{11} = 319.3\ V_0 + 73{,}270{,}000\,\theta_0 \quad \text{[41]}$$

From Equations [35] through [38], the following boundary conditions are obtained at point 11 (shaft simply supported in the bearing)

$$(\theta_{11})_{\text{span 2}} = (\theta_{11})_{\text{span 1}}$$
$$(y_{11})_{\text{span 2}} = (y_{11})_{\text{span 1}} = 0$$
$$(M_{11})_{\text{span 2}} = (M_{11})_{\text{span 1}}$$

Placing y_{11} equal to zero in Equation [40] gives V_0 in terms of θ_0. Hence V_0 may be eliminated from Equations [39] and [41]. Then by virtue of the foregoing boundary conditions, the following values apply to the initial point for span 2

$$\theta_{11} = 0.561\,\theta_0$$
$$y_{11} = 0$$
$$M_{11} = 4{,}240{,}000\,\theta_0$$

Because of the unknown bearing reaction, the shearing force V_{11} for span 2 is not known. Hence the calculations for span 2 are made in terms of the two unknowns, V_{11} and θ_0. On the tabular form this is done by making the calculations in two parts with the following initial conditions

$$\text{I}\begin{cases} V_{11} = 1.000 \\ \theta_{11} = y_{11} = M_{11} = 0 \end{cases} \qquad \text{II}\begin{cases} V_{11} = y_{11} = 0 \\ M_{11} = 4{,}240{,}000 \\ \theta_{11} = 0.561 \end{cases}$$

The calculations for span 2 are carried out in the same manner as for span 1. They have not been included in this paper because of space limitations. From these calculations the following equations are obtained for V_{19}, the shearing force at an infinitesimal distance beyond the point of attachment of the 19th disk, and M_{19}, the bending moment at point 19

$$V_{19} = 1.523 V_{11} + 688{,}400\,\theta_0 \quad \text{[42]}$$

$$M_{19} = 21.469 V_{11} + 7{,}470{,}000\,\theta_0 \quad \text{[43]}$$

Since point 19 represents the free end of the rotor, the following boundary conditions apply

$$V_{19} = 0$$

$$M_{19} = 0$$

In general, only one of these conditions can be satisfied. Only if the assumed speed is exactly equal to a critical speed will both conditions be satisfied. Placing V_{19} equal to zero in Equation [42] and solving for M_{19} in terms of θ_0 in Equation [43] yields the following value for M_{19}

$$M_{19} = -2{,}230{,}000\,\theta_0$$

Since M_{19} is not equal to zero, the assumed speed of 5000 rpm does not represent a critical speed. A series of calculations similar to the one just discussed have been made for this rotor at different assumed speeds. The values of M_{19} obtained from these calculations have been plotted against assumed speed in Fig. 3. In plotting these values of M_{19} the slope θ_0 at the left-hand end of the rotor is arbitrarily placed equal to unity. (Any value may be assigned to θ_0 since, at a critical speed, the rotor is in a state of indifferent equilibrium.) The first three values of speed required to make M_{19} equal to zero are as follows:

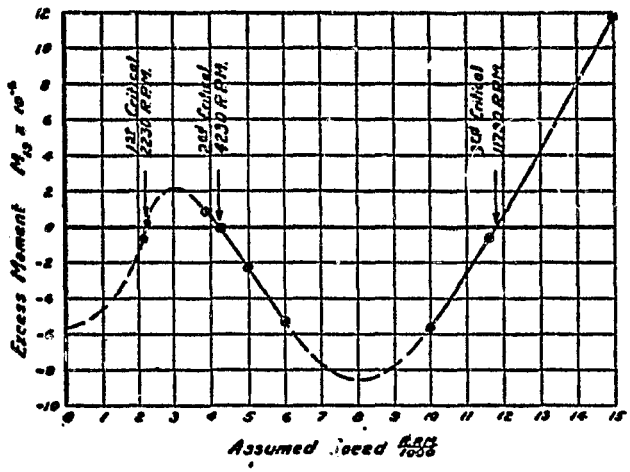

FIG. 3 PLOT OF EXCESS BENDING MOMENT VERSUS ASSUMED SPEED

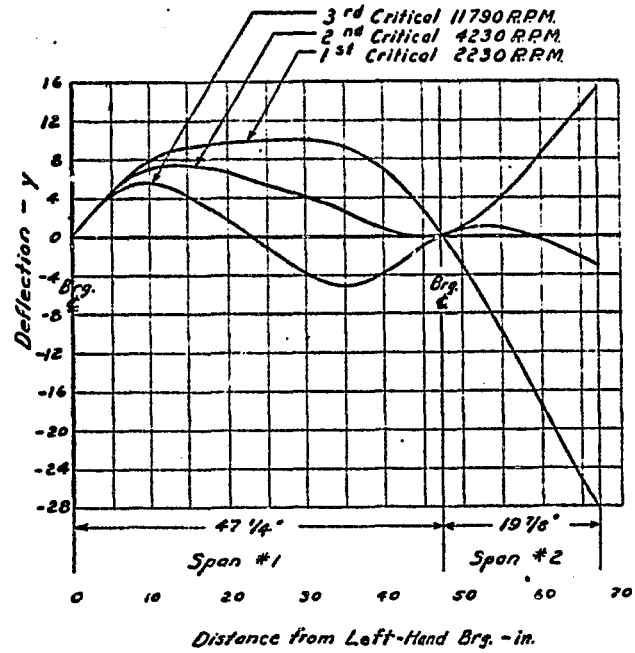

FIG. 4 DEFLECTION CURVES FOR FIRST, SECOND, AND THIRD CRITICAL SPEEDS

Critical speed 1 = 2230 rpm
Critical speed 2 = 4230 rpm
Critical speed 3 = 11,790 rpm

The deflection diagram may be readily plotted for any assumed speed, since an equation of the form of Equation [40] may be obtained from the tabular calculation for every point along the rotor. The deflection curves for the first three critical speeds have been plotted in Fig. 4.

EFFECT OF MASS MOMENT OF INERTIA OF DISKS

Assume that values of mass moment of inertia, both polar and diametral, have been assigned to the disks of the idealized system. The effect of the mass moment of inertia may be readily taken into account on the tabular form. It is necessary, however, to differentiate between the nonrotating and rotating cases.

Nonrotating Case. For a rotor which is vibrating in a transverse plane at a natural frequency, a rotary inertia effect is involved. Consider a disk on a vibrating shaft at the instant of maximum amplitude, as shown in Fig. 5. Let the deflection of the disk center of gravity be denoted by y, the angle of rotation by ϕ, and the frequency of vibration by ω. The force F and the moment M which must be exerted on the disk with respect to its center of gravity are

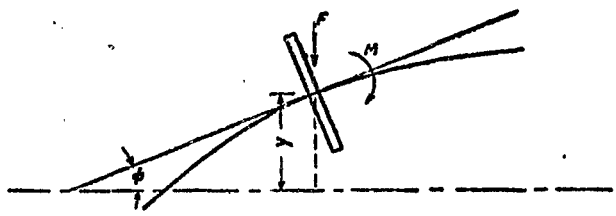

FIG. 5

$$F = m\omega^2 y \quad \ldots\ldots [44]$$

$$M = B\omega^2\phi \quad \ldots\ldots [45]$$

where B is the mass moment of inertia of the disk about an axis through the center of gravity and normal to the axis of symmetry.

The force and the moment which the disk exerts on the shaft will have magnitudes equal to the foregoing values, but will have directions opposite to those shown in Fig. 5.

Equation [44] requires that there be a change in shearing force in the shaft at the point of attachment of the disk proportional to the deflection, the proportionality factor being $m\omega^2$. This has already been incorporated in the calculation procedure. Equation [45] requires that there be a change in bending moment at the point of attachment of the disk proportional to the angle ϕ, the proportionality factor being $B\omega^2$. In terms of the notation employed on the tabular form Equation [45] becomes

$$\Delta M = -B\omega^2\theta \quad \ldots\ldots [46]$$

where the slope θ has been substituted for the angle ϕ. (This is permissible for small angles.)

Rotating Case. For a rotor which is whirling at a critical speed, a gyroscopic effect is involved. Consider a balanced disk, as shown in Fig. 6, the center of gravity of which is whirling in a circular path of radius y at a speed ω. Let the axis of the disk make a constant angle ϕ with the rotation axis. Assume that there is no rotation of the disk relative to the rotating plane formed by the disk axis and the rotation axis. This means that a point Q, for example, which is the outside point on the periphery of the disk will remain the outside point.

The components of rotation about the axes a and b are $\omega \cos \phi$ and $\omega \sin \phi$, respectively. Since axes a and b are principal axes of inertia for the disk, the components of angular momentum H_a and H_b are given by the following formulas

$$H_a = A\omega \cos \phi$$

$$H_b = B\omega \sin \phi$$

where A and B are the mass moments of inertia of the disk about axes a and b, respectively.

The moment which must act on the disk about the center of gravity to sustain the prescribed motion is equal to the time rate of change of the resultant angular momentum H

$$M = \frac{dH}{dt} = H_y\omega \quad \ldots\ldots [47]$$

where H_y is the component of H normal to the axis of rotation

$$H_y = H_a \sin \phi - H_b \cos \phi$$

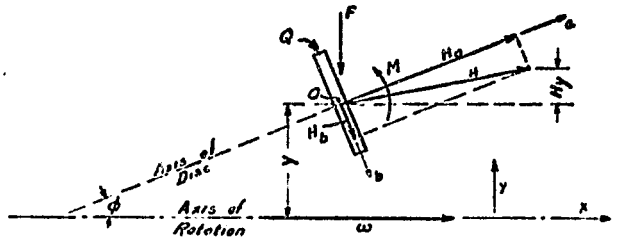

FIG. 6

or

$$H_y = (A - B)\omega \sin \phi \cos \phi \quad \ldots\ldots [48]$$

Substituting Equation [48] in Equation [47], and placing sin $\phi = \phi$ and cos $\phi = 1$ (permissible for small angles) gives

$$M = (A - B)\omega^2\phi \quad \ldots\ldots [49]$$

The direction of this moment is in the direction of the change of momentum, as indicated in Fig. 6. It will be noted that the direction of this moment is opposite to that shown in Fig. 5, for the nonrotating case. In addition to the moment M, given by Equation [49], a centripetal force F, as given by Equation [44], is required to maintain the prescribed motion.

The force and the moment which the disk exerts on the shaft will be equal in magnitude to F and M in Fig. 6, but opposite in direction.

Expressing Equation [49] in terms of the notation on the tabular form gives the expression

$$\Delta M = (A - B)\omega^2\theta \quad \ldots\ldots [50]$$

If the disks of the idealized system have appreciable mass moment of inertia, then the bending-moment diagram, shown in Fig. 1, must be modified as indicated in Fig. 7. Because of the finite change in bending moment which occurs at each point according to Equation [50], there will be two values of bending moment at each point. Thus in Fig. 7, M_{1L} signifies the bending moment at an infinitesimal distance to the left of the point of attachment of the disk and M_{1R} the bending moment at an infinitesimal distance to the right.

The last two columns on the form, Table 1, have been added so that the effect of the mass moment of inertia of the disks may be incorporated into the calculation. The heading of column 18 applies to the rotating case. If a nonrotating case is to be handled, the symbol A should be deleted from the heading, according to Equation [46]. The values of ΔM obtained by Equation [46] or Equation [50] are tabulated in column 4 of the form, the values being entered on the horizontal lines. (The values of ΔM due to the shearing force in the shaft sections are entered in the space between the lines.) This dual set of values for ΔM gives rise to two values of bending moment at each point in column 5. The first value is entered just above the horizontal line bearing the point number, and the second value just below. The rest of the calculation is then the same as the sample shown in Table 1.

The mass moments of inertia A and B for a flat solid disk are given by the following equations

$$A = \frac{\pi phD^4}{32} \quad \ldots\ldots [51]$$

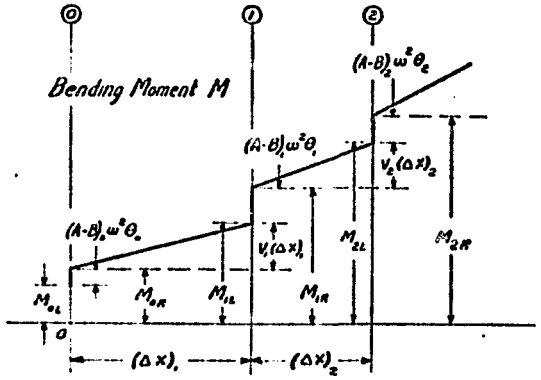

FIG. 7 BENDING-MOMENT DIAGRAM FOR SYSTEM OF FIG. 1, WHERE THE DISKS HAVE APPRECIABLE MASS MOMENT OF INERTIA

$$B = \frac{\pi phD^4}{64}\left[1 + \frac{4}{3}\left(\frac{h}{D}\right)^2\right] \quad \ldots\ldots [52]$$

If the thickness h of the disk is small compared to the diameter D, then $A \cong 2B$, and the proportionality factors between moment and slope in Equations [46] and [50] become equal in magnitude but opposite in sign.

For the nonrotating case, the natural frequencies obtained by neglecting the mass moment of inertia are decreased if the effect of the mass moment of inertia is considered. For the rotating case, the critical speeds are increased by taking into account the mass moment of inertia provided that $A > B$.

CONCLUSIONS

The tabular-calculation method presented in this paper gives an exact solution for the critical speeds of the idealized system. Hence the accuracy of the method in so far as an actual rotor is concerned depends entirely on how closely the idealized system and the idealized boundary conditions represent the actual rotor and its bearings.

ACKNOWLEDGMENT

The author wishes to express his appreciation to Dr. H. Poritsky of the Engineering General Division of the General Electric Company, Schenectady, N. Y., for originally outlining the general method of attacking this problem and for his suggestions and comments.

BIBLIOGRAPHY

1 "Mechanical Vibrations," by J. P. Den Hartog, McGraw-Hill Book Company, Inc., New York, N. Y., 1940, pp. 194–196.

2 "On the Strength of Shafting When Exposed Both to Torsion and End Thrust," by A. G. Greenhill, Proceedings of The Institution of Mechanical Engineers, 1883, pp. 182–225.

3 "On the Whirling and Vibration of Shafts," by S. Dunkerley, Philosophical Transactions of the Royal Society of London, series A, vol. 185, 1894, pp. 279–360.

4 Reference (1), pp. 222–237.

5 "Strength of Materials, Part I," by S. Timoshenko, D. Van Nostrand Company, Inc., New York, N. Y., 1940, pp. 72–74.

6 "A New Method of Calculating Natural Modes of Uncoupled Bending Vibration of Airplane Wings and Other Types of Beams," by N. O. Myklestad, *Journal of the Aeronautical Sciences*, vol. 11, no. 2, April, 1944, pp. 153–162.

END OF REFERENCE

92

REFERENCE

93

MYKELSTAD, N. O.: NUMERICAL ANALYSIS OF FORCED VIBRATIONS OF BEAMS. J. APPL. MECH., VOL. 20, NO. 11, MAR. 1953.

Numerical Analysis of Forced Vibrations of Beams

By N. O. MYKLESTAD,[1] URBANA, ILL.

In this paper a simple tabular method is developed by which the vibration amplitudes, bending moments, and shear forces of a beam of variable but symmetrical cross section, carrying any number of concentrated masses and acted on by any number of harmonically varying forces, can be found. The driving forces must all have the same frequency but the phase angles may be different. The method is an extension of the one employed by the author to find natural modes of vibration of beams, but in the case of forced vibration only one application of the tabular calculations is necessary, making it essentially a far simpler problem than that of finding the natural modes. Internal damping of the beam material is easily considered and should always be taken into account if there is any danger that the forced frequency is near any one of the natural frequencies.

Introduction

IN the present numerical analysis it is assumed that the beam is subjected to bending in one plane only and that it does not twist during vibration. The mass of the beam must be concentrated at discrete points along the elastic axis and the number of such points will depend on the number of concentrated driving forces as well as on the accuracy desired. The driving forces must all be harmonic and of the same frequency, but need not be in phase. They are conveniently written in the form $\bar{F}\,e^{i\omega t}$, where $\bar{F} = F\,e^{i\alpha}$ is the complex amplitude of a force with real amplitude F and phase angle α with respect to the rotating vector $e^{i\omega t}$. The internal damping is considered by assuming a complex damping factor $2b$ and multiplying each of the elastic coefficients by the quantity $e^{-2bi} = \cos 2b - i \sin 2b$, or $1 - 2bi$ if b is a small quantity and extreme accuracy is not required. All the deflections, slopes, shearing forces, bending moments, and so on, entering the problem will now be harmonic but with complex amplitudes. The term $e^{i\omega t}$ may then be canceled out as usual and only the complex amplitudes used in the calculations.

The beam is divided into sections with concentrated masses at the boundaries, and the elastic coefficients for the nth section are defined as follows: If the left end of the section is clamped and a unit bending moment applied to the right end the slope at this end will be v_{Mn} and the deflection d_{Mn}; while a unit force at the right end would give a slope v_{Fn} and deflection d_{Fn}. For a uniform section of length l and flexural rigidity EI these quantities would be

$$v_M = \frac{l}{EI} \quad [1]$$

$$v_F = d_M = \frac{l^2}{2EI} \quad [2]$$

$$d_F = \frac{l^3}{3EI} \quad [3]$$

Also, $\bar{v}_M = v_M\,e^{-2bi}$, $\bar{v}_F = \bar{d}_M = v_F\,e^{-2bi}$, $\bar{d}_F = d_F\,e^{-2bi}$, where $2b$ is the complex damping factor. For a nonuniform section more accurate formulas are derived elsewhere.[2]

Beam With Free End

A beam with free end is shown schematically in Fig. 1, where the free end is at the right and the base is at the left end, which may be either free, hinged, or clamped. Fig. 2 shows the nth section of the beam in its extreme position when the free end of

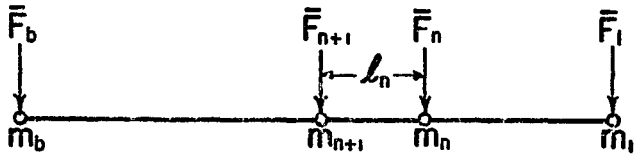

FIG. 1

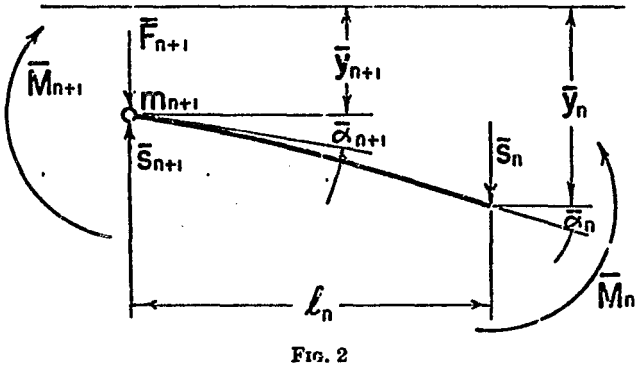

FIG. 2

the beam itself has a deflection $\bar{\delta}$ and a slope $\bar{\varphi}$. The slope and deflection at station n are then $\bar{\alpha}_n$ and $\bar{y}_n$, respectively, while the shearing force immediately to the left of mass m_n is $\bar{S}_n$ and the bending moment $\bar{M}_n$. If these quantities are known at station n they can be found at station $n + 1$ by means of the following equations

$$\bar{S}_{n+1} = \bar{S}_n + m_{n+1}\,\omega^2\,\bar{y}_{n+1} + \bar{F}_{n+1} \quad [4]$$

$$\bar{M}_{n+1} = \bar{M}_n - l_n\bar{S}_n \quad [5]$$

$$\bar{\alpha}_{n+1} = \bar{\alpha}_n - \bar{v}_{Fn}\,\bar{S}_n + \bar{v}_{Mn}\,\bar{M}_n \quad [6]$$

---

[1] Professor of Theoretical and Applied Mechanics, University of Illinois. Mem. ASME.

Contributed by the Applied Mechanics Division and presented at the Fall Meeting, Chicago, Ill., September 8–11, 1952, of THE AMERICAN SOCIETY OF MECHANICAL ENGINEERS.

Discussion of this paper should be addressed to the Secretary, ASME, 29 West 39th Street, New York, N. Y., and will be accepted until April 10, 1953, for publication at a later date. Discussion received after the closing date will be returned.

NOTE: Statements and opinions advanced in papers are to be understood as individual expressions of their authors and not those of the Society. Manuscript received by ASME Applied Mechanics Division, May 19, 1952. Paper No. 52—F-12.

[2] "Vibration Analysis," by N. O. Myklestad, McGraw-Hill Book Company, Inc., New York, N. Y., 1944, p. 201.

$$\bar{y}_{n+1} = \bar{y}_n - l_n \bar{\alpha}_{n+1} - \bar{d}_{Fn} \bar{S}_n + \bar{d}_{Mn} \bar{M}_n \quad [7]$$

By substituting for $\bar{\alpha}_{n+1}$ from Equation [6] in Equation [7] this becomes

$$\bar{y}_{n+1} = \bar{y}_n - l_n \bar{\alpha}_n + \bar{u}_{Fn} \bar{S}_n - \bar{u}_{Mn} \bar{M}_n \quad [7a]$$

where

$$\bar{u}_{Fn} = l_n \bar{v}_{Fn} - \bar{d}_{Fn} \quad [8]$$

$$\bar{u}_{Mn} = l_n \bar{v}_{Mn} - \bar{d}_{Mn} \quad [9]$$

For a uniform beam section this gives

$$u_{Fn} = \frac{l_n^3}{6EI} \quad [8a]$$

$$u_{Mn} = \frac{l_n^2}{2EI} \quad [9a]$$

and $\bar{u}_F = u_F e^{-2bi}$, $\bar{u}_M = u_M e^{-2bi}$. Owing to the linear character of these equations each of the foregoing quantities can be written as a linear function of the slope $\bar{\varphi}$ and deflection $\bar{\delta}$ at the free end of the beam. This gives

$$\bar{S}_n = -\bar{G}_{\varphi n} \bar{\varphi} + \bar{G}_{\delta n} \bar{\delta} + \bar{G}_n \quad [10]$$

$$\bar{M}_n = \bar{G}'_{\varphi n} \bar{\varphi} - \bar{G}'_{\delta n} \bar{\delta} - \bar{G}_n' \quad [11]$$

$$\bar{\alpha}_n = \bar{f}_{\varphi n} \bar{\varphi} - \bar{f}_{\delta n} \bar{\delta} - \bar{f}_n \quad [12]$$

$$\bar{y}_n = -\bar{g}_{\varphi n} \bar{\varphi} + \bar{g}_{\delta n} \bar{\delta} + \bar{g}_n \quad [13]$$

where the minus signs have been introduced merely to make the coefficients $\bar{G}$, $\bar{G}'$, $\bar{f}$ and $\bar{g}$ positive for most practical problems, which makes the tabular calculations somewhat easier. Substituting Equations [10] to [13] in Equations [4] to [7a], and equating like terms, results in the following system of equations

$$\bar{G}_{\varphi n+1} = \bar{G}_{\varphi n} + m_{n+1} \omega^2 \bar{g}_{\varphi n+1} \quad [14]$$

$$\bar{G}_{\delta n+1} = \bar{G}_{\delta n} + m_{n+1} \omega^2 \bar{g}_{\delta n+1} \quad [15]$$

$$\bar{G}_{n+1} = \bar{G}_n + m_{n+1} \omega^2 \bar{g}_{n+1} + \bar{F}_n \quad [16]$$

$$\bar{G}_{\varphi n+1}' = \bar{G}'_{\varphi n} + l_n \bar{G}_{\varphi n} \quad [17]$$

$$\bar{G}_{\delta n+1}' = \bar{G}'_{\delta n} + l_n \bar{G}_{\delta n} \quad [18]$$

$$\bar{G}_{n+1}' = \bar{G}_n' + l_n \bar{G}_n \quad [19]$$

$$\bar{f}_{\varphi n+1} = \bar{f}_{\varphi n} + \bar{v}_{Fn} \bar{G}_{\varphi n} + \bar{v}_{Mn} \bar{G}'_{\varphi n} \quad [20]$$

$$\bar{f}_{\delta n+1} = \bar{f}_{\delta n} + \bar{v}_{Fn} \bar{G}_{\delta n} + \bar{v}_{Mn} \bar{G}_{\delta n}' \quad [21]$$

$$\bar{f}_{n+1} = \bar{f}_n + \bar{v}_{Fn} \bar{G}_n + \bar{v}_{Mn} \bar{G}_n' \quad [22]$$

$$\bar{g}_{\varphi n+1} = \bar{g}_{\varphi n} + l_n \bar{f}_{\varphi n} + \bar{u}_{Fn} \bar{G}_{\varphi n} + \bar{u}_{Mn} \bar{G}_{\varphi n}' \quad [23]$$

$$\bar{g}_{\delta n+1} = \bar{g}_{\delta n} + l_n \bar{f}_{\delta n} + \bar{u}_{Fn} \bar{G}_{\delta n} + \bar{u}_{Mn} \bar{G}_{\delta n}' \quad [24]$$

$$\bar{g}_{n+1} = \bar{g}_n + l_n \bar{f}_n + \bar{u}_{Fn} \bar{G}_n + \bar{u}_{Mn} \bar{G}_n' \quad [25]$$

The boundary conditions at the free end now require that $\bar{\alpha}_1 = \bar{\varphi}$, $\bar{y}_1 = \bar{\delta}$, $\bar{S}_1 = m_1 \omega^2 \bar{\delta} + \bar{F}_1$, and $\bar{M}_1 = 0$; which gives

$$\bar{f}_{\varphi 1} = 1 \qquad \bar{f}_{\delta 1} = 0 \qquad \bar{f}_1 = 0 \quad [26]$$

$$\bar{g}_{\varphi 1} = 0 \qquad \bar{g}_{\delta 1} = 1 \qquad \bar{g}_1 = 0 \quad [27]$$

$$\bar{G}_{\varphi 1} = 0 \qquad \bar{G}_{\delta 1} = m_1 \omega^2 \qquad \bar{G}_1 = \bar{F}_1 \quad [28]$$

$$\bar{G}_{\varphi 1}' = 0 \qquad \bar{G}_{\delta 1}' = 0 \qquad \bar{G}_1' = 0 \quad [29]$$

It is now possible to proceed from the free end of the beam to the base, and by satisfying the boundary conditions at the base, the values of $\bar{\varphi}$ and $\bar{\delta}$ can be obtained. The shearing forces, bending moments, slopes, and deflections may then be obtained from Equations [10] to [13].

Free-Free-Beam

In this case the base of the beam is completely free and the boundary conditions become $\bar{S}_b = \bar{M}_b = 0$. Equations [10] and [11] then give

$$\bar{G}_{\varphi b} \bar{\varphi} - \bar{G}_{\delta b} \bar{\delta} = \bar{G}_b \quad [30]$$

$$\bar{G}_{\varphi b}' \bar{\varphi} - \bar{G}_{\delta b}' \bar{\delta} = \bar{G}_b' \quad [31]$$

from which are found

$$\bar{\varphi} = \frac{\bar{G}_b' \bar{G}_{\delta b} - \bar{G}_b \bar{G}_{\delta b}'}{\bar{G}_{\varphi b}' \bar{G}_{\delta b} - \bar{G}_{\varphi b} \bar{G}_{\delta b}'} \quad [32]$$

$$\bar{\delta} = \frac{\bar{G}_{\varphi b} \bar{G}_b' - \bar{G}_{\varphi b}' \bar{G}_b}{\bar{G}_{\varphi b}' \bar{G}_{\delta b} - \bar{G}_{\varphi b} \bar{G}_{\delta b}'} \quad [33]$$

Cantilever Beam

In this case the base of the beam is clamped and the boundary conditions become $\bar{\alpha}_b = \bar{y}_b = 0$. Equations [12] and [13] then give

$$\bar{f}_{\varphi b} \bar{\varphi} - \bar{f}_{\delta b} \bar{\delta} = \bar{f}_b \quad [34]$$

$$\bar{g}_{\varphi b} \bar{\varphi} - \bar{g}_{\delta b} \bar{\delta} = \bar{g}_b \quad [35]$$

from which are found

$$\bar{\varphi} = \frac{\bar{g}_b \bar{f}_{\delta b} - \bar{f}_b \bar{g}_{\delta b}}{\bar{g}_{\varphi b} \bar{f}_{\delta b} - \bar{f}_{\varphi b} \bar{g}_{\delta b}} \quad [36]$$

$$\bar{\delta} = \frac{\bar{f}_{\varphi b} \bar{g}_b - \bar{g}_{\varphi b} \bar{f}_b}{\bar{g}_{\varphi b} \bar{f}_{\delta b} - \bar{f}_{\varphi b} \bar{g}_{\delta b}} \quad [37]$$

Simply Supported Beam

For a simply supported beam it is merely necessary to replace Equations [10] to [13] by the following

$$\bar{S}_n = \bar{G}_{\varphi n} \bar{\varphi} - \bar{G}_{Rn} \bar{R}_a + \bar{G}_n \quad [38]$$

$$\bar{M}_n = -\bar{G}_{\varphi n}' \bar{\varphi} + \bar{G}_{Rn}' \bar{R}_a - \bar{G}_n' \quad [39]$$

$$\bar{\alpha}_n = -\bar{f}_{\varphi n} \bar{\varphi} + \bar{f}_{Rn} \bar{R}_a - \bar{f}_n \quad [40]$$

$$\bar{y}_n = \bar{g}_{\varphi n} \bar{\varphi} - \bar{g}_{Rn} \bar{R}_a + \bar{g}_n \quad [41]$$

Substituting these equations in Equations [4] to [7a] and equating like terms gives a system of equations identical with Equations [14] to [25], except that the subscript δ is replaced by the subscript R. The boundary conditions at the right end now become

$$\bar{G}_{\varphi 1} = 0 \qquad \bar{G}_{R1} = 1 \qquad \bar{G}_1 = 0 \quad [42]$$

$$\bar{G}_{\varphi 1}' = 0 \qquad \bar{G}_{R1}' = 0 \qquad \bar{G}_1' = -\bar{M}_a \quad [43]$$

$$\bar{f}_{\varphi 1} = 1 \qquad \bar{f}_{R1} = 0 \qquad \bar{f}_1 = 0 \quad [44]$$

$$\bar{g}_{\varphi 1} = 0 \qquad \bar{g}_{R1} = 0 \qquad \bar{g}_1 = 0 \quad [45]$$

in which it has been assumed that $\bar{S}_1 = -\bar{R}_a$, $\bar{M}_1 = \bar{M}_a$ (where $\bar{M}_a$ may be due to an overhang but is usually zero), $\bar{\alpha}_1 = -\bar{\varphi}$, and $\bar{y}_1 = 0$.

At the left end of the beam, which is now the base, the boundary conditions are $\bar{y}_b = \bar{M}_b = 0$, and Equations [41] and [39] then give

$$-\bar{g}_{\varphi b} \bar{\varphi} + \bar{g}_{Rb} \bar{R}_a = \bar{g}_b \quad [46]$$

$$-\bar{G}_{\varphi b}'\,\bar{\varphi} + \bar{G}_{Rb}'\,\bar{R}_a = \bar{G}_b' \quad \ldots\ldots [47]$$

From these two simultaneous equations in $\bar{\varphi}$ and $\bar{R}_a$ are obtained

$$\bar{\varphi} = \frac{\bar{g}_b\,\bar{G}_{Rb}' - \bar{G}_b'\,\bar{g}_{Rb}}{\bar{G}_{\varphi b}'\,\bar{g}_{Rb} - \bar{g}_{\varphi b}\,\bar{G}_{Rb}'} \quad \ldots\ldots [48]$$

$$\bar{R}_a = \frac{\bar{G}_{\varphi b}'\,\bar{g}_b - \bar{g}_{\varphi b}\,\bar{G}_b'}{\bar{G}_{\varphi b}'\,\bar{g}_{Rb} - \bar{g}_{\varphi b}\,\bar{G}_{Rb}'} \quad \ldots\ldots [49]$$

Examples

1 As an example of a free-free beam consider a three-cylinder reciprocating engine resting on flexible supports. The mass is all concentrated at the centers of the cylinders and the crank angle is 120 deg, so that the primary reciprocating inertia force at cylinder 2 is 120 deg behind cylinder 1 and cylinder 3 is 240 deg behind cylinder 1. The amplitude of the exciting force is $F_1 = 1000$ lb at $\omega = 100$ radians per sec which gives $\bar{F}_2 = 1000\,e^{-2\pi i/3} = 1000\,(\cos 120 - i \sin 120) = -500 - 866i$, and $\bar{F}_3 = 1000\,(\cos 240 - i \sin 240) = -500 + 836\,i$. The three concentrated masses are calculated to be $m_1 = 2$ lb-sec^2/in., $m_2 = 1.5$ lb-sec^2/in., and $m_3 = 3$ lb-sec^2/in., and the cast-iron frame of the engine may be considered equivalent to a uniform beam of $I = 10$ in.^{4} and $E = 15 \times 10^6$ psi. With a cylinder spacing of $l = 10$ in. this gives $v_M = (10/150) \times 10^{-6} = 0.00667 \times 10^{-6}$ lb^{-1} in.$^{-1}$, $v_F = u_M = (100/300) \times 10^{-6} = 0.3333 \times 10^{-6}$ lb^{-1}, and $u_F = (1000/900) \times 10^{-6} = 1.111 \times 10^{-6}$ in./lb. The damping in the structure is equivalent to a complex damping factor of $2b = 0.30$, giving $\cos 2b = 0.955$ and $\sin 2b = 0.2956$. The complex elastic coefficients become

$$\bar{u}_F \times 10^6 = \begin{cases} 1.011 \\ -0.3284 \end{cases} \qquad \bar{u}_M \times 10^6 = \begin{cases} 0.3183 \\ -0.09852 \end{cases}$$

$$\bar{v}_F \times 10^6 = \begin{cases} 0.3183 \\ -0.09852 \end{cases} \qquad \bar{v}_M \times 10^6 = \begin{cases} 0.06367 \\ -0.01971 \end{cases}$$

With these values for the fundamental quantities columns 1 to 14 of Table 1 are completed. Equations [32] and [33] then give

$$\bar{\varphi} = \begin{cases} -0.00295740 \\ 0.00189416 \end{cases} \qquad \bar{\delta} = \begin{cases} -0.0354599 \\ 0.0208169 \end{cases}$$

This means that at the front end of the engine the maximum deflection is $\delta = |\bar{\delta}| = 0.0411$ in. and the maximum slope is $\varphi = |\bar{\varphi}| = 0.00351$ radians $= 0.201$ deg. In column 15 the bending moments are worked out, and the fact that it is zero at station b is a check on the values for $\bar{\varphi}$ and $\bar{\delta}$. The maximum bending moment is $M_2 = |\bar{M}_2| = 5070$ in-lb. If the engine is bolted to a rigid foundation the vibrating motion of the engine and foundation together, considered as a free body, can easily be found by merely equating the elastic coefficients to zero and adding the mass of the foundation to that of the engine.

2 A 2-in-diam steel shaft carries four disks as shown in Fig. 3.

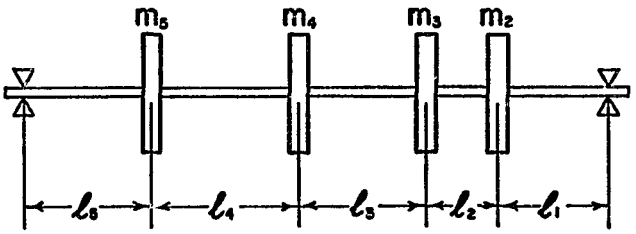

Fig. 3

The disks have slight eccentricities that all lie in the same plane but not necessarily to the same side of the axis of the shaft. The shaft rotates with an angular velocity $\omega = 316.228$ radians per sec, giving $\omega^2 = 100{,}000$, and all the fundamental data for the system are given in Table 2. The exciting forces are the inertia forces $m\omega^2\rho \cos \omega t$, where ρ is the eccentricity which may be either positive or negative, and it is desired to find the deflection curve for the shaft during rotation.

Solution: Since the deflections during rotation are identical to the amplitude of lateral vibration with exciting forces given by $m\omega^2\rho \cos \omega t$, where ω is the angular velocity of rotation, the method of this section may be used. In Table 3 the amplitudes coefficients are worked out, and Equations [48] and [49] then give

$$\varphi = 0.00134303 \text{ and } R_a = 145.760 \text{ lb}$$

TABLE 1

	1	2	3	4	5
n	$\frac{m\omega^2}{10^6}$	$\bar{v}_\varphi = (2) + l\,(3) + \bar{u}_M\,(4) + \bar{u}_F(5)$ for $n-1$	$\bar{f}_\varphi = (3) + \bar{v}_M\,(4) + \bar{v}_F\,(5)$ for $n-1$	$\bar{G}_\varphi' \times 10^{-6} = (4) + l\,(5)$ for $n-1$	$\bar{G}_\varphi \times 10^{-6} = (5)_{n-1} + (1)\,(2)$
1	0.02 0	0 0	1 0	0 0	0 0
2	0.015 0	10 0	1 0	0 0	0.15 0
3	0.03 0	20.1592 −0.04927	1.04775 −0.01478	1.5 0	0.754776 −0.001478

	15	6	7	8	9
n	$\bar{M} \times 10^{-6} = \bar{\varphi}\,(4) - \bar{\delta}\,(8) - (13)$	$\bar{v}_\delta = (6) + l\,(7) + \bar{u}_M(8) + \bar{u}_F\,(9)$ for $n-1$	$\bar{f}_\delta = (7) + \bar{v}_M(8) + \bar{v}_F\,(9)$ for $n-1$	$\bar{G}_\delta' \times 10^{-6} = (8) + l\,(9)$ for $n-1$	$\bar{G}_\delta \times 10^{-6} = (9)_{n-1} + (1)\,(6)$
1	0 0	1 0	0 0	0 0	0.02 0
2	−0.00290802 −0.00416338	1.02192 −0.006568	0.006366 −0.001970	0.2 0	0.0353183 −0.00009852
3	0 0	1.18060 −0.057681	0.030352 −0.009424	0.553183 −0.0009852	0.0708983 −0.00182895

	10	11	12	13	14
n	$\frac{\bar{F}}{10^6}$	$\bar{v} = (11) + l\,(12) + \bar{u}_M\,(13) + \bar{u}_F\,(14)$ for $n-1$	$\bar{f} = (12) + \bar{v}_M\,(13) + \bar{v}_F\,(14)$ for $n-1$	$\bar{G}' \times 10^{-6} = (13) + l\,(14)$ for $n-1$	$\bar{G} \times 10^{-6} = (14)_{n-1} + (10) + (1)(11)$
1	0.001 0	0 0	0 0	0 0	0.001 0
2	−0.0005 −0.000866	0.00106111 −0.0003284	0.0003183 −0.00009852	0.01 0	0.00051592 −0.000870926
3	−0.0005 0.000866	0.00708916 −0.0033925	0.0010334 −0.0006236	0.0151592 −0.0087926	0.00024659 −0.00010670

TABLE 2

n	m	l	$u_M \times 10^4$	$u_F \times 10^4$	$v_M \times 10^4$	$v_F \times 10^4$	$F \times 10^{-4}$
1	0	25	0.2720	1.105	0.01062	0.1330	0
2	0.25	15	0.04775	0.238	0.00637	0.0478	0.01
3	0.4	20	0.03480	0.569	0.00850	0.0852	−0.05
4	0.35	10	0.0212	0.0711	0.00425	0.0213	0.03
5	0.3	30	0.19130	1.9060	0.01275	0.1912	0.02
6	0						0

TABLE 3

	1	2	3	4	5
	$\frac{m\omega^2}{10^{-4}}$	$g_\varphi = (2) + l\,(3) + u_M\,(4) + u_F\,(5)$ for $n-1$	$f_\varphi = (3) + v_M\,(4) + v_F\,(5)$ for $n-1$	$G_\varphi' \times 10^{-4} = (4) + l\,(5)$ for $n-1$	$G_\varphi \times 10^{-4} = (5)_{n-1} + (1)\,(2)$
n					
1	0	0	1	0	0
2	2.5	25	1	0	62.5
3	4.0	54.875	3.9875	937.5	282.0
4	3.5	374.582	35.9826	6577.5	1593.04
5	3	987.116	97.8687	22507.9	4554.39
6	0	16909.5	1255.64	159139.6	4554.39

	15	6	7	8	9
	$y = \varphi\,(2) - R_a \times 10^{-4}\,(6) + (11)$	$g_R = (6) + l\,(7) + u_M\,(8) + u_F\,(9)$ for $n-1$	$f_R = (7) + v_M\,(8) + v_F\,(9)$ for $n-1$	$G_R' \times 10^{-4} = (8) + l\,(9)$ for $n-1$	$G_R \times 10^{-4} = (9)_{n-1} + (1)\,(6)$
n					
1	0	0	0	0	1
2	0.01747	1.1050	0.1330	25	3.7625
3	0.00044	5.1892	0.4721	81.4375	24.5194
4	−0.00689	35.4886	3.2534	571.8255	148.73
5	−0.00568	90.2200	8.8516	2059.13	420.890
6	0	1552.38	115.579	14685.8	420.890

	10	11	12	13	14
	$\frac{F}{10^4}$	$\gamma = (11) + l\,(12) + u_M\,(13) + u_F\,(14)$ for $n-1$	$f = (12) + v_M\,(13) + v_F\,(14)$ for $n-1$	$G' \times 10^{-4} = (13) + l\,(14)$ for $n-1$	$G \times 10^{-4} = (14)_{n-1} + (10) + (1)\,(11)$
n					
1	0	0	0	0	0
2	0.01	0	0	0	0.01
3	−0.05	0.00283	0.000478	0.15	−0.03048
4	0.03	0.0073168	−0.000843896	−0.4596	0.0251288
5	0.02	−0.00907910	−0.00226196	−0.208312	0.0178915
6	0	−0.0826867	−0.00149708	0.328433	0.0178915

With these values the deflections are worked out in column 15 of Table 3 and there appears to be a node very close to station 3.

It is interesting to compare the deflections y with the corresponding values of the eccentricity ρ, which values are easily found to be $\rho_2 = 0.004$ in., $\rho_3 = -0.0125$ in., $\rho_4 = 0.00857$ in., and $\rho_5 = 0.00667$ in. The centers of gravity of the disks then move in circles with radii $\rho_2 + y_2 = 0.02147$ in., $\rho_3 + y_3 = -0.01206$ in., $\rho_4 + y_4 = 0.00168$ in., and $\rho_5 + y_5 = 0.00099$ in., where a negative radius merely means a phase shift of 180 deg. If the stationary shaft were loaded with the static forces $m\omega^2(\rho + y)$ the deflection curve should be identical to that obtained in column 15 of Table 3, which fact may be used as a check on the calculations.

In the present example all the exciting forces were in phase and damping was neglected. If the eccentricities of the disks had been in different directions it would be necessary to use complex amplitudes and the deflections would then be out of phase with each other just as in Example 1.

END OF REFERENCE

REFERENCE

94

THOMSON, W. T.: MATRIX SOLUTION FOR THE VIBRATION OF NONUNIFORM BEAMS. J. APPL. MECH., VOL. 17, NO. 3, SEPT. 1950.

Matrix Solution for the Vibration of Nonuniform Beams

By W. T. THOMSON,[1] MADISON, WIS.

A matrix method for the determination of natural frequencies of any nonuniform beam is presented. It accomplishes the same task as that of Myklestad's tabular method with the added advantage of simplicity of formulation. Included is a procedure for the case where the nonuniform beam is represented by a series of uniform sections.

Nomenclature

The following nomenclature is used in the paper:

S_i = shear at position just to the left of station i
M_i = moment at i
θ_i = slope at i
y_i = deflection at i
α_{Si}, α_{Mi} = angular displacement of i with respect to a tangent at $i + 1$, due to unit shear and unit moment at i
d_{Si}, d_{Mi} = linear displacement of i with respect to a tangent at $i + 1$, due to unit shear and unit moment at i
m_i = mass at i
ω = frequency in radians/sec
l_i = length of section i
$\beta_i^4 = \dfrac{m_i\omega^2}{E_iI_i}$

Introduction

Myklestad's tabular method[2] is probably the most successful method of determining the natural frequencies of nonuniform beams. The method is used successfully in the vibration analysis of airplane wings and fuselages, bridges, critical speeds of shafts, and so forth. The uniqueness of the method lies in the fact that the shape of the vibration curve need not be assumed and higher modes of vibration are obtained readily.

Myklestad's method assumes the mass distribution to be represented by concentrated masses at several stations along the beam. The stiffness coefficients for each section of the beam between stations are determined from the actual stiffness curve of the beam by the area-moment principle (see Computation Procedure). The geometric and equilibrium equations are then transformed to a tabular computational scheme by somewhat tedious algebraic substitutions which can be avoided by the matrix method.

The Matrix Method

In problems of beam vibrations, the four quantities involved in the solution are the shear, moment, slope, and deflection at any point along the beam. In the matrix method, these quantities at any station $i + 1$ must be expressed in terms of corresponding quantities at the adjacent station i.

From the diagram of Fig. 1 the quantities of interest can be expressed by the following equations.[2,3]

$$S_{i+1} = S_i + m_{i+1}\omega^2 y_{i+1} \quad [1]$$

$$M_{i+1} = l_i S_i + M_i \quad [2]$$

$$\theta_{i+1} = -\alpha_{Si} S_i - \alpha_{Mi} M_i + \theta_i \quad [3]$$

$$y_{i+1} = -d_{Si} S_i - d_{Mi} M_i - l_i\theta_{i+1} + y_i \quad [4]$$

y_{i+1} and θ_{i+1} on the right side of Equations [1] and [4] are now replaced by quantities at i by substituting Equation [3] in [4], and then Equation [4] in [1]. Arranged in matrix form, these equations become

$$\begin{bmatrix} S_{i+1} \\ M_{i+1} \\ \theta_{i+1} \\ y_{i+1} \end{bmatrix} = \begin{bmatrix} 1 + m_{i+1}\omega^2(\alpha_{Si}l_i - d_{Si}) & m_{i+1}\omega^2(\alpha_{Mi}l_i - d_{Mi}) & -l_i m_{i+1}\omega^2 & m_{i+1}\omega^2 \\ l_i & 1 & 0 & 0 \\ -\alpha_{Si} & -\alpha_{Mi} & 1 & 0 \\ (\alpha_{Si}l_i - d_{Si}) & (\alpha_{Mi}l_i - d_{Mi}) & -l_i & 1 \end{bmatrix} \begin{bmatrix} S_i \\ M_i \\ \theta_i \\ y_i \end{bmatrix} \quad [5]$$

The shear, moment, slope, and deflection at $i + 1$ are now in terms of corresponding quantities at i, and the quantities in the square matrix are all in terms of mass, length, and stiffness of the section for any chosen frequency ω. Having determined the square matrix for each section, the quantities at i may be replaced by quantities at $i - 1$, etc., the final equation becoming

$$\begin{bmatrix} S_n \\ M_n \\ \theta_n \\ y_n \end{bmatrix} = \begin{bmatrix} A_{11} & A_{12} & A_{13} & A_{14} \\ A_{21} & A_{22} & A_{23} & A_{24} \\ A_{31} & A_{32} & A_{33} & A_{34} \\ A_{41} & A_{42} & A_{43} & A_{44} \end{bmatrix} \begin{bmatrix} S_0 \\ M_0 \\ \theta_0 \\ y_0 \end{bmatrix} \quad [6]$$

The square matrix of Equation [6] is obtained by multiplying all the square matrices of the form shown in Equation [5] where the ij-term is obtained by multiplying the ith row by the jth column.

Equation [6] holds for any boundary conditions, some of which are discussed in the section which follows.

Cantilever Beam. With the free and fixed ends at 0 and n, respectively, the boundary conditions become

$$S_0 = M_0 = \theta_n = y_n = 0$$

Substituting into Equation [6]

---

[1] Associate Professor of Mechanics, Department of Mechanics, College of Engineering, University of Wisconsin. Mem. ASME.

[2] "New Method of Calculating Natural Modes of Uncoupled Bending Vibrations," by N. O. Myklestad, *Journal of the Aeronautical Sciences*, vol. 11, 1944, pp. 153–162.

Contributed by the Applied Mechanics Division and presented at the Annual Meeting, New York, N. Y., November 27–December 2, 1949, of The American Society of Mechanical Engineers.

Discussion of this paper should be addressed to the Secretary, ASME, 29 West 39th Street, New York, N. Y., and will be accepted until October 10, 1950, for publication at a later date. Discussion received after the closing date will be returned.

Note: Statements and opinions advanced in papers are to be understood as individual expressions of their authors and not those of the Society. Paper No. 49—A-11.

[3] "Mechanical Vibrations," by W. T. Thomson, Prentice Hall, Inc New York, N. Y., 1948, p. 172.

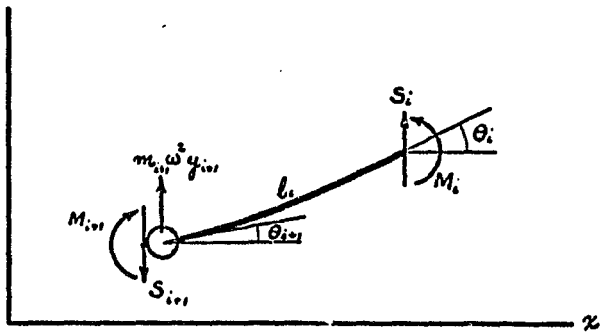

FIG. 1 FREE-BODY DIAGRAM OF SECTION i

$$A_{23}\theta_0 + A_{24}y_0 = 0$$
$$A_{43}\theta_0 + A_{44}y_0 = 0$$

Eliminating θ_0 and y_0, the frequency equation becomes

$$-\frac{A_{43}A_{24}}{A_{23}} + A_{44} = 0 \quad \ldots\ldots\ldots\ldots\ldots [7]$$

Beams With Hinged Ends. The boundary conditions are

$$M_0 = M_n = y_0 = y_n = 0$$

Thus from Equation [6]

$$A_{21}S_0 + A_{23}\theta_0 = 0$$
$$A_{41}S_0 + A_{43}\theta_0 = 0$$

and the frequency equation becomes

$$-\frac{A_{41}A_{23}}{A_{21}} + A_{43} = 0 \quad \ldots\ldots\ldots\ldots\ldots [8]$$

An Airplane Wing. Placing station 0 at the wing tip and the fuselage at n, the boundary conditions for the symmetric and antisymmetric modes become

(*a*) Symmetric modes

$$S_0 = M_0 = S_n = \theta_n = 0$$

From Equation [6]

$$A_{13}\theta_0 + A_{14}y_0 = 0$$
$$A_{33}\theta_0 + A_{34}y_0 = 0$$

and the frequency equation is

$$-\frac{A_{13}A_{34}}{A_{33}} + A_{14} = 0 \quad \ldots\ldots\ldots\ldots\ldots [9]$$

(*b*) Antisymmetric modes

$$S_0 = M_0 = M_n = y_n = 0$$

Equation [6] then yields

$$A_{23}\theta_0 + A_{24}y_0 = 0$$
$$A_{43}\theta_0 + A_{44}y_0 = 0$$

leading to the frequency equation

$$-\frac{A_{23}A_{44}}{A_{43}} + A_{24} = 0 \quad \ldots\ldots\ldots\ldots\ldots [10]$$

Equations [9] and [10] correspond to $S_n = 0$ and $M_n = 0$, i.e., the shaking force and shaking moment necessary to maintain vibration at resonance is zero.

COMPUTATION PROCEDURE

Numerical computations are carried out by first assuming a frequency ω and computing the elements of the square matrix, Equation [5], for each section of the beam. It should be noted that only the first row of Equation [5] depends on ω. Multiplying out the square matrices from n to 0, the matrix elements A_{ij} of Equation [6] are obtained and substituted into the frequency equation. Repeating with other values of ω, the natural frequencies are determined where the curve for the frequency equation passes through zero.

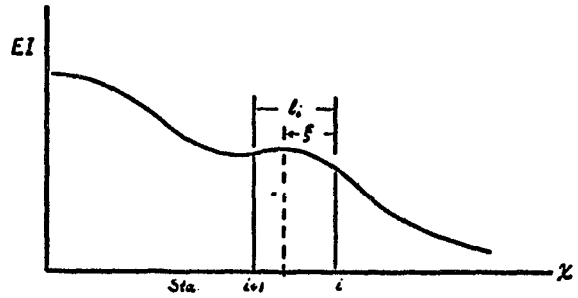

FIG. 2

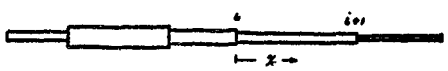

FIG. 3

Stiffness. The stiffness coefficients are determined by the area-moment principle. Referring to Fig. 2, they are

$$\alpha_{Mi} = \int_0^{l_i} \frac{d\xi}{EI}$$

$$\alpha_{Si} = d_{Mi} = \int_0^{l_i} \frac{\xi d\xi}{EI}$$

$$d_{Si} = \int_0^{l_i} \frac{\xi^2 d\xi}{EI}$$

If the EI-curve between stations is assumed to be a straight line these equations reduce to the expressions of Myklestad.[2]

Nonuniform Beam Represented by a Series of Uniform Sections. If the beam is represented by a series of uniform sections as in Fig. 3, the differential equation for the ith section becomes

$$\frac{d^4y}{dx^4} - \beta_i^4 y = 0$$

with the solution

$$y_{i+1} = \frac{1}{2}(\cosh \beta_i l_i + \cos \beta_i l_i)y_i + \frac{1}{2\beta_i}(\sinh \beta_i l_i + \sin \beta_i l_i)y_i'$$
$$+ \frac{1}{2\beta_i^2}(\cosh \beta_i l_i - \cos \beta_i l_i)y_i'' + \frac{1}{2\beta_i^3}(\sinh \beta_i l_i - \sin \beta_i l_i)y_i'''$$

Differentiating, the quantities at $i + 1$ can be expressed in terms of corresponding quantities at i by the matrix equation

$$\begin{bmatrix} y_{i+1} \\ y'_{i+1} \\ y''_{i+1} \\ y'''_{i+1} \end{bmatrix} = \begin{bmatrix} a & b/\beta_i & c/\beta_i^2 & d/\beta_i^3 \\ \beta_i^3 d & a & b/\beta_i & c/\beta_i^2 \\ \beta_i^2 c & \beta_i d & a & b/\beta_i \\ \beta_i^3 b & \beta_i^2 c & \beta_i d & a \end{bmatrix} \begin{bmatrix} y_i \\ y'_i \\ y''_i \\ y'''_i \end{bmatrix}$$

where

$$a = \frac{1}{2}(\cosh \beta_i l_i + \cos \beta_i l_i)$$

$$b = \frac{1}{2}(\sinh \beta_i l_i + \sin \beta_i l_i)$$

$$c = \frac{1}{2}(\cosh \beta_i l_i - \cos \beta_i l_i)$$

$$d = \frac{1}{2}(\sinh \beta_i l_i - \sin \beta_i l_i)$$

Thus the solution can be put in the form of Equation [6] with the corresponding frequency equations.

END OF REFERENCE

REFERENCE

95

SATCHWELL, D. L.: MORE ACCURATE BALANCING FOR HIGH-SPEED ROTORS. MACHINE DESIGN, VOL. 37, SEPT. 16, 1965.

COURTESY OF MACHINE DESIGN JOURNAL

COPY 1

8.2-0-0 DF.

More Accurate Balancing for

HIGH-SPEED ROTORS

A66-16433

When balanced components are assembled into high-speed rotors, subsequent balancing of the assembly can do more harm than good. It can distrurb component balance which leads to excessive shaft bending at operational speeds. This article shows how and when random selection of individually balanced components can provide better balanced rotors, particularly at high speed, than rotors balanced after assembly.

LEWIS RESEARCH CENTER
Aerospace Safety Research
and Data Institute
MAR 1 1972
CLEVELAND, OHIO

DAVID L. SATCHWELL
Sr. Development Engineer
Garrett Corp.
AiResearch Industrial Div., Los Angeles, Calif.

IN balancing high-speed rotating machinery, it is common practice to balance separately the individual components of a rotor assembly, and then to balance the rotor, when completely assembled, in a process called "assembly balancing". Assembly balancing may be sufficient when operational speeds are low. However, as operational speeds increase, unbalances in individual rotor members, created during assembly balancing, cause bending forces significantly larger than at (lower) balancing speed.

For example, consider a wheel in a high-speed rotor assembly, Fig. 1. After the wheel is balanced separately, it is fixed in place in the assembly where its un-normal faces cause a displacement e of its center of mass. ("Un-normal" faces are out of normal with respect to the axes of parts of which they are features.) The assembly is out of bal-

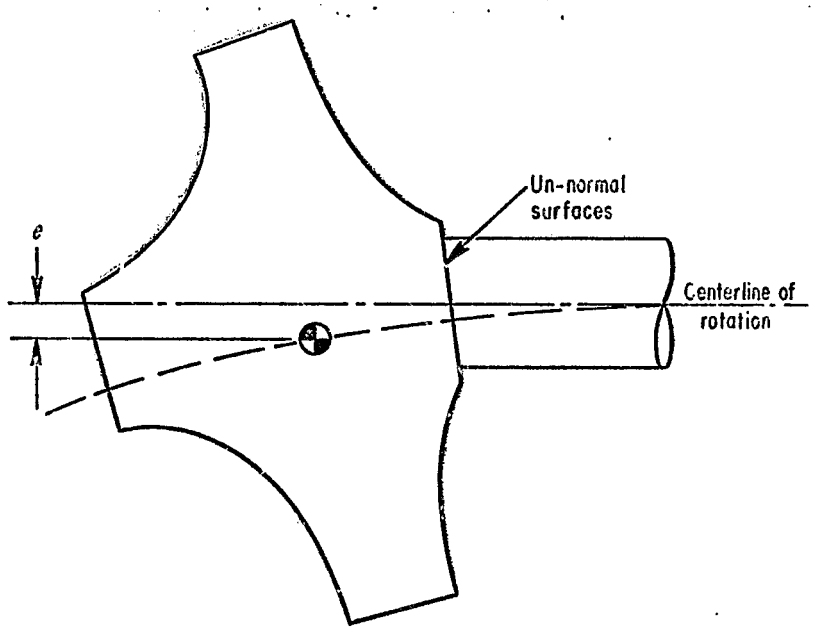

Fig.1- Effect of un-normal surfaces on rotor wheel.

LIBRARY COPY
MAR 20 1972
LEWIS RESEARCH CENTER

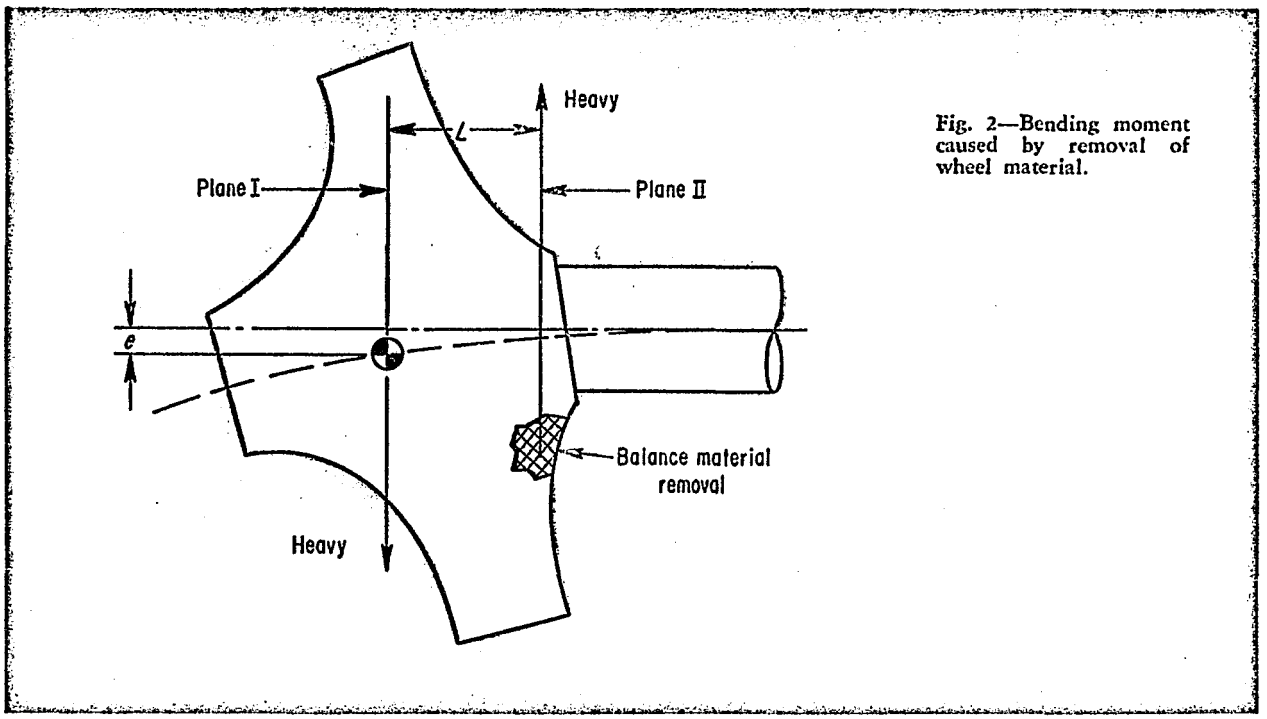

Fig. 2—Bending moment caused by removal of wheel material.

ance an amount equal to the weight of the wheel times the displacement *e* in a plane through the center of mass and normal to the rotational axis of the assembly, Plane I, Fig. 2.

To balance the assembly, material should be removed from the plane of the eccentric mass on the heavy side of the assembly—in this case, from Plane I in the wheel. But often it is difficult to remove material in the plane of the eccentric mass, so material is removed from some convenient plane—in this case, Plane II, Fig. 2. The assembly appears to be balanced statically when mounted on knife edges. It may even appear to be balanced dynamically at balancing machine speeds. But the wheel itself is heavy in two distinct planes (I and II) and forms a couple such that the bending moment equals the distance *L* between the unbalance planes times the weight of unbalance. At operating speed, this bending moment will cause bending of the shaft. This will cause the center of mass of the wheel to be displaced still farther from the centerline of rotation.

Much of this undesirable shaft bending can be eliminated by a simple method which involves component balancing alone. Individual components are balanced separately to good accuracy in the same configuration in which they will operate, they are selected arbitrarily and assembled squarely, and then no further balancing is done.

In practice, component balancing has been found to reduce not only the functional unbalance, but to reduce bearing-system energy loss. It allows interchangeability of parts and provides simplified parts handling. In tests, the level of unbalance that results from component balancing has been less, at operational speeds, than the unbalance that results when assembly balancing follows balancing of individual parts.

Differences between individual parts require variations in the method of component balancing and in the amount of remaining unbalance, but an example is given here to describe a typical method of balancing and to show how accurately parts must be balanced.

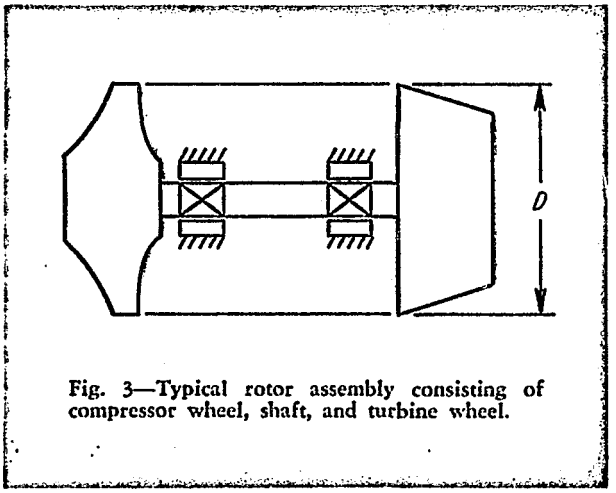

Fig. 3—Typical rotor assembly consisting of compressor wheel, shaft, and turbine wheel.

A double overhung rotor, Fig. 3, must operate at speeds through and beyond the first critical shaft speed. For this example, *D* is rotor diameter, in., and *N* is rotational speed, rpm. When DN^2 is greater than 2×10^{10}, component balancing is recommended. An increase in shaft stiffness, to place the first critical shaft resonance speed above the operational speed, will allow the increase of DN^2 value and still allow assembly balancing.

When parts are biplanar balanced (that is, balanced in each of two planes by separating those planes on a balancing machine), successful operation is obtained when center-of-gravity displacement from the centerline of rotation does not exceed 0.0002 in. in each plane.

END OF REFERENCE

REFERENCE

96

ESHLEMAN, R. L.: PROCEDURES FOR CALCULATING NATURAL FREQUENCIES OF SHAFTING SYSTEMS. IITRI-K6086, IIT RESEARCH INSTITUTE TECHNOLOGY CENTER, 1967. (AVAILABLE FROM DDC AS AD-811785.)

THIS REFERENCE HAS A LIMITED DISTRIBUTION AND MAY NOT BE REPRODUCED.

END OF REFERENCE

96

REFERENCE

97

BRUNNER, J. J.: ANALYSIS AND EXPERIMENTAL VERIFICATION OF AXIAL THRUST ON THE M-1 LIQUID OXYGEN TURBOPUMP. REP. AGC 8800-51, AEROJET GENERAL CORP. (NASA CR-54817), 1966.

8.2-0-0

N66-23563

NASA CR 54817
AGC 8800-51

COPY 1

N66-23563

ANALYSIS AND EXPERIMENTAL VERIFICATION OF AXIAL THRUST ON THE M-1 LIQUID OXYGEN TURBOPUMP

By

J. J. Brunner

CLEVELAND, OHIO

LIBRARY COPY

JUN 12 1966

LEWIS LIBRARY, NASA
CLEVELAND, OHIO

Prepared for

National Aeronautics and Space Administration

Contract NAS 3-2555

AEROJET-GENERAL CORPORATION

SACRAMENTO, CALIFORNIA

NOTICE

This report was prepared as an account of Government sponsored work. Neither the United States, nor the National Aeronautics and Space Administration (NASA), nor any person acting on behalf of NASA:

A.) Makes any warranty or representation, expressed or implied, with respect to the accuracy, completeness, or usefulness of the information contained in this report, or that the use of any information, apparatus, method or process disclosed in this report may not infringe privately owned rights, or

B.) Assumes any liabilities with respect to the use of, or for damages resulting from the use of any information, apparatus, method or process disclosed in this report.

As used above, "person acting on behalf of NASA" includes any employee or contractor of NASA, or employee of such contractor, to the extent that such employee or contractor of NASA, or employee of such contractor prepares, disseminates, or provides access to, any information pursuant to his employment or contract with NASA, or his employment with such contractor.

Requests for copies of this report should be referred to:

National Aeronautics and Space Administration
Office of Scientific and Technical Information
Attention: AFSS-A
Washington, D. C. 20546

NASA CR-54817
AGC 8800-51

TECHNOLOGY REPORT

ANALYSIS AND EXPERIMENTAL VERIFICATION OF AXIAL THRUST ON THE M-1 LIQUID OXYGEN TURBOPUMP

Prepared for

NATIONAL AERONAUTICS AND SPACE ADMINISTRATION

April 15, 1966

CONTRACT NAS 3-2555

Prepared by:

AEROJET-GENERAL CORPORATION
LIQUID ROCKET OPERATIONS
SACRAMENTO, CALIFORNIA

AUTHOR: J. J. Brunner

APPROVED: W. E. Campbell
Manager
M-1 Turbopump Project

Technical Management:

NASA LEWIS RESEARCH CENTER
CLEVELAND, OHIO

TECHNICAL MANAGER: M. M. Bailey
K. L. Baskin
C. F. Zalabak

APPROVED: W. F. Dankhoff
M-1 Project Manager

ABSTRACT

Axial thrust characteristics of two oxidizer turbopump assemblies are presented and evaluated over a representative range of speed, flow, and suction pressure. Estimates of thrust changes resulting from impeller backvane modifications and thrust verification tests conducted with a three-eighths size subscale pump are discussed. All tests were conducted with liquid nitrogen as the pumping fluid and either gaseous nitrogen or gas generator (H_2O_2) turbine drive. The turbopump consists of a centrifugal pump directly driven by a single-stage impulse turbine. The shaft is supported in rolling contact, propellant cooled bearings. The 27,000 shp turbopump has a nominal head generating capability of 3400 ft. The 28.5-in. unshrouded impeller produced a maximum thrust of approximately 70,000 lb towards suction. Net thrust was measured using calibrated sleeve-mounted strain gages.

during turbopump operation when high energy vibrations are available to reduce the apparent coefficients of friction in the system. Knowledge of the post-test no-load transmitter output and the shape of the calibration curve allowed construction of an accurate calibration curve for each test and the measured values of thrust were determined upon that basis.

C. THRUST CALCULATION

1. Pump Thrust

The net axial pump thrust is equal to the difference between the total integrated frontside pressure force and the total backside force. The force resulting from the change in momentum of the flow passing through the impeller eye is often neglected because of its relatively minor effect upon the net thrust. The momentum force acts away from suction and if considered in calculations it must be added to the pressure load of the frontside.

The momentum force can be expressed as follows:

$$F_{Mt} = \frac{\dot{w}}{g} V_{m,1} \qquad \text{Equation (4)}$$

At the typical data point presented in Table I F_{Mt} is 1680 lb. This amounts to 2.7% of the thrust calculated by pressure integration.

During the first test series, pump thrust was determined by graphical integration of pressure profiles. The products of pressure and radius for each pressure tap location (see Figure 13) were plotted versus radius and the points for the frontside and backside were fitted with a smooth curve as shown in Figure 14. The shaded differential area of the two profiles was then determined with a planimeter and the thrust was calculated by applying the proper scale factor to convert square inches into pounds.

In equation form

$$F_{AX,pump} = 2\pi \left[\int_{R_{SH}}^{R_2} P_{BV}(r)\ r\ dr - \int_{o}^{R_2} P_{HC}(r)\ r\ dr \right]$$

(Thrust towards suction is considered positive.)

Because speed levels were increased during later tests and thrust values approached appreciable magnitudes, the need for a more rapid method of thrust computations became necessary for post-test evaluation and/or making quick decisions prior to retesting. The method devised is based upon straight line point-to-point pressure profiles. Frontside and backside forces were determined by numerical integration of the area elements. The procedure is set up in tabulated form and presented in Table III.

$$P_{BV}(r)\ r\ dr \quad ; \quad P_{HC}(r)\ r\ dr$$

TABLE III (Sheet 1 of 2)

PUMP THRUST CALCULATION BY NUMERICAL INTEGRATION
OF STRAIGHT LINE PRESSURE PROFILES

INPUT DATA

Parameter	Units	Test No. 9A	Test No. 9C	Test No. 10B
Time	sec	4.43	~ 8,500	10.400 10.900
POS 6	psia	111.7	102.0	103.5
POHC 1	psia	110.0	106.6	136.5
POHC 2	psia	118.0	132.5	156.6
POHC 3	psia	150.5	198.5	255.5
POHC 4	psia	261.0	465.7	569.0
POHC 5	psia	343.4	675.0	810.0
POBV 1	psia	125.1	154.5	193.0
POBV 2	psia	136.0	190.2	239.7
POBV 3	psia	166.0	270.0	337.3
POBV 4	psia	228.7	407.0	507.4
POBV 5	psia	308.3	596.0	726.3
POBV 6	psia	353.4	708.5	858.0
RPF 0 = 9.75 x POS 6	lb/in.	1090	994	1010
RPF 1 = 9.75 x POHC 1	lb/in.	1072	1040	1330
RPF 2 = 10.21 x POHC 2	lb/in.	1210	1353	1599
RPF 3 = 11.04 x POHC 3	lb/in.	1665	2190	2820
RPF 4 = 12.46 x POHC 4	lb/in.	3255	5800	7090
RPF 5 = 14.25 x POHC 5	lb/in.	4890	9630	11530
RPB 0 = 2.5 x POBV 1	lb/in.	312.5	387	483
RPB 1 = 5.75 x POBV 1	lb/in.	720.0	890	1100
RPB 2 = 8 x POBV 2	lb/in.	1089	1520	1915
RPB 3 = 9.9 x POBV 3	lb/in.	1643	2670	3340
RPB 4 = 11.8 x POBV 4	lb/in.	2700	4800	5980
RPB 5 = 13.75 x POBV 5	lb/in.	4240	8200	10000
RPB 6 = 14.42 x POBV 6	lb/in.	5090	10200	12400

TABLE III (Sheet 2 of 2)

PUMP THRUST CALCULATION BY NUMERICAL INTEGRATION
OF STRAIGHT LINE PRESSURE PROFILES

PROCEDURE

Equation	Test No.	9A	9C	10B
	Time	4.43	~ 8.500	10.400 10.900
FRONTSIDE FORCE, FF				
1. 4.875 RPF 0		5320	4850	4920
2. 0.23 (RPF 1 + RPF 2)		526	550	673
3. 0.415 (RPF 2 + RPF 3)		1193	1470	1830
4. 0.71 (RPF 3 + RPF 4)		3500	5660	7040
5. 0.895 (RPF 4 + RPF 5)		7280	13800	16680
6. Σ (1 to 5)		17819	26330	31143
7. FF = $2\pi\Sigma$(1 to 5) (lb)		112000	165500	195800
BACKSIDE FORCE, FB				
8. 1.625 (RPB 0 + RPB 1)		1680	2075	2570
9. 1.125 (RPB 1 + RPB 2)		2035	2710	3390
10. 0.95 (RPB 2 + RPB 3)		2590	3980	5000
11. 0.95 (RPB 3 + RPB 4)		4125	7100	8850
12. 0.975 (RPB 4 + RPB 5)		6760	12690	15580
13. 0.25 [0.746 (RPB 6 - RPB 5) + 2RPB 5]		2275	4470	5290
14. Σ (8 to 13)		19,465	33025	40680
15. FB = $2\pi\Sigma$(8 to 13) (lb)		122200	207500	255500
16. F_{AX} = FB - FF (lb)		10200	42000	59700

SYMBOL	R IN.
$P_{o BV1}$	5.75
$P_{o BV2}$	8.00
$P_{o BV3}$	9.90
$P_{o BV4}$	11.80
$P_{o BV5}$	13.75
$P_{o BV6}$	14.42

SYMBOL	R IN.
$P_{o CH1}$	9.75
$P_{o CH2}$	10.21
$P_{o CH3}$	11.04
$P_{o CH4}$	12.46
$P_{o CH5}$	14.25
$P_{o CH6}$	15.12

BACKVANE INLET RADIUS : R_{BV4} = 8.00 IN FOR B/U #1
R_{BV4} = 10.00 IN FOR B/U #2

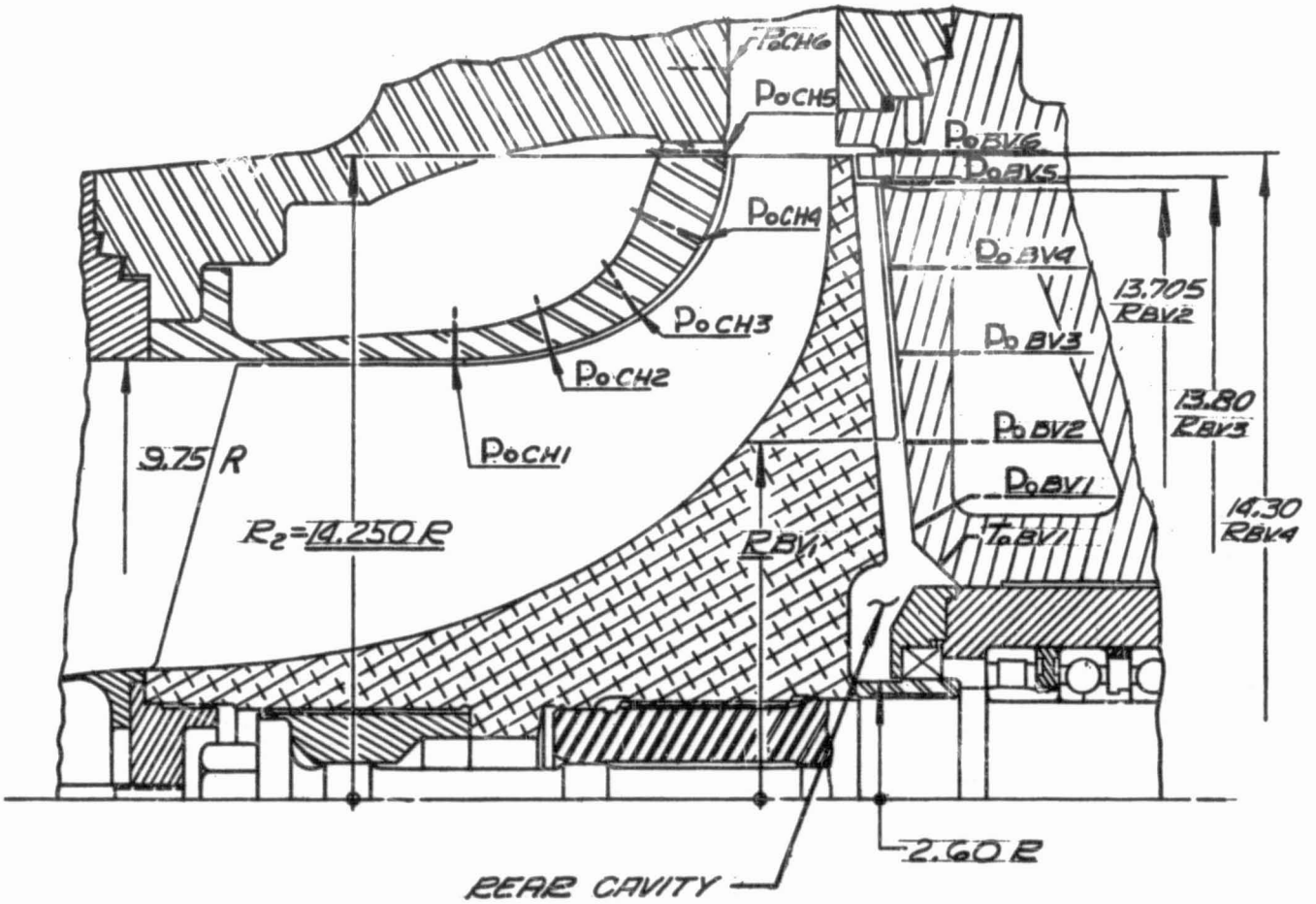

Figure 13

STATIC PRESSURE TAP LOCATION

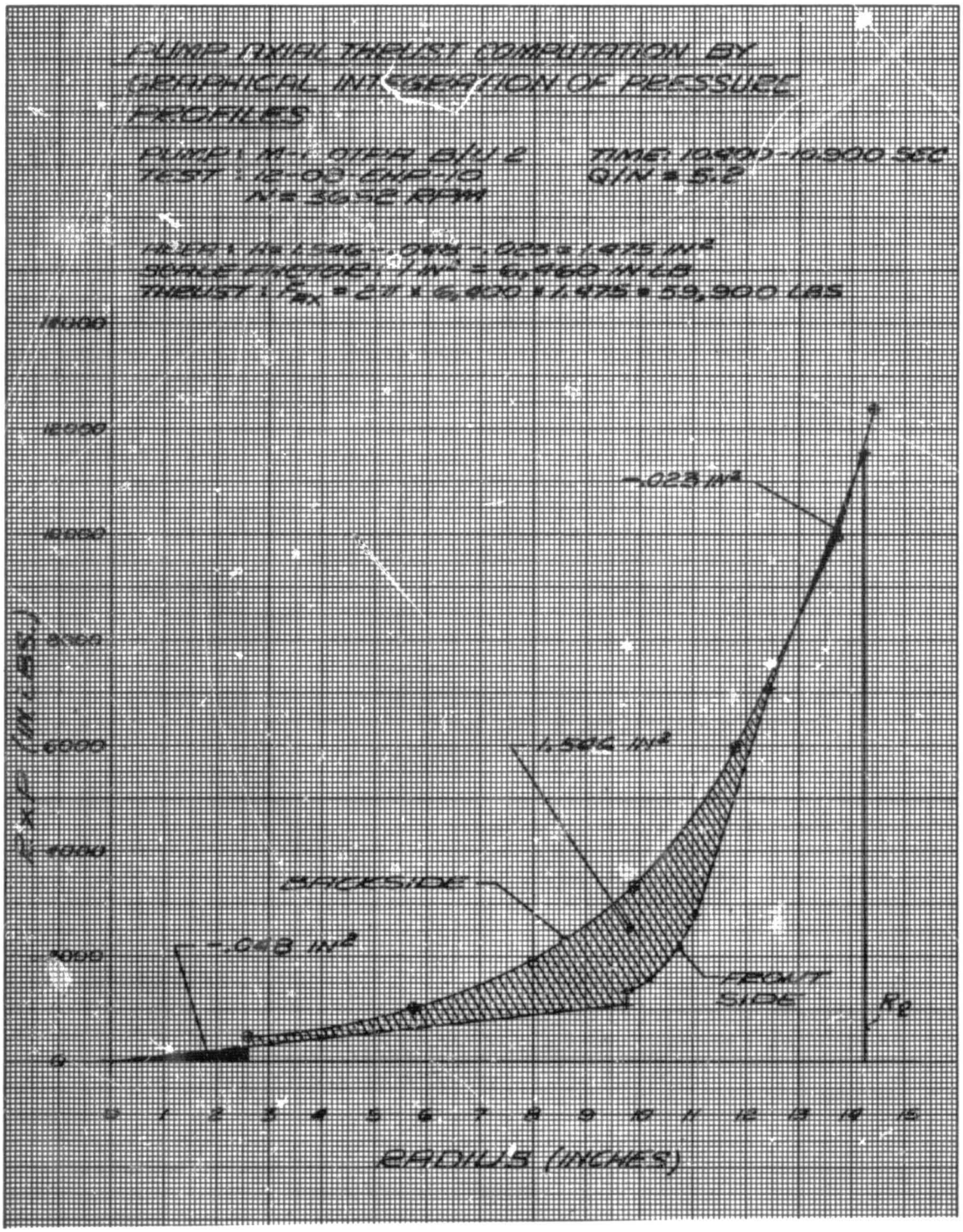

Figure 14

PUMP AXIAL THRUST COMPUTATION BY GRAPHICAL INTEGRATION OF PRESSURE PROFILES

A third and fourth method were derived from the above method to determine the effect of smoothed pressure profiles on axial thrust. Because curve fitting of the inflected frontside pressure profile by analytical methods is rather complex, the pressure force of the impeller frontside was calculated from straight line pressure profiles according to the second method. In the third method, the backside pressure force was calculated from a curve-fitted profile consisting of two parabolic sections for the vaned and vaneless sections. In the fourth method, the backvane pressure profile was based upon parabolic sections representing the theoretical hydraulic gradient between the measured pressures. All thrust data plotted was obtained from the computer program for data reduction. The computer method used for computation of axial thrust was based upon curve fitted frontside and backside pressure profiles. The procedures and results of the various methods are summarized in Table IV.

The lower magnitudes obtained with the third and fourth methods reflect the combination of curve fitted backside and straight line frontside pressure profiles. Results of the first, second, and fifth methods fall within 2.6% of their average value.

2. Turbine Thrust

Turbine thrust is dependent upon inlet pressure, turbine flow rate, pressure ratio, and the properties of the drive gas. In general, axial thrust of an impulse turbine is relatively low at design conditions. However, under off-design conditions, as in the case of this turbine operating with gaseous nitrogen drive, thrust magnitudes can be significant.

Turbine thrust was computed from pressure forces on both sides of the rotor disc. The thrust caused by gas friction in the rotor blades was neglected because it was in all cases smaller than 1000 lb for gas generator (hydrogen-oxygen) drive and smaller than 500 lb for gaseous nitrogen drive.

a. Thrust with Gaseous Nitrogen Turbine Drive

Test results from the first test series confirmed evidence of an expected rotor exit swirl, which caused large pressure losses in the exhaust cone and consequently, a lower than desired pressure ratio across the turbine. The swirl created a large pressure gradient behind the disc and thereby caused a thrust component downstream. This partly compensated for the decrease in turbine thrust caused by the decrease in pressure ratio. A similar exit swirl was experienced on the Model II scale turbine tested by NASA/LeRC. Test data indicated a large reduction in pressure towards the center of the exhaust side of the disc and a large thrust downstream. No provision was made during initial tests of the first series to measure such a pressure distribution; therefore, the representative pressure on the downstream side of the disc was determined from the pressure gradient measured on the scale turbine.

The pressure force acting on the inlet side of the rotor was estimated from the single pressure probe P_{GOTD} (Figure 15) in the hub area of the disc. Radial equilibrium was assumed at the nozzle exit and the nozzle discharge

TABLE IV

PUMP THRUST CALCULATIONS
COMPARISON OF METHODS AND RESULTS

PUMP: OTPA, B/U 2, N = 3652 rpm, Q/N = 5.2, P_S = 103.5 psia

Method	Procedure	Pressure Profiles	Frontside Force (lb)	Backside Force (lb)	Thrust[1] (lb)
1	Graphical Integration	Curve fitted frontside and backside.	--	--	59,900
2	Numerical Integration	Straight lines frontside and backside.	195,800	255,500	59,700
3	Numerical Integration	Straight lines on frontside, parabolic sections on backside.	195,800	252,847	57,047
4	Numerical Integration	Straight lines on frontside, curve fitted backside.	195,800	251,370	55,750
5	Computer Integration	Curve fitted frontside and backside.	--	--	61,500

(1) Momentum force neglected.
Pressure profiles to above data point are presented in Figure 14 in terms of radius times pressure.

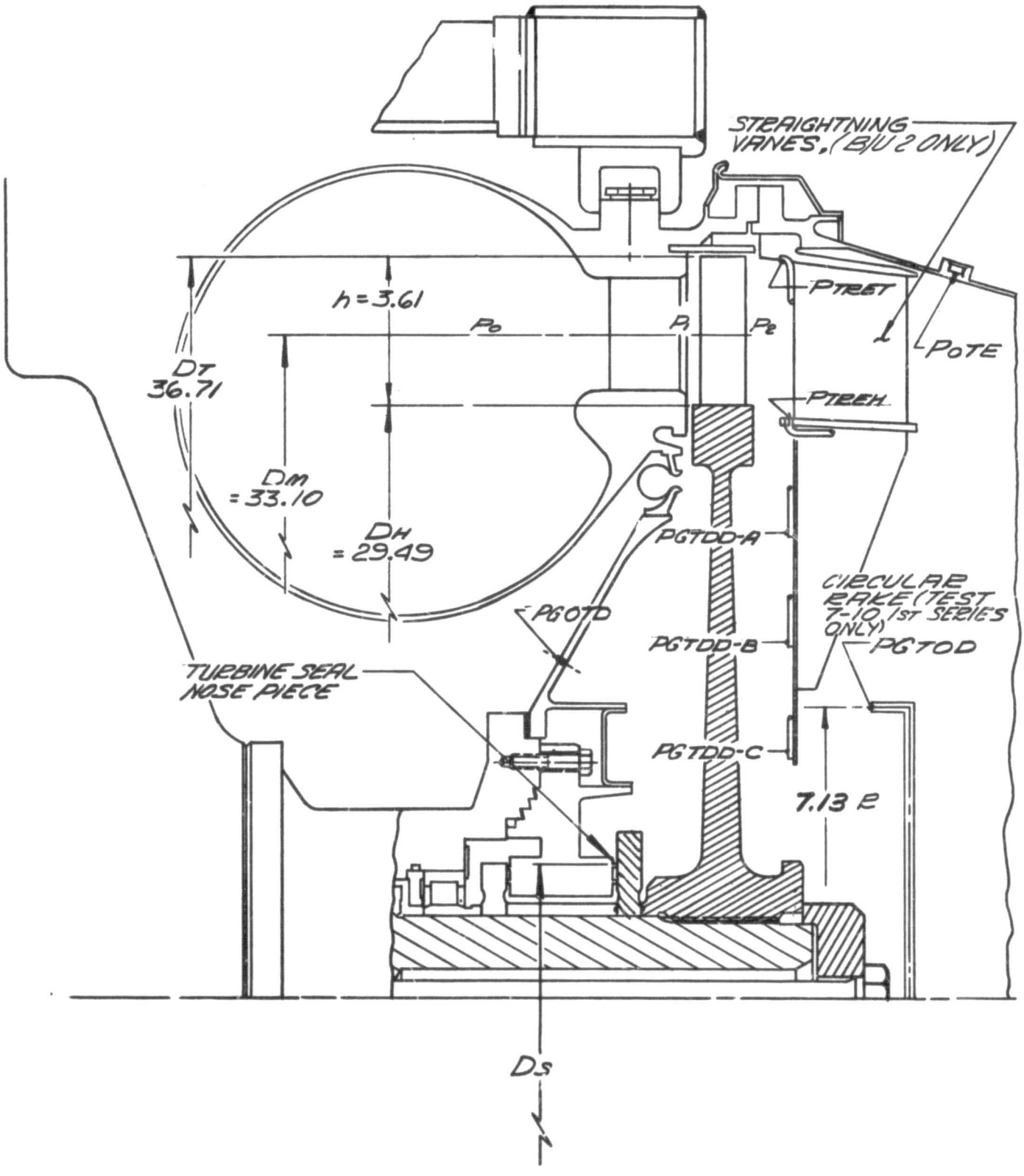

Figure 15

M-1 OTPA MODEL I TURBINE ROTOR MAIN DIMENSIONS AND INSTRUMENTATION LOCATIONS

pressure P_1 was calculated by multiplying the measured pressure P_{GOTD} with a radial equilibrium factor of 1.11. P_{GOTD} was considered representative of the mean pressure acting against the upstream side of the disc because the pressure tap is located close to the appropriate center of pressure.

The pressure force F_u towards the pump was determined for Test No. 1 through 6 of the first test series from the wall static pressure P_{OTE1} in the exhaust cone. The swirl effect was considered by multiplying the pressure force obtained by a correction factor K_{F_u} of 0.855 determined from NASA scale turbine data.

Pressure force towards the pump, uncorrected, $F_u' = A_2 P_{OTE1}$

Pressure force towards the pump, corrected for swirl effect, $F_u = K_{F_u} A_2 P_{OTE1}$

Pressure force towards the exhaust, $F_D = A_{1H} P_{1H} + A_B P_1$

Net turbine thrust = $F_u - F_D = K_{F_u} A_2 P_{OTE1} - A_{1H} P_{1H} - A_B P_1$

Whereby: (see Figure 15)

$A_{1H} = \pi/4 (D_H^2 - D_S^2) = 647.5$ in.^{2} (Hub area, inlet side)

$P_{1H} = P_{GOTD}$ (Rotor inlet pressure, hub, inlet side)

$P_1 = 1.11 P_{GOTD}$ (Rotor inlet pressure at the mean diameter)

$A_B = \pi D_{m\,h} = 375$ in.^{2} (blade area)

$A_2 = \pi/4 D_T^2 = 1060$ in.^{2} (Total area, exhaust side)

Test No. 7 through 10 of the first series were conducted with a circular rake installed on the exhaust side of the rotor hub with pressure pickups located on a 7.13-in. radius.

A linear pressure profile was assumed through P_{OTE}, and P_{GTOD} and the pressure force towards suction was then determined by integration of the profile.

$$F_{u2} = 2\pi \int rp(r)\, dr$$

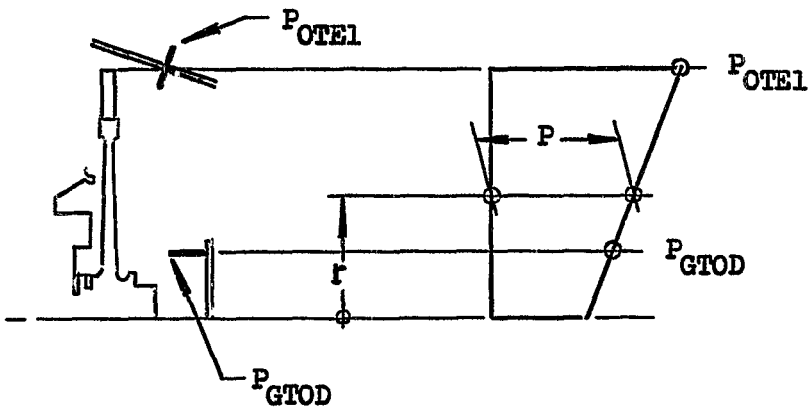

The pressure force towards suction for a specific case (Test 6.0-04-EHP-9) determined by the different methods described above compare as follows:

Pressure force towards suction, uncorrected.	F_u'	= 67,300 lb
Pressure force towards suction, corrected for swirl effect on the basis of NASA data.	F_{u_1}	= 57,500 lb
Pressure force towards suction, based upon circular rake data and wall static exhaust pressure.	F_{u_2}	= 54,000 lb

The correction factor K_{F_u}, applicable to this data was verified from the above results

$$K_{F_u} = \frac{F_{u_2}}{F_u'} = 0.805$$

When straightening vanes were installed on Buildup No. 2 to eliminate the exit swirl, additional static taps were provided to measure the pressure distribution on the downstream side of the disc. With these new instrumentation stations, the computation of the pressure force towards suction was greatly simplified and yielded more representative magnitudes. The force was calculated as follows:

$$F_u = A_{2H}\, P_{GTDD_{mean}} + 1/2\, A_B\, (P_{TRET} + P_{TREH})$$

Whereby: $A_{2H} = \pi/4\ D_{H_2}^2$ and $A_B = \pi\, D_m\, h$

Test results from the second test series showed no significant variation of the three pressure measurements P_{GTDD} behind the turbine disc. This indicated that the swirl was eliminated. Thus, the mean value of the three pressures P_{GTDD} was used for calculating turbine thrust. Turbine pressures are listed for a typical data point in Table I.

b. Thrust with Gas Generator (Hydrogen-Oxygen) Turbine Drive

The turbine operated with a pressure ratio of approximately 2.4 with gas generator drive and the small exhaust orifice (240-in.^{2}). A comparison of the mean exhaust pressure with the calculated inlet pressure based upon radial equilibrium indicated impulse conditions $P_1 = P_2$. Under those circumstances, thrust was directly computed from the pressure forces acting upon the turbine disc. Thrust resulting from some negative reaction at the disc and some positive reaction at the blade tip partly cancelled each other so that their difference was considered insignificant. The thrust equation was reduced to:

$$F_{AX} = A_{2H} P_{GTDD_{mean}} - A_{1H} P_{GOTD}$$

Under impulse conditions, thrust was always positive or directed towards the pump because of the effect of radial equilibrium upon the upstream side of the rotor.

Pressure ratios of approximately 3.5 were obtained with the large exhaust orifice of 314-in.^{2}. The rotor operated with some reaction because of the high pressure ratio. New radial equilibrium factors were calculated for the upstream side of the disc for gas generator Tests No. 13 and 14. A correction factor was obtained that was nearly identical to the one obtained for gaseous nitrogen turbine drive (1.11). Axial thrust was computed similar to the method derived for gaseous nitrogen drive.

$$F_{AX} = A_{2H} P_{GTOD_{mean}} + \frac{1}{2} A_B (P_{TRET} + P_{TREH}) - P_{GOTD} (A_{1H} + KA_B)$$

Whereby:

K = radial equilibrium factor.

3. Thrust Predictions

a. Initial Estimates

The thrust direction predicted for the interim impeller was towards the pump. However, for gaseous nitrogen turbine drive, a downward turbine thrust direction was expected. The net thrust of these two estimates was predicted to be towards the pump, even though downward thrust was possible at low pump speeds. A bearing orientation to give load sharing towards the pump was then chosen for the following reasons.

(1) Net thrust was predicted in a direction towards pump suction.

(2) Poor performance of the backvane diffuser would result in increased thrust towards pump suction.

(3) Tests with gas generator drive as intended for this unit would have no turbine thrust, and, hence, net thrust toward the pump. At these higher speeds, thrust prediction errors would be better accommodated with the bearing orientation chosen.

b. The Ideal Pump Thrust

Pump thrust predictions for full speed operation (with gas generator turbine drive) were based upon thrust values established from low speed tests (with gaseous nitrogen turbine drive) and on the following assumptions:

(1) Affinity laws hold true (static headrise varies directly with speed squared; efficiency remains constant).

(2) Fluid Temperature remains constant (no change in friction losses).

(3) Fluid density is not dependent upon pressure.

(4) Reynolds number effects are negligible.

The idealized thrust was calculated from front and backside pressure forces derived as follows:

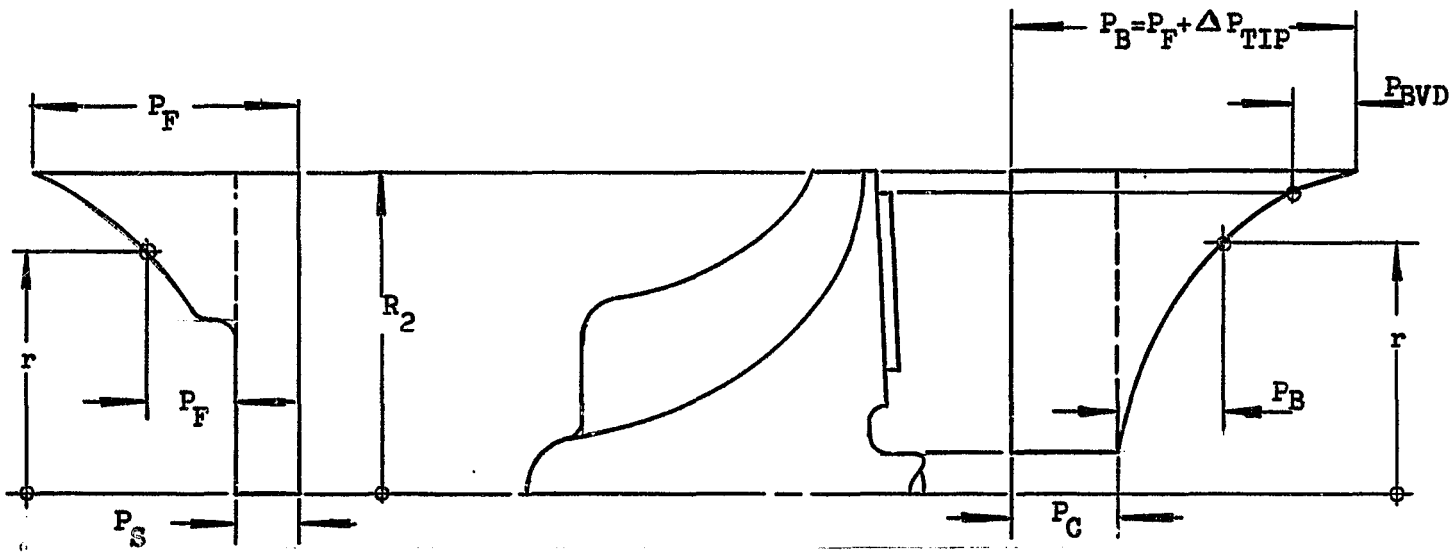

ΔP_{TIP} = Pressure Gradient Across Impeller Discharge = $(P_B - P_F)$

Frontside pressure force:

$$F_F = F_s + \Delta F_F = P_s A_F + K_{fF} N^2 \int_0^{R_2} \psi_F(r)\, r\, dr$$

Backside pressure force:

$$F_B = F_c + \Delta F_B = P_C A_B + K_{fB} N^2 \int_{R_{SH}}^{R_2} \psi_B(r)\, r\, dr$$

As explained in Section III.A. the cavity pressure P_c is equal to the suction pressure, plus the pressure rise of the frontside, plus the pressure difference at the discharge, and minus the pressure rise of the backside.

$$P_c = P_s + \Delta P_F + \Delta P_{TIP} - \Delta P_B$$

The pressure difference at the discharge $\Delta P_{TIP} = P_{OBV6} - P_{OHC5}$ is assumed to stay proportional with N^2.

Thus:

$$P_C = P_s + K_{p,F}\, \psi_F N^2 + K_{p,TIP}\, \psi_{TIP}\, N^2 - K_{p,B}\, \psi_B\, N^2$$

$$= P_s + N^2 (K_{p,F}\, \psi_F + K_{p,TIP}\, \psi_{TIP} - K_{p,B}\, \psi_B)$$

Substituting this expression into the equation for the backside pressure force:

$$F_B = \left[P_s + N^2 (K_{p,F}\, \psi_F + K_{p,TIP}\, \psi_{TIP} - K_{p,B}\, \psi_B) \right] A_B$$

$$+ K_{f,B}\, N^2 \int_{R_{SH}}^{R_2} \psi_B(r)\, r\, dr$$

Neglecting the momentum force

$$F_{AX} = F_B - F_F$$

$$= A_B \left[P_s + N^2 \left(K_{p,F} \dot{\psi}_F + K_{p,TIP} \dot{\psi}_{TIP} - K_{p,B} \dot{\psi}_B \right) \right.$$

$$+ K_{f,B} N^2 \int_{R_{SH}}^{R_2} \psi_B (r) \, r \, dr - P_s A_F - K_{f,F} N^2 \int_o^{R_2} \psi_F (r) \, r \, dr$$

$$= P_s (A_B - A_F) + N^2 \left[A_B \left(K_{p,F} \dot{\psi}_F + K_{p,TIP} \dot{\psi}_{TIP} - K_{p,B} \dot{\psi}_B \right) \right.$$

$$\left. + K_{f,B} \int_{R_{SH}}^{R_2} \psi_B (r) \, r \, dr - K_{f,F} \int_o^{R_2} \psi_F (r) \, r \, dr \right]$$

Equation (5)

This equation shows that if $A_B = A_F$, the thrust is directly proportional to N^2 and suction pressure P_s cancels out. The thrust component caused by suction pressure F_{SH} can be expressed in terms of the shaft area $A_{SH} = A_F - A_B$.

Thus: $F_{SH} = P_s (A_F - A_B) = P_s A_{SH}$.

Thrust, F_{SH}, can be removed from Equation (5) so that the resulting expression becomes directly a function of speed squared.

$$F_{AX} + F_{SH} = F_{AX} + P_s A_{SH} = f (N^2)$$

Knowing F_{SH} and a thrust value at low speed, the ideal thrust at full speed can be calculated from the following relationship:

$$\frac{F_{AX2} + P_s A_{SH}}{F_{AX1} + P_s A_{SH}} = \left[\frac{N_2}{N_1} \right]^2$$

and

$$F_{AX2} = \left[\frac{N_2}{N_1} \right]^2 (F_{AX1} + P_s A_{SH}) - P_s A_{SH}$$

Equation (6)

The ideal pump thrust based upon actual measured or estimated values (F_{AX1}) at the prespin speed of 2100 rpm is plotted versus speed for 85%, 100%, and 120% of design Q/N on Figure 16. The characteristics shown are exponential curves $F_{AX} = N^n$ with (n) approaching 2 at high magnitudes of F_{AX}. This reflects the effect of the thrust component caused by suction pressure $P_S A_{SH}$, which becomes negligible at very high thrust values.

The scale factors to relate ideal thrust at full speed from thrust data at prespin (N_1 = 2100 rpm, N_2 = 3635 rpm, and constant suction pressure P_s = 115 psia) are:

$$F_{AX2} \text{ at } 85\% \text{ DES } Q/N = F_{AX1} \times \left[\frac{N_2}{N_1}\right]^{2.135} \qquad (F_{AX1} = 17{,}500 \text{ lb})$$

$$F_{AX2} \text{ at } 100\% \text{ DES } Q/N = F_{AX1} \times \left[\frac{N_2}{N_1}\right]^{2.17} \qquad (F_{AX1} = 14{,}000 \text{ lb})$$

$$F_{AX2} \text{ at } 120\% \text{ DES } Q/N = F_{AX1} \times \left[\frac{N_2}{N_1}\right]^{2.22} \qquad (F_{AX1} = 12{,}000 \text{ lb})$$

4. Accuracy

When calculating pump thrust, a very accurate analytical procedure could yeild an axial thrust value far from the value obtained experimentally. For example, if an axial balance of 30,000 lb towards the impeller eye is desired and a frontside force of approximately 230,000 lb is underestimated by as little as 3% and a backside force of approximately 260,000 lb is overestimated by 3%, the measured thrust could be off by 50% of the analytical estimate. This can also apply to turbine thrust, although pressure forces on the rotor are of much smaller magnitudes; however, they are acting upon larger areas.

The above is an example that perfect agreement between predicted and measured thrust is strictly incidental, especially if pressure distributions or thrust values at different operating points are unknown. For large pumps, where margins between nominal and maximum safe operating thrust loads result in lower percentages than with smaller size pumps, it becomes necessary to conduct a partial speed test to verify estimates before attempting full speed operation.

Variations in the magnitudes of pressure forces could result from circumferential pressure variations. As illustrated in Figures 17, 18, and 19, the pressures $P_{OHC\ 6\ A\ -\ F}$ along the impeller periphery show a variation of approximately $\pm$ 10%. However, it was believed that the thrust calculated from pressure forces is representative because the tip pressures $P_{OHC\ 5}$ and $P_{OBV\ 6}$ were measured in areas of average circumferential pressure (Figures 17 through 19).

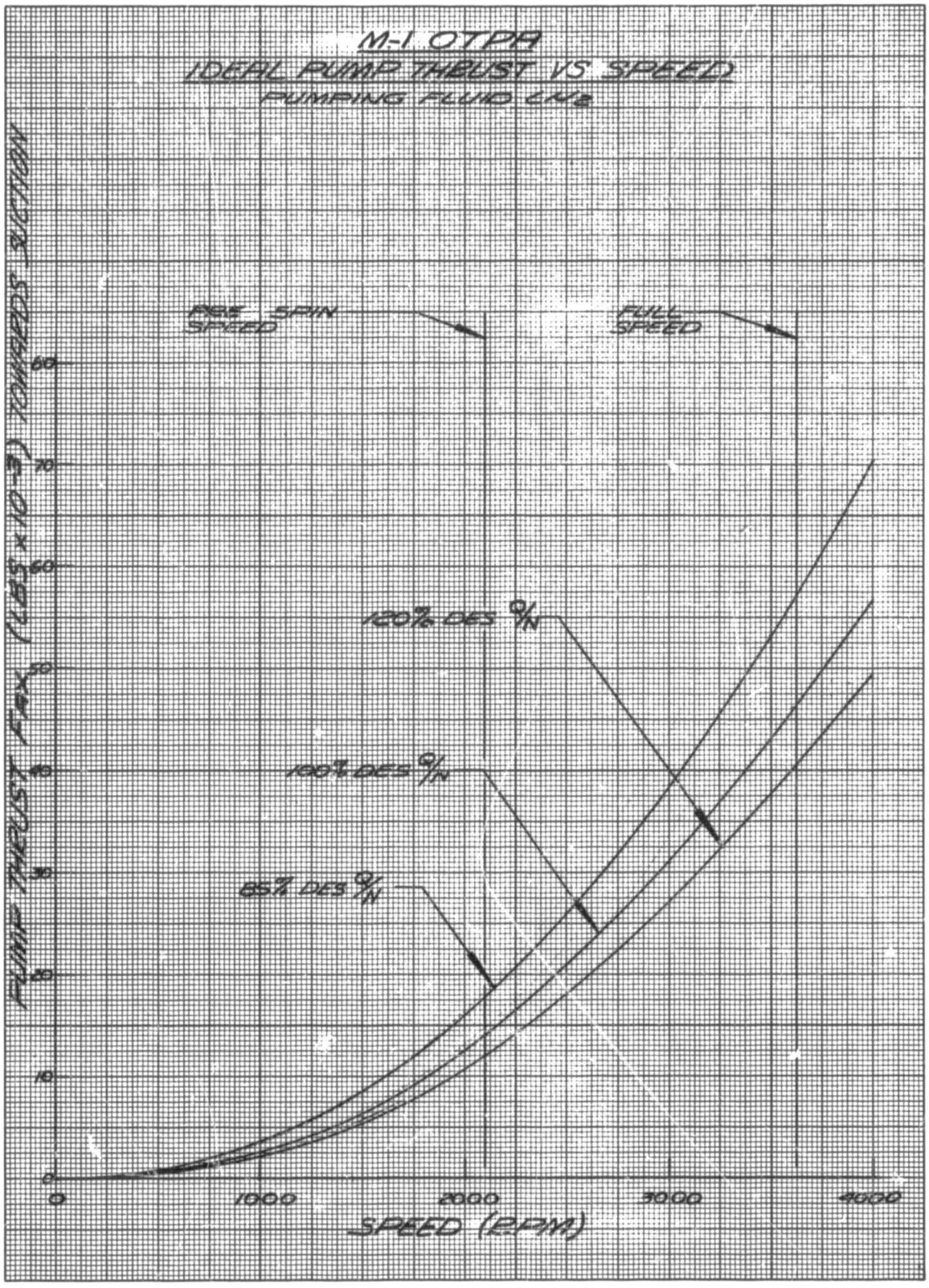

Figure 16

M-1 OTPA IDEAL PUMP THRUST VS SPEED

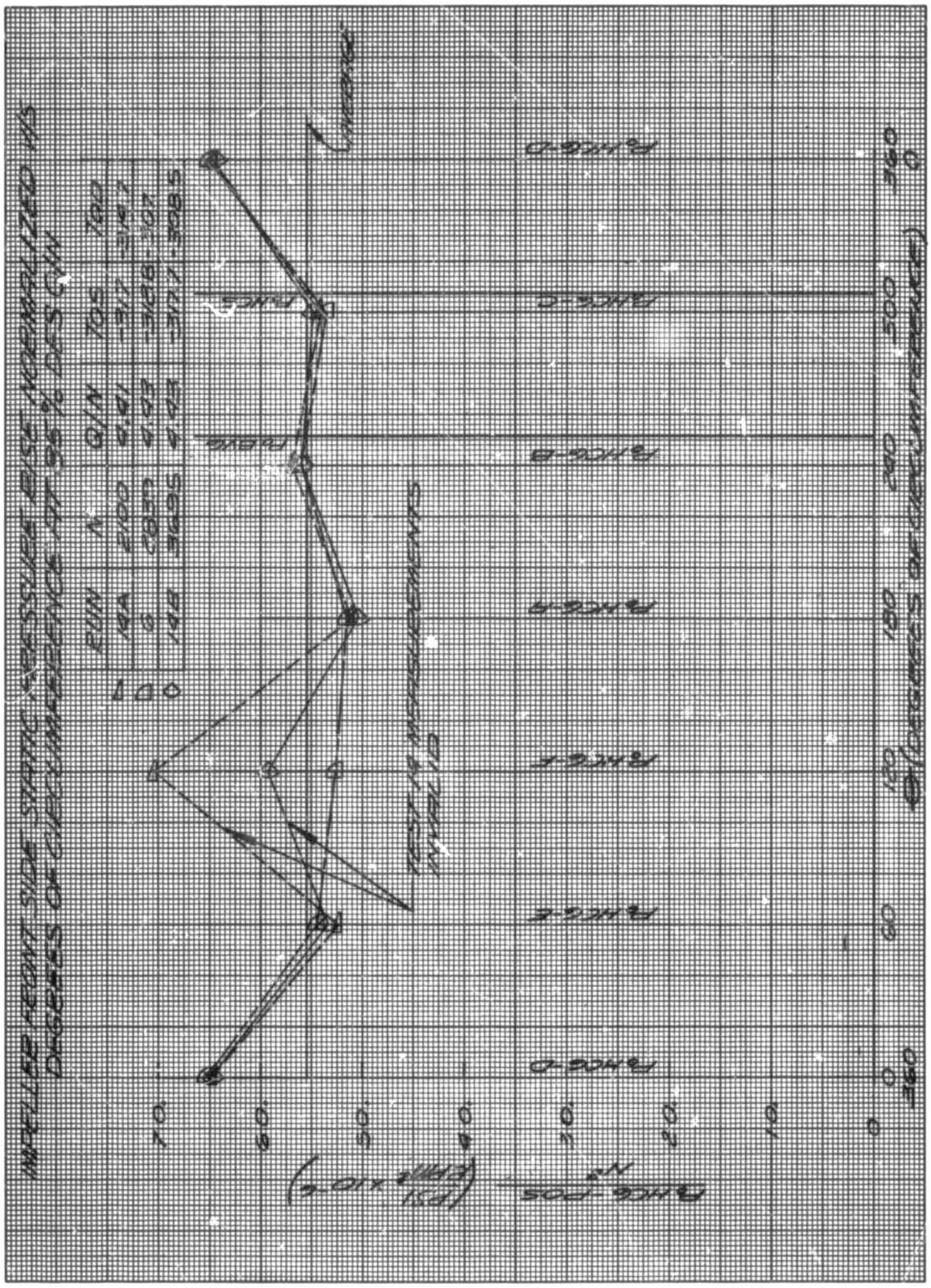

Figure 17

IMPELLER FRONTSIDE NORMAL STATIC PRESSURE RISE VS
DEGREES OF CIRCUMFERENCE AT 85% OF DESIGN Q/N

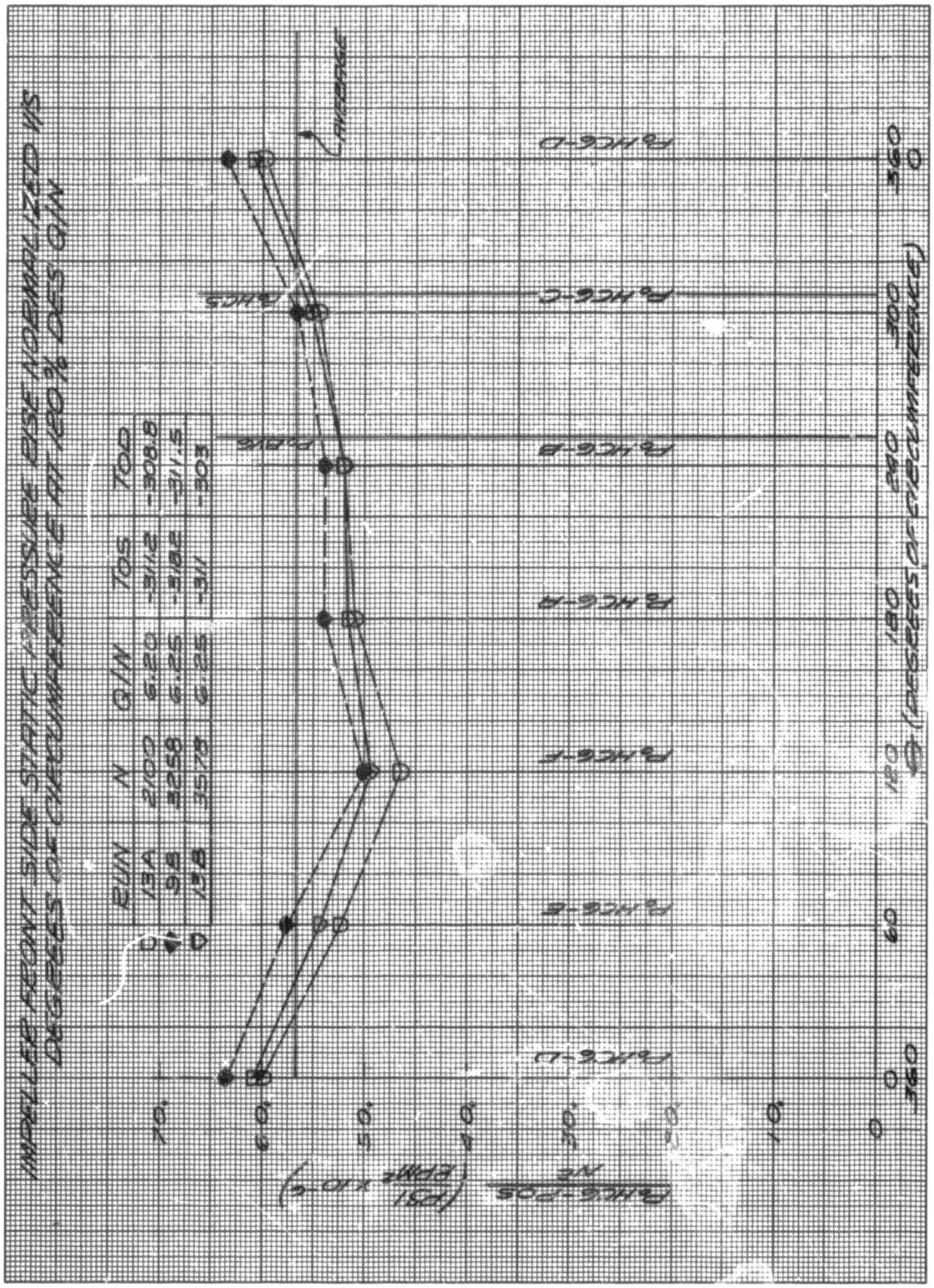

Figure 18

IMPELLER FRONTSIDE STATIC PRESSURE RISE NORMALIZED vs DEGREES OF CIRCUMFERENCE AT 120% OF DESIGN Q/N

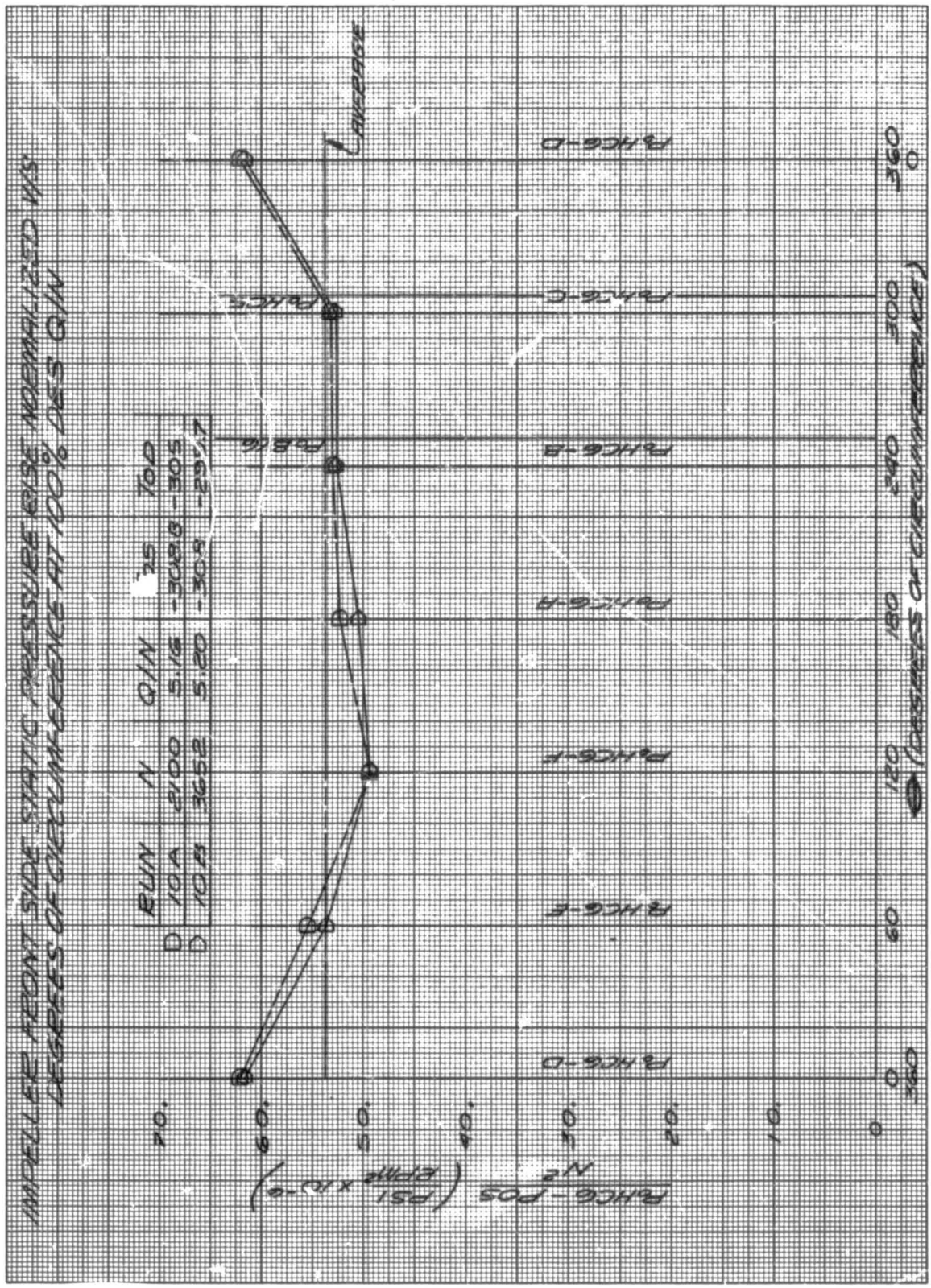
IMPELLER FRONT SIDE STATIC PRESSURE RISE NORMALIZED WITH
RUN 101 102 103 104 105
N/D 0.5 0.6 0.7 0.8 0.9
Q/N 100 85 70 55 40
Pt/ρ(N/60)²D² - COS (2πf/N x (θ-α)) vs DEGREES OF CIRCUMFERENCE (θ)
Pt/ρ(N/60)²D² - COS (2πf/N x (θ-α))
Pt/ρ(N/60)²D²
Pt/ρ(N/60)²D²
Pt/ρ(N/60)²D²

END OF REFERENCE

97

REFERENCE

98

PINKEL, I. I.; HARTMANN, M. J.; HAUSER, C. H.; MILLER, M. J.; RUGGERI, R. S.; AND SOLTIS, R. F.: PUMP TECHNOLOGY. SELECTED TECHNOLOGY FOR THE PETROLEUM INDUSTRY. NASA SP-5053, 1965.

NASA SP-5053

CONFERENCE ON SELECTED TECHNOLOGY for the PETROLEUM INDUSTRY

LEWIS RESEARCH CENTER

CLEVELAND, OHIO

DECEMBER 8-9, 1965

NATIONAL AERONAUTICS AND SPACE ADMINISTRATION

NASA SP-5053

CONFERENCE ON SELECTED TECHNOLOGY for the PETROLEUM INDUSTRY

Lewis Research Center
Cleveland, Ohio
December 8-9, 1965

Scientific and Technical Information Division 1966
NATIONAL AERONAUTICS AND SPACE ADMINISTRATION
Washington, D.C.

CONTENTS

		PAGE
	FOREWORD	*iii*
	INTRODUCTION Walter T. Olson	1
I.	*COMBUSTION* Richard S. Brokaw, Frank E. Belles, Bruce J. Clark, and Frank J. Zeleznik	5
II.	*SOME DEVELOPMENTS IN AEROSPACE HEAT TRANSFER* Robert Siegel, Robert W. Graham, Vernon H. Gray, John R. Howell, and William L. Jones	25
III.	*HYDRODYNAMICS OF LIQUID SURFACES* Edward W. Otto	45
IV.	*SURFACE PHYSICS AND CHEMISTRY* Robert A. Lad	67
V.	*MAGNETICS AND SUPERCONDUCTIVITY* Edmund E. Callaghan	73
VI.	*PUMP TECHNOLOGY* I. Irving Pinkel, Melvin J. Hartmann, Cavour H. Hauser, Max J. Miller, Robert S. Ruggeri, and Richard F. Soltis	81
VII.	*LUBRICANTS, BEARINGS, AND SEALS* Edmond E. Bisson, William J. Anderson, Robert L. Johnson, Erwin V. Zaretsky, and Lawrence P. Ludwig	103
VIII.	*STORAGE AND HANDLING OF CRYOGENIC FLUIDS* Donald L. Nored, Glen Hennings, Donald H. Sinclair, Gordon T. Smith, George R. Smolak, and Andrew J. Stofan	125
IX.	*TECHNOLOGY UTILIZATION* Breene M. Kerr, Melvin S. Day, George J. Howick, Richard L. Lesher, and Howard L. Timms	155
	AUTHORS	*167*

VI Pump Technology

I. Irving Pinkel, Melvin J. Hartmann, Cavour H. Hauser, Max J. Miller, Robert S. Ruggeri, and Richard F. Soltis
Lewis Research Center

Attention is focused in this discussion on some of the technological advances in turbomachinery research and development which the petroleum industry, with its widely diverse technology, might find useful. The research and development on turbomachinery being conducted by the NASA Lewis Research Center and supported by this center through contract to industry and universities include effort on such components as compressors, turbines, and pumps and on materials used in their construction. Because of the large total effort involved, the following discussion is limited to only a selected portion of the overall effort in order that the work can be described in sufficient detail to reveal its scope and quality.

The subject chosen is that of high-performance pumps and the role of cavitation in defining pump performance limits. NASA interest in this subject stems from the need to minimize the structural weight of space vehicles to provide a corresponding increase in payload capability. The dependence of payload capability on pump performance can be illustrated by considering the principal components of a typical upper stage of a space vehicle shown in figure VI–1. The largest components by far are the propellant tanks, the wall thickness of which is determined primarily by tank pressure, although other factors are involved. For space vehicles in which the tank wall thickness is determined by propellant pressure, lower tank pressures allow lower vehicle weights.

In order to prevent propellant boiling, the tank pressure must be greater than the vapor pressure of the propellant. Propellants that have a high vapor pressure, for example, liquid hydrogen, are often carried at a tank pressure only a few pounds per square inch greater than the vapor pressure. Under these conditions, the propellant is in a near-boiling state.

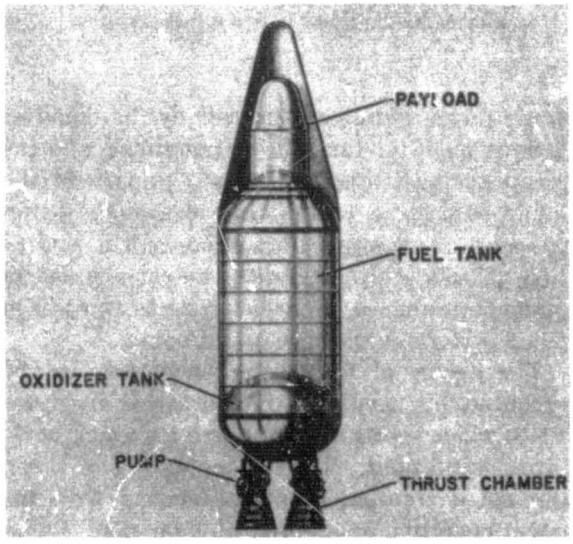

Figure VI–1.—Liquid-fueled rocket vehicle.

The difficulty in pumping a near-boiling liquid can be described by use of a simplified diagram of a rocket stage, as illustrated in figure VI–2, which shows one propellant tank, the thrust chamber, and the pump which delivers the propellant from the tank to the thrust chamber. A portion of a typical centrifugal pump rotor (and blading) often used in liquid rocket systems is also shown. The propellant tank is assumed to contain a near-boiling liquid. The

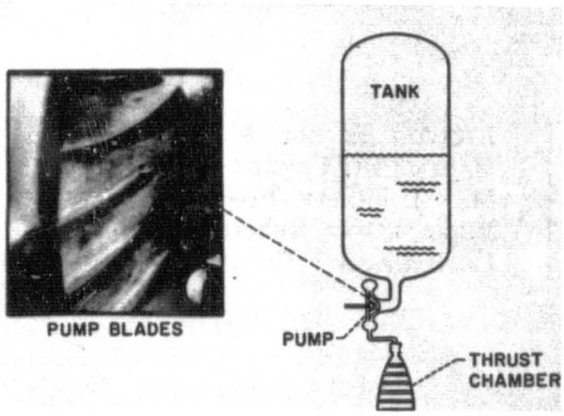

FIGURE VI–2.—Pump in liquid rocket system.

static pressure drop experienced by the liquid as it flows from the tank to the pump and into the pump passages usually causes a portion of the liquid to flash to vapor (boil) within the pump passages. This vapor formation, called cavitation, if sufficiently extensive, can cause a loss in pump performance. In rocket systems, this loss in pump performance can be catastrophic.

The degree of flow disturbance that can be produced by cavitation is illustrated in figure VI–3, which shows a pump operating under cavitating conditions. The photograph was taken through a transparent pump housing with the pump operating at a speed of 3000 rpm. Pump cavitation can be categorized into two basic types according to location, blade-tip cavitation and blade-surface cavitation. The first type is vapor formation that occurs because of flow through the clearance region between the blade tip and the pump casing (fig. VI–3). In general, blade-tip cavitation does not appreciably affect pump performance; however, blade-surface cavitation can degrade pump performance severely. The blade-surface cavitation shown in figure VI–3 disturbed the flow in the carefully designed flow passages of the pump sufficiently to degrade pump performance severely.

The requirement that rocket propellants be pumped under the conditions of lowest possible tank pressure (i. e., in a near-boiling state) can be discussed with reference to the Centaur space vehicle shown in figure VI–4. Centaur will be used as an upper stage on an Atlas booster to lift Surveyor to the Moon. Surveyor is designed to soft-land an instrumented package on the Moon to sample and to analyze the surface of the Moon and to make other measurements in preparation for manned landing a few years hence. The Centaur vehicle is 10 feet in diameter and about 16 feet long (cylindrical portion only) and uses liquid hydrogen as fuel. The fuel tank pressure is only 2.0 pounds per square inch greater than the vapor pressure of liquid hydrogen. This additional pressure above the vapor pressure is provided by the injection of helium gas at the top of the tank. Helium is used because it does not liquefy at the very low temperature of liquid hydrogen (about −423° F). The helium is carried separately in heavy high-pressure spheres at the bottom of the vehicle (fig. VI–4). If the tank pressure had to be raised an additional 2.0 pounds per square inch to avoid pump cavitation and assure good liquid-hydrogen pump performance, the extra thickness of tank wall required to support the added pressure and the additional helium plus the helium system would raise the structural and system weight several hundred pounds. This extra weight would reduce the payload by an equal amount and make it too low for the Surveyor mission.

The discussion presented herein, therefore, deals with the problems of pumping near-boiling liquids with modern high-performance pumps.

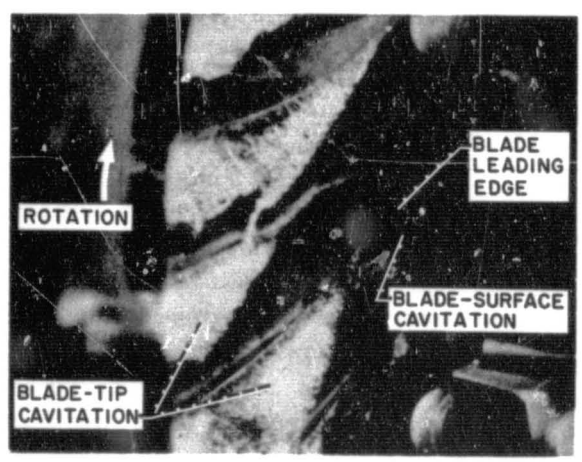

FIGURE VI–3.—Pump cavitation.

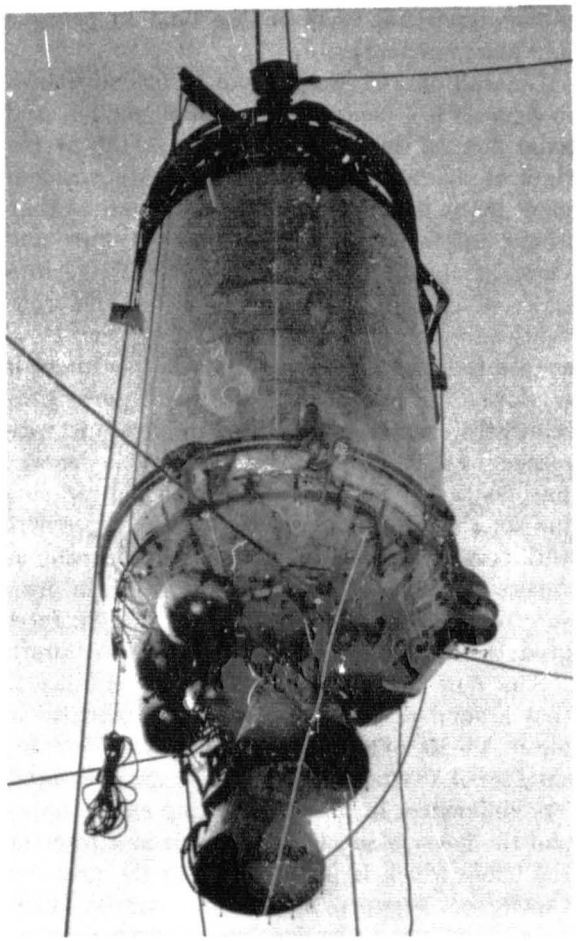

FIGURE VI–4.—Centaur space vehicle.

Subjects covered include the limiting effects of cavitation on pump performance, the approach to pump design that helps to overcome some of these limitations, methods for predicting pump performance under cavitating conditions for various liquids, cavitation damage, and pump flow instabilities with and without cavitation.

TYPES OF ROCKET PUMP

One of the two principal types of pumps used for handling rocket propellants is the centrifugal pump shown in figure VI–5. Basically, the centrifugal pump consists simply of a set of blades mounted on a rotating hub or rotor which is supported by a shaft and bearings and is generally driven by a turbine. Pumping work is done on the fluid by the rotor as the fluid flows radially outward through passages between the blading. The fluid is collected in a volute and delivered at high pressure.

Within limits, the work done on the fluid and thus the pressure at the discharge can be increased by increasing the rotational speed of the pump. If the desired pressure is higher than that which can be achieved by a single rotor, it is necessary to pass the propellant through additional rotor stages. Staging centrifugal pump rotors, however, requires elaborate ducting and an increased number of bearing supports, and heavy pumps result. A sketch of a typical multistage centrifugal pump is presented in figure VI–6. Thus, when the required discharge pressure is greater than can be attained by use of a single

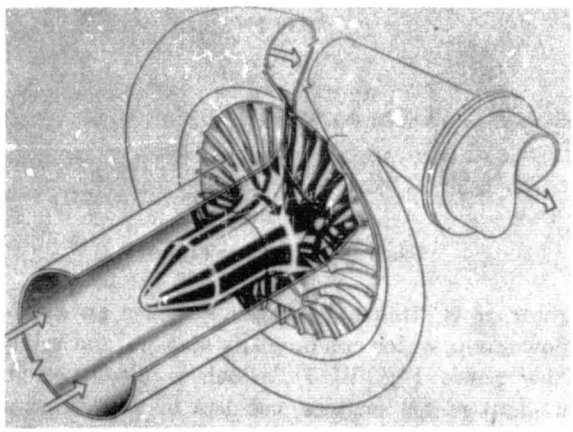

FIGURE VI–5.—Centrifugal pump.

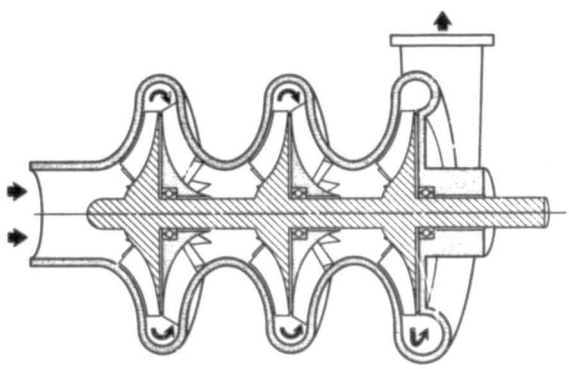

FIGURE VI–6.—Multistage centrifugal pump.

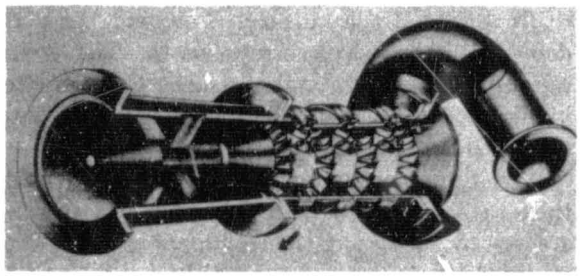

FIGURE VI–7.—Multistage axial-flow pump.

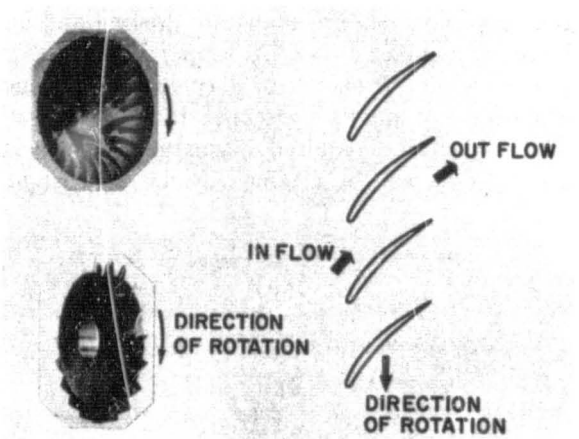

FIGURE VI–8.—Pump blades.

rotor, it is often advantageous to use an axial-flow pump, which can be easily staged. The axial-flow pump (fig. VI–7), which is also used in modern rocket engines, consists of a succession of rows of rotor blades and stator blades. The rotor blades, all of which are mounted on the same rotating drum, do work on the fluid being pumped, and the stator blades turn the flow into the desired direction for the next rotor stage. Although the pressure rise per stage of the axial pump is less than that of a centrifugal stage, the ease with which successive stages can be added to the axial-flow type allows a more compact high-pressure pump.

PUMP-FLOW ANALYSIS

Before the discussion of the manner in which cavitation degrades pump performance and the approach to design that is used to achieve a high degree of cavitation tolerance in pumps, it may be appropriate to review the manner in which pumps do useful work on the fluid to produce flow and pressure rise.

Rotors from the two types of pumps are shown in figure VI–8, centrifugal in the upper left and axial flow in the lower left. The sketch at the right of the figure represents a two-dimensional view of the blades for either type pump as they would appear unwrapped from the hub and viewed from the blade tips. The similarity to a series of aircraft wings can be noted. On conventional aircraft (fig. VI–9), the wing is so shaped that the air flowing immediately under it is slowed to less than flight speed and, consequently, experiences a rise in pressure with respect to that of the approaching air, as denoted by plus signs. The air adjacent to the top surface of the wing experiences a drop in pressure with respect to that of the approaching air, as denoted by minus signs. This difference in pressure on the upper and the lower wing surfaces produces the lift force that supports the aircraft.

The flow around pump blades is similar to that around a wing, as shown schematically in figure VI–10. The pressure variation along the surfaces of a typical pump blade is also presented. The differences in pressure existing on the upper and the lower blade surfaces result in a force on the blade which is proportional to the area between the pressure distribution curves. Conversely, an equal reaction force is exerted on the fluid by the pump blade, and, because the blade moves in the direction of force, work is done on the fluid. This work produces flow and a pressure rise across the blade row.

It is important to note that smooth flow must exist over the entire blade surface to produce the desirable large pressure differences. On the high-pressure side (lower surface), smooth flow can

FIGURE VI–9.—Wing analogy.

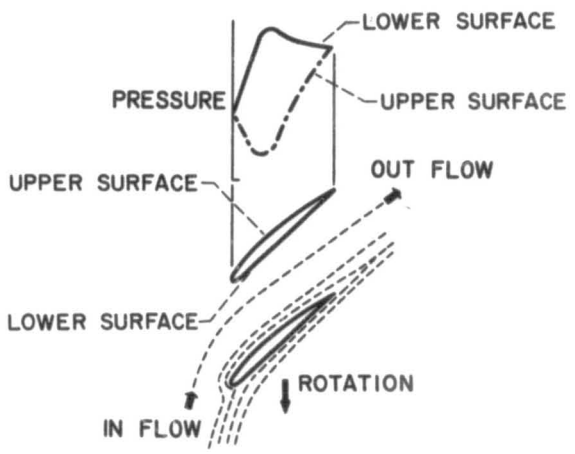

FIGURE VI–10.—Typical pump blade pressure distribution.

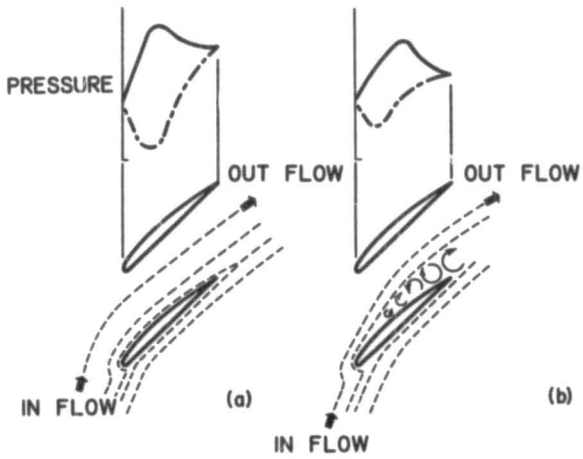

(a) Normal flow. (b) Separated flow.

FIGURE VI–11.—Pump blade pressure distribution for normal and separated flow.

be easily maintained, because this surface faces the oncoming flow which must stream around it. Maintaining smooth flow over the upper surface of the blade, however, is a critical matter. The flow adheres to the upper surface under the influence of low pressures, or suction, which exist on this surface. The flow over the upper surface of a pump blade can be easily disturbed and may detach, or separate, from the surface, as illustrated in figure VI–11. The desired suction on the upper surface is then partly lost over that portion of the blade where separation occurs. This loss is reflected by a change in the pressure distribution diagram. A comparison of the pressure distribution diagrams of figure VI–11 for smooth flow and separated flow shows that the area within the diagram is always less with flow separation. Because the suction on the top surface of the blade accounts for about half the force on the blade, partial loss of this suction reduces the blade force; hence, the pump work capability of the blade decreases. This decrease in pump work appears as a lowered pressure rise across the pump. Because flow separation disturbs the entire flow within the pump passage, the pressure distribution on the pressure surface of the blade is also affected, as noted in figure VI–11.

PUMPING NEAR-BOILING FLUIDS

As mentioned previously, the presence of extensive amounts of vapor (cavitation) in the pump limits pump performance. This problem of cavitation and its effect on pump performance becomes increasingly more critical as the fluid entering the pump approaches the near-boiling condition. In order to illustrate the effects of cavitation on flow conditions about pump blades, blade pressure distributions with and without cavitation are compared in figure VI–12. The

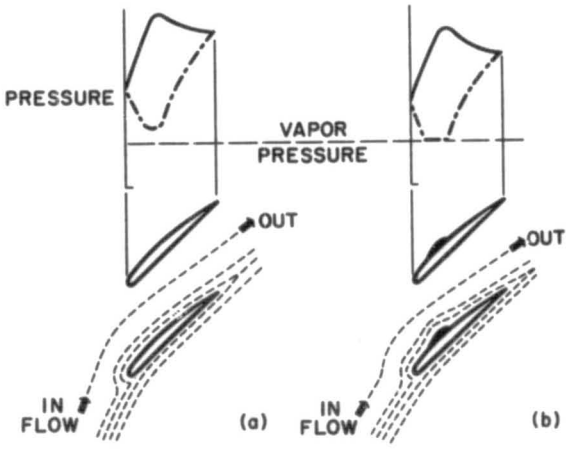

(a) Noncavitating. (b) Limited cavitation.

FIGURE VI–12.—Blade pressure distributions with and without cavitation.

horizontal dashed line represents the vapor pressure of the incoming fluid. If the inlet pressure is sufficiently high, the blade surface pressures are everywhere greater than the liquid vapor pressure. However, if inlet pressure is reduced sufficiently, local pressures on the suction surface of the blade are reduced to the fluid vapor pressure, and cavitation occurs. Because the pressure on the suction surface of the blade cannot be less than the vapor pressure of the liquid immediately adjacent to the vapor cavity, a loss in blade force results. This loss corresponds to the reduced area of the pressure distribution diagram, as illustrated by the right-hand diagram of figure VI–12.

As inlet pressure is further reduced, the cavitated region on the suction surface of the blade grows until the flow adjacent to the vapor cavity can no longer follow the sharp curvature at the downstream end of the vapor cavity, as illustrated by the right-hand diagram of figure VI–13. As noted in the figure, the flow separates from the blade, and a large part of the highly desirable suction is lost. The presence of cavitation causes a decrease in blade pressures on the lower surface because of disturbed flow in the channel between blades, as was the case for separated flow without cavitation (fig. VI–11). The greatly reduced area of the pressure diagram is

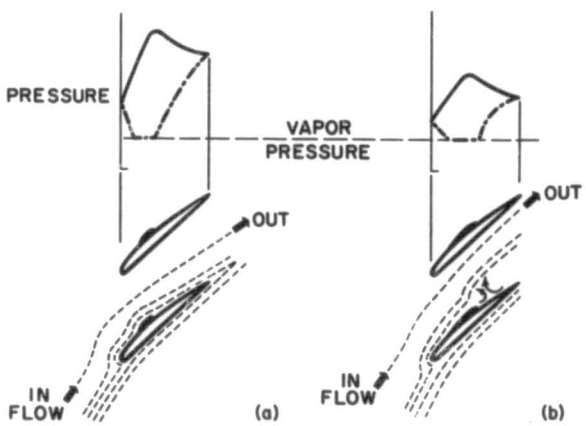

(a) Limited cavitation. (b) Severe cavitation.

FIGURE VI–13.—Blade pressure distributions with two degrees of cavitation.

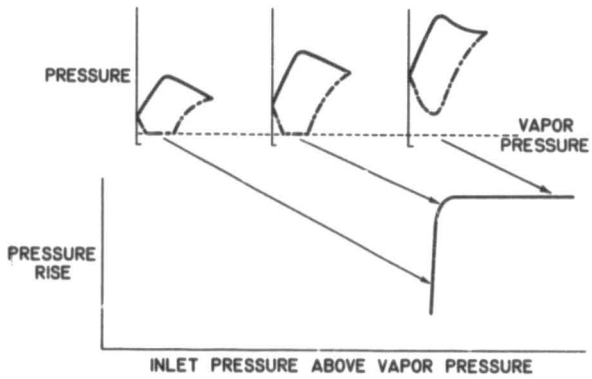

FIGURE VI–14.—Pump performance.

indicative of the large decrease in pumping work that can occur with extensive cavitation.

For fixed operating conditions, the difference between the pressure of the fluid entering the pump and the liquid vapor pressure is the factor which determines whether cavitation will occur in a given pump. The pressure rise provided by a high-performance pump for various values of inlet pressure above the vapor pressure is presented in figure VI–14. If the margin of inlet pressure above vapor pressure is adequate, cavitation is avoided and the desired pressure rise is attained. Reduction in inlet pressure below a critical value first produces cavitation of an extent just sufficient to cause a slight decrease in pump performance, as represented by the center pressure diagram of figure VI–14. Further reduction in inlet pressure leads to rapid deterioration of pump performance because of extensive cavitation and accompanying flow separation from the suction surface of the blade.

Photographs of pump flow corresponding to the three regimes of operation depicted in figure VI–14 are presented in figure VI–15. Cavitation-free flow, moderate cavitation at the point of performance dropoff, and extensive cavitation associated with a large performance loss are illustrated in figures VI–15(a), (b), and (c), respectively. With moderate cavitation (fig. VI–15(b)) where the pump operated just above the point of severe performance falloff, both blade-tip cavitation and suction-surface cavitation are evident. Although the blade-tip cavitation is quite prominent, it had no appreciable effect on

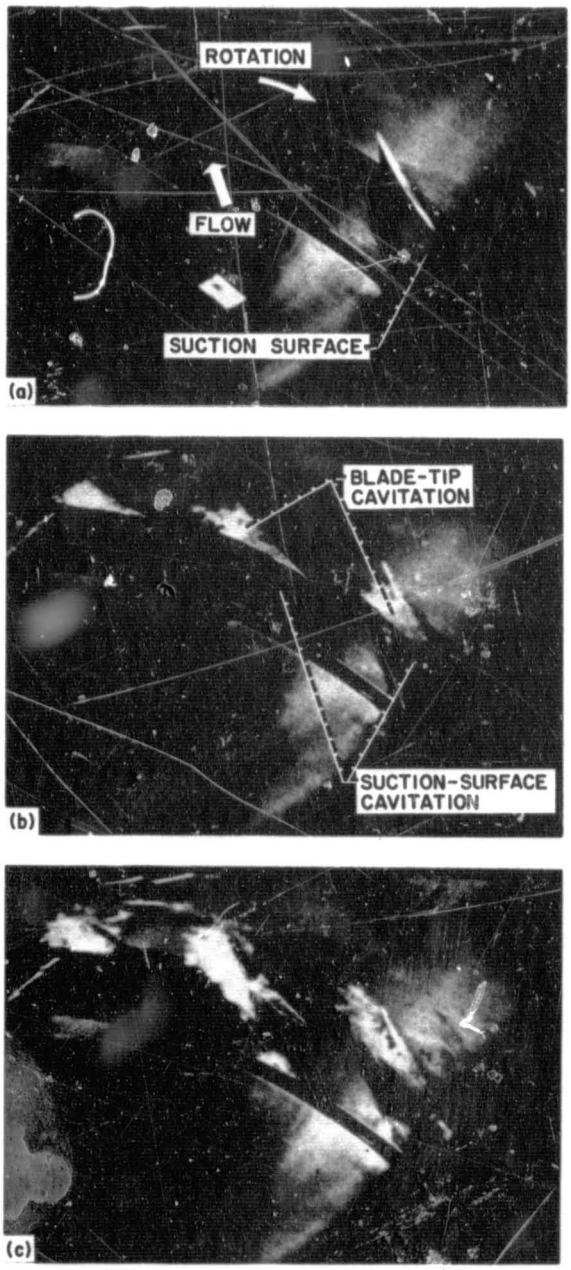

(a) Cavitation-free flow.
(b) Moderate cavitation.
(c) Extensive cavitation.

Figure VI–15.—Various degrees of cavitation.

pump blade performance. As inlet pressure was reduced, blade-surface cavitation continued to grow, as shown in figure VI–15(c). With this large amount of vapor present on the suction surface, the pump no longer operated effectively.

Unfortunately, for high-pressure-rise, high-speed pumps, the falloff in performance with extensive cavitation occurs at pump inlet pressures considerably greater than the low tank pressures required for some rocket applications.

INDUCERS

The problem of pumping from low-pressure tanks (i. e., near-boiling fluids) has been alleviated to a large extent through the design of a prepumping stage, which operates satisfactorily even under conditions of extensive cavitation. Such a prepumping stage is called an inducer. A typical inducer is presented in figure VI–16. The three exceptionally long blades are mounted on the hub in a manner approximating a helix. Inducers are generally located immediately upstream from the main pump and rotate on the same shaft as the main stage rotor. A typical inducer—axial-flow-pump combination is shown in figure VI–17 and the pressure rise through the various stages is illustrated schematically in figure VI–18. The inducer is only required to produce a pressure rise sufficient to allow the first axial-flow stage to operate free of cavitation.

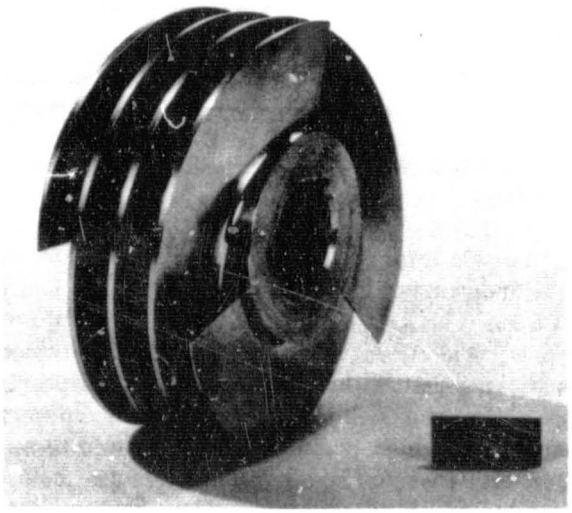

FIGURE VI–16.—Inducer.

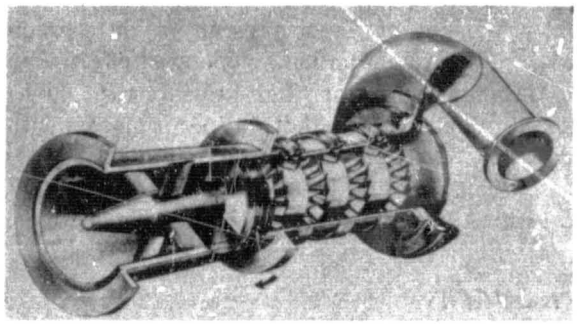

FIGURE VI–17.—Axial-flow pump with inducer.

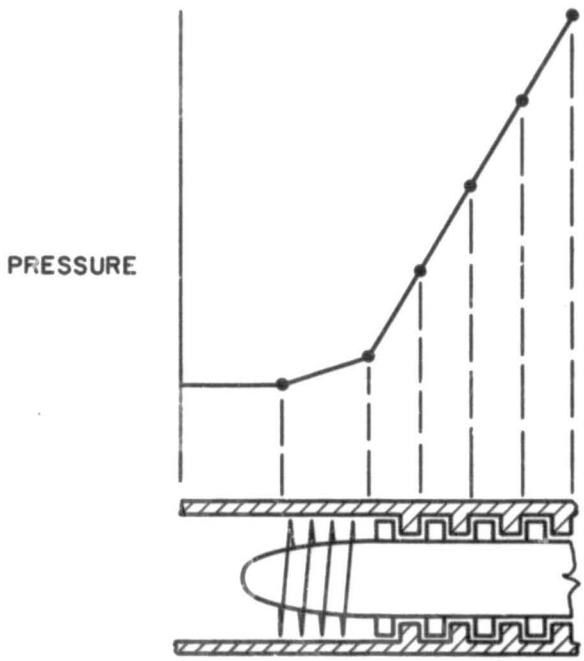

FIGURE VI–18.—Pressure rise in axial-flow pump with inducer.

The basis for the large cavitation tolerance of the inducer is illustrated qualitatively in figure VI–19. The long blades are shown in simplified form. The noncavitating pressure distribution indicates that with proper design the pressures on the suction side of the blade do not dip very deeply; the inlet pressure is thus allowed to approach close to liquid vapor pressure before cavitation is encountered. The diagram also shows that the largest pressure differences exist on the forward portion of the blade; thus, when operating without cavitation, the forward part of the blade does most of the pumping work. At low inlet pressures, cavitation and flow separation occur on the forward portion of the blade, but, because of the length and the hydrodynamic design of the blades, the separated flow reattaches to the blade surface behind the cavity to reestablish the desired blade force. Although the pressure forces on the forward portion of the blade have decreased, the forces exerted by the rear portion of the blade have increased. This compensating effect results in the same total area within the pressure diagram, denoted by the crosshatched areas; hence, blade pumping performance is maintained despite extensive cavitation. In order to illustrate the performance gains realized by use of an inducer, a comparison of the cavitation performance limit of a pump with and without an inducer is presented in figure VI–20. The addition of an inducer lowered the inlet pressure requirement for the pump to a value much closer to the liquid vapor pressure. Like the pump, however, the inducer is also limited by cavitation, as shown by the drop-off in performance.

An example of the amount of cavitation an inducer can tolerate with no appreciable loss in performance is shown in figure VI–21. The cavitation-free flow noted in the rearward channels between blades is associated with the pressure rise through the inducer, which causes the vapor to condense. In most cases, the use of

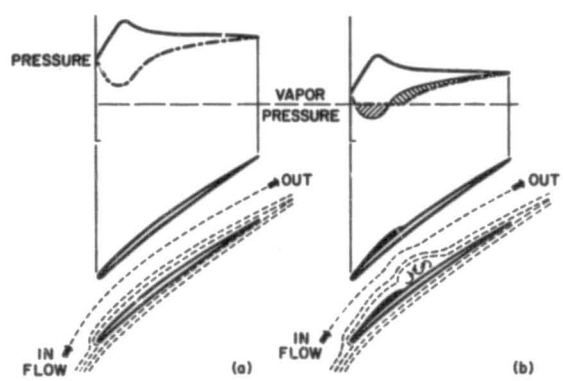

(a) Noncavitating. (b) Cavitating.

FIGURE VI–19.—Inducer blade pressure distributions.

inducers in rocket-engine pumps has allowed a reduction in propellant tank pressure sufficient to permit reasonable structural weights.

TYPICAL ROCKET PUMPS

Pump technology has made great strides in recent years. The liquid-hydrogen rocket-engine pump shown in figure VI–22, for example, provides a flow rate of 8000 gallons per minute and a pressure rise of 1400 pounds per square inch

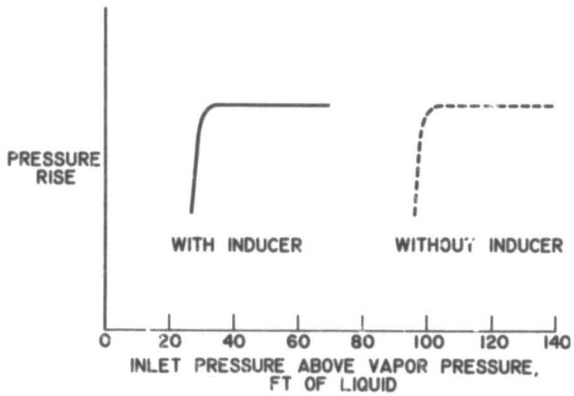

FIGURE VI–20.—Pump performance.

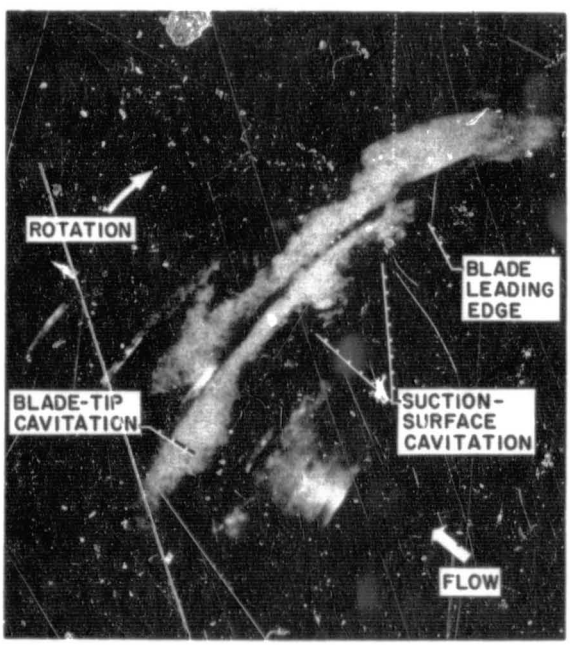

FIGURE VI–21.—Cavitating inducer.

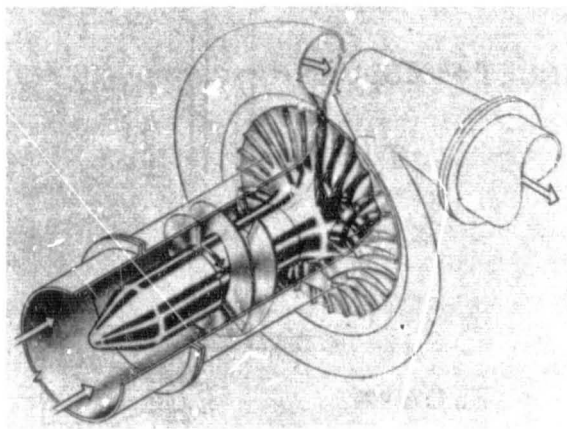

FIGURE VI–22.—Centrifugal pump with inducer.

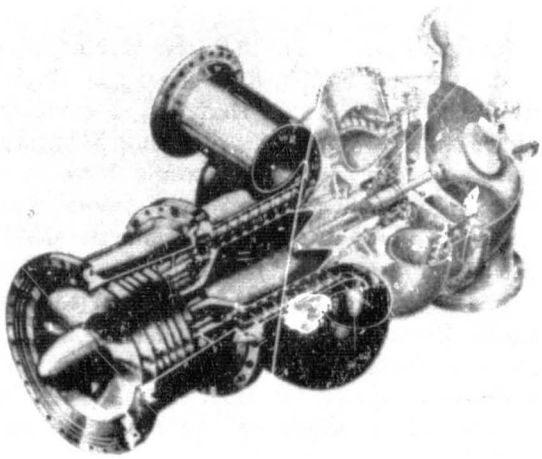

FIGURE VI–23.—Axial-flow liquid-hydrogen pump.

and requires about 9000 horsepower. The pressure rise across the pump is equivalent to raising the hydrogen to a height of over 50 000 feet. The technical sophistication of this pump can be realized from the fact that the 9000 horsepower is absorbed in useful work by a pump rotor that is about 8 inches in diameter and 8 inches long.

An axial-flow rocket pump for handling liquid hydrogen is shown in figure VI–23. This pump, developed for an advanced 1.5-million-pound-thrust engine, consists of an inducer and several axial-flow stages and is about 17 inches in diameter. It pumps 65 000 gallons of liquid hydrogen per minute to a pressure in excess of 1500

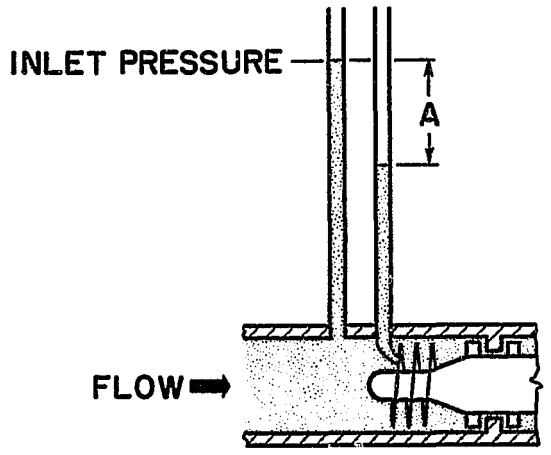

FIGURE VI-24.—Schematic pressure measurements.

pounds per square inch. The drive turbine, which produces over 90 000 horsepower, is directly connected to the pump shaft. If a cavitating inducer of the type shown could not be utilized, the pump rotational speed would have to be substantially reduced, and many more stages would have been required to obtain the desired discharge pressure. In addition, the pump diameter would have had to be increased to about 5 feet. Because the pump would have been required to rotate more slowly than the drive turbine, a massive speed-reduction gear box capable of transmitting 90 000 horsepower would have been required.

EFFECTS OF FLUID PROPERTIES ON CAVITATION PERFORMANCE

The aerospace program has provided high-performance pumps that operate well when near-boiling fluids are handled. For the most part, these pumps were proven with the use of rocket propellants such as kerosene, liquid oxygen, liquid hydrogen, and liquid fluorine. Because the cavitating performance of a pump can change with the liquid being pumped, the industrial designer is faced with the problem of having to determine cavitating performance with other liquids, that is, liquids of his interest. Specifically, the problem is that of predicting the lowest possible inlet pressure that can be established at the pump inlet while maintaining good pump performance.

The Lewis Research Center is presently engaged in several experimental and theoretical studies directed toward solving this prediction problem. Before the results of these studies are discussed, some basic observations with regard to pumps which handle different liquids under cavitating conditions should be noted in the interest of clarity.

Consider the schematic diagram of figure VI-24, which shows an inlet, pump inducer, and main pump of either axial or centrifugal type. It is assumed that the volume flow and the pump rotational speed for which the pump performs well are specified. It is also assumed that the inducer is operating under the condition of maximum tolerable cavitation; that is, any further reduction of inlet pressure would result in unacceptable pump performance. Pump inlet pressure is measured by a manometer containing the same liquid as that being pumped. A similar manometer symbolically measures the pressure on the suction surface of the blade in the cavitation zone. The basic observation is that the difference in level A between the two manometers shown is the same for all liquids for a given pump operating under the conditions specified. This observation is supported by theory and experience with cavitating pumps in which liquids of widely diverse physical properties were used. Once the pressure head difference A is established by some prior experience with the pump, it can be considered known.

Because the manometer on the inducer is in the cavitation zone, it measures the vapor pressure of the local liquid. For some liquids, this vapor pressure is essentially the same as the vapor pressure of the liquid entering the pump, which is known. For this case, the inlet pressure required is simply the sum of the head difference A and the known liquid vapor pressure. With some fluids, however, there is a beneficial effect, which is derived from the local cooling of the fluid adjacent to the cavitation zone. This cooling allows lower than expected inlet pressure requirements for these fluids. The difference in inlet pressure requirements with and without cavitation cooling is illustrated in figure VI-25.

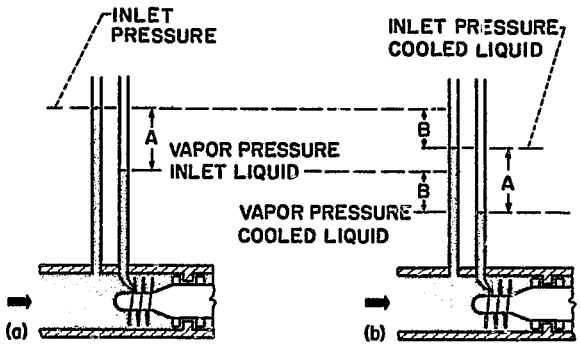

(a) No cavitation cooling. (b) Cavitation cooling.

FIGURE VI–25.—Cavitation cooling effect on pump inlet pressure.

Since the vapor pressure decreases with the lower temperature, the manometer on the inducer would read a vapor pressure which is lower than that of the incoming liquid by an amount B. Under these conditions, the inlet pressure can be lowered a corresponding amount, since it is sufficient to maintain the fixed pressure head differential A greater than the vapor pressure of the cooler liquid.

The cooling that occurs with cavitation present on the suction surface of an inducer blade is illustrated in figure VI–26. Heat is required to generate the vapor that fills the cavity, and this heat must be drawn from the surrounding liquid. Because of the high fluid velocities involved, the time required for the liquid and the vapor to traverse the cavitated region on the blade is very short. As a result, the amount of liquid which supplies the heat to form vapor is actually confined to a thin liquid film adjacent to the cavity, as shown. Because the amount of liquid involved is relatively small, a substantial cooling of the liquid film can occur in some cases. This cooling causes a drop in the vapor pressure of the liquid and a corresponding drop in the cavity pressure. As the temperature is decreased from that of the bulk liquid to that of the cooled film, a vapor-pressure drop occurs, as shown in the vapor-pressure—temperature curve of figure VI–26.

The magnitude of the vapor-pressure drop can be estimated by setting up a heat balance between the heat required for vaporization and the heat drawn from the surrounding liquid film, as follows:

Heat required for vaporization = Heat drawn from liquid film

$$\rho_v V_v L = (\Delta T)\, A h \rho_L C_L \qquad (1)$$

$$\text{Vapor-pressure drop} = K \left(\frac{\rho_v}{\rho_L} \frac{L}{C_L} \frac{dp}{dT}\right) \left(\frac{\rho_L C_L}{k}\right)^m U^n \qquad (2)$$

The mass of vapor generated is the product of the vapor volume V_v and vapor density ρ_v. This product multiplied by the heat of vaporization L is the heat required for vaporization. The heat drawn from the liquid film is equal to the mass of the film, given by the film area A, its average thickness h, and liquid density ρ_L, multiplied by its specific heat C_L and the film temperature drop ΔT.

The average thickness of the cooled liquid film depends on the heat-transfer process and can be expected to change with fluid properties and flow conditions. By introducing these heat-transfer effects and expressing the temperature drop ΔT in terms of a vapor-pressure drop through the vapor-pressure—temperature relations, equation (1) can be expressed as in equation (2). The term K is a proportionality constant that depends on the hydrodynamic characteristics of the flow device, such as a pump or inducer. The term dp/dt is the slope of the vapor-pressure—temperature curve at the bulk liquid temperature of interest. The last two terms are heat-transfer factors. The first of these is the inverse of the liquid thermal diffusivity and contains the ther-

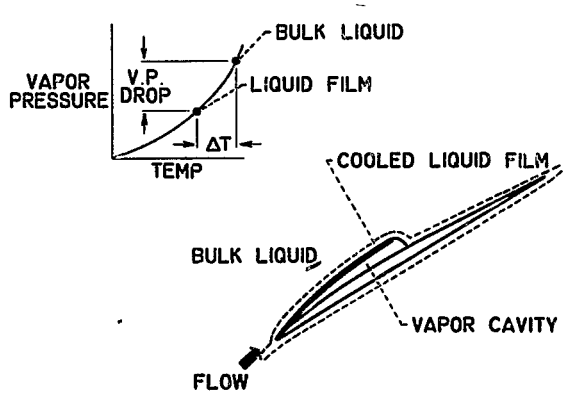

FIGURE VI–26.—Cavitation cooling.

mal conductivity of the liquid k, liquid density, and specific heat. The term U is a characteristic velocity, which can be the average velocity of the liquid relative to the blade. The exponents m and n depend on the heat-transfer process accompanying cavitation.

Because the minimum volume of vapor necessary to cause performance dropoff for a given pump is essentially the same for all liquids, comparisons of vapor-pressure drop are made on the basis of the same cavity size. For this case, a fixed relation exists between vapor volume V_v and film area A over which vaporization occurs. The terms V_v and A, therefore, do not appear explicitly in the vapor-pressure drop equation but are included in the constant K. Except for the constant K and velocity U, all terms are fluid properties.

In order to check the validity of this theoretical equation, it was necessary to conduct cavitation studies in such a way that the pressures and the temperatures within the cavitated region of various liquids could be measured directly. Because of the difficulty of making such measurements on a rotating pump blade, a venturi was used (fig. VI–27). The inside walls of the venturi are shaped to approximate the suction surface of a pump blade. With noncavitating flow, the pressure distribution on the venturi wall (lower part of fig. VI–27) is a useful approximation of the distribution on a pump blade. When the inlet pressure is lowered sufficiently to cause cavitation, vapor cavities are formed in the region of lowest pressure; the

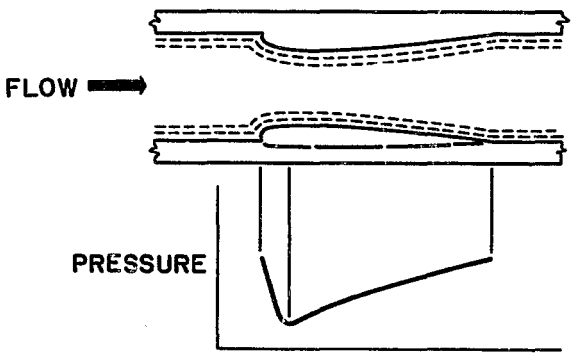

FIGURE VI–27.—Venturi.

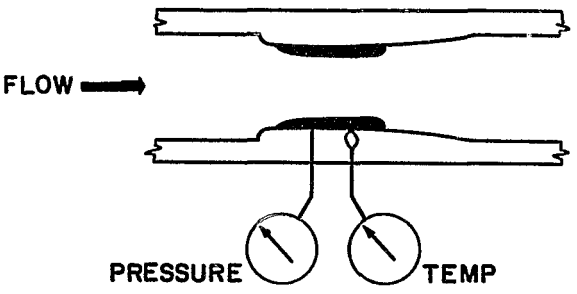

FIGURE VI–28.—Venturi with cavitation.

cavities then collapse downstream where the pressure increases, as shown schematically in figure VI–28. Temperatures and pressures within the annulus of vapor formed under cavitating conditions were measured simultaneously by means of thermocouples that protruded into the cavity and pressure taps located on the adjacent wall.

The fluids used in these studies were Freon 114, liquid nitrogen, and water in order to provide a wide spread in physical properties of the test fluids. Each fluid was studied over a range of flow velocity, temperature, and cavity length. Cavity length was determined by direct observation through the transparent walls of the venturi.

For all conditions studied, the measured cavity pressures corresponded to the vapor pressure at the measured temperatures. Cavity pressures as much as 6 pounds per square inch less than the vapor pressure of the incoming fluid were measured. This drop in vapor pressure corresponded to a 10° F drop in temperature accompanying cavitation.

Some of the measured vapor-pressure-drop data obtained with Freon 114 in the venturi study were used to evaluate the exponents and the constant K in the theoretical vapor-pressure-drop equation. The experimentally determined values for m, n, and K, respectively, are 0.5, 0.85, and 0.008; thus, the vapor-pressure-drop equation for the venturi is

$$\text{Vapor-pressure drop} = 0.008\left(\frac{\rho_v}{\rho_L}\frac{C_L}{L}\frac{dp}{dT}\right)\left(\frac{\rho_L C_L}{k}\right)^{0.5} U^{0.85} \quad (3)$$

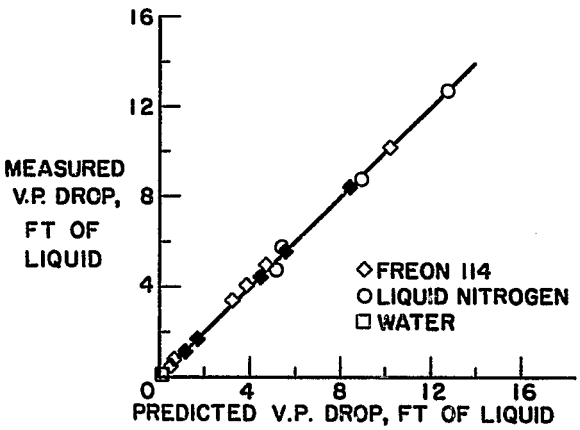

FIGURE VI–29.—Prediction of vapor-pressure drop.

With m, n, and K established by experiment, the vapor-pressure drop in the cavity can be computed for any liquid, the physical properties of which are known. The equation was used to predict the vapor-pressure drop for liquid nitrogen, water, and Freon 114 at different values of flow velocity and liquid temperature for the venturi. Some typical results are presented in figure VI–29, which compares the measured and the predicted vapor-pressure drops from equation (3). Some measured values of cavitation vapor-pressure drop for Freon 114 and liquid nitrogen at various temperatures, and flow velocities are listed in table VI–1. All the values listed are for a fixed cavity size. For conditions studied, room-temperature water showed essentially no vapor-pressure drop. In fact, all the water data obtained covering the temperature range from 40° to 120° F can be represented by the single datum point shown at the extreme low end of the curve (fig. VI–29). The solid symbols are representative Freon 114 data used to evaluate the unknowns in the equation. These points, of course, fall on the curve. The good agreement obtained between predicted and measured values indicates the equation, with the experimentally determined exponents of 0.5 and 0.85, to be quite general. The constant K, however, must still be evaluated for each different flow device.

TABLE *VI–1.—Measured Vapor-Pressure Drop*

Liquid	Temperature, °F	Flow velocity, ft/sec	Measured vapor-pressure drop, ft of liquid
Freon 114	6	32	0.9
Freon 114	20	32	1.8
Freon 114	59	32	5.1
Freon 114	79	32	8.5
Nitrogen	—320	32	8.8
Freon 114	78	44	10.2
Nitrogen	—320	42	12.5

The equation was used to predict the cavitation vapor-pressure drop for other liquids (fig. VI–30). The bar graph shows predicted vapor-pressure drops for several liquids, computed for the liquid temperatures shown. The 75° F water and the liquid-nitrogen results are repeated from figure VI–29 for comparative purposes. Although room-temperature water showed essentially no vapor-pressure drop, and drop for 450° F water is quite large, about 130 feet of water. This drop is due primarily to the large increase in vapor density and slope of the vapor-pressure —temperature curve at the higher temperatures. The vapor-pressure drop for two commercial liquids, liquid methane at the normal boiling point and methyl alcohol at 180° F, is about the same as for nitrogen. Liquid hydrogen, which is of interest as a rocket fuel, shows large vapor-pressure drops; from 130 feet of hydrogen at its normal boiling point of −423° F (37° R) to more

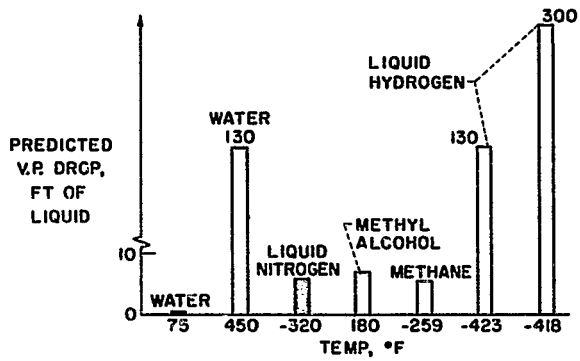

FIGURE VI–30.—Predicted vapor-pressure drops for Venturi.

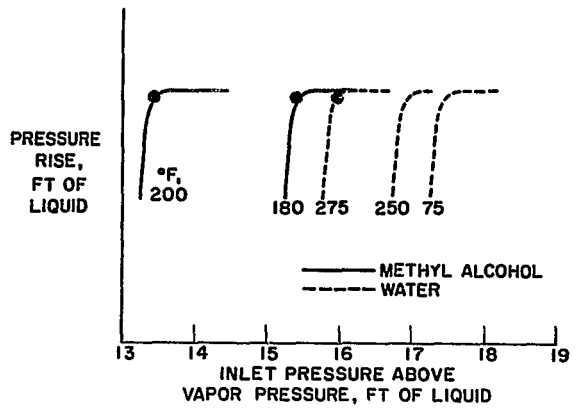

FIGURE VI–31.—Pump performance with water and methyl alcohol.

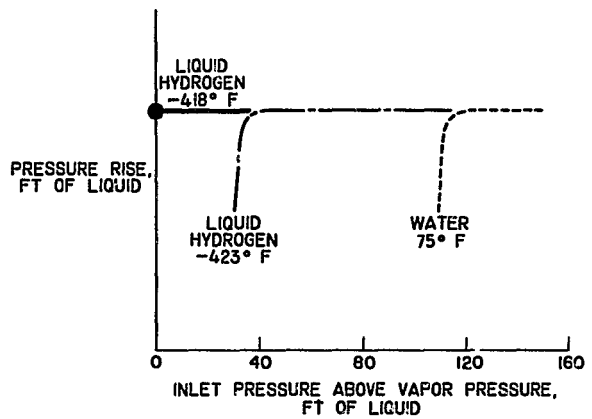

FIGURE VI–32.—Pump performance with water and liquid hydrogen.

than 300 feet of hydrogen at −418° F (42° R), an increase in temperature of only 5° F.

The utility of the vapor-pressure-drop equation for pumps was checked by using it to predict the cavitating performance limit for a small centrifugal pump handling hot water and methyl alcohol. A comparison of pump performance obtained with these liquids at various temperatures but for the same operating conditions is presented in figure VI–31, which shows pump pressure rise plotted as a function of inlet pressure above vapor pressure. The performance data obtained for the pump operated at 75° and 250° F water were used to evaluate the constant K in the equation

$$\text{Vapor-pressure drop} = K\left(\frac{\rho_v}{\rho_L}\frac{L}{C_L}\frac{dp}{dT}\right)\left(\frac{\rho_L C_L}{k}\right)^{0.5} U^{0.85}$$

which uses the exponents of 0.5 and 0.85 established in the venturi study. This equation was then used to predict the inlet pressure requirements (for the same small loss in pressure rise) for 275° water and 180° and 200° F methyl alcohol. The predicted values, shown by the solid symbols, are in good agreement with the experimental results.

The vapor-pressure-drop equation predicted a large drop in vapor pressure for cavitating liquid hydrogen as compared with room-temperature water (fig. VI–30). Figure VI–32 shows the performance of a pump operated at the same flow conditions in both water and liquid hydrogen. As anticipated from the cavitation-cooling studies, the margin of inlet pressure above vapor pressure at which the pump performance declined is much lower for the liquid hydrogen than for the cold water. For the same rotational speed and flow rate, the analysis also predicted that an increase of only 5° F in liquid-hydrogen temperature (from −423° to −418° F) would enable satisfactory operation of this pump at zero margin of inlet pressure above vapor pressure, that is, with the incoming liquid at its boiling point. This predicted point is indicated by the solid symbol. When the pump was operated under these conditions, pump performance was sustained when the hydrogen entering the inlet was boiling, as indicated by the solid line. Measured and predicted pump performance are thus in good agreement.

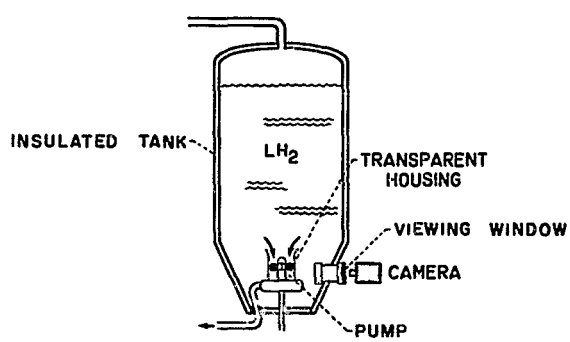

FIGURE VI–33.—Hydrogen-pump test arrangement.

Photographs of the pump operating at 20 000 rpm under cavitating conditions in −418° F liquid hydrogen were obtained with the experimental arrangement shown in figure VI–33. The pump, encased in a transparent housing, was photographed through an evacuated window tube, which was directly immersed in the tank of liquid hydrogen. Figure VI–34(a) shows the pump operating with a moderate degree of cavitation. It was impossible to obtain good photographs of inducer cavitation for the condition of zero margin of inlet pressure above vapor pressure. As the tank pressure (or pump inlet pressure) is progressively reduced, the tank pressure reaches the vapor pressure of the hydrogen,

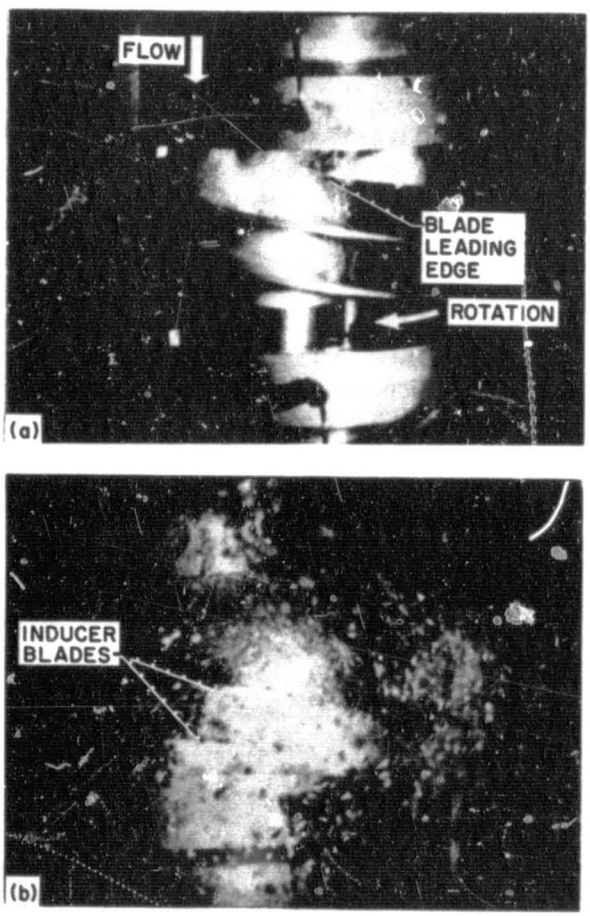

(a) Moderate cavitation.
b) Operation with boiling liquid hydrogen.

FIGURE VI–34.—Inducer cavitation in liquid hydrogen at −418° F.

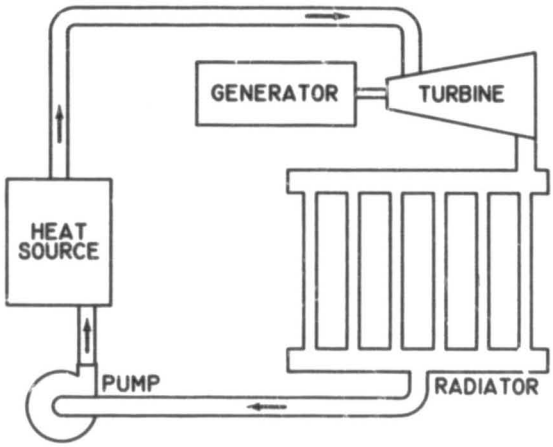

FIGURE VI–35.—Turbogenerator space power system.

and the liquid boils throughout the tank. The resulting vapor bubbles occurring between the window and the pump housing restrict the view of the inducer as shown in figure VI–34(b). Under the conditions shown in figure VI–34(b), the pump continued to produce a satisfactory pressure rise (fig. VI–32).

The present method for predicting pump cavitation performance for various liquids has been examined with only a limited number of liquids; however, because the test liquids had widely diverse physical properties, the general utility of the method is regarded with confidence. Present Lewis programs are exploring this subject further.

CAVITATION DAMAGE

Another and perhaps more familiar aspect of cavitation in industrial pumps is the structural failure that it can cause. In pumps used for rocket engines, cavitation damage is not a problem because the duration of the engine operation is so short. Pumps used in turbogenerator electric power systems on space vehicles, however, will be required to operate continuously unattended for a year or more. A schematic diagram of such a system is shown in figure VI–35. The system generates electrical power by means of a turbine-driven generator and uses a metal vapor, such as sodium or potassium, as the working fluid. After leaving the turbine, the

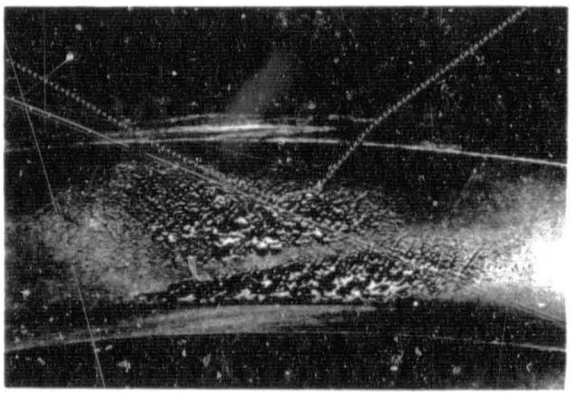

FIGURE VI–36.—Pump blade cavitation damage.

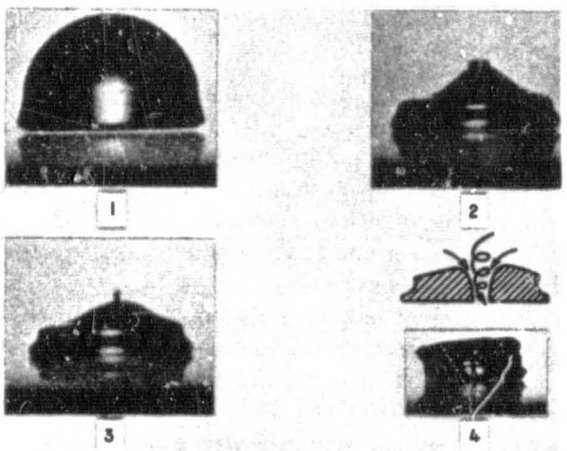

FIGURE VI–37.—Vapor bubble collapse mode. (Courtesy A. T. Ellis, California Institute of Technology, and T. B. Benjamin, University of Cambridge.)

spent vapor is condensed in the radiator. The condensate is returned to the boiler by a pump. Since this condensate is in a near-boiling condition, a cavitation problem also exists with liquid sodium or potassium. That a cavitation-damage problem exists is evident from the photograph of a pump blade presented ir figure VI–36. The view shows the blade surface near the outlet of a mixed-flow impeller. The pump was tested at the Pratt & Whitney CANEL installation under cavitating conditions in liquid potassium at a temperature of 1400° F for 350 hours. If the severe pitting shown had been allowed to continue, blade failure would have eventually resulted. The need for cavitation damage research is clear.

Cavitation damage occurs on a fluid-containment surface, such as a pump blade, where adjacent vapor cavities rapidly collapse. Although various studies have shown that pure vaporous cavities can collapse rapidly and at high energy levels, the basic mechanics of damage by imploding vapor bubbles is not clearly established. Recent research, however, has revealed one way in which cavitation damage occurs. Figure VI–37 shows the successive phases of an imploding cavitation bubble near a solid surface. The first photograph shows a cavitation bubble adjacent to a surface somewhat as it would appear moving along the suction surface of a pump blade. As the bubble moves into a zone of higher pressure, the vapors within condense rapidly. The collapsing bubble takes odd shapes. In collapsing (photographs 2, 3, and 4), a jet of liquid is formed, which pierces the bubble and impinges on a small area of the adjacent blade surface. Careful scrutiny of the photographs of the impinging jet suggests that the jet is in rapid rotation. The center of the jet appears in the photographs as a dark core which extends above the bubble.

Lewis has sponsored research on materials that resist cavitation damage. Studies of cavitation damage with the use of alkali-metal pumps are supplemented by work with a magnetostrictive vibratory device which closely simulates pump-blade damage. This device (fig. VI–38) consists of two principal parts, a magnetostrictive vibrator, and a test specimen which is driven by the vibrator. Cavitation damage is produced on the

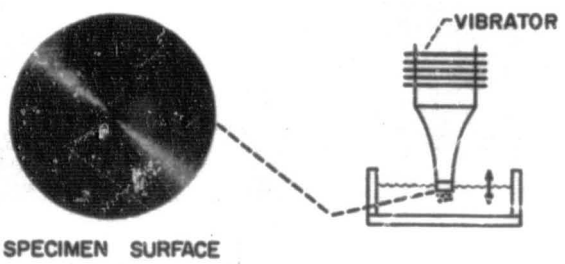

FIGURE VI–38.—Magnetostrictive cavitation damage apparatus.

surface of the 0.5-inch-diameter circular specimen, which is submerged in liquid and caused to vibrate at high frequency. On each upstroke, vapor bubbles are formed near the surface of the specimen. These bubbles collapse with high energy on the ensuing downstroke. The device provides a practical method for making rapid, accurate, and detailed measurements of the rate of weight loss for a given material.

The cavitation erosion rates for a number of materials, tested over a range of conditions, are presented in figures VI–39 and VI–40. Rate of weight loss in milligrams per hour is plotted as a function of exposure time in hours. The curve of figure VI–39 is for 304L stainless steel tested in 80° F water; the curve of figure VI–40 is for 316 stainless steel tested in 400° F liquid sodium. The curves are similar in that the damage rate is small initially, rises sharply, and then falls off to a constant, steady-state rate. Comparisons between various materials are made in the steady-state zone. The damage rate differs for the various materials. In water, for example, soft aluminum is eroded by cavitation about 60 times faster than stainless steel. The resistance of several refractory alloys, TZM, T–222, and columbium 132M has been studied in liquid sodium. These alloys maintain their strength at the high temperatures of interest in space power systems. In 400° F sodium, the resistance of these materials to cavitation damage (based on steady-state values) is comparable with that of 316 stainless steel. Stellite 6B, a cobalt-base alloy, is remarkably resistant to damage. After 14 hours

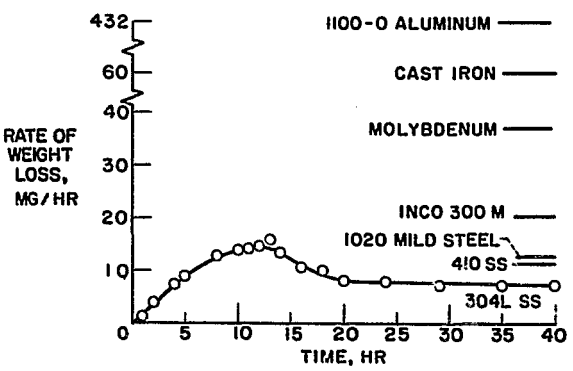

FIGURE VI–39.—Cavitation damage rate in water at 80° F.

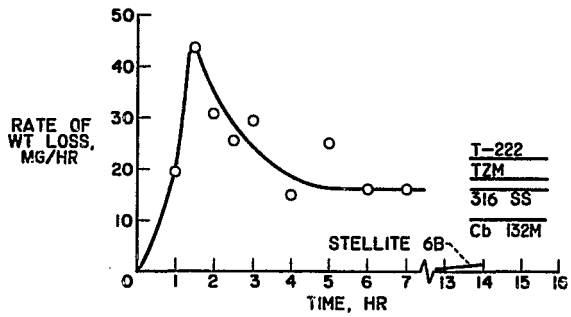

FIGURE VI–40.—Cavitation damage rate in liquid sodium at 400° F.

of exposure, weight loss was only beginning to become measurable. Because of its high cost and difficulty of fabrication, it is impractical to fabricate an entire pump rotor of Stellite. An inlay of Stellite in the most damage-prone area of the blading, however, might greatly extend pump life.

In order to determine which physical properties of the material are important in determining the resistance to cavitation damage, it is important to consider the mechanism of damage. Basically, the containment material is exposed to the jet impingement and pressure shock waves of imploding bubbles on or very near its surface. Damage resistance, then, is a measure of the capacity of a material to absorb this mechanical attack before fracture or pitting occurs. Thus, high values of yield strength, ultimate tensile strength, hardness, and ductility (percentage of elongation to fracture) are beneficial in providing resistance to cavitation damage.

In space powerplant systems, operation at high temperature levels is desirable; thus, it is important to consider the effect of fluid temperature on the rate of cavitation damage. The rate of damage for three materials immersed in liquid sodium at temperatures of 400°, 1000°, and 1500° F are compared in figure VI–41. All the data presented were obtained with the liquid sodium at atmospheric pressure. The greatly reduced rate of damage observed at 1500° F occurs despite the fact that the specimen materials have less strength at this higher temperature. This reduced damage is attributed to the high vapor pressure of sodium at 1500° F, which causes the

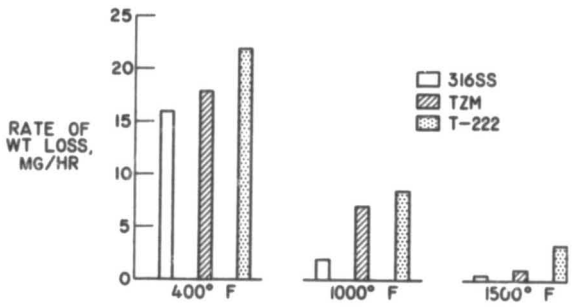

FIGURE VI–41.—Effect of temperature on cavitation damage rate in liquid sodium.

cavitation bubbles to collapse with less violence. For space power systems, it may be desirable to pump sodium at 1500° F or greater; thus, the reduced damage rate at high temperature is favorable.

Cavitation-damage data obtained thus far allow the arrangement of materials in the order of their resistance to cavitation damage with some degree of confidence. Further studies are being conducted to obtain a better understanding of the basic phenomena as well as the practical problems associated with cavitation damage.

FLOW INSTABILITY

Cavitation can cause pump damage in an entirely different manner; it can lead to flow instabilities, which produce strong pressure fluctuations in the pump. These pressure fluctuations can vibrate some of the pump parts to failure.

Photographs of flow oscillations induced by cavitation in a pump inducer (operating in water) were obtained by use of the arrangement shown in figure VI–42. The inducer was encased in a transparent housing, and nylon tufts attached to the housing wall were used to indicate local flow direction. A photograph showing the arrangement of tufts and inducer blading is also shown in the figure. Under normal flow conditions, the tufts ahead of the rotor indicate flow directly into the inducer. Tufts in the rotor area indicate the flow turned in the direction of inducer rotation. Flow oscillations that can occur with cavitation are presented in figure VI–43. With the inducer operating at a tolerable level of cavitation (fig. VI–43(a)), steady flow is indicated. As inlet pressure is reduced (fig. VI–43(b)), cavitation becomes more severe and the flow unsteady, as indicated by oscillations of those tufts ahead of the rotor. A further reduction of inlet pressure results in extreme cavitation (fig. VI–43(c)), and the entire flow pulses violently. In some instances, periodic flow reversals were indicated by all the tufts.

Figure VI–44 shows an inducer blade failure which occurred after a few minutes of operation in the presence of severe flow instability. These studies indicate that while inducers can operate satisfactorily with some degree of cavitation, flow instabilities caused by extreme cavitation can result in pump failure.

Pump instabilities can also occur in the absence of cavitation, and in some instances, these instabilities may lead to an erroneous diagnosis of difficulties in pumping systems. The manner in which these instabilities arise in cavitation-free flow can be illustrated by an examination of the flow in the channels between pump blades. Diagrams of the flow streamlines and the velocity profile in the flow channels of a centrifugal pump are presented in figure VI–45. The advancing face of the blade is the pressure surface (denoted by +), and the trailing face is the suction surface (denoted by −); thus, the pressure varies across the flow channel. A corresponding variation in flow velocity across the channel exists as diagramed with the highest velocities corresponding to the lowest pressures. The velocity distribution shown is for a well-designed pump

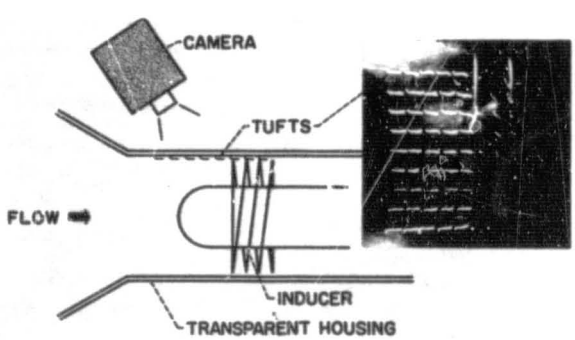

FIGURE VI–42.—Experimental arrangement for flow instability study.

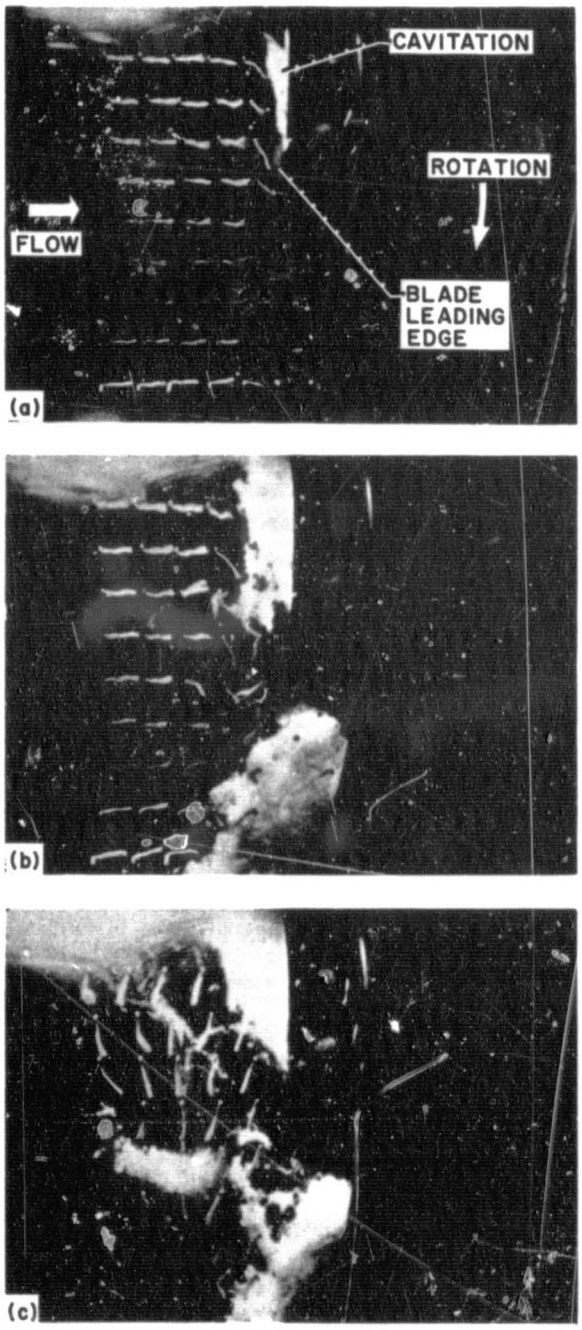

(a) Mild cavitation.
(b) Severe cavitation.
(c) Extreme cavitation.

FIGURE VI–43.—Cavitation-induced flow instability.

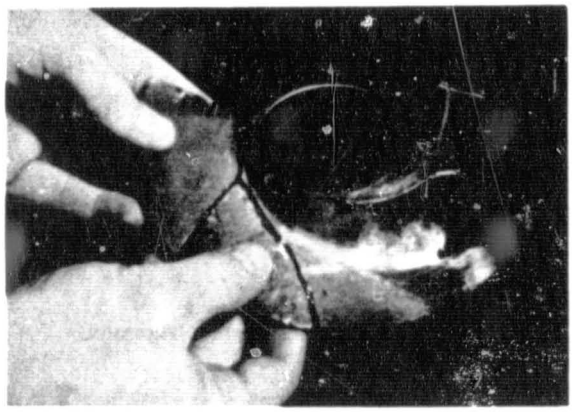

FIGURE VI–44.—Inducer blade failure.

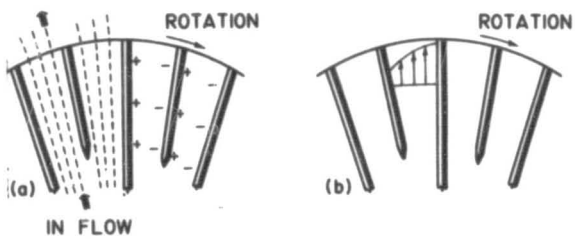

(a) Flow streamlines. (b) Velocity profile.

FIGURE VI–45.—Flow between pump blades.

operated at design conditions. Velocity distribution can be controlled by varying the hub contour, blade height and thickness, circumferential spacing, and blade curvature.

In a pump of poor design, the flow velocity may drop to zero or even become negative on the high-pressure side of the flow passage, as shown in figure VI–46. A negative velocity means that the local flow is opposed to the main stream direction. These local flow reversals produce a whirling eddy, which disturbs the flow, as indicated by the marked distortion of the streamlines. Unfortunately, these eddies are unstable. Eddies are continually generated, grow as they move outward through the blade passage, and are then washed downstream to produce a rhythmic fluctuation in pump delivery pressure and flow rate. Such oscillations can build to destructive magnitudes in pumps and associated plumbing systems.

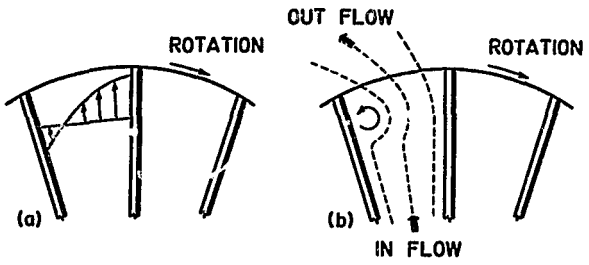

(a) Velocity profile. (b) Flow streamlines.

FIGURE VI-46.—Eddy flow.

Instabilities can also occur in a well-designed pump, if it is operated too far below the design flow rate. At low flow rates, eddies form and flow oscillations occur in a manner similar to that for a poorly designed pump. The stream flow field within a pump rotor can be determined by theoretical calculation procedures. Such a calculation can be used to determine the useful operating range of a well-designed pump; that is, the point of onset of flow oscillation that may occur as the flow is throttled can be predicted.

This analytical prediction technique has been programed in FORTRAN language for digital computing. Some pump manufacturers have obtained this program from Lewis and have used it to design and analyze the flow conditions within their pumps. The computer deck and necessary instructions are available upon request. It is referred to as a "Quasi-three-dimensional flow solution for centrifugal pump impellers." The analytical program is sufficiently flexible to allow calculation of velocity distributions in other internal flow devices, such as inlets, diffusers, or elbows.

CONCLUDING REMARKS

The foregoing discussion of the role of cavitation in defining pump performance treats one phase of NASA work on high-performance pumps. Companion work includes studies on the design of high pressure-rise blading for centrifugal and axial-flow pumps and high-work turbines for driving these pumps. These studies make extensive use of the compressor and turbine technology developed earlier for jet engines. Most of this work is documented in NASA reports dating from 1958.

Present NASA work on rotating machinery extends from large components for aircraft jet engines to small, high-speed turbines and compressors suited for turbogenerated electrical power systems in space that use gases such as argon and neon as the working fluid. The high efficiencies attained in turbines and compressors ranging in size to one as small as 3 inches in diameter represents a new advance in the technology of these machines. The wide range of information developed should include many areas of interest to the machine designers who serve the petroleum industry.

BIBLIOGRAPHY

Pumps and Inducers

CROUSE, JAMES E.; MONTGOMERY, JOHN C.; AND SOLTIS, RICHARD F.: Investigation of the Performance of an Axial-Flow-Pump Stage Designed by the Blade-Element Theory—Design and Overall Performance. NASA TN D-591, 1961.

CROUSE, JAMES E.; SOLTIS, RICHARD F.; AND MONTGOMERY, JOHN C.: Investigation of the Performance of an Axial-Flow-Pump Stage Designed by the Blade-Element Theory—Blade-Element Data. NASA TN D-1109, 1961.

HARTMANN, MELVIN J.; AND BALL, CALVIN L.: New Problems Encountered with Pumps and Turbines. Proceedings of the NASA-University Conference on the Science and Technology of Space Exploration, Vol. 2, NASA SP-11, 1962, pp. 23-35.

OSBORN, WALTER M.: Noncavitating and Cavitating Performance of a Liquid-Fluorine Pump Designed by Stream-Filament Method. NASA TM X-722, 1963.

SANDERCOCK, DONALD M.; SOLTIS, RICHARD F.; AND ANDERSON, DOUGLAS A.: Cavitation and Noncavitation Performance of an 80.6° Flat-Plate Helical Inducer at Three Rotational Speeds. NASA TN D-1439, 1962.

SOLTIS, RICHARD F.: Some Visual Observations of Cavitation in Rotating Machinery. NASA TN D-2681, 1965. (Technical Film Supplement C-239 available on request.)

SOLTIS, RICHARD F.: ANDERSON, DOUGLAS A.; AND SANDERCOCK, DONALD M.: Investigation of the Performance of a 78° Flat-Plate Helical Inducer. NASA TN D-1170, 1962.

Cavitation

JACOBS, ROBERT B.; MARTIN, KENNETH B.; AND HARDY, RICHARD J.: Direct Measurement of Net Positive Suction Head. Rep. No. 5500, National Bureau of Standards, July 18, 1957.

RUGGERI, ROBERT S.; AND GELDER, THOMAS F.: Cavitation and Effective Liquid Tension of Nitrogen in a Tunnel Venturi. NASA TN D-2088, 1964.

STAHL, H. A.; AND STEPANOFF, A. J.: Thermodynamic Aspects of Cavitation in Centrifugal Pumps. ASME Trans., vol. 78, Nov. 1956, pp. 1691–1693.

WILCOX, W. W.; MENG, P. R., AND DAVIS, R. L.: Performance of an Inducer-Impeller Combination at or Near Boiling Conditions for Liquid Hydrogen. Vol. 8 of Advances in Cryogenic Eng., K. D. Timmerhaus, ed., Plenum Press, 1963, pp. 446–455.

Cavitation Damage

KULP, ROBERT S.; AND ALTIERI, JAMES V.: Cavitation Damage of Mechanical Pump Impellers Operating in Liquid Metal Space Power Loops. NASA CR-165, 1965.

THIRUVENGADAM, A.; PREISER, H. S.; AND RUDY, S. L.: Cavitation Damage in Liquid Metals. Tech. Prog. Rep. 467-3, Hydronautics, Inc. (NASA CR-54459), 1965.

END OF REFERENCE

Card #22

REFERENCE

99

RUGGERI, R. S.; AND MOORE, R. D.: METHOD FOR PREDICTION OF PUMP CAVITATION PERFORMANCE FOR VARIOUS LIQUIDS, LIQUID TEMPERATURES, AND ROTATIVE SPEEDS, NASA TN D-5292, 1969.

8.2-0-0 V.S

NASA TECHNICAL NOTE

NASA TN D-5292

NASA TN D-5292

COPY 2

LEWIS RESEARCH CENTER
Aerospace Safety Research
and Data Institute
FEB 4 1972
CLEVELAND, OHIO

METHOD FOR PREDICTION OF PUMP CAVITATION PERFORMANCE FOR VARIOUS LIQUIDS, LIQUID TEMPERATURES, AND ROTATIVE SPEEDS

84.0°
71.3°
68.0°

by Robert S. Ruggeri and Royce D. Moore

Lewis Research Center
Cleveland, Ohio

LIBRARY COPY
LEWIS LIBRARY, NASA
CLEVELAND, OHIO

NATIONAL AERONAUTICS AND SPACE ADMINISTRATION • WASHINGTON, D. C. • JUNE 1969

NASA TN D-5292

METHOD FOR PREDICTION OF PUMP CAVITATION PREFORMANCE FOR VARIOUS LIQUIDS, LIQUID TEMPERATURES, AND ROTATIVE SPEEDS

By Robert S. Ruggeri and Royce D. Moore

Lewis Research Center
Cleveland, Ohio

NATIONAL AERONAUTICS AND SPACE ADMINISTRATION

For sale by the Clearinghouse for Federal Scientific and Technical Information
Springfield, Virginia 22151 – CFSTI price $3.00

ABSTRACT

A method for predicting the cavitation performance of pumps with various liquids, liquid temperatures, and rotative speeds is presented. Both theoretical and experimental studies used in formulating the method are discussed. Good agreement was obtained in comparisons between experimental and predicted results of cavitation performance for several pumps operated in liquids that exhibit a wide range of physical properties. Use of the method requires that two sets of test data be available for the pump and operating conditions of interest, but these data need not be for the same liquid, temperature, or pump speed. Numerical examples are presented.

METHOD FOR PREDICTION OF PUMP CAVITATION PERFORMANCE FOR VARIOUS LIQUIDS, LIQUID TEMPERATURES, AND ROTATIVE SPEEDS

by Robert S. Ruggeri and Royce D. Moore

Lewis Research Center

SUMMARY

A method that predicts the cavitation performance for pumps and inducers is presented. The present study shows that the method consistently provided good agreement between experimental and predicted performance for an inducer and five different pumps operated with a variety of liquids that have widely diverse physical properties. Use of the method requires that two sets of appropriate test data be available for each pump and operating condition of interest. These test data need not necessarily be for the same liquid, liquid temperature, or rotative speed. At least one set of data, however, must provide measurable thermodynamic effects of cavitation. From these reference tests, accurate predictions of cavitation performance for a given pump can be made for other liquids, liquid temperatures, and/or rotative speeds. Predictions are made on the basis of flow similarity with cavitation and, thus, predicted values apply to the same conditions of flow coefficient and pump cavitation performance level used in obtaining the reference test data.

INTRODUCTION

Cavitation, which is the formation and collapse of vaporous cavities in flowing liquids, can degrade the performance of pumps and other hydraulic equipment. Because cavitation is a vaporization process that involves heat and mass transfer, the physical properties of the liquid and its vapor and the flow conditions can affect the cavitation process and thus the cavitation performance of hydraulic equipment as well. The combined effects of fluid properties, flow conditions, and heat transfer, termed thermodynamic effects of cavitation, can improve cavitation performance. For example, cavitation studies with pumps and venturis (refs. 1 to 10) have shown that, for certain liquids and/or liquid temperatures, the net positive suction head (NPSH) requirements can be signifi-

cantly less than that obtained for room-temperature water. (NPSH is defined as the total pressure above vapor pressure at the inlet to a pump.) This improvement (decrease) in inlet pressure requirements is attributed to the varying degrees of evaporative cooling associated with the cavitation process. Because of the evaporative cooling, the cavity pressure and the vapor pressure of the liquid adjacent to the cavity are decreased relative to the vapor pressure of the bulk liquid. This decrease in cavity pressure retards the rate of further vapor formation, thereby allowing the pump to operate at lower values of NPSH than would otherwise be possible. The NPSH requirement for a pump operating at a given head rise and flow condition is reduced by the amount corresponding to the decrease in cavity pressure. The accurate prediction of thermodynamic effects of cavitation is therefore essential to an optimum flow system that is designed to operate with cavitation.

Various analyses that relate thermodynamic effects of cavitation to pump performance have been proposed (refs. 1 to 7). Although these studies are useful in predicting trends, their applicability is somewhat limited because either (1) the analysis does not predict quantitative values or (2) the experimental data used did not adequately cover the range of fluid properties and flow conditions of current interest, particularly in the aerospace field. Also, existing analyses do not account for effects of heat transfer, flow velocity (and its relation to heat transfer), or pump scale.

Subsequent to the studies of references 1 to 7, several investigations have been conducted to study in detail the thermodynamic effects of cavitation and its relation to the cavitation performance of various flow devices such as venturis, pumps, and pump inducers (refs. 9 to 12). From venturi studies, a method for predicting thermodynamic effects of cavitation as a function of the liquid used, liquid temperature, flow velocity, and body scale for a given venturi design was formulated in references 10 and 11. Use of the method requires reference data obtained by experiment. The method, based primarily on Freon-114 cavitation results, was later demonstrated to be applicable to the prediction of cavitation performance for pumps and inducers (refs. 9, 13, and 14). The applicability of the method was extended over a wide range of fluid properties and flow conditions by conducting a subsequent cavitation study using liquid hydrogen (ref. 15) in a venturi of identical design to that previously used. These hydrogen data were then used in conjunction with other available cavitation data for the same venturi design to re-evaluate the exponents of the prediction equation. The new exponents, which are now based on a wider range of variables, are reported in reference 16. The resulting slight changes have little effect on predicted results of references 9, 13, and 14.

The objective of this study was to present, in a comprehensive and detailed manner, a method for the prediction of cavitation performance for pumps and inducers. The method presented is based on, and is an extension of, the method already reported in reference 16 for venturis. It is applicable to various liquids, liquid temperatures, and pump rotative speeds. A prerequisite to this prediction method is that similarity of the cavitating flow over the suction surface of the blade be maintained for all conditions to

which the method is applied. Use of the method requires that two sets of appropriate test data be available for each pump and operating condition of interest.

Cavitation performance data for several research and commercial pumps, obtained with a variety of liquids over a range of conditions, are compared with predicted results using the derived method. Selective data for an inducer and two centrifugal pump impellers operated with liquid hydrogen are presented and compared with predictions to show magnitude changes in thermodynamic effects of cavitation with hydrogen temperature, pump speed, flow coefficient, and geometric design. A discussion on the implementation of the method, including numerical examples, is also presented.

ANALYSIS

Development of Basic Relations

Cavitation similarity parameters. - The conventional cavitation parameter for dynamic similarity of cavity flow is of the form

$$K \equiv \frac{h_0 - h_v}{\frac{V_0^2}{2g}} \tag{1}$$

where free-stream static-pressure head h_0 and free-stream velocity V_0 are those required to produce a given amount of cavitation, and h_v is the vapor pressure head corresponding to free-stream temperature. (Symbols are defined in appendix A.) Equation (1) is based on the assumption that the cavity surface is at a constant pressure equal to free-stream vapor pressure. However, because of the thermodynamic effect of cavitation, cavity pressure can be significantly less than free-stream vapor pressure. In the case of liquid hydrogen, cavity pressures can be less than free-stream vapor pressure by several hundred feet of liquid (refs. 15 and 16). Thus, a more general cavitation parameter is one in which h_v in equation (1) is replaced by the actual cavity pressure h_c. However, venturi cavitation studies have shown that, within a given fixed cavity, the pressure varies with axial distance (refs. 10, 12, and 16), and thus it becomes necessary to specify a particular reference cavity pressure. Herein, as in references 10, 11, and 16, the minimum cavity pressure head $h_{c,min}$, which occurs near the cavity leading edge, is used to define a modified cavitation parameter for developed cavities; namely,

$$K_{c,\,min} = \frac{h_0 - h_{c,\,min}}{\frac{V_0^2}{2g}} = K + \frac{h_v - h_{c,\,min}}{\frac{V_0^2}{2g}} = K + \frac{\Delta h_v}{\frac{V_0^2}{2g}} \qquad (2)$$

In the absence of thermodynamic effects of cavitation, cavity pressure corresponds to free-stream vapor pressure ($\Delta h_v = 0$) and thus $K_{c,\,min} = K$. The usefulness of $K_{c,\,min}$ as a similarity parameter has been demonstrated by the studies of references 10 and 16 wherein it was shown that, for fixed-size cavities in a given venturi design ($\Delta X/D$ = Constant), the modified parameter $K_{c,\,min}$ remained essentially constant for different liquids, liquid temperatures, flow velocities, and venturi scales, whereas the corresponding K values, which are based on stream vapor pressure, varied widely. For constant values of $K_{c,\,min}$ and V_0 in equation (2), a change in the minimum cavity pressure $h_{c,\,min}$ (maximum depression) results in an equal change in stream static pressure under conditions of flow similarity. As discussed later in this section, this direct correspondence between $h_{c,\,min}$ and h_0 provides the basis for use of equation (2) in the prediction of cavitation performance (free-stream static-pressure requirements) for devices such as pumps and inducers.

The magnitude of cavity pressure depression is a complex function of body geometry, flow velocity, and the heat- and mass-transfer processes involved, as well as the physical properties of the liquid and its vapor. Because of the complexity of the cavitation process, the value of $h_{c,\,min}$ or Δh_v is not generally known or predictable for any arbitrary flow device, liquid, and/or flow situation. However, performance predictions for a given flow device can be made indirectly by experimentally determining a reference value of Δh_v and, thus, $K_{c,\,min}$ by using practically any convenient combination of test liquid, liquid temperature, or flow velocity that yields a measurable Δh_v. Then by use of the method detailed in references 10, 11, 16, and herein, predicted values of Δh_v, relative to the reference test value, are calculated for other liquids, liquid temperatures, and/or flow velocities of interest. With the experimentally determined value of $K_{c,\,min}$, which remains constant for geometrically similar cavities, the free-stream static-pressure requirement h_0 is predicted by use of equation (2).

Geometric similarity of the cavitated region is essential to the use of $K_{c,\,min}$ for prediction purposes. In a given pump or inducer, cavitation performance is of course dependent on the vapor cavity volume present within the blade passages, although the presence of small vapor cavities on the suction surface of the blade will not necessarily affect the performance. It is reasonable to assume that, for operation of a pump at a constant flow coefficient (similarity of entering flow), the cavity on the suction surface of the blade, and thus the vapor volume corresponding to a specified head-rise coefficient ratio ψ/ψ_{NC}, is essentially constant irrespective of the liquid, liquid temperature, and/or rotative speed. This criterion of fixed-vapor cavity volume, together with the

previously discussed constancy of $K_{c,\,min}$, allows the prediction method developed for venturis to be extended to pumps and inducers. The prediction method, as applied to pumps, is described in the following section.

Similarity relations for pumps. - Pump cavitation performance is generally presented in terms of the net positive suction head (NPSH) required at a specified ratio of the head-rise coefficient with cavitation to that without cavitation (ψ/ψ_{NC}). The NPSH is defined as the margin of fluid total head above fluid vapor pressure head at the pump inlet; or in terms of inlet static-pressure head and velocity head,

$$NPSH = h_0 + \frac{V_1^2}{2g} - h_v$$

In terms of net positive suction head, equation (2) may be written as

$$\frac{V_1^2}{2g}(K_{c,\,min} + 1.0) = h_0 + \frac{V_1^2}{2g} - h_v + \Delta h_v$$

or

$$K_{c,\,min} = \frac{NPSH + \Delta h_v}{\frac{V_1^2}{2g}} - 1.0 \qquad (3)$$

where V_1 in the preceding equations is analogous to V_0 for venturis. Because the value of $K_{c,\,min}$ is constant for geometrically similar cavities in a given flow device, it follows (from eq. (3)) that

$$\frac{NPSH_{ref} + (\Delta h_v)_{ref}}{NPSH + \Delta h_v} = \left[\frac{(V_1)_{ref}}{V_1}\right]^2 \qquad (4)$$

where the subscript ref denotes a reference value that must be established by experiment. With flow similarity, the fluid velocity at the pump inlet is proportional to pump rotative speed N, and thus equation (4) may be expressed as

$$\frac{NPSH_{ref} + (\Delta h_v)_{ref}}{NPSH + \Delta h_v} = \left(\frac{N_{ref}}{N}\right)^2 \qquad (5)$$

Equation (5) may be used to predict the required NPSH for a particular pump operated with cavitation at a fixed flow coefficient and head coefficient ratio but with changes in liquid, liquid temperature, and/or rotative speed. For a fixed rotative speed, equation (5) reduces to

$$NPSH_{ref} - NPSH = \Delta h_v - (\Delta h_v)_{ref} \tag{6}$$

which states that a change in NPSH requirements for different liquids and/or liquid temperatures is equal to the change in the maximum pressure depression Δh_v within the cavitated region.

The procedure for estimating Δh_v, required for use in equations (5) and (6), is discussed in the following section.

Determination of Cavity Pressure Depressions

Thermodynamic effects of cavitation. - A method for estimating values of Δh_v for untested liquids and conditions from known reference values was previously reported for venturis in references 10, 11, and 16. However, the pertinent results that lead to the development of the prediction method for pumps presented herein are included for convenience and clarity.

The previously mentioned reduction in pressure (below free-stream vapor pressure) within cavitated regions of various liquids is attributed to evaporative cooling of a thin layer of liquid adjacent to the cavity. This cooling causes a decrease in the vapor pressure of the affected liquid layer and a corresponding decrease in cavity pressure provided that the liquid and its vapor are locally in thermodynamic equilibrium and no permanent gases are present.

Heat balance. - The magnitude of cavity pressure depression can be estimated by setting up (as an initial step) a heat balance between the heat required for vaporization and the heat drawn from the liquid surrounding the cavity; that is,

$$\rho_v \mathscr{V}_v L = \rho_l \mathscr{V}_l C_l (\Delta T) \tag{7}$$

where $\mathscr{V}_l$ represents the volume of the thin layer of liquid that is cooled during vaporization. The cooled layer of liquid is only a fraction of the total liquid flow. For small changes in temperature of the liquid layer, the temperature drop ΔT may be expressed as

$$\Delta T = \Delta h_v \left(\frac{1}{\frac{dh_v}{dT}} \right)$$

where dh_v/dT is the slope of the vapor pressure-temperature curve. With the use of this relation equation (7) becomes

$$\Delta h_v = \frac{\rho_v}{\rho_l} \frac{\gamma_v}{\gamma_l} \frac{L}{C_l} \left(\frac{dh_v}{dT} \right) \tag{8}$$

An accurate solution of equation (8), which accounts for changes in fluid properties as the equilibrium temperature drops because of vaporization, is presented in reference 10. Values of Δh_v as a function of the vapor- to liquid-volume ratio based on the solution of reference 10 are presented in figure 1 for liquid hydrogen, water, butane, and

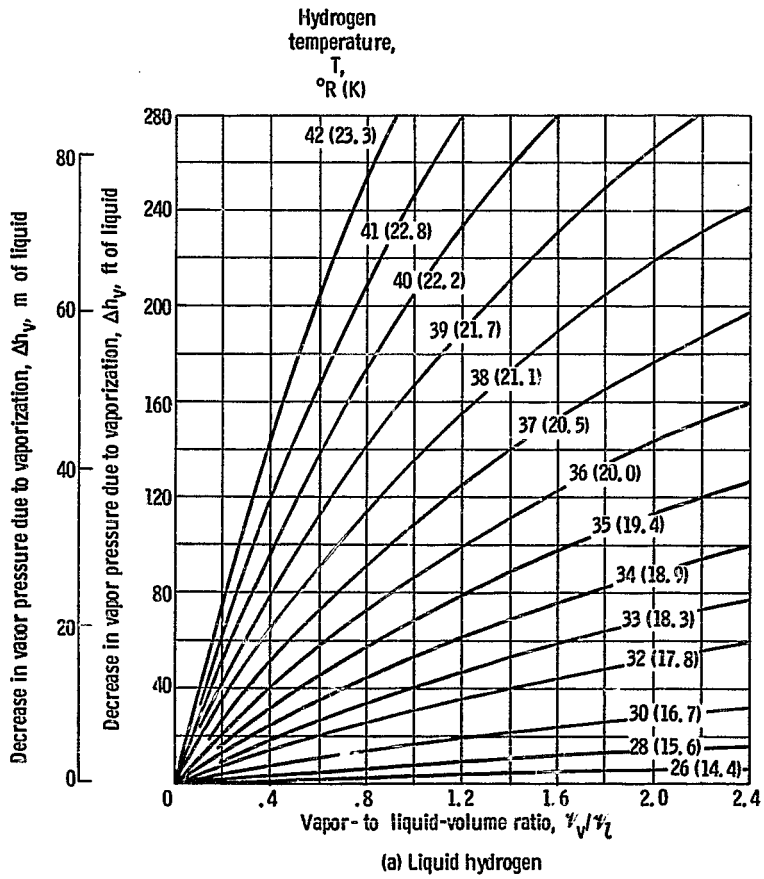

(a) Liquid hydrogen

Figure 1. - Vapor pressure depression as function of vapor- to liquid-volume ratio for various liquids and liquid temperatures.

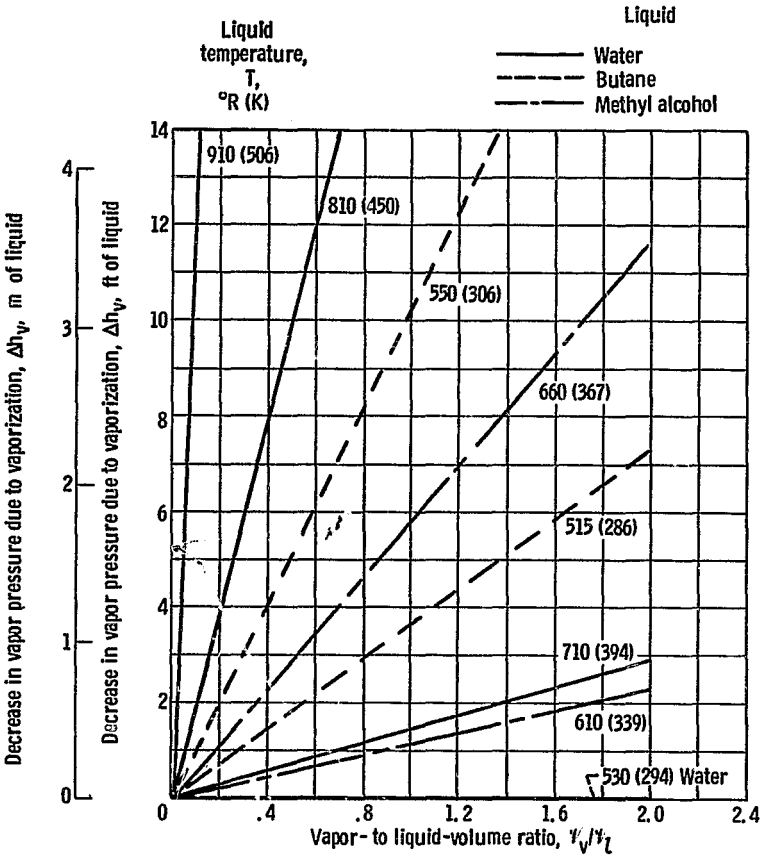

(b) Water, butane, and methyl alcohol.

Figure 1. - Concluded.

methyl alcohol at various temperatures. For a given value of γ_v/γ_l, the depression in cavity pressure can vary by several orders of magnitude depending on liquid and liquid temperature.

An approximate solution of equation (8) is obtained through the use of the Clausius-Clapeyron equation to approximate the slope of the vapor pressure-temperature curve. The Clausius-Clapeyron equation states that

$$\frac{\Delta h_v}{\Delta T} = \frac{\mathcal{J}}{\rho_l} \frac{L}{T(\nu_v - \nu_l)} \frac{g_c}{g} \tag{9}$$

where ν_v and ν_l are the specific volume of the vapor and liquid, respectively. Except near the critical temperature, $\nu_l \ll \nu_v$ and thus ν_l can be neglected. Setting $\nu_l = 0$ and substituting for $\Delta h_v/\Delta T$ (eq. (9)) in equation (8) gives

$$\Delta h_v \cong J\left(\frac{\rho_v}{\rho_l}\right)^2 \left(\frac{L^2}{C_l T}\right)\left(\frac{\mathscr{V}_v}{\mathscr{V}_l}\right)\left(\frac{g_c}{g}\right) \tag{10}$$

This expression provides a useful and close approximation of the curves presented in figure 1.

The vapor- to liquid-volume ratio $\mathscr{V}_v/\mathscr{V}_l$ in any real flow situation is not known and cannot be measured directly, and thus the values of this ratio from figure 1 are used only in a relative sense. Useful predictions for geometrically similar cavities have been made by experimentally establishing an effective or reference value of $\mathscr{V}_v/\mathscr{V}_l$ through the determination of cavity-pressure depressions Δh_v for one flow device, liquid, temperature, and velocity. Then values of $\mathscr{V}_v/\mathscr{V}_l$ for other geometrically similar flow devices, liquids, liquid temperatures, and flow velocities are estimated relative to this reference value, as described subsequently. With these predicted values of $\mathscr{V}_v/\mathscr{V}_l$ and figure 1, determination of Δh_v relative to reference data is possible.

Estimation of vapor- to liquid-volume ratio and cavity-pressure depression. - Theoretical analyses, coupled with experimental venturi cavitation results (refs. 10, 11, and 16), led to the development of the following expression relating the reference and predicted values of vapor- to liquid-volume ratio:

$$\left(\frac{\mathscr{V}_v}{\mathscr{V}_l}\right)_{pred} = \left(\frac{\mathscr{V}_v}{\mathscr{V}_l}\right)_{ref} \left(\frac{\alpha_{ref}}{\alpha}\right)^{1.0} \left(\frac{V_1}{V_{1,ref}}\right)^{0.8} \left(\frac{D}{D_{ref}}\right)^{0.2} \left[\frac{\left(\frac{\Delta X}{D}\right)}{\left(\frac{\Delta X}{D}\right)_{ref}}\right]^{0.3} \tag{11}$$

As previously discussed in the section Similarity relations for pumps, pump inlet velocity V_1 is proportional to pump rotative speed N under conditions of flow similarity. Also, for a given pump operated at a constant flow coefficient φ and a constant value of ψ/ψ_{NC}, cavity length (ΔX of eq. (11)) is considered to remain essentially constant for various liquids, liquid temperatures, and pump rotative speeds. Thus, when applied to a particular pump, equation (11) becomes

$$\left(\frac{\mathscr{V}_v}{\mathscr{V}_l}\right)_{pred} = \left(\frac{\mathscr{V}_v}{\mathscr{V}_l}\right)_{ref} \left(\frac{\alpha_{ref}}{\alpha}\right)^{1.0} \left(\frac{N}{N_{ref}}\right)^{0.8} \tag{12}$$

With $(\mathscr{V}_v/\mathscr{V}_l)_{pred}$ established, relative to the known reference value, the corresponding Δh_v value may be determined from either equation (10) or from the curves of

Δh_v against γ_v/γ_l similar to those of figure 1 for any liquid or liquid temperature of interest. With Δh_v known, the NPSH requirements may then be predicted by use of equation (5) (eq. (6) if N = constant). It should be emphasized that, because of the implied assumption of flow similarity used in this analysis, a predicted value of required NPSH applies only to the particular pump and the specific operating conditions of φ and ψ/ψ_{NC} used to obtain the required test data.

For pumps, the direct measurement of $(\Delta h_v)_{ref}$, needed for use in the prediction equations, is not feasible. However, an estimate of Δh_v is possible without measuring cavity pressure directly. For a particular pump, this estimation requires that two sets of experimental data be obtained to determine the NPSH requirement at each value of ψ/ψ_{NC} and flow coefficient φ of interest. These tests need not necessarily be for the same liquid, liquid temperature, or pump rotative speed; however, at least one of these must yield measurable thermodynamic effects of cavitation. Measured values of NPSH and rotative speed N from one of the two test conditions are arbitrarily chosen as the reference values in equation (5). Because both Δh_v and $(\Delta h_v)_{ref}$ are unknown, an iterative procedure is required for the solution of equation (5). First, a value of $(\Delta h_v)_{ref}$ is assumed. The corresponding $(\gamma_v/\gamma_l)_{ref}$ can be obtained from equation (10) (or equivalent curves of fig. 1). The predicted γ_v/γ_l for the second test condition is then calculated from equation (12), and the corresponding value of Δh_v is then obtained from equation (10) (or equivalent curves of fig. 1). Successive calculations are made until the values of Δh_v and $(\Delta h_v)_{ref}$ satisfy equation (5). With the value of $(\Delta h_v)_{ref}$ once determined, values of Δh_v and, consequently, the NPSH requirements can be predicted for other liquids, liquid temperatures, or pump rotative speeds by the use of equation (5). As indicated in the preceding paragraph, the predicted values apply only to a particular pump and specific values of ψ/ψ_{NC} used to obtain the necessary test data (i.e., values of ψ/ψ_{NC} and φ corresponding to $\Delta h_{v,ref}$).

Further details on the implementation of the prediction method are presented in appendix B. Numerical examples, which use test data obtained under various conditions, are included.

APPARATUS AND PROCEDURE

The test rotors used in the present study are shown in figure 2. Some of the geometric features of each rotor are also presented in the figure. The flat-plate helical inducer (fig. 2(a)) is the same as that described fully in reference 9. The centrifugal pump impeller with the 2.67-inch (6.78-cm) inlet blade tip diameter, herein termed impeller A (fig. 2(b)), is described in reference 17. The other centrifugal impeller (inlet blade tip

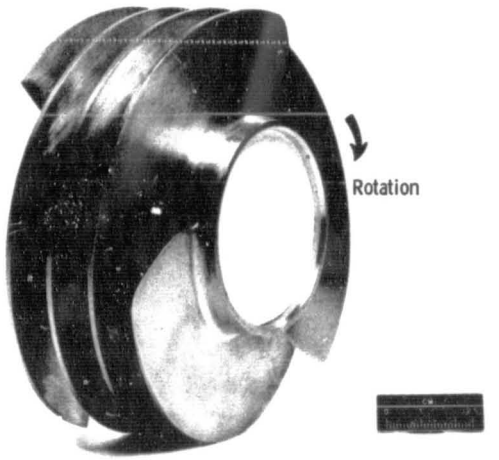

C-67-423

(a) Flat-plate helical inducer. Tip diameter, 4.986 inches (12.66 cm); hub diameter, 2.478 inches (6.29 cm); number of blades, 3; inlet tip blade angle, 84° (from axial direction).

$\tan(90-84) = .105$

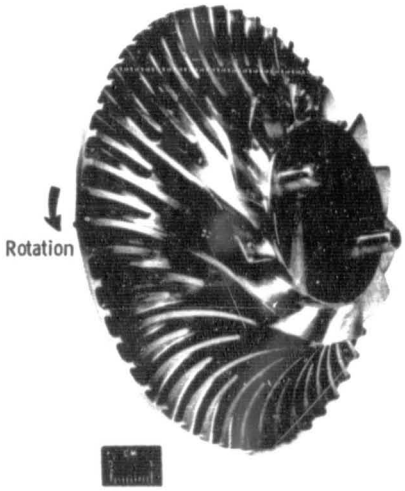

C-67-1782

(b) Impeller A, centrifugal pump. Inlet blade tip diameter, 2.67 inches (6.78 cm); hub diameter at inlet, 1.87 inches (4.75 cm); overall diameter, 4.56 inches (11.58 cm); number of blades, 12; number of splitter vanes, 12 primary and 24 secondary; inlet tip blade angle, 71.3° (from axial direction).

$\tan(90-71.3) = .338$

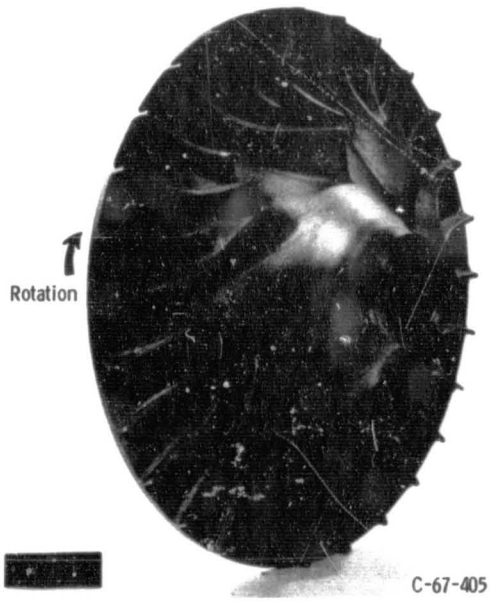

C-67-405

(c) Impeller B, centrifugal pump. Inlet blade tip diameter, 3.86 inches (9.80 cm); hub diameter, 1.54 inches (3.91 cm); overall diamter, 7.44 inches (18.90 cm); number of blades, 7; number of splitter vanes, 7 primary and 14 secondary; inlet tip blade angle, 68° (from axial direction).

$\tan(90-68) = .404$

Figure 2. Test rotors.

diam, 3.86 in. or 9.80 cm), herein termed impeller B, is shown in figure 2(c) and is described in reference 18. The impellers used for this study were those for which sufficient data were available to check the prediction method. They do not necessarily represent the best designs for good cavitation performance. The rotors were tested in the liquid-hydrogen test facilities located at the NASA Plum Brook Station.

The test procedure used to obtain the data was the same for the three rotors. Throughout each test run, the liquid temperature, rotative speed, and flow coefficient were held constant. The NPSH was steadily reduced from a value corresponding to noncavitating conditions ($\psi/\psi_{NC} = 1.0$) to a value that corresponds to about $\psi/\psi_{NC} = 0.7$. This same procedure was used for each liquid temperature, rotative speed, and flow coefficient studied.

RESULTS AND DISCUSSION

The prediction method was applied to an axial-flow inducer and several centrifugal pump impellers. These rotors were operated in several different liquids at various liquid temperatures. Experimental and predicted cavitation performance results are compared for (1) an inducer operated in liquid hydrogen at various temperatures, (2) two centrifugal pump impellers operated at various values of flow coefficient and rotative speed in constant-temperature hydrogen, and (3) several small commercial centrifugal pumps operated in a variety of liquids, each over a temperature range. Experimental data for the commercial pumps are taken from references 1 and 2.

Inducer Cavitation Performance

The cavitation performance for the 4.986-inch- (12.664-cm-) diameter research inducer shown in figure 2(a) is presented in figure 3. The data are for liquid hydrogen at temperatures from 27.5° to 36.6° R (15.3 to 20.3 K) and for constant values of flow coefficient and rotative speed. As expected, for a given value of the head-rise coefficient ratio ψ/ψ_{NC}, the required NPSH decreases rapidly with increasing hydrogen temperature. The performance results obtained at 27.5° and 31.7° R (15.3 and 17.6 K) were arbitrarily chosen as reference test data to predict the NPSH requirements for hydrogen at 34.3° and 36.6° R (19.1 and 20.3 K). The predicted NPSH requirements (dashed lines of fig. 3) agree with experimental results.

The magnitude of the thermodynamic effects of cavitation realized at the various temperatures for ψ/ψ_{NC} of 0.9 and 0.8 are listed in table I. For both values of ψ/ψ_{NC}, the Δh_v values increased rapidly with increasing temperature.

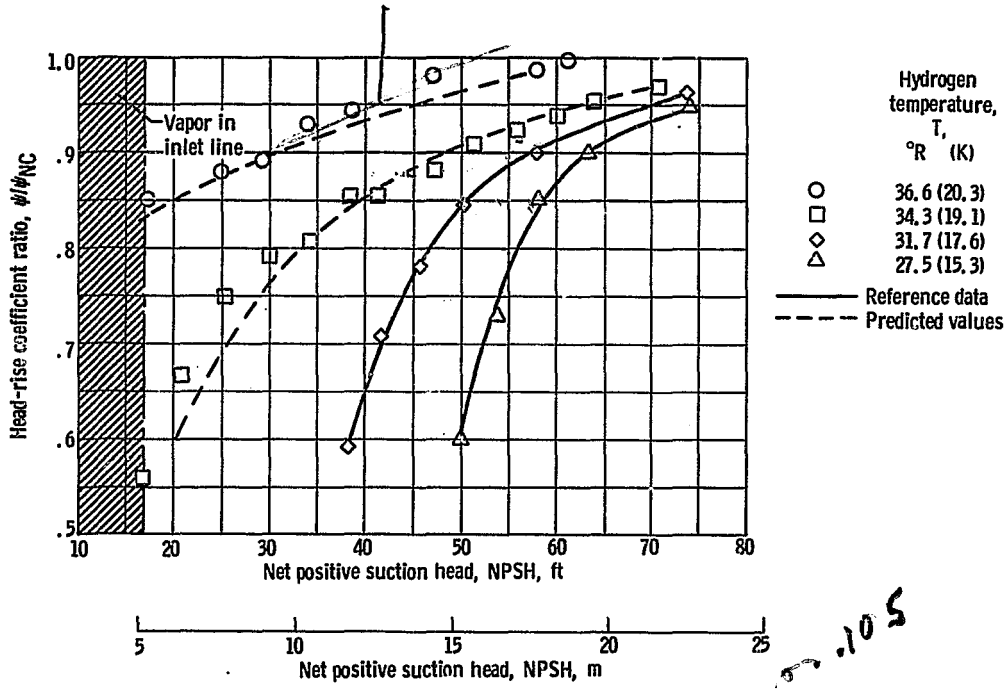

Figure 3. - Comparison of experimental and predicted inducer cavitation performance for an inducer in hydrogen at constant rotative speed of 20 000 rpm and flow coefficient of 0.074.

The data of table I also show that the values of Δh_v increase with decreasing values of the head coefficient ratio ψ/ψ_{NC}. A decrease in the value of ψ/ψ_{NC} implies an increase in the length of cavity present within the blade passages. The analysis shows that Δh_v should increase with cavity length ΔX under otherwise fixed conditions (see eq. (11)). Thus, the trend noted in table I is expected.

At a relatively low value of NPSH, depending on the pump design and mode of operation, a condition can be reached where the static pressure in the inlet line becomes equal to the vapor pressure of the entering liquid. As a result, vapor forms in the inlet line,

TABLE I. - INDUCER CAVITY-PRESSURE DEPRESSION VALUES

[Rotative speed, 20 000 rpm; flow coefficient, 0.074.]

Head-rise coefficient ratio, ψ/ψ_{NC}	Hydrogen temperature, T, °R (K)			
	27.5 (15.3)	31.7 (17.6)	34.3 (19.1)	36.6 (20.3)
	Cavity-pressure depression, Δh_v, ft of liquid (m of liquid)			
0.9	2.0 (0.6)	8.1 (2.5)	17.3 (5.3)	35.0 (10.7)
.8	2.2 (0.7)	11.5 (3.5)	24.0 (7.3)	----------

and any further reductions in NPSH produce increasing amounts of vapor that are ingested by the pump. For the inducer performance data of figure 3, this condition of boiling in the inlet line occurred at an NPSH of about 17 feet (5.2 m). The data for 36.6° R (20.3 K) show that the test inducer was capable of pumping boiling hydrogen while maintaining about 85 percent of the noncavitating head-rise coefficient.

With vapor present in the inlet line, the requirement of flow similarity with respect to reference test conditions is, in general, not met; and thus the present method is not applicable to this mode of operation. The subject of two-phase flow in the inlet line and its effect on inducer cavitation performance in hydrogen is discussed in references 19 and 20.

Pump Cavitation Performance

Impeller A. - Cavitation performance for the 2.67-inch- (6.78-cm-) inlet diameter centrifugal impeller operated in hydrogen at a near-constant temperature of 37.2° R

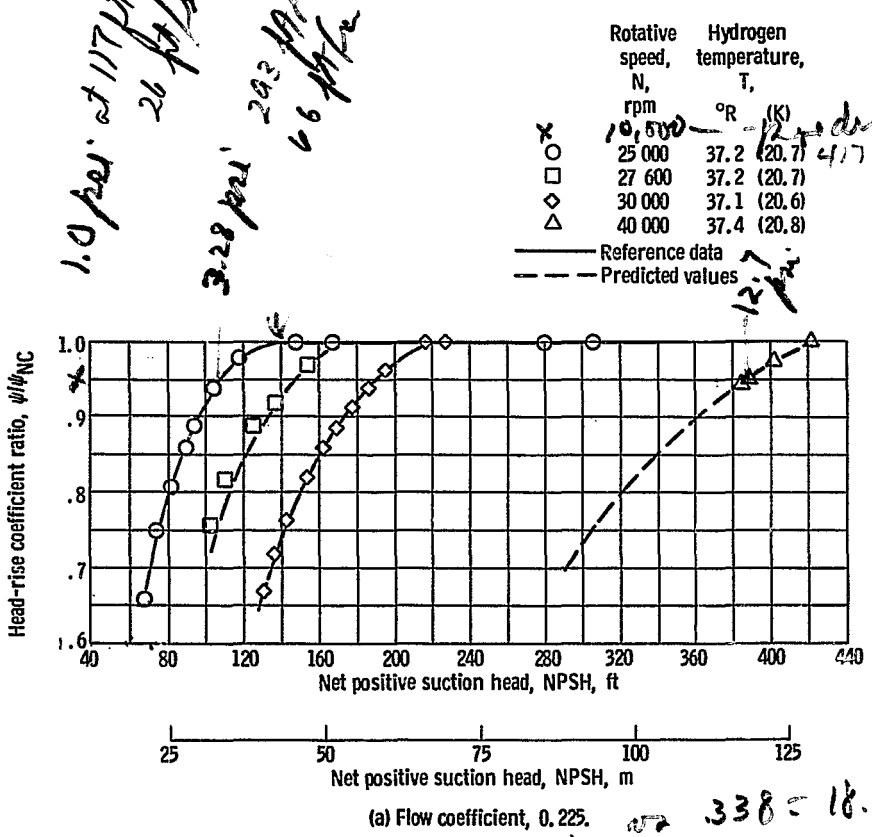

(a) Flow coefficient, 0.225.

Figure 4. - Comparison of experimental and predicted cavitation performance for impeller A in liquid hydrogen.

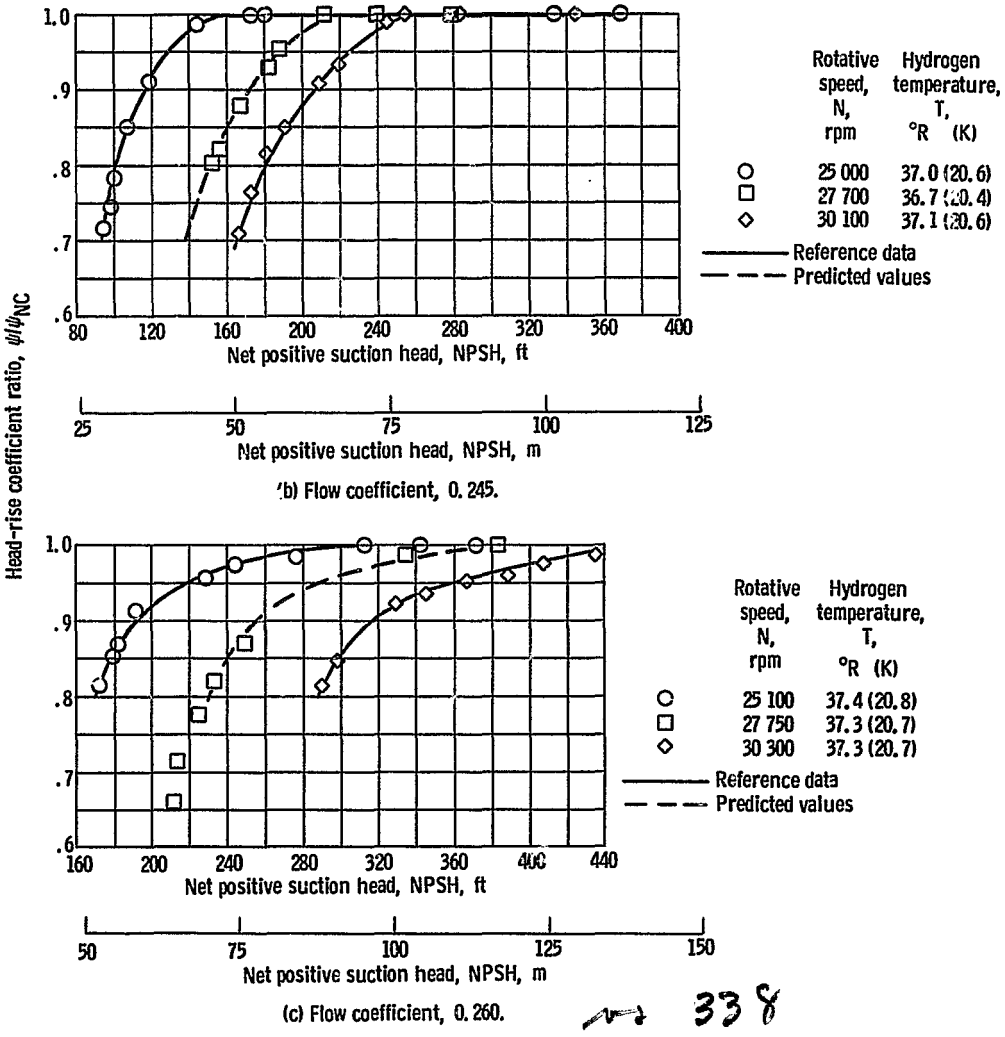

(b) Flow coefficient, 0.245.

(c) Flow coefficient, 0.260.

Figure 4. - Concluded.

(20.7 K) is presented in figure 4 for speeds from 25 000 to 40 000 rpm and flow coefficients of 0.225, 0.245, and 0.260. The predicted cavitation performance curves (dashed lines) are all in excellent agreement with the experimental data.

The values of Δh_v realized for this impeller (from data of fig. 4) are listed in table II for a head-rise coefficient ratio of 0.9. Thermodynamic effects of cavitation increased significantly with increasing pump rotative speed. At a flow coefficient of 0.245, the Δh_v value for N = 27 700 rpm is lower than the Δh_v value for N = 25 000 rpm. This apparent lower value of Δh_v is the result of the lower test liquid temperature for this particular set of performance data (see fig. 4(b)).

The thermodynamic effects of cavitation also varied considerably with changes in flow coefficient (table II). This trend was also observed in reference 9. The results of

TABLE II. - IMPELLER A CAVITY-PRESSURE DEPRESSION VALUES

[Nominal hydrogen temperature, 37.2° R (20.7 K); head-rise coefficient ratio, 0.9.]

Flow coefficient, φ	Nominal rotative speed, N, rpm			
	25 000	27 700	30 000	40 000
	Cavity-pressure depression, Δh_v, ft of liquid (m of liquid)			
0.225	98 (29.9)	103 (31.4)	106 (32.3)	133 (40.5)
.245	112 (34.1)	111 (33.8)	127 (38.7)	---
.260	110 (33.5)	114 (34.8)	122 (37.2)	---

reference 21 indicate that the magnitude of thermodynamic effects of cavitation is a function of the noncavitating wall pressure distribution. Since changes in flow coefficient affect the pressure distribution on the pump blades, this variation in thermodynamic effects with flow coefficient is to be expected.

Because of the rapid change in the physical properties of hydrogen with temperature, the seemingly small variation in temperature of about 0.3° R (0.2 K) between the various performance curves, as in figure 4(a), must be accounted for if reasonably accurate predictions are to be realized. For N = 40 000 rpm and $\psi/\psi_{NC} = 0.9$, for example, the predicted value of NPSH would have been 380 feet (115.8 m) of hydrogen instead of 361 feet (110.0 m) if the temperature for all the performance curves of figure 4(a) had been assumed to be constant at 37.1° R (20.6 K).

Impeller B. - Experimental and predicted results for the 3.86-inch- (9.80-cm-) inlet diameter impeller operated in hydrogen at nearly constant temperature for three rotational speeds are presented in figure 5. The predicted cavitation performance (dashed line) is in good agreement with the experimental data. As with pump impeller A, the thermodynamic effects of cavitation increase significantly with pump speed, as can be noted by the Δh_v values listed in table III. However, for a comparable hydrogen temperature, the magnitudes of the thermodynamic effects for this impeller exceed the largest value noted for either the inducer or impeller A. The reason for these large changes in thermodynamic effects of cavitation with rotor design is not known at present.

An examination of the Δh_v values of tables I to III show conclusively that thermodynamic effects of cavitation in liquid hydrogen are substantial. These effects depend on liquid temperature, rotor type and geometric design, rotative speed, flow coefficient φ, and, to some extent, head-rise coefficient ratio ψ/ψ_{NC}.

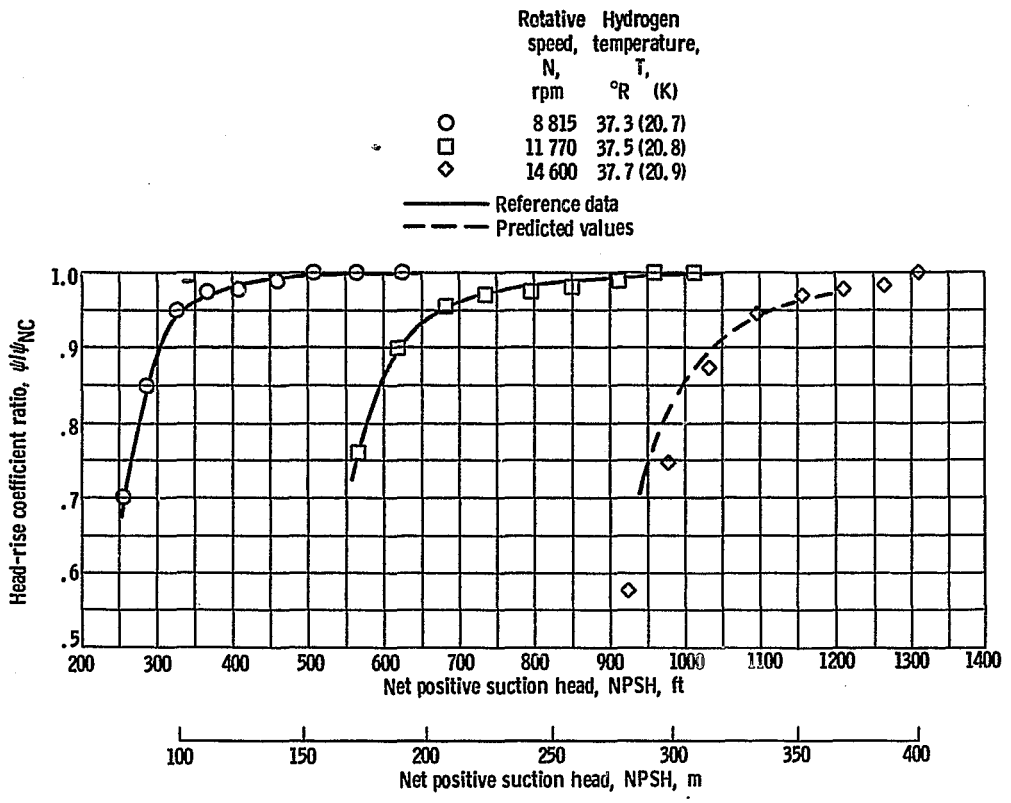

Figure 5. - Comparison of experimental and predicted cavitation performance for impeller B in liquid hydrogen. Flow coefficient, 0.44.

TABLE III. - IMPELLER B CAVITY-PRESSURE DEPRESSION VALUES

[Flow coefficient, 0.44; head-rise coefficient ratio, 0.9.]

Rotative speed, N, rpm	Hydrogen temperature, T		Cavity-pressure depression, Δh_v	
	°R	K	ft of liquid	m of liquid
8 815	37.3	20.7	141	43.0
11 770	37.5	20.8	171	52.1
14 600	37.7	20.9	199	60.7

Commercial pumps. - The prediction method was also used to predict the cavitation performance for several small commercial pumps operated in a variety of liquids at various temperatures. The measured and predicted NPSH requirements for three single-stage centrifugal units pumping water, methyl alcohol, butane, and Freon-11 are compared in table IV. The NPSH values listed are taken from references 1 and 2. All values are for a head-rise coefficient ratio ψ/ψ_{NC} of 0.97, a pump speed of about 3550 rpm, and the operating point of best efficiency. The two reference test values of

TABLE IV. - COMPARISONS OF MEASURED AND PREDICTED PUMP CAVITATION PERFORMANCE

[Nominal rotative speed, 3550 rpm; head-rise coefficient ratio, 0.97.]

Pump	Liquid	Temperature, T		Net positive suction head, NPSH			
		^{o}R	K	ft		m	
				Measured (±0.5 ft)	Predicted	Measured (±0.2 m)	Predicted
I (ref. 2)	Water	534	297	[a]17.5	----	[a]5.3	---
		600	333	17.5	17.5	5.3	5.3
		670	372	17.5	17.4	5.3	5.3
		710	394	[a]17.0	----	[a]5.2	---
		735	408	16.0	16.5	4.9	5.0
		756	420	13.3	15.6	4.1	4.8
	Methyl alcohol	560	311	17.5	17.4	5.3	5.3
		611	339	16.7	16.8	5.1	5.1
		641	356	15.5	15.3	4.7	4.7
		663	368	13.5	13.3	4.1	4.1
II (ref. 1)	Water	530	294	12.3	11.8	3.7	3.6
		710	394	[a]11.0	----	[a]3.4	---
		760	422	8.6	8.7	2.6	2.7
	Butane	495	275	9.8	10.2	3.0	3.1
		515	286	[a]8.8	----	[a]2.7	---
		540	300	5.1	5.6	1.6	1.7
		550	306	3.5	3.4	1.1	1.0
	Freon-11	545	303	10.2	10.5	3.1	3.2
		580	322	8.4	8.1	2.6	2.5
III (ref. 1)	Water	530	294	[a]12.0	----	[a]3.7	---
		750	417	[a]9.5	----	[a]2.9	---
		785	436	6.0	6.0	1.8	1.8
		870	483	[b]2.0	0	0.6	0

[a]Reference test data.

[b]Estimated accuracy of 2.0 ft (0.6 m).

NPSH listed for each pump (noted by (a)) were arbitrarily chosen to determine reference values of vapor- to liquid-volume ratio $(\forall_v/\forall_l)_{ref}$ and subsequently $(\Delta h_v)_{ref}$ for use in the prediction method. The predicted results are in excellent agreement with the experimental data. In fact, except for the 756° R (420 K) water data for pump I, the predicted values are all within the experimental accuracy of measured NPSH values.

For pump III operated in 870° R (483 K) water, the predicted NPSH value is zero, which implies that this pump should have been capable of satisfactory operation at an NPSH value sufficiently low to cause vapor to form in the inlet line. Reference 2 states that there were indeed indications of flashing in the inlet line at rated flow.

As a consequence, the listed NPSH value of 2.0 feet (0.6 m) of water was actually determined by extrapolation of performance data obtained at less-than-design flow rates. This set of data, as well as the hydrogen data of figure 3, illustrates that it is possible to pump boiling liquids satisfactorily if the fluid being pumped has sufficiently high thermodynamic effects of cavitation.

CONCLUDING REMARKS

The method for predicting the cavitation performance of pumps presented herein provided consistently good agreement between predicted and experimental results for several different pumps operated in liquids having widely diverse physical properties. Use of the method requires that two sets of test data, at least one of which provides measurable thermodynamic effects, be available for the pump and operating conditions of interest. However, the test data need not necessarily be for the same liquid, liquid temperature, or pump rotative speed. From these reference tests, accurate predictions of cavitation performance for a given pump can be made for any liquid, liquid temperature, and pump rotative speed provided that a condition of flow similarity is maintained.

The method also has useful application in the generalization of experimental data obtained with liquids that exhibit substantial thermodynamic effects of cavitation. Pump studies involving a particular liquid, for example, need not be conducted at precise values of liquid temperature or rotative speed since, by use of the present method, the data can be normalized or adjusted to any convenient liquid temperature or pump speed. Use of the prediction method may provide substantial reductions in the cost and development time required for new pump designs, particularly for those used in the aerospace field. It should be possible to conduct development testing at reduced speed using convenient or easy-to-handle liquids that exhibit thermodynamic effects of cavitation, such as Freon or high-temperature water; from these tests, the cavitation performance for the liquid and operating condition of interest may be predicted.

Although additional studies are required to prove the validity of the method to size effects for geometrically similar pumps, additional substantial savings are possible if the method can be used to accurately predict the cavitation performance for a full-scale pump from test results obtained for smaller prototypes.

Lewis Research Center,
National Aeronautics and Space Administration,
Cleveland, Ohio, March 27, 1969,
128-31-32-12-22.

APPENDIX A

SYMBOLS

C_l	specific heat of liquid, Btu/(lbm)(^oR); J/(kg)(K)
D	characteristic body dimension, in.; cm
g	local acceleration due to gravity, 32.163 ft/sec^2; 9.80 m/sec^2
g_c	dimensional constant, 32.174 (ft)(lbm)/(sec^2)(lbf); 1.0 (m)(kg)/(sec^2)(N)
ΔH	pump or inducer head rise, ft of liquid; m of liquid
h_c	pressure in cavitated region, ft of liquid abs; m of liquid abs
h_0	free-stream or pump inlet static pressure, ft of liquid abs; m of liquid abs
h_v	vapor pressure corresponding to free-stream temperature, ft of liquid abs; m of liquid abs
Δh_v	decrease in vapor pressure due to vaporization, ft of liquid; m of liquid
J	mechanical equivalent of heat, 778 (ft)(lbf)/Btu
K	developed cavitation parameter based on free-stream vapor pressure, $(h_0 - h_v)/(V_0^2/2g)$
$K_{c,min}$	developed cavitation parameter based on minimum cavity pressure, $(h_0 - h_{c,min})/(V_0^2/2g)$
k	thermal conductivity of saturated liquid, (Btu)(ft)/(hr)(ft^2)(^oR); J/(m)(sec)(K)
L	latent heat of vaporization, Btu/lbm; J/kg
N	rotative speed, rpm
T	free-stream liquid temperature, ^oR; K
ΔT	decrease in local equilibrium temperature due to vaporization, ^oR; K
U_T	blade tip velocity, ft/sec; m/sec
V_0	free-stream velocity, ft/sec; m/sec
V_1	mean axial inlet velocity, ft/sec; m/sec
$\mathscr{V}_l$	volume of saturated liquid, cu ft; cu m
$\mathscr{V}_v$	volume of saturated vapor, cu ft; cu m
ΔX	length of cavitated region, in.; cm
α	thermal diffusivity, $k/\rho_l C_l$, ft^2/hr; m^2/hr

$7.71 \times 10^{-3} \frac{ft^2}{hr}$ for H_2

ν_l specific volume of saturated liquid, cu ft/lbm; cu m/kg

ν_v specific volume of saturated vapor, cu ft/lbm; cu m/kg

ρ_l saturated liquid density, lbm/cu ft; kg/cu m

ρ_v saturated vapor density, lbm/cu ft; kg/cu m

φ flow coefficient, V_1/U_T

ψ head-rise coefficient, $\Delta H/U_T^2$

Subscripts:

min minimum

NC noncavitating

pred predicted value

ref reference value obtained from experimental tests

APPENDIX B

NUMERICAL EXAMPLES

Example 1 - Prediction Based on Test Data Obtained for a Given Liquid at Various Temperatures

Cavitation performance curves are available for an inducer operated at a constant flow coefficient and rotative speed in liquid hydrogen at 27.5° and 31.7° R (15.3 and 17.6 K); see figure 3.

To be determined is the inducer NPSH required for 36.6° R (20.3 K) liquid hydrogen at a head-rise coefficient ratio of 0.9 for the same operating conditions.

From the analysis presented earlier,

$$\frac{NPSH_{ref} + (\Delta h_v)_{ref}}{NPSH + \Delta h_v} = \left(\frac{N_{ref}}{N}\right)^2 \tag{B1}$$

and

$$\left(\frac{\nu_v}{\nu_l}\right)_{pred} = \left(\frac{\nu_v}{\nu_l}\right)_{ref} \left(\frac{N}{N_{ref}}\right)^{0.8} \left(\frac{\alpha_{ref}}{\alpha}\right)^{1.0} \tag{B2}$$

With 27.5° R (15.3 K) hydrogen data arbitrarily chosen for reference conditions, the values of NPSH for a head-rise coefficient ratio of 0.9 (from fig. 3) are

$$NPSH_{ref} = 63.5 \text{ ft } (19.4 \text{ m}) \quad \text{for } T_{ref} = 27.5^\circ \text{ R } (15.3 \text{ K})$$

$$NPSH = 57.4 \text{ ft } (17.5 \text{ m}) \quad \text{for } T = 31.7^\circ \text{ R } (17.6 \text{ K})$$

For this example, $N_{ref} = N$; $\alpha_{ref} = 7.71 \times 10^{-3}$ square feet per hour (7.16×10^{-4} m^2/hr); $\alpha = 7.23 \times 10^{-3}$ square feet per hour (6.71×10^{-4} m^2/hr). Substitution of these values into equations (B1) and (B2) yields

$$\Delta h_v - (\Delta h_v)_{ref} = 6.1 \text{ ft } (1.9 \text{ m})$$

and

$$\left(\frac{\nu_v}{\nu_l}\right) = 1.07 \left(\frac{\nu_v}{\nu_l}\right)_{ref}$$

An iterative solution of these two expressions using the curves of figure 1(a) results in the following:

$$\left(\frac{\nu_v}{\nu_l}\right)_{ref} = 0.25$$

and

$$(\Delta h_v)_{ref} = 2.0 \text{ ft } (0.6 \text{ m})$$

For hydrogen at 36.6° R (20.3 K), $\alpha = 6.69 \times 10^{-3}$ square feet per hour (6.22×10^{-4} m^2/hr). With the use of this value for α and the foregoing reference value for $(\nu_v/\nu_l)_{ref}$ in equation (B2), the predicted $(\nu_v/\nu_l)_{pred}$ for 36.6° R (20.3 K) hydrogen is

$$\left(\frac{\nu_v}{\nu_l}\right)_{pred} = 0.25\ (1.0)\left(\frac{7.7 \times 10^{-3}}{6.69 \times 10^{-3}}\right) = 0.29$$

From figure 1(a), the corresponding value for Δh_v is 35.0 feet (10.7 m). The predicted value of required NPSH for 36.6° R (20.3 K) hydrogen is obtained by substitution of the reference values and Δh_v into equation (B1); thus,

$$\text{NPSH} = 63.5 + 2.0 - 35.0 = 30.5 \text{ ft } (9.3 \text{ m})$$

The corresponding measured value of NPSH is about 30.0 feet (9.1 m).

Example 2 - Prediction Based on Test Data Obtained with a Given Liquid at Different Temperatures and Pump Rotative Speeds

Cavitation performance curves are available for a pump handling 37.2° R (20.7 K) hydrogen at 25 000 rpm and 37.1° R (20.6 K) hydrogen at 30 000 rpm at a constant flow coefficient of 0.225 (see fig. 4(a)).

To be determined is the pump NPSH required with 37.4° R (20.8 K) hydrogen for a head-rise coefficient ratio of 0.95, a pump speed of 40 000 rpm, and the same flow coefficient.

With the data for 25 000 rpm abitrarily taken as reference conditions, the NPSH values for a head-rise coefficient ratio of 0.95 (from fig. 4(a)) are

$$NPSH_{ref} = 107.5 \text{ ft } (32.8 \text{ m}) \quad \text{for } 25\,000 \text{ rpm} = N_{ref}$$

$$NPSH = 190.0 \text{ ft } (57.9 \text{ m}) \quad \text{for } 30\,000 \text{ rpm} = N$$

Substitution of these values in equations (B1) and (B2) yields

$$(\Delta h_v)_{ref} - 0.695\,\Delta h_v = 24.5 \text{ ft } (7.5 \text{ m})$$

$$\left(\frac{\nu_v}{\nu_l}\right) = 1.16 \left(\frac{\nu_v}{\nu_l}\right)_{ref}$$

An iterative solution of the two preceding expressions using the curves of figure 1(a) results in the following reference values: (Note: for this example, changes in α (eq. (B2)) are negligible; but effects of small changes in hydrogen temperature are accounted for in the use of curves of fig. 1.)

$$\left(\frac{\nu_v}{\nu_l}\right)_{ref} = 0.80; \quad (\Delta h_v)_{ref} = 98.0 \text{ ft } (29.9 \text{ m}) \quad \text{at } 25\,000 \text{ rpm}$$

Substituting $(\nu_v/\nu_l)_{ref}$ into equation (B2) gives the value of $(\nu_v/\nu_l)_{pred}$ for 40 000 rpm

$$\left(\frac{\nu_v}{\nu_l}\right)_{pred} = 0.8 \left(\frac{40\,000}{25\,000}\right)^{0.8} = 1.17 \quad \text{where } \alpha = \alpha_{ref}$$

From figure 1(a), the corresponding value of Δh_v at 37.4° R (20.8 K) is 134.0 feet (40.8 m). Substituting for Δh_v and N in equation (B1) and solving for NPSH yields

$$(NPSH)_{pred} = \frac{107.5 + 98.0}{\left(\frac{25\,000}{40\,000}\right)^2} - 134.0 = 392.1 \text{ ft } (119.5 \text{ m})$$

The corresponding measured value from figure 4(a) is about 387 feet (118.0 m).

Example 3 - Prediction Based on Test Data Obtained Using Different Liquids

The NPSH requirements are given for pump II (table IV) handling 710° R (394 K) water and 515° R (286 K) butane at fixed operating conditions (3550 rpm and ψ/ψ_{NC} = 0.97).

To be determined is the pump NPSH required for 550° R (306 K) butane under the same operating conditions.

With the water data arbitrarily chosen for reference, the NPSH values (from table IV) are

$$NPSH_{ref} = 11.0 \text{ ft } (3.4 \text{ m}) \quad \text{for } 710^\circ \text{ R } (394 \text{ K}) \text{ water}$$

$$NPSH = 8.8 \text{ ft } (2.7 \text{ m}) \quad \text{for } 515^\circ \text{ R } (286 \text{ K}) \text{ butane}$$

Values of liquid thermal diffusivity α are 6.60×10^{-3} square feet per hour (6.13×10^{-4} m^2/hr) for 710° R (395 K) water and 4.02×10^{-3} square feet per hour (3.73×10^{-4} m^2/hr) for 515° R (286 K) butane. Substituting the foregoing values of NPSH and α into equations (B1) and (B2) yields

$$\Delta h_v - (\Delta h_v)_{ref} = 2.2 \text{ ft } (0.7 \text{ m})$$

$$\left(\frac{\psi_v}{\psi_l}\right) = 1.64 \left(\frac{\psi_v}{\psi_l}\right)_{ref}$$

An iterative solution of the above relations using the curves of figure 1(b) gives

$$\left(\frac{\psi_v}{\psi_l}\right)_{ref} = 0.49; \quad (\Delta h_v)_{ref} = 0.7 \text{ ft } (0.2 \text{ m})$$

Substituting $(\rho_v/\rho_l)_{ref}$ into equation (B2) yields the predicted value of (ρ_v/ρ_l) for 550^o R (306 K) butane

$$\left(\frac{\rho_v}{\rho_l}\right)_{pred} = 0.49\ (1.0)\left(\frac{6.60\times10^{-3}}{4.02\times10^{-3}}\right) = 0.80$$

for butane, $\alpha_{550^o\ R\ (306\ K)} = \alpha_{515^o\ R\ (286\ K)}$. From figure 1(b), the corresponding value of Δh_v is 8.3 feet (2.5 m). Thus, from equation (B1), the predicted NPSH for pump II (table IV) pumping 550^o R (306 K) butane at 3550 rpm and a head-rise coefficient ratio of 0.97 is

$$NPSH_{pred} = 11.0 + 0.7 - 8.3 = 3.4\ ft\ (1.0\ m)$$

From table IV, the corresponding measured NPSH is 3.5 feet (1.1 m).

REFERENCES

1. Salemann, Victor: Cavitation and NPSH Requirements of Various Liquids. J. Basic Eng., vol. 81, no. 2, June 1959, pp. 167-180.

2. Spraker, W. A.: The Effects of Fluid Properties on Cavitation in Centrifugal Pumps. J. Eng. Power, vol. 87, no. 3, July 1965, pp. 309-318.

3. Wilcox, Ward W.; Meng, Phillip R.; and Davis, Roger L.: Performance of an Inducer-Impeller Combination at or Near Boiling Conditions for Liquid Hydrogen. Advances in Cryogenic Engineering. Vol. 8, K. D. Timmerhaus, ed., Plenum Press, Inc., 1963, pp. 446-455.

4. Jacobs, Robert B.: Prediction of Symptoms of Cavitation. J. Res. Natl. Bur. Std., sec. C, vol. 65, no. 3, July-Sept. 1961, pp. 147-156.

5. Stahl, H. A.; and Stepanoff, A. J.: Thermodynamic Aspects of Cavitation in Centrifugal Pumps. Trans. ASME, vol. 78, no. 8, Nov. 1956, pp. 1691-1963.

6. Stepanoff, A. J.: Cavitation in Centrifugal Pumps with Liquids Other Than Water. J. Eng. Power, vol. 83, no. 1, Jan. 1961, pp. 79-90.

7. Stepanoff, A. J.: Cavitation Properties of Liquids. J. Eng. Power, vol. 86, no. 2, Apr. 1964, pp. 195-200.

8. Ball, Calvin L.; Meng, Phillip R.; and Reid, Lonnie: Cavitation Performance of 84° Helical Pump Inducer Operated in 37° and 42° R Liquid Hydrogen. NASA TM X-1360, 1967.

9. Meng, Phillip R.: Change in Inducer Net Positive Suction Head Requirement with Flow Coefficient in Low Temperature Hydrogen (27.9° to 36.6° R). NASA TN D-4423, 1968.

10. Gelder, Thomas F.; Ruggeri, Robert S.; and Moore, Royce D.: Cavitation Similarity Considerations Based on Measured Pressure and Temperature Depressions in Cavitated Regions of Freon-114. NASA TN D-3509, 1966.

11. Moore, Royce D; and Ruggeri, Robert S.: Venturi Scaling Studies on Thermodynamic Effects of Developed Cavitation of Freon-114. NASA TN D-4387, 1968.

12. Ruggeri, Robert S.; and Gelder, Thomas F.: Cavitation and Effective Liquid Tension of Nitrogen in a Tunnel Venturi. NASA TN D-2088, 1964.

13. Pinkel, I. Irving; Hartmann, Melvin J.; Hauser, Cavour H.; Miller, Max J.; Ruggeri, Robert S.; and Soltis, Richard F.: Pump Technology. Selected Technology for the Petroleum Industry. NASA SP-5053, 1966, pp. 81-101.

14. Ruggeri, Robert S.; Moore, Royce D.; and Gelder, Thomas F.: Method for Predicting Pump Cavitation Performance. Paper presented at the ICRPG Ninth Liquid Propulsion Symposium, St. Louis, Oct. 25-27, 1967.

15. Hord, Jesse; Edmonds, Dean K.; and Millhiser, David R.: Thermodynamic Depressions Within Cavities and Cavitation Inception in Liquid Hydrogen and Liquid Nitrogen. Rep. 9705, National Bureau of Standards (NASA CR-72286), Mar. 1968.

16. Moore, Royce D.; and Ruggeri, Robert S.: Prediction of Thermodynamic Effects of Developed Cavitation Based on Liquid-Hydrogen and Freon-114 Data in Scaled Venturi. NASA TN D-4899, 1968.

17. Urasek, Donald C.: Investigation of Flow Range and Stability of Three Inducer-Impeller Pump Combinations Operating in Liquid Hydrogen. NASA TM X-1727, 1969.

18. Miller, Max J.; and Soltis, Richard F.: Detailed Performance of a Radial-Bladed Centrifugal Pump Impeller in Water. NASA TN D-4613, 1968.

19. Meng, Phillip R.; and Connelly, Robert E.: Investigation of Effects of Simulated Nuclear Radiation Heating on Inducer Performance in Liquid Hydrogen. NASA TM X-1359, 1967.

20. Urasek, Donald C.; Meng, Phillip R.; and Connelly, Robert E.: Cavitation Performance of 80.6° Helical Inducer in Liquid Hydrogen. NASA TN D-5258, 1969.

21. Moore, Royce D.; Ruggeri, Robert S.; and Gelder, Thomas F.: Effects of Wall Pressure Distribution and Liquid Temperature on Incipient Cavitation of Freon-114 and Water in Venturi Flow. NASA TN D-4340, 1968.

NASA-Langley, 1969 — 15 E-4832

END OF REFERENCE

99

REFERENCE

100

NUMACHI, F.: EFFECT OF SURFACE ROUGHNESS ON CAVITATION PERFORMANCE OF HYDROFOILS - REPORT 3. TRANS. ASME, SER. B, J. BASIC ENG., VOL. 89, NO. 1, MAR. 1967.

F. NUMACHI
Professor Emeritus,
Tôhoku University,
Institute of High Speed Mechanics,
Sendai, Japan.
Mem. ASME

Effect of Surface Roughness on Cavitation Performance of Hydrofoils—Report 3

As a sequel to the first and second reports of the present series of experiments intended to gain knowledge on the effect of surface roughness on hydromechanical characteristics, particularly cavitation performance, the author has this time taken up the case of striations in the direction parallel to the chord, to determine their effect on cavitation efficiency and profile performance in general, for comparison with that of spanwise striations which were the subject of the preceding two reports.

Introduction

KNOWLEDGE of the effect on hydromechanical characteristics, particularly efficiency, of the surface roughness of blades and guidevanes of hydraulic machinery has frequently been demanded for their direct implications on the manufacture of actual hydraulic components. Following the work covered by the first two reports [1, 2][1] in the current series, in which roughness produced by striations in the direction of span was the subject, this present study deals with the case of striations in the direction of chord, to determine their effect on cavitation performance, for comparison with the previous results.

In the preceding experiments, the maximum roughness tested was 25S in the scale[2] specified by the Japanese Industrial Standards [3, 4], but in view of the occurrence in actual practice of even rougher surfaces on hydraulic turbines and pumps, a specimen of 35S was also tested on this occasion.

The first experiment carried out this time with 25S specimen resulted in a larger drag and smaller lift produced by the chordwise as compared to the previous spanwise striations. Investigation into the cause of this unexpected result revealed that it was the result of the incorrect method of finishing the specimen, and the method of specimen preparation was improved. Experience of the invalid experiment with the incorrect specimen is also reported here in the hope that it might be found to have some value for reference in practice.

The Clark Y 11.7 percent profile was adopted for the specimens in the present series, for the reason that its cavitation characteristics have already been thoroughly studied in the past [1, 2, 6, 7, 8]. Details of the profile form have been fully described before [6]. The specimens were again of chord and span both measuring 70 mm.

The experimental procedure has also been previously explained [6]. Various environmental factors constituting the conditions of experiment were held the same as for the previous experiments so as to eliminate their effect in making comparisons: Content of air a/a_s = 1.05–1.06 [9], static head H_s = 3.3 m.aq, water temperature t_w = 19 or 22 deg C.

[1] Numbers in brackets designate References at end of paper.

[2] The ASA scale [5] specifies center line average roughness, determined by the average height of protuberances above the surface center line. Correspondence between the Japanese and American standards is as follows:

JIS	0.2S	25S	35S
ASA	2μ in	125μ in.	160μ in.

Contributed by the Fluids Engineering Division and presented at the Winter Annual Meeting, New York, N. Y., November 27–December 1, 1966, of THE AMERICAN SOCIETY OF MECHANICAL ENGINEERS. Manuscript received at ASME Headquarters, August 8, 1966. Paper No. 66—WA/FE-26.

Record of Invalid Experiment

Roughness of Striations in the Direction of Chord

The method adopted for preparing the specimens and finishing their surface [10], as well as that for measuring the surface roughness [1, 2] has already been reported, and will not be repeated here. The specimen in question, intended to represent a roughness of 25S (which we will hereafter call C25S′) was made by first finishing the surface to 0.2S (which, as ascertained by the procedure described in the preceding report [1], is amply smooth to be regarded as hydrodynamically smooth), and then passing it over once with a 25S file in the direction of chord.

While it was subsequently found upon measurement that the actual roughness of this specimen was 26S and not 25S as intended, this was not the cause of the unexpected results from the specimen, since an inaccuracy of this extent in striations in the same direction has been verified by experiment covering spanwise striations [1] to be immaterial (affecting the cavitation performance by less than 0.2 percent).

Performance Curves

Performance curves for the C25S′ were obtained and compared with those for the specimens with 25S striations in the direction of span and with the hydrodynamically smooth 0.2S specimens from the previous experiments [1]. The results are presented graphically in Figs. 1–4. Explanations concerning the meaning of these curves has already been explained in detail [1], and it should suffice to recall that:

Lift coefficient $C_a = A/\frac{1}{2}\rho v^2 F$
Drag coefficient $C_w = W/\frac{1}{2}\rho v^2 F$
Cavitation coefficient $k_d = (p - p_d)/\frac{1}{2}\rho v^2$

where A, W: Lift and drag, respectively; ϵ = drag-lift ratio; p = pressure of flow; p_d = vapor pressure; v = flow velocity; F = blade surface = chord × span; ρ = density of water; α_0 = angle of incidence; λ_0 = position of cavitation head, measured from leading edge of blade; λ = position of cavitation tail, similarly measured; l = chord length.

With respect to zones around the profile:

Zone I: Vacuum (back) side, toward leading edge (head)
Zone II: Pressure (belly) side, toward head
Zone III: Back side, toward trailing edge (tail)
Zone IV: Belly side, toward tail

The curves marked I, II, . . . and so on, indicate the conditions of cavitation incipience in the respective zones.

It can be concluded from the data that:

(i) The effect on lift coefficient of striations along the chord

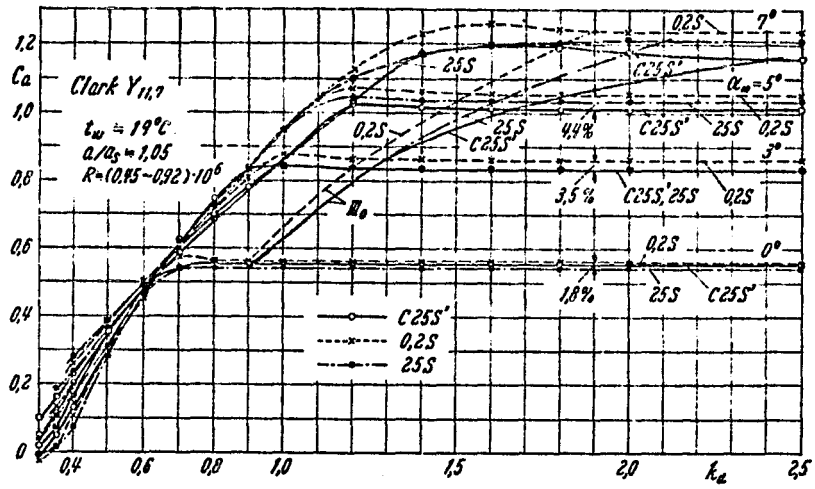

Fig. 1 Relation of lift coefficient C_a to cavitation coefficient k_d for different surface roughness

C25S′: Striations in direction of chord
25S: Striations in direction of span
0.2S: Hydrodynamically smooth surface

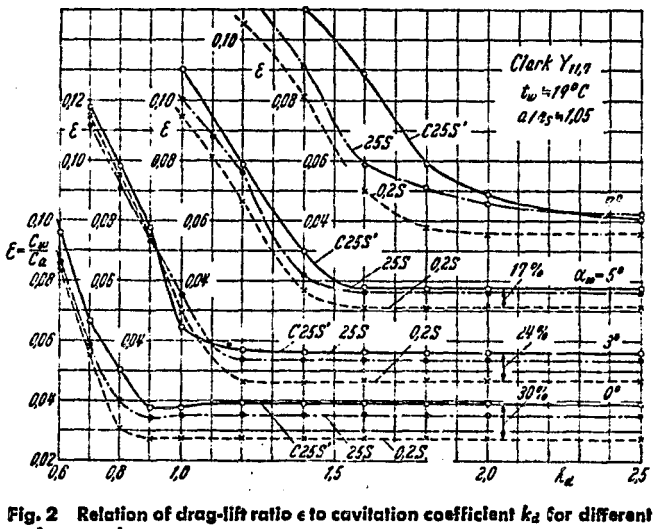

Fig. 2 Relation of drag-lift ratio ε to cavitation coefficient k_d for different surface roughness

C25S′: Striations in direction of chord
25S: Striations in direction of span
0.2S: Hydrodynamically smooth surface

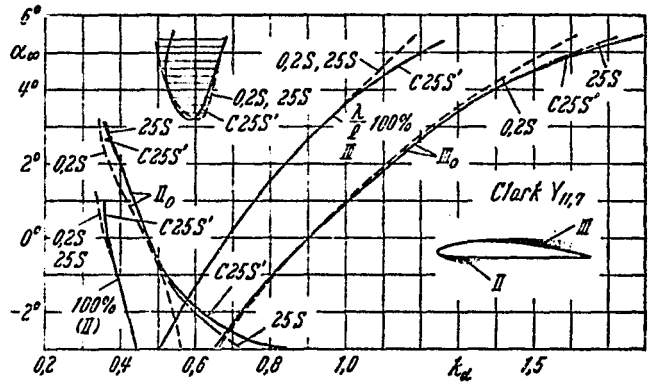

Fig. 3 Modes of cavitation occurrence on surfaces of different roughness. Same specimens as Figs. 1 and 2

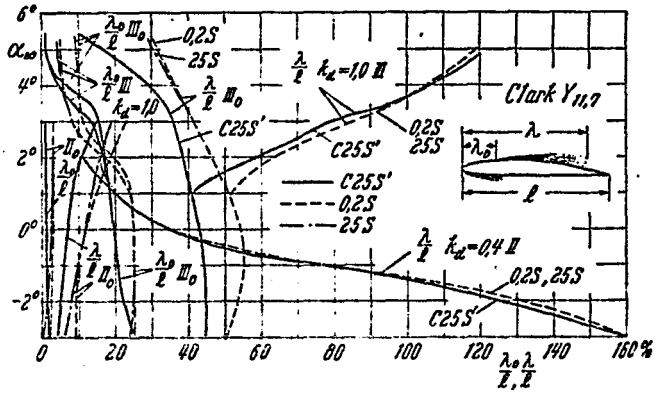

Fig. 4 Change in position of cavitation head and tail with different surface roughness for various incidence angles α_∞

λ_0: Position of cavitation head
λ: Position of cavitation tail (both in distance from leading edge, in percentage of chord length)

(C25S′) are greater than that of spanwise striations measured with 25S. For example, at $\alpha_\infty = 5$ deg the reduction of lift by the roughness was 4.4 percent with C25S′ (chordwise) and 2.2 percent with 25S (spanwise).

(ii) A similarly unexpected result was obtained for increase in drag coefficient.

(iii) Cavitation incipience properties were found to be generally similar between the two forms of striation, though locally, for instance, in Zone III when $\alpha_\infty > 4.5$ deg and in Zone II when $\alpha_\infty < -1$ deg, the C25S′ tended to induce cavitation somewhat earlier than the 25S.

(iv) The positions of head (λ_0) and tail (λ) of incipient cavitation were both found to be nearer the leading edge with C25S′ as compared to 25S.

Search for the Cause of Inverted Results

Since the results obtained indicating that striation in the direction of chord (C25S′) affected drag and lift more than spanwise striations (25S) were the reverse of what was expected, the experiments were repeated to ascertain that there was no error in measurement. Observation of photographs of the cavitating area, as undertaken in previous studies [1, 2], and examination by high-speed cinematography (8000 frames/sec) to compare the behavior of cavitation bubbles, both failed to provide a plausible explanation. Available literature of possible pertinence was scanned but found to provide no clue.

In order to examine whether drag—and consequently lift—was really affected more by chordwise than spanwise striations, the author undertook to test the hydrodynamic resistance of cylindri-

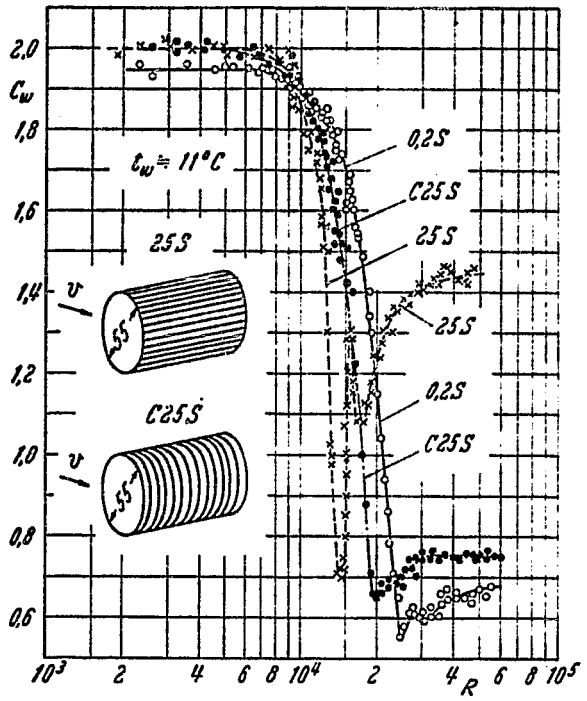

Fig. 5 Drag behavior of cylinders striated in different directions in different surface roughness

cal specimens. Two cylinders, both 55 mm diameter and 70 mm long, were finished with their surfaces roughened to 25S, one with axially oriented and the other with circumferential striations, and the two were tested in the same cavitation tunnel [6] under identical conditions. One end of the cylinder was solidly inplanted on the circular mounting forming part of the tunnel wall and imparting the forces acting on the cylinder to the measuring balance behind it. The free end of the specimen cylinder had a 0.05-mm clearance between it and the opposite wall.

In the velocity range covered by the present series of studies, both laminar and turbulent boundary layers exist simultaneously [1], and so in this side experiment the drag was measured in the region around the critical Reynolds number to cover both forms of boundary layer. Inducement of cavitation was avoided by appropriate manipulation of static pressure, and with flow velocity varied between 0.6 and 12 m/s, Reynolds numbers in the range $(0.2\text{–}5.5)\cdot 10^5$ could be realized. The results are shown in Fig. 5.

It is seen that in a cylindrical specimen, drag is evidently increased to no greater extent by striations parallel to flow than across flow. It was thought logical to presume that this should also apply to hydrofoils, and that the results obtained with the C25S′ specimen described earlier should therefore be attributed to causes other than the direction of striation. Based on this consideration, the specimen was reexamined.

Reexamination of Specimen

To verify uniform roughness over the whole specimen surface, the C25S′ had been subjected to the inspection procedure already described [1], i.e., oscillographic recording of surface irregularities sensed by contact probe (as specified by JIS [3, 4] at 10 different positions along the span). The point nearest the leading edge was 14 mm from the head (20 percent of chord) for the reason that measurement was awkward in the immediate vicinity of the blade edge. This region had been inspected visually and had appeared to present no particular anomaly.[3]

[3] Measurements of roughness had been undertaken until this stage of the study series by Assistant Prof. R. Ōba and his assistant, and those after this stage as well as performance measurements throughout the whole series of studies, by Assistants I. Chida and R. Satō.

Nevertheless, it was recalled that it was precisely this zone around the leading edge where roughness had its greatest effect on blade performance [2]. The zone in question was therefore reexamined visually with the aid of a microscope eyepiece (magnifying power about 10 times), and in effect, some irregularity in roughness was detected near the leading edge.

The area in question is shown in the photos (2)–(5) in Fig. 6, which represent a magnification of about 7 times. These pictures should be compared with photo (1) showing a regular surface near the center of the back side under similar magnification. Photo (2) reveals a thin ridge running spanwise, and photo (4), a wider rib, while photos (3) and (5) indicate the existence of discontinuities in the striations. (The anomalies should be more clearly grasped by comparison with the illustrations in Fig. 6, representing correct specimen surfaces.)

From the foregoing observations, it was concluded that the increased drag presented by the C25S′ must be attributed to the surface anomalies existing in the vital zone near the leading edge.

The fact that such anomalies, so small as to elude detection by casual visual inspection, should under certain circumstances have appreciable effect on performance persuaded the author to spare some lines for an account of the foregoing negative experience, particularly considering that surface roughness and deviations of form in such minor amount occur even in laboratory specimens, not to speak of test models reproducing actual turbines and pumps.

Improved Method of Roughening Specimen Surface and Results of Measurement

Striations in Direction of Span

There had not been any particular problem felt in obtaining the required roughness in the specimens for the experiments reported previously [1, 2], in which the striations were in the direction of span. For the different degrees of roughness tested, that is, up to 25S, the striations were obtained by passing an emery cloth or file in the spanwise direction over surfaces finished to 0.2S. The roughness of 35S, taken up this time, could not be produced by file, and a circular grinder (specification A-24-P-m-v)[4] was used for the purpose. Irregular protuberances that might exist on the grinder surface were first removed by lightly passing the grinder surface with a diamond tool, and consequent fouling of the grinder surface then cleaned by dresser brush. The grinder was then turned manually at 60–80 rpm and the test specimen held against it with a sweeping motion. The specimens thus prepared were designated 35S (spanwise striations) and C35S (chordwise striations).

Striation in Direction of Chord

It was clear from the experience described previously that it was not proper to prepare the zone near the leading edge simply by filing. The following method was consequently devised. As shown in Fig. 7, the specimen sides were held between lathe centers z_1 and z_2 at points 2.8 mm from the leading edge (position $x/l = 4$ percent—see Fig. 6 for reference). A piece of 60-mesh emery cloth PP was held against the leading part of the specimen blade and immobilized. The handle H on the face plate C_1 attached with the support S was then turned manually so as to revolve the specimen surface around the edge thus swept parallel to chord, within a zone extending about 5 mm along chord on the back side

[4] The grinder was 350 mm diameter by 50 mm thick. Japanese grinder specifications compared with those of the Norton Co. (U. S.) are as follows:

	Japan Industrial Standard	Norton
Nature of grain	A	A
Mesh	24	24
Hardness (binder strength)	P	P
Composition (ratio between grains and binder)	m	4–9
Binder	V	V

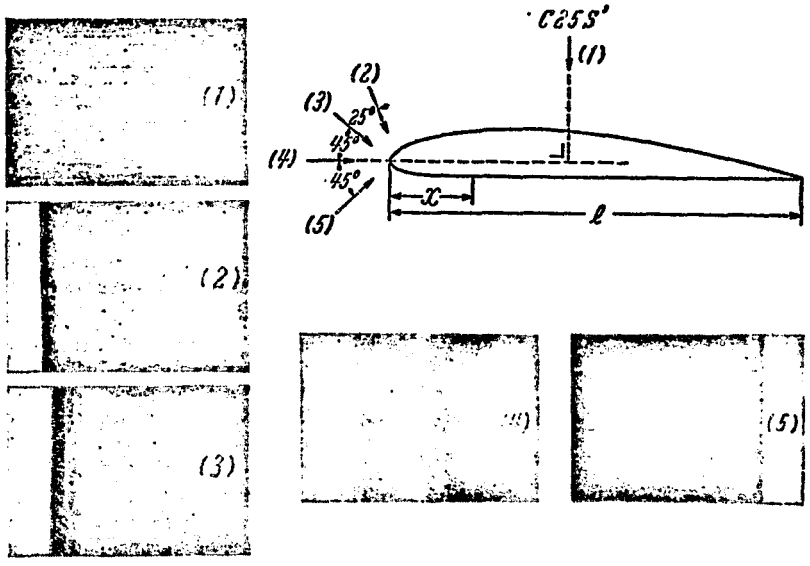

Fig. 6 Anomalies in roughened surface of C25S'

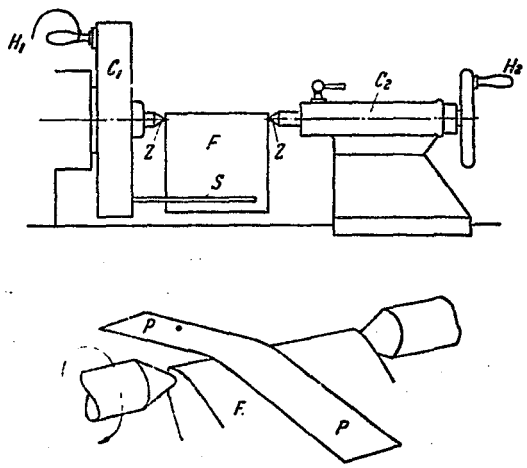

Fig. 7 Improved method of striating leading edge zone in chordwise direction

F: Hydrofoil, PP: Emery cloth

(x/l = 7.1 percent) and 3 mm on the belly side (x/l = 4.3 percent). The remaining surface toward tail was swept once with a 300 mm long very coarse square file. The resulting correct specimen was designated C25S (and distinguished from the previous incorrect C25S').

The C35S was prepared in a similar manner except for the use of 40-mesh emery cloth and, as already explained, grinder instead of file.

Inspection of Roughness

The surfaces were first photographed as in the case of C25S' for examination of roughness uniformity. The resulting pictures are shown in Fig. 8, where the photos (1)–(5) are views from the same angles as the corresponding photos in Fig. 6. No anomalies to break the uniformity are discernible from this microscopic examination. To ascertain that there was no effect from the difference in method of striation between the zone near the leading edge and the rest of the specimen surface, the actual roughness of these two parts of the surface was measured according to Japanese Industrial Standards with a Kosaka SD_6 surface inspecting machine, which follows the surface with a contact needle. The surface was thus examined on both back and belly sides at ten different points on each side. Typical oscillograms are shown in Figs. 9–11. Comparison of the oscillograms taken of the surface near the leading edge (x/l = 0 and x/l = 7.1 percent) and

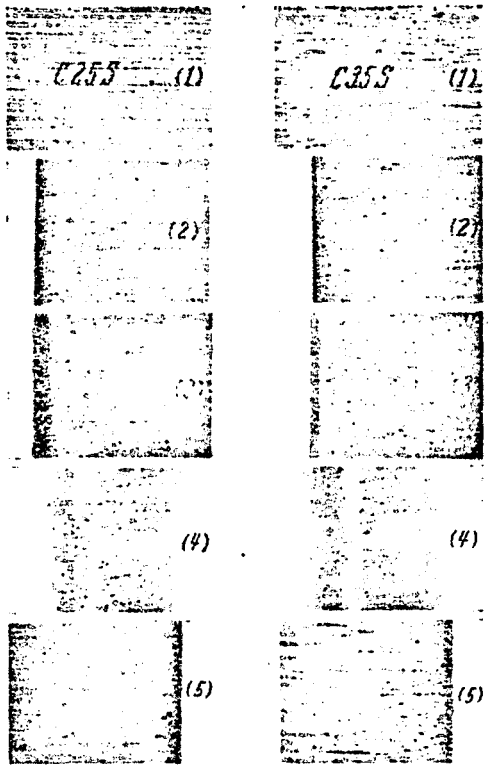

Fig. 8 Regular roughness on surface of C25S and C35S obtained by improved method of striation

other parts indicated no appreciable difference in roughness either in the ridge profiles or in their average height. While neither ASA nor JIS (Japanese Standards) specify in their roughness standards the pitch of the ridges forming the irregularities, the number of striations per mm were counted in the present instance, as shown in Table 1.

Striations thus are somewhat more closely distributed when made by emery cloth than by file, but this amount of difference can be considered negligible.

Results of roughness measurements similarly undertaken on C25S' are presented in Fig. 11(c). The surface irregularities near the leading edge around x = 0 were 34–38μ high. The pitch, while being 7.7 and 8 per mm, respectively, in the main portion of the back and belly, and thus similar to values for

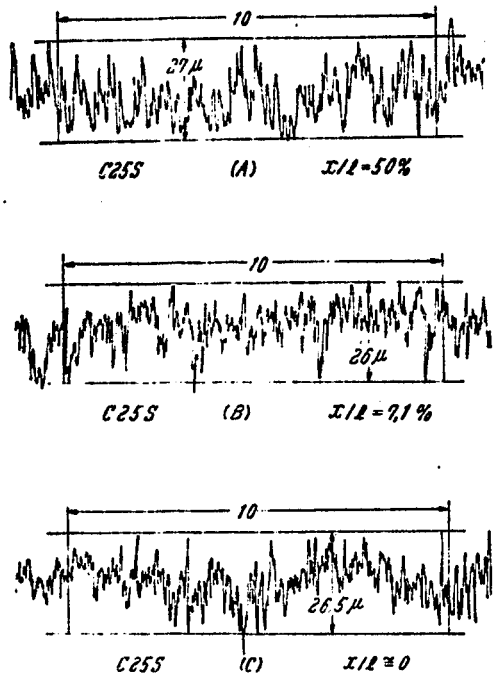

Fig. 9 Oscillographs of specimen surface (C25S)

(A) Central area, back side (x/l = 50 percent)
(B) Zone near leading edge, back side (x/l = 7.1 percent)
(C) Tip of leading edge (x/l ≒ 0)
μ:1/1000 mm

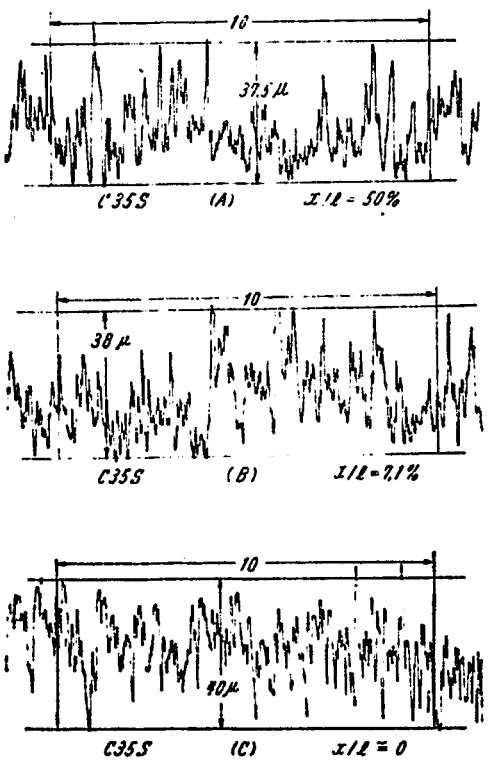

Fig. 10 Oscillographs of specimen surface (C35S)

(A) Central area, back side (x/l = 50 percent)
(B) Zone near leading edge, back side (x/l = 7.1 percent)
(C) Tip of leading edge (x/l ≒ 0)
μ:1/1000 mm

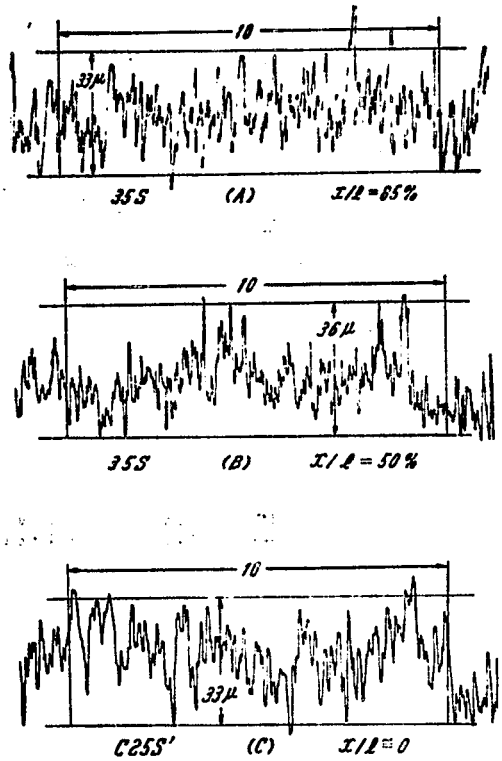

Fig. 11 Oscillographs of specimen surface (35S and C25S')

(A) Central area, back side (x/l = 85 percent), 35S
(B) Central area, belly side (x/l = 50 percent), 35S
(C) Tip of leading edge (x/l ≒ 0), C25S'
μ:1/1000 mm

Table 1 Number of striations f per unit length
x: Distance from blade head
l: Chord length

		Suction side					Pressure side
x/l %		0	4,3	7,1	50,0	85,0	50,0
C25S	f	9,2	8,8	8,7	7,9		7,8
C35S		6,3	6,1	5,9	5,6		5,7
C25S'		5,2	7,6	7,9	7,7		8,0
35S						6,2	6,1

C25S, is 5.2 per mm around $x = 0$, which is much nearer the value of C35S than C25S.

Experimental Results

The results obtained are presented in the form already described earlier in this report [1].

Lift Coefficient

Difference Owing to Direction of Striations. Fig. 12 shows curves relating the lift coefficient C_a to cavitation coefficient k_d for 25S roughness profiles striated in both spanwise (25S) and chordwise (C25S) directions. Similar curves for 35S profiles appear in Fig. 13. In both figures, reference curves are also shown indicating the values of the hydrodynamically smooth 0.2 specimen.

The results correct the invalid data obtained from the previous experiments with the C25S' specimen, and provide the expected answer that a smaller effect on lift is presented by chordwise compared to spanwise striations.

Difference Owing to Degree of Roughness. Comparison between the curves for 25S in Fig. 12 and that for 35S in Fig. 13 will pro-

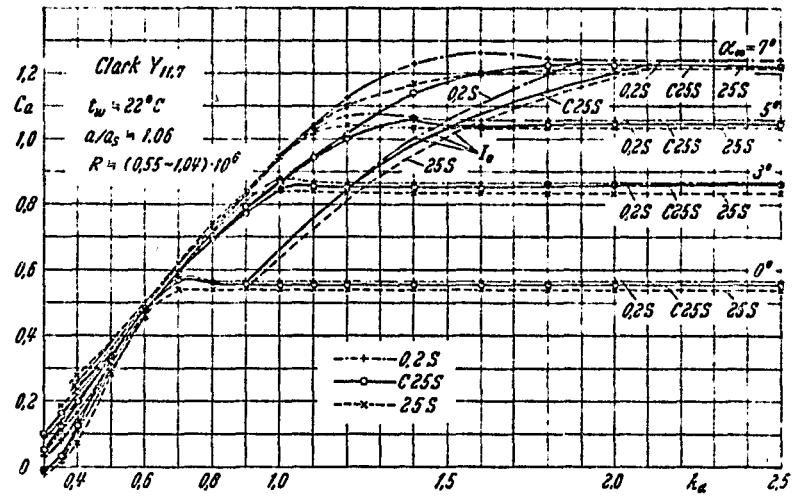

Fig. 12 Relation of lift coefficient C_a to cavitation coefficient k_d for different roughness—effect of direction of striation (specimen roughness 25S)

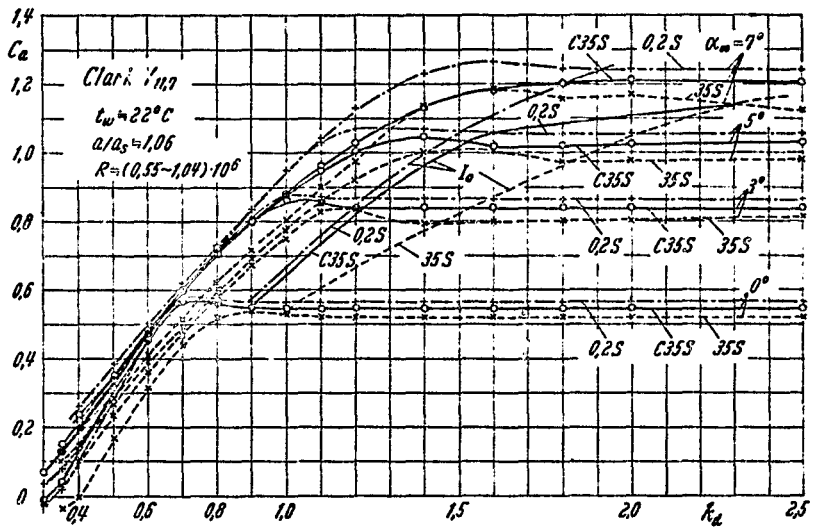

Fig. 13 Relation of lift coefficient C_a to cavitation coefficient k_d for different roughness—effect of direction of striation (specimen roughness 35S)

vide an indication of the difference caused by varying roughness in the spanwise direction, and in the same token, difference in the chordwise direction should be clear from a similar comparison between the curves for C25S and C35S. Further comparison with specimens of intermediate roughnesses 1.5S and 6S can be made by reference to the previous report [1].

Drag-Lift Ratio

In theoretical calculations on the efficiency of axial flow turbines and pumps as well as ship propellers, the drag-lift ratio is more commonly used than the actual value of the drag itself, and for this reason we will save space by omitting graphic representation of drag coefficient, and only present the drag-lift ratio in Figs. 14 and 15 in the form of curves relating $\epsilon = C_w/C_a$ to cavitation coefficient k_d.

Comparisons Based on Lift Coefficient and Drag-Lift Ratio

In Table 2 are given the percentage decreases of lift coefficient ΔC_a as well as increases of drag coefficient ΔC_w and of drag-lift ratio $\Delta\epsilon$ over the smooth 0.2S specimen caused by varying roughness, as observed in the range free of cavitation. The sequence between the specimens for degree of affectation by roughness varies somewhat according to incidence angle when basing the comparison on ΔC_a and ΔC_w, but based on $\Delta\epsilon$ the general sequence is

35S—C35S—C25S′—25S—C25S

with roughness effect diminishing from left to right.

In the range of incidence angle $\alpha_\infty > 6$ deg however, the order is reversed between 25S and C25S′ (cf. Fig. 2—$\alpha_\infty = 7$ deg, $k_d = 2.5$). The cause of this inversion may be attributed to the fact that in roughening the surface, an area along a line on the pressure side near the leading edge became flattened (cf. bright portion seen in photo (5), Fig. 6). This resulted in a diminished camber which in turn reduced both lift (cf. Fig. 1) and drag coefficients, but in the particular case of $\alpha_\infty \geq 6$ deg, the effect must have been significantly less pronounced on ΔC_w than on ΔC_a (cf. Table 2).

Cavitation Stalling

An important parameter governing the performance of axial turbines and pumps is the point where development of cavitation causes a sharp drop in output. This point has been defined on the

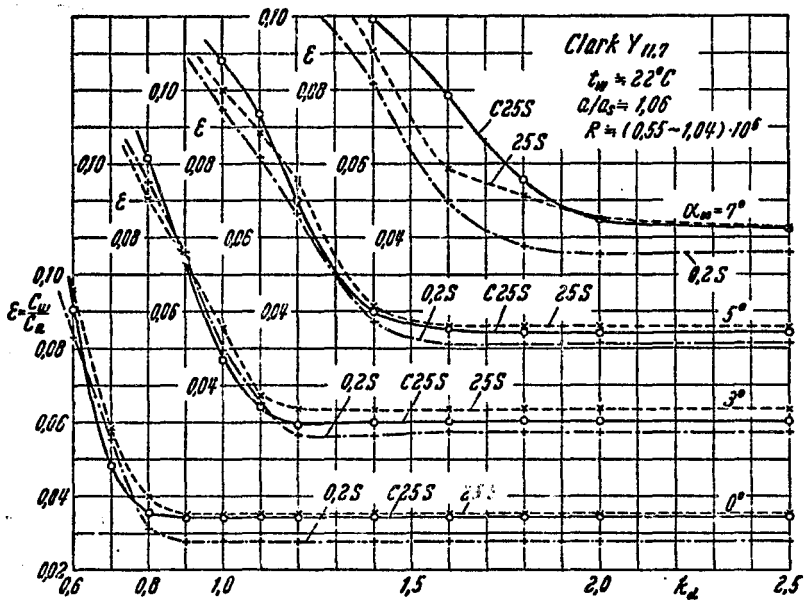

Fig. 14 Relation of drag-lift ratio ε to cavitation coefficient k_d for different roughness—effect of direction of striation (specimen of roughness 25S)

$C_a - k_d$ curve by the intersection of straight lines extending the horizontal and sloped arms of this curve, and the k_d-value of this intersection has been designated the cavitation stalling point k_{Ba} [1].

Up to a roughness of 25S, as already reported [1, 2], no appreciable effect of roughness has been discernible on k_{Ba}, but curves relating k_{Ba} to (not reproduced here) reveal that shifting of the stalling point is quite evident when the roughness reaches 35S.

Effect of Surface Roughness on Hydromechanical Efficiency

The calculations performed in the preceding studies [1] were repeated with the use of the same theoretical equation. The highest and lowest values of drag-lift ratio obtained in the present study were adopted in calculating the theoretical hydraulic efficiency, for comparison with that of the hydrodynamically smooth 0.2S specimen. The resulting reduction in the highest and lowest values of efficiency, $\Delta\eta_R$, are given in Table 3, together with the corresponding values of drag lift ε adopted for the calculations. The ranges chosen for k_c, k_u, and m were the same as in the preceding calculations [1]. The expression for efficiency, η_R, which was employed in reference [1] was developed in reference [11] and is given by

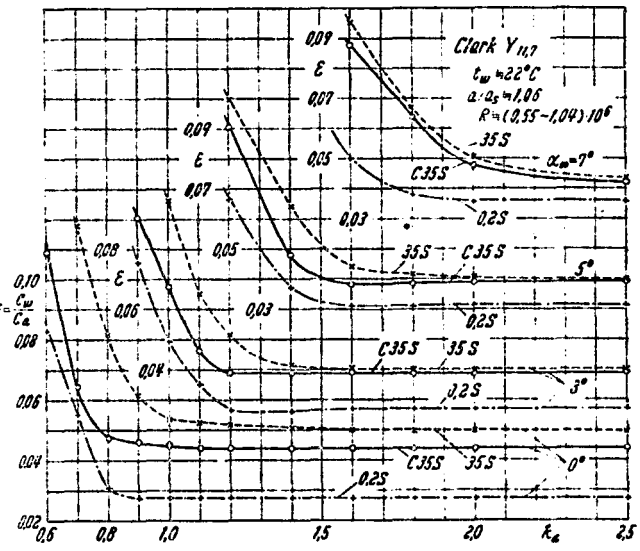

Fig. 15 Relation of drag-lift ratio ε to cavitation coefficient k_d for different roughness—effect of direction of striation (specimen of roughness 35S)

$$\eta_R = \frac{1}{1 + \frac{2\epsilon k_c}{k_u}\left(\frac{m}{1+m}\right) - \frac{\epsilon}{k_c k_u}\left(\frac{m}{1+m}\right) + \frac{\epsilon m^3}{8k_c k_u^3(1+m)} + \left(\frac{2\epsilon k_u}{3k_c}\right)\frac{m^2+m+1}{m(m+1)}}$$

where

$$k_u = \frac{u_a}{\sqrt{2gH_a}}$$

$$k_c = \frac{c_m}{\sqrt{2gH_a}}$$

$m = D_e/D_i$

u_a = linear velocity of runner periphery

c_m = partial velocity of flow in the direction of axis

D_e, D_i = outer and inner diameters, respectively, of runner

H_a = water head on runner or impeller

It can be concluded from this table that $\Delta\eta_R$ assumes values that cannot be ignored. It should also be noted that, while the

Table 2 Percentage decrease of lift coefficient ΔC_a and corresponding increase of drag-lift ratio $\Delta\varepsilon$ over the smooth specimen caused by varying roughness

Profile		C25S	25S	C25S'	35S	35S
$\alpha_m = 0°$	ΔC_a	1.8	2.7	1.8	3.5	7.1
$k_d = 1.0$	ΔC_w	22.6	22.6	35.5	58	81
	$\Delta\varepsilon$	24.8	28.4	38.0	64.3	94.4
$\alpha_m = 3°$	ΔC_a	0.6	3.5	3.5	3.9	7.5
$k_d = 1.6$	ΔC_w	10.6	19.1	29.7	38.3	36.2
	$\Delta\varepsilon$	11.0	23.2	38.1	42.3	47.1
$\alpha_m = 5°$	ΔC_a	1.0	1.9	4.3	2.8	7.1
$k_d = 2.0$	ΔC_w	7.6	12.1	15.7	21.2	21.2
	$\Delta\varepsilon$	8.6	14.1	20.1	24.6	30.3
$\alpha_m = 7°$	ΔC_a	1.6	2.0	7.2	6.8	7.6
$k_d = 3.0$	ΔC_w	15.7	15.7	3.4	14.6	10.1
	$\Delta\varepsilon$	11.4	18.1	11.4	20.3	20.3

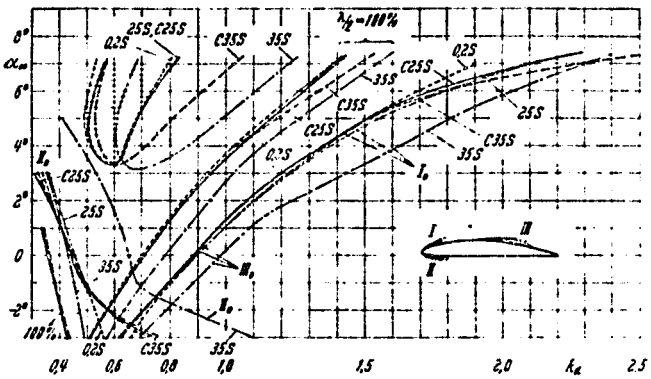

Fig. 16 Modes of cavitation occurrence on surface of different roughness

Table 3 Reduction of hydraulic efficiency ($\Delta\eta_R$) of axial-flow turbines and pumps owing to blade surface roughness

	ε	$\Delta\eta_R$ %
C25S	0,0300 ~ 0,0330	0,7 ~ 2,5
25S	0,0335 ~ 0,0350	1,2 ~ 2,9
C25S′	0,0358 ~ 0,0382	1,8 ~ 4,4
C35S	0,0385 ~ 0,0425	1,9 ~ 5,9
35S	0,0400 ~ 0,0460	2,3 ~ 7,2
0,2S	0,0265 ~ 0,0300	

difference between 25S and C25S is only about 0.5 percent, this difference between spanwise and chordwise striations reaches 1.3 percent with a roughness of 35S. This is an indication that cases may arise that should call for consideration on the direction of applying the file when finishing the surfaces of hydraulic machines and specimens.

Cavitation Inception and Initial Cavitation

Manner of Onset and Size of Initial Cavitation. Fig. 16 is a graphical representation of the conditions of cavitation incipience in the different zones (marked by I_0, II_0, and III_0) of the different specimens tested (relation between incidence angle α_∞ and cavitation coefficient k_d). Also shown in the same figure are curves indicating the conditions under which cavitation develops to the point where its tail reaches the trailing edge of the blade ($\lambda/l = 100$ percent), beyond which cavitation erosion need no longer be feared. The curves in the upper left-hand corner delimit zones of violent vibration caused on the specimens, with the zone relevant to 0.2S shaded in as an example.

The curves in Fig. 17 indicate the positions of head, λ_0, and tail, λ, of incipient cavitation according to incidence angle. The manner in which the onset of cavitation and vibrations are advanced (value of k_d increased) by surface roughness is clear from these figures. The tendency of the cavitation head and tail to be displaced slightly forward by roughness is again visible, as it was in the previous cases [1].

While minute examination of the curves in Figs. 16 and 17 should reveal partial departures from the sequence cited earlier of the specimens arranged according to the extent of cavitation performance deterioration by surface roughness, it may safely be concluded that the sequence generally holds for all four characteristic parameters (point of inception, violent vibrations, displacement of incipient cavitation head, λ_0, and tail, λ), when account is taken of the inaccuracies inherent in the visual determination of λ_0 and λ, and the convincing results obtained with the 35S specimens.

Stringlike Cavitation. With surfaces rougher than 0.2S, incipient cavitation in the zones I and II near the leading edge presents an unstable stringlike form which upon only very slight development (as soon as λ/l exceeds a certain value λ_s/l), assumes the ordinary

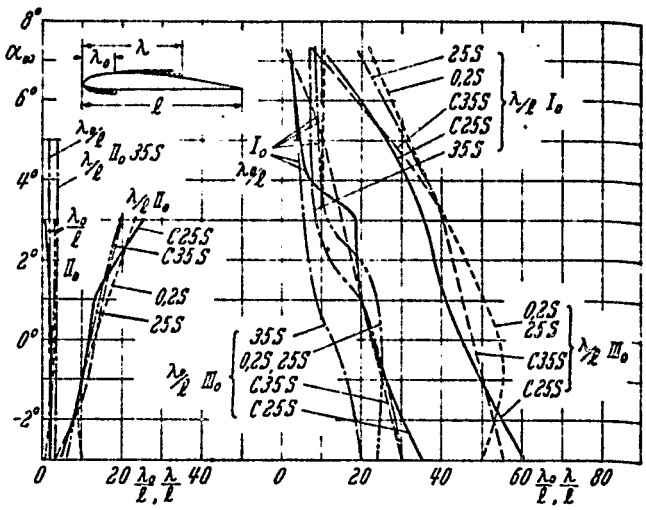

Fig. 17 Change in position of cavitation head (λ_0) and tail (λ) with different surface roughness

form of cavitation which to the naked eye appears to spread uniformly over the span. The stringlike cavitation is particularly clearly observed in specimens with surface rougher than 25S. Typical values of the transition point to ordinary cavitation, i.e., λ_s/l, is roughly as follows:

Specimen		Zone I (back) λ_s/l (percent)		Zone II (belly) λ_s/l (percent)
C25S	α_∞ = 5 deg	40	α_∞ = 3 deg	40
25S	α_∞ = 7 deg	15	α_∞ = −3 deg	10
C35S	α_∞ = 5 deg	40	α_∞ = 3 deg	50
35S	α_∞ = 7 deg	20	α_∞ = −3 deg	10

Stringlike cavitation appears also at other angles of incidence, with transition at correspondingly lower degrees of development. Cavitation coefficients at the transition points will be obtained from reference to Figs. 16 and 17.

The foregoing results would indicate that stringlike cavitation appearing near the leading blade edges of axial-flow turbines and pumps could be attributed to excessive surface roughness. A typical form of stringlike cavitation is illustrated in Fig. 18.

Conclusions

1 For equal degree of roughness, both lift and drag-lift ratio are affected less by striations oriented chordwise than by spanwise striations (Figs. 12—15).

2 When preparing rough surface specimens, anomaly in the striations are liable to be caused on the rounded surface near the leading edge, even in producing striations in the chordwise direction (cf. C25S′) if done by ordinary filing methods, and almost undetectable anomalies in this zone can appreciably affect cavitation performance. The inverted results obtained with specimen C25S′ which registered roughness effects greater than 25S contrary to expectation was the result of such extremely minor anomalies (Figs. 1, 2, 6, and 11).

3 Striations in the same direction affect performance in accordance with the degree of roughness, as is quite naturally expected, and the sequence of specimens arranged in the order of smaller effect on drag-lift ratio is:

C25S—25S—C25S′—C35S—35S

though for incidence angles exceeding 6 deg, drag-lift ratio is greater with C25S than with 25S.

4 Cavitation stalling point is not appreciably affected by roughness up to 25S, but is significantly advanced (cavitation coefficient smaller) in the case of 35S (spanwise striation).

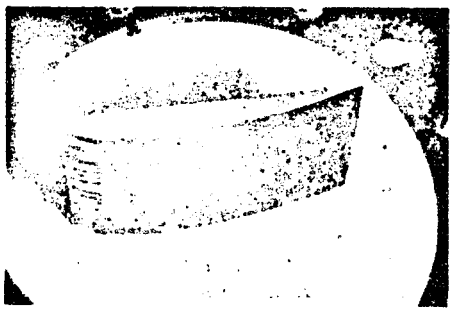

Fig. 18 Stringlike incipient cavitation

5 The effect on the hydraulic efficiency of axial-flow turbines and pumps, estimated from the present results, indicated lowering of efficiency ranging up to 5.9 percent with C35S and 7.2 percent with 35S compared with the hydrodynamically smooth 0.2S specimen, and the difference of 1.3 percent seen between the two 35S specimens according to direction of striation would point toward the possible occurrence of cases that should call for consideration on the direction of applying the file when finishing blade surfaces.

6 Cavitation onset and violent vibrations appear to be advanced (value of critical k_d increased) by roughness, Fig. 16.

7 Roughness tends to displace both head and tail of incipient cavitation toward the leading edge, Fig. 17. The tendencies cited under 6 and 7 previously appear somewhat ambiguous in the results from the 25S specimens, but are unmistakably evident with the 35S.

8 Beyond a certain roughness, incipient cavitation takes an unstable stringlike form, which assumes the ordinary form of cavitation upon slight development of the cavitation, Fig. 18. It may be inferred from this that the stringlike cavitation observed in actual turbines and pumps could be attributed to insufficiently smooth blade surface.

Acknowledgment

The author wishes to acknowledge the services offered by Mr. I. Chida and Mr. R. Satō, Assistants of the Institute, and the work done by Assistant M. Hongō in preparing the drawings and templates for the blade specimens. Mention must also be made of the assistance provided by the staff of the Institute's workshop in devising and implementing the methods for striating the blade surfaces.

References

1 F. Numachi, R. Ōba, and I. Chida, "Effect of Surface Roughness on Cavitation Performance of Hydrofoils—Report 1," JOURNAL OF BASIC ENGINEERING, TRANS. ASME, Series D, vol. 87, 1965, pp. 495–503; *Reports of the Institute of High Speed Mechanics*, Japan, vol. 16, 1964–1965, pp. 137–158.

2 F. Numachi, R. Ōba, and I. Chida, "Effect of Surface Roughness on Cavitation Performance of Hydrofoils—Report 2," Symposium on Cavitation in Fluid Machinery, Winter Annual Meeting of ASME, Chicago, November 7–12, 1965, pp. 16–31.

3 Japan Industrial Standard, JIS, B 0601.

4 Japan Industrial Standard, JIS, B 0651, B 0652.

5 ASA, B 46-1, 1955, Surface Roughness, Waviness and Lay.

6 F. Numachi, "Kraftmessungen an vier Flügelprofilen bei Hohlsog," *VDI-Forschung*, vol. 11, 1940, pp. 303–308.

7 F. Numachi, K. Tsunoda, and I. Chida, "Cavitation Tests on Clark Y Profiles of Several Thickness Ratio," *Reports of the Institute of High Speed Mechanics*, Japan, vol. 8, 1957, pp. 47–65.

8 F. Numachi and I. Chida, "Effect of Static Pressure Differences on the Cavitation Characteristics of Hydrofoil Profils," Rept. 1–3, *Reports of the Institute of High Speed Mechanics*, Japan, vol. 5, 1955, pp. 37–49; vol. 7,1956, pp. 123–134; vol. 11, 1959–1960, pp. 89–101.

9 F. Numachi, "Über die Kavitationsentstehung mit besonderem Bezug auf den Luftgehalt des Wassers," *Ingenieur-Archiv*, Berlin, vol. 7, 1936, pp. 396–406.

10 F. Numachi and H. Sakai, "Method of Producing Hydrofoil Profile Test-Pieces for Cavitation Tests," *Reports of the Institute of High Speed Mechanics*, Japan, vol. 7, 1956, pp. 189–201.

11 F. Numachi, "On the Hydraulic Efficiency of Propeller Turbines and Propeller Pumps (Report 2, On Aerofoil Theory of Propeller Turbines and Propeller Pumps)," *Technol. Reports*, Tōhoku Imperial University, vol. 9, 1930, pp. 231–253.

END OF REFERENCE

100

REFERENCE

101

KING, J. A.; AND FARREL, E. C.: THE TRANSIENT PERFORMANCE OF A HYDRAULIC TURBINE-DRIVEN INDUCER: COMPUTER PREDICTIONS AND TEST VERIFICATION. REP. R-7747, ROCKETDYNE. (NASA CR-72518), 1969.

JUL 7 '69

5/5 L Farrell

8.2-0-0

N69-23693

N69-23693

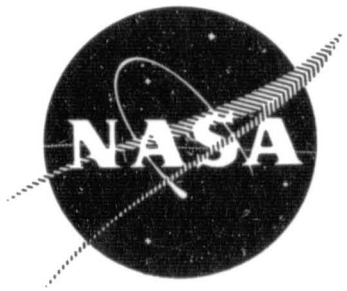

NASA CR-72518
R-7747

Aerospace Safety Research
and Data Institute
NOV 5 1971
CLEVELAND, OHIO

THE TRANSIENT PERFORMANCE OF A HYDRAULIC-TURBINE-DRIVEN INDUCER: COMPUTER PREDICTIONS AND TEST VERIFICATION

LIBRARY COPY

JUL 7 1969

LEWIS LIBRARY, NASA
CLEVELAND, OHIO

by

J. A. King and E. C. Farrel

ROCKETDYNE
A DIVISION OF NORTH AMERICAN ROCKWELL CORPORATION

prepared for

NATIONAL AERONAUTICS AND SPACE ADMINISTRATION

NASA Lewis Research Center
Contract NAS3-10280
W. A. Rostafinski, Project Manager

NOTICE

This report was prepared as an account of Government-sponsored work. Neither the United States, nor the National Aeronautics and Space Administration (NASA), nor any person acting on behalf of NASA:

A. Makes any warranty or representation, expressed or implied, with respect to the accuracy, completeness, or usefulness of the information contained in this report, or that the use of any information, apparatus, method, or process disclosed in this report may not infringe privately owned rights; or

B. Assumes any liabilities with respect to the use of, or for damages resulting from the use of, any information, apparatus, method or process disclosed in this report.

As used above, "person acting on behalf of NASA" includes any employee or contractor of NASA, or employee of such contractor, to the extent that such employee or contractor of NASA or employee of such contractor prepares, disseminates, or provides access to any information pursuant to his employment or contract with NASA, or his employment with such contractor.

Requests for copies of this report should be referred to

National Aeronautics and Space Administration
Scientific and Technical Information Facility
P.O. Box 33
College Park, Md. 20740

NASA CR-72518
R-7747

FINAL REPORT

THE TRANSIENT PERFORMANCE OF A HYDRAULIC-TURBINE-DRIVEN INDUCER: COMPUTER PREDICTIONS AND TEST VERIFICATION

by

J. A. King and E. C. Farrel

ROCKETDYNE
A DIVISION OF NORTH AMERICAN ROCKWELL CORPORATION
Canoga Park, California 91304

prepared for

NATIONAL AERONAUTICS AND SPACE ADMINISTRATION

February 1969

CONTRACT NAS3-10280

NASA Lewis Research Center
Large Engine Technology Branch
Cleveland, Ohio
W. A. Rostafinski, Project Manager

SUMMARY

The purpose of the contract was the development of a computer program that would predict the transient performance of a low-speed inducer driven by a partial-flow, hydraulic turbine. Two programs, an analog and a digital, were developed that will do this. To check the accuracy of the programs, an inducer-turbine unit was designed, fabricated, and tested. Steady-state performance maps of the inducer, the turbine, and the high-pressure pump were made from existing data and by synthetic mapping procedures. These maps were used in the computer programs to predict the acceleration performance of the unit in the system in which it was eventually tested. The computer programs were also used to make parametric studies to determine the effect of selected changes in the system, and to investigate several inducer-turbine combinations in simulated rocket engine installations. From the results of these studies, the following conclusions were drawn:

1. The inducer acceleration would be satisfactory for the planned test series and also actual rocket engine installation.
2. The preinducer rotating moment of inertia has a significant effect upon the starting performance (the lower the inertia, the better the start).
3. The fluid inertia (ratio of line length to area) of the pump coupling line for a remote location of the preinducer has an effect upon the starting performance (the lower the inertia, the better the performance).
4. The proportions (length and area) of the return line to the turbine and the type of turbine (impulse or reaction) do not significantly affect the transient performance of the unit.
5. The use of a preinducer in a rocket engine feed system is feasible with a proper starting sequence. The result is lower allowable tank pressures and, thus, reduced tank wall weights, or possible elimination of the tank pressurization system.

The inducer-turbine was tested in water with the high-pressure pump being driven by an electric motor. Steady-state H-Q and cavitation tests were run both with and without a signal generator in the system. Acceleration tests, both rapid and slow, were made from idle to full speed. Transient tests to simulate the throttling of a rocket were also made. Tests were made with the preinducer in both close-coupled and remote positions.

The cavitation tests showed that the suction specific speeds of the inducer-pump combination at 80, 100, and 120 percent design Q/N were 70,000, 63,600, and 54,600, respectively. These were based on the through flow and the speed of the main pump.

From the results of the acceleration, simulated throttling, and flowrate pulsing tests, the following conclusions were drawn:

1. The computer models developed for the design and parametric studies do accurately simulate the acceleration and simulated throttling transients of a hydraulic-turbine-driven inducer.
2. Inertia of the fluid in the inducer is important in predicting the inducer exit pressure drop during the initial portion of the inducer acceleration.
3. Inlet and outlet compliances assigned to the inducer have no effect on the inducer acceleration performance for the acceleration times tested.
4. Low-frequency dynamic characteristics can be described with an inducer inlet compliance variable with inducer net positive suction pressure.

INTRODUCTION

A major objective in turbopump design is to minimize turbopump weight; this can best be done by using high rotative speeds. A second major objective is to operate reliably at low suction pressures; this is very difficult to accomplish with high-speed turbomachinery. However, the objective can be met by using a low-speed inducer upstream of the high-speed pump to generate sufficient head to prevent the main pump from cavitating under any operating conditions. The low-speed inducer can be driven in a variety of ways, one of which is by using part of the high-pressure discharge flow from the main pump to power a hydraulic turbine that drives the inducer. The research program under this contract is concerned with the theory, design, construction, and testing of such a partial-flow, hydraulic-turbine-driven, low-speed inducer. Of particular interest is the ability of this inducer to perform as required during conditions of rapid pump acceleration, throttling, and shutdown. Can the transient performance of the inducer be predicted accurately? And if so, what are the variables that most affect this transient performance?

The purpose of this contract is the development of analog and digital computer programs that will accurately predict the transient performance (including the low-frequency dynamic effects) of a low-speed inducer driven by a partial-flow, hydraulic turbine. The programs then will be used to investigate the transient behavior of several inducer-turbine combinations in a particular system and to determine the effect of selected parameter changes in the system on this transient behavior. The validity of the computer programs will be verified by designing, constructing, and testing a turbine-driven inducer to determine its steady-state and transient characteristics in water. The test results will then be compared with the predicted results. If necessary, the mathematical model will be refined to include measured rather than assumed constants.

GENERAL DESCRIPTION OF THE SYSTEM

Figure 1 shows a section of a typical LOX/liquid hydrogen rocket with the thrust chamber at the bottom. Mounted on either side of the thrust chamber are the high-speed LOX and liquid hydrogen turbopumps. The spheres in the upper portion of the figure represent the tanks, the egg-shaped sphere at the bottom being the LOX tank. The duct from the LOX tank to the turbopump is fairly short.

The tank at the top of the figure is the fuel tank, which is connected to the turbopump by a relatively long line. The hydraulic-turbine-driven inducer is shown in this line near the fuel pump. High-pressure liquid is taken from the exit of the high-pressure pump, and passes through the return line into the hydraulic turbine, which drives an inducer (low-speed pump). Flows from the turbine and the inducer blend before entering the high-speed pump.

The low-speed inducer is designed so that it will not cavitate even at very low pressures. At sea level takeoff, the pressures both inside and outside the tanks are very nearly atmosphere. As the rocket leaves the earth's atmosphere, the pressure on the outside of the tanks approaches zero. If pressure is maintained within the tanks, the tanks tend to explode. To prevent this, fairly thick and heavy walls are necessary. If the pressure inside the tanks is allowed to fall, the fluid pressure also falls and the liquids start to boil. High-speed pumps are unable to pump such a low-pressure fluid; they cavitate and stop producing the pressure necessary for the rocket engine to provide its thrust.

While the rocket engine is firing, the pumps are continually removing liquid from the tanks, which tends to pull a vacuum on the vessels. To prevent this, the tanks must be pressurized by additional equipment onboard the vehicle. This can take the form of a boiler, in which hot gas from the thrust chamber is used to boil liquid in a heat exchanger and the resultant hot gas is returned to the top of the tank. The amount of gas returned

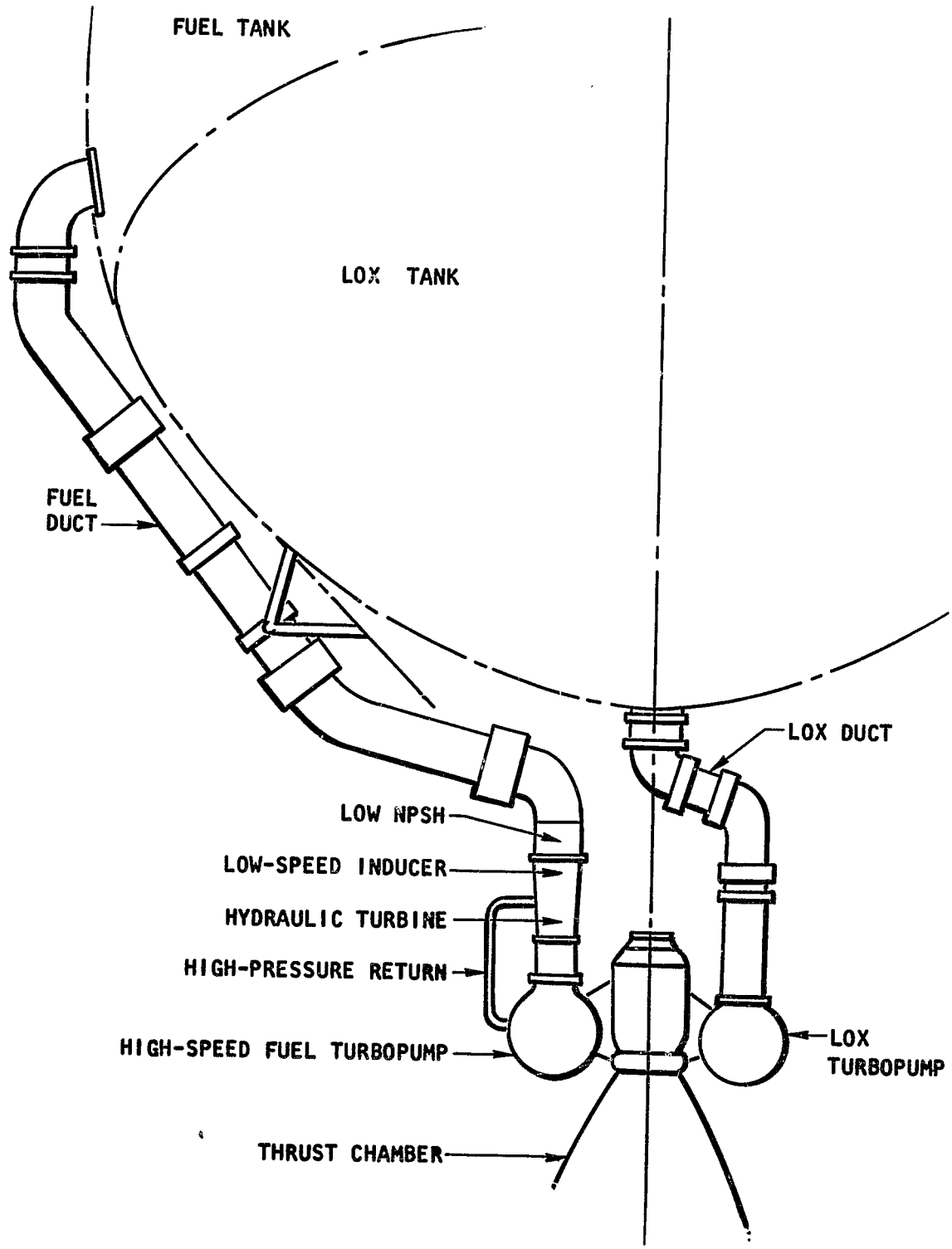

Figure 1. Liquid Oxygen/Liquid Hydrogen Rocket Engine

involves a metering or control system, as well as checkout and monitoring systems, and the entire package is heavy and expensive, resulting in a loss of specific impulse.

The hydraulic-turbine-driven inducer shown in Fig. 1 can theoretically operate at pressures sufficiently low that tank pressurization is unnecessary, producing enough pressure to prevent the high-speed pump from cavitating. The unit, therefore, offers potentially thinner and lighter tank walls, elimination of the heavy and expensive pressurization system, and more flexibility. As can be seen from Fig. 1, the unit could be mounted in a remote position far up the duct, which might result in smaller and lighter ducting. It also provides a means of controlling and possibly eliminating a source of POGO-type oscillations by changing the natural frequency of the feed system as related to that of the vehicle structure.

DESIGN OF A PARTIAL-FLOW, HYDRAULIC-TURBINE-DRIVEN INDUCER

HYDRODYNAMIC DESIGN

Nomenclature

D = diameter, inches

D_m = mean diameter, inches

ΔH = head rise, feet

HP = horsepower

N = rotational speed, rpm

N_{ss} = suction specific speed, $N_{ss} = N\sqrt{Q}/(NPSH)^{3/4}$

NPSH = net positive suction head, feet

ΔP = pressure rise, lb/sq in.

Q = volume flow, gal/min

W = weight flow, lb/sec

φ = flow coefficient

Design Points for LO_2 and Water

The contract specified that, at the design point, the inducer NPSH should be 8 feet, in water, and that its characteristics were to be compatible with those of the J-2 oxidizer pump, which was to serve as the high-pressure pump. A J-2 fuel pump inducer design modified to a larger scale was to be used for the preinducer design. These basic "ground rules" did not fix the size or the speed of the unit. Calculations were made on a variety of sizes, with both NPSH and facility limitations being considered. The calculations indicated that the inlet diameter of the inducer should be about 10 inches. Accordingly, a standard-size pipe was selected; the pipe was schedule 40 stainless with an OD of 10.750 inches and an ID of 10.020 inches.

The optimum flow coefficient of the J-2 fuel pump inducer is 0.07, and the inlet diameter of the pipe is 8.015 inches. It was desired to have the same value of Q/ND^3 for the modified inducer. For the J-2:

$$\varphi = 0.2292\ Q/N$$

$$\frac{Q}{ND^3} = \frac{\varphi}{0.2292D^3} = \frac{0.07}{(0.2292)(8.015)^3} = \frac{1}{1685.88192}$$

For the preinducer in water:

$D = 10.020$ inches; NPSH = 8 feet; $N_{ss} = 40{,}000$ (44,250 from test data)

$(NPSH)^{3/4} = (8)^{3/4} = 4.75682847$

$N\sqrt{Q} = (40{,}000)(4.75682847) = 190{,}273.1388$

$$\frac{Q}{ND^3} = \frac{Q\sqrt{Q}}{N\sqrt{Q}\ D^3} = \frac{Q\sqrt{Q}}{(190{,}273.1388)(10.020)^3} = \frac{1}{1685.88192}$$

$Q\sqrt{Q} = 113{,}541.2036$; $Q = 2344.79$; $N = 3929.40$

The inducer head was obtained from a curve of the test data, so the complete values for the preinducer design point in water are:

Q = 2345 gpm	ΔH = 171 feet
N = 3930 rpm	ΔP = 74.2 psi
φ = 0.07	HP = 135
N_{ss} = 40,000	W = 326 lb/sec
NPSH = 8 feet	

The ratio of the pipe size is R = 10.020/8.015 = 1.25. So every dimension of the scaled-up inducer is 1.25 times that of the J-2 fuel pump inducer.

Although the design point of the preinducer provided some indication of the flow through the high-pressure pump (inducer flow plus recirculation flow), it did not fix the head and speed of the pump. These variables were open to arbitrary selection. It was decided that if the final unit successfully passed all its tests, it might, with a few modifications, be made available for an actual rocket engine test. Rocketdyne has made many studies on uprated J-2 engines, and the version on which the preinducer would be of most use is the 265K engine. On this engine, the LO_2 pump speed would increase by an approximate ratio of 265:200. The NPSH, therefore, would increase by the square of this ratio, or 1.756. A preinducer would be desirable if such an engine were ever tested. Calculations showed that a 265K engine would require a throughflow of 3314 gpm and a head of 3258 feet. The preinducer running on such an engine would operate at the following values:

Q	= 3314 gpm	ΔH	= 342 feet
N	= 5554 rpm	ΔH	= 168.2 psi
W	= 523 lb/sec	HP	= 434
NPSH	= 16 feet		

Under these conditions, the high-pressure pump would produce a head of 2916 feet and a flow of 4090 gpm at a speed of 10,560 rpm. At the design point in water, the corresponding head of the high-pressure pump is 1459 feet at a flow of 2893 gpm and a speed of 7471 rpm.

Inducer Guide Vanes

The inducer imparts a large amount of whirl to the fluid so that the guide vanes must turn the fluid through an angle of 59.6 degrees to remove all the rotation. It was decided that the best way to accomplish this was to use a scaled-up model of the stator following the J-2 fuel pump inducer (Fig. 15 page 29). This row of 19 airfoils removes 35.6 degrees of rotation and converts most of the velocity head into static pressure. The remaining 24 degrees of rotation is removed by a second

cascade containing 19 double-circular-arc blades, each with a chord of 4 inches and a maximum thickness of 0.4 inch. Each vane has 5 holes of 1/4-inch diameter for the passage of the return flow to the turbine. The total area of these holes is 4.6633 sq in. and the flow through them is 549 gpm with a resultant velocity of 37.7 ft/sec and a velocity head of 22 feet.

The 19 blade stator following the J-2 fuel pump inducer was carefully designed to avoid cavitation; test results have shown that the inducer cavitates first.

Hydraulic Turbine Design

Preliminary calculations were made on several types of turbines. These included a partial admission turbine driving a shrouded inducer through the shroud and a full-admission turbine driving the inducer through a shaft. A three-stage, full-admission turbine was the most promising. In 1966, under Contract Nonr 4507(00) for the Office of Naval Research, Dr. O. E. Balje' issued a Rocketdyne report (R-6805) that presented the results of a study program for the prediction of turbine performance. In the Performance Diagrams section of this report is a figure giving the optimum performance of full-admission axial-flow turbines. This diagram is shown reproduced in Fig. 2 . To put the values into the same units as used by Dr. Balje' we have for the LOX conditions

$$D = 5.816/12 = 0.48467 \text{ feet}; \quad Q = 122.30/70.79 = 1.727645 \text{ cfs}$$

$$\sqrt{Q} = 1.31440; \quad N = 5554.31 \text{ rpm}$$

$$Had^{1/4} = (805.17)^{1/4} = (28.37552)^{1/2} = 5.326868$$

$$Had^{3/4} = 151.15265$$

$$D_s = \frac{(0.48467)(5.326868)}{1.3144} = 1.9642$$

$$N_s = \frac{(5554.31)(1.3144)}{151.15265} = 48.30$$

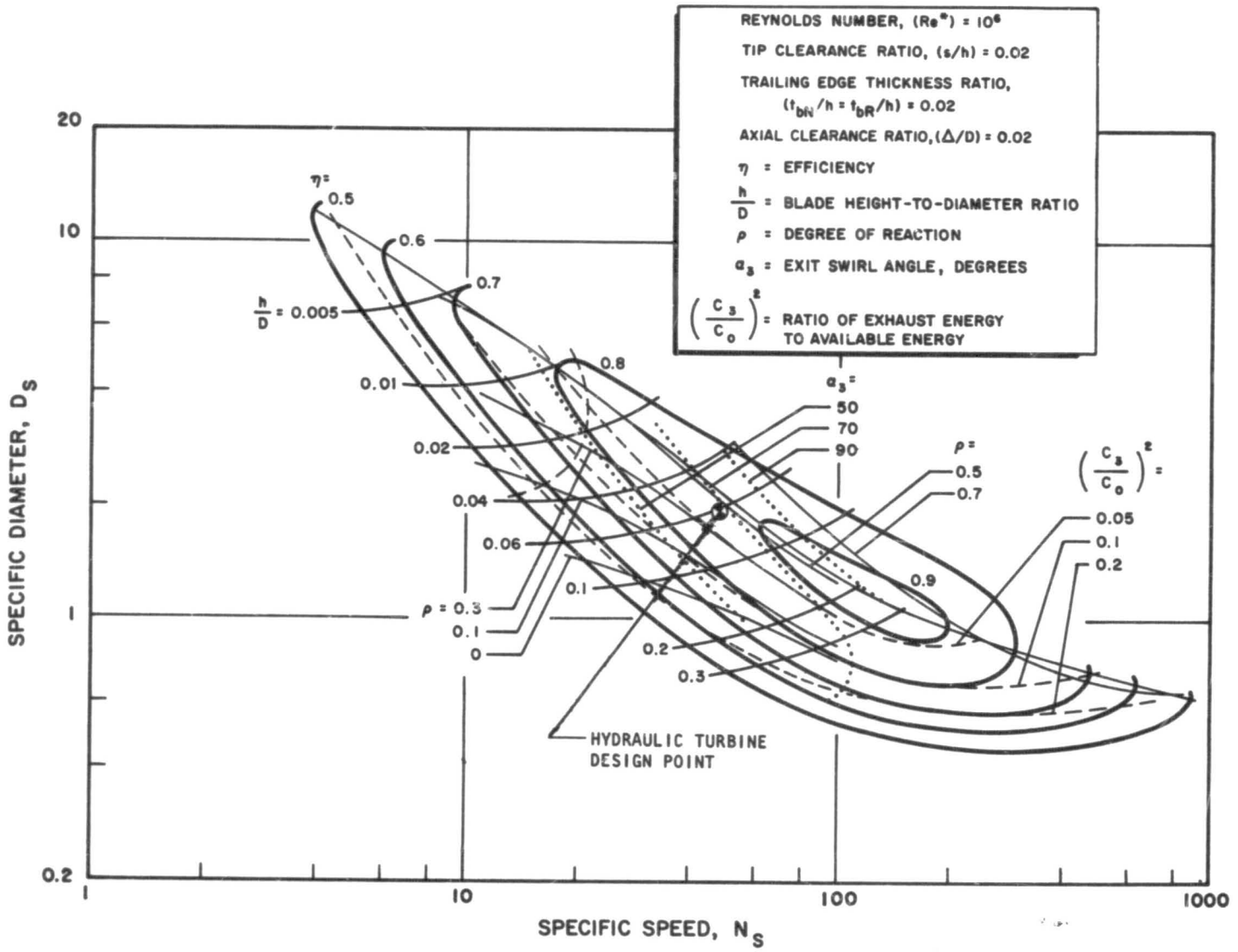

Figure 2. Optimum Performance of Full-Admission, Axial-Flow Turbines

On this map is shown the operating point of the three-stage hydraulic turbine with a predicted efficiency of over 85 percent. A partial-admission turbine would have an efficiency of approximately half this value and would, thus, require twice the recirculated flow. Additional advantages of the full-admission turbine are:

1. A more easily maintained tip clearance
2. A better dynamically balanced unit
3. A smaller rotating diameter with little or no increase in unit length
4. An unshrouded inducer that is easier to manufacture. Shrouding would change the performance of the J-2 inducer.
5. Seal diameters and speeds that are lower

In view of these advantages, it was decided to use the full-admission turbine.

A generous allowance was made for the head drop in the return line between the high-pressure pump and the turbine. This permitted the insertion of a flowmeter for measuring the return flow and a valve for controlling the speed of the turbine. The remaining head was assumed to drop uniformly across the three stages. This gave a head drop across each stage of 403 feet in water with an Euler head of 325 feet. The resultant Euler efficiency was approximately 80 percent. The resultant turbine flow to provide the inducer design horsepower was 549 gpm. Figure 3 shows the velocity diagram for the three-stage turbine. Figures 4 through 7 show the shapes of the nozzles and rotors as defined by the turbine designer.

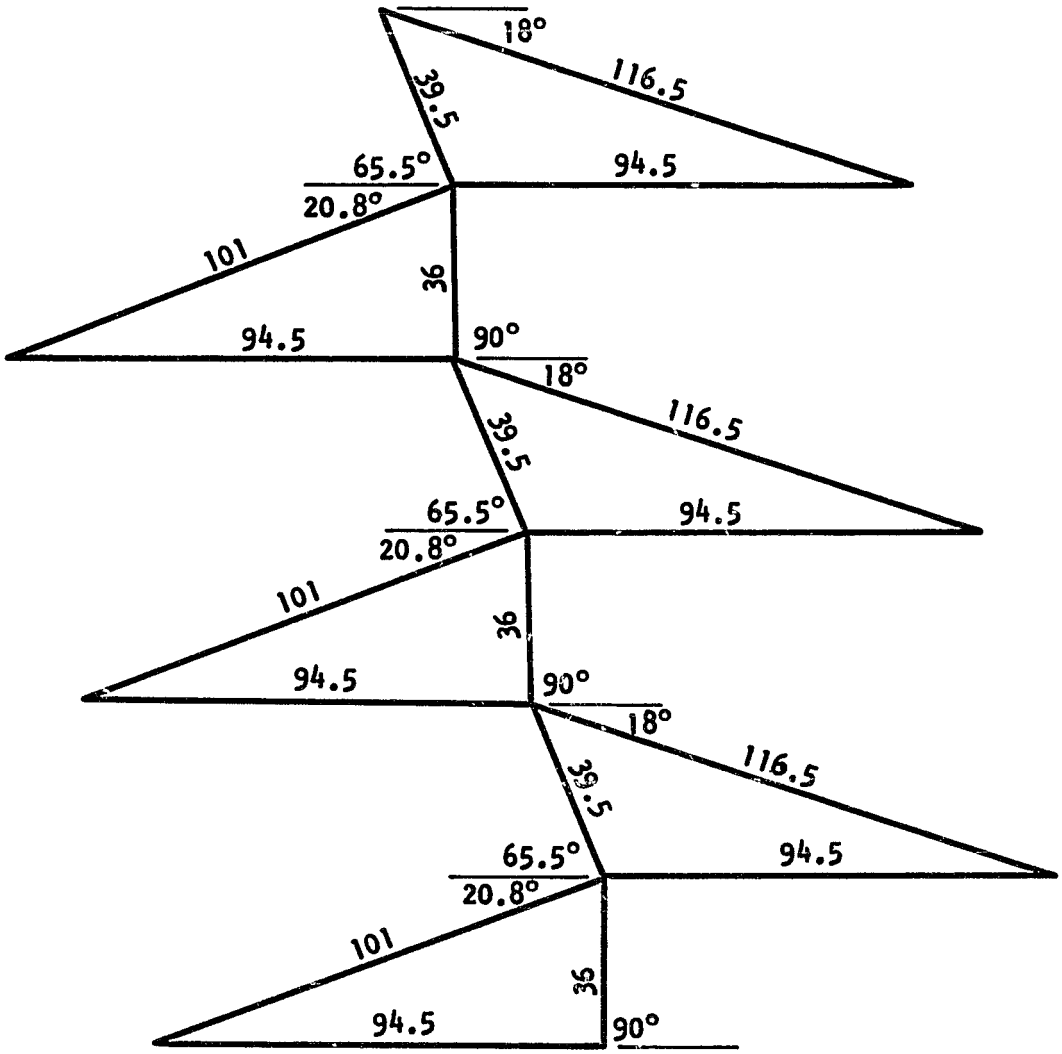

Figure 3. Preinducer Hydraulic Turbine (H_2O) Velocity Diagram

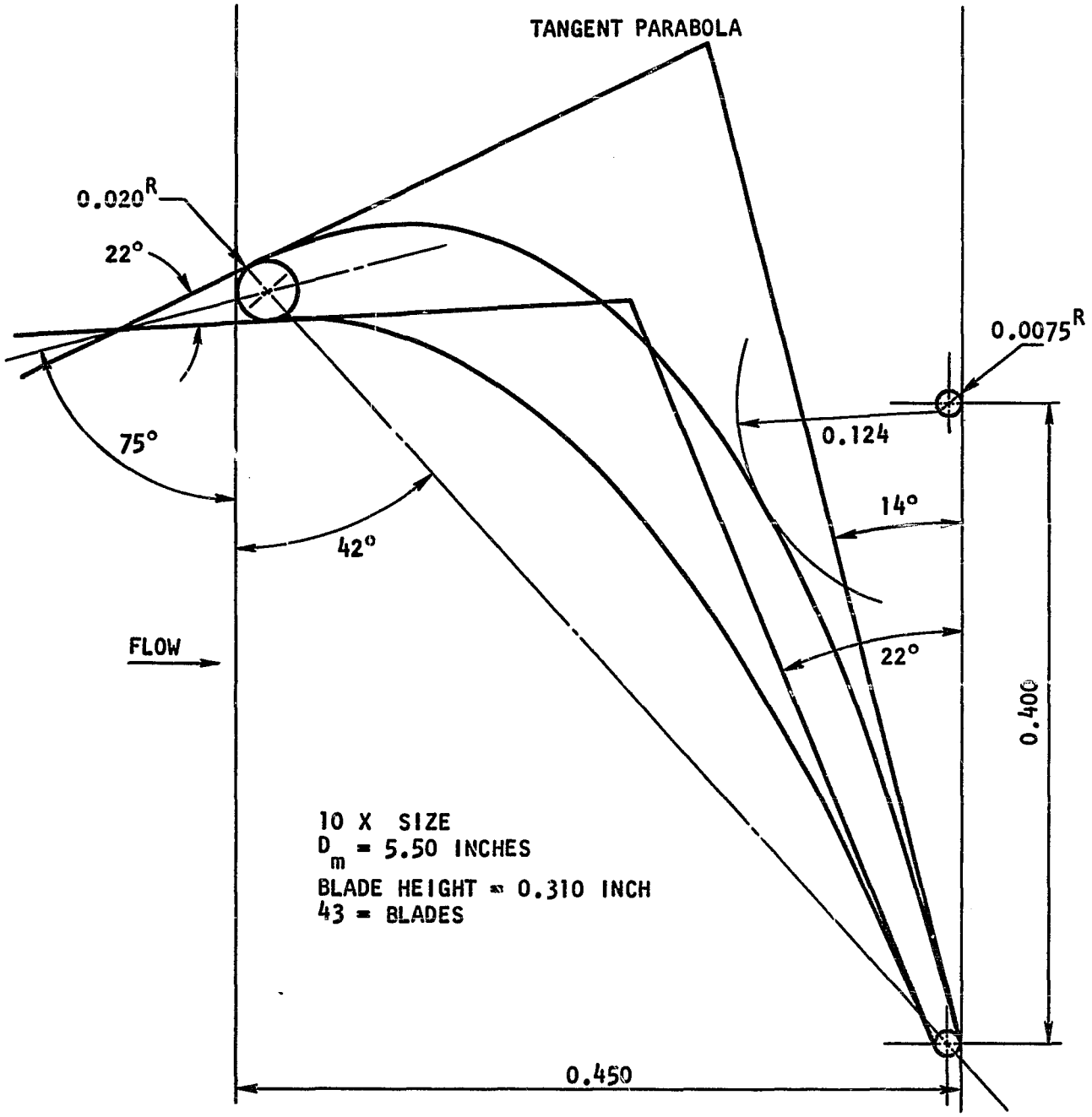

Figure 4. Preinducer Turbine Nozzle

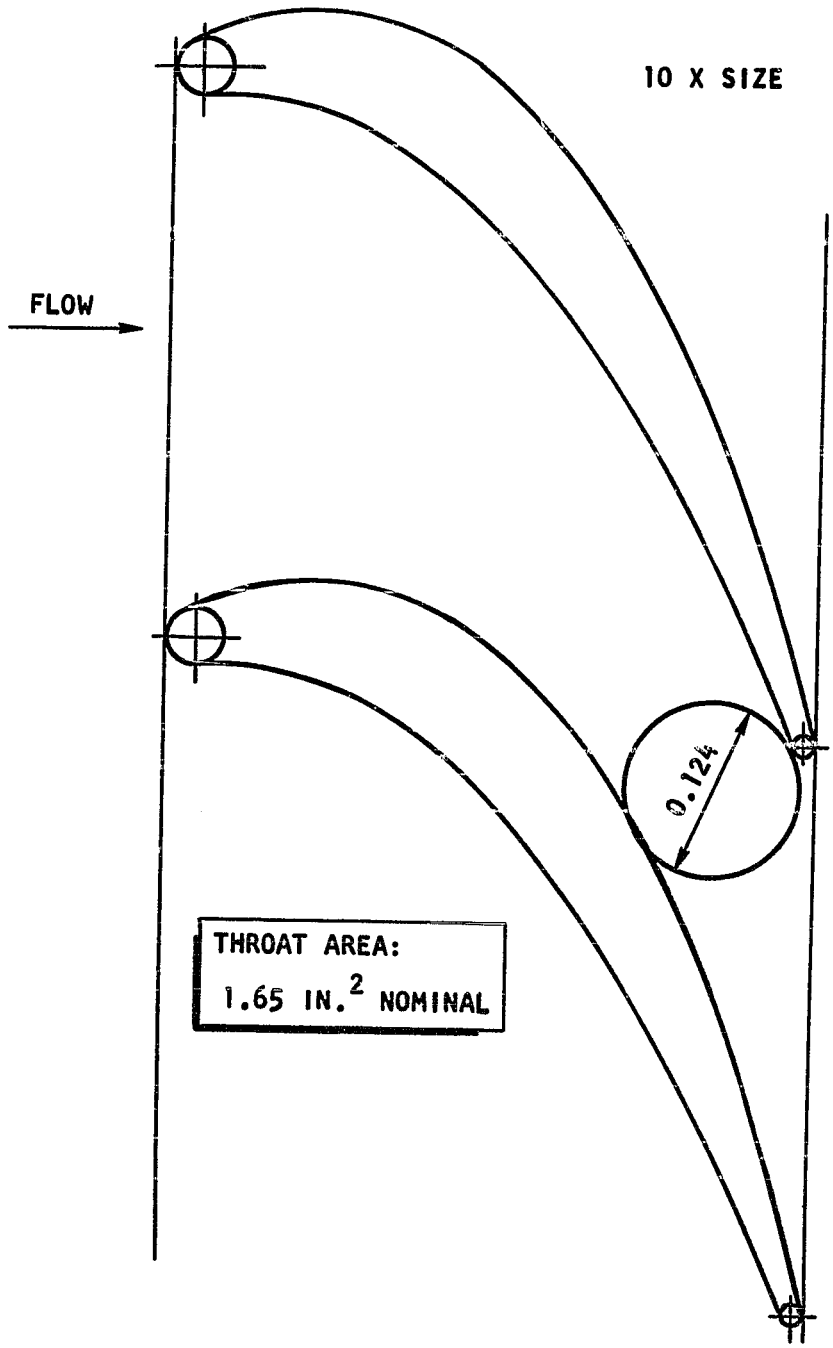

Figure 5. Preinducer Turbine Nozzle

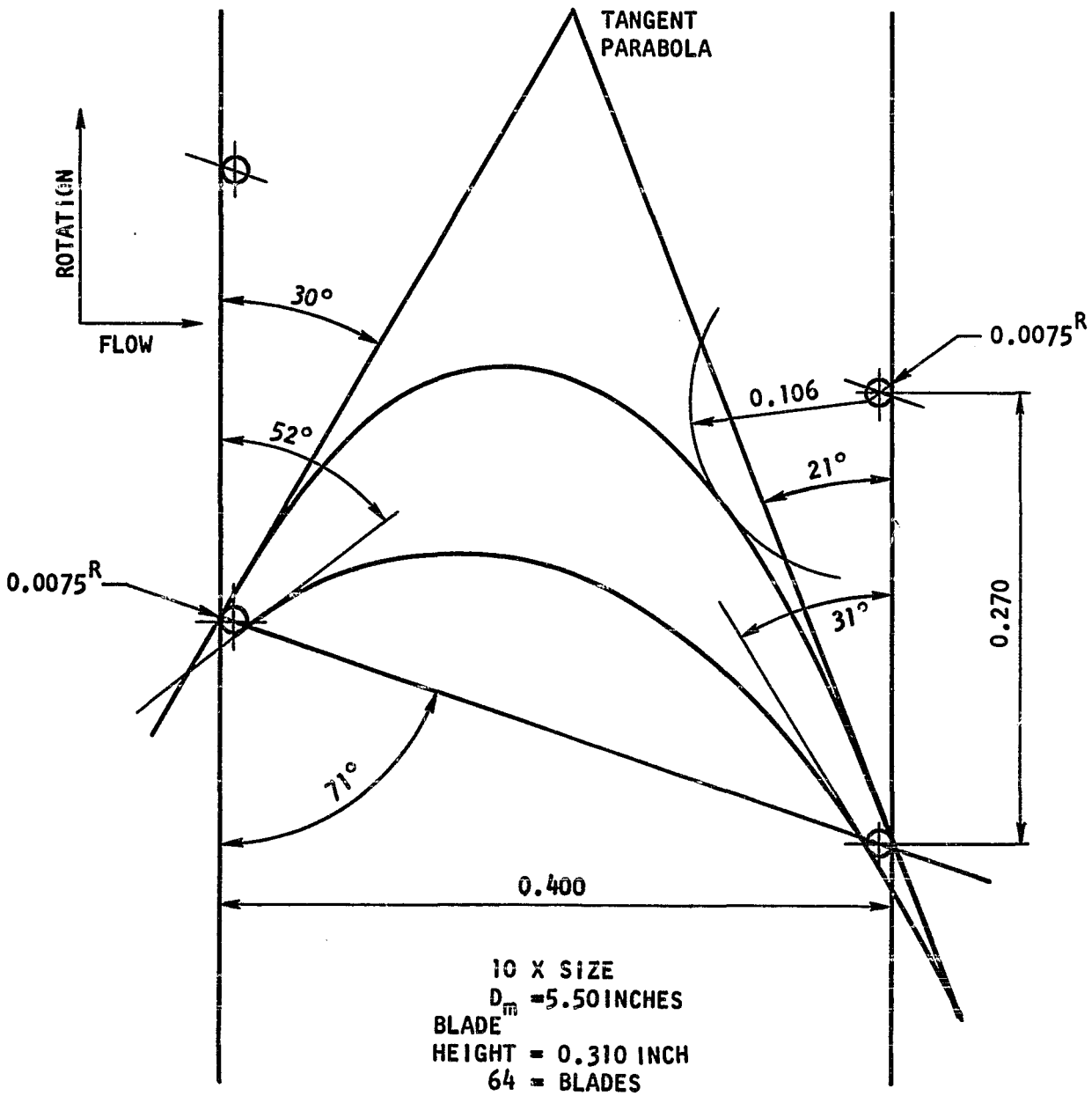

Figure 6. Preinducer Turbine Rotor

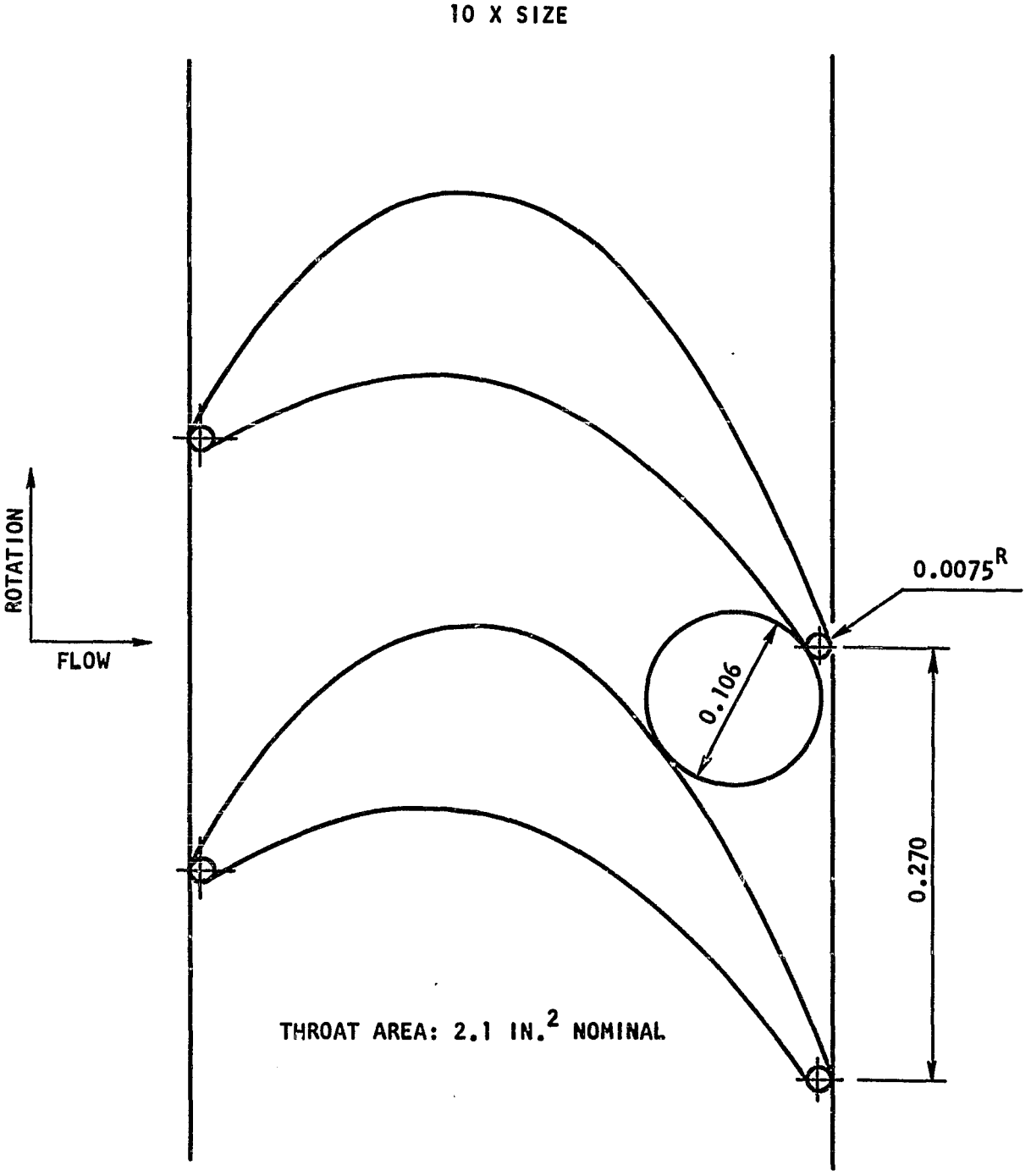

Figure 7. Preinducer Turbine Rotor

Steady-State Maps

The computer programs required steady-state performance maps of the various components as inputs. These include the head, flow, efficiency, and NPSH as a function of speed for both the inducer and the high-pressure pump and the torque, pressure drop and flow as a function of speed for the hydraulic turbine. The high-pressure pump (J-2 oxidizer pump) and the J-2 fuel pump inducer have both been tested at Rocketdyne. Figure 8 shows the nondimensional H-Q performance of the high-pressure pump while Fig. 9 and 10 give the efficiency and NPSH. The nondimensional H-Q and efficiency of the preinducer are shown in Fig. 11, and the cavitation performance is shown in Fig. 12. The H-Q map was taken from calibration tests made on J-2 fuel pumps at full speed in liquid hydrogen. The inlet head was the total head at the inlet of the pump; the discharge head was measured with a static wall tap at the discharge of the stator row that follows the inducer. To this static head was added the head corresponding to the axial component of velocity. It was assumed that the static pressure remained constant through the second row of vanes of the preinducer (the losses were equal to the velocity head recovery associated with the removal of the fluid rotation). The map, thus, includes the effect of incidence on the first row of stators and is accurate at off-design conditions except at low flows. At low flows the J-2 fuel pump stalls and testing is terminated. The low-flow predictions were based on the results of an air rig test of the inducer without the following stators. The losses through the stators were estimated. The maps for the preinducer have been modified by the affinity laws to account for the fact that the inducer is 1.25 times as large as the J-2 fuel pump inducer.

It was necessary to calculate the turbine map because no data were available. The calculated map was based on the following assumptions:

1. The turbine is of the full-admission, repeating-stage type.
2. The flow is two-dimensional and the design is fixed by a velocity diagram at only one radius.
3. The flow is incompressible.

Figure 8. J-2 Oxidizer Pump Performance

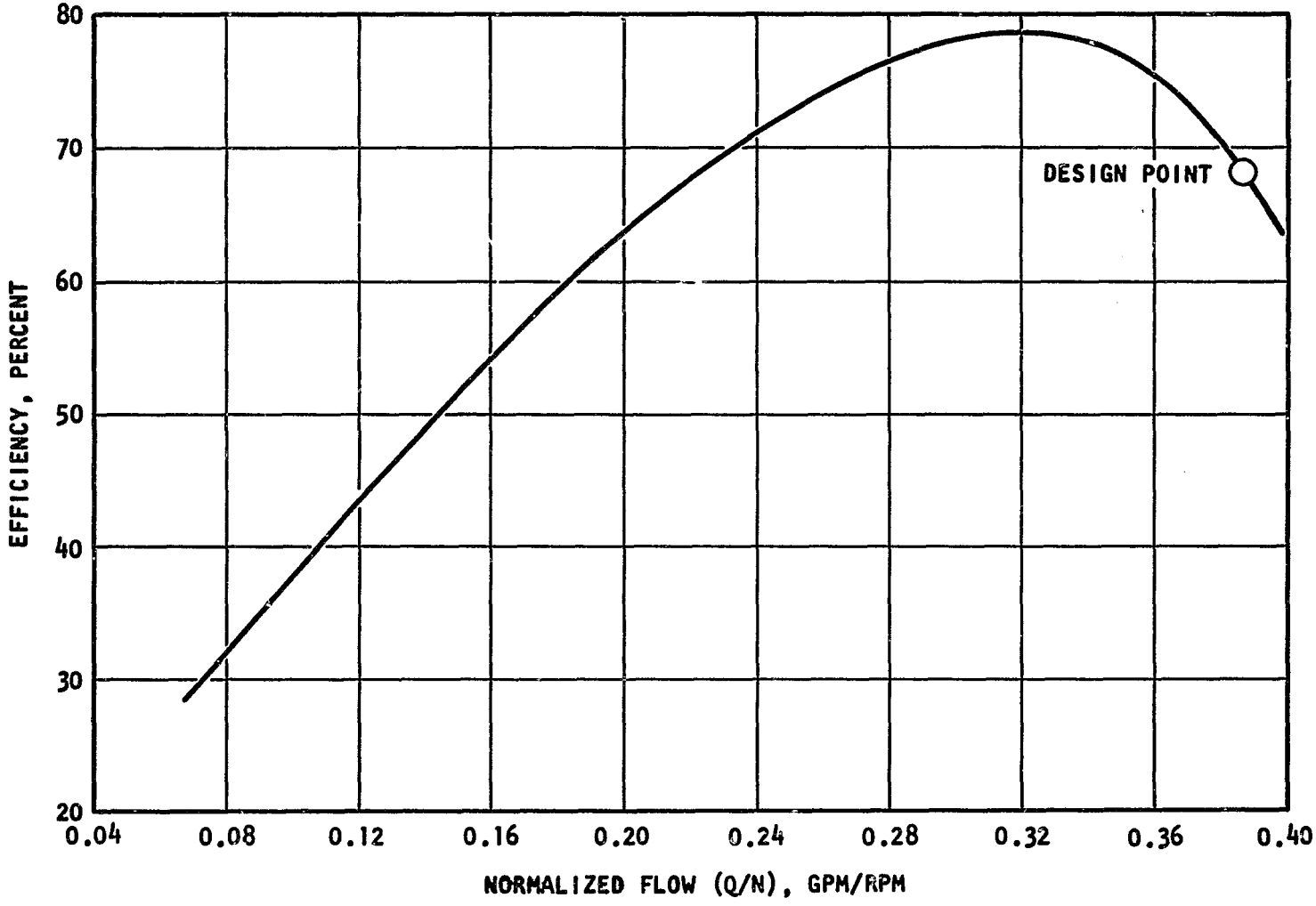

Figure 9. J-2 Oxidizer Pump Performance

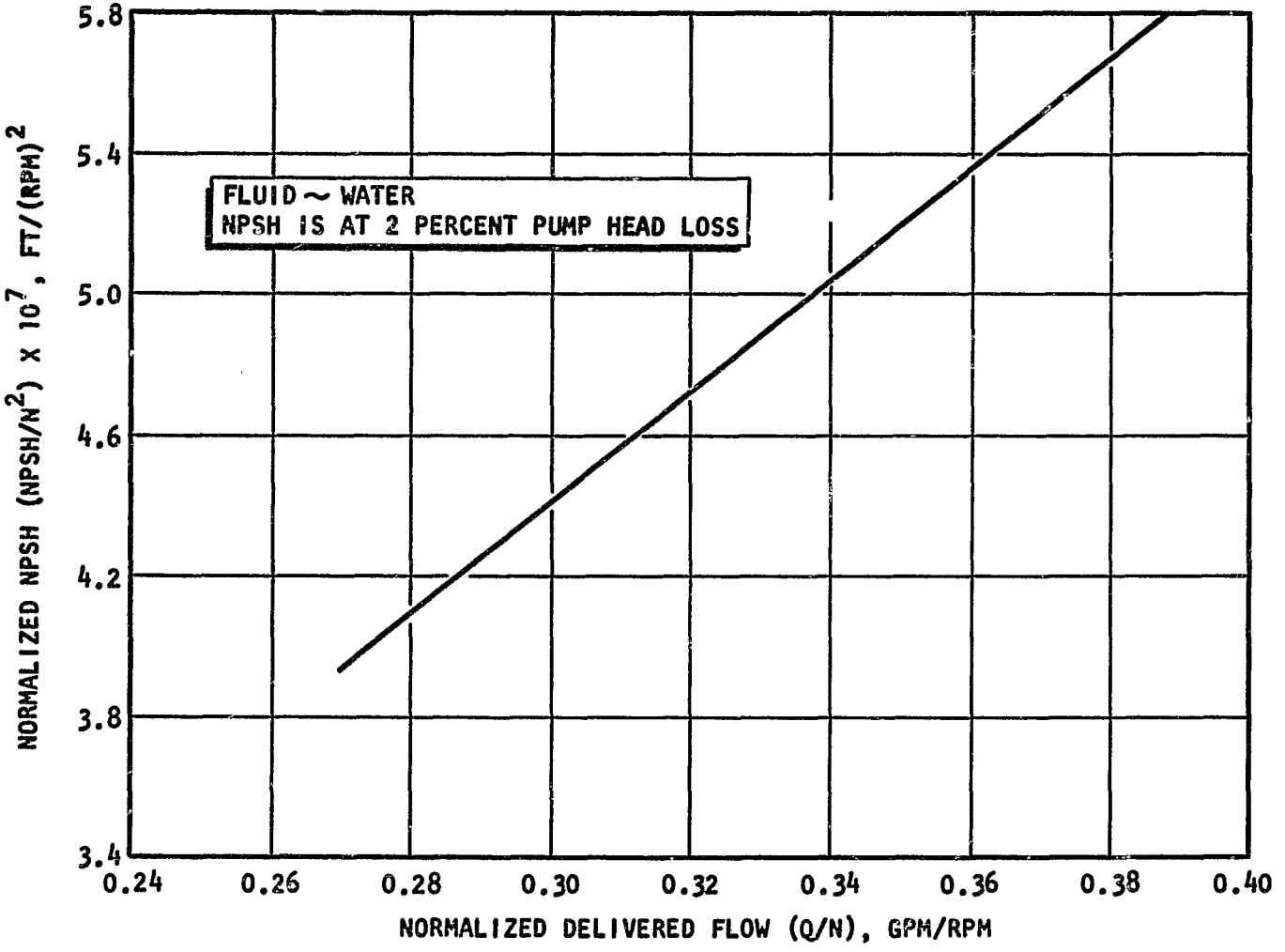

Figure 10. J-2 Oxidizer Pump Suction Performance

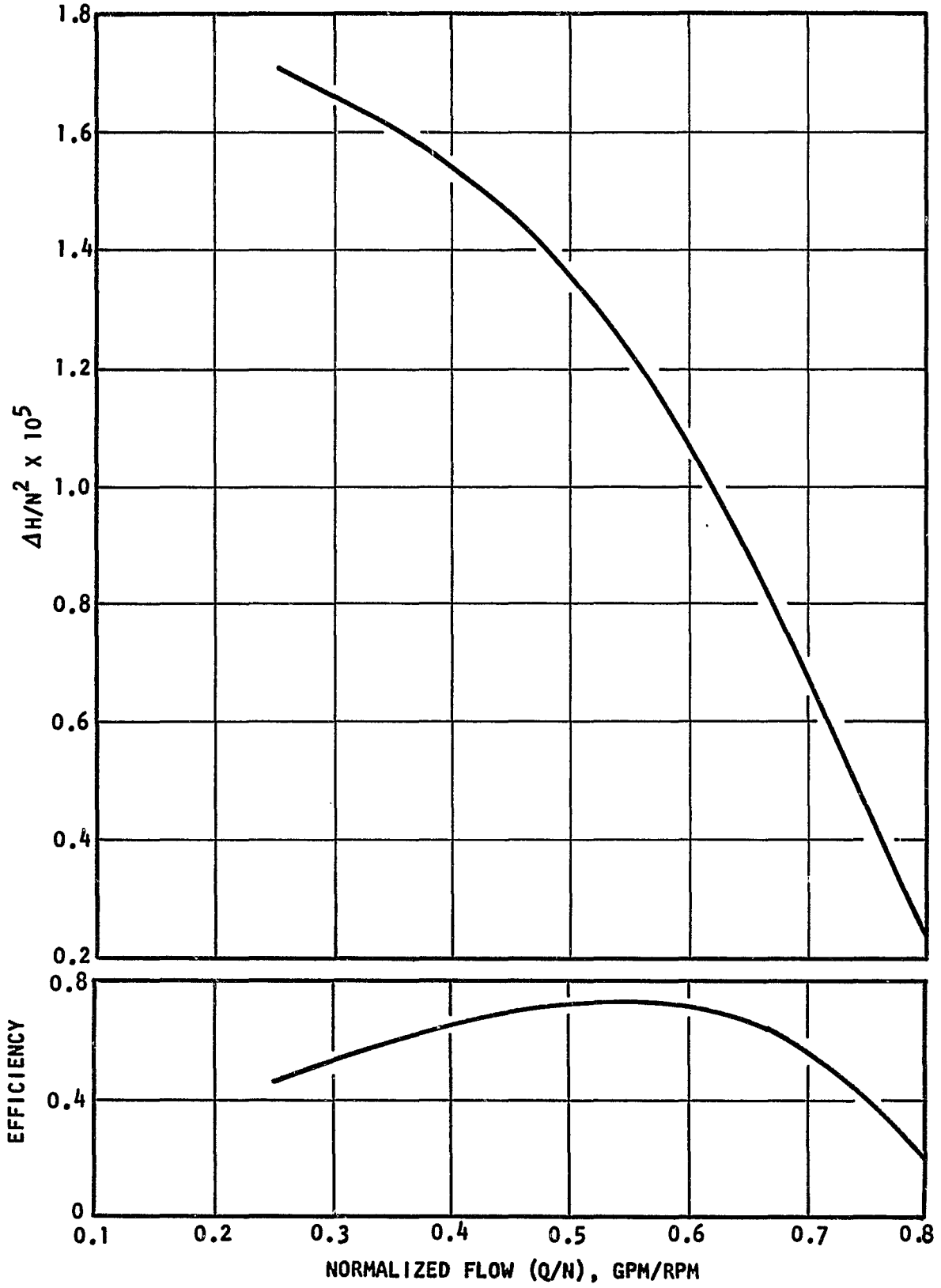

Figure 11. J-2 Oxidizer Preinducer Predicted Performance

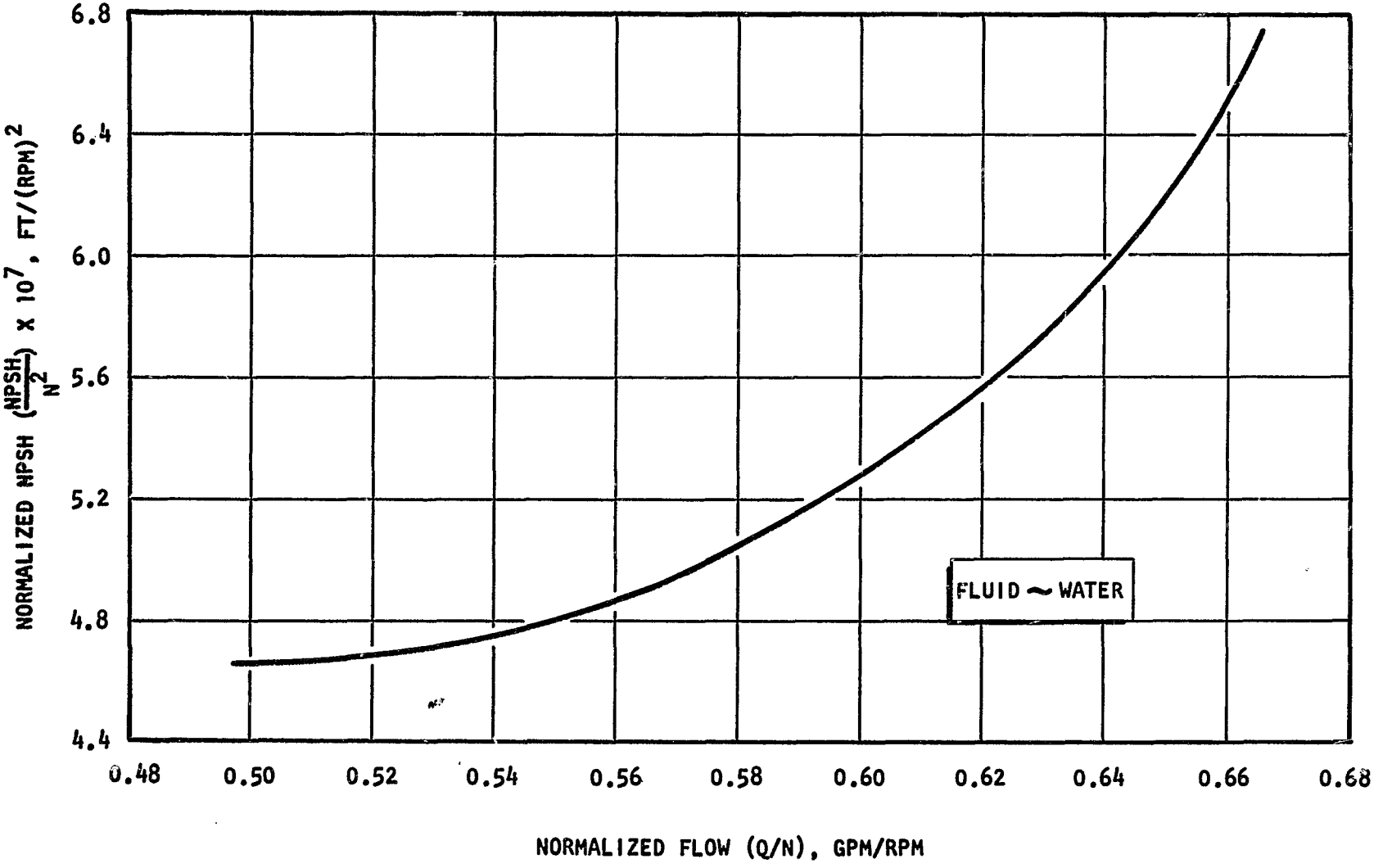

Figure 12. J-2 Oxidizer Preinducer Predicted Suction Performance

4. The nozzle and rotor discharge angles as determined by the basic velocity diagram at the design point are attained by a properly designed set of blades; at off-design points these angles remain unchanged (the deviation angle is not affected by incidence angle).

5. The efficiency at the design point is known (by calculation or estimation). This efficiency is expressed as a loss coefficient applied to the nozzle and rotor spouting velocities; this loss coefficient is held constant at all off-design points. It also is assumed that additional losses are caused by positive or negative incidence angles on both rotor and stator at off-design points. These losses are equal to the velocity head of the component normal to the design inlet velocity vector.

With these assumptions, it was a simple matter to set up the equations and write an IBM program to calculate turbine maps. Figures 13 and 14 show the maps generated by the program. The curve for the three-stage turbine is for the actual turbine. The curves for the two- and four-stage turbines were made for parametric studies of the effect of the degree of turbine reaction on the transient performance of the unit. The two-stage turbine was close to being a pure impulse turbine (11.72 percent reaction); the three-stage turbine had 41.14 percent reaction, and the four-stage turbine had 55.86 percent. At first, it was assumed that all turbines had the same axial velocity at the design point. However, this assumption for the two-stage turbine produced too flat an angle leaving the nozzle. This angle (with the tangent) was increased to 14 degrees by increasing the axial velocity.

MECHANICAL DESIGN

A cross section of the preinducer is shown in Fig. 15, with the major hardware components identified. Flow enters the inducer from the left

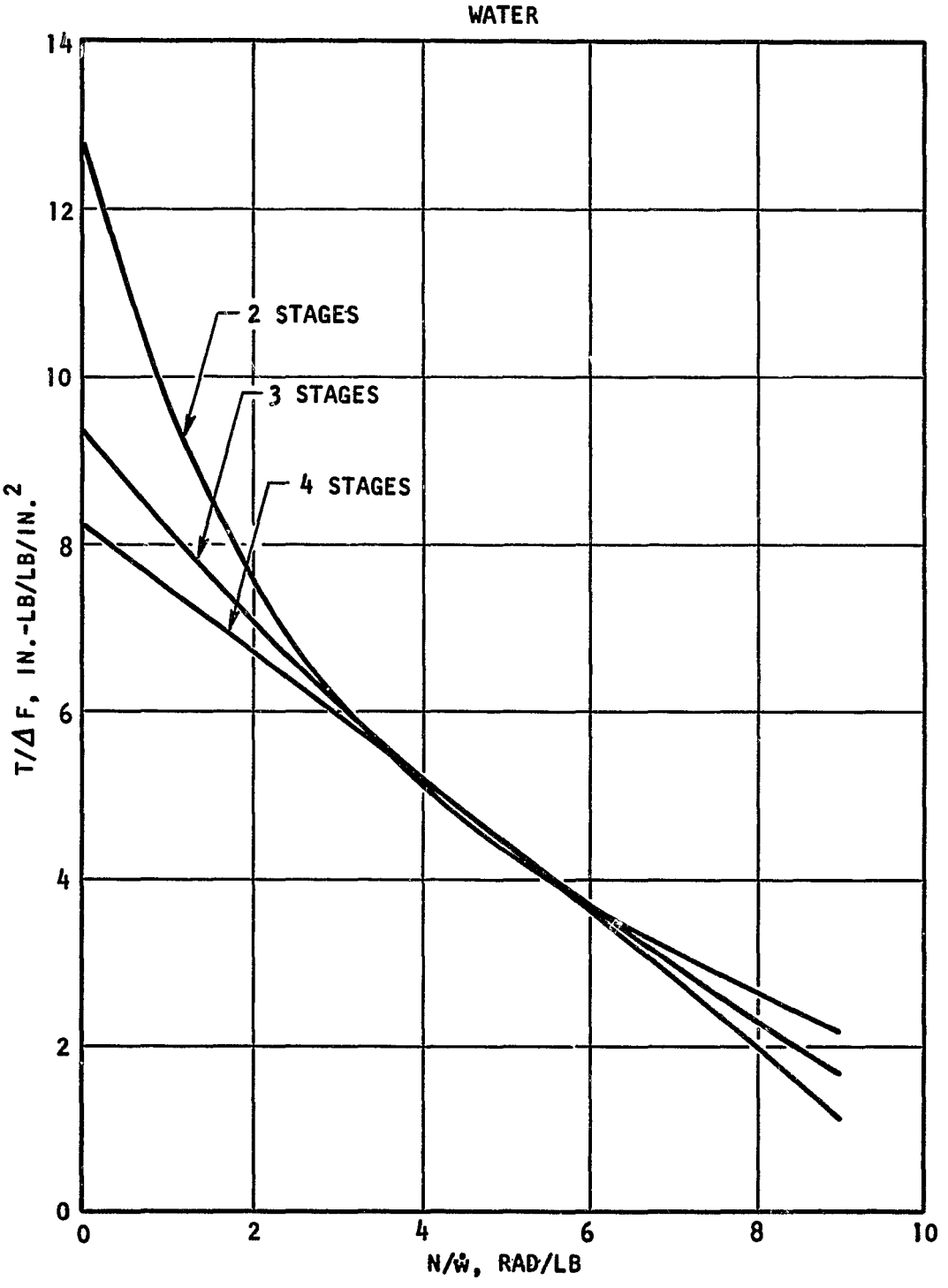

Figure 13. Torque of Preinducer Hydraulic Turbine in Water

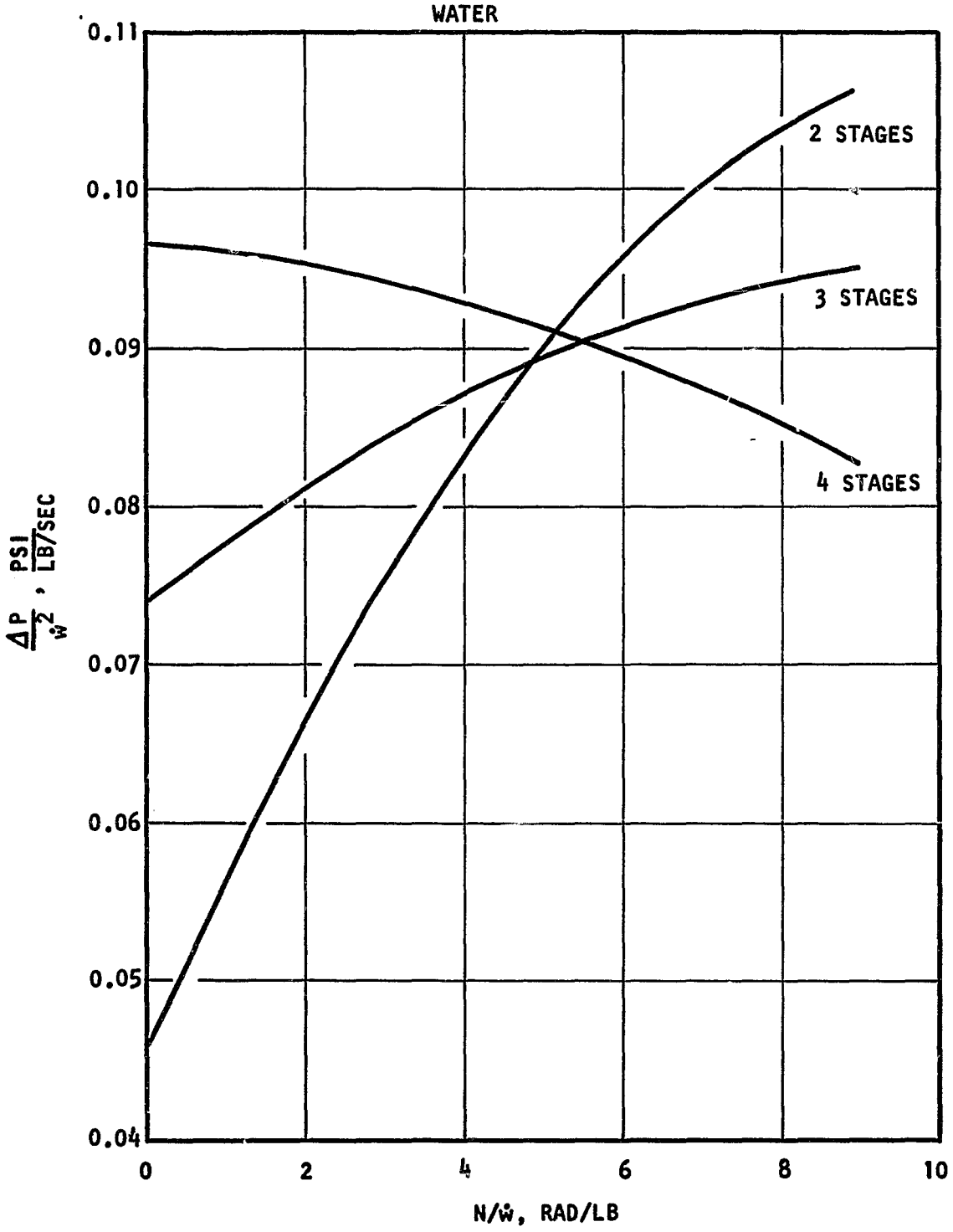

Figure 14. Pressure-Flow Curve of Preinducer Hydraulic Turbine in Water

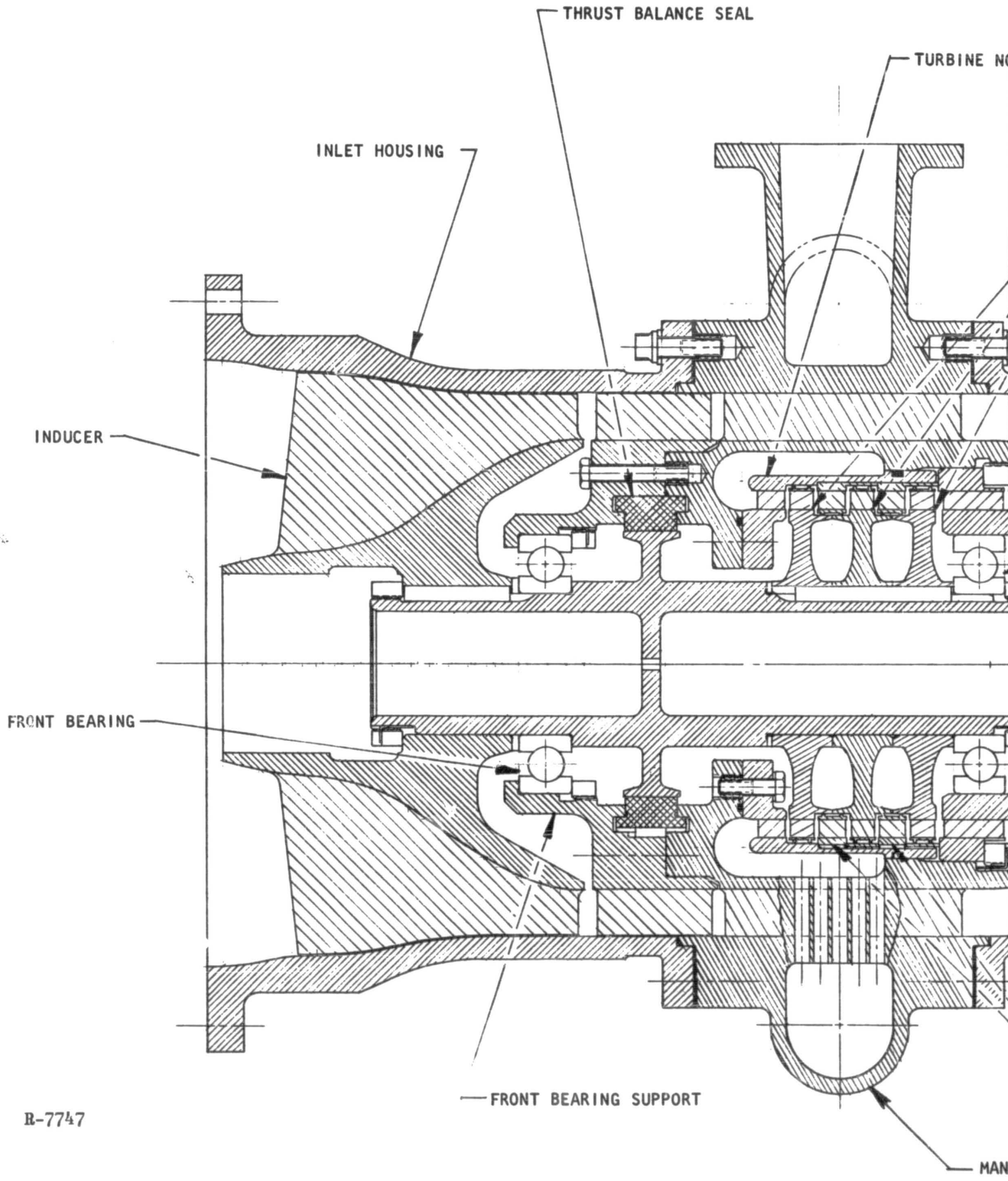
THRUST BALANCE SEAL
TURBINE NO
INLET HOUSING
INDUCER
FRONT BEARING
FRONT BEARING SUPPORT
MAN

R-7747

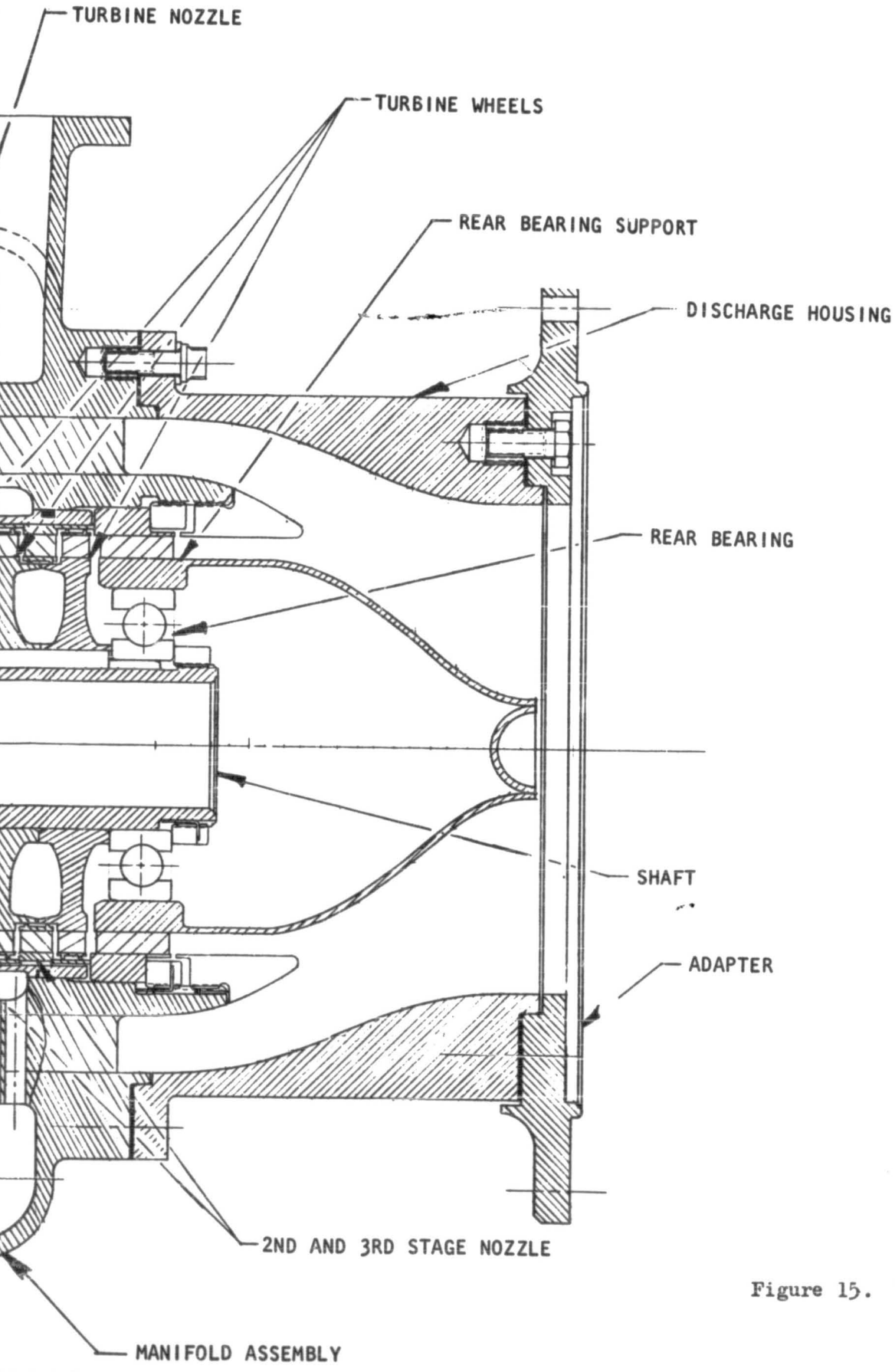

Figure 15. Preinducer Cross Section

and is discharged into a two-row cascade. Most of the whirl is removed by the first row of 19 airfoils; the remaining whirl is removed by the second row. The second row of vanes is used also as a structural member to support the bearings and the walls of the turbine. The turbine is driven by high-pressure fluid from the discharge of the high-pressure pump. This fluid enters a circumferential manifold through a single inlet and is distributed around the outer periphery from which it passes to the inner circumferential manifold through 5 radial holes drilled in each of the 19 vanes. After the fluid has expelled its energy in the turbine, it blends with the inducer discharge flow and enters the high-pressure pump.

The rotor assembly was a flightweight design so that realistic rotor dynamics would be displayed. A critical speed analysis indicated that no critical speed problems would exist throughout the operating range. If a conservative bearing spring rate of 10^5 lb/in. were assumed, the critical speed would be greater than 14,000 rpm. Other numbers pertinent to the rotating assembly are listed below:

Weight	15.67 pounds
Center of Gravity	5.58 inches from inducer end at the hub
Moment of Inertia in Roll	0.2402 lb-in.-sec^2
Diametral Moment of Inertia	0.5563 lb-in.-sec^2

The axial thrust of the turbine is in the aft direction; it exceeds the forward thrust of the inducer. The thrust difference is compensated by a thrust balance disk which senses the inducer discharge pressure on the forward side and the turbine nozzle discharge pressure on the aft side. The diameter of the disk is such that a balance is obtained at the design point.

In contrast to the rotor assembly, the housings are heavy to simplify machining and to provide a sturdy support for the rotor.

Inlet Housing

The inlet housing converges the flow from the facility ducting to the inducer inlet OD. It is also the inducer housing and contains the speed pickup. The speed pickup is a Bently transducer located at the inducer blade leading edge OD. The inlet housing wall was left thick to minimize machining costs. As a result of this, the stress level in the housing from both operating and mounting loads is low. The inlet housing was machined from a 6061-T651 aluminum alloy hand forging.

Inducer

The inducer is a scaled-up version of the J-2 fuel pump inducer. It has an inlet diameter of 9.75 inches, and an exit diameter of 9.0625 inches; it has four full and four partial blades. It is machined from a 7075-T73 aluminum alloy hand forging. A pilot diameter and inducer nut are used for retention to the shaft with a single key to transmit torque. The centrifugal blade loading stresses are quite low; the hydrodynamic blade loading is the largest, being approximately half the blade design capability. The maximum possible weight has been removed from the inducer hub to keep the rotor assembly flightweight. A photograph of the inducer with the first row of diffuser vanes resting on top (for the photographer's convenience) is shown in Fig. 16.

Front Bearing Support

The front bearing support incorporates the diffuser vanes as an integral part. It has a retention flange for the thrust balance labyrinth seal. The bearing support is bolted to the manifold assembly, and the bearing is installed in the conventional manner with a bearing shoulder, nut, and lock tab washer. It is machined from a 6061-T651 aluminum alloy hand forging.

Manifold Assembly

The manifold assembly consists of the outer manifold, the second row of diffuser vanes, and the outer shell of the turbine. The vanes, along

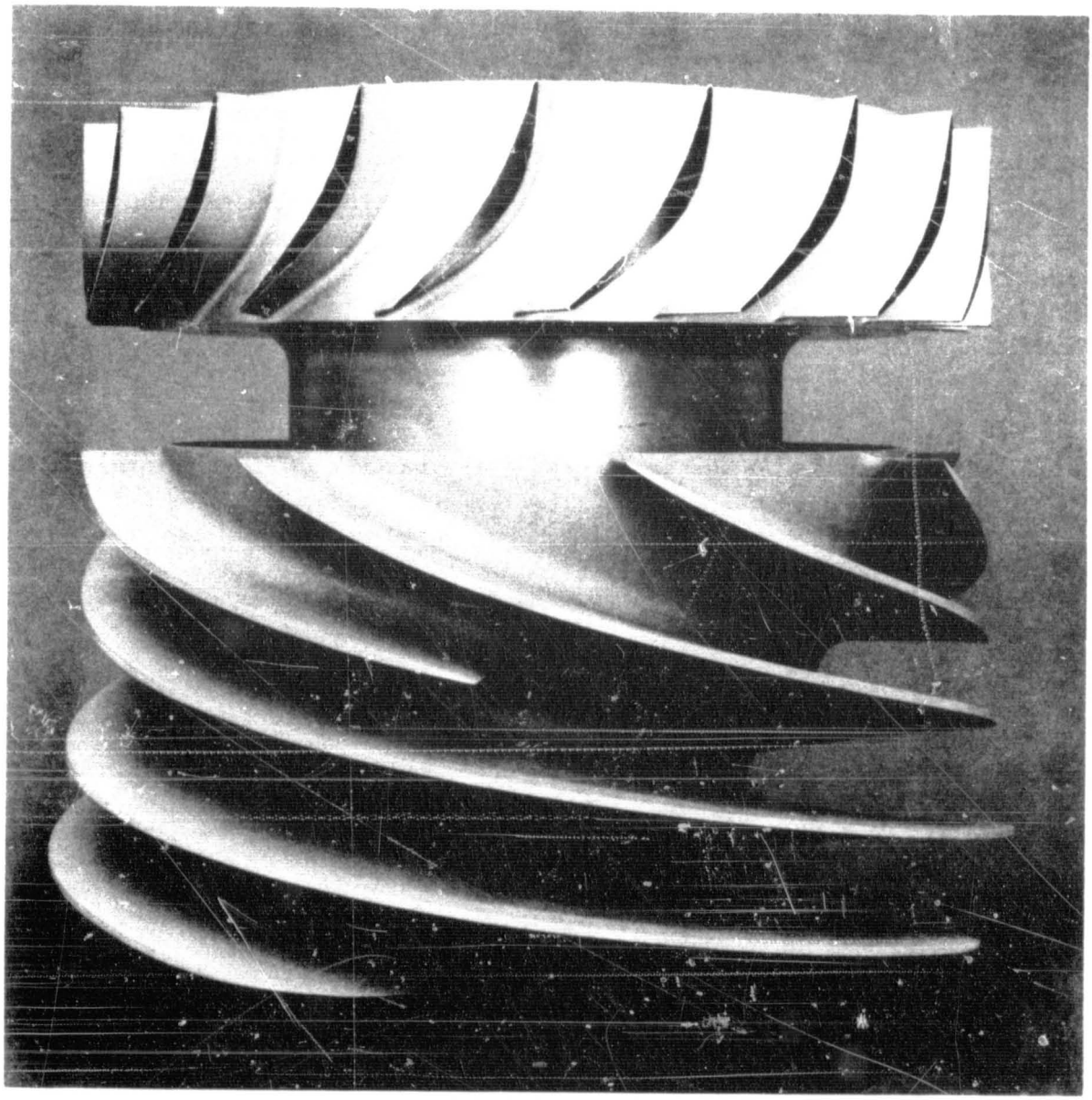

1CT62-8/19/68-C1D

Figure 16. Inducer and First Row of Diffuser Vanes

with the two walls, were machined from solid 6061 aluminum stock, and the five radial fluid passage holes then were drilled in each vane. The manifold inlet and the manifold ring were separately machined from 6061, then the entire assembly was welded together. This was followed by heat treat and final machining. The maximum stress in this assembly occurs at the elliptical section of the inlet. At the maximum operating pressure, this stress is half the capability of the material. The assembly was proof pressure tested to 925 psi. The maximum stress at this pressure in the elliptical section was calculated to be approximately two-thirds the capability of the material. Figure 17 is a photograph of the manifold assembly.

Shaft

An aluminum shaft was selected over the conventional steel shaft because the stress levels in the shaft were low. The shaft is hollow; the result is a lightweight low-inertia shaft for fast acceleration response and good rotor dynamics. The shaft was machined from a 6061 aluminum alloy bar. The thrust balance disk was machined as an integral part of the shaft. The finished shaft was heat treated to a T6 condition as per MIL-H-6088. It was hard anodized at the bearing journals and thrust balance seal surface to a thickness of 0.0010 inch. The remaining surface of the shaft was hard anodized to a thickness of 0.0002 to 0.0003 inch. The shaft threads were dry film lubricated to prevent galling.

Turbine Nozzle

The turbine nozzle was machined from 6061-T651 aluminum alloy. There are 43 vanes in the nozzle ring. A cylinder that retains the second- and third-stage nozzle ring was welded to the outer shroud of the turbine nozzle. The turbine nozzle was bolted to the manifold assembly by a flange that was machined on the inner shroud. The split lines between turbine nozzle and the manifold assembly were sealed with O-rings. The highest stress occurs as hoop compression in the welded-on cylinder. This stress is approximately half the material capability. A photograph of the nozzle is shown in Fig. 18.

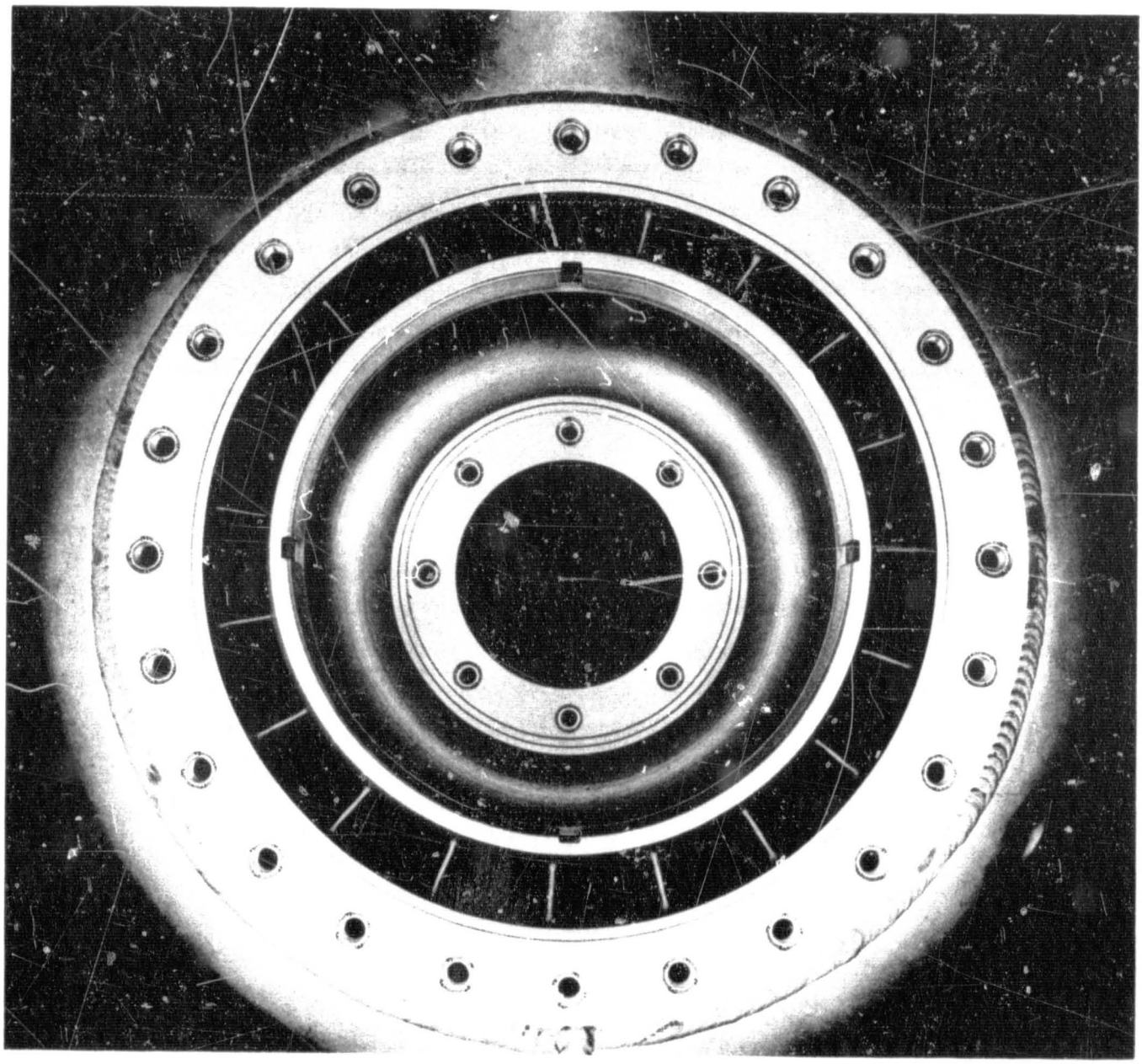

1CT62-8/19/68-C1B

Figure 17. Manifold Vane Assembly

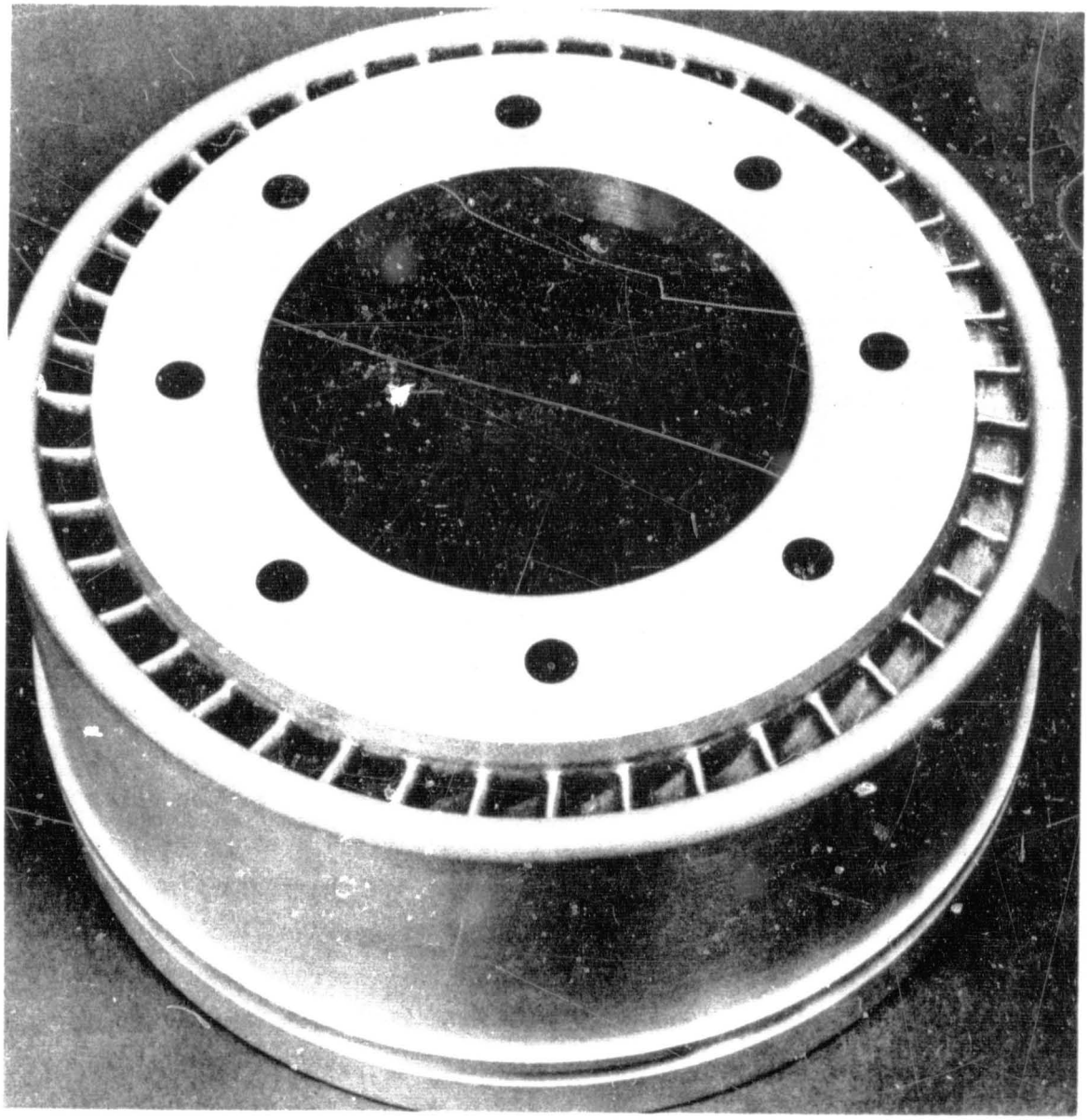

1CT62-8/19/68-C1A

Figure 18. First-Stage Turbine Nozzle

Second- and Third-Stage Nozzles

The second- and third-stage nozzles are identical and interchangeable. Their flow passage is the same as that of the first-stage nozzle. They were machined from 6061-T651 aluminum alloy; two lips were machined on the inner periphery of the inner shroud to form a seal and reduce fluid leakage between the stationary nozzle and the rotating wheel rim. The nozzle torque is restrained by keying each nozzle stage at the outer shroud to the cylinder of the turbine nozzle. The maximum stress in each nozzle stage is in bending at the vane tips where the torque resistance is transferred from each vane into the outer shroud. The stress level in this area is less than half the design capability.

Turbine Wheels

The three turbine wheels are identical except for the spacing rim. The center wheel has the spacing rim on each side, while the first- and third-stage wheels have the rim removed from the front and back side, respectively. The turbine blades were machined without an outer shroud and as an integral part of the disk. The outer shrouds were installed with a dip braze over the blade tips. Two lips were machined on the outer periphery of each shroud to form a seal to reduce fluid leakage over the wheel OD. The turbine wheels are keyed to the shaft. The nozzle-to-wheel clearance is set with a spacer between the first-stage wheel hub and the shaft shoulder. The wheels are held on the shaft by the rear bearing nut. The three turbine wheels were machined from 6061-T651 aluminum alloy and heat treated to a T6 condition after the dip brazing process. The highest stress occurs at the blade roots, and this stress is well within the design capability. Figure 19 is a photograph of two of the turbine rotors. The rotor on the left shows the discharge edges of the blades while the rotor on the right shows the leading edges.

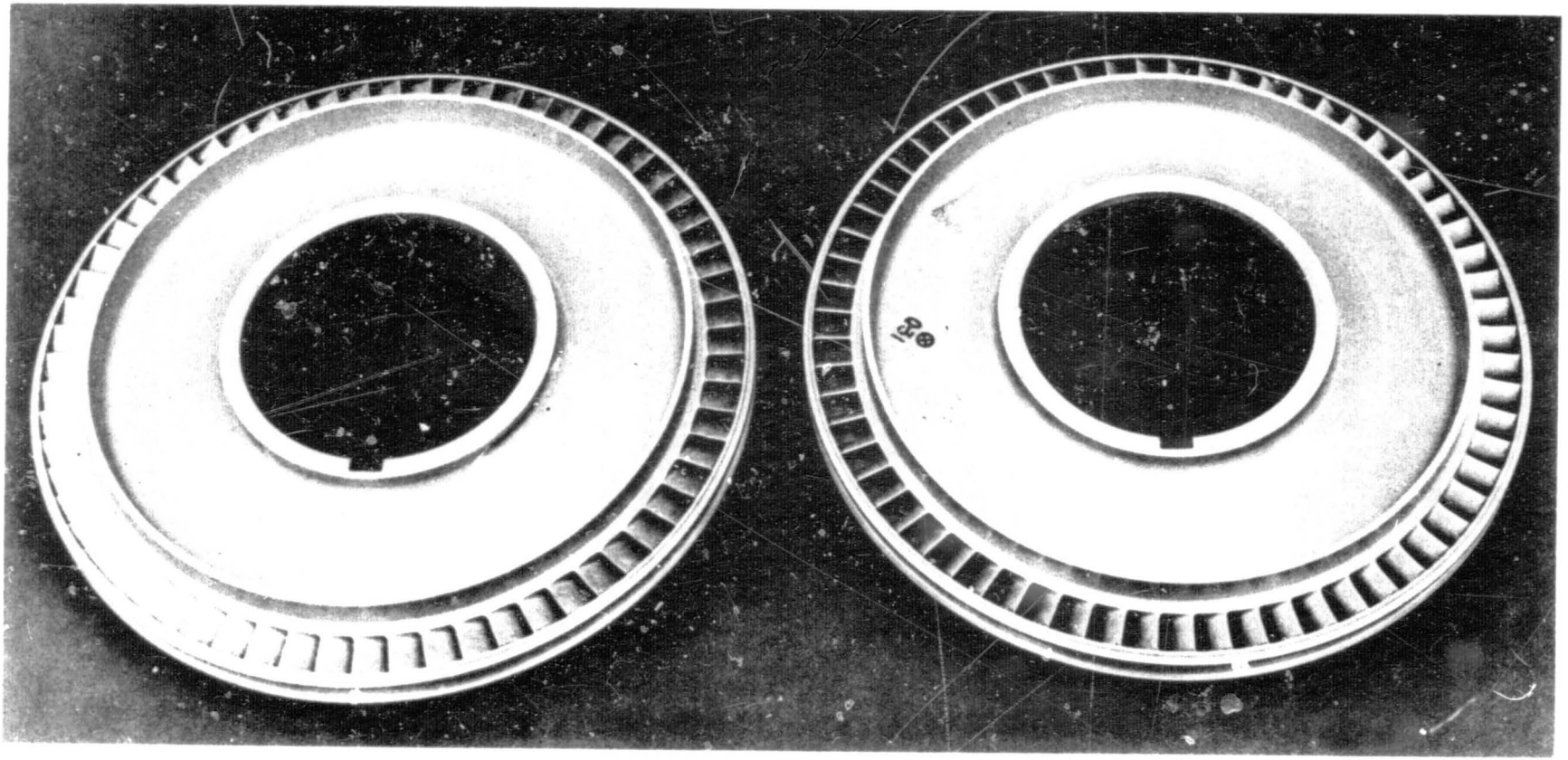

1CT62-8/19/68-C1C

Figure 19. Turbine Rotors

Rear Bearing Support

The rear bearing support was machined from 6061 aluminum alloy. The discharge cone was formed from 6061 aluminum sheet and welded to the bearing support. Fifteen vanes are used in the fluid passageway to transmit the bearing loads into the manifold assembly. These vanes are straight and radial and remove any rotation remaining in the fluid. The bearing support is held in place by a single, large-diameter retaining nut.

Discharge Housing

The discharge housing coverges the flow passage from the inducer discharge diameter to the J-2 oxidizer inlet diameter. It was machined from a 6061-T651 aluminum alloy hand forging. The stress level here, as in the inlet housing, is low because the walls were left thick to minimize machining costs.

Bearings

Two ball bearings were used to support the rotor assembly, one aft of the inducer and one aft of the turbine. The two bearings used are the same bearings used in the J-2 oxidizer turbopump. 440-C steel was used for the race and ball material. The bearing cage was made of Armalon with riveted aluminum side bands. Axial retention is maintained on both the inner and outer races of the front bearing. The rear bearing is retained at the inner race only while the outer race is allowed to move axially. The front bearing is lubricated by fluid leakage through the balance disk seal. The rear bearing is lubricated with turbine discharge fluid. This fluid flows to the low pressure inlet through a controlling orifice in the center of the shaft.

Thrust Balance Piston

The thrust balance piston was incorporated into the design to counteract the axial thrust produced by the turbine. The rotating thrust balance piston was machined as an integral part of the shaft. The stationary seal is a smooth cylindrical part machined from Kel-F. The pressure differential across the piston produces a force on the piston opposite that of the rotating assembly.

Adapter

The preinducer discharge housing bolt circle is smaller in diameter than the J-2 oxidizer turbopump inlet flange bolt circle. The preinducer was installed next to the turbopump and also in a remote position upstream of the turbopump. Because of these installation locations, the adapter was incorporated to eliminate large bolt circle diameter flanges on the facility ducting and preinducer discharge. The adapter was machined from 6061-T6 aluminum alloy plate. The stresses in this part are low.

END OF REFERENCE

101

REFERENCE

102

FARQUHAR, J.; LINDLEY, B. K.; AND ROSTAFINISKI, W. A.: TRANSIENT PUMPING PERFORMANCE OF A TWO SPEED, HYDRAULIC TURBINE DRIVEN/INDUCER SYSTEM. AIAA PAPER 69-551, JUNE 1969.

THIS REFERENCE IS MATERIAL THAT IS READILY AVAILABLE AND THEREFORE THE CONTENTS HAVE NOT BEEN REPRODUCED.

END OF REFERENCE

102

REFERENCE

103

FARQUHAR, J.; LINDLEY, B. K.; McKINNEY, E. B.; OLSON, G. K.; AND BUCKMANN, P. S.: INDUCER DYNAMICS: FULL-FLOW, FULL-ADMISSION HYDRAULIC TURBINE DRIVE, REP. AGC 7977-T1, AEROJET GENERAL CORP. (NASA CR-72378), 1969.

THIS REFERENCE IS MATERIAL THAT IS READILY AVAILABLE AND THEREFORE THE CONTENTS HAVE NOT BEEN REPRODUCED.

END OF REFERENCE

103

REFERENCE

104

BAIR, E. K.; AND CAMPBELL, W. E.: EVALUATION OF A TWIN-SPOOL HYDROGEN TURBOPUMP AT ZERO NPSP. J. SPACECRAFT & ROCKETS, VOL. 7, NO. 1, JAN. 1970.

THIS REFERENCE IS MATERIAL THAT IS READILY AVAILABLE AND THEREFORE THE CONTENTS HAVE NOT BEEN REPRODUCED.

END OF REFERENCE

104

Card #23

REFERENCE

105

BISSON, E. E.; AND ANDERSON, W. J.: ADVANCED BEARING TECHNOLOGY, NASA SP-38, 1964.

REFERENCE

NASA SP-38

COPY 2

ADVANCED BEARING TECHNOLOGY

LEWIS RESEARCH CENTER
Aerospace Safety Research
and Data Institute
JAN 25 1971
CLEVELAND, OHIO

NATIONAL AERONAUTICS AND SPACE ADMINISTRATION

NASA SP-38

ADVANCED BEARING TECHNOLOGY

By
EDMOND E. BISSON
AND
WILLIAM J. ANDERSON
Lewis Research Center, Cleveland, Ohio

Office of Scientific and Technical Information 1964
NATIONAL AERONAUTICS AND SPACE ADMINISTRATION
Washington, D.C.

PREFACE

THIS BOOK is an outgrowth of a set of lecture notes originally published for an advanced course on bearing technology at the University of California at Los Angeles. Its objectives are twofold:

(1) To present an exposition of the fundamentals of (a) friction and wear, (b) fluid film bearings, and (c) rolling-element bearings

(2) To demonstrate, through discussion of selected research results, how fundamental principles can be applied to the solution of unique and advanced bearing problems involving environmental factors such as extreme temperature, radiation, high vacuum, and corrosive fluids

The book is devoted primarily, in the examples and the discussion of research results, to advanced bearing problems; for example, the current and anticipated bearing problems in aircraft, in missiles, and in spacecraft are covered in some detail. The principles established and enunciated herein are, however, not limited in their application to advanced bearing problems. On the contrary, these principles apply equally well to mundane and ordinary bearing problems.

Many of the research investigations described herein were a part of the exploratory research program being conducted at the laboratories of the NASA Lewis Research Center by the authors and their colleagues. This research program was designed to explore the fundamentals in advanced problem areas and to establish basic principles, where possible, in these advanced areas. Application of these basic principles is possible not only within the advanced areas but under ordinary conditions as well.

The two chapters of this book that were written by guest authors are natural outgrowths of the lectures that they originally gave as part of the advanced course on bearing technology.

The authors are indebted to the members of the Lubrication and Wear and Editorial Branches of the Lewis Research Center for their assistance in reviewing and editing the manuscript. In particular, the assistance of Robert L. Johnson in technical matters and Margaret C. Appleby in editorial matters is appreciated.

CONTENTS

CHAPTER		PAGE
1	INTRODUCTION AND DEFINITION OF NEWER PROBLEM AREAS by Edmond E. Bisson	1
2	BOUNDARY LUBRICATION by Edmond E. Bisson	15
3	HYDRODYNAMIC LUBRICATION by William J. Anderson	63
4	HYDROSTATIC LUBRICATION by William J. Anderson	97
5	GAS-LUBRICATED BEARINGS by J. S. Ausman	109
6	ROLLING-ELEMENT BEARINGS by William J. Anderson	139
7	LIQUID LUBRICANTS by Douglas H. Moreton	175
8	NONCONVENTIONAL LUBRICANTS by Edmond E. Bisson	203
9	FRICTION AND BEARING PROBLEMS IN THE VACUUM AND RADIATION ENVIRONMENTS OF SPACE by Edmond E. Bisson	259
10	FRICTION OF METALS, LUBRICATING COATINGS, AND CARBONS IN LIQUID NITROGEN AND HYDROGEN by Edmond E. Bisson	289
11	EXTREME-TEMPERATURE BEARINGS by William J. Anderson	309
12	FATIGUE IN ROLLING-ELEMENT BEARINGS by William J. Anderson	371
13	LIQUID METALS AS WORKING FLUIDS FOR POWER GENERATION SYSTEMS TO BE USED IN SPACE by Edmond E. Bisson	451
14	LUBRICATION OF BEARINGS WITH LIQUID METALS by William J. Anderson	469
	AUTHOR INDEX	497
	SUBJECT INDEX	503

CHAPTER 6

Rolling-Element Bearings

By WILLIAM J. ANDERSON

IN CONTRAST TO HYDRODYNAMIC BEARINGS, which depend for low-friction characteristics on a fluid film between the journal and the bearing surfaces, rolling-element bearings employ a number of balls or rollers that roll in an annular space. To some extent, these rollers help to avoid gross sliding and the high coefficients of friction that are associated with sliding. The term rolling element is used to describe this class of bearing because the contact between the rolling elements and the races or rings consists more of sliding than of actual rolling. A rolling contact implies no interfacial slip; this condition is seldom maintained because of material elasticity and geometric factors. Rolling-element bearings ordinarily consist of two races or rings (the inner race and the outer race), a set of rolling elements (either balls or rollers), and a separator (sometimes called a cage or retainer) for keeping the set of rolling elements approximately equally spaced.

Rolling-element bearings offer the following advantages when they are compared with hydrodynamic bearings: (1) low starting friction, (2) low operating friction, which is comparable to hydrodynamic bearings at low speeds and somewhat less at high speeds, (3) less sensitivity to interruptions in lubrication than hydrodynamic bearings, and (4) a capability of supporting combined loads with several types of bearings. In this latter respect, rolling-element bearings are more versatile than hydrodynamic bearings, which usually can support only radial or thrust loads.

Rolling-element bearings also have the following disadvantages: (1) They occupy more space in the radial direction than do hydrodynamic bearings and (2) they have a finite fatigue life because of repeated stresses at the ball-race contacts, which is in contrast to hydrodynamic bearings that usually offer an almost infinite fatigue life.

SYMBOLS

a	semimajor axis of contact ellipse, in.
b	semiminor axis of contact ellipse, in.
C	specific dynamic capacity, lb
C_o	specific static capacity, lb
CF	centrifugal force
D,d	ball or rolling-element diameter, in.
E	Young's modulus of elasticity, lb/sq in., or pitch diameter, in.
$E(\epsilon)$	complete elliptic integral of the second order
F	sliding friction force, lb
f	coefficient of sliding friction
g,ϵ,μ,ν,τ	functions used in calculation of Hertz stresses
H	heat generated, in.-lb/sec
I	moment of inertia, (in.-lb)(sec^2)
$K(\epsilon)$	complete elliptic integral of the first order
L	life, millions of revolutions
l	length of line contact or rolling element, in.
M	moment, in.-lb
n	load-life exponent
P	normal ball load, lb
Q	load distribution factor
R	radius, in.
S	normal stress, lb/sq in.
V	linear velocity, in./sec
W	bearing load, lb
x,y,z	coordinates
x_0	location of rolling band
Z	number of balls
α	contact angle, deg
β	angle between load vector and bearing radial plane, deg, or angle between rolling elements, deg
γ	angle between rolling axis and tangent plane at outer-race contact, deg
δ	normal approach or deflection, in.
θ	elastic constant
ξ	coefficient of rolling resistance
σ	Poisson's ratio
ω	angular velocity, radians/sec
Subscripts:	
a	axial, body a
B	ball
b	body b
c	cage or separator

f	frictional
G	gyroscopic
IR,i	inner race
m	mean
max	maximum
OR,o	outer race
r	radial, rolling
s	spin
x	in direction of x-axis
y	in direction of y-axis
z	in direction of z-axis

BEARING TYPES

The various types of rolling-element bearings may be placed in two broad categories; the first of these is ball bearings. The most common types of ball bearings are as follows:

(1) Deep groove or Conrad
(2) Angular contact
(3) Self-alining
(4) Duplex
(5) Ball thrust

A typical deep-groove ball bearing is shown in figure 6–1. This bearing has moderately high radial-load capacity and moderate thrust-load capacity. Figure 6–2 shows an angular-contact bearing. This bearing has a higher thrust-load capacity than a deep-groove bearing, but it can carry thrust load in only one direction. A self-alining ball bearing with the outer-race groove ground to a spherical shape is illustrated in figure 6–3(a). This bearing has a relatively low load capacity but is insensitive to shaft and to housing misalinements.

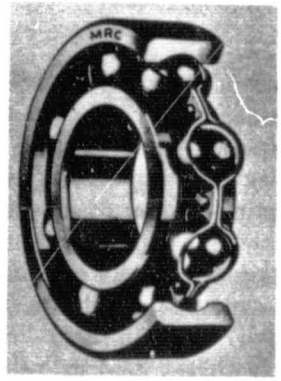

FIGURE 6–1.—Deep-groove ball bearing. (Courtesy Marlin Rockwell Corporation.)

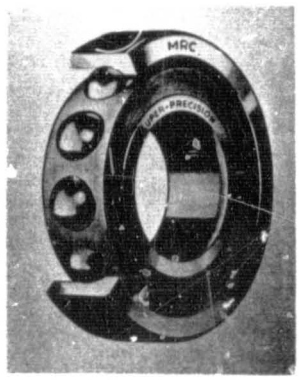

FIGURE 6–2.—Angular-contact ball bearing. (Courtesy Marlin Rockwell Corporation.)

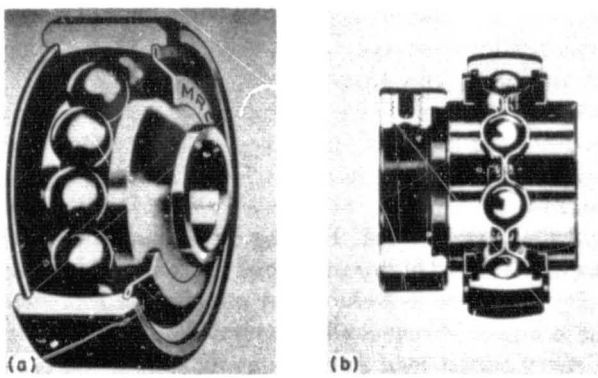

(a) Groove of outer race ground to spherical shape.
(b) Outside diameter of outer race ground to fit spherical housing.
FIGURE 6–3.—Self-alining ball bearing. (Courtesy Marlin Rockwell Corporation.)

Figure 6–3(b) shows a second type of self-alining ball bearing with the self-alining feature obtained by grinding the outer-race outside diameter in a spherical shape to fit a spherical housing. This bearing has a higher load capacity than the bearing in figure 6–3(a), but care must be taken to maintain freedom of movement between the outer race and the housing.

Angular-contact bearings are usually used in pairs in duplex mounts. Different types of duplex mounts are shown in figure 6–4(a) (back to back) and in figure 6–4(b) (face to face). These two arrangements make it possible to carry thrust load in either direction. Bearings are so manufactured as matched pairs that, when they are mated and the races made flush, each bearing is preloaded slightly. This pre-

loading provides greater stiffness and helps to prevent ball skidding with acceleration at light load. When a high unidirectional thrust load must be carried, a duplex tandem mount (fig. 6–4(c)) is used. With careful manufacture and installation, a tandem bearing pair may have a thrust capacity as high as 1.8 times the capacity of a single bearing. A thrust ball bearing is shown in figure 6–5. This bearing has a high thrust capacity but is limited to low speeds because of the high degree of sliding in the ball-race contacts.

The second broad category is that of roller bearings. Common types are

(1) Cylindrical
(2) Tapered
(3) Spherical
(4) Needle

Cylindrical-roller bearings (fig. 6–6) are best suited of all roller-bearing types for high-speed operation. These bearings carry only radial load, and they are frequently used where freedom of movement of the shaft in the axial direction must be provided because of differential expansion. Tapered-roller bearings (fig. 6–7) and spherical-roller bearings (fig. 6–8) are high-load-capacity low-speed roller bearings with combined radial-load and thrust-load capability. Needle bearings (fig. 6–9) are capable of carrying high loads and are useful in applications where limited radial space is available.

While rolling-element bearings are usually equipped with a separator, in some instances they are not. Bearings without separators are

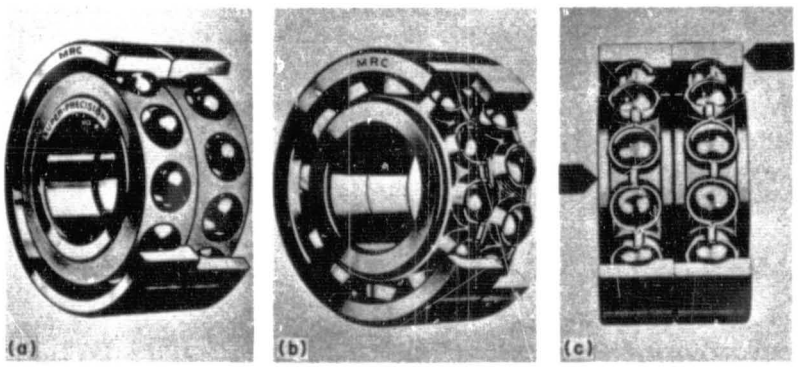

(a) Mounted back to back.
(b) Mounted face to face.
(c) Mounted in tandem.

FIGURE 6–4.—Duplex angular-contact ball bearing. (Courtesy Marlin Rockwell Corporation.)

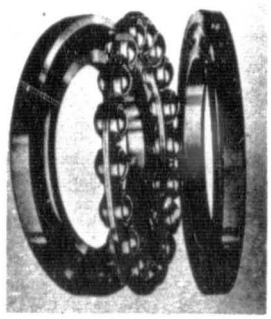

FIGURE 6–5.—Thrust ball bearing. (Courtesy Marlin Rockwell Corporation.)

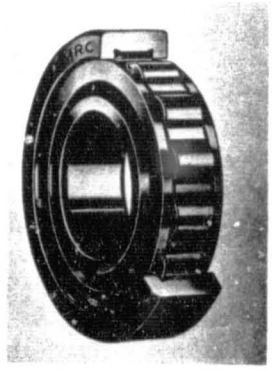

FIGURE 6–6.—Cylindrical-roller bearing. (Courtesy Marlin Rockwell Corporation.)

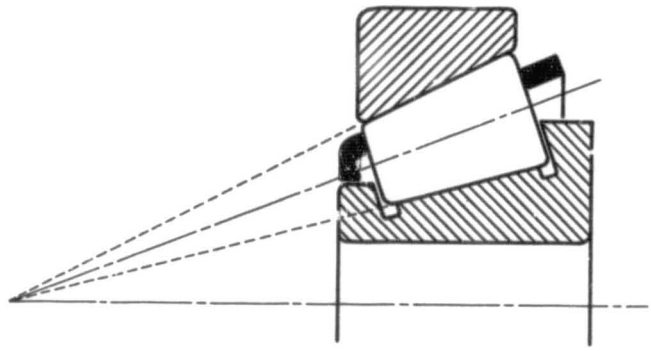

FIGURE 6–7.—Tapered-roller bearing.

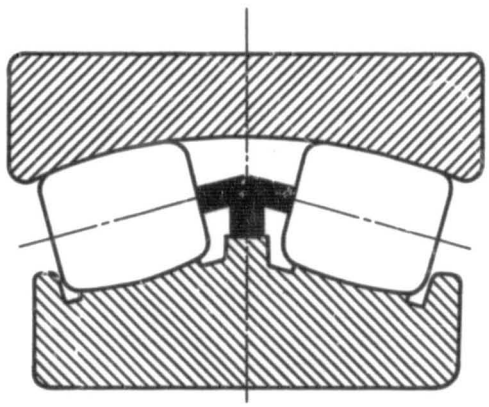

FIGURE 6–8.—Spherical-roller bearing.

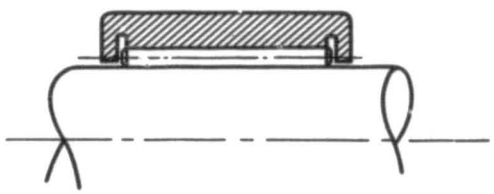

FIGURE 6–9.—Needle bearing with shaft as inner race.

usually termed full-complement bearings. A common type of full-complement roller bearing is the needle bearing. In some low-speed applications where load capacity is of primary importance, full-complement ball bearings are used. In this type of bearing, the annular space between the races is packed with the maximum number of balls.

ROLLING FRICTION

The concepts of rolling friction are important as the characteristics and behavior of rolling-element bearings depend on rolling friction. The theories of Reynolds (ref. 1) and of Heathcote (ref. 2) were previously well accepted as correctly explaining the origin of rolling friction for a ball in a groove. The energy lost in rolling was believed to be that required to overcome the interfacial slip which occurs because of the curved shape of the contact area. As shown in figure 6–10, the ball rolls about the x-axis and makes contact with the groove from a to b. If the groove is fixed, then for zero slip over the contact

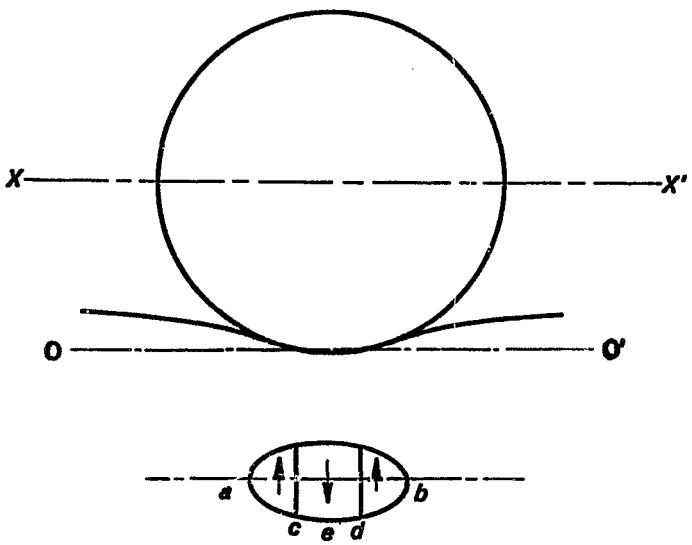

FIGURE 6–10.—Differential slip due to curvature of contact ellipse.

area no point within the area should have a velocity in the direction of rolling. The surface of the contact area is curved, however, so that points a and b are at different radii from the x-axis than are points c and d. For an inelastic ball, points a and b must have different velocities with respect to the x-axis than do points c and d because the velocity of any point on the ball relative to the x-axis equals the angular velocity ω times the radius from the x-axis. Slip must occur at various points over the contact area unless the body is so elastic that yielding can take place in the contact area to prevent this interfacial slip. The theory of Reynolds and later of Heathcote assumed that this interfacial slip took place, and that the forces required to make a ball roll were those forces required to overcome the friction due to this interfacial slip. In the contact area, rolling without slip will occur at a specific radius from the x-axis. Where the radius is greater than this radius to the rolling point, slip will occur in one direction, and, where it is less than the radius to this rolling point, slip will occur in the other direction. In figure 6–10 the lines to points c and d represent the approximate location of the rolling bands, and the arrows shown in the three portions of the contact area represent the directions of interfacial slip when the ball is rolling into the paper.

The location of the two rolling bands relative to the axis of the contact ellipse can be obtained by means of a summation of the forces acting on the ball in the direction of rolling. With reference to figure 6–11, these forces are

$$2F_2 - F_1 = \tfrac{1}{3}P \tag{6-1}$$

The forces F_1 and F_2 represent sliding friction forces. From the Hertz theory of contact stresses, which will be discussed more fully later, the pressure pattern over the contact area is ellipsoidal so that the pressure variation along any axis is elliptical. When this assump-

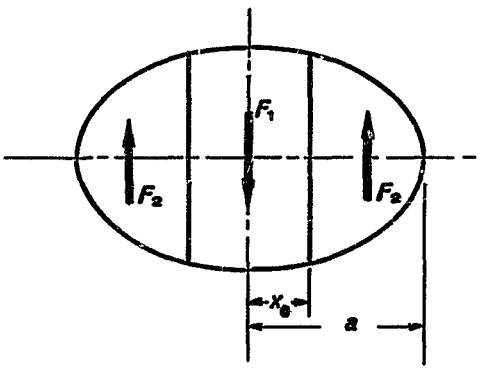

Figure 6–11.—Friction forces in contact ellipse.

tion of the pressure variation is used, F_1 and F_2 are obtained by integrating the pressure times the coefficient of friction over the particular area on which these forces act. These integrals are

$$F_1 = 2\left(\frac{3Pf}{2\pi ab}\right)\int_0^{x_0}\int_{-b\left(1-\frac{x^2}{a^2}\right)^{1/2}}^{b\left(1-\frac{x^2}{a^2}\right)^{1/2}}\left(1-\frac{x^2}{a^2}-\frac{y^2}{b^2}\right)^{1/2}dy\,dx \tag{6-2}$$

$$F_2 = \frac{3Pf}{2\pi ab}\int_{x_0}^{a}\int_{-b\left(1-\frac{x^2}{a^2}\right)^{1/2}}^{b\left(1-\frac{x^2}{a^2}\right)^{1/2}}\left(1-\frac{x^2}{a^2}-\frac{y^2}{b^2}\right)^{1/2}dy\,dx \tag{6-3}$$

Equations (6–2) and (6–3) can be integrated with standard integrals:

$$F_1=\frac{3Pf}{2a}\left(x_0-\frac{x_0^3}{3a^2}\right) \tag{6–4}$$

$$F_2=\frac{3Pf}{4a}\left(\frac{2a}{3}+\frac{x_0^3}{3a^2}-x_0\right) \tag{6–5}$$

Substituting equations (6–4) and (6–5) into equation (6–1) and simplifying yield

$$3\left(\frac{x_0}{a}\right)-\left(\frac{x_0}{a}\right)^3=1-\frac{\xi}{f} \tag{6–6}$$

For bearing steels, the ratio of ξ/f is so small that

$$\frac{x_0}{a}\cong 0.347 \tag{6–7}$$

Eldredge (ref. 3) determined the following expression for the force required to overcome the friction due to interfacial slip:

$$F=\frac{fP}{12}\left(\frac{2a}{D}\right)^2 \tag{6–8}$$

Recent work done by Eldredge and Tabor (refs. 4 to 6) and by Drutowski (ref. 7) indicates that the greater portion of rolling resistance results from elastic hysteresis losses in the metal rather than from friction due to interfacial slip.

Palmgren, in reference 8 and in a discussion to reference 6, states that loss of energy due to interfacial slip constitutes a large portion of the rolling resistance. Thus, Palmgren and Tabor appeared to disagree; however, a closer examination of the experimental data on which Palmgren based his conclusions reveals that Palmgren's work was done with full bearings and that a great deal of slippage occurs in practically all bearings, as shown in the discussion of kinematics of roller bearings. This slippage accounts for the greater portion of the

energy lost in a rolling bearing. The gross sliding in the contact areas between the rolling elements and the races in a rolling bearing, however, is differentiated from the interfacial slip that was first discussed by Heathcote and which is discussed by Tabor in his basic work on rolling resistance. Actually, both Tabor and Palmgren appear to be correct; the controversy arises because they are talking about different things. Tabor discussed basic rolling resistance, which is a factor in the total energy lost in a rolling bearing, and Palmgren discussed the friction that arises from gross sliding in the contact areas, which is far greater than the loss due to hysteresis effects.

FRICTION LOSSES IN ROLLING BEARINGS

Some of the factors that affect the magnitude of friction losses in rolling bearings are

(1) Bearing size
(2) Bearing type
(3) Bearing design
(4) Load (magnitude and type, either thrust or radial)
(5) Speed
(6) Oil viscosity
(7) Oil flow

In a specific bearing, friction losses consist of

(1) Sliding friction losses in the contacts between the rolling elements and the raceways
(2) Hysteresis losses due to the damping capacity of the raceway and the ball material
(3) Sliding friction losses between the separator and its locating race surface and between the separator pockets and the rolling elements
(4) Shearing of oil films between the bearing parts and oil churning losses caused by excess lubricant within the bearing

The relative magnitude of each of these friction losses depends on the bearing type and design, the lubricant, and the type of lubrication.

Palmgren (ref. 8) presents friction coefficients for various types of bearings that may be used for rough calculations of bearing torque. These values were computed at a bearing load that will give a life of 1×10^9 revolutions for the respective bearings. As the bearing load approaches zero, the friction coefficient becomes infinite because the

bearing torque remains finite. Friction coefficients given by Palmgren in reference 8 are given in the following table:

Bearing	Friction coefficient
Self-alining ball	0.0010
Cylindrical roller, with flange-guided short rollers	.0011
Thrust ball	.0013
Single-row deep-groove ball	.0015
Tapered and spherical roller, with flange-guided rollers	.0018
Needle	.0045

All these friction coefficients are referenced to the bearing bore.

Palmgren (ref. 8) and Muzzoli (ref. 9) attempted to relate all the factors that influence rolling-bearing torque. Palmgren outlined a method for computing the torque of several types of bearings by calculating the zero-load torque and the sliding and the hysteresis losses due to the load. Muzzoli's equation for bearing torque is discussed in reference 10, page 84. A number of factors in these equations must be known in order to make them useful. The validity depends on the accuracy with which some of these factors are determined.

CONTACT STRESSES

The contact of two solid, curved elastic bodies at a point or along a line results in elastic and sometimes plastic deformation of the bodies at the contact. The contact areas become finite in extent as a result of this deformation and consist of circular, elliptical, or rectangular areas. Hertz (ref. 11) investigated mathematically the shape and size of the pressure area and the distribution of stress over the contact area. The relations that were developed by Hertz agree with experimental results for bodies in static contact where the dimensions of the projected contact area are small in comparison with the radii of the bodies.

The derivations of the Hertz equations are complex and only a brief summary of the results will be given herein. The various equations obtained by Hertz together with charts of the various functions that appear in the Hertz equations are given in references 8, 12, and 13.

For point contact under a load P, a pressure area with semiaxes a and b results. Hertz gives the dimensions of the pressure area in terms of the transcendental functions μ and ν as

$$a=\mu g \tag{6-9}$$

$$b=\nu g \tag{6-10}$$

where

$$g=\left[\frac{3P(\theta_a+\theta_b)}{8\left(\frac{1}{R_{a,1}}+\frac{1}{R_{a,2}}+\frac{1}{R_{b,1}}+\frac{1}{R_{b,2}}\right)}\right]^{1/3} \tag{6-11}$$

The subscripts 1 and 2 refer to planes that are orthogonal to the tangent plane and contain the major and minor axes of the contact ellipse. The sign of each radius is positive if the center of curvature is in the body and is negative if the center of curvature is outside the body.

The elastic constants θ_a and θ_b for the two bodies are functions of the modulus of elasticity E and of Poisson's ratio σ:

$$\theta_a=\frac{4(1-\sigma_a^2)}{E_a} \tag{6-12}$$

$$\theta_b=\frac{4(1-\sigma_b^2)}{E_b} \tag{6-13}$$

For point contact of steel ($E=29\times10^6$; Poisson's ratio $\sigma=1/4$), the mean compressive stress $S_m\equiv P/\pi ab$ is

$$S_m=\frac{15079\left(\frac{1}{R_{a,1}}+\frac{1}{R_{a,2}}+\frac{1}{R_{b,1}}+\frac{1}{R_{b,2}}\right)^{2/3}P^{1/3}}{\mu\nu} \tag{6-14}$$

The stress in point contact varies as the cube root of the normal force. Functions μ and ν are related through the auxiliary angle ϵ as

$$\cos\epsilon=\frac{\nu}{\mu} \tag{6-15}$$

and

$$\nu=\left[\frac{2E(\epsilon)\cos\epsilon}{\pi}\right]^{1/3} \tag{6-16}$$

The angle ϵ is found from the relation

$$\cos\tau=1-\frac{2[K(\epsilon)-E(\epsilon)]\cot^2\epsilon}{E(\epsilon)} \tag{6-17}$$

where

$$\cos\tau=\frac{\frac{1}{R_{a,1}}-\frac{1}{R_{a,2}}+\frac{1}{R_{b,1}}-\frac{1}{R_{b,2}}}{\frac{1}{R_{a,1}}+\frac{1}{R_{a,2}}+\frac{1}{R_{b,1}}+\frac{1}{R_{b,2}}} \tag{6-18}$$

Complete elliptic integrals of the first and second orders $K(\epsilon)$ and $E(\epsilon)$ have the modulus sin ϵ:

$$K(\epsilon)=\int_0^{\pi/2}\frac{d\varphi}{(1-\sin^2\epsilon\sin^2\varphi)^{1/2}} \tag{6-19}$$

$$E(\epsilon)=\int_0^{\pi/2}(1-\sin^2\epsilon\sin^2\varphi)^{1/2}\,d\varphi \tag{6-20}$$

The functions μ and ν are usually plotted with cos τ for easy calculation.

The compressive stress at any point on the contact area (fig. 6-12) is equal to the ordinate of a semiellipsoid of revolution erected on the contact area as a base. At any point x, the stress y is

$$S=\frac{3P}{2\pi ab}\left(1-\frac{x^2}{a^2}-\frac{y^2}{b^2}\right)^{1/2} \tag{6-21}$$

The maximum compressive stress that acts at the center of the contact area is

$$S_{max}=\frac{3P}{2\pi ab}=\frac{3}{2}S_m \tag{6-22}$$

For line contact if the total load is distributed evenly along the length l, the semiwidth of the pressure rectangle is

$$b=\left[\frac{P(\theta_a+\theta_b)}{\pi l\left(\frac{1}{R_a}+\frac{1}{R_b}\right)}\right]^{1/2} \tag{6-23}$$

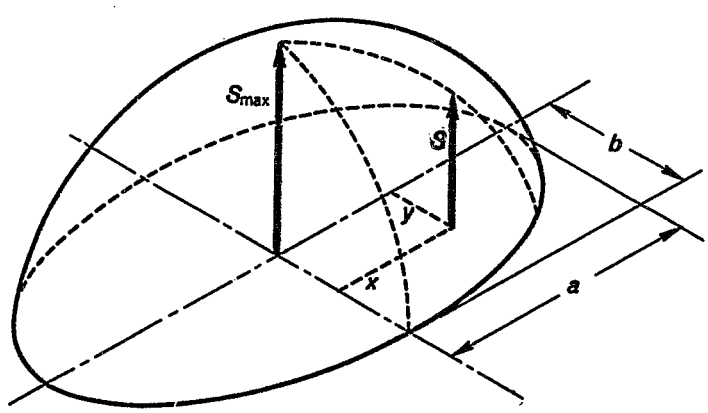

FIGURE 6-12.—Stress ellipsoid.

and the mean compressive stress is

$$S_m=\frac{P}{2bl} \tag{6-24}$$

For steel, the semiwidth of the pressure rectangle is

$$b=0.00028692\left[\frac{P}{l\left(\frac{1}{R_a}+\frac{1}{R_b}\right)}\right]^{1/2} \tag{6-25}$$

and the mean stress is

$$S_m=1742.6\left[\frac{P}{l}\left(\frac{1}{R_a}+\frac{1}{R_b}\right)\right]^{1/2} \tag{6-26}$$

The compressive stress at a distance y from the center of the contact line to the edge is equal to the ordinate of a cylinder erected with the contact line as a base. Then

$$S=\frac{2P}{\pi lb}\left[1-\left(\frac{y}{b}\right)^2\right]^{1/2} \tag{6-27}$$

The maximum stress is

$$S_{max}=\frac{2P}{\pi lb} \tag{6-28}$$

The maximum stress is $4/\pi$ or 1.273 times the mean stress.

Thus, for point contact, the stress varies as the cube root of the normal force, and the maximum stress is 1.5 times the mean stress. For line contact, the stress varies as the square root of the normal force, and the maximum stress is 1.273 times the mean stress.

In addition to the surface compressive stresses, the stresses that exist in the interior of each contacting body in the region near the contact area are of interest. Subsurface stresses for point contact have been determined by several investigators including Thomas and Hoersch (ref. 14). An outline of their derivation together with charts, which facilitate easy calculation, is given in reference 13.

Consider an elementary particle at a depth z below the pressure surface and located on the z-axis as shown in figure 6–13. There are three principal stresses S_x, S_y, and S_z that act on the particle.

As shown in figure 6–13, the z-axis is directed normal to the surface, and the x-axis is in the direction of the major axis. The three principal stresses are plotted against the depth from the surface in figure 6–14. The principal stresses are all compressive and diminish in intensity with greater depth from the surface. At a value of z/b

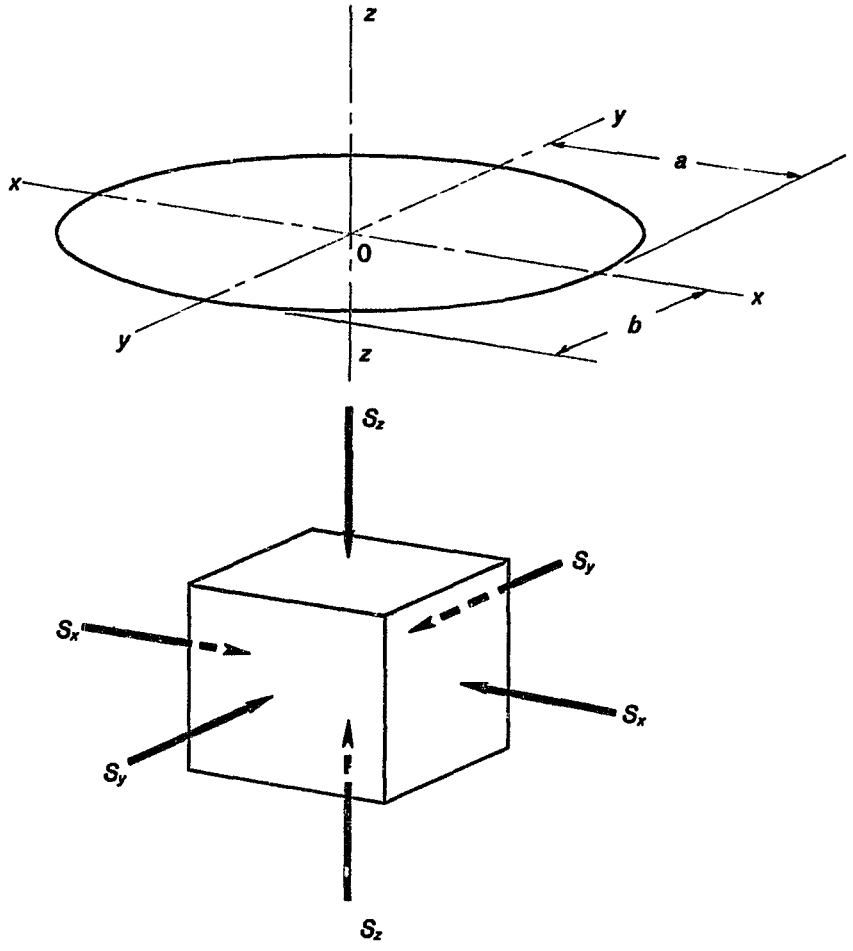

FIGURE 6–13.—Contact ellipse and coordinate axes.

of about 1.5, S_y becomes slightly tensile. The stress S_y diminishes more rapidly than does S_x, and the maximum shear stress, which is one-half the difference between any two principal stresses, is determined by the stresses S_z and S_y. The maximum value of τ occurs below the surface, as shown in figure 6–14. Since ductile materials fail in shear, material failures might originate below the surface. This failure has been observed and will be discussed fully in chapter 12.

DEFORMATIONS

In addition to knowing the stresses set up within the components of rolling bearings by the bearing loads, knowing the amount the bearing components will elastically deform under load is important.

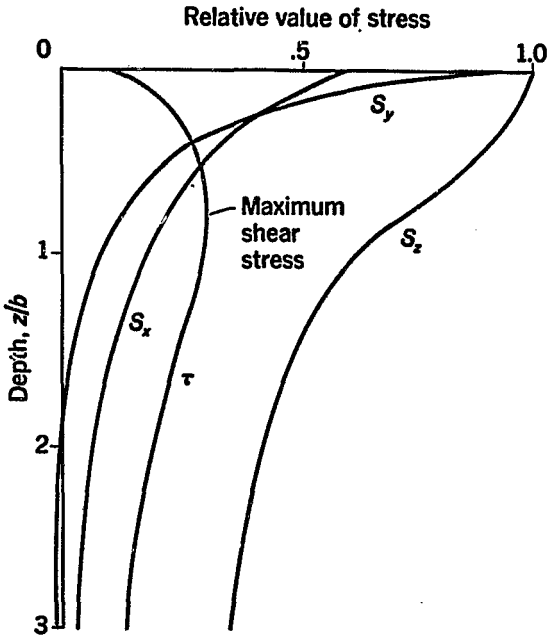

FIGURE 6-14.—Relative value of three principal stresses and of shear stress with depth from surface.

This problem was also solved by Hertz (ref. 15). The normal approach δ of two bodies in point contact (ref. 13) is

$$\delta=\frac{3P(\theta_a+\theta_b)}{8\pi a}K(\epsilon) \tag{6-29}$$

Substituting in equations (6-9), (6-10), (6-11), and (6-16) yields

$$\delta=\frac{0.192417(\theta_a+\theta_b)^{2/3}K(\epsilon)\cos^{2/3}\epsilon}{[E(\epsilon)]^{1/3}}\left[\sum\left(\frac{1}{R}\right)\right]^{1/3}P^{2/3} \tag{6-30}$$

Reference 13 contains charts that facilitate solving normal approach problems. For bodies of steel with a Poisson's ratio of ¼ and a Young's modulus of 29 million,

$$\delta=7.8107\times10^{-6}\frac{K(\epsilon)\cos^{2/3}\epsilon}{[E(\epsilon)]^{1/3}}\left(\frac{1}{R_{a,1}}+\frac{1}{R_{a,2}}+\frac{1}{R_{b,1}}+\frac{1}{R_{b,2}}\right)^{1/3}P^{2/3} \tag{6-31}$$

The compressive deformation in line contact cannot be simply expressed. Palmgren (ref. 8) gives an expression for the approach between the axis of a finite-length cylinder compressed between two infinite plane-surfaced bodies and a distant point in either of the support bodies:

$$\delta=0.39(\theta_a+\theta_b)^{0.9}\frac{P^{0.9}}{L^{0.8}} \tag{6-32}$$

Equation (6-32) may be applied to roller bearings. From equation (6-32), for line contact, the radius of curvature of the roller does not affect the deflection.

Equations (6-12), (6-13), (6-30), (6-31), and (6-32) show that the normal approach of two bodies in contact depends on the normal load, the geometry, and certain material constants. The calculation of deflections in a complete bearing requires a knowledge of its geometry, material, and the radial and the axial components of load. From the load components, the load on the most heavily loaded rolling element must be calculated. Exact calculations of deflection are complex and tedious.

In general, when both radial and axial loads are applied to a bearing inner ring, the ring will be displaced both axially and radially. The direction of the resultant displacement, however, may not coincide with the direction of the load vector. If α is the bearing contact angle defined as the angle between a line drawn through the ball contact points and the radial plane of the bearing (fig. 6-15), and β is the angle between the load vector and the radial plane, then the relation between the radial displacement δ_r and the axial displacement δ_a is given in figure 6-16 (ref. 8). With a thrust load, $\tan\alpha/\tan\beta=0$, and the resulting displacement is in the axial direction ($\delta_r=0$). For a radial displacement ($\delta_a=0$), $\tan\alpha/\tan\beta=0.823$ for point contact and 0.785 for line contact. A radial load can be applied to single-row bearings only when $\alpha=0$ in which case the displacement is also radial.

Palmgren (ref. 8) gives the deflection formuals, which are approximately true for standard bearings, under load conditions that give radial deflection. For self-alining ball bearings,

$$\delta_r=\frac{2.53\times10^{-5}}{\cos\alpha}\left(\frac{P^2}{d}\right)^{1/3} \tag{6-33}$$

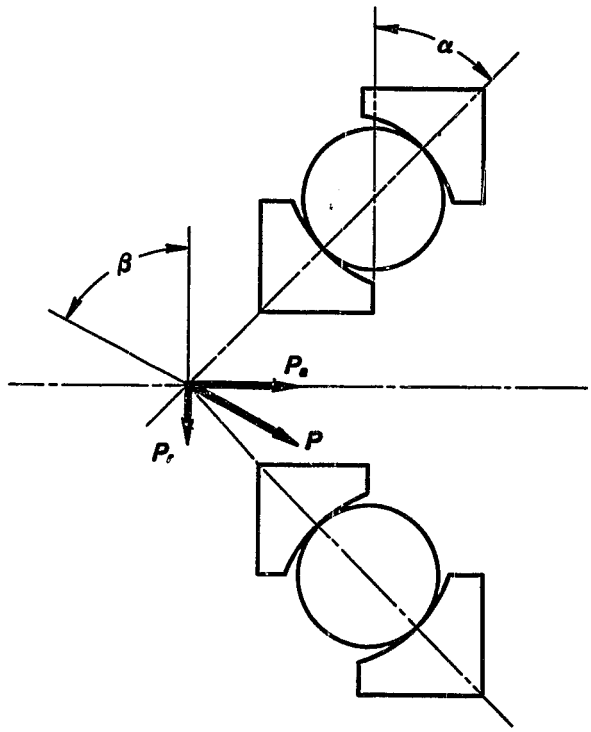

FIGURE 6–15.—Bearing-contact angle α and load-vector direction β.

For deep-groove and angular-contact bearings,

$$\delta_r = \frac{1.58 \times 10^{-5}}{\cos \alpha} \left(\frac{P^2}{d} \right)^{1/3} \tag{6-34}$$

For roller bearings with point contact at one race and line contact at the other,

$$\delta_r = \frac{4.31 \times 10^{-6}}{\cos \alpha} \frac{(P^3)^{1/4}}{L^{1/2}} \tag{6-35}$$

For roller bearings with line contact at both raceways,

$$\delta_r = \frac{8.73 \times 10^{-7}}{\cos \alpha} \frac{P^{0.9}}{L^{0.8}} \tag{6-36}$$

With axial load, the corresponding equations are

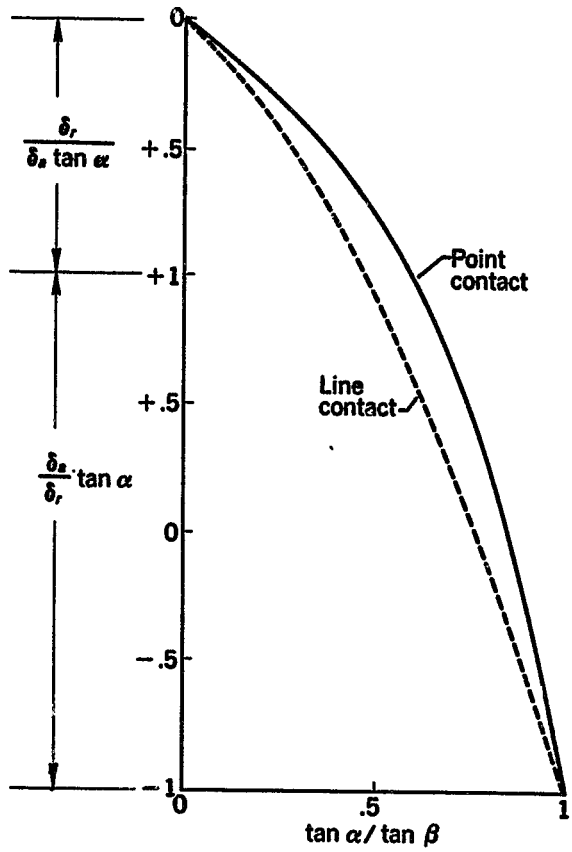

FIGURE 6–16.—Relation between contact angle α and load-vector direction β and axial and radial bearing deflections.

$$\delta_a = \frac{2.53 \times 10^{-5}}{\sin \alpha} \left(\frac{P^2}{d}\right)^{1/3} \tag{6-33a}$$

$$\delta_a = \frac{1.58 \times 10^{-5}}{\sin \alpha} \left(\frac{P^2}{d}\right)^{1/3} \tag{6-34a}$$

$$\delta_a = \frac{4.31 \times 10^{-6}}{\sin \alpha} \frac{(P^3)^{1/4}}{l^{1/2}} \tag{6-35a}$$

$$\delta_a = \frac{8.73 \times 10^{-7}}{\sin \alpha} \frac{P^{0.9}}{l^{0.8}} \tag{6-36a}$$

All deflections are in inches and are for zero clearance bearings. The load on the most heavily loaded rolling element P is in pounds, and the rolling-element diameter d is in inches.

KINEMATICS

Normal Speeds

The relative motion of the separator, the balls, and the races of a ball bearing is important to understand the performance of this type of bearing. If ω_i is the angular velocity of the inner race, then the velocity of point A (fig. 6–17) is

$$V_A=\omega_i\overline{AB} \tag{6–37}$$

Similarly, if ω_o is the angular velocity of the outer race, then the velocity of point C is

$$V_C=\omega_o\overline{CD} \tag{6–38}$$

From geometry,

$$\overline{AB}=\frac{E}{2}-\frac{d}{2}\cos\alpha \tag{6–39}$$

and

$$\overline{CD}=\frac{E}{2}+\frac{d}{2}\cos\alpha \tag{6–40}$$

The velocity of the ball center V_0 is

$$V_0=\frac{1}{2}(V_A+V_C) \tag{6–41}$$

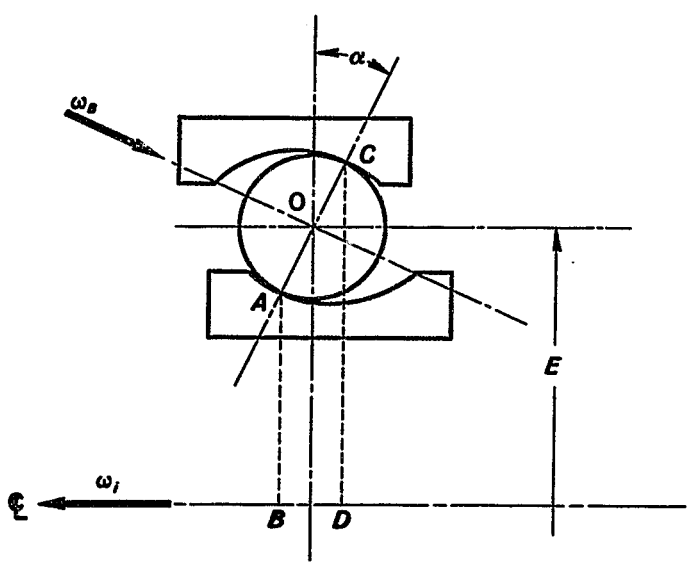

FIGURE 6–17.—Relation for derivation of retainer angular velocity.

Substituting equations (6–37) and (6–38) into equation (6–41) gives

$$V_0=\frac{1}{2}\left[\frac{\omega_i}{2}(E-d\cos\alpha)+\frac{\omega_o}{2}(E+d\cos\alpha)\right] \tag{6–42}$$

The angular velocity of the separator or ball set ω_c about the shaft axis is

$$\omega_c=\frac{V_0}{E/2} \tag{6–43}$$

Then

$$\omega_c=\frac{1}{2}\left[\omega_i\left(1-\frac{d\cos\alpha}{E}\right)+\omega_o\left(1+\frac{d\cos\alpha}{E}\right)\right] \tag{6–44}$$

The speed of the separator when the outer race is fixed is

$$\omega_c=\frac{\omega_i}{2}\left(1-\frac{d\cos\alpha}{E}\right) \tag{6–45}$$

For $\alpha<90°$, the separator speed is always less than half the shaft speed. When both races rotate, the speed of the inner race relative to the separator is

$$\omega_{i/c}=\omega_i-\omega_c=\frac{1}{2}(\omega_i-\omega_o)\left(1+\frac{d\cos\alpha}{E}\right) \tag{6–46}$$

The speed of the outer race relative to the separator is

$$\omega_{o/c}=\omega_o-\omega_c=\frac{1}{2}(\omega_o-\omega_i)\left(1-\frac{d\cos\alpha}{E}\right) \tag{6–47}$$

From equations (6–46) and (6–47), the speed of the inner race relative to the separator is always greater than that of the outer race relative to the separator. A point on the inner-race ball track will receive a greater number of stress cycles per unit time than will a point on the outer race.

For ball bearings that operate at nominal speeds, the centrifugal force on the balls is so negligible that the only forces that keep the ball in equilibrium are the two contact forces. For such conditions, the contact forces are equal and opposite, and the inner- and the outer-race contact angles are approximately equal. Even when the

two contact angles are equal, true rolling of the ball can occur only at one contact. As shown in figure 6–18, the ball is rolling about axis $0A$, and true rolling occurs at the inner-race contact B but not at the outer-race contact C.

If the ball has an angular velocity ω_B about the axis $0A$, then it has a rolling component ω_r and a spin component $\omega_{s,o}$ relative to the outer race as shown in figure 6–19. The frictional heat generated at the ball-race contact, where slip takes place, is

$$H_f=\omega_s M_s \tag{6–48}$$

where M_s is the twisting moment required to cause slip. Poritsky, Hewlett, and Coleman (ref. 16) integrated the friction force over the contact ellipse to obtain M_s as

$$M_s=\frac{3}{8}fPaE(\epsilon) \tag{6–49}$$

When $b/a=1$, $\epsilon=0°$ and $E=\pi/2$. When $b/a=0$, $\epsilon=90°$ and $E=1$. For the same P, M_s will be greater for the ellipse with the greater

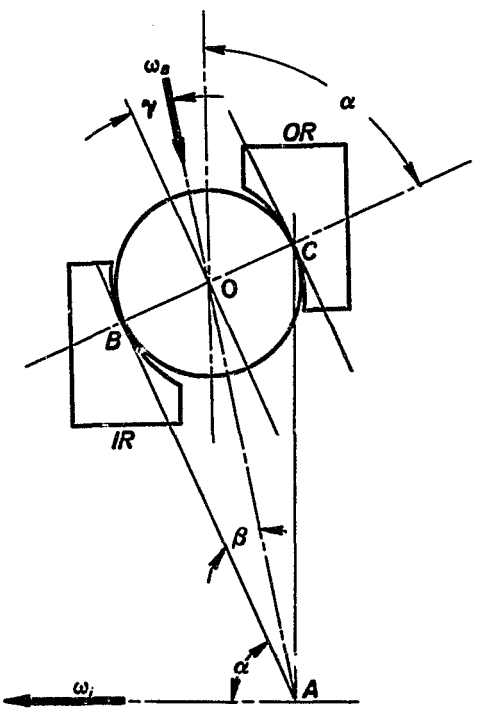

FIGURE 6–18.—Relation for derivation of ball-spin velocity with inner-race control.

eccentricity because the increase in a is greater than the decrease in E. In a given ball bearing that operates under a given speed and load, rolling will always take place at one race and spinning at the other. Rolling will take place at the race where M_s is greater because of the greater gripping action. This action is referred to as ball

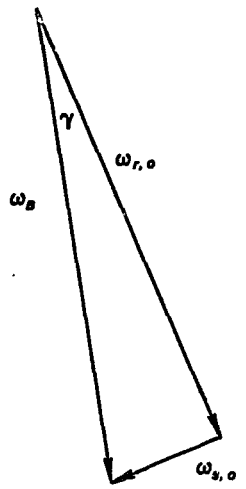

FIGURE 6–19.—Rolling and spinning components of ball velocity at outer race

control. If a bearing is designed with equal race curvatures (race curvature is defined as the ratio of the race-groove radius in a plane normal to the rolling direction to the ball diameter) and the operating speed is such that centrifugal forces are negligible, spinning will usually occur at the outer race (fig. 6–18). This spinning results from the fact that the inner-race contact ellipse has a greater eccentricity than the outer-race contact ellipse.

The frictional heat generated at the ball-race contact where spinning takes place accounts for a significant portion of the total bearing friction loss. The closer the race curvatures, the greater the frictional heat developed. On the other hand, open race curvatures, which reduce friction, also increase the maximum contact stresses and, consequently, reduce the bearing fatigue life. (See chapter 12.)

High Speeds

At high speeds, the centrifugal force developed on the balls becomes significant, and the contact angles at the inner and the outer races are no longer equal. Jones (ref. 17) presents a method for calculating inner- and outer-race contact angles in bearings that operate at high speed. This divergence of contact angles tends to increase the angular velocity of spin between the ball and the slipping race and

to aggravate the problem of heat generation. Figure 6–20 illustrates contact geometry at high speed in a ball bearing with ball control at the inner race. The velocity diagram of the ball relative to the outer race remains the same as in figure 6–19 except that γ has become greater and the magnitude of $\omega_{s,o}$ has increased.

Since the magnitude of P_o becomes greater with increasing centrifugal force, ball control probably will be shifted to the outer race unless the race curvatures are adjusted to prevent this. Figure 6–21 illustrates ball control at the outer race. The velocity of the ball relative to the inner race is shown in figure 6–22. The inner-race angular velocity ω_i must be subtracted from the angular velocity of the ball ω_B to obtain the velocity of the ball relative to the inner race $\omega_{B/i}$. The spin component of the ball relative to the inner race is then $\omega_{s,i}$. In most instances, $\omega_{s,i}$ will be greater than $\omega_{s,o}$ so that great care must be taken in designing a ball bearing for a high-speed application where heat generation is critical. Reference 17 can be used to calculate the two operating contact angles for various values of assumed race curvature. The spinning moments given by equation (6–49) can be calculated to determine which race will have ball control. The heat generated because of ball spin (eq. (6–48)) can

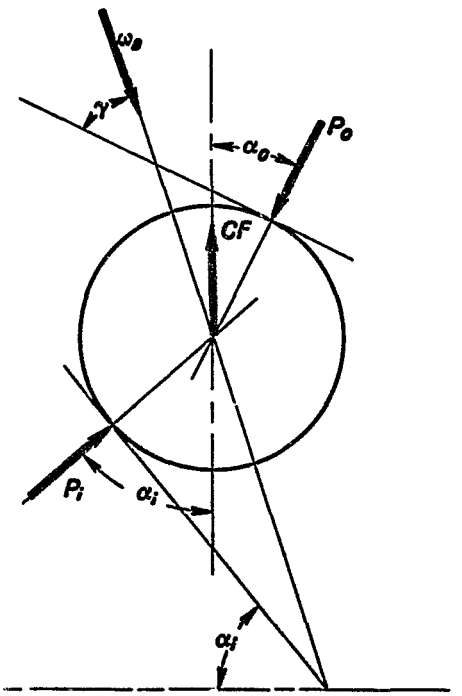

FIGURE 6–20.—Forces that act on ball in bearing at high rotative speeds. Ball control at inner race.

be calculated by solving for the value of ω_s in velocity diagrams similar to figure 6–19 or 6–22.

A further cause of possible ball skidding in lightly loaded ball bearings that operate at high speed is the gyroscopic moment that acts on each ball. If the contact angle α is other than zero, there will be a component of spin about the axis through 0 normal to the paper in figure 6–18, and a gyroscopic couple will develop. The magnitude of this moment M_G will be

$$M_G = I\omega_B\omega_c \sin(\alpha+\beta_1) \qquad (6\text{–}50)$$

where I is the moment of inertia of a ball about the axis through 0 and ω_c is given by equation (6–45). For the ball shown in figure 6–18, the gyroscopic moment will tend to rotate the ball clockwise in the plane of the paper. Rotation will be resisted by the friction forces at the inner- and the outer-race contacts, which are fP_i and fP_o, respectively. Whether or not slip takes place depends on the magnitude of the bearing load. In lightly loaded bearings that operate at high speeds, slippage is a possibility.

LOAD DISTRIBUTION

When a ball bearing is subjected to a radial load, the balls are not equally loaded. At best, only half the balls are loaded at any given

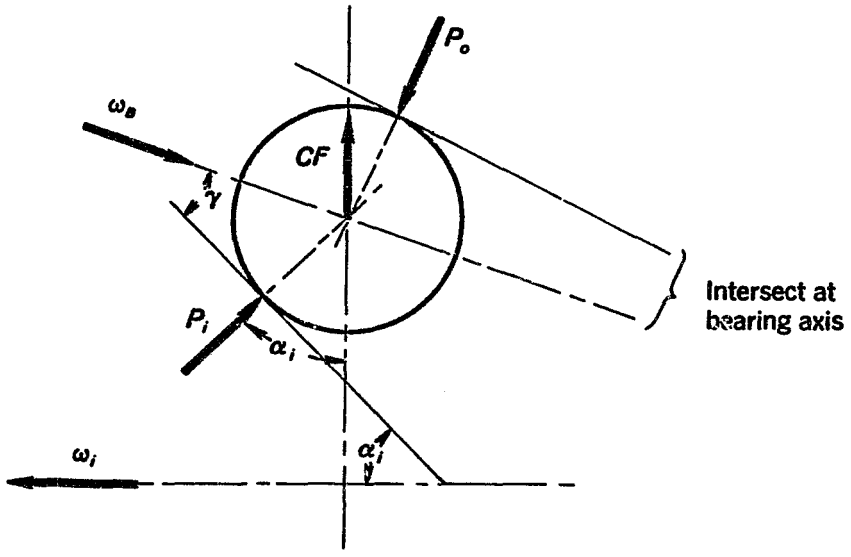

FIGURE 6–21.—Forces that act on ball in bearing at high rotative speeds. Ball control at outer race.

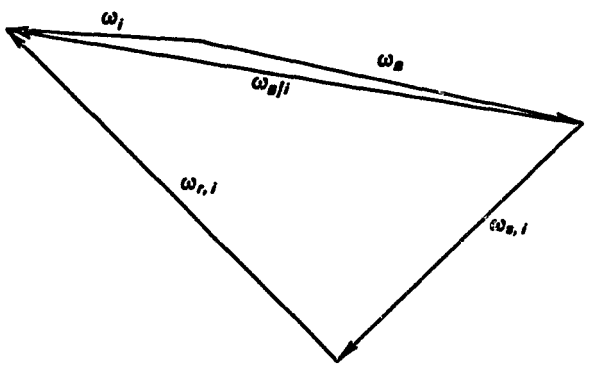

FIGURE 6–22.—Velocity diagram for computing ball-spin velocity for ball control at inner race.

time, and the actual load on each of the loaded balls depends on its position in the bearing relative to the load vector.

Stribeck (ref. 18) investigated the load distribution in radially loaded bearings and developed an expression for the most heavily loaded ball. For static equilibrium of the bearing in figure 6–23,

$$W_r = P_1 + 2P_2 \cos \beta + 2P_3 \cos 2\beta + \ldots \qquad (6\text{–}51)$$

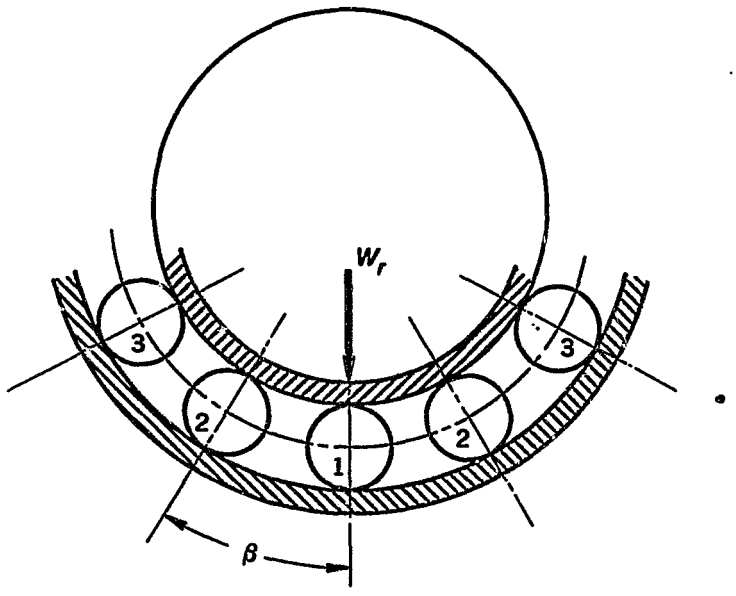

FIGURE 6–23.—Relation used to calculate distribution of ball load due to a radial load W_r.

The normal approach between two surfaces in point contact is proportional to $P^{2/3}$:

$$\frac{\delta_2}{\delta_1}=\left(\frac{P_2}{P_1}\right)^{2/3} \tag{6-52}$$

or

$$\frac{P_2}{P_1}=\left(\frac{\delta_2}{\delta_1}\right)^{3/2} \tag{6-53}$$

If the races remain circular,

$$\delta_2=\delta_1 \cos \beta \tag{6-54}$$

and

$$\delta_3=\delta_1 \cos 2\beta \tag{6-55}$$

Then

$$\frac{P_2}{P_1}=(\cos \beta)^{3/2} \tag{6-56}$$

and

$$\frac{P_3}{P_1}=(\cos 2\beta)^{3/2} \tag{6-57}$$

Substituting equations (6-56), (6-57), etc., into equation (6-51) gives

$$W_r=P_1[1+2(\cos \beta)^{5/2}+2(\cos 2\beta)^{5/2}+\ldots] \tag{6-58}$$

If Z equals the number of balls,

$$\beta=\frac{360}{Z} \tag{6-59}$$

The quantity in brackets in equation (6-58) is called the load-distribution factor Q, which depends only on Z. Stribeck found that the quantity Z/Q remained approximately constant at 4.37. To allow for possible uncircularity of the balls and the races and for bearing clearance, Stribeck took the value of Z/Q to be 5. Then

$$P_1=P_{max}=W_r \frac{5}{Z} \tag{6-60}$$

In an axially loaded bearing, all the balls are equally loaded so that

$$P_{max}=\frac{W_a}{Z \sin \alpha} \tag{6-61}$$

For combined load conditions, the maximum ball load depends on the initial contact angle and the magnitudes of W_r and W_a.

SPECIFIC DYNAMIC CAPACITY AND LIFE

In ordinary bearing applications where extreme speeds and temperatures are not present, a properly installed and lubricated bearing will fail because of material fatigue. The repeated stresses developed in the contact areas between the rolling elements and the races eventually result in failure of the material, which manifests itself as a fatigue crack. The fatigue crack propagates until a piece of the race or rolling-element material spalls out and produces the failure. Many bearings fail because of reasons other than fatigue, but in ordinary applications these failures are considered avoidable if the bearing is properly handled, installed, and lubricated and is not overloaded.

If a number of similar bearings are tested to fatigue at a specific load, there is a wide dispersion of life among the various bearings. For a group of 30 or more bearings, the ratio of the longset to the shortest life may be of the order of 20 or more. A curve of life as a function of the percent of bearings that failed can be drawn for any group of bearings. For a group of 30 or more bearings, the longest life would be of the order of four or five times the average life. The term life, as used in bearing catalogs, usually means the life that is exceeded by 90 percent of the bearings. This is the so-called B–10 or 10-percent life. The 10-percent life is one-fifth the average of 50-percent life for a normal life-dispersion curve.

If two groups of identical bearings are run to fatigue at two different loads, the life varies inversely as the nth power of the load:

$$\frac{L_2}{L_1}=\left(\frac{W_1}{W_2}\right)^n \tag{6-62}$$

For point contact $n=3$ and for line contact $n=4$. For point contact, then,

$$\frac{W_1}{W_2}=\left(\frac{L_2}{L_1}\right)^{1/3} \tag{6-63}$$

$$W_1L_1^{1/3}=W_2L_2^{1/3}=\text{constant} \tag{6-64}$$

If W in equation (6–64) is a radial load that acts on a radial bearing and L is a million revolutions with rotation of the inner race, then the constant in equation (6–64) is the specific dynamic capacity. The specific dynamic capacity for thrust bearings is determined if W is a thrust load.

In terms of the specific dynamic capacity C,

$$L=\left(\frac{C}{P}\right)^3 \tag{6-65}$$

where L is the life in millions of revolutions and P is the equivalent load. In general, ball bearings support both radial and thrust loads, and formulas for obtaining the equivalent load P in terms of radial and thrust loads are given for various bearing types in most bearing catalogs.

The bearing-design factors that affect the specific dynamic capacity are the race conformities, the rolling-element dimensions, and the number of rolling elements. Recent research has shown that the bearing material and both the lubricant viscosity and the base stock can have marked effects on fatigue. The original bearing-fatigue investigations, which include those of Palmgren (ref. 8), were made before the advent of the extreme temperatures and speeds to which rolling bearings are now subjected. As a result, the great majority of bearings were made of SAE 51100 or SAE 52100 alloys and wide variations in material-fatigue strength were not encountered. In addition, all rolling bearings were lubricated with a mineral oil such as SAE 30 or with a mineral-base soap grease so that the effect of the lubricant on fatigue was not important enough to be included among the parameters affecting fatigue life.

This problem will be discussed in chapter 12 along with formulas for calculating dynamic capacity.

SPECIFIC STATIC CAPACITY

From considerations of allowable permanent deformation, there is a limit to the load that a bearing can support while not rotating. The maximum load that a bearing can be permitted to support when not rotating is called the specific static capacity. It is arbitrarily defined as the load that will produce a permanent deformation of the race and the rolling element at a contact of 0.0001 times the rolling-element diameter. When permanent deformations exceed this value, bearing vibration and noise increase noticeably when the bearing is subsequently rotated under lesser loads. Specific static capacity is determined by the maximum rolling-element load and the race conformity at the contact.

As a result of this definition of the specific static capacity C_o, a bearing can be loaded above the specific static capacity as long as this load is applied only when the bearing is rotating. The permanent deformations that occur during rotation will be distributed evenly around the periphery of the races and will not be harmful until they become more extensive.

Static and dynamic load capacities are normally given for all bearings in bearing catalogs.

LUBRICATION

The term lubrication, in the broadest sense, means the effective reduction of friction between surfaces in relative motion. Some sort of lubrication must be provided to rolling-element bearings to ensure successful operation. In many rolling-element bearing applications, the externally applied lubricant serves both as a lubricant and as a coolant and, in a few extreme cases, strictly as a coolant. These applications include extreme speeds, elevated temperatures, and operation in fluids such as fuels or propellants that are not ordinarily considered to be lubricants. Unusual applications will be considered separately and conventional lubrication techniques will be discussed here. Conventional lubrication techniques can be divided into three broad categories:

(1) Grease lubrication
(2) Solid oil lubrication
(3) Oil-air-mist lubrication

Grease Lubrication

Lubricating greases consist of a lubricating oil and a thickener. Grease-lubricated bearings are generally used for moderate operating conditions and bearings that are required to operate for extended periods of time without relubrication. Conventional greases are limited in temperature to about 250° F and in DN value (product of bearing bore in mm and speed in rpm) to about 250,000, although recent research on synthetic greases has extended the temperature limit beyond 450° F and grease-lubricated bearings have been run successfully at DN values as high as 1 million. Grease-lubricated bearings with double seals are used advantageously with contaminating conditions. Since the bearing cavity is charged with the grease, torque values are not as low as with an oil-lubricated bearing. Greases cannot be used if heat flow to the bearing is significant enough to require a circulating flow of lubricant to remove the heat.

The thickeners used in conventional greases are usually sodium, calcium, or lithium soaps, although barium, strontium, and aluminum soaps are used if water resistance is important. In recent years, thickeners of inorganic materials such as bentonite clay have been used in synthetic greases.

Lime-base or calcium-soap greases are insoluble in water and are only suitable for use to about 130° F because of their low melting points. Their consistency is buttery and they have a tendency to channel or to separate from the part to be lubricated as a result of centrifugal forces. The calcium-soap greases, for this reason, are more satisfactory for use in sleeve bearings than in rolling bearings.

Soda-base or sodium-soap greases are more stable than calcium-

693-489 O-64—12

soap greases and are suitable for temperatures to about 200° F. They are water soluble in contrast to the lime-base greases, which are insoluble in water. The structure is spongelike so they do not tend to channel. They are widely used in rolling bearings. Aluminum-base greases are water insoluble and do not tend to channel. They are stable to fairly high temperatures but are somewhat more expensive than lime- and soda-base greases.

Lithium-soap greases have been used recently because of their desirable characteristics over a wide temperature range and their good oxidation resistance.

Common greases ordinarily use petroleum oils such as SAE 20 or 30. Low-temperature greases may use less viscous oils, and high-temperature greases may use more viscous oils. Synthetic greases that use silicones, diesters, polyglycols, and other synthetic oils are used for applications above 250° F.

Solid-Oil Lubrication

Solid-oil lubrication with a recirculating system is normally employed for high-speed applications especially when a considerable amount of heat must be removed from the bearing. An example is the lubrication system used in turbojet engines for the rotor bearings. The high power loss in the bearings plus the flow of heat to the bearings from hot engine parts makes it necessary to use high oil flows to maintain allowable bearing temperatures. While the oil acts as a coolant, the high flow rates frequently aggravate the problem by increasing the rate of heat generation due to oil churning.

Oil jets or nozzles are normally used to introduce the oil in the form of a high-velocity stream directed at the face of the bearing. The most efficient lubrication and cooling is obtained when the jet is directed at the space between the retainer and the inner race. Multiple jets spaced around the periphery are used to reduce circumferential temperature gradients in bearings that support high radial loads.

Oil is normally drained from both sides of the bearing to minimize oil churning losses. If bearing temperature is critical, the oil may be drained only from the side opposite the oil jet, which forces all the oil to flow through the bearing and increases the cooling efficiency. This method is sometimes referred to as puddling.

Oil-Air-Mist Lubrication

At extremely high speeds where any appreciable quantity of oil present in the bearings would cause an intolerable power loss due to oil churning, utilization of oil-mist lubrication is necessary. Small-bore bearings that operate in the speed range from 50,000 to above 100,000 rpm are usually lubricated with oil mist. The effect of oil

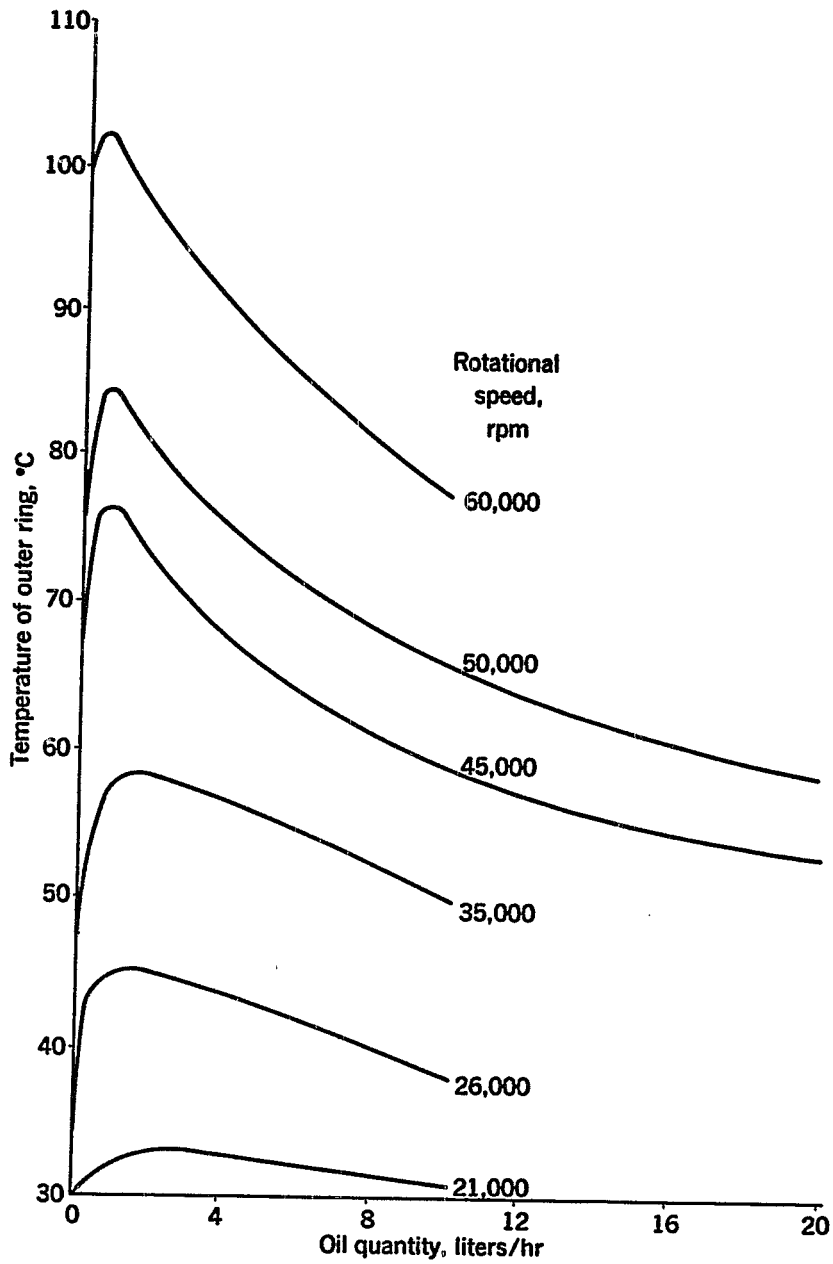

FIGURE 6-24.—Relation between bearing temperature and oil supplied for 6202-size deep-groove ball bearing (15-mm-diam. bore); radial clearance, approximately 20 microns; radial load, 0.4 kilogram; axial load, 4 kilograms. (From ref. 19.)

flow on bearing power loss for a wide range of oil flows can be surmised from the data reported in reference 19 and shown in figure 6–24. In the low oil-flow range, the bearing operating temperature increases with increasing oil flow, which indicates that churning losses increase faster than cooling effectiveness. In the high oil-flow range the cooling effectiveness increases faster than the churning losses, which results in a gradual decrease in the bearing operating temperature. The bearing power loss, however, continues to increase throughout the entire range of oil flows.

Oil-mist systems are noncirculating; the oil is passed through the bearing once and then discarded. Extremely low oil flows are required for the lubrication function exclusive of cooling. Commercial oil-mist generators are available for systems that contain one to many bearings. Since the required oil flows are low, a nominal capacity sump is adequate for supplying a multiple-bearing system for an extended period of time.

Data on the minimum oil-flow requirements of ball bearings are presented in reference 20. Ball bearings with 75-millimeter bore operated satisfactorily at 12,000 rpm, 400° F, and 1000-pound-thrust load with oil flows as low as 0.003 pound per minute.

REFERENCES

1. Reynolds, O.: On Rolling Friction. Phil. Trans. Roy. Soc. (London), vol. 166, 1876, pp. 155–174.
2. Heathcote, H. L.: The Ball Bearing in the Making, Under Test and in Service. Proc. Inst. Automotive Eng., vol. 15, 1921, pp. 569–702.
3. Eldredge, K. R.: Rolling Friction of Spheres on Surfaces. Ph. D. Thesis, Cambridge Univ., 1952.
4. Eldredge, K. R., and Tabor, D.: The Mechanism of Rolling Friction. I. The Plastic Range. Proc. Roy. Soc. (London), ser. A, vol. 229, no. 1177, Apr. 21, 1955, pp. 181–198.
5. Tabor, D.: The Mechanism of Rolling Friction. II. The Elastic Range. Proc. Roy. Soc. (London), ser. A, vol. 229, no. 1177, Apr. 21, 1955, pp. 198–220.
6. Tabor, D.: The Mechanism of "Free" Rolling Friction. Lubrication Eng., vol. 12, no. 6, Nov.–Dec. 1956, pp. 379–386.
7. Drutowski, Richard C.: Energy Losses of Balls Rolling on Plates. Record of Proc. Instr. Ball Bearing Conf., sponsored by New Departure, General Motors Corp., Cleveland (Ohio), Mar. 26–27, 1958, pp. 97–116.
8. Palmgren, A.: Ball and Roller Bearing Engineering, third ed., SKF Industries, Inc., 1959.
9. Muzzoli, M.: Ricerche di ingegneria, Sept.–Oct. 1934.
10. Wilcock, D. F., and Booser, E. R.: Bearing Design and Application. McGraw-Hill Book Co., Inc., 1957.
11. Hertz, H.: The Contact of Elastic Bodies. Gesammelte Werke, vol. 1, 1881.
12. Allan, R. K.: Rolling Bearings. Sir Isaac Pitman & Sons, Ltd., 1945.

13. JONES, A. B.: New Departure—Analysis of Stresses and Deflections. Vols. I–II. New Departure Div., Gen. Motors Corp., 1946.
14. THOMAS, HOWARD R., and HOERSCH, VICTOR A.: Stresses Due to the Pressure of One Elastic Solid Upon Another with Special Reference to Railroad Rails. Bull. 212, Eng. Exp. Station, Univ. Illinois, 1930.
15. LOVE, A. E. H: Mathematical Theory of Elasticity. Fourth ed., Dover Pub., 1944, p. 197.
16. PORITSKY, H., HEWLETT, C. W., JR., and COLEMAN, R. E., JR.: Sliding Friction of Ball Bearings of the Pivot Type. Jour. Appl. Mech., vol. 14, no. 4, Dec. 1947, pp. 261–268.
17. JONES, A. B.: The Life of High-Speed Ball Bearings. Trans. ASME, vol. 74, no. 5, July 1952, pp. 695–699; discussion, pp. 699–703.
18. STRIBECK, R.: Ball Bearings for Various Loads. Trans. ASME, vol. 29, 1907, pp. 420–463; discussion, pp. 464–467.
19. GETZLAFF, G.: The Behavior of Rolling Bearings at Very High Running Speeds. Eng. Digest, vol. 13, no. 11, Sept. 1952, pp. 379–384.
20. SCHULLER, FREDRICK T., and ANDERSON, WILLIAM J.: Operating Characteristics of 75 Millimeter Bore Ball Bearings at Minimum Oil Flow Rates over a Temperature Range to 500° F. Lubrication Eng., vol. 17, no. 6, June 1961, pp. 291–298.

CHAPTER 11

Extreme-Temperature Bearings

By WILLIAM J. ANDERSON

EXTREME-TEMPERATURE BEARINGS ARE OF INTEREST (1) at temperatures from −65° F down to temperatures approximating those of liquid helium, a few degrees above absolute zero, and (2) at temperatures of 400° F and above, up to an absolute maximum of 3000° F.

For the low temperatures, one of the lubrication problems involves operating bearings in turbomachinery that pumps high-energy cryogenic propellants for chemical rockets. Lubrication with conventional oils in many of these applications may not be practicable because of the difficulty of raising the ambient temperature of the bearing to keep the oil hot enough so that it can be pumped. Even if heating is possible, the use of coventional lubrication systems may necessitate long overhung shafts to isolate the bearing from the cold region. These systems usually lead to various design and critical speed problems. Although not directly related to bearings, shaft seals are an additional problem. Many dynamic sealing problems can be alleviated or eliminated completely by operating the bearings in the working fluid. When reliable operation can be accomplished with bearings lubricated and cooled by the working fluid, shaft seals and bearing lubrication systems can be greatly simplified. This simplification results in an appreciable reduction of complexity, weight, and cost. Specific applications in the cryogenic region require bearings to operate at very high speeds with light to heavy loads for relatively short times as in turbopumps or at moderate speeds and loads as in cooling-system pumps.

At elevated temperatures, bearing applications include low rotative speed or oscillating conditions at very high loads, such as airframe control bearings for supersonic aircraft. Other applications at high temperatures involve high rotative speeds with loads ranging from

low to high. An example of this application would be small high-speed turbomachinery with bearings located close to hot turbines. Jet-engine rotor bearings for supersonic aircraft also operate hot at high DN values and loads. In these engines limited cooling capacity and high stagnation temperatures result in high ambient temperatures around the bearings.

The approaches to bearing operating problems in these two areas will be discussed separately. The results obtained by various investigators in this field will be examined. Problems in the cryogenic temperature region will be discussed first.

SYMBOLS

a	semimajor axis of contact ellipse, in.
b	semiminor axis of contact ellipse, in.
CF	centrifugal force on ball, lb
d	ball diameter, in.
E	bearing unit pitch diameter, in.
$E(k)$	complete elliptic integral of the second kind
f	race curvature
M_1	torque about bearing axis, in.-lb
M_s	ball spin moment, in.-lb
n	number of balls
P	normal ball load, lb
Q	oil flow, lb/min
Q_s	heat generated between balls and race due to ball spin, Btu/min
r	race-ball groove radius, in.
T	bearing thrust load, lb
V_B	linear velocity of inner-race ball contact, in./sec
W	thrust load, lb
$\alpha_1,\alpha_2,\gamma,\Delta,\theta$	angles, defined on figures, deg
β	contact angle under load, deg
β'	initial mounted no-load contact angle, deg
β_i	inner-race contact angle at load and speed, deg
β_o	outer-race contact angle at load and speed, deg
μ_s	coefficient of sliding friction
ω	angular velocity of a ball about its rolling axis, radian/sec

Subscripts:

i	inner race
o	outer race
R	rolling
s	spinning

LOW-TEMPERATURE BEARINGS

When bearings are operated in cryogenic fluids such as liquid nitrogen, liquid oxygen, or liquid hydrogen, ample cooling capacity is available. These fluids are poor boundary lubricants, however, so that the problem is one of preventing surface damage in sliding and in rolling contact. Before a rolling bearing can be operated successfully in an application where the lubrication is marginal, two principal problems must be overcome. First, the integrity of the surfaces in rolling and in sliding contact must be maintained. Therefore, the bearings should be made of materials that tend to exhibit minimum wear and maximum resistance to galling and to surface welding in sliding. Second, the heat generated within the bearing must be removed to maintain an equilibrium operating condition and to prevent a total loss of bearing operating clearance that could result in bearing seizure. The bearing material and design must be chosen to minimize heat generation within the bearing in order to provide a maximum assurance of success. There are two principal sources of heat generation within a ball bearing: (1) the sliding friction between the retainer and its locating race and the retainer and the balls, and (2) the friction due to ball spin in the ball-race contact area. Bearings must be designed to minimize both of these sources of heat generation to obtain maximum performance in cryogenic fluids. Therefore, retainer materials selected for test should be chosen from among those that exhibit low friction coefficients and good resistance to wear as determined by cryogenic friction and wear tests. These tests are much less expensive to conduct than full-scale bearing tests. A background of knowledge in friction and wear of candidate materials is necessary to conduct a bearing experimental program intelligently. To minimize heat generation due to ball spin losses requires an examination of various design parameters such as ball diameter and race curvatures to determine the amount of heat generation due to ball spinning.

Friction and Wear Experiments

References 1 and 2 present the results of friction and wear experiments in both liquid nitrogen and liquid hydrogen. These results indicate that filled Teflon compositions show promise for cryogenic applications. In reference 1, 25 percent glass-fiber-filled Teflon sliding against 304 stainless steel in liquid nitrogen showed low wear at sliding velocities to 6000 feet per minute. In this material, the Teflon provides the lubrication while the glass fibers are added to increase structural strength.

Early Bearing Experiments

Some of the early bearing experiments in cryogenic fluids are reported in reference 3. The authors started out with SAE 52100 steel bearings. These radial bearings had pressed steel separators and gave only limited service in liquid nitrogen and liquid hydrogen. In all these bearings, mechanical failures occurred in the separator. Further experiments with ½-inch and 15-millimeter-bore SAE 52100 steel angular-contact bearings equipped with cotton-cloth phenolic-laminated separators showed that successful operation could be obtained at speeds from 3300 to 8000 rpm. These experiments indicated, however, that 52100 steel, because of its lack of corrosion resistance, is not an ideal ball and race material for cryogenic applications where thermal cycling back to room temperature is apt to occur. When cycling does occur, condensation may form on the bearing surfaces, and since they are free from organic contaminants, corrosion may take place. Additional experiments were conducted with bearings that had races and balls made of 440C stainless steel, and satisfactory operation was obtained for 262 hours in liquid hydrogen at 12,000 rpm. Other bearings in these experiments were operated successfully at 3300 rpm for running times in excess of 4700 hours. Although the bearings in reference 3 were run at nominal speeds and light loads, the results indicated that with proper design and good choice of retainer materials bearing operation at very high DN values was a distinct possibility. A more systematic investigation of the operation of 10-millimeter-bore bearings at 3150 rpm under a thrust load of 144 pounds in liquid nitrogen was conducted in reference 4. In reference 4, bearings with cotton-cloth phenolic laminate, Teflon-coated steel, filled Teflon machined, Teflon-coated grade A phosphor bronze, grade A phosphor-bronze retainers, and full-complement bearings with alternate undersize 440C balls were investigated. Among the cotton-cloth phenolic laminates were inner-ring-riding retainers, outer-ring-riding retainers, and ball-riding retainers. With the exception of the machined retainers of filled Teflon material, all the other retainer configurations gave life results from 0.4 to 20 hours. The bearings with filled Teflon retainers operated without failure for 1000 hours. The criterion of failure used in these experiments was excessive torque.

High-Speed Bearing Experiments

In contrast to the work reported in references 3 and 4, which was aimed at the development of bearings with long lives at nominal running speeds, the work of reference 5 is directly related to bearings for high-speed turbomachinery with short-duration lives. The objective of the work reported in reference 5 was to study the performance as well as the operating limitations of ball bearings in liquid

hydrogen for running times of 1 hour at DN values to 1.5×10^6. In reference 5, both retainer material and bearing design were studied. The retainer material that performed best was again the filled Teflon material, which agrees with the results obtained in references 3 and 4. Among the bearing-design parameters investigated in reference 5 were the effects of diametral clearance, ball size, and bearing race curvatures on the limiting speed when bearings were submerged in liquid hydrogen and operated under thrust loads from 100 to 500 pounds. The majority of the work in reference 5 was conducted with 40-millimeter ball bearings, which were operated successfully at speeds to 42,000 rpm. A detailed discussion of the approach to the problem of heat generation in the ball-race contact is presented in reference 5. An approximate analysis was made of the effects of bearing design parameters on the amount of heat generation in the ball-race contact. This analysis showed that open-race curvatures reduce the amount of heat generation due to ball spin. Therefore, higher limiting speeds can be obtained with bearings designed for minimum heat generation. An additional important factor was shown to be ball diameter, which is discussed in reference 5.

Heat generation due to ball spin.—In a ball bearing that operates under any load condition other than radial, ball spinning, in addition to rolling, occurs at the ball-race contacts. If the bearing is operated at high speed, the centrifugal force on the balls creates an additional load at the outer-race contact. The effect of centrifugal force is to shift the contact points between the balls and the races from those at lower speeds. The result is an increase in the operating contact angle at the inner race. The normal ball load at the outer-race contact can be expressed by

$$P_o=CF\cos\beta_o+\frac{T\cos(\beta_i-\beta_o)}{n\sin\beta_i} \tag{11-1}$$

(ref. 6), whereas the ball load at the inner-race contact is

$$P_i=\frac{T}{n\sin\beta_i} \tag{11-2}$$

Usually the ball will have either outer-race or inner-race control, that is, rolling at one race contact without spin and spinning plus rolling at the other race contact. The frictional moment created by ball spin in the pressure ellipse at the ball-race contact can be expressed approximately as

$$M_s=\frac{3}{8}\mu_s PaE(k) \tag{11-2a}$$

(See ref. 7.) The ball will roll at the race contact where the value of the friction moment is the greater.

An approximate analysis to determine the heat generated in the ball-race contact of a thrust-loaded ball bearing is outlined in reference 8 for inner-race rotation where gyroscopic moments are neglected and the ball rolls on one race without spin. The following assumptions are made in this analysis:

(1) The effective ball rolling radius r at operating conditions is the unstressed radius $d/2$.

(2) In computing the spin moment M_s, the linear slip velocities in the direction of rolling that occur because of the curvature of the contact ellipse are small compared with the slip velocities due to ball spin.

(3) Gyroscopic moments are insufficient to cause ball slip.

(4) The rotating radial load that results from shaft unbalance at high speeds is neglected.

From figure 11–1(a) for inner-race control,

$$V_B=\omega_i\left(\frac{E}{2}-\frac{d}{2}\cos\beta_i\right) \tag{11–3}$$

$$\tan\alpha_1=\frac{\sin\beta_1}{\frac{E}{d}-\cos\beta_i} \tag{11–4}$$

$$\frac{1}{2}(\gamma+\alpha_2)=\frac{1}{2}(\pi-\theta) \tag{11–5}$$

$$\tan\frac{1}{2}(\gamma-\alpha_2)=\frac{\frac{E}{d}-\sin(\beta_i+\alpha_1)}{\frac{E}{d}+\sin(\beta_i+\alpha_1)}\tan\frac{1}{2}(\gamma+\alpha_2) \tag{11–6}$$

$$\alpha_2=\frac{1}{2}(\gamma+\alpha_2)-\frac{1}{2}(\gamma-\alpha_2) \tag{11–7}$$

$$\omega=\frac{\omega_i\sin\beta_i}{(\tan\alpha_1+\tan\alpha_2)\cos\alpha_1} \tag{11–8}$$

$$\omega_{s,o}=\omega\sin(\beta_i+\alpha_1-\beta_o) \tag{11–9}$$

$$Q_{s,o}=n\omega_{s,o}M_{s,o} \tag{11–10}$$

When equation (11–10) is converted to torque about the bearing axis,

$$M_{1,o}=\frac{Q_{s,o}}{\omega_i} \tag{11–11}$$

where, from reference 7

$$M_{s,o}=\frac{3}{8}\mu_s P_o a_o E(k_o) \tag{11-12}$$

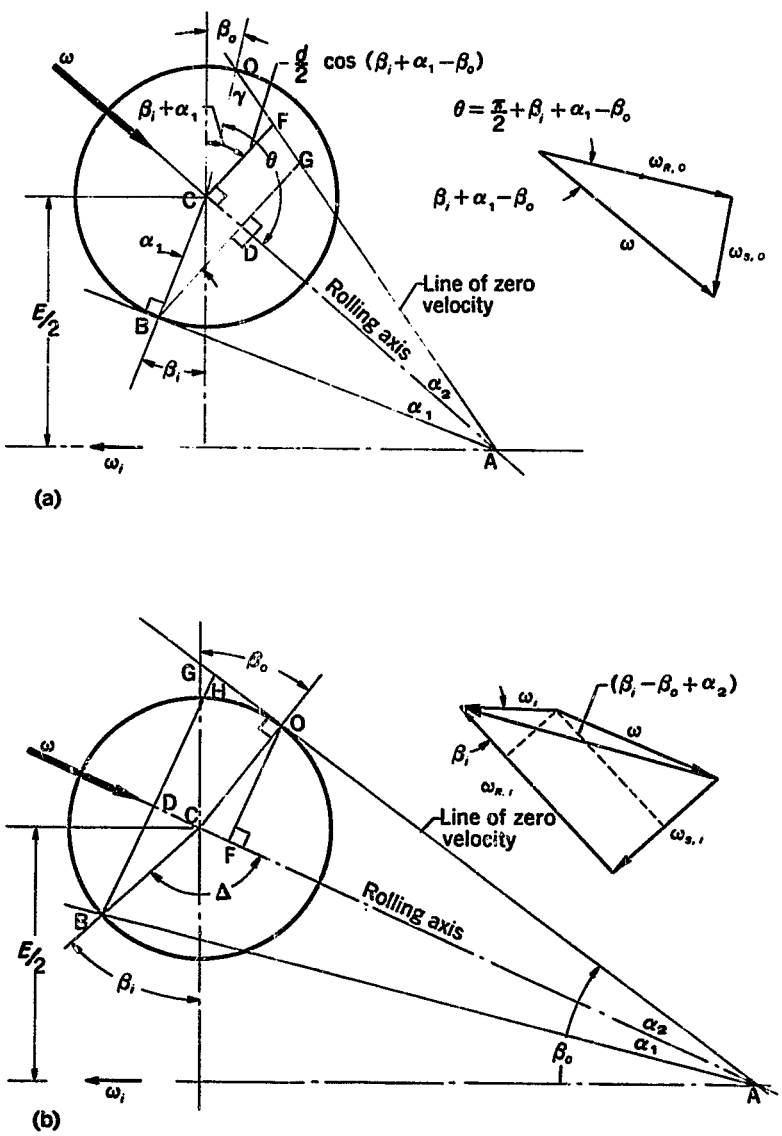

(a) Inner-race control.
(b) Outer-race control.

FIGURE 11-1.—Bearing geometric relations used to calculate heat generation due to ball spinning. (From ref. 5.)

From figure 11–1(b) for outer race control,

$$V_B=\omega_i\left(\frac{E}{2}-\frac{d}{2}\cos\beta_i\right) \tag{11–3}$$

$$\tan\alpha_2=\frac{\sin\beta_o}{\frac{E}{d}+\cos\beta_o} \tag{11–13}$$

$$\Delta=\frac{\pi}{2}+\beta_i-\beta_o+\alpha_2 \tag{11–14}$$

$$\sin\alpha_1=\frac{\sin\Delta}{\left\{1+\left[\frac{\frac{E}{d}}{\sin(\beta_o-\alpha_2)}\right]^2-2\left[\frac{\frac{E}{d}}{\sin(\beta_o-\alpha_2)}\right]\right\}^{1/2}} \tag{11–15}$$

$$\omega=\frac{\omega_i\left(\frac{E}{d}-\cos\beta_i\right)\Big/(\sin\alpha_1+\tan\alpha_2\cos\alpha_1)}{\left\{1+\left[\frac{\frac{E}{d}}{\sin(\beta_o-\alpha_2)}\right]^2-2\left[\frac{\frac{E}{d}}{\sin(\beta_o-\alpha_2)}\right]\cos\Delta\right\}^{1/2}} \tag{11–16}$$

$$\omega_{s,i}=\omega\sin(\beta_i-\beta_o+\alpha_2)+\omega_i\sin\beta_i \tag{11–17}$$

$$Q_{s,i}=n\omega_{s,i}M_{s,i} \tag{11–18}$$

When equation (11–18) is converted to torque about the bearing axis,

$$M_{l,i}=\frac{Q_{s,i}}{\omega_i} \tag{11–19}$$

where, from reference 7

$$M_{s,i}=\frac{3}{8}\mu_s P_i a_i E(k_i) \tag{11–20}$$

Calculations were made on a digital computer for 40-millimeter-bore bearings of an extremely light series (1908 with 0.250-in.-diam. balls) and an extra light series (108 with 0.375-in.-diam. balls). Four race-curvature combinations were assumed, and calculations were made for thrust loads of 100, 200, and 300 pounds, initial contact angles of 5°, 10°, 15°, and 20°, and a rotative speed of 40,000 rpm (1.6 million DN). The results are shown in table (11–I).

A value of 0.56 was used for the sliding friction coefficient in calculating heat generation. This value was obtained in reference 2 for 440C sliding on 440C in liquid hydrogen. Since the heat-generation

TABLE 11–I.—TORQUE DEVELOPED ABOUT BEARING AXIS DUE TO BALL SPIN[a]

(a) 108-Series bearing: ball diameter, 0.375 in.; pitch diameter, 2.111 in.; coefficient of sliding friction, 0.56; angular velocity of inner race, 4190 radian/sec

Race curvature	f_i=0.51, f_o=0.58				f_i=0.51, f_o=0.56				f_i=0.52, f_o=0.54				f_i=0.54, f_o=0.52			
Initial mounted contact angle, β', deg	5	10	15	20	5	10	15	20	5	10	15	20	5	10	15	20
Inner-race contact angle at 300 lb, β_i, deg	18.8	24.0	32.7	44.5	20.1	24.8	32.5	42.7	19.1	22.3	27.4	34.0	16.5	18.8	22.5	27.0
Thrust load, T, lb	Torque about bearing axis, M_t, lb-in.															
100	2.143	2.095	2.132	2.314	2.143	2.099	2.106	2.214	1.698	1.653	1.620	1.612	1.356	1.319	1.285	1.259
200	4.830	4.755	4.755	4.978	4.941	4.755	4.755	4.904	3.752	3.698	3.789	3.648	2.931	2.894	2.853	2.831
300	7.579	7.504	7.467	7.616	7.579	7.504	7.467	7.579	5.870	5.795	5.758	5.758	4.569	4.532	4.495	4.458

(b) 1908-Series bearing: ball diameter, 0.250 in.; pitch diameter, 2.001 in.; coefficient of sliding friction, 0.56; angular velocity of inner race, 4190 radian/sec

Race curvature	f_i=0.51, f_o=0.58				f_i=0.51, f_o=0.56				f_i=0.52, f_o=0.54				f_i=0.54, f_o=0.52			
Initial mounted contact angle, β', deg	5	10	15	20	5	10	15	20	5	10	15	20	5	10	15	20
Inner-race contact angle at 300 lb, β_i, deg	[c]13.2	[c]15.1	[c]17.0	31.7	[c]14.1	21.1	25.7	32.0	18.6	21.0	24.8	29.8	17.2	19.2	22.4	26.4
Thrust load, T, lb	Torque about bearing axis, M_t, lb-in.															
100	1.839	1.831	1.850	1.939	1.835	1.831	1.846	1.910	1.419	1.412	1.412	1.423	1.096	1.092	1.092	1.092
200	3.789	3.789	3.789	3.864	3.789	3.789	3.789	3.884	2.916	2.912	2.920	2.946	2.259	2.255	2.251	2.262
300	2.964[b]	3.299[b]	3.864[b]	5.832	3.407[b]	5.795	5.795	5.832	4.458	4.458	4.458	4.458	3.462	3.448	3.433	3.440

[a] From ref. 5.
[b] Inner-race control, ball spinning at outer race.
[c] Outer-race contact angle β_o.

calculations are all relative and are used for comparative purposes only, the actual coefficient of friction is unimportant.

For the 108-series bearings, ball control was at the outer race for all combinations of race curvature and thrust load chosen. For the 1908-series bearings, ball control was at the outer race for all combinations except four. Ball control is at the inner race for a thrust load of 300 pounds and the following sets of curvatures and contact angles:

(1) $f_i=0.51$
$f_o=0.58$
$\beta=5°$, 10°, and 15°

(2) $f_i=0.51$
$f_o=0.56$
$\beta=5°$

Inner-race ball control is desirable because it results in relatively low friction torque due to ball spin.

At a specific thrust load, the values of M_1 do not change appreciably with initial mounted contact angle when control is at the outer race. The torque developed decreases with increasing race curvature at the spinning contact and is not affected by curvature at the rolling contact. This fact is apparent since close values of ball-race conformities (i.e., approaching 0.50) result in high rates of heat generation. The operating contact angle is given for a thrust load of 300 pounds. The operating contact angle and the angular velocity of ball spin increase with increasing initial mounted contact angle for all race-curvature combinations shown. Torque developed at the inner-race contact of the 108-series bearing with $f_i=0.52$ and $f_o=0.54$ at thrust loads of 100 and 200 pounds is greater than that developed in the 1908-series with the same race curvatures, which indicates the importance of ball diameter.

The importance of ball spin losses can be noted by comparing the results for the two series bearings shown on figure 11–2. The 1908-series bearings with inner- and outer-race curvatures of 0.54 operated to higher limiting DN values than did the 108-series bearings with inner- and outer-race curvatures of 0.52 and 0.54, respectively, over the entire range of thrust loads investigated. The results of these tests appear to indicate that ball-spin losses are important.

In addition to ball diameter and race curvatures, another bearing design parameter, which was found to be important in reference 5, was bearing diametral clearance. Limiting DN values increased with diametral clearance for 108-series bearings with two different retainer materials as shown in figure 11–3.

Bearing experiments in cryogenic and other propellants.—Reference 9 contains some data on the operation of rolling bearings in liquid hydrogen, liquid oxygen, nitrogen tetroxide, and RP–1, a kerosene base

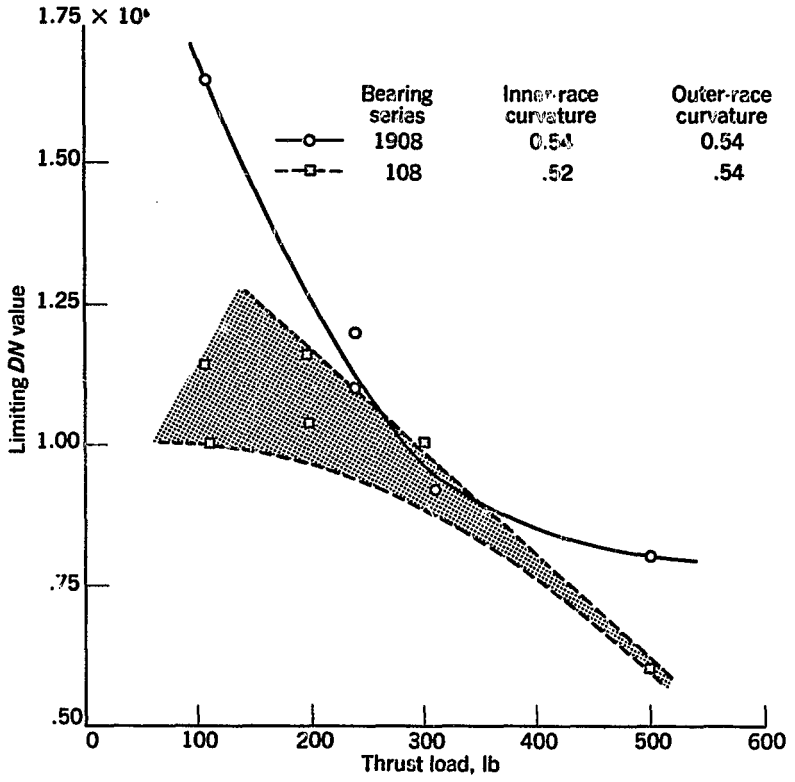

FIGURE 11-2.—Limiting DN value as function of thrust load for 108-series and 1908-series bearings with filled Teflon retainers. (From ref. 5.)

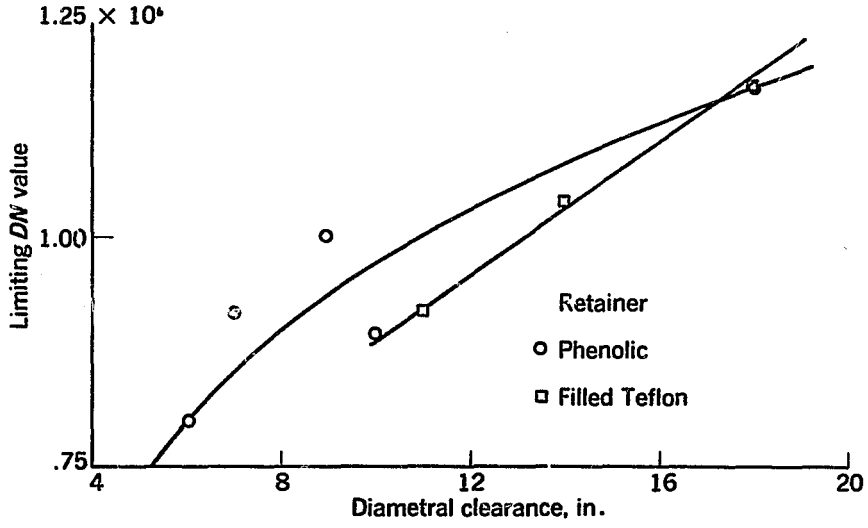

FIGURE 11-3.—Limiting DN value as function of diametral clearance for 108-series bearings with two different retainer materials. (From ref. 5.)

rocket fuel. As in references 4 and 5, the best results in the cryogenic propellants were obtained with bearings having glass-filled Teflon retainers and glass-supported Teflon retainers. The bearings used in this investigation were extra light (100 series) and light (200 series) with bore sizes from 35 to 45 millimeters. These bearings were run at speeds to 6400 rpm in liquid oxygen and nitrogen tetroxide and at 25,000 rpm in liquid hydrogen. These speeds correspond to the actual shaft speeds in a turbopump unit that pumps liquid oxygen and liquid hydrogen. In liquid hydrogen, bearings with several different types of metallic retainers all failed within a few minutes after starting. Likewise, in liquid oxygen and nitrogen tetroxide, bearings with metallic retainers had very short lives. Severe wear and galling caused failure.

Bearings with phenolic retainers were operated with some success in both liquid oxygen and liquid hydrogen. In liquid hydrogen, a speed of 20,000 rpm was successfully obtained. A tendency for the bearing to exhibit chatter at low shaft speeds existed, however, because of the high friction coefficient between the steel and the phenolic cage. Bearings with glass-supported Teflon retainers were operated successfully for almost 10 hours at 25,000 rpm in liquid hydrogen, 9 hours in liquid oxygen, and almost 5 hours in nitrogen tetroxide at 6400 rpm. In liquid oxygen successful operation was also obtained with a bearing that had a ribbon steel separator with a 0.010-inch coating of Teflon on the retainer parts. This bearing was run for 1 hour at 6400 rpm.

Some discrepancies existed in results obtained in various unpublished researches on the operation of rolling bearings in liquid oxygen. In some instances (ref. 9), no severe oxidation of the bearing, races, or balls was evident, and in unpublished tests, severe oxidation occurred. This discrepancy or anomaly in results has not been clarified, but there appears to be some evidence which indicates that the presence of moisture on the bearing is extremely critical. The presence of any moisture may cause severe corrosion in a highly reactive medium such as liquid oxygen. The problem of maintaining surface integrity is, of course, quite different in a reducing environment such as liquid hydrogen than it is in a highly oxidizing environment such as liquid oxygen. In liquid hydrogen, the temperature reached at the sliding asperities would be sufficient for the reactions between the hydrogen and any oxide films to ultimately produce clean nascent metals. Clean metals have characteristically poor friction and wear properties and gall readily. In a highly reactive oxidant, such as liquid oxygen, the opposite is true. Here the problem is one of controlling surface corrosion. Again the asperity temperatures would be sufficient to cause reaction between the oxygen and the metal at the asperities so that the maintenance of protective oxide films should not be a problem.

Discussion of Results

The general bearing design philosophy for bearings which are to be used in cryogenic applications is to design for minimum heat generation. The sources of heat generation are at the sliding surfaces between the retainer and the races, the retainer and the balls, and in the sliding contact between the balls and the races. Materials with good friction and wear properties such as filled Teflon should be used to reduce heat generation at the retainer sliding surfaces. For high-speed applications, reinforcement of retainers made of these materials with thin shrouds of either aluminum or stainless steel is necessary. For high-speed applications where loads are not too heavy and where heat generation is very critical, open-race curvatures and very liberal diametral clearances must be used. The open-race curvatures do reduce the load capacity of the bearing somewhat, but they also effect an appreciable reduction in the heat generation at these contacts; this extends the limiting speed at which the bearings can be successfully operated. Because centrifugal forces become predominant at extreme speeds and nominal loads, very light series bearings with small balls are found to have a higher load carrying capacity than heavier series bearings. This is in contrast to normal, conventionally lubricated bearing applications where the load capacity increases as the bearing series becomes heavier. A corrosion-resistant ball and race material, such as the ferritic tool steel 440C, is recommended rather than the standard bearing material SAE 52100 steel, which is subject to corrosion.

HIGH-TEMPERATURE BEARINGS

Applications and Problems

In the high-temperature region, applications include those at low rotative speeds or oscillating motion and very high load, such as airframe control bearings for supersonic aircraft, and applications at high rotative speeds with loads ranging from low to high. High rotative-speed applications include small high-speed turbomachinery with hot bearings located close to hot turbines and jet-engine rotor bearings for supersonic aircraft where limited cooling capacity and high stagnation temperatures result in high ambient temperatures.

The three major problems that are encountered in operating rolling-contact bearings at high temperatures are materials, lubricants, and bearing designs. These problems will be discussed in order.

Materials

Requirements.—The material problem involves obtaining materials that have adequate hot hardness, good oxidation resistance if the atmosphere is oxidizing, and good dimensional stability at high

CHAPTER 12

Fatigue in Rolling-Element Bearings

By WILLIAM J. ANDERSON

SYMBOLS

A constant in Weibull equation, e ln A is vertical intercept on Weilbull plot when $L=1$
a half axis of pressure ellipse in direction normal to rolling direction, in.
C specific dynamic capacity
D rolling-element diameter, in.
d diameter, in.
E bearing-pitch diameter, in.
e slope of Weibull plot
F probability that a crack will occur
f_c coefficient dependent on material and bearing type
i number of rows of rolling elements
L life in millions of revolutions
l length of raceway contact, in.
l_a roller length, in.
N angular velocity, rpm
n millions of stress cycles
n load-life exponent
P bearing or system thrust load, lb
P_e bearing equivalent load, lb
p pressure, lb/sq in.
R rolling-element profile radius normal to direction of rolling
r race groove radius normal to direction of rolling
S probability of survival
T temperature
t time
V stressed volume

W bearing load, lb
y_E standardized excess life
y_T standardized theoretical life
z number of balls per row
z_o depth to maximum shear stress
α contact angle
β slope of pressure-viscosity curve
μ_o viscosity at atmospheric pressure, lb-sec/sq in.
μ_p viscosity at pressure p, lb-sec/sq in.
σ stress, psi
τ_o maximum shear stress, psi
ω_s angular spin velocity
Subscripts:
i inner
m pitch
o outer

SPECIFIC DYNAMIC CAPACITY

In chapter 6, the life dispersion, the load-life relations, and the meaning of specific dynamic capacity, or load rating, of rolling bearings were discussed. These three factors must be understood to predict the life of a given bearing in a specific application. Formulas for calculating the specific dynamic capacity must be available because large groups of bearings cannot be tested experimentally to determine the expected life for every application.

Lundberg-Palmgren Theory

Much of the analytical and the experimental work, which has resulted in specific-dynamic-capacity formulas, was done by Palmgren (ref. 1) and Lundberg and Palmgren (ref. 2). An empirical method for determining specific dynamic capacity is presented in reference 1, and a more refined method, based on statistics, is presented in reference 2.

The life formula developed in reference 2 is based on the known fact that, the more concentrated the stress is, the greater the endurance. Weibull's investigations (refs. 3 and 4) have resulted in a statistical theory of strength based on the theory of probability, where the dependence of strength on volume is explained by the dispersion in material strength. Therefore, the dependence on volume caused by the dispersion in material strength must be considered. Weibull's theory, however, assumes that the first crack that forms eventually leads to a break. Many bearing races were examined and were found to contain numerous subsurface cracks that never progressed to failure; thus Weibull's assumption is questionable. Therefore, the depth z_o, at which the maximum shear stress occurs, must also be

considered. According to Weibull's theory, the logarithm of the inverse of the probability of survival is proportional to the magnitude of the stressed volume. This relation results from the multiplicative law, which states that the probability of failure of the whole is equal to the product of the probabilities of failure of the parts. In equation form, the life formula is therefore

$$\ln \frac{1}{S} = F(\tau_o, n, z_o)V \tag{12-1}$$

where

S probability of survival
F probability that a crack will occur
τ_o maximum shear stress
n number of stress cycles in millions
V stressed volume

The function F can be expressed as a power function:

$$F(\tau_o, n, z_o) \sim \frac{\tau_o^c n^e}{z_o^h} \tag{12-2}$$

where c, e, and h are exponents to be determined experimentally.

An arbitrary expression for V is

$$V = a z_o l \tag{12-3}$$

where

a half axis of pressure ellipse in direction normal to rolling direction
length of raceway

From equations (12-1) to (12-3)

$$\ln \frac{1}{S} \sim \frac{\tau_o n^e a l}{z_o^{h-1}} \tag{12-4}$$

The Lundberg-Palmgren dynamic capacity is developed from equation (12-4). The exponents in equation (12-4) are determined from the dispersion of bearing lives, the dependence of life on load, and the dependence of the specific dynamic capacity on bearing size. Lundberg and Palmgren extended the Hertz theory to calculate the shear-stress amplitude in a plane parallel to the direction of rolling and used this amplitude to determine the dependence of dynamic capacity on conformity between rolling elements and races. Their theory of fatigue strength is based on the assumption that the maximum shear stress in the plane parallel to the direction of rolling is the stress that causes failure. Other investigators believe that either the maximum orthogonal or the maximum octahedral shear stress is the stress that causes failure. Extensive studies in this area are needed.

The derivations of dynamic-capacity formulas in reference 2 are complex. Their principal value is that they improve the theoretical understanding of the relations between the statistical nature of bearing fatigue and bearing-load capacity. The empirical approach used by Palmgren in reference 1 is more direct and will be outlined herein. Weibull (ref. 5) postulated that the fatigue lives of a homogeneous group of rolling-element bearings are dispersed according to the following relation:

$$\ln \ln \frac{1}{S} = e \ln \frac{L}{A} \tag{12–5}$$

where L represents life in millions of revolutions and e is the dispersion exponent (slope of the Weibull plot) or a measure of the scatter in bearing lives. Experimental results confirm that bearing lives conform well to the Weibull distribution, at least at survival probabilities ranging from 0.5 to 0.9. Bearing-fatigue data will plot as a straight line with the coordinates given by equation (12–5), commonly known as Weibull coordinates.

The factors upon which the specific dynamic-load rating depends are the following:

(1) The size of the rolling elements
(2) The number of rolling elements per row
(3) The number of rows of rolling elements
(4) The conformity between the rolling elements and the races
(5) The contact angle under load
(6) The properties of the material
(7) The properties of the lubricant
(8) The operating temperature
(9) The operating speed

Factors 1 through 5 are considered in standard capacity formulas. The remaining factors will be discussed later.

According to the Hertz theory, the load-carrying capacity should be proportional to the square of the rolling-element diameter. From extensive experimental data, Palmgren (ref. 1) found that capacity varied as $D^{1.8}$ for balls up to about 25 millimeters in diameter and as $D^{1.4}$ for balls larger than 25 millimeters in diameter.

For a constant bearing load, the normal force between a rolling element and a race will be inversely proportional to the number of rolling elements. Therefore, for a constant number of stress cycles at a point, the capacity is proportional to the number of rolling elements. On the other hand, the number of stress cycles per revolution is also proportional to the number of rolling elements, so that for a constant rolling-element load the capacity for point contact is inversely proportional to the cube root of the number of rolling

elements. This comes from the inverse cubic relation between load and life for point contact. Then the capacity varies with

$$\frac{z}{z^{1/3}}=z^{2/3}$$

Multiple-row bearings with i rows of balls may be considered as a combination of i single-row bearings. From equation (12–5) and the theory of probability, the following relation between the life of a multirow bearing and the lives of the i individual rows is obtained:

$$\frac{1}{L^e}=\frac{1}{L_1^e}+\frac{1}{L_2^e}+\cdots+\frac{1}{L_i^e} \tag{12–6}$$

Then

$$\frac{1}{L^e}=\frac{i}{L_i^e} \tag{12–7}$$

If each row of the bearing is loaded with a load equal to the specific dynamic-load rating of one row C_i, then $L_i=1$ and, from equation (12–7),

$$L^e=\frac{1}{i} \tag{12–8}$$

or

$$L=\frac{1}{i^{1/e}} \tag{12–9}$$

The load on the entire bearing is iC_i. In chapter 6, the load-life relation was given as

$$L=\left(\frac{C}{P_e}\right)^n \tag{12–10}$$

where P_e is the equivalent bearing load. In this case,

$$P_e=iC_i \tag{12–11}$$

From equations (12–9) to (12–11),

$$\left(\frac{C}{iC_i}\right)^n=\frac{1}{i^{1/e}} \tag{12–12}$$

or

$$C=C_i\, i^{1-(1/en)} \tag{12–13}$$

For ball bearings, $n=3$ and e is approximately 1.1, so that the capacity of multirow bearings varies as $i^{0.7}$. For radial ball bearings, the normal force between a ball and a race varies as $1/\cos\alpha$, so that the capacity is proportional to $\cos\alpha$. The influence of the degree of conformity, bearing type, and internal dimensions is expressed by

$f_c/(\cos \alpha)^{0.3}$. Therefore the capacity of a radial ball bearing varies as $(i \cos \alpha)^{0.7}$.

For thrust ball bearings, the normal force between a ball and a race varies as $1/\sin \alpha$, so that the capacity is proportional to $\sin \alpha$ or to $\cos \alpha \tan \alpha$. When the influences of the degree of conformity, of bearing type, and of internal dimensions are included, the capacity of a thrust ball bearing varies as $(i \cos \alpha)^{0.7} \tan \alpha$.

For roller bearings with line contact, the exponent in the life equation is 4, so that the capacity varies as $z^{3/4}$. From equation (12–13) with $n=4$, the capacity of multirow-roller bearings is found to vary as $i^{0.78}$. Theoretically, the capacity of roller bearings should be proportional to $l_a D_a$. Experimental data indicate that capacity varies as $l_a^{0.78} D_a^{1.07}$.

The formulas for specific dynamic capacity as developed by Palmgren (ref. 1) and Lundberg and Palmgren (ref. 2) are as follows:

(1) For radial ball bearings with $D<25$ millimeters,

$$C=f_c(i \cos \alpha)^{0.7} z^{2/3} D^{1.8} \tag{12–14}$$

(2) For radial ball bearings with $D>25$ millimeters,

$$C=f_c(i \cos \alpha)^{0.7} z^{2/3} D^{1.4} \tag{12–15}$$

(3) For radial roller bearings,

$$C=f_c(i \cos \alpha)^{0.78} z^{3/4} D^{1.07} l_a^{0.78} \tag{12–16}$$

(4) For thrust ball bearings with $\alpha \neq 90°$,

$$C=f_c(i \cos \alpha)^{0.7} (\tan \alpha) z^{2/3} D^{1.8} \tag{12–17}$$

(5) For thrust roller bearings with $\alpha \neq 90°$,

$$C=f_c(i \cos \alpha)^{0.78} (\tan \alpha) z^{3/4} D^{1.07} l_a^{0.78} \tag{12–18}$$

(6) For thrust ball bearings with $\alpha=90°$,

$$C=f_c i^{0.7} z^{2/3} D^{1.8} \tag{12–19}$$

(7) For thrust roller bearings with $\alpha=90°$,

$$C=f_c i^{0.78} z^{3/4} D^{1.07} l_a^{0.78} \tag{12–20}$$

The coefficient f_c depends on the material and the bearing type. For ordinary bearing steels such as SAE 52100 with mineral-oil lubrication, f_c can be evaluated by using tables 12–I and 12–II.

Deviations From the Weibull Distribution

Until recently the analysis of bearing-fatigue data was based on the primary importance of two lives, the L_{10} and L_{50} (the lives at failure probabilities of 10 and 50 percent). As previously stated, the Weibull distribution (eq. (12–5)) predicts the life dispersion of bearings within the failure-probability range from 10 to 50 percent with satisfactory accuracy. Catalog ratings of bearings are based on the L_{10} and L_{50} lives.

Requirements for high-reliability mechanisms in space vehicles and other applications have made it necessary to investigate life dispersion at very low probabilities of failure. Bearing-fatigue data are, for the most part, taken from relatively small samples, so that the reliability cannot be determined accurately.

A true fit with the Weibull distribution would imply a zero minimum life, and knowing whether such a true fit exists over the entire range of failure probabilities from 0 to 100 percent is important.

Tallian (ref. 6) analyzed a composite sample of 2500 rolling-element bearings and concluded that a good fit was obtained in the failure probability region between 10 and 60 percent. Outside this region, experimental life is longer than the Weibull prediction. In the early failure region, bearings were found to behave as shown in figure 12–1.

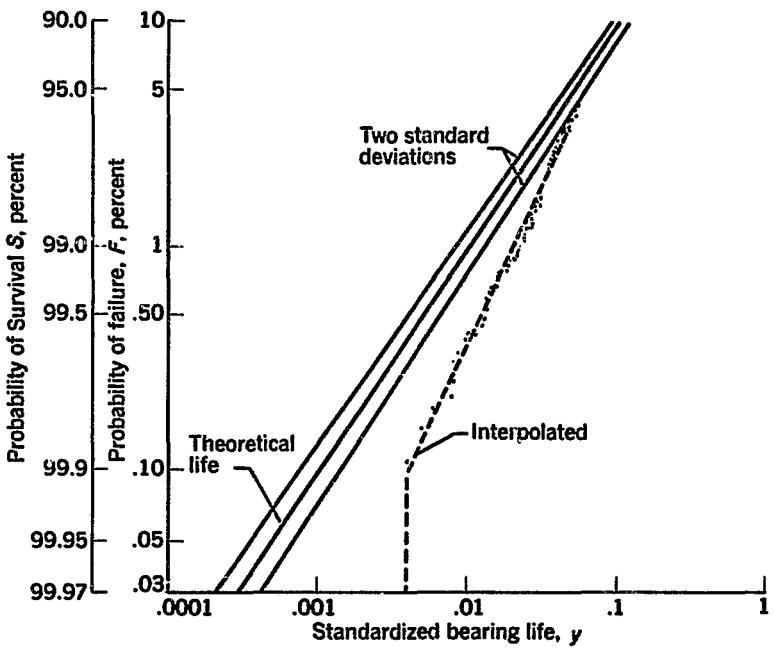

FIGURE 12–1.—Life distribution in early failure region. (From ref. 6.)

693-499 O-64—25

TABLE 12-I.—CONVENTIONAL BEARING TYPES [a]

[Units in kg and mm.]

Function	Point contact of ball bearings	Line contact of roller bearings
C	$f_c f_a i^{0.7} z^{2/3} D^{1.8}$	$f_c f_a i^{7/9} z^{3/4} D^{29/27} l_{a,i}^{7/9}$
f_c	$g_c f_1 f_2 \left(\frac{2r_i}{2r_i - D}\right)^{0.41}$	$g_c f_1 f_2$
g_c	$\left[1+\left(\frac{C_i}{C_o}\right)^{10/3}\right]^{-0.3}$	$\left[1+\left(\frac{C_i}{C_o}\right)^{9/2}\right]^{-2/9}$
C_i/C_o	$f_3 \left(\frac{r_i}{r_o}\frac{2r_o - D}{2r_i - D}\right)^{0.41}$	$f_3 \left(\frac{l_{a,i}}{l_{a,o}}\right)^{7/9}$

	Radial	Thrust		Radial	Thrust	
		$\alpha \neq 90°$	$\alpha = 90°$		$\alpha \neq 90°$	$\alpha = 90°$
γ	$\frac{D \cos \alpha}{d_m}$		$\frac{D}{d_m}$	$\frac{D \cos \alpha}{d_m}$		$\frac{D}{d_m}$
f_a	$(\cos \alpha)^{0.7}$	$(\cos \alpha)^{0.7} \tan \alpha$	1	$(\cos \alpha)^{7/9}$	$(\cos \alpha)^{7/9} \tan \alpha$	1
f_1	3. 7–4. 1	6–10		18–25	36–60	
f_2	$\frac{\gamma^{0.3}(1-\gamma)^{1.39}}{(1+\gamma)^{1/3}}$		$\gamma^{0.3}$	$\frac{\gamma^{2/9}(1-\gamma)^{29/27}}{(1+\gamma)^{1/3}}$		$\gamma^{2/9}$
f_3	$104 f_4$	f_4	1	$1.14 f_4$	f_4	1
f_4	$\left(\frac{1-\gamma}{1+\gamma}\right)^{1.72}$			$\left(\frac{1-\gamma}{1+\gamma}\right)^{38/37}$		

[a] From refs. 1 and 2.

TABLE 12–II.—POINT AND LINE CONTACT OF ROLLER BEARINGS [a]

[$C=C_i[1+(C_i/C_o)^4]^{1/4}$; units in kg and mm.]

Function	Radial bearing	Thrust bearing		Radial bearing	Thrust bearing	
		$\alpha \neq 90°$	$\alpha=90°$		$\alpha \neq 90°$	$\alpha=90°$
	Inner race			Outer race		
γ	$\frac{D\cos\alpha}{d_m}$		$\frac{D}{d_m}$	$\frac{D\cos\alpha}{d_m}$		$\frac{D}{d_m}$
	Line contact C_i			Point contact C_o		
C_i or C_o	$f_1 f_2 f_a i^{7/9} z^{3/4} D^{29/27} l_{a.t}^{7/9}$			$f_1 f_2 f_a \left(\frac{2R}{D}\frac{r_o}{r_o-R}\right)^{0.41} i^{0.7} z^{3/4} D^{1.8}$		
f_a	$(\cos\alpha)^{7/9}$	$(\cos\alpha)^{7/9}\tan\alpha$	1	$(\cos\alpha)^{0.7}$	$(\cos\alpha)^{0.7}\tan\alpha$	1
f_1	18–25	36–60		3. 5–3. 9	6–10	
f_2	$\frac{\gamma^{2/9}(1-\gamma)^{29/27}}{(1+\gamma)^{1/3}}$		$\gamma^{2/9}$	$\frac{\gamma^{0.3}(1+\gamma)^{1.29}}{(1-\gamma)^{1/3}}$		$\gamma^{0.3}$

	Point contact C_i			Line contact C_o		
C_i or C_o	$f_1 f_2 f_a \left(\frac{2R}{D}\frac{r_i}{r_i - R}\right)^{0.41} i^{0.7} Z^{2/3} D^{1.8}$			$f_1 f_2 f_a i^{7/9} Z^{3/4} D^{29/27} l_{se}^{7/9}$		
f_a	$(\cos\alpha)^{0.7}$	$(\cos\alpha)^{0.7}\tan\alpha$	1	$(\cos\alpha)^{7/9}$	$(\cos\alpha)^{7/9}\tan\alpha$	1
f_1	3.7–4.1	6–10		15–22	36–60	
f_2	$\frac{\gamma^{0.3}(1-\gamma)^{1.39}}{(1+\gamma)^{1/3}}$		$\gamma^{0.3}$	$\frac{\gamma^{2/9}(1+\gamma)^{29/27}}{(1-\gamma)^{1/3}}$		$\gamma^{2/9}$

[a] From refs. 1 and 2.

The following table provides expressions for excess life in the early failure region:

Probability of survival, S, percent	Standardized theoretical life, y_T	Standardized life, y_T+y_E	Assumed behavior of points in figure 12–1
$S \geq 99.9$	$y_T \leq 0.001$	$y_T+y_E=0.004$	Points approach vertical asymptote
$99.9>S \geq 95$	$0.001<y_T<0.05$	$\ln (y_T+y_E) = 0.690 \ln 0.328y_T$	Points fit sloping interpolated straight line in Weibull plot
$95>S>40$	$0.05<y_T<0.9$	$y_E=0.013$	Points deviate from theoretical Weibull line by constant excess life

In the previous table, taken from reference 6, y_T represents the theoretical standardized life as obtained from reference 7, and y_E is the excess standardized life. The standardized life y is

$$y=\left(\frac{L}{A}\right)^e \tag{12–21}$$

In terms of the standardized life, equation (12–5) is written

$$S=\exp(-y) \tag{12–22}$$

When data are reduced, y is calculated from the following equation:

$$y=\left(\frac{L}{L_{50}}\right)^e \ln 2 \tag{12–23}$$

The expected life at very low probabilities of failure can be calculated with equation (12–23) to obtain y_T and the expressions given in the previous table for the sum of y_T and y_E. The sum of y_T and y_E at a specific survival probability gives the expected life.

OPERATING VARIABLES

Limitations of the Capacity Formulas

The capacity formulas for various types of bearings given by equations (12–14) to (12–20) are valid only for bearings of conventional steel lubricated with mineral oils when they are operated at nominal speeds. Since the development of the Lundberg-Palmgren capacity

formulas, many bearing applications exist in which rolling bearings are required to operate under extreme conditions of speed and temperature with a variety of lubricants and lubrication techniques. These operating conditions have made the development of new bearing materials necessary. In order to design bearing systems intelligently, the effects of bearing materials and lubricants, as well as speed and temperature, on fatigue life and load capacity have been investigated. The effects of various processing and operating variables will be discussed.

Among the processing variables that will be discussed are material composition, melting technique, hardness, fiber orientation, and contact angle. The operating variables to be discussed are load, speed, lubricant type (base stock), which includes dry-powder lubricants, lubricant viscosity, and temperature. Each of these processing and operating variables has an effect on fatigue. This effect must be known in order to design the best bearing-lubricant combination for a given set of operating conditions and to predict accurately its performance under fatigue conditions. Obtaining rolling fatigue data is expensive because many bearings must be tested so that the scatter in life can be treated statistically. The cost factor plus the urgent need for rolling-element-bearing fatigue data has stimulated the development of several bench-type fatigue testers. These testers obtain fatigue data quickly and economically with easily fabricated specimens such as balls or cylindrical rods. Many of the data reported herein were obtained on bench-type fatigue testers, which produce fatigue failures similar to those obtained in full-scale bearings at a reduction in time and cost.

Load

All experimental evidence obtained to date indicates that the inverse cubic relation between load and life, which was found to exist for point contact with conventional bearing materials with mineral-oil lubrication, is approximately true for other materials and lubricants and for bench-type fatigue testers used for studying the effects of different variables on rolling-element-bearing fatigue. Butler and Carter (ref. 8) report fatigue data obtained with 52100 steel balls in the fatigue spin rig. A description of this apparatus is given in reference 9. Balls of SAE 52100 steel were tested at maximum Hertz compressive stresses of 600,000, 675,000, and 750,000 psi in the fatigue spin rig. Weibull plots (given in ref. 8) were made for each of these three lots of ball specimens, and the results were plotted as the applied maximum Hertz stress against ball life at the 10-percent failure point (fig. 12–2). The slope of this line is 10.4. Normal full-scale bearing data produce a slope of approximately 9,

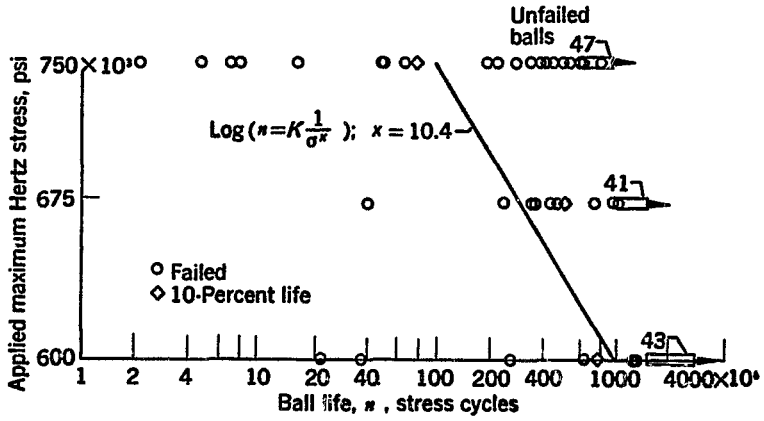

FIGURE 12–2.—Variation of ball life with applied stress for SAE 52100 balls. Room temperature; lubrication, SAE 10 mineral oil; fatigue spin rig. (From ref. 8.)

which corresponds to a load-life exponent of 3. These results indicate that the load- or stress-life relation in the fatigue spin rig approximates that which would be expected in full-scale bearings.

In reference 10 the relation of stress and life was investigated for two separate lots of crystallized glass ceramic balls using a five-ball fatigue tester. Crystallized glass ceramic balls taken from specimen lot A were run at maximum Hertz stresses of 265,000, 295,000, and 330,000 psi. Weibull plots (given in ref. 10) were made at each of these stress levels, and the 10- and 50-percent lives were determined from these Weibull plots. The plot of stress against life for specimen lot A is shown in figure 12–3(a). The stress-life exponent at the 10-percent level is 13.8 and at the 50-percent level is 11.6. For this particular material, the sensitivity of life to applied stress is slightly greater than that for steels. The results for specimen lot B, which were tested at maximum Hertz stresses of 265,000 and 330,000 psi, are shown in figure 12–3(b). Here the stress-life exponents are 10.6 at the 10-percent level and 10.5 at the 50-percent level. Again, these results indicate a slightly greater sensitivity of life to applied stress for this ceramic material than for steels.

For both the SAE 52100 steel and the ceramic material investigated, the load- or stress-life relation in two different types of bench fatigue testers approximate those for steels in full-scale bearing tests.

Barwell and Scott (ref. 11) used a four-ball fatigue tester to determine the load-life relation for five different lubricants. These lubricants were an aircraft mineral oil, a water glycol, a hydraulic petroleum oil, a chlorinated diphenyl, and a synthetic polyester.

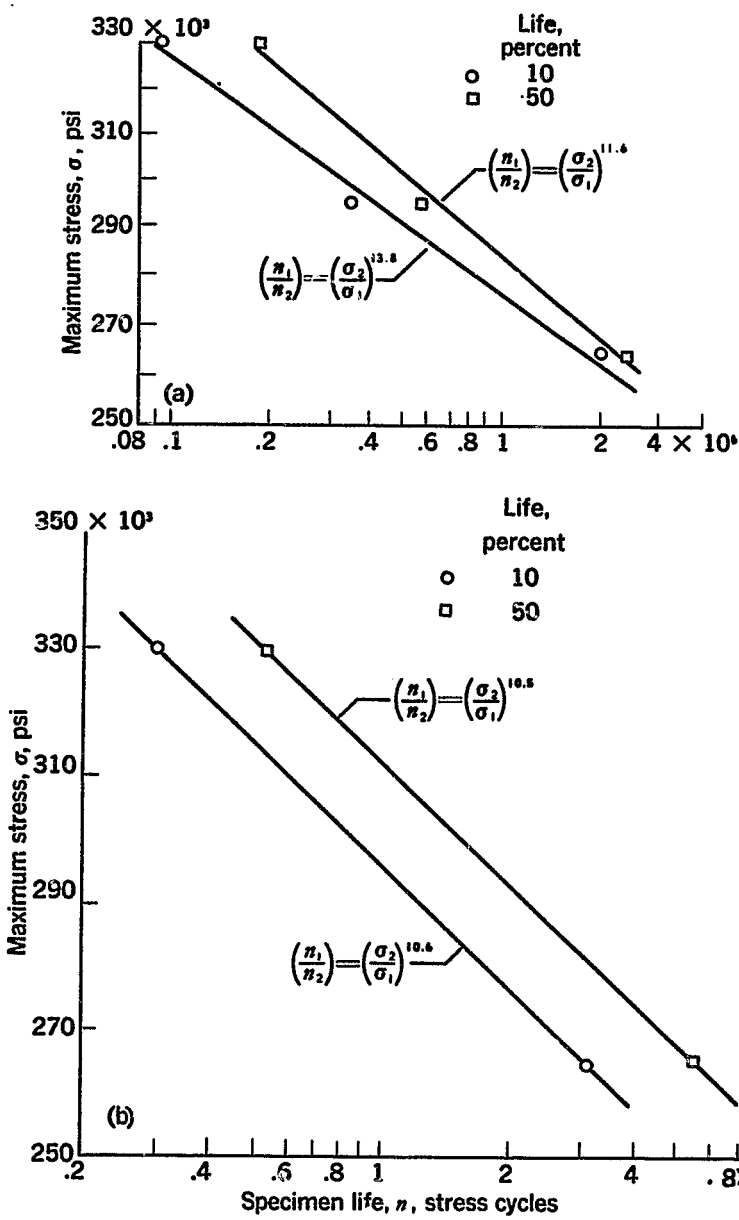

(a) Specimen lot A.

(b) Specimen lot B.

FIGURE 12-3.—Variation of ball life with applied stress for crystallized glass ceramic balls. Room temperature; synthetic diester lubricant; five-ball fatigue tester, contact angle, 40°. (From ref. 10)

The results of tests of standard ½-inch-diameter balls at maximum Hertz stresses of 660,000 to 950,000 psi are shown in figure 12–4. For all five lubricants, the inverse cubic load-life relation was found to be true. The life used in these tests was the average time to failure. Further load-life tests were conducted by Scott in reference 12 at 200° C (392° F) by use of a synthetic diester lubricant and T–1 tool-steel balls. These results are shown in table 12–III. Again, the inverse cubic relation was true.

Cordiano, Cochran, and Wolfe (ref. 13) report fatigue tests with 217-size angular-contact ball bearings that were flood lubricated with four oils. These oils included a mineral oil and three combustion-resistant hydraulic fluids: a phosphate ester, a phosphate ester base, and a water-glycol base. Bearings were run at thrust loads of 12,900 and 8600 pounds with the phosphate lubricants and at an additional load of 4300 pounds with the water-base glycol. The load-life relations obtained are plotted in figure 12–5. The exponents vary from 2.7 for the glycol to 4.2 for the phosphate ester.

Fatigue life varies inversely as the third to fourth power of the load for a variety of materials and lubricants (refs. 8 and 10 to 13). This relation apparently will exist for new bearing materials and lubricants.

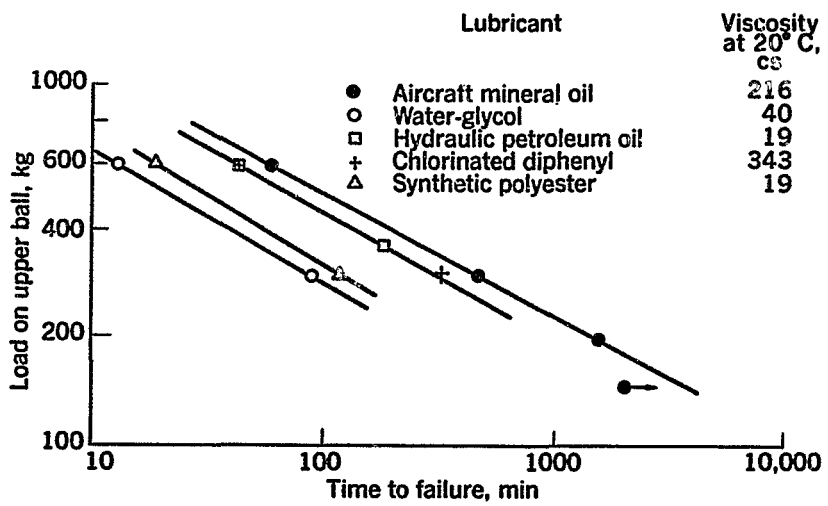

FIGURE 12–4.—Effect of load on time to failure for various lubricants. (From ref. 11.)

TABLE 12–III.—TEST RESULTS WITH DIESTER-TYPE SYNTHETIC LUBRICANT [a]

Test	Load on upper ball, kg	Temperature, ° C		Time to failure, min	Average time to failure, min	$t^{1/3}W$
		Start	Finish			
1	600	202	197	8	8.6	1229
2	600	202	202	7	8.6	1229
3	600	202	206	5	8.6	1229
4	600	201	200	8	8.6	1229
5	600	202	202	10	8.6	1229
6	600	198	195	11	8.6	1229
7	600	195	192	11	8.6	1229
8	500	203	202	13	14.3	1214
9	500	202	202	12	14.3	1214
10	500	202	203	13	14.3	1214
11	500	202	202	14	14.3	1214
12	500	201	197	17	14.3	1214
13	500	204	202	17	14.3	1214
14	400	202	201	32	31	1257
15	400	201	198	32	31	1257
16	400	203	202	24	31	1257
17	400	202	206	28	31	1257
18	400	201	201	24	31	1257
19	400	201	205	27	31	1257
20	400	205	198	36	31	1257
21	400	204	199	36	31	1257
22	400	202	202	40	31	1257

[a] From ref. 12.

Lubricant Base Stock

The need for lubricants with better oxidative and thermal stability has stimulated research on the synthesis of many synthetic compounds that offer promise as high-temperature lubricants. Rolling-element fatigue data are needed with these new lubricants, for new oils cannot be used with any confidence without some knowledge of their effect on the fatigue behavior of bearing steels.

In reference 11, fatigue tests with ½-inch-diameter balls were conducted with 26 different lubricants. The life results with five of these lubricants are shown in figure 12–4. Of these five oils, the aircraft mineral oil showed the best life and the water-based glycol showed the poorest life. Viscosity differences among these lubricants, however, make an unbiased comparison impossible since lubricant viscosity has a marked effect on fatigue life. The experiments of reference 11 were conducted at maximum Hertz stress levels up to 950,000 psi, where considerable plastic deformation occurs. This deformation makes the validity of extrapolating these data to lower stress levels questionable.

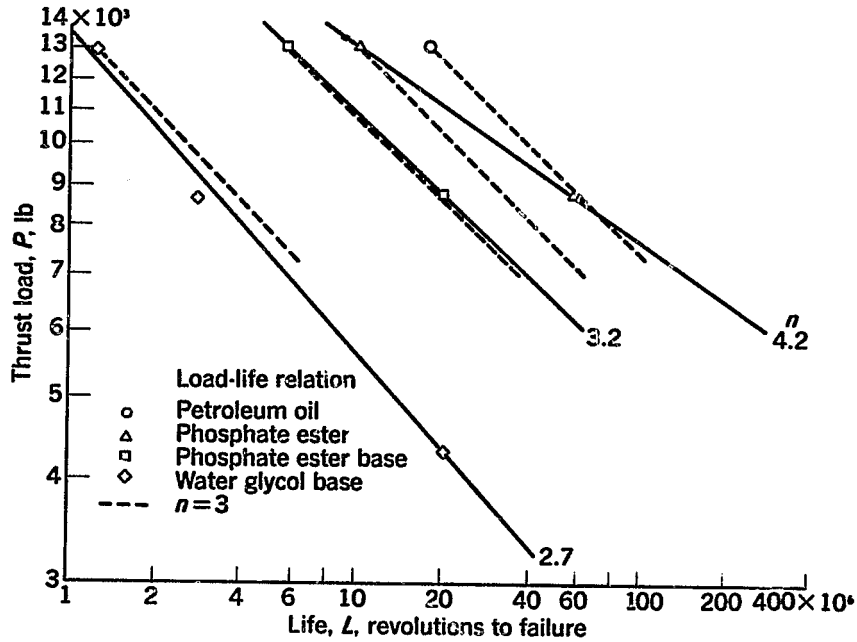

FIGURE 12–5.—Load-life relation of bearings operated in four hydraulic fluids; LP^n=constant. (From ref. 13.)

Table 12–IV shows data obtained with 13 of the lubricants tested in reference 11. Again, viscosity differences make unbiased comparisons

TABLE 12–IV.—VISCOSITY AND AVERAGE LIFE FOR DIFFERENT LUBRICANTS [a]

Type of lubricant	Viscosity at 20° C, cs	Average life, mln
Aircra' mineral oil	216	59
Mineral-base hydraulic oil with additives	89	42
Hydraulic petroleum oil	19	40
Synthetic silicate ester	17	32
Nonflammable synthetic polyester	19	18
Phosphate ester	174	67. 5
Chlorinated diphenyl	343	40
Nonflammable water-base glycol	40	13
Polyalkalene glycol	16	11
Dimethyl siloxane	1. 6	58
Silicone	52	64
Triercsyl phosphate	97	48
Naphthenic-base oil	53	51

[a] From ref. 11.

difficult, but some general conclusions can be made. The mineral oils, which include the aircraft mineral oil, a hydraulic oil, and a naphthenic-base oil, appear to give good fatigue life. The nonflammable water glycol and the polyalkylene glycol appear to give the poorest fatigue results. Somewhat better are the synthetic polyester and the synthetic silicate. The (dimethyl) siloxane, despite its low viscosity, gave good life, and the silicone appeared to be one of the best lubricants. Closer control of viscosity among the various base stocks is necessary before more definitive conclusions can be drawn.

Fatigue lives of ½-inch-diameter test balls were determined at a maximum Hertz stress of 830,000 psi with two different greases in reference 12. These results are shown in table 12–V. The mineral-

TABLE 12–V.—AVERAGE TIME TO FAILURE FOR GREASES [a]

[Maximum Hertz stress, 830,000 psi; test temperature, 200° C.]

Lubricant	Average time to failure, min	Remarks
Lithium-base grease	93	Bearing surface and balls clean and bright
Experimental silicone grease containing chlorine	36	Balls dull with etched surface appearance

[a] From ref. 12.

oil lithium-base grease gave significantly better fatigue life than the experimental silicone grease that contained chlorines. These tests were conducted at 200° C (392° F).

Baughman (ref. 14) conducted fatigue tests using the rolling-contact fatigue tester. In this tester, the test specimen is a ½-inch-diameter cylindrical rod, which is stressed between two crowned cylinders, each 7.5 inches in diameter. Fatigue results with a synthetic diester (14.2 cs at 100° F), a mineral oil (10.2 cs at 100° F), and a methylphenyl silicone (10.8 cs at 100° F) are shown in figure 12–6. These results were obtained with M–1 tool steel at a maximum Hertz stress of 725,000 psi. Ten-percent fatigue lives for the silicone, mineral oil, and diester were 4.0, 2.2, and 1.1 million stress cycles, respectively. Figure 12–7 shows a plot of the log log of the 50-percent life plotted against the log of the viscosity at 80,000 psi for these three lubricants. Fatigue life appears to be related to the actual viscosity existing in the high-pressure region.

Experiments similar to those of reference 14 are reported in references 15 and 16. Five different base-stock lubricants, each with an atmospheric pressure viscosity of about 10 centistokes at 100° F were

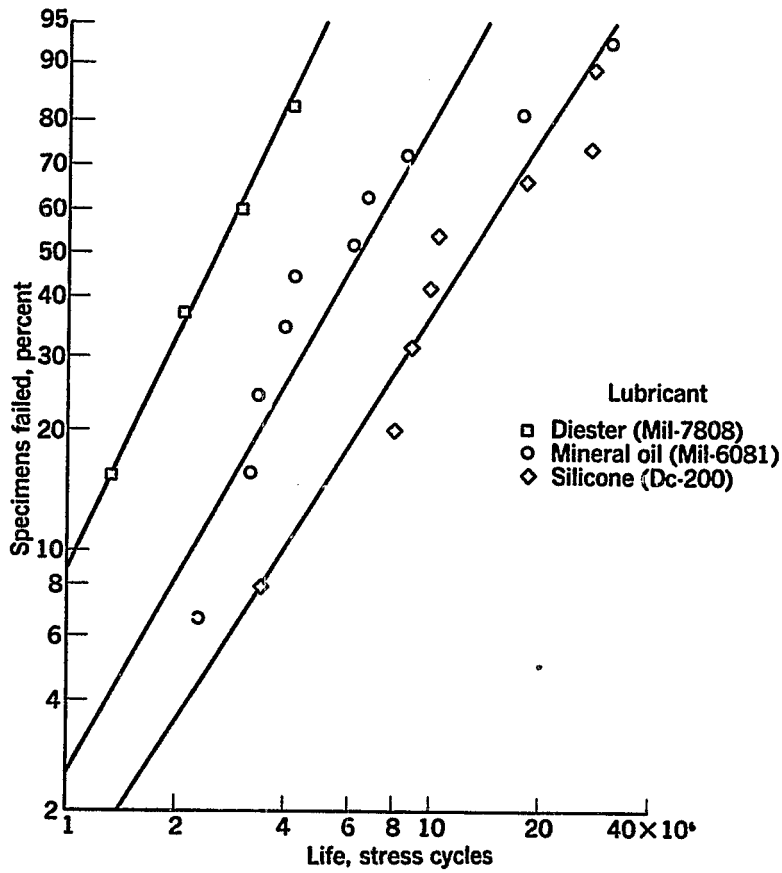

FIGURE 12–6.—Weibull plot of data from rolling-contact fatigue tester on M–1 tool steel when tested with three different lubricants. Maximum Hertz stress, 725,000 psi; room temperature. (From ref. 14.)

used in these experiments. AISI M–1 balls were tested at a maximum Hertz stress of 725,000 psi in the fatigue spin tester. Figure 12–8 shows the fatigue-life results. These data are summarized in table 12–VI. Again, as in reference 14, the silicone gave the best life, followed by the mineral oil, the polyalkylene glycol, the sebacate, and the dioctyl adipate.

Figure 12–9 shows the 10-percent-life data from figure 12–8 plotted against the pressure-viscosity coefficients for the five lubricants. The pressure-viscosity coefficient is defined as the slope of the curve of the log of absolute viscosity plotted against pressure. Since there is some curvature in each of these plots, the initial slope is used. The pressure viscosity is assumed to be given approximately by an equation of the following type:

$$\mu_p = \mu_o \times 10^{\beta p} \qquad (12\text{–}24)$$

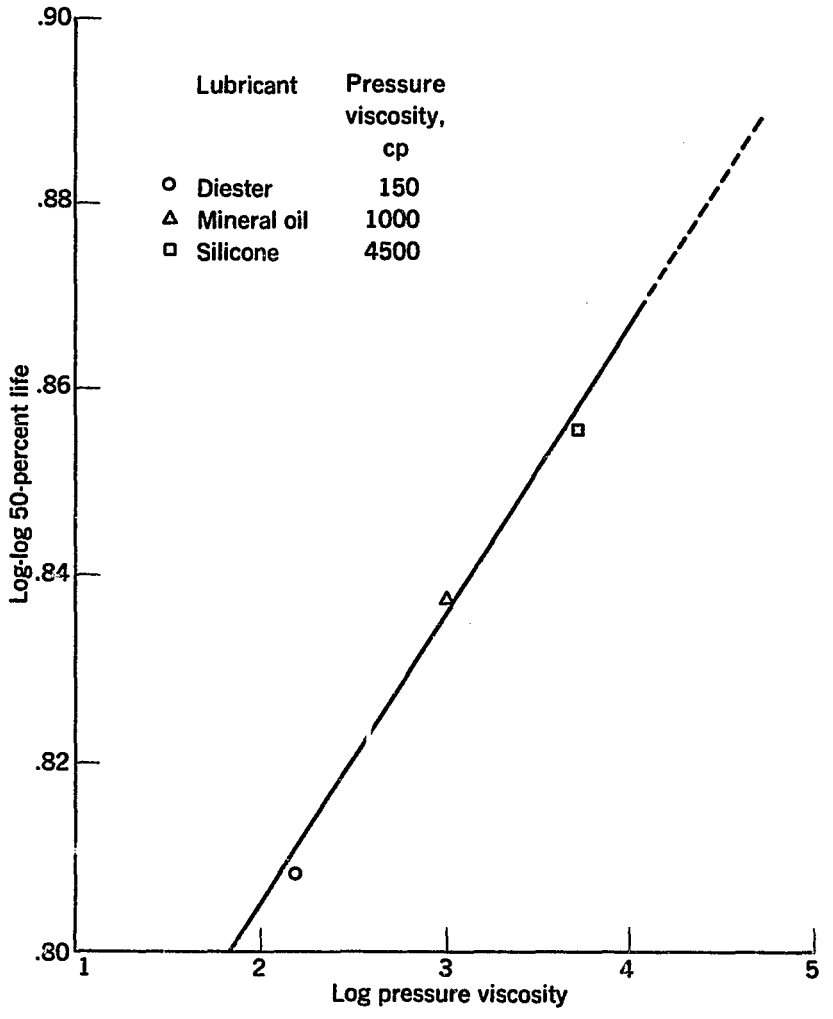

FIGURE 12–7.—Relation between lubricant viscosity at 80,000 psi and fatigue life of M–1 tool steel. Temperature, 210° F. (From ref. 14.)

Values of β shown in table 12–VI were obtained from reference 17 for all but the adipate oil. The curve of figure 12–9 indicates that fatigue life increases with increasing pressure-viscosity coefficient. Since the initial viscosities of these five lubricants were all approximately 10 centistokes, the actual viscosities under pressure would be expected to vary as the pressure-viscosity coefficient. The good correlation of figure 12–9 may indicate that actual viscosity is a variable of prime importance in determining fatigue life.

TABLE 12–VI.—FATIGUE LIVES OF ½-INCH AISI M–1 TOOL-STEEL BALLS LUBRICATED WITH VARIOUS BASE-STOCK FLUIDS [a]

[Test temperature, 100° F; maximum Hertz compressive stress, 725,000 psi.]

Lubricant	Pressure-viscosity coefficient, β, 1/psi	Specimens tested	Failures	Runouts	10-percent failure life, stress cycles	50-percent failure life, stress cycles
Methyl silicone	8.35×10^{-5}	26	5	21	106×10^{6}	$17,000\times10^{6}$ [b]
Paraffinic mineral oil	5.38	28	14	14	18	660
Glycol	3.28	16	11	5	7.6	167
Sebacate	2.52	22	15	7	5.2	200
Adipate	Unavailable	26	12	14	2.4	1,000

[a] From ref. 15.
[b] Extrapolated.

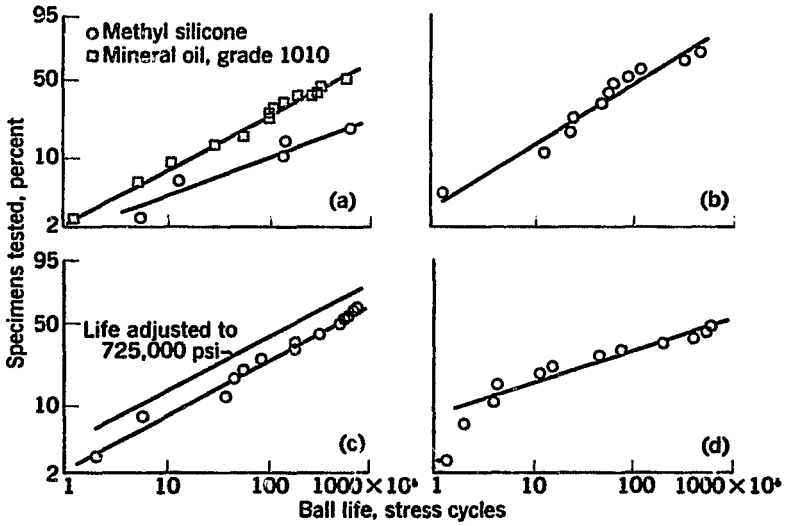

(a) Mineral oil and silicone. (b) Polyalkylene glycol.
(c) Sebacate. Maximum Hertz stress, 650,000 psi. (d) Adipate.

FIGURE 12–8.—Fatigue life of AISI M–1 tool-steel balls with various base stock lubricants. Test temperature, 100° F; maximum Hertz stress, 725,000 psi; fatigue spin tester. (From ref. 16.)

Fatigue tests with full-scale 217-size angular-contact ball bearings, lubricated with three combustion-resistant hydraulic fluids and a mineral oil, are reported in reference 18. These bearings were run at 2150 rpm, 12,900-pound thrust load, and flood lubricated with the oil outlet temperature adjusted to 150° to 160° F. Viscosities of the test oils are given in table 12–VII. The life results obtained are summarized in table 12–VIII. Comparison of modal lives with that of mineral oil shows that life with the phosphate ester is 58 percent,

TABLE 12–VII.—LUBRICANTS USED IN FATIGUE TESTS OF ANGULAR-CONTACT BALL BEARINGS [a]

Lubricant	Viscosity, Saybolts Seconds Universal at—	
	100° F	210° F
Petroleum oil	182	44.3
Phosphate ester	214	42.3
Phosphate ester base	231.4	44.2
Water-glycol base	280.2	69.5

[a] From ref. 18.

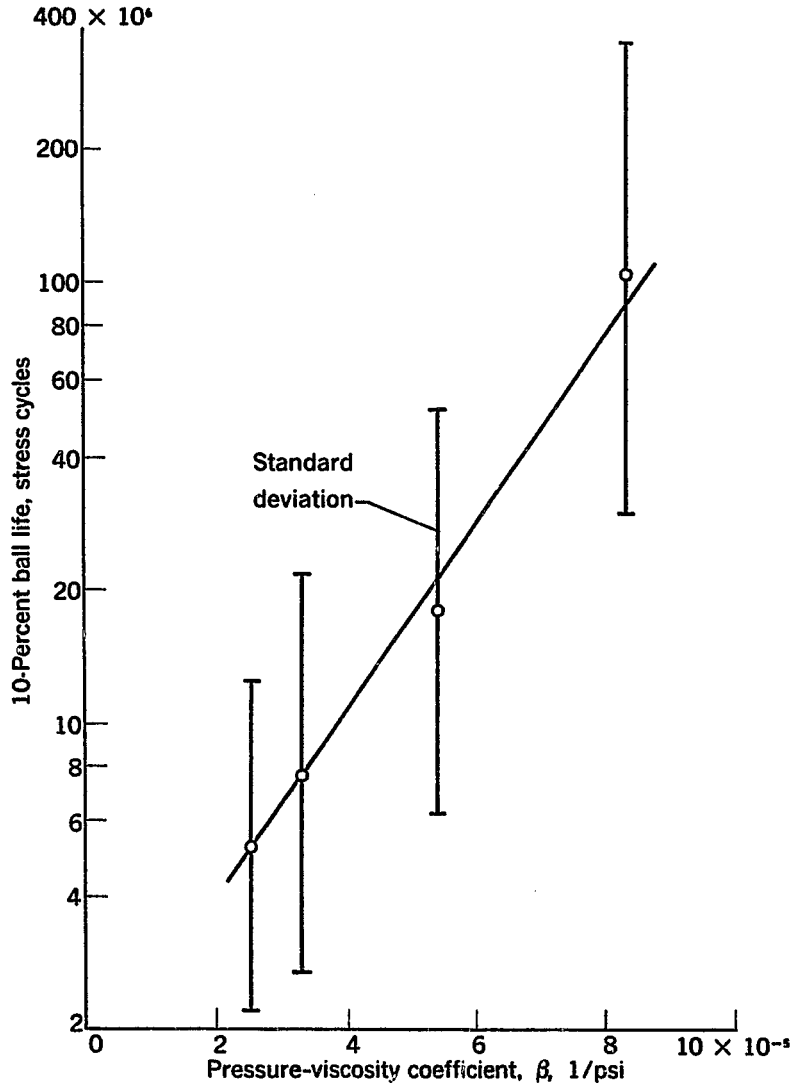

FIGURE 12–9.—Life of AISI M–1 tool-steel ball as function of pressure-viscosity coefficient. Test temperature, 100° F; aximum Hertz stress, 725,000 psi; fatigue spin tester. (From ref. 16.)

life with the phosphate ester base is 31 percent, and life with the water-glycol base is only 6 percent.

Reference 13 presents additional fatigue data obtained with the lubricants used in reference 18 at 200° F and at various loads. Fatigue life at 200° F was slightly lower than at 150° F for both the phosphate ester and the phosphate ester base lubricants. Attempts were made in reference 13 to determine the causes for the life differences

TABLE 12-VIII.—MODAL AND MEDIAN LIVES OF ANGULAR-CONTACT BALL BEARINGS OPERATED IN PETROLEUM OIL AND THREECOMBUSTION-RESISTANT FLUIDS[a]

Lubricant	Life, revolutions		Relative life	
	Modal	Median	Modal	Median
Petroleum oil	18.6×10^6	24.9×10^6	1.00	1.00
Phosphate ester	10.7	13.5	.58	.54
Phosphate ester base	5.8	6.8	.31	.27
Water-glycol base	1.2	1.3	.06	.05

[a] From ref. 18.

shown by the various fluids. Pressure-viscosity relations for the oils were detemined at three temperatures and at pressures up to 50,000 psi by use of a rolling-ball viscometer to determine whether a correlalation existed between pressure viscosity and fatigue life. The results are shown in figure 12–10. The rise in viscosity with pressure for the phosphate ester base and phosphate ester fluids is similar to that for the petroleum oil but at a greater rate. In contrast, the relatively flat pressure-viscosity curves for the water-glycol-base fluid indicate that the relatively low viscosity of this fluid at high pressures may be a contributing factor to the poor fatigue life with this fluid. There is no correlation between pressure-viscosity coefficient and fatigue life, however, since the coefficients for the other three lubricants are in reverse to the fatigue lives. Thus, the data from bench tests in references 15 and 16 indicate that a correlation exists between pressure-viscosity coefficient and fatigue life, and the bearing data of reference 13 indicate that it does not. More work is necessary to establish the degree to which pressure-viscosity and other rheological properties affect fatigue life.

Rounds (ref. 19) has conducted an extensive investigation of the fatigue properties of many lubricants by use of a four-ball-type apparatus and ½-inch-diameter SAE 51100 test balls. Tests were conducted at a maximum Hertz stress of 1.2×10^6 psi, 1582 rpm, and 200° F. The extrapolation of these data to the lower stress levels that exist in bearings is questionable because of the extent of plastic deformation that occurs at Hertz stresses in the region of 10^6 psi. Some 60 base oils were selected from 11 different chemical classes that include mineral oils and most of the commonly used synthetic fluids. Figure 12–11 shows some fatigue-life data plotted against visciosty for mineral oils and several polyphenyl ethers. Figure 12–12 shows similar data obtained with a group of esters. Fatigue lives reported are relative to the life obtained with an Mil–L–7808C oil. All the ethers and all the esters with the exception of two high-viscosity diabasic acid

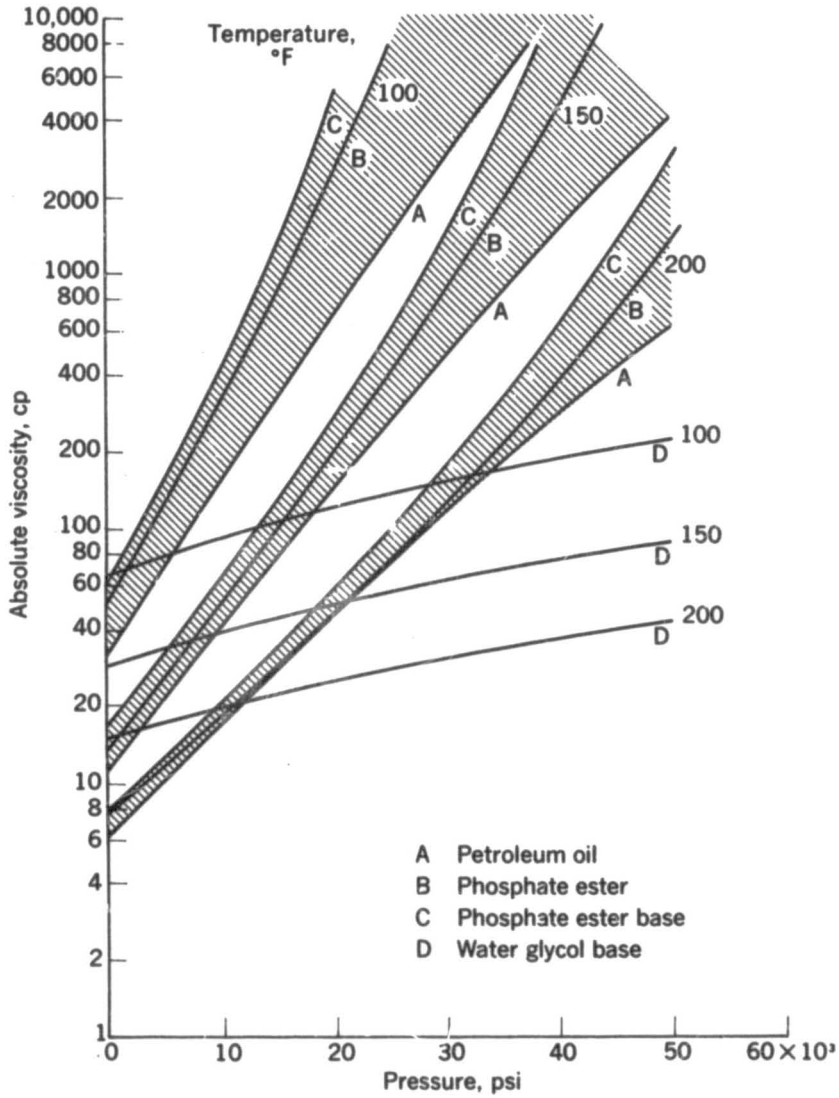

FIGURE 12–10.—Pressure-viscosity isotherms of four hydraulic fluids. (From ref. 13.)

esters showed better fatigue lives than the mineral oils when compared on the basis of similar viscosities.

Figure 12–13 shows fatigue data obtained with alcohols, polyglycols, and acids. The fatigue performance of the fatty acids is very poor, and the higher viscosity polyglycols show poor fatigue life. The fatigue performance of silicones is shown in figure 12–14. In

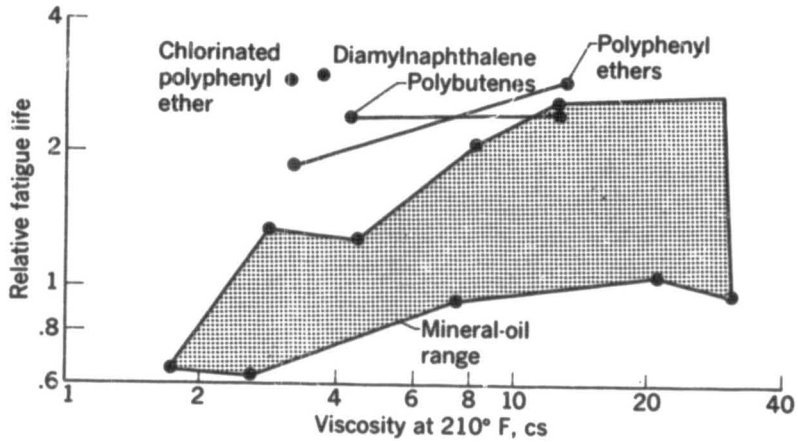

FIGURE 12–11.—Effect of polyphenyl ether and hydrocarbon lubricants on fatigue life. (From ref. 19.)

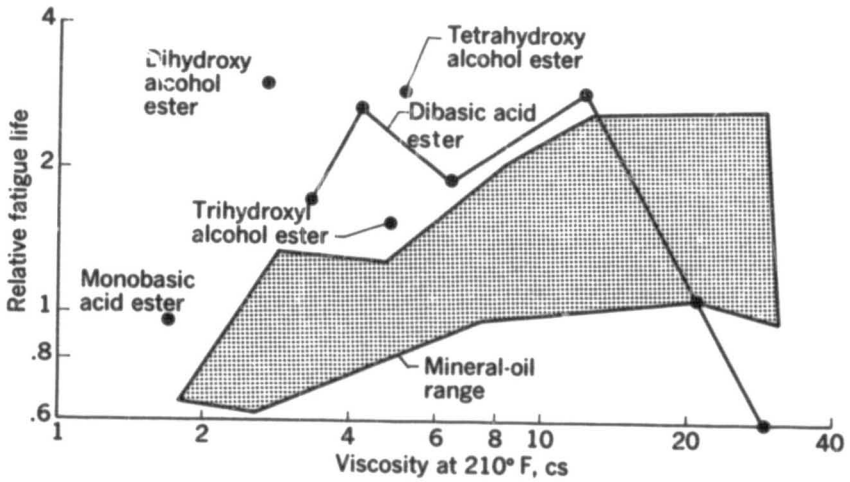

FIGURE 12–12.—Effect of ester lubricants on fatigue life. (From ref. 19.)

general, the performance of the silicones is good although the performance of the methylphenyl silicone with polyglycol chains is extremely poor. Most fatigue data obtained with silicone oils, such as those of references 11 and 15, indicate that silicones give superior fatigue performance.

Data obtained with phosphate esters and halogenated hydrocarbons are shown in figure 12–15. The phosphate esters gave good fatigue life but the other lubricants in this group gave poor fatigue life. Note the contrast in relative fatigue performance of the phos-

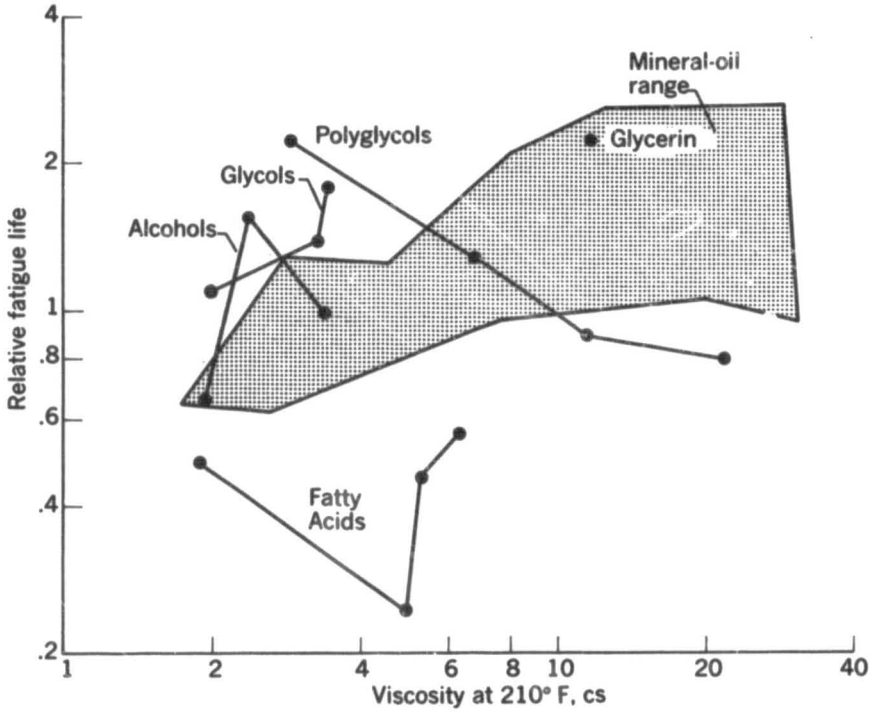

FIGURE 12–13.—Effect of alcohol, polyglycol, and acid lubricants on fatigue life. (From ref. 19.)

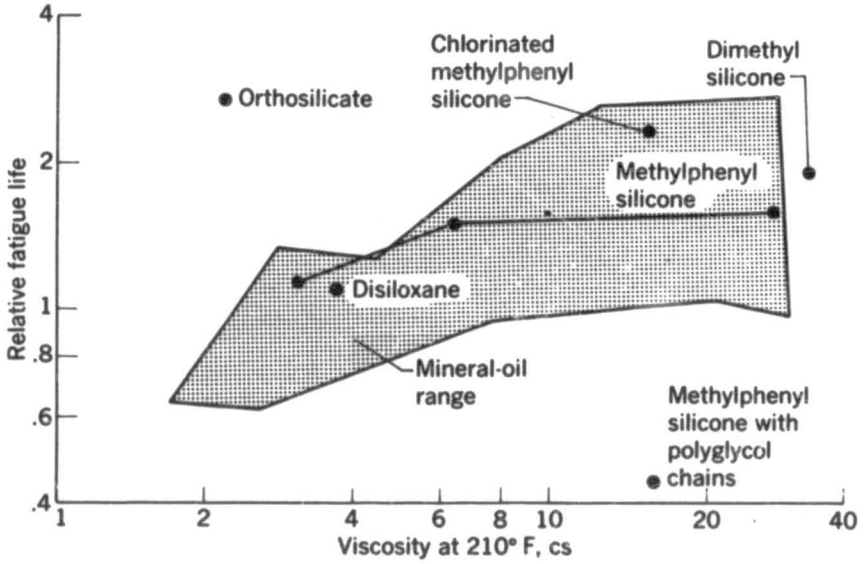

FIGURE 12–14.—Effect of silicone and related fluid lubricants on fatigue life (From ref. 19.)

phate ester in these tests and in the full-scale bearing tests of reference 13, where the phosphate ester gave poorer fatigue life than a mineral oil.

Among the mineral oils investigated in reference 19, the naphthenic oils showed consistently better fatigue life than paraffinic oils. These data are shown in figure 12–16.

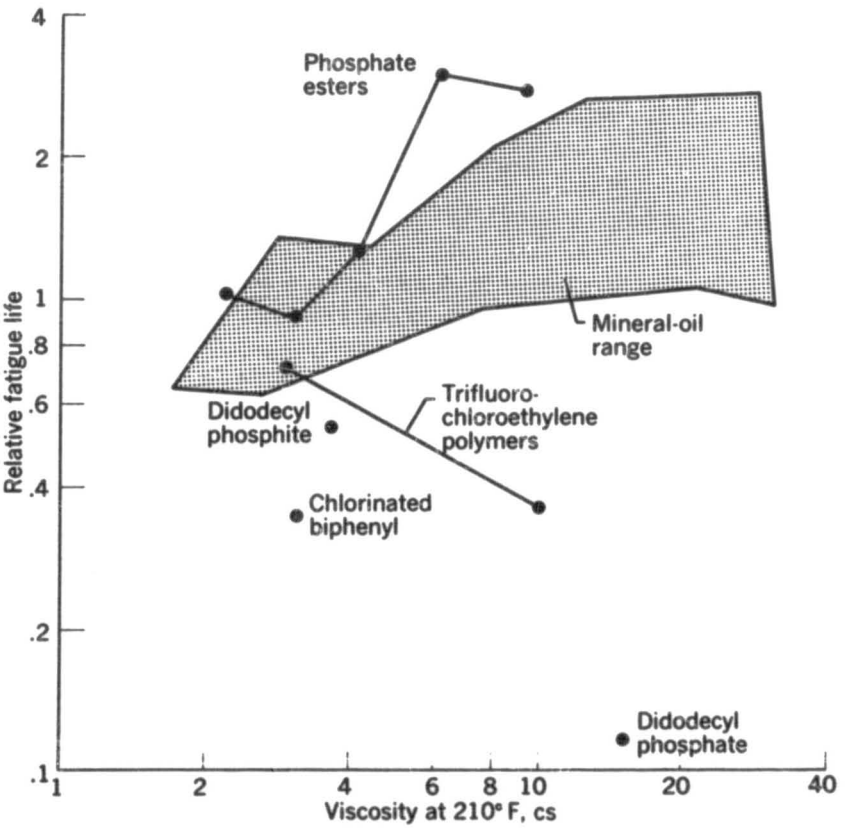

FIGURE 12–15.—Effect of phosphate ester and halogenated hydrocarbon lubricants on fatigue life. (From ref. 19.)

An analysis of the data of reference 19 showed that several factors significantly affect fatigue life. The effects of viscosity will be discussed more fully later. One factor of importance appears to be the physical shape of the average molecule in the lubricant. Fa-

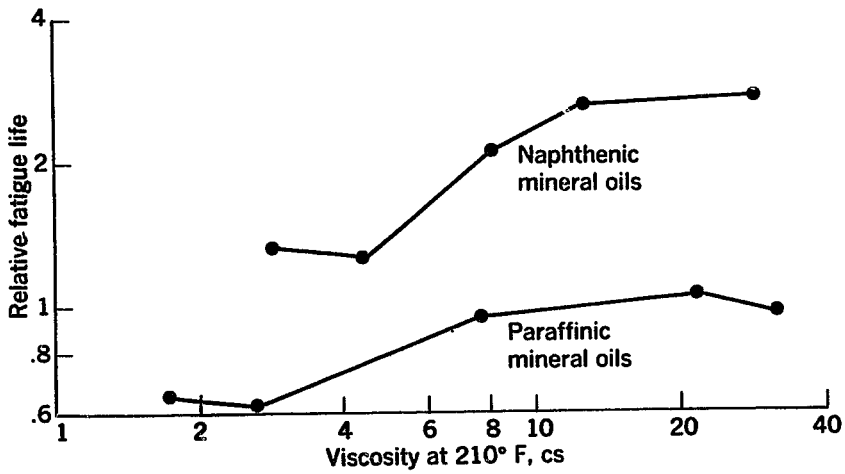

FIGURE 12-16.—Effect of mineral-oil lubricants on fatigue life. (From ref. 19.)

tigue life seems to be affected by the number of aromatic or naphthenic rings in the molecule as shown in the following table:

Base oil type	Average number of rings per molecule	Relative fatigue life at 6-cs viscosity
Fatty acids	0	0.54
Paraffinic mineral oils	1–2	.87
Naphthenic mineral oils	2–3	1.62
Polyphenyl ethers	4–5	2.32

The presence of ring structures in other classes of fluids is apparently beneficial to fatigue life. Phosphate esters with aryl groups gave better life than those with alkyl groups. The ring structure in phthalic acid may account for the better fatigue life with di(2-ethylhexyl)phthalate than with di(2-ethylhexyl)sebacate. In the alcohol series, the ring compound cyclohexane gave better life than the straight-chain alcohols. Except for the chlorinated biphenyl and a substituted silicone, all fluids containing ring structures gave longer lives than the paraffinic oils and many were superior to the naphthenic mineral oils. Ring structures tend to make the molecule more compact, which suggests that compactness of the molecule is beneficial to fatigue life.

Increasing the polarity or reactivity of the molecule appears to be detrimental to fatigue life. Changing the hydroxyl group in oleyl

alcohol to the more polar carboxyl group in oleic acid decreased the relative life from 1.01 to 0.23; with the phosphorous compounds, life decreased progressively in going from tri(2-ethylhexyl)phosphate to the strongly acid didecyl phosphate. Esters, in which the polar carboxyl and hydroxyl groups of the reacted acid and alcohol have been effectively neutralized, generally gave longer lives than did either of the reactants used to make the ester. Examples include isodecyl pelargonate, which was superior to *n*-decyl alcohol and pelargonic acid, and dipropylene glycol dipelargonate, which was superior to dipropylene glycol and pelargonic acid.

An exception to this rule appears to be the chlorinated compounds. The addition of reactive chlorine compounds to mineral oil reduced life but chlorinating either the polyphenyl ether or the methylphenyl silicone increased life.

Scott (ref. 20) made a more extensive study of the effect of additives on lubricant fatigue life. A four-ball tester was used and tests were run at a maximum Hertz stress of 950,000 psi. A paraffinic mineral oil was used as a reference fluid, and several additives of the extreme-pressure type were added to the paraffin oil, first in normal percentages, and then in greater than normal percentages. Table 12–IX sum-

TABLE 12–IX.—BALL FATIGUE LIVES FOR PARAFFINIC MINERAL-OIL LUBRICANT AND VARIOUS ADDITIVES [a]

[With 600-kg load and normal additive concentrations.]

Lubricant	Additive	Average time to failure, min
Paraffinic mineral oil	None	41
	1 percent dibutyl phosphite	42
	1 percent tricresyl phosphate	40
	1 percent chlorinated wax	35
	0.36 percent elemental sulfur	58
	0.36 percent elemental sulfur + 10 percent lead naphthenate	50
	1 percent graphite	109
	1 percent molybdenum disulfide	79

[a] From ref. 20.

marizes the results obtained with conventional amounts of additives. None of the five extreme-pressure additives reduced fatigue life any significant amount from that obtained with the base oil. The addition of 1 percent graphite or 1 percent molybdenum disulfide improved fatigue life. These results will be discussed fully in the section on solid lubricants.

The addition of greater than normal percentages of chlorinated wax and dibutyl phosphite produced a sharp reduction in fatigue life as shown in table 12–X. The addition of 10 percent tricresyl phosphate,

TABLE 12–X.—BALL FATIGUE LIVES WITH LUBRICANTS HAVING GREATER THAN NORMAL ADDITIVE CONCENTRATIONS*

Lubricant	Additive	Average time to failure, min
Paraffinic mineral oil	None	41
	5 percent chlorinated wax	14
	10 percent chlorinated wax	5½
	10 percent dibutyl phosphite	8
	10 percent tricresyl phosphate	43
100-percent tricresyl phosphate	None	48

*From ref. 20.

however, did not reduce fatigue life, and fatigue life with 100 percent tricresyl phosphate was comparable to that with the paraffin oil. Therefore, in lubrication systems where a single lubricant is used to lubricate both bearings and gears, tricresyl phosphate appears to be the most suitable extreme-pressure additive. It is effective as a gear additive and will not reduce bearing fatigue life.

Effect of Water in Lubricant

Some very interesting experiments to determine the effect of water content in the lubricant on rolling fatigue were conducted in reference 21. Tests were conducted in a four-ball-type apparatus at 1500 rpm using both standard 1.5-percent-chromium steel balls and also 12-percent-chromium stainless-steel balls. The maximum Hertz stress level was about 1×10^6 psi. Five lubricants, which are widely used in the lubrication of ball bearings, were chosen for testing. A description of the test oils is given in table 12–XI. The water content of each lubricant was varied over a wide range by a series of four treatments:

(1) Dry—The oil was dried over metallic sodium for 24 hours before test.

(2) As received.

(3) Saturated with water before test—A sample of the oil was thoroughly shaken with an equal volume of water and then allowed to settle 24 hours. The oil was carefully decanted for the test.

(4) Supersaturated with water during test—To ensure excess water

TABLE 12–XI.—LUBRICANTS USED IN BALL FATIGUE TESTS [a]

Lubricant	Type, composition, and description of lubricant	Viscosity at 20° C, cs
A	Compounded oil containing 94 percent mineral oil and 6 percent refined rape-seed oil	2200
B	Compounded oil containing 90 percent mineral oil and 10 percent blown rape-seed oil	600
C	Refined mineral oil containing 0.5 percent tricresyl phosphate as antiwear additive. Antioxidant, anticorrosive, and antifoam additives may be present	75
D	An oil containing extreme-pressure additives	90
E	Mineral oil formulated for use in aircraft engines	200

[a] From ref. 21.

during test, a small quantity (1 ml) of water was added to the lubricant bath immediately after the start of each test.

The moisture content of each oil in each condition is shown in table 12–XII. Moisture contents varied from essentially 0 to

TABLE 12–XII.—WATER CONTENT OF OILS AFTER VARIOUS TREATMENTS [a]

Lubricant	Water content, percent by weight			
	Lubricant condition			
	(1)	(2)	(3)	(4)
A	0.01	0.027	0.15	6.86
B	0	.022	.034	3.33
C	0	.052	.060	6.80
D	----	0	0	5.63
E	0	.033	-------	5.11

[a] From ref. 21.

almost 7 percent by weight. A summary of the fatigue lives of commercial EN 31 steel balls obtained with the various lubricants is presented in table 12–XIII. A considerable reduction in fatigue life occurs with all the oils with increasing water content as shown in figure 12–17. The fatigue results with the stainless-steel balls lubricated with three of the oils are summarized in table 12–XIV. The stainless-steel balls showed no reduction in fatigue life with increasing

TABLE 12–XIII.—FATIGUE LIFE WITH COMMERCIAL STEEL BALLS [a]

Lubricant	Mean fatigue life, min			
	Lubricant condition			
	(1)	(2)	(3)	(4)
A	157	124	123	51
B	123	110	102	54
C	82	62	54	36
D	-------	53	47	16
E	107	60	-------	34

[a] From ref. 21.

water content. The fatigue life of the stainless-steel balls, however, was no better than the fatigue life of the EN 31 balls with supersaturated oils. The fatigue life was, in fact, much shorter with lubricant A.

The reduction in fatigue life of the EN 31 balls with increasing lubricant-water content together with the lack of this effect with the stainless-steel balls suggests that corrosion fatigue may be an important factor in causing rolling fatigue. With oils A, B, and E, the track surface on EN 31 balls was bright and failure occurred as a single small pit, which was independent of the water content. Oils C and D, which contained reactive additives, produced stained or

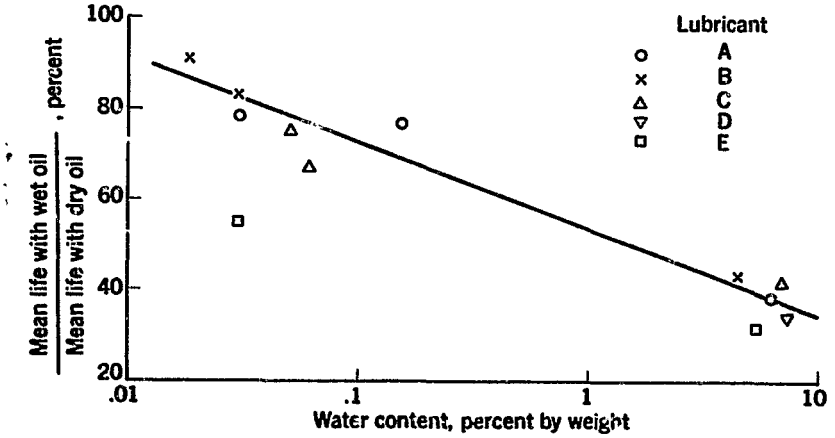

FIGURE 12–17.—Effect of water content of lubricant on mean life of balls. (See table 12–XI for definition of lubricant.) (From ref. 21.)

TABLE 12–XIV.—TESTS WITH STAINLESS-STEEL BALLS [a]

Lubricant	Lubricant condition	Mean life, min	Standard deviation, min	Coefficient of variation, percent	Number of tests
A	(1)	34	8	24	5
	(2)	35	10	29	10
	(3)	------	------	------	------
	(4)	31	7.5	24	14
D	(1)	------	------	------	------
	(2)	16	4	25	8
	(3)	------	------	------	------
	(4)	16	5	31	5
E	(1)	33	14	42	7
	(2)	32	5.5	17	12
	(3)	------	------	------	------
	(4)	33	1.5	5	6

[a] From ref. 21.

dull tracks, and supersaturation of these oils produced roughening of the surface. Almost continuous pitting appeared under these conditions. The stainless-steel balls had generally bright surfaces and no differences were observed with oils with different water contents.

Effect of additives in lubricants containing water.—In an attempt to extend fatigue life of lubricants containing water, Grunberg and Scott (ref. 22) conducted ball fatigue tests with various additives added to the base oils. Two oils were chosen for these tests, which were conducted under the same conditions of speed and stress as those of reference 21. A description of these oils is given in table 12–XV. Five

TABLE 12–XV.—BASE LUBRICANTS USED IN BALL FATIGUE TESTS [a]

Code letter	Lubricant	Viscosity, cs		
		At 25° C	At 50° C	At 60° C
F	Blend of two high-viscosity index components from a Venezuelan source	636	134	82
G	Distillate from a Venezuelan source	14.4	6.5	5.1

[a] From ref. 22.

different conditions of water content were used. Conditions (1), (2), and (3) were the same as those in reference 21. Condition (4) was supersaturation with ½ milliliter of water added before test, and condi-

tion (5) was the same as condition (4) in reference 21 (1 ml of water added before test). The fatigue lives obtained with the two lubricants in five conditions of saturation without additives are shown in table 12–XVI.

TABLE 12–XVI.—EFFECT OF WATER CONTENT ON FATIGUE LIFE [a]

Lubricant	Mean fatigue life, min				
	Lubricant condition				
	(1)	(2)	(3)	(4)	(5)
F	121	63	55	26	21
G	65	48	44	10	6

[a] From ref. 22.

The following additives were used:

(1) Isoamyl alcohol, 3 percent
(2) Oleic acid, 2 percent, a fatty acid
(3) Triethanolamine, 2 percent, an amine
(4) Imidazoline derivative, 2 percent, a dewatering agent
(5) Sarkosine derivative, 2 percent, a dewatering agent
(6) Phenoxy-acetic acid, 2 percent, a dewatering agent
(7) Sodium dodecane sulfonate, 0.5 percent, a typical detergent
(8) 0.5-Percent sodium nitrite plus 0.5-percent sodium benzoate, corrosion inhibitors

The fatigue results obtained with the base oils and the base oils with various additives are summarized in table 12–XVII. The addition of 3-percent isoamyl alcohol partially counteracted the deleterious effects of the presence of water in spite of the fact that the addition of the alcohol lowered the viscosity considerably.

Both oleic acid and triethanolamine lowered the fatigue life under conditions of water saturation (condition 3) and raised the fatigue life under conditions of high supersaturation. The data obtained with these two additives indicate that fatigue life is independent of water content. Of the three dewatering agents (imidazoline and sarkosine derivatives and phenoxy-acetic acid), only the imidazoline derivative was effective in improving fatigue life under all conditions tested. The sarkosine derivative and the phenoxy-acetic acid actually decreased fatigue life.

In reference 22, post-test examinations showed that the ball tracks were a brownish color under highly supersaturated conditions but were bright and polished when a surface active agent was added.

TABLE 12-XVII.—MEAN FATIGUE LIFE AS FUNCTION OF WATER CONTENT AND ADDITIVE CONTENT [a]

Lubricant	Additive	Mean fatigue life, min				
		Lubricant condition				
		(1)	(2)	(3)	(4)	(5)
Base oil F		121	63	55	26	21
	3 percent isoamyl alcohol	-----	----	93	33	---
	2 percent oleic acid	-----	----	33	----	32
	2 percent triethanolamine	-----	----	40	----	38
	2 percent imidazoline derivative	-----	----	70	----	37
	2 percent sarkosine derivative	-----	----	----	----	18
	2 percent phenoxyacetic acid	-----	----	----	----	17
	0.5 percent sodium benzoate and 0.5 percent sodium nitrite	-----	----	----	----	23
	0.5 percent sodium dodecane sulfonate	-----	----	----	----	29
Base oil G		65	48	44	10	6
	3 percent isoamyl alcohol	-----	----	50	34	----
	2 percent oleic acid	-----	----	27	----	23
	2 percent triethanolamine	-----	----	29	----	26
	2 percent imidazoline derivative	-----	----	50	----	17
	2 percent sarkosine derivative	-----	----	----	----	4
	2 percent phenoxyacetic acid	-----	----	----	----	8
	0.5 percent sodium benzoate and 0.5 percent sodium nitrite	-----	----	----	----	7
	0.5 percent sodium dodecane sulfonate	-----	----	----	----	4

[a] From ref. 22.

In the absence of additives under supersaturated conditions, electron photomicrographs revealed that the track surface was covered with fine pits and debris. This pitting is strong evidence of corrosion fatigue and of the likelihood that corrosion promoted fatigue pitting.

Lubricant Viscosity

The most important single property of a lubricant in its effect on

fatigue is viscosity. Fatigue data that treat the effects of viscosity will be dealt with as a separate operating variable. From the data obtained by Rounds (ref. 19), figure 12–16 shows the effect of viscosity on life for both paraffinic and naphthenic mineral oils over the range from 1.7 to 30 centistokes viscosity at 210° F. For both naphthenic and paraffinic base oils, the fatigue life doubles for a tenfold increase in viscosity at 210° F. Further gains in life, however, would not seem to result from increasing the viscosity above 30 centistokes. There do not appear to be sufficient data among some of the other classes of lubricants studied in reference 19 to evaluate the effects of viscosity. The dibasic acid esters (fig. 12–12) show an erratic and inconclusive trend. The polyglycols (fig. 12–13) show a decrease in fatigue life with an increase in viscosity. The methylphenyl silicones (fig. 12–14) show a fairly constant fatigue life with varying viscosity.

Scott (ref. 23) corroborated Rounds' data on the effects of viscosity on life for mineral oils and silicone oils (fig. 12–18). The mineral-oil results shown in figure 12–18, which were obtained in a four-ball fatigue tester, suggest that life increases at a rate approximately proportional to the 0.3 power of the viscosity. The silicone oils show no change in life with viscosity, which agrees with Rounds' data. The polyalkylene glycols, however, exhibit a small increase in life with viscosity, which contradicts the results obtained by Rounds.

Carter and Anderson (refs. 15 and 16) obtained data in the fatigue spin tester with M–1 tool-steel balls and four paraffinic mineral oils, which indicated that fatigue life varied approximately as the 0.2 power of viscosity. These oils varied in viscosity from 5.1 to 119.1 centistokes at 100° F. A more complex, but more versatile, equation was fitted to the results for life against viscosity in references 15 and 16 by consideration of extreme-value theory. Since each failure results from the weakest point on the running track, all other points

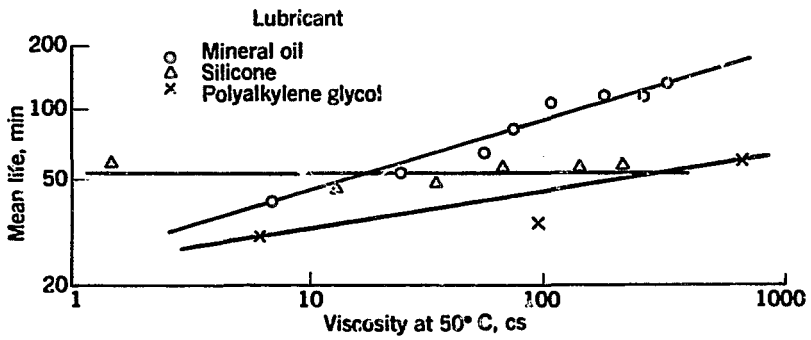

FIGURE 12–18.—Effect of lubricant viscosity on fatigue life with various types of lubricants. (From ref. 23.)

on the track are of necessity stronger; thus, the fatigue lives observed are a series of extreme values for all the infinitesimal areas of the running tracks. An extreme-value analysis results in an equation of the form

$$\ln \ln \frac{1}{S}=(0.625+0.007\sqrt{\mu_o}) \ln\left(\frac{L\times 10^{-8}}{5+0.42\sqrt{\mu_o}}\right) \tag{12–25}$$

where L is the life in millions of stress cycles. Equation (12–25) can be used to calculate the life as a function of viscosity at any level of survival, but calculations can be made more expedient by expressing equation (12–25) in the following exponential form:

$$S=\epsilon^{-\left(\frac{L\times 10^{-8}}{5+0.42\sqrt{\mu_o}}\right)^{(0.625+0.007\sqrt{\mu_o})}} \tag{12–26}$$

where ϵ is the Naperian base.

Equations (12–5) and (12–25) are similar in form. The constant e in equation (12–5) has been replaced by the function $0.625+0.007\sqrt{\mu_o}$ in equation (12–25) and the constant A by the function $\frac{10^{-8}}{5+0.42\sqrt{\mu_o}}$. The two constants e and A in the Weibull equation are obtained from experimental data for standard material bearings lubricated with a mineral oil. From equation (12–25), e and A are not constants but functions of viscosity. The function e represents the slope of the Weibull plot, and since

$$e=0.625+0.007\sqrt{\mu_o} \tag{12–27}$$

viscosity has a very small effect on the Weibull slope or scatter in life. The life at any survival level, however, is affected markedly by viscosity as shown by

$$A=\frac{10^{-8}}{5+0.42\sqrt{\mu_o}} \tag{12–28}$$

The 10- and 50-percent lives obtained in references 15 and 16 are plotted in figure 12–19 together with the simple exponential relations and the more versatile extreme-value relations. The exponential relations fit the data points well over the range of viscosities that were used, but they predict zero life at zero viscosity, which is unrealistic. The extreme-value relations also fit the data points well and are probably more correct for extrapolation because they predict a finite life at zero viscosity.

Barwell and Scott (ref. 11) in their four-ball investigation of several different types of lubricants found that life increased with increasing

viscosity with straight mineral oils, naphthenic base oils, and polyalkylene glycols, but not with silicone oils. The results for mineral

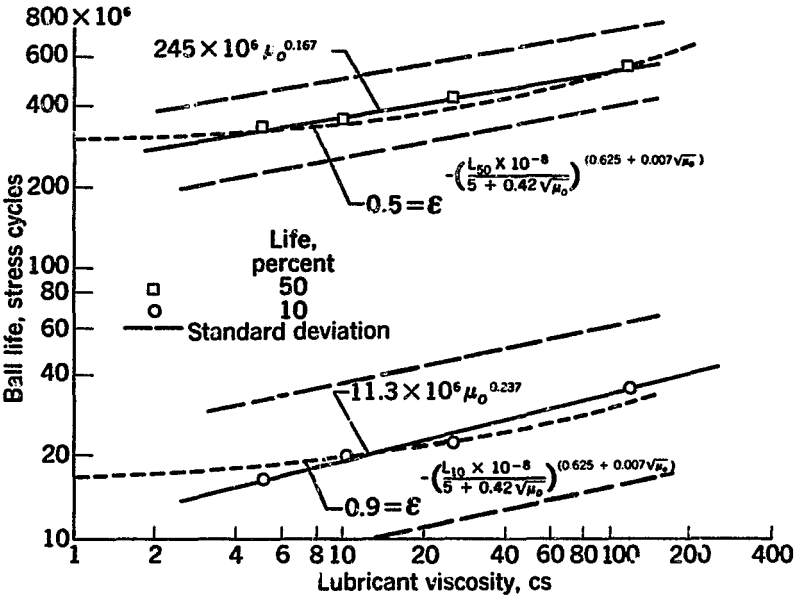

FIGURE 12–19.—Variation of fatigue life with lubricant viscosity. (From ref. 16.)

oils are shown in figure 12–20. These results are similar to those obtained in references 15, 16, 19, and 23.

Another approach to the study of the effect of lubricant viscosity on fatigue was taken by Baughman (ref. 14). He determined the actual viscosities of several test lubricants at 80,000 psi and found a correlation between this viscosity and fatigue life. These results, obtained in the rolling-contact tester, in which the test specimen is a cylindrical rod, are shown in figure 12–7. The log of life is a linear function of the log of viscosity.

Fatigue tests with full-scale roller bearings are reported by Otterbein in reference 24. Lubricants used were as follows:

(1) SAE 30 motor oil
(2) Five synthetic diesters (Mil–L–7808 oils)
(3) A polyester with a viscosity approximating that of SAE 30 motor oil
(4) SAE 10w motor oil
(5) A silicone oil

Figure 12–21 shows average life on a relative scale plotted against viscosity. A general trend exists toward longer life with higher viscos-

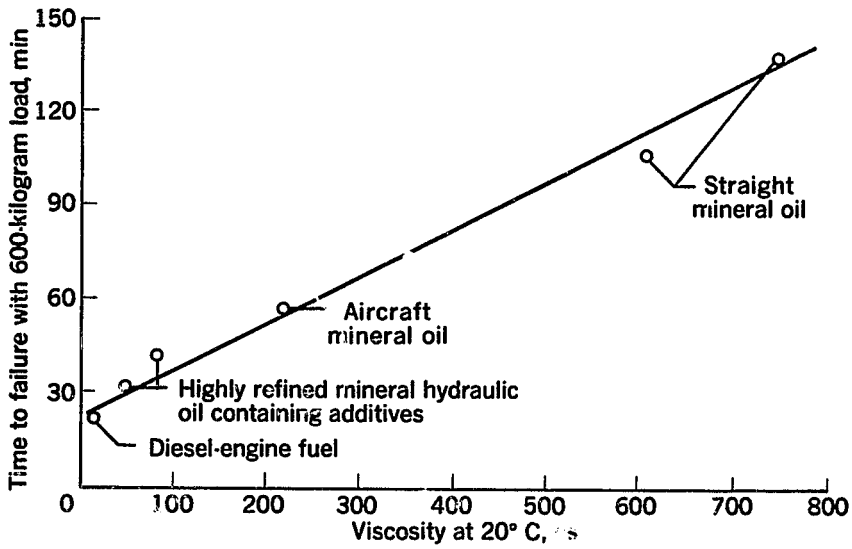

FIGURE 12–20.—Effect of viscosity on life of hydrocarbon lubricants. (From ref. 11.)

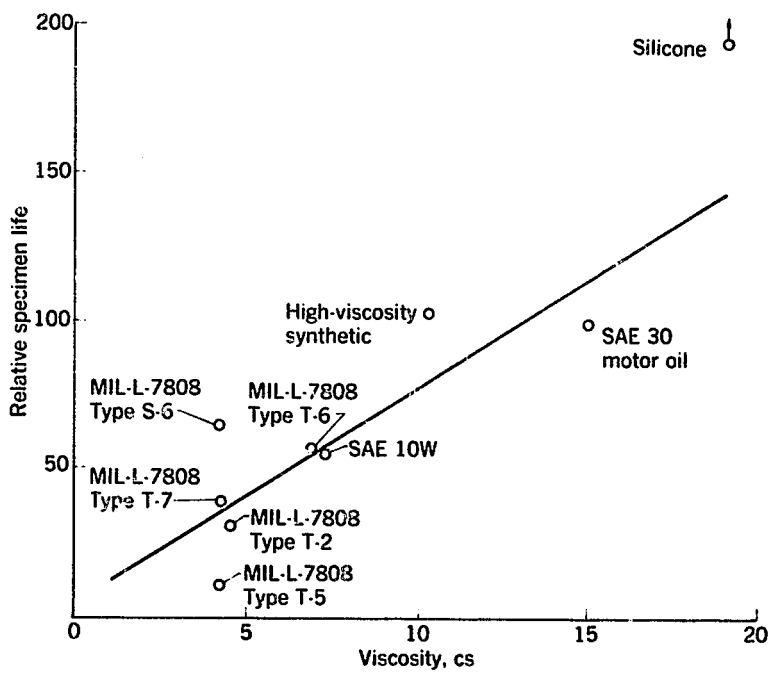

FIGURE 12–21.—Effect of viscosity on roller-bearing fatigue life. (From ref. 24.)

ity, although there is considerable scatter even among lubricants of the same type such as the diesters. Also, the silicone appears to have produced a much longer life than its viscosity would warrant.

Otterbein concluded that low-viscosity lubricants are detrimental to fatigue life and that additives such as viscosity improvers or thickeners are not effective in increasing the life with low-viscosity base oils. He also noted that some low-viscosity lubricants tend to produce shallow surface pitting that resembles corrosion fatigue. The cause of this shallow pitting was not determined.

Fatigue life in both bench tests and full-scale bearings appears to improve with viscosity for almost all the classes of fluids tested. The silicones appear to be an exception and exhibit approximately constant fatigue life over a range of viscosities. Life at the higher viscosities appears to level off in some instances, but more work with high-viscosity oils is needed to corroborate this. Life has been found to vary as the 0.2 to 0.3 power of viscosity for mineral oils over the range of viscosities investigated.

Discussion of Results With Lubricants

The reasons for the variation in life with viscosity and with base stock are not known. In addition to its function as a lubricant for sliding surfaces and as a coolant, the lubricant may influence the stress distribution and thus influence the maximum stress that occurs in the contact zone between a ball and a race. Since fatigue life for point contact varies inversely as the maximum stress raised to the ninth or tenth power, small reductions in the maximum contact stress would produce significant increases in life.

Way (ref. 25) proposed that increasing viscosity results in longer fatigue life because forcing a more viscous lubricant into an incipient fatigue crack is difficult. In fatigue tests of steel rollers, Way found that (1) a lubricant must be present if pitting is to take place, and (2) pitting can be prevented if the lubricant is of a viscosity above a certain critical value, which depends on the load.

Way's theory that the lubricant acts as a wedge offers a plausible explanation for those applications in which fatigue cracks originate at the surface. As discussed in chapter 6, however, the maximum shear stress occurs, in most applications, below the surface. Since the maximum shear stress is the stress considered most damaging, many fatigue cracks may originate in the subsurface. Evidence in the literature shows that this is true. Subsurface structural changes due to cyclical stresses were observed by both Jones (ref. 26) and Carter (ref. 15). The change in structure resulted from additional tempering of the martensite and is believed to be caused by a combination of thermal and strain energy. Carter (ref. 15) observed that many fine

cracks developed in the areas of structural change and that these cracks generally became enlarged and elongated with longer running times. Many instances of fatigue failures that originate at inclusions or other material defects in the subsurface region of high shear stress have been observed; thus fatigue failures may originate either in the subsurface or on the surface. Therefore, Way's theory does not completely explain the role of the lubricant in fatigue.

Viscosity of lubricants varies with pressure, and various lubricants have different pressure-viscosity characteristics. The actual viscosity under pressure is a function of the initial viscosity and of the pressure-viscosity coefficient. The pressure-viscosity coefficient has a greater effect on the actual viscosity under pressure than does the atmospheric pressure viscosity. Therefore, for lubricants in the normal viscosity range, the pressure-viscosity coefficient is of prime importance in determining the actual viscosity under pressure.

Several attempts have been made to treat analytically the problem of lubricated nonconforming bodies in contact under high pressure. This is the so-called elastohydrodynamic problem, which requires the simultaneous solution of energy, elasticity, hydrodynamic, and viscosity equations for an exact solution. Simplifying assumptions must be made to make a numerical solution feasible on a digital computer.

Dörr (ref. 27) obtained a solution for the pressure distribution between an infinitely long roller and a race. His results predict a decrease in maximum contact pressure with an increase in viscosity, but his assumption of constant viscosity may affect the validity of the results. Other notable contributors to the solution of the elastohydrodynamic problem are Grubin (ref. 28), Petrusevich (ref. 29), Poritsky (ref. 30), and Weber and Saafeld (ref. 31); however, none of the solutions in these references is completely satisfactory.

A numerical solution to the two-dimensional problem of elastic cylinders is presented by Dowson and Higgenson in reference 32. Their findings indicate that the maximum contact pressure when a lubricant is present is about the same as the Hertzian pressure. The only significant variations in the pressure distribution from the Hertzian when a lubricant is present occur at the inlet and the exit of the load zone where the pressures are low. Dowson and Higgenson assumed that the viscosity varied exponentially with pressure and simultaneously solved the Reynolds and the elasticity equations.

Sternlicht, Lewis, and Flynn (ref. 33) present a number of solutions to the two-dimensional problem of rollers in contact. These solutions contain varying degrees of simplifying assumptions. For specific minimum film thickness, rolling velocity, viscosity, and variation of viscosity with temperature and pressure, the following load capacities were obtained:

Viscosity	Load capacity, lb/in.	
	Rigid surfaces	Elastic surfaces
Constant	140	450
$f(p)$	320	12, 000
$f(p, T)$	232	9, 780

From this comparison, the influence of pressure on viscosity and on surface deformation increases the load-carrying capacity significantly, while temperature decreases the load-carrying capacity.

The results of reference 33 agree with those of reference 32 in that the elastohydrodynamic pressure distribution was found to be similar to the Hertzian pressure distribution. The results of reference 33 are based on a simultaneous solution of the Reynolds, the energy, and the elasticity equations with the assumption that viscosity varies with both pressure and temperature. While the stresses were found not to vary with various lubricant viscosity-pressure-temperature functions, the temperature distributions did vary. Reference 33 hypothesizes that temperature gradients produce thermal stresses that must be considered in conjunction with normal pressures in order to determine maximum shear stress. Thus, the lubricant that produces lower thermal gradients within the contact zone will yield longer fatigue life in rolling contact.

Full-scale bearing-fatigue tests with two lubricants were conducted in reference 33, which confirmed the analysis. The oil that produced the lower temperature gave longer fatigue life.

Lubricants do not appear to affect fatigue life because of direct influences on the pressure distribution. Thermal effects may be important as may other lubricant properties such as chemical stability, chemical activity, or bulk modulus. In the experiments of references 15 and 16, the best fatigue life was obtained with the least reactive lubricants (silicone and mineral oil), and the poorest fatigue life was obtained with the most reactive lubricants (adipate and sebacate). Further experimental fatigue work with lubricants is necessary to define the important lubricant properties.

Temperature

Temperature and its effect on fatigue life are of extreme interest because of the many high-temperature applications in which bearings are expected to perform satisfactorily over extended periods of time. The effects of temperature are reflected on both the lubricant and on

Card #24

the material. Decreasing viscosity will, in most instances, result in decreased fatigue life. Since the viscosity of lubricants decreases with rising temperature, an increase in temperature would be expected to be detrimental to fatigue life. The hardness of bearing materials is reduced as temperatures rise, and this is detrimental to fatigue life, as shown in the discussion of PROCESSING VARIABLES.

Carter (ref. 15) reports fatigue data obtained with M–1 steel balls and a sebacate lubricant at 100°, 250°, and 450° F in the fatigue spin tester. Weibull plots of these data are shown in figure 12–22. These results show a reduction in early failure lives with an increase in test temperature. On the basis of the relation between life and lubricant viscosity given in reference 15, $L_1/L_2=(\mu_{o,1}/\mu_{o,2})^{0.2}$, some reduction in life could be anticipated because of the change in viscosity. Table 12–XVIII shows the theoretical reduction in ball life due to viscosity reduction alone. The observed lives were less than those expected if viscosity of the lubricant were the only variable that affected fatigue life. The difference between the observed and the theoretical lives is probably caused by the amplification at the high test temperatures of other factors that affect fatigue life. No significant changes in the appearance of the test tracks with temperature were noted. In particular, there was no evidence of chemical corrosion present on any of the specimens.

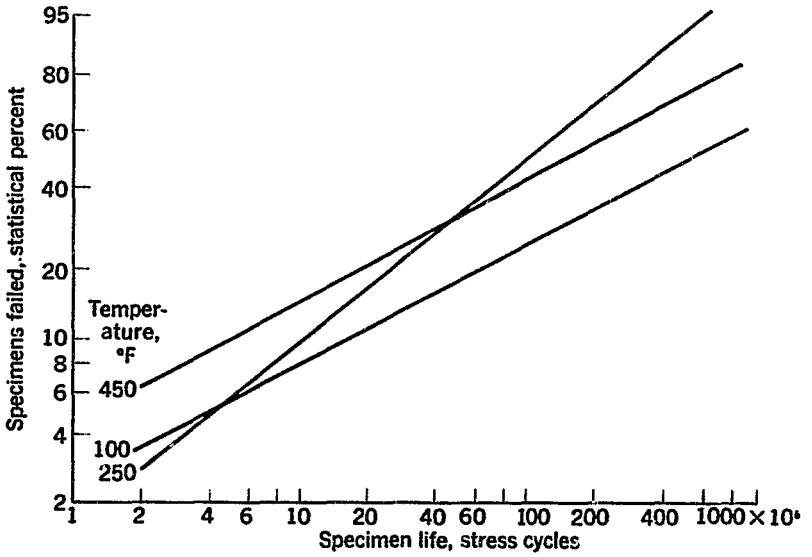

FIGURE 12–22.—Fatigue life for ½-inch-diameter AISI M–1 tool-steel balls at various test temperatures. Lubricant, di(2-ethylhexyl)sebacate; maximum Hertz compressive stress, 650,000 psi. (From ref. 15.)

TABLE 12-XVIII.—FATIGUE LIFE FOR ½-INCH AISI M-1 BALLS AT VARIOUS TEMPERATURES [a]

[Lubricant, di(2-ethylhexyl)sebacate; maximum Hertz compressive stress, 650,000 psi.]

Temperature, °F	Lubricant viscosity, cs	Observed 10 percent life, stress cycles	Theoretical 10 percent life, stress cycles
100	13.5	15.7×10^6	[a] 15.7×10^6
250	3.8	10.2	[b] 12.2
450	1.66	4.75	[b] 10.3

Temperature, °F	Life ratio, observed / theoretical	Observed 50 percent life, stress cycles	Theoretical 50 percent life, stress cycles	Life ratio, observed / theoretical
100	1	580×10^6	[b] 580×10^6	1
250	.84	109	[c] 450	.24
450	.46	160	[c] 382	.42

[a] From ref. 15.
[b] Assumed the same as observed life.
[c] Based on relation $L_1/L_2=(\mu_{o,1}/\mu_{o,2})^{0.2}$, where L is life in stress cycles and μ_o is lubricant viscosity.

Post-test sectioning of the test specimens of reference 15 revealed a metallurgical transformation in the subsurface shear zone. This transformation increased with increase in number of test cycles and in temperature. Jones (ref. 26) reported a deterioration of metallurgical structure in the subsurface zone of maximum shear for SAE 52100 steel bearings. This transformation consisted of a further tempering of the martensite and resulted from the accumulation of hysteresis energy in the zone of high shear stress. The structure of the transformed M-1 steel that was reported by Carter in reference 15 has not been definitely identified. The deterioration of structure in the subsurface shear zone may be one of the factors that contributed to the loss in fatigue life at higher test temperatures.

Fatigue tests of crystallized glass ceramic (Pyroceram) balls are reported in reference 34. These tests were conducted at test temperatures of 80° and 700° F in the five-ball fatigue tester at 330,000 psi maximum Hertz stress with a highly refined paraffinic mineral oil. The fatigue life at 700° F was approximately one-fourth that at 80° F (fig. 12-23). The viscosity of the test oil was 107 centistokes at 100° F and 1.1 centistokes at 700° F. If the life-viscosity relation of reference 15 is used, this difference in viscosity would produce a reduction in life of about 3½ to 1. Thus, the observed loss in fatigue life at the higher temperature could be accounted for by changes in

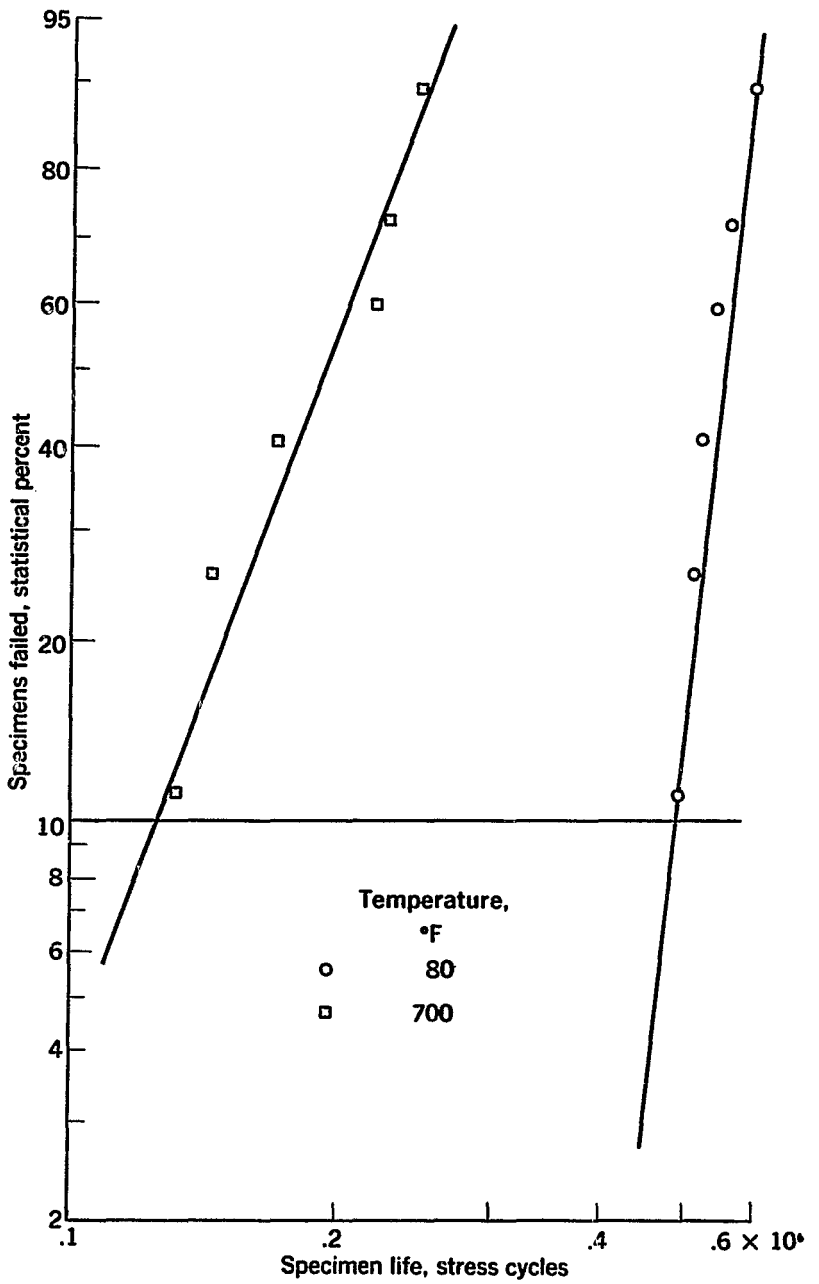

FIGURE 12-23.—Rolling-element-contact fatigue life of crystallized glass ceramic balls as function of temperature. Contact angle, 40°; lubricant, mineral oil; maximum Hertz stress, 330,000 psi. (From ref. 34.)

lubricant properties, so that a deterioration of the Pyroceram material did not necessarily occur.

Otterbein (ref. 24) found that roller-bearing fatigue life decreased steadily with an increase in temperature over the temperature range from 120° to 300° F when a single diester oil was used as the lubricant. The relative life was a linear function of viscosity, as shown in figure 12–24. These data show a stronger relation between life and viscosity than do the data of Scott (ref. 23) or Carter (ref. 15) because two variables, viscosity and temperature, are present in figure 12–24. Decreasing viscosity and increasing temperature both contribute to a loss in fatigue life. An increase in temperature from 120° to 250° F results in a drop in relative life from 70 to 20, which is a decrease of about 70 percent. The significant effect that operating temperature has on fatigue life is thus apparent.

Further data on the effects of temperature on full-scale ball-bearing fatigue life are shown in table 12–XIX. These data are from reference 37, which reports the results of a comprehensive investigation of the effects of melting practice and other variables on ball-bearing fatigue life. This work includes some of the early investigations into the fatigue properties of tool steels. Data were obtained with 45-millimeter-bore ball bearings under a radial load, and results are expressed in terms of the basic AFBMA load capacity for conventionally lubricated SAE 52100 steel bearings. Bearings of three tool steels, M–10,

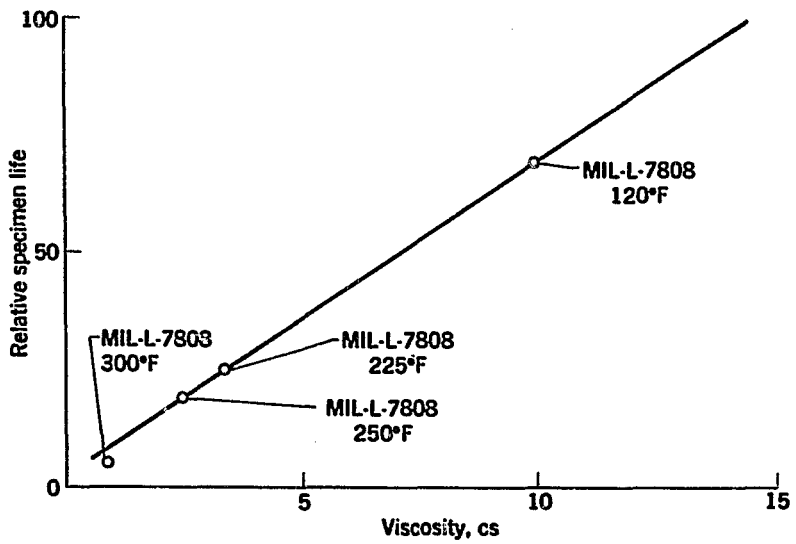

FIGURE 12–24.—Effect of viscosity on ball-bearing life. (From ref. 24.)

TABLE 12-XIX.—BEARING LOAD RATINGS FOR TOOL STEELS [a]

Melting practice	Tool steel	Temperature, °F	Rating as percent AFBMA basic load rating, based on	
			10-percent life	50-percent life
Basic arc	M-10	Room	77	70
	M-10	450	64	64
	M-1	Room	83	91
	M-1	Room	76	78
	M-1	450	60	54
Induction vacuum	M-1	Room	132	122
Induction vacuum	M-1	450	64	77
Consumable vacuum	M-50	Room	144	126
Consumable vacuum	M-50	450	93	100

[a] From ref. 37.

M-1, and M-50, were tested at room temperature and at 450° F. The reduction in load ratings from room temperature to 450° F are believed to be caused principally by the lubricant; the bearings at room temperature were lubricated by a mineral-based grease and those at 450° F by a synthetic diester. A discussion of the effects of melting practice will be given in the section PROCESSING VARIABLES.

Solid Lubricants

Because of the requirement that rolling-element bearings operate at temperatures above the range in which organic liquid lubricants are usable, solid lubricants such as graphite and molybdenum disulfide (MoS_2) have been considered as lubricants for rolling-element bearings. The effectiveness of solid lubricants in preventing failures other than those due to fatigue is discussed in chapter 11. Some data on the influence of solid lubricants on rolling fatigue are contained in references 12, 15, and 20. In reference 15, fatigue tests of ½-inch-diameter M-1 steel balls were conducted in the fatigue spin tester with the following lubricants:

(1) Polyalkylene glycol at 100° F
(2) Synthetic sebacate at 450° F
(3) Polyalkylene glycol plus 0.2 percent molybdenum disulfide at 100° F
(4) Polyalkylene glycol plus 0.2 percent molybdenum disulfide at 450° F
(5) Dry graphite at 450° F

The fatigue results for these five lubricants are given as Weibull plots

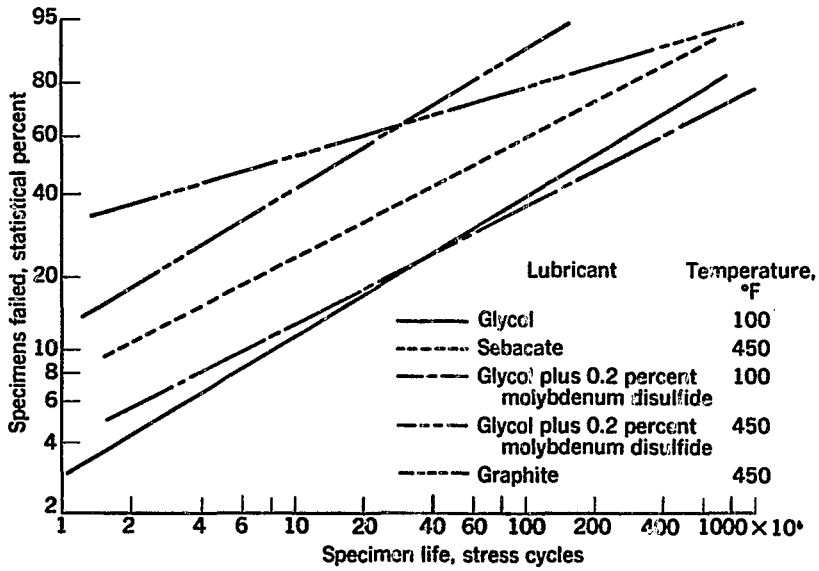

FIGURE 12–25.—Fatigue life for ½-inch-diameter AISI M–1 tool-steel balls with various lubricants. Maximum Hertz compressive stress, 725,000 psi. (From ref. 15.)

in figure 12–25. Fatigue lives obtained with the glycol and the suspension of glycol and MoS_2 at 100° F are almost identical, which indicates no effect from the presence of the MoS_2. The suspension of glycol and MoS_2 produced a poorer fatigue life at 450° F. The glycol was chosen as a carrier for the MoS_2 because it evaporates at 350° F and leaves no residue. Thus, at 450° F, the lubricant present was essentially dry MoS_2 powder. Fatigue tests with dry graphite and air dust produced even poorer fatigue life as shown in figure 12–25. The results with a synthetic sebacate at 450° F are shown for comparison with the graphite and the MoS_2 results. Fatigue life with the synthetic sebacate was better than with the dry-powder lubricants by a factor of at least five.

Either physical or chemical factors could have been responsible for the poor fatigue life with the dry-powder lubricants. Since graphite is quite different from MoS_2 chemically but similar physically, different results would be expected if chemical activity were a major factor. The similar life results with graphite and MoS_2 seem to preclude chemical effects. Post-test examination of the test balls run with dry-powder lubricants revealed two annular bands of small spalls located at the rolling bands rather than the usual single track-centered spall obtained in tests with liquid lubricants. Examination of the dry powders revealed a maximum particle size of about 25 microns.

This size is believed to be sufficiently large for the particles to act as stress raisers in the regions where they were not sheared. The appearance of the spalls in the rolling bands apparently confirms this, since the relative motion of the two surfaces is perpendicular to the plane of the surfaces in the rolling bands. The stress on the lubricant particles would be purely compressive in these regions and, because of the quasi-hydrostatic loading, the particles could carry compressive stresses higher than their yield strength.

The theory that the dry-lubricant particles produce high, localized compressive stresses in the bands of pure rolling is a hypothetical one, but one that is supported by substantial evidence which indicates that some localized stress raiser that is not present in fluid lubricants is present with dry lubricants. The unique appearance of the spalling, the intense localized incipient matrix damage confined to the region of the unique spalling, and the short lives support this theory. The stress-raising effects that were noted in these tests may not be present to such an extent in full-scale rolling-element bearings because better conformity exists between balls and races and because relative sliding of the surfaces is greater.

Scott (ref. 12), in four-ball tests conducted at 200° C (392° F) and at a maximum Hertz stress of 830,000 psi, reported improvements in fatigue life with MoS_2 and graphite suspensions in oils. The average time to failure with two silicone oils was 36 and 23 minutes (table 12–XX). A suspension of MoS_2 in a soap-thickened silicone fluid, 2- and 10-percent suspensions of graphite in mineral oil, and a MoS_2 paste in a mineral-oil carrier generally extended fatigue life. Dry MoS_2 was beneficial to fatigue life, but dry graphite and a mixture of dry graphite and lead oxide produced fatigue lives equal to or less than those with the liquid lubricants. With the dry MoS_2, failure was caused by a progressive surface roughening rather than by the appearance of a surface pit. The particle size of the dry powders used in reference 12 was not given, but possibly they were smaller than those used in reference 15.

Further tests of solid lubricants by Scott are reported in reference 20. The results of these tests, which were conducted at a maximum Hertz stress of 10^6 psi, are shown in table 12–XXI. These tests were conducted with solid lubricants in the form of dry powders and dispersed in various media; however, the particle size of the dry powders was not given. The results with MoS_2 were considerably better than those with graphite, which agree with reference 12. Better results were achieved when MoS_2 was suspended in a mineral-oil carrier than when it was suspended in water. Dilution of the paste-like suspension of MoS_2 in water resulted in severe reduction of life.

TABLE 12-XX.—FATIGUE LIFE RESULTS WITH VARIOUS LUBRICANTS [a]

[Maximum Hertz stress, 830,000 psi; test temperature, 200° C.]

Lubricant	Average time to failure, min	Remarks
Typical conventional silicone	36	Considerable amount of wear on upper ball; bottom balls dull
Experimental silicone intended for use at −50° C and above; contains chlorine	23	Normal pitting failure; single small pit
Suspension of molybdenum disulfide in soap-thickened silicone fluid; lubricant formulated to combine thermal and physical properties of silicone with lubricating potentialities of molybdenum disulfide	50	Considerable amount of wear on upper ball; bottom balls dull
Experimental lubricant: 2 percent graphite in special mineral oil	55	Normal pitting failure
10 percent graphite in thin mineral-oil base	41	Normal pitting failure
Dry graphite power	26	Considerable wear and damage, bottom balls black
Dry graphite powder with graphite-coated balls	20	Bottom ball from previous test used
Mixture of dry graphite and lead oxide in ratio 1:2	36	Considerable wear and severe damage; bottom balls black
Dry molybdenum disulfide	98	Considerable wear
Molybdenum disulfide in paste form with mineral-oil carrier	135	Normal pitting failure

[a] From ref. 12.

The results of the experiments conducted in references 12, 15, and 20 indicate that solid lubricants can be beneficial to fatigue and that MoS_2 appears to be better than graphite. Suspensions of solids in conventional lubricants give better results than dry powders or aqueous suspensions. Particle size appears to be critical with submicron size particles that are necessary for good fatigue results.

Speed

Conventional calculations of bearing life are based on the fatigue of the components due to the externally applied loads. At high

TABLE 12-XXI.—EFFECT OF SOLID LUBRICANTS ON BALL FATIGUE LIFE [a]
[Maximum Hertz stress, 10^6 psi.]

Description of lubricant	Duration of test, min	Remarks
N, suspension of larger particle variety of molybdenum disulfide in water; soft cream consistency	105 115 80 110	Test to failure
N, diluted 1:2 with water	120 120 80	Test to failure
N, diluted 1:5 with water	12 8 9 6 5	Test to failure; two test balls fractured
N, diluted 1:9 with water	4 4 3	Test to failure
Molybdenum disulfide in paste form in mineral-oil carrier	120 150 285	No failure
Suspension of molybdenum disulfide in soap-thickened silicone fluid	50 60 120 160	No failure by normal pitting; considerable wear in every instance; bearing track had abraded appearance
2 percent by weight conventional graphite in mineral oil	124 130 131 75 105	Test to failure
10 percent by weight colloidal graphite in petroleum base	75 63 65 100	Test to failure
Dry molybdenum disulfide	145 210 240	No failure
Dry graphite	13 15 10	Test to failure; considerable damage to upper ball; lower balls black color
Dry graphite	17 15	Test to failure; lower balls from above test apparently covered with graphite layer used as upper ball
Dry graphite lead oxide mixture, 1:2	18 15 20	Test to failure; considerable wear and damage to upper ball
Graphite suspension in alcohol	55 32 35	Test to failure; considerable damage to upper ball; alcohol evaporated and test ran almost dry

[a] From ref. 20.

speed, the centrifugal force on the balls increases the load at the outer-race contact. In addition, bearing temperature may rise with increasing speed and may produce an effect on fatigue life.

Jones (ref. 35) analyzed the effects of high speed on both radial-loaded and thrust-loaded bearings. In radial ball bearings under radial load, the effect of speed is to reduce life because the centrifugal force on the balls increases the probability of failure of the outer race. These results are shown in figure 12–26 for a 209-size bearing operating under a 400-pound radial load. The divergence between the calculated static load life and the high-speed life increases with increasing speed.

In angular-contact bearings, which operate under thrust load,

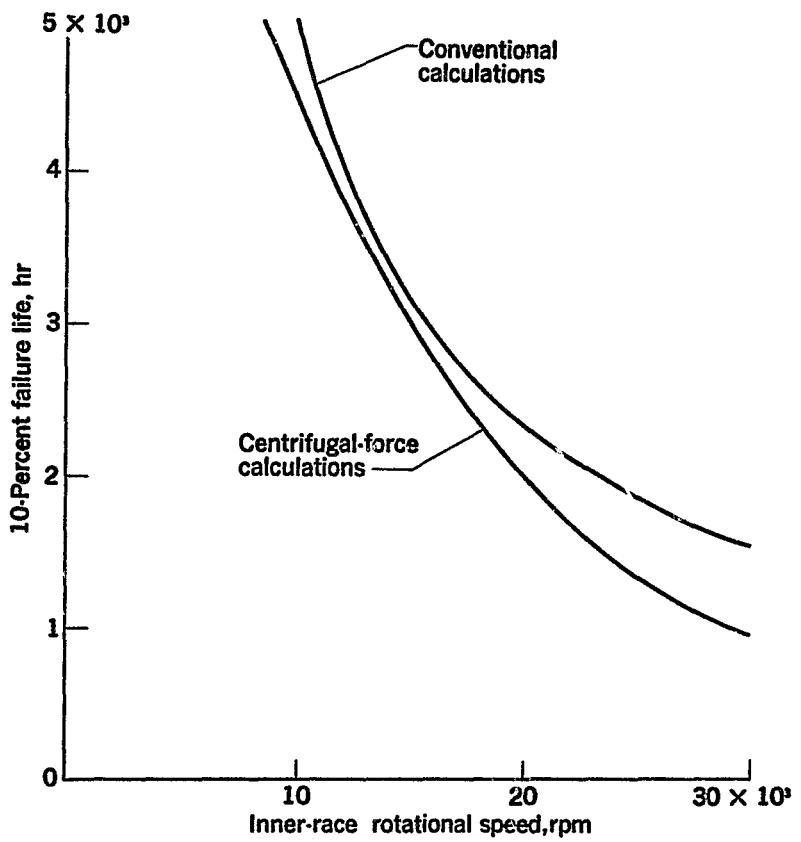

FIGURE 12–26.—Ten-percent failure life as function of speed as calculated by conventional means and with consideration of centrifugal force for 209-size bearing with nine balls of ½-inch diameter; race curvatures: inner, 51 percent; outer, 52 percent; 400-pound radial load. (From ref. 35.)

centrifugal loading of the balls increases the inner-race contact angle and reduces the stress at the inner-race contacts. Thus, the relative probabilities of outer- and inner-race failure are different from those calculated from static load conditions, and bearing life is accordingly different. Calculations made for a 214-size bearing that operates at 10,200 rpm with an initial contact angle of about 20° are shown in figure 12–27. The ratio of life for load at high speed to that for static load is plotted against thrust load. At zero external load, the life ratio is effectively zero because the total load originates from centrifugal forces. The life ratio increases with increasing thrust load and is greater than 1 at thrust loads above about 500 pounds. Thus, the changes in contact angle produced by the high speed theoretically increase the bearing fatigue life. Experimental results are needed to confirm these analyses.

The load capacity of a bearing increases as the rolling-element diameter (or the bearing series) is increased. This theory is true only in the nominal speed range. At extreme speeds, higher loads may be carried with a lighter series bearing because of the predominance of centrifugal forces on the rolling elements; an example is discussed in chapter 11. The Marlin-Rockwell Corporation has developed the following criterion for establishing the limiting speed of thrust-loaded ball bearings:

$$\frac{EN^3D^3}{\cos^3\alpha} < 31\times10^8 \qquad (12\text{–}29)$$

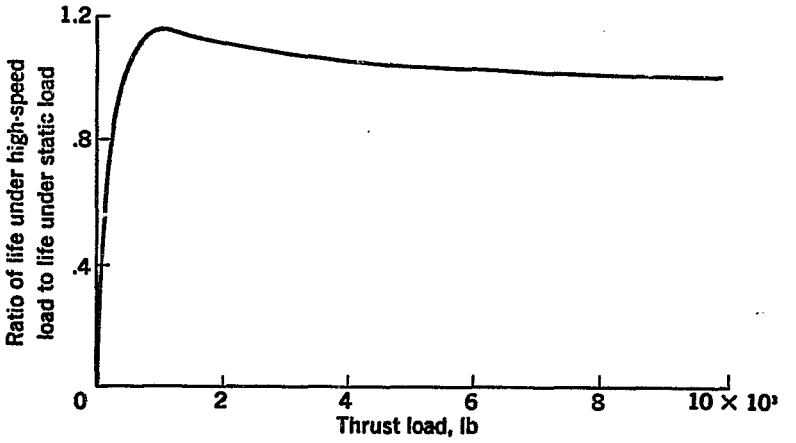

FIGURE 12–27.—Ten-percent failure life for load at high speed relative to life for static load as function of thrust load for 214-size bearing with 16 balls of 11/16-inch diameter; contact angle α, 19.64°; race curvatures: inner, 51 percent; outer, 52 percent; inner race rotating at 10,200 rpm. (From ref. 35.)

693-499 O-64—28

The term D^3, which is proportional to the mass of a rolling element, appears in the inequality. The expression in the numerator is akin to a centrifugal force multiplied by an angular velocity since it contains terms equivalent to a radius, an angular velocity cubed, and a mass.

Zaretsky, Anderson, and Parker (ref. 36) ran fatigue tests of ½-inch M–1 balls in the five-ball fatigue tester at 5000 and 10,000 rpm at a contact angle of 30°. In a series of fatigue tests at 10,000 rpm at various contact angles (ref. 36), life decreased with increasing contact angle at a constant normal load. The significance of these results will be discussed later, but of importance here is the fact that, as contact temperature increased, fatigue life decreased. Contact temperature at 5000 rpm was lower than at 10,000 rpm so that, on the basis of temperature, a longer fatigue life would be expected at the lower speed. A 5000-rpm life was predicted from the 10,000 rpm data and measured contact temperatures. As shown in figure 12–28, the predicted life is almost identical to the actual life at 5000 rpm. These experiments were conducted under conditions where centrifugal loads were not present, and the appearance of the specimens after test indicated that hydrodynamic lubrication may not have existed. Contact tempera

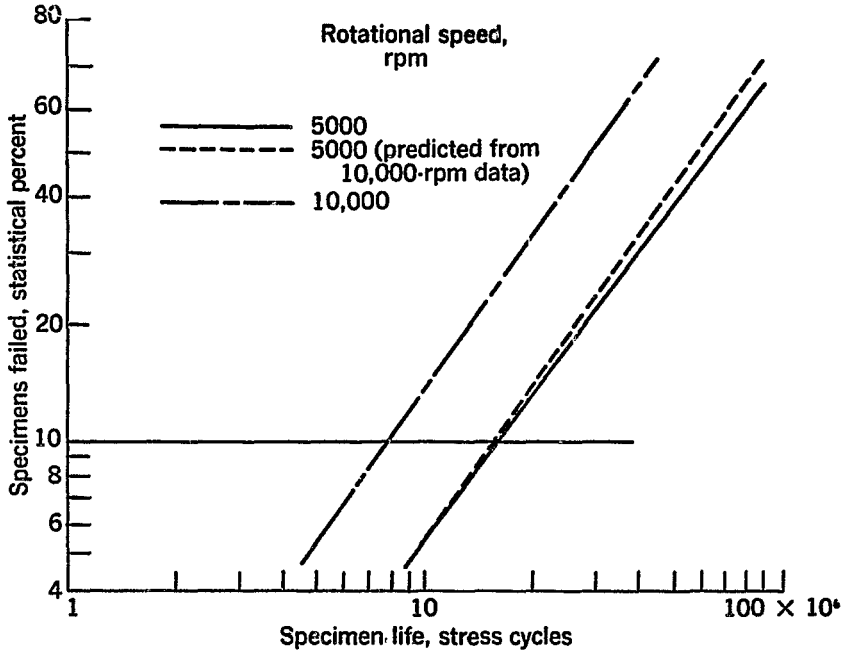

FIGURE 12–28.—Rolling-element-contact fatigue life at 5000 and 10,000 rpm of AISI M–1 tool-steel balls for contact angle of 40°. Initial maximum Hertz stress, 800,000 psi; race temperature, 120° F. (From ref. 36.)

ture appears to be an important variable that is influenced by speed, but further experimental data are needed to confirm this hypothesis.

PROCESSING VARIABLES

In addition to the environmental or operating variables, processing variables such as material and melting technique, material hardness, material fiber orientation, and contact angle also affect fatigue.

Material and Melting Technique

Morrison, Walp, and Remorenko (ref. 37) thoroughly investigated the effects of melting practice with vacuum-melted 52100 steel and with both air and vacuum melts of several tool steels. For reference, the nominal analyses of a number of bearing materials are given in table 12–XXII. Table 12–XXIII, from reference 37, shows some data obtained with induction and consumable-electrode vacuum-melted 52100 steel. Load ratings are given in terms of the AFBMA basic load rating. Specimens were inner rings of 6309-size bearings or outer rings of 1309-size self-alining bearings. These data show, generally, that consumable-electrode melting produces material with better fatigue properties than induction vacuum melting. Unpublished results obtained by other investigators generally confirm that consumable-electrode vacuum-melting produces the most consistent high-quality bearing material. A partial explanation may be that a refractory crucible is used in the induction-melting process with the result that refractory particles sometimes get into the melt. In the consumable-electrode-melting process, the ingot is used as one terminal of the arc, and the process is completely clean.

Results with tool steels, obtained in reference 37, are shown in table 12–XIX. In addition to the two vacuum-melting techniques, several heats of material were basic-arc air melted. The air-melted M–10 and M–1 materials were deficient in load-carrying capacity. At room temperature, load capacities based on the 50-percent life ranged from 70 to 91 percent. At 450° F with synthetic diester lubrication, the load capacities were even poorer. The induction-vacuum-melted M–1 was superior to the standard AFBMA rating at room temperature, but quite poor at 450° F. Only the consumable-vacuum-melted M–50 was comparable to or better than the standard at both room temperature and at 450° F.

The authors of reference 37 state that little correlation was found with cleanliness as determined by inclusion ratings obtained from the Jernkontoret chart in that the improvement in life was not commensurate with improvements in cleanliness. This conclusion was generally confirmed by Carter (ref. 15), who conducted ball-fatigue tests of 10 different materials in the fatigue spin rig. The life results of these tests are shown in a bar graph in figure 12–29. All these materials

TABLE 12–XXII.—NOMINAL ANALYSIS OF BEARING MATERIALS

Steel	Analysis, percent by weight										
	C	P (max)	S (max)	Mn	Si	Cr	V	W	Mo	Al	Co
SAE 52100	1.00	0.025	0.025	0.35	0.30	1.45	----	-----	----	----	----
AISI M–1	.80	.030	.030	.30	.30	4.00	1.00	1.50	8.00	----	----
AISI M–50	.80	.030	.030	.30	.25	4.00	1.00	-----	4.25	----	----
AISI M–2	.83	.030	.030	.30	.30	3.85	1.90	6.15	5.00	----	----
AISI M–10	.85	.030	.030	.25	.30	4.00	2.00	-----	8.00	----	----
AISI T–1	.70	.030	.030	.30	.25	4.00	1.00	18.00	----	----	----
AISI MV–1	.80	.030	.030	.30	.25	4.10	1.10	-----	4.25	----	----
Al steel (MHT)	1.03	.025	.025	.35	.35	1.50	----	-----	----	1.36	----
L.A.T.S. (Haimo)	.65	.030	.030	.27	1.20	4.6	.55	-----	5.2	----	----
TMT	1.00	.025	.025	.50	1.00	1.45	----	-----	.30	.08	----
440C	1.03	.018	.014	.48	.41	17.3	.14	-----	.50	----	----
WB49	1.07	.006	.007	.30	.02	4.4	2.0	6.8	3.9	----	5.2

TABLE 12-XXIII.—TEST RESULTS FOR VACUUM-MELTED SAE 52100 STEEL [a]

Approximate ingot size, in.	Melting practice	Rating, percent AFBMA basic load rating	
		10-percent life	50-percent life
5½-in. diam.	Induction vacuum	95	90
5½-in. diam.	Induction vacuum	108	112
6 in. sq	Induction vacuum	71	83
	Induction vacuum	100	97
	Induction vacuum	95	93
	Induction vacuum	91	94
	Induction vacuum	80	90
9⅝ in. sq	Induction vacuum	103	103
9⅝ in. sq	Induction vacuum	126	123
16-in. diam.	Consumable electrode	124	116
16-in. diam.	Consumable electrode	106	112

[a] From ref. 37.

had inclusion ratings of 1 in the A and D categories of the Jernkontoret rating system, but within that group each material was given a rating of excellent, good, fair, or poor based on the metallographer's judgment. The air-melted materials tested by Carter included SAE 52100, M–1, MHT, TMT, M–10, T–1, MV–1, and M–50. Among these materials, no particular correlation between cleanliness and fatigue life was noted. Two heats of M–1 steel, one air melt, and one vacuum melt were tested with a glycol lubricant. The vacuum melt M–1 produced significantly better fatigue life. The two modified SAE 52100 base alloys (MHT with 1-percent aluminum and TMT with 1-percent silicon) showed an improvement over standard SAE 52100. With the addition of these deoxidizers, fewer short-lived failures were obtained, and the scatter in life was reduced.

Balls of several materials were fatigue tested by Jackson (ref. 38) in a modified one-ball fatigue tester. These data are shown in figure 12–30. Metallurigical data obtained with balls with the lowest and highest life from each series are shown in table 12–XXIV. Good cleanliness does not ensure good fatigue life although the M–50, which was quite clean, had the best fatigue life. The MHT, which was quite dirty, had good fatigue life, whereas the Halmo, which was fairly clean, had poor life. Jackson found that life can vary appreciably for several apparently similar heats of the same material, which agrees with the findings of the authors of reference 37 (table 12–XXIII). Note, for example, on table 12–XXIII, the load-capacity data for bearing groups 5 and 6. These are two groups of bearings made from the same heat poured to the same ingot size, and yet bearing group 6 had a 15 percent greater capacity than did group 5

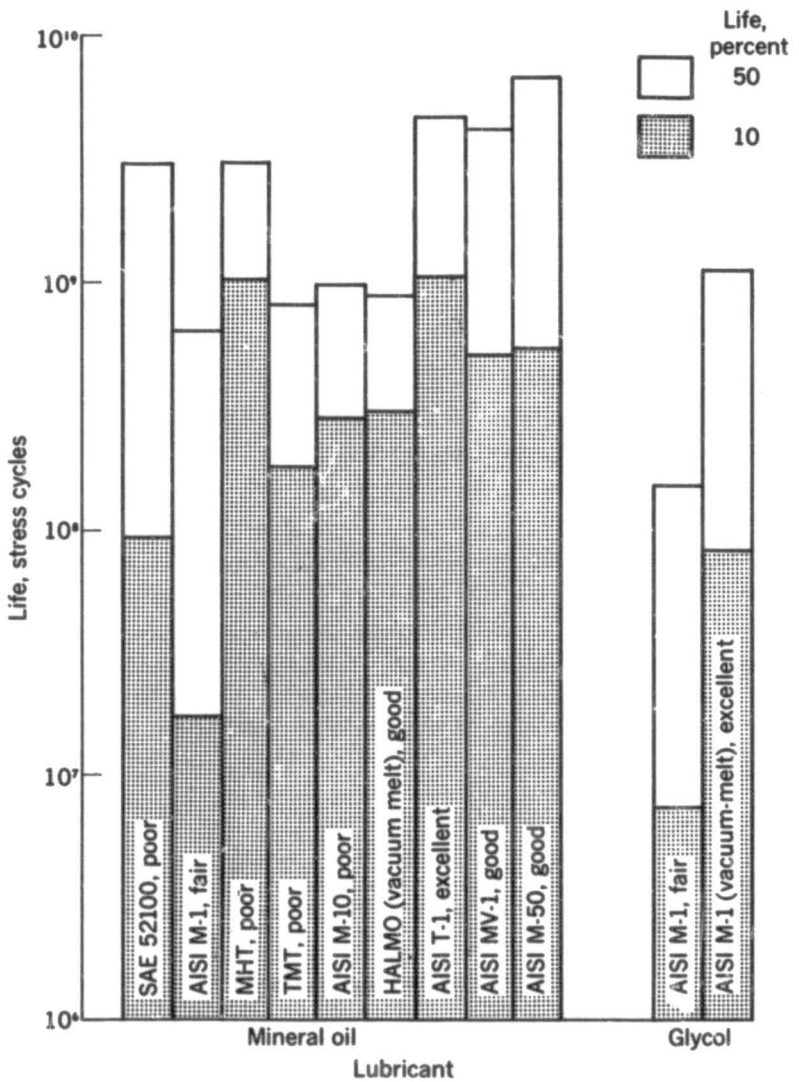

FIGURE 12–29.—Summary of fatigue-life data giving material and cleanliness ranking within A–1 and D–1 Jernkontoret ratings. (From ref. 15.)

based on the 50-percent life. A 15-percent difference in capacity corresponds to a 50-percent difference in life.

The important conclusions regarding the effects of material and melting technique on fatigue from the data of references 15, 37, and 38 are as follows:

(1) The standard Jernkontoret cleanliness measurements are not sufficient to establish relative quality.

TABLE 12-XXIV.—METALLURGICAL OBSERVATIONS OF FATIGUE SPECIMENS[a]

[Lowest- and highest-life balls from each series.]

Steel	Lot	Series [b]	Jernkontoret cleanliness rating [c]	ASTM grain size [d]	Carbide distribution	Polarity, deg [e]	Life, stress cycles
SAE 52100	19A	16	2D thin	20	None	60	0.1×10^6
	19A	16	2D thin	20	None	60	35
Al steel (MHT)	21A	17	3D thick	20	Light	45	42
	21A	17	3D thick	20	Light	90	45
440C	18	11	2D thin	13	Light	0	1.3
	18	11	2D thin	13	Light	0	47
L.A.T.S. (Halmo)	3	10	1D thin	8	Heavy	30	11
	3	10	1D thin	7	Heavy	75	41
AISI M-50	23	20 A and B	Very clean	10	Heavy	30	26
	23	20 A and B	Very clean	10	Medium	45	103
	25	22	Very clean	10	Light	60	33
	25	22	Very clean	10	Light	45	176
	25A	19	1C thin	10	Heavy	30	6
	25A	19	1C thin	10	Heavy	75	53
	4	6, 8	Very clean	13	Light	15	17
	4	6, 8	Very clean	15	Light	0	116
	26	18	Very clean	13	Light	45	35
	26	18	Very clean	13	Medium	0	80
	26	21	Very clean	13	Light	0	15
	26	21	Very clean	13	Light	30	37

[a] From ref. 38.
[b] Lowest-life ball in each series is listed first.
[c] By comparison with ASTM E45-51 charts.
[d] Intercept method.
[e] Degrees between failure pit and pole as determined by deep etch.

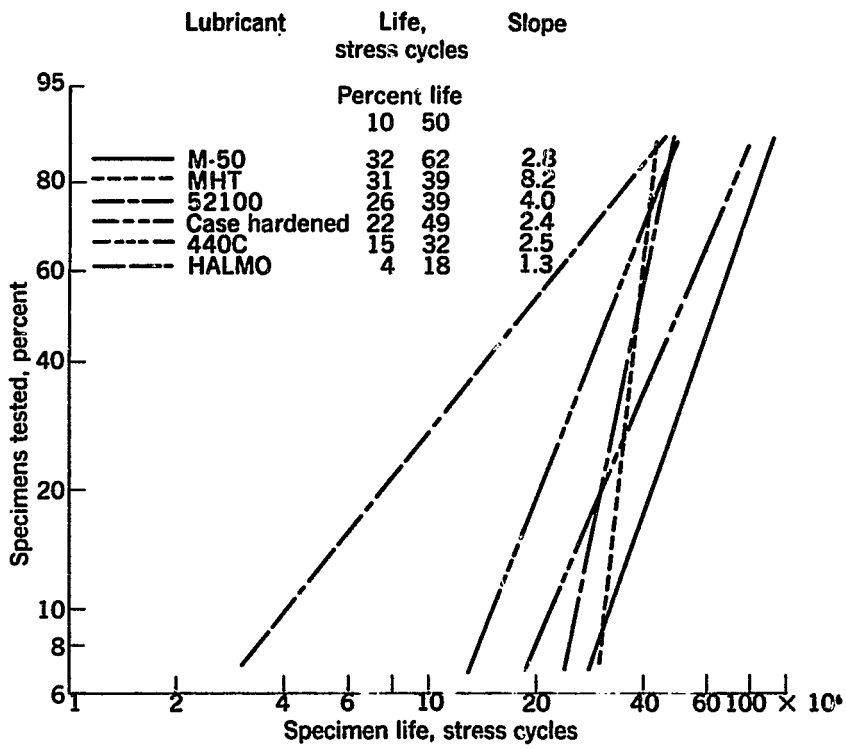

FIGURE 12-30.—Best results obtained with each of six materials tested. (From ref. 38.)

(2) Vacuum melting appears to improve fatigue life but not in proportion to the improvement in cleanliness, and consumable-electrode vacuum melting produces the most consistently good material.

(3) Vacuum melting does not reduce the number of early failures, since the scatter in life is about the same with vacuum-melted materials as with air-melted materials.

(4) The material M–50, especially vacuum-melted M–50, appears to have good fatigue life (refs. 37 and 38).

Hardness

Material hardness is of prime importance because a minimum hardness is required to prevent brinelling and plastic flow in the race grooves. In addition, hardness varies with temperature. Knowing how fatigue life varies with hardness is necessary so that the secondary effects of temperature can be assessed. Hardness is intimately associated with heat treatment and structure and therefore is of general interest in studying rolling-element fatigue.

Early work on the effect of hardness on bearing life was reported by Irwin (ref. 39). Four groups of SAE 52100 207-size bearings were fatigue tested and produced the results shown in figure 12–31. A continuous improvement in fatigue life was noted over the hardness range from Rockwell C–59 to C–63. The life data shown in figure 12–31 were replotted in terms of relative capacity as a function of hardness and are shown in figure 12–32. Also shown in figure 12–32 are plots of hardness and temperature for SAE 52100, MHT, and M–50. When the hardness and relative-capacity curve is assumed the same for all three materials, the relative capacity can be calculated for each material at any temperature over the range for which hardnesses are given. At 400° F, for example, the Rockwell hardnesses of 52100, MHT, and M–50 are C–57.4, C–59.1, and C–60.8, respectively; these hardnesses produce relative capacities of 65, 86, and 95 percent, respectively. The importance of maintaining high hardness is thus evident.

Jackson (ref. 38) conducted fatigue tests of three groups of M–50 balls in a modified one-ball fatigue tester. These data, which are

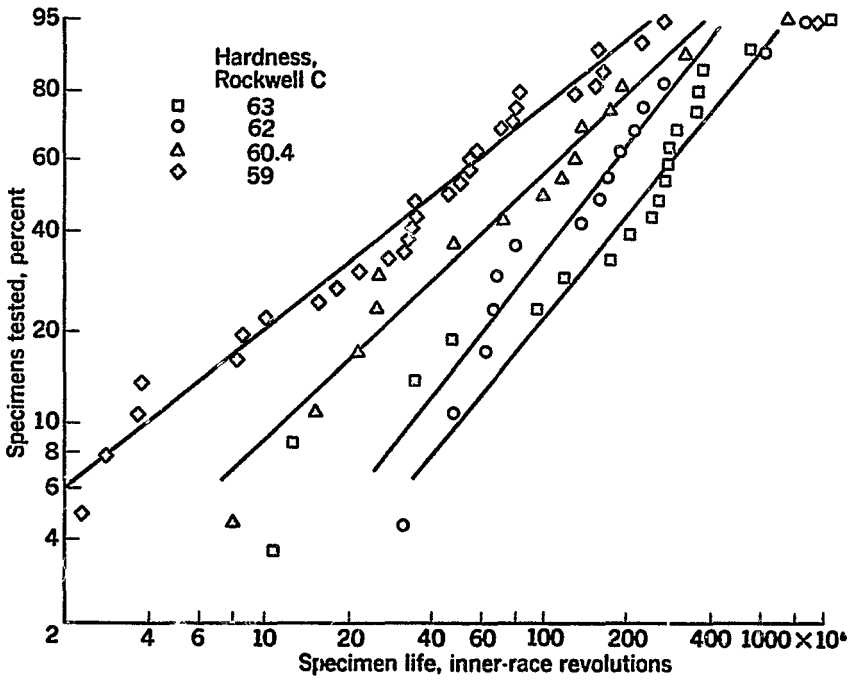

FIGURE 12–31.—Ball-bearing fatigue life at four hardness levels. (From ref. 39.)

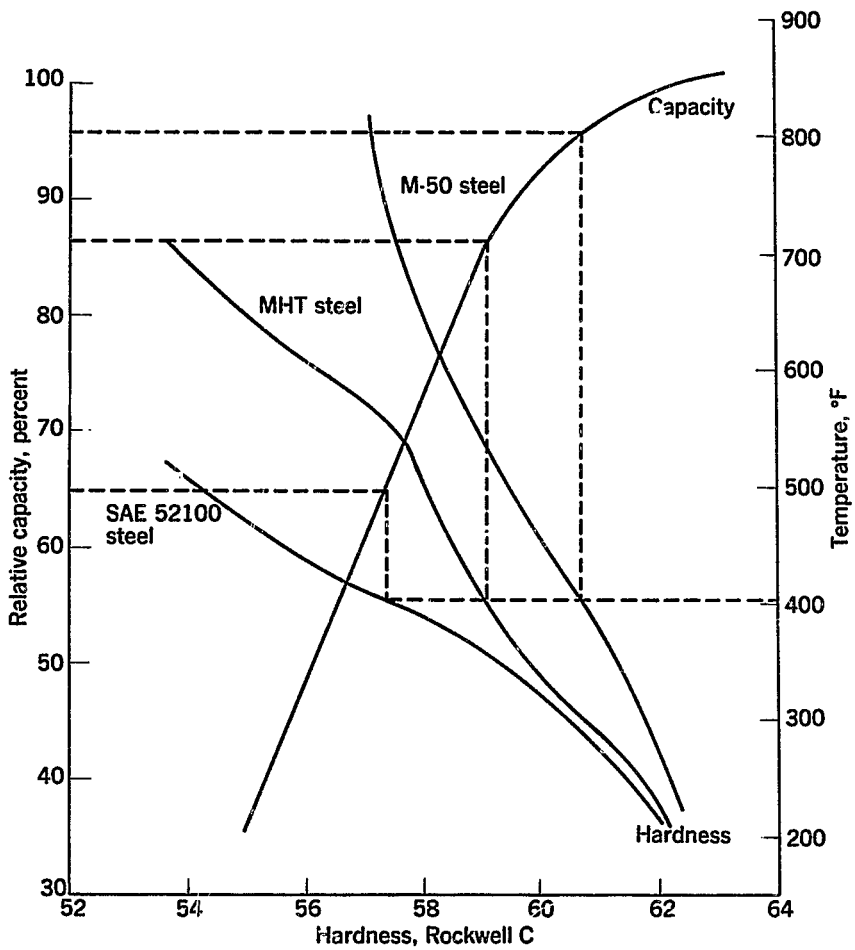

FIGURE 12–32.—Relation between temperature, hardness, and bearing load capacity for three materials. (From ref. 39.)

shown in figure 12–33, indicate a continuous increase in fatigue life with increasing hardness over the hardness range from Rockwell C–60 to C–63.5. The improvement in life over this hardness range is greater than one order of magnitude. Similar data were obtained by Zaretsky and Anderson (ref. 40) for M–1, M–50, and Halmo steel balls in the fatigue spin tester and for WB–49 steel balls in the five-ball fatigue tester. These data are summarized in figure 12–34. Fatigue life for each of these materials increased continuously with increasing hardness over the ranges of hardness investigated. For these four materials, the 10-percent fatigue life at the highest hardness was 3 to 15 times the life at the lowest hardness. These data

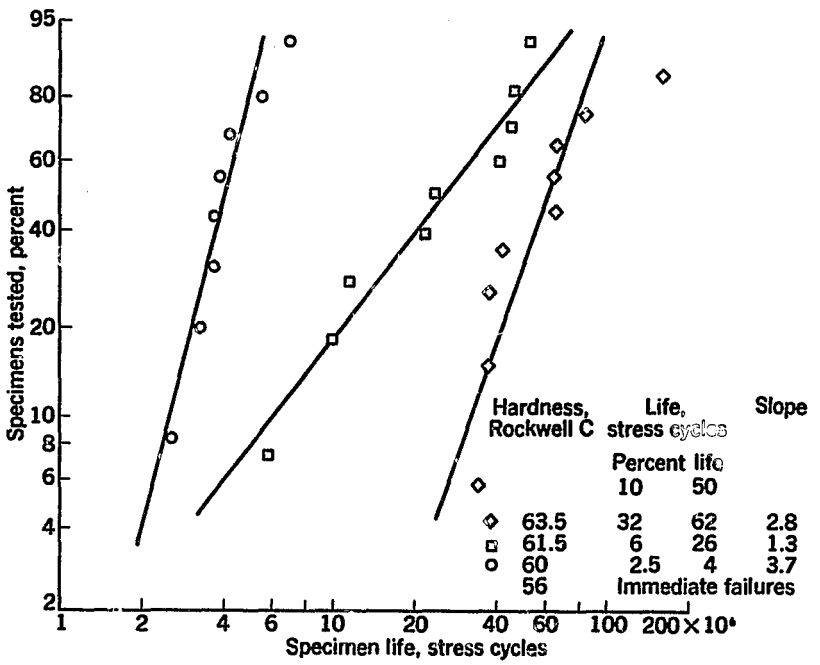

FIGURE 12–33.—Effect of hardness on fatigue life. One lot of M–50 retempered Lubricant, fresh Mil-L-7808C. (From ref. 38.)

from reference 41 are plotted in terms of relative capacity in figure 12–35. The capacity of the softest of each of the materials varied from 70 to 40 percent of the capacity of the hardest material of each alloy. Thus, a few points of hardness can easily double the load capacity of a given material.

Baughman (ref. 42) conducted fatigue tests on M–50 specimens in the rolling-contact tester to determine the effects of hardness, surface finish, and grain size on fatigue life. Four tests were conducted at each combination of grain size, hardness, surface finish, and stress level. This number of tests for each combination of variables is a bare minimum; justification is based on previously published reproducibility studies (ref. 14). A statistical analysis was used to determine the influence of each variable on the 10-percent life. Because of the small number of data points obtained in reference 14, the validity of the conclusions is questionable.

The effect of grain size at various hardness levels and values of surface finish is shown in figure 12–36. Large grains (indicated by a small grain-size number) are beneficial, especially in the high hardness range. The sensitivity of the 10-percent life to grain size diminishes as the hardness is lowered. Life appears to improve with surface

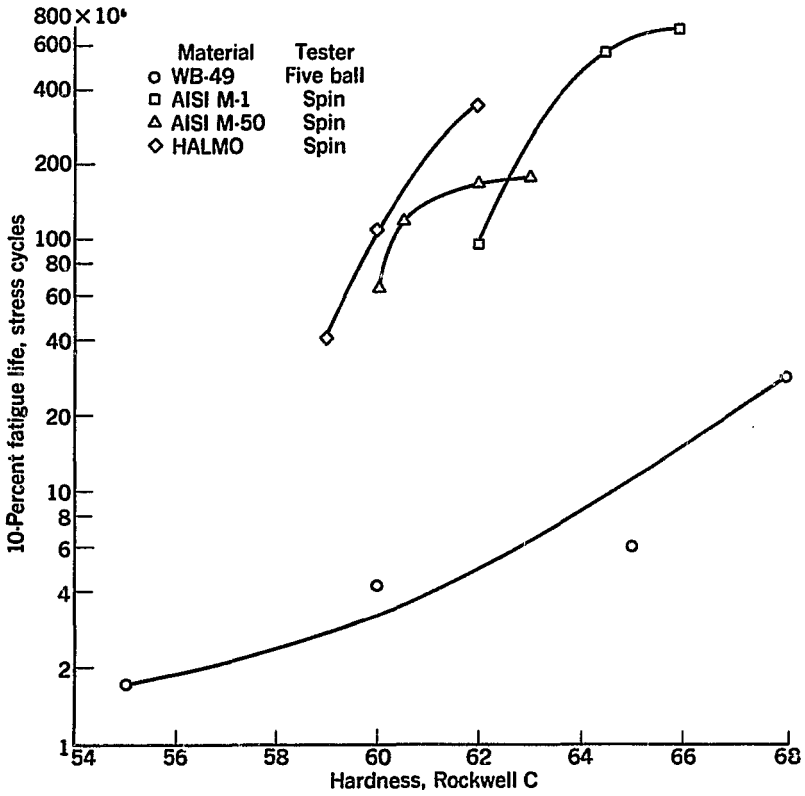

FIGURE 12–34.—Ten-percent fatigue failure life as function of hardness for four tool steels. (From ref. 40.)

finish since the upper bound on life is formed by the 2 rms surface finish (fig. 12–37). As the surface is roughened, life decreases. As with grain size, the sensitivity of 10-percent life to surface finish diminishes as the hardness is lowered. The effect of hardness on the 10-percent life at various values of grain size is shown in figure 12–38. At the larger grain sizes, a continuous improvement in 10-percent life with increasing hardness is indicated over the entire range of hardness investigated. As the grain size decreases, the 10-percent life peaks at an intermediate hardness. For example, at a grain size of 10 and a surface finish of 2 rms, the maximum life occurs at a hardness of Rockwell C–62. The sensitivity of 10-percent life to hardness decreases with decreasing grain size.

Figure 12–39 (ref. 42) shows the effect of hardness on 10-percent life at various values of surface finish. The sensitivity of 10-percent life to hardness is greatest at the finest surface finish and diminishes as

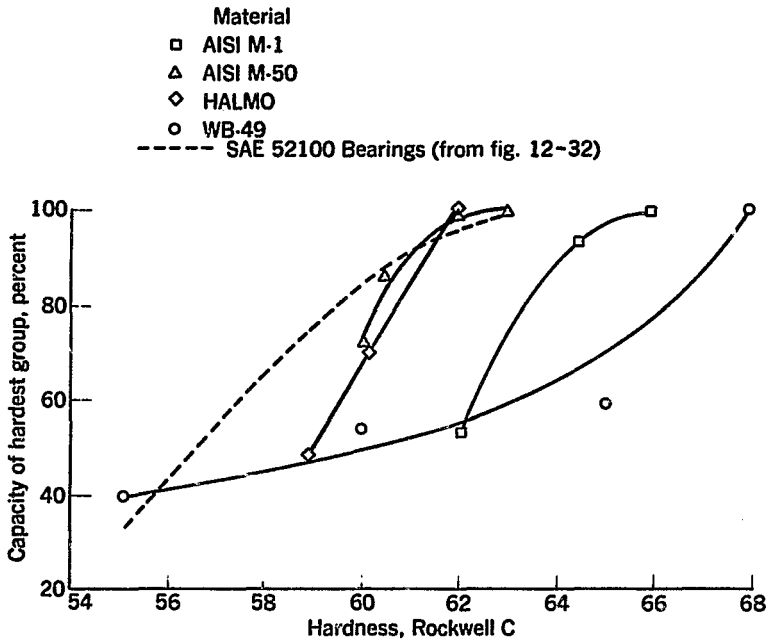

FIGURE 12-35.—Relative load-carrying capacity of bearing steel balls tempered to different hardness levels. (From ref. 41.)

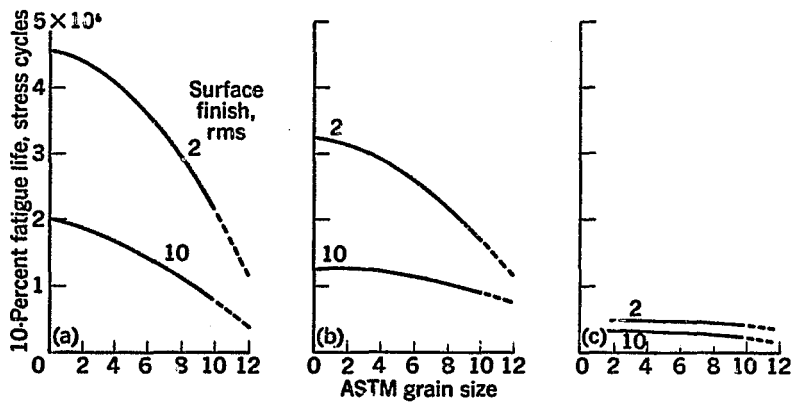

(a) Hardness, Rockwell C-62½. (b) Hardness, Rockwell C-58. (c) Hardness, Rockwell C-54.

FIGURE 12-36.—Effect of grain size on 10-percent fatigue life for various hardnesses and surface finishes. (From ref. 42.)

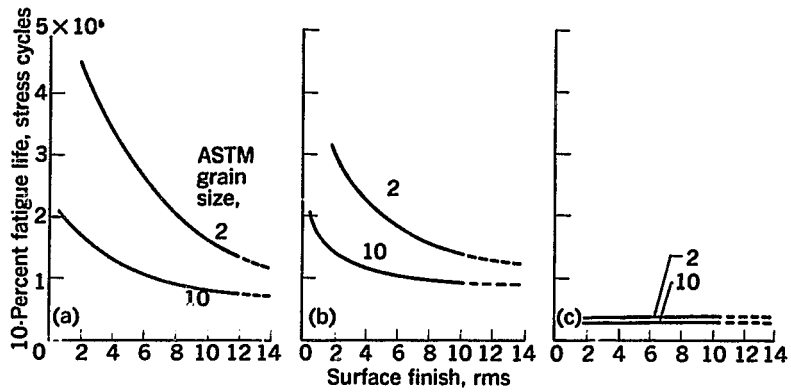

(a) Hardness, Rockwell C–62¼. (b) Hardness, Rockwell C–58. (c) Hardness, Rockwell C–54.

FIGURE 12–37.—Effect of finish on 10-percent fatigue life for various hardnesses and grain sizes. (From ref. 42.)

the surface becomes rougher. Life appears to improve continuously over the entire range of hardnesses at the finer values of surface finish and to peak at an intermediate hardness level at the coarsest surface finish. For example, at a surface finish of 10 rms and a grain size of 2, the maximum 10-percent life occurs at a hardness of Rockwell C–62. From the results of reference 42, maximum 10-percent life for M–50 steel is obtained at maximum hardness (Rockwell C–64 in this investigation), the finest surface finish, and the largest grain size.

From the mass of fatigue data accumulated with materials of various hardnesses, maximum fatigue life is obtained with the highest hardness material. Highest hardness means the maximum hardness obtainable with reasonable heat-treatment procedures. This conclusion appears to be true for the various iron-base alloys, which are candidates for bearing materials for service at temperatures up to 1000° F. In most instances, the rate of increase of fatigue life (or load capacity) with increasing hardness diminished at higher hardness values, which indicates tha further increases in hardness would produce little benefit in extended life.

Fiber Orientation

The races and rolling elements of most rolling-element bearings are formed by forging. Any metallic object formed by forging generally possesses a fiber flow pattern that reflects the flow of metal during the forming operation. Nonmetallic inclusions are progressively elongated during each forming operation from the ingot to the final bearing-element shape, and although the desired metallic crystalline

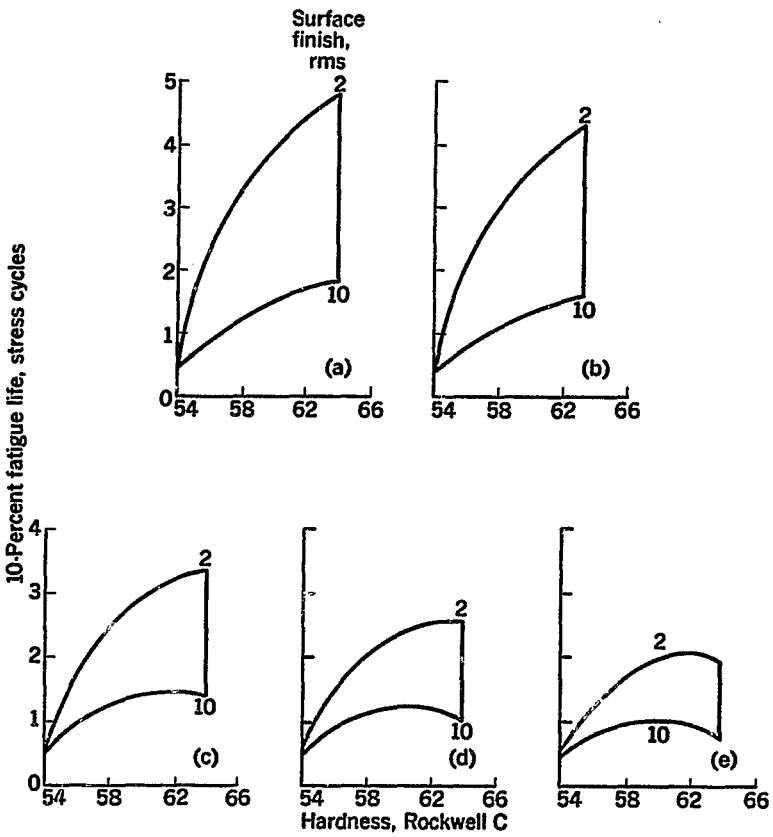

(a) ASTM grain size, 2. (b) ASTM grain size, 4.

(c) ASTM grain size, 6. (d) ASTM grain size, 8. (e) ASTM grain size, 10.

FIGURE 12-38.—Effect of hardness on 10-percent fatigue life for various grain sizes and surface finishes. (From ref. 42.)

structure is obtained by heat treatment, the inclusions retain their accumulated elongation pattern. This pattern is best described as fibrous in appearance; hence the term fiber flow lines. The type of forging used to produce rolling-element bearing components determines the fiber pattern that exists in these bearing parts. The effect on fatigue of the orientation of fibers with respect to the surface being tested is reported in references 15 and 41.

In particular, steel balls are usually fabricated by upsetting between hemispherical dies. This fabrication technique produces a fiber flow pattern with two diametrically opposed areas having fibers oriented approximately perpendicular to the surface. These areas are commonly known as the poles. The excess metal extruded from between

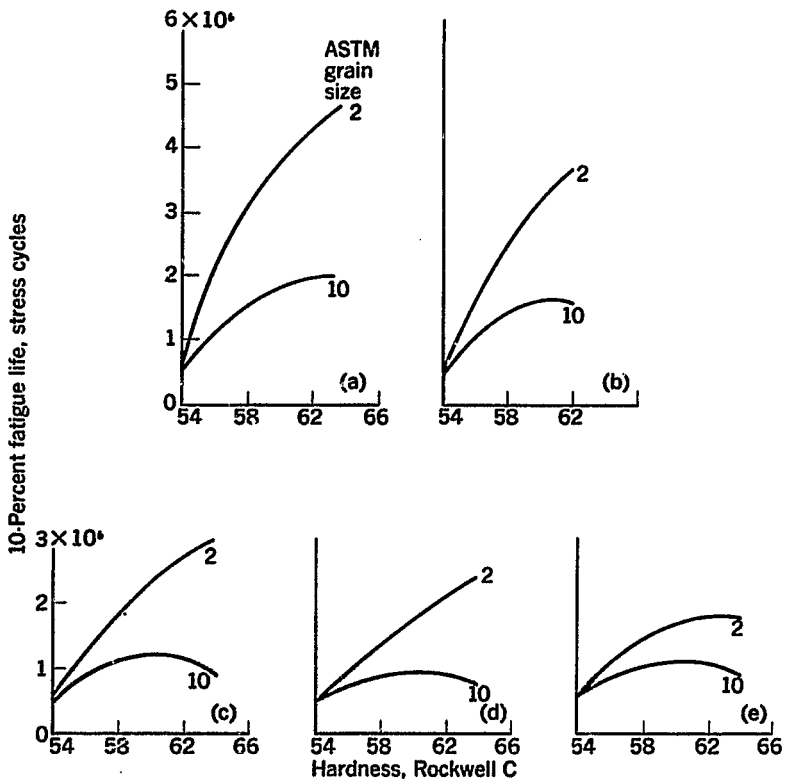

(a) Surface finish, 2 rms. (b) Surface finish, 4 rms.

(c) Surface finish, 6 rms. (d) Surface finish, 8 rms. (e) Surface finish, 10 rms.

FIGURE 12–39.—Effect of hardness on 10-percent fatigue life for various grain sizes and surface finishes. (From ref. 42.)

the two dies produces a thin band of perpendicularly oriented fiber when the flashing at the die parting line is removed. This line, when present, is commonly termed the equator. Thus, a typical ball has several surface areas with varying fiber orientation.

The initial effect of fiber orientation on fatigue life (ref. 15) was carried out in the spin tester using two lots of SAE 52100 balls. Each of these two lots of balls was modified during manufacture by a 0.050-inch hole drilled diametrically through it. This predetermined the axis of rotation and enabled one lot to be run over the poles and the other on the equator. The results obtained from these tests are shown in figure 12–40. The results are shown as a bar graph, because most of the balls run on the equator did not fail after 10^9 stress cycles. The 10-percent life obtained from the balls run over the poles was of the order of 17×10^6 stress cycles. These results indicate a significant

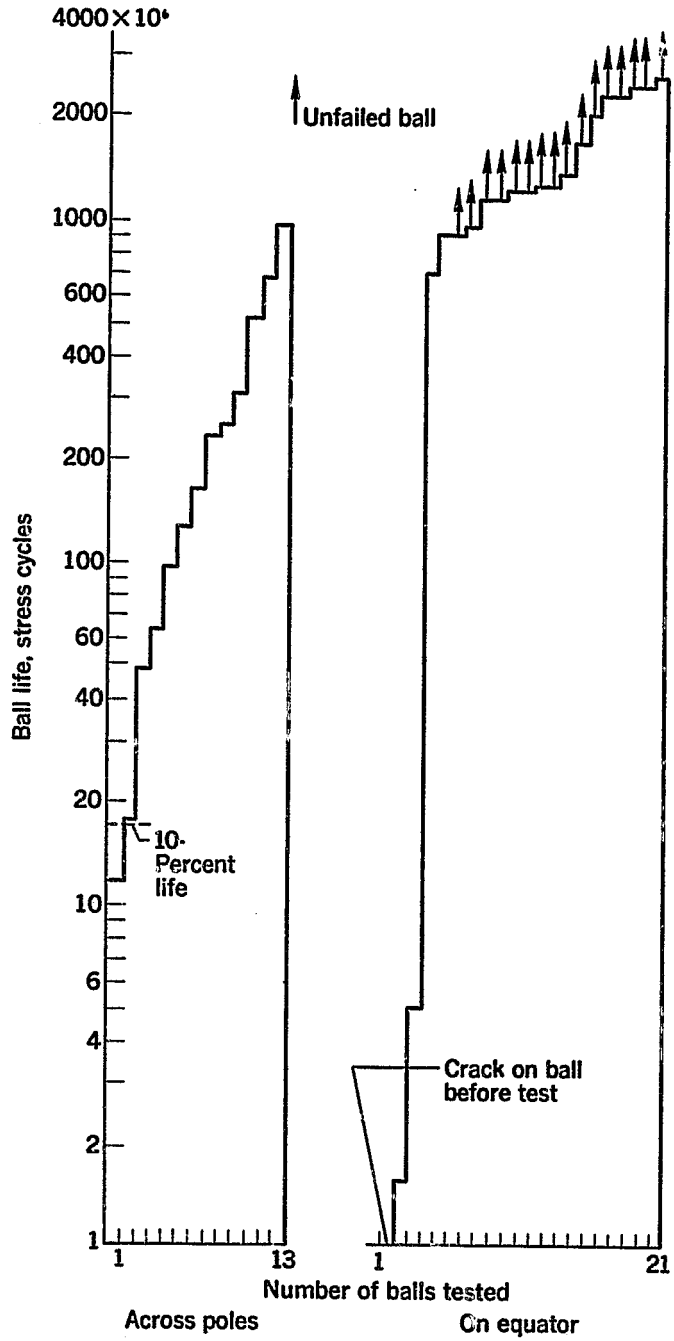

FIGURE 12–40.—Comparison of tests in which SAE 52100 balls ran on equator and across poles. Room temperature; synthetic diester lubricant; maximum Hertz compressive stress, 714,000 psi. (From ref. 41.)

693-499 O-64—29

improvement in fatigue life when the test track did not pass through the poles.

Fatigue data obtained with 10 different ball materials (ref. 15) were then examined with respect to the location of specific spalls on the ball test specimens. Each of the ball specimens was destructively etched after testing to indicate the location of the failure relative to the pole areas. From these data, a plot of failure density against ball latitude starting at 0° at the equator and going 90° to the center of each pole was made. These data (fig. 12–41) indicate that a small increase in

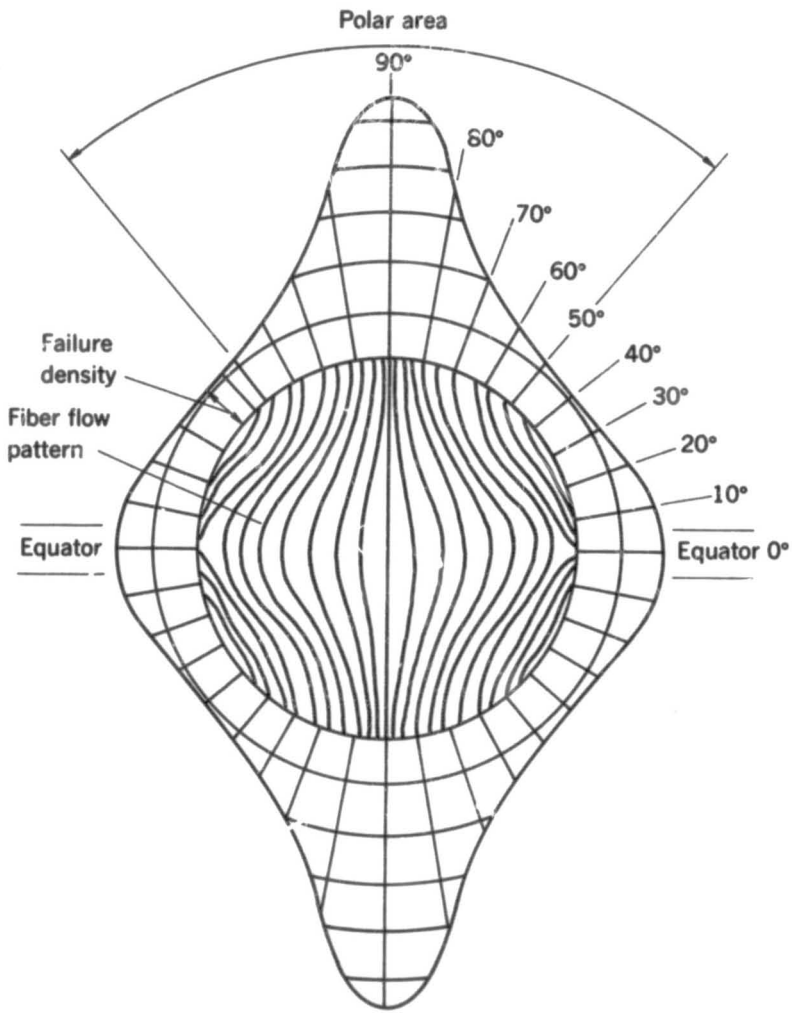

FIGURE 12–41.—Failure density as function of ball latitude (for 211 failures and 10 materials). (From ref. 41.)

failure density occurs at the equator where the thin band of perpendicular fiber exists, and a very significant increase in failure density occurs in the polar areas or regions where fiber is essentially perpendicular to the test surface.

Specimens with controlled fiber flow were obtained by machining race cylinders from a billet of AISI T–1 steel at various angles to the direction of forging to obtain better control of fiber orientation than is available in ordinary test balls. As shown in figure 12–42, three cylinders were machined with axes parallel to, at 45° to, and perpendicular to the direction of fiber flow. The first cylinder had fiber flow parallel to the test surface (0° cylinder), the second had fiber orientation that ranged continuously from parallel to 45° to the test surface (0° to 45° cylinder), and the third had fiber orientation that ranged continuously from parallel to perpendicular to the test surface (0° to 90° cylinder). For each of these three test cylinders, approximately 60 failures were obtained. The fatigue-life results for the three special test cylinders are given in figure 12–43. The 0° cylinder had the best life, while the 0° to 45° and 0° to 90° cylinders had approximately equal lives. The difference in 10-percent lives represents about two standard deviations. These data indicate that there is a significant difference in life between the 0° cylinder and the other two cylinders.

In addition to the fatigue-life data obtained from these cylinders, further evidences of the effect of fiber orientation on fatigue were obtained by examining failure density as a function of fiber-orientation angle. In both the 0° to 45° and 0° to 90° cylinders, there are four similar 90° quadrants so that the data could be condensed into one equivalent quadrant. The equivalent quadrant was then divided into four zones for the 0° to 45° cylinder and five zones for the 0° to 90° cylinder, and the number of failures in each zone were counted. The resulting histograms are shown in figure 12–44. This figure shows

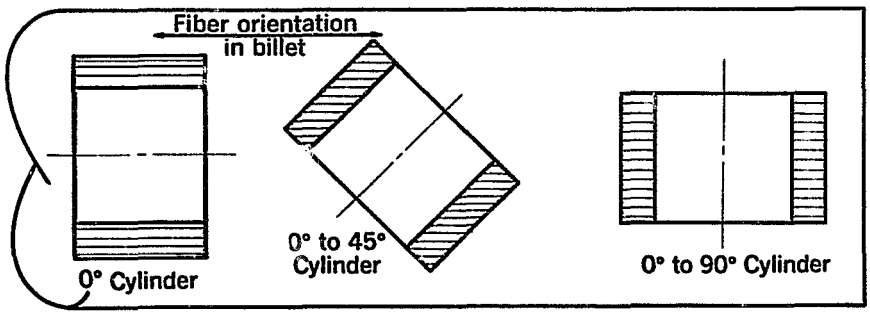

FIGURE 12–42.—T–1 tool-steel-cylinder orientation in billet stock. (From ref. 41.)

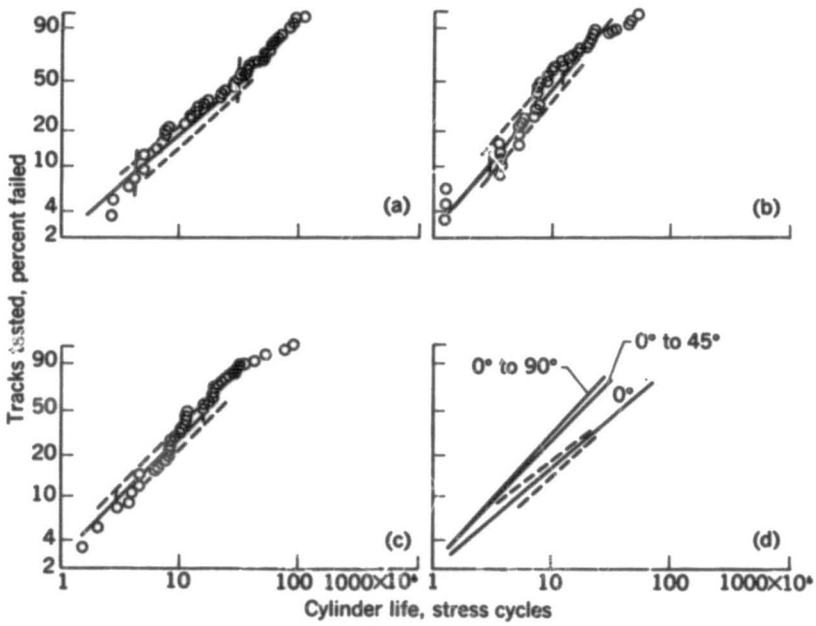

(a) 0° cylinder. (b) 0° to 45° cylinder.

(c) 0° to 90° cylinder. (d) Comparison of three cylinders.

FIGURE 12–43.—Fatigue life data for specially oriented T–1 tool-steel cylinders. Dashed line indicates standard deviation. Room temperature; lubricant, SAE 10 mineral oil; maximum Hertz compressive stress, 750,000 psi. (From ref. 41.)

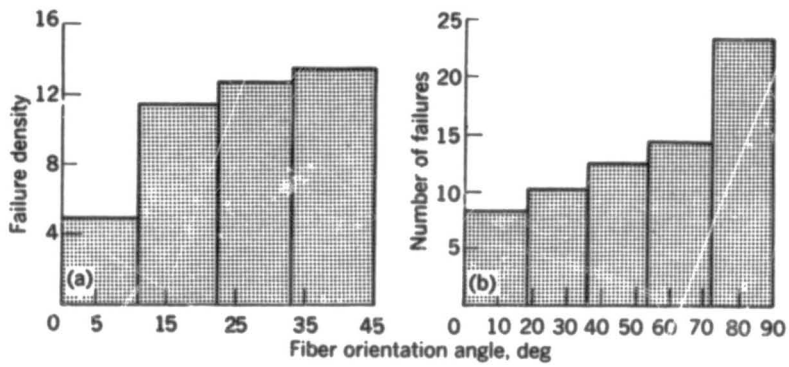

(a) 0° to 45° cylinder. (b) 0° to 90° cylinder.

FIGURE 12–44.—Variation in failure density with fiber-orientation angle in the 0° to 45° and 0° to 90° T–1 tool steel cylinders. (From ref. 41.)

that for both cylinders, the failure density is significantly higher in the regions of greater fiber-orientation angles than in the regions where

the fibers are oriented almost parallel to the test surface. Thus both life and failure-density data indicate that large fiber-orientation angles are detrimental to rolling-contact fatigue.

Jackson (ref. 38) also found that a greater than expected failure incidence occurred in the polar areas of ball specimens. These data are shown in table 12–XXIV.

To summarize the fiber orientation results obtained in references 15, 38, and 41 with ball and cylinder specimens, it would appear that better life could be obtained with rolling-element bearings if forging processes are used, which result in parts having fiber flow parallel or nearly so to the test surface.

Contact Angle

Palmgren (ref. 1) and Lundberg and Palmgren (ref. 2) suggest that the load-carrying capacity of a thrust bearing increases as a function of increasing contact angle. As contact angle is increased for a constant bearing thrust load, the normal ball load is decreased. Since the Lundberg-Palmgren theory predicts constant life with constant normal ball load, fatigue life should increase. Unpublished ball-fatigue data obtained from Pratt & Whitney Aircraft for specimens in the one-ball tester indicate that at contact angles of 30° to 55°, fatigue life decreases with increasing contact angle at constant normal ball load. These data, therefore, imply a quantitative discrepancy between the theory and the experimental results. Further experiments to determine the effect of contact angle on fatigue are reported in reference 36. The five-ball fatigue tester was used in these experiments with tests conducted at contact angles of 10°, 20°, 30°, and 40°. The Pratt & Whitney tests, in the one-ball tester, were conducted using V-grooved rollers with the V-groove angle changed to vary the contact angle. The fatigue-life results obtained by Pratt & Whitney and in reference 36 are summarized in figure 12–45. A smooth curve results when the data from both testers are plotted against contact angle, with life at constant contact stress that shows a continuous decrease with increasing contact angle. These life data were converted to thrust-load capacity and compared with the predicted thrust-load capacity as shown in figure 12–46. Again, the data for the two testers plot as a smooth curve. The experimental capacity agrees well with the predicted capacity at contact angles up to 30°. At contact angles above 30°, the experimental capacity is less than the predicted capacity, and the deviation increases as contact angle is increased.

The discrepancy between thrust capacity as predicted by the Lundberg-Palmgren theory and experimental results may be due to one or more of several factors. As contact angle is increased, the ball

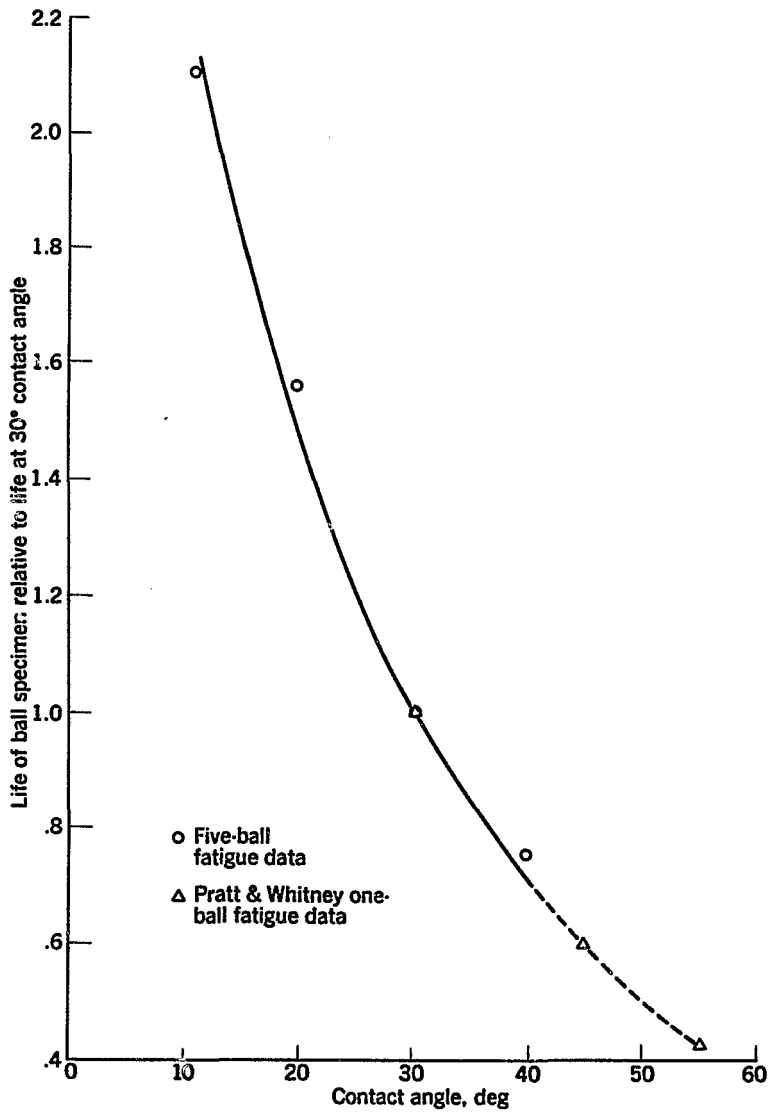

FIGURE 12–45.—Effect of contact angle at constant stress and stress volume on life of ball specimen relative to life at 30° contact angle. (From ref. 36.)

spin velocity (and, therefore, the relative sliding between ball and race) is increased. The variation of life with relative angular spin velocity is shown in figure 12–47. As contact angle, and thus spin velocity, are increased, the rate of heat generation rises. An increase in contact temperature, which has already been shown to be detrimental to fatigue life, results. Increased friction and heat generation

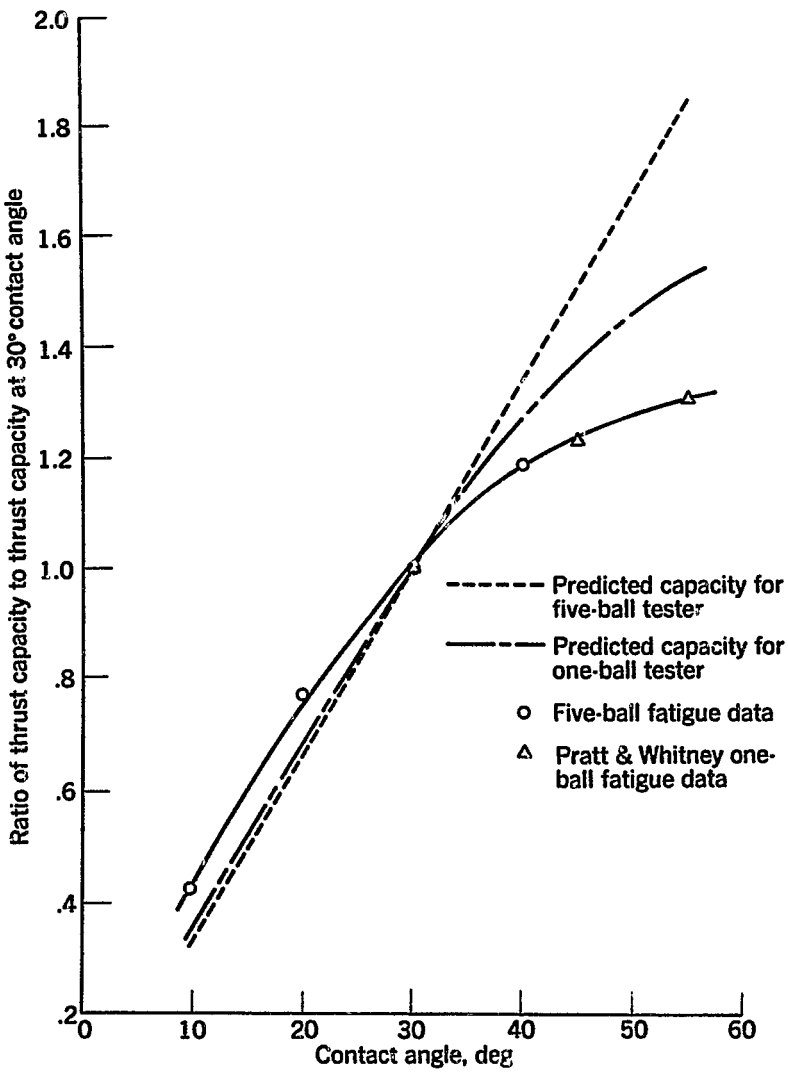

FIGURE 12–46.—Increase in thrust capacity relative to thrust capacity at 30° measured experimentally and as predicted by the Lundberg-Palmgren equation. (From ref. 36.)

can also increase the shearing stresses for two bodies in contact. The effects of friction coefficient on shearing stresses are treated theoretically by Smith and Liu (ref. 43) and those of heat generation by Melan (ref. 44). The authors of reference 33 discuss possible effects of thermal stresses.

Another factor, which may be relevant, is the effect of sliding on viscosity and other rheological properties of the lubricant film. Sibley

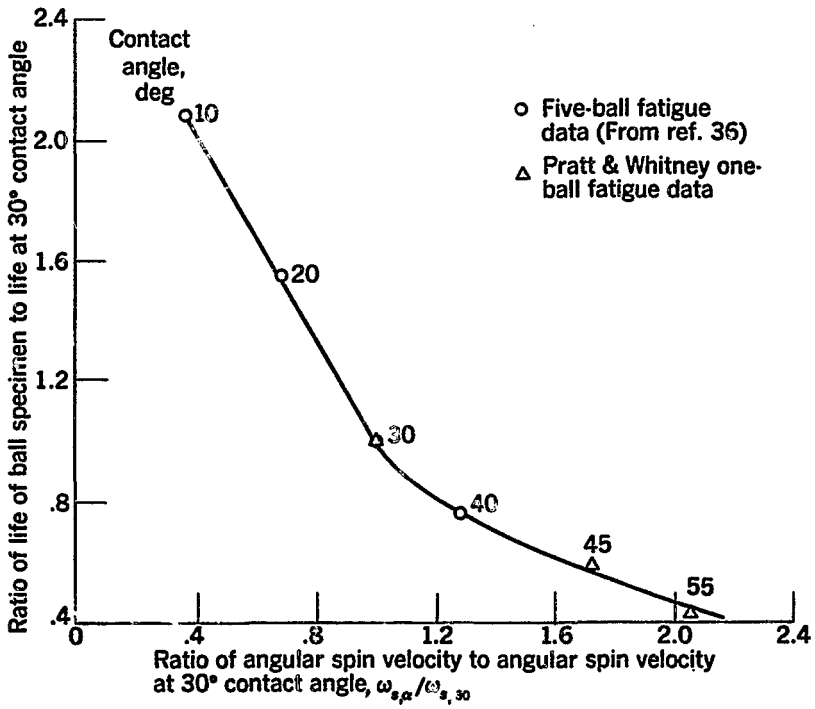

FIGURE 12–47.—Life of ball specimen relative to life at 30° contact angle against angular spin velocity relative to angular spin velocity at 30° contact angle at constant stress and stress volume.

and Orcutt (ref. 45) show experimentally that the geometry of the contact area of two rolling surfaces changes with lubricant shear rate and temperature. Further investigations with carefully controlled variables are necessary to define the importance of rheological properties on fatigue life.

REFERENCES

1. PALMGREN, A.: Ball and Roller Bearing Engineering. Third ed., SKF Industries, Inc., 1959.
2. LUNDBERG, G., and PALMGREN, A.: Dynamic Capacity of Rolling Bearings. Acta Polytech., Mech. Eng. Ser., vol. 1, no. 3, 1947.
3. WEIBULL, W.: A Statistical Theory of the Strength of Materials. Proc. Roy. Swedish Academy Eng. Sci., no. 151, 1939.
4. WEIBULL, W.: The Phenomenon of Rupture in Solids. Proc. Roy. Swedish Academy Eng. Sci., no. 153, 1939.
5. WEIBULL, W.: A Statistical Representation of Fatigue Failures in Solids. Trans. Roy. Inst. Tech., no. 27, Stockholm (Sweden), 1949.
6. TALLIAN, T.: Weibull Distribution of Rolling Contact Fatigue Life and Deviations Therefrom. Trans. ASLE, vol. 5, no. 1, Apr. 1962, pp. 183–196.

7. LIEBLEIN, J., and ZELEN, M.: Statistical Investigation of the Fatigue Life of Deep-Groove Ball Bearings. Jour. Res. Nat. Bur. Standards, vol. 57, no. 5, Nov. 1956, pp. 273–316.
8. BUTLER, ROBERT H., and CARTER, THOMAS L.: Stress-Life Relation of the Rolling-Contact Fatigue Spin Rig. NACA TN 3930, 1957.
9. MACKS, E. F.: The Fatigue Spin Rig—A New Apparatus for Rapidly Evaluating Materials and Lubricants for Rolling Contact. Lubrication Eng., vol. 9, no. 5, Oct. 1953, pp. 254–258.
10. CARTER, THOMAS L., and ZARETSKY, ERWIN V.: Rolling-Contact Fatigue Life of a Crystallized Glass Ceramic. NASA TN D-259, 1960.
11. BARWELL, F. T., and SCOTT, D.: Effect of Lubricant on Pitting Failure of Ball Bearings. Engineering, vol. 182, no. 4713, July 6, 1956, pp. 9–12.
12. SCOTT, D.: Lubricants at Higher Temperatures: Assessing the Effects on Ball Bearing Failures. Engineering, vol. 185, no. 4811, May 23, 1958, pp. 660–662.
13. CORDIANO, H. V., COCHRAN, E. P., JR., and WOLFE, R. J.: A Study of Combustion Resistant Hydraulic Fluids as Ball Bearing Lubricants. Lubrication Eng., vol. 12, no. 4, July–Aug. 1956, pp. 261–266.
14. BAUGHMAN, R. A.: Experimental Laboratory Studies of Bearing Fatigue. Paper 58-A-235, ASME, 1958.
15. CARTER, THOMAS L.: A Study of Some Factors Affecting Rolling-Contact Fatigue Life. NASA TR R-60, 1960.
16. ANDERSON, W. J., and CARTER, T. L.: Effect of Lubricant Viscosity and Type on Ball Fatigue Life. Trans. ASLE, vol. 1, no. 2, Oct. 1958, pp. 266–272.
17. Anon.: Viscosity and Density of Over 40 Lubricating Fluids of Known Composition at Pressures to 150,000 PSI and Temperatures to 425° F. Vol. II. ASME, 1953.
18. CORDIANO, H. V., COCHRAN, E. P., JR., and WOLFE, R. J.: Effect of Combustion Resistant Hydraulic Fluids on Ball Bearing Fatigue Life. Preprint 55-LUB-21, ASME, 1955.
19. ROUNDS, F. G.: Effects of Base Oil Viscosity and Type on Bearing Ball Fatigue. Preprint 61 LC-13, ASLE, 1961.
20. SCOTT, D.: Study of the Effect of Lubricant on Pitting Failure of Balls. Proc. of Conf. on Lubrication and Wear, Inst. Mech. Eng., 1957, pp. 463–468.
21. GRUNBERG, L., and SCOTT, D.: The Acceleration of Pitting Failure by Water in the Lubricant. Jour. Inst. Petroleum, vol. 44, no. 419, Nov. 1958, pp. 406–410.
22. GRUNBERG, L., and SCOTT, D.: The Effect of Additives on the Water-Induced Pitting of Ball Bearings. Jour. Inst. Petroleum, vol. 46, no. 440, Aug. 1960, pp. 259–266.
23. SCOTT, D.: The Effect of Lubricant Viscosity on Ball Bearing Fatigue Life. Rep. LDR 44/60, Dept. of Sci. and Ind. Res., Nat. Eng. Lab., Dec. 1960.
24. OTTERBEIN, MARK E.: The Effect of Aircraft Gas Turbine Oils on Roller Bearing Fatigue Life. Trans. ASLE, vol. 1, no. 1, Apr. 1958, pp. 33–40.
25. WAY, STEWART: Pitting Due to Rolling Contact. Jour. Appl. Mech., vol. 2, no. 1, June 1935, pp. A49–A58; discussion, pp. A110–A114.
26. JONES, A. B.: Metallographic Observations of Ball Bearing Fatigue Phenomena. Symposium on Testing of Bearings, ASTM, 1947, pp. 35–48; discussion, pp. 49–52.
27. DÖRR, J.: Schmiermitteldruck und Randverformungen des Rollenlagers Ing. Archiv, bd. XXII, 1954, pp. 171–193.

28. GRUBIN, A. N., and VINOGRADOVA, I. E., eds.: Investigation of the Contact of Machine Components. CTS-235, Dept. Sci. and Ind. Res. (British), 1949. (Trans. of Russian book.)
29. PETRUSEVICH, A. E. (I. C. Lecompte, trans.): Basic Conclusions from the Contact-Hydrodynamic Theory of Lubrication Greases. Reps. Acad. Sci. USSR, Dept. Tech. Sci., no. 2, Feb. 1951, pp. 209–223. (Bur. Ships Trans. 480.)
30. PORITSKY, H.: Lubrication of Gear Teeth, Including the Effect of Elastic Displacement. Paper Presented at ASLE Nat. Symposium on Fundamentals of Friction and Lubrication in Eng., 1952.
31. WEBER, C., and SAAFELD, K.: Schmierfilm bei Walzen mit Verformung. Zs. angew. Math. Mech., bd. 34, 1954, p. 54.
32. DOWSON, D., and HIGGINSON, G. R.: A Numerical Solution to the Elasto-Hydrodynamic Problem. Jour. Mech. Eng. Sci., vol. 1, no. 1, 1959, pp. 6–15.
33. STERNLICHT, B., LEWIS, P., and FLYNN, P.: Theory of Lubrication and Failure of Rolling Contacts. Jour. Basic Eng. (Trans. ASME), ser. A, vol. 83, no. 2, June 1961, pp. 213–226.
34. ZARETSKY, ERWIN V., and ANDERSON, WILLIAM J.: Rolling-Contact Fatigue Studies with Four Tool Steels and a Crystallized Glass Ceramic. Jour. Basic Eng. (Trans. ASME), ser. D, vol. 83, no. 4, Dec. 1961, pp. 603–612.
35. JONES, A. B.: The Life of High-Speed Ball Bearings. Trans. ASME, vol. 74, no. 5, July 1952, pp. 695–703.
36. ZARETSKY, E. V., ANDERSON, W. J., and PARKER, R. J.: The Effect of Contact Angle on Rolling-Contact Fatigue and Bearing Load Capacity Trans. ASLE, vol. 5, no. 1, Apr. 1962, pp. 210–219.
37. MORRISON, T. W., WALP, H. O., and REMORENKO, R. P.: Materials in Rolling-Element Bearings for Normal and Elevated (450° F) Temperatures. Trans. ASLE, vol. 2, no. 1, Apr. 1959, pp. 129–146.
38. JACKSON, E. G.: Rolling Contact Fatigue Evaluation of Bearing Materials and Lubricants. Trans. ASLE, vol. 2, no. 1, 1959, pp. 121–128.
39. IRWIN, ARTHUR S.: Effect of Bearing Temperature on Capacities of Bearings of Various Materials. Paper Presented at ASME Lubrication Symposium, New York (N.Y.), Mar. 14–15, 1960.
40. ZARETSKY, E. V., and ANDERSON, W. J.: Relation between Rolling-Contact FatigueLife and Mechanical Properties for Several Aircraft Bearing Steels. Trans. ASTM, vol. 60, 1960, pp. 627–649.
41. BIDWELL, J. B.: Rolling Contact Phenomena. Elsevier Pub. Co., 1962, pp. 317–345.
42. BAUGHMAN, R. A.: Effect of Hardness, Surface Finish, and Grain Size on Rolling-Contact Fatigue Life of M-50 Bearing Steel. Jour. Basic Eng. (ASME Trans.), ser. D, vol. 82, no. 2, June 1960, pp. 287–294.
43. SMITH, J. O., and LIU, C. K.: Stresses Due to Tangential and Normal Loads on an Elastic Solid with Application to Some Contact Stress Problems. Jour. Appl. Mech., vol. 20, no. 2, June 1953, pp. 157–166.
44. MELAN, E.: Wärmespannungen in einer Scheibe infolge einer Wandernden Wärmequelle. Ingenieur-Archiv, bd. 20, 1952, pp. 46–48.
45. SIBLEY, L. B., and ORCUTT, F. K.: Elasto-Hydrodynamic Lubrication of Rolling-Contact Surfaces. ASLE Trans., vol. 4, no. 2, Nov. 1961, pp. 234–249.

END OF REFERENCE

105

REFERENCE

106

LIQUID ROCKET ENGINE TURBOPUMP BEARINGS, NASA SP-8048, 1971.

NASA
SPACE VEHICLE
DESIGN CRITERIA
(CHEMICAL PROPULSION)

NASA SP-8048

COPY 2

LIQUID ROCKET ENGINE TURBOPUMP BEARINGS

LEWIS RESEARCH CENTER
Aerospace Safety Research
and Data Institute
JAN4 1971
CLEVELAND, OHIO

MARCH 1971

NATIONAL AERONAUTICS AND SPACE ADMINISTRATION

FOREWORD

NASA experience has indicated a need for uniform criteria for the design of space vehicles. Accordingly, criteria are being developed in the following areas of technology:

Environment
Structures
Guidance and Control
Chemical Propulsion

Individual components of this work will be issued as separate monographs as soon as they are completed. This document, part of the series on Chemical Propulsion, is one such monograph. A list of all monographs issued prior to this one can be found on the last page of this document.

These monographs are to be regarded as guides to design and not as NASA requirements, except as may be specified in formal project specifications. It is expected, however, that these documents, revised as experience may indicate to be desirable, eventually will provide uniform design practices for NASA space vehicles.

This monograph, "Liquid Rocket Engine Turbopump Bearings," was prepared under the direction of Howard W. Douglass, Chief, Design Criteria Office, Lewis Research Center; project management was by Harold W. Schmidt and Lionel Levinson. The monograph was written by Myles F. Butner of Rocketdyne Division, North American Rockwell Corporation, and was edited by Russell B. Keller, Jr. of Lewis. To assure technical accuracy of this document, scientists and engineers throughout the technical community participated in interviews, consultations, and critical review of the text. In particular, Fred R. Mallaire of Aerojet-General Corporation, Robert L. Thomas of Pratt and Whitney Aircraft Division, United Aircraft Corporation, and William J. Anderson and Herbert W. Scibbe of the Lewis Research Center individually and collectively reviewed the text in detail.

Comments concerning the technical content of this monograph will be welcomed by the National Aeronautics and Space Administration, Lewis Research Center (Design Criteria Office), Cleveland, Ohio 44135.

March 1971

GUIDE TO THE USE OF THIS MONOGRAPH

The purpose of this monograph is to organize and present, for effective use in design, the significant experience and knowledge accumulated in development and operational programs to date. It reviews and assesses current design practices, and from them establishes firm guidance for achieving greater consistency in design, increased reliability in the end product, and greater efficiency in the design effort. The monograph is organized into two major sections that are preceded by a brief introduction and complemented by a set of references.

The State of the Art, section 2, reviews and discusses the total design problem, and identifies which design elements are involved in successful design. It describes succinctly the current technology pertaining to these elements. When detailed information is required, the best available references are cited. This section serves as a survey of the subject that provides background material and prepares a proper technological base for the *Design Criteria* and Recommended Practices.

The *Design Criteria,* shown in italic in section 3, state clearly and briefly what rule, guide, limitation, or standard must be imposed on each essential design element to assure successful design. The *Design Criteria* can serve effectively as a checklist of rules for the project manager to use in guiding a design or in assessing its adequacy.

The Recommended Practices, also in section 3, state how to satisfy each of the criteria. Whenever possible, the best procedure is described; when this cannot be done concisely, appropriate references are provided. The Recommended Practices, in conjunction with the *Design Criteria,* provide positive guidance to the practicing designer on how to achieve successful design.

Both sections have been organized into decimally numbered subsections so that the subjects within similarly numbered subsections correspond from section to section. The format for the Contents displays this continuity of subject in such a way that a particular aspect of design can be followed through both sections as a discrete subject.

The design criteria monograph is not intended to be a design handbook, a set of specifications, or a design manual. It is a summary and a systematic ordering of the large and loosely organized body of existing successful design techniques and practices. Its value and its merit should be judged on how effectively it makes that material available to and useful to the designer.

CONTENTS

	Page
1. INTRODUCTION	1
2. STATE OF THE ART	4
3. DESIGN CRITERIA and Recommended Practices	31
REFERENCES	69
GLOSSARY	73
NASA Space Vehicle Design Criteria Monographs Issued to Date	77

SUBJECT	STATE OF THE ART		DESIGN CRITERIA	
BEARING ASSEMBLY DESIGN	*2.1*	4	*3.1*	31
Load Capability	*2.1.1*	5	*3.1.1*	31
Speed Capability	*2.1.2*	12	*3.1.2*	31
Stiffness	*2.1.3*	13	*3.1.3*	32
Misalignment Tolerance	*2.1.4*	14	*3.1.4*	32
Bore	*2.1.5*	14	*3.1.5*	33
Internal Clearance	*2.1.6*	14	*3.1.6*	34
Cooling	*2.1.7*	16	*3.1.7*	34
Bearing Mounting	*2.1.8*	18	*3.1.8*	40
Bearing Materials	*2.1.9*	19	*3.1.9*	46
Testing	*2.1.10*	23	*3.1.10*	52
BEARING COMPONENT DESIGN	*2.2*	23	*3.2*	52
Rolling Element Design	*2.2.1*	23	*3.2.1*	52
Race Design	*2.2.2*	25	*3.2.2*	59
Cage Design	*2.2.3*	28	*3.2.3*	63

LIST OF FIGURES

Figure	Title	Page
1	Split-inner-ring ball bearing	7
2	Angular-contact ball bearings	7
3	Roller bearing applications	8-9
4	Balance piston bearing systems	10
5	Balance piston system clearances, loads, and deflections	11
6	Race crowning to allow for misalignment in roller bearings	15
7	Race-retention methods	20
8	Poisson's effect of heavy radial load	21
9	Bearing clamping to eliminate fretting	21
10	Roller crowning	25
11	Ball bearing unloading chute	29
12	Types of lubrication jets	38
13	Inner race fits, ABEC-5	41
14	Outer race fits, ABEC-5	42
15	Shaft shoulder design	43
16	Housing or shaft shoulder height sizing	45
17	Provisions for race removal	45
18	Required clamping force	47
19	Ball size basic proportions	53
20	Roller size basic proportions	54
21	Roller dimension terms and symbols	58
22	Shoulder configuration terms and symbols	58

Page

23 Bearing race average diameters 60
24 Ball bearing race shoulder height 62
25 Ball bearing raceway edge relief 62
26 Cage construction 64-65
27 Coolant flow channels 66

LIST OF TABLES

Table Title Page

I Comparison of Turbopump Bearings 4
II Summary of Current Turbopump Bearing Capabilities 6
III Speed Limits for Bearings 12
IV Curvature and Contact Angle for Specific Design Goals Using Ball Bearings 26
V Bearing Misalignment Capabilities 33
VI Corrosion Resistant Race and Rolling Element Materials 48
VII Recommended Cage Materials 51
VIII Roller Bearing Capacity Reduction Caused by Bearing Misalignment 59

LIQUID ROCKET ENGINE TURBOPUMP BEARINGS

1. INTRODUCTION

Bearing requirements for liquid propellant rocket engine turbopumps have forced advances in a specialized branch of bearing technology to fulfill the special and unusual operating conditions of speed, load, life, and environment. Advances in technology presently are being pursued to develop longer life bearings, roller bearings cooled by propellants, higher speed bearings, bearings for service with liquid fluorine, and solution of ball speed variation problems. Also in progress are bearing-material development programs for space environments, applications with heat soakback, hot restarts, and extended exposures to propellants at elevated temperatures.

These advances in bearing technology rely heavily on empirical results of testing under actual or simulated operating environments. In addition, computer calculations are utilized extensively to evaluate the effects of speed, geometry, and loading on bearing life, stresses, and deflections, and to determine bearing spring rates used for shaft dynamics calculations.

Presently, rolling contact bearings are utilized almost exclusively in preference to fluid film bearings because of the following characteristics:

- Large capacity-to-volume ratio
- Ability to operate independently of external pressurizing systems
- Ability to operate satisfactorily after ingesting foreign material
- Tolerance for short periods of coolant/lubrication starvation
- High radial spring rate
- Low heat generation and coolant/lubrication consumption

The development of bearings satisfactory for use with rocket engine turbopumps has depended on the solution of a number of basic problems in bearing design:

(1) Use of nonlubricants for cooling high-speed, high-load bearings has required specialized bearing geometry, careful material selection, adequate coolant quantity, and control of manufacturing processes.
(2) Maintaining quality control of bearings has required adequate specifications for physical properties of what may often be new materials, for material identification, for confirmation of material integrity, for cleaning and packaging, and for inspection of new bearing physical dimensions.
(3) Obtaining shaft dynamic response through design control of the bearing stiffness has required that bearing detail design be performed as part of the basic turbo-

pump layout selection input. Computerized analyses of bearings and shaft systems make possible the rapid evaluation of trial designs.

(4) Permanent race and rolling element dimensional changes that occur when bearings are chilled to cryogenic temperatures have been eliminated by the use of stabilizing chill cycles prior to final machining.

(5) Rolling element size changes due to thermal effects or wear remain a problem. There is some experimental evidence that race relief (unloading chute) may be a solution for ball bearings.

(6) Cage wear problems largely have been overcome by the use of low-friction materials to provide the lubricating function, use of adequate clearances, use of sufficient web thickness to allow for wear, material properties control, and manufacturing quality control.

(7) Damage and wear caused by skidding of rolling elements operating at high speed and low load have been controlled by the use of suitable axial or radial preloading.

Prevention of bearing problems is more effective and less costly than their cure. It is essential that the bearing designer participate in turbopump preliminary design by aiding the mechanical designer in basic decisions that influence the bearing application and overall reliability. In this capacity, the bearing designer should

- Reduce the DN value of the bearings to a minimum
- Minimize the number of bearings used
- Guide the mechanical designer in selecting the proper bearing type
- Secure hydraulic balancing of impeller forces
- Select bearing materials with appropriate chemical and mechanical properties
- Provide for mechanical balancing
- Provide adequate clean coolant supply
- Assure practical means for bearing assembly
- Avoid design practices that lead to severe misalignment and the detrimental combination of radial and thrust load

These provisions are more easily incorporated as integral design features before the design is hardened than as adjustments after detailing is underway.

After a firm turbopump layout has been adopted, the bearing designer should review design details of pump parts affecting bearings, e.g., fits, finishes, and race clamping; perform detailed examination of specimens from bearing tests to detect any need for bearing design improvements; and examine bearings from component (turbopump hot fire) and engine tests to verify that the bearing design is adequate for the actual operating conditions of load, alignment, and cooling. This step is mandatory because accurate prediction of pump loads and temperatures is extremely difficult.

The material that follows has been divided into two categories: (1) the fundamental problems involved in bearing assembly design; and (2) the problems involved in the design of the three basic bearing components—the rolling element, the race, and the cage.

These problems are considered in the order and manner in which the designer must handle them. The designer must first choose a bearing assembly design that will meet all the needs of the proposed application and then design the components to meet the needs of the assembly. In all cases, there is cross-feed between these two design efforts, and accordingly this monograph frequently cross-references and dovetails related material.

2. STATE OF THE ART

2.1 Bearing Assembly Design

Turbopump shafts are generally supported at two bearing positions. These are placed as closely as possible to major rotating components to reduce radial movement and to control critical speeds. Ball bearings (Conrad-type, angular-contact, and split-inner-ring) and cylindrical roller bearings are used because of their capabilities in load, speed, stiffness, and misalignment tolerances (see table I). Film bearings have found limited use in specialized applications. Tapered roller bearings, needle bearings, and pure-

TABLE I.—Comparison of Turbopump Bearings

Bearing type	Advantages	Disadvantages	Primary condition for use
Conrad-type ball	Any combination of radial and thrust direction; large misalignment capability; moment load capacity	Limited number of balls; two-piece cage necessary	Combined load; two-direction thrust loads
Angular-contact ball	Thirty percent more capacity than similar size Conrad; one-piece cage	Predominant thrust required; one-direction capacity; lower misalignment tolerances than Conrad	High speed, high load; single-direction thrust
Split-ring ball	Thirty percent more thrust capacity than similar size Conrad; one-piece cage; two-direction thrust capability; lower axial clearance through use of gothic arch	Predominant thrust required; lower misalignment tolerance than Conrad	Two-direction thrust
Cylindrical roller	Much higher radial capacity than ball bearing; provides axial freedom of shaft; higher radial stiffness than ball bearings; one-piece cage	No axial load capacity; roller ends wear in nonlubricating coolants; lower misalignment tolerance than ball bearings	High radial capacity without axial restraint; high radial stiffness
Balance piston	High thrust capacity	Must be protected from thrust loads during start; has no capacity without pressure; must be carefully designed for stable operation	Pump shaft thrust exceeds rolling bearing capacity

thrust ball bearings have not been used in rocket engine turbopumps because of their limited speed capabilities.

Table II presents a summary of current turbopump bearing practice and state of the art regarding bearing type, size, speed, load, coolant use, and other factors relevant to displaying bearing capabilities.

The first consideration in the design or selection of a bearing is its directional loading capability for the intended application. Then, for bearings that are to be used at high speeds, relationships of speed-load-life that account for centrifugal force must be used. Further, because bearing radial stiffness is a controlling factor in critical speed control, it is often a primary consideration in bearing type selection and bearing location on the turbopump shaft.

2.1.1 Load Capability

Currently, Conrad-type ball bearings are often used because of their ability to support a combined radial and axial load, a thrust load in both axial directions, and moment loading. Their capacity depends on the number of balls, which is limited by the assembly method. Also, they require a two-piece cage, which limits their speed capability.

Split-inner-ring ball bearings and angular-contact bearings, which have approximately 30 percent more thrust capacity than Conrad-type bearings, are used singly or in tandem to support heavy axial loads. The advantages offered by split-inner-ring bearings are the use of a one-piece cage, two-way thrust load capability, and the ability to lower the total end play of the bearing through the use of the gothic arch inner race. This latter feature makes a predominant thrust load requirement for satisfactory operation. A predominant radial load results in a change from a normal operation (fig. 1(a)) to a three-point contact (fig. 1(b)), and consequent race-ball distress. Design considerations are given in reference 1, pp. 44 and 45. Angular-contact ball bearings are used only for predominantly axial loads so that ball contact with the low shoulder does not occur (fig. 2(a)). A conservative rule of thumb for split-ring and angular-contact bearings is to ensure that the thrust load is always twice the radial load.

Tandem duplexed ball bearings are used when the thrust load is greater than the capability of a single bearing with ball size maximized to centrifugal limits. Two or three bearings are used to share the loading (ref. 2). To ensure load sharing, face flushness, bore and outside diameters, and contact angles are specified within close limits in each set of bearings; selective assembly may be used rather than extremely tight tolerances. Duplexed ball bearings with opposing contact angles are used to limit axial deflection and to obtain increases in bearing radial spring rate (figs. 2(b) and 2(c)). Preloaded springs are often used to avoid thermal loading of the bearings.

TABLE II.–Summary of Current Turbopump Bearing Capabilities

Bearing type	Bore, mm	Materials			Load, lb_f		Speed, 10^3 rpm	Coolant		Experience		Maximum test hours per bearing (no failure)	Maximum temperature, °F
		Ball or roller	Races	Cage	Axial	Radial		Fluid	Flowrate, gpm	Turbopump	Test rig		
Ball	35	Halmo	Halmo	S-Monel	1,400	1350	40	RP-1	0.2	X		5	800
Ball	70	52100	52100	AMS 4616	5,900	4700	6.8	RP-1	0.1	X		1.75	250
Tandem Ball	130	52100	52100	AMS 4616	55,000	0	5.5	RP-1	4.0	X		20	350
Roller	35	4620	4620	AMS 4616	0	3700	40.0	RP-1	0.2	X		5	350
Roller	70	52100	52100	AMS 4616	0	4000	6.8	RP-1	0.1	X		1.75	250
Roller	170	11	11	AMS 4616	0	500	5.5	RP-1	1	X		100	800
Ball	40	K5H[1]	440-C	25% GFT[2]	2,700	NA	40	50-50[3]	14		X	0.2	NA
Ball	45	K-96[4]	K-96	Graphite[12]	300	0	25	50-50	1.1		X	0.6	NA
Roller	40	440-C	440-C	25% GFT	0	500	40	50-50	8 to 10		X	0.2	NA
Ball	45	440-C	440-C	Armalon	330	0	25	EDA[5]	1.5		X	1	NA
Ball	45	440-C	440-C	Armalon	315	0	25	B_5H_9[6]	1		X	0.4	NA
Ball	45	440-C	440-C	Armalon	800	100	28.3	Liquid hydrogen	100	X		6	-350
Ball	45	440-C	440-C	Armalon	300	0	34.5	Liquid hydrogen	10		X	9	NA
Ball	50	440-C	440-C	Armalon	3,000	NA	24	Liquid hydrogen	20	X		3	NA
Ball	60	440-C	440-C	Armalon	800	100	28.3	Liquid hydrogen	20	X		6	-350
Ball	65	440-C	440-C	Armalon	2,200	100	31.5	Liquid hydrogen	40	X		3	-350
3 Tandem Ball	110	440-C	440-C	Armalon	36,000	NA	13.3	Liquid hydrogen	150		X	0.75	NA
Ball	150	440-C	440-C	Armalon	1,000	0	20	Liquid hydrogen	150		X	0.5	NA
Ball	200	440-C	440-C	Armalon	5,000	0	15	Liquid hydrogen	150		X	1.6	NA
Roller	50	440-C	440-C	Armalon	0	2000	24	Liquid hydrogen	20	X		3	NA
Roller	120	440-C	440-C	Armalon	0	5000	13.3	Liquid hydrogen	26		X	1.63	NA
Ball	35	440-C	440-C	Rulon	0 to 400	150	30	Gaseous hydrogen	0.02 to 0.2 lb/sec	X		5.5	-400 to +60
Ball	40	440-C	440-C	Rulon	140	200	30	Gaseous hydrogen	0.03 lb/sec	X		5.5	-400 to +60
Ball	45	440-C	440-C	Armalon	300	0	34.5	Gaseous hydrogen	0.1 lb/sec		X	9	NA
Roller	30	440-C	440-C	7	0	300	12	Gaseous hydrogen	NA	X		5.5	-60
Roller	40	440-C	440-C	7	0	200	12	Gaseous hydrogen	0.02 lb/sec	X		5.5	-60
Ball	45	440-C	440-C	Armalon	330	0	25	IRFNA[8]	5 gpm		X	1	NA
Ball	40	440-C	440-C	25% GFT	1,500	NA	40	N_2O_4	5 to 15		X	0.25	NA
Ball	45	440-C	440-C	Armalon	330	0	25	N_2O_4	2 to 5		X	1	NA
Ball	50	K5H	440-C	25% GFT	2,500	NA	25	N_2O_4	5 to 15		X	0.25	NA
Roller	40	440-C	440-C	25% GFT	0	1000	40	N_2O_4	5 to 15		X	0.25	NA
Ball	45	440-C	440-C	Armalon	500	0	25	Liquid oxygen	5		X	15	-250
Ball	60	440-C	440-C	Armalon	3,500	0	8.8	Liquid oxygen	10	X		6	-250
Ball	110	440-C	440-C	Armalon	18,000	NA	4	Liquid oxygen	8.5		X	0.9	NA
Roller	105	440-C	440-C	Armalon	0	3750	4	Liquid oxygen	2		X	2	NA
Ball	45	440-C	440-C	K-Monel	400	0	3.6	Liquid fluorine	Submerged		X	1	NA
Ball	45	K162B[9]	440-C	K-Monel	400	0	3.6	Liquid fluorine	Submerged		X	1	NA
Ball	50	440-C	440-C	BN440[10]	400 to 12	0	20	Liquid fluorine	12 to 20		X	0.5	-293

[1]Tungsten-titanium carbide
[2]Glass-filled teflon
[3]UDMH-N_2H_4 (50-50 mixture)
[4]Tungsten carbide
[5]Ethylene diamine
[6]Pentaborane
[7]Plated lead on silver on AMS 4616
[8]Inhibited red fuming nitric acid
[9]Titanium carbide
[10]Berylco Nickel 440
[11]Bower 315
[12]U.S. graphite, grade 2

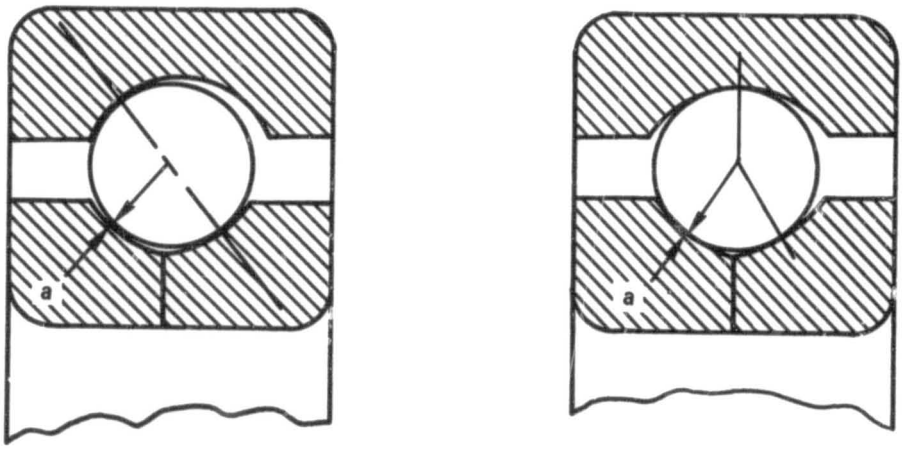

(a) Normal operation (clearance at a)

(b) Three-point contact (wiping contact at a)

Figure 1.—Split-inner-ring ball bearing.

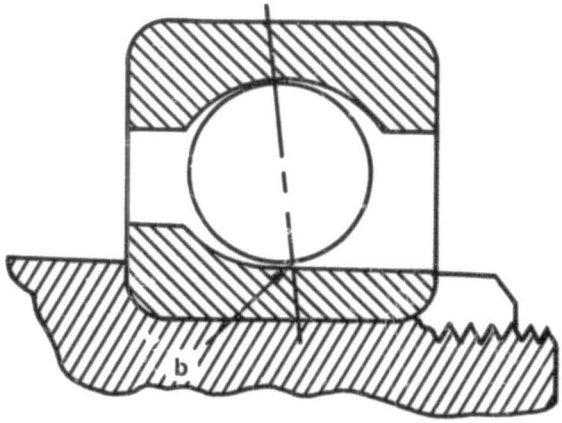

(a) Low shoulder contact at b

(b) Duplex DB (back-to-back)

(c) Duplex DF (face-to-face)

Figure 2.—Angular-contact ball bearings.

Cylindrical roller bearings possess several times the radial capacity and stiffness of ball bearings. They are used only for radial loading; axial loads are taken by ball bearings axially connected to the roller bearing shaft (fig. 3(a)). Occasional uses of roller bearings

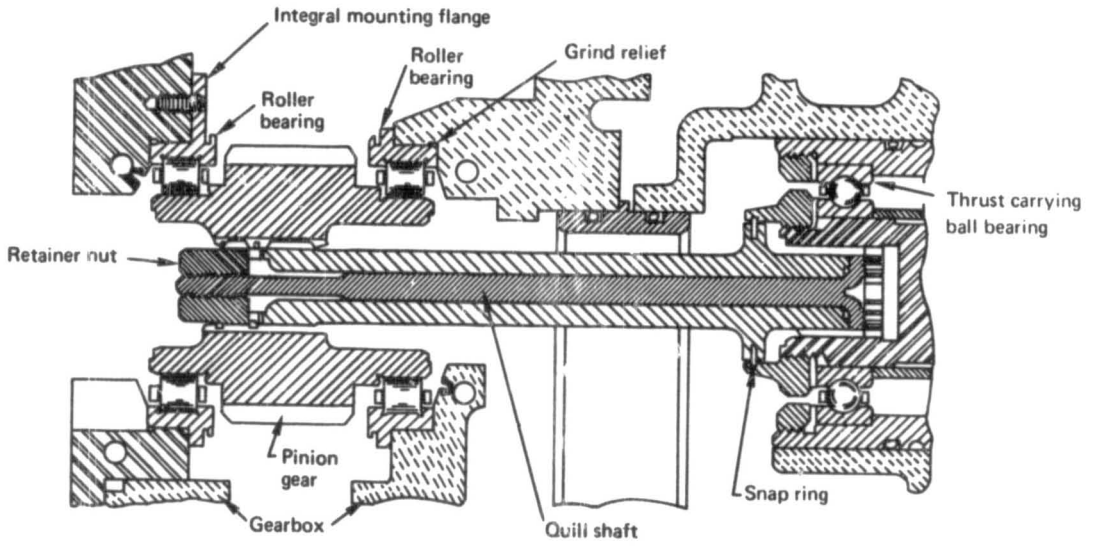

(a) Elimination of thrust load from roller bearing

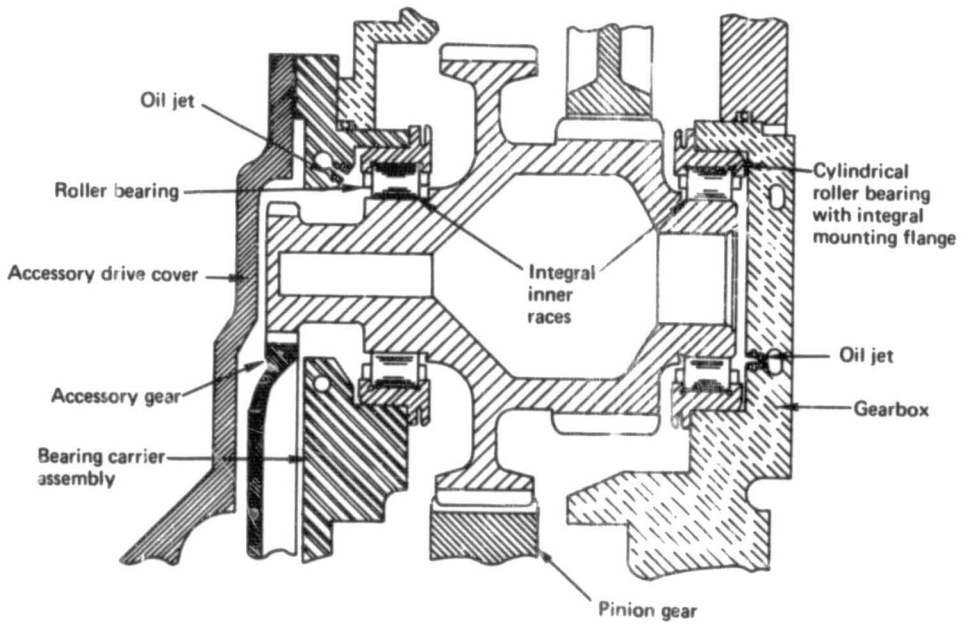

(b) Cylindrical roller bearings used for axial location

Figure 3.—Roller bearing applications.

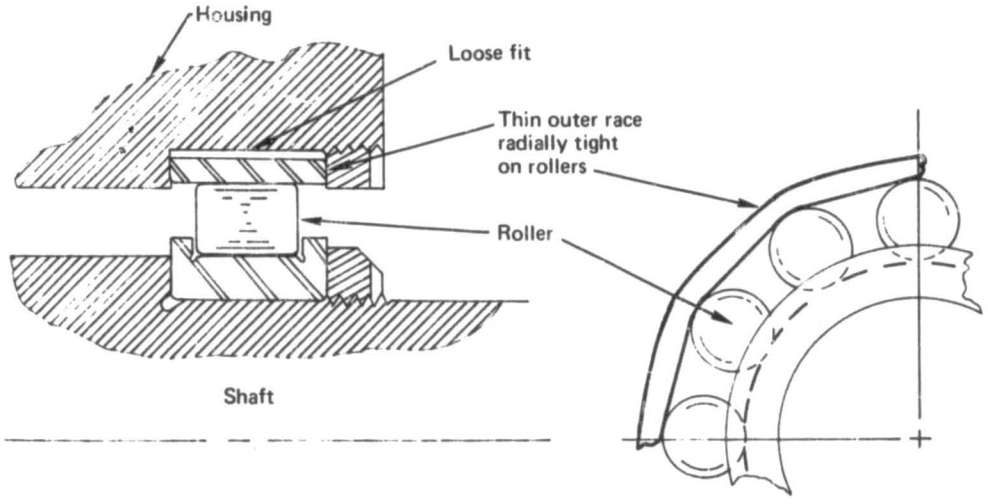

(c) Radially tight roller bearing

Figure 3.—Concluded. Roller bearing applications.

for axial loads are limited to handling the loads that result from providing axial location for rotating components (fig. 3(b)). Roller bearings with negative diametral clearance can be used for propellant-cooled service (liquid hydrogen) (fig. 3(c)) (ref. 8, pp. 505-518).

Film bearings (e.g., balance pistons) are prevented from rubbing contact during startup until sufficient pressure is generated to lift the bearing. Figure 4 shows typical balance piston and bearing configurations. Figure 5(a) is a schematic of the balance piston/bearing arrangement; while figure 5(b) is a load-deflection diagram with corresponding clearances and deflections. The values will vary with individual turbopump designs; however, the basic objective is to prevent balance piston contact from occurring (fig. 5(b), V and VI). This is accomplished by selecting gaps 3, 4, 5, and 6 in fig. 5(a), so that the loads at V and VI exceed the net pump shaft loads when insufficient fluid is pumped for balance piston operation.

When the need for adequate directional load support capability has been satisfied, the requirement that the bearing possess sufficient load capacity must then be considered. Load capacity is a direct function of bearing size unless high-speed effects predominate. For low-speed applications ($DN < 0.5 \times 10^6$), the bearing is sized by selecting a sufficiently large bearing from manufacturers' catalogs. For high-speed applications, this method is inadequate. To determine the necessary capacity for required life, the designer must resort to load-life-speed relationships that account for centrifugal, inertial, and friction forces.

The relations for dynamic analysis of ball and roller bearings accounting for speed effects are derived in reference 3. This analysis has been programmed for digital computers, making possible rapid determination of high-speed bearing stresses, life, stiffness, dynamic forces, and velocities.

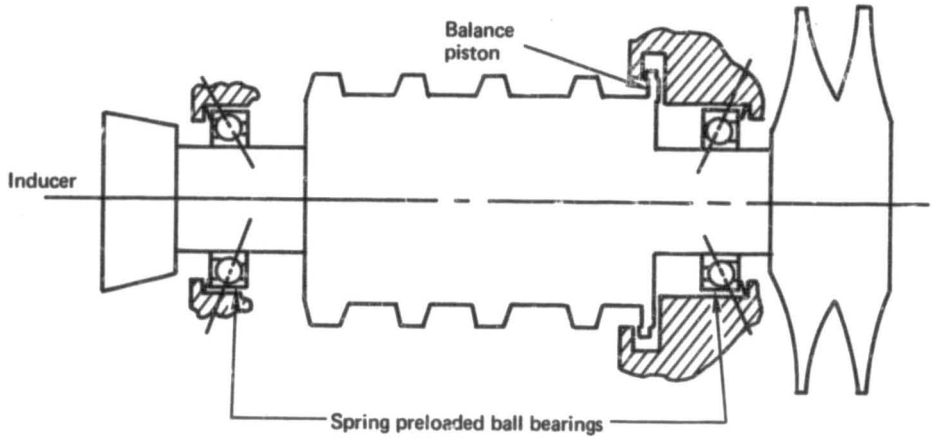

(a) Mark 15–F turbopump

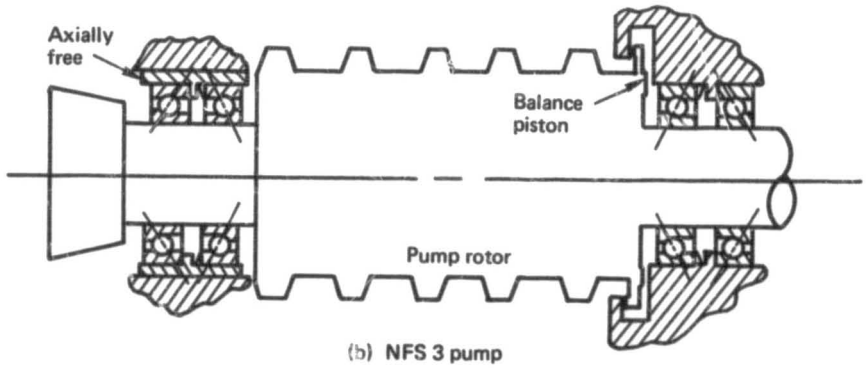

(b) NFS 3 pump

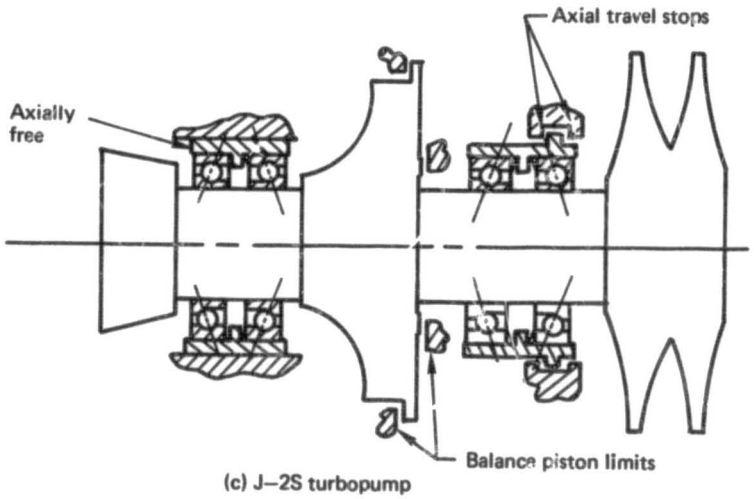

(c) J–2S turbopump

Figure 4.—Balance piston bearing systems.

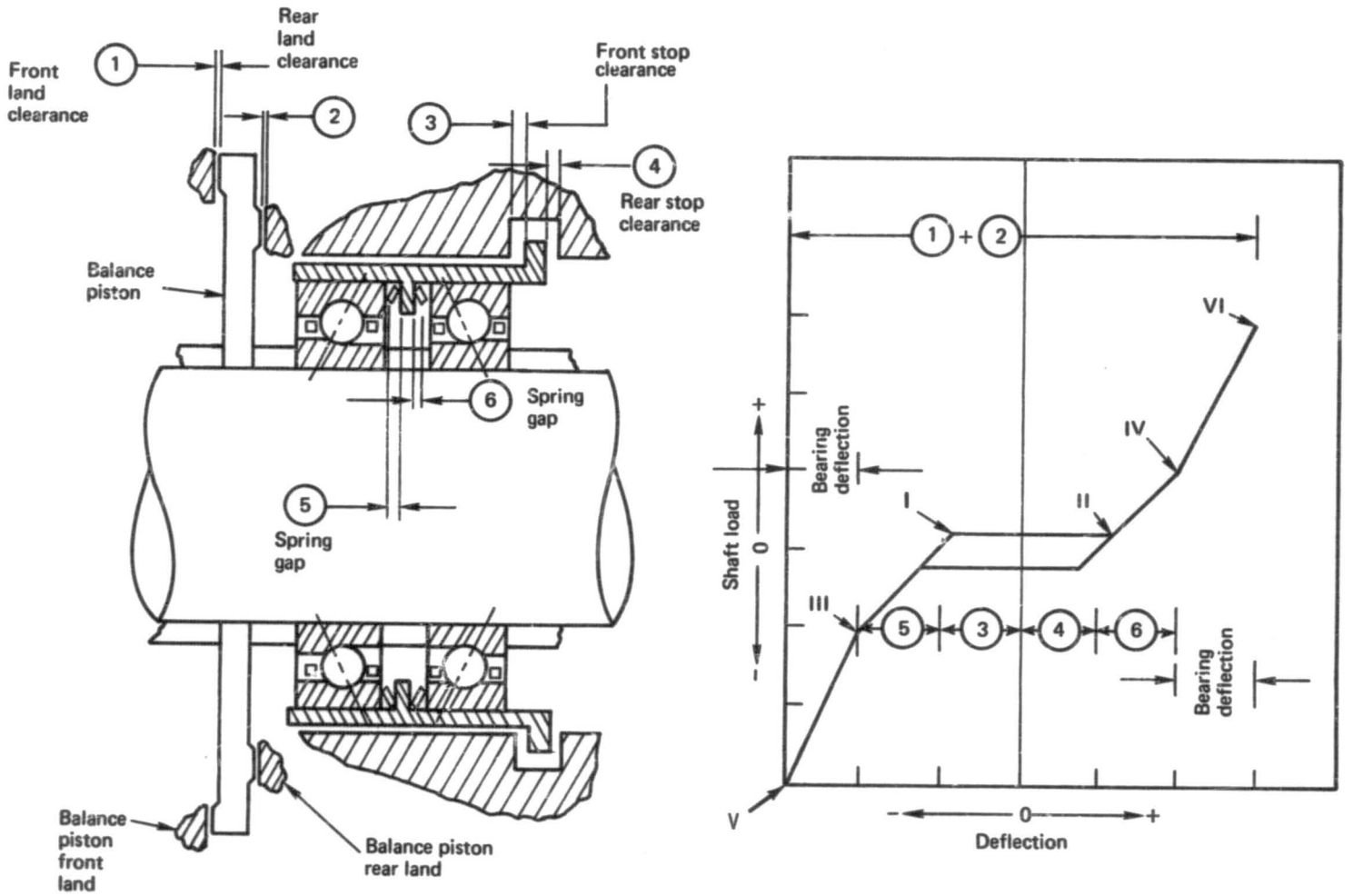

(a) Balance piston schematic

(b) Load and deflection chart

Figure 5.—Balance piston system clearances, loads, and deflections.

Turbopump required service life is usually 1 to 2 hours. Bearings are sized for this service by specifying a calculated B_{10} fatigue life (including speed effects) that exceeds turbopump life by an arbitrary factor (usually 10). This conservative value is used not only to prevent fatigue failures, but also to compensate for other undefined life-reducing factors such as the low lubricity of most propellant/coolants. B_{10} fatigue life is the operating time that 90 percent of identical bearings will exceed without fatigue failure. It is calculated by relating the stress cycles of a new design to the statistically analyzed results of repeated fatigue tests on controlled test bearings. Most bearing manufacturers present basic life data on their bearings; however, their life rating methods do not include effects of centrifugal force. These effects are considered in the general analysis (ref. 3).

2.1.2 Speed Capability

DN value (product of bearing bore in millimeters and shaft speed in rpm) is used as the general measure of bearing speed because it is simple, easy to compute, and is widely understood and accepted. DN is not completely descriptive of speed severity as it does not account for rolling element size or bearing internal geometry; however, no entirely acceptable substitute for DN has been proposed.

Table III lists the approximate maximum speeds that have been achieved for bearings in operational turbopumps and experimental programs using the coolant shown. Maximum attainable speeds have not been established for each bearing type and coolant. However, it is reasonable to expect that the speed levels in table III can be exceeded provided that the propellant coolant has a higher rank as a lubricant than the given coolant (sec. 2.1.7).

TABLE III.—Speed Limits for Bearings

Bearing type	Existing maximum turbopump DN, million	Existing maximum test DN, million	Limiting factor	Test coolant
Conrad-type ball	1.6	1.6	Cage weakness	Liquid hydrogen
Angular-contact ball	2.05	3.0 (ref. 4)	Heat generation	Liquid hydrogen
Cylindrical roller	1.6	1.6	Roller guidance, cage slippage	RP-1

In turbopump designs, bearing speeds near the ultimate bearing speed capability are avoided because operation near this limit makes all aspects of alignment, loading, cooling, lubrication, and manufacturing variables critical to success; the slightest departure

from ideal conditions may result in failure. Therefore, to gain reliability, DN values are held to the lowest possible levels consistent with pump requirements.

It should be noted also that a finite minimum load (inherent application loads or preloads) is required at each bearing speed to prevent gross skidding of rolling elements and consequent damage to bearing surfaces. The minimum required load is a function of materials, bearing geometry, lubrication, and acceptable life reduction. Dynamic analyses of bearing performance (ref. 3) are required to determine the skidding tendencies of an application. A discussion of roller bearing skidding appears in reference 1, pp. 321-328.

The sensitivity of bearings to speed, load, and life changes (as are often required in uprating) is illustrated in the two examples below:

(1) Conrad bearings with phenolic cages, entirely satisfactory for turbine shaft thrust bearing service at 1.2×10^6 DN in Atlas and Thor vehicle turbopumps, had to be replaced by split-inner-ring bearings with one-piece bronze cages when the speed and load were increased by approximately 10 percent for service in the H-1 engine.
(2) Extended service life requirements in J-2 engine fuel pump bearings operating at 1.6×10^6 DN caused failures of two-piece, riveted cages made of Armalon (glass-fabric-supported polytetrafluoroethylene (PTFE)). The substitution of a one-piece (otherwise identical) cage resulted in satisfactory service.

2.1.3 Stiffness

Bearing stiffness is a controlling factor in shaft dynamics (critical speed control). Therefore, bearing detail design calculations are often made and used as background information for decision making during selection of the shaft layout. Dynamic analyses (ref. 3) programmed for digital computers are used to determine quickly the radial stiffness of candidate bearing designs for the expected range of loads and speeds. Bearing type, preloading, mounting, and shaft layout selections are often determined on the basis of calculated bearing spring rates (stiffness). Roller bearings are sometimes used to obtain adequate stiffness (1.5 to 2.0×10^6 lb/in.) when subcritical operation is required, e.g., in throttled engines. Supercritical operation can be obtained by the use of soft mountings for bearings, thus depressing criticals to below operating speeds.

On one particular experimental turbopump a radial stiffness of 120,000 lb/in. was required for critical speed control. Analysis indicated that at the desired lower preload limit of 40 lb, the radial stiffness had dropped off to 20,000 lb/in.; the solution required increasing the preload to 60 lb minimum even though this reduced the calculated fatigue life of the bearing. This type of compromise often is required in a high-speed, relatively lightly loaded ball bearing because the centrifugal force per ball is large relative to the total ball loads.

2.1.4 Misalignment Tolerance

Misalignment tolerance of ball bearings can be increased by providing sufficient cage pocket clearance (ref. 5) to allow for circumferential advance and retard of ball position caused by ball speed variation (BSV). Excessive BSV results in cage pocket wear and heating. In reference 6, the detrimental effects of BSV are discussed and methods are provided for calculating BSV. Some designers prefer to use elliptical ball pockets. With this technique, only the circumferential cage pocket clearance is increased while the standard axial cage pocket clearance is unchanged; this practice prevents cage wobble and consequent land wear. Digital computer programs based on the original work presented in reference 3 are used to compute cage-rolling element forces and rolling element excursions that determine the required minimum clearance.

Roller bearing misalignment results in capacity loss caused by edge loading of the rollers. Misalignment tolerance is increased by crowning the outer race (fig. 6) (ref. 7). In general, the misalignment imposed on turbopump bearings is minimized by proper shaft and housing design and manufacturing techniques such as line-boring of gear cases.

2.1.5 Bore

Turbopump bearing bores have ranged from 8 to 170 millimeters, and testing has been conducted on bearings with 200 millimeter bore. The preferred bore size is the smallest diameter that satisfies the shaft strength, stiffness, and bearing capacity requirements. For extremely high-speed applications, an increase in bore size will not always result in an increase in bearing load capacity because centrifugal loading of the rolling elements increases faster than capacity as size increases. In such cases, tandem duplex thrust bearings are utilized (e.g., in the turbopumps for the F-1 and M-1 engines).

Placing splines inside bearings is avoided because the bore must expand to accommodate two torque-carrying shaft sections. In addition, uneven expansion of torque-carrying splines tends to distort bearing races into cone shapes; this results in roller skewing and consequent end wear.

2.1.6 Internal Clearance

Unfitted diametral clearances are specified with allowances made for all causes of diametral clearance loss. Except as noted below, care is taken to prevent the occurrence of negative clearance, which almost always results in sudden catastrophic failure. Press fits, centrifugal growth, material properties (such as Poisson's ratio), and thermally induced differential growths are all considered in establishing design clearances.

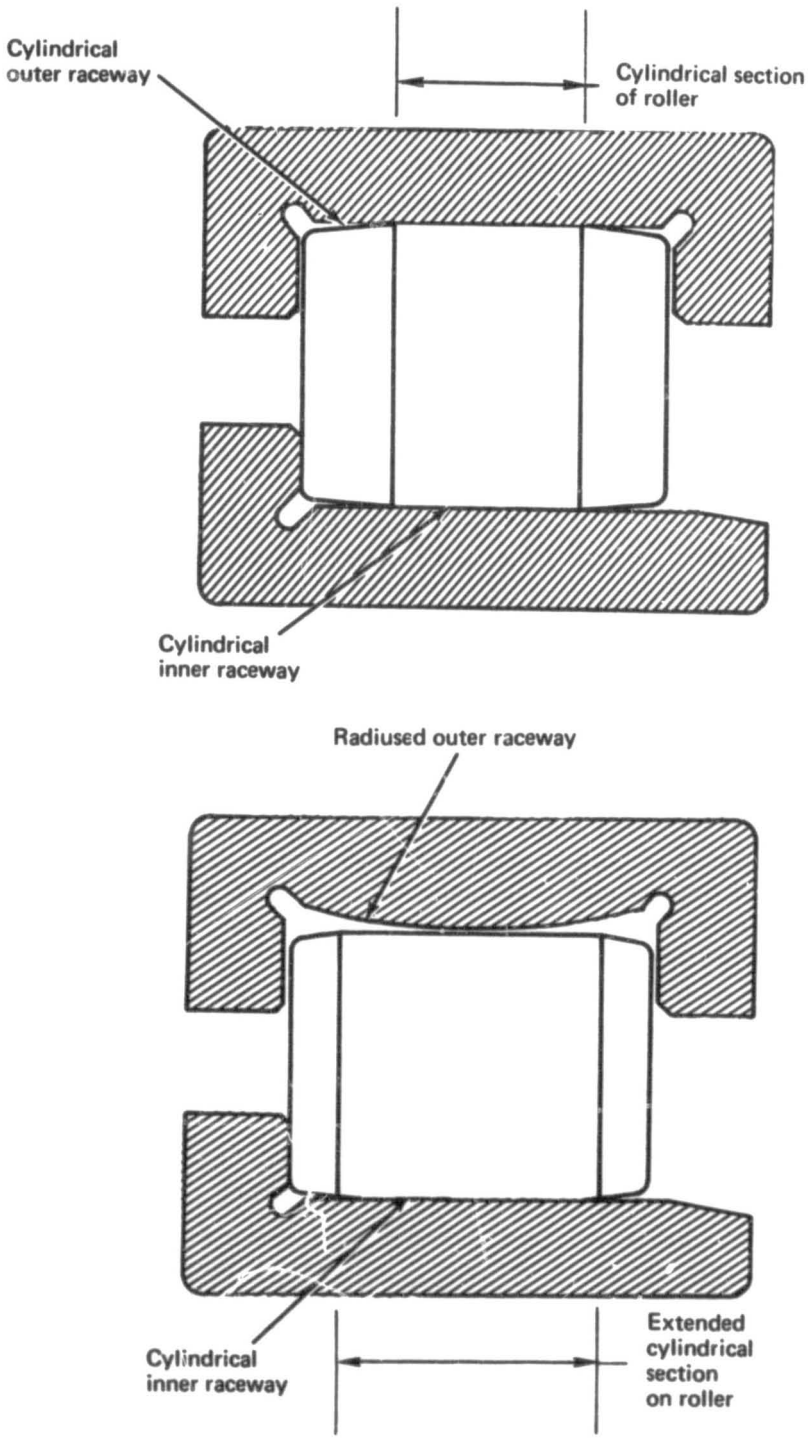

Figure 6.—Race crowning to allow for misalignment in roller bearings.

Roller bearings are sometimes designed utilizing radial preloading where light-load, high-speed conditions will result in excessive roller skidding and wear. Preloading techniques include elastically deforming the outer races out of round (ref. 1, p. 323) and use of zero or negative diametral clearance. Special design considerations for radially tight bearings are given in the unclassified appendix of reference 8, vol. III pp. 505-518. In utilizing zero or negative clearance, extreme care must be taken to ensure that sufficient cooling is available to prevent a self-aggravated thermal growth loading cycle that will rapidly result in a complete bearing seizure.

2.1.7 Cooling

Table II summarizes current bearing cooling practice. Most turbopump bearings are cooled with pumped propellant. A small quantity of the total pump flow is bled from a high-pressure region of the pump, flows through the bearings, and re-enters into a low-pressure area of the pump or at the pump inlet. An investigation of the bearing lubricating ability of various liquid rocket propellants (ref. 18) resulted in the following ranking (in descending order): RP-1, liquid oxygen, liquid hydrogen, N_2O_4, IRFNA, EDA, UDMH, N_2H_4, and 50-50 N_2H_4-UDMH.

A few turbopumps still use conventional lubrication that requires a separate tanking and circulation system. Oil systems in use include recirculating (Titan) and once-through overboard-drain (Atlas and Thor).

Coolant effects.—Roller end wear of cylindrical roller bearings is aggravated when roller bearings are used with chemically reducing coolants such as liquid hydrogen and the amines (50-50 mixture of UDMH and hydrazine). Roller end wear does not appear to be severe with liquid oxygen and is insignificant with N_2O_4 (refs. 2, 9, and 10). The use of dissimilar roller and race materials will reduce the end wear significantly even with chemically reducing coolants (ref. 9).

For high-speed turbopumps, angular-contact ball bearings with one-piece, outer-land-riding cages made from self-lubricating materials containing PTFE are preferred. These bearings have been tested successfully at speeds to 3.0×10^6 DN (ref. 4) (table II).

Development of roller bearings for propellant-cooled high-speed use requires special considerations in clearances, guidance, and roller skidding prevention (refs. 2, 8, 9, and 10).

Coolant quantity.—Coolant quantity is established by heat balance calculations confirmed or modified by testing. Typical values for coolant flow range from 0.1 gpm of RP-1 for low-load, low-speed bearings to 150 gpm of liquid hydrogen for large, high-speed bearings (table II). With roller bearings cooled by liquid hydrogen, increasing coolant flow above that required for heat balance has reduced roller end wear.

Coolant delivery system.—Jets of lubricant carefully targeted to the gap between the inner race and cage are used for the more viscous conventional oils and most RP-1 systems (fig. 3(b)). The effectiveness of this lubrication system depends on the accuracy of the jet targeting and the elimination of other possible reasons for failure of adequate lubricant to reach all necessary areas of the bearing. Churning losses are less than those with flooded lubrication systems, decreasing the flowrate required (especially with viscous fluids where $\mu > 1$ centistoke) and thereby decreasing the payload penalty of the lubrication system. Additional coolant flow is sometimes directed through slots in the bearing races or shaft under the races. Most lubrication systems for highly loaded power transmissions used at low ambient pressures (altitudes of 100,000 ft or more) are pressurized to 2 psia to provide lubricant circulation by windage. Otherwise, lubricants may not reach critical areas of the bearing and the bearing will fail.

Tests with the Atlas and Thor engine transmissions have demonstrated that outer-land cage-equipped ball and roller bearings with direct lubrication jet cooling can operate successfully at very low ambient pressure (2 mm Hg). The Agena engine employs an unpressurized splash-lubricated gear transmission (no lubrication jets) that has operated successfully at 0.2 psia.

Flooded through-flow systems are generally used for propellant-cooled bearings for two reasons:

(1) There is less chance of blockage of jets with particles of foreign matter, or with pieces of ice in cryogenic systems.
(2) Churning losses and heating are small because of the low viscosity of most propellants.

Coolant quality (liquid/vapor fraction).—Attempts are made to maintain the coolant at 100-percent liquid condition at the bearings because this increases the cooling effectiveness. When the fluid temperature in the pump is above the critical temperature, the pressure is sometimes altered to be above the critical pressure (ref. 11). Gaseous hydrogen has been used in the RL-10 engine turbopump as a bearing coolant; flowrate was found to be critical to successful bearing operation.

Contamination.—Chemical contamination of propellant systems is controlled by applying cleanliness standards similar to MSFC-SPEC-164 (developed for liquid-oxygen systems) (ref. 12), which controls particle size, particle number, and nonvolatile residue. In addition, passivation by controlled exposure to fluorine gas is required for components intended for service in liquid fluorine or in FLOX (mixture of liquid fluorine and liquid oxygen).

When bearings are not corrosion resistant, water is excluded from the bearing. In oil and RP-1 systems, this is accomplished by use of water-displacing preservatives; in cryogenic systems, by use of dry gas purges (MIL-P-27401B nitrogen (ref. 13) or MIL-P-27407 helium (ref. 14)) or desiccants (MIL-D-3464D (ref. 15)).

Filters and screens are used to prevent blockage of lubricant jets and damage to bearings by particulate contamination. In RP-1 and oil systems, 40-micron filters are used, while screens with 10-micron openings are used in the flooded coolant system in the J-2 engine liquid-oxygen turbopump. The J-2 engine fuel pump uses no filter or screen, but relies on centrifugal force to separate particles from the coolant and prevent contamination of the bearings.

The RL-10 engine turbopump depends upon the initial cleanliness of components and system. In the Titan II, turbine exhaust gases used to pressurize the gear box generate sludge in the lubricant (MIL-L-7808 (ref. 16)); replaceable filters are used in the turbopumps to remove this sludge. A bypass check valve is used to prevent lubricant starvation if the filter clogs.

2.1.8 Bearing Mounting

Interference fits.—A light press fit between the rotating race and its mounting is maintained to prevent relative motion and consequent fretting. For heavy radial loads, heavier press fits are required. Some applications (H-1 engine turbopump; Thor and Atlas vehicle turbopumps) experienced extremely heavy radial loads, and creeping of races could not be prevented by clamping. The problem was solved by making the inner races integral with the gears (figs. 2(a) and 3(b)).

Maximum interference fits are held below the fit that causes inner race fracture. Interference fits up to 0.001 in./in. of bore diameter are used without problems.

Sliding fits.—Spring-preload bearings and axially floating bearings as used in the turbopumps for the J-2 engine require loose-fit outer races to maintain axial freedom. When sticking of the outer races, coupled with shortening of the rotor due to the Poisson effect of centrifugal force, caused loss of preload and shaft dynamic problems in the engine fuel pump, looser fits for the bearings and increased preload were used.

Bearing mounting surfaces.—Shaft journals and housing bores generally are chrome plated to prevent galling and fretting of the surfaces due to the relative motion of the races or assembly press fitting. This practice is mandatory for Inconel and Monel shafts used in cryogenic pumps. Titanium shafts cannot be chrome plated, but the contraction is similar to 440-C steel; therefore, lighter fits are possible, and galling because of assembly and disassembly is minimal. SAE 4130 steel shaft journals hardened to 40 R_c generally do not gall even with heavy press fits.

Corner radius interference.—Interference of the bearing bore and outer diameter corners with the shaft shoulder corner radius is prevented by use of a grind relief (fig. 3(a)).

Mounting surface accuracy.—The mounting surface accuracy (roundness of cylindrical surfaces, taper of diameters, and axial runouts of shoulders) is maintained by specifying tolerances equivalent to ABEC 5 or RBEC 5 (AFBMA Standards (ref. 17)). Looser tolerances would destroy the accuracy obtained from the bearing design.

Shoulder heights.—Shaft and housing shoulder heights are chosen to provide sufficient compressive strength to transmit clamping loads through the solid race sections without bending the race and possibly pinching the rollers. Normally, 0.050 in. or more of the bearing race face is exposed to allow pulling of the bearing. When this is not possible, bearings are provided with grooves or they are disassembled by pulling through the rolling elements, a practice that often damages the bearing.

Race retention.—Rotating races are retained by nut clamping (fig. 7(a)) or tension bolting (fig. 7(b)). Early designs that relied on press fit alone were altered when race walking caused fretting of the journals and axial displacement of the races.

Snap rings for turbopump bearing race retention have been abandoned because of the possibility of removal by centrifugal force, shock, and vibration.

When either of the bearing races rotates relative to a heavy radial load, the clamping load must be large enough to prevent race creep. Figure 8 illustrates the Poisson effect on the inner race of a heavy radial load. This rotating "bulge" of metal caused severe fretting of Atlas turbopump gear bearing inner races. Extremely strong retainers did not stop the fretting. The final solution was to make the inner races integral with the gear (figs. 3(a), (b)).

The bearing-retaining nut or tension bolt is designed and applied to provide clamping loads large enough to prevent the stack of components from loosening under thrust, bending, or thermal effects. Clamping loads as large as 50,000 pounds are used in the bearing tension bolt in the J-2S engine. A clamping-nut torque of 800 ft-lb is used in the F-1 engine turbopump. A case of severe fretting of the gear and bearing race mating surfaces (fig. 9) in the Atlas sustainer turbopump was eliminated entirely by increasing the clamping-nut torque to 200 ft-lb.

2.1.9 Bearing Materials

Corrosion resistance.—Bearings are made of corrosion resistant materials for propellant-cooled applications. Races and rolling elements are made of 440-C steel; cages are made of plastics, and occasionally are reinforced with corrosion resistant steel (CRES) or aluminum. Standard noncorrosion-resistant materials (52100, tool series) are protected during idle periods by preservatives. Grade 440-C steel, the most com-

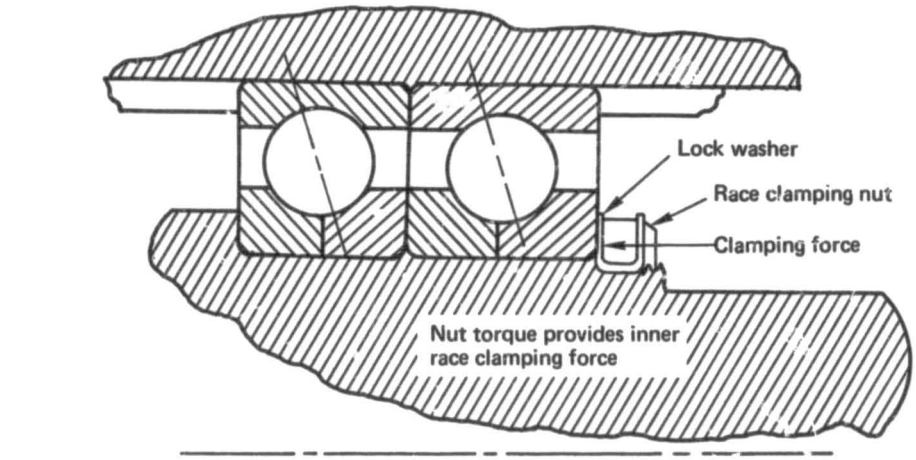

(a) Nut clamping

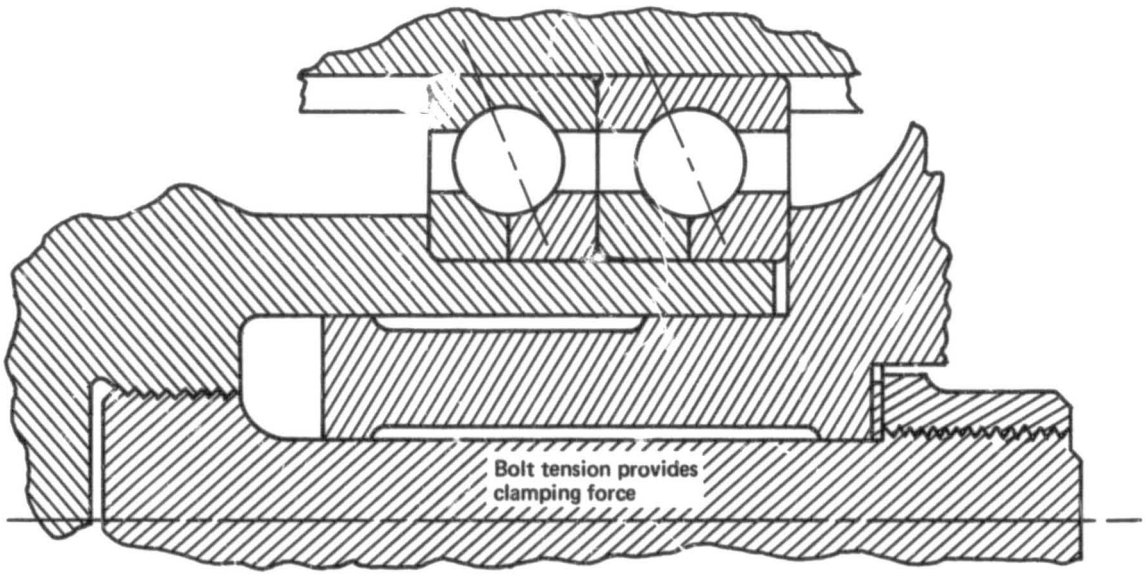

(b) Bolted retention

Figure 7.—Race-retention methods.

monly used race material for propellant-cooled applications, is not entirely corrosion resistant, and investigations are underway to discover a substitute; none has been found with the combination of hardness, corrosion resistance, fatigue life, and availability displayed by 440-C. Nickel-based alloys are corrosion resistant, but soft. Sintered carbides are corrosion resistant and hard, but brittle. Stellite Star-J has been investigated as a cryogenic bearing material, but testing has not produced design recommendations.

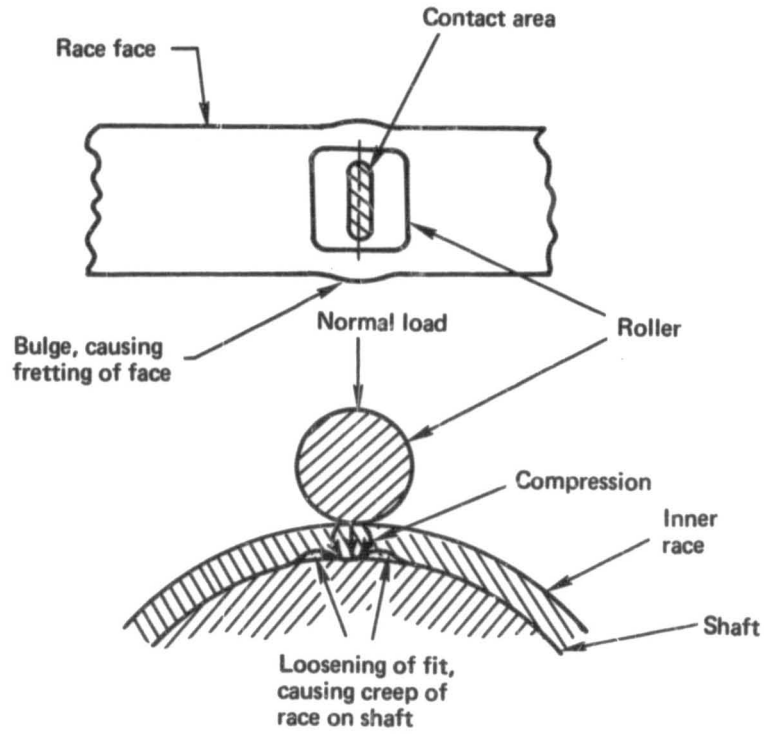

Figure 8.—Poisson's effect of heavy radial load.

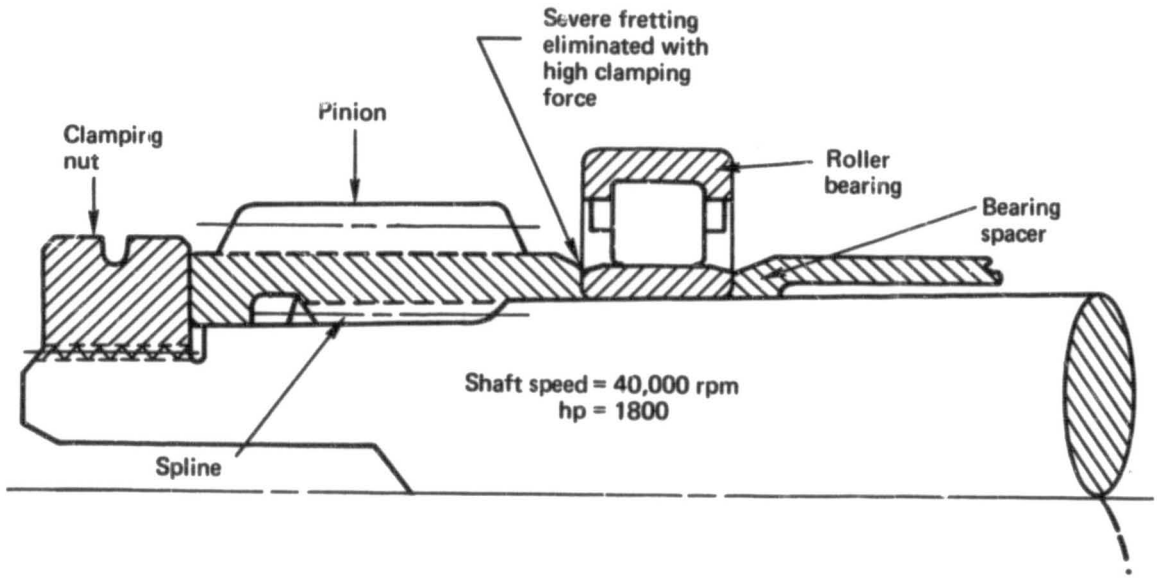

Figure 9.—Bearing clamping to eliminate fretting.

Hardness.—Since full capaciy requires a minimum hardness of 58 R_c, few materials qualify as full capacity race and rolling element materials. In addition to the materials that appear in table II, M-10 and M-50 tool steel have been used. To date, materials softer than 58 R_c have not been used in turbopump bearings. Extensive testing would be required to provide reasonable confidence in the life capabilities of softer materials.

Adhesion resistance.—Adequate resistance to adhesion between the rolling element and race is attained for most propellant environments using 440-C (table III). Oil and RP-1 pose no problems for 52100 or tool steels. However, 440-C displayed adhesive degradation of races and balls when cooled by strong reducers (N_2H_4, UDMH, and mixtures of both) (refs. 18 and 19). In reference 9, however, successful testing of the same material combinations is reported. Additional testing is required in this area of conflicting results. As noted earlier the use of dissimilar race and rolling element materials reduces wear rates in chemically reducing coolant environments (ref. 9).

Dimensional stability.—Stabilization by repeated cycles of chilling with liquid nitrogen and then tempering has successfully eliminated dimensional changes noted in liquid-oxygen and liquid-hydrogen bearings. Stabilizing chill cycles are part of most cryogenic bearing design specifications for 440-C bearings. Requirements for stabilization procedures for nickel-based alloys and carbides are not known.

Grinding burns.—Grinding burns once were a source of dimensional changes and internal stresses that resulted in race fracture. These have been largely eliminated by more rigid controls of grinding-wheel grit speed and feed and of coolant type and amount. Nital etch will detect grinding burns in 52100 and 4620 steels, but no satisfactory test has been proposed for grinding burn detection for 440-C steel. (Picric etch has been proposed as a detection method, but its effectiveness has not been proven.) Grinding burns are not a significant problem area if effective quality control methods are used to ensure proper processing.

Material cleanliness.—Vacuum melted steels are used extensively for race and rolling elements to ensure freedom from nonmetallic inclusions and consequent increase in fatigue life (refs. 20 and 21). Consumable electrode vacuum melting (CEVM) is preferred, as it produces more consistently clean steel than can be obtained by use of other vacuum melting processes. The reduction in nonmetallic inclusions obtained by vacuum melting also reduces the possibility of chemical attack by reactive propellants.

Cage material friction.—Low-friction materials are used for cages; those used for propellant lubrication provide their own lubricity and in addition may lubricate the rolling surfaces by transfer of a low-friction film from cage to balls to raceway (ref. 22). Table II presents the cage materials used with the various propellant/coolants. An exception in the self-lubricating quality sought for propellant-cooled service is the K-Monel and other high-nickel alloys used with liquid fluorine. It is possible that low-shear-strength nickel fluorides form on the cage and provide a slick film on the surface. Testing is continuing on bearings cooled by liquid fluorine.

2.1.10 Testing

Bearing designs are subjected to full-scale empirical tests in test rigs or in turbopumps to evaluate coolant flow and geometric configurations including tolerance range. Great care is taken to assure that test conditions simulate as closely as possible the expected operating condition. Bearings often are made separable to permit periodic inspection of bearing components during test programs.

Subscale tests of rolling element, race, and cage materials are often used for screening candidate new materials. The value of these tests is limited by the accuracy of simulation of the actual bearing operating conditions; therefore, the results of simple rolling and sliding tests must be interpreted with care and confirmed with full-scale tests.

Rolling contact tests.—Subscale rolling contact screening tests are used to select bearing race and rolling element materials for later fabrication of full-scale bearings. An example of this procedure is illustrated in reference 19 where a Barwell conversion of the Shell four-ball machine was used to screen various rolling contact material combinations.

Sliding friction tests.—Simple button riders held in contact with a spinning plate have been used extensively in cage material screening tests (refs. 18 and 19). The information from the testing described in reference 23 was used directly in selecting successful cage materials for liquid-hydrogen and liquid-oxygen service for the J-2 engine turbopumps.

2.2 Bearing Component Design

2.2.1 Rolling Element Design

Ball and roller element complements (size and number) are selected by performing dynamic analyses of candidate bearing designs (ref. 3), with the following considerations:

- Maximum ball or roller size is limited to the diameter whose further increase results in a decrease in capacity because of centrifugal force effects (contact stress, spinning and sliding). Ball sizes for turbopump bearings range from about 3/16 to 7/8 in. diameter; roller sizes range from approximately 1/4 to 1 in. diameter. Where capacity requirements exceed the increase available by increasing diameter, tandem duplexed bearings are used. Minimum ball or roller size is limited to the diameter that results in an adequately strong cage cross section and adequate coolant flow. Cage radial thickness of 0.100 in. and coolant flow radial space of 0.070 in. are generally the minimum used for bearings of over 40-mm bore.

- The maximum number of rolling elements is limited by cage web thickness considerations. It was found (ref. 9) that for nonmetallic, propellant-cooled bearing cages, a minimum cage web thickness of 0.150 in. is desirable. Metallic cages can utilize narrower bars because of greater strength. In addition, metallic cages are not adaptable to sacrificial wear as are low-friction, nonmetallic cages because metallic wear debris is potentially more detrimental to the bearing.
- The minimum number of rolling elements is not a usual design goal. The typical minimum number occurs in a Conrad-type bearing; the space between balls is slightly less than ball diameter.

Ball and roller diameter uniformity.—Ball and roller size variation is limited in new bearings to 10 to 20 microinches (μ in.). Excessive size variation leads to orbital velocity variation that results in cage distress. Ball quality criteria have been standardized by industry into AFBMA standard grades. These grades specify diameter uniformity among individual balls (in a bulk container) and ball roundness in an individual ball. Balls for turbopump bearings are usually AFBMA grade 10 (AFBMA Standards (ref. 24)).

Ball and roller roundness.—Ball and roller roundness is specified to limits of 10 to 20 μ in. to ensure smooth running bearings and load sharing among rolling elements. Excessive size variation will result in heavy cage wear and potential fatigue failure.

Ball and roller surface finish.—AFBMA Standards are utilized to specify ball quality; in addition to roundness and size variation, these standards also control ball surface finish. The AFBMA grade 10 specified for turbopump bearing balls controls the surface finish to 1.0 μ in. arithmetic average (AA) maximum.

Presently, a roller finish must be specified separately as there is no AFBMA standard for rollers. Typical roller surface finishes are 4 μ in. AA on outer diameters and 6 μ in. AA on the roller ends.

Roller guidance.—Roller guidance is extremely important to satisfactory wear performance of rollers and is ensured by control of the following design features:

(1) Roller length/diameter ratio of 1 is preferred; 1.3 is used as a maximum.
(2) Roller ends are held square within 0.0001 in. of the total indicated runout.
(3) Roller bearing race shoulders are 14 to 20 percent of the roller diameter, providing a guiding contact chord of 75 percent of the roller diameter.
(4) Roller end clearance between guiding lips in the guiding raceway may range from 0.0002 to 0.0020 in. in turbopump bearings. (Care is taken to avoid roller pinch from clamping loads.) Roller end clearance uniformity within an individual bearing assembly is assured by specifying roller length to be uniform within 0.0002 in.
(5) Roller corner radii concentricity control of 0.002 in. TIR (total indicated runout) is necessary to avoid roller cage wear caused by roller unbalance. Bearing manufacturers are now developing techniques that will enable them to supply rollers with the end radii concentric within 0.0005 in. TIR.

Roller corner radii.—Roller corner radii are controlled so that the maximum value still results in adequate roller guidance, but the minimum does not interfere with race shoulder corner radii. Typical turbopump bearing roller corner radii are controlled to be within the range 0.020 to 0.030 in.

Roller end relief (crowning).—To prevent stress concentration at the roller end, rollers are crowned (fig. 10) an amount slightly greater than the elastic deflection of the heaviest loaded roller. In addition to the amount for end relief, crowning provides an allowance for misalignment.

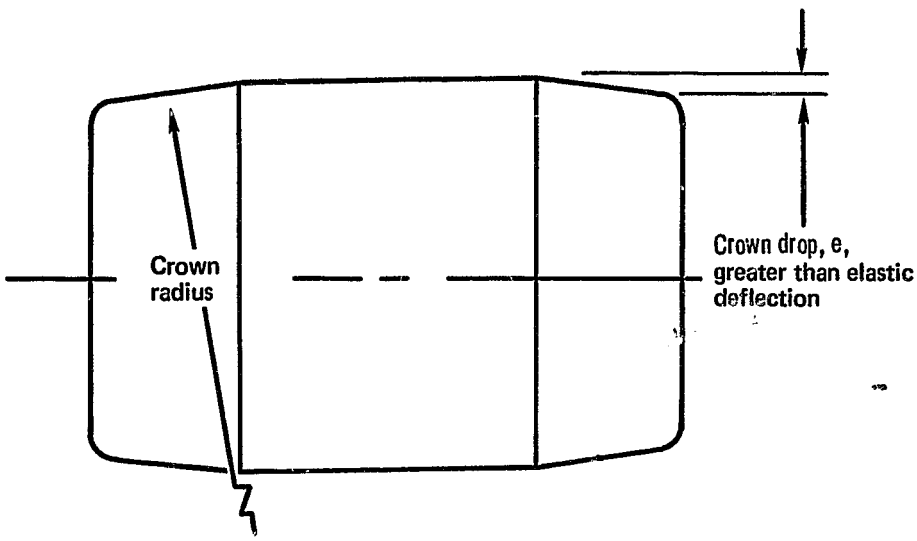

Figure 10.—Roller crowning.

2.2.2 Race Design

Race cross section.—A race cross section thickness less than 0.04 times the mean diameter promotes brittle fracture of 440-C races used in liquid-hydrogen service, and therefore greater thicknesses are used.

Ball bearing transverse race curvature.—Transverse race radii less than 51 percent of the ball diameter result in such wide contacts that excessive spinning and sliding occur. The breakover point where closer curvature results in excessive heat generation rate varies with speed and bearing size. In a bearing with close curvatures, small changes in clearance make large proportional changes in contact angle. The bearing geometry is quite sensitive to manufacturing tolerances, and dimension variations that would be insignificant in a bearing with 54 percent curvatures would make rapid changes in diametral clearance and contact angle in a bearing with 51 percent curvatures.

To reduce heat generation in high-speed ball bearings, race curvatures are made wider than the normal 51 to 53 percent. The maximum race curvature presently used in turbopumps (J-2 engine fuel pump) is 59 percent. A further increase in curvature increases stress and decreases capacity, with diminishing returns in spin reduction.

Inner (F_i) and outer (F_o) race curvatures are varied independently to achieve specific design goals as indicated in table IV. Most rules and guidelines used are the

TABLE IV.—Curvature and Contact Angle for Specific Design Goals Using Ball Bearings

Goal	Bearing design parameter		
	*F_o	F_i	β, degrees
Maximum thrust capacity	Minimum ~0.52	Minimum ~0.52	Maximum ~35
Maximum radial capacity	Minimum ~0.52	Minimum 0.52	Minimum ~12
Minimum contact angle divergence ($\beta_i - \beta_o$)	Maximum ~0.59	Maximum ~0.59	Minimum ~12 to 15
Minimum torque	Maximum ~0.59	Maximum ~0.59	Minimum 12 to 15
Maximum radial stiffness	Minimum 0.52	Minimum 0.52	Minimum 12 to 15
Inner race control	Maximum >0.54	Minimum <0.54	Minimum 12 to 15

*F = race radius divided by ball diameter.

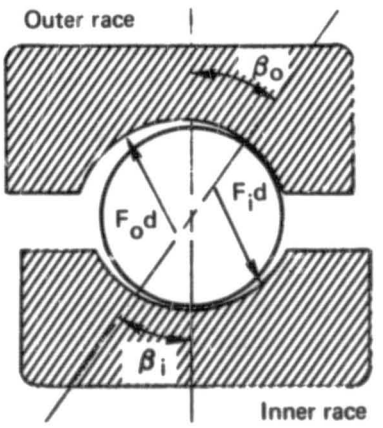

result of analysis, with little if any empirical confirmation in full-scale bearings. In general, if a combination performs satisfactorily during testing, the design is adopted and no further experiments are performed, partly because testing, especially with cryogenic coolants, is extremely expensive. Some results of rig testing at extremely high speed (ref. 4) have indicated that designing for minimum heat generation allows operation at 3 x 10^6 DN with large (150 to 200 mm) bearings. In general, bearings for liquid-hydrogen service are required to operate at high speed because of the low density of hydrogen. These bearings are therefore designed for a low-heat-generation maximum-speed capability.

Optimum high-speed bearing design seeks to minimize the detrimental inertial effects of speed. This requires minimizing initial contact angle β to reduce the dynamic contact angle divergence $(\beta_i - \beta_o)$. Large total curvatures $(F_o + F_i - 1)$ permit lower contact angle while maintaining a required safe diametral clearance (see sec. 2.1.6).

Within the total curvature required for adequate clearance, inner and outer race curvature can be varied, and the designer is free to select a beneficial combination F_o/F_i. There is theoretical justification for attempting to obtain inner race control (IRC) (refs. 25 and 26) by setting $F_i < F_o$. IRC exists when rolling action is maintained at the inner race contact and spinning occurs predominantly at the outer race contact. The advantage of IRC is that it produces less bearing torque than ORC (outer race control) and allows small F_i, resulting in lower contact stress and longer inner race fatigue life. The limitation to the benefits obtained in this way are that (1) it is difficult to obtain IRC in bearings of over 50 mm bore, and (2) at extremely high speeds, the centrifugal force acting on the balls makes the outer race stress the more significant life-controlling factor. In general, in extremely high-speed bearings F_o is made less than F_i. This reduces heat generation caused by ball spinning at the inner race contact without unduly affecting bearing fatigue life, which is limited primarily by the outer race because of centrifugal ball forces.

Race finish.—Although extremely fine finishes are possible, the following finishes are easily attainable and give satisfactory service:

Direction	Surface[1] roughness	Waviness[1,2]	
		17 to 330 peaks/revolution	4 to 17 peaks/revolution
Raceway, circumferential	6 μ in. AA	30 μ in.	60 μ in./30° circumferential arc
Raceway, transverse	30 μ in. AA	NA	NA
Cage land, circumferential	25 μ in. AA	75 μ in.	NA

[1]See ASA B46.1 - 1962 (ref. 27) for surface texture definitions.

[2]Waviness is normally defined as the maximum peak-to-valley dimension; however, waviness of bearing races is often defined as the average deviation from a nominal surface (see ref. 27).

Some users require even finer finishes in special cases. Bearing manufacturers can obtain a transverse finish of 6μ in. AA with resulting improvement in circumferential finish. Production techniques for providing these finer finishes are under development.

Surface finish refinement promotes formation of elastohydrodynamic (EHD) films, provides smooth bearing operation, increases fatigue life, and aids in the formation of transfer films (ref. 22). Actual formation of EHD films is unlikely in turbopump bearings regardless of the raceway finish because the viscosity of the propellant/coolants is low. (For a review of current EHD technology, see ref. 28, pp. 36-37.) Although fatigue life generally increases with finer finishes, some preliminary results of single-ball fatigue testing indicate there may be a decrease in fatigue life when race finishes are reduced below 5μ in. AA.

Ball bearing shoulder configuration.—Ball bearing shoulder heights are specified as a percent of ball diameter, the value being derived from analyses that describe the dynamic position of the ball and the size of the contact ellipse. The shoulder height is specified high enough to contain the contact ellipse under all anticipated loading conditions. Normal ball bearing shoulder heights vary from 18 to 22 percent. High-speed ball bearings with low contact angles often have much lower shoulders, some only 12 percent.

To provide a safety factor for overloads, the race edge is relieved to prevent ball creasing. The value of edge relief was shown in tests of highly loaded thrust bearings for the F-1 engine turbopump; ball bearings with edge relief survived axial loads that resulted in approximately 0.030 in. excursion of theoretical contact ellipse length beyond the race edge. Bearings with no relief or inferior edge relief failed immediately.

Race relief.—Cage problems caused by ball size variation in bearings under constant thrust load are not solved simply by enlarging ball pocket size. Rather than alternately advancing and retarding from a nominal position, different size balls tend to continue to advance or retard, applying excessive forces on the cage. In limited testing at 2.0 x 10^6 DN in liquid hydrogen, a small raceway relief or unloading chute (fig. 11) 0.003 in. deep by 0.300 in. long was effective in reducing the cage forces.

2.2.3 Cage Design

Cage strength.—Cages made of weak or brittle materials are often stiffened and strengthened with metal shrouds or reinforcing bands. Cages of serviceable strength have thus been constructed from otherwise unsatisfactory materials such as filled PTFE compositions (ref. 9). The early Armalon (glass-fabric-supported PTFE) cages were reinforced with aluminum side bands, but subsequent testing and practice have shown Armalon to be rigid and strong enough at cryogenic temperatures to be satisfactory even when unsupported.

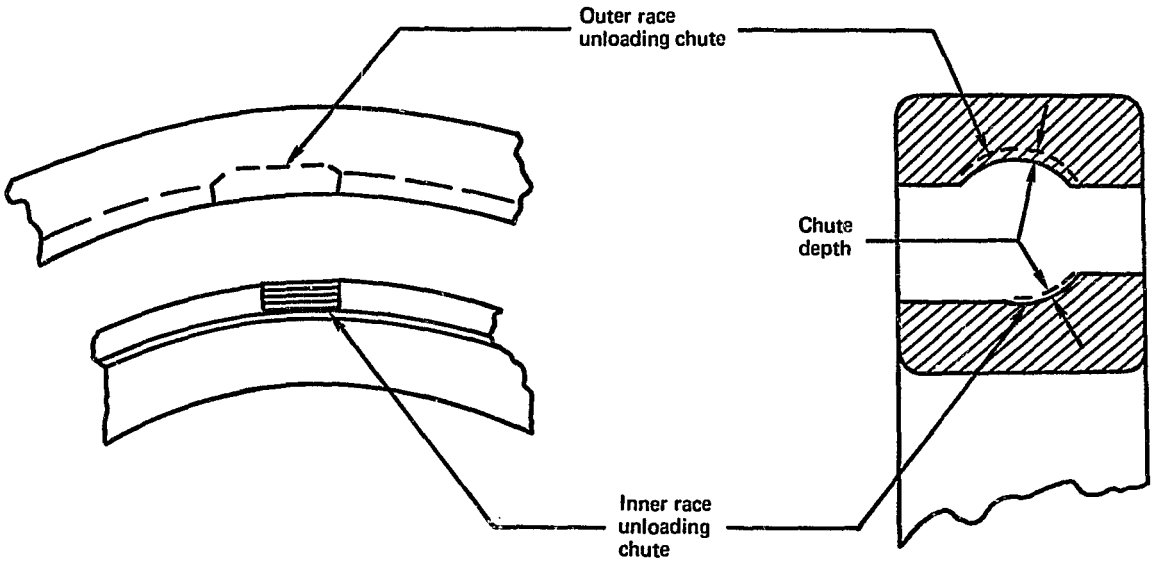

Figure 11.—Ball bearing unloading chute.

Coolant flow area.—Cages are designed with minimum cross section to allow free through-flow of coolant. Minimum radial thickness of Armalon cages used for liquid-hydrogen and liquid-oxygen bearings has been 0.100 in. for cages approximately 3.5 in. in mean diameter and 0.150 in. for cages approximately 8 in. in mean diameter. Cages of weaker materials are made thicker or are reinforced; metallic cages are usually no thinner than Armalon cages in order to preserve a generous contact area for the rolling element in the ball pockets or to avoid off-center contact with rolling elements.

Cage–rolling element contact.—The cage pocket contact with the ball or roller is usually centered at the rolling-element complement pitch line to avoid jamming or deflecting the cage as the rolling element tends to "climb" over the cage web. This is not mandatory, because in some applications the cage makes contact above the pitch line with satisfactory results. Limitations generally are not explored, and changes are made only if difficulty is encountered.

Web thickness.—Cage web thicknesses of less than 0.150 in. are unsatisfactory for propellant-cooled bearings. Metallic cage webs can be made thinner, but minimum thicknesses must be determined by testing because of differences in operating severity.

Guiding land clearance.—Cage guiding land clearance is maintained at some positive value for all operating conditions, but ge erally has a minimum value of approximately 0.010 in. Larger clearances are occasionally necessary to allow ball advance and retard because of misalignment or combined load (ref. 6). Standard land clearances can be used if the circumferential cage pocket clearance is sufficient to allow ball excursions.

Pocket clearance.—Cage-ball pocket clearance is extremely important in cases of misalignment or combined load (refs. 5 and 6). Pocket clearances of 0.025 to 0.035 in. are often used when some ball speed variation is expected. Elliptical cage pockets with major ellipse diameter in the circumferential direction are sometimes used when low transverse pocket clearance is desired to prevent cage wobble.

Cage sides protrusion.—Total cage widths are normally limited so that the cage side does not protrude beyond the bearing faces during operation. Countersunk or counterbored rivet-head sockets are often used instead of flat surfaces for the rivet heads to reduce cage width and still maintain the cage sidewall thickness that will provide adequate strength.

Cage rivet tightness.—Cage rivet fit and tension are carefully controlled to prevent loosening of rivets. Plating is not allowed between cage halves or under rivet heads. Rivet and cage materials are thermally matched to prevent loosening by differential response to changes in temperature. The diameters and lengths of cage rivets are established to obtain rivet stretch sufficient to maintain tightness while not deforming the cage or side plate material.

3. DESIGN CRITERIA and Recommended Practices

3.1 Bearing Assembly Design

3.1.1 Load Capability

The bearing shall be suitable for supporting the type and magnitude of the predicted loading (radial only, one-direction axial only, two-direction axial only, and combined radial and axial loads).

Bearings fulfilling the load direction requirements shown in table I should be analyzed for dynamic characteristics (including speed effects) by methods given in reference 3. The most favorable configuration and internal geometry should then be established on the basis of fatigue life, heat generation, stiffness, coolant suitability, and misalignment tolerance. It is recommended that bearings for turbopump service display a calculated minimum B_{10} fatigue life of 10 times the required turbopump life.

3.1.2 Speed Capability

The bearing shall satisfy the speed requirements of the application.

The use of any bearing type that dynamic analysis shows has either of the following weaknesses should be avoided: (1) an outer race inadequate to survive fatigue induced by centrifugal force of the rolling elements; or (2) a cage whose structural capacity is exceeded by centrifugal force or is subject to unsatisfactory dynamic interaction such as excessive sliding and heat generation of the rolling elements and races. The limitation on the last condition is difficult to define quantitatively because it is subject to improvement by changes in loading, cooling, and geometry.

Experience to date in the design of bearings for high-speed applications provides a basis for the following recommendations:

(1) One-piece cages should be used for speeds over 1.0×10^6 DN.
(2) Angular-contact ball bearings should be used for speeds between 1.0 and 3.0×10^6 DN.
(3) Reference 8 should be consulted for maximum speeds with cylindrical roller bearings.
(4) Rolling element bearings should not be used for speeds over 3.0×10^6 DN without prior testing.

3.1.3 Stiffness

Through a dynamic analysis of performance under operating conditions of speed and load, the proposed bearing design shall exhibit stiffness adequate for the intended use.

Digital computer programs based on the generalized bearing analysis presented in reference 3 should be used to analyze bearing designs; such programs provide a means for quickly performing complex calculations that would be prohibitively time consuming to perform by hand.

If the stiffness of a proposed design is inadequate, another design or loading condition must be evaluated. For example, assume that a proposed design of a single ball bearing has too low a radial stiffness; any of the following design alternatives will yield a stiffer bearing:

(1) Increase the size of the bearing.
(2) Increase the axial preload.
(3) Decrease the contact angle.
(4) Change the design to incorporate a greater number of smaller diameter balls.
(5) Substitute a duplex pair of ball bearings for the single bearing.
(6) Substitute a roller bearing for the ball bearing.
(7) Lengthen rollers (see sec. 3.2.1.5 for precautions on maximum roller length/diameter ratio).

3.1.4 Misalignment Tolerance

The misalignment capabilities of the bearing design shall exceed the misalignment imposed by the application.

The misalignment imposed on the bearing in the turbopump design should be minimized. The maximum recommended stationary race misalignment of common bearing types is presented in table V.

The misalignment tolerance in ball bearings can be maximized by providing adequate circumferential cage pocket clearance to allow for orbital ball speed variation (BSV). In reference 6 Barish discusses the cause and effects of BSV and proposes a means of calculating the cage clearance required to minimize cage distress caused by BSV.

A roller crown should be provided in roller bearings to reduce the loss of capacity caused by the edge loading of the rollers (see sec. 3.2.1.7).

TABLE V.—Bearing Misalignment Capabilities

Bearing type	Misalignment capability		
	(1)	(2)	(3)
Conrad-type (ref. 6)	0°15′	0°25′	—
Angular-contact, spring preload (ref. 6)	0° 2′	0°10′	—
Angular-contact, rigid preload	—	—	0°0′
Cylindrical roller bearing (ref. 20)	—	—	0°5′
Split-inner-ring (ref. 20)	0° 2′	—	—

Notes:

(1) Cage-guiding land and ball-ball pocket clearances: 0.005 to 0.015 in.

(2) Cage-guiding land and ball-ball pocket clearances: 0.025 to 0.035 in.

(3) No clearances specified.

3.1.5 Bore

The bearing bore shall be sufficiently small to reduce the detrimental effects of high speed.

The bearing with the smallest diameter that meets shaft strength and stiffness requirements should be utilized.

When analyzing the shaft stiffness to determine the minimum bearing bore, the stiffening effect of spacers, races, and clamping forces should be included; this effect may allow a smaller bearing size to be used.

The maximum allowable bearing bore is limited by the centrifugal loading on the materials of the rolling elements at design speed. A tandem set of ball thrust bearings should be used when the capacity of a single be ing is inadequate but an increase in bearing bore would result in a loss of capacity because of centrifugal loading.

Do not put a spline inside a bearing. A spline generally enlarges the required bore and may result in inner race taper distortion produced by spline tooth loads.

3.1.6 Internal Clearance

Internal clearance in rolling bearings shall not become negative.

The unfitted diametral clearance should be specified to maintain positive operating diametral clearance by using the formula

$$C_d = C_o + C_f + C_t + C_c$$

where

C_d = Unfitted diametral clearance
C_o = Operating diametral clearance, which should be (1) the results of the contact angle and curvatures, or (2) 0.0005 in. minimum
C_f = Clearance change caused by press fitting (see sec. 3.1.8)
C_t = Clearance change caused by the temperature difference between the inner and outer race. Measured values or heat-transfer analysis results should be used. If temperatures are unknown, use the following guideline values when the inner race is warmer than the outer race:

Bearing DN, millions	ΔT,°F
0.5	0
0.5 to 1.0	50
1.0 to 1.5	100
1.5 to 3.0	150

C_c = Clearance reduction caused by the centrifugal growth of the inner race (calculated by the methods of ref. 29, pp. 214-221).

Exceptions to the rule for maintaining positive diametral clearances should be considered in applications where roller skidding may occur because of insufficient radial load. Testing then must confirm that the cooling provided is adequate to establish stable safe temperature levels (ref. 8).

3.1.7 Cooling

3.1.7.1 Coolant Effects

The bearing type shall be suitable for and appropriate to the coolant available.

Ball bearings are preferable to roller bearings for nonlubricating coolant applications where the ball bearings are adequate for the required load capacity, speed capacity, and stiffness. Full-scale bearing tests should confirm the use of cylindrical roller bearings particularly in applications involving chemically reduced coolants.

The most favorable bearing design for propellant lubrication is the angular-contact ball bearing; the relieved shoulder provides good coolant circulation, and the separable feature of the bearing allows full cleaning and cleanliness verification that would be impossible with a Conrad-type bearing. Alternatively, a split-inner-ring bearing should be used where thrust load capacity is required in both directions.

3.1.7.2 Coolant Quantity

The flowrate of bearing coolant shall be sufficient to maintain temperatures that do not endanger bearing integrity.

Positive through-flow of bearing coolant should be of sufficient quantity to maintain acceptably low temperatures throughout the bearing system. The required quantity can be determined as follows:

(1) Estimate the heat-generation rate of the bearing by utilizing the results of dynamic analyses, or use an effective friction coefficient applied to bearing dimensions and load. For jet- or mist-lubricated applications involving oil and RP-1, use the following effective friction coefficients (refs. 30 and 31) applied at the bearing bore radius:

Bearing type	Rolling friction coefficient
Ball bearing, radial load	0.0015
Ball bearing, axial load	0.0018
Cylindrical roller bearing	0.0010

As bearing speed increases, the value used for friction coefficient should be increased to allow for churning; the increased value may be as much as twice the original value for jet-lubrication applications and up to ten times the original for flooded-lubrication systems.

For ball bearings with combined load, the conservative approach is to add the effects of the radial and axial loading. For close determination of the effective friction coefficient, test the actual bearing.

(2) Estimate the heat input from external sources such as turbine heat, heat from the atmosphere (for cryogenic coolants), or frictional heat from seals, gears, or other mechanical devices associated with the bearings.

(3) Determine the allowable heat capacity of the coolant.

For storable propellants, subtract the maximum expected inlet temperature from the maximum desirable fluid temperature (that which assures no degradation of the fluid) to obtain the minimum anticipated useable temperature differential.

Multiply the ΔT found by the specific heat of the fluid to obtain the heat capacity per unit of mass allowable.

For cryogenic coolants, determine the enthalpy change for constant pressure heating that will maintain desirable fluid temperature (preferably liquid).

(4) Divide the total heat input from (1) and (2) by the allowable heat capacity of the fluid from (3). The result is the minimum quantity (flowrate of coolant required).

3.1.7.3 Coolant Delivery System

The coolant-system configuration shall not result in excessive heat generation.

The choice between a jet-fed and a flooded-lubricant system should be based on avoiding excessive heat generation caused by churning of the fluid.

Flooded-lubricant/coolant systems should be chosen for propellant-cooled bearings. Most flooded-lubrication systems return the coolant to the pump low pressure area, so the flow of coolant does not represent a complete loss.

All passage areas should be maximized to avoid restriction caused by contamination.

The flow on the downstream side of bearing should be throttled. This is particularly desirable in cryogenic cooling systems to maximize pressure and thereby inhibit vaporization.

Cumulative foaming of a lubricant in a recirculating lube system can be prevented by selecting a foam-resistant coolant and by providing adequate stay time in the oil sump to allow gas escape. Testing may be required to obtain optimum balance between foam control and system compactness.

In a recirculating lubrication system, a scavenge pump should be provided with a capacity four times the lubricant flowrate.

The flow system should be designed with the fewest possible turns, crevices, and dead-ended areas to facilitate maintenance of liquid conditions throughout the bearing area.

The return point for the coolant should be chosen so that it causes the least disturbance to the pump hydrodynamic performance.

The coolant should be taken from the cleanest area, and when possible centrifugal force should be used to exclude particles from the flow system.

Jet or mist feed should be used for coolants other than the pumped propellants.

In conventional lubricant or RP-1 systems, ample coolant exit passages from the bearing area should be provided. A simple rule of thumb is to use four times the area required for liquid flow to allow for foaming.

In noncryogenic coolant systems, submergence of the bearing in stagnant coolant or preservative can be prevented by placing the drain at the lowest point of the system.

Positive through-flow of coolant can be ensured by employing a slinger adjacent to the bearing.

The jet should be placed as close to the bearing as practical to ease targeting. Large-diameter small-cross-section O-rings should not be used as static seals for lubrication jet rings; they become clipped easily during installation. Standard-cross-section O-rings should be used when possible.

3.1.7.3.1 Jet Targeting

Lubrication jets shall direct the coolant to the area between the inner race and the cage.

To ensure that the stream of coolant always enters the area between the inner race and cage, a tolerance stackup of all related parts should be performed. Correct targeting of the jet can be obtained by (1) shimming a bayonet type jet to strike a scribed line on plastic target or (2) controlling closely the jet angle and diameter tolerances for fixed lubrication jet rings (fig. 12). All possible reasons for mistargeting the stream must be eliminated. Jets should be checked for flowrate and for stream separations that would make a significant portion of the flow ineffective.

Outer-land-riding cages should be utilized to increase the target area (the gap between inner race and cage).

If the use of inner-land-riding cages is unavoidable, the bearing area should be pressurized to 2 psig minimum with gas (such as nitrogen) so that sufficient windage occurs to ensure distribution of the lubricant.

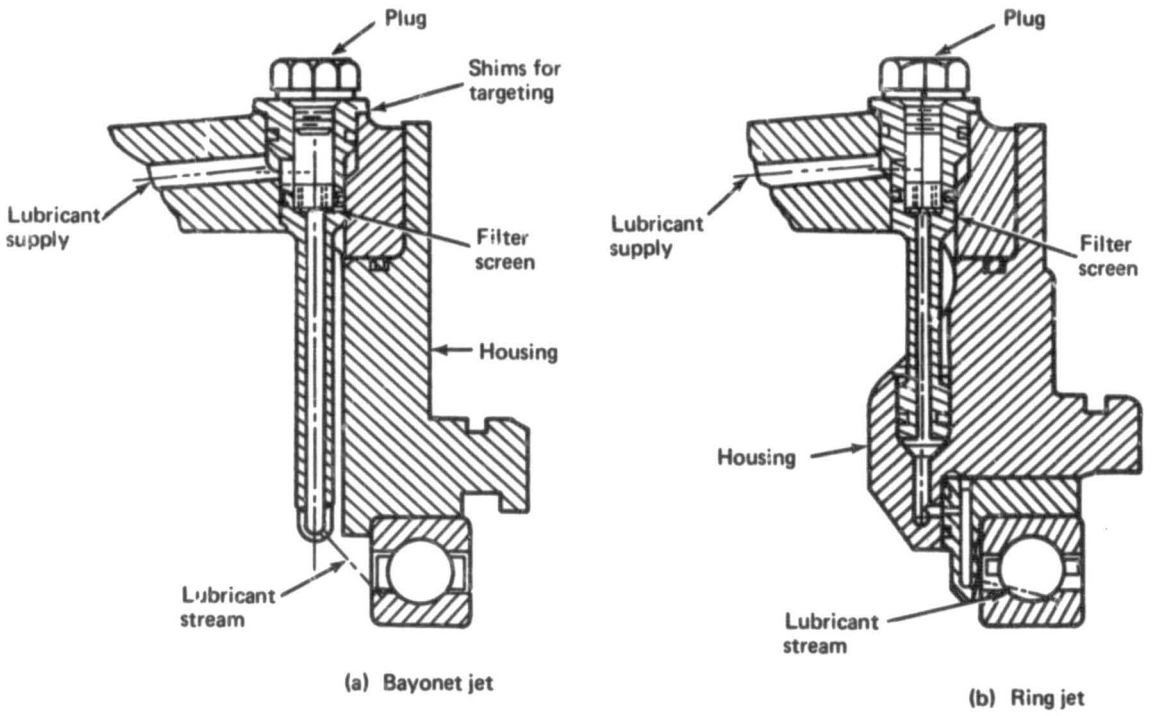

Figure 12.—Types of lubrication jets.

3.1.7.4 Coolant Quality (Liquid/Vapor Fraction)

For maximum cooling effectiveness, the coolant shall exist in the liquid state throughout the bearing area.

The cryogenic coolant pressure and temperature should be maintained to ensure a liquid state at the inlet to the bearing.

If the temperature of the fluid is above the critical temperature, the pressure of the coolant should be maintained above the critical pressure level (ref. 11).

3.1.7.5 Contamination

3.1.7.5.1 Chemicals

There shall be no material chemically incompatible with the coolant in any propellant-cooled bearing system.

Bearing components should be cleansed in nonpetroleum solvents before assembly. Chlorinated or fluorinated hydrocarbons may be used; with either, ensure adequate ventilation and minimum exposure of personnel.

The particle count and NVR (nonvolatile residue) requirements developed for liquid oxygen systems in specification MSFC-SPEC-164 (ref. 12), which controls the contamination per square foot of component, should be enforced as follows:

Particle size	Number allowed per ft^2
175 to 700 microns	5
700 to 2500 microns	1
> 2500 microns	0
Nonvolatile residue	1 mg/ft^2 maximum

Passivation of all systems using fluorine or FLOX should be provided (ref. 32, pp. 212-317).

3.1.7.5.2 Water

No water shall be in the bearing area during idle periods.

Bearings cooled by RP-1 and conventional lubricants should be protected during idle periods by coating with water-displacing preservatives. Suitable preservatives should be similar to compounds that meet MIL-L-16173 (ref. 33). The preservative selected must be compatible with all materials it may contact (e.g., leaked propellant, products of combustion, etc.).

Water vapor should be excluded from propellant-cooled bearings by sealing the system from the atmosphere.

To prevent the entry of water and to remove water from propellant-cooled bearing cavities, purging with dry nitrogen is recommended. Dry helium gas should be used for purging liquid hydrogen systems. In cryogenic coolant systems, the purge must be maintained during chilled periods to prevent ice formation.

3.1.7.5.3 Particulate Matter

No particulate matter that might damage the bearing or plug the lubrication passages or jets shall contaminate the lubrication system.

The solvents used in cleaning bearings should be passed through 10μ filters. Preservatives and greases should be passed through filters with a minimum size opening of 40μ; finer filters may remove the active ingredients of preservatives. Coolant delivery passages should be equipped with screens or filters having a mesh size of 40μ or less. When designing lubrication jets, a provision for chip cleanout after machining should be included.

Press fits should not be used as static seals for lubrication jets or lubrication jet rings because metal chips shaved off during the pressing operation may later clog the jet orifices.

For systems subject to oil sludging from combustion products, replaceable filters are recommended. A bypass valve should be provided to avoid complete oil starvation should the filter clog.

3.1.8 Bearing Mounting

3.1.8.1 Interference Fits

The fit between the rotating race and its shaft (inner race rotation) or its housing (outer race rotation) shall be tight enough at all operating temperatures to prevent relative motion and consequent fretting, but shall not be so tight at any anticipated temperature that brittle fracture of the raceways results.

Care should be taken to obtain the minimum possible interference fit of the bearing race that will prevent relative rotation at operating temperature. The selection of room temperature shaft and housing dimensions should follow the steps outlined below:

(1) Determine the fit required at operating temperature. Choose the fit shown for the race rotation (inner or outer) and the bore size shown in figure 13 for inner races and figure 14 for outer races.
(2) Calculate the effect of differential contraction or expansion on the operating temperature of the shaft and housing materials.
(3) Determine the interference necessary to prevent creeping caused by the Poisson effect of rolling element loads (ref. 31, pp. 122-123).
(4) Use integral races where possible if extra-heavy interference fits are required.
(5) Calculate the inner ring tensile stress resulting from the interference fit for both ambient and operating temperatures. Use the methods of reference 34, Vol. II, pp. 161-170. Modify the fit to reduce the interference if, under any temperature condition, the tensile stress approaches the strength of the race material. Consider that race materials have very small elongation before fracture.

3.1.8.2 Sliding Fits

Spring preloaded races requiring axial freedom to maintain preload shall have sliding fits at all operating temperatures.

Outer races of spring preloaded bearings should be fit at operating temperature as shown in the lower curve of figure 14. Differential contraction or expansion should be compensated for to determine manufacturing dimensions.

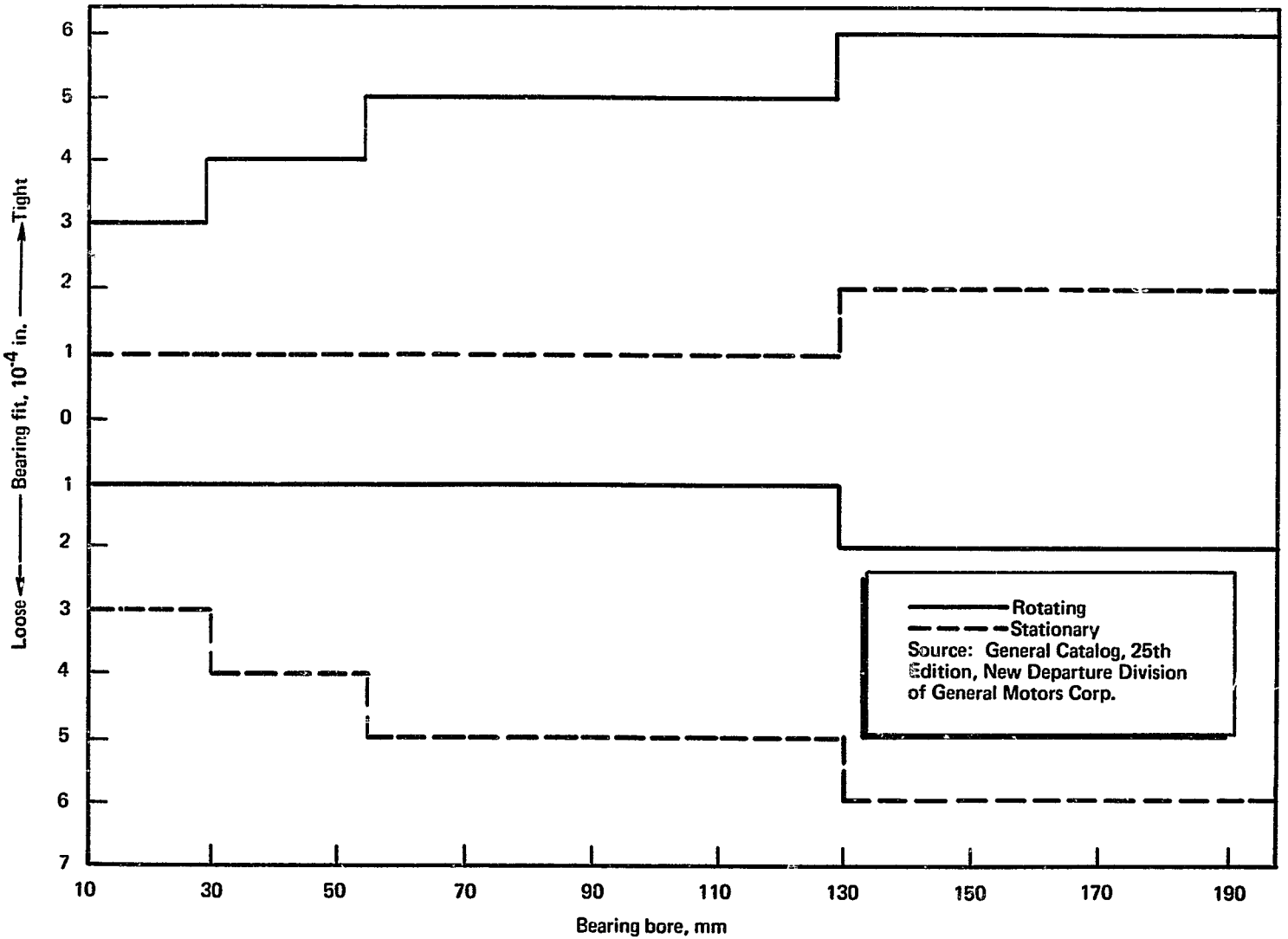

Figure 13.—Inner race fits, ABEC-5.

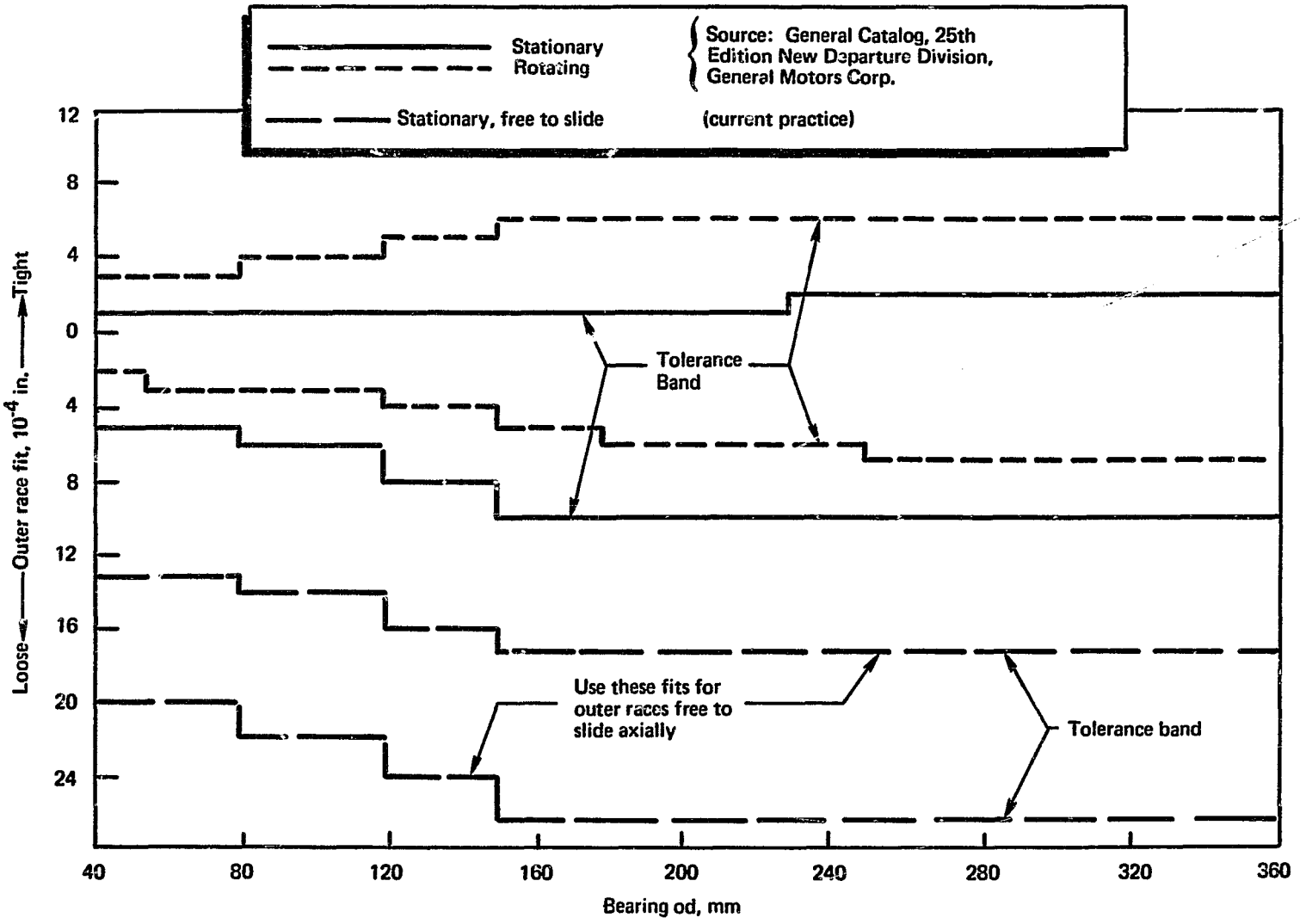

Figure 14.—Outer race fits, ABEC-5.

3.1.8.3 Bearing Mounting Surfaces

Shaft journals and housing bores shall not be subject to galling and fretting.

Galling and fretting of shaft journals and housing bores that may result from repeated assembly or from relative motion of axially free races should be prevented by one of the following practices:

(1) Chrome plate journals and bores. The recommended practice is to plate with hard dense (not decorative or porous) chrome per Federal Specification QQ-C-320 (ref. 35). The plating should be thick enough to attain 0.002 to 0.006 in. of chrome after grinding. Finish grind the plating to a finish of 16μ in. AA. This practice is essential for journals and bores made of Inconel and Monel to prevent galling with 440-C bearing rings.
(2) When using 4130, 4340, or 9310 steel for shafts and housings mounting bearings made of SAE 52100 and SAE 4620, harden journals and bores to 40 R_c minimum.
(3) When titanium shafts are used, install the bearing with a light press fit.

3.1.8.4 Corner Radii Interference

Shaft shoulder corner radii shall not interfere with raceway corner radii.

To ensure that the shaft shoulder radii do not interfere with the raceway corner radii one of the following practices should be utilized:

(1) Use a grind relief (fig. 15(a)) instead of corner radius at the shaft shoulder (fig. 15(b)) when this does not cause an excessive concentration of shaft stress.

(a) Shaft shoulder with grind relief

(b) Shaft shoulder with corner radius

Figure 15.—Shaft shoulder design.

(2) Specify that the corner radius of shaft R_s shall be smaller than the minimum bearing corner radius R_B (fig. 15(b)).

3.1.8.5 Mounting Surface Accuracy

The concentricity and normality of the bearing mounting surfaces shall be consistent with and adequate for the bearing alignment requirements.

Shaft diametral tolerances should be compatible with the class of precision of the bearing specified (ABEC 5, RBEC 5, or ABEC 7).

A maximum taper control of 50μ in. per inch should be specified for interference-fitted journals and housing bores.

A surface finish of 16μ in. AA should be specified for bearing journals and housing bores.

The concentricity of housing bores and normality of housing shoulders that will result in a maximum misalignment, including runouts of faces, should be specified as follows:

(1) Conrad-type bearings with loose cage or no thrust—0° 25′
(2) Conrad-type bearings or angular-contact bearings with loose cage—0° 15′
(3) Thrust-load-carrying ball bearings and cylindrical roller bearings—0° 5′

Shaft shoulder normality should be compatible with the bearing tolerance. The following values should be used as guidelines:

Bearing bore, mm	Shoulder normality, inches TIR
0 to 80	0.0003
80 to 120	0.0004
120 to 200	0.0005

3.1.8.6 Shoulder Heights

Shaft and housing shoulder heights shall be sized for sufficient axial support of the race, and shall allow removal of the bearing.

When using commercially available bearings, shaft and housing shoulder heights should be chosen from the heights recommended in the manufacturers' catalog. For most rocket engine turbomachinery applications, the guidelines below should be used:

(1) The shaft or housing shoulder should be larger than the maximum bearing race corner radius (fig. 16). Conversely, the corner bearing race corner radius should be smaller than the minimum shoulder height.
(2) The contact area between the shaft shoulder and race face should be sufficient to keep the compressive stress below the compressive yield strength of the shoulder material under clamping thrust loads.

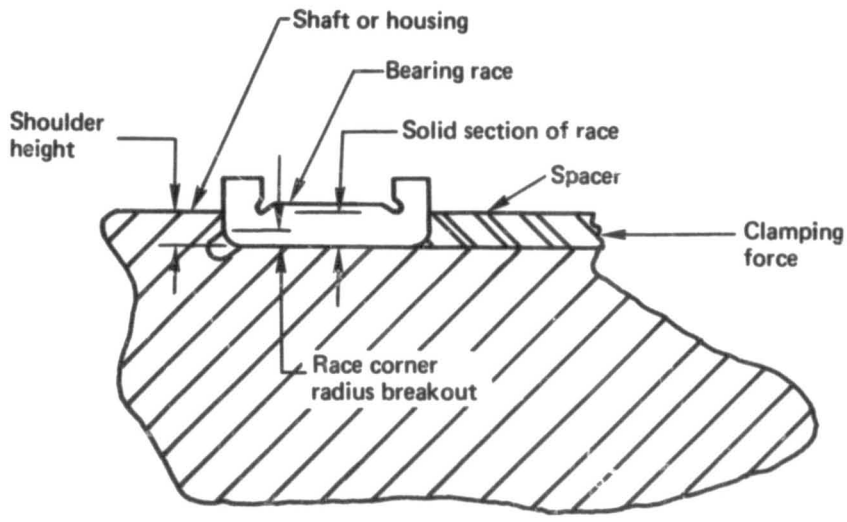

Figure 16.—Housing or shaft shoulder height sizing.

(3) Shoulder diameters that will put the clamping load through the solid race section should be chosen; any condition that may result in shoulder bending should be avoided (see fig. 16).

(4) The shoulder should be smaller than the race face by a sufficient margin for puller tool contacts (fig. 17(a)) or another means of bearing removal, e.g., puller grooves in races (fig. 17(b)) or jack screw holes in flanges, should be provided.

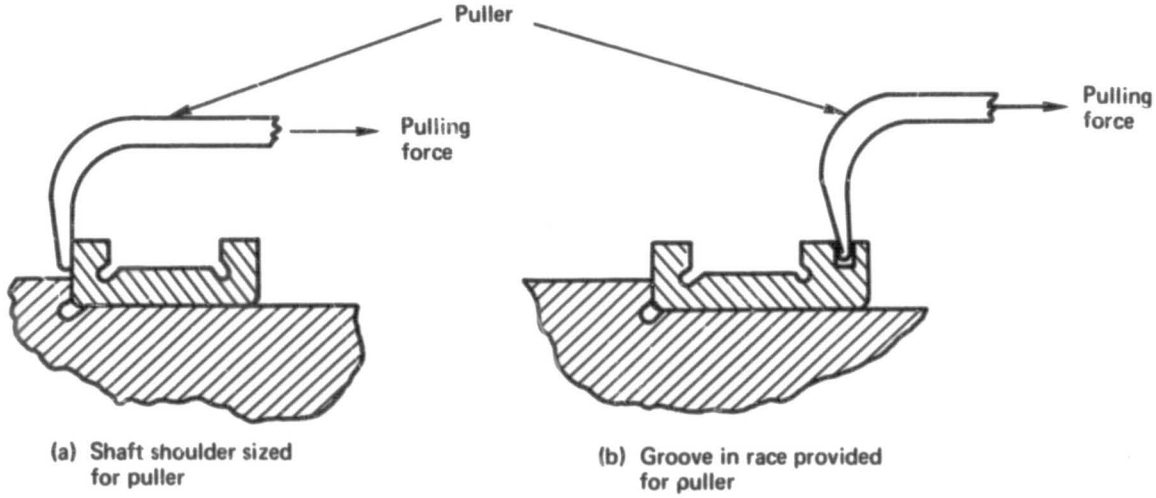

Figure 17.—Provisions for race removal.

3.1.8.7 Race Retention

Race retention methods shall maintain proper support and clamping loads for all thermal and loading conditions including friction, vibration, and shock.

The elastic deflection imposed by clamping devices should be sufficient to maintain a clamping force for any loading that will occur over the thermal range expected in the application. Snap rings should be avoided. The required nut torque should be calculated from the thread dimensions and force relations shown in reference 36, section 3. p. 48.

Bearing retaining clamping loads should be set so that the compressive stress exceeds the tensile bending stress induced in the shaft caused by bending (fig. 18). Failure to accomplish this will result in heavy fretting of the mating surfaces (ref. 7).

3.1.8.7.1 Clamping Loads

Clamping loads applied to bearing races with heavy rotating loads shall be sufficient to prevent both race creeping and fretting resulting from the Poisson effect of the individual rolling element loads and loosening of the stackup of parts resulting from bending of the shaft.

The clamping load required to prevent creeping caused by the race-widening Poisson effect of concentrated compressive loads at the rolling element positions should be determined by experiment. This clamping load may be impossible to attain at extremely high radial loads; the only solution then is to utilize integral inner races, which completely eliminates the problem.

Locking devices, e.g., bendup washers or tabs bent into slots to prevent loosening of clamping nuts, should be included. Tabs should be bent in the same direction as the centrifugal force on the rotating locks.

3.1.9 Bearing Materials

3.1.9.1 Corrosion Resistance

The rolling element, race, and cage materials shall be resistant to or protected from corrosion under all operating conditions.

AISI 440-C corrosion resistant steel is recommended for most propellant-cooled bearing applications. While no known material ideally fulfills the requirements of hardness, ductility or toughness, machinability, and availability, 440-C best meets the requirements with the fewest limitations.

Other bearing materials should be considered for propellant-lubricated applications where more complete corrosion resistance is required. Table VI presents a few of the possible materials choices, with some properties and disadvantages.

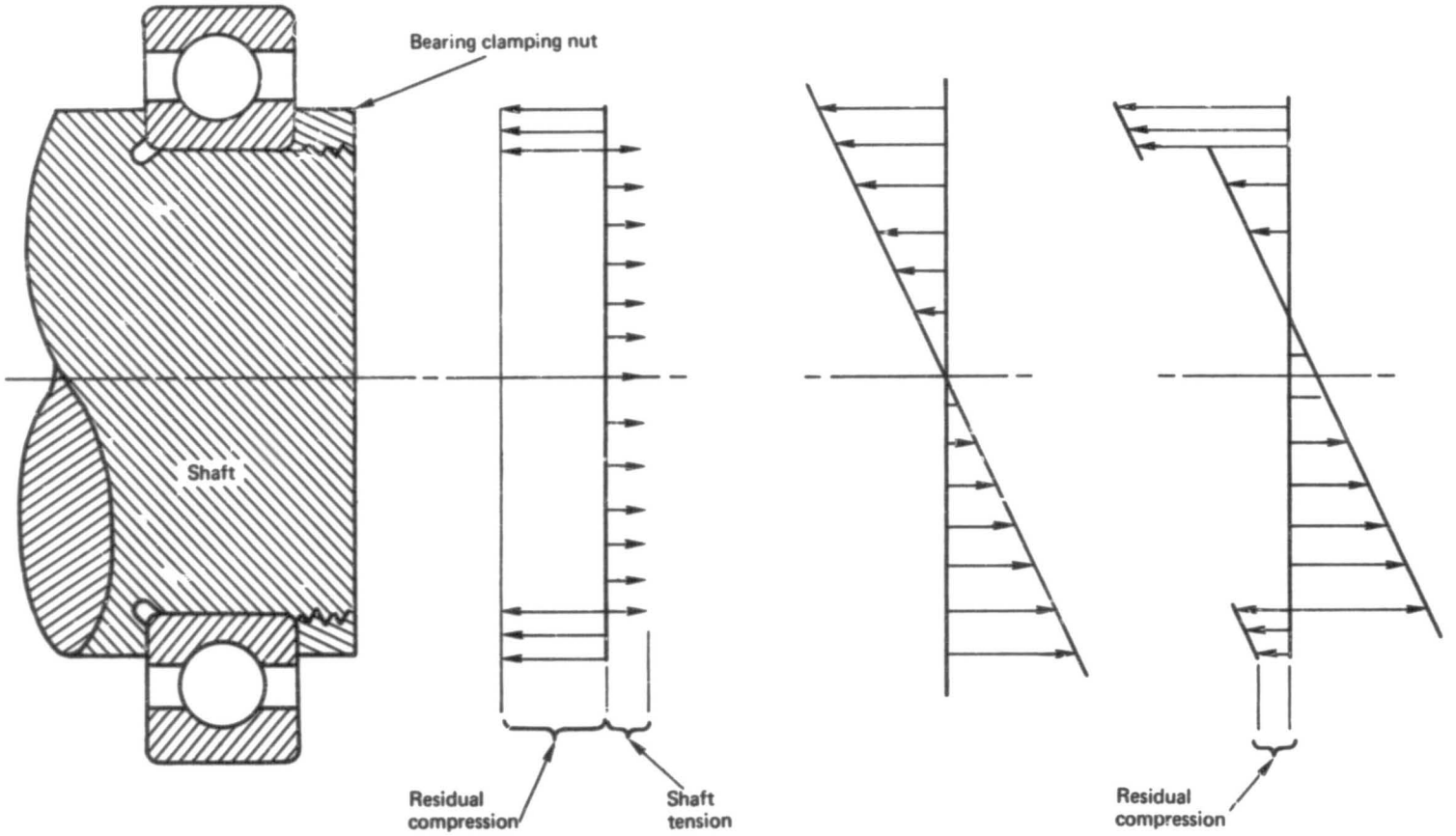

Figure 18.—Required clamping force.

TABLE VI.—Corrosion Resistant Race and Rolling Element Materials

Temperature range, °F	Designation	Hardening	Maximum hardness, R_c	Disadvantages
−423 to 700	440-C	Through	60	Brittleness; not completely corrosion resistant
−423 to 1200	Haynes 25	Work hardened	55	Low hardness; limited availability; high cost
−425 to 68*	Stellite Star-J	Cast chill cast	52 61	Lack of test experience; high cost
	Stellite 19	Cast chill cast	49 55	Low hardness
	Stellite 3	Cast chill cast	51 59	Low hardness
−423 to 68*	Titanium Carbide K162B	Through	76	Brittleness; high modulus resulting in high stresses; high cost; difficult to fabricate
−423 to 68*	Tungsten Carbide	Through	76	Brittleness; high modulus; heavier than steel

*For hot hardness, the manufacturer's data should be consulted, then capacity adjustment should be applied according to the relationship given in section 3.1.9.2.

For RP-1 or conventional-lubricant cooled bearings, the use of standard bearing materials is recommended, with a provision for corrosion protection with preservatives. Materials that should be considered are

(1) SAE 52100
(2) Tool steels: M-10 and M-50
(3) SAE 4620 carburizing
(4) Proprietary steels as recommended by bearing suppliers

3.1.9.2 Hardness

Rolling element and race materials shall possess sufficient hardness to prevent plastic deformation under all loading conditions.

The capacity rating of bearing steels based on their hardness at operating temperature converted to tensile strength should be determined according to the relationship

$$\text{Capacity} \approx (\text{ultimate tensile strength})^n$$

where

$n = 3$ for ball bearings
$n = 2$ for roller bearings
$2 < n < 3$ for crowned roller bearings

See reference 37 for a more detailed discussion of hardness effect on capacity of rolling surfaces.

Fatigue properties of nonferrous bearing materials (e.g., sintered carbides, ceramics, nickel alloys) should be determined by test.

To obtain maximum fatigue life, a differential hardness that makes rolling elements harder than the races by 1 to 2 points R_c (ref. 38) should be specified. Inherently, balls will be a few points harder than races because of the effect of smaller mass in heat treatment.

3.1.9.3 Adhesion Resistance

The rolling element and race materials shall resist adhesion during rolling contact in the presence of the selected coolant.

440-C CRES is suitable for use as a race and ball material with the following propellant/coolants (ref. 18):

Fuels	Oxidizers
RP-1	Liquid oxygen
Liquid hydrogen	IRFNA
B_5H_9	Liquid fluorine

Tests should be conducted under simulated operating conditions before using 440-C in bearings cooled by the following propellants:

N_2H_4 (hydrazine)
Ethylene diamine
UDMH
50 percent UDMH–50 percent N_2H_4

3.1.9.4 Dimensional Stability

Raceway materials for cryogenic bearings shall not change dimensionally during use.

To obtain dimensional stability for 440-C races, repeated chilling and tempering cycles should be performed before final finishing operations.

A recommended stabilization procedure for 440-C intended for cryogenic service is

(1) Temper to +325° to +350° F.
(2) Cold soak in liquid nitrogen (−320° F) for 30 minutes minimum.
(3) Temper again to +325° to +350° F before final grinding.

3.1.9.5 Grinding Burns

Raceways shall not be subject to grinding burns.

Grinding coolant flow, feed rate, and grinding wheel composition should be controlled by the manufacturer to preclude grinding burns in raceways. Suspected grinding burns can be detected with Nital etch on carburizing steel. Ensure that the acid is neutralized and that surface effects are removed by final finishing.

3.1.9.6 Cage Materials—Friction

Sliding friction of cage materials against rolling elements and races shall not result in excessive forces and heat generation.

Table VII presents cage materials recommended for use because they display good frictional characteristics with the indicated propellant, i.e., the coefficient of friction is between 0.05 and 0.15.

Bearing cages for bearings cooled by RP-1 or conventional lubricants should follow aircraft bearing practice, as follows:

Temperature range, °F	Material
−65 to 250	Linen-supported phenolic resin
−65 to 600	Silver-plated iron silicon bronze
	Silver-plated 4130 or 6414 steel
−65 to 1000	Oxide-coated S-Monel

TABLE VII.—Recommended Cage Materials

Oxidizer	Fuel	Cage material				
		Armalon[2]	Salox M[3]	Rulon A[4]	25 percent GFT[5]	K-Monel
	Amines[1]				X	
	B_5H_9	X				
	Liquid hydrogen	X	X	X	X	
	Gaseous hydrogen		X	X		
N_2O_4					X	
IRFNA		X				
Liquid oxygen		X	X	X		
FLOX[6] or liquid fluorine						X

[1] N_2H_4, UDMH, or 50-50 mixture
[2] Mandrel-wrapped, glass-fabric-supported PTFE
[3] 40 percent bronze-powder-filled PTFE
[4] 15 percent glass-fiber-filled PTFE
[5] 25 percent glass-fiber-filled PTFE
[6] Mixture of liquid fluorine and liquid oxygen

3.1.9.7 Materials Cleanliness

Materials used for races and rolling elements shall be free of nonmetallic inclusions.

Consumable-electrode vacuum-melted materials should be specified for race and rolling elements.

3.1.10 Testing

Bearing tests shall confirm the adequacy of the design.

Full-scale testing.—Full-scale bearing tests simulating operating environment should confirm design adequacy prior to production use of the bearing. Test sequences should confirm bearing life and structural integrity over the entire range of turbopump speed and load conditions. The dimensions of the test bearing should cover the range of manufacturing tolerances, particularly diametral clearance.

Rolling contact tests.—Modified Shell Four-Ball (Barwell) Tester (ref. 19), NASA Five-Ball Tester (ref. 38), or similar subscale testers should be used to determine the rolling contact performance of candidate materials for untried coolants.

Sliding friction tests.—The use of simple sliding tests, e.g., a button on a rotating disk (ref. 23), is recommended to shorten significantly the search for low-friction, long-wearing cage materials.

The results of subscale rolling and sliding friction tests will indicate the most fruitful avenues of investigation for full-scale bearing tests, thus shortening the total design cycle.

3.2 Bearing Component Design

3.2.1 Rolling Element Design

3.2.1.1 Size

The ball or roller diameter shall be sufficiently large to obtain the required bearing capacity, adequate cage radial thickness, and adequate coolant flow area; the diameter shall be less than that which reduces capacity because of increased centrifugal force.

The number and size of rolling elements should be optimized by selecting from iterated dynamic analyses the most favorable of candidate bearing design geometries. Bearing manufacturers' catalogs represent optimized dimensions for most conditions and are therefore a good starting point for special design optimization. Figure 19 presents the approximate ball diameter/pitch diameter ratio versus bore for the various cross-section series for standard ball bearings; figure 20 presents the same information for roller bearings.

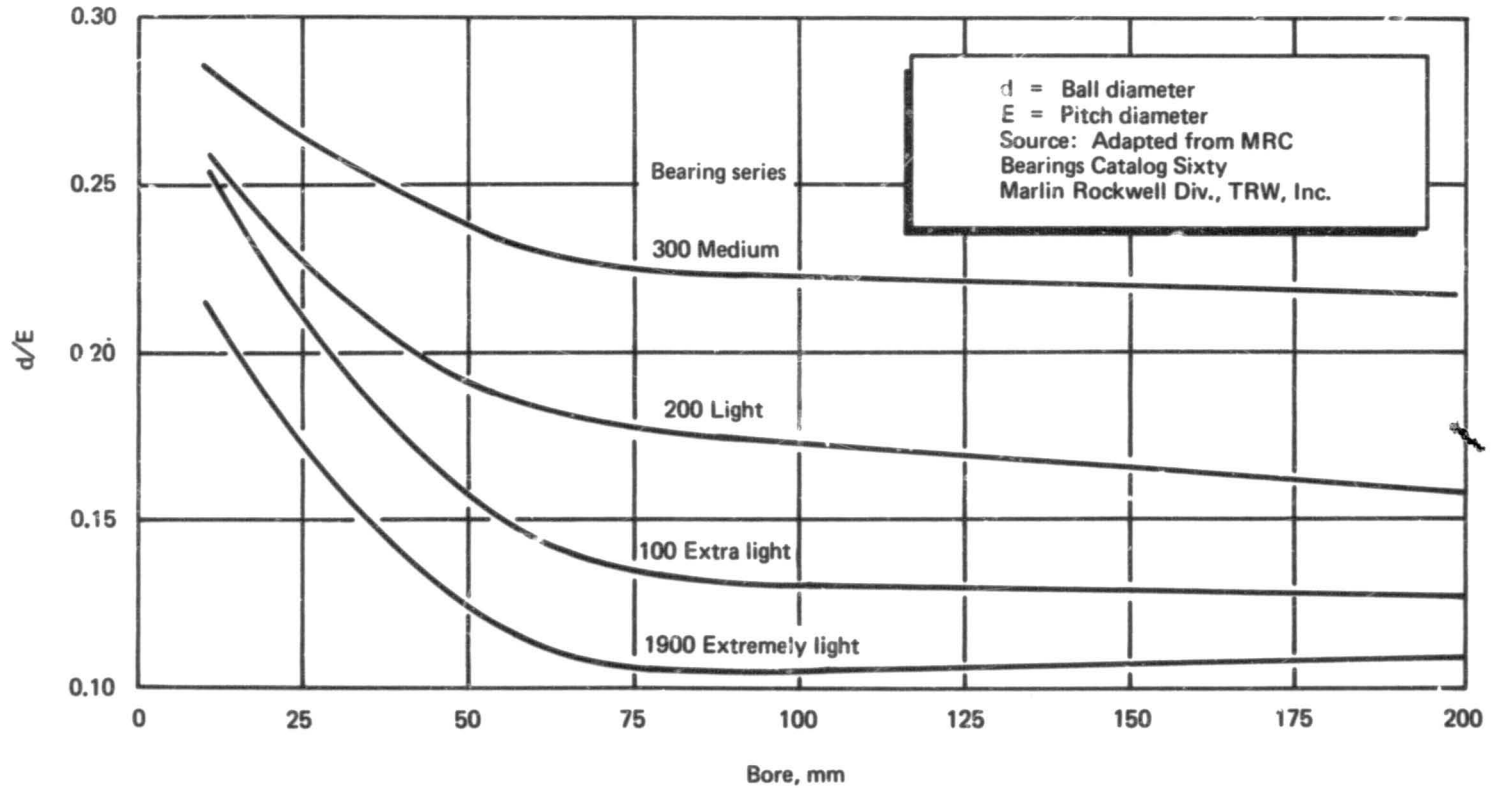

Figure 19.—Ball size basic proportions.

Card #25

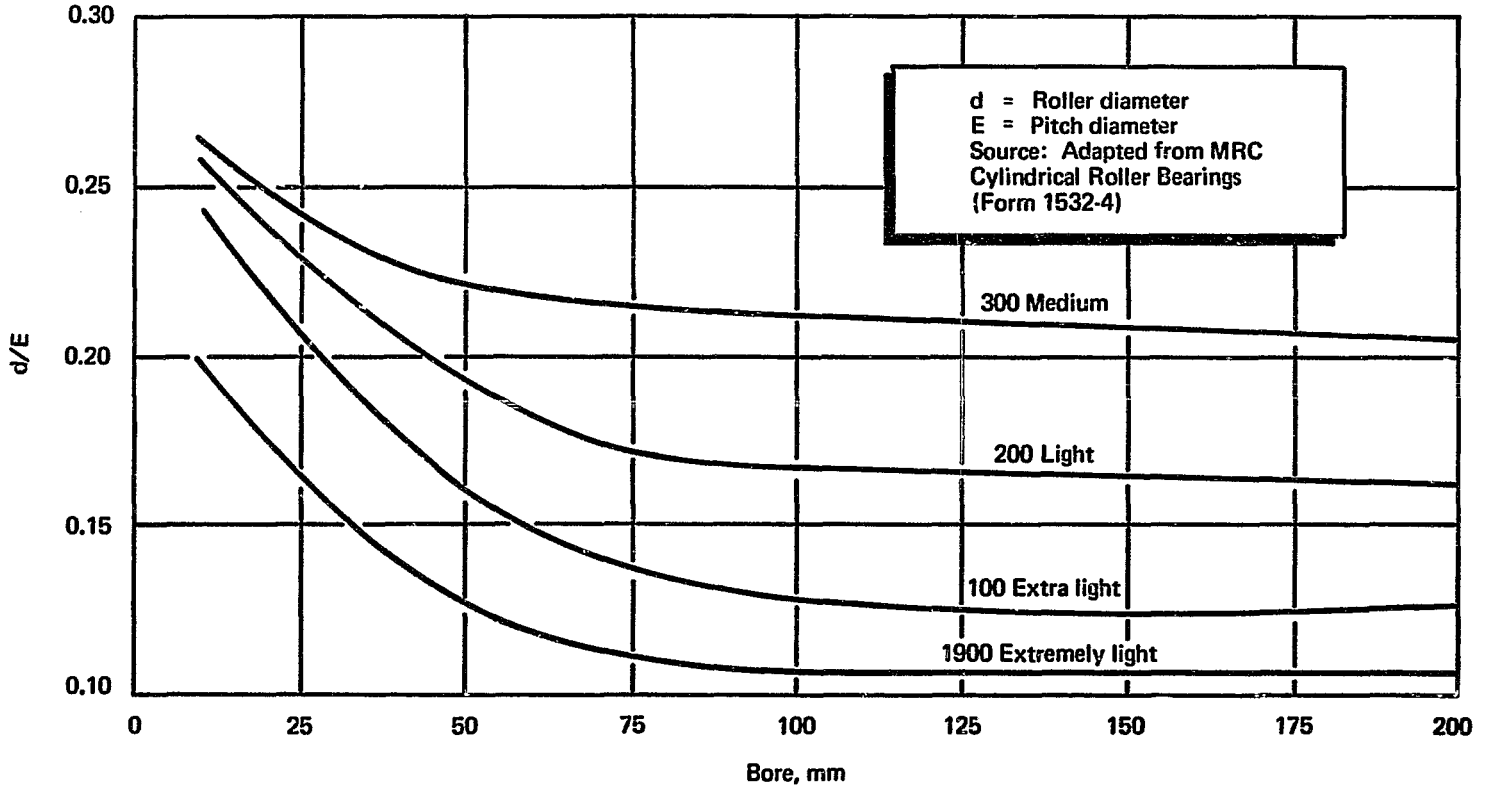

Figure 20.—Roller size basic proportions.

Maximum ball size.—Since centrifugal force varies as d^3 and capacity varies as $d^{1.8}$, the maximum desirable ball size will result. An acceptable rule of thumb proposed by Barish is to limit the ball size so that the following inequality holds:

$$\frac{\text{Sum of ball centrifugal forces}}{\text{500 hr capacity at speed}} \leq \begin{matrix} 2 \text{ for air-melt steels, or} \leq 2.88 \\ \text{for vacuum-melted steels} \end{matrix}$$

If finer determination of maximum ball size is required, iterated calculations of fatigue life should be made for proposed bearing designs varying ball size and number (see sec. 3.2.1.2); the ball size that results in the required life of the bearing should be selected.

Minimum ball/roller size.—In minimizing rolling element size, sufficient size must be maintained to provide both structure for a cage of adequate strength and an area adequate for through-flow of coolant. In lieu of test experience to the contrary, the following guidelines are suggested for minimum proportions:

(1) Minimum cage radial thickness > 0.090 for nonmetallic cages

(2) $\dfrac{\text{Minimum cage radial thickness}}{\text{Cage average diameter}} \geq 0.015$

(3) $\dfrac{\text{Minimum open area for through-flow}}{\text{Bearing pitch diameter}} \geq 0.03$

Smaller dimensions should be subjected to development testing.

3.2.1.2 Number of Rolling Elements

The number of rolling elements shall be sufficient to give smooth bearing operation, but shall not exceed the quantity that results in the minimum allowable cage web thickness.

The maximum number of rolling elements should be determined so that the cage web thickness is not less than 0.150 inch for nonmetallic cages nor less than 0.070 inch for metallic cages. If the wear life of the cage is shown by testing to be insufficient, the number of rolling elements should be reduced.

The usual goal in bearing design is to maximize the number. If minimization is required for a special consideration, a rule of thumb is that the spacing between rolling elements should not be greater than the diameter of an individual element. To evaluate the effect of a minimum number of elements, the radial displacements caused by passing the elements through the radial load zone should be calculated, and their effects on shaft dynamics should be determined. For axial load, the polygonal distortion of the outer race (ref. 39, case 9, p. 158) should be calculated, and the harm that may result from the deflections should be determined.

3.2.1.3 Ball and Roller Diameter Uniformity

The ball or roller diameters within a bearing shall be sufficiently uniform to prevent ball speed variation and provide loading uniformity among individual balls or rollers.

Ball diameter tolerances should be specified as follows:

Bearing DN, millions	AFBMA grade balls	Maximum out of round, μ in.	Maximum size variation, μ in.
0 to 0.75	25	25	50
0.75 to 1.5	10	10	20
1.5 to 3.0	5	5	10

Where extremely smooth operation is required, the finer grades should be specified.

Specifications for roller size uniformity and cylindrical roundness should be equivalent to the AFBMA standards for balls.

3.2.1.4 Ball and Roller Surface Finish

The surface finish of rolling elements shall be fine enough to produce adequate load distribution in the contact area.

Ball finishes should be controlled by specifying the appropriate AFBMA grade. Roller outside-diameter maximum roughness should be specified as 4μ in. AA, and the roller ends as 6μ in. AA.

3.2.1.5 Roller Guidance

Roller guidance shall be adequate to prevent skewing and consequent roller end wear.

For roller bearings with diametral clearance, roller end play in the guiding lips must be maintained at a positive low value. The minimum end play should provide some allowance for thermal growth of the roller; the maximum end play should be limited to prevent a large roller skew angle. Suggested limits are 0.0005 to 0.002 in., with uniform length within 0.0002 in. for all rollers in one bearing assembly.

For specialized roller bearing applications, tests will be required to determine end play limits (ref. 8).

Shoulder height should be specified to contact the roller at approximately 75 percent of its diameter excluding corner radii. Suggested limits for shoulder height are 14 to 20 percent of the roller diameter.

Roller length/diameter ratio should be near unity for the best guidance. For a compromise between adequate stiffness and roller guidance, a maximum l/d ratio of 1.23:1 (ref. 40) should be used.

Parallelism of race guiding lips should be within 0.0002 inch.

Roller ends should be specified as square within 0.0001 in. TIR to prevent wear at the high points and aid in roller guidance.

3.2.1.6 Roller Corner Radii

3.2.1.6.1 Size

Roller corner radii shall be small enough to result in sufficient roller end contact bearing area but large enough to avoid interference with race corner radii.

Maximum roller end radii breakout height (b, fig. 21) should be less than one-half the shoulder height (h, fig. 22(a)) to preserve the roller end bearing area. Roller corner radii (r, fig. 21) should be greater than the race shoulder corner radius (R, fig. 22(b)).

3.2.1.6.2 Runout

Roller corner radii shall not cause unbalance of roller.

Roller corner radii runout should be controlled to 0.002 in. TIR to prevent excessive unbalance in high-speed bearings.

3.2.1.7 Roller End Relief (Crowning)

Roller end relief shall prevent compressive stress concentration at the ends of the rollers because of maximum anticipated misalignment.

Crown drop (e, fig. 21) should be greater than the elastic deflection of the heaviest loaded roller. The elastic deflection should be calculated using the method shown in reference 41. Crowning plus blending (as shown in fig. 21) should be used to prevent stress concentrations.

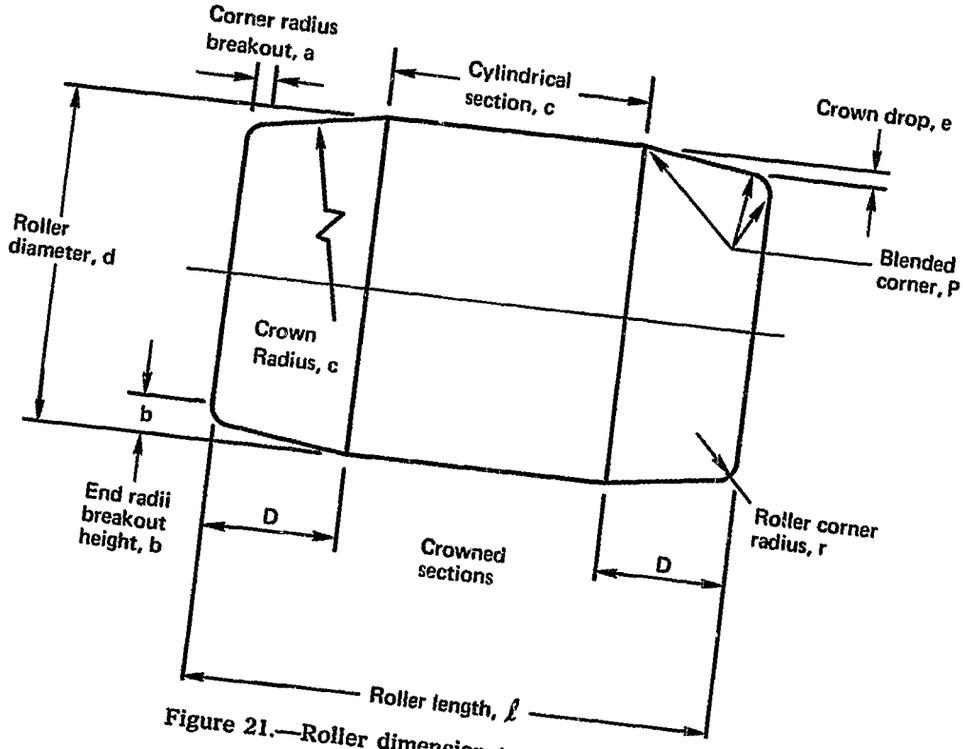

Figure 21.—Roller dimension terms and symbols.

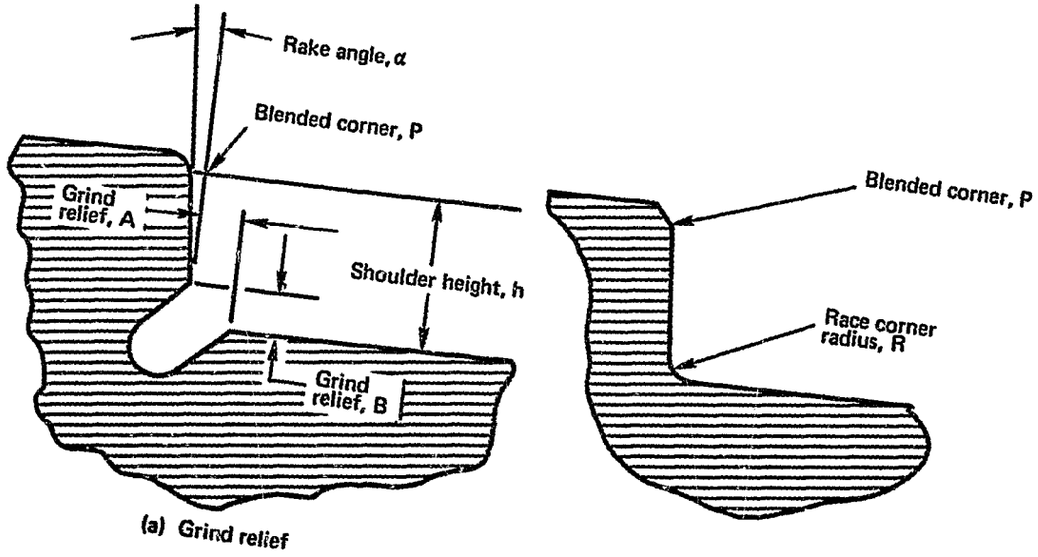

Figure 22.—Shoulder configuration terms and symbols.

If misalignment beyond 0°5′ exists in the application, the methods given by Harris (ref. 41) should be used to calculate the crown drop required to avoid edge loading. Blending of all such boundaries should be specified as shown in figure 21.

If no design control of roller crown is available, the dynamic capacity of the bearing should be derated as indicated in table VIII.

TABLE VIII.—Roller Bearing Capacity Reduction Caused by Bearing Misalignment*

Location misalignment, in./in.	Percent of basic dynamic capacity	Deflection misalignment, in./in.	Percent of basic dynamic capacity
0.0003	99.4	0.0003	97.5
0.0005	99.1	0.0005	96.0
0.0007	98.6	0.0007	94.4
0.0010	98.0	0.0010	91.8
0.0020	95.6	0.0014	88.3
0.0030	93.1	0.0018	84.2
0.0040	90.6	0.0022	79.6
0.0060	84.8	0.0026	74.4
0.0080	77.9	0.0030	67.9
0.0100	69.2		

*From Catalog AR-59, Rollway Bearing Co., Inc., Syracuse, N. Y., 1959.

3.2.2 Race Design

3.2.2.1 Cross Section

The race cross section shall be sufficiently massive to prevent brittle fracture of the race.

Races should be proportioned so the ratio of raceway thickness to mean raceway diameter does not fall below 0.05. For bearing raceways with lands (fig. 23) the average diameter D_{avg} and average cross-section radial thickness t_{avg} should be used.

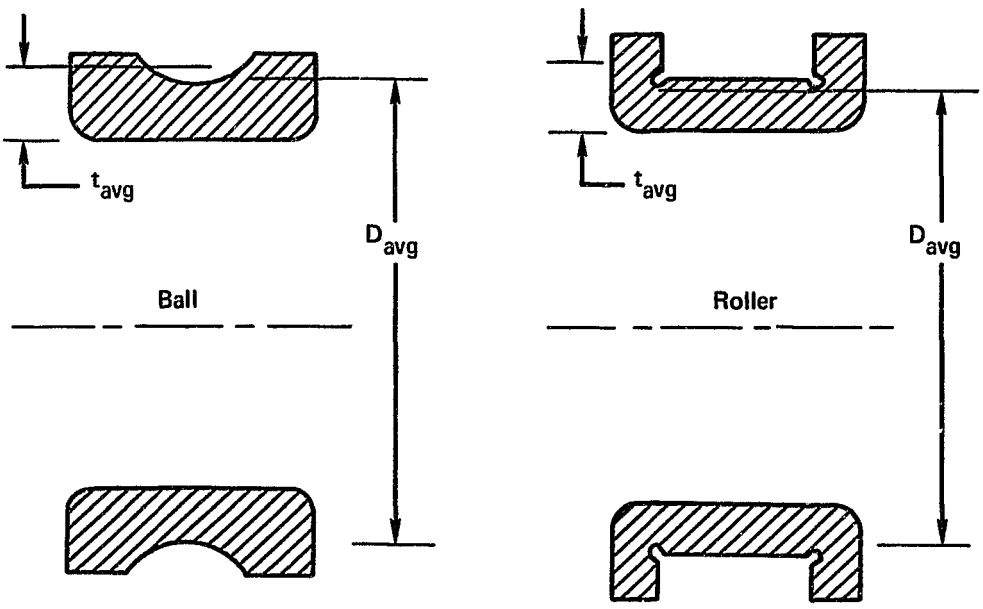

Figure 23.—Bearing race average diameters.

3.2.2.2 Ball Bearing Transverse Race Curvature

Race radii (curvatures) shall conform to ball radii closely enough to achieve the required load capacity, and yet not so closely that excessive nonrolling action (spinning and sliding of the balls) will occur and result in excessive heat generation and wear.

Race curvatures must be combined with ball size and the required diametral clearance to obtain the required fatigue life with acceptable ball spin. See reference 37 for the effect of sliding on fatigue life.

Determine whether the basic goals of the bearing design are minimum rolling friction torque or maximum capacity. For speeds in excess of 1.5×10^6 DN, bearings should be designed for minimum torque.

Perform dynamic analyses of candidate bearing designs, using a range of values for race curvatures. Suggested limits are 0.51 to 0.60. Select that bearing design with longest fatigue life or minimum friction torque consistent with the primary design goal.

For minimum friction torque, maximize curvatures with the limitation that adequate fatigue life should be maintained. Larger curvatures will result in smaller contact areas, less heat generation, but higher contact stress; consider that fatigue life varies inversely with the ninth power of stress.

If maximum capacity or high fatigue life is the objective, curvatures should be minimized but the minimum race curvature must not be so small that an excessively large contact angle will result from the requirements for diametral clearance (see sec. 3.1.6). A large initial contact angle will result in a large contact-angle divergence ($\beta_i - \beta_o$) under high-speed operation (ref. 3) resulting in excessive ball spin, heating, sear, and surface degradation. For static geometric relationships, see reference 34, Vol. I, pp. 1-4.

The race curvatures F_o (outer race) and F_i (inner race) should be varied independently to achieve the optimum overall effect for high-speed bearings (table IV).

For optimum high-speed bearing design, the minimum total curvature ($F_o + F_i - 1$) should be chosen so that initial contact angle is minimized, while the required diametral clearance (see sec. 3.1.6) is preserved. Minimum initial contact angle will result in minimized dynamic contact-angle divergence ($\beta_i - \beta_o$), and higher bearing radial stiffness.

IRC should be obtained for the specific bearing design, speed, and load by choosing a curvature combination F_o/F_i (refs. 25 and 26) so that $F_i < F_o$. It should be recognized that IRC is very difficult to achieve consistently with large bearings (50 mm bore) and high-speed bearings ($DN > 1.3 \times 10^6$). Whenever possible, however, the benefits of IRC should be obtained by using curvatures chosen as follows:

Curvature	Maximum value	Minimum value
F_o	That giving adequate fatigue life	That resulting in desirable β_o, P_D and equal fatigue lives for individual races
F_i	That required for IRC	

3.2.2.3 Race Finish

Raceway finish for ball or roller bearings shall be sufficiently smooth both circumferentially and axially to assure predictable stress distribution and smooth operation.

The currently acceptable race finishes provided in section 2.2.2 should be specified. Finer finishes should be considered if elastohydrodynamic (EHD) lubrication is to be used (ref. 28, pp. 36-39).

3.2.2.4 Ball Bearing Race Shoulder Configuration

The shoulder configuration for a ball bearing race shall prevent damage to balls under all normal loading conditions.

Using the results of the dynamic analysis, the minimum race shoulder height (fig. 24) should be specified large enough to contain the ball contact ellipse at all loading conditions and should provide a 50-percent overload safety factor. As an added precaution, an edge relief should be provided at the race shoulder as shown in figure 25.

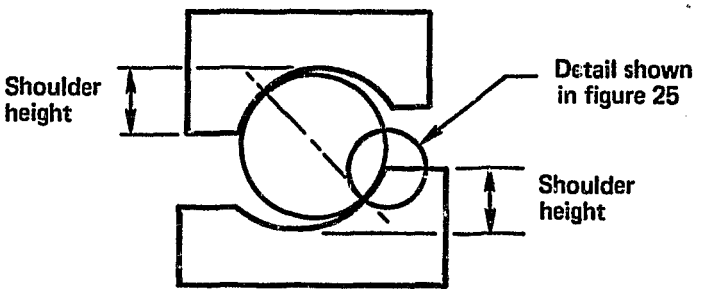

Figure 24.—Ball bearing race shoulder height.

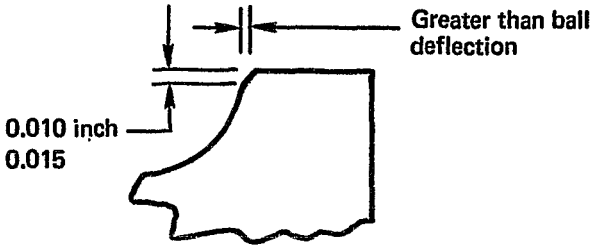

Figure 25.—Ball bearing raceway edge relief.

3.2.2.5 Roller Bearing Shoulder Configuration

The shoulder configuration of a cylindrical roller bearing shall provide proper roller guidance, minimize roller end wear, and prevent stress concentrations.

The corner configuration employing grind relief (fig. 22(a)) is preferred because this design eliminates possible interference of the radiused corner with roller corner radius (r, fig. 21).

The rake angle α should be 0° 15′ to 0° 45′.

The shoulder height h should be 14 to 20 percent of the roller diameter to provide proper guidance.

Maximum axial grind relief A (fig. 22(a)) should be less than roller end radius breakout a in figure 21.

The maximum radial grind relief B (fig. 22(a)) should be less than the corner radius breakout height b in figure 21.

3.2.3 Cage Design

3.2.3.1 Cage Strength

The cage design shall possess sufficient strength and rigidity to maintain rolling element spacing and to withstand hoop stress from centrifugal force.

A one-piece cage design should be specified whenever possible. A supporting structure should be provided for all cages made of nonmetallic materials except those having fabric reinforcement (i.e., glass-fabric-supported PTFE (Armalon) and linen-supported phenolic). The supporting structure should be a full metal shroud or reinforced band design (fig. 26). The shroud material must be undercut to prevent contact with rolling elements or race land. A supporting structure for two-piece cages made of Armalon should be provided. The supporting structure can be full metal shrouds for inner-land-riding cages or riveted side bands for outer-land-riding cages.

Minimum allowable radial thickness must be determined individually for each application and cage material. A suggested minimum radial thickness dimension for cages made of unsupported nonmetallic materials is 0.090 in. A suggested minimum ratio of thickness to mean diameter is 0.015 in. Thinner sections should be tested prior to any use in production turbomachinery.

3.2.3.2 Coolant Flow Area

The cage shall allow free flow of coolant through the bearings.

Free through-flow of coolant can be assured by providing one of the following design features:

(1) Outer-land-riding cage with slim cross section (fig. 27(a)).
(2) Inner-land-riding cage with coolant flow cutouts (ref. 9) (fig. 27(b)).
(3) Outer-land-riding cage with flow cutouts (fig. 27(c) and (d)).

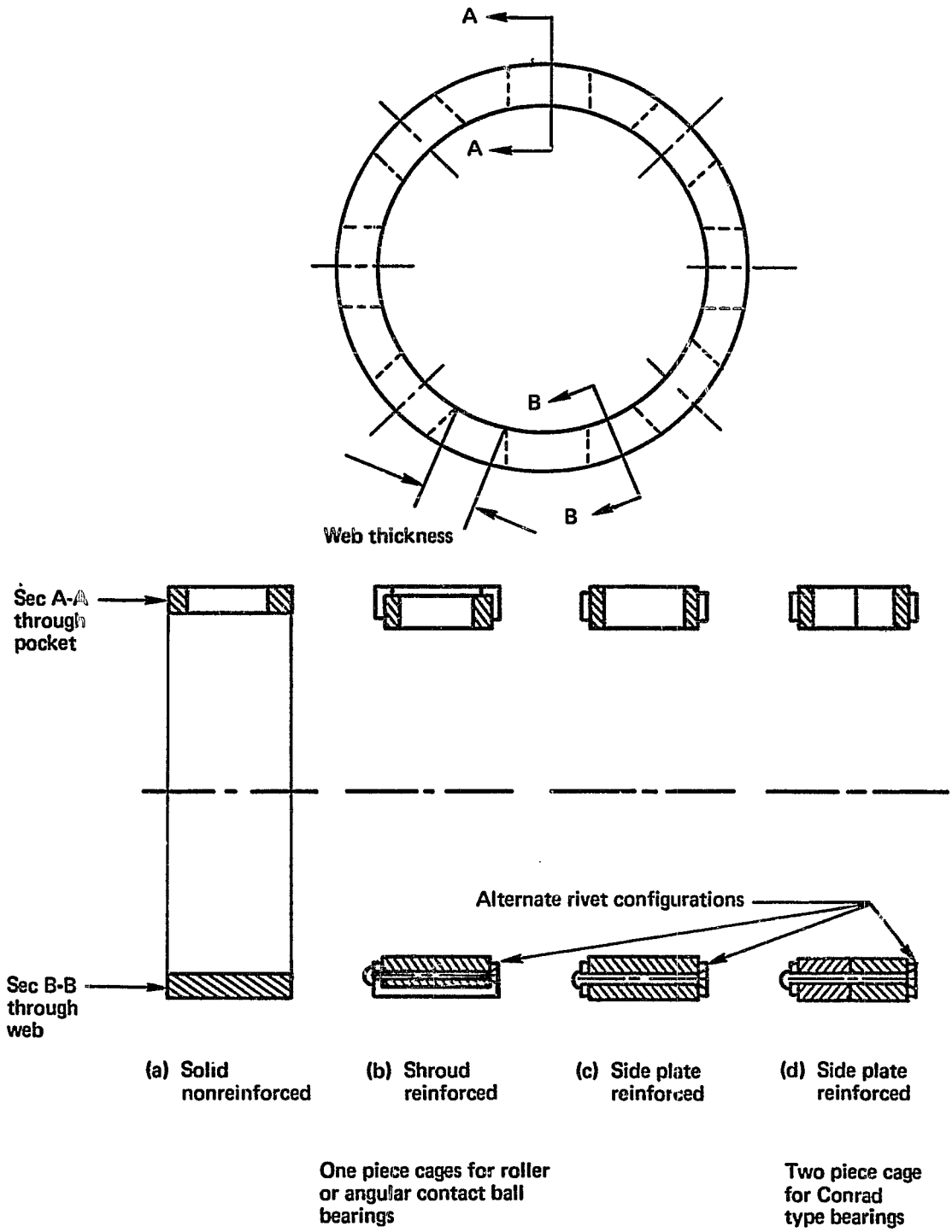

Figure 26.—Cage construction.

(e) Ball retaining cage

(f) Roller retaining cage

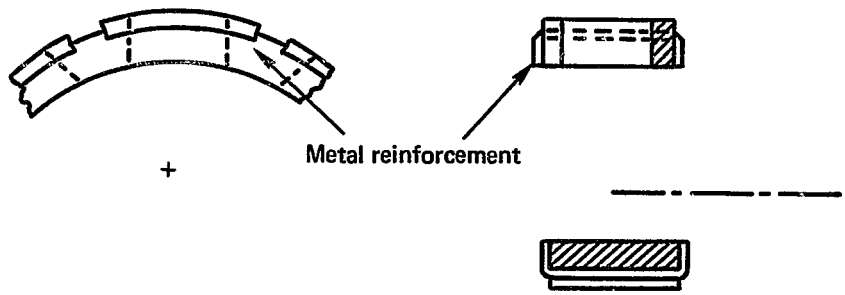

(g) Outer land riding shrouded cage (ref. 1)

Figure 26.—Concluded. Cage construction.

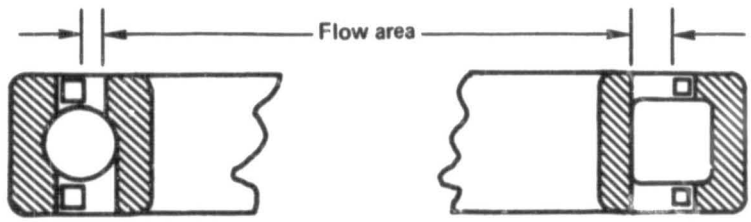

Thin cage, no flow channels

(a)

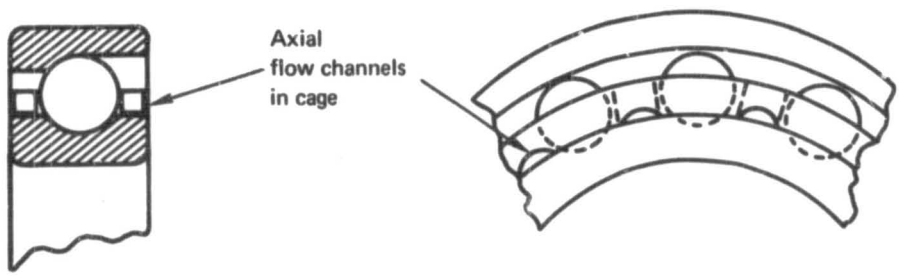

(b)

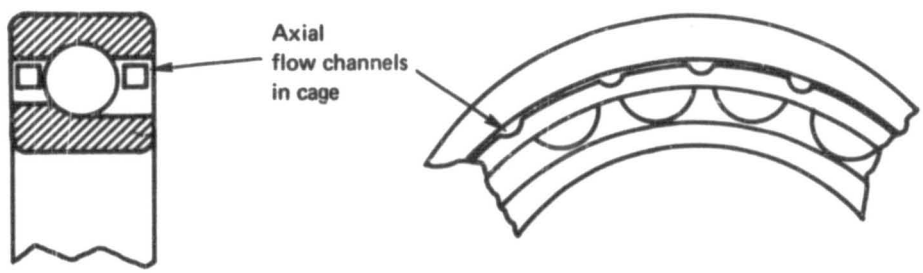

(c)

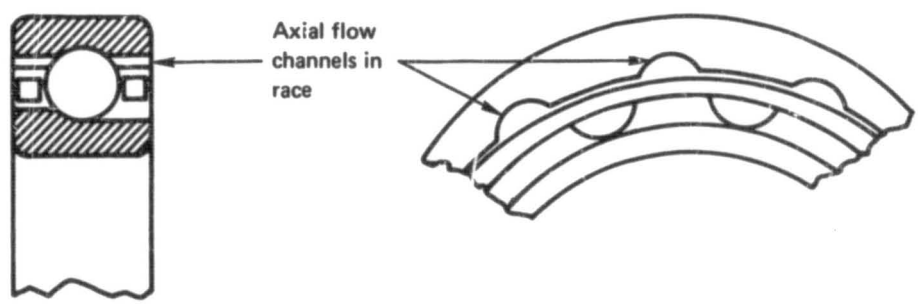

(d)

Figure 27.—Coolant flow channels.

3.2.3.3 Cage-Rolling Element Contact

The cage pocket surface shall meet the rolling element so that the rolling elements do not tend to "climb over" or deform the cage web.

The cage pocket surface should meet the rolling element at its pitch diameter to avoid a wedging action of the rolling element that could deform the cage.

3.2.3.4 Web Thickness

The cage web shall be thick enough to provide adequate strength with allowances for wear.

The following guides (see fig. 26) should be used where test results are not available:

(1) Minimum cage web thickness for metallic cages should be 0.070 in.
(2) Minimum cage web thickness for nonmetallic cages should be 0.150 in. (ref. 9).

3.2.3.5 Guiding Land Clearance

Cage guiding land clearance shall be adequate at all operating temperatures and rotating speeds.

A minimum cage guiding land clearance of 0.003 in./in. of guiding land diameter under all operating conditions should be provided; allowances for differential thermal growth of cage and race material and for centrifugal growth of race and cage material should be included.

3.2.3.6 Pocket Clearance

Cage pocket clearance in ball bearings shall be sufficient to allow ball advance and retard due to combined load or misalignment. Roller bearing cage pocket clearances shall not become negative.

Testing may be required to select the optimum clearance. The following can be used as guidelines:

(1) Cage pocket clearance for ball bearings under combined axial and radial load or misalignment should be 0.035 in./in. of ball diameter.
(2) Cage pocket clearance for ball bearings under normal alignment and thrust only or radial only should be 0.025 in./in. of ball diameter.

(3) Cage pocket clearance for roller bearings: 0.025 in./in. roller diameter (circumferential); 0.005 in./in. of roller length (axial).
(4) Cage half register in a Conrad-type bearing should be sufficiently accurate that cage pocket clearance is maintained.
(5) Elliptical cage pockets should be used to reduce axial cage clearance and still obtain adequate circumferential clearance.

3.2.3.7 Cage Sides Protrusion

The cage side shall not make contact with components adjacent to the bearing.

A tolerance stackup of cage position should be performed allowing for extremes of ball dynamic position, cage clearances, and cage dimensions. If cage protrusion occurs, either ensure that no components can come in contact with the cage by specifying their position or minimize protrusion by using countersunk rivet heads or reducing cage width. If cage width is reduced, ensure that the cage structure is not unduly weakened.

3.2.3.8 Cage Rivet

A cage rivet shall provide positive tension throughout the design temperature range without overstressing the cage material.

To size the rivet diameter and length, take into account the compressive strength of cage material, the tensile strength of the rivet material, and the elastic moduli, Poisson's ratio, and thermal expansion properties for both materials. Appropriate analyses should demonstrate that under all operating conditions the rivet will provide a positive tension without yielding the cage material.

REFERENCES

1. Harris, T. A.: Rolling Bearing Analysis. John Wiley and Sons, 1966.

2. Purdy, C. C.: Design and Development of Liquid Hydrogen Cooled 120 mm Roller, 110 mm Roller and 110 mm Tandem Ball Bearings for M-1 Fuel Turbopump. NASA CR-54826, AGC 8800-27, Aerojet-General Corp., Feb. 1966.

3. Jones, A. B.: A General Theory for Elastically Constrained Ball and Radial Roller Bearings Under Arbitrary Load and Speed Conditions. J. Basic Eng., Vol. 82, June 1960, pp. 309-320.

*4. Butner, M. F.; and Wagner, D. A.: Liquid Hydrogen Cooled Bearings for Three Million DN. Unpublished, May 1968.

*5. Butner, M. F.: Mark 3 Number Two Bearing Distress Investigation. Unpublished, May 1963.

6. Barish, Thomas: Ball Speed Variation in Ball Bearing and Its Effects on Cage Design. Lubrication Engineering, vol. 25, no. 3, Mar. 1969, pp. 110-116.

*7. Barish, Thomas: Ball and Roller Bearings for Rocket Pumps. Unpublished, June 1962.

8. Atherton, R. R.: Air Force Reusable Rocket Engine Program. AFRPL-TR-69-3, XRL 129-P-1, PWA FR-2972, Pratt & Whitney Aircraft, Jan. 1969. (Confidential)

9. Anon.: Advanced Rocket Engine—Storable Phase 1 Interim Final Report. AFRPL TR 67-75, parts 1, 2, 3 (Unclassified). Aerojet-General Corp., Aug. 1967. (Confidential)

10. Young, M. W.; and Kirby, L. F.: Development of Liquid Oxygen Cooled 110 mm Roller and Tandem Ball Bearings at up to 0.5 x 10^6 DN Values for the Oxidizer Turbopump of the M-1 Engine. NASA CR-54816, AGC 880-23, Aerojet-General Corp., Mar. 1966.

11. Roesch, E.; and Paternak, T.: Development of Large Size Bellows Face Type Seals for Liquid Oxygen and Oxygen/Hydrogen Hot Gas Service at Moderate to High Pressures. NASA CR-54818, AGC 8800-16, Aerojet-General Corp., Feb. 10, 1966.

*Available in the Dossier for Design Criteria Monograph for Liquid Rocket Engine Turbopump Bearings. Unpublished, 1968. Collected source material available for inspection at Lewis Research Center, Cleveland, Ohio.

12. Anon.: Cleanliness of Components for Use in Oxygen, Fuel, and Pneumatic Systems. MSFC-SPEC-164, Apr. 16, 1962, Amend. 4, July 27, 1964.

13. Anon.: Propellant Pressurizing Agent, Nitrogen. MIL-P-27401B, Sept. 19, 1962.

14. Anon.: Propellant Pressurizing Agent, Helium. MIL-P-27407, Amend. 1, Jan. 8, 1965.

15. Anon.: Desiccants, Activated, Bagged, Packaging, Use and Static Dehumidification. MIL-D-3464D, May 17, 1966.

16. Anon.: Lubricating Oil, Aircraft Turbine Engine, Synthetic Base. MIL-L-7808, Rev. G, Amend. 1, Nov. 15, 1969.

17. Anon.: AFBMA Standards—Ball and Roller Bearing Tolerances. AFBMA Standards, Sec. 3, Rev. 8, Mar. 1965.

18. Butner, M. F.: Final Report, Propellant Lubrication Properties Investigation. Report No. WADD-TR-61-77 (AD 259143), June 1961.

19. Butner, M. F.: Propellant Lubrication Properties Investigation, Final Report. Report No. WADD-TR-61-77 part II (AD 403699), Mar. 1963.

20. Wills, William H., Jr.: Vacuum Melting Benefits Steel Users. Metal Progress, vol. 92, no. 5, Nov. 1967, pp. 60-64.

21. Erickson, John A.: Degassing and Consumable-Electrode Remelting Improve Bearings. Metal Progress, vol. 92, no. 5, Nov. 1967, pp. 69-73.

22. Brewe, David E.; Scibbe, Herbert W.; and Anderson, William J.: Film Transfer Studies of Seven Ball Bearing Retainer Materials in 60° R (33° K) Hydrogen Gas at 0.8 Million DN Value. NASA TN D-3730, 1966.

23. Wisander, D. W.; Maley, C. R.; and Johnson, R. L.: Wear and Friction of Filled Polytetrafluoroethylene Compositions in Liquid Nitrogen. ASLE Transactions, vol. 2, no. 1, 1959, pp. 58-66.

24. Anon.: AFBMA Standards for Balls. AFBMA Standards, Sec. 10, Rev. 5, Dec. 1964.

25. Mayer, J. T.; and Litzler, T. C.: An Approximate Determination of the Effects of Geometry on Ball Bearing Torque and Fatigue Life. NASA TN D-2792, 1965.

26. Bisson, Edmund; and Anderson, William J.: Advanced Bearing Technology, NASA SP-38, 1965.

27. Anon.: Surface Texture. ASA B46.1-1962, Dec. 21, 1965.

28. Anderson, W. J.; and Zaretsky, E. V.: Rolling-Element Bearings. Bearings Reference Issue, Machine Design, ch. 5, vol. 40, no. 14, June 13, 1968, pp. 22-39.

29. Timoshenko, S.: Strength of Materials. Part II, Advanced Theory and Problems. Third Ed., D. Van Nostrand Company, Inc., 1956, pp. 214-221.

*30. Barish, T.: The Fundamentals of Ball Bearing Design. Unpublished, 1957.

31. Palmgren, Arvid: Ball and Roller Bearing Engineering, Third Ed., SKF Industries, Inc., 1959.

32. Schmidt, Harold W.: Handling and Use of Fluorine-Oxygen Mixtures in Rocket Systems. NASA SP-3037, 1967.

33. Anon.: Corrosion-Preventive Compound, Solvent Cut-back, Cold-Application. MIL-L-16173, Rev. D, Amend. 2, Nov. 19, 1968.

34. Jones, A. B.: Analysis of Stresses and Deflections. Vol. I and II. General Motors Corp., New Departure Div., 1946.

35. Anon.: Chromium Plating (Electrodeposited). Federal Specification QQ-C-320, Rev. a, July 25, 1967.

36. Baumeister, Theodore, Ed.: Marks' Mechanical Engineers' Handbook. Sixth Ed., McGraw-Hill Book Co., Inc., 1958, pp. 3-48.

37. Barish, Thomas: How Sliding Affects Life of Rolling Surfaces. Machine Design, vol. 32, no. 21, Oct. 13, 1960, pp. 189-194.

38. Zaretsky, Erwin V.; et al.: Bearing Life and Failure Distribution as Affected by Actual Component Differential Hardness. NASA TN-D-3101, 1965.

39. Roark, R. J.: Formulas for Stress and Strain. Third Ed., McGraw-Hill Book Co., Inc., 1954.

40. Carney, J. A.: M-1 Fuel Pump Turbine End Roller Bearing Design and Evaluation. Unpublished, June 1964.

41. Harris, T. A.: Misaligned Roller Bearings. Machine Design, vol. 40, no. 20, Aug. 29, 1968, pp. 98-101.

*Available in the Dossier for Design Criteria Monograph for Liquid Rocket Engine Turbopump Bearings. Unpublished, 1968. Collected source material available for inspection at Lewis Research Center, Cleveland, Ohio.

REFERENCE 106

PAGE 72 BLANK

GLOSSARY

MATERIAL DESIGNATIONS

Common designation as used in Monograph	Specification or other identification
Armalon	Glass-fabric-supported PTFE (Teflon). Normal form for bearing cages in mandrel wrapped tubing. Trade mark of E. I. duPont. To be fully defined, the density, size of weave, and mechanical properties must be specified.
AMS 4616	Silicon-bronze alloy.
Bower 315	Alloy steel used for high-temperature roller bearings. Composition is specified by Bower Roller Bearing Division of Federal-Mogul-Bower, Inc., Detroit, Michigan.
BN 440	Commercial beryllium-nickel alloy made by Kawecki Berylco Industries, Inc.
CRES	Corrosion resistant steel.
EDA	Ethylene diamine.
GFT	Glass-filled Teflon: PTFE with random glass fibre content, specified in percent by volume.
Halmo	Alloy steel used for high-temperature bearings by New Departure-Hyatt Division of General Motors Corporation.
Haynes 25	Cobalt-chromium-nickel alloy covered under AMS 5796.
IRFNA	Inhibited red fuming nitric acid.
K-Monel	Nickel-copper alloy conforming to AMS 4676 and Federal Specification QQ-N-286, Class A annealed.
K-5H	Sintered tungsten—titanium carbide material (Kennametal, Inc.).
K-96	Sintered tungsten-carbide material with cobalt binder manufactured by Kennametal, Inc., Latrobe, Pennsylvania.
K-162B	Sintered titanium-carbide material with nickel-molybdenum binder (Kennametal, Inc.).

M-10	AISI designation for molybdenum-steel alloys.
M-50	AISI designation for molybdenum-steel alloys.
PTFE	Chemical composition: Polytetrafluoroethylene. Commercial name: Teflon.
Rulon A	PTFE (Teflon) with random glass fibre content 15 percent by volume. T. F. Dixon Company, Bristol, Rhode Island.
Salox M	Commercial designation for PTFE filled with 40 percent bronze powder.
S-Monel	Nickel-copper alloy conforming to Navy Specification 46N7, Class B.
Stellite	Commercial cobalt-chromium-nickel alloys manufactured by Haynes Stellite Corporation.
UDMH	Unsymmetrical dimethyl hydrazine.
50-50	Mixture: 50 percent N_2H_4-50 percent UDMH.
4130	AISI designation for low alloy carbon steel.
6414	Premium quality AISI 4340 steel.

ORGANIZATIONS

Abbreviation	Identification
ABEC	Annular Bearing Engineering Committee of the AFBMA. ABEC-1, -3, -5, -7, -9 are progressively more precise tolerance specifications for ball bearings.
AFBMA	Anti-friction Bearing Manufacturers Association.
AISI	American Iron and Steel Institute.
AMS	Aerospace Material Specifications published by SAE.
ASA	American Standards Association.
RBEC	Roller Bearing Engineering Committee of the AFBMA. RBEC-1, -5, etc. are progressively more precise tolerance specifications for roller bearings.
SAE	Society of Automotive Engineers.

MISCELLANEOUS TERMINOLOGY

Term or symbol	Definition
AA	Arithmetic average.
$\beta_i - \beta_o$	Difference between inner race contact angle β_i and outer race contact angle β_o that occurs under dynamic conditions.
B_{10}	Expression for bearing fatigue life defined as the operating time that 90 percent of identical bearings will exceed without fatigue failure.
BSV	Ball speed variation.
C_c	Clearance reduction due to centrifugal growth of inner race.
C_d	Unfitted diametral clearance.
C_f	Clearance change due to press fitting.
C_o	Operating diametral clearance that should be selected in the original design.
C_t	Clearance change caused by temperature difference between races.
circumferential	Lying in a plane perpendicular to the shaft centerline.
D_{avg}	Average raceway diameter.
DN	Product of bearing bore in millimeters and shaft speed in revolutions per minute.
d	Diameter of ball or roller.
E	Pitch diameter of ball complement.
EHD	Elastohydrodynamic.
F_i	Inner transverse race curvature: inner race radius divided by ball diameter.

F_o	Outer transverse race curvature: outer race radius divided by ball diameter.
$F_o + F_i - 1$	Expression for total bearing curvature.
FLOX	Fluorine-oxygen mixture.
IRC	Inner race control.
NVR	Nonvolatile residue.
ORC	Outer race control.
R_c	Hardness on the Rockwell C scale.
TIR	Total indicated runout.
t_{avg}	Average cross-section radial thickness of race.
transverse	Lying in a plane containing the shaft centerline.
windage	Circulation or pumping of fluids caused by impeller action of rotating components. That is, a gas contained in a cavity with shafts, gears, or bearings will circulate within the cavity by windage.

END OF REFERENCE

106

REFERENCE

107

SCIBBE, H. W.: BEARINGS AND SEALS FOR CRYOGENICS FLUIDS. NASA TM X-52415, 1968.

#2

NASA TECHNICAL MEMORANDUM

NASA TM X-52415

NASA TM X-52415

LEWIS RESEARCH CENTER
Aerospace Safety Research
and Data Institute
FEB 5 1973
CLEVELAND, OHIO

BEARINGS AND SEALS FOR CRYOGENIC FLUIDS

by H. W. Scibbe
Lewis Research Center
Cleveland, Ohio

TECHNICAL PAPER presented at Fuels and Lubricants
Meeting sponsored by the Society of Automotive Engineers
Cleveland, Ohio, November 13, 1967

NATIONAL AERONAUTICS AND SPACE ADMINISTRATION · WASHINGTON, D.C. · 1968

BEARINGS AND SEALS FOR CRYOGENIC FLUIDS

by H. W. Scibbe

Lewis Research Center
Cleveland, Ohio

TECHNICAL PAPER presented at

Fuels and Lubricants Meeting
sponsored by the Society of Automotive Engineers
Cleveland, Ohio, November 13, 1967

NATIONAL AERONAUTICS AND SPACE ADMINISTRATION

BEARINGS AND SEALS FOR CRYOGENIC FLUIDS

by H. W. Scibbe

Lewis Research Center

Cleveland, Ohio.

E-3453

ABSTRACT

Bearings and seals in rocket engine turbopumps operate directly in the cryogenic propellant. Special design and lubricating techniques are required since ordinary oils and greases become glasslike solids at these extremely cold temperatures. The bearing load carrying surfaces are lubricated by thin transfer films. The lubricant is provided by the bearing cage which is usually fabricated from a self-lubricating Teflon compound. Material compatibility and wear are the important factors for face contact seals in these cryogenic fluids. Carbon, normally used in seal nosepieces, has violent reactions when run in liquid fluorine, an extremely chemically active fluid. Wear at the rubbing contact is minimized when the seal is designed for positive face separation with acceptable leakage.

X-52415

turbopump components, including the bearings to preclude failure of an expensive and complex rocket engine system. Total bearing run time is usually 4 or 5 hours including system checkout and engine static firing tests.

Ball-Race Materials

In addition to the high compressive strength and hardness requirements necessary in bearing steels, properties such as corrosion resistance, dimensional stability, and low-temperature ductility are required for ball and race materials used at cryogenic temperatures. Conventional SAE 52100 bearing steel and AISI 440C stainless steel have both been used successfully as ball and race materials in cryogenic bearings applications (3,4,and 5). The 440C stainless steel exhibits properties similar to those of 52100 steel at these low temperatures, but is generally preferred because of its better corrosion resistance.

Early bearing experiments in liquid nitrogen and liquid hydrogen indicated that corrosion formed on SAE 52100 balls and races when thermal cycling back to room temperature occurred (3). During thermal cycling, condensation forms on the bearing surfaces, and, since they are cleaned free of protective oil or grease, they readily corrode.

Dimensional instability is produced in bearing steels, such as 440C stainless, as the result of appreciable amounts (10 to 15 percent by volume) of retained austenite in the crystalline structure after heat treatment. Conversion of the unstable austenite to martensite can result in an increase in physical bearing dimensions. The transformation to martensite is delayed and usually occurs during bearing service. This is particularly

true when the bearings are operated at temperatures below that of the quenching bath, such as in cryogenic applications. Retained austenite in 440C stainless steel may be as large as 30 percent by volume depending on the austenitizing temperature, the quenching time, and the quenching bath temperature. To convert the retained austenite to martensite the steel is subcooled to -100° F or lower, immediately after quenching. Subcooling is followed by tempering to stabilize the newly formed martensite. When specifications require a minimum amount (3 percent or less) of retained austenite in the final structure, a second subcool and tempering cycle is performed. To insure maximum dimensional stability in 440C stainless and other bearing steels that will be used in cryogenic applications, subcooling followed by tempering is now generally specified as part of the heat cycle.

Although 440C stainless steel exhibits an increase in tensile (compressive) strength and hardness at cryogenic temperatures, it also experiences an increase in brittleness and a decrease in impact strength. Specific data on the low-temperature ductility of 440C is not readily available, however it may be assumed that the balls and races do retain some ductility, even at temperatures as low as liquid hydrogen (-423° F). Ring cracking has been observed in several cryogenic bearing applications, [5] probably as a result of excessive shrink fits between the 440C races and the shaft or housing materials. The results of preliminary experiments, with the bearings operating immersed in liquid nitrogen and hydrogen, indicated that the differential contraction rates of the various materials used can, upon cooling, affect bearing running clearance [4]. The ball-race materials,

the bearing mounting materials, and the mounting clearances therefore should be selected so as to minimize the reduction in bearing diametral clearance at the cryogenic temperature.

Since the required life of bearings operating in cryogenic turbopumps is only a few hours, rolling element fatigue is not considered a major cause of failure. It is generally recommended however, that the maximum Hertz compressive stress in the ball-race contacts be limited to 350 000 pounds per square inch. The primary cause of ball bearing failure in hydrogen turbopumps has been excessive heat generation. The major sources of heat generation in the bearings are the ball spinning friction in the ball-race contact areas and the rubbing friction between the cage and balls, and the cage locating surface on one of the races. The heat generated within the bearing must be removed to assure an equilibrium operating condition and to prevent a total loss in operating clearance that results in seizure.

The measured, room-temperature, diametral and cage clearances in hydrogen turbopump bearings should be two to three times those required in high-speed oil lubricated bearings. The actual clearances specified are largely dependent upon the bearing size, the maximum operating speed, and the relative contraction rates between the ball-race and cage materials as the turbopump assembly is cooled to liquid hydrogen temperature (-423° F) [4].

Bearing Lubrication by Transfer Films

In a conventional lubrication system for ball bearings, surface integrity in the ball-race contact is maintained and surface welding prevented by the presence of contaminant surface films or by a lubricant that separates the surface asperities.

Operation in liquid hydrogen is considerably more difficult because, as previously mentioned, conventional lubricants cannot be used and contaminant low shear films cannot be readily formed on the surfaces in a reducing atmosphere. To facilitate the formation of a transfer film on the balls and race grooves that prevents contact between the clean nascent metals, the bearings must be equipped with a cage constructed of a self-lubricating material. The surfaces that require lubrication in a ball bearing are shown in figure 1. The surfaces that require lubrication immediately when the shaft begins to rotate are those where pure sliding contact occurs, at the cage locating surface on the inner race and at the ball-cage contacts. These surfaces are easy to lubricate because they are in direct contact with the lubricant (cage material). The ball-race contacts where rolling with sliding takes place also require some lubricant, but lubrication here is more difficult. It has been speculated that lubrication at the ball-race contacts is obtained through transfer films also provided by the cage material. The film-transfer process is illustrated in figure 2. As the bearing rotates, the balls rub the self-lubricating cage. The cage material or lubricant transfers to the ball and is subsequently transferred by the ball to the race grooves as thin films.

The best lubricant used to date for cryogenic applications has been Teflon (polytetrafluoro ethylene). Teflon provides low friction at the bear-sliding contacts, but it cannot be used in its pure form as a cage material because of poor strength properties and because of its tendency to cold flow even under the lightest loads. Teflon also has poor thermal conductivity which becomes a problem at high cage speeds, where heat generation in the

bearing may become detrimental to successful operation. Teflon must therefore be compounded with other materials (fillers) to give it these desirable properties.

Experiments have been conducted with 40-millimeter-bore ball bearings operating in -400° F gaseous hydrogen at 20 000 rpm and 200 pound thrust load. The bearings have operated satisfactorily for total running times up to 10 hours (6 and 7). Transverse profile traces were made on the inner-race grooves to measure the film buildup from transferred cage material and determine the extent of race wear. Cage materials that exhibited good film-transfer capability with long wear lives were (1) a laminated glass cloth with Teflon binder, (2) a glass-fiber-filled Teflon, and (3) a bronze-filled Teflon. These three cage materials and the measurement of the transfer films are discussed in the following paragraphs.

Measurement of transfer films. - A profile tracing technique was used to study the formation and life histories of the transfer films on the bearing inner races. Several different cage materials were investigated. A cross-section of the bearing inner-race groove and a typical profile trace are shown in figure 3. As the stylus traces the race groove contour, a highly magnified profile trace is produced as shown in the lower portion of figure 3. Of particular interest is the ball-track region where lubrication is required. The horizontal line shown on the profile trace is the original race groove contour. The area of profile trace above the line is transfer film (lubricant) and the shaded area below the line is race wear. Successive profile traces were made at intervals of approximately 2 hours running time to study the history of the transfer films.

Laminated-glass-cloth-with-Teflon-binder cage material (38 percent glass cloth, 62-percent Teflon). - This material is currently used in several turbopump bearings. It is quite strong because of its laminated structure. Typical inner-race profile traces of a bearing using this cage material are shown in figure 4. Illustrated is the life history of the transfer film for approximately ten hours total running time. After running for 284 minutes (fig. 4(c)) a fairly good film of lubricant has been deposited on the inner race. The scratches that appear in the film are indicative of abrasion caused by the glass in the cage material. With continued running, the film breaks down and wear of the inner race surface begins (fig. 4(d)). Race wear progresses with time and, after 10 hours running, the bearing is in danger of failing. The cause of the film breakdown and the large amount of race wear is probably abrasion by the glass fibers which are shredded from the cage material. This postulated abrasive-wear process is illustrated in figure 5. Shown are alternate layers of glass cloth and Teflon. The ball rotates and wears away the softer Teflon material. The Teflon is deposited in the race groove as the lubricant film. After a short time the Teflon has worn back leaving the glass cloth exposed to the rubbing action of the balls. Continued running results in film breakdown, caused by glass fibers which are shredded away from the cloth and embedded into the film. The film is worn away faster than it can be reformed by the Teflon and drastic race groove wear results, which eventually causes bearing failure.

Glass-fiber-filled Teflon cage material (15-percent glass fiber, 85-percent Teflon). - In order to provide more Teflon and reduce the possibility of film destruction through abrasion, a second material was selected for

evaluation. The progressive profile traces of the inner-race groove of a bearing using a 15-percent glass fiber, 85-percent Teflon cage is shown in figure 6. This material has good film forming capability and the film life appears to be somewhat longer than that of the glass cloth-Teflon laminated material. Its thermal conductivity is quite poor, however, so that adequate heat rejection becomes a problem at high bearing speeds.

Bronze-filled Teflon cage material (30-percent bronze powder, 70-percent Teflon). - To improve the thermal conductivity of the cage material, Teflon has been compounded with metals such as bronze, copper, or silver. Bearings with bronze-Teflon cages have had excellent success in film transfer evaluation runs at 20 000 rpm. This material has shown fairly good film formation with no apparent wear of the inner-race groove as illustrated in figure 7.

The total cage wear, given as percent weight loss of the original weight, was 0.25 percent or less for the three materials discussed. This wear value is extremely low for a total bearing run time of approximately 10 hours [6].

Bearing Cage Design

A second consideration for ball bearing cages used in liquid hydrogen turbopumps is their design. In addition to the self-lubricating feature, other properties of the cage material such as mechanical strength, structural rigidity, and wear resistance must be acceptable.

Mechanical strength at cryogenic temperatures must be accompanied with a good strength-to-weight ratio. Materials that do not have sufficient strength by themselves should be reinforced on their outer surfaces with metal shrouds.

Structural rigidity is required because the cage material must be rigid

enough to withstand deformation, but not become so brittle at cryogenic temperatures that it fails by cracking.

In addition to the strength and rigidity requirements, the material must have good wear resistance. In order that material wear resistance be used to its full advantage, the cage must be designed with proper ball-pocket and cage-locating (land) clearances.

Inner-race located cage design. - Three designs used successfully for inner-race located cages are shown in figure 8. These designs were used in 40 millimeter ball bearings run in -400° F hydrogen gas at 20 000 rpm and 200 pound thrust load. Of the three designs illustrated in figure 8 the one selected for a particular turbopump bearing is usually dependent upon the strength and the strength-to-weight ratio of the cage body materials at the cryogenic temperature.

Outer-race located cage design. - Other cage designs that have been used successfully in the NERVA [8] (Nuclear Engine for Rocket Vehicle Application) and other [5] turbopump bearings are shown in figure 9. The conventionally designed cage (fig. 9(a)) has a heavy cross-section with reinforcing side plates, similar to the inner-race located design shown in figure 8(b). Because of the large rotating mass the cage generates considerable heat at the outer-race locating surface.

The thin-line, lighter weight design shown in figure 9(b) is flexible and sufficiently strong because it depends on the rigidity of the outer race for reinforcement. The open design also permits greater thru-flow of liquid hydrogen and therefore results in better cooling efficiency of the bearing than does the conventional cage design. The laminated-glass-cloth-with-Teflon-

binder cage material has been used successfully with the thin-line design in several turbopump bearings (5 and 8).

Cage clearances. - As indicated previously (p.7), the cage clearances specified for hydrogen turbopump bearings are somewhat dependent upon the relative contraction rates between the ball-race and cage materials, as the bearing is cooled to -423° F. The total linear contraction from 70 to -423° F for 440C stainless steel, ball and race material, is approximately 0.0019 inch per inch (9). In contrast the contraction for 100 percent TFE (polytetrafluoroethylene) Teflon is 0.0215 inch per inch (10) more than an order of magnitude greater over the same temperature range. Filler materials added to Teflon resin will reduce the total contraction depending upon the shape of the fillers, whether they are fibrous or spherical, the amount added in weight percent, and their coefficients of contraction. Fibrous fillers (glass fibers) produce the greatest reduction in contraction in the direction perpendicular to the molding pressure; spherical fillers (bronze powder) tend to equalize contraction in both directions (11). The laminated-glass-cloth-with-Teflon-binder material has the greatest contraction in the direction of the glass cloth layers. Filled Teflon cages are usually made from molded tube stock with the molding pressure direction parallel to the axis of the tube (cage). The laminated Teflon cages are also made from tube stock. The tube is made by continuously wrapping glass cloth on a mandrel and binding the successive layers together with Teflon resin.

The total contraction from 70 to -423° F of several filled Teflon and the laminated-glass-cloth Teflon materials are given in table II. The materials shown are similar to cage materials discussed previously. It can

be noted that the glass-fiber-filled and the laminated-glass-cloth Teflon materials exhibit anisotropic contraction with respect to the cage radial and width directions. The radial direction is perpendicular to direction of molding pressure for the glass-fiber-filled material and through the glass cloth layers for the laminated-glass-cloth material, as noted in table II. The bronze filled Teflon has the same contraction in both directions. Contraction in the radial direction will decrease the cage locating clearances, for inner-race located cages, whereas contraction in the width direction will decrease ball-pocket clearances. With filler materials or glass cloth layers, the total contraction of the Teflon cage materials shown in table II, range from four to eight times greater than that for the 440C ball and race material.

Typical locating-race and ball pocket clearances for seven cage materials are shown in table III. The first four cages listed are fabricated from Teflon based materials and have contraction properties similar to those described above. Their inner-race locating clearances range from 0.017 to 0.038 inch and the ball-pocket clearances from 0.014 to 0.026 inch.

The relative contraction of cage reinforcing materials such as aluminum and stainless steel can also affect cage clearances at cryogenic temperatures. The total contraction for 2024 aluminum is about 0.0042 in per inch, whereas that for AISI 410 or 416 stainless steel is approximately 0.0019 inch per inch, from 70° to -423° F [10], which is the same as the 440C ball and race material.

In table III bearing cages using materials 1, 3, and 7 were reinforced with aluminum. Cages fabricated from materials 5 and 6 used stainless steel

shrouds. A glass-fiber-filled Teflon cage (material 3, table III) supported with a riveted aluminum shroud experienced ball pocket cracking after running about 8 hours in -400° F hydrogen gas. The cracking was partly caused by the different contraction rates between the glass-fiber-filled Teflon body (0.0164 in./in.) and the aluminum shroud (0.0042 in./in.). A more complete analysis of the cage failure is discussed in the following section.

Cage failure mechanisms. - An example of a brittle failure of a cage material (material 7, table III) is illustrated in figure 10(a). The molybdenum disulphide-(MoS_2) filled-polyimide cage experienced complete failure after running only 22 minutes in hydrogen gas at -400° F. The cage design was similar to that shown in figure 8(c).

When an inner-race located cage is cooled to cryogenic temperature, insufficient clearance at the locating race will cause binding and the excessive heat generated at the surface may lead to cage failure. Bearing 23-S in table III is an example of a cage with insufficient clearance. In the initial run the bearing was brought to a complete stop from 5000 rpm with a 200 pound applied load.

The combination of a larger-than-required inner-race clearance and poor wear resistance can also result in cage failure. A silver composite cage (bearing 11-5, table III) fitted with a stainless steel shroud experienced this type of failure. The bearing had run in -400° F hydrogen gas at 20 000 rpm and 200 pounds for 138 minutes. The bearing after test is shown in figure 10(b). During bearing operation the shroud had rubbed on the outer-race land and moved relative to the cage body. The balls wore into the shroud and jammed the bearing.

Although a cage material may have good wear resistance, failure can result from structural deficiency in the material even when reinforcing is used. The delamination of the laminated-glass-cloth-with-Teflon-binder cage material is shown in figure 10(c). After running 349 minutes, this cage delaminated between two ball pockets. Delamination probably resulted from insufficient Teflon binder between the cloth layers, or from an improper curing technique during lamination.

The glass-fiber-filled Teflon cage material reinforced with a riveted aluminum shroud also showed structural weakness. After running 464 minutes, cracks appeared in a ball pocket of the cage (fig. 10(d)). It is speculated that the cracks resulted from the difference in contraction rates between the Teflon cage body and the aluminum shroud. The body shrank away from the shroud when the bearing was cooled to -400° F. When the bearing was subsequently run at high speed, centrifugal growth of the body between rivets caused fracture of the cage at the thin web section. Subsequent runs were made in -400° F hydrogen gas with other bearings using glass-fiber-filled Teflon cages without aluminum shrouds. No pocket cracking occurred in these cages when the bearings were run at speeds to 40 000 rpm.

Heat Generated Within a Ball Bearing

The problem of operating at high speed in a marginal lubricating fluid is that of maintaining a heat balance within the bearing. A heat balance can be accomplished by designing the bearing for minimum heat generation and then removing the heat generated with the hydrogen coolant (liquid or gas). One of the major sources of heat generation in a ball bearing operating under thrust load is the spinning which occurs in the contact between the balls

and one race. Spinning occurs between the balls and one race in all ball bearings that operate under a thrust or combined thrust and radial load.

Heat generation due to change in contact angle. - As shown in figure 11, a bearing under thrust load operates at same contact angle, β. At low speeds, the contact angles β are equal at the inner and outer race contacts (fig. 11(a)). When the bearing is operated at high speed, ball centrifugal force creates an additional load at the outer race contact which results in unequal contact angles at the inner and outer race contacts (fig. 11(b)). The magnitude of this difference in operating contact angles further increases ball spinning and consequently more heat is generated by the bearing.

Effect of bearing design and geometric factors on heat generation. - An analysis was made and programmed on a digital computer to determine the design and geometric factors that influence heat generation rates in a high speed ball bearing operating in liquid hydrogen. The computer results, which were supported experimentally with data from the bearing test program, indicate that the following factors contribute to lower heat generation rates: (1) open race curvatures (i.e., larger value for ratio of race groove radius to ball diameter than for bearingsdesigned for oil lubrication), (2) small ball diameter, (3) ball spinning at the race with larger curvature.

The results of the computer program for ball bearings of 40 millimeter bore size with two different ball diameters and using two race curvature combinations are shown in table IV. The heat generated due to ball spin is converted to shaft torque. The torque values are for ball spin at the inner race contact, and are for a 100 pound thrust load (T) at a shaft speed (N) of 40 000 rpm with an initial contact angle (β) of 10 degrees. The ball-spin friction coefficient (f) of 0.56 is for 440C stainless steel sliding

on itself at liquid hydrogen temperature (-423° F). The 108 series bearings have a 0.375-inch-ball diameter and the 1908 series have a 0.250-inch-ball diameter. The 108 series bearings have larger values of torque for both race curvature combinations due to the greater heat generated by the larger ball size. Increasing the race curvature at the spinning contact from 0.51 to 0.52 causes the torque values to decrease for both the 108 and 1908 bearings. Note that the large decrease in torque from the 108 bearing with an inner-race curvature of 0.51 to the 1908 bearing with an inner-race curvature of 0.52 is a function of both ball size and race curvature.

The turbopump for the Nerva engine has a design speed of 24 000 rpm. The pump ball bearings are 40 millimeter angular contact type (210 series) and operate at a rated thrust load of 2000 pounds [8]. A computer analysis similar to that described for the 40 millimeter bearing above, was made for the 210 series bearings to indicate the effect of several race curvature combinations on ball spin torque. The torque values are plotted in figure 12 for shaft speeds from 15 000 to 30 000 rpm. They are plotted for ball spin at the outer-race contact using three race curvature combinations at a thrust load of 2000 pounds, and an initial contact angle of 20 degrees. Increasing the outer-race curvature from 0.52 to 0.54 decreased the torque approximately 40 percent throughout the speed range. Increasing the outer-race curvature to 0.58 decreased the torque approximately 70 percent from the 0.52 curve. An effect of ball centrifugal force on the outer-race contact can be seen in the lowest curve. The ball spinning changes from outer race to inner race at approximately 27 000 rpm. This transition occurs because at the higher rotative speeds, ball centrifugal force increases and the balls

grip the 0.58 outer-race contact more firmly. Ball spinning, therefore, occurs at the 0.54 inner-race contact and considerably more heat is generated. This transition from spinning at the outer-race contact to spinning at the inner-race contact would not occur as long as the shaft speed of 24 000 rpm is not appreciably exceeded. In the Nerva turbopump bearing test program, several bearings with 0.52 outer - 0.52 inner-race curvatures and the 0.54 outer - 0.58 inner-race curvatures have been run in liquid hydrogen at 24 000 rpm at thrust loads to 2000 pounds, for operating times up to 90 minutes. These bearings were run with force-fed liquid hydrogen thru flow.

Thrust bearing configuration for high DN values. - For the first three shaft sizes shown in table V , the bearings operate at DN values (bearing bore in mm times shaft speed in rpm) to 2 million. As the ball diameter increases, the ball centrifugal force at the outer-race contact increases for these three bearings. As indicated previously in table IV, larger ball diameters adversely affect heat generation rates in a bearing operating at high speed. A conventional series 250 millimeter bore bearing is fitted with 2.375-inch diameter balls. As shown in table V, the centrifugal force per ball at a DN value of 4 million is 17 300 pounds. This load value exceeds the capacity of the ball-race contact.

One solution to problems of ball centrifugal force at high DN values, is to use smaller diameter balls. This concept is illustrated by comparing the centrifugal force of 0.625- and 0.875-inch diameter balls for the 150 and 200 millimeter bore bearings, respectively with that for the 250 millimeter bore size. For a bearing with a DN value of approximately 4 million, reducing the ball diameter from 2.375 to 0.625 inch decreases ball centrifugal force by a factor of 30.

The load capacity of a ball bearing operating under thrust load is proportional to the product of the number of balls (n) and the square of the ball diameter (d^2). In order that the load capacity not be appreciably reduced when decreasing the ball diameter, it is necessary therefore to increase the number of balls in the bearing. There is a practical limit for reducing ball diameter or increasing the number of balls and that is the cage strength, especially between adjacent ball pockets. If the cage annular cross-section is reduced excessively it may break at high speed because of inadequate strength.

FACE CONTACT SEAL DESIGN FOR LIQUID FLUORINE TURBOPUMPS

Face Contact Seals

In some turbopump applications rotating shaft seals are required. These turbopump designs contain various cryogenic fluids at pressures different from the surrounding space. Intolerable leakage of the fluid along the shaft is avoided by means of dynamic seals [2].

Face contact seals, which are the most common type of seal in use today, exist in a variety of forms, but most have the essential arrangement shown in figure 13. The sketch in the upper right-hand corner shows the location of a seal on a pump shaft sealing pump outlet pressure P_1. The seal consists of two main parts, (1) a seal seat which is fixed to the shaft and rotates with it, and (2) a nosepiece flexibly attached to the stationary shaft housing. A piston ring secondary seal permits axial movement of the nosepiece. A sealing dam is formed by the nonrotating nosepiece which is held by a force from the spring and the sealed fluid pressure in rubbing contact or close proximity to the rotating seal seat. The sealing gap is

END OF REFERENCE

107

REFERENCE

108

YOUNG, M. W.; AND KIRBY, L. F.: DEVELOPMENT OF LIQUID OXYGEN COOLED 110MM ROLLER AND TANDEM BALL BEARINGS AT UP TO .5 X 10^6 DN VALUES FOR THE OXIDIZER TURBOPUMP OF THE M-1 ENGINE. REP. AGC 8800-23, AEROJET GENERAL CORP. (NASA CR-54816), 1966.

N66-19031

NCC-19031

NASA CR 54816
AGC 8800-23

COPY

DEVELOPMENT OF LIQUID OXYGEN COOLED 110MM ROLLER AND TANDEM BALL BEARINGS AT UP TO .5 x 10^6 DN VALUES FOR THE OXIDIZER TURBOPUMP OF THE M-1 ENGINE

LEWIS RESEARCH CENTER
Aerospace Safety Research
and Data Institute
NOV 5 1971
CLEVELAND, OHIO

By

M. W. Young
L. F. Kirby

Prepared for

National Aeronautics and Space Administration

Contract NAS 3-2555

JUL 7 1963
LEWIS LIBRARY, NASA
CLEVELAND, OHIO

AEROJET-GENERAL CORPORATION

SACRAMENTO, CALIFORNIA

NOTICE

This report was prepared as an account of Government sponsored work. Neither the United States, nor the National Aeronautics and Space Administration (NASA), nor any person acting on behalf of NASA:

A.) Makes any warranty or representation, expressed or implied, with respect to the accuracy, completeness, or usefulness of the information contained in this report, or that the use of any information, apparatus, method or process disclosed in this report may not infringe privately owned rights, or

B.) Assumes any liabilities with respect to the use of, or for damages resulting from the use of any information, apparatus, method or process disclosed in this report.

As used above, "person acting on behalf of NASA" includes any employee or contractor of NASA, or employee of such contractor, to the extent that such employee or contractor of NASA, or employee of such contractor prepares, disseminates, or provides access to, any information pursuant to his employment or contract with NASA, or his employment with such contractor.

Requests for copies of this report should be referred to:

National Aeronautics and Space Administration
Office of Scientific and Technical Information
Attention: AFSS-A
Washington, D. C. 20546

NASA CR-54816
AGC 8800-23

TECHNOLOGY REPORT

DEVELOPMENT OF LIQUID OXYGEN COOLED 110MM ROLLER AND TANDEM BALL BEARINGS AT UP TO .5 x 10^6 DN VALUES FOR THE OXIDIZER TURBOPUMP OF THE M-1 ENGINE

Prepared for

NATIONAL AERONAUTICS AND SPACE ADMINISTRATION

March 11, 1966

CONTRACT NAS 3-2555

Prepared by:

AEROJET-GENERAL CORPORATION
LIQUID ROCKET OPERATIONS
SACRAMENTO, CALIFORNIA

AUTHORS: M. W. Young
L. F. Kirby

APPROVED: W. E. Campbell
Manager
M-1 Turbopump Project

Technical Management:

NASA LEWIS RESEARCH CENTER
CLEVEIAND, OHIO

TECHNICAL MANAGEMENT: K. L. Baskin
M. M. Bailey

APPROVED: W. F. Dankhoff
M-1 Project Manager

ABSTRACT

A development program for the purpose of evaluating the suitability of the bearing package designed for the M-1 liquid oxygen turbopump was completed. The test results indicate that the bearing performance is adequate as compared with that predicted during the design phase. The 110 mm roller and tandem ball bearings were demonstrated at $.5 \times 10^6$ DN values, radial loads of 15,000 lb and thrust loads up to 70,000 lb (twice the rated load). Liquid oxygen and liquid nitrogen were used as coolants; bearing materials were 440C stainless steel with armalon cages.

I. SUMMARY

This report describes the activity and results of the program to develop liquid oxygen cooled bearings for use in the oxidizer turbopump of the M-1 Engine. The objectives of this development program were to obtain bearing operational information and to qualify the bearings for use in the turbopump.

The basic bearing configuration selected for use in the turbopump consisted of a single 110 mm roller bearing on the output (pump) end, a single 105 mm roller bearing on the input (turbine) end, and a tandem set of two 110 mm ball bearings mounted between those on the common shaft. The shaft and housing were sized to provide radial interference fits on the roller bearings and ball bearing inner races, and clearance fits on the ball bearing outer races. The coolant supply system was basically a "total immersion system", but coolant jets were provided to assure circulation through the bearings.

Design operating requirements were as follows:

		Output Roller	Input Roller	Tandem Ball
Load	lb	15,000	7,000	35,000
Speed	rpm	3,720	3,720	3,720
Acceleration	rpm/sec	7,200	7,200	7,200

Five basic test setups, ranging in complexity from a turbine-driven, single-bearing tester to the complete turbopump system were used during the program. These testers provided the capability to simulate turbopump operation on multiple combinations of ball and roller bearings under controlled conditions of load, acceleration, speed, and coolant properties.

Early testing of commercially-available thrust bearings yielded valuable operational information such as pre-test cooling requirements, load and speed control relationships, and tester capability. The results of the testing also indicated that tests of a large number of bearing configurations were unnecessary in selecting a bearing design suitable for the intended loads, speed, and acceleration. The test program was modified to concentrate effort upon the qualification of tandem thrust bearings manufactured by the New Departure Corp. and roller bearings produced by SKF Industries, Inc. Qualification testing provided bearing life information at turbopump operating conditions. Load sharing tests performed with the tandem thrust bearings received special attention because good load sharing would contribute to safe turbopump operation at off-design conditions. A special qualification test series was conducted using liquid nitrogen as the bearing coolant because early turbopump testing would be conducted using liquid nitrogen to simulate a propellant.

Performance of all preferred-configuration bearings was excellent, with life in excess of 5000 sec at design radial and axial loads in liquid oxygen and of at least 200 sec at or near 100% axial overload at DN values of $.5 \times 10^6$. Performance using liquid nitrogen as a coolant was equally satisfactory. The excellent post-test condition of the bearings used in the first turbopump test series demonstrated that component test results are directly applicable to the turbopump.

II. INTRODUCTION

In the M-1 liquid oxygen turbopump, power is transmitted through a single shaft connecting the pump impeller to the turbine rotor. Therefore, the power transmission components are located between the liquid oxygen pump and the hot gas turbine. The extreme complexity of seals, heaters, and auxiliary pumping systems required for conventional oil lubrication made it desirable that the bearings be cooled with liquid oxygen. The requirement that the shaft system be rigid enough to prevent interference between rotating and static parts under load dictated that the bearing minimum size should be approximately 110 mm bore and that axially rigid ball bearings be used to support end thrust.

The development of the bearing system which was selected as indicated is the subject of this report, which describes the effort and results obtained during the program conducted by Aerojet-General Corporation under Contract NAS3-2555 to the National Aeronautics and Space Administration.

III. BEARING DEVELOPMENT PROGRAM

A. DEVELOPMENT PROGRAM OBJECTIVES

The bearing development program was planned to yield operational information concerning liquid oxygen cooled bearings such as the required coolant flow rate and pressure, cooling rate (chilldown time), malfunction behavior (temperature rise, torque increase, vibration level), and purging or drying requirements; and to survey the performance (load-life relationship) of a large number of bearings produced by different manufacturers. Results of very successful early testing indicated that the survey testing was unnecessary, and the program was modified to concentrate effort upon qualification of the preferred configuration thrust bearing (P/N 281642/700797), turbine end roller bearing (P/N 281643), and pump end roller bearing (P/N 281644) for use in the turbopump. The qualification test program was planned to provide bearing life information at varying conditions of load, load direction, load sharing, load application rate, speed, acceleration, coolant flow rate, coolant pressure, coolant properties (liquid oxygen and liquid nitrogen), and initial (pre-test) temperature.

B. BEARING CONFIGURATION

1. Arrangement of Bearings in the Turbopump

a. Assembly Arrangement

Bearings were arranged as shown in **Figures 1 and 2 on a** common shaft with a 110 mm bore x 170 mm O.D. x 28 mm long roller bearing on the pump (output) end, a 105 mm bore x 160 mm O.D. x 26 mm long roller bearing on the turbine (input) end, and with the tandem set of two 110 mm bore x 170 mm O.D. x 28 mm long ball thrust bearings located between the roller bearings, adjacent to the pump end roller.

The bearings/shaft assembly was encased in a common (one-piece) housing to provide positive control of relative radial position and alignment of the roller bearings.

b. Mounting and Fits

The bearings were mounted on the shaft with the required spacers and jet rings and clamped in **place** by a lock nut.

Bearing fits (inner race to shaft and outer race to housing) were the same for all manufacturers' bearings. Fits between shafts or housings and prototype bearings were as follows:

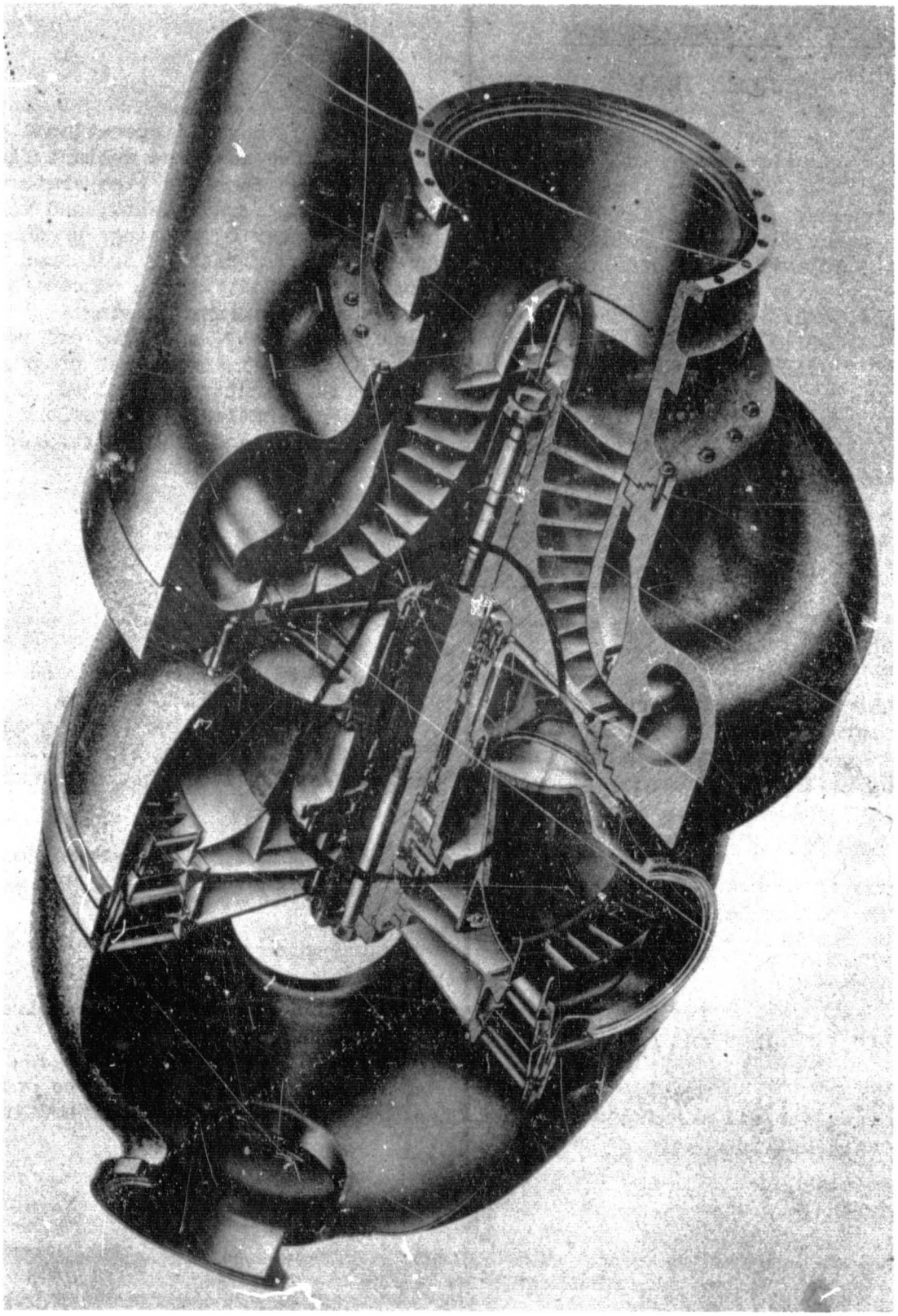

Figure 1

Oxidizer Turbopump Assembly

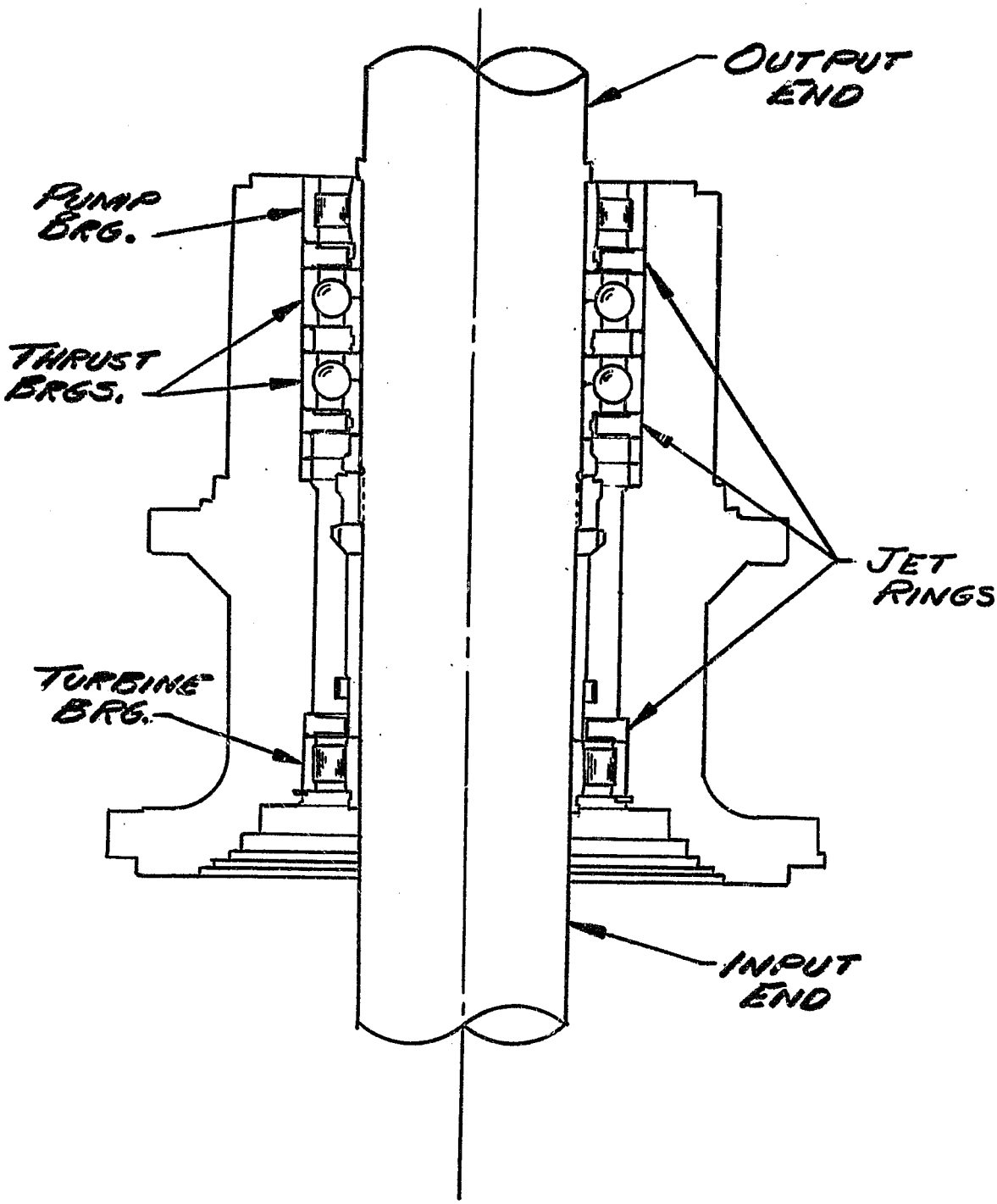

Figure 2

Turbopump Power Transmission

Type of Bearing	Diametral Fit Inner Race to Shaft (in.) Ambient Temperature	Diametral Fit Inner Race to Shaft (in.) Operating Temperature(-287°F)	Diametral Fit Outer Race to Housing (in.) Ambient Temperature	Diametral Fit Outer Race to Housing (in.) Operating Temperature(-287°F)
Pump Roller P/N 281644	0.0017/0.0023 Tight	0.0004/0.0010 Tight	0.0003/0.0012 Loose	0.0015/0.0024 Tight
Turbine Roller P/N 281643	0.0017/0.0023 Tight	0.0004/0.0010 Tight	0.0003/0.0012 Loose	0.0013/0.0022 Tight
Thrust Bearing P/N 281642	0.0012/0.0018 Tight	0.0001 Loose/ 0.0005 Tight	0.0131/0.0146 Loose	0.0104/0.0119 Loose

Assembly of the bearings was facilitated by heating the bearings to 300°F/350°F before installation to overcome the interference fit between the inner race and shaft.

c. Coolant System

Coolant was supplied to the bearings through jet rings which direct the coolant directly on the rolling elements. The jet ring passage has an annular distribution channel with axial exit, cylindrical spray nozzles.

The jet rings were arranged in the turbopump (Figure 2) with one ring between the pump end roller bearing and the adjacent thrust bearing supplying coolant through five 0.050-in. diameter holes to the roller bearing and through fifteen 0.050-in. diameter holes to the thrust bearing; one jet ring supplied the lower thrust bearing through fifteen 0.050-in. diameter holes; and one jet ring with five 0.050-in. diameter holes supplied coolant to the turbine end roller bearing.

The jet rings were designed to supply coolant to dissipate the heat generated at design radial and thrust loads at the approximate rates of 1.4 gpm per bearing for the radial bearings and 5.7 gpm per bearing for the thrust bearings(1).

2. Operating Conditions

a. Thrust Bearings

Tandem thrust bearings were manufactured by two vendors: the New Departure Corp. (P/N 281642 and 700797) and Industrial Tectonics, Inc. (P/N 288280). Thrust bearings P/N 281642 and 700797 are identical except for

(1) Dubief, J., Heat Generation in Annular Contact Ball Bearings Under Axial Load, Report RMR 0075, Aerojet-General, 16 January 1963.

being matched for load sharing in opposite directions relative to their orientation in the turbopump. Single thrust bearings were manufactured by the same vendors: the New Departure Corp. (P/N EX31000C) and Industrial Tectonics, Inc. (P/N 288140).

The operating conditions for the tandem bearings were as follows:

Operating Condition	P/N 281642 and 700797	P/N 288280
Thrust Load (Sharing Direction), lb	35,000	40,000
Thrust Load (Reverse Direction), lb	8,000	5,000
Overload (Sharing Direction), lb	39,000	44,000
Overload (Reverse Direction), lb	9,000	5,500
Speed, rpm	3,720	3,720
Overspeed, rpm	4,000	4,000
Acceleration Rate, rpm/sec	7,200	7,200
Coolant Flow Rate, gpm/Bearing	5.72	5.72
Coolant Pressure, psig	450	450
Coolant Temperature, LN_2, °F	-320	-320
Coolant Temperature, LO_2, °F	-297	-297

b. Radial Bearings

Radial load roller bearings were manufactured by the SKF Industries, Inc., with the following operational requirements:

Operating Condition	Pump Bearing P/N 281644	Turbine Bearing P/N 281643
Radial Load, lb	15,000	7,000
Radial Overload, lb	16,500	8,000
Speed, rpm	3,720	3,720
Overspeed, rpm	4,000	4,000
Acceleration Rate, rpm/sec	7,200	7,200

Operating Condition	Pump Bearing P/N 281644	Turbine Bearing P/N 281643
Coolant Flow Rate, gpm	1.394	1.394
Coolant Pressure, psig	450	450
Coolant Temperature, LO_2, °F	-297	-297
Coolant Temperature, LN_2, °F	-320	-320

3. Design Data

a. Thrust Bearings

(1) New Departure Corp. (ND)

Two separate bearings were manufactured by New Departure for the bearing evaluation program: a single thrust bearing and a tandem thrust bearing set.

The single bearing (P/N EX31000C) had a nonseparable outer race, ball, and cage assembly with a split inner race without puller grooves. The tandem bearing (P/N 281642/700797) was made up of two bearings matched for optimum load sharing. The bearings were completely separable with puller grooves on the inner races.

Both bearings were made with the same materials, AISI 440C Stainless Steel races and balls and Armalon 405C-116 cages. Design details of these bearings are as follows:

	P/N 281642/700797	P/N EX31000C
Type	Duplex Tandem	Single
Size	110 mm x 170 mm x 28 mm	110 mm x 170 mm x 28 mm
No. of Balls	19	18
Size of Balls	3/4 in.	25/32 in.
Class	ABEC5	ABEC5
Contact Angle	20°	25°
Race Curvature	52% Inner, 52% Outer	52% Inner, 56% Outer

	P/N 281642/700797	P/N EX31000C
Radial Clearance at Ambient Temperature	0.0038/0.0042	0.0115/0.0119
End Play	0.017/0.023	0.049/0.053
Cage Design	One Piece, Reinforced with Aluminum Side Plates	One Piece, Reinforced with Aluminum Side Plates

(2) Industrial Tectonics, Inc. (ITI)

Two separate bearings were made for the bearing evaluation program by ITI, a single thrust bearing (P/N 288140) and a tandem thrust bearing (P/N 288280). The bearings were similar in design and made of the same material, AISI 440C Stainless Steel races and balls and Armalon 405C-116 cages. The cage design incorporated a controlled ball drop. Design details of these bearings are as follows:

	P/N 288280	P/N 288140
Type	Duplex Tandem	Single
Size	110 mm x 170 mm x 28 mm	110 mm x 170 mm x 28 mm
No. of Balls	20	19
Size of Balls	23/32	3/4
Class	ABEC7	ABEC7
Contact Angle	30°	27.5°
Race Curvature	53% Inner, 52% Outer	52% Inner, 54% Outer
Radial Clearance at Ambient Temperature	0.0063/0.0069	0.0083/0.0087
End Play	0.020/0.025	0.0223/0.0255
Cage Design	One Piece, Reinforced with Aluminum Side Plates	One Piece, Reinforced with Aluminum Side Plates

b. Radial Bearings

Pump and the turbine-end radial bearings were manufactured by SKF Industries, Inc. These radial bearings also used 440C race and roller material and Armalon 405C-116 cages.

Design details of these bearings are as follows:

	P/N 281643	P/N 281644
Size	105 mm x 160 mm x 26 mm	110 mm x 170 mm x 28 mm
No. of Rollers	19	19
Size of Rollers	15 mm dia., 17 mm long	16 mm dia., 16 mm long
Roller Configuration	Crowned	Crowned
Class	ABEC 5	ABEC 5
Diametral Clearance at Ambient Temperature	0.0029 to 0.0033	0.0030 to 0.0034
Cage Design	One Piece, Reinforced with Aluminum Side Plates	One Piece, Reinforced with Aluminum Side Plates

4. Operating Stresses (Prototype Bearings)

a. Thrust Bearings

An analysis was made to determine the contact, hoop, and radial stresses at ambient and operating temperatures for the two-bearing tandem stack (P/N 281642); the total shared load was assumed to be 33,000 lb. This study was made under two loading conditions: 50%/50% load sharing and 60%/40% load sharing. The results are shown in Table I.

The dynamic contact angles of 34.1 degrees on the inner race and 33.8 degrees on the outer race for the prototype bearing at 4000 rpm and 16,500-lb load results in the contact ellipse being confined well within the design shoulder height.

b. Roller Bearings

An analysis of hoop and compressive stresses was completed for roller bearings P/N 281644 (pump end) and P/N 281643 (turbine end) at ambient temperature with no load at operating temperature and design load. Stresses were calculated using maximum interference fits. The results were as follows:

	P/N 281644		P/N 281643	
	Operating Temperature		Operating Temperature	
	Ambient	-287°F	Ambient	-287°F
Radial Load, lb	0	17,680	0	9,970
Inner Race Hoop Stress, psi	13,500	500	16,800	1,240
Inner Race Radial Stress, psi	*1520	*144	*1880	*139
Outer Race Tangential Stress, psi	0	6,070	0	3,880
Outer Race Radial Stress, psi	0	*610	0	*810
Inner Race Contact Stress, psi	0	264,000	0	204,000
Outer Race Contact Stress, psi	0	235,000	0	182,000

*Compressive stress

TABLE I

CALCULATED STRESSES FOR M-1 LIQUID OXYGEN THRUST BEARING P/N 281642

Temperature (°F)	Single Row Load (lb)	Speed (rpm)	Free Cont. Angle (Deg)	Mounted Cont. Angle (Deg)	Dynamic Cont. Angle (Degrees) On Inner Race	Dynamic Cont. Angle (Degrees) On Outer Race	Radial Interference (in.)	Max. Comp. Stress (Hertz) (psi)	Tangential Stress (Hoop) Inner Race (psi)	Radial Stress Inner Race (psi)	Clamping Load on Inner Race (lb)	Load Sharing
68	0	0	23	20.75	--	--	0.0011	--	6,750	*1,170	10,492	
-297	0	0	23	22.5	--	--	0.0002	--	1,230	*213	58,682	
-297	16,500	4,000	23	22.1	34.10	33.8	0.0002	347,690	1,230	*213	58,682	50%/50%
-297	20,000	4,000	23	22.1	34.10	33.8	0.0002	410,000	1,230	*213	58,682	60%/40%

*Compressive Stress

END OF REFERENCE

108

REFERENCE

109

CLEANLINESS OF COMPONENTS FOR USE IN OXYGEN, FUEL AND PNEUMATIC SYSTEMS. MSFC-SPEC-164A, NASA GEORGE C. MARSHALL SPACE FLIGHT CENTER, OCT. 1970.

A00030-6

MSFC-SPEC-164A
October 1, 1970
SUPERSEDING
MSFC-SPEC-164
April 16, 1962

GEORGE C. MARSHALL SPACE FLIGHT CENTER

NATIONAL AERONAUTICS AND SPACE ADMINISTRATION

HUNTSVILLE, ALABAMA

CLEANLINESS OF COMPONENTS FOR USE IN OXYGEN, FUEL, AND PNEUMATIC SYSTEMS, SPECIFICATION FOR

1. SCOPE

1.1 Scope. - This specification covers the cleanliness levels of components used in oxygen, pneumatic, and fuel systems of space vehicles and associated ground support equipment.

1.2 Classification. - The cleanliness level and inspection procedures as specified shall be applicable to the types and classes, classified according to configuration and materials, as follows:

Type I - Tubing, rigid[1]

Class 1 - Corrosion resistant, 300 series, steel

Class 2 - Aluminum alloy

Type II - Flexible hose assemblies[2]

Class 1 - Teflon lined

Class 2 - All metal

---

[1]Tubing, as defined for the purpose of this classification, shall include rigid tubing in sizes up through 2-inch outside diameter. Tubing having a diameter greater than 2 inches shall be considered as miscellaneous components (type III).

[2]Flexible hose assemblies, as defined for the purpose of this classification, shall include braided hoses in sizes up through 2-inch inside diameter. Flexible hoses with a diameter greater than 2 inches shall be considered as miscellaneous components (type III).

Type III - Miscellaneous components

Class 1 - Metallic and teflon

Class 2 - Nonmetallic

Type IV - Control assemblies[3]

Type V - Containers, metallic

2. APPLICABLE DOCUMENTS

2.1 The following documents, of the issue in effect on date of invitation for bids, form a part of this specification to the extent specified herein.

SPECIFICATIONS

Federal

O-H-765	Acid, Hydrochloric (Muriatic), Technical Grade.
O-H-795	Hydrofluoric Acid, Technical.
O-M-232	Methyl Alcohol, Methanol.
O-N-350	Nitric Acid, Technical.
O-O-670	Orthophosphoric Acid.
O-S-642	Sodium Phosphate, Tribasic, Technical, Anhydrous, Dodecahydrate, and Monohydrate.
BB-N-411	Nitrogen.
UU-T-81	Tags, Shipping and Stock.
PPP-T-60	Tape, Pressure-Sensitive Adhesive, Waterproof for Packaging and Sealing.

[3]Control assemblies shall include such items as valves, regulators, pressure switches, and temperature control switches.

Military

MIL-D-16791	Detergents, Nonionic.
MIL-P-27401	Propellant Pressurizing Agent, Nitrogen.
MIL-T-27602	Trichloroethylene, Oxygen Propellant Compatible, (By Flushing Methods).
MIL-C-81302	Cleaning Compound, Solvent, Trichlorotrifluoroethylene.
MIL-T-81533	1, 1, 1 - Trichloroethane (Methyl Chloroform) Inhibited, Vapor Degreasing.

George C. Marshall Space Flight Center

MSFC-SPEC-106	Testing Compatibility of Materials for Liquid Oxygen Systems.
MSFC-SPEC-217	Trichloroethylene, Technical.
MSFC-SPEC-234	Nitrogen, Space Vehicle Grade.
MSFC-SPEC-237	Solvent, Precision Cleaning Agent.
MSFC-SPEC-456	Film, Transparent, Plastic, LOX Compatible, Gas and Contamination Barrier.
MSFC-SPEC-471	Solvent, 1, 1, 1 - Trichloroethane, High Purity, Inhibited.

STANDARDS

George C. Marshall Space Flight Center

MSFC-STD-246	Design and Operational Criteria of Controlled Environment Areas.
MSFC-STD-343	Preservation, Packaging, Packing, Marking, Handling, and Shipping of Space Vehicle Components, Parts, and Associated Equipment, General Standard for.

PROCEDURE

George C. Marshall Space Flight Center

MSFC-PROC-404 Gases, Drying and Preservation, Cleanliness Level and Inspection Methods.

(Copies of specifications, standards, drawings, and publications required by contractors in connection with specific procurement functions should be obtained from the procuring activity or as directed by the contracting officer.)

3. REQUIREMENTS

3.1 Production cleaning and preservation process approval. - The cleaning and preservation process and the type equipment to be used shall be left to the discretion of the manufacturer; however, approval of the process and the type of equipment to be used shall be obtained from the procuring activity prior to cleaning and handling. The utilization of a recommended procedure will not guarantee acceptance of the end product. The contractor shall be required to submit to the contracting officer a statement in writing containing the following information:

(a) Processing materials to be used. This shall include, as applicable, trade names, specifications, chemical and physical properties.

(b) Processing equipment and cleaning procedures to be used.

(c) Quality assurance provisions to be utilized. This shall include in process control procedures to prevent built-in contamination or latent corrosion.

(d) Preservation methods and preservation materials to be used.

(Preservation methods proposed shall reflect the requirements presented in Standard MSFC-STD-343.)

(e) Controlled environment levels to be maintained for cleaning, assembly, handling, and test.

3.2 Materials. - Processing and protection materials used shall be as specified herein, on the drawing, or of a quality approved by the procuring activity (see 3.1).

3.2.1 Test and cleaning solvents. - Normally the selection of cleaning solvents is left to the discretion of the cleaning activity (see 3.1). However, selected solvents shall be compatible with the item being cleaned (e.g., methyl alcohol, O-M-232, is compatible with and shall be used to clean or test Kel-F materials; but, chlorinated solvent, such as

trichloroethylene and trichloroethane, are not compatible with titanium alloys and shall not be used unless specifically approved by the procuring activity). Test and cleaning solvents are subject to rapid chemical decomposition when exposed to even small quantities of water or dissimilar solvents which result in adverse effects on both metallic and nonmetallic materials. Every effort shall be made to prevent contamination of solvents with water or dissimiliar solvents.

NOTE

Due to degradation caused by mixtures of some solvent-water or dissimiliar solvents, parts or components subjected to the solvents specified herein during cleaning or testing operations shall be thoroughly dried with drying gas (see 3.2.2) prior to and subsequent to a water or dissimiliar solvent flush.

3.2.1.1 Test solvent. - Test solvents shall conform to Specification, type I of MIL-C-81302, type I of MIL-T-27602, type I or type II of MSFC-SPEC-217, MSFC-SPEC-237, or MSFC-SPEC-471 and shall meet the following requirements.

(a) The nonvolatile residue shall be not greater than 0.010 gram (g) per 500 milliliters (ml) at 221 ± 9 degrees Fahrenheit (°F) when tested in accordance with 4.4.3.2.

(b) There shall be no particle over 175 microns in any dimension and no more than 5 particles from 100 to 175 microns in size when tested in accordance with 4.4.3.1.

3.2.1.2 Cleaning solvent.

3.2.1.2.1 Vapor degreasing. - Unless otherwise approved in accordance with 3.1, solvents used for vapor degreasing cleaning processes shall conform to: type I of MIL-T-27602, MIL-C-81302, MIL-T-81533, type I or type II of MSFC-SPEC-217, or MSFC-SPEC-237.

NOTE

The 1, 1, 1 trichloroethane (inhibited) covered by Specification MIL-T-81533 is intended for vapor degreasing where air pollution regulations preclude the use of other materials.

3.2.1.2.2 Immersion cleaning solvents. - Unless otherwise approved in accordance with 3.1, solvents used for immersion cleaning process shall conform to: type I of MIL-T-27602, type I of MIL-C-81302, type I or type II of MSFC-SPEC-217, MSFC-SPEC-237, or MSFC-SPEC-471 and shall meet the nonvolatile residue content as specified for test solvents (see 3.2.1.1).

3.2.1.3 Fluids. - Fluids other than fluids in controlled environment areas (see 3.2.13) that contact cleaned surfaces after final cleaning or testing for cleanliness shall, as a minimum, meet the requirements for test solvents (see 3.2.1.1) for liquids and drying gas (see 3.2.2) for gases.

3.2.2 Drying, testing or preservation gas. - Gases used in drying, testing, or preservation processes shall conform to the cleanliness and quality assurance requirements for gases as specified in Procedure MSFC-PROC-404.

3.2.2.1 Nitrogen - Nitrogen gas used in the drying or preservation processes shall conform to type I, class 1, grade B of BB-N-411; to type I of MIL-P-27401; or to type I of MSFC-SPEC-234, and shall meet the requirements of 3.2.2.

3.2.2.2 Air. - Air used in the drying or preservation processes shall conform to the requirements specified in 3.2.2.

3.2.3 Filter paper. - Filter paper shall be either approved membrane (10 micron pore size, or less) or fiber type (e.g., Whatman No. 42, 45 MM) and shall be compatible with the fluids being tested.

3.2.4 Trisodium phosphate. - Trisodium phosphate used in the cleaning process shall conform to Specification O-S-642.

3.2.5 Nitric acid. - Nitric acid used in the cleaning process shall conform to Specification O-N-350.

3.2.6 Phosphoric acid. - Phosphoric acid used in the cleaning process shall conform to Specification O-O-670.

3.2.7 Hydrochloric acid. - Hydrochloric acid if used in the cleaning process shall conform to Specification O-H-765.

3.2.8 Hydrofluoric acid. - Hydrofluoric acid if used in the cleaning process shall conform to Specification O-H-795.

3.2.9 Detergent cleaning agent. - Detergent cleaning agents used in the cleaning process shall conform to Specification MIL-D-16791.

3.2.10 Demineralized water. - Demineralized water, if specified for rinsing or testing operations, shall contain no particle over 175 microns in any dimension and no more than 5 particles from 100 to 175 microns in size when tested in accordance with 4.4.3.1. The minimum specific resistance of the water shall be 50,000 ohms with a pH rating between 6.0 and 8.0.

3.2.11 Tape. - Tape used to secure and reinforce protective covers shall conform to Specification PPP-T-60.

3.2.12 Protective materials and devices. - Protective materials and devices that serve as contamination barriers in contact with or exposed to significant surfaces shall be compatible with the applicable service media (e.g. oxygen systems per MSFC-SPEC-106). Prior to use, the materials or devices shall be cleaned and dried to a level compatible with the component cleanliness requirement. Under normal usage, the materials or devices shall be lint free, and shall not delaminate, peel, disintegrate, slough or otherwise deteriorate in a manner that will contaminate the cleaned item. (See MSFC-SPEC-456).

3.2.13 Controlled areas. - Final cleaning, testing, assembly, packaging, and analysis of components cleaned in accordance with this specification shall be performed in an environmentally controlled area compatible with the component cleanliness requirements (see 3.1.e). Standard MSFC-STD-246 will be used by the procuring activity to evaluate the applicable environmentally controlled area.

3.3 Precleaning.

3.3.1 Precleaning. - Dust and grit, scale, corrosion, grease, oil, and other major soils shall be removed and a pressure test performed as applicable prior to final cleaning.

3.3.2 Precleaning and surface treatment. - Metallic items shall be treated (cleaning, passivating, and coating processes) to prevent latent corrosion and contamination. Items that do not lend themselves to this type of treatment, as an assembled item, shall be treated prior to assembly. Surface treated areas imparied during fabrication and assembly shall be reprocessed, as required, to restore the original protective finish.

3.4 Tubing and hoses.

3.4.1 Particle size limitations. - Tubing and hoses used in onboard and ground support equipment oxygen[4], fuel, or pneumatic systems shall be

---

[4]Oxygen, as defined for the purpose of this specification, shall include both gaseous and liquid forms.

cleaned to comply with the limits specified herein. Particles of contamination per square foot of component surface area (see 6.3) shall not exceed the following limits:

(a) No particle[5] greater than 2500 microns in any dimension.

(b) One particle between 700 and 2500 microns.

(c) Five particles between 175 and 700 microns.

3.4.2 Nonvolatile-residue content.

3.4.2.1 Oxygen systems. - The nonvolatile-residue contamination on the significant surfaces[6] of the tubing and hoses used in oxygen systems shall be not greater than 0.001 g per square foot of surface area as determined by analysis of the reliability test solution tested in accordance with 4.4.2.2.

3.4.2.2 Fuel systems. - No nonvolatile residue requirement.

3.4.2.3 Pneumatic systems.

3.4.2.3.1 Onboard systems. - The cleaning procedure shall completely remove all traces of oil, wax and gum, and other organic soils as determined by visual examination or any other test method determined acceptable by the procuring activity.

3.4.2.3.2 Ground support equipment systems. - The nonvolatile-residue contamination on the significant surfaces of tubing and hoses used in ground support equipment pneumatic systems shall be not greater than 0.001 g per square foot of surface area as determined by analysis of the reliability test solution tested in accordance with 4.4.2.2.

3.4.3 Rinsing. - Cleaned tubes and hoses shall be rinsed, as applicable, to remove cleaning and preparation chemicals. The cleaned and rinsed tube and hose surfaces shall register a pH within a range from 6.0 to 8.0.

---

[5]Particles, as defined for the purpose of this specification, shall include all foreign material whether it is metallic or non-metallic.

[6]Significant surfaces, as defined for the purpose of this specification, shall include all component surfaces that may come in contact with the respective service medium.

3.4.4 Drying. - Tubes and hoses shall be thoroughly dried by flowing prefiltered drying gas (see 3.2.2) through the tubes and hoses. The effluent gas shall not exhibit moisture pickup or measurable concentrations of residual organic solvents when tested in accordance with 4.4.2.3. Miscellaneous items, control assemblies, and large containers that do not lend themselves to this type of drying or testing procedures shall be dried and tested in accordance with procedures approved by the procuring activity (see 3.1).

3.4.5 Protection. - Tubes and hoses shall be protected by sealing openings with approved coverings (see 3.2.12) and secured with tape (see 3.2.11). Tubes and hoses to be shipped or stored after cleaning shall be placed in visually clean bags. The interior of the bags and parts shall be purged with an inert drying gas (see 3.2.2) to assure an inert storage package. The bags shall be completely sealed. The sealed bags shall be overpacked as necessary to prevent damage to the bags, tubes, hoses, or integral parts. Desiccants, when required for additional corrosion protection shall not be placed in such a manner as to recontaminate the cleaned surfaces of components. Provisions shall be made for monitoring desiccants. Other packaging materials compatible with the applicable service media may be used; however, the gas purging and overpackaging requirements shall be as listed above. If alternate methods are used, prior approval of the materials and procedures shall be obtained from the procuring activity.

3.5 Tubing, rigid.

3.5.1 Corrosion-resistant steel.

3.5.1.1 Particle size limitations. - Corrosion-resistant steel tubing used in onboard and ground support equipment oxygen, fuel, or pneumatic systems shall be cleaned to meet the requirements specified in 3.4.1.

3.5.1.2 Nonvolatile-residue content.

3.5.1.2.1 Oxygen systems. - The nonvolatile-residue contamination shall be no greater than as specified in 3.4.2.1.

3.5.1.2.2 Fuel systems. - No nonvolatile-residue requirements.

3.5.1.2.3 Pneumatic system.

3.5.1.2.3.1 Onboard systems. - The cleaning procedure shall be as specified in 3.4.2.3.1.

3.5.1.2.3.2 Ground support equipment systems. - The nonvolatile-residue contamination shall be not greater than that specified in 3.4.2.3.2.

3.5.1.3 Rinsing. - Tubing shall be rinsed as specified in 3.4.3.

3.5.1.4 Drying. - Tubing shall be dried as specified in 3.4.4.

3.5.1.5 Protection. - Tubing shall be protected as specified in 3.4.5.

3.5.1.6 Recommended procedure. - A cleaning, rinsing, and drying procedure that has been found acceptable to the procuring activity for cleaning corrosion-resistant steel tubing to the levels specified herein is as follows:

(a) Circulate an approved inhibited nonetch alkaline cleaning solution (e.g. Turco 4215 - Concentration 10 plus or minus 2 oz per gallon, or equal) at 160 plus or minus 10 degrees F, through the tubing or hoses for a minimum of 10 minutes. The circulation rate shall be not less than 20 tubing or hose volumes of liquid per minute.

(b) Flush tubing thoroughly with large quantities of tap water for a minimum of 10 minutes at room temperature.

(c) Circulate a solution of 10 plus or minus 2.0 percent by weight a nitric acid, conforming to Specification O-N-350, at 170 to 190 degrees F, through the tubing for a minimum of 5 minutes and maximum of 10 minutes.

(d) Flush thoroughly with large quantities of demineralized water (see 3.2.10) in the manner described in step (b).

(e) Dry tubing thoroughly with a drying gas (see 3.2.2) in accordance with procedure specified in 3.4.4 or by a vacuum drying process.

3.5.2 Aluminum alloy.

3.5.2.1 Particle size limitations. - Aluminum alloy tubing used in onboard and ground support equipment oxygen, fuel, or pneumatic systems shall be cleaned to meet requirements specified in 3.4.1.

3.5.2.2 Nonvolatile-residue content.

3.5.2.2.1 Oxygen systems. - The nonvolatile-residue contamination shall be not greater than that specified in 3.4.2.1.

3.5.2.2.2 Fuel systems. - No nonvolatile residue requirements.

3.5.2.2.3 Pneumatic systems.

3.5.2.2.3.1 Onboard systems. - The cleaning procedure shall be as specified in 3.4.2.3.1.

3.5.2.2.3.2 Ground support equipment systems. - The nonvolatile residue contamination shall be not greater than that specified in 3.4.2.3.2.

3.5.2.3 Rinsing. - Tubing shall be rinsed as specified in 3.4.3.

3.5.2.4 Drying. - Tubing shall be dried as specified in 3.4.4.

3.5.2.5 Protection. - Tubing shall be protected as specified in 3.4.5.

3.5.2.6 Recommended procedure. - A cleaning, rinsing, and drying procedure that has been found acceptable to the procuring activity for cleaning aluminum alloy tubing to the levels specified herein is as follows:

(a) Circulate a solution as described in step (a) for corrosion-resistant steel tubing (see 3.5.1.6).

(b) Flush tubing thoroughly with large quantities of tap water in the same manner as described in step (b) for corrosion-resistant steel (see 3.5.1.6).

(c) Circulate a solution of 3.0 to 5.0 percent nitric acid, conforming to Specification O-N-350, through the tubing at 85 to 95 degrees F for a minimum of 5 minutes and a maximum of 7 minutes. A solution of 5 plus or minus 0.5 percent by weight of phosphoric acid conforming to Specification O-O-670 at 160 to 180 degrees F may be used for removing heavy soils that cannot be removed with the nitric acid solution. In such cases circulate the solution through the tubing for a minimum of 5 minutes and a maximum of 7 minutes.

(d) Flush tubing thoroughly with large quantities of demineralized water (see 3.2.10) in the same manner as described in step (d) for corrosion-resistant steel tubing (see 3.5.1.6).

(e) Dry the tubing thoroughly as described in step (e) for corrosion-resistant steel tubing in 3.5.1.6.

3.6 Flexible hose assemblies.

3.6.1 Teflon lined.

3.6.1.1 Particle size limitations. - Teflon-lined flexible hoses used in onboard and ground support equipment oxygen, fuel, and pneumatic systems shall be cleaned to meet requirements specified in 3.4.1.

3.6.1.2 Nonvolatile-residue content.

3.6.1.2.1 Oxygen systems. - The nonvolatile-residue contamination shall be not greater than that specified in 3.4.2.1.

3.6.1.2.2 Fuel systems. - No nonvolatile-residue requirement.

3.6.1.2.3 Pneumatic systems.

3.6.1.2.3.1 Onboard systems. - The cleaning procedure shall be as specified in 3.4.2.3.1.

3.6.1.2.3.2 Ground support equipment systems. - The nonvolatile-residue contamination shall be not greater than that specified in 3.4.2.3.2.

3.6.1.3 Rinsing. - Hoses shall be rinsed as specified in 3.4.3.

3.6.1.4 Drying. - Hoses shall be dried as specified in 3.4.4.

3.6.1.5 Protection. - Hoses shall be protected as specified in 3.4.5.

3.6.1.5.1 Recommended procedure. - A cleaning, rinsing, and drying procedure that has been found acceptable to the procuring activity to meet the levels specified herein for teflon-lined flexible-hose assemblies is as follows:

(a) Brush interior of components thoroughly for 10 to 15 minutes with a nylon brush and 0.5 percent detergent and water solution at a temperature of 122 (plus or minus 9) degrees F.

(b) Flush interior of hoses for 2 to 5 minutes with demineralized water (see 3.2.10) at room temperature.

(c) Vacuum dry or purge with prefiltered drying gas (see 3.2.2).

(d) Flush with solvent conforming to requirements specified in 3.2.1.2.2.

(e) Purge with prefiltered drying gas conforming to the requirements of 3.2.2.

(f) Vacuum dry internal and external surfaces.

3.6.2 All metal hose.

3.6.2.1 Particle size limitations. - All metal flexible-hose assemblies used in onboard and ground support equipment oxygen, fuel, and pneumatic systems shall be cleaned to meet requirements specified in 3.4.1.

3.6.2.2 Nonvolatile-residue content.

3.6.2.2.1 Oxygen systems. - The nonvolatile-residue contamination shall be not greater than that specified in 3.4.2.1.

3.6.2.2.2 Fuel systems. - No nonvolatile-residue requirement.

3.6.2.2.3 Pneumatic systems.

3.6.2.2.3.1 Onboard systems. - The cleaning procedure shall be as specified in 3.4.2.3.1.

3.6.2.2.3.2 Ground support equipment systems. - The nonvolatile-residue contamination shall be not greater than that specified in 3.4.2.3.2.

3.6.2.3 Rinsing. - All metal flexible-hose assemblies shall be rinsed as specified in 3.4.3.

3.6.2.4 Drying. - All metal flexible-hose assemblies shall be dried as specified in 3.4.4.

3.6.2.5 Protection. - All metal flexible-hose assemblies shall be protected from recontamination by sealing all openings with approved secured closures, placing the assemblies in polyethylene bags, purging bags with a dry oil-free gas to assure an inert package during storage, heat-sealing both ends of bags, and overpacking as necessary to prevent recontamination or damage during handling and storage.

3.6.2.6 Recommended procedure. - Cleaning, rinsing, and drying procedures that have been found acceptable to the procuring activity to meet the levels specified herein for all metal flexible-hose assemblies are as follows:

(a) Ultrasonic cleaning.

*1. Clean hose assemblies in an ultrasonic cleaning tank equipped with a recirculating system utilizing a 10 micron filter. The solution shall be a detergent cleaning agent (see 3.2.9) and demineralized water (see 3.2.10).

*2. Rinse by flushing with demineralized water.

3. Vacuum dry or purge with prefiltered dry, oil-free gas.

4. Flush with solvent conforming to the requirements specified in 3.2.1.2.2.

*5. Purge with prefiltered drying gas conforming to the requirements of 3.2.2.

*6. Vacuum dry internal and external surfaces.

(b) Detergent cleaning.

*1. Brush interior of flexible hose assemblies thoroughly for 10 to 15 minutes with a nylon brush and 0.5 percent detergent and water solution at a temperature of 122 plus or minus 9 degrees F.

*2. Flush for 2 to 5 minutes with demineralized water (see 3.2.10) at room temperature.

3. Vacuum dry or purge with prefiltered drying gas (see 3.2.2).

4. Flush with solvent conforming to the requirements specified in 3.2.1.2.2.

*5. Purge with prefiltered drying gas conforming to the requirements of 3.2.2.

*6. Vacuum dry internal and external surfaces.

NOTE

Steps preceded by * are only steps recommended for fuel systems. All steps are applicable to recommended procedure for oxygen and pneumatic systems.

3.7 Miscellaneous components.

3.7.1 Metallic and Teflon.

3.7.1.1 Particle size limitations. - Miscellaneous metallic and teflon components used in onboard and ground support equipment oxygen, fuel, and pneumatic systems shall be cleaned to meet requirements specified in 3.4.1.

3.7.1.2 Nonvolatile-residue content.

3.7.1.2.1 Oxygen systems. - The nonvolatile-residue contamination shall be not greater than that specified in 3.4.2.1.

3.7.1.2.2 Fuel systems. - No nonvolatile-residue requirements.

3.7.1.2.3 Pneumatic systems. -

3.7.1.2.3.1 Onboard systems. - The cleaning procedure shall be as specified in 3.4.2.3.1.

3.7.1.2.3.2 Ground support equipment systems. - The nonvolatile-residue contamination shall be not greater than that specified in 3.4.2.3.2.

3.7.1.3 Rinsing. - Miscellaneous metallic and teflon components shall be rinsed as specified in 3.4.3.

* 3.7.1.4 Drying. - Miscellaneous metallic and teflon components shall be dried as specified in 3.4.4.

3.7.1.5 Protection. - All significant surfaces or openings to surfaces that will contact the applicable service medium of miscellaneous metallic and teflon components shall be protected from recontamination by sealing the surfaces or openings with approved coverings (see 3.2.12) and secured with tape (see 3.2.11) or other approved methods. The protected components shall be placed in visually clean bags (bags purged with drying gas - see 3.2.2), completely sealed to assure an inert package during storage, and overpacked as necessary to prevent damage during storage and handling. If alternate methods are used, prior approval of the materials (other than materials conforming to Specification MSFC-SPEC-456) and procedures shall be obtained from the procuring activity (see 3.1). See 3.4.5 for use of desiccants.

3.7.1.6 Recommended procedure. - Due to various types and complexities of components covered under this classification, no recommended procedure is included. Contractors shall submit respective procedure for approval in accordance with 3.1.

3.7.2 Nonmetallic components.

3.7.2.1 Particle size limitations. - Nonmetallic miscellaneous components shall be cleaned in such a manner that all visible foreign contamination will be removed.

3.7.2.2 Freedom from oils and greases. - The cleaning procedure shall be as specified in 3.4.2.3.1.

3.7.2.3 Rinsing. - Nonmetallic components shall be rinsed as specified in 3.4.3.

3.7.2.4 Drying. - Nonmetallic components shall be dried as specified in 3.4.4.

3.7.2.5 Protection. - Nonmetallic components shall be protected as specified in 3.7.1.5.

3.7.2.6 Recommended procedure. - Due to various types and complexities of components covered under this classification, no recommended procedure is included. Contractors shall submit procedure for approval in accordance with 3.1.

3.8 Control assemblies.

3.8.1 Metallic control assemblies or assembly components.

3.8.1.1 Particle size limitations. - Requirements for metallic control components and assemblies used in onboard and ground support equipment oxygen, fuel, or pneumatic systems shall be as specified in 3.4.1.

3.8.1.2 Nonvolatile residue content.

3.8.1.2.1 Oxygen systems. - The nonvolatile-residue contamination shall be no greater than as specified in 3.4.2.1.

3.8.1.2.2 Fuel systems. - No nonvolatile-residue requirement.

3.8.1.2.3 Pneumatic systems.

3.8.1.2.3.1 Onboard systems. - The cleaning procedure shall be as specified in 3.4.2.3.1.

3.8.1.2.3.2 Ground support equipment systems. - The nonvolatile-residue contamination shall be no greater than specified in 3.4.2.3.2.

3.8.1.3 Rinsing. - Metallic control components and assemblies shall be rinsed as specified in 3.4.3.

3.8.1.4 Drying. - Metallic control components and assemblies shall be dried as specified in 3.4.4.

3.8.1.5 Protection. - Metallic control components and assemblies shall be protected as specified in 3.7.1.5.

3.8.1.6 Recommended procedure. - Due to various types and complexities of components covered under this classification, no recommended procedure is included. Contractors shall submit respective procedure for approval in accordance with 3.1.

NOTE

Many control assemblies are cleaned and inspected as metallic and nonmetallic parts, then assembled. Cleaning and testing of control assemblies, by flushing with liquids or purging with gases are not generally recommended. However, if applicable, the contractor shall include, as a part of the cleaning and preservation processes (see 3.1), procedures for cleaning, handling, assembling, protecting, and testing of assembled components.

3.8.2 Nonmetallic control assembly components.

3.8.2.1 Particle size limitations. - Nonmetallic control assembly components shall be cleaned as specified in 3.7.2.1.

3.8.2.2 Freedom from oils and greases. - The cleaning procedure shall be as specified in 3.4.2.3.1.

3.8.2.3 Rinsing. - Nonmetallic control assembly components shall be rinsed as specified in 3.4.3.

3.8.2.4 Drying. - Nonmetallic control assembly components shall be dried as specified in 3.4.4.

3.8.2.5 Protection. - Nonmetallic control assembly components shall be protected as specified in 3.7.1.5.

3.8.2.6 Recommended procedure. - Due to various types and complexities of components covered under this classification, no recommended procedure is included. Contractors shall submit respective procedure for approval in accordance with 3.1. (See NOTE 3.8.1.6)

3.9 Containers (metallic).

3.9.1 Liquid and pneumatic.

3.9.1.1 Particle size limitation. - Liquid and pneumatic containers shall be cleaned to meet the cleanliness limits specified herein based on the specified sampling plan (see 4.4.1.4.1). Particles of contamination per square foot of surface area (area exposed to the service medium (see 6.3)) shall not exceed the following limits:

(a) No particle greater than 2500 microns in any direction.

(b) One particle between 700 and 2500 microns.

(c) Five particles between 175 and 700 microns.

3.9.1.2 Nonvolatile-residue content.

3.9.1.2.1 Oxygen containers. - The nonvolatile-residue contamination on the significant surfaces of oxygen containers (according to component surface area) shall be not greater than 0.005 g per square foot as determined by analysis of the test solution of 4.4.1.4.2 in accordance with 4.4.2.2.

3.9.1.2.2 Fuel containers. - No nonvolatile-residue requirement.

3.9.1.2.3 Pneumatic containers.

3.9.1.2.3.1 Onboard systems. - The cleaning procedure shall completely remove all traces of oil, wax, gum, and other organic soils as determined by visual examination or any other test method determined acceptable by the procuring activity.

3.9.1.2.3.2 Ground support equipment systems. - The nonvolatile-residue contamination on the significant surfaces of ground support equipment pneumatic system containers (according to component surface area) shall be not greater than 0.001 g per square foot as determined by analysis of the test solution of 4.4.1.3 in accordance with 4.4.2.2.

3.9.1.3 Rinsing. - Liquid and pneumatic containers shall be adequately rinsed to remove cleaning and preparation chemicals.

3.9.1.4 Drying. - Inner surfaces of liquid and pneumatic containers shall be thoroughly dried as evidenced by no moisture pickup in prefiltered gas (see 3.2.2) passing through the container.

3.9.1.5 Protection. - Immediately after drying, liquid and pneumatic container openings shall be covered with approved precleaned dry covers secured in a manner to prevent detachment or damage during handling, storage, or shipment. Covers shall be designed to facilitate tank-venting and to prevent recontamination of the tank interior.

3.9.1.6 Recommended procedure. - Due to size of containers and the complexity of construction, no recommended procedure is submitted. The contractor shall submit procedures for approval in accordance with 3.1. However, the procedure and materials used shall be such that harmful residue cannot be entrapped within the container.

3.10 Marking. - Unless otherwise specified by the procuring activity, cleaned components shall be marked with tags conforming to type C, Specification UU-T-81, and shall contain the following information:

(a) Part or identification number.

(b) Contractor identification.

(c) Contractor cleaning and packaging procedure identification (number, title, etc.)

(d) Date of cleaning.

(e) Title, date, and number of this specification.

(f) Service medium or intended use of component.

(g) Manufacturer's serial number.

4. QUALITY ASSURANCE PROVISIONS

4.1 The supplier is responsible for the performance of all inspection requirements as specified herein. Except as otherwise specified, the supplier may utilize his own or any other inspection facilities and services acceptable to the Government. Inspection records of the examination and tests shall be kept complete and available to the Government as specified in the contract or order. The Government reserves the right to perform any of the inspections set forth in the specification where such inspections are deemed necessary to assure supplies and services conform to prescribed requirements.

4.2 Sampling, acceptance inspection.

4.2.1 Visual inspection. - The sample for the inspection of 4.3.1 and 4.3.2, as applicable, shall consist of all cleaned components.

4.2.2 Reliability sample. - Unless otherwise specified, a quantitative analysis reliability sample for the test of 4.4 consisting of a minimum of 5-percent of the items cleaned, but not less than one sample for each group of 20 or less (except as noted in 4.2.2.2 and 4.2.2.3) of the items cleaned, shall be selected at random by Government inspection from production items that have been cleaned, examined in accordance with 4.3, and found acceptable. The sample shall be selected in a manner that will provide maximum representation of the affected lot. The reliability sample and the segment of production that it represents shall be clearly identified as specified by the procuring activity.

4.2.2.1 Small components. - The reliability sample for small components (components having a significant surface area less than 1.0 square foot) shall consist of a sufficient number of components to make up 1 square foot (minimum) of surface area. When the total quantity of items

procured have a combined surface area less than 1.0 square foot, a quantity (sufficient to make up 1.0 square foot of surface area) of clean stock items shall be used in preparation of the reliability sample or upon written request by the contractor to the procuring activity, a special test procedure will be furnished.

4.2.2.2 Containers. - All containers submitted for acceptance shall be inspected for size of particles of contamination. All oxygen and pneumatic containers shall be inspected for nonvolatile residue contamination.

4.2.2.3 Rigid tubing. - The reliability of the cleaning procedure for rigid tubing shall be determined and the cleaning process qualified as specified herein. After qualification of the procedure and equipment, reliability sampling shall be left to the discretion of the procuring activity. Samples for the applicable tests of 4.4 to determine conformance to 3.5.1.1, 3.5.1.2, 3.5.2.1, and 3.5.2.2, as applicable, and qualification of the cleaning process and cleaning equipment to be used in production cleaning shall be selected as follows:

(a) Select a minimum of 5 cleaned tubes a minimum of 3 feet long and having a minimum combined significant surface area of 1.0 square foot from each size (diameter) and type (corrosion resistant steel or aluminum alloy) tube to be cleaned. Select test samples from tubes cleaned in accordance with the exact procedures and utilizing the equipment approved in accordance with 3.1.

(b) Upon satisfactory qualification (conformance of samples from step (a) to meet the requirements of 3.5.1.1, 3.5.1.2, 3.5.2.1, and 3.5.2.2 when tested in accordance with 4.4) of the cleaning procedure and equipment, periodic spot checks in addition to the inspection of 4.3 will be made to insure that the cleaning procedures continue to be effective.

4.3 Acceptance inspection. - Except as specified herein, acceptance inspection shall be performed on applicable components used for the space vehicle and associated ground support equipment.

4.3.1 Examination. - Surfaces of all cleaned components that will contact the respective service medium shall be visually inspected for the presence of contaminants such as moisture, corrosion, scale, dirt, oil, grease, and similar foreign material. A flashlight or borescope may be required to examine internal surfaces. Components, such as small diameter tubing (1/2-inch diameter or less), having limited accessibility to visual examination shall be accepted or rejected on the basis of the reliability inspections. The presence of contamination shall require a reliability test (see 4.4) to determine acceptance or rejection, however, components

that do not lend themselves to a solvent-rinse test method shall be accepted or rejected on the basis of visual examination of other methods approved by the procuring activity (see 3.1). Scale-free discoloration due to welding and passivation is permitted. All components shall also be examined to determine conformance to paragraph 3.10.

4.3.2 Acidity or alkalinity. - External and internal surfaces of cleaned and rinsed components shall be tested with pH-indicating paper while the component is still wet from the last rinse or after wetting the test surface with a few drops of distilled water to determine that the surface acidity or alkalinity registers a pH between 6.0 and 8.0. The pH-indicating paper shall be sensitive to the requirement specified above.

4.4 Reliability tests. - Cleaned components selected by the Government inspector for reliability tests shall be subjected to all examinations and tests specified herein. The visual examinations of 4.3.1 and 4.3.2, as applicable, shall precede the reliability tests.

4.4.1 Preparation of test solution. - Preparation of test solution (see 3.2.1.1) for oxygen, fuel, and pneumatic system components, that lend themselves to solvent cleaning, shall be as specified herein.

4.4.1.1 Small components. - A 500 ml, (minimum) test solution to determine particle population (particles greater than 175 microns in size) and the nonvolatile residue on the significant surfaces of small components (less than 1.0 square foot in surface area) selected for reliability tests shall be prepared as follows:

(a) Divide the 500 ml, test solution (see 3.2.1) into quantities in proportion to the surface area of the individual components used to make up 1.0 square foot of surface area (see 4.2.2.1).

(b) Flush each component with proportionate share of test solution.

(c) Collect the flushing solvent for the analysis of 4.4.2.1 and 4.4.2.2 as applicable.

(d) Thoroughly dry components after completion of flushing operation.

4.4.1.2 Components 1.0 square foot to 5.0 square feet in surface area. - A 500 ml, (nominal) test solution to determine the particle population (particles greater than 175 microns in size) and the nonvolatile residue on the significant surfaces of the reliability samples selected from components having significant surface areas from 1.0 square foot through 5.0 square feet shall be prepared by flushing the

test solvent (see 3.2.1.1) over the significant surfaces and collecting the solvent for the analysis of 4.4.2.1 and 4.4.2.2 as applicable. The component shall be thoroughly dried after completion of flushing operation.

4.4.1.3 Components with surface areas greater than 5.0 square feet. - The test solution to determine the particle population (particles greater than 175 microns in size) and nonvolatile residue on the significant surfaces of the reliability sample (see 4.2.2 and 4.2.2.2) from components, except for containers specified in 4.4.1.4, having significant surface areas greater than 5.0 square feet shall be prepared as follows:

(a) Flush the significant surfaces with 100 ml, (maximum) of test solvent per square foot of surface area.

(b) Collect the flushing solvent.

(c) If more than 500 ml, of test solvent is used, the flushings shall be thoroughly agitated and a 500 ml, sample shall be taken from the total quantity of flushing solution for the quantitative analysis of 3.4.2.1 and 4.4.2.2, as applicable.

(d) The component shall be thoroughly dried after the flushing operation (step (a)).

4.4.1.4 Containers, oxygen and fuel. - The samples for determining the presence of excessive large particles and nonvolatile-residue on significant surfaces of oxygen and fuel containers, as applicable, shall be determined as specified herein.

4.4.1.4.1 Particle size. - The particle size determination, based on a cleaning procedure utilizing a high-pressure liquid spray, with a rotating nozzle traversing the length of the container-interior, shall be obtained as follows:

(a) With container in vertical position, traverse the interior of the container with a spray utilizing demineralized water (see 3.2.10) or an acceptable substitute at a minimum flow rate of 40 gallons per minute (gpm) and a pump pressure of 250 (plus or minus 50) pounds per square inch. The pressure drop between the pump discharge and the spray nozzle shall be not greater than 20 pounds per square inch gage (psig).

(b) From a continuous flow of test medium through the sampling line (a funnel-shaped flange located at the bottom of the container), take a minimum of five 500 ml samples. The samples shall be taken at equally spaced intervals (vertical positions of the spray nozzle) during the rinsing operation.

(c) A 500 ml sample of the rinsing medium, to determine conformance to 3.2.10 or specified purity of acceptable substitute, shall be taken at the beginning and at the end of the rinsing period. The samples shall be taken from a sampling line for the rinsing medium located as near the spray nozzle as practical.

4.4.1.4.2 Nonvolatile-residue (oxygen containers only). - The nonvolatile-residue contamination sample for oxygen containers shall be prepared by one of the following methods:

(a) Vertical position (spray operation).

(1) With container in vertical position, traverse the interior of the container with a spray utilizing trichloroethylene (see 3.2.1.1) or an acceptable substitute at a minimum flow rate of 5 gpm and a pump pressure of 60 plus or minus 10 psig.

(2) From a continuous flow of test medium through the sampling line (a funnel-shaped flange located at the bottom of the container), take a minimum of five 1000 ml samples. The samples shall be taken at equally spaced intervals (vertical positions of the spray nozzle) during the rinsing operation.

(3) A 500 ml sample of the rinsing medium, to determine conformance to 3.2.1.1 or specified purity of acceptable substitute, shall be taken at the beginning and at the end of the rinsing period. The samples shall be taken from a sampling line for the rinsing medium located as near the spray nozzle as practical.

(b) Horizontal position (barrel-roll operation).

(1) Place the container in a horizontal position and fill with sufficient amount of test solvent

to completely cover all projecting surfaces. The total weight of solvent used in any one complete rotating cycle shall be determined prior to introduction into the container.

(2) Sample the rinsing solvent before and during approved intervals in the rotation cycle.

(3) Conduct tests in accordance with 4.4.2.2 to determine the total nonvolatile-residue pickup.

(4) Continue rotation of the container until the increase in the nonvolatile-residue during an approved interval of rotation, is 2 milligrams (mg) or less per liter of solution.

(5) If the total compound nonvolatile-residue per square foot of significant surface area is greater than 0.005 g per square foot of surface area, the container shall be recleaned.

(6) The test solvent shall be drained from the container and the interior thoroughly dried prior to application of protection.

NOTE

Alternate test methods and sampling procedures may be used with prior approval by the procuring activity.

4.4.2 Tests.

4.4.2.1 Particle size analysis. - Each sample reliability test solution from 4.4.1.1, 4.4.1.2, 4.4.1.3, and 4.4.1.4.1 shall be filtered through filter paper (see 3.2.3) and the residue examined for particulate under 10 to 45 power microscope. The larger particles (175 microns in any dimension and greater) shall be measured with a filter micrometer and the contamination per square foot of surface area calculated to determine the reliability of the visual examination of 4.3.1 and conformance to 3.5.1.1, 3.5.2.1, 3.6.1.1, 3.6.2.1, 3.7.1.1, 3.8.1.1, and 3.9.1.1, as applicable. Alternate methods of determining reliability may be used by the contractor with prior approval by the procuring activity (see 3.1).

4.4.2.2 Nonvolatile-residue. - The filtered sample (500 ml nominal volume) of 4.4.2.1 from oxygen and applicable pneumatic components or a

500 ml sample from 4.4.1.4.2 shall be analyzed for nonvolatile residue content to determine reliability of the examinations of 4.3.1 and conformance to 3.5.1.2.1, 3.5.1.2.3.2, 3.5.2.2.1, 3.5.2.2.3.2, 3.6.1.2.1, 3.6.1.2.3.2, 3.6.2.2.1, 3.6.2.2.3.2, 3.7.1.2.1, 3.7.1.2.3.2, 3.8.1.2.1, 3.8.1.2.3.2, 3.9.1.2.1, and 3.9.1.2.3.2 as follows:

(a) Transfer 500 ml of the solvent into a clean degreased 800 ml beaker.

(b) Evaporate the solvent to 10 to 20 ml volume in a steam bath.

(c) Transfer the solvent to a constant-weight (within 0.3 mg) tared 30 ml weighing bottle, weighed to the nearest 0.1 mg.

(d) Continue evaporation to a volume of 5 plus or minus 0.5 ml. Do not let the solvent evaporate to dryness.

(e) Place the weighing bottle in a constant temperature oven at 221 to 230 degrees F for 1.5 hours.

(f) Cool weighing bottle in a desiccator and then weigh to the nearest 0.1 mg.

(g) Return the weighing bottle to the constant temperature oven for one-half hour.

(h) Repeat (f). If the difference between the weights is greater than 0.3 mg, repeat step (g) until the difference between successive weighing is 0.3 mg or less.

(i) Compare the results obtained from used solvent with the results obtained from unused solvent. The difference between the weights shall be not greater than the increase specified for the affected item (based on surface area and total amount of solvent used for testing).

4.4.2.3 Drying. - Unless otherwise approved by the procuring activity, the reliability of the drying procedure for items subjected to liquids during cleaning or drying procedures shall be determined by testing the sample of 4.2.2 before and after the tests of 4.4.2.1 and 4.4.2.2. The presence of surface moisture and residual organic solvents on the cleaned, tested, and dried items shall be tested as follows:

(a) Flow prefiltered drying gas through or over the affected surfaces of the item being tested.

(b) Monitor the dew point of the drying gas entering and leaving the affected item to determine presence of moisture on cleaned and dried surfaces. Any moisture pickup in the drying gas that has flowed through or over the affected surfaces shall necessitate additional drying prior to packaging or application of protective coverings.

(c) Monitor the effluent drying gas with a halogen detector to determine if affected surfaces are free from residual organic solvents. If no measurable concentrations are indicated by the halogen detector, the affected surfaces shall be considered free from excessive residual organic solvents. Any measurable concentrations in the drying gas that has flowed through or over the affected surfaces shall necessitate additional drying prior to packaging or application of protective coverings.

NOTE

Additional verification may be required to ascertain the dryness of components having deep recesses and entrapment areas. Certification shall be made by a quality assurance representative that approved drying procedures (proven by adequate tests) for the affected component has been followed.

4.4.3 Solvent control checks.

4.4.3.1 Particle size. - At least once daily while being used, particle size control tests shall be conducted on solvent to determine conformance to 3.2.1.1. Filter 500 ml of solvent through filter paper (see 3.2.3) and examine for particulate in accordance with 4.4.2.1. Alternate methods of determining particle count may be used with prior approval of the procuring activity.

4.4.3.2 Nonvolatile-residue. - At least once daily while being used, nonvolatile-residue content tests shall be conducted on solvent to determine conformance to 3.2.1.1. Test procedure specified in 4.4.2.2 for a 500 ml sample shall be used.

4.5 Rejection and resubmittal.

4.5.1 Individual rejection. - Components that fail the visual inspection of 4.3.1 or the test of 4.3.2, as applicable, shall be rejected and reprocessed.

4.5.2 Lot rejection. - If any reliability sample fails to meet the requirements specified herein, a second sample, twice the size of the first, shall be selected and tested. If any item from the second sample fails to meet the requirements specified herein, the entire lot represented by the sample shall be rejected.

4.5.3 Resubmittal. - Before resubmittal of rejected lots, full particulars concerning previous rejection and corrective measures taken to prevent recurrence of the failure shall be made available to the procuring activity.

5. PREPARATION FOR DELIVERY

Not applicable.

6. NOTES

6.1 Intended use. - The procedures, cleaning levels, and preservation methods covered by this specification are intended for use in cleaning, inspecting, and protecting of components used in oxygen, pneumatic, and fuel systems of space vehicles and associated ground support equipment.

6.2 Ordering data. - Procurement documents should specify the following:

(a) Title, number, and date of this specification.

(b) Whether preproduction approval is required (see 3.1).

(c) Cleanliness level required.

6.3 Surface area. - The standard unit (area) used for determination of contamination levels is 1.0 square foot of significant surface area (area that will contact the service medium). Exact calculations of surface areas are not mandatory. Approximate surface area calculations acceptable to the Government inspector may be used.

Notice. - When Government drawings, specifications, or other data are used for any purpose other than in connection with a definitely related Government procurement operation, the United States Government thereby incurs no responsibility nor any obligation whatsoever; and the fact that the Government may have formulated, furnished, or in any way supplied the said drawings, specifications, or other data is not to be

regarded by implication or otherwise as in any manner licensing the holder or any other person or corporation, or conveying any rights or permission to manufacture, use, or sell any patented invention that may be in any way related thereto.

Custodian:	Preparing activity:
NASA - George C. Marshall Space Flight Center	George C. Marshall Space Flight Center

NASA—MSFC—C

END OF REFERENCE

109

Card #26

REFERENCE

110

COE, H. H.; SCIBBE, H. W.; AND PARKER, R. J.: PERFORMANCE OF 75-MILLIMETER-BORE BEARINGS TO 1.8 MILLION DN WITH ELECTRON-BEAM-WELDED HOLLOW BALLS. NASA TN D-5800, 1970.

NASA TECHNICAL NOTE NASA TN D-5800

NASA TN D-5800

PERFORMANCE OF 75-MILLIMETER-BORE BEARINGS TO 1.8 MILLION DN WITH ELECTRON-BEAM-WELDED HOLLOW BALLS

by Harold H. Coe, Herbert W. Scibbe, and Richard J. Parker

Lewis Research Center
Cleveland, Ohio 44135

NATIONAL AERONAUTICS AND SPACE ADMINISTRATION • WASHINGTON, D. C. • MAY 1970

1. Report No. NASA TN D-5800	2. Government Accession No.	3. Recipient's Catalog No.
4. Title and Subtitle PERFORMANCE OF 75-MILLIMETER-BORE BEARINGS TO 1.8 MILLION DN WITH ELECTRON-BEAM-WELDED HOLLOW BALLS		5. Report Date May 1970 6. Performing Organization Code
7. Author(s) Harold H. Coe, Herbert W. Scibbe, and Richard J. Parker		8. Performing Organization Report No. E-5442
9. Performing Organization Name and Address Lewis Research Center National Aeronautics and Space Administration Cleveland, Ohio 44135		10. Work Unit No. 126-15 11. Contract or Grant No. 13. Type of Report and Period Covered Technical Note
12. Sponsoring Agency Name and Address National Aeronautics and Space Administration Washington, D.C. 20546		14. Sponsoring Agency Code

15. Supplementary Notes

16. Abstract

An experimental investigation was performed with two series (115 and 215) of 75-mm-bore ball bearings using hollow balls as the rolling elements. Similar bearings using solid balls were also tested and the data compared. The bearings were tested at 500- and 1000-lb (2200- and 4400-N) thrust loads at shaft speeds up to 24 000 rpm (1.8×10^6 DN). The results showed only slight differences in torque and outer-race temperature between the hollow ball bearings and the corresponding solid ball bearings. The 11/16-in.- (17.5-mm-) diameter AISI M-50 steel hollow balls, for use with the series 215 bearings, were tested in a five-ball fatigue tester. The resulting fatigue life was significantly less than expected. The balls failed in flexure fatigue because of a stress concentration in the weld area.

17. Key Words (Suggested by Author(s))	18. Distribution Statement
Bearing Hollow balls Electron-beam welded Fatigue life	Unclassified - unlimited

19. Security Classif. (of this report)	20. Security Classif. (of this page)	21. No. of Pages	22. Price *
Unclassified	Unclassified	23	$3.00

*For sale by the Clearinghouse for Federal Scientific and Technical Information Springfield, Virginia 22151

PERFORMANCE OF 75-MILLIMETER-BORE BEARINGS TO 1.8 MILLION DN WITH ELECTRON-BEAM-WELDED HOLLOW BALLS

by Harold H. Coe, Herbert W. Scibbe, and Richard J. Parker

Lewis Research Center

SUMMARY

Experiments were performed to compare the operating characteristics of ball bearings using hollow balls as the rolling elements with similar bearings using solid balls.

Two series (115 and 215) of 75-millimeter-bore bearings were tested with thrust loads of 500 and 1000 pounds (2200 and 4400 N) at shaft speeds up to 24 000 rpm or 1.8×10^6 DN (bearing bore in mm times shaft speed in rpm). The series 115 bearings used 1/2-inch- (12.7-mm-) diameter SAE 52100 steel balls. The hollow balls used with these bearings had a 0.100-inch (2.5-mm) wall thickness (21-percent weight reduction). The series 215 bearings used 11/16-inch- (17.5-mm-) diameter balls, and the AISI M-50 steel hollow balls had a 0.060-inch (1.5-mm) wall thickness (56-percent weight reduction).

The results of the tests with the series 115 bearings showed very little difference in torque or outer-race temperature between the bearings with the hollow balls and those with the solid balls. The tests with the series 215 bearings showed that the torque and outer-race temperature of the bearings with the hollow balls were slightly lower than those with the solid balls over the range of test conditions.

The results from a previous investigation showed that rolling-element fatigue life of the 1/2-inch- (12.7-mm-) diameter hollow balls was not significantly different from that of solid balls of the same material. The fatigue life of the 11/16-inch- (17.5-mm-) diameter hollow balls, determined in the NASA five-ball fatigue tester at a maximum Hertz stress of 700 000 psi (4.82×10^9 N/m^2), was significantly less than that of previously run solid balls. The 11/16-inch (17.5-mm) hollow balls in the fatigue tests and in the series 215 bearing tests failed by flexure fatigue. Cracks initiated at the inner diameter of the ball at a stress concentration in the weld area and propagated through the wall, usually terminating in a spall on the outer surface.

INTRODUCTION

Recent developments in gas turbine engines, such as advanced compressor design, high-temperature materials, and increased power output, have resulted in a requirement for larger shaft diameters and higher main shaft bearing speeds (ref. 1). Bearings in current production aircraft turbine engines operate in the range from 1.5 to 2 million DN (bearing bore in mm times shaft speed in rpm). Engine designers anticipate that, during the next decade, turbine bearing DN values will have to increase to the range of 2.5 to 3 million. It is speculated that, after 1980, turbine engine developments may require bearing DN values as high as 4 million.

When ball bearings are operated at DN values above 1.5 million, centrifugal forces produced by the balls can become significant. The resulting increase in Hertz stresses at the outer-race-ball contacts can seriously affect bearing fatigue life (ref. 2).

Operation at high DN values also results in high heat generation. Excessive heat generation can result from ball skidding (ref. 3) or ball spinning (ref. 4). The heat generated within the bearing must be removed, or a loss in operating clearance will occur and the bearing will fail. Refinements in bearing internal geometry, such as the use of smaller diameter balls, larger diametral clearances, or more open race curvatures, can effectively reduce heat generation and/or centrifugal force. The degree of improvement is limited, however, since the geometrical changes that reduce heat generation will generally reduce fatigue life (ref. 5).

Another possible solution to problems caused by ball centrifugal force or excessive heat generation is the use of hollow balls in the bearing. Obviously, removal of a large percentage of the mass from the ball will reduce the centrifugal force. In reference 6, an analysis was made that predicted some advantages of hollow balls over solid balls in a high-speed thrust bearing. The analysis showed that when hollow balls with an outer- to inner-diameter ratio of 1.25 (51-percent weight reduction) were used at a DN value of 3 million, the ball spin-to-roll ratio was reduced by as much as 25 percent. (Ball spin-to-roll ratio is an indication of the total rolling and spinning torque. The lower this ratio, the lower the bearing ball-spin torque and, thus, the lower the heat generation.)

The feasibility of fabricating hollow balls by electron-beam welding two hemispherically formed shells has been adequately demonstrated (refs. 7 to 9). In reference 9, rolling-element fatigue tests were conducted with 1/2-inch- (12.7-mm-) diameter solid and hollow balls made from SAE 52100 consumable-electrode vacuum-melted steel. The hollow balls had a 0.100-inch (2.54-mm) wall thickness (21-percent weight reduction). The fatigue lives of these hollow balls compared favorably with those of the 1/2-inch (12.7-mm) solid balls fabricated from the same heat of material. From the limited number of hollow ball failures, it was concluded that the weld zone was not appreciably

weak in fatigue. It was also determined that the weld zone had a hardness and microstructure similar to that of the parent material in the ball.

The objectives of the present investigation were to (1) determine experimentally the operating characteristics of a full-scale bearing using hollow balls as the rolling elements, (2) compare the torque and outer-race temperature data of a bearing with the hollow balls with data of a similar bearing with solid balls, and (3) determine the fatigue lives of hollow balls with a weight reduction of approximately 50 percent.

Bearing tests were conducted with two series (115 and 215 series) of 75-millimeter-bore deep-groove ball bearings using both hollow and solid balls. The bearings were operated at thrust loads of 500 and 1000 pounds (2200 and 4400 N) at speeds to 24 000 rpm (1.8×10^6 DN) using air-oil-mist lubrication. The hollow balls for the series 115 bearings had a 1/2-inch- (12.7-mm-) diameter and a 0.100-inch (2.54-mm) wall thickness (a weight reduction of 21.7 percent from that of the solid balls). The hollow balls for the series 215 bearings had a 11/16-inch (17.5-mm) diameter and a 0.060-inch (1.5-mm) wall thickness (a weight reduction of 56.5 percent from that of the solid balls).

The NASA five-ball fatigue tester was used to determine the life of the 11/16-inch-(17.5-mm-) diameter hollow balls. Tests were conducted at a maximum Hertz stress of 700 000 psi (4.82×10^9 N/m^2), a shaft speed of 10 600 rpm, and a contact angle of 34.5°.

APPARATUS AND INSTRUMENTATION

Bearing Test Rig

A cutaway view of the bearing test apparatus is shown in figure 1. A variable-speed, direct-current motor drives the test bearing shaft through a gear speed increaser. The ratio of the test shaft speed to the motor shaft speed was 14.

The test shaft was supported and cantilevered at the driven end by two oil-jet-lubricated ball bearings. The test bearing was thrust loaded by a pneumatic cylinder through an externally pressurized gas thrust bearing.

Bearing torque was measured with an unbonded strain-gage force transducer connected to the periphery of the test bearing housing, as shown in figure 1. This torque was recorded continuously by a millivolt potentiometer. The estimated accuracy of the data recording system was ±0.05 pound-inch (0.006 N-m).

Bearing outer-race temperature was measured with two iron-constantan thermocouples located as shown in figure 1. The estimated accuracy of the temperature measuring system was about ±2° F (±1 K).

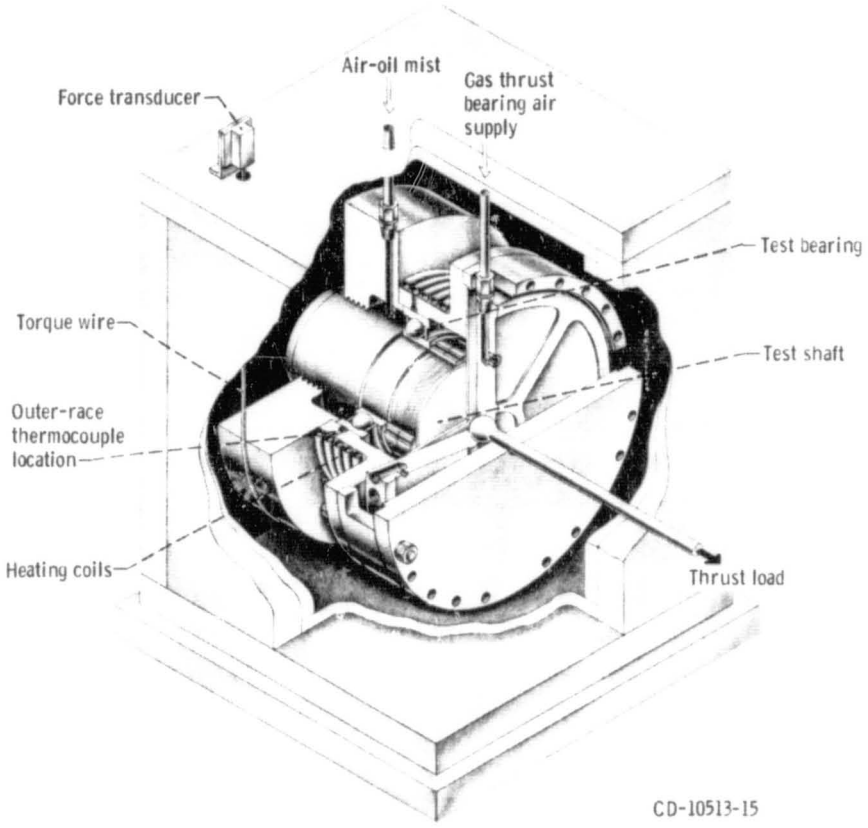

Figure 1. - Bearing test apparatus.

Test Bearing Lubrication System

The test bearing was lubricated by an air-oil mist introduced to the bearing as shown in figure 1. The air-oil-mist generating system (fig. 2) was used previously for a minimum oil flow investigation (ref. 10). The pressurized tank fed oil through the capillary tube into the air line downstream from a Venturi. A jet of high-velocity air generated by the Venturi atomized a metered flow of oil from the capillary into an air-oil mist. The mist then flowed to the test bearing lubricator through plastic tubing. The oil flow rates ranged from 0.01 to 0.07 pound per minute (0.8×10^{-4} to 5.3×10^{-4} kg/sec). The lubricant used in this investigation was a super-refined naphthenic mineral oil with a viscosity of 75 centistokes at 100° F (75×10^{-6} m^2/sec at 311 K).

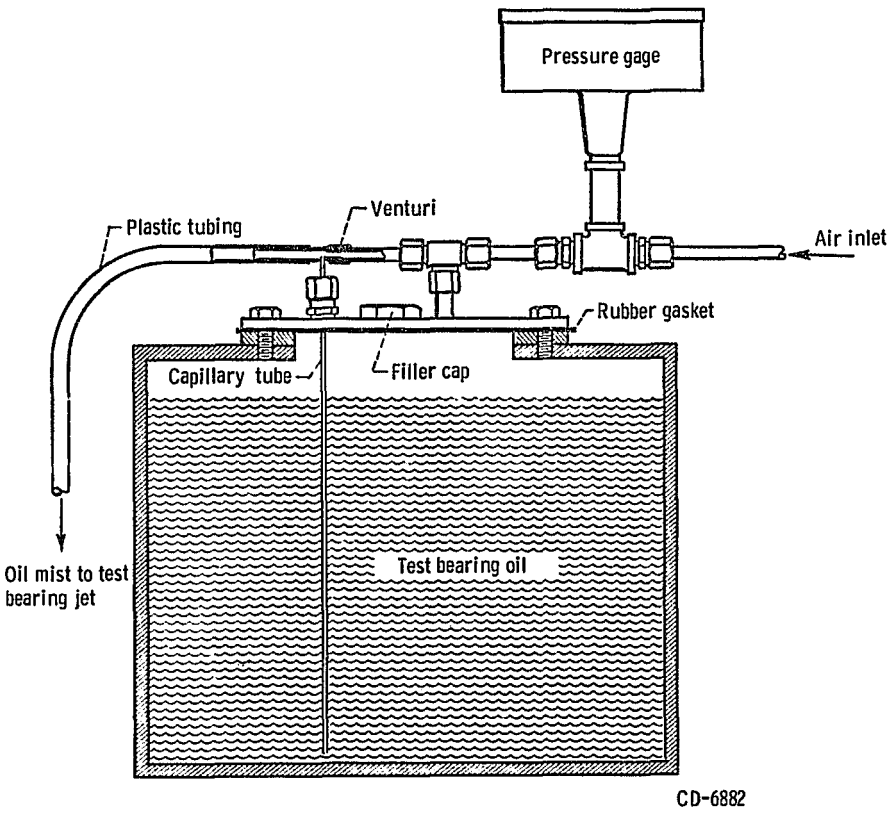

Figure 2. - Air-oil-mist test bearing lubrication system.

Five-Ball Fatigue Tester

The NASA five-ball fatigue tester was used for the hollow ball fatigue tests. The apparatus (fig. 3) is identical to that used in reference 9 and is described in detail in reference 11. This fatigue tester consists essentially of an upper test ball pyramided on four lower support balls that are positioned by a separator and are free to rotate in an angular-contact raceway. The load is applied to the upper test ball through a vertical shaft that drives the ball assembly. The operation of the test ball and raceway is analogous to that of the inner and outer races of a bearing, respectively. The separator and the lower support balls function like the cage and the balls in a bearing, respectively.

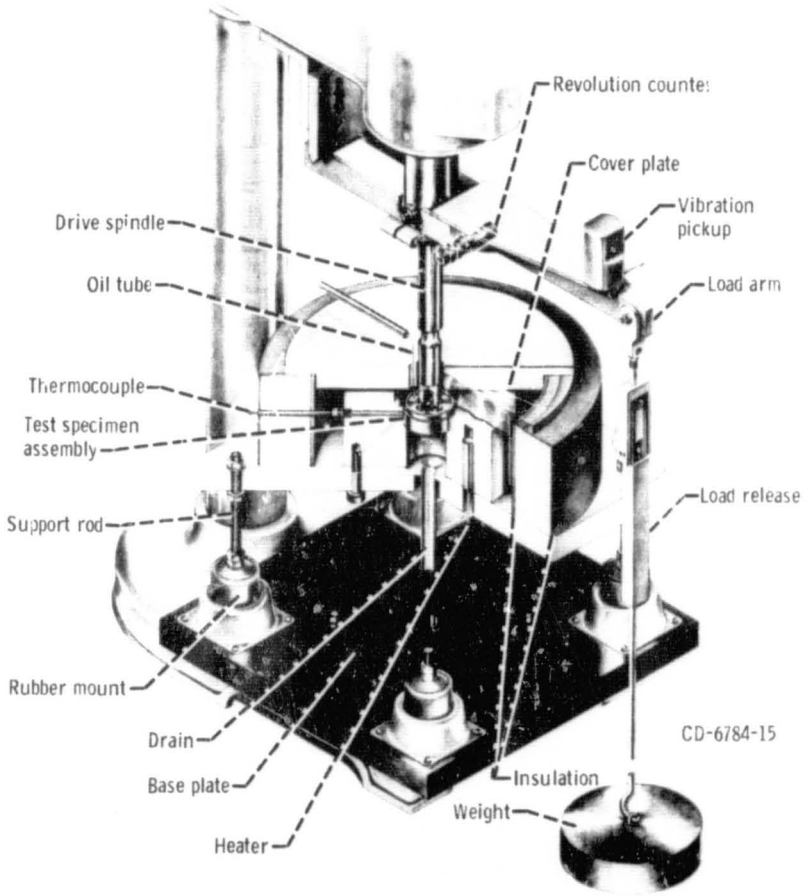

(a) Cutaway view of five-ball fatigue tester.

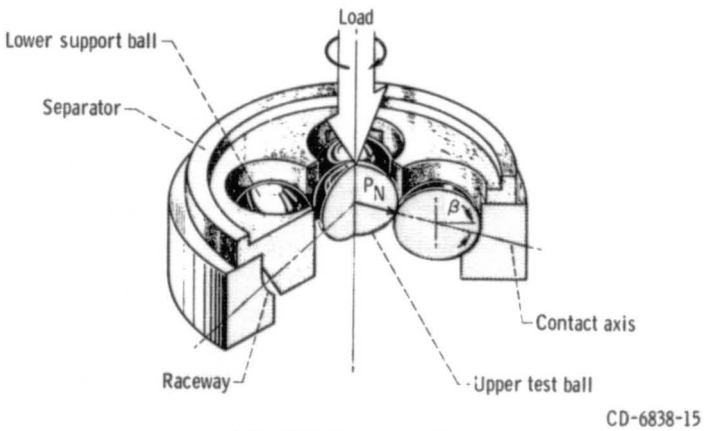

(b) Test specimen assembly.

Figure 3. - Five-ball fatigue tester.

Test Bearings and Hollow Balls

The test bearing specifications are listed in table I. Two series (115 and 215) of 75-millimeter-bore deep-groove ball bearings were used with both solid and hollow balls. The series 115 bearings used 1/2-inch- (12.7-mm-) diameter balls, and the series 215 bearings used 11/16-inch- (17.5-mm-) diameter balls. The test bearings are shown in figure 4.

The 1/2-inch- (12.7-mm-) diameter hollow balls had a wall thickness of 0.100 inch (2.5 mm). The ratio of the outside to the inside diameter was 1.67, and the weight reduction was 21.7 percent from that of a solid ball. The hollow 1/2-inch- (12.7-mm-) diameter balls were made from SAE 52100 consumable-electrode vacuum-melted (CVM) steel.

The 11/16-inch- (17.5-mm-) diameter hollow balls had a wall thickness of 0.060 inch (1.5 mm). This is an outside- to inside-diameter ratio of 1.2 with a weight reduction of 56.5 percent from that of a solid ball. The 11/16-inch (17.5-mm) hollow balls were fabricated from AISI M-50 CVM steel.

TABLE I. - DEEP-GROOVE 75-MILLIMETER-BORE BEARING SPECIFICATIONS

Bearing[a]				Ball							
Series	Outer diameter, mm	Radial clearance		Number per bearing	Outside diameter		Wall thickness		Material[b]	Weight reduction, percent	Ratio of outside to inside diameter
		in.	mm		in.	mm	in.	mm			
115	115	0.0027	0.069	14	0.500	12.7	Solid	Solid	SAE 52100	----	----
115	115	.0027	.069	14	.500	12.7	0.100	2.5	SAE 52100	21.7	1.67
215	130	.0020	.051	11	.6875	17.5	Solid	Solid	AISI M-2	----	----
215	130	.0020	.051	11	.6875	17.5	.060	1.5	AISI M-50	56.5	1.21

Race			Retainer		
Curvature		Material[b]	Design	Locating surface	Material
Inner	Outer				
0.54	0.54	SAE 52100	One piece, machined	Inner race	Silver-plated bronze
.54	.54				
.53	.53	AISI M-2	Two piece, machined, riveted	Outer race	Annealed AISI M-2
.53	53				

[a]Grade ABEC-5.

[b]Consumable-electrode vacuum-melted.

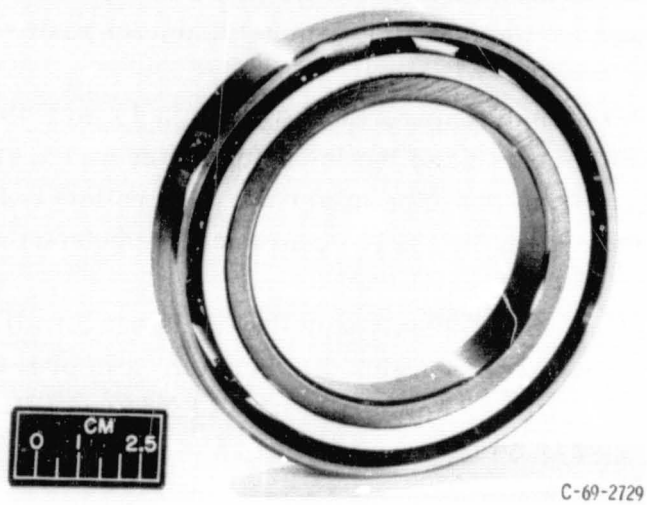

C-69-2729

(a) Series 115: separable at outer race; one-piece cage construction; cage material, silver-plated iron-silicon-bronze.

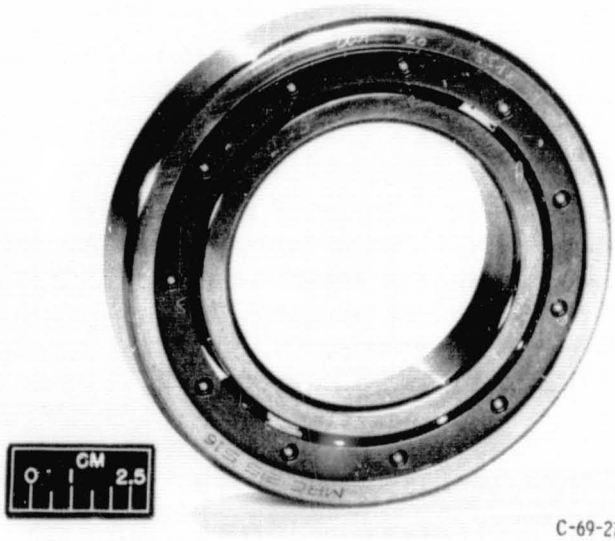

C-69-2728

(b) Series 215: deep groove; two-piece machined cage construction; cage material, AISI M-2 tool steel.

Figure 4. - Test bearings.

TABLE II. - CHEMICAL ANALYSIS OF HOLLOW BALL MATERIALS

Material[a]	C	Si	Mn	S	P	W	Cr	V	Mo	Co	Ni	Cu
	Analysis, wt.%											
SAE 52100	1.03	0.26	0.34	0.005	0.010	----	1.53	----	0.03	----	0.05	0.08
AISI M-50	.79	.22	.23	.004	.008	0.02	4.05	1.04	4.20	0.02	.04	.02

[a]Consumable-electrode vacuum-melted.

TABLE III. - HOLLOW BALL MATERIAL HEAT TREATMENT

[Consumable-electrode vacuum-melting process.]

Material	Anneal after electron-beam welding	Austenitize	Quench	Temper			Nominal Rockwell C hardness
				First	Second	Third	
SAE 52100	Heat to 1475° F (1079 K) Hold for 7 hours[a] Furnace cool to 300° F (422 K) at 20° F per hour (6.5 K/hr) Air cool to room temperature	1550° F (1118 K) for 12 minutes	Oil to room temperature	1020° F (822 K) for 180 minutes	1045° F (836 K) for 120 minutes[c]	1050° F (838 K) for 120 minutes	65
AISI M-50	Heat to 1550° F (1118 K) Hold for 2 hours[b] Furnace cool to 1050° F (838 K) at 50° F per hour (10 K/hr) Air cool to room temperature	2065° F (1403 K) for 6 minutes	Molten salt to 1050° F (838 K) Air cool to room temperature	275° F (408 K) for 60 minutes	----------	----------	63.5

[a]In spent cast iron chips.
[b]In stainless-steel bag.
[c]Subzero cool to -150° F (172 K) for 2 hr.

A chemical analysis of the material from which each size hollow ball was made is given in table II. The heat treatment schedule for each material is given in table III.

PROCEDURE

Bearing Tests

Each test bearing was run in for 1 hour with a 250-pound (1100-N) thrust load, a shaft speed of 6000 rpm, and an air-oil-mist flow rate of about 0.010 pound per minute (0.8×10^{-4} kg/sec). After run-in, the air-oil-mist flow rate was increased to 0.037 pound per minute (2.8×10^{-4} kg/sec), the thrust load was set at 500 pounds (2200 N), and the shaft speed was increased to 10 000 rpm. Each bearing was operated at this initial condition until temperature equilibrium was achieved. Equilibrium was assumed for each data point when the bearing outer-race temperature reading had not changed more than 1° F (2 K) over a 10-minute interval.

After the initial data point was taken at a speed of 10 000 rpm and a thrust load of 500 pounds (2200 N), the shaft speed was increased in increments of 2000 rpm while the

TABLE IV. - LUBRICANT FLOW RATE

Shaft speed, rpm	Thrust load, lb (N)			
	500 (2200)		1000 (4400)	
	Oil flow rate[a]			
	lb/min	kg/sec	lb/min	kg/sec
10 000	0.037	0.00028	0.037	0.00028
12 000	.037	.00028	.037	.00028
14 000	.037	.00028	.037	.00028
16 000	.046	.00035	.062	.00047
18 000	.062	.00047	.073	.00055
20 000	.073	.00055	-----	-------
22 000	.073	.00055	-----	-------
24 000	.073	.00055	-----	-------

[a]Oil introduced to bearing as an air-oil mist.

load was maintained constant. The lubricant flow rate was increased with the shaft speed, as shown in table IV. The technique described in reference 12 was used to determine the flow rates required. Outer-race temperature and bearing torque were recorded for each shaft speed. Data points were taken until outer-race temperature equilibrium could not be attained. This procedure was repeated for the 1000-pound (4400-N) thrust load tests. The highest maximum Hertz stress was about 280 000 psi (1.9×10^9 N/m^2) at the ball-race contacts for the series 115 bearings and about 250 000 psi (1.7×10^9 N/m^2) for the series 215 bearings.

Fatigue Tests

Fatigue tests were conducted in the five-ball fatigue tester at a maximum Hertz stress of 700 000 psi (4.82×10^9 N/m^2). The drive-shaft speed was 10 600 rpm, and the contact angle (indicated by β in fig. 3) was 34.5°. Tests were run continuously for 300 hours, or until failure of the upper test ball or a lower support ball occurred. The outer-race temperature stabilized at about 145° F (336 K) with no heat added. The 11/16-inch- (17.5-mm-) diameter hollow balls were run with 1/2-inch (12.7-mm) solid AISI M-50 lower support balls with a Rockwell C hardness of 64 to 64.5. The lubricant was identical to the super-refined naphthenic mineral oil used in the bearing tests.

Post-Test Inspection

After the testing, the bearings were disassembled, cleaned, and inspected for damage.

After the fatigue tests, the hollow balls with failures were cleaned and examined. The balls were electropolished to determine the location of the weld, the orientation of the weld relative to the ball track, and the proximity of the spall to the weld area.

Some balls were sectioned through and parallel to the track. The sections were polished and photomicrographs were taken.

RESULTS AND DISCUSSION

Bearing Tests

Two series (115 and 215) of 75-millimeter-bore ball bearings were tested with solid and hollow rolling elements to determine their operating characteristics. The results of tests with the series 115 bearings are shown in figure 5. Very little difference existed

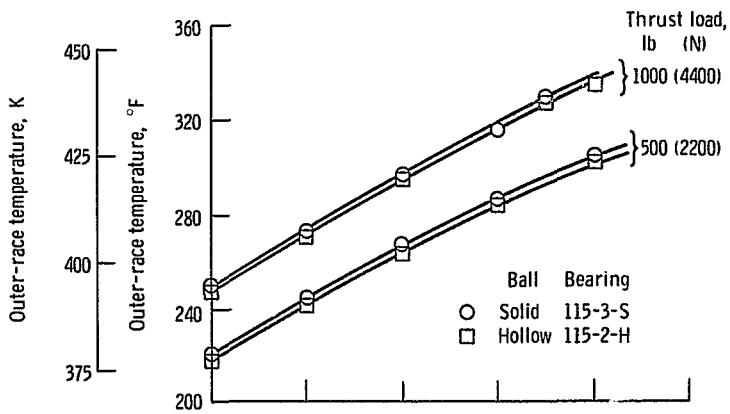

(a) Outer-race temperature as function of shaft speed.

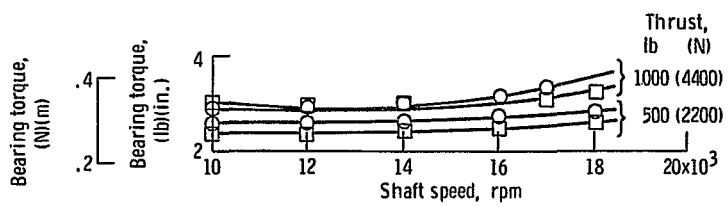

(b) Bearing torque as function of shaft speed.

Figure 5. - Comparison of performance data of series 115 75-millimeter bearings using both solid and hollow balls. Ball diameter, 1/2 inch (12.7 mm); ball material, SAE 52100 steel; bearing specifications given in table I.

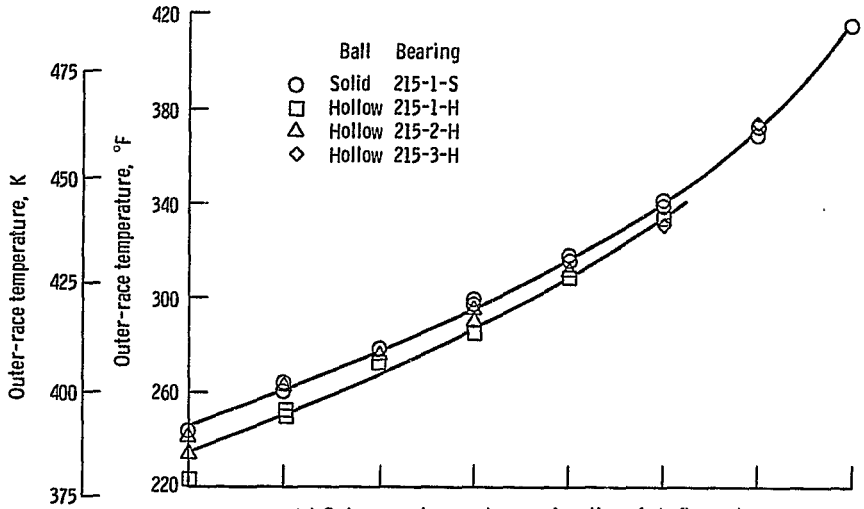

(a) Outer-race temperature as function of shaft speed.

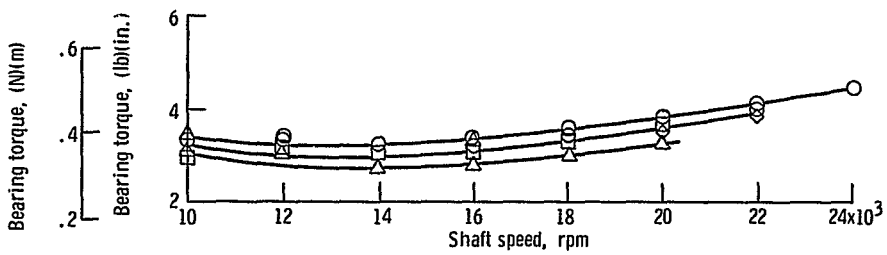

(b) Bearing torque as function of shaft speed.

Figure 6. - Comparison of performance data of series 215 75-millimeter bearings using both solid and hollow balls. Ball diameter, 11/16 inch (17.5 mm); ball material, AISI M-2 for solid balls and AISI M-50 for hollow balls; thrust load, 500 pounds (2200 N); bearing specifications given in table I.

in either the outer-race temperature (fig. 5(a)) or the total bearing torque (fig. 5(b)) between the bearing with the solid balls and the bearing with the hollow balls over the range of shaft speeds investigated.

The results of tests with the series 215 bearings are shown in figure 6. The curves of outer-race temperature (fig. 6(a)) and bearing torque (fig. 6(b)) against speed show that the hollow ball bearings had slightly lower values than the solid ball bearing for the range of shaft speeds investigated.

Post-Test Inspection of Bearings

Visual inspection of the series 115 bearings revealed that the solid and hollow balls, races, and retainers were in very good condition with no apparent wear.

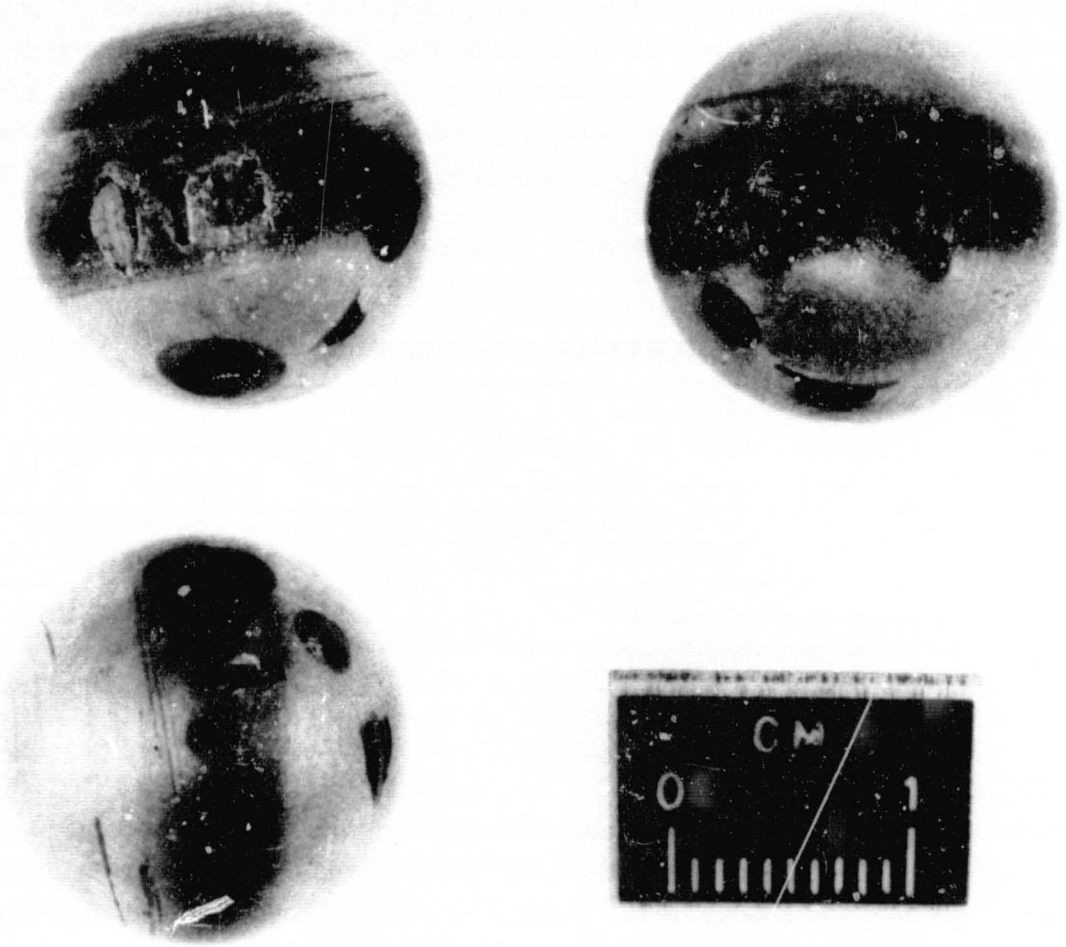

C-69-170

(a) Balls from bearing 215-1-H showing external spalls.

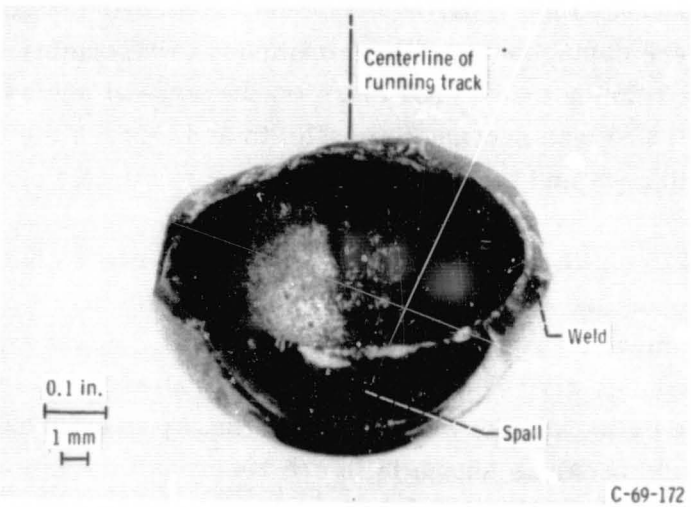

C-69-172

(b) Ball from bearing 215-3-H showing complete fracture.

Figure 7. - Typically damaged hollow balls from series 215 bearings.

Inspection of the series 215 bearings, however, revealed extensive damage to the hollow balls. A photograph showing typical damage experienced by the balls is presented in figure 7. The ball damage ranged from spalling (fig. 7(a)) to complete fracture (fig. 7(b)). The spalls were all on the running track. The ball in figure 7(b) fractured into two halves at the weld. The track was perpendicular to the weld, and a spall was right at the weld. The total running times and damage to the hollow balls of each bearing are summarized in table V.

TABLE V. - SUMMARY OF BALL DAMAGE OF SERIES 215 BEARINGS

Bearing	Running time, hr	Condition of balls
215-1-H	[a]13.6	Nine spalled balls
215-2-H	8.6	One spalled ball that broke when bearing was dissembled
215-3-H	4.1	One fractured ball, four spalled balls, and one ball with surface crack

[a]Bearing apparently ran for about 3 hr after first spall occurred.

One ball from bearing 215-1-H had 14 spalls around its circumference (fig. 8(a)). After this ball was sectioned and examined, it was determined that the ball track coincided with the plane of the weld, as shown in figures 8(a) and (b). Further examination of this ball revealed many cracks on the internal surface, across the weld, as shown in figure 8(c). This ball was then sectioned parallel to and through the track, and the specimen was polished. A composite of several photomicrographs, shown in figure 8(d), reveals a pattern of cracks extending from the inside of the ball to the outside surface spalls.

Other balls that were damaged were electropolished to determine the orientation of the weld relative to the running track. All these tracks were at angles from 45° to 90° to the weld. Every ball that was sectioned parallel to and through the track revealed cracks between the weld area and the outside surface, and example of which is shown in figure 9.

It was not apparent from these photographs whether the cracks had originated at the outside surface and propagated inward or had originated at the inside surface and propagated outward through the wall, resulting in a surface spall. However, several balls that did not show any surface distress were sectioned parallel to and through the ball track. In each of these balls, cracks were revealed that apparently had originated at the inside surface in the weld area, as shown in figure 10.

Several observations on the integrity of the weld were made. Microhardness readings were taken on a sectioned ball in the weld zone and in the parent material. A vari-

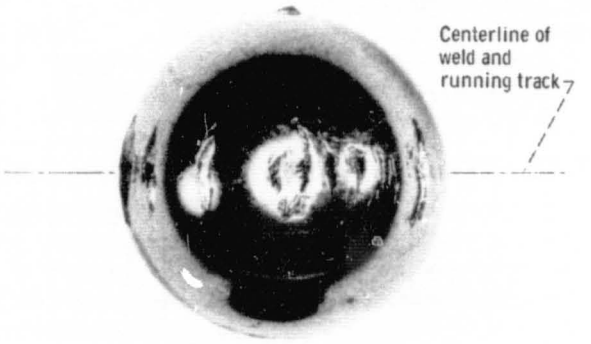

C-69-173

(a) View of external surface showing multiple spalls.

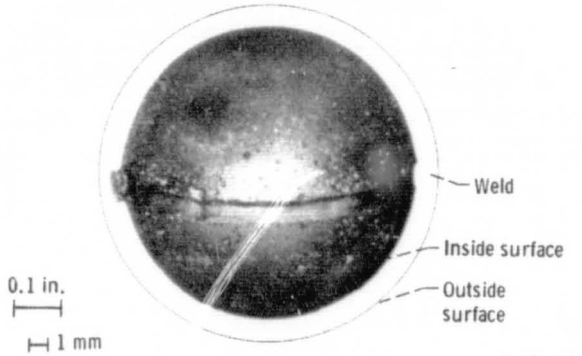

C-69-174

(b) View of internal surface showing weld.

Figure 8. - Ball from bearing 215-1-H with running track directly on weld area.

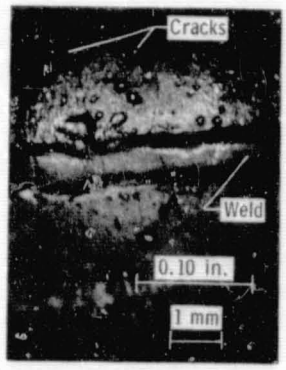

(c) Closeup view of weld bead showing cracks on internal surface, across weld.

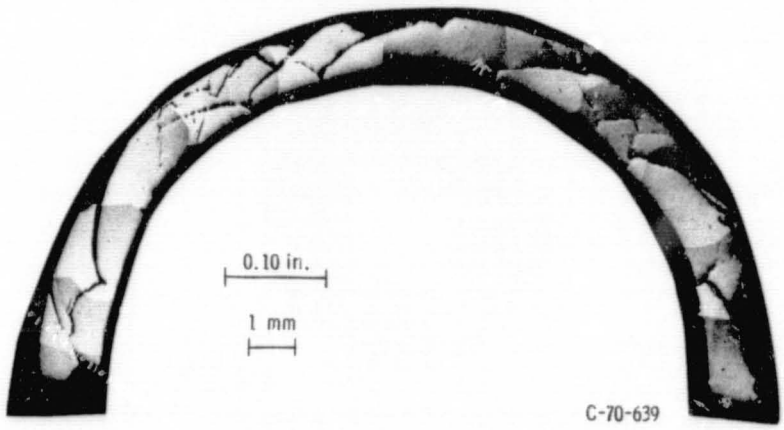

(d) Composite of photomicrographs of ball sectioned parallel to and through both running track and weld.

Figure 8. - Concluded.

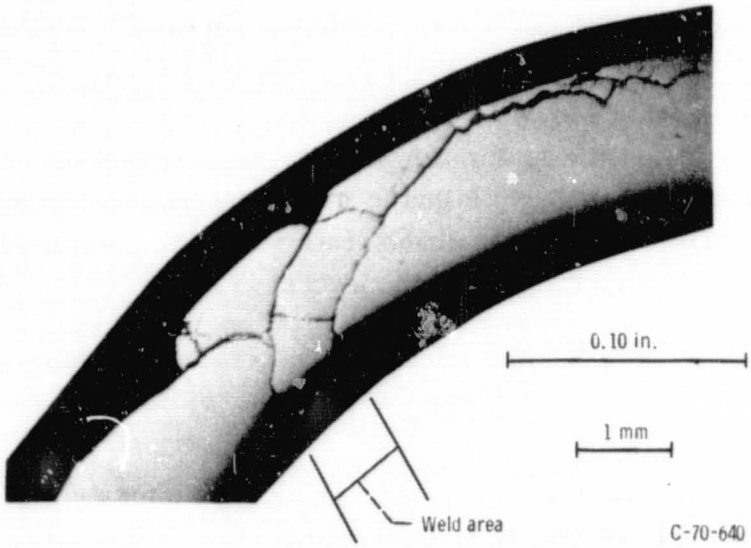

Figure 9. - Sectional view showing typical cracks between weld area and outside surface of ball. Section taken parallel to and through running track.

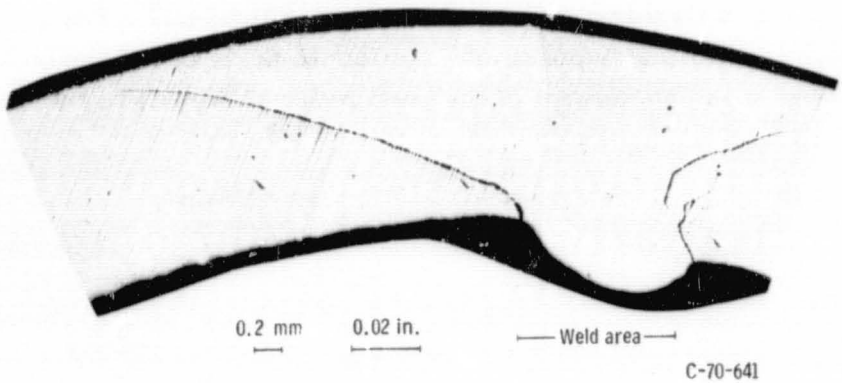

Figure 10. - Section of typical ball (from bearing 215-1-H) on which no surface spalls were evident. Cracks shown originated at weld area. Section taken parallel to and through running track.

ation in Rockwell C hardness of about one point was observed. A very slight difference in microstructure was observed, but this difference was not considered significant.

The electron-beam weld appeared to be of good quality and proper technique. The bead on the inside surface of the balls, however, varied in thickness around the circumference. There was considerable spatter of material on the inside surface of the ball. In some sectioned specimens, the wall thickness was slightly less adjacent to the weld than in the remainder of the wall.

Two hollow balls that had not been run in a bearing were examined by X-ray techniques, and no cracks were observed. Three hollow balls that had been run in a bearing but had no apparent surface defects were then examined by X-ray, and cracks in the weld area were observed in all three.

From the aforementioned examination, it was concluded that the hollow balls from the series 215 bearings had probably failed in flexure because of a stress concentration in the region of the weld. This stress concentration appeared in nearly all cases to be caused by the notch formed at the edge of the weld bead.

Fatigue Tests

The results of fatigue tests with 1/2-inch- (1.27-mm) diameter balls in the NASA five-ball fatigue tester are presented in reference 9. The fatigue lives of those hollow balls (0.100-in. or 2.54-mm wall thickness) compared favorably with solid balls of the same material. It was concluded that the weld zone material on the hollow balls was not significantly weaker in fatigue than the solid parent material.

The results of fatigue tests with the 11/16-inch- (17.5-mm-) diameter hollow balls (0.060-in. or 1.5-mm wall thickness) are presented in figure 11. The balls were run in the five-ball fatigue tester under conditions similar to those of reference 9. Figure 11 is a plot of the log-log of the reciprocal of the probability of survival as a function of the log

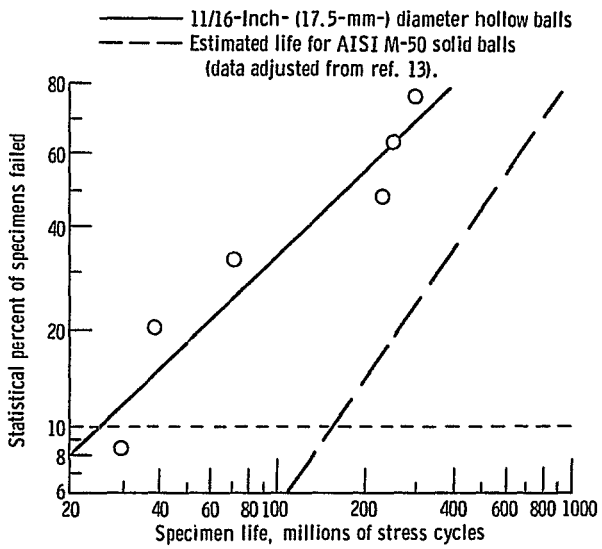

Figure 11. - Rolling-element fatigue life of AISI M-50 steel hollow and solid upper balls in five-ball fatigue tester. Maximum Hertz stress, 700 000 psi (4.82×10^9 N/m^2); speed, 10 600 rpm; lubricant, naphthenic mineral oil; no heat added.

of the stress cycles to failure (Weibull coordinates). For convenience, the ordinate is the statistical percent of specimens failed. For comparison, data for M-50 steel solid balls from reference 13 were adjusted for differences in stressed volume and contact stress and were plotted in figure 11. The fatigue lives are obviously much lower for the hollow balls than for the solid balls.

Post-Test Inspection of Fatigue Balls

The 11/16-inch- (17.5-mm-) diameter hollow balls that had been tested on the five-ball fatigue tester were electropolished to determine the orientation of the weld. On each of the six failed balls, the running track crossed the weld. The fatigue spall on five of these six balls was adjacent to or directly on the weld. The spall on the other ball was clearly away from the weld area. On the one ball that had no fatigue spall after 530 million stress cycles (300 hr), the running track did not cross the weld.

Four of the failed balls with the spall adjacent to the weld were sectioned parallel to and through the running track. In each ball, a crack connected the outside surface spall to the inside surface and passed through the weld area. A typical crack is shown in figure 12.

From the width, shape, and pattern of these cracks, it was concluded that they initiated at the inner surface of the ball and propagated to the outer surface, resulting in a spall that resembled those of classical subsurface rolling-element fatigue. It was also concluded that these hollow balls had probably failed in flexure because of a stress con-

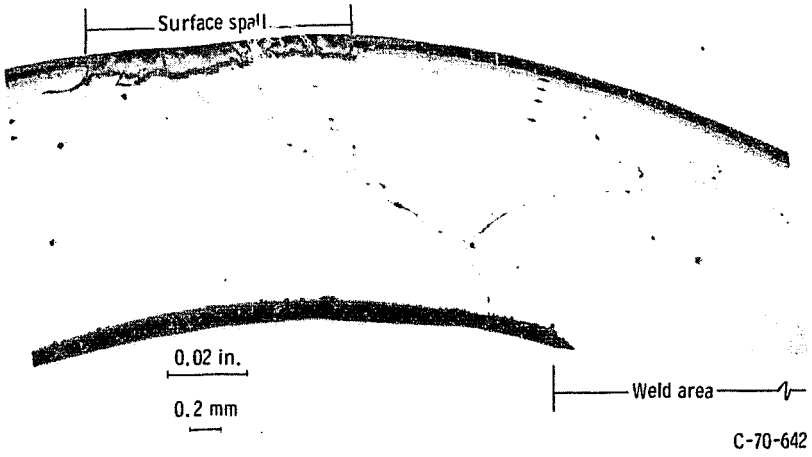

Figure 12. - Typical section through junction of weld and running track showing crack connecting inside of wall with spall on outer surface. AISI M-50 steel 11/16-inch- (17.5-mm-) diameter hollow ball (upper test ball in five-ball fatigue tester). Maximum Hertz stress, 700 000 psi (4.82×10^9 N/m^2); etchant, Picral-hydrochloric acid.

centration in the region of the weld, like the balls in the series 215 bearings. Again, the stress concentration appeared to be at the notch formed at the edge of the weld at the ball inner diameter.

The ball with the spall away from the weld area was also sectioned through the spall, parallel to the running track. No cracks were seen connecting the spall and the inner surface of the ball. This failure was apparently not a result of flexure of the wall and most probably was classical subsurface fatigue.

CONCLUDING REMARKS

The results of reference 9 showed that 1/2-inch- (12.7-mm-) diameter SAE 52100 steel hollow balls, with an outside- to inside-diameter ratio of 1.6, compared favorably with solid balls in fatigue tests. However, the 11/16-inch- (17.5-mm-) diameter M-50 steel hollow balls, with a diameter ratio of 1.2 reported herein, did not compare well with solid balls in fatigue tests. The fact that the balls were of different material and size should not have made any significant difference in the fatigue comparisons. These results suggest that the diameter ratio of 1.2 results in a wall that is too flexible for use in a bearing ball.

The series 115 hollow ball bearings (diameter ratio = 1.6) did not have any ball failures but showed no marked improvement in torque or temperature over the solid ball bearings over the range of shaft speeds tested. Although the series 215 hollow ball bearings (diameter ratio = 1.2) had ball failures, they did show some improvement in torque and temperature over the solid ball bearings. However, a combination of the air-oil-mist lubrication system and the temperature limitation of the SAE 52100 steel limited the testing of the series 115 bearings to moderate speeds. This does not preclude the possibility that some improvement in torque or temperature would be noted if the bearing could have been operated at higher shaft speeds.

A number of problems are inherent in the manufacture of hollow balls that are to be used in bearings. Two significant problems are the difficulty in (1) maintaining uniform wall thickness and (2) controlling the weld penetration around the periphery of the ball. Therefore, the balls will almost always have an unbalance and/or a slightly different stiffness at the weld. Under dynamic conditions, these factors could adversely affect the life of the ball.

The hollow ball failures reported herein originated at a stress concentration at the ball inner diameter. It may therefore be concluded that, where stress raisers exist,

early failures will result when the wall of a hollow ball is sufficiently thin and flexure becomes significant.

SUMMARY OF RESULTS

An experimental investigation was conducted to determine the operating characteristics of ball bearings using hollow balls as the rolling elements. Similar bearings using solid balls were also tested and the data compared. Two series (115 and 215) of 75-millimeter-bore deep-groove ball bearings were operated at shaft speeds up to 24 000 rpm (1.8×10^6 DN) with thrust loads of 500 and 1000 pounds (2200 and 4400 N). The series 115 bearings used 1/2-inch- (12.7-mm-) diameter balls with a 0.100-inch (2.54-mm) wall thickness, and the series 215 bearings used 11/16-inch- (17.5-mm-) diameter balls with a 0.060-inch (1.5-mm) wall thickness. The torque and outer-race temperature data of the bearings with the hollow balls were compared with data of similar bearings with solid balls. Tests were conducted in the NASA five-ball fatigue tester to determine the life of the 11/16-inch- (17.5-mm-) diameter hollow balls. The following results were obtained:

1. The 11/16-inch- (17.5-mm-) diameter hollow balls failed by flexure fatigue. Cracks initiated at the inner diameter at a stress concentration in the weld area and propagated through the wall, terminating in a spall on the outer surface.

2. The rolling-element fatigue life of the 11/16-inch- (17.5-mm-) diameter hollow balls, determined at a maximum Hertz stress of 700 000 psi (4.82×10^9 N/m^2), was significantly less than lives predicted from previously run AISI M-50 solid steel balls. The hollow balls from the fatigue tests appeared to have failed in flexure, like the hollow balls from the series 215 bearings.

3. The torques and outer-race temperatures of the series 115 hollow ball bearings operating at speeds up to 18 000 rpm (1.35×10^6 DN) were not significantly different from those of the series 115 solid ball bearings.

4. The torque and outer-race temperature of the series 215 hollow ball bearings were slightly lower than the values for the series 215 solid ball bearings at corresponding test conditions.

Lewis Research Center,
National Aeronautics and Space Administration,
Cleveland, Ohio, March 3, 1970,
126-15.

NASA-Langley, 1970 — 15 E-5442

ERRATA

NASA Technical Note D-5800

PERFORMANCE OF 75-MILLIMETER-BORE BEARINGS TO 1.8 MILLION DN WITH ELECTRON-BEAM-WELDED HOLLOW BALLS

by Harold H. Coe, Herbert W. Scibbe, and Richard J. Parker
May 1970

The following list should appear as page 22:

REFERENCES

1. Brown, P. F.: Discussion of Paper Previously Published in ASLE Trans. (Ref. 6 below). ASLE Trans., vol. 12, no. 3, July 1969, pp. 204-205.
2. Jones, A. B.: The Life of High-Speed Ball Bearings. ASME Trans., vol. 74, no. 5, July 1952, pp. 695-703.
3. Kilman, Peter S.: High Speed Ball Bearings-Limitation and Thrust Requirements. Lubri. Eng., vol. 20, no. 4, Apr. 1964, pp. 151-154.
4. Bisson, Edmond E.; and Anderson, William J.: Advanced Bearing Technology. NASA SP-38, 1964, pp. 159-164, 311-321.
5. Mayer, John T.; and Litzler, Thomas C.: An Approximate Determination of the Effects of Geometry on Ball-Bearing Torque and Fatigue Life. NASA TN D-2792, 1965.
6. Harris, T. A.: On the Effectiveness of Hollow Balls in High-Speed Thrust Bearings. Trans. ASLE, vol. 11, no. 4, Oct. 1968, pp. 290-294.
7. Eklund, P. R.: Test on a Three-Inch Hollow Ball. Research and Technology Briefs, Air Force Flight Dynamics Laboratory, vol. 55, no. 10, Nov. 1966.
8. Hanau, Heinz; et al: New Concepts in Bearing Designs and Applications. Industrial Tectonics, Inc., 1965, pp. 20-33.
9. Scibbe, Herbert W.; Parker, Richard J.; and Zaretsky, Erwin V.: Rolling-Element Fatigue Life of SAE 52100 Steel Hollow Balls. NASA TN D-3832, 1967.
10. Glenn, Dean C.; and Anderson, William J.: Minimum-Oil-Flow Requirements of High-Speed Ball Bearings at Temperatures to 800° F. NASA TN D-1994, 1963.

NASA-Langley, 1970

Issued 10-12-70

11. Carter, Thomas L.; Zaretsky, Erwin, V.; and Anderson, William J.: Effect of Hardness and Other Mechanical Properties on Rolling-Contact Fatigue Life of Four High-Temperature Bearing Steels. NASA TN D-270, 1960.

12. Nemeth, Zolton N.; and Anderson, William J.: Effect of Speed, Load, and Temperature on Minimum-Oil-Flow Requirements of 30- and 75-Millimeter-Bore Ball Bearings. NASA TN D-2908, 1965.

13. Parker, Richard J.; and Zaretsky, Erwin V.: Rolling-Element Fatigue Life of Ausformed M-50 Steel Balls. NASA TN D-4954, 1968.

END OF REFERENCE

110

REFERENCE

111

COE, H. H.; SCIBBE, H. W.; AND ANDERSON, W. J.: EVALUATION OF CYLINDRICALLY HOLLOW (DRILLED) BALLS IN BALL BEARINGS AT DN VALUES TO 2.1 MILLION. NASA TN D-7007, 1971.

NASA TECHNICAL NOTE

NASA TN D-7007

NASA TN D-7007

EVALUATION OF CYLINDRICALLY HOLLOW (DRILLED) BALLS IN BALL BEARINGS AT DN VALUES TO 2.1 MILLION

by Harold H. Coe, Herbert W. Scibbe, and William J. Anderson

Lewis Research Center
Cleveland, Ohio 44135

NATIONAL AERONAUTICS AND SPACE ADMINISTRATION • WASHINGTON, D. C. • MARCH 1971

1. Report No.	2. Government Accession No.	3. Recipient's Catalog No.
NASA TN D-7007		

4. Title and Subtitle	5. Report Date
EVALUATION OF CYLINDRICALLY HOLLOW (DRILLED) BALLS IN BALL BEARINGS AT DN VALUES TO 2.1 MILLION	March 1971
	6. Performing Organization Code
7. Author(s)	8. Performing Organization Report No.
Harold H. Coe, Herbert W. Scibbe, and William J. Anderson	E-5889
	10. Work Unit No.
9. Performing Organization Name and Address	126-15
Lewis Research Center National Aeronautics and Space Administration Cleveland, Ohio 44135	11. Contract or Grant No.
	13. Type of Report and Period Covered
12. Sponsoring Agency Name and Address	Technical Note
National Aeronautics and Space Administration Washington, D. C. 20546	14. Sponsoring Agency Code

15. Supplementary Notes

16. Abstract

An experimental investigation was conducted with 75-mm-bore bearings using hollow (drilled) balls as the rolling elements. Similar bearings using solid balls were also tested and the data compared. The bearings were operated with a 500-lb (2200-N) thrust load at shaft speeds up to 28 000 rpm (2.1×10^6 DN). The torque and temperature of the bearings with the drilled balls (50 percent weight reduction) were significantly lower than those of the solid-ball bearings. No test bearing failures occurred with total running times of up to 107 hr.

17. Key Words (Suggested by Author(s))	18. Distribution Statement
Bearings Hollow ball bearing High speed bearing	Unclassified - unlimited

19. Security Classif. (of this report)	20. Security Classif. (of this page)	21. No. of Pages	22. Price*
Unclassified	Unclassified	17	$3.00

*For sale by the National Technical Information Service, Springfield, Virginia 22151

EVALUATION OF CYLINDRICALLY HOLLOW (DRILLED) BALLS IN BALL BEARINGS AT DN VALUES TO 2.1 MILLION

by Harold H. Coe, Herbert W. Scibbe, and William J. Anderson

Lewis Research Center

SUMMARY

An experimental investigation was conducted to evaluate a bearing with cylindrically hollow (drilled) balls as the rolling elements. Ball bearings having a 75-millimeter bore and either solid or drilled balls were tested with a thrust load of 500 pounds (2200 N) at shaft speeds up to 28 000 rpm or 2.1×10^6 DN (bearing bore in mm times shaft speed in rpm). The 11/16-inch-(17.5-mm-) diameter hollow balls had a 0.42-inch-(10.7-mm-) diameter hole drilled through the center to effect a 50-percent weight reduction. Test data with the drilled-ball and solid-ball bearings were compared.

The test results showed that the drilled-ball bearing operated satisfactorily over the range of conditions investigated. The outer-race temperatures and torques of the drilled-ball bearings were significantly lower than those of the solid-ball bearings, when the lubricant flow rate was greater than 0.4 pound per minute (3×10^{-3} kg/sec). A drilled-ball bearing was still operating satisfactorily after 107 hours accumulated running time, including 66 hours at DN values of at least 1.5×10^6. It was concluded that the drilled-ball bearing concept offers potential for high-speed applications.

INTRODUCTION

Recent trends in gas turbine design and development have been toward engines with higher thrust-to-weight ratios, which result in a requirement for higher shaft speeds and larger shaft diameters (ref. 1). Bearings in current production aircraft turbine engines operate in the range from 1.5 to 2.0 million DN (bearing bore in mm times shaft speed in rpm). Engine designers anticipate that turbine bearing DN values will have to increase to 2.5 to 3.0 million by 1980. It is speculated that turbine engine developments after 1980 may require bearing DN values as high as 4.0 million.

When ball bearings are operated at DN values above 1.5 million, centrifugal forces produced by the balls can become significant. The resulting increase in Hertz stresses at the outer-race ball contacts can seriously shorten bearing fatigue life (ref. 2).

A possible solution to problems with high-speed bearings would be to reduce the mass of the ball and thereby reduce the centrifugal force (ref. 3). One method of reducing ball mass is to form a hollow ball by welding two hemispherical shells together (ref. 4). Tests were conducted with 75-millimeter-bore bearings with 11/16-inch-(17.5-mm-) diameter spherically hollow balls having a 0.060-inch (1.5-mm) wall (refs. 5 and 6). The hollow balls in these tests failed by flexure fatigue due to a stress concentration in the weld area. These balls had a weight reduction of 56 percent. Two other significant problems with spherically hollow balls, mentioned in references 5 and 6, are the difficulty in (1) maintaining uniform wall thickness and (2) controlling the weld penetration around the periphery of the ball. These problems would cause the balls to have an unbalance and/or a slightly different stiffness at the weld.

Another method of reducing ball mass is to machine a concentric hole through the ball. This method alleviates the possible problems of ball unbalance because the hole concentricity can be maintained very accurately. Additionally, a very smooth surface finish can be achieved, without the irregularities present in the area of a weld.

The objectives of this investigation were (1) to experimentally evaluate a ball bearing with "drilled" or cylindrically hollow balls as the rolling elements and (2) to compare torque and outer-race temperature data of a bearing with drilled balls with data of a similar bearing with solid balls over a range of operating conditions.

Tests were conducted with 75-millimeter-bore, deep-groove ball bearings using either solid or drilled balls. The bearings were operated at a thrust load of 500 pounds (2200 N) at speeds to 28 000 rpm (2.1 million DN) with either air-oil-mist or oil-jet lubrication. The bearings used 11/16-inch-(17.5-mm-) diameter balls. The drilled balls were made by electric-discharge machining (EDM) a 0.42-inch-(10.7-mm-) diameter hole through the center of a solid ball to effect a 50-percent weight reduction. Pins through the cage and the balls were used to prevent ball misorientation.

APPARATUS AND INSTRUMENTATION

Bearing Test Rig

A cutaway view of the bearing test apparatus is shown in figure 1. A variable-speed, direct-current motor drives the test bearing shaft through a gear speed increaser. The ratio of the test shaft speed to the motor shaft speed was 14. The limiting speed of the test shaft was 28 000 rpm.

The test shaft was supported and cantilevered at the driven end by two oil-jet-lubricated ball bearings. The test bearing was thrust loaded by a pneumatic cylinder through an externally pressurized gas thrust bearing. The gas bearing was used so that the test bearing torque could be measured.

Bearing torque was measured with an unbonded strain-gage force transducer connected to the periphery of the test bearing housing, as shown in figure 1. This torque was recorded continuously by a millivolt potentiometer. The estimated accuracy of the data recording system was ±0.05 pound-inch (0.006 N-m).

Bearing outer-race temperature was measured with two iron-constantan thermocouples located as shown in figure 1. The estimated accuracy of the temperature measuring system was about $\pm 2^{\circ}$ F (±1 K).

Test Bearing Lubrication System

The test bearing was lubricated by either an air-oil mist or an oil jet introduced to the bearing as shown in figure 1. The air-oil-mist generating system is shown in figure 2. The pressurized tank fed oil through the capillary tube into the air line downstream from a Venturi. A jet of high-velocity air generated by the Venturi atomized a metered flow of oil from the capillary into an air-oil mist. The mist then flowed to the test bearing lubricator through plastic tubing. After the initial tests with the air-oil mist, a recirculating oil lubrication system was installed. The oil flow rates for the air-oil mist tests ranged from 0.01 to 0.07 pound per minute (0.8×10^{-4} to 5×10^{-4} kg/sec). The flow rates for the oil-jet lubrication tests ranged from 0.4 to 2.0 pounds per minute (3×10^{-3} to 15×10^{-3} kg/sec).

The lubricant used in this investigation was a superrefined naphthenic mineral oil with a viscosity of 75 centistokes at 100° F (75×10^{-6} m^2/sec at 311 K).

Test Bearings and Drilled Balls

The test bearing specifications are listed in table I. The bearings were 75-millimeter-bore, deep-groove ball bearings with 11/16-inch-(17.5-mm-) diameter balls. The two-piece, machined cages were outer-race riding. One shoulder of the inner race was removed for the drilled-ball bearings to make the bearing separable. Photographs of the bearings are shown in figure 3.

A section view of the modified bearing showing details of the drilled ball and the restraining pin is presented in figure 4. Each ball has a 0.42-inch-(10.7-mm-) diameter concentric hole machined through the center. This size hole results in a weight reduction of 50 percent from that of a solid ball. Each ball is retained in the cage by a 0.125-inch-

(3.2-mm-) diameter pin made from stainless-steel tubing which prevents the edge of the hole from riding on the race groove. The pin is sized to allow the ball to turn to its contact angle. The pin is located at approximately the center of the ball pocket at the pitch diameter of the bearing.

PROCEDURE

The bearings were tested with both air-oil-mist and oil-jet lubrication. Each test bearing was run in for 1 hour with a 250-pound (1100-N) thrust load, a shaft speed of 6000 rpm, and an air-oil-mist flow rate of about 0.010 pound per minute (0.8×10^{-4} kg/sec). After run-in for the air-oil-mist tests, the flow rate was increased to 0.037 pound per minute (2.8×10^{-4} kg/sec), the thrust load was set at 500 pounds (2200-N), and the shaft speed was increased to 10 000 rpm. Each bearing was operated at this initial condition until temperature equilibrium was achieved. Equilibrium was assumed for each data point when the bearing outer-race temperature reading had not changed more than 1° F (2 K) over a 10-minute interval.

After the initial data point was taken at a speed of 10 000 rpm and a thrust load of 500 pounds (2200 N), the shaft speed was increased in increments of 2000 rpm while the load was maintained constant. The maximum hertz stress of the solid-ball bearing at 28 000 rpm was approximately 250 000 psi (1.7×10^{9} N/m^2) at the outer-race - ball contact. The lubricant flow rate was increased with the shaft speed, as shown in table II. The technique described in reference 7 was used to determine the flow rates required. Outer-race temperature and bearing torque were recorded for each shaft speed. Data points were taken until outer-race temperature equilibrium could not be attained.

Two types of tests were conducted with oil-jet lubrication. In the first type, the procedure just given was repeated with a constant oil flow rate of about 1 pound per minute (8×10^{-3} kg/sec). For the second type of tests, the procedure was used until the shaft speed was 20 000 rpm. Then, at a constant shaft speed, the oil flow rate was changed. The oil flow rate was first increased to about 2 pounds per minute (15×10^{-3} kg/sec) and then decreased to about 0.4 pound per minute (3×10^{-3} kg/sec), in about 10 increments. Equilibrium data were taken at each flow rate. A final check point was then taken at about 1 pound per minute (8×10^{-3} kg/sec) to make certain that the bearing operating characteristics had not changed.

RESULTS AND DISCUSSION

Two 75-millimeter-bore bearings with cylindrically hollow (drilled) balls were operated with a 500-pound (2200-N) thrust load over a range of shaft speeds to 28 000 rpm

(2.1 million DN), using either air-oil-mist or oil-jet lubrication. Similar bearings with solid balls were also tested under the same conditions. Outer-race temperature and torque data for the drilled-ball bearings were compared with similar data for the solid-ball bearings.

Air-Oil-Mist Lubrication Tests

The results of the bearing tests with air-oil-mist lubrication are presented in figure 5. The drilled-ball bearing 4SRH had a significantly lower outer-race temperature than the solid-ball bearing (1S). The temperature of bearing 3SRH was also lower at the lower shaft speeds but was the same as that of the solid-ball bearing at the higher speeds. The difference in the outer-race temperatures of the two drilled-ball bearings was probably due to the difference in radial internal clearance (see table III). The differences in torque were considered insignificant.

Oil-Jet Lubrication Tests

Two types of tests were conducted with oil-jet lubrication. In the first type, the oil flow rate was held constant while the shaft speed was varied. In the second type, the shaft speed was maintained constant while the oil flow rate was varied.

Variable shaft-speed tests. - The results of the variable shaft speed tests with oil-jet lubrication are presented in figure 6. The outer-race temperature and bearing torque are significantly lower for the drilled-ball bearings than for the solid-ball bearings.

The tests were run several times, and the values presented are the averages of all runs. The scatter in the temperature data was very small, as shown in figure 6. The agreement between the two drilled-ball bearings was very good over the range tested, although the torque of bearing 3SRH was deviating toward higher values at the higher shaft speeds.

During testing, a critical speed of the test shaft was encountered at about 8000 rpm (as the speed was increased from 6000 to 10 000 rpm), which caused a rise in the recorded bearing torque. This influence on bearing torque still existed somewhat at 10 000 rpm, as the values for all three bearings were slightly high at that point.

The lower outer-race temperatures for the drilled-ball bearings reflected lower surface temperatures of the balls and were probably due to two factors. These were (1) the lower ball mass, which resulted in lower heat generation, and (2) additional cooling surface, which was available with the hole through the interior of the ball. Comparison of figures 5 and 6 shows that the bearing temperatures with oil-jet lubrication averaged about 70° F (40 K) cooler than with air-oil-mist lubrication over the same speed range.

Comparison of figures 5 and 6 also shows that the bearing torques increased about 3 or 4 times with the increase in the oil flow rate of from 15 to 100 times when going from mist to jet lubrication. The bearing torque was more sensitive to shaft speed with jet lubrication because of the additional oil churning losses.

Variable oil flow tests. - The results of the variable oil flow rate tests are presented in figure 7. The torque and temperature of the drilled-ball bearing remained lower than those of the solid-ball bearing over the range tested. The changes in outer-race temperature were greater at the lower flow rates, as would be expected, since the oil was functioning as a coolant (flow rate much greater than that required for lubrication). With cooling, the outer-race temperature varied inversely with coolant flow rate. Therefore, a small change in oil flow rate will produce a greater change in outer-race temperature at low flow rates than at high flow rates.

The bearing torque doubled with a fivefold increase in oil flow rate. The rate of increase in torque was lower at the higher flow rates, as the bearing was becoming saturated with oil.

Bearing Post-Test Inspection

Visual inspection of the drilled-ball bearings showed that the balls and races were still in good condition. There was no evidence of abnormal ball-race tracking or skidding in either bearing.

The cages were also in good condition, although there was slight wear on the outside diameter in the area of the land, as shown in figure 8. The wear was not considered excessive. Wear of the pins was observed, however, as shown in figures 9 and 10. Most of the pins from bearing 3SRH showed moderate wear, but two pins had heavier wear. Pins from bearing 3SRH are shown in figure 9. Most of the pins from bearing 4SRH had light wear, but three had very heavy wear. Typical pins from bearing 4SRH are shown in figure 10. It is assumed that the wear was caused by the edge of the concentric hole. The stainless-steel tubing pins were free to turn in the cage.

The total running times for each drilled-ball bearing are shown in tables IV and V. Note that bearing 3SRH (table IV) was still operating satisfactorily after 107 hours accumulated running time, including 66 hours at DN values of at least 1.5×10^6. This compares with the fact that the same size spherically hollow ball bearings in reference 5 failed after 4 to 10 hours running time.

CONCLUDING REMARKS

It was expedient to modify an existing bearing for these tests to evaluate the drilled-ball bearing. Therefore, the bearing in this report should obviously not be considered an optimum design.

The wear of the pins could certainly have been reduced by using a hardened material. The results with the stainless-steel tubing however, do point out that pin wear could be a problem.

It should be noted that the tests reported herein were limited to the speed range of the test apparatus and not limited by the test bearings. Since the drilled-ball bearing performed quite well over the range of conditions tested, it was concluded to be not only a workable concept, but one worthy of further investigation. The drilled-ball bearing has potential for high-speed application.

SUMMARY OF RESULTS

An experimental investigation was conducted to evaluate a drilled-ball bearing. Two 75-millimeter-bore bearings having balls with a 50-percent weight reduction were operated with a 500-pound (2200-N) thrust load at speeds to 28 000 rpm (2.1 million DN). Weight reduction was achieved by drilling a 0.42-inch- (10.7-mm-) diameter concentric hole through each 11/16-inch- (17.5-mm-) diameter ball. Test results were evaluated by comparing the torque and temperature of the drilled-ball bearing with data of a similar bearing with solid balls over a range of operating conditions. The following results were obtained.

1. The drilled-ball bearings operated satisfactorily over the range of conditions investigated with both mist and jet lubrication.

2. The torques and outer-race temperatures of the drilled-ball bearing were significantly lower than those of a similar bearing with solid balls when the lubricant flow rates were greater than 0.4 pound per minute (3×10^{-3} kg/sec).

3. A drilled-ball bearing was still operating satisfactorily after 107 hours accumulated running time, including 66 hours at DN values of at least 1.5×10^{6}.

Lewis Research Center,
National Aeronautics and Space Administration,
Cleveland, Ohio, October 14, 1970,
126-15.

REFERENCES

1. Brown, P. F.: Discussion of Paper Previously Published in ASLE Trans. (Ref. 3 below). ASLE Trans., vol. 12, no. 3, July 1969, pp. 204-205.

2. Jones, A. B.: The Life of High-Speed Ball Bearings. Trans. ASME, vol. 74, no. 5, July 1952, pp. 695-703.

3. Harris, T. A.: On the Effectiveness of Hollow Balls in High-Speed Thrust Bearings. ASLE Trans., vol. 11, no. 4, Oct. 1968, pp. 290-294.

4. Scibbe, Herbert W.; Parker, Richard J.; and Zaretsky, Erwin V.: Rolling-Element Fatigue Life of SAE 52100 Steel Hollow Balls. NASA TN D-3832, 1967.

5. Coe, Harold H.; Scibbe, Herbert W.; and Parker, Richard J.: Performance of 75-Millimeter-Bore Bearings to 1.8 Million DN with Electron-Beam-Welded Hollow Balls. NASA TN D-5800, 1970.

6. Coe, Harold H.; Parker, Richard J.; and Scibbe, Herbert W.: Evaluation of Electron-Beam Welded Hollow Balls for High-Speed Ball Bearings. Paper 70-Lubs-17, ASME, May 1970.

7. Nemeth, Zolton N.; and Anderson, William J.: Effect of Speed, Load, and Temperature on Minimum-Oil-Flow Requirements of 30- and 75-Millimeter-Bore Ball Bearings. NASA TN D-2908, 1965.

TABLE I. - BEARING SPECIFICATIONS

Bore diameter, mm	75
Radial clearance, in. (mm)	0.0016 to 0.0024 (0.041 to 0.061)
Number of balls	11
Ball diameter,[a] in. (mm)	0.6875 (17.5)
Ball and race material,[b, c]	AISI M-2
Race curvature, inner and outer	0.53
Retainer locating surface	Outer race
Retainer material	Annealed AISI M-2

[a]Hole size of drilled balls was 0.420 in. (10.7 mm).
[b]Consumable-electrode vacuum melted.
[c]Ball material for one drilled-ball bearing was SAE 52100.

TABLE II. - LUBRICANT FLOW RATE

Shaft speed, rpm	Oil flow rate[a]	
	lb/min	kg/sec
10 000	0.037	0.00028
12 000	.037	.00028
14 000	.037	.00028
16 000	.046	.00035
18 000	.062	.00047
20 000	.073	.00055
22 000	.073	.00055

[a]Oil introduced to bearing as an air-oil mist.

TABLE III. - RADIAL INTERNAL CLEARANCE MEASURED AFTER TEST

Bearing number	Ball type	Clearance	
		in.	mm
1S	Solid	0.0023	0.058
6S	Solid	.0024	.061
3SRH	Drilled	.0036	.091
4SRH	Drilled	.0024	.061

TABLE IV. - ACCUMULATED RUNNING TIME

FOR BEARING 3SRH

Shaft speed, rpm	Time at speed, min		
	Air-oil-mist runs	Oil-jet runs	Total
6 000	337	128	465
10 000	241	424	665
12 000	178	111	289
14 000	213	66	279
16 000	313	78	391
17 000	----	11	11
18 000	269	78	347
20 000	3724	114	3838
22 000	----	140	140
	Total 5275	1150	6425

TABLE V. - ACCUMULATED RUNNING TIME FOR

BEARING 4SRH

Shaft speed, rpm	Time at speed, min		
	Air-oil-mist runs	Oil-jet runs	Total
6 000	75	288	363
10 000	78	799	877
12 000	110	250	360
14 000	9	320	329
15 000	---	8	8
16 000	36	288	324
18 000	37	321	358
20 000	77	922	999
22 000	---	52	52
24 000	---	45	45
25 000	---	46	46
26 000	---	75	75
27 000	---	54	54
28 000	---	51	51
29 000	---	14	14
	Total 422	3533	3955

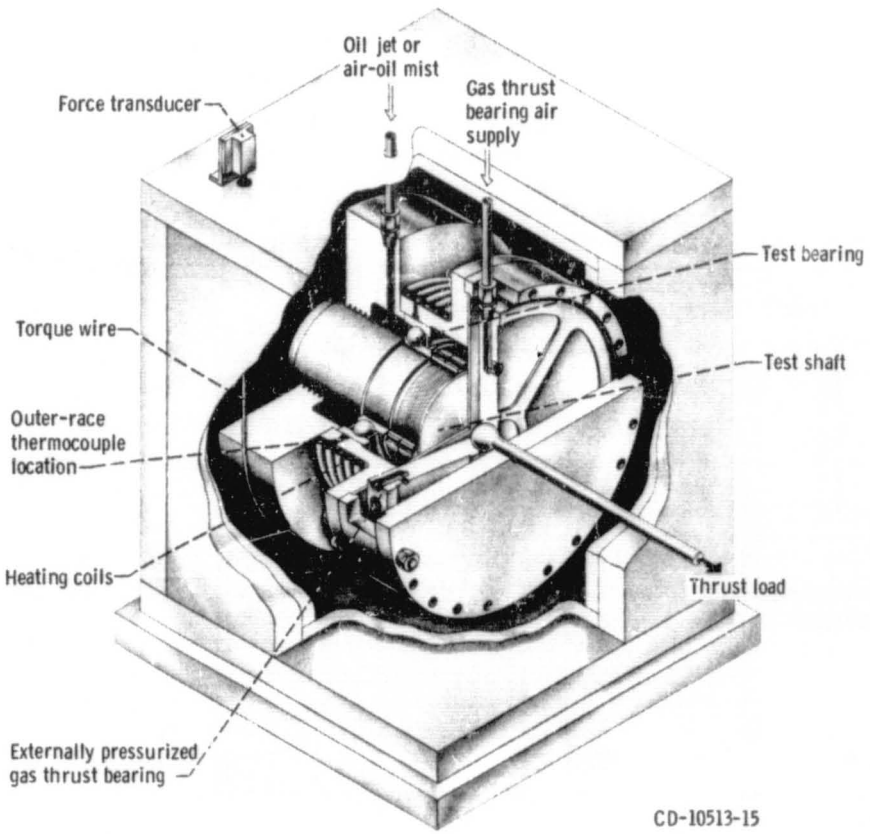

Figure 1. - Bearing test apparatus.

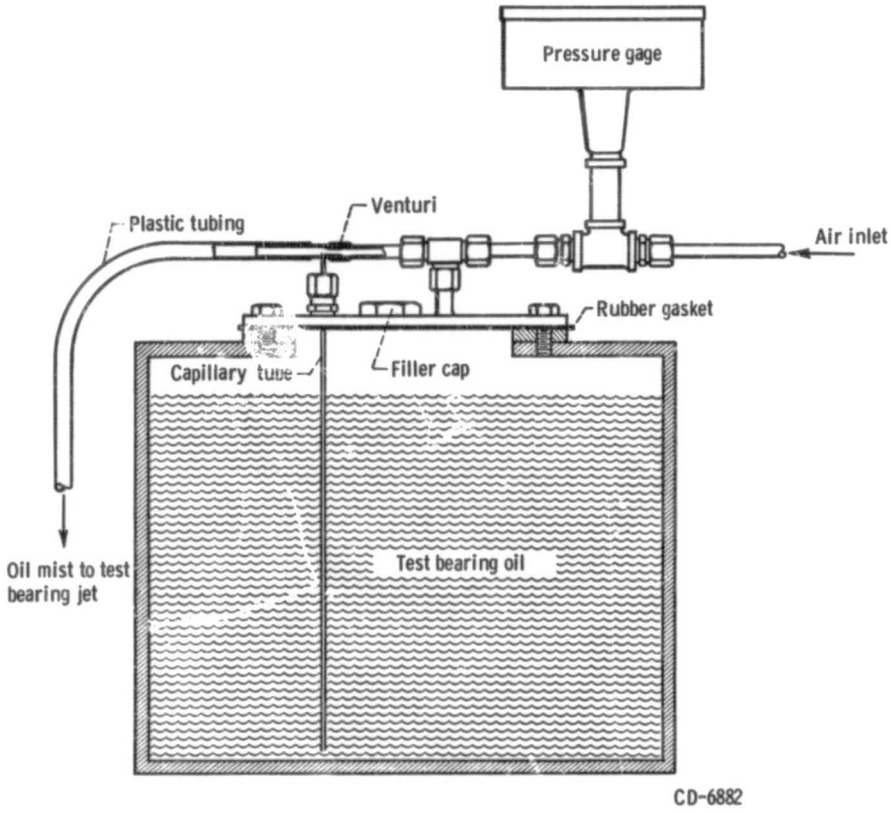

Figure 2. - Air-oil-mist test bearing lubrication system.

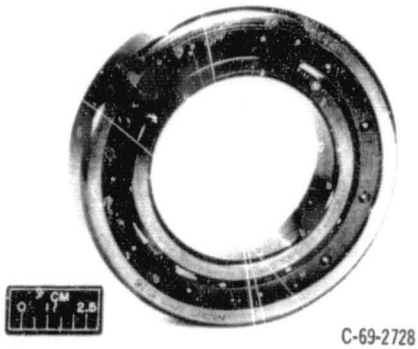

C-69-2728

(a) Assembled solid-ball bearing.

C-69-1256

(b) Disassembled cylindrically hollow (drilled) ball bearing.

Figure 3. - Test bearings. Type, deep groove; material, AISI M-2 tool steel; cage construction, two-piece machined.

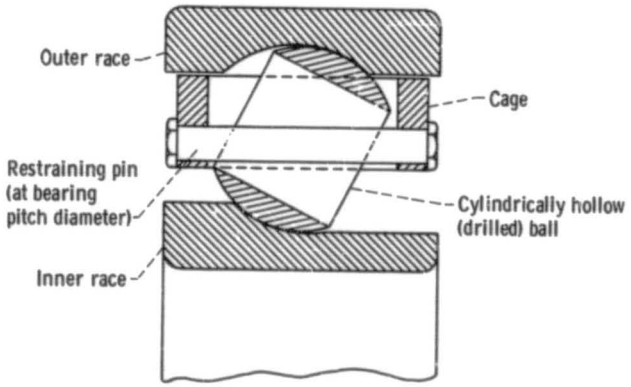

Figure 4. - Section view of test bearing with hollow ball.

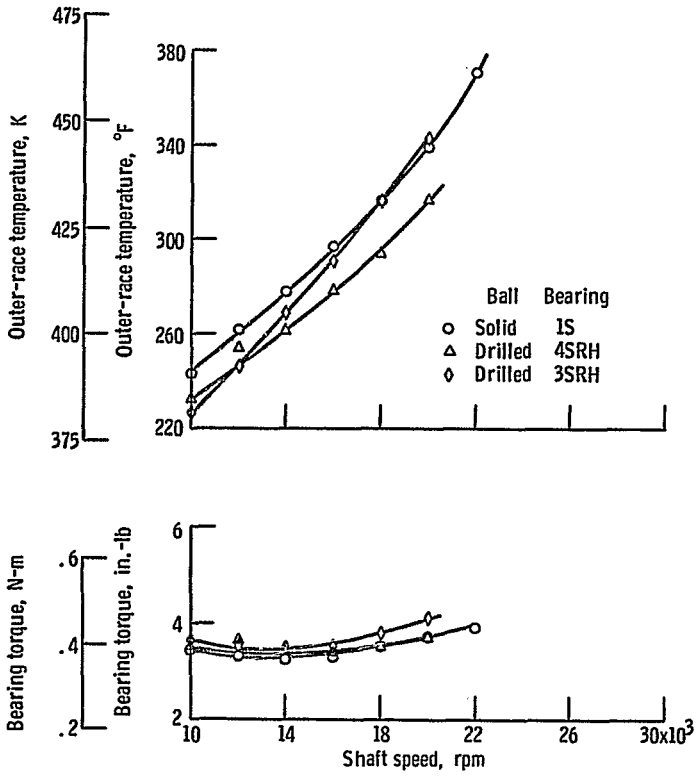

Figure 5. - Comparison of performance data of 75-millimeter-bore bearings using both solid and cylindrically hollow (drilled) balls with air-oil-mist lubrication. Oil flow rate, 0.01 to 0.07 pound per minute (0.8×10^{-4} to 5×10^{-4} kg/sec).

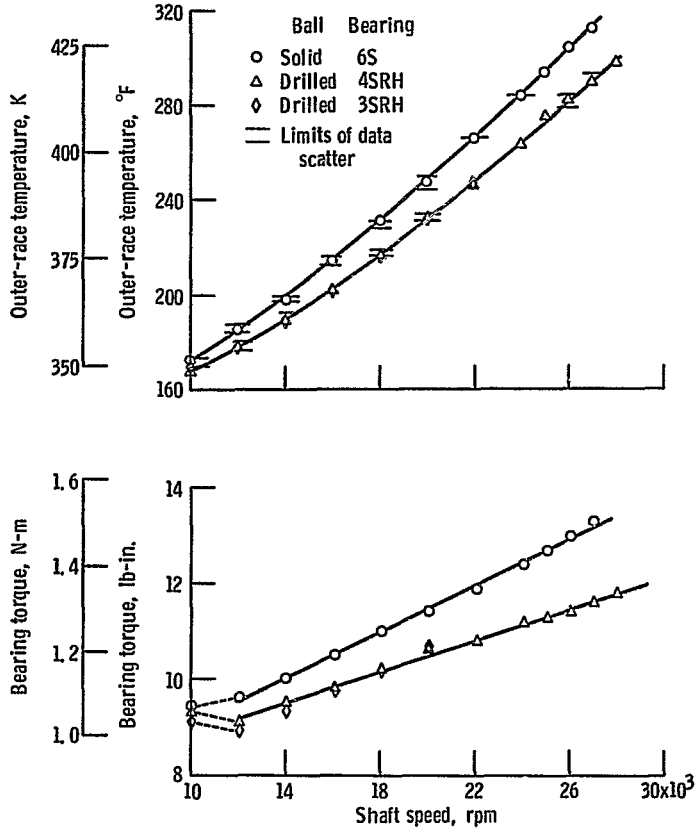

Figure 6. - Comparison of performance data of 75-millimeter-bore bearings using both solid and drilled balls, with jet lubrication. Oil flow rate, 0.95 pound per minute (7.2×10^{-3} kg/sec).

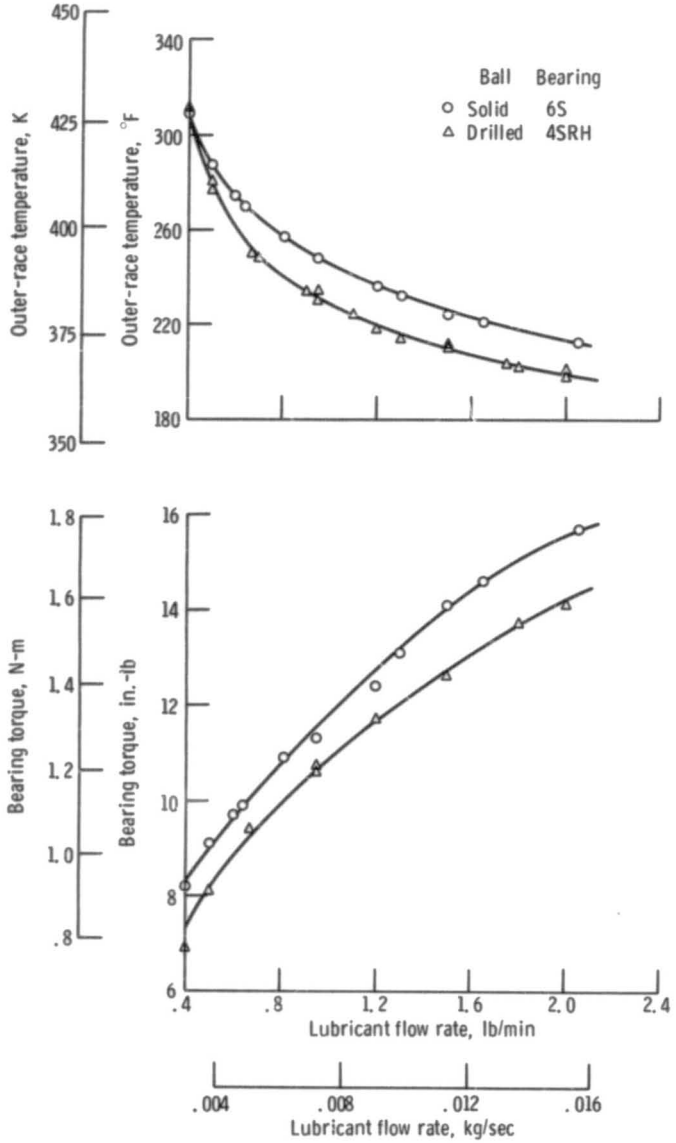

Figure 7. - Bearing performance as function of lubricant flow rate. Oil inlet temperature, 110° F (316 K); shaft speed, 20 000 rpm; thrust load, 500 pounds (2200 N).

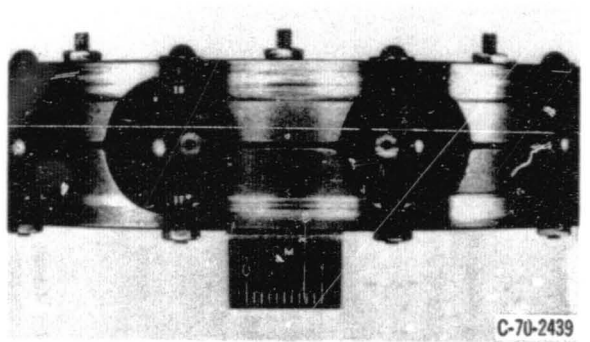

(a) Bearing 3SRH.

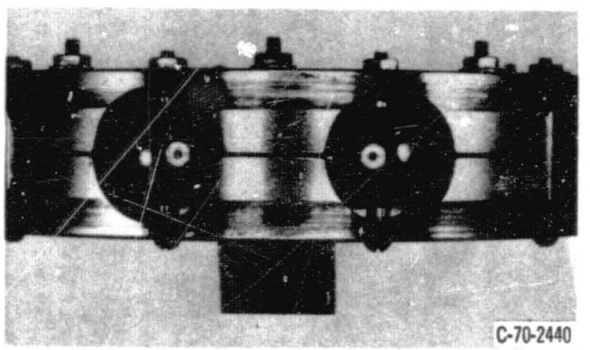

(b) Bearing 4SRH.

Figure 8. - Post-test view of drilled-ball bearing retainers showing area of light wear from outer-race land contact.

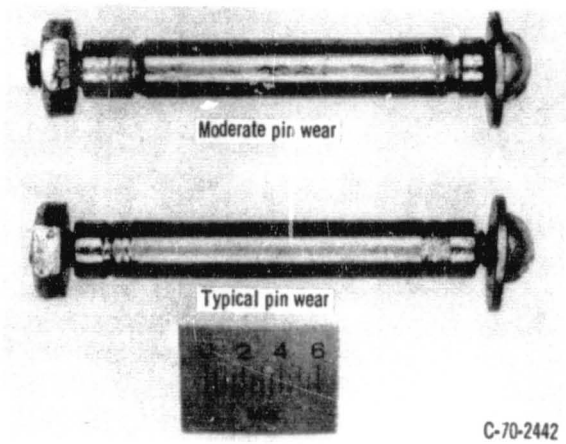

Figure 9. - Pins from bearing 3SRH after 107 hours of running, including 66 hours at DN values of at least $1.5X10^6$. Maximum speed, 22 000 rpm.

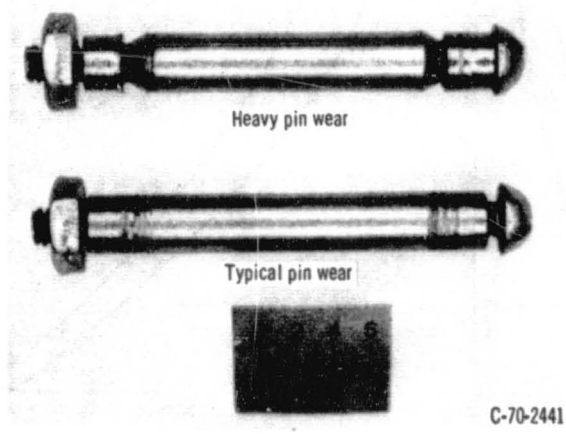

Figure 10. - Pins from bearing 4SRH after 66 hours of running, including 22 hours at DN values of at least $1.5X10^6$. Maximum speed, 29 000 rpm.

NASA-Langley, 1971 —— 15 E-5889

END OF REFERENCE

111

REFERENCE

112

LUDWIG, L. P.: SELF-ACTING AND HYDRODYNAMIC SHAFT SEALS. NASA TM X-68214, 1973.

NASA TECHNICAL MEMORANDUM

NASA TM X-68214

NASA TM X-68214

SELF-ACTING AND HYDRODYNAMIC SHAFT SEALS

by Lawrence P. Ludwig
Lewis Research Center
Cleveland, Ohio 44135

TECHNICAL PAPER proposed for presentation at
Seal Education Course of the Annual Meeting of the
American Society of Lubrication Engineers
Chicago, Illinois, April 30-May 3, 1973

SELF-ACTING AND HYDRODYNAMIC SHAFT SEALS

by Lawrence P. Ludwig

National Aeronautics and Space Administration
Lewis Research Center
Cleveland, Ohio 44135

ABSTRACT

Self-acting and hydrodynamic seals are described. The analytical procedures are outlined for obtaining a seal force balance and the operating film thickness. Particular attention is given to primary ring response (seal vibration) to rotating seat face runout. This response analysis revealed three different vibration modes. Proposed applications of self-acting seals in gas turbine engines and in rocket vehicle turbopumps are described. Also experimental data on self-acting face seals operating under simulated gas turbine conditions are given; these data show the feasibility of operating the seal at conditions of 345 newtons per square centimeter (500 psi) and 152 meters per second (500 ft/sec) sliding speed.

E-7406

INTRODUCTION

Considerable effort has been put into development of self-acting and hydrodynamic seals because conventional contact seals cannot meet the ever increasing pressure, temperature and speed requirements of some modern and advanced rotating equipment. As an example, in advanced aircraft gas turbine operation, seal speeds are expected to reach 183 meters per second (600 ft/sec), and pressures may reach 345 newtons per square centimeter (500 psi) (ref. 1).

The present solution to severe operating conditions is to use clearance seals such as labyrinths; these seals are reliable but carry performance penalties because of high leakage.

In advanced industrial compressors, pressures to 3450 newtons per square centimeter (5000 psi) are under consideration. The current sealing system for these high pressures usually is a liquid buffer bushing that requires a high pressure pump and electric drive motor (also for fail-safe reasons a backup pump and motor is required). These compressor seal systems with their allied plumbing and controls take up considerable space and can cost as much as the compressor.

Thus, there is a need for reliable, low leakage shaft seals that require no external controls or equipment and that can operate at the pressures, temperatures and speeds of advanced machines. Recent studies

(carbon) wear was insignificant (see fig. 35). Typical leakage values are shown in table IV.

In order to check the effect of starting and stopping, the seal was subjected to 40 starts and stops with room-temperature air at 69 newtons per square centimeter (100 psi). The seal speed was increased from 0 to 76 meters per second (0 to 250 ft/sec) in about 15 seconds. The seal was then allowed to coast to a stop in about 25 seconds. A comparison of the surface profile traces before and after the 40 starts and stops revealed carbon wear to be less than 1.27 micrometers (0.00005 in.).

Rocket Engine Turbopump Applications

In rocket engine turbopumps, shaft seals are used to seal propellants such as liquid oxygen and hot hydrogen gas. Experience has shown that the shaft seal system is a very critical item and seal failure can result in total destruction of the vehicle. Figure 36 shows a typical rocket engine seal system used in current practice. The purpose of the system is to separate liquid oxygen at pressures as high as 310 newtons per square centimeter (450 psi) from the hot turbine gas at 689 newtons per square centimeter (1000 psi). The seal system consists of three sealing areas with a central helium purge and a dual vent.

The liquid oxygen seal is a conventional rubbing contact seal with a bellows secondary seal. Oxygen is prevented from leaking past the helium seal by the purge flow of helium, and both the oxygen and helium pass out the vent indicated in figure 36. A similar action occurs on the hot hydrogen gas side. However, the hydrogen gas seals are conventional ring (clearance) seals. The helium purge seals are also conventional ring (clearance) seals.

In the seal system such as depicted in figure 36 there are a number of problem areas, the most critical of which is compatibility of the seal material with liquid oxygen. Therefore, as indicated, welded bellows designs are very often used. Another problem area has been wear life. The typical wear life is now in the range of 2 to 3 hours, which is a satisfactory margin for the current rocket vehicles. However, for the shuttle vehicle a total life of 10 hours is needed with a start-stop (mission) capability of 100. Clearly, the current seal technology is not adequate for the shuttle life requirements; and the self-acting seal may provide a solution.

An advanced seal system is under development (fig. 37) with a hydrodynamic seal for liquid oxygen and a self-acting circumferential seal for the helium. The seal for liquid oxygen is a hydrodynamic type with Regleigh step type thrust bearing geometry. Instead of a bellows secondary, a carbon piston ring is used. Liquid oxygen pressure is near

345 newtons per square centimeter (500 psi) and seal sliding speed about 137 meters per second (450 ft/sec). The predicted operating film thickness is 0.00076 centimeters (0.0003 in.).

The helium purge seal is a circumferential seal modified to have self-acting geometry similar to that shown in figure 38. This self-acting geometry, as in the case of the self-acting face seal, acts to maintain positive separation between the rotating shaft and the non-rotating carbon rings. The helium gas pressure is 35 to 69 newtons per square centimeter (50 to 100 psi). In comparison, the clearance ring seal shown in the conventional configuration (fig. 36) has a leakage rate 50 times greater. Thus, by use of the self-acting helium seals, the on-board helium inventory can be reduced and significant weight saving will acrue because of the smaller tanks and lines.

SUMMARY

Self-acting and hydrodynamic seals and their potential applications in gas turbine engines and in rocket engine turbopumps are described. In particular the analytical procedure is given for predicting the operating film thickness of a 16.76 centimeter (6.6 in.) diameter seal designed for gas turbine applications. The analysis and subsequent operation of this seal under simulated gas turbine conditions revealed the following:

1. Analysis

a. Noncontact operation with acceptable leakage is predicted at the selected four design conditions of idle, takeoff, climb, and cruise.

b. The operating film thickness ranged between 0.00046 and 0.00119 centimeter (0.00018 and 0.00047 in.) for the four design conditions.

c. The calculated seal leakage rates ranged between 0.01 and 0.40 scmm (0.4 and 14.0 scfm) for the four design conditions.

d. For a typical operating condition, noncontact operation was predicted under the assumption of a 2-milliradian face deformation. Gas leakage was about twice that for parallel-face operation.

2. Experiment-Simulated Engine Operation

a. The self-acting seal ran without rubbing contact during all of the simulated engine operating conditions. Of particular interest was that noncontact operation was maintained at the advanced engine conditions of a 152-meter-per-second (500 ft/sec) sliding speed, a 345 newtons per square centimeter (500 psi) sealed pressure differential, and a 811 K (1000° F) sealed air temperature.

b. The leakage rates during endurance tests ranged from 0.79 to 1.63 standard cubic meters per minute (28 to 57.5 scfm).

c. Self-acting geometry wear due to rubbing contact proved to be insignificant.

d. Two seal wear problems were noted. These are (1) fretting wear of the secondary ring (piston ring) and (2) erosion of the seal dam (primary seal) by hard particles.

e. Wear due to starts and stops proved to be insignificant. For 40 starts and stops wear was less than 1.27 micrometers (0.00005 in.).

REFERENCES

1. Anon., "Aircraft Propulsion," NASA SP-259 (1971).

2. Parks, A. J., McKibbin, R. H., Ng, C. C. W., and Slayton, R. M., "Development of Main-shaft Seals for Advanced Air Breathing Propulsion Systems," Pratt & Whitney Aircraft Rep. PWA-3161, NASA CR-72338 (1967).

3. Povinelli, V. P., and McKibbin, A. H., "Development of Mainshaft Seals for Advanced Air Breathing Propulsion Systems - Phase II," Pratt & Whitney Aircraft Rep. PWA-3933, NASA CR-72737 (1970).

4. Orcutt, F. K., "An Investigation of the Operation and Failure of Mechanical Face Seals," Presented at the 4th International Conference on Fluid Sealing, British Hydromechanics Research Association, Cranfield, Bedford, England (1969).

5. Mayer, E., "High Duty Mechanical Seals for Nuclear Power Stations," Paper A5, Presented at the 5th International Conference on Fluid Sealing, British Hydromechanics Research Association, Cranfield, Bedford, England (1971).

6. Mayer, E., "Thermodynamics in Mechanical Seals," Presented at the 4th International Conference on Fluid Sealing, British Hydromechanics Research Association, Cranfield, Bedford, England (1969).

7. Ludwig, L. P., and Johnson, R. L., "Design Study of Shaft Face Seal with Self-Acting Lift Augmentation. III - Mechanical Components," NASA TN D-6164 (1971).

8. Brown, P. F., "A Glossary of Seal Terms," Special Publication SP-1, American Society of Lubrication Engineers.

9. Ludwig, L. P., Zuk, J., and Johnson, R. L., "Design Study of Shaft Face Seal with Self-Acting Lift Augmentation. IV - Force Balance," NASA TN D-6568 (1972).

END OF REFERENCE

112

REFERENCE

113

HADY, W. F.; ALLEN, G. P.; AND JOHNSON, R. L.: WEAR AND FRICTION OF MECHANICAL CARBONS IN LIQUID OXYGEN AS INFLUENCED BY TRANSFER FILMS. ASLE TRANS., VOL. 6, NO. 3, JULY 1963.

8.0-8-0...

SEP 13 '63

COPY 1

Reprinted from
ASLE TRANSACTIONS 6, 201-208 (1963)
Academic Press Inc.
Printed in U.S.A.

RP-5

Wear and Friction of Mechanical Carbons in Liquid Oxygen as Influenced by Transfer Films

By WILLIAM F. HADY (ASLE),[1] GORDON P. ALLEN (ASLE),[1] and ROBERT L. JOHNSON (ASLE)[2]

Experimental wear and friction studies were conducted with a series of mechanical carbons sliding against metal surfaces in liquid oxygen (—298 F) at sliding velocities to 6500 feet per minute and a load of 1000 gm. The data reported shows that dense highly graphitic carbons have potential use as seal and bearing materials for liquid oxygen applications.

High density graphitic carbons with a greater oxidation resistance and a greater capability of forming a transfer film gave the lowest wear and friction. Metals that form the most stable oxide films promote greater adherence of the graphite to the mating surface. Impregnated carbons must be selected with caution because frictional heating generated during sliding can initiate hazardous reactions between oxygen and certain unstable organic compounds.

Introduction

MECHANICAL carbons are being used in seals and bearings to operate over a wide range of temperatures and environments. One area employing carbons is in liquid oxygen applications; however, the basis for selecting particular types of carbon for use in oxygen is inadequately defined. The stringent compatibility requirement imposed by the liquid oxygen environment limits the selection of impregnated carbons to be used to those of known stability in oxygen. Any unstable organic compound in the carbon could react violently with the oxygen when sufficient heat is generated during sliding. Earlier friction and wear investigations have shown that mechanical carbons can be used as self-lubricating materials for aircraft turbine engines at high temperatures of 700 F (*1, 2*) as well as in turbopump applications for rocket propulsion at liquid hydrogen temperatures, —423 F (*3*). It is feasible, therefore, that a carbon with or without adjuncts can be selected to perform satisfactorily in liquid oxygen and provide the necessary low friction and low wear required.

The low wear of mechanical carbons, as experienced in the more conventional applications, where air, moisture, or other vapors are present, is attributed to the self-lubricating characteristics of the carbon. It has been reported (*4*), that effective lubrication is accomplished only when an oriented surface layer of graphitic carbon is established on the mating surface, which in effect results in a sliding combination of carbon on carbon rather than carbon on metal.

Reference (*1*) hypothesized that graphite lubrication depends primarily upon adherence of the graphite to the metal mating surface. This adherence can be achieved by the presence of intermediate films of adsorbed moisture, gases, or by the presence of an oxide film on one or both of the surfaces to be lubricated. The more common theory for the mechanism of graphite lubrication, which suggests the shearing of interlamellar adsorption films between the graphite platelets, does not consider affinity or adhesion of graphite to the lubricated surfaces. Earlier liquid oxygen studies (*5*) have indicated that oxide films are beneficial in minimizing wear and friction in metal–metal combinations. Therefore, since beneficial oxide films form readily on metal surfaces in liquid oxygen and graphite effectively lubricates oxidized metals (*1*), it is likely that films of graphite on the mating surface will develop readily and lubrication will be enhanced. Such film formation is essential for the lubrication to provide low wear and friction as required in dynamic seals and bearings.

The objectives of this investigation were (a) to determine the influence of graphite content on wear and friction of carbon bodies, (b) to determine the influence of adjuncts to carbon bodies on wear and friction, (c) to investigate what effect, if any, the free energy of formation of metal oxides of the mating surfaces has on wear and friction of graphite, and (d) to suggest improved seal materials for liquid oxygen turbopump applications. Carbons with varied amounts of graphite content as well as carbons modified by means of adjuncts were run in sliding contact against metals having different oxidation characteristics in liquid oxygen at —298 F. Data were obtained with a 1/16-inch-radius rider speci-

LIBRARY COPY
SEP 13 1963
LEWIS LIBRARY, NASA
CLEVELAND, OHIO

Contributed by the ASLE Technical Committee on Seals and Packings and presented at the Annual Meeting of the American Society of Lubrication Engineers held in New York, April, 1963.

[1] Research Engineer, NASA, Lewis Research Lab, 2100 Brookpark Road, Cleveland 35, Ohio.

[2] Head, Lubrication Section, NASA, Lewis Research Lab.

men sliding on a flat surface of a rotating 2½-inch-diameter disk. Runs were made with specimens submerged in liquid oxygen at surface speeds ranging from 1000 to 6500 feet per minute and a normal load of 1000 gm.

Apparatus and procedure

The apparatus used in this investigation is shown schematically in Fig. 1. The basic elements are a rotating disk specimen (2½-inch-diameter) and a stationary

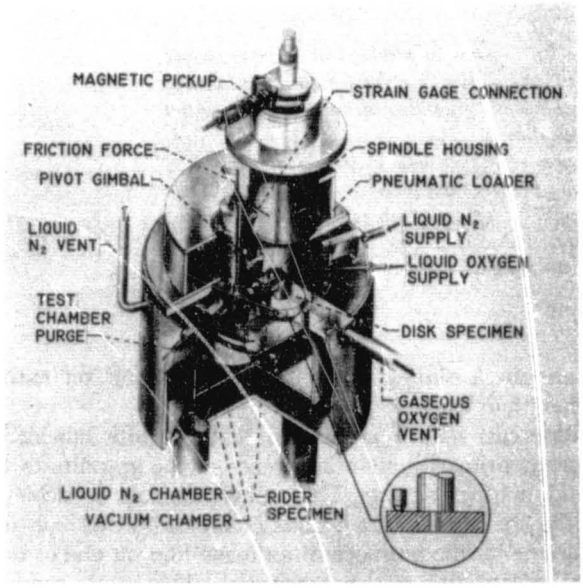

FIG. 1. Liquid oxygen friction apparatus

hemispherically tipped rider specimen (3/16-inch-radius) in sliding contact with the disk (see inset). The disk is rotated by a variable speed electric motor through a gear box speed increaser coupled to the specimen shaft. Disk speed is monitored by a magnetic pickup whose output is fed into a digital readout instrument.

The rider specimen is loaded against the disk by a pneumatic operated piston on the end of a gimbal mounted arm. Through this arm, pressurizing gas (dry He) is supplied. The arm is linked to a strain gage assembly for measurement of frictional force.

The apparatus consists of two sections which may be separated for changing specimens. The lower section consists of four separate chambers: The inner chamber, or test chamber, is located within a "jacket" which may be filled with liquid nitrogen for cooling. This cooling jacket is surrounded by a vacuum chamber to reduce the boil-off rate of the cooling and test fluids. The outermost chamber, or spill chamber, surrounds the three chambers and provides safe operation in the event excess amounts of the test fluid should escape. The upper section is a vacuum jacket through which passes the disk specimen drive shaft housing and the rider specimen arm assembly. A series of carbon face seals are employed to seal around the drive shaft and flexible bellows are used to seal the rider arm assembly. Fluorinated hydrocarbon oils are used to lubricate the gear box and the support bearings in the shaft housing to prevent a reaction of the oil with the liquid oxygen in case the shaft seals fail.

The test fluid, liquid oxygen in this investigation, passes through a coil within the cooling jacket before entering the test chamber near the bottom. In tests where the test fluid initially is in the gaseous state, the coil would condence the gas into the liquid state. Excess liquid and vapor are vented by a line leaving from a point near the top of the chamber. The liquid level within the test chamber is monitored by a capacitance probe and recorded on a circular chart capacitance recorder.

The cooling jacket is filled with liquid nitrogen and vented by two diametrically opposite lines. The coolant level is monitored with a carbon resistance probe, a full jacket being indicated by a sharp drop in output when the coolant absorbs the heater output.

SPECIMEN PREPARATION AND TEST PROCEDURE

The nonimpregnated carbon rider specimens were cleaned by soaking them in ACS certified acetone for 5 hours and placed in a vacuum (10^{-3} mm Hg) for 10 hours.

In cleaning the impregnated carbons it was discovered that in some cases the above procedure caused the impregnants to be leached out when they were placed in the vacuum. Therefore, the impregnated carbons were cleaned by wiping them with a soft cloth saturated with ACS certified acetone before being placed in the vacuum. All the carbon specimens were then stored in a desiccator until used.

The nonplated disk specimens used in this experiment were circumferentially finished to a surface roughness of 4–8 microinches RMS. The plated specimens, 440-C hardened to 52-54 R_c, were ground and lapped to 4–8 microinches RMS before plating (Table 1). The various platings were electro-deposited from electrolytes held in absorbent materials attached to portable electrodes (*6*).

All the disk specimens were then given the following cleaning treatment: (a) immersion in an ultrasonic cleaning tank filled with water, for ½ hour; (b) thorough rinsing with ACS certified acetone; (c) polishing with moist levigated alumina on a soft cloth; and (d) thorough rinsing with distilled water. The remaining water was removed using filter paper. Each disk specimen was prepared just prior to being placed in the test chamber.

After the desired liquid oxygen level was attained, the disk specimen was brought up to speed and the normal load was applied. Duration of runs was 60 minutes or less depending on the stability of operation. The frictional force was measured continuously by resistance strain gages mounted on a dynamometer ring whose output was fed into a recording potentiometer.

TABLE 1
Physical and Chemical Properties of Metal Disk Materials Used in This Study

Disk		Plate thick. (in.)	Standard hardness (BHN)[a]	Surface finish (μin. RMS)	$-\Delta F_{-298F}$[b]
Solid	Plate				
	Au	0.0030	110	4.2	0.30
Ag			36	6.2	7
	Ag	.0038	85	4.2	7
	Rh	.0020	925	4.0	20
Cu			82	6.2	35
	Cu	.0034	175	4.0	35
Co			101	8.4	55
	Co	.0015	—	8.4	55
Ni			68	5.5	56
	Ni	.0046	379	4.5	56
Fe			66	4.8	63
	Sn	.0042	<5	3.6	67
	Zn	.0035	50	12.0	82
Cr			120	8.4	87
	Cr	.0042	733	4.2	87
Ti			175	7.2	110
440-C			20-54 R_c	4.0-8.0	

[a] At 75 F.
[b] Reference (*10*) (Kcal per gram atom of O_2).

Rider wear was obtained by measuring the wear scar diameter and calculating the wear volume.

Results and discussion

Influence of Graphite Content on Wear and Friction

The importance of graphite content on the wear of carbon riders is demonstrated in Fig. 2. The carbon riders were run in sliding contact with 440-C stainless steel and chromium plate in liquid oxygen at 2300 feet per minute and a 1000-gm load. Rider wear decreased with increasing graphite content; the fully graphitized carbons gave the lowest wear against either 440-C stainless steel or chromium plate. In both series the wear of the amorphous carbons was about 20 times that of the fully graphitized carbon. Mechanical carbons that have operated successfully in liquid nitrogen and liquid hydrogen (*3*) have wear rates on the order of 10^{-11} inch^3 per foot of sliding, which is comparable to the wear rate of the 20% graphite sliding on chromium plate (Fig. 2) in this investigation.

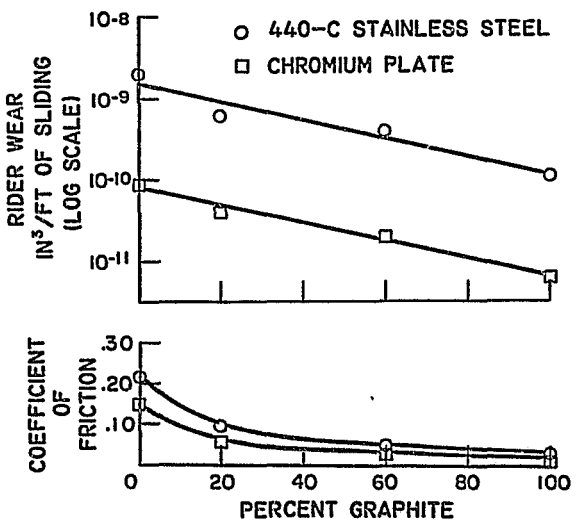

FIG. 2. Effect of graphite content on the lubricating properties of carbons in liquid oxygen (2300 fpm; 1000-gm load; duration, 1 hour).

The low wear exhibited by the fully graphitized carbon specimens is attributed in part to their greater resistance to oxidation than those carbons of lower graphite content.

It has been reported that amorphous carbon begins to oxidize in air at 622 F and that graphitic carbon begins to oxidize in air at 842 F (*7*). It would therefore appear that, in the highly oxidative environment of this investigation, even though the temperature is at —298 F, the sliding interface temperatures were sufficient to promote a more rapid and extensive oxidation of the carbons containing little graphite and resulted in excessive corrosive wear.

It appears also that, in this investigation, the greater capability of the fully graphitized materials to form a transfer film of graphite on the metal mating surface is important in reducing rider wear. Visual inspection of the disk specimens showed that an adherent graphite film was noted best with the fully graphitized rider run on chromium plate. It was also observed that the carbons of lower graphite content did not transfer sufficient graphite to the mating surface so that the carbon was continually sliding on bare metal surfaces. As a result, the lower graphitic carbons were more susceptible to wear by abrasive processes as well as oxidation. Figure 3 is a set of photomicrographs showing rider wear scars and the transfer film of graphite on the mating chromium plate surfaces.

The distinct separation of the two curves is very significant as it points out the importance of oxides being present on the metal surfaces when graphite is to be used as a lubricant in the absence of moisture or water vapor. The selection, therefore, of mating surfaces takes on increased importance when designing dynamic seals for liquid oxygen applications. Previous friction and wear studies with graphite at elevated temperatures (*1*) suggested that the presence of beneficial oxide films promoted an affinity of the graphite for the metal mating surface and was a requirement of graphite lubrication in unconventional systems. The 20-fold reduction in wear between the two curves was the basis for a more exhaustive study as to the role played by oxide films in graphite lubrication for liquid oxygen applications. These results will be presented and discussed subsequently.

Coefficient of friction data (bottom of Fig. 2) show a downward trend as the amount of graphite is increased

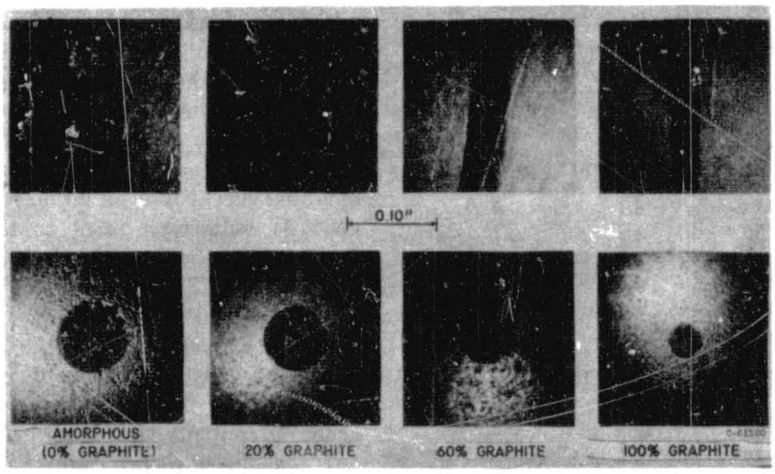

FIG. 3. Disk (top) and rider (bottom) wear areas of nonimpregnated carbons with various graphite content sliding on chromium plate in liquid oxygen (load, 1000 gm; sliding velocity, 2300 fpm; duration, 1 hour).

from 0 to 100%. The values reported are the values of friction after stabilization has occurred. The importance of graphite content in reducing friction is easily shown since the drop in friction, comparing the amorphous carbon to the 20% graphite carbon, is very pronounced: 0.22–0.10, when sliding on 440-C stainless steel and 0.10–0.06 when sliding on chromium plate. With further increases in graphite content, further reductions in the coefficient of friction are experienced with values reaching about 0.03 for the fully graphitized carbons sliding on 440-C and chromium plate.

Frictional force is the product of the effective shear area in sliding and the shear strength of the interface film (*8*). The harder amorphous carbons, having higher shear strength than the graphitic carbons, usually give minimum shear areas. The addition of minor amounts (20–30%) of graphite to the amorphous carbon usually gives an optimum combination of low shear strength (from the graphite) and low shear area (from the amorphous carbon matrix) that results in minimum friction. In liquid oxygen, however, the lowest friction values were obtained with the fully graphitic carbons. It is probable that the relative influence of the cryogenic temperature on the shear area (as determined by hardness) and the chemical behavior of the oxygen on the formation of adsorbates for easy surface shear, may have altered the optimum composition.

The data of Fig. 4 are presented to show that high starting torques can be experienced with carbons of low graphite content and that for systems where high starting torques cannot be tolerated, fully graphitized carbons can provide low starting friction without extensive run-in periods. The values of friction attained after run-in are those shown in Fig. 2.

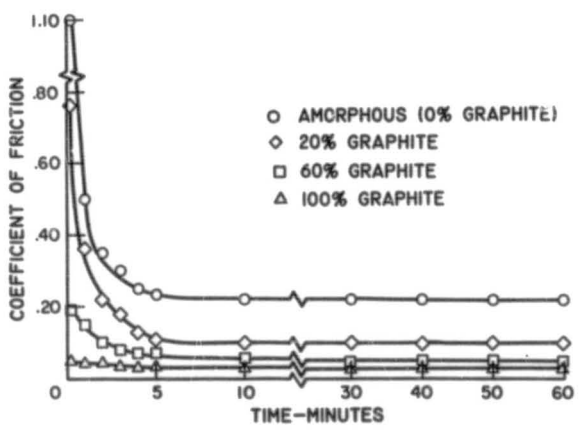

FIG. 4. Effect of graphite content on the friction of carbon on 440-C stainless steel in liquid oxygen (2300 fpm; 1000-gm load; duration, 1 hour).

INFLUENCE OF METAL MATING HARDNESS ON GRAPHITE WEAR AND FRICTION

The differences in wear as noted in Fig. 2 between the 440-C stainless steel and the chromium plate suggested that hardness of the mating surface, usually considered important to wear of carbon type seal materials, may be responsible for the lower wear of carbons on chromium plate. A series of runs was therefore made with a hardenable stainless steel (type 440-C) of various hardnesses obtained by altering the heat treatment. In using one base metal, the variables of oxidation resistance and composition were eliminated. The data of Fig. 5 are presented to show that hardness of the mating surface from 20 to 54 Rockwell-C had no significant effect on the wear of the fully graphitized carbons when run in liquid oxygen. From this it can be deduced that graphite rider wear in liquid oxygen is influenced more by the oxidation resistance and composition of the mating surface than hardness.

Figure 5 data also show that the coefficient of friction

of a fully graphitized carbon sliding of 440-C of various hardnesses remained constant within the scope of this investigation.

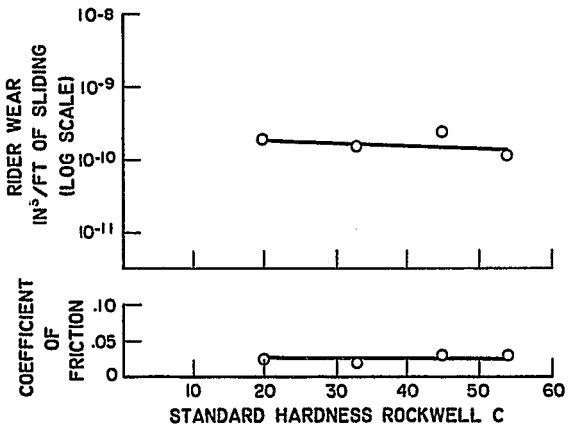

FIG. 5. Effect of surface hardness of 440-C stainless steel on the lubricating properties of graphite in liquid oxygen (2300 fpm; 1000-gm load; duration, 1 hour).

INFLUENCE OF SLIDING VELOCITY ON GRAPHITE WEAR AND FRICTION

The dissipation of frictional heat generated during sliding contact by dynamic seals in liquid oxygen could become of prime concern where substantial surface speeds are encountered. The additional heat experienced at the higher sliding velocities could increase the oxidation of the fully graphitized carbons which would lead to increased corrosive wear. A series of tests was conducted to show the effect of sliding velocity on the wear of a fully graphitized carbon rider sliding on 440-C stainless steel in liquid oxygen. Data of Fig. 6 present wear per unit distance of sliding at velocities from 1000 to 6500 feet per minute and a load of 1000 gm.

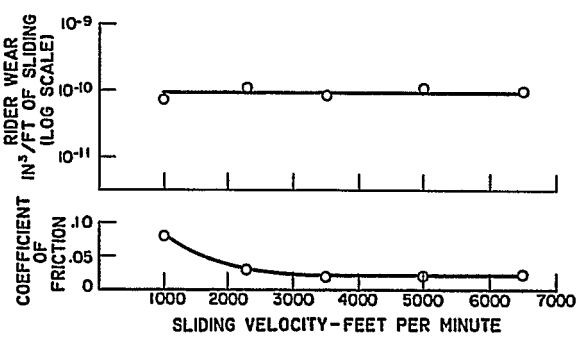

FIG. 6. Effect of sliding velocity on the lubricating properties of graphite sliding on 440-C stainless steel in liquid oxygen (1000-gm load; duration, 1 hour).

In this investigation, sliding velocity had no significant effect on graphite rider wear. Further increases in surface speeds, however, could bring about increased wear as the interface temperatures could become sufficiently high and cause extensive oxidation of the graphite. With the addition of adjuncts to the base graphite (to increase the oxidation resistance and improve physical properties) higher surface speeds may be tolerable. The selection of adjuncts is limited, however, to those that will remain stable in the highly oxidizing environment.

The coefficient of friction (bottom of Fig. 6) shows a decreasing trend to 3000 feet per minute, after which it remains constant within the limits of this investigation. The reduction in friction between 1000 and 3000 feet per minute (0.08–0.03) is not significant as both values are well below 0.10.

THE INFLUENCE OF IMPREGNANTS ON WEAR AND FRICTION

Two series of impregnated carbons, a 20% graphite base grade, and a 100% graphite base grade were run against 440-C stainless steel in liquid oxygen to study the effects of various impregnants on wear and friction of these carbons. The unimpregnated base grades were run against themselves for a comparison [note (A), Figs. 7 and 8].

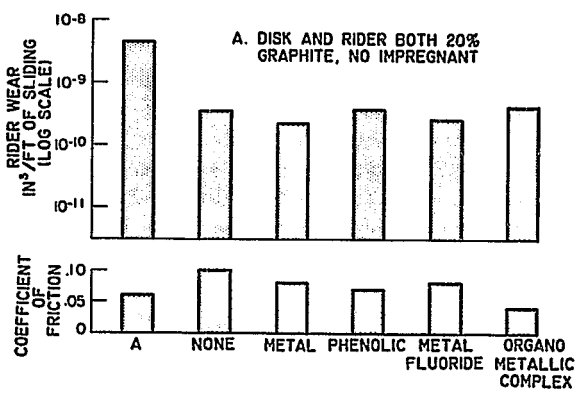

FIG. 7. Effect of impregnants on the lubricating properties of a 20% graphite sliding on 440-C stainless steel in liquid oxygen (2300 fpm; 1000-gm load; duration, 1 hour).

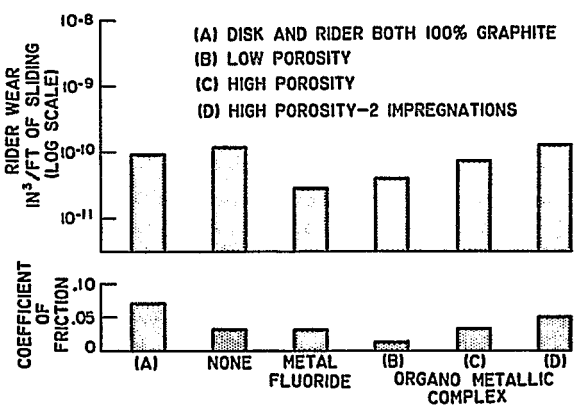

FIG. 8. Effect of impregnants on the lubricating properties of a 100% graphite sliding on 440-C stainless steel in liquid oxygen (2300 fpm; 1000-gm load; duration, 1 hour).

The wear data for the 20% graphite series, presented in Fig. 7, show that the impregnant had little effect on the wear of the carbon rider. The carbon with metal impregnation had the lowest wear: 2.2×10^{-10} inch^3 per foot of sliding for this series of runs.

The coefficients of friction of the variously impregnated 20% graphite riders are presented at the bottom of Fig. 7. The addition of the impregnants had no significant effect on the frictional properties of the carbons used in this investigation. The organo-metallic complex impregnated carbon had the lowest coefficient of friction (0.04) for this series.

The data in Fig. 8 show the effect of impregnants on the wear and friction of a 100% graphite rider sliding on 440-C in liquid oxygen. In general, additive impregnants did not significantly influence wear; however, the metal fluoride impregnant and the organo-metallic complex impregnant in a low porosity carbon did reduce wear by a factor of approximately 3. The metal fluoride impregnant had the lowest wear of the two: 3×10^{-11} inch^3 per foot of sliding.

This reduction in carbon rider wear indicates the oxidation resistance of the carbon was increased with the addition of the impregnant. The wear reduction is an indication of the importance of corrosive wear. The impregnant also acts to encourage a more rapid rate of graphite transfer to the metal surface which in turn reduces adhesive wear. It is important to note that the graphite riders of high porosity carbons with organo-metallic complexes (single and double impregnations) had higher wear than the low porosity graphite rider having the same impregnant.

Figure 8 also presents coefficients of friction for the same series of impregnations. The high density, organo-metallic complex, graphite rider sliding on 440-C stainless steel in liquid oxygen gave the lowest friction coefficient, 0.01.

From the results of Figs. 7 and 8, high density (low porosity) 100% graphite mechanical carbons can be considered for bearings and seals in liquid oxygen applications. The selection of impregnants should be made with caution, however, and should be limited to those having known stability with liquid oxygen.

THE INFLUENCE OF MATING SURFACE ON WEAR AND FRICTION

Friction and wear studies (*9*) at elevated temperatures to 700 F hypothesized that in the absence of adsorbed water or vapor, the continual presence of a proper oxide on one or both of the lubricated surfaces influenced the adherence of graphite to the mating surface and affected good graphite lubrication. A series of tests, therefore, was made to explore this hypothesis by sliding 100% unimpregnated graphite riders on various metal surfaces in liquid oxygen. These data are shown on Figs. 9 (solids) and 10 (platings).

The abscissa, free energy of formation of the oxide, in

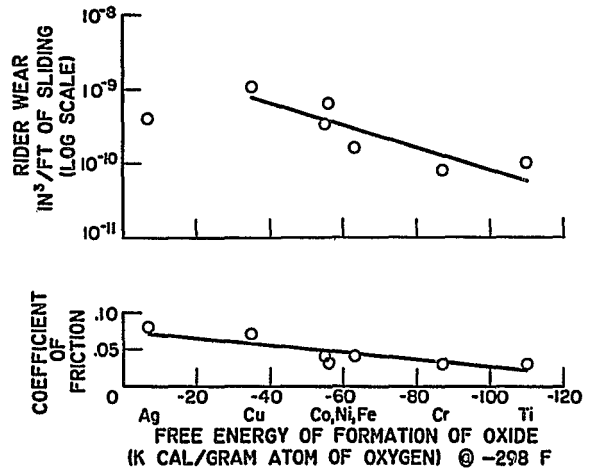

FIG. 9. Effect of metal oxide formation on the lubricating properties of a 100% graphite sliding on various solid metals in liquid oxygen (2300 fpm; 1000-gm load; duration, 1 hour).

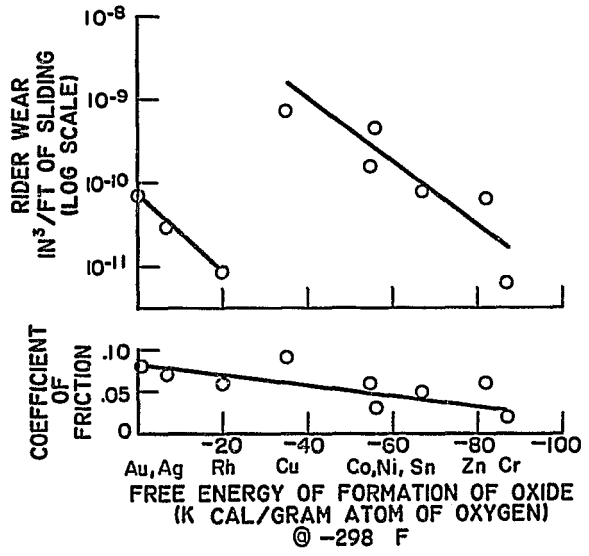

FIG. 10. Effect of metal oxide formation on the lubricating properties of 100% graphite sliding on various metal plates in liquid oxygen (2300 fpm; 1000-gm load; duration, 1 hour).

kcal per gram atom oxygen, is a measure of the ease with which the various metal oxides can form at liquid oxygen temperatures. (The more negative the value, the more stable the oxide.) The relative position of the standard free energies of formation for the oxides of the metals studied were in the same order over the entire temperature range that could be expected to result from local frictional heating on the surfaces. Reference (*8*) indicates that under conditions of boundary lubrication more favorable than in the present experiments, surface temperatures 900 F above the ambient might be obtained. On that basis, in these experiments, interface temperatures of about 600 F could be postulated. The surface temperatures, therefore, can be expected to range from the ambi-

ent of —298 to 600 F. The values used in plotting the relative position of the oxides formed were extrapolated from graphs down to —298 F, liquid oxygen temperature (*10*).

The data of Figs. 9 and 10 show a downward trend in graphite rider wear as the free energy formation of the oxide becomes more negative. This downward trend in wear is more pronounced with the plated specimens (Fig. 10) than with the solid disk specimens (Fig. 9). The break in the curve for the plated specimens, i.e., in separating the precious metals from the remaining specimens, could be caused by the presence of a contaminant, co-deposited from the electrolyte with the metal, remaining on the surface of the disk. Any contamination present in studies of this nature can have marked effect on the wear and frictional properties of the materials under investigation. The coefficient of friction also shows a downward trend with both the plated and solid disk specimens as the oxides that are formed become increasingly stable.

Those metals forming the more stable oxides developed transfer films from the graphitic carbon bodies (mechanical carbons); such films provided the most effective lubrication. The stability of the film is associated with the formation of a chemical bond between the graphite and the metal oxide. During sliding contact, penetration of the fluid (O_2) adsorbed on the surface would be achieved. Thus, with the mechanical carbon and the oxide-coated metal in intimate contact, a chemical reaction to form a carbon-oxygen-metal complex can occur. Conditions favorable for such reaction are that the contacting solids are under pressure (the yield strength of the softer slider material) and that sufficient frictional energy is available for reaction. The kinetics of such reactions are impossible to define because of transient conditions that are characteristic of sliding contact. The present reference to free energy relationships indicate the relative stabilities of potential chemical bonds in the postulated carbon-oxygen-metal complex. The chemical bonding energy is associated with stability of adhering graphitic carbon films on the mating metal surfaces as described herein. Thus, the sliding process was one of graphite sliding on a graphite film rather than graphite on nascent metal.

With those metals forming less stable oxides, it is thought that the graphite rider, through a chemical reaction, removes the bonded oxygen from the metal surface resulting in the formation of carbon monoxide or carbon dioxide. In these experiments, those metal oxides having a less negative ΔF than either carbon monoxide or carbon dioxide showed little or no graphite transferred to the mating surface. It is thought that in the liberation of these gases the nascent metal surfaces reoxidized from time to time leading to a corrosive type wear mechanism for the graphite rider. It appears that as the metal oxides become less stable, the degree of corrosive and adhesive wear increases.

Summary of results

An experimental wear and friction investigation of mechanical carbons for seals and bearings was conducted in an environment of liquid oxygen. The following results were obtained:

(1) Highly graphitic mechanical carbons had better wear and friction properties in liquid oxygen than more commonly used materials which have low graphite content. Of the graphitic materials tested, performance was best with those having high density (low porosity). Low wear values for graphitic carbon are attributed in part to its greater oxidation resistance in comparison with amorphous carbon. Also important to both wear and friction is the greater capability of the graphitic materials to form a transfer film of carbon on the metal mating surface; optimum performance appears to occur when a continuous transfer film is present on the mating metal so that the solid carbon can slide on a carbon film.

(2) Chromium plate was a better mating surface than any of the other metal platings, pure metals, or 440-C. Observations in these and other carbon wear studies suggest that the metal oxide films are of primary importance in effecting graphite lubrication. Metals forming the most stable and dense oxide films appear to perform best. The presence of these metal oxides on the mating surface promotes adherence of a beneficial transfer film of graphite from the mechanical carbons in sliding contact.

(3) Additive impregnants to mechanical carbons did not have a significant effect on wear and friction. Erratic data was experienced with impregnated carbons as compared to data for the nontreated base grade carbons; this was attributed to treatment inconsistencies. Where the use of treated carbons is preferred they should be impregnated in very nearly the final form so that the most effectively treated material will not be removed by machine finishing.

(4) Hardness of the mating 440-C material was varied from 20 to 54 Rockwell-C without significant influences on wear and friction of fully graphitized carbon rider specimens.

(5) Sliding velocity from 1000 to 6500 feet per minute had no significant effect on rate of wear or friction of fully graphitized carbon rider specimens when run on 440-C.

(6) Carbon wear problems are less severe in these liquid oxygen experiments than in liquid hydrogen studies made previously. A potential reaction hazard exists, however, with carbons in sliding contact at high surface speeds in liquid oxygen. Dense, highly graphitic materials have the greatest resistance to initiating such an oxidation reaction; any impregnants used to improve the performance of mechanical carbons in liquid oxygen applications must, therefore, have known stability in oxygen.

REFERENCES

1. BISSON, E. J., JOHNSON, R. L., and ANDERSON, W. J., "Friction and Lubrication with Solid Lubricants at Temperatures to 1000 F with Particular Reference of Graphite," Inst. Mech. Eng. Conf. on Lubrication and Wear. Paper no. 23, Oct. 1957.
2. PETERSON, M. B., and JOHNSON, R. L., "Friction Studies of Graphite and Mixtures with Several Metallic Oxides and Salts at Temperatures to 1000 F," *NACA (Natl. Aeron. Space Admin.) Tech. Note* 3657, 1956.
3. WISANDER, D. W., and JOHNSON, R. L., "Wear and Friction of Impregnated Carbon Seal Materials in Liquid Nitrogen and Hydrogen," *In* "Advances in Cryogenic Engineering," (K. D. Timmerhouse, ed.), Vol. 6, Plenum Press, Inc., New York, 1961.
4. SAVAGE, R. H., "Physically and Chemically Adsorbed Films in the Lubrication of Graphite Sliding Contacts," *Ann. N. Y. Acad. Sci.* **53**, 362-869 (1951).
5. HADY, W. F., ALLEN, G. P., and JOHNSON, R. L., "Boundary Lubrication Characteristics of a Typical Bearing Steel in Liquid Oxygen." *NASA (Natl. Aeron. Space Admin.) Tech Note* **1580**, 1962.
6. HUGHES, H. D., "Practical Brush-Plating," *Inst. Met. Finishing, Trans.* **33**, 424-442 (1955-56).
7. MANTELL, CHARLES L., "Industrial Carbon," 2nd ed., Van Nostrand, Princeton, N. J., 1946.
8. BOWDEN, F. P., and TABOR, D., "The Friction and Lubrication of Solids," Oxford Univ. Press (Claredon), London and New York, 1950.
9. SWIKERT, M. A., and JOHNSON, R. L., "Wear of Carbon-Type Seal Materials with Varied Graphite Content," *ASLE Trans.* **1**, 115-120 (1958).
10. GLASSNER, A., "The Thermochemical Properties of the Oxides, Fluorides, and Chlorides to 2500 K," Argonne National Laboratory Publication, ANL-5750.

LEWIS RESEARCH CENTER
Aerospace Safety Research
and Data Institute
DEC 3 1970
CLEVELAND, OHIO

END OF REFERENCE

113

REFERENCE

114

HADY, W. F.; ALLEN, G. P.; SLINEY, H. E.; AND JOHNSON, R. L.: FRICTION, WEAR, AND DYNAMIC SEAL STUDIES IN LIQUID FLUORINE AND LIQUID OXYGEN. NASA TN D-2453, 1964.

AUTHOR'S PERSONAL COPY

NASA TECHNICAL NOTE

NASA TN D-2453

NASA TN D-2453

LEWIS RESEARCH CENTER
Aerospace Safety Research
and Data Institute
FEB 5 1973
CLEVELAND, OHIO

FRICTION, WEAR, AND DYNAMIC SEAL STUDIES IN LIQUID FLUORINE AND LIQUID OXYGEN

by W. F. Hady, G. P. Allen,
H. E. Sliney, and R. L. Johnson

Lewis Research Center
Cleveland, Ohio

NATIONAL AERONAUTICS AND SPACE ADMINISTRATION • WASHINGTON, D. C. • AUGUST 1964

FRICTION, WEAR, AND DYNAMIC SEAL STUDIES IN LIQUID FLUORINE AND LIQUID OXYGEN

By W. F. Hady, G. P. Allen, H. E. Sliney, and R. L. Johnson

Lewis Research Center
Cleveland, Ohio

NATIONAL AERONAUTICS AND SPACE ADMINISTRATION

For sale by the Office of Technical Services, Department of Commerce,
Washington, D.C. 20230 -- Price $0.50

FRICTION, WEAR, AND DYNAMIC SEAL STUDIES IN LIQUID FLUORINE AND LIQUID OXYGEN

by W. F. Hady, G. P. Allen, H. E. Sliney, and R. L. Johnson

Lewis Research Center

SUMMARY

Friction and wear studies were conducted with four material combinations run submerged in liquid oxygen and in liquid fluorine to determine their potential as dynamic seal components for fluorine turbopump applications. The friction and wear experiments were conducted with a 3/16-inch-radius hemispherically tipped rider sliding in a circumferential path on the flat surface of a rotating 2½-inch-diameter disk.

The seals used in this investigation had a flame-sprayed Al_2O_3 nosepiece (0.006 to 0.008 in. thick) and were run against a mating disk of TiC cermet or a fused coating of CaF_2 + LiF + NiF_2 on Al_2O_3 submerged in liquid fluorine.

Results indicated that the presence of a fluoride film, either as an applied fused coating (CaF_2 + LiF + NiF_2) or as a film formed during sliding (NiF_2 on the TiC cermet or possibly aluminum fluoride (AlF_3) on Al_2O_3) in liquid fluorine, was beneficial in reducing the friction and wear of the Al_2O_3 riders. The seal experiments in liquid fluorine showed that flame-sprayed Al_2O_3 sliding against the TiC cermet or a fused coating of CaF_2 + LiF + NiF_2 on Al_2O_3 are potential seal materials for fluorine turbopump applications.

INTRODUCTION

The potential use of liquid fluorine as the oxidizer for high-thrust rocket engines imposes critical problems for sliding contact seals in turbopumps. To date little information is available to aid in the selection of sliding contact seal materials for use in liquid fluorine. Materials that have been used successfully in seals for liquid hydrogen and liquid oxygen applications have also been used in liquid fluorine with some problems. The successes that have been achieved can generally be attributed to the use of a sweep gas across the seal face, which reduces contact of the seal materials with fluorine (ref. 1).

Instances of violent explosions have occurred, however, with both oxygen and fluorine where carbons have been used and the ignition source has been

traced to the seal areas. Compatibility studies have shown that "amorphous" carbon will react violently with very low concentrations of fluorine in nitrogen and that graphitic carbon, after prolonged soaking, will also react violently (refs. 2 to 4). Applications, therefore, should be avoided where contact of the carbon with liquid fluorine is possible. Material combinations must be selected that will be compatible with fluorine during sliding contact and will provide the low wear and friction necessary for dynamic seals. Such selections can be based on well-known chemical thermodynamic principles and on experimental reaction rate and compatibility studies (refs. 5 to 7). Reactive-gas lubrication studies (ref. 8) showed that controlled reaction rates (i.e., limiting the degree of corrosion) were useful in providing effective lubrication. It is possible, therefore, that materials that have low reaction rates or are able to resist excessive corrosion with fluorine may also form beneficial lubricating films.

The following investigation was accomplished in three phases: (1) friction and wear studies in liquid oxygen of material combinations expected to be chemically stable in fluorine, (2) friction and wear studies of these combinations in liquid fluorine, and (3) full-scale seal studies of these combinations in liquid fluorine at surface speeds and loads representative of a pump application.

MATERIAL SELECTION

The solid materials used in this investigation were selected primarily for their resistance to fluorine attack. The TiC cermet and Al_2O_3 were selected because of hardness, resistance to wear, and chemical stability in fluorine. The nickel-chrome alloy that contains approximately 55 percent nickel was selected as the substrate for the fused fluoride coating (62 BaF_2 + 38 CaF_2, eutectic) because of its hardness and the tight bond formed between this coating and nickel-chrome alloys. Anticipated shear properties of passivation films in sliding contact were also important in the selection of materials.

The two fused fluoride coatings (76 CaF_2 + 23 LiF + 1 NiF_2 and 62 BaF_2 + 38 CaF_2) were selected because they are very stable compounds that would not be chemically affected by liquid fluorine. These fused fluoride coatings have also shown considerable promise as solid lubricants in other extreme environments (ref. 9).

APPARATUS AND PROCEDURE

The apparatus used in the first two phases of this investigation is shown schematically in figure 1. The basic elements are a rotating disk specimen ($2\frac{1}{2}$-in. diam.) and a stationary hemispherically tipped rider specimen (3/16-in. rad.) in sliding contact with the disk (see inset). The disk is rotated by a variable speed electric motor through a gearbox speed increaser coupled to the specimen shaft. Disk speed is monitored by a magnetic pickup whose output is fed into a digital readout instrument.

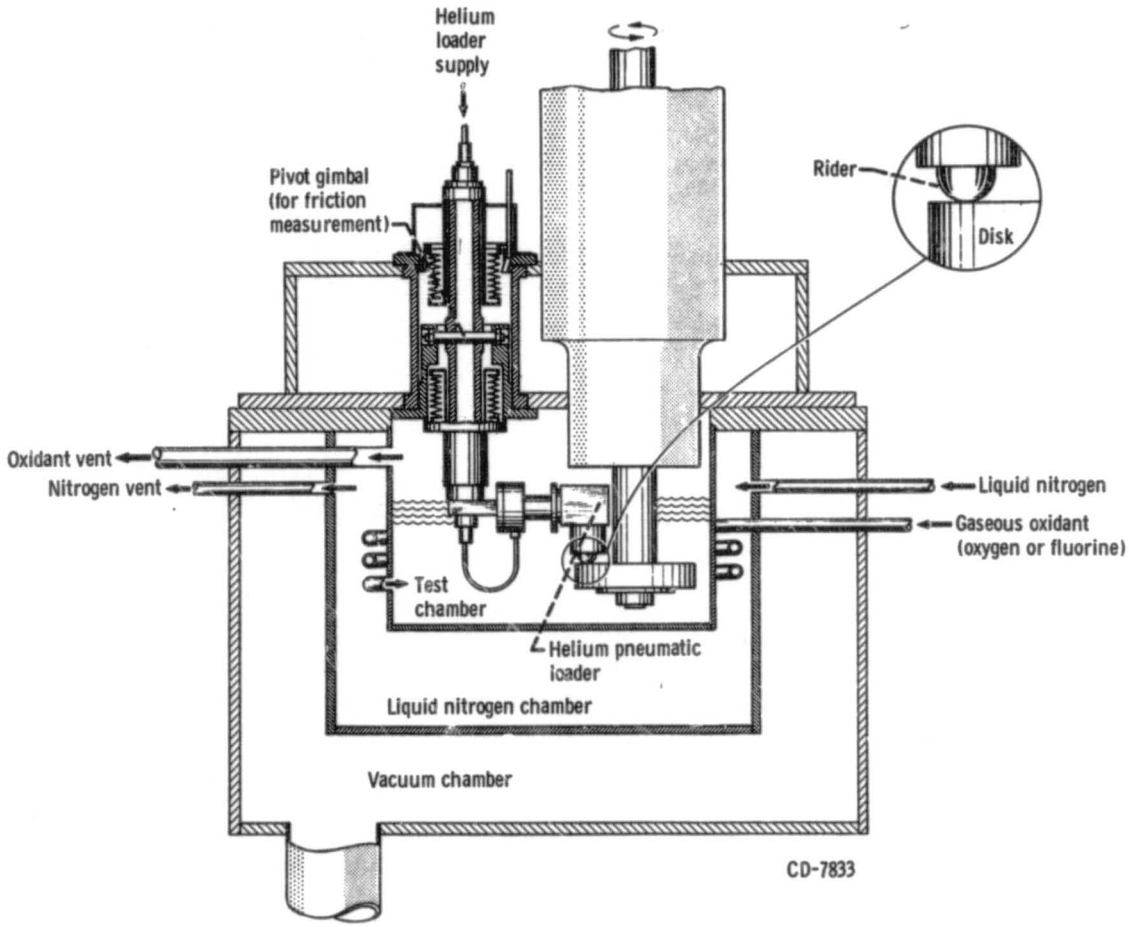

Figure 1. - Liquid oxidant friction apparatus.

The rider specimen is loaded against the disk by a pneumatically operated piston on the end of a gimbal mounted arm. Through this arm pressurizing gas (dry helium) is supplied. The arm is linked to a strain gage assembly for measurement of frictional force.

The apparatus consists of two sections (lower and upper) that may be separated for changing specimens. The lower section consists of four separate chambers. The inner chamber, or test chamber, is located within a "jacket" that is filled with liquid nitrogen for cooling and condensing the test gas. This cooling jacket is surrounded by a vacuum chamber to reduce the boiloff rate of the cooling and test fluids. The outermost or spill chamber (not shown in fig. 1) surrounds the three chambers and would provide safe operation if excess amounts of the test fluid should escape. The upper section is a vacuum jacket through which pass the disk specimen drive shaft housing and the rider specimen arm assembly. A series of face seals are used to prevent leakage of the oxidant along the drive shaft. Located in the upper half of the bearing housing are two carbon face seals used primarily to prevent leakage of the cooling oil. Within the housing that extends down into the test chamber is a double-face seal that is purged with helium set at a pressure slightly higher than the test chamber pressure. The upper half of this double seal consists

of graphite running against a nickel-chrome alloy, and the lower half consists of Al_2O_3 running against a fused fluoride coating (BaF_2 + CaF_2) on the nickel-chrome alloy. Flexible bellows are used to seal the load beam assembly. Fluorinated hydrocarbon oils are used to lubricate the gearbox and the support bearings in the shaft housing to minimize the possibility of reaction of the oil with the test fluid in case the shaft seals fail.

The test gas, oxygen or fluorine, passes through a coil within the cooling jacket before entering the test chamber near the bottom. In these tests the test fluid is initially in the gaseous state; the coil, at liquid nitrogen temperature, condenses the gas into the liquid state. Excess liquid and vapor are vented by a line leaving from a point near the top of the chamber. The liquid level within the test chamber is monitored by a capacitance probe.

The cooling jacket is filled with liquid nitrogen and vented by two diametrically opposite lines. The coolant level is monitored with a carbon resistance probe.

After the desired liquid level was attained, the disk specimen was brought up to speed and the normal load was applied. When possible, experiment duration was 1 hour. The frictional force was measured continuously by resistance strain gages mounted on a dynamometer ring whose output was fed into a recording potentiometer. After completion of a run, rider wear was obtained by measuring the wear scar and calculating the wear volume.

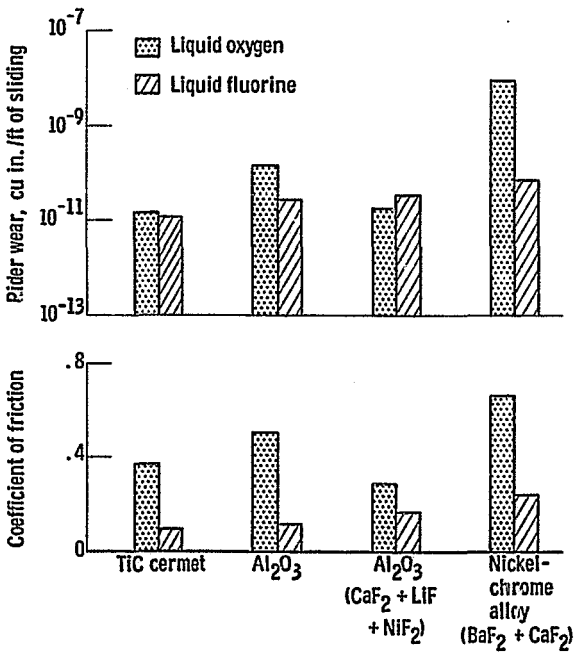

Figure 2. - Friction and wear of aluminum oxide riders sliding on various materials in liquid oxygen and liquid fluorine. Sliding velocity, 2300 feet per minute; load, 1000 grams.

For the seal experiments a housing adapter was made that contained the test seal. A 1/16-inch purge line was connected to the housing adapter, which maintained a 2-pound-per-square-inch pressure differential across the test seal.

SPECIMEN PREPARATION

For the friction and wear experiments, the solid Al_2O_3 riders and disks were scrubbed with levigated alumina, rinsed with distilled water, rinsed with alcohol, dried, and then rinsed with a solvent (1,1,1 trichloroethane) just prior to testing. The TiC cermet disk specimens were also cleaned in this manner. The fused fluoride coatings were prepared in a hydrogen atmosphere furnace at 1900° F, stored in a dessicator, and finally rinsed with a solvent (1,1,1 trichloroethane) before being placed in the friction apparatus.

For the fluorine seal experiments, the mating disk specimens were cleaned and prepared as described previously. The experimental seal assemblies were previously cleaned and passivated (exposed to fluorine gas to form a "passive" surface film). Upon assembly the flame-sprayed Al_2O_3 nosepieces were wiped with a soft cloth saturated with the solvent.

RESULTS AND DISCUSSION

Friction and Wear Experiments

Data were obtained in liquid oxygen and in liquid fluorine with Al_2O_3 riders sliding on four disk materials: (1) nickel-bonded TiC cermet, (2) solid Al_2O_3, (3) 76 CaF_2 - 23 LiF - 1 NiF_2 film on Al_2O_3 (1 NiF_2 was used as a coloring agent in order to differentiate between the fluoride coating and the Al_2O_3 substrate), and (4) 62 BaF_2 - 38 CaF_2 (eutectic) film on a nickel-chrome alloy. The friction and wear results are presented in table I and figure 2; these results are representative of a number of runs.

TABLE I. - EXPERIMENTAL DATA FOR FRICTION AND WEAR OF MATERIALS IN LIQUID OXYGEN AND LIQUID FLUORINE

[Riders, aluminum oxide; sliding velocity, 2300 feet per minute; load, 1000 grams.]

Disk material composition	Coating composition and thickness	Test liquid	Total run time, min	Rider wear rate, cu in./ft of sliding	Disk substrate wear rate, cu in./ft of sliding	Friction coefficient, f	Remarks
TiC cermet (52 Ti, 5 Mo, 25 Ni, 4.5 Cb, 13.2 C, 0.3 Ta)	None	Oxygen	60	0.015×10^{-9}	1.180×10^{-9}	0.37	Friction erratic; polished wear scars
	None	Fluorine	[a]23	0.012×10^{-9}	0.120×10^{-9}	<0.10	Friction steady; surface reaction film NiF_2 identified
Al_2O_3	None	Oxygen	60	0.140×10^{-9}	Negligible	0.50	Friction erratic; polished wear scars
	None	Fluorine	60	0.028×10^{-9}	Negligible	0.12	Friction steady; polished wear scars
Al_2O_3	76 CaF_2, 23 LiF, 1 NiF_2 0.0025 in.	Oxygen	62.5	0.015×10^{-9}	Negligible	[b]0.29	Friction steady; film failed at approximately 61.5 min
	76 CaF_2, 23 LiF, 1 NiF_2 0.003 in.	Fluorine	[a]45	0.033×10^{-9}	Negligible	0.17	Friction steady
Nickel-chrome alloy (53 Ni, 3.2 Ti, 19 Cr, 12 Fe, 11 Co, 1.6 Al, 10 Mo)	62 BaF_2, 38 CaF_2 0.0025 in.	Oxygen	59	8.300×10^{-9}	Excessive	0.66	Film failed immediately
	62 BaF_2, 38 CaF_2 0.002 in.	Fluorine	[a]20	0.076×10^{-9}	0.011×10^{-9}	0.24	Friction steady

[a]Test terminated because of low liquid fluorine level.

[b]Coefficient of friction after film failure, 0.50.

The results obtained indicate that liquid fluorine is potentially a better boundary lubricating media than liquid oxygen for the material combinations selected for this investigation. The low coefficients of friction in fluorine are attributed to the formation of beneficial metal fluoride films on the mating surfaces. The rider wear rates, cubic inches per foot of sliding, are in general of the same order of magnitude with the exception of the $BaF_2 + CaF_2$ eutectic coating on the nickel-chrome alloy run in liquid oxygen, which is approximately three hundred times greater. Resistance to oxidation by liquid oxygen and to fluoridation by liquid fluorine as well as hardness of the substrate materials are thought to be responsible for the low rider wear in these experiments. It appears that the corrosive and abrasive wear that could be expected in the highly corrosive environments were minimized by the careful selection of materials.

Previously reported liquid oxygen studies (refs. 10 and 11) showed that the presence of a proper oxide film on one of the mating surfaces was beneficial in effecting good lubrication. In this study it appears that the presence of a fluoride film, either an applied fused fluoride film in liquid oxygen or a fluoride film formed during sliding in liquid fluorine, is also beneficial in reducing wear and friction.

Friction and Wear with Surface Reaction Films

The results for Al_2O_3 sliding against either the TiC cermet or Al_2O_3 show a reduction in rider wear, friction coefficient, and disk wear in liquid fluorine as compared with liquid oxygen (table II and fig. 2). Photographs of

TABLE II. - EXPERIMENTAL SEAL DATA IN LIQUID FLUORINE

[Nosepiece, flame-sprayed aluminum oxide; sliding velocity, 2300 feet per minute; pressure difference, 2 lb/sq in.]

Disk material	Coating composition and thickness	Face load,[a] lb	Total run time, min	Nosepiece wear, cu in./ft of sliding	Disk substrate wear rate, cu in./ft of sliding	Remarks
TiC cermet	None	21	20	28.00×10^{-9}	7.000×10^{-9}	Surface speed, 80 ft/min
	None	15	40	6.85×10^{-9}	0.152×10^{-9}	Surface reaction; film NiF_2 identified
Al_2O_3	76 CaF_2, 23 LiF, 1 NiF_2 0.0015 in.	15	60	$<0.80\times10^{-9}$	Negligible	Trace amounts of applied fluoride film detected on wear track

[a]Calculated load at cryogenic temperature taking into account differential thermal contraction of assembly.

these two material combinations after running in oxygen and in fluorine can be seen in figures 3 and 4. Of the two sliding combinations, Al_2O_3 sliding against Al_2O_3 showed the greatest improvement in that rider wear was reduced by a factor of 5 and the coefficient of friction was reduced from 0.50 in oxygen to 0.12 in fluorine. While the combination of Al_2O_3 sliding on the TiC cermet shows no appreciable change in rider wear, the friction coefficient is reduced from 0.37 in oxygen to 0.10 in fluorine. It is important to note that continuous friction traces recorded during these runs showed that sliding was very smooth and steady in liquid fluorine as compared with the liquid oxygen, in which sliding was very rough and friction coefficient varied as much as ±0.05.

X-ray diffractions of the disk specimen wear tracks were taken after runs in the test fluids to determine whether a reaction film had formed on the materials. Nickel fluoride was identified as being present on the wear track

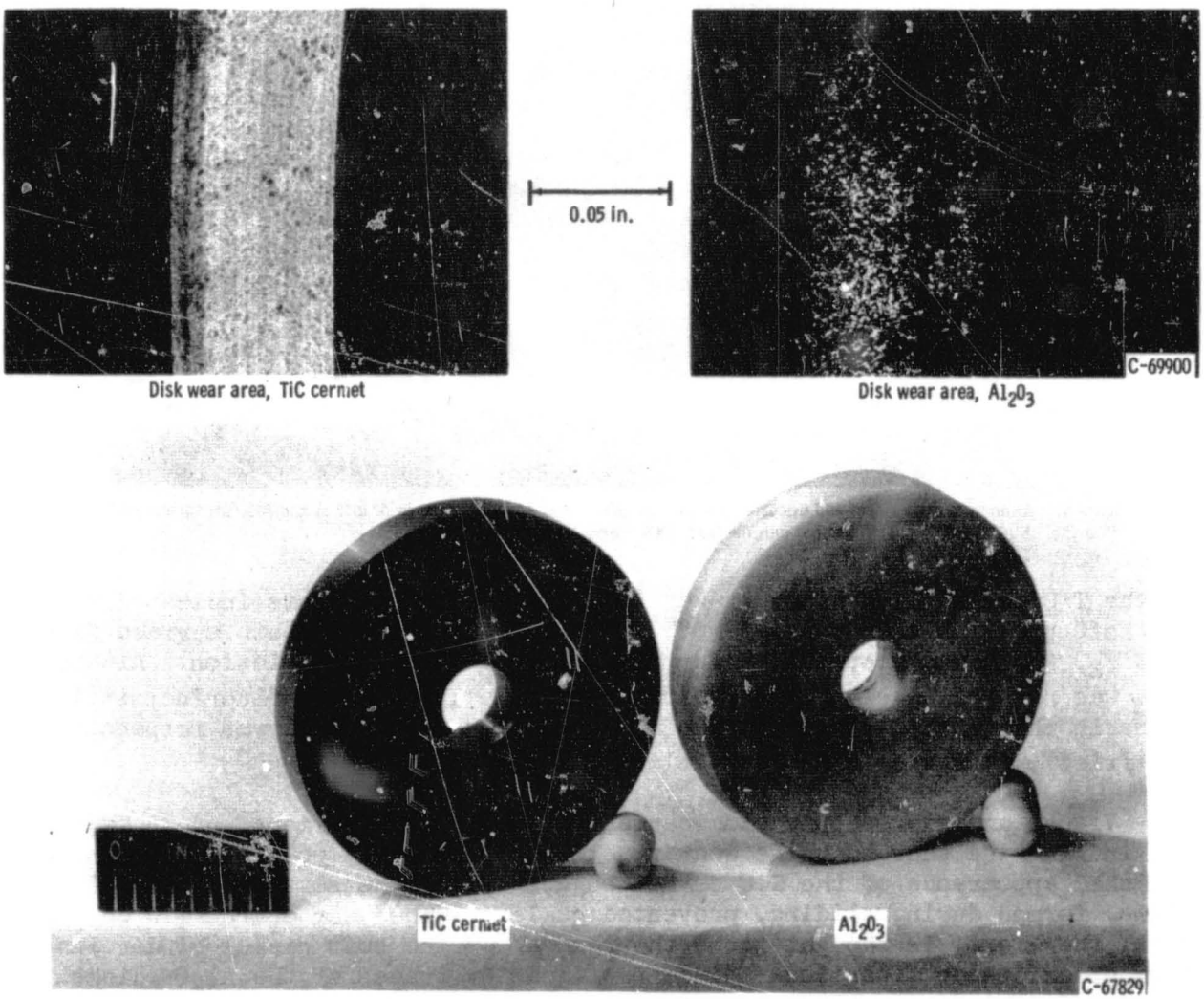

Disk wear area, TiC cermet

Disk wear area, Al_2O_3

Figure 3. - Aluminum oxide riders and uncoated titanium carbide cermet and aluminum oxide disk specimens run submerged in liquid oxygen. Sliding velocity, 2300 feet per minute; load, 1000 grams.

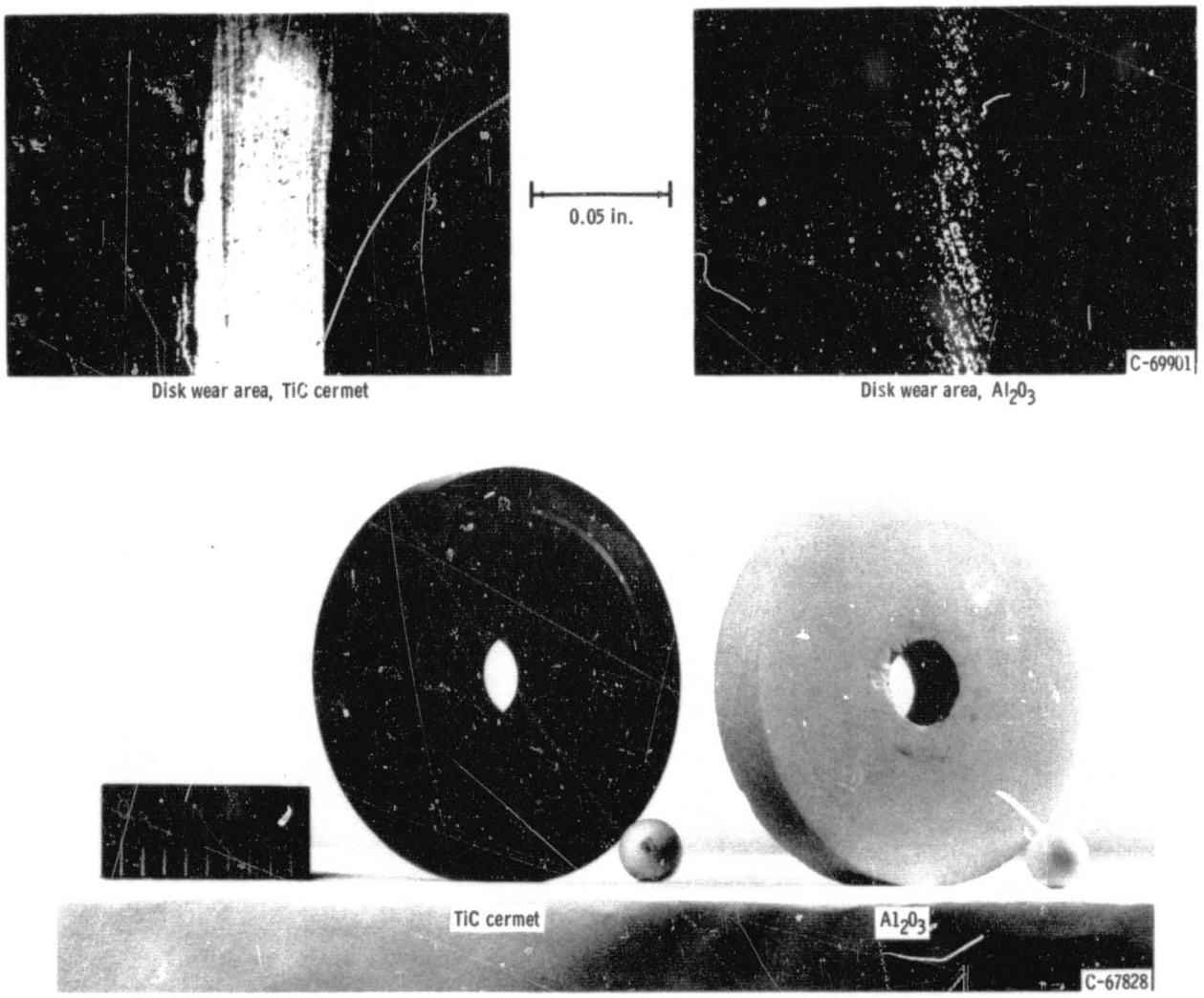

Figure 4. - Aluminum oxide riders and uncoated titanium carbide cermet and aluminum oxide disk specimens run submerged in liquid fluorine. Sliding velocity, 2300 feet per minute; load, 1000 grams.

of the TiC cermet disk after it was in liquid fluorine. This indicated that the soft nickel binder reacted with the fluorine to form a thin surface film of NiF_2, which was responsible for the low coefficient of friction. Although AlF_3 was not positively identified on the Al_2O_3 disk run in fluorine, it is probable that a thin AlF_3 film was formed during sliding and was responsible for friction and wear characteristics.

Visual and microscopic examinations of the disk specimens run in oxygen and in fluorine show that the wear tracks are smooth and polished. The highly polished appearance of the TiC cermet suggests that the soft intermediate films, formed during sliding, prevented galling. The wear of the TiC cermet disk, therefore, is thought to be the removal of the soft nickel binder in the form of oxides or fluorides. Since profilometer traces of the Al_2O_3 disks indicated no appreciable wear in liquid fluorine, it is thought that the rider tip, being continually subjected to high interface temperatures, contributed

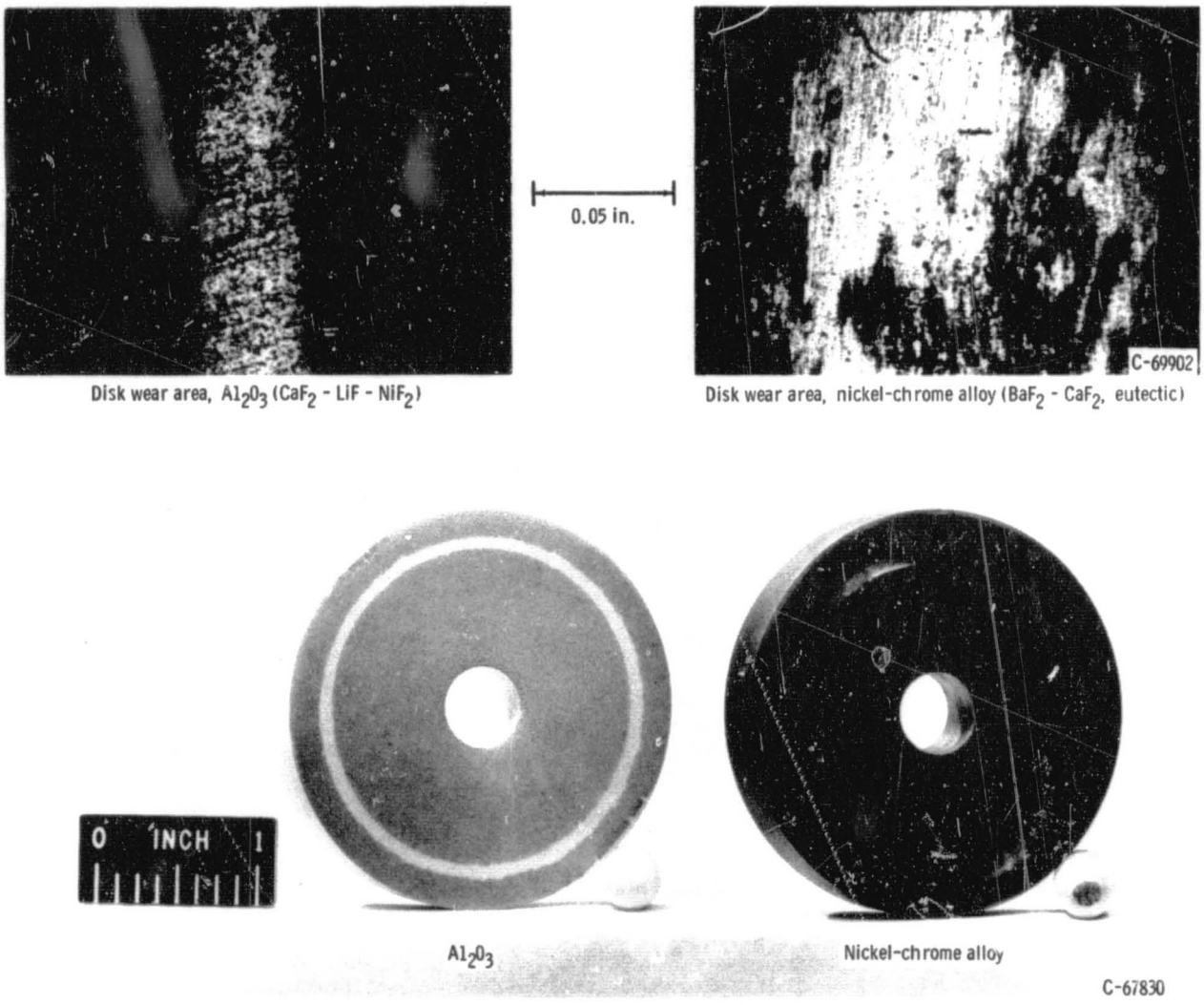

Disk wear area, Al_2O_3 (CaF_2 - LiF - NiF_2)

Disk wear area, nickel-chrome alloy (BaF_2 - CaF_2, eutectic)

Figure 5. - Aluminum oxide riders and coated aluminum oxide and nickel-chrome disk specimens run submerged in liquid oxygen. Sliding velocity, 2300 feet per minute; load, 1000 grams.

most to the formation of the fluoride film. Because of its performance, both in liquid oxygen and in fluorine, the combination of Al_2O_3 sliding against the TiC cermet was selected as one of the material combinations for the fluorine seal phase of this investigation.

Friction and Wear with Applied Surface Films

The results of the applied fluoride coatings on either Al_2O_3 or the nickel-chrome alloy indicated that these coatings show promise in oxygen and in fluorine (table I and fig. 2). In general, the experiments showed the films performed at least as well in fluorine as they did in oxygen.

The CaF_2 + LiF + NiF_2 on Al_2O_3 appears capable of providing an effective mating surface for the Al_2O_3 rider in oxygen. When the results of this coat-

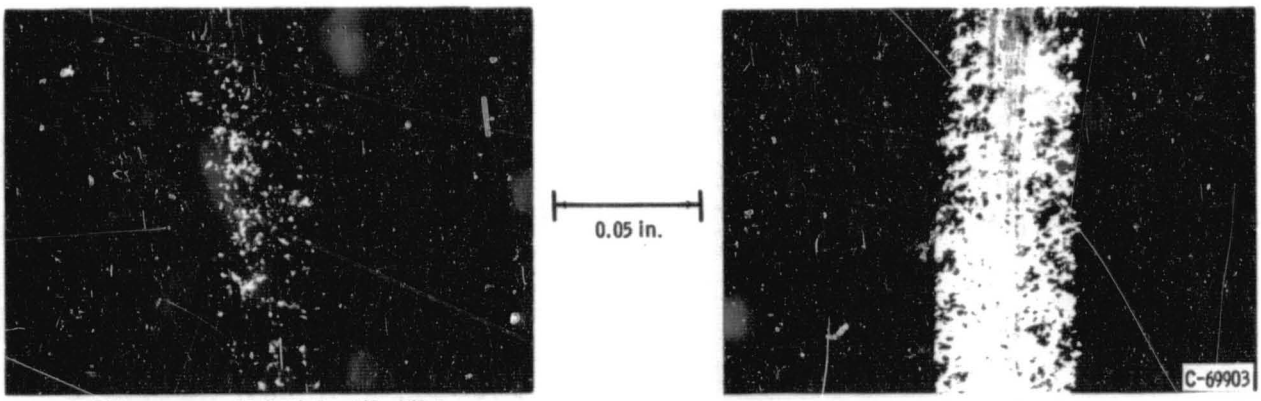

Disk wear area, Al_2O_3 (CaF_2 - LiF - NiF_2)

Disk wear area, nickel-chrome alloy (BaF_2 - CaF_2, eutectic)

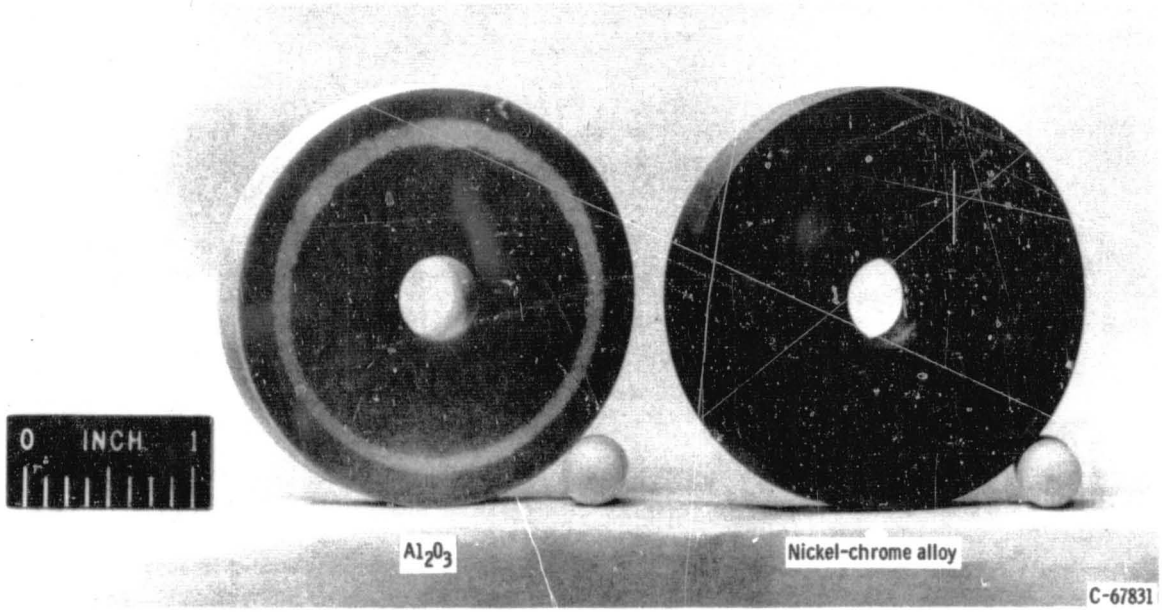

Figure 6. - Aluminum oxide riders and coated aluminum oxide and nickel-chrome disk specimens run submerged in liquid fluorine. Sliding velocity, 2300 feet per minute; load, 1000 grams.

ing are compared with the results of the uncoated Al_2O_3 (fig. 1) run in oxygen, it is noted that the friction coefficient was reduced from 0.50 to 0.29 by the coating. In fluorine, however, this fluoride coating on Al_2O_3 showed a higher friction coefficient (0.17) than the uncoated Al_2O_3 (0.12). Continuous friction traces recorded during runs in both oxygen and fluorine indicated that sliding was smooth and steady with the coating.

The Al_2O_3 rider wear in oxygen and in fluorine is essentially the same, and, although there is evidence of apparent coating failure (figs. 5 and 6), surface profile traces of the disk wear tracks show the wear of the Al_2O_3 substrate to be negligible. Because of the performance shown in the friction and wear experiments both in oxygen and in fluorine the CaF_2 + LiF + NiF_2 on Al_2O_3 was selected as a mating material for the Al_2O_3 nosepiece for the fluorine seal studies.

The applied film of BaF_2 + CaF_2 on the nickel chrome showed a great variance in performance when comparing the runs in oxygen and in fluorine. The runs in oxygen indicated that the film failed immediately and resulted in a deep grooving of the nickel-chrome substrate (fig. 5) as well as excessive Al_2O_3 rider wear (table I and fig. 2); the rider also showed evidence of metal transfer. The friction coefficient for this run remained high, and the recorded friction trace indicated very rough sliding and erratic contact.

In liquid fluorine, however, disk and rider wear are appreciably less (table I and fig. 2). Surface profile traces indicated very little wear to the nickel-chrome substrate. It is quite possible that NiF_2 was formed during sliding as was the case for the TiC cermet run in fluorine; however, X-ray diffraction did not detect its presence. The reduction in rider wear and disk wear and the low friction coefficient (0.24) are thought to be due to the effectiveness of the applied eutectic fluoride coating. Photographs of this combination after running in liquid fluorine are shown in figure 6.

Seal Experiments

From the friction and wear study, the material combinations of Al_2O_3 sliding against the TiC cermet and Al_2O_3 sliding against a fused coating (CaF_2 + LiF + NiF_2) on Al_2O_3 were selected as the materials to be used in the dynamic seal experiments in liquid fluorine (table II).

The stationary, flame-sprayed Al_2O_3 nosepiece was attached to a machined beryllium copper bellows that had a spring rate of 1000 pounds per inch and was run against the mating disk while submerged in liquid fluorine. The required experimental test conditions were as follows: sliding velocity, 2300 feet per minute; face load, 15 pounds; pressure differential across the seal, 2 pounds per square inch. In these seal experiments, the low pressure differential did not prevent the sealing surfaces from being wetted by liquid fluorine.

Two minor modifications to the friction and wear apparatus were required before the dynamic seal studies could be made (fig. 7). These modifications consisted in removing the loader assembly and redesigning the lower seal housing to incorporate the housing of the experimental seal. In addition, a helium purge line was connected between the load beam and the seal housing. This helium purge line was used to pressurize internally the experimental seal and to maintain a 2-pound-per-square-inch pressure differential across the seal. The results of the seal studies are presented in table II and figure 8.

In the first attempt to run a full-scale seal in fluorine it was found that the desired surface speed could not be attained because of insufficient power to drive the shaft. The overloading of the drive unit was caused by the high (21-lb) face load on the seal. As a result, this experiment was terminated after 20 minutes. Surface profile traces of the TiC cermet disk

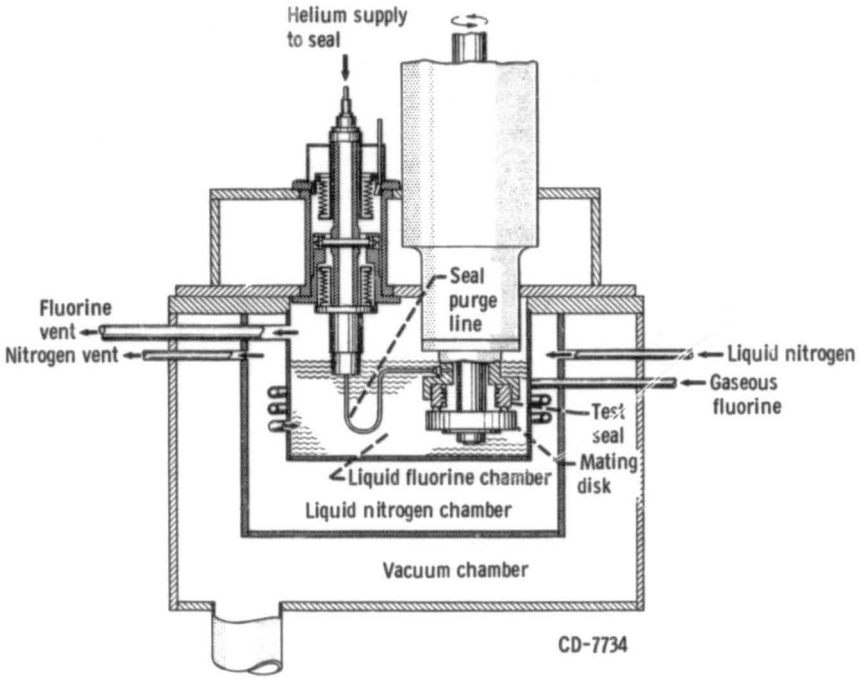

Figure 7. - Liquid fluorine seal test apparatus.

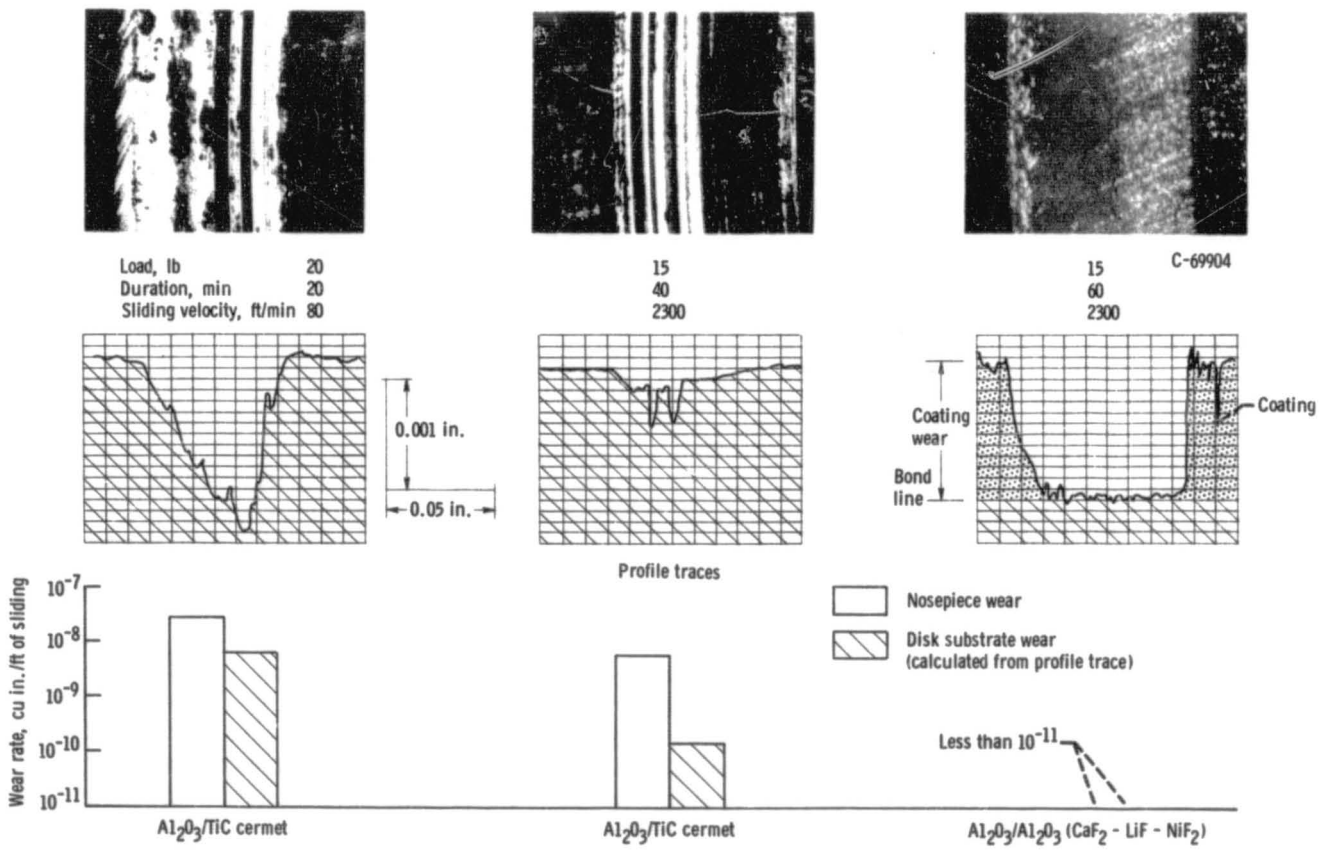

Figure 8. - Wear of seal materials obtained during seal experiments in liquid fluorine.

(fig. 8) indicated that a deep groove had been worn in the disk. The measurements of the Al_2O_3 nosepiece also indicated considerable wear in addition to visible edge chipping. Photographs of the seal components for this experiment can be seen in figure 9.

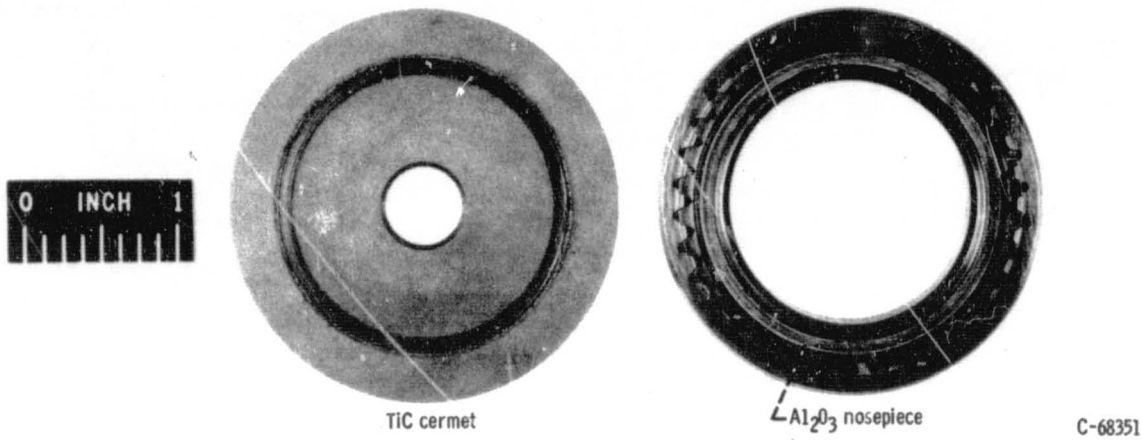

Figure 9. - Seal components; flame-sprayed aluminum oxide sliding against a titanium carbide cermet in liquid fluorine. Sliding velocity, 80 feet per minute; load, 21 pounds; duration, 20 minutes.

The second seal experiment was run after a modification to the drive unit was accomplished as well as calculations of expected seal face loading due to contraction of the shaft. This experiment was run successfully for 40 minutes at 2300 feet per minute and a face load of 15 pounds. Surface profile traces of the TiC cermet disk indicated a reduction in disk wear as compared with the first seal experiment (fig. 8). The Al_2O_3 nosepiece also showed less wear and less edge chipping. The seal components (fig. 10) are shown after completion of the experiment in fluorine.

The final seal experiment, that of Al_2O_3 running against a fused coating of CaF_2 + LiF + NiF_2 on Al_2O_3, was run successfully for 60 minutes. Visual examination of the mating disk indicated apparent loss of the film; however, X-ray diffraction showed that traces of the fused fluoride coating were present in the wear track. Surface profile traces of the mating disk indicated that there was no measurable wear of the Al_2O_3 substrate (fig. 8). Figure 11 shows the seal components used in the third seal experiment after 60 minutes of running in liquid fluorine. The results of the seal experiments indicated that Al_2O_3 sliding against either the fused fluoride film on Al_2O_3 or the TiC cermet are acceptable material combinations for fluorine seal applications. Proper pressure balancing of the seal is required, however, to prevent excessive face loading, which can cause catastrophic seal wear and local fragmentation of Al_2O_3.

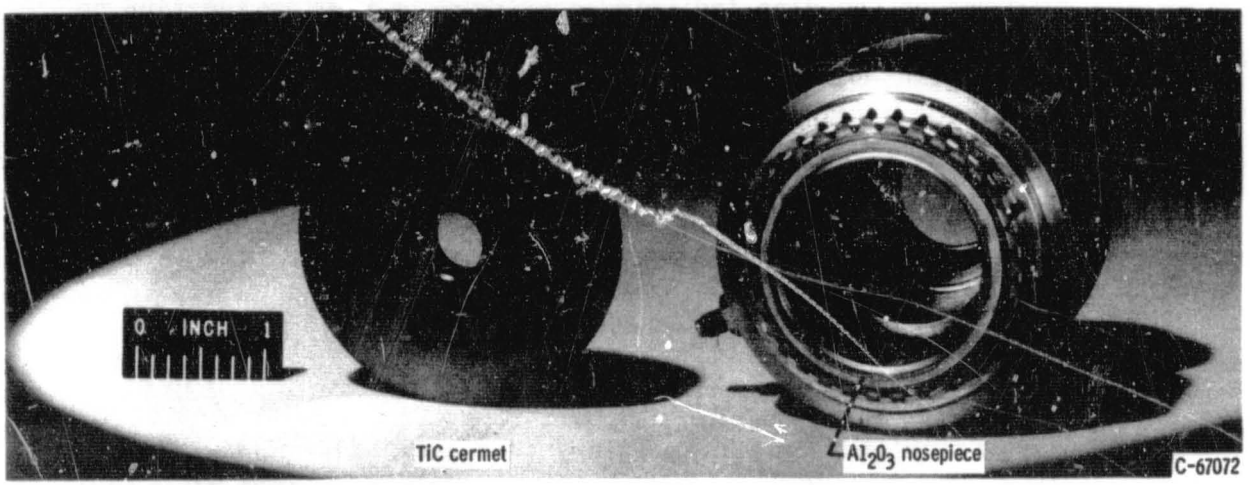

Figure 10. - Seal components; flame-sprayed aluminum oxide sliding against a titanium carbide cermet in liquid fluorine. Sliding velocity, 2300 feet per minute; load, 15 pounds; duration, 40 minutes.

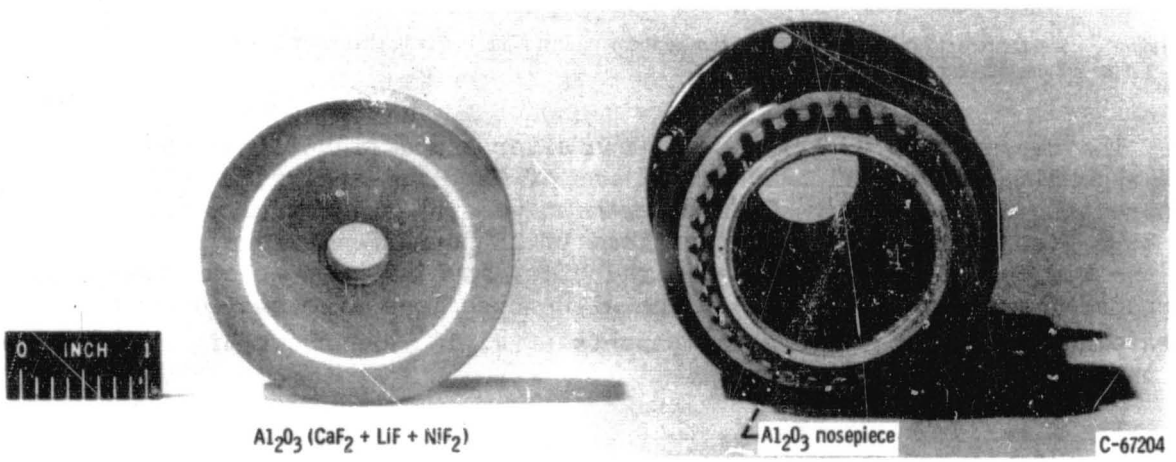

Figure 11. - Seal components; flamed-sprayed aluminum oxide sliding against 76 CaF_2 + 23 LiF + 1 NiF_2 on aluminum oxide in liquid fluorine. Sliding velocity, 2300 feet per minute; load, 15 pounds; duration, 60 minutes.

SUMMARY OF RESULTS

From the data obtained with aluminum oxide (Al_2O_3) in sliding contact with several mating surfaces submerged in liquid oxygen or in liquid fluorine in friction, wear, and dynamic seal studies, the following results were noted:

1. The Al_2O_3 sliding against either the titanium carbide cermet or a fused fluoride film on Al_2O_3 are potentially useful seal material combinations for liquid fluorine turbopump applications.

2. The presence of a fluoride film, either as an applied film (calcium fluoride (CaF_2) - lithium fluoride (LiF) - nickel fluoride (NiF_2)) or a film formed during sliding (NiF_2) is beneficial in reducing friction and wear of

materials in liquid fluorine.

3. With the same sliding combination in this investigation, the coefficient of friction was generally lower in liquid fluorine than in liquid oxygen.

Lewis Research Center
National Aeronautics and Space Administration
Cleveland, Ohio, June 4, 1964

REFERENCES

1. Osborn, Walter M.: Noncavitating and Cavitating Performance of a Liquid-Fluorine Pump Designed by Stream-Filament Method. NASA TM X-722, 1963.

2. Schmidt, Harold W.: Reaction of Fluorine with Carbon as a Means of Fluorine Disposal. NACA RM E57E02, 1957.

3. Ruff, Otto, und Bretschneider, Otto: Die Zusammensetzung und Bildungswarme der aus Norit und aus SiC Gebildeten Kohlenstoss-Fluoridgemische. Zs. Anorg. und Allgem. Chem., Bd. 217, Heft 1, 1934, pp. 19-21.

4. Simons, J. H., and Block, L. P.: Fluorocarbons. The Reaction of Fluorine with Carbon. Jour. Am. Chem. Soc., vol. 61, 1939, pp. 2962-2966.

5. Price, Harold G., Jr., and Douglass, Howard W.: Nonmetallic Material Compatibility with Liquid Fluorine. NACA RM E57G18, 1957.

6. Schmidt, Harold W.: Compatibility of Metals with Liquid Fluorine at High Pressures and Flow Velocities. NACA RM E58D11, 1958.

7. Godwin, Thomas W., and Lorenzo, Carl F.: Ignition of Several Metals in Fluorine. Preprint 740-58, Am. Rocket Soc., Inc., 1958.

8. Buckley, Donald H., and Johnson, Robert L.: Inhibiting Corrosive Wear in Lubrication with Halogenated Gases at 1500° F by Use of Competitive Reactions and Other Methods. ASLE Trans., vol. 4, no. 1, Apr. 1961, pp. 33-38.

9. Sliney, Harold E., Strom, Thomas N., and Allen, Gordon P.: Fused Fluoride Coatings as Solid Lubricants in Liquid Sodium, Hydrogen, Vacuum, and Air. NASA TN D-2348, 1964.

10. Hady, William F., Allen, Gordon P., and Johnson, Robert L.: Boundary Lubrication Characteristics of a Typical Bearing Steel in Liquid Oxygen. NASA TN D-1580, 1963.

11. Hady, William F., Allen, Gordon P., and Johnson, Robert L.: Wear and Friction of Mechanical Carbons in Liquid Oxygen as Influenced by Transfer Films. Paper 63AM 5B-3, ASLE, 1963.

END OF REFERENCE

114

REFERENCE

115

BERND, L. H.: SURVEY OF THE THEORY OF MECHANICAL FACE SEALS, PART 1 - CHARACTERISTICS OF SEALS. LUBRI. ENG., VOL. 24, NO. 10, OCTOBER 1968.

Survey of the Theory of Mechanical Face Seals—

Part I Characteristics of Seals

L. H. BERND
General Electric Research & Development Center

A brief review is presented of various theories and approaches that have been followed seeking to explain the functioning of face seals, and improve their operation. The known, essential characteristics of a radial face seal are summarized. The performance and inherent limitations of a seal are discussed in terms of the axial forces on the seal faces and the character of the lubrication between the mating faces.

Considerable explorative work has been done over the past decade, spurred by Denny's experiments showing that hydrodynamic pressure generation (increased load bearing) and inward pumping (reduced leakage) can take place in a seal. Definite approaches involving different mechanisms have emerged. The status is that the dominant mechanisms have not been fully studied, isolated, and reduced to useable, universal parameters. Hence, the conscious exploitation of these mechanisms to obtain improved sealing lies largely ahead in most cases.

Presented at the 23rd ASLE Annual Meeting in Cleveland, May 6–9, 1968

INTRODUCTION

The purpose of this article is to review the status of face seal theory. Mechanical face seals have been used in industry since the early nineteen hundreds. They are unique in their ability to seal with negligible leakage under severe conditions, and consume relatively little frictional energy. They are reliable, have long life, and require no maintenance. Their major application is to seal liquids under pressure.

The function of a face seal is to prevent leakage where a rotating shaft pierces a housing or wall. The basic concept involved appears simple at first thought. Two smooth faces, one a rotating ring affixed to the shaft, the other a stationary ring secured to the housing, are pressed together. This decreases the clearance between the faces, thus decreasing the size of the leakage path to limit or prevent fluid leakage.

The realization that this seal is in many respects a complex device; that boundary lubrication, cavitation, or a full fluid film can exist between the faces depending upon conditions; that conceivably various different mechanisms can act to provide load bearing between the faces (as well as prevent leakage); are thoughts of relatively recent origin. Indeed, the past decade has seen considerable exploration of the face seal as a fluid film device, motivated by the hopeful expectation of improv-

NOMENCLATURE

A_h = Nominal area of contact between seal faces
A_p = Area of rear of seal exposed to pressure of fluid being sealed
b = Width of seal face = $R_2 - R_1$
c = Constant
F_f = Friction force
F_h = Force on seal face
F_p = Hydrostatic force
F_s = Spring force
f = Coefficient of friction
h = Mean clearance between seal faces
N = Rotational speed
P = Pressure
P_p = Fluid pressure being sealed
Q = Leakage rate between seal faces
R_1 = Inner radius of seal face
R_2 = Outer radius of seal face
Z = Viscosity
(ZN/P) = Duty parameter

β Balance of seal
η $1 - \beta$, a measure of seal balance
σ External pressure applied to seal face
τ Shear stress on seal faces

ing the operation of the seal. Nevertheless, the theory of face seals has not in toto progressed to the point of providing a general, useable, "textbook" type of rational design approach based on analytical foundations. The scope of existing, comprehensive studies is somewhat limited; many important areas still lie unexplored, both analytically and experimentally. The range of major studies is blocked out in Fig. 1.

Thus, even though certain mechanistic approaches are well advanced, it cannot as yet be said whether the face seal as it basically stands today—evolved largely by trial and error testing—has resulted in about the best seal possible when used properly; or whether advances such as longer life, lower leakage, operation at greater extremes of rotational speed or fluid pressure, can ultimately be obtained.

Undoubtedly a primary reason for this slow advance is the small dimensions of a face seal making direct examination of a lubricating or sealing mechanism exceedingly difficult. Furthermore, the wide range of conditions possible as to seal materials, dimensions, alignment, fluid pressures, bearing loads, rotational speeds; as well as the difficulty in assuming what may or may not be a dominant mechanism (or mechanisms) confuse the issue. Small differences in dimensions as well as manufacturing tolerances may produce considerable variations in performance. Judging by progress over the past decade, one may expect continued exploration and increasing knowledge, leading to a slow evolution of design techniques.

A seal is also a thrust bearing. Thus it has the same basic problems as a bearing, as well as additional requirements stemming from its sealing function. A review of theory must include as evidence the performance of a seal, show how this is related to physical form, and the lubrication regimes that exist. Boundary lubrication fundamentals are important to a class of seals; practice here is well established. Mixed and fluid film lubrication are also found in seals. For these, the hydrodynamic generation of pressure for load bearing and sealing between faces is an interesting, as well as speculative subject.

Initially, the theories or approaches applied to face seal design were simple. For example:

1. It is an intuitively obvious concept that seal faces can be forced together to prevent leakage. Thus it seemed reasonable to design by experimentally increasing the external load on the faces until leakage became tolerable, seeking a compromise versus increasing wear and shorter life.
2. Surface tension acting at the interface between liquid and air, at the low-pressure edge of the seal faces, creates a pressure differential to contain the liquid. The sealing pressure so created can be computed, knowing the surface tension, and assuming that the maximum gap width between seal faces is equal to the sum of the waviness of the two face surfaces (*6*). For common fluids, sealing pressure in the order of 25 to 50 psi can thus be inferred.
3. In high speed seals, centrifugal force acting on fluid present between seal faces that are not in physical contact can be used to oppose the hydrostatic pressure causing inward radial leakage (*7*).

In contrast, much of the recent literature is concerned with how the physical features of face seals possessing liquid films between the faces are related to seal performance. How important are these features? Should they be modified? Thus, for example, are better or more poorly finished surfaces desirable? Can distortion, vibration, and eccentricity and misalignment be put to advantageous use?

In summation, practical knowledge of boundary lubrication in a seal is far more advanced than knowledge of hydrodynamic effects. That is, it is possible to design a seal and select suitable face materials from the standpoint of friction and wear. It is not possible on a broad basis to select or isolate specific hydrodynamic pressure generating mechanisms to be used, and thereby deliberately create load bearing pressure with pressure variations to oppose leakage. An exception to this would be the use of centrifugal force in a high speed seal.

CHARACTERISTICS OF A MECHANICAL FACE SEAL

Performance Limits

The practical operating limits of seals are generally stated to be as follows:

Pressure—Figure 2 is a compilation from the published data of various seal manufacturers of the pressures that can be sealed readily with a face seal. Important is the fact that higher pressures can be sealed with balanced seals than with unbalanced seals. Typical maximum pressures for unbalanced seals are in the order of one to two hundred psi. Balanced seals are used up to pressures in the order of 1000 psi or more.

This originally raised the question why relatively small changes in balancing can alter the maximum sealing pressure so (*1*). This difference in duty can be ascribed to the different lubricating regimes that can exist between the seal faces.

Face Speed—Manufacturers' recommendations are for maximum shaft speeds in the 6000 rpm to 15,000 rpm range. The maximum speed noted for any face seal is about 30,000 rpm.

Life—In conservative refinery practice, typical seal life is noted as being about 2000-8000 hr (*9*). In domestic water pumps, life is probably in the order of 15,000 hr, i.e., 2 years of continuous service. For very high face velocities and poor lubrication, such as for a cryogenic liquid seal in a rocket engine turbopump, life may be only a matter of minutes.

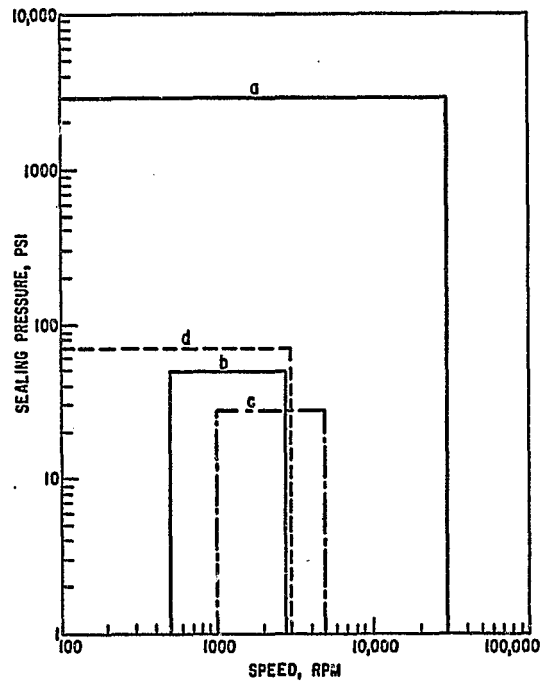

Fig. 1—Range of major studies (pressure sealed vs. speed).

Leakage—Existing data is unreliable since in practice a liquid may often evaporate before it can be measured. For a "properly" designed seal, anticipated leakage can range from "zero" to about 10 cc/min. Leakage is generally reported to increase with speed. Some find the converse: a stationary seal leaks badly, but improves in sealing with increasing speed.

Essential Physical Features of Mechanical Face Seals

Empirical experience has produced features common to all mechanical face seals. These features are:

1. Sealing is accomplished by holding two mating, annular faces together.
2. The faces are pressed together by light spring loading, and by fluid pressure acting on the rear of one of the sealing faces. The amount of fluid pressure so employed varies according to the "balance" of the seal.
3. The two annular surfaces in contact are made from dissimilar materials capable of operation under boundary lubrication conditions. Low coefficients of friction, good heat conductivity, are sought to prevent high temperatures and breakdown of face materials.
4. The face seal mating surfaces are lapped flat to within a 2–5 light bands of flatness (24 to 60 microinches); the resultant finish (surface roughness) is approximately 10 to 20 microinches.

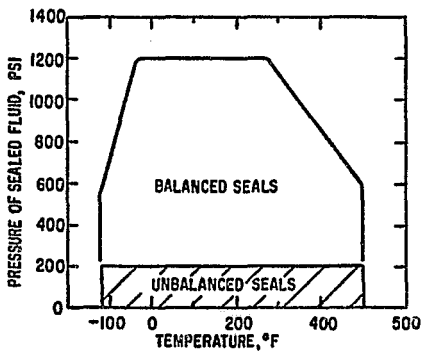

Fig. 2—Approximate outline of seal operating conditions recommended by manufacturers (pressure vs. temperature).

5. A certain minimum amount of roughness and/or waviness of the seal faces should be considered an essential feature of a seal. Excessively rough surfaces can make for high coefficients of friction, excessive wear and for short life. However, exceedingly smooth surfaces have resulted in the failure of seals and bearings. The ability to provide load bearing is lost. Such failure has been attributed to the lack of hydrodynamic pressure generation that variations in surface height would have produced, or the inability of the surfaces to retain a lubricant (*11*).
6. The shaft mounted face is flexibly mounted and sealed to the shaft so that the mating faces are held in contact in spite of shaft vibration or eccentricity.
7. Auxiliary "static" seals, usually "O" rings, are provided to seal the mating faces to the shaft or machinery housing.

Cross-sections of several typical types of face seals are given in Fig. 3.

BALANCE

Axial Forces on a Seal

It is necessary to consider the axial forces acting on a seal face in order to define the "balance" of a seal and relate balance to seal performance. Two external forces act to press the seal faces together. They are:

1. A hydrostatic force F_p, proportional to the pressure being sealed P_p. Most of the load on the faces is produced in this way by the fluid being sealed.
2. A spring force F_s. This force is relatively small. It is used to ensure contact between the faces before the pressure being sealed has been built up. The spring force must be large enough to overcome the static friction F_f of the "O" ring.

Fluid pressure between the seal faces (when fluid is present between the faces to exert pressure) opposes these external forces, and acts to separate the seal faces. This pressure can be due primarily to leakage flow across the faces, and be determined by the characteristics of the flow process acting to produce a pres-

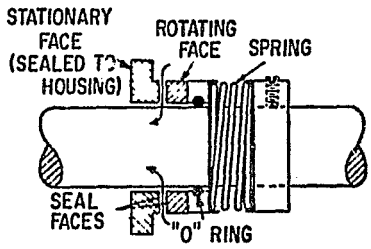

Fig. 3a—Unbalanced seal—cross section.

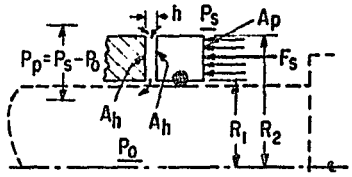

Fig. 3b—Unbalanced seal—schematic.

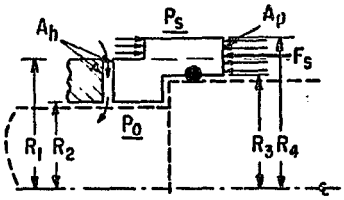

Fig. 3c—"Balanced" seal—schematic.

h =CLEARANCE BETWEEN MATING SEAL FACES
F_s =SPRING FORCE
P_p =NET HYDROSTATIC PRESSURE OF FLUID BEING SEALED-PSI $(P_s - P_0)$
P_0 =EXTERNAL, AMBIENT PRESSURE
P_s = INTERNAL PRESSURE

Fig. 3—Typical seals.

sure drop. If the faces are close enough, and speeds high enough, hydrodynamic pressure generation caused by surface irregularities or other causes should be superposed on this pressure drop. If however, the faces are pressed tightly together, fluid should be excluded, as evidenced by a lack of fluid pressure as reported by Mayer (2).

For the first case, suppose that the seal faces are parallel and separated by fluid. Then laminar leakage for a continuous liquid film between the faces, results in a linear pressure distribution between inlet and outlet (Fig. 4). This follows when the width of the seal face is small with respect to the radius of the seal, and a constant viscosity is assumed. The net force F_h acting on the rotating seal face due to this leakage pressure is $(P_p/2)A_h$, where A_h is the contact area of a face.

Unbalanced Seal

The unbalanced seal is the simplest form of seal (Fig. 3a). It is fitted to a shaft of constant diameter. As a consequence, the contact area A_h between the sealing faces is equal to the area A_p on the rear of the sealing ring upon which the hydrostatic pressure of the fluid being sealed acts (Fig. 3b). Presumably, the pressure limit for sealing is reached when the external load $F_s + F_p$ is sufficiently large with respect to the opposing pressure within the fluid film between the faces to force the faces together; produce considerable physical contact and boundary lubrication; with attendant high friction, heat release and wear.

Balanced Seal

To overcome the pressure limitation of a few hundred psi, a seal is "balanced" by using a stepped shaft (Fig. 3c). This reduces the loading on the seal faces resulting from the hydrostatic pressure P_p. The usual limit to balancing is about one third. One third of the pressure is balanced out, leaving two-thirds of the hydrostatic pressure (P_p) act on the seal face. That is:

$$F_p = (1 - \beta)P_p A_p = \tfrac{2}{3}P_p A_p, \qquad [1]$$

where β is termed the amount of balance. Alternately, $(1 - \beta) = \eta$ is also used to designate the extent of balance (*10*).

Should the balancing limit of $\beta = \frac{1}{3}$ be much exceeded, it has been found that the seal faces tend to be in an unstable condition (*9*). Balancing can only be carried so far, i.e., up to $\beta = \frac{1}{2}$ as an ideal limit. For a β larger than this, once the faces are slightly forced apart by motion, misalignment, flashing of liquid into vapor, dirt, etc., the faces will open further by themselves, and subsequently be unable to close.

To see why this should be so, let us consider the axial forces that act on the seal. For the seal gap (h) not to open, the sum of the axial forces must act to press the faces together. That is:

$$(F_s + F_p) > F_h$$

For a linear pressure distribution between the seal faces:

$$[F_s + (1 - \beta)P_p A_p] > \frac{P_p}{2} A_h \qquad [2]$$

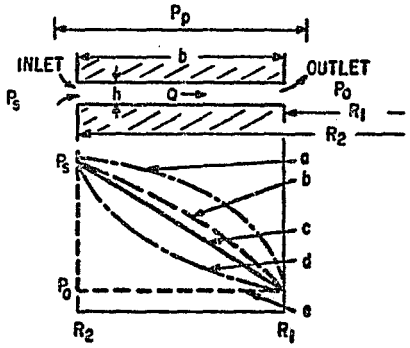

LEGEND:
a. CLEARANCE (h) DECREASING IN DIRECTION OF FLOW
b. PARALLEL FACES, $(R_2 - R_1)/R_2$ NOT SMALL
c. PARALLEL FACES, $b \ll R_2, R_1$
d. CLEARANCE (h) INCREASING IN DIRECTION OF FLOW
e. CLEARANCE (h) = 0 PERFECT CONTACT, Q=0

Fig. 4—Pressure between seal faces due to leakage.

Neglecting a relatively small F_s:

$$(1 - \beta)P_pA_p > \frac{P_p}{2}A_h$$

For $\beta = \frac{1}{3}$:

$$(1 - \beta) = \frac{2}{3} > \frac{1}{2}\frac{A_h}{A_p}$$

$$\frac{2}{3} > \frac{1}{2}$$

A_h in practice is only slightly larger than A_p. This shows therefore, that a ⅓ balance acts to provide a net force keeping the faces together, and that a much greater degree of balance cannot do so.

Actually, to keep the faces together, the net static forces acting on the seal ($F_s + F_p + F_h$) must be greater than zero for various reasons. There must be a margin sufficient to overcome vibration, part misalignment, and "O" ring friction. In addition, the leakage pressure term ($P_p/2$) may increase (or decrease) because the seal faces may cease to be parallel under operating conditions because of wear, thermal gradients and deformation under load.

Suppose it were possible to press the seal faces tightly together, leaving no gap ($h = 0$), so that full contact with no leakage were achieved. Then the net fluid pressure between the faces due to the leakage of fluid between them would approach zero (Fig. 4). Or, suppose that the leakage clearance diverged in the direction of flow to reduce the net fluid pressure. Under these conditions a balance larger than $\beta = \frac{1}{3}$ would be possible. The fact that a $\beta = \frac{1}{3}$ has been stated to work satisfactorily until the faces move apart (*9, 1*) implies that the average fluid pressure between faces can be less than $P_p/2$.

FRICTION

One expects friction in a seal to follow the trends found in other bearing elements, where different lubricating regimes exist depending upon conditions. These regimes are customarily termed boundary lubrication, mixed film lubrication, and full film lubrication. Different coefficients of friction are found in each regime. This is sketched in Fig. 5 versus the "duty parameter" (ZN/P).

Boon, Honingh and Van Rijssen (*12*) state that they have tested many seals. They consider Fig. 6 to be typical of the frictional characteristics of the seals they have tested when sealing a liquid. Figure 7 gives dry friction for the same seal. It is quite different in character. The "wet" seal friction in Fig. 6 initially decreases with load, then increases greatly as the load is further increased. The friction values obtained are representative of the transition between full film, mixed and boundary lubrication. The fact that lower friction values occur at about $\eta = 0.5$ to 0.8 ($\eta = 0.7$ for $\beta = 0.3$ balance), and that higher friction is found at $\eta = 1.0$

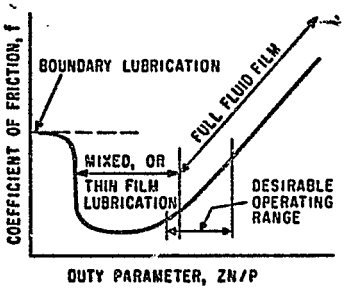

Fig. 5—Lubrication regimes (friction vs. duty parameter).

($\eta = 1$ for an unbalanced seal, i.e., $\beta = 0$), ties in nicely with the need to use a balanced seal when sealing against high pressures. This points out that balancing a seal decreases friction by changing dry friction to lubrication with a liquid film.

If a fluid film has been obtained by balancing, the gap width should increase. This is apparently confirmed since the authors note: "For $\eta = 0.5$ the friction is quite low, but the seal leaks a little." The implication is that the improved ability of a balanced seal to handle higher pressure and obtain a lower effective coefficient of friction is attained at the cost of leakage, and that this leakage then brings in to play the following effects:

1. Fluid pressure between faces due to leakage.
2. Hydrodynamic bearing action, because of the presence of liquid, to enable higher unit loads to be borne by the seal faces.

Fogg, in tests on a parallel thrust bearing (*13*), obtained data giving a relation between the coefficient of friction (f) and high values of (ZN/P) in the full fluid regime of

$$f = c(ZN/P)^{1/2} \qquad [3]$$

where c is a constant.

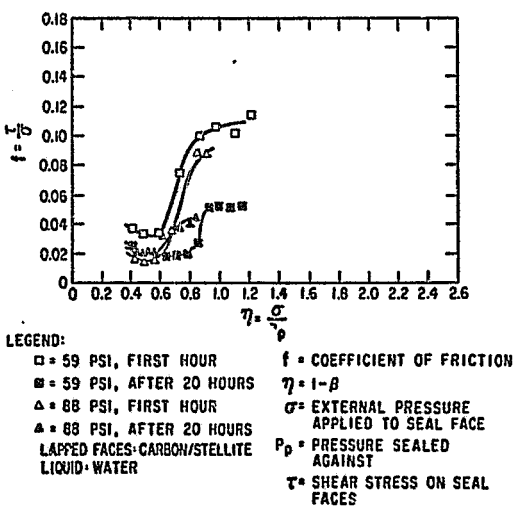

Fig. 6—Typical wet running friction of a face seal.

It is possible to show that the exponent for (ZN/P) should be approximately ½ if the hydrodynamic pressure generating mechanism is reducible to the Reynolds equation without side leakage; i.e., if pressure generation were due primarily to fluid viscosity acting in a converging clearance. This relation should hold for large values of (ZN/P) when the ratio of clearance to variations in surface height is large. As the bearing surfaces approach at low values of (ZN/P), the exponent should decrease.

Nau (*14, 15*) has compared face clearance and friction/duty parameter data from tests of various seal, and seal-like geometries. He notes that in some cases (*3*) and (*4*) the exponent is one-half, whereas in others (*5*) and (*16*), an entirely different relation holds. Thus it would appear that different mechanisms have been observed to act in the fluid lubrication regime.

REFERENCES

(*1*) Mayer, E., "Unbalanced Mechanical Seals for Liquids," Paper E2[1], April 1961.

(*2*) Mayer, E., "Leakage and Friction of Mechanical Seals with Special Consideration of Hydrodynamic Mechanical Seals," Paper E3[1], April 1961.

(*3*) Summer-Smith, D., "Laboratory Investigation of the Performance of a Radial Face Seal," Paper D1[1], April 1961.

(*4*) Ishiwata, H. and Hirabayashi, H., "Friction and Sealing Characteristics of Mechanical Face Seals," Paper D5[1], April 1961.

(*5*) Denny, D. F., "Some Measurements of Fluid Pressures Between Plane Parallel Thrust Surfaces with Special Reference to Radial Face Seals," *Wear*, V.4, 1960.

(*6*) Brkich, A., "Mechanical Seals Theory and Criteria for Their Design," *Prod. Eng.* V.21, April 1950.

(*7*) Huhn, D., "Theory of Fluid Sealing," Paper D2[1], April 1961.

(*8*) Lymer, A., "Mechanical Sealing as It Stands Today," *Engineering*, V.194, April 21, 1961.

(*9*) Wood, T. H., "Mechanical Shaft Seals in the Chemical Industry," *Trans. Instn. Chem. Eng.*, V.32, 1954.

(*10*) Schoenherr, K., "Design Terminology for Mechanical End Face Seals," *SAE Trans.*, V.74, Paper 650301, 1966.

(*11*) Fuller, D. D., "Theory and Practice of Lubrication for Engineers," John Wiley and Sons, 1956, p. 160.

(*12*) Boon, E. F., Honingh, S., Van Rijssen, D. C., "Some Notes on Seals for Rotating Shafts," Proceedings Fourth World Petroleum Congress, Rome 1955, Carlo Colombo.

(*13*) Fogg, A., "Fluid Film Lubrication of Parallel Thrust Surfaces," *Instn. of Mech. Eng.*, V.155, 1946.

(*14*) Nau, B. S., "Some Recent Results in Fluid Sealing Research," 1962 International Fluid Power Conference.

(*15*) Nau, B. S., "Hydrodynamic Lubrication in Face Seals," Third BHRA International Conference on Fluid Sealing, April 1967, Paper E5.

(*16*) Reiner, M., "The Centripetal Pump Effect in a Vacuum Pump," *Proc. Roy Soc.* A247.

[1] Designates British Hydromechanics Research Association (BHRA) International Conference on Fluid Sealing, April 1961.

END OF REFERENCE

115

REFERENCE

116

RUSSEL, T. E.; ALLEN, G. P.; LUDWIG, L. P.; AND JOHNSON, R. L.: GAS TURBINE FACE SEAL THERMAL DEFORMATION AND COMPUTER PROGRAM FOR CALCULATION OF AXISYMMETRIC TEMPERATURE FIELD. NASA TN D-5605, 1969.

8.4-0-0
DON FORNEY
8-6
(216)

NASA TECHNICAL NOTE

NASA TN D-5605

NASA TN D-5605

COPY 2

LEWIS RESEARCH CENTER
Aerospace Safety Research
and Data Institute
FEB 7 1972
CLEVELAND, OHIO

GAS TURBINE FACE SEAL THERMAL DEFORMATION AND COMPUTER PROGRAM FOR CALCULATION OF AXISYMMETRIC TEMPERATURE FIELD

by Terrence E. Russell, Gordon P. Allen, Lawrence P. Ludwig, and Robert L. Johnson

Lewis Research Center
Cleveland, Ohio

LIBRARY COPY
FEB 5 1970
LEWIS LIBRARY, NASA
CLEVELAND, OHIO

NATIONAL AERONAUTICS AND SPACE ADMINISTRATION • WASHINGTON, D. C. • DECEMBER 1969

1. Report No. NASA TN D-5605	2. Government Accession No.	3. Recipient's Catalog No.
4. Title and Subtitle GAS TURBINE FACE SEAL THERMAL DEFORMATION AND COMPUTER PROGRAM FOR CALCULATION OF AXISYMMETRIC TEMPERATURE FIELD		5. Report Date December 1969 6. Performing Organization Code
7. Author(s) Terrence E. Russell, Gordon P. Allen, Lawrence P. Ludwig, and Robert L. Johnson		8. Performing Organization Report No. E-4389
9. Performing Organization Name and Address Lewis Research Center National Aeronautics and Space Administration Cleveland, Ohio 44135		10. Work Unit No. 126-15 11. Contract or Grant No. 13. Type of Report and Period Covered Technical Note
12. Sponsoring Agency Name and Address National Aeronautics and Space Administration Washington, D.C. 20546		14. Sponsoring Agency Code
15. Supplementary Notes		

16. Abstract

A computer program, which is general and can be applied to a variety of steady-state thermal problems, is presented in detail. The program is written in FORTRAN IV language. Application of the program to a specific mainshaft seal design is illustrated; both computer input and output data are given. A sample problem, having an exact solution, is also given as a means of demonstrating program accuracy.

17. Key Words (Suggested by Author(s))

Seal
Computer program
Heat transfer
Temperature
Steady state
Axisymmetric
Thermal deformation

18. Distribution Statement

Unclassified - unlimited

19. Security Classif. (of this report)	20. Security Classif. (of this page)	21. No. of Pages	22. Price *
Unclassified	Unclassified	110	$3.00

*For sale by the Clearinghouse for Federal Scientific and Technical Information
Springfield, Virginia 22151

CONTENTS

Page

SUMMARY 1

INTRODUCTION 1

SYMBOLS 2

DISCUSSION OF THERMAL DEFORMATION IN SEALS 5

ANALYSIS OF TEMPERATURE FIELDS IN AXISYMMETRICAL BODIES 8

LIMITATIONS AND SCOPE 15

CONCLUDING REMARKS 16

APPENDIXES

A - COMPUTER PROGRAM 17

Preparation of Input Data 17

Computer Input 19

Computer Output 31

Standard output of results 31

Program error messages 32

Program Symbols and Definitions 32

Conductance matrix CE(NJPTS, 4) 33

Boundary conductance matrix H(NBPT, 10) 34

Conduction data matrix TD1(NJPTS, 19) 34

TD2 list for subroutine SN1, type 2 (forced convection), subtype 1 (duct flow, liquid) 35

TD2 list for subroutine SN2, type 2 (forced convection), subtype 2 (sides of rotors) 35

TD2 list for subroutine SN3, type 2 (forced convection), subtype 3 (radial seal gap) 36

TD2 list for subroutine SN4, type 2 (forced convection), subtype 4 (concentric cylinders) 37

TD2 list for subroutine SN5, type 2 (forced convection), subtype 5 (flat plate) 37

TD2 list for subroutine FC1, type 3 (free convection), subtype 1 (horizontal cylinder) 38

TD2 list for subroutine FC2, type 3 (free convection), subtype 2 (vertical cylinder or plane) 38

TD2 list for subroutine FC3, type 3 (free convection), subtype 3 (liquid film cooling, gravity flow) 39
TD2 list for subroutine RA1, type 4 (radiation) 39
TD2 list for subroutine SC1, type 5 (specified heat transfer coefficient) 40
TD2 list for subroutine VT1, type 6 (varying temperature forced convection), subtype 1 (duct flow, liquid) 40
TD2 list for subroutine VT2, type 6 (varying temperature forced convection), subtype 2 (radial seal gap) 40
Flow Charts and Program Listing 41
B - CHANGING OF BOUNDARY CONDITION COEFFICIENTS 73
Substitution of a Different Coefficient 73
Addition of New Coefficients 74
C - COMPUTER PROGRAM APPLICATION TO MAINSHAFT SEAL 75
Seal Description 75
Computer Output for Sample Problem 81
D - HEAT TRANSFER COEFFICIENT EQUATIONS 98
Radiation 98
Liquid Film Cooling 98
Other Free Convection Coefficients 98
Use of Local Coefficients 99
Flat Plate 99
Duct Flow, Liquid 99
Concentric Cylinders 100
Rotors 100
Derivation of Equations for the Rotor Coefficients 100
E - SAMPLE THERMAL PROBLEM FOR COMPARISON WITH EXACT SOLUTION 103

REFERENCES 107

GAS TURBINE FACE SEAL THERMAL DEFORMATION AND COMPUTER PROGRAM FOR CALCULATION OF AXISYMMETRIC TEMPERATURE FIELD

by Terrence E. Russell, Gordon P. Allen, Lawrence P. Ludwig, and Robert L. Johnson

Lewis Research Center

SUMMARY

The effects of seal deformation on seal balance are pointed out. In particular, divergent sealing faces are shown to be undesirable. As a first step in determining sealing face deformation, a computer program is presented for calculating the temperature field in the arbitrary body of revolution with arbitrary thermal boundary conditions. The program, which is written in FORTRAN IV language for an IBM 7094 digital computer, is general and can be applied to a variety of problems. Application of the program to a specific gas turbine mainshaft seal is demonstrated in detail; both computer input and output data are given. The program is also used to solve an example problem which has an exact solution; thus a partial check on program accuracy is provided.

INTRODUCTION

Face seals in advanced gas turbine engines will be subjected to temperatures, pressures, and sliding surface speeds higher than that of current engine practice. Increases in temperature arise from continuing increases in flight speed and turbine inlet temperature (ref. 1), increases in pressure result from use of higher pressure ratio compressors, and increases in surface speeds are due in part to increases in shaft diameter needed to carry increases in torque. As an example, proposed advanced engines have seal sliding speeds to 500 feet per second (127 m/sec) (ref. 2) as compared to 350 feet per second (88.9 m/sec) in engines in current use. In order to cope with these higher temperatures, pressures, and speeds, the contacting-type face seal may be replaced with noncontacting face seals such as the hydrostatic and hydrodynamic type (ref. 3). However, regardless of the type of face seal used, deformation of the sealing faces, due to thermal gradients, pressures, and centrifugal forces, will have significant effects on seal performance (ref. 4). In particular, deformations due to thermal gradients are a

Card #27

major problem area. The first step in determining thermal deformation is calculation of temperature distribution in the seal assembly. Such calculation by computer program is the subject of this report. The specific objectives of this study were to (1) present in detail a computer program for calculation of temperature distribution in axisymmetric bodies, (2) show how the computer program is applied to mainshaft seal thermal analysis, and (3) demonstrate program accuracy by comparison with a thermal problem having an exact solution.

The computer program for calculation of temperature distribution is written in FORTRAN IV computer language for use on an IBM 7094 digital computer. The program is quite general and can be applied to a variety of axisymmetric body problems. The calculation procedure requires that these bodies be divided into an arbitrary finite number of axisymmetric volume elements or nodes. These nodes need not be equal in cross section. The program will take into account contact resistance at the interface between nodes and will also account for material properties that vary from node to node. Also provisions are made in the program to handle varying gas temperatures along the seal boundaries and internal viscous heat generation within the fluid at the boundaries.

SYMBOLS

A	area, ft^2
A_x	cross section area, ft^2
a	outer radius of rotor or stator, ft
C	thermal conductance, Btu/(sec)(^oF)
C_f	skin friction coefficient
C_M	torque coefficient
C_p	specific heat, Btu/(lbm)(^oF)
D	hydraulic diameter, ft
D_L	characteristic length for liquid film cooling, ft
d	differential
F	function of
f	view factor for radiation
Gr	Grashof number
Gr_D	Grashof number based on diameter, $D_o^3 g_o(T_b - T_s)/\nu_f^2 T_f$
Gr_L	Grashof number based on length, $L^3 g_o(T_b - T_s)/\nu_f^2 T_f$

g_o	gravitational acceleration, ft/sec^2
H	convective conductance, Btu/(sec)(^{o}F)
h	heat transfer coefficient, Btu/(ft^2)(sec)(^{o}F)
K	β/ω
k	thermal conductivity, Btu/(ft)(sec)(^{o}F)
L	length of cylinder or surface, ft
Δl	axial length, in. or ft
N	radiative conductance, Btu/(sec)(^{o}F)
Nu	Nusselt number, hD_L/k
P_w	wetted perimeter, ft
Pr	Prandtl number
Pr_f	Prandtl number of boundary film, $\left[C_p\mu/k\right]_f$
Q	heat flux, Btu/sec
q	internal heat generation, Btu/sec
q_f	fluid internal heat generation, Btu/sec
R	thermal resistance, (sec)(^{o}F)/Btu
R_c	contact resistance, (sec)(^{o}F)/Btu
Re	Reynolds number
Re_c	critical Reynolds number for transition
Re_v	Reynolds number based on total velocity, $\left(\sqrt{\omega^2 r^2 + V_a^2}\right)_s \Big/ \nu_f$
Re_w	Reynolds number based on mass flow, $W_a D/\mu_f$
Re_x	Reynolds number based on flow length, $V_\infty X/\nu_f$
Re_ω	Reynolds number based on rotation, $\omega r^2/\nu_f$
r	radial coordinate, ft
Δr	radial width, in. or ft
r_{av}	average radius of element, in. or ft
r_i	inner radius of annulus between cylinders, ft
r_o	outer radius of annulus between cylinders, ft
s	clearance (e.g., seal gap), ft

T temperature, ^{o}F

T_{av} average (or film) temperature, ^{o}F

T_{in} temperature entering fluid element, ^{o}F

T_{out} temperature leaving fluid element, ^{o}F

T_{∞} bulk fluid temperature, ^{o}F

Ta_f Taylor number of boundary film, $\omega r s^{3/2} / \nu_f^{3/2}$

V_a axial velocity, ft/sec

V_R linear velocity of inner cylinder, ft/sec

V_{tot} total fluid velocity, ft/sec

V_{∞} free stream velocity, ft/sec

W mass flow rate, lbm/sec

W_a mass flow per square foot of cross section, W/A_x, lbm/(ft^2)(sec)

w over-relaxation factor

X flow length, ft

z axial coordinate, ft

α coefficient of thermal expansion

β angular velocity of fluid, rad/sec

∂ partial derivative

Δ difference

ϵ emissivity for radiation

μ absolute viscosity, lbm/(ft)(sec)

ν kinematic viscosity, ft^2/sec

ρ density, lbm/ft^3

τ_t tangential shear stress at wall, lbf/in.^{2}

ω rotor angular velocity, rad/sec

Subscripts:

b at fluid bulk temperature

c convective

e environment

ei between element and environment

es	from environment to element
f	at boundary film temperature
i	element
j	neighbor element of i
ji	between neighbor and element
k	environment "area" affecting element i by radiation
ki	between environment "area" k and element
ℓ	environment "area" affecting element i by convection
ℓam	laminar
ℓi	between environment "area" ℓ and element
r	radiation
s	surface
se	from element to environment
tr	transition
turb	turbulent

DISCUSSION OF THERMAL DEFORMATION IN SEALS

Figure 1 is a schematic drawing of a gas turbine mainshaft seal for bearing sumps. The seal restricts leakage of surrounding high temperature, high pressure gas into the

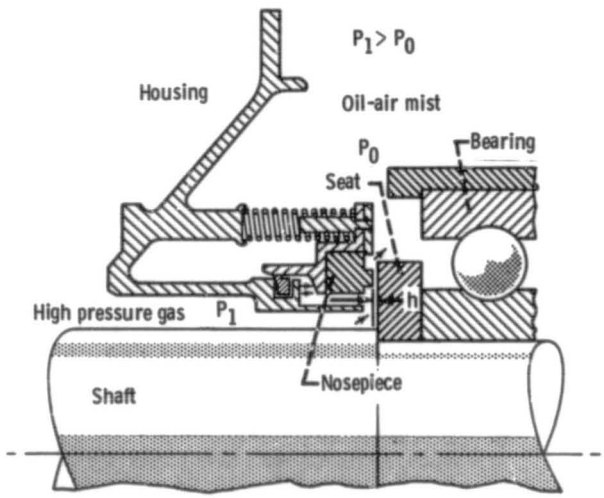

Figure 1. - Mainshaft seal for bearing sump in gas turbine engine.

sump. The gas leakage, through the seal into the sump, acts as a sweep gas which helps prevent oil leakage. However, it is desirable to minimize this gas leakage, since the hot gas degrades the lubricant and adds to the cooling requirements of the lubricant system.

Seal leakage and wear are grossly affected by seal force balance and it has been recognized that deformation of the sealing faces (which form the dam) can have a significant effect on the seal force balance (ref. 5). A discussion of seal force balancing can be found in reference 6. The manner in which the sealing face deformation affects the seal force balance and stability of a conventional face seal is discussed in reference 7. In general, thermal deformations cause the seal faces (dam) to form a nonparallel leakage path, and the pressure within these sealing faces is greatly dependent on the shape (convergent or divergent) of this leakage path; thus the force balance is affected by the thermal deformation.

Thermal gradients usually produce sealing gaps divergent from the dam inside diameter to the outside diameter. Thus, it is usually advantageous to locate the higher pressure at the seal outside diameter since this will result in convergence with respect to the leakage direction. However, many face seals are designed with the higher pressure at

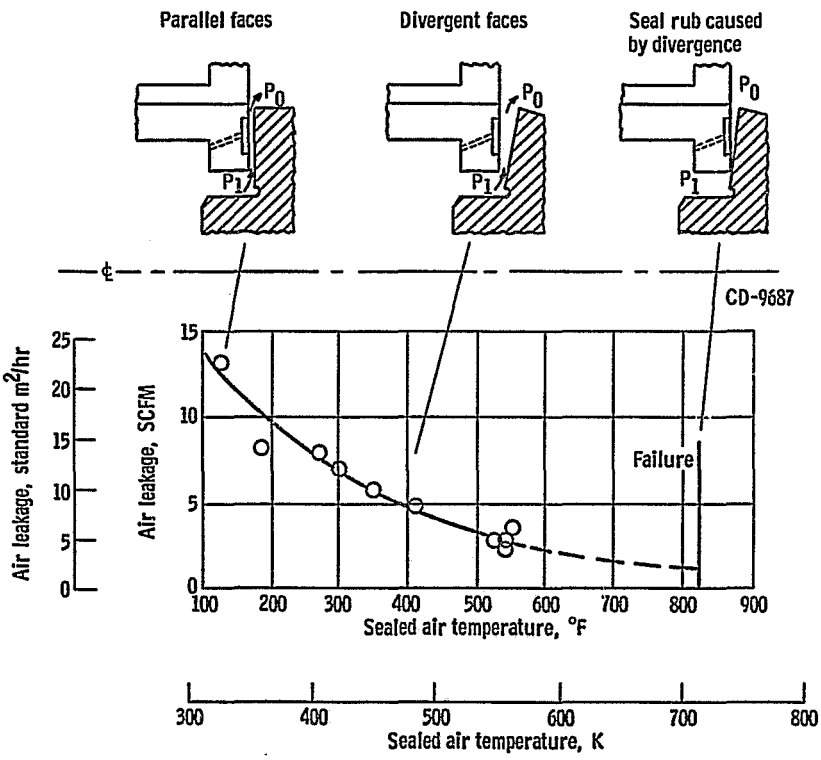

Figure 2. - Effect of thermal deformation on air leakage of orifice compensated hydrostatic seal. Sliding speed, 200 feet per second (61.0 m/sec); pressure differential, 100 pounds per square inch (6.89×10^4 N/m^2). (Data from ref. 4.)

the dam inside diameter and the gas turbine face seal is an example of this construction practice. The advantage of placing the higher pressure gas at the dam inside diameter puts the oil mist at the outside diameter; thus centrifugal force also acts to prevent oil leakage.

Thermal deformation also affects operation of hydrostatic seals. Figure 2, from reference 4, shows the effect of sealing face deformation on leakage through a hydrostatic seal operating at 200 feet per second (61.0 m/sec) and 100 pounds per square inch (6.89×10^4 N/m^2) pressure differential. With a sealed air temperature of 120° F (322 K), the seal leakage is approximately 13 SCFM (0.0062 standard m^3/sec) and as the air tem-

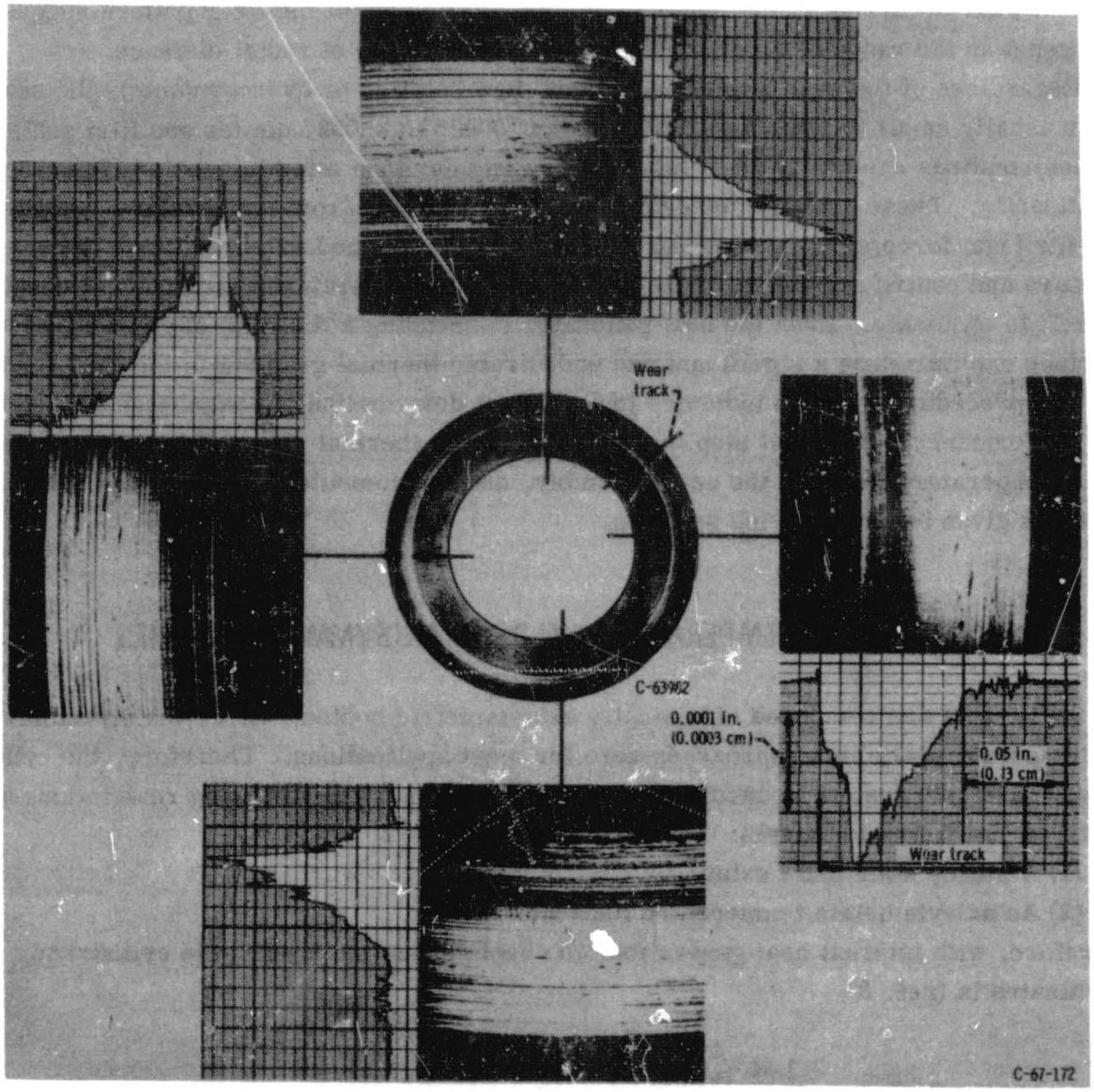

Figure 3. - Overall wear pattern, surface profile traces, and photomicrographs of tungsten carbide seal seat. Sodium temperature, 1000° F (538° C); operating time, 4 hours; sliding velocity, 79 feet per second (24 m/sec); pressure, 50 pounds per square inch gage (34 N/cm^2 gage). Data from ref. 6.)

perature is increased, the leakage decreases. This leakage decrease is due to increasing angular deformation of the sealing gap. The result is that the seal runs with closer clearance. Eventually as the air temperature increases still further, the deformation causes the inside diameter of the nosepiece to rub against the seal seat and failure occurs.

Seal thermal deformation effects have also been noticed in other applications. As an example, reference 6 reports that the main problem in sealing liquid sodium with a face contact seal was thermal deformation of the sealing faces. Some results of this study are repeated in figure 3 which shows the wear pattern made by a nosepiece sliding against a seal seat. Surface profile traces have been taken at intervals around the wear track. These profile traces show that the sealing faces were not parallel during operation, the greatest wear occurring at the inside diameter. The slope of the wear pattern suggests a divergence in the range of 0.006 inch per inch (0.006 m/m) of radial distance.

Regardless of the seal type (face contact, hydrostatic, or hydrodynamic), the sealing gap is usually small (0.0001 to 0.0010 in. or 0.00025 to 0.0025 cm for gas film seals) and deformations can easily be of the same magnitude, thus affecting seal performance significantly. These sealing face deformations could arise from temperature, pressure, or centrifugal force effects. Careful design can minimize undesirable effects due to pressure and centrifugal force. Deformations due to temperature gradients are usually difficult to eliminate. Even the heat generated in shearing a thin film of gas within the interface can introduce a significant and undesirable thermal gradient in the seal rings.

The preceding evidence indicates that thermal deformation can significantly affect seal performance. The first step in analysis of these thermal deformations is calculation of the temperature fields in the seal assembly, and the computer program for these calculations is given in the following sections.

ANALYSIS OF TEMPERATURE FIELDS IN AXISYMMETRIC BODIES

Shaft seals are composed of basically axisymmetric bodies. Also, the circumferential temperature gradient approaches zero for most applications. Therefore, the cylindrical coordinate system is used as a basis for analysis. The following restrictions are placed on the thermal analysis:

(1) A steady state must exist.

(2) An axisymmetric temperature field must exist.

Therefore, with internal heat generation, the heat conduction equation in cylindrical coordinates is (ref. 8)

$$\frac{1}{r}\frac{\partial}{\partial r}\left(kr\frac{\partial T}{\partial r}\right)+\frac{\partial}{\partial z}\left(k\frac{\partial T}{\partial z}\right)+q(r,z)=0 \qquad (1)$$

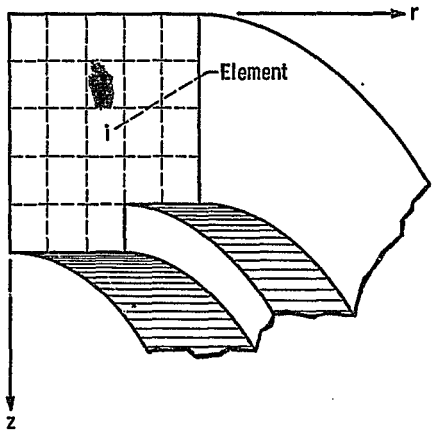

Figure 4. - Seal axisymmetric nosepiece subdivided into finite number of three-dimensional axisymmetric volume elements.

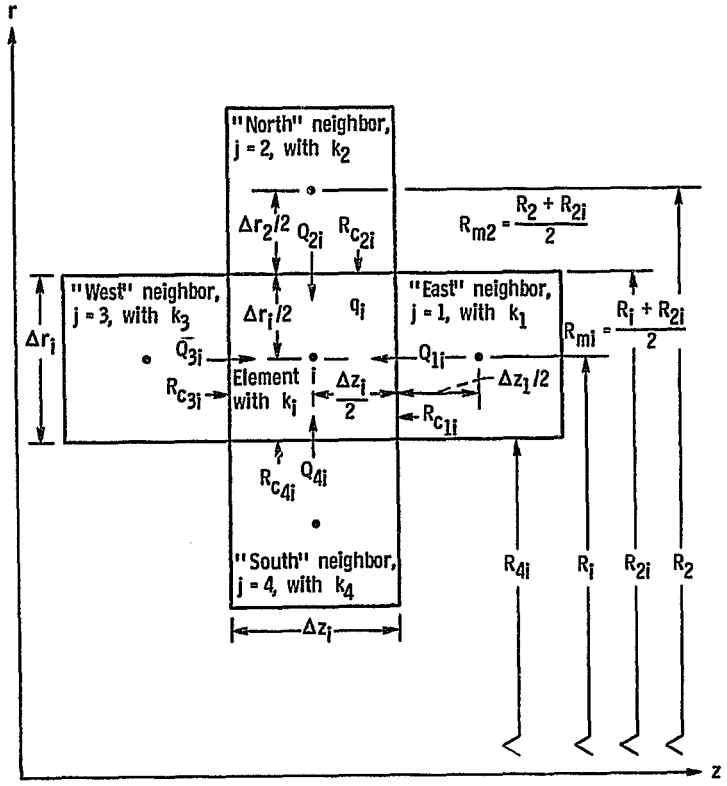

Figure 5. - Typical interior (i^{th}) element and its four neighbor elements.

where r is the radial coordinate, k is thermal conductivity, z is the axial coordinate, T is temperature, and q is internal heat generation.

Equation (1), which makes no restrictions of constant thermal conductivity k, can be approximated by a finite difference numerical approach in which thermal conductivity is held constant over small regions. In this finite difference approach, each of the axisymmetric bodies, which comprise the seal, is subdivided into a finite number of three-dimensional axisymmetric volume elements of rectangular cross section (see fig. 4). These elements need not be equal in cross-sectional area. In general, there will be P elements of which m are elements whose temperature is obtained by solving a heat balance equation and P - m are elements in which the temperature is specified. Figure 4 indicates the position of a typical interior element (i^{th} element). The numbers assigned to the neighboring elements will be determined in the construction of the element pattern, but for the purpose of developing the heat balance equation these neighboring elements are numbered 1, 2, 3, and 4 (see fig. 5).

For the numerical solution, the application of the law of conservation of energy at each volume element allows good generality to be maintained. Referring to figure 5, a heat balance for steady-state conduction at element i results in the following difference equation:

$$Q_{1i} + Q_{2i} + Q_{3i} + Q_{4i} + q_i = 0$$

where the Q_{ji} terms are the heat fluxes from the neighboring elements or

$$C_{1i}(T_1 - T_i) + C_{2i}(T_2 - T_i) + C_{3i}(T_3 - T_i) + C_{4i}(T_4 - T_i) + q_i = 0 \tag{2a}$$

in which the conductances C_{ji} are computed as follows with reference to figure 5:

$$\left.\begin{aligned} R_{1i} = \frac{1}{C_{1i}} &= \frac{\frac{\Delta z_1}{2}}{2\pi R_1 \, \Delta r_1 k_1} + \frac{\frac{\Delta z_i}{2}}{2\pi R_i \, \Delta r_i k_i} + R_{c_{1i}} \\ R_{2i} = \frac{1}{C_{2i}} &\cong \frac{\frac{\Delta R_i}{2}}{2\pi R_{mi} \, \Delta z_i k_i} + \frac{\frac{\Delta R_2}{2}}{2\pi R_{m2} \, \Delta z_2 k_2} + R_{c_{2i}} \end{aligned}\right\} \tag{2b}$$

where R_{ji} is thermal resistance. As an example, for heat conduction from neighbor element 1 to the i^{th} element, the resistance is made up of the resistance of one-half that of the i^{th} element plus one-half that of neighbor element 1 plus the contact resistance $R_{c_{ji}}$. Thus the calculated temperature is that of the element center. However, the thermal conductivity assigned to the whole element volume is the value at the temperature of the element center.

Equation (2a) can be stated concisely as

$$\sum_{j=1}^{4} C_{ji}(T_j - T_i) + q_i = 0 \tag{3}$$

where i is the element under consideration, the j's are its four neighboring elements, and $1 \leq i \leq m$. At the outer surfaces of the axisymmetric bodies, which comprise the seal, the i^{th} element will have less than four solid neighbor elements but will have environmental radiation and convection effects on the external surface (or surfaces) (fig. 6). This means that some of the j neighbors are replaced by environmental regions which are identified as the k^{th} area for radiation and the ℓ^{th} area for convection. It should be noted that an external surface could have both radiation and convection effects. The k^{th} and ℓ^{th} areas would, therefore, be superimposed.

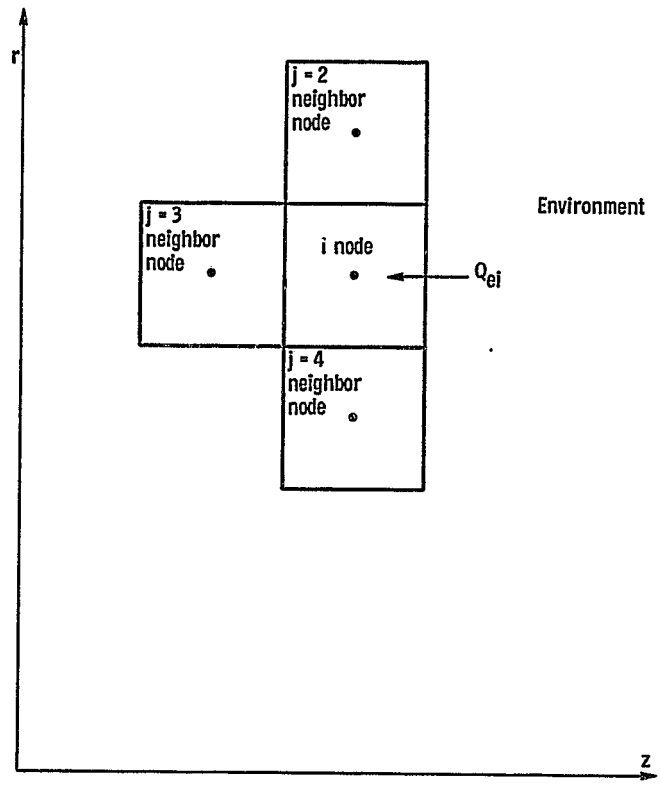

Figure 6. - Typical element with environment convection and/or radiation to one surface.

An i^{th} element could have radiation on more than one face. This radiation heat flux is

$$Q_{ki} = \sum_{k=1}^{4} N_{ki}(T_k - T_i) \tag{4}$$

An i^{th} element could have more than one face with convective effects

$$Q_{\ell i} = \sum_{\ell=1}^{4} H_{\ell i}(T_\ell - T_i) \tag{5}$$

Combining equations (3), (4), and (5) results in the difference equation for the heat balance of the i^{th} element:

$$\underbrace{\sum_{j=1}^{4} C_{ji}(T_j - T_i)}_{\text{Conduction}} + \underbrace{\sum_{k=1}^{4} N_{ki}(T_k - T_i)}_{\text{Radiation}} + \underbrace{\sum_{\ell=1}^{4} H_{\ell i}(T_\ell - T_i)}_{\text{Convection}} + \underbrace{\dot{q}_i}_{\substack{\text{Internal} \\ \text{heat} \\ \text{genera-} \\ \text{tion}}} = 0 \qquad (6)$$

It should be noted that equation (6) establishes the convention that heat flowing from an element has a negative value and heat flowing into an element has a positive value.

In addition to the boundary conditions of radiation and convection, two other boundary surface conditions arepossible. The heat flux may be a specified function

$$Q_{ei} \begin{cases} = K_{ei} A \left(\frac{\partial T}{\partial r}\right)_i \\ = C_{ei}\left(\frac{\partial T}{\partial r}\right) \\ \text{or} \\ = C(r, z) \end{cases} \qquad (7)$$

where $C(r, z) = 0$ for a perfectly insulated surface. Or the heat transfer coefficient may be a specified value such as

$$h_{ei} = f(r, z) \quad (\text{or } H_{ei} = f(r, z)) \qquad (8)$$

Also the temperature of any element may be specified as

$$T_i = f(r, z) \qquad (9)$$

The program has the special feature of calculating varying gas temperatures in flow over a surface or in small passages. In addition, heat generated within a fluid, such as that due to viscous shear in the sealing interfaces, can be accounted for. Referring to figure 7 reveals the heat balance for the center fluid element is

$$WC_p(T_{in} - T_{out}) + h_1 A_1 (T_{s1} - T_{in}) + h_2 A_2 (T_{s2} - T_{in}) + q_f = 0 \qquad (10)$$

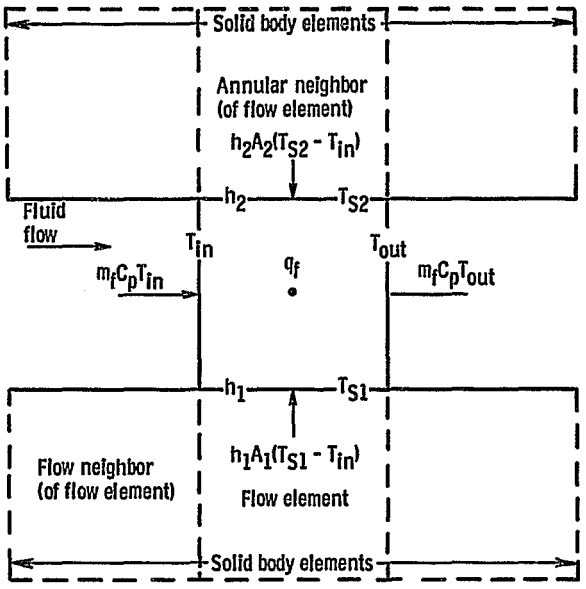

Figure 7. - Fluid volume element for varying temperature forced convection heat transfer.

in which q_f is the internal heat generated. Equation (10) enters into the element heat balance (eq. (6)) only through the determination of the fluid temperature.

Returning to the element heat balance (eq. (6)) matrix notation can be used to express this system of linear equations as follows:

$$\underbrace{-\sum_{j=1}^{4} C_{ji}T_j + \left(\sum_{j=1}^{4} C_{ji} + \sum_{k=1}^{4} N_{ki} + \sum_{\ell=1}^{4} H_{\ell i}\right)}_{[A]} \underbrace{T_i}_{\{T\}} = \underbrace{\sum_{k=1}^{4} N_{ki}T_k + \sum_{\ell=1}^{4} H_{\ell i}T_\ell - q_i}_{\{TL\}} \tag{11}$$

where [A] is the $m \times m$ conductance matrix, $\{T\}$ is the $m \times 1$ temperature vector, and $\{TL\}$ is the $m \times 1$ thermal load vector.

In equations (6) and (11) it should be noted that, for interior elements, the N_{ki} and $H_{\ell i}$ terms vanish; also numbers are assigned to the j^{th} elements.

The matrix [A] can be shown to be real, symmetric, and positive definite. The temperatures are obtained using the successive over-relaxation technique. By introducing the over-relaxation factor w, the successive over-relaxation algorithm is given for the temperature at the i^{th} element at the $(K + 1)^{th}$ iteration by:

$$a_{i,i}T_i^{K+1} = a_{i,i}T_i^K + W\left[-\sum_{j=1}^{i-1} a_{i,j}T_j^{K+1} - \sum_{j=i+1}^{m} a_{i,j}T_j^K + (TL)_i - a_{i,i}T_i^K\right]$$

where

$$1 \leq W < 2 \quad \text{and} \quad 1 < i \leq m$$

and

$$a_{i,i} = \left(\sum_{j=1}^{4} C_{ji} + \sum_{k=1}^{4} N_{ki} + \sum_{\ell=1}^{4} H_{\ell i}\right) \qquad \text{diagonal term of } i^{th} \text{ row in matrix [A]}$$

$$a_{i,j} = -C_{ji} = a_{j,i} \qquad \text{off-diagonal terms of } i^{th} \text{ row in matrix [A]}$$

$$(TL)_i = \sum_{k=1}^{4} N_{ki}T_k + \sum_{\ell=1}^{4} H_{\ell i}T_\ell + q_i \qquad i^{th} \text{ thermal load term}$$

This system of m equations is iteratively solved until a specified level of convergence is obtained.

The boundary condition conductances N_{ki} and $H_{\ell i}$ are calculated with the aid of the empirical relations listed in table I and discussed later.

LIMITATIONS AND SCOPE

This program has a present capacity of 400 volume elements, 200 boundary condition elements, 95 varying temperature boundary elements (see Computer Input in appendix A), and 15 different materials. Several minor limitations are discussed in the section on input where the parameters involved are introduced. The program is designed for an IBM 7094 digital computer and is written in FORTRAN IV language.

Provision is made for adding subroutines to calculate additional boundary condition coefficients without interrupting the sequence of statement numbers or altering present statements. Up to four forced convection, five free convection, and two varying tempera-

TABLE I. - BOUNDARY HEAT TRANSFER COEFFICIENTS

Heat transfer type	Geometry and fluid	Regime	Coefficient equation
Forced convection	Duct flow, liquid	Laminar	$h = 1.24\,(k_f/D)(Re_w Pr_f D/X)^{1/3}$
		Turbulent	$h = 0.023\,(k_f/D)Re_w^{0.8}Pr_f^{0.4}\left[1 + 0.3\,(D/X)^{0.7}\right]$
		Transition	$h_{tr} = h_{lam} + (h_{turb} - h_{lam})(Re - 2500)/4500$
	Sides of rotors, liquid or gas	Laminar	$h = 0.574\,(k_f/r)(s/r)^{0.1}Re_\omega^{0.5}Pr_f^{1/3}/(\beta/\omega)$
		Turbulent	$h = 0.01826\,(k_f/r)(s/r)^{0.1}Re_\omega^{0.8}Pr_f^{1/3}/(\beta/\omega)$
	Radial seal gap, liquid or gas	Laminar	$h = 2\,(k_f/s)Pr_f^{1/3}$
		Turbulent	$h = 0.0297\,(k_f/r)(r/s)^{1/6}Re_\omega^{3/4}Pr_f^{1/3}$
	Concentric cylinders, liquid or gas	Turbulent	$h = \frac{k}{\Delta r}\left[0.015\,Re_d^{0.8}Pr_f^{1/3}\left(\frac{r_o}{r_i}\right)^{0.46} + 0.092\,Ta_f^{2/3}Pr_f^{1/3}\right]$
	Flat plate, liquid or gas	Laminar	$h = 0.332\,(k/X)Re_x^{1/2}Pr_f^{1/3}$
		Turbulent	$h = 0.0288\,(k/X)Re_x^{0.8}Pr_f^{1/3}$
Free convection	Horizontal cylinder, liquid or gas	Laminar	$h = 0.53\,(k_f/D_o)(Gr_{D,f}Pr_f)^{1/4}$
		Turbulent	$h = 0.13\,(k_f/D_o)(Gr_{D,f}Pr_f)^{1/3}$
	Vertical cylinder or plane	Laminar	$h = 0.44\,(k_f/X)(Gr_{D,f}Pr_f)^{1/4}$
		Turbulent	$h = 0.13\,(k_f/X)(Gr_{D,f}Pr_f)^{1/3}$
	Liquid film cooling, gravity flow	--------	$h = 2C_p(W/L)/\pi D_l$
Radiation	Any surface	--------	$h_r = \frac{q}{A\,\Delta T} = \frac{\sigma\epsilon_e(1-\epsilon_s)F_{es}\left(T_e^3 + T_e^2T_s + T_eT_s^2 + T_s^3\right)}{1 - F_{es}F_{se}(1-\epsilon_e)(1-\epsilon_s)}$

ture conditions can be added by writing appropriate subroutines and by adding the required statements in subroutine CQN. The CQN statements required can be deduced from the portions labeled for present coefficients. Changes and some limitations are discussed in more detail in appendix B.

The present coefficient equations are based on properties evaluated at the boundary film temperature (average of bulk fluid and surface temperatures). Unless the initial temperature estimates (required as a starting point) are very close to the final temperatures calculated, the input required will have to be changed and the problem rerun at least once to obtain the best results.

CONCLUDING REMARKS

The program, which is written in FORTRAN IV language for an IBM 7094 digital computer, is general and can be applied to a variety of axisymmetric problems. Various convection and radiation boundary conditions which can be used are given in the mathematical formulation. The program listing and flowcharts for steady-state thermal solution of an axisymmetric solid in cylindrical coordinates are given. Computer program application to a nosepiece assembly is given in detail. Additional demonstration of the program is provided in a comparison of the program solution to the exact solution for a finite cylinder. This comparison shows a maximum error of 15 percent when a coarse mesh is used. Thus a partial check on program accuracy is provided.

Lewis Research Center,
National Aeronautics and Space Administration,
Cleveland, Ohio, July 10, 1969,
126-15.

APPENDIX A

COMPUTER PROGRAM

Preparation of Input Data

The recommended first step is the preparation of the element pattern. For the seal analyzed in appendix C, a layout of the seal assembly five times actual size was used. There is no restriction on the numbering sequence except the use of consecutive numbers (i.e., every number from 1 to P), but it is preferable to use an orderly system in order to avoid confusion and to expedite assembling the data required for input. The drawing also includes, for convenience, the radial dimension and mean radius of each element row and the axial dimension of each column.

Adjacent elements should have the same common dimension. Slight variations will not cause appreciable errors if a contact resistance is added to compensate for the increased conduction path length of off-center nonmatching elements.

Also, for convenience, the boundary conditions (pressure, temperature, fluid, and so forth, needed to determine the values of required properties) are included. The materials of the various parts are included in a table (on the drawing if room is available).

The items of data required are listed in the following section on computer input. A compact outline of most items can be obtained from the section Program Symbols and Definitions or from table II. The conduction element matrix (TD1) and boundary coefficient lists (TD2) include input data.

TABLE II. - SUMMARY OF TD2 LISTS FOR SUBROUTINES TO CALCULATE COEFFICIENTS

[Parameters in parentheses are calculated in subroutine. Except for TD2(20) of SN3 and VT2 and TD2(11) of FC1 and FC2, parameters after hA are merely to make writing FORTRAN expression for h easier.]

TD2 word or subscript	Subroutine											
	SN1 (duct flow, liquid)	SN2 (sides of rotors)	SN3 (radial seal gap)	SN4 (concentric cylinders)	SN5 (flat plate)	FC1 (horizontal cylinder)	FC2 (vertical cylinder or plane)	FC3 (liquid film cooling, gravity flow)	RA1 (radiation)	SC1 (specified heat transfer coefficient)	VT1 (varying temperature duct flow, liquid)	VT2 (varying temperature radial seal gap)
1	T_b	T_b	T_b	T_b	T_b	T_b	T_b	T_b	T_e	T_b or T_e	T_b	T_b
2	k_f	k_f	k_f	k_f	k_f	k_f	k_f	W/L	f_{es}	h	k_f	k_f
3	$C_{p,f}$	$C_{p,f}$	$C_{p,f}$	$C_{p,f}$	$C_{p,f}$	$C_{p,f}$	$C_{p,f}$	C_p	f_{se}	(hA)	$C_{p,f}$	$C_{p,f}$
4	μ_f	μ_f	μ_f	μ_f	μ_f	μ_f	μ_f	D_L	ϵ_e	--------	μ_f	μ_f
5	W_a	ν_f	ν_f	ν_f	ν_f	ν_f	ν_f	(h)	ϵ_s	--------	W	ν_f
6	D	r_{av}	r_{av}	r_o	X	D	L	(hA)	(h)	--------	D	r_{av}
7	X	s	s	r_i	V_∞	(Pr_f)	(Pr_f)	------	(hA)	--------	X	s
8	---------	ω	ω	ω	(Re_x)	(Gr_D)	(Gr_L)	------	$(1 - \epsilon_e)$	--------	Annular neighbor conduction number	ω
9	---------	a	a	V_a	(Pr_f)	(h_f)	(h_f)	------	$(1 - \epsilon_s)$	--------	Flow neighbor conduction number	a
10	---------	*	----	(Re_v)	(h)	(hA)	(hA)	------	$\left(\frac{T_e^4 - T_s^4}{T_e - T_s}\right)$	--------	Combining flow indicator	Combining flow indicator
11	---------	(Re_ω)	----	$\left(Pr_f^{1/3}\right)$	(hA)	$(Pr_f Gr_D)$	$(Pr_f Gr_D)$	------	--------	--------	Flow initiation indicator	Flow initiation indicator
12	---------	$\left(Pr_f^{1/3}\right)$	----	(h_f)	-----	(ΔT)	(ΔT)	------	--------	--------	A_x	Annular neighbor conduction number
13	(Re_w)	(h_f)	----	(hA)	-----	(T_{av})	(T_{av})	------	--------	--------	(Re_w)	Flow neighbor conduction number
14	(Pr_f)	(hA)	----	(V_R)	-----	(k_f/D)	(k_f/L)	------	--------	--------	(Pr_f)	W
15	(h_f)	(k_f/r_{av})	(Re_ω)	$\left(V_{tot}^2\right)$	-----	--------	--------	------	--------	--------	(h_f)	(Re_ω)
16	(hA)	$\left([s/r_{av}]^{0.1}\right)$	$\left(Pr_f^{1/3}\right)$	(V_{tot})	-----	--------	--------	------	--------	--------	(hA)	$\left(Pr_f^{1/3}\right)$
17	(D/X)	(K)	(Re_c)	(s)	-----	--------	--------	------	--------	--------	(D/X)	(Re_c)
18	(k_f/D)	----------	(h_f)	------	-----	--------	--------	------	--------	--------	(k_f/D)	(h_f)
19	$\left([(D/X)]^{0.7}\right)$	----------	(hA)	------	-----	--------	--------	------	--------	--------	$\left([D/X]^{0.7}\right)$	(hA)
20	---------	----------	(Heat generation factor)	------	-----	--------	--------	------	--------	--------	---------	(Heat generation factor)

*Rotor or stator flag (zero for rotor, nonzero for stator).

Computer Input

The data input of a problem is submitted to the computer on the cards described in this section. Unless specifically stated, no input card may be omitted.

Item 1: Title card (72H)

word 1	columns 1 to 72	Title of problem being run

Item 2: Output control (LO) card (10I6) for obtaining printouts in addition to that listed in the section Computer Output

word 1	columns 1 to 6	A nonzero integer causes printout of the conduction matrix (TD1 table) input
word 2	columns 7 to 12	A nonzero integer causes printout of the boundary conductance matrix (H(NBPT,J),J=1,9)
word 3	columns 13 to 18	A nonzero integer causes printout of the element temperatures for the next to last iteration (unless execution terminated by reaching maximum number of iterations) for comparison with temperatures of last iteration
word 4	columns 19 to 24	Leave blank. This word is set within the program to cause printout of the convergence criterion (Item 5, word 4) and of the temperature change for each element at each N^{th} iteration; N is specified by word 2 of the Run data card (Item 4).
word 5	columns 25 to 30	A nonzero integer causes printout of the boundary condition input matrix (TDA and TD2 lists)
word 6	columns 31 to 36	Not used
word 7	columns 37 to 42	Not used
word 8	columns 43 to 48	A nonzero integer causes the final element temperatures to be punched on cards for use as initial estimates for another run
word 9	columns 49 to 54	A nonzero integer causes thermal expansions to be punched on cards for use in other programs (e.g., a stress analysis)

word 10	columns 55 to 60	A nonzero integer causes printout of element temperatures and heat fluxes after each iteration. Also thermal expansion data (α, T, α ΔT) are printed. This option is meant only for debugging data and should not be included for a standard run.

Item 3: Miscellaneous options (NI) card (5I6)

word 1	columns 1 to 6	Number of cases (designs) to be analyzed. If only one case, this word may be left blank.

No other words now used; leave blank.

Item 4: Run data (RD) card (5F6.0)

word 1	columns 1 to 6	Over-relaxation factor w ($1 \leq w < 2$)
word 2	columns 7 to 12	Reference temperature for thermal expansion (α ΔT)
word 3	columns 13 to 18	The interval N required for word 4 of the LD card (Item 2)

No other words now used.

Item 5: Case data (CD) card (10F6.0)

word 1	columns 1 to 6	Number of elements (400 maximum at present)
word 2	columns 7 to 12	Number of boundary elements (200 maximum at present)
word 3	columns 13 to 18	Maximum number of iterations allowed for a run
word 4	columns 19 to 24	Temperature convergence criterion. The maximum change in temperature of any element from one iteration to the next that is considered an acceptable error.
word 5	columns 25 to 30	Not used
word 6	columns 31 to 36	Starting temperature for varying temperature flow 1 (see varying temperature under boundary condition input (Item 10))
word 7	columns 37 to 42	Starting temperature for varying temperature flow 2

word 8	columns 43 to 48	Not used
word 9	columns 49 to 54	To avoid numerical instability due to low flow rates in the varying temperature calculation, the boundary elements are subdivided. The number of subdivisions is specified between 1 and 100 in this word.
word 10	columns 55 to 60	Not used

Item 6: Thermal conductivity data cards

The thermal conductivity of each material is treated as a power series function of temperature ($k = AT^0 + BT^1 + \ldots + NT^m$). Provision is made for curve fitting up to 15 materials. The coefficients required are computed by an auxiliary program (or, of course, by hand) from available data. The degree of fit of a curve is defined as the highest power of temperature appearing in the function. Thus, a linear fit is degree 1; a constant conductivity is degree 0; and so forth.

The auxiliary program is designed to produce fits of all degrees up to 11 from which the best agreement with a set of average values of k is selected as the function to be used. Therefore, words 4 and 5 were included to avoid exceeding the computer capacity when the higher powers of temperature occurred. Later it was somewhat arbitrarily decided to limit the maximum degree of fit to five in view of data scatter due to variation between material lots. The primary reason was to increase the number of materials possible and to save computer storage space.

Card 1 (5F10.0)

word 1	columns 1 to 10	Upper temperature limit of curve fit
word 2	columns 11 to 20	Material code number. Each material must be assigned a number so that the correct properties will be used in the program.
word 3	columns 21 to 30	Degree of fit (0 to 5)
word 4	columns 31 to 40	Thermal conductivity scaling factor. At present, this is 1.
word 5	columns 41 to 50	Temperature scaling factor. At present, this is 1.

Card 2 (6E13.6) - The coefficients of the equation: A in columns 1 to 13, B in columns 14 to 26, and so forth.

Card 3 (blank card) - If less than 15 materials are used, a blank card must be inserted following the last conductivity card in order to terminate the reading of data.

Item 7: Mean coefficient of linear thermal expansion cards

The remarks made about conductivity (see Item 6) also apply to expansion.

Card 1 (5F10.0)

word 1	columns 1 to 10	Upper temperature limit of curve fit
word 2	columns 11 to 20	Material code number
word 3	columns 21 to 30	Degree of fit (0 to 5)
word 4	columns 31 to 40	Thermal expansion scaling factor. At present, this is 1.
word 5	columns 41 to 50	Temperature scaling factor. At present, this is 1.

Card 2 (6E13.6) - The coefficients of the equation as in Item 6.

Card 3 (blank card) - To terminate data read in for less than 15 materials (see Item 6).

Item 8: Conduction matrix data (TD1) card (F4.0, 1X, F7.4, 2F5.3, 1X, 4F4.0, F3.0, 4F7.0) - 1 card per element; element numbers in numerical order

word 1	columns 1 to 4	Element conduction number
word 2	columns 6 to 12	Mean element radius, r_{av}, in.
word 3	columns 13 to 17	Element radial width, Δr, in.
word 4	columns 18 to 22	Element axial length, Δl, in.
word 5	columns 24 to 27	East neighbor conduction number, j_1
word 6	columns 28 to 31	North neighbor conduction number, j_2
word 7	columns 32 to 35	West neighbor conduction number, j_3
word 8	columns 36 to 39	South neighbor conduction number, j_4
word 9	columns 40 to 42	Material code number (see Item 6, word 2)
word 10	columns 43 to 49	East contact resistance, $R_{c_{1,i}}$, (sec)(^{o}F)/Btu
word 11	columns 50 to 56	North contact resistance, $R_{c_{2,i}}$, (sec)(^{o}F)/Btu
word 12	columns 57 to 63	West contact resistance, $R_{c_{3,i}}$, (sec)(^{o}F)/Btu
word 13	columns 64 to 70	South contact resistance, $R_{c_{4,i}}$, (sec)(^{o}F)/Btu

Item 9: Initial temperature cards (16F5.0) - Put 16 initial element temperatures per card.

words 1 to 16	columns 1 to 5, 6 to 10, 11 to 15, and so forth	Initial element temperatures (^{o}F) are listed in sequence from 1 to the total number of elements: elements 1 to 16 on the first card, elements 17 to 32 on the second, and so forth.

Item 10: Boundary heat transfer cards

Each boundary element requires an indicator card. Following the indicator card is a set of one or more cards for each boundary condition associated with the element. A partial outline is presented in table II. This sequence is repeated for each boundary element.

Card 1: Boundary indicator card (3I6) - 1 card per element

word 1	columns 1 to 16	Boundary number of the element. In addition to the comduction numbers which are assigned to the elements, each boundary element is given a boundary number. Any convenient order of numbering can be used. This is for convenience in preparing data.
word 2	columns 7 to 12	Conduction number of the boundary element. Most computation is based on the conduction number.
word 3	columns 13 to 18	Boundary heat transfer type code number for first basic type associated with the element. Code numbers are as follows: (1) Specified heat flux - the net flux for all faces for which it is specified. If this type is associated with a node, it must appear first; but the other types need not appear in any fixed order. (2) Forced convection (3) Free convection (4) Radiation (5) Specified heat transfer coefficient (6) Specified temperature - By definition this will be the only condition for an element; the program considers only its effect on adjacent elements.

Card 2: Index card (for each condition: basic type or subtype)

This card has two forms. Form A is used for specified parameters (types 1 and 7) which require no additional cards. Form B (TDA) is used for the remaining types which do require additional cards.

Form A for specified heat flux (I5, E13.6, I6)

word 1	columns 1 to 5	Conduction number of element
word 2	columns 6 to 18	Heat flux, Btu/sec
word 3	columns 19 to 24	A nonzero integer if other types or subtypes associated with the node follow; blank (or 0) if no types or subtypes follow.

Form A for specified temperature (I5, 1X, F6.0)

word 1	columns 1 to 5	Conduction number of element
word 2	columns 7 to 12	Temperature of element, ^{o}F

Form B (6F6.0, F12.0) - These (TDA) cards are the same for all types using them.

word 1	columns 1 to 6	Conduction number of element
word 2	columns 7 to 12	Heat transfer type (2 to 6)
word 3	columns 13 to 18	Heat transfer subtype code number. (For additions or substitutions see limitations and scope.)

Subtype code numbers for type 2 (forced convection) are as follows:

(1) Duct flow, liquid - for explanation see headings under additional cards
(2) Sides of rotors
(3) Radial seal gap
(4) Concentric cylinders
(5) Flat plate
(6) to (9) for additional subtypes

Subtype code numbers for type 3 (free convection) are as follows:

(1) Horizontal cylinder
(2) Vertical cylinder or plane
(3) Liquid film cooling, gravity flow
(4) to (8) for additional subtypes

		Subtype code numbers for type 6 (varying temperature forced convection) are as follows: (1) Duct flow, liquid (2) Radial seal gap (3) to (4) for additional subtypes Types 4 and 5, at present, have no subtypes; so word 3 = 0.
word 4	columns 19 to 24	Nonzero number if other types or subtypes follow
word 5	columns 25 to 30	Number of items to be read from the remaining cards for this condition
word 6	columns 31 to 36	Area indicator code number specifies to which face of the element the condition applies; these numbers are as follows: (1) East face (2) North face (3) West face (4) South face (5) Specified area - used for special cases such as a small duct passing through an element or a boundary at an appreciably nonparallel or nonnormal angle to the axis. Since conductive resistance is assumed to be negligible compared with boundary film resistance, the problem of location does not occur.
word 7	columns 37 to 48	If a specified area (code number 5 in word 6) is used, the value in square feet is placed here; otherwise, this word is left blank.

For types 2 to 6, the following additional cards are needed as shown under types 4 and 5 and the subtypes of types 2, 3, and 6. Card 1 is the indicator card described previously. Card 2 is the TDA card for the type or subtype. The properties are evaluated at the temperature indicated by the equations in table I.

Steady-state forced convection (type 2):

Subtype 1 - Duct flow, liquid

Card 3 (7F11.0)

word 1	columns 1 to 11	Fluid bulk temperature, ^{o}F

word 2	columns 12 to 22	Thermal conductivity, Btu/(ft)(sec)(^{o}F)
word 3	columns 23 to 33	Specific heat, Btu/(lbm)(^{o}F)
word 4	columns 34 to 44	Absolute viscosity, lbm/(ft)(sec)
word 5	columns 45 to 55	Mass flow per square foot of cross section, lbm/(ft^2)(sec)
word 6	columns 56 to 66	Hydraulic diameter, $4A_x/P_w$, ft
word 7	columns 67 to 77	Flow length (distance from start of duct to center of element), ft

Subtype 2 - Sides of rotors (see Use of Local Coefficients in appendix D)

Card 3 (7F11.0)

word 1	columns 1 to 11	Fluid bulk temperature, ^{o}F
word 2	columns 12 to 22	Thermal conductivity, Btu/(ft)(sec)(^{o}F)
word 3	columns 23 to 33	Specific heat, Btu/(lbm)(^{o}F)
word 4	columns 34 to 44	Absolute viscosity, lbm/(ft)(sec)
word 5	columns 45 to 55	Kinematic viscosity, ft^2/sec
word 6	columns 56 to 66	Average radius of element, ft
word 7	columns 67 to 77	Gap between rotor and stator, ft

Card 4 (3F11.0)

word 1	columns 1 to 11	Rotor angular velocity, rad/sec
word 2	columns 12 to 22	Outer radius of rotor or stator, ft
word 3	columns 23 to 33	Rotor or stator flag (zero for rotor, nonzero for stator)

Subtype 3 - Radial seal gap

Card 3 (7F11.0)

word 1	columns 1 to 11	Fluid bulk temperature, ^{o}F
word 2	columns 12 to 22	Thermal conductivity, Btu/(ft)(sec)(^{o}F)
word 3	columns 23 to 33	Specific heat, Btu/(lbm)(^{o}F)
word 4	columns 34 to 44	Absolute viscosity, lbm/(ft)(sec)

word 5	columns 45 to 55	Kinematic viscosity, ft^2/sec
word 6	columns 56 to 66	Average radius of element, ft
word 7	columns 67 to 77	Gap between rotor and stator, ft

Card 4 (2F11.0)

word 1	columns 1 to 11	Rotor angular velocity, rad/sec
word 2	columns 12 to 22	Outer radius of rotor or stator, ft

Subtype 4 - Concentric cylinders (inner cylinder rotating)

Card 3 (7F11.0)

word 1	columns 1 to 11	Fluid bulk temperature, ^oF
word 2	columns 12 to 22	Thermal conductivity, Btu/(ft)(sec)(^oF)
word 3	columns 23 to 33	Specific heat, Btu/(lbm)(^oF)
word 4	columns 34 to 44	Absolute viscosity, lbm/(ft)(sec)
word 5	columns 45 to 55	Kinematic viscosity, ft^2/sec
word 6	columns 56 to 66	Outer radius of annulus between cylinders, ft
word 7	columns 67 to 77	Inner radius of annulus, ft

Card 4 (2F11.0)

word 1	columns 1 to 11	Rotational velocity of inner cylinder, rad/sec
word 2	columns 12 to 22	Axial flow velocity, ft/sec

Subtype 5 - Flat plate

Card 3 (7F11.0)

word 1	columns 1 to 11	Fluid bulk temperature, ^oF
word 2	columns 12 to 22	Thermal conductivity, Btu/(ft)(sec)(^oF)
word 3	columns 23 to 33	Specific heat, Btu/(lbm)(^oF)
word 4	columns 34 to 44	Absolute viscosity, lbm/(ft)(sec)
word 5	columns 45 to 55	Kinematic viscosity, ft^2/sec
word 6	columns 56 to 66	Flow length (distance from start of plate to center of element), ft
word 7	columns 67 to 77	Velocity of bulk fluid, ft/sec

Free convection (type 3):

Subtype 1 (horizontal cylinder) or 2 (vertical cylinder or plane), gas - identical except for the characteristic length used

Card 3 (6F11.0)

word 1	columns 1 to 11	Fluid bulk temperature, ^{o}F
word 2	columns 12 to 22	Thermal conductivity, Btu/(ft)(sec)(^{o}F)
word 3	columns 23 to 33	Specific heat, Btu/(lbm)(^{o}F)
word 4	columns 34 to 44	Absolute viscosity, lbm/(ft)(sec)
word 5	columns 45 to 55	Kinematic viscosity, ft^2/sec
word 6	columns 56 to 66	Subtype 1: hydraulic diameter, ft Subtype 2: flow length (distance from start of flow to top of surface of which element is a part), ft

Subtype 3 - Liquid film cooling, gravity flow

Card 3 (4F11.0)

word 1	columns 1 to 11	Fluid film temperature, ^{o}F
word 2	columns 12 to 22	Mass flow per unit length (at a right angle to flow direction), lbm/(ft)(sec)
word 3	columns 23 to 33	Specific heat, Btu/(lbm)(^{o}F)
word 4	columns 34 to 44	Flow length (distance from point where flow starts to where it leaves surface (e.g., one-half circumference of horizontal cylinder)), ft

Graybody radiation (type 4):

Card 3 (4F11.0)

word 1	columns 1 to 11	Environmental temperature, ^{o}F
word 2	columns 12 to 22	View factor, environment to surface
word 3	columns 23 to 33	View factor, surface to environment
word 4	columns 34 to 44	Emissivity of environment
word 5	columns 45 to 55	Emissivity of surface

Specified heat transfer coefficient (type 5):

Card 3 (2F11.0)

word 1	columns 1 to 11	Fluid bulk (or environmental) temperature, ^{o}F
word 2	columns 12 to 22	Heat transfer coefficient, Btu/(ft^2)(sec)(^{o}F)

Varying temperature forced convection (type 6):

Subtype 1 - Varying temperature duct flow, liquid

Card 3 (7F11.0)

word 1	columns 1 to 11	Fluid bulk temperature, ^{o}F
word 2	columns 12 to 22	Thermal conductivity, Btu/(ft)(sec)(^{o}F)
word 3	columns 23 to 33	Specific heat, Btu/(lbm)(^{o}F)
word 4	columns 34 to 44	Absolute viscosity, lbm/(ft)(sec)
word 5	columns 45 to 55	Mass flow per square foot of cross section, lbm/(ft^2)(sec)
word 6	columns 56 to 66	Hydraulic diameter, $4A_x/P_w$, ft
word 7	columns 67 to 77	Flow length (distance from start of duct to center of element), ft

Card 4 (4F11.0)

word 1	columns 1 to 11	Conduction number of annular neighbor (element on other boundary of flow if flow is between two elements). If none, leave blank.
word 2	columns 12 to 22	Conduction number of flow neighbor (element upstream of element under consideration). If this is the first element along the flow, leave blank.
word 3	columns 23 to 33	Combined flow indicator (see remarks at end of this subtype)
word 4	columns 34 to 44	Flow initiation indicator (see remarks at end of this subtype)
word 5	columns 45 to 55	Cross section of duct, ft^2

There is provision in the program for varying temperature flows of two starting temperatures. Any number of varying temperature flows can be handled subject to the fol-

lowing additional restrictions. The program will handle only one such boundary condition per element. The number of elements with varying temperature flows cannot exceed half the number of boundary elements (95) at present. There can be no more than five combined flows (explained later).

The flow initiation indicator distinguishes the two starting temperatures. If 1 is used, the starting temperature is word 1, Card 2 of Item 5 (Case data). If 2 is used, the starting temperature is word 2, Card 2 of Item 5.

If two flows (limit of program) combine at a boundary element to form a new flow, this element is a combined flow element. For a combined flow element, the flow initiation indicator must be zero. Five such combinations are permitted by the program. An additional card is then required.

Card 5 (2I6) - only for combined flow elements

word 1	columns 1 to 6	Conduction number of one upstream neighbor element
word 2	columns 7 to 12	Conduction number of other upstream neighbor element

Subtypes - Varying temperature radial seal gap

Card 1 (7F11.0)

word 1	columns 1 to 11	Fluid bulk temperature, ^{o}F
word 2	columns 12 to 22	Thermal conductivity, Btu/(ft)(sec)(^{o}F)
word 3	columns 23 to 33	Specific heat, Btu/(lbm)(^{o}F)
word 4	columns 34 to 44	Absolute viscosity, lbm/(ft)(sec)
word 5	columns 45 to 55	Kinematic viscosity, ft^2/sec
word 6	columns 56 to 66	Average radius of element, ft
word 7	columns 67 to 77	Gap between rotor and stator, ft

Card 2 (7F11.0)

word 1	columns 1 to 11	Rotor angular velocity, rad/sec
word 2	columns 12 to 22	Outer radius of rotor, ft
word 3	columns 23 to 33	Combined flow indicator
word 4	columns 34 to 44	Flow initiation indicator
word 5	columns 45 to 55	Annular neighbor conduction number

word 6	columns 56 to 66	Flow neighbor conduction number
word 7	columns 67 to 77	Mass flow, lbm/sec

Card 5 (2I6) - only for combined flow elements

word 1	columns 1 to 6	Conduction number of one upstream neighbor element
word 2	columns 7 to 12	Conduction number of other upstream neighbor element

Computer Output

Standard output of results. - The standard output of the program is obtained with all list options (Item 2 of Computer Input) set at zero with the possible exception of the punch options (words 8 and 9). This output is as follows:

Item 1: Problem title
Item 2: Printout options (see input Item 2)
Item 3: Miscellaneous options (see input Item 3)
Item 4: Run data (see input Item 4)
Item 5: Case data (see input Item 5)
Item 6: Thermal conductivity curve fit coefficients for each material
Item 7: Thermal expansion curve fit coefficients for each material
Item 8: Element starting temperature estimates
Item 9: Varying temperature boundary element dimensionless coefficient, hA/WC_p
Item 10: Varying temperature boundary element fluid internal heat generation
Item 11: Conduction number and preceding element conduction numbers for each combined flow element
Item 12: Conduction number, varying temperature number, and flow code for varying temperature boundary elements
Item 13: Element steady-state temperatures
Item 14: Boundary element forced convection, free convection, radiation, and varying temperature convection conductances
Item 15: Varying temperature boundary condition fluid temperatures
Item 16: Element thermal conductivities
Item 17: Element heat fluxes to neighbor elements
Item 18: Element conductances to neighbor elements
Item 19: Element boundary conductance sums and boundary heat flux sums
Item 20: Element free thermal expansion, $\alpha \Delta T$

An illustration of the output can be found in the listing for the sample problem in appendix C.

Program error messages. - The program includes checks of some of the input to ensure correct relations. First, the conductivity (TD1) cards are checked for numerical order of conduction numbers. Once this has been achieved, a check is made for neighbor agreement. For example, if element 10 has element 11 listed as east neighbor, element 11 must have element 10 as west neighbor, assuming this is the correct relation. When the neighbor agreement is complete, a check is made of boundary index cards to ensure numerical order of boundary numbers. Then a check is made to see that the conduction number(s) on the element boundary index card(s) agree with the conduction number on the indicator card. Also there is a check for agreement of the boundary number corresponding to an element conduction number with the conduction number corresponding to the element boundary number.

Program Symbols and Definitions

AFN(NTF)	conduction number of varying temperature element annular neighbor
ALPHA(15, 11)	thermal expansion curve fit matrix (input Item 6)
CE(NJPTS, 4)	neighbor conductance matrix
GFN(NTF)	conduction number of varying temperature element flow neighbor
H(NBPTS, 9)	boundary conductance matrix
JBNT(JBPT)	boundary number of element JBPT
JBP	conduction number of boundary element (in card check)
JBPT	conduction number of boundary element, NBND(NBP)
JNTF(JVPT)	varying temperature number of element JVPT
JPT	conduction number of element
JVPT	conduction number of varying temperature element, NODE(NTF)
MATL(15, 11)	thermal conductivity curve fit matrix (input Item 5)
NAT(NDR)	conduction number of one adjacent element upstream of NDR
NBDIM	maximum number of boundary elements accepted by program
NBND(NBP)	conduction number of boundary element NBP
NBP	boundary number of boundary element
NBPTS	actual number of boundary elements

NBR(NTR)	flow number (input Item 10, Card 4, word 3) of varying temperature element
NBT(NDR)	conduction number of other adjacent element upstream of NDR
NDIM	maximum number of conduction elements accepted by program
NDR	combination number of combined flow varying temperature element
NITS	maximum number of iterations allowed for analysis
NJPTS	actual number of conduction elements
NM(NDR)	conduction number of combined flow element NDR
NODE(NTF)	conduction number of varying temperature element NTF
NTF	varying temperature number of varying temperature boundary element
NTR	noncombining flow number of varying temperature element
NVDIM	maximum number of varying temperature elements accepted
QF(NTF)	fluid shear heat generation at varying temperature element NTF
Q(JBPT)	sum of boundary heat fluxes of conduction element JBPT
SUMH(NBPT)	sum of boundary conductances of boundary element NBPT
SUMT(NBPT)	sum of boundary heat fluxes of boundary element NBPT
TBND(NTF)	fluid temperature at varying temperature boundary element
TCF(NTF)	dimensionless coefficient of varying temperature element, kA/WC_p
TDA(7)	index card (input Item 10, Card 2) list
TD1(NJPTS, 19)	conduction data matrix
TD2(20)	properties cards (input Item 10, Card(s) 3 and those following) list
THEXP(JPT)	element thermal expansion, $\alpha \Delta T$
T(JPT)	initial temperature estimate for element JPT
TS(INC)	fluid temperature calculation by subdivision of boundary element

Conductance matrix CE(NJPTS, 4). - The symbols for conductance matrix CE(NJPTS, 4) are as follows:

CE(JPT, 1)	conductance between conduction element JPT and east neighbor
CE(JPT, 2)	conductance between conduction element JPT and north neighbor
CE(JPT, 3)	conductance between conduction element JPT and west neighbor
CE(JPT, 4)	conductance between conduction element JPT and south neighbor

Boundary conductance matrix H(NBPTS, 9). - The symbols for boundary conductance matrix H(NBPTS, 9) are as follows:

H(NBPT, 1)	specified heat flux
H(NBPT, 2)	sum of forced convection (including specific coefficient) conductances
H(NBPT, 3)	sum of forced convection conductance × fluid temperature
H(NBPT, 4)	sum of free convection conductances
H(NBPT, 5)	sum of free convection conductance × fluid temperature
H(NBPT, 6)	sum of radiation "conductances"
H(NBPT, 7)	sum of radiation "conductance" × environmental temperature
H(NBPT, 8)	sum of varying temperature conductances
H(NBPT, 9)	sum of varying temperature conductance × fluid temperature

Conduction data matrix TD1(NJPTS, 19). - The symbols for conduction data matrix TD1(NJPTS, 19) are as follows:

TD1(JPT, 1)	element conduction number
TD1(JPT, 2)	mean element radius
TD1(JPT, 3)	element radial width, Δr
TD1(JPT, 4)	element axial length, $\Delta \ell$
TD1(JPT, 5)	east neighbor conduction number, j_1
TD1(JPT, 6)	north neighbor conduction number, j_2
TD1(JPT, 7)	west neighbor conduction number, j_3
TD1(JPT, 8)	south neighbor conduction number, j_4
TD1(JPT, 9)	material code number
TD1(JPT, 10)	east contact resistance, $R_{c_{1i}}$
TD1(JPT, 11)	north contact resistance, $R_{c_{2i}}$
TD1(JPT, 12)	west contact resistance, $R_{c_{3i}}$
TD1(JPT, 13)	south contact resistance, $R_{c_{4i}}$
TD1(JPT, 14)	east and west boundary areas (added during run)
TD1(JPT, 15)	north boundary area (added during run)
TD1(JPT, 16)	south boundary area (added during run)
TD1(JPT, 17)	boundary condition type code number (added during run)

TD1(JPT,18) thermal conductivity (added during run)

TD1(JPT,19) element temperature (added during run)

TD2 list for subroutine SN1, type 2 (forced convection), subtype 1 (duct flow, liquid). - The TD2 list is as follows:

TD2(1) fluid bulk temperature, T_b

TD2(2) boundary film thermal conductivity, k_f

TD2(3) boundary film specific heat, $C_{p,f}$

TD2(4) boundary film absolute viscosity, μ_f

TD2(5) fluid mass flow per square foot of cross section, W_a

TD2(6) duct hydraulic diameter, D

TD2(7) length from start of flow to center of element, X

TD2(8) not used in order to obtain compatability with VT1

TD2(9) not used in order to obtain compatability with VT1

TD2(10) not used in order to obtain compatability with VT1

TD2(11) not used in order to obtain compatability with VT1

TD2(12) not used in order to obtain compatability with VT1

TD2(13) Reynolds number (calculated in subroutine), Re_w

TD2(14) Prandtl number (calculated in subroutine), Pr_f

TD2(15) heat transfer coefficient (calculated in surboutine), h_f

TD2(16) conductance across boundary film (calculated in subroutine), hA

TD2(17) hydraulic diameter/flow length (calculated in subroutine), D/X

TD2(18) conductivity/hydraulic diameter (calculated in subroutine), k_f/D

TD2(19) 0.7 power of TD2(16) (calculated in subroutine), $(D/X)^{0.7}$

TD2 list for subroutine SN2, type 2 (forced convection), subtype 2 (sides of rotors). - The TD2 list is as follows:

TD2(1) fluid bulk temperature, T_b

TD2(2) boundary film thermal conductivity, k_f

TD2(3) boundary film specific heat, $C_{p,f}$

TD2(4) boundary film absolute viscosity, μ_f

TD2(5) boundary film kinematic viscosity, ν_f

TD2(6) average radius of element, r_{av}

TD2(7) clearance between rotor and stator, s

TD2(8) rotor angular velocity, ω

TD2(9) outer radius of rotor, a

TD2(10) rotor or stator flag (zero for rotor, nonzero for stator)

TD2(11) Reynolds number (calculated in subroutine), Re_{ω}

TD2(12) cube root of Prandtl number (calculated in subroutine), $Pr_f^{1/3}$

TD2(13) heat transfer coefficient (calculated in subroutine), h_f

TD2(14) conductance across boundary film (calculated in subroutine), hA

TD2(15) conductivity/average radius (calculated in subroutine), k_f/r_{av}

TD2(16) 0.1 power of clearance/average radius (calculated in subroutine), $(s/r_{av})^{0.1}$

TD2(17) fluid angular velocity/rotor angular velocity (calculated in subroutine), K

TD2 list for subroutine SN3, type 2 (forced convection), subtype 3 (radial seal gap). - The TD2 list is as follows:

TD2(1) fluid bulk temperature, T_b

TD2(2) boundary film thermal conductivity, k_f

TD2(3) boundary film specific heat, $C_{p,f}$

TD2(4) boundary film absolute viscosity, μ_f

TD2(5) boundary film kinematic viscosity, ν_f

TD2(6) average radius of element, r_{av}

TD2(7) clearance between rotor and stator, s

TD2(8) rotor angular velocity, ω

TD2(9) outer radius of rotor, a

TD2(10) not used to obtain compatability with VT2

TD2(11) not used to obtain compatability with VT2

TD2(12) not used to obtain compatability with VT2

TD2(13) not used to obtain compatability with VT2

TD2(14) not used to obtain compatability with VT2

TD2(15) Reynolds number (calculated in subroutine), Re_{ω}

TD2(16) cube root of Prandtl number (calculated in subroutine), $Pr_f^{1/3}$

TD2(17) critical Reynolds number (calculated in subroutine), Re_c

TD2(18) heat transfer coefficient (calculated in subroutine), h_f

TD2(19) conductance from center of seal gap to surface (calculated in subroutine), hA

TD2(20) heat generation factor (calculated in subroutine)

TD2 list for subroutine SN4, type 2 (forced convection), subtype 4 (concentric cylinders). - The TD2 list is as follows:

TD2(1) fluid bulk temperature, T_b

TD2(2) boundary film thermal conductivity, k_f

TD2(3) boundary film specific heat, $C_{p,f}$

TD2(4) boundary film absolute viscosity, μ_f

TD2(5) boundary film kinematic viscosity, ν_f

TD2(6) outer radius of annulus between cylinders, r_o

TD2(7) inner radius of annulus between cylinders, r_i

TD2(8) angular velocity of inner rotating cylinder, ω

TD2(9) axial flow velocity, V_a

TD2(10) Reynolds number (calculated in subroutine), Re_v

TD2(11) cube root of Prandtl number (calculated in subroutine), $Pr_f^{1/3}$

TD2(12) heat transfer coefficient (calculated in subroutine), h_f

TD2(13) conductance across boundary film (calculated in subroutine), hA

TD2(14) linear velocity of inner cylinder (calculated in subroutine), V_R

TD2(15) square of total fluid velocity (calculated in subroutine), V_{tot}^2

TD2(16) total fluid velocity (calculated in subroutine), V_{tot}

TD2(17) annular clearance (calculated in subroutine), s

TD2 list for subroutine SN5, type 2 (forced convection), subtype 5 (flat plate). - The TD2 list is as follows:

TD2(1) fluid bulk temperature, T_b

TD2(2) boundary film thermal conductivity, k_f

TD2(3) boundary film specific heat, $C_{p,f}$

TD2(4) boundary film absolute viscosity, μ_f

TD2(5) boundary film kinematic viscosity, ν_f

TD2(6) length from start of flow to center of element, X

TD2(7) bulk fluid velocity, V_∞

TD2(8) Reynolds number (calculated in subroutine), Re_x

TD2(9) Prandtl rumber (calculated in subroutine), Pr_f

TD2(10) heat transfer coefficient (calculated in subroutine), h

TD2(11) conductance across boundary film (calculated in subroutine), hA

TD2 list for subroutine FC1, type 3 (free convection), subtype 1 (horizontal cylinder). - The TD2 list is as follows:

TD2(1) fluid bulk temperature, T_b

TD2(2) boundary film thermal conductivity, k_f

TD2(3) boundary film specific heat, $C_{p,f}$

TD2(4) boundary film absolute viscosity, μ_f

TD2(5) boundary film kinematic viscosity, ν_f

TD2(6) diameter of cylinder, D

TD2(7) Prandtl number (calculated in subroutine), Pr_f

TD2(8) Grashof number (calculated in subroutine), Gr_D

TD2(9) heat transfer coefficient (calculated in subroutine), h_f

TD2(10) conductance across boundary film (calculated in subroutine), hA

TD2(11) Prandtl number × Grashof number (calculated in subroutine), $Pr_f Gr_D$

TD2(12) fluid to surface temperature difference (calculated in subroutine), ΔT

TD2(13) average (or film) temperature (calculated in subroutine), T_{av}

TD2(14) conductivity/cylinder outside diameter (calculated in subroutine), k_f/D

TD2 list for subroutine FC2, type 3 (free convection), subtype 2 (vertical cylinder or plane). - The TD2 list is as follows:

TD2(1) fluid bulk temperature, T_b

TD2(2) boundary film thermal conductivity, k_f

TD2(3) boundary film specific heat, $C_{p,f}$

TD2(4) boundary film absolute viscosity, μ_f

TD2(5) boundary film kinematic viscosity, ν_f

TD2(6) total height of surface, L

TD2(7) Prandtl number (calculated in subroutine), Pr_f

TD2(8) Grashof number (calculated in subroutine), Gr_L

TD2(9) heat transfer coefficient (calculated in subroutine), h_f

TD2(10) conductance across boundary film (calculated in subroutine), hA

TD2(11) Prandtl number × Grashof number (calculated in subroutine), $Pr_f Gr_D$

TD2(12) fluid to surface temperature difference (calculated in subroutine), ΔT

TD2(13) average temperature (calculated in subroutine), T_{av}

TD2(14) conductivity/surface height (calculated in subroutine), k_f/L

TD2 list for subroutine FC3, type 3 (free convection), subtype 3 (liquid film cooling, gravity flow). - The TD2 list is as follows:

TD2(1) fluid bulk temperature, T_b

TD2(2) mass flow of liquid per unit length normal to flow, W/L

TD2(3) fluid specific heat, C_p

TD2(4) flow length (e.g., one-half circumference of horizontal cylinder), D_L

TD2(5) heat transfer coefficient (calculated in subroutine), h

TD2(6) conductance from surface to liquid (calculated in subroutine), hA

TD2 list for subroutine RA1, type 4 (radiation). - The TD2 list is as follows:

TD2(1) environmental temperature, T_e

TD2(2) view factor from environment to element surface, f_{es}

TD2(3) view factor from element surface to environment, f_{se}

TD2(4) emissivity of environment, ϵ_e

TD2(5) emissivity of element surface, ϵ_s

TD2(6) radiation coefficient (calculated in subroutine), h

TD2(7) "conductance" from element surface to environment (calculated in subroutine), hA

TD2(8) reflectivity of environment (calculated in subroutine), $1 - \epsilon_e$

TD2(9) reflectivity of element surface (calculated in subroutine), $1 - \epsilon_s$

TD2(10) difference between fourth powers of temperatures/temperature difference (calculated in subroutine), $\left(T_e^4 - T_s^4\right)/\left(T_e - T_s\right)$

TD2 list for subroutine SC1, type 5 (specified heat transfer coefficient). - The TD2 list is as follows:

TD2(1) fluid bulk (or environmental) temperature, T_b (or T_e)

TD2(2) specified heat transfer coefficient, h

TD2(3) conductance between surface and bulk fluid (calculated in main program), hA

TD2 list for subroutine VT1, type 6 (varying temperature forced convection), subtype 1 (duct flow, liquid). - The TD2 list is as follows:

TD2(1) fluid bulk temperature, T_b

TD2(2) boundary film thermal conductivity, k_f

TD2(3) boundary film specific heat, $C_{p,f}$

TD2(4) boundary film absolute viscosity, μ_f

TD2(5) fluid mass flow per square foot of cross section, W_a

TD2(6) duct hydraulic diameter, D

TD2(7) length from start of flow to center of element, X

TD2(8) annular neighbor conduction number

TD2(9) flow neighbor conduction number

TD2(10) combining flow indicator code number

TD2(11) flow initiation indicator code number (must be zero for combined flow element)

TD2(12) duct cross section, A_x

TD2(13) Reynolds number (calculated in subroutine), Re_w

TD2(14) Prandtl number (calculated in subroutine), Pr_f

TD2(15) heat transfer coefficient (calculated in subroutine), h_f

TD2(16) conductance across boundary film (calculated in subroutine), hA

TD2(17) hydraulic diameter/flow length (calculated in subroutine), D/X

TD2(18) conductivity/hydraulic diameter (calculated in subroutine), k_f/D

TD2(19) 0.7 power of TD2(16) (calculated in subroutine), $(D/X)^{0.7}$

TD2 list for subroutine VT2, type 6 (varying temperature forced convection), subtype 2 (radial seal gap). - The TD2 list is as follows:

TD2(1) fluid bulk temperature, T_b

TD2(2) boundary film thermal conductivity, k_f

TD2(3)	boundary film specific heat, $C_{p,f}$
TD2(4)	boundary film absolute viscosity, μ_f
TD2(5)	boundary film kinematic viscosity, ν_f
TD2(6)	average radius of element, r_{av}
TD2(7)	clearance between rotor and stator, s
TD2(8)	rotor angular velocity, ω
TD2(9)	outer radius of rotor, a
TD2(10)	combining flow indicator code number
TD2(11)	flow initiation indicator code number (must be zero for combined flow element)
TD2(12)	annular neighbor conduction number
TD2(13)	flow neighbor conduction number
TD2(14)	fluid mass flow rate, W
TD2(15)	Reynolds number (calculated in subroutine), Re_ω
TD2(16)	cube root of Prandtl number (calculated in subroutine), $Pr_f^{1/3}$
TD2(17)	critical Reynolds number (calculated in subroutine), Re_c
TD2(18)	heat transfer coefficient (calculated in subroutine), h_f
TD2(19)	conductance from center of seal gap to surface (calculated in subroutine), hA
TD2(20)	heat generation factor (calculated in subroutine)

Flow Charts and Program Listing

The flow charts for the main routine (SEAL2) and subroutines CQN and QT are presented in figures 8, 9, and 10. A listing of the program is as follows:

```
$IBFTC SEAL2

C
C       STEADY STATE HEAT TRANSFER ANALYSIS OF AXISYMMETRIC SYSTEMS TO
C       INCLUDE VARYING FLUID TEMPERATURES ALONG BOUNDARIES APPLIED TO
C       ADVANCED AIR BREATHING ENGINE SEAL DESIGN
C
        DIMENSION TD1(400,19),T(400),CE(400,4),Q(400),THEXP(400),TD2(20)
        DIMENSION H(200,9),SUMH(200),SUMT(200),NBND(200),TBND(95)
        DIMENSION LD(10),NI(5),RD(5),CD(10),TDA(7),MATL(15,11),NODE(95)
        DIMENSION ALPHA(15,11),JNTF(400)
        COMMON/BLK1/JBNT(400),KAN(200),NTF,NDR,NTR,QF(95),NQR
        COMMON/BLK2/TCF(95),BFN(95),AFN(95),NBR(95),NM(5),NAT(5),NBT(5)
        REAL MATL
C
  101 FORMAT(1H1)
  102 FORMAT(F4.0,1X,F7.4,2F5.3,1X,4F4.0,F3.0,4F7.0)
  103 FORMAT(1HO,10X,43HCONDUCTION (TD1) CARD ORDER ERROR, CARD NO.,I3,2
     2X,5HWRONG)
  104 FORMAT(1HO,10X,23HNABOR ERROR FOR ELEMENT,I4,3X,6HAND/OR,I4)
  105 FORMAT(1HO,45X,30HCONDUCTION ELEMENT TABLE (TD1)//(5X,I4,2X,7(2X,I
     22,1H,,1PE11.4)/10X,6(2X,I2,1H,,1PE11.4)//))
  106 FORMAT(16F5.0)
  107 FORMAT(1H1,50X,29HELEMENT STARTING TEMPERATURES//)
  108 FORMAT(10(2X,I3,1X,F6.1))
  109 FORMAT(25X,74HBOUNDARY COEFFICIENT MATRIX -(H*A)BTU/F.SEC AND (H*A
     2*T-B) OR W*C-P BTU/SEC//1X,11HBNDRY COND.,2X,10HFIXED FLUX,6X,17HF
     3ORCED CONVECTION,10X,15HFREE CONVECTION,14X,9HRADIATION,12X,19HVAR
     4.TEMP.CONVECTION/1X,11HELEM. ELEM.,6X,1HW,11X,3HH*A,8X,7HH*A*T-B,8
     5X,3HH*A,8X,7HH*A*T-B,8X,3HH*A,8X,7HH*A*T-E,8X,3HH*A,8X,5HW*C-P//(1
     6X,2(I4,1X),1X,9(1X,E12.5)))
  110 FORMAT(1HO,30X,58HVAR.TEMP.CONVECTION DIMENSIONLESS COEFFICIENTS (
     2H*A/W*C-P)//(6(1X,2I4,1H,,1PE11.4)))
  111 FORMAT(1HO,45X,36HFLUID SHEAR HEAT GENERATION, BTU/SEC//(6(1X,2I4,
     21H,,1PE11.4)))
  112 FORMAT(1HO,2X,10HDATA TIME=,F7.4,2X,7HMINUTES)
  113 FORMAT(1H1,20X,61HTEMPERATURES (F) AND HEAT FLUXES (BTU/SEC) FOR E
     2ACH ITERATION)
  114 FORMAT(3(4X,I3,1H,,1PE14.7,2X,1PE14.7))
  115 FORMAT(1H1,30X,32HCONVERGENCE CRITERIA, ITERATION=,I4//23X,8HCOND.
     2NO.,6X,9HNEW TEMP.,10X,9HOLD TEMP.,9X,10HDIFFERENCE,8X,9HMAX.DIFF.
     3//)
  116 FORMAT(1HO,2X,42HCONVERGENCE CRITERION NOT MET, ITERATIONS=,I6)
  117 FORMAT(1HO,2X,43HCONVERGENCE CRITERION ACHEIVED, ITERATIONS=,I6)
  118 FORMAT(1H1,20X,56HELEMENT(AT CENTER) TEMPERATURES (DEGREES F), ITE
     2RATIONS=,I6//)
  119 FORMAT(6(2X,I4,1H,,1PE14.7))
  120 FORMAT(1H1,9X,102HELEMENT FORCED CONVECTION, FREE CONVECT., RADIAT
     2ION AND VAR.TEMP.CONVECT. CONDUCTANCES(H*A)   BTU/HR.F//)
  121 FORMAT(16X,2I6,4E19.7)
  122 FORMAT(1H1,45X,38HVAR.TEMP.CONVECTION BOUNDARY TEMPS.(F)//(6(1X,2I
     24,1H,,1PE11.4)))
  123 FORMAT(1H1,42X,43HELEMENT THERMAL CONDUCTIVITIES  BTU/HR.FT.F//)
```

```
  124 FORMAT(3X,35HELEMENT ENWS CONDUCTION HEAT FLUXES,2X,I3,4(2X,E14.7)
     2,2X,6HBTU/HR)
  125 FORMAT(15X,45HELEMENT ENWS CONDUCTANCES TO NABORS(BTU/HR.F)//(10X,
     2I4,4(2X,E14.7)))
  126 FORMAT(1HO,10X,104HELEMENT BOUNDARY NO, CONDUCTION NO, BNDRY CONDU
     2CTANCE(H*A) SUM(BTU/HR.F) AND BNDRY HEAT FLUX SUM(BTU/HR)//(3(3X,2
     3I4,2X,E14.7,2X,E14.7)))
  127 FORMAT(1H1,40X,43HELEMENT FREE THERMAL EXPANSION,ALPHA*(T-TO)//)
  128 FORMAT(6E13.6)
C
C
      CALL TIME 1 (START)
C
C     READ RUN PARAMETERS
   60 DO 1 J=1,10
      LD(J)=0
    1 CD(J)=0.
      DO 2 J=1,5
      NI(J)=0
    2 RD(J)=0.
      DO 3 J=1,15
      DO 3 K=1,11
      MATL(J,K)=0.
    3 ALPHA(J,K)=0.
      NK=0
      CALL CDA(LD,NI,RD,CD,MATL,ALPHA)
      IF (NK.NE.0) GO TO 99
C
      NDIM=400
      NBDIM=200
      NVDIM=95
      NJPTS=CD(1)
      NBPTS=CD(2)
      NITS=CD(3)
      NK=0
C
C     ZERO COMMON STORAGE
      DO 5 JPT=1,NJPTS
      T(JPT)=0.0
      Q(JPT)=0.0
      JBNT(JPT)=0
      JNTF(JPT)=0
      THEXP(JPT)=0.0
      DO 4 J=1,4
    4 CE(JPT,J)=0.0
      DO 5 J=1,19
    5 TDT(JPT,J)=0.0
C
      DO 6 NBPT=1,NBPTS
      NBND(NBPT)=0
      SUMH(NBPT)=0.0
      SUMT(NBPT)=0.0
      DO 6 J=1,9
    6 H(NBPT,J)=0.0
C
      DO 7 K=1,NVDIM
```

```
      QF(K)=0.0
      TCF(K)=0.0
      GFN(K)=0.0
      AFN(K)=0.0
      NBR(K)=0
      NODE(K)=0
      TEND(K)=0.0
C
      DO 8 K=1,5
      NM(K)=0
      NAT(K)=0
    8 NBT(K)=0
C
C     READ ELEMENT GEOMETRY DATA, CHECK CARD ORDER
      DO 10 JPT=1,NJPTS
      READ(5,102) (TD1(JPT,J),J=1,13)
C
      NPC=TD1(JPT,1)
      IF (JPT-NPC) 9,10,9
    9 WRITE(6,103) JPT
      NK=1
   10 CONTINUE
      IF (NK.NE.0) GO TO 99
C
C     CHECK FOR CONDUCTANCE NABOR ERRORS
      NK=0
      DO 15 JPT=1,NJPTS
      DO 15 J=5,8
      N=TD1(JPT,J)
      IF (N) 14,15,11
   11 IF (JPT-N) 12,14,12
   12 RJPT=JPT
      JN=J-4
      GO TO (13,213,313,413),JN
   13 IF (RJPT-TD1(N,7)) 14,15,14
  213 IF (RJPT-TD1(N,8)) 14,15,14
  313 IF (RJPT-TD1(N,5)) 14,15,14
  413 IF (RJPT-TD1(N,6)) 14,15,14
   14 WRITE(6,104) JPT,N
      NK=1
   15 CONTINUE
      IF (NK.NE.0) GO TO 99
C
      IF (LD(1).EQ.0) GO TO 16
      WRITE(6,101)
      WRITE(6,105) (JPT,(J,TD1(JPT,J),J=1,13),JPT=1,NJPTS)
C
C     COMPUTE ELEMENT BOUNDARY AREAS, CONVERT TD1 DATA TO FEET
   16 DO 17 JPT=1,NJPTS
      RO=TD1(JPT,2)+TD1(JPT,3)/2.
      RI=TD1(JPT,2)-TD1(JPT,3)/2.
      TC1(JPT,14)=.04363323*TD1(JPT,2)*TD1(JPT,3)
      TD1(JPT,15)=.04363323*TD1(JPT,4)*RO
      TC1(JPT,16)=.04363323*TD1(JPT,4)*RI
      TC1(JPT,2)=TD1(JPT,2)/12.
      TC1(JPT,3)=TD1(JPT,3)/12.
```

```
   17 TD1(JPT,4)=TD1(JPT,4)/12.
C
C     READ INITIAL TEMPERATURE GUESSES, CURVE FIT CONDUCTIVITIES
      READ(5,106) (T(JPT),JPT=1,NJPTS)
      WRITE(6,107)
      WRITE(6,108) (JPT,T(JPT),JPT=1,NJPTS)
      DO 18 JPT=1,NJPTS
      TD1(JPT,19)=T(JPT)
   18 CALL FIT(TD1,JPT,NDIM,MATL)
C
C     READ BOUNDARY CONDITION DATA AND COMPUTE COEFFICIENTS
      IF (LD(5).NE.0) WRITE(6,101)
      NK=0
      NTF=0
      NCR=0
      NTR=0
      DO 19 NBPT=1,NBPTS
   19 CALL CON(NBPT,NBDIM,H,NBND,TBND,TD1,TDA,TD2,NDIM,T,LD,NK,NVDIM,NOD
     1E,JNTF)
      IF (NK.NE.0) GO TO 99
C
C     CON PRINTOUT
      IF (LD(2).EQ.0) GO TO 20
      WRITE(6,101)
      WRITE(6,109) (NBPT,NBND(NBPT),(H(NBPT,J),J=1,9),NBPT=1,NBPTS)
   20 IF (NTF.EQ.0) GO TO 21
      WRITE(6,101)
      WRITE(6,110) (J,NODE(J),TCF(J),J=1,NTF)
      WRITE(6,111) (J,NODE(J),QF(J),J=1,NTF)
C
C     PERFORM ITERATIVE ANALYSIS
   21 CALL TIME 1 (TEX)
      TDAT=(TEX-START)/3600.
      WRITE(6,112) TDAT
      NCC=0
      NPRT=RD(3)
C
      DO 29 NIT=1,NITS
      NK=0
      NCR=0
      NTF=0
      NOR=1
      NTR=0
      NCC=NCC+1
      LD(4)=0
      DO 22 NBPT=1,NBPTS
   22 KAN(NBPT)=0
C
C     BOUNDARY CONDITION ITERATION
      DO 23 NBPT=1,NBPTS
      JBPT=NBND(NBPT)
      CALL QT(NBPT,NBDIM,NDIM,JBPT,H,SUMT,SUMH,TD1,TBND,T,CD,NVDIM,NIT,N
     1DCF,JNTF)
   23 Q(JBPT)=SUMT(NBPT)
C
C     OVER-RELAXATION
```

```
      NQR=0
      DO 24 JPT=1,NJPTS
   24 CALL TATS(TD1,JPT,NDIM,NBND,NBDIM,Q,T,H,RD,LD,CE,NK)
      IF (NK.NE.0) GO TO 99
C
      IF (LD(10).EQ.0) GO TO 25
      WRITE(6,113)
      WRITE(6,114) (JPT,T(JPT),Q(JPT),JPT=1,NJPTS)
C
C     CHECK FOR CONVERGENCE, CORRECTION OF TD1 TEMPERATURES
   25 ERR=CD(4)
      IF (NIT.EQ.NITS) GO TO 30
      IF (NCC.NE.NPRT) GO TO 26
      NCC=0
      LD(4)=1
      WRITE(6,115) NIT
   26 DO 27 JPT=1,NJPTS
   27 CALL CONCHK(JPT,NDIM,TD1,ERR,LD,NK,T)
      IF (NK) 28,31,28
C
C     RECALC. K FROM NEWEST TEMP.
   28 DO 29 JPT=1,NJPTS
      TD1(JPT,19)=T(JPT)
   29 CALL FIT(TD1,JPT,NDIM,MATL)
C
   30 WRITE(6,116) NIT
      GO TO 33
   31 WRITE(6,117) NIT
C
C     TEMPERATURE PRINTOUT
      IF (LD(3)) 32,33,32
   32 NITM1=NIT-1
      WRITE(6,118) NITM1
      WRITE(6,119) (JPT,TD1(JPT,19),JPT=1,NJPTS)
   33 WRITE(6,118) NIT
      WRITE(6,119) (JPT,T(JPT),JPT=1,NJPTS)
      IF (LD(8).NE.0) PUNCH 106, (T(JPT),JPT=1,NJPTS)
C
C     CONVERT FROM SEC.TO HRS.
      DO 34 NBPT=1,NBPTS
      SUMT(NBPT)=SUMT(NBPT)*3600.
      SUMH(NBPT)=SUMH(NBPT)*3600.
      DO 34 J=2,8,2
   34 H(NBPT,J)=H(NBPT,J)*3600.
C
C     PRINT OUT BOUNDARY CONDUCTANCES(H*A)
      WRITE(6,120)
      WRITE(6,121) (NBPT,NBND(NBPT),(H(NBPT,J),J=2,8,2),NBPT=1,NBPTS)
C
C     PRINT OUT VAR.TEMP.BOUNDARY TEMPS.
      IF (NTF.NE.0) WRITE(6,122) (J,NODE(J),TBND(J),J=1,NTF)
C
C     PRINT OUT ELEMENT THERMAL CONDUCTIVITIES
      DO 35 JPT=1,NJPTS
   35 TD1(JPT,18)=TD1(JPT,18)*3600.
      WRITE(6,123)
```

```
      WRITE(6,119) (JPT,TD1(JPT,18),JPT=1,NJPTS)
C
C     COMPUTE AND WRITE HEAT FLUXES
      DO 36 JPT=1,NJPTS
      DO 36 K=1,4
   36 CE(JPT,K)=CE(JPT,K)*3600.
C
      WRITE(6,101)
      DO 48 JPT=1,NJPTS
      NE=TD1(JPT,5)
      IF (NE) 38,37,38
   37 QJE=0.0
      GO TO 39
   38 QJE=CE(JPT,1)*(T(NE)-T(JPT))
   39 NN=TD1(JPT,6)
      IF (NN) 41,40,41
   40 QJN=0.0
      GO TO 42
   41 QJN=CE(JPT,2)*(T(NN)-T(JPT))
   42 NW=TD1(JPT,7)
      IF (NW) 44,43,44
   43 QJW=0.0
      GO TO 45
   44 QJW=CE(JPT,3)*(T(NW)-T(JPT))
   45 NS=TD1(JPT,8)
      IF (NS) 47,46,47
   46 QJS=0.0
      GO TO 48
   47 QJS=CE(JPT,4)*(T(NS)-T(JPT))
   48 WRITE(6,124) JPT,QJE,QJN,QJW,QJS
C
      WRITE(6,101)
      WRITE(6,125) (JPT,(CE(JPT,J),J=1,4),JPT=1,NJPTS)
C
C     PRINT OUT BOUNDARY CONDUCTANCE SUMS AND HEAT FLUX SUMS
      WRITE(6,101)
      WRITE(6,126) (NBPT,NBND(NBPT),SUMH(NBPT),SUMT(NBPT),NBPT=1,NBPTS)
C
C     THERMAL EXPANSION CALCN. AND PRINTOUT
      IF (LD(10).NE.0) WRITE(6,101)
      DO 49 JPT=1,NJPTS
      CALL FIT2(TD1,NDIM,JPT,ALPHA,THEXP)
   49 CALL DEFORM(JPT,NDIM,TD1,RD,LD,THEXP)
      WRITE(6,127)
      WRITE(6,119) (JPT,THEXP(JPT),JPT=1,NJPTS)
      IF (LD(9).NE.0) PUNCH 128,(THEXP(JPT),JPT=1,NJPTS)
C
C     CHECK FOR ADDTL.CASES
      IF (NI(1)-1) 99,99,50
   50 GO TO 60
C
   99 CALL EXIT
      STOP
      END
```

```
$IBFTC CDAM

      SUBROUTINE CDA(LD,NI,RD,CD,MATL,ALPHA,NK)
C
C     PROBLEM PARAMETER INPUT, CONDUCTIVITY AND EXPANSION INPUT
C
      DIMENSION LD(10),NI(5),RD(5),CD(10),MATL(15,11),ALPHA(15,11)
      DIMENSION FILE(11),WCOM(12)
      REAL MATL
C
  101 FORMAT(12A6)
  102 FORMAT(1H1,29X,12A6//)
  103 FORMAT(10I6)
  104 FORMAT(1HO,13X,3HLD=,10(3X,I2,1H,I3))
  105 FORMAT(1HO,13X,3HNI=,5(3X,I2,1H,I3))
  106 FORMAT(10F6.0)
  107 FORMAT(1HO,13X,3HRD=,5(3X,I2,1H,1PE13.6))
  108 FORMAT(1HO,13X,3HCD=,5(3X,I2,1H,1PE13.6)/16X,5(3X,I2,1H,1PE13.6))
  109 FORMAT(1HO,2X,58HNO.CONDUCTION OR BOUNDARY ELEMENTS EXCEEDS ALLOTE
     2D STORAGE)
  110 FORMAT(5F10.0)
  111 FORMAT(6E13.6)
  112 FORMAT(1HO,59X,11HDATA FOR K./(17X,6(2X,I2,1PE14.7)))
  113 FORMAT(1HO,59X,15HDATA FOR ALPHA./(17X,6(2X,I2,1PE14.7)))
C
      READ(5,101) WCOM
      WRITE(6,102) WCOM
C
C     GENERAL DATA
      READ(5,103) (LD(J),J=1,10)
      WRITE(6,104) (J,LD(J),J=1,10)
      READ(5,103) (NI(I),I=1,5)
      WRITE(6,105) (I,NI(I),I=1,5)
      READ(5,106) (RD(I),I=1,5)
      WRITE(6,107) (I,RD(I),I=1,5)
      READ(5,106) (CD(J),J=1,10)
      WRITE(6,108) (J,CD(J),J=1,10)
      IF (400.-CD(1)) 2,1,1
    1 IF (200.-CD(2)) 2,3,3
    2 WRITE(6,109)
      NK=1
      GO TO 11
C
C     CONDUCTIVITY DATA
    3 DO 6 L=1,15
      READ(5,110) (FILE(NCQ),NCQ=1,5)
      IF (FILE(1)) 4,7,4
    4 MN=FILE(2)
      NP6=FILE(3)+6.
      READ(5,111) (FILE(NCQ),NCQ=6,NP6)
      DO 5 NCQ=1,NP6
    5 MATL(MN,NCQ)=FILE(NCQ)
```

```
     6 WRITE(6,112) (NCQ,FILE(NCQ),NCQ=1,NP6)
C
C       EXPANSION DATA
     7 DO 10 I=1,15
       READ(5,110) (FILE(NCQ),NCQ=1,5)
       IF (FILE(1)) 8,11,8
     8 MN=FILE(2)
       NP6=FILE(3)+6.
       READ(5,111) (FILE(NCQ),NCQ=6,NP6)
       DO 9 NCQ=1,NP6
     9 ALPHA(MN,NCQ)=FILE(NCQ)
    10 WRITE(6,112) (NCQ,FILE(NCQ),NCQ=1,NP6)
    11 RETURN
       END



$IBFTC FITM

       SUBROUTINE FIT(TD1,JPT,NDIM,MATL)
C
C      FIT CONDUCTIVITY (K) FROM POLYNOMINAL CURVE
C
       DIMENSION TD1(NDIM,19),COS(5),CALC(6),MATL(15,11)
       REAL MATL
C
   101 FORMAT(1H0,20X,41HTEMPERATURE EXCEEDS CURVE FIT LIMIT FOR K)
C
       TEMP= TD1(JPT,19)
       MAN = TD1(JPT,9)
       DO 1 NCQ=1,5
     1 COS(NCQ)= MATL(MAN,NCQ)
       IF(TEMP-COS(1)) 3,3,2
     2 WRITE(6,101)
       GO TO 9
     3 NOP = COS(3)
       NOP1=NOP+1
       DO 4 NCQ=1,NOP1
       LC = 5+NCQ
     4 CALC(NCQ)= MATL(MAN,LC)
       IF(COS(3)) 6,5,6
     5 Y= CALC(1)*COS(4)
       GO TO 8
     6 Y = CALC(NOP1)
       TEM1 = TEMP*COS(5)
       DO 7 NPY=1,NOP
       J2 = NOP1-NPY
     7 Y= CALC(J2)+Y*TEM1
       Y = Y*COS(4)
     8 TD1(JPT,18)=Y
C
     9 RETURN
       END
```

```
$IBFTC CQNM

      SUBROUTINE CQN(NBPT,NBDIM,H,NBND,TBND,TDL,TDA,TD2,NDIM,T,LD,NK,NVD
     1IM,NODE,JNTF)
C
C     COMPUTE HEAT TRANSFER COEFFICIENTS
C
      DIMENSION H(NBDIM,9),NBND(NBDIM),TBND(NVDIM),TDA(7),TD2(20)
      DIMENSION TDL(NDIM,19),T(NDIM),LD(10),NODE(NVDIM),JNTF(NDIM)
      COMMON/BLK1/JBNT(400),KAN(200),NTF,NDR,NTR,QF(95),NQR
      COMMON/BLK2/TCF(95),GFN(95),AFN(95),NBR(95),NM(5),NAT(5),NBT(5)
C
  101 FORMAT(3I6)
  102 FORMAT(1H0,15X,60HBOUNDARY INDICATOR CARD ORDER ERROR,   BOUNDARY
     2ELEMENT NO.=,I4,11H CARD READS,I4)
  103 FORMAT(I5,1X,F6.0)
  104 FORMAT(1H0,10X,71HBOUNDARY INDEX (TYPE 1 OR 7) CARD ORDER ERROR,
     2CONDUCTION ELEMENT NO.=,I4,11H CARD READS,I4)
  105 FORMAT(I5,E13.6,I6)
  106 FORMAT(6F6.0,F12.0)
  107 FORMAT(7F11.0)
  108 FORMAT(1H0,10X,71HBOUNDARY INDEX (TYPE 2 TO 6) CARD ORDER ERROR,
     2CONDUCTION ELEMENT NO.=,I4,11H CARD READS,I4)
  109 FORMAT(1H0,2X,8HELEMENT=,F4.0,2X,5HTYPE=,F2.0,2X,8HSUBTYPE=,F2.0,2
     2X,5HNEXT=,F2.0,2X,11HITEMS READ=,F3.0,3X,10HAREA CODE=,F2.0,2X,13H
     3SPECIAL AREA=,E12.5,1X,7HSQ.FEET)
  110 FORMAT(1H0,2X,17HDUCT FLOW, LIQUID/2X,4HT-B=,F5.0,2X,4HK-F=,E11.4,
     22X,4HC-P=,E11.4,2X,3HMU=,E11.4,2X,10HMASS FLOW=,E11.4,2X,7HD-HYDR=
     3,E11.4,2X,7HL-FLOW=,E11.4/2X,3HRE=,E11.4,2X,3HPR=,E11.4,9X,8HH COE
     4FF=,E14.7,2X,11HCOEFF*AREA=,E14.7)
  111 FORMAT(1H0,2X,15HSIDES OF ROTORS/2X,4HT-B=,F5.0,2X,4HK-F=,E11.4,2X
     2,4HC-P=,E11.4,2X,3HMU=,E11.4,2X,3HNU=,E11.4,2X,5HR-AV=,E11.4,2X,4H
     3GAP=,E11.4,2X,6HOMEGA=,F6.0/4HR-O=,E11.4,2X,5HFLAG=,F2.0,9X,3HRE=,
     4E11.4,2X,8HPR**1/3=,E11.4,2X,8HH COEFF=,E14.7,2X,11HCOEFF*AREA=,E1
     54.7)
  112 FORMAT(1H0,2X,15HRADIAL SEAL GAP/2X,4HT-B=,F5.0,2X,4HK-F=,E11.4,2X
     2,4HC-P=,E11.4,2X,3HMU=,E11.4,2X,3HNU=,E11.4,2X,5HR-AV=,E11.4,2X,4H
     3GAP=,E11.4,2X,6HOMEGA=,F6.0/2X,4HR-O=,E11.4,15X,3HRE=,E11.4,2X,8HP
     4R**1/3=,E11.4,2X,5HRE-C=,E11.4/2X,8HH COEFF=,E14.7,2X,11HCOEFF*ARE
     5A=,E14.7)
  113 FORMAT(1H0,2X,20HCONCENTRIC CYLINDERS/2X,4HT-B=,F5.0,2X,4HK-F=,E11
     2.4,2X,4HC-P=,E11.4,2X,3HMU=,E11.4,2X,3HNU=,E11.4,2X,4HR-O=,E11.4,2
     3X,4HR-I=,E11.4,2X,6HOMEGA=,F6.0/2X,5HV-AX=,E11.4,15X,3HRE=,E11.4,2
     4X,8HPR**1/3=,E11.4,2X,8HH COEFF=,E14.7,9X,11HCOEFF*AREA=,E14.7)
  114 FORMAT(1H0,2X,10HFLAT PLATE/2X,4HT-B=,F5.0,2X,4HK-F=,E11.4,2X,4HC-
     2P=,E11.4,2X,3HMU=,E11.4,2X,3HNU=,E11.4,2X,7HL-FLOW=,E11.4,2X,7HV-F
     3LOW=,E11.4/2X,3HRE=,E11.4,2X,3HPR=,E11.4,9X,8HH COEFF=,E14.7,2X,11
     4HCOEFF*AREA=,E14.7)
C
C     FUTURE FORCED CONVEC.COEFF.FORMATS (115-8)
  119 FORMAT(1H0,2X,39HHORIZONTAL CYLINDER OR VERTICAL SURFACE/2X,4HT-B=
     2,F5.0,2X,4HK-F=,E11.4,2X,4HC-P=,E11.4,2X,3HMU=,E11.4,2X,3HNU=,E11.
```

```
     34,2X,17HL-FLOW OR D-HYDR=,E11.4/2X,3HPR=,E11.4,2X,3HGR=,E11.4,9X,8
     4HH COEFF=,E14.7,2X,11HCOEFF*AREA=,E14.7)
  120 FORMAT(1HO,2X,19HLIQUID FILM COOLING/2X,4HT-B=,F5.0,2X,4HW/L=,E11.
     24,2X,4HC-P=,E11.4,2X,7HL-FLOW=,E11.4,10X,8HH COEFF=,E14.7,2X,11HCO
     3EFF*AREA=,E14.7)
C
C      FUTURE FREE CONVEC.COEFF.FORMATS (121-5)
  126 FORMAT(1HO,2X,9HRADIATION/2X,4HT-E=,F5.0,2X,10HFACTOR-SE=,E11.4,2X
     2,10HFACTOR-ES,E11.4,2X,8HEMIS.-E=,E11.4,2X,8HEMIS.-S=,E11.4/2X,8HH
     3 COEFF=,E14.7,2X,11HCOEFF*AREA=,E14.7)
  127 FORMAT(1HO,2X,21HSPECIFIED COEFFICIENT/2X,4HT-B=,F5.0,2X,8HH COEFF
     2=,E14.7,5X,11HCOEFF*AREA=,E14.7)
  128 FORMAT(1HO,2X,26HVAR.TEMP.DUCT FLOW, LIQUID/2X,4HT-B=,F5.0,2X,4HK-
     2F=,E11.4,2X,4HC-P=,E11.4,2X,3HMU=,E11.4,2X,10HMASS FLOW=,E11.4,2X,
     37HD-HYDR=,E11.4,2X,7HL-FLOW=,E11.4/2X,9HANN.NBR.=,F4.0,2X,9HFLOW N
     4BR=,F4.0,2X,7HFLAG-C=,F2.0,2X,7HFLAG-I=,F2.0,2X,6HX-SEC=,E11.4/2X,
     53HRE=,E11.4,2X,3HPR=,E11.4,6X,8HH COEFF=,E14.7,2X,11HCOEFF*AREA=,E
     614.7)
  129 FORMAT(1HO,2X,24HVAR.TEMP.RADIAL SEAL GAP/2X,4HT-B=,F5.0,2X,4HK-F=
     2,E11.4,2X,4HC-P=,E11.4,2X,3HMU=,E11.4,2X,3HNJ=,E11.4,2X,5HR-AV=,E1
     31.4,2X,4HGAP=,E11.4,2X,6HOMEGA=,F6.0/2X,4HR-O=,E11.4,2X,7HFLAG-C=,
     4F2.0,2X,7HFLAG-I=,F2.0,2X,9HANN.NBR.=,F4.0,2X,9HFLO.NBR.=,F4.0,2X,
     510HMASS FLOW=,E11.4/2X,3HRE=,E11.4,2X,8HPR**1/3=,E11.4,2X,5HRE-C=,
     6E11.4,9X,8HH COEFF=,E14.7,2X,11HCOEFF*AREA=,E14.7/2X,14HHT.GEN.FAC
     7TOR=,E12.5)
C
C      FUTURE VAR.TEMP.COEFF.FORMATS (130-1)
  132 FORMAT(1HO,2X,38HCOMBINED FLOW ELEMENT, CONDUCTION NO.=,I4,2X,24HF
     2LOW FROM COND.ELEMENTS ,I3,4HAND ,I4)
C
C      FUTURE COEFF.SUBPROGR.FORMATS (115-8(FORCED),121-5(FREE),130-1
C      (VAR.TEMP.)
C
C      READ INDICATOR CARD, CHECK ORDER
       READ(5,101) NBP,NBND(NBP),INDB
       IF (NBPT-NBP) 1,2,1
     1 WRITE(6,102) NBPT,NBP
       NK=1
C
C      SET PARAMETERS
     2 JBPT=NBND(NBP)
       JBNT(JBPT)=NBPT
       TD1(JBPT,17)=INDB
C
C      SPECIFIED TEMPERATURE
       IF (INDB.NE.7) GO TO 4
       READ(5,103) JBP,T(JBP)
       IF (JBP.NE.JBPT) GO TO 3
       TD1(JBPT,19)=T(JBP)
       GO TO 99
     3 WRITE(6,104) JBPT,JBP
       NK=1
       GO TO 99
C
     4 GO TO (5,7,7,7,7,7),INDB
C
```

```
C       SPECIFIED HEAT FLUX
      5 READ(5,105) JBP,H(NBPT,1),IADDQ
        IF (JBP.EQ.JBPT) GO TO 6
        WRITE(6,104) JBPT,JBP
        NK=1
      6 IF (IADDQ.EQ.0) GO TO 99
C
C       BOUNDARY AREAS
      7 AE=TD1(JBPT,14)
        AN=TD1(JBPT,15)
        AS=TD1(JBPT,16)
C
C       READ DATA FOR TYPES 2 TO 6
     90 READ(5,106) (TDA(J),J=1,7)
        NITM=TDA(5)
        READ(5,107) (TD2(J),J=1,NITM)
C
C       CHECK CONDUCTION NO.MATCH
        JBP=TDA(1)
        IF (JBP-JBPT) 8,9,8
      8 WRITE(6,108) JBPT,JBP
        NK=1
      9 IF (NK.NE.0) GO TO 99
C
        ITYPE=TDA(2)
        GO TO (99,10,29,46,48,55),ITYPE
C
C       FORCED CONVECTION
     10 ISTYPE=TDA(3)
        GO TO (11,13,15,17,19),ISTYPE
C
C       DUCT FLOW, LIQUID
     11 CALL SN1(TDA,TD2,AE,AN,AS)
        H(NBPT,2)=H(NBPT,2)+TD2(16)
        H(NBPT,3)=H(NBPT,3)+TD2(16)*TD2(1)
        IF (LD(5).EQ.0) GO TO 12
        WRITE(6,109) (TDA(J),J=1,7)
        WRITE(6,110) (TD2(J),J=1,7),(TD2(K),K=13,16)
     12 IF (TDA(4)) 90,99,90
C
C       SIDES OF ROTORS
     13 CALL SN2(TDA,TD2,AE,AN,AS)
        H(NBPT,2)=H(NBPT,2)+TD2(14)
        H(NBPT,3)=H(NBPT,3)+TD2(14)*TD2(1)
        IF (LD(5).EQ.0) GO TO 14
        WRITE(6,109) (TDA(J),J=1,7)
        WRITE(6,111) (TD2(J),J=1,14)
     14 IF (TDA(4)) 90,99,90
C
C       RADIAL SEAL GAP
     15 CALL SN3(TDA,TD2,AE,AN,AS)
        H(NBPT,2)=H(NBPT,2)+TD2(19)
        H(NBPT,3)=H(NBPT,3)+TD2(19)*TD2(1)
        IF (LD(5).EQ.0) GO TO 16
        WRITE(6,109) (TDA(J),J=1,7)
        WRITE(6,112) (TD2(J),J=1,9),(TD2(K),K=15,19)
```

```
   16 IF (TDA(4)) 90,99,90
C
C      CONCENTRIC CYLINDERS
   17 CALL SN4(TDA,TD2,AE,AN,AS)
      H(NBPT,2)=H(NBPT,2)+TD2(13)
      H(NBPT,3)=H(NBPT,3)+TD2(13)*TD2(1)
      IF (LD(5).EQ.0) GO TO 18
      WRITE(6,109) (TDA(J),J=1,7)
      WRITE(6,113) (TD2(J),J=1,13)
   18 IF (TDA(4)) 90,99,90
C
C      FLAT PLATE
   19 CALL SN5(TDA,TD2,AE,AN,AS)
      H(NBPT,2)=H(NBPT,2)+TD2(11)
      H(NBPT,3)=H(NBPT,3)+TD2(11)*TD2(1)
      IF (LD(5).EQ.0) GO TO 20
      WRITE(6,109) (TDA(J),J=1,7)
      WRITE(6,114) (TD2(J),J=1,11)
   20 IF (TDA(4)) 90,99,90
C
C      FOR FUTURE SUBROUTINES (4 MORE) (STATEM. NOS 21-2,23-4,25-6,27-8)
C
C      FREE CONVECTION
   29 ISTYPE=TDA(3)
      GO TO (30,32,34),ISTYPE
C
C      HORIZONTAL CYLINDER
   30 CALL FC1(TDA,TD2,AE,AN,AS,T,JBPT,NDIM)
      H(NBPT,4)=H(NBPT,4)+TD2(10)
      H(NBPT,5)=H(NBPT,5)+TD2(10)*TD2(1)
      IF (LD(5).EQ.0) GO TO 31
      WRITE(6,109) (TDA(J),J=1,7)
      WRITE(6,119) (TD2(J),J=1,10)
   31 IF (TDA(4)) 90,99,90
C
C      VERTICAL PLANE OR CYLINDER
   32 CALL FC2(TDA,TD2,AE,AN,AS,T,JBPT,NDIM)
      H(NBPT,4)=H(NBPT,4)+TD2(10)
      H(NBPT,5)=H(NBPT,5)+TD2(10)*TD2(1)
      IF (LD(5).EQ.0) GO TO 33
      WRITE(6,109) (TDA(J),J=1,7)
      WRITE(6,119) (TD2(J),J=1,10)
   33 IF (TDA(4)) 90,99,90
C
C      LIQUID FILM COOLING, GRAVITY FLOW
   34 CALL FC3(TDA,TD2,AE,AN,AS)
      H(NBPT,4)=H(NBPT,4)+TD2(6)
      H(NBPT,5)=H(NBPT,5)+TD2(6)*TD2(1)
      IF (LD(5).EQ.0) GO TO 35
      WRITE(6,109) (TDA(J),J=1,7)
      WRITE(6,120) (TD2(J),J=1,6)
   35 IF (TDA(4)) 90,99,90
C
C      FOR FUTURE SUBROUTINES (5 MORE) (STATEM. 36-7,38-9,40-1,42-3,44-5)
C
C      RADIATION
```

```
   46 CALL RA1(TDA,TD2,AE,AN,AS,T,JBPT,NDIM)
      H(NBPT,6)=H(NBPT,6)+TD2(7)
      H(NBPT,7)=H(NBPT,7)+TD2(7)*TD2(1)
      IF (LD(5).EQ.0) GO TO 47
      WRITE(6,109) (TDA(J),J=1,7)
      WRITE(6,126) (TD2(J),J=1,7)
   47 IF (TDA(4)) 90,99,90
C
C     SPECIFIED COEFFICIENT
   48 NCR=TDA(6)
      GO TO (49,50,49,51,52),NCR
   49 AF=AE
      GO TO 53
   50 AF=AN
      GO TO 53
   51 AF=AS
      GO TO 53
   52 AF=TDA(7)
   53 TD2(3)=TD2(2)*AF
      H(NBPT,2)=H(NBPT,2)+TD2(3)
      H(NBPT,3)=H(NBPT,3)+TD2(3)*TD2(1)
      IF (LD(5).EQ.0) GO TO 54
      WRITE(6,109) (TDA(J),J=1,7)
      WRITE(6,127) (TD2(J),J=1,3)
   54 IF (TDA(4)) 90,99,90
C
C     VARIABLE TEMPERATURE FORCED CONVECTION
   55 NTF=NTF+1
      ISTYPE=TDA(3)
      GO TO (56,57),ISTYPE
C
C     VAR.TEMP.DUCT FLOW, LIQUID
   56 CALL SN1(TDA,TD2,AE,AN,AS)
      H(NBPT,8)=TD2(16)
      H(NBPT,9)=TD2(5)*TD2(3)*TD2(12)
      TBND(NTF)=TD2(1)
      TCF(NTF)=H(NBPT,8)/H(NBPT,9)
      AFN(NTF)=TD2(8)
      GFN(NTF)=TD2(9)
      NODE(NTF)=JBPT
      JXPT=NODE(NTF)
      JNTF(JXPT)=NTF
      IF (LD(5).EQ.0) GO TO 60
      WRITE(6,109) (TDA(J),J=1,7)
      WRITE(6,128) (TD2(J),J=1,16)
      GO TO 60
C
C     VAR.TEMP.RADIAL SEAL GAP
   57 CALL SN3(TDA,TD2,AE,AN,AS)
      TBND(NTF)=TD2(1)
      H(NBPT,8)=TD2(19)
      H(NBPT,9)=TD2(14)*TD2(3)
      TCF(NTF)=H(NBPT,8)/H(NBPT,9)
      AFN(NTF)=TD2(12)
      GFN(NTF)=TD2(13)
      NODE(NTF)=JBPT
```

```
      JXPT=NODE(NTF)
      JNTF(JXPT)=NTF
C
C     FLUID SHEAR HEAT GENERATION
      OMRP=TD2(8)*TD2(8)*TD1(JBPT,2)*TD1(JBPT,2)
      QF(NTF)=TD2(20)*.0000399416*TD2(4)*OMRP*TD1(JBPT,14)/TD2(7)
C
      IF (LD(5).EQ.0) GO TO 60
      WRITE(6,109) (TDA(J),J=1,7)
      WRITE(6,129) (TD2(J),J=1,20)
      GO TO 60
C
C     FOR FUTURE SUBROUTINES (2 MORE) (STATEMENTS 58,59)
C
C     FLOW INITIATION ELEMENT
   60 IF (TD2(11).EQ.0.) GO TO 61
      NTR=NTR+1
      NBR(NTR)=TD2(11)
      GO TO 62
C
C     COMBINED FLOW ELEMENT
   61 IF (TD2(10).EQ.0.) GO TO 62
      NDR=NDR+1
      READ(5,101) NAT(NDR),NBT(NDR)
      WRITE(6,132) JBPT,NAT(NDR),NBT(NDR)
      NM(NDR)=JBPT
   62 IF (TDA(4)) 90,99,90
C
   99 RETURN
      END
```

```
$IBFTC SN1M

      SUBROUTINE SN1(TDA,TD2,AE,AN,AS)
C
C     HEAT TRANSFER COEFFICIENTS FOR LIQUIDS IN DUCTS
C
      DIMENSION TD2(20),TDA(7)
C
C     COMPUTE REYNOLDS AND PRANDTL NUMBERS
      TD2(13)=TD2(5)*TD2(6)/TD2(4)
      TD2(14)=TD2(3)*TD2(4)/TD2(2)
C
C     LAMINAR OR TURBULENT COEFFICIENT
      TD2(17)=TD2(6)/TD2(7)
      TD2(18)=TD2(2)/TD2(6)
      TD2(19)=TD2(17)**.7
      IF (TD2(13)-2500.) 1,1,2
    1 TD2(15)=1.24*TD2(18)*(TD2(13)*TD2(14)*TD2(17))**(1./3.)
      GO TO 5
    2 IF (TD2(13)-7000.) 4,3,3
    3 TD2(15)=.023*TD2(18)*(TD2(13)**.8)*(TD2(14)**.4)*(1.+.3*TD2(19))
      GO TO 5
    4 TD2(15)=.5*((7000.-TD2(13))/4500.)*1.24*(TD2(13)*TD2(14)*TD2(17))*
     2*(1./3.)+.5*((TD2(13)-2500.)/4500.)*.023*TD2(18)*(TD2(13)**.8)*(TD
     32(14)**.4)*(1.+.3*TD2(19))
C
C     COEFFICIENT*AREA
    5 NCR=TDA(6)
      GO TO (6,7,6,8,9),NCR
    6 AF=AE
      GO TO 10
    7 AF=AN
      GO TO 10
    8 AF=AS
      GO TO 10
    9 AF=TDA(7)
   10 TD2(16)=AF*TD2(15)
      RETURN
      END
```

```
$IBFTC SN2M

      SUBROUTINE SN2(TDA,TD2,AF,AN,AS)
C
C     HEAT TRANSFER COEFFICIENTS FOR FLUID MOVING RELATIVE TO RADIAL
C     SURFACE   SEPERATE BOUNDARY LAYERS
C
      DIMENSION TD2(20),TDA(7)
C
C     REYNOLDS AND PRANDTL NUMBERS
      TD2(11)=TD2(8)*TD2(6)*TD2(6)/TD2(5)
      TD2(12)=(TD2(3)*TD2(4)/TD2(2))**(1./3.)
C
C     LAMINAR OR TURBULENT COEFFICIENT
      TD2(15)=TD2(2)/TD2(6)
      TD2(16)=(TD2(7)/TD2(6))**.1
      IF (TD2(11)-158000.) 1,1,4
C
C     LAMINAR
    1 IF (TD2(10).EQ.0.) GO TO 2
      TD2(17)=.50185-.6508*TD2(7)/TD2(9)
      GO TO 3
    2 TD2(17)=.49815+.6508*TD2(7)/TD2(9)
    3 TD2(13)=.574*TD2(15)*TD2(16)*(TD2(11)**.5)*TD2(12)/TD2(17)
      GO TO 7
C
C     TURBULENT
    4 IF (TD2(10).EQ.0.) GO TO 5
      TD2(17)=.48558-.35778*TD2(7)/TD2(9)
      GO TO 6
    5 TD2(17)=.51442+.35778*TD2(7)/TD2(9)
    6 TD2(13)=.01826*TD2(15)*TD2(16)*(TD2(11)**.8)*TD2(12)/TD2(17)
C
C     COEFFICIENT*AREA
    7 NCR=TDA(6)
      GO TO (8,9,8,10,11),NCR
    8 AF=AF
      GO TO 12
    9 AF=AN
      GO TO 12
   10 AF=AS
      GO TO 12
   11 AF=TDA(7)
   12 TD2(14)=AF*TD2(13)
      RETURN
      END
```

```
$IBFTC SN3M

      SUBROUTINE SN3(TDA,TD2,AF,AN,AS)
C
C     HEAT TRANSFER COEFFICIENTS FOR ROTOR AND STATOR WITH SMALL
C     CLEARANCE   MERGED BOUNDARY LAYERS
C
      DIMENSION TD2(20),TDA(7)
C
C     REYNOLDS AND PRANDTL NUMBERS
      TD2(15)=TD2(8)*TD2(6)*TD2(6)/TD2(5)
      TD2(16)=(TD2(3)*TD2(4)/TD2(2))**(1./3.)
C
C     LAMINAR OR TURBULENT COEFFICIENT
      TD2(17)=366.34*((TD2(9)/TD2(7))**(10./9.))
      IF (TD2(15)-TD2(17)) 1,1,2
    1 TD2(18)=2.*TD2(2)*TD2(16)/TD2(7)
      TD2(20)=1.
      GO TO 3
    2 TD2(18)=.0297*(TD2(2)/TD2(6))*((TD2(6)/TD2(7))**(1./6.))*TD2(16)*(
     1TD2(15)**.8)
      TD2(20)=.0002286*(TD2(17)**1.5)*((TD2(7)/TD2(6))**(5./3.))
C
C     COEFFICIENT*AREA
    3 NCR=TDA(6)
      GO TO (4,5,4,6,7),NCR
    4 AF=AF
      GO TO 8
    5 AF=AN
      GO TO 8
    6 AF=AS
      GO TO 8
    7 AF=TDA(7)
    8 TD2(19)=AF*TD2(18)
      RETURN
      END
```

```
$IBFTC SN4M

      SUBROUTINE SN4(TDA,TD2,AE,AN,AS)
C
C     HEAT TRANSFER COEFFICIENTS FOR FLOW BETWEEN CONCENTRIC CYLINDERS
C     INNER ROTATING, NO AXIAL FLOW EFFECT ON BOUNDARY LAYERS
C
      DIMENSION TD2(20),TDA(7)
C
C     TURBULENT COEFFICIENT
      TD2(11)=(TD2(3)*TD2(4)/TD2(2))**(1./3.)
      TD2(14)=TD2(8)*.5*(TD2(6)+TD2(7))
      TD2(15)=TD2(14)*TD2(14)+TD2(9)*TD2(9)
      TD2(16)=SQRT(TD2(15))
      TD2(17)=TD2(6)-TD2(7)
      TD2(10)=2.*TD2(17)*TD2(16)/TD2(5)
      TD2(12)=(TD2(2)/TD2(17))*(.015*(TD2(10)**.8)*TD2(11)*((TD2(6)/TD2(
     17))**.46)+.052*(TD2(14)**(2./3.))*TD2(17)*TD2(11)/TD2(5))
C
C     COEFFICIENT*AREA
      NCR=TDA(6)
      GO TO (1,2,1,3,4),NCR
    1 AF=AE
      GO TO 5
    2 AF=AN
      GO TO 5
    3 AF=AS
      GO TO 5
    4 AF=TDA(7)
    5 TD2(13)=AF*TD2(12)
      RETURN
      END
```

```
$IBFTC SN5M
      SUBROUTINE SN5(TDA,TD2,AE,AN,AS)
C
C     HEAT TRANSFER COEFFICIENTS FOR FLOW OVER FLAT PLATES
C
      DIMENSION TD2(20),TDA(7)
C
C     REYNOLDS AND PRANDTL NUMBERS
      TD2(8)=TD2(7)*TD2(6)/TD2(5)
      TD2(9)=(TD2(3)*TD2(4)/TD2(2))**(1./3.)
C
C     LAMINAR OR TURBULENT COEFFICIENT
      IF(TD2(8)-500000.) 1,1,2
    1 TD2(10)=.332*TD2(2)*(TD2(8)**.5)*TD2(9)/TD2(6)
      GO TO 3
    2 TD2(10)=.0288*TD2(2)*(TD2(8)**.8)*TD2(9)/TD2(6)
C
C     COEFFICIENT*AREA
    3 NCR=TDA(6)
      GO TO (4,5,4,6,7),NCR
    4 AF=AE
      GO TO 8
    5 AF=AN
      GO TO 8
    6 AF=AS
      GO TO 8
    7 AF=TDA(7)
    8 TD2(11)=AF*TD2(10)
      RETURN
      END
```

```
$IBFTC FC1M

      SUBROUTINE FC1(TDA,TD2,AF,AN,AS,T,JBPT,NDIM)
C
C     HEAT TRANSFER COEFFICIENTS FOR HORIZ.CYLINDER FREE CONVECTION
C
      DIMENSION TDA(7),TD2(20),T(NDIM)
C
      TD2(12)=ABS(TD2(1)-T(JBPT))
      TD2(13)=.5*(TD2(1)+T(JBPT))+459.7
      TD2(14)=TD2(2)/TD2(6)
C
C     PRANDTL AND GRASHOF NUMBERS
      TD2(7)=TD2(3)*TD2(4)/TD2(2)
      TD2(8)=TD2(6)*TD2(6)*TD2(6)*32.174*TD2(12)/(TD2(5)*TD2(5)*TD2(13))
      TD2(11)=TD2(7)*TD2(8)
C
C     LAMINAR OR TURBULANT COEFFICIENT
      IF (TD2(11)-.1E+10) 1,1,2
    1 TD2(9)=.53*TD2(14)*TD2(11)**(1./4.)
      GO TO 3
    2 TD2(9)=.13*TD2(14)*TD2(11)**(1./3.)
C
C     COEFFICIENT*AREA
    3 NCR=TDA(6)
      GO TO (4,5,4,6,7),NCR
    4 AF=AF
      GO TO 8
    5 AF=AN
      GO TO 8
    6 AF=AS
      GO TO 8
    7 AF=TDA(7)
    8 TD2(10)=AF*TD2(9)
      RETURN
      END
```

```
$IBFTC FC2M
      SUBROUTINE FC2(TDA,TD2,AE,AN,AS,T,JBPT,NDIM)
C
C     HEAT TRANSFER COEFFICIENTS FOR VERT. SURFACE FREE CONVECTION
C
      DIMENSION TDA(7),TD2(20),T(NDIM)
C
      TD2(12)=ABS(TD2(1)-T(JBPT))
      TD2(13)=.5*(TD2(1)+T(JBPT))+459.7
      TD2(14)=TD2(2)/TD2(6)
C
C     PRANDTL AND GRASHOF NUMBERS
      TD2(7)=TD2(3)*TD2(4)/TD2(2)
      TD2(8)=TD2(6)*TD2(6)*TD2(6)*32.174*TD2(12)/(TD2(5)*TD2(5)*TD2(13))
      TD2(11)=TD2(7)*TD2(8)
C
C     LAMINAR OR TURBULANT COEFFICIENT
      IF (TD2(11)-.1E+10) 1,1,2
    1 TD2(9)=.44*TD2(14)*TD2(11)**(1./4.)
      GO TO 3
    2 TD2(9)=.13*TD2(14)*TD2(11)**(1./3.)
C
C     COEFFICIENT*AREA
    3 NCR=TDA(6)
      GO TO (4,5,4,6,7),NCR
    4 AF=AE
      GO TO 8
    5 AF=AN
      GO TO 8
    6 AF=AS
      GO TO 8
    7 AF=TDA(7)
    8 TD2(10)=AF*TD2(9)
      RETURN
      END
```

```
$IBFTC FC3M

      SUBROUTINE FC3(TDA,TD2,AE,AN,AS)
C
C     HEAT TRANSFER COEFFICIENTS FROM HORIZONTAL CYLINDER TO LIQUID
C     FILM (GRAVITY FLOW)
C
      DIMENSION TD2(20),TDA(7)
C
      TD2(5)=TD2(2)*TD2(3)/TD2(4)
      NCR=TDA(6)
      GO TO (1,2,1,3,4),NCR
    1 AF=AE
      GO TO 5
    2 AF=AN
      GO TO 5
    3 AF=AS
      GO TO 5
    4 AF=TDA(7)
    5 TD2(6)=AF*TD2(5)
      RETURN
      END



$IBFTC RA1M

      SUBROUTINE RA1(TDA,TD2,AE,AN,AS,T,JBPT,NDIM)
C
C     RADIATION(THERMAL)-GRAY BODY
C
      DIMENSION TDA(7),TD2(20),T(NDIM)
C
      TAE=TD2(1)
      TAS=T(JBPT)
      TD2(8)=1.-TD2(4)
      TD2(9)=1.-TD2(5)
      TD2(10)=TAE*TAE*TAE+TAE*TAE*TAS+TAE*TAS*TAS+TAS*TAS*TAS
      TD2(6)=4.83E-13*TD2(4)*TD2(9)*TD2(2)*TD2(10)/(1.-(TD2(2)*TD2(3)*TD
     12(8)*TD2(9)))
      NCR=TDA(6)
      GO TO (1,2,1,3,4),NCR
    1 AF=AE
      GO TO 5
    2 AF=AN
      GO TO 5
    3 AF=AS
      GO TO 5
    4 AF=TDA(7)
    5 TD2(7)=AF*TD2(6)
      RETURN
      END
```

```
$IBFTC QTM

      SUBROUTINE QT(NBPT,NBDIM,NDIM,JBPT,H,SUMT,SUMH,TDI,TBND,T,CD,NVDIM
     1,NIT,NODE,JNTF)
C
C     COMPUTE BOUNDARY HEAT FLUXES
C
      DIMENSION H(NBDIM,9),SUMT(NBDIM),SUMH(NBDIM),TDI(NDIM,19)
      DIMENSION TBND(NVDIM),T(NDIM),CD(10),TS(100),JNTF(NDIM)
      COMMON/BLK1/JBNT(400),KAN(200),NTF,NDR,NTR,QF(95),NQR
      COMMON/BLK2/TCF(95),GFN(95),AFN(95),NBR(95),NM(5),NAT(5),NBT(5)
C
  101 FORMAT(1H0,2X,39HCOMBINED FLOWS ELEMENT, COMBINATION NO.,I2,3X,12H
     2CONDUCT.NO.=,I3,3X,10HBNDRY.NO.=,I3,3X,31HPREVIOUS ELEMENT VAR.TEM
     3P.NOS.=,I3,2X,3HAND,I4)
  102 FORMAT(1H0,2X,19HCONDUCT.ELEMENT NO.,I4,3X,20HVAR.TEMP.ELEMENT NO.
     2,I4,3X,10HFLOW CODE=,I2)
C
      SUMT(NBPT)=0.0
      SUMH(NBPT)=0.0
      ITYPE=TDI(JBPT,17)
      IF (ITYPE.NE.7) GO TO 1
      GO TO 99
C
C     SPECIFIED FLUX
    1 IF (H(NBPT,1).EQ.0.) GO TO 2
      SUMT(NBPT)=H(NBPT,1)
C
C     FORCED CONVECTION (INCL.SPECIFIED COEFF.)
    2 IF (H(NBPT,2).EQ.0.) GO TO 3
      SUMH(NBPT)=H(NBPT,2)
      SUMT(NBPT)=SUMT(NBPT)+H(NBPT,3)-H(NBPT,2)*T(JBPT)
C
C     FREE CONVECTION
    3 IF (H(NBPT,4).EQ.0.) GO TO 4
      SUMH(NBPT)=SUMH(NBPT)+H(NBPT,4)
      SUMT(NBPT)=SUMT(NBPT)+H(NBPT,5)-H(NBPT,4)*T(JBPT)
C
C     RADIATION
    4 IF (H(NBPT,6).EQ.0.) GO TO 5
      SUMH(NBPT)=SUMH(NBPT)+H(NBPT,6)
      SUMT(NBPT)=SUMT(NBPT)+H(NBPT,7)-H(NBPT,6)*T(JBPT)
C
C     VARYING TEMPERATURE
    5 IF (H(NBPT,8).EQ.0.) GO TO 99
      NTF=NTF+1
      NPT=0
      LHN=0
      QFI=0.
      SUMH(NBPT)=SUMH(NBPT)+H(NBPT,8)
      IF (KAN(NBPT).EQ.0) GO TO 6
      SUMT(NBPT)=SUMT(NBPT)+H(NBPT,8)*(TBND(NTF)-T(JBPT))
```

```
C
     6 JNPT=AFN(NTF)
       JLHN=GFN(NTF)
       TS=0.
       IF (JNPT.EQ.0) GO TO 7
       NPT=JBNT(JNPT)
     7 IF (JLHN.EQ.0) GO TO 8
       LHN=JNTF(JLHN)
     8 IF (NM(NDR)-JBPT) 14,9,14
C
C      COMBINED FLOWS
     9 JNFR=NAT(NDR)
       JNFS=NBT(NDR)
       IF (JNFR.EQ.0) GO TO 10
       NFR=JBNT(JNFR)
       JAT=JNTF(JNFR)
       GO TO 11
    10 NFR=0
       TBND(NFR)=0.
       H(NFR,9)=0.
    11 IF (JNFS.EQ.0) GO TO 12
       NFS=JBNT(JNFS)
       JBT=JNTF(JNFS)
       GO TO 13
    12 NFS=0
       TBND(NFS)=0.
       H(NFS,9)=0.
    13 IF ((NIT-1).EQ.0) WRITE(6,101) NDR,JBPT,NTF,JAT,JBT
C
C      STARTING TEMP.FOR COMBINED FLOWS ELEMENT TEMP.CALC.
       COMBF=H(NFR,9)+H(NFS,9)
       PNFR=H(NFR,9)*TBND(NFR)/COMBF
       PNFS=H(NFS,9)*TBND(NFS)/COMBF
       STEMP=PNFR+PNFS
       NDR=NDR+1
       GO TO 18
C
C      STARTING TEMP.ORDINARY FLOW ELEMENT
    14 NTR=NTR+1
       NER=NBR(NTR)
       IF ((NIT-1).EQ.0) WRITE(6,102) JBPT,NTR,NBR(NTR)
       IF (LHN.NE.0) GO TO 17
       GO TO (15,16),NER
    15 STEMP=CD(6)
       GO TO 18
    16 STEMP=CD(7)
       GO TO 18
    17 STEMP=TBND(LHN)
C
    18 IF (KAN(NBPT).NE.0) GO TO 99
C
C      CALC.TEMP.CHANGE
       HINC=TCF(NTF)/CD(9)
       IF (QF(NTF).EQ.0.) GO TO 19
       QF1=QF(NTF)/(H(NBPT,9)*CD(9))
    19 NCD=CD(9)
```

```
      IF (NPT.NE.0) GO TO 22
C
C     TEMP.CHANGE-NO ANN.NABOR
      DO 21 INC=1,NCD
      IF (INC.NE.1) GO TO 20
      TS(INC)=STEMP+HINC*(T(JBPT)-STEMP)+QF1
      GO TO 21
   20 TS(INC)=TS(INC-1)+HINC*(T(JBPT)-TS(INC-1))+QF1
   21 CONTINUE
      TBND(NTF)=TS(INC)
      GO TO 25
C
C     TEMP.CHANGE-ANNULAR NABOR
   22 HANC=H(NPT,8)/(H(NPT,9)*CD(9))
      DO 24 INC=1,NCD
      IF (INC.NE.1) GO TO 23
      TS(INC)=STEMP+HINC*(T(JBPT)-STEMP)+HANC*(T(JNPT)-STEMP)+QF1
      GO TO 24
   23 TS(INC)=TS(INC-1)+HINC*(T(JBPT)-TS(INC-1))+HANC*(T(JNPT)-TS(INC-1)
     1)+QF1
   24 CONTINUE
      TBND(NTF)=TS(INC)
      TBND(NPT)=TBND(NTF)
      KAN(NPT)=1
   25 SUMT(NBPT)=SUMT(NBPT)+H(NBPT,8)*(TBND(NTF)-T(JBPT))
   99 RETURN
      END
```

```
$IBFTC TATSM

      SUBROUTINE TATS(TD1,JPT,NDIM,NBND,NBDIM,Q,T,H,RD,LD,CE,NK)
C
C     OVER-RELAXATION AND NEW TEMPERATURE CALCULATION
C
      DIMENSION TD1(NDIM,19),CE(NDIM,4),LD(10),RD(5)
      DIMENSION NBND(NBDIM),Q(NDIM),T(NDIM),H(NBDIM,9)
      COMMON/BLK1/JBNT(390),KAN(190),NTF,NDR,NTR,QF(95),NQR
C
  101 FORMAT(1HO,5X,58HERROR IN BNDRY AND COND.NO CORRESP.(TATS CHECK OF
     2ITERATION,I6,13H)COND.ELEMENT,I4,25HGIVES BNDRY NO OF ELEMENT,I4)
C
      HSUM=0.
C
C     EAST CONDUCTANCE
      NE= TD1(JPT,5)
      IF (NE) 2,1,2
    1 CE(JPT,1)=0.C
      GO TO 3
    2 CE(JPT,1)=1./(TD1(JPT,4)/(2.*TD1(JPT,14)*TD1(JPT,18))+TD1(NE,4)/(2
     1.*TD1(NE,14)*TD1(NE,18))+TD1(JPT,10))
*C
C     NORTH CONDUCTANCE
    3 NN=TD1(JPT,6)
      IF (NN) 5,4,5
    4 CE(JPT,2)=0.C
      GO TO 6
    5 CE(JPT,2)=1./(2.*TD1(JPT,3)/(TD1(JPT,18)*(3.*TD1(JPT,15)+TD1(JPT,1
     16)))+2.*TD1(NN,3)/(TD1(NN,18)*(3.*TD1(NN,16)+TD1(NN,15)))+TD1(JPT,
     21))
C
C     WEST CONDUCTANCE
    6 NW=TD1(JPT,7)
      IF (NW) 8,7,8
    7 CE(JPT,3)=0.C
      GO TO 9
    8 CE(JPT,3)=1./(TD1(JPT,4)/(2.*TD1(JPT,14)*TD1(JPT,18))+TD1(NW,4)/(2
     1.*TD1(NW,14)*TD1(NW,18))+TD1(JPT,12))
*C
C     SOUTH CONDUCTANCE
    9 NS= TD1(JPT,8)
      IF (NS) 11,10,11
   10 CE(JPT,4)=0.C
      GO TO 12
   11 CE(JPT,4)=1./(2.*TD1(JPT,3)/(TD1(JPT,18)*(3.*TD1(JPT,16)+TD1(JPT,1
     15)))+2.*TD1(NS,3)/(TD1(NS,18)*(3.*TD1(NS,15)+TD1(NS,16)))+TD1(JPT,
     213))
C
   12 NTD=TD1(JPT,17)
      IF(NTD.EQ.7) GO TO 99
C
```

```
C       COMPUTE RESIDUAL, OVER-RELAX
        RES=CE(JPT,1)*(T(NE)-T(JPT))+CE(JPT,2)*(T(NN)-T(JPT))+CE(JPT,3)*(T
       1(NW)-T(JPT))+CE(JPT,4)*(T(NS)-T(JPT))+Q(JPT)
        CSUM=CE(JPT,1)+CE(JPT,2)+CE(JPT,3)+CE(JPT,4)
C
        WRES=RD(1)*RES
C
C       COMPUTE NEW TEMPERATURE
        IF (Q(JPT)) 13,15,13
   13   NBPT=JBNT(JPT)
        JBPT=NBND(NBPT)
        IF (JBPT.EQ.JPT) GO TO 14
        WRITE(6,101) NIT,JPT,JBPT
        NK=1
        GO TO 99
   14   HSUM=H(NBPT,2)+H(NBPT,4)+H(NBPT,6)+H(NBPT,8)
   15   T(JPT)=T(JPT)+WRES/(CSUM+HSUM)
C
   99   RETURN
        END
```

```
$IBFTC FITA

      SUBROUTINE FIT2(TD1,NDIM,JPT,ALPHA,THEXP)
C
C     FIT EXPANSION COEFFICIENT FROM POLYNOMINAL CURVE
C
      DIMENSION TD1(NDIM,19),COS(5),CALC(6),ALPHA(15,11),THEXP(NDIM)
C
  101 FORMAT(1HO,20X,45HTEMPERATURE EXCEEDS CURVE FIT LIMIT FOR ALPHA)
C
      TEMP= TD1(JPT,19)
      MAN = TD1(JPT,9)
      DO 1 NCO=1,5
    1 COS(NCO)= ALPHA(MAN,NCO)
      IF(TEMP-COS(1)) 3,3,2
    2 WRITE(6,101)
      GO TO 9
    3 NOP = COS(3)
      NOP1=NOP+1
      DO 4 NCO=1,NOP1
      LC = 5+NCO
    4 CALC(NCO)= ALPHA(MAN,LC)
      IF(COS(3)) 6,5,6
    5 Y= CALC(1)*COS(4)
      GO TO 8
    6 Y = CALC(NOP1)
      TEM1 = TEMP*COS(5)
      DO 7 NPY=1,NOP
      J2 = NOP1-NPY
    7 Y= CALC(J2)+Y*TEM1
      Y = Y*COS(4)
    8 THEXP(JPT)=Y
C
    9 RETURN
      END
```

```
$IBFTC CONCHC

      SUBROUTINE CONCHK(JPT,NDIM,TD1,ERR,LD,NK,T)
C
C     CHECK FOR CONVERGENCE OF OVER-RELAXATION CALC.
C
      DIMENSION TD1(NDIM,19),LD(10),T(NDIM)
C
  101 FORMAT(24X,I4,4(5X,E14.7))
C
      DIFF=T(JPT)-TD1(JPT,19)
      IF (ABS(DIFF).LE.ERR) GO TO 1
      NK=1
    1 IF (LD(4).EQ.0) GO TO 9
      WRITE(6,101) JPT,T(JPT),TD1(JPT,19),DIFF,ERR
C
    9 RETURN
      END



$IBFTC DEFRMM

      SUBROUTINE DEFORM(JPT,NDIM,TD1,RD,LD,THEXP)
C
C     COMPUTE FREE THERMAL EXPANSION  ALPHA*DELTA TEMP
C
      DIMENSION TD1(NDIM,19),THEXP(NDIM),RD(5),LD(10)
C
  101 FORMAT(1H0,10X,16HELEMENT COND.NO=,I4,3X,6HALPHA=,E13.6,3X,5HTEMP=
     2,F12.5,3X,14HALPHA*(T1-T0)=,E13.6)
C
      TIN=RD(2)
      DELTEM=TD1(JPT,19)-TIN
      A=THEXP(JPT)
      ACT=THEXP(JPT)*DELTEM
      THEXP(JPT)=ACT
      IF (LD(10).EQ.0) GO TO 99
      WRITE(6,101) JPT,A,TD1(JPT,19),THEXP(JPT)
C
   99 RETURN
      END
```

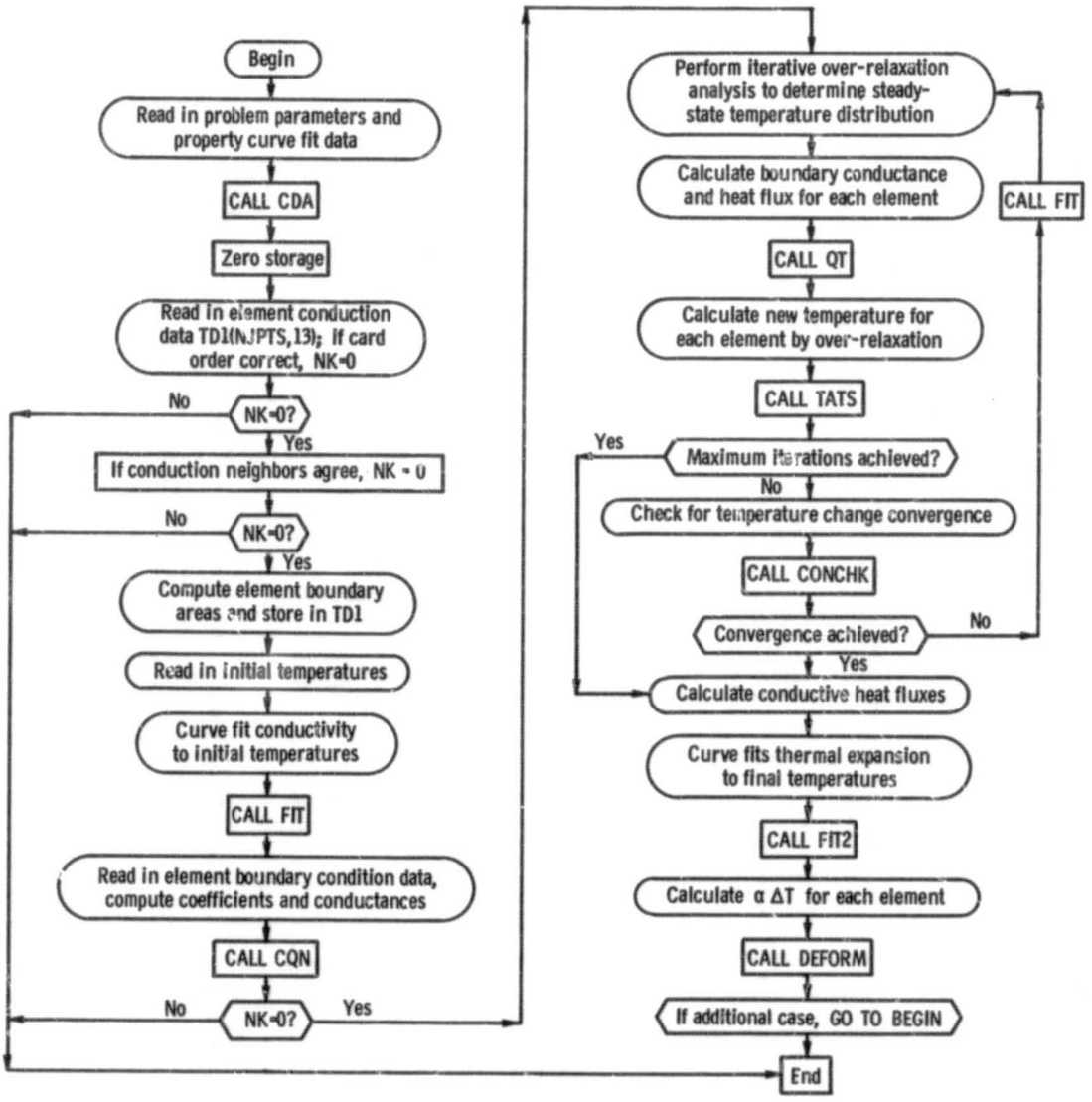

Figure 8. - Flow chart for main route SEAL2.

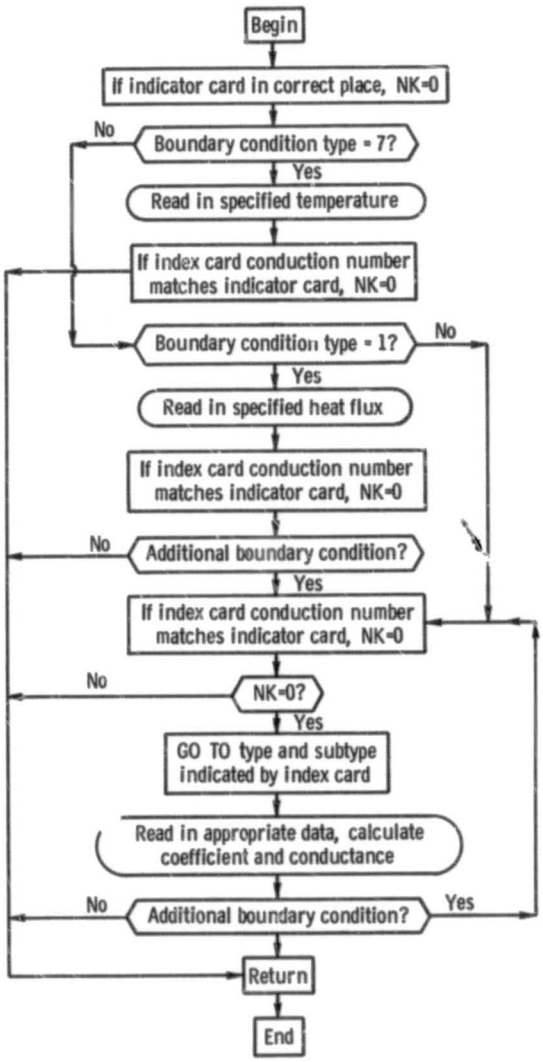

Figure 9. - Flow chart for subroutine CQN.

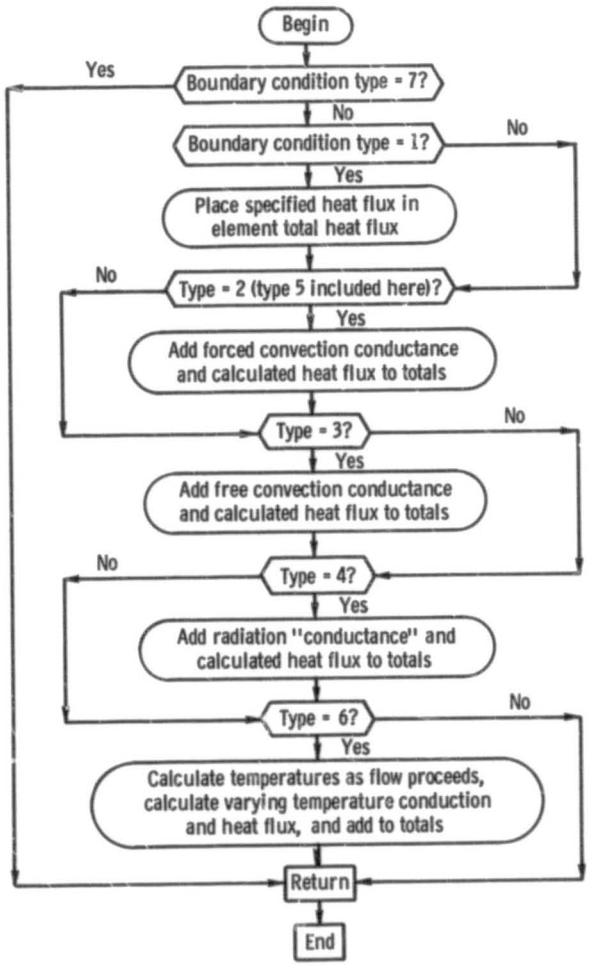

Figure 10. - Flow chart for subroutine QT.

APPENDIX B

CHANGING OF BOUNDARY CONDITION COEFFICIENTS

The program is designed to make the addition or substitution of equations for heat transfer coefficients relatively easy. The coefficients, the products of coefficient times boundary area and the products of coefficient times boundary area times bulk fluid (or environmental) temperature are calculated in subroutines SN1, SN2, SN3, SN4, SN5, FC1, FC2, FC3, and RA1.

The varying temperature coefficients, at present, use subroutines SN1 and SN3. Other calculations for the varying temperature boundary conditions are performed in subroutines CQN and QT.

Substitution of a Different Coefficient

To substitute a new expression for one of those presently used, the appropriate subroutine is rewritten using the present words in the TD2 list for the output (coefficient, etc.). This assumes that the same properties or at least the same number of properties are required. If not, the number of items to be read in must be changed in subroutine CQN. Also the TD2 words used for output must be changed in the coefficient subroutine as well as in subroutine CQN. The appropriate formats of subroutine CQN must also be changed to reflect the TD2 changes.

The TD2 list of a varying temperature condition must be compatible with the TD2 list of the coefficient subprogram used. Thus, if subroutine SN1 is changed to require more input data, subroutine VT1 (see table II) must also be changed. The output, which is common to both, must use the same new TD2 words.

TD2 word changes for a varying temperature subroutine must be made in subroutine QT as well as in subroutine CQN. Wherever a TD2 word (e.g., TD2(15)) appears in the varying temperature sections of subroutines CQN and QT, the new word must be substituted.

Also the two indicator flag words (TD2(10) and TD2(11)) must be the same for all VT (varying temperature) conditions. The calculations involving the flags require this. The sections in subroutines CQN and QT handling the temperature change along the flow and the effect of flow combination use the flags to control the flow in the subroutines. If one or both of the flag words are changed for one VT condition, it (they) must be changed for all conditions and the new word(s) must be used in subroutines CQN and QT.

A word of warning should be added. As implied previously, the TD2 list is used for both input to and output from the coefficient subroutines. This table is dimensioned for 20 items. If more are needed, the dimensions in SEAL2, CQN, and the coefficient subroutines must be increased.

Addition of New Coefficients

If an additional boundary condition is desired, a new subroutine must be written. A varying temperature condition involves the precautions mentioned under substitution. Also the TD2 list capacity must be remembered.

Also, for an added condition, a section must be added to subroutine CQN. This section will be analogous to the subtype sections already present. The products of coefficient times area and of coefficient times area times bulk fluid temperature must be stored in the correct places in the conductance matrix. An output format for the TD2 list must be composed. Unused statement and format numbers are provided for this purpose.

APPENDIX C

COMPUTER PROGRAM APPLICATION TO MAINSHAFT SEAL

Seal Description

This appendix is presented as an application of the computer program to a specific seal design. Figure 11 shows a schematic of a mainshaft seal being developed for gas-

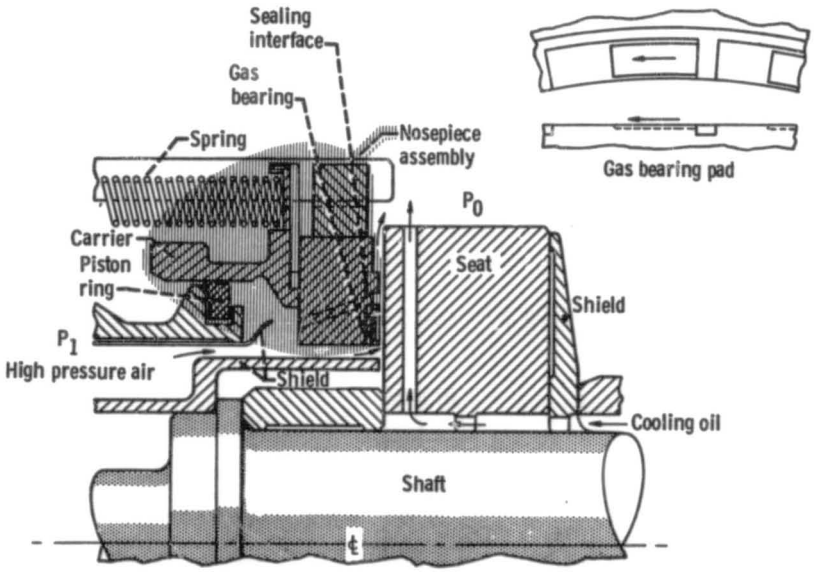

Figure 11. - Face seal with self-acting gas bearing for lift augmentation.

turbine engines. This is a face-type seal with a self-acting gas bearing which acts to prevent rubbing contact when deformation of the sealing faces occurs.

In figure 12(a) a modified version of the nosepiece assembly is presented and the boundary conditions are shown. This modification is for the purpose of concentrating on the mechanics of the program application.

Figure 12(b) shows the element schematic including conduction numbers and dimensions. A portion of the seal plate is included since it influences the temperature of the airflow through the seal gap and therefore has an effect on the nosepiece temperature. Also a portion of the piston ring and its holder, which form a conduction path to the nosepiece carrier, are included.

The numbering sequence starts with the nosepiece assembly since this is the region of interest for this problem. The desired printout is therefore available at the beginning of

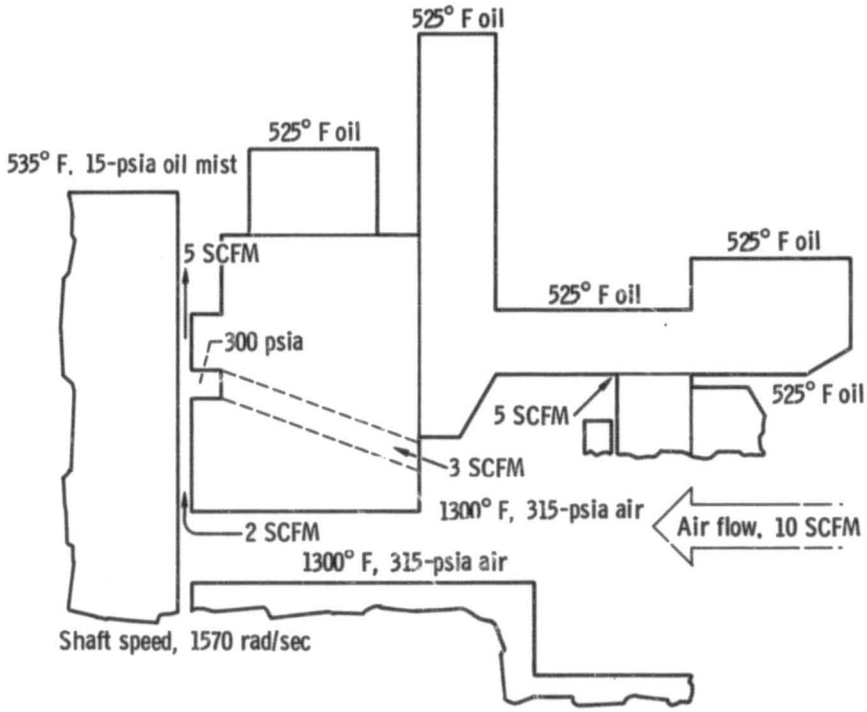

(a) Modification of and boundary conditions for nosepiece assembly of seal depicted in figure 11.

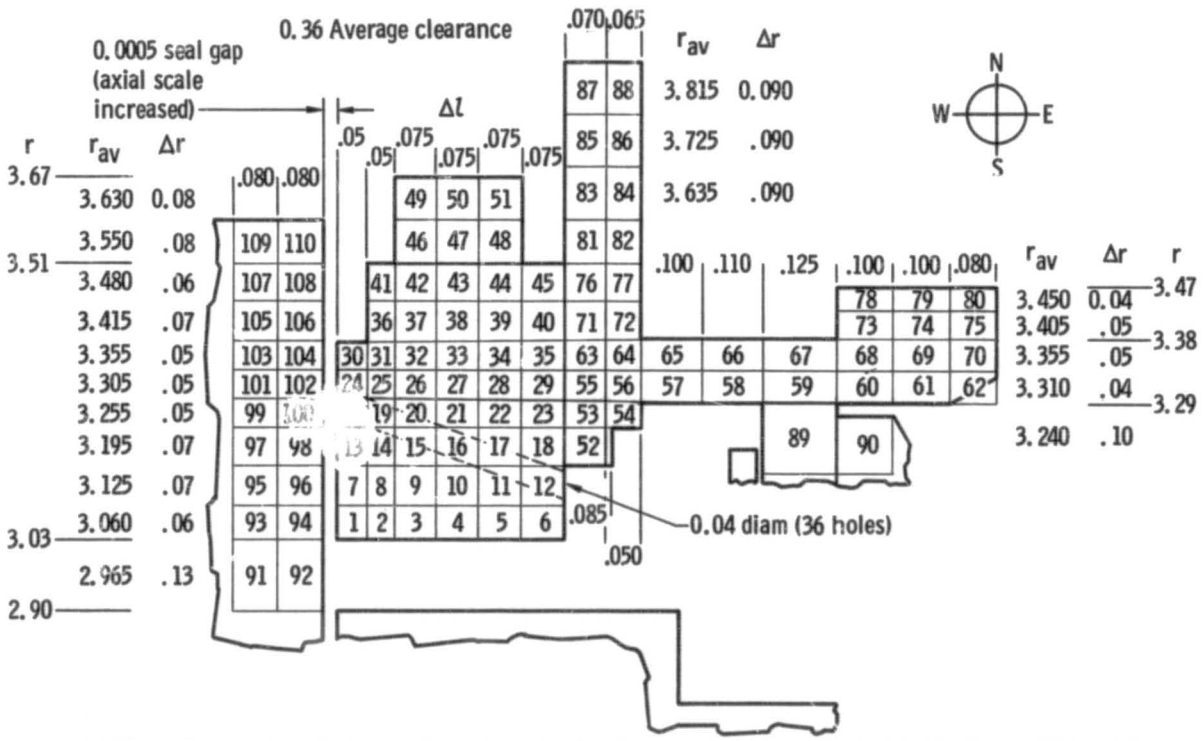

(b) Dimensions and conductance element numbering for nosepiece assembly depicted in figure 12(a). (All dimensions in inches.)

Figure 12. - Example problem.

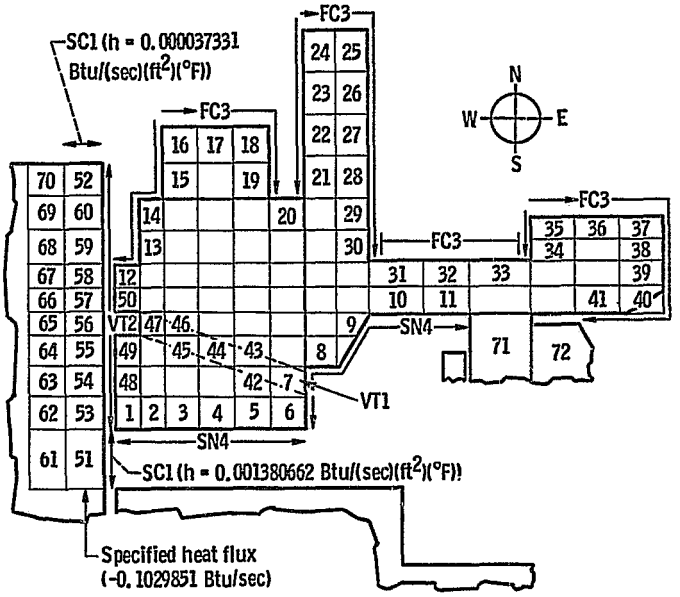

(c) Boundary element numbering and boundary heat transfer conditions for nosepiece assembly depicted in figure 12(a).

Figure 12. - Concluded.

each section of output, and the remaining elements can be ignored. The piece by piece numbering is not necessary; any convenient order could be used.

Figure 12(c) shows the boundary numbers and the subroutines used to calculate the heat transfer coefficients. Here again, the sequence is a matter of convenience and the nosepiece assembly is numbered first. Numbers 1 to 11 are assigned to the region where concentric cylinder flow (SN4) is assumed. Conduction element 56 was ignored since only a relatively tiny part is a boundary of the piece. Numbers 12 to 41 were assigned to the liquid film cooled (FC3) boundaries. The varying temperature duct flow (VT1) is numbered next. Since conduction element 12 already has a boundary number (7), the sequence continues with 42 assigned to conduction element 11. The method used is an approximation to avoid the complexities involved if conduction elements 18 and 14 are included as should be done. For the varying temperature seal gap (VT2) flow, numbers 48 to 50 were assigned to the nosepiece elements not already given boundary numbers.

For the seal plate, the east face of conduction element 92 and the north face of 110 were assigned coefficients. The south face of 92 was assigned a heat flux. These values were obtained from a thermal analysis of the seal shown in figure 11. Boundary numbers 53 to 60 were assigned to the seal plate elements exposed to seal gap flow. The remaining boundary numbers, 61 to 72, were assigned to elements given specified temperatures obtained from the previous analysis mentioned.

The title and parameter cards (Items 1 to 5 under Computer Input in appendix A) were filled out as indicated in the first section of the printout. Also in this section, Items 6

and 7, the thermal conductivity and expansion data, are indicated.

Next are the conduction element cards (input Item 8). These are shown in the second section of printout (conduction element table). Words 1 to 8 of each card are obtained from the information in figure 12(b). In word 9, three materials were used. The nosepiece was material number 1. The piston ring and its holder were material number 3. The remaining parts were material number 2. The last four words are contact resistances.

It should be noted that each contact resistance must appear twice since the program ignores neighbor contact resistance in computing heat fluxes. Thus for elements 42 and 46, the contact resistance appears in word 11 (north contact resistance) of element 42 and in word 13 (south contact resistance) of element 46. Contact resistances between parts were calculated using a "conductance coefficient" ($h_c = 0.2$) for conductance across the interface. The resistance between elements 90 and 60 was the difference between the resistance of the air gap and the resistance of an equal volume of material number three (element 90 uses the same mean radius and radial width as element 89). The resistance between mismatched elements (elements 52 and 54 were changed in axial length to approximate the actual dimensions in the region) was calculated as illustrated in figure 13. It was assumed that the larger i^{th} element (e.g., 52) has a conduction path length of d' rather than $\Delta r/2$ as in figure 5. The area was based on $\Delta \ell_m$ rather than $\Delta \ell_i$. The contact resistance was the difference between $d'/2\pi r_m \Delta \ell_m$ and $\Delta r_i/4\pi r_m \Delta \ell_i$.

The initial temperature estimates (input Item 9) follow the conduction cards. These values were obtained from a previous analysis in order to reduce the computer time required. However, any reasonable estimates can be used including the use of one temperature for all elements.

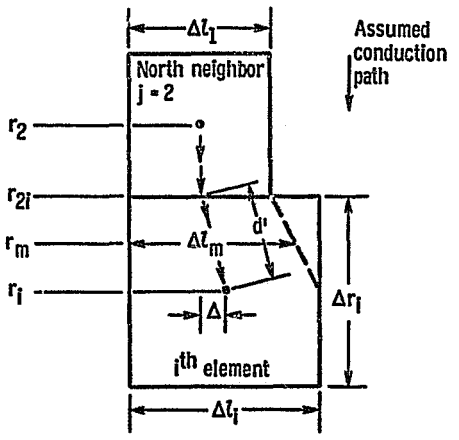

Figure 13. - Outline of calculation of contact resistance between elements of different axial dimensions. $d' = \sqrt{\Delta^2 + (\Delta \ell_i/2)^2}$; $\Delta \ell_m = (\Delta \ell_1 + \Delta \ell_2)/2$.

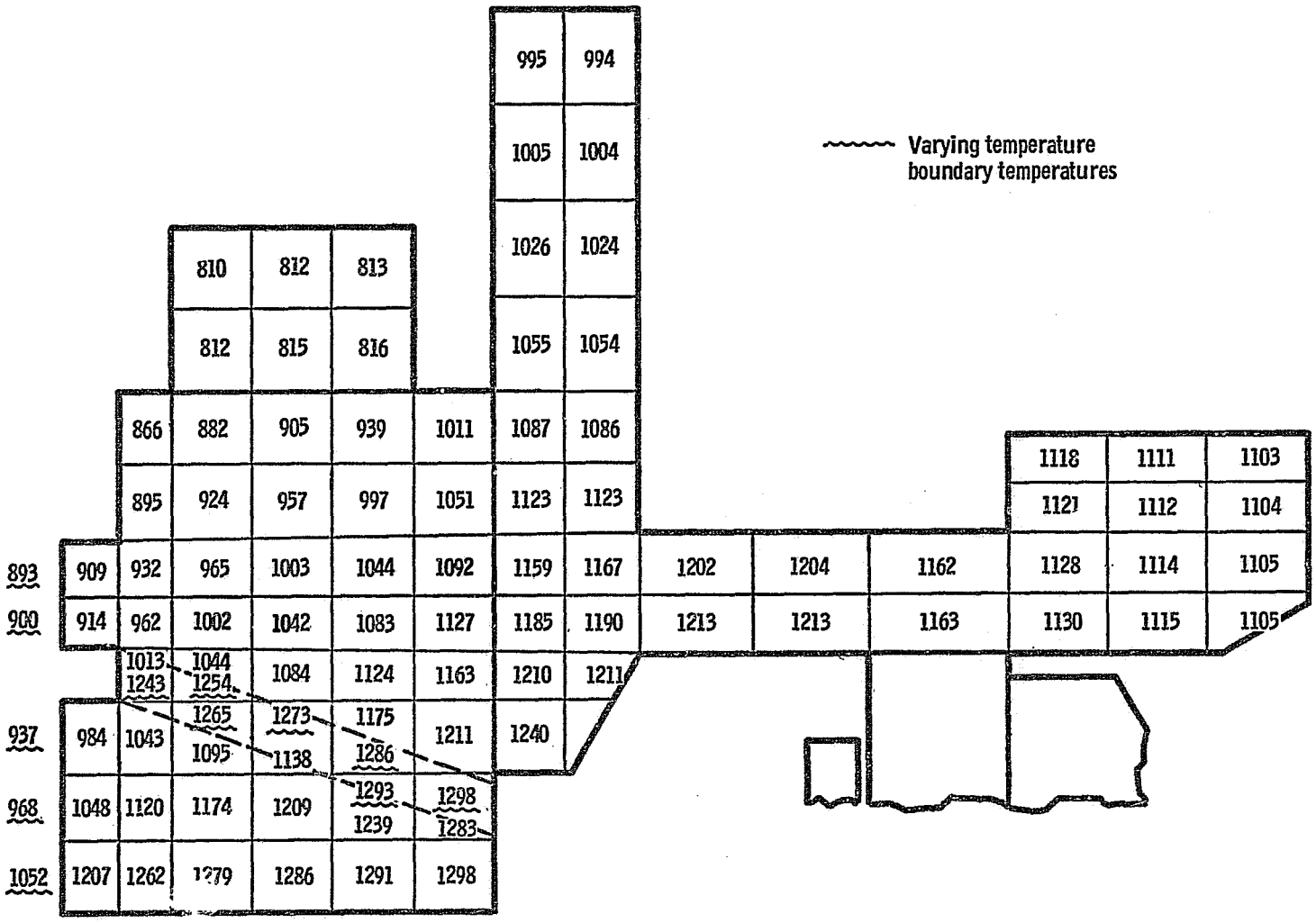

Figure 14.- Example problem of temperature distribution in °F for nosepiece assembly of seal depicted in figure 11.

The boundary heat transfer cards (input Item 9) are assembled element by element. The boundary numbers determine the order of the sets. A set consists of the indicator card for the element followed by the index card, plus any others required, for each "side" of the element that is a boundary. The indicator cards do not appear in the printout but the order of the other cards for each element is indicated in the section of printout following the initial temperatures. This section, as well as the conduction element table, are not standard output items but are included to indicate the cards required. Some calculated values (Reynolds or Prandtl numbers and the following items for each element side) are included in this printout.

In preparing the varying temperature boundary cards, the region at which the flows joined required the use of approximations because the program permits only one varying temperature condition per element. Boundary element 47 (fig. 12(c)) was assumed to be affected only by the duct flow. For boundary elements 49 and 50, special areas (code number 5) were used with the sums of the appropriate faces as the area values. Element 56 was made the combined flow element with 47 and 55 (conduction numbers 19 and 98) as the upstream elements.

The film cooled (FC3) boundary was another area where approximations were involved. It was assumed that flows originated at the northwest corners of boundary elements 16 (two 0.018 lbm/sec), 24 (two 0.018 lbm/sec), and 35 (two 0.012 lbm/sec) (see fig. 12(c)). The flows were assumed to be either toward or parallel to the axis except for elements 20 and 31 to 33. The arrows outlining the region indicate this. Elements 20 and 31 to 33 had flow around the circumference and were the only elements where the equation properly applied. For the other elements, the flow length was taken as the sum of the element sides over which the flow occurred and the length perpendicular to flow was the average circumference for the side.

After all cards were prepared and assembled, a preliminary run was made to check for errors. The LD card (input Item 2) options (or words) 1, 2, and 5 were used. Limits of 1 minute and 100 iterations were set. The results of the final run are presented in the sections of printout starting with the element center temperatures. These temperatures and the varying temperature boundary temperatures are also plotted in figure 14. Improved results could be obtained by using fluid properties based on the new film temperatures calculated from the results. This applies especially to the varying temperature flows where the properties were based on the initial flow temperatures (1300° F).

Computer Output for Sample Problem

```
                    SAMPLE PROBLEM# MAINSHAFT SEAL NOSEPIECE

 ID=    1, 1     2, 1     3, 1     4, -0     5, 1     6, -0     7, -0     8, -0     9, -0    10, -0

 NT=    1, 1     2, -0    3, -0    4, -0     5, -0

 RO=    1, 1.5000000E 00     2, 7.0000000E 01     3, 1.0000000E 02     4,-0.              5,-0.

 CO=    1, 1.1000000E 02     2, 7.2000000E 01     3, 1.0000000E 03     4, 5.0000000E-02   5,-0.
        6, 1.3000000E 03     7, 1.3000000E 03     8,-0.                9, 2.0000000E 01   10,-0.

                                                  DATA FOR ALPHA.
        1 1.5000000E 03   2 1.0000000E 00   3 1.0000000E 00   4 1.0000000E 00   5 1.0000000E 00   6 1.3500000E-06
        7 1.5000000E-09

                                                  DATA FOR ALPHA.
        1 1.8000000E 03   2 2.0000000E 00   3 1.0000000E 00   4 1.0000000E 00   5 1.0000000E 00   6 2.9447000E-06
        7 2.5400000E-09

                                                  DATA FOR ALPHA.
        1 1.6000000E 03   2 3.0000000E 00   3 2.0000000E 00   4 1.0000000E 00   5 1.0000000E 00   6 7.0200000E-06
        7 8.6071429E-10   8 3.5714290E-13


                                CONDUCTION ELEMENT TABLE (TD1)

 1    1, 1.C000E 00   2, 3.0600E 00   3, 6.0000E-02   4, 5.0000E-02   5, 2.0000E 00   6, 7.0000E 00   7, 0.
      8, 0.           9, 1.0000E 00  10,-0.           11,-0.          12,-0.          13,-0.

 2    1, 2.C000E 00   2, 3.0600E 00   3, 6.0000E-02   4, 5.0000E-02   5, 3.0000E 00   6, 8.0000E 00   7, 1.0000E 00
      8,-0.           9, 1.0000E 00  10,-0.           11,-0.          12,-0.          13,-0.

 3    1, 3.0000E 00   2, 3.0600E 00   3, 6.0000E-02   4, 7.5000E-02   5, 4.0000E 00   6, 9.0000E 00   7, 2.0000E 00
      8,-0.           9, 1.0000E 00  10,-0.           11,-0.          12,-0.          13,-0.

 4    1, 4.C000E 00   2, 3.0600E 00   3, 6.0000E-02   4, 7.5000E-02   5, 5.0000E 00   6, 1.0000E 01   7, 3.0000E 00
      8,-0.           9, 1.0000E 00  10,-0.           11,-0.          12,-0.          13,-0.

 5    1, 5.C000E 00   2, 3.0600E 00   3, 6.0000E-02   4, 7.5000E-02   5, 6.0000E 00   6, 1.1000E 01   7, 4.0000E 00
      8,-0.           9, 1.0000E 00  10,-0.           11,-0.          12,-0.          13,-0.

 6    1, 6.C000E 00   2, 3.0600E 00   3, 6.0000E-02   4, 7.5000E-02   5, 0.           6, 1.2000E 01   7, 5.0000E 00
      8,-0.           9, 1.0000E 00  10,-0.           11,-0.          12,-0.          13,-0.

 7    1, 7.C000E 00   2, 3.1250E 00   3, 7.0000E-02   4, 5.0000E-02   5, 8.0000E 00   6, 1.3000E 01   7, 0.
      8, 1.0C00E 00   9, 1.0000E 00  10,-0.           11,-0.          12,-0.          13,-0.

 8    1, 8.C000E 00   2, 3.1250E 00   3, 7.0000E-02   4, 5.0000E-02   5, 9.0000E 00   6, 1.4000E 01   7, 7.0000E 00
      8, 2.0C00E 00   9, 1.0000E 00  10,-0.           11,-0.          12,-0.          13,-0.

 9    1, 9.0000E 00   2, 3.1250E 00   3, 7.0000E-02   4, 7.5000E-02   5, 1.0000E 01   6, 1.5000E 01   7, 8.0000E 00
      8, 3.0C00E 00   9, 1.0000E 00  10,-0.           11,-0.          12,-0.          13,-0.

10    1, 1.C000E 01   2, 3.1250E 00   3, 7.0000E-02   4, 7.5000E-02   5, 1.1000E 01   6, 1.6000E 01   7, 9.0000E 00
      8, 4.0C00E 00   9, 1.0000E 00  10,-0.           11,-0.          12,-0.          13,-0.

11    1, 1.1000E 01   2, 3.1250E 00   3, 7.0000E-02   4, 7.5000E-02   5, 1.2000E 01   6, 1.7000E 01   7, 1.0000E 01
      8, 5.0C00E 00   9, 1.0000E 00  10,-0.           11,-0.          12,-0.          13,-0.

12    1, 1.2000E 01   2, 3.1250E 00   3, 7.0000E-02   4, 7.5000E-02   5, 0.           6, 1.8000E 01   7, 1.1000E 01
      8, 6.0C00E 00   9, 1.0000E 00  10,-0.           11,-0.          12,-0.          13,-0.

13    1, 1.3000E 01   2, 3.1950E 00   3, 7.0000E-02   4, 5.0000E-02   5, 1.4000E 01   6, 0.           7, 0.
      8, 7.0C00F 00   9, 1.0000E 00  10,-0.           11,-0.          12,-0.          13,-0.

14    1, 1.4000E 01   2, 3.1950E 00   3, 7.0000E-02   4, 5.0000E-02   5, 1.5000E 01   6, 1.9000E 01   7, 1.3000E 01
      8, 8.C00F 00    9, 1.0000E 00  10,-0.           11,-0.          12,-0.          13,-0.

15    1, 1.5000E 01   2, 3.1950E 00   3, 7.0000E-02   4, 7.5000E-02   5, 1.6000E 01   6, 2.0000E 01   7, 1.4000E 01
      8, 9.0C00F 00   9, 1.0000E 00  10,-0.           11,-0.          12,-0.          13,-0.

16    1, 1.6000F 01   2, 3.1950E 00   3, 7.0000F-02   4, 7.5000E-02   5, 1.7000E 01   6, 2.1000E 01   7, 1.5000E 01
      8, 1.0000E 01   9, 1.0000E 00  10,-0.           11,-0.          12,-0.          13,-0.
```

```
17    1, 1.7000E 01   2, 3.1950E 00   3, 7.0000E-02   4, 7.5000E-02   5, 1.8000F 01   6, 2.2000E 01   7, 1.6000E 01
      8, 1.1C00F 01   9, 1.0000E 00  10,-0.          11,-0.          12,-0.          13,-0.

18    1, 1.8000E 01   2, 3.1950E 00   3, 7.0000E-02   4, 7.5000E-02   5, 5.2000E 01   6, 2.3000E 01   7, 1.7000E 01
      8, 1.2C00E 01   9, 1.0000E 00  10, 5.1200F 02  11,-0.          12,-0.          13,-0.

19    1, 1.9000E 01   2, 3.2550E 00   3, 5.0000E-02   4, 5.0000E-02   5, 2.0000F 01   6, 2.5000E 01   7, 0.
      8, 1.4C00F 01   9, 1.0000E 00  10, 0.          11,-0.          12,-0.          13,-0.

20    1, 2.C000E 01   2, 3.2550E 00   3, 5.0000E-02   4, 7.5000E-02   5, 2.1000E 01   6, 2.6000E 01   7, 1.9000E 01
      8, 1.5C00E 01   9, 1.0000E 00  10,-0.          11,-0.          12,-0.          13,-0.

21    1, 2.1000E 01   2, 3.2550E 00   3, 5.0000E-02   4, 7.5000E-02   5, 2.2000E 01   6, 2.7000E 01   7, 2.0000E 01
      8, 1.6000E 01   9, 1.0000E 00  10,-0.          11,-0.          12,-0.          13,-0.

22    1, 2.2000F 01   2, 3.2550E 00   3, 5.0000E-02   4, 7.5000E-02   5, 2.3000E 01   6, 2.8000E 01   7, 2.1000E 01
      8, 1.7C00F 01   9, 1.0000E 00  10,-0.          11,-0.          12,-0.          13,-0.

23    1, 2.3000F 01   2, 3.2550F 00   3, 5.0000E-02   4, 7.5000E-02   5, 5.3000E 01   6, 2.9000E 01   7, 2.2000E 01
      8, 1.8C00E 01   9, 1.0000E 00  10, 7.0400E 02  11,-0.          12,-0.          13,-0.

24    1, 2.4000E 01   2, 3.3050E 00   3, 5.0000E-02   4, 5.0000E-02   5, 2.5000E 01   6, 3.0000E 01   7, 0.
      8, 0.           9, 1.0000E 00  10, 0.          11,-0.          12,-0.          13,-0.

25    1, 2.5000E 01   2, 3.3050E 00   3, 5.0000E-02   4, 5.0000E-02   5, 2.6000E 01   6, 3.1000E 01   7, 2.4000E 01
      8, 1.9C00E 01   9, 1.0000E 00  10,-0.          11,-0.          12,-0.          13,-0.

26    1, 2.6000E 01   2, 3.3050E 00   3, 5.0000E-02   4, 7.5000E-02   5, 2.7000E 01   6, 3.2000E 01   7, 2.5000E 01
      8, 2.0C00F 01   9, 1.0000E 00  10,-0.          11,-0.          12,-0.          13,-0.

27    1, 2.7000E 01   2, 3.3050E 00   3, 5.0000E-02   4, 7.5000E-02   5, 2.8000E 01   6, 3.3000E 01   7, 2.6000E 01
      8, 2.1C00F 01   9, 1.0000E 00  10,-0.          11,-0.          12,-0.          13,-0.

28    1, 2.8000E 01   2, 3.3050F 00   3, 5.0000E-02   4, 7.5000E-02   5, 2.9000E 01   6, 3.4000E 01   7, 2.7000E 01
      8, 2.2C00E 01   9, 1.0000E 00  10,-0.          11,-0.          12,-0.          13,-0.

29    1, 2.9000E 01   2, 3.3050E 00   3, 5.0000E-02   4, 7.5000E-02   5, 5.5000E 01   6, 3.5000E 01   7, 2.8000E 01
      8, 2.3C00F 01   9, 1.0000E 00  10, 6.9300E 02  11,-0.          12,-0.          13,-0.

30    1, 3.0000F 01   2, 3.3550E 00   3, 5.0000E-02   4, 5.0000E-02   5, 3.1000E 01   6, 0.           7, 0.
      8, 2.4C00F 01   9, 1.0000E 00  10, 0.          11,-0.          12,-0.          13,-0.

31    1, 3.1000F 01   2, 3.3550F 00   3, 5.0000E-02   4, 5.0000E-02   5, 3.2000E 01   6, 3.6000E 01   7, 3.0000E 01
      8, 2.5C00F 01   9, 1.0000E 00  10,-0.          11,-0.          12,-0.          13,-0.

32    1, 3.2000F 01   2, 3.3550E 00   3, 5.0000E-02   4, 7.5000E-02   5, 3.3000E 01   6, 3.7000E 01   7, 3.1000E 01
      8, 2.6C00E 01   9, 1.0000E 00  10,-0.          11,-0.          12,-0.          13,-0.

33    1, 3.3000E 01   2, 3.3550E 00   3, 5.0000E-02   4, 7.5000E-02   5, 3.4000E 01   6, 3.8000E 01   7, 3.2000E 01
      8, 2.7C00F 01   9, 1.0000E 00  10,-0.          11,-0.          12,-0.          13,-0.

34    1, 3.4000E 01   2, 3.3550E 00   3, 5.0000E-02   4, 7.5000E-02   5, 3.5000E 01   6, 3.9000E 01   7, 3.3000E 01
      8, 2.8C00F 01   9, 1.0000E 00  10,-0.          11,-0.          12,-0.          13,-0.

35    1, 3.5000E 01   2, 3.3550E 00   3, 5.0000E-02   4, 7.5000E-02   5, 6.3000E 01   6, 4.0000E 01   7, 3.4000E 01
      8, 2.9C00E 01   9, 1.0000E 00  10, 6.8800E 02  11,-0.          12,-0.          13,-0.

36    1, 3.6000F 01   2, 3.4150E 00   3, 7.0000E-02   4, 5.0000E-02   5, 3.7000E 01   6, 4.1000E 01   7, 0.
      8, 3.1C00E 01   9, 1.0000E 00  10, 0.          11,-0.          12,-0.          13,-0.

37    1, 3.7000E 01   2, 3.4150E 00   3, 7.0000E-02   4, 7.5000E-02   5, 3.8000E 01   6, 4.2000E 01   7, 3.6000E 01
      8, 3.2C00F 01   9, 1.0000E 00  10,-0.          11,-0.          12,-0.          13,-0.

38    1, 3.8000F 01   2, 3.4150E 00   3, 7.0000E-02   4, 7.5000E-02   5, 3.9000E 01   6, 4.3000E 01   7, 3.7000E 01
      8, 3.3C00F 01   9, 1.0000E 00  10,-0.          11,-0.          12,-0.          13,-0.

39    1, 3.9000E 01   2, 3.4150E 00   3, 7.0000E-02   4, 7.5000E-02   5, 4.0000E 01   6, 4.4000E 01   7, 3.8000E 01
      8, 3.4C00F 01   9, 1.0000E 00  10,-0.          11,-0.          12,-0.          13,-0.

40    1, 4.C000E 01   2, 3.4150E 00   3, 7.0000E-02   4, 7.5000E-02   5, 7.1000E 01   6, 4.5000E 01   7, 3.9000E 01
      8, 3.5C00E 01   9, 1.0000E 00  10, 4.7900F 02  11,-0.          12,-0.          13,-0.

41    1, 4.1000F 01   2, 3.4800E 00   3, 6.0000E-02   4, 5.0000F-02   5, 4.2000E 01   6, 0.           7, 0.
      8, 3.6C00F 01   9, 1.0000E 00  10, 0.          11,-0.          12,-0.          13,-0.
```

42 1. 4.2000E 01 2. 3.4800E 00 3. 6.0000E-02 4. 7.5000E-02 5. 4.3000E 01 6. 4.6000E 01 7. 4.1000E 01
8. 3.7000E 01 9. 1.0000E 00 10.-0. 11. 4.3500E 02 12.-0. 13.-0.

43 1. 4.3000E 01 2. 3.4800E 00 3. 6.0000E-02 4. 7.5000E-02 5. 4.4000E 01 6. 4.7000E 01 7. 4.2000E 01
8. 3.8000E 01 9. 1.0000E 00 10.-0. 11. 4.3500E 02 12.-0. 13.-0.

44 1. 4.4000E 01 2. 3.4800E 00 3. 6.0000E-02 4. 7.5000E-02 5. 4.5000E 01 6. 4.8000E 01 7. 4.3000E 01
8. 3.9000E 01 9. 1.0000E 00 10.-0. 11. 4.3500E 02 12.-0. 13.-0.

45 1. 4.5000E 01 2. 3.4800E 00 3. 6.0000E-02 4. 7.5000E-02 5. 7.6000E 01 6. 0. 7. 4.4000E 01
8. 4.0000E 01 9. 1.0000E 00 10. 5.4900E 02 11. 0. 12.-0. 13.-0.

46 1. 4.6000E 01 2. 3.5500E 00 3. 8.0000E-02 4. 7.5000E-02 5. 4.7000E 01 6. 4.9000E 01 7. 0.
8. 4.2000E 01 9. 2.0000E 00 10. 0. 11.-0. 12.-0. 13. 4.3500E 02

47 1. 4.7000E 01 2. 3.5500E 00 3. 8.0000E-02 4. 7.5000E-02 5. 4.8000E 01 6. 5.0000E 01 7. 4.6000E 01
8. 4.3000E 01 9. 2.0000E 00 10.-0. 11.-0. 12.-0. 13. 4.3500E 02

48 1. 4.8000E 01 2. 3.5500E 00 3. 8.0000E-02 4. 7.5000E-02 5. 0. 6. 5.1000E 01 7. 4.7000E 01
8. 4.4000E 01 9. 2.0000E 00 10.-0. 11.-0. 12.-0. 13. 4.3500E 02

49 1. 4.9000E 01 2. 3.6300E 00 3. 8.0000E-02 4. 7.5000E-02 5. 5.0000E 01 6. 0. 7. 0.
8. 4.6000E 01 9. 2.0000E 00 10.-0. 11.-0. 12.-0. 13. 0.

50 1. 5.0000E 01 2. 3.6300E 00 3. 8.0000E-02 4. 7.5000E-02 5. 5.1000E 01 6. 0. 7. 4.9000E 01
8. 4.7000E 01 9. 2.0000E 00 10.-0. 11.-0. 12.-0. 13.-0.

51 1. 5.1000E 01 2. 3.6300E 00 3. 8.0000E-02 4. 7.5000E-02 5. 0. 6. 0. 7. 5.0000E 01
8. 4.8000E 01 9. 2.0000E 00 10.-0. 11.-0. 12.-0. 13.-0.

52 1. 5.2000E 01 2. 3.1950E 00 3. 7.0000E-02 4. 8.5000E-02 5. 0. 6. 5.3000E 01 7. 1.8000E 01
8. 0. 9. 2.0000E 00 10. 0. 11. 1.6000E 00 12. 5.1200E 02 13.-0.

53 1. 5.3000E 01 2. 3.2550E 00 3. 5.0000E-02 4. 7.0000E-02 5. 5.4000E 01 6. 5.5000E 01 7. 2.3000E 01
8. 5.2000E 01 9. 2.0000E 00 10.-0. 11. 0. 12. 7.0400E 02 13. 1.6000E 00

54 1. 5.4000E 01 2. 3.2550E 00 3. 5.0000E-02 4. 5.0000E-02 5. 0. 6. 5.6000E 01 7. 5.3000E 01
8. 0. 9. 2.0000E 00 10.-0. 11. 2.2000E 00 12. 0. 13. 0.

55 1. 5.5000E 01 2. 3.3050E 00 3. 5.0000E-02 4. 7.0000E-02 5. 5.6000E 01 6. 6.3000E 01 7. 2.9000E 01
8. 5.3000E 01 9. 2.0000E 00 10.-0. 11. 0. 12. 6.9300E 02 13. 0.

56 1. 5.6000E 01 2. 3.3050E 00 3. 5.0000E-02 4. 6.5000E-02 5. 5.7000E 01 6. 6.4000E 01 7. 5.5000E 01
8. 5.4000E 01 9. 2.0000E 00 10.-0. 11.-0. 12. 0. 13. 2.2000E 00

57 1. 5.7000E 01 2. 3.3100E 00 3. 4.0000E-02 4. 1.0000E-01 5. 5.8000E 01 6. 6.5000E 01 7. 5.6000E 01
8. 0. 9. 2.0000E 00 10.-0. 11.-0. 12.-0. 13. 0.

58 1. 5.8000E 01 2. 3.3100E 00 3. 4.0000E-02 4. 1.1000E-01 5. 5.9000E 01 6. 6.6000E 01 7. 5.7000E 01
8. 0. 9. 2.0000E 00 10.-0. 11.-0. 12.-0. 13. 0.

59 1. 5.9000E 01 2. 3.3100E 00 3. 4.0000E-02 4. 1.2500E-01 5. 6.0000E 01 6. 6.7000E 01 7. 5.8000E 01
8. 8.9000E 01 9. 2.0000E 00 10.-0. 11.-0. 12.-0. 13. 2.7900E 02

60 1. 6.0000E 01 2. 3.3100E 00 3. 4.0000E-02 4. 1.0000E-01 5. 6.1000E 01 6. 6.8000E 01 7. 5.9000E 01
8. 9.0000E 01 9. 2.0000E 00 10.-0. 11.-0. 12.-0. 13. 5.4438E 05

61 1. 6.1000E 01 2. 3.3100E 00 3. 4.0000E-02 4. 1.0000E-01 5. 6.2000E 01 6. 6.9000E 01 7. 6.0000E 01
8. 0. 9. 2.0000E 00 10.-0. 11.-0. 12.-0. 13. 0.

62 1. 6.2000E 01 2. 3.3100E 00 3. 4.0000E-02 4. 8.0000E-02 5. 0. 6. 7.0000E 01 7. 6.1000E 01
8. 0. 9. 2.0000E 00 10.-0. 11.-0. 12.-0. 13.-0.

63 1. 6.3000E 01 2. 3.3550E 00 3. 5.0000E-02 4. 7.0000E-02 5. 6.4000E 01 6. 7.1000E 01 7. 3.5000E 01
8. 5.5000E 01 9. 2.0000E 00 10.-0. 11.-0. 12. 6.8300E 02 13.-0.

64 1. 6.4000E 01 2. 3.3550E 00 3. 5.0000E-02 4. 6.5000E-02 5. 6.5000E 01 6. 7.2000E 01 7. 6.3000E 01
8. 5.6000E 01 9. 2.0000E 00 10.-0. 11.-0. 12. 0. 13.-0.

65 1. 6.5000E 01 2. 3.3550E 00 3. 5.0000E-02 4. 1.0000E-01 5. 6.6000E 01 6. 0. 7. 6.[illegible]0E 01
8. 5.7000E 01 9. 2.0000E 00 10.-0. 11.-0. 12.-0. 13.-0.

66 1. 6.6000E 01 2. 3.3550E 00 3. 5.0000E-02 4. 1.1000E-01 5. 6.7000E 01 6. 0. 7. 6.5000E 01
8. 5.8000E 01 9. 2.0000E 00 10.-0. 11.-0. 12.-0. 13.-0.

```
67    1, 6.7000E 01   2, 3.3550E 00   3, 5.0000E-02   4, 1.2500E-01   5, 6.8000E 01   6, 0.           7, 6.6000E 01
      8, 5.9000E 01   9, 2.0000E 00  10,-0.           11,-0.          12,-0.          13,-0.

68    1, 6.8000E 01   2, 3.3550E 00   3, 5.0000E-02   4, 1.0000E-01   5, 6.9000E 01   6, 7.3000E 01   7, 6.7000E 01
      8, 6.0000E 01   9, 2.0000E 00  10,-0.           11,-0.          12,-0.          13,-0.

69    1, 6.9000E 01   2, 3.3550E 00   3, 5.0000E-02   4, 1.0000E-01   5, 7.0000E 01   6, 7.4000E 01   7, 6.8000E 01
      8, 6.1000E 01   9, 2.0000E 00  10,-0.           11,-0.          12,-0.          13,-0.

70    1, 7.0000E 01   2, 3.3550E 00   3, 5.0000E-02   4, 8.0000E-02   5, 0.           6, 7.5000E 01   7, 6.9000E 01
      8, 6.2000E 01   9, 2.0000E 00  10,-0.           11,-0.          12,-0.          13,-0.

71    1, 7.1000E 01   2, 3.1450E 00   3, 7.0000E-02   4, 7.0000E-02   5, 7.2000E 01   6, 7.6000E 01   7, 4.0000E 01
      8, 6.3000E 01   9, 2.0000E 00  10,-0.           11,-0.          12, 4.7900E 02  13,-0.

72    1, 7.2000E 01   2, 3.1450E 00   3, 7.0000E-02   4, 6.5000E-02   5, 0.           6, 7.7000E 01   7, 7.1000E 01
      8, 6.4000E 01   9, 2.0000E 00  10,-0.           11,-0.          12, 0.          13,-0.

73    1, 7.3000E 01   2, 3.0450E 00   3, 5.0000E-02   4, 1.0000E-01   5, 7.4000E 01   6, 7.8000E 01   7, 0.
      8, 6.8000E 01   9, 2.0000E 00  10,-0.           11,-0.          12,-0.          13,-0.

74    1, 7.4000E 01   2, 3.0450E 00   3, 5.0000E-02   4, 1.0000E-01   5, 7.5000E 01   6, 7.9000E 01   7, 7.3000E 01
      8, 6.9000E 01   9, 2.0000E 00  10,-0.           11,-0.          12,-0.          13,-0.

75    1, 7.5000E 01   2, 3.0450E 00   3, 5.0000E-02   4, 8.0000E-02   5, 0.           6, 8.0000E 01   7, 7.4000E 01
      8, 7.0000E 01   9, 2.0000E 00  10,-0.           11,-0.          12,-0.          13,-0.

76    1, 7.6000E 01   2, 3.4800E 00   3, 6.0000E-02   4, 7.0000E-02   5, 7.7000E 01   6, 8.1000E 01   7, 4.5000E 01
      8, 7.1000E 01   9, 2.0000E 00  10,-0.           11,-0.          12, 5.4900E 02  13,-0.

77    1, 7.7000E 01   2, 3.4800E 00   3, 6.0000E-02   4, 6.5000E-02   5, 0.           6, 8.2000E 01   7, 7.6000E 01
      8, 7.2000E 01   9, 2.0000E 00  10,-0.           11,-0.          12, 0.          13,-0.

78    1, 7.8000E 01   2, 3.4500E 00   3, 4.0000E-02   4, 1.0000E-01   5, 7.9000E 01   6, 0.           7, 0.
      8, 7.3000E 01   9, 2.0000E 00  10,-0.           11,-0.          12,-0.          13,-0.

79    1, 7.9000E 01   2, 3.4500E 00   3, 4.0000E-02   4, 1.0000E-01   5, 8.0000E 01   6, 0.           7, 7.8000E 01
      8, 7.4000E 01   9, 2.0000E 00  10,-0.           11,-0.          12,-0.          13,-0.

80    1, 8.0000E 01   2, 3.4500E 00   3, 4.0000E-02   4, 8.0000E-02   5, 0.           6, 0.           7, 7.9000E 01
      9, 7.5000E 01   9, 2.0000E 00  10,-0.           11,-0.          12,-0.          13,-0.

81    1, 8.1000E 01   2, 3.5500E 00   3, 8.0000E-02   4, 7.0000E-02   5, 8.2000E 01   6, 8.3000E 01   7, 0.
      8, 7.6000E 01   9, 2.0000E 00  10,-0.           11,-0.          12,-0.          13,-0.

82    1, 8.2000E 01   2, 3.5500E 00   3, 8.0000E-02   4, 6.5000E-02   5, 0.           6, 8.4000E 01   7, 8.1000E 01
      8, 7.7000E 01   9, 2.0000E 00  10,-0.           11,-0.          12,-0.          13,-0.

83    1, 8.3000E 01   2, 3.6350E 00   3, 9.0000E-02   4, 7.0000E-02   5, 8.4000E 01   6, 8.5000E 01   7, 0.
      8, 8.1000E 01   9, 2.0000E 00  10,-0.           11,-0.          12,-0.          13,-0.

84    1, 8.4000E 01   2, 3.6350E 00   3, 9.0000E-02   4, 6.5000E-02   5, 0.           6, 8.6000E 01   7, 8.3000E 01
      8, 8.2000E 01   9, 2.0000E 00  10,-0.           11,-0.          12,-0.          13,-0.

85    1, 8.5000E 01   2, 3.7250E 00   3, 9.0000E-02   4, 7.0000E-02   5, 8.6000E 01   6, 8.7000E 01   7, 0.
      8, 8.3000E 01   9, 2.0000E 00  10,-0.           11,-0.          12,-0.          13,-0.

86    1, 8.6000E 01   2, 3.7250E 00   3, 9.0000E-02   4, 6.5000E-02   5, 0.           6, 8.8000E 01   7, 8.5000E 01
      8, 8.4000E 01   9, 2.0000E 00  10,-0.           11,-0.          12,-0.          13,-0.

87    1, 8.7000E 01   2, 3.8150E 00   3, 9.0000E-02   4, 7.0000E-02   5, 8.8000E 01   6, 0.           7, 0.
      8, 8.5000E 01   9, 2.0000E 00  10,-0.           11,-0.          12,-0.          13,-0.

88    1, 8.8000E 01   2, 3.8150E 00   3, 9.0000E-02   4, 6.5000E-02   5, 0.           6, 0.           7, 8.7000E 01
      8, 8.6000E 01   9, 2.0000E 00  10,-0.           11,-0.          12,-0.          13,-0.

89    1, 8.9000E 01   2, 3.2400E 00   3, 1.0000E-01   4, 1.2500E-01   5, 9.0000E 01   6, 5.9000E 01   7, 0.
      8, 0.           9, 3.0000E 00  10,-0.           11, 2.7900E 02  12,-0.          13,-0.

90    1, 9.0000E 01   2, 3.2400E 00   3, 1.0000E-01   4, 1.0000E-01   5, 0.           6, 6.0000E 01   7, 8.9000E 01
      8, 0.           9, 3.0000E 00  10,-0.           11, 5.4438E 05  12,-0.          13,-0.

91    1, 9.1000E 01   2, 2.9650E 00   3, 1.3000E-01   4, 8.0000E-02   5, 9.2000E 01   6, 9.3000E 01   7, 0.
      8, 0.           9, 2.0000E 00  10,-0.           11, 0.          12,-0.          13,-0.
```

92	1, 9.2000E 01	2, 2.9650E 00	3, 1.3000E-01	4, 8.0000E-02	5, 0.	6, 9.4000E 01	7, 9.1000E 01		
	8, 0.	9, 2.0000E 00	10,-0.	11,-0.	12,-0.	13,-0.			
93	1, 9.3000E 01	2, 3.0600E 00	3, 6.0000E-02	4, 8.0000E-02	5, 9.4000E 01	6, 9.5000E 01	7, 0.		
	8, 9.1000E 01	9, 2.0000E 00	10,-0.	11,-0.	12,-0.	13,-0.			
94	1, 9.4000E 01	2, 3.0600E 00	3, 6.0000E-02	4, 8.0000E-02	5, 0.	6, 9.6000E 01	7, 9.3000E 01		
	8, 9.2000E 01	9, 2.0000E 00	10,-0.	11,-0.	12,-0.	13,-0.			
95	1, 9.5000E 01	2, 3.1250E 00	3, 7.0000E-02	4, 8.0000E-02	5, 9.6000E 01	6, 9.7000E 01	7, 0.		
	8, 9.3000E 01	9, 2.0000E 00	10,-0.	11,-0.	12,-0.	13,-0.			
96	1, 9.6000E 01	2, 3.1250E 00	3, 7.0000E-02	4, 8.0000E-02	5, 0.	6, 9.8000E 01	7, 9.5000E 01		
	8, 9.4000E 01	9, 2.0000E 00	10,-0.	11,-0.	12,-0.	13,-0.			
97	1, 9.7000E 01	2, 3.1950E 00	3, 7.0000E-02	4, 8.0000E-02	5, 9.8000E 01	6, 9.9000E 01	7, 0.		
	8, 9.5000E 01	9, 2.0000E 00	10,-0.	11,-0.	12,-0.	13,-0.			
98	1, 9.8000E 01	2, 3.1950E 00	3, 7.0000E-02	4, 8.0000E-02	5, 0.	6, 1.0000E 02	7, 9.7000E 01		
	8, 9.6000E 01	9, 2.0000E 00	10,-0.	11,-0.	12,-0.	13,-0.			
99	1, 9.9000E 01	2, 3.2550E 00	3, 5.0000E-02	4, 8.0000E-02	5, 1.0000E 02	6, 1.0100E 02	7, 0.		
	8, 9.7000E 01	9, 2.0000E 00	10,-0.	11,-0.	12,-0.	13,-0.			
100	1, 1.0000E 02	2, 3.2550E 00	3, 5.0000E-02	4, 8.0000E-02	5, 0.	6, 1.0200E 02	7, 9.9000E 01		
	8, 9.8000E 01	9, 2.0000E 00	10,-0.	11,-0.	12,-0.	13,-0.			
101	1, 1.0100E 02	2, 3.3050E 00	3, 5.0000E-02	4, 8.0000E-02	5, 1.0200E 02	6, 1.0300E 02	7, 0.		
	8, 9.9000E 01	9, 2.0000E 00	10,-0.	11,-0.	12,-0.	13,-0.			
102	1, 1.0200E 02	2, 3.3050E 00	3, 5.0000E-02	4, 8.0000E-02	5, 0.	6, 1.0400E 02	7, 1.0100E 02		
	8, 1.0000E 02	9, 2.0000E 00	10,-0.	11,-0.	12,-0.	13,-0.			
103	1, 1.0300E 02	2, 3.3550E 00	3, 5.0000E-02	4, 8.0000E-02	5, 1.0400E 02	6, 1.0500E 02	7, 0.		
	8, 1.0100E 02	9, 2.0000E 00	10,-0.	11,-0.	12,-0.	13,-0.			
104	1, 1.0400E 02	2, 3.3550E 00	3, 5.0000E-02	4, 8.0000E-02	5, 0.	6, 1.0600E 02	7, 1.0300E 02		
	8, 1.0200E 02	9, 2.0000E 00	10,-0.	11,-0.	12,-0.	13,-0.			
105	1, 1.0500E 02	2, 3.4150E 00	3, 7.0000E-02	4, 8.0000E-02	5, 1.0600E 02	6, 1.0700E 02	7, 0.		
	8, 1.0300E 02	9, 2.0000E 00	10,-0.	11,-0.	12,-0.	13,-0.			
106	1, 1.0600E 02	2, 3.4150E 00	3, 7.0000E-02	4, 8.0000E-02	5, 0.	6, 1.0800E 02	7, 1.0500E 02		
	8, 1.0400E 02	9, 2.0000E 00	10,-0.	11,-0.	12,-0.	13,-0.			
107	1, 1.0700E 02	2, 3.4800E 00	3, 6.0000E-02	4, 8.0000E-02	5, 1.0800E 02	6, 1.0900E 02	7, 0.		
	8, 1.0500E 02	9, 2.0000E 00	10,-0.	11,-0.	12,-0.	13,-0.			
108	1, 1.0800E 02	2, 3.4800E 00	3, 6.0000E-02	4, 8.0000E-02	5, 0.	6, 1.1000E 02	7, 1.0700E 02		
	8, 1.0600E 02	9, 2.0000E 00	10,-0.	11,-0.	12,-0.	13,-0.			
109	1, 1.0900E 02	2, 3.5500E 00	3, 8.0000E-02	4, 8.0000E-02	5, 1.1000E 02	6, 0.	7, 0.		
	8, 1.0700E 02	9, 2.0000E 00	10,-0.	11,-0.	12,-0.	13,-0.			
110	1, 1.1000E 02	2, 3.5500E 00	3, 8.0000E-02	4, 8.0000E-02	5, 0.	6, 0.	7, 1.0900E 02		
	8, 1.0800E 02	9, 2.0000E 00	10,-0.	11,-0.	12,-0.	13,-0.			

ELEMENT STARTING TEMPERATURES

1 1097.0	2 1110.0	3 1123.0	4 1163.0	5 1205.0	6 1251.0	7 1042.0	8 1157.0	9 1080.0	10 1127.0
11 1172.0	12 1223.0	13 1016.0	14 1130.0	15 1052.0	16 1100.0	17 1141.0	18 1174.0	19 1040.0	20 1053.0
21 1090.0	22 1129.0	23 1158.0	24 943.0	25 947.0	26 1054.0	27 1085.0	28 1120.0	29 1146.0	30 941.0
31 946.0	32 1053.0	33 1085.0	34 1113.0	35 1138.0	36 1058.0	37 1065.0	38 1086.0	39 1108.0	40 1132.0
41 1062.0	42 1073.0	43 1086.0	44 1101.0	45 1120.0	46 1005.0	47 1007.0	48 1009.0	49 985.0	50 987.0
51 989.0	52 1181.0	53 1179.0	54 1180.0	55 1177.0	56 1177.0	57 1179.0	58 1175.0	59 1169.0	60 1165.0
61 1163.0	62 1162.0	63 1174.0	64 1175.0	65 1176.0	66 1174.0	67 1169.0	68 1165.0	69 1163.0	70 1163.0
71 1172.0	72 1173.0	73 1164.0	74 1163.0	75 1163.0	76 1170.0	77 1171.0	78 1164.0	79 1163.0	80 1162.0
81 1169.0	82 1169.0	83 1167.0	84 1167.0	85 1166.0	86 1166.0	87 1165.0	88 1165.0	89 1107.0	90 1060.0
91 871.0	92 881.0	93 869.0	94 877.0	95 866.0	96 872.0	97 864.0	98 868.0	99 861.0	100 865.0
101 860.0	102 864.0	103 858.0	104 860.0	105 856.0	106 858.0	107 856.0	108 856.0	109 853.0	110 854.0

```
 ELEMENT=  1.  TYPE=2.  SUBTYPE=4.  NEXT=1.  ITEMS READ= 9.   AREA CODE=4.  SPECIAL AREA=-0.          SQ.FEET

 CONCENTRIC CYLINDERS
T-B=1300.  K-F= 0.1018E-04  C-P= 0.2679E 00  MU= 0.2683E-04  NU= 0.5593E-04  R-O= 0.2525E 00  R-I= 0.2417E 00  OMEGA= 1570.
V-AX= 0.3134E 00              RE= 0.1502E 06  PR**1/3= 0.8903E 00  H COEFF= 0.9706356E 00          COEFF*AREA= 0.6616322E-02

 ELEMENT=  1.  TYPE=6.  SUBTYPE=2.  NEXT=0.  ITEMS READ=14.   AREA CODE=3.  SPECIAL AREA=-0.          SQ.FEET

 VAR.TEMP.RADIAL SEAL GAP
T-B=1062.  K-F= 0.9654E-05  C-P= 0.2647E 00  MU= 0.2562E-04  NU= 0.4990E-04  R-AV= 0.2550E 00  GAP= 0.4333E-04  OMEGA= 1570.
R-O= 0.2992E 00  FLAG-C=0.  FLAG-I=2.  ANN.NBR.= 94.  FLO.NBR.=  0.  MASS FLOW= 0.2382E-02
RE= 0.2046E 07  PR**1/3= 0.8890E 00  RE-C= 0.6754E 07          H COEFF= 0.3961579E 00  COEFF*AREA= 0.3173645E-02
HT.GEN.FACTOR= 0.10000E 01

 ELEMENT=  2.  TYPE=2.  SUBTYPE=4.  NEXT=0.  ITEMS READ= 9.   AREA CODE=4.  SPECIAL AREA=-0.          SQ.FEET

 CONCENTRIC CYLINDERS
T-B=1300.  K-F= 0.1021E-04  C-P= 0.2680E 00  MU= 0.2690E-04  NU= 0.5632E-04  R-O= 0.2525E 00  R-I= 0.2417E 00  OMEGA= 1570.
V-AX= 0.3134E 00              RE= 0.1492E 06  PR**1/3= 0.8904E 00  H COEFF= 0.9672406E 00          COEFF*AREA= 0.6393880E-02

 ELEMENT=  3.  TYPE=2.  SUBTYPE=4.  NEXT=0.  ITEMS READ= 9.   AREA CODE=4.  SPECIAL AREA=-0.          SQ.FEET

 CONCENTRIC CYLINDERS
T-B=1300.  K-F= 0.1024E-04  C-P= 0.2682E 00  MU= 0.2696E-04  NU= 0.5664E-04  R-O= 0.2525E 00  R-I= 0.2417E 00  OMEGA= 1570.
V-AX= 0.3134E 00              RE= 0.1483E 06  PR**1/3= 0.8905E 00  H COEFF= 0.9643760E 00          COEFF*AREA= 0.9562416E-02

 ELEMENT=  4.  TYPE=2.  SUBTYPE=4.  NEXT=0.  ITEMS READ= 9.   AREA CODE=4.  SPECIAL AREA=-0.          SQ.FEET

 CONCENTRIC CYLINDERS
T-B=1300.  K-F= 0.1033E-04  C-P= 0.2687E 00  MU= 0.2716E-04  NU= 0.5774E-04  R-O= 0.2525E 00  R-I= 0.2417E 00  OMEGA= 1570.
V-AX= 0.3134E 00              RE= 0.1455E 06  PR**1/3= 0.8907E 00  H COEFF= 0.9549769E 00          COEFF*AREA= 0.9469218E-02

 ELEMENT=  5.  TYPE=2.  SUBTYPE=4.  NEXT=0.  ITEMS READ= 9.   AREA CODE=4.  SPECIAL AREA=-0.          SQ.FEET

 CONCENTRIC CYLINDERS
T-B=1300.  K-F= 0.1042E-04  C-P= 0.2692E 00  MU= 0.2736E-04  NU= 0.5890E-04  R-O= 0.2525E 00  R-I= 0.2417E 00  OMEGA= 1570.
V-AX= 0.3134E 00              RE= 0.1427E 06  PR**1/3= 0.8910E 00  H COEFF= 0.9452609E 00          COEFF*AREA= 0.9372877E-02

 ELEMENT=  6.  TYPE=2.  SUBTYPE=4.  NEXT=1.  ITEMS READ= 9.   AREA CODE=1.  SPECIAL AREA=-0.          SQ.FEET

 CONCENTRIC CYLINDERS
T-B=1300.  K-F= 0.1051E-04  C-P= 0.2698E 00  MU= 0.2759E-04  NU= 0.6018E-04  R-O= 0.2550E 00  R-I= 0.2417E 00  OMEGA= 1570.
V-AX= 0.                      RE= 0.1727E 06  PR**1/3= 0.8912E 00  H COEFF= 0.9318566E 00          COEFF*AREA= 0.7465160E-02

 ELEMENT=  6.  TYPE=2.  SUBTYPE=4.  NEXT=0.  ITEMS READ= 9.   AREA CODE=4.  SPECIAL AREA=-0.          SQ.FEET

 CONCENTRIC CYLINDERS
T-B=1300.  K-F= 0.1051E-04  C-P= 0.2698E 00  MU= 0.2759E-04  NU= 0.6018E-04  R-O= 0.2525E 00  R-I= 0.2417E 00  OMEGA= 1570.
V-AX= 0.3134E 00              RE= 0.1396E 06  PR**1/3= 0.8912E 00  H COEFF= 0.9348986E 00          COEFF*AREA= 0.9270129E-02

 ELEMENT= 12.  TYPE=2.  SUBTYPE=4.  NEXT=1.  ITEMS READ= 9.   AREA CODE=1.  SPECIAL AREA=-0.          SQ.FEET

 CONCENTRIC CYLINDERS
T-B=1300.  K-F= 0.1045E-04  C-P= 0.2694E 00  MU= 0.2745E-04  NU= 0.5940E-04  R-O= 0.2608E 00  R-I= 0.2417E 00  OMEGA= 1570.
V-AX= 0.                      RE= 0.2543E 06  PR**1/3= 0.8911E 00  H COEFF= 0.9354691E 00          COEFF*AREA= 0.8928836E-02

 ELEMENT= 12.  TYPE=6.  SUBTYPE=1.  NEXT=0.  ITEMS READ=12.   AREA CODE=5.  SPECIAL AREA= 0.23562E-02 SQ.FEET

 VAR.TEMP.DUCT FLOW, LIQUID
T-B=1285.  K-F= 0.1042E-04  C-P= 0.2693E 00  MU= 0.2738E-04  MASS FLOW= 0.5685E 01  D-HYDR= 0.3333E-02  L-FLOW= 0.3125E-02
ANN.NBR.=  0.  FLOW NBR=  0.  FLAG-C=0.  FLAG-I=1.  X-SEC= 0.3142E-03
RE= 0.6920E 03  PR= 0.7074E 00          H COEFF= 0.3122549E-01  COEFF*AREA= 0.7357350E-04

 ELEMENT= 52.  TYPE=2.  SUBTYPE=4.  NEXT=1.  ITEMS READ= 9.   AREA CODE=1.  SPECIAL AREA=-0.          SQ.FEET

 CONCENTRIC CYLINDERS
T-B=1300.  K-F= 0.1036E-04  C-P= 0.2689E 00  MU= 0.2725E-04  NU= 0.5824E-04  R-O= 0.2662E 00  R-I= 0.2417E 00  OMEGA= 1570.
V-AX= 0.4726E 00              RE= 0.3366E 06  PR**1/3= 0.8908E 00  H COEFF= 0.9456614E 00          COEFF*AREA= 0.9228304E-02

 ELEMENT= 52.  TYPE=2.  SUBTYPE=4.  NEXT=0.  ITEMS READ= 9.   AREA CODE=4.  SPECIAL AREA=-0.          SQ.FEET

 CONCENTRIC CYLINDERS
T-B=1300.  K-F= 0.1036E-04  C-P= 0.2689E 00  MU= 0.2725E-04  NU= 0.5824E-04  R-O= 0.2633E 00  R-I= 0.2417E 00  OMEGA= 1570.
V-AX= 0.4726E 00              RE= 0.2949E 06  PR**1/3= 0.8908E 00  H COEFF= 0.9450770E 00          COEFF*AREA= 0.1107619E-01

 ELEMENT= 54.  TYPE=2.  SUBTYPE=4.  NEXT=1.  ITEMS READ= 9.   AREA CODE=1.  SPECIAL AREA=-0.          SQ.FEET

 CONCENTRIC CYLINDERS
T-B=1300.  K-F= 0.1036E-04  C-P= 0.2689E 00  MU= 0.2725E-04  NU= 0.5824E-04  R-O= 0.2712E 00  R-I= 0.2417E 00  OMEGA= 1570.
V-AX= 0.4726E 00              RE= 0.4050E 06  PR**1/3= 0.8908E 00  H COEFF= 0.9476610E 00          COEFF*AREA= 0.6729633E-02

 ELEMENT= 54.  TYPE=2.  SUBTYPE=4.  NEXT=0.  ITEMS READ= 9.   AREA CODE=5.  SPECIAL AREA= 0.17617E-02 SQ.FEET

 CONCENTRIC CYLINDERS
T-B=1300.  K-F= 0.1036E-04  C-P= 0.2689E 00  MU= 0.2725E-04  NU= 0.5824E-04  R-O= 0.2692E 00  R-I= 0.2417E 00  OMEGA= 1570.
V-AX= 0.4726E 00              RE= 0.3787E 06  PR**1/3= 0.8908E 00  H COEFF= 0.9467012E 00          COEFF*AREA= 0.1667804E-02

 ELEMENT= 57.  TYPE=2.  SUBTYPE=4.  NEXT=0.  ITEMS READ= 9.   AREA CODE=4.  SPECIAL AREA=-0.          SQ.FEET

 CONCENTRIC CYLINDERS
T-B=1300.  K-F= 0.1036E-04  C-P= 0.2689E 00  MU= 0.2724E-04  NU= 0.5818E-04  R-O= 0.2742E 00  R-I= 0.2417E 00  OMEGA= 1570.
V-AX= 0.4726E 00              RE= 0.4524E 06  PR**1/3= 0.8908E 00  H COEFF= 0.9497571E 00          COEFF*AREA= 0.1384408E-01

 ELEMENT= 58.  TYPE=2.  SUBTYPE=4.  NEXT=0.  ITEMS READ= 9.   AREA CODE=4.  SPECIAL AREA=-0.          SQ.FEET

 CONCENTRIC CYLINDERS
T-B=1300.  K-F= 0.1035E-04  C-P= 0.2688E 00  MU= 0.2722E-04  NU= 0.5807E-04  R-O= 0.2742E 00  R-I= 0.2283E 00  OMEGA= 1570.
V-AX= 0.9321E 00              RE= 0.6228E 06  PR**1/3= 0.8908E 00  H COEFF= 0.9274974E 00          COEFF*AREA= 0.1664599E-01
```

```
 ELEMENT= 30.  TYPE=3.  SUBTYPE=3.  NEXT=1.  ITEMS READ= 4.   AREA CODE=2.  SPECIAL AREA=-0.          SQ.FEET

 LIQUID FILM COOLING
T-B= 525.  W/L= 0.1000E-01  C-P= 0.5030E 00  L-FLOW= 0.8849E 00          H COEFF= 0.5684258E-02  COEFF*AREA= 0.4191581E-04

 ELEMENT= 30.  TYPE=6.  SUBTYPE=2.  NEXT=0.  ITEMS READ=14.  AREA CODE=3.  SPECIAL AREA=-0.          SQ.FEET

 VAR.TEMP.RADIAL SEAL GAP
T-B= 955.  K-F= 0.9048E-05  C-P= 0.2611E 00  MU= 0.2423E-04  NU= 0.1571E-03  R-AV= 0.2796E 00  GAP= 0.4333E-04  OMEGA= 1570.
R-D= 0.2992E 00  FLAG-C=0.  FLAG-I=2.  ANN.NBR.=104.  FLO.NBR.= 24.  MASS FLOW= 0.5954F-02
RE= 0.7811E 06  PR**1/3= 0.8876E 00  RE-C= 0.6754E 07          H COEFF= 0.3706926E 00  COEFF*AREA= 0.2713275E-02
HT.GEN.FACTOR= 0.10000E 01

 ELEMENT= 36.  TYPE=2.  SUBTYPE=3.  NEXT=0.  ITEMS READ= 4.   AREA CODE=3.  SPECIAL AREA=-0.          SQ.FEET

 LIQUID FILM COOLING
T-B= 525.  W/L= 0.1000E-01  C-P= 0.5030E 00  L-FLOW= 0.2339E 00          H COEFF= 0.2150492E-01  COEFF*AREA= 0.2243075E-03

 ELEMENT= 41.  TYPE=3.  SUBTYPE=3.  NEXT=1.  ITEMS READ= 4.   AREA CODE=2.  SPECIAL AREA=-0.          SQ.FEET

 LIQUID FILM COOLING
T-B= 525.  W/L= 0.1000E-01  C-P= 0.5030E 00  L-FLOW= 0.9189E 00          H COEFF= 0.5473936E-02  COEFF*AREA= 0.4191739E-04

 ELEMENT= 41.  TYPE=3.  SUBTYPE=3.  NEXT=0.  ITEMS READ= 4.   AREA CODE=3.  SPECIAL AREA=-0.          SQ.FEET

 LIQUID FILM COOLING
T-B= 525.  W/L= 0.1000E-01  C-P= 0.5030E 00  L-FLOW= 0.2339E 00          H COEFF= 0.2150492E-01  COEFF*AREA= 0.1959231E-03

 ELEMENT= 46.  TYPE=3.  SUBTYPE=3.  NEXT=0.  ITEMS READ= 4.   AREA CODE=3.  SPECIAL AREA=-0.          SQ.FEET

 LIQUID FILM COOLING
T-B= 525.  W/L= 0.2000E-01  C-P= 0.5030E 00  L-FLOW= 0.2450E 00          H COEFF= 0.4106122E-01  COEFF*AREA= 0.5088240E-03

 ELEMENT= 49.  TYPE=3.  SUBTYPE=3.  NEXT=1.  ITEMS READ= 4.   AREA CODE=2.  SPECIAL AREA=-0.          SQ.FEET

 LIQUID FILM COOLING
T-B= 525.  W/L= 0.1500E-01  C-P= 0.5030E 00  L-FLOW= 0.9608E 00          H COEFF= 0.7852831E-02  COEFF*AREA= 0.9431286E-04

 ELEMENT= 49.  TYPE=3.  SUBTYPE=3.  NEXT=0.  ITEMS READ= 4.   AREA CODE=3.  SPECIAL AREA=-0.          SQ.FEET

 LIQUID FILM COOLING
T-B= 525.  W/L= 0.2000E-01  C-P= 0.5030E 00  L-FLOW= 0.2450E 00          H COEFF= 0.4106122E-01  COEFF*AREA= 0.5202905E-03

 ELEMENT= 50.  TYPE=3.  SUBTYPE=3.  NEXT=0.  ITEMS READ= 4.   AREA CODE=2.  SPECIAL AREA=-0.          SQ.FEET

 LIQUID FILM COOLING
T-B= 525.  W/L= 0.1500E-01  C-P= 0.5030E 00  L-FLOW= 0.9608E 00          H COEFF= 0.7852831E-02  COEFF*AREA= 0.9431286E-04

 ELEMENT= 51.  TYPE=3.  SUBTYPE=3.  NEXT=1.  ITEMS READ= 4.   AREA CODE=1.  SPECIAL AREA=-0.          SQ.FEET

 LIQUID FILM COOLING
T-B= 525.  W/L= 0.5000E-02  C-P= 0.5030E 00  L-FLOW= 0.2450E 00          H COEFF= 0.1026531E-01  COEFF*AREA= 0.1300726E-03

 ELEMENT= 51.  TYPE=3.  SUBTYPE=3.  NEXT=0.  ITEMS READ= 4.   AREA CODE=2.  SPECIAL AREA=-0.          SQ.FEET

 LIQUID FILM COOLING
T-B= 525.  W/L= 0.1500E-01  C-P= 0.5030E 00  L-FLOW= 0.9608E 00          H COEFF= 0.7852831E-02  COEFF*AREA= 0.9431286E-04

 ELEMENT= 48.  TYPE=3.  SUBTYPE=3.  NEXT=0.  ITEMS READ= 4.   AREA CODE=1.  SPECIAL AREA=-0.          SQ.FEET

 LIQUID FILM COOLING
T-B= 525.  W/L= 0.5000E-02  C-P= 0.5030E 00  L-FLOW= 0.2450E 00          H COEFF= 0.1026531E-01  COEFF*AREA= 0.1272060E-03

 ELEMENT= 45.  TYPE=3.  SUBTYPE=3.  NEXT=0.  ITEMS READ= 4.   AREA CODE=2.  SPECIAL AREA=-0.          SQ.FEET

 LIQUID FILM COOLING
T-B= 525.  W/L= 0.2000E-01  C-P= 0.5030E 00  L-FLOW= 0.9189E 00          H COEFF= 0.1094787E-01  COEFF*AREA= 0.1257522E-03

 ELEMENT= 81.  TYPE=3.  SUBTYPE=3.  NEXT=0.  ITEMS READ= 4.   AREA CODE=3.  SPECIAL AREA=-0.          SQ.FEET

 LIQUID FILM COOLING
T-B= 525.  W/L= 0.1500E-01  C-P= 0.5030E 00  L-FLOW= 0.2361E 00          H COEFF= 0.3195680E-01  COEFF*AREA= 0.3960034E-03

 ELEMENT= 83.  TYPE=3.  SUBTYPE=3.  NEXT=0.  ITEMS READ= 4.   AREA CODE=3.  SPECIAL AREA=-0.          SQ.FEET

 LIQUID FILM COOLING
T-B= 525.  W/L= 0.1500E-01  C-P= 0.5030E 00  L-FLOW= 0.2361E 00          H COEFF= 0.3195680E-01  COEFF*AREA= 0.4561709E-03

 ELEMENT= 85.  TYPE=3.  SUBTYPE=3.  NEXT=0.  ITEMS READ= 4.   AREA CODE=3.  SPECIAL AREA=-0.          SQ.FEET

 LIQUID FILM COOLING
T-B= 525.  W/L= 0.1500E-01  C-P= 0.5030E 00  L-FLOW= 0.2361E 00          H COEFF= 0.3195680E-01  COEFF*AREA= 0.4674653E-03

 ELEMENT= 87.  TYPE=3.  SUBTYPE=3.  NEXT=1.  ITEMS READ= 4.   AREA CODE=2.  SPECIAL AREA=-0.          SQ.FEET

 LIQUID FILM COOLING
T-B= 525.  W/L= 0.1500E-01  C-P= 0.5030E 00  L-FLOW= 0.1010E 01          H COEFF= 0.7466601E-02  COEFF*AREA= 0.8802897E-04

 ELEMENT= 87.  TYPE=3.  SUBTYPE=3.  NEXT=0.  ITEMS READ= 4.   AREA CODE=3.  SPECIAL AREA=-0.          SQ.FEET

 LIQUID FILM COOLING
T-B= 525.  W/L= 0.1500E-01  C-P= 0.5030E 00  L-FLOW= 0.2631E 00          H COEFF= 0.2867731E-01  COEFF*AREA= 0.4296282E-03

 ELEMENT= 88.  TYPE=3.  SUBTYPE=3.  NEXT=1.  ITEMS READ= 4.   AREA CODE=1.  SPECIAL AREA=-0.          SQ.FEET

 LIQUID FILM COOLING
T-B= 525.  W/L= 0.2500E-01  C-P= 0.5030E 00  L-FLOW= 0.2669E 00          H COEFF= 0.4711502E-01  COEFF*AREA= 0.7058523E-03

 ELEMENT= 88.  TYPE=3.  SUBTYPE=3.  NEXT=0.  ITEMS READ= 4.   AREA CODE=2.  SPECIAL AREA=-0.          SQ.FEET
```

```
 LIQUID FILM COOLING
T-R= 525.  W/L= 0.1500E-01  C-P= 0.5030E 00  L-FLOW= 0.1010E 01          H COEFF= 0.7466601E-02  COEFF*AREA= 0.8174119E-04

 ELEMENT= 86.  TYPE=3.  SUBTYPE=3.  NEXT=0.  ITEMS READ= 4.  AREA CODE=1.  SPECIAL AREA=-0.          SQ.FEET

 LIQUID FILM COOLING
T-R= 525.  W/L= 0.2500E-01  C-P= 0.5030E 00  L-FLOW= 0.2669E 00          H COEFF= 0.4711502E-01  COEFF*AREA= 0.6892005E-03

 ELEMENT= 84.  TYPE=3.  SUBTYPE=3.  NEXT=0.  ITEMS READ= 4.  AREA CODE=1.  SPECIAL AREA=-0.          SQ.FEET

 LIQUID FILM COOLING
T-R= 525.  W/L= 0.2500E-01  C-P= 0.5030E 00  L-FLOW= 0.2669E 00          H COEFF= 0.4711502E-01  COEFF*AREA= 0.6725486E-03

 ELEMENT= 82.  TYPE=3.  SUBTYPE=3.  NEXT=0.  ITEMS READ= 4.  AREA CODE=1.  SPECIAL AREA=-0.          SQ.FEET

 LIQUID FILM COOLING
T-R= 525.  W/L= 0.2500E-01  C-P= 0.5030E 00  L-FLOW= 0.2669E 00          H COEFF= 0.4711502E-01  COEFF*AREA= 0.5838417E-03

 ELEMENT= 77.  TYPE=3.  SUBTYPE=3.  NEXT=0.  ITEMS READ= 4.  AREA CODE=1.  SPECIAL AREA=-0.          SQ.FEET

 LIQUID FILM COOLING
T-R= 525.  W/L= 0.2500E-01  C-P= 0.5030E 00  L-FLOW= 0.2669E 00          H COEFF= 0.4711502E-01  COEFF*AREA= 0.4292470E-03

 ELEMENT= 72.  TYPE=3.  SUBTYPE=3.  NEXT=0.  ITEMS READ= 4.  AREA CODE=1.  SPECIAL AREA=-0.          SQ.FEET

 LIQUID FILM COOLING
T-R= 525.  W/L= 0.2500E-01  C-P= 0.5030E 00  L-FLOW= 0.2669E 00          H COEFF= 0.4711502E-01  COEFF*AREA= 0.4525801E-03

 ELEMENT= 65.  TYPE=3.  SUBTYPE=3.  NEXT=0.  ITEMS READ= 4.  AREA CODE=2.  SPECIAL AREA=-0.          SQ.FEET

 LIQUID FILM COOLING
T-R= 525.  W/L= 0.1200E-01  C-P= 0.5030E 00  L-FLOW= 0.8849E 00          H COEFF= 0.6821110E-02  COEFF*AREA= 0.1005979E-03

 ELEMENT= 66.  TYPE=3.  SUBTYPE=3.  NEXT=0.  ITEMS READ= 4.  AREA CODE=2.  SPECIAL AREA=-0.          SQ.FEET

 LIQUID FILM COOLING
T-R= 525.  W/L= 0.1100E-01  C-P= 0.5030E 00  L-FLOW= 0.8849E 00          H COEFF= 0.6252684E-02  COEFF*AREA= 0.1014363E-03

 ELEMENT= 67.  TYPE=3.  SUBTYPE=3.  NEXT=0.  ITEMS READ= 4.  AREA CODE=2.  SPECIAL AREA=-0.          SQ.FEET

 LIQUID FILM COOLING
T-R= 525.  W/L= 0.1200E-01  C-P= 0.5030E 00  L-FLOW= 0.8849E 00          H COEFF= 0.6821110E-02  COEFF*AREA= 0.1257474E-03

 ELEMENT= 73.  TYPE=3.  SUBTYPE=3.  NEXT=0.  ITEMS READ= 4.  AREA CODE=3.  SPECIAL AREA=-0.          SQ.FEET

 LIQUID FILM COOLING
T-R= 525.  W/L= 0.1000E-01  C-P= 0.5030E 00  L-FLOW= 0.2298E 00          H COEFF= 0.2188860E-01  COEFF*AREA= 0.1454094E-03

 ELEMENT  78.  TYPE=3.  SUBTYPE=3.  NEXT=1.  ITEMS READ= 4.  AREA CODE=2.  SPECIAL AREA=-0.          SQ.FEET

 LIQUID FILM COOLING
T-R= 525.  W/L= 0.1500E-01  C-P= 0.5030E 00  L-FLOW= 0.9084E 00          H COEFF= 0.8305812E-02  COEFF*AREA= 0.1257561E-03

 ELEMENT= 78.  TYPE=3.  SUBTYPE=3.  NEXT=0.  ITEMS READ= 4.  AREA CODE=3.  SPECIAL AREA=-0.          SQ.FEET

 LIQUID FILM COOLING
T-R= 525.  W/L= 0.1000E-01  C-P= 0.5030E 00  L-FLOW= 0.2298E 00          H COEFF= 0.2188860E-01  COEFF*AREA= 0.1317997E-03

 ELEMENT= 79.  TYPE=3.  SUBTYPE=3.  NEXT=0.  ITEMS READ= 4.  AREA CODE=2.  SPECIAL AREA=-0.          SQ.FEET

 LIQUID FILM COOLING
T-R= 525.  W/L= 0.1500E-01  C-P= 0.5030E 00  L-FLOW= 0.9084E 00          H COEFF= 0.8305812E-02  COEFF*AREA= 0.1257561E-03

 ELEMENT= 80.  TYPE=3.  SUBTYPE=3.  NEXT=1.  ITEMS READ= 4.  AREA CODE=1.  SPECIAL AREA=-0.          SQ.FEET

 LIQUID FILM COOLING
T-R= 525.  W/L= 0.1500E-01  C-P= 0.5030E 00  L-FLOW= 0.2325E 00          H COEFF= 0.3245161E-01  COEFF*AREA= 0.1954037E-03

 ELEMENT= 80.  TYPE=3.  SUBTYPE=3.  NEXT=0.  ITEMS READ= 4.  AREA CODE=2.  SPECIAL AREA=-0.          SQ.FEET

 LIQUID FILM COOLING
T-R= 525.  W/L= 0.1500E-01  C-P= 0.5030E 00  L-FLOW= 0.9084E 00          H COEFF= 0.8305812E-02  COEFF*AREA= 0.1006049E-03

 ELEMENT= 75.  TYPE=3.  SUBTYPE=3.  NEXT=0.  ITEMS READ= 4.  AREA CODE=1.  SPECIAL AREA=-0.          SQ.FEET

 LIQUID FILM COOLING
T-R= 525.  W/L= 0.1500E-01  C-P= 0.5030E 00  L-FLOW= 0.2325E 00          H COEFF= 0.3245161E-01  COEFF*AREA= 0.2155812E-03

 ELEMENT= 70.  TYPE=3.  SUBTYPE=3.  NEXT=0.  ITEMS READ= 4.  AREA CODE=1.  SPECIAL AREA=-0.          SQ.FEET

 LIQUID FILM COOLING
T-R= 525.  W/L= 0.1500E-01  C-P= 0.5030E 00  L-FLOW= 0.2325E 00          H COEFF= 0.3245161E-01  COEFF*AREA= 0.2375287E-03

 ELEMENT= 62.  TYPE=3.  SUBTYPE=3.  NEXT=1.  ITEMS READ= 4.  AREA CODE=1.  SPECIAL AREA=-0.          SQ.FEET

 LIQUID FILM COOLING
T-R= 525.  W/L= 0.1500E-01  C-P= 0.5030E 00  L-FLOW= 0.2325E 00          H COEFF= 0.3245161E-01  COEFF*AREA= 0.1874742E-03

 ELEMENT= 62.  TYPE=3.  SUBTYPE=3.  NEXT=0.  ITEMS READ= 4.  AREA CODE=4.  SPECIAL AREA=-0.          SQ.FEET

 LIQUID FILM COOLING
T-R= 525.  W/L= 0.1000E-01  C-P= 0.5030E 00  L-FLOW= 0.8613E 00          H COEFF= 0.5840C09E-02  COEFF*AREA= 0.6706822E-04

 ELEMENT= 61.  TYPE=3.  SUBTYPE=3.  NEXT=0.  ITEMS READ= 4.  AREA CODE=4.  SPECIAL AREA=-0.          SQ.FEET

 LIQUID FILM COOLING
T-R= 525.  W/L= 0.5000E-02  C-P= 0.5030E 00  L-FLOW= 0.8613E 00          H COEFF= 0.2920005E-02  COEFF*AREA= 0.4191764E-04

 ELEMENT= 11.  TYPE=6.  SUBTYPE=1.  NEXT=0.  ITEMS READ=12.  AREA CODE=5.  SPECIAL AREA= 0.16115E-02 SQ.FEET
```

```
 VAR.TEMP.DUCT FLOW, LIQUID
T-B=1255.  K-F= 0.1035E-04  C-P= 0.2688E 00  MU= 0.2721E-04  MASS FLOW= 0.5685E 01  D-HYDR= 0.3333E-02  L-FLOW= 0.7885E-02
ANN.NBR.=  0.  FLOW NBR= 12.  FLAG-C=0.  FLAG-I=1.  X-SEC= 0.3142E-03
RE= 0.6965E 03  PR= 0.7069E 00       H COEFF= 0.2280963E-01  COEFF*AREA= 0.3675772E-04

 ELEMENT= 17.  TYPE=6.  SUBTYPE=1.  NEXT=0.  ITEMS READ=12.   AREA CODE=5.  SPECIAL AREA= 0.16115E-02 SQ.FEET

 VAR.TEMP.DUCT FLOW, LIQUID
T-B=1240.  K-F= 0.1028E-04  C-P= 0.2684E 00  MU= 0.2705E-04  MASS FLOW= 0.5685E 01  D-HYDR= 0.3333E-02  L-FLOW= 0.1133E-01
ANN.NBR.=  0.  FLOW NBR= 11.  FLAG-C=0.  FLAG-I=1.  X-SEC= 0.3142E-03
RE= 0.7006E 03  PR= 0.7064E 00       H COEFF= 0.1982752E-01  COEFF*AREA= 0.3195205E-04
 ELEMENT= 16.  TYPE=6.  SUBTYPE=1.  NEXT=0.  ITEMS READ=12.   AREA CODE=5.  SPECIAL AREA= 0.23562E-02 SQ.FEET

 VAR.TEMP.DUCT FLOW, LIQUID
T-B=1210.  K-F= 0.1019E-04  C-P= 0.2679E 00  MU= 0.2685E-04  MASS FLOW= 0.5685E 01  D-HYDR= 0.3333E-02  L-FLOW= 0.1643E-01
ANN.NBR.=  0.  FLOW NBR= 17.  FLAG-C=0.  FLAG-I=1.  X-SEC= 0.3142E-03
RE= 0.7057E 03  PR= 0.7059E 00       H COEFF= 0.1755946E-01  COEFF*AREA= 0.4160923E-04

 ELEMENT= 15.  TYPE=6.  SUBTYPE=1.  NEXT=0.  ITEMS READ=12.   AREA CODE=5.  SPECIAL AREA= 0.15087E-02 SQ.FEET

 VAR.TEMP.DUCT FLOW, LIQUID
T-B=1180.  K-F= 0.1003E-04  C-P= 0.2673E 00  MU= 0.2661E-04  MASS FLOW= 0.5685E 01  D-HYDR= 0.3333E-02  L-FLOW= 0.2103E-01
ANN.NBR.=  0.  FLOW NBR= 16.  FLAG-C=0.  FLAG-I=1.  X-SEC= 0.3142E-03
RE= 0.7121E 03  PR= 0.7053E 00       H COEFF= 0.1514010E-01  COEFF*AREA= 0.2435057E-04

 ELEMENT= 20.  TYPE=6.  SUBTYPE=1.  NEXT=0.  ITEMS READ=12.   AREA CODE=5.  SPECIAL AREA= 0.15087E-02 SQ.FEET

 VAR.TEMP.DUCT FLOW, LIQUID
T-B=1165.  K-F= 0.1009E-04  C-P= 0.2673E 00  MU= 0.2661E-04  MASS FLOW= 0.5685E 01  D-HYDR= 0.3333E-02  L-FLOW= 0.2497E-01
ANN.NBR.=  0.  FLOW NBR= 15.  FLAG-C=0.  FLAG-I=1.  X-SEC= 0.3142E-03
RE= 0.7121E 03  PR= 0.7053E 00       H COEFF= 0.1524155E-01  COEFF*AREA= 0.2299492E-04

 ELEMENT= 19.  TYPE=6.  SUBTYPE=1.  NEXT=0.  ITEMS READ=12.   AREA CODE=5.  SPECIAL AREA= 0.15708E-02 SQ.FEET

 VAR.TEMP.DUCT FLOW, LIQUID
T-B=1150.  K-F= 0.1006E-04  C-P= 0.2671E 00  MU= 0.2655E-04  MASS FLOW= 0.5685E 01  D-HYDR= 0.3333E-02  L-FLOW= 0.2843E-01
ANN.NBR.=  0.  FLOW NBR= 20.  FLAG-C=0.  FLAG-I=1.  X-SEC= 0.3142E-03
RE= 0.7137E 03  PR= 0.7051E 00       H COEFF= 0.1456088E-01  COEFF*AREA= 0.2287223E-04

 ELEMENT=  7.  TYPE=6.  SUBTYPE=2.  NEXT=0.  ITEMS READ=14.   AREA CODE=3.  SPECIAL AREA=-0.          SQ.FEET

 VAR.TEMP.RADIAL SEAL GAP
T-B= 975.  K-F= 0.9329E-05  C-P= 0.2628E 00  MU= 0.2488E-04  NU= 0.4696E-04  R-AV= 0.2604E 00  GAP= 0.4333E-04  OMEGA= 1570.
R-D= 0.2992E 00  FLAG-C=0.  FLAG-I=2.  ANN.NBR.= 96.  FLO.NBR.=  1.  MASS FLOW= 0.2382E-02
RE= 0.2267E 07  PR**1/3= 0.8883E 00  RE-C= 0.6754E 07          H COEFF= 0.3824877E 00  COEFF*AREA= 0.3650757E-02
HT.GEN.FACTOR= 0.10000E 01

 ELEMENT= 13.  TYPE=6.  SUBTYPE=2.  NEXT=0.  ITEMS READ=14.   AREA CODE=5.  SPECIAL AREA= 0.16805E-01 SQ.FEET

 VAR.TEMP.RADIAL SEAL GAP
T-B= 945.  K-F= 0.9431E-05  C-P= 0.2634E 00  MU= 0.2511E-04  NU= 0.4919E-04  R-AV= 0.2675E 00  GAP= 0.9152E-03  OMEGA= 1570.
R-D= 0.2992E 00  FLAG-C=0.  FLAG-I=2.  ANN.NBR.= 98.  FLO.NBR.=  7.  MASS FLOW= 0.2382E-02
RE= 0.2284E 07  PR**1/3= 0.8885E 00  RE-C= 0.2278E 06          H COEFF= 0.2927813E 00  COEFF*AREA= 0.4920307E-02
HT.GEN.FACTOR= 0.19315E 01

 ELEMENT= 24.  TYPE=6.  SUBTYPE=2.  NEXT=0.  ITEMS READ=14.   AREA CODE=5.  SPECIAL AREA= 0.14366E-01 SQ.FEET

 VAR.TEMP.RADIAL SEAL GAP
T-B=1005.  K-F= 0.9170E-05  C-P= 0.2618E 00  MU= 0.2451E-04  NU= 0.2928E-04  R-AV= 0.2744E 00  GAP= 0.1078E-02  OMEGA= 1570.
R-D= 0.2992E 00  FLAG-C=0.  FLAG-I=2.  ANN.NBR.=102.  FLO.NBR.=100.  MASS FLOW= 0.5954E-02
RE= 0.4037E 07  PR**1/3= 0.8879E 00  RE-C= 0.1900E 06          H COEFF= 0.4274941E 00  COEFF*AREA= 0.6141509E-02
HT.GEN.FACTOR= 0.18512E 01

 ELEMENT= 92.  TYPE=5.  SUBTYPE=0.  NEXT=0.  ITEMS READ= 2.   AREA CODE=1.  SPECIAL AREA=-0.          SQ.FEET

 SPECIFIED COEFFICIENT
T-B=1300.  H COEFF= 0.1380662E-02      COEFF*AREA= 0.2322056E-04

 ELEMENT=110.  TYPE=5.  SUBTYPE=0.  NEXT=1.  ITEMS READ= 2.   AREA CODE=2.  SPECIAL AREA=-0.          SQ.FEET

 SPECIFIED COEFFICIENT
T-B= 535.  H COEFF= 0.3733100E-04      COEFF*AREA= 0.4678121E-06

 ELEMENT=110.  TYPE=6.  SUBTYPE=2.  NEXT=0.  ITEMS READ=14.   AREA CODE=1.  SPECIAL AREA=-0.          SQ.FEET

 VAR.TEMP.RADIAL SEAL GAP
T-B= 900.  K-F= 0.8707E-05  C-P= 0.2590E 00  MU= 0.2345E-04  NU= 0.8278E-03  R-AV= 0.2958E 00  GAP= 0.8375E-02  OMEGA= 1570.
R-D= 0.2992E 00  FLAG-C=0.  FLAG-I=2.  ANN.NBR.=  0.  FLO.NBR.=108.  MASS FLOW= 0.5954E-02
RE= 0.1659E 06  PR**1/3= 0.8869E 00  RE-C= 0.1947E 05          H COEFF= 0.2106143E-01  COEFF*AREA= 0.2609898E-03
HT.GEN.FACTOR= 0.16334E 01

 ELEMENT= 94.  TYPE=6.  SUBTYPE=2.  NEXT=0.  ITEMS READ=14.   AREA CODE=1.  SPECIAL AREA=-0.          SQ.FEET

 VAR.TEMP.RADIAL SEAL GAP
T-B=1062.  K-F= 0.9147E-05  C-P= 0.2617E 00  MU= 0.2446E-04  NU= 0.4423E-04  R-AV= 0.2550E 00  GAP= 0.4333E-04  OMEGA= 1570.
R-D= 0.2992E 00  FLAG-C=0.  FLAG-I=2.  ANN.NBR.=  1.  FLO.NBR.=  0.  MASS FLOW= 0.2382E-02
RE= 0.2308E 07  PR**1/3= 0.8878E 00  RE-C= 0.6754E 07          H COEFF= 0.3748462E 00  COEFF*AREA= 0.3002915E-02
HT.GEN.FACTOR= 0.10000E 01

 ELEMENT= 96.  TYPE=6.  SUBTYPE=2.  NEXT=0.  ITEMS READ=14.   AREA CODE=1.  SPECIAL AREA=-0.          SQ.FEET

 VAR.TEMP.RADIAL SEAL GAP
T-B= 975.  K-F= 0.8979E-05  C-P= 0.2604E 00  MU= 0.2396E-04  NU= 0.4261E-04  R-AV= 0.2604E 00  GAP= 0.4333E-04  OMEGA= 1570.
R-D= 0.2992E 00  FLAG-C=0.  FLAG-I=2.  ANN.NBR.=  7.  FLO.NBR.= 94.  MASS FLOW= 0.2382E-02
RE= 0.2498E 07  PR**1/3= 0.8874E 00  RE-C= 0.6754E 07          H COEFF= 0.3657236E 00  COEFF*AREA= 0.3490747E-02
HT.GEN.FACTOR= 0.10000E 01

 ELEMENT= 98.  TYPE=6.  SUBTYPE=2.  NEXT=0.  ITEMS READ=14.   AREA CODE=1.  SPECIAL AREA=-0.          SQ.FEET
```

```
 VAR.TEMP.RADIAL SEAL GAP
T-R= 945.  K-F= 0.8847E-05  C-P= 0.2599E 00  MU= 0.2377E-04  NU= 0.4245E-04  R-AV= 0.2663E 00  GAP= 0.4333E-04  OMEGA= 1570.
R-O= 0.2992E 00  FLAG-C=0.  FLAG-I=2.  ANN.NBR.= 13.  FLO.NBR.= 96.  MASS FLOW= 0.2382E-02
RE= 0.2623E 07  PR**1/3= 0.8872E 00  RE-C= 0.6754E 07          H COEFF= 0.3623054E 00  COEFF*AREA= 0.3535583E-02
HT.GEN.FACTOR= 0.10000E 01

 ELEMENT=100.  TYPE=6.  SUBTYPE=2.  NEXT=0.  ITEMS READ=14.  AREA CODE=1.  SPECIAL AREA=-0.          SQ.FEET

 VAR.TEMP.RADIAL SEAL GAP
T-R=1050.  K-F= 0.9090E-05  C-P= 0.2614E 00  MU= 0.2433E-04  NU= 0.4552E-04  R-AV= 0.2713E 00  GAP= 0.4208E-02  OMEGA= 1570.
R-O= 0.2992E 00  FLAG-C=1.  FLAG-I=0.  ANN.NBR.= 0.  FLO.NBR.= 98.  MASS FLOW= 0.5954E-02
RE= 0.2539E 07  PR**1/3= 0.8877E 00  RE-C= 0.4183E 05          H COEFF= 0.2351904E 00  COEFF*AREA= 0.1670160E-02
HT.GEN.FACTOR= 0.18866E 01

 COMBINED FLOW ELEMENT. CONDUCTION NO.= 100  FLOW FROM COND.ELEMENTS  98AND  19

 ELEMENT=102.  TYPE=6.  SUBTYPE=2.  NEXT=0.  ITEMS READ=14.  AREA CODE=1.  SPECIAL AREA=-0.          SQ.FEET

 VAR.TEMP.RADIAL SEAL GAP
T-R=1005.  K-F= 0.9981E-05  C-P= 0.2607E 00  MU= 0.2408E-04  NU= 0.5563E-04  R-AV= 0.2754E 00  GAP= 0.4333E-04  OMEGA= 1570.
R-O= 0.2992E 00  FLAG-C=0.  FLAG-I=2.  ANN.NBR.= 24.  FLO.NBR.=100.  MASS FLOW= 0.5954E-02
RE= 0.2141E 07  PR**1/3= 0.8875E 00  RE-C= 0.6754E 07          H COEFF= 0.3679046E 00  COEFF*AREA= 0.2652736E-02
HT.GEN.FACTOR= 0.10000E 01

 ELEMENT=104.  TYPE=6.  SUBTYPE=2.  NEXT=0.  ITEMS READ=14.  AREA CODE=1.  SPECIAL AREA=-0.          SQ.FEET

 VAR.TEMP.RADIAL SEAL GAP
T-R= 955.  K-F= 0.8852E-05  C-P= 0.2599E 00  MU= 0.2378E-04  NU= 0.1497E-03  R-AV= 0.2796E 00  GAP= 0.4333E-04  OMEGA= 1570.
R-O= 0.2992E 00  FLAG-C=0.  FLAG-I=2.  ANN.NBR.= 30.  FLO.NBR.=102.  MASS FLOW= 0.5954E-02
RE= 0.8197E 06  PR**1/3= 0.8872E 00  RE-C= 0.6754E 07          H COEFF= 0.3625071E 00  COEFF*AREA= 0.2653361E-02
HT.GEN.FACTOR= 0.10000E 01

 ELEMENT=106.  TYPE=6.  SUBTYPE=2.  NEXT=0.  ITEMS READ=14.  AREA CODE=1.  SPECIAL AREA=-0.          SQ.FEET

 VAR.TEMP.RADIAL SEAL GAP
T-R= 935.  K-F= 0.8799E-05  C-P= 0.2596E 00  MU= 0.2366E-04  NU= 0.8472E-03  R-AV= 0.2846E 00  GAP= 0.4208E-02  OMEGA= 1570.
R-O= 0.2992E 00  FLAG-C=0.  FLAG-I=2.  ANN.NBR.= 0.  FLO.NBR.=104.  MASS FLOW= 0.5954E-02
RE= 0.1501E 06  PR**1/3= 0.8871E 00  RE-C= 0.4183E 05          H COEFF= 0.2275467E-01  COEFF*AREA= 0.2373432E-03
HT.GEN.FACTOR= 0.17420E 01

 ELEMENT=108.  TYPE=6.  SUBTYPE=2.  NEXT=0.  ITEMS READ=14.  AREA CODE=1.  SPECIAL AREA=-0.          SQ.FEET

 VAR.TEMP.RADIAL SEAL GAP
T-R= 915.  K-F= 0.8746E-05  C-P= 0.2593E 00  MU= 0.2354E-04  NU= 0.8360E-03  R-AV= 0.2900E 00  GAP= 0.4208E-02  OMEGA= 1570.
R-O= 0.2992E 00  FLAG-C=0.  FLAG-I=2.  ANN.NBR.= 0.  FLO.NBR.=106.  MASS FLOW= 0.5954E-02
RE= 0.1579E 06  PR**1/3= 0.8870E 00  RE-C= 0.4183E 05          H COEFF= 0.2318910E-01  COEFF*AREA= 0.2112670E-03
HT.GEN.FACTOR= 0.16882E 01
```

BOUNDARY COEFFICIENT MATRIX -(H*A)BTU/F.SEC AND (H*A*T-B) OR W*C-P BTU/SEC

BNDRY ELEM.	COND. ELEM.	FIXED FLUX W	FORCED CONVECTION H*A	FORCED CONVECTION H*A*T-B	FREE CONVECTION H*A	FREE CONVECTION H*A*T-B	RADIATION H*A	RADIATION H*A*T-E	VAR.TEMP.CONVECTION H*A	VAR.TEMP.CONVECTION W*C-P
1	1	0.	0.64163E-02	0.83412E 01	0.	0.	0.	0.	0.31736E-02	0.63061E-03
2	2	0.	0.63939E-02	0.83120E 01	0.	0.	0.	0.	0.	0.
3	3	0.	0.95624E-02	0.12431E 02	0.	0.	0.	0.	0.	0.
4	4	0.	0.94692E-02	0.12310E 02	0.	0.	0.	0.	0.	0.
5	5	0.	0.93729E-02	0.12185E 02	0.	0.	0.	0.	0.	0.
6	6	0.	0.16735E-01	0.21756E 02	0.	0.	0.	0.	0.	0.
7	12	0.	0.89288E-02	0.11607E 02	0.	0.	0.	0.	0.73574E-04	0.15308E 01
8	52	0.	0.20304E-01	0.26396E 02	0.	0.	0.	0.	0.	0.
9	54	0.	0.83974E-02	0.10917E 02	0.	0.	0.	0.	0.	0.
10	57	0.	0.13634E-01	0.17724E 02	0.	0.	0.	0.	0.	0.
11	58	0.	0.14646E-01	0.19040E 02	0.	0.	0.	0.	0.	0.
12	30	0.	0.	0.	0.41916E-04	0.22006E-01	0.	0.	0.27133E-02	0.15546E-02
13	36	0.	0.	0.	0.22431E-03	0.11776E 00	0.	0.	0.	0.
14	41	0.	0.	0.	0.23784E-03	0.12487E 00	0.	0.	0.	0.
15	46	0.	0.	0.	0.50882E-03	0.26713E 00	0.	0.	0.	0.
16	49	0.	0.	0.	0.61460E-03	0.32267E 00	0.	0.	0.	0.
17	50	0.	0.	0.	0.94313E-04	0.49514E-01	0.	0.	0.	0.
18	51	0.	0.	0.	0.22439E-03	0.11780E 00	0.	0.	0.	0.
19	48	0.	0.	0.	0.12721E-03	0.66783E-01	0.	0.	0.	0.
20	45	0.	0.	0.	0.12575E-03	0.66020E-01	0.	0.	0.	0.
21	81	0.	0.	0.	0.39600E-03	0.20790E 00	0.	0.	0.	0.
22	83	0.	0.	0.	0.45617E-03	0.23949E 00	0.	0.	0.	0.
23	85	0.	0.	0.	0.46747E-03	0.24542E 00	0.	0.	0.	0.
24	87	0.	0.	0.	0.51766E-03	0.27177E 00	0.	0.	0.	0.
25	88	0.	0.	0.	0.78759E-03	0.41349E 00	0.	0.	0.	0.
26	86	0.	0.	0.	0.68920E-03	0.36183E 00	0.	0.	0.	0.
27	84	0.	0.	0.	0.67255E-03	0.35309E 00	0.	0.	0.	0.
28	82	0.	0.	0.	0.58384E-03	0.30652E 00	0.	0.	0.	0.
29	77	0.	0.	0.	0.42925E-03	0.22535E 00	0.	0.	0.	0.
30	72	0.	0.	0.	0.45258E-03	0.23760E 00	0.	0.	0.	0.
31	65	0.	0.	0.	0.10060E-03	0.52814E-01	0.	0.	0.	0.
32	66	0.	0.	0.	0.10144E-03	0.53254E-01	0.	0.	0.	0.
33	67	0.	0.	0.	0.12575E-03	0.66017E-01	0.	0.	0.	0.
34	73	0.	0.	0.	0.14541E-03	0.76340E-01	0.	0.	0.	0.
35	78	0.	0.	0.	0.25756E-03	0.13522E 00	0.	0.	0.	0.
36	79	0.	0.	0.	0.12576E-03	0.66022E-01	0.	0.	0.	0.
37	80	0.	0.	0.	0.29601E-03	0.15540E 00	0.	0.	0.	0.
38	75	0.	0.	0.	0.21558E-03	0.11318E 00	0.	0.	0.	0.
39	70	0.	0.	0.	0.23753E-03	0.12470E 00	0.	0.	0.	0.
40	62	0.	0.	0.	0.25454E-03	0.13363E 00	0.	0.	0.	0.
41	61	0.	0.	0.	0.41918E-04	0.22007E-01	0.	0.	0.	0.

42	11	0.	0.	0.	0.	0.	0.	0.	0.36758E-04	0.43011E-03
43	17	0.	0.	0.	0.	0.	0.	0.	0.31952E-04	0.47940E-03
44	16	0.	0.	0.	0.	0.	0.	0.	0.41609E-04	0.47849E-03
45	15	0.	0.	0.	0.	0.	0.	0.	0.24351E-04	0.47740E-03
46	20	0.	0.	0.	0.	0.	0.	0.	0.22995E-04	0.47740E-03
47	19	0.	0.	0.	0.	0.	0.	0.	0.22872E-04	0.47713E-03
48	7	0.	0.	0.	0.	0.	0.	0.	0.36508E-02	0.62599E-03
49	13	0.	0.	0.	0.	0.	0.	0.	0.49203E-02	0.62744E-03
50	24	0.	0.	0.	0.	0.	0.	0.	0.61415E-02	0.15591E-02
51	92	-0.10299E 00	0.23221E-04	0.30187E-01	0.	0.	0.	0.	0.	0.
52	110	0.	0.46781E-06	0.25028E-03	0.	0.	0.	0.	0.26099E-03	0.15424E-02
53	94	0.	0.	0.	0.	0.	0.	0.	0.30029E-02	0.62337E-03
54	96	0.	0.	0.	0.	0.	0.	0.	0.34907E-02	0.62025E-03
55	98	0.	0.	0.	0.	0.	0.	0.	0.35355E-02	0.61908E-03
56	100	0.	0.	0.	0.	0.	0.	0.	0.15702E-02	0.15561E-02
57	102	0.	0.	0.	0.	0.	0.	0.	0.25527E-02	0.15523E-02
58	104	0.	0.	0.	0.	0.	0.	0.	0.26534E-02	0.15476E-02
59	106	0.	0.	0.	0.	0.	0.	0.	0.23736E-03	0.15457E-02
60	108	0.	0.	0.	0.	0.	0.	0.	0.21127E-03	0.15438E-02
61	91	0.	0.	0.	0.	0.	0.	0.	0.	0.
62	93	0.	0.	0.	0.	0.	0.	0.	0.	0.
63	95	0.	0.	0.	0.	0.	0.	0.	0.	0.
64	97	0.	0.	0.	0.	0.	0.	0.	0.	0.
65	99	0.	0.	0.	0.	0.	0.	0.	0.	0.
66	101	0.	0.	0.	0.	0.	0.	0.	0.	0.
67	103	0.	0.	0.	0.	0.	0.	0.	0.	0.
68	105	0.	0.	0.	0.	0.	0.	0.	0.	0.
69	107	0.	0.	0.	0.	0.	0.	0.	0.	0.
70	109	0.	0.	0.	0.	0.	0.	0.	0.	0.
71	89	0.	0.	0.	0.	0.	0.	0.	0.	0.
72	90	0.	0.	0.	0.	0.	0.	0.	0.	0.

VAR.TEMP.CONVECTION DIMENSIONLESS COEFFICIENTS (H*A/W*C-P)

1 1, 5.0327E 00	2 12, 1.5299E-01	3 30, 1.7453E 00	4 11, 7.6561E-02	5 17, 6.6650E-02	6 16, 8.5960E-02
7 15, 5.1007E-02	8 20, 4.8167E-02	9 19, 4.7937E-02	10 7, 5.8320E 00	11 13, 7.8418E 00	12 24, 3.9393E 00
13 110, 1.6921E-01	14 94, 4.8172E 00	15 96, 5.6280E 00	16 98, 5.7110E 00	17 100, 1.0733E 00	18 102, 1.7089E 00
19 104, 1.7145E 00	20 106, 1.5355E-01	21 108, 1.3685E-01			

FLUID SHEAR HEAT GENERATION, BTU/SEC

1 1, 3.0329E-02	2 12, 0.	3 30, 3.1501E-02	4 11, 0.	5 17, 0.	6 16, 0.
7 15, 0.	8 20, 0.	9 19, 0.	10 7, 3.6591E-02	11 13, 3.6094E-03	12 24, 2.2674E-03
13 110, 4.8837E-04	14 94, 2.8952E-02	15 96, 3.5241E-02	16 98, 3.7368E-02	17 100, 5.6112E-04	18 102, 2.9926E-02
19 104, 3.0920E-02	20 106, 8.1461E-04	21 108, 7.1239E-04			

DATA TIME= 0.1306 MINUTES

CONDUCT.ELEMENT NO. 1 VAR.TEMP.ELEMENT NO. 1 FLOW CODE= 2

CONDUCT.ELEMENT NO. 12 VAR.TEMP.ELEMENT NO. 2 FLOW CODE= 1

CONDUCT.ELEMENT NO. 30 VAR.TEMP.ELEMENT NO. 3 FLOW CODE= 2

CONDUCT.ELEMENT NO. 11 VAR.TEMP.ELEMENT NO. 4 FLOW CODE= 1

CONDUCT.ELEMENT NO. 17 VAR.TEMP.ELEMENT NO. 5 FLOW CODE= 1

CONDUCT.ELEMENT NO. 16 VAR.TEMP.ELEMENT NO. 6 FLOW CODE= 1

CONDUCT.ELEMENT NO. 15 VAR.TEMP.ELEMENT NO. 7 FLOW CODE= 1

CONDUCT.ELEMENT NO. 20 VAR.TEMP.ELEMENT NO. 8 FLOW CODE= 1

CONDUCT.ELEMENT NO. 19 VAR.TEMP.ELEMENT NO. 9 FLOW CODE= 1

CONDUCT.ELEMENT NO. 7 VAR.TEMP.ELEMENT NO. 10 FLOW CODE= 2

CONDUCT.ELEMENT NO. 13 VAR.TEMP.ELEMENT NO. 11 FLOW CODE= 2

CONDUCT.ELEMENT NO. 24 VAR.TEMP.ELEMENT NO. 12 FLOW CODE= 2

CONDUCT.ELEMENT NO. 110 VAR.TEMP.ELEMENT NO. 13 FLOW CODE= 2

CONDUCT.ELEMENT NO. 94 VAR.TEMP.ELEMENT NO. 14 FLOW CODE= 2

CONDUCT.ELEMENT NO. 96 VAR.TEMP.ELEMENT NO. 15 FLOW CODE= 2

CONDUCT.ELEMENT NO. 98 VAR.TEMP.ELEMENT NO. 16 FLOW CODE= 2

COMBINED FLOWS ELEMENT, COMBINATION NO. 1 CONDUCT.NO.=100 BNDRY.NO.= 17 PREVIOUS ELEMENT VAR.TEMP.NOS.= 16 AND 9

CONDUCT.ELEMENT NO. 102 VAR.TEMP.ELEMENT NO. 17 FLOW CODE= 2

CONDUCT.ELEMENT NO. 104 VAR.TEMP.ELEMENT NO. 18 FLOW CODE= 2

CONDUCT.ELEMENT NO. 106 VAR.TEMP.ELEMENT NO. 19 FLOW CODE= 2

CONDUCT.ELEMENT NO. 108 VAR.TEMP.ELEMENT NO. 20 FLOW CODE= 2

CONVERGENCE CRITERIA, ITERATION= 100

COND.NO.	NEW TEMP.	OLD TEMP.	DIFFERENCE	MAX.DIFF.
1	0.1207188E 04	0.1207189E 04	-0.9002686E-03	0.5000000E-01
2	0.1262054E 04	0.1262066E 04	-0.1525879E-02	0.5000000E-01
3	0.1279193E 04	0.1279195E 04	-0.2044678E-02	0.5000000E-01
4	0.1285989E 04	0.1285991E 04	-0.2151489E-02	0.5000000E-01
5	0.1290989E 04	0.1290990E 04	-0.1678467E-02	0.5000000E-01
6	0.1298350E 04	0.1298050E 04	-0.3662109E-03	0.5000000E-01
7	0.1047630E 04	0.1047635E 04	-0.5157471E-02	0.5000000E-01
8	0.1120079E 04	0.1120038E 04	-0.9185791E-02	0.5000000E-01
9	0.1173756E 04	0.1173768E 04	-0.1269531E-01	0.5000000E-01
10	0.1209530E 04	0.1209544E 04	-0.1362610E-01	0.5000000E-01
11	0.1239491E 04	0.1239502E 04	-0.1098633E-01	0.5000000E-01
12	0.1283117E 04	0.1283120E 04	-0.3250122E-02	0.5000000E-01
13	0.9841284E 03	0.9841373E 03	-0.8911133E-02	0.5000000E-01
14	0.1043133E 04	0.1043151E 04	-0.1814270E-01	0.5000000E-01
15	0.1095047E 04	0.1095072E 04	-0.2456665E-01	0.5000000E-01
16	0.1138706E 04	0.1138733E 04	-0.2659607E-01	0.5000000E-01
17	0.1175654E 04	0.1175677E 04	-0.2363586E-01	0.5000000E-01
18	0.1211240E 04	0.1211257E 04	-0.1673889E-01	0.5000000E-01
19	0.1013473E 04	0.1013504E 04	-0.3154755E-01	0.5000000E-01
20	0.1044790E 04	0.1044827E 04	-0.3697205E-01	0.5000000E-01
21	0.1084893E 04	0.1084932E 04	-0.3944397E-01	0.5000000E-01
22	0.1124159E 04	0.1124195E 04	-0.3547668E-01	0.5000000E-01
23	0.1163354E 04	0.1163381E 04	-0.2624512E-01	0.5000000E-01
24	0.9142733E 03	0.9142952E 03	-0.2188873E-01	0.5000000E-01
25	0.9630659E 03	0.9631024E 03	-0.3651428E-01	0.5000000E-01
26	0.1002695E 04	0.1003742E 04	-0.4723358E-01	0.5000000E-01
27	0.1043344E 04	0.1043395E 04	-0.5065918E-01	0.5000000E-01
28	0.1084042E 04	0.1084088E 04	-0.4553223E-01	0.5000000E-01
29	0.1127134E 04	0.1127168E 04	-0.3353882E-01	0.5000000E-01
30	0.9091563E 03	0.9091920E 03	-0.2575684E-01	0.5000000E-01
31	0.9330364E 03	0.9330827E 03	-0.4633331E-01	0.5000000E-01
32	0.9659154E 03	0.9659751E 03	-0.5961609E-01	0.5000000E-01
33	0.1004118E 04	0.1004181E 04	-0.6332397E-01	0.5000000E-01
34	0.1045186E 04	0.1045242E 04	-0.5645752E-01	0.5000000E-01
35	0.1092378E 04	0.1092418E 04	-0.4060364E-01	0.5000000E-01
36	0.8963174E 03	0.8963848E 03	-0.6735992E-01	0.5000000E-01
37	0.9249237E 03	0.9250017E 03	-0.7803345E-01	0.5000000E-01
38	0.9584554E 03	0.9585373E 03	-0.8094788E-01	0.5000000E-01
39	0.9984394E 03	0.9985108E 03	-0.7141113E-01	0.5000000E-01
40	0.1051777E 04	0.1051825E 04	-0.4855347E-01	0.5000000E-01
41	0.8576335E 03	0.8577148E 03	-0.8129120E-01	0.5000000E-01
42	0.8835890E 03	0.8836909E 03	-0.1019058E 00	0.5000000E-01
43	0.9070508E 03	0.9071563E 03	-0.1055069E 00	0.5000000E-01
44	0.9411399E 03	0.9412338E 03	-0.9381104E-01	0.5000000E-01
45	0.1011581E 04	0.1011636E 04	-0.5464172E-01	0.5000000E-01
46	0.8149281E 03	0.8150896E 03	-0.1614914E 00	0.5000000E-01
47	0.8176213E 03	0.8177812E 03	-0.1599426E 00	0.5000000E-01
48	0.8188905E 03	0.8190473E 03	-0.1567459E 00	0.5000000E-01
49	0.8127623E 03	0.8129218E 03	-0.1594925E 00	0.5000000E-01
50	0.8151225E 03	0.8152804E 03	-0.1579361E 00	0.5000000E-01
51	0.8159731E 03	0.8161280E 03	-0.1548691E 00	0.5000000E-01
52	0.1239837E 04	0.1239845E 04	-0.7919312E-02	0.5000000E-01
53	0.1210087E 04	0.1210098E 04	-0.1136780E-01	0.5000000E-01
54	0.1210826E 04	0.1210837E 04	-0.1107788E-01	0.5000000E-01
55	0.1185108E 04	0.1185122E 04	-0.1371765E-01	0.5000000E-01
56	0.1189948E 04	0.1189961E 04	-0.1325989E-01	0.5000000E-01
57	0.1212945E 04	0.1212958E 04	-0.1272583E-01	0.5000000E-01
58	0.1212910E 04	0.1212927E 04	-0.1690674E-01	0.5000000E-01
59	0.1163028E 04	0.1163059E 04	-0.3027344E-01	0.5000000E-01
60	0.1131052E 04	0.1131106E 04	-0.4396057E-01	0.5000000E-01
61	0.1115488E 04	0.1115537E 04	-0.4867554E-01	0.5000000E-01
62	0.1105840E 04	0.1105889E 04	-0.4917908E-01	0.5000000E-01
63	0.1159076E 04	0.1159092E 04	-0.1539612E-01	0.5000000E-01
64	0.1166984E 04	0.1166998E 04	-0.1463318E-01	0.5000000E-01
65	0.1202627E 04	0.1202641E 04	-0.1374817E-01	0.5000000E-01
66	0.1204443E 04	0.1204461E 04	-0.1806641E-01	0.5000000E-01
67	0.1163022E 04	0.1163053E 04	-0.3030396E-01	0.5000000E-01
68	0.1128746E 04	0.1128790E 04	-0.4391479E-01	0.5000000E-01
69	0.1114913E 04	0.1114961E 04	-0.4800415E-01	0.5000000E-01
70	0.1105842E 04	0.1105890E 04	-0.4837036E-01	0.5000000E-01
71	0.1123232E 04	0.1123249E 04	-0.1690674E-01	0.5000000E-01
72	0.1123547E 04	0.1123583E 04	-0.1597595E-01	0.5000000E-01
73	0.1121688E 04	0.1121733E 04	-0.4518127E-01	0.5000000E-01
74	0.1113244E 04	0.1113292E 04	-0.4743958E-01	0.5000000E-01
75	0.1105152E 04	0.1105199E 04	-0.4751587E-01	0.5000000E-01
76	0.1087554E 04	0.1087571E 04	-0.1757813E-01	0.5000000E-01
77	0.1086031E 04	0.1086048E 04	-0.1666260E-01	0.5000000E-01
78	0.1118345E 04	0.1118390E 04	-0.4495239E-01	0.5000000E-01
79	0.1111852E 04	0.1111898E 04	-0.4653931E-01	0.5000000E-01
80	0.1104256E 04	0.1104302E 04	-0.4646301E-01	0.5000000E-01
81	0.1055370E 04	0.1055387E 04	-0.1722717E-01	0.5000000E-01
82	0.1053932E 04	0.1053999E 04	-0.1670837E-01	0.5000000E-01
83	0.1026047E 04	0.1026064E 04	-0.1692200E-01	0.5000000E-01
84	0.1024745E 04	0.1024763E 04	-0.1649475E-01	0.5000000E-01
85	0.1005677E 04	0.1005693E 04	-0.1657867E-01	0.5000000E-01
86	0.1004407E 04	0.1004423E 04	-0.1618195E-01	0.5000000E-01
87	0.9953152E 03	0.9953313E 03	-0.1615906E-01	0.5000000E-01
88	0.9939358E 03	0.9939516E 03	-0.1577759E-01	0.5000000E-01
89	0.1107000E 04	0.1107000E 04	0.	0.5000000E-01
90	0.1060000E 04	0.1060000E 04	0.	0.5000000E-01
91	0.8710000E 03	0.8710000E 03	0.	0.5000000E-01
92	0.8726228E 03	0.8726228E 03	-0.7629395E-05	0.5000000E-01
93	0.8690000E 03	0.8690000E 03	0.	0.5000000E-01
94	0.8791839E 03	0.8791839E 03	0.	0.5000000E-01
95	0.8560000E 03	0.8560000E 03	0.	0.5000000E-01

96	0.8760228E 03	0.8760228E 03	-0.7629395E-05	0.5000000E-01
97	0.8640000E 03	0.8640000E 03	0.	0.5000000E-01
98	0.8712150E 03	0.8712150E 03	-0.1525879E-04	0.5000000E-01
99	0.8610000E 03	0.8610000E 03	0.	0.5000000E-01
100	0.8661229E 03	0.8661230E 03	-0.2288818E-04	0.5000000E-01
101	0.8500000E 03	0.8500000E 03	0.	0.5000000E-01
102	0.8573022E 03	0.8573022E 03	-0.1525879E-04	0.5000000E-01
103	0.8580000E 03	0.8580000E 03	0.	0.5000000E-01
104	0.8648023E 03	0.8648024E 03	-0.7629395E-05	0.5000000E-01
105	0.8560000E 03	0.8560000E 03	0.	0.5000000E-01
106	0.8599932E 03	0.8599932E 03	0.	0.5000000E-01
107	0.8550000E 03	0.8550000E 03	0.	0.5000000E-01
108	0.8572584E 03	0.8572584E 03	0.	0.5000000E-01
109	0.8530000E 03	0.8530000E 03	0.	0.5000000E-01
110	0.8554687E 03	0.8554687E 03	0.	0.5000000E-01

CONVERGENCE CRITERION ACHEIVED, ITERATIONS= 131

ELEMENT(AT CENTER) TEMPERATURES (DEGREES F), ITERATIONS= 130

1. 1.2073900E 03	2. 1.2621996E 03	3. 1.2792890E 03	4. 1.2860528E 03	5. 1.2910258E 03	6. 1.2980559E 03
7. 1.0485211E 03	8. 1.1208364E 03	9. 1.1743483E 03	10. 1.2099351E 03	11. 1.2397363E 03	12. 1.2831623E 03
13. 9.8575897E 02	14. 1.0444335E 03	15. 1.0960944E 03	16. 1.1394177E 03	17. 1.1759955E 03	18. 1.2112994E 03
19. 1.0149709E 03	20. 1.0458352E 03	21. 1.0853686E 03	22. 1.1243037E 03	23. 1.1633123E 03	24. 9.1654068E 02
25. 9.6442071E 02	26. 1.0033938E 03	27. 1.0435496E 03	28. 1.0839858E 03	29. 1.1269771E 03	30. 9.1070828E 02
31. 9.3385793E 02	32. 9.6617658E 02	33. 1.0039886E 03	34. 1.0448881E 03	35. 1.0920869E 03	36. 8.9623836E 02
37. 9.2457432E 02	38. 9.5786542E 02	39. 9.9780642E 02	40. 1.0513206E 03	41. 8.6706945E 02	42. 8.8259656E 02
43. 9.0588249E 02	44. 9.4004122E 02	45. 1.0109861E 03	46. 8.1260896E 02	47. 8.1532953E 02	48. 8.1665190E 02
49. 8.1047188E 02	50. 8.1286117E 02	51. 8.1376455E 02	52. 1.2397408E 03	53. 1.2099419E 03	54. 1.2106788E 03
55. 1.1849299E 03	56. 1.1857669E 03	57. 1.2127559E 03	58. 1.2126390E 03	59. 1.1629276E 03	60. 1.1303272E 03
61. 1.1146724E 03	62. 1.1050158E 03	63. 1.1588738E 03	64. 1.1667836E 03	65. 1.2024228E 03	66. 1.2041541E 03
67. 1.1625215E 03	68. 1.1280120E 03	69. 1.1141088E 03	70. 1.1050314E 03	71. 1.1230080E 03	72. 1.1233525E 03
73. 1.1209323E 03	74. 1.1124499E 03	75. 1.1043562E 03	76. 1.0873188E 03	77. 1.0858072E 03	78. 1.1175932E 03
79. 1.1110728E 03	80. 1.1034779E 03	81. 1.0551364E 03	82. 1.0537560E 03	83. 1.0258155E 03	84. 1.0245209E 03
85. 1.0054487E 03	86. 1.0041852E 03	87. 9.9509299E 02	88. 9.9371971E 02	89. 1.1070000E 03	90. 1.0600000E 03
91. 8.7099999E 02	92. 8.7280047E 02	93. 8.6899999E 02	94. 8.7969958E 02	95. 8.6600000E 02	96. 8.7711291E 02
97. 8.6400000E 02	98. 8.7383481E 02	99. 8.6099999E 02	100. 8.7193322E 02	101. 8.5999999E 02	102. 8.7032722E 02
103. 8.5799999E 02	104. 8.6634888E 02	105. 8.5599999E 02	106. 8.6073503E 02	107. 8.5500000E 02	108. 8.5761781E 02
109. 8.5300000E 02	110. 8.5565917E 02				

ELEMENT(AT CENTER) TEMPERATURES (DEGREES F), ITERATIONS= 131

1. 1.2071726E 03	2. 1.2620373E 03	3. 1.2791568E 03	4. 1.2859512E 03	5. 1.2909592E 03	6. 1.2980433E 03
7. 1.0475390E 03	8. 1.1199171E 03	9. 1.1735314E 03	10. 1.2092899E 03	11. 1.2392973E 03	12. 1.2830393E 03
13. 9.8397093E 02	14. 1.0428129E 03	15. 1.0946141E 03	16. 1.1382373E 03	17. 1.1752374E 03	18. 1.2109470E 03
19. 1.0129158E 03	20. 1.0441371E 03	21. 1.0841971E 03	22. 1.1235345E 03	23. 1.1628938E 03	24. 9.1388655E 02
25. 9.6242095E 02	26. 1.0018606E 03	27. 1.0424498E 03	28. 1.0832400E 03	29. 1.1265452E 03	30. 9.0871111E 02
31. 9.3221766E 02	32. 9.6486228E 02	33. 1.0030300E 03	34. 1.0441905E 03	35. 1.0916644E 03	36. 8.9512587E 02
37. 9.2354479E 02	38. 9.5702671E 02	39. 9.9717945E 02	40. 1.0509228E 03	41. 8.6619644E 02	42. 8.8178763E 02
43. 9.0518625E 02	44. 9.3948340E 02	45. 1.0106195E 03	46. 8.1207172E 02	47. 8.1479235E 02	48. 8.1611814E 02
49. 8.0994133E 02	50. 8.1232901E 02	51. 8.1323395E 02	52. 1.2397008E 03	53. 1.2098909E 03	54. 1.2105354E 03
55. 1.1848719E 03	56. 1.1857191E 03	57. 1.2127252E 03	58. 1.2126175E 03	59. 1.1625043E 03	60. 1.1303005E 03
61. 1.1146448E 03	62. 1.1049883E 03	63. 1.1588108E 03	64. 1.1667315E 03	65. 1.2023893E 03	66. 1.2041306E 03
67. 1.1624979E 03	68. 1.1279854E 03	69. 1.1140814E 03	70. 1.1050041E 03	71. 1.1229402E 03	72. 1.1232921E 03
73. 1.1209056E 03	74. 1.1124227E 03	75. 1.1043292E 03	76. 1.0872511E 03	77. 1.0857446E 03	78. 1.1175565E 03
79. 1.1110459E 03	80. 1.1034512E 03	81. 1.0550741E 03	82. 1.0536952E 03	83. 1.0257570E 03	84. 1.0244533E 03
85. 1.0053927E 03	86. 1.0041295E 03	87. 9.9503828E 02	88. 9.9366528E 02	89. 1.1070000E 03	90. 1.0500000E 03
91. 8.7099999E 02	92. 8.7262275E 02	93. 8.6899999E 02	94. 8.7918385E 02	95. 8.6600000E 02	96. 8.7602273E 02
97. 8.6400000E 02	98. 8.7121484E 02	99. 8.6099999E 02	100. 8.6512252E 02	101. 8.5999999E 02	102. 8.5730202E 02
103. 8.5799999E 02	104. 8.6480223E 02	105. 8.5599999E 02	106. 8.5999316E 02	107. 8.5500000E 02	108. 8.5725842E 02
109. 8.5300000E 02	110. 8.5546871E 02				

ELEMENT FORCED CONVECTION, FREF CONVECT., RADIATION AND VAR.TEMP.CONVECT. CONDUCTANCES(H*A) BTU/HR.F

1	1	0.2309876E 02	0.	0.	0.1142512E 02
2	2	0.2301797E 02	0.	0.	0.
3	3	0.3442470E 02	0.	0.	0.
4	4	0.3408918E 02	0.	0.	0.
5	5	0.3374236E 02	0.	0.	0.
6	6	0.6024704E 02	0.	0.	0.
7	12	0.3214381E 02	0.	0.	0.2648646E 00
8	52	0.7309619E 02	0.	0.	0.
9	54	0.3023077E 02	0.	0.	0.
10	57	0.4908268E 02	0.	0.	0.
11	58	0.5272555E 02	0.	0.	0.
12	30	0.	0.1508969E 00	0.	0.9767791E 01
13	36	0.	0.8075071E 00	0.	0.
14	41	0.	0.8562257E 00	0.	0.
15	46	0.	0.1831766E 01	0.	0.
16	49	0.	0.2212572E 01	0.	0.
17	50	0.	0.3395263E 00	0.	0.
18	51	0.	0.8077877E 00	0.	0.
19	48	0.	0.4579416E 00	0.	0.
20	45	0.	0.4527078E 00	0.	0.

21	81	0.	0.1425612E 01	0.	0.
22	83	0.	0.1642215E 01	0.	0.
23	85	0.	0.1682875E 01	0.	0.
24	87	0.	0.1863566E 01	0.	0.
25	88	0.	0.2835336E 01	0.	0.
26	86	0.	0.2481122E 01	0.	0.
27	84	0.	0.2421175E 01	0.	0.
28	82	0.	0.2101830E 01	0.	0.
29	77	0.	0.1545289E 01	0.	0.
30	72	0.	0.1629288E 01	0.	0.
31	65	0.	0.3621526E 00	0.	0.
32	66	0.	0.3651705E 00	0.	0.
33	67	0.	0.4526907E 00	0.	0.
34	73	0.	0.5234740E 00	0.	0.
35	78	0.	0.9272007E 00	0.	0.
36	79	0.	0.4527218E 00	0.	0.
37	80	0.	0.1065631E 01	0.	0.
38	75	0.	0.7760924E 00	0.	0.
39	70	0.	0.8551035E 00	0.	0.
40	62	0.	0.9163529E 00	0.	0.
41	61	0.	0.1509035E 00	0.	0.
42	11	0.	0.	0.	0.1323278E 00
43	17	0.	0.	0.	0.1150274E 00
44	15	0.	0.	0.	0.1497932E 00
45	15	0.	0.	0.	0.8766205E-01
46	20	0.	0.	0.	0.8278172E-01
47	19	0.	0.	0.	0.8234002E-01
48	7	0.	0.	0.	0.1314272E 02
49	13	0.	0.	0.	0.1771311E 02
50	24	0.	0.	0.	0.2210943E 02
51	92	0.8359403E-01	0.	0.	0.
52	110	0.1684123E-02	0.	0.	0.9395632E 00
53	94	0.	0.	0.	0.1081050E 02
54	96	0.	0.	0.	0.1256669E 02
55	98	0.	0.	0.	0.1272810E 02
56	100	0.	0.	0.	0.6012575E 01
57	102	0.	0.	0.	0.9549869E 01
58	104	0.	0.	0.	0.9552101E 01
59	106	0.	0.	0.	0.8544354E 00
60	108	0.	0.	0.	0.7605613E 00
61	91	0.	0.	0.	0.
62	93	0.	0.	0.	0.
63	95	0.	0.	0.	0.
64	97	0.	0.	0.	0.
65	99	0.	0.	0.	0.
66	101	0.	0.	0.	0.
67	103	0.	0.	0.	0.
68	105	0.	0.	0.	0.
69	107	0.	0.	0.	0.
70	109	0.	0.	0.	0.
71	89	0.	0.	0.	0.
72	90	0.	0.	0.	0.

VAR.TEMP.CONVECTION BOUNDARY TEMPS.(F)

1	1, 1.0516E 03	2	12, 1.2976E 03	3	30, 8.9297E 02	4	11, 1.2933E 03	5	17, 1.2857E 03	6	16, 1.2734E 03
7	15, 1.2645E 03	8	20, 1.2541E 03	9	19, 1.2428E 03	10	7, 9.6841E 02	11	13, 9.3688E 02	12	24, 8.9985E 02
13	110, 9.1990E 02	14	94, 1.0620E 03	15	95, 9.7500E 02	16	98, 9.4500E 02	17	100, 7.5451E 02	18	102, 1.0050E 03
19	104, 9.5500E 02	20	106, 9.4192E 02	21	108, 9.3149E 02						

ELEMENT THERMAL CONDUCTIVITIES BTU/HR.FT.F

1, 3.3891022E 00	2, 3.2509139E 00	3, 3.2088574E 00	4, 3.1923199E 00	5, 3.1801741E 00	6, 3.1630672E 00
7, 3.8219351E 00	8, 3.6198994E 00	9, 3.4764545E 00	10, 3.3836611E 00	11, 3.3075424E 00	12, 3.1933524E 00
13, 4.0075200E 00	14, 3.8354569E 00	15, 3.5894391E 00	16, 3.5702831E 00	17, 3.4719671E 00	18, 3.3794140E 00
19, 3.9220373E 00	20, 3.8316448E 00	21, 3.7183625E 00	22, 3.6100353E 00	23, 3.5044902E 00	24, 4.2211350E 00
25, 4.0721750E 00	26, 3.9544748E 00	27, 3.8364705E 00	28, 3.7210288E 00	29, 3.6018636E 00	30, 4.2373451E 00
31, 4.1643429E 00	32, 4.0647814E 00	33, 3.9511351E 00	34, 3.8314753E 00	35, 3.6975774E 00	36, 4.2799824E 00
37, 4.1911136E 00	38, 4.0884663E 00	39, 3.9582653E 00	40, 3.8122348E 00	41, 4.3720887E 00	42, 4.3222151E 00
43, 4.2483087E 00	44, 4.1419617E 00	45, 3.9287386E 00	46, 7.3044968E 01	47, 7.3021833E 01	48, 7.3010582E 01
49, 7.3063127E 01	50, 7.3042787E 01	51, 7.3035095E 01	52, 6.9873211E 01	53, 7.0071213E 01	54, 7.0066240E 01
55, 7.0239279E 01	56, 7.0206575E 01	57, 7.0052282E 01	58, 7.0052993E 01	59, 7.0391088E 01	60, 7.0512513E 01
61, 7.0721455E 01	62, 7.0789098E 01	63, 7.0416341E 01	64, 7.0362301E 01	65, 7.0121414E 01	66, 7.0109738E 01
67, 7.0391131E 01	68, 7.0628570E 01	69, 7.0725393E 01	70, 7.0788989E 01	71, 7.0663680E 01	72, 7.0561235E 01
73, 7.0677786E 01	74, 7.0736992E 01	75, 7.0793731E 01	76, 7.0914325E 01	77, 7.0925013E 01	78, 7.0701363E 01
79, 7.0746629E 01	80, 7.0799901E 01	81, 7.1144552E 01	82, 7.1154514E 01	83, 7.1358092E 01	84, 7.1357505E 01
85, 7.1508669E 01	86, 7.1518073E 01	87, 7.1585967E 01	88, 7.1596256E 01	89, 7.5937494E 01	90, 7.2999994E 01
91, 7.2554519E 01	92, 7.2541301E 01	93, 7.2570832E 01	94, 7.2488013E 01	95, 7.2595346E 01	96, 7.2513555E 01
97, 7.2611717E 01	98, 7.2552767E 01	99, 7.2536321E 01	100, 7.2594343E 01	101, 7.2644534E 01	102, 7.2584701E 01
103, 7.2660978E 01	104, 7.2605148E 01	105, 7.2577646E 01	106, 7.2644590E 01	107, 7.2685690E 01	108, 7.2567381E 01
109, 7.2702194E 01	110, 7.2681825E 01				

ELEMENT ENMS CONDUCTION HEAT FLUXES	1	0.3500629E 03	-0.7173817E 03	0.	0.	BTU/HR
ELEMENT ENMS CONDUCTION HEAT FLUXES	2	0.8493505E 02	-0.5087063E 03	-0.3500629E 03	0.	BTU/HR
ELEMENT ENMS CONDUCTION HEAT FLUXES	3	0.2787327E 02	-0.6604753E 03	-0.8493505E 02	0.	BTU/HR
ELEMENT ENMS CONDUCTION HEAT FLUXES	4	0.2045288E 02	-0.4715087E 03	-0.2787327E 02	0.	BTU/HR
ELEMENT ENMS CONDUCTION HEAT FLUXES	5	0.2879872E 02	-0.3134156E 03	-0.2045288E 02	0.	BTU/HR
ELEMENT ENMS CONDUCTION HEAT FLUXES	6	0.	-0.8908973E 02	-0.2879872E 02	0.	BTU/HR
ELEMENT ENMS CONDUCTION HEAT FLUXES	7	0.6164732E 03	-0.2938891E 03	0.	0.7173817E 03	BTU/HR
ELEMENT ENMS CONDUCTION HEAT FLUXES	8	0.3610744E 03	-0.3393345E 03	-0.6164732E 03	0.6087063E 03	BTU/HR
ELEMENT ENMS CONDUCTION HEAT FLUXES	9	0.1872781E 03	-0.5007160E 03	-0.3470744E 03	0.6604753E 03	BTU/HR
ELEMENT ENMS CONDUCTION HEAT FLUXES	10	0.1532962E 03	-0.4375617E 03	-0.1872781E 03	0.4715087E 03	BTU/HR
ELEMENT ENMS CONDUCTION HEAT FLUXES	11	0.2173733E 03	-0.3846594E 03	-0.1532962E 03	0.3134156E 03	BTU/HR
ELEMENT ENMS CONDUCTION HEAT FLUXES	12	0.	-0.4201151E 03	-0.2173733E 03	0.8908973E 02	BTU/HR
ELEMENT ENMS CONDUCTION HEAT FLUXES	13	0.5401655E 03	0.	0.	0.2938891E 03	BTU/HR
ELEMENT ENMS CONDUCTION HEAT FLUXES	14	0.3636212E 03	-0.1628458E 03	-0.5401655E 03	0.3393345E 03	BTU/HR
ELEMENT ENMS CONDUCTION HEAT FLUXES	15	0.2471701E 03	-0.3992199E 03	-0.3636212E 03	0.5007160E 03	BTU/HR
ELEMENT ENMS CONDUCTION HEAT FLUXES	16	0.2033787E 03	-0.4140727E 03	-0.2471701E 03	0.4375617E 03	BTU/HR
ELEMENT ENMS CONDUCTION HEAT FLUXES	17	0.1909676E 03	-0.3849976E 03	-0.2033787E 03	0.3846594E 03	BTU/HR
ELEMENT ENMS CONDUCTION HEAT FLUXES	18	0.1187314E 03	-0.3479073E 03	-0.1909676E 03	0.4201151E 03	BTU/HR
ELEMENT ENMS CONDUCTION HEAT FLUXES	19	0.1545259E 03	-0.3466769E 03	0.	0.1628458E 03	BTU/HR
ELEMENT ENMS CONDUCTION HEAT FLUXES	20	0.1717864E 03	-0.4238508E 03	-0.1646259E 03	0.3992199E 03	BTU/HR
ELEMENT ENMS CONDUCTION HEAT FLUXES	21	0.1637377E 03	-0.4061137E 03	-0.1717864E 03	0.4140727E 03	BTU/HR
ELEMENT ENMS CONDUCTION HEAT FLUXES	22	0.1590473E 03	-0.3803781E 03	-0.1637377E 03	0.3869976E 03	BTU/HR
ELEMENT ENMS CONDUCTION HEAT FLUXES	23	0.1437275E 03	-0.3326274E 03	-0.1590473E 03	0.3479073E 03	BTU/HR
ELEMENT ENMS CONDUCTION HEAT FLUXES	24	0.3481610E 03	-0.3816319E 02	0.	0.	BTU/HR
ELEMENT ENMS CONDUCTION HEAT FLUXES	25	0.2184400E 03	-0.2168363E 03	-0.3481610E 03	0.3466769E 03	BTU/HR
ELEMENT ENMS CONDUCTION HEAT FLUXES	26	0.1823687E 03	-0.3878909E 03	-0.2184400E 03	0.4238508E 03	BTU/HR
ELEMENT ENMS CONDUCTION HEAT FLUXES	27	0.1777793E 03	-0.4016309E 03	-0.1823687E 03	0.4061137E 03	BTU/HR
ELEMENT ENMS CONDUCTION HEAT FLUXES	28	0.1828759E 03	-0.3855568E 03	-0.1777793E 03	0.3803781E 03	BTU/HR
ELEMENT ENMS CONDUCTION HEAT FLUXES	29	0.1833797E 03	-0.3328724E 03	-0.1828759E 03	0.3326274E 03	BTU/HR
ELEMENT ENMS CONDUCTION HEAT FLUXES	30	0.1734538E 03	0.	0.	0.3816319E 02	BTU/HR
ELEMENT ENMS CONDUCTION HEAT FLUXES	31	0.1882795E 03	-0.2317683E 03	-0.1734538E 03	0.2168363E 03	BTU/HR
ELEMENT ENMS CONDUCTION HEAT FLUXES	32	0.1789737E 03	-0.3787090E 03	-0.1882795E 03	0.3878909E 03	BTU/HR
ELEMENT ENMS CONDUCTION HEAT FLUXES	33	0.1875667E 03	-0.4104379E 03	-0.1789737E 03	0.4016309E 03	BTU/HR
ELEMENT ENMS CONDUCTION HEAT FLUXES	34	0.2092321E 03	-0.4072054E 03	-0.1876667E 03	0.3855568E 03	BTU/HR
ELEMENT ENMS CONDUCTION HEAT FLUXES	35	0.2169110E 03	-0.3396829E 03	-0.2092321E 03	0.3328724E 03	BTU/HR
ELEMENT ENMS CONDUCTION HEAT FLUXES	36	0.2405199E 03	-0.1736076E 03	0.	0.2317683E 03	BTU/HR
ELEMENT ENMS CONDUCTION HEAT FLUXES	37	0.2312853E 03	-0.3696520E 03	-0.2405199E 03	0.3787090E 03	BTU/HR
ELEMENT ENMS CONDUCTION HEAT FLUXES	38	0.2698817E 03	-0.4491997E 03	-0.2312853E 03	0.4104379E 03	BTU/HR
ELEMENT ENMS CONDUCTION HEAT FLUXES	39	0.3487814E 03	-0.4862198E 03	-0.2698817E 03	0.4072054E 03	BTU/HR
ELEMENT ENMS CONDUCTION HEAT FLUXES	40	0.3335038E 03	-0.3244261E 03	-0.3487814E 03	0.3396829E 03	BTU/HR
ELEMENT ENMS CONDUCTION HEAT FLUXES	41	0.1184190E 03	0.	0.	0.1736076E 03	BTU/HR
ELEMENT ENMS CONDUCTION HEAT FLUXES	42	0.1461514E 03	-0.3975692E 03	-0.1184190E 03	0.3696520E 03	BTU/HR
ELEMENT ENMS CONDUCTION HEAT FLUXES	43	0.2097017E 03	-0.5129126E 03	-0.1461514E 03	0.4491997E 03	BTU/HR
ELEMENT ENMS CONDUCTION HEAT FLUXES	44	0.4181535E 03	-0.6947881E 03	-0.2097017E 03	0.4862198E 03	BTU/HR
ELEMENT ENMS CONDUCTION HEAT FLUXES	45	0.3136507E 03	0.	-0.4181535E 03	0.3244261E 03	BTU/HR
ELEMENT ENMS CONDUCTION HEAT FLUXES	46	0.3939557E 03	-0.2742551E 03	0.	0.3975692E 03	BTU/HR
ELEMENT ENMS CONDUCTION HEAT FLUXES	47	0.1919342E 03	-0.3170224E 03	-0.3939557E 03	0.5129126E 03	BTU/HR
ELEMENT ENMS CONDUCTION HEAT FLUXES	48	0.	-0.3711374E 03	-0.1919342E 03	0.6947881E 03	BTU/HR
ELEMENT ENMS CONDUCTION HEAT FLUXES	49	0.3536301E 03	0.	0.	0.2742551E 03	BTU/HR
ELEMENT ENMS CONDUCTION HEAT FLUXES	50	0.1340007E 03	0.	-0.3536301E 03	0.3170224E 03	BTU/HR
ELEMENT ENMS CONDUCTION HEAT FLUXES	51	0.	0.	-0.1340007E 03	0.3711374E 03	BTU/HR
ELEMENT ENMS CONDUCTION HEAT FLUXES	52	0.	-0.4289205E 04	-0.1107314E 03	0.	BTU/HR
ELEMENT ENMS CONDUCTION HEAT FLUXES	53	0.7408617E 02	-0.4220089E 04	-0.1437275E 03	0.4289205E 04	BTU/HR
ELEMENT ENMS CONDUCTION HEAT FLUXES	54	0.	-0.2627680E 04	-0.7408617E 02	0.	BTU/HR
ELEMENT ENMS CONDUCTION HEAT FLUXES	55	0.4363274E 03	-0.4473862E 04	-0.1830797E 03	0.4220089E 04	BTU/HR
ELEMENT ENMS CONDUCTION HEAT FLUXES	56	0.1470416E 04	-0.3662107E 04	-0.4363274E 03	0.2627680E 04	BTU/HR
ELEMENT ENMS CONDUCTION HEAT FLUXES	57	-0.4984610E 01	-0.2809042E 04	-0.1470416E 04	0.	BTU/HR
ELEMENT ENMS CONDUCTION HEAT FLUXES	58	-0.2076528E 04	-0.2536940E 04	0.4984610E 01	0.	BTU/HR
ELEMENT ENMS CONDUCTION HEAT FLUXES	59	-0.1398827E 04	-0.2196907E 01	0.2076528E 04	-0.6777360E 03	BTU/HR
ELEMENT ENMS CONDUCTION HEAT FLUXES	60	-0.7669700E 03	-0.6339728E 03	0.1398827E 04	-0.4648849E 00	BTU/HR
ELEMENT ENMS CONDUCTION HEAT FLUXES	61	-0.5262595E 03	-0.1545058E 03	0.7669700E 03	0.	BTU/HR
ELEMENT ENMS CONDUCTION HEAT FLUXES	62	0.	0.3467910E 01	0.5262595E 03	0.	BTU/HR
ELEMENT ENMS CONDUCTION HEAT FLUXES	63	0.7254982E 03	-0.4933809E 04	-0.2160110E 03	0.4473862E 04	BTU/HR
ELEMENT ENMS CONDUCTION HEAT FLUXES	64	0.2665624E 04	-0.5602479E 04	-0.7254982E 03	0.3662107E 04	BTU/HR
ELEMENT ENMS CONDUCTION HEAT FLUXES	65	0.1021304E 03	0.	-0.2665624E 04	0.2809042E 04	BTU/HR
ELEMENT ENMS CONDUCTION HEAT FLUXES	66	-0.2186558E 04	0.	-0.1021304E 03	0.2536940E 04	BTU/HR
ELEMENT ENMS CONDUCTION HEAT FLUXES	67	-0.1899557E 04	0.	0.2186558E 04	0.2196907E 01	BTU/HR
ELEMENT ENMS CONDUCTION HEAT FLUXES	68	-0.8631382E 03	-0.1671667E 04	0.1899557E 04	0.6339728E 03	BTU/HR
ELEMENT ENMS CONDUCTION HEAT FLUXES	69	-0.5267930E 03	-0.3920681E 03	0.8631382E 03	0.1545058E 03	BTU/HR
ELEMENT ENMS CONDUCTION HEAT FLUXES	70	0.	-0.1277191E 03	0.5267930E 03	-0.3467910E 01	BTU/HR
ELEMENT ENMS CONDUCTION HEAT FLUXES	71	0.4245203E 02	-0.4693337E 04	-0.3335038E 03	0.4983009E 04	BTU/HR
ELEMENT ENMS CONDUCTION HEAT FLUXES	72	0.	-0.4585237E 04	-0.4246203E 02	0.5602479E 04	BTU/HR
ELEMENT ENMS CONDUCTION HEAT FLUXES	73	-0.4731506E 03	-0.3833292E 03	0.	0.1671667E 04	BTU/HR
ELEMENT ENMS CONDUCTION HEAT FLUXES	74	-0.5072814E 03	-0.3645066E 03	0.4781506E 03	0.3920681E 03	BTU/HR
ELEMENT ENMS CONDUCTION HEAT FLUXES	75	0.	-0.1860999E 03	0.5072814E 03	0.1277191E 03	BTU/HR
ELEMENT ENMS CONDUCTION HEAT FLUXES	76	-0.1730384E 03	-0.4207191E 04	-0.3136507E 03	0.4693337E 04	BTU/HR
ELEMENT ENMS CONDUCTION HEAT FLUXES	77	0.	-0.3891766E 04	0.1730384E 03	0.4585237E 04	BTU/HR
ELEMENT ENMS CONDUCTION HEAT FLUXES	78	-0.3332247E 03	0.	0.	0.3833292E 03	BTU/HR
ELEMENT ENMS CONDUCTION HEAT FLUXES	79	-0.4315122E 03	0.	0.3332247E 03	0.3645066E 03	BTU/HR
ELEMENT ENMS CONDUCTION HEAT FLUXES	80	0.	0.	0.4315122E 03	0.1860999E 03	BTU/HR
ELEMENT ENMS CONDUCTION HEAT FLUXES	81	-0.2161438E 03	-0.3235988E 04	0.	0.4207191E 04	BTU/HR
ELEMENT ENMS CONDUCTION HEAT FLUXES	82	0.	-0.2996551E 04	0.2161438E 03	0.3891766E 04	BTU/HR
ELEMENT ENMS CONDUCTION HEAT FLUXES	83	-0.2343526E 03	-0.2179990E 04	0.	0.3235988E 04	BTU/HR
ELEMENT ENMS CONDUCTION HEAT FLUXES	84	0.	-0.2021472E 04	0.2343526E 03	0.2996551E 04	BTU/HR
ELEMENT ENMS CONDUCTION HEAT FLUXES	85	-0.2349137E 03	-0.1137354E 04	0.	0.2179990E 04	BTU/HR
ELEMENT ENMS CONDUCTION HEAT FLUXES	86	0.	-0.1067466E 04	0.2349137E 03	0.2021472E 04	BTU/HR
ELEMENT ENMS CONDUCTION HEAT FLUXES	87	-0.2617961E 03	0.	0.	0.1137354E 04	BTU/HR
ELEMENT ENMS CONDUCTION HEAT FLUXES	88	0.	0.	0.2617961E 03	0.1067466E 04	BTU/HR
ELEMENT ENMS CONDUCTION HEAT FLUXES	89	-0.5287456E 04	0.6777360E 03	0.	0.	BTU/HR
ELEMENT ENMS CONDUCTION HEAT FLUXES	90	0.	0.4648849E 00	0.5287456E 04	0.	BTU/HR
ELEMENT ENMS CONDUCTION HEAT FLUXES	91	0.2969990E 03	-0.1927497E 03	0.	0.	BTU/HR
ELEMENT ENMS CONDUCTION HEAT FLUXES	92	0.	0.5320201E 03	-0.2969990E 03	0.	BTU/HR
ELEMENT ENMS CONDUCTION HEAT FLUXES	93	0.8875800E 03	-0.4339453E 03	0.	0.1927497E 03	BTU/HR
ELEMENT ENMS CONDUCTION HEAT FLUXES	94	0.	-0.4567316E 03	-0.8875800E 03	-0.6320201E 03	BTU/HR
ELEMENT ENMS CONDUCTION HEAT FLUXES	95	0.1041136E 04	-0.2746592E 03	0.	0.4339453E 03	BTU/HR
ELEMENT ENMS CONDUCTION HEAT FLUXES	96	0.	-0.5594095E 03	-0.1041136E 04	0.4567316E 03	BTU/HR
ELEMENT ENMS CONDUCTION HEAT FLUXES	97	0.7665407E 03	-0.4905089E 03	0.	0.2746592E 03	BTU/HR
ELEMENT ENMS CONDUCTION HEAT FLUXES	98	0.	-0.8320146E 03	-0.7665407E 03	0.6594095E 03	BTU/HR
ELEMENT ENMS CONDUCTION HEAT FLUXES	99	0.3952253E 03	-0.1996018E 03	0.	0.4905089E 03	BTU/HR

ELEMENT ENWS CONDUCTION HEAT FLUXES 100	0.	0.2352648E 03	-0.3962253E 03	0.8320146E 03	BTU/HR
ELEMENT ENWS CONDUCTION HEAT FLUXES 101	0.5734788E 03	-0.4053579E 03	0.	0.1996018E 03	BTU/HR
ELEMENT ENWS CONDUCTION HEAT FLUXES 102	0.	-0.5062507E 03	-0.5734788E 03	-0.2352648E 03	BTU/HR
ELEMENT ENWS CONDUCTION HEAT FLUXES 103	0.5424470E 03	-0.3434600E 03	0.	0.4053579E 03	BTU/HR
ELEMENT ENWS CONDUCTION HEAT FLUXES 104	0.	-0.8253795E 03	-0.5424470E 03	0.5062507E 03	BTU/HR
ELEMENT ENWS CONDUCTION HEAT FLUXES 105	0.4539583E 03	-0.1614701E 03	0.	0.3434600E 03	BTU/HR
ELEMENT ENWS CONDUCTION HEAT FLUXES 106	0.	-0.4414204E 03	-0.4539583E 03	0.8253795E 03	BTU/HR
ELEMENT ENWS CONDUCTION HEAT FLUXES 107	0.2243036E 03	-0.3058020E 03	0.	0.1614701E 03	BTU/HR
ELEMENT ENWS CONDUCTION HEAT FLUXES 108	0.	-0.2735725E 03	-0.2243036E 03	0.4414204E 03	BTU/HR
ELEMENT ENWS CONDUCTION HEAT FLUXES 109	0.3335688E 03	0.	0.	0.3058020E 03	BTU/HR
ELEMENT ENWS CONDUCTION HEAT FLUXES 110	0.	0.	-0.3335688E 03	0.2735725E 03	BTU/HR

ELEMENT ENWS CONDUCTANCES TO NABORS(BTU/HR.F)

1	0.6380464E 01	0.4493929E 01	0.	0.
2	0.4961302E 01	0.4283041E 01	0.6380464E 01	0.
3	0.4102397E 01	0.6252999E 01	0.4961302E 01	0.
4	0.4084020E 01	0.6150550E 01	0.4102397E 01	0.
5	0.4066258E 01	0.6066671E 01	0.4084020E 01	0.
6	0.	0.5945660E 01	0.4066258E 01	0.
7	0.8517389E 01	0.4623222E 01	0.	0.4493929E 01
8	0.6473546E 01	0.4400986E 01	0.8517389E 01	0.4283041E 01
9	0.5237299E 01	0.6344815E 01	0.6473546E 01	0.6252999E 01
10	0.5108618E 01	0.6158279E 01	0.5237299E 01	0.6150550E 01
11	0.4967171E 01	0.6004682E 01	0.5108618E 01	0.6066671E 01
12	0.	0.5825843E 01	0.4967171E 01	0.5945660E 01
13	0.9179930E 01	0.	0.	0.4623222E 01
14	0.7019563E 01	0.5446862E 01	0.9179930E 01	0.4400986E 01
15	0.5666012E 01	0.7908951E 01	0.7019563E 01	0.6344815E 01
16	0.5496713E 01	0.7662297E 01	0.5666012E 01	0.6158279E 01
17	0.5347800E 01	0.7446346E 01	0.5496713E 01	0.6004682E 01
18	0.4129233E 01	0.7240057E 01	0.5347800E 01	0.5825843E 01
19	0.5272871E 01	0.6861634E 01	0.	0.5446862E 01
20	0.4288229E 01	0.1002559E 02	0.5272871E 01	0.7908951E 01
21	0.4162387E 01	0.9727925E 01	0.4288229E 01	0.7662297E 01
22	0.4040905E 01	0.9439952E 01	0.4162387E 01	0.7446346E 01
23	0.3058222E 01	0.9151030E 01	0.4040905E 01	0.7240057E 01
24	0.7173489E 01	0.7373895E 01	0.	0.
25	0.5538589E 01	0.7179228E 01	0.7173489E 01	0.6861634E 01
26	0.4493030E 01	0.1048401E 02	0.5538589E 01	0.1002559E 02
27	0.4358385E 01	0.1018080E 02	0.4493030E 01	0.9727925E 01
28	0.4222955E 01	0.9873525E 01	0.4358385E 01	0.9439952E 01
29	0.3138867E 01	0.9543145E 01	0.4222955E 01	0.9151030E 01
30	0.7378956E 01	0.	0.	0.7373895E 01
31	0.5767553E 01	0.6248674E 01	0.7378956E 01	0.7179228E 01
32	0.4692822E 01	0.9165828E 01	0.5767553E 01	0.1048401E 02
33	0.4556075E 01	0.8927738E 01	0.4692822E 01	0.1018080E 02
34	0.4407302E 01	0.8661914E 01	0.4556075E 01	0.9873525E 01
35	0.3217019E 01	0.8337477E 01	0.4407302E 01	0.9543145E 01
36	0.8463673E 01	0.6000853E 01	0.	0.6248674E 01
37	0.6907766E 01	0.8852423E 01	0.8463673E 01	0.9165828E 01
38	0.6721378E 01	0.8665041E 01	0.6907766E 01	0.8927738E 01
39	0.6489764E 01	0.8427264E 01	0.6721378E 01	0.8661914E 01
40	0.6630875E 01	0.8049619E 01	0.6489764E 01	0.8337477E 01
41	0.7595242E 01	0.	0.	0.6000853E 01
42	0.6246157E 01	0.5702704E 01	0.7595242E 01	0.8852423E 01
43	0.6114262E 01	0.5674195E 01	0.6246157E 01	0.8665041E 01
44	0.5878220E 01	0.5631959E 01	0.6114262E 01	0.8427264E 01
45	0.4092969E 01	0.	0.5878220E 01	0.8049619E 01
46	0.1448029E 03	0.1287345E 03	0.	0.5702704E 01
47	0.1447688E 03	0.1286951E 03	0.1448029E 03	0.5674195E 01
48	0.	0.1286794E 03	0.1447688E 03	0.5631959E 01
49	0.1481057E 03	0.	0.	0.1287345E 03
50	0.1480773E 03	0.	0.1481057E 03	0.1286961E 03
51	0.	0.	0.1480773E 03	0.1286794E 03
52	0.	0.1438851E 03	0.4129233E 01	0.
53	0.9951651E 02	0.1686754E 03	0.3058222E 01	0.1438851E 03
54	0.	0.1256288E 03	0.9951651E 02	0.
55	0.9001584E 02	0.1716679E 03	0.3138867E 01	0.1686754E 03
56	0.6391423E 02	0.1593078E 03	0.9001584E 02	0.1256288E 03
57	0.4625108E 02	0.2717758E 03	0.6391423E 02	0.
58	0.4143682E 02	0.2989272E 03	0.4625108E 02	0.
59	0.4343676E 02	0.3411765E 03	0.4143682E 02	0.1221050E 02
60	0.4898949E 02	0.2738342E 03	0.4343676E 02	0.6612817E-02
61	0.5449790E 02	0.2742306E 03	0.4898949E 02	0.
62	0.	0.2195874E 03	0.5449790E 02	0.
63	0.9159468E 02	0.1389386E 03	0.3217019E 01	0.1716679E 03
64	0.7475564E 02	0.1289722E 03	0.9159468E 02	0.1593078E 03
65	0.5865224E 02	0.	0.7475564E 02	0.2717758E 03
66	0.5252016E 02	0.	0.5865224E 02	0.2989272E 03
67	0.5503968E 02	0.	0.5252016E 02	0.3411766E 03
68	0.6207817E 02	0.2361166E 03	0.5503968E 02	0.2738342E 03
69	0.6905060E 02	0.2363741E 03	0.6207817E 02	0.2742306E 03
70	0.	0.1892597E 03	0.6905060E 02	0.2195874E 03
71	0.1206709E 03	0.1315060E 03	0.4630875E 01	0.1389386E 03
72	0.	0.1221184E 03	0.1206709E 03	0.1289722E 03
73	0.5636644E 02	0.2645487E 03	0.	0.2361166E 03
74	0.6267794E 02	0.2647491E 03	0.5636644E 02	0.2363741E 03
75	0.	0.2119648E 03	0.6267794E 02	0.1892597E 03
76	0.1148658E 03	0.1307518E 03	0.4392969E 01	0.1315060E 03
77	0.	0.1214300E 03	0.1148658E 03	0.1221184E 03
78	0.5110266E 02	0.	0.	0.2645487E 03
79	0.5681803E 02	0.	0.5110266E 02	0.2647491E 03
80	0.	0.	0.5681803E 02	0.2119648E 03

81	0.1567415E 03	0.1103788E 03	0.	0.1307518E 03
82	0.	0.1025086E 03	0.1567415E 03	0.1214300E 03
83	0.1810977E 03	0.1070493E 03	0.	0.1103788E 03
84	0.	0.9941604E 02	0.1810977E 03	0.1025086E 03
85	0.1859730E 03	0.1098429E 03	0.	0.1070493E 03
86	0.	0.1020110E 03	0.1859730E 03	0.9941604E 02
87	0.1906733E 03	0.	0.	0.1098429E 03
88	0.	0.	0.1906733E 03	0.1020110E 03
89	0.1124991E 03	0.122105JE 02	0.	0.
90	0.	0.6512817E-02	0.1124991E 03	0.
91	0.1830213E 03	0.9637487E 02	0.	0.
92	0.	0.9532843E 02	0.1830213E 03	0.
93	0.8715561E 02	0.1446484E 03	0.	0.9637487E 02
94	0.	0.1444846E 03	0.8715561E 02	0.9532843E 02
95	0.1038774E 03	0.1372846E 03	0.	0.1446484E 03
96	0.	0.1371515E 03	0.1038774E 03	0.1446846E 03
97	0.1062448E 03	0.1635030E 03	0.	0.1372846E 03
98	0.	0.1633861E 03	0.1062448E 03	0.1371515E 03
99	0.7734957E 02	0.1996018E 03	0.	0.1635030E 03
100	0.	0.1994623E 03	0.7734957E 02	0.1633861E 03
101	0.7853696E 02	0.2026789E 03	0.	0.1996018E 03
102	0.	0.2025175E 03	0.7853696E 02	0.1994620E 03
103	0.7974536E 02	0.1717300E 03	0.	0.2026789E 03
104	0.	0.1716296E 03	0.7974536E 02	0.2025176E 03
105	0.1136839E 03	0.1614701E 03	0.	0.1717300E 03
106	0.	0.1614117E 03	0.1136839E 03	0.1716296E 03
107	0.9931902E 02	0.1529010E 03	0.	0.1614701E 03
108	0.	0.1528598E 03	0.9931902E 02	0.1614117E 03
109	0.1351181E 03	0.	0.	0.1529010E 03
110	0.	0.	0.1351181E 03	0.1528598E 03

ELEMENT BOUNDARY NO. CONDUCTION NO. BNDRY CONDUCTANCE(H*A) SUM(BTU/HR.F) AND BNDRY HEAT FLUX SUM(BTU/HR)

1	1	0.3452368E 02	0.3673041E 03	2	2	0.2301797E 02	0.8738152E 03	3	3	0.3442470E 02	0.7174999E 03
4	4	0.3403918E 02	0.4788905E 03	5	5	0.3374236E 02	0.3050405E 03	6	6	0.6024704E 02	0.1173793E 03
7	12	0.3240867E 02	0.5083548E 03	8	52	0.7309619E 02	0.4407473E 04	9	54	0.3023077E 02	0.2701465E 04
10	57	0.4908268E 02	0.4783502E 04	11	58	0.5272555E 02	0.4607039E 04	12	30	0.9918687E 01	-0.2117325E 03
13	36	0.8075071E 00	-0.2988954E 03	14	41	0.8562257E 00	-0.2921620E 03	15	46	0.1831765E 01	-0.5259372E 03
16	49	0.2212572E 01	-0.6305592E 03	17	50	0.3395263E 00	-0.9757187E 02	18	51	0.8077877E 00	-0.2328694E 03
19	48	0.4579416E 00	-0.1333307E 03	20	45	0.4527078E 00	-0.2198511E 03	21	81	0.1425612E 01	-0.7556872E 03
22	83	0.1042215E 01	-0.8223586E 03	23	85	0.1682875E 01	-0.8084487E 03	24	87	0.1863565E 01	-0.8759558E 03
25	88	0.2835336E 01	-0.1328835E 04	26	86	0.2481122E 01	-0.1188790E 04	27	84	0.2421175E 01	-0.1209293E 04
28	82	0.2101830E 01	-0.1111237E 04	29	77	0.1545289E 01	-0.8665199E 03	30	72	0.1629288E 01	-0.9747977E 03
31	65	0.3621520E 00	-0.2453197E 03	32	66	0.3651705E 00	-0.2480004E 03	33	67	0.4526907E 00	-0.2385933E 03
34	73	0.5234740E 00	-0.3119478E 03	35	78	0.9272007E 00	-0.5494400E 03	36	79	0.4527218E 00	-0.2553218E 03
37	80	0.1069631E 01	-0.6164296E 03	38	75	0.7760924E 00	-0.4496235E 03	39	70	0.8551035E 00	-0.4959753E 03
40	62	0.9163529E 00	-0.5314868E 03	41	61	0.1509035E 00	-0.8898155E 02	42	11	0.1323278E 00	0.7143526E 01
43	17	0.1150274E 00	0.1270090E 02	44	16	0.1497932E 00	0.2023887E 02	45	15	0.8755205E-01	0.1488822E 02
46	20	0.8278172E-01	0.1737837E 02	47	19	0.8234032E-01	0.1892660E 02	48	7	0.1314272E 02	-0.1340006E 04
49	13	0.1771311E 02	-0.8361237E 03	50	24	0.2210943E 02	-0.3101982E 03	51	92	0.8359403E-01	-0.3353232E 03
52	110	0.9412473E 00	0.5999754E 02	53	94	0.1081050E 02	0.1976333E 04	54	96	0.1255659E 02	0.1243815E 04
55	98	0.1272810E 02	0.9391448E 03	56	100	0.6012575E 01	-0.6710515E 03	57	102	0.9549849E 01	0.1314995E 04
58	104	0.9552101E 01	0.8615781E 03	59	106	0.8544354E 00	0.6999946E 02	60	108	0.7605613E 00	0.5645594E 02
61	91	0.	0.	62	93	0.	0.	63	95	0.	0.
64	97	0.	0.	65	99	0.	0.	66	101	0.	0.
67	103	0.	0.	68	105	0.	0.	69	107	0.	0.
70	109	0.	0.	71	89	0.	0.	72	90	0.	0.

ELEMENT FREE THERMAL EXPANSION,ALPHA*(T-TO)

1,	3.9943291E-03	2,	3.8658456E-03	3,	3.9524164E-03	4,	3.9870181E-03	5,	4.0126103E-03	6,	4.0483390E-03
7,	2.8556995E-03	8,	3.1911310E-03	9,	3.4823287E-03	10,	3.6046590E-03	11,	3.7522281E-03	12,	3.9722755E-03
13,	2.5828532E-03	14,	2.8350141E-03	15,	3.0655976E-03	16,	3.2660188E-03	17,	3.4404786E-03	18,	3.6127419E-03
19,	2.7056181E-03	20,	2.8408324E-03	21,	3.0186332E-03	22,	3.1978439E-03	23,	3.3818226E-03	24,	2.2963979E-03
25,	2.4931405E-03	26,	2.658463oE-03	27,	2.8334589E-03	28,	3.0143082E-03	29,	3.2117509E-03	30,	2.2755398E-03
31,	2.3697116E-03	32,	2.5032663E-03	33,	2.6533292E-03	34,	2.8410915E-03	35,	3.0522736E-03	36,	2.2218305E-03
37,	2.3348097E-03	38,	2.4709482E-03	39,	2.5386291E-03	40,	2.8706202E-03	41,	2.1094527E-03	42,	2.1597587E-03
43,	2.2616254E-03	44,	2.3992145E-03	45,	2.6958183E-03	46,	3.7161562E-03	47,	3.7349236E-03	48,	3.7443777E-03
49,	3.7014799E-03	50,	3.7179224E-03	51,	3.7241565E-03	52,	7.1276395E-03	53,	6.8596904E-03	54,	6.8563255E-03
55,	6.6382a7dE-03	56,	6.6809345E-03	57,	6.9849771E-03	58,	6.8840256E-03	59,	6.4430768E-03	60,	6.1566581E-03
61,	6.0338784E-03	62,	5.9527183E-03	63,	5.4110420E-03	64,	6.4797431E-03	65,	6.7929769E-03	66,	5.3084495E-03
67,	6.4430209E-03	68,	6.1467721E-03	69,	6.0291285E-03	70,	5.9528487E-03	71,	6.1039015E-03	72,	5.1053804E-03
73,	6.0867442E-03	74,	6.0151572E-03	75,	5.9471924E-03	76,	5.8047992E-03	77,	5.7923142E-03	78,	5.0585200E-03
79,	6.0035700E-03	80,	5.9398372E-03	81,	5.5406761E-03	82,	5.5294732E-03	83,	5.3046070E-03	84,	5.2942355E-03
85,	5.1431972E-03	86,	5.1332539E-03	87,	5.0519350E-03	88,	5.0511997E-03	89,	8.7216585E-03	90,	8.2503362E-03
91,	4.1307d89E-03	92,	4.1424658E-03	93,	4.1164160E-03	94,	4.1898140E-03	95,	4.0948945E-03	96,	4.1569745E-03
97,	4.0809723E-03	98,	4.1323342E-03	99,	4.3591272E-03	100,	4.0957727E-03	101,	4.0519889E-03	102,	4.1042293E-03
103,	4.0377277E-03	104,	4.0863148E-03	105,	4.3234867E-03	106,	4.0519401E-03	107,	4.0163739E-03	108,	4.0324449E-03
109,	4.0021635E-03	110,	4.0197072E-03								

01 EXIT IN SEAL2

APPENDIX D

HEAT TRANSFER COEFFICIENT EQUATIONS

The equations used to calculate boundary heat transfer coefficients are mostly obtained from books by McAdams (ref. 9) and by Kreith (ref. 10).

Radiation

The radiation equation is based on information from chapter 4 of Kreith and chapter 5 of McAdams. The basic expression is in terms of the heat flux but can also be expressed as

$$h = \frac{Q}{A\ \Delta T}$$

The number of properties required is reduced by substitution of others as explained in the references.

Liquid Film Cooling

The gravity-flow liquid film cooling equation can be found in chapter 9 of McAdams. Strictly, it applies only to flow over horizontal cylinders. However, in the program, it is also used for flow down vertical surfaces.

Other Free Convection Coefficients

The two other free convection subtype expressions are obtained from a study of chapter 7 of McAdams and of chapter 7 of Kreith. They are actually for nonenclosed spaces, but are considered acceptable for two reasons. First, the boundaries at which free convection occurs are far enough from the parts of interest (seal plate and nosepiece) that they have little influence. Second, the knowledge of coefficients in enclosed spaces appears to be limited and to be expressed in terms of overall coefficients.

Comparison of the two conditions (table I) shows the equations for turbulent flow are identical and those for laminar flow differ only in the constant used. Transition from laminar to turbulent flow is considered to occur at $GrPr = 10^9$ (ref. 9).

Card #28

Use of Local Coefficients

The expression for free convection at vertical surfaces is for a local coefficient instead of an average as is the case for the other cases already mentioned.

The program deals with small sections of boundary surfaces. There are few, if any, places where a fully established velocity profile (e.g., in duct flow) or boundary film (e.g., in flat plate flow) exists in seal applications. In the problem of appendix C, as an example, the use of a local coefficient is generally preferable.

While free convection around a horizontal cylinder should properly be considered a circumferential flow, the assumption of an axisymmetric temperature distribution implies a uniform coefficient around the circumference as well as along the cylinder.

The conversion of average coefficients to local coefficients is based on text and equations in chapter 6 of Kreith.

Flat Plate

These coefficients and the critical Reynolds number for laminar turbulent transition are obtained directly from chapter 6 of Kreith's book.

Duct Flow, Liquid

For the most accurate result, the equation used for duct flow depends on the shape of the cross section and on the viscosity of the fluid. However, McAdams and also Jakob (ref. 11) indicate that the use of pipe flow equations with an equivalent (hydraulic) diameter is acceptable.

In the example of appendix C, the only fluid flowing in a duct is a synthetic oil with a viscosity in the range covered by McAdams recommended equation for turbulent flow. The laminar flow expression as well as that for turbulent flow are taken from chapter 9 of McAdams.

McAdams' data indicate that transition from laminar to turbulent flow can be considered as occurring over the Reynolds number range between 2500 and 7500. Kreith and also Jakob agree with the overall trend during transition. The equation presented in table I seems to be an acceptable approximation of the coefficient in this range.

Concentric Cylinders

This expression is obtained from reference 12. The experimental conditions are similar to those found in the problem of appendix C. One assumption is made in the problem; the axial flow has a negligible effect on the boundary film. This seems reasonable for the high rotational speed and the low axial flow velocities. Therefore, the entrance effect term is dropped.

Rotors

The equations for the remaining two flow types are derived from the results of reference 13. While the completely shrouded disk used does not duplicate the flow in a seal gap, no work applicable to laminar flow (the most probable regime in a seal gap) has yet been found. Also the derivation involves using the Reynolds analogy so the resulting expressions are only rough approximations.

In applying the results, the assumption is made that one or the other of the following situations exists:

(1) The clearance between the side of a rotating part and the housing or other stationary part is so small that the boundary layers are merged at all times (seal gap).

(2) The clearance is large enough that the boundary layers are separate at all times (sides of rotors). This should be a good approximation of the situation in the problem of appendix C except for the seal gap.

The laminar to turbulent transition for the sides of rotors case occurs at a Reynolds number of 158 000. For the seal gap case, the critical Reynolds number is a function of the ratio of gap clearance to rotor outer radius, that is,

$$Re_c = \frac{366.34}{\left(\frac{S}{r_o}\right)^{1019}}$$

Derivation of Equations for the Rotor Coefficients

The Reynolds analogy (ref. 14)

$$Nu = \frac{C_f Re Pr^{1/3}}{2} \tag{D1}$$

requires an expression for the wall shear stress τ_t because the skin friction coefficient

$$C_f = \frac{2\tau_t}{\rho V_\infty^2} \tag{D2}$$

The torque coefficients C_M obtained in reference 13 are, in effect, functions of τ_t; that is

$$C_M = \frac{8\pi}{\rho\omega^2 a^5} \int_0^a r^2 \tau_t \, dr \tag{D3}$$

A general form of the equation for shear stress in a pipe (ref. 14, p. 509)

$$\tau_t = A\rho^v \omega^w r^x \nu^y s^z \tag{D4}$$

is used to obtain the following expression for the torque coefficient:

$$C_M = \frac{8\pi A}{3 + X} \frac{\rho^{v-1} \nu^y s^z}{\omega^{2-w} a^{2-x}} \tag{D5}$$

This is matched with an empirical equation from reference 13 to evaluate the constant A and the coefficients of the properties. Substitution in equations (D4), (D2), and (D1) gives an expression for the Nusselt number. The heat transfer coefficient h is a factor of the Nusselt number; that is,

$$Nu = \frac{h r_{av}}{k}$$

The free stream velocity V_∞ must still be evaluated. For the seal gap with merged boundary layers, $V_\infty = r\omega/2$. For the case of separated boundary layers, the difference between the free stream velocity and the rotor velocity is required for a rotating part. For a nonrotating part, of course, the difference is the free stream velocity $V_\infty = \beta r$. Information in reference 13 indicates that β is a function of the rotor angular velocity and the ratio s/a, or that $\beta = K\omega$ where $K = F(s/a)$. Evaluating the data presented yields the following expressions for K (the coefficient equation can be expressed in terms of K, see table I):

$$\left.\begin{aligned} K_{stator} &= 0.50185 - 0.6508\left(\frac{s}{a}\right) \\ K_{rotor} &= 0.49815 + 0.6508\left(\frac{s}{a}\right) \end{aligned}\right\} \text{laminar flow}$$

$$\left.\begin{aligned} K_{stator} &= 0.48558 - 0.35778\left(\frac{s}{a}\right) \\ K_{rotor} &= 0.51442 + 0.35778\left(\frac{s}{a}\right) \end{aligned}\right\} \text{turbulent flow}$$

APPENDIX E

SAMPLE THERMAL PROBLEM FOR COMPARISON WITH EXACT SOLUTION

To demonstrate the accuracy of the program, the following sample problem (see fig. 15) was solved.

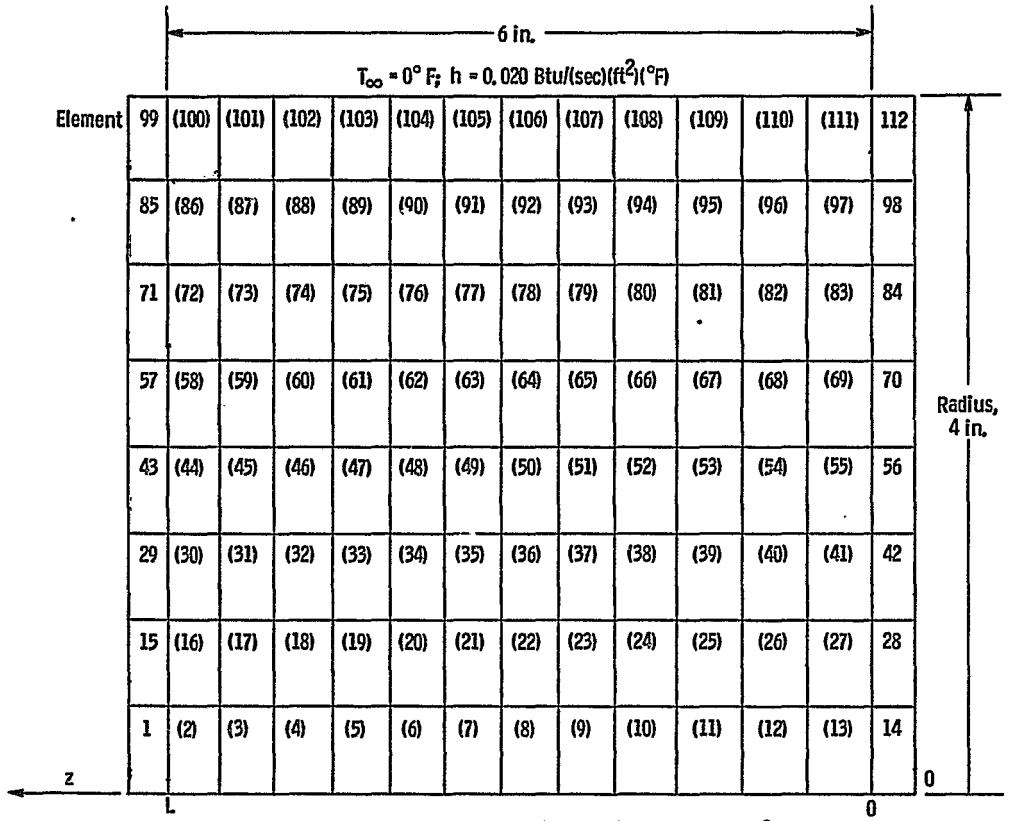

Figure 15. - Thermal sample problem. Solid cylinder with right end (z = 0) held at 200° F and left end (z = L) held at 0° F. Right side boundary elements (i.e., 14, 28, 42, 56, 70, 84, 98, and 112) held at 200° F. Left side elements held at 0° F.

For the finite cylinder with $0 \leq r \leq a$ and $0 \leq z \leq L$,

$$z = 0 \text{ held at } 200^{\circ} \text{ F (366 K)}$$

$$z = L \text{ held at } 0^{\circ} \text{ F (255 K)}$$

Forced convection into a medium at $T_\infty = 0^{\circ}$ F (255 K) occurs at $r = a$.

For an exact solution, the temperature has to satisfy the following equation for an isotropic homogeneous solid:

$$\frac{\partial^2 T}{\partial r^2} + \frac{1}{r}\frac{\partial T}{\partial r} + \frac{\partial^2 T}{\partial z^2} = 0 \qquad 0 \le r \le a,\ 0 \le z \le L$$

which is subject to the following boundary conditions:

$$T = 0^{\circ} F\ (255\ K) \text{ at } z = L \text{ and } 0 \le r \le a$$

$$T = 200^{\circ} F\ (366\ K) \text{ at } z = 0 \text{ and } 0 \le r \le a$$

$$k\frac{\partial T}{\partial r} + hT = 0 \text{ at } r = a \text{ and } 0 < z < L$$

If the following definitions are used:

J_0 Bessel function of first kind, zero order

J_0' derivative with respect to its arguments

α root of equation $\alpha J_0'(\alpha a) + h_c J_0(\alpha a) = 0$

the exact solution is given by

$$T = T_\infty \sum_{n=1}^{\infty} \frac{2h_c J_0(r\alpha_n)\sinh\left[(L - z)\alpha_n\right]}{a\left(h_c^2 + \alpha_n^2\right) J_0(a\alpha_n)\sinh(L\alpha_n)} \qquad \text{(E1)}$$

For the numerical solution, a coarse mesh of 112 elements was chosen. As indicated in figure 15, the 96 elements between $z = 0$ and $z = L$ had 0.5-inch (1.27-cm) radial and axial dimensions. The 16 elements constituting boundary conditions had 0.25-inch (0.635-cm) axial dimensions.

The temperatures were calculated by means of the program and of equation (E1). The following values were required to obtain solutions:

a = 4.0 in. (10 cm) h_c = 0.020 Btu/(sec)(ft^2)(^{o}F); 0.0098 cal/(sec)(cm^2)(^{o}C)

L = 6.0 in. (15 cm) k = 0.00361 Btu/(sec)(ft)(^{o}F); 0.0537 cal/(sec)(cm)(^{o}C)

The results are shown in figure 16 and table III. The maximum error using this coarse mesh is 15 percent. A finer mesh would be expected to show a lesser error.

(Element)	(99)	(100)	(101)	(102)	(103)	(104)	(105)	(106)	(107)	(108)	(109)	(110)	(111)	(112)
Exact solution	0	2.71	8.23	14.09	20.55	27.90	36.50	46.81	59.50	75.54	96.55	125.55	169.61	200
Program solution		2.57	7.26	12.94	19.22	26.41	34.90	45.17	57.91	74.15	95.52	124.93	163.09	
	(85)	(86)	(87)	(88)	(89)	(90)	(91)	(92)	(93)	(94)	(95)	(96)	(97)	(92)
	0	3.23	9.81	16.80	24.48	33.19	43.33	55.42	70.11	88.35	111.44	141.15	178.86	200
		3.11	8.65	15.39	22.84	31.34	41.34	53.36	68.12	86.59	110.16	140.81	175.96	
	(71)	(72)	(73)	(74)	(75)	(76)	(77)	(78)	(79)	(80)	(81)	(82)	(83)	(84)
	0	3.70	11.23	19.21	27.95	37.82	49.23	62.66	78.72	98.13	121.68	149.99	182.68	200
		3.55	9.87	17.54	25.99	35.60	46.82	60.18	76.33	96.06	120.32	150.00	180.94	
	(57)	(58)	(59)	(60)	(61)	(62)	(63)	(64)	(65)	(66)	(67)	(68)	(69)	(70)
	0	4.10	12.45	21.27	30.90	41.71	54.09	68.49	85.39	105.30	128.59	155.30	184.74	200
		3.92	10.88	19.32	28.59	39.09	51.25	65.58	82.62	102.98	127.19	155.50	183.40	
	(43)	(44)	(45)	(46)	(47)	(48)	(49)	(50)	(51)	(52)	(53)	(54)	(55)	(56)
	0	4.43	13.44	22.94	33.28	44.80	57.90	72.95	90.34	110.38	133.22	158.65	185.99	200
		4.21	11.68	20.72	30.62	41.77	54.62	69.60	87.19	107.81	131.73	158.87	184.78	
	(29)	(30)	(31)	(32)	(33)	(34)	(35)	(36)	(37)	(38)	(39)	(40)	(41)	(42)
	0	4.67	14.19	24.20	35.06	47.10	60.69	76.16	93.82	113.84	136.25	160.77	186.77	200
		4.41	12.24	21.70	32.04	43.65	56.95	72.35	90.25	110.96	134.58	160.89	185.58	
	(15)	(16)	(17)	(18)	(19)	(20)	(21)	(22)	(23)	(24)	(25)	(26)	(27)	(28)
	0	4.84	14.69	25.04	36.24	48.62	62.52	78.23	96.02	115.99	138.10	162.03	187.22	200
		4.53	12.57	22.28	32.88	44.75	58.30	73.93	91.99	112.71	136.13	161.97	186.00	
	(1)	(2)	(3)	(4)	(5)	(6)	(7)	(8)	(9)	(10)	(11)	(12)	(13)	(14)
	0	4.93	14.94	25.47	36.83	49.37	63.42	79.25	97.08	117.02	138.97	162.62	187.41	200
		4.57	12.68	22.47	33.15	45.11	58.75	74.45	92.55	113.27	136.63	162.31	186.14	

Figure 16. - Thermal sample problem showing thermal distribution.

TABLE III. - THERMAL SAMPLE PROBLEM COMPARISON WITH EXACT SOLUTION

Element number	Exact temperature, °F	Calculated temperature, °F	Percent error	Element number	Exact temperature, °F	Calculated temperature, °F	Percent error
2	4.925	4.571	7.19	58	4.097	3.920	4.32
3	14.943	12.682	15.13	59	12.448	10.883	12.57
4	25.465	22.471	11.76	60	21.270	19.322	9.16
5	36.830	33.150	9.99	61	30.903	28.592	7.48
6	49.372	45.109	8.63	62	41.707	39.088	6.28
7	63.415	58.746	7.36	63	54.087	51.250	5.25
8	79.246	74.446	6.06	64	68.487	65.576	4.25
9	97.082	92.548	4.67	65	85.394	82.621	3.25
10	117.018	113.272	3.20	66	105.298	102.978	2.20
11	138.969	136.631	1.68	67	128.585	127.185	1.09
12	162.620	162.308	.19	68	155.300	155.304	.13
13	187.408	186.137	.68	69	184.744	183.395	.73
16	4.841	4.532	6.38	72	3.695	3.552	3.87
17	14.691	12.573	14.42	73	11.230	9.868	12.13
18	25.044	22.281	11.03	74	19.210	17.536	8.71
19	36.240	32.876	9.28	75	27.954	25.986	7.06
20	48.619	44.749	7.96	76	37.822	35.598	5.88
21	63.515	58.303	6.74	77	49.226	46.819	4.89
22	73.233	73.932	5.50	78	62.661	60.178	3.96
23	96.016	91.985	4.20	79	78.724	76.328	3.04
24	115.990	112.708	2.83	80	98.134	96.063	2.11
25	138.096	136.134	1.42	81	121.684	120.316	1.12
26	162.028	161.968	.04	82	149.987	150.003	.11
27	187.216	186.004	.65	83	182.681	180.937	.95
30	4.670	4.412	5.52	86	3.227	3.106	3.75
31	14.188	12.242	13.72	87	9.811	8.650	11.83
32	24.202	21.702	10.33	88	16.797	15.391	8.37
33	35.056	32.041	8.60	89	24.477	22.837	6.70
34	47.102	43.654	7.32	90	33.187	31.344	5.55
35	60.690	56.952	6.16	91	43.330	41.338	4.60
36	76.162	72.354	5.00	92	55.415	53.359	3.71
37	93.815	90.252	3.80	93	70.114	68.116	2.85
38	113.843	110.955	2.54	94	88.353	86.586	2.00
39	136.253	134.579	1.23	95	111.444	110.157	1.15
40	160.767	160.892	.08	96	141.150	140.806	.24
41	186.765	185.584	.63	97	178.863	175.963	1.62
44	4.425	4.207	4.93	100	2.705	2.574	4.84
45	13.437	11.678	13.09	101	8.227	7.260	11.75
46	22.941	20.716	9.70	102	14.091	12.941	8.16
47	33.276	30.616	7.99	103	20.551	19.220	6.48
48	44.802	41.774	6.76	104	27.899	26.411	5.33
49	57.897	54.618	5.66	105	36.497	34.896	4.39
50	72.951	69.603	4.59	106	46.814	45.168	3.52
51	90.343	87.192	3.49	107	59.503	57.913	2.67
52	110.384	107.809	2.33	108	75.544	74.148	1.85
53	133.215	131.727	1.12	109	96.548	95.518	1.07
54	158.647	158.871	.14	110	125.551	124.981	.45
55	185.989	184.781	.65	111	169.610	163.090	3.84

REFERENCES

1. Bisson, Edmond E.; and Anderson, William J.: Advanced Bearing Technology. NASA SP-38, 1964.
2. Schevchenko, Richard P.: Shaft, Bearing and Seal Systems for a Small Engine. Paper 670064, SAE, Jan. 1967.
3. Cheng, H. S.; Chow, C. Y.; and Wilcock, D. F.: Behavior of Hydrostatic and Hydrodynamic Noncontacting Face Seals. Paper 67-WA/Lub-19, ASME, Nov. 1967.
4. Parks, A. J.; McKibbin, R. H.; Ng, C. C. W.; and Slayton, R. M.: Development of Main Shaft Seals for Advanced Air Breathing Propulsion Systems. Rep. PWA-3161, Pratt and Whitney Aircraft (NASA CR-72338), Aug. 14, 1967.
5. Austin, R. M.; and Fisher, M. J.: A Hydrostatic Seal for Boiler Feed Pumps. Paper E-4, 2nd International Conference on Fluid Sealing, the British Hydromechanics Research Association, Apr. 1964.
6. Ludwig, Lawrence P.; Strom, Thomas N.; Allen, Gordon P.; and Johnson, Robert L.: Improving Performance of Face Contact Seal in Liquid Sodium (400° to 1000° F) by Incorporation of Spiral-Groove Geometry. NASA TN D-3942, 1967.
7. Johnson, Robert L.; and Ludwig, Lawrence P.: Shaft Face Seal with Self-Acting Lift Augmentation for Advanced Gas Turbine Engines. NASA TN D-5170, 1969.
8. Carslaw, H. S.; and Jaeger, J. C.: Conduction of Heat in Solids. Second ed., Clarendon Press, Oxford, 1959.
9. McAdams, William H.: Heat Transmission. Third ed., McGraw-Hill Book Co., Inc., 1954.
10. Kreith, Frank: Principles of Heat Transfer. International Textbook Co., 1958.
11. Jakob, Max: Heat Transfer. Vol. I. John Wiley & Sons, Inc., 1949.
12. Tachibana, Fujio; and Fukui, Sukeo: Convective Heat Transfer of the Rotational and Axial Flow Between Two Concentric Cylinders. Bull. Japan Soc. Mech. Eng., vol. 7, no. 26, 1964, pp. 385-391.
13. Daily, J. W.; and Nece, R. E.: Chamber Dimension Effects on Induced Flow and Frictional Resistance of Enclosed Rotating Disks. J. Basic Eng., vol. 82, no. 1, Mar. 1960, pp. 217-232.
14. Schlichting, Hermann (J. Kestin, trans.): Boundary Layer Theory. Fourth ed., McGraw-Hill Book Co., Inc., 1960.

NASA-Langley, 1969 — 33 E-4389

END OF REFERENCE

116

REFERENCE

117

ROBINSON, R. P.; AND BURTON, R.: TEMPERATURE GRADIENTS IN SEAL RINGS: A METHOD OF ANALYSIS. PROCEEDINGS OF THE FOURTH INTERNATIONAL CONFERENCE ON FLUID SEALING. A. L. KING, B. S. NAU AND H. S. STEPHENS, EDS., BRITISH HYDROMECHANICS RES. ASSOC. (ENGLAND), 1969.

THIS MATERIAL HAS BEEN APPROVED FOR PUBLICATION PER LETTER FROM MAXINE E. HENSLEY, AMERICAN SOCIETY OF LUBRICATION ENGINEERS TO JOANNE FOLK DATED AUG. 19, 1974.

Proceedings of the Fourth International Conference on Fluid Sealing

LIBRARY COPY
LEWIS LIBRARY
CLEVELAND, OHIO

Philadelphia, U. S. A.
1969

Temperature Gradients in Seal Rings: A Method of Analysis

R. P. ROBINSON AND R. BURTON
Flexibox Ltd.
Manchester, U. K.

Presented at the Fourth International Conference on Fluid Sealing held in conjunction with the 1969 ASLE Annual Meeting in Philadelphia, Pa. This paper sponsored by the British Hydro Mechanics Research Association.

A numerical method, based on the well known relaxation technique, is described for determining temperature distributions in seal rings. The method is one which can be applied to seal rings of non-uniform cross sectional shape and is particularly suitable to digital methods of solution.

Choice and quantitative application of thermal boundary conditions to the analysis are discussed in relation to operation conditions encountered by mechanical seals in the field.

Illustrations of temperature distributions in non-dimensional form, in actual seal rings, which have been calculated by this method, are included. The usefulness of these results to the seal designer in dealing with the twin problems of thermal distortion and frictional heat removal, are discussed.

INTRODUCTION

The increasing need for mechanical seals to handle duties beyond the reach of other sealing methods, for example, on multiple stage pipeline pumps or sealing liquids near to boiling point, has, in recent year, caused seal designers to pay more attention than hitherto to the hydrodynamic and thermodynamic aspects of seal technology.

Whereas in the past it has often been sufficient to adapt a particular seal, or range of seals to handle stiffer duties, merely by following certain largely empirical rules, it is becoming increasingly necessary to make use of all that modern technology has to offer in analytical techniques when designing a new seal. This is particularly true in the design of the contact faces of a mechanical seal where several factors, in addition to the already well known ones, such as material combination and degree of hydraulic balance, can influence the performance of the seal. Of these, distortion of the contact faces and frictional heat removel are among the most significant.

Distortion of the faces is particularly important because the concept of hydraulic balance depends for its validity on the assumption that the opposing faces remain plane and parallel. Any transient conic distortion of either one or both faces of a seal, which has fully bedded in

NOMENCLATURE

b	Radial width of contact face
D	Mean diameter of contact face
f	Coefficient of friction
G	Grashof number
h	Surface heat transfer coefficient between seal ring and cooling medium
k	Thermal conductivity of seal ring material
l	Length of mesh line between intersections
l_o	Length of mesh line outside seal profile (= k/h)
Nu	Nusselt number
Pr	Prandtl number
q	Rate of heat input to seal ring
Re	Reynolds number relating to flow in annulus
R	Reynolds number relating to speed of rotation of seal ring
Rs	Reynolds number relating to cross flow over rotating seal ring
T	Temperature at a point within seal ring profile
TO	Temperature of cooling medium
$\overline{T}$	Non-dimensional quantity defining an isotherm
ΔT	Temperature differential over one mesh width at contact face
U	Linear velocity of rotating contact face
W	Total load on contact face
μ	Absolute viscosity

after running under a particular set of conditions, can cause a dramatic change in balance, often sufficiently severe to bring about complete failure of the seal owing to hydraulic over-balance. The causes of distortion are in the main twofold. Thermal gradients contribute, as do mechanical forces caused by hydraulic pressures, spring loads and mounting methods which, in varying degree, act on all seal rings. The problem of mechanical forces is outside the scope of this analysis and is only mentioned here in order to indicate the nature of the overall problem confronting the seal designer.

Frictional heat removal from the seal faces is linked with thermal distortion in so far as the thermal gradients causing distortion are generated by the heat input at the contact face and heat removal at the cooled surfaces of a seal ring. The importance of heat removal in relation to the duty being handled by a mechanical seal has been described by Lymer and Greenshields (1). It is sufficient to say here that the more detailed the knowledge available regarding heat flow and temperatures with a seal ring, the better, when designing seal rings for arduous duties.

The following analysis presents a method where by a complete map of the temperatures throughout a seal ring can be determined for a given set of operating conditions, thus enabling both thermal distortion and heat removal characteristics of the seal ring to be estimated with a fair degree of accuracy.

ANALYSIS

Fig. 1 shows a typical arrangement of a balanced mechanical seal. Although the description which follows has been built around the floating (and rotating) member of such a seal, it will become evident that the method of approach can be applied with equal facility to other forms of seal ring, whether they be stationary or rotating members.

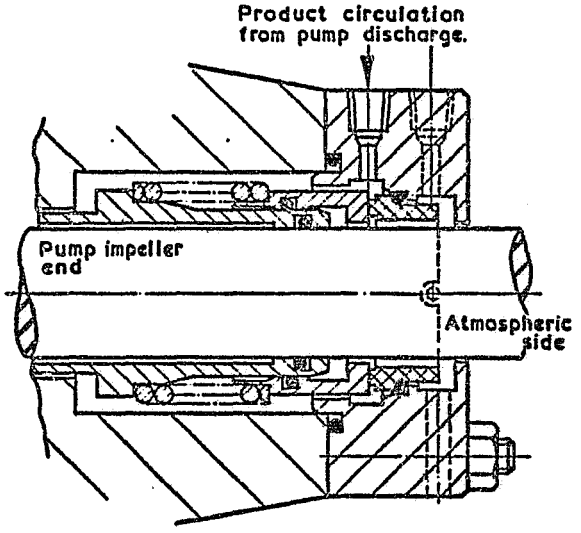

FIG. 1 BALANCED MECHANICAL SEAL.

The method of solution is based on the relaxation method for solving problems of two-dimensional heat conduction in solids, which is described in most modern text books on thermdynamics (2). In order to apply the method to heat flow in a seal ring, some simplifying assumptions and modifications to the better known techniques are introduced.

Two Dimensional Heat Flow

The seal ring is considered as being opened out into a flat section of uniform thickness πD. Two dimensional heat flow is, therefore, assumed over the radial cross section and the analysis is only strictly true for rings whose radial thickness is small in relation to diameter which, fortunately, is the case for most seal rings.

Insulated Surfaces

In applying the relaxation method, square blocks of material of unit thickness can be considered to be replaced by conducting rods, which are represented as lines in a uniform mesh, as shown in Fig. 2. At an insulated surface, heat is transferred parallel to the surface, but not through it. The equivalent mesh lines are, therefore, omitted where these would pass through, or touch an insulated surface. The material adjacent to the surface is represented by lines parallel to the surface and disposed half a mesh width from it.

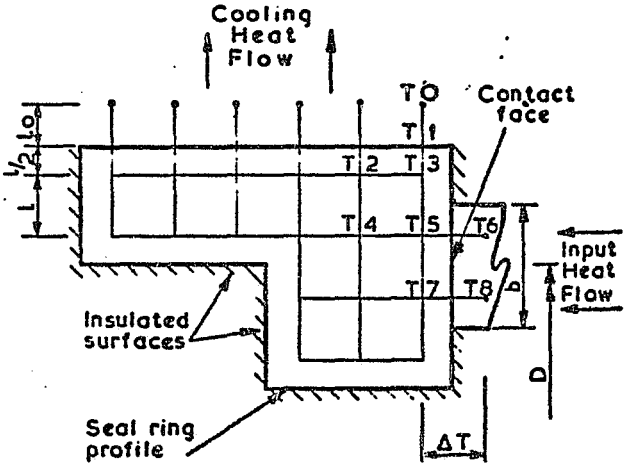

FIG. 2 RELAXATION MESH.

Cooled Surfaces

Where heat passes through a surface, the mesh is extended through it into the cooling medium. For most seal rings, the cooling medium is the sealed fluid and this may be continuously circulated through the seal chamber, in order to assist cooling. At the cooled surface, the mesh length is modified in order to allow for the heat transfer characteristics from the seal ring sur-

face to the cooling medium. This correction is calculated as follows:

$$\ell o = k/h$$

Such a change in local mesh length also involves a modification to the relaxation calculation. For example, referring to Fig. 2, the corrected value of T3 is calculated from the equation.

$$\frac{TO - T3}{\ell o + \ell/2} + \frac{T2 - T3}{\ell} + \frac{T5 - T3}{\ell} = 0$$

The actual value of surface temperature, on completion of the relaxation calculations, is obtained by interpolation. For example, again referring to Fig. 2:-

$$\frac{T1 - TO}{\ell o} = \frac{T3 - TO}{\ell o + \ell/2}$$

Heat Input

A proportion of the frictional heat generated by the seal enters the ring through the contact face area. The actual proportion varies with the type of seal, being dependent on the relative heat removal properties of the two opposing seal rings. With the type of seal shown in Fig. 1, employing metal rotary and carbon stationary seal rings, it is reasonable to assume that almost the whole of the generated heat is removed via the rotating seal ring.

Assuming the heat flux to be uniform over the contact face area, heat flow into the ring is given by the equation

$$q = \pi k D \Delta T \, b/\ell \qquad (1)$$

where ΔT is the temperature drop over each of the one or more mesh lines of length ℓ which pass through the contact face, as in Fig. 2.

In order for the conducting rod analogy to remain true in this region, the ratio b/ℓ must be made an integer, whose magnitude depends on the number of mesh blocks and, hence, conducting rods, chosen to represent the contact face. The width of contact face can thus be seen to be a major factor in the fittings of a suitable mesh for calculation purposes, to the seal ring as a whole.

When carrying out the relaxation calculation, the temperature difference ΔT, calculated from Eq. (1), is held constant over the contact face mesh, i. e. in Fig. 2:

$$(T6 - T5) = (T8 - T7) = \Delta T$$

As for cooled surfaces of the ring, the actual surface temperature at the contact face can be interpolated on completion of the relaxation calculation.

Calculation of Temperature Distribution

Assuming that the boundary conditions for a given seal ring, including rate of heat input, are known, a suitable mesh is applied to its radial cross section, remembering to make the ratio b/ℓ an integer, and ΔT is calculated from Eq. (1). The temperature of the cooling medium, which is usually the sealed fluid, is applied at the appropriate mesh points and provisional estimates made of the temperatures at the other mesh intersections. Using the relaxation technique, successive approximations are then made until a final steady state solution is obtained.

The resultant temperature distribution will depend for its accuracy and detail on the size of mesh chosen and on the choise of boundary conditions. In Fig. 2, for reasons of clarity, the size of mesh shown is much coarser than would normally be used in practice.

GENERAL SOLUTION

The analysis, in the form thus far described, would be extremely tedious were it to be carried out in full for every individual case requiring examination. In designing seals, it is usual to find that the cross sectional shapes of seal rings fall into a fairly limited number of recognisable patterns, which can be analysed according to their shape, as follows.

Assuming the thermal conductivity of a given ring is constant throughout its cross section, all temperature gradients within the ring are directly proportional to the input temperature gradient $\Delta T/\ell$. The temperature difference between any any two points in the ring is given by the product of average temperature gradient and distance between the points. The distance between two similar points within seal ring/contact face combinations, differing in size but identical in shape, is proportional to any given linear dimension, fo for example, contact face width b.

Hence $(T - TO)$ is proportional to $\Delta T \, b/\ell$

but from Eq. (1) $\frac{\Delta T \, b}{\ell} = \frac{q}{\pi k D}$

and therefore $T - TO = \overline{T} \frac{q}{kD} \qquad (2)$

where $\overline{T}$ is:

(a) a non-dimensional quantity defining an isotherm in a seal ring/contact face combination of particular cross sectional profile.

(b) independent of the physical size of that profile and its associated mean diameter D.

(c) not entirely independent of thermal conductivity k, owing to the heat transfer correction at cooling surfaces, but for ferrous materials and normal rotating speeds the variation is small.

Determination of T

From Eqs. (1) and (2)

$$T = \frac{T - TO}{\pi \Delta T} \quad \frac{\ell}{b}$$

Note that D does not appear in this equation

In order to determine the temperature distribution in terms of $\overline{T}$ for a particular seal ring shape and relative width of contact face, it is thus necessary to assume typical cooling boundary conditions, fit a suitable relaxation mesh to the radial section and assuming a purely arbitrary value of ΔT, calculated the corresponding values of (T - TO) as before. $\overline{T}$ is then found for each point in the mesh by applying Eq. (3) with the, previously assumed, arbitrary value of ΔT. Isotherms, or lines of constant $\overline{T}$, are dtermined by interpolation.

Examples of rather simplified typical seal ring shapes, analysed in this way, ar shown in Figs. 3, 4 & 5. The effect on temperature distribution of change in cross sectional shape and width of contact face can be seen in these illustrations. Applying Eq. (2) to these, or similar figures prepared for other types of seal ring, provides a ready means of determining actual temperature distributions for a wide variety of operating conditions.

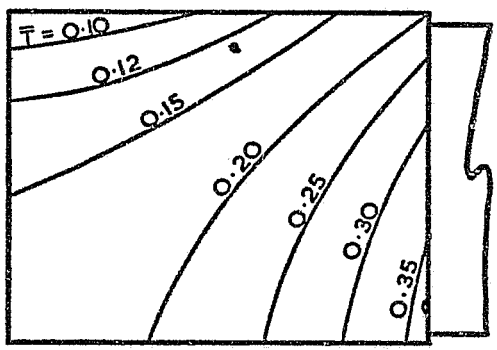

FIG. 3 ISOTHERMS IN SEAL RING WIDE FACED.

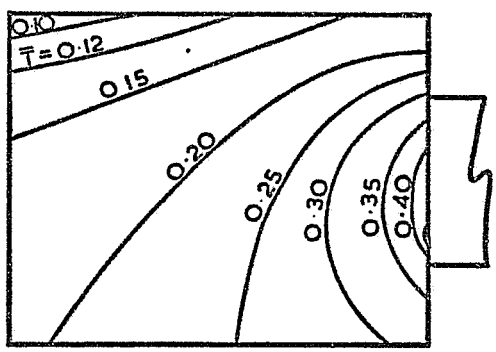

FIG. 4 ISOTHERMS IN SEAL RING NARROW FACED.

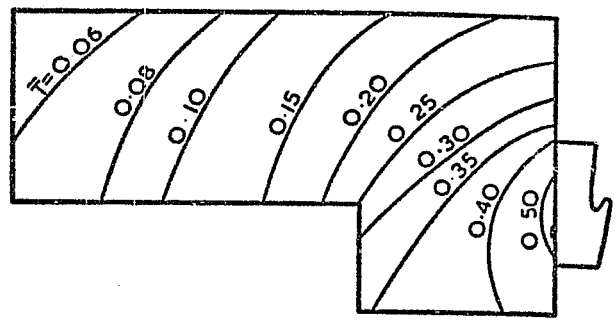

FIG. 5 ISOTHERMS IN BALANCED SEAL RING.

CHOICE OF BOUNDARY CONDITIONS

Cooled Surfaces

As already pointed out, the cooling medium surrounding a seal ring is invariably the sealed fluid itself. This may be contained in a "dead end" sealing chamber, in which case heat is transferred from the seal ring surface to the fluid and thence to the walls of the chamber, both being convective processes. Alternatively, the sealed fluid may be circulated through the sealing chamber, as is often the case with mechanical seals used on centrifugal pumps, where a tapping from pump discharge allows fluid to circulate through the sealing chamber, or stuffing box, and return to suction via a close clearance bushing at the inboard end of the seal. Such an arrangement is shown in Fig. 1.

It can thus be seen that both natural and forced convection heat transfer can apply to a seal ring, varying with the mechanical arrangement. A further complication arises by virtue of the fact that one of the opposing pair of seal rings rotates. This introduces another form of forced convection which, apart from its obvious effects on the rotating ring, may have some influence on the stationary ring also, again depending on the mechanical arrangement. In any individual case, the decision regarding the form of heat transfer applicable to the ring must, therefore, be left to the skill of the seal designer and his interpretation of the conditions surrounding the seal.

It is fairly safe to say that the relatively low surface coefficients, usually associated with pure natural convection, are seldom met with in mechanicla seals, except possibly in the case of narrow gaps caused by fitting tolerances. These are usually, however, best considered as special cases of heat transfer by conduction, which leaves to be considered the two forms of forced convection mentioned above.

Convective heat transfer by forced circulation of the sealed fluid through an annular gap between the stationary seal ring and the wall of the sealing chamber is a common method employed for seal ring cooling. Surface coeffi-

cients can be calculated from the equation for flow in an annulus (3).

$$Nu = 0.023\ (Re)^{0.8}\ (Pr)^{0.4} \qquad (4)$$

By using high flow rates quite high surface coefficients can be obtained and Fig. 6 shows some typical values for a seal operating in water.

Convection coefficients associated with rotating seal rings are, on the other hand, less dependent on rate of circulation flow, being governed largely by the speed of rotation. Dorfman (4) suggests the following equation for calculating surface coefficients of rotating cylinders

$$Nu = 0.135\ (2R^2 + Rs^2 + G)\ Pr^{0.33} \qquad (5)$$

Other researchers (5) (6) give similar results. Figure 7 shows typical values of surface heat coefficient due to rotation, calculated from Eq. (5), allowing for a modest rate of circulation flow over the seal ring. These values are based on the same sealing conditions as used to determine Fig. 6 and thus give some indications of the relative effectiveness of the two forms of convective cooling.

The high values of heat transfer coefficient indicated by Figs. 6 and 7 lend some justification to the assumption used in the relaxation analysis, that those surfaces of the sea- ring not subject to similar conditions, are considered to be insulated.

Heat Input

Eqs. (1) and (2) depend for their practical usefulness on the value given to the rate of heat input at the contact face q which, assuming this to be the total heat generated at the contact faces, is given by

$$q = f\ W\ U \qquad (6)$$

The coefficient of friction f is the one indeterminate factor in Eq. (6). The works of Summers-Smith (7) and Ishiwata and Hirabayashi (8), which was discussed later by Nau (9), suggests that for seals operating in the hydrodynamic region

$$f \left\{\frac{\mu Ub}{W}\right\}^{-0.5} = \text{constant} \qquad (7)$$

This in itself is not much help, since the constant still requires determination and in any case it is by no means certain that all seals operate in the hydrodynamic region.

For the present, at least, it remains up to the seal designer to gather his information as best he may, preferably by actual measurements in the laboratory on the seal types with which he is concerned. Currently accepted values for friction coefficient on mechanical seals in commercial use varv from 0. 02 to 0. 10.

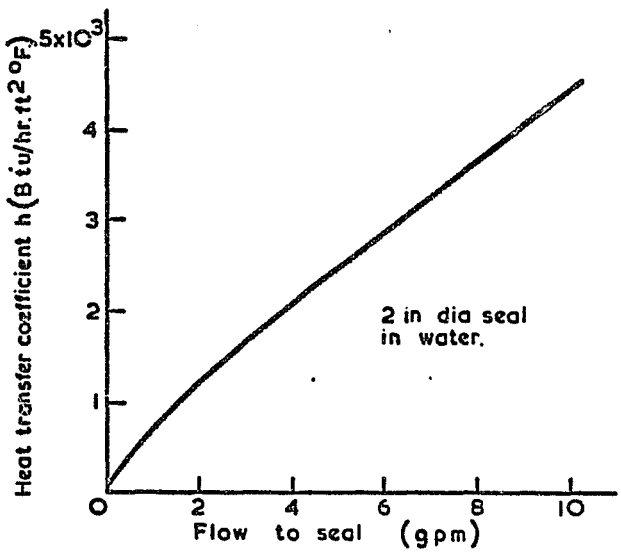

FIG. 6 HEAT TRANSFER COEFFICIENTS STATIONARY SEAL RINGS.

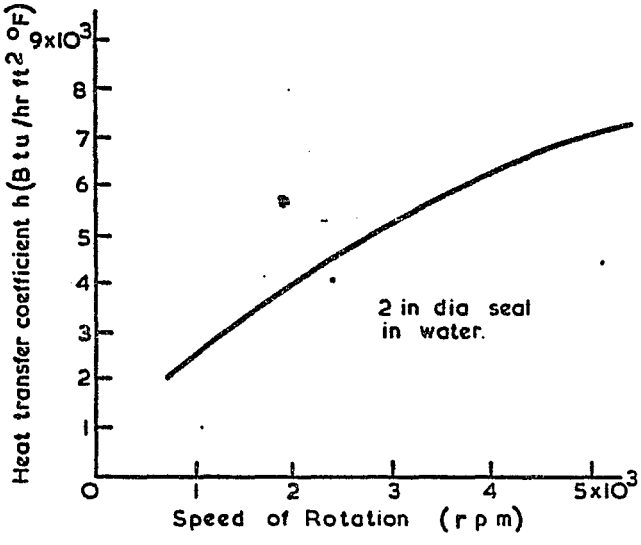

FIG. 7 HEAT TRANSFER COEFFICIENTS ROTATING SEAL RINGS.

Some difficulty arises when removal of the generated heat is shared by both seal rings. In such cases the problem can be solved by analysing each seal ring independently for arbitrarily assumed proportions of the total heat generated and using an iterative technique to arrive at a common values of contact face temperature.

APPLICATION TO DESIGN

It must be admitted that, whilst having a detailed map of the temperature distributions in a seal ring goes a long way toward analysing the problem of thermal distortion, it is really only a half way stage in the whole operation. In order to fully examine the effects of temperature distribution and the complementary mechanical and hydraulic loadings in terms of distortion of the contact face, it is necessary to solve the resultant complex strain pattern arising from these

factors. Some work has been done by Fisher (10) Watson (11) and Nau (12) towards this end.

Illustrations such as Figs, 3, 4 & 5 do, however, provide the seal designer with a qualitative appreciation of the influence of temperature gradients in relation to the structural shape of the sea- ring and assist him in choosing the best design for the particular purpose in hand.

With regard to frictional heat removal on the other hand, a detailed knowledge of the thermal characteristics of the seal ring is invaluable, particularly when sealing liquids near to their boiling point. It is useful also to be able to correlate the material and structural shape of the seal ring with the conditions under which it operates, in order to select which ring should be of the higher conductivity material.

For instance, it can be shown that for most common pumping duties, where carbon versus metallic seal faces are used, that the lowest temperature difference between the contact faces and seal liquid occurs when the metallic ring is placed in the region of highest surface heat transfer. Reference to Figs. 6 and 7 shows that this can most conveniently be done by making the metallic ring the rotary component. In order to achieve the same results with the metallic ring stationary, would need very high cooling flow rates, with the consequent increased possibility of erosion damage being suffered by the seal or its auxilliary components.

The full potential of the method of analysis described, could be realised by programming on a digital computer, to which it is ideally suited. Alternatively, in the absence of this facility, a number of illustrations on the lines of Figs. 3, 4 and 5 can be prepared to cover the principle types of applications of seal rings with which the designer is concerned.

By selecting the illustration most nearly fitting the shape of the seal ring in question and in conjunction with Eq. (2), these would then provide a reasonably accurate and speedily applied design method for predicting the temperature gradients in the ring and, in particular, the temperature difference between contact faces and sealed liquid.

ACKNOWLEDGEMENTS

The authors wish to thank the Directors of Flexibox Limited, for permission to publish this paper.

REFERENCES

1. Lymer, A, and Greenshields, A. L. "Thermal aspects of mechanical seals." Paper presented at the first Pumping exhibition and conference, Earls Court, London. 13pp. (June, 15th-17th, 1965).
2. Rogers, G. F. C. and Mayhew, Y. R. "Engineering thermodynamics work and heat transfer." Longmans, London. (1957)
3. McAdams, W. H. "Heat transmission." 3rd Edition McGraw-Hill Book Co. Inc., New York. pp. 219 & 241. (1954).
4. Dorfman, L. A. "Hydrodynamic resistance and the heat loss from rotating solids." Book transl. from Russian by Prof. N. Kemmer. pp. 182-7. Published by Oliver & Boyd Ltd. (1963).
5. Seban, R. A. and Johnson, H. A. "Heat transfer from a rotating cylinder in oil." NASA- Memo No. 4-22-59W.
6. Theordorsen, T. and Regier, A. "Experiments on the drag of revolving discs, cylinders and streamline rods at high speed." Report No. NACA REP. 793 (1944).
7. Summers-Smith, D. "Laboratory investigation of the performance of a radial-face seal." Paper presented at the 1st International conference on Fluid Sealing, Ashford, Kent. Organised by British Hydromechanics Research Association. Paper No. D1. 12pp. (April, 1961).
8. Ishiwata, H. and Hirabayashi, H. "Friction and sealing characteristics of mechanical seals." Paper presented at the 1st International conference on Fluid Sealing, Ashford, Kent. Organised by British Hydromechanics Research Association. Paper No. D5. 10pp. (April. 1961)
9. Nau, B. S. "Hydrodynamic lubrication in face seals." B. H. R. A. Report No. TN 843. 36pp. 36 figs. (July, 1965).
10. Fisher, M. J. "Analysis of the deformation of the balanced ring in high pressure radial-face seals." Paper presented at the 1st International conference on Fluid Sealing, Ashford, Kent. Organised by British Hydromechanics Research Association. Paper No. D4. 9pp. (April, 1961).
11. Watson, R. D. "Performance testing of conical-face high pressure rotary shaft seals." Atomic Energy of Canada, Limited. Report No. AECL-2551, 33pp. (November, 1965).
12. Nau, B. S. "Calculation of distortions in mechanical seals." B. H. R. A. Report No. 954. 10pp. 10 figs. (May, 1968).

END OF REFERENCE

117

REFERENCE

118

STROM, T. N.; LUDWIG, L. P.; AND HUDELSON, J. C.: VIBRATION OF SHAFT FACE SEALS AND STABILIZING EFFECT OF VISCOUS AND FRICTION DAMPING. NASA TN D-5161, 1969.

Ref 30 #*

NASA TECHNICAL NOTE NASA TN D-5161

NASA TN D-5161

LEWIS RESEARCH CENTER
Aerospace Safety Research
and Data Institute
FEB5 1973
CLEVELAND, OHIO

VIBRATION OF SHAFT FACE SEALS AND STABILIZING EFFECT OF VISCOUS AND FRICTION DAMPING

by Thomas N. Strom, Lawrence P. Ludwig, and John C. Hudelson

Lewis Research Center
Cleveland, Ohio

NATIONAL AERONAUTICS AND SPACE ADMINISTRATION • WASHINGTON, D. C. • APRIL 1969

NASA TN D-5161

VIBRATION OF SHAFT FACE SEALS AND STABILIZING EFFECT OF VISCOUS AND FRICTION DAMPING

By Thomas N. Strom, Lawrence P. Ludwig, and John C. Hudelson

Lewis Research Center
Cleveland, Ohio

NATIONAL AERONAUTICS AND SPACE ADMINISTRATION

For sale by the Clearinghouse for Federal Scientific and Technical Information
Springfield, Virginia 22151 – CFSTI price $3.00

ABSTRACT

In inert and reducing environments both at room and elevated temperatures, undamped seals operated with severe vibration which caused early bellows fatigue and high leakage rates of a 1.57-inch (3.99-cm) mean diameter seal operating to speeds of 165 feet per second (50.3 m/sec) at 24 000 rpm. Friction damping by mechanical dampers and the viscous damping by oil in the bellows were both effective in maintaining seal stability. Nosepiece temperatures caused by the sliding contact were high enough to reduce hardness of the mating seal seats.

VIBRATION OF SHAFT FACE SEALS AND STABILIZING EFFECT OF VISCOUS AND FRICTION DAMPING

by Thomas N. Strom, Lawrence P. Ludwig, and John C. Hudelson

Lewis Research Center

SUMMARY

Shaft face seals of 1.57 inch (3.99 cm) mean diameter with a bellows secondary seal were operated in inert and reducing gaseous environments. Starting temperatures ranged from 75° to 800° F (297 to 700 K) and sliding speeds ranged to 165 feet per second (50.3 m/sec) at 24 000 rpm. A study was made of seal stability (nosepiece vibration) as affected by both friction and viscous damping. The studies showed that undamped bellows seals have a very strong tendency for the nosepiece to vibrate in an unstable manner at high frequency (400 Hz) and high amplitudes (0.010 in. or 0.025 cm). This severe vibration allows excessive leakage because of the large nosepiece amplitudes and can cause early bellows failure. In contrast, seals with either friction (mechanical dampers) or viscous damping operated in a stable manner from 75° to 800° F (297 to 700 K) and to sliding speeds of 165 feet per second (50.3 m/sec) at 24 000 rpm. Stable seals, when operating without lubrication, however, had high (>700° F or 644 K) nosepiece temperatures; lubricated seals had significantly lower nosepiece temperatures. Results of allied studies showed that the temperature generated by the sliding contact can be high enough to reduce seat metal hardness.

INTRODUCTION

Small shaft face seals of 1.57 inches (3.99 cm) mean sliding diameter with a bellows secondary seal are being used in small gas turbine engines, rocket turbopumps, and turbosuperchargers. These seals operate at high shaft speeds (to 60 000 rpm) in a hot (to 900° F or 755 K) gaseous environment. In the case of gas turbine engines, the hot gases are oxidizing; in rocket turbopump drives the gases are reducing; and in turbosuperchargers the gases are either oxidizing or reducing, depending on load. In these gaseous environments, an undamped bellows seal with one of its natural frequencies

near shaft rotational frequency could operate in an unstable manner; that is, the seal nosepiece (stator) could vibrate and cause a marked increase in seal leakage (ref. 1). More significantly, reference 2 reports severe nosepiece vibrations, for seals operating in liquid nitrogen, at frequencies not in resonance with shaft speed. In the study of reference 2, the vibration amplitude of the nosepiece was measured to be as large as 0.037 inch (0.094 cm) with predominant frequencies of 500 to 600 hertz. With such large amplitudes, the leakage past the nosepiece sealing dam is excessive; the high frequencies, coupled with the large amplitudes, quickly induce bellows fatigue failures.

The source or forcing function which induces the nosepiece vibration could be shaft axial vibration (ref. 3), seat face runout (ref. 3), or frictional forces at the seal sliding interface. Of these three sources, the data of reference 2 suggests that the severe vibrations are more readily caused by frictional forces at the sliding interface. Thus the coefficient of friction associated with sliding material combinations and the environment may affect seal vibration. For instance, it has been recognized (ref. 4) that carbon-graphites have lower friction coefficients in oxidizing environments than in inert or reducing environments. Thus, larger frictional forces may exist in inert or reducing environments.

The objectives of this study were to (1) determine if a shaft face seal (undamped) operates unstably (nosepiece vibration) in inert and reducing environments, (2) determine the effect of friction (coulomb) and viscous damping on seal vibration and leakage rate, and (3) measure seal temperature induced by high-speed operations.

Shaft face seals to 1.57 inches (3.99 cm) mean diameter at the sliding interface were operated to speeds of 165 feet per second (50.3 m/sec) at 24 000 rpm in inert and reducing environments. Both friction and viscous damping were employed to inhibit vibration. The sealed pressure differentials were generally small in the range of 2 pounds per square inch (1.38 N/cm^2). Vibration amplitude, frequency, leakage rate, and temperature were measured.

APPARATUS AND PROCEDURE

Typical Application

Figure 1 is a schematic drawing of a typical application of a shaft face seal in a rocket engine turbopump. The function of the face seal is to restrict the leakage of hot products of combustion into the area containing the oil lubricated support bearings. The bellows secondary seal acts to hold the nosepiece in sliding contact against the rotating seat and permits axial displacements due to thermal expansion.

Room Temperature Apparatus, Nitrogen Gas Environment

For seal vibration studies at room temperature the application depicted in figure 1 was simulated by the apparatus of figure 2. A nitrogen gas environment was used. The shaft which carries the rotating seat is the stub end of a high-speed grinding spindle. The test seal has an insert cemented to the nosepiece inside diameter, and a displacement probe monitors the axial movement (vibration) of this insert. As a second means of sensing vibration, subminiature accelerometers were also cemented to this insert. A circumferential shaft riding seal was used to form a cavity which was pressurized with nitrogen gas to a gage pressure of 2 pounds per square inch (1.38 N/cm^2). Leakage through the seal was measured by a rotating drum wet test meter. Temperature of the carbon-graphite seal nosepiece was measured by means of thermocouples embedded in the carbon-graphite. The thermocouple wire size was small, 0.003 inch (0.0076 cm), in order not to interfere with seal dynamics. No external heating was used; thus any increase in the carbon-graphite temperature was due to sliding at the interface. In some runs, Mil-L-7808D lubricant was introduced through a feed tube at the rate of 1 cubic centimeter per minute

Elevated Temperature Apparatus

In tests at ambient temperatures to 300° F (700 K), the apparatus sketched in figure 3 was employed. The rotating seat was mounted on a gas bearing supported spindle and face runout was held within 0.0005 inch (0.0018 cm) full indicator runout (FIR). The nosepiece and bellows assembly carried by the housing could be positioned axially, thus changing the amount of bellows compression. The seal assembly and gas environment was heated by means of an induction coil surrounding the seal support housing. Leakage through the seal was collected in the enclosure and measured by passing the leakage through a wet test meter. Mil-L-7808D lubricant could be supplied by means of a small tube (fig. 3) directing lubricant flow to the seal interface. Shaft speed was monitored by a magnetic pickup and counter. One of the gases used in the elevated temperature apparatus was termed products of combustion (POC) which had the following analysis: 24.7 percent CH_4, 0.7 percent CO, 0.7 percent CO_2, 40.0 percent H_2, 25.7 percent N_2, and 8.2 percent H_2O.

Face Seal With Bellows Secondary

Figure 4 consists of schematics of the shaft face seals used in sealing nitrogen gas and products of combustion. The nosepiece was carbon-graphite impregnated with silver, and the seat was 17-4 PH stainless steel. A 300 series stainless steel was used for the seal housing, nosepiece carrier, and bellows. To establish the seal operating length, the bellows spring rate was measured, and the results are given in figure 5 for an undamped bellows seal (fig. 4(a)). In operation, the initial operating seal length was set at 0.525 inch (1.333 cm). Because of the shaft and housing mounting arrangement, thermal expansion tended to reduce the seal length with the result that the operating seal length varied typically from 0.525 to 0.505 inch (1.33 to 1.28 cm) during the run. These lengths were within the range specified by the manufacturer. If the bellows did not relax, the bellows force ranged between 7.5 and 12.0 pounds (33.4 and 53.4 N). Seals with and without dampers have similar spring rates since the damper exerts only a small frictional force on the bellows. In several runs a plastic diaphragm was attached to the nosepiece (fig. 4(c)); thus lubricant could be added only to the bellows and the interface would remain unlubricated, or vice versa.

Procedure

Room temperature and elevated temperature runs were made both with and without Mil-L-7808D lubricant. Seal components were cleaned ultrasonically in alcohol prior to assembly and rinsed off with alcohol after assembly. Leakage rates, temperatures, pressures, seal vibration, and speed were continuously recorded on magnetic tape.

RESULTS AND DISCUSSION

Seal Stability, Bellows Face Seals Without Mechanical Dampers

Table I lists the results obtained when operating a face seal with a bellows secondary (fig. 4(a)) without a friction damper. Inspection of the data indicate that the seal is

(1) Unstable (nosepiece vibrates) when operated without lubrication (runs 1 and 6)

(2) Stable when lubricant is present in the bellows and at the sliding interface (runs 3 and 4) before start of rotation (Lubricant flow was 1 cm^3/min throughout the run.)

(3) Stable when the sliding interface (carbon nosepiece) is lubricated (no lubricant in bellows) (run 5)

(4) Stable when the bellows contains lubricant (no lubricant at interface) (run 7)

As an example of unstable operation, figure 6 shows the transducer outputs of proximity, accelerometer, and pressure probes for the first 100 milliseconds of run 1. Within 3 milliseconds after the start of rotation both the accelerometer and proximity probes indicate the onlet of severe vibration. The proximity probe shows 0.010-inch (0.025-cm) displacement. This amplitude was maintained throughout the run and may have been larger if the proximity probe had not limited the nosepiece travel (also see fig. 2). In general, the frequency was high (700 Hz or higher) during startup and shutdown, but at steady speed operation of 24 000 rpm, the vibration frequency was near rotational frequency (400 Hz). This frequency-to-shaft-speed relation is illustrated in figures 7 and 8. These figures show in detail the vibration frequencies during shutdown. In run 2 (table I) rotation was started with no lubricant and starting lubricant flow after 60 seconds of operation made no detectable change in vibration amplitude or frequency at 24 000 rpm, however the peak frequency at shutdown was lower (fig. 8) than that for the run without lubricant. Except for this peak frequency difference, the two runs were identical.

The seals without mechanical dampers showed the same vibration characteristics in the elevated temperature apparatus as in the room temperature apparatus. The lubricated seals operated in a stable manner, and the unlubricated seals operated in an unstable manner. Table II lists the pertinent data for runs with nitrogen gas and with products of combustion (see APPARATUS AND PROCEDURE section). In these runs the lubricant was added before the start of rotation and was not supplied during operation. As a result, the lubricant evaporated near the end of the 600° and 800° F (589 and 700 K) temperature runs and unstable operation occurred.

Seal Stability, Bellows Face Seals With Mechanical Dampers

Bellows face seals with a mechanical damper (fig. 4(b)) were run in both the room temperature apparatus and the elevated temperature apparatus. The mechanical damper consisted of a thin steel band which rubs against the bellows outside diameter; the resulting friction serves to dampen vibration. The seals with a mechanical damper ran in a stable manner for unlubricated and lubricated operation in nitrogen gas at room temperature and in both nitrogen gas and products of combustion at elevated temperature. These data are given in table III. No unstable operation occurred with these damped seals.

Effect of Vibration on Seal Leakage

Inspection of the data in tables I and II reveal a marked increase in leakage rate when the seal operates in an unstable manner. For example (in table I) the leakage rate is less than 100 standard cubic centimeters per minute (SCCM) for stable operation and is 27 500 standard cubic centimeters per minute for unstable operation. This high leakage rate is due to the nosepiece vibration amplitude which was measured to be 0.010 inch (0.025 cm). There was evidence that the proximity probe was limiting the vibration amplitude (nosepiece insert hitting the probe). When the proximity probe had greater clearance, amplitudes of 0.030 inch (0.076 cm) were indicated.

Unstable seal operation did not cause any extremely detrimental carbon wear or damage; therefore, post-test leakage rates were low and could not be used as a criterion for determining whether the mode of prior seal operation was stable or unstable.

Seal Nosepiece Temperatures

Figure 9 shows carbon nosepiece temperature as a function of operating time. All of the runs of figure 9 were started at room temperature and no external heat was added; therefore, the increase in the nosepiece temperature is due solely to sliding contact at the seal dam. The bellows face seals with mechanical dampers operated without lubrication in a stable manner, but the nosepiece temperature exceeded 700° F (644 K) (limit of recording equipment) very quickly (160 sec in one case and 290 sec in the other) and the maximum temperature reached is unknown. However, when the seal was lubricated at 1 cubic centimeter per minute of lubricant flow, a level-off temperature of 560° F (566 K) was attained. Unstable seal operation results in lower nosepiece temperature (370° F or 461 K) because of intermittent contact. The data indicate that temperatures due to unlubricated sliding contact are high enough to reduce the hardness of the rotating seat, and reduction in seat hardness can lead to excessive wear. As an example, in an allied experiment, a 1.5-inch (2.93-cm) mean diameter seal was operated at 250 feet per second (76 m/sec) in an argon and oil mist environment. The seal seat material was 440 C stainless steal. Hardness measurements on the seal wear track after operation were 53 Rockwell C as compared to the original 57 Rockwell C. Such a reduction in hardness would require a tempering temperature of 1000° F (811 K) (ref. 5). The wear track on the seat was 0.0045 inch (0.0114 cm) deep after 30 hours of operation.

Bellows Fatigue

It is recognized that, in many applications, bellows face seals operate for thousands of hours without bellows fatigue. It is significant, therefore, when bellows fatigue is reached in only seconds of unstable operation. Figure 10 shows the time-temperature history of three seals. One which operated in an unstable mode at room temperature for 630 seconds suffered a 0.015 inch (0.038 cm) reduction (relaxation) in bellows length. The seal which operated unstably at 600° F (589 K) failed within 17.8 seconds; and the seal which operated unstably at 800° F (700 K) failed within 4.4 seconds.

SUMMARY OF RESULTS

Shaft face seals of 1.57-inch (3.99-cm) mean sliding diameter with a bellows secondary seal were run in inert and reducing gaseous environments. Measurements were made of seal stability (nosepiece vibration), leakage rate, and nosepiece temperature. The effect of viscous and coulomb damping on seal stability were studied at temperatures to 800° F (700 K) and sliding speeds to 165 feet per second (50.3 m/sec). The pertinent results are as follows:

1. Seal stability (vibration)

   a. Seals without either friction damping or viscous damping have a very strong tendency to operate in an unstable mode at high frequencies.

   b. Seals with either friction damping or viscous damping operate in a stable manner (no vibration).

   c. For unstable operation the predominant frequency of vibration was near that of shaft rotational frequency (400 Hz) with excursions to near 700 hertz (or higher) during start and stop.

2. Leakage rates: Seals which operated unstably had large (0.010 in. or 0.025 cm) nosepiece vibration amplitudes; hence, leakage rates were excessive.

3. Nosepiece temperature

   a. Unlubricated seals operating in a stable manner and at the manufacturers' recommended bellows compression generated high (>700° F or >644 K) carbon temperatures because of sliding contact at the interface; lubricated seals operating in a stable manner generated much lower (560° F or 566 K) nosepiece temperature.

   b. Temperatures generated by sliding contact can be high enough to reduce the hardness of the seal seat material.

4. Bellows fatigue: Seals operating in an unstable manner cause bellows relaxation at low temperature (75° F or 297 K) operation and bellows cracking in very short periods of operation (4 sec) at elevated temperatures such as 800° F (700 K).

Lewis Research Center,
National Aeronautics and Space Administration,
Cleveland, Ohio, January 24, 1969,
120-27-04-21-22.

REFERENCES

1. Blair, R. W.; Johnson, D. L.; and Morley, J. P.: Metal Bellows Seals. Lubr. Eng., vol. 17, no. 10, Oct. 1961, pp. 470-475.
2. Hudelson, John C.: Dynamic Instability of Undamped Bellows Face Seals in Cryogenic Liquid. NASA TN D-3198, 1966.
3. Hart, Franklin D.; and Zorowski, Carl F.: Onset of Mechanical Separation In Bellows - Supported Rotary Face Seals. Paper 65-GTP-4, ASME, Feb. 1965.
4. Bisson, E. E.; Johnson, R. L.; and Anderson, W. J.: On Friction and Lubrication at Temperatures to 1000° F with Particular Reference to Graphite. Paper 57-Lub-1, ASME, Oct. 1957.
5. Lyman, Taylor, ed.: Heat Treating, Cleaning and Finishing. Vol. 2 of Metals Handbook. 8th ed., ASM, 1964.

TABLE I. - BELLOWS FACE SEAL WITHOUT MECHANICAL DAMPER; OPERATION IN ROOM TEMPERATURE APPARATUS

[Sealed gas, nitrogen; operating speed, 24 000 rpm; sliding speed at mean diameter of sliding dam, 165 ft/sec (50.3 m/sec).]

Run number	Run time, sec	Lubrication	Sealed pressure		Leakage rate, SCCM[a]			Nosepiece temperature		Operation	Vibration frequency, Hz
			lbf/in.^{2}	N/cm^2	Pretest at 5 lbf/in.^{2} (3.4 N/cm^2)	Dynamic	Post test at 5 lbf/in.^{2} (3.4 N/cm^2)	^{o}F	K		
1	300	None	[b]0.80	[b]0.55	<10	27 500	12	380	466	Unstable	450
2	300	None at start; lubricant added 60 sec into run	[b]0.80	[b]0.55	12	26 500	10	395	475	Unstable	395
3	360	Lubricant flow started 60 sec before start of run	2	1.38	10	<100	<10	524	546	Stable	---
4	540	Lubricant flow started 60 sec before start of run	2	1.38	<10	<100	<10	590	583	Stable	---
5	60	No lubricant in bellows; carbon wetted with lubricant	2	1.38	---	----	---	---	---	Stable	---
6	30	None	2	1.38	---	----	---	---	---	Unstable	---
7	60	No lubricant on carbon nosepiece, lubricant in bellows	2	1.38	---	----	---	---	---	Stable	---

[a]Leakage rate related to standard conditions of 14.7 lbf/in.^{2} (10.1 N/cm^2) and 68^{o} F (293 K); SCCM = standard cm^3/min.
[b]High leakage due to unstable operation caused reduction in sealed pressure from 2 to 0.8 lbf/in.^{2} (1.38 to 0.55 N/cm^2).

TABLE II. - BELLOWS FACE SEAL WITHOUT MECHANICAL DAMPER; OPERATION IN ELEVATED TEMPERATURE APPARATUS

Run number	Run time, sec	Lubrication	Sealed pressure		Sealed gas	Nosepiece temperature				Shaft speed, rpm	Leakage rate, SCCM[a]			Operation
			lbf/in.^{2}	N/cm^2		Starting		Maximum			Pretest at 5 lbf/in.^{2} (3.4 N/cm^2)	Dynamic	Post test at 5 lbf/in.^{2} (3.4 N/cm^2)	
						°F	K	°F	K					
8	67	None	2	1.38	N_2	80	300	340	444	5 000	<10	18 500	-----	Stable 4.8 sec; unstable 62.2 sec
9	68	None	2	1.38	N_2	140	333	332	440	5 000	----	17 200	-----	Unstable
10	210	Lubricant added before start of run[b]	2	1.38	N_2	80	300	---	---	5 000	----	650	-----	Stable
	110	↓				---	---	---	---	10 000	----	765	-----	↓
	170					---	---	---	---	15 000	----	700	633	
11	65	Lubricant added before start of run[b]	2	1.38	N_2	89	305	210	372	15 000	770	905	790	Stable
	79	↓	↓	↓	↓	200	366	368	460	↓	790	730	870	↓
	74					400	478	416	486		870	<500	-----	
	84					500	533	516	542		470	<500	-----	↓
	40					600	589	659	621		220	[d]17 200	-----	Unstable after 22 sec due to evaporation of lubricant
12	66	None	2	1.38	N_2	200	366	429	494	15 000	<10	<500	410	Stable 64.6 sec; unstable 1.4 sec
13	4.5	None	2	1.38	N_2	200	366	---	---	3 000	410	-----	1 600	Unstable 4 sec
14	10	None	2	1.38	POC[d]	400	478	---	---	3 000	1340	13 000	86	Stable 3.5 sec; unstable 6.5 sec
15	80	Lubricant added before start of run[b]	2	1.38	POC[d]	400	478	448	504	15 000	----	1 180	-----	Stable
	80	↓	4	2.76	↓	---	---	487	526	↓	----	1 570	-----	↓
	80		6	4.14		---	---	603	590		----	1 350	-----	
	70		8	5.58		---	---	675	630		----	1 735	-----	
	188	↓	2	1.38	↓	---	---	548	560	↓	----	<500	160	↓
16	80	Lubricant added before start of run[b]	2	1.38	POC[d]	600	589	665	625	15 000	<500	388	-----	Stable
	80	↓	4	2.76	↓	↓	↓	685	636	↓	----	429	-----	↓
	60		6	4.14				754	674		----	456	-----	
	60		8	5.52				812	706		----	741	-----	
	64	↓	2	1.38	↓	↓	↓	799	699	↓	----	<500	190	↓
17	6.6	No lubricant added	2	1.38	POC[d]	800	700	---	---	3 000	<500	-----	[e]7 500	Stable 2.2 sec; unstable when lubricant evaporated
18	220	Lubricant added	2	1.38	POC[d]	800	700	---	---	15 000	[e]7130	7 690	[e]12 000	Stable operation, bellows cracked during instability of run 17

[a]Leakage rate related to standard conditions of 14.7 lbf/in.^{2} (10.1 N/cm^2) and 68° F (293 K); SCCM = standard cm^3/min.

[b]2 cm^3 of lubricant was added to bellows region (see fig. 3) before rotation. No further lubricant was added during run.

[c]After 22 sec.

[d]POC = products of combustion: 24.7 percent CH_4, 0.7 percent CO, 0.7 percent CO_2, 40.0 percent H_2, 25.7 percent N_2, and 8.2 percent H_2O.

[e]Cracked in bellows.

TABLE III. - RESULTS OF OPERATION OF BELLOWS FACE SEAL WITH MECHANICAL DAMPER

[Sealed pressure, 2 lbf/in.^{2} (1.38 N/cm^2).]

Run number	Run time, sec	Lubrication	Sealed gas	Nosepiece temperature				Shaft speed, rpm	Leakage rate, SCCM[a]			Operation
				Starting		Maximum			Pretest at 5 lbf/in.^{2} (3.4 N/cm^2)	Dynamic	Post test at 5 lbf/in.^{2} (3.4 N/cm^2)	
				°F	K	°F	K					
Room temperature apparatus												
19	300	None	N_2	75	297	---	---	24 000	<10	<100	<10	Stable
20	300	None	N_2	75	297	---	---	24 000	<10	<100	<10	Stable
21	300	None	N_2	75	297	---	---	24 000	<10	<100	<10	Stable
22	300	None	N_2	75	297	>700	>644	24 000	<10	<100	<10	Stable
23	300	None	N_2	75	297	>700	>644	24 000	<10	<100	<10	Stable
24	300	Lubricated	N_2	75	297	370	461	24 000	<10	<100	<10	Stable
25	480	Lubricated	N_2	75	297	562	568	24 000	<10	<100	<10	Stable
Elevated temperature apparatus												
26	66	None	N_2	74	296	285	414	15 000	<10	<500	<10	Stable
	67	↓	↓	200	366	374	463	↓	---	530	---	↓
	116			400	478	555	564		---	<500	---	
	77			500	533	610	594		---	<500	---	
	69			600	589	649	616		---	500	---	
	312			600	589	797	698		---	220	---	
27	68	None	POC[d]	300	422	519	544	15 000	86	<500	100	Stable
	68	↓	↓	600	589	721	656	↓	106	596	20	↓
	313			714	652	780	689		---	<500	95	
	280			796	698	871	739		133	<500	---	

[a]Leakage rate related to standard conditions of 14.7 lbf/in.^{2} (10.1 N/cm^2) and 68° F (293 K); SCCM = standard cm^3/min.

[b]POC = products of combustion: 24.7 percent CH_4, 0.7 percent CO, 0.7 percent CO_2, 40.0 percent H_2, 25.7 percent N_2, and 8.2 percent H_2O.

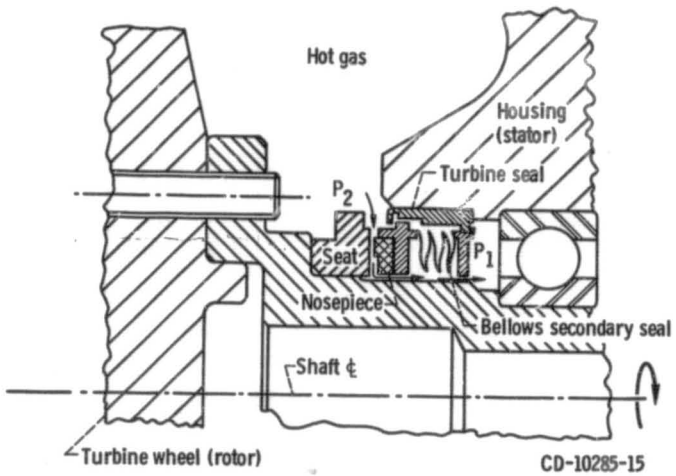

Figure 1. - Cross-sectional view of face seal in turbopump.

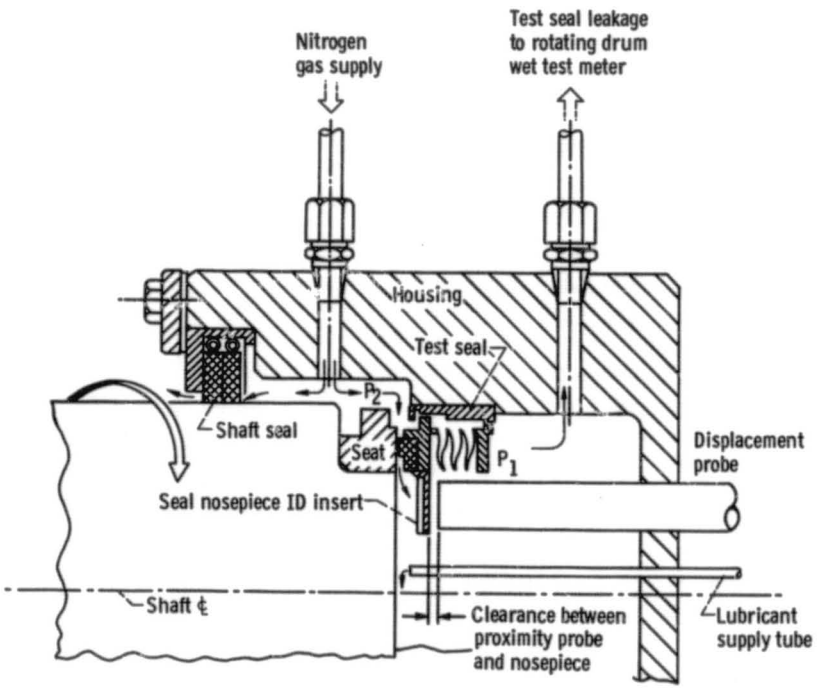

Figure 2. - Cross-sectional view of room temperature seal test apparatus.

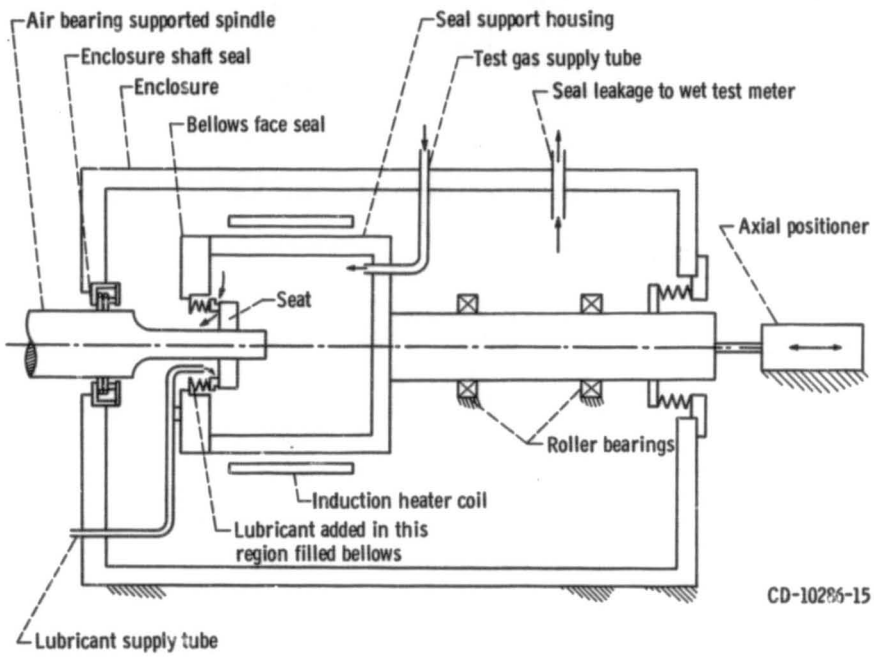

Figure 3. - Elevated temperature seal test apparatus.

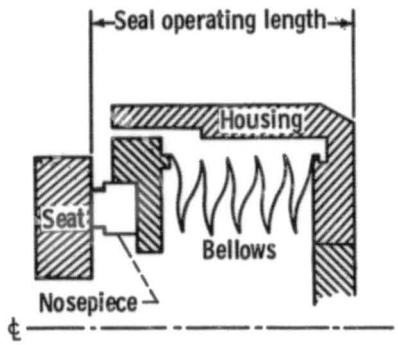

(a) Face seal with bellows secondary seal.

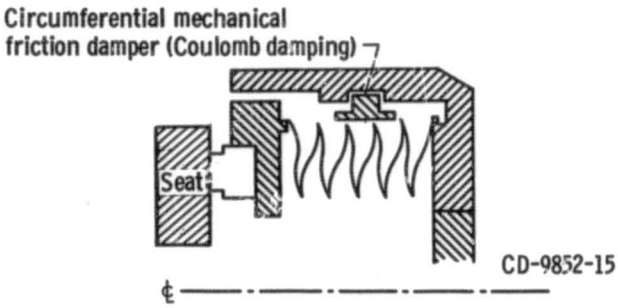

(b) Face seal with damper on bellows.

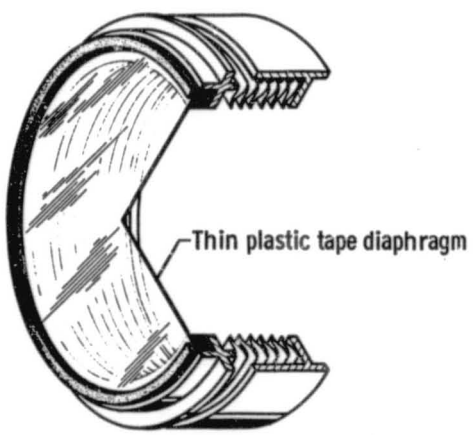

(c) Bellows face seal with diaphragm to separate interface area from bellows area.

Figure 4. - Shaft face seals.

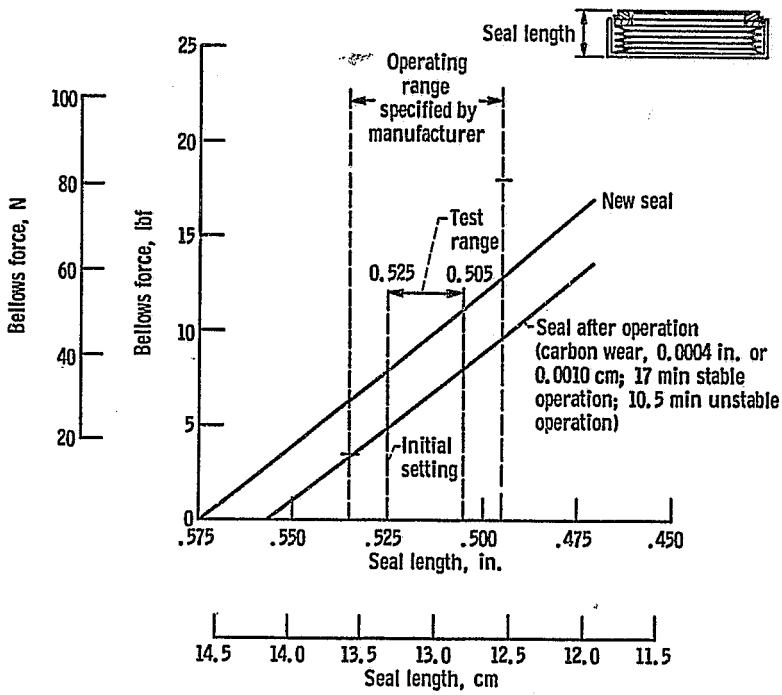

Figure 5. - Bellows spring rate.

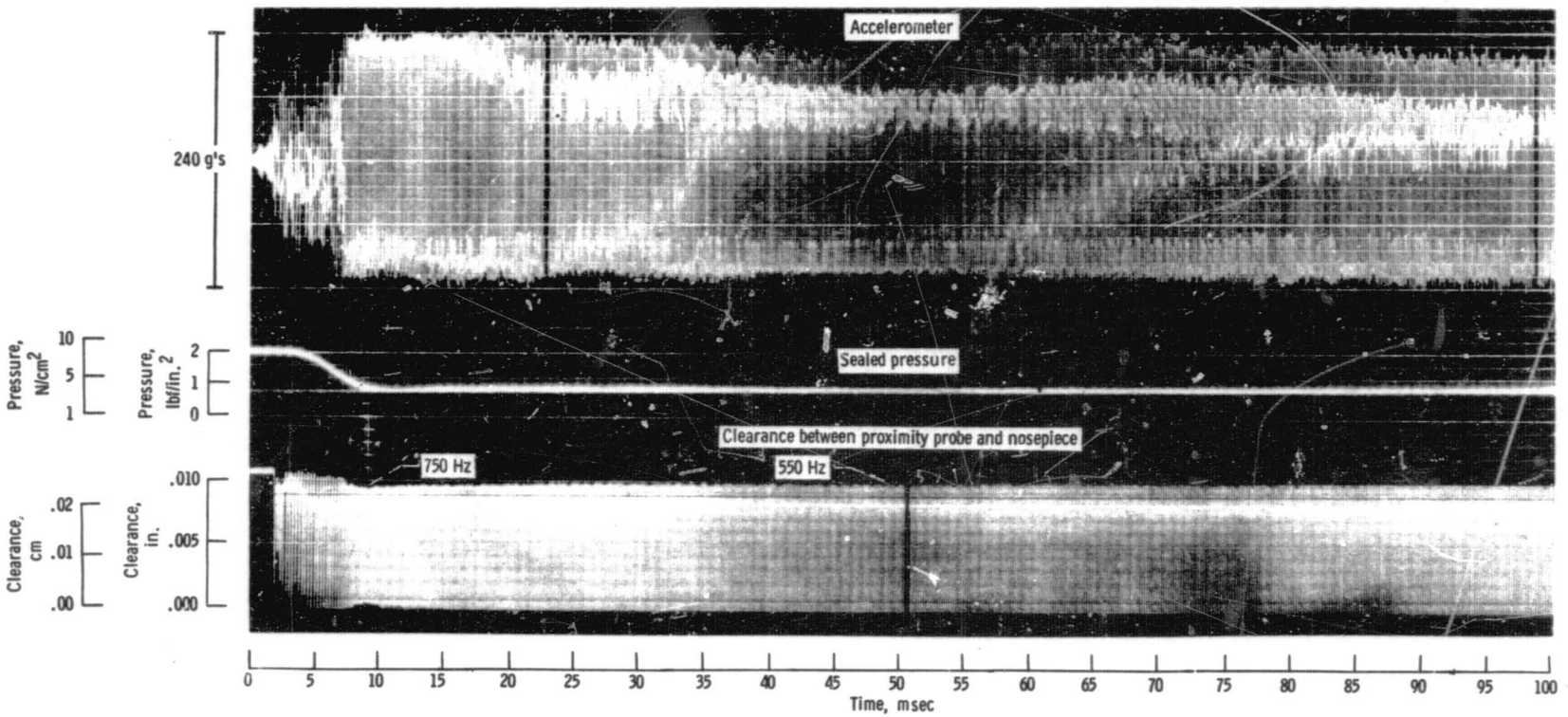

Figure 6. - Typical transducer outputs of accelerometer, pressure, and proximity probe for a seal during unstable operation. No lubricant; sealed gas, nitrogen at room temperature.

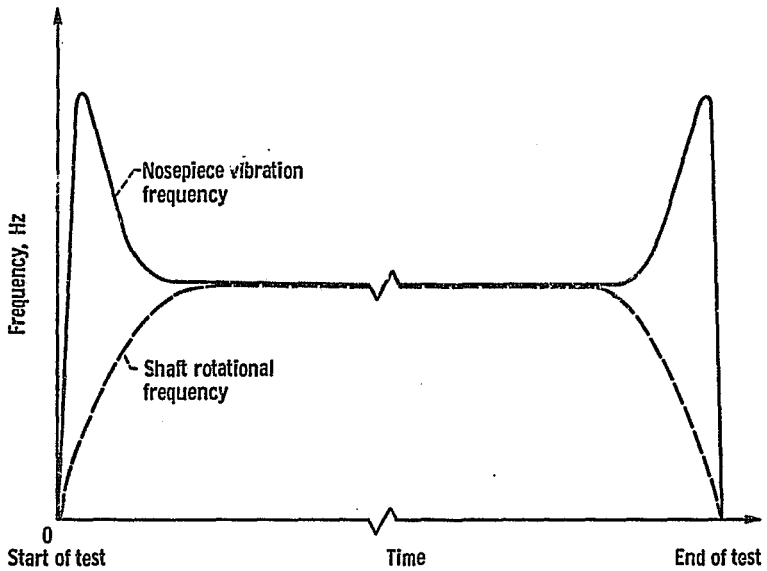

Figure 7. - Typical nosepiece and shaft rotational frequency relation exhibited during unstable seal operation. Sealed gas, nitrogen; no external heat added; no lubricant.

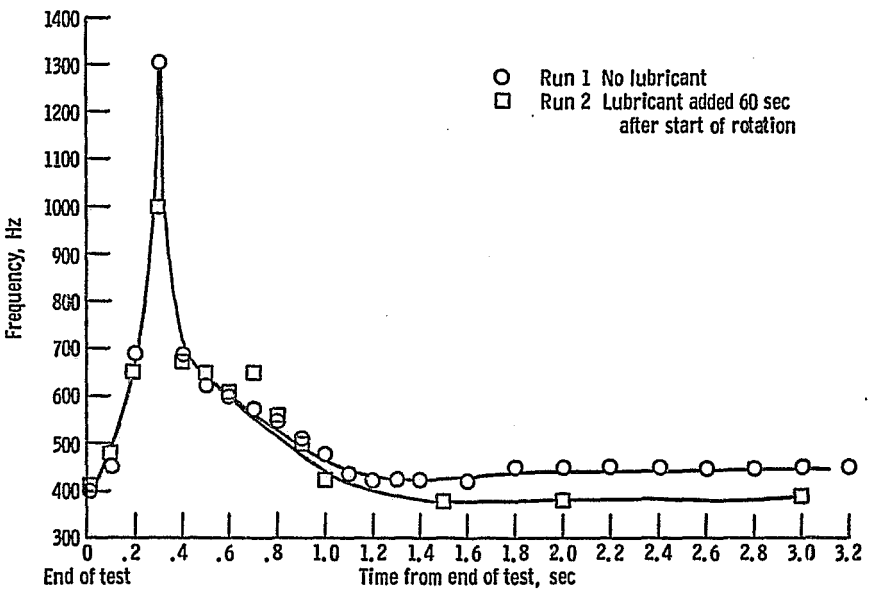

Figure 8. - Predominate seal vibrational frequency during shutdown.

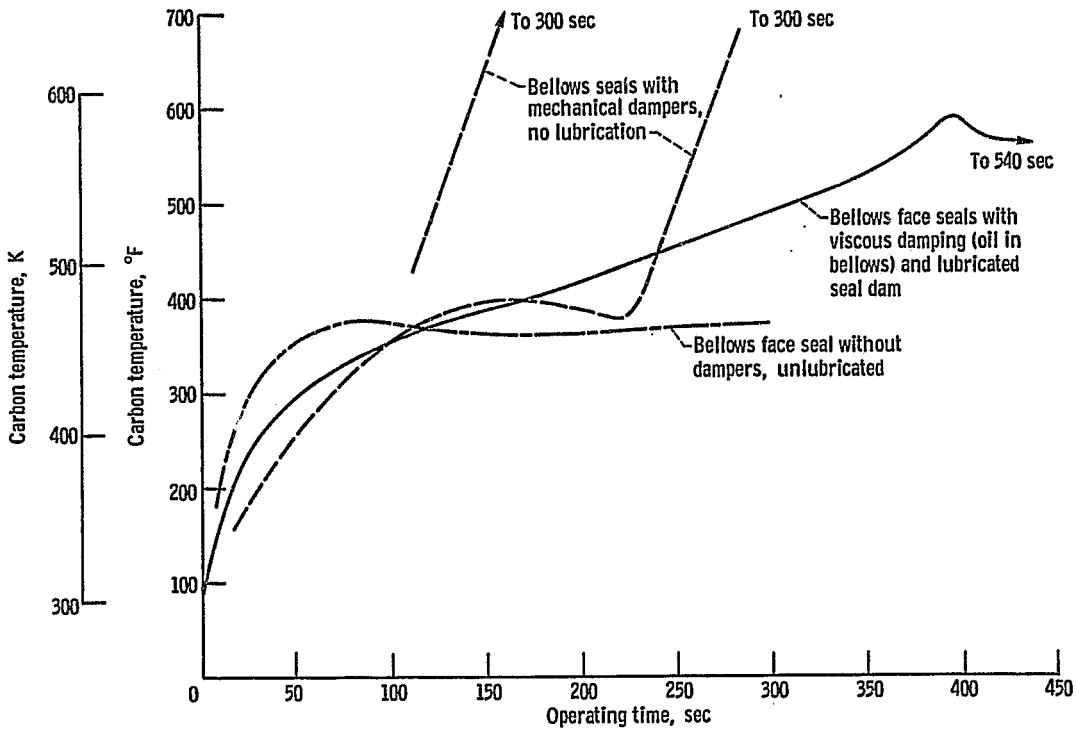

Figure 9. - Carbon nosepiece temperatures. Sealed gas, nitrogen; shaft speed, 24 000 rpm; no external heat.

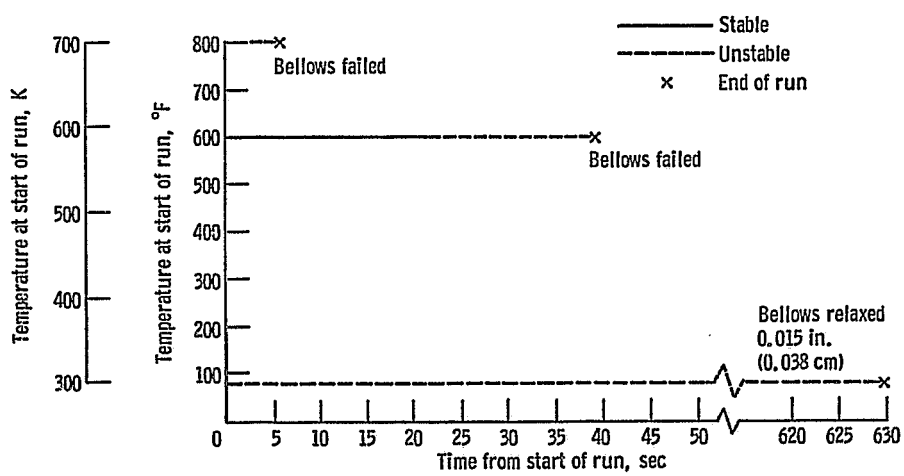

Figure 10. - Bellows fatigue as function of time and temperature. No lubrication; no mechanical or viscous damping.

NASA-Langley, 1969 — 15 E-4830

END OF REFERENCE

118

REFERENCE

119

KAUFFMANN, W. M.: SAFE OPERATION OF OXYGEN COMPRESSORS. CHEMICAL ENGINEERING, VOL. 76, NO. 23, OCT. 20, 1969.

REPRINTED BY SPECIAL PERMISSION FROM CHEMICAL ENGINEERING, OCTOBER 20, 1969, COPYRIGHT (C), 1969, BY McGRAW-HILL, INC., NEW YORK, NY 10036.

C71-04360

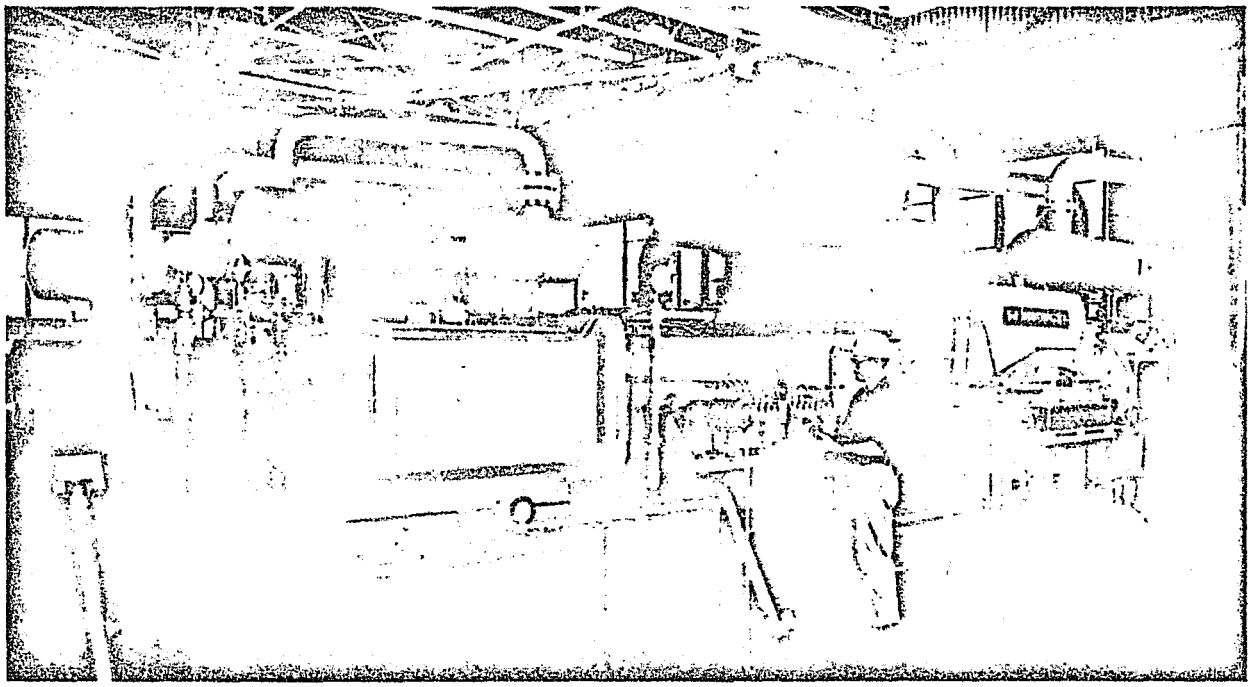

Safe Operation Of Oxygen Compressors

When only fingerprints on a cylinder can cause a violent fire, what special design features, fabrication precautions and maintenance procedure are required to keep oxygen compressors operating safely?

WILLIAM M. KAUFFMANN, Consulting Engineer

Supervisors and engineers who operate oxygen compressors are usually aware of the safety precautions required. Too often, however, because compressors are the heart of oxygen operations, they are overhauled on a crash basis. When this happens, supervisors become tempted to expedite repairs by taking shortcuts on the seemingly tedious procedures and precautions that are always recommended by manufacturers for the servicing of oxygen-handling compressors.

Continual shifting of operations personnel and turnover in millwrights and mechanics also create situations that result in dangerous relaxations of established safety practices.

Oxygen equipment should not be treated casually. Although oxygen serves man in the air he breathes and the water he drinks, in its pure form it is a potentially violent oxidant.*

Once, a vendor representative, called into a plant to supervise the reassembling of an oxygen com-

* Bulletin No. 259, which has been issued by the U. S. Dept. of Labor in its Environmental and Chemical Hazard Series and which deals with the use and handling of compressed gasses, offers valuable information on the hazards of oxygen; copies of it can be obtained from the U. S. Government Printing Office, Washington, D. C.

pressor, arrived to find millwrights installing the piston with bare hands. When his protests went unheeded, he left abruptly. Shortly afterwards, a telegram arrived at his office informing him that the compressor had burned and was a total loss. Fingerprint grease on the piston had contaminated the cylinder sufficiently to cause ignition.

Safe Maintenance and Operation

Engineers and maintenance personnel should know not only what to guard against in oxygen compressor maintenance and operations, but also what manufacturers provide in the way of a safe compressor, from both the standpoint of design and fabrication.

Specifically, the following questions will be answered:

- What design features and fabrication procedures that contribute to safe, reliable compressor operation should operating and maintenance personnel know about especially?
- What should supervisors know to keep oxygen compressors operating efficiently and safely?
- What kind of repair program will contribute to safe and efficient compressor operation?

A repair program and procedures for safe startup and operation will be reviewed. This will cover preparation for overhaul, inspection procedure and work schedule, contaminant detection and evaluation, assembly procedure, and starting up and running in the compressor.

Design for Safety

Compressors for oxygen service differ from other types because they incorporate the following major features: (1) nonlubricated components, including TFE* piston rings, piston-rider rings and rod packing; (2) extended frame housing with a sealed and vented packing section and double oil-scraper rings; (3) special nonlubricated valve assemblies; (4) TFE-fitted diaphragm unloaders; and (5) TFE-honed cylinders.

The cylinder of a modern oxygen compressor is designed to operate with components made of self-lubricating materials such as glass-filled TFE.

For additional protection, the cylinder is also separated from the compressor frame by an extra-long distance piece. Also, an oil slinger, clamped on the piston rod, blocks off contaminants that may pass the scraper rings of the crankcase (Fig. 1). The distance piece is long enough that the oil slinger travels full stroke in the housing. A double distance piece with an oil slinger in each provides additional safety.

Finishes are finer and tolerances closer than in lubricated compressors because mating surfaces of self-lubricating materials cannot otherwise seal off small extrusion leakage. Cylinder bores are honed

* Tetrafluoroethylene, also Teflon.

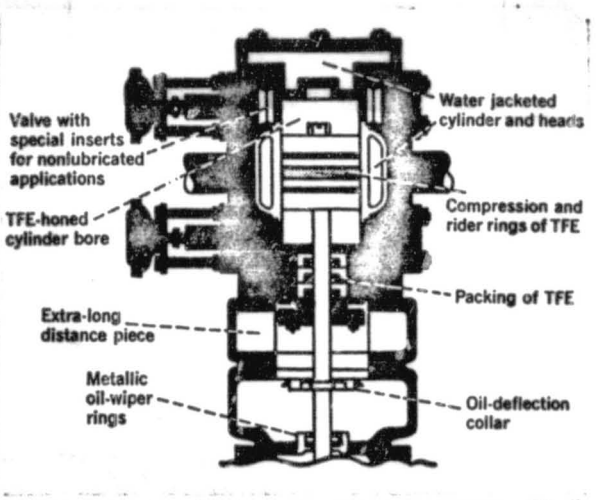

INTERNALS of nonlubricated oxygen compressor—Fig. 1

to a 10-to-20 microin. finish, then with TFE to provide a compatible wearing surface.

Cylinders are rust-proofed with a coating of manganese phosphate, which permeates the iron surface and renders it impervious to oxidation. Piston rods are normally surface hardened in the packing area (to a nominal hardness of 55 Rockwell C); and ground to an 8-to-15 microin. finish.

Ring and Rider-Ring Assembly

Wearing parts of cylinders for oxygen service are mostly of glass-filled TFE. The trend is to solid (one piece) piston-rider, or wear, rings. Two types of jointless rider rings are now mostly used, both appropriately nicknamed "rubberband." One type is expanded and forced over the piston and into the ring grove by means of a taper mandrel. If correctly installed, this ring contracts fully into the groove in an hour or less. The other type, already expanded on a mandrel whose inside diameter is slightly larger than that of the piston, is pressed off the mandrel onto the piston and into the groove. If the ring contracts too slowly, heat is applied to it.

The most widely accepted nonlubricated piston-ring configuration is the step-cut (or butt-cut) one-piece piston ring. This type is usually selected for oxygen service because of ease of assembly, low cost and simplicity of parts replacement. Because spring expander rings are not required, the possibility of metal-to-metal contact is eliminated if ring wear is excessive. For pressures above 1,500 psi., special designs that provide pressure balancing extend ring life.

Valves and Unloaders

Valves for nonlubricated operation are equipped with replaceable TFE nubs at the ends of the strip profiles. Valve seats and guards, at both suction

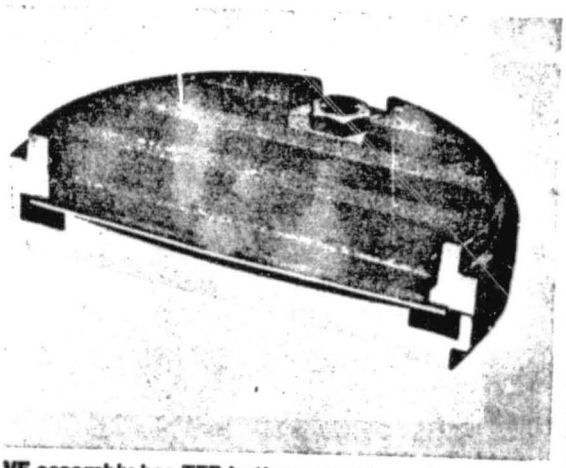

VALVE assembly has TFE buttons at strip ends—Fig. 2

and discharge, are also chemically treated to resist oxidation (Fig. 2).

Load control in oxygen compressors is accomplished by external diaphragm-operated unloading elements, which consist of a springloaded finger assembly that prevents the strips from seating during unloading. The sliding members of the actuating elements are guided in TFE sleeves, which provide lubrication.

The external diaphragm casing is mounted above the unloading assembly, and the actuating stem is sealed with TFE packing. Because the seal gland is open to the atmosphere, it can be easily inspected while the compressor is operating.

Building in Safety

The key to operational safety is the "clean room" of the compressor manufacturer. It is here that all compressor parts that will come in contact with oxygen are cleaned (with a special detergent solution), inspected, assembled and protectively wrapped. Cylinders, ports and passages are rustproofed, and openings sealed and bores protected with a special vapor-inhibiting paper.

Protection often extends to double wrapping of parts in the special vapor-inhibiting paper, and covering everything with an outer-wrap of polyethylene, which is held in place with a special waterproof tape suitable for oxygen service.

Before shipment, cylinders and openings are charged with a special vapor-inhibiting powder that prevents the accumulation of moisture and condensation in them.

Installation for Safety

Setting up a compressor in a plant requires continuing checks for cleanliness. Parts that will come in contact with oxygen should be thoroughly chipped or shot-blasted to remove all weld slag, scale and other deleterious substances. Acid cleaning to remove rust should follow dipping in a stripping tank to take off paint or other coatings.

After acid cleaning and phosphatizing, the parts should be dried and protective coating applied. Flanged openings should be blanked off with heavy gaskets. Each pipe and pressure vessel prefabricated by the manufacturer should be tagged to show that it has been cleaned and protected for oxygen service. Such protection should not be taken off until after the last connection has been made.

Intercoolers, aftercoolers and interstage piping should be similarly handled.

No Shortcuts in Preparation

More time will be needed to properly service and overhaul an oxygen compressor than, for instance, an air compressor, except for the crankcase, which can be handled routinely. This is because the gear in the crankcase does not come in contact with oxygen, which is why it is oil lubricated.

However, special procedures must be followed when stripping down cylinders, removing pistons and piston rods, valves and unloader assemblies.

Preparations for servicing critical parts should be made before disassembly, including the following:

- Work tables should be clean and completely covered with the special vapor-inhibiting paper, which should be secured with a tape suitable for oxygen service.
- Cleaning tanks should be provided for two separate rinses of an inhibited 1,1,1-trichloroethane solution. A tank containing fluid for blacklight inspections for contamination should also be available.
- Tools should be thoroughly cleaned in the aforementioned tanks and placed in a clean location. Before the tools are used, they should be checked for contamination under the blacklight, and periodically afterwards.
- All compressor parts that will contact oxygen should only be handled by millwrights who wear clean, white cotton-canvas gloves, especially after the parts have been cleaned and when they are being assembled.
- Clothing worn by the maintenance crew should be clean and free of grease or oil.
- A 3,200-3,800 angstrom blacklight should be on hand for examining parts after they have been cleaned.
- Dry nitrogen should also be available for blowing off or drying parts. Compressed air from the plant system should never be used for cleaning or drying parts.

Inspections at Overhauls

Systematic inspection is mandatory before and during the assembling of the cylinder and its associated parts. For finding contamination, a 3,200-3,800 angstrom blacklight is indispensable. The light will

reveal hydrocarbon or dirt contamination as a fluorescent smear, smudge or blot. Contaminated parts must be cleaned until the fluorescence disappears.

The cleaning fluid should also be checked periodically. This can be done by placing a sample of it on a blotter and examining it under the blacklight. Contaminants in excess of 100 ppm. will cause the fluid to glow, in which case it should be replaced.

Parts and tools should be inspected under a blacklight during the assembling of the compressor, and contamination removed by cleaning and scrubbing. Brushes should be of bronze or stainless steel, never of a synthetic material. (A typical overhauling of an oxygen compressor consists of the steps shown in the box on this page.)

Starting Up Is Critical

Oxygen compressors are normally started up on dry nitrogen. Atmospheric air should never be used. The nitrogen should not only be dry, but also should have been compressed by a machine that also does not require lubrication so as to eliminate the possibility of hydrocarbon contamination.

During the startup, the upper and lower valve should be left out of each cylinder. Water jackets should also be filled, then the water flow stopped. Next, the compressor should be turned over by hand several times. The crankcase oil should be checked for proper type and level.

Before starting the compressor, make sure the suction and discharge valves have been properly placed in the cylinder. Serious damage and loss of capacity can result if they are improperly installed. Also, check that the valve locking screws are tight and the gaskets correctly in place, both for the valve seats and valve covers.

Bump the motor by power and check for proper rotation. If it is correct, bump the motor again; count three seconds; then press the stop button. All this time, be checking the oil pressure gage. By the time the compressor stops, oil pressure should register on the gage. If it does, start the compressor again. If the driver is a synchronous motor, be sure the exciter is on when it synchronizes. Check that proper field d.c. amperage is applied either through fixed taps or manual rheostat control. Check the motor nameplate for the a.c. voltage and amperage and the d.c. voltage and amperage required to properly operate the motor.

Run the compressor for five minutes, observing all the gages. Then shut it down by tripping the oil pressure switch. This tests whether it is properly wired into the stop circuit. Also check bearings, connecting rods and piston rods for abnormal heat.

Next, start the compressor again and run it for 10 minutes. Then shut it down again for the aforementioned checks. If everything appears to be satisfactory, start it again and run it for 20 minutes before shutting it down and repeating the heat check. If the temperatures are acceptable, start it up and run it for one hour before shutting down and repeating the heat check.

The piston rod temperature should not rise over 140 F. They usually run fairly hot in nonlubricated packing. By now, the water jackets will show signs of warming. Flow should be adjusted as required until pressure begins to build up.

If the compressor is two stage, the first stage valves should now be installed and the machine started up again. After the second stage has been blown through for 10 minutes, the compressor should be shut down and the second stage valves installed.

The final discharge bypass to the first stage should now be opened and dry nitrogen admitted. The compressor should then be started again and nitrogen circulated around the loop for about two hours or until the pressure rises to approximately 10 psi. Then the compressor should be shut down and the heat check repeated.

Finally, start the compressor again and begin closing the bypass of the suction valve to build up pressure. Admit additional nitrogen to hold 2-to-6 psi. suction pressure. After checking operating conditions, build up the load 10%/hr. of the final discharge, while at the same time maintaining the proper suction pressure.

After the proper loading at the final discharge has been reached and the compressor is running satisfactorily, unload and load it to check out the unloader elements. Be sure interstage pressure is correct for multistage machines.

Adjust the water flow through the cylinders so that the outlet temperature from the final stage will be from 110-to-115 F. Crankcase oil temperatures should be about 120-to-140 F. After operating con-

Oxygen Compressor Overhauling Checklist

- ☐ Removing valves, covers and gaskets, which must be protected from dirt and moisture.
- ☐ Taping unloader-pipe openings with special tape.
- ☐ Removing and tagging water lines.
- ☐ Removing the cylinder head.
- ☐ Opening the frame to expose the piston rod and crosshead.
- ☐ Tramming the rod to the crosshead and checking the crosshead guide clearance; tramming is not necessary if the piston rod is flanged-bolted to the crosshead.
- ☐ Loosening the lock and crosshead nut and removing the rod and piston.
- ☐ Removing packing, cases and oil scraper rings.
- ☐ Inspecting and measuring the cylinder bore.
- ☐ Checking piston grooves for wear, and the rings for end gaps.
- ☐ Checking the piston rod for runout and wear at packings.
- ☐ Servicing valves and replacing worn parts.

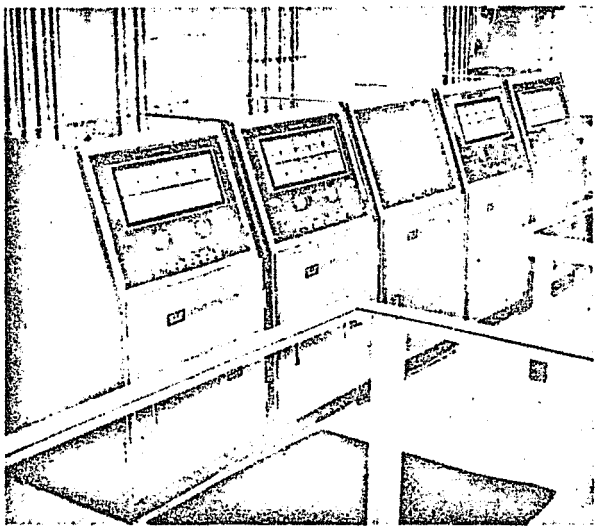

CENTRALIZED stations improve safety control—Fig. 3

ditions are satisfactory on dry nitrogen, oxygen can be introduced into the compressor.

It is important to continue a close watch of all the operational data, including especially the pressures and temperatures of water and oil and at the interstage coolers and the final discharge.

Continuing Maintenance Assures Safety

Once an oxygen compressor has been put into operation, it should be the object of a rigorous preventive maintenance program. Vendor representatives who specialize in overhauling oxygen compressors are usually available to train plant personnel in preventive maintenance practices. Often overlooked is the valuable guidance in the proper maintenance of oxygen compressors offered in manufacturers' instruction booklets.

Safe compressor operations demand alert and conscientious maintenance. Compressor fires have resulted because valves and packing rings were not correctly assembled or installed. Inoperable safety devices have also led to considerable damage. Such devices should be checked frequently to ensure their proper operation.

During normal operation, the following items should be vigilantly checked: cooling water flow; crankcase oil level, pressure and temperature; operation of controls and control pressure; suction and discharge pressures and temperatures; unusual noises; and motor loading and temperature.

If a portable blacklight is available, checking the piston rod between the frame and the cylinder will reveal the presence of contamination in the distance piece, such as that which would appear if the scraper rings became worn. Such inspections should be scheduled according to length of service and to accommodate work schedules.

Fires have been caused by cylinder hot spots when cylinder-jacket water passages have become clogged with sludge or scale. Jackets, coolers and the packing-case cooling system should be inspected each time the compressor is overhauled. Clean surfaces will result in cooler operation and greater safety. Water treatment is essential to control scale and sediment deposits.

A daily log of compressor operations is essential for maintenance efficiency, especially with multistage units. At least the following should be recorded: (1) suction, discharge and interstage temperatures and pressures; (2) inlet, outlet and interstage water jacket temperatures; (3) temperature and pressure of lubricating oil to frame bearings; (4) motor load, amperage and voltage; (5) ambient temperature; and (6) date and time.

From such a log, a supervisor can note changes in pressure or temperature that signal a malfunction in the system. Prompt corrective action often can prevent serious trouble later.

Frequent checks of the open housing between the cylinder and crankcase with a blacklight for possible contamination and oil carryover from the crankcase into the housing should also be continued.

Safety Devices Offer Insurance

Compressor safety controls are rapidly being incorporated into centralized control stations. Such controls offer the means for the rapid assessment of a malfunction and its location. They may also automatically initiate alarms and shutdowns. One set of points may be set up to set off an alarm and trigger an amber warning light; then, if the malfunction continues, the alarm sounds a second time, actuates a red light and shuts down the compressor. Another set of more-critical points may actuate an alarm and red light and shut down the compressor immediately (Fig. 3).

The following conditions are generally arranged to lead to only a delayed shutdown: excessive interstage gas temperature; low oil level in crankcase; high final-discharge gas temperature or pressure; and excessive frame oil temperature.

An immediate alarm and shutdown is usually arranged for the following conditions: failure of frame oil pressure; excessive vibration; and lack of cooling water flow. ■

Meet the Author

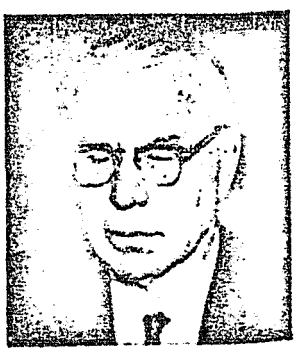

William M. Kauffmann, now a consultant (2577 Nottingham Dr., Parma, Ohio 44134), was formerly a regional representative in customer service for Worthington Corp. During his 31 yrs. with Worthington, he had also been manager of research and chief engineer of its engine division.

A holder of a mechanical engineering degree from Armour Tech (now Illinois Institute of Technology), he is a member of ASME, National Society of Professional Engineers and Society of Automotive Engineers.

END OF REFERENCE

119

REFERENCE

120

SMITH, G. M.: HIGH PERFORMANCE SPACE SHUTTLE AUXILIARY PROPELLANT VALVE PROGRAM. REP. R-9078, ROCKETDYNE DIV., ROCKWELL INTERNATIONAL. (NASA CR-120976), 1973.

8.5-0-0

N73 24516

HS

NASA CR-120976

R-9078

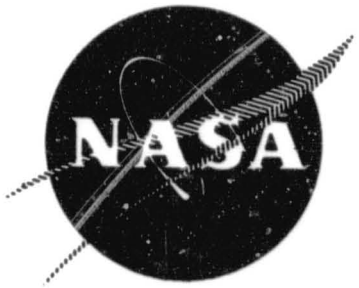

HIGH-PERFORMANCE SPACE SHUTTLE AUXILIARY PROPELLANT VALVE PROGRAM

By

G. M. Smith

LEWIS RESEARCH CENTER
Aerospace Safety Research
and Data Institute
AUG 31 1973
CLEVELAND, OHIO

ROCKETDYNE DIVISION
ROCKWELL INTERNATIONAL

prepared for

NATIONAL AERONAUTICS AND SPACE ADMINISTRATION

NASA-Lewis Research Center
NAS3-14350
Rudy E. Grey, Project Manager

NOTICE

This report was prepared as an account of Government-sponsored work. Neither the United States, nor the National Aeronautics and Space Administration (NASA), nor any person acting on behalf of NASA:

A. Makes any warranty of representation, expressed or implied, with respect to the accuracy, completeness, or usefulness of the information contained in this report, or that the use of any information, apparatus, method, or process disclosed in this report may not infringe privately-owned rights; or

B. Assumes any liabilities with respect to the use of, or for damages resulting from the use of, any information, apparatus, method or process disclosed in this report.

As used above, "person acting on behalf of NASA" includes any employee or contractor of NASA, or employee of such contractor, to the extent that such employee or contractor of NASA or employee of such contractor prepares, disseminates, or provides access to any information pursuant to his employment or contract with NASA, or his employment with such contractor.

Requests for copies of this report should be referred to

National Aeronautics and Space Administration
Scientific and Technical Information Facility
P.O. Box 33
College Park, Md. 20740

1. Report No.	2. Government Accession No.	3. Recipient's Catalog No.
NASA CR-120976		

4. Title and Subtitle	5. Report Date
HIGH-PERFORMANCE SPACE SHUTTLE AUXILIARY PROPELLANT VALVE PROGRAM	June 1973
	6. Performing Organization Code
7. Author(s)	8. Performing Organization Report No.
G. M. Smith	R-9078
	10. Work Unit No.
9. Performing Organization Name and Address	
Rocketdyne Division, Rockwell International Canoga Park, California 91304	11. Contract or Grant No. NAS3-14350
	13. Type of Report and Period Covered
12. Sponsoring Agency Name and Address	Contractor Report
National Aeronautics and Space Administration Washington, D. C. 20546	14. Sponsoring Agency Code

15. Supplementary Notes

Project Manager, Rudy E. Grey, NASA-Lewis Research Center, Cleveland, Ohio

16. Abstract

Several potential valve closures for the space shuttle auxiliary propulsion system (SS/APS) have been investigated analytically and experimentally in a modeling program. The most promising of these were analyzed and experimentally evaluated in a full-size functional valve test fixture of novel design.

The engineering investigations conducted for both model and scale evaluations of the SS/APS valve closures and functional valve fixture are described. Preliminary designs, laboratory tests, and overall valve test fixture designs are presented, and a final recommended flightweight SS/APS valve design is presented.

17. Key Words (Suggested by Author(s))	18. Distribution Statement
Valve Closures Long Life Fast Response Low Leakage	

19. Security Classif. (of this report)	20. Security Classif. (of this page)	21. No. of Pages	22. Price*
Unclassified	Unclassified	326	

* For sale by the National Technical Information Service, Springfield, Virginia 22151

SS/APS VALVES PROGRAM

ANALYSIS AND CONCEPTUAL DESIGN

The design requirements of Table I established the need for: (1) basic valve mechanism and closure concept studies and (2) an initial valve design trade study from which the contract effort would draw its direction. Based on these results, model closure concepts were analyzed and designed along with a unique closure screening tester to enable an evaluation of merit of the various closure concepts. These initial analyses and conceptual designs, then, pointed the way for a logical progression of effort toward the final program objectives: SS/APS flightweight valve design.

TRADE STUDY

Valving Concepts Study

A trade study covering past and potential performance of closures, actuators, seals, and other related supporting parts was initially a major item of effort. The trade study used the design requirements of Table I on a "no exceptions" basis to establish evaluation criteria for use in review of the various concepts. These criteria consisted of primary criteria selected on the basis of fundamental requirements, avoiding specific constraints that would limit the scope of a preliminary trade study. Secondary criteria were compiled on the basis of hardware and operational considerations for a more refined screening of candidate design concepts. Design concepts reviewed were listed in broad categories of single poppet valves, single rotary valves, miscellaneous valves, and bipropellant valves.

The actual valving types considered in the trade study are shown in Table II, with corresponding actuation concepts shown in Table III. Conventional butterfly, ball, and blade valves could not meet the long-life, low-leakage requirements because of seal wear factors. The diaphragm materials available would not meet the temperature requirements, and the spool valve basically will leak too much to be considered. Electric motors for the size and response required are too cumbersome and heavy and a direct solenoid of the size needed is not feasible from power, weight, and response considerations.

The question of monopropellant versus bipropellant valves was then considered. In any discussion of linked bipropellant and monopropellant valves, one of the primary topics involves weight of the respective valves. Typically, a bipropellant valve assembly will weigh less than two monopropellant valves for the same service. An immediate reduction in complexity and weight is achieved with a linked bipropellant valve since it uses a single pilot valve, a single housing, a single actuator, and a single position indicator, as opposed to two each for two monopropellant valves. For fast-response hydrogen and oxygen service, a bipropellant valve will use hydrogen for actuation, the pilot being intermediate in size between a pilot for a hydrogen monopropellant valve and a pilot for an oxygen monopropellant valve. Additionally, a bipropellant valve, even with its mechanical linkage, will represent fewer total parts than two monopropellant valves.

TABLE I - DESIGN REQUIREMENTS

Valve Type	Single or bipropellant
Propellants	Hydrogen (1) Oxygen (2)
Operating Temperature Range	200 to 850 R (111 to 472 K)
Propellant Temperature Range	
Hydrogen	200 to 800 R (111 to 444.5 K)
Oxygen	250 to 800 R (139 to 444.5 K)
Propellant Pressures at Valve Inlet	
High-Pressure System	400 ±50 psia (276 ±34.5 N/cm^2)
Low-Pressure System	20 ±5 psia (13.8 ±3.5 N/cm^2)
Pressure Drop (Maximums):	
High Pressure	
Fuel	5 psi at 0.69 lb/sec and 540 R (3.5 N/cm^2 at 0.313 kg/sec and 300 K)
Oxidizer	5 psi at 2.76 lb/sec and 540 R (3.5 N/cm^2 at 1.25 kg/sec and 300 K)
Low Pressure	
Fuel	1 psi at 1.14 lb/sec and 540 R (0.69 N/cm^2 at 0.52 kg/sec and 300 K)
Oxidizer	1 psi at 2.86 lb/sec and 540 R (0.69 N/cm^2 at 1.3 kg/sec and 300 K)
Actuation Requirements	
Pneumatic Pressure	TBD (to be determined)
Hydraulic	TBD
Electrical	TBD
Opening and Closing Response	Total time (delay and travel) from signal to end of motion = 30 milliseconds maximum Travel (motion) = 15 milliseconds maximum
Internal Leakage	0.102 scim (100 scc/hr) with gaseous helium at operating pressure and temperature per items 4 and 5
External Leakage	3.66×10^{-6} scim (1×10^{-6} scc/sec) with gaseous helium at operating pressures and temperature
Operating Life (Goal)	1,000,000 cycles
Environmental Conditions	
Vibration	TBD
Acceleration Loads	TBD
Acoustic	TBD

Maintenance - There shall be no maintenance of components during the design life period

Size and Weight - Design to minimum

Proof Pressure - 1.5 times operating pressure

Burst Pressure - 1.33 times proof pressure

Failure Criteria - The valve shall fail-safe close under normal operating conditions

Gaseous hydrogen derived from the vaporization of liquid hydrogen per MIL-P-27201
Gaseous oxygen derived from the vaporization of liquid oxygen per MIL-P-25508A

TABLE II - VALVE CONCEPTS

- Butterfly
- Ball
- Blade
- Butterfly or Ball (Retracting Seat)
- Poppet
- Diaphragm
- Spool

TABLE III - ACTUATION CONCEPTS

- Electric Motor
- Direct Solenoid
- Hydraulic
- Pneumatic (Helium)
- Pneumatic (Propellant)

These considerations also lead to some other conclusions. Replacement of a single valve can be accomplished with a monopropellant valve configuration, so that a single valve failure replacement is simple. However, the bipropellant valve with its single pilot, indicator, and housing represents a simple installation from a total valve standpoint.

Sequencing of propellants is another important area of consideration. The bipropellant valve, due to its mechanical linkage, provides *positive* propellant sequencing. This is not possible with two independently actuated monopropellant valves. For propellant-actuated monopropellant valves, timing of one valve relative to the other will vary if propellant temperatures vary with respect to each other. Monopropellant valves, therefore, require thermal compensation to maintain timing; even so, this does not ensure *positive* sequencing as achieved with a linked bipropellant valve.

Monopropellant valves can accommodate a gross change of fuel or oxidizer lead or lag; the bipropellant valve is much less flexible. The most important aspect of the entire sequencing discussion, however, is the fact that *positive* mechanical linking of a bipropellant valve precludes thruster damage or destructive due to delay or fail to open of one of the propellant valves. In addition, the linked bipropellant valve will produce the optimum integrated mixture ratio for pulse performance, giving better pulse performance with less total propellant consumption.

Only certain concepts of monopropellant valves require bellows, diaphragms, or dynamic seals for operation. However, a linked bipropellant valve of any design will require a bellows or a zero leak dynamic shaft seal to achieve positive propellant isolation for explosion safety. For long-life capability, considerably more bellows technology effort will be required to ensure a reliable bipropellant valve design. In addition to the problem of propellant isolation for explosion safety, thermal isolation must be maintained between gaseous hydrogen and gaseous oxygen propellants since cold gaseous hydrogen in near proximity to gaseous oxygen would result in liquefaction of a portion of the gaseous oxygen. This condition would be extremely hazardous at thruster startup.

Because of the problems associated with propellant isolation and bellows technology, the "no exceptions" approach to the APS design requirements favored an hydraulically actuated poppet valve design concept with flat metal-to-metal closure seat-seal for the high-pressure system, while an hydraulically actuated valve with radial-arc displacement, a flexible metal seal, and metal seat was favored for the low-pressure system. The favored concepts are shown in Fig. 2 and 3, respectively.

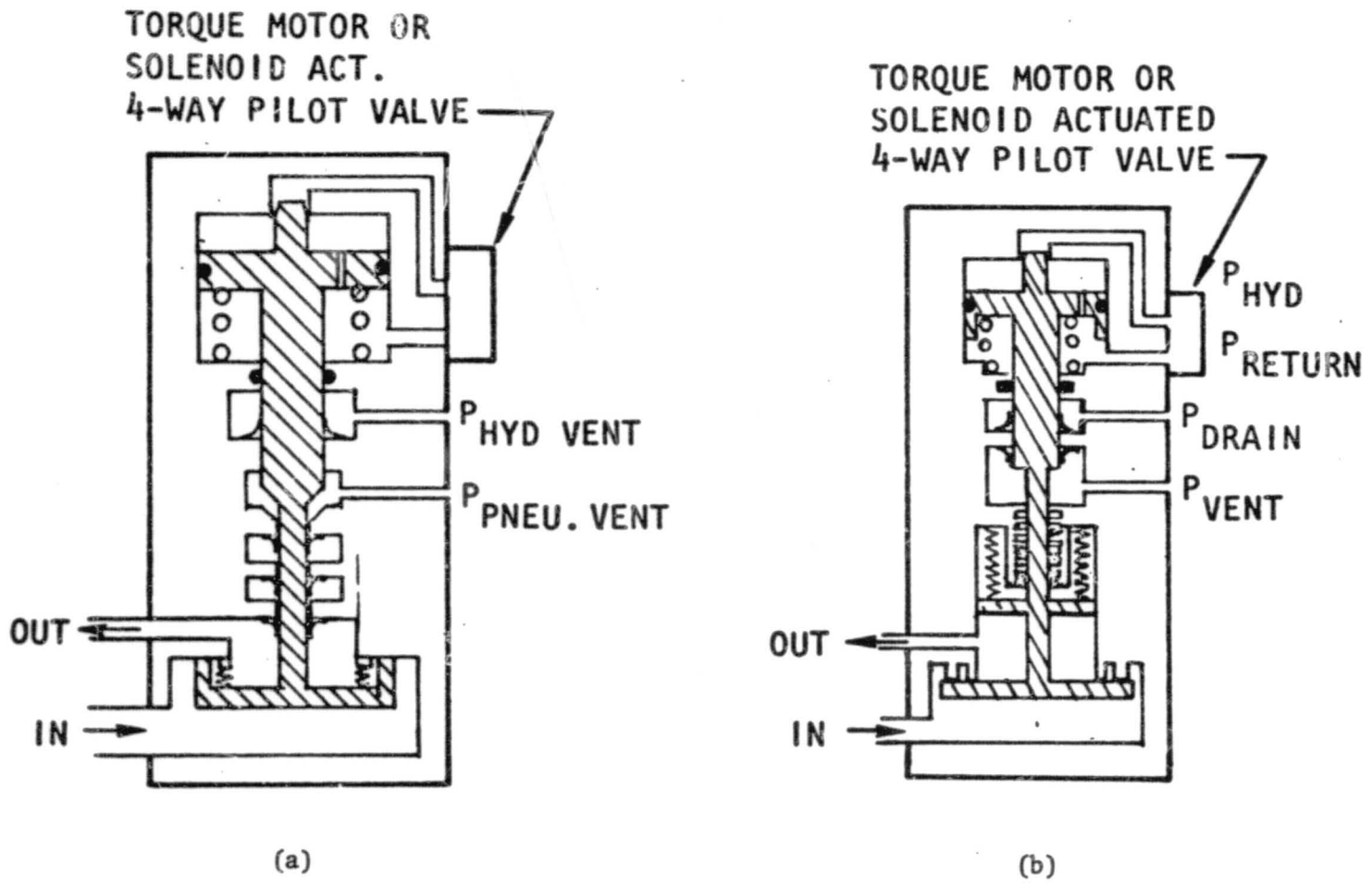

Figure 2. Preliminary High-Pressure Trade Study Configurations

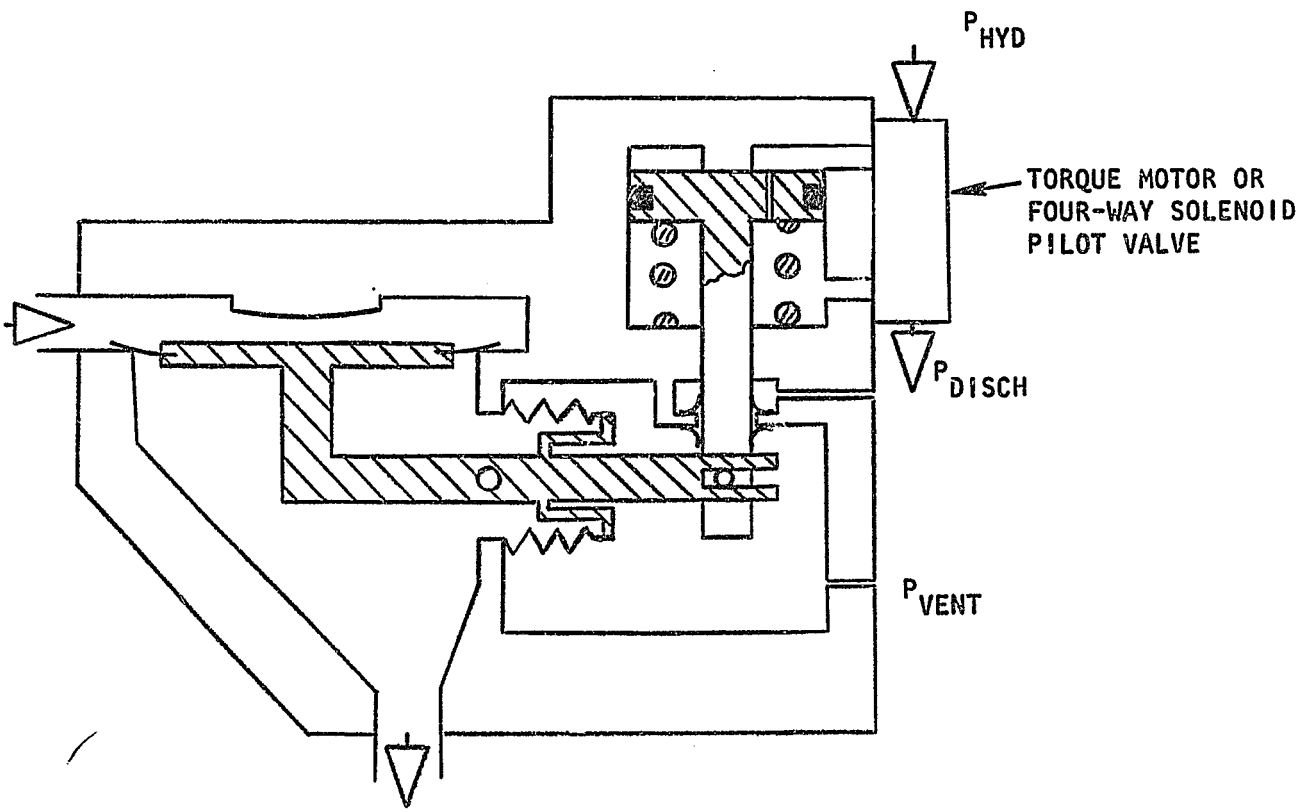

Figure 3. Preliminary Low-Pressure Trade Study Configuration

The design concept shown schematically in Fig. 2b has the same hydraulic actuator and impact-snubbing features as the concept of Fig. 2a. With the valve in or near its closed position, a contoured pintle attached to the actuator piston restricts the flow passage between the opening side of the piston and the pilot valve. When the main valve is beginning to open, or when it is approaching its seat during a closing transient, the restricted flow passage limits the hydraulic fluid volumetric displacement and, consequently, limits the initial valve-opening velocity as well as the valve-closing impact velocity against the poppet seat and mechanical stop.

The velocity-snubbing features at and near each end of the valve stroke do not impede the attainment of high velocities at intermediate valve displacements, as required for satisfying the response-timing requirements. The poppet stem dynamic seal is a metal bellows with an all-metal labyrinth seal for redundancy. The flat-faced poppet seat has an inner annular surface for sealing and an outer annular surface for absorbing impact energy.

Poppet valve full stroke is limited by a piston displacement stop in the hydraulic actuator. When the piston is at or near full stroke, the piston skirt restricts the pilot valve flow passage in the cylinder wall to restrict hydraulic fluid flow and, consequently, limit piston displacement velocity. The piston mechanical stop can be designed with a relatively large contact surface area and high impact momentum absorption capacity, compared to the poppet and seat, and can be designed so that minor deformation at the stop does not impair actuator functional integrity. Velocity snubbing is, therefore, less critical in the opening direction than in the closing direction, and less precision is required for opening impact velocity control.

Use of a contoured pintle attached to the piston, for impact velocity snubbing when the valve is closing, provides for adequate precision in closing-velocity contouring for as great a percentage of the piston full stroke as is required in obtaining full stroke within 0.015 second but with the slowest obtainable poppet-to-seat impact velocity.

Use of a high-pressure hydraulic operating fluid and a double-acting piston actuator contributes to minimizing the mass of the moving parts to minimize impact momentum, and contributes to precise control of velocity profiles in both directions of motion. The load stiffness and dashpot damping characteristics inherent in hydraulic actuators minimize rebound and repeated contact at the poppet closure seal.

When propellant inlet pressure is applied, it acts against the poppet seat cross section to increase the net closing force. Maximum poppet seat stress for sealing is obtained at maximum inlet pressure. As the valve begins to open and flow, the resulting increase in outlet pressure acts on the differential between seat cross-section area and bellows seal effective area to supply an opening force that increases as valve displacement increases. This regenerative-force assisting actuation ensures positive, continuous, chatter-free stroking in the presence of dynamic flow forces. As the valve begins to close, and outlet flow is throttled by the poppet, the reduction in outlet pressure decreases the net force opposing deactuation, and smooth closing is ensured.

During tests and checkouts with inlet pressures not applied, propellant pressure regenerative forces are not present, and the hydraulic differential pressure acting on the piston is different during checkouts from what it is during system operation. However, with hydraulic actuation, the piston can be sized to minimize variations in piston differential pressure related to variations in seal friction and to temperature-related variations in mechanical spring rates. Variations in response timing and in impact momentum can thereby be minimized throughout the full envelope of test and operating conditions.

The poppet valve stem primary dynamic seal is an internally vented metal bellows. The bellows is shielded from direct impingement of valve effluent and from direct exposure to effluent turbulence by locating the bellows in a semi-enclosed cavity. Acting as the primary dynamic seal, the bellows provides for compliance with the program design requirement for essentially zero external leakage.

Because a bellows seal will be vulnerable to fatigue failure in a valve designed for 1,000,000 full-stroke, 0.015-second, on-off cycles in a not-yet-defined vibration environment, the poppet stem guide is designed as a secondary dynamic seal. The guide is shown schematically as a series of close-fitting lands with small intermediate gas expansion volumes. An alternate stem seal concept appears in Fig. 2a. Secondary seal design emphasis would be on long cycle-life with minimum leakage in the event of a bellows leakage failure.

As the stem dynamic seals are isolated from propellant inlet pressure, a primary stem seal leakage failure would result in closely limited leakage only when the valve is in operation. A seal leakage failure will not result in a valve operational failure.

Figure 2b illustrates a flat-faced, metal-to-metal poppet and seat with two concentric seat lands. Contact between the poppet and the inner land provides the closure seal. When the poppet is seated on the inner land, there is a few ten-thousandths of an inch clearance between the poppet and the outer land. When the valve is open and is stroking to the closed position, angularity between the plane of the poppet sealing surface and the plane of the inner seat land sealing surface results in impact at the seat outer land. The potential for sealing surface impact deformation or abrasion is thereby minimized. This poppet and seat concept places the design emphasis on poppet guiding to minimize scuffing of the poppet against the seat as seating occurs.

Figure 3 illustrates a design concept for an hydraulically actuated, normally closed shutoff valve with a closure seal designed for low pressure. Valve closure sealing is effected by an initially flat, thin, annular metal section, deflected in contact with a seat in the valve housing.

The actuator is isolated from the propellant flow path by a metal bellows dynamic seal attached to a pivoted rocket arm in the valve lifting mechanism. A relatively large-diameter, low-lift valve with radial-arc displacement is indicated.

When the valve is open and flowing, the bellows dynamic seal is pressurized internally. As bellows elements have lower allowable pressure differentials with the internal pressure higher than they do with the external pressure higher, the concept of Fig. 3 is more applicable to the low-pressure propellant system than it is to the high-pressure system.

Additionally, the valve closure-seal design concept is more applicable to the low-pressure propellant system than it is to the high-pressure system.

Relatively high actuation forces related to large valve sizes are accompanied by relatively low actuation velocities related to low valve lifts. Use of an hydraulic actuator provides for fast response with relatively high power levels, and impact velocity snubbing can be obtained.

When propellant inlet pressure is applied, it acts against the valving element to increase the closing force. Maximum closure-seal stress for sealing is obtained at maximum inlet pressure. As the valve begins to open and flow, the resulting pressure increase in the valve body cavity that is ported for outflow acts against the valving element in the opening direction. This supplemental force (as a function of displacement) ensures positive, continuous, chatter-free actuation. Similarly, when the valve is open and flowing and begins to close, throttling of the valve flow results in a displacement-related reduction in pressure force opposing closing, and smooth deactuation is ensured.

Because a bellows seal will be vulnerable to fatigue failure in a valve designed for 1,000,000, full-stroke, 0.015-second, on-off cycles in a not-yet-defined vibration environment, the vent cavity to which the bellows is exposed is designed for a restricted outflow. A bellows seal leakage failure will result in limited external leakage only when the valve is in operation. A seal-leakage failure will not result in a valve operational failure.

The actuator piston ring seal is for leakage deterrance only, and appreciable degradation of that seal is tolerable. Minor degradation of the piston rod seal with extensive cycling may be tolerable provided that the seal drain cavity and wiper seals are designed to prevent hydraulic leakage into the valve body vent cavity.

Heat Soakback and Venting

In order to ensure that the use of non-metallics in the valves was a safe approach, a thermal analysis of the thrusters was performed. A preliminary system soakback analysis was conducted for a typical thruster assembly to determine the transient temperature response of various components after shutdown. In particular, the effect of soakback to the fuel and oxidizer valves was studied using a simplified thermal model.

A simplified soakback model of the thruster assembly can be used advantageously for preliminary screening of valve-chamber-injector interaction. A typical schematic of such a simplified thermal model is shown in Fig. 4 for the double-wall, regeneratively cooled thruster concept.

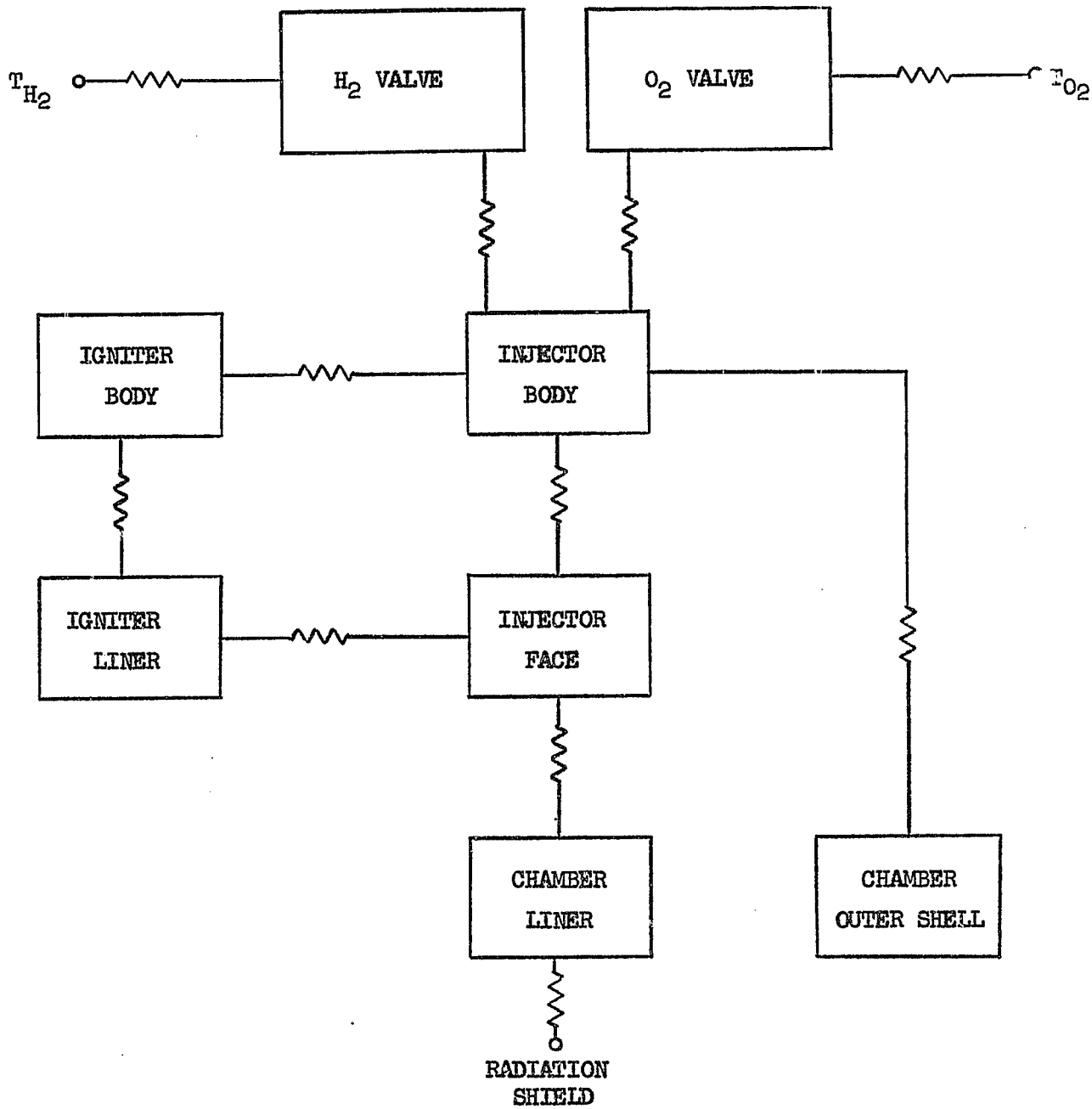

Figure 4. Schematic of a Simplified Thermal Soakback Model for a Regeneratively Cooled Thruster

In essence, the thruster assembly is represented by a nodal network comprised of the various components or subcomponents necessary to provide accurate soakback temperature response results. In the selected simplified model, the thrust chamber is represented by the combustion-gas liner and outer shell. The injector is divided into face and body subcomponents and the igniter is also divided into hot-wall liner and outer body. Each of the valves is represented individually.

The thermal resistances between the various nodes (components) are calculated based on the relative geometries, wall thickness, and materials of the various components. In particular, the thermal resistance between the injector and valves can be readily varied to simulate the effects of close-coupled or standoff valves on the resultant valve soakout temperatures.

The results of the analysis for close-mounted (but not integrated) valves are presented in Fig. 5, assuming a regeneratively cooled, double-wall thrust chamber. The hydrogen valve temperature increases about 100 F (311 K) within 1 hour after shutdown. The oxygen valve temperature increases about 70 F (294 K) in a similar time period. The primary heat input is from the thrust chamber hot-wall NARloy-Z liner, which is seen to cool down from its initial soakout value of 600 F (589 K) to -100 F (200 K) in 1 hour. The injector face plate also contributes to the head load to the valve. The initial temperatures at shutdown are based on nominal average steady-state operating temperatures of the various components.

It was apparent from this preliminary investigation that the magnitude of the soakback could be reduced by thermally isolating the chamber from the injector and/or by isolating the valves from the injector manifold. Studies into the impact of valve isolation were also made and showed very promising results. For this initial nalysis, it was assumed that a 1-inch-long (2.54 cm), 0.5-inch (1.27 cm) -diameter steel bellows with 0.010-inch (0.0254 cm) wall thickness was integrated between the valve and injector body. The equivalent line length of the bellows was taken as 6 inches (15.24 cm). The resulting effective thermal resistance between valve and injector was about a factor of 100 higher than for the close-mounted valves.

The resulting soakback temperature response is presented in Fig. 6. It is apparent that in 6 hours (21,600 seconds), the hydrogen and oxygen valve temperature increases by only 15 and 10 F (264 and 261 K), respectively. Thus the use of non-metallics such as Teflon was considered a safe approach.

In the event that the gaseous propellants themselves would be used as the valve(s) actuating fluid, it was necessary to ensure that no adverse effects would occur as a result of venting those fluids. Initial investigation revolved around venting the propellant gas into a lower-pressure area on the thruster manifolds. However, this created the situation that as manifold pressure rose to near valve inlet pressures, a large valve actuator was needed to maintain force balances necessary for valve full-open conditions. In turn, these large actuators caused the response of the valves to be slowed by time-consuming venting and pressurizing of the larger actuator cavities. Computer studies with the DAP4H system (to be discussed later in this report) showed that

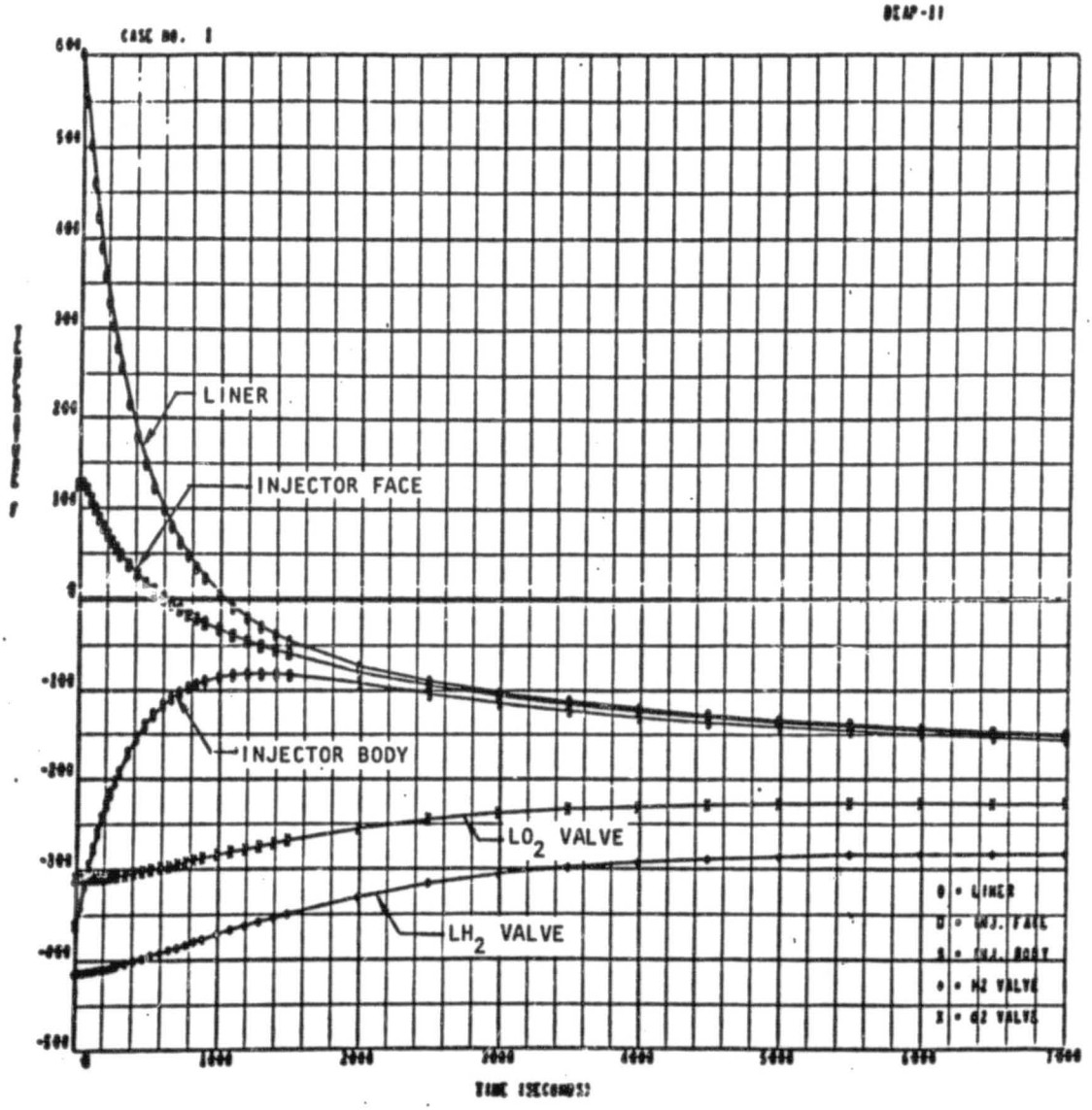

Figure 5. The Effect of Soakback on the Temperature of Various Thruster Components (Close-Mounted Valves)

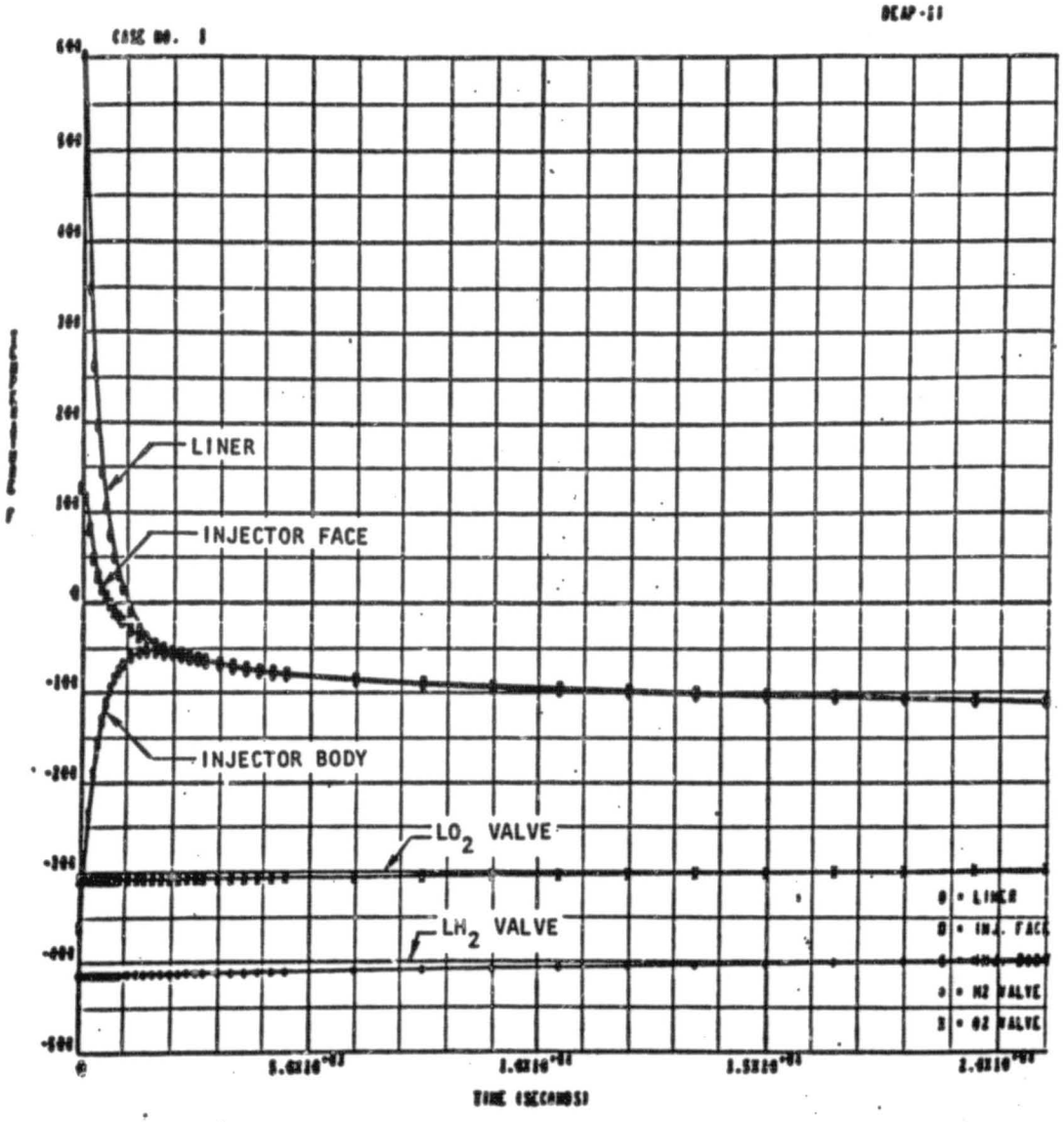

Figure 6. The Effect of Soakback on the Temperature of Various Thruster Components (Standoff Valves)

sonic nozzles could be incorporated into the injector just downstream of the valves, giving a low-pressure area for actuation gas venting, and also giving good pressure recovery for proper injection pressures. Thus, the valve actuators were not required to be so large, and response could be met. Venting into the respective propellant ducts prevents the hazardous situation of possible mixing of propellants. Thus, it was determined that on any flighweight engine, this approach could be used successfully.

ANALYTICAL LEAKAGE MODEL

Leakage past valve seats results from a combination of leakage paths consisting of surface roughness, surface flaws (scratches, nodules, etc.), deviation from pure geometrical surfaces (e.g., flat, sphere, cone) and non-conformance between sealing lands due to entrapped contamination, unsymmetrical loading, or warpage from temperature change or stress. Some of these factors can be analytically treated by comparison of measured and predicted leakage for idealized models. The value in this approach is that sealing performance can be related to specific causes through surface inspection tracers and microscopic examination using interference techniques. Relating cause and effect thereby provides the basis for design modification and improvement.

A variety of valve poppet and seat configurations have been tested and results correlated with measured surface conditions (Ref. 1 through 4 and 6). For aerospace applications, leakage is in the laminar-molecular range with surface roughness for metal-to-metal closures less than 2 microinches AA (5.08×10^{-6} cm). Even with entrapped solid particles causing sealing land separation, leakage is laminar except for contaminants normally termed "foreign objects." Significant variation from expected leakage can usually be traced to one or more of the aforementioned causes for increased gap.

Several attempts have been made to provide a theoretical basis to relate valve seat load with leakage (Ref. 1, 6, and 7). While allowing a better understanding of the problem, these attempts have failed because there is not a sufficiently accurate means to measure the myriad "real world" surface and geometrical features and, even if they could be measured, the strain interaction between these features would require a costly three-dimensional finite element stress analysis. Wear-related surface changes present an even more complex problem because existing wear data are not related to surface texture (Ref. 8). Consequently, each valve seat of a type or configuration must be load-leakage tested and cycled to characterize its performance. With multiple tests to establish a mean or normal condition, the correlation of leakage with geometry, before and after specific tests, will provide a basis to define overall limitations and capabilities.

The following paragraphs present a general discussion of valve seat geometry and means for predicting leakage through various flaws. The flow equations are presented with a typical example and the section is concluded with flow curves of theoretical model seat leakage versus gap, or height.

Nomenclature

Nomenclature used in subsequent discussion and analyses is as follows:

- A = area, sq in.
- C = discharge coefficient
- D = hydraulic diameter, inches
- D_e = effective pressure balance diameter
- D_s = mean seat diameter
- f = friction coefficient
- g = gravitational acceleration constant, 1.39×10^6 in./min^2 (3.5306×10^6 cm/min^2)
- h_o = taper height, inches
- h_e = equivalent parallel plate channel height, inches
- h_p = parallel plate channel height, inches
- k = ratio of specific heats
- L or X = channel length, inches
- M = entrance Mach number
- P = static pressure, psia
- Q = volumetric flow at standard conditions of temperature (T_s = 530 R, 294 K) and pressure (P_s = 14.7 psia, 10.13 N/cm^2), in.^{3}/min, or for compressible flow, scim
- R_i = inside diameter, inches
- R_o = outside diameter, inches
- R = gas constant, in./R
- Re = Reynolds number
- T = static temperature, R
- V = velocity, in./min
- W = channel width or perimeter, inches

Greek Symbols

- ω = weight flowrate, lb/min
- μ = viscosity, lb-min/in.^{2}
- ρ = density, lb/in.^{3}
- λ = mean molecular free path, inches
- β = pressure profile factor

Subscripts

1 = inlet or entrance conditions

2 = outlet or discharge conditions

o = stagnation conditions

s = standard conditions

i = incompressible

c = compressible

Geometry of Valve Seating

The performance of a valve seat is intimately related to the geometrical configuration of the seating surfaces. While a large variety of configurations are employed, the fundamental flat, conical, and spherical geometries can be identified in most cases. This stems from the simplicity of these shapes which are attendant with natural fabrication processes. The three configurations are shown in Fig. 7 with the parameters and equations combining basic geometry and load for the definition of apparent seat stress (S).

Superimposed upon real valve seating surfaces is a variety of other smaller geometries which often have a greater influence on the closure than the more obvious gross configuration. Most apparent is surface texture which includes the machining errors of roughness, waviness, pits, nodules, and scratches. However, often overlooked and of more subtle influcence is the geometry of the seat land. While a seat land may be specified by engineering drawing or fabrication process, perfect conformability of mating surfaces is impossible and deviations are difficult to define or prove precisely; hence, the actual contact dimensions may be quite different than planned and also may change with seat load. Because leakage is inversely dependent upon real contact land dimensions, it follows that variation of these dimensions will also have an effect on leakage.

Land geometry is identical in cross section for the flat and conical configurations. For spherical seating, the only difference is the definition of a land width on a curved surface which is usually narrow; thus, except for this one difference, the seat land is the same for all three configurations. The land, which may be on the seat, poppet or both, is composed of three basic parts as illustrated below:

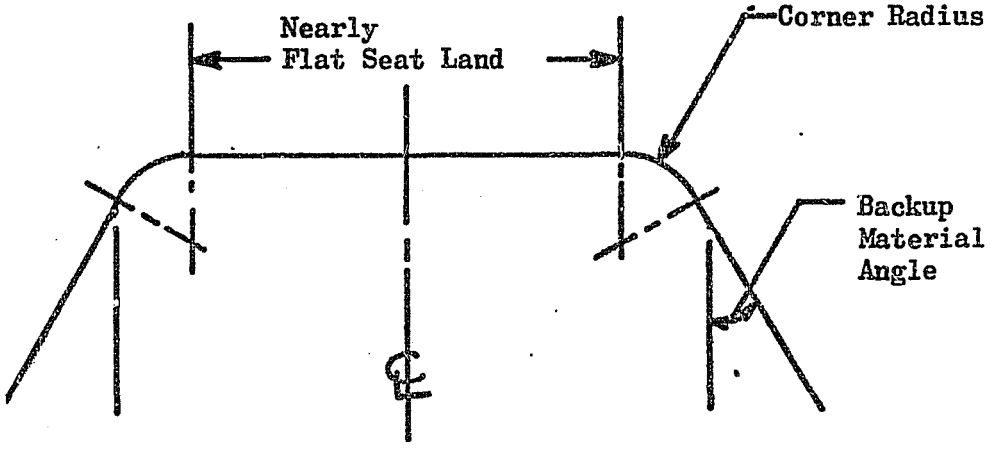

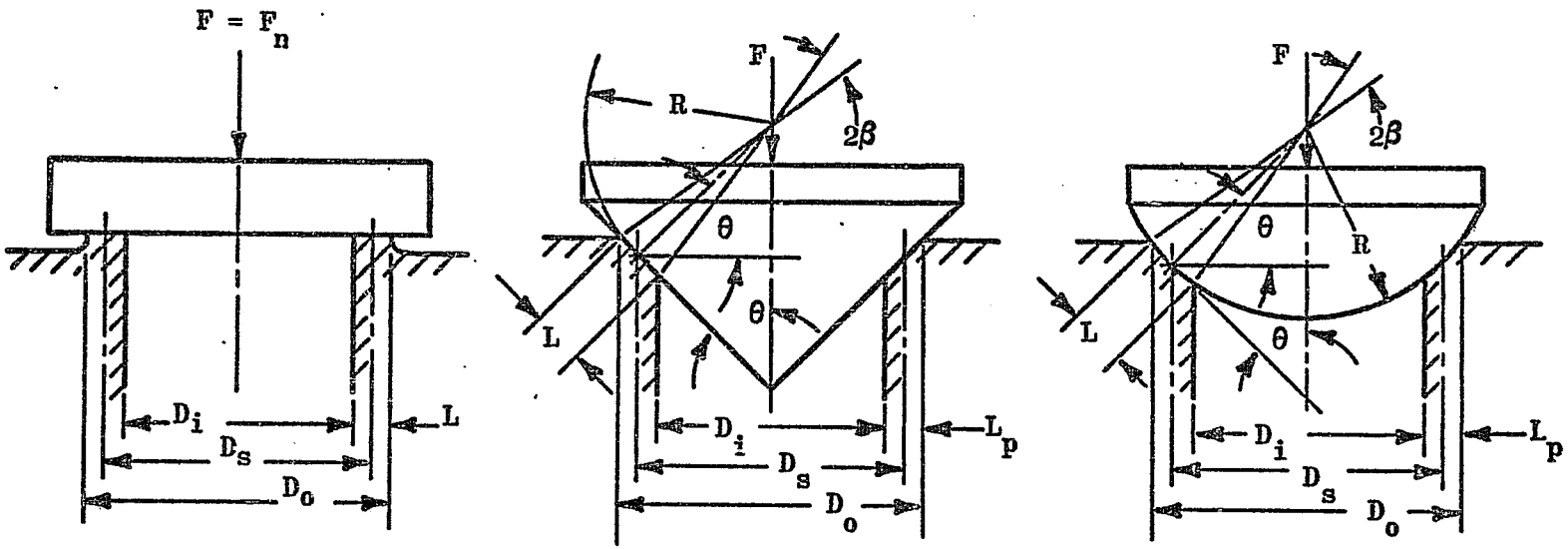

$L = 1/2\ (D_o - D_i)$

$D_s = 1/2\ (D_o + D_i) = D_i + L$

$A_s = \pi D_s L$

$$S \equiv \frac{F}{A_s} \equiv \frac{F}{\pi D_s L}$$

$L_p = 1/2\ (D_o - D_i) = L \sin\theta$

$L = 2R \tan\beta \cong 2\beta R$

$D_s = D_i + L_p$

$A_s = \pi D_s L$

$A_{sp} = \pi D_s L_p$

$F_n = F/\sin\theta$

$F_r = F/\tan\theta$

$$S \equiv \frac{F}{A_{sp}} \equiv \frac{F_n}{A_s}$$

$L = 2\beta R$

$L_p = 1/2\ (D_o - D_i) \cong L \sin\theta$

$D_s = 2R \cos\theta$

$A_s = \pi D_s L$

$A_{sp} = \pi D_s L_p$

$$S \equiv \frac{F_n}{A_s} \equiv \frac{F}{A_{sp}}$$

Figure 7. Flat, Conical, and Spherical Seating Equations

Each of these parts may take many forms and combinations too numerous to depict. The backup material angle on most flat seats is zero (but may approach 90 degrees) whereas for 45-degree conical or spherical seating, it is normally 45 degrees (but also may approach 90 degrees). The "flat land" may be flat, concave, or convex with symmetry near its own centerline or to the seat diameter. Corner radii also vary over a considerable range from a mere ragged discontinuity formed by intersecting surface roughnesses to the opposite extreme of a complete sphere (ball in cone).

Seating Gap

The seating gap under a no-load condition is a result of variation in the above land geometry combined with dimensional and positional errors. In many cases, the real length of land contact is a complex function of the load, being formed elastically with each contact. The seat land may have been developed through plastic flow of an initially sharp edge with subsequent deformations predominantly elastic. Where the land is plastically formed, the resultant contact shape is largely indeterminate. With defined simple curved shapes, however, a Hertz stress analysis may be used to predict the elastically loaded configuration. In any case, a definite land length does exist under the slightest load, and the term "sharp seat" is a relative generalization.

Dimension errors result in deviations from true form and nonconformity between poppet and seat lands. Symmetrical errors may create only a taper gap with full contact at the roughness level around the periphery; however, errors of roundness always result in a through-gap. Even with symmetrical errors, as exemplified by differential radii in spherical seating, a finite load must be applied to establish a minimal land for adequate sealing or else leakage could be in the nozzle regime and, thus, much greater than for the laminar condition.

It is notable that unlike the flat poppet and seat (for which it is relatively simple to obtain near-perfect conformity), the conical and spherical designs necessitate a match of physical dimensions, i.e., the included angle for the cone and radius for the sphere. As a result, these configurations will almost always have a taper gap from a few microinches to thousandths of an inch, depending upon size and fabrication and measurement precision. For constrained flat and conical seats, parallelism and axis tilt are usual positional errors. Freedom from this error is the advantage of the spherical seat.

Superimposed upon the seat land, and causing gaps which may only be reduced but never closed, are the surface textural errors of roughness, waviness, modules, pits, and scratches. Thus, a variety of geometrical errors cause conformal gaps in seating which must be reduced through load deformation of the "high" material.

Equivalent Flow Paths for Surface Deviations

The deviations of seating geometry that result in leakage may be broadly divided into the following:

1. Gross abnormalities of geometry such as out-of-parallel plates; broad curvatures measured as a deviation from a flat plane; and spherical, out-of-round, or tapered mating surfaces

2. Parameters of surface texture, i.e., roughness, waviness, nodules, pits, and scratches

The leakage flow through these various surface deviations may be indirectly approximated by computing the equivalent flow path of each deviation for that portion of the seating surface it occupies. Valve seat leakage takes place mainly in the laminar and, to a lesser extent, in the molecular flow regimes. In laminar flow between parallel plates, the defining parameters are the channel length or the radial land width (L), peripheral width ($W = \pi D_s$), and separation height cubed (h^3). The same conditions hold for molecular flow except the separation height is squared (h^2).

Because the surface deviations considered herein are very close approximations of parallel plates, the flow may be imagined to travel through discrete radial channels of varying height which may be integrated to arrive at an equivalent parallel plate separation (h_e).

In these calculations, advantage is taken of the fact that the majority of flow occurs through the larger spaces so that small nonradial flows may be neglected. It has also been assumed that the seat land width is sufficiently narrow with respect to the ID to neglect radial flow divergence.

Simplified Chordal Equations. In analyses of various curved geometries, the expression for the chordal height often occurs as shown below:

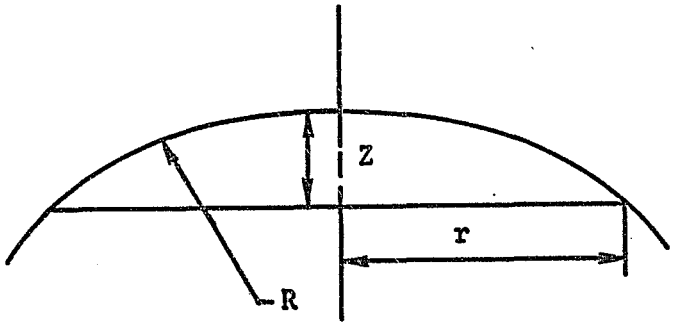

The equation defining this geometry is:

$$r = \sqrt{2RZ - Z^2} \cong \sqrt{2RZ}$$

$$Z \cong \frac{r^2}{2R}$$

For most analyses herein, R is much larger than Z; therefore, the approximate relation may be used with small error as shown below:

R/Z	Error, percent
25.4	1.0
5.4	5.0
2.9	10.0

Gross Geometry Deviations. Valve seat leakage caused by gross separations in the interface is mainly laminar, but may be turbulent channel or nozzle flow. While a large number of surface deviations are possible, there is a great similarity between the various gap shapes which allows the consideration of maximum gap and equivalent height to be reduced to a reasonable few. These may often be superimposed to obtain approximate results for composite shapes. In the case of taper gaps (h_o), a physical separation of the seating surfaces (h_p) is assumed to exist due to surface texture or other errors.

Out-Parallel Flat Poppet and Seat. For this case, the seating surfaces are assumed perfectly smooth and flat with flow perfectly radial. The flow may be imagined to follow a large but finite number of radial stream channels which may be summed to obtain the total flow through the gap. Because laminar flow varies as the height cubed, it follows that the predominant flow path is through the widest gap. The analytical model and describing equations are shown below:

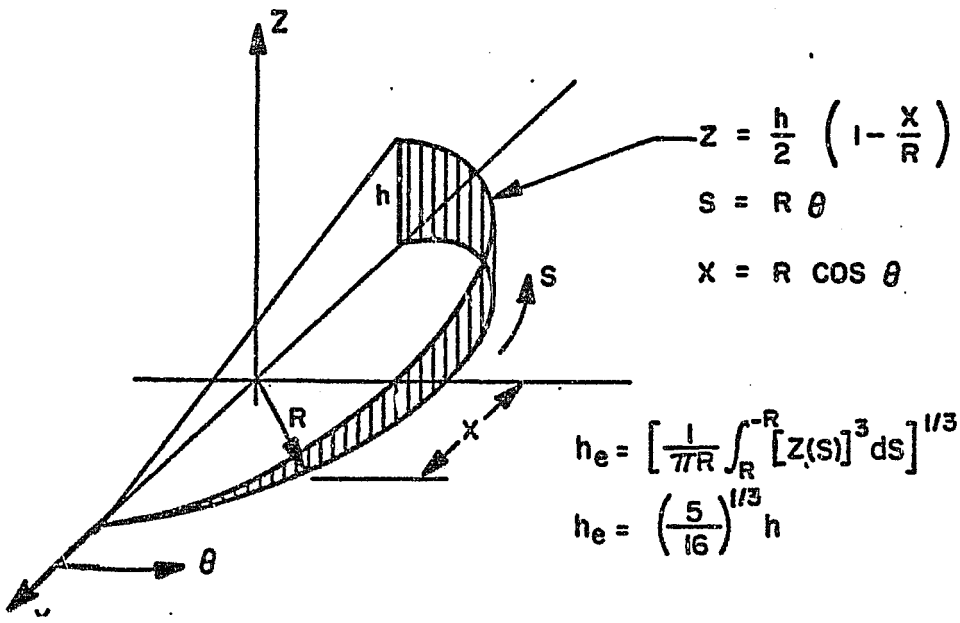

As curve Z is one-half of a sine wave when unwrapped, the same result is obtained by integrating Z over the length πR. It can be shown for this model that the assumption of perfect radial flow results in small error because more than 90 percent of the total flow discharges from the wide 180 degrees of the periphery, leaving less than 10 percent of the flow involved in the contact regions where the flow is partially circumferential.

Sinusoidal Gap Separations. The flat poppet and seat have one or both surfaces cylindrically out-of-flat (egg-shaped poppet) and, also, out-of-round conical, and spherical seating surfaces all have gaps which are basically sinusoidal regardless of the number of lobes. Consequently, integration of these shapes yields the same results obtained for the flat out-of-parallel case above, i.e.:

$$h_e = \left(\frac{5}{16}\right)^{1/3} h$$

where h is the maximum gap.

Axially Symmetrical Tapered Seating. Taper between poppet and seat is usual for nearly all forms of seating involving matching surfaces. It results in flat seating from customary convex (or, to a lesser extent, concave) machining errors, as schematically shown below:

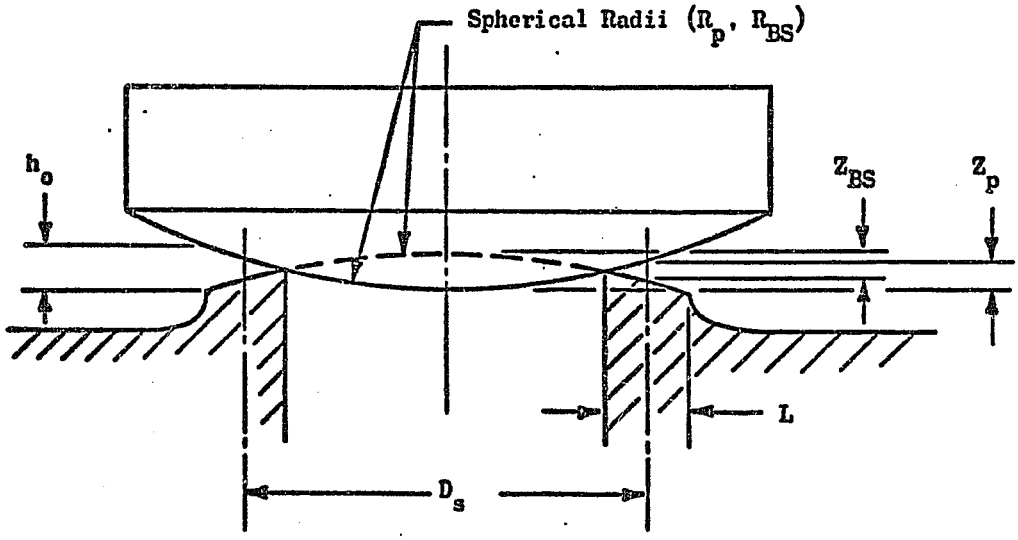

For flatness errors (Z_1 and Z_2) measured nominally at the mean seat diameter (D_s), the taper gap (h_o) is derived from the simplified chordal equation as:

$$h_o \cong \frac{4L}{D_s} (Z_p + Z_{BS})$$

with the appropriate sign applied to Z for concave or convex conditions.

A more unusual symmetrical form error is the crowned surface which might occur from excessive polishing of a flat, conical, or even spherical seat, thus dubbing the edges. Although the actual shape is often elliptical, the geometry may be approximately described by the chordal equation. A similar seating configuration occurring naturally is the ball in a wide conical seat (elastic contact only). Taper gaps from these configurations are shown below:

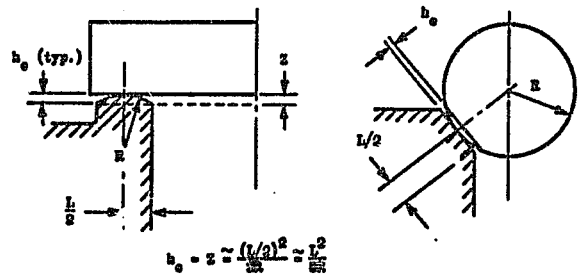

As previously noted, a more serious problem exists for the conical and spherical surfaces because of the conformal dependence upon physical dimensions. For conical seating, the seat gap is a function of the land width (L) and differential seating or half angle ($\Delta\theta$) between poppet and seat; thus, $h_o = \Delta\theta L$.

With spherical seating, the taper gap is related to the differential (ΔR) between the poppet (R_p) and ball seat (R_{BS}) spherical radii. The exact equation is cumbersome in that small differences necessitate a computer solution. However, simplification is possible for seating half-angle (θ) between 15 and 75 degrees, and land with (L) is small with respect to the basic spherical radius (R). Applicable terms are shown in the following sketch for the case where (R_{BS}) is greater than (R_p). The approximate solution for (h_o) is derived from the sine law with (L) assumed a straight line.

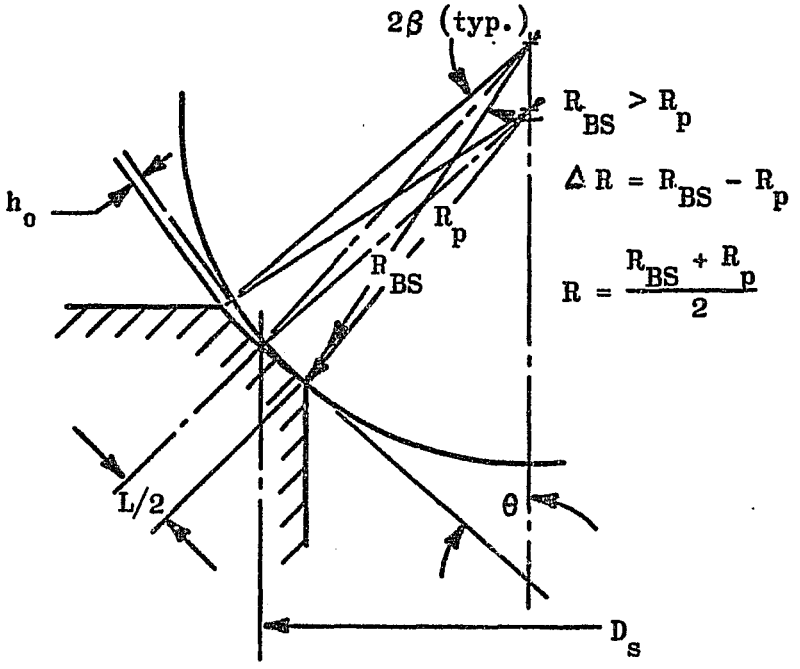

$$h_o \cong \frac{\Delta RL}{R_p \tan(\theta \pm \beta)} = \frac{\Delta DL}{D \tan(\theta \pm \beta)}$$

$$\beta \cong \frac{L}{2R} : (+) \text{ for } R_{BS} > R_p ; (-) \text{ for } R_p > R_{BS}$$

$$\theta = \arccos \frac{D_s}{2R}$$

In terms of the differential between ball and seat spherical diameters (ΔD) and mean seat diameter (D_s):

$$h_o \cong \frac{\Delta DL \cos\theta}{D_s \tan(\theta \pm \beta)} = \Delta\theta L$$

Taper gap data are plotted in Fig. 8 in terms of the taper angle ($\Delta\theta$). Consideration of experimental data has shown that the usual tolerance angular differential of 1/2 to 1.0 degree would, in most cases, result in unacceptable large taper gaps.

The problem now is to describe the taper gap (h_o) in leakage parameter terms. For the ideal case of perfectly smooth, flat, or round surfaces, there would be no leakage. Roughness and/or geometry errors do, however, cause a separation which, due to the very narrow contact land, may be assumed to offer negligible resistance to flow (unless the taper gap is very large, in which case the leakage would result from a nozzle flow condition). With some gap, the problem is resolved to one of simple tapered flow. The equivalent separation for this case will be presented in the Leakage Flow Analysis section. The simple integration averaging process may not be used for channel height varying along the flow direction. Comparison of laminar flow factors is illustrated in Fig. 9 for two cases noted as "linear" and "taper" flow. For the linear case, h does not vary in the direction of land width (L), and the cubical average (h_g) is obtained as previously shown. For taper flow, the basic flow equation must be integrated with L to obtain an equivalent path height. There is a small difference between the two flow factors at (h_p/h_o) ratios greater than one; thus, the more universal M_L factor may be used to approximate complex surface geometry. Below this value, however, taper flow should be considered as the defining parameter and N_L used to compute the flow.

Surface Texture Deviations. Except in rare instances, loaded on-seat leakage will be laminar and, for gases, may reach molecular levels. The basic leak path is through the interstices formed by contacting waviness and/or roughness. Additional leakage components of possible significance may be through nodule created gaps, radial scratches, or a density of interconnecting pits. As with gross geometry deviations, weighted averages of the maximum spacing height (h) can be computed for various regular geometric wave forms.

Surface Roughness and Waviness. The geometrical terms and equations used to describe model surfaces are summarized in the sinusoidal representation shown in Fig. 10. The height (h) and wave length (λ) can be assumed to represent various other wave forms and exist as waviness or roughness, or a combination of both. For example, a sinusoidal curve of smaller (h) and (λ) can be superimposed upon the sine wave shown. In addition, these waves can be imagined to be either linear into the paper or undulating in a similar fashion as that indicated resulting in a three-deimensional series of "hills and valleys" which contain a smaller version of the same. For the fine surfaces under consideration (h = 0.5 to 20 microinches [1.27 x 10^{-6} to 50.8 x 10^{-6} cm]), the average asperity angle (Φ) will seldom exceed 4 degrees, and sharp lapping scratches do not have slope angles much greater than 10 degrees.

Various averages have been computed from the equations shown in Fig. 10 for a number of regular geometric wave forms (Fig. 11). These factors may be used to estimate the variations between surfaces and the possible effects on leakage performance.

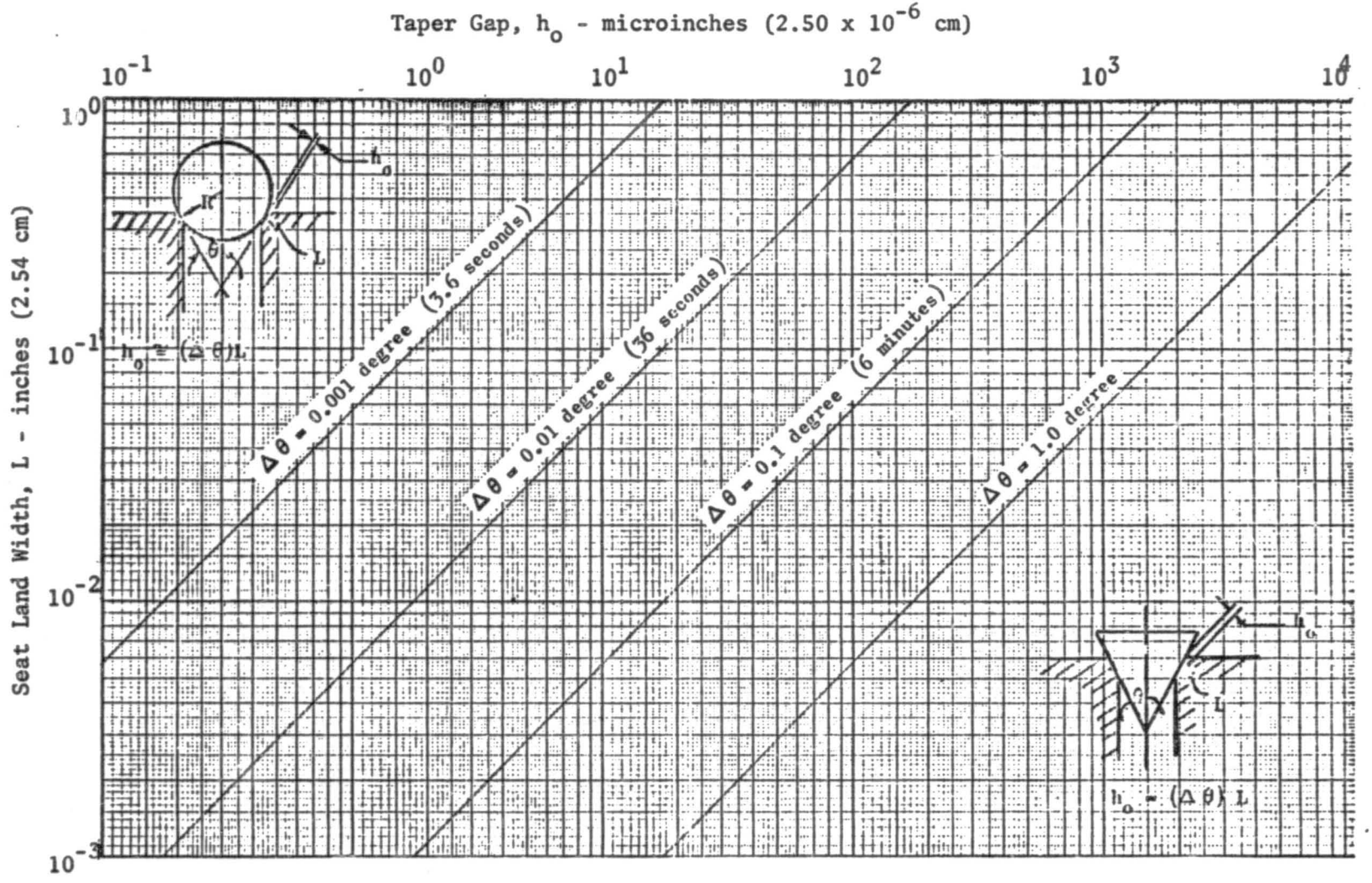

Figure 8. Taper Gap for Flat, Conical, and Spherical Seating

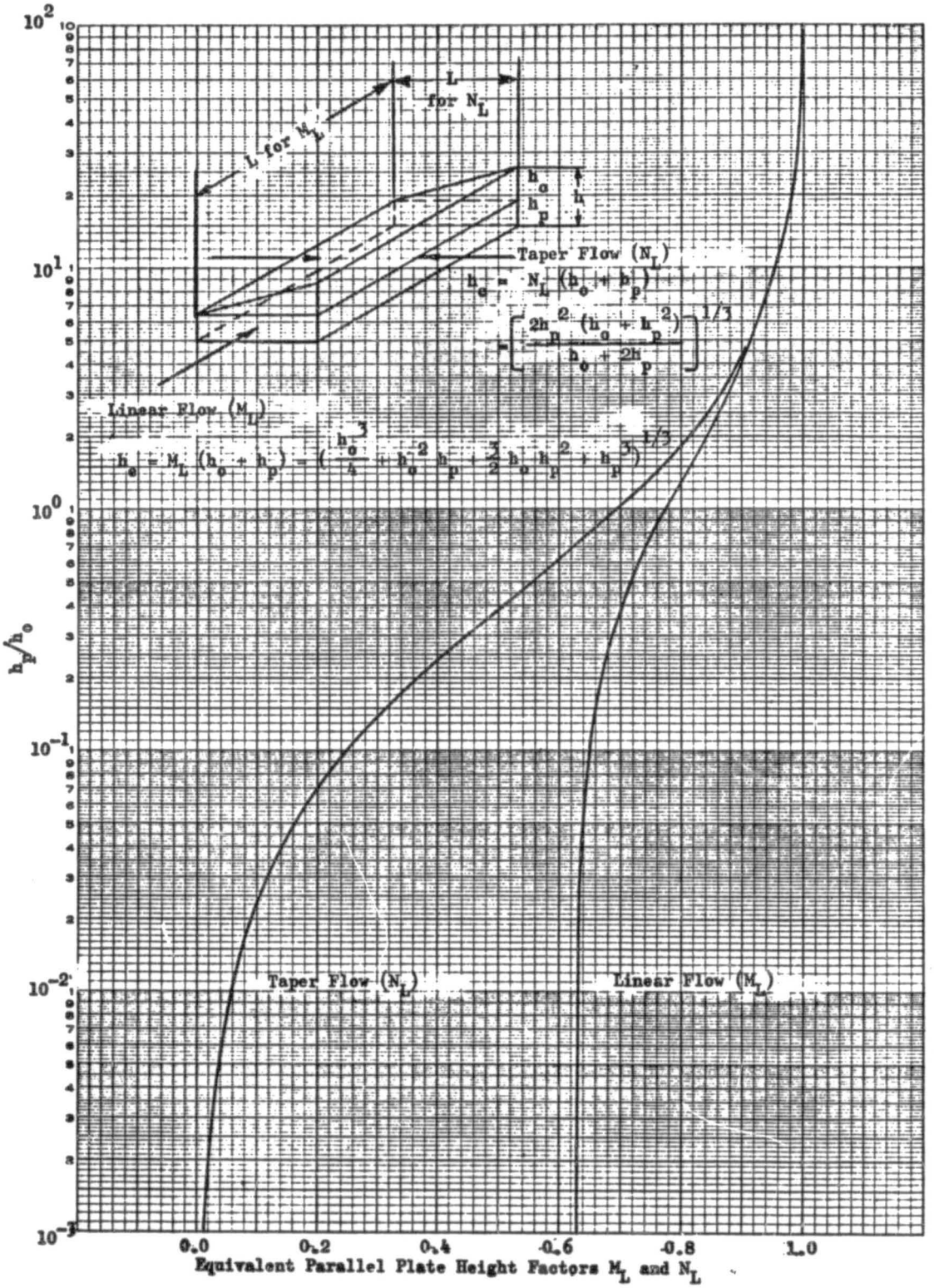

Figure 9. Laminar Flow Factors

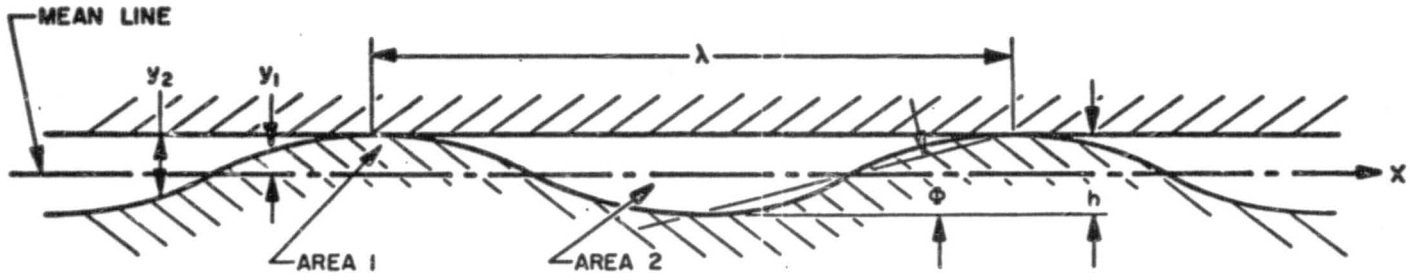

$$AA = \frac{1}{\lambda}\int_0^{\lambda} |y_1|\,dx \; ; \; rms = \left[\frac{1}{\lambda}\int_0^{\lambda} y_1^2\,dx\right]^{1/2}$$

$$h_{eL} = \left[\frac{1}{\lambda}\int_0^{\lambda} y_2^3\,dx\right]^{1/3} \; ; \; h_{eM} = \left[\frac{1}{\lambda}\int_0^{\lambda} y_2^2\,dx\right]^{1/2}$$

Average Asperity Angle $\Phi \simeq \frac{2h}{\lambda}$

Location of Mean Line Defined by Area 1 = Area 2

Figure 10. Model Surface Geometry With Defining Equations

WAVE FORM: h = 1	M_L*	M_M*	AA	rms	$\frac{h}{AA}$	$\frac{h}{rms}$	$\frac{G}{h}$	$\frac{G}{AA}$	$\frac{rms}{AA}$
UNIFORMLY RANDOM 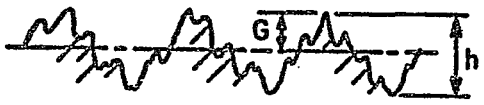	---	---	0.2	0.25	5.0	4.0	0.5	2.5	1.25
ROUND CRESTED PARABOLIC	0.523	---	0.256	0.298	3.91	3.36	0.333	1.29	1.16
SHARP CRESTED PARABOLIC	0.770	---	0.256	0.298	3.91	3.36	0.667	2.60	1.16
SINUSOIDAL	0.678	0.612	0.318	0.353	3.14	2.83	0.5	1.57	1.11
SAW TOOTH 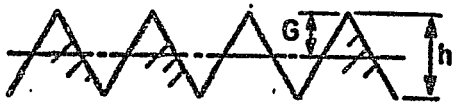	0.630	0.578	0.25	0.289	4.0	3.46	0.5	2.0	1.16
SQUARE 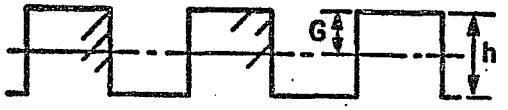	1.0	1.0	0.5	0.5	2.0	2.0	0.5	1.0	1.0

*$h_{eL} = M_L h$; $h_{eM} = M_M h$

Figure 11. Average Height Values for Various Wave Forms

Scratches. The remaining surface defects pertinent to valve seating are scratches, nodules, and pits in decreasing significance. Because of the difficulty associated with defining these defects, they take on a much greater importance than is commensurate with their usual contribution to leakage. Of particular significance in this respect are scratches. The definition of the relative effect of scratches (and other defects) upon leakage may be estimated through comparison of their size-number contribution to total leakage as compared with other deviations.

The analytical model considered is the seat land having one radial scratch, as shown below:

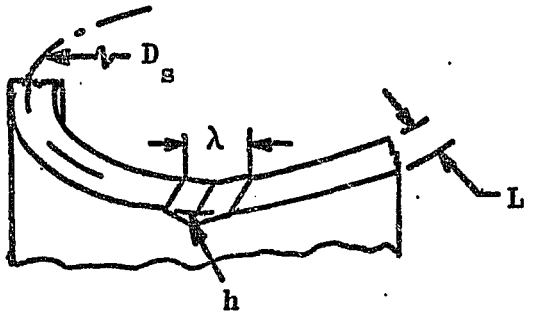

The equivalent height for the sawtooth configuration from Fig. 11 is:

$$h_{eL} = 0.63\ h \text{ and } h_{eM} = 0.58\ h$$

Scratch density (β_s) relates the one-radial-scratch model to the usual case of many radial scratches; thus:

$$\beta_s \equiv \frac{n\lambda}{\pi D_s} \quad \text{or} \quad n = \frac{\pi D_s \beta_s}{\lambda}$$

where Q for many scratches of average width (λ) equals (n) times (Q_s) for one scratch. Scratch leakage, computed for correlation with experimental data, is shown in Fig. 12 with the reduced flow equation and applicable data.

Nodules. Contaminants and nodules have a highly load-sensitive effect on leakage due to their usually small contact area. Uniformly dispersed over the seating area, the separation height is merely the parallel plate configuration. However, one nodule will cause the out-of-parallel positional error previously discussed. In this case, contact will occur at the roughness height of the two surfaces and the equivalent height must be determined for the combined gaps (i.e., M_L in Fig. 9 where h_p is the equivalent combined roughness height, and h_o the out-of-parallel gap).

Pits. Few localized pits not bridging the seat land will have little effect on leakage. A uniform distribution of pits will tend to reduce the effective land width since they offer negligible flow resistance (large relative h).

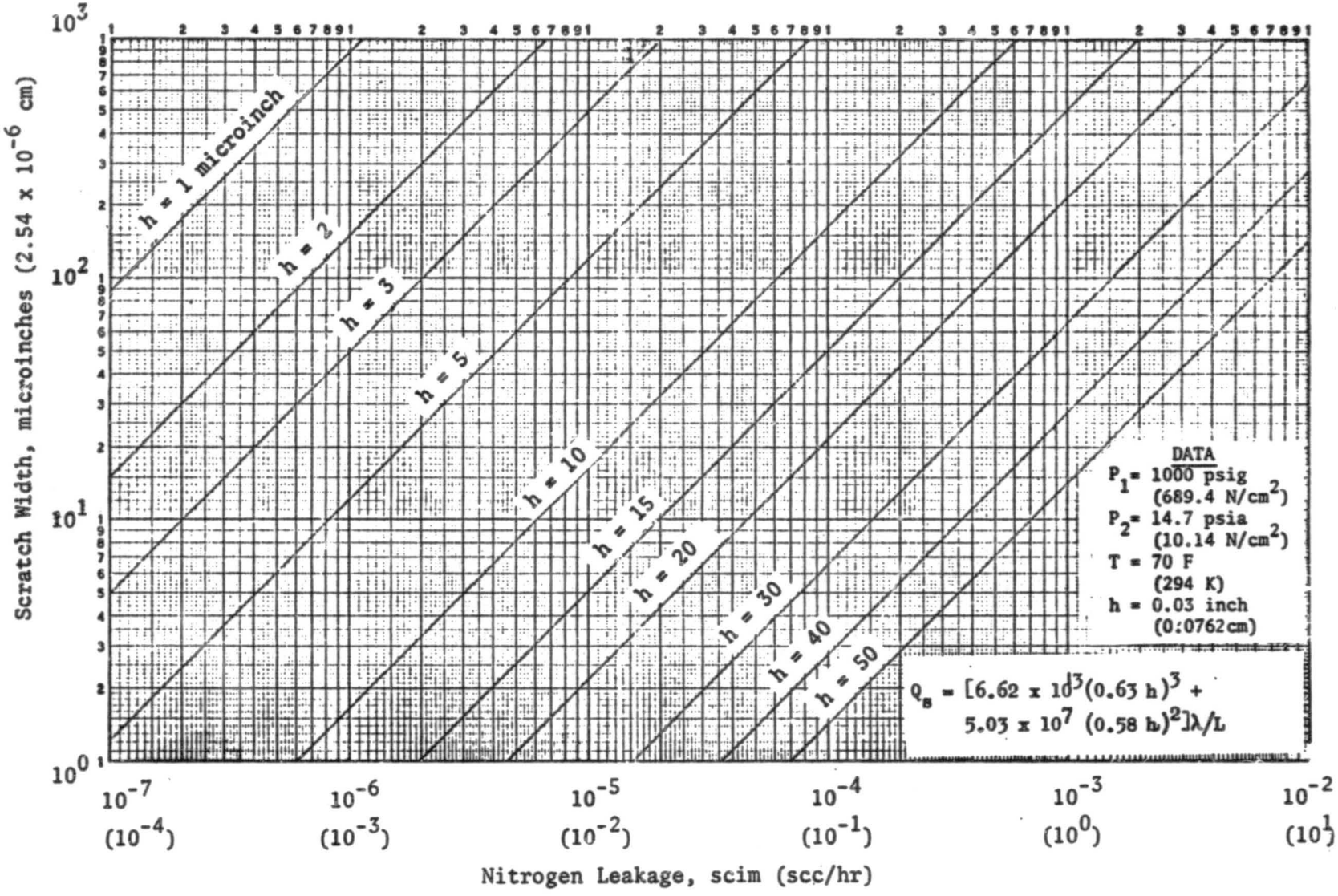

Figure 12. Single Scratch Leakage, Q_s

Leakage Flow Analysis

In considering the leakage and flow across a valve seat, a number of equations must be taken into account. These range from the nozzle equation which generally applies to the wide open valve to the viscous and molecular flow equations applicable under seated conditions. The equations derived in this section are presented for compressible and noncompressible fluids for flow through parallel plates. The equations are equally applicable to flat, conical, and spherical valve configurations because the near and on-seated passage configurations approximate the parallel plate model. Because of the importance of the laminar flow regime, the special case of taper in the direction of flow is also considered.

A specific example of nitrogen flow through a model valve seat is presented which shows how each flow regime blends into the next to build the overall flow-leakage characteristic curve. As the flow regime boundaries are not sharply defined, the example additionally illustrates the range over which the various equations may be applied.

Nozzle Flow. The compressible and incompressible flow equations derive from the basic Euler momentum relationship. The Euler equation gives the following relationship between velocity, pressure, and density:

$$\frac{V^2}{2g} + \int \frac{dP}{\rho} = \text{constant}$$

For the incompressible consideration, density (ρ) is constant, and the resultant relationship is known as the Bernoulli equation. If the inlet velocity is neglected, the following equation evolves for flow of an incompressible fluid through a nozzle:

$$\omega = CA \sqrt{2\, g\, \rho\, (P_1 - P_2)}$$

This equation requires a discharge coefficient (C) to correct the ideal frictionless flow to the actual case. The discharge coefficient is a function of the specific configuration being considered; therefore, it is derived from empirical data.

For the specific application of this equation to a valve configuration, area (A) is the minimum flow opening expressed as a function of the stroke height (h_p) and the minimum seat perimeter. This substitution can be made in the nozzle and the turbulent channel equations. For circular valve seats where the radial land width (L) is small with respect to the ID, it is convenient to assume a mean seat perimeter $W = \pi D_s$, where (D_s) is the mean seat diameter.

With compressible flow, the density is not constant and, therefore, the integral of dP/ρ must be evaluated for specific assumptions. For an adiabatic, frictionless process considering a perfect gas, the following equation is derived:

$$\omega = \frac{CAP_1}{\sqrt{RT_1}} \sqrt{gk \left(\frac{2}{k+1}\right)^{k+1/k-1}}$$

As in the case of the incompressible flow, a discharge coefficient is required to account for the irreversibility of flow. The above equation further assumes that choked or sonic flow exists across the nozzle.

In practice, leakage is most often expressed in terms of a volumetric flow. For compressible fluids, where density is a variable function of pressure and temperature, standard conditions (P_s, T_s, ρ_s) must be defined. The conversion relationship for all fluids is:

$$Q = \frac{\omega}{\rho_s} = \omega \frac{RT_s}{P_s}$$

Therefore, for both incompressible and compressible flow at standard conditions, the weight and volumetric flows differ by a constant.

The nozzle equations can be applied to a poppet valve configuration (similar to an orifice) from the wide-open condition to the near-seated position. When the valve closure height has decreased to the position where wall friction at the seating surface (and, thus, land length) is significant, the nozzle regime terminates and turbulent channel flow commences. There is no precise point at which nozzle flow terminates, the transition being a complex function of the particular channel geometry and Reynolds number. However, in general, if the length-to-height ratio is 10 or greater, channel flow is imminent.

Turbulent Channel Flow. In this flow regime, the same basic continuity and momentum considerations hold with the addition of a term for the effects of friction. In the case of an incompressible fluid, the basic Bernoulli equation is modified to the form:

$$\Delta P = \frac{fL}{D} \frac{\rho V^2}{2g}$$

where flow is defined by continuity as:

$$\omega = \rho A V$$

The first equation expresses differential pressure as a function of friction factor (f) and velocity (V). The friction factor is related to velocity through empirical parametric curves of friction versus Reynolds number and wall roughness. The solution to these equations is by trial and error.

The equations for flow in the turbulent channel regime were developed for flow-through circular tubes. To apply the equations to other channel configurations, the tube diameter in these equations must be expressed in terms of hydraulic diameter (D). Hydraulic diameter is defined as four times the ratio of the cross-sectional area to the wetted perimeter. For parallel plates, the hydraulic diameter is equal to twice the plate spacing ($2h_p$).

The equations used to compute compressible fluid flow in this regime are obtained from Shapiro (Ref. 9). They assume an adiabatic constant-area flow and include the effects of internal fluid and wall friction and fluid momentum. To compute the weight flowrate, two equations are required. The first is a relationship between entrance Mach number (M) and fraction factor (f) for the condition of choked flow at the exit of the valve seat channel (M = 1):

$$\frac{fL}{D} = \frac{1-M^2}{kM^2} + \frac{k+1}{2k} \ln \frac{(k+1)\ M^2}{2\left(1+\frac{k-1}{2} M^2\right)}$$

As in the incompressible case, the solution of this equation is by trial and error. Shapiro's text gives considerable assistance in the solution of this equation by tabulating fL/D versus Mach number, thus permitting interpolation of desired information. For the subsonic solution, reference is made to Shapiro's text.

Once the entrance Mach number and density are determined, they are used in the continuity equation to compute the weight flowrate based on the inlet conditions:

$$\omega = \rho\ AM\ \sqrt{k\ g\ RT}$$

The equations in this section are confined to the turbulent flow regime, i.e., Reynold numbers greater than 2000. However, these equations can be extended into the initial portion of the laminar flow regime where fluid momentum is still an important consideration. In this case, the friction factor is a linear function of Reynolds number and is given for the parallel plate consideration as:

$$f = 96/Re \quad \text{and} \quad Re > 500$$

The defining equation for Reynolds number is:

$$Re = \frac{VD\rho}{\mu g}$$

As before, (D) refers to the hydraulic diameter for other than round configurations. For the parallel plate consideration of a circular valve seat, this equation may be reduced to:

$$Re = \frac{2\omega}{W\mu g}$$

Laminar Flow. The analysis of fluid flow in this regime assumes that the temperature is constant (isothermal), that the fluid momentum effects are negligible, and that viscous shear forces govern the flow, i.e., Reynolds number less than 500. These assumptions result in the Poiseuille equation for flow through stationary flat plates (Ref. 11):

$$-\frac{dP}{dX} = \frac{12\ \mu\ V_{average}}{h^2}$$

By using the continuity equation, the relationship is reduced to express the viscous flow through flat plates:

$$\omega = \frac{\rho W h_p^3 (P_1 - P_2)}{12\mu L}$$

For a compressible gas, thermal effects are present; however, the assumption of isothermal condition can be made because of the small channel thickness and low velocity. The compressible version of the Poiseuille equation is obtained by integration of the pressure profile across the seat land and assumption of a perfect gas; therefore,

$$\omega = \frac{W h_p^3 (P_1^2 - P_2^2)}{24\mu LRT}$$

This same basic relationship can be derived for flow between circular flat plates. This equation contains the natural log of the radius ratio which accounts for radial divergence of the flow and is as follows:

$$\omega = \frac{\pi h_p^3}{12\mu \ln \frac{R_o}{R_i}} \left(\frac{P_1^2 - P_2^2}{RT}\right)$$

Normally, this divergence can be neglected as the R_o/R_i ratio is close to unity.

For the special case where convergent or divergent taper exists between seating surfaces, the equivalent parallel plate separation becomes:

$$h_e = \frac{2h_p^2 (h_o + h_p)^2}{h_o + 2h_p}$$

where (h_p) is the separation at the narrow end of the land (L) and ($h_o + h_p$) the separation at the wide end. Thus, for $h_o = 0$, $h_e^3 = h_p^3$.

Transition and Molecular Flow. The determination of molecular flow involves the application of the kinetic theory of gases. A flow equation derived (Ref. 12) for the molecular regime is:

$$Q = \frac{4}{3} \frac{V_a}{\int_o^L \frac{H}{A^2} dL} (P_1 - P_2)$$

This equation relates the flow (Q) to the mean molecular speed (V_a), differential pressure ($P_1 - P_2$), and geometry where (H) is the channel perimeter. When this basic relationship is applied to parallel planes, the equation has the form:

$$\omega = \frac{4}{3}\sqrt{\frac{2}{\pi}} \frac{W h_p^2}{L} \frac{(P_1 - P_2)}{\sqrt{\frac{RT}{g}}}$$

There exists a transition region where both molecular and laminar (viscous) flow effects are operating. The limits of these regions are approximately defined by the ratio of mean free path of the molecule (λ') to the characteristic dimension of the channel (h_p) when:

λ'/h_p <0.01, flow is viscous

λ'/h_p is 0.01 to 1.0, transitional flow exists

λ'/h_p >1.0, flow is molecular

From kinetic theory of gases, the mean free path of gas molecules is given as:

$$\lambda' \cong \frac{\delta\mu\sqrt{RTg}}{P}$$

where δ is a constant. At atmospheric pressure and 70 F (294 K) the computed value of δ is nearly constant (~1.8) for nitrogen, helium, argon, and hydrogen gases. Assuming at high pressures that P is the mean channel pressure, the average mean free path reduces to:

$$\overline{\lambda'} = \frac{3.6\ \mu\sqrt{RTg}}{P_1 + P_2}$$

The separation at midtransition flow may be found by equating the molecular and laminar flow equations, and is given by:

$$h_p = \frac{25.5\ \mu\sqrt{RTg}}{P_1 + P_2}$$

The corresponding ratio of $\overline{\lambda'}/h_p$ is 0.14. A modified equation proposed for flow in the transition region is:

$$\omega_{total} = \omega_{viscous} + \varepsilon\omega_{molecular}$$

The molecular flow factor (ε) is generally close to unity. It takes into consideration such items as the difference in gases and physical properties of the passage walls. For simplicity and in lieu of explicit test data, (ε) has been assumed as unity.

Throughout the entire range of laminar and molecular flow, the flowrate computed from each of the specific equations will predominate in its applicable regime of flow. Thus, the summation equation above may be used without regard to regime boundary since the flow computed for the regime outside of its range will be negligible (see Sample Computation below).

Sample Computation

To illustrate how the previously developed flow equations are used, the following sample computation is presented. The seat model selected is the 1-inch configuration used in the off-seat leakage tests. A cross section of this seat configuration is shown in Fig. 13. Flow is from the inside (ID) to the outside (OD) of the 0.060-inch (0.1524 cm) flat seat land. Leakage has been computed for nitrogen gas at a 100-psig (68.95 N/cm^2) inlet pressure, a 70 F (294 K) inlet gas temperature, and a 14.7-psia (10.14 N/cm^2) outlet pressure.

Figure 14 presents the leakage spectrum for the sample computation. The various flow regimes, i.e., nozzle, turbulent channel, laminar, transitional, and molecular are identified on the curve. Also, the limits of each regime are shown. A range of theoretical parametric data has been computed for various pressures and gases and is presented with the Model Leakage section.

The following parameters are known values for this seat configuration and are used in the flow equations to compute the noted leakage characteristics:

Discharge Coefficient	$C = 0.95$
Gravitational Acceleration Constant	$g = 1.39 \times 10^6$ in./min^2 (3.5306×10^6 cm/min^2
Specific Heat Ratio	$k = 1.14$
Channel Length or Land Width	$L = 0.060$ in. (0.1524 cm)
Inlet Pressure	$P_1 = 114.7$ psia (79.07 N/cm^2)
Discharge Pressure	$P_2 = P_s = 14.7$ psia (10.13 N/cm^2)
Gas Constant	$R = 663$ in./R
Absolute Temperature	$T_1 = T_s = 530$ R (294.4 K)
Channel Perimeter (πD_s)	$W = 2.95$ in. (7.493 cm)
Absolute Viscosity	$\mu = 4.40 \times 10^{-11}$ lb-min/in.^{2} (7.944×10^{-13} N-sec/cm^2)

Nozzle Flow. For a compressible fluid flowing sonically, the following equation is used:

$$Q = \frac{RT_s}{P_s}\left[\frac{C\ Wh_p\ P_1}{\sqrt{RT_1}}\sqrt{gK\left(\frac{2}{k+1}\right)^{k+1/k-1}}\right]$$

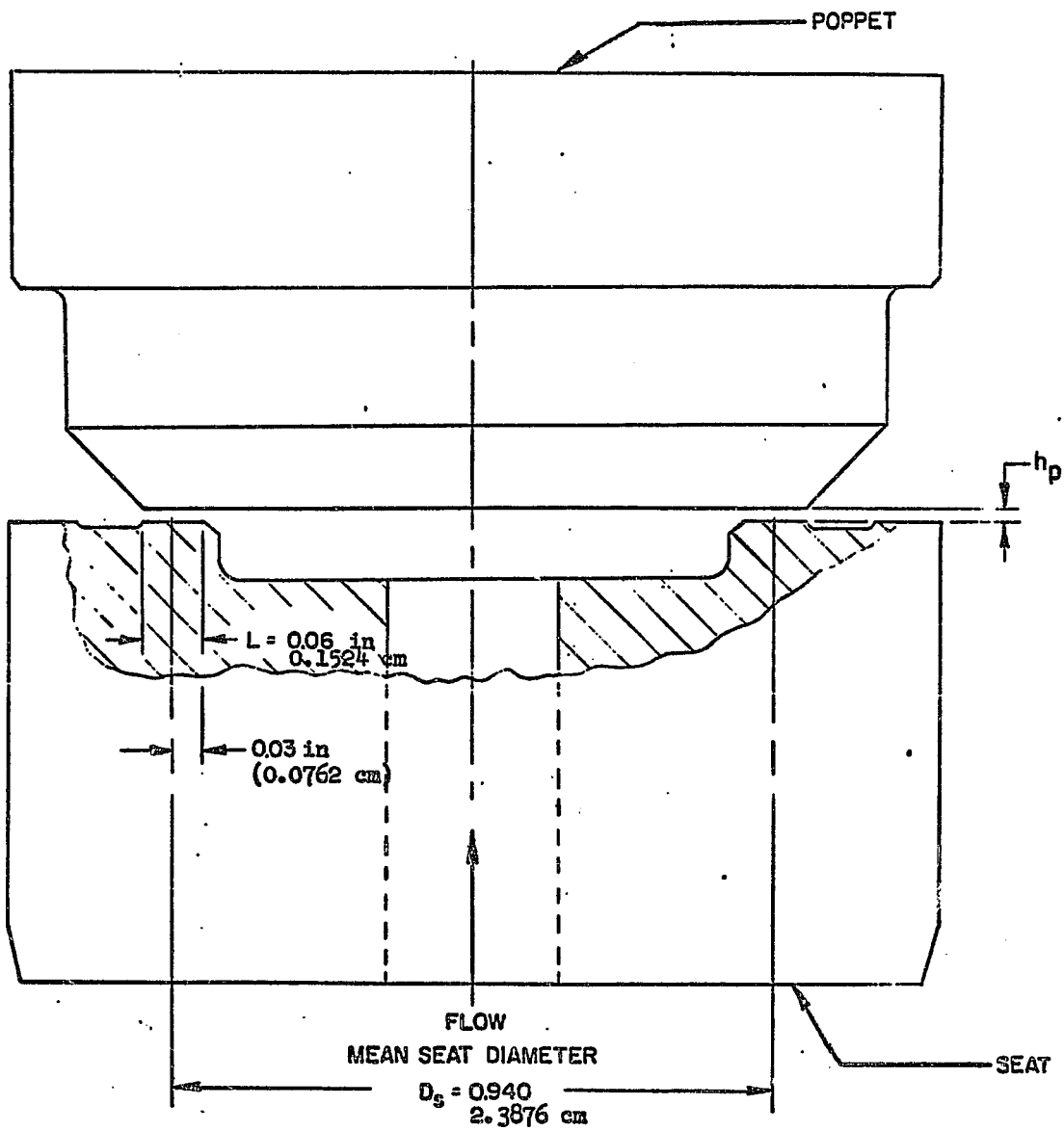

Figure 13. Typical 1.0-Inch (2.54 cm) Poppet and Seat Model

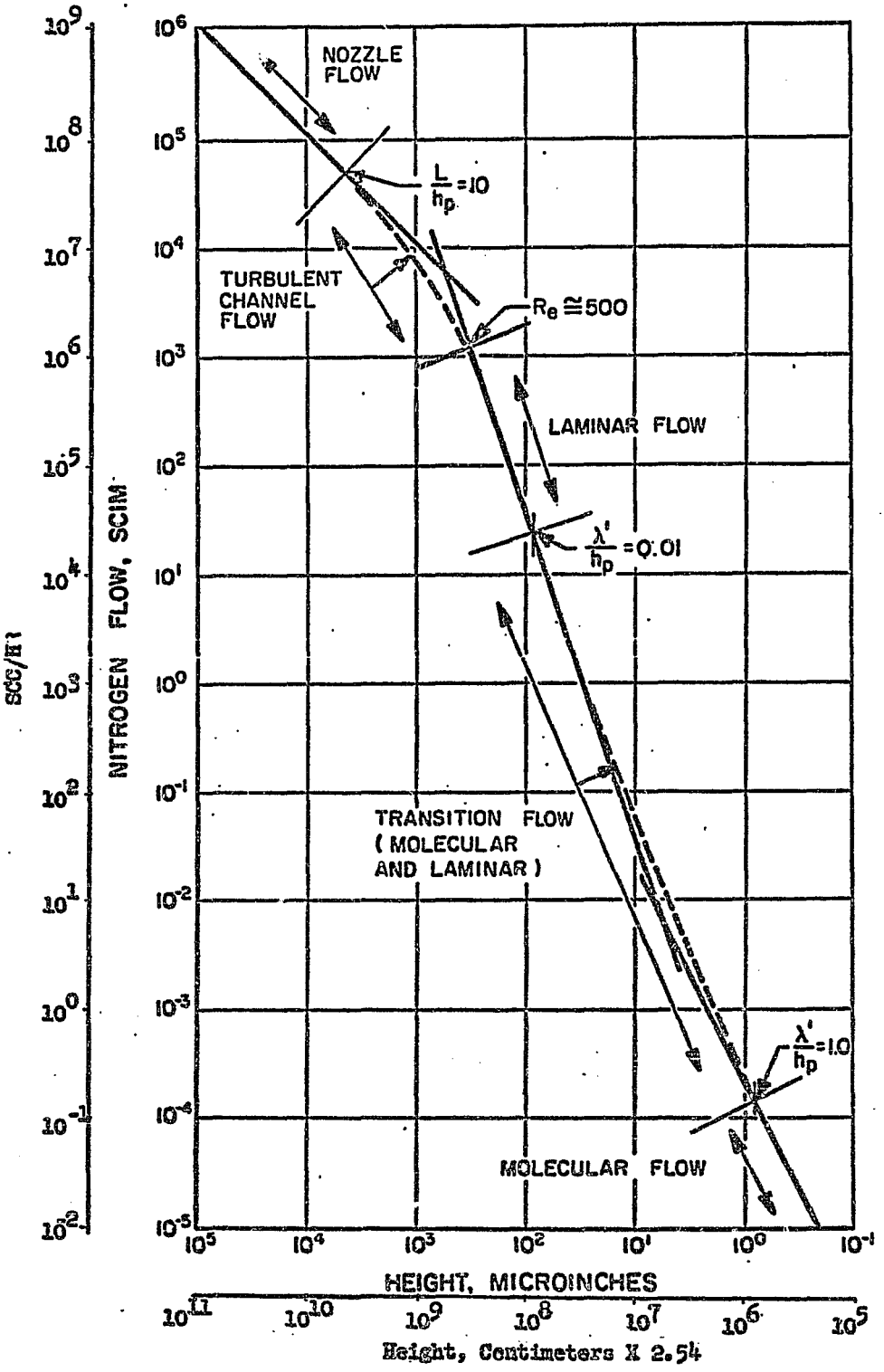

Figure 14. Theoretical Nitrogen Flow Through the Valve Model Shown in Fig. 13

Using the assumptions and data outlined:

$$Q = 1.045 \times 10^7 \, h_p$$

The orifice flow ceases, and turbulent channel flow commences at a height (h_p) of approximately 6 x 10^3 microinches 0.01524 cm (Fig. 14). The land width is 0.060 (0.1524 cm) inch, giving an L/h_p ratio of 10 for the break point.

Turbulent Channel Flow. Flow in this regime is defined by a curve on log-log paper; therefore, a sample calculation of one point will illustrate the method used. Leakage is computed for a stroke height (h_p) of 0.001 inch (0.00254 cm) in the following steps:

1. Hydraulic diameter, $D = 2h_p$ = 0.002 inch (0.00508 cm)
2. A friction coefficient (f) is estimated at 0.040. This is the starting point for the trial and error solution; (f) will be verified at the conclusion of this computation.
3. Compute $fL/D = fL/2h_p = 1.20$
4. Using Table B-4, Ref. 9, and the equation:

$$\frac{fL}{D} = \frac{1 - M^2}{kM} + \frac{k+1}{2k} \ln \frac{(k+1) M^2}{2 \left(1 + \frac{k-1}{2} M^2\right)}$$

   yields entrance Mach number (M_1) = 0.49.

5. Assuming an isentropic entrance condition, entrance static pressure (P_1) can be computed from the following equation (Ref. 9) where P_o is the stagnation (total) pressure of 114.7 psia (79.08 N/cm^2) and M^o is the entrance Mach number:

$$\frac{P_o}{P_1} = \left(1 + \frac{k-1}{2} M^2\right)^{k/k-1}$$

   therefore, static entrance pressure (P_1) = 97.3 psia (67.09 N/cm^2)

6. Again, assuming isentropic conditions, the entrance static temperature (T_1) is computed from the following equation for a total temperature (T_o) of 530 R (294 K)

$$\frac{T_o}{T_1} = 1 + \frac{k-1}{2} M^2$$

   therefore, static temperature (T_1) = 506 R (281 K)

7. The following series of equations are used to compute the flow (Q) in the channel:

$$V_1 = M\sqrt{kg\ RT_1}$$

$$\rho_1 = \frac{P_1}{RT_1}$$

$$A = Wh_p$$

$$\omega = \rho_1 AV_1$$

$$Q = \omega \frac{RT_s}{P_s}$$

from which the flow (Q) = 8090 scim (7.95×10^6 scc/hr)

8. To prove the flow computation, the originally estimated friction coefficient (f) is checked. Reynolds number is first computed:

$$Re = \frac{DV_1\rho_1}{\mu g} = 3.76 \times 10^3$$

Using the computed value for Reynolds number, a friction coefficient is determined from the Moody diagram. The friction coefficient determined from this curve is close enough to the original estimate of 0.040 so that a recomputation is not necessary.

The curve plotted from this and other data points is shown as a dashed line in Fig. 14. This flow regime extends into the initial portion of laminar flow, i.e., Re below 2000 where fluid momentum is still an important consideration.

Laminar Flow. Laminar flow for nitrogen gas is computed from the Poiseuille equation in the following form:

$$Q = \frac{RT_s}{P_s}\left[\frac{Wh_p^{\,3}(P_1^{\,2} - P_2^{\,2})}{24\ \mu\ L\ RT}\right]$$

Using the assumptions and data outlined:

$$Q = 4.08 \times 10^{13}\ (h_p^{\,3})$$

Transition and Molecular Flow. The equation used to compute leakage in the molecular regime is as follows:

$$Q = \frac{RT_s}{P_s}\left[\frac{4}{3}\ \frac{2}{\pi}\ \frac{Wh_p^{\,2}(P_1 - P_2)}{L\sqrt{RT/g}}\right]$$

Using the assumptions and data outlined:

$$Q = 2.49 \times 10^{8} \ (h_p^{\ 2})$$

This flow regime is plotted on the lower right of Fig. 14. The dashed line connecting the laminar and molecular flow regimes is simply the sum of the two leakage values. Therefore, the transition equation is:

$$Q_{transition} = Q_{laminar} + Q_{molecular}$$

The boundaries of this transition regime are defined by the following limits:

$$\overline{\lambda'}/h_p = 0.01 \text{ to } 1.0$$

The molecular mean free path (λ') is 3.61 (9.17 x 10^{-6} cm) microinches for nitrogen at standard conditions (70 F (294 K) and 14.7 (10.13 N/cm^2) psia). For a mean pressure of 50 psig, $\overline{\lambda'}$ = 0.82 microinch (2.08 x 10^{-6} cm).

The corresponding height limitation of the transition regime is between 0.82 and 82 microinches (2.08 x 10^{-6} and 2.08 x 10^{-4} cm) with the point of equal laminar-molecular flow at 6.05 microinches 1.54 x 10^{-5} cm (Fig. 14).

Model Leakage

Theoretical nitrogen leakage for a flat poppet and seat model employed in screening tests is presented in Fig. 15 through 17. Helium leakage in the laminar regime will be nearly the same as nitrogen since the viscosity of nitrogen and helium are close.

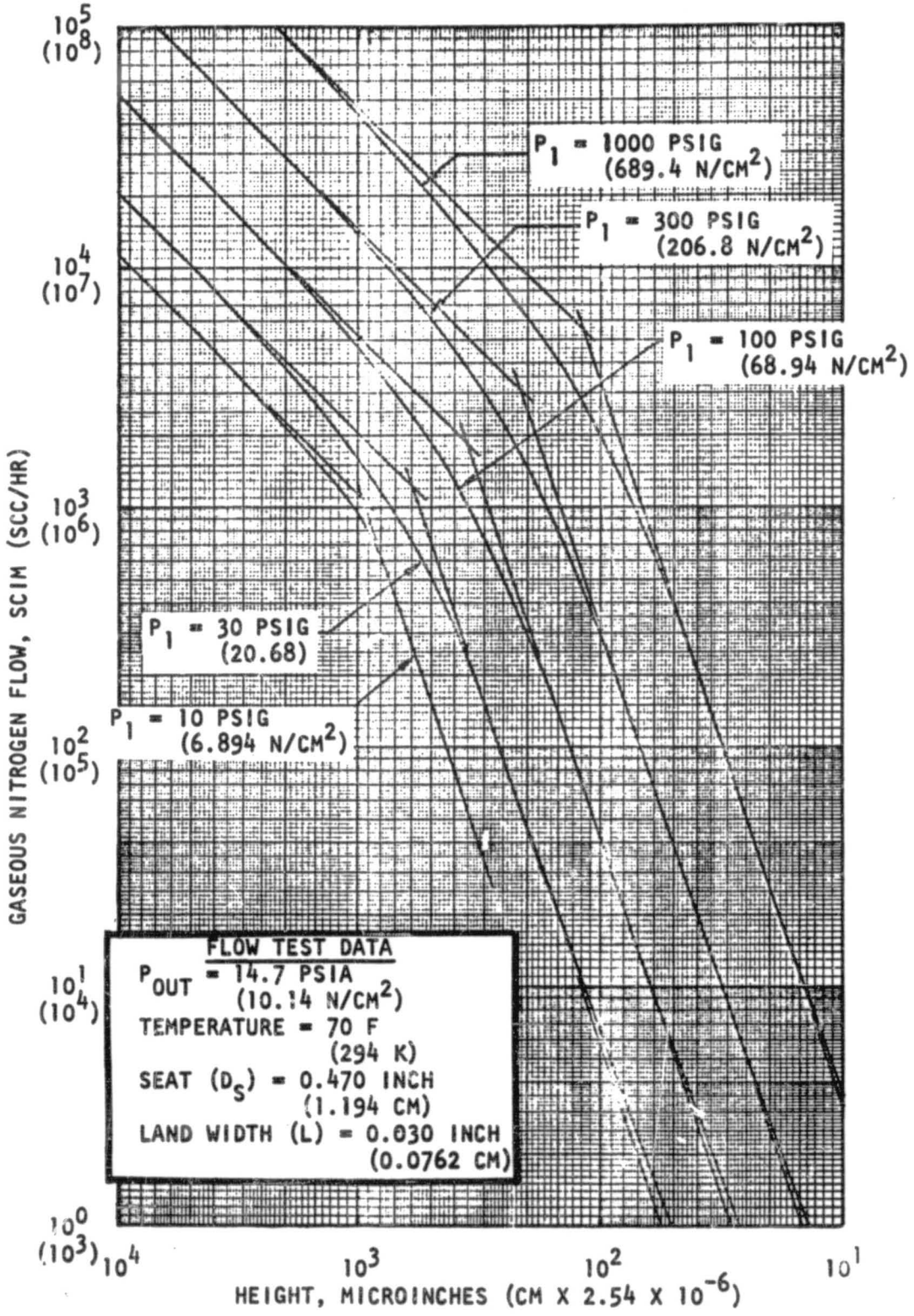

Figure 15. Theoretical Seat Leakage, Part 1

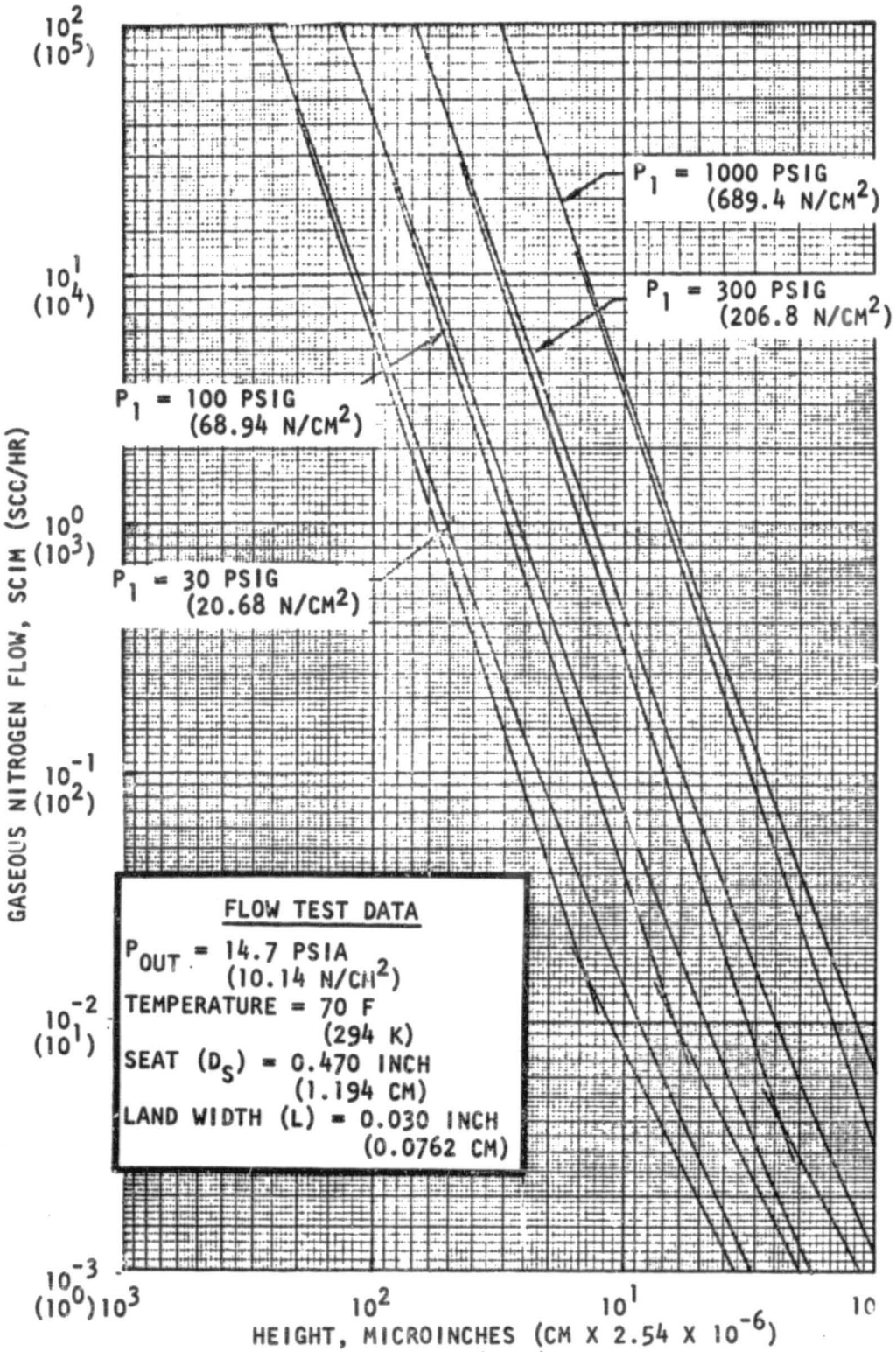

Figure 16. Theoretical Seat Leakage, Part 2

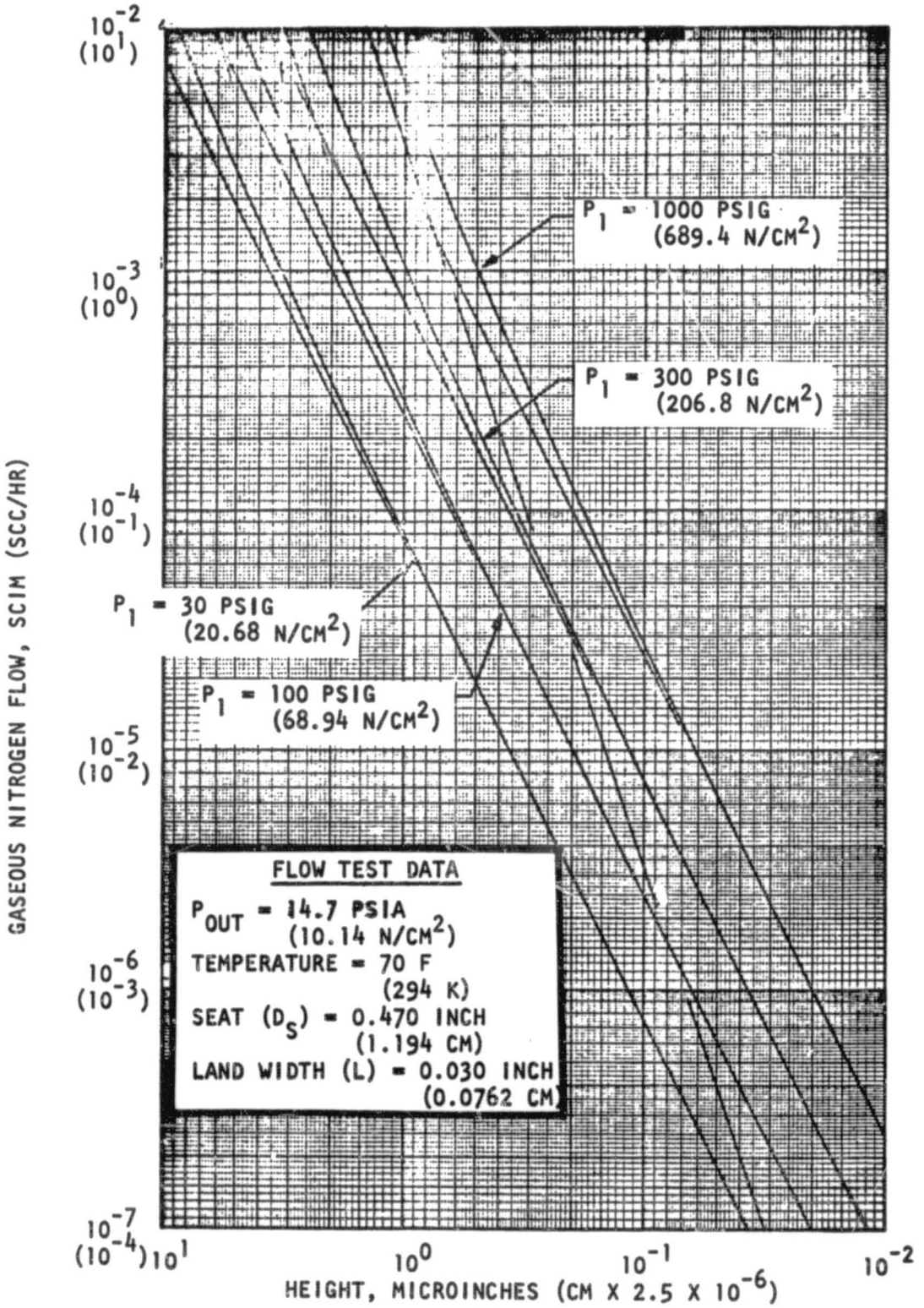

Figure 17. Theoretical Seat Leakage, Part 3

END OF REFERENCE

120

Card #29

REFERENCE

121

SCHWARTZBERG, F. R.; OSGOOD, S. H.; BRYANT, C.; AND KNIGHT, M.: CRYOGENIC MATERIALS DATA HANDBOOK. MARTIN MARIETTA CORP., 1970. VOL. 1 - SECTIONS A, B, AND C, REVISED. AFML-TDR-64-280-VOL. 1-REV.; AD-713619. VOL. 2 - SECTIONS D, E, F, G, H, AND I, REVISED. AFML-TDR-64-280-VOL. 2-REV.; AD-713620.

THIS REFERENCE IS MATERIAL THAT IS READILY AVAILABLE AND THEREFORE THE CONTENTS HAVE NOT BEEN REPRODUCED.

END OF REFERENCE

121

REFERENCE

122

TELLIER, G. F.: POPPET AND SEAT DESIGN DATA FOR AEROSPACE VALVES. AFRPL-TR-66-147, AIR FORCE ROCKET PROPULSION LAB. (AD-488480), 1966.

AUG 7 '67

X67-14599

X67-14599
AD-488480
8.5-0-6

POPPET AND SEAT DESIGN DATA FOR AEROSPACE VALVES

COPY 1

Technical Report AFRPL-TR-66-147

July 1966

LEWIS RESEARCH CENTER
Aerospace Safety Research
and Data Institute
APR 11 1972
CLEVELAND, OHIO

Air Force Rocket Propulsion Laboratory
Research and Technology Division
Air Force Systems Command
Edwards, California

Project No. 6753, Task No. 675304

(Prepared under Contract No. AF04(611)-9712 by Rocketdyne Division of North American Aviation, Inc., Canoga Park, California.
G. F. Tellier, Author)

This document is subject to special export controls and each transmittal to foreign governments or foreign nationals may be made only with prior approval of AFRPL (RPRP), Edwards, California 93523.

NOTICES

Qualified users may obtain copies of this report from the Defense Documentation Center.

Defense Documentation Center release to the Office of Technical Services is not authorized.

When U.S. Government drawings, specifications, or other data are used for any purpose other than a definitely related Government procurement operation, the Government thereby incurs no responsibility or any obligation whatsoever, and the fact that the Government may have formulated, furnished, or in any way supplied the said drawings, specifications, or other data, is not to be regarded by implication or otherwise, or in any manner licensing the holder or any other person or corporation, or conveying any rights or permission to manufacture, use, or sell any patented invention that may in any way be related thereto.

If this copy is not needed, return to AFRPL (RPRPD), Edwards, California.

APPROVED FOR PUBLIC RELEASE; DISTRIBUTION UNLIMITED, AFRPL LTR., 22 MAR 73, TAB, 73-10, PP.A7.

POPPET AND SEAT DESIGN DATA FOR AEROSPACE VALVES

85

Technical Report AFRPL-TR-66-147

July 1966

Air Force Rocket Propulsion Laboratory
Research and Technology Division
Air Force Systems Command
Edwards, California

Project No. 6753, Task No. 675304

(Prepared under Contract No. AF04(611)-9712 by Rocketdyne Division of North American Aviation, Inc., Canoga Park, California, G. F. Tellier, Author)

This document is subject to special export controls and each transmittal to foreign governments or foreign nationals may be made only with prior approval of AFRPL (RPRP), Edwards, California 93523.

ABSTRACT

Presented herein is a description of the work accomplished in providing fundamental sealing data on metal-to-metal seat and poppet valving elements. The reported effort supplements and updates initial results published as Technical Documentary Report No. RPL-TDR-64-68, "Rocket Engine Valve Poppet and Seat Design Data," dated May 1964.

The program involved experimental and analytical studies of the detailed aspects of valve seating. Flat, conical, and spherical test models were fabricated with particular emphasis placed on documentation of fabrication methods and description of the resultant surfaces. Model stress-leakage characteristics, as a function of surface texture, geometry, coatings, and material variations were experimentally investigated. The resulting information is presented in graphical form supported by inspection evidence from which test surface condition and features were deduced. Mathematical models relating surface texture and resulting deformation characteristics are formulated to provide understanding of the leakage path closure mechanism and extrapolation of experimental stress-leakage data.

Additionally, cyclic effects on model sealing capabilities were investigated. A simplified analysis relating tester and model configuration with anticipated dynamic loading characteristics is developed and further extended by digital programming techniques.

A high degree of correlation was obtained between the analytical predictions and the test results. From cycle tests of representative models at various impact levels, corrosion fretting was determined to be a fundamental mode of surface degradation and, from these results, an optimum seating configuration evolved.

Errors of Form

These errors refer to deviation of the nominal surface from perfect geometry and do not include surface texture. Definitions for tolerances of form are given in MIL-STD-8C.

MEASURING METHODS AND DEVICES

A brief review of surface measuring devices will include only instruments capable of measuring at the level significant to this study.

Stylus Instruments

The most common method of measuring surface roughness is by moving a cone-shaped diamond stylus over the surface and translating its vertical motion to a value of average deviation from the mean. Factors which affect the resulting reading include the radius of the stylus, its force upon the surface, and the reference surface or skid upon which the tracer is supported. Error may be introduced because of mechanical vibration and electrical limitations. The almost universally used devices use stylus tracers with electrical amplification and may be grouped as follows.

Continuously Averaging Instantaneous Readout. This is a tracer-type instrument using either the standard 0.0005-inch radius stylus or the 0.0001-inch stylus for fine finishes. Vertical movements of the stylus are converted into voltage and amplified to actuate a direct-reading dial. These readings are in rms or arithmetical average with the lower limit of surface discrimination down to about 1 microinch. This device shows variations in average roughness height but does not indicate asperity configuration or wavelength greater than the set cutoff value.

Permanent Record. This is an electromechanical stylus instrument for measuring and recording roundness, flatness, roughness, scratches, flaws, and total profiles. For a linear reference, a precision flat is employed;

for round surfaces, an ultra-precision spindle is used. Magnified readings or traces are recorded on a chart with vertical magnifications of up to 50,000 times, enabling discriminate study of geometry and minute surface variations including waviness and asperity angle.

Probably the most important factor contributing to misinterpretation of surface roughness is the stylus tip radius size. It is obvious that some valleys and cracks cannot be reached by stylus tips of 0.0005- and 0.0001-inch radius found in most instruments. Also, these instruments evaluate the roughness along a thin line which undermines accuracy because the three-dimensional aspect is not taken into account. This situation might be minimized by traversing in various directions and also by having knowledge of the distribution of the irregularities.

Interesting comparisons have been made of various tip radii effects on similar surfaces (Ref. 3). Results showed that, for a turned surface, the 0.001-inch stylus read 53-microinch AA finish while the 0.0001-inch stylus gave a reading of 52-microinch AA, hardly a significant difference. But in three ground surfaces, the blunter instrument could not bottom consistently, therefore giving smaller measurements. For these surfaces, the 0.001-inch radius tip measured 1.6-microinch AA for the first, 5.5 for the second, and 22 for the third. The 0.0001-inch tip measured 1.8-, 7-, and 31-microinch AA, respectively. The difference in stylus effect is more pronounced in the rougher finishes for those ground surfaces.

The precision of stylus instruments was tested by comparison with standards which were constructed and measured optically by Bickel (Ref. 4). One observation was the effect of the tracer radius in interpreting sharp corners as being rounded (Fig. 4).

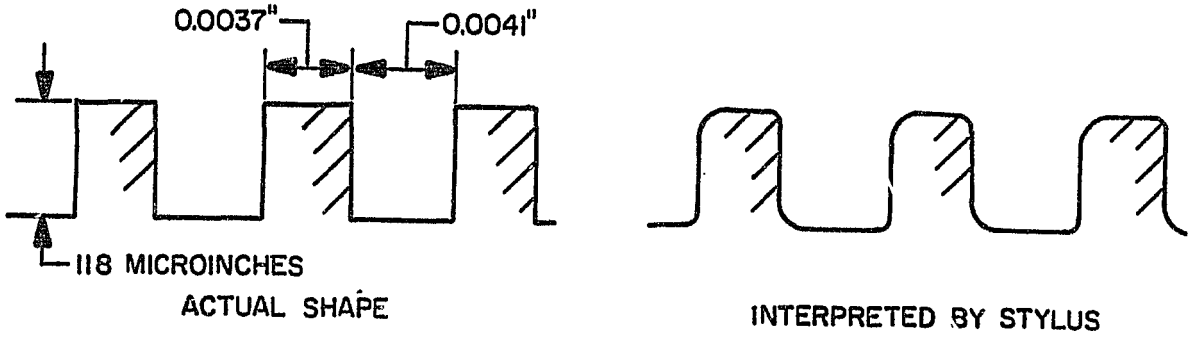

Figure 4. Stylus Interpretation of a Rectangular Shape

While profiles of simple sine wave shapes could be accurately followed by the stylus, the combined form of rectangular shapes upon a sine wave (Fig. 5) could not be contoured satisfactorily.

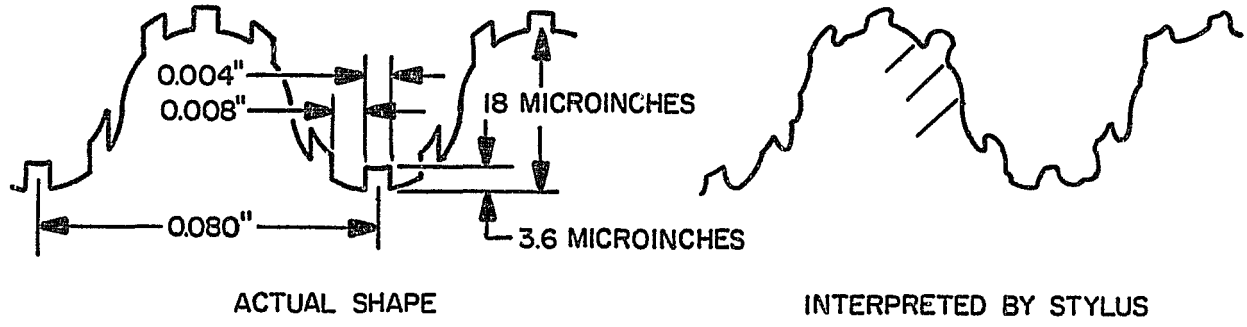

Figure 5. Stylus Interpretation of a Combination Shape

Table 1 indicates the results obtained by Bickel in a comparison of three stylus instruments (set at the cutoff values noted) while measuring rectangular profiles similar to those shown in Fig. 4.

TABLE 1

COMPARISON OF ARITHMETICAL AVERAGING INSTRUMENTS (MICROINCHES AA)

Calculated	Instrument A, 0.030 inch	Instrument B, 0.060 inch	Instrument C, 0.030 inch
2.7	2.6	2.36	3.2
25.0	25.6	26.4	30.0
58.0	57.0	53.3	68.0
120.0	124.0	128.0	136.0

A calculated curve which relates the stylus radius error with the average roughness height of precision reference specimens used to calibrate these instruments is found in Appendix C of Ref. 1. The reference specimen profile is made up of a series of known sizes of peaks and valleys having included angles of 150 degrees. For example, use of stylus tips having 0.0005- and 0.0001-inch radii for a reference specimen of a 4-microinch AA results in errors of 77 and 12 percent, respectively, indicating the relative capability of each tip radius to bottom the 150-degree included angle.

In measuring errors of form, the precision spindle electromechanical stylus instrument providing a profile record has generally replaced the more simple two and three point comparitor methods. (See Ref. 5 for a comprehensive collection of papers on roundness measurement.) Where lobing and nonsymmetrical errors exist, this is the only technique which will give valid results. However, as with all measuring methods, familiarity with potential errors and correct interpretation of the profile is necessary to obtain accurate and repeatable results. Of particular importance is the proper alignment of the basic reference of the part being measured with respect to the measuring datum. In the case of flat parts, the nominal surface must be parallel with a plane perpendicular to the spindle axis so that recorded deviations are totally from the part and not from setup errors. The mean axis of cylindrical parts must be coincident with

the axis of the spindle or an error in roundness will be superimposed upon the profile. For example, a perfectly round part will present a sine wave linear trace when located eccentrically from the spindle axis. Furthermore, interpretation of numerical values can be geometrically misleading due to high vertical magnification (5×10^4). Dips in the profile trace of round surfaces are significant only of a small change in radius and not actual depressions in the surface (neglecting surface texture).

Taper Sectioning

Taper sectioning is a method whereby the surface roughness is magnified by slicing (grinding and lapping) the surface at an oblique angle. The magnification of the surface asperities of a taper section is a function of the taper angle, e.g., if the section is cut at 2.3 degrees, the vertical dimension would be 25 times the horizontal. Most materials require hard surface electroplating to prevent damage when cutting. This method of surface study is most accurate when the irregularities are wedge-shaped or produced by unidirectional processes. When ground surfaces of this type are viewed, they appear as jagged, sharp peaks with an irregular pattern. Lapped multidirectional surfaces are very difficult to evaluate because they include pits, gouges, and material that appears to be floating on the surface. Evidently, what is seen considering various sized cones as the surface makeup will depend on the sectioning angle and at what point it cuts each cone.

Excellent taper sectioning can be seen in Plate I of Ref. 6 and pages 191 and 192 of Ref. 7. These microphotographs show the irregular contour of various finishes on metal surfaces. One particular photo (Ref. 7) shows a 1.6-microinch-rms surface whose vertical dimensions are optically magnified to 10,000X. The surface appears to be less jagged than other photos of higher rms values. A taper section microphotograph (Ref. 7) shows a surface finished by loose-abrasive lapping. It is unique in that no definite trace can be observed, rather what is seen are outlines of

cones or "mountains" of various sizes superimposed and scattered throughout. Analysis of such surfaces would be difficult even though the surface can be microscopically resolved to 1 microinch.

Optical Interference

The use of the principle of light wave interference makes it possible to measure surface finishes to a high degree of precision. Monochromatic light is directed through a transparent material with an accurate flat side which lies on the surface being inspected (Fig. 6). The two surfaces are separated by a thin "wedge" of air. Light waves are reflected from the work piece and the optical flat surfaces so that waves in phase produce bands of light and, conversely, when they are out of phase the waves interfere, producing dark bands. Alternate bands of light and dark approximately the same width appear at right angles to the direction of the air wedge. The bands give the effect of a contour map, decreasing in width and increasing in number as the wedge separation distance increases. Conversely, on a flat surface the bands will appear straight and parallel. The distance from a point on one band to the next band is equal to 1/2 of the wave length of the light used. The waviness and jaggedness of the interference bands are an indication of the surface irregularity and can be measured.

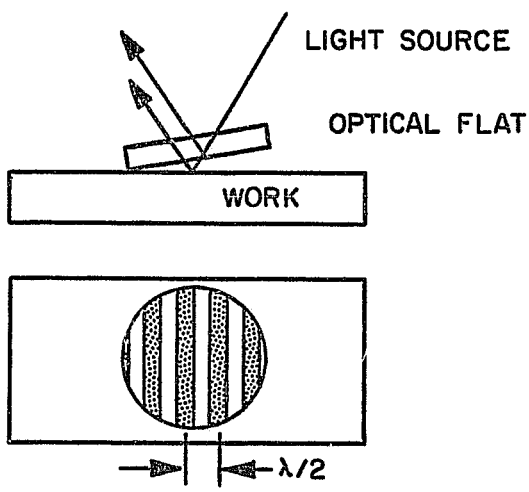

Figure 6. Light Interference With an Optical Flat

Optical Flats. Optical flats are precision glass or quartz plates that are flat to less than 0.000001 inch, and utilize optical interference between the specimen and the optical flat as shown in Fig. 6. Normally, a source of monochromatic light is used. Some of the light sources available are white light with a wave length (λ) of approximately 20 microinches, yellow-orange light at 23.2 microinches, and green light at 21.5 microinches.

Microinterferometry. Microinterferometry is the use of the optical flat and monochromatic light source with a microscope, which gives a very sensitive method of measuring surface roughness. The instruments incorporating this principle are known as interference microscopes or microinterferometers. The Zeiss instrument (Ref. 8), with magnification lenses of 80X, 200X, and 480X, uses a reference mirror on one side of the optical flat and two light beams. Various reflecting powers are available so the brightness of the test piece can be matched, giving sharp fringes.

This type of equipment is best applied on highly finished or glossy surfaces where the deviation of surface heights is within a few light wave lengths. Coarse surfaces cause the contour lines to become very close together and interpretation very difficult.

Multiple-Beam Interferometry. Most of the advances toward the high degree of sensitivity of the multiple-beam interferometry method of measuring surface contour have been made recently. Surfaces of the optical flat and the specimen (if nonreflective) are coated with silver having a high reflecting coefficient and also a high transmission coefficient so that incident light will be reflected back and forth resulting in an interference pattern of all these beams (Ref. 9 and 10). The relatively wide bands usually observed in other optical methods are reduced to thin lines which are able to reveal fine detail down to 0.02 microinch when sufficient horizontal resolution is available.

Electron Microscope

The high resolving power of the electron microscope makes it useful for the determination of fine finishes. Its main difficulty is that the electrons must pass through the specimen before striking a photographic plate, thereby limiting its use to thin sections. Another drawback is the necessity of using high vacuum and strong electron beams which can cause physical changes in certain specimens (Ref. 11).

The surface roughness is estimated by light and dark areas on the photographic plate. Electrons hitting high spots have a longer path to travel so that a smaller portion of them will pass through. The relative density on the photo plate is an indication of the variation of surface height.

In certain instances (thick sections), it is impractical to use the actual specimen so plastic replicas of the surface are used. The surface is coated with a film which is then stripped off and examined. In practice, resolution down to 0.2 microinch or magnification of 10,000 diameters (Ref. 12) is usual, although linear magnification of 50,000 is possible with this type of instrument under optimum conditions. Excellent microphotographs of polished surfaces obtained by this technique can be seen on pages 188 and 189 of Ref. 11.

The disadvantages of the replica technique can be avoided by the electron reflection method where the surface is viewed obliquely and the surface protuberances are seen in profile. This method, studied by Halliday (Ref. 13), is shown to be particularly suitable for the examination of surfaces on which the irregularities are small; therefore, ground, lapped, finely abraded and polished surfaces can be studied.

Profile or Light Section Microscope

This simple optical method gives a detail picture of the surface but only of a very thin plane. The light source provided through a narrow slit falls on the specimen at an angle of 45 degrees to the surface of the

specimen. Seen in the optical system is a cross section of local irregularities made by a line of light following the surface contour (Fig. 7).

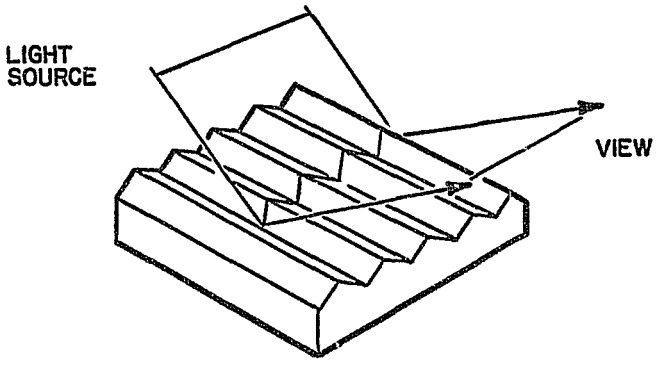

Figure 7. Principle of the Light Section Microscope

The smallest irregularity visible is on the order of the wave length of light or microinches (Ref.11). Sensitivity of this method is between 20 and 1600 microinches in deviation from the plane surface. It is considerably less sensitive than interferometry, being based on simple magnification rather than interference.

CHARACTERISTICS OF REAL SURFACES

To visualize real surfaces properly requires the ability to think small coupled with first-hand experience. There are many variations possible in ground and lapped surfaces because of the complexity of even the most regular fine finishes. Some idea of the scope of the topography can be obtained with the analogy of a plowed field or a mountainous terrain. Metal surface asperities undergo transformations similar to erosion as the surface is made smooth. Peaks are removed, and the remaining slopes become less steep.

Dimensions

Real surface dimensions are measured normally in microinches or millionths of an inch with nearly 40 microinches to the micron (10^{-6} meters) and 250 Angstrom units to the microinch. Metal valve seats are normally finished to less than 16 microinches AA by grinding and lapping, which places the upper peak-to-valley measurement at less than 100 microinches (0.0001 inch). At the other end of the spectrum, the lower limit of interest is in the vicinity of 1 microinch based on current-day achievements.

To describe the surface geometry more completely, an angle is often associated with surface asperities. This angle is the slope of individual undulations relative to the nominal surface. Except for machine-induced regularities, the asperity slope has wide variation from minute fraction of a degree to approaching the vertical, depending upon the scale of roughness viewed. As with mountainous terrain, large-scale undulations have shallow angles, and range from a gross flat characteristic of one gradual curve to periodic waviness. Superimposed upon the larger undulations are smaller and smaller facets (analogous to individual mountain peaks), and the smaller the facet viewed, the larger the slope angle may be.

A detailed examination of ground, lapped, and abraded surfaces was undertaken by Halliday (Ref. 13) using reflection-electron microscopy. Micrographs of aluminum, copper, mild steel, and hardened tool steel show asperity slope angles and heights from 0.1 degree and 0.4 microinch for electropolished aluminum to 30 degrees and 70 microinches for ground, hardened steel. Finer surfaces of approximately a 10-microinch height had corresponding asperity angles of about 1 to 2 degrees. This places the base dimensions of these asperities between 100 and 1000 microinches.

Rabinowicz (Ref. 14) describes results of absorption methods used for deducing real surface area. It is noted that relatively smooth surfaces obtained by rolling or electropolishing have real areas only slightly greater than projected; however, a metal surface obtained by an abrasion process has a total area nearly three times its projected area. The significance is that for the latter surface the angular inclines would have to be quite large, the average slope angle being 70 degrees.

Configuration

It has often been assumed that the irregularities or asperities of finishes that have been ground or lapped multidirectionally are generally cone shaped. They begin in the shape of wedges, scratches, etc., but are slowly rounded as cuts are taken radially. Examining any one irregularity microscopically would show smaller irregularities pointing to a situation of flatness not being possible in an absolute sense.

Bowden and Taber (Ref. 6) describe investigations of yield pressure as a function of the included angle or a single, cone-shaped asperity in an analysis of the plasticity characteristics of the cone.

Other surface investigators in various experiments concluded that meaningful results are possible when assuming conical asperity shapes (Ref. 15, 16, 17, and 18). Archard (Ref. 15) discussed some interesting data of an experiment by Halliday who, by reflection-electron microscopy, measured the slopes of surface irregularities of various steel and copper cylinders that were rough-etched and rolled against each other with contact force high enough to cause plastic flow. The resultant maximum slope angle measured 1.2 degrees, and the minimum 0.8 degree. Archard's conclusions suggested that asperities of angles more than some calculable amount will plastically yield until they reach the shallow, low, wide-base shapes measured above. These asperities of small slope will elastically deform into the surface until sufficient bearing area is developed to support the applied load.

Many of the approximations of the conical shape and size can be applied to the pyramidal shape. This shape can be assumed to result if a surface is finished by a process involving abrasion or cutting in two directions normal to each other. In unidirectional processes such as turning or superfinishing the wedge-shape irregularity results. Scratches fall into this category. As the wedge shapes become shorter in length as in grinding, they approach more closely the pyramidal shapes.

The geometry of spherical-shaped asperities has been assumed by Archard (Ref. 15), Kragelsky (Ref. 19), and Bowden and Tabor (Ref. 6) in contact analyses where this idealized configuration lessened the mathematical difficulties involved. It is probable that, among the various shapes suggested, the spherical one is most unlikely to occur except in unique cases. However, with a situation of worn, broken, or deformed peak points, almost any shape asperity may approximate the sphere if only at its tip.

There is little information on the statistical distribution of asperities of fine surfaces. The surface of the most finely finished material can be described as irregular if very sensitive instruments are used to examine it. Indications are that all surfaces contain random irregularities of various sizes with scratches, cracks, and intermittent flaws. Application of distribution laws can only be done theoretically with approximation as the result.

A paper by Reason (Ref. 20) shows profile charts of two actual surfaces whose profiles do not appear congruent but having similar AA values. These inconsistencies have been recognized by researchers in the field (Ref. 4, 21 and 7) in considering the multitudinous variables affecting surface geometry; it has been suggested by Reason (Ref. 20) that, for some surfaces, the process of manufacturing may need to be specified with the AA used as a simple controlling measure. This approach is obviously applicable to many critical valve sealing surfaces.

Visual Appearance

In describing real surfaces, a great deal of importance is often placed on visual effects and what is assumed from them. At best, the resolving power of optical microscopes is 6.7 microinches*, and no configurations smaller than this dimension can be clearly seen. Matte surfaces contain irregularities smaller than 40 microinches set at random angles so as to scatter the majority of light. The darker the surface the more scattered

*1/3 wave length of maximum intensity

the light and, thus, rougher the surface. Conversely, polished surfaces have broad areas which reflect a great deal of light similar to a mirror; however, in normal terms of peak-to-valley roughness, both surfaces can have the same average value.

Attempting to judge surface texture on a purely visual basis is generally misleading. Matte surfaces will tend to hide defects and scratches. However, a smooth appearing, mirror-like surface may contain relatively large undulations.

Composition

The surface layer is composed of a mixture of absorbed gases, metallic oxides, and various other contaminants in amounts depending upon past history. It is these contaminants which maintain sufficient separation between mating surfaces to preclude welding. Bowden and Tabor (Ref. 6) indicate that freshly lapped or ground metals (iron, nickel, chromium, and aluminum) will acquire a layer of oxide between 10 and 100 Angstroms thick in about 5 minutes or less. It is the breakdown of these oxides and other films which lead to wear and galling or seizure.

Because of the work-hardening nature of the finishing process, the hardness of the surface layer will be greater than the base metal. Soft, work-hardenable materials will have a larger increase than hardened steels. In addition, hardness within the crystalline grain structure of metals may vary considerably. This can induce roughness between contacting surfaces under loaded conditions.

CONTACT AREA AND LOADING EFFECTS

If two relatively smooth surfaces are brought together, contact will take place only in isolated spots. The irregular nature of the surfaces will permit stable touching at three points of contact until increased load causes a combination of plastic flow of the initially contacted asperities and elastic deformation of the supporting base material.

Gross areas of contact may be completely defined when the contact is curvilinear as in bearings and curved rollers, etc. The Hertz theory of elastic contacts (Ref. 22) describes a contact stress distribution which allows computation of gross bearing area, maximum stress, and deformation. Nominally flat surfaces, which are not perfectly flat, do not have well-defined regions of gross contact until loads are such as to bring the geometric total of the bearing surfaces in intimate contact. Even then the real contact area is only a relatively small percentage of the gross or apparent bearing area because of surface roughness.

In their study of friction and lubrication, Bowden and Tabor (Ref. 6) have evolved contact theories to describe the real contact area between metal surfaces. These are based upon observed evidence that: (1) real contact area increases in direct proportion to applied load, and (2) friction force, while independent of apparent area, is a function of the real area of contact. If the contacting asperities are assumed in a state of full plasticity and welded at contact, the force required to shear the welds would be the friction force. The real area of contact is defined by the plastic flow pressure (P_m), or stress, of the surface asperities and load (W), so that:

$$A_r = \frac{W}{P_m}$$

The plastic flow pressure has been evaluated for pyramidal and spherical shapes and, for the shallow slope angles normal for asperities, is related to the elastic limit (Y) by a constant. It is, therefore, independent of the applied load; for fully work-hardened metal:

$$_m \cong 2.8Y$$

The real area of contact is also defined by the material shear strength (S) and friction force (f) as

$$A_r = \frac{f}{S}$$

and it follows that the friction coefficient:

$$\mu = \frac{f}{W} = \frac{A_r S}{A_r P_m} = \frac{S}{P_m}$$

This relationship has been experimentally correlated for a number of different materials. Considering that valve seats normally work well below the yield strength, it is apparent that the real areas of contact computed from the above equation would result in a very small percentage of the apparent area in real contact. If it can be assumed that the apparent contact area (A_a) is defined, the ratio of real to apparent area is equal to the ratio of apparent stress (S_a) to plastic flow pressure (P_m), or:

$$\frac{A_r}{A_a} = \frac{W/P_m}{W/S_a} = \frac{S_a}{P_m} = \frac{S_a}{2.8Y}$$

A typical hardened valve seat (Y = 250,000 psi) operating at 10,000-psi apparent stress would then have a real contact area equal to 1.4 percent of the apparent contact seating area.

In flat surface experiments (Ref. 6), two steel surfaces (lapped flat within a few fringes) of 0.124 and 3.25 sq in. were brought together under various loads, and the electrical resistance between them was measured to determine the real contact area. Results for the 3.25-sq in. pair are duplicated as follows:

Load, pounds	Apparent Stress, psi	n Contacts	Diameter of Each Contact, inches	Fraction of Area in Contact	R, 10^{-5} ohms
4.4	1.35	3	0.004	1/100,000	50.0
11.0	3.38	5	0.005	1/40,000	25.0
44.0	11.4	9	0.007	1/10,000	9.0
220.0	68.0	22	0.009	1/2,000	2.5
1100.0	338.0	35	0.017	1/400	0.9

The results indicate real area proportional to load. However, the range of apparent stress is far below valve seat stresses.

Through analysis of wear experiments, Archard (Ref. 15) has concluded that real surfaces support their loads predominantly in an elastic manner with only a small percentage of the contacts undergoing plastic flow. Friction between real surfaces has been experimentally proved to be proportional to the real area of contact. Archard has examined mathematical models of spherical surface protuberances pressing on a flat plate and has shown that real contact area is a power function of the load or

$$A \propto W^n$$

where $n = 2/3$ for a single protuberance (Hertz) and approaches unity for numerous protuberances. This conclusion was also reached by Kragelsky (Ref.19). Consequently, it was concluded (Ref. 15) that surface welding was a consequence of singular encounters occurring infrequently, and the more typical event is an elastic contact in which protuberances separate without damage. The elastic event thus determines friction and not welding as concluded by Bowden and Tabor.

In substantiation of his views, Archard describes the results of reflection electron microscopic examination (Ref. 13) of some metal surfaces (aluminum, copper, iron, nickel, steel, etc.) pressed flat (base metal plastically flowed) by a carefully polished, hardened-steel anvil. It was shown that the resulting slopes of the asperities were in all cases less than 1.2 degrees and, following compression, were entirely elastic in that the asperities could be pressed just flat without plastic flow. Moreover, in experiments involving phase contrast microscopy observation of nominally flat, ground, polished, and lapped specimens against a metallized gloss surface, Dyson and Hirst (Ref. 23) concluded that the bearing area may be comprised of considerably more points of contact than noted by Bowden and Tabor. Instead of 9 contacts at a 0.007-inch diameter and 44 pounds, they measured many contacts of only a "few microns" (0.0001 to 0.0002 inch) under similar conditions. This evidence supports Archard's hypothesis of bearing area increasing directly with load through an increase in number of contacts.

The elastic theory would suggest that low slopes of irregularities of the fine finishes being considered applicable to valve seats would preclude the occurrence of plastic flow. The significance here is important when considering the effect of removing the load which allows, in this reversible process, a return to the original state of the surface.

Further substantiation of Archard's views of elastic behavior of surface asperities are provided by O'Connor (Ref. 24) in examining the role of asperities in transmitting tangential forces. An idealized surface with a sinusoidal profile is assumed in contact with a flat surface of the same material under an average pressure. For purely elastic deformation, the Hertz theory indicates real to apparent area of contact

$$\frac{A_r}{A_a} = 0.684 \left(\frac{P}{E}\ \frac{\lambda}{h}\right)^{1/2}$$

with

$$\frac{\lambda}{h} > 1.27\ \frac{EP}{Y^2}$$

as required microgeometry for elastic behavior

where

A_a = apparent area

A_r = real area

E = elastic modulus

h = peak-to-valley height of surface asperities

P = average Hertz contact pressure

Y = yield strength

λ = wave length of surface asperities

For full plasticity, the required load is approximately 75 times that re-required for initial yield; therefore, the criterion for fully plastic behavior is:

$$\frac{\lambda}{h} < 0.017 \frac{EP}{Y^2}$$

Microscopic examination of several surfaces varying from rough-and-soft (λ/h of 5 and DPH* 145) to smooth-and-hard (λ/h of 30 and DPH 700) indicated a general correlation with the above analysis, i.e., the asperities of the soft material yielded plastically while the hard surface indicated no signs of yielding, either directly or with profile records. These experiments were performed using a normal load of 13,440 pounds between two surfaces, one of which was flat and the finish varied, and the other curved to a 30-inch radius with the surface hard and polished. The high, normal load resulted in elastic contact circles of approximately a 1/2-inch diameter and maximum contact pressures for the hard and soft materials of 83,000 and 53,000 psi, respectively. Although the asperities of the soft material yielded, its real area of contact was only slightly larger than the harder specimen. The A_r/A_a values for the soft metal that were calculated and microscopically measured was 0.28 at the center or maximum pressure area, whereas the calculated value for the harder material was 0.20.

The paper concludes that the majority of surface irregularities of typical engineering surfaces are deformed elastically, or at least do not reach the condition of full plasticity. Under these conditions, the area of real contact is determined by the surface topograph (λ/h) as well as hardness of the material, and is appreciably greater than a purely plastic analysis would suggest.

Generally supporting the theory that surfaces deform under load in a predominantly elastic mode is a significant collection of papers from the Soviet Union (Ref. 25), summarizing the results of studies on contact area. Of particular importance was the conclusion that real bearing area

*DPH = Vickers diamond pyramid hardness number

increases with load as a function of increasing number of contacting asperities with the growth of individual asperity contacts contributing little to the total area. (It should be noted, however, that when the real bearing area becomes an appreciable fraction of the apparent area, the concept of individual contacting asperities fails and real area must increase with increase in the size of individually contacted asperities.)

The above concepts are generally supported by Greenwood (Ref. 26) who examined the influence of asperity distribution statistics upon contact area and compliance between rough surfaces and flats. He proposes a "plasticity index" for surfaces with spherical asperities which predicts elastic contact at heaviest loads for "polished and well run-in" surfaces. (This index is much the same as that of O'Conner's previously presented.)

SURFACE DAMAGE AND WEAR

The vast literature on friction and wear attests to the complexity of this subject. The purpose of this section is not to summarize the literature which has been accomplished by recognized authorities (Ref. 6, 27, 14 and 28), but to present a synopsis of related data which might lead toward an understanding of cyclic seating effects upon the closure geometry and leakage.

Elastic theory has shown that, for direct normal contact, material failure initially occurs below the surface. As tangential forces are applied, the maximum shearing stress moves up toward the surface (Ref. 29) and, with sufficient friction, exists at the surface. Overcoming frictional forces, interfacial slip with wear results.

For most valve seats, a period of cyclic service usually results in some change in the leakage characteristic. When leakage decreases with cycles, a "run or wear-in" process is thought of and for the converse, a "wear-out." A change in the leakage characteristic certainly denotes a change in the seating compliance (since seat loads are fixed) and, in the absence of changing external forces, a change in the surface profile. The converse

assumption of constant leakage representing constant surface profile is not likely because the probable interplay between surface roughness, macroelastic and plastic strains due to contaminants and edge contacts, and wear from interfacial shear.

Plastic Strains

Substrate plastic strains with attendant change of geometrical form are a complex function of the impulse load and its distribution. Valve seating members having errors of form (taper, out-of-roundness, or parallelism) or which are imperfectly guided may be subject to such deformations depending upon the amount of error. Because of the geometrical complexity of most valve seating errors, a theoretical treatment for stress distribution which might allow an elastic design approach is generally not available (see Seating Analysis section for treatment of this subject).

Where initial impacts cause plastic deformation, subsequent cycles under like conditions will produce predominantly elastic deformation since the material has been deformed and strengthened to an equilibrium state. Interfacial compliance will be affected in proportion to the amount and location of plastically displaced material because this material must henceforth be elastically deformed by the fixed seat load. If the displaced material is above the plane of seating, leakage will be increased. Conversely, if material has been pressed into the seating plane, a decrease in leakage will result.

Experience has shown that, for functional valves, leakage is generally reduced with cycles up to some point, holds constant, and then increases. This characteristic involves a combination of plastic strain of the surface asperities and supporting substrate along with a wear process. The amount of leakage change and corresponding cycles is related to the surface profile and roughness, seating errors, material properties, and impact energy.

Valve seats undergoing plastic flow with each cycle ("brute-force" approach) generally have a relatively low cyclic capacity due to work hardening of the interface material. With work hardening and a fixed seat load, leakage might be expected to increase with cycles, ending in abrupt failure from surface fatigue. This is not to say such valves do not seal well. Indeed, many industrial valves hold very low leakage levels but at the expense of weight, heavy seat loads and short life.

Other valves employing liquid metal as interfacial material have been investigated (Ref. 30) and found to be capable of holding molecular leakage levels. However, many severe technological problems need to be overcome before a reliable cyclic capability is developed.

Wear

Because of the above complexities and the difficulties of measuring the minute dimensions associated with even large leakage changes, very little factually correlated experimental data on the mechanism of valve failures have been documented. Consequently, the many descriptions and hypotheses of seating mechanisms and subsequent failure modes are largely conjectural (including some of the preceding discussion). This leaves little from which to draw any conclusion as to the predominant wear process in seating.

A review of the literature has indicated that,while the laws of friction have been fairly well substantiated, there are no satisfactory laws for wear. As a result, the design of equipment considering wear must be based upon direct experimental evidence and guided by the documented test data of many researchers.

Rabinowicz (Ref. 14) describes four basic types of wear as:

1. Adhesive wear. This is the most common form of wear. Junctions are formed between sliding surfaces which subsequently shear in either of the two metals or at the interface, depending upon relative strengths.

2. Abrasive wear. Surfaces are worn by the plowing action of hard particles.

3. Corrosive wear. Surface films formed by a corrosive environment are worn away so that corrosion continues.

4. Surface fatigue wear. Repeated high contact loads induce surface and subsurface cracks which eventually break up the surface leaving relatively large pits.

Wear has also been more generally divided into its most predominant forms by Tabor (Ref. 28) as mild and severe wear. Below a certain load, it has been observed that interfacial shear occurs and wear is small (mild wear); above this load, wear rises catastrophically to values that may be many times greater (severe wear). In severe wear, the loss of material is mainly due to subsurface shearing of the weaker metal.

When wear is due mainly to the shearing of junctions (i.e., adhesive wear), an empirical relation for the value of wear per unit distance of travel is:

$$Z = \frac{KW}{3p}$$

where (K) represents the percent of friction junctions producing wear, (W) is the applied load, and (p) is the hardness of the wearing surface. Tabulated values for (K) show that the wear rate between two surfaces is reduced by: (1) use of hard materials, and (2) use of materials with low interaction, i.e., unlike materials of low solubility.

The above relationship does not, however, provide any information about the change in surface texture with wear. Rabinowicz (Ref. 14) has shown that, in some cases, wear particle sizes can be predicted on the basis of elastic surface energy and hardness properties. Considerable data have been abstracted from the literature and combined with experimental results in application of this theory to sliding metallic seals (Ref. 31). While the theory has been correlated for experiments using soft metals, no data are given for the various combinations of harder metals known to have the best wear characteristics.

Fretting. In many cases, wear takes place in various combinations and degrees. One of these which has received considerable attention is fretting, or more commonly, fretting corrosion. A thorough summary of fretting prepared by Harry Diamond Laboratories (Ref. 32) describes the test methods, results, and conclusions from over 200 reports obtained from the English literature.

Fretting is caused by small oscillatory tangential motions between two materials. The process normally involves relatively large numbers of cycles, occurs over a wide range of loads, and is usually accompanied by a formation of corrosion products which are a function of material and environment. The mechanism of fretting appears to be a wear process involving adhesion that is further accelerated by corrosion and abrasive wear from the corrosion products. However, fretting has been produced in literally all material combinations and various atmospheres (including a vacuum); therefore, corrosion is not necessarily a part of the process. Fretting corrosion factors (Ref. 32) of potential significance to poppet and seat design are listed below:

1. Load. As load on the test part is increased without changing other factors, relative slip gradually decreases. Weight loss (due to wear) has corresponding increase, reaches a maximum, and then decreases to zero when the parts are sufficiently loaded to preclude slip.

2. Slip Amplitude. Fretting is generally recognized to occur from oscillating motions between 5×10^{-8} and 10^{-2} inches. In general, the wear rate is proportional to the slip amplitude.

3. Slip Frequency and Duration. While fretting wear is not greatly dependent upon the frequency of oscillations, it is proportional to the total number of oscillations. Therefore, parts subject to the higher frequencies would be expected to suffer the greatest wear (assuming constant slip amplitude).

4. Temperature. Fretting increases with lower temperatures with the worst condition reported for steel in air at -240 F. Fretting has also been produced at -300 F. Between 32 and 300 F, fretting

was almost constant. It would appear that high surface temperatures do not generally occur due to fretting (see bibliography in Ref. 32 for specific materials).

5. Atmosphere. Oxidation is an important consideration in determining the amount of damage; hence, the presence of oxygen and water vapor affect the rate of fretting. For ferrous materials, it is essentially the controlling factor in the damage process. Increases in wear of from 3 to 10 times have been observed for changes in atmosphere from nitrogen to air. However, tests made in a vacuum indicate that even though oxidation is suppressed, damage may be increased. Tests in a helium atmosphere indicate damage is caused almost entirely by metal transfer.

6. Materials. In general, softer materials fret more than hard materials. Metals which form hard, abrasive oxides (such as aluminum, chromium, and tin) are particularly susceptible. Aluminum and stainless steel form hard oxide debris (Al_2O_3 and Cr_2O_3), and also very rapidly oxidize and absorb oxygen upon exposure to fresh air. Stainless steel is reported as being the most susceptible of all materials to fretting. (While literally all materials fret to some degree, even with lubrication, it would appear that the extent must be determined for a specific application, choosing materials most suitable.)

7. Surface Roughness. In general, the finer the surface the more susceptible to fretting wear. No data have been reported on terminal surface roughnesses produced by fretting.

In the case of curved contact surfaces such as bearings, it has been shown that fretting can result from small tangential loads, even though there is no gross slipping (Ref. 24, 33, 34 and 35). Because of the elliptical pressure distribution under normal load between curved surfaces, a small annular area at the edge of contact exists in which any externally applied tangential force must exceed the frictional restraining force. This is caused by the elastic lateral deformation in the higher loaded central area of the contact which governs the total motion between the contacting parts. Thus, as the contact pressure diminishes

to zero toward the contact edge, a point is reached where the frictional force from local normal load is exceeded by the tractive force. Tractive forces between curved surfaces can be applied externally as a straight tangential load or couple.

Another more subtle source of interfacial tractive forces occurs when materials are pressed together which do not deform laterally in like fashion due to either unlike configuration or different elastic properties (shear modulus and Poisson's ratio). Goodman (Ref. 36) has described analytically the second case occurring between normally loaded, perfectly rough spheres.

Even when like materials were used in cyclic normal loading between spheres, fretting has been observed (Ref. 33). However, this was attributed to the likely possibility that the vibration within the cycling apparatus caused small tangential forces to be applied to the contact area.

Contamination

For the most part, the stringent weight and performance requirements for rocket engine control valves has precluded the brute force approach to seating. The survey of numerous valve designs in the initial program effort (Ref. 37) and other component development and test programs (Ref. 38, 39 and 66) has shown the need for hard poppets and seats with light seat loads and close guidance of moving members. The consequence is a requirement for finer surfaces, narrower seat lands with an attendant increased sensitivity to contamination.

Reference 41 presents a comprehensive summary of contamination, its nature, externally viewed effects (sticking poppets, leakage, etc.), cleaning and control methods, and considerations in design. Review of this and other literature will show that little has been accomplished in quantitatively defining either the source/volume of contaminants or their effect on valve seating. Consequently, filtration and cleaning requirements are based upon generalization of contamination sensitivity and availability

of commercial products rather than detailed knowledge of the real problem. This is manifest in numerous failure reports citing contamination as the cause of malfunction.

SURFACE-FINISHING METHODS

Surface-finishing methods capable of generating surface quality and precision applicable to rocket engine control valve seating are turning, grinding, lapping, and polishing. While turning and grinding may not generally be associated with the very smooth surfaces, roughness as low as 2-microinch AA for turning, and 1-microinch AA for grinding is possible (Ref. 1).

A survey of the literature indicates that little information relating a specific finishing operation with the resultant surface texture has been published. This is particularly true for surfaces commensurate with precision valve sealing, i.e., less than 16-microinch AA. It is suspected that considerable unpublished information exists but is not disseminated for proprietary (competitive) reasons.

Most researchers consider the noted operations from a production basis and are concerned with the economical removal of metal. However, the literature does document operation fundamentals, theories of the metal cutting mechanism and some process effects on the workpiece and general surface texture-metal removal relationships.

Turning

To produce a precision-turned surface the machine tool must be in excellent condition. However, even the best conventional machines are inadequate for some purposes. The duPont Company, for instance, has applied the hydrostatic gas-lubricated bearing principle to several machine tools. One, with a design target of producing 4-inch-diameter hemispheres true within ±25 microinches has turned aluminum parts of this type round within approximately 1-microinch with a 2-microinch rms roughness (Ref. 42).

Other considerations regarding the turned surface are:

1. In general, the higher the cutting speed, the smaller the roughness (Ref. 43).
2. Lapped cutting tools have a sharper, more uniform cutting edge (Ref. 44). (It follows that improved surface roughness results.)
3. For a given cutting condition, improved surface roughness will result with successive changes from high-speed steel, to carbide to ceramic and diamond tools (Ref. 45).
4. The conglomerate of welded chip particles forming on the cutting tool face called "bue" (built-up edge) is detrimental to surface texture. Increased cutting speeds reduce this formation and its detrimental effect (Ref. 45 and 46).
5. Surface temperature at the tool tip is quite high with observed values greater than 500 F and increases with cutting speed. Tool wear and surface texture deterioration are accelerated with temperature increases (Ref. 47, 48, and 49). (This implies that workpiece surface metallurgical transformations are likely.)

Grinding

In the grinding process, metal is removed in chip form although very brittle materials may disintegrate into dust particles. Three distinct actions are involved: (1) rubbing, where some abrasive grains do little more than elastically deform the surface, (2) plowing, when there is insufficient interference between grain and work, and the metal is simply plastically pushed aside, and (3) cutting or chip removal (Ref. 50 and 51).

Grinding as a mechanical process is almost unique in the creation of very high interface temperatures. The heat, however, is conducted more quickly into the workpiece than through the interface between the work and grinding fluid. Thus, all the fluid can do is remove the heat from the workpiece after it has produced whatever change it can induce. While plastic deformation produces residual compressive stresses, the heating action

results in tensile stresses. Furthermore, hard metals may be tempered to a lesser hardness or increased hardness may be caused by transformation of austenite to martensite or by cold-working the austenite. Thus, the properties of the metal surface may be radically different from the unaffected substrata. The temperature present during the cutting action cannot be deduced from the spark stream or surface discolorations. Since wheel trailing edge cutting may remove oxides, the absence of an oxide film does not necessarily mean that excessive temperatures were not generated (Ref. 50).

The two principal ingredients of a grinding wheel are the abrasive grains and the bond which holds them together. The three abrasive grains most commonly used are aluminum oxide, silicon carbide, and diamond, which are available in several varieties differing primarily in friability, a measure of fracturing ease to provide new cutting elements. Wheel bonds employed are vitrified clay (most commonly used), organic materials, and metal (Ref. 50). From the recommended uses and applications (Ref. 43), it would appear that, for hard valve sealing surfaces, a soft organic bond such as shellac with diamond grit (minimal wear, hence, consistent cutting) might provide an optimum cutting combination. However, no references were noted relating grinding process and specific wheel to the roughness produced.

Lapping

Lapping is an abrasion process used to establish size, geometry, or fine texture at extremely small tolerance levels. In the production flat lapping operation, surface roughness of 2- to 3-microinch AA is usually achieved using close-grained cast-iron laps. While it is commonly believed that the lap should be softer than the workpiece, production lapping of soft steels and nonferrous metals such as aluminum and copper with cast-iron laps is successfully accomplished (Ref. 44).

The soft-lap philosophy presumes the lapping action is performed by embedded abrasive. However, some question as to the exact cutting mechanism exists. Hawxhurst (Ref. 44) indicates that the amount of embedded

abrasive is negligible, does little cutting, and is removed by subsequent cleaning. This theory suggests the lapping action to be one of occasional cutting by rolling or suspended abrasive particles.

In another experiment (Ref. 52) the amount of abrasive embedded in the lapped workpiece was measured by radiation techniques. It was found, for example, that tool steel lapped with 11- to 28-micron silicon carbide having a vehicle-to-abrasive ratio of 18:1 on a cast-iron plate and following a 3-minute scrub under running water, retained approximately 24,000 abrasive particles/sq in. Although not measured, it was concluded that the cast-iron lap employed had also retained a significant amount of abrasive.

True chips are formed in the lapping process until the abrasive particle size approaches the 8-micron dimension. With smaller sizes, it is believed that the process is limited to plastic deformation without chip formation (Ref. 53). However, recent experiments (Ref. 54 and 55) suggest a mechanism for cutting at this level.

The most commonly used abrasives are manufactured silicon carbide and aluminum oxide which are preferred over natural abrasives since they have low impurity level and exhibit definite hardness, toughness, and friability properties. Aluminum oxide, for instance, is available in as many as five types varying in the noted properties. Other natural abrasives predominantly used are corundum, emery, and garnet (Ref. 43).

In the lapping process, the abrasive is suspended in a carrying agent or vehicle which is designed to suspend the abrasive particles, cool the working surfaces, float or lubricate the workpiece, and carry off spent abrasive and chips produced by the operation. The vehicle is generally a petroleum base of low viscosity with additives which increase body, strength, and cohesion to keep the abrasive in suspension. Water-soluble vehicles are also used (Ref. 44).

Abrasive size grading is based on National Bureau of Standards criteria and specified by a number which represents the approximate number of openings per linear inch in the screen or mesh used for grading. Grades

smaller than 400-mesh size are specified in micron ranges (Ref. 44). (An elutriation process is used for smaller size grading where mesh straining or sieving is impractical. Diamond compound, for instance, is available in the 0- to 0.1-micron range. Shape grading is apparently a function of industry competition.) An indication of potential surface roughness and the relationship of grain size and grade for diamond abrasive is shown below (Ref. 56):

Grade No.	Grain Size, micron	Grit Size Mesh, equivalent	Microinch AA	
			Metal Lap	Soft Lap
	(For fast stock removal)			
60	35 to 85	230	20 to 25	3 to 4
45	30 to 60	325	10 to 15	2 to 3
30	20 to 40	600	6 to 8	1 to 1.5
	(General purpose)			
15	8 to 22	1,200	4 to 5	0.5 to 0.75
9	6 to 12	2,000	3 to 4	0.5
6	4 to 8	3,000	3	0.4
	(Finest select work)			
3	1 to 5	8,000	2	0.2
1	0 to 2	14,500	1	0.0+
1/2	0 to 1	50,000	0.5	0.00

Polishing

It is common practice to brighten metal surfaces by rubbing them against a series of successively finer abrasives, generally by machine operations. The resultant surface, however, depends largely upon the way the abrasive is used. If the abrasive is firmly bonded to a cloth, paper, or similar backing, a surface containing obvious scratches which diffuse light, causing a somewhat dull appearance, is generally produced; this is considered an abraded surface. If, however, the same abrasive is used as an unbonded slurry on a soft cloth pad, it may produce a bright mirrorlike appearance on the polished surface (Ref. 54 and 55).

The nature of the polished surface and the mechanism of producing it is still subject to discussion. Beilby postulated that material was smeared over the surface to fill in the pre-existing irregularities, leaving a surface covered with an amorphous-like layer. This Beilby layer theory has for some time been the accepted mechanism of polishing. Bowden and Hughes refined the theory by proposing a thermally activated process where asperities are locally melted and deposited in adjacent depressions, thus gradually filling them and leveling the surface.

Samuels (Ref. 54 and 55) in reporting these developments, however, suggests that new evidence indicates polishing is primarily a cutting mechanism. This theory considers plastic shearing of surface layers, gradually cutting away the irregularities, and replacing them by a set of much finer ones. The resultant surface is compression-plastically deformed and fully crystalline; a Beilby layer is not formed.

It should be noted that, while polishing with soft-cloth pads can improve a metal surface, unlike lapping on a precision flat surface, it will not correct errors of form.

NEAR-SEATED TESTS

Parametric test data were obtained for comparison with theoretically predicted flow and force balance characteristics of parallel plate poppet and seat models. These investigations included leakage measurement of nitrogen, helium, and argon gases for the nozzle, turbulent channel, laminar, and transition-molecular regimes of flow. For force-balance analysis, the pressure profile was determine in the nozzle, turbulent channel, and laminar flow regimes.

Flow and pressure-distribution tests were performed using the flat poppet and 1-inch seat configuration of Test Model A. Land dimensions for this model are nearly identical with those used for the sample calculation in the Leakage Flow Analysis section. Interpreted surface texture and land dimensions for Model A are presented in Table 4. The multidirectionally lapped texture of the seat is illustrated in Fig. 105. Seat corner conditions along with a typical pressure tap used in pressure distribution tests are shown in the microinterference photo (Fig. 106). The diamond-lapped and polished-poppet surface texture is shown in Fig. 107. These surfaces, having a combined average PTV roughness of less than 10 microinches, are thus suitable for correlation tests down to the electrical contact leakage nominal (h_p) value of 20 microinches.

NEAR-SEATED FLOW TESTS

Leakage flow from 10^{-1} to 10^{4} scim was measured for poppet stroke (h_p) ranging from approximately 20 microinches to 0.006 inch. Data were obtained at 30-, 100-, 300-, and 1000-psig inlet pressure levels with nitrogen and, for comparison, tests were also performed at 100 psig with helium and argon gases. All test results were corrected to standard conditions of 14.7 psia and 70 F.

The correlation of test and theoretical data is shown in Fig. 381 through 389 by an overlay of test data points on computed curves. Data for preparation of these curves were presented in the noted sample calculation.

Gas properties assumed are tabulated below; hydrogen gas has been included for correlation use in the next section. As gas viscosities do not change appreciably with pressure, the values shown are based upon 70 F and 500 psia which is the average for the 1000-psig inlet pressure test condition used predominantly in the test program.

Gas	K	R, in./R	μ, lb-min/in.^{2}	Figure Number
Nitrogen	1.4	663	4.40×10^{-11}	381, 382, and 383
Helium	1.66	4630	4.70×10^{-11}	384 and 385
Argon	1.67	464	5.66×10^{-11}	386 and 387
Hydrogen	1.4	9210	2.15×10^{-11}	388 and 389

To minimize confusion, the theoretical curves, computed from the equations outlined in the Leakage Flow Analysis section, are continuously plotted while the actual test data points are represented by symbols. Because the theoretical trend of the nozzle to the laminar transition (turbulent channel regime) is sufficiently shown by the 30- and 100-psig data of Fig. 381, these curves were not computed for the 300- and 1000-psig nitrogen tests nor for the other gases.

The reference used in all of the flow data is the point where electrical contact occurs. This position represents approximately 20 microinches height when equated to flow between two flat plates. The physical determination of this point in the test setup involves some error. Based on comparative measurement with the Merz (and other instruments), it was determined that the micrometer adjustment for position is sensitive to approximately ±2 microinches. In addition to this, there is a possible error because of an out-of-parallel condition between the poppet and seat; however, experiments have shown that this error can be controlled to less than 10 microinches. Contamination can also introduce error into the evaluation of electrical contact. Contamination is an elusive variable which is relatively easy to detect but extremely difficult to accurately evaluate. Generally, the test setup was torn down and the poppet and seat cleaned (or refinished) when contamination was detected. In summary,

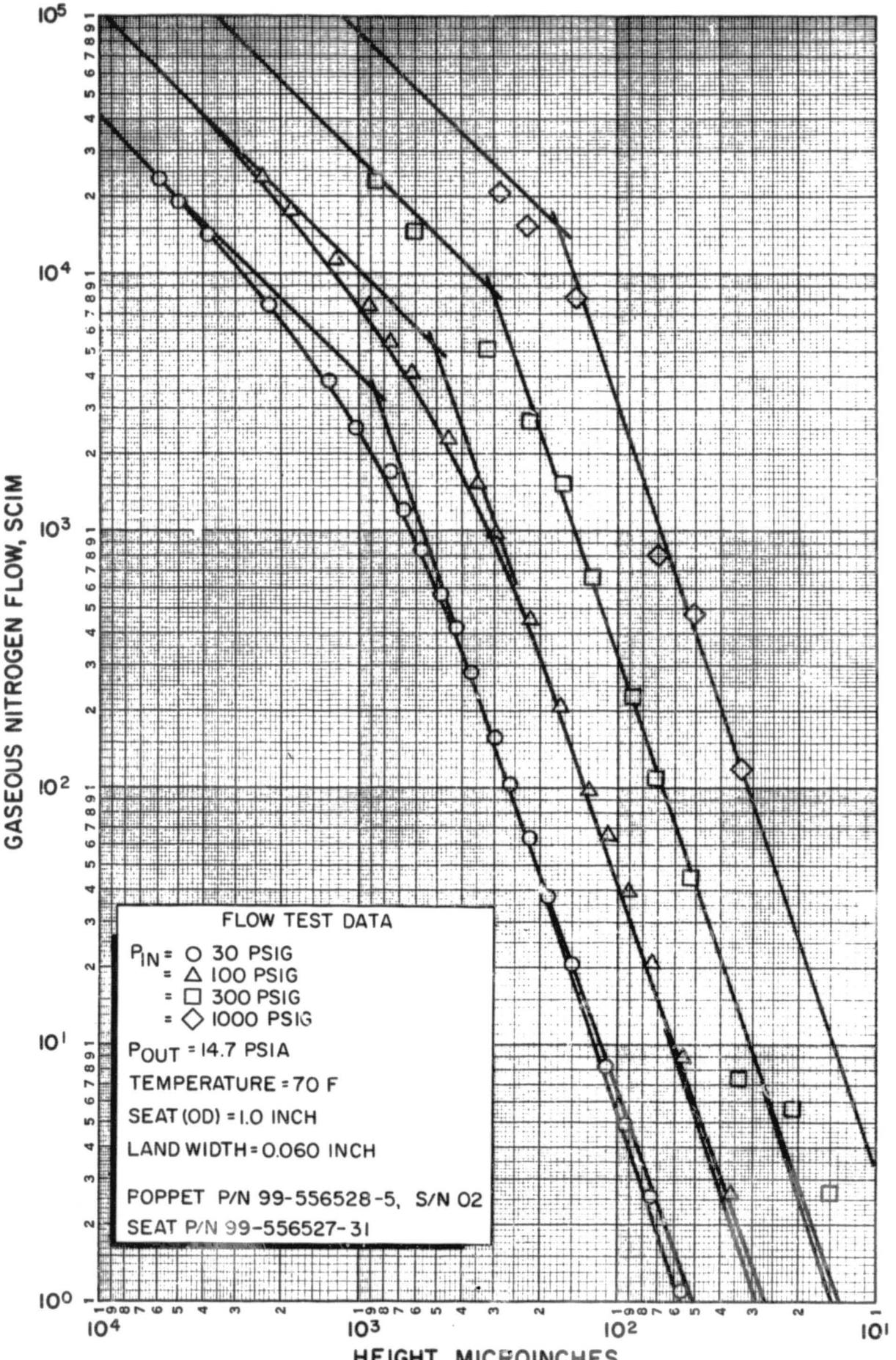

Figure 381. Nitrogen Flow Data, Part 1

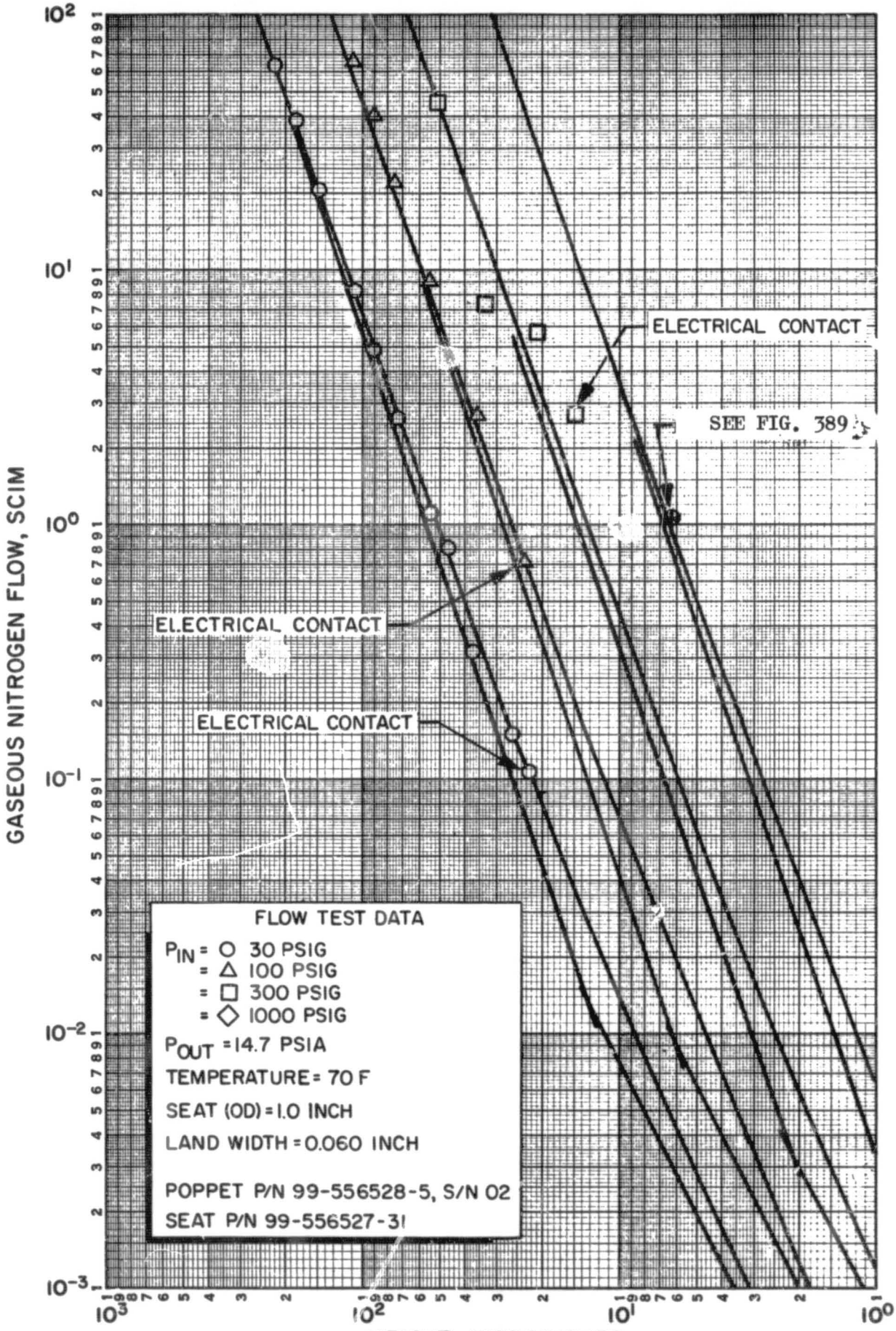

Figure 382. Nitrogen Flow Data, Part 2

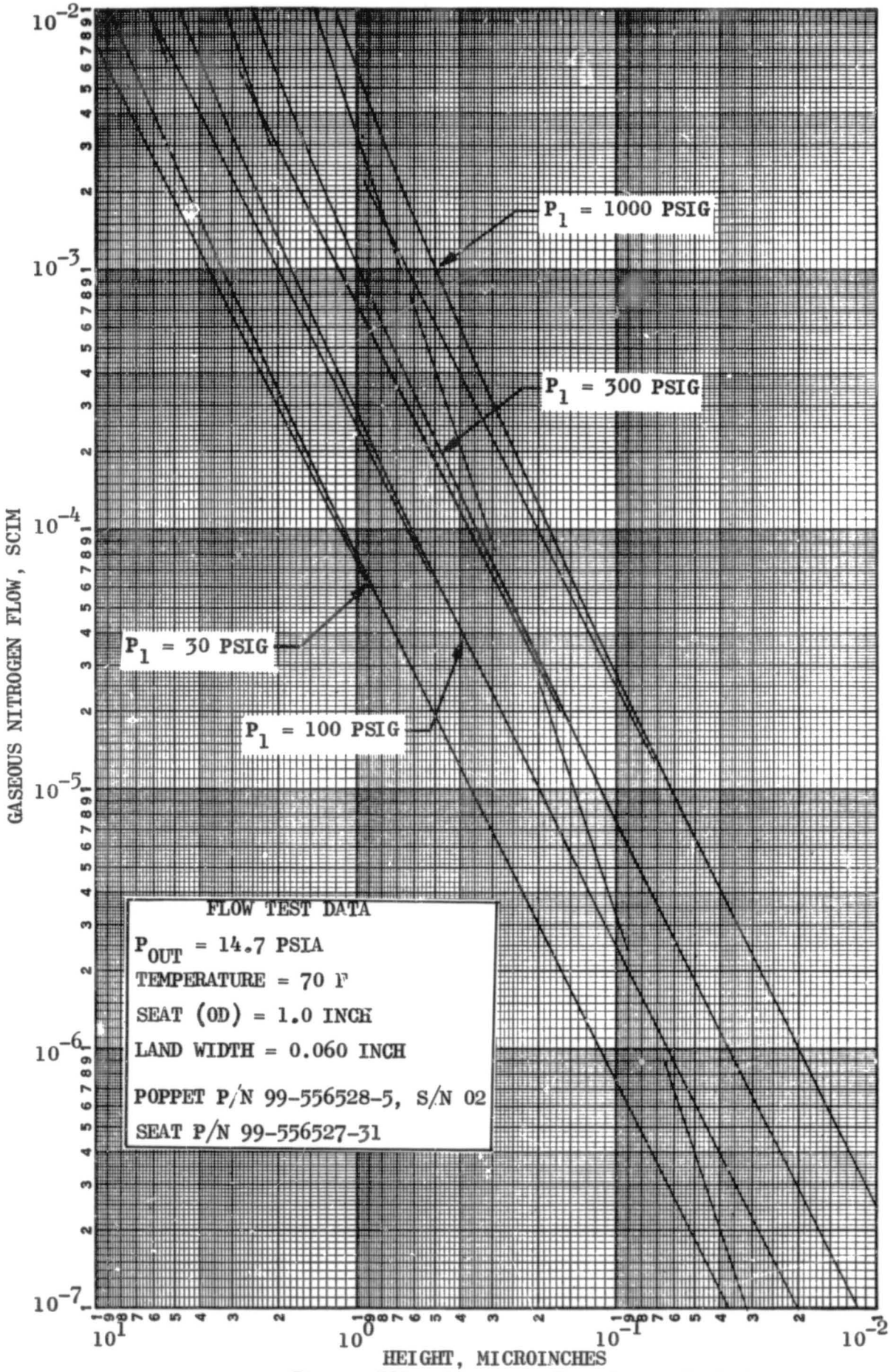

Figure 383. Nitrogen Flow Data, Part 3

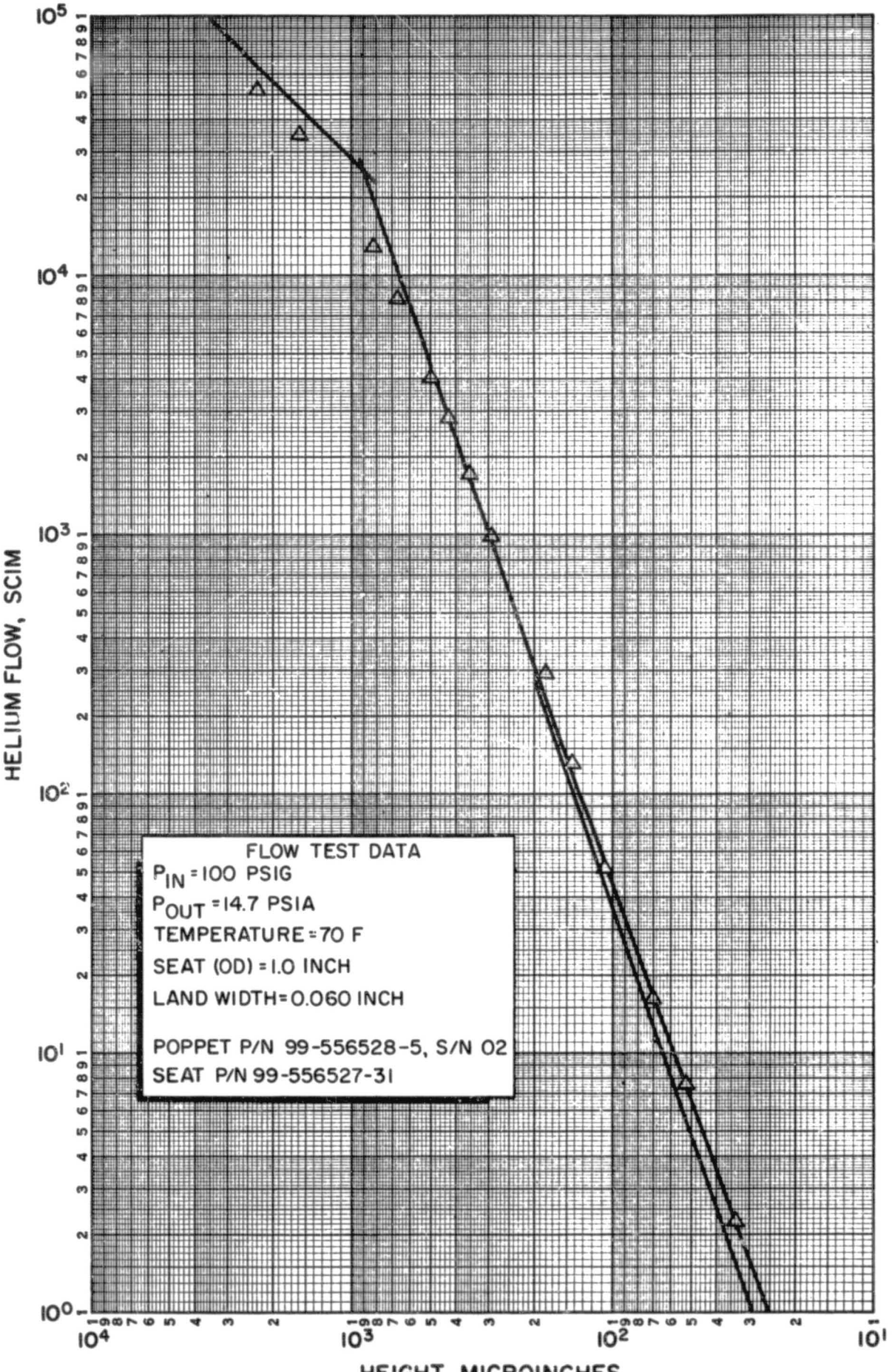

Figure 384. Helium Flow Data, Part 1

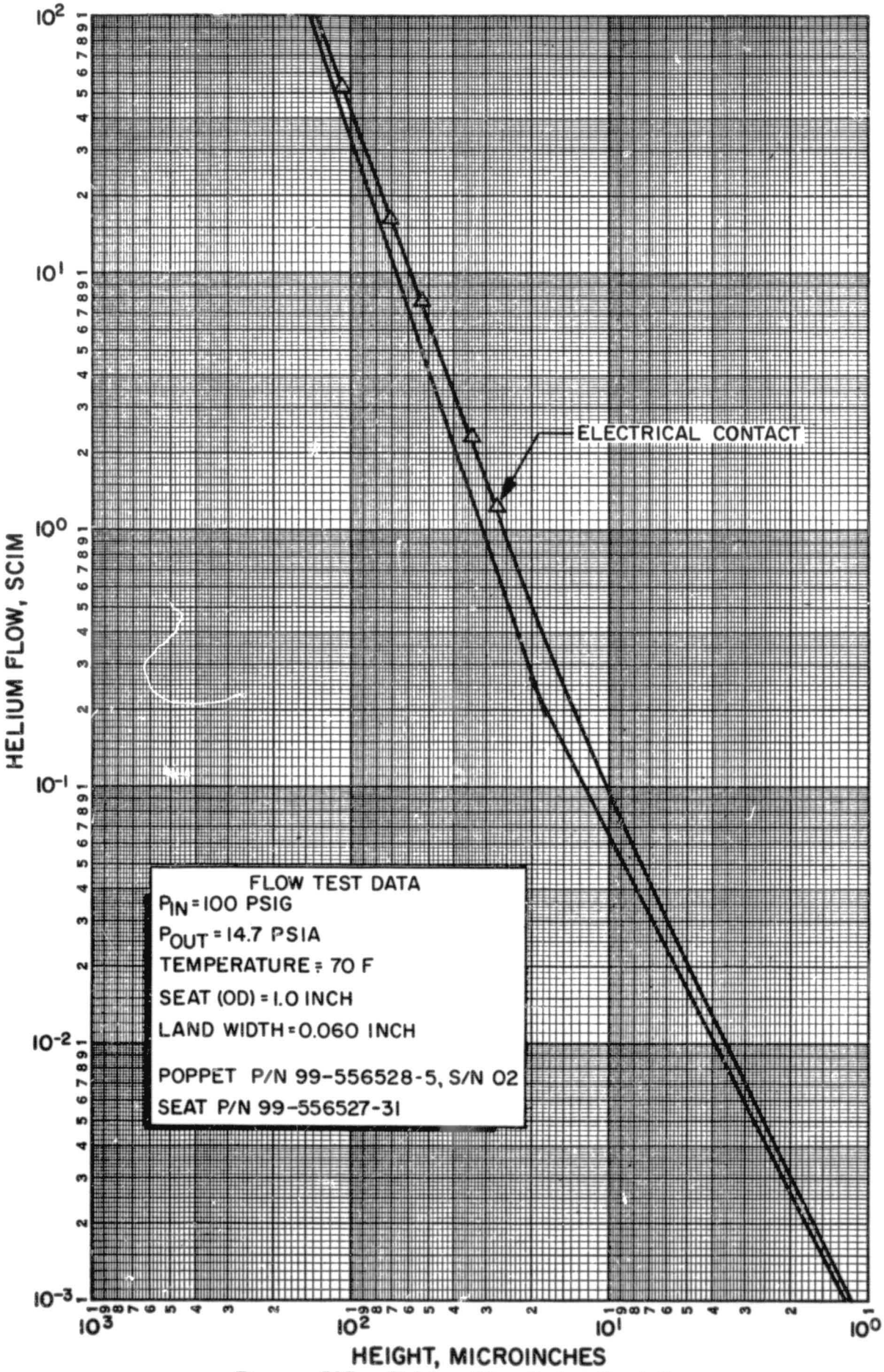

Figure 385. Helium Flow Data, Part 2

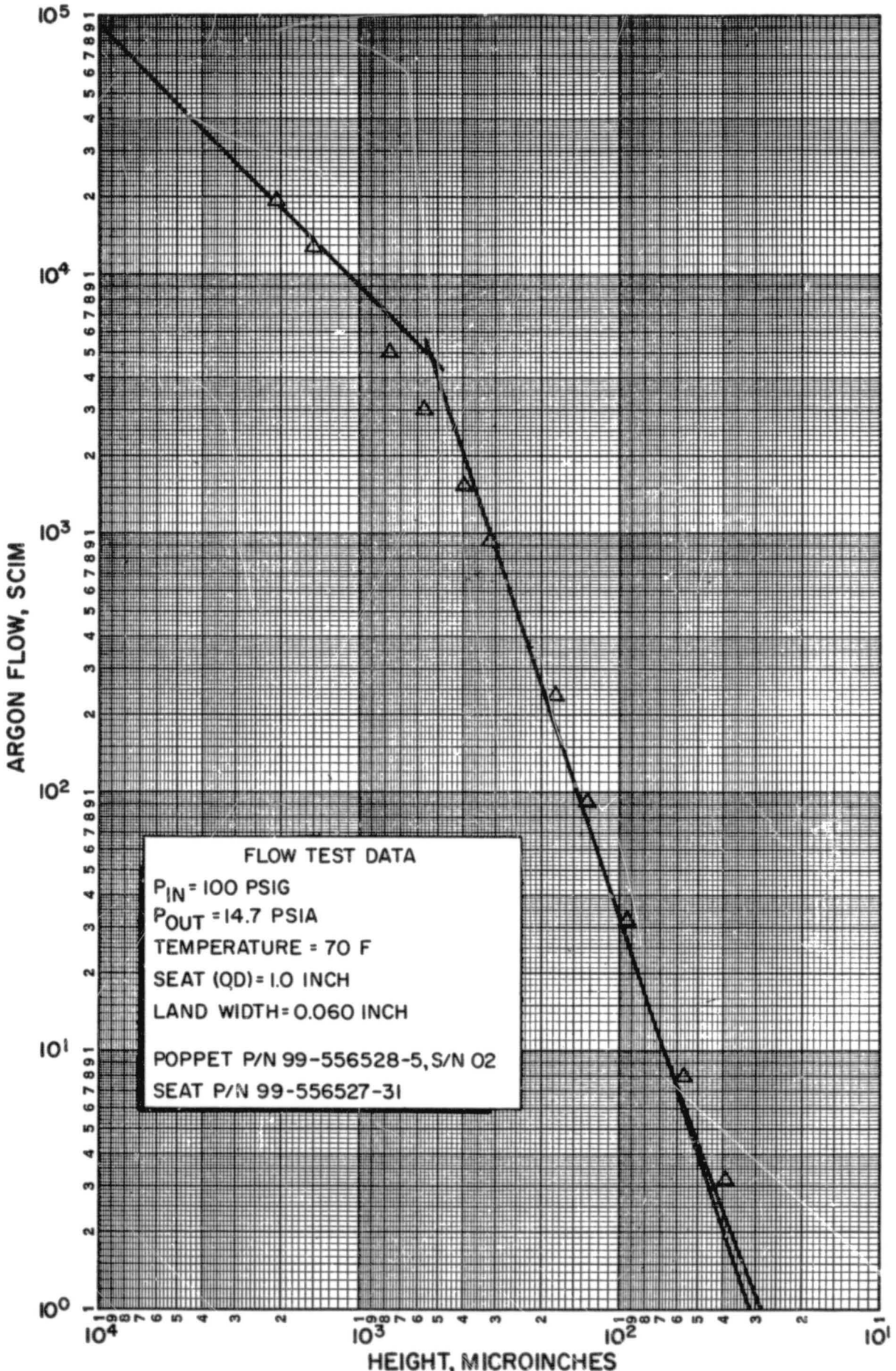

Figure 386. Argon Flow Data, Part 1

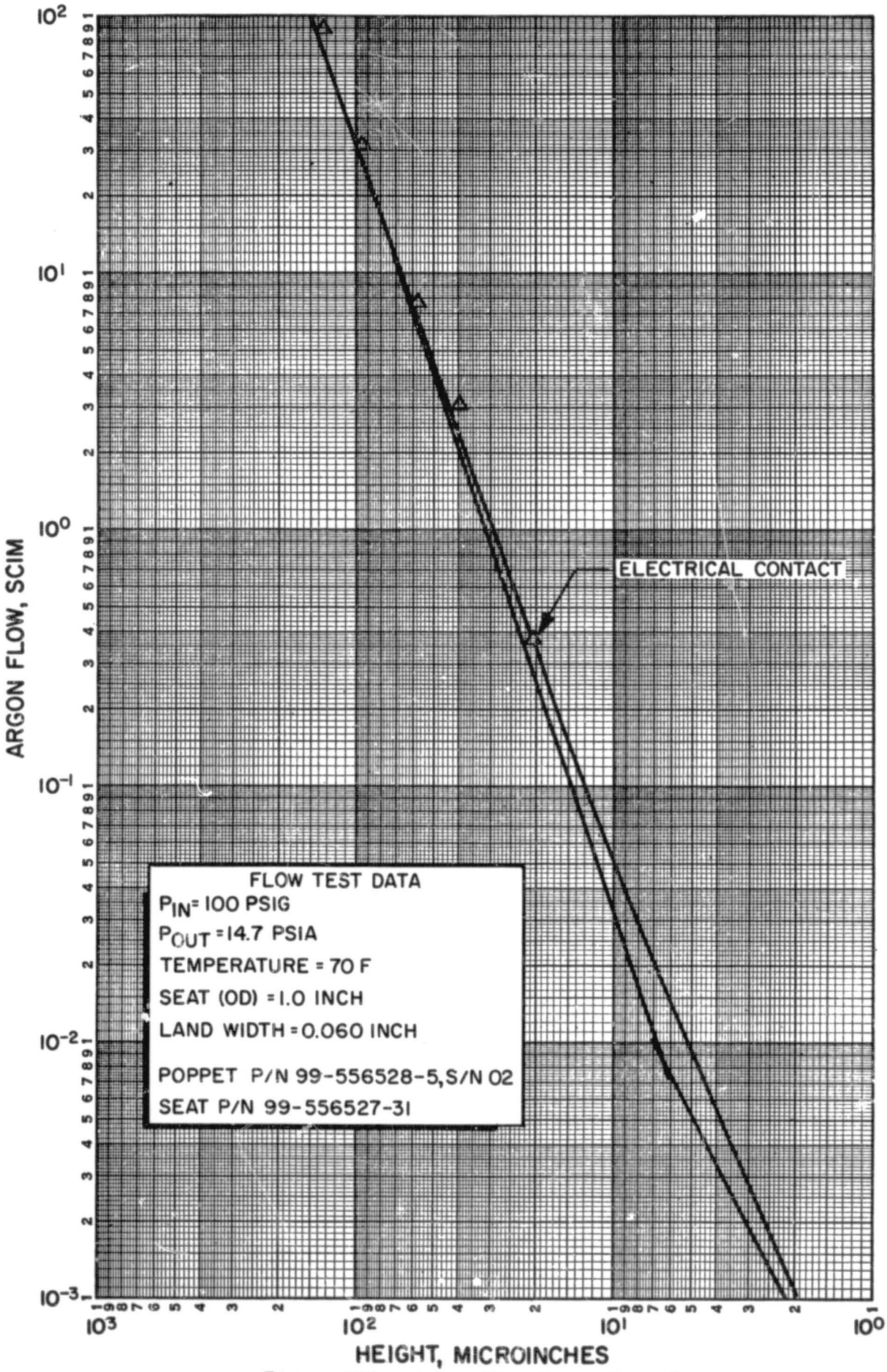

Figure 387. Argon Flow Data, Part 2

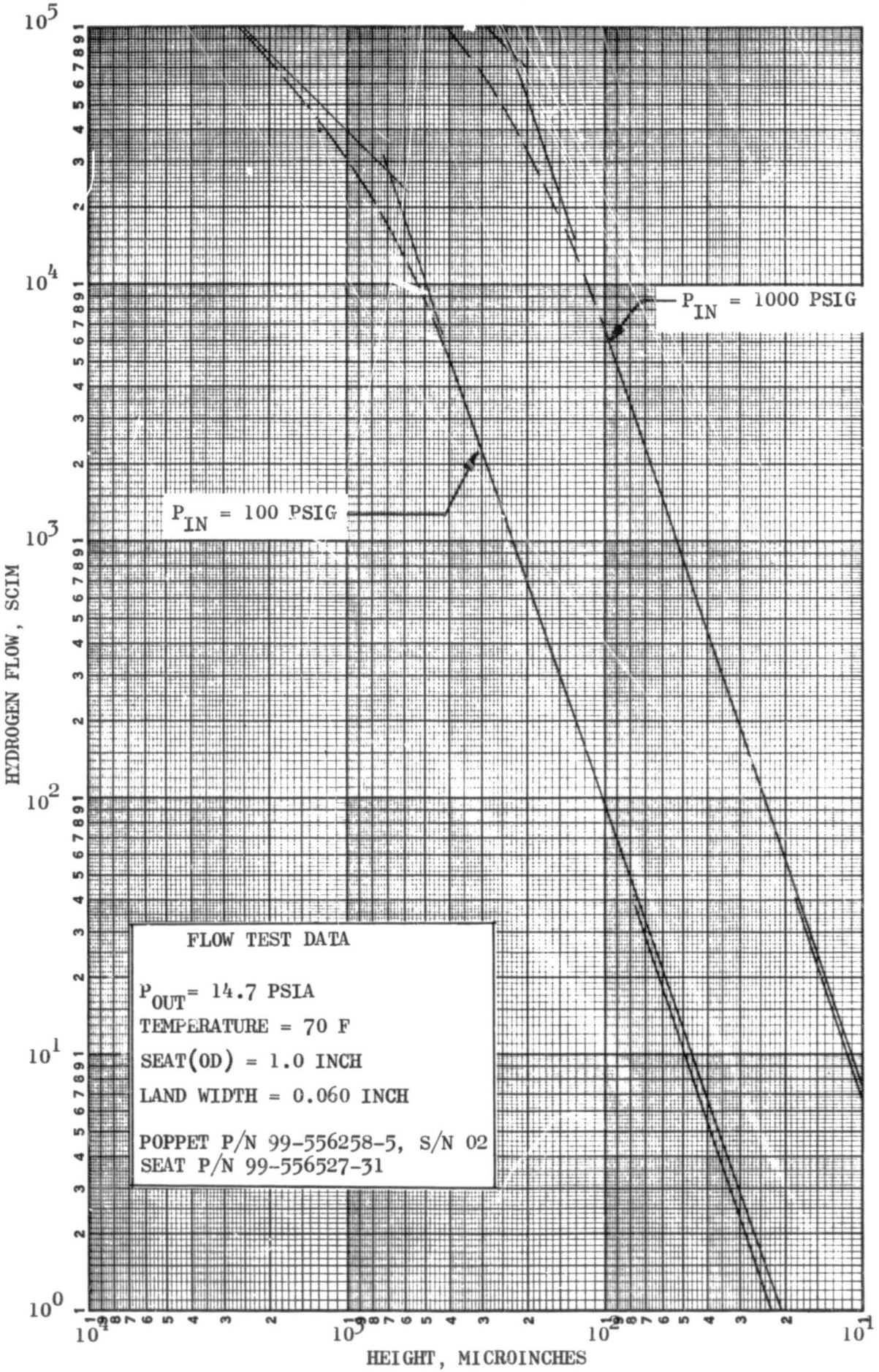

Figure 388. Hydrogen Flow Data, Part 1

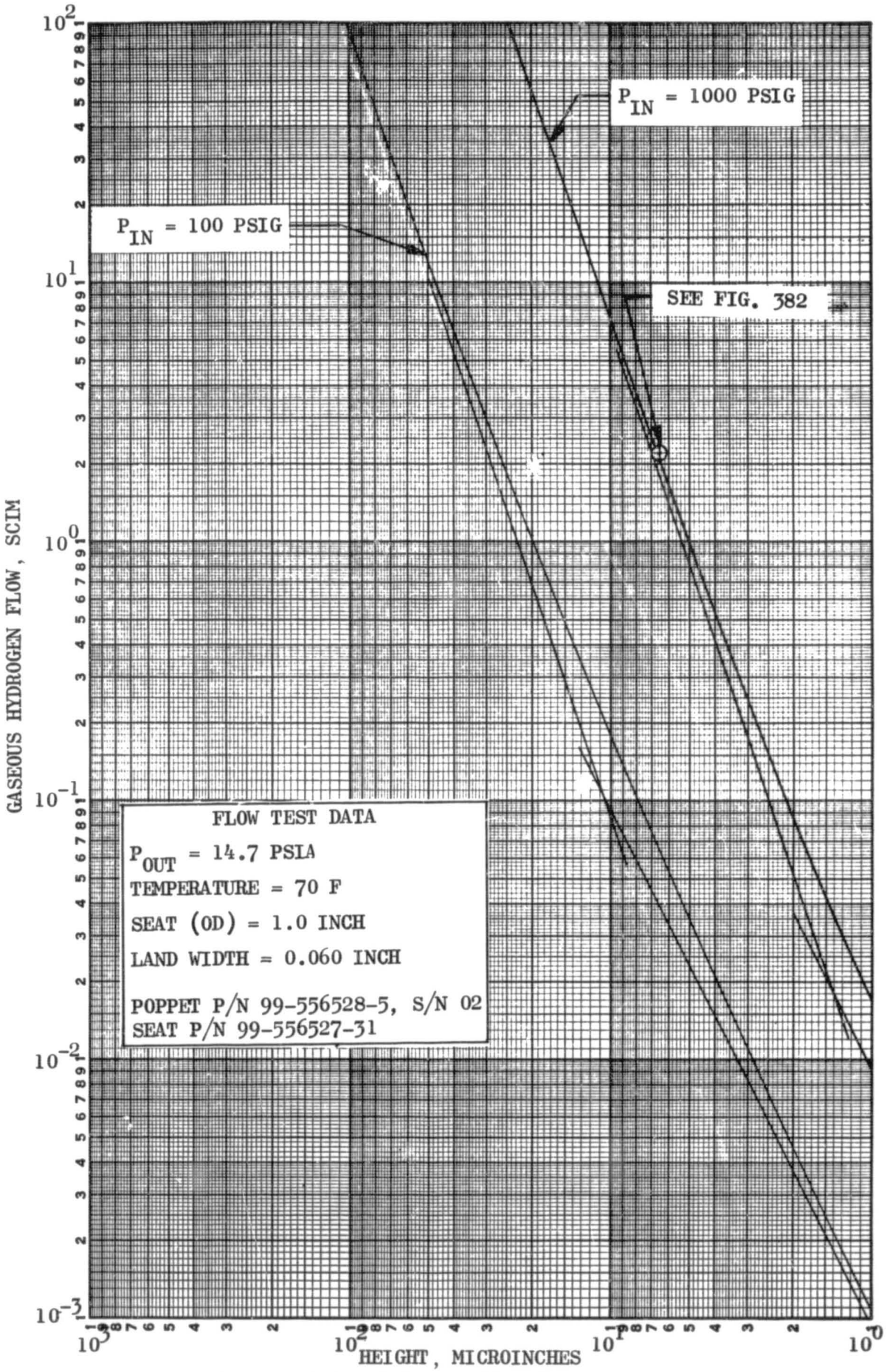

Figure 389. Hydrogen Flow Data, Part 2

it appears that the point of electrical contact could vary by as much as 10 microinches. An examination of the test data showed a range from 20 to 27 microinches. These data points were determined by placing the flow at electrical contact on the theoretical flow curve to establish the smooth plate height (h_p).

Except for the reference point of electrical contact, the experimental and theoretical flow data are plotted independent of each other. Within the 5-percent plot and test accuracy there is a high degree of correlation between experimental and theoretical data through several orders of magnitude of flow. The correlation was found throughout the pressure range and gas media investigated. The flow regimes covered include nozzle, turbulent channel, laminar, and approaching the region of molecular flow. (A detail examination of these flow regimes appears in the Leakage Flow Analysis section where a specific example, illustrating how each flow regime blends into the next to build the overall flow-leakage characteristic curve, is presented.) Some data scatter resulted at the high-pressure conditions (300 and 1000 psig) because of the difficulty in controlling poppet position with the micrometer head at these higher pressures and resultant loads. In the 1000-psig condition, control pressure was necessary to enable the adjustment of the micrometer. Consequently, no electrical contact point was established because of the difficulty in maintaining a sufficiently precise load balance.

If the near-seated test data are examined for the significant flow characteristic, laminar flow is selected as being the most representative regime. When the laminar flow curves are compared for each of the three gases, the flow does not vary by more than 30 percent for any given height (h_p). This is verified by the laminar equation for volumetric flow which shows that flow is a function of viscosity only. (Viscosity for the common gases varies by, at most, 2:1 for any given pressure and temperature.) The significance of this observation is that if leakage data are known for one particular gas, it will serve as an estimate for most any other gas of interest. As the predominant characteristic for system leakages is laminar flow, the rate of change of bottle storage pressure will be a function of gas viscosity and thus essentially the same for most gases.

END OF REFERENCE

122

REFERENCE

123

LIQUID ROCKET VALVE ASSEMBLIES. NASA SPACE VEHICLE DESIGN CRITERIA (CHEMICAL PROPULSION). NASA SP-8097, 1973.

NASA
SPACE VEHICLE
DESIGN CRITERIA
(CHEMICAL PROPULSION)

NASA SP-8097

LEWIS RESEARCH CENTER
Aerospace Safety Research
and Data Institute
JUN 20 1974
CLEVELAND, OHIO

LIQUID ROCKET VALVE ASSEMBLIES

NOVEMBER 1973

NATIONAL AERONAUTICS AND SPACE ADMINISTRATION

GUIDE TO THE USE OF THIS MONOGRAPH

The purpose of this monograph is to organize and present, for effective use in design, the significant experience and knowledge accumulated in development and operational programs to date. It reviews and assesses current design practices, and from them establishes firm guidance for achieving greater consistency in design, increased reliability in the end product, and greater efficiency in the design effort. The monograph is organized into two major sections that are preceded by a brief introduction and complemented by a set of references.

The State of the Art, section 2, reviews and discusses the total design problem, and identifies which design elements are involved in successful design. It describes succinctly the current technology pertaining to these elements. When detailed information is required, the best available references are cited. This section serves as a survey of the subject that provides background material and prepares a proper technological base for the *Design Criteria* and Recommended Practices.

The *Design Criteria*, shown in italics in section 3, state clearly and briefly what rule, guide, limitation, or standard must be imposed on each essential design element to assure successful design. The *Design Criteria* can serve effectively as a checklist of rules for the project manager to use in guiding a design or in assessing its adequacy.

The Recommended Practices, also in section 3, state how to satisfy each of the criteria. Whenever possible, the best procedure is described; when this cannot be done concisely, appropriate references are provided. The Recommended Practices, in conjunction with the *Design Criteria*, provide positive guidance to the practicing designer on how to achieve successful design.

Both sections have been organized into decimally numbered subsections so that the subjects within similarly numbered subsections correspond from section to section. The format for the Contents displays this continuity of subject in such a way that a particular aspect of design can be followed through both sections as a discrete subject.

The design criteria monograph is not intended to be a design handbook, a set of specifications, or a design manual. It is a summary and a systematic ordering of the large and loosely organized body of existing successful design techniques and practices. Its value and its merit should be judged on how effectively it makes that material available to and useful to the designer.

a latch used during static testing that engaged at launch and prevented the valve from opening. Static-test valve latches were removed from later Atlas vehicles to preclude the recurrence of such a failure.

Proper sequencing is important, and operational safeguards are established to ensure that the valve is not inadvertently actuated before the latch is released; otherwise, linkage may be distorted and the latching mechanism may be damaged. Figure 22 illustrates two methods for latching a butterfly disk.

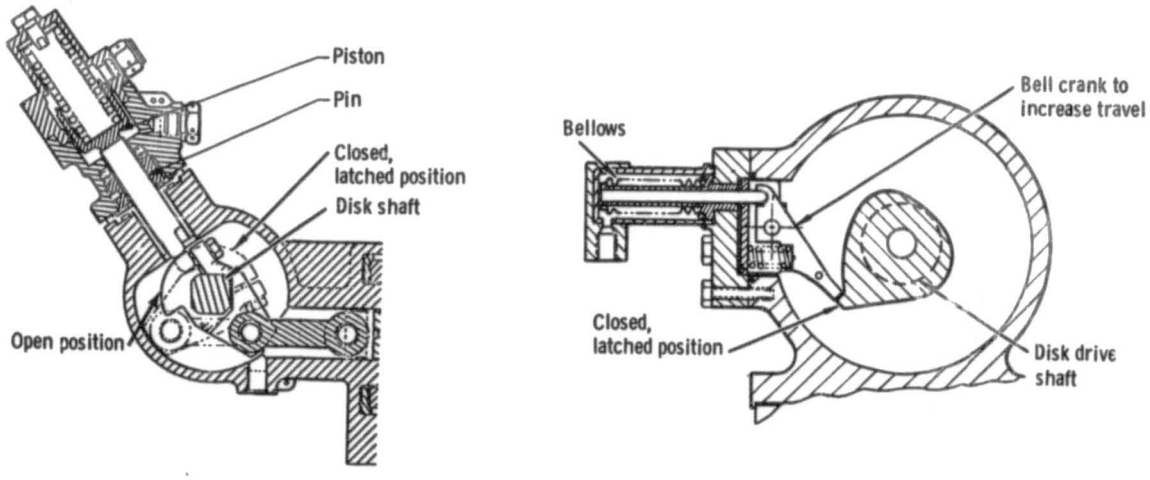

(a) Piston-actuated direct-acting pin.

(b) Bellows-actuated latch.

Figure 22. - Cross-section drawings of latching mechanisms for a butterfly disk.

2.3.8 Filtering

Filtering of pneumatic and hydraulic supplies for engine control systems is accepted practice in all propulsion systems. Filters are also preferred in pneumatic actuator vent ports upstream of control orifices to ensure that the orifice does not become plugged. The rating of filters in pneumatic and hydraulic systems in some present propulsion systems is shown below:

System	Components Protected	Filter Rating
J-2 pneumatic-control package	Regulator and solenoid valves	10 μm
LMDE tank pressurization	Regulator and solenoid valves	15 μm absolute
LMAE tank pressurization	Regulator and solenoid valves	15 μm absolute

Filters also are used to catch the debris from explosive-actuated valves. Such filters are installed either integral with the valve in the downstream section of the housing or in the downstream line upstream of any critical components.

In present boosters, in which exposure of valves is relatively short and only one engine burn is required, filters generally are not employed in the propellant feed system; instead, reliance is placed on system cleanliness and filtering of propellants as they are transferred to the vehicle. Valves in such unfiltered systems must be tolerant of contamination.

In upper-stage vehicles and landing craft, where the propulsion system is designed for restart capability, or in reaction control systems with long coast periods between engine burns, leakage requirements are very stringent (on the order of 5 cm^3/hr helium). To ensure reliable valve operation and engine performance, filters must be provided. Filter selection is based on minimum clearances in the valve and the tolerance of the seating material; however, the filter micron rating is selected to provide an adequate margin of safety. For example, filter specifications for RCS engines in the 25- and 50-lbf (111 and 222 N) thrust range were based on minimum diametral clearances of 0.002 to 0.003 in. (0.05 to 0.08 mm) in the poppet guides. The 304C-mesh filters [10 μ (10 μm) nominal, 25 μ (25 μm) absolute] were installed integral with the valve inlet housing. However, valve sticking occurred, and it was necessary to expand the poppet guide (armature bore) clearances to 0.008 to 0.009 in. (0.20 to 0.23 mm) to ensure reliable valve operation. Filters for the LMDE feed system have a filtration rating of 40 μ (40 μm) nominal (60 μ [60 μm] absolute) and are located upstream of the quad-redundant valves. On the LMAE, the inlet filters for the quad-redundant propellant valve have an absolute filtration rating of 200 μ (200 μm).

The optimum filter for a given liquid or pneumatic flow system is dependent on (1) the largest particle size that can be tolerated by system components such as valves and injectors, (2) the amount of contaminant and the particle size of the contaminants that the filter must stop during the service life, and (3) the maximum pressure drop that can be tolerated by the flow system during its mission life. Detailed design information for filters is presented in reference 41. Filters usually are considered separate components; however, they are often

incorporated into the body of a valve to reduce weight and envelope and to provide positive exclusion of contaminants from critical areas of the valve when the system is open. The benefit gained by filters in a flow system must be evaluated against the weight, envelope, and pressure-drop penalties to the system.

2.3.9 Purging, Draining, and Flushing

Incorporation of ports and fittings in the body housing of the valve assembly to purge, drain, or flush may be a system requirement as well as a valve requirement. Valve actuators may require special draining provisions if the actuation fluid is propellant and the control system utilizes a pressure-ladder sequence. On engine shutdown, the closing side of the actuator will be filled with propellant. All propellant from the closing-side actuator cavity must be drained, since any residual propellant remaining in the actuator will affect valve timing on subsequent valve operation. A pretest check to ensure complete drainage is made.

On the H-1 engine, erratic closing time on the thrust-chamber main valves was traced to residual fuel remaining in the closing side of the actuators. When the engine was vertical, drainage was complete. When the engine was gimbaled and thus tilted off the center line, residuals were not drained; these residuals caused the valve to close more rapidly on the subsequent test. Procedures were revised to ensure complete draining. The importance of locating the drain port or line to prevent trapping residuals in any possible engine position is evident.

In propulsion systems using toxic or corrosive propellants, draining or flushing is necessary to ensure personnel safety and reliable operation of the valve on subsequent tests. Although special fittings may not be included in a small RCS valve assembly, the valve assembly is flushed and purged through the valve inlet fitting to eliminate residuals after the valve is exposed to propellant. Special fixtures are used to hold the valve in the proper position, and the flushing or purging systems are maintained at acceptable cleanliness levels. These flushing and purging operations are a post-test procedure and are not part of the engine mission duty cycle.

On the LOX valve for the F-1 gas generator, an accumulation of water around the bellows used for loading the ball seats froze, and the resulting high seal load and friction affected valve timing. A routine vacuum-dry cycle on the engine bootstrap system was required to prevent condensed moisture in the system from accumulating in the valve.

System purges at engine start or shutdown may be directed through a valve housing, since the volume just downstream of the valving element often represents the extreme end of a line to be cleared of residuals. The orientation of the inlet or outlet port on the housing usually is determined by the position of the valve in the normal engine test position or position on the vehicle, because these ports often are located at a low point. On the main

END OF REFERENCE

123

REFERENCE

124

ENGINEERING MEMO - HAMILTON STANDARD DIV. OF UNITED AIRCRAFT CORP. TO NASA MSC. SUBJECT: SILICONE "O" SEALS-PLSS AND OPS HIGH PRESSURE OXYGEN APPLICATIONS. AUG. 12, 1970.

THIS MATERIAL HAS BEEN APPROVED FOR PUBLICATION PER LETTER FROM JAMES V. CORREALE, NASA LYNDON B. JOHNSON SPACE CENTER TO JOANNE FOLK DATED SEPT. 24, 1974.

F689C 4/65

Hamilton Standard DIVISION OF UNITED AIRCRAFT CORPORATION
WINDSOR LOCKS, CONNECTICUT

ENGINEERING MEMORANDUM

E.M. NO. NA-SS-4487
DATE August 12, 1970
PAGE 1 OF 6
☒ REPLY NOT REQUESTED
☐ REPLY REQUESTED BY (DATE)
PROGRAM/WPI NO.
AFFECTS:

SPECIFICATION: See Paragraph	N/A
SCHEDULE: See Paragraph	N/A
WEIGHT: See Paragraph	N/A
COST: See Paragraph	N/A

TO National Aeronautics and Space Administration
Manned Spacecraft Center
Crew Systems Division
2101 NASA Boulevard
Houston, Texas 77058

Attention: Mr. M. A. Carson, EC-6
Apollo EVA Systems Section

SUBJECT

Silicone "O" seals - PLSS and OPS High Pressure O_2 Applications

REFERENCE NA-SS-3552 Dated February 6, 1969

1.0 INTRODUCTION

Due to the Apollo 13 flight malfunction, Hamilton Standard was directed to conduct a review of critical hardware used in the EMU. As part of this study, the use of silicone rubber "O" seals was rereviewed to verify its acceptability. Silicone rubber meets all of the criteria defined by NASA document MSC-PA-D-67-13 (Category "D") for selection of nonmetallics for the Apollo spacecraft except that of GOX Pneumatic and Mechanical Impact. This requirement has been waivered via the reference Engineering Memorandum.

This engineering memorandum summarizes the rationale including the test background used to select silicone "O" seals for the PLSS and OPS applications.

2.0 SEAL APPLICATIONS

Silicone rubber "O" rings are used throughout the OPS and in numerous locations within the high pressure O_2 portions of the PLSS. Figures 1, 2 and 3 are cross sectional drawings which show all high pressure sealing areas within the OPS. Figures 4 and 5 provide an enlarged cross section of the typical static sealing application within the OPS and the typical dynamic sealing applications within the OPS and PLSS. Figures 6, 7 and 8 are cross sectional drawings which depict the high pressure sealing areas within the PLSS which utilize silicone "O" seals and Figure 9 is an enlarged cross section of the typical static sealing applications within the PLSS.

3.0 SEAL MATERIAL SELECTION

During the early phases of the Apollo program silicone "O" seals were utilized for the high O_2 pressure applications in the PLSS and Emergency Oxygen system. The material was selected because of the favorable experience gained during the Mercury and Gemini programs where silicone rubber was utilized for high pressure O_2 applications. Subsequent to the Apollo 7 fire and imposition of the NASA specifications (NASA non-metallic specifica-

Nothing contained herein shall be deemed to alter the terms of any Purchase Order or Contract between Hamilton Standard and the addressee. This EM is not a Contract Change Commitment. Changes in contract task, schedules, prices or specifications that may result from this EM require further written agreement and authorization by an authorized representative of Hamilton Standard and the addressee.

3.0 Continued

tions MSC-PA-D-66-3A and ASPO-RQ70-D67-5A) all of the silicone seals in the high pressure PLSS and OPS applications were replaced by viton A. The viton seals were found to be functionally unsuitable and silicone rubber "O" seals were re-instituted.

3.1 Viton Seal Experience

Table 1 provides a seal failure summary for viton-A "O" seals incurred on the OPS program. The failures were characterized by seal swelling, blistering, splitting and extrusion. Seal failure was attributed to gas saturation of the Viton and its subsequent inability to relieve internal seal pressure during OPS depressurization, resulting in seal rupture.

3.2 Seal Materials Survey

Following the viton seal malfunctions a materials search was conducted to find a replacement material. The following materials were considered:

Viton D-80 - rejected because of similarity to Viton A.

Fluorel - rejected because of similarity to Viton A and because of similar failures when used in the OPS Test Stand.

Fluorosilicone - rejected because of lack of experience and test data for high O_2 pressure applications.

CNR - rejected because of poor compressive set characteristics and lack of test background in high O_2 pressure applications.

Silicone - recommended because of extensive experience in applications similar to the OPS and because of successful performance in a series of ignition tests conducted at Hamilton Standard. In addition the OPS was designed for minimum ignition potential as the nonmetallics (seals) are heat sinked and are not exposed directly to the gas stream.

3.3 Experience with Silicone Seals

Table 1 presents a summary of cummulative operating experience with gas pressures of 5000 psi or greater recorded at the time of the seal material change. Since then the OPS has accumulated an additional 501 hours of operation at pressure. There have been no functional, leakage or ignition anomalies experienced with high pressure oxygen system configurations using silicone seals.

Nothing contained herein shall be deemed to alter the terms of any Purchase Order or Contract between Hamilton Standard and the addressee. This EM is not a Contract Change Commitment. Changes in contract task, schedules, prices or specifications that may result from this EM require further written agreement and authorization by an authorized representative of Hamilton Standard and the addressee.

3.4 Silicone Seal Off Design Tests

3.4.1 Because of the viton seal failures experienced during OPS Regulator DVT PDA and Qualification (Ref. Table 2), Hamilton Standard initiated a program to determine the cause of the seal degradation. At the outset of the investigation it was hypothesized that the failures were due to nitrogen saturation of seals and subsequent inability of the seal to release entrapped gas during rapid depressurization. The initial seal evaluation tests were inconclusive as to the cause of the failure; therefore, the DVT regulator was rebuilt after seal failure using Viton seals and was tested under stringent controls of test gas (oxygen) and depressurization rates. The DVT unit failed after approximately 70 hours of operation with oxygen. The failure was characterized by low regulation, increased regulation hysteresis, and, as the investigation continued, excessive leakage at the shut-off valve.

These results revealed that failure could occur even on units exposed only to oxygen and depressurization rates consistent with those obtained during normal operation. The seal evaluation test program was modified to run comparison tests between Viton A and silicone seals. The test results (ref. Table 3) indicate that the Viton seals are susceptible to damage under test conditions which simulate actual usage, whereas, the silicone seals are undamaged when exposed to the same conditions. Figure 10 defines the test fixture used during the seal evaluation tests.

To further verify the performance of the silicone seals, the DVT regulator was completely rebuilt after the second failure of the Viton seals, using silicone seals and the unit was subjected to the regulator flow cycling (1010 cycles), shut-off valve cycling (500 cycles, minimum functional and leakage tests. Test results indicate there was no damage to the silicone seals.

With functional performance of the silicone seals verified, additional testing was conducted to demonstrate that the silicone seals, as used in the OPS, were acceptable from an ignition standpoint.

3.4.2 The off design ignition test program evaluated the static and dynamic sealing configuration utilized in the OPS. The test set up for this series of tests is shown in Figure 11.

3.4.2.1 Four test fixtures duplicating typical internal OPS sealing configurations as shown in Figure 12 were used to conduct a total of 19 static seal tests. The fixtures were assembled with silicone seals less the Δ seal rings and the back-up ring normally used in the flight configuration. Each test was conducted by subjecting the fixture to a sudden pressure increase of 10,000 psi oxygen vs a nominal 5880 psi OPS pressure with an estimate pressurization time of .008 sec to 7000 psi (Reference Appendix I, Figure 3. The test series included increasing the diametral seal clearance beyond allowable drawing tolerances until severe extrusion of the seal occurred

Nothing contained herein shall be deemed to alter the terms of any Purchase Order or Contract between Hamilton Standard and the addressee. This EM is not a Contract Change Commitment. Changes in contract task, schedules, prices or specifications that may result from this EM require further written agreement and authorization by an authorized representative of Hamilton Standard and the addressee.

3.4.2.1 Continued

with resultant gas leakage. Test results are shown in Table 4. There was no evidence of ignition during all of the tests.

3.4.2.2 The dynamic seal configuration was evaluated using an OPS regulator. A total of 3 tests were conducted on the OPS regulator stem seal modified by removing the teflon cup seal (chevron seal) and both backup rings from the lower valve stem. The stem was also reworked to increased diametral clearance between the valve stem and regulator body 6 times larger than normal part tolerance to allow seal extrusion. The regulator, with the shut-off valve open, was subjected to a sudden oxygen pressure increase of 8500 psi vs a nominal OPS working pressure of 5880 psi with an estimated pressurization time of 0.122 sec to 6300 psi. (Reference Appendix I, Figure). The test rig solenoid-pneumatic piston valve (V_1), reference Figure 11, used for this test series had an opening time of 0.1 second. The test results are presented in Table 4. The regulator was subsequently disassembled and examined for evidence of ignition. Seal extrusion was noted; however, there was no evidence of ignition.

3.5 Pressurization Mode Analysis

The current review of silicone seal applications consisted of reviewing the seal test program, specifically the seal ignition test series, to substantiate the adequacy of silicone seal when exposed to high pressure oxygen. The review included (1) an analysis of normal OPS pressurization rates vs imposed pressurization rate during the seal ignition testing to insure the test conditions were more severe than actual flight conditions, and (2) a study to determine any failure/operational modes which could result in a more rapid pressurization rate downstream of the OPS shut-off valve than previously tested or exposed during flight operation.

3.5.1 Appendix I provides the analytical comparison of pressurization rate for normal OPS operation and for the seal ignition tests. The results verify that the test conditions imposed were more severe than under actual OPS useage.

3.5.2 The failure/operational mode analysis consisted of reviewing all possible combinations of single point anomalies that could result in an increase to the pressurization rate experienced downstream of the shut-off valve. Specifically, the areas considered were as follows:

A. Increase Valve Actuation Rate

The actuation rate considered in the analysis (ref. enclosure 1) was based on one second being required to go from the full off to the full on position of the OPS actuator. This is believed to be conservative. While this is not a failure mode, it is a means by which more rapid pressurization could be induced and was considered as part of this study.

Nothing contained herein shall be deemed to alter the terms of any Purchase Order or Contract between Hamilton Standard and the addressee. This EM is not a Contract Change Commitment. Changes in contract task, schedules, prices or specifications that may result from this EM require further written agreement and authorization by an authorized representative of Hamilton Standard and the addressee.

3.5.2 Continued

B. "0" Seal Leakage Around OPS Shut-Off Valve

Pressure buildup rate would be less than that experienced during normal actuation as the flow area around the shut-off valve with seals and backup rings removed is less than the flow area of the full open valve.

C. Clogged Heater Passage

Pressurization rate would be greater if the heater passage downstream of the OPS shut-off valve was clogged significantly. Clogging is not considered possible as the assembly is cleaned to "no particles greater than 90 micron" and the porting leading to the passage contains a 12 micron absolute filter.

D. Shut-Off Valve Open Due to Impact or Shock Loading

This is not possible as the valve is spring loaded and pressure loaded closed with resulting closing forces far in excess of any that shock loading could induce.

E. Primary Static Seal Failing Suddenly and Grossly

This condition would result in a rapid pressure increase at the secondary seal. This failure is not possible as tests have shown that the seals cannot fail in this manner with the closely controlled clearances utilized in the OPS design.

The preceding review did not reveal any operational/failure mode which would result in a pressurization rate downstream of the shut-off valve more rapid than experienced during normal operation of the OPS.

4.0 SUMMARY

Silicone "0" seals are suitable for the OPS and PLSS high pressure oxygen applications. This conclusion is based on the following:

A. Unable to induce seal ignition even with:

1) seal backup rings removed
2) plug to housing diametrical clearance increased to 5 times the nominal or 2 times the maximum allowed for flight hardware
3) oxygen pressurization rates up to 20 times the rates predicted during mission usage
4) oxygen pressure levels 1.4 times the maximum mission levels
5) seal extrusion and leakage occurring

B. Total logged and estimated operating experience with silicone "0" seals, at operating pressures in excess of 5000 psi for the Mercury,

Nothing contained herein shall be deemed to alter the terms of any Purchase Order or Contract between Hamilton Standard and the addressee. This EM is not a Contract Change Commitment. Changes in contract task, schedules, prices or specifications that may result from this EM require further written agreement and authorization by an authorized representative of Hamilton Standard and the addressee.

4.0 Continued

Gemini and Apollo space programs, exceeding 19,500 hours, with no ignition failures attributable to the use of silicone rubber.

C. The seals in the OPS and PLSS are heat sinked and are not exposed directly to the flow stream.

D. The OPS and PLSS high pressure oxygen storage subsystems utilize redundant "O" seals.

F. H. Goodwin
Engineering Manager
Apollo EMU

for J. C. Beggs
Program Manager
Apollo EMU

FHG/DP/cbh

Nothing contained herein shall be deemed to alter the terms of any Purchase Order or Contract between Hamilton Standard and the addressee. This EM is not a Contract Change Commitment. Changes in contract task, schedules, prices or specifications that may result from this EM require further written agreement and authorization by an authorized representative of Hamilton Standard and the addressee.

Appendix I

Predicted Seal Pressurization Rates

Oxygen pressure versus time for OPS seal mission conditions and silicone seal ignition tests were calculated to verify that testing was more severe than mission use. The results of the analysis indicate that the pressurization rates experienced during the seal ignition tests were approximately 20 times greater than the rates predicted for mission use.

OPS System Normal Operation

The OPS high pressure oxygen system is defined by the following schematic:

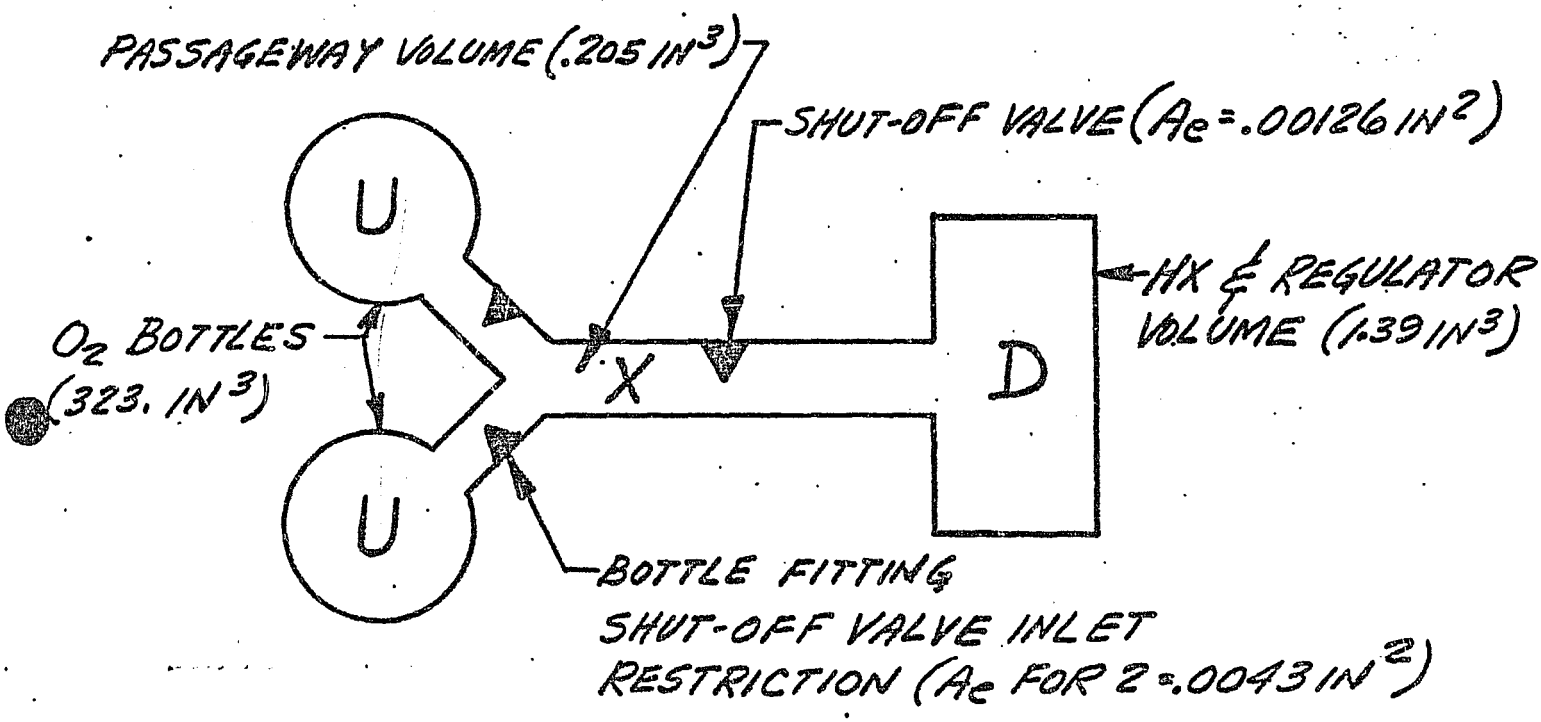

High pressure oxygen is stored in the bottles (U) and at 5880 psi and 70°F, the shut-off valve is normally in the closed position and pressure in chamber D is ambient.

1.0 seconds was assumed for full travel of the shut-off valve actuator and 0.12 seconds of that time is required to produce maximum flow area for the shutoff valve.

Appendix I (Continued)

Three iterations were utilized to obtain the curve of Figure 1 which shows pressure vs time at the regulator:

I. For the first 0.12 seconds the shut-off valve area is varying linearly from 0.000 to 0.00126 in^2. During this phase gas flow through the valve is always sonic and the flow rate is increasing.

II. With the valve area a constant, sonic flow continues to time 0.1342 seconds (pressure in chamber D = 4120 psi) and flow rate is constant.

III. From 0.1342 seconds till volume D pressure is 5880 psi the gas flow is subsonic and the flow rate is decreasing.

Assumptions

1. Bottle pressure is constant at 5880 psi
2. Isothermal process
3. Passageway pressure (P_x) is constant.

Ignition Test With Simulated Fill Valve

The test item and system are defined by the following schematic:

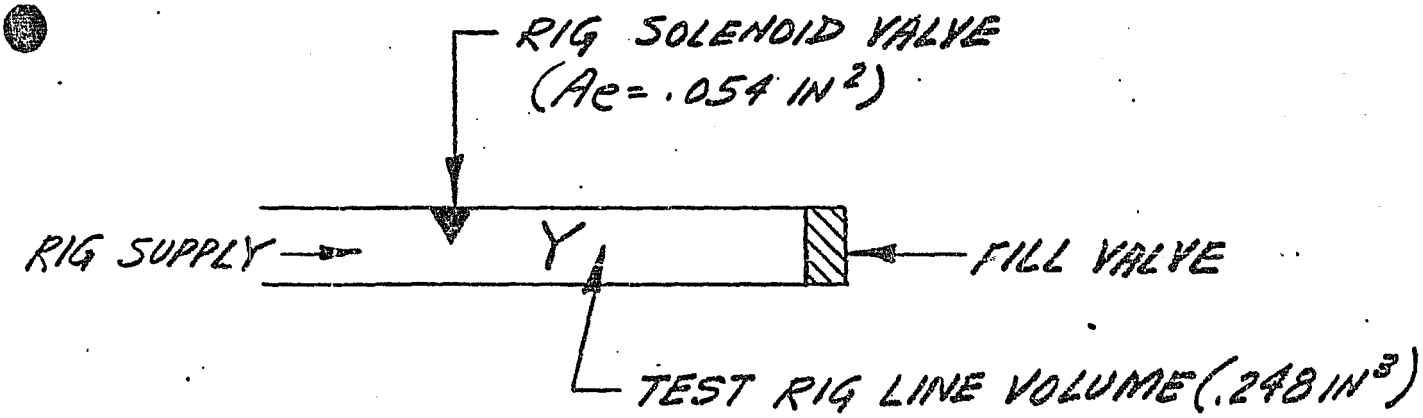

Appendix I (Continued)

High pressure oxygen is stored in the rig supply at 10,000 psi, the rig solenoid valve is closed, chamber Y is at ambient pressure and the fill valve is attached to the rig line.

The rig solenoid valve fully opens in 0.10 seconds with the valve area varying linearly with stroke.

Two iterations were utilized to obtain the curve of Figure 2 which shows pressure vs time at the fill valve.

I. For 0.1 seconds the rig solenoid valve area is varying linearly from 0.000 to 0.054 in^2. During the part of this phase, gas flow through the valve is sonic and the flow rate is increasing. (By referring to Figure 2, it will be seen that the pressure of chamber Y will be equal to rig pressure before the valve is fully open.)

II. With the rig solenoid valve area still increasing the critical pressure in chamber Y will be reached and the gas flow will be subsonic.

Assumptions

1. Rig supply pressure constant at 10,000 psi
2. Isothermal process

Ignition Test with OPS Regulator

The test item and system are defined by the following schematic:

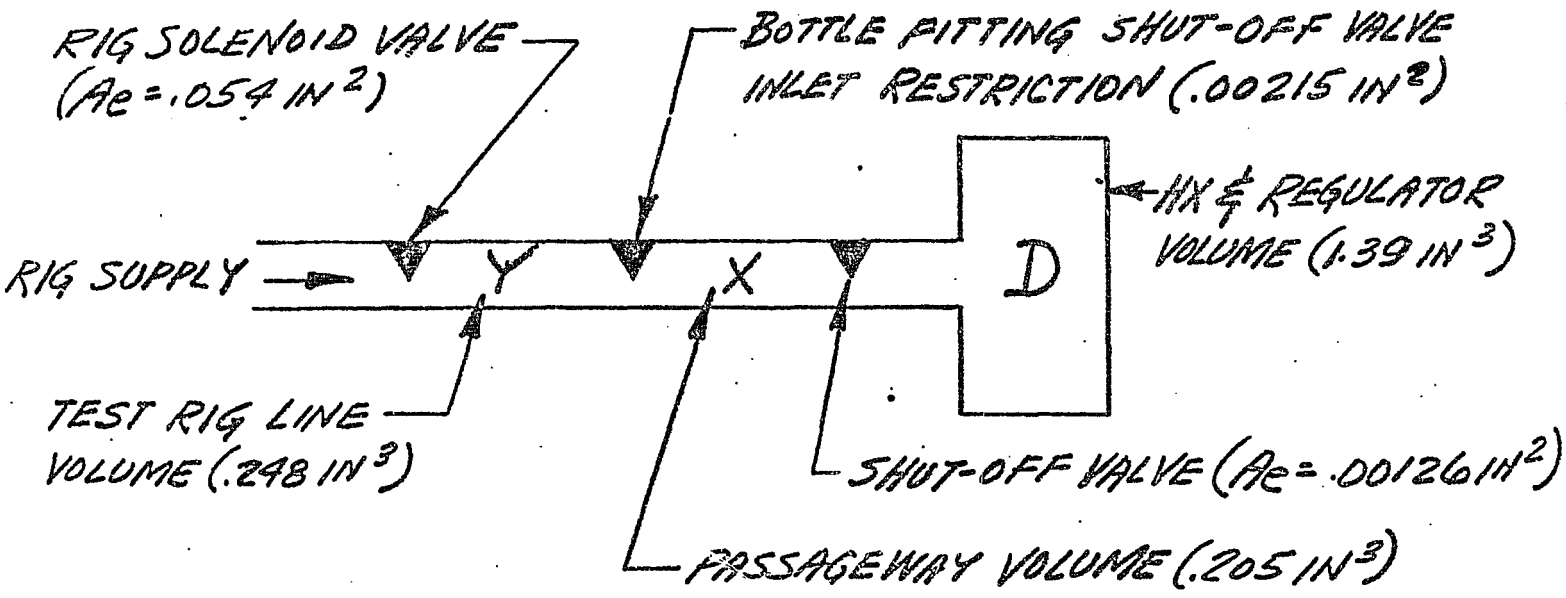

Appendix I (Continued)

High pressure oxygen is stored in the Rig Supply at 8500 psi, the rig solenoid valve is closed, the shut-off valve is open (A_e = .00126 in^2) and chambers Y, X and D are at ambient pressure.

The rig solenoid valve fully opens in 0.1 seconds with the valve area varying linearly with stroke.

Three iterations were utilized to obtain the curve of Figure 3 which shows pressure vs time at the regulator:

I. For 0.1 seconds the rig solenoid valve area is increasing from .000 to .054 in^2. During part of this phase gas flow thru the valve, the shut-off valve inlet restriction and the shut-off valve is sonic.

II. With the rig solenoid valve area still increasing, the critical pressure will be reached in chamber Y and the gas flow across the rig solenoid valve will be subsonic. However, the flow across the two restrictions downstream will still be sonic.

III. With the rig solenoid valve fully open (A_e = .054 in^2) flow at all restrictions is changing from sonic to subsonic.

Assumptions

1. Rig supply pressure constant at 8500 psi
2. Isothermal process

FIGURE 1

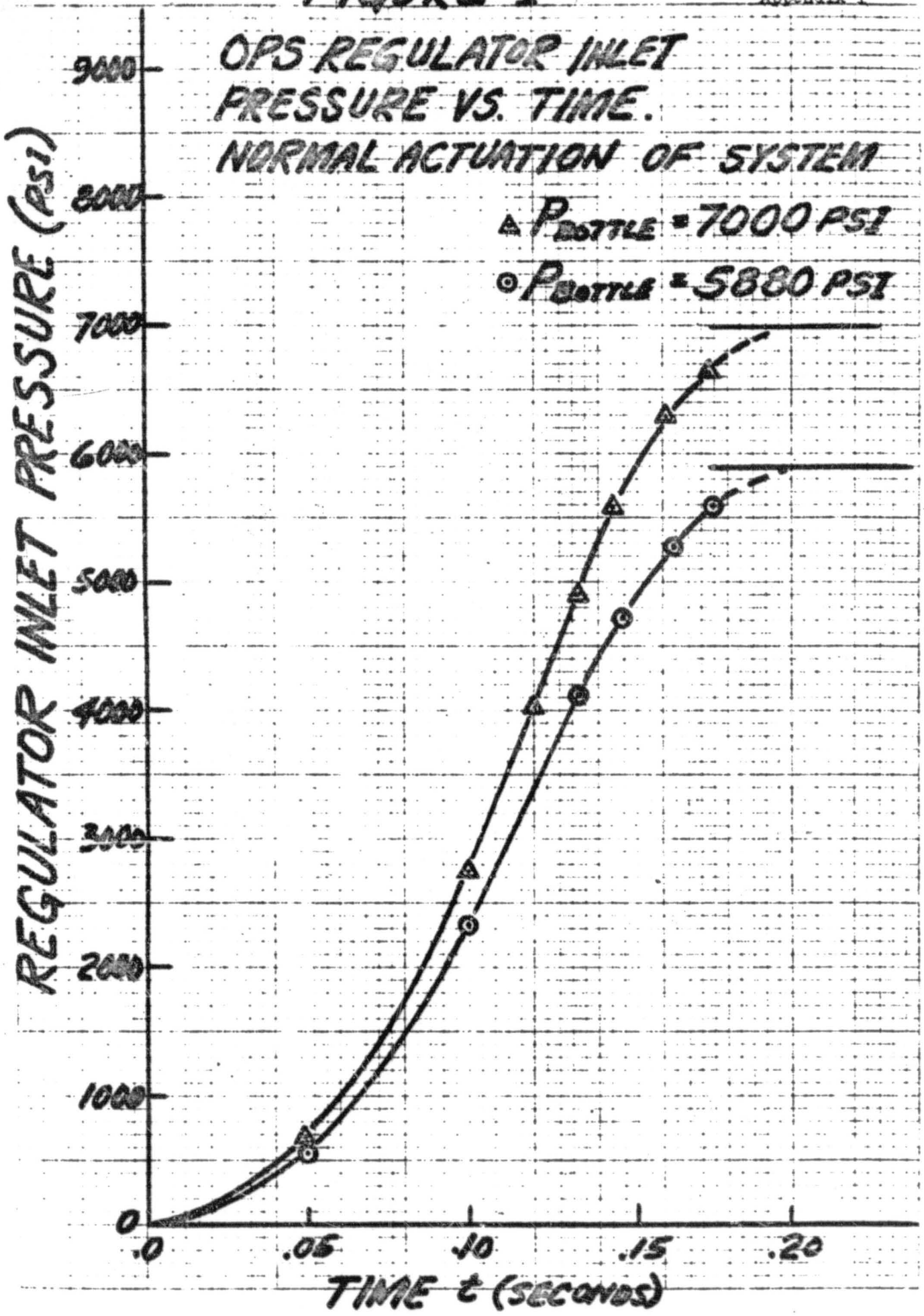
OPS REGULATOR INLET PRESSURE VS. TIME.
NORMAL ACTUATION OF SYSTEM
△ P_{BOTTLE} = 7000 PSI
⊙ P_{BOTTLE} = 5880 PSI
REGULATOR INLET PRESSURE (PSI)
9000
8000
7000
6000
5000
4000
3000
2000
1000
0
.0
.05
.10
.15
.20
TIME t (SECONDS)

FIGURE 2

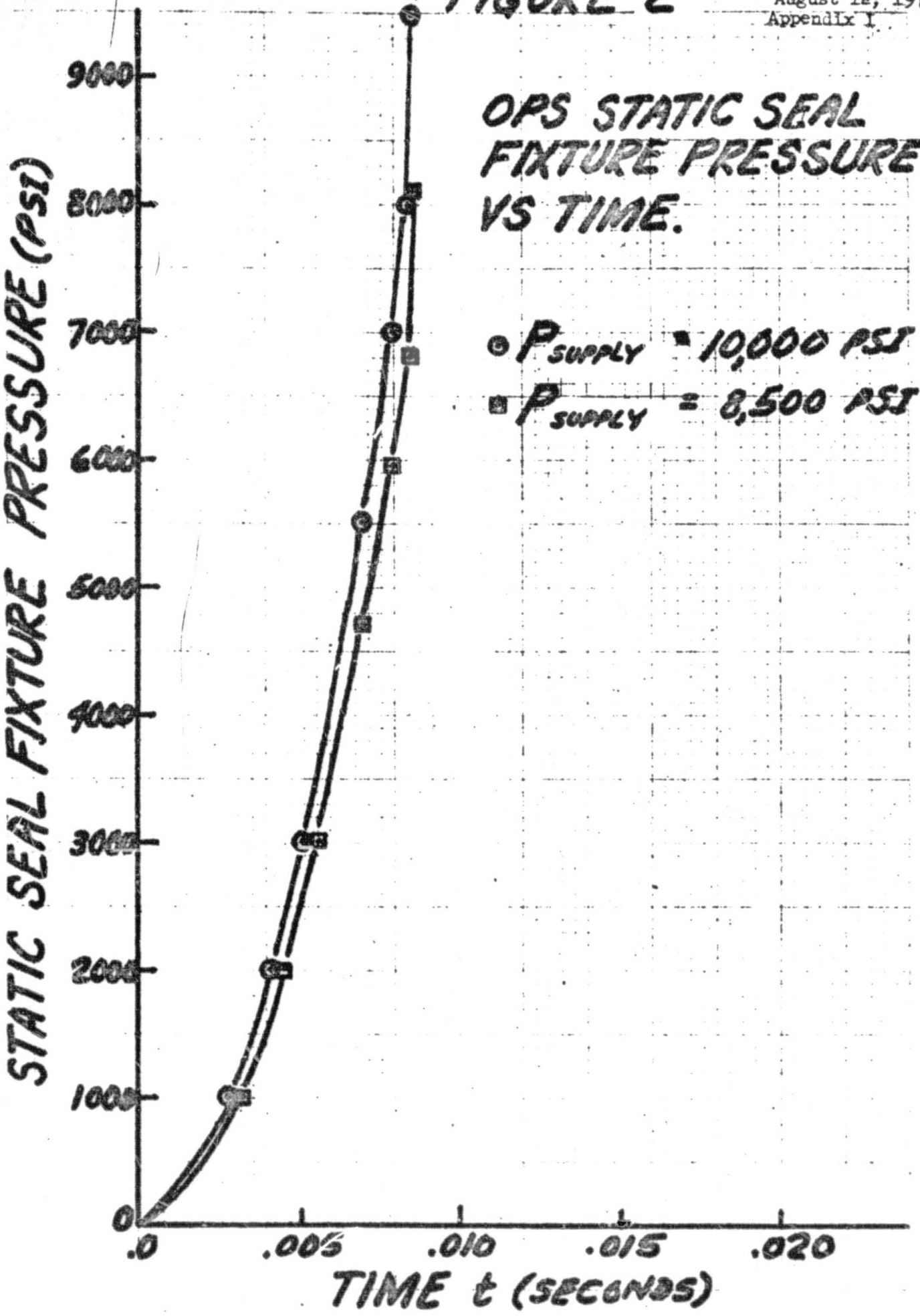
OPS STATIC SEAL FIXTURE PRESSURE VS TIME.
● P_{SUPPLY} = 10,000 PSI
■ P_{SUPPLY} = 8,500 PSI
STATIC SEAL FIXTURE PRESSURE (PSI)
9000
8000
7000
6000
5000
4000
3000
2000
1000
0
.0
.005
.010
.015
.020
TIME t (SECONDS)

FIGURE 3
OPS IGNITION TEST
REGULATOR CHAMBER PRESSURE VS. TIME

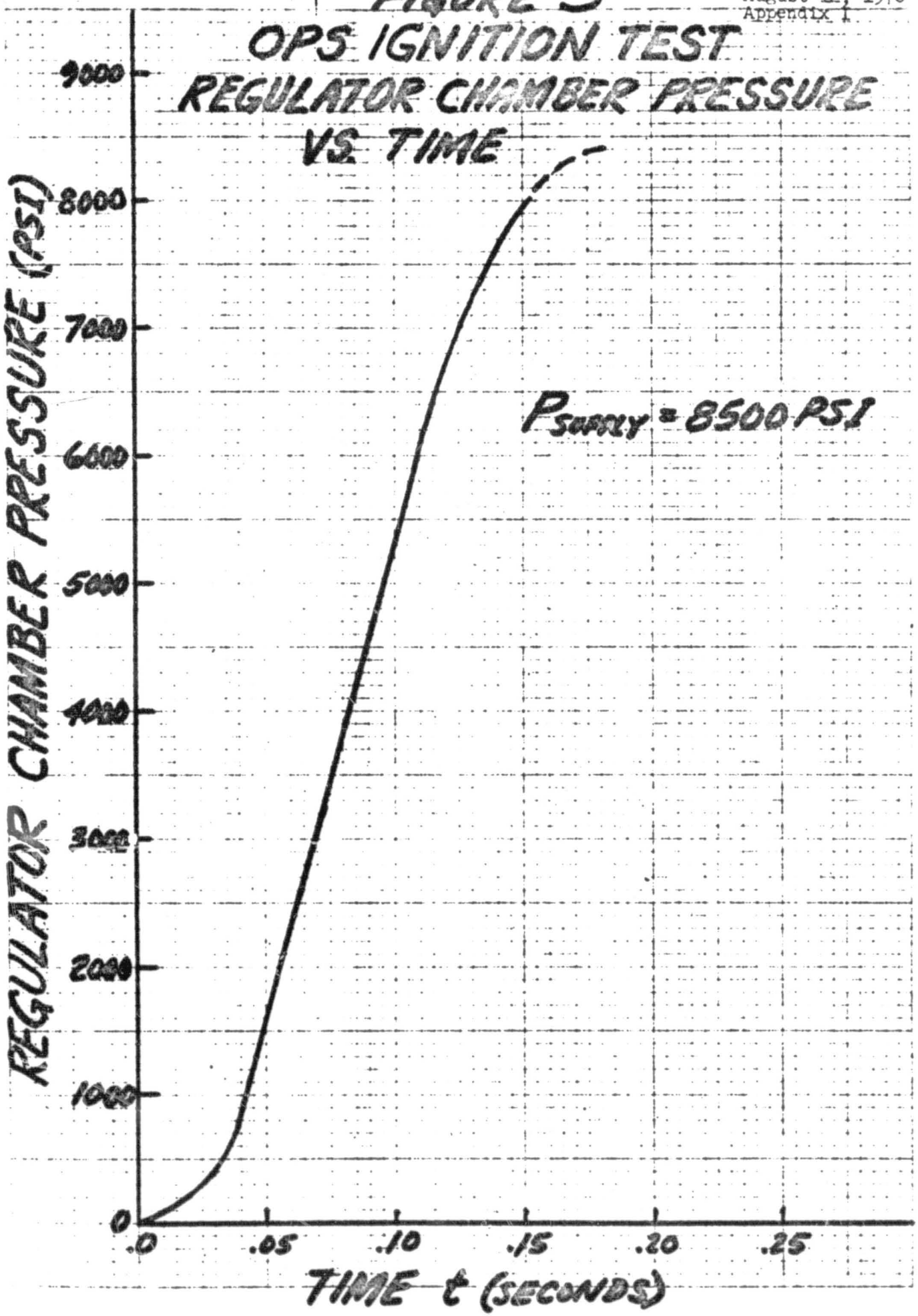

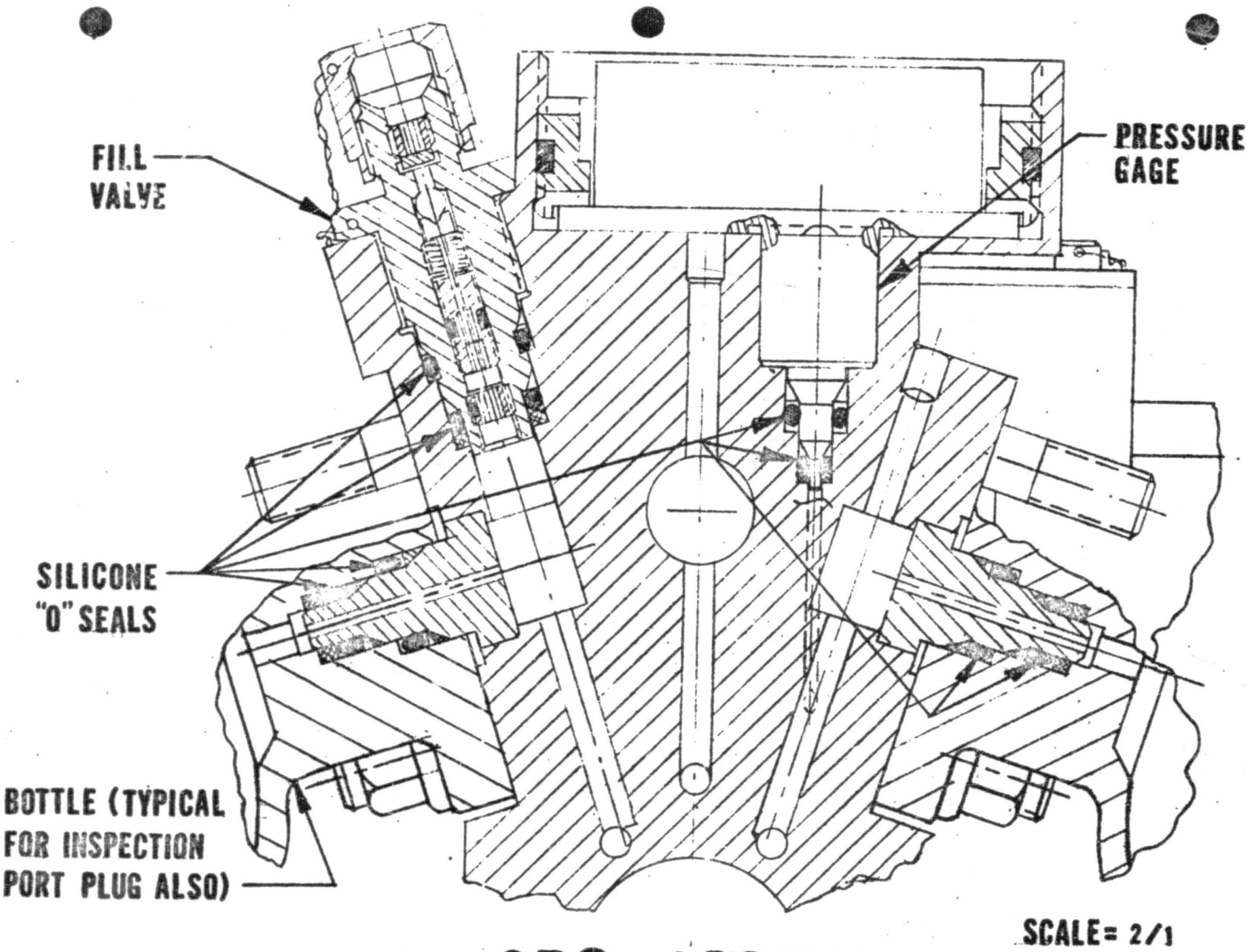

OPS ASSEMBLY

FIGURE 1

MA-SS-4487
August 12, 1970

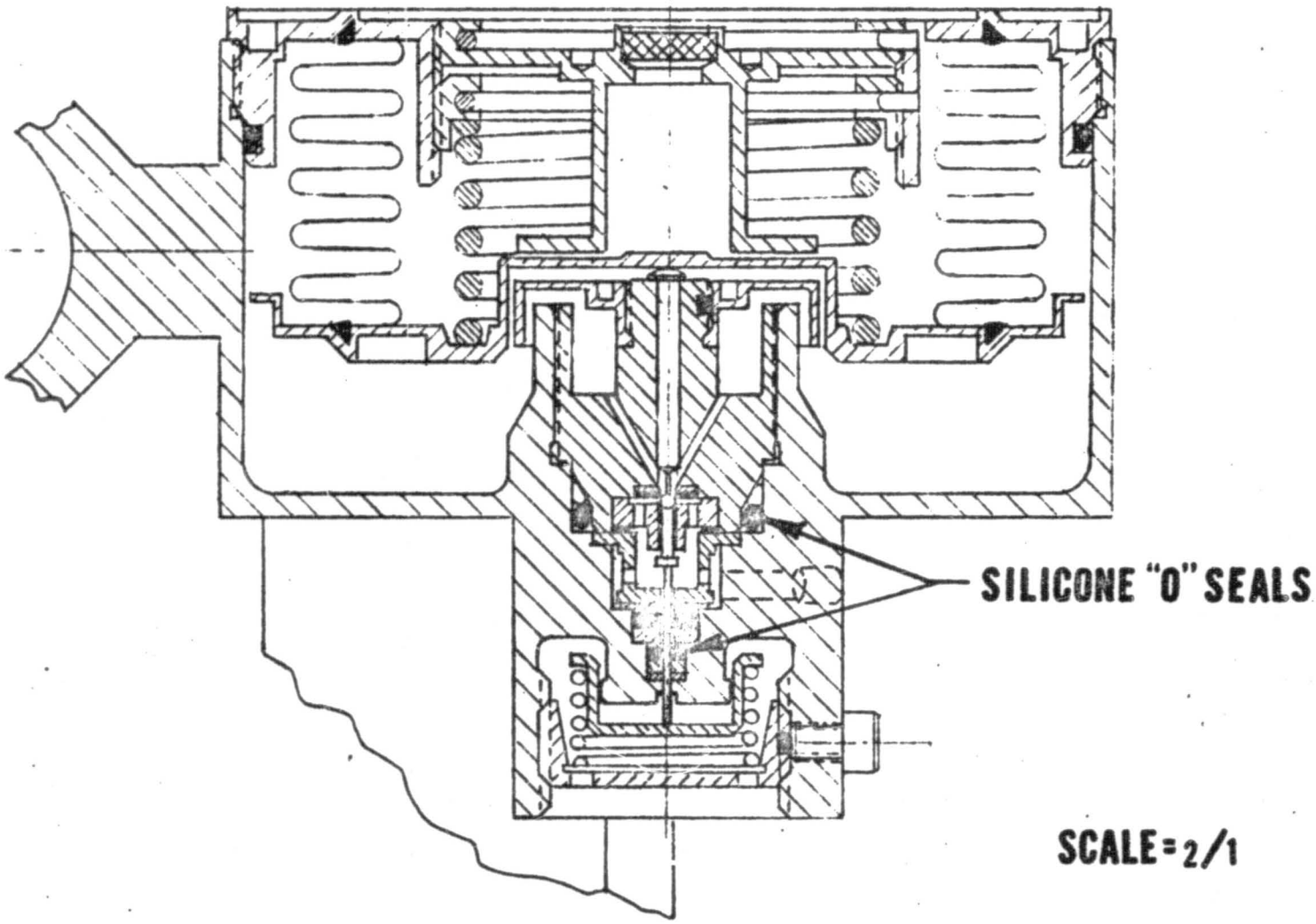

OPS REGULATOR

FIGURE 2

NA-SS-4487
August 12, 1970

OPS SHUT-OFF VALVE

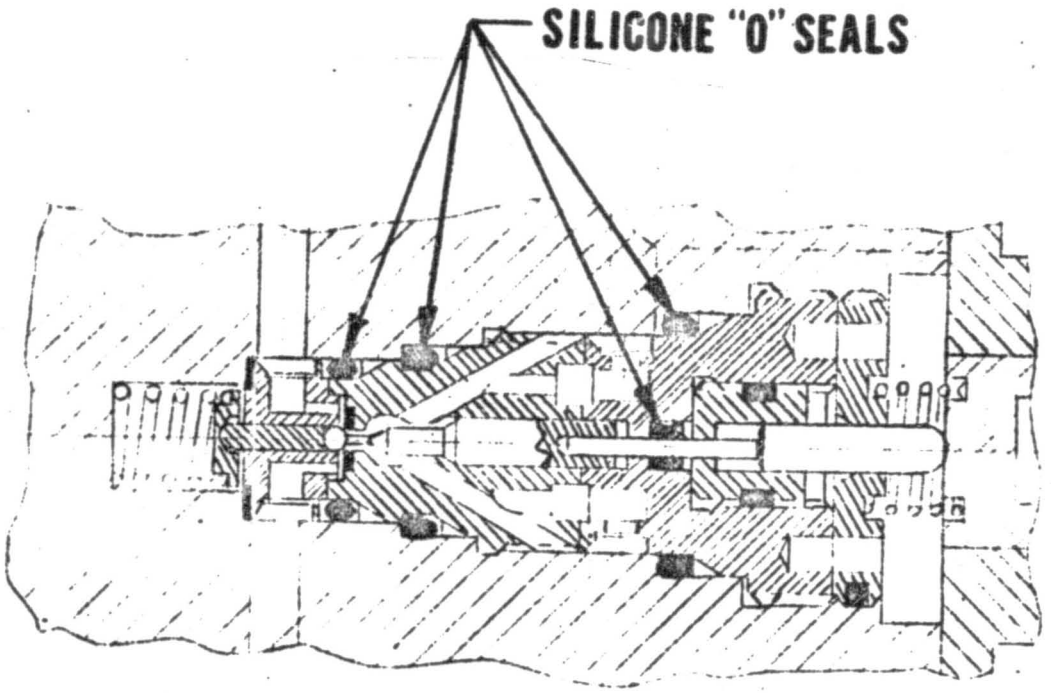

SCALE = 2/1

FIGURE 3

MA-SS-4487
August 12, 1970

OPS TYPICAL STATIC SEAL APPLICATION

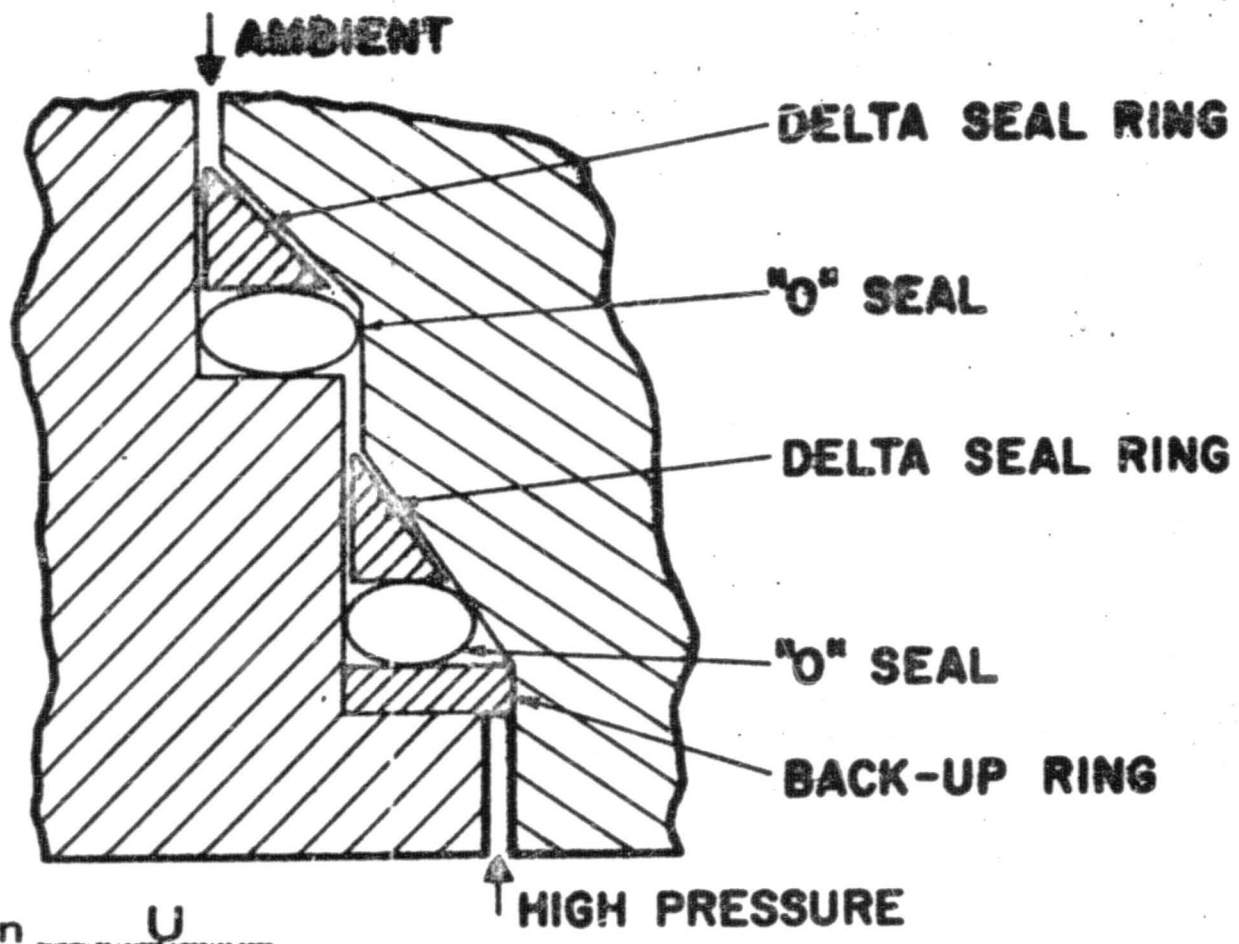

Hamilton Standard
DIVISION OF UNITED AIRCRAFT CORP
UA

FIGURE 4

August 12, 1970

TYPICAL DYNAMIC SEAL APPLICATION

OPS AND PLSS

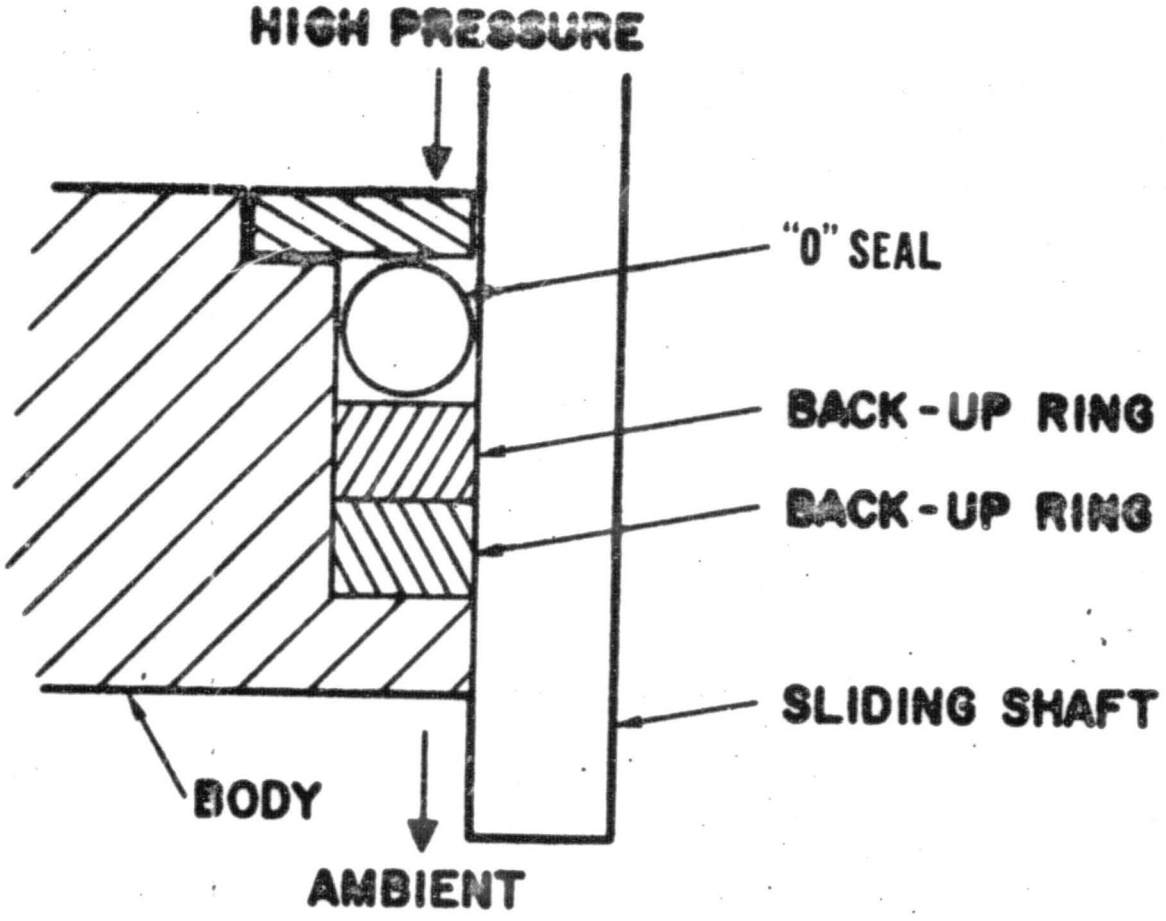

Hamilton Standard — Division of United Aircraft Corp.

FIGURE 5

NA-SS-4487
August 12, 1970

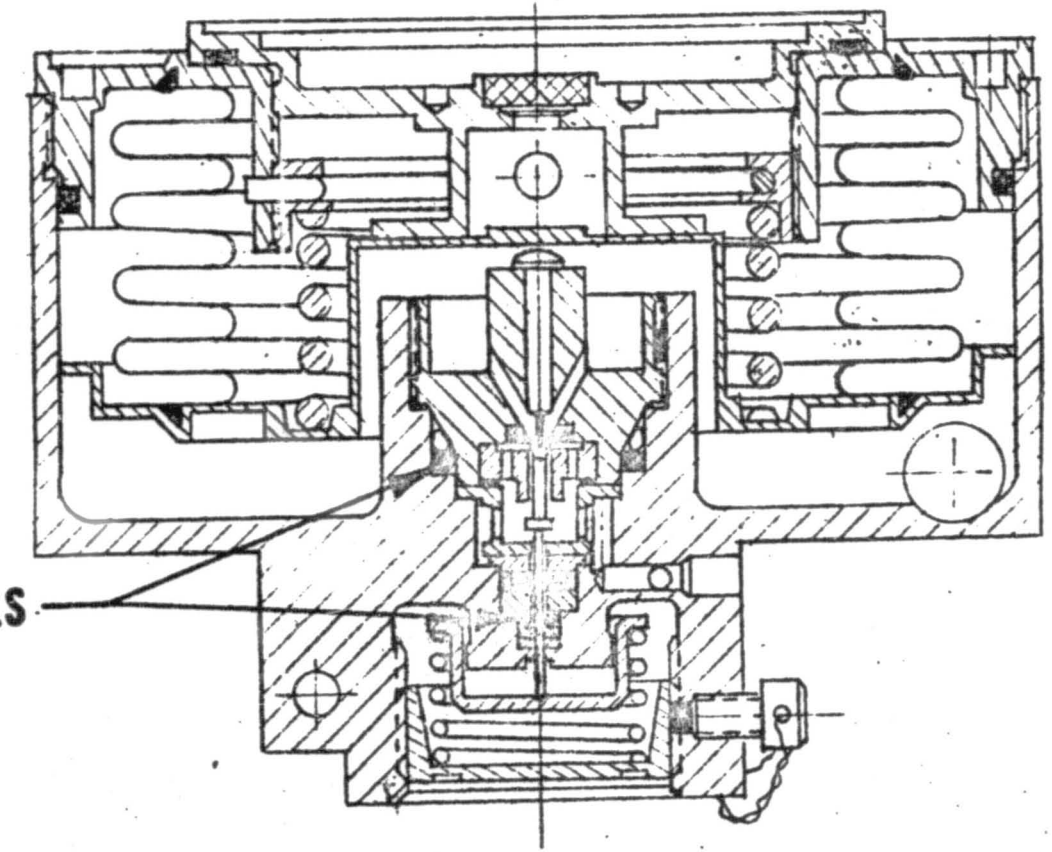

SCALE = 2/1

PLSS PRIMARY REGULATOR

FIGURE 6

MA-SS-4487
August 12, 1970

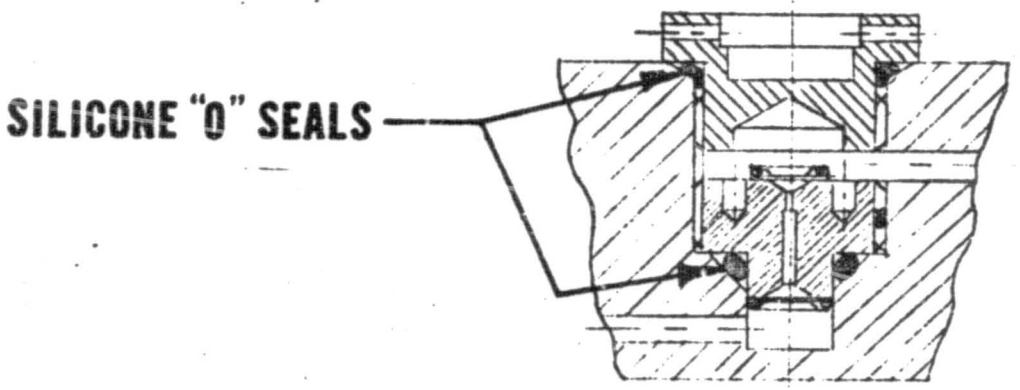

FLOW LIMIT ORIFICE

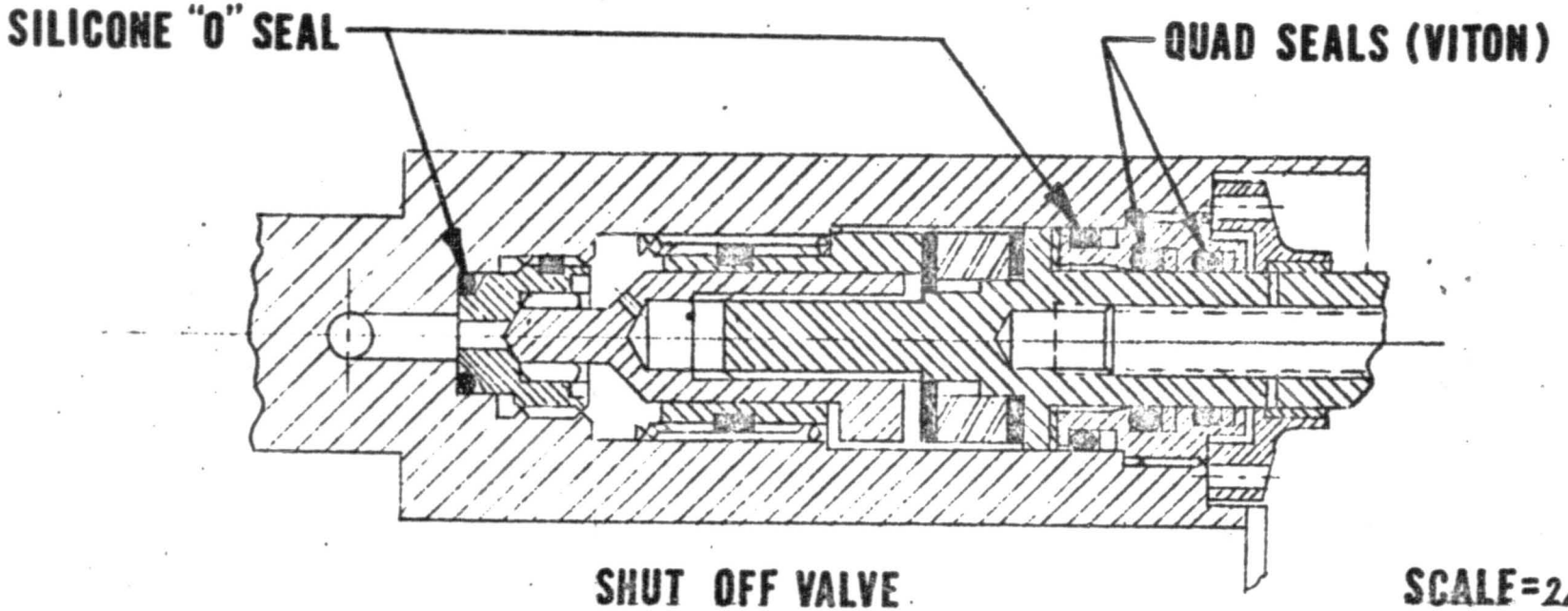

SHUT OFF VALVE

SCALE=2/1

PLSS PRIMARY REGULATOR

FIGURE 7

NA-SS-4487
August 12, 1970

PLSS STATIC SEALS

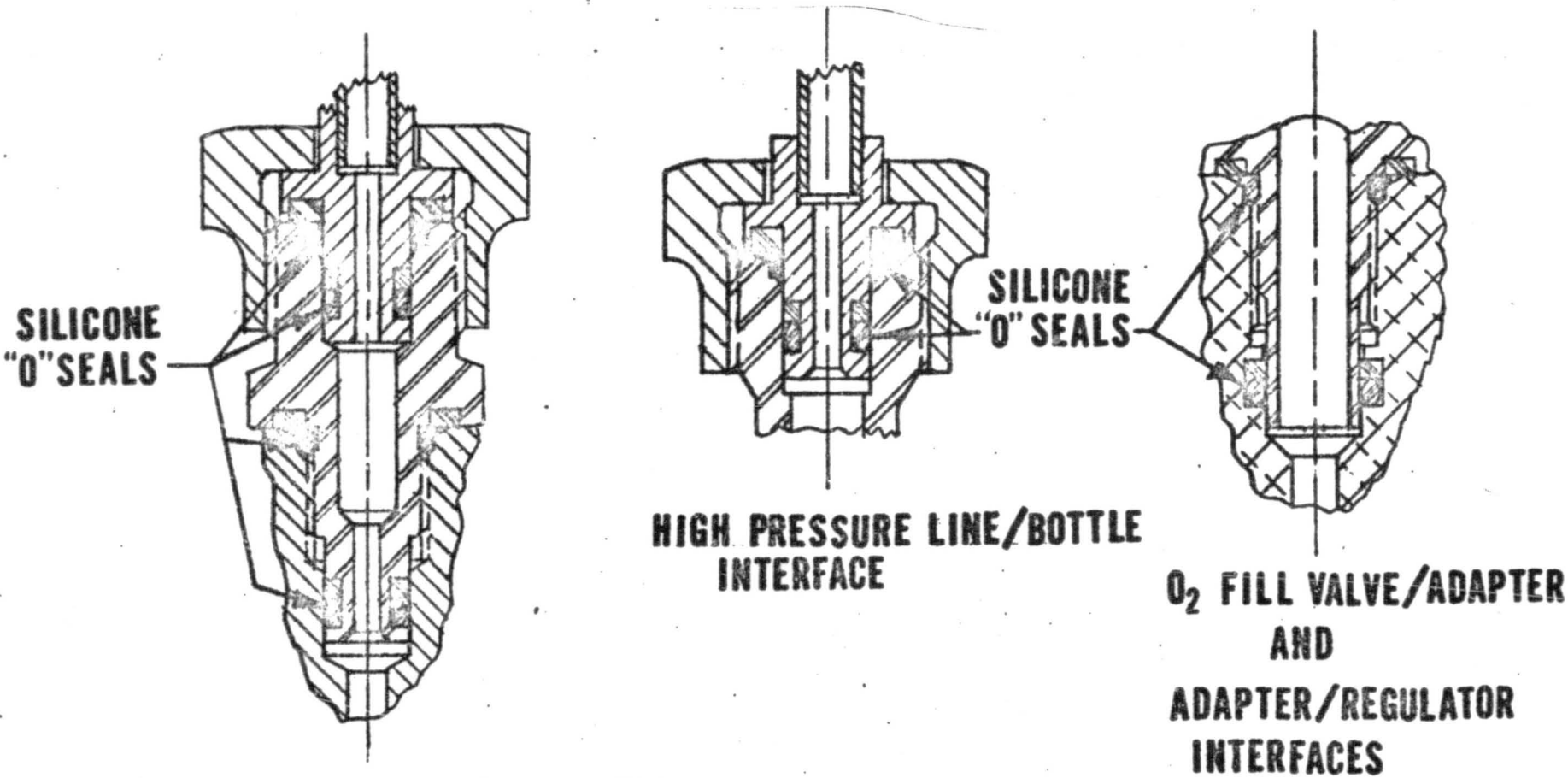

SCALE = 2/1

August 12, 1970

FIGURE 8

PLSS TYPICAL STATIC SEAL APPLICATIONS

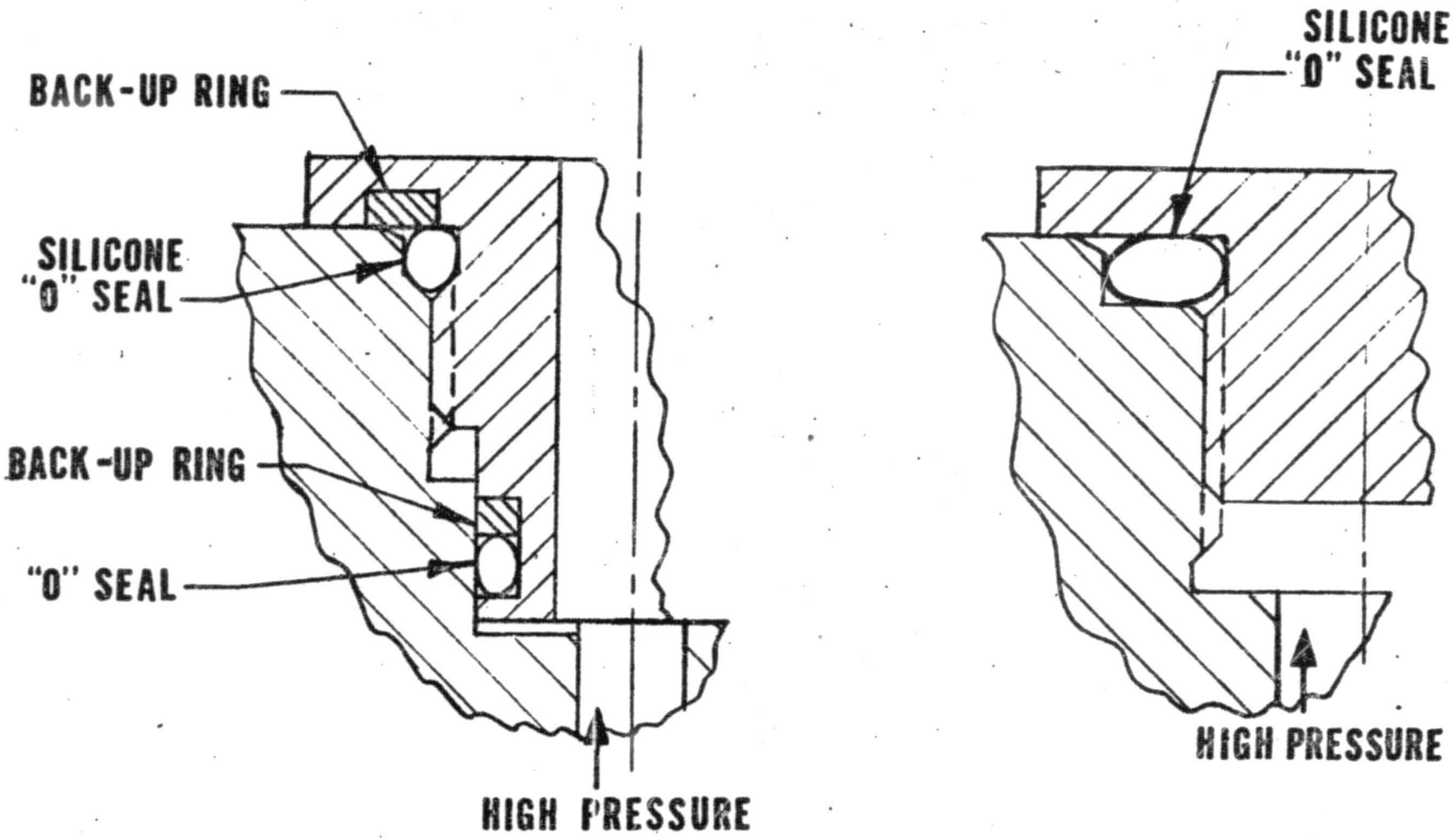

FIGURE 9

NA-SS-4487
August 12, 1970

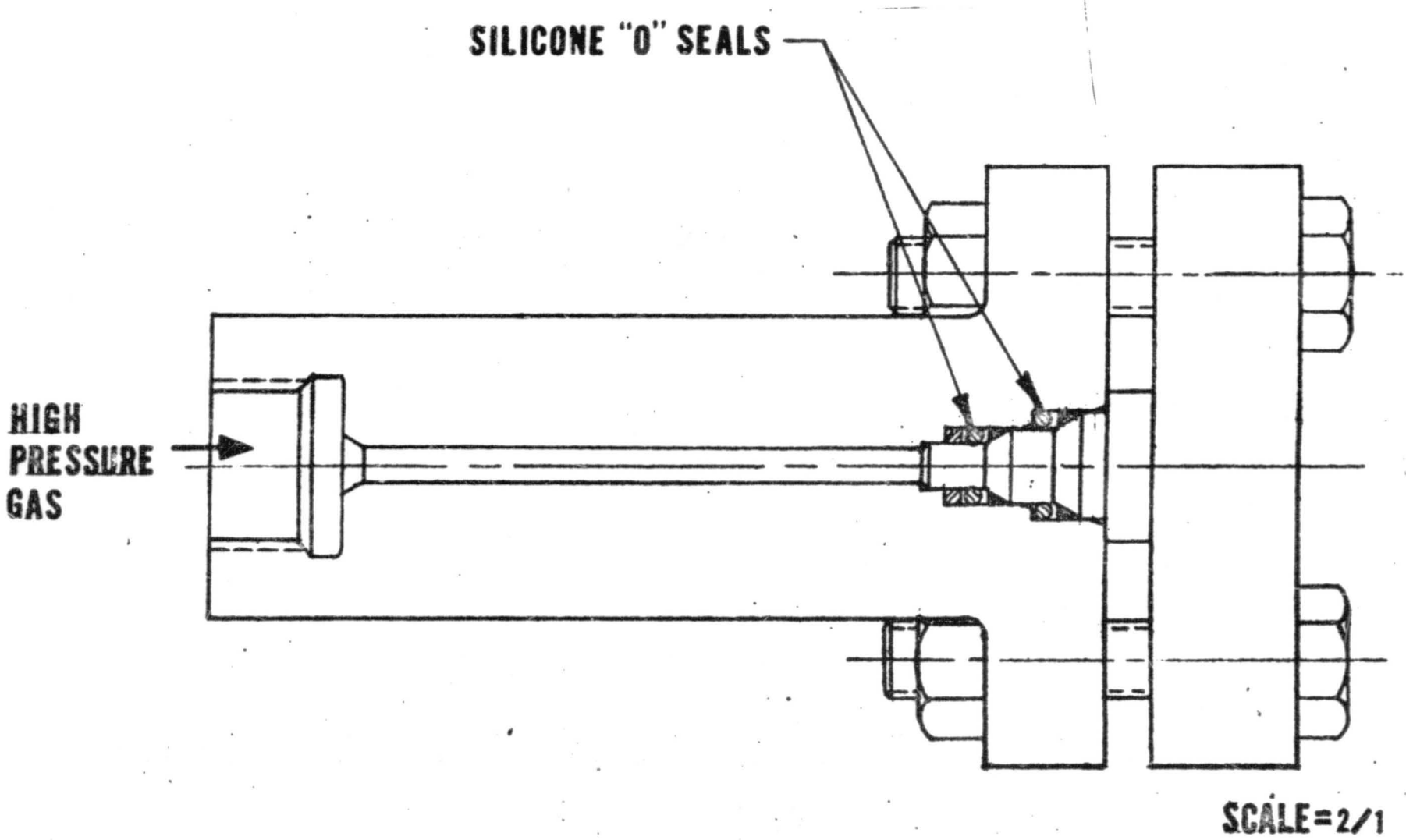

"O" SEAL TEST FIXTURES

(B1, B2, B3, B4)

FIGURE 10

NA-SS-4487
August 12, 1970

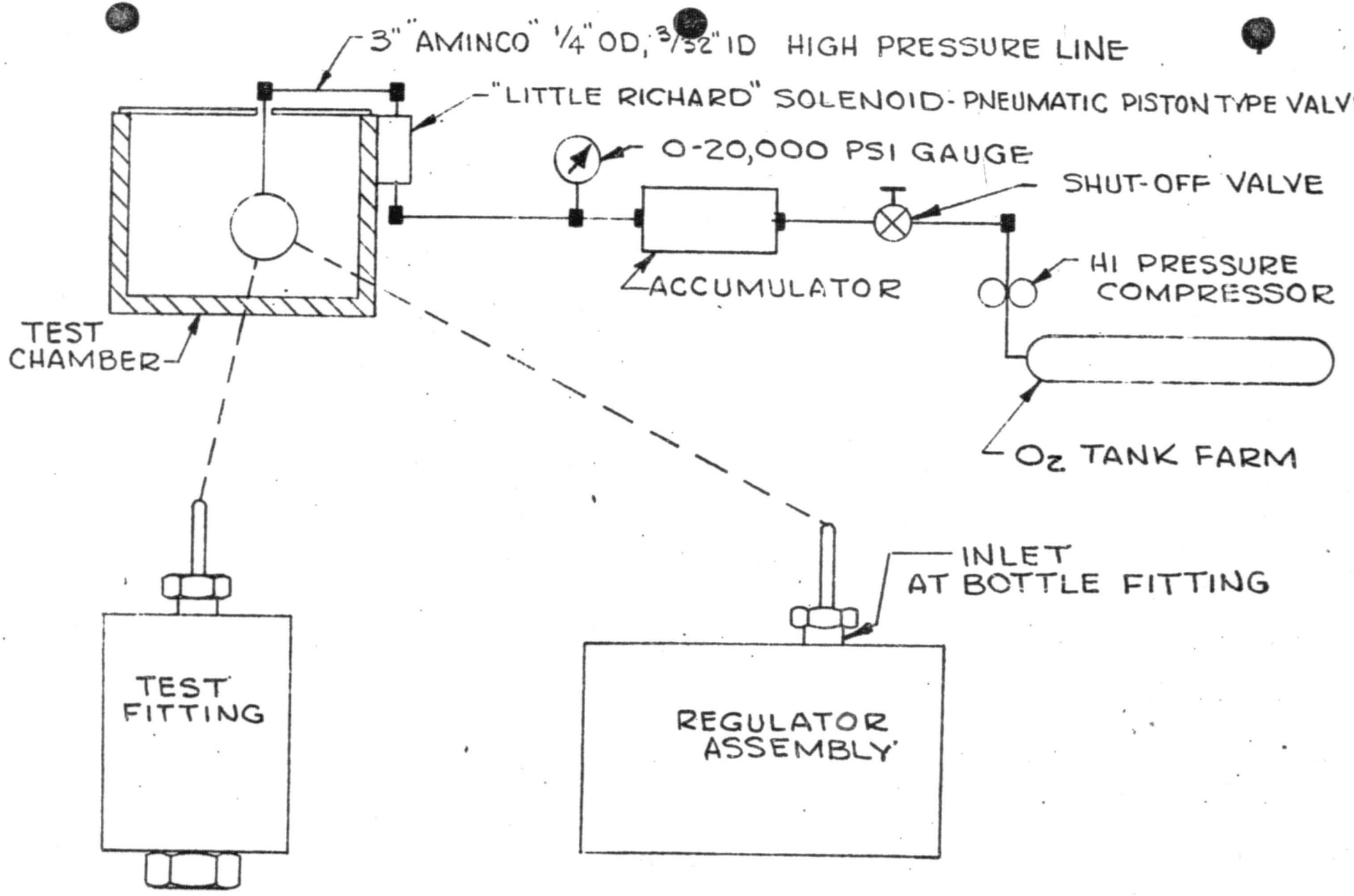

SEAL IGNITION TEST RIG SET UP

FIGURE 11

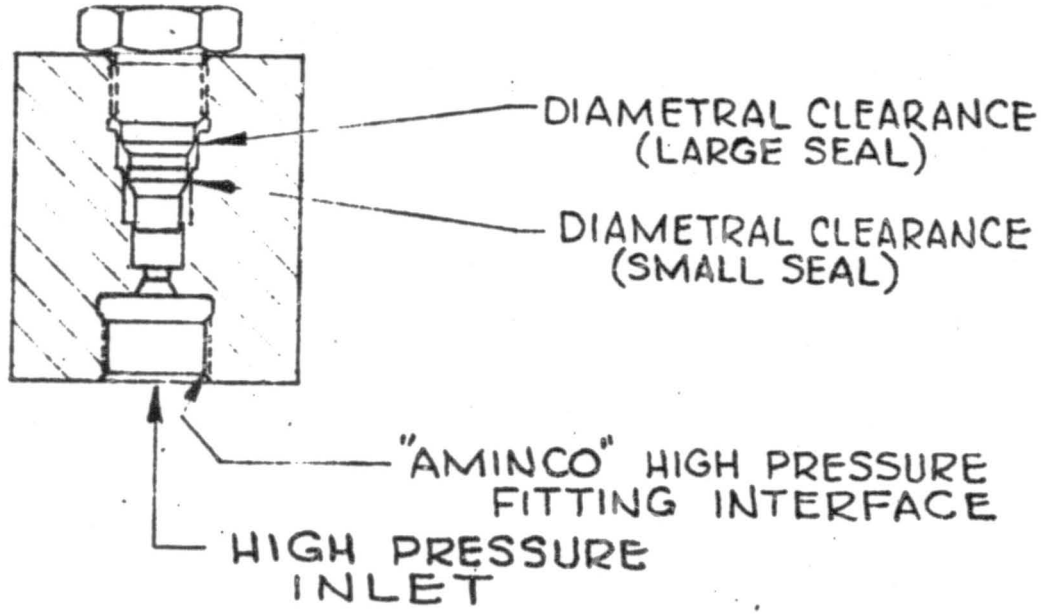

STATIC SEAL TEST FIXTURE
CROSS SECTION - SCALE: 1/1
(REFERENCE NA-SS-3052, FIXTURES A-1, A-2, A-3, A-4)

FIGURE 12

TABLE 1

Total logged and estimated hours of operating experience with gas pressures at 5000 psi or greater

System	Seal Material	Dynamic	Static
Mercury	Silicone	900	1,400
Gemini	Silicone	3,500	10,000
OSS	Silicone	150	240
EOS	Silicone	865	1,444
OPS	Silicone	284	301
OPS	Viton A	413	1,532

TABLE 2

VITON SEAL FAILURE SUMMARY

Test	Description and Total Test Time	Observations	Remarks
1) Vendor PAT	Excessive leakage of Seals resulted in pressure build up under High Pressure gage causing Regulator Body failure at the gage. (20 hrs.)	'O' seals were swollen and ruptured - Theory: Seal damage caused by rapid depressurization.	Test procedures were revised to limit depressurization rate. Pressure-relief porting was provided at gage.
2) HSD DVT	Excessive external leakage at pressure gage (80 hrs. - initial test) (30 hrs. after replacing seals)	Δ rings were split, 'O' rings swollen, & ruptured, one ring found "nibbled" by split in Δ ring, one 'O' ring bad at assy. - Theory: Improper Δ ring Mat'l, Improper inspection, seal damage due to use of N2 and Rapid depressurization.	Inspection procedures were revised - Test Plans were revised to eliminate use of N2 and to limit depressurization rate. Analysis of Δ rings was initiated.
3) HSD DVT	Leakage at Regulator Valve Stem (110 hrs.)	Several Δ rings were Split 'O' rings were swollen, blistered and deformed Theory: improper Δ ring Mat'l, Seal Damage due to use of N2 and Rapid depressurization.	Seal evaluation program initiated - DVT unit was rebuilt and tested with only O_2 and controlled depressurization.
4) HSD DVT	Leakage at Shut-off Valve Stem (61 hrs.)	'O' rings exhibited cracking, blistering and extrusion, extrusion of Backup Ring. Theory: Failures due to Seal Mat'l.	Unit Rebuilt with Silicone Seals and KEl-F Δ rings and Backup Rings. Unit completed DVT using O_2 with no failures.
5) HSD QUAL/DESIGN S/N 001	OFF Regulation Degradation (37 hrs.)	'O' rings exhibited extrusion, rupture, blistering. Δ rings were fractured. Theory: failures due to Seal Mat'l.	Design Review of 'O' rings and Δ rings indicates change should be made to Silicone 'O' rings and KEl-F Δ rings.

August 12, 1970

TABLE 2 (Cont'd)

VITON SEAL FAILURE SUMMARY

Test	Description and Total Test Time	Observations	Remarks
6) HSD PDA	High Regulation Pressure (30 hrs.)	Unit disassembled - Seal in regulator found swollen - only anomaly Theory: Swollen Seal restricted lower valve stem movement.	Regulators with Silicone Seals did not exhibit similar failures.
7) HSD Seal Evaluation	(See Table 3)	Viton Seals exhibit blisters, splits, pressure setting and swelling regardless of test gas or depressurization rate.	Silicone Seals did not exhibit similar failures.
8) HSD Rig 19	Repeated Leakage of Filter Seals and Regulator Seals (15-30 hrs.)	Seal damage - Split, tears, blisters and swelling.	Failures occur with Viton or Flourel Seals - N2 or O2 as test gas.

OPS Seal Tests

Table 3

Date	Fixture No.	Gas	Press psi	Time Cycle	Bleed Down Rate psi/min	Seal Mat'l.	No. Cycle	Damage
10/12	B1	N_2	10,360	5 min	1000	Viton	1	
		N_2	7,000	12 hr	1000	A	1	
10/12	B2	N_2	10,360	5 min	1000	Viton	1	
		N_2	7,000	12 hr	200	A	1	
10/12	B3	N_2	10,400	5 min	200	Viton	1	
		N_2	7,000	12 hr	1000	A	1	
10/12	B4	N_2	10,400	5 min	200	Viton	1	
		N_2	7,000	12 hr	200	A	1	
10/15	B1	N_2	10,500	5 min	1000	Viton	1	
		O_2	7,000	12 hr	1000	A	1	
10/15	B2	N_2	10,500	5 min	1000	Viton	1	
		O_2	7,000	12 hr	200	A	1	
10/15	B3	N_2	10,500	5 min	200	Viton	1	
		O_2	7,000	12 hr	1000	A	1	
10/15	B4	N_2	10,500	5 min	200	Viton	1	
		O_2	7,000	12 hr	200	A	1	
10/18	B1	N_2	10,150	5 min	1000	Viton A	1	
10/18	B2	N_2	10,350	5 min	700	Viton A	1	
10/18	B3	N_2	10,350	5 min	400	Viton A	1	
10/18	B4	N_2	10,350	5 min	200	Viton A	1	
10/18	B1	N_2	10,350	5 min	1000	Viton	1	
		O_2	7,050	4 hr	1000	A	6	
10/18	B2	N_2	10,350	5 min	1000	Viton	1	
		O_2	7,000	4 hr	200	A	6	
10/18	B3	N_2	10,350	5 min	200	Viton	1	
		O_2	7,000	4 hr	1000	A	6	
10/18	B4	N_2	10,350	5 min	200	Viton	1	
		O_2	7,000	4 hr	200	A	6	

Table 3 (Continued)

Date	Fixture No.	Gas	Press psi	Time Cycle	Bleed Down Rate psi/min	Seal Mat'l.	No. Cycle	Damage
10/24	B1	N_2	10,350	5 min	1000	Viton A	1	
		N_2	7,000	8 hr	1000		6	
10/24	B2	N_2	10,350	5 min	1000	Viton A	1	
		N_2	7,000	8 hr	200		6	
10/24	B3	N_2	10,350	5 min	200	Viton A	1	
		N_2	7,000	8 hr	1000		6	
10/24	B4	N_2	10,350	5 min	200	Viton A	1	
		N_2	7,000	8 hr	200		6	
10/29	B3	N_2	10,350	6 min	1000	Silicon	3	None
10/29	B2	N_2	10,350	6 min	1000	Silicon	1	None
10/29	B4	N_2	10,350	6 min	200	Silicon	1	
		N_2	7,000	8 hr	200	Silicon	6	None
10/29	B1	N_2	10,350	6 min	1000	Silicon	3	
11/5		N_2	10,000	½ hr	1500-2000		97	None
11/5	B3	N_2	10,000	½ hr	1500-2000	Viton A	97	Minimal
11/	B2	O_2	7,000	8 hr	6000-7000	Silicon	5	None
11/18	B4	O_2	7,000	8 hr	6000-7000	Viton A	5	Minimal
11/20	B1	O_2	7,000	12 hr	5000-10,000		1	
	150-155°F	O_2	7,000	36 hr	5000	Silicon	1	None
		O_2	7,000	8 hr	5000		1	
11/20	B3	O_2	7,000	12 hr	5000-10,000		1	Sm. seal swollen
	165-168°F	O_2	7,000	36 hr	5000	Viton A	1	Lg. seal starting to
		O_2	7,000	8 hr	5000		1	extrude at ID & OD of Δ seal
11/23	B1	O_2	7,000	41 hr		Viton A	1	Sm. seal swollen, many busters & one split lg. seal press. set against Δ seal
	26 hr 15				No vacu. bake			
11/23	B3	O_2	7,000	41 hr		Viton A	1	Sm. seal swollen & one buster. Lg. seal press. set against Δ seal
	26 hr 15							
11/29	B1	O_2	7,000	70.5 hr	7000	Silicon	1	None
11/29	B3	O_2	7,000	70.5 hr	7000	Viton A	1	Small seal swollen & one buster

TABLE 4

SILICONE 'O' SEAL IGNITION TESTING

Test No.	Test Item	Test Description	Pressure (O_2)	Diametral Clearance Large Seal/Small Seal	Results
1	Fixture A_1	Small and large 'O' Seals installed less Δ Seals and Backup ring	Sudden application of 10,000 psi	.0025/.0016	No Damage
2	Fixture A_2	Small and large 'O' Seals installed less Δ Seals and Backup ring	Sudden application of 10,000 psi	.0021/.0023	No Damage
3	Fixture A_3	Small and large 'O' Seals installed less Δ Seals and Backup ring	Sudden application of 10,000 psi	.0040/.0026	Ridge on small 'O' Seals only.
4	Fixture A_4	Small and large 'O' Seals installed less Δ Seals and Backup ring	Sudden application of 10,000 psi	.0025/.0025	No Damage
5	Fixture A_1	Small 'O' Seal deleted. Large 'O' Seal installed less Δ Seal and Backup ring	Sudden application of 10,000 psi	.0056	Ridge on 'O' Seal
6	Fixture A_2	Small 'O' Seal deleted. Large 'O' Seal installed less Δ Seal and Backup ring	Sudden application of 10,000 psi	.0040	Ridge on 'O' Seal

August 12, 1970

TABLE 4 (Cont'd)

SILICONE 'O' SEAL IGNITION TESTING

Test No.	Test Item	Test Description	Pressure (O_2)	Diametral Clearance Large Seal/Small Seal	Results
7	Fixture A_3	Small 'O' Seal deleted. Large 'O' Seal installed less △Seal and Backup ring	Sudden application of 10,000 psi	.0048/	Ridge on 'O' Seal
8	Fixture A_4	Small 'O' Seal deleted. Large 'O' Seal installed less △Seal and Backup ring	Sudden application of 10,000 psi	.0057/	Ridge on 'O' Seal
9	Fixture A_1	Large 'O' Seal deleted. Small 'O' Seal installed less △Seals and Backup rings	Sudden application of 10,000 psi	/.0029	Small gouge - Ridge on 'O' Seal
10	Fixture A_2	Large 'O' Seal deleted. Small 'O' Seal installed less △Seals and Backup rings	Sudden application of 10,000 psi	/.0040	Ridge on 'O' Seal
11	Fixture A_3	Large 'O' Seal deleted. Small 'O' Seal installed less △Seals and Backup rings	Sudden application of 10,000 psi	/.0049	Ridge on 'O' Seal
12	Fixture A_4	Large 'O' Seal deleted. Small 'O' Seal installed less △Seals and Backup rings	Sudden application of 10,000 psi	/.0057	Ridge & slight cut on 'O' Seal - possible beginning of extrusion.

TABLE 4 (Cont'd)

SILICONE 'O' SEAL IGNITION TESTING

Test No.	Test Item	Test Description	Pressure (O_2)	Diametral Clearance Large Seal/Small Seal	Results
13	Fixture A_1	Large 'O' Seal deleted. Small 'O' Seal installed less Δ Seal and Backup ring.	Sudden application of 10,000 psi	/.0114	Approx. 360° ring torn out of 'O' seal (the ridge extruded). Pressure decay indicates seal developed leak. No ignition.
14	Fixture A_2	Large 'O' Seal deleted. Small 'O' Seal installed less Δ Seal and Backup ring.	Sudden application of 10,000 psi	/.0116	Approx. 360° ring torn out of 'O' seal (the ridge extruded). Pressure decay indicates seal developed leak. No ignition.
15	Fixture A_3	Large 'O' Seal deleted. Small 'O' Seal installed less Δ Seal and Backup ring.	Sudden application of 10,000 psi	/.0116	Approx. 360° ring torn out of 'O' seal (the ridge extruded). Pressure decay indicates seal developed leak. No ignition.
16	Fixture A_4	Large 'O' Seal deleted. Small 'O' Seal installed less Δ Seal and Backup ring.	Sudden application of 10,000 psi	/.0116	Approx. 360° ring torn out of 'O' seal (the ridge extruded). Pressure decay indicates seal developed leak. No ignition.
17	Fixture A_1	Small 'O' Seal deleted. Large 'O' Seal installed less Δ Seal and Backup ring.	Sudden application of 10,000 psi	.0113/	Approx. 360° ring torn out of 'O' seal (the ridge extruded). Pressure decay indicates seal developed leak. No ignition.
18	Fixture A_3	Small 'O' Seal deleted. Large 'O' Seal installed less Δ Seal and Backup ring.	Sudden application of 10,000 psi	.0118/	Approx. 360° ring torn out of 'O' seal (the ridge extruded). Pressure decay indicates seal developed leak. No ignition.

TABLE 4 (Cont'd)

SILICONE 'O' SEAL IGNITION TESTING

Test No.	Test Item	Test Description	Pressure (O_2)	Diametral Clearance Large Seal/Small Seal	Results
19	Fixture A_4	Small 'O' Seal deleted. Large 'O' Seal installed less △ Seal and Backup ring.	Sudden application of 10,000 psi	.0117/	Approx. 360° ring torn out of 'O' seal (the ridge extruded). Pressure decay indicates seal developed leak. No ignition.
20	Regulator	Dynamic Seal at regulator Stem installed less Backup Rings	Sudden to 8500 psi	/.012	Seal extruded. No evidence of ignition.
21	Regulator	Dynamic Seal at regulator Stem installed less Backup Rings	Sudden to 8500 psi	/.012	Seal extruded. No evidence of ignition.
22	Regulator	Dynamic Seal at regulator Stem installed less Backup Rings	Sudden to 8500 psi	/.012	Seal extruded. No evidence of ignition.

END OF REFERENCE

Card #30

REFERENCE

125

POWER PIPING. ASA B31.1, ANSI, 1973.

THIS REFERENCE IS COPYRIGHTED MATERIAL AND THEREFORE
THE CONTENTS HAVE NOT BEEN REPRODUCED FROM THE TEXT.

END OF REFERENCE

125

REFERENCE
126

PETROLEUM REFINERY PIPING. B31.3, ANSI, 1973.

THIS REFERENCE IS COPYRIGHTED MATERIAL AND THEREFORE
THE CONTENTS HAVE NOT BEEN REPRODUCED FROM THE TEXT.

END OF REFERENCE

126

REFERENCE
127

STANDARD METHOD OF TEST FOR BRITTLENESS TEMPERATURE OF PLASTICS AND ELASTOMERS BY IMPACT. PART 27 OF ASTM ANNUAL STANDARDS. ASTM DESIGNATION D 746-72, 1973.

THIS REFERENCE IS COPYRIGHTED MATERIAL AND THEREFORE THE CONTENTS HAVE NOT BEEN REPRODUCED FROM THE TEXT.

END OF REFERENCE

127

REFERENCE

128

BASS, R. L.; AND HOLSTER, J. L.: BELLOWS VIBRATION WITH INTERNAL CRYOGENIC FLOWS. TRANS. ASME, SER. B: J. ENG. IND., VOL. 94, NO. 1, FEBRUARY 1972.

R. L. BASS
Senior Research Engineer.

J. L. HOLSTER
Research Engineer.

Department of Mechanical Sciences,
Southwest Research Institute,
San Antonio, Texas

Bellows Vibration With Internal Cryogenic Fluid Flows[1]

The flow-induced vibrations of metal bellows with internal cryogenic flow are examined experimentally, and analytical techniques are given to predict vibration suppression characteristics. Heat transfer is shown to create local vaporization inside the convolutes which kills the primary source of bellows vibration, vortex shedding. The reduction in vibration amplitude is shown to be a function of the state properties of the liquid inside the bellows and the heat transfer rate into the liquid. External damping from frost, ice, or condensed liquid, which can appear on the bellows exterior, is discussed, and a method for estimating the reduction in vibration severity with external condensation is presented.

Introduction

Flow-induced vibrations in fluid ducting systems such as metal bellows, have for some time, been a problem for aerospace applications. There are known instances where flow-induced vibrations of bellows have resulted in fatigue failures which forced the premature shutdown of critical fluid systems.

A great deal of the current knowledge of bellows flow-induced longitudinal vibrations is presented in references [1 and 2],[2] where the flow excitation phenomena responsible for bellows vibration has been established as a dynamic coupling between a vortex shedding process and the bellows convolute motion. The process of periodic vortex formation and shedding is a boundary layer instability which causes a corresponding periodic pressure to be exerted on the bellows convolutions. The amplitude of the alternating pressure is proportional to the free-stream stagnation pressure ($1/2\rho_f V_s^2$) and its effect is considered as a net force applied at the tip of each convolution. If the frequency of the vortex shedding coincides with some bellows longitudinal mode frequency, then a resonance occurs and the bellows convolutions experience an axial vibratory displacement. This convolution vibratory displacement causes a corresponding stress, and the magnitude of this stress is dependent on the convolution geometry.

In reference [1], an analysis is presented for determining bellows vibratory stresses and a special "Stress Indicator," developed to aid in rapidly judging the severity of bellows flow-induced vibrations, is discussed. This parameter is essentially an approximation of a more exact form for bellows vibrations and is given by

$$\text{Stress Indicator} = \left(\frac{C_F Q}{N_P}\right)\left(\frac{h}{t}\right)^2 (1/2\rho_f V_s^2) \qquad (1)$$

Using values for C_F, a vortex force coefficient, and Q, a dynamic amplification factor, the stress indicator can be quickly calculated for any situation. Bellows fatigue life as a function of Stress Indicator has also been compiled as an aid to the designer.

This state-of-the-art of bellows vibrations was derived from experimental and analytical studies of free bellows and flex hose, and resulted in the development of an acceptable analytical model of bellows flow-induced vibrations. However, the work is not complete in that (*a*) the results are not adequate for gas flows where acoustical resonances have a significant influence and (*b*) where cryogenic liquids are the flow media, so that heat transfer and/or external damping play an important role.

The importance of cryogenic flow effects was discovered from investigations into the cause of a flex hose failure (J-2 engine, ASI fuel line) on Saturn flight AS-502; this is reported by Daniels and Fargo in reference [3]. Their results raised questions about the relative importance of heat transfer and external damping caused by liquid condensation on the bellows flow excitation process.

With cryogenic liquids, heat transfer effects as well as other influences must be considered so that an understanding of the flow-induced vibrations in flexible metal bellows can be obtained. The consequences of heat transfer in the case of cryogenic flow in bellows are of particular interest, since large temperature differences exist between the flowing liquid and the bellows environment which can lead to a phase change near the inside bellows wall creating a change in the bellows flow response. In addition to vapor effects, frost buildup or liquid condensation on

---

[1] Research sponsored by NASA-Marshall Space Flight Center, under Contract NAS8-21133.

[2] Numbers in brackets designate References at end of paper.

Contributed by the Design Engineering Division and presented at the Vibrations Conference, Toronto, Canada, September 8–10, 1971, of The American Society of Mechanical Engineers. Manuscript received at ASME Headquarters, May 11, 1971. Paper No. 71-Vibr-14.

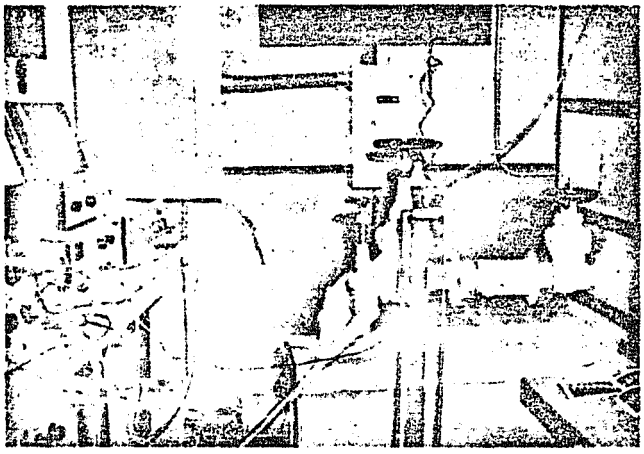

Fig. 1 Cryogenic flow loop with insulation

Table 1 Test bellows—dimensional data (in in.)

Bellows # 1		Bellows # 2	
I. D. = 1.49	h = .312	I. D. = 1.49	h = .36
O. D. = 2.22	λ = .345	O. D. = 2.22	λ = .187
Dm = 1.85	σ = .125	Dm = 1.85	σ = .125
N_c = 7	t = .013	N_c = 7	t = .013
N_p^c = 1	LL = 2.75	N_p^c = 1	LL = 1.5
Bellows # 3		Bellows # 4	
I. D. = 1.46	h = .27	I. D. = 1.46	h = .25
O. D. = 2.02	λ = .22	O. D. = 2.02	λ = .282
Dm = 1.74	σ = .144	Dm = 1.74	σ = .144
N_c = 8	t = .013	N_c = 8	t = .013
N_p^c = 1	LL = 1.52	N_p^c = 1	LL = 1.95
Bellows # 5		Bellows # 6	
I. D. = 1.46	h = .28	I. D. = 1.49	h = .345
O. D. = 2.02	λ = .156	O. D. = 2.22	λ = .250
Dm = 1.74	σ = .125	Dm = 1.85	σ = .125
N_c = 8	t = .013	N_c = 7	t = .013
N_p^c = 1	LL = 1.25	N_p^c = 1	LL = 2.0

ID = internal diameter
OD = outside diameter
Dm = mean diameter
N_c = number of convolutes
N_p^c = number of plys
h_p = convolute height
λ = convolute pitch
σ = convolute tip width (internal)
t = ply thickness
LL = live length

the outside bellows surface will affect the heating rate and add damping to the bellows structure, influencing its operating characteristics. Also, the change in the bellows structural characteristics at extremely low temperatures, in contrast to conditions tested in air and water at near ambient conditions, must be considered.

The remainder of this paper is devoted to a discussion summarizing the results of an investigation into the factors that alter the vibration characteristics of bellows flowing a cryogenic liquid. Details of this work are given in reference [4].

Experimental Program

Experimental Facility and Instrumentation. A special cryogenic flow loop shown in Fig. 1 was designed and fabricated for the purposes of this study. All bellows installed in the cryogenic flow loop were instrumented to monitor 1 the upstream fluid temperature, 2 the downstream fluid temperature, 3 the bellows metal or skin temperature, and 4 the surrounding temperature of the environment in which the bellows were placed.

Bellows static pressure and pressure drop were also recorded during the tests. Dynamic strain was monitored through the use of constantan foil gages, calibrated for low-temperature conditions and mounted on the first convolution tip of each bellows.

Experimental Results. The cryogenic flow loop was utilized to study bellows flow excitation for a number of fluid and surrounding conditions. To obtain a comparison of bellows response with liquid nitrogen (LN_2) versus water, tests were conducted with identical bellows using both mediums, and with heat transfer effects maintained at a minimum. Heat transfer effects with LN_2 were then studied by controlling the bellows environmental conditions (temperature, frost buildup, and convection rate), and recording the strain levels at different flow rates and pressures. Six different test bellows were utilized, and dimensional data for these bellows are given in Table 1.

Testing of bellows with liquid nitrogen revealed that the bellows vibrational amplitudes were dependent on the bellows operating static pressure. In order to induce vibrations of the lower modes, the bellows pressure had to be increased such that the state of the fluid in the bellows was adjusted into the liquid phase away from the liquid-vapor line.

The effect of increasing the bellows static pressure can be seen in Fig. 2. The maximum strain level was recorded versus the bellows pressure at various values of the tank system vapor pressure (P_T). In all cases, it can be seen that the strain increased with increasing bellows pressure (P_B) up to a maximum where it leveled off and became invariant with further increases in bellows pressure. The results in Fig. 2 were typical of all bellows tested with liquid nitrogen.

A direct comparison of flow-induced vibration phenomena between LN_2 and water, in which heat transfer effects were minimized, was obtained for identical test bellows. The resultant data, therefore, reflect basically any possible difference in the vibrations because of differences in the two flow media or be-

Nomenclature

C_F = vortex force coefficient
f = bellows vibrational frequency
h_i = inside convection coefficient
h_0 = outside convection coefficient
K_f = thermal conductivity of frost
K_w = thermal conductivity of wall
l = bellows length for heat transfer model
P_B = bellows pressure
$P_{B\max}$ = bellows pressure at maximum strain
$P_{B\min}$ = bellows pressure at zero strain
P_v = vapor pressure
P_T = tank vapor pressure
P_d = stream dynamic pressure
Q = dynamic amplification factor, a measure of damping
q = heat transfer
r_m = mean bellows radius
R = resistance to heat transfer
t_f = frost thickness
t_w = wall thickness
T_{f0} = outside frost temperature
T_s = stream temperature
T_w = wall temperature
V_s = flow velocity
ρ_s = condensate fluid density
ρ_f = internal fluid density
σ_m = cavitation number at maximum strain
σ_0 = cavitation number at zero strain
ϵ = empirical constant ($\epsilon = 0.25$)
δ = space between convolute tips

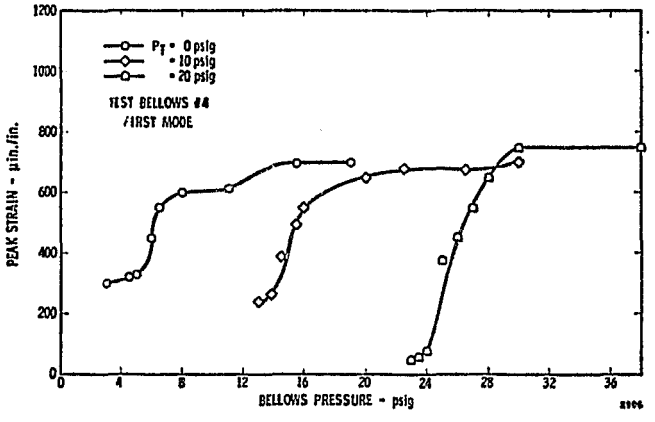

Fig. 2 Pressure sensitivity of flow excited bellow (#4) with LN_2 flow

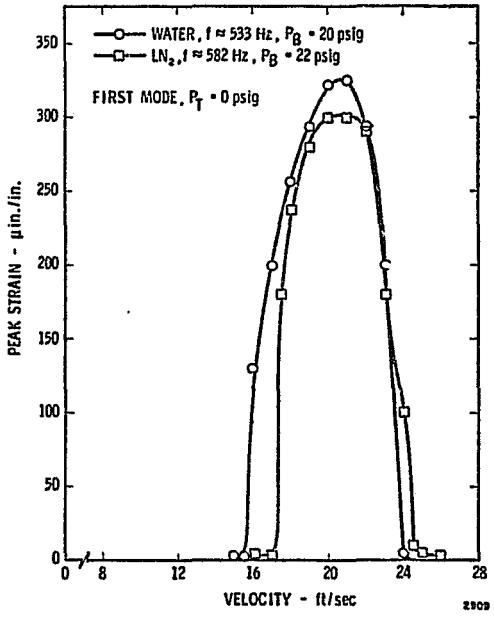

Fig. 3 Comparison of flow-induced vibration with water and LN_2, bellows #6

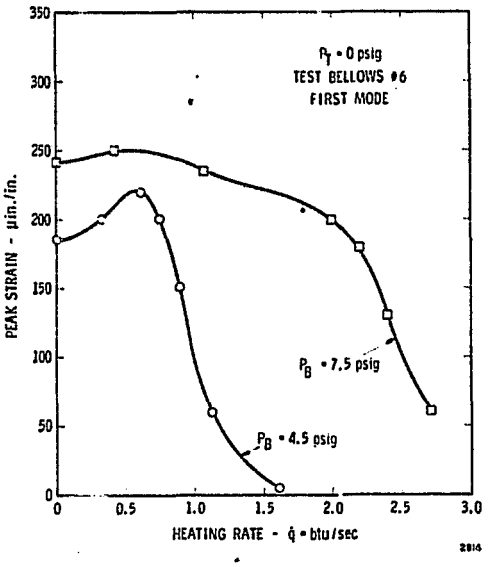

Fig. 4 Effect of heating rate on maximum strain level

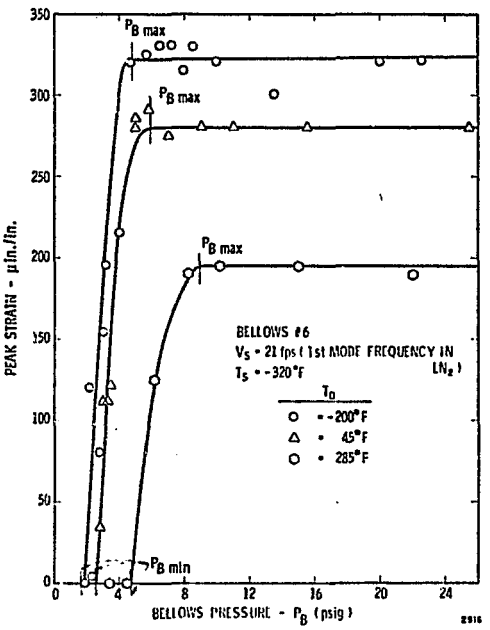

Fig. 5 Effects of heat transfer on bellows pressure at zero and maximum strain

cause of bellows material property changes with temperature. Each bellows was tested with conditions sufficient to ensure maximum vibration strain and typical flow-induced vibration test results for the first longitudinal mode, with both water and LN_2 flows, are given in Fig. 3. The data presented in Fig. 3 show good agreement of the peak flow-induced strain levels for the two test liquids. In each case, the maximum strain is greater for water flow than for the LN_2 flow. This is to be expected since LN_2 is less dense than the water; hence, the excitation force, which is proportional to $\frac{1}{2}\rho_f V_s^2$, is reduced. Comparing the results for all bellows geometries tested, the agreement is sufficiently good to conclude that there are no major discrepancies between flow induced vibration results for water and LN_2, *if no cavitation suppression occurs and no external damping media are allowed to form.*

Quantitative information on the effects of heat addition during operation of flow-excited bellows was obtained by passing hot air over the bellows convolutes and recording bellows strain versus heating rate. With the bellows operating at a velocity which produced maximum excitation of the first mode, the heating rate was increased with time, and the resulting strain amplitude was recorded. Results shown in Fig. 4 indicate that increasing the heating rate produced a corresponding decrease in strain until the vibration was completely suppressed. The results in Fig. 4 for large transient heating rates are not typical of bellows environmental conditions, since bellows usually operate under conditions of approximately steady-state heat transfer, but do indicate the possible effects from heat transfer.

Additional tests were conducted to determine the bellows strain response with constant heat input. Three conditions of heating were utilized by producing three levels of environmental temperature (T_0). For each environmental temperature, the bellows were operated at flow velocities corresponding to peak excitation of the first vibrational mode, and strain data were obtained over a range of operating pressures. No frost or condensation was allowed to build up on the bellows external surface. The strain response versus operating pressure shown in Fig. 5 indicated that there is some minimum pressure at which the bellows vibrated and produced maximum flow-induced strain. This pressure is indicated as $P_{B\max}$ in Fig. 5 and is, then, the lowest operating pressure at which maximum strain occurs. As the pressure is decreased below $P_{B\max}$, the strain amplitude decreases rapidly until zero strain is recorded at $P_{B\min}$, the highest operating pressure for no flow-induced vibration. Below

P_{Bmin}, no condition of flow excitation is observed. These results indicate that under conditions of constant heat transfer there is a minimum operating pressure which allows flow excitation to occur and produce vibrational strains in the bellows structure. The results in Fig. 5 also show that as additional heat is added to the bellows, i.e., increasing T_0, the values of P_{Bmax} and P_{Bmin} are also increased.

The bellows flow velocities required to produce peak flow-induced strain remained unchanged with the different heat transfer rates used in this study. An investigation of the theoretical bellows frequency change with large structural temperature changes supported the experimental results, showing that no frequency shift occurred with different levels of bellows temperature since insignificant changes in Young's modulus and the elemental model mass occurred.

Analysis

Heat Transfer. The experimental results presented in the preceding section indicate that heat transfer to a flowing cryogen through a bellows wall can change the flow-induced response of the bellows. In order to gain a better understanding of the heat transfer effects, and to obtain a method for predicting the operating conditions at which the bellows response characteristics are altered, a heat transfer model was developed to predict temperature distributions across the bellows between the environment and the flowing medium. A knowledge of this distribution, combined with a defining cavitation number, allowed the operating pressures at the initial points of maximum and minimum dynamic strain to be correlated and predicted. The effect of frost formation of these pressures was also obtained, and a limiting frost thickness was determined for different environmental conditions.

The bellows geometry, for purposes of setting up the heat transfer model, was assumed to be a thin-walled cylinder of radius, r_m, equal to the mean radius of the bellows and of length, l, corresponding to the actual expanded length along the convoluted surface.

The heat transfer was assumed to be one-dimensional, steady-state conduction and convection in the radial direction of the thin-walled cylinder, with no conduction along its length.

The heat transferred between the bellows environment, at temperature T_0, and the flowing liquid at T, is given by

$$q = \frac{T_0 - T_s}{R} \tag{2}$$

where

$$R = R_1 + R_2 + R_3 + R_4 \tag{3}$$

is the total resistance to heat transfer. The resistances are (R_1) the convection resistance between the environment and the outside surface (frost or wall), (R_2) the conduction resistance of the frost at thickness t_f and having a thermal conductivity K_f, (R_3) the conduction resistance of the wall at thickness t_w with thermal conductivity K_w, and (R_4) is the convection resistance between the inside wall and the free stream.

In order to obtain heating rates and temperatures, a knowledge of the inside and outside convection coefficients, h_i and h_0, are required as well as the bellows geometry, and thermal conductivity, K_w, and the frost conditions, t_f and K_f. One of the most difficult parameters to estimate is the inside heat transfer coefficient, h_i, which depends on the state of the cryogenic fluid in the convolutes. The experimental heat transfer results for LN_2 show that wall temperatures remain within 1 to 5 deg F of the cryogenic liquid saturation temperature for heat transfer rates typical of those to be expected in actual situations. Therefore, forced convection heat transfer with minimum boiling was used to represent the heat transfer between the inside bellows wall and the flowing cryogen, and the work of Nunner (reference [5]) was used to estimate h_i. Reference [5] is considered ideal for estimating h_i since results are shown to fit experimental data taken on pipes artificially roughened by attaching various sizes of rings to the inside surface. The rings are directly analogous to the convoluted section of a bellows. If excessive rates of heat transfer result in large-scale nucleate or film boiling, then other methods of estimating h_i must be used.

The outside convection coefficient, h_0, can be determined from correlations for the forced flow of air over cylinders or from the literature when natural convection or condensation is considered.

Pressure at Peak and Zero Strain. The bellows inside wall temperature i determined by

$$T_{wi} = T_s + qR_4 \tag{4}$$

Knowing T_{wi}, an estimate of the bellows operating pressure at peak and zero strain can be obtained from a set of cavitation numbers defined as

$$\sigma_m = \frac{P_{Bmax} - P_v @ T_{wi}}{P_d} \text{ (Cavitation number at peak strain)} \tag{5}$$

$$\sigma_0 = \frac{P_{Bmin} - P_v @ T_{wi}}{P_d} \text{ (Cavitation number at zero strain)} \tag{6}$$

where P_v at T_{wi} is the vapor pressure corresponding to the inside wall temperature, and P_d is the stream dynamic pressure. The cavitation numbers at peak and zero strain, together with the inside wall temperature, flow velocity, and density, allow P_{Bmax} and P_{Bmin} to be calculated.

A knowledge of the cavitation number is required so that an estimate of the operating pressures at peak and zero strain may be made. The experimental P_{Bmax} and P_{Bmin} data together with the heat transfer model (which yields P_v at T_{wi}) allow σ_m and σ_0 to be determined.

Vapor pressures corresponding to T_{wi} calculated from the model, and combined with experimental values of P_{Bmax} and P_{Bmin}, were used to determine σ_0 and σ_m from equations (5) and (6). The results are presented in Fig. 6. These cavitation numbers are reasonable when considering that initial cavitation usually occurs between zero and one. The results indicate that when operating conditions are such that the cavitation number nears σ_m initial cavitation begins and vibrations are damped, and, when σ_0 is approached, vibrational amplitudes are completely suppressed.

The cavitation numbers, together with the heat transfer analysis, have been used to predict P_{Bmax} and P_{Bmin} under more general conditions than those tested. The results shown in Figs. 7 and 8 indicate that the largest resistance to heat transfer from the environment to the fluid flowing in a bellows occurs from the outside convection characteristics, h_0, and from the insulating effect from the frost. The thin bellows wall offers little resistance

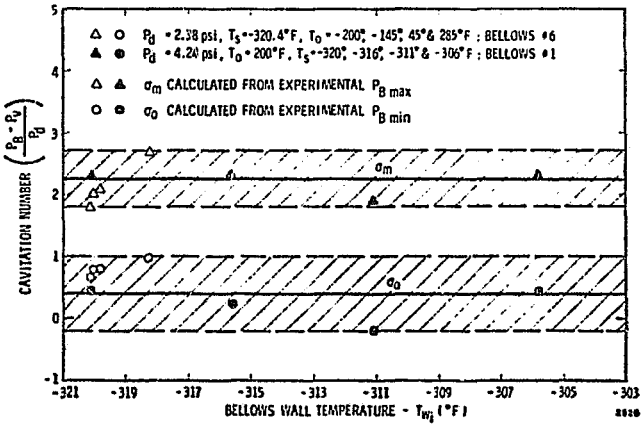

Fig. 6 Experimental cavitation numbers at maximum strain (σ_m) and at zero strain (σ_0)

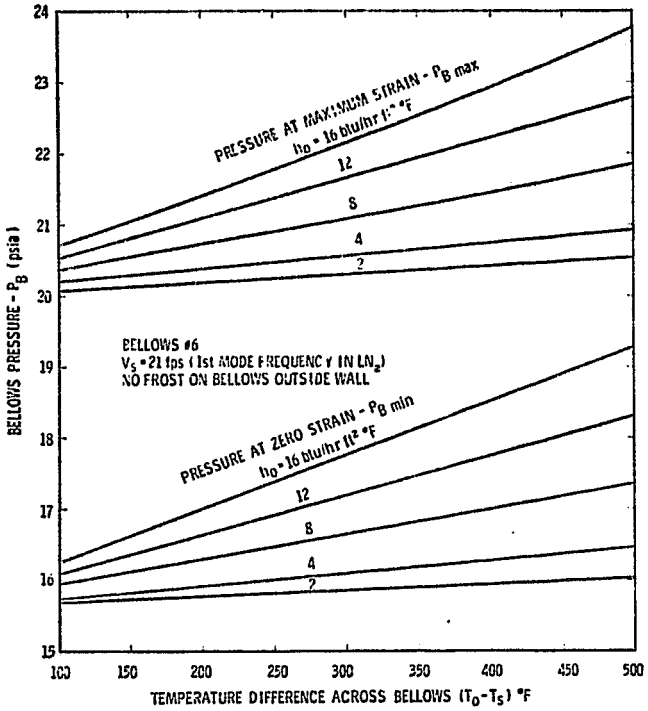

Fig. 7 Bellows pressure at zero and maximum strain with no frost on wall

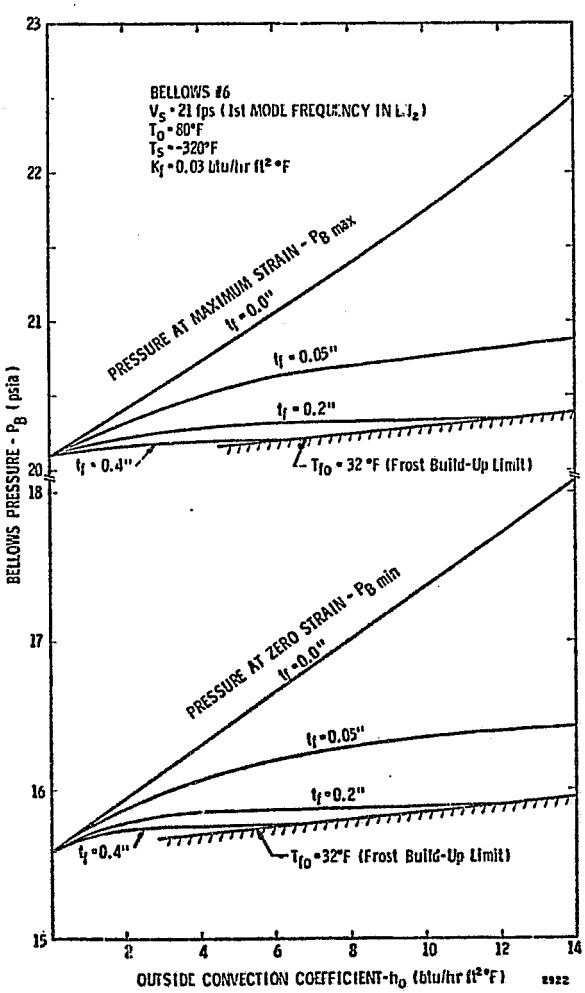

Fig. 8 Bellows pressure at zero and maximum strain with frost built-up

to heat flow, and the inside convection resistance is small because of the forced flow over the rough convoluted surface.

The results of this analysis for no frost formation are presented in Fig. 7 for a bellows flowing LN_2 at a velocity corresponding to the first mode frequency, and with no frost formation on the bellows exterior surface. The results indicate that promoting heat transfer, by increasing T_0 or h_0, will result in a corresponding increase in the bellows pressure to insure vibrational strains.

The effects of frost formation are presented in Fig. 8 for the same flow conditions as for the no-frost case. In this case, environmental temperature is held constant at 80 deg F, and the effects of frost thickness with varying outside convection conditions are presented. The limiting frost thickness is determined by examining the frost temperature at the outside surface as given by

$$T_{fo} = T_{wi} + qR_2. \tag{7}$$

When the frost thickness has increased to a point where the temperature drop across the frost is such that $T_{fo} = 32$ deg F, then no additional frost buildup will occur. The limiting thickness will depend on the total heat transfer, q, as determined from the environmental and stream conditions. This maximum thickness is shown in Fig. 8. The results indicate that: 1 for a given convection coefficient, h_0, frost buildup significantly insulates the bellows, reducing $P_{B\min}$ and $P_{B\max}$ and 2 increasing h_0 at a given frost thickness results in an increase in $P_{B\max}$ and $P_{B\min}$.

All results presented in this paper are for velocities corresponding to the first vibrational mode. No data have been taken at higher mode frequencies to confirm the accuracy of this analysis. In general, the analysis should be adequate to yield an accurate estimate of operating pressures, to insure that cavitation does not occur under a given environmental situation.

In the case of condensation on the bellows exterior, the heat transfer may be increased over that for typical forced convection rates alone. This results from an increase in the outside heat transfer coefficient, h_0, due to the condensation process. While the results presented in Figs. 7 and 8 represent heat transfer rates for both natural and forced convection, the present analysis is also valid for condensation if the outside convection coefficient is determined appropriately. In this case, no frosting will occur and large operational static pressures will be required to insure maximum strain levels. However, when the liquified gases are allowed to collect on the outside of the convolutes, external damping can create a significant reduction in vibrational response even when the flow in the bellows is supercritical and no cavitation can occur.

External Damping. The prior discussions have been devoted primarily to one mechanism, heat transfer, which can suppress bellows flow excitation where cryogenic liquids are the flow media. Another possible suppression mechanism where cryogens are the flow media is the extra damping introduced by the external buildup of some combination of ice, frost, or condensed air.

Frost buildup alone on a bellows with an internal cryogen flow has a minor to negligible effect on the amplitude of flow-induced vibrations. Several experiments were conducted to determine if the vibration was suppressed by frost formation, and, in all cases where frost *alone* was present, no truly significant reduction was noted even for heavy frost buildups. Therefore the frost buildup offers negligible resistance to convolute motion but does add thermal insulation.

External ice buildup with internal cryogen flow may or may not cause suppression of the flow-induced vibrations. If the ice buildup is of sufficient magnitude so that the spaces between the convolutes are largely filled with ice, then no vibrations will occur. When thinner ice coatings are present, low energy vibrations are completely suppressed, but high energy level vibrations cause the ice coating to crack and fall off so that the original or undamped (external damping) vibration amplitude is restored.

Bellows damping, because of the presence of an external liquid, can be quite significant, and such a condition generally occurs when air condenses on the bellows exterior. Experiments were conducted under simulated conditions employing external water damping on bellows flowing water and air. In addition, an analysis was performed to develop a mathematical model for this type of damping.

Vibratory motion of the convolutes causes the external liquid to be periodically forced in and out of the space between the convolutes, and the external period fluid motion produces a damping force on the vibrating convolutes. This force, because of the turbulent dissipation mechanism, is proportional to the convolute relative velocity to the second power. Based on this hypothesis, a model was developed for the convolute vibrations for a case where external damping alone is present (no conventional damping). The results have been formulated in terms of a Stress Indicator equation, to be compatible with earlier results. Since some conventional damping is always present, the Stress Indicator, SI_e for external damping only, does not indicate the true bellows flow-induced stress level, but only the external damping limited part. The true or correct Stress Indicator is a combination of the conventional value (equation (1)) and the external damping value (SI_e) and is given by the expression

$$SI_c = \frac{1}{\frac{1}{SI} + \frac{1}{SI_e}} \tag{8}$$

where

SI = Stress Indicator for Conventional Damping (equation (1))

and

$$SI_e = \frac{\epsilon \delta t E N_P}{f h^3} \left(\frac{C_f P_d}{\rho_e} \right)^{1/2} \tag{9}$$

The use of equation (8) allows an accurate estimate of the reduced bellows vibration response when an internal cryogen flow creates condensation on the bellows exterior.

Summary and Conclusions

Results of the present investigation of bellows flow-induced vibrations where a cryogen is the flow media have demonstrated that the phenomena are predictable by the method presented in reference [1], except for two important limiting cases. First, if boiling and/or cavitation occurs in the bellows, vibrations will be suppressed. Second, the presence of an external buildup of ice or condensing liquid can also suppress the vibrations. The data in reference [1] provide an upper-limit prediction of vibration amplitudes, and the phenomena described herein are vibration, suppression mechanisms.

From the standpoint of a designer or test engineer, it is important that these possible suppression mechanisms be recognized so that the worst-case condition is examined in any design or test activity. The case history reported in reference [3] is dramatic evidence of the importance of recognizing these suppression mechanisms.

The results and conclusions reported herein are based on a large volume of experimental data and observations obtained in the present test program. However, testing did not include condensation heat transfer or supercritical flow conditions. While the present test data provide valuable information in an area where data are limited, additional effort is needed to more fully understand all aspects of bellows flow response with both sub- and supercritical internal cryogenic flows undergoing different forms of heating and damping. Present results which relate bellows flow response to heat transfer rates, external liquid damping and the internal cryogenic state properties should prove valid, regardless of the mechanism responsible for heat flow. Additional experimental data should substantiate this conclusion.

References

1 Gerlach, C. R., and Schroeder, E. C., "Study of Minimum Pressure Loss in High Velocity Duct Systems," Interim Technical Report No. 1, Contract NAS8-21133, Southwest Research Institute, July 1969.

2 Gerlach, C. R., "Flow-Induced Vibrations of Metal Bellows," JOURNAL OF ENGINEERING FOR INDUSTRY, TRANS. ASME, Series B, Vol. 91, No. 4, Nov. 1969, pp. 1196–1202.

3 Daniels, C. M., and Fargo, C. G., "Fatigue Failure in Metal Bellows Due to Flow-Induced Vibrations," Technical Support Package (TSP 69-10071) for NASA Technical Brief 69-10071.

4 Gerlach, C. R., Bass, R. L., Holster, J. L., and Schroeder, E. C., "Flow-Induced Vibrations of Bellows with Internal Cryogenic Fluid Flows," Interim Technical Report No. 2, Contract NAS8-21133, Southwest Research Institute, Aug. 1970.

5 Nunner, W., "Warmenbergang und Druckabfall in Rauhen Rohren," VDI-Forschungsheft, 1956, p. 455.

END OF REFERENCE

128

REFERENCE

129

SACK, L. E.: ANALYSIS OF FLOW-INDUCED VIBRATION ASSOCIATED WITH BELLOWS CONVOLUTIONS. ROCKETDYNE, NORTH AMER. ROCKWELL, IL8112-3175, DEC. 1968.

THIS MATERIAL HAS BEEN APPROVED FOR PUBLICATION PER LETTER FROM L. E. SACK TO JOANNE FOLK DATED AUG. 29, 1974.

INTERNAL LETTER

NORTH AMERICAN ROCKWELL CORPORATION
AEROSPACE AND SYSTEMS GROUP

I.L. 8112-3175

Date . 19 December 1968

TO . Those Listed
Address .

FROM . L. E. Sack
Address . D/596-112
AC-15

Phone . 3257

Subject . Analysis of Flow Induced Vibrations Associated with Bellows Convolutions

SUMMARY

An analysis was made of the dynamic response and fluid excitation required to characterize flex hose fatigue failures associated with single convolution modes of flow induced vibrations.

The essential dynamic consideration presented is that the response characteristics for the single convolution modes are the result of coupling between the structural dynamics of the convolutions and the dynamics of the fluid within the convolutions.

The excitation due to fluid flow within the flex line is described as being capable of exciting a band of response frequencies where the boundaries of the excitation frequencies are proportional to velocity. The lower frequency excitations are generally associated with vortex shedding within the turbulent boundary layer. The higher frequency, and potentially much stronger excitation, is associated with a convection frequency in the turbulent boundary layer. The convection frequency is defined as the characteristic frequency associated with the fluid velocity flowing past equally spaced wall irregularities, (the convolutions).

If a resonance can potentially exist, a discussion is presented on a technique of estimating the energy levels associated with the resonance; the energy available can then be translated to a stress level in the part. When the expected stress level is known, a quantitative evaluation can then be made to determine if the stress level exceeds the alternating stress the part is capable of withstanding without experiencing high cycle fatigue failure.

INTRODUCTION

The two flex line failures that occurred on the Apollo/Saturn 502 flight led to an extensive program of testing and analysis. The testing and analytical program was initiated in an attempt to understand why the particular flex line in question would experience repeated failure in flight after having accumulated an extensive history of successful ground level operation. The only obvious difference between ground level and flight operation was the ambient pressure; the 14 psi difference did not seem to be a reasonable explanation for the cause of failure in a metal flex line with approximately 1100 psi internal operating pressure.

In support of the total failure evaluation effort, a program of experimental testing and analysis was initiated. The objectives of the program were; (1) to gain an understanding of the flex line failure mode, (2) to provide insight necessary to interpret the test data obtained from flow testing, and (3) to determine if all

flex lines needed to be flow tested to prove their reliability.

DEFINITION OF THE SYSTEM

The flex lines that failed on the Apollo/Saturn 502 flight were nominal 0.5 inch internal diameter convoluted bellows innercore with an external restraint of braided wire as shown in Figure 1. The fluid flowing through the flex line was hydrogen at approximately 50 degrees R.(-410 degrees F.) and a nominal pressure of 1100 psia.

Initial component tests (following the flight failure) were at first unable to fail the flex line at flowrates thought to represent reasonable flight limits. These tests were performed with ground level air as the flex line environment. The inability to produce a flex line failure mode in ground level testing led to the speculation that the only reasonable difference, the air environment, was affording some means of "protecting" the flex line.

Tests were then made with the flex line sealed in a vacuum chamber, (typical external pressures were equivalent to less than 50 microns of mercury). When tested in a vacuum environment, the flex line would repeatedly fail at flowrates within the expected operating range. Accelerometers mounted on the ends of the flex line indicated high amplitude vibration would develop over discrete ranges of flowrate. The frequency of vibration was typically at approximately 20,000 Hz; 20KHz is a frequency typical of the nth accordian modes of the bellows or one of the single convolution modes of the bellows. The single convolution modes of bellows motion would seem reasonable for braided hoses because of the severe mechanical interference that exists between the braid and convolution crown. The mechanical interference would put extremely high damping on any modes of vibration that required motion of the crown.

Since the motion of concern was assumed to involve the single convolution modes, the flex hose could be analyzed by considering only a portion of the total flex line. As a practical compromise, a system as illustrated on Figure 2 was analyzed; this system must not only include the effects of the structural dynamics, but must also be capable of evaluating the dynamics of the fluid that is associated with the structure. The total response characteristics of the system were evaluated by analytically analyzing the combined system response of the component elements. The primary components considered were the structure and the fluid within the structure. The excitation characteristics of the fluid were determined by evaluating experimental and test data; the data were obtained from flow testing of actual flex lines and from water table testing of 2-dimensional models. The dual role played by the fluid in effecting both the response and the excitation is important to keep in mind as the individual elements of the system are discussed.

System Dynamic Response

The convolution structural dynamics are associated with the mechanical vibration of the convolutions that make up the flex line. For a braided flex line, the mechanical interference between the convolution crowns and the braid results in restricting the relative motion of the crowns. With the convolution crown motion restricted, the fundamental vibration characteristics of the bellows can be adequately approximated

by the vibration characteristics of a single convolution or a differential equation as illustrated in Fig. 3.

The forcing function to the mechanical motion results from convolution root drag (as a result of the boundary layer disturbance), and any pressure oscillation that may exist in the convolution cavity (Fig. 3).

The points to keep in mind concerning the mechanical vibration are that:

1. The structural dynamics can be characterized by an equivalent mechanical spring-mass system, and thus have a resonant frequency, and

2. That the mechanical motion can be influenced by the fluid trapped in the convolution spaces.

The convolution fluid dynamics are associated with flow in and out of the space between the bellows convolutions as well as pressure oscillations within the convolution. For the high frequency fluid dynamics of interest, the effective compressibility in the cavity is important. The effective compressibility of the cavity results from a combination of the fluid compressibility and the elasticity of the cavity walls. The effective mass of the fluid is characterized by the inertance of the fluid flow as the fluid is accelerated in and out of the convolution cavity. When the walls of the cavity are fixed, the fluid dynamics are characterized by the classical Helmholtz resonant cavity. The expressions relating fluid flow, pressure, compressibility, and mass are presented in Fig. 4. When the walls of the cavity are allowed to move, the influence of the rate of change in cavity volume can be expressed by including wall motion in the expression that relates a change in cavity pressure to flowrate into and out of the cavity (see the first equation in Fig. 4).

The points to keep in mind concerning the convolution fluid dynamics are that:

1. The fluid can be characterized by an equivalent spring mass system and thus has a resonant frequency.

2. Thst the fluid dynamic behavior can be influenced by motion of the structural system.

Now after some discussion of the fluid and structural elements, the combined fluid-structural system can be examined.

The dynamic system, made up of a combination of the convolution structural dynamics and the convolution fluid dynamics, can be represented by an equivalent spring mass analogy. The analogy, as presented in Fig. 5, illustrates how the fluid spring-mass elements are related to the structural spring-mass system. The resulting two-degree of freedom fluid-structural system indicates how the response of the total system can be influenced by elements of the system or by changes in these elements. A characteristic of a two-degree of freedom system, as illustrated, is that the observed system resonant frequencies are not the same as the frequencies characteristic of the resonant systems analyzed individually.

The fluid-structural response frequencies associated with the combined system are the resonant frequencies of concern with respect to a fluid flow excitation. Once the

resonant response frequencies have been computed, the next step is to compute the excitation frequencies expected.

System Excitation

The excitation frequencies are a result of boundary layer disturbance. The type of boundary layer disturbance is not fully understood, but present evidence indicates that at least two types of boundary layer disturbances can be expected.

Work by Dr. Gerlach, at Southwest Research Institute, has indicated the importance of vortex shedding to the excitation of bellows vibrations (Ref. 1). The vortex shedding frequency will fall in a frequency range characterized by Strouhal Numbers in the range of 0.1 to 0.5. The vortex shedding frequency, f_e can be related to the Strouhal Number N_S, by the fluid velocity v, and some characteristic dimension of the convolution geometry, σ_l, thus

$$f_E = \frac{N_s V}{\sigma_l}$$

From Dr. Gerlach's range of $N_S = 0.1$ to 0.5, and his suggestion of using d_1 as illustrated on Fig. 6 for σ_l, the vortex shedding frequency range becomes

$$f_E = \frac{0.1\ V}{d_1} \text{ to } \frac{0.5\ V}{d_1}$$

Work at Rocketdyne, that includes testing and analysis of a large number of braided flex hoses and testing of a model in a two-dimensional water table, has resulted in establishing that an excitation frequency exists in addition to the ones associated with vortex shedding. The frequency relationship established by the Rocketdyne effort, and will be referred to as the convection frequency, can be characterized by an oscillation wave length that is twice the convolution pitch distance. The convection frequency has consistently resulted in exciting higher vibration levels in braided flex lines than have the vortex shedding frequencies. Definitions of the pitch distance, d_2, as well as the convolution dimension, d_1, are given in Fig. 6. With the oscillation wave length equal to twice the pitch distance, the excitation frequency becomes:

$$f_E = \frac{V}{2\ d_2}$$

(where: v = stream velocity

d_2 = bellows pitch distance)

The observed frequency results from the rate at which the wave length that corresponds to the distance between 2 convolutions is "convected" or moved past a convolution root; the frequency is thus a function of the stream velocity, v. An equally likely convection frequency would be associated with a wave length equal to the distance between convolutions, but the only system response likely would be "in phase" flow in and out of adjacent cavities. In phase flow of all cavities is unlikely from continuity considerations, therefore this mode is believed to be non-existent.

In addition to the possible excitation frequency defined above, the fluid-structural response frequencies have been found to be potentially excited at twice the excitation

frequency. The "double frequency" response results from the non-linearities associated with the drag force being a function of velocity squared (Fig. 6). Thus, to include the possibility of "double frequency" response to the convection frequency excitation, the effective excitation frequency range must be extended to $f_E = 2.0 \left(\frac{V}{2d_2}\right)$. To be consistent with the potential excitation frequencies associated with both the vortex shedding frequency and fluid "convection" frequency, the excitation frequency limits are assumed to be:

$$f_E = \frac{0.1V}{d_1} \qquad \text{to} \qquad f_E = 2.0 \left(\frac{V}{2d_2}\right)$$

A convenient method of determining the existence of a potential resonance is through use of an "interference chart". Typical "interference charts" are illustrated in Fig. 7. These charts are constructed by plotting the response and excitation frequency limits on a grid of frequency vs fluid velocity. If both the response and excitation frequencies interfere with the operating velocity range, a potential resonance is defined to exist.

The existence of a resonance does not automatically mean that the flex line will fail when "on resonance". The part will fail only if the endurance limit of the material is exceeded for the number of cycles accumulated. Therefore, to evaluate if a flex line can potentially fail when a flow induced resonance is experienced, the fatigue failure potential must be determined.

Endurance Limit Analysis

The endurance limit analysis compares the maximum alternating stress expected by a flex line to the endurance limit of the flex line material. The technique of computing the maximum alternating stress must assume that the maximum load conditions exist. As an initial step, an alternating fluid velocity is assumed to exist; the velocity assumed has a maximum dynamic velocity that is twice the mean fluid velocity (Fig. 8). The load due to dynamic or an alternating velocity is computed. The computed load, resulting from drag force and pressure oscillations, is a function of (1) the convolution geometry, (2) the fluid density, and (3) the fluid velocity. Next, the stress per unit load is computed. The stress per unit load is a function only of the convolution geometry.

The above computations are of a static nature and do not account for any dynamic gain. When a resonant system is operated "on resonance", the system damping plays a role in defining the maximum potential amplitude. Unless otherwise specified, a dynamic gain of 100 (corresponding to a damping ratio of 0.005) was assumed for computations made at Rocketdyne.

The maximum alternating stress, if on resonance, is computed as:

$$\sigma = (\text{Force}) \times (\text{Stress/Unit Force}) \times 100$$

The resulting stress is then compared to a "design value" of material endurance limit. The design value being used is a value that is 50 percent of the average high cycle

fatigue failure value for the material and the temperature of concern. If the computed stress is less than the design endurance limit stress, the flex line is considered to be satisfactory even though a resonance may exist.

There is some indication from experimental data that the dynamic gain term for single ply bellows could be as high as 200; for multiple ply bellows the dynamic gain could be in the range of 30 - 50. More data need to be obtained before definite dynamic gain terms can be stated.

Explanation of Flex Line Failure on Apollo Saturn 502

The anomaly of the flex line that would fail in a vacuum environment, but would not fail in an environment of ground level air, can now be explained. As was subsequently determined, a major difference between ground level and altitude operation was that with a normal ground level environment, liquid air would condense on the exterior surface of the flex line. The hydrogen flowing within the flex line was at a temperature of -410 degrees F and is a temperature well below that required to condense nitrogen or oxygen out of the air.

Water table testing of a flex line cross-sectional model indicated that very little circulation existed between the fluid within the convolutions and the main stream fluid. In the presence of heat transfer the "trapped" fluid within the convolutions would stabilize at a fluid state different than when no heat transfer existed, (as in a vacuum). The change in hydrogen fluid properties due to the difference in heat transfer was shown analytically to result in a change in the convolutions fluid-structural response dynamics. The resulting vibration response was significantly more severe when no heat transfer (associated with condensing air) was present; thus the condensing air resulted in "protecting" the flex line in air testing. The difference in flex line response amplitude could be simulated even though the boundary layer excitation phenomena were the same for both air and vacuum testing. The frequency of the excitation phenomena correlated exactly with the "double " frequency response of the coupled fluid-structural system to the convection frequency.

For the particular flex line involved in the Apollo/Saturn 502 failure, the environment of air in ground level development testing had afforded a means of "protecting" the flex hose by reducing the response amplitude. For flex lines in general, a clarification should be made. Flex line vibration response can be effected by external influences such as condensation or heat transfer, but the resulting changes in observed vibration response amplitude may have different trends for different flex lines. Since the change in response amplitude is the result of a change in the dynamic "tuning" of the flex line, the change in response could either increase or decrease when the external influence (such as heat transfer,) becomes significant.

CONCLUSIONS

The analysis performed was accomplished by; (1) formulating and mechanizing an analog computer model of the fluid-structural dynamics associated with a bellows convolution, and by (2) analyzing experimental data obtained from controlled testing of braided flex hoses. The analysis resulted in verifying that the failures were due to resonant response characteristics of the bellows convolutions being excited by a boundary layer disturbance that had frequency content proportional to the fluid velocity.

The resonant response characteristics were found to be a function of both the structural dynamics associated with the convolutions themselves, and the fluid dynamics associated with the fluid "trapped" in the spaces between the convolutions (Figure 2). The excitation, or energy input, results from the unstable fluid boundary layer that is established as a function of the convolution geometry and the fluid velocity. Thus, as illustrated in Figure 2, the fluid in the bellows plays a role in defining both the response characteristics of the fluid-structural system, and in defining the excitation occurring as a result of the boundary layer phenomenon.

J. Thompson JT
G. K. Cooper GKC

L. Sack
Dynamic Analysis Unit

LS:vc
Encl:
Figures (8)

REFERENCES:
Gerlach, C.R., "Flow Induced Vibration of Bellows" etc.

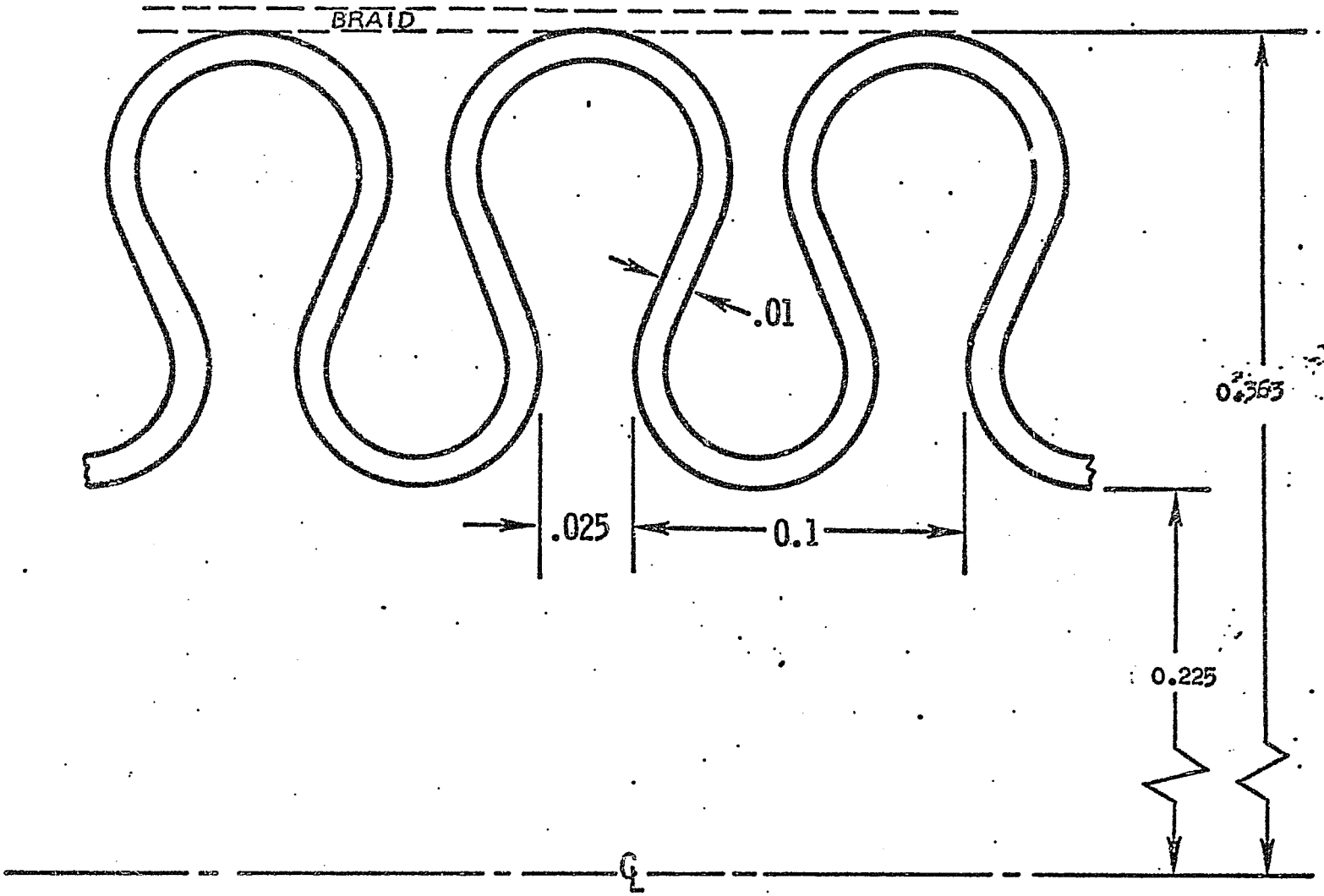

FIGURE 1. TYPICAL GEOMETRY OF A FLEXIBLE BELLOWS INNERCORE

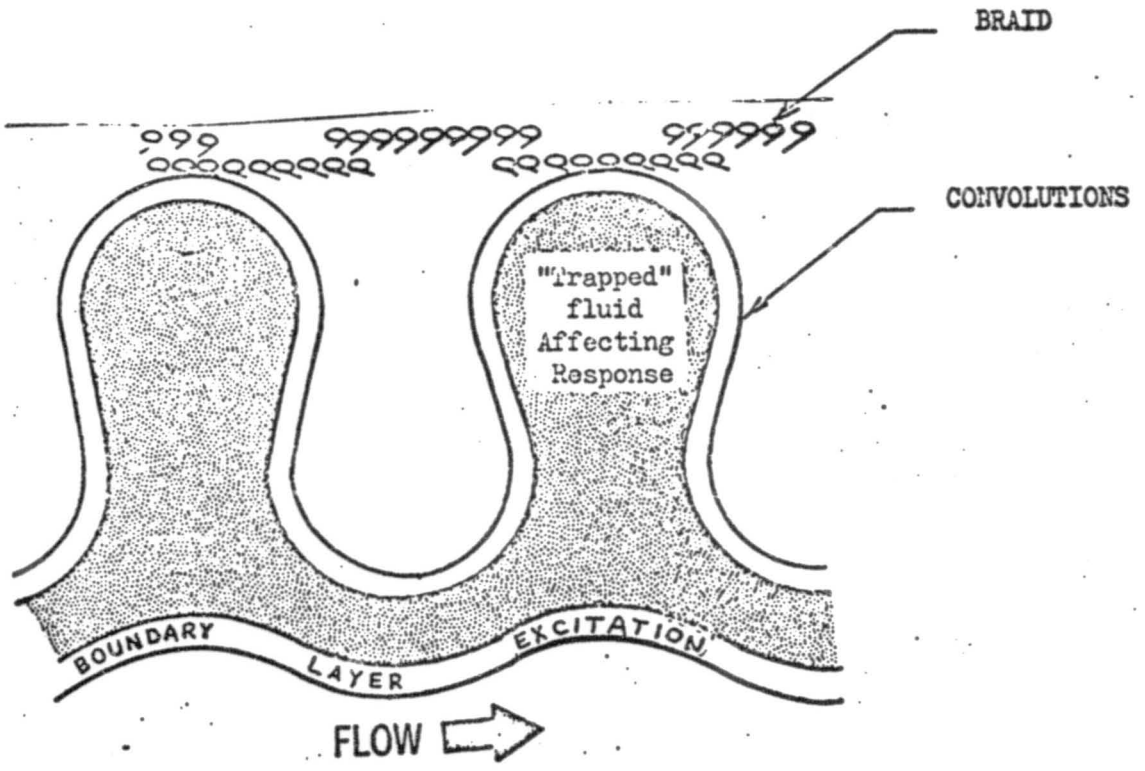

FIGURE 2. SCHEMATIC OF SYSTEM THAT IS BEING ANALYZED

CONVOLUTION STRUCTURAL MOTION

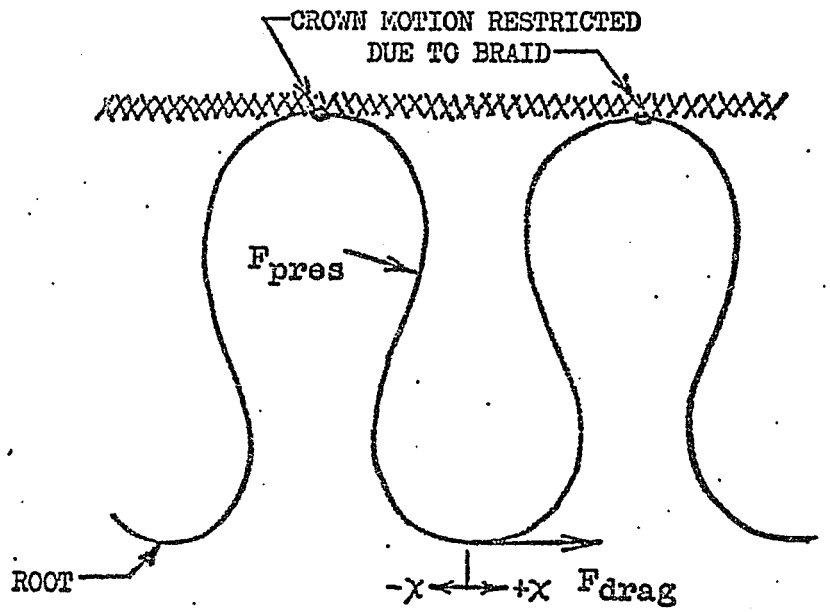

- Equation of motion for single convolution

$$\frac{d^2X}{dt^2} + A_1\frac{dX}{dt} + A_2X = F_{drag} + F_{pres}$$

- Where

  $F_{drag} \propto \rho v^2$

  A_1 is a damping coefficient

  A_2 is a function of structural natural frequency

FIGURE 3. ILLUSTRATION OF CONVOLUTION STRUCTURAL MOTION

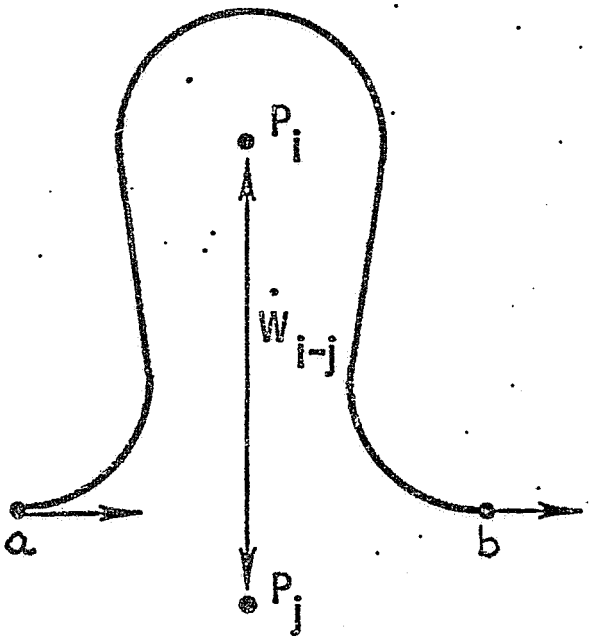

$$\frac{dP_i}{dt} = \frac{\beta}{\bar{W}_i}\left[\dot{W}_{i-j} + C_1\left(\frac{dX_a}{dt} - \frac{dX_b}{dt}\right)\right]$$

$$\frac{d\dot{W}_{i-j}}{dt} = \frac{Ag}{\ell}\left[P_j - P_i - R\dot{W}_{i-j}\right]$$

$$f_H = \frac{1}{2\pi}\sqrt{\frac{Ag\beta}{\ell \bar{W}}} \quad \text{(REF.)}$$

WHERE

P_i = PRESSURE AT NODE i, LB/IN^2

$\dot{W}_{i-j}$ = FLOWRATE BETWEEN NODES i & j, LB/SEC

f_H = RESONANT FREQUENCY OF FLUID IN CAVITY, HZ

β = EFFECTIVE BULK MODULUS AT NODE i, LB/IN^2

$\bar{W}$ = AVERAGE WEIGHT OF FLUID AT NODE i LB

$X_{a,b}$ = CONVOLUTION ROOT DISPLACEMENT, IN

C_1 = CONSTANT RELATING WALL MOTION & FLUID DISPLACED

A = EFFECTIVE FLOW AREA IN AND OUT OF CONVOLUTION

ℓ = EFFECTIVE LENGTH OF CAVITY

R = FLUID DAMPING TERM

FIGURE 4. SCHEMATIC AND RELATED EQUATION FOR CONVOLUTION FLUID DYNAMICS

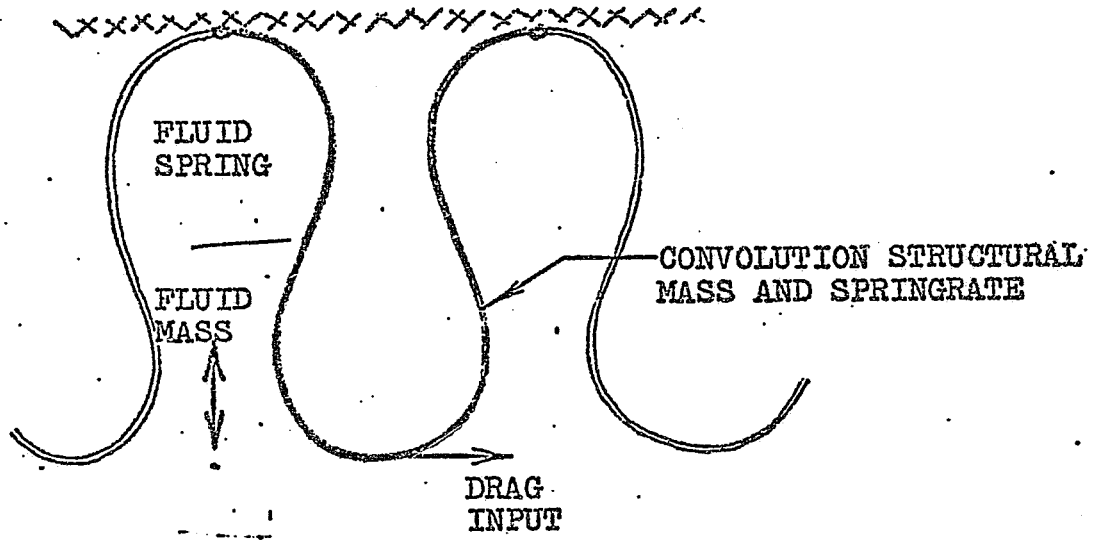

(a) SYSTEM SCHEMATIC

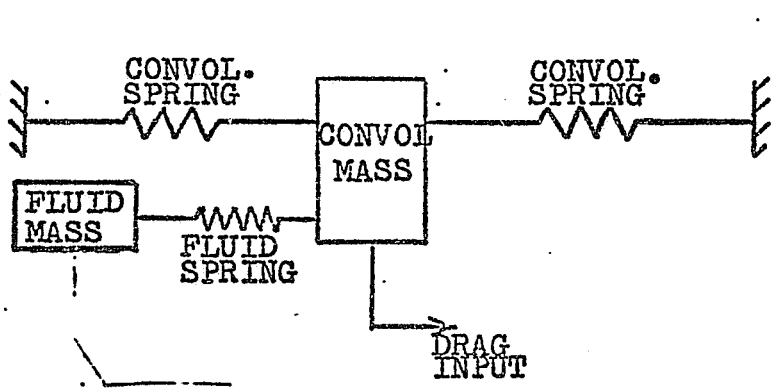

(b) SYSTEM ANALOGY

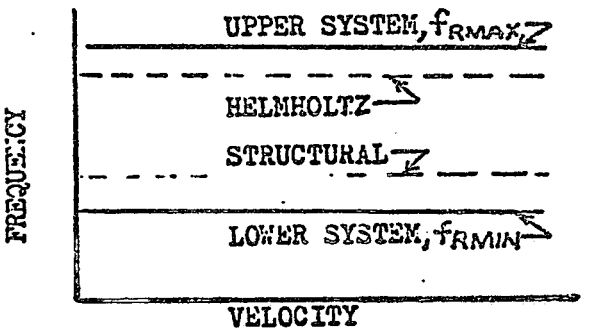

(c) FREQUENCY RELATIONSHIPS

FIGURE 5. SCHEMATIC AND MECHANICAL ANALOGY OF COMBINED FLUID-STRUCTURAL SYSTEM

- FREQUENCY RANGE ASSOCIATED WITH VORTEX SHEDDING

$$f_E = \frac{0.1\ v}{d_1} \longrightarrow \frac{0.5\ v}{d_1}$$

- ROCKETDYNE TEST EXPERIENCE HAS DEMONSTRATED CONVECTION FREQUENCY EXCITATION IS LIKELY AT

$$f_E = \frac{v}{2d_2}$$

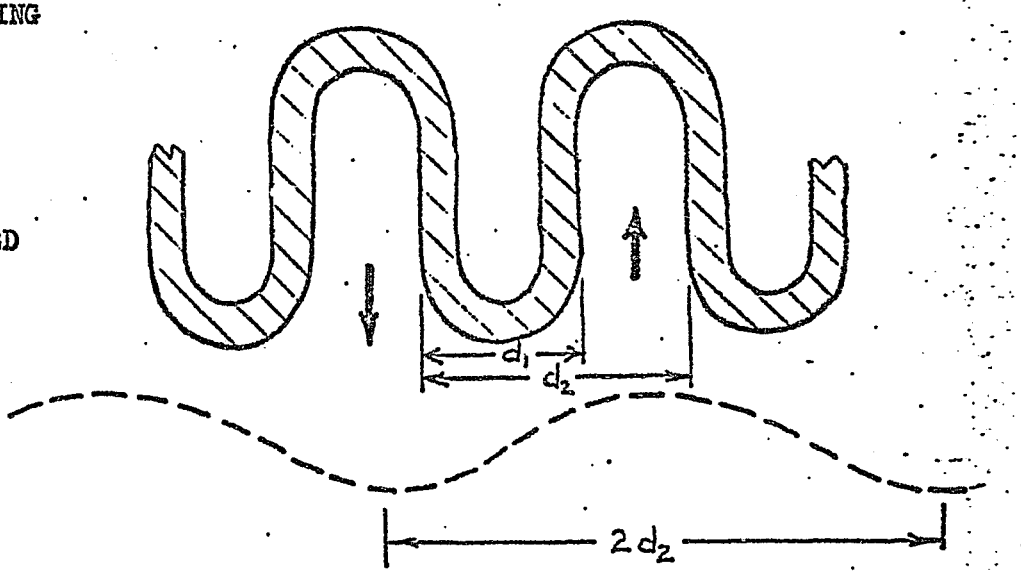

- ROCKETDYNE TEST EXPERIENCE AND ANALYSIS INDICATES POTENTIAL RESPONSE AT TWICE EXCITATION FREQUENCY DOUBLE FREQUENCY RESPONSE CAN BE ILLUSTRATED BY RELATING DRAG FORCE TO THE SQUARED VELOCITY OSCILLATION

$$v \propto \sin wt$$

$$\text{Drag Force} \propto v^2 \propto \sin^2 wt \propto \cos 2wt$$

- THEREFORE, LIMITS USED ARE

$$f_E = \frac{0.1\ v}{d_1} \longrightarrow 2\left(\frac{v}{2d_2}\right)$$

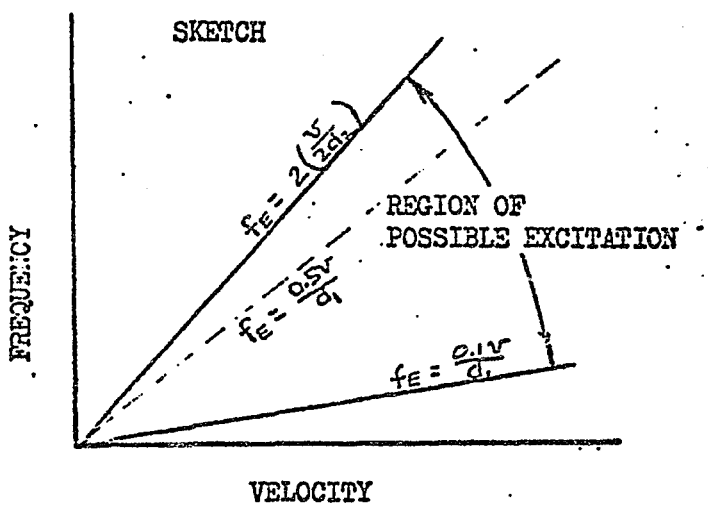

FIGURE 6. DEVELOPMENT OF EXCITATION FREQUENCY SPECIFICATION

- POTENTIAL RESONANCE CAN BE EVALUATED BY COMPARING THE FOLLOWING
  - OPERATING RANGE OF VELOCITIES
  - RESPONSE FREQUENCIES OF FLUID-STRUCTURAL SYSTEM
  - EXCITATION FREQUENCIES AS A FUNCTION OF VELOCITY

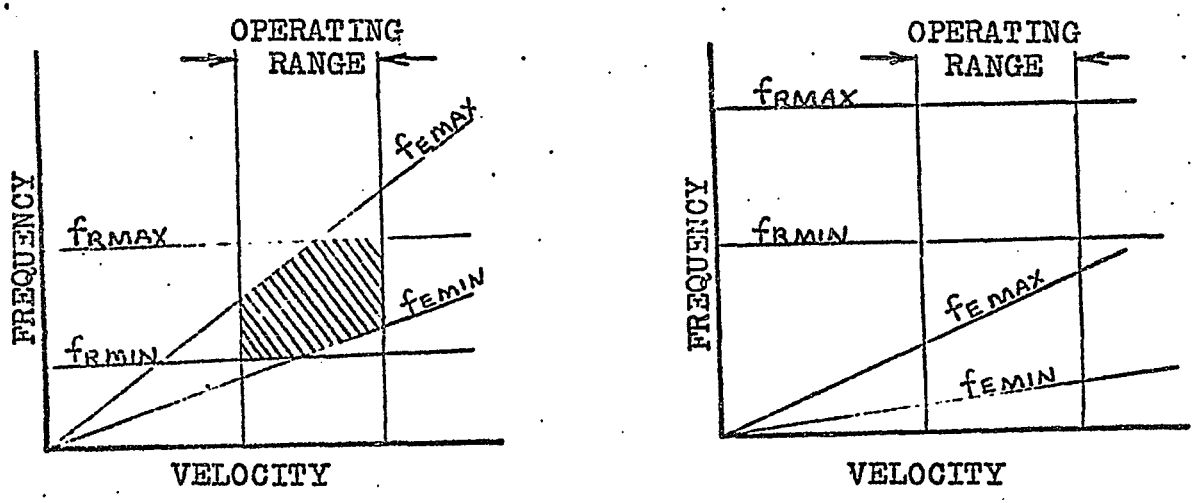

LINE HAS POTENTIAL RESONANCE

NO RESONANCE POSSIBLE

FIGURE 7. ILLUSTRATION OF FREQUENCY INTERFERENCE CHARTS

- EVALUATE FATIGUE FAILURE POTENTIAL IF RESONANCE CONDITION IS POTENTIAL
  - ASSUME EXCITATION

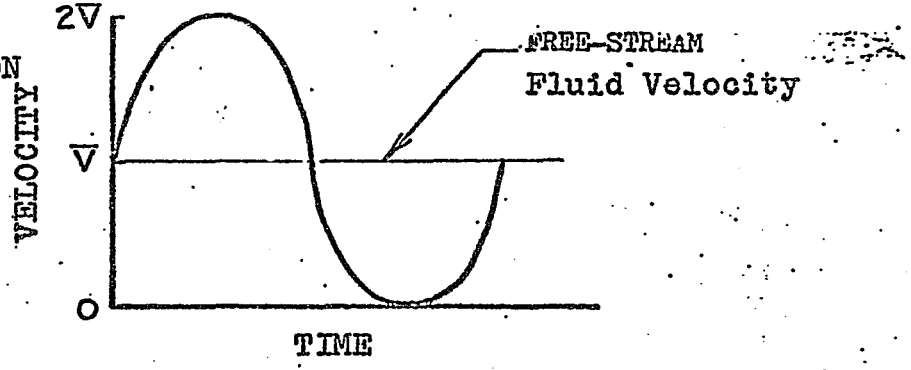

  - COMPUTE STATIC FORCE, $F = f(\text{geometry, fluid, } \bar{V})$
  - COMPUTE STRESS PER UNIT FORCE, $\sigma/F_1 = f(\text{geometry})$
  - DEFINE DYNAMIC GAIN FOR OPERATING "ON RESONANCE"

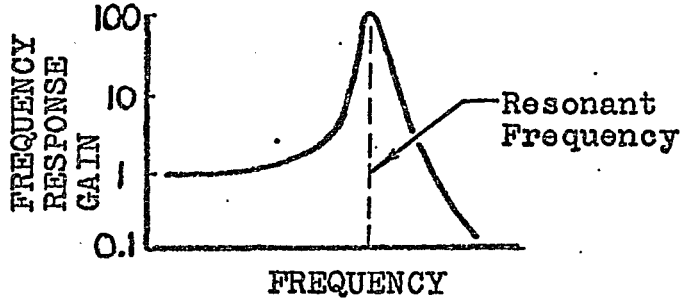

  - COMPUTE MAXIMUM EXPECTED STRESS IF "ON RESONANCE," $\sigma = F \times \sigma/F_1 \times 100$
  - COMPARE COMPUTED STRESS TO "DESIGN VALUE" OF MATERIAL ENDURANCE LIMIT

FIGURE 8. SUMMARY OF STEPS REQUIRED FOR THE ENDURANCE LIMIT ANALYSIS

END OF REFERENCE

129

REFERENCE

130

F-1 FLEXIBLE LINE FLOW-INDUCED VIBRATION VERIFICATION PROGRAM. R-7897, ROCKETDYNE, NORTH AMER. ROCKWELL, JULY 1969.

THIS MATERIAL HAS BEEN APPROVED FOR PUBLICATION PER LETTER FROM GUY B. JACKSON, NASA GEORGE C. MARSHALL SPACE FLIGHT CENTER TO JOANNE FOLK DATED AUG. 27, 1974.

FILE COPY

Rocketdyne
North American Rockwell

6633 Canoga Avenue,
Canoga Park, California 91304

R-7897

F-1 FLEXIBLE LINE FLOW-INDUCED VIBRATION VERIFICATION PROGRAM FINAL REPORT

NAS8-18734
G.O. 09143

PREPARED BY

Rocketdyne Engineering
Canoga Park, California

APPROVED BY

J. R. Hale
F-1 Senior Project Engineer

NO. OF PAGES 50 & viii REVISIONS DATE 10 July 1969

DATE	REV. BY	PAGES AFFECTED	REMARKS

FORM R13-G REV. 5-59

INTRODUCTION

At the direction of NASA, an analysis was conducted on all F-1 engine flexible lines to determine their susceptibility to flow-induced vibration fatigue failures in the convoluted bellows sections. This report summarizes the results of the analysis and subsequent test programs conducted.

SUMMARY

All flexible lines on the F-1 engine were categorized according to operating environment and failure criticality, i.e., (I) risk to astronaut, (II) risk to vehicle, (III) delay in launch, and (IV) noncritical. Those lines identified in categories I and II which had operating environments that possibly could produce flow vibrations (as mutually agreed upon by NASA and Rocketdyne) were flow tested. These lines were flow tested to either 10 percent beyond the 3-sigma minimum and maximum engine operating range or to model specification requirements, whichever was greater. Of the 41 different flexible lines on the F-1 engine 10 lines were selected for flow test. All flow tested lines satisfactorily completed the tests. The results of the program led to the conclusion that no evidence of detrimental flow-induced bellows oscillations exists for F-1 engine flexible lines on Vehicle 503 and subsequent.

CONCLUSIONS AND RECOMMENDATIONS

1. No detrimental flow-induced bellows oscillations exist in any of the flexible lines on Vehicle 503 and subsequent.
2. The design analysis described in Appendix C should be used in the design analysis of all new F-1 engine flexible lines to ensure that they are not susceptible to flow-induced fatigue failures.

APPENDIX B, SUPPLEMENT A

HEAT EXCHANGER GASEOUS OXYGEN OUTLET AND HELIUM OUTLET LINES, FLOW ANALYSIS RELATIVE TO FLOW-INDUCED BELLOWS VIBRATION

BASIC VELOCITY CHARACTERISTICS

Average velocity across the bellows inside diameter is of prime consideration, relating directly to flow-induced vibration excitation frequency. (See Appendix C for an analysis of flow-induced resonant vibration.) In systems having a liquid flow medium, the flowrate relates proportionally to velocity; therefore, the flowrate is an adequate parameter to control during resonance dwell tests. On the other hand, in a gas system which includes a heat exchanger that, due to flowrate changes and carbon accumulation, continually changes the amount of heat added to the gas, velocity cannot be considered directly proportional to the mass flowrate.

$$v = \frac{\dot{w}}{\rho A}$$

where

- v = velocity
- $\dot{w}$ = weight flowrate
- ρ = density
- A = area

density is:

$$\rho = (f)\ P, T$$

where

- P = pressure
- T = temperature

If the heat input to the heat exchanger and the flowrate are held constant, outlet gas temperature continually decreases with time due to carbon fouling of the heat exchanger coils. The resultant increase in outlet density causes a decreasing velocity vs accumulated time on the heat exchanger. If a point of flow-induced vibration is experienced at a particular flowrate it would not, therefore, be expected to exist at that same flowrate with increasing test time.

It can be seen that if flow-induced vibration occurs at a flowrate near the high end of the flowrate range when a new or clean coil heat exchanger is used, the resonant condition would not be maintained as heat exchanger test time was accumulated if the prescribed flowrate range was held constant.

Another point of consideration is the rate of flowrate increase. If a rapid rate of flowrate increase occurs, the outlet velocity increases significantly for a short period of time. The relatively warm outlet gas, caused by the initial low flowrate, is accelerated until the cooler gas, caused by the higher gas flowrate, displaces it and approaches a new steady-state condition. This temperature lag temporarily causes a higher-than-normal outlet gas velocity during flowrate increasing transient periods, making rate of flowrate change an important consideration in searching for flow-induced vibration. It was, therefore, concluded that the vehicle flight conditions should be simulated during the flow tests.

HEAT EXCHANGER OUTLINE VELOCITY CHARACTERISTICS AT STAGE INTERFACE

Vehicle flight data showed an increasing gaseous oxygen mass flowrate during flight; however, volumetric flowrate was calculated for flight and found to be approximately constant. (Figure 3 shows a 17-percent increase in $\dot{V}$ with a 57-percent increase in $\dot{w}$.) This means that the gaseous oxygen bellows velocity on a vehicle is approximately constant during flight even though $\dot{w}$ is increasing.

$$\dot{V} = \frac{\dot{w}}{\rho} = vA \qquad \dot{V} = \text{volumetric flowrate}$$

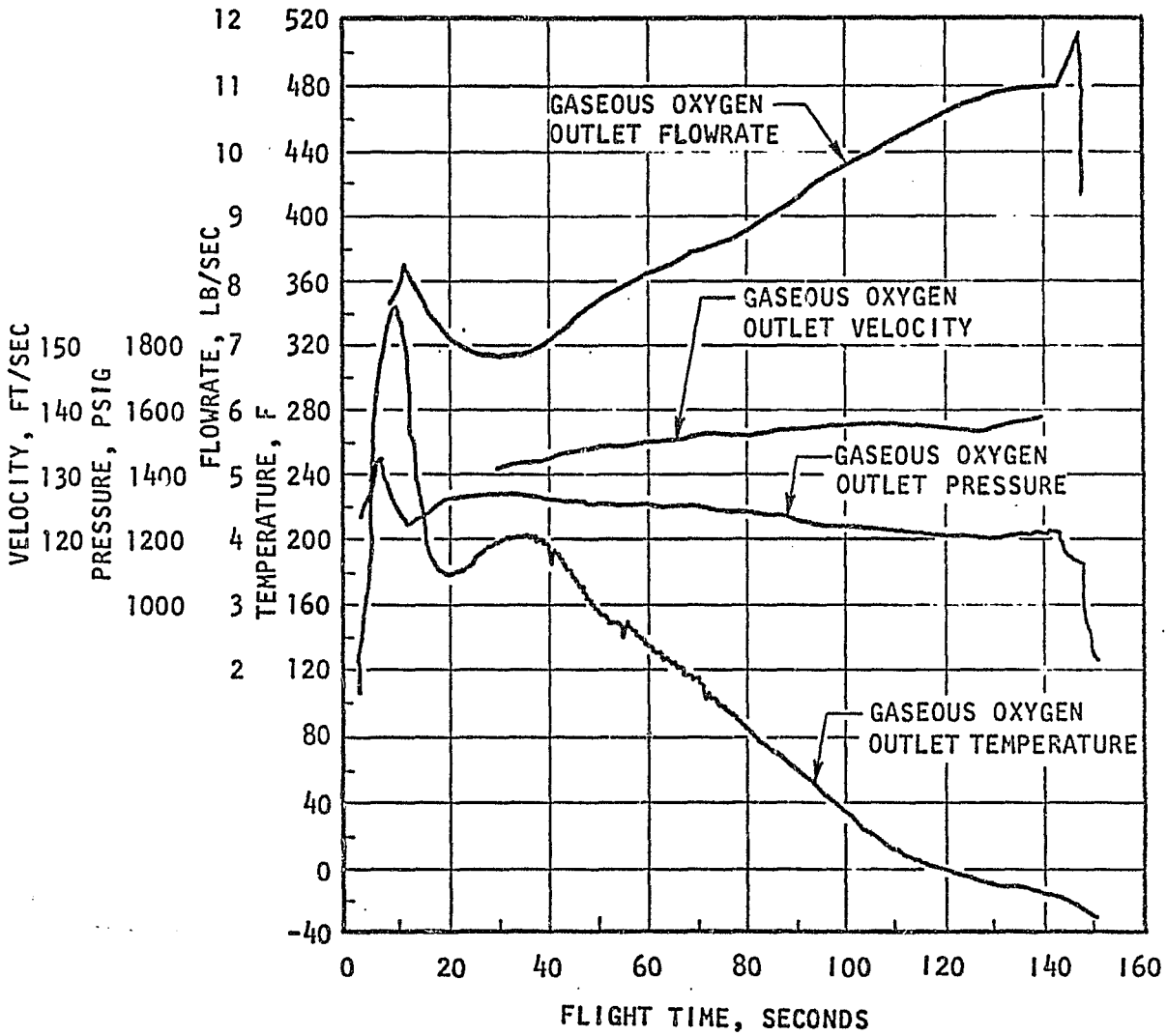

Figure 3. Gaseous Oxygen Outlet Line Characteristics

Assuming $\dot{V}$ to be a constant and A is a constant area, then velocity, v, must also be constant.

Relating this to heat exchanger operation, $\dot{w}$ must increase to maintain a constant velocity as heat exchanger time is accumulated.

Figure 3 shows actual flight data demonstrating this condition during Vehicle AS-502 flight on the gaseous oxygen pressurization system.

GASEOUS OXYGEN LINE BELLOWS FLOW ANALYSIS

The resonance search and dwell flow tests established the threshold of flow-induced vibration at approximately 215 ft/sec velocity, or 1.9 ft^3/sec volumetric flowrate. Figure 4 is a chart of response vs gaseous oxygen velocity. Maximum response occurred at about 235 ft/sec velocity or 2.07 ft^3/sec volumetric flowrate.

The maximum velocity was 142 ft/sec, and maximum volumetric flowrate in the line was 1.26 ft^3/sec for any one heat exchanger during steady-state flight conditions on Vehicle AS-502. Average total volumetric flowrate required for Vehicle AS-502 was 5.9 ft^3/sec, or 1.18 ft^3/sec from each heat exchanger. Differences in heat exchanger volumetric output, neglecting differences in system heat exchanger outlet pressure due to configuration, is caused by the difference in accumulated test time and resultant carbon fouling and carbon accumulation rate of the heat exchangers. If all new or carbon cleaned heat exchangers were used on a vehicle, they would tend to balance and produce an average of approximately 1.18 ft^3/sec volumetric flowrate for each heat exchanger.

If all the heat exchangers had heavily carbon fouled coils with approximately the same accumulated test time, a balanced condition would again exist and an output flowrate of approximately 1.18 ft^3/sec for each heat exchanger would prevail. The extreme flowrate condition would occur if

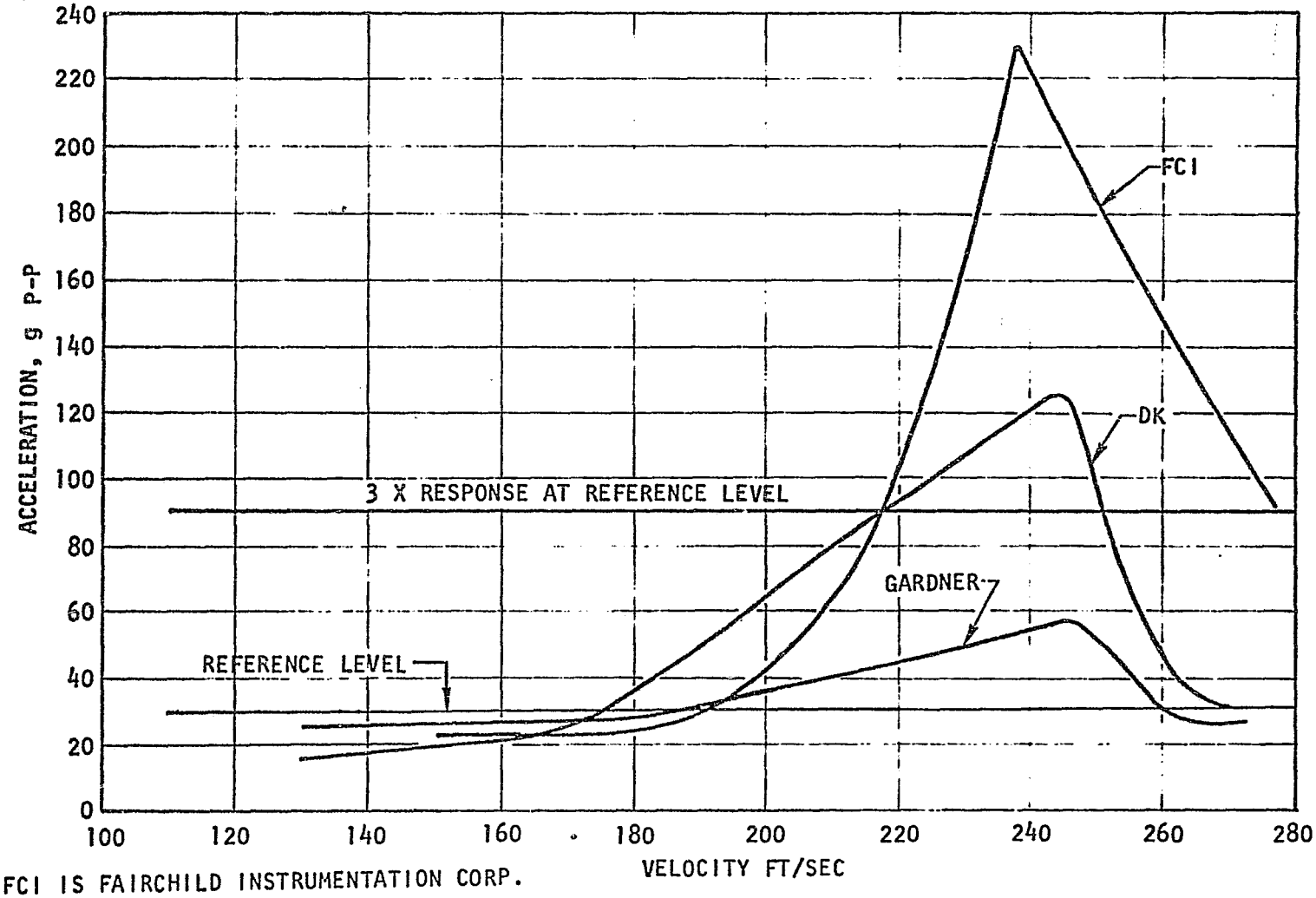

FCI IS FAIRCHILD INSTRUMENTATION CORP.
DK IS DK CORP.

Figure 4. Response vs Gaseous Oxygen Velocity

one new or clean coil heat exchanger were used along with four heavily carbon fouled heat exchangers. Heat exchanger outlet pressures must equalize, neglecting system differences, on all heat exchangers because they are all connected to a common stage manifold. The maximum heat exchanger pressure drop, which controls the flowrate, experienced on Vehicle AS-502 would produce a volumetric flowrate of 1.8 ft^3/sec and a gas velocity of 204 ft/sec in the outlet lines bellows of a new or carbon cleaned heat exchanger if only one new heat exchanger were used. This is on the threshold of flow-induced resonant vibration, but would not produce a significant response.

HELIUM OUTLET BELLOWS FLOW ANALYSIS

The resonance search and dwell flow tests established that flow-induced vibration could occur at gas velocities above 250 ft/sec in the helium outlet line bellows; however, the vibration acceleration amplitude in all cases was comparatively low, below 80 g P-P. This low acceleration amplitude confirms the analysis on the helium outlet bellows, which indicates low acceleration amplitude flow-induced vibration with gas velocities below 1000 ft/sec. A review of Vehicle AS-502 flight data shows velocities no greater than 850 ft/sec. These velocity data are approximated, however, since only total flowrate from all five heat exchangers was recorded. To obtain this flowrate the total flowrate was assumed to be evenly divided between the heat exchangers. Also, the outlet parameters, temperature and pressure, necessary to calculate velocity were recorded for only two heat exchangers.

The highest velocity recorded during the EFL flow test program was 650 ft/sec as compared to 850 ft/sec for Vehicle AS-502 even though the flowrate was in excess of 1.0 lb/sec as compared to 0.4 to 0.75 lb/sec in flight.

The reason for the velocity differences is the helium inlet pressure and resultant gas density used in the flow tests as compared to the flight values. The flow test pressures were controlled within the model specification limits, whereas the Vehicle AS-502 operated below these limits (Fig. 5).

Since the analysis technique developed and confirmed during the flow test program indicated that these lines were not susceptible to flow-induced vibration even at the higher velocities experienced in flight, it was concluded that additional flow tests were unnecessary.

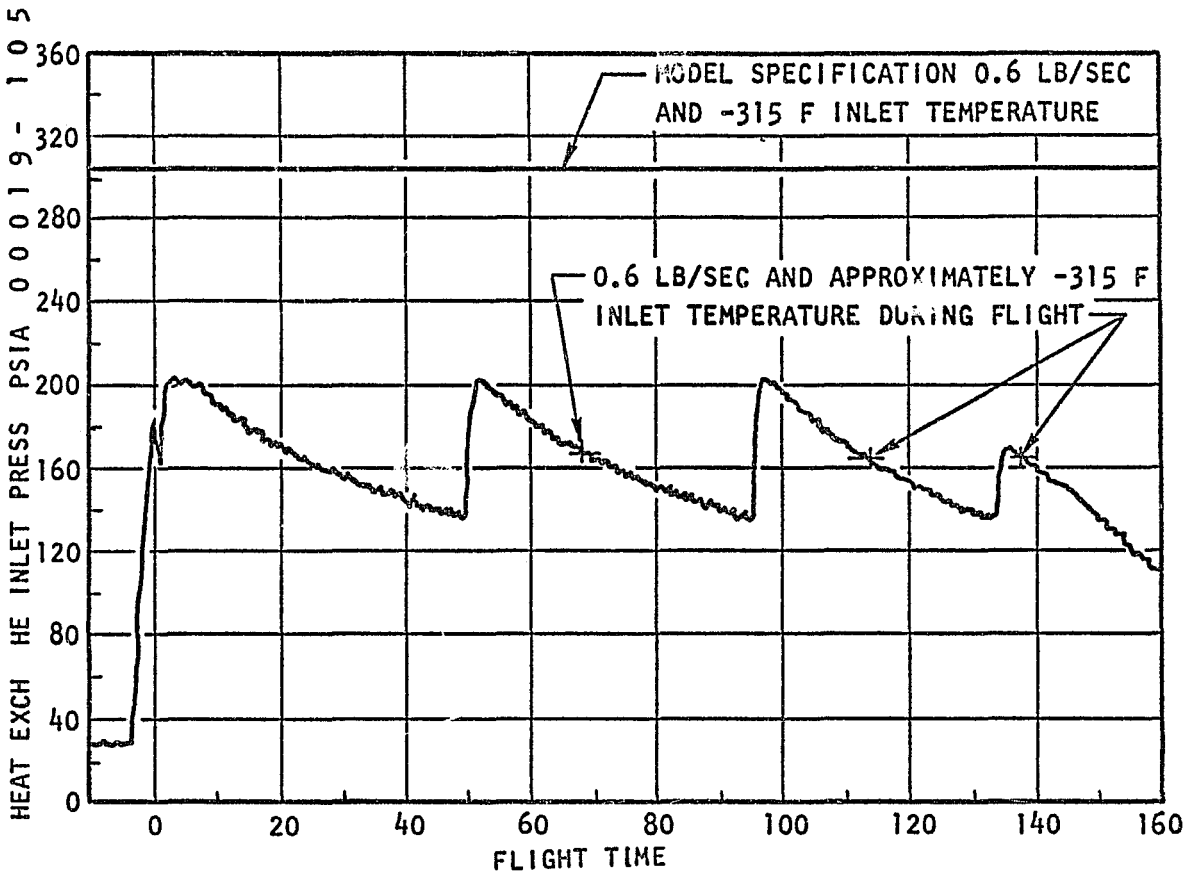

MODEL SPECIFICATION NOMINAL CALIBRATION REQUIREMENTS:

FLOW RATE	0.6 LB/SEC
INLET TEMPERATURE	-345 F
INLET PRESSURE	250 PSIA

MODEL SPECIFICATION REQUIREMENTS RELATED TO INLET TEMPERATURE OF -315 F WHICH IS THE APPROXIMATE CONDITION DURING FLIGHT AT 0.6 LB/SEC ARE:

FLOWRATE	0.6 LB/SEC
INLET TEMPERATURE	-315 F
INLET PRESSURE	305 PSIA

Figure 5. Helium Inlet Pressure vs Flight Time

APPENDIX C

ANALYSIS OF FLOW-INDUCED VIBRATIONS ASSOCIATED WITH BELLOWS CONVOLUTIONS

The objectives of the analysis were: (1) to gain an understanding of the flexible line failure mode, (2) to provide insight necessary to interpret the test data obtained from flow testing, and (3) to determine whether all flexible lines needed to be flow tested to prove their reliability.

This flow-induced vibration analysis presentation is not considered adequate to use for performing a complete analysis, and is presented here only to provide the reader with general knowledge of the methods used in analyzing the F-1 flexible lines. A complete, detailed report on flow-induced, vibration-fatigue, bellows failure analysis is being prepared and will be available before the end of 1969.

The analysis performed was accomplished by (1) formulating and mechanizing an analog computer model of the fluid-structural dynamics associated with a bellows convolution, and by (2) analyzing experimental data obtained from controlled testing of braided flexible hoses. The analysis resulted in verifying that the failures were due to resonant response characteristics of the bellows convolutions being excited by a boundary layer disturbance that had a frequency content proportional to the fluid velocity.

The resonant response characteristics were found to be a function of both the structural dynamics associated with the convolutions themselves, and the fluid dynamics associated with the fluid "trapped" in the spaces between the convolutions (Fig. 6). The excitation, or energy input, results from the unstable fluid boundary layer that is established as a function of the convolution geometry and the fluid velocity. Thus, as illustrated in Fig. 6, the fluid in the bellows plays a role in defining both the response characteristics of the fluid-structural system, and in defining the excitation occurring as a result of the boundary layer phenomenon. The dual role played by the fluid in effecting both the response and the excitation is important to keep in mind as the individual elements of the system are discussed.

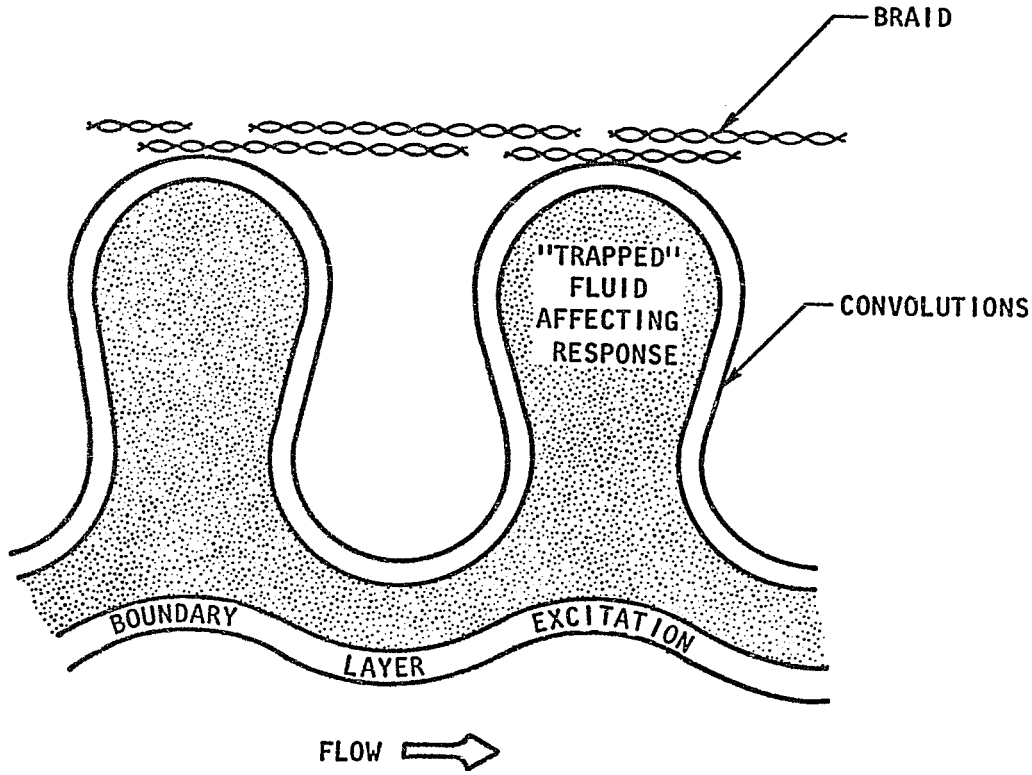

Figure 6. System Being Considered

SYSTEM DYNAMIC RESPONSE

Convolution Structural Dynamics

The convolution structural dynamics are associated with the mechanical vibration of the convolutions that make up the flexible line. For a braided flexible line, the mechanical interference between the convolution crowns and the braid results in restricting the relative motion of the convolution crowns.

With the convolution crown motion restricted, the fundamental vibration characteristics of the bellows can be adequately approximated by the vibration characteristics of a single convolution or a differential equation, as illustrated in Fig. 7).

The forcing function to the mechanical motion results from convolution root drag (as a result of the boundary layer disturbance), and any pressure oscillation that may exist in the convolution cavity (Fig. 7).

The points to keep in mind concerning the mechanical vibration are that:

1. The structural dynamics can be characterized by an equivalent mechanical spring-mass system, and thus have a resonant frequency.
2. The mechanical motion can be influenced by the fluid trapped in the convolution spaces.

Convolution Fluid Dynamics

The convolution fluid dynamics are associated with flow in and out of the space between the bellows convolutions as well as pressure oscillations within the convolution. For the high-frequency fluid dynamics of interest, the effective compressibility in the cavity is important. The effective

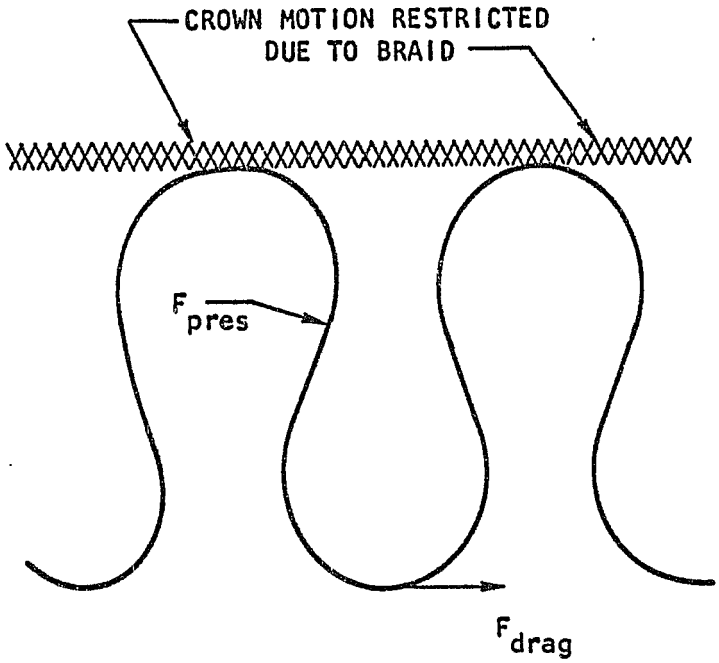

$$\frac{d^2X}{dt^2} + A_1 \frac{d\,X}{dt} + A_2X = B_1 \cdot F_{drag} + B_2 \cdot F_{pres}.$$

where:

$F_{drag} \propto \rho v^2$

X = convolution root displacement, inches

t = time

A_1 = damping coefficient

A_2 = frequency coefficient

B_1 = constant relating root drag to motion

F_{drag} = root drag

B_2 = constant relating convolution pressure to motion

F_{pres} = force due to convolution pressure differential

ρ = fluid density

v = fluid velocity

Figure 7. Convolution Structural Motion

compressibility of the cavity results from a combination of the fluid compressibility and the elasticity of the cavity walls. The effective mass of the fluid is characterized by the inertance of the fluid flow as the fluid is accelerated in and out of the convolution cavity. When the walls of the cavity are fixed, the fluid dynamics are characterized by the classical Helmhotz resonant cavity. The expressions relating fluid flow, pressure, compressibility, and mass are illustrated on Fig. 8 When the walls of the cavity are allowed to move, the influence of the rate of change in cavity volume can be expressed by including wall motion in the expression that relates a change in cavity pressure to flowrate into and out of the cavity (see the first equation on Fig. 8).

The points to keep in mind concerning the convolution fluid dynamics are that:

1. The fluid can be characterized by an equivalent spring-mass system and thus has a resonant frequency.
2. The fluid dynamic behavior can be influenced by motion of the structural system.

Now after some discussion of the fluid and structural elements, the combined fluid-structural system can be examined.

Dynamic System

The dynamic system, made up of a combination of the convolution structural dynamics and the convolution fluid dynamics, can be represented by an equivalent spring mass analogy. The analogy, as presented in Fig. 9, illustrates how the fluid spring-mass elements are related to the structural spring-mass system. The resulting two-degree of freedom fluid-structural system indicates how the response of the total system can be influenced by elements of the system or by changes in these elements. A characteristic of a two-degree of freedom system, as illustrated, is that the

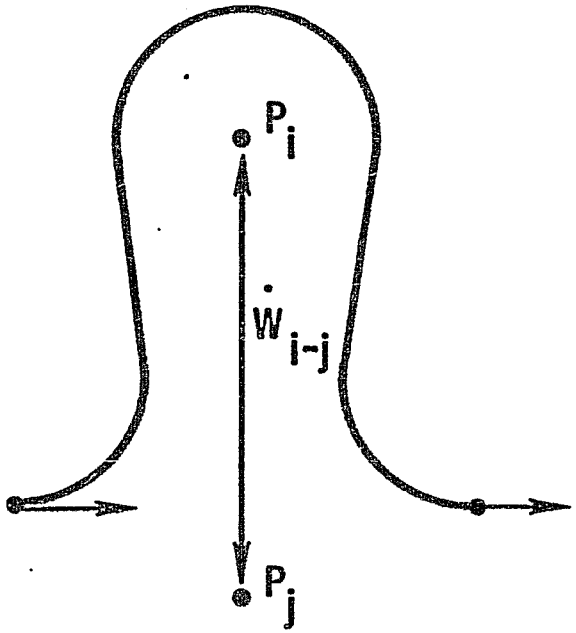

$$\frac{dP_i}{dt} = \frac{\beta_i}{\bar{W}_i}\left[\dot{W}_{i-j} + C_1\left(\frac{dX_A}{dt} - \frac{dX_B}{dt}\right)\right]$$

$$\frac{d\dot{W}_{i-j}}{dt} = \frac{Ag}{\ell}\left[P_j - P_i - R\,\dot{W}_{i-j}\right]$$

$$f_H = \frac{1}{2\pi}\sqrt{\frac{Ag\beta}{\ell\,\bar{W}}}$$

WHERE:

P_i = PRESSURE AT NODE i, LB/IN^2

$\dot{W}_{i-j}$ = FLOWRATE BETWEEN NODES i & j, LB/SEC

f_H = RESONANT FREQUENCY OF FLUID IN CAVITY, HZ

β_i = FLUID BULK MODULUS AT NODE i, LB/IN^2

$\bar{W}$ = AVERAGE WEIGHT OF FLUID AT NODE i, LB

$X_{A,B}$ = CONVOLUTION ROOT DISPLACEMENT, IN

C_1 = CONSTANT RELATING WALL MOTION & FLUID DISPLACED

A = EFFECTIVE FLOW AREA IN AND OUT OF CONVOLUTION

ℓ = EFFECTIVE LENGTH OF CAVITY

R = FLUID DAMPING TERM

Figure 8. Convolution Fluid Dynamics

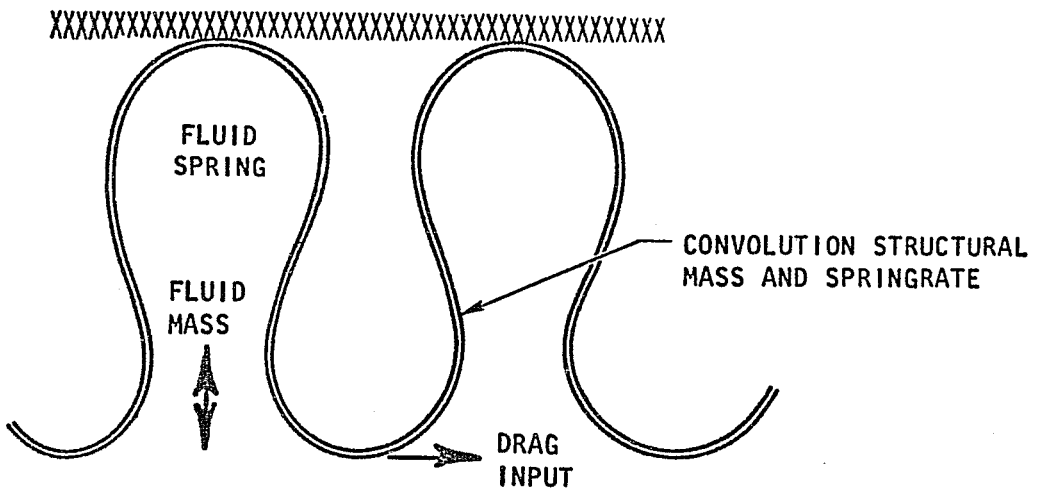

● SYSTEM SCHEMATIC

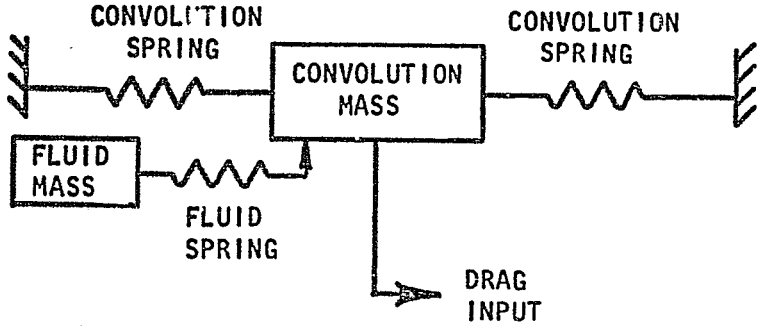

● SYSTEM ANALOGY

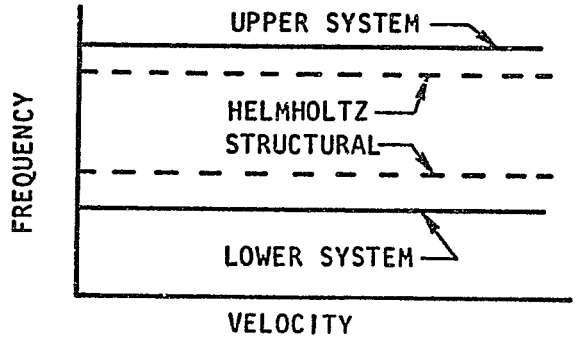

● FREQUENCY RELATIONSHIPS

Figure 9. Combined Fluid-Structural System

observed system resonant frequencies are not the same as the frequencies characteristic of the resonant systems analyzed individually.

The fluid-structural response frequencies associated with the combined system are the resonant frequencies of concern with respect to a fluid flow excitation. Once the resonant response frequencies have been computed, the next step is to compute the excitation frequencies expected.

SYSTEM EXCITATION

The excitation frequencies are a result of boundary layer disturbance. The type of boundary layer disturbance is not fully understood, but present evidence indicates that at least two types of boundary layer disturbance can be expected.

Work by Dr. Gerlach at Southwest Research Institute has indicated the important of vortex shedding and that the vortex shedding frequency will fall in a frequency range characterized by Strouhal numbers in the range of 0.1 to 0.5. The vortex shedding frequency is a function of the Strouhal number, the fluid velocity, and the convolution geometry.

Work at Rocketdyne, which includes testing and analysis of a large number of braided flex hoses and testing of a model in a two-dimensional water table, has resulted in establishing that an excitation frequency exists in addition to the ones associated with vortex shedding. The frequency relationship established by the Rocketdyne effort can be characterized by an oscillation wave length that is twice the convolution pitch distance. (Definitions of the pitch distance, d_2, as well as the convolution dimension, d_1, are given in Fig. 10.) With the oscillation wave length equal to twice the pitch distance, the oscillation frequency becomes:

$$f = \frac{0.5v}{d_2}$$

- NASA REQUIREMENTS

$$f_E = \frac{0.1\ v}{d_1} \rightarrow \frac{0.5\ v}{d_1}$$

- ROCKETDYNE TEST EXPERIENCE HAS DEMONSTRATED RESONANCE LIKELY AT

$$f_E = \frac{v}{2d_2}$$

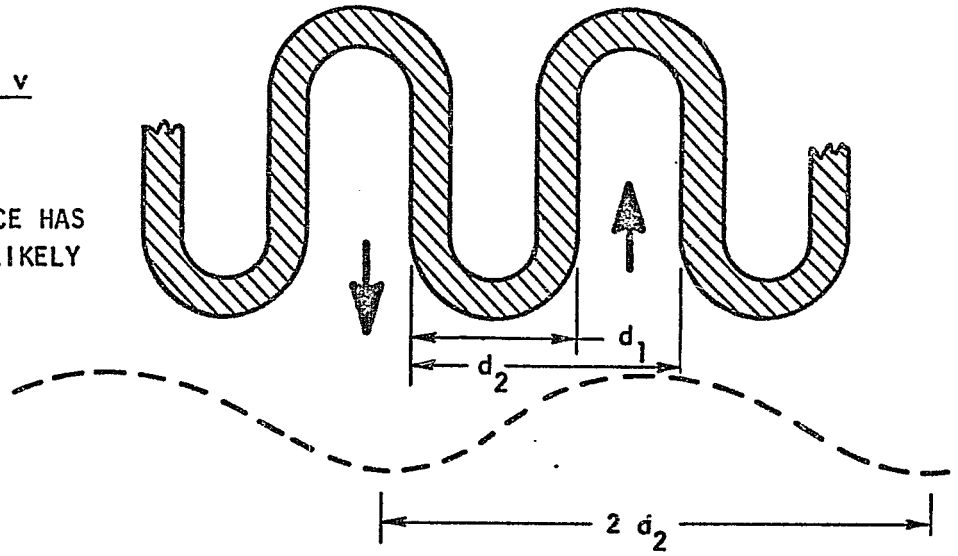

- ROCKETDYNE TEST EXPERIENCE AND ANALYSIS INDICATES POTENTIAL RESPONSE AT TWICE EXCITATION FREQUENCY

$v \alpha \sin wt$

DRAG FORCE $\alpha\ v^2 \alpha \sin^2 wt \alpha \cos 2wt$

- THEREFORE, LIMITS USED ARE

$$f_E = \frac{0.1\ v}{d_1} \longrightarrow \frac{2(0.5v)}{d_2}$$

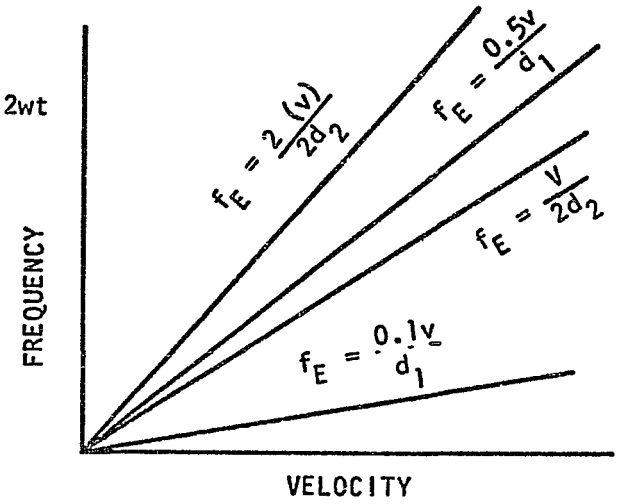

Figure 10. Excitation Frequency

where

v = stream velocity

d_2 = bellows pitch distance

The observed frequency results from the rate at which the wave length is "convected" or moved past a convolution root; the frequency is thus a function of the stream velocity (v).

In addition to the possible excitation frequency defined above, the fluid-structural response frequencies have been found to be potentially excited at twice the excitation frequency. The double frequency excitation results from the nonlinearities associated with the drag force being a function of velocity squared (Fig. 10). To be consistent with the potential excitation frequencies associated with both the vortex shedding frequency and fluid "convection" frequency, the excitation frequency limits are assumed to be:

$$f_E = \frac{0.1v}{d_1} \quad \text{to} \quad \frac{2.0\ (0.5v)}{d_2}$$

A convenient method of determining the existence of a potential resonance is through use of an "interference chart." Typical interference charts are illustrated in Fig. 11. These charts are constructed by plotting the response and excitation frequency limits on a grid of frequency vs fluid velocity. If both the response and excitation frequencies interfere with the operating velocity range, a potential resonance is defined to exist.

The existence of a resonance does not automatically mean that the flexible line will fail when "on resonance." The part will fail only if the endurance limit of the material is exceeded for the number of cycles accumulated. Therefore, to evaluate whether a flexible line can potentially fail when a flow-induced resonance is experienced, the fatigue failure potential must be evaluated.

POTENTIAL RESONANCE CAN BE EVALUATED BY COMPARING THE FOLLOWING

- OPERATING RANGE OF VELOCITIES
- RESPONSE FREQUENCIES OF FLUID-STRUCTURAL SYSTEM
- EXCITATION FREQUENCIES AS A FUNCTION OF VELOCITY

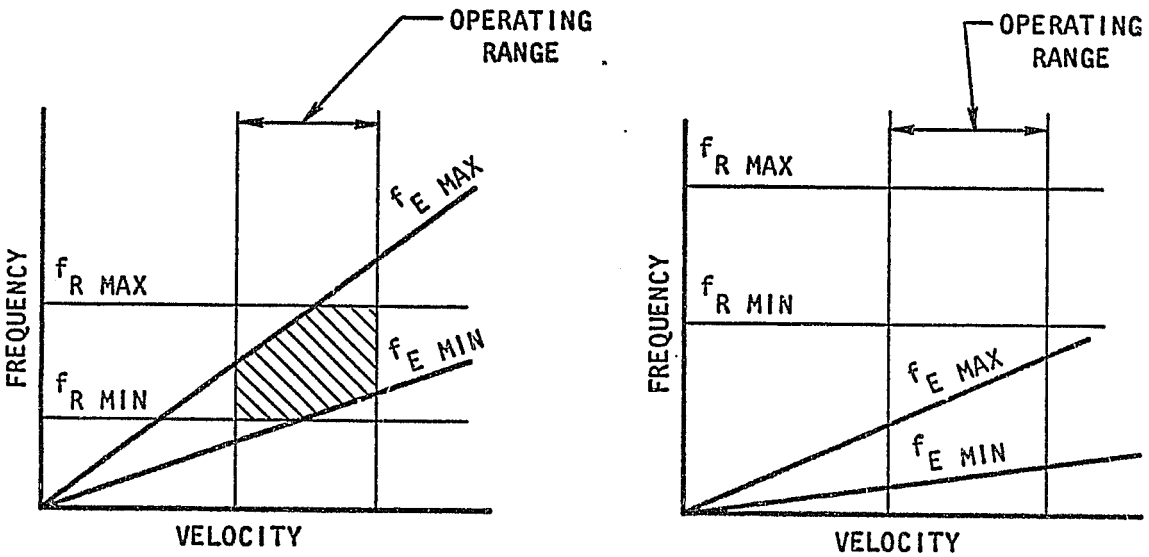

Figure 11. Frequency Interference Chart

ENDURANCE LIMIT ANALYSIS

The endurance limit analysis compares the maximum alternating stress expected by a flexible line to the endurance limit of the flexible line material. The technique of computing the maximum alternating stress must assume that the maximum load conditions exist. As an initial step, an alternating fluid velocity is assumed to exist; the velocity assumed has a maximum dynamic velocity that is twice the mean fluid velocity (Fig. 12). The load due to dynamic or an alternating velocity is computed. The computed load, resulting from drag force and pressure oscillations, is a function of (1) the convolution geometry, (2) the fluid density, and (3) the fluid velocity. Next, the stress per unit load is computed. The stress per unit load is a function only of the convolution geometry.

The above computations are of a static nature and do not account for any dynamic gain. When a resonant system is operated "on resonance," the system damping plays a role in defining the maximum potential amplitude. Unless otherwise specified, a dynamic gain of 100 (corresponding to a damping ratio of 0.005) was assumed for computations made at Rocketdyne.

The maximum alternating stress, if on resonance, is computed as:

$$\sigma = (\text{Force}) \dot{x} (\text{Stress/Unit Force}) \times 100$$

The resulting stress is then compared to a "design value" of material endurance limit. The design value being used is a value that is 50 percent of the average high cycle fatigue failure value for the material and the temperature of concern. If the computed stress is less than the design endurance-limit stress, the flexible line is considered to be satisfactory even through a resonance may exist.

- EVALUATE FATIGUE FAILURE POTENTIAL IF RESONANCE CONDITION IS POTENTIAL
  - ASSUME EXCITATION

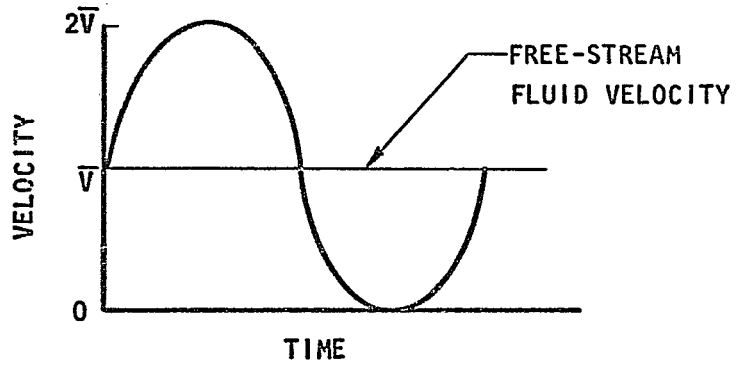

  - COMPUTE STATIC FORCE, $F = f$ (GEOMETRY, FLUID, $\bar{V}$)
    WHERE $\bar{V}$ = AVERAGE FLUID VELOCITY
  - COMPUTE STRESS PER UNIT FORCE, $\sigma_1 / F_1 = f$ (GEOMETRY)
  - DEFINE DYNAMIC GAIN FOR OPERATING "ON RESONANCE"

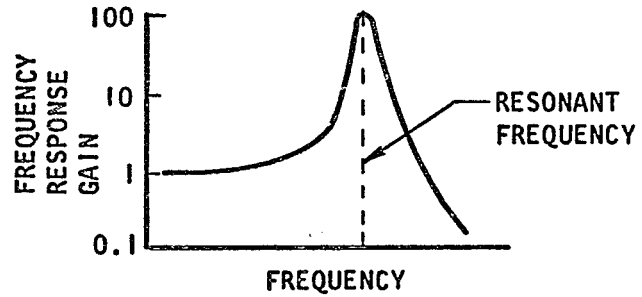

  - COMPUTE MAXIMUM EXPECTED STRESS IF "ON RESONANCE," $\sigma = F \times \sigma_1 / F_1 \times 100$
  - COMPARE COMPUTED STRESS TO "DESIGN VALUE" OF MATERIAL ENDURANCE LIMIT

Figure 12. Endurance Limit Analysis

SUMMARY OF F-1 FLEXIBLE LINE ANALYSIS

Table 4 summarizes the resonant frequency analysis performed on all F-1 flexible hoses and bellows. The fuel high-pressure duct bleed line is the only line on the F-1 engine deemed marginal by this analysis. Flow-induced vibration was detected during flow tests as predicted; however, the lines were tested at maximum response for 2250 seconds without failure.

TABLE 4

F-1 FLEXIBLE HOSES AND BELLOWS RESONANT FREQUEN

Item	NAS-Number	Description	Supplier	Material	Analytically Determined Structural Frequencies, cps		Number of Plys	Maximum Velocity Analyzed ft/sec	Boundary Layer Excitation Frequency, cps		Combined Fluid-Struct Response Frequency, c	
					Accordion	Convolution			Minimum	Maximum	Minimum	Maxi
	Category I											
1	NAS-26744	Gas Generator Fuel Feed Bootstrap	Fair	-	-	-	-	108	Lined	-	-	-
	NAS-26744	Gas Generator Fuel Feed Bootstrap	Arrow	-	-	-	-	108	Lined	-	-	-
	Catetory II											
1	NAS-26743	Gas Generator LOX Feed Duct End	Fair	-	-	-	-	84	Lined	-	-	-
	NAS-26743	Gas Generator LOX Feed Duct End	DK	-	-	-	-	84	Lined	-	-	-
2	NAS-26743	Gas Generator LOX Feed Valve End	Fair	-	-	-	-	84	Lined	-	-	-
	NAS-26743	Gas Generator LOX Feed Valve End	DK	-	-	-	-	84	Lined	-	-	-
3	NAS-260142	Heat Exchanger Helium Inlet	Fair	718	708	8184	3	200	0	14400	708	1455
	NAS-260142	Heat Exchanger Helium Inlet	DK	718	1213	13076	2	200	0	14400	1213	1605
	NAS-260091	Heat Exchanger Helium Inlet	Fair	718	708	8184	3	200	0	14400	708	1455
	NAS-260091	Heat Exchanger Helium Inlet	DK	718	1213	13076	2	200	0	14400	1213	1605
4	NAS-260142	Heat Exchanger Helium in Wrap-Around	Fair	718	708	8184	3	200	0	14400	708	1455
	NAS-260142	Heat Exchanger Helium in Wrap-Around	DK	718	1213	13076	2	200	0	14400	1213	1605
	NAS-260091	Heat Exchanger Helium in Wrap-Around	Fair	718	708	8184	3	200	0	14400	708	1455
	NAS-260091	Heat Exchanger Helium in Wrap-Around	DK	718	1213	13076	2	200	0	14400	1213	1605
5	NAS-260143	Heat Exchanger Helium Outlet	Fair	718	719	8012	3	850	0	61320	719	2823
	NAS-260143	Heat Exchanger Helium Outlet	DK	718	1178	12018	3	850	0	57849	1178	2936
	NAS-260092	Heat Exchanger Helium Outlet	Fair	718	719	8012	3	850	0	61320	719	2823
	NAS-260092	Heat Exchanger Helium Outlet	DK	718	1200	12959	2	850	0	57849	1200	2861
6	NAS-260143	Heat Exchanger Helium Outlet Wrap-Around	Fair	718	719	8012	3	850	0	61320	719	2823
	NAS-260143	Heat Exchanger Helium Outlet Wrap-Around	DK	718	1178	12018	3	850	0	57849	1178	2936
	NAS-260092	Heat Exchanger Helium Outlet Wrap-Around	Fair	718	719	8012	3	850	0	61320	719	2823
	NAS-260092	Heat Exchanger Helium Outlet Wrap-Around	DK	718	1200	12959	2	850	0	57849	1200	2861
7	NAS-26753	Heat Exchanger Helium Bypass	ANA	321	Braid[1]	17687	1	151.8	0	12740	12131	2021
	NAS-26753	Heat Exchanger Helium Bypass	AVI	321	Braid	21973	1	151.8	0	14140	15196	2098
8	NAS-260159	Heat Exchanger LOX Inlet	ANA	321	Braid	17687	1	3[illegible].6	0	3206	3626	5553
	NAS-260159	Heat Exchanger LOX Inlet	AVI	321	Braid	26121	1	[illegible]3.1	0	3633	7717	6784
	NAS-26757	Heat Exchanger LOX Inlet	TITE	321	Braid	17352	1	4[illegible].8	0	4369	3273	5449
	NAS-26757	Heat Exchanger LOX Inlet	AVI	321	Braid	26121	1	43.1	0	3633	7717	6784
9	NAS-260144	Heat Exchanger GOX Outlet	Fair	718	643	9383	4	250	0	16552	643	1250
	NAS-260144	Heat Exchanger GOX Outlet	DK	718	913	12792	3	250	0	17860	913	1884
	NAS-260093	Heat Exchanger GOX Outlet	Fair	718	643	9383	4	250	0	16552	643	1250
	NAS-260093	Heat Exchanger GOX Outlet	DK	718	913	12792	3	250	0	17860	913	1884
	NAS-260093	Heat Exchanger GOX Outlet	Gardner	718	900	9710	4	250	0	17280	900	2338
10	NAS-260144	Heat Exchanger GOX Outlet Wrap-Around	Fair	718	643	9383	4	285	0	18870	643	1250
	NAS-260144	Heat Exchanger GOX Outlet Wrap-Around	DK	718	913	12792	3	285	0	20350	913	1884
	NAS-260093	Heat Exchanger GOX Outlet Wrap-Around	Fair	718	643	9383	4	285	0	18870	643	1250
	NAS-260093	Heat Exchanger GOX Outlet Wrap-Around	DK	718	913	12792	3	285	0	20350	913	1884
	NAS-260093	Heat Exchanger GOX Outlet Wrap-Around	Gardner	718	900	9710	4	285	0	19700	900	2338
11	NAS-260162	Heat Exchanger LOX Bypass	ANA	321	Braid	25900	1	9.7	0	1276	5065	8443
	NAS-260162	Heat Exchanger LOX Bypass	AVI	321	Braid	30829	1	12.0	0	1152	8143.5	8403
	NAS-260162	Heat Exchanger LOX Bypass	ANA	321	Braid	25900	1	9.9	0	1309	5091.8	8436
	NAS-260162	Heat Exchanger LOX Bypass	AVI	321	Braid	30829	1	12.0	0	1152	8143.5	8403
12	19-458784	Fuel Pump Balance Cavity Bleed Return	Weath.	321	-	-	-	12.2	Teflon Tubing	-	-	-
	19-458784	Fuel Pump Balance Cavity Bleed Return	TITE	321	-	-	-	12.2	Teflon Tubing	-	-	-
13	19-461020	Fuel Pump Balance Cavity Supply	Weath.	321	-	-	-	95	Teflon Tubing	-	-	-
14	NAS-260116	Hydraulic Cutoff Valve to Inlet Elbow	DK	321	Braid	5664	2	16.2	0	1263.6	1120.8	1806
	NAS-260116	Hydraulic Cutoff Valve to Inlet Elbow	FMH	321	Braid	30656	1	16.2	0	1360.8	7395.1	5556
	NAS-260083	Hydraulic Cutoff Valve to Inlet Elbow	DK	321	Braid	5665	2	16.2	0	1263.6	1352	1915
	NAS-260083	Hydraulic Cutoff Valve to Inlet Elbow	FMH	321	Braid	25046	1	16.2	0	1360.8	6539.8	5133
15	NAS-260048	Fuel Drain	Fair	321	1562	16915	1	-	0	145.7	1562	4206
16	408848	Turbopump Bearing Lube Drain	ANA	321	Braid	32399	1	2.52	0	231	10659.9	8397
17	19-457645	Turbine Bearing Supply	ANA	321	Braid	32325	1	6.77	0	286.9	9254.8	9334
18	19-457648	Turbine Bearing Return	ANA	321	Braid	32399	1	3.7	0	310.8	11031.8	8338
19	NAS-26927	Heat Exchanger Duct	Arrow	-	-	-	-	780	Lined	-	-	-
	NAS-26927	Heat Exchanger Duct	Arrow	-	-	-	-	780	Lined	-	-	-

[1] Braid restricts accordion motion

[2] Based on criteria agreed on prior to development of analytical method

BLE 4

RESONANT FREQUENCY ANALYSIS SUMMARY

ayer ency, cps	Combined Fluid-Structure Response Frequency, cps		Endurance Limit Analysis, psi		Analysis Summary: Flow Resonance Search Not Required Because of				Analysis Indicates Resonance Search Required	Part Flow Resonance Searched(2)
Maximum	Minimum	Maximum	Maximum Expected	Maximum Allowed	Lined Bellows	Drain System or Dead End Service	Excitation and Response Frequency Do Not Couple	Stress Below Endurance Limit		
-	-	-	-	-	///					
-	-	-	-	-	///					
-	-	-	-	-	///					
-	-	-	-	-	///					
-	-	-	-	-	///					
-	-	-	-	-	///					
14400	708	14557	7097	33000				///		///
14400	1213	16058	3264	33000				///		///
14400	708	14557	7099	33000				///		///
14400	1213	16058	3264	33000				///		///
14400	708	14557	7097	33000				///		///
14400	1213	16058	3264	33000				///		///
14400	708	14557	7097	33000				///		///
14400	1213	16058	3264	33000				///		///
61320	719	28239	20540	27750				///		///
57849	1178	29364	10105	27750				///		///
61320	719	28239	20540	27750				///		///
57849	1200	28611	10016	27750				///		///
61320	719	28239	20540	27750				///		///
57849	1178	29364	10105	27750				///		///
61320	719	28239	20540	27750				///		///
57849	1200	28611	10016	27750				///		///
12740	12131	20213	1381	45000				///		///
14140	15196	20983	1967	45000			///	///		///
3206	3626	55535	9052	44000			///	///		///
3633	7717	67844	8756	44000			///	///		///
4369	3273	54497	17957	44000			///	///		///
3633	7717	67844	8756	44000			///	///		///
16552	643	12501	23300	27750				///		///
17860	913	18848	23700	27750				///		///
16552	643	12501	23300	27750				///		///
17860	913	18848	23700	27750				///		///
17280	900	23384	20900	27750				///		///
18870	643	12501	26500	27750				///		///
20350	913	18848	27000	27750				///		///
18870	643	12501	26500	27750				///		///
20350	913	18848	27000	27750				///		///
19700	900	23384	23800	27750				///		///
1276	5065	84431.4	370	42000			///			
1152	8143.5	84037.5	540	42000			///			
1309	5091.8	84360.3	289	42000			///			
1152	8143.5	84037.3	540	42000			///			
-	-	-	-	-						
-	-	-	-	-						
-	-	-	-	-						
1263.6	1120.8	18067.2	2824.5	22500				///		
1360.8	7395.1	55567.8	361.6	22500			///			
1263.6	1352	19155.0	2824.5	22500			///			
1360.8	6539.8	51338.2	361.8	22500			///			
145.7	1562	42063	41	22500		///				
231	10659.9	83976.6	60.9	22500			///			
286.9	9254.8	93349.3	58.8	22500			///			
310.8	11031.8	83385.1	135.6	22500			///			
-	-	-	-	-	///					
-	-	-	-	-	///					

TABLE 4

(Concluded)

Item	NA5-Number	Description	Supplier	Material	Analytically Determined Structural Frequencies, cps		Number of Plys	Maximum Velocity Analyzed ft/sec	Boundary Layer Excitation Frequency, cps	
					Accordion	Convolution			Minimum	Maximum
	Category II (Continued)									
20	RD271-3005-0200	3-Way Override Inlet	ANA	-	-	-	1	No Flow	-	-
	RD271-3005-0200	3-Way Override Inlet	TITE	-	-	-	1	No Flow	-	-
21	RD271-3005-0200	3-Way Override Outlet	ANA	-	-	-	1	No Flow	-	-
	RD271-3005-0200	3-Way Override Outlet	TITE	-	-	-	1	No Flow	-	-
22	RE271-3001-	Turbine Outlet Pressure (instrumentation)	ANA	-	-	-	1	No Flow	-	-
	RE271-3001-	Turbine Outlet Pressure (instrumentation)	TITE	-	-	-	1	No Flow	-	-
23	RE271-3001-	GOX Return Pressure (instrumentation)	ANA	-	-	-	1	No Flow	-	-
	RE271-3001-	GOX Return Pressure (instrumentation)	TITE	-	-	-	1	No Flow	-	-
24	NA5-260213	Dual Thrust LOX Inlet	ANA	321	Braid[1]	41509	1	35	0	4620
25	NA5-260214	Dual Thrust LOX Outlet	ANA	321	Braid	41509	1	35	0	4620
26	NA5-260233	Dual Thrust Warmant	ANA	321	Braid	30573	3	20.8	0	2994
	NA5-260233	Dual Thrust Warmant	ANA	321	Braid	30573	3	20.8	0	2994
27	RE271-3001-0080	Fuel Bleed High Pressure Duct	ANA	321	Braid	60750	1	200	0	36000
	RE271-3001-0060	Fuel Bleed High Pressure Duct	TITE	321	Braid	118450	1	157	0	25434
	Category III									
1	NA5-260163	Hypergol Manifold to Thrust Chamber	ANA	321	Braid	31891	1	91.4	0	8250
	407877	Hypergol Manifold to Thrust Chamber	ANA	321	Braid	38018	1	91.4	0	8250
2	NA5-26882	LOX Dome Purge - Wrap-Around	ANA	321	Braid	30277	1	284	0	44330
3	NA5-260050	Hydraulic Ground Support - Engine to Four-Way	ANA	321	Braid	11188	1	20.8	0	1625
	NA5-260050	Hydraulic Ground Support - Engine to Four-Way	TITE	321	Braid	29874	1	20.8	0	2000
4	NA5-260145	Hydraulic Supply Wrap-Around	Fair	718	643	9383	4	57.5	0	3966
	NA5-260145	Hydraulic Supply Wrap-Around	DK	718	913	14938	3	57.5	0	4525
	NA5-260094	Hydraulic Supply Wrap-Around	Fair	718	643	9383	4	57.5	0	3966
	NA5-260094	Hydraulic Supply Wrap-Around	DK	718	913	17659	3	57.5	0	4525
	NA5-260094	Hydraulic Supply Wrap-Around	Gardner	718	643	9710	4	57.5	0	4140
5	NA5-260146	Hydraulic Return Wrap-Around	Fair	718	719	8012	3	47.9	0	3340
	NA5-260146	Hydraulic Return Wrap-Around	DK	718	1072	11790	3	47.9	0	3249
	NA5-260095	Hydraulic Return Wrap-Around	Fair	718	719	8012	3	47.9	0	3340
	NA5-260095	Hydraulic Return Wrap-Around	DK	718	1072	14660	3	47.9	0	3249
6	NA5-260158	Hydraulic Ground Return	TITE	321	Braid	10778	1	18.2	0	1642
	NA5-260158	Hydraulic Ground Return	DK	321	Braid	12064	1	18.2	0	1752
	NA5-26756	Hydraulic Ground Return	DK	321	Braid	8806	2	18.2	0	1642
	NA5-26756	Hydraulic Ground Return	TITE	321	Braid	11869	1	18.2	0	1752
7	NA5-26851	Turbopump LOX Seal Purge Wrap-Around	ANA	321	Braid	38018	1	20.1	0	1807.5
8	NA5-26883	Thrust Chamber Prefill Wrap-Around	ANA	321	Braid	25484	1	21.3	0	4096
9	NA5-26884	Purge, Cocoon Condition Wrap-Around	ANA	321	Braid	25484	1	122	0	25360
	Category IV									
1	NA5-260049	LOX Drain	Fair	-	-	-	1	No Flow	-	-
2	RE271-3001-	Gas Generator Injector to Combustor Seal Vent	ANA	-	-	-	1	No Flow	-	-
	RE271-3001-	Gas Generator Injector to Combustor Seal Vent	TITE	-	-	-	1	No Flow	-	-
3	RE271-3001-	Gas Generator Combustor to Turbine Seal Vent	ANA	-	-	-	1	No Flow	-	-
	RE271-3001-	Gas Generator Combustor to Turbine Seal Vent	TITE	-	-	-	1	No Flow	-	-
4	RE271-3001-	Helium Supply Pressure (instrumentation)	ANA	-	-	-	1	No Flow	-	-
	RE271-3001-	Helium Supply Pressure (instrumentation)	TITE	-	-	-	1	No Flow	-	-
5	RE271-3001-	Helium Return Pressure (instrumentation)	ANA	-	-	-	1	No Flow	-	-
	RE271-3001-	Helium Return Pressure (instrumentation)	TITE	-	-	-	1	No Flow	-	-

[1] Braid restricts accordion motion

[2] Based on criteria agreed on prior to development of analytical method

TABLE 4

(Concluded)

Boundary Layer Excitation Frequency, cps		Combined Fluid-Structure Response Frequency, cps		Endurance Limit Analysis, psi		Analysis Summary					
						Flow Resonance Search Not Required Because of					
Minimum	Maximum	Minimum	Maximum	Maximum Expected	Maximum Allowed	Lined Bellows	Drain System or Dead End Service	Excitation and Response Frequency Do Not Couple	Stress Below Endurance Limit	Analysis Indicates Resonance Search Required	Part Flow Resonance Searched(2)
-	-	-	-	-	-		//////				
-	-	-	-	-	-		//////				
-	-	-	-	-	-		//////				
-	-	-	-	-	-		//////				
-	-	-	-	-	-		//////				
-	-	-	-	-	-		//////				
-	-	-	-	-	-		//////				
-	-	-	-	-	-		//////				
0	4620	7005.9	97825.4	4846.9	22500			//////	//////		//////
0	4620	7005.9	97825.4	4846.9	42000			//////	//////		//////
0	2994	8272.5	92067	1484.4	22500			//////	//////		
0	2994	8272.5	92067	1484.4	22500			//////	//////		
0	36000	16770	175240	73500	22500					//////	//////
0	25434	49632	218590	41500	22500			//////			//////
0	8250	11313	8365	31091	22500			//////			//////
0	8250	13789	81817	31091	22500			//////			//////
0	44330	11094	39075	19127	22500				//////		
								//////	//////		
0	1625	3465	50423	2073	22500						
								//////	//////		
0	2000	8391	76831	1332	22500						
0	3966	643	30421	11283	27750				//////		
0	4525	913	42122	8776	27750				//////		
0	3966	643	30431	11283	27750				//////		
0	4525	913	40731	8776	27750				//////		
0	4140	643	31319	10594	27750				//////		
0	3340	719	24776	26950	27750				//////		
0	3249	1072	34483	14052	27750				//////		
0	3340	719	24776	26950	27750				//////		
0	3249	1072	35761	11963	27750				//////		
0	1542	2899	46309	1963	22500			//////	//////		
0	1752	2568	41487	2779	22500			//////	//////		
0	1542	1853	26502	4319	22500			//////	//////		
0	1752	2550	43673	2064	22500			//////	//////		
0	1807.5	17859	38209	15.9	22500			//////	//////		
0	4096	4342	93570	2439	22500			//////	//////		
0	25360	17565	30005	789	21000				//////		
-	-	-	-	-	-		//////				
-	-	-	-	-	-		//////				
-	-	-	-	-	-						
-	-	-	-	-	-		//////				
-	-	-	-	-	-						
-	-	-	-	-	-		//////				
-	-	-	-	-	-						
-	-	-	-	-	-		//////				
-	-	-	-	-	-						
-	-	-	-	-	-		//////				
-	-	-	-	-	-						
-	-	-	-	-	-		//////				
-	-	-	-	-	-						
-	-	-	-	-	-		//////				
-	-	-	-	-	-						

REFERENCES

1. F-1 Component Qualification Report No. 409262-401, "Hose Assembly, Flex-Bleed Line, No. 2 Fuel."

2. IL 68/17 to R. L. Ludeman from C. A. Russell, dated 17 July 1968.

3. IL 68/86 "Recommended Procedure for Monitoring Resonance During Flow Tests" to C. M. Daniels from E. Mogil, dated 16 July 1968.

4. 68R1852, "F-1 Bellows Verification" to F. A. Stewart from R. J. Fontaine, dated 2 July 1968.

END OF REFERENCE

130

REFERENCE

131

HULBERT, L. E.; KEITH, R. E.; AND TRAINER, T. M.: STATE-OF-THE-ART SURVEY OF METALLIC BELLOWS AND DIAPHRAGMS FOR AEROSPACE APPLICATIONS. BATTELLE MEMORIAL INST., 1965. (AFRPL-TR-65-215).

AFRPL-TR-65-215

X66-16966

STATE-OF-THE-ART SURVEY OF METALLIC BELLOWS AND DIAPHRAGMS FOR AEROSPACE APPLICATIONS

Dr. L. E. Hulbert, Dr. R. E. Keith, and T. M. Trainer
Battelle Memorial Institute
Columbus, Ohio

TECHNICAL REPORT NO. AFRPL-TR-65-125

November 1965

Air Force Rocket Propulsion Laboratory
Research and Technology Division
Air Force Systems Command
Edwards Air Force Base
California

NOTICES

Qualified users may obtain copies of this report from the Defense Documentation Center.

Defense Documentation Center release to the Office of Technical Services is not authorized.

When U. S. Government drawings, specifications, or other data are used for any purpose other than a definitely related Government procurement operation, the fact that the Government may have formulated, furnished, or in any way supplied the said drawings, specifications, or other data, is not to be regarded by implication or otherwise, or in any manner licensing the holder or any other person or corporation, or conveying any rights or permission to manufacture, use, or sell any patented invention that may in any way be related thereto.

If this copy is not needed, return to AFRPL (RPRPD), Edwards, California, 93523.

NOW APPROVED FOR PUBLIC RELEASE, DISTRIBUTION UNLIMITED
PER AF RPL LETTER DATED MAY 5, 1971, TAB 71-16, PP.A3

ABSTRACT

A 2-1/2-year program has been undertaken to establish analytical design procedures, stress-analysis methods, techniques for manufacturing control, and other factors essential to the successful design and fabrication of metallic bellows and diaphragms. The initial phase of the program has included a state-of-the-art survey to assist in the determination of the best means of accomplishing the over-all program objectives. This report summarizes the results of the survey and presents recommendations for the remainder of the program. An annotated bibliography of 376 references is included.

FABRICATION TECHNOLOGY

The extent to which the service performance of bellows and diaphragms achieves the design predictions is strongly dependent upon the quality of the materials from which they are fabricated and the care taken in their manufacture. Material defects, weld discontinuities, forming irregularities, and postfabrication damage can all result in locally high stresses that may lead to premature failure. In this section, the present state of the art with respect to materials, manufacturing methods, and inspection will be discussed.

Materials

Typical materials for formed, welded, and deposited bellows are discussed. So many materials are suitable for machined bellows that they are not included. Diaphragms can be made from any of the materials listed for formed, welded, and deposited bellows.

Formed Bellows Materials

Materials for formed bellows, shown in Table 3, must be weldable and formable. Although smaller bellows are usually made from seamless tubing, most bellows over an inch or two in diameter are made from sheet or strip formed into a cylinder and longitudinally seam welded. Whether the strip or sheet is purchased to any special tolerances depends upon the end application of the bellows. When the spring rate is not critical--bellows intended for expansion joints, for example--the customary 10 percent mill thickness tolerance is satisfactory. When the deflection characteristics must be more carefully controlled, materials may be selected from warehouse stock. In this way, thickness may be controlled to within about 5 percent on a given order. Rerolled materials from specialty metal fabricators provide the best commercially obtainable thickness tolerances. Bellows manufacturers using rerolled materials claim thickness tolerances of ±0.0001 inch. A more commonly quoted tolerance is ±0.00025 inch over a 20-inch strip width.

TABLE 3. TYPICAL FORMED-BELLOWS MATERIALS

Alloy	Crystal Structure
Solution-strengthened alloys	
Alpha brass	Face-centered cubic
Copper	"
Stainless steels, Types 304, 321, 347	"
Titanium, commercially pure and Alpha alloys	Hexagonal close packed
Inconel	Face-centered cubic
Precipitation-hardened alloys	
Beryllium copper	Face-centered cubic
Inconel 718	"
Aluminum, 7075 alloy	"
Transformation-hardened alloy	
Titanium, Alpha-Beta alloys	Hexagonal close packed - body-centered cubic

Opinions differ among manufacturers as to the desirability of a bright surface finish on the starting material. Some manufacturers note an improvement in the fatigue life of bellows produced from bright-finished material (No. 2B finish), while others see no difference. Some manufacturers also claim that the bright-finished material, containing more cold work than the dull, or matte-finished material (No. 2D finish), is more difficult to form. There is a trend toward the use of bright-finished material arising from the alleged tendency of inspectors to pass shiny bellows and reject dull bellows.

Although there is some disagreement, most manufacturers see no effect of "grain", or preferred orientation, in their starting material. The common materials from which formed bellows are fabricated, when produced under good control, are nearly isotropic, so preferred orientation does not appear to be a serious problem.

END OF REFERENCE

131

REFERENCE

132

FITTINGS, MC, CLASSIFICATION OF DEFECTS. MSFC-STD-437, NASA GEORGE C. MARSHALL SPACE FLIGHT CENTER, FEBRUARY 11, 1965.

MSFC-STD-437
February 11, 1965

GEORGE C. MARSHALL SPACE FLIGHT CENTER

NATIONAL AERONAUTICS AND SPACE ADMINISTRATION

STANDARD

FITTINGS, MC, CLASSIFICATION OF DEFECTS

GEORGE C. MARSHALL SPACE FLIGHT CENTER

NATIONAL AERONAUTICS AND SPACE ADMINISTRATION

STANDARD

FITTINGS, MC, CLASSIFICATION OF DEFECTS

1. SCOPE

1.1 This standard establishes a classification of defects applicable to non-conforming characteristics of MC fittings and shall be used as the minimum requirements for inspection functions responsible for acceptance inspection operations.

1.2 For each MC fitting this standard lists characteristics and applicable code numbers.

2. REFERENCED DOCUMENTS

2.1 The following documents form a part of this standard to the extent specified herein. Unless otherwise indicated, the issue in effect on date of invitation for bids or request for proposals shall apply.

SPECIFICATIONS

George C. Marshall Space Flight Center

MSFC-SPEC-143	Fittings, Flared Tube, Pressure Connections.

STANDARDS

Military

MIL-STD-105	Sampling Procedures and Tables for Inspection by Attributes.

George C. Marshall Space Flight Center

MC 124	Nut, Coupling.
MC 125	Sleeve, Flared Tube Fitting.

5.3 Classification of defects for Flared Tube Connection, Fitting End, MC 172.

5.3.1 Sealing surface.

Classification	Code	Characteristic
Critical	1	Roundness 360° - Maximum deviation shall not exceed 0.0003 in 360°
Critical	2	Roundness 60° - Maximum acceptable accumulative deviation shall not exceed 0.00010 in any 60° of arc
Critical	3	Roundness 15° - Maximum rate of deviation shall be less than 0.00010 in 15° or less of arc
Critical	4	Concavity (none allowable)
Critical	5	Surface finish - Steel parts - 8 ✓ Aluminum parts - 16 ✓
Critical	6	Surface imperfections (Tool chatter marks, tool runoff marks, steps, offsets, flat spots, cracks, checks, scratches, ridges, indentations, etc.)
Major	101	Sealing surface shall be concentric with thread pitch diameter T within 0.003 total indicator reading
Major	102	Angle 37° ± 0° 15'
Minor B	301	Convexity exceeding 0.0005
Minor B	302	Radius 0.015 ± 0.005 (two places)

5.3.2 Threads.

Classification	Code	Characteristic
Major	103	Pitch diameter
Major	104	Squareness between thread axis and face of hex shall not exceed H dimension
Major	107	More than two partial threads (style G only)
Minor A	201	Major diameter
Minor A	205	F diameter shall be concentric with thread pitch diameter T within 0.005 total instrument reading (style E only)
Minor A	230	Length of full thread (style E only)
Minor B	303	Angle 45° ± 5° (two places)

END OF REFERENCE

132

REFERENCE

133

HENSON, F. M.: AN EVALUATION OF GASKETS, SEALS, AND JOINTS FOR AEROSPACE HARDWARE. AEROJET-GENERAL CORP. (NASA CR-93784), 1967.

THIS REFERENCE HAS A LIMITED DISTRIBUTION AND MAY NOT BE REPRODUCED.

END OF REFERENCE

133

REFERENCE

134

PIPING AND TUBING TECHNOLOGY. NASA SP-5903(02).

NASA SP-5903 (02)

REFERENCE

TECHNOLOGY UTILIZATION

LEWIS RESEARCH CENTER
Aerospace Safety Research
and Data Institute
MAR 7 1972
CLEVELAND, OHIO

N72-13420

PIPING AND TUBING TECHNOLOGY

A COMPILATION

NATIONAL AERONAUTICS AND SPACE ADMINISTRATION

Foreword

The National Aeronautics and Space Administration has established a Technology Utilization Program for the dissemination of information on technological developments which have potential utility outside the aerospace community. By encouraging multiple application of the results of its research and development,. NASA earns for the public an increased return on the investment in aerospace research and development programs.

This publication is part of a series intended to provide such technical information. The devices, methods, and techniques presented have resulted from the great variety of requirements that have been encountered in the aerospace program. The handling of fluids has encompassed a wide range of materials, and has covered a spectrum from low to high pressures and from cryogenic to elevated temperatures.

The document is divided into four sections. The first section includes a number of fittings, couplings, and connectors that have been useful in joining tubing and piping and various systems. Section two presents a family of devices used where flexibility and/or vibration damping are necessary. The third section contains a number of devices found useful in the regulation and control of fluid flow. In the last section, shop hints to aid in maintenance and repair procedures such as cleaning, flaring and swaging of tubes, etc., are presented.

Additional technical information on individual tools and techniques can be requested by circling the appropriate number on the Reader Service Card included in this compilation.

Unless otherwise stated, NASA contemplates no patent action on the technology described.

We appreciate comment by readers and welcome hearing about the relevance and utility of the information in this compilation.

Ronald J. Philips, *Director*
Technology Utilization Office
National Aeronautics and Space Administration

NOTICE • This document was prepared under the sponsorship of the National Aeronautics and Space Administration. Neither the United States Government nor any person acting on behalf of the United States Government assumes any liability resulting from the use of the information contained in this document, or warrants that such use will be free from privately owned rights.

For sale by the National Technical Information Service, Springfield, Virginia 22151 — Price $1.00

Section 1. Fittings, Couplings, and Connectors

PIPE JOINTS REINFORCED IN PLACE WITH FITTED ALUMINUM SLEEVES

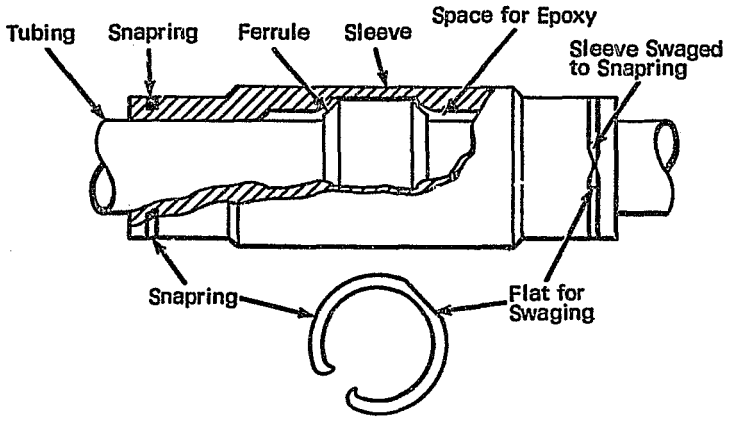

A new technique can be used to reinforce solder-sealed ferrule joints in installed small-diameter aluminum tubing. A fitted aluminum sleeve is placed over the joint using specially designed tools.

The reinforcement sleeve (see fig.) is made in two longitudinal halves for easy installation over the joint ferrule and a contiguous section of tubing. Epoxy cement is used to seal and bond the sleeve tightly around the joint assembly. Snaprings inserted in circumferential grooves position and hold the sleeve halves together. Each snapring is ground to a flat at the crown, allowing the shield metal to be swaged over the ring at the flat area. The snaprings are quickly and accurately installed in one of the sleeve halves by means of a special die and swaging punch, the free ends of the rings protrude equally beyond the cut edges of the sleeve half.

The inside of the sleeve is machined to the contour of the ferrule joint, with clearance to accommodate the epoxy cement. A sufficient length of sleeve is provided to allow an ample contact surface for sealing and bonding between the sleeve and tubing on both sides of the ferrule. Grooves for the snaprings are cut around the outside diameter of the sleeve near each end. The sleeve is then cut in half lengthwise with a 0.05 cm (0.02 in.) mill saw to form two identical shells.

Immediately prior to permanent installation over a joint, both shells of the sleeve are completely coated on the inside cleared surfaces with a commercial epoxy resin. The clamping action of the snaprings aids in distributing the epoxy resin, and any excess expelled from the sleeve can be removed before jelling occurs (within 8 hours at room temperature). The epoxy resin normally cures to standard test strength in approximately 24 hours. Centering and installation of the shielding over joints in constricted working areas are greatly facilitated with specially designed centering and insertion tools. The insertion tool positions the sleeve halves over the tubing joint and locks them in place in a single, one-handed operation.

Although the method was specifically designed for solder-sealed ferrule joints in small-diameter aluminum tubing, the approach is adaptable to a variety of tubing sizes, materials, and joints. Tubing joints reinforced by this method have withstood considerable torsion, tension, and vibra-

tion stresses at moderately elevated temperatures. In tests for resistance to mechanical abuse, tubing and joint assemblies were bent to failure. All failures occurred in the tubing rather than in the reinforced joint.

Source: I. Cortex, Jr., J. Siegfried, and O. Wobig
Manned Spacecraft Center
(MSC-11109)

Circle 1 on Reader Service Card.

HIGH-PRESSURE COUPLING FOR UNTHREADED, UNFLARED TUBES

A high-pressure coupling connects to any straight, unflared, and unthreaded tubing, without deforming or otherwise damaging the tubing. The coupling (see fig.) grips the tube wall tightly

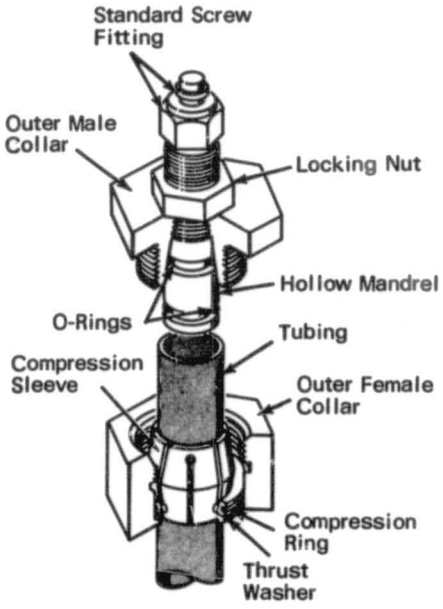

between an external compression sleeve and an internal hollow mandrel, and is adaptable to standard screw fittings for test stand attachment.

The mandrel portion is inserted in the tubing with two O-rings installed. The outer female collar, thrust washer, and compression ring are then placed over the tubing. The tapered and slotted compression sleeve is slid onto the tubing, with its forward taper fitting inside the compression ring taper and the tube end flush with the rear portion of the sleeve. The outer male collar is threaded onto that portion of the hollow mandrel which extends from the tube and into the female threads of the outer female collar.

As the male collar advances into the female collar, its internal taper forces the compression sleeve to deform because of the longitudinal slots in the sleeve. The resultant compressive radial force on the tube outer wall, supported from within the tube by the hollow mandrel, causes the tube to be gripped firmly by the coupling.

A locking nut is then threaded onto the plug thus formed, and the test stand adapter or connector is attached. Pressure is transmitted from the test apparatus to the tubing through the hollow mandrel.

Source: J. A. Stein of
North American Rockwell Corp.
under contract to
Manned Spacecraft Center
(MSC-600)

No further documentation is available.

METHOD FOR REINFORCING TUBING JOINTS

A joint repair technique permits resealing or reinforcing leaking or weak tubing joints without removing the failing member from the system. A split longitudinal aluminum shield with an epoxy resin coating is used in conjunction with sectioned nuts that slip over the tubing and mate with the threaded ends of the split shield.

The shield is threaded on each end with stand-

ard pipe threads and is designed with a small space adjacent to each side of the ferrule location to ensure a continuous circumferential epoxy seal. The

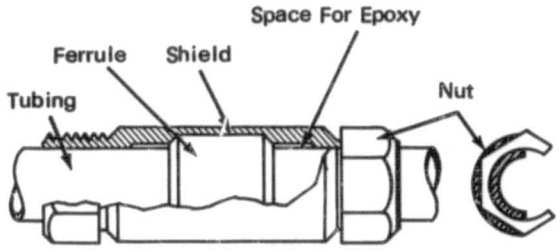

aluminum shield is halved longitudinally with a slit saw, and a generous coating of epoxy resin is applied to the inner surfaces of each half. Nuts to fit the pipe-threaded ends of the shield are sectioned (see fig.) to just slip over the tubing, the shield halves are clamped together over the joint, and the nuts are attached and drawn up on the shield and threads. For increased strength and clamping action, two such nuts can be applied at each end of the shield. In this case, the nuts should be so sectioned that their open portions lie on opposite sides of the shield.

Source: W. S. Lee and J. Kinzler
Manned Spacecraft Center
(MSC-11108)

Circle 2 on Reader Service Card.

SELF-SEALING FITTING FOR INJECTION AND SAMPLING OF LIQUIDS

A standard AN fitting has been modified to accept a blunt-ended hypodermic needle for insertion into a liquid system so that material may be either introduced into or withdrawn from the system without danger of contamination. This technique greatly reduces the quantities required to obtain representative system samples, and has been successfully used for taking contamination control samples from a fluid system located in an unclean area.

As shown in the sketch, a standard AN fitting is modified by the introduction of two compression wafers of silicone rubber with a durometer hardness of approximately 40. Each washer is punctured through its center by a very short slit. The wafers are then installed in the fitting so that the slits are at right angles to each other to form a cross. A short piece of flared thick-wall tubing is inserted into the fitting on top of the compression wafers, and a standard AN "B" nut is installed and tightened to compress the wafers. The blunt needle is then inserted through the wafer slits, without permitting any leakage or contamination.

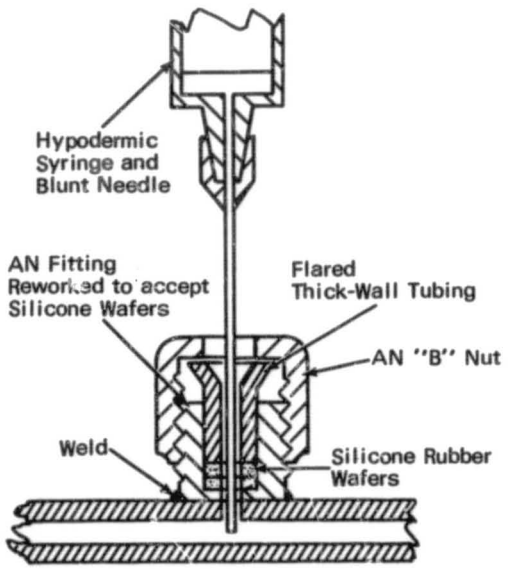

Source: C. W. Overbey of
North American Rockwell Corp.
under contract to
Manned Spacecraft Center
(MSC-15005)

No further documentation is available.

A QUICK DISCONNECT FOR CRYOGENIC FLUID LINES

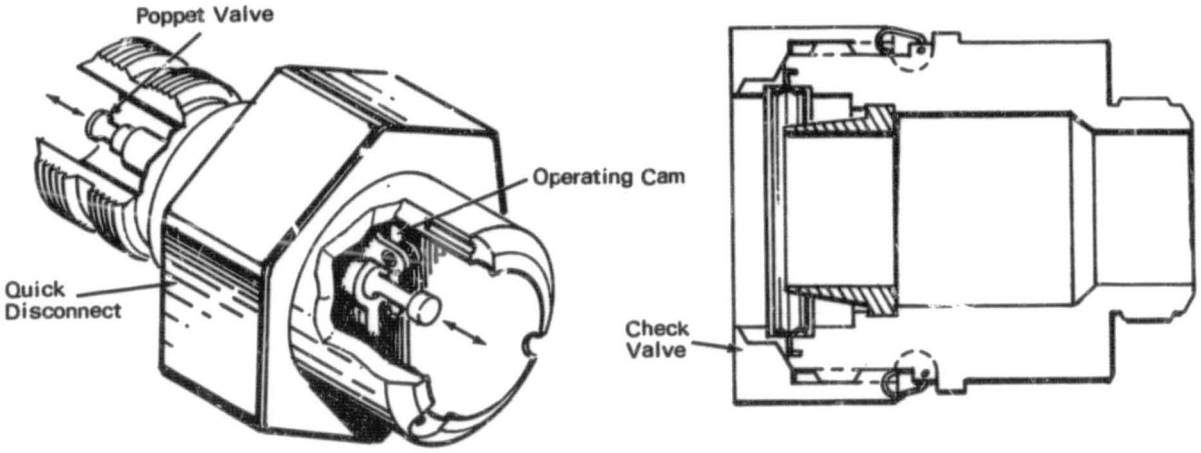

A cam-operated valve can be used for handling fluids at cryogenic temperatures and at very low pressures. The valve (see fig.) is part of a quick-disconnect coupling designed to implement the separation of a space vehicle liquid fluid system and its umbilically-connected ground supply facility.

The cam-lever actuated poppet valve has been used in conjunction with a ground half-disconnect to overcome LOX tank ullage pressure decay caused by "cryo-pumping" resulting from the temperature differential across the LH_2/LOX tanks and He-pressurized common bulkhead. The cam actuates the normally closed airborne half-poppet to the open position when the ground half-disconnect coupling is engaged, and maintains an evacuated system while providing a thermal barrier in the disengaged position.

Source: E. J. Castaldo and P. J. Formolo of
North American Rockwell Corp.
under contract to
Marshall Space Flight Center
(MFS-16622)

Circle 3 on Reader Service Card.

ELBOW FITTING WITH SELF-LOCKING COUPLING NUT

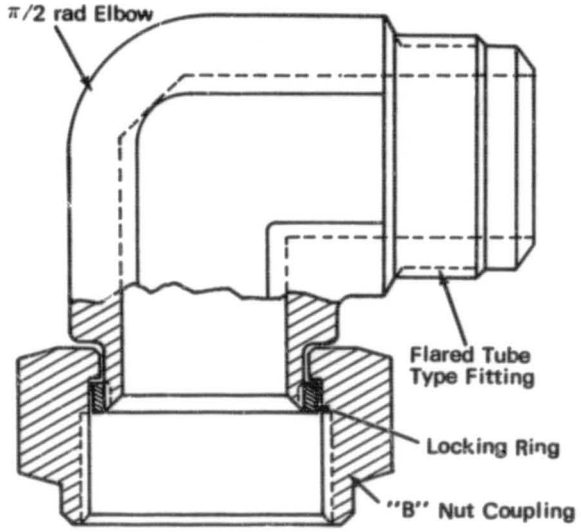

A $\pi/2$ rad (90°) elbow fitting can swivel 2π rad (360°) in one plane for more effective alignment with mating hardware, yet may be secured in place without the usual locking devices. On existing elbow assemblies, the fitting and locknut are secured by means of a locking wire inserted through a hole in the nut and a channel in the fitting. When torqued beyond a certain point, such an arrangement will shear the wire, swage the fitting groove, or mutilate the channel, all of which are undesirable.

This improved technique (see fig.) uses a left-hand threaded locking ring to ensure secure attachment of the locknut to the fitting. Sufficient surface area is obtained on the face of the locking ring to support the compression sur-

face of the locknut, thus maintaining a 2π rad (360°) pressure on the sealing areas of the fitting. This eliminates the requirement for the locking wire.

Source: F. L. Broadwick of
The Chrysler Corp.
under contract to
Marshall Space Flight Center
(MFS-14366)

Circle 4 on Reader Service Card.

LIGHTWEIGHT HOSE ASSEMBLY WITH HIGH FLEXIBILITY AND STRENGTH

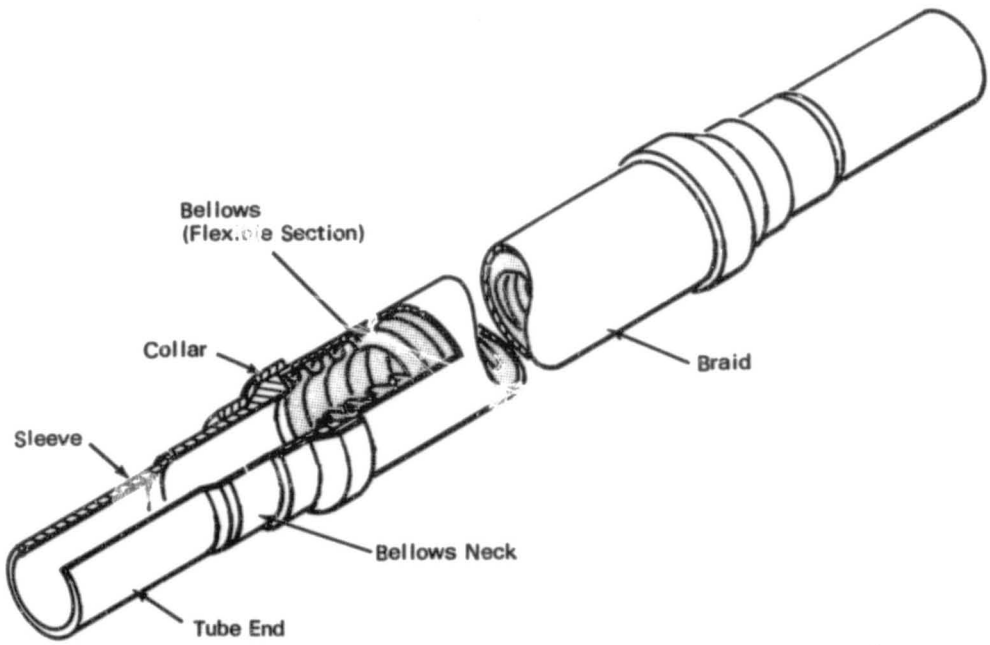

A new hose design incorporates flexible sections fastened to reinforcement braid. The assembly is lightweight and flexible, is useful in high- and low-pressure oxygen, helium, and hydrogen systems, and can withstand pressures from 689.5 kN/m^2 (100 psi) to 22,064 kN/m^2 (3200 psi) and temperatures from 294.25 K (70° F) to 58.15 K (−423° F).

The all-metal hose assembly consists of a flexible section, sleeves, reinforcement braid, collars, and tube ends (see fig.). The flexible section is an annular, continuous convoluted bellows. An overlapping, double-row resistance weldment joins the end sleeves to the bellows neck, which fits snugly within the inside diameter of the sleeve. The weldment is trimmed, still leaving a pressure-tight joint, and the resulting end is subsequently butt welded to the tube ends. The stainless steel braid is then assembled over the flexible section which is compressed in a fixture to its required length. The braid is formed over the sleeve conical shoulder, and a collar is positioned over and against the braid at the sleeve cone area. This provides a clamping action which is maintained by swaging and heliarc welding the collar and the braid to the sleeve.

Source: L. L. Bessing of
North American Rockwell Corp.
under contract to
Marshall Space Flight Center
(MFS-1831)

Circle 5 on Reader Service Card.

FUSIBLE METAL USED IN HIGH-PRESSURE PIPE JOINT

A simple method increases the pressure handling capabilities of threaded pipe joints and renders them practically impervious to thermal transient conditions. Conventional flanged joints usually fail in the extremes of these two areas.

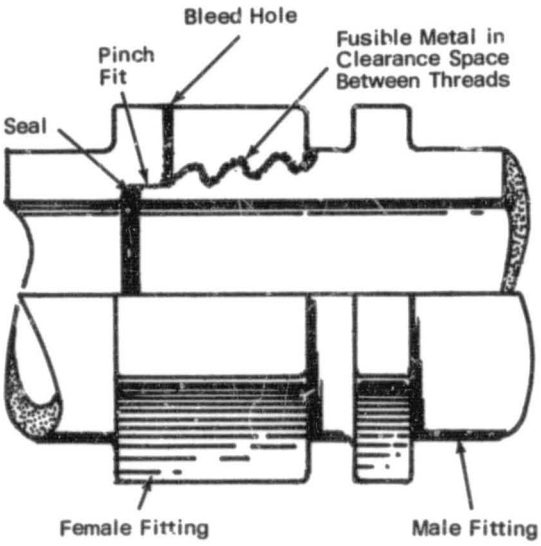

In this application, the joint is assembled dry to the proper seal compression and fusible metal is flowed into the threaded area, filling the void space between the threads. A bleed hole is used as an exit for any gas trapped during the filling process. The joint can be disassembled by heating it while expelling the fusible metal by applying pressurized gas to either end of the threaded joint. For joints where one part cannot be rotated relative to the other, or where a precise angular relationship is required, a left-hand/right-hand threaded turnbuckle-type double joint can be used.

Source: R. E. Meyer of
Pratt & Whitney Aircraft
under contract to
Marshall Space Flight Center
(MFS-21176)

No further documentation is available.

Section 2. Flexible Devices and Vibration Damping

PLASTIC TUBING PROTECTS FLEXIBLE COPPER HOSE

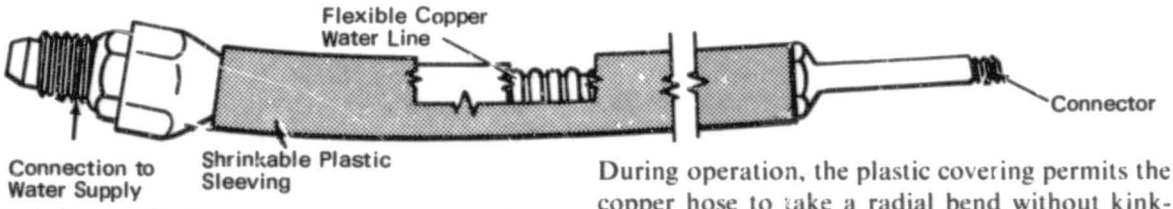

Reinforcing flexible copper purge and coolant hoses with a sleeve of high-temperature shrinkable plastic has proven to be an excellent protective measure in a severe vibration condition, such as testing a rocket engine. Similar flexible copper coolant lines can be used in automotive applications.

The flexible copper hose is inserted into a slightly larger plastic tube. Sufficient heat is then applied to shrink the plastic until it assumes the contour of the hose in intimate contact. During operation, the plastic covering permits the copper hose to take a radial bend without kinking, and prevents it from taking a permanent bend (setting). The plastic covering also serves as a reinforcement of the joint between the hose and fitting.

Source: B. E. Mellgren of
North American Rockwell Corp.
under contract to
Marshall Space Flight Center
(MFS-772)

No further documentation is available.

END OF REFERENCE

134

REFERENCE

135

RATHBUN, F. O., JR., ED.: SEPARABLE CONNECTOR DESIGN HANDBOOK (TENTATIVE): DESIGN CRITERIA FOR ZERO LEAKAGE CONNECTORS FOR LAUNCH VEHICLES. GENERAL ELECTRIC CO. (NASA CR-64944), 1964.

X65-19662
NASA CR-64944

ADVANCED TECHNOLOGY LABORATORIES

X65-19662
LEWIS RESEARCH CENTER
Aerospace Safety Research and Data Institute
JUN 13 1972
CLEVELAND, OHIO

DISTRIBUTION UNLIMITED PER NASA TECHNICAL DIRECTIVE 75-101, 11-5-74

Available from NASA to NASA offices, NASA centers, and NASA contractors only.

SEPARABLE CONNECTOR DESIGN HANDBOOK (TENTATIVE)

LIBRARY COPY
LEWIS LIBRARY, NASA
CLEVELAND, OHIO

EDITED BY

F. O. RATHBUN, JR.

Contract NAS 8-4012

December 1, 1964

CR64944

GENERAL ELECTRIC

DISTRIBUTION UNLIMITED PER
NASA TECHNICAL DIRECTIVE
75-101, 11-5-74

SEPARABLE CONNECTOR DESIGN HANDBOOK (TENTATIVE)

CONTRACT NAS 8-4012

Design Criteria
For Zero Leakage Connectors
For Launch Vehicles

Edited by

F. O. Rathbun, Jr.

Prepared for

PROPULSION AND VEHICLE ENGINEERING DIVISION
GEORGE C. MARSHALL SPACE FLIGHT CENTER
NATIONAL AERONAUTICS AND SPACE ADMINISTRATION
HUNTSVILLE, ALABAMA

Prepared by

Advanced Technology Laboratories
General Electric Company
Schenectady, New York

Sponsored by

Missile and Space Division
General Electric Company
Philadelphia, Pennsylvania

NASA Technical Manager
C. C. Wood (M-P&VE-PT)

December 1, 1964

PREFACE

By

L. G. Gitzendanner

The purpose of this handbook is to aid in the design and/or selection of separable fluid connectors. Since fluid connectors must be designed for handling various fluids, for a large range of temperatures, for a range of pressures, and for various environmental conditions, there can be many designs for connectors. However, it is possible to present the basic approach that one may follow in designing or selecting a connector for a particular application. Discussion of the phenomena associated with connectors is included to help the designer avoid oversights, be able to better judge the cause and nature of past difficulties, and, in general, to better appreciate the fundamentals involved.

The Connector Design Handbook is divided into seven chapters. Chapter 1, "Fundamental Considerations of Separable Connector Design," presents a general discussion of the problems to be considered in separable connector design and is based on the laws of physics and an appreciable amount of experimental data.

Chapters 2 and 3, "Flanged Connector Design" and "Threaded Connector Design," give specific design procedures for establishing the geometric dimensions of separable connectors. Design examples, which illustrate the step-by-step mathematical manipulations necessary to finalize a design, are included in each chapter. The design and analysis equations given are based on an elastic stress analysis and have been checked for accuracy within the limitations of the physical assumptions. While ultimate verification of the procedures must await repetitive application of the procedures for a multitude of sizes, pressures, and temperatures, the procedure has been used to effect one threaded connector design (for 4700 psi, 1440°F service) and four possible flange configurations for a ten inch connector (750 psi, 700°F).

Chapter 4, "Pressure-Energized Cantilever Seals and Hollow Metallic O-Rings," also based on elastic stress analyses, gives detailed equations and nomographs for direct and final design of cantilever-type pressure-energized seals. Equations for determining the displacement characteristics of hollow metallic O-rings are also presented.

Chapter 5, "Leakage Measurement Techniques," presents techniques and standards for the determination of the leakage characteristics of fluid connectors under development. The procedures outlined have proven successful over a period of two and one half years in a fluid connector development program.

Material properties useful to a designer are given in Chapter 6, "Material Properties and Compatibility." Included are the mechanical properties of elastomers, plastics, and some structural materials. Compatibility of materials with typical contained fluids is also discussed. This chapter should be a convenient reference for the more commonly required information. All data listed is from accredited sources which are referenced.

Chapter 7, "Catalog of Seals," lists seal configurations and materials particularly applicable to aerospace applications. Each entry is based on experimental results obtained using the leakage test procedures given in Chapter 5. As new configurations are proven and new materials are shown to be successful, additional entries can be made in this catalog.

It is believed that employment of the fundamental considerations listed and use of the analysis and design procedures given will result in connectors which will satisfy most requirements. Where unusually mild or unusually severe environments, or other extreme requirements are included, it may be advantageous or necessary to develop modifications to the equations and procedures, in which case an understanding of the principles underlying the procedures given will be helpful.

The Handbook is at present considered "tentative" in that insufficient use has been given its contents to date. When the applicability and utility of the various procedures have been proven by usage, the volume will be considered "final." Comments pertinent to the contents of the Handbook should be directed to Mr. C.C. Wood, M-P&VE-PT, Marshall Space Flight Center, National Aeronautics and Space Administration, Huntsville, Alabama.

Section 2

FLANGED CONNECTOR DESIGN

by

S. Levy

2.0 Introduction

This Section presents a more rigorous way of analyzing flanged connectors than has commonly been used in the past. It obtains a more complete picture of how stresses and deformations are distributed and thus makes possible better optimization. It provides a detailed design procedure for lap flanges. It also makes use of more criteria for acceptability of a particular design than has been done heretofore. Although this portion of the Handbook has been carefully assembled many of the features are new, and therefore should be considered preliminary until experience and use confirm or modify the procedure presented.

The analytical procedures indicate new configurations which show advantages over present configurations for some applications. Some of these configurations are described in Section 2.6, pages 2 - 54.

The basic analytical procedure presented in this Section makes use of equilibrium and compatibility conditions to obtain a solution. In the appendices, Section 2.9, the basic formulas are presented in a form best adapted to connector analysis. These formulas are adapted to either hand or digital computer computation. Where a computer is to be used exclusively, an energy approach is simpler. To this end, Section 2.7 (page 2 - 57) shows techniques for programming a computer for an energy analysis of connectors.

Preliminary design procedures are presented for each basic type of connector so that the trial configuration can be a fair approximation to the final design. Since these procedures necessarily make fixed assumptions regarding the distribution of redundant loads, they must be considered as giving only an approximation to the best configuration, and may indeed be unconservative.

The effects of frictional forces at the gasket, between loose and lap flanges, and elsewhere, are taken into account. Since gasket sliding is a major consideration if "zero leakage" is a design goal, it is felt that this mechanism must be considered. Friction elsewhere has marked effects on the sealing force at the gasket and thus also effects leakage performance.

The effects of eccentric loading on the bolts is included in the analysis. This factor is an important consideration in choosing between flanges having no contact outside the bolt circle and those having such contact.

2.0.1 When To Use Flanged Connectors

Flanged connectors are used for joining larger sizes of pipes while tube connectors are used for smaller sizes. Ordinarily the change over from one type to the other occurs at a diameter of about one inch. The transition is dictated by torque requirements on the bolts. If flanged connectors are used for very small pipes the bolts become too small for reliable torquing. On

the other hand if a tubing connector were used for very large pipes, the wrenches would need to be unreasonably large. In very high-pressure systems the axial loads are so high that the transition from tube to flange connectors might occur at sizes below one inch; while, with very low pressures the size could be somewhat greater than one inch.

2.0.2 Material Choice for Flanged Connectors

Materials for use in flanged connectors must first be selected on the basis of their compatibility with the fluids being transferred. Secondly, they must have an appropriate strength at the temperatures and other environmental conditions to which they will be subjected. Finally, weight, weldability, low expansion coefficient, low creep, corrosion resistance, ease of machining, fatigue strength, ductility, stiffness, etc., may be important material considerations in a particular design. Necessary information on materials of interest in fluid connector design is provided in Section 6 of this Handbook.

Selection of flange materials for connectors used in missiles has in the past largely been limited to stainless steels and aluminum alloys. Bolt and loose flange materials need not have as great a compatibility with missile fluids and therefore offer a greater range of selection.

Where the gasket is not a vendor item, it is recommended that tests be performed to determine the seating and minimum operating gasket forces. Where sealing is the result of plastic flow of the gasketing material, a sealing stress of about 2.75 times the yield stress is indicated in Section 1 (page 1-6), "Fundamental Considerations of Separable Connector Design." To keep bolt forces low, therefore, it is desirable that the gasket be thin. Ordinarily once a "seal" has been made, the gasket force may be reduced up to about half (the exact value of the reduction will depend on the sealing mechanism and is best determined by test) before its ability to maintain "zero leakage" is lost. This consideration governs the seal width since the initial gasket force must be large enough so proof and operating loads do not reduce it below the minimum value permitted.

Where sealing is achieved by mating surfaces whose finish is in the microinch range, the material selection should emphasize wear resistance. Thus the loss in finish, with repeated use and with the "working" which accompanies assembly as well as temperature and pressure changes, will be minimized.

Lubricants to reduce the coefficient of friction between bolt and nut, and at other contact points, are important because variability in this factor is a primary source of variability in the force at the gasket to achieve sealing. The lubricant should be selected to be compatible and to give the lowest possible friction coefficients between rubbing parts.

2.0.3 Environmental Conditions

Some of the environmental conditions to which a fluid connector is subjected primarily affect the material properties or the material integrity. These include:

a. Chemical interaction; i.e., LOX sensitivity or corrosion resistance.
b. Radiation

c. Temperature; i.e., change in mechanical properties with temperature or loss of heat treatment, etc.

Other environmental conditions also cause the connector to deform. These include:

a. Fluid pressure.
b. Axial load or bending moment on pipe.
c. Thermal expansion.
d. Creep
e. Vibration, shock, water-hammer.

The first group of environmental conditions primarily affect material selection, while the second group primarily affect the detailed geometric design.

2.0.4 Interaction of Flanges and Seal

The choice of a seal determines the assembly preload and the load to be maintained under various operating conditions. Shear O-rings, knife edges, and other wedging-type seals, as compared with flat gaskets, permit about twice as large a ratio between the gasket load at assembly and when operating. Pressure-energized seals, such as the metal O-ring or the Naflex types, are ordinarily contained so that the primary load path bypasses the seal. Such seals place limits on the permissible flange separation at the seal and may also place limits on the permissible relative radial "scrubbing" between flanges.

For flange re-usability it is important that the seal material be softer than the flange material. Surface finish of the flange at the gasket has a moderate effect on the gasket force required for sealing.

Where welding, or some other manufacturing process,is expected to result in a small lack of flange flatness, variable flange rolling or variable gasket compression must make up the difference.

2.0.5 Input Parameters Needed by Flange Designer

The flanges will be subjected to bolt forces, gasket forces, pressure, and pipe forces. The pipe forces include not only the hydrostatic end load from internal pressure but also axial load and bending moment from the pipe supports, Ref 2.3, or from vibration, shock or water-hammer, Ref 2.1. For purposes of design,it will often be adequate to combine the pipe forces into an "equivalent" axisymmetric axial load causing axial pipe stresses equal to the maximum axial fiber stress under the actual axial load (including hydrostatic end load) plus twice the bending moment. (The doubling of the bending effect is an estimate based on the results on pages 47-49 of Ref 2.3 which show a factor of one is unconservative).

In addition to loads,the flange designer must know the operating pressures and temperatures and the time over which satisfactory performance must be maintained.

Combining this information with a knowledge of the fluids, special environmental factors, and re-usability requirements, the flange designer can

select materials and proceed with a detailed design of the flanges.

The input parameters required are therefore:

a. Pipe size and fluid identification.
b. Pipe axial load and bending moment.
c. Fluid pressure-temperature-time history.

2.0.6 Flange Type

A floating (or loose) flange is used when it is necessary to join sections of pipe for which it is not possible to be sure the bolt holes of adjoining flanges will line up.

No contact outside the bolt circle has been standard practice in the ASME codes. Occasionally it is found desirable, however, to have contact outside the bolt circle. Typical cases are:

a. Where a pressure energized seal is being used and such a configuration provides convenient containment for the seal as well as preventing flange rolling.

b. Where internal pressure is low and the pipe wall is so thin that it affords little restraint to flange rolling.

c. Where control of gasket thickness is good enough to provide the planned sharing of bolt load between the gasket and the contact outside the bolt circle.

d. Where floating flanges might roll excessively.

In the case where the flanges are in contact outside the bolt circle, there is little flange rolling and therefore the bolts are loaded more squarely. This effect permits the use of bolt loads closer to the yield stress times the root cross-sectional area than the 25 percent permitted in the ASME code in the case of flanges with no contact outside the bolt circle. The decreased bolt size permits smaller flange dimensions when there is contact outside the bolt circle.

Present design experience with flanges having contact outside the bolt circle is insufficient to provide a simple guide to predict when they may be prefereable to those having no such contact. In the cases listed above it appears to be desirable to perform design studies with both types.

2.0.7 Organization of Section 2

After selecting the flange type, steps in the flange design will be considered in the following sequence:

a. Selection of materials for the flanges, bolts, and gaskets.

b. Identification of design values for gasket forces, internal pressure, temperature, and pipe loads for assembly, proof test, and various operating conditions.

c. Determination of mechanical property values for the materials taking account of the effect of temperature and time under load.

d. Estimation of a preliminary design layout.

e. Calculation of stresses and deformations for the preliminary design.

f. Modification of the design to bring stresses and deformations to design values.

2.0.8 Limitations of Section 2

The analysis is based on linear elastic theory. Therefore, no account is taken of localized yielding which may result from the addition of design stresses to the residual stresses which may have been left during flange manufacture. In the case of ductile materials, it may frequently be desirable to apply initial high bolt forces causing some yielding in the hub region. When the bolt force is released the resulting residual stress pattern may be such that the creep resistance is improved at lower bolt loads, Ref 2.6. The analysis given here applies only after this initial yielding has taken place.

Creep is not considered directly in Section 2. Instead, it is taken into account to a limited degree by using reduced values of allowable stresses. Creep will be more pronounced in highly stressed areas, so that some redistribution of stress will occur. It is recommended that the reduced value of stress, if any, be that for which a 10 percent relaxation of stress will occur during the time the connector is subjected to surge pressure at temperature. Since only localized areas of the connector are at maximum stress, this requirement should result in a much smaller reduction in bolt and gasket loads in the connector, probably less than five percent.

2.1 Design Procedure

Design procedures for axisymmetric flanged connectors are presented in various standards, in ASME papers, Ref 2.4, and in the Taylor Forge Bulletin, Ref 2.2. These procedures embody a number of rational formulas together with design rules and approximations based on past experience.

Perhaps the most significant difference imposed by launch vehicle use is that "zero leakage" must be maintained whereas previously it was sufficient to prevent "large scale leakage". From the point of view of flange design, this means that a substantial gasket load is required even at the highest pressures. A second difference is that the temperature range is wider from cryogenic values to those for hot gases. A third difference is that weight is a far more important requirement for missile applications than it would be for connectors used on the ground. A fourth difference is that dynamic forces in a missile apply substantial loads to the connector. Finally, it is likely to be more difficult to retighten bolts and thus compensate for creep effects.

The design procedure presented herein will have fewer approximations in the formulas than those given previously and will include design rules based on

launch vehicle experience. The computations will determine deformations as well as stresses since in some cases excessive deformation is the reason for poor performance. A detailed design procedure is presented here for lap flanges; whereas, in the past these were frequently "estimated" with resulting excessive deformations and stresses.

2.1.1 Material Properties

Compatibility with the fluid is a primary requisite of the flange material. Table 6.5 in Section 6 of this manual provides information on the chemical compatibility of various flange materials with propellants in a static environment. It can be used as an indicator of the materials having the best probability of being compatible in the presence of abrasion or other severe mechanical environments.

Mechanical properties are given in Tables 6.1 to 6.3 of Section 6. Table 6.3 shows, for example, that in the 1500°F temperature range only nickel alloys and stainless steels have suitable properties. Table 6.1 shows that, at room temperature, aluminum alloys are quite competitive on a strength/weight basis.

Not all materials are suitable for use at cryogenic temperatures since they may become too brittle or experience phase transformations that make them unsuitable. Some steels, for example, become unsuitable at as high a temperature as 0°F, with the 300 series of stainless steels conditionally suitable at cryogenic temperature. Nickel alloys and aluminum alloys are suitable for service at liquid helium temperatures.

2.1.2 Design Loads

Maximum and minimum gasket forces for zero leakage must ordinarily be obtained empirically. If the gasket is a vendor item, the manufacturer can frequently provide values. Factors affecting the gasket force are the gasket material, the surface finish of the flanges, and the flange contour, i.e. flat or knife-edges. On the basis of limited results in Section 1.2.1.6 it appears that flat gaskets require stresses of about 2.75 times the yield stress to achieve "zero leakage". The gasket force can then be reduced roughly a third before the "zero leakage" state is lost. (With knife-edge type gaskets the permissible reduction is closer to two-thirds). The initial gasket load must be large enough so that the application of pressure and pipe loads will not reduce it below the limiting minimum value.

Pressure energized gaskets are usually "contained". As a result there will be flange-to-flange contact. In such a case the force at the flange-to-flange contact can drop to nearly zero without impairing the gasket performance.

Internal pressure is zero during assembly. During proof test it will be 1.5 times the maximum operating pressure, in the absence of other specifications. The connector must also withstand all pressure and temperature combinations anticipated during its service life. Pressure surges can cause increased momentary pressure in the pipe line when valves are opened, Ref 1, Chapter 62. Although these might, under adverse circumstances, double the pressure, it seems that in general a 50 percent increase is a generous design margin for this purpose.

Card #31

Pipe load is ordinarily considered to be the result of hydrostatic end force in the case of ground installations. In a launch vehicle system, however, it can also be affected by relative displacement of the pipe supports during launch vehicle flexing and by dynamic forces resulting from vibration or shock. Ref 2.1, Chapter 63, shows that dynamic forces of 50 to 100 times the static forces due to gravity can be expected. Thus, it is important to place pipe supports close enough to keep the static forces due to gravity at low levels. In the absence of other specifications, it will be assumed in this handbook that the pipe supports are placed closely enough to prevent the dynamic forces from adding a load having an effect greater than that of the hydrostatic end force. In the absence of specific surge information, fluid surging will be considered able to add 50 percent to the pressure. Thus, the design value of the internal pressure and equivalent pipe load is taken as,

$p = 1.5\ p_{max.oper.}$ during operation with surges ($lb/in.^2$)

$P = 2.5\ \pi R^2\ p_{max.\ oper.}$ during operation with surges (lb.)

(Note: In these equations the 0.5 factor is for a nominal surge factor of 50 percent. With specific surge information this factor should be replaced by the actual value)

For pipe with less than 1.5" O.D.

$p = 2.0\ p_{max.\ oper.}$ during proof test ($lb/in.^2$)

$P = 2.0\ \pi R^2\ p_{max.\ oper.}$ during proof test (lb.)

$p = 4.0\ p_{max.\ oper.}$ during burst test ($lb/in.^2$) (2.1)

$P = 4.0\ \pi R^2\ p_{max.\ oper.}$ during burst test (lb.)

For pipe with greater than 1.5" O.D.

$p = 1.5\ p_{max.oper.}$ during proof test ($lb/in.^2$)

$P = 1.5\ \pi R^2\ p_{max.\ oper.}$ during proof test (lb.)

$p = 2.5\ p_{max.oper.}$ during burst test ($lb/in.^2$)

$P = 2.5\ \pi R^2\ p_{max.\ oper.}$ during burst test (lb.)

$p_{max.oper}$ = maximum operating internal pressure ($lb/in.^2$)

In Eq.2.2, the bending moment effect is doubled in line with the results in Chapter 47 of Ref 2.3.

No additional margin is added above the added 50 percent required for surges during operation and 100 percent (Eq. 2.2) required for dynamic loads. These added loads are present for only a short portion of the life of the connector and thus provide a substantial margin to cover creep, fatigue, thermal transients, etc.

Creep is presently not well understood. It may have a significant effect

when surge pressure is present for long time periods at high temperature. To remove the effects of early creep, the practice of retightening the bolts over a period of several days after initial assembly is recommended. In the case of ductile flange materials it is sometimes advantageous to initially tighten bolts enough to cause some yielding at the hub-flange junction and thereby achieve a more favorable residual stress distribution, Ref 2.6. Such procedures, however, require thorough experimental verification of their effect on creep in a particular installation. Flanges, bolts, and hubs designed by the procedures in this handbook will have stresses below the yield range at all times and therefore will probably have little long-time creep. Excepting for connectors which must operate for long periods of time at high temperatures under their most severe loading conditions, it is recommended that long-time creep be considered negligible for launch vehicle applications. This is done in this handbook. A reduced allowable stress can be used in design if experience indicates creep is significant. This stress should be that for which a 10 percent relaxation in stress will occur during a time equal to the life required under surge pressure conditions at temperature.

2.1.3 Design Requirements

The octahedral stress at any position in the bolts, flanges, or hub is given by

$$\sigma_o = \sqrt{\frac{1}{2}}\sqrt{(\sigma_1 - \sigma_2)^2 + (\sigma_2 - \sigma_3)^2 + (\sigma_1 - \sigma_3)^2}$$

where

σ_1, σ_2, σ_3 = hoop, axial and radial stresses respectively.

The requirement to be satisfied is:

$$\sigma_o < \sigma_{allow} \qquad (2.3)$$

where

σ_{allow} = The allowable stress. The yield stress at temperature is taken as σ_{allow} where creep is not important. Where creep is significant, σ_{allow} is taken as the stress for which a 10 percent relaxation in stress will occur during a time equal to the time during which surge pressure is acting at temperature. (It should be noted that standards which permit only 25 percent of the yield stress for bolt materials do not consider bolt bending as is done here. The inclusion of bolt bending is in fact a stricter requirement in many cases). The presence of cyclical loads may require a reduction of allowable stress, however, the margin for surges and dynamic loads in Eq. 2.1 provides substantial fatigue life even when the yield stress is taken as the allowable stress.

The stresses at locations of high stress in a connector are generally a combination of axial and bending stresses. As a result, so long as the connector materials have some ductility, Eq. 2.3 is conservative, since exceeding σ_{allow} moderately merely results in a stress redistribution, rather than failure.

Deformations under load must be such that no interference of parts results. Loose-ring, floating, flanges must be particularly checked for excessive rotation. Lap flanges may also rotate excessively.

The gasket force must always exceed its minimum permitted value.

2.2 Flanges with No Contact Outside the Gasket Circle

The most widely used flanged connector is that having no contact outside the gasket circle. Use will be made of the elastic interaction of the bolts, flanges, hubs, gasket and pipes under the various applied loads to arrive at an optimum design configuration. The design procedure involves selecting a preliminary design layout, analyzing for stresses and deformations under the various loading conditions, using the results to select an improved design layout, reanalyzing, and remodifying until an efficient design is attained. Every effort has been made to make the preliminary design procedure a good one. However, for simplicity, only a few parameters can be considered at a time. Thus, the highly complex interactions of the connector parts can only be accounted for approximately in the preliminary design phase. At least one or two cycles of the analysis-redesign procedure are essential if an optimum configuration is to be achieved.

The detailed design procedure is presented here in a form suitable for hand computation so that the procedures can be clearly understood. It is also in a form which can readily be translated to digital computer language either in part or total. Where many connectors must be designed, use of a digital computer recommends itself both from the point of view of accuracy in the many numerical computations involved as well as cost in repeating computations to achieve an optimum configuration.

2.2.1 Preliminary Design Layout - Integral Flanges

a. Determine the pipe size, wall thickness, and material to either side of the connector. Select materials for the connector halves to be the same as the corresponding pipes except for possible differences in heat treatment or alloying compounds to improve creep, fatigue, or yield strength. Check that the pipe wall thickness satisfies Section 2.4.1 c.

Select a connector sealing system whose maximum permissible load exceeds its minimum permissible load for "zero leakage" by at least $2.5\,\pi R_G^2\, p_{max\ oper.}$, the estimated reduction in gasket load during operation.

Determine:

1. Details of the seal -- material, thickness, diameters, etc.
2. Axial load, (G_I) needed to make an effective seal.
3. Axial load, (G_M) needed to maintain a seal at operating temperature

(See Section 2.1.2 for guidance on selecting gasket loads).

b. Determine the initial bolt load, (B_I), as the greater of the two values:

(G_I) or

$(G_M) + 2.5\pi R_G^2 p_{max.oper.}$

where R_G is the average radius of the seal and $p_{max.oper.}$ is the maximum nominal operating pressure (no surges). The factor of 2.5 is an empirical value included to allow for pressure surges, bending moments and axial forces imposed on the system, in addition to bolt load caused by normal pressure.

Select a bolt material and determine its yield stress at maximum operating temperature. In selecting bolt material desirable factors include: high strength, coefficient of expansion compatible with flange material coefficient, and suitability over the entire temperature range low end as well as high end.

Determine (A_B), the minimum permissible bolt total area at the root of of the threads.

$$(A_B) = \frac{5 \cdot (B_I)}{(S_B)}$$

where (S_B) is the yield strength of the bolt material at maximum working temperature. The factor 5 is included to allow for the increase in stress (over that caused by straight tension) due to the normally present bolt bending. For arriving at a preliminary design, it is assumed that the rigidity of the seal system is enough greater than the rigidity of the bolt-flange system that the bolt stress is relatively unaffected by pipe vibration forces and pressure changes and no factor need be included for fatigue.

c. Use Table 2.1, Column 2, to select a bolt size. Enter Column 1, in the appropriate thread-type column, at a value equal to or just larger than the ratio $(A_B)/(R_{BC})$ where (R_{BC}) is an estimated bolt circle radius. The bolt size is given in Column 2. Columns 3 through 7 give other data related to bolt size.

Check to see that the estimated value of (R_{BC}) was reasonable by applying the formula

$$(R_{BC}) = R + (\text{Col. } 5) + (\text{Col. } 7) \times \sqrt{(S_B)/(S_F)}$$

where $(S_B)/(S_F)$ is the ratio of yield stresses for the bolt and flange materials, R is the inner radius of the pipe, and (R_{BC}) is the bolt circle radius. If (R_{BC}) is sufficiently changed that using it in Column 1 of Table 2.1 results in a different bolt size selection, recheck using the new bolt size.

Table 2.1 is based on standard bolts. The use of internal wrenching bolts or special thin-wall wrenches would, generally, result in a design using a larger number of smaller bolts and a reduction in overall connector size and weight.

Select an integral number of bolts, n, such that n is as small as possible while satisfying the relationship:

$n \geq (A_B)/(\text{Col. } 3)$

Check that (R_{BC}) satisfies the relationship:

$$(R_{BC}) \geqq \left(\frac{m}{2\pi}\right) \text{ (Col. 4)}$$

If it does not, it will be necessary to increase (R_{BC}) enough to meet this requirement, while leaving the number and size of bolts unchanged.

d. Select a flange thickness (H_I) and a hub thickness (T_I) based on,

$$(H_I) = \text{(Col. 7)} \times \sqrt{(S_B)/(S_F)} = (T_I)$$

Select a flange outer radius, (R_{OL}), given by,

$$(R_{OL}) = (R_{BC}) + \text{(Col. 6)}$$

Select a radius for the large end of the hub, (R_{HI}), given by,

$$(R_{HI}) = R + (T_I)$$

e. Select a hub length (L_I) given by

$$(L_I) = \sqrt{(R/2)\left[(T_I) + (T_P)\right]}$$

where (T_P) is pipe wall thickness.

Determine the hub slope (S_H), given by,

$$(S_H) = (L_I)/\left[(T_I) - (T_P)\right]$$

If $(S_H) < 3$, it may be necessary to modify the hub by adding a section with a reduced taper. The details of the reduced taper hub are dictated by welding limitations and should be made to satisfy good welding practice, but not to add unnecessarily to weight. In general, and in the absence of welding information which would be specific or indicate a different design to be better, the hub adjacent to the pipe should have a taper not exceeding 1:3 and a length of at least four pipe wall thicknesses. Thus, in the absence of specific data, make:

$$(L_T) = 4(T_P)$$

$$(R_T) = R + \left(2\tfrac{1}{3}\right)(T_P)$$

(Refer to Figure 2.2)

Add welding details to drawing.

Add fillet radii to limit stress concentration at:

1. Transition of flange to hub. Make the fillet radius between 0.1 and 0.2 (T_I).

2. Transition of hub to reduced taper hub, if used, and to pipe.

Make the fillet radius between 0.1 and 0.2 (T_p)

f. Choose a lubricant for the bolt-nut-flange interfaces to give the lowest possible coefficient of friction.

Specify bolt torque and torqueing procedure.

Bolt torque is given approximately by,

$$T = \left(\frac{1}{2}\,\mu_N + \frac{3}{4}\,\mu_F\right)\, d\left[\frac{(B_I)}{n}\right]$$

where d is the nominal bolt diameter (i.e., 5/8 inch, 1 inch, etc.), μ_N is the coefficient of friction between the bolt and nut, and μ_F is coefficient of friction between flange and nut.

A torqueing pattern should be specified which will avoid uneven tightening. A suggested pattern for an eight-bolt assembly is to tighten in the order 1, 5, 3, 7, 2, 6, 4, 8; repeating this pattern for the following loads:

1. Finger tight.
2. Bolt 1 brought to 1/4 rated torque or 1/3 turn increment, whichever is reached first, and all bolts brought to approximately same torque in stated order. If necessary repeat 1/3 turn increments till 1/4 rated torque is reached.
3. Repeat for 1/2 T (but not to exceed 1/6 turn increments).
4. Repeat for 3/4 T (but not to exceed 1/6 turn increments).
5. Repeat for rated torque (but not to exceed 1/6 turn increments) and repeat sequence for rated torque until no bolt continues to tighten when rated torque is applied.

The correct values of μ to use depend on materials and the lubricant, if any, that is used. Guide values are given in Table 2.2 . Combinations of materials which may gall should be avoided if possible. It is best to determine the actual relationship between bolt torque and bolt load by test in actual flanges since in use the bolt load is applied eccentrically as a result of flange cocking. In addition the coefficient of friction is variable from one application to another. In some cases bolt load may be set more accurately by tightening the nut an appropriate number of turns, depending on overall connector flexibility.

g. Select coefficients of friction for the contact between gasket and flange. An approximate value for this is 0.5 if test values are unobtainable.

h. Add dimensional tolerances in accord with standard shop practice except that sealing face flatness tolerance should not exceed 0.1 times the expected compression of the gasket.

i. Select loading conditions for which a detailed analysis to be described is required. These would normally include,

1. Initial assembly-

   Given - Bolt force (B_I)
   Axial load P and internal pressure p are zero
   Temperature is room temperature

   Determine - Initial stretch C of bolt-flange-pipe system as well as stresses and deformations

2. Maximum operating conditions

   Given - Initial stretch C from above solution
   $p = 1.5\ p_{max\ oper.}$
   $P = 2.5\pi\ R^2 p_{max\ oper.}$
   Temperature, operating temperature.

3. Other severe environmental conditions, if present.

Compute the stresses and the deflections that develop in the above trial design for the various loading conditions in accordance with Section 2.2.2. Determine whether any deflection is excessive. Determine whether at any point the octahedral stress, σ_o, multiplied by the appropriate stress concentration factor is either: 1) in excess of the yield stress at maximum temperature reduced by appropriate factors for fatigue and relaxation; or 2) is appreciably lower than this value. (For a few materials yield stress is lower at a lower temperature. In these cases, the lowest yield stress in the intended operating range should be used).

Factors to be used are:

Place	Purpose	Factor
Flange -	For stress concentration at fillet.	1.3
	For fatigue (assuming gasket has appreciably less compliance than bolt-flange system).	1.0
	For stress relaxation.	Select factor based on service life at high temperature. For most designs 1.0 is appropriate. See Section 2.0.8
Hub	For stress concentration at flange fillet	1.3
	Elsewhere on hub	1.0

Place	Purpose	Factor
Hub	For fatigue	Select factor based on material, steady-state stress, alternating component due to vibration and desired life. If not specifically determined use factor of 2.0.
	For stress relaxation.	Select factor based on service life at high temperature. For most designs 1.0 is appropriate. Section 2.0.8.
Bolts	For stress concentration	1.0
	For fatigue (see note for flange)	1.0
	For stress relaxation.	Select factor based on service life at high temperature. For most designs 1.0 is appropriate. See Section 2.0.8.

(Note: Complete steps i through ℓ before attempting to complete a modified design).

j. Check for load on the gasket under design conditions and determine whether this load exceeds (G_M), the gasket load required to maintain a seal. If gasket load drops too much, it is an indication of excessive deformation due to pressure. It can be corrected by using a higher initial gasket load with correspondingly higher initial bolt load. These in turn result in corresponding increases in flange and bolt dimensions. (Complete steps i through (ℓ) before attempting to complete a modified design).

k. If under design loads octahedral stress multiplied by the stress concentration factor is greater than the yield stress reduced by the fatigue and relaxation factors, modify the design as follows:

Overstressed Part	Action
Bolt	Infrequent occurrence. Recheck calculations for error. New trial design if appropriate using more bolt area.
Flange or hub near flange	Increase thickness by a factor equal to half the overstress factor.
Hub, near pipe	Modify hub to join pipe with decreased taper, either by increasing hub length or by using hub with two or more graduated tapers.

ℓ. If octahedral stress is lower than permissible, this indicates the preliminary design is too conservative. The reverse action of step k should be taken.

TABLE 2.1

Estimation of Bolt Size and Number of Bolts*

(1) (Total Bolt Area) (Bolt Circle Radius)			(2)	(3) Root Area			(4)	(5)	(6)	(7) Flange Thickness Factor		
Fine	Coarse	8 Thread	Bolt Size	Fine	Coarse	8 Thread	Bolt Spacing**	Radial Eccen.	Edge Distance	Fine	Coarse	8 Thread
(in)	(in)	(in)	(in)	(in^2)	(in^2)	(in^2)	(in)	(in)	(in)	(in)	(in)	(in)
.273	.225	---	1/4	.0326	.0269	---	3/4	1/2	3/8	.161	.147	---
.406	.352	---	5/16	.0524	.0454	---	13/16	9/16	7/16	.209	379	---
.508	.426	---	3/8	.0809	.0678	---	1	5/8	1/2	.246	.225	---
.609	.521	---	7/16	.1090	.0953	---	1-1/8	11/16	9/16	.283	.262	---
.748	.633	---	1/2	.1486	.126	---	1.25	.81	.62	.340	.313	---
1.007	.845	---	5/8	.2400	.202	---	1.50	.94	.75	.426	.390	---
1.262	1.083	---	3/4	.3513	.302	---	1.75	1.12	.81	.521	.482	---
1.464	1.278	---	7/8	.4805	.419	---	2.06	1.25	.94	.592	.553	---
1.743	1.537	1.537	1	.6245	.551	.551	2.25	1.37	1.06	.676	.634	.634
2.040	1.740	1.828	1-1/8	.8118	.693	.728	2.50	1.50	1.12	.765	.706	.723
2.29	1.988	2.08	1-1/4	1.024	.890	929	2.81	1.75	1.25	.876	.815	.836
2.69	2.16	2.37	1-3/8	1.260	1.054	1.155	3.06	1.87	1.37	.981	.878	.921
2.94	2.50	2.71	1-1/2	1.521	1.294	1.405	3.25	2.00	1.50	1.058	.976	1.015

*Derived from Ref. 2, page 27, and other sources.

**This spacing can be reduced with internal wrenching bolts or by use of special thin-wall wrenches. When this is done, an appreciable reduction in flange weight is possible since the bolt size can be reduced one or two sizes.

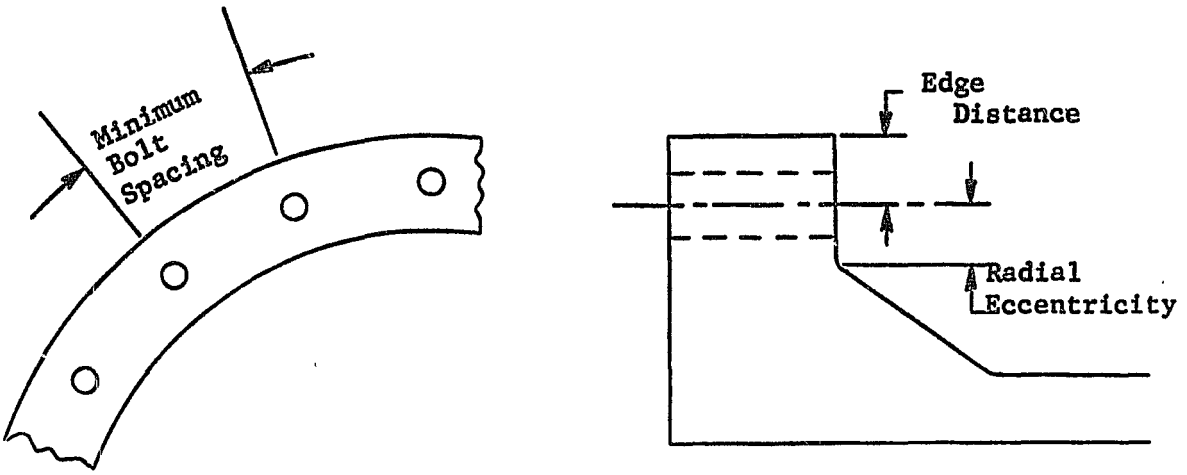

Figure 2.1. Bolt Clearances. See Table 2.1 for Values.

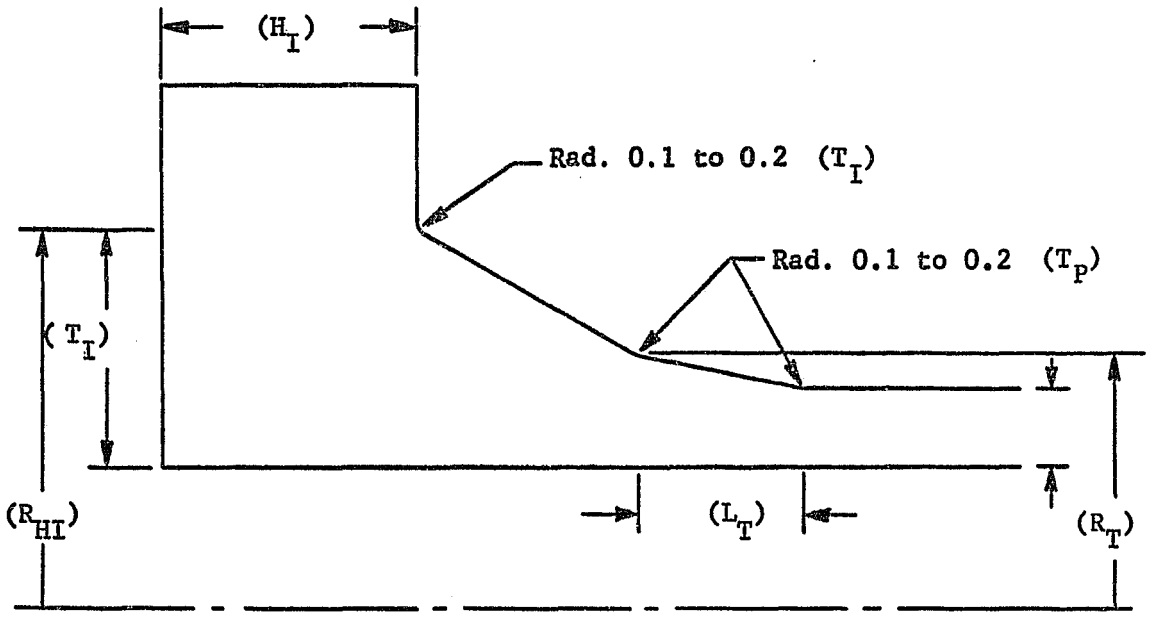

Figure 2.2. Double-Taper Hub Initial Dimensions.

Table 2.2

APPROXIMATE FRICTION COEFFICIENTS

Lubricated Steel on Steel	0.1
Dry Steel on Steel	0.7
Lubricated Aluminum on Steel	0.2
Dry Aluminum on Steel	0.6
Lubricated Aluminum on Aluminum	0.1
Dry Aluminum on Aluminum	1.0

2.2.2 Integral Flanges With No Contact Outside the Gasket Circle Detailed Analysis

An elastic analysis is achieved by satisfying equilibrium and compatibility conditions at the pipe-hub and flange-hub interfaces as well as at the flange-bolt and flange-gasket interfaces. From the elastic analysis, deformations and stresses are obtained at all locations of interest. In the following discussion, the flange is considered to be a plate and the pipe and hub are considered to be cylindrical shells. The bolts are considered to be eccentrically loaded by the flanges at their radially inward side because of flange rotation. The gasket is considered elastic.

The solution in regard to the hub and flange ring is basically a step-by-step process. Thus, the solution of a large number of simultaneous equations is avoided. Starting at the small end of the hub Section 2.2.2.1 proceeds stepwise down the hub. At each step, values are obtained for the wall shear, wall moment, radial deflection, and slope in terms of the wall moment and wall shear at the small end of the hub and the pressure, p, axial load, P, and expansion $\alpha\Delta$ T. Then in Section 2.2.2.2 the solution proceeds similarly from the inner to the outer radius of the flange ring. Finally, the wall moment and the wall tension are set to zero at the outer radius of the flange ring and the resulting two simultaneous equations for the moment and shear at the small end of the hub are solved in terms of p, P, $\alpha\Delta$T, (B or C) and Q_{gf}.

The solution in regard to the influence of bolt and gasket stiffness is found in Sections 2.2.2.3 and 2.2.2.4. Here three simultaneous equations must be solved. One of these equations involves compatibility of the bolt stretch, gasket compression, and flange ring deflection. The other two equations involve compatibility of the radial displacements of the flange rings and gasket at their points of contact. Solution of these equations gives the values of (B or C) and the gasket friction force on each face of the gasket in terms of p, P, $\alpha\Delta$ T. With these the hub and flange ring forces are obtained at the small end of the hub and elsewhere and the corresponding stresses are also obtained.

Because of the length of the computation and the fact that it involves the solution of simultaneous equations, it is recommended that five or more

significant figures be maintained in the numerical computation.

2.2.2.1 Pipe Stiffness Including Hub

With cylindrical shell theory, Appendix 2A, it can readily be shown that the deflection and slope of the wall at the end of a long pipe due to wall moment, wall shear, axial force, pressure, and temperature is

$$u = \left(\frac{R\beta^2}{\pi Et}\right) M + \left(\frac{R\beta}{\pi Et}\right) Q + \left(\frac{R^2}{Et}\right) p - \left(\frac{\nu}{2\pi Et}\right) P + R\alpha\Delta T \qquad (2.4)$$

$$\theta = \left(\frac{2R\beta^3}{\pi Et}\right) M + \left(\frac{R\beta^2}{\pi Et}\right) Q \qquad (2.5)$$

(When the radii to inner and outer pipe walls differs much from R, Eqs. 2A-1 and 2A-2 should be used.)

With cylindrical shell theory for a pipe segment it can be shown (Appendix 2B) that the deflection, slope, wall moment, and wall shear at one end are given in terms of those at the other end and the internal pressure, axial load, and temperature change as

$$Q_r = + K_4 Q_\ell + 2\beta K_1 M_\ell + \left(\frac{\pi Et}{R\beta^2}\right) K_2 \theta_\ell + \left(\frac{2\pi Et}{R\beta}\right) K_3 u_\ell - \left(\frac{2\pi R}{\beta}\right) p K_3 + \left(\frac{\nu}{R\beta}\right) K_3 P - \left(\frac{2\pi Et}{\beta}\right) \alpha\Delta T K_3 \qquad (2.6)$$

$$M_r = -\left(\frac{1}{\beta}\right) K_3 Q_\ell + K_4 M_\ell - \left(\frac{\pi Et}{R\beta^3}\right) K_1 \theta_\ell - \left(\frac{\pi Et}{R\beta^2}\right) K_2 u_\ell + \left(\frac{\pi R}{\beta^2}\right) K_2 p - \left(\frac{\nu}{2R\beta^2}\right) P K_2 + \left(\frac{\pi Et}{\beta^2}\right) \alpha\Delta T K_2 \qquad (2.7)$$

$$\theta_r = - \left(\frac{R\beta^2}{\pi Et}\right) K_2 Q_\ell + \left(\frac{2\beta^3 R}{\pi Et}\right) K_3 M_\ell + K_4 \theta_\ell - 2\beta K_1 u_\ell + \left(\frac{2\beta R^2}{Et}\right) K_1 p - \left(\frac{\beta\nu}{\pi Et}\right) K_1 P + 2\beta R\alpha\Delta T K_1 \qquad (2.8)$$

$$u_r = - \left(\frac{R\beta}{\pi Et}\right) K_1 Q_\ell + \left(\frac{R\beta^2}{\pi Et}\right) K_2 M_\ell + \left(\frac{1}{\beta}\right) K_3 \theta_\ell + K_4 u_\ell + \left(\frac{R^2}{Et}\right)(1-K_4) p - \left(\frac{\nu}{2\pi Et}\right)(1-K_4) P + R(1-K_4)\alpha\Delta T \qquad (2.9)$$

Where subscripts "r" and "ℓ" refer to "right" and "left" ends of the segment respectively.

$$\beta^4 = 3\,(1-\nu^2)\,/R^2t^2 \qquad (2.10)$$

$$K_1 = \left(\frac{\beta^3L^3}{3}\right)\,(1 - \beta^4L^4/210),\ \beta L<1 \qquad (2.11)$$

$$K_2 = \beta^2L^2\,(1-\beta^4L^4/90),\ \beta L<1 \qquad (2.12)$$

$$K_3 = \beta L\,(1-\beta^4L^4/30)\ ,\beta L<1 \qquad (2.13)$$

$$K_4 = 1 - \beta^4L^4/6 + L^8/2520\ ,\beta L<1 \qquad (2.14)$$

Where L = length of pipe segment (in.).
(For values of β L greater than one or for the case where the inner and outer pipe walls have radii much different from R use Appendix 2B).

The theory for tapered hubs is available only for hubs with a linear taper. Even in the case of a linear taper, taking account of all four hub variables, that is, radius, length, and thickness at each end, becomes quite cumbersome. To avoid these difficulties the following procedures will be used:

a. Divide the hub into a small number of cylindrical segments as shown by the dotted lines in Figure 2.3. The cylinders should approximate the hub dimensions. Three should ordinarily suffice.

b. Obtain Eqs. 2.6 to 2.14 for each segment.

c. Use Eqs. 2.4 and 2.5 to obtain the deflection and rotation at the small end of the hub in terms of the wall moment and wall shear at this location.

d. Take the slope and wall shear obtained in (c) as the values at the left side of the first hub segment from the small end of the hub. Take the moment and deflection obtained in (c) and add to them.

$$\Delta M_1 = (P/2)\ (\text{thickness of wall of first segment} - \text{thickness of wall of pipe})$$

$$\Delta u_1 = (\alpha\Delta T/2)\ (\text{thickness of wall of first segment} - \text{thickness of wall of pipe}).$$

to obtain the moment and deflection at the left side of the first hub segment. (No correction is used for Δu_1 if R is used in place of the mid-thickness radius in Eqs. 2.4 and 2.6 to 2.9).

e. With the results obtained in (b) for the first hub segment and in (d) for deflection, slope, wall shear, and wall moment at the left side of this segment, corresponding values at the right side of this segment are obtained from Eqs. 2.6 to 2.9.

f. Take the slope and wall shear obtained in (e) as the values at the left side of the second hub segment. Take the moment and deflection obtained in (e) at the right side of the first segment and add to them

$$\Delta M_2 = (P/2)\ (\text{thickness of wall of second segment} - \text{thickness of wall of first segment})$$
$$\Delta u_2 = (\alpha \Delta T/2)\ (\text{thickness of wall of second segment} - \text{thickness of wall of first segment})$$

to obtain the moment and deflection at the left side of the second hub segment.

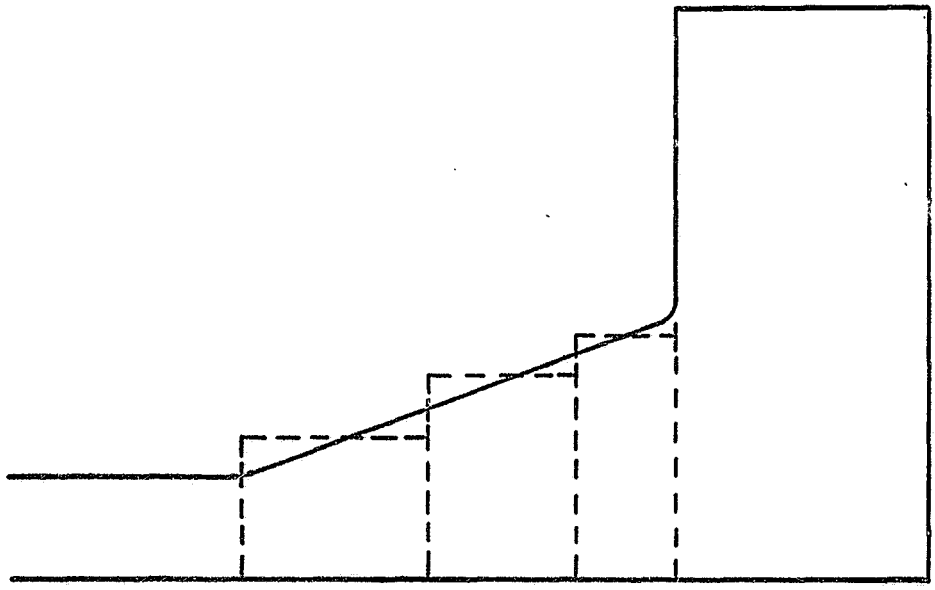

Figure 2.3. Approximate Hub by a Small Number of Cylindrical Segments, shown dotted. (As the number of segments used increases, the wall moment and wall shear as well as the deformations, converge to the values obtained using the theory for a nonuniform wall thickness.)

g. With the results obtained in (b) for the second hub segment and in (f) for values at the left side of the second segment, values at the right side of the second segment are obtained.

h. Repeat steps (f) and (g) for the third and any additional segments giving the moment, M_{Hub}, shear, Q_{Hub}, deflection, and slope at the large end of the hub in terms of the moment and shear at the small end of the hub and p, P, $\alpha\Delta T$.

2.2.2.2 Flange Ring Stiffness

Bolt holes reduce the stiffness of the flange ring. In Ref 2.6 it is shown that the increase in flexibility due to the bolt holes is approximately given by

$$f = \frac{1}{1 - nd^2/\pi(R_{OF}^2 - R^2)} \tag{2.15}$$

Thus, f is equal to the ratio of the flange ring volume without bolt holes to the flange ring volume had the bolt holes been square. Eq. 2.15 is confirmed experimentally in Ref 2.6 for the case of flange rotation.

Regarding stress, it is shown in Ref 2.6 that the weakening effect of the bolt holes occurs at points where the circumferential bending moment is reduced so that there is negligible effect on flange hoop stresses.

All the forces from the hub and gasket are considered, as well as the internal pressure, to cause a resultant radial force, axial force, and moment at the bottom of the flange ring given by,

$$\text{Flange bottom axial force} = \text{bolt pull, } B \tag{2.16}$$

$$\text{Flange bottom radial force, } Q_R = Q_{Hub} + Q_{gf} - 2\pi Rph \tag{2.17}$$

$$\text{Flange bottom moment, } M_R = M_{Hub} - G(R_G - R) - t_{Hub}P/2 + \left(\frac{h}{2}\right) Q_{gf} - \left(\frac{h}{2}\right) Q_{Hub} - \left(\frac{\pi p}{3}\right)(R_G - R)(2R_G^2 - RR_G - R^2) \tag{2.18}$$

Where Figure 2.4 gives sign conventions and symbols.

Q_{Hub} is the total circumferential wall shear force in the hub at the hub-flange interface.

M_{Hub} is the total circumferential wall moment in the hub at the hub-flange interface.

t_{Hub} is the hub thickness at the flange.

Q_{gf} is the frictional force applied by the gasket.

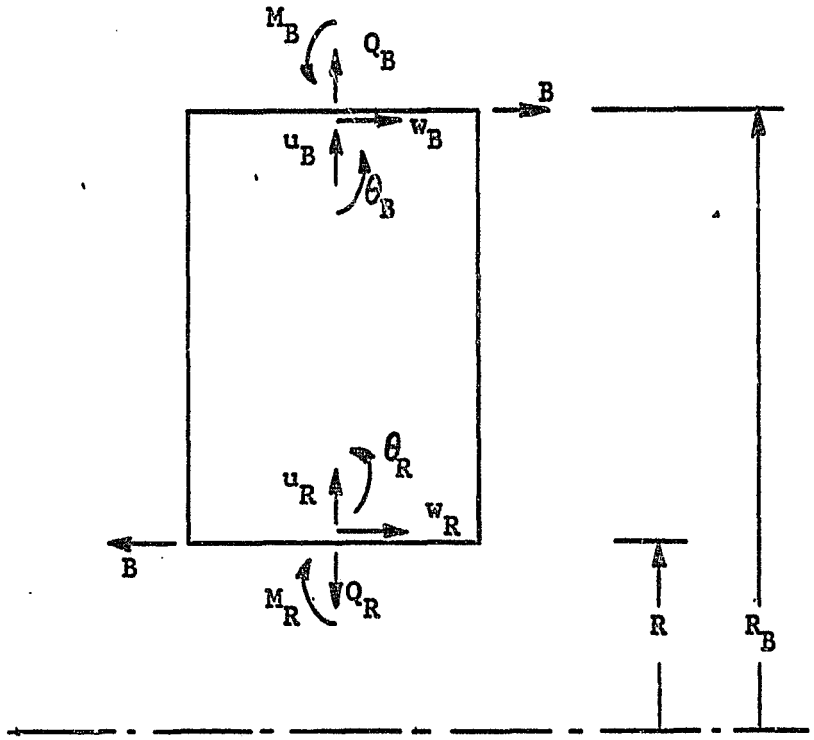

Figure 2.4. Flange Ring Below Line of Action of Bolt Load. (For flanges having no contact outside the bolt circle, R_B is the radius to the circle that is tangent to the inside of the bolts, i e., the radius to the bolt center minus the bolt radius.

The displacements at the bottom of the flange ring are taken as

$$\theta_R = \theta_{Hub}, \quad u_R = u_{Hub} + (h/2)\,\theta_{Hub} - t_{Hub}\,\alpha\Delta T/2 \tag{2.19}$$

The last term in Eq 2.19 is omitted if R is used in place of the mid-thickness radius in Eqs. 2.4 and 2.6 to 2.9 .

The corresponding values at the line of action of the bolts are obtained from the values at the flange bottom (Eqs. 2.16 to 2.19) by the use of Appendix 2 C as,

$$Q_B = 1/2\left[(1+\nu)\frac{R_B}{R} + (1-\nu)\frac{R}{R_B}\right] Q_R + \left(\frac{\pi Eh}{f}\right)\left(\frac{R_B}{R} - \frac{R}{R_B}\right) {}_1R - \left(\frac{\pi Eh}{f}\right)\left(\frac{R_B}{R} - \frac{R}{R_B}\right) R\,\alpha\Delta T \tag{2.20}$$

$$M_B = 1/2\left[(1+\nu)\frac{R_B}{R} + (1-\nu)\frac{R}{R_B}\right] M_R + \left(\frac{\pi Eh^3}{12f}\right)\left(\frac{R_B}{R} - \frac{R}{R_B}\right)\theta_R + \left[(1-\nu)\left(\frac{R_B^2 - R^2}{4R_B}\right) + \left(\frac{1+\nu}{2}\right) R_B \log\left(\frac{R_B}{R}\right)\right] B \tag{2.21}$$

$$\theta_B = \left[\frac{3f(1-\nu^2)}{\pi E h^3}\right]\left(\frac{R_B}{R} - \frac{R}{R_B}\right) M_R + 1/2\left[(1-\nu)\frac{R_B}{R} + (1+\nu)\frac{R}{R_B}\right]\theta_R$$

$$+\left[\frac{3(1-\nu^2)fR_B}{\pi E h^3}\right]\left[-\left(\frac{R_B^2 - R^2}{2R_B^2}\right) + \log\left(\frac{R_B}{R}\right)\right] B \qquad (2.22)$$

$$u_B = \left[\frac{f(1-\nu^2)}{4\pi E h}\right]\left[\frac{R_B}{R} - \frac{R}{R_B}\right] Q_R + 1/2\left[(1-\nu)\frac{R_B}{R} + (1+\nu)\frac{R}{R_B}\right] u_R$$

$$+ 1/2\,(1+\nu)\left[\frac{R_B}{R} - \frac{R}{R_B}\right] R\alpha\Delta T \qquad (2.23)$$

where $B = P + G + \pi p (R_G^2 - R^2)$ (2.24)

R_B = radius to center of bolts minus radius of bolts for flanges which do not touch outside the bolt circle. For flanges that do touch outside the bolt circle, R_B is the radius to the center of the bolts. (2.25)

Proceeding to the top of the flange ring, it is known that the moment and shear at this location are zero. Using the values at the bolt circle given by Eqs. 2.20 to 2.23 in the equations of Appendix 2C, Eqs. 2C.3 and 2C.5 give

$$0 = \left(\frac{\pi E h}{f}\right)\left[\frac{R_{OF}}{R_B} - \frac{R_B}{R_{OF}}\right] u_B + 1/2\left[(1+\nu)\frac{R_{OF}}{R_B} + (1-\nu)\frac{R_B}{R_{OF}}\right] Q_B$$

$$-\left(\frac{\pi E h}{f}\right)\left[\frac{R_{OF}}{R_B} - \frac{R_B}{R_{OF}}\right] R_B \alpha \Delta T \qquad (2.26)$$

$$0 = \left(\frac{\pi E h^3}{12f}\right)\left[\frac{R_{OF}}{R_B} - \frac{R_B}{R_{OF}}\right]\theta_B + 1/2\left[(1+\nu)\frac{R_{OF}}{R_B} + (1-\nu)\frac{R_B}{R_{OF}}\right] M_B \qquad (2.27)$$

Equations 2.26 and 2.27 are solved simultaneously to give the pipe wall moment and the pipe wall shear at the hub junction in terms of the bolt load, pressure, temperature change, axial force, and gasket forces. If Eqs. 2.26 and 2.27 are rewritten and denote the coefficients by symbols K_{10}, K_{11}, etc.,

$$0 = K_{10}M + K_{11}Q + K_{12}B + K_{13}p + K_{14}\alpha\Delta T + K_{15}P + K_{16}G + K_{17}Q_{gf}$$

$$0 = K_{20}M + K_{21}Q + K_{22}B + K_{23}p + K_{24}\alpha\Delta T + K_{25}P + K_{26}G + K_{27}Q_{gf}$$

When these equations are solved simultaneously for M and Q

$$M = \left[\frac{K_{21}}{K_{11}K_{20}-K_{10}K_{21}}\right]\left[\; K_{12}B + K_{13}p + K_{14}\alpha\Delta T + K_{15}P + K_{16}G + K_{17}Q_{gf} \;\right]$$

$$- \left[\frac{K_{11}}{K_{11}K_{20} - K_{10}K_{21}}\right]\left[\; K_{22}B + K_{23}p + K_{24}\alpha\Delta T + K_{25}P + K_{26}G + K_{27}Q_{gf} \;\right]$$

$$Q = -\left[\frac{K_{20}}{K_{11}K_{20} - K_{10}K_{21}}\right]\left[\; K_{12}B + K_{13}p + K_{14}\,\alpha\Delta T + K_{15}P + K_{16}G + K_{17}Q_{gf} \;\right]$$

$$+ \left[\frac{K_{10}}{K_{11}K_{20} - K_{10}K_{21}}\right]\left[\; K_{22}B + K_{23}p + K_{24}\alpha\Delta T + K_{25}P + K_{26}G + K_{27}Q_{gf} \;\right]$$

From the solution for M and Q at the pipe-hub interface, the loads and deformations in the left flange-hub-pipe combination are determined. A similar procedure is used for the right flange-hub-pipe combination starting from the smaller end of the hub and working towards the flange ring top. In the case of the right flange-hub-pipe combination, sign conventions are a mirror image of the left flange-hub-pipe combination. As a result, radial displacement is again outward and axial displacement is towards the gasket.

The axial deflection of the flange at the bolts in respect to the gasket circle is obtained from Eq. 2C-9 as

$$w_B - w_G = \left[\frac{3fB(1-\nu^2)}{4\pi Eh^3}\right]\left[2R^2\left(\frac{R_B^2 - R_G^2}{R_B^2 - R^2}\right)\log\left(\frac{R_B}{R}\right) + \left(\frac{3+\nu}{1+\nu}\right)\left(R_B^2 - R_G^2\right)\right.$$
$$\left. -2R_G^2\log\left(\frac{R_B}{R_G}\right) + 4\left(\frac{1+\nu}{1-\nu}\right)\left(\frac{R_B^2R^2}{R_B^2 - R^2}\right)\log\left(\frac{R_B}{R_G}\right)\log\left(\frac{R_B}{R}\right)\right]$$

$$+ \left[\frac{6fM_R(1-\nu^2)}{\pi Eh^3}\right]\left[\frac{R\left(R_B^2 - R_G^2\right)}{2\,(1+\nu)\left(R_B^2 - R^2\right)} + \frac{RR_B^2}{(1-\nu)(R_B^2 - R^2)}\log\left(\frac{R_B}{R_G}\right)\right]$$

$$- \left[\frac{6fM_B(1-\nu^2)}{\pi Eh^3}\right]\left[\frac{R_B\left(R_B^2 - R_G^2\right)}{2\,(1+\nu)\left(R_B^2 - R^2\right)} + \frac{R_BR^2}{(1-\nu)(R_B^2 - R^2)}\log\left(\frac{R_B}{R_G}\right)\right] \qquad (2.28)$$

The radial displacement of the flange at the gasket is obtained from Eqs. 2C.14 and 2C.15 as

$$u_G = \left[\frac{R_G^2 + R^2 - \nu\left(R_G^2 - R^2\right)}{2\pi R_G E h \left(R_B^2 - R^2\right)}\right] fR_B Q_B - \left[\frac{R_B^2 + R_G^2 + \nu\left(R_B^2 - R_G^2\right)}{2\pi R_G E h \left(R_B^2 - R^2\right)}\right] fRQ_R$$

$$+R_G \alpha \Delta T - \left[\frac{3R\left(R_B^2 + R_G^2 + \nu\left(R_B^2 - R_G^2\right)\right)}{\pi R_G E h^2 \left(R_B^2 - R^2\right)}\right] fM_R$$

$$+ \left[\frac{3R_B\left(R_G^2 + R^2 - \nu\left(R_G^2 - R^2\right)\right)}{\pi R_G E h^2 \left(R_B^2 - R^2\right)}\right] fM_B$$

$$- \left[\frac{3Bf}{2\pi R_G E h^2}\right]\left[R_G^2 (1 - \nu^2) \log\left(\frac{R_B}{R_G}\right) + R_G^2 (1 - \nu)\right.$$

$$\left. + \frac{R_G^2\left(R^2 (1 - \nu^2)\right)}{R_B^2 - R^2} \log\left(\frac{R_B}{R}\right) + \frac{R_B^2 R^2 (1 + \nu)^2}{R_B^2 - R^2} \log\left(\frac{R_B}{R}\right)\right] \quad (2.29)$$

2.2.2.3 Bolt and Gasket Stiffness

The effective bolt shortening is from Eq. 2D-1

$$w_{BB} = \left(\frac{20}{\pi}\right)\left(\frac{L_B}{nEd^2}\right)B + (2h+h_G)\alpha_B \Delta T - C - h\alpha_F \Delta T \quad (2.30)$$

(The last terms in Eqs. (2.30) and (2.31) account for the flange expansion between edge and mid-thickness)

The axial compression of the gasket is from Eq. 2E-1

$$W_{GG} = \left(\frac{hG}{2\pi g R_G E_G}\right) G - h_G \alpha_G \Delta T - h\alpha_F \Delta T \quad (2.31)$$

The radial displacement of the gasket is obtained from Eq. 2E-2 as

$$u_{GT} = \left(\frac{R_G}{2\pi g h_G E_G}\right) Q_{gf}$$

$$+ \left(\frac{R_G}{2\pi g h_G E_G}\right) Q_{gf}$$

$$+ \left[\frac{R_G\left(R_G - g/2\right)}{g E_G}\right] p + R_G \alpha_G \Delta T \quad (2.32)$$

Where both right and left gasket frictions are positive outwards in acting on the gasket.

2.2.2.4 Interaction of Flange, Bolts, and Gasket - Integral Flanges.

The sum of the axial deflections of the two flanges, Eq. 2.28, the effective bolt shortening, Eq. 2.30, and the gasket compression, Eq. 2.31, must remain constant in the absence of bolt tightening or creep. This provides an equation involving the initial system extension constant C.

$$w_{BB} + w_{GG} + (w_B - w_G)_{\text{Left flange}} + (w_B - w_G)_{\text{Right flange}} = 0 \qquad (2.33)$$

Equating the gasket radial displacements, Eq. 2.32, to the corresponding flange values, Eq. 2.29, gives two additional equations.

$$(u_G)_{\text{Left flange}} = u_{GT} \qquad (2.34)$$

$$(u_G)_{\text{Right flange}} = u_{GT} \qquad (2.35)$$

These equations can be solved simultaneously with Eq. 2.33 and Eq. 2.24 to give the gasket force G, bolt pull B (or when initially tightened the constant C) and the gasket friction forces. If the resulting values for gasket friction exceed the gasket friction coefficient times the gasket force, this indicates that sliding actually occurs. In that case, the two radial deflection equations (Eqs. 2.34 and 2.35) are replaced by

$$Q_{gf\ \text{left}} = -Q_{gf\ \text{right}} = \pm \mu_G G \qquad (2.36)$$

the sign depending on the relative direction of sliding.

The value of the constant C is now evaluated at the initial tightening conditions by setting p, P, ΔT equal zero, and B = (B_I). Using this value of C and the design load values, the load distribution in the flange and the hub and the deformations are found.

The bolt stress is given by Eq. 2D.3.

Maximum hoop compressive stresses in the flange ring occur at the inner radius away from the hub. From Eq. 2C.13 we have

$$\sigma_{\text{Hoop, Flange, Max}} = \left[\frac{R_B Q_B}{\pi h}\right]\left[\frac{1}{R_B^2 - R^2}\right] - \frac{Q_R (R_B^2 + R^2)}{2\pi R h (R_B^2 - R^2)} \qquad \text{(continue)}$$

$$-\left[\frac{3B}{2\pi h^2}\right]\left[(1+\nu)\left(\frac{2R_B^2}{R_B^2 R^2}\right)\log\left(\frac{R_B}{R}\right) + (1-\nu)\right]$$

$$-\left(\frac{3M_R}{\pi R h^2}\right)\left(\frac{R_B^2+R^2}{R_B^2-R^2}\right) + \left(\frac{6R_B M_B}{\pi h^2}\right)\left(\frac{1}{R_B^2-R^2}\right) \qquad (2.37)$$

At this location,

$$\sigma_{Axial} = \sigma_{Radial} = -p \qquad (2.38)$$

The radial stress in the hub and pipe can be taken as zero. The hoop stress in the hub and pipe is given by using Eqs. 2.4 or 2.9 to obtain u (here used to denote radial deflection generally), and substituting in

$$\sigma_{Hoop\ pipe} = \left(\frac{E}{R_{mid\text{-}thickness}}\right)\left(u + \frac{\nu}{2\pi Et}P\right) - E\alpha\Delta T \qquad (2.39)$$

where t is the actual thickness rather than that of the substitute cylindrical segments. The axial stress in the hub and pipe is given by using Eq. 2.7 to obtain M (here used to denote wall moment generally) and substituting in

$$\sigma_{Axial\ pipe} = \left(\frac{P}{2\pi t R_{mid\text{-}thickness}}\right) \pm \left(\frac{6M}{2\pi t^2 R_{mid\text{-}thickness}}\right) \qquad (2.40)$$

(The value will be greatest when the sign before M in Eq. 2.40 is minus since the value of M is ordinarily negative in the hub region when there is no contact outside the bolt circle. The thickness t in Eq. 2.40 is the actual thickness, not that of the substitute segments.)

Comparing the stresses with the allowable values indicates where additional thickness is needed and where thickness can be removed. Since the connector is a redundant structure, additions of material at either hub or flange tend to affect stresses everywhere but have the greatest affect locally. It is recommended that thickness changes be in direct proportion to half the difference of stress from the allowable values. Comparing the gasket load with the minimum permitted indicates whether an increase in initial bolt load or general thickening is needed. Similarly distortion limits may require thickening.

2.3 Integral Flange - Contact Outside Bolt Circle

An integral flange connector with contact at a raised region outside the gasket circle, (Figure 2.5) is frequently applied where the gasket is contained in a pocket. The use of raised regions near the flange edge and the gasket is preferred to a flat flange since it makes the gasket contact stiffer. Use will be made of an elastic analysis to achieve an optimum design configuration.

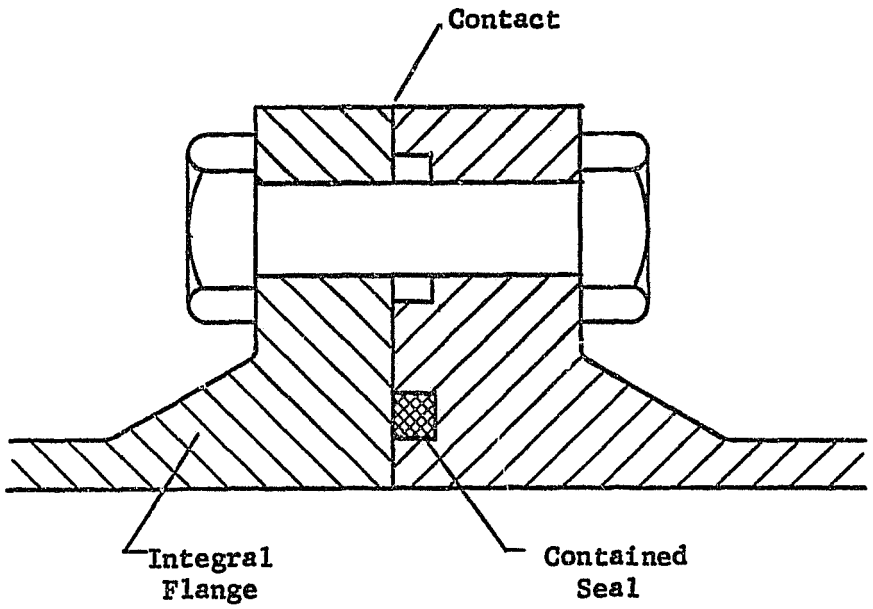

Figure 2.5. Integral Flange Connector with Contact Outside Gasket Circle.

The design procedure involves selecting a preliminary design layout, analyzing for stresses and deformations under the various loading conditions, using the results to select an improved design layout, reanalyzing, and remodifying, until an efficient design is attained. Every effort has been made to make the preliminary design procedure a good one. However, for simplicity, only a few parameters can be considered at a time. Thus,the highly complex interactions of the connector parts can only be accounted for approximately in the preliminary design phase. At least one or two cycles of the analysis-redesign procedure are essential if an optimum configuration is to be achieved.

The detailed design procedure is presented here in a form suitable for hand computation so that the procedures can be clearly understood. It is also in a form which can readily be translated to digital computer language either in part or total. Where many connectors must be designed, use of a digital computer recommends itself both from the point of view of accuracy in the many numerical computations involved as well as cost in repeating computations to achieve an optimum configuration.

2.3.1 Preliminary Design Layout - Contact Outside Bolt Circle

a. Determine the pipe size, wall thickness, and material to either side of the connector. Select materials for the connector halves to be the same as the corresponding pipes except for possible differences in heat treatment or alloying compounds to improve creep, fatigue,or yield strength.

   Select a connector sealing system whose maximum permissible load exceeds its minimum permissible load for "zero leakage" by at

least $2.5\pi R_G^2 p$ max. oper., the estimated reduction in gasket load during operation.

b. Set the initial bolt load (B_I) equal to twice the value in (b) of Section 2.2.1. (This assumes equal load division during assembly between the gasket region and a raised outboard region of the flange. Set the minimum total bolt area (A_B) at the root of the threads equal to the ratio of initial bolt load to yield stress of the bolt material.

$$(A_B) = (B_I)/(S_B)$$

c. Use Table 2.1 to select the bolt size and number of bolts. Enter this table in Column 1 at a value just larger than the ratio of the minimum total bolt area (A_B) to an estimated bolt circle radius (R_{BC}). The bolt size is given in Column 2. The corresponding number of bolts is obtained by dividing the minimum total bolt area by the root area per bolt, Column 3, and rounding up to a convenient integral number. If this number, when multiplied by the minimum bolt spacing in Column 4, exceeds the bolt circle in circumference, it will be necessary to increase (R_{BC}) slightly keeping the same bolt size and number of bolts.

d. Select a flange thickness (H_I) from Column 7 of Table 2.1 such that

$$(H_I) = (\text{Col. } 7)\sqrt{3(S_B)/(S_F)}$$

e. Select a flange outer radius (R_{OL}) given by $(R_{OL}) = 2(R_{BC})-R$. Provide a raised bearing surface at outer edge of the flange based on Col. 1 of Table 2.1. Let the radial width of this raised surface be $(R_{BS}) = 0.1$ Col.1. Let the height of this raised bearing surface be $(H_B) \geq 0.002$ Col. 1. Let the flange be raised at the gasket region to match the raised bearing surface at the outer edge. Contain the gasket.

f. Select a hub thickness at the flange of $(T_I) = 2.5\, Rp_{max.oper.}/\sigma_{allow.}$

(The value 3.28 in place of 2.5 for the coefficient would be such that if the flange neither deflected radially nor rotated, the maximum axial hub stress at the inside radius would equal the allowable when the internal pressure was $1.5_{max.oper.}$ and the axial load was $2.5\pi R^2 p_{max.oper.}$. The reduction to 2.5 gives an adjustment for the fact that the flange ring deflects and rotates somewhat, and the hub tapers more rapidly. Check that $(R_{BC}) > R+1.2(T_I)$ + Col.5 of Table 2.1. Increase (R_{BC}) if necessary.)

g. Same as (e), (f), (g), and (h) Section 2.2.1.

h. Same as (i), (j), (k), (ℓ), Section 2.2.1, except perform computation in accordance with Section 2.3.2 instead of 2.2.2.

2.3.2 Integral Flanges With Contact Outside the Gasket Circle - Detailed Analysis

The elastic analysis is based on satisfying equilibrium and compatibility conditions at the pipe-hub, flange-hub, flange-gasket, flange-bolt, and flange-flange interfaces. The methods presented in connection with Section 2.2.2 are used here as well. From the analysis deformations and stresses are obtained for all the loading conditions of interest. Usually the bolts are considered to be squarely loaded since flange rolling should be low with contact outside the bolt circle. The gasket is considered contained so there is flange-to-flange contact in the gasket region as well as at the flange edges.

The solution in regard to the hub and flange ring is again a step-by-step process. Thus the solution of a large number of simultaneous equations is avoided. Starting at the small end of the hub, calculations are made stepwise down the hub as described in Section 2.3.2.1. At each step, solutions are obtained for the wall shear, wall moment, radial deflection, and wall slope in terms of the wall moment, M, and wall shear, Q, at the small end of the hub and the pressure, p, the axial load, P, and the local expansion, $\alpha\Delta$ T. Then, in Section 2.3.2.2 solutions are obtained similarly from the inner to the outer radius of the flange ring. Finally, the frictional force is balanced at the contacting outer edge of the flanges and the resulting two equations are solved for M and Q in terms of p, P, $\alpha\Delta$ T, (B or C), F, and the friction forces at the gasket and outer flange regions.

The solution in regard to the influence of bolt and gasket stiffness is found in Sections 2.3.2.3 and 2.3.2.4. Here four simultaneous equations must be solved. Two of these involve compatibility of the bolt stretch and flange ring deformations at the gasket and outer flange regions. The other two involve equilibrium of the frictional forces between the two flanges in the gasket and outer flange regions. Solution of these equations gives the values of (B or C) and the normal and friction forces at the gasket and outer flange regions in terms of p, P, and $\alpha\Delta$ T. With these M and Q are obtained. Stresses and deformations at all portions of the connector can then be computed.

Because of the length of the computation and the fact that it involves the solution of simultaneous equations, it is recommended that five or more significant figures be maintained in the numerical computation.

2.3.2.1 Pipe and Hub Stiffness

This portion of the analysis is identical with that in Section 2.2.2.1 for flanges with no contact outside the gasket circle.

2.3.2.2 Flange Ring Stiffness

Bolt holes reduce the stiffness of the flange. In the case of a flange having contact outside the bolt circle, the largest flange stresses are radial and are maximum at the bolt circle. In the absence of better data, the increase in flexibility will be considered as being inversely proportional to the uncut circumference at the bolt circle.

$$f = 2\pi R_B / (2\pi R_B - nd) \qquad (2.41)$$

where R_B = radius to the circle through the bolt centers for flanges having contact outside the bolt circle.

Regarding radial flange stress, the same factor f will be taken as the ratio of actual stress to that computed neglecting bolt holes. In line with the discussion in Section 2.2.2.2, no factor will be applied to the flange hoop stress.

The forces from the hub and gasket as well as the internal pressure are considered to cause a resultant axial force at the bottom of the flange ring.

Equations 2.16 through 2.23 apply to the case of the flange having contact outside the bolt circle, if B is replaced by (B-F) in Eqs. 2.16, 2.21, and 2.22.

Proceeding now to the flange portion between the bol circle and the outer edge, it is known that the moment and tension at the outer edge balance the flange friction Q_{OF} at the outer edge. Using Appendix 2C, Eqs. 2C.3 and 2C.5 give

$$Q_{OF} = \left(\frac{\pi Eh}{f}\right)\left(\frac{R_{OF}}{R_B} - \frac{R_B}{R_{OF}}\right) u_B + \left(\frac{1}{2}\right)\left[(1+\nu)\frac{R_{OF}}{R_B} + (1-\nu)\frac{R_B}{R_{OF}}\right] Q_B$$

$$- \left(\frac{\pi Eh}{f}\right)\left(\frac{R_{OF}}{R_B} - \frac{R_B}{R_{OF}}\right) R_B \alpha \Delta T \qquad (2.42)$$

$$\left(\frac{h}{2}\right) Q_{OF} = M_{OF} = \left(\frac{\pi Eh^3}{12f}\right)\left(\frac{R_{OF}}{R_B} - \frac{R_B}{R_{OF}}\right)\theta_B + \left(1/2\right)\left[(1+\nu)\frac{R_{OF}}{R_B} + (1-\nu)\frac{R_B}{R_{OF}}\right] M_B$$

$$-\left(\frac{R_B}{4}\right)\left(\frac{R_{OF}}{R_B} - \frac{R_B}{R_{OF}}\right)\left[(1-\nu) + 2(1+\nu)\left(\frac{R_{OF}^2}{R_{OF}^2 - R_B^2}\right)\log\left(\frac{R_{OF}}{R_B}\right)\right] F \qquad (2.43)$$

Equations 2.42 and 2.43 are solved simultaneously to give the pipe wall moment and the pipe wall shear at the small end of the hub in terms of the bolt load, pressure, temperature change, axial force, and forces at the flange-to-flange contacts.

From these the loads and deformations in the left flange-hub-pipe combination are determined. From Eq. 2C.9.

$$(w_B - w_G) = \left[\frac{3f(1-\nu^2)(B-F)}{4\pi Eh^3}\right]\left[2R^2\left(\frac{R_B^2 - R_G^2}{R_B^2 - R^2}\right)\log\left(\frac{R_B}{R}\right) + \right.$$

$$\left(\frac{3+\nu}{1+\nu}\right)\left(R_B^2 - R_G^2\right) - 2R_G^2 \log\left(\frac{R_B}{R_G}\right)$$

$$\left. +4\left(\frac{1+\nu}{1-\nu}\right)\left(\frac{R_B^2 R^2}{R_B^2 - R^2}\right)\log\left(\frac{R_B}{R_G}\right)\log\left(\frac{R_B}{R}\right)\right]$$

$$+\left[\frac{6f(1-\nu^2)M_R}{\pi Eh^3}\right]\left[\frac{R\left(R_B^2 - R_G^2\right)}{2(1+\nu)\left(R_B^2 - R^2\right)} + \frac{RR_B^2}{(1-\nu)\left(R_B^2 - R^2\right)}\log\left(\frac{R_B}{R_G}\right)\right]$$

$$-\left[\frac{6f(1-\nu^2)M_B}{\pi Eh^3}\right]\left[\frac{R_B\left(R_B^2 - R_G^2\right)}{2(1+\nu)\left(R_B^2 - R^2\right)} + \frac{R_B R^2}{(1-\nu)\left(R_B^2 - R^2\right)}\log\left(\frac{R_B}{R_G}\right)\right] \qquad (2.44)$$

$$(w_B - w_{OF}) = \left[\frac{3fF}{4\pi Eh^3}\right]\left[(1-\nu)(3+\nu)\left(R_{OF}^2 - R_B^2\right) + 4(1+\nu)^2\left(\frac{R_{OF}^2 R_B^2}{R_{OF}^2 - R_B^2}\right)\log^2\left(\frac{R_{OF}}{R_B}\right)\right]$$

$$-\left[\frac{3fM_B}{\pi Eh^3}\right]\left[(1-\nu)R_B + 2(1+\nu)\left(\frac{R_B R_{OF}^2}{R_{OF}^2 - R_B^2}\right)\log\left(\frac{R_{OF}}{R_B}\right)\right]$$

$$+\left[\frac{3fQ_{OF}}{2\pi Eh^2}\right]\left[(1-\nu)R_{OF} + 2(1+\nu)\left(\frac{R_B^2 R_{OF}}{R_{OF}^2 - R_B^2}\right)\log\left(\frac{R_{OF}}{R_B}\right)\right] \qquad (2.45)$$

The radial displacement of the gasket region of the flange is given by Eq. 2.29 with the term B replaced by (B-F).

The radial displacement of the outer flange region is given by Eqs. 2C-14 and 2C-15.

$$u_{OF} = \left[\frac{R_{OF}^2 + R_B^2 - \nu\,(R_{OF}^2 - R_B^2)}{2\pi Eh\,(R_{OF}^2 - R_B^2)}\right] fQ_{OF} - \left[\frac{R_{OF}R_B}{\pi Eh(R_{OF}^2 - R_B^2)}\right] fQ_B$$

$$- \left[\frac{6R_{OF}R_B}{\pi Eh^2\,(R_{OF}^2 - R_B^2)}\right] fM_B + 3\left[\frac{R_{OF}^2 + R_B^2 - \nu\,(R_{OF}^2 - R_B^2)}{2\pi Eh\,(R_{OF}^2 - R_B^2}\right] fQ_{OF}$$

$$+\left(\frac{3R_{OF}}{2\pi Eh^2}\right)\left[1-\nu + 2(1+\nu)\left(\frac{R_B^2}{R_{OF}^2 - R_B^2}\right)\log\left(\frac{R_{OF}}{R_B}\right)\right] fF + R_{OF}\Delta T \qquad (2.46)$$

A similar procedure is used for the right flange-hub-pipe combination starting from the smaller end of the hub and working towards the flange ring top. Sign conventions for the right combination are a mirror image of those for the left combination. As a result radial displacement is again outward, and axial displacement is towards the gasket. The friction forces at the outer flange and gasket regions must satisfy the relations,

$$Q_{OF\ Left} + Q_{OF\ Right} = 0 \qquad (2.47)$$

$$Q_{gf\ Left} + Q_{gf\ Right} = 0 \qquad (2.48)$$

2.3.2.3 Bolt and Gasket Stiffness

The axial extension of the bolt and gasket regions is from Eq. 2D.2 and 2E.1.

$$w_{BB} = \left(\frac{4}{\pi}\right)\frac{L_B B}{nEd^2} + 2\,h\alpha_B\Delta T - C - h\alpha_F\Delta T \qquad (2.49)$$

$$w_{GG} = -\,h\alpha_F\Delta T$$

The last term in Eq. 2.49 accounts for the expansion of the flange between edge and midthickness.

2.3.2.4 Interaction of Bolts and Flanges - Contact Outside the Gasket Circle.

The sum of the axial deflections of the two flanges between the gasket and the bolt circle plus the bolt stretch must remain constant in the absence of bolt tightening or creep. Similarly, the sum of the axial deflections of the two flanges between the flange edge and the bolt circle plus the bolt stretch must remain constant. These two equations involve the initial system tightening constant, C, and the force, F, at the flange edge. Thus

$$w_{GG}+w_{BB}+(w_B-w_G)_{\text{Left Flange}}+(w_B-w_G)_{\text{Right Flange}}=0 \qquad (2.50)$$

$$w_{GG}+w_{BB}+(w_B-w_{OF})_{\text{Left Flange}}+(w_B-w_{OF})_{\text{Right Flange}}=0 \qquad (2.51)$$

If there is no slipping between gasket regions of the two flanges,

$$u_{G\ \text{Left Flange}}=u_{G\ \text{Right Flange}} \qquad (2.52)$$

If there is no slipping in the outer flange region,

$$u_{OF\ \text{Left Flange}}=u_{OF\ \text{Right Flange}} \qquad (2.53)$$

Solving simultaneously Eqs. 2.50, 2.51, 2.52, 2.53 and

$$B=G+F+P+\pi\left(R_G^2-R^2\right)p \qquad (2.54)$$

gives the gasket force, G, the bolt pull, B (or when initially tightened the constant C), the outer flange force, F, and the friction forces in the "gasket area" and the "outer edge of flange" area. If the resulting values for either friction force exceed the coefficient of friction times the corresponding normal force, G or F, this is an indication that sliding actually occurs in this area. In case sliding occurs at the gasket area, replace Eq. 2.52 by

$$Q_{gf\ \text{Left}}=-Q_{gf\ \text{Right}}=\pm\mu G \qquad (2.55)$$

and repeat the computations, the sign in Eq. 2.55 depending on the relative direction of sliding. In case sliding occurs in the outer flange region, replace Eq. 2.53 by

$$Q_{OF\ \text{left}}=-Q_{OF\ \text{right}}=\pm\mu F \qquad (2.56)$$

and repeat the computation,

where again the sign depends on the relative direction of sliding.

The value of the constant, C, is evaluated at the initial tightening condition by setting p, P, ΔT equal to zero and $B = (B_I)$. Using this value of C and the design load values, the load and deformation distributions in the flanges and hub are obtained.

The bolt stress is given by Eq. 2D.4.

The maximum hoop stress in the flange is given by one of the Eqs. 2C.10 to 2C.13. However, it is likely to be quite small so it may be taken as zero for conventional designs.

The radial stress in the flange at the bolt circle is given by either Eqs. 2C.16 or 2C.17 as

$$\sigma_{Radial} = \left[\frac{Q_B}{2\pi R_B h} \pm \frac{3M_B}{\pi R_B h^2}\right] f \qquad (2.57)$$

where the sign is chosen to give the largest value of the radial stress and the multiplying factor f is obtained from Eq. 2.41.

The hoop and axial stresses in the hub and pipe are given by Eqs. 2.39 and 2.40. In the case of flanges contacting outside the bolt circle, the sign before M in Eq. 2.40 is most critical when it is positive.

Comparing the stresses with the allowable values indicates where additional thickness is needed and where thickness can be removed. If the gasket load drops below the minimum permitted, an increase in initial bolt load or general thickening may be beneficial. Similarly distortion limits may require thickening. Where increased thickening is used, the change in thickness should be in proportion to half the difference between values obtained and allowable values.

2.4 Loose Flange - No Contact Outside Bolt Circle

A widely used form of flange connector is one having one integral flange and one loose flange Figure 2.6. The loose flange permits bolt holes to be matched more readily than with two integral flange connectors. The loose flange in turn bears on a lap flange (ferrule). Use will be made of the elastic interaction of the bolts, flanges, hubs, gasket and pipes under the various applied loads to arrive at an optimum design configuration.

The design procedure involves selecting a preliminary design layout, analyzing for stresses and deformations under the various loading conditions, using the results to select an improved design layout, reanalyzing, and remodifying until an efficient design is attained. Every effort has been made to make the preliminary design procedure a good one. However, for simplicity, only a few parameters can be considered at a time. Thus, the highly complex interactions of the connector parts can only be accounted for approximately in the preliminary design phase. At least

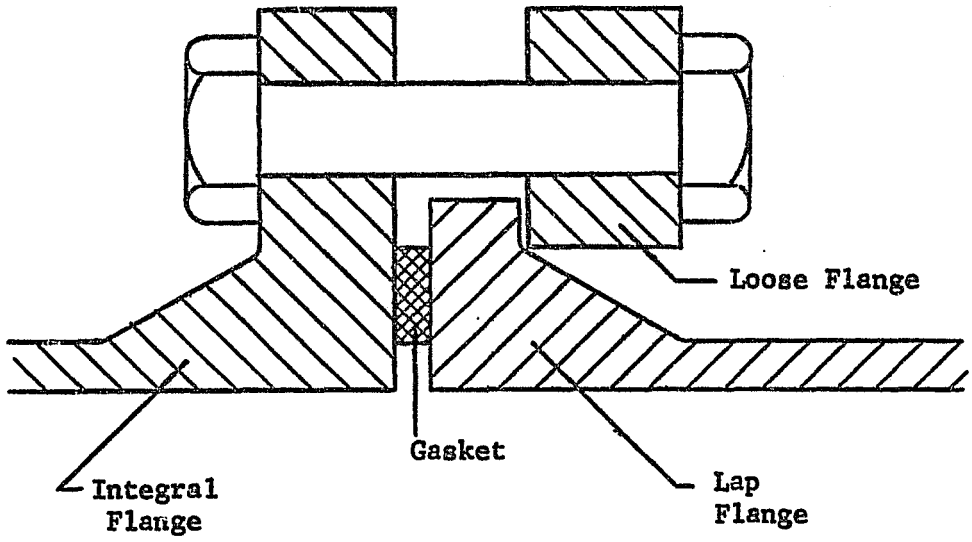

Figure 2.6. Loose Flange - No Contact Outside Bolt Circle.

Table 2.3

ESTIMATION OF LAP AND LOOSE FLANGE DIMENSIONS

1	2	3	4	5	6
Pipe wall thickness / Inner pipe radius	Hub thickness at flange(lap) / Pipe wall thickness	Outer flange (lap) radius / Inner pipe radius	Max.Oper. Pressure / Allowable stress in pipe wall	Hub length (lap) / Inner pipe radius	Loose flange inner radius / Inner pipe radius
0.01	5.60	1.077	0.0072	0.183	1.067
0.03	5.40	1.225	0.0216	0.318	1.195
0.05	5.24	1.364	0.0362	0.409	1.314
0.07	5.08	1.496	0.0507	0.485	1.426
0.09	4.96	1.626	0.0655	0.550	1.536
0.11	4.84	1.749	0.080	0.611	1.64
0.13	4.74	1.871	0.095	0.665	1.74
0.15	4.66	1.988	0.110	0.717	1.84
0.17	4.58	2.09	0.125	0.766	1.92
0.19	4.51	2.20	0.140	0.812	2.01
0.21	4.44	2.32	0.155	0.857	2.11
0.23	4.37	2.44	0.170	0.898	2.21
0.25	4.31	2.55	0.186	0.942	2.30
0.27	4.25	2.65	0.200	0.98	2.38
0.29	4.20	2.76	0.216	1.02	2.47
0.31	4.16	2.86	0.231	1.06	2.55
0.33	4.12	2.97	0.246	1.10	2.64
0.35	4.08	3.06	0.262	1.13	2.71
0.37	4.04	3.16	0.277	1.17	2.79
0.39	4.00	3.26	0.292	1.20	2.87

one or two cycles of the analysis-redesign procedure are essential if an optimum configuration is to be achieved.

The detailed design procedure is presented here in a form suitable for hand computation so that the procedures can be clearly understood. It is also in a form which can readily be translated to digital computer language either in part or total. Where many connectors must be designed, use of a digital computer recommends itself both from the point of view of accuracy in the many numerical computations involved as well as cost in repeating computations to achieve an optimum configuration.

2.4.1 Preliminary Design Layout - Integral and Loose Flanges - No Contact Outside Bolt Circle.

A preliminary design layout is selected as follows:

a. Proceed with steps (a) to (ℓ) of Section 2.2.1 for the bolts and integral flange portion of the connector.

b. Choose a lubricant and friction coefficient for the contact between loose flange and lap flange. Some approximate friction coefficients are given in Table 2.2. A low friction coefficient will usually be preferable.

c. Check the pipe wall thickness at the small end of the hub* from Table 2.3 by entering in Col. 4 with the ratio of maximum operating pressure to allowable stress in the pipe and setting

$$(T_P) = \text{R Col. 1}$$

Take the hub thickness at the junction with the lap flange as

$$(T_L) = (T_P)\ \text{Col. 2}$$

Take the outer flange radius of the lap flange as

$$(R_{OL}) = \text{R Col. 3}$$

Take the thickness of the lap flange as

$$(H_L) = (T_P)\ \text{Col. 2}$$

Let the fillet at the junction of hub and lap flange have a radius of 0.1 to 0.2 (T_L).and the fillet at the junction of hub and pipe have a radius of 0.1 to 0.2 (T_P).

Take the basic hub length as

$$(L_H) = \text{R Col. 5}$$

* Exceeds by a small margin the value obtained.

This will generally give a hub having a greater slope than 3:1 so a welding taper as described in Section 2.2.1, e should be added.

d. Same as 2.2.1,h.

e. Take the inner radius of the loose flange from Table 2.3 as

$$(R_{ILF}) = \text{R Col. 6}$$

f. Take the outer radius of the loose flange from the value for the integral flange as (R_{OF}).

g. Using the values determined for the integral flange of the connector of

(B_I) = initial bolt load
(R_{BC}) = radius to bolt center
d = bolt diameter

determine the loose flange thickness as

$$(H_F) = \sqrt{\frac{(B_I)}{(S_{FL})}\left[\frac{(R_{BC})-(R_{ILF})-(d-t)/2}{(R_{OF})-(R_{ILF})}\right]}$$

where (S_{FL}) is the allowable stress in the loose flange material.. (Since the loose flange is not in contact with the fluid, it may be of higher strength material than the "integral" or "lap stub" flanges).

Ordinarily the loose flange dimensions will be such that the bolt clearance makes a hub inappropriate. The "loose" flange "lap" "stub" combination should be checked to assure satisfaction of the bolt clearance requirement, Col. 5 of Table 2.1. If necessary, increase the loose flange thickness above the value computed here to satisfy the clearance requirement.

2.4.2 Loose Flange - No Contact Outside Bolt Circle - Detailed Analysis

The elastic analysis is based on satisfying equilibrium and compatibility conditions at the various interfaces. The methods in Section 2.2 are used. From the analysis, deformations and stresses are obtained for all the loading conditions of interest. The bolts in this case are eccentrically loaded because of flange rolling.

The solution in regard to the integral hub and flange ring is basically a step-by-step process. Starting at the small end of the hub, solutions are obtained stepwise down the hub and up the flange ring as described in Section 2.3.2.1. Setting the wall moment and wall tension to zero at the outer radius of the flange ring, the resulting two simultaneous equations are solved for the moment and shear in the pipe wall at its junction with the integral flange hub in terms of p, P, $\alpha\Delta T$, (B or C), and Q_{gf}.

the integral flange hub in terms of p, P, $\alpha\Delta T$, (B or C), and $Q_{Gasket\ friction}$.

The solution in regard to the lap flange is similar. Starting at the small end of the lap-flange hub, solutions are obtained stepwise along the hub to the lap flange and then up the lap-flange ring as described in Section 2.4.2.2. Placing the forces between lap and loose flanges in equilibrium, the resulting two simultaneous equations are solved for the moment and shear in the pipe wall at its junction with the lap-flange hub in terms of p, P, $\alpha\Delta T$, (B or C), Q_{gf}, and the friction forces between the loose and lap flanges.

The solution in regard to the loose flange is based on the assumption of no loose-flange hub. (Lap flanges designed as described here make loose-flange hubs inappropriate). Starting at the inner radius of the loose flange the solution in Section 2.4.2.4 proceeds stepwise to the outer radius. Placing the wall moment and wall tension to zero and solving the resulting two simultaneous equations, gives the radial displacement and rotation of the inner radius of the loose-flange ring in terms of (B or C), $\alpha\Delta T$, and the friction force between loose and lap flanges.

The solutions in regard to bolt and gasket stiffness are given in Section 2.4.2.3.

In Section 2.4.2.5 the interaction of the various connector parts is considered by solving four simultaneous equations. The first involves compatibility of the bolt stretch, gasket compression, and flange ring deflections. The other three involve equilibrium of frictional forces at the two flange-gasket contacts and at the contact of lap and loose flanges. Solution of these equations gives the values of (B or C) and the three friction forces. With these the stresses and deformations are also obtained.

2.4.2.1 Pipe, Hub, and Flange Stiffness of Integral Flange.

The flexibility of the integral pipe-hub-flange combination is computed by using Sections 2.2.2.1 and 2.2.2.2 directly. These give the deformations and stresses for this portion in terms of the bolt load, pressure, temperature change, axial force and gasket frictional force.

2.4.2.2 Pipe, Hub, and Flange Stiffness of Lap Flange

A similar procedure to Sections 2.2.2.1 is applied starting from the smaller end of the flange hub and working towards the larger end. For the lap-flange ring, the procedure in Section 2.2.2.2, Eqs. 2.15 to 2.19, is followed, except for the following difference. Since the lap-flange ring has no holes, in place of Eq. 2.15

$$f = 1 \qquad (2.58)$$

At the outer radius of the lap flange, the axial force, P_R, equals the bolt force B and the radial force is

$$Q_{OL} = -Q_{LF} \tag{2.59}$$

and the moment is

$$M_{OL} = \left(\frac{h}{2}\right)\ (Q_{LF}) \tag{2.60}$$

Usually the loose flange rolls inward with respect to the lap flange so

$$Q_{LF} = \mu_{OL} B \tag{2.61}$$

Using Appendix 2C

$$Q_{OL} = (\pi Eh)\left[\frac{R_{OL}}{R} - \frac{R}{R_{OL}}\right] u_R + 1/2 \left[(1+\nu)\ \frac{R_{OL}}{R} + (1-\nu)\ \frac{R}{R_{OL}}\right] Q_R$$
$$-(\pi Eh)\left[\frac{R_{OL}}{R} - \frac{R}{R_{OL}}\right] R\alpha\Delta T \tag{2.62}$$

$$M_{OL} = \left(\frac{\pi Eh^3}{12}\right)\left[\frac{R_{OL}}{R} - \frac{R}{R_{OL}}\right]\Theta_R + 1/2 \left[(1+\nu)\ \frac{R_{OL}}{R} + (1-\nu)\frac{R}{R_{OL}}\right] M_R \tag{2.63}$$
$$+\left[\frac{R_{OL}}{R} - \frac{R}{R_{OL}}\right]\left[1-\nu+2(1+\nu)\left(\frac{R_{OL}^2}{R_{OL}^2 - R^2}\right)\log\left(\frac{R_{OL}}{R}\right)\right] B$$

Equations 2.59 to 2.63 are solved simultaneously to give the wall moment and wall shear at the small end of the hub. The values are obtained in terms of the bolt load, pressure, temperature change, axial force, gasket force, and frictional forces.

2.4.2.3 Bolt and Gasket Stiffness

The axial extension of the bolt is obtained from Eq. 2D.1 as

$$w_{BB} = \left(\frac{20}{\pi}\right)\left[\frac{L_B}{nEd^2}\right] B - C + \left[h_G + (H_I) + (H_L) + (H_F)\right] \alpha_B \Delta T$$
$$-\left[(H_L) + (H_I)/2 + (H_F)/2\right] \alpha_F \Delta T \tag{2.64}$$

The axial compression of the gasket is obtained from Eq. 2E.1 as

$$w_{GG} = \left[\frac{h_G}{2\pi g R_G E_G}\right] G - \left[\left(H_L\right) + \left(H_I\right)/2 + \left(H_F\right)/2\right] \alpha_F \Delta T$$

$$- h_G \alpha_G \Delta T \qquad (2.65)$$

The radial gasket displacement is given by Eq. 2.32.

2.4.2.4 Loose Flange Stiffness

The loose flange stiffness is obtained similarly to the integral flange stiffness. Assuming no hub, subscript ILF is taken to indicate the inner radius of the loose flange and set

Loose-flange-bottom axial force = bolt pull, B (2.66)

Loose-flange-bottom radial force, $Q_{ILF} = -Q_{LF}$ (2.67)

Loose-flange-bottom moment, $M_{ILF} = -(1/2)(H_F)(Q_{LF})$

$$- B(R_{OL} - R_{ILF}) \qquad (2.68)$$

The displacements at the bottom of the loose-flange ring are taken as

$$\Theta_{ILF}, \quad u_{ILF}$$

The corresponding values at the line of action of the bolts are given by use of Appendix 2C. In this case, the flexibility factor due to the bolt holes is

$$f = 1/\left[1 - nd^2/\pi\left(R_{OF}^2 - R_{ILG}^2\right)\right] \qquad (2.69)$$

Equations 2.20 to 2.25 of Section 2.2.2.2 apply, except R_{ILF}, replaces R, Q_{ILF} replaces Q_R, u_{ILF} replaces u_R, Θ_{ILF} replaces Θ_R, and M_{ILF} replaces M_R.

Equations 2.26 and 2.27 apply directly and are solved simultaneously to give the radial wall displacement and wall rotation at the inner radius of the loose flange in terms of the bolt load, temperature change, and loose-flange friction. From these the loads and deformations in the loose flange are determined.

2.4.2.5 Interaction of Flanges, Bolts and Gasket - Loose Flange Without Contact Outside Bolt Circle.

The sum of the axial deflections of the flanges, the bolt stretch, Eq. 2.30 and the gasket compression, Eq.2.31 must remain constant in the absence of bolt tightening or creep. This provides an equation involving the initial system extension C.

$$(w_{BB} + w_{GG}) + (w_B - w_G)_{\text{Integral Flange}} + (w_{OL} - w_G)_{\text{Lap flange}}$$

$$+ (w_B - w_{OL})_{\text{Loose flange}} = 0 \qquad (2.70)$$

In this expression the first term is obtained from Eqs. 2.64 and 2.65. The second term is obtained from Eq. 2.28 with f from Eq. 2.15, M_R for the integral flange, and h equal (H_I). The third term is obtained from Eq. 2.28 with f equal one, subscript OL replacing subscript B, h equal (H_L), and M_R for the lap flange. The last term is obtained from Eq. 2.28 with h equal (H_F), subscript OL replacing subscript G, subscript ILF replacing subscript R, R_{ILF} replacing R, and f obtained from Eq. 2.69.

The radial displacement of the integral flange at the gasket is obtained from Eq. 2.29 with f given by Eq. 2.15, h equal (H_L), and Q_R, M_R, M_B the values for the integral flange. Equating this to the value in Eq. 2.32 gives an equation applying when there is no gasket slip.

$$u_G(\text{Integral}) = u_{GT} \qquad (2.71)$$

The radial displacement of the lap flange at the gasket is obtained from Eq. 2.29 with f equal one, h equal (H_L), M_R and Q_R the values for the lap flange, and subscript OL replacing subscript B. Equating this to the value in Eq. 2.32 gives another equation applying when there is no gasket slip.

$$u_G(\text{Lap}) = u_{GT} \qquad (2.72)$$

The two equations 2.71 and 2.72 involving gasket frictions are solved simultaneously with Eq. 2.70 to give the bolt pull, B, (or when initially tightened the constant C) and the gasket friction forces. The gasket force is obtained from Eq. 2.25. If the resulting values for gasket friction exceed the friction coefficient times the gasket force, G, this indicates that sliding actually occurs. In that event, one or both equations involving radial displacement are replaced by Eqs. 2.36.

The radial displacement of the loose flange at the point of contact with the lap flange is obtained from Eq. 2.29 with h equal (H_F), subscript OL replacing subscript G, subscript ILF replacing subscript R, R_{ILF} replacing R, and using the value of f in Eq. 2.69.

The radial displacement of the lap flange at the point of contact with the loose flange is obtained from Eq. 2.29 with h equal (H_L), subscript OL replacing subscripts G and B, f equal one, and reversing the signs of the last three terms in Eq. 2.29 involving B and the two moments.

If these two radial deflections do not show a relative radial displacement inwards of the loose flange with respect to the lap flange, the value of the frictional force between them will be less than μ B and is found by equating the radial deflections of the loose and lap flanges at their point of contact and solving the simultaneous equations again for the value of Q_{LF}.

The value of the constant C is now evaluated at the initial tightening conditions by setting p, P, $\Delta T=0$, and $B=G=(B_I)$. Using this value of C and the load values corresponding to proof test and various operating conditions, the load distribution in the flanges, hubs, bolts, etc. are found. Deformations are also found and should be checked to see that rolling of the loose or lap flanges is not excessive and that the proper assumptions regarding friction (sliding or not) have been used for all loadings.

The bolt stress is given by Eq. 2D.3. The maximum stress in the integral flange is given by Eq. 2.37 and 2.38. For the loose flange the maximum hoop stress is given by Eq. 2.37 with R replaced by R_{ILF} and subscript R replaced by subscript ILF. The axial and radial stresses in the loose flange are usually negligible. For the lap flange the maximum stress is given by Eq. 2.37 and 2.38 with subscript B replaced by subscript OL. The hoop stress in the hub and pipe for the integral and lap flanges is given by Eq. 2.39 Axial stress in the hubs and pipe is given by Eq. 2.40.

Comparing the stresses and deformations with allowable values indicates where thickness changes may be desirable. Comparing the gasket loads with the minimum permitted values indicates when a higher initial bolt load may be required. In general the thickness changes should be in proportion to half the desired stress or deformation changes.

2.5 Loose Flange - Contact Outside Bolt Circle

Where contact outside the bolt circle is desirable it may be necessary to provide a loose flange so that bolt holes can be aligned. Such a connector design is considered in Figure 2.7. The lap flange should always be checked for excessive rolling in such a design.

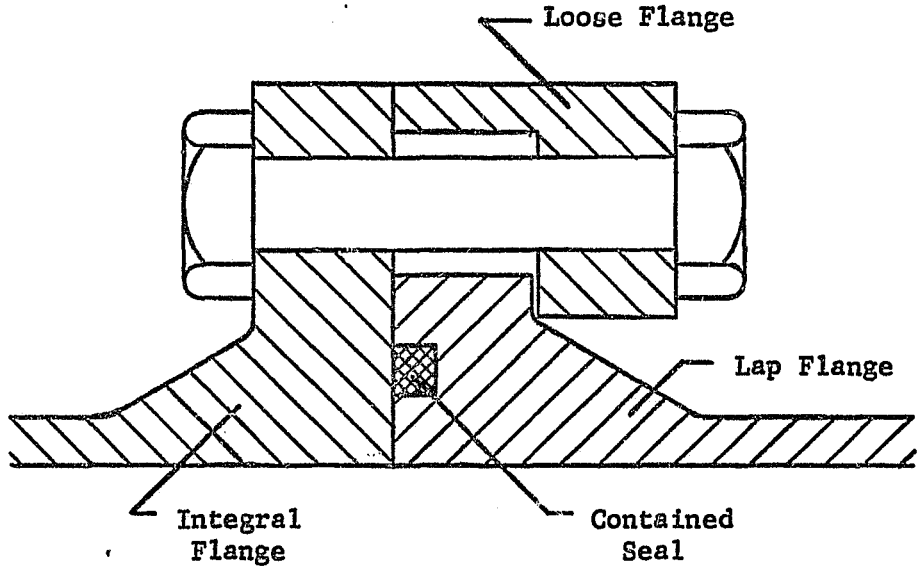

Figure 2.7. Loose Flange - With Contact Outside Bolt Circle

The design procedure involves selecting a preliminary design layout, analyzing for stresses and deformations under the various loading conditions using the results to select an improved design layout, reanalyzing, and remodifying until an efficient design is attained. Every effort has been made to make the preliminary design procedure a good one. However, for simplicity, only a few parameters can be considered at a time. Thus, the highly complex interactions of the connector parts can only be accounted for approximately in the preliminary design phase. At least one or two cycles of the analysis-redesign procedure are essential if an optimum configuration is to be achieved.

The detailed design procedure is presented here in a form suitable for hand computation so that the procedures can be clearly understood. It is also in a form which can readily be translated to digital computer language either in part or total. Where many connectors must be designed, use of a digital computer recommends itself both from the point of view of accuracy in the many numerical computations involved as well as cost in repeating computations to achieve an optimum configuration.

2.5.1 Preliminary Design Layout - Loose Flange - Contact Outside Bolt Circle

(a) For the integral flange and bolts and gasket, steps (a) through (f) of Section 2.3.1 and steps (e) through (ℓ) of Section 2.2.1 are followed, except perform detailed computations as described in Section 2.5.2.

(b) For the lap flange, follow steps (b) through (d) of Section 2.4.1.

c. For the loose flange, let the outer radius be the same as that of the integral flange. Provide a lip at the outer radius whose depth is sufficient to reach the integral flange and whose inner radius clears the bolt. Let the inner radius of the loose flange clear the lap flange hub. Take the thickness equal to that of the integral flange.

2.5.2 Detailed Analysis - Loose Flange - Contact Outside Bolt Circle

2.5.2.1 Integral Flange, Hub and Pipe

These are treated exactly as described in Sections 2.3.2.1 and 2.3.2.2.

2.5.2.2 Lap Flange, Hub and Pipe

These are treated exactly as described in Section 2.4.2.2.

2.5.2.3 Bolt and Gasket Deformation

The axial extension of the bolt is obtained from Eq. 2D.2 as (considering the gasket contained),

$$w_{BB} = \left(\frac{4}{\pi}\right)\left[\frac{L_B}{nEd^2}\right]B\text{-}C + \left[\left(H_I\right) + \left(H_L\right) + \left(H_F\right)\right]\alpha_B\Delta T$$

$$- \left[\left(H_L\right) + \left(H_I\right)/2 + \left(H_F\right)/2\right]\alpha_F\Delta T \qquad (2.73)$$

The axial compression of the gasket is obtained from Eq. 2E.1 (considering the gasket contained) as,

$$w_{GG} = -\left[\left(H_L\right) + \left(H_I\right)/2 + \left(H_F\right)/2\right]\alpha_F\Delta T \qquad (2.74)$$

2.5.2.4 Loose Flange Stiffness

Assuming no hub, subscript ILF is taken to indicate the inner radius of the loose flange and set

Loose flange bottom axial force = B-F (2.75)

Loose flange bottom radial force = $Q_{ILF} = -Q_{LF}$ (2.76)

Loose flange bottom moment = $M_{ILF} = -(1/2)\left(H_F'\right)\left(Q_{LF}\right)$ (2.77)

Take θ_{ILF} and u_{ILF} as the inner displacements.

The flexibility factor is given by Eq. 2.41. The values at the bolt circle are obtained from Eqs. 2.20 to 2.24 with R_{ILF} replacing R, (B-F) replacing B, subscript ILF replacing subscript R, and h equal $\left(H_F'\right)$.

Proceeding now to the flange portion between the bolt circle and the outer edge, the only force at the outer edge is the flange friction. Eqs. 2.42 and 2.43 apply directly with h equal (H_F) and f given by Eq. 2.41.

2.5.2.5 Interaction of Bolts and Flanges - Loose Flange with Contact Outside Bolt Circle

The axial deflections of the flanges and bolts must remain compatible. In the absence of bolt tightening, Eq. 2.70 applies directly. In this expression, w_{BB} is obtained from Eq. 2.73 and w_{GG} from Eq. 2.74. The second term is obtained from Eq. 2.44 with f from Eq. 2.41, M_R for the integral flange, and h equal (H_I). The third term is obtained from Eq. 2.28 with f equal one, subscript OL replacing subscript B, (B-F) replacing B, M_R for the lap flange, and h equal (H_L). The last term is obtained from Eq. 2.28 with f from Eq. 2.41, (B-F) replacing B, subscript OL replacing subscript G, subscript ILF replacing subscript R, R_{ILF} replacing R, and h equal (H_F).

Similarly Eq. 2.51 for compatibility at the outer flange region applies directly. Again w_{BB} is obtained from Eq. 2.73 and w_{GG} from Eq. 2.74. The third term in this expression is obtained from Eq. 2.45 with f given by Eq. 2.41, M_B the value for the integral flange, and h equal (H_I). The last term in the expression is given by Eq. 2.45 with f given by Eq. 2.41, M_B the value for the loose flange, and h equal (H_F).

The radial displacement compatibility in the outer flange regions is expressed by Eq. 2.53. The term on the left side of this expression is obtained from Eq. 2.46 using Q_B and M_B for the integral flange, f from Eq. 2.41, and h equal (H_I). The term on the right side of Eq. 2.53 is obtained from Eq. 2.46 using Q_B and M_B for the loose flange, f from Eq. 2.41, and h equal (H_F).

The radial displacement compatibility in the gasket region is expressed by Eq. 2.52. The term on the left side of this expression is obtained from Eq. 2.29 with M_B, Q_B, M_R, Q_R the values for the integral flange, (B-F) replacing B, f given by Eq. 2.41, and h equal (H_I). The term on the right side of Eq. 2.52 is given by Eq. 2.29 with f equal one, subscript OL replacing subscript B, (B-F) replacing B, M_R and Q_R for the lap flange, and h equal (H_L).

The gasket force is given by Eq. 2.54. The loose-flange frictional force will ordinarily be inwards with respect to the lap flange so

$$Q_{lf} = \mu_{OL} (B\text{-}F) \qquad (2.78)$$

Using Eqs. 2.51, 2.52, 2.53, 2.70 and 2.78 simultaneously makes it possible to solve for (B or C), F, G, and the three frictional forces. If the resulting value of Q_{gf} exceeds $\mu_G G$, the corresponding compatibility equation is replaced by Eq. 2.55 with appropriate sign. If the resulting value of Q_{OF} exceeds $\mu_{OF} F$, the corresponding compatibility equation is replaced by Eq. 2.56 with appropriate sign.

Equation 2.78 applies if there is relative inward sliding of the loose flange on the lap flange. A check should be made to assure that this occurs by computing the radial displacements of the two flanges at their points of contact. The radial displacement of the lap flange is obtained from Eq. 2.29 by replacing B by (B-F), replacing subscripts G and B by subscript OL, setting f equal one, h equal (H_L), reversing the signs of the last three terms involving (B-F), M_{OL}, M_R, and using the values of M_R and Q_R for the lap flange. The radial displacement of the loose flange u_{OL} (Loose) is obtained from Eq. 2.29 by replacing subscript G with subscript OL, subscript R with subscript ILF, R with R_{ILF} B with (B-F), and using h equal (H_F), f from Eq. 2.41, M_B, Q_B for the loose flange. In the event the relative sliding is not as assumed, Eq. 2.78 is replaced by

$$u_{OL}\ (\text{Lap}) = u_{OL}\ (\text{Loose}) \tag{2.79}$$

The value of the constant, C, is now evaluated at the initial tightening conditions by setting p, P, ΔT=0, and B= (B_I). Using this value of C and the design load, stress and deformation distributions in the connector are found. At this point, it is again desirable to check that the proper assumptions on friction (sliding or not) have been used.

The bolt stress is given by Eq. 2D.4 . The hoop stress in the flanges is given by one of Eqs. 2C.10 to 2C.13. However, it is likely to be quite small. The radial flange stress is given by Eq. 2.57. The hoop and axial stresses are given for the hubs and pipes by Eqs. 2.39 and 2.40. In the case of the integral flange, Eq. 2.40 is most critical with the sign before M positive, while for the lap flange the negative sign is more critical.

Comparing stresses with allowable values indicates where thickness changes are needed. If the gasket load drops below the minimum permissible value, an increase in bolt load, an increase in flange height, or a general thickening would be beneficial. If the lap flange has greater roll than the gasket can tolerate, the roll can be reduced by increasing the thickness of the lap flange and its hub.

Each set of changes in geometry must be reanalyzed until a satisfactory configuration is found.

2.6 Other Configurations

The methods presented here are suitable for analyzing connectors which are different from the conventional ones considered in the previous sections. Some of these are sketched in Figure 2.8. Their possible advantages and disadvantages are discussed below.

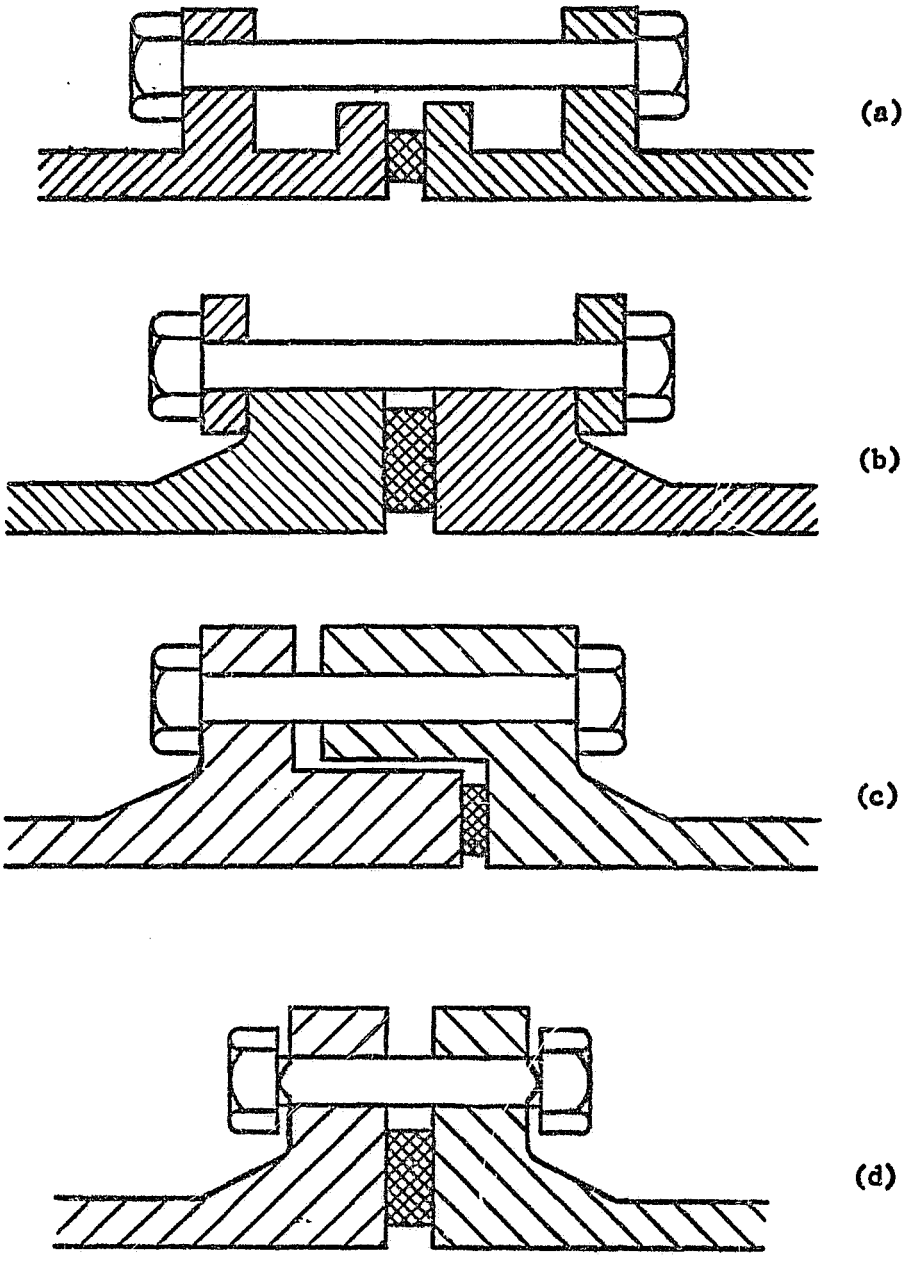

Figure 2.8. Other Connector Configurations

(a) This configuration restrains flange rolling by having the pipe to both sides of each flange. "Barrelling" should be materially less. Thermal effects may be increased somewhat because of the increased bolt length. Weight is saved in flange width but lost again in increased bolt length.

(b) This configuration recognizes that the bolts bear only near their inner side when the flanges can roll. This design increases flange thickness while reducing flange height, thus saving weight for the same stiffness and stress levels. The increased bolt length counterbalances this weight saving. The purpose of a "loose" flange is achieved without the flexibility of "loose" flanges.

(c) Interlocked flanges increase the rolling stiffness of each flange without any overall weight increase. For the same strength and stiffness weight can be saved. The joint loses symmetry however and is somewhat more difficult to machine.

(d) By providing a slight protuberance on the flange at the bolt-centerline circle, it is possible to load the bolts more squarely, even in the presence of flange rolling, than would otherwise be possible. Bolt stresses would thereby be substantially reduced. Bearing stresses under the bolt head and nut would be large, however, high bearing stresses also occur with eccentric loading by a flange which has rolled. The reduction in bolt area permits the use of smaller bolts and thus reduces the overall flange dimensions.

2.7 Other Analytical Methods

Connectors of the types described above can also be analyzed by Castigliano's Theorem. In this approach the strain energy of all the component elements is determined in terms of the applied and redundant loads. The component strain energies are then summed giving a quadratic function in the loads. The derivatives of this function with respect to the redundant loads, when set equal to zero, give a set of simultaneous equations which can be solved for the redundant loads. The derivatives with respect to the applied loads give the deflections at these loads. This approach can readily be adapted to include friction and temperature effects. Appendices 2F, 2G, and 2H give expressions for the energy in cylindrical and ring segments and in the bolts.

To include friction effects where no sliding is anticipated, the friction force is allowed to be a redundant load. To include friction where sliding is anticipated, the friction force is taken as the friction coefficient times the normal force. In each case, the original assumption can be checked by comparing the force with the maximum possible where no sliding is assumed, or by checking the direction of sliding where sliding has been assumed.

The application of Castigliano's Theorem is simple in principle for a structure made up of cylindrical and ring elements. However, it involves a large amount of numerical computation both in obtaining the energies and in solving the resulting simultaneous equations. Therefore, is is particularly

well suited to machine computation where simplicity in formulation is of prime importance, whereas drudgery in computation is of no moment since it can be accomplished by machine.

2.8 References

2.1 Levy, S., ed.,"Environmental Effects", Design Criteria for Zero-Leakage Connectors for Launch Vehicles, Vol. 6, TIS Report No. 63GL46, (NASA Contract NAS 8-4012), March 15, 1963.

2.2 "Modern Flange Design", Taylor Forge Bulletin 502, (4th Edition), 1961.

2.3 Levy, S.,ed., "Design of Connectors", Design Criteria for Zero-Leakage Connectors for Launch Vehicles, Vol. 4, TIS Report No. 63GL44, (NASA Contract NAS 8-4012), March 15, 1963.

2.4 "Pressure Vessels and Piping Design Collected Papers 1927-1959", ASME

2.5 Goodman, T.P., ed., "Summary, Conclusions, and Design Examples", Design Criteria for Zero-Leakage Connectors for Launch Vehicles, Vol.1, TIS Report No. 63GL41, (NASA Contract NAS 8-4012), March 15, 1963

2.6 Bernhard, H. J., "Flange Theory and the Revised Standard B.S. 10:1962-Flanges and Bolting for Pipes, Valves and Fittings", (paper presented to the Institution of Mechanical Engineers in London) October 1963.

2.7 McCalley, R.B.,Jr., and Kelly, R.G., "Tables of Functions for Short Cylindrical Shells", Paper No. 56-F-5, (presented at ASME Fall Meeting in Denver, Colorado, 1956. (Can be consulted at Engineering Societies' Library).

2.8 Timoshenko, S., Theory of Elasticity, McGraw-Hill Book Co., 1934.

2.9 Timoshenko, S., Theory of Plates and Shells, McGraw-Hill Book Co., 1940.

2.10 Tentative Structural Design Basis for Reactor Pressure Vessels and Directly Associated Components, distributed by OTS, Department of Commerce, PB151987, 1 December 1958, Revision with Addendum No. 1, 27 February 1959, (See also NR-S-1 issued March 1961).

Section 3

THREADED CONNECTOR DESIGN

by

John Wallach

3.0 Selection of Connector

The selection of the correct connector for a given application is not only a question of choosing a connector to meet all of the technical design requirements, but also a question of the time and money available. This section is primarily concerned with the design of a technically optimized connector. It is a custom designed connector for a particular application and requires more time and money than an "off-the-shelf" standard connector. Therefore, whenever a standard connector will meet all the design requirements it should be used.

The current commercial connectors can usually be grouped as flared-tube connectors, swaged-tube connectors, or flanged-tube connectors. The flared-tube connector is subject to leakage unless a soft gasket is used, to gross deformation due to an excessive hoop stress in the union if it is overtorqued, and to fatigue failure at the root of the flare. The swaged-tube connector is subject to leakage unless a gasket is used and to fatigue failure in the swage. The flanged-tube connector is subject to leakage unless a gasket is used and to fatigue failure where the flanged section is attached to the tubing. Each type of connector has many advantages, some of which are peculiar to a certain connector design. The listing necessary to point out these features is too long to include here. Also, some connectors seal effectively with the use of ultrafine machined sealing surfaces rather than a soft gasket. However, the latter method of sealing is considered more reliable.

In case a standard connector will not meet the design requirements, a custom connector can be designed using the design procedure given in this Section. This will result in a technically optimized connector for the particular application. However, if over a period of time a large number of custom designed connectors are required, the design procedure can be automated by the use of a digital computer. Also, if the connectors required can be grouped according to their design requirements, it is possible to design a number of standard connectors so that one standard connector will meet the design requirements of a particular grouping. The use of standard connectors makes possible the stocking of connectors for immediate use.

3.1 Design Requirements

The threaded connector design begins with an accurate statement of the design requirements. These are the input quantities to the design procedure. At this stage of the design, it has already been decided that a separable connector is to be used and that a threaded connector rather than a flanged connector is applicable. The threaded connector is chosen when the tubing

outside diameter is one inch or less and the assembly torque required is not excessively large (under 2400 inch pounds).

The detailed design input requirements are:

a. Tubing
   - Material
   - Outside diameter, D_t
   - Inside diameter, d_t

b. Fluid contained in the tubing
   - Name and chemical composition
   - Operating pressure, P_o
   - Constant pressure, P_k
   - Cyclical pressure, P_c
   - Number of cycles of pressure, N_p
   - Temperature, T_g

c. Environmental conditions
   - Surrounding fluid
   - Ambient pressure, P_a
   - Ambient temperature, T_a

d. External loads
   - Constant force, F_k
   - Cyclical force, F_c
   - Number of cycles of force, N_f
   - Constant transverse moment, m_k
   - Cyclical transverse moment, m_c
   - Number of cycles of moment, N_m

e. Allowable leakage level

These design requirements are determined for each critical operating condition, both steady state and transient. A table of operating conditions and input parameters helps to keep the operating conditions separate. For each operating condition, a check of each parameter is necessary so that the value of the parameter in the table is the correct one for that condition.

In the following sections, reference is usually made to only one operating condition. This condition is very general and includes all of the design input parameters. Based on these parameters, a set of formulas have been derived for the determination of the connector dimensions.

By repeated use of the design procedure for each operating condition and the selection of the most conservative design, a connector design meeting all of the design requirements is generated. Wherever possible, the prior elimination of those operating conditions leading to nonconservative designs will greatly reduce the design effort.

3.2 Connector Configuration

The connector consists of a flange, union, seal and nut. The typical connector configuration is illustrated in Figure 3.1.

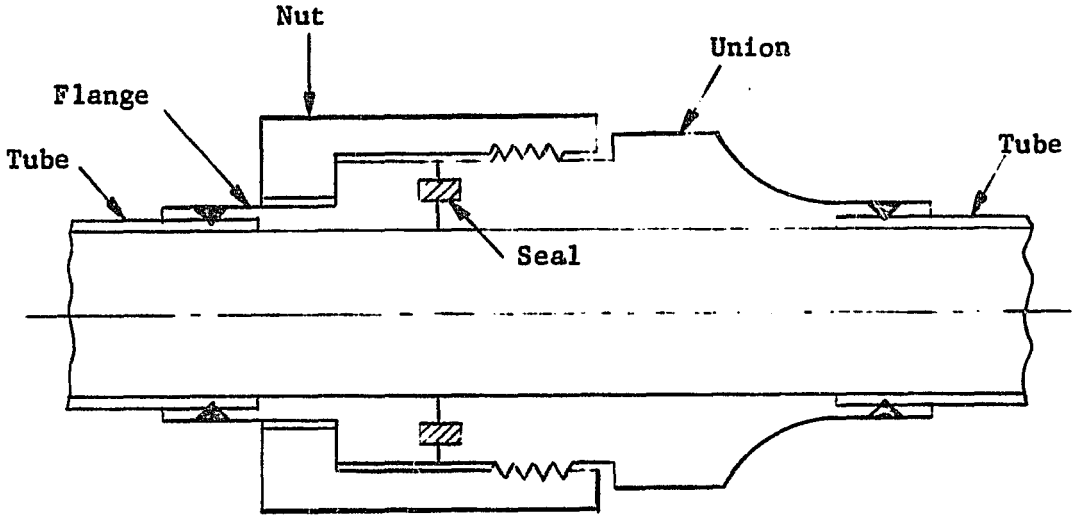

Figure 3.1 Typical Connector Configuration

The connector design separates the various connector functions. The attachments to the tube are made between the flange and the tube, and the union and the tube by welding. The separable part of the connector consists of the flange, nut, and union. Flats are provided on the nut and the union for wrench jaws. The seal is placed between the flange and the union. The compressive load path is from the flange to the union (not through the seal), and the tensile load path is through the nut.

3.3 Seal

The seal consists of either two flange and union surfaces properly prepared or a removable gasket and its companion sealing surfaces on the flange and the union. There is no one seal that can be successfully used in every application. However, certain types of seals can be used in specific

environments. Most of the gaskets for these seals are commercially available, and the seal can be designed from the manufacturer's catalog. A complete discussion of seals is included in Sections 1 and 4 of this Handbook.

3.4 Attachment to Tubing

The attachment of the connector to the tube must be structurally sound, leakproof, and compatible with the fluid contained. The method which best fits these requirements is welding. Swaging is not reliably leak-proof and brazing is limited because of compatibility and temperature problems. Welding, in general, also presents many problems when used in launch vehicle systems. However, a great deal of effort has already gone into the solution of these problems and satisfactory methods are being developed.

One such welding method, which has been developed and is recommended for use in this connector design, is discussed in Refs. 1 and 2. The method described is a tube-to-tube connection, but is applicable to the connector-to-tube connection shown in Figure 3.2. The tubing is slid into the connector

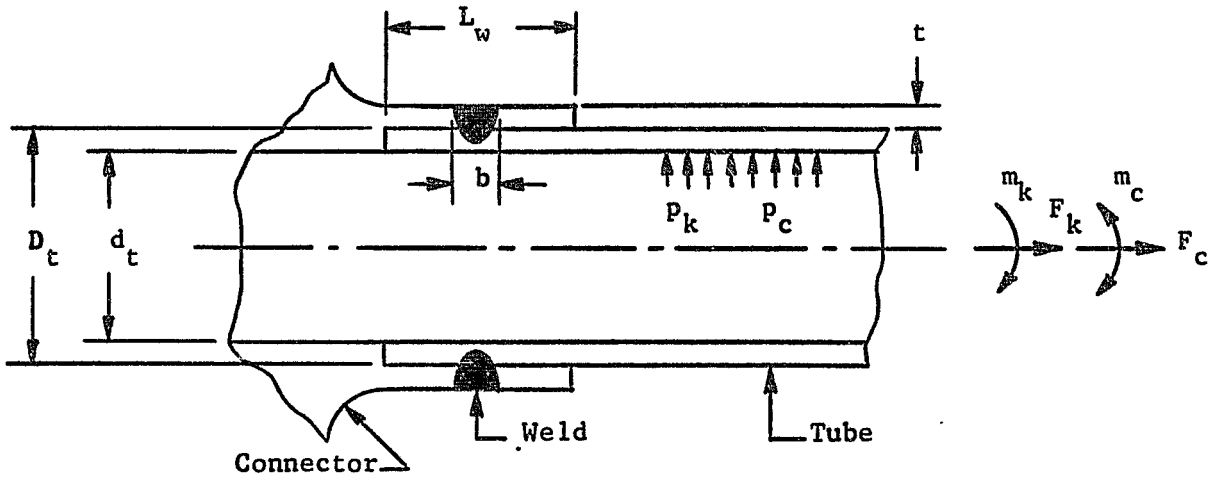

Figure 3.2 Connector-to-tubing Weld

socket and swaged into the socket. The weld is formed by melting the connector and tube materials together. The radial thickness of the socket is assumed equal to the tube thickness. However, the thickness and length, L_w, of the socket are determined by the materials to be welded, the type of weld, and the loading.

The structural integrity of the weld is so largely dependent on the type of weld, welding procedure, and connector and tube materials, that a separate yield strength, B_y, fracture strength, B_u, and fatigue strength, B_n, are determined for the weld. The strengths are expressed in pounds per linear inch of weld circumference. With these strengths known for the critical operating conditions (the strengths are temperature dependent) the structural integrity of the weld can be checked.

To prevent yielding.

$$\frac{H_m}{D_t}\left[0.3183(F_k+F_c)+0.25d_t^{\,2}(p_k+p_c)+\frac{1.273}{D_t}(m_k+m_c)\right]\leq B_y \qquad (3.1)$$

To prevent fracture.

$$\frac{H_m}{D_t}\left[0.3183(F_k+F_c)+0.25d_t^{\,2}(p_k+p_c)+\frac{1.273}{D_t}(m_k+m_c)\right]\leq B_u \qquad (3.2)$$

To prevent fatigue failure.

$$\frac{H_f}{D_t}\left[0.3183\left(\frac{F_k}{B_u}+\frac{F_c}{B_u}\right)+0.25d_t^{\,2}\left(\frac{p_k}{B_u}+\frac{p_c}{B_n}\right)+\frac{1.273}{D_t}\left(\frac{m_k}{B_u}+\frac{m_c}{B_n}\right)\right]\leq 1 \qquad (3.3)$$

There is no inconsistency between Eqs. 3.1 and 3.2, because only one of these equations will be used for any one operating condition.

3.5 Flange

3.5.1 Flange Configuration

The flange consists of three elements. The socket is provided for the mechanical attachment of the tube to the flange. A hub increases the distance between the weld and the seal in order to prevent thermal distortion of the flange ring during welding and to provide a smoother transition between the flexible socket and the rigid flange ring. The flange ring provides a bearing surface for the nut, an interface between the flange and the union for the seal and compressive load, and the structural rigidity to maintain the seal. The three elements and the nomenclature associated with the detailed dimensions of each element are shown in Figure 3.3.

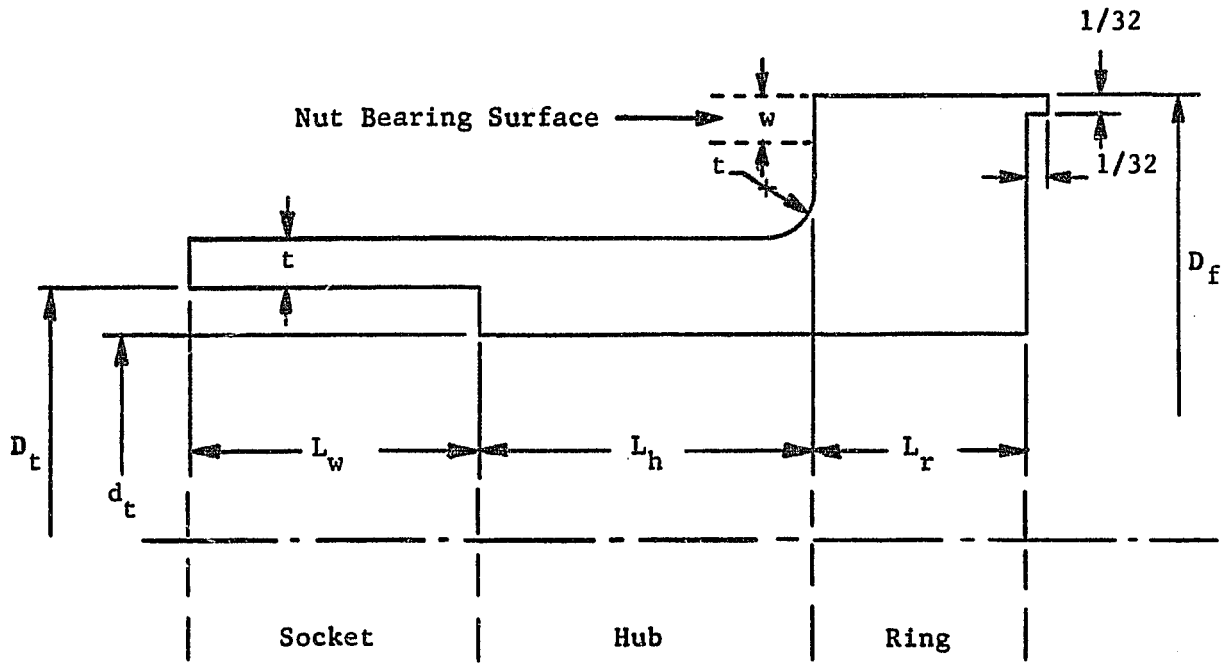

Figure 3.3 Flange Elements

All of the dimensions are chosen on the basis of a thorough stress and vibration analysis. This analysis is done in two steps and possibly a number of iterations. The structural analysis depends on the prior knowledge of the preload applied when tightening the nut. However, the preload depends on prior determination of the structural response of the connector by a structural analysis. Therefore, it is necessary to make an initial estimate of the connector dimensions. Then the preload is determined using these dimensions. The dimensions are then calculated on the basis of a thorough structural analysis using the calculated preload, and the preload is recalculated using the more accurate dimensions. This iterative calculation of connector dimensions and preload is continued until the change in dimensions and preload is negligible. If the second of two consecutive preload calculations results in a preload within five percent of the previous calculation, then the connector is adequately designed for the second preload and the calculations may be stopped.

3.5.2 Approximate Flange Dimensions

The following dimensions are necessary for the calculation of the preload. As stated above, the preload must be calculated before a final determination of flange dimensions is possible.

The length of the transition section of the flange is

$$L_h = 1.5\ (D_t+2t-d_t) \qquad (3.4)$$

The outside diameter of the flange ring, D_f, is the largest of the following:

$$(D_f)_1 = D_t + 6t$$

$$(D_f)_2 = D_t + 4t + 1/8$$

$$(D_f)_3 = D_g + 2t + 1/16$$

$$(D_f)_4 = D_g + 3/16 \qquad (3.5)$$

D_f = the largest of $(D_f)_1$, $(D_f)_2$, $(D_f)_3$, or $(D_f)_4$

The length of the flange ring is approximated by making it equal to the radial width.

$$L_r = 1/2\ (D_f - d_t) \qquad (3.6)$$

The radial bearing length of the nut on the flange, w, is equal to t or 1/16", whichever is larger.

$$w = \text{larger of } (t \text{ or } 1/16") \qquad (3.7)$$

3.6 Union

3.6.1 Union Configuration

The union provides the seal interface, the threads to engage the nut, a set of wrenching flats, and a tube socket. The seal configuration and dimensions are in accordance with Sections 1 or 4. The union configuration and dimensions are given in this section. Figure 3.4 shows the details and dimensional nomenclature for the union. The outside and inside diameters (D_g and d_g) and axial length (L_g) of the seal are shown for reference.

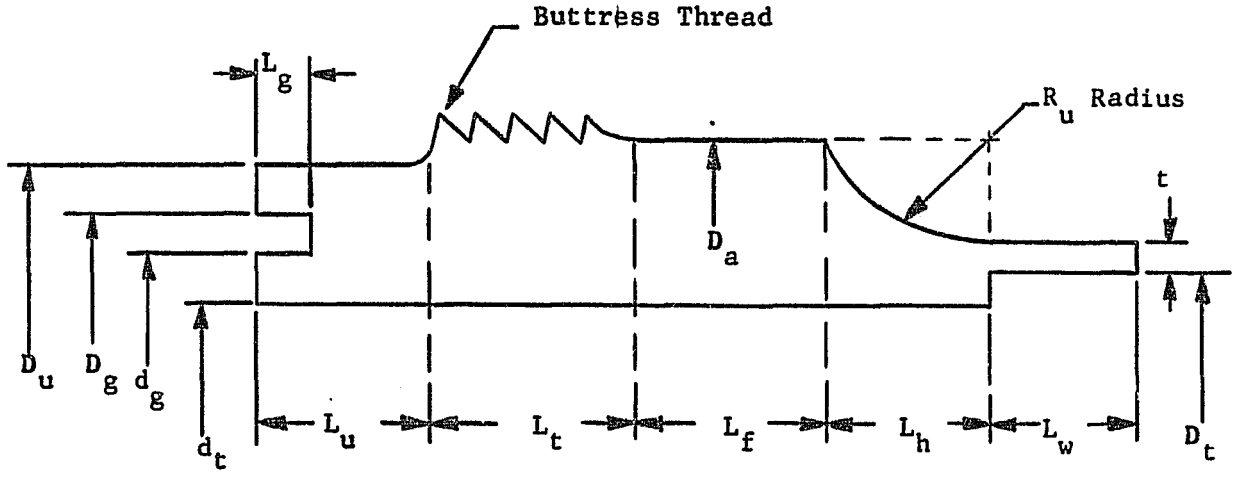

Figure 3.4 Union Dimensions

3.6.2 Union Dimensions

The union dimensions are determined by the mating parts and by the loads imposed. As the loading is not known until the preload has been calculated, the union dimensions and those of the mating parts can not be finalized at this stage of the design. In this Section the union dimensions are determined without a thorough stress analysis. In Section 3.10, after a complete structural analysis the dimensions will be checked.

The union diameter, D_u, is to be a snug sliding fit inside the lip on the flange face. In this way the union is located on the flange and radial motion between the two is prevented.

$$D_u = D_f - 1/16 \tag{3.8}$$

The length, L_u, is to be long enough so that the load on the threads is distributed uniformly over the union-to-flange contact area. So L_u is taken equal to the depth of the seal recess, L_g.

$$L_u = L_g \tag{3.9}$$

The union and nut thread is an American standard buttress screw thread (ASA B 1.9-1953). The nominal size of the thread, D_b, is chosen so that the minimum minor diameter of the nut is larger than D_f, and the nut will freely slide over the flange.

$$D_b \geq D_f + 1.2/n \tag{3.10}$$

The recommended thread sizes, number of threads, lengths of thread engagement, and lengths of threads are given in Table 3.1. These recommendations are based on a structural analysis of the Buttress thread using the formulas of Ref. 3.

Table 3.1

RECOMMENDED BUTTRESS THREAD SIZES

Nominal Size Inch D_b		Number of Threads Per Inch n	Length of Engagement Inch L_e	Length of Thread Inch L_t
From	To			
0	1/2	20	1/4	5/16
1/2	3/4	16	5/16	3/8
3/4	1	12	3/8	7/16
1	1-1/4	10	7/16	1/2
1-1/4	2	8	9/16	5/8
2	3	8	11/16	3/4

The next portion of the union provides a place to put a wrench so that the nut can be tightened on the union. In order to facilitate cutting of the threads, the diameter across corners of the wrenching flats is taken slightly less than the minor diameter of the thread on the union. The diameter across flats, D_a, is given by the following inequality:

$$D_t+2t \leq D_a \leq 0.866\ D_b - \frac{1.219}{n} - 0.017 \qquad (3.11)$$

The largest D_a which satisfies Eq. 3.11 and is a standard size for an open end or camloc wrench is chosen. Then L_f is chosen equal to the thickness of the wrench head.

The next section of the union provides a transition between the wrenching flats and the tube socket. A radius, R_u, is used to reduce the stress concentration.

$$R_u = 1/2\ (D_a - D_t) - t \qquad (3.12)$$

The tube socket on the union is identical to that on the flange. The same final dimensions are used for both. The flange tube socket is discussed in Sections 3.5 and 3.9..

3.7 Nut

3.7.1 Nut Configuration

The nut provides the tension necessary to compress the seal at assembly and to maintain this compression under all operating conditions. The ring of the nut bears on the ring of the flange,and the threads on the nut engage the threads of the union. Wrenching flats are provided on the outside diameter of the nut. Figure 3.5 shows the details and dimensional nomenclature for the nut.

3.7.2 Nut Dimensions

Most of the nut dimensions have been determined in the preceding sections. All of the nut dimensions except the outside diameter, D_n, and length of the ring, L_n, are determined by the mating parts. These remaining dimensions are estimated in this section so that the preload can be calculated. Then the dimensions are checked on the basis of a structural analysis, Section 3.9..

The nominal size of the thread, number of threads per inch, length of thread engagement, and length of thread are the same as for the union, Section 3.6.2. Based on these dimensions the inside diameter of the nut, d_s, is chosen equal to the maximum major diameter of the thread.

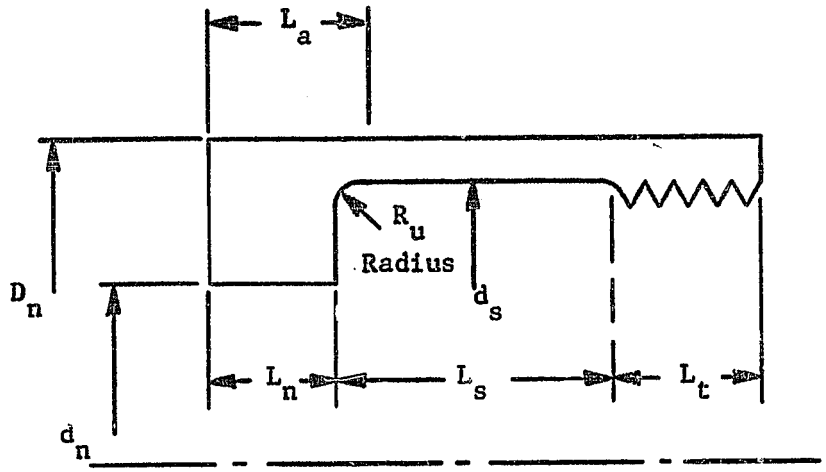

Figure 3.5 Nut Configuration

$$d_s = D_b + \frac{0.208}{n} + 0.014 \tag{3.13}$$

The length of the shell part of the nut is determined by the mating parts.

$$L_s = L_r + L_u + L_e - L_t \tag{3.14}$$

The inner diameter of the ring part of the nut is determined by the flange dimensions.

$$d_n = D_f - 2w \tag{3.15}$$

The small radius, R_n, is used to decrease the stress concentration.

$$R_n = 1/2(d_s - D_f) \tag{3.16}$$

The basic outside diameter of the nut, D_n, is also the diameter across flats of the wrenching flats provided on the nut. The value of D_n

$$D_n \geq d_s + D_u - d_t \tag{3.17}$$

chosen is the smallest standard diameter across the flats for a nut that satisfies Eq. 3.17. The wrenching flats are located at the ring end of the nut and the length of the flats, L_a, is taken equal to the thickness of a standard wrench head.

The length of the ring, L_n, is taken equal to the radial thickness.

$$L_n = 1/2\ (D_n - d_n) \tag{3.18}$$

3.8 Preload

Preloading of the connector at assembly is essential to proper operation of the connector. Too small a preload in the connector will result in leakage and too large a preload will result in overstressing the connector. The use of the proper preload is also important in the stress calculations. The use of too small a preload in the calculations will result in a leaky connector and the use of too large a preload will result in an over-designed and overweight connector.

The preloading of a connector at assembly can be considered a two-step operation. First, the nut is tightened until the seal is sufficiently compressed and the flange and union come into contact. The axial force necessary is referred to as the seating force, F_s. At this point a seal has been effected. That is, the seal is designed so that the compressive force to bring the flange and union into contact is more than adequate to make the seal leak-tight.

The second step of the connector preloading is to increase the flange-to-union contact force to a value large enough to maintain the flange-to-union contact during all operating conditions. As the flange and union remain in contact at all times, the only axial movement the seal experiences is the elastic deformation of the flange and union faces. The seal is also protected from relative radial motions as long as the friction force between the flange and the union is not exceeded by the radial forces occurring during operation of the connector. For this reason, a minimum compressive force between the flange and union is maintained at all times.

3.8.1 Seal Force

Two forces are important to the seal. These are the force to effect a leak-tight seal at assembly and the minimum allowable force that will assure a leak-tight connector during operation. Sometimes an amount of compression rather than the force is specified. For instance, a rubber O-ring vendor usually recommends the amount of compression to effect the initial seal. In this case the force is very small, and it is more meaningful to specify the compression. However, in cases where the force to effect the seal is not negligible with respect to the preload, the force must be considered.

The connector being designed depends on a direct flange-to-union contact to carry the major portion of the compressive load. Only during assembly, before the union seats on the flange, does the seal take all the compressive load. Once the union seats on the flange, practically all of the increase in compressive load is taken by the union to flange interface. Therefore, the load on the seal when the flange is just touching the union must be large enough to effect a seal. However, the force should be only as large as necessary to reliably effect a seal at each assembly. Also, the force should be larger than the minimum allowable force for maintaining a leak-tight seal. This is usually the case. That is, for nearly all seals, the force to effect the seal is larger than the force to maintain the seal.

Thus, the sealing forces can be reduced to one force, the seating force F_s. This is the force necessary to bring the flange and union into direct contact. In the succeeding design procedure it is assumed that F_s is just large enough to reliably effect a seal at each assembly and is larger than the force necessary to maintain the seal during operation. The determination of F_s may be by analysis, test, or experience, depending upon the seal. For some seals the vendor will recommend the force to effect the seal and the force necessary to maintain the seal. In case the compression rather than the force is specified and the force is significant the force is determined from the compression. If the force is insignificant, as for a rubber O-ring, F_s is set equal to zero and the connector is designed only in accordance with the necessary compression.

3.8.2 Preload Calculation

The assembly preload, F_p, is chosen so that the load on the seal, F_g is always equal to or greater than the seating force, F_s. To choose the preload, first the axial spring constant, G_n, for the nut is calculated. Then the force on the seal is calculated for each critical operating condition, and from these results the necessary preload is calculated.

3.8.2.1 Spring Constant for the Nut

The spring constant for the nut is calculated on the basis of a thorough structural analysis. Because of the complexity of the analysis and the need to determine the forces and moments at the critical nut locations in order to calculate the stresses, the spring constant is calculated from a set of linear simultaneous equations. The numerical work involved in solving this set of equations is formidable, and the use of a digital computer is recommended. No programming will be necessary at most computer facilities as they will already have a program for linear simultaneous equations in operation. The coefficients in the equations can also be evaluated with the use of a digital computer, if this is desirable.

The nut was separated into a ring and three shells for the structural analysis, Figure 3.6. The deflections, rotations, forces, and moments are shown in Figure 3.6 in a positive sense. The externally applied load, F_n, acts on the nut ring and on the threads. The force on the threads is assumed to be divided equally between two finite locations. Because of the small thread angle there is no radial component of F_n on the threads. The following set of equations will allow the calculations of the deflections, rotations, forces, and moments due to a unit axial force (F_n=1). From these results the spring constant is calculated. The set of equations is written in a condensed form and the coefficients of the variables and constant terms, C_i, are written separately in Section 3.11.1.

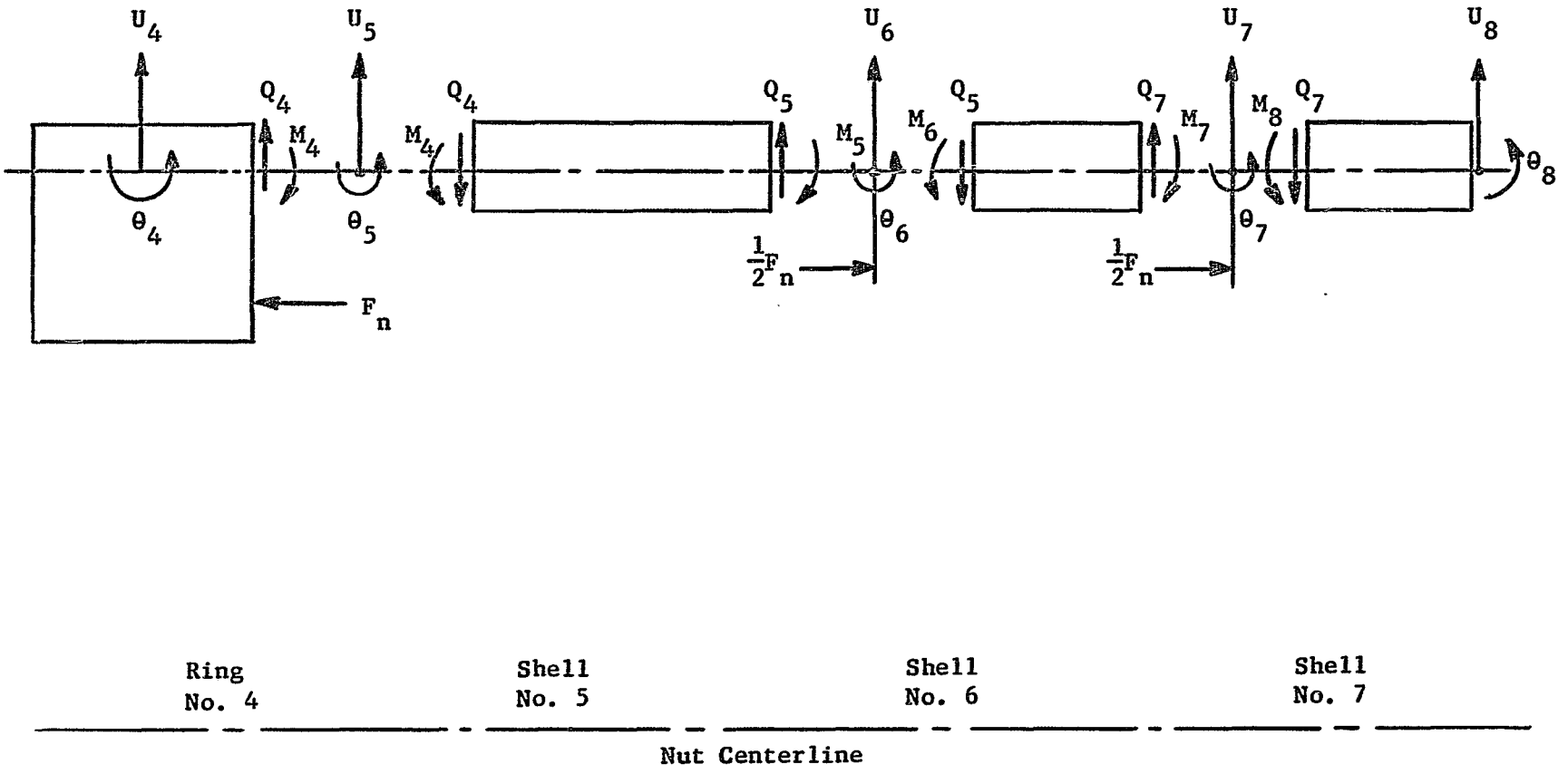

Figure 3.6 Separation of Nut for Structural Analysis

$$u_4 - u_5 + C_1\theta_4 = 0$$

$$u_4 + C_2Q_4 = 0$$

$$C_3u_5 - C_4u_6 + C_5\theta_5 + C_6\theta_6 + C_7Q_4 = C_8$$

$$C_4u_5 - C_3u_6 + C_6\theta_5 + C_5\theta_6 + C_7Q_5 = - C_8$$

$$-C_5u_5 + C_6u_6 - C_9\theta_5 - C_{10}\theta_6 + C_7M_4 = C_{11}$$

$$C_6u_5 - C_5u_6 + C_{10}\theta_5 + C_9\theta_6 + C_7M_5 = C_{11}$$

$$C_{12}u_6 - C_{13}u_7 + C_{14}\theta_6 + C_{15}\theta_7 + C_{16}Q_5 = C_{17}$$

$$C_{13}u_6 - C_{12}u_7 + C_{15}\theta_6 + C_{14}\theta_7 + C_{16}Q_7 = -C_{17}$$

$$-C_{14}u_6 + C_{15}u_7 - C_{18}\theta_6 - C_{19}\theta_7 + C_{16}M_6 = C_{20}$$

$$C_{15}u_6 - C_{14}u_7 + C_{19}\theta_6 + C_{18}\theta_7 + C_{16}M_7 = C_{20}$$

$$C_{21}u_7 - C_{22}u_8 + C_{23}\theta_7 + C_{24}\theta_8 = 0$$

$$C_{25}u_7 - C_{26}u_8 + C_{21}\theta_7 + C_{22}\theta_8 = 0$$

$$C_{26}u_7 - C_{25}u_8 + C_{22}\theta_7 + C_{21}\theta_8 + C_{27}Q_7 = 0$$

$$-C_{22}u_7 + C_{21}u_8 - C_{24}\theta_7 - C_{23}\theta_8 + C_{27}M_8 = 0$$

$$\theta_4 - \theta_5 + C_{28}Q_4 + C_{29}M_4 = 0$$

$$C_{30}\theta_4 + C_{31}Q_4 + C_{32}M_4 = C_{33}$$

$$M_5 - M_6 = C_{34}$$

$$M_7 - M_8 = C_{34} \qquad (3.19)$$

Having solved Eq. 3.19, it is possible to calculate the spring constant for the nut directly.

$$\frac{1}{G_n} = -0.25\,(D_n + d_s - 2d_n - 2w)\,\theta_4 + 0.125\,(D_n + d_s - 2D_b + \frac{1.2}{n})\,(\theta_6 + \theta_7) + \frac{1.273(L_s + L_t) - 0.7417\,L_e}{E_n\,(D_n^2 - d_s^2)} \qquad (3.20)$$

The spring constant is a linear function of the modulus of elasticity, E_n, which is temperature dependent. Therefore, a different value of the spring constant is calculated for each nut temperature. This is easily done by calculating the spring constant at room temperature and then using Eq. 3.21 to calculate the spring constants at various temperatures.

$$G_n(\text{operating temperature}) = G_n(\text{room temperature})\,\frac{E_n\,(\text{operating temperature})}{E_n\,(\text{room temperature})} \qquad (3.21)$$

3.8.2.2 Seal Force Calculation

The use of direct contact between the flange and the union to transmit the major portion of the compressive load means that the force on the seal during operation does not appreciably increase over F_s, the seating force. Therefore, it is more meaningful to calculate the force F_3, and moment, M_3, between the flange and the union. The seal force, F_g, is some function of this force and moment, and this functional relationship depends on the seal, flange face, and union face.

$$F_g = \text{function}\,(F_3, M_3) \qquad (3.22)$$

To determine M_3 for any operating condition a thorough structural analysis of the flange and union was made. Because of the complexity of the analysis and the need to determine the forces and moments at various locations for the subsequent stress calculation, the result of the analysis is a set of linear simultaneous equations. Again, it is recommended to use a digital computer for their solution.

The flange was separated into three shells and the union was separated into two shells as shown in Figure 3.7. The deflections, rotations, forces, and moments are shown in a positive sense. The nut force, F_n, acts on the flange and the union. Because of the comparative

rigidity of the union, it was possible to assume the nut force concentrated at one point, with negligible error. The flange and union are also loaded by an axial force F_a, and internal pressure, p. The axial force is a composite of a constant and cyclical axial pressure force, an externally applied axial force, and an externally applied transverse moment. The maximum value of F_a for a particular operating condition is calculated from Eq. 3.23. In this equation some of the forces may be zero for a particular operating condition.

$$F_a = (F_k + F_c) + .7854\, D_t^{\,2}\,(p_k + p_c) + \frac{4}{D_t + t}\,(m_k + m_c) \qquad (3.23)$$

For each critical operating condition F_a may be different and may require a separate calculation. This is also true for G_n, the pressure ($p = p_k + p_c$), and the temperature of the various connector parts. Having determined the nut spring constant, and the loads and temperatures for each critical operating condition the next step is to calculate M_3 for a unit preload ($F_p = 1$) for each operating condition. This requires the solution of the following set of simultaneous equations for each operating condition. The set of equations is written in a condensed form and the coefficients of the variables and constant terms, c_i, are written separately in Section 3.11.2.

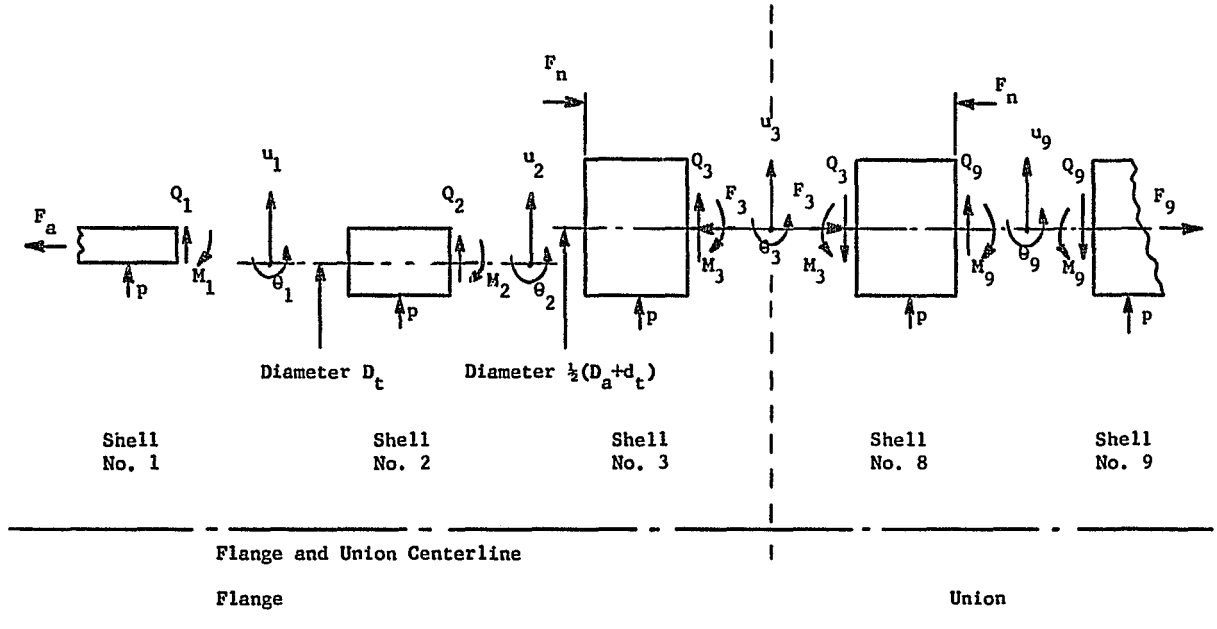

Figure 3.7. Separation of Flange and Union for Structural Analysis

$$C_{35}u_1 - C_{36}u_2 + C_{37}\theta_1 + C_{38}\theta_2 + C_{39}Q_1 + C_{40}Q_2 + C_{41}M_2 = C_{42} \qquad (3.24)$$

$$C_{43}u_1 - C_{44}u_2 + C_{45}\theta_1 + C_{46}\theta_2 + C_{47}Q_2 + C_{48}M_1 + C_{49}M_2 = C_{50}$$

$$C_{44}u_1 - C_{43}u_2 + C_{46}\theta_1 + C_{45}\theta_2 + C_{51}Q_2 + C_{52}M_2 = C_{53}$$

$$C_{36}u_1 - C_{35}u_2 + C_{38}\theta_1 + C_{37}\theta_2 + C_{54}Q_2 + C_{55}M_2 = -C_{42}$$

$$u_1 + C_{56}Q_1 + C_{57}M_1 = C_{58}$$

$$C_{60}u_2 - C_{61}u_3 + C_{62}\theta_2 + C_{63}\theta_3 + C_{64}Q_2 + C_{65}F_n = C_{66}$$

$$C_{67}u_2 - C_{59}u_3 + C_{63}\theta_2 + C_{62}\theta_3 + C_{68}Q_3 - C_{65}F_n = C_{69}$$

$$C_{71}u_2 - C_{72}u_3 + C_{73}\theta_2 + C_{74}\theta_3 + C_{75}M_2 + C_{76}F_n = C_{77}$$

$$C_{78}u_2 - C_{70}u_3 + C_{74}\theta_2 + C_{73}\theta_3 + C_{79}M_3 + C_{80}F_n = C_{81}$$

$$C_{82}u_3 - C_{83}u_9 + C_{84}\theta_3 + C_{85}\theta_9 + C_{86}Q_3 + C_{87}F_n = C_{88}$$

$$C_{83}u_3 - C_{82}u_9 + C_{85}\theta_3 + C_{84}\theta_9 + C_{86}Q_9 - C_{87}F_n = -C_{88}$$

$$C_{89}u_3 - C_{90}u_9 + C_{91}\theta_3 + C_{92}\theta_9 + C_{93}M_3 + C_{94}F_n = C_{95}$$

$$C_{90}u_3 - C_{89}u_9 + C_{92}\theta_3 + C_{91}\theta_9 - C_{93}M_9 + C_{96}F_n = C_{97}$$

$$u_9 + C_{98}Q_9 + C_{99}M_9 = C_{100}$$

$$\theta_1 + C_{101}Q_1 + C_{102}M_1 = 0$$

$$\theta_9 - C_{99}Q_9 + C_{103}M_9 = 0$$

$$F_n = C_{104}$$

Then F_3 is calculated from Eq. 3.25.

$$F_3 = C_{104} - F + \frac{\pi}{4}\left[D_t^2 - d_t^2 - \frac{1}{4}(D_g + d_g - 2d_t)(D_g + d_g + 2d_t)\right] p \qquad (3.25)$$

After which, F_g is calculated using Eq. 3.22. The operating condition giving the smallest F_g, that is the smallest compressive force (it may be the largest tensile force), is the most critical operating condition. This is the condition which determines F_p.

M_3 is linearly related to F_p in the following manner.

$$M_3 = A_3 + A_4 F_p \tag{3.26}$$

By repeating the solution of Eqs. 3.24 and 3.25 for the most critical operating condition with $F_p = 0$, the constants A_1 and A_3 are determined.

$$\begin{aligned} A_1 &= (F_3)_{F_p=0} \\ A_3 &= (M_3)_{F_p=0} \end{aligned} \tag{3.27}$$

From the previous calculation of M_3 where $F_p = 1$ the other constants are determined.

$$\begin{aligned} A_2 &= (F_3)_{F_p=1} - A_1 \\ A_4 &= (M_3)_{F_p=1} - A_3 \end{aligned} \tag{3.28}$$

Then substituting Eqs. 3.26 in Eq. 3.22 gives F_g as a function of only F_p.

$$F_g = \text{function } (F_p) \tag{3.29}$$

F_g is equal to F_s times a safety factor. Thus, with F_s and the safety factor known, the preload is determined by solving Eq. 3.29 for F_p.

3.8.3 Assembly Torque Calculation

The most common method of setting the preload at assembly is by torquing the nut to a specified torque value using a torque wrench. The accuracy of this method depends on the accuracy of the torque wrench, skill of the mechanic, and accurate knowledge of the friction factors. The torque required to obtain a given preload is calculated from Eq. 3.30 where f_t is the friction factor for the nut and union threads and f_n is the friction factor for the bearing surface between the nut and flange.

$$W = \frac{F_p}{2n} \left\{ .3183 + nf_n (d_n + W) + \frac{n^2 D_b^2 - 1.2nD_b + .4613}{\frac{nD_b - .6}{1.007\, f_t} - .3183} \right\} \tag{3.30}$$

3.9 Stress Analysis

The preload was determined without any regard to the stresses in the connector. Therefore, the next step in the design procedure is a calculation of the stresses at the critical operating conditions. There is no assurance that the operating condition determining the preload will also result in the most severe stress condition and it is therefore necessary to consider each operating

condition which is suspected of causing an adverse stress condition. For each operating condition the deflections, rotations, forces and moments of the flange and union are calculated using Eq. 3.24, and the value of F_p previously determined. The calculation also gives the value of F_n for each operating condition. As the deflections, rotations, forces,and moments of the nut were calculated for a unit force F_n, as part of the spring constant calculation, it is possible to use these values in the stress calculations by simply multiplying them by the appropriate value of F_n. This assumes that the spring constant calculation was performed for every operating condition of interest. Otherwise the spring constant calculation is made for those operating conditions not previously considered.

Thus the maximum deflections, rotations, forces, and moments are known throughout the connector for each critical operating condition. It is noted that the maximum loading conditions have been used in the preceding calculations. In the calculation of F_a by Eq. 3.23, the maximum mean (or constant) load and the maximum amplitude of the cyclic load, for a particular operating condition, were added together. This method of calculation results in the determination of the peak stresses and the calculation is necessary for the static load analysis discussed in the next section. However, for the vibration analysis a separate mean value and cyclic amplitude of the total load, F_a, is necessary. Thus, a mean value of F_a and a cyclic value of F_a are calculated for each operating condition using Eq. 3.23. Again the deflections, rotations, forces, moments and F_n are calculated separately for the constant and cyclic load for each operating condition using Eq. 3.24. Then the results of the spring constant calculation are again used to obtain the deflections, rotations, forces, and moments for the nut for the constant and cyclic loadings separately.

In the following sections the static load and vibration analysis of the connector design are discussed. The stress formulas are for the static and cyclic stresses at various connector locations for one particular operating condition. After the stress calculations have been made for each critical operating condition,the operating condition resulting in the largest stresses is chosen. The connector design is then optimized using this operating condition as outlined in Section 3.9.3.

3.9.1 Static Stress Analysis

The static stress analysis is performed to prevent yielding of the connector during any operating condition (including the proof test), to prevent fracture during the burst test, and to reduce the connector weight to a minimum. Two failure criteria are used; one for yielding and one for fracture. For the yielding criteria,the shear distortion energy theory is most appropriate for this design procedure. Further, as the material properties are usually expressed as uniaxial stresses for yielding the effective stress, S, is chosen as the calculated parameter in applying the shear distortion energy theory. This effective stress can be compared directly with the uniaxial test data to determine whether yielding will occur. The effective stress, calculated for a triaxial stress field, is the uniaxial stress which would result in the same amount of shear distortion energy as would the triaxial stress field.

In the following sections of the static stress analysis the stress formulas given are for the effective stress at the critical connector locations.

The effective stresses calculated should be multiplied by a safety factor (equal to or larger than 1.1) before comparing them to the uniaxial yield strengths. It is also important to determine the temperature at the connector location under consideration and to use the proper values of the yield and fracture strength.

The complexity of the fracture strength calculation makes it impractical to carry it out. The nonlinearity of the stress-strain curve in the region between yielding and fracture is contrary to the basic assumption in the preceding analysis. A nonlinear analysis is too complex. Therefore, fracture is prevented by choosing a ductile material whose fracture strength is sufficiently larger than its yield strength to meet the design requirements.

3.9.1.1 Flange

Before proceeding with the stress calculations the deflections and rotations of the various parts of the connector are reviewed to see whether they are consistent with the proper functioning of the connector. After correcting any inconsistencies, the stresses are calculated using the following formulas. The subscript on the effective stress refers to the flange location of the stress. These locations are noted in Figure 3.8.

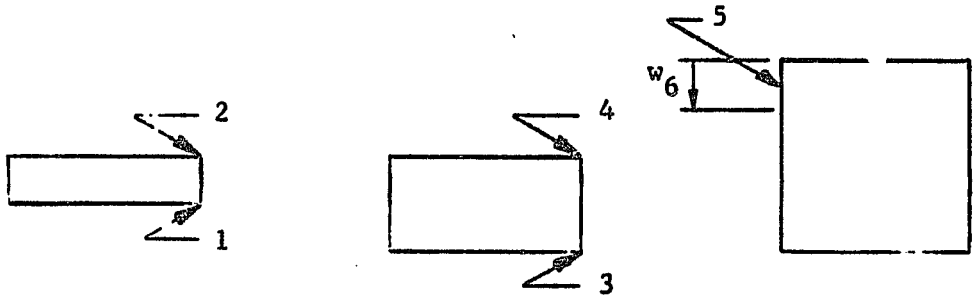

Figure 3.8 Location of Flange Stresses Calculated

The square of the effective stress is calculated because it is more convenient to present the stress formulas this way. The σ_h and σ_r are the hoop and radial thermal stresses respectively. These are only important during thermal transients and are calculated using the methods of Ref. 4.

Location 1

$$S_1^2 = \left\{ \frac{1.414E_f}{D_t} u_1 - \frac{0.4502}{t(D_t + t)} F_a + \frac{8.486}{t^2} M_1 - 0.07778p + 0.7071 \sigma_h \right\}^2$$
$$+ \left\{ - \frac{1.273}{t^2} M_1 + \frac{1.414Ef}{D_t} u_1 + \frac{0.06751}{t(D_t + t)} F_a + 0.6293p + 0.7071 (\sigma_h - \sigma_r) \right\}^2$$
$$+ \left\{ \frac{0.5177}{t(D_t + t)} F_a - \frac{9.759}{t^2} M_1 + 0.7071p - 0.7071 \sigma_r \right\}^2 \qquad (3.31)$$

Location 2

$$S_2^2 = \left\{ \frac{1.414E_f}{D_t} u_1 - \frac{0.1576}{t(D_t + t)} F_a - \frac{2.97}{t^2} M_1 - 0.07778p + 0.7071\sigma_h \right\}^2$$

$$+ \left\{ \frac{1.273}{t^2} M_1 + \frac{1.414E_f}{D_t} u_1 + \frac{0.06751}{t(D_t + t)} F_a - 0.07778p + 0.7071\ (\sigma_h - \sigma_r) \right\}^2$$

$$+ \left\{ \frac{0.2251}{t(D_t + t)} F_a + \frac{4.243}{t^2} M_1 - 0.7071\sigma_r \right\}^2 \qquad (3.32)$$

Location 3

$$S_3^2 = \left\{ \frac{1.414E_f}{D_t} u_2 - \frac{0..6302}{(D_t + 2t)^2 - d_t^2} F_a + \frac{11.88}{(D_t + 2t - d_t)^2} M_2 \right.$$

$$\left. + 0.7071\sigma_h + \left[\frac{0.495(D_t^2 - d_t^2)}{(D_t + 2t)^2 - d_t^2} - 0.07778 \right] p \right\}^2$$

$$+ \left\{ \frac{1.414E_f}{D_t} u_2 + \frac{0.2701}{(D_t + 2t)^2 - d_t^2} F_a + 0.7071\ (\sigma_h - \sigma_r) - \frac{5.092}{(D_t + 2t - d_t)^2} M_2 \right.$$

$$\left. + \left[0.6293 - \frac{0.2121\ (D_t^2 - d_t^2)}{(D_t + 2t)^2 - d_t^2} \right] p \right\}^2$$

$$+ \left\{ \frac{0.9003}{(D_t + 2t)^2 - d_t^2} F_a - \frac{16.97}{(D_t + 2t - d_t)^2} M_2 - 0.7071\sigma_r \right.$$

$$\left. + \frac{2.828\ t\ (D_t + t)}{(D_t + 2t)^2 - d_t^2} p \right\}^2 \qquad (3.33)$$

Location 4

$$S_4^2 \left\{ \frac{1.414E_f}{D_t} u_2 - \frac{1.224}{(D_t + 2t)^2 - d_t^2} F_a - \frac{23.08}{(D_t + 2t - d_t)^2} M_2 \right.$$

$$\left. + 0.7071\ \sigma_h + \left[\frac{0.9617(D_t^2 - d_t^2)}{(D_t + 2t)^2 - d_t^2} - 0.07778 \right] p \right\}^2$$

$$+ \left\{ \frac{1.414E_f}{D_t} u_2 + \frac{0.2701}{(D_t + 2t)^2 - d_t^2} F_a + 0.7071\ (\sigma_h - \sigma_r) \right. \qquad (3.34)$$

(continued)

$$+\frac{5.092}{(D_t + 2t - d_t)^2} M_2 - \left[0.07778 + \frac{0.2121(D_t^2 - d_t^2)}{(D_t + 2t)^2 - d_t^2}\right] p \Bigg\}^2$$

$$+\left\{\frac{1.494}{(D_t + 2t)^2 - d_t^2} F_a - \frac{1.174\ (D_t^2 - d_t^2)}{(D_t + 2t)^2 - d_t^2}\ p + \frac{28.17}{(D_t + 2t - d_t)^2} M_2\right.$$

$$\left. -0.7071\sigma_r \right\}^2 \qquad (3.34)$$

Location 5

$$S_5^2 = \left\{\frac{1.414E_f}{D_t} u_2 - \frac{0.1576}{w(D_f - w)} F_n - 0.07778\ p + 0.7071\sigma_h \right\}^2$$

$$+\left\{\frac{1.414E_f}{D_t} u_2 + \frac{0.06752}{w(D_f - w)} F_n - 0.07778\ p + 0.7071\ (\sigma_h - \sigma_r)\right\}^2$$

$$+\left\{\frac{0.2251}{w\ (D_f - w)} F_n - 0.7071\sigma_r \right\}^2 \qquad (3.35)$$

3.9.1.2 Union

The locations of stresses calculated in the union are shown in Figure 3.9.

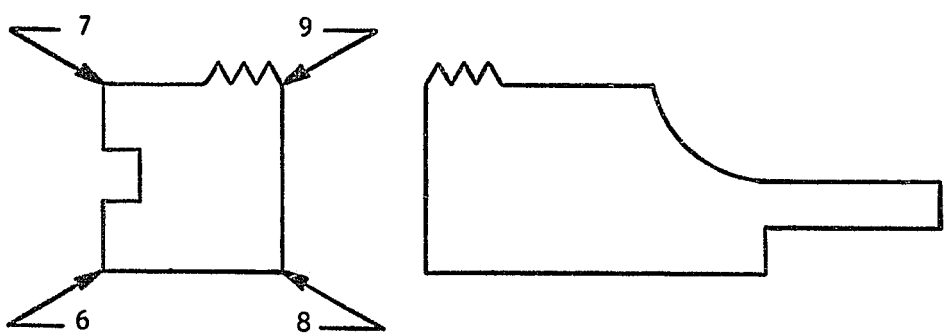

Shell No. 8

Union Centerline

Figure 3.9. Location of Union Stresses Calculated

The stresses at locations 6 and 7 depend on whether there is full contact between the flange face and the union face or whether there is separation of the faces at the inside diameter. The stress formulas assume full face contact. These formulas, when used with an appropriate safety factor, can be used for design calculations even when there is less than full face contact.

Location 6

$$S_6^2 = \left\{ \frac{2.828E_u}{D_t + d_t} u_3 - \frac{0.2701}{D_u^2 - d_t^2} (F_n - F_a) + \frac{0.9003}{D_u^2 + d_g^2 - D_g^2 - d_t^2} F_3 \right.$$

$$\left. + \frac{11.88 (D_u - d_t)}{(D_u - d_t)^3 - (D_g - d_g)^3} M_3 + \left[0.6293 - \frac{0.2121(D_t^2 - d_t^2)}{D_u^2 - d_t^2} \right] p + 0.7071\sigma_h \right\}^2$$

$$+ \left\{ \frac{2.828E_u}{D_u + d_t} u_3 - \frac{0.2701}{D_u^2 - d_t^2} (F_n - F_a) + 0.7071 (\sigma_h - \sigma_r) \right.$$

$$\left. - \frac{5.092 (D_u - d_t)}{(D_u - d_t)^3 - (D_g - d_g)^3} M_3 + \left[0.6293 - \frac{0.2121 (D_t^2 - d_t^2)}{D_u^2 - d_t^2} \right] p \right\}^2$$

$$+ \left\{ \frac{0.9003}{D_u^2 + d_g^2 - D_g^2 - d_t^2} F_3 + \frac{16.97 (D_u - d_t)}{(D_u - d_t)^3 - (D_g - d_g)^3} M_3 + 0.7071\sigma_r \right\}^2 \quad (3.36)$$

Location 7

$$S_7^2 = \left\{ \frac{2.828E_u}{D_u + d_t} u_3 - \frac{0.2701}{D_u^2 - d_t^2} (F_n - F_a) + \frac{0.9003}{D_u^2 + d_g^2 - D_g^2 - d_t^2} F_3 \right.$$

$$\left. - \frac{11.88 (D_u - d_t)}{(D_u - d_t)^3 - (D_g - d_g)^3} M_3 - \left[0.07778 + \frac{0.2121(D_t^2 - d_t^2)}{D_u^2 - d_t^2} \right] p + 0.7071\sigma_h \right\}^2$$

$$+ \left\{ \frac{2.828E_u}{D_u + d_t} u_3 - \frac{0.2701}{D_u^2 - d_t^2} (F_n - F_a) + 0.7071 (\sigma_h - \sigma_r) \right.$$

$$\left. + \frac{5.092 (D_u - d_t)}{(D_u - d_t)^3 - (D_g - d_g)^3} M_3 - \left[0.07778 + \frac{0.2121 (D_t^2 - d_t^2)}{D_u^2 - d_t^2} \right] p \right\}^2$$

$$+ \left\{ \frac{0.9003}{D_u^2 + d_g^2 - D_g^2 - d_t^2} F_3 - \frac{16.97 (D_u - d_t)}{(D_u - d_t)^3 - (D_g - d_g)^3} M_3 + 0.7071\sigma_r \right\}^2 \quad (3.37)$$

Location 8

$$S_8^2 = \left\{ \frac{2.828E_u}{D_u + d_t} u_9 - \frac{0.6302}{(D_u^2 - d_t^2)} F_a + \frac{11.88}{(D_u - d_t)^2} M_9 + 0.7071\sigma_h \right.$$

$$\left. + \frac{2.521\, D_u + 1.261\, d_t - 3.782 D_b + \frac{2.269}{n}}{(D_u + d_t)\,(D_u - d_t)^2} F_n + \left[\frac{0.495(D_t^2 - d_t^2)}{D_u^2 - d_t^2} - 0.07778 \right] p \right\}^2$$

$$+ \left\{ \frac{2.828E_u}{D_u + d_t} u_9 + \frac{0.2701}{D_u^2 - d_t^2} F_a + 0.7071\,(\sigma_h - \sigma_r) - \frac{5.092}{(D_u - d_t)^2} M_9 \right.$$

$$\left. + \frac{1.621\, D_b - \frac{0.9724}{n} - 1.081\, D_u - 0.5403\, d_t}{(D_u + d_t)\,(D_u - d_t)^2} F_n + \left[0.6293 - \frac{0.2121(D_t^2 - d_t^2}{D_u^2 - d_t^2} \right] p \right\}^2$$

$$+ \left\{ \frac{0.9003}{D_u^2 - d_t^2} F_a - \frac{16.97}{(D_u - d_t)^2} M_9 - 0.7071\sigma_r \right.$$

$$\left. + 0.7071 \frac{D_u^2 - D_t^2}{D_u^2 - d_t^2} p + \frac{5.402D_b - 3.601D_u - 1.801d_t - \frac{3.241}{n}}{(D_u + d_t)\,(D_u - d_t)^2} F_n \right\}^2 \qquad (3.38)$$

Location 9

$$S_9^2 = \left\{ \frac{2.828E_u}{D_u + d_t} u_9 - \frac{1.531}{D_u^2 - d_t^2} F_a - \frac{28.85}{(D_u - d_t)^2} M_9 + 0.7071\sigma_h \right.$$

$$+ \left[\frac{1.202(D_t^2 - d_t^2)}{D_u^2 - d_t^2} - 0.07778 \right] p$$

$$\left. + \frac{9.183D_b - 3.061D_u - 6.122d_t - \frac{5.51}{n}}{(D_u + d_t)\,(D_u - d_t)^2} F_n \right\}^2 \qquad (3.39)$$

(continued)

$$+\left\{\frac{2.828E_u}{D_u + d_t}\ u_9 + \frac{0.2701}{D_u^2 - d_t^2} F_a + 0.7071\ (\sigma_h - \sigma_r - \sigma_t)\right.$$

$$\left. - \frac{1.621D_b - \frac{0.9724}{n} - 0.5402D_u - 1.08d_t}{(D_u + d_t)\ (D_u - d_t)^2} F_n - \left[.07778 + \frac{0.2121(D_t^2 - d_t^2)}{D_u^2 - d_t^2}\right] p + \frac{5.092}{(D_u - d_t)^2} M_9\right\}^2$$

$$+\left\{\frac{1.801}{(D_u^2 - d_t)^2} F_a - \frac{10.8D_b - 3.601D_u - 7.202d_t - \frac{6.482}{n}}{(D_u + d_t)\ (D_u - d_t)^2} F_n\right.$$

$$\left. + \frac{33.94}{(D_u - d_t)^2} M_9 - \frac{1.414\ (D_t^2 - d_t^2)}{D_u^2 - d_t^2} p - 0.7071\ (\sigma_r + \sigma_t)\right\}^2 \qquad (3.39)$$

where the maximum bending stress in the thread, σ_t, is:

$$\sigma_t = \frac{1.053C_{105}F_n\ (1 - C_{106} + C_{106} \cosh C_{105})}{L_e\ (D_b - \frac{6}{n})\ \sinh C_{105}} \qquad (3.40)$$

and C_{105} and C_{106} are given in Section 3.11.3.

3.9.1.3 Nut

The locations of stresses calculated in the nut are shown in Figure 3.10.

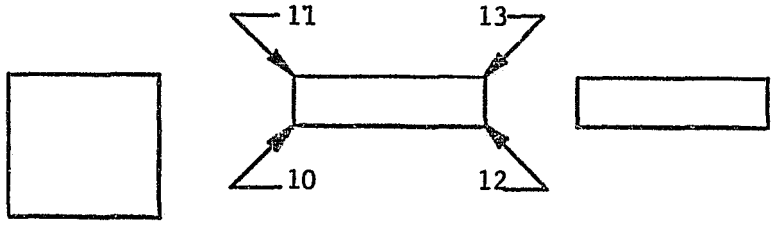

Ring No. 4 Shell No. 5 Shell No. 6 and 7

Nut Centerline

Figure 3.10. Location of Nut Stresses Calculated

Location 10

$$S_{10}^2 = \left\{ \frac{2.828E_n}{D_n + d_s} u_5 - \frac{1.278}{D_n^2 - d_s^2} F_n + \frac{24.1}{(D_n - d_s)^2} M_4 + 0.7071\sigma_h \right\}^2$$

$$+ \left\{ - \frac{5.092}{(D_n + d_s)^2} M_4 + \frac{2.828E_n}{D_n + d_s} u_5 + \frac{0.2701}{D_n^2 - d_s^2} F_n + 0.7071 \ (\sigma_h - \sigma_r) \right\}^2$$

$$+ \left\{ \frac{1.549}{D_n^2 - d_s^2} F_n - \frac{29.19}{(D_n - d_s)^2} M_4 - 0.7071\sigma_r \right\}^2 \qquad (3.41)$$

Location 11

$$S_{11}^2 = \left\{ \frac{2.828E_n}{D_n + d_s} u_5 - \frac{0.6302}{D_n^2 - d_s^2} F_n - \frac{11.88}{(D_n - d_s)^2} M_4 + 0.7071\sigma_h \right\}^2$$

$$+ \left\{ \frac{5.092}{(D_n - d_s)^2} M_4 + \frac{2.828E_n}{D_n + d_s} u_5 + \frac{0.2701}{D_n^2 - d_s^2} F_n + 0.7071 \ (\sigma_h - \sigma_r) \right\}^2$$

$$+ \left\{ \frac{0.9003}{D_n^2 - d_s^2} F_n + \frac{16.97}{(D_n - d_s)^2} M_4 - 0.7071\sigma_r \right\}^2 \qquad (3.42)$$

Location 12

$$S_{12}^2 = \left\{ \frac{2.828E_n}{D_n + d_s} u_6 - \frac{1.531}{D_n^2 - d_s^2} F_n + \frac{28.85}{(D_n - d_s)^2} M_5 + 0.7071\sigma_h \right\}^2$$

$$+ \left\{ - \frac{5.092}{(D_n - d_s)^2} M_5 + \frac{2.828E_n}{D_n + d_s} u_6 + \frac{0.2701}{D_n^2 - d_s^2} F_n + 0.7071 \ (\sigma_h - \sigma_t - \sigma_r) \right\}^2$$

$$+ \left\{ \frac{1.801}{D_n^2 - d_s^2} F_n - \frac{33.94}{(D_n - d_s)^2} M_5 - 0.7071 \ (\sigma_t + \sigma_r) \right\}^2 \qquad (3.43)$$

where σ_t is given by Eq. 3.40.

Location 13

$$S_{13}^2 = \left\{ \frac{2.828E_n}{D_n + d_s} u_6 - \frac{0.6302}{D_n^2 - d_s^2} F_n - \frac{11.88}{(D_n - d_s^2} M_5 + 0.7071\sigma_h \right\}^2$$

$$+ \left\{ \frac{5.092}{(D_n - d_s)^2} M_5 + \frac{2.828E_n}{D_n + d_s} u_6 + \frac{0.2701}{D_n^2 - d_s^2} F_n + 0.7071 (\sigma_h - \sigma_r) \right\}^2$$

$$+ \left\{ \frac{0.9003}{D_n^2 - d_s^2} F_n + \frac{16.97}{(D_n - d_s)^2} M_5 - 0.7071\sigma_r \right\}^2 \qquad (3.44)$$

3.9.1.4 Assembly Stresses

During assembly there are usually only two static loads, the axial preload, F_p, and the torque, W. The connector stresses due to the preload are calculated in the same manner as the stresses for any operating condition. The major differences are that F_a and p are zero.

However, the stresses due to the applied torque on the nut and union are calculated separately. The stress in the length L_f of the union (See Figure 3.4) is:

$$S_{14} = \frac{0.2676W(D_a + 20.42d_t)}{L_f D_a (D_a - d_t)^2} \left\{ 1 - e^{-\frac{1.914L_f}{(D_a + d_t)^{3/4}}} \cos\left[\frac{1.914L_f}{(D_a + d_t)^{3/4}} \right] \right\}$$

$$+ \frac{24M_9}{(D_a - d_t)^2} \qquad (3.45)$$

The effective stresses in the nut due to F_p and W can be calculated using the formulas of Section 3.9.1.3. The required values of σ_n in S_{10} and S_{11} can be gained from Eqs. 3.46 and 3.47. Normally there are no thermal stresses during assembly (σ_h and σ_r = 0); but even if there are, these can be added to the stresses calculated below.

$$(\sigma_h)_{10} = - \frac{1.635\ W\ (D_n + d_s)}{D_n(L_a - L_n)\ (D_n - d_s)^2} \cdot \frac{1}{1 + \frac{L_n(D_n - d_n)^3\ (D_n + d_s)^3}{(L_a - L_n)\ (D_n - d_s)^3\ (D_n + d_n)^3}} \qquad (3.46)$$

$$(\sigma_h)_{11} = - (\sigma_h)_{10} \qquad (3.47)$$

If S_{14} is too large compared to the yield strength, D_a is increased to the next standard wrench size and S_{14} is again calculated. Likewise, if the nut stresses are too large, D_n is increased to the next standard wrench size and the stresses are calculated again.

3.9.2 Fatigue Analysis

The fatigue analysis also depends on the use of the effective stress in order to use the fatigue data from uniaxially loaded specimens as a criterion for the triaxially loaded connector. However, the effective stress calculations are done in two parts. First the effective stress due to the constant (or mean) axial force and pressure, S_k, is calculated. Then the effective stress due to the amplitude of the cyclical axial force and pressure, S_c, is calculated. These calculations are readily done using the formulas of the preceding section.

Thus, for each stress location, an equivalent fatigue stress is calculated using Eq. 3.48. All of the stresses refer to only

$$S_f = \frac{S_c}{1 - \frac{S_k}{S_u}} \tag{3.48}$$

one stress location and S_c amd S_k were both calculated using the same formula from the preceding section. The equivalent fatigue stress is then compared to the fatigue strength, S_n, for the number of fatigue cycles, N, desired. A factor of safety of 1.1 or larger is applied to S_f.

$$H_f S_f \leq S_n \tag{3.49}$$

S_f must satisfy Eq. 3.49

3.9.3 Connector Modifications

In order to choose the most severe operating condition the stresses calculated in the previous sections are tabulated in the manner shown below for each operating condition.

Table 3.2

FORMAT FOR COMPILATION OF STRESS CALCULATIONS

Operating Condition _____

(1) Stress Location	(2) S_m	(3) S_f	(4) H_m	(5) H_f	(6) S_y	(7) S_n	(8) $H_m S_m / S_y$	(9) $H_f S_f / S_n$
1								
2								
3								
4								
.								
.								
.								

Table 3.3. Format for Optimization of Connector Design for Most Severe Operating Condition

(1) Stress Location	(2) S_m	(3) S_f	(4) H_m	(5) H_f	(6) S_y	(7) S_n	(8) $H_m S_m / S_y$	(9) $H_f S_f / S_n$	Recommended Changes in Parameters to Change Stresses. Prime Denotes New Dimension.
1									$t' = [(8) \text{ or } (9)]^{2/3} t$ or $L_h' = [(8) \text{ or } (9)] L_h$
2									$t' = [(8) \text{ or } (9)]^{2/3} t$ or $L_h' = [(8) \text{ or } (9)] L_h$
3									$(D_t - d_t + 2t') = [(8) \text{ or } (9)]^{2/3} (D_t - d_t + 2t)$ or $L_h' = [(8) \text{ or } (9)] L_h$
4									$(D_t - d_t + 2t') = [(8) \text{ or } (9)]^{2/3} (D_t - d_t + 2t)$ or $L_h' = [(8) \text{ or } (9)] L_h$
5									$w' = [(8) \text{ or } (9)] w$
6									$(D_u' - d_t) = [(8) \text{ or } (9)]^{2/3} (D_u - d_t)$ or $L_u' = [(8) \text{ or } (9)] L_u$
7									$(D_u' - d_t) = [(8) \text{ or } (9)]^{2/3} (D_u - d_t)$ or $L_u' = [(8) \text{ or } (9)] L_u$
8									$(D_u' - d_t) = [(8) \text{ or } (9)]^{2/3} (D_u - d_t)$
9									$(D_u' - d_t) = [(8) \text{ or } (9)]^{2/3} (D_u - d_t)$
10									$(D_n' - d_s) = [(8) \text{ or } (9)]^{2/3} (D_n - d_s)$ or $L_n' = [(8) \text{ or } (9)]^{1/2} L_n$
11									$(D_n' - d_s) = [(8) \text{ or } (9)]^{2/3} (D_n - d_s)$ or $L_n' = [(8) \text{ or } (9)]^{1/2} L_n$
12									$(D_n' - d_s) = [(8) \text{ or } (9)]^{2/3} (D_n - d_s)$
13									$(D_n' - d_s) = [(8) \text{ or } (9)]^{2/3} (D_n - d_s)$

From this tabulation the most severe operating condition is chosen by choosing the condition which has the largest value in Column 8 or 9 of Table 3.3. The connector design is then optimized for this operating condition as discussed in the remainder of this Section. Once this optimization is complete, another check is made (by a table such as Table 3.2, if necessary) to make sure that the chosen operating condition is still the most severe. If another operating condition is the most severe, the optimizing procedure is repeated.

The table is expanded for the most severe condition to include the calculation of the dimensional parameters to be changed in order to optimize the design, see Table 3.3. In Table 3.3 the largest value in Column 8 or 9 is checked in the following inequality.

$$0.9 \leq [\,(8) \text{ or } (9)\,] \leq 1.0 \qquad (3.50)$$

If the inequality is not satisfied, the parameter recommended in the table is changed. Then the second largest value in Column 8 or 9 is checked in Eq. 3.50. If this does not satisfy the inequality, the parameter recommended in the table is changed, but only if it was not changed in the previous step. The procedure is continued with the third largest value of Column 8 or 9, the fourth largest and on till all values have been considered. Then the preload and stress calculations are repeated, the most severe operating condition is selected and the changes in parameters are again calculated. This procedure is continued until the largest algebraic stresses of the most severe operating condition satisfy Eq. 3.50.

3.10 Testing

Each new connector design is tested. The extent of the testing is determined by the design requirements and past experience with similar designs. The testing serves a twofold purpose: prove the new design meets all the specifications and gain experience for future designs. The type of tests depends upon the design, and care is necessary to be certain that the operating conditions are duplicated and accurate measurements are taken.

3.11 Appendix

3.11.1 Coefficients for the nut spring constant calculation

The values for the Ks are given in Section 3.11.4.

$$C_1 = L_n/2$$

$$C_2 = -\frac{D_n\,[.0875(D_n + d_s)^2 + .65\,d_n^2]}{L_n E_n\,(D_n^2 - d_n^2)}$$

$$C_3 = K_5 \text{ where } h = 1/2\,(D_n - d_s)$$

$$\ell = L_s + L_t - .72\,L_e$$

$$r = 1/4\,(D_n + d_s)$$

$$C_4 = K_6 \text{ where } (h, \ell, r)_4 = (h, \ell, r)_3$$

END OF REFERENCE

135

REFERENCE

136

REFRIGERATION PIPING. B31.5, ANSI, 1966.

THIS REFERENCE IS COPYRIGHTED MATERIAL AND THEREFORE THE CONTENTS HAVE NOT BEEN REPRODUCED FROM THE TEXT.

END OF REFERENCE

136

REFERENCE

137

MECHANICAL/ELECTRICAL PROCESS SYSTEMS. PART B - TESTING OF PRESSURE SYSTEMS. CH. 6 OF NASA LEWIS OPERATIONAL SAFETY MANUAL. 1966.

THIS MATERIAL HAS BEEN APPROVED FOR PUBLICATION PER MEMORANDUM FROM ROY A. MAURER, NASA LEWIS RESEARCH CENTER TO JOANNE FOLK DATED AUG. 22, 1974.

LEWIS OPERATIONAL SAFETY MANUAL

CHAPTER 6 - MECHANICAL/ELECTRICAL PROCESS SYSTEMS

PART B - TESTING OF PRESSURE SYSTEMS - ASME DESIGNS

1. SCOPE

a. The test procedures as outlined in this Part are to serve as the Lewis safety standard for the testing of components and pressure systems. Work done by either contract or NASA personnel shall be done in accordance with this Part. Cognizant Lewis supervisors, inspectors and Area Safety Committees shall insure that these procedures are carried out by either NASA or contract labor. It is conceivable that these standard procedures will not represent the best possible test program or sequence for every system to be tested. When such deviations or modifications to the outlined test procedure seem advantageous, they should be referred to the cognizant Area Safety Committee for approval.

b. This policy and Pressure Testing Procedure Part does not apply to vessels regulated by the Interstate Commerce Commission.

c. In the Plum Brook Reactor Area, any A. E. C. or other standards approved especially for nuclear installations and operations for that area take precedence over this Part.

d. The "Design Engineer" as used in this Part is the person signing the drawing or writing the specification. Where the work involves existing systems or components, the "Design Engineer" shall be a qualified individual who has been duly authorized to design such systems and components.

e. Design engineers, project engineers, fabrication and installation personnel all have responsibility for obtaining appropriate supervisory approval and for bringing proposed pressure components and systems testing procedures to the attention of the proper Area Safety Committee. All Pneumatic Pressure Testing must have the previous approval of the cognizant Area Safety Committee.

f. This Part supersedes all previous issues related to ASME pressure testing.

TABLE VIII. SUGGESTED MAXIMUM TORQUE VALUES FOR FASTENERS OF DIFFERENT MATERIALS

BOLT SIZE	LOW CARBON STEEL	18-8 ST. ST.	BRASS	SILICON BRONZE	ALUMINUM 24ST-4	316 ST. ST.	MONEL
	in.-lbs.	in.-lbs.	in.-lbs.	in.-lbs.	in.-lbs.	in.-lbs.	in.-lbs.
2-56	2.2	2.5	2.0	2.3	1.4	2.6	2.5
2-64	2.7	3.0	2.5	2.8	1.7	3.2	3.1
3-48	3.5	3.9	3.2	3.6	2.1	4.0	4.0
3-56	4.0	4.4	3.6	4.1	2.4	4.6	4.5
4-40	4.7	5.2	4.3	4.8	2.9	5.5	5.3
4-48	5.9	6.6	5.4	6.1	3.6	6.9	6.7
5-40	6.9	7.7	6.3	7.1	4.2	8.1	7.8
5-44	8.5	9.4	7.7	8.7	5.1	9.8	9.6
6-32	8.7	9.6	7.9	8.9	5.3	10.1	9.8
6-40	10.9	12.1	9.9	11.2	6.6	12.7	12.3
8-32	17.8	19.8	16.2	18.4	10.8	20.7	20.2
8-36	19.8	22.0	18.0	20.4	12.0	23.0	22.4
10-24	20.8	22.8	18.6	21.2	13.8	23.8	25.9
10-32	29.7	31.7	25.9	29.3	19.2	33.1	34.9
1/4"-20	65.0	75.2	61.5	68.8	45.6	78.8	85.3
1/4"-28	90.0	94.0	77.0	87.0	57.0	99.0	106.0
5/16"-18	129	132	107	123	80	138	149
5/16"-24	139	142	116	131	86	147	160
3/8"-16	212	236	192	219	143	247	266
3/8"-24	232	259	212	240	157	271	294
7/16"-14	338	376	317	349	228	393	427
7/16"-20	361	400	327	371	242	418	451
1/2"-13	465	517	422	480	313	542	584
1/2"-20	487	541	443	502	328	565	613
9/16"-12	613	682	558	632	413	713	774
9/16"-18	668	752	615	697	456	787	855
5/8"-11	1000	1110	907	1030	715	1160	1330
5/8"-18	1140	1244	1016	1154	798	1301	1482
3/4"-10	1259	1530	1249	1416	980	1582	1832
3/4"-16	1230	1490	1220	1382	958	1558	1790
7/8"-9	1919	2328	1905	2140	1495	2430	2775
7/8"-14	1911	2318	1895	2130	1490	2420	2755

TABLE VIII. SUGGESTED MAXIMUM TORQUE VALUES FOR FASTENERS (Cont.) OF DIFFERENT MATERIALS

BOLT SIZE	LOW CARBON STEEL	18-8 ST. ST.	BRASS	SILICON BRONZE	ALUMINUM 24ST-4	316 ST. ST.	MONEL
	in.-lbs.	in.-lbs.	in.-lbs.	in.-lbs.	in.-lbs.	in.-lbs.	in.-lbs.
1"-8	2832	3440	2815	3185	2205	3595	4130
1"-14	2562	3110	2545	2885	1995	3250	3730
	ft.-lbs.	ft.-lbs.	ft.-lbs.	ft.-lbs.	ft.-lbs.	ft.-lbs.	ft.-lbs.
1-1/8"-7	340	413	337	383	265	432	499
1-1/8"-12	322	390	318	361	251	408	470
1-1/4"-7	432	523	428	485	336	546	627
1-1/4"-12	396	480	394	447	308	504	575
1-1/2"-6	732	888	727	822	570	930	1064
1-1/2"-12	579	703	575	651	450	732	840

This table of torque values is reprinted by courtesy of the H. M. Harper Company. The table is intended as a guide only. Tests were conducted on dry or near dry products. Mating parts were wiped clean of chips and foreign matter.

END OF REFERENCE

137

REFERENCE

138

BRAZING MANUAL. AMERICAN WELDING SOCIETY, INC., 1963.

THIS REFERENCE IS COPYRIGHTED MATERIAL AND THEREFORE
THE CONTENTS HAVE NOT BEEN REPRODUCED FROM THE TEXT.

END OF REFERENCE

REFERENCE

139

REYNOLDS, W. C.: INVESTIGATION OF IGNITION TEMPERATURES OF SOLID METALS. NASA TN D-182, 1959.

2.1-1

LEWIS RESEARCH CENTER
Aerospace Safety Research
and Data Institute
OCT 20 1971
CLEVELAND, OHIO

NASA TN D-182

TECHNICAL NOTE
D-182

INVESTIGATION OF IGNITION TEMPERATURES OF SOLID METALS

By W. C. Reynolds

Stanford University

NATIONAL AERONAUTICS AND SPACE ADMINISTRATION

WASHINGTON

October 1959

1A

NATIONAL AERONAUTICS AND SPACE ADMINISTRATION

TECHNICAL NOTE D-182

INVESTIGATION OF IGNITION TEMPERATURES OF SOLID METALS

By W. C. Reynolds

SUMMARY

The ignition temperature of a solid metal is related through a thermal definition of ignition to the rate of oxidation and to the radiation and convection heat-transfer parameters. The mechanisms of oxidation are reviewed and the factors which influence ignition temperatures are discussed. Reasonable agreement between theoretical and experimental ignition temperatures is demonstrated. Experimental ignition temperatures for several metals are presented.

INTRODUCTION

For many years the maximum safe operating temperatures for metals have been determined from strength considerations. However, some metals have been known to ignite and burn at what would normally be structurally safe temperatures. It seems, then, that failure by ignition and burning may, in some cases, precede failure by structural weakening with temperature and that the possibility of ignition must be considered in the design of high-temperature metal apparatus.

The advent of high-speed flight has brought about increased interest in the problem of metal ignition. At flight speeds typical of modern aircraft and missiles, aerodynamic heating causes extremely high skin temperatures. The danger of ignition is increased in regions behind shock waves where temperatures and pressures are exceptionally high. Other fields where metal ignition is of interest include the design of gas turbines, high-temperature furnaces, gas-cooled nuclear reactors, and rocket motors.

Obviously there are many factors which enter into the problem of ignition and burning. The mechanisms involved are entirely different, and the distinction between ignition and burning must be kept clear. Ignition is brought about by the exothermal oxidation reaction between the solid metal and its gaseous environment. Consequently, it is believed that the phenomenon of ignition is quite closely related to the relatively slow oxidation that occurs on all metals at low temperatures ("rusting"). Burning, on the other hand, may proceed by any of

TABLE 3

IGNITION TEMPERATURES OF SOLID METALS

Metal	Ignition temperature, °F	Source	Gas	Pressure, atm
Mild steel	2,240 to [a]2,330	(b)	Air,(c)	1 to 7
W	2,270 to [a]2,350	(b)	Air,(c)	1 to 7
Ta	2,260 to [a]2,340	(b)	Air,(c)	1 to 7
Ti alloys:				
RC-70	2,880 to [a]2,960	(b)	Air,O_2	1 to 7
RS-70	2,890 to [a]2,940	(b)	Air,O_2	1 to 7
RS-110-A	2,860 to [a]2,910	(b)	(d),O_2	1 to 7
RS-110-BX	2,850 to [a]2,920	(b)	(d),O_2	1 to 7
Stainless steels:				
430	2,460 to [a]2,490	(b)	(d),O_2	1 to 7
302	(e)	(b)	Air,O_2	1 to 7
Cu	(e)	(b)	Air,O_2	1 to 7
Ni	(e)	(b)	Air,O_2	1 to 7
Ni alloys:				
Inconel	(e)	(b)	Air,O_2	1 to 7
Inconel X	(e)	(b)	Air,O_2	1 to 7
Be alloys:				
Berylco 10	1,750 to 1,760	(b)	Air,O_2	1 to 7
Berylco 25	(e)	(b)	Air,O_2	1 to 7
Mg	1,171	ref. 6	O_2	1 to 10
Mg alloys:				
20% Al	936	ref. 7	O_2	1
70% Zn	1,004	ref. 7	O_2	1
25% Ni	934	ref. 7	O_2	1
20% Sb	1,099	ref. 7	O_2	1
63% Al	862	ref. 7	O_2	1
Fe	1,706	ref. 9	O_2	1
Sr	1,328	ref. 9	O_2	1
Ca	1,022	ref. 9	O_2	1
Th	932	ref. 9	O_2	1
Ba	347	ref. 9	O_2	1
Mo	1,400	ref. 9	O_2	1
U	608	ref. 10	O_2	1
Ce	608	ref. 11	O_2	1
Al	(e)	ref. 9	O_2	1
Zn	(e)	ref. 9	O_2	1
Pb	(e)	ref. 9	O_2	1
Sn	(e)	ref. 9	O_2	1
Bi	(e)	ref. 9	O_2	1
Li	(e)	ref. 9	O_2	1
Cd	(e)	ref. 9	O_2	1
Na	(e)	ref. 9	O_2	1
K	(e)	ref. 9	O_2	1

[a]Brightness temperature.

[b]Present investigation.

[c]Not tested in oxygen, but probably ignites in oxygen at about the same temperature.

[d]Does not ignite in air.

[e]Melts before igniting.

TABLE 6

TANK TESTS WITH TANTALUM

Run	Model specifications			Gas	Pressure, atm	Ambient temperature, °F	Humidity, lb H_2O / lb air	Power at failure, w	Brightness ignition temperature, °F
	Length, in.	Width, in.	Thickness, in.						
1	1	1/4	0.02	Air	1	74	0.006	[a]100	2,300 ± 20
2	1	1/4	.02	Air	1	74	.006	----	2,260 ± 20
3	1	1/4	.02	Air	2	74	.006	----	2,330 ± 20
4	1	1/4	.02	Air	2	74	.006	----	2,310 ± 20
5	1	1/4	.02	Air	3	74	.006	----	2,320 ± 20
6	1	1/4	.02	Air	3	74	.006	----	2,260 ± 20
7	1	1/4	.02	Air	4	74	.006	----	2,340 ± 20
8	1	1/4	.02	Air	4	74	.006	----	2,340 ± 20
9	1	1/4	.02	Air	4	74	.006	----	2,300 ± 20
10	1	1/4	.02	Air	4	74	.006	----	2,310 ± 20
11	1	1/4	.02	Air	5	74	.006	----	2,280 ± 20
12	1	1/4	.02	Air	5	74	.006	----	2,300 ± 20
13	1	1/4	.02	Air	6	74	.006	----	2,320 ± 20
14	1	1/4	.02	Air	6	74	.006	----	2,280 ± 20
15	1	1/4	.02	Air	7	74	.006	----	2,290 ± 20
16	1	1/4	.02	Air	7	74	.006	----	2,290 ± 20
17	1	1/4	.02	Air	8	74	.006	----	2,320 ± 20
18	1	1/4	.02	Air	8	74	.006	----	2,330 ± 20

[a]Nominal.

TABLE 7

TANK TESTS WITH TITANIUM RC-70

Run	Model specifications			Gas	Pressure, atm	Ambient temperature, °F	Humidity, lb H_2O / lb air	Power at failure, w	Brightness ignition temperature, °F
	Length, in.	Width, in.	Thickness, in.						
1	1.5	1/8	0.020	O_2	1	70	------	101	2,930 ± 30
2	1.5	1/8	.020	O_2	1	70	------	114	2,880 ± 30
3	1.5	1/4	.067	O_2	2	70	------	1,150	2,940 ± 30
4	1.5	1/8	.067	O_2	3	70	------	460	2,910 ± 20
5	1.5	1/8	.040	O_2	4	70	------	295	2,890 ± 20
6	1.5	1/8	.040	O_2	4	70	------	300	2,930 ± 20
7	1.5	1/4	.067	O_2	5	70	------	1,220	2,930 ± 20
8	1.5	1/8	.010	O_2	6	70	------	-----	2,895 ± 20
9	1.25	1/4	.067	O_2	7	70	------	840	2,900 ± 30
10	1.5	1/4	.067	O_2	7	70	------	940	2,880 ± 30
11	1.5	1/4	.010	Air	1	63	0.0080	-----	2,910 ± 20
12	1.5	1/4	.010	Air	2	63	.0080	-----	2,900 ± 30
13	1.5	1/4	.010	Air	3	63	.0080	-----	2,910 ± 20
14	1.5	1/4	.010	Air	4	63	.0080	-----	2,890 ± 30
15	1.5	1/4	.010	Air	5	63	.0080	-----	2,920 ± 20
16	1.5	1/4	.010	Air	6	63	.0080	-----	2,940 ± 20
17	1.5	1/4	.010	Air	7	63	.0080	-----	2,920 ± 20
18	1.5	1/4	.067	He	1	63	------	-----	[a]3,010 ± 20

[a]Melted.

TABLE 8

WIND-TUNNEL TEST OF TITANIUM RC-70

Run	Model specifications			Mach number	Humidity of jet, $\frac{\text{lb } H_2O}{\text{lb dry air}}$	Stagnation temperature, °F	Power at failure, w	Brightness ignition temperature, °F
	Length, in.	Width, in.	Thickness, in.					
1	1.88	0.138	0.067	1.25	0.00184	163	1,670	2,950 ± 10
2	1.88	.202	.067	1.25	.00184	197	1,800	2,880 ± 20
3	1.88	.237	.067	1.25	.00184	163	2,210	2,950 ± 20
4	1.88	.237	.067	1.25	.00184	140	1,900	2,960 ± 20

TABLE 9

TANK TESTS WITH TITANIUM RS-70

Run	Model specifications			Gas	Pressure, atm	Ambient temperature, °F	Humidity, lb h_2O / lb dry air	Power at failure, w	Brightness ignition temperature, °F
	Length, in.	Width, in.	Thickness, in.						
1	1.5	3/16	0.025	O_2	1	71	------	311	2,920 ± 20
2	1.5	3/16	.025	O_2	3	71	------	281	2,940 ± 10
3	1.5	3/16	.025	O_2	4	71	------	307	2,920 ± 20
4	1.5	3/16	.025	O_2	5	71	------	285	2,940 ± 10
5	1.5	3/16	.025	O_2	6	71	------	307	2,930 ± 20
6	1.5	3/16	.025	O_2	7	71	------	281	2,890 ± 20
7	1.5	3/16	.025	Air	1	73	0.0062	298	2,930 ± 30
8	1.5	3/16	.025	Air	1	73	.0062	304	2,970 ± 30
9	1.5	3/16	.025	Air	1	73	.0062	298	3,000 ± 30
10	1.5	3/16	.025	Air	3	73	.0062	298	3,010 ± 30
11	1.5	3/16	.025	Air	5	73	.0062	298	2,930 ± 30
12	1.5	3/16	.025	Air	7	73	.0062	310	2,960 ± 30

TABLE 10

WIND-TUNNEL TESTS OF TITANIUM RS-70

Run	Model specifications			Mach number	Humidity of jet, $\frac{\text{lb } H_2O}{\text{lb dry air}}$	Stagnation temperature, ^oF	Brightness ignition temperature, ^oF
	Length, in.	Width, in.	Thickness, in.				
1	1.88	0.188	0.025	1.25	0.00184	105	2,950 ± 30
2	1.88	.188	.025	1.25	.00184	105	2,940 ± 30

TABLE 11

TANK TESTS WITH TITANIUM RS-110-A

Run	Model specifications			Gas	Pressure, atm	Ambient temperature, °F	Humidity, lb H_2O / lb dry air	Power at failure, w	Brightness ignition temperature, °F
	Length, in.	Width, in.	Thickness, in.						
1	1.5	3/16	0.025	O_2	1	71	------	282	2,890 ± 20
2	1.5	3/16	.025	O_2	3	71	------	300	2,890 ± 30
3	1.5	3/16	.025	O_2	5	71	------	331	2,890 ± 10
4	1.5	3/16	.025	O_2	7	71	------	328	2,910 ± 20
5	1.5	3/16	.025	O_2	8	71	------	307	2,860 ± 20
6	1.5	3/16	.025	Air	1	73	0.0081	288	[a]3,260 ± 100
7	1.5	3/16	.025	Air	1	73	.0081	260	[a]3,260 ± 50
8	1.5	3/16	.025	Air	3	73	.0081	325	[a]3,110 ± 50
9	1.5	3/16	.025	He	1	70	------	330	[a]3,040 ± 50

[a]Melted.

TABLE 12

WIND-TUNNEL TESTS OF TITANIUM RS-110-A

Run	Model specifications			Mach number	Humidity of jet, $\frac{\text{lb } H_2O}{\text{lb dry air}}$	Stagnation temperature, ^oF	Brightness ignition temperature, ^oF
	Length, in.	Width, in.	Thickness, in.				
1	1.88	0.188	0.025	1.25	0.00184	140	[a]2,760 ± 30
2	1.88	.188	.025	1.25	.00184	140	[a]2,720 ± 30
3	1.88	.188	.010	1.25	.00184	140	[a]3,040 ± 30
4	1.88	.188	.010	1.25	.00184	140	[a]3,060 ± 30

[a]Melted.

TABLE 13

TANK TESTS WITH TITANIUM RS-110-BX

Run	Model specifications			Gas	Pressure, atm	Ambient temperature, °F	Humidity, lb H_2O / lb dry air	Power at failure, w	Brightness ignition temperature, °F
	Length, in.	Width, in.	Thickness, in.						
1	1.5	3/16	0.025	O_2	1	70	------	248	2,910 ± 20
2	1.5	3/16	.025	O_2	1	70	------	260	2,850 ± 20
3	1.5	3/16	.025	O_2	3	70	------	272	2,920 ± 20
4	1.5	3/16	.025	O_2	5	70	------	265	2,900 ± 20
5	1.5	3/16	.025	O_2	7	70	------	282	2,890 ± 20
6	1.5	3/16	.025	O_2	8	70	------	300	2,890 ± 20
7	1.5	3/16	.025	Air	1	70	0.0075	264	[a]3,280 ± 50
8	1.5	3/16	.025	Air	1	68	------	---	[a]3,150 ± 30
9	1.5	3/16	.025	Air	1	68	------	---	[a]3,040 ± 30
10	1.5	3/16	.025	Air	5	70	.0075	306	[a]3,050 ± 50
11	1.5	3/16	.025	Air	8	70	.0075	278	[a]3,270 ± 50

[a]Melted.

TABLE 14

WIND-TUNNEL TESTS OF TITANIUM RS-110-BX

Run	Model specifications			Mach number	Humidity of jet, $\frac{\text{lb } H_2O}{\text{lb dry air}}$	Stagnation temperature, ^oF	Brightness ignition temperature, ^oF
	Length, in.	Width, in.	Thickness, in.				
1	1.88	0.188	0.025	1.25	0.00184	140	2,940 ± 20
2	1.88	.188	.025	1.25	.00184	140	2,880 ± 20
3	1.88	.188	.025	1.25	.00184	140	2,830 ± 20
4	1.88	.188	.025	1.26	.00184	140	2,850 ± 20
5	1.88	.188	.025	1.25	.00184	140	3,050 ± 20
6	1.88	.188	.010	1.25	.00184	140	2,930 ± 20
7	1.88	.188	.010	1.25	.00184	140	2,910 ± 20
8	1.88	.188	.010	1.25	.00184	140	2,950 ± 20
9	1.88	.188	.010	1.25	.00184	140	2,950 ± 20
10	1.88	.188	.010	1.25	.00184	140	2,930 ± 20

Card #32

TABLE 15

TANK TESTS WITH STAINLESS STEEL 430

Run	Model specifications			Gas	Pressure, atm	Ambient temperature, °F	Humidity, lb H_2O / lb dry air	Power at failure, w	Brightness ignition temperature, °F
	Length, in.	Width, in.	Thickness, in.						
1	1.75	3/16	0.025	O_2	1	67	------	243	2,470 ± 20
2	1.75	3/16	.025	O_2	1	67	------	233	2,490 ± 20
3	1.75	3/16	.025	O_2	3	67	------	223	2,480 ± 20
4	1.75	3/16	.025	O_2	5	67	------	205	2,460 ± 20
5	1.75	3/16	.025	O_2	5	67	------	205	2,470 ± 20
6	1.75	3/16	.010	O_2	7	67	------	---	2,480 ± 20
7	1.75	3/16	.025	Air	1	67	0.0065	261	[a]2,670 ± 30
8	1.75	3/16	.025	Air	1	67	.0065	284	[a]2,680 ± 30
9	1.75	3/16	.025	Air	4	67	.0065	244	[a]2,710 ± 30
10	1.75	3/16	.025	Air	7	67	.0065	294	[a]2,720 ± 30

[a]Melted.

TABLE 16

WIND-TUNNEL TEST OF STAINLESS STEEL 430

Run	Model specifications			Mach number	Humidity of jet, $\frac{\text{lb } H_2O}{\text{lb dry air}}$	Stagnation temperature, ^{o}F	Brightness ignition temperature, ^{o}F (a)
	Length, in.	Width, in.	Thickness, in.				
1	1.88	0.188	0.025	1.25	0.00184	110	2,730 ± 20
2	1.88	.188	.025	1.25	.00184	107	2,780 ± 40

[a]Model melted.

TABLE 17

TANK TESTS WITH STAINLESS STEEL 302

Run	Model specifications			Gas	Pressure, atm	Ambient temperature, °F	Humidity, lb H_2O / lb dry air	Power at failure, w	Brightness ignition temperature, °F (a)
	Length, in.	Width, in.	Thickness, in.						
1	1.5	3/16	0.025	O_2	1	71	------	254	2,600 ± 30
2	1.5	3/16	.025	O_2	1	71	------	259	2,550 ± 30
3	1.5	3/16	.025	O_2	3	71	------	255	2,500 ± 20
4	1.5	3/16	.025	O_2	5	71	------	266	2,520 ± 20
5	1.5	3/16	.025	O_2	7	71	------	255	2,520 ± 20
6	1.5	3/16	.025	O_2	8	71	------	247	2,510 ± 20
7	1.5	3/16	.025	Air	1	71	0.0050	292	2,550 ± 20
8	1.5	3/16	.025	Air	1	71	.0050	320	2,510 ± 20
9	1.5	3/16	.025	Air	3	71	.0050	296	2,550 ± 20
10	1.5	3/16	.025	Air	5	71	.0050	289	2,540 ± 20
11	1.5	3/16	.025	Air	8	71	.0050	310	2,590 ± 20

[a]Model melted.

END OF REFERENCE

139

REFERENCE
140

SYSTEM SAFETY. AFSC DESIGN HANDBOOK DH 1-6, THIRD ED., JUL. 1971.

THIS REFERENCE HAS A LIMITED DISTRIBUTION AND MAY NOT BE REPRODUCED.

END OF REFERENCE

140

REFERENCE

141

JUSTL, O. J.: DEVELOPMENT OF SEAL MATERIAL FOR OXYGEN SYSTEMS. TECH. REPT. 28-22, MARE ISLAND NAVAL SHIPYARD, 1972. (AVAILABLE FROM DDC AS AD-891963L.)

THIS MATERIAL HAS BEEN APPROVED FOR PUBLICATION PER LETTER FROM J. B. ALFERS, NAVAL SHIP ENGINEERING CENTER TO JOANNE FOLK DATED JULY 18, 1974.

Technical Report No. 28-22
24 February 1972

DEVELOPMENT OF SEAL MATERIAL FOR OXYGEN SYSTEMS

Otto J. Justl

Rubber Laboratory

Laboratory Division
MARE ISLAND NAVAL SHIPYARD
VALLEJO, CALIFORNIA 94592

THIS DOCUMENT MAY BE FURTHER DISTRIBUTED BY ANY HOLDER ONLY WITH SPECIFIC PRIOR APPROVAL OF THE COMMANDER, NAVAL SHIP ENGINEERING CENTER, HYATTSVILLE, MD., 20782

ABSTRACT

The purpose of this investigation was to develop a rubber compound for fabricating seals for use in oxygen systems. Seal failures have been noted in such systems. The Rubber Laboratory attributes these failures to high compression set and/or porosity of the rubber compound due to expansion of the dissolved oxygen upon sudden release of pressure.

Sixty compounds based on fluorocarbon rubbers which have high autocombustion temperatures were evaluated. Of this group of compounds, Rubber Laboratory formulation 377-262, made from fluorocarbon rubber Viton D-80, appeared to be the most promising. O-rings molded from this compound had a compression set value of only 7 percent after 7 days at 74°F, which is a remarkably low value for fluorocarbon rubber compounds. These O-rings when subjected to 3000 psig oxygen pressure for 96 hours at 74°F did not deteriorate, blister, or have excessive swell upon sudden release of pressure.

Specification requirements based on the physical properties of this compound are proposed.

After this work was completed, the Rubber Laboratory was advised by E. I. du Pont de Nemours & Co., the manufacturer of Viton D-80, that this rubber would no longer be made. It is possible that a compound can be developed from another fluorocarbon rubber to meet the specification requirements.

ADMINISTRATIVE INFORMATION

RDT&EN Subproject SF 35 543 002

Task No. 907

Project Manager: E. A. Bukzin, Code 0342, Naval Ship Systems Command

Technical Agent: D. Pratt, Code 6101E, Naval Ship Engineering Center

hardness, compression set at 74°F and the effect of rapid blowdown after 96 hours under 3000 psig oxygen pressure.

7. Examination of the data in Appendix 1 shows that the best compounds of this group for high pressure oxygen seals were 377-195 made from Viton D-80 and 377-202 made from Fluorel 2160. These were the only compounds which were not blistered after the rapid blowdown of high pressure oxygen gas and which had a reasonably low compression set at 74°F.

SPONTANEOUS IGNITION TEMPERATURE

8. The Naval Ship Research and Development Laboratory (NSRDL) at Annapolis has developed a test for determining the spontaneous ignition temperature of materials in high pressure oxygen, reference (e). A small specimen of the material is placed in a strong container, and the container is pressurized with oxygen to 1500 psig. The temperature in the container is then slowly raised until the specimen ignites. The temperature at which this occurs is the spontaneous ignition temperature. The higher this temperature, the more suitable the material is for service in high pressure oxygen.

9. O-rings made from Viton D-80 compound 377-231, Fluorel 2160 compounds 377-202 and 377-234 and Viton E-60 compound 377-238 were sent to NSRDL for measurement of their spontaneous ignition temperatures. The temperatures found in reference (f) are tabulated below. Also given is the spontaneous ignition temperature reported by NSRDL for a Buna N (nitrile rubber) compound. The O-rings commonly used for sealing joints in oil and gas systems are made from Buna N.

Compound	Spontaneous ignition temperature, °F
377-202 (Fluorel LCS 2160 with blanc fixe)	575
377-231 (Viton D-80 with Philblack E)	515
377-234 (Fluorel LCS 2160 with United SPF)	523
377-238 (Viton E-60 with Philblack E)	520
Buna N	363

10. Fluorel 2160 compound 377-202 with the mineral pigment loading gave the highest spontaneous ignition temperature. All four fluorocarbon rubber compounds had values over 500°F as compared to 363°F for a Buna N rubber compound. This test confirmed that fluorocarbon rubber compounds have high spontaneous ignition temperatures compared to conventional rubbers. Mineral pigment loading increased the spontaneous ignition temperature over carbon black loading but at the sacrifice of other physical properties (see Appendix 1).

FURTHER DEVELOPMENT OF COMPOUND AND SPECIFICATION

11. As pointed out in paragraph 7, Viton D-80 compound 377-195 and Fluorel 2160 compound 377-202 were the best of the compounds in the screening test. The Viton D-80 compound had better tensile properties than the Fluorel 2160 compound. In view of this, 377-195 and another Viton D-80 compound, 377-262, which was similar except for curing agents, were subjected to additional tests to confirm their suitability for the intended service and to establish specification requirements. Compound 377-262 was designed to arrive at a higher state of cure than 377-195 and therefore to have a lower compression set.

12. Compounds 377-195 and 377-262 were tested for the following properties:

a. Initial tensile properties, hardness, tension set and specific gravity.

b. Tensile properties, hardness, compression set and specific gravity after aging in high pressure oxygen.

APPENDIX 2

PROPERTIES OF VULCANIZED VITON D-80 COMPOUNDS AND PROPOSED SPECIFICATION REQUIREMENTS
(Page 1 of 2 pages)

Stock No. 377-	195	262	
Viton D-80	100	100	
Thermax (N990)	30	30	
Maglite D	10	10	
Calcium hydroxide	3	-	
Barium carbonate	-	5	
Diak No. 5	1	1.5	
Cure Press: minutes/°F	30/330	30/330	
Oven: hours/°F	24/400	24/400	
Properties			**Proposed specification requirements**
Initial			
Tensile strength, psi*	2150	1640	1300 minimum
Ultimate elongation, %*	200	140	110 minimum
Hardness, Shore A, 15 sec***	79	80	80 ± 5
Tension set, %*	4	4	8 maximum
Specific gravity	1.90	1.93	
After aging in high pressure oxygen (3000 psig, for 168 hours at 200°F			
Retention of tensile strength, %*	89	97	80 minimum
Retention of ultimate elongation, %*	108	111	80 minimum
Change in Shore A hardness, 15 sec***	0	0	± 5 maximum
Compression set, %**	24	9	15 maximum
Change in specific gravity	.00	.00	-.03 to +.01
After 96 hours at 74°F in 3000 psig oxygen followed by rapid blowdown			
Increase in inside diameter, %*	13	10	15 maximum
Appearance*	no blisters	no blisters	no blisters

* Test performed on ARP 568-229 O-rings
** Test performed on ARP 568-331 O-rings
*** Test performed on cylindrical specimens, 2 inch diameter x 0.25 inch thick

PROPERTIES OF VULCANIZED VITON D-80 COMPOUNDS AND PROPOSED SPECIFICATION REQUIREMENTS
(Page 2 of 2 pages)

Properties	195	262	Proposed specification requirements
After 96 hours at 32°F in air			
Compression set, 10 sec reading, %**	57	35	45 maximum
30 min reading, %	30	16	25 maximum
After 168 hours at 74°F in air			
Compression set, 30 min reading, %**	14	7	12 maximum
After 168 hours at 200°F in distilled water			
Retention of tensile strength, %*	94	108	90 minimum
Retention of ultimate elongation, %*	113	137	90 minimum
Change in Shore A hardness, 15 sec***	+8	+4	0 to +10
Volume change, %*	+4	+3	0 to +8
After 70 hours at 180°F in 5% trisodium phosphate solution			
Retention of tensile strength, %*	93	118	90 minimum
Retention of ultimate elongation, %*	100	133	90 minimum
Change in Shore A hardness, 15 sec***	+1	+1	0 to +5
Volume change, %*	+4	+3	0 to +6
After 168 hours at 74°F in Freon PCA			
Retention of tensile strength, %*	67	74	60 minimum
Retention of ultimate elongation, %*	87	96	70 minimum
Change in Shore A hardness, 15 sec***	-10	-8	-15 to +0
Volume change, %*	+24	+25	0 to +30
Corrosion and adhesion to Monel (70 Ni-30 cu) after 2 weeks contact at > 90% relative humidity and 74°F			
Appearance of metal surface*	smooth	smooth	No pitting or roughening of metal
Adhesion of rubber to metal*	none	none	No adhesion to metal

*Test performed on ARP 568-229 O-rings
**Test performed on ARP 568-331 O-rings
***Test performed on cylindrical specimens, 2 inch diameter x 0.25 inch thick

APPENDIX 2

END OF REFERENCE

141

REFERENCE

142

CURRY, J. E.: STATUS REPORT ON LIQUID OXYGEN SEAL INVESTIGATION. NASA TM X-53183, 1964.

THIS REFERENCE IS MATERIAL THAT IS READILY AVAILABLE AND THEREFORE THE CONTENTS HAVE NOT BEEN REPRODUCED.

END OF REFERENCE

142

REFERENCE

143

FLUOROCARBON PLASTICS. MATERIALS AND PROCESS MANUAL NO. 215. MATERIALS IN DESIGN ENGINEERING, FEB. 1964.

THIS REFERENCE IS COPYRIGHTED MATERIAL AND THEREFORE THE CONTENTS HAVE NOT BEEN REPRODUCED FROM THE TEXT.

END OF REFERENCE

143

REFERENCE

144

JOY, L. A.; AND BAUMER, R. E.: SAFETY ASPECTS OF USING OXYGEN IN A HAZARDOUS ENVIRONMENT. ENGINEERING REPT. 037-70, AEROJET LIQUID ROCKET CO., 1970.

THIS MATERIAL HAS BEEN APPROVED FOR PUBLICATION PER LETTER FROM M. S. LIPSON TO JOANNE FOLK DATED AUG. 23, 1974.

Enclosure #2

DATE: 16 NOVEMBER 1970

AEROJET LIQUID ROCKET COMPANY
SYSTEMS ENGINEERING SECTION

ENGINEERING REPORT NUMBER 037-70

SAFETY ASPECTS OF USING OXYGEN IN A HAZARDOUS ENVIRONMENT

Prepared By:

L. A. Joy
Equipment Design Group
Systems Engineering Section
Test & Product Support Department

Approved By:

R. E. Baumer, Supervisor
Equipment Design Group
Systems Engineering Section
Test & Product Support Department

I. INTRODUCTION:

Bulk oxygen has long been recognized as a potentially hazardous fluid. With the advent of modern aviation and space programs there has been considerable information gained regarding the safe handling and application of liquid oxygen. This information has been presented in many individual reports and several major reports that attempt to consolidate the information into a single "application and handling" document. The most recent and comprehensive report of this type is,

CHEMICAL ROCKET/PROPELLANT HAZARDS

by the JANNAF Hazards Working Group - Chemical Propulsion Information Agency (CPIA). The Johns Hopkins University applied Physics Laboratory, 8621 Georgia Ave - Silver Springs, Maryland.

CPIA Publication No. 194 - May 1970

This report is the result of a joint effort by the major government agencies affiliated with aviation and space programs, Army, Navy, Air Force, and NASA. It compiles up to date state-of-the art information pertaining to the safe use hazardous fluids. Chapter 18 - Liquid Oxygen is presented in Enclosure I. It is recommended that this report be considered as a basic reference for liquid oxygen handling procedures and designs. Deviations from its recommendations should only be made after competent engineering review.

A review of USBM literature concerning coal dust explosion indicates that this is a complex condition and influenced by many other factors in addition to oxygen content. It is felt that this topic is beyond the scope of this particular report and should be reviewed in a separate study.

B. Filters

As noted earlier in this report, the presence of contaminants in the oxygen systems may cause serious trouble and consequently filters are frequently used. Oxygen filters must be treated in a different manner than routine filters. In most systems filters are allowed to "load-up" until the pressure loss across the element reaches an undesireable point and then they are cleaned. With oxygen filters it must be remembered that the unit is filtering and storing contaminants. If the stored contaminants include a high precentage of hydrocarbons, which may be increasing with each use, the filter can become a "bomb".

For maximum safety in hazardous conditions the system designer and operators should consider two items.

(1) Assume that the filter may explode and locate or guard it accordingly.

(2) Clean the filter at regular short intervals of use.

C. Lox Transfer Operations

If the making and breaking of transfer piping connections is to be made in hazardous conditions an additional factor should be kept in mind. Estimates by experienced field operations indicate that a leak at the connection will occur 20% to 50% of the time. This is due to the change in seal and joint clearances as the system undergos thermal distortions with the admission of the cryogenic fluid into the ambient piping. This becomes a routine occurrence and it is of no great hazard in liquid rocket operations for two reasons:

END OF REFERENCE

144

REFERENCE

145

McKINELY, C.; AND WANG, E. S. J.: HYDROCARBON-OXYGEN SYSTEMS SOLUBILITY. ADVANCES IN CRYOGENIC ENGINEERING, VOL. 4. K. D. TIMMERHAUS, ED., PLENUM PRESS, INC., 1960.

THIS REFERENCE IS MATERIAL THAT IS READI[illegible]ABLE
AND THEREFORE THE CONTENTS HAVE NOT BEEN [illegible]ODUCED.

END OF REFERENCE

145

REFERENCE

146

FASSELL, W. M., JR.; GULBRASEN, L. B.; LEWIS, J. R.; AND HAMILTON, J. H.: IGNITION TEMPERATURES OF MAGNESIUM AND MAGNESIUM ALLOYS. J. MET., VOL. 3, JUL. 1951.

Ignition Temperatures of Magnesium And Magnesium Alloys

by

W. Martin Fassell, Jr.
Leonard B. Gulbransen
John R. Lewis
and
J. Hugh Hamilton

A simple reproducible method was developed for determining the ignition temperatures of magnesium and magnesium alloys and by this method magnesium and over 100 magnesium alloys were measured. The ignition temperature of magnesium was determined in O_2-SO_2, O_2-N_2 mixtures and in O_2 from 0.166 to 10 atm pressure. The ignition temperature of magnesium is generally lowered by alloying and increased by an increase in oxygen pressure.

WITH the expanded use of magnesium alloys in industry, ignition temperatures are of considerable importance, especially in heat treating and for service at elevated temperatures. Magnesium alloys exhibit a relatively slow linear oxidation rate up to temperatures near the melting point.[1] At some critical temperature the rate of oxidation becomes extremely rapid. This high rate of oxidation is accompanied by the emission of light and additional characteristics suggesting a flame.

The literature concerning the ignition temperatures of magnesium and magnesium alloys is relatively incomplete and the values reported by various authors are not in agreement. The most probable reasons for this are: 1—The absence of a suitable definition of ignition, and 2—the need of a standardized method of determining the ignition temperatures of inflammable metals and alloys.

W. M. FASSELL, JR. is Assistant Professor, Department of Metallurgy, University of Utah, Salt Lake City. L. B. GULBRANSEN is Instructor, Department of Metallurgy, Colorado School of Mines, Golden. J. R. LEWIS, Member AIME, is Head, Department of Metallurgy, University of Utah. J. H. HAMILTON, Member AIME, is Director, Engineering Experiment Station, University of Utah.

Discussion on this paper, TP 3070E, may be sent, 2 copies, to AIME by Sept. 1, 1951. Manuscript, Aug. 28, 1950; revision, Dec. 28, 1950. St. Louis Meeting, February 1951.

This paper is a report of work done under contract with the Technical Command, Chemical Corps, U. S. Army.

The exact date of the discovery of the fact that magnesium will ignite and burn is unknown. It is likely that H. Davey encountered this property of the metal during its preparation in 1809. The first reference in the literature specifically on ignition of magnesium is by Lenze, Metz, and Rubens.[2] They investigated the inflammability of certain magnesium alloys. Brown[3,4] reported that magnesium ribbon will ignite in air at 507°C by what was called the rising temperature method. Hartman, Nagy, and Brown[5] reported that magnesium powder ignites from 475° to 560°C depending on particle size. According to Guise, Mars, and Wilson[6] prolonged heating in air at 427°C of common casting magnesium alloy causes it to ignite. Samples of magnesium alloys were placed directly in the flame of a torch by Carapella and Shaw.[7] These investigators obtained some evidence of melting prior to ignition. For commercial magnesium, they reported an ignition temperature of 650°C. Their values varied from 450° to 800°C for magnesium alloys. Willmore and Peterson[8] studied the effect of air velocity, humidity, rate of heating, and foreign metal contact on the ignition temperature of magnesium. They conclude that melting is not a prerequisite for ignition and that the conditions which influence ignition are complex and difficult to analyze.

The only quantitative theoretical treatment of the ignition temperatures of magnesium and magnesium

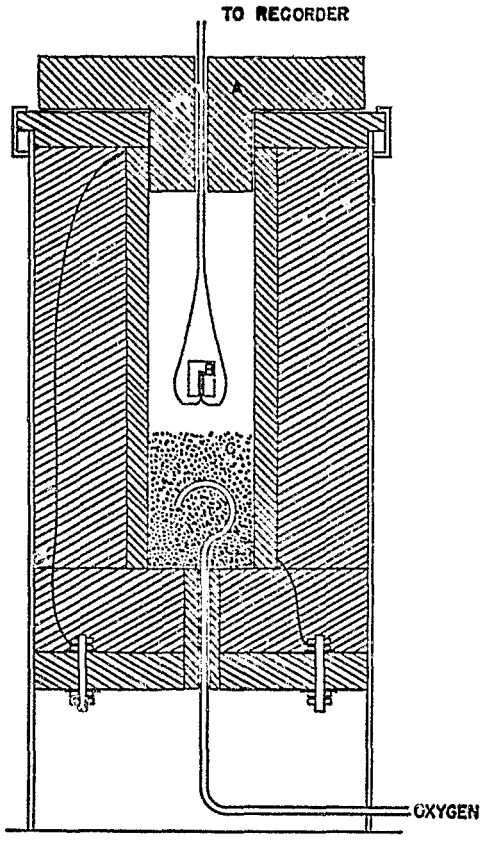

Fig. 2—Furnace used in ignition temperature experiments.

±5°C) on any given alloy composition. In addition, the ignition temperature is not influenced by complicating factors such as the Constable effect[11] ("self heating" of the sample); size of sample, within reasonable limits; rate of flow of oxygen; time of exposure; and rate of heating.

Measurement of Ignition Temperature

The alloy samples were melted in a small induction furnace, cast in a preheated split steel mold (½ in. diam x 3 in.) and turned on a lathe to 0.375 in. and cut into ½ in. lengths. Power cross feeds of 0.0018 in. per revolution were used to insure uniform surface conditions on all samples. A hole was drilled coaxially ⅜ in. deep with a No. 47 wire gage drill to provide a well for the thermocouple.

The hot junction of the thermocouple was inserted into the well of the alloy sample to be tested and the lead wires doubled back to form a U-shaped cradle so that only the junction was in contact with the sample.

Throughout the investigation the ignition temperatures were determined by measuring the temperature of the sample with a chromel-alumel thermocouple (28 gage) connected to a Leeds and Northrop Micromax recorder.

The schematic arrangement of the furnace (Hoskins Type FA120) with the sample in position is shown in Fig. 2. This equipment was used in all ignition temperature determinations in oxygen, oxygen-nitrogen, and oxygen-sulphur dioxide mixtures at atmospheric pressure.

With the sample in position, the flow of pure oxygen or oxygen mixture was started through the bottom of the furnace and adjusted to a rate of 250 ml per min. (The ignition temperature of pure magnesium was found to remain constant at flow rates from 50 to 500 ml per min.)

After 5 min the furnace was turned on (voltage to furnace held constant at 100 v, i.e. 83 pct rated voltage). Heating was continued until the recorder showed a sharp increase in rate of temperature rise, indicating ignition. After completion of the test, the tangential intersection of the two branches of the heating curve was plotted and the temperature of ignition evaluated.

Oxygen was used for the majority of the ignition temperature determinations. While this does not duplicate the conditions during heat treatment, it does provide comparative results between magnesium and its alloys. When air was substituted for oxygen, somewhat erratic temperatures were obtained, but with oxygen no such difficulty occurred and usually the mean variation did not exceed 2°C.

The ignition temperatures of the following systems have been determined: Mg, Mg-Ag, Mg-Bi, Mg-Co, Mg-Ca, Mg-Ni, Mg-Sb, Mg-Pb, Mg-Zn. In addition a number of other binary alloys have been studied in certain regions as well as a number of

Table II. Ignition Temperatures of Magnesium and Magnesium Alloys in Oxygen at Atmospheric Pressure

Composition, Pct Alloying Element	Ignition Temperature, °C	Composition, Pct Alloying Element	Ignition Temperature, °C	Composition, Pct Alloying Element	Ignition Temperature, °C
Pure EMCO Mg	623	Mg-Ca		Mg-Zn	
		1.0	624	19.07	523
		2.0	630	19.33	530
Mg-Al		5.0	633	19.91	552
5.67	558			30.14	513
5.88	527	Mg-In		30.2	534
11.43	530	10.0	613	31.74	524
13.97	535	20.0	593	33.48	524
18.17	502	30.0	586	51.13	588
26.04	514			60.72	542
33.25	515	Mg-Li		69.73	535
38.65	560	0.3	553	76.9	541
53.7	535	0.8	578	89.33	538
63.15	462	4.0	513		
80.33	None	8.0	514	Mg-Al-Zn	
82.72	to	11.4	518	1.21 Al	610
93.73	900			1.12 Zn	
		Mg-Mn			
Mg-Ag		1.0	621	2.16 Al	585
4.8	550	2.0	616	2.07 Zn	
9.04	537	3.0	631		
14.12	540			3.14 Al	575
		Mg-Ni		3.27 Zn	
		5.0	510		
Mg-Bi		10.0	517	4.23 Al	544
10.0	500	20.0	508	4.19 Zn	
20.0	548				
		Mg-Sb		3.18 Al	576
		1.20	582	4.98 Zn	
Mg-Cd		4.38	585		
7.15	612	5.22	588	5.95 Al	560
8.35	597	9.0	588	3.58 Zn	
10.78	588	21.6	593		
12.54	593	29.1	586	6.10 Al	543
14.07	595			6.02 Zn	
15.75	603	Mg-Si			
17.86	587	1.83	610	10.69 Al	549
20.98	596	3.15	625	14.26 Zn	
23.05	587				
25.31	607	Mg-Sn		Mg-Al-Cd	
[illegible]	[illegible]	0.39	576	14.75 Al	534
33.19	578	10.52	560	11.26 Cd	
35.10	586	11.34	556		
41.17	571	20.33	571	9.5 Al	514
44.09	559	22.31	574	4.98 Cd	
50.93	541	25.62	574		
61.40	517			Mg-Cd-Ag	
62.30	522			22.9 Cd	570
71.80	535	Mg-Pb		0.33 Ag	
80.73	533	16.24	575		
90.52	551	29.97	565	15.3 Cd	560
		45.98	553	1.77 Ag	
		58.26	504		
Mg-Co				24.9 Cd	592
1.0	617			2.22 Ag	
5.0	616	Mg-Zn			
		3.04	595	26.77 Cd	567
		4.81	552	2.3 Ag	
Mg-Cu		5.23	546		
10.3	537	9.25	509	Mg-Cd-Zn	
20.5	519	10.34	537	19.9 Cd	553
30.76	532	12.5	558	2.78 Zn	

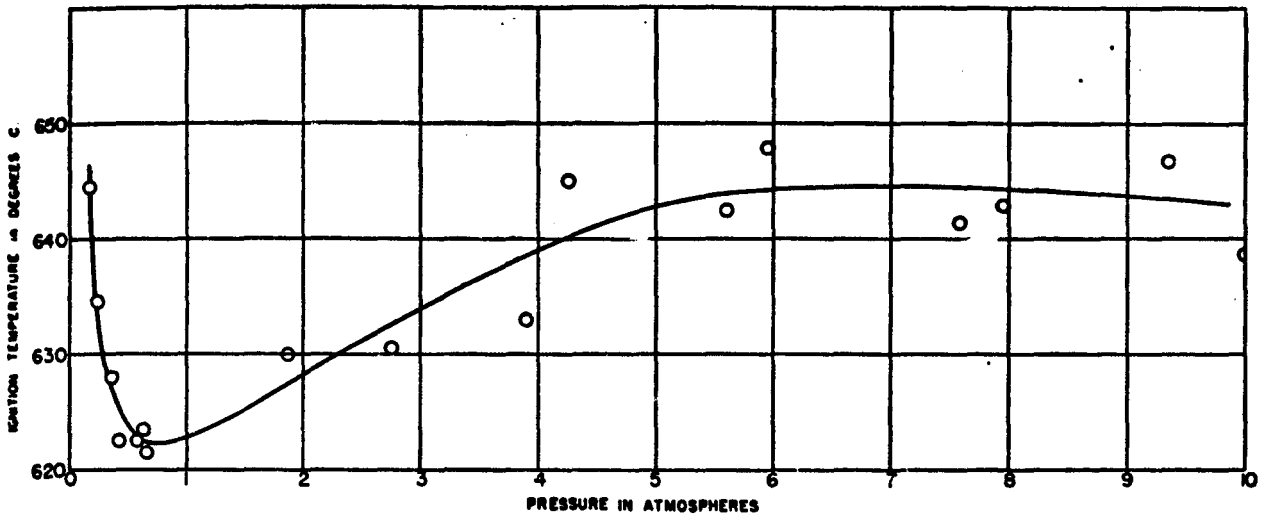

Fig. 6—Ignition temperature of magnesium with respect to oxygen pressure.

performed in this laboratory indicate that the ignition temperature of magnesium is lowered appreciably by contact with aluminum, nickel, and 70-30 brass. Silver and plain carbon steel did not affect the ignition temperature. The samples were prepared by drilling a hole through a piece of pure magnesium followed by reaming with a 2/0 taper pin reamer. The dissimilar metal in the form of a pin was driven in and the ends turned off thus giving a perfect contact. The values of the ignition temperatures of pure magnesium in contact with other metals are presented in Table VII (oxygen atmosphere).

Discussion of Results

The method developed for the determination of the ignition temperatures of magnesium and magnesium alloys is simple and reproducible. As an illustration of the accuracy of this test, ten samples of magnesium of the same lot were run in oxygen by four different individuals over a period of six months. The average ignition temperature obtained from this series of tests was:

$$623°C \pm 0.5°C$$

The ignition temperature of magnesium generally is lowered by the addition of alloying elements providing the melting point (liquidus) is lower than pure magnesium. Ignition of magnesium alloys may occur at temperatures either above or below the melting point indicating that the conclusions of Carapella and Shaw[4] are not generally valid. The Mg-Cd system, Fig. 3, is an excellent example of this effect. The melting point of the alloy has some influence on the ignition temperature, but it is not the only factor that must be considered. This is discussed in detail in ref. 14.

One rather unusual observation was made of the magnesium and magnesium alloy samples just prior to ignition. Normally the oxide coating present is white in color. However, just an instant before ignition occurs, the oxide coating turns a dark brown or black color. Once the color change occurs, ignition follows immediately.

A correlation exists between the rates of linear oxidation and the ignition temperatures of magnesium alloys. Sufficient data to justify its presentation is available only on the Mg-Al system. Qualitatively, however, all of the alloy compositions investigated by Leontis and Rhines show the same relationship. Table VIII shows the correlation of the linear oxidation rates and the ignition temperatures of some Mg-Al alloys.

The ignition temperature of magnesium in oxygen-sulphur dioxide mixtures increases from 623°C at zero percent SO_2 to approximately the melting point of magnesium (650°C) at 1.7 pct SO_2. From 1 to 5.8 pct SO_2 no further increase is observed. Qualitatively, at least, it is well known that high concentrations of SO_2 prevent the ignition of magnesium at temperatures considerably above the melting point. Thus, a further increase in the ignition temperature would be expected at concentrations above 5.8 pct SO_2 which was the maximum concentration investigated in this work.

The results obtained on the time-delay of the ignition of magnesium show that if the furnace or bath

Table VI. The Ignition Temperature of Magnesium in Oxygen as a Function of Pressure

Oxygen Pressure, Atm	Ignition Temperature, °C	Average Ignition Temperature
0.166	643 645	644.5
0.234	636 633	634.5
0.365	628 628	628
0.42	622 623	622.5
0.58	623 622	622.5
0.64	623 624	623.5
0.688	621 622	621.5
1.0	10 at 623	623
1.865	630 630 629 631	630
2.75	633 628	630.5
3.9	635 631	633
4.25	645 645	645
5.6	644 641	642.5
5.95	649 647	648
7.68	641 642	641.5
7.95	641 644 644	643
9.35	647 647	647
10.0	640 638 638	638.8

Table VII. Ignition Temperatures of Magnesium in Contact with Other Metals

Sample	Contact Metal	Ignition Temperature, °C
Mg		623
Mg	Ni	598
Mg	Ag	623
Mg	70-30 brass	538
Mg	Steel	623
Mg	Al	823

END OF REFERENCE

146

REFERENCE

147

WOLFHARD, H. G.; GLASSMAN, I.; AND GREEN, L., EDS.: HETEROGENOUS COMBUSTION. PROGRESS IN ASTRONAUTICS AND AERONAUTICS. VOLUME 15. ACADEMIC PRESS, 1964.

THIS MATERIAL HAS BEEN APPROVED FOR PUBLICATION PER LETTERS FROM IRVIN GLASSMAN DATED OCT. 21, 1974 AND MARIAN McGRATH, ACADEMIC PRESS, INC. DATED AUG. 6, 1974 TO JOANNE FOLK.

Heterogeneous Combustion

Edited by

Hans G. Wolfhard
Research and Engineering Support Division,
Institute for Defense Analyses, Washington, D. C.

Irvin Glassman
Guggenheim Laboratories for Aerospace Propulsion Sciences,
Department of Aerospace and Mechanical Sciences,
Princeton University, Princeton, New Jersey

Leon Green Jr.
Research and Technology Division,
Air Force Systems Command, Washington, D. C.

A Selection of Technical Papers
based mainly on
the American Institute of Aeronautics and Astronautics
Heterogeneous Combustion Conference
held at Palm Beach, Florida
December 11-13, 1963

ACADEMIC PRESS · NEW YORK · LONDON · 1964

PREFACE

In the strictest sense heterogeneous combustion is defined as combustion supported by heterogeneous chemical reaction. Examples of heterogeneous reactions include a gas reacting with another gas on a solid surface or reacting with the surface itself. In general use the subject of heterogeneous combustion is considered in a much broader context. If, in any aspect of the combustion process, more than one physical state exists, then the over-all process is considered heterogeneous. By this definition the burning of solid propellants which first gasify and then react homogeneously would be a heterogeneous problem, as would be the case of two liquid propellants reacting in the liquid phase and having gaseous products. However, in this book the primary concern is with certain condensed state diffusion flames which involve the combustion of solids and liquids in gaseous atmospheres. In essence, droplet burning is considered as a heterogeneous phenomenon, even though the principal energy release may be the result of homogeneous gas-phase reactions. Any condensed-phase diffusion flame meets the requirement of this definition.

Gas-phase diffusion flames, or for that matter gaseous premixed and decomposition flames, can take on heterogeneous characteristics as well, if they are supported by heterogeneous reactions or create a condensed phase. The paper by Markstein which is related to metal vapor-oxygen systems fits this classification, as do the papers which describe diborane-oxygen combustion.

Not only do all papers in this volume fall within the general definition, but they also are related to three topics of great current interest to the combustion and chemical propulsion fields. In fact, these topics--combustion of metals, hybrid rockets, and condensation--bear a direct relationship to each other.

The hybrid rocket motor is one in which both liquid and solid propellants are used. The solid component is usually a singly perforated cylinder but can take any shape similar to unrestricted solid propellant grains. The liquid is injected in the open port area of the grain at a position close to the forward end or, in some cases, in a chamber volume ahead of the forward end of the grain. After ignition, the liquid apparently is vaporized due to the heat release from the ignition phase, and further combustion between the vapor and gasifying solid proceeds

by a diffusion flame. This diffusion mechanism is different from that mentioned earlier in that the stagnant conditions usually assumed for particles no longer exist, and fluid mechanical considerations become important.

In addition to the feature of controllability, hybrid rocket motors gain a performance advantage over solid propellant rockets in their ability to contain conveniently large quantities of high-energy metals and metal compounds, such as Al, Mg, Be, Zr, BeH_2, $AlLiH_4$, etc. These materials are dispersed uniformly in the solid grain as in metallized composite solid propellants. The performance advantage of hybrids can be realized only if the metals and metal compounds burn efficiently within the motor. Metal combustion leads to high boiling point products in which much of the available heat is obtained from the latent heat of condensation of these products. For efficient performance, then, not only must the metals burn completely, but the product oxide must condense within the motor as well. Thus, condensation phenomena are of great importance in metallized systems.

In the initial section of the book are some of the first published works on the analytical determination of metal burning rates, the various flame mechanisms of aluminum and magnesium, the combustion of aluminum in carbon dioxide atmospheres, and the ignition temperature of beryllium. Two other papers are concerned with the high-temperature oxidation of molybdenum, tungsten, graphite, and boron nitride, which are considered protective, high-temperature materials. Such knowledge of high-temperature surface oxidation contributes directly to the knowledge of the over-all combustion process of metals. For, as pointed out by two groups, Glassman and his co-workers and Friedman and Maček, it is the initial oxidation of the particle surface which controls the ignition of the metal. This fact is particularly significant in practical propellant systems. Similarly, the study on the combustion of zirconium hydride-uranium fuel rods, which was motivated by the problem of dispersing radioactive materials during atmospheric re-entry, contributes information on the various models of metal combustion which have been proposed.

The physical state in which the metal element is introduced into the combustion chamber does not affect the theoretical performance obtainable in metallized propellant systems. Thus, if it is difficult to obtain high efficiencies with metal particles, then, perhaps, the metal can be introduced in various other forms, such as a liquid alkyl-metal compound, a polymeric substance containing a metallic element in the chain, etc. The possibilities of this approach lead to various studies which contribute both directly and indirectly to the understanding of metal combustion phenomena. The oxidation and flame studies with diborane and its alkyl derivatives are of particular interest, as are the reaction studies between boron and nitrogen compounds. A contribution to this latter problem is made here by Seklemian and Lawrence, who isolate the adduct formed between pentaborane and hydrazine by running the

reaction in very dilute solutions of cyclohexane. Bauer et al. consider the oxidation of diethyldiborane under explosive and nonexplosive conditions. Wolfhard et al. report flame speed data for diborane. Their observations on the BO spectra found in the flames leads one to believe that BO is present only as an intermediate. Pyrolysis of the alkyls is considered by Skinner and Snyder, who report experimental data on diborane, and by Takima and Marsel, who discuss the mechanisms for the decomposition of the aluminum alkyls.

Papers in the third section of this volume deal with some aspects of the over-all hybrid combustion process, which from Green's introductory review is seen to center about the problem of heat and mass addition at the fluid-solid interface. Refinement of the simplified theory employed in this review by introduction of boundary-layer growth considerations is discussed by Marxman et al., and experimental results are compared. Courtney et al. report spectroscopic observations of hybrid burning. Their results give insight as to the thickness of the flame zone. Houser and Peck discuss the role of surface pyrolysis in determining solid phase regression rates. McAlevy discusses various modeling techniques that could prove valuable not only for hybrids, but also for composite solid propellants. Williams in a theoretical analysis considers the boundary-layer distribution of trace species, such as those found in an ablation or surface combustion process. In their paper Chen and Toong consider evaporation with combustion in a well-defined aerodynamic configuration.

Fundamental to many of the studies previously mentioned is the formation and growth of the condensed particle (B_2O_3, B, BN, Al, MgO, etc.). Theoretical and experimental studies of nucleation and condensation phenomena are reviewed in many of the papers in the last section. Most deal with compounds classically used in such investigations; however, one by Courtney reports some initial work on a metal oxide system.

This volume undoubtedly contains one of the largest and most interesting collections of recent papers on metal and hybrid combustion. Most were presented at the AIAA Heterogeneous Combustion Conference in December 1963.

Irvin Glassman
Princeton University, Princeton, N. J.

Leon Green Jr.
Air Force Systems Command, Washington, D. C.

Hans G. Wolfhard
Institute for Defense Analyses, Washington, D. C.

July 1964

between a horizontal and a vertical electrode, this particular configuration being convenient for flame spectroscopy and photography.

Table 1 Highest brightness temperatures reached by aluminum wires in oxygen

Pressure	Brightness temperature, °K	
	Anodized wire	Clean wire
50 mm Hg	2000	1800 no ignition
100 mm Hg	2010 all	1890 no ignition
300 mm Hg	2010 tests	2000 ignited
1 atm	2025 ignited	2025 ignited
4 atm	2025	2025 ignited
10 atm	2025	2025 ignited
20 atm	2025	2025 ignited

The wires that failed to ignite broke on the long vertical leg close to the top electrode where the oxide coating apparently had not grown thick enough at the low oxygen pressure to support the weight of the melted aluminum wire.

It is significant that the brightness temperature of the wire at ignition was independent of pressure and that it was the same for the anodic oxide coating as for the oxide coating which grew as the wire was heated. These observations offer further substantiation for the suggested ignition mechanism.

Combustion Mechanisms

A composite map of the burning mechanisms of aluminum wires observed in oxygen-argon mixtures is shown in Fig. 7. The observations on which it is based were made at pressures of 100, 300, and 500 mm Hg, 15,30,45,90,120,150,180 and 225 psia at values of the oxygen mole fraction varying in steps of 0.1 between 0 and 1. Runs at 300 and 375 psia were made at X_{O_2} = 0.3,0.5,0.7 and 1. Runs at 450 psia were made at X_{O_2} = 0.2,0.3,0.4,0.5,0.7 and 1. Additional low-pressure tests were carried out at 50 mm Hg for X_{O_2} = 0.3,0.5,0.6,0.7 and 0.8.

Region 1: The combustion in this region was very similar to that observed in region 1 for magnesium.

END OF REFERENCE

147

REFERENCE

148

JAKOWSKY, J. J.; AND BUTZLER, E. W.: OXYGEN-OIL EXPLOSIONS. PRELIMINARY REPORT 11. SPONTANEOUS IGNITION OF METALS IN OXYGEN UNDER PRESSURE. BM-RI-2521, BUREAU OF MINES, SEPT. 1923.

Bureau of Mines, Reports of Investigation
RI-2521
R.I.
Serial No. 2521
September, 1923.

3.1-0-0

REPORTS OF INVESTIGATIONS

DEPARTMENT OF THE INTERIOR -- BUREAU OF MINES

OXYGEN-OIL EXPLOSIONS.

Preliminary Report II. Spontaneous Ignition of Metals in Oxygen under Pressure.

By J. J. Jakowsky* and E. W. Butzler**.

This preliminary report deals with the effects of oxygen pressure on the ignition temperature and combustibility of iron, copper, brass and lead. It is the second of a series which will present the results of an investigation being made by the Bureau of Mines, on oxygen-oil explosions. The purpose of this research is to obtain technical data that will serve as a basis for safety precautions. A general outline of the problem has been given in the first report (Serial 2507).

The present experiments were undertaken to determine (1) the relationship between oxygen pressure and the ignition temperature of the metals most frequently used in high-pressure oxygen apparatus; and (2), the metals most suitable, as regards safety and freedom from combustion, for use in high-pressure oxygen systems. A study was made of the relation between ignition temperature and pressure for iron, copper, and brass, which are the three materials usually employed, and for lead.

Apparatus Used.

The gas apparatus used in these experiments consisted essentially of the following equipment (See Figure 1):

A 200-cubic foot cylinder of compressed oxygen from an air liquefaction and reduction process was connected by means of copper tubing to a release valve, a pressure gage for indicating the pressure in the bomb, and the bomb.

The bomb was an old Parr calorimeter bomb which had been altered, as shown in Figure 2, to allow the wire (e) to be inserted, this wire comprising the material to be tested in the bomb. The lead-in through the bomb consisted of a brass piece threaded on the under side and fastened with a heavy nut. This construction was adopted because of the high pressure to be used. Suitable lead washers were used as packing to make a gas-tight joint. The brass piece was drilled and tapered to hold the fiber insulation (b), through the center of which passed the insulated terminal (a). The wire was placed across the terminals of

* Assistant engineer, Bureau of Mines, Department of the Interior.
** Assistant to physicist, Bureau of Mines.

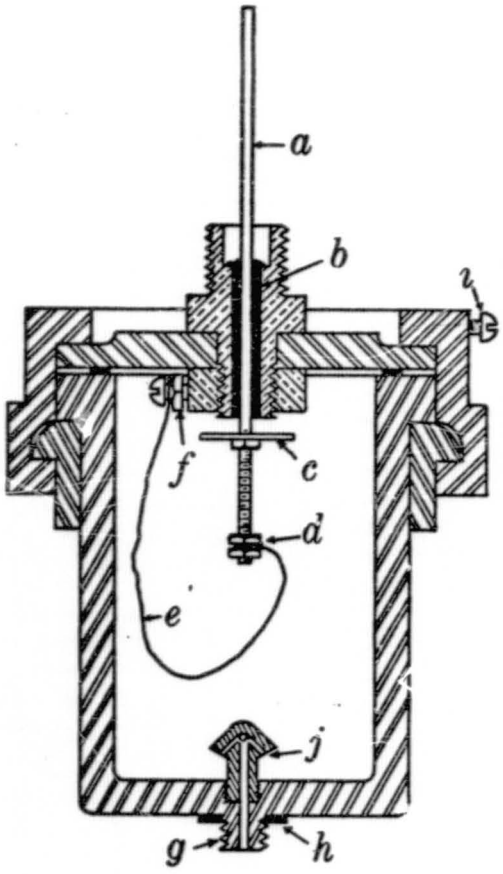

Fig. 2
Oxygen chamber

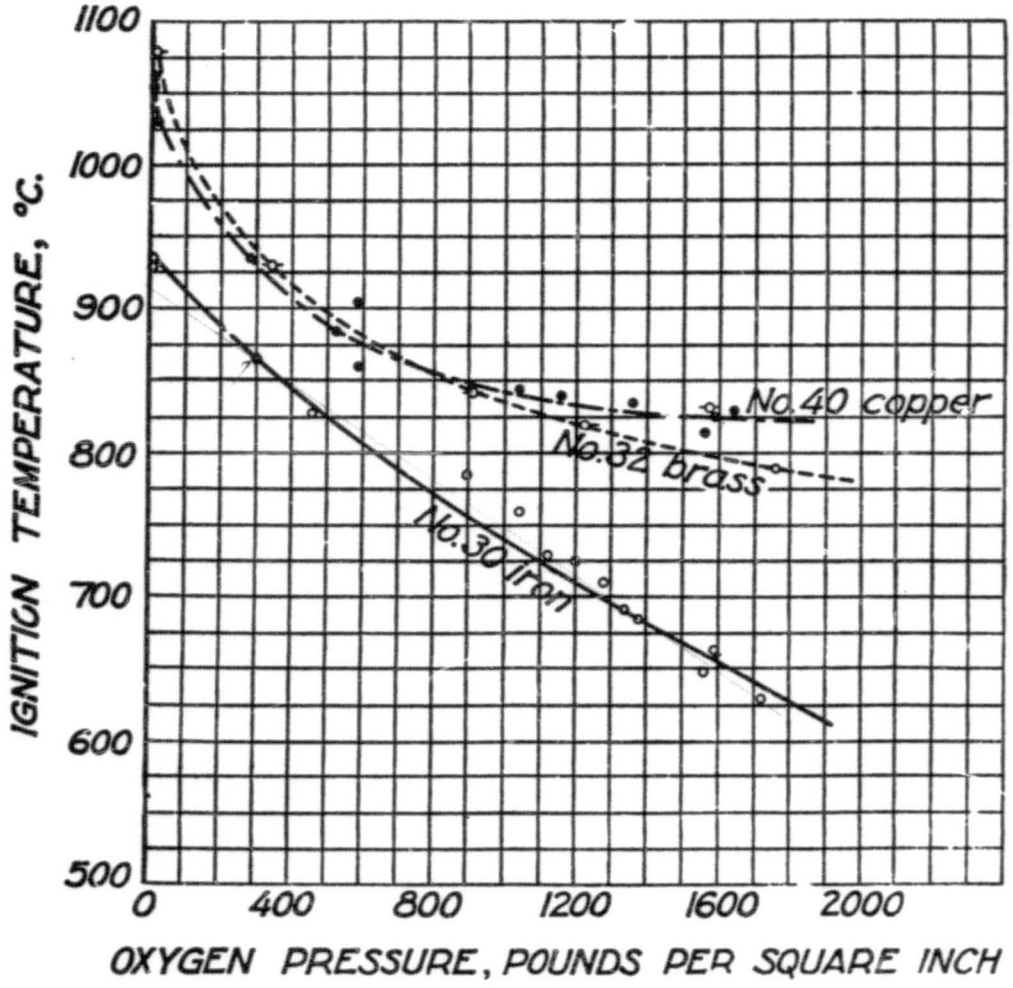

Fig. 3
Apparent relation between ignition temperature and oxygen pressure

END OF REFERENCE

148

REFERENCE

149

GROVES, W. E.: SAFE HANDLING OF LARGE QUANTITIES OF GASEOUS OXYGEN IN STEEL PIPELINES. IRON AND STEEL ENGR., VOL. 42, NO. 1, JAN. 1965.

COURTESY OF IRON AND STEEL ENGINEERS JOURNAL

Safe Handling of Large Quantities of Gaseous Oxygen in Steel Pipelines

by W. E. GROVES
Engineer, Gas Products Production
Linde Div.
Union Carbide Corp.
New York, N. Y.

A clean pipeline, judicious use of filters, adiabatic compression temperature, application of organic material and correct selection of metal components and pipes are all necessary considerations in the safe operation of an oxygen steel pipeline.

TRANSMISSION of gaseous oxygen by pipeline has expanded very rapidly in the last decade. Pipelines are now the accepted means of supplying large consumers in the metallurgical and chemical industries. As the demands of large consumers have increased, the maximum pressure and maximum gas velocity in gaseous oxygen pipelines have also increased. Low-carbon steel pipe is normally used for these pipelines. Since low-carbon steel pipe can burn in oxygen, it has been necessary to learn how to design, install and operate steel pipelines in gaseous oxygen service in order to avoid fires. This has been accomplished by studying the combustion of metals and organic materials in oxygen, by determining the causes of ignition in oxygen pipelines and by analyzing past oxygen pipeline fires.

In a gaseous oxygen pipeline there are at least three sources of ignition energy:

1. Potential energy of oxygen gas.
2. Kinetic energy of oxygen gas.
3. Energy introduced into pipeline in the form of work on a component of the pipeline.

The potential energy of the gas can provide ignition energy when a valve is suddenly opened between a high-pressure and a low-pressure section. This results in very rapid compression of the low-pressure gas, and can theoretically produce temperatures approaching the adiabatic compression temperature.

The kinetic energy of the gas can provide ignition energy by accelerating entrained particulate matter and impacting it against valve disks or other objects protruding into the gas stream, scraping it along the surface of the pipe or rubbing the particles against one another. The kinetic energy of the gas stream can also provide ignition energy by vibrating a thin membrane protruding into the oxygen stream, by vibrating a loose gasket between flanges or by tearing loose a valve disk, filter screen or some other part of the pipeline and carrying this part down the pipeline.

Opening or closing a valve can produce ignition energy by impacting a small piece of material between the disk and seat of the valve, and by producing friction between valve parts.

In addition to recognizing the sources of ignition energy, one must also have some understanding of the combustion of materials in oxygen.

COMBUSTION OF MATERIALS IN OXYGEN

Organic materials—Organic materials are combustible in air; therefore, it is natural to expect them to be com-

TABLE I
Combustibility Data for Organic Materials

Material	Combustibility Data		
	Ignition temperature in 2000-psig oxygen, F*	Impact producing ignition after immersion in liquid oxygen, ft-lb*	Heat of combustion, Btu per lb
Rubber bonded compressed asbestos sheet gasket material	270 to 340	41 to 114	2250 to 3030
Fluorocarbon oils, greases and solids	750 to 930**	114**	2000 to 3000
Pipe and joint compounds	570 to 930	30 to 114	0*** to 10,000
Synthetic rubber materials	340 to 640	21 to 114	6750 to 15,300

* These data obtained by test methods described in International Acetylene Association publication entitled "Anti-Friction Compounds for Use with Gaseous Oxygen."
** Maximum capacity of test equipment.
*** Indicates material did not ignite in Parr calorimeter.

bustible in oxygen. Combustion tests have been run on organic materials for 30 years and the combustion data have been used as an aid in determining the safety of specific applications of organic materials in oxygen service. Actually, if at all possible, inorganic materials are used and organic materials are only used where inorganic materials will not perform satisfactorily.

The first test indicated the ignition temperature under the test conditions of organic material in 2000-psi oxygen. The second test determined the impact necessary to produce ignition after immersion in and while still saturated with liquid oxygen. The third test measured the heat of combustion of the material. A fourth test provided a visual observation of the burning of the material in oxygen at atmospheric pressure. Experience in evaluating the results of these tests and in their practical application is a very important part of their usefulness.

Should there be a case where one does not believe that the results of the four combustion tests together with experience provide sufficient information to establish the safety of using an organic material for a given application, a full scale combustion test was conducted. In the full scale test, the material was ignited in the piece of equipment in which it is to be used and at the oxygen pressure at which it is to be used and the results of burning the organic material were observed.

Table I presents the results of combustibility tests for four classes of organic materials commonly used in oxygen pipelines. Table I is presented only to indicate the wide range of test results obtained. It is not intended to indicate that materials having test results within these ranges are satisfactory for any particular application in oxygen pipelines. This table shows the outstanding resistance to combustion in oxygen of the fluorocarbon materials. This is, of course, the characteristic which makes these materials suitable for many applications in oxygen service.

In addition to data on the ignition of organic materials, data on the ignition and combustion of metals are required. Before presenting this data on metals, some consideration must be given to the combustion of metals.

Metal Combustion—As a result of experimental investigation, a review of the literature and a study of oxygen pipeline fires, an initial understanding of the burning of metals has been obtained. This burning can be divided into two phases: ignition and combustion. Ignition is the first phase. It precedes combustion and encompasses that period during which the metal temperature increases from ambient to the temperature at which combustion begins. Combustion is that phase in which the metal combines with oxygen rapidly enough to produce light and heat.

The resistance of a metal to ignition depends on several factors including the activation energy necessary to reach the ignition temperature, the thermal conductivity of the metal, the characteristic of the oxide that forms on the metal surface before the ignition temperature is reached, and the mass and shape of the particular piece of metal.

Some metals reach their ignition temperature before they reach their melting point. Other metals melt before they ignite, or ignite at about the melting point. In experimental work it has been difficult, because of the techniques and equipment used, to determine in many instances whether the ignition or the melting occurred first.

Variation of the ignition temperature of brass, copper

TABLE II
Ignition Temperature of Metals in Oxygen

Metal	Ignition temperature, F				Resistance to ignition	Rate of combustion
	Oxygen pressure					
	0 psig	500 psig	1000 psig	1800 psig		
Copper①	1984*	1625	1535	1481	1 (most resistant)	4 (does not propagate combustion)
430 stainless steel②	2490	...	...	...	2	2
Mild steel②,③	2330	2020	1835	1700	3	3
Iron①	1706	1517	1364	1166	...	...
Aluminum	1220*	...	...	...	4 (least resistant to ignition)	1 (burns most rapidly)

* Melting temperature.
① Bureau of Mines Report No. 2313.
② NASA Technical Note D-182.
③ Linde investigation.

END OF REFERENCE

149

REFERENCE

150

GROSSE, A. V.; AND CONWAY, J. B.: COMBUSTION OF METALS IN OXYGEN. INDUS. ENG. CHEM., VOL. 50, NO. 4, APR. 1958.

A. V. GROSSE and J. B. CONWAY[1]
Research Institute, Temple University, Philadelphia, Pa.

Combustion of Metals in Oxygen

The basic aim of the work was to develop a technique for producing and utilizing high temperature sources. Combustion of aluminum yields a source of high intensity thermal radiation. Powdered metal-oxygen flames are highly effective in cutting through thick sections of concrete and ceramic materials.

In 1948 the Research Institute of Temple University established a High Temperature Laboratory to study and develop methods for producing high temperatures (about 3000° C.). The basic objective was to establish techniques for producing, confining, maintaining, and controlling high temperatures, and ultimately to apply this experience in studying chemical and physical phenomena in this temperature region. Most previous work has dealt with chemical reactions of substances in the gaseous, liquid, or solid phases (*2, 7–11, 17, 32, 33*). The combustion of metals was convenient and effective for producing high temperatures and was studied in considerable detail.

The dictionary defines combustion as "any chemical process accompanied by the evolution of light and heat." Oxygen need not be one of the reacting substances; the reaction of hydrogen with fluorine is as truly a combustion as the reaction of hydrogen with oxygen. The combustion of metals therefore designates reactions of metals which evolve heat and light. The work described is limited to combustion in which the metals react with molecular oxygen. Reactions with other gases, including ozone, are described in separate articles.

Although metals are not generally looked upon as fuels, they must be classified with such solid combustibles as coal and wood. Their combustion differs from that of wood in the formation of reaction products (metallic oxides) which are solid at room temperature. Their heats of combustion and ignition temperatures, however, are of the same order of magnitude as those of various solid nonmetallic fuels (interpreted as applying to reactions with oxygen; these values differ for combustion in fluorine or some other atmosphere). The heats of combustion of some common combustibles and typical metals listed in Table I are from the recent compilation of Brewer (*3*). On a pound basis the metals liberate about as much heat as carbon, methane, and acetylene; hydrogen is very high because of its low atomic weight. On a gram-mole or gram-atom basis the same is true, hydrogen now being near the bottom of the list.

The first experiments on combustion of metals were those of von Ingenn-Hausz in 1782, in which heated spirals of iron and steel were plunged into oxygen (*26*). These experiments demonstrated that certain metals could be made to burn in oxygen to produce highly luminous flames generating large quantities of heat and light. These characteristics of metal combustion have been primarily responsible for numerous practical applications of this fundamental reaction. The operation of a photo-

Table I. Heats of Combustion

Fuel	Combustion Product	At. or Mol. Wt.	Kcal./G. Mole Fuel	Kcal./Gram Fuel	B.T.U./Lb. Fuel	Kcal./Gram O_2
H_2	$H_2O(l)$	2.016	68.3	33.9	61,000	4.27
C	CO_2	12.0	94.05	7.83	14,100	2.94
CH_4	CO_2, H_2O	16.03	212.7	13.3	24,000	3.32
C_2H_2	CO_2, H_2O	26.02	310.5	11.9	21,400	3.88
CO	CO_2	28.0	67.6	2.41	4,340	4.22
Li	Li_2O	6.94	71.3	10.25	18,500	8.93
Na	Na_2O	22.997	49.7	2.16	3,900	6.25
Be	BeO	9.02	147.0	16.3	29,400	9.2
Mg	MgO	24.32	143.7	5.9	11,600	9.0
Ca	CaO	40.08	151.7	3.79	6,820	9.4
Sr	SrO	87.6	140.8	1.61	2,900	8.8
Ba	BaO	137.4	133.0	0.97	1,750	8.4
B	B_2O_3	10.8	152.7	14.1	25,400	6.4
Al	Al_2O_3	26.97	200.1	7.43	13,400	8.3
Th	ThO_2	232.1	293.2	1.26	2,300	9.15
Ti	Ti_2O_3	47.9	181.5	3.79	6,820	7.6
Zr	ZrO_2	91.2	261.8	2.87	5,160	8.2
Fe	FeO	55.85	63.2	1.13	2,000	3.9
Co	CoO	58.94	57.0	0.97	1,750	3.6
Ni	NiO	58.69	58.0	0.99	1,780	3.6
Si	SiO_2	28.06	210.2	7.5	13,500	6.6
Sb	Sb_2O_3	121.76	83.5	0.69	1,240	3.5
Bi	Bi_2O_3	209.0	69.0	0.33	594	2.88
Hf	HfO_2	178.6	266.0	1.49	2,680	8.3

History of Combustion of Metals

Author	Lit.	Remarks
Baker and Strong	(*1*)	Burner fed with finely divided Al powder dispersed in O_2
Cueilleron and Scartazzini	(*13*)	
Scartazzini	(*30*)	
Bunsen and Roscoe	(*4*)	Measurements of radiant energy emitted by combustion of metals
Forsythe and Easley	(*15*)	
Van Liempt and de Vriend	(*35*)	
Cassel, Das Gupta, and Guruswamy	(*5*)	Factors affecting flame propagation through dust clouds
Coffin	(*6*)	Burning times of Mg ribbons in various atmospheres
Hart and Tomlinson	(*18*)	Use of finely divided metals in explosives
Hartmann, Nagy, Brown, and Jacobson	(*19–21*)	Ignition characteristics and limits of flammability of metal dust dispersions
Rasor	(*29*)	Patent for use of powdered metal as fuel for propulsion of submarines
Wolfhard and Parker	(*34*)	Optical measurements on stationary flame of Al and Mg flakes suspended in air, color temp. of 3600° C. recorded
Zenghelis	(*35*)	Burning Al in MgO crucible, qualitative measurements of combustion temperature

[1] Present address, Aircraft Nuclear Propulsion Department, General Electric Co., Evendale, Ohio.

capacities for the liquid phase are usually a little higher than those for the solid phase. The biggest error is made when data are not available on boiling temperature, latent heats of vaporization, or the oxide species which exist at high temperatures.

As Figure 10 shows, the combustion temperatures are periodic functions of the atomic number of the element. The maxima are the metals of Groups II, III, and IV. In the first period beryllium has the highest combustion temperature; in the second, aluminum; in the third, calcium (and probably scandium); in the fourth and fifth, zirconium and hafnium, respectively; and in the last, thorium. The minimum combustion temperatures are obviously obtained with the nonmetals, the absolute or trivial minima being the noble gases, as they do not combine with oxygen. There are secondary minima in the transition group metals, occurring with the monetary metals—copper, silver, and gold—and the last members of the noble metals such as nickel, palladium, and platinum; intermediate maxima, probably at germanium, tin, and bismuth, also occur with the transition metals. Figure 10 gives a general correlation of the combustion temperatures of metals. Some of the values are only estimates (usually indicated with a ?), but the whole relationship will not change appreciably when better data are available.

Flame temperatures are a function of total pressure. High pressures increase the boiling point of the oxide, so that higher flame temperatures are also obtained even where the oxide decomposes on vaporization. The combustion of aluminum at 10 atm. results in a flame temperature of 4400° K., compared to 3800° K. at 1 atm.

Ignition Temperature of Metals

In general, the rates of oxidation of metals follow the Arrhenius equation; the rate of oxidation is increased with increase in temperature, the exact relationship depending upon the energy of activation of the reaction. As the heat released is directly proportional to the reaction rate, this also exhibits the same temperature dependence. A temperature is eventually reached at which the heat generated begins to exceed the heat dissipated to the surroundings, the ensuing autogenous temperature rise brings the material to the glow or flame point, and the metal is said to have ignited. This is termed the ignition temperature and should be a characteristic property of the metal, similar to melting point, density, and tensile strength. The fact that it is not ordinarily so considered is due to the apparent discrepancies in the values reported by various investigators. However, most of these discrepancies are undoubtedly due to failure to reproduce test conditions in every detail; in all probability once a firm definition of ignition temperature is accepted, the precision and accuracy of successive and independent measurements will be enhanced. It is already accepted that the factors to be investigated as they affect ignition temperatures are: purity of the metal, gas composition including moisture content, pressure, velocity past the surface, state of subdivision, previous history of the metal, and apparatus and technique.

The mechanism of oxidation is also usually affected by temperature, in that the rate law which applies is different for different temperature ranges. It seems to be generally accepted, at least for pure metals (although not experimentally verified in every case), that oxidation proceeds exponentially with time at low temperatures, parabolically at intermediate temperatures, and linearly at high temperatures. The temperature ranges corresponding to these mechanisms are, of course, different for different metals. Cubicciotti (*12*) has cited for a few metals the temperature at which the oxidation changes from parabolic to linear—for thorium, calcium, and aluminum, 350°, 400°, and 500° C., respectively. It is not clear if there is any correlation between this transformation temperature and the ignition temperature. Thorium and calcium ignite (in oxygen) about 100° C. above this temperature, but aluminum has an ignition temperature at least 600° C. above its parabolic to linear transition temperature. Perhaps this transition must take place before ignition, although such a statement lacks experimental verification.

The ignition temperature as defined is dependent upon the rates of heat generation and of heat dissipation. It would seem plausible, therefore, to expect a correlation between ignition temperature and the rates of oxidation, at least when the oxidation is linear. This follows from the fact that the higher the rate of linear oxidation, the more heat is produced per unit time and hence the lower the temperature at which ignition can occur (differences in heat dissipation due to differing oxide properties are ignored). Such a correlation has been noted by Fassell and others (*14*) for various magnesium alloys. The linear oxidation rate of each alloy at 475° C. was tabulated with the corresponding ignition temperature; as the oxidation rate increased, the ignition temperature decreased. Such a correlation, although perhaps applicable to a given alloy system, has not been shown to metals in general.

Table IV. Adiabatic Combustion Temperatures in Oxygen at 1-Atm. Pressure

Metal	Adiabatic Comb. Temp., ° K.	Metal	Adiabatic Comb. Temp., ° K.
Al	3800	Cr	3300
Mg	3350	Mo	3000
Li	2600	W	3200
Na	2000	Mn	3400
K	1700	Zn	2200
Be	4300	Ca	1700
Ca	3800	Si	2500
Sr	3500	Sn	2700
Ba	3000	Pb	1800
B	2900	Sb	1700
Th	4700	Bi	2000
Ti	3300		
Hf	4800		
Zr	4800		
Fe	3000		

As the ignition temperatures of metals have been studied only sparingly, the factors affecting ignition have not been clearly defined nor has the mechanism been fully explained. However, it is certain that metals can be divided into three classes based on their ignition temperatures: (1) metals that ignite at or below their melting points, (2) the metals that ignite after they melt (magnesium is an example of Class I and aluminum of Class II), and (3) metals that have no ignition temperature (silver, mercury, platinum).

Some recently measured ignition temperatures are shown in Table V with data of Mellor (*27*). A single piece of the metal weighing about 10 grams was

Table V. Ignition Temperatures of Metals in Oxygen

Metal	M. P., ° C.	Ignition Temp., ° C. This work	Ignition Temp., ° C. Mellor
Li	179	190	180
Na	97.8	118	100[a]
K	63	69	70[a]
Rb	39	...	...
Cs	28	...	30[a]
Mg	650	625	540
Ca	850	550	300
Sr	771	720	...
Ba	720	175	...
B	2100	...	700[b]
Al	660	>1000	580
Ti	1730	...	610
Zr	1845	...	1400[a]
Th	1800	500	400[b]
Ta	2996	...	600
Cr	1900	...	2000
Mo	2620	750	500–600
Fe	1535	930	...
Zn	419	900	505[b]
Cd	321	760	...
Sn	232	865	2700[a,b]
Pb	327	870	...
Sb	630	650	1600[a,b]
Bi	271	775	1600[a,b]

[a] Estimated from remarks of Mellor.
[b] Ignition in air not oxygen.

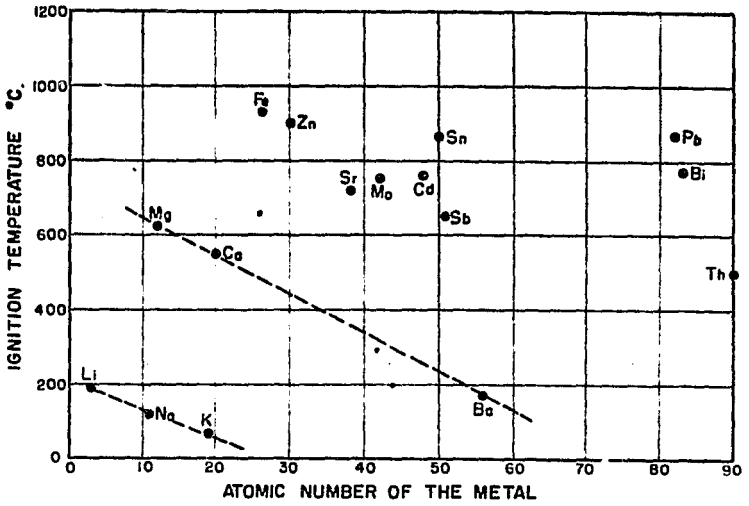

Figure 11. Ignition temperatures should be considered a characteristic property, as shown by the periodicity of the ignition temperatures at 1.0 atm. *vs.* atomic weight

Table VI. Classification of Metals According to Ignition Temperature

Metal	M. P., ° C.	Ignition Temp., ° C.	P. and B. Ratio
Class I, Ignition at or below Melting Point			
Mg	650	623	0.81
Th	1800	500	1.35
Ca	850	550	0.64
Fe	1535	930	2.10
Sr	771	720	0.61
Ba	720	175	0.67
Mo	2620	750	...
Class II, Ignition above Melting Point			
Al	660	1000	1.28
Zn	419	900	1.55
Sn	232	865	1.32
Pb	327	870	1.31
Bi	271	775	1.20
Sb	630	650	1.44
Cd	321	760	1.21
Li	179	190	0.58
Na	97.8	118	0.55
K	63	69	0.45

placed in an Alundum crucible contained in a Type FD 104 Hoskins electric furnace and heated to a predetermined temperature in an argon atmosphere (a Chromel-Alumel thermocouple inside the crucible next to the sample gave the temperature). When the temperature became uniform, a stream of oxygen was fed to the top of the crucible to sweep the argon away and expose the metal to oxygen (the velocity of the jet was very low). A sight-glass enabled visual observation of the sample to determine if ignition was obtained. If the sample did not ignite, a new specimen was used and the procedure repeated until ignition was obtained (accuracy no better than ±10° C.).

The metals studied are divided into two classes in Table VI and tabulated with their Pilling and Bedworth ratio (*28*). All Class II metals listed have melting points above 650° C., Class I metals have melting points below 660° C. It appears that the alkali metals belong to Class II, while the metals of the magnesium group belong to Class I. It might be reasoned that metals whose Pilling and Bedworth ratio is greater than 1.0 (indicating protective oxide film) should not ignite until after they melt and their mobility in the liquid states causes rupture of the oxide film. This reasoning is in accord with Table VI, where all the Class II metals indicate a ratio greater than 1.0 (improved experimental accuracy might relocate the alkali metals in Class I, although there is no reason why a metal with a nonprotective oxide should not melt before it ignites).

The ignition temperatures of the alkali metals decrease from lithium to potassium and a plot of ignition temperature *vs.* atomic number for this group is linear. A similar plot for the magnesium group is also linear, but strontium is much too high, suggesting that this value may be in error. The ignition temperature of strontium from the plot should be about 360° C. instead of 720° C. as given in Table V.

That ignition temperatures should be considered a characteristic property is supported by the periodicity shown in Figure 11. This variation is similar to that noted in similar plots of melting and boiling points and heats of formation.

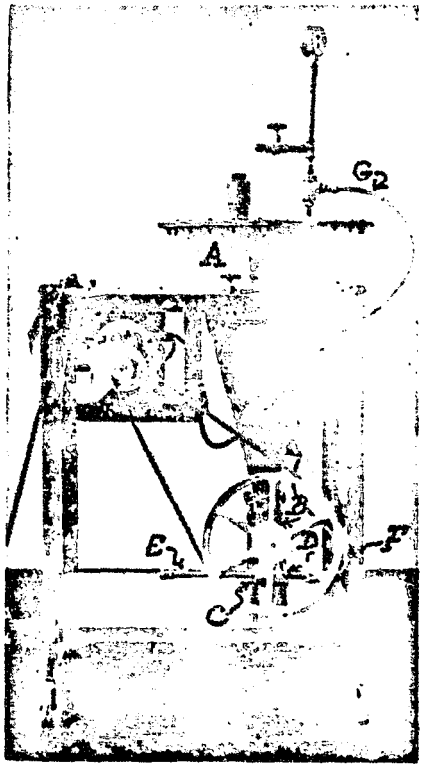

Figure 12. Early model of powdered metal feed device

Powdered-Metal Flames

Powdered metals dispersed in oxygen or air form explosive mixtures with ignition temperatures lower than those of the corresponding bulk metal. As might be expected, these mixtures have ignition temperatures, limits of flammability, and minimum energies for ignition just as do the explosive mixtures formed by the gaseous combustibles such as acetylene, propane, and hydrogen. Their flammability and explosibility have been reported in considerable detail (*19–27*), in an attempt to evaluate all factors affecting flame propagation.

The similarity between powdered metal–oxygen (or air) dispersions and combustible gas-oxygen (or air) mixtures

Table VII. Operating Data for Powdered-Metal Flames

Metal	Oxide Formed	Ignition Temp., ° C.	Min. Explosive Concn., Gram Metal/Liter Air	Stoichiometric Composition G. metal/ l. O_2	G. metal/ g. O_2
Al	Al_2O_3	645	0.025	1.6	1.12
Mg	MgO	520	0.020	2.14	1.5
Fe	FeO	315	0.105	5.0	3.5
	Fe_2O_3	...	0.105	3.33	2.3
Ti	TiO_2	480	0.045	2.14	1.5
	Ti_2O_3	...	0.045	2.87	2.0
Si	SiO_2	775	0.16	1.25	0.88
Mn	MnO	450	0.21	4.9	3.43
Zr	ZrO_2	Room temp.	0.04	4.1	2.87

END OF REFERENCE

150

REFERENCE

151

LAURENDEAU, N. M.; AND GLASSMAN, I.: IGNITION TEMPERATURES OF METALS IN OXYGEN ATMOSPHERES. COMB. SCI. TECH., VOL. 3, 1971.

THIS MATERIAL HAS BEEN APPROVED FOR PUBLICATION PER LETTER FROM EDMUND H. IMMERGUT (GORDON AND BREACH) TO JOANNE FOLK DATED SEPT. 18, 1974.

Combustion Science and Technology, 1971, Vol. 3, pp. 77–82

© Gordon and Breach, Science Publishers Ltd.
Printed in Belfast, N. Ireland

Ignition Temperatures of Metals in Oxygen Atmospheres

N. M. LAURENDEAU AND I. GLASSMAN

Guggenheim Laboratories, Princeton University, Princeton, New Jersey

Abstract—The ignition temperature of ten common non-toxic metals has been determined experimentally in an oxygen environment. In this investigation a induction furnace facility that emphasized the pre-ignition surface oxidation effects upon the ignition temperature was used. The bulk ignition temperatures of barium, bismuth, calcium, iron, lead, magnesium, molybdenum, strontium, tin, and zinc were found and compared to the previous results of Grosse and Conway. The differences in the results are attributed to how the heating cycle is carried out and how the cycle affects the surface oxide coat.

I. INTRODUCTION

In the past decade, the use of metals as a chemical fuel in rocket propulsion devices has stimulated new interest in the combustion and ignition of pure metal species. Investigation showed that in particular early quantitative modeling of ignition processes was applicable to a few limited cases (Mellor, 1967). A qualitative model of heterogeneous ignition, postulated by Mellor (1967), [see also Glassman *et al.* (1970)], has been used to explain much of the phenomena inherent to the ignition of nearly all metals. Unfortunately, neither a quantitative extension of this model, nor any other quantitative work, can be verified, due to the limited data available on the ignition temperature of various metals. The present investigation attempted to fill this need via an experimental determination of the bulk ignition temperature of ten common non-toxic metals in a pure oxygen atmosphere.

II. THEORETICAL BACKGROUND

The general model of heterogeneous metal ignition has been discussed at length by Mellor (1967) and modified to a degree by Laurendeau (1968). This work was reviewed by Glassman, *et al.* (1970). Only those qualitative concepts useful in the present investigation are repeated here.

As in other heterogeneous systems, metals are known to be capable of self-heating to ignition in an oxidizing atmosphere, under the proper circumstances. The model of Mellor (1967) showed that an unstable equilibrium *surface* temperature, characteristic of the self-heating potential of a particular metal particle, could be defined. This temperature is the so-called critical temperature, T_{crit}, which is defined as the lowest initial surface temperature from which the surface may self-heat to reach the steady-state combustion configuration. T_{crit} is commonly called the spontaneous ignition temperature in the literature, but here is labeled the critical temperature in order to avoid confusion with the experimental ignition temperature. The ignition temperature, T_{ign}, is experimentally defined to be that temperature at which there occurs the most rapid rate of change with time of both light intensity and sample temperature, i.e., the flame appears. This distinction between the critical temperature and the ignition temperature is made to allow for the possibility of the existence of a self-heating or ignition delay time.

Metal ignition is inherently more complicated than the heterogeneous ignition of other simple fuel-oxidizer systems due to the formation of solid phase products on the surface during the pre-ignition process. Isothermal oxidation experiments have shown that, in general, the metal oxide film is protective at lower temperatures, and non-protective at higher temperatures. This phenomenon usually is explained by assuming that the oxide film has either become porous or has cracked and hence offers no protection at higher temperatures to further oxidation of the surface by the surrounding oxidizing environment. The temperature at which the oxide surface becomes non-protective is called the transition temperature, T_{trans}. Below this temperature, simple low temperature metal oxidation occurs.

Usually, the non-protective nature of the oxide film is characterized by an isothermal surface reaction rate independent of both time and, hence, the amount of metal previously consumed in the reaction. Thus, T_{trans} can also be defined as the

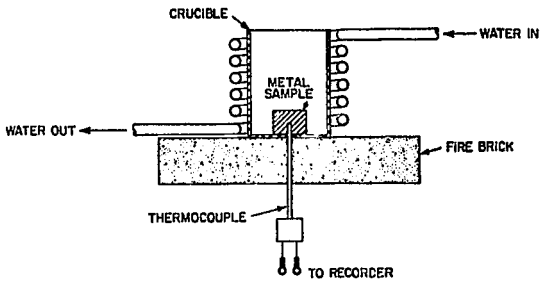

FIG. 2. Schematic of experimental configuration for induction heating.

of S/V coincides with the middle of the bulk range as determined by Mellor (1967). Table I lists alphabetically all ten metals used in the present investigation, along with their purity, average geometrical dimensions, and average surface to volume ratio (S/V).

Before all tests, most metal samples were washed in hexane and allowed to dry and degas in a room temperature environment for 24 hrs. The three metals, barium, calcium, and strontium, which oxidize quickly at room temperatures, were stored and machined under mineral oil. In early experiments, they were washed in hexane for one hour at room temperature and then degassed in a vacuum desiccator for at least 24 hrs. In later experiments, each sample was put into a vapor degreaser using liquid freon for approximately three minutes just prior to the experimental run.

TABLE I

Simple Dimensions of Experimental Metals

Metal	Purity (%)	Diameter (cm)	Length (cm)	S/V (mm $^{-1}$)
Ba	99.99	2.14	1.83	0.239
Bi	99.999	1.23	2.57	0.365
Ca	99.5	2.37	1.0	0.365
Fe	99.9	2.52	1.0	0.264
Pb	99.999	1.27	2.60	0.357
Mg	99.96	2.38	1.0	0.285
Mo	99.95	1.59	2.06	0.306
Sr	99.0	1.64	1.75	0.309
Sn	99.999	1.24	2.58	0.366
Zn	99.9	1.90	1.71	0.277

IV. RESULTS AND DISCUSSION

Table II lists the ignition temperatures to the nearest 5 degrees of the metals investigated. Considering the unknown effects of certain environmental factors, a scatter of ±25 is considered satisfactory.

A. *The effect of ambient pressure*

The present investigation was not expected to demonstrate a large variation in ignition temperature with pressure since the pressure range studied was restricted experimentally to one order of magnitude. An exception was zinc whose ignition temperature varied with pressure due to the effect of the boiling point (Glassman, *et al.* (1970), Laurendeau (1968)). Large variations in T_{ign} may certainly occur over a large pressure range, however. For example, titanium is reported to have a T_{ign} of 1300–1600 °C in the 15–200 psia range, and a T_{ign} of 850–1300 °C in the 200–700 psiz range.

TABLE II

Metal Bulk Ignition Temperatures

Metal	Pressure	Ignition temperatures (C)	Average ign. temp (°C)
Ba	300 torr	550, 560, 620, 630,	590 ± 45
	1 atm	480, 510, 570, 650	550 ± 90
	5 atm	535, 540, 600	560 ± 30
Bi	300 torr	780, 805, 810, 825	805 ± 25
	1 atm	715, 735, 750, 750	735 ± 20
	5 atm	715, 735, 760	735 ± 25
Ca	300 torr	790, 795, 800, 800	795 ± 5
	1 atm	785, 785, 805	790 ± 10
	5 atm	760, 775, 805	780 ± 20
Fe	300 torr	1310, 1320, 1330	1320 ± 10
	1 atm	1300, 1310, 1340	1315 ± 20
	5 atm	1285, 1300, 1315	1300 ± 15
Pb	300 torr	845, 850, 860	850 ± 5
	1 atm	845, 855, 860	850 ± 5
	5 atm	810, 830, 840	825 ± 15
Mg	300 torr	630, 635, 635	635 + 5
	1 atm	630, 640, 640	635 ± 5
	5 atm	620, 620, 620	620
Mo	300 torr	795, 795, 810, 810	800 ± 10
	1 atm	780, 785, 785	780 ± 5
	5 atm	740, 765, 765, 785	765 ± 25
Sr	300 torr	985, 1015, 1160	1055 ± 85
	1 atm	935, 1115, 1175	1075 ± 120
	5 atm	1125, 1150, 1165	1150 ± 20
Sn	300 torr	975, 1005, 1015	1000 ± 20
	1 atm	910, 945, 965	940 ± 25
	5 atm	910, 955, 990, 1000	965 ± 45
Zn	300 torr	815, 835, 840, 880	840 ± 30
	1 atm	895, 905, 920	905 ± 15
	5 atm	1090, 1140, 1150, 1165	1135 ± 35

As for titanium, most metals are expected to show a decrease in ignition temperature as oxidizer pressure is increased, since the surface reaction rate would be expected to increase. In the present study, this trend is observed only in certain metals. A T_{trans} controlled metal (zinc), which always exhibits a protective oxide coating, or any metal producing an extremely thick oxide coat (strontium), may not be influenced by oxidizer pressure, or may have the opposite behavior. Although the present data are not conclusive, to a degree they do support the hypothesis that critical temperature controlled metals have ignition temperatures that generally decrease with increasing pressure. (Laurendeau (1970) discusses the support given by Mellor's model to these conclusions.) Thus, one may conclude here that the variation of the ignition temperature with pressure may be the result of whether a particular metal is critical or transition temperature controlled.

B. *Effect of heating technique*

The bulk ignition data obtained would appear to be consistent with what one suspects in comparison with other data when the procedures for obtaining the data are evaluated in the context of the simple model described earlier. Table III lists the present results and other results. Except for the work at the Temple Research Institute very little other data are available. The Temple results were obtained by using a resistance furnace at an ambient gas temperature of one atmosphere. The results were reputed to be reproducible to within ±5 °C. However, the metals in this case were heated in an inert gas atmosphere to a specific temperatures, and then exposed to a flowing oxygen stream. Thus, the oxide buildup is a minimum, if any, and the ignition temperature more closely corresponds to the critical temperature.

In the present experiments and in the others reported in Table III, there is slow heating in an oxygen atmosphere and there can be a buildup of an oxide layer. It is in the understanding of the character of this oxide layer that one can explain the differences between the data in Table 3. As a convenience for the explanation to follow, specific data about the metals used are accumulated in Table IV.

TABLE III

Comparison of Bulk Ignition Temperatures[a]

Metal	Present results (T C)	Temple Research Institute results[b]	Other results
Ba	550 ± 90	175	
Bi	735 ± 20	775	
Ca	790 ± 10	550	805[c], 704–743[d]
Fe	1315 ± 20	930	
Pb	850 ± 5	870	
Mg	635 ± 5	623	640[c], 623–630[e]
Mo	780 ± 5	750	
Sr	1075 ± 120	720	
Sn	940 ± 25	865	
Zn	905 ± 15	900	

[a] 1 atm pressure, all temperature in C.
[b] Conway and Kirschenbaum (1954), Grosse and Conway (1958).
[c] Mellor (1967).
[d] Reynolds (1959).
[e] Fassell *et al.* (1951).

TABLE IV

Fundamental Temperatures of Interest for Metals*

Metal	Metal oxide (T °C)	Metal melting point (T C)	Metal oxide melting point (T °C)	Metal boiling point (T C)	Metal boiling point (T C)	Transition temperature (T °C)
Ba	BaO	710	1923	1527	2000	17
Bi	Bi_2O_3	271	860	1470	1890	—
Ca	CaO	848	2580	1240	2850	400
Fe	FeO	1536	1420	2872	—	1200
Pb	PbO	328	897	1753	1516	550
Mg	MgO	650	2800	1105	3600	450
Mo	MoO_3	2620	795	4507	1155	700
Sr	SrO	774	2430	1366	3000	—
Sn	SnO_2	232	1127	2260	1850	475
Zn	ZnO	419	1975	907	—	700

* Taken and extrapolated from Mellor (1967), JANAF (1965), Kubaschewski and Hopkins (1951), Hodgman (1964), Kage and Laby (1966), Kofstad (1966), and Hauffe (1965).
Boiling points are for 760 torr.

Consider first those metals for which the ignition temperatures from the two primary investigations reported in Table III are, within experimental error, the same. These include bismuth, lead, magnesium, molybdenum, and zinc. Zinc is easily explained through its dependence on total pressure via the metal boiling point. The other materials have a very thin oxide coat that is non-protective at lower temperatures due to a combination of low metal melting point, low T_{trans}, and low oxide melting points, which limit the protective qualities of the oxide shell (see Table IV).

Now, the fact that a particular metal has a thin porous oxide coat explains why the ignition temperature for such metals are in excellent agreement. This type of oxide layer does not prevent the natural diffusion of oxygen to the surface of the parent metal. Thus, no matter whether heating is accomplished in an inert or oxidizing atmosphere, the oxide coat cannot have any influence on the results. This observation, along with the nearness of the melting point of the oxide to the measured ignition temperature in some cases, accounts for the good agreement between the present work and Temple work for bismuth, lead, magnesium, and molybdenum. Indeed, other results obtained by heating in an oxygen atmosphere with a resistance furnace (Fassell, *et al.* (1951)) indicate that magnesium has an ignition temperature that is very reproducible under varying environmental conditions.

Consider now those metals for which the ignition temperatures listed in Table III are different. These include the alkaline earth metals, barium, calcium, strontium, and iron and tin. All of these metals, when heated in an oxidizing environment, either develop a highly protective oxide coat (iron) under the conditions of the experiment, or their oxide layers are so thick that they hinder the ignition process by allowing only a small fraction of the needed oxygen to the metal substrate, and thus delay the actual ignition of the metal (tin, strontium, especially). In addition, the above metals, excluding iron, undergo a large amount of self-heating when suddenly exposed to an oxygen atmosphere. This characteristic alone could easily account for the disagreement in the two investigations, especially for barium and calcium. Based on these observations, any differences in the ignition temperatures between the two sets of data may perhaps be attributed solely to whether an inert or oxidizing atmosphere was used in the metal heating cycle of the ignition process.

The oxidizing environment in the present investigation leads to higher ignition temperatures for the five metals discussed above (see Table III). Tin and strontium have thick oxides which hinder ignition and cause large variations in the measured ignition temperature. The oxide layer in the strontium runs is so thick, that it supports molten strontium, as would a crucible. Barium and calcium undergo an extraordinary amount of self-heating. Hence, the Temple measurements must be very near the critical temperature for these metals. Barium is particularly susceptible to the instabilities of the critical temperature, and thus gives rise to large variations in the measured ignition temperature.

The results for calcium are quite reproducible because of the consistency of its oxide layer in different experimental runs. The present results compare well with the data of Mellor (1967) who found an average ignition temperature at 1 atm. of 805 °C. Reynolds' results (1959) in a flowing stream of *air* also give comparable ignition temperatures over 700 °C. His data, although lower due to the removal of the room temperature oxide scale, are significant, for they indicate a higher ignition temperature for calcium when heated in an oxidizing atmosphere in a completely different type of ignition environment.

The above results, especially for calcium, indicate that a consistent bulk ignition temperature can be defined for most metals, independent of the method of heating, but dependent on ambient pressure and the type of oxidizing environment.

C. *The relation between ignition and combustion*

Visual observations of the ignition and subsequent combustion of the above metals generally substantiated Glassman's criterion (Glassman, 1959, 1960). If the boiling point of the metal oxide is greater than that of the parent metal, then combustion occurs on the metal surface. Barium, calcium, magnesium, strontium, and zinc all burned in the vapor phase, while the rest burned on the surface. Bismuth (see Table IV) proved the only exception to the above combustion criterion, but its initial burning appeared to be in the vapor phase with subsequent degradation to the surface.

There appears to be little correlation between the type of combustion (surface or vapor-phase) and whether a particular metal is critical or transition temperature controlled. Other visual observations are discussed in detail by Laurendeau (1968).

END OF REFERENCE

151

REFERENCE

152

MELLOR, A. M.: HETEROGENEOUS IGNITION OF METALS: MODEL AND EXPERIMENT. PH.D. THESIS, PRINCETON UNIVERSITY. (NASA CR-93541), 1967.

MAY 4 '70 3.1-0-0 D.F.

N69-36133

HETEROGENEOUS IGNITION OF METALS: MODEL AND EXPERIMENTS

A. M. Mellor, 1967

Published on demand by
UNIVERSITY MICROFILMS
University Microfilms Limited, High Wycomb, England
A Xerox Company, Ann Arbor, Michigan, U.S.A.

COPY 1 LIBRARY COPY
JUL 1 1970
LEWIS RESEARCH CENTER, NASA
CLEVELAND, OHIO

HETEROGENEOUS IGNITION OF METALS:

MODEL AND EXPERIMENT

by

Arthur McLeod Mellor

Submitted By: Arthur M. Mellor
Arthur M. Mellor

Approved By: Irvin Glassman
Irvin Glassman
Professor of Aerospace Sciences

A dissertation submitted to the Department of Aerospace and Mechanical Sciences of Princeton University in partial fulfillment of requirements for the degree of Doctor of Philosophy.

Guggenheim Laboratories for the Aerospace Propulsion Sciences
Department of Aerospace and Mechanical Sciences
PRINCETON UNIVERSITY
Princeton, New Jersey

1967

protective oxidation rates are observed at low temperatures in the Zr-air reaction (see Table 8).

8. Titanium

a. Critical Temperatures

Hill et al. (213) measured spontaneous ignition temperatures for Ti in O_2 and in air. For bulk Ti samples of S/V = 2.56 mm^{-1}, the values are 1150°C in 33.3 atm of O_2 and 1592°C in 1 atm of air. Unfortunately, no ignition delay times are given.

The transition temperature of the Ti-O_2 system has only been estimated within the pressure range 10^{-3} through 760 torr, and was taken as 900°C. Subject to this large pressure difference and noting that a spontaneous ignition rather than critical temperature was reported by Hill et al. (213), it may be concluded that the critical temperature also controls in the ignition of bulk Ti in O_2.

b. Ignition Temperatures

Littman et al. (241) studied the ignition of Ti bars broken in tension in O_2; as has been mentioned previously, this experiment falls outside the scope of the present report.

Literature ignition temperatures are shown in Table 21 and Fig. 15. Few conclusions can be drawn for Ti in the various gases, as a transition temperature is available only in O_2. Some of the expected trends with respect to sample size and with respect to type of experiment are seen in the table and figure.

TABLE 21.

LITERATURE IGNITION TEMPERATURES FOR TITANIUM

Reference	Stated Size	Gas Pressure	Sample Condition	Ignition Temperature, °C
Oxygen				
(194)	2.25-7.88 mm^{-1}	3.3 atm	B	1315
		20 atm		815
Nitrogen				
(203)	<44 μ	1 atm?	QP	700
	<74 μ	1 atm?	QP	900
(228)	445 mm^{-1}	1 atm?	QP	760
(210)	1200-6000 mm^{-1}	flowing	QP	830
Air				
(205)	---	1 atm?	DD	480
(209)	1-5 μ	1 atm	QP	625
(206)	<40 μ	1 atm?	DD	401
(203)	<44 μ	1 atm?	QP	475
(206)	40-53 μ	1 atm?	DD	425
	<66 μ	1 atm?	DD	412
(203)	<74 μ	1 atm?	QP	460
(204)	<149 μ	1 atm?	DD	480
			QP	460
Carbon Dioxide				
(203)	<44 μ	1 atm?	QP	685
	<74 μ	1 atm?	QP	680
(204)	<149 μ	1 atm?	QP	680
(210)	1200-6000 mm^{-1}	flowing	QP	670
(228)	445 mm^{-1}	1 atm?	QP	550
(194)	2.25-7.88 mm^{-1}	20 atm	B	1520

Note that the results of Hill et al. (213) and of Dean and Thompson (194) on the ignition of bulk Ti in O_2 are in disagreement: according to these investigators, a spontaneous ignition temperature at 33.3 atm is 1150°C (213), and the ignition temperature at 20 atm is 815°C and at 3.3 atm is 1315°C (194), that is, an inconsistent pressure trend is reported. Perhaps a pressure dependence of the transition temperature has come into play here.

A final item is that Riehl and co-workers (242) could not ignite bulk Ti at a temperature less than 1200°C in a H_2/air flame at a pressure of about 1.67 atm.

9. Tantalum

a. Critical Temperatures

In oxidation experiments with bulk Ta (S/V = 0.845 mm^{-1}) in 1 atm of O_2, Albrecht et al. (157) reported an ignition delay time of 15 min at 1250°C. Ignition was instantaneous at 1300°C. Since the transition temperature is much below these values (500°C), it is concluded that the ignition of Ta in O_2 is controlled by the critical temperature.

b. Ignition Temperatures

Reported ignition temperatures for Ta in O_2 and air are shown in Table 22. Cowgill and Stringer (159,243) listed a value of 1000°C in O_2 for a slightly smaller sample than that used in Ref. (157). Since these authors noted that the sample burst into flame

TABLE 22.

LITERATURE IGNITION TEMPERATURES FOR TANTALUM

Reference	Stated Size	Gas Pressure	Sample Condition	Ignition Temperature, °C
Oxygen				
(159), (243)	4.2 mm^{-1}	---	B	1000
(157)	0.845 mm^{-1}	1 atm	B	1300
Air				
(203)	<44 μ	1 atm?	DD	630
			QP	300
(220)	4.32 mm^{-1}	1-7 atm	B	1238-1282[1]

[1] Brightness temperature.

when O_2 was admitted at 1000°C, this value may actually be a critical temperature as a result of sample self-heating during the transient filling period.

The bulk air results (220) are consistent with the air transition temperature of 800°C; lower ignition temperatures observed in DD and QP experiments are most likely a result of sample self-heating, as was the case for similar experiments with Zr and Ti.

Evidently in this experimental environment the critical temperature of Mo is extremely high (perhaps due to large heat losses from the samples), and interferred with the oxidation experiments.

b. Ignition Temperatures

In Table 23 literature ignition temperatures for Mo in O_2 and air are listed. Excellent agreement is seen between the O_2 transition temperature of 725°C and the bulk ignition temperatures.

In air, the DD result is above the air transition temperature (595°C), but the QP datum is below this value, probably due to the low critical temperature associated with QP experiments.

TABLE 23.

LITERATURE IGNITION TEMPERATURES FOR MOLYBDENUM

Reference	Stated Size	Gas Pressure	Sample Condition	Ignition Temperature, °C
Oxygen				
(177)	2.33 mm^{-1}	1 atm	B	750
(196), (200)	≈10 g	1 atm	B	750
(36)	---	6.7 atm	B	725
Air				
(203)	< 74 μ	1 atm?	DD	720
			QP	360

On the basis of the ignition temperature data, no further conclusion may be drawn as to which of the transition and critical temperatures controls the bulk ignition of Mo.

11. Silicon

No indications of Si self-heating or spontaneous ignition are present in the literature. Furthermore, very few ignition data are available for Si (Table 24). As transition temperatures have been estimated only for the Si-O_2 and Si-H_2O systems, no conclusion can be drawn from the data listed in Table 24.

TABLE 24.

LITERATURE IGNITION TEMPERATURES FOR SILICON

Reference	Stated Size	Gas Pressure	Sample Condition	Ignition Temperature, °C
Nitrogen				
(203)	<53 μ	1 atm?	QP	1000
(204)	<149 μ	1 atm?	QP	1000
Air				
(203)	<53 μ	1 atm?	QP	950
	<74 μ	1 atm?	QP	790
(204)	<149 μ	1 atm?	QP	950
			DD	775
Carbon Dioxide				
(203)	<53 μ	1 atm?	QP	1000
(204)	<149 μ	1 atm?	QP	1000

END OF REFERENCE

152

REFERENCE

153

HILL, P. R.; ADAMSON, D.; FOLAND, D. H.; AND BRESSETTE, W. E.: HIGH TEMPERATURE OXIDATION AND IGNITION OF METALS. NACA RM L55L23B, 1956.

APR 2 56

[redacted]

NACA RM L55L23b

COPY 1

NACA

REF. (3)

RESEARCH MEMORANDUM

HIGH-TEMPERATURE OXIDATION AND IGNITION OF METALS

By Paul R. Hill, David Adamson, Douglas H. Foland,
and Walter E. Bressette

Langley Aeronautical Laboratory
Langley Field, Va.

LIBRARY COPY

MAR 28 1956

LEWIS LIBRARY, NACA
CLEVELAND, OHIO

DECL. RA
OCT 3 1957

CLASSIFIED DOCUMENT

This material contains information affecting the National Defense of the United States within the meaning of the espionage laws, Title 18, U.S.C., Secs. 793 and 794, the transmission or revelation of which in any manner to an unauthorized person is prohibited by law.

NATIONAL ADVISORY COMMITTEE
FOR AERONAUTICS

WASHINGTON
March 26, 1956

[redacted]

NATIONAL ADVISORY COMMITTEE FOR AERONAUTICS

RESEARCH MEMORANDUM

HIGH-TEMPERATURE OXIDATION AND IGNITION OF METALS

By Paul R. Hill, David Adamson, Douglas H. Foland,
and Walter E. Bressette

SUMMARY

A study of the high-temperature oxidation of several aircraft construction materials was undertaken to assess the possibility of ignition under high-temperature flight conditions. Tests have been made both in open and closed jets, and, in addition, the burning of metals has been observed under static conditions in a pressurized vessel containing either air, oxygen, or nitrogen. When heated in an atmosphere of oxygen or when heated and plunged into a supersonic airstream, titanium, iron, carbon steel, and common alloys such as 4130 were found to have spontaneous-ignition temperatures in the solid phase (below melting) and they melted rapidly while burning. Inconel, copper, 18-8 stainless steel, Monel, and aluminum could not be made to ignite spontaneously at temperatures up to melting with the equipment available. Magnesium ignited spontaneously in either type of test at temperatures just above the melting temperature.

A theory for the spontaneous ignition of metals, based on the first law of thermodynamics, is presented. Good correlation was obtained between calculated spontaneous-ignition temperatures and values measured in supersonic jet tests.

There appears at the present time to be no need for concern regarding the spontaneous ignition of Inconel, the stainless steels, copper, aluminum, or magnesium for ordinary supersonic airplane or missile applications where the material temperature is kept within ordinary structural limits or at least below melting. For hypersonic applications where the material is to be melted away to absorb the heat of convection, the results of the present tests do not apply sufficiently to allow a conclusion.

INTRODUCTION

In the engineering of missiles or other aircraft to fly at extremely high speeds it has been customary to choose materials that retain strength at design temperature. More recently, designers who have been concerned with aircraft under transient thermal conditions have planned to use the skin as a heat sink and, in some extreme cases, to use the heat of fusion, or melting, as a possible means of absorbing the aerodynamic heating.

$$Q_O = Q_{CONV} + Q_{RAD}$$

$$\frac{134500}{\delta} e^{-\frac{42170}{T}} = 1.32 \frac{k}{d} R^{.5} N_{PR}^{.4} (T_{AW} - T) + 0.000048\epsilon \left(\frac{T}{100}\right)^4 \quad (2)$$

Conduction is omitted because the rods were quite uniformly heated. The first term represents oxidation and is taken from equation (1). The second term is Sibulkin's theory for the heat transfer on a hemispherical nose, which, in this case, had a diameter of 3/8 inch. The last term is the usual expression for radiation. The value of emissivity was taken as 0.88. The unknown quantity T, the surface temperature for equilibrium conditions, appears in each term. The solutions of this equation for oxide thicknesses of 0.0001 and 0.001 are plotted in figure 4. The theory shows a slight rise in spontaneous-ignition temperature with airspeed because the convection represents a loss. The measured spontaneous-ignition temperatures also show a slight rise with speed at the higher speed range. At 150 ft/sec, no ignition was obtained although the specimens were heated to near melting. Insufficient oxygen, together with nitrogen enrichment of the boundary layer, seems to be the most probable cause of the failure to ignite at low airspeed, although reduced erosion may possibly affect the result.

Some nonferrous materials such as Inconel and copper were tested to temperatures approaching melting in a supersonic blowdown jet with a stagnation temperature of 600° F, without obtaining ignition. The same results were obtained from the simple heated-wire tests in an atmosphere of oxygen. Figure 5 shows temperature-time histories for wires of several materials tested in oxygen at 500 lb/sq in. abs. Although the Inconel and copper were heated until they melted, no ignition was obtained. The rate of oxidation of these materials was too small to be measured by the techniques used. The break in the titanium curve is not associated with oxidation but is believed to result from the heat absorption by the alotropic transformation. When the electric power was cut off at 2,100° F the titanium spontaneously ignited and burned vigorously. Titanium was also found to burn vigorously in an atmosphere of pure nitrogen as well as in an atmosphere of air. The spontaneous ignition temperature in air at a pressure of 1 atmosphere was 2,900° F. Magnesium was observed to ignite when it melted, possibly because some of the protective oxide coating was floated off.

CONCLUSIONS

Tests of low-carbon steel and several other materials heated artificially in wind tunnels, in air jets, and under static conditions in atmospheres of air, oxygen, and nitrogen indicate the following:

END OF REFERENCE

153

REFERENCE

154

DEAN, L. E.; AND THOMPSON, W. R.: IGNITION CHARACTERISTICS OF METALS AND ALLOYS. ARS J., VOL. 31, NO. 7, JUL. 1961.

9 Cohen, C. B. and Reshotko, E., "The Compressible Laminar Boundary Layer with Heat Transfer and Arbitrary Pressure Gradient," NACA Rep. 1294, 1956.
10 Gazley, Jr., C., "Theoretical Evaluation of the Turbulent Skin Friction and Heat Transfer on a Cone in Supersonic Flight," General Electric Co. Rep. R49A0524, 1949.
11 Schlichtling, H., *Boundary Layer Theory*, McGraw-Hill Book Co., N. Y., 1955, Ch XXIIc.
12 Welsh, Jr., W. E. and Witte, A. B., "A Comparison of Analytical and Experimental Local Heat Fluxes in Liquid-Propellant Rocket Thrust Chambers," Jet Propulsion Laboratory TR 32-43, California Institute of Technology, Feb. 1 1961.

Ignition Characteristics of Metals and Alloys

L. E. DEAN[1] and W. R. THOMPSON[2]

Aerojet-General Corp. Sacramento, Calif.

The ignition characteristics of engine structural metals and alloys as influenced by the composition and pressure of the ambient atmosphere are of immediate interest to propulsion design engineers. Tubular test sections of the stainless steel, cobalt and nickel alloys, besides aluminum, copper and titanium were resistance heated in controlled atmospheres of oxygen, carbon dioxide and an equal mixture of these gases. Tube and gas temperatures obtained were correlated with color motion picture coverage of the manner in which the tube heated and failed. Stainless steels and cobalt alloys ignited within the melting point range of each material. Nickel alloys did not ignite until the melting point was reached. The rate of combustion increased with oxygen content. Stainless steels with a high nickel content appear most suited for applications at high temperatures in an oxidizing atmosphere.

THE ADVENT of nuclear energy and rocket propulsion has focused attention on the need for a more complete understanding of the mechanisms involved in the high temperature oxidation and ignition of metals in comparatively short time periods. The factors of metal composition and fabrication history, metal temperature and the composition, pressure and superficial velocity of the ambient atmosphere must be considered in any systematic evaluation of such ignition processes. In selecting materials to resist rapid oxidation, however, due emphasis must be given to other necessary metal prerequisites, including high thermal conductivity and tensile strength, low density, high melting point, ease of fabrication, and availability at reasonable cost.

Oxidation Mechanisms

Most metals and alloys, when exposed to an oxidizing atmosphere, undergo a chemical reaction with the oxidizing component of the gas phase, forming an oxide film or scale on the surface of the metal. The physical and chemical reactions controlling oxidation (e.g., the rate at which the oxide forms and the nature of its bond to the metal surface) are complex functions of a number of variables. These include not only the chemical composition and physical state of the metal surface, and the geometry of the metal object, but also environmental factors (i.e., the chemical composition and fluid-dynamical characteristics of the gaseous environment and the pressure and temperature of the entire system).

Those metals that form a nonporous oxide film which adheres tightly to the base metal are immune to further oxidation. Ignition of the metal will not normally occur unless this protective film is broken. Nickel and aluminum have this desirable characteristic. However, if the oxide film is porous, or does not adhere to the base metal, oxidation will occur. This results in destruction of the metal through complete conversion to the oxide form. Ignition occurs more readily for metals forming such films. Mild steel, molybdenum and titanium have these characteristics. For most common metals, under ambient atmospheric conditions, such oxidation rates are comparatively slow.

Oxidation is an exothermic reaction. For slow rates of oxidation (e.g., the rusting of steel) the heat of reaction at the surface of the metal is dissipated principally by conduction to the bulk of the metal and by convection to the atmosphere. The metal temperature thus remains essentially at the ambient level. If, however the rate of oxidation is so rapid that

Presented at the ARS 15th Annual Meeting, Washington, D. C., Dec. 5-8, 1960.
[1] Head, Physical Research Section, Research and Material Dept., Liquid Rocket Plant. Member ARS.
[2] Senior Engineer, Advanced Research Div., Azusa, Calif. Member ARS.
[3] Numbers in parentheses indicate References at end of paper.

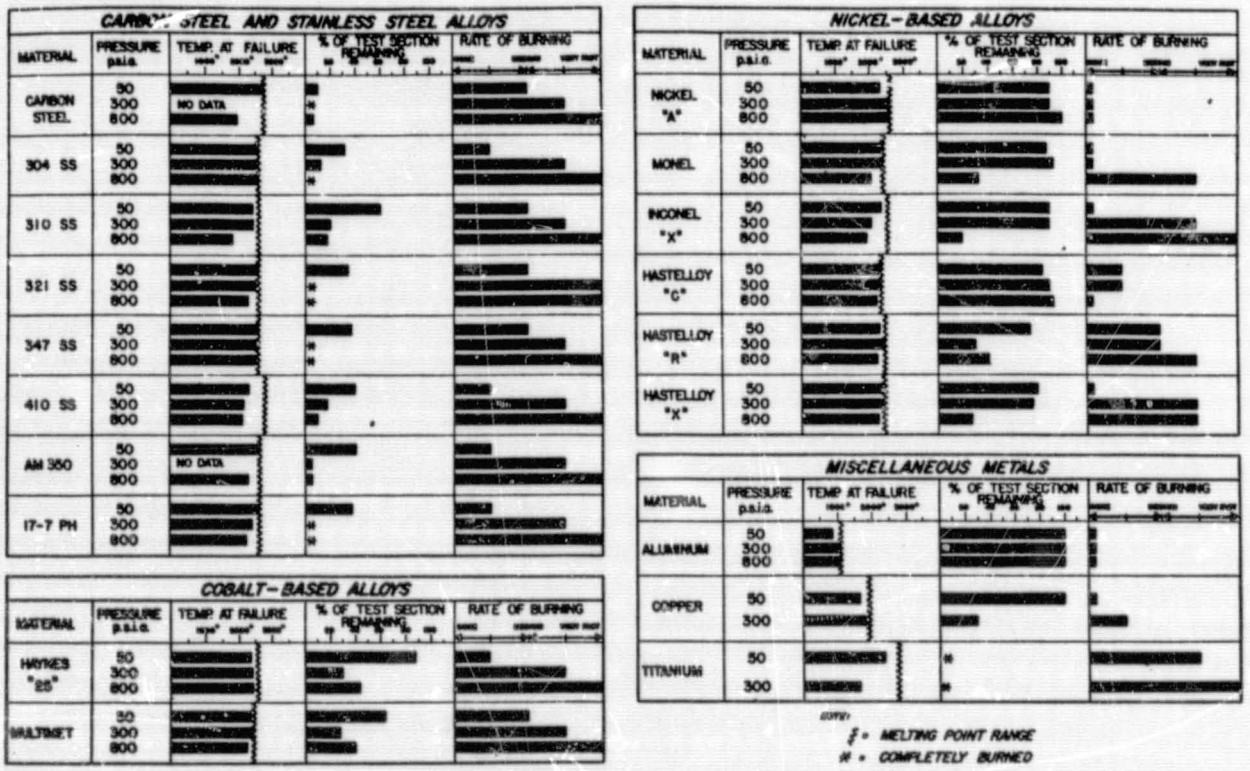

Fig. 9 Test summary in oxygen atmosphere

may ignite. These results indicate that ignition of titanium is also dependent upon the condition of the oxide film and consequently upon the particular testing technique employed. Of all the metals tested, titanium proved to be the most reactive metal at elevated temperatures regardless of the composition of the atmosphere.

Conclusions

The results of this investigation are graphically summarized in Fig. 8, in which the effect of gas composition at a constant pressure is shown, and in Fig. 9, in which the effect of pressure upon tubes in an oxygen atmosphere is noted. The following general conclusions are indicated.

The ignition of stainless steels (containing nickel) occurred within the melting point ranges of the alloys during tests in an oxygen atmosphere. Steel alloys, with no nickel content ignited at temperatures below their melting points. The rates of burning and destruction of the test sections increased with increasing oxygen concentrations.

Most of the nickel based alloys did not ignite until the melting point was reached. Nickel A did not ignite in oxygen, and, whereas ignition was noted for the other alloys at elevated pressures, the rate of burning of Nickel A was generally less severe than that observed for the ferrous based alloys.

Cobalt based alloys ignited at temperatures within their melting point range. The rates of burning were similar to those of the iron based alloys; however, the resulting damage to the test sections was less severe.

Ignition did not occur with the aluminum alloy studied. A copper test section ignited when tested in oxygen at the 300 psia pressure level. Titanium was the most reactive of all the metals tested, and was the only metal which ignited in an atmosphere of carbon dioxide.

From these test results it is concluded that stainless steels with a high nickel content are the most suitable material for the manufacture of such items as rocket engine combustion chambers. This metal is especially adaptable where high temperature environment plus resistance to oxidation reactions are major controlling factors.

References

1 Fassell, W. M., Gulbransen, L. B., Lewis, J. R. and Hamilton, J. F., "Ignition Temperatures of Magnesium and Magnesium Alloys," *J. Metals*, vol. 3, March 1940, pp. 522–528.

2 Grosse, A. V. and Conway, J. B., "Combustion of Metals in Oxygen," *Ind. and Eng. Chem.*, vol 50, April 1958, pp. 663–672.

3 Mellor, J. W., *Treatise on Inorganic and Theoretical Chemistry*, Longmans, Green and Co., N. Y., 1946.

4 Reynolds, W. C., "Investigation of Ignition Temperatures of Solid Metals," NASA Tech. Note TN D-182, Oct. 1959.

5 Hill, P. R., Adamson, D., Fuland, D. H. and Bressette, W. E., "High-Temperature Oxidation and Ignition of Metals," NACA Rep. L55I23b, Research Mem. RM, March 1956.

6 "The Reaction of Metal in Oxidizing Gases at High Temperatures," Aerojet-General Rep. AGC-IDO-28000, Azusa, Calif., April 30, 1957.

7 Harrison, P. L., "The Combustion of Titanium and Zirconium," *Seventh Symposium (International) on Combustion*, Butterworths Scientific Publications, London, Eng.

8 Sidgwick, N. V., *The Chemical Elements and Their Compounds*, Oxford University Press, N. Y., 1950.

9 Moeller, T., *Inorganic Chemistry*, John Wiley and Sons, N. Y., 1952.

END OF REFERENCE

154

REFERENCE

155

NONMETALLIC MATERIALS DESIGN GUIDELINES AND TEST DATA HANDBOOK. NASA TM X-67639, 1970. (AVAILABLE FROM DDC AS AD-889181L.)

THIS REFERENCE HAS A LIMITED DISTRIBUTION AND MAY NOT BE REPRODUCED.

END OF REFERENCE

155

REFERENCE
156

GUTER, M.: IGNITION IN HIGH PRESSURE OXYGEN.
S&T MEMO 13/50, BRITISH MINISTRY OF AVIATION, 1967.

S & T MEMO 13/50

LEWIS RESEARCH CENTER
Aerospace Safety Research
and Data Institute
OCT 1[illegible] 1972
CLEVELAND, OHIO

N71-00073

IGNITION IN HIGH PRESSURE OXYGEN

by

M. GUTER

GPO PRICE $ _____

CFSTI PRICE(S) $ _____

Hard copy (HC) 3.00

Microfiche (MF) .65

ff 653 July 65

REPORT OF WORK CARRIED OUT BY THE
BRITISH OXYGEN CO. LTD. UNDER
MINISTRY OF SUPPLY CONTRACT

FACILITY FORM 602

N67-27788 _____
(ACCESSION NUMBER) (THRU)

56 3
(PAGES) (CODE)

_____ 33
(NASA CR OR TMX OR AD NUMBER) (CATEGORY)

FIRST ISSUED IN JUNE, 1950
BY TPA 3, MINISTRY OF SUPPLY

RE-ISSUED FEBRUARY, 1967
BY
TECHNICAL INFORMATION AND LIBRARY SERVICES

MINISTRY OF AVIATION

U.D.C. No. 536.46 : 541.126 : 661.937

R. & D. Report No. 1312

Copy No.

THE BRITISH OXYGEN COMPANY LIMITED

RESEARCH AND DEVELOPMENT DEPARTMENT

REPORT

TITLE

IGNITION IN HIGH PRESSURE OXYGEN

Author: M. Guter

Date: 1st June, 1950

Issued by: A.M. Clark

Approved by: P.H. Sykes

1(b)3. - Silicone Greases.

Three Silicone greases were examined in oxygen at pressures up to 250 atmospheres. The ignition temperatures are given in Table 8 and show that the ignition temperatures obtained at any given pressure in a flow of oxygen are greater than under static conditions. Similar results were obtained with D.C.Fluid 200 CSTKS 100. Grease D.C.41 appears to be the most resistant of the three silicone greases examined but its ignition temperatures are lower than those reported previously for the Acheson compound G.30 and for anti-seize and sealing compound AN-C-86.

TABLE 8.

Ignition Temperatures of Silicone Greases.

Silicone Material	Pressure ats	Flow F (2 l/min) or Static S	Ignition Temperature - °C		
			Individual Results.	Average	Standard deviation
Plug Cock grease	50	S	243, 249, 259	250	-
	250	S	285, 300, 280	288	-
	50	F	265, 330, 318, 272, 296, 280, 300, 278, 294.	293	21
	175	F	230, 238, 257, 253, 230, 265.	245	15
Grease D.C.33	50	S	209, 220, 210.	213	-
		F	272, 243, 251, 259.	256	12
	250	S	181, 190, 189.	187	-
		F	233, 181, 189, 222, 222, 218.	211	21
Grease D.C.41	1	S	no ignitions up to 520°C.	-	-
		F	502, 500, 493, 502, 500, 500.	499	4
	50	S	300, 344, 375, 370, 367, 252.	335	49
		F	360, 368, 350, 360, 371, 350.	360	9
	100	S	274, 220, 215, 200, 282, 308.	250	44
		F	312, 302, 312, 328, 283, 317.	309	15

Grease D.C.33. was also examined in air flowing at 2 litres/minute at pressures up to 250 atmospheres. Results given in Table 9 show that there is no appreciable change in ignition temperature with increasing pressure and that the ignition temperatures in air are higher than in oxygen by 30° at 50 atmospheres pressure and by 70° at 250 atmospheres pressure.

TABLE 9.

Ignition Temperatures of Silicone Grease D.C.33 in air

Pressure ats.	Ignition Temperature - °C		
	Individual Results.	Average	Standard Deviation
50	281, 271, 283, 283, 338, 254, 307.	287	27
100	293, 284, 257, 283, 257, 217.	265	28
175	256, 272, 260, 268, 270, 210, 233.	253	23
250	300, 241, 250, 289, 296, 303, 280.	280	25

In experiment No.1151 in which Grease D.C.41 was under examination, ignition of the material in the reaction tube was followed by an explosion in the copper tube connecting the bomb to the exit control valve. The copper tube was burst in several places. The incident is described in Appendix II.

Class I - DISCUSSION.

An examination of the ignition temperatures of the materials reported in this section leads to the following conclusions:-

1. Spontaneous ignition did not occur. No materials included in this section ignited unless heated to 180°C even at the highest oxygen pressure.

2. The ignition temperature fell with increasing oxygen pressure but the effect was not marked at pressures above 50 atmospheres up to the maximum of 250 atmospheres. At high pressures rate of flow of oxygen within the range examined had a minor effect.

3. Of the liquid materials examined the Aroclors are clearly the most resistant to ignition. Whether these materials are safe to use regularly in high pressure oxygen systems is of course not decided by ignition temperature alone; it is not unreasonable to suggest, however, that the Aroclors, if their other properties are satisfactory, may be suitable for use as lubricants and hydraulic fluids in oxygen systems.

4. The Acheson compounds G.30 and C.T.2. and the Ministry Anti-seize Compound AN-C-86 have high ignition temperatures unaffected by pressure and should be safe to use in oxygen systems. Judged by ignition temperature they are to be preferred to the Silicone materials.

S.H.Brooks in U.S.A. Bureau of Mines Reports of Investigations No.2555 entitled "Spontaneous Ignition of Oils in Oxygen under Pressure" reports the ignition temperatures he obtained for a few oils. Brooks used a static method in which small samples of oil distributed on pure asbestos were placed inside a steel bomb of 4 ccs capacity and heated until ignition took place. The point at which ignition occurred was determined by listening with headphones for the explosion which accompanied the ignition. The work is also described by M.D.Hersey in a paper entitled "A Study of the Oxygen-Oil Explosion Hazard" from which the following ignition temperatures are taken:-

Oil	Ignition Temp. °C
Kerosene	175
Mobiloil A	170
Sperm	135
Linseed	120

The effect of heating rate was examined at 175 atmospheres, when it was found that increasing the rate so that the sample was raised through 100° in one minute reduced the ignition temperature from 245° to 177°C. The results are given in Table 16 and in all cases were obtained using the normal heating rate in a flow of oxygen of 2 litres/minute, except one series of experiments at 175 atmospheres at the faster heating rate. The inner lining of two neoprene hoses, one for oxygen and one for acetylene, made by the British Tyre and Rubber Company to their specification 1219, was also examined in 100 atmospheres at a flow rate of 2 litres/minute. The average ignition temperatures were 304° and 312°C respectively, which is about 20° above the ignition temperature under identical conditions of the neoprene lining tube submitted by the Ministry.

TABLE 16.

Ignition Temperatures of Neoprene Lining Tube

Pressure	Ignition Temperatures - °C			
	With fabric	Without fabric		
ats.	Average	Individual results.	Average	Standard deviation
50	229	300, 312, 300, 315, 300, 307.	306	7
100	176	279, 292, 292, 285, 275, 290.	285	7
175	191	264, 245, 238, 243, 251, 230.	245	12
		Fast heating rate 178, 176, 168, 168, 180, 190.	177	8
250	165	249, 245, 189, 162, 170, 248, 175.	205	44

The materials were also examined by the 'pot' test and the minimum ignition temperatures were as follows:-

Neoprene lining tube with fabric	- 330°C
Neoprene lining tube without fabric	- 380°C
BTR Specification 1219 oxygen hose	- 370°C
BTR Specification 1219 acetylene hose	- 370°C

II(b)3. - High Pressure Oxygen Hose BTR Specification 1180.

The inner lining of this hose manufactured for use in high pressure oxygen systems was examined at 100 and 250 atmospheres in a flow of oxygen. No ignitions were obtained at 250 atmospheres when the heating rate was the same as that used in the experiments at 100 atmospheres; hard carbonised residues were obtained. When, however, the heating rate was increased ignition occurred quite readily at about 175°C. The increase in heating rate was not very great; at the faster rate the sample was warmed from 60 to 160° in one and a half minutes.

The results are shown in Table 17.

TABLE 17.

Ignition Temperatures of H.P.Oxygen Hose
BTR Specification 1180.

Pressure ats	Heating rate	Ignition Temperatures - °C		
		Individual results.	Average	Standard deviation
100	Normal (100-200° in 2 mins)	314, 330, 333, 346, 300, 330.	325	16
250	Normal	Four non-ignitions. Samples heated to 320°C	-	-
	Fast	179, 181, 190, 172, 168, 161.	175	10

II(b)4 - Siebe Gorman Hose.

A sample of single covered wire reinforced high pressure hose used by the Siebe Gorman Company was received for examination. In special experiments Messrs. Siebe Gorman had succeeded in causing ignition of identical hose by adiabatic compression.

The material was examined at 100 and 250 atmospheres in oxygen flowing at 2 litres/minute. The results given in Table 18 show a marked reduction in ignition temperature at the higher pressure. The 'pot' ignition temperature was 400°C.

TABLE 18.

Ignition Temperatures of Siebe Gorman Hose.

Pressure ats.	Ignition Temperatures - °C		
	Individual results.	Average.	Standard deviation
100	378, 375, 368, 379, 372, 379.	375	4
250	147, 148, 170, 141, 128, 168.	150	16

II(b)5 - Silicone Rubber.

This material was examined at 50 and 175 atmospheres in a flow of oxygen and at 250 atmospheres under static conditions. The ignition temperatures are quite high and like the other Silicone materials reported in Class I are not greatly affected by increases in pressure. The material failed to ignite in the 'pot' test at 500°C.

TABLE 19

Ignition Temperatures of Silicone Rubber.

Pressure ats	Flow (F) (2 l/min) or Static (S)	Ignition Temperatures - °C		
		Individual results.	Average.	Standard deviation
50	F	355, 351, 360.	355	5
175	F	297, 333, 290, 331, 330, 265.	306	28
250	S	315, 330, 340, 315.	326	12

II(c) - Carbon Blacks.

Three samples of carbon blacks used in rubber compounding were examined in oxygen at 100 atmospheres flowing at 2 litres/minute in February 1949. The results are given in Table 20.

TABLE 20.

Ignition Temperatures of Carbon Blacks.

Material	Ignition Temperature - °C		
	Individual results	Average	Standard deviation
Lamp Black	309, 320, 314, 296, 281, 293.	302	15
Thermatomic Black	340, 308, 331, 335, 343, 339.	333	13
Gastex Black S.R.F.	301, 310, 305, 309, 312, 303.	307	4

Lamp Black was re-examined in September 1949; the ignition temperatures are given in Table 21 and are considerably greater at 100 atmospheres than the results obtained in February 1949. The heating rates used in both sets of experiments were the same and in all cases quite sharp breaks were obtained in the temperature-time curves. The samples were received as powders in air-tight tins. It is difficult to explain the discrepancy between the results obtained in February and September, but it is reasonably certain that pressure in the range 100 - 250 atmospheres does not have a marked effect on ignition temperature and that the carbon blacks have relatively high ignition temperature in high pressure oxygen.

TABLE 21.

Ignition Temperatures of Lamp Black obtained in September 1949.

Pressure ats.	Ignition Temperature - °C		
	Individual results.	Average	Standard deviation
50	373, 435. (failed to ignite in four tests)		
100	419, 396, 376, 378, 385, 399.	392	16
175	380, 390, 391, 371, 402, 402.	386	13
250	410, 375, 351, 361, 329, 317.	357	32

Class II - DISCUSSION.

Natural and synthetic rubber hoses are used in both high and low pressure oxygen systems. In high pressure systems the hoses are used mainly as flexible connections for charging cylinders. Fires in such high pressure systems have been reported but no detailed accounts are available of such incidents and they are believed to be infrequent. Fires in low pressure hoses used with oxy-acetylene welding equipment are more common. The fires usually occur after a 'flashback', i.e. hot gases are forced back from the torch into the supply hose where they may cause a hose to ignite.

As rubber hoses are frequently used in oxygen systems considerable work was carried out to determine the ignition characteristics of typical hose materials. The results presented

CLASS III - POLYMERS.

The following materials have been included in this Section:-

1. Polythene.
2. Teflon.
3. Kel-F.
4. Polyvinylchloride.
5. Polyvinyl-alcohol.
6. Nylon, *
7. Perspex. *
8. Buna. *
9. Red Vulcanised Fibre *
10. Resin-bonded fabric *
11. Tufnol.

* indicates that the material was submitted by the Ministry of Supply.

The first eight materials have all been developed in recent years; Kel-F, in fact, is not yet readily available. The last three materials are included in this section because the bonding material is often a polymer and like the other materials included in this section they may be machined to form seats and gaskets in high pressure oxygen systems.

III.1. - Polythene (Polyethylene).

Small block samples were cut from a $\frac{1}{2}$" rod of polythene and examined in oxygen at 2 litres/minute and in air at 2 to 10 litres/minute. The average ignition temperatures are given in Table 22 in which the standard deviations are shown in brackets. It will be seen that, with either oxygen or air, pressure in the range 50 to 250 atmospheres has little effect on ignition temperature, nor is there any big difference between the results with air at 10 litres/minute, and the results at 2 litres/minute, although it is interesting to note that in all cases ignition temperatures were slightly lower at the higher gas rate.

The 'pot' ignition temperature was 380°C.

TABLE 22.

Ignition Temperatures of Polythene.
(Standard deviation in brackets)

Pressure ats.	Mean Ignition Temperature in Air. °C				Mean Ignition Temp. in Oxygen. °C	
	Flow rate - litres/min. 2		10		Flow rate - l/min 2	
50	231	(13)	218	(10)	235	(16)
100	222	(31)	201	(20)	205	(10)
175	255	(12)	208	(9)	171	(19)
250	222	(33)	215	(27)	203	(16)

Samples of Polythene seats for oxygen regulators were examined in block form at 100 atmospheres as received, and after storage for three days at 50°C in oxygen at 100 atmospheres. It will be seen from Table 23 that the ignition temperature of these Polythene seats increased on ageing.

TABLE 23.

Ignition Temperatures of Polythene Seats.

Pressure ats.	Ignition Temperature - °C			
	As received		After accelerated ageing	
	Individual results.	Average	Individual results.	Average
100	142, 151, 191, 173, 152, 155.	161	200, 195, 188, 187, 210, 193.	196

III.2. - Teflon (Tetrafluoroethylene polymer).

This interesting material was examined in the bomb in block form and as shavings up to pressures of 250 atmospheres. Experiments were carried out in a static atmosphere and in a flow of oxygen at 2 litres/minute, but in no case was ignition recorded although the samples were heated to 350°C. In all cases the residue was translucent when removed from the bomb, but on cooling became opaque and indistinguishable from samples that had not been heated in oxygen. It was possible, however, to ignite teflon in oxygen at 1 atmosphere in the 'pot' test at abnormally high temperatures. The material could be seen burning feebly in oxygen preheated to 530°C. The results of the 'pot' test are shown in Table 24 in which 'x' indicates failure to ignite.

TABLE 24.

'Pot' Ignition Temperatures of Teflon.

Temperature °C	Ignition Time seconds	Frequency
520	x x x	0/3
530	60, 72, 70.	3/3
550	30, 28.	2/2

III.3 - Kel-F (Monochloro trifluoro-ethylene polymer).

A sample of this new material was obtained from America. Unlike Teflon it is a transparent thermoplastic, the physical properties of which can be modified by suitable treatment.

There was insufficient for high pressure tests but a little of the material was examined by the 'pot' test, when it was found to ignite at 600°C, but not at 560°C. It may be that the exact 'pot' ignition temperature is below 600°C, but it is clear that Kel-F has a higher ignition temperature than Teflon as determined by the 'pot' test. The detailed results are given in Table 25, in which 'x' indicates failure to ignite. As with Teflon the material burned feebly when ignition did occur.

TABLE 25.

'Pot' Ignition Temperatures of Kel-F

Temperature °C	Ignition Time seconds	Frequency
560	x x x	0/3
600	23, 16, 18	3/3

III.4 - Polyvinylchloride (PVC).

(a) Unplasticised:

Some polyvinylchloride in powder form, obtained from Messrs. I.C.I. Limited, was examined in high pressure oxygen flowing at 2 litres/minute. The results given in Table 26 show that the ignition temperature of PVC falls from 444° at 1 atmosphere to 204° at 100 atmospheres and 161° at 250 atmospheres; pressure clearly had a marked effect on ignition temperature, but increases in pressure above 100 atmospheres did not greatly reduce the ignition temperature.

TABLE 26.

Ignition Temperatures of Polyvinylchloride. (Unplasticised)

Pressure ats.	Ignition Temperature - °C		
	Individual Results.	Average	Standard deviation
1	425, 450, 471, 431.	444	21
50	229, 249, 250, 239, 259, 246.	245	9
100	229, 224, 198, 210, 185, 181.	204	20
175	170, 162, 171, 162, 228, 165.	160	31
250	178, 154, 157, 158, 159, 162.	161	5

(b) Plasticised:

A sample of polyvinylchloride plasticised with tricresyl phosphate was received from the Research Association of British Rubber Manufacturers and examined in block form. The results given in Table 27 show that the plasticised material has a slightly higher ignition temperature than the unplasticised.

The 'pcc' ignition temperature of the plasticised was 450°C.

TABLE 27.

Ignition Temperatures of Polyvinylchloride. (Plasticised)

Pressure ats.	Ignition Temperature - °C		
	Individual Results.	Average	Standard deviation
50	266, 265, 280, 273, 275, 284.	274	7
100	241, 248, 248, 231, 250, 246.	244	7
250	175, 170, 200, 209, 193, 198.	191	15

III.5 - Polyvinyl-alcohol.

The first material examined, a polyvinyl-alcohol manufactured in Germany, containing phosphoric acid, had a surprisingly high ignition temperature, as can be seen from Table 28. In order to decide if resistance to ignition were conferred by the phosphoric acid, tests were carried out on specially prepared specimens free from this addition. The ignition temperatures of the latter material are shown in comparison with those of the German material in Table 28.

It will be seen that at 100 atmospheres the German material has an ignition temperature that is more than 200° higher than the material containing no phosphoric acid. At 250 atmospheres the German material failed to ignite up to temperatures of 320°C and when the samples were removed from the bomb they were in a semi-molten state with some clear liquid lying at the bottom of the boat. On cooling a brittle black residue was obtained.

TABLE 28.

Ignition Temperatures of Polyvinyl Alcohol.

Pressure	Ignition Temperature - °C			
	German sample containing phosphoric acid.		Material made at Morden containing no phosphoric acid	
ats.	Individual results.	Average	Individual results.	Average
50	443, 440, 421, 430, 390, 410.	422	300, 298, 305, 375, 361, 318, 309.	324
100	429, 442, 480, 450, 454, 472.	455	279, 237, 239, 245, 250, 225.	246
250	Failed to ignite in four experiments up to 320°C.		Not examined.	

Small samples of polyvinyl alcohol phosphorylated with phosphorus oxychloride ($POCl_3$) were prepared and examined at 250 atmospheres in oxygen in the high pressure bomb. Under these conditions the material failed to ignite at temperatures up to 350°C. The material ignited when examined by the 'pot' test at the very high temperature of 660°C. The corresponding ignition temperature for the polyvinyl alcohol before phosphorylation was 420°C.

III.6 - Nylon.

Nylon in the form of a small bar was received from the Ministry of Supply and examined in a static atmosphere and in a flow of oxygen at 2 litres/minute. The 'pot' ignition temperature of this material was 500°C and it will be seen from Table 29 that there is a marked decrease in ignition temperature as pressure is increased; at 50 atmospheres the ignition temperature was 328°C; at 100 atmospheres 249°C and at 175 atmospheres 188°C. Ignition temperature increased slightly to 219°C when the pressure was increased to 250 atmospheres. It will be seen from the table that very often only three experiments were carried out at each pressure as the amount of material available for test was small. There is no significant difference between the ignition temperatures determined under static experiments compared with the results obtained under flow conditions.

TABLE 29.

Ignition Temperatures of Nylon.

Pressure	Ignition Temperature - °C			
	Static		Flow	
ats.	Individual results.	Average.	Individual results	Average
50	321, 321, 330.	324	325, 330, 330.	328
100	252, 340, 255, 160, 210	243	235, 251, 261.	249
175	-	-	160, 203, 200.	188
250	-	-	180, 220, 221, 255.	219

END OF REFERENCE

156

REFERENCE

157

HUST, J. G.; AND CLARK, A. F.: A SURVEY OF COMPATABILITY OF MATERIALS WITH HIGH PRESSURE OXYGEN SERVICE. REPT. 275.03-72-11, NBS INSTITUTE FOR BASIC STANDARDS, CRYOGENICS DIVISION, OCT. 1972.

3.0-0-0

Final Report 275.03-72-11

on

A Survey of Compatibility of Materials with High Pressure Oxygen Service

prepared for

National Aeronautics and Space Administration
George C. Marshall Space Flight Center
Huntsville, Alabama

LEWIS RESEARCH CENTER
Aerospace Safety Research
and Data Institute
OCT 23 1973
CLEVELAND, OHIO

October 1972

NASA Order Number H-9 2180A
Principal Technical Representative
John G. Austin
Huntsville, Alabama

Prepared by

J. G. Hust and A. F. Clark
Cryogenics Division
Institute for Basic Standards
National Bureau of Standards
Boulder, Colorado 80302

THIS REPORT FOR SPONSOR OFFICIAL USE ONLY AND

IS NOT TO BE RELEASED TO DDC OR CLEARINGHOUSE

MAY BE DISTRIBUTED AND REFERENCED PER
PHONE CONVERSATION WITH J. G. AUSTIN
AND GEORGE MANDEL ON 2/28/73.

IMPORTANT NOTICE

The results of this report are not to be used for advertising or promotional purposes, or to indicate endorsement or disapproval of the product(s) by the National Bureau of Standards.

A Survey of Compatibility of Materials with High Pressure Oxygen Service

I. Introduction

The Cryogenics Division of the National Bureau of Standards (NBS-CD) was recently requested by the Marshall Space Flight Center of the National Aeronautics and Space Administration (NASA-MSFC) to perform a survey and assess the existing state of knowledge regarding compatibility of materials with high pressure oxygen. Particular emphasis is to be placed on past practical operational and research experience.

Material compatibility, in general, implies a harmonious coexistence of all the materials of a system. The lack of such compatibility can lead to undesirable and sometimes disastrous results. For example, the chemical reaction of a combustible material with oxygen in a system results in corrosion, burning, or even explosion. It is clear that the general definition of incompatibility encompasses many phenomena. In this study, however, we have restricted ourselves to the consideration of materials exposed to high pressure oxygen. Because only high pressures are considered, any man-related incompatibilities are ignored. The harmonious coexistence of materials in a high pressure oxygen system implies the physical containment of the oxygen as well as the lack of significant chemical reactions with the oxygen. Thus compatible materials are defined, in this study, as those materials or combinations of materials with sufficient mechanical strength to withstand the high pressures and whose properties are not significantly degraded by the presence of oxygen. We will pay particular attention to the ease with which any degradation is initiated (reaction sensitivity), the rate at which degradation progresses (reaction intensity), and the sources of degradation

initiation (ignition sources). The dependence of these parameters on physical properties, such as thermal conductivity, specific heat, density, and heat of combustion, as well as system characteristics, such as pressure, pipe wall thickness, total mass, radius of pipe bends, and surface roughness, is considered. It is to be noted that the dependence on pressure is the primary consideration here; however, the interdependence of the effects of these characteristics makes it essentially impossible to analyze any one separately.

The objective of this survey is to gather the available information on the compatibility of materials with oxygen as applied to the production, transport, and applications experience of high pressure liquid and gaseous oxygen and to compile this material into a usable reference report. High pressure is here defined to be above about 2000 to 3000 psia. Since high pressure projections sometimes can be made from lower pressure data, some low pressure data are also included. Low pressure data are included if they are considered helpful to a better understanding of the behavior at high pressures.

It is anticipated that this technical input to NASA-MSFC will assist in the establishment of practical and safe, but not stifling, guidelines in the future use of high pressure oxygen. It is hoped that such guidelines will eventually be commonly accepted throughout NASA, other government agencies, and the commercial sector as well.

Recently, Clark (1971) of NBS performed a survey on oxygen compatibility of materials at ordinary pressures. Information from Clark's report which is especially applicable to high pressure application will be repeated for convenience. Surveys of oxygen related accidents have been conducted recently by Ordin (1971) and Johnson (1970) for NASA and by McQuaid and Cole (1972) for the Navy. Each of these surveys indicate a surprisingly high rate of accidents caused by material incompatibility. The surveys by Ordin and Johnson covered

NASA, some Air Force, and some related contractor records. Ordin reported 20% of the mishaps with liquid oxygen and 36% of the mishaps with gaseous oxygen involved material incompatibility. Johnson reported 56% were caused by the presence of oxygen incompatible materials. In many cases more than one factor was involved in the mishaps. For example, procedural errors were involved in 78% of the mishaps and design errors were present in 63% of the mishaps according to Ordin. Even though material incompatibility with oxygen was present in fewer instances than procedural or design error, the percentage due to incompatibility is significantly large and it is expected to be even higher in high pressure oxygen systems. It is also noted that the accident rate due to material incompatibility in high pressure gaseous oxygen is almost twice that in liquid oxygen.

McQuaid and Cole's (1972) survey indicates an accident in a Navy compressed gas system due to spontaneous ignition every four weeks during the period January 1968 to May 1971. They do not indicate what proportion of these are due to material incompatibility, but do state that material failure accounts for about half of these accidents; the cause of the other half is unknown. No accidents are attributed to design failure or personnel error. From this information one can not rule out that a sizable proportion may be due to material incompatibility.

Recent trends in NASA, military, and commercial use of liquid (LOX) and gaseous (GOX) oxygen point toward use of higher pressures. With this increased use to 10,000 psi and higher, compatibility considerations are of paramount importance. Deep concern with safety is rightfully prevalent throughout the field, both by the producer and the user. This survey will better define material incompatibility problems and hazards caused by the use of high pressure LOX and GOX. This report contains recommended guidelines in later sections which will hopefully allow the necessary flexibility and compromise between cost - effectiveness and

safety. Also included is a tabulation and assessment of available high pressure compatibility data and an indication of the availability of equipment. The next section is a discussion of the compatibility parameters affecting the selection of materials for high pressure oxygen service. Following sections include discussions on structural integrity, chemical compatibility, and experimental tests and data which characterize the relative compatibility of different materials.

II. Material Selection

The selection of a given material to fulfill a specified function in high pressure oxygen service must be based both on its physical-mechanical properties as well as its chemical properties. The principal chemical property of interest here is its potential reactivity with oxygen. The relevant physical-mechanical properties are primarily strength and plastic deformation properties. For example the plastic deformation of polytetrafluoroethylene may make it unusable for a valve seat material at sufficiently high pressure and copper may be too weak for a pressure chamber, even though they may be judged chemically compatible with oxygen. Also, the designer needs to consider that plastics and nearly all metals become more brittle at LOX temperatures. Other properties such as specific heat, thermal conductivity, density, and thermal diffusivity influence material compatibility. For example, nickel-copper alloys are rapidly replacing stainless steel in high pressure oxygen systems because of the increased thermal conductivity and diffusivity of the nickel-copper alloys. The higher thermal conductivity results in lower reaction sensitivity. Also, mechanical properties may be altered in the presence of high pressure oxygen, e.g. crack propagation may be enhanced.

Several good reviews of lower pressure oxygen compatibility have been written. Many of these contain information basic to the understanding of the higher pressure phenomena. The most recent review is by Clark (1971);

Card #33

APPENDIX I - HIGH PRESSURE OXYGEN COMPATIBILITY DATA

PURE METALS

Reference	Materials	Test Pressure (psi)	Ignition Temp. (K)	Test Temp. (K)	Mechanical Impact Energy (kg m)	Mechanical Impact Reaction Rate	Pneumatic Impact Reaction Rate	Specimen Thickness (in)	Flash Point (K)	Fire Point (K)	Environment
Jakowsky and Butzler (1923)	Copper	15	1325								GOX
		400	1180								GOX
		800	1130								GOX
		1200	1110								GOX
		1600	1100								GOX
		2000	1100								GOX
"	Iron	15	1210								GOX
		400	1120								GOX
		800	1050								GOX
		1000	1015								GOX
		1200	980								GOX
		1600	925								GOX
		2000	870								GOX

ALLOYS

Reference	Materials	Test Pressure (psi)	Ignition Temp. (K)	Test Temp. (K)	Mechanical Impact Energy (kg m)	Mechanical Impact Reaction Rate	Pneumatic Impact Reaction Rate	Specimen Thickness (in)	Flash Point (K)	Fire Point (K)	Environment
Austin (1972)	Aluminum 6061-T6	100		90	10	3/7		.032			LOX
		100		90	10	16/20		.032			LOX
		100		90	7.4	4/20		.032			LOX
		100		90	10	0/20		.063			LOX
		100		90	10	0/20		.063			LOX
		500		90	10	0/20		.063			LOX
		500		90	10	0/20		.063			LOX
		1000		90	10	0/20		.063			LOX
		1500		90	10	0/20		.063			LOX
		50		300	10	0/20		.032			GOX
		100		300	10	9/20		.032			GOX
		100		300	10	0/20		.032			GOX
		500		300	10	6/20		.032			GOX
		500		300	10	0/20		.032			GOX
		500		300	10	0/6		.032			GOX
		1000		300	10	0/20		.032			GOX
		1000		300	10	0/6		.032			GOX
Austin (1972)	Aluminum 2014-T6	500		90	10	3/20		.063			LOX
		1000		90	7	0/20		.063			LOX
		1000		90	5	0/20		.063			LOX
		1400		90	5	6/20		.063			LOX
		100		90	10	0/20		.090			LOX
		500		90	10	0/20		.090			LOX
		1400		90	5	0/20		.090			LOX
		250		300	10	0/20		.063			GOX
		500		300	10	0/20		.063			GOX
		500		300	5	6/20		.063			GOX
		500		300	10	0/20		.063			GOX
		500		300	10	0/20		.063			GOX
		500		300	10	0/20		.063			GOX
		500		300	10	0/20		.063			GOX
		500		300	10	2/20		.063			GOX
		1000		300	10	2/3		.063			GOX
		1000		300	5	2/20		.063			GOX

ALLOYS cont.

Reference	Materials	Test Pressure (psi)	Ignition Temp. (K)	Test Temp. (K)	Mechanical Impact Energy (kg m)	Mechanical Impact Reaction Rate	Pneumatic Impact Reaction Rate	Specimen Thickness (in)	Flash Point (K)	Fire Point (K)	Environment
Austin (1972)	Aluminum 2219-T87	50		90	10	0/20		.063			LOX
		100		90	10	0/20		.063			LOX
		500		90	10	1/2		.063			LOX
		1000		90	7.62	0/20		.063			LOX
		1000		90	5.54	0/20		.063			LOX
		500		90	10	0/20		.070			LOX
		500		90	10	0/20		.090			LOX
		500		300	10	0/20		.063			GOX
		500		300	5.54	0/20		.063			GOX
		1000		300	10	1/3		.063			GOX
		1000		300	7.62	0/20		.063			GOX
		1000		300	5.54	0/20		.063			GOX
		1000		300	5	0/20		.063			GOX
		1400		300	10	1/2		.063			GOX
		1400		300	9.02	0/20		.063			GOX
		1400		300	7.62	0/20		.063			GOX
		1400		300	5.54	0/20		.063			GOX
Austin (1972)	Ferrous Alloy A286	100		90	10	0/20		.020			LOX
		500		90	10	0/20		.020			LOX
		1000		90	10	0/20		.020			LOX
		1500		90	10	0/20		.020			LOX
		100		90	10	0/20		.050			LOX
		500		90	10	0/20		.050			LOX
		1000		90	10	0/20		.050			LOX
		1500		90	10	0/20		.050			LOX
		100		300	10	0/20		.020			GOX
		500		300	10	0/20		.020			GOX
		1000		300	10	2/20		.020			GOX
		1000		300	10	0/20		.020			GOX
		1000		300	9.02	0/20		.020			GOX
		1500		300	10	8/20		.020			GOX
		1500		300	9.02	4/20		.020			GOX
		1500		300	8.34	0/20		.020			GOX
		1500		300	7.62	0/20		.020			GOX

ALLOYS cont.

Reference	Materials	Test Pressure (psi)	Ignition Temp. (K)	Test Temp. (K)	Mechanical Impact Energy (kg m)	Mechanical Impact Reaction Rate	Pneumatic Impact Reaction Rate	Specimen Thickness (in)	Flash Point (K)	Fire Point (K)	Environment
Austin (1972)	304 Stainless Steel	15		90	10	0/30		.063			LOX
		15		90	10	0/20		.063			LOX
		100		90	10	0/20		.063			LOX
		500		90	10	0/20		.063			LOX
		1000		90	10	0/20		.063			LOX
		1500		90	10	0/20		.063			LOX
		15		90	10	0/20		.090			GOX
		100		300	10	0/20		.090			GOX
		500		300	10	0/20		.090			GOX
		1000		300	10	0/20		.090			GOX
		1500		300	10	2/20		.090			GOX
		1500		300	9.02	0/20		.090			GOX
		1500		300	8.34	0/20		.090			GOX
Austin (1972)	PH 15-7 Stainless Steel	100		90	10	0/20		.030			LOX
		500		90	10	0/20		.030			LOX
		1000		90	10	3/20		.030			LOX
		1000		90	9.02	0/20		.030			LOX
		1000		90	8.34	0/20		.030			LOX
		1500		90	10	5/20		.030			LOX
		1500		90	9.02	0/20		.030			LOX
		1500		90	8.34	0/20		.030			LOX
		100		90	10	0/20		.050			LOX
		500		90	10	0/20		.050			LOX
		1000		90	10	2/20		.050			LOX
		1500		90	10	3/20		.050			LOX
		1500		90	9.02	0/20		.050			LOX
		1500		90	8.34	0/20		.050			LOX
		100		90	10	0/20		.090			LOX
		500		90	10	0/20		.090			LOX
		1000		90	10	0/20		.090			LOX

ALLOYS cont.

Reference	Materials	Test Pressure (psi)	Ignition Temp. (K)	Test Temp. (K)	Mechanical Impact Energy (kg m)	Mechanical Impact Reaction Rate	Pneumatic Impact Reaction Rate	Specimen Thickness (in)	Flash Point (K)	Fire Point (K)	Environment
Austin (1972)	17-7 PH Stainless Steel	15		90	10	2/20		.030			LOX
		15		90	10	0/20		.030			LOX
		1500		90	10	0/20		.030			LOX
		100		90	10	0/20		.063			LOX
		500		90	10	0/20		.063			LOX
		1000		90	10	0/20		.063			LOX
		1500		90	10	0/20		.063			LOX
		15		90	10	0/20		.070			LOX
		100		90	10	0/20		.070			LOX
		500		90	10	0/20		.070			LOX
		1000		90	10	0/20		.070			LOX
		1500		90	10	0/20		.070			LOX
		100		300	10	0/20		.039			GOX
		500		300	10	0/20		.030			GOX
		1000		300	10	0/20		.030			GOX
		100		300	10	0/20		.063			GOX
		500		300	10	0/20		.063			GOX
Austin (1972)	Stainless Steel 21Ni-6Cr-9Mn	100		90	10	0/20		.030			LOX
		500		90	10	0/20		.030			LOX
		1000		90	10	0/20		.030			LOX
		1500		90	10	0/20		.020			LOX
		100		90	10	0/20		.063			LOX
		500		90	10	0/20		.063			LOX
		1000		90	10	0/20		.063			LOX
		1500		90	10	0/20		.063			LOX
		100		90	10	0/20		.085			LOX
		500		90	10	0/20		.085			LOX
		1000		90	10	0/20		.085			LOX
		1500		90	10	0/20		.085			LOX
		100		300	10	0/20		.031			GOX
		500		300	10	0/20		.031			GOX
		1000		300	10	0/20		.031			GOX
		1500		300	10	0/20		.031			GOX
Austin (1972)	Stainless Steel 22Ni-13Cr-5Mn	100		90	10	0/20		.050			LOX
		500		90	10	0/20		.050			LOX
		1000		90	10	0/20		.050			LOX
		1500		90	10	0/20		.050			LOX
		100		300	10	0/20		.050			GOX
		500		300	10	0/20		.050			GOX
		1000		300	10	0/20		.050			GOX
		1500		300	10	0/20		.050			GOX

ALLOYS cont.

Reference	Materials	Test Pressure (psi)	Ignition Temp. (K)	Test Temp. (K)	Mechanical Impact Energy (kg m)	Mechanical Impact Reaction Rate	Pneumatic Impact Reaction Rate	Specimen Thickness (in)	Flash Point (K)	Fire Point (K)	Environment
Austin (1972)	Haynes alloy 186	100		90	10	0/20		.063			LOX
		500		90	10	0/20		.063			LOX
		1000		90	10	0/20		.063			LOX
		1500		90	10	0/20		.063			LOX
		100		90	10	0/20		.090			LOX
		500		90	10	0/20		.090			LOX
		1000		90	10	0/20		.090			LOX
		1500		90	10	0/20		.090			LOX
		100		300	10	0/20		.063			GOX
		500		300	10	0/20		.063			GOX
		1000		300	10	0/20		.063			GOX
		1500		300	10	0/20		.063			GOX
		100		300	10	0/20		.090			GOX
		500		300	10	0/20		.090			GOX
		1000		300	10	0/20		.090			GOX
		1500		300	10	0/20		.090			GOX
Austin (1972)	301 Stainless Steel	100		90	10	0/20		.125			LOX
		500		90	10	0/20		.125			LOX
		1000		90	10	0/20		.125			LOX
		1500		90	10	0/20		.125			LOX
		100		300	10	0/20		.125			GOX
		500		300	10	0/20		.125			GOX
		1000		300	10	0/20		.125			GOX
		1500		300	10	0/20		.125			GOX
Austin (1972)	Inconel 600	15		90	10	0/20		.031			LOX
		15		90	10	0/20		.031			LOX
		15		90	10	0/20		.090			LOX
		100		300	10	0/20		.031			GOX
		500		300	10	0/20		.031			GOX
		1000		300	10	0/20		.031			GOX
		1500		300	10	0/20		.031			GOX
		100		300	10	0/20		.063			GOX
		500		300	10	0/20		.063			GOX
		1000		300	10	0/20		.063			GOX
		1500		300	10	0/20		.063			GOX
		100		300	10	0/20		.093			GOX
		500		300	10	0/20		.093			GOX
		1000		300	10	0/20		.093			GOX
		1500		300	10	0/20		.093			GOX

ALLOYS cont.

Reference	Materials	Test Pressure (psi)	Ignition Temp. (K)	Test Temp. (K)	Mechanical Impact Energy (kg m)	Mechanical Impact Reaction Rate	Pneumatic Impact Reaction Rate	Specimen Thickness (in)	Flash Point (K)	Fire Point (K)	Environment
Austin (1972)	Inconel 718	50		90	10	0/20		.125			LOX
		100		90	10	0/20		.125			LOX
		500		90	10	0/20		.125			LOX
		1000		90	10	0/20		.125			LOX
		1500		90	10	0/20		.125			LOX
		500		300	10	0/20		.063			GOX
		50		300	10	0/20		.125			GOX
		100		300	10	0/20		.125			GOX
		500		300	10	0/20		.125			GOX
		1000		300	10	0/20		.125			GOX
		1500		300	10	0/20		.125			GOX
		10000			10	0/20		.012			GOX
Austin (1972)	Inconel 750	100		90	10	0/20		.062			LOX
		500		90	10	0/20		.062			LOX
		1000		90	10	0/20		.062			LOX
		1500		90	10	0/20		.062			LOX
		100		300	10	0/20		.062			GOX
		500		300	10	0/20		.062			GOX
		1000		300	10	0/20		.062			GOX
		1500		300	10	0/20		.062			GOX
Austin (1972)	Monel 400	15		90	10	0/20		.031			LOX
		15		90	10	0/20		.063			LOX
		100		300	10	0/20		.031			GOX
		500		300	10	0/20		.031			GOX
		1000		300	10	0/20		.031			GOX
		1500		300	10	2/20		.031			GOX
		1500		300	9.02	0/20		.031			GOX
		1500		300	9.02	0/20		.031			GOX
		1500		300	8.34	0/20		.031			GOX
		1500		300	8.34	0/20		.031			GOX
		100		300	10	0/20		.062			GOX
		500		300	10	0/20		.062			GOX
		1000		300	10	0/20		.062			GOX
		1500		300	10	3/20		.062			GOX
		1500		300	9.62	0/20		.062			GOX
		1500		300	8.34	0/20		.062			GOX
		100		300	10	0/20		.090			GOX
Austin (1972)	Inconel 625	10000		420	10	0/20		.05			GOX
	K-Monel	10000		300	10	0/20		.05			GOX
"	Inconel 718 brazed with	10000		300	10	0/20		.05			GOX
"	Nicrobraze alloy										

ALLOYS cont.

Reference	Materials	Test Pressure (psi)	Ignition Temp. (K)	Test Temp. (K)	Mechanical Impact Energy Reaction (kg m) Rate	Pneumatic Impact Reaction Rate	Specimen Thickness (in)	Flash Point (K)	Fire Point (K)	Environment
Jakowsky and Butzler(1923)	Brass	15	1350							GOX
		400	1190							GOX
		800	1130							GOX
		1200	1090							GOX
		1600	1070							GOX
		2000	1050							GOX

HALOGENATED COMPOUNDS

Reference	Materials	Test Pressure (psi)	Ignition Temp. (K)	Test Temp. (K)	Mechanical Impact Energy (kg m)	Mechanical Impact Reaction Rate	Pneumatic Impact Reaction Rate	Specimen Thickness (in)	Flash Point (K)	Fire Point (K)	Environment
Jamison (1970)	Fluorel 1059	2000		297	2.8	0/12					GOX
Pippen and Stradling (1971)	Fluorel	5							668	None	GOX
		25							680	728	GOX
		50							645	700	GOX
		50							581	581	GOX
		100							548	548	GOX
		500							506	506	GOX
		1000							506	506	GOX
		1500							505	505	GOX
		2000							494	494	GOX
Marzani (1968a) (1968b)	Polychloro-trifluor-ethylene (CTFE)	4000	700								GOX GOX GOX GOX GOX
Jamison (1970)	KEL-F Bar Stock	2000		299	1.4	0/18					GOX
Pippen and Stradling (1971)	KEL-F-81	5							745	None	GOX
		25							698	None	GOX
		50							693	724	GOX
		500							639	639	GOX
		1000							647	647	GOX
		1500							643	643	GOX
		2000							647	647	GOX
McQuaid (1972)	CTFE	3800	685								GOX
Marzani (1968a)	Polytetra-fluoro-ethylene (Teflon)(TFE)	4025	735								GOX
Jamison (1970)	TFE	2000		289	2.8	0/21					GOX
"	TFE tubing	2000		286	1.4	0/21					GOX

HALOGENATED COMPOUNDS cont.

Reference	Materials	Test Pressure (psi)	Ignition Temp. (K)	Test Temp. (K)	Mechanical Impact Energy (kg m)	Mechanical Impact Reaction Rate	Pneumatic Impact Reaction Rate	Specimen Thickness (in)	Flash Point (K)	Fire Point (K)	Environment
Pippen and Stradling (1971)	Glass Filled Teflon	500			1.4	1/?					GOX
		1000			1.4	1/1					GOX
		2500					0/4				GOX
"	Teflon	5							None	None	GOX
		25							741	None	GOX
		50							754	None	GOX
		50							735	735	GOX
		100							733	733	GOX
		200							728	728	GOX
		500							707	707	GOX
		1000							645	645	GOX
		1500							637	637	GOX
		2000							660	660	GOX
"	Virgin Teflon Sheet	4000					0/4				GOX
		4500					4/4				GOX
		5000			.34	0/4					GOX
Jamison (1970)	T-EMS372 (J.L. Dore)	2000		289	1.4	0/21					GOX

NON-HALOGENATED PLASTICS

Reference	Materials	Test Pressure (psi)	Ignition Temp. (K)	Test Temp. (K)	Mechanical Impact Energy (kg m)	Mechanical Impact Reaction Rate	Pneumatic Impact Reaction Rate	Specimen Thickness (in)	Flash Point (K)	Fire Point (K)	Environment
Austin (1972)	Electrofilm 2306	100		90	1.4	0/20					LOX
		500		90	1.4	0/20					LOX
		1000		90	1.4	0/20					LOX
		1500		90	1.4	0/20					LOX
		100		300	1.4	0/20					GOX
		500		300	1.4	0/20					GOX
		1000		300	1.4	0/20					GOX
		1000		300	1.2	0/20					GOX
		1000		300	1.1	0/20					GOX
		1500		300	1.4	4/20					GOX
		1500		300	1.2	0/20					GOX
		1500		300	1.1	0/20					GOX
"	Electrofilm 2396	100		90	1.4	0/20					LOX
		100		90	1.4	0/20					LOX
		500		90	1.4	0/20					LOX
		500		90	1.4	0/20					LOX
		1000		90	1.4	0/20					LOX
		1000		90	1.4	0/20					LOX
		1500		90	1.4	0/20					LOX
		1500		90	1.4	0/20					LOX
		100		300	1.4	0/20					GOX
		100		300	1.4	0/20					GOX
		500		300	1.4	0/20					GOX
		500		300	1.4	0/20					GOX
		1000		300	1.4	0/20					GOX
		1000		300	1.4	0/20					GOX
		1500		300	1.4	0/20					GOX
		1500		300	1.4	6/20					GOX
		1500		300	1.2	5/20					GOX
"	Electrofilm 2406	100		90	1.4	0/20					LOX
		500		90	1.4	0/20					LOX
		1000		90	1.4	0/20					LOX
		1500		90	1.4	0/20					LOX
		100		300	1.4	0/20					GOX
		500		300	1.4	0/20					GOX
		1000		300	1.4	0/20					GOX
		1500		300	1.4	0/20					GOX

NON-HALOGENATED PLASTICS cont.

Reference	Materials	Test Pressure (psi)	Ignition Temp. (K)	Test Temp. (K)	Mechanical Impact Energy (kg m)	Mechanical Impact Reaction Rate	Pneumatic Impact Reaction Rate	Specimen Thickness (in)	Flash Point (K)	Fire Point (K)	Environment
Austin(1972)	Epoxy Fiberglass	15		90	1.4	20/20		.050			LOX
		15		90	1.1	20/20		.050			LOX
		15		90	0.76	20/20		.050			LOX
		15		90	0.48	20/20		.050			LOX
		15		90	0.19	4/20		.050			LOX
		15		90	0.094	2/20		.050			LOX
		100		300	1.4	15/20		.050			GOX
		100		300	1.1	20/20		.050			GOX
		100		300	0.76	5/20		.050			GOX
		100		300	0.67	2/20		.050			GOX
		100		300	0.57	0/20		.050			GOX
		100		300	0.48	0/20		.050			GOX
		500		300	0.67	2/5		.050			GOX
		500		300	0.57	0/20		.050			GOX
		1000		300	0.57	1/6		.050			GOX
		1500		300	0.57	1/1		.050			GOX
Pippen and Stradling (1971)	Gemon 3010 Polymide laminate	4000			1.4	0/4	0/4				GOX
		4500			1.4	1/3	0/1				GOX
Guter(1967)	German Buna Solid Black	15	737								GOX
		300	588								GOX
		750	622								GOX
Pippen and Stradling (1971)	Glass Fabric	5000			1.4	0/4					GOX
Jamison (1970)	Lexan 1100 (Polycarbonate)	2000		297	2.8	0/22					GOX
"	Nylon	2000		299	2.8	0/21					GOX
Guter(1967)	Nylon	750	601								GOX
		1500	522								GOX
		2625	461								GOX
		3750	492								GOX
Pippen and Stradling (1971)	Nylon Sheet	5							665	None	GOX
		25							677	684	GOX
		50							664	664	GOX
		50							570	570	GOX
		100							548	548	GOX
		500							507	507	GOX
		1087							494	494	GOX

NON-HALOGENATED PLASTICS cont.

Reference	Materials	Test Pressure (psi)	Ignition Temp. (K)	Test Temp. (K)	Mechanical Impact Energy (kg m)	Mechanical Impact Reaction Rate	Pneumatic Impact Reaction Rate	Specimen Thickness (in)	Flash Point (K)	Fire Point (K)	Environment
McQuaid(1972)	Nylon '66' (Valve Seat)	2400	458								GOX
"	Nylon '66'	200	575								GOX
Guter(1967)	Perpex Block and Shavings	750	562								GOX
		1500	557								GOX
		2625	464								GOX
		3750	497								GOX
Marzani (1968a)	Polyethylene	2525	452								GOX
		2400	449								GOX
		2350	449								GOX
		750	452								GOX
		325	457.5								GOX
		325	457.5								GOX
		250	>740.5								GOX
		250	>699								GOX
"	70% Polyethylene 30% Fiberglass	2350	458								GOX
Marzani (1968a)	85% Polymide 15% Graphite	3350	618								GOX
Schwinghamer (1971)	Polymide #3	50				0					GOX
		100				29%					GOX
		500				100%					GOX
		1000				100%					GOX
Marzani (1968a)	Polymide	3350	620								GOX
McQuaid(1972)	Polymide	3375	622								GOX
Guter(1967)	Polythene	750	508								GOX
		1500	478								GOX
		2625	444								GOX
		3000	476								GOX

NON-HALOGENATED PLASTICS cont.

Reference	Materials	Test Pressure (psi)	Ignition Temp. (K)	Test Temp. (K)	Mechanical Impact Energy (kg m)	Mechanical Impact Reaction Rate	Pneumatic Impact Reaction Rate	Specimen Thickness (in)	Flash Point (K)	Fire Point (K)	Environment
Marzani (1968a)	Polyvinylidene Fluoride	2975	560								GOX
"	Polyurethane	2725	560								GOX
"	Polyurethane Foam, Renticulated	2650	491								GOX
"	Polyurethane Foam Renticulated, Fire Retardant	2450	471								GOX
McQuaid (1972)	Polyurethane Foam, Renticulated	2725	522								GOX
Marzani (1968a)	Polyurethane Foam, Fire Retardant	2450	471								GOX
Guter(1967)	Polyvinyl Alcohol (with H_3PO_4)	750	695								GOX
		1500	728								GOX
		3375	593								GOX
"	Polyvinyl Chloride (unplasticized)	15	717								GOX
		750	518								GOX
		1500	477								GOX
		2625	433								GOX
		3375	434								GOX

NON-HALOGENATED PLASTICS cont.

Reference	Materials	Test Pressure (psi)	Ignition Temp. (K)	Test Temp. (K)	Mechanical Impact Energy (kg m)	Mechanical Impact Reaction Rate	Pneumatic Impact Reaction Rate	Specimen Thickness (in)	Flash Point (K)	Fire Point (K)	Environment
Guter(1967)	Polyvinyl Chloride (plasticized)	750	547								GOX
		1500	517								GOX
		3375	464								GOX
"	Tufnol	750	564								GOX
		1500	521								GOX
		2625	444								GOX
Jamison (1970)	Vespel (Polyamide)	2000		297	2.8	2/38					GOX
		2000		297	1.4	0/42					GOX
Pippen and Stradling (1971)	Vespel SP-1	5							None	None	GOX
		25							722	None	GOX
		50							722	None	GOX
		50							755	755	GOX
		100							724	724	GOX
		500							658	658	GOX
		1000							619	619	GOX
		1500							588	588	GOX
		2000							582	582	GOX
"	Vespel SP-21	5							569	None	GOX
		25							784	None	GOX
		50							548	None	GOX
		50							774	774	GOX
		100							766	766	GOX
		500							718	718	GOX
		1000							660	660	GOX
		1500							620	620	GOX
		2000							605	605	GOX
Marzani (1968b)	Vespel SP-1 Polyimide	3325	621								GOX

SEALANTS, THREAD, COMPOUNDS, AND LUBRICANTS

Reference	Materials	Test Pressure (psi)	Ingition Temp. (K)	Test Temp. (K)	Mechanical Impact Energy (kg m)	Mechanical Impact Reaction Rate	Pneumatic Impact Reaction Rate	Specimen Thickness (in)	Flash Point (K)	Fire Point (K)	Environment
Guter(1967)	Aircraft Lubricating Oil DE 2472 B/O	15	582								GOX
		300	513								GOX
		750	498								GOX
		1500	483								GOX
		2625	475								GOX
		3750	480								GOX
Jamison(1970)	Andox C Oil	2000		299	1.4	0/21					GOX
Nihart and Smith(1964)	Aroclor 1254	2000	649								GOX
		7500	628								GOX
"	Burnil Brand Microplates	2000	>773								GOX
		7500	>773								GOX
"	Dixon's Flake Graphite No. 1	2000	>773								GOX
		7500	>773								GOX
Jamison(1970)	Dow Corning 33 Grease	2000		297	1.4	0/20					GOX
Pippen and Stradling (1971)	Drilube 822	5							721	None	GOX
		25							648	677	GOX
		50							608	608	GOX
		50							561	561	GOX
		100							576	576	GOX
		500							525	525	GOX
		1000							511	511	GOX
		1500							473	473	GOX
		2000							483	483	GOX
Nihart and Smith(1964)	Everlube No. 811	2000	489								GOX
		7500	523								GOX
Austin(1972)	Everlube No. 811	100		90	10	0/20		.030			LOX
		500		90	10	0/20		.030			LOX
		1000		90	10	0/20		.030			LOX
		1500		90	10	0/20		.030			LOX
		100		300	10	0/20		.030			GOX
		500		300	10	0/20		.030			GOX
		1000		300	10	0/20		.030			GOX
		1500		300	10	0/20		.030			GOX

SEALANTS, THREAD, COMPOUNDS, AND LUBRICANTS cont.

Reference	Materials	Test Pressure (psi)	Ignition Temp. (K)	Test Temp. (K)	Mechanical Impact Energy (kg m)	Mechanical Impact Reaction Rate	Pneumatic Impact Reaction Rate	Specimen Thickness (in)	Flash Point (K)	Fire Point (K)	Environment
Austin(1972)	Everlube No. 811 B-2	100		90	10	0/20		.030			LOX
		500		90	10	0/20		.030			LOX
		1000		90	10	0/20		.030			LOX
		1500		90	10	2/20		.030			LOX
		1500		90	9	0/20		.030			LOX
		1500		90	8.3	0/20		.030			LOX
		100		300	10	0/20		.030			GOX
		500		300	10	0/20		.030			GOX
		1000		300	10	0/20		.030			GOX
		1500		300	10	0/20		.030			GOX
"	Everlube No. 812	100		90	10	0/20		.030			LOX
		500		90	10	0/20		.030			LOX
		1000		90	10	0/20		.030			LOX
		1500		90	10	0/20		.030			LOX
		100		300	10	0/20		.030			GOX
		500		300	10	0/20		.030			GOX
		1000		300	10	0/20		.030			GOX
		1500		300	10	0/20		.030			GOX
Nihart and Smith(1964)	Fluorinated Hydrocarbon	50				0					GOX
		100				20 %					GOX
		500				50 %					GOX
		1000				66.6%					GOX
Austin(1972)	Fluorolube GR 290	100		90	10	0/20		.030			LOX
		500		90	10	0/20		.030			LOX
		1000		90	10	0/20		.030			LOX
		1500		90	10	0/20		.030			LOX
		100		300	10	0/20		.030			GOX
		500		300	10	0/20		.030			GOX
		1000		300	10	0/20		.030			GOX
		1500		300	10	8/20		.030			GOX
		1500		300	9	5/20		.030			GOX
		1500		300	8.3	0/20		.030			GOX
		1500		300	7.6	0/20		.030			GOX

SEALANTS, THREAD, COMPOUNDS, AND LUBRICANTS cont.

Reference	Materials	Test Pressure (psi)	Ingition Temp. (K)	Test Temp. (K)	Mechanical Impact Energy (kg m)	Mechanical Impact Reaction Rate	Pneumatic Impact Reaction Rate	Specimen Thickness (in)	Flash Point (K)	Fire Point (K)	Environment
Austin(1972)	Halocarbon 4-11ES	100		90	10	0/20		.030			LOX
		500		90	10	0/20		.030			LOX
		1000		90	10	0/20		.030			LOX
		1500		90	10	0/20		.030			LOX
		100		300	10	0/20		.030			GOX
		500		300	10	0/20		.030			GOX
		1000		300	10	0/20		.030			GOX
		1500		300	10	0/20		.030			GOX
"	Halocarbon 10-25E	100		90	10	0/20		.030			LOX
		500		90	10	0/20		.030			LOX
		1000		90	10	0/20		.030			LOX
		1500		90	10	0/20		.030			LOX
		100		300	10	0/20		.030			GOX
		500		300	10	0/20		.030			GOX
		1000		300	10	0/20		.030			GOX
		1500		300	10	12/20		.030			GOX
		1500		300	8.3	2/20		.030			GOX
		1500		300	7.6	0/20		.030			GOX
		1500		300	7.0	0/20		.030			GOX
"	Halocarbon 14-25	100		90	10	0/20		.030			LOX
		500		90	10	0/20		.030			LOX
		1000		90	10	0/20		.030			LOX
		1500		90	10	0/20		.030			LOX
		100		300	10	0/20		.030			GOX
		500		300	10	0/20		.030			GOX
		1000		300	10	0/20		.030			GOX
		1500		300	10	2/20		.030			GOX
		1500		300	9	0/20		.030			GOX
		1500		300	8.3	0/20		.030			GOX
"	Halocarbon 14-25ES	100		90	10	0/20		.030			LOX
		500		90	10	0/20		.030			LOX
		1000		90	10	0/20		.030			LOX
		1500		90	10	0/20		.030			LOX
		100		300	10	0/20		.030			GOX
		500		300	10	0/20		.030			GOX
		1000		300	10	0/20		.030			GOX
		1500		300	10	0/20		.030			GOX

SEALANTS. THREAD. COMPOUNDS. AND LUBRICANTS cont.

Reference	Materials	Test Pressure (psi)	Ingition Temp. (K)	Test Temp. (K)	Mechanical Impact Energy (kg m)	Mechanical Impact Reaction Rate	Pneumatic Impact Reaction Rate	Specimen Thickness (in)	Flash Point (K)	Fire Point (K)	Environment
Austin(1972)	Halocarbon 11-14E	100		90	10	0/20		.030			LOX
		500		90	10	0/20		.030			LOX
		1000		90	10	0/20		.030			LOX
		1500		90	10	0/20		.030			LOX
		100		300	10	0/20		.030			LOX
		500		300	10	0/20		.030			GOX
		1000		300	10	0/20		.030			GOX
		1500		300	10	0/20		.030			GOX
"	Halocarbon 11-21E	100		90	10	0/20		.030			LOX
		100		90	10	0/20		.030			LOX
		500		90	10	0/20		.030			LOX
		1500		90	10	0/20		.030			LOX
		100		300	10	0/20		.030			GOX
		500		300	10	0/20		.030			GOX
		1000		300	10	0/20		.030			GOX
		1500		300	10	0/20		.030			GOX
"	Halocarbon 11-21ES	100		90	10	0/20		.030			LOX
		500		90	10	0/20		.030			LOX
		1000		90	10	0/20		.030			LOX
		1500		90	10	0/20		.030			LOX
		100		300	10	0/20		.030			GOX
		500		300	10	0/20		.030			GOX
		1000		300	10	0/20		.030			GOX
		1500		300	10	0/20		.030			GOX
"	Halocarbon 13-21ES	100		90	10	0/20		.030			LOX
		500		90	10	0/20		.030			LOX
		1000		90	10	0/20		.030			LOX
		1500		90	10	0/20		.030			LOX
		100		300	10	0/20		.030			GOX
		500		300	10	0/20		.030			GOX
		1000		300	10	0/20		.030			GOX
		1500		300	10	0/20		.030			GOX
Nihart and Smith(1964)	Halocarbon Grease Series 25-10	2000, 7500	704								
"	Halocarbon Oil Series 13-21	2000, 7500	708								GOX
											GOX

SEALANTS, THREAD, COMPOUNDS, AND LUBRICANTS cont.

Reference	Materials	Test Pressure (psi)	Ignition Temp. (K)	Test Temp. (K)	Mechanical Impact Energy (kg m)	Mechanical Impact Reaction Rate	Pneumatic Impact Reaction Rate	Specimen Thickness (in)	Flash Point (K)	Fire Point (K)	Environment
Nihart and Smith(1964)	High Purity Goop	2000, 7500	684								GOX
Austin(1972)	Inlox 44	100		90	10	0/20		.030			LOX
		500		90	10	0/20		.030			LOX
		1000		90	10	0/20		.030			LOX
		1500		90	10	0/20		.030			LOX
		100		300	10	0/20		.030			GOX
		500		300	10	0/20		.030			GOX
		1000		300	10	0/20		.030			GOX
		1500		300	10	0/20		.030			GOX
Jamison(1970)	Invelco 33F Grease	2000		294	10	0/20					GOX
Nihart and Smith(1964)	KEL-F 90 Grease	2000	708								GOX
		7500	708								GOX
Austin(1972)	Krytox 280-AB	100		90	10	0/20		.030			LOX
		500		90	10	0/20		.030			LOX
		1000		90	10	0/20		.030			LOX
		1500		90	10	0/20		.030			LOX
		100		300	10	0/20		.030			GOX
		500		300	10	0/20		.030			GOX
		1000		300	10	0/20		.030			GOX
		1500		300	10	0/20		.030			GOX
Pippen and Stradling(1971)	Krytox 240 AC Grease	5							621	None	GOX
		25							429	None	GOX
		50							None	None	GOX
		50							739	739	GOX
		100							731	731	GOX
		500							725	725	GOX
		1000							689	689	GOX
		1500							703	703	GOX
		2000							689	689	GOX
"	Krytox 240 AC Grease	5000		300	1.4	0/4	0/4				GOX
Jamison(1970)	Krytox 240 AC Grease	2000		297	1.4	0/20					GOX

SEALANTS, THREAD, COMPOUNDS, AND LUBRICANTS cont.

Reference	Materials	Test Pressure (psi)	Ignition Temp. (K)	Test Temp. (K)	Mechanical Impact Energy (kg m)	Mechanical Impact Reaction Rate	Pneumatic Impact Reaction Rate	Specimen Thickness (in)	Flash Point (K)	Fire Point (K)	Environment
Nihart and Smith(1964)	Linde Green Pipe Joint Compound	2000	629								GOX
		7500	635								GOX
"	50-50 Soft Solder	2000	>773								GOX
		7500	>773								GOX
Brooks(1923)	Linseed Oil	0-3200	394								GOX
Pippen and Stradling (1971)	L9/3T Grease	5							641	None	GOX
		25							671	678	GOX
		50							685	685	GOX
		50							588	588	GOX
		100							551	551	GOX
		500							518	518	GOX
		1000							512	512	GOX
		1500							506	506	GOX
		2000							515	515	GOX
Nihart and Smith(1964)	Mano Pipe and Joint Compound	2000	633								GOX
		7500	695								GOX
"	MolyKote Z	2000, 7500	550								GOX
"	Oxweld Anti-Friction Compound No. 54	2000	510								GOX
		7500	503								GOX
"	Oxweld Anti-Friction Compound No. 64	2000, 7500	683								GOX
"	Oxylube No. 703	2000	511								GOX
		7500	463								GOX
"	Rectorseal No. 15	2000	647								GOX
		7500	628								GOX
Guter(1967)	Silicone D.C. Fluid 200 CSTICS 100	750	561								GOX
		3750	474								GOX

ELASTOMERS

Reference	Materials	Test Pressure (psi)	Ignition Temp. (K)	Test Temp. (K)	Mechanical Impact Energy (kg m)	Reaction Rate	Pneumatic Impact Reaction Rate	Specimen Thickness (in)	Flash Point (K)	Fire Point (K)	Environment
Pippin and Stradling (1971)	Burma-N Rubber	5000		300	0.34	0/4	0/4				GOX
		1500		300	0.34	0/4	2/4				GOX
		2000		300	0.34	0/4	4/4				GOX
"	Butyl Rubber	5							650	None	GOX
		25							619	619	GOX
		50							617	617	GOX
		50							503	503	GOX
		100							494	494	GOX
		500							453	453	GOX
		1000							439	439	GOX
		1500							431	431	
		2000									
Nihart and Smith (1964)	Duroid 5600	7500	742								GOX
	Duroid 5650	7500	725								GOX
	Duroid 5870	7500	730								GOX
	Duroid 5813	7500	736								GOX
		2000	701								
McQuaid (1972)	Ethylene Propylene Rubber	2475	456.5								GOX
Marzani (1968)	Ethylene Propylene Rubber	2500	457								GOX
"	Ebonite	750	455								GOX
		1500	435								GOX
		2625	417								GOX
		3750	419								GOX
Jamison (1970)	Ethylene - Propylene Rubber-EMS 388 (EPR)	2000		294	1.4	8/9					GOX
Pippen and Stradling (1971)	Fluorosilicone Elastomer	2500		300			0/4				GOX
		3000		300	1.4	0/2	1/4				GOX
		3500		300			1/2				GOX
		4000		300	1.4	0/2	1/2				GOX
		4500		300			4/4				GOX
		5000		300	1.4	0/8					GOX

ELASTOMERS cont.

Reference	Materials	Test Pressure (psi)	Ignition Temp. (K)	Test Temp. (K)	Mechanical Impact Energy (kg m)	Mechanical Impact Reaction Rate	Pneumatic Impact Reaction Rate	Specimen Thickness (in)	Flash Point (K)	Fire Point (K)	Environment
Schwinghamer (1971)	Fluorinated Silicone	50				50%					GOX
		100				50%					GOX
		500				100%					GOX
		1000				100%					GOX
Pippen and Stradling (1971)	Fluorosilicone L-449-6	5							644	682	GOX
		25							653	653	GOX
		50							639	639	GOX
		50							548	548	GOX
		100							544	544	GOX
		500							529	529	GOX
		1000							498	498	GOX
		1500							465	465	GOX
		2000							463	463	GOX
Guter (1967)	Hycar Lining Tube	750	643								GOX
		1500	646								GOX
		2625	473								GOX
		3750	435								GOX
"	I.C.I. Standard Rubber	750	598								
		1500	589								
		3750	470								
"	I.C Sta. Rub.	750	524								
		1500	409								
		2625	408								
		3750	407								
Nihart and Smith (1964)	KEL-F 81	7500	701				1/1				GOX
	KEL-F Elastomer 3700	7500	610								GOX
	KEL-F Elastomer 5500	7500	620								GOX
Guter (1967)	Natural Rubber Hose	750	584								GOX
		1500	451								GOX
		2625	406								GOX

ELASTOMERS cont.

Reference	Materials	Test Pressure (psi)	Ignition Temp. (K)	Test Temp. (K)	Mechanical Impact Energy (kg m)	Mechanical Impact Reaction Rate	Pneumatic Impact Reaction Rate	Specimen Thickness (in)	Flash Point (K)	Fire Point (K)	Environment
McQuaid (1972)	Neoprene (Valve Diaphragm)	2300	454								GOX
	Neoprene	1000		300			0/4				GOX
		1500		300			2/3				GOX
		4500		300			4/4				GOX
		5000		300	0.34	0/4					GOX
Guter (1967)	Neoprene	750	579								GOX
		1500	558								GOX
		2625	518								GOX
		3750	478								GOX
Pippen and Stradling (1971)	Neoprene	5							611	None	GOX
		25							600	602	GOX
		50							649	649	GOX
		50							507	507	GOX
		100							506	506	GOX
		500							496	496	GOX
		1000							496	496	GOX
		1500							460	460	GOX
		2000							465	465	GOX
"	Red Fiber Sheet	5000		300	0.34	0/4					GOX
		1500		300		0/4					GOX
		2000		300		1/2					GOX
		2500		300		1/2					GOX
		3000		300		4/4					GOX
Guter (1967)	Red Vulcanized Fiber Block	15	648								
		750	545								
		1500	493								
		2625	483								
		3750	485								
Guter (1967)	Red Vulcanized Fiber Shavings	15	625								
		750	546								
		1500	488								
		2625	462								
		3750	418								
	Rubber Diaphragms	750	503								GOX
		1500	448								GOX
		3750	410								GOX

ELASTOMERS cont.

Reference	Materials	Test Pressure (psi)	Ignition Temp. (K)	Test Temp. (K)	Mechanical Impact Energy (kg m)	Mechanical Impact Reaction Rate	Pneumatic Impact Reaction Rate	Specimen Thickness (in)	Flash Point (K)	Fire Point (K)	Environment
Nihart and Smith (1964)	Rulon A	7500	737								GOX
	Rulon B	7500	736								GOX
"	Rulon C	7500	735								GOX
Jamison (1970)	Si Elastomer SE-342	2000		294	1.4	4/20					GOX
"	Si Elastomer	2000		297	1.4	5/9					GOX
Pippen and Stradling (1971)	Silicone Elastomer	1000		300	1.4	0/4					GOX
		1500		300	1.4	1/2					GOX
		2000		300	1.4	4/4					GOX
		3000		300			0/4				GOX
		3500		300			4/4				GOX
		4500		300	0.34	0/4					GOX
		5000		300	0.34	1/2					GOX
"	Silicone C-Ring	5							None	None	GOX
		25							684	702	GOX
		50							688	688	GOX
		50							610	610	GOX
		100							656	656	GOX
		500							527	527	GOX
		1000							496	496	GOX
		1500							503	503	GOX
		2000							501	501	GOX
Jamison (1970)	Silicone Rubber Primer A-4094	2000		299	1.4	0/21					GOX
"	Primer SS-4004	2000		297	1.4	3/6					GOX
Schwinghamer (1971)	Silicone	50				50%					GOX
		100				100%					GOX
		500				100%					GOX
		1000									GOX
Jamison (1970)	Silicone 5537	20		296.5	2.8	0/21					GOX
		100		299.5	2.8	3/9					GOX
		2000		296.5	1.4	7/16					GOX
Guter (1967)	Silicone Rubber	750-3750	598								GOX

ELASTOMERS cont.

Reference	Materials	Test Pressure (psi)	Ignition Temp. (K)	Test Temp. (K)	Mechanical Impact Energy (kg m)	Mechanical Impact Reaction Rate	Pneumatic Impact Reaction Rate	Specimen Thickness (in)	Flash Point (K)	Fire Point (K)	Environment
Nihart and Smith (1964)	Teflon (virgin)	7500	740				1/1				GOX
	Teflon (100 x)	7500	688								GOX
"	Viton A (virgin)	7500	578				2/2				GOX
	Viton B (virgin)	7500	593								GOX
Jamison (1970)	Viton V-EMS-338	2000		299	1.4	0/20					GOX
"	Viton A-HS-757A	2000		299	1.4	0/20					GOX
"	Viton B	2000		200	1.4	0/21					GOX
Pippen and Stradling (1971)	Viton Rubber	3500		300			0/4				GOX
		4000		300	.34	0/1	1/3				GOX
		5000		300	.34	0/4					GOX
"	Viton A	5							621	None	GOX
		25							610	740	GOX
		50							660	714	GOX
		50							590	590	GOX
		100							583	583	GOX
		500							540	540	GOX
		1000							523	523	GOX
		1500							518	518	GOX
		2000							515	515	GOX

MISCELLANEOUS

Reference	Materials	Test Pressure (psi)	Ignition Temp. (K)	Test Temp. (K)	Mechanical Impact Energy (kg m)	Mechanical Impact Reaction Rate	Pneumatic Impact Reaction Rate	Specimen Thickness (in)	Flash Point (K)	Fire Point (K)	Environment
Jamison(1970)	Armstrong A-2	2000		294	1.4	4/20					GOX
	Activator A	100		294	1.4	0/22					GOX
Marzani (1968a)	Asbestos, TFE, MOS_2 Phenolic Resin	2250	446.5								GOX
"	Asbestos Cloth TFE Phenolic Resin	2200	432.5								GOX
"	Asbestos Cloth Graphite, Phenolic Resin	2200	430								GOX
"	Carbon Graphite-Copper	3275	607								GOX
"	Carbon Graphite - Silver	3200	588								GOX
"	Carbon Graphite-Babbit	3100	576.5								GOX
Pippen and Stradling (1971)	Epibond 70-1768	500		300	1.4	4/4					GOX
		1000		300			0/4				GOX
		1500		300			1/2				GOX
		2000		300			1/3				GOX
Jamison(1970)	Epibond 123	2000		297	1.4	5/9					GOX
	Hardner 931	100		297	1.4	0/21					GOX
Pippen and Stradling (1971)	2T Epoxy	4500		300	.34	0/4					GOX
		5000			.34	1/3	0/4				GOX
"	EA-40 Epoxy	3500		300			0/1				GOX
		4000		300			0/4				GOX
		4500		300			4/4				GOX
Marzani (1968a)	Laminated Glass-Filled Epoxy	2500	460								GOX

MISCELLANEOUS cont.

Reference	Materials	Test Pressure (psi)	Ignition Temp. (K)	Test Temp. (K)	Mechanical Impact Energy (kg m)	Reaction Rate	Pneumatic Impact Reaction Rate	Specimen Thickness (in)	Flash Point (K)	Fire Point (K)	Environment
Austin(1972)	Epoxy	15		90	10	20/20		0.05			LOX
	Fiberglass	15		90	7.62	20/20		0.05			LOX
		15		90	5.54	20/20		0.05			LOX
		15		90	3.46	20/20		0.05			LOX
		15		90	1.38	4/20		0.05			LOX
		15		90	0.68	2/20		0.05			LOX
		100		300	10	15/20		0.05			GOX
		100		300	7.62	20/20		0.05			GOX
		100		300	5.54	20/20		0.05			GOX
		100		300	4.86	2/20		0.05			GOX
		100		300	4.17	0/20		0.05			GOX
		100		300	3.46	0/20		0.05			GOX
		500		300	4.86	2/5		0.05			GOX
		500		300	4.17	0/20		0.05			GOX
		1000		300	4.17	1/6		0.05			GOX
		1500		300	4.17	1/1		0.05			GOX
Guter(1967)	GACO Seats	750	673								GOX
	Grade H22	1500	604								GOX
		3750	455								GOX
Marzani (memo)	Graphite	3800	724								GOX
Guter(1967)	Lamp Black	750	646								GOX
Jamison (1970)	Locktite Grade C	2000		294	1.4	0/20					GOX
Pippen and Stradling (1971)	FLV Viton Cement	25							None	None	GOX
		50							701	701	GOX
		50							617	617	GOX
		100							632	632	GOX
		500							574	574	GOX
		1000							559	559	GOX
		1500							507	507	GOX
		2000							516	516	GOX
Jamison (1970)	RTV	2000		297	1.4	4/4					GOX
Guter(1967)	Resin Bonded Fabric	750	483								GOX
		1500	474								GOX
		3750	434								GOX
Jamison (1970)	Scot Weld Structural	2000		297	1.4	2/19					GOX
"	Viton Cement Coating Material	2000		299	1.4	0/20					GOX

END OF REFERENCE

157

REFERENCE

158

ATTWOOD, H. C.; AND ALLEN, G. R.: ON THE SPONTANEOUS IGNITION TEMPERATURE OF ORGANIC MATERIALS IN OXYGEN. C.P. NO. 1172, BRITISH MINISTRY OF DEFENCE (AVIATION SUPPLY), 1971.

N72-12957

3.0-0-0 D.F.

C.P. No. 1172 H.S.

MAR 17 '72

COPY

C.P. No. 1172

MINISTRY OF DEFENCE (AVIATION SUPPLY)

AERONAUTICAL RESEARCH COUNCIL

CURRENT PAPERS

On the Spontaneous Ignition Temperature of Organic Materials in Oxygen

by

Hilda C. Attwood and G. R. Allen

Engineering Physics Dept., R.A.E., Farnborough

REPRODUCTION RESTRICTIONS OVERRIDDEN
NASA Scientific and Technical Information Facility

REFERENCE COPY
MAR 17 1972
NASA
CLEVELAND, OHIO

LONDON: HER MAJESTY'S STATIONERY OFFICE

1971

PRICE 50p NET

U.D.C. 541.126 : 661.937

CP No.1172*
May 1970

ON THE SPONTANEOUS IGNITION TEMPERATURE OF ORGANIC MATERIALS IN OXYGEN

by

Hilda C. Attwood
G. R. Allen

SUMMARY

Doubts have been expressed on the significance of the current 'Bomb' and 'Pot' tests used to measure the spontaneous ignition temperature of organic materials in high and low pressure oxygen. An investigation by the British Oxygen Company to explore some of these doubts and to test new materials is described and the results are discussed. Suggestions are made for improved 'Bomb' and 'Pot' test procedures, and for investigations into the basic nature of ignition processes and the relationship between laboratory tests and field conditions.

---

* Replaces RAE Technical Report 70083 - ARC No.32376.

CONTENTS

		Page
1	INTRODUCTION	3
2	EXPERIMENTAL DETAIL	3
	2.1 British Oxygen Co. Ltd. 'Bomb' test	3
	2.2 British Oxygen Co. Ltd. 'Pot' test	4
	2.3 Outline of investigation	4
3	RESULTS OF TESTS BY THE BRITISH OXYGEN CO. LTD.	7
4	DISCUSSION OF BRITISH OXYGEN CO. LTD.'S RESULTS	8
	4.1 Spread of results	9
	4.2 Ageing of nylon	9
	4.3 New materials	10
	4.4 Effect of powders	10
	4.5 Comparison of 'Bomb' and 'Pot' tests	10
5	FURTHER CONSIDERATIONS OF MATERIAL COMPATIBILITY WITH OXYGEN	12
	5.1 Basic work	12
	5.2 Interim standard test	13
6	CONCLUSIONS AND RECOMMENDATIONS	14
Acknowledgements		15
Appendix A	Fires/explosions in oxygen valves	17
Appendix B	Statistical analysis of results	19
Tables 1-6		21-26
References		27
Illustrations		Figures 1-7
Detachable abstract cards		-

1 INTRODUCTION

1.1 After several incidents of fire in high pressure oxygen equipment, which are outlined in Appendix A, the suitability of certain materials for use in oxygen was reconsidered. Probably the most important physical property involved is the spontaneous ignition temperature (SIT) of a material in oxygen.

The main U.K. reference for SITs of materials in high and low pressure oxygen is the Ministry of Supply Memorandum S & T 13/50 [1], but this report, being issued in 1950, includes no data on modern materials. Furthermore SITs at atmospheric pressure were measured by a 'Pot' test whereas a 'Bomb' test was used at all higher pressures; both tests are detailed in sections 2.1 and 2.2. Hence the apparent large reduction in SIT which occurs for some materials as the oxygen pressure is increased from 1 atm to 5 atm and above, could be due, wholly or in part, to the different methods of test. Some means of correlating the results of the two tests is obviously desirable.

1.2 In the six incidents leading to this study it was possible that wear by moving parts could have generated particles of material, or that 'ageing' of a material either naturally with time, or by contamination, might have occurred. The effects of these factors on SIT had not been investigated in either the 'Bomb' or the 'Pot' tests. To help clarify the above points an R.A.E. contract was placed with British Oxygen Company Ltd. to explore the above effects on the SIT of selected materials; most of which are relatively new and are intended for use in future oxygen equipment. At about the same time a Mintech contract was placed with Bristol University, for a paper study of test techniques and means of assessing material compatability with oxygen, which are currently used in the U.K. and the U.S.A.

1.3 In this Report the two methods of test used by B.O.C. Ltd., the factors investigated, and the materials tested, are outlined in section 2. The test results are presented in section 3 and discussed in section 4. The more fundamental aspects of this work are linked with the work of Bristol University in section 5. Conclusions and recommendations are given in section 6.

2 EXPERIMENTAL DETAIL

2.1 British Oxygen Co. Ltd. 'Bomb' test

The high pressure oxygen test, referred to as the 'Bomb' test, is substantially the same as that used by Guter in 1950 and is fully described

in S & T 13/50 [1]. The 'Bomb' and the associated test apparatus are shown diagrammatically in Figs.1 and 2. The temperature in the 'Bomb' is increased at a rate of approximately 20°C per minute and is recorded continuously. Ignition is indicated by a sudden increase in this temperature.

2.1.1 Use with static gas, pressure in excess of 1 atmosphere

The glass boat, containing a sample of material weighing 60 mg is positioned in the 'Bomb' so that it is directly beneath the thermocouple tip, midway along the heating element. The nose plug is tightened into the 'Bomb' chamber which is then purged with oxygen at 5 atm pressure. The chamber is then filled with oxygen to approximately 90% of the required test pressure. Heating is commenced and the temperature recorded. The pressure increases with the temperature, and any excess gas is vented through a manually operated valve in the outlet pipe.

When either ignition occurs, or a temperature of 400°C is reached, the heating is switched off. After the system has cooled to 100°C the gas is vented and the test sample examined.

2.1.2 Flowing gas at 1 atmosphere pressure

A weighed sample is positioned in the 'Bomb' as above. A flowmeter is then connected to the outlet and the flow adjusted to either 0.2 l/min or 2.0 l/min. The meter is then disconnected, but the constant mass flow of oxygen is maintained and is vented to a fume cupboard. The heating is then switched on and the experiment continued as above.

2.2 British Oxygen Co. Ltd. 'Pot' test

A diagram of the test apparatus, which is fully described elsewhere[1] is given in Fig.3. The temperature of the oxygen in the open ended tube or 'Pot' is maintained at a predetermined value to within ±2°C for 15 minutes. A sample of material, weighing 60 mg is placed on a Pyrex glass spoon and is then lowered into the gas stream. If no ignition is seen within two minutes the test is repeated with a fresh sample of material. Samples are tested for gas temperature increments of 5°C, either until ignition occurs or until a temperature of 400°C is reached.

2.3 Outline of investigation

2.3.1 Aims

The materials and the test conditions were chosen in order to investigate the following factors:

(i) The spontaneous ignition temperature of nylon, and of the sealing compound ZX32: both of which were suspect materials in recent fire incidents.

(ii) The effect of 'ageing', either with time or by contamination, on the spontaneous ignition temperature of nylon used in R.A.F. line valves.

(iii) The comparison of the results of the 'Bomb' and the 'Pot' tests, both at atmospheric pressure, (see section 1.1).

(iv) The difference in SIT between powdered samples and block samples of equal weight of the same material.

(v) The spontaneous ignition temperature of the materials listed in section 2.3.3, most of which are relatively new and are intended for use in future equipment. These materials were chosen after consultation with several firms which have design and/or production contracts from Mintech HQ.

2.3.2 Test schedule

The conditions of each test are detailed in the results shown in Figs.4, 5 and 6 and are outlined below:

SIT of materials measured by 'Pot' test

60 mg block samples of each material, listed in section 2.3.3 were tested at atmospheric pressure with an oxygen flow rate of 2 l/min. 60 mg powdered samples of each solid material were also tested in the same conditions. The required number of samples to establish the ignition temperature, or to reach the 400°C temperature limit of the apparatus, were used. The SIT was 'established' when the first three samples tested at one temperature, all ignited.

SIT of materials measured by the 'Bomb' test

Six 60 mg block samples of each material listed in section 2.3.3 were tested in static oxygen at 10 atm and 130 atm above atmospheric pressure, as these are the working pressures of aircraft LOX and high pressure gas systems respectively. Some of the materials were also tested at 5 atm and 50 atm above atmospheric pressure. Six 60 mg powdered samples of each solid material were also tested under the same conditions as the block samples.

So that the 'Bomb' and 'Pot' tests could be compared, 60 mg samples, in block and powder form of most materials, were tested in the 'Bomb' at 1 atm pressure in flowing gas. A flow of 2 l/min was used to give the same mass flow as in the 'Pot' test. Because of differences in the sizes of the two test

apparatuses, some tests were repeated in the 'Bomb' with a flow of 0.2 l/min, so that the gas velocity was the same as in the 'Pot' test.

2.3.3 Classification of materials

The materials tested fall into four main groups:

Group A - Nylon

(i) New Nylon 66.

(ii) Used Nylon 66 (valve seats of high pressure line valves removed from R.A.F. aircraft because of stripped threads etc.).

(iii) A new type of nylon designated B100.

Group B - Lubricants and sealing compounds

(i) Rocol MA-1 (water based, molybdenum disulphide with organic soap).

(ii) Rocol dry film lubricant (water based, molybdenum disulphide, sodium silicate).

(iii) Acheson Industries Ltd. ZX32 (DAG517. A suspension of graphite in a non-flammable fluid).

(iv) Silicone grease XG315 (equivalent to MS33).

Group C - Elastomers and thermoplastic materials

(i)	ICI, silicone rubbers (room temperature vulcanised)	Silcoset 100 Silcoset 106
(ii)	Midland Silicones Ltd., silicone rubbers	Silastomer S2453 Silastomer S2475
(iii)	Dow Corning, silicone rubber	Silastic 55
(iv)	J. Walker & Co. Ltd., (PTFE molybdenum disulphide fibre glass mixture).	Fluolion G15M

Group D - Adhesives

(i)	Midland Silicones Ltd., silicone adhesive	MS2705
(ii)	Douglas Kane Ltd., shaft locking compound.	Loktite D.

2.3.4 Preparation of materials

All samples as received from the suppliers were handled with clean, oil free tools. Block samples were cut into 60 mg portions using clean degreased cutters. Powders were made by means of a new degreased file cooled in liquid nitrogen. A separate file was kept for each material to prevent cross contamination. Only that portion of the powder which would pass through a size 30 mesh, but not through a size 85 mesh was used in the tests as this was thought to be representative of the size of particle which could be formed inside valves etc. by general wear. One exception was however made: because only a limited supply of used nylon was available the powder was graded by size 30 and size 200 mesh for this material only.

3 RESULTS OF TESTS BY THE BRITISH OXYGEN CO. LTD.

The spontaneous ignition temperature of each sample of material is shown diagrammatically in Figs.4, 5 and 6. Detailed results of 'Pot' tests, illustrating test procedure, are given in Fig.7. A summary is given in Table 1.

The most noticeable features of the results are:

(i) The wide range of measured SIT for certain nominally identical sample and test conditions, especially in the 'Bomb' test.

(ii) The low SIT of some powdered 'aged' samples of nylon.

(iii) The increase in the SIT of several silicone materials with increasing oxygen pressure.

Wherever possible a statistical analysis has been made to assess the significance levels of the effects of various factors on SIT. Details of the analysis are given in Appendix B and the results presented in Tables 2 to 6. As some of the results were indefinite, being stated as 'above 400°C' the validity of the findings is uncertain, but some trends, summarised in the table on the following page are apparent.

Test	Material	Factor giving lowest statistically significant SIT	Factor giving lowest individual SIT
Comparison of 'Pot' at 2.0 1/min and 'Bomb' at 0.2 and 2.0 1/min 1 atm.	Silicones Loktite D	'Bomb' 'Pot'	'Bomb' 'Bomb'
Comparison of flow rates in 'Bomb' test	Silicones Loktite D	High flow No significant difference	High flow Low flow
Effect of pressure on 'Bomb' test	Silicones (not XG315) XG315 and Nylon Loktite D	Low pressure High pressure Low pressure	Low pressure High pressure Low pressure
Comparison of block and powder 11 atm static 11 atm static 1 atm flowing 51 atm static 131 atm static	 Silicones Nylon Silicones Nylon Nylon	 Block Block Powder Powder Powder	 Block Block Powder Both same Powder
Effect of age and use	Nylon	Used material	Used material

4 DISCUSSION OF BRITISH OXYGEN CO. LTD.'S RESULTS

It is apparent that the nature of the test, whether 'Bomb' or 'Pot', static gas or flowing gas, and that the condition of the test sample, whether in block or powder form, new or used, can considerably affect the SIT of a material. However no generalizations regarding the differences between 'Bomb' and 'Pot' tests, or block and powder samples, can be made. For instance most silicone materials have a lower SIT in the 'Bomb' at atmospheric pressure, than in the 'Pot' at atmospheric pressure. The reverse is true for three powdered samples of nylon, and for Loktite D when the flow through the 'Bomb' is 2 1/min, these materials do not contain silicone. Similarly powdered materials may have either a higher or lower SIT than blocks of materials, depending upon the oxygen pressure. Additionally nominally identical tests on six samples yielded a wide range of SITs in some cases; and the results of the 'Bomb' test at 1 atm varied significantly with the velocity of oxygen. These factors are discussed separately in the following sections.

4.1 Spread of results

An interesting and so far inexplicable feature of the 'Bomb' test results which does not occur with those of the 'Pot' test is the wide range of measured values for certain nominally identical conditions. It is presumed that generally the SIT of a material is measured for comparison with some predetermined lowest limit of acceptability, and hence some method of interpreting the spread of results is needed. If the distribution of SITs about the mean value is random, then 95% of all samples of material can be expected to have an SIT within two standard deviations of the mean measured SIT, hence 97½% will have an SIT above the 'mean minus two s.ds' temperature.

It is therefore suggested that if the mean SIT minus two standard deviations, is equal to or greater than a specified critical temperature, then the material is acceptable. With this mode of interpreting the results there is a 2½% or less probability that the actual SIT of any single sample falls below the acceptance level.

Although 2½% might at first sight seem to be high, it must be remembered that first this probability of a sample having an SIT less than the predetermined lowest acceptable value will apply only to borderline materials; it is expected that many materials will have SITs much higher than the critical temperature in which cases any risk will be negligible.

Secondly, if a material only just passes the acceptability test then for a fire to occur the 2½% or less of items having SITs less than the critical temperature must coincide with an occurrence of abnormally high temperature. As normal precedures for using oxygen equipment are designed to prevent such occurrences, high temperatures are expected to be rare, hence the probability of fire, even with borderline materials, should be very much less than 2½%.

4.2 Ageing of nylon

The results (Table 2) indicate that the SIT of nylon can significantly decrease over a period of time in use in a high pressure oxygen system. The exact cause of this reduction is not known, but it is suggested that either the nylon undergoes some physical or chemical change when used continually in high pressure oxygen, or small amounts of contamination build up on the surface of the nylon: the ignition of such contaminants could release sufficient energy to ignite the nylon. Both of these suggested mechanisms have received limited study in the U.S.A. One investigator[2] showed that after prolonged storage in oxygen some materials are degraded physically and chemically,

however, no measurement of resultant SIT was attempted. Another investigator[3] showed that, as would be expected, material of high SIT can be ignited if a material of low SIT burns on its surface, and a 'promoted ignition test' based on this mechanism, was devised.

This ageing effect was probably a contributory cause to some of the fires listed in Appendix A.

4.3 New materials

The increase in the SIT with increase in oxygen pressure of all except one silicone material is the reverse of the findings of 1950[1] for materials not containing silicone. This, together with the fact that the lowest SIT was 300°C indicates that wider use of silicone materials could be encouraged in high pressure oxygen systems. However, only limited tests have been performed and the effect of ageing has not been investigated. More comprehensive tests would be needed before any definite conclusions could be reached.

4.4 Effect of powdering

As can be seen in Table 3 some materials which can be powdered give significantly different SITs in the powder form than in block form. However, the effect of powdering varies amongst materials and for a given material, depends upon test technique and oxygen pressure. No consistent pattern of behaviour could be found, nor could the change of SIT with powdering be explained. As particles of a material could be produced in manufacture and assembly, or in use, then the change of SIT with powdering can considerably affect the overall compatibility of the material with oxygen systems. Tests of material compatibility with oxygen should therefore include the SIT of both block and powder samples (section 5.2).

The reduction in SIT at high pressure, of 'aged' nylon, due to powdering may have been a contributory factor to the fires which sparked off this investigation.

4.5 Comparison of 'Bomb' and 'Pot' tests

From Figs.4, 5 and 6 it can be seen that, with the exception of one sample of nylon, the measured SIT of all solid materials was lower in the 'Bomb' at 1 atm than in the 'Pot' at 1 atm. Similarly for lubricants, sealants and adhesives, although the statistical analysis detailed in Table 4 shows no significant differences, there is some indication that the 'Bomb' gives lower

measured SITs than does the 'Pot'. Hence, the apparent large reduction in SIT of some materials, which was noted in S & T 13/50 [1] as the pressure increases from 1 atm in the 'Pot' to higher pressures in the 'Bomb', can be attributed, in part, to change in test technique. Hence when comparing materials for compatibility with oxygen, effects of test technique cannot be neglected.

The conditions of the 'Bomb' and 'Pot' tests are compared with one another, and with actual conditions from which a fire might arise, in Table 5. The two major differences at atmospheric pressure are flow rate and heating rate. From Figs.4, 5 and 6 and Table 5 it will be noted that a change of flow rate in the 'Bomb' can cause a change in measured SIT; for solids a decrease in SIT accompanies an increase in flow rate, but for lubricants, sealants and adhesives an increase in flow rate causes an increase in SIT. Although the two flow rates in the 'Bomb' were chosen to give either the same gas velocity or the same mass flow as in the 'Pot' test, neither set of 'Bomb' test results at 1 atm correlated with the 'Pot' test results.

Some of the differences could be attributed to the wide difference in heating rates. Whereas in the 'Pot' tests a material is lowered into hot gas and a relatively rapid rate of heating ensues, in the 'Bomb' test the material and the 'Bomb' are heated simultaneously and slowly. Thus in the 'Pot' there is little opportunity for gaseous material to evolve and accumulate at a sample temperature below that of the gas, but in the 'Bomb' test there is ample time for vapours to be generated and accumulated, and a combustible mixture might be formed and ignited at a temperature lower than the 'Pot' ignition temperature. Also it is possible that during the 20 minute heating period in the 'Bomb' some of the evolved vapours decompose to materials which have SITs different from the SIT of the original vapours. Such vapours might have a lower or higher SIT than the original vapour and could accelerate or inhibit the onset of fire. Alternatively, slow heating might produce slow, but not self sustaining, ignition which could lead to the test sample being surrounded by a layer of incombustible vapour.

Accumulation of vapour during the heating process can be affected by the rate of flow of oxygen through the apparatus, as high flows will tend to sweep away any vapour. In the 'Pot' test it is expected that, because of rapid heating and relatively fast flow rates, any evolved vapour will be swept away rapidly, very little decomposition will occur and only when a high temperature is attained will combustion occur. However, in the 'Bomb' the sweeping away of

any vapour would remove either ignitable material or inhibitors, thus increasing the flow rate of oxygen would in the first case increase the SIT by removing ignitable vapour, and in the second case reduce SIT by removing an inhibiting blanket of vapour. The former might apply to Loktite and silicone adhesive, the latter to silicone grease, Silicoset 100 powder, and Silastic 55 powder.

Obviously the above discussion is conjectural and there is relatively little data on the increase or decrease of SIT with flow rate. Equally obviously the 'Bomb' and 'Pot' tests cannot be correlated, nor is there any ready general explanation of the differences. Hence the 'Pot' test alone, which rarely gives the lowest SIT at atmospheric pressure, is not suitable for assessing the behaviour of a material at 1 atm or at higher oxygen pressures. Additionally as shown in Table 5, neither test fully represents the nature of ignition processes which are likely to occur in oxygen systems. As these two tests are generally accepted in the U.K. as the standard means of measuring SIT and hence of assessing material compatibility with oxygen, then further study of these, and other test techniques is desirable.

5 FURTHER CONSIDERATIONS OF MATERIAL COMPATIBILITY WITH OXYGEN

When choosing a material for use in oxygen the overriding question, once mechanical suitability and absence of toxic hazards and odour have been established, is whether or not the material is a fire hazard. This problem is generally resolved in the U.K. by measuring the SIT of the material using the 'Bomb' and 'Pot' test methods. But, as shown in section 4.5 the results of these two tests can be widely and inexplicably different, and, as illustrated in Table 5 neither test fully represents actual ignition processes. Despite this no other standard test or set of tests, by which to measure material compatibility with oxygen, in respect of fire prevention, is known to exist in the U.K. Clearly some such test is desirable. However, the work reported here, and the investigation made at Bristol University indicate that a considerable amount of basic work would be necessary before a standard laboratory test could be established and correlated with field conditions.

5.1 Basic work

There are four major parameters which are thought to affect ignition of material, and which would need investigating.

(i) The temperature, often localised, of the material and its immediate surroundings.

(ii) The chemical condition of the material, e.g. surface oxide layer.

(iii) The physical condition of the material, e.g. surface contamination, block or powder for solids, thick or thin layers for liquids.

(iv) The oxygen pressure.

The first three of these parameters are thought to be controlled by:

(v) The energy involved in the triggering process, e.g. friction, impact, etc.

(vi) The rate of application of energy.

(vii) The gas flow round the material which can remove unignited vapour or products of combustion, and can affect local temperatures.

(viii) The specific heat of the material and its surroundings.

(ix) The thermal conductivity of the material and its surroundings.

(x) The thermal absorption and emission characteristics of the material and its surroundings.

The extent and seriousness of the propagation of fire depends upon many of the above factors and also on:

(xi) The calorific value of the material.

Any basic work on these factors would almost certainly need to be related to the conditions likely to occur in actual oxygen systems.

5.2 Interim standard test

Any study as outlined above would be complex and lengthy. It is therefore suggested that an interim standard test should be adopted. Although the 'Pot' test gives results which are more consistent than those of the 'Bomb' test it is usable only at 1 atm pressure and there are no reliable means of extrapolating the results to higher pressures. Also in most, but not all, cases, the 'Pot' SIT is higher than the 'Bomb' SIT; and it is the lowest measured SIT which is particularly important in assessing material compatibility with oxygen. It is therefore suggested that the 'Pot' test, and a modified 'Bomb' test both be used as interim standards, new materials being tested over a full range of conditions and subsequent quality control tests being made for only a few selected conditions, namely those for which the material has its lowest SIT.

The range of initial test conditions for the interim standard test should include:

(i) (a) Block and powder samples for a solid.

(b) Thick and thin films for a liquid or grease.

(ii) Oxygen pressures of 0, 4, 9, 49 atm above atmospheric pressure and then at 50 atm intervals up to the maximum working pressure of the material, in the 'Bomb' test, atmospheric pressure in the 'Pot' test.

(iii) A realistic range of flow rates of oxygen.

(iv) A range of sample heating rates.

Wherever this test shows that two materials appear equally suitable then the one with the lowest calorific value should be used, as this material would be least likely to ignite, or to propagate ignition if contamination having a lower SIT caught fire, the violence of any fire will therefore be minimum.

Unpublished work at R.A.E. has shown that when a manually operated valve is suddenly opened, so allowing high pressure gas to enter a closed region which was initially at low pressure, transient temperatures up to 300°C can be attained. As such sudden temperature increases could occur in actual oxygen systems, item (iv) above might include sudden insertion of a sample into a pre-heated 'Bomb'. However, as the 'Pot' test showed that sudden heating of a sample at 1 atm tends to give higher SITs than the slower heating rates of the 'Bomb' test, and as rapid insertion of samples would necessitate modification of existing 'Bomb' test apparatus, it is thought that item (iv) could be limited to those heating rates currently obtainable with existing apparatus.

In view of the compression temperatures measured at R.A.E. it is suggested that the critical ignition temperature for assessing material compatibility with medium and high pressure oxygen should be at least 300°C. Any material which might ignite below this temperature in normal working conditions, should be deemed to be incompatible with oxygen in those conditions. Spread of experimentally measured SITs should be interpreted as suggested in section 4.1, that is, if the mean measured SIT, minus twice the standard deviation of the measured SITs is above the critical temperature (300°C) for all proposed working conditions, then the material is compatible with oxygen.

6 CONCLUSIONS AND RECOMMENDATIONS

(1) The dependence of the spontaneous ignition temperature, SIT, of a material on test techniques such as heating rate and gas flow rate, and on sample conditions such as powder or block, new and clean or used and 'aged', has been demonstrated; but no consistent trends were apparent (sections 4.1 to 4.5).

(2) Previously reported large decreases in SIT with increase in pressure above atmospheric are likely to have been partly caused by the change in test technique (section 4.5). With few exceptions the 'Pot' test gives higher SITs than the 'Bomb' test, hence the use of the 'Pot' test alone, to assess the suitability of materials for use in oxygen, cannot be recommended.

(3) Nylon is not recommended for use in high pressure oxygen. Even when new or unused its SIT can be below 300°C (section 3), and wear and 'ageing' during use can apparently lower the SIT to 155°C (section 4.2). These could have been contributory factors to the six fires from which this investigation stemmed.

(4) ZX32 a material suspected in one fire, did not ignite in any test.

(5) The SITs of several relatively new silicone materials have been measured and generally increase with an increase in oxygen pressure (section 4.3 and Fig.5). As this is the reverse of the behaviour of many non-silicone materials tested in 1950[1], silicone materials might well be used more widely in high pressure oxygen systems. However, only limited tests have been made so far: further investigation would be necessary before any definite conclusions could be drawn.

(6) The need for a test or set of tests by which to define the compatibility of a material with oxygen has been discussed (section 5) and a programme of work aimed at establishing such a test has been outlined (section 5.1). An interim standard test has been proposed (section 5.2) and a method of interpreting any spread of results suggested (sections 5.2 and 4.1).

ACKNOWLEDGEMENTS

The authors would like to thank Dr. T. J. Webster and Mr. W. O. Keeping of British Oxygen Company Limited for their considerable help and cooperation in preparing the test programme and in carrying out the experimental work. They would also like to thank all those concerned in selecting the list of materials to be tested, and in supplying samples. They acknowledge permission from British Oxygen Company Limited to reproduce Figs.1, 2 and 3 in this Report.

Table 1

RANGE OF SPONTANEOUS IGNITION TEMPERATURES, °C, OF MATERIALS IN OXYGEN

Material	'Pot' test 2 l/min 1 atm	'Bomb' test			
		2 l/min 1 atm	0.2 l/min 1 atm	Static	
				11 atm	131 atm
Nylon 66					
New block	395 to >400	>400	>400	335 to 385	285 to 315
New powder	>400	>400	>400	>400	275 to 310
6 year old block				290 to >400	275 to 360
4-6 year old powder*				355 to >400	215 to 270
1-5 year old block				300 to 320	250 to 320
Up to 7 year old powder*				350 to >400	155 to 315
Nylon B100					
New block				335 to >400	305 to 355
New powder				355 to >400	265 to 350
Silcoset 100 block	>400	370 to >400		320 to 370	>400
Silcoset 100 powder	385	315 to 355	345 to 400	355 to 375	>400
Silcoset 106 block	>400	>400		>400	>400
Silcoset 106 powder	>400	>400		>400	>400
Silastomer S2453 block	>400	>400		305 to 395	>400
Silastomer S2453 powder	380 to 395	305 to 320		360 to 370	>400
Silastomer S2475 block	400	360 to 400		335 to 375	>400
Silastomer S2475 powder	375	295 to 310		345 to 355	380 to >400
Silastic 55 block	>400	>400	>400	365 to 380	>400
Silastic 55 powder	>400	345 to 370	375 to 395	370 to 385	>400
Fluolion block	>400	>400	>400	>400	>400
Fluolion powder	>400	>400	>400	>400	>400
Rocol MA-1					305 to 330
Rocol dry film lubricant	>400	>400	>400	>400	>400
Silicon grease XG315	>400	375 to 400	>400	275 to 355	255 to >400
Sealing compound ZX32	>400	>400	-	>400	>400
Silicon adhesive MS2705	340 to 345	290 to >400	345 to >400	290 to 360	310 to 330
Loktite D	220 to 230	>400	190 to >400	170 to 210	230 to 280

* Powder graded by mesh sizes 30 and 200; all other powders graded by mesh sizes 30 and 85.

N 72 - 12957
British

END OF REFERENCE

158

REFERENCE

159

KUCHTA, J. M.; LITCHFIELD, E. L.; AND FURNO, A. L.: FLAMMABILITY OF MATERIALS IN HYPERBARIC ATMOSPHERES, FINAL REPORT. REP. NO. 4016, BUREAU OF MINES, 1967.

Appropriation 7560370
Division of Hospital and
Medical Facilities
Public Health Service
Department of Health, Education
and Welfare

EXPLOSIVES RESEARCH CENTER

FLAMMABILITY OF MATERIALS IN HYPERBARIC ATMOSPHERES

FINAL REPORT NO. 4016
August 30, 1967

BUREAU OF MINES, PITTSBURGH, PA.

UNITED STATES
DEPARTMENT OF
THE INTERIOR

UNITED STATES
DEPARTMENT OF THE INTERIOR
BUREAU OF MINES
Pittsburgh, Pennsylvania

FLAMMABILITY OF MATERIALS IN HYPERBARIC ATMOSPHERES

FINAL REPORT

August 30, 1967

by

Joseph M. Kuchta
Elton L. Litchfield
Aldo L. Furno

APPROVED:

Robert W. Van Dolah
Research Director
Explosives Research Center

FLAMMABILITY OF MATERIALS IN HYPERBARIC ATMOSPHERES

FINAL REPORT

August 30, 1967

ABSTRACT

To evaluate the potential fire hazards of combustible solids in hyperbaric atmospheres, hot plate ignition temperatures, flame spread rates, and minimum ignition energies were determined for various materials. The combustibles included cotton sheeting, cotton sheeting treated with fire retardants, cotton balls, paper drapes, conductive rubber sheeting, blanket wool, polyvinyl chloride sheet, Plexiglas sheet, cellulose sheet, wood strips and dowels, and a Nomex fabric. Air, oxygen, and various oxygen-nitrogen atmospheres were employed at pressures from 1 to 6 atmospheres. Determinations for selected combustibles were also made in oxygen at reduced pressures.

The hot plate ignition temperatures of the combustibles correlated reasonably well with the oxygen partial pressure. Flame spread rates were also correlated with oxygen partial pressure; however, the rates tended to depend more upon oxygen percentage than upon total pressure. A noteworthy finding was that materials treated with certain fire retardants can ignite in oxygen-enriched atmospheres at lower temperatures than untreated materials. Ignitions of combustible solid materials by electrical sparks or arcs were obtained in several instances with electrical energies comparable to those which a human may discharge under conditions of low humidity (10 to 20 mj). In addition, minimum ignition energy requirements were investigated for several anesthetic agents including cyclopropane, diethyl ether, divinyl ether, trichloroethylene, Fluoromar, Fluothane, and chloroform.

TABLE 2. - Minimum Hot Plate Ignition Temperatures of 9 Combustible Materials in Oxygen-Nitrogen Mixtures at Various Total Pressures.

Material		Ignition Temperature, °C Total Pressure, atmospheres 1	2	3	6
Cotton sheeting	Air	465	440(425)[2]	385	365
	42% O_2, 58% N_2	390	370	355	340
	100% O_2	360	345	340	325
Cotton sheeting, treated[1]	Air	575	520(510)	485(350)	370(325)
	42% O_2, 58% N_2	390(350)	335	315	295
	100% O_2	310	--	300	285
Conductive rubber sheeting	Air	480	395	370	370
	42% O_2, 58% N_2	430	365	350	350
	100% O_2	360	--	345	345
Paper drapes	Air	470	455	425	405
	42% O_2, 58% N_2	430	--	400	370
	100% O_2	410	--	365	340
Nomex fabric	Air	>600	>600	>600	560
	42% O_2, 58% N_2	550	540	510	495
	100% O_2	520	505	490	470
Polyvinyl chloride sheet	Air	>600	--	495	490
	42% O_2, 58% N_2	575	--	370	350
	100% O_2	390	--	350	325
Plexiglas	Air	595	--	520(395)	450(400)
	42% O_2, 58% N_2	525	--	425(370)	390(385)
	100% O_2	430	--	--	--
Cellulose Acetate	Air	>600(520)	--	535(504)	470
	42% O_2, 58% N_2	525	--	410	380
	100% O_2	425	--	400	375
Blanket Wool	Air	>600	--	565	520
	42% O_2, 58% N_2	555	--	495	455
	100% O_2	500	--	450	400

1/ Cotton sheeting treated with Du Pont X-12 fire retardant; amount of retardant equal to 12 percent of cotton specimen weight.

2/ Values in parentheses indicate temperature at which material glowed.

rate of burning and flame spread will tend to be approximately the same, at least for relatively thin specimens. Higher rates should result from the 45° angle method or the vertical method[19/] (with upward propagation) because of buoyancy effects; the latter method gives less reproducible results and is generally used for materials of low combustibility. In the present work, most of the data were obtained by the 45° angle method in a 2-foot diameter steel sphere as described in Appendix 4; the burning rack was similar to that specified in reference 16.

Table 3 compares data which were obtained for the burning of cotton sheeting (4.72 oz/sq.yd.) specimens by different methods in air at atmospheric pressure. The flame spread rates (in/sec) refer to the propagation of the flame front over the top surface and length of the specimen; the burning rates (in/sec) refer to the linear rates of material burning or charring in the same direction as stated above. As expected, the lowest flame spread rate was obtained with the specimen burning downward in a vertical position (0.05 in/sec) and the highest rate with the burning upward (2.1 in/sec). The rate by the latter method was nearly 3 times as high as that found by the 45° angle method and approximately 20 times higher than that observed by the horizontal method. In comparison, the burning rates by the vertical method (burning upward) and the 45° angle method differed only slightly and were noticeably lower than the corresponding flame spread rates.

TABLE 3. - Rates of Burning and Flame Spread by Various Methods for Cotton Sheeting in Air at One Atmosphere Pressure.

	Flame Spread, in/sec	Burning Rate, in/sec
Burning Upward in Vertical Position	2.1	0.5
" Downward " "	0.05	(~0.05)
" Upward at 45° Angle	0.8	0.45
" in Horizontal Position	0.10	--

Flame spread rates from experiments conducted in open air differed little from the corresponding values found in the sphere. Also, analyses of the gases in the sphere before and after burning indicated that the oxygen depletion was less than 15 percent of the initial concentration for most of the materials examined in air or oxygen at atmospheric pressure. The exceptions were the heavy weight materials like the conductive rubber sheeting (14.75 oz/sq.yd.) which consumed excessive quantities of oxygen. However, experiments with an oxidant flow of ~10 liters per minute indicated that the flame spread rate was not greatly affected by the oxygen depletion. This can be explained by the fact that the oxygen percentage of the atmosphere did not change greatly during the fraction of the burning period when

19/ Federal Spec. CCC-T-191b, Method 5902, Textile Test Methods, Fire Resistance of Cloth, Vertical, May 15, 1961.

TABLE 4. - Flame Spread Rates of 10 Combustible Materials in Various Oxygen-Nitrogen Mixtures and at Various Total Pressures.

Oxygen Vol. %	Cotton Sheeting	Cotton Sheeting, Treated[1/]	Conductive Rubber Sheeting	Paper Drapes	Nomex	Blanket Wool	Polyvinyl Chloride Sheet	Plexiglas Sheet	Cellulose Acetate Sheet	White Pine Strips
					Flame Spread Rate, in/sec					
					One Atmosphere					
14	NB[2/]	NB	NB	NB	NB	--	--	--	--	--
21	0.8	NB	NB	2.0	NB	NB	--	0.2	NB	0.2
42	1.8	0.9	1.0	3.3	0.8	0.5	0.4	0.5	0.4	0.6
100	3.2	1.7	1.3	7.7	1.7	(~100)[3/]	1.0	--	1.1	1.1
					Two Atmospheres					
14	NB	NB	NB	--	NB	--	--	--	--	--
21	1.2	NB	NB	--	0.5	--	--	--	--	--
42	2.6	1.4	1.4	--	--	2.5	0.6	0.8	--	--
					Three Atmospheres					
14	NB	--	NB	1.8	NB	--	--	--	--	--
21	2.0	--	0.8	3.5	0.6	--	NB	0.6	--	0.4
42	3.7	--	2.3	7.1	1.0	--	0.8	--	--	1.6
					Six Atmospheres					
14	1.4	NB	NB	1.8	NB	--	--	--	--	--
21	3.0	NB	1.8	4.0	0.7	NB	NB	1.4	NB	0.7
42	5.1	2.9	2.5	10.0	1.2	7.1	--	--	--	2.5

1/ Cotton sheeting treated with Du Pont X-12 fire retardant; amount of retardant equal to 12 percent of cotton specimen weight.

2/ NB - No sustained burning beyond a distance $\leq$ 1 inch from the point of ignition.

3/ Approximate rate observed when flame flashed across the nap of the material following ignition.

TABLE 5. - Flame Spread Rates of 8 Combustible Materials in 100 Percent Oxygen at Various Pressures.

Pressure, Atmospheres	Cotton Sheeting	Cotton Sheeting 12% X-12	Conductive Rubber	Paper Drapes	Nomex	Blanket Wool	PVC	Cellulose Acetate
			Flame Spread Rate, in/sec					
0.21	1.0	0.5	0.6	2.6	0.5	--	0.3	0.4
0.35	1.3	--	--	--	--	--	--	--
0.42	--	0.8	0.8	4.0	1.0	10.0	0.6	0.7
0.84	2.6	--	--	--	--	--	--	--
1.00	3.2	1.7	1.3	7.7	1.7	~100.0	1.0	1.1
2.52	11.0	--	2.3	--	2.5	--	--	--

END OF REFERENCE

159

REFERENCE

160

COOK, G. A.; MEIERER, R. E.; AND SHIELDS, B. M.:
COMBUSTIBILITY TESTS ON SEVERAL FLAME-RESISTANT FABRICS
IN COMPRESSED AIR, OXYGEN-ENRICHED AIR, AND PURE OXYGEN.
TEXT. RES. J., VOL. 37, NO. 7, JULY 1967.

UNCLASSIFIED

3.0-9-1

AD 658 953

COMBUSTIBILITY TESTS ON SEVERAL FLAME-RESISTANT FABRICS IN COMPRESSED AIR, OXYGEN-ENRICHED AIR, AND PURE OXYGEN

Gerhard A. Cook, et al.

Union Carbide Corporation
Tonawanda, New York

July 1967

NOV 10 1970
CLEVELAND, OHIO

Processed for . . .

DEFENSE DOCUMENTATION CENTER
DEFENSE SUPPLY AGENCY

LIBRARY COPY

NOV 10 1970

LEWIS LIBRARY, NASA
CLEVELAND, OHIO

CLEARINGHOUSE
FOR FEDERAL SCIENTIFIC AND TECHNICAL INFORMATION

U. S. DEPARTMENT OF COMMERCE / NATIONAL BUREAU OF STANDARDS / INSTITUTE FOR APPLIED TECHNOLOGY

UNCLASSIFIED

AD 658953
$3.00

Reprinted from TEXTILE RESEARCH JOURNAL, Vol. 37, No. 7, July, 1967
Printed in U. S. A.

1967

Combustibility Tests on Several Flame-Resistant Fabrics in Compressed Air, Oxygen-Enriched Air, and Pure Oxygen

Gerhard A. Cook, Robert E. Meierer, and Bruce M. Shields

Union Carbide Corporation, Linde Division Research Laboratory
Tonawanda, New York

C-35847-B

Introduction

There is increasing concern with fire safety in pressurized chambers to be occupied by human beings. The chamber may be filled with compressed air or with oxygen-enriched compressed air. Such atmospheres are encountered by patients and hospital personnel in hyperbaric oxygen chambers and by divers in decompression chambers. Deep-sea divers also make use of oxygen diluted with helium

We have undertaken an experimental study to augment available information on the subject of fire

Reproduced by the
CLEARINGHOUSE
for Federal Scientific & Technical
Information Springfield Va. 22151

9

safety in confined spaces. One of the first problems encountered by those who are responsible for diving or other hyperbaric activities is the choice of cloth for making clothing, bed sheets, pillow and mattress covers, etc for use by those who are to be in the chamber. Therefore, the first phase of our study included combustion tests on samples of various cloth fabrics in air, with and without oxygen enrichment, at pressures varying from one to ten atm. We give herein an account of our work on this first phase.

We also give the results of tests made on the same fabrics in 100% oxygen. These findings are of interest, among other things, in connection with aerospace travel; American astronauts have in the past, at least, made their space flights in cabins filled with essentially undiluted oxygen.

In the last few years, many papers have been published on fire safety in isolated chambers and on the combustion rates of certain fabrics. Only a few of these publications can be cited here.

There is a good review by Roth [8]. An extensive paper by Harter [5] gives the details of a fatal fire experienced in a decompression chamber of the Experimental Diving Unit of the U. S. Navy. The interesting results of experiments carried out by Turner, Segal, Yanda, and Moore in a hyperbaric oxygen chamber in the Hospital of the Good Samaritan, Los Angeles, have been reported [9, 10, 11]. Also of interest is the work by Coleman [1] and by Wraight and Thomas [12] on the flammability of cloth fabrics, and the experiments with manikins and dead pigs carried out by Denison, Ernsting, and Creswell at the Royal Air Force Institute of Aviation Medicine in England [3].

Studies of combustion in 100% oxygen at reduced pressures have been published by Hall and Fang [4] and by Huggett, Von Elbe, Haggerty, and Grossman [6].

Equipment and Technique

The pressure vessel used for our experiments is made of stainless steel; it is 6 in. in I.D. by 20 in. long. The head closure easily fits in place and seals on a Viton O-ring with a rotation of only one-eighth of a turn. Thus, new samples may be rapidly installed and tested.

The vessel is equipped with a 2-in.-diameter laminated-glass window which has a working pressure of 600 psig (about 1350 fsw[1]). The vessel also has a 600 psig bursting disc, located on the side opposite that in which the window is located.

Attached to the center of the head closure is a ¼-in.-diameter rod on which are mounted the sample holder, the wires which bring electrical power to the igniter, and the thermocouple wires. The wires are brought into the vessel through Conax pressure fittings in the head closure. Combustion rates are measured between two thermocouple junctions 12.8 cm apart, attached to the sample holder. The latter has a series of brass pins at half inch intervals to keep the sample strip in position while being tested.

The combustion chamber can be used at any angle from horizontal (0°) to vertical (90°). The sample is ignited at one end by an igniter made of Chromel resistance wire: when the chamber is mounted at an angle greater than zero with the horizontal, the igniter is always at the lower end of the sample, so that the flame will travel upwards. The igniter is heated by a measured quantity of electricity. A 28-gage Chromel-Alumel thermocouple is welded to the Chromel igniter to measure the approximate temperature. The measured temperature tends to be somewhat lower than the actual ignition temperature, because the thermocouple has some cooling effect on that portion of the igniter to which it is welded.

To make a test, the sample and sample holder are sealed inside the pressure vessel. The latter is evacuated. The gas mixture to be tested, prepared in a separate cylinder and analyzed in advance, is bubbled through water and then admitted to the experimental vessel until the pressure is one atm. abs. The water bubbler is then bypassed, and dry gas is added until the desired total pressure is reached.

The burning-rate data given in the tables are the actual rates measured by us. Burning rates vary, not only with pressure, gas composition, and the angle at which the sample is held, but also with the size, shape, and weight of the samples, the weave of the cloth, the humidity in the chamber, and other factors. The rates given are therefore relative, and are useful principally for purposes of comparison.

Combustion of Paper in Compressed Air

Preliminary tests (to be described in a future publication) on paper strips 6 mm wide and 16 cm long showed the following.

[1] fsw = feet of seawater = 0.445 lb/in.^{2}

1. The burning rate is lowest when the sample is held in the horizontal position, highest in the vertical position, and intermediate in other positions.

2. There is little or no change in the burning rate in air, as the pressure is increased, when the sample is held horizontally (0°), but when the sample is held at an angle greater than 0°, an increase in the pressure has the effect of increasing the burning rate, at least up to a pressure of 148 psia (300 fsw) and up to an angle of 75°. The increase in rate with increase in pressure (compared with the rate at atmospheric pressure) is greatest at an angle of 45°. In the vertical (90°) position, the burning rate of paper is highest. Erratic flaming takes place, so that the measured rates are reproducible only within rather large limits.

3. At all angles, the temperature required to ignite paper decreases as the pressure increases.

We concluded that the best angle at which to compare the burning rates of various materials is 45°, although the most hazardous burning condition exists when the flammable materials are in the vertical position.

Results for Cloth Fabrics in Compressed Air (20.95% [2] Oxygen)

A description of the fabrics tested is given toward the end of this paper.

Ignition and burning tests were made on cloth strips about 12 mm wide and 16 cm long. This size is smaller than the one used in most standard tests and was chosen to obviate the necessity of using a flowing gas to keep the oxygen concentration fairly constant and to keep the size of the pressure vessel (and therefore the quantity of special gas mixtures needed) reasonably small.

Table I gives some of the measured ignition temperatures. As can be seen, the reproducibility of the measurements was rather poor. In the case of both treated and untreated cotton, the ignition temperature falls rapidly as the pressure increases, but this effect is much less marked with wool. Within the experimental error, change of pressure showed no increase in the ignition temperature of Nomex.

Tables II and III list the measured rates of combustion of the fabrics when the sample strips were held at 45° and at 90°, respectively. In general, the rates are higher in the vertical position. The rates with Roxel cotton were difficult to reproduce.

[2] All percentages are by volume.

TABLE I. Ignition Temperatures for Vertical Cloth Strips in Compressed Air

Total pressure, psia	Measured ignition temperature, °F				
	Cotton broadcloth	Roxel broadcloth	Wool	Nomex	Teflon TFE
14.7	950 980	840 980	1000 1010 1050	955 1080 1125	—
26	—	—	—	1005	—
37	—	—	—	890	—
59	710 800	710	930	920 930 980	1195
81	—	—	—	970 980 1055	—
104	680	700 705	910	980 1090	—
148	680	635 665	965	895 990 1000	1115

The fact that an ignition temperature is given in this table does not mean that the fabric continued to burn after ignition. See Tables II, III, V, and VI for data on burning rates.

Each temperature in the table is for a separate test.

TABLE II. Burning Rate of Cloth Strips Held at an Angle of 45° in Compressed Air

Total pressure, psia	Burning Rate, cm/sec				
	Cotton Terry cloth	Cotton broadcloth	Roxel cotton broadcloth	Wool	Nomex
14.7	0.58 0.71	1.16 1.76	*, †, ‡	*, ‡	‡‡
37	1.65	2.41	*	*	‡
59	3.56	7.88	*	0.71	0.22 ‡
104	5.78, ††	11.82 ††	*	0.70 0.74	‡
126	—	—	*	—	—
148	8.97, ††	**, ††, ††	6.84, *, *, *	*	‡

** Rate was too fast to measure.
†† In another test, rate was also too fast to measure.
* Sample ignited with a strong flame which extinguished itself before reaching the last thermocouple.
‡ Same as *, except that flame was weak.
† Sample did not ignite, even in contact with the igniter.
Repeated footnote symbols signify repeated experiments.

Effect of Pressure on Burning Rates in Air

When the sample was held at an angle of 45° and, in some cases, when held at 90°, increasing the air pressure up to about 148 psia (300 fsw) increased the combustion rate of the samples.

As can be seen in Table IV, when the pressure of the air is increased, the partial pressure of oxygen

TABLE III. Burning Rate for Vertical Cloth Strips in Compressed Air

Total pressure, psia	Burning rate, cm/sec		
	Roxel cotton broadcloth	Wool	Nomex
14.7	*	2.08, ‡	*
26			0.52
37	*		0.85
48	*		
59	†	2.52	0.77, ‡
70	**		
81	**		*
104	‡, **	2.17	0.66, ‡
126	**		0.91
148	2.92, 3.10, 3.21, ‡, ††, ‡‡	1.04	*

Cotton terry cloth and cotton broadcloth burned too rapidly to make rate measurements.

Teflon cloth ignited (to give a small blue flame) in contact with the igniter at pressures of 59 psia (100 fsw) and above, but was self-extinguishing beyond the igniter.

Beta Fiberglas fabric neither ignited nor burned.

* Fabric ignited, but flame extinguished itself before a rate could be measured with the thermocouples.

‡ The flame climbed all the way to the top; no clear thermocouple peaks were seen on the recorder chart due to the height of the initial flame.

† Flamed up high while igniter was on, but then extinguished itself; no smoldering observed.

** Flamed up high while igniter was on, then smoldered part of the way up the strip.

†† Similar to **, but smoldered all the way to the top.

‡‡ Even though the burning rates measured between the thermocouples were not very great, the sample flamed too high for safety.

increases. This would explain why the burning rate increases, if it were not for the fact that the partial pressure of the diluent nitrogen increases in exactly the same proportion as that of oxygen. It must therefore be concluded that, at a nitrogen percentage of about 79%, the increased damping effect of nitrogen when the total pressure is increased is less than the increased burning effect of oxygen. We have found that this is no longer true at pressures much above about 150 psia; at the higher pressures, the rate of combustion in air seems to stay fairly constant as the pressure is increased.

TABLE IV. Equivalent Pressures and Partial Pressures of Oxygen for Various Conditions

Total pressure			Partial pressure of oxygen, atm	
fsw	psia	atm, abs	air	25% O_2
0	14.7	1.00	0.21	0.25
25	25.8	1.76	0.37	0.44
50	37.0	2.51	0.53	0.63
75	48.1	3.27	0.69	0.82
100	59.2	4.03	0.84	1.01
125	70.3	4.79	1.00	1.20
150	81.5	5.54	1.16	1.38
200	103.7	7.06	1.48	1.77
250	126.0	8.57	1.80	2.14
300	148.2	10.1	2.11	2.52

Results for Cloth Fabrics at Higher Oxygen Percentages

Each of the fabrics that appeared to be reasonably safe in compressed air was tested in a mixture of 24.9% oxygen and 75.1% nitrogen. These tests were made because there are times when divers in decompression chambers and patients in hyperbaric hospital chambers breathe 100% oxygen gas through face masks. It is possible that oxygen leaking out through the masks into the chamber might enrich the air so that the resultant oxygen concentration would be greater than the 20.95% which is normally present in air.

The results for 24.9% oxygen are given in Table V. It is seen that wool and Roxel cotton both burned rapidly. These fabrics, although they are safer than untreated cotton in compressed air, do not have the extra safety factor that is desirable for use in compressed air that might be slightly enriched in oxygen.

The fabrics that survived the 24.9% oxygen experiment were tested in mixtures of 30.9% oxygen

TABLE V. Burning Rates for Vertical Cloth Strips at 25% and Higher Oxygen Percentages

Total pressure, psia	Burning rate, cm/sec				
	Roxel cotton broadcloth, 24.9% O_2	Nomex			Teflon
		24.9% O_2	30.9% O_2	30.97% O_2	41.3% O_2
14.7	*	1.13	†	‡	‡
26	—	—	†	—	—
37	6.43	1.54	1.19	—	—
59	6.67	1.33 1.61 2.06	2.48	‡	0.63
104	*	1.00 1.36	†	‡	1.27
148	*	1.97	†	‡	2.55

The diluent in all cases was nitrogen.

In 24.9% O_2, wool and untreated cotton broadcloth burned so rapidly that the rate could not be measured.

In 24.9% O_2, Teflon gave a small blue flame in contact with the igniter, but there was no combustion beyond the igniter.

Beta Fiberglas did not burn at all.

* Sample burned so rapidly that the rate could not be measured.

† Although the rate of combustion of the main part of the strip was low, the initial flame was so high that the second thermocouple was heated at the same time as the first; hence, no rate could be measured.

‡ Flame extinguished itself before reaching the last thermocouple.

and 69.1% nitrogen. The results are also given in Table V. At 30.9% oxygen, Nomex fabric flared up rapidly, although the combustion of the main part of the strip was still slow. Teflon fabric burned a distance of a few centimeters, but the flame always went out before the whole strip was burned. At 41.3% oxygen, the strips of Teflon fabric burned slowly all the way.

Results in Oxygen

Experiments in oxygen were carried out as follows.

1. The test vessel was evacuated.
2. In the case of the runs at an angle of 45°, water vapor was admitted to a pressure within about 2 mm Hg of the vapor pressure of water at room temperature. For tests at 90°, no water vapor was admitted.
3. Pure oxygen was then admitted to the desired pressure.

In the hope of obtaining a good comparison, all the fabrics were tested in oxygen at an angle of 45°. However, all the flame-resistant fabrics except Teflon and Beta Fiberglas burned so erratically and flamed up so high that the rates could not be measured, even at oxygen pressures as low as 0.21 atm.

Teflon and Beta Fiberglass were also tested in pure oxygen in the vertical position. The results with Teflon are given in Table VI. In the vertical position, the burning rate became fairly rapid at a pressure of 0.84 atm, but the flame did not appear to be very hot.

Beta Fiberglas cloth showed no signs of combustion, even at a pressure of 2.12 atm of undiluted oxygen in the vertical position.

Description of Fabrics

A description of the fabrics tested and some comments on the results are given below.

Cotton

White cotton terry cloth (8.1 oz/yd²) and a white light-weight cotton broadcloth (3.1 oz/yd²) were both tested. The terry cloth was tested just as received from the retailer. The broadcloth was a part of a shirt which had been laundered many times before it was cut up into samples for the burning tests. Both burned too rapidly in the vertical position to give rates that could be measured in our equipment, even at atmospheric pressure. In the vertical position, the fuzz (nap) rapidly burned off the terry cloth; meanwhile, the main body of the cloth burned at a somewhat lower rate. At 45° the nap did not flame up, and the burning rate could be measured; this burning rate for terry cloth turned out to be lower than for the light-weight broadcloth.

TABLE VI. Burning Rate of Tedon Cloth in Oxygen*

Partial pressure of O_2, atm†	Burning rate, cm/sec, at an angle of	
	45°	90°
0.21	‡	‡
0.53	‡	**
0.84	0.73	2.60, ††
1.16	1.42	—
1.48	0.63	3.02, ††
2.12	1.23	3.47

* The oxygen contained water vapor for the 45° angle tests, but was dry for the vertical tests. The oxygen was the standard U. S. P. gas, containing 99.6% oxygen and 0.4% argon.
† See Table IV for corresponding air pressures.
‡ Burned only at and near the igniter, then extinguished itself.
** Smoldered for 5 cm after the igniter, then extinguished itself.
†† In another run the strip smoldered and curled for its entire length.
Note: Repetition of a symbol represents a separate test.

Roxel Fabric

A sample of white Roxel cotton cloth (5.4 oz/yd²) was supplied by Hooker.[3] Roxel is the trade name for cellulosic fabric finished with tetrakis (hydroxymethyl)phosphonium chloride (THPC) in a proprietary system developed by Hooker, based on work originally done [7] at the Southern Regional Research Laboratory of the U. S. Department of Agriculture. The flame-retardant finish will withstand repeated laundering. Roxel fabric is commercially available at prices slightly higher than those of cotton.

When the flame from a match (or cigarette lighter) was brought in contact with the lower end of a strip of Roxel held vertically in the air of the room, the fabric burned while heated by the flame, but combustion stopped as soon as the match or lighter was withdrawn. During the burning, the Roxel gave off irritating fumes. With regard to these fumes, the following information was supplied to us by Hooker: During charring of THPC-treated cotton at 400°C,

[3] See the last paragraph under Acknowledgments for a list of the complete names and addresses of companies that supplied us samples and information.

END OF REFERENCE

REFERENCE

161

PIPPEN, D. L.; AND STRADLING, J. S.: MATERIALS TESTING IN A GASEOUS OXYGEN ENVIRONMENT. PAPER PRESENTED AT 74TH NATIONAL MEETING, A.I.CH.E. (NEW ORLEANS, LA), MAR. 1973.

ABSTRACT

Materials Testing in a Gaseous Oxygen Environment

David L. Pippen

Jack S. Stradling

The techniques developed at the NASA White Sands Test Facility for testing materials in a gaseous oxygen environment are discussed. Propagation rate, flash and fire point, electrical arc ignition, and pneumatic and mechanical impact sensitivity test equipment are described. Each test method provides a rapid means for evaluating materials for possible use in oxygen environments or for material screening. The test systems described can be used with various gas mixtures as well as with 100 percent oxygen. The data from test techniques described were used for determining the compatibility of materials used in the low and high pressure oxygen systems of the Apollo spacecraft and will continue to be employed in support of Skylab and Shuttle test requirements.

Table 2--Flash and Fire Point Test Results

Material	Test Pressure (psia)	Flash Point (°F)	Fire Point (°F)	Test Chamber*
Nylon Sheet	5	740	None	L
	25	760	773	L
	50	568	568	H
	100	529	529	H
	500	464	464	H
	1087	432	432	H
Silicone O-Ring	5	None	None	L
	25	774	806	L
	50	639	639	H
	100	723	723	H
	500	490	490	H
	1000	434	434	H
	1500	447	447	H
	2000	444	444	H
Fluorel Sheet	20	800	807	H
	50	790	790	H
	100	767	767	H
	250	723	723	H
	500	712	712	H
	1000	648	648	H
	1500	629	629	H
	2000	616	616	H
	3000	603	603	H
Vespel SP-21	5	566	None	L
	25	953	None	L
	50	935	935	H
	100	921	921	H
	500	835	835	H
	1000	730	730	H
	1500	658	658	H
	2000	631	631	H

* L = 50 psia maximum low pressure test chamber
H = 3000 psia maximum high pressure test chamber

END OF REFERENCE

161

REFERENCE

162

HUGGETT, C.; VON ELBE, G.; AND HAGGERTY, W.: THE COMBUSTIBILITY OF MATERIALS IN OXYGEN-HELIUM AND OXYGEN-NITROGEN ATMOSPHERES. REP. SAM-TR-66-85, ATLANTIC RES. CORP., 1966.

SAM-TR-66-85

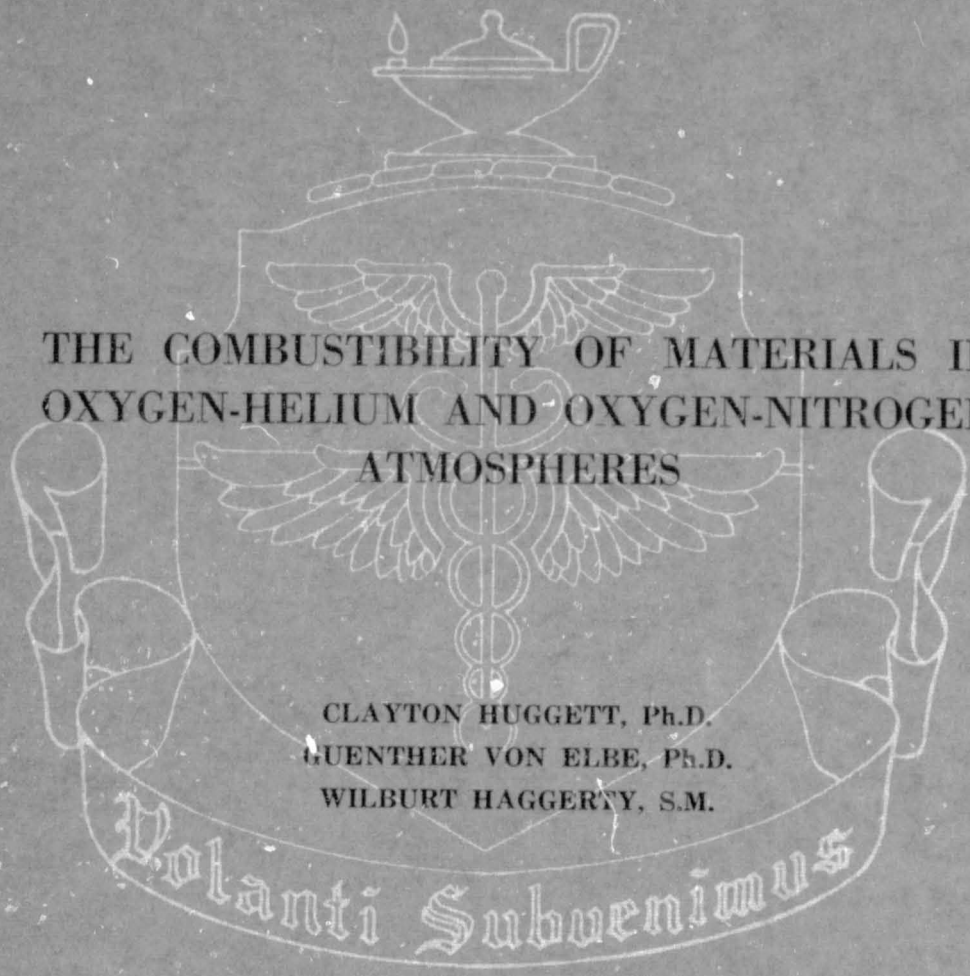

THE COMBUSTIBILITY OF MATERIALS IN OXYGEN-HELIUM AND OXYGEN-NITROGEN ATMOSPHERES

CLAYTON HUGGETT, Ph.D.
GUENTHER VON ELBE, Ph.D.
WILBURT HAGGERTY, S.M.

December 1966

USAF School of Aerospace Medicine
Aerospace Medical Division (AFSC)
Brooks Air Force Base, Texas

Qualified requesters may obtain copies of this report from DDC. Orders will be expedited if placed through the librarian or other person designated to request documents from DDC.

When U. S. Government drawings, specifications, or other data are used for any purpose other than a definitely related government procurement operation, the government thereby incurs no responsibility nor any obligation whatsoever; and the fact that the government may have formulated, furnished, or in any way supplied the said drawings, specifications, or other data is not to be regarded by implication or otherwise, as in any manner licensing the holder or any other person or corporation, or conveying any rights or permission to manufacture, use, or sell any patented invention that may in any way be related thereto.

Distribution of this document is unlimited.

THE COMBUSTIBILITY OF MATERIALS IN OXYGEN-HELIUM AND OXYGEN-NITROGEN ATMOSPHERES

CLAYTON HUGGETT, Ph.D.
GUENTHER VON ELBE, Ph.D.
WILBURT HAGGERTY, S.M.

ABSTRACT

The energy required for ignition of various materials and the rate at which flames spread over the surface after ignition were determined in oxygen-nitrogen and oxygen-helium mixtures in order to assess the fire hazards associated with proposed space cabin atmospheres.

It was found that flames spread more rapidly in oxygen-helium mixtures than in comparable oxygen-nitrogen mixtures. The experimental data correlated well with the specific heats of the gas mixtures per mole of oxygen, indicating that the flame temperature is the dominant factor in determining flame spread rates. A theoretical model of flame spread was developed.

Slightly more energy was required to ignite materials in oxygen-helium than in oxygen-nitrogen mixtures; however, the difference was small enough so as not to reduce significantly the fire hazards, especially since the flames spread more rapidly once the material was ignited.

It was concluded that fire hazards are greater in oxygen-helium atmospheres than in oxygen-nitrogen atmospheres.

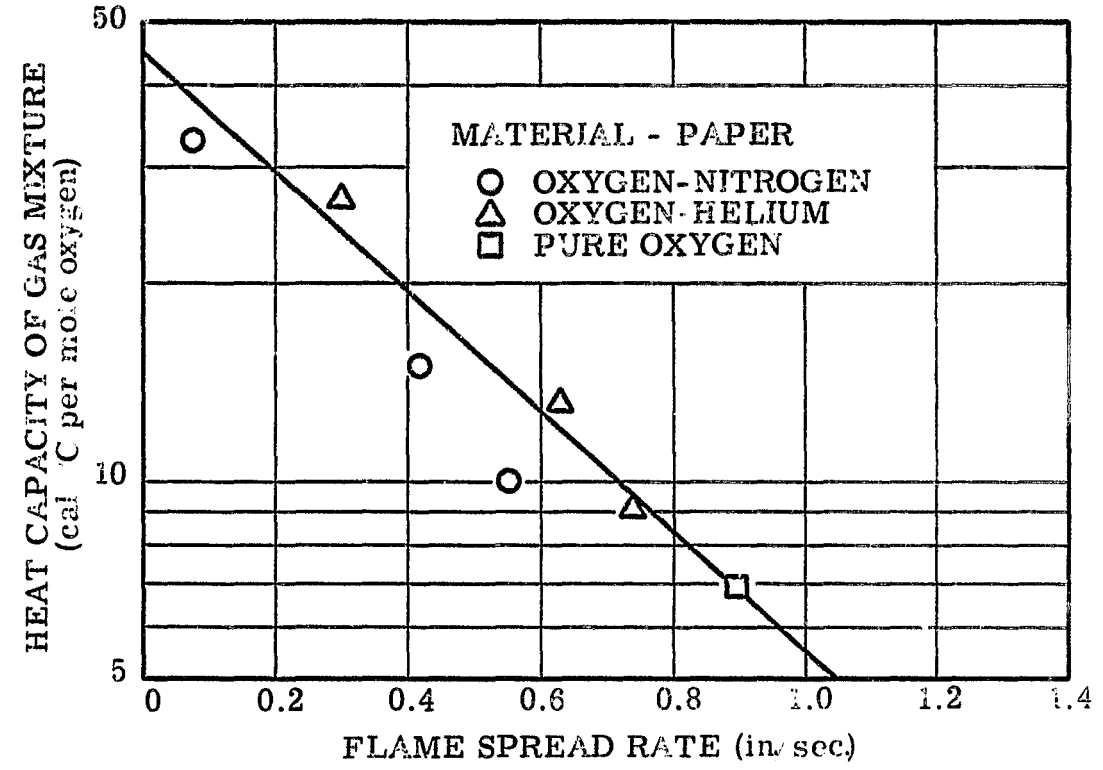

FIGURE 2

Flame spread rate for paper versus heat capacity of atmosphere.

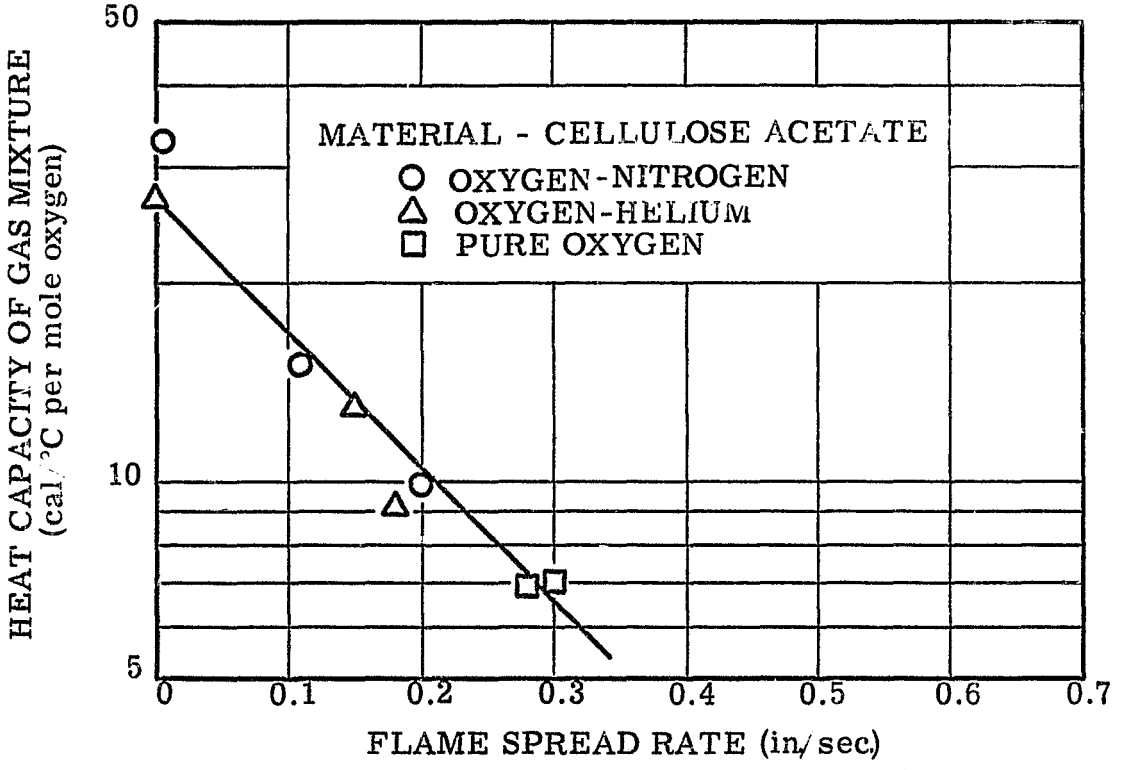

FIGURE 3

Flame spread rate for cellulose acetate versus heat capacity of atmosphere.

END OF REFERENCE

162

REFERENCE

163

HUGGETT, C.; VON ELBE, G.; HAGGERTY, W.; AND GROSSMAN, J.: THE EFFECTS OF 100% OXYGEN AT REDUCED PRESSURE ON THE IGNITIBILITY AND COMBUSTIBILITY OF MATERIALS. SAM-TR-65-78, ATLANTIC RESEARCH CORP. (AD-477338), 1965.

COPY 3 c. 3

AD 477 338

THE EFFECTS OF 100% OXYGEN AT REDUCED PRESSURE ON THE IGNITIBILITY AND COMBUSTIBILITY OF MATERIALS

Clayton Huggett, et al

Aerospace Medical Division (AFSC)
Brooks Air Force Base, Texas

December 1965

LEWIS RESEARCH CENTER
Aerospace Safety Research
and Data Institute
NOV 12 1970
CLEVELAND, OHIO

3.4-0-0
6.2-0-0

LIBRARY COPY
NOV 12 1970
LEWIS LIBRARY, NASA
CLEVELAND, OHIO

SAM-TR-65-78

(40)
1-8
RC

AD No. 477338 $3.00
Clearinghouse FOR FEDERAL SCIENTIFIC & TECHNICAL INFORMATION FILE COPY

THE EFFECTS OF 100% OXYGEN AT REDUCED PRESSURE ON THE IGNITIBILITY AND COMBUSTIBILITY OF MATERIALS

CLAYTON HUGGETT, Ph.D., et al.

DDC
RELEASED
FEB 14 1966
DDC-IRA E

December 1965

USAF School of Aerospace Medicine
Aerospace Medical Division (AFSC)
Brooks Air Force Base, Texas

Reproduced by the
CLEARINGHOUSE
for Federal Scientific & Technical
Information Springfield Va. 22151

37

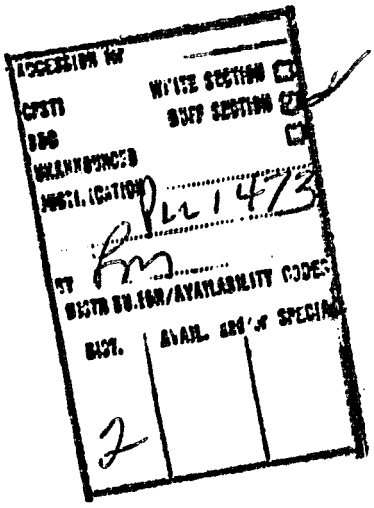

Qualified requesters may obtain copies of this report from DDC. Orders will be expedited if placed through the librarian or other person designated to request documents from DDC.

When U. S. Government drawings, specifications, or other data are used for any purpose other than a definitely related government procurement operation, the government thereby incurs no responsibility nor any obligation whatsoever; and the fact that the government may have formulated, furnished, or in any way supplied the said drawings, specifications, or other data is not to be regarded by implication or otherwise, as in any manner licensing the holder or any other person or corporation, or conveying any rights or permission to manufacture, use, or sell any patented invention that may in any way be related thereto.

NO LIMITATION PER AF SAM LETTER DATED 7-11-67,
TAB 68-1, PP. A5

ABSTRACT

An investigation was conducted to determine the effect of prolonged exposure to an atmosphere of 100% oxygen at a pressure of 258 mm. Hg on the fire hazards associated with space cabin materials. The ignitibility and combustibility of standard reference materials and samples of materials normally found in space cabin simulators were determined both before and after a 30-day exposure to such an oxygen atmosphere.

The experimental results show that flame spreads over the surfaces of materials much faster in the 258 mm. Hg oxygen atmosphere than in air. Some materials which would not sustain combustion in air burned vigorously in the oxygen atmosphere. Prolonged storage in the oxygen atmosphere had no appreciable effect on the flame spread rate. However, the geometry and composition of the material influenced this rate significantly. No major differences were found in the energies required for ignition of materials in air, in oxygen, or after storage in oxygen.

Proper selection of materials used in construction of space cabins and simulators can significantly reduce fire hazards.

equivalent partial pressure of oxygen (160 mm. Hg), indicating the magnitude of the effect of the inert nitrogen in air.

The outcome of this initial series of tests confirms that the process by which flames spread over the surfaces of materials is a very complex one. The geometry of the surface was found to be a very important parameter. As noted from the results of this test series, flames propagate along sharp corners or edges approximately five times faster than over a flat smooth surface. Although several methods of preventing burning of the edges were developed, none was adaptable to the storage tests. The aluminum silicate paste became very brittle during storage and flaked off the samples. The metal strips were too bulky to fit into the storage tubes and were not adaptable to many of the geometries involved in the space cabin samples. This applies also to geometries such as flat sheets or cylindric rods. It was therefore decided to conduct the storage tests with specimens (0.5 inch wide by 4 inches long) cut from the samples and to permit the flame to run along the edges. Admittedly, the flame spread rates would not be as reproducible as desired, but any gross differences in rates before and after storage would be detectable.

Flame spread rates over standard samples. The rates at which flames spread over the surface of standard materials in air at normal barometric pressure, in pure oxygen at 258 mm. Hg absolute, and in the oxygen atmosphere after prolonged storage in oxygen are shown in table XI. The flame spread rates in air were very consistent over different portions of the same specimen. The flame spread rates in the oxygen atmosphere, however, varied over different portions of the same

TABLE XI

Effect of oxygen and storage in oxygen on flame spread rates over various materials (edges not inhibited)

Material	Flame spread rate (in./sec.)		
	In air	In 258 mm. oxygen	
		Before storage	After 30-day storage
Butyl rubber	0.006	0.40 ± 0.04	0.31 ± 0.04
Canvas duck	NP	0.25 ± 0.05	—
Cellulose acetate	0.012	0.28 ± 0.12	0.24 ± 0.12
Kel-F	NI	NI	NI
Natural rubber	0.010	0.61 ± 0.05	0.61 ± 0.08
Neoprene rubber	NI	0.32 ± 0.04	0.25 ± 0.05
Nylon 101	NI	0.19 ± 0.05	0.15 ± 0.01
Plexiglas	0.005	0.35 ± 0.01	0.24 ± 0.01
Polyethylene	0.014	0.25 ± 0.05	0.36 ± 0.06
Polypropylene	0.010	0.35 ± 0.01	0.36 ± 0.12
Polystyrene	0.032	0.80 ± 0.20	0.51 ± 0.01
Polyvinyl chloride	NI	0.10 ± 0.01	0.06 ± 0.01
Silicone rubber	NI	0.14 ± 0.01	0.14 ± 0.01
Teflon	NI	NI	NI
Viton A	NI	0.003 ± 0.002	0.01 ± 0.005

All samples except canvas duck, 3 by ½ by ⅛ in.; canvas duck, 3 by ½ by 1/80 in.

NP — No sustained propagation of flame.

NI — No ignition of material.

TABLE XII

Effect of oxygen and storage in oxygen on flame spread rates over various space cabin materials (edges not inhibited)

Material	Flame spread rate (in./sec.)		
	In air	In 258 mm. oxygen	
		Before storage	After 30-day storage
Aluminized Mylar tape	—	1.95	—
Aluminized vinyl tape	NI	3.1 ± 0.4	3.0 ± 0.4
Asbestos insulating tape	NI	0.08	0.05
Chapstick	NI	1.82	—
Cotton shirt fabric	NP	1.50 ± 0.05	2.10 ± 0.3
Electrical insulating resin	NI	0.27	0.20
Electrical terminal board	NI	0.06 ± 0.01	0.06 ± 0.01
Fiberglas insulating tape	NI	4.2 ± 0.6	2.0 ± 0.8
Foam cushion material	0.19	12.4	11.3
Foamed insulation	0.002	2.2 ± 0.2	3.0 ± 0.3
Food packet, aluminized paper	NI	0.28 ± 0.05	0.26 ± 0.05
Food packet, brown aluminum	NI	0.7 ± 0.30	0.8 ± 0.20
Food packet, plastic	0.33	0.55	0.47
Glass wool	NI	NI	NI
Masking tape	0.17	1.82	—
Paint, 3-M velvet	NI	0.15 ± 0.01	0.31 ± 0.02
Paint, Capon ivory	NI	0.38 ± 0.04	0.35 ± 0.02
Paint, Pratt & Lambert, grey	NI	0.60 ± 0.2	0.24
Pump oil	NI	0.89	—
Refrigeration oil	NI	0.82 ± 0.07	—
Rubber tubing	0.03	0.24	0.25 ± 0.05
Silicone grease	NI	0.92	—
Solder, rosin core	NI	0.18	0.25
Sponge, washing	0.07	8.1 ± 0.1	10 ± 2
Teflon pipe sealing tape	NI	NI	NI
Teflon tubing	NI	NI	NI
Tygon tubing	0.18	0.50 ± 0.05	0.52 ± 0.05
Wire, Mil W76B, orange	NI	0.57 ± 0.05	0.54
Wire, Mil W76B, blue	NI	—	0.57
Wire, Mil W76B, yellow	NI	—	0.54
Wire, Mil W16878, green	NI	NI	NI
Wire, Mil W16878, black	NI	NI	NI
Wire, Mil W16878, yellow	NI	NI	NI
Wire, Mil W16878, white	NI	NI	NI
Wire, misc., white, 3/32 dim.	NI	0.33	0.25
Wire, misc., black. 3/16	NI	—	0.40
Wire, misc., brown, 7/32	NI	0.51 ± 0.05	—
Wire, misc., yellow, 7/64	NI	0.89	—
Wire, misc., yellow, 5/32	NI	0.41	—

NP -- No sustained propagation of flame.

NI — No ignition of material.

oxygen pressure, and pressure changes were followed by means of mercury manometers. After completion of the storage tests the samples were reweighed and the weight change recorded. A sample of natural rubber was stored under a pressure of 160 mm. Hg of oxygen. The results of these tests are shown in table XIII. The pressure in the sample tube containing natural rubber decreased from 160 mm. Hg to 129 mm. Hg during the 252-day

END OF REFERENCE

163

REFERENCE

164

KIMZEY, J. H.: FLAMMABILITY DURING WEIGHTLESSNESS.
NASA TM X-58001, 1966.

NASA TECHNICAL MEMORANDUM

NASA TM X-58001

FLAMMABILITY DURING WEIGHTLESSNESS

By John Howard Kimzey
Manned Spacecraft Center
Houston, Texas

FACILITY FORM 602

N66 29225 (ACCESSION NUMBER)

(THRU) 1

17 (PAGES)

(CODE) 33

TMX-58001 (NASA CR OR TMX OR AD NUMBER)

(CATEGORY)

Presented to
the Twelfth Annual Technical Meeting
of the Institute of Environmental Sciences
San Diego, California, April 13, 1966

GPO PRICE $ _____

CFSTI PRICE(S) $ _____

Hard copy (HC) 1.00

Microfiche (MF) .50

ff 653 July 65

NATIONAL AERONAUTICS AND SPACE ADMINISTRATION

May 1966

FLAMMABILITY DURING WEIGHTLESSNESS

By John Howard Kimzey, NASA-Manned Spacecraft Center

INTRODUCTION

A series of experiments was conducted to learn the effects of weightlessness or "zero gravity" on a flame. This program was undertaken so that the seriousness of an accidental fire in a spacecraft may be evaluated, and means of controlling such an event may be developed. Many materials in a spacecraft are flammable. A fire could result from any number of malfunctions in the 100-percent-oxygen environment.

Only two instances were found in the literature regarding flammability in zero gravity. In 1956, Kumagai and Isoda reported on combustion of liquid droplets in a falling chamber. Data showed that as the droplet diameter decreased the flame diameter increased. Time was less than one-third second. Next, Hall in 1963 observed a burning candle in aircraft tests with intervals reported to be as long as 25 to 28 seconds. He concluded that the coloration change to deep blue, and some thermocouple data, indicated a somewhat hotter flame than in lg. Both of these earlier workers indicated that a steady-state condition existed.

ZERO-G FLAMMABILITY-PHASE I

A comparison between a flame in lg and zero-g environments is indicated in figure 1. In lg burning of paraffin (shown in the left side) a series of events takes place simultaneously. Solid material is converted to a gas, thereby absorbing energy. The gas physically mixes with the surrounding atmosphere and, in chemically reacting with the oxygen, liberates energy. Hot gas products are formed: carbon dioxide, carbon monoxide, water vapor and a long list of minor constituents ranging from hydrogen to complex acids, alcohols, and other organic compounds. These products are formed through various intermediates including atoms and free radicals. The high temperature of these gases contributes to their low density. The gases rise out of the flame zone, allowing more oxygen to enter and mix with the fuel gases. Thus a steady state is possible and the flow-in can be equated to the flow-out. The

TABLE II. - BURNING RATES IN lg AND ZERO-g

Fuel[1]	Rate of burning, inch per second					
	lg			Zero-g		
	15 psia air	5 psia oxygen	15 psia oxygen	15 psia air	5 psia oxygen	15 psia oxygen
Neoprene	0.0	0.2	0.4	-	0.10	-
Silicone	0.04	0.5	1.1	0.0	0.08	-
Teflon	0.0	-	-	-	0.00	-
Polyurethane	-	0.6	0.7	0.0	0.08	0.15
Dacron[2]	-	0.6	0.7	-	0.08	0.15

Note:

1. Fuel is tubular (#10 AWG I.D.) and threaded over a steel or ceramic mandrel.

2. Dacron thread is wrapped around polyurethane.

3. Ignition is provided by electric resistance coil.

4. Temperature of atmosphere is 65 ± 5° F.

END OF REFERENCE

164

REFERENCE

165

DAWN, F. S.: NONMETALLIC-MATERIALS DEVELOPMENT FOR SPACECRAFT APPLICATIONS. CONFERENCE ON MATERIALS FOR IMPROVED FIRE SAFETY. NASA SP-5096, 1971.

Lowdermilk

NASA SP-5096

CONFERENCE ON MATERIALS FOR IMPROVED FIRE SAFETY

MANNED SPACECRAFT CENTER

HOUSTON, TEXAS

MAY 6–7, 1970

NATIONAL AERONAUTICS AND SPACE ADMINISTRATION

NASA SP-5096

CONFERENCE ON MATERIALS FOR IMPROVED FIRE SAFETY

MANNED SPACECRAFT CENTER
HOUSTON, TEXAS
MAY 6–7, 1970

Technology Utilization Office
1971
NATIONAL AERONAUTICS AND SPACE ADMINISTRATION
Washington, D.C.

FOREWORD

The Manned Spacecraft Center was pleased to host the NASA Conference on Materials for Improved Fire Safety which was held May 6–7, 1970. This document is a compilation of papers presented at the conference and represents the culmination of several years of effort by NASA and industry which was directed toward the common objective of minimizing the fire hazard in manned spacecraft and in some other related areas. One of the more serious problem areas in the Apollo program was the flammability of nonmetallic materials. The effective and timely solution of this problem area resulted from much of the effort reported herein and contributed greatly toward the successful achievement of landing men on the Moon and returning them safely to Earth.

Each year on Earth the loss in property and human lives resulting from fire is enormous. The materials developed for improved fire safety and the many lessons and knowledge gained in the course of conducting this research and development are quite extensive and should find many direct and useful applications in industrial, commercial, and domestic areas. With the judicious and proper application of such information it should be possible to make a large step toward minimizing this age-old hazard to mankind.

ROBERT R. GILRUTH
Director
Manned Spacecraft Center

CONTENTS

	Page
SESSION I—FLAMMABILITY REQUIREMENTS AND TEST TECHNIQUES	
The Combustion Process	3
Manned Spacecraft Nonmetallic-Materials Flammability Selection Criteria and Requirements	9
Development of Materials Screening Tests for Oxygen-Enriched Environments	23
Flammability Testing of Components	29
Flammability Tests for Apollo Command Module and Lunar Module Mockups	43
SESSION II—MATERIALS DEVELOPMENT	
Nonmetallic-Materials Development for Spacecraft Applications	57
Development and Applications of Fluorel	65
Development and Application of Flame-Resistant Polymers and Composites	73
Development of Nonflammable Potting Compounds for Spacecraft	83
New Materials for Manned Spacecraft, Aircraft, and Other Applications	91
The Performance of Lightweight Plastic Foams Developed for Fire Safety	103
Intumescence: An In Situ Approach to Thermal Protection	111
SESSION III—CONFIGURATION CONTROL AND MATERIALS APPLICATIONS	
Nonmetallic-Material Configuration Control in the Apollo Spacecraft	123
Apollo Spacecraft Nonmetallic Materials Applications	129
The Effects of Gravity on Flammability	137
Apollo Applications of Beta Fiber Glass	141
Apollo Space-Suit Materials	145
Fire Safety Design of a Mobile Quarantine Facility	151
Fire and Safety Materials Utilization at the John F. Kennedy Space Center	155
Fire Extinguishment in Hypobaric and Hyperbaric Environments	163
SESSION IV—SPECIAL TESTS	
Manned Spacecraft Electrical Fire Safety	173
Special Flammability Test Techniques	179
Specialized Testing and Evaluation of Space-Suit Materials	187
Development of an Oxygen Impact-Testing Method	191
Odor Test	203
Toxicology of Spacecraft Materials	207
Flammability Control in the Oxygen Environment of the Apollo Guidance and Navigation Equipment	211
GLOSSARY	219

TABLE XVII.—*Flammability Test Results on Typical Apollo Nonmetallic Materials*

[Silicone ignitor, 100 percent oxygen]

Materials	Burn rate, in./sec				
	Top ignition		Bottom ignition		
	16.5 psia	6.2 psia	16.5 psia	[a]16.5 psia	6.2 psia
Beta	[b]NI	NI	NI	NI	NI
Teflon	SE	SE	.55	.30	.30
PBI	.20	.16	.41	.35	.30
Asbeston	[c]SE	SE	SE	SE	SE
Nomex	.33	.16	1.00	.60	.60
Viton	SE	SE	SE	SE	SE
Fluorel	SE	SE	SE	SE	SE
CNR	SE	SE	SE	SE	SE
Velcro [d]	.02	.01	.50	.37	.35

[a] 60 percent oxygen, 40 percent nitrogen.
[b] NI—No ignition.
[c] SE—Self-extinguishing.
[d] Astro Velcro.

TABLE XVIII.—*Offgassing Characteristics of New Materials*

Materials	Total organic, μg/g	Carbon monoxide, μg/g	Odor
Durette	0.6	3.0	0.2
Polysulfone	.9	.2	1.0
Fluorinated polyurethane	89.0	8.0	.6
Polyquinoxaline	.5	4.3	1.3
Asbestos foam	4.1	3.7	1.7
Fypro	1.0	4.0	.7

ant plastic for helmet-visors and instrument panels. Flame-resistant plastic films for thermal insulations and packaging materials also are needed. In addition, the development of flame-resistant organic fibers, elastic fibers, finer diameter glass fibers, elastomers, coatings, adhesives, films, and fasteners is continuing with emphasis on improved physical properties.

Many of the materials developed for the Apollo Program are in commercial and military use. Interchanges of information are taking place with the aircraft industry, which is interested in building improved flame-resistant airplane interiors, with the U.S. Army for possible use as flameproof, inflatable-portable hospitals, and with the U.S. Navy for potential sea laboratory applications. Other potential applications are noted in table XX.

REFERENCES

1. NAIMER, JACK: Apollo Applications of Beta Fiber Glass. Paper presented at the NASA Conference on Materials for Improved Fire Safety (Houston, Tex.), May 1970.
2. SUPKIS, DANIEL E.: Development and Applications of Fluorel. Paper presented at the NASA Conference on Materials for Improved Fire Safety (Houston, Tex.), May 1970.
3. SAUERS, DALE G.: Development and Application of Flame-Resistant Polymers and Composites. Paper presented at the NASA Conference on Materials for Improved Fire Safety (Houston, Tex.), May 1970.
4. ANON: Apollo Spacecraft Nonmetallic Materials Requirements. MSC-PA-D-67-13, Feb. 1968.
5. KATSIKAS, C. J.; AND LEVINE, J. H.: Manned Spacecraft Nonmetallic-Materials Flammability Selection Criteria and Requirements. Paper presented at the NASA Conference on Materials for Improved Fire Safety (Houston, Tex.), May 1970.

END OF REFERENCE

165

Card #34

REFERENCE

166

RADNOFSKY, M. I.: NEW MATERIALS FOR MANNED SPACECRAFT, AIRCRAFT, AND OTHER APPLICATIONS. CONFERENCE ON MATERIALS FOR IMPROVED FIRE SAFETY. NASA SP-5096, 1971.

REFERENCE

NASA SP-5096
(N72-16409)

COPY 2

CONFERENCE ON MATERIALS FOR IMPROVED FIRE SAFETY

LEWIS RESEARCH CENTER
Aerospace Safety Research
and Data Institute

MANNED SPACECRAFT CENTER

HOUSTON, TEXAS

MAY 6–7, 1970

NATIONAL AERONAUTICS AND SPACE ADMINISTRATION

NASA SP-5096

CONFERENCE ON MATERIALS FOR IMPROVED FIRE SAFETY

MANNED SPACECRAFT CENTER
HOUSTON, TEXAS
MAY 6–7, 1970

Technology Utilization Office 1971
NATIONAL AERONAUTICS AND SPACE ADMINISTRATION
Washington, D.C.

NOTICE • This document was prepared under the sponsorship of the National Aeronautics and Space Administration. Neither the United States Government nor any person acting on behalf of the United States Government assumes any liability resulting from the use of the information contained in this document, or warrants that such use will be free from privately owned rights.

For sale by the Superintendent of Documents,
U.S. Government Printing Office, Washington, D.C. 20402
Price $2.25
STOCK NUMBER 3300 0390
Library of Congress Catalog Card Number 79-611768

CONTENTS

	Page
SESSION I—FLAMMABILITY REQUIREMENTS AND TEST TECHNIQUES	
The Combustion Process	3
Manned Spacecraft Nonmetallic-Materials Flammability Selection Criteria and Requirements	9
Development of Materials Screening Tests for Oxygen-Enriched Environments	23
Flammability Testing of Components	29
Flammability Tests for Apollo Command Module and Lunar Module Mockups	43
SESSION II—MATERIALS DEVELOPMENT	
Nonmetallic-Materials Development for Spacecraft Applications	57
Development and Applications of Fluorel	65
Development and Application of Flame-Resistant Polymers and Composites	73
Development of Nonflammable Potting Compounds for Spacecraft	83
New Materials for Manned Spacecraft, Aircraft, and Other Applications	91
The Performance of Lightweight Plastic Foams Developed for Fire Safety	103
Intumescence: An In Situ Approach to Thermal Protection	111
SESSION III—CONFIGURATION CONTROL AND MATERIALS APPLICATIONS	
Nonmetallic-Material Configuration Control in the Apollo Spacecraft	123
Apollo Spacecraft Nonmetallic Materials Applications	129
The Effects of Gravity on Flammability	137
Apollo Applications of Beta Fiber Glass	141
Apollo Space-Suit Materials	145
Fire Safety Design of a Mobile Quarantine Facility	151
Fire and Safety Materials Utilization at the John F. Kennedy Space Center	155
Fire Extinguishment in Hypobaric and Hyperbaric Environments	163
SESSION IV—SPECIAL TESTS	
Manned Spacecraft Electrical Fire Safety	173
Special Flammability Test Techniques	179
Specialized Testing and Evaluation of Space-Suit Materials	187
Development of an Oxygen Impact-Testing Method	191
Odor Test	203
Toxicology of Spacecraft Materials	207
Flammability Control in the Oxygen Environment of the Apollo Guidance and Navigation Equipment	211
GLOSSARY	219

New Materials for Manned Spacecraft, Aircraft, and Other Applications

MATTHEW I. RADNOFSKY

Manned Spacecraft Center

The NASA nonmetallic-materials development program has achieved a high degree of fire safety within the Apollo spacecraft. When properly adapted for other uses, many of the nonflammable and fire-resistant materials developed by NASA should make a significant contribution toward fireproofing aircraft and other interiors.

Although the overall objectives of fireproofing a spacecraft cabin are similar to those of fireproofing an aircraft interior, some significant differences merit consideration in the final selection of materials. The spacecraft crew bay contains a closed environment, while an aircraft cabin contains a ventilated, open environment. Therefore, considerations of odor and toxic offgassing are much more critical for spacecraft than for aircraft. In addition, manned spacecraft to date have operated in space with a 100-percent-oxygen atmosphere, while most aircraft operate with an air or mixed-air-and-oxygen atmosphere. This factor has severely limited the use of materials in spacecraft interiors because very few nonmetallic materials exist that will not burn in oxygen.

When materials for aircraft are selected, other considerations are of greater importance. Foremost among these considerations is durability. Because of the relatively short usage time in currently operational spacecraft, compromises have been made in this area in favor of improved fire safety. Functional utility for the duration of a single mission (with adequate margins) has been an acceptable criterion. However, nonmetallic materials that will withstand the rigors of repetitive usage are required for aircraft. With the advent of increasingly long space missions, the variation in durability criteria between aircraft and spacecraft lessens.

For the airlines, aesthetic considerations are almost as important as durability. To date, this factor has been of little concern in spacecraft-interior design. However, aesthetic considerations become important with increasingly long space missions.

While many of the fibrous materials used in the spacecraft cannot be dyed and are available only in white or varying shades of brown, methods of coloring fire-resistant fibers are being sought actively by industry. The applicability of many of the recently developed nonflammable and fire-retardant spacecraft materials for many commercial-aircraft items such as curtains, upholstery, carpets, decorative panels, cabinets, paper products, oxygen lines (and associated equipment such as masks), and straps is reviewed and discussed in this paper.

FIBROUS MATERIALS

Asbestos Fiber

Undoubtedly, the highest degree of nonflammability can be obtained with inorganic fibers such as asbestos and fiber glass. Asbestos, a natural mineral fiber, is not used in any exposed areas of the spacecraft, however, because of a tendency to shed particulate matter. This shedding is caused by the short staple length of the individual fibers,

TABLE XLV.—*Fabric-Characteristics Summary*

Fabric	Weight, oz/sq yd [a]	Combustion rate, in./sec						Physical				
		Air	10 psia 35 percent oxygen, 65 percent nitrogen	6.2 psia oxygen	16.5 psia oxygen	16.5 psia 60 percent oxygen, 40 percent nitrogen	Elongation, percent [b]	Breaking strength (warp), lb/in. [b]	Tear strength, g [c]	Wear resistance, number of cycles [d]	Folding endurance, number of cycles [e]	Stiffness, in/lb [f]
Nylon	6.9	[n] NA	NA	0.78	NA	NA	22	350	>6400	174	>5000	0.002
Beta 4190B	6.5	0	0	0	0	0	8.1	106	2400	148	>5000	.003
Beta 4484/Teflon	6.1	0	0	0	0	0	8.9	142	>6400	151	>5000	.003
Teflon—bleached T162-42	8.7	NA	0.29	.13	0.435	NA	67	59	5100	93	>5000	.0002
Teflon—natural	16.9	NA	NA	.21	.725	NA	56	172	5400	343	>5000	.002
Nomex (HT 90-40)	6 2	NA	.121	.63	1.00	NA	40	325	>6400	689	>5000	.001
Nomex—treated—$POCl_3Br_2$	7.3	NA	NA	.42	NA	NA	10	128	3000	353	>5000	.004
Polybenzimidazole—untreated	5.0	NA	NA	.003	.009	NA	20	149	4600	206	>5000	.004
Polybenzimidazole—treated—$POCl_3$	8.0	0	NA	0	NA	NA	60	188	>6400	234	>5000	.002
Polybenzimidazole—treated—$POCl_3Br_2$	5.9	NA	NA	.14	NA	NA	20	184	5700	721	>5000	.002
Durette (X-400)	6.2	NA	[p] SE	.31	.813	NA	30	138	5900	126	>5000	.0003
X-410	5.0	NA	SE	.29	NA	NA	14	200	3000	96	>5000	.001
X-420	5.6	NA	NA	.30	NA	NA	13.3	124	4100	93	>5000	.002
Nickel chromium (Karma cloth or Chromel-R)	18.0	0	0	0	0	0	NA	176	5400	869	>5000	.008
Fypro 5007/7	6.0	0	.29	.7	NA	0.8	24	154	3800	836	>5000	.003
Kynol fiber	NA	NA	.27 (SE)	.71 (SE)	NA	5.0 (SE)	20	[q] 1.7	NA	NA	>5000	NA

[a] Physical test method according to Federal Standard (FED STD) 191, method 5041.
[b] Physical test method according to FED STD 191, method 5104.
[c] Physical test method according to FED STD 191, method 5132.
[d] Physical test method according to FED STD 191, method 5302.
[e] Physical test method according to American Society for testing materials specification ASTM-D 2176.
[f] Physical test method according to FED STD 191, method 5202.
[g] Physical test method according to FED STD 191, method 5306 (C517 wheel).
[h] Physical test method according to FED STD 191, method 5304 (600-grit paper).
[i] Physical test method according to FED STD 191, method 5450.

characteristics						Outgassing						
Abrasion, number of cycles (g)	Abrasion, number of cycles (h)	Air permeability, $ft^3/ft^2/min$ (i)	Electrostatic charge, nanocoulombs (j)	Thermal conductivity, cal/sec-cm^2 (°C/cm) (k)	Sample thickness, in. (l)	Odor (m)	Carbon monoxide, μg/g	Total organics, μg/g	Cost, dollars	Availability	Supplier
2468	870	7.98	8.0	1.49×10^{-4}	0.0145	12	1.2	0.0003	3/yd	Commercial	Stern and Stern
198	85	.5	2.0	1.69×10^{-4}	.008	NA	NA	NA	6/yd	Commercial	Owens-Corning
125	1200	22.7	18.0	1.2×10^{-4}	.008 to .009	NA	NA	NA	10/yd	Available on special order	Owens-Corning
584	600	4.8	20.0	2.1×10^{-4}	.009	0.9	.7	34.0	30/yd	Commercial	NA
1075	1952	11.2	32.0	1.8×10^{-4}	.018	1.7	4.2	9.0	30/yd	Commercial	E. I. du Pont
943	260	4.9	8.0	1.58×10^{-4}	.013	7	.4	1.0	8/yd	Commercial	Stern and Stern
450	227	10.9	.06	1.6×10^{-4}	.014	NA	NA	NA	6/yd[o]	Experimental	Dynatech
629	143	98.5	40.0	3.0×10^{-5}	.0135	5	2.4	3.0	200/lb	Government use only	Celanese
2481	1651	26.9	2.6	3.2×10^{-5}	.017	NA	NA	NA	6/yd[o]	Experimental	Dynatech
1200	1500	38.7	2.4	4.8×10^{-5}	.014	NA	NA	NA	NA	Experimental	Monsanto
467	116	89.1	2.0	1.3×10^{-4}	.012	NA	3.7	0	25 to 50/yd	Being evaluated	Monsanto
145	65	28.9	18.0	1.8×10^{-4}	.0118	11	2.8	1.0	NA	Experimental	Monsanto
100	350	43.4	.01	2.0×10^{-4}	.013	NA	NA	NA	NA	Experimental	Monsanto
2034	977	68.8	0	NA	.010	NA	NA	NA	150 to 1500/lb	Available on special order	Fabric Research Laboratory
217	41	49	12	2.0×10^{-4}	.015	.7	4.0	1.0	6.50/yd	Commercial	Travis Mills
NA	NA	NA	NA	NA	NA	NA	NA	NA	5/lb	Commercial	Carborundum

[j] Physical test method according to Sweeney test method.
[k] Physical test method according to Cenco-Fitch test method.
[l] Physical test method according to FED STD 191, method 5030.
[m] Physical test method according to MSC specification MSC-PA-D-67-13; 2.5 or lower is acceptable.
[n] Not available.
[o] Treated.
[p] Self-extinguished.
[q] Breaking tenacity, g/denier.

TABLE XLIX.—*Characteristics of Fluorocarbon Elastomers*

Material	Combustion rate, in/sec [a]				Physical characteristics						
	10 psia 35 percent oxygen, 65 percent nitrogen	6.2 psia oxygen	16.5 psia oxygen	16.5 psia 60 percent oxygen, 40 percent nitrogen	Elongation, percent [b]	Tensile strength, psi [b]	Tear strength, lb/in. [c]	Embrittlement temperature, °F [d]	Specific gravity [e]	Durometer, Shore A [f]	Hydrogen permeability, l/m²/24 hr [g]
Fluorel 1059 L-23171-1	[i] NA	[i] SE	NA	NA	210	2045	122	NA	1.99	71	NA
Fluorel 1071	NA	NA	SE	NA	200	1370	55	−50	2.03	55	NA
Fluorel 1076	NA	SE	SE	NA	350	1250	77	−85	1.97	45	NA
Fluorel 1079K	NA	SE	[i] 0.040	NA	300	1523	75	−90	2.02	49	NA
Fluorel L-3203-6	NA	NA	SE	NA	75	1558	128	NA	2.11	97	NA
Fluorel L-3251-3	NA	SE	SE	NA	75	1820	61.5	NA	2.08	96	NA
Fluorel L-3203-6 RL 3550, 25 percent asbestos.	NA	NA	SE	NA	25	100	128	NA	1.94	97	NA
Viton 238-12-1	NA	[i] SE	[i] .030	NA	NA	613	NA	NA	NA	NA	NA
Viton 238-26-1	NA	0.016	[i] .025	SE	230	800 to 1240	95	[m] −65	2.11	57	NA
Viton 238-97-1 on Beta	NA	.037	NA	NA	NA	NA	NA	NA	NA	NA	NA
Viton 238-46-1	NA	NA	.016	NA	NA	NA	NA	NA	NA	NA	NA
Viton 238-46-2	[i] SE	[i] SE	[i] SE	NA	500	1587	156.2	−222	2.0	70	0
Viton 238-98-1 [n]	NA	[i] SE	NA	NA	70	765	NA	NA	NA	[o] 50	NA
Viton 238-99-1 [p]	NA	[i] SE	[i] SE	NA	NA	NA	NA	NA	NA	[q] 40	NA
Viton DR-8380	NA	[i] SE	.016	NA	400	1720	140.0	−50	NA	82	0
Carboxy nitroso rubber	[r] NI	NI	NI	NI	NA	NA	NA	NA	NA	NA	NA
Polyquinoxaline, laminated	NA	SE	.007	SE	NA	1700	NA	−323	NA	NA	NA
Fluorinated urethane	NA	NA	NA	SE	NA	NA	NA	NA	1.87	100	NA
Polyimide laminate	NA	NA	NI	NA	NA	5200	NA	NA	1.75	NA	NA

[a] Tissue ignitor. All listed materials are nonflammable in air.
[b] Physical test method according to American Society for Testing Materials (ASTM) standard D 412.
[c] Physical test method according to ASTM standard 624.
[d] Physical test method according to MSC test method.
[e] Physical test method according to FED STD 601, method 14011.
[f] Physical test method according to ASTM standard D 2240.
[g] Physical test method according to ASTM standard D 815.
[h] Physical test method according to FED STD 191, method 5030.
[i] Not available.

Physical characteristics		Outgassing						
Shrinkage, percent (d)	Sample thickness, in. (h)	Odor	Carbon monoxide, μg/g	Total organics, μg/g	Cost, dollars	Application	Availability	Supplier
NA	0.070	1.3	2.7	1.0	2000/lb	Hoses and headrests	Commercial	Mosites Rubber, Raybestos-Manhattan.
3.3 (k4.4)	.075	1.4	.9	1.0	3750/lb	Tubes and hoses	Commercial	Mosites Rubber.
3.7 (k4.6)	.080	.4	.5	1.0	3750/lb	Tubes and hoses	Commercial	Mosites Rubber.
6 (k6)	.069	1.2	.4	1.0	3750/lb	Tubes and hoses	Commercial	Mosites Rubber.
NA	NA	1.0	.7	1.0	2220/lb	Nonflammable coatings	Commercial	Raybestos-Manhattan.
NA	NA	1.2	1.3	3.0	2220/lb	Boot soles (softer than L-3203-6)	Commercial	Raybestos-Manhattan.
NA	NA	NA	NA	NA	130.39/gal	Fireproof coating	Commercial	Raybestos-Manhattan.
0	.125	.8	.4	0	NA	Tubing, hoses, and molded parts	Commercial	E. I. du Pont
0	.125	.9	.4	0	19.35/lb	Tubing, hoses, and molded parts	Commercial	E. I. du Pont
NA	NA	NA	NA	NA	NA	Fireproof coating	Commercial	E. I. du Pont
NA	NA	NA	NA	NA	NA	Tubing, hoses, and molded parts	Commercial	E. I. du Pont
NA	.125	.5	.4	0	37.10/lb	Tubing, hoses, and molded parts	Commercial	E. I. du Pont
NA	.0055	NA	NA	NA	NA	Fireproof coating	Commercial	E. I. du Pont
NA	NA	NA	NA	NA	NA	Conformal coating	Commercial	E. I. du Pont
NA	.125	1.0	.6	.4	NA	Extruded elastomer	Commercial	Detroit Rubber
NA	NA	2.7	1.0	24.0	500/lb[s]	Nonflammable, solvent-resistant elastomer	Not currently being produced	Thiokol Chemical
NA	.125	NA	NA	NA	900/gal	Structural composite	Commercial	Narmco Research and Development Division, Whittaker Corp.
NA	NA	.6	8.0	89.0	1800/lb[s]	Flame-resistant, flexible adhesive	NASA contracts only	Narmco Research and Development Division, Whittaker Corp.
NA	.125	NA	NA	NA	5.97/sq yd	Structural composite.	Commercial	E. I. du Pont

[j] Self-extinguished.
[k] With grain.
[l] Silicone ignitor.
[m] Centigrade.
[n] Stability (viscosity 50 cP)—no change in 14 days.
[o] Shore D.
[p] Stability—no change in 14 days.
[q] Shore C.
[r] No ignition.
[s] Approximate.

END OF REFERENCE

166

REFERENCE

167

JOHNSON, J. E.; AND WOODS, F. J.: FLAMMABILITY IN UNUSUAL ATMOSPHERES, PART II - SELECTED MATERIALS IN OXYGEN-NITROGEN AND OXYGEN-HELIUM MIXTURES AT PRESSURES UP TO 315 PSIA. NRL-6606, NAVAL RESEARCH LABORATORY, 1967. (AVAILABLE FROM DDC AS AD-823059L.)

THIS MATERIAL HAS BEEN APPROVED FOR PUBLICATION PER LETTER FROM JAMES E. SULLIVAN, NAVAL RESEARCH LABORATORY TO JOANNE FOLK DATED SEPT. 13, 1974.

NRL Report 6606

Flammability in Unusual Atmospheres
Part 2 - Selected Materials in Oxygen-Nitrogen and Oxygen Helium Mixtures at Pressures up to 315 PSIA

LEWIS RESEARCH CENTER
Aerospace Safety Research
and Data Institute
NOV 20 1974
CLEVELAND, OHIO

September 22, 1967

NAVAL RESEARCH LABORATORY
Washington, D.C.

SEE INSIDE OF COVER FOR DISTRIBUTION RESTRICTIONS

Each transmittal of this document outside the agencies of the U.S. Government must have prior approval of Director, Naval Research Laboratory, Washington, D.C. 20390.

PREVIOUS REPORT IN THIS SERIES

"Flammability in Unusual Atmospheres, Part 1—Preliminary Studies of Materials in Hyperbaric Atmospheres Containing Oxygen, Nitrogen and/or Helium," J. E. Johnson and F. J. Wooda, NRL Report 6470, Oct. 5[illegible], 1966

NRL Report 6606

Flammability in Unusual Atmospheres
Part 2 - Selected Materials in Oxygen-Nitrogen and Oxygen Helium Mixtures at Pressures up to 315 PSIA

F. J. Woods and J. E. Johnson

Fuels Branch
Chemistry Division

September 22, 1967

NAVAL RESEARCH LABORATORY
Washington, D.C.

Table 6
Combustion of High Temperature Nylon (Nomex) in Mixtures
Containing 41% Oxygen

Total Pressure (psia)	Warp Direction				Fill Direction			
	41% O_2/N_2		41% O_2/He		41% O_2/N_2		41% O_2/He	
	Ignition Delay (sec)	Burn Rate (cm/sec)	Ignition Delay (sec)	Burn Rate (cm/sec)	Ignition Delay (sec)	Burn Rate (cm/sec)	Ignition Delay (sec)	Burn Rate (cm/sec)
15	10.0	0.64	22.4	0.54	12.0	0.52	24.6	0.48
65	5.1	1.02	24.0	0.89	-	-	22.2	0.79
115	5.8	1.87	18.0	1.76	6.8	1.43	15.8	1.04
215	5.0	3.2	15.0	2.31	-	-	-	-
315	4.2	5.77	14.9	2.82	-	-	8.9	1.58

Only two instances of the effect of helium versus nitrogen as the inert gas in the flammability of solid materials have been found (10,12) other than that from this Laboratory (6). Klein (12) concluded that the burning rate of cotton cloth in atmospheres of oxygen and helium differs very little from atmospheres of oxygen and nitrogen at pressures of 0.5 atm. or less. Huggett, et al. (10), concluded that nitrogen is more effective than helium in reducing flame spread rate (at 760 mm Hg and less). In our earlier work (6) it was observed that "most of the materials tested had a decidedly greater burning rate in the helium mixtures than in nitrogen mixtures." In the present work this statement can still be made (Fig. 9), but in one important case shown in Fig. 10, high temperature nylon (FM-9) burned much faster in 41% O_2/N_2 than in 41% O_2/He. This case is discussed in more detail in the next section of this report.

EFFECT OF THE NATURE OF THE MATERIAL

The first report of this series (6) clearly indicated that materials vary in their degree of flammability — from highly flammable (easily ignitable and fast burning) to nonflammable under the test conditions. However, the effect of variables, such as pressure and diluent, on flammability is influenced by the nature of the material being studied. The following studies will confirm these facts.

A temperature-resistant nylon (FM-9) was studied in 41% O_2 mixtures in both nitrogen and helium up to total pressures of 315 psia. The data are given in Table 6 and a comparative plot in Fig. 10 shows increased burning rates for Nomex nylon in 41% O_2/N_2 over helium. In contrast with this data Fig. 6 shows that filter paper burned faster in 41% O_2/He than in 41% O_2/N_2.

In Fig. 11 a plot is made comparing rates for Nomex and the filter paper (FM-1) in 41% O_2/N_2. This graph shows that Nomex burned much faster than filter paper in this atmosphere at higher pressures. For example, at 315 psia Nomex burned about four times as fast as the filter paper. The significance of this difference is underscored by the fact that Nomex would not burn in ordinary air (21% O_2) even at 315 psia, whereas the filter paper ignited readily in air at pressures as low as 8 psia. The differences in pyrolysis rates between Nomex nylon and paper under various conditions probably account for their different flammability behavior. Plans have been made to study this phase of the work in more detail.

END OF REFERENCE

167

REFERENCE

168

NOTARDONATO, J. J.; BURKHARD, L. A.; AND COCHRAN, T. H.: EFFECTS OF PRESSURE, OXYGEN CONCENTRATION, AND FORCED CONVECTION ON THE FLAME SPREAD RATE OF PLEXIGLASS, NYLON, AND TEFLON. NASA TN D-7555, 1974.

NASA TECHNICAL NOTE

NASA TN D-7555

NASA TN D-7555

EFFECTS OF PRESSURE, OXYGEN CONCENTRATION, AND FORCED CONVECTION ON FLAME SPREAD RATE OF PLEXIGLAS, NYLON, AND TEFLON

by Julius J. Notardonato, Leo A. Burkhardt, and Thomas H. Cochran

Lewis Research Center
Cleveland, Ohio 44135

NATIONAL AERONAUTICS AND SPACE ADMINISTRATION • WASHINGTON, D. C. • FEBRUARY 1974

1. Report No.	2. Government Accession No.	3. Recipient's Catalog No.
NASA TN D-7555		

4. Title and Subtitle	5. Report Date
EFFECTS OF PRESSURE, OXYGEN CONCENTRATION, AND FORCED CONVECTION ON FLAME SPREAD RATE OF PLEXIGLAS, NYLON, AND TEFLON	February 1974
	6. Performing Organization Code
7. Author(s) Julius J. Notardonato, Leo A. Burkhardt, and Thomas H. Cochran	8. Performing Organization Report No. E-7611
	10. Work Unit No. 502-28
9. Performing Organization Name and Address Lewis Research Center National Aeronautics and Space Administration Cleveland, Ohio 44135	11. Contract or Grant No.
	13. Type of Report and Period Covered Technical Note
12. Sponsoring Agency Name and Address National Aeronautics and Space Administration Washington, D.C. 20546	14. Sponsoring Agency Code

15. Supplementary Notes

16. Abstract

Experiments were conducted in which the burning of cylindrical materials in a flowing oxidant stream was studied. Plexiglas, nylon, and Teflon fuel specimens were oriented such that the flames spread along the surface in a direction opposed to the flowing gas. Correlations of flame spread rate were obtained that were power law relations in terms of pressure, oxygen concentration, and gas velocity.

17. Key Words (Suggested by Author(s))	18. Distribution Statement
Polymeric Combustion Flame spread rate Oxygen safety	Unclassified - unlimited Cat. 33

19. Security Classif. (of this report)	20. Security Classif. (of this page)	21. No. of Pages	22. Price*
Unclassified	Unclassified	26	$3.00

* For sale by the National Technical Information Service, Springfield, Virginia 22151

TABLE I. - EFFECTS OF PRESSURE ON

FLAME SPREAD RATE

[Oxygen concentration, 1.0 mole fraction.]

Fuel	Test	Gas velocity, cm/sec	Gas pressure, atm	Average flame spread rate, cm/sec
Plexiglas	1	21	1.0	1.32
	2	16	3.3	2.29
	3	16	6.8	3.64
	4	16	6.8	3.78
	5	18	21.8	8.50
	6	16	47.8	17.00
	7	16	75.2	25.20
	8	16	6.8	2.78
Nylon	1	25	1.0	0.50
	2	16	3.6	.96
	3	↓	6.9	1.57
	4		6.9	1.46
	5		6.7	1.39
	6		20.6	2.41
	7	18	20.6	2.83
	8	20	34.3	5.29
	9	16	34.9	3.25
	10	↓	34.6	4.21
	11		35.4	3.04
	12		47.8	9.48
	13		62.4	8.21
	14		75.4	8.51
Teflon	1	17	6.6	0.03
	2	16	20.9	.35
	3	16	34.2	.47
	4	15	35.1	.24
	5	16	34.4	.35
	6	16	47.8	.25
	7	15	61.9	.66
	8	14	75.2	.71

TABLE II. - EFFECTS OF OXYGEN CONCENTRATION ON FLAME SPREAD RATE

Fuel	Test	Gas velocity, cm/sec	Gas pressure, atm	Oxygen concentration, mole fraction	Average flame spread rate, cm/sec
Plexiglas	9	13	6.8	0.905	2.55
	10	15	7.3	.824	2.54
	11	16	7.1	.738	1.75
	12	13	6.8	.579	1.83
	13	14	6.8	.351	.77
	14	14	6.8	.239	.30
Nylon	15	21	6.6	0.943	1.37
	16	14	7.5	.892	1.07
	17	16	7.5	.808	.93
	18	16	6.6	.717	.70
	19	16	6.6	.600	.66
	20	14	7.2	.552	.67
	21	16	6.6	.324	.24
Teflon	9	13	7.4	0.905	0.01
	10	15	7.1	.824	.01
	11	15	7.4	.695	(a)
	12	15	6.9	.583	(a)
	13	13	6.9	.526	(a)

[a]No flame propagation apparent in these tests.

TABLE III. - EFFECTS OF GAS VELOCITY ON FLAME SPREAD RATE

[Oxygen concentration, 1.0 mole fraction.]

Fuel	Test	Gas velocity, cm/sec	Gas pressure, atm	Average flame spread rate, cm/sec
Plexiglas	15	15	6.8	2.86
	16	33	6.6	4.27
	17	67	6.6	5.69
	18	161	6.6	6.34
	19	305	6.8	4.16
	20	701	7.1	.89
	21	884	7.1	.34
	22	146	6.8	5.90
	23	17	21.1	9.29
	24	23	21.6	8.13
	25	49	19.7	13.54
	26	111	21.4	13.54
	27	167	21.4	14.78
	28	405	19.9	4.64
	29	14	35.1	11.61
	30	28	33.7	16.25
	31	52	34.7	15.48
	32	113	36.0	19.12
	33	176	35.7	18.10
	34	300	34.7	15.48
	35	15	66.9	25.60
	36	28	68.9	29.56
	37	28	68.6	21.67
	38	60	69.9	29.56
	39	130	68.8	46.45
	40	157	68.6	36.12
Nylon	22	36	6.6	2.37
	23	79	6.6	2.43
	24	149	7.2	2.88
	25	305	6.9	1.54
	26	589	6.8	.93
	27	853	6.9	.19
	28	137	6.8	1.39
	29	128	6.9	1.46
	30	18	21.2	4.58
	31	27	21.2	3.92
	32	48	19.7	6.00
	33	116	21.4	5.00
	34	170	21.7	6.50
	35	275	21.9	2.62
	36	404	19.9	9.94
	37	14	34.6	6.25
	38	28	33.7	7.56
	39	52	34.9	5.80
	40	111	36.0	11.61
	41	174	35.7	10.84
	42	301	34.2	19.12
	43	14	67.9	9.03
	44	28	69.1	13.00
	45	58	69.9	20.32
	46	119	67.9	20.32
	47	158	68.4	40.64
Teflon	14	27	21.6	0.13
	15	49	19.7	.09
	16	112	21.4	.08
	17	14	35.6	.23
	18	28	33.7	.17
	19	53	35.2	.17
	20	113	36.0	.16
	21	174	36.3	.36
	22	14	67.3	.63
	23	28	69.4	.44
	24	59	70.1	.24
	25	127	68.4	.50
	26	155	68.6	.37

TABLE IV. - EFFECTS OF PRESSURE ON MASS CONSUMPTION RATE

[Gas velocity, 16 cm/sec; oxygen concentration, 1.0 mole fraction.]

Fuel	Test	Gas pressure, atm	Mass consumption rate, g/sec
Teflon	1	8.0	0.165
	2	36.5	.265
	3	70	.365
Nylon	1	8.0	0.120
	2	36.5	.125
	3	70	.195

END OF REFERENCE

168

REFERENCE

169

NEUSTEIN, R. A.; MADER, P. P.; COLOMBO, G. V.; AND RICHARDSON, D. E.: THE EFFECT OF ATMOSPHERE SELECTION AND GRAVITY ON BURNING RATE AND IGNITION TEMPERATURE. McDONNELL DOUGLAS REPORT DAC-62431, OCTOBER 1968. (N70-10589).

THIS REFERENCE IS MATERIAL THAT IS READILY AVAILABLE AND THEREFORE THE CONTENTS HAVE NOT BEEN REPRODUCED.

END OF REFERENCE

169

REFERENCE
170

WHITAKER, D. H.: EFFECTS OF ACCELERATION UPON COMBUSTION RATE TEST, NOMEX STANDARD CLOTH. REP. TF-WSTF-111A, WHITE SANDS TEST FACILITY. (AVAILABLE AS CR-129442), 1967.

THIS REFERENCE HAS A LIMITED DISTRIBUTION AND MAY NOT BE REPRODUCED.

END OF REFERENCE

170